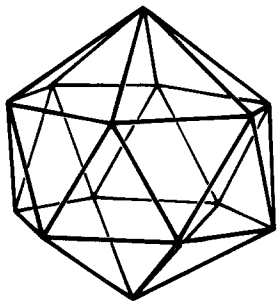

POLYHEDRON

The International Journal for Inorganic and Organometallic Chemistry

Founding Editor
Sir Geoffrey Wilkinson

Executive Editors
G. Christou
C. E. Housecroft

PERGAMON

POLYHEDRON

Aims and Scope

Polyhedron will publish original, fundamental, experimental and theoretical work of the highest quality in the major areas of inorganic and organometallic chemistry. These areas include synthetic and reaction chemistry, kinetics and mechanisms of reaction, bioinorganic chemistry, photochemistry and the use of metal and organometallic compounds in stoichiometric and catalytic synthesis of organic compounds. Papers concerned solely with stability constants determined by potentiometric titration data unsupported by other e.g. spectroscopic techniques will not be acceptable nor will solvent extraction data unless supported by other data of interest to inorganic chemists.

Back Issues: Back issues of all previously published volumes are available direct from Elsevier Science offices (Oxford and New York). Complete volumes and single issues can be purchased for 1991–1997. Earlier issues are available in high quality photo-duplicated copies as complete volumes only. Back volumes on microfilm are available from UMI, 300 North Zeeb Road, Ann Arbor, MI 48106, U.S.A.

Copyright © 1998 Elsevier Science. All rights reserved
This journal and the individual contributions contained in it are protected by the copyright of Elsevier Science, and the following terms and conditions apply to their use:

Photocopying. Single photocopies of single articles may be made for personal use as allowed by national copyright laws. Permission of the publisher and payment of a fee is required for all other photocopying, including multiple or systematic copying, copying for advertising or promotional purposes, resale, and all forms of document delivery. Special rates are available for educational institutions that wish to make photocopies for non-profit educational classroom use.

In the U.S.A., users may clear permissions and make payment through the Copyright Clearance Center Inc., 222 Rosewood Drive, Danvers, MA 01923, U.S.A. In the U.K., users may clear permissions and make payment through the Copyright Licensing Agency Rapid Clearance Service (CLARCS), 90 Tottenham Court Road, London W1P 9HE, U.K. In other countries where a local copyright clearance centre exists, please contact it for information on required permissions and payments.

Derivative Works. Subscribers may reproduce tables of contents or prepare lists of articles including abstracts for internal circulation within their institutions. Permission of the publishers is required for resale or distribution outside the institution. Permission of the publisher is required for all other derivative works, including compilations and translations.

Electronic Storage. Permission of the publisher is required to store electronically any material contained in this journal, including any article or part of an article. Contact the publisher at the address indicated.

Except as outlined above, no part of this publication may be reproduced, stored in a retrieval system or transmitted in any form or by any means, electronic, mechanical, photocopying, recording or otherwise, without prior written permission of the publisher.

Disclaimer. No responsibility is assumed by the Publisher for any injury and/or damage to persons or property as a matter of products liability, negligence or otherwise, or from any use or operation of any methods, products, instructions or ideas contained in the material herein.

Although all advertising material is expected to conform to ethical standards, inclusion in this publication does not constitute a guarantee or endorsement of the quality or value of such product or of the claims made of it by its manufacturer.

♾™ The paper in this publication meets the minimum requirements of American National Standard for Information Sciences—Permanence of Paper for Printed Library Materials, ANSI Z39.48-1984.

The Item-fee Code for this publication is: 0277–5387/98 $19.00 + 0.00

ContentsDirect, the ***free*** e-mail alerting service, delivers the table of contents for this journal directly to your PC, prior to publication. The quickest way to register for **ContentsDirect** is via the Internet at: **http://www.elsevier.nl/locate/ContentsDirect.** If you don't have access to the Internet you can register for this service by sending an e-mail message to cdsubs@ elsevier.co.uk— specifying the title of the publication you wish to register for.

Pergamon

Polyhedron Vol. 17, Nos. 13–14, p. iii, 1998
Elsevier Science Ltd. Printed in Great Britain

CONTRIBUTORS TO THIS ISSUE

(Chief Author's name(s) in bold)

Almond, M. J. 2301
Alyea, E. C. 2231
Amador, U. 2373
Araya, E. 2225
Atherton, Z. 2257
Atwood, D. A. 2237
Baenziger, N. C. 2379
Balmaseda, J. 2353
Banerjee, P. 2313
Baricelli, P. 2289
Barquín, M. 2373
Basuli, F. 2191
Batt, R. V. 2173
Belokon, A. I. 2309
Bennett, W. E. 2379
Benzo, F. 2295
Bergman, J. 2153
Bhattacharya, S. 2191, 2313
Bian, G.-q. 2267
Bridgeman, A. J. 2279
Brown, K. L. 2213
Bullivant, D. P. 2173
Cancela, J. 2373
Cardin, C. J. 2301
Casas, J. S. 2249
Castellano, E. E. 2249
Cheng, S. 2213
Chen, X. 2271
Chen, Y.-T. 2363
Chiu, H.-T. 2187
Chuang, S.-H. 2187
Clifford, T. 2167
Connolly, J. 2331
Dai, J. 2267
Díaz, C. 2225
Ding, M. 2327
Dinjus, E. 2199
Doyle, J. R. 2379
Drew, M. G. B. 2301
Dutta, A. 2313
Edwards, D. A. 2321
Elkington, K. E. 2173
Ferguson, G. 2231
Fernandez-Bertran, J. 2353
Gao, S. 2243
García-Tasende, M. S. 2249
González Garmendia, M. J. 2373
Gelling, A. 2141
Genge, A. R. J. 2331
Görls, H. 2199
Gomez, A. 2353
Goodgame, D. M. L. 2257
Guerrero, J. 2289
Gu, Z.-X. 2363
Hay, R. W. 2167, 2337
Hibbs, D. E. 2141
Hill, M. S. 2237
Hill, S. E. 2173
Hilton, J. 2173
Hoskins, G. M. 2321
Houghton, T. J. 2173
Hovell, M. 2173
Hursthouse, M. B. 2141
Kannan, S. 2231
Katahira, D. A. 2257
Kessler, V. G. 2309
Kiss, E. 2167
Kivekäs, R. 2153
Kuchta, L. 2161
Kuroda-Sowa, T. 2207, 2267
Laitalainen, T. 2153
Lee, G.-H. 2187
Lin, H.-K. 2363
Lin, Y. 2327
Liu, Q. 2327
Li, B. 2243
Loechel, C. 2167
Luo, X. 2271
Maekawa, M. 2207, 2267
Mahon, M. F. 2321
Malik, K. M. A. 2141
Marek, J. 2161
Marques, H. M. 2213
Mendoza, C. 2295
Menzer, S. 2257
Miller, S. 2337
Molloy, K. C. 2321
Morris, S. 2301
Moya, S. A. 2289
Munakata, M. 2207, 2267
Muñoz-Hernández, M.-A. 2237
Nikitin, K. V. 2309
O'Donnell, P. S. 2379
Orrell, K. G. 2141
Osborne, A. G. 2141
Palaniandavar, M. 2179
Pardey, A. J. 2289
Pastene, R. 2289
Patel, B. 2345
Peng, S.-M. 2187
Peng, S.-M. 2191
Pope, S. J. A. 2331, 2345
Queirolo, M. 2295
Quintana, G. 2353
Quintanilla, J. 2373
Reguera, E. 2353
Reid, G. 2331, 2345
Rice, D. A. 2301
Rudolph, G. R. G. 2321
Sánchez, A. 2249
Santa Ana, M. A. 2225
Schwendt, P. 2161
Sienra, B. 2295
Šik, V. 2141
Soboroff, D. M. 2379
Song, Y. 2271
Sordo, J. 2249
Suenaga, Y. 2207
Sundberg, M. R. 2153
Su, X.-C. 2363
Švančárek, P. 2161
Thomas, K. R. J. 2179
Tsai, C.-E. 2187
Uggla, R. 2153
Velusamy, M. 2179
Vidarte, M. J. 2249
Wallwork, S. C. 2173
White, A. J. P. 2257
Williams, D. J. 2257
Xing, Y. 2327
Xu, Q.-f. 2267
Yi, T. 2243
Zevaco, T. A. 2199
Zhou, S. 2271
Zhou, Z.-F. 2363
Zhu, L. 2271
Zhu, S.-R. 2363
Zubavichus, Y. 2301

Pergamon

Polyhedron Vol. 17, Nos. 11–12, p. iii, 1998
Elsevier Science Ltd. Printed in Great Britain

CONTRIBUTORS TO THIS ISSUE

(Chief Author's name(s) in bold)

Ahlgrén, M. 2073
Akbar Ali, M. 1803
Alvarez, B. 2029
Balema, V. P. 2087
Batista, A. A. 2013
Becker, U. 1983
Beddoes, R. L. 1997
Beynek, N. 2137
Blake, A. J. 1897
Bodini, M. E. 2109
Boyle, T. J. 1959
Bryan, J. C. 1803
Buschmann, H.-J. 1891
Butcher, R. J. 1803, 2037
Cano, M. 2115
Castellano, E. E. 2013
Chattopadhyay, S. K. 1897
Chen, X.-F. 1883
Choi, K.-Y. 1975
Chung, C.-S. 2127
Clegg, W. 1923
Cocco, M. T. 2065
Coe, B. J. 1997
Copia, G. E. 2109
Dantz, D. A. 1891
Darkwa, J. 1811
Dean, P. A. W. 1937
de Oliveira, L. A. A. 2013
del Valle, M. A. 2109
Dou, J.-M. 1877
Duan, C.-Y. 1883
Dunbar, K. R. 2049
Edelmann, F. T. 2043
Fabrizi de Biani, F. 1795
Fernández, E. J. 2029
Ferreira, A. G. 2013
Fraser, I. 1931
Fukushima, Y. 1943
Ghosh, S. 1897
Gimeno, M. C. 2029
Glidewell, C. 1795
Govan, N. 2079
Guillaumont, R. 1991
Haiduc, I. 2043
Han, Y. 2095
Hay, R. W. 1931, 2079
Hennig, L. 2087
Heras, J. V. 2115
Hey-Hawkins, E. 2087
Hirohata, M. 1943
Holah, D. G. 2101
Horsburgh, L. 1923
Hossain, M. 1897
Hu, C.-H. 1877
Huang, X.-Y. 1863
Hughes, A. N. 2101
Ibers, J. A. 2105
Ibrahim, N. E. H. 1803
Ionova, G. 1991
Jain, V. K. 2037
James, M. 1843
Jasinski, J. M. 1803
Jasinski, J. P. 1803
Jezierska, J. 1831
Jiang, Z.-H. 1953
Jin, R.-S. 1877
Jones, P. G. 2029
Kai, F. 1943
Kashiwabara, K. 1817
Kawaguchi, H. 1843
Koenig, J. 1795
Kroczewska, D. 1831
Kura, G. 1907
Kurzak, B. 1831
Laguna, A. 2029
Lahiri, G. K. 1913
Lai, C.-Y. 2127
Lan, W.-J. 2127
Li, **W.** 1877
Liao, D.-Z. 1953
Lin, S.-T. 2021
Liu, **Q.** 1863
Liu, S.-H. 1883
López-de-Luzuriaga, J. M. 2029
Longridge, J. J. 1871
Lundeen, C. 2101
Ma, J. 1883
Madic, C. 1991
Magnuson, V. R. 2101
Magull, J. 1983
Maji, M. 1897
Marsh, S. J. 1795
Matsumoto, N. 1943
Matsumoto, T. 1943
McDonald, C. I. 1997
McPartlin, M. 2137
Mimura, M. 1943
Min, N.-B. 1883
Miyazaki, Y. 1907
Monge, A. 2115
Mulvey, R. E. 1923
Munshi, P. 1913
Murphy, B. P. 2137
Nakajima, K. 1817
Narayan, S. 2037
Noltemeyer, M. 2043
Onnis, V. 2065
Ovejero, P. 2115
Pakkanen, T. A. 2073
Pakkanen, T. T. 2073
Pedrotty, D. M. 1959
Pinilla, E. 2115
Pink, M. 2087
Ponticelli, G. 2065
Rawson, J. M. 1871
Ross, M. J. 1923
Rowlings, R. B. 1923
Ruiz, F. A. 2115
Sakamoto, J. 1907
Samanta, R. 1913
Scheer, M. 1983
Schmidt, H.-G. 2043
Schollmeyer, E. 1891
Scott, B. 1959
Scowen, I. J. 2137
Shen, Q. 2009
Shen, H.-Y. 1953
Sheu, R.-S. 2021
Sieler, J. 2087
Silvestru, C. 2043
Smith, D. M. 2105
Soimasuo, M. 2073
Soto, C. 2109
Spanu, A. 2065
Spiccia, **L.** 1851
Sun, B.-W. 1953
Sun, J. 2009
Sun, J.-S. 2049
Sunatsuki, Y. 1943
Suzuki, T. 1817
Taguchi, N. 1817
Takagi, H. D. 1817
Tan, X. S. 2095
Tang, W. X. 2095
Tatsumi, K. 1843
Thomas, M. S. 1811
Uzelmeier, C. E. 2049
Vittal, J. J. 1937
Wang, C. 2127
Wang, G.-L. 1953
Wang, H.-G. 1953
Wang, Y.-J. 2021
Wang, Y.-M. 2021
Ward, D. L. 2049
Wei, J.-D. 1877
West, B. O. 1851
Wilson, V. 1923
Wohnrath, K. 2013
Xiang, D. F. 2095
Xu, Y.-H. 1883
Xu, Z. 1863
Yan, S.-P. 1953
Yao, H.-J. 1877
Yao, X.-K. 1953
You, X.-Z. 1863, 1883
Yuan, **F.** 2009
Yu, K. B. 2095
Zanello, P. 1795
Zhang, Q. 1851
Zhang, S. W. 2095
Zheng, P.-J. 1877
Ziller, J. W. 1959
Zou, J.-Z. 1863
Zukerman-Schpector, J. 2013

Pergamon

Polyhedron Vol. 17, No. 10, p. iii, 1998
Elsevier Science Ltd. Printed in Great Britain

CONTRIBUTORS TO THIS ISSUE

(Chief Author's name(s) in bold)

Andruh, M. 1787
Aravamudan, G. 1659
Banerjee, R. 1693
Baricelli, P. J. 1621
Bastida, R. 1759
Bélanger-Gariépy, F. 1747
Benvenutti, E. V. 1627
Beyer, L. 1601
Bhattacharya, A. K. 1693
Bolos, C. A. 1779
Buffy, J. J. 1791
Cimpoesu, M. 1787
Cingolani, A. 1677
Crespo, M. 1651
Cruywagen, J. J. 1741
de Blas, A. 1759
Ding, **L.** 1725
D'Olieslager, J. 1773
Drozdov, A. 1677
Faure, R. 1747
Fenton, D. E. 1759
Fleming, J. S. 1705
Font-Bardía, M. 1651, 1735
Fraser, I. 1611
Fronczek, F. R. 1617
Fun, H.-K. 1659
Garland, M. T. 1729
Ghosh, B. K. 1735
Gilliams, B. 1773
Glowiak, T. 1767
Görller-Walrand, C. 1773
Goeminne, A. M. 1715
Goldberg, I. 1659
Granifo, J. 1729
Hatzidimitriou, A. 1779
Hay, R. W. 1611
Herman, G. G. 1715
Heyns, J. B. B. 1741
Hong, F.-E. 1643
Hueso-Ureña, F. 1747
Isovitsch, R. A. 1617
Itoh, H. 1637
Ito, S. 1637
Jeffery, J. C. 1705
Klička, R. 1631
Koe, J. R. 1791
Koman, M. 1767
Kumar, R. K. 1659
Kumar, S. R. 1699
Leadbeater, N. E. 1755
Lewis, J. 1755
Liao, F.-L. 1643
Lippens, W. 1715
Longo, C. 1621
Lopez, F. 1621
Macías, A. 1759
Maji, D. 1693
Mann, K. L. V. 1705
Marchetti, F. 1677
Maverick, A. W. 1617
McCleverty, J. A. 1705
Mediavilla, M. 1621
Melník, **M.** 1767
Mondal, A. B. 1693
Monfort, M. 1735
Moreno-Carretero, M. N. 1747
Moronta, D. 1621
Moya, S. A. 1621
Nishida, Y. 1637
Nishino, S. 1637
Ohba, S. 1637
Owen, N. C. 1611
Pardey, A. J. 1621
Pauwels, T. F. 1715
Pettinari, C. 1677
Pillai, P. K. 1699
Pineda, D. 1621
Platas, C. 1759
Powell, D. R. 1791
Psillakis, E. 1705
Raithby, P. R. 1755
Rennie, M.-A. 1755
Resino, I. 1735
Ribas, J. 1735
Rodríguez-Blas, T. 1759
Rodríguez-Navarro, J. A. 1747
Rodríguez, A. 1759
Rohwer, E. A. 1741
Salas-Peregrín, J. M. 1747
Schoutens, K. 1773
Seidelman, O. 1601
Seshasayee, M. 1659
Šindelář, Z. 1631
Sivakumar, K. 1659
Smékal, Z. 1631
Solans, X. 1651, 1735
Stager, C. V. 1787
Stanica, N. 1787
Sun, S.-Y. 1643
Thornton, P. 1631
Troyanov, S. I. 1677
Vega, A. 1729
Wang, S.-L. 1643
Ward, M. D. 1705
Warrier, K. G. K. 1699
West, R. 1791
Wu, Y. J. 1725
Zawislak, L. I. 1627
Zhou, D. P. 1725

Pergamon

Polyhedron Vol. 17, No. 9, p. iii, 1998
Elsevier Science Ltd. Printed in Great Britain

CONTRIBUTORS TO THIS ISSUE

(Chief Author's name(s) in bold)

Álvarez-Larena, A. 1591
Baker, P. K. 1407
Bhattacharya, S. 1525
Burlov, A. S. 1547
Chen, Z.-N. 1535
Chen, Y.-G. 1541
Chiarizia, R. 1471
Choi, K.-Y. 1415
Choi, S. N. 1415
Clark, A. I. 1407
Clegg, W. 1591
Dai-Zheng, L. 1587
D'Alpaos, M. 1481
Dong, Y.-B. 1579
Drew, M. G. B. 1407
Duran, M. L. 1547
Durrant, M. C. 1407
Ecclestone, T. 1435
Escandar, G. M. 1517
Escrivà, E. 1495
Ferraro, J. R. 1471
Folgado, J.-V. 1495
Gantzel, P. K. 1511
Garcia-Vazquez, J. A. 1547
Garcia, J. A. 1471
Garnovskii, A. D. 1547
Garnovskii, D. A. 1547
Geng-Lin, W. 1587
Ghosh, P. 1525
Goher, M. A. S. 1561
Gonzàlez-Duarte, P. 1591
Guang-Ming, Y. 1587
Guo, J. 1541
Hashimoto, M. 1463
Hendrickson, D. N. 1511
Herlinger, A. W. 1471
Hu, Q.-M. 1579
James, M. 1571
Juan, S. 1587
Kanbara, Y. 1463
Kang, B.-S. 1535
Kawaguchi, H. 1571
Kitamura, Y. 1449
Kobayashi, T. 1553
Kunita, M. 1553
Laurie, S. H. 1435
Ledesma, G. N. 1517
Leiva, A. 1591
Li, Y.-K. 1579
Li, Y.-T. 1423
Liao, D.-Z. 1423
Litkowska, H. 1477
Liu, J.-F. 1541
Liu, Y. 1541
López, G. 1503
March, R. 1591
Mautner, F. A. 1561
Meng, L. 1541
Moriguchi, Y. 1463
Murakami, S. 1449
Nibu, T. 1463
Nishida, Y. 1553
Odamura, T. 1463
Ohba, S. 1553
Okuno, T. 1553
Patroniak-Krzyminiewska, V. 1477
Piniella, J. F. 1591
Pons, J. 1591
Pope, M. T. 1541
Pramanik, K. 1525
Pramanik, N. C. 1525
Radecka-Paryzek, W. 1477
Rein, F. N. 1439
Richards, R. L. 1407
Rodríguez, V. 1503
Romero, J. 1547
Ruiz, J. 1503
Sakata, K. 1463
Sallomi, I. J. 1429
Server-Carrió, J. 1495
Shaheen, A. J. 1429
Shibata, A. 1449
Shi-Ping, Y. 1587
Sierra, M. G. 1517
Solans, X. 1591
Song, L.-C. 1579
Sousa, A. 1547
Suh, I.-H. 1415
Sun, J. 1579
Sun, Z. 1511
Suzuki, T. 1553
Su, C.-Y. 1535
Symons, M. C. R. 1435
Taiwo, F. A. 1435
Tatsumi, K. 1571
Toma, H. E. 1439
Tsuge, A. 1463
Tušek-Božić, L. 1481
Vicente, C. 1503
Yan, C.-W. 1423
Yu, K.-B. 1535
Zhang, H.-X. 1535
Zheng, Y.-J. 1423
Zong-Hui, J. 1587

Pergamon

Polyhedron Vol. 17, No. 8, p. iii, 1998
Elsevier Science Ltd. Printed in Great Britain

CONTRIBUTORS TO THIS ISSUE

(Chief Author's name(s) in bold)

Abdul Malik, K. M. 1329
Abram, U. 1303
Abram, S. 1303
Adams, M. E. 1289
Alberto, R. 1303
Bau, R. 1281
Baxter, I. 1329
Beattie, J. K. 1343
Butcher, R. J. 1317
Chatterjee, M. 1369
Chaudhuri, N. Ray 1217, 1363
Chen, X.-L. 1381
Choi, K.-Y. 1241
Darr, J. A. 1329
Das, D. 1363
Dilworth, J. R. 1303
Dorsey, B. T. 1289
Exarchos, G. 1257
Fun, H. K. 1211
Gardner, N. 1267
Garoufis, A. 1281
Ghosh, A. 1217
Ghosh, S. 1369
Gourbatsis, S. 1281
Gupta, A. 1231
Gutiérrez-Zorrilla, J. M. 1247
Hadjiliadis, N. 1281
Hambley, T. W. 1343
Hursthouse, M. B. 1329
Jain, V. K. 1317
Jung, W.-S. 1223
Kamatchi, P. 1397
Kandaswamy, M. 1397
Kasselouri, S. 1281
Keerthi, K. D. 1387
Kelly, R. S. 1289
Kim, J.-K. 1223
Kim, S.-D. 1223
Klepetko, J. A. 1343
Lahiri, G. K. 1387
Laskar, I. R. 1363
Lee, S. T. 1211
Lei, P. 1381
Liang, W. 1323
Liao, D.-Z. 1311
Li, Y.-T. 1311
Liu, S. 1323
Lucas, C. R. 1323
Luque, A. 1247
Lutz, F. 1281
Mak, T. C. W. 1369, 1375
Malachowski, M. R. 1289
Martínez-Ripoll, M. 1247
Masters, A. F. 1343
McAleese, J. 1329
Miller, D. O. 1323
Milletti, M. C. 1267
Mingos, D. M. P. 1329
Mondal, A. 1217
Mostafa, G. 1217, 1363
Nyburg, S. C. 1257
Parameswary, M. 1211
Park, S.-H. 1267
Parker, M. J. 1289
Perlepes, S. P. 1281
Prasad, R. L. 1231
Qiao, Q.-L. 1381
Raju, K. M. 1355
Ramalingam, K. 1211
Reddy, K. H. 1355
Reddy, M. R. 1355
Robinson, S. D. 1257
Román, P. 1247
Ryu, H. 1241
Santra, B. K. 1387
Schibli, R. 1303
Shawkataly, O. b. 1211
Sivakumar, K. 1211
Skarżewskia, J. 1231
Su, Y.-Z. 1311
Suh, I.-H. 1241
Tan, X. S. 1375
Tang, W. X. 1375
Tian, L. 1275
Turner, P. 1343
Vitoria, P. 1247
Vogt, A. 1231
Welch, A. J. 1363
Wery, A. S. J. 1247
Wołowiec, S. 1231, 1295
Wong, W.-T. 1217
Wu, B.-M. 1369
Xiang, D. F. 1375
Xue, F. 1375
Yan, C.-W. 1311
Yan, S.-Y. 1381
Yu, W. 1275
Zhan, L. 1381
Zhao, B. 1275
Zhou, Z. 1275

Pergamon

Polyhedron Vol. 17, No. 4, p. iii, 1998
Elsevier Science Ltd. Printed in Great Britain

CONTRIBUTORS TO THIS ISSUE

(Chief Author's name(s) in bold)

Arrowsmith, S.	421	Hintermaier, F.	483	Rogers, R. D.	603
Batsanov, A.	421	Ho, D. M.	607	Runde, W. H.	599
Beck, W.	483	Hudson, E. A.	599	Sanmartín, J.	413
Beer, P. D.	405	Hu, Q.-M.	469	Santini, C.	561
Benito, A.	491	Jordan IV, G. T.	589	**Shen, Q.**	519
Bermejo, M. R.	413	Jovanović, T.	399	Sivý, J.	539
Blower, P. J.	513	**Kee, T. P.**	433	**Song, L.-C.**	469
Bobbo, T.	475	Kettmann, V.	539	Soto, J.	491
Boricha, V. P.	443	Lee, G. H.	449	**Sousa, A.**	413
Brechbiel, M. W.	603	**Leung, W.-H.**	457	**Srinivas, D.**	443
Campana, C. F.	617	Lewis, J. S.	513	Subramanian, P. S.	443
Cattalini, L.	475	Li, G. Q.	607	Sun, J.	519
Chand, S.	507	Liao, F.-L.	547	Švajlenová, O.	539
Chen, Z.	405	Lin, Y.	555	Tait, C. D.	599
Chim, J. L. C.	457	Liu, Q.	555	Tang, Y.	429
Chung, Y. H.	449	Liu, Y. H.	449	**Tan, M.**	429
Chung, C.-S.	547	Lloris, J. M.	491	Taylor, R. J.	433
Clark, D. L.	599	Logan, N.	421	**Teo, B. K.**	617
Coll, R. K.	507	**Mahamid, I. Al**	599	Tošić, M. S.	399
Conradson, S. D.	599	Mak, T. C. W.	497	Traldi, P.	531
Cotton, F. A.	589	Mandal, S. K.	607	**Tušek-Božić, L.**	531
Ćurić, M.	531	Marangoni, G.	475	**Vasić, V. M.**	399
Dang, H.	617	Marchetti, F.	561	Visentin, F.	475
Daniels, L. M.	589	**Martínez-Máñez, R.**	491	Vujisić, Lj. S.	399
Dashti-Mommertz, A.	523	**McAuliffe, C. A.**	413	Wang, S.-L.	547
Dave, P. C.	443	McIndoe, J. S.	507	Wang, Y.	449
Ding, M.	555	Miliani, M.	561	**Wei, H. H.**	449
Dinjus, E.	613	Mitchell, M. C.	433	**Wei, P.-R.**	497
Dove, M. F. A.	421	**Murillo, C. A.**	589	Werner, B.	523
Drew, M. G. B.	405	Nedeljković, J. M.	399	Wong, W.-T.	457
Fernández, M. I.	413	**Neumüller, B.**	523	Wu, D.-D.	497
Fondo, M.	413	Neu, M. P.	599	Wu, M.-C.	457
Friebel, C.	539	Olsen, G. M.	577	Xing, Y.	555
Gale, P. A.	405	**Orchin, M.**	607	Yao, Y.	519
Gan, **X.**	429	Palmer, P. D.	599	Ye, N.	603
Görls, H.	613	Pariya, C.	547	**Zevaco, T. A.**	613
Govan, N.	463	Pellei, M.	561	**Zhang, H.**	617
Hay, R. W.	463	**Pettinari, C.**	561	Zheng, X.	429
Heath, J. A.	405	**Pitteri, B.**	475	Zhou, Z.-Y.	497
Henderson, W.	577	**Planalp, R. P.**	603	Zhu, Y.-H.	469
Hess, N. J.	599	**Plesch, G.**	539	Zweit, J.	513

Publisher's Note

As from January 1998, *Polyhedron* will no longer publish a "Communications" section. Instead, a new periodical, *Inorganic Chemistry Communications*, is being launched and distributed to all *Polyhedron* subscribers.

The change has been dictated by several factors, one of which is the obvious need for a specialized periodical covering the swift publication of hot research results. The project has received sustained support from scientists, and will be managed in coordination and parallel with other Elsevier inorganic chemistry journals.

Another reason for the launch of *Inorganic Chemistry Communications* is the imperative need to publish communications within 8–10 weeks. The exercise has proved to be very difficult when regular articles and rapid papers are combined within the same cover. The separate publication of both sections will technically help to achieve the targeted publication times.

Finally, it should be mentioned that communications and regular articles do not serve exactly the same purpose. Communications aim to function as an efficient early notice board on current research whereas articles constitute the essential detailed validation of the findings. By binding the two sections under separate covers, readers will clearly obtain what they expect to find in these volumes.

From January 1998, all submissions to the "Communications" section of *Polyhedron* will be channelled to *Inorganic Chemistry Communications*. Authors will be informed of this change and offered the choice of publishing their paper in *Inorganic Chemistry Communications*, withdrawing it, or having it published as a regular article in *Polyhedron*. It is important to note that the circulation of *Inorganic Chemistry Communications* is also being extended to subscribers of *Inorganica Chimica Acta*, *Polyhedron* and the *Journal of Organometallic Chemistry*, thus these papers will reach an audience that far surpasses the initial expectations of the authors.

The Publisher

Pergamon

Polyhedron Vol. 17, Nos. 2–3, p. iii, 1998
Elsevier Science Ltd. Printed in Great Britain

CONTRIBUTORS TO THIS ISSUE

(Chief Author's name(s) in bold)

Adams, K. J. 341
Akamatsu, T. 235
Alyea, E. C. 275
Ansari, M. A. 299
Bardwell, D. A. 211
Batsanov, A. S. 367
Batten, S. R. 373
Blanco, L. M. 381
Boni, G. 261
Burlov, A. S. 381
Bu, X.-H. 289
Campo, J. 275
Cao, X.-C. 289
Cerrada, E. 295
Chen, W. 289
Chen, Z.-N. 331
Constable, E. C. 243
Constable, E. C. 395
Contant, R. 357
Couchman, S. M. 211
Crabtree, S. P. 367
Demartin, F. 305
Deplano, P. 305
Devillanova, F. A. 305
Dieck, T. 381
Edwards, A. J. 243
Evans, W. J. 299
Fenga, P. G. 313
Garnovskii, A. D. 381
Garnovskii, D. A. 381
Giovani, W. F. D. 313
Goubitz, K. 281
Grimmbacher, T. 267
Gu, J. 231
Haire, G. R. 243
Hannon, M. J. 243
Heinemann, F. W. 351
Henderson, W. 221
Horwood, E. L. 373
Howard, J. A. K. 367
Huang, X. 331
Isaia, F. 305
Jeffery, J. C. 211, 373
Kang, B.-S. 331
Karaböcek, N. 319
Karaböcek, S. 319
Kharisov, B. I. 381
Kilner, M. 367
Koch, K. R. 267
Korovina, L. V. 381
Kräuter, G. 391
Kuznetsova, L. I. 381
Laguna, M. 295
Łasocha, W. 281
Liang, K. 231
Lima, E. C. 313
Lippolis, V. 305
Liu, Q.-T. 331
Maher, J. P. 211
Mathur, V. K. 325
McCaffrey, L. J. 221
McGrath, T. D. 341
Mercuri, M. L. 305
Michaut, J. P. 357
Moïse, C. 261
Neumann, O. 351
Nicholson, B. K. 221
Nishida, Y. 235
Ohba, S. 235
Opozda, E. M. 281
Otter, C. A. 211
Park, S. 325
Planalp,R. P. 325
Petrič, M. 255
Piludu, S. 305
Pohleven, F. 255
Raithby, P. R. 243
Rees, L. H. 373
Rees, W. S. 391
Romero, J. R. 313
Roncin, J. 357
Sacht, C. 267
Sakamoto, M. 235
Sasaki, Y. 235
Schenk, H. 281
Šegedin, P. 255
Shi, J.-C. 331
Śledziewska, E. 281
Sorolla, P. A. 295
Steinborn, D. 351
Sunny, S. K. 391
Thomas, C. 289
Tommasino, J. B. 357
Tsuchiya, K. 235
Turel, I. 255
Verani, G. 305
Wagner, J.-P. 351
Ward, M. D. 211, 373
Weichmann, H. 351
Welch, A. J. 341
Wen, T.-B. 331
White, A. J. P. 255
Whittle, B. 373
Williams, D. J. 255
Xu, D. 231
Xu, L. 231
Xu, Y. 231
Zhang, R.-H. 289
Ziller, J. W. 299

Pergamon

Polyhedron Vol. 17, No. 1, p. iii, 1998
Elsevier Science Ltd. Printed in Great Britain

CONTRIBUTORS TO THIS ISSUE

(Chief Author's name(s) in bold)

Abram, S.	131	**Green, M. L. H.**	119	Nishide, T.	105
Abram, U.	131	Haggerty, B. S.	1	Obadović, D. Ž.	27
Aguas, M. D.	49	Hawash, N. M.	199	**Pan, Y.**	69
Alyea, E. C.	11	Hayashi, S.	55	**Parkin, I. P.**	49
Andrade, C.	173	Helgason, O.	149	Pérez-Flores, J.	193
Arancibia, M.	173	Heo, N. H.	55	Pettinari, C.	17
Arias, J. L.	193	Huang, X.	69	Popkov, Y.	145
Asada, H.	105	Hu, Q.-M.	35	Putanov, P.	27
Baraona, R.	159	Imbalzano, A.	125	Qiu, W.	75
Ben Cheikh, R.	185	**Iskander, M. F.**	199	Rheingold, A. L.	1
Berry, F. J.	149	Jackman, M.	153	Rosas, N.	193
Bilsborrow, R.	149	**Jin, T.-Z.**	43	Salmón, M.	193
Bohra, R.	163	Ji, L.	75	Santini, C.	17
Bonnet, M. C.	185	**Kiš, E.**	27	**Sella, A.**	63
Bošković, G.	27	Kiurski, J.	27	Shakya, R. P.	11
Bovio, B.	17	Kokozay, V. N.	85	shen, **Y.**	69
Cabrera, A.	193	**Korovin, Y.**	145	Shen, J.-Y.	35
Campos, M.	159	Kovbasyuk, L. A.	85	Shevchuk, S.	145
Casey, M.	153	Lee, M.-H.	55	Skelton, B. W.	85
Cecchi, P.	17	Lewkebandara, T. S.	1	Skinner, S. J.	149
Cerva, A.	93	Linert, W.	85	**Song, L.-C.**	35
Chaabouni, R.	185	**Liu, S.-X.**	81	Sun, X.	69
Chaves, S.	93	Li, X.	75	Tashima, S.	207
Chernega, A. N.	119	**Lobbia, G. G.**	17	Timmons, D. J.	179
Coombe, G. C.	49	Lomić, G.	27	Toledo, I.	173
Cotton, F. A.	179	**Lu, T.**	75	Torayama, H.	105
Crivelli, I.	173	Maichle-Mössmer, C.	131	**Vassilyeva, O. Yu.**	85
Cusumano, M.	125	Mao, Z.	75	**Velasco, L.**	193
Dahan, F.	185	Marchetti, F.	17	Wang, R.-Y.	43
Delgado, R.	93	Marco, J. F.	149	Williams, V. C.	119
Devereux, M.	153	Marinković-Nedučin, R.	27	**Winter, C. H.**	1
Dhammani, A.	163	Massoud, S. S.	199	Wu, X.-Y.	35
Dong, G.	69	Matsushita, T.	105	Xu, G.-X.	43
El-Sayed, L.	199	Maunder, G. H.	63	Yap, G. P. A.	1
Espinosa-Pérez, G.	193	McCann, M.	153	Yu, K.	75
Ferguson, G.	11	McKarns, P. J.	1	**Zamudio, W.**	159
Fujiwara, M.	105	Meehan, P. R.	11	Zhao, J.-J.	43
Galsworthy, J. R.	119	Mehrotra, R. C.	163	Zheltvay, I.	145
Gao, S.	81	**Mikuriya, M.**	207	Zhou, X.-G.	43
Giannetto, A.	125	Nazarenko, N.	145	Zhou, Z.-Y.	43

Pergamon

Polyhedron Vol. 17, No. 4, p. iii, 1998
Elsevier Science Ltd. Printed in Great Britain

CONTRIBUTORS TO THIS ISSUE

(Chief Author's name(s) in bold)

Arrowsmith, S.	421	Hintermaier, F.	483	Rogers, R. D.	603
Batsanov, A.	421	Ho, D. M.	607	Runde, W. H.	599
Beck, W.	483	Hudson, E. A.	599	Sanmartín, J.	413
Beer, P. D.	405	Hu, Q.-M.	469	Santini, C.	561
Benito, A.	491	Jordan IV, G. T.	589	**Shen, Q.**	519
Bermejo, M. R.	413	Jovanović, T.	399	Sivý, J.	539
Blower, P. J.	513	**Kee, T. P.**	433	**Song, L.-C.**	469
Bobbo, T.	475	Kettmann, V.	539	Soto, J.	491
Boricha, V. P.	443	Lee, G. H.	449	**Sousa, A.**	413
Brechbiel, M. W.	603	**Leung, W.-H.**	457	**Srinivas, D.**	443
Campana, C. F.	617	Lewis, J. S.	513	Subramanian, P. S.	443
Cattalini, L.	475	Li, G. Q.	607	Sun, J.	519
Chand, S.	507	Liao, F.-L.	547	Švajlenová, O.	539
Chen, Z.	405	Lin, Y.	555	Tait, C. D.	599
Chim, J. L. C.	457	Liu, Q.	555	Tang, Y.	429
Chung, Y. H.	449	Liu, Y. H.	449	**Tan, M.**	429
Chung, C.-S.	547	Lloris, J. M.	491	Taylor, R. J.	433
Clark, D. L.	599	Logan, N.	421	**Teo, B. K.**	617
Coll, R. K.	507	**Mahamid, I. Al**	599	Tošić, M. S.	399
Conradson, S. D.	599	Mak, T. C. W.	497	Traldi, P.	531
Cotton, F. A.	589	Mandal, S. K.	607	**Tušek-Božić, L.**	531
Ćurić, M.	531	Marangoni, G.	475	**Vasić, V. M.**	399
Dang, H.	617	Marchetti, F.	561	Visentin, F.	475
Daniels, L. M.	589	**Martínez-Máñez, R.**	491	Vujisić, Lj. S.	399
Dashti-Mommertz, A.	523	**McAuliffe, C. A.**	413	Wang, S.-L.	547
Dave, P. C.	443	McIndoe, J. S.	507	Wang, Y.	449
Ding, M.	555	Miliani, M.	561	**Wei, H. H.**	449
Dinjus, E.	613	Mitchell, M. C.	433	**Wei, P.-R.**	497
Dove, M. F. A.	421	**Murillo, C. A.**	589	Werner, B.	523
Drew, M. G. B.	405	Nedeljković, J. M.	399	Wong, W.-T.	457
Fernández, M. I.	413	**Neumüller, B.**	523	Wu, D.-D.	497
Fondo, M.	413	Neu, M. P.	599	Wu, M.-C.	457
Friebel, C.	539	Olsen, G. M.	577	Xing, Y.	555
Gale, P. A.	405	**Orchin, M.**	607	Yao, Y.	519
Gan, **X.**	429	Palmer, P. D.	599	Ye, N.	603
Görls, H.	613	Pariya, C.	547	**Zevaco, T. A.**	613
Govan, N.	463	Pellei, M.	561	**Zhang, H.**	617
Hay, R. W.	463	**Pettinari, C.**	561	Zheng, X.	429
Heath, J. A.	405	**Pitteri, B.**	475	Zhou, Z.-Y.	497
Henderson, W.	577	**Planalp, R. P.**	603	Zhu, Y.-H.	469
Hess, N. J.	599	**Plesch, G.**	539	Zweit, J.	513

Pergamon

Polyhedron Vol. 17, No. 7, p. v, 1998
Elsevier Science Ltd. Printed in Great Britain

CONTRIBUTORS TO THIS ISSUE

(Chief Author's name(s) in bold)

Abram, S.	1133	Gómez-Sal, P.	1055, 1081	Nakayama, Y.	1065
Abram, U.	1133	Gómez, R.	1055	**Nozaki, K.**	1159
Alberto, R.	1133	Gonçalves, I. S.	1091	**Okuda, J.**	1035, 1073
Amor, F.	1073	Guzei, I. A.	1037	Paterniti, D. P.	1177
Anwander, R.	1195	**Härter, P.**	1141	Peters, F.	1149
Atwood, J. D.	1177	Hahn, C.	1183	**Poli, R.**	1115
Barnes, C. E.	1045	Herdtweck, E.		Rheingold, A. L.	1037
Barz, M.	1121		1121, 1141, 1149, 1195	Riermeier, T. H.	1165
Beller, M.	1165	Hinz, I.	1103	Rogge, W.	1203
Bender-Gresse, M.	1115	Hiyama, T.	1159	**Romão, C. C.**	1091
Calvo, M.	1081	**Hughes, R. P.**	1037	**Royo, P.**	1055, 1081
Ciruelos, S.	1055	Hultzsch, K. C.	1073	Scherer, W.	1149, 1165
Collange, E.	1115	Kaden, T. A.	1133	Schibli, R.	1133
Cuenca, T.	1055	Kociok-Köhn, G.	1103	Schubiger, P. A.	1133
Drew, M. G. B.	1091	Kühn, F. E.	1091	Sieler, J.	1183
duPlooy, K. E.	1073	Latzel, K.	1141	Spaniol, T. P.	1073
Eberle, T.	1073	Lopes, A. D.	1091	Spiegler, M.	1141
Egli, A.	1133	Maddock, S. M.	1037	Tani, K.	1065
Eppinger, J.	1195	Mägerlein, W.	1165	**Taube, R.**	1183
Félix, V.	1091	Manzanero, A.	1055, 1081	**Thiel, W. R.**	1121
Feist, M.	1103	**Mashima, K.**	1065	**Wagner, M.**	1149
Filippou, A. C.	1103	Mattamana, S.	1115	**Weiß, J.**	1203
Fischer, R. A.	1203	Müller, T. E.	1165	Winter, J. G.	1103
Försterling, F. H.	1045	Nakamoto, K.	1159	Yasutomi, M.	1159
Fukumoto, H.	1065	Nakamura, A.	1065		

Publisher's Note

As from January 1998, *Polyhedron* will no longer publish a "Communications" section. Instead, a new periodical, *Inorganic Chemistry Communications*, is being launched and distributed to all *Polyhedron* subscribers.

The change has been dictated by several factors, one of which is the obvious need for a specialized periodical covering the swift publication of hot research results. The project has received sustained support from scientists, and will be managed in coordination and parallel with other Elsevier inorganic chemistry journals.

Another reason for the launch of *Inorganic Chemistry Communications* is the imperative need to publish communications within 8–10 weeks. The exercise has proved to be very difficult when regular articles and rapid papers are combined within the same cover. The separate publication of both sections will technically help to achieve the targeted publication times.

Finally, it should be mentioned that communications and regular articles do not serve exactly the same purpose. Communications aim to function as an efficient early notice board on current research whereas articles constitute the essential detailed validation of the findings. By binding the two sections under separate covers, readers will clearly obtain what they expect to find in these volumes.

From January 1998, all submissions to the "Communications" section of *Polyhedron* will be channelled to *Inorganic Chemistry Communications*. Authors will be informed of this change and offered the choice of publishing their paper in *Inorganic Chemistry Communications*, withdrawing it, or having it published as a regular article in *Polyhedron*. It is important to note that the circulation of *Inorganic Chemistry Communications* is also being extended to subscribers of *Inorganica Chimica Acta*, *Polyhedron* and the *Journal of Organometallic Chemistry*, thus these papers will reach an audience that far surpasses the initial expectations of the authors.

The Publisher

Pergamon

Polyhedron Vol. 17, Nos. 5–6, p. vii, 1998
Elsevier Science Ltd. Printed in Great Britain

CONTRIBUTORS TO THIS ISSUE

(Chief Author's name(s) in bold)

Abboud, K. A. 725
Andersen, R. A. 953
Ansari, M. A. 869
Archer, L. 713
Arndt, P. 845
Arunasalam, V. C. 641
Atwood, D. A. 811
Baroni, T. E. 759
Barron, A. R. 983
Baxter, I. 625, 641
Beatty, A. M. 781
Bengtsson-Kloo, L. A. 965
Bergman, R. G. 803
Beswick, M. A. 745
Bois, C. 821
Boncella, J. M. 725
Bott, S. G. 879, 983
Bott, C. 737
Budzichowski, T. A. 705, 857
Buhro, W. E. 781
Cai, S. 749
Carmalt, C. J. 977
Chisholm, M. H. 623, 705, 857
Clegg, W. 659, 993
Corriu, R. 925
Cotton, F. A. 959
Cowley, A. H. 977
Coxall, R. A. 659
Cummins, C. C. 675
Darr, J. A. 641
Davis, W. M. 749
Deacon, G. B. 791
Decken, A. 977
Drake, S. R. 625, 641
Duesler, E. 713
Errington, R. J. 659
Evans, W. J. 869
Eve, T. M. 725
Fanwick, P. E. 769, 773
Fokken, S. 943
Folting, K. 857
Francis, J. A. 983
Fryzuk, M. D. 947
Gade, L. H. 737
Gatehouse, B. M. 791
Gehrhus, B. 999
Giesbrecht, G. R. 947
Glenny, M. W. 851
Goel, S. C. 781
Gruhn, N. E. 705
Guérin, F. 917
Hampden-Smith, M. J. 713
Harmer, C. N. 745
Haubrich, S. T. 791
Hellmann, K. W. 737
Heppert, J. A. 759
Hill, M. S. 811
Hoffman, D. M. 879
Hollingsworth, J. A. 781
Hopkins, A. D. 745
Horsburgh, L. 993
Howard, W. A. 803
Hubert-Pfalzgraf, L. G. 821
Huffman, J. C. 857
Hursthouse, M. B. 641, 625
Ireland, J. 791
Johnson, S. A. 947
Just, O. 1001
Kang, H.-C. 943
Kempe, R. R. 749
Kempe, R. 845
Kessler, V. G. 899, 965
Kickham, J. E. 947
Kirmse, R. 845
Koide, Y. 983
Kolesnichenko, V. 759
Lappert, M. F. 999
Lawrenz, E. T. 791
Liable-Sands, L. M. 759
Lichtenberger, D. L. 705
Love, J. B. 947
Maatta, E. A. 969
Mackenzie, F. M. 993
Malik, K. M. A. 625, 641
Massa, W. 943
Mathur, C. 1005
Mathur, S. 1005
McBurnett, B. G. 977
McConville, D. H. 917
McPartlin, M. 737
Mehrotra, R. C. 689
Mingos, D. M. P. 625, 641
Mulvey, R. E. 993
Neumayer, D. A. 977
Nielson, A. J. 851
Odom, A. L. 675
Okuda, J. 943
Otway, and D. J. 625
Paver, M. A. 745
Plakatouras, J. C. 625
Profilet, R. D. 773
Raithby, P. R. 745
Raston, C. L. 935
Rees, Jr, W. S. 1001
Rheingold, A. E. 759
Rheingold, A. L. 891
Rickard, C. E. F. 851
Rickman, B. 725
Ridland, J. 659
Riley, P. N. 773
Robinson, K. D. 781
Rothwell, I. P. 769, 773
Salberg, M. M. 773
Schmitz, A. 879
Schrock, R. R. 749
Schumann, H. 1001
Scowen, I. J. 737
Seib, L. 759
Sherwood, J. M. 659
Shevelkov, A. V. 965
Silverman, J. S. 977
Singh, A. 689
Sirio, C. 821
Skelton, B. W. 935
Spannenberg, A. 845
Stewart, J. L. 953
Streib, W. E. 857
Su, **K.** 891
Tcheboukov, D. E. 899
Terry, K. W. 891
Tiedtke, D. B. 705, 857
Tillack, A. 845
Tilley, T. D. 891
Tolhurst, V.-A. 935
Turevskaya, E. P. 899
Turova, N. Ya. 899
Vecchio, O. D. 917
Veith, M. 1005
Vilardo, J. S. 769
Wang, S. 831
Weimann, R. 1001
Wei, P. 811
Wheeler, D. E. 969
White, A. H. 935
Wright, D. S. 745
Wu, J.-F. 969
Yanovskaya, M. I. 899
Yanovsky, A. I. 899
Yap, G. P. A. 759
Yokochi, A. 959
Zhuang, W.-W. 879
Ziller, J. W. 869

Pergamon

PII: S0277-5387(97)00309-4

Polyhedron Vol. 17, No. 1, pp. 1–9, 1998
© 1997 Elsevier Science Ltd
All rights reserved. Printed in Great Britain
0277-5387/98 $19.00+0.00

Adducts of titanium tetrachloride with organosulfur compounds. Crystal and molecular structures of $TiCl_4(C_4H_8S)_2$ and $(TiCl_4)_2(CH_3SSCH_3)$

T. Suren Lewkebandara,[a] Peggy J. McKarns,[a] Brian S. Haggerty,[b] Glenn P. A. Yap,[b] Arnold L. Rheingold,[b] and Charles H. Winter[a]*

[a]Department of Chemistry, Wayne State University, Detroit, Michigan 48202, U.S.A.

[b]Department of Chemistry, University of Delaware, Newark, Delaware 19716, U.S.A.

(Received 21 May 1997; accepted 3 July 1997)

Abstract—Treatment of titanium tetrachloride with a range of organothiols affords adducts of the formula $TiCl_4(HSR)_2$ in 77–89% yields. Reaction of titanium tetrachloride with organic sulfides gives sulfide adducts of the formula $TiCl_4(SR_2)_2$ in 87–98% yields. These complexes are volatile and monomeric with cis-organosulfur ligands. Treatment of titanium tetrachloride with methyl disulfide affords the adduct $(TiCl_4)_2(CH_3SSCH_3)$ in 98% yield, which adopts a dinuclear structure with a Ti_2Cl_8 core and a bridging disulfide ligand. The crystal structures of $TiCl_4(C_4H_8S)_2$ and $(TiCl_4)_2(CH_3SSCH_3)$ were determined. The relevance of these observations to the chemical vapor deposition of titanium disulfide and trisulfide films is discussed. © 1997 Elsevier Science Ltd

Keywords: titanium disulfide; titanium trisulfide; titanium tetrachloride; chemical vapor deposition.

Titanium disulfide is one of the desirable cathode materials for lithium batteries [1]. Titanium disulfide films have also been used as a solid lubricant due to weak Van der Waals interactions between adjacent layers in the lattice [2]. The majority of Chemical Vapor Deposition (CVD) routes to titanium disulfide films are based on the reaction between titanium tetrachloride and hydrogen sulfide, organic sulfides, or disulfides [3–5]. Schleich [4] has recently disclosed that the CVD reaction between titanium tetrachloride and di-tert-butyl disulfide affords titanium trisulfide films at temperatures between 200–260°C, mixtures of titanium trisulfide and titanium disulfide films between 260–400°C, and titanium disulfide films above 400°C. In contrast, di-tert-butyl sulfide reacted with titanium tetrachloride at $\geqslant$260°C to give titanium disulfide films. Recently we reported a new atmospheric pressure CVD process for titanium disulfide films, which relies upon the reaction of titanium tetrachloride with organothiols at temperatures $\geqslant$200°C, and affords highly pure, crystallographically oriented, stoichiometric, adhesive coatings [6]. We subsequently disclosed that complexes of the formula $TiCl_4(HSR)_2$ (R = alkyl) constitute the first single-source precursors for the CVD of titanium disulfide films [7]. Significant aspects of the processes based upon organothiols include a large drop in the minimum deposition temperature for titanium disulfide film deposition ($\geqslant$200°C versus $\geqslant$400°C for hydrogen sulfide) and the fact that no carbon or chlorine impurities were detected in the films.

The differences observed between the use of organothiols, organosulfides, and organodisulfides in the deposition of titanium disulfide films raise the possibility that there are corresponding variations in the reactions between titanium tetrachloride and the respective sulfur sources. Since there is very little known about the reactivity of titanium tetrachloride toward organosulfur compounds [8–11], we have initiated an investigation of the solution coordination chemistry of titanium tetrachloride with sulfur

* Author to whom correspondence should be addressed.

donors. Herein we describe the reaction of titanium tetrachloride with several sulfides and disulfides and also report the crystal structures of two complexes.

EXPERIMENTAL

General considerations

All manipulations were performed under an inert atmosphere using either glovebox or Schlenk line techniques. Hexane was distilled from sodium. Chloroform-*d* and dichloromethane-d_2 was dried over activated 4 Å molecular sieves. Titanium tetrachloride and the organosulfur compounds were used as received from Aldrich Chemical Co.

^{1}H NMR and ^{13}C{^{1}H} NMR spectra were obtained at 300 or 75 MHz in chloroform-*d* or dichloromethane-d_2. Infrared spectra were obtained using Nujol as the medium. Elemental analyses were performed by Midwest Microlab, Indianapolis, IN. Melting points were obtained on a Haake-Buchler HBI digital melting point apparatus and are uncorrected.

Preparation of $TiCl_4(HSC_6H_{11})_2$ (**1**)

A 200-cm^3 Schlenk flask was charged with titanium tetrachloride (2.00 cm^3, 18.2 mmol), dichloromethane (30 cm^3), and a stir bar and was fitted with a septum. The solution was cooled to 0°C, and cyclohexylthiol (4.46 cm^3, 36.48 mmol) was added by syringe to afford a clear, deep yellow solution. The solution was allowed to reach ambient temperature and was stirred for 2 h. The volatiles were pumped off and the resultant yellow solid was extracted with hexane (100 cm^3) and filter through a 2 cm pad of Celite to afford a clear, yellow solution. This solution was kept at −20°C, to afford needle shaped yellow crystals of **1**. The supernatant was removed by cannulation and the crystals were vacuum dried (5.96 g, 84% based upon titanium tetrachloride): m.p. 78°C (dec with sublimation); IR (Nujol, cm^{-1}) 2492 (m, S—H stretch), 1340 (w), 1263 (w), 1210 (w), 1022 (w), 995 (m), 886 (w), 875 (w), 809 (w), 755 (s, broad), 727 (s), 667 (w); ^{1}H NMR ($CDCl_3$, 23°C, δ) 3.11 (m, C*H*SH), 2.33 (s, S—*H*), 2.06 (m, CH_2), 1.74 (m, CH_2), 1.60 (m, CH_2), 1.35 (m, CH_2); ^{13}C{^{1}H} NMR ($CDCl_3$, 23°C, ppm) 42.60 (s, *C*HSH), 36.68 (s, 2 *C*H_2), 26.09 (s, 2 *C*H_2), 25.16 (s, *C*H_2). Found: C, 33.82; H, 5.68. Calc. for $C_{12}H_{24}Cl_4S_2Ti$: C, 34.14; H, 5.73%.

Preparation of $TiCl_4(HSC_5H_9)_2$ (**2**)

A 100-cm^3 Schlenk flask was charged with cyclopentylthiol (0.20 cm^3, 1.83 mmol), hexane (15 cm^3), a stir bar and was fitted with a rubber septum. This solution was cooled to 0°C, and titanium tetrachloride (0.1 cm^3, 0.91 mmol) was added *via* a syringe to give a clear, deep yellow solution. This solution was allowed to reach ambient temperature and stirred for 2 h. The solution was placed at −20°C for 6 h to afford yellow crystals of **2**. The solvent was transferred and the crystals were vacuum dried to afford **2** (0.28 g, 78% based upon titanium tetrachloride): m.p. 60°C (dec. with sublimation); IR (Nujol, cm^{-1}) 2520 (m, S—H), 2505 (m, S—H), 1310 (s), 1261 (s), 1236 (m), 1158 (w), 1089 (w), 1020 (m), 794 (s), 715 (s); ^{1}H NMR ($CDCl_3$, 23°C, δ) 3.53 (m, C*H*SH), 2.95 (s, S*H*), 2.09 (s, CH_2), 1.72 (s, CH_2), 1.57 (s, CH_2); ^{13}C{^{1}H} NMR ($CDCl_3$, 23°C, ppm) 44.52 (s, *C*HSH), 36.25 (s, 2CH_2), 24.57 (s, 2*C*H_2). Found: C, 30.26; H, 4.99. Calc. for $C_{10}H_{20}Cl_4S_2Ti$: C, 30.48; H, 5.12%.

Preparation of $TiCl_4(C_4H_8(SH)_2)$ (**3**)

A 100-cm^3 Schlenk flask was charged with 2,3-butanedithiol (0.86 cm^3, 6.9 mmol), dichloromethane (10 cm^3), and a stir bar and was fitted with a rubber septum. This solution was cooled to 0°C, and titanium tetrachloride (0.75 cm^3, 6.90 mmol) was added *via* a syringe to give a yellow solution. The solution was allowed to reach ambient temperature and was stirred for 3 h. This solution was filtered through a 2 cm pad of Celite to give a clear, yellow solution. Hexane (75 cm^3) was carefully layered on the dichloromethane layer. The system was allowed to equilibrate for 24 h. The solvent was decanted by cannula and the crystals were vacuum dried to afford **3** as yellow rods (1.87 g, 87% based on titanium tetrachloride): m.p. 98°C (dec); IR (Nujol, cm^{-1}) 2724 (w), 2678 (w), 2518 (s, S—H), 1443 (s), 1381 (s), 1325 (m), 1294 (w), 1257 (w), 1236 (w), 1221 (w), 1144 (m), 1092 (m), 1061 (w), 1051 (w), 1040 (w), 994 (w), 983 (w), 968 (w), 958 (w), 865 (s), 828 (w), 766 (w), 715 (w), 679 (w), 642 (w); ^{1}H NMR ($CDCl_3$, 23°C, δ) 3.95 (m, C*H*), 3.72 (broad s, S—H), 3.59 (m, C*H*), 3.55 (broad s, S—*H*), 1.67 (d, J = 5.7 Hz, CH_3), 1.58 (d, J = 6.9 Hz, CH_3); ^{13}C{^{1}H} ($CDCl_3$, 23°C, ppm) 52.10 (broad s, *C*H), 49.38 (broad s, *C*H), 22.68 (s, *C*H_3), 18.43 (s, *C*H_3). Found: C, 15.46; H, 3.24. Calc. for $C_4H_{10}Cl_4S_2Ti$: C, 15.40; H, 3.23%.

Preparation of $TiCl_4(HSCH_2CH_2CH_3)_2$

A 5-mm NMR tube was charged with titanium tetrachloride (0.010 cm^3, 0.090 mmol) and chloroform-*d* (0.70 cm^3) and was fitted with a rubber septum. *n*-Propylthiol (0.020 cm^3, 0.20 mmol) was added into the NMR tube by syringe to afford a bright yellow solution of $TiCl_4(HSCH_2CH_2CH_3)_2$: ^{1}H NMR ($CDCl_3$, 23°C, δ) 3.15 (broad s, S—*H*), 2.97 (t, CH_2CH$_2$CH$_3$, J = 6.9 Hz), 1.78 (sextet, CH$_2$CH_2CH$_3$, J = 7.2 Hz), 1.04 (t, CH$_2$CH$_2$CH_3, J = 7.5 Hz); ^{13}C{^{1}H} NMR ($CDCl_3$, 23°C, ppm) 34.23 (s, *C*H$_2$CH$_2$CH$_3$), 25.09 (s, CH$_2$*C*H$_2$CH$_3$), 12.98 (s, CH$_2$CH$_2$*C*H$_3$).

Preparation of $TiCl_4(HSCH(CH_3)_2)_2$

In a fashion similar to $TiCl_4(HSCH_2CH_2CH_3)_2$, titanium tetrachloride (0.010 cm^3, 0.090 mmol) and isopropylthiol (0.020 cm^3, 0.20 mmol) were reacted to afford a bright yellow solution of $TiCl_4(HSCH(CH_3)_2)_2$ in chloroform-*d* (0.70 cm^3): ^1H NMR ($CDCl_3$, 23°C, δ) 3.29 (m, *H*SCH$(CH_3)_2$), 2.12 (broad s, HSC*H*$(CH_3)_2$), 1.35 (d, $J = 6.6$ Hz, HSCH$(CH_3)_2$); $^{13}C\{^1H\}$ NMR ($CDCl_3$, 23°C, ppm) 33.16 (s, HS*C*H$(CH_3)_2$), 26.92 (s, HSCH$(CH_3)_2$).

Preparation of $TiCl_4(SC_4H_8)_2$ (**4**)

A 100-cm^3 Schlenk flask was charged with titanium tetrachloride (0.10 cm^3, 0.91 mmol), hexane (30 cm^3), a stir bar and was fitted with a rubber septum. The contents were cooled to 0°C and tetrahydrothiophene (0.16 cm^3, 1.8 mmol) was added by syringe to afford an orange solution. This solution was stirred for 1.5 h and the volatiles were pumped off to afford **4** as an orange solid (0.29 g, 87% based on titanium tetrachloride): m.p. 132°C (with sublimation); IR (Nujol, cm^{-1}) 1438 (s), 1424 (m), 1405 (w), 1304 (m), 1252 (s), 1204 (w), 1128 (m), 1090 (broad, w), 1066 (m), 1013 (s), 955 (m), 879 (w), 869 (w), 798 (s), 659 (m); ^1H NMR ($CDCl_3$, 23°C, δ) 3.35 (t, $J = 6.0$ Hz, SC*H*$_2$), 2.13 (m, SCH$_2$C*H*$_2$); $^{13}C\{^1H\}$ NMR ($CDCl_3$, 23°C, ppm) 39.90 (s, S*C*H$_2$), 29.81 (s, SCH$_2$*C*H$_2$). Found: C, 24.95; H, 4.28. Calc. for $C_8H_{16}Cl_4S_2Ti$: C, 26.25; H, 4.41%.

Preparation of $TiCl_4(SC_5H_{10})_2$ (**5**)

In a fashion similar to the preparation of **1**, titanium tetrachloride (0.10 cm^3, 0.91 mmol) and pentamethylene sulfide (0.19 cm^3, 1.8 mmol) were reacted to afford **5** as an orange solid (0.35 g, 97% based on titanium tetrachloride): m.p. 127°C (with sublimation); IR (Nujol, cm^{-1}) 1453 (s), 1435 (s), 1420 (s), 1367 (w), 1352 (m), 1346 (m), 1336 (m), 1300 (m), 1266 (m), 1258 (m), 1231 (m), 1210 (m), 1202 (m), 1143 (w), 1095 (m), 1064 (m), 1013 (m), 966 (s), 961 (s), 894 (s), 838 (w), 828 (w), 813 (m), 739 (w), 719 (w), 678 (w), 645 (w), 636 (m); ^1H NMR ($CDCl_3$, 23°C, δ) 3.11 (t, $J = 6.0$ Hz, SC*H*$_2$), 1.92 (m, C*H*$_2$), 1.62 (m, C*H*$_2$); $^{13}C\{^1H\}$ NMR ($CDCl_3$, 23°C, ppm) 37.97 (s, S*C*H$_2$), 27.02 (s, *C*H$_2$), 25.42 (s, C*H*$_2$). Found: C, 30.41; H, 5.13. Calc. for $C_{10}H_{20}Cl_4S_2Ti$: C, 30.48; H, 5.12%.

Preparation of $TiCl_4((CH_3)_2S)_2$ (**6**)

In a fashion similar to the preparation of **1**, titanium tetrachloride (3.0 cm^3, 27.4 mmol) and dimethyl sulfide (4.02 cm^3, 54.7 mmol) were reacted to afford **6** as an orange solid (8.41 g, 98% based on titanium tetrachloride): m.p. 79–82°C; IR (Nujol, cm^{-1}) 1597 (w), 1426 (s), 1422 (s), 1411 (m), 1366 (w), 1325 (w), 1303 (w), 1258 (m), 1104 (w), 1095 (w), 1089 (w), 1066 (w), 1062 (w), 1028 (m), 1019 (m), 978 (w), 970 (w), 922 (w), 916 (w), 796 (m); ^1H NMR ($CDCl_3$ 23°C, δ) 2.54 (s, C*H*$_3$); $^{13}C\{^1H\}$ NMR ($CDCl_3$, 23°C, ppm) 25.00 (s, *C*H$_3$). Found: C, 15.17; H, 3.75. Calc. for $C_4H_{12}Cl_4S_2Ti$: C, 15.30; H, 3.85%.

Preparation of $(TiCl_4)_2(CH_3SSCH_3)$ (**7**)

A 250-cm^3 Schlenk flask was charged with titanium tetrachloride (3.0 cm^3, 27.4 mmol), hexane (60 cm^3), and a stir bar and was fitted with a rubber septum. The contents were cooled to 0°C and dimethyl disulfide (4.93 cm^3, 54.7 mmol) was added *via* a syringe to afford an orange solution. This solution was stirred for 1.5 h and the volatiles were pumped off to afford **7** as a yellow-brown solid (6.34 g, 98% based on titanium tetrachloride): m.p. 63–64°C (dec. with sublimation); IR (Nujol, cm^{-1}) 1605 (w), 1446 (s), 1408 (w), 1365 (w), 1257 (w), 1084 (w), 1075 (w), 1058 (w), 1022 (w), 799 (m); ^1H NMR ($CDCl_3$, 23°C, δ) 2.56 (s, C*H*$_3$); $^{13}C\{^1H\}$ NMR ($CDCl_3$, 23°C, ppm) 23.20 (s, *C*H$_3$). Found: C, 5.12; H, 1.27. Calc. for $C_2H_6Cl_8S_2Ti_2$: C, 5.07; H, 1.28%.

Crystal structure determinations of **4** *and* **7**

Crystals of **4** and **7** were grown by sublimation. Suitable crystals were selected and mounted in nitrogen-flushed, thin-walled capillary tubes. The unit-cell parameters were obtained by the least-squares refinement of the angular settings of 25 reflections ($20° \leqslant 2\theta \leqslant 25°$). The systematic absences in the diffraction data for **4** are consistent with the space groups *Pnma* and $Pn2_1a$; for **7**, $P\bar{1}$ and $P1$. *E*-statistics suggested the centrosymmetric alternative for **4** and the non-centrosymmetric space group for **7**. The space group assignments were verified subsequently through further refinement. The η parameter refined to 0.87(7), indicating that the absolute structure has been determined for **7**.

Structure **4** was solved by direct methods while **7** was solved with a sharpened Patterson map. Both structures were completed by subsequent difference Fourier syntheses and were refined by full-matrix least-squares procedures. The tetrahydrothiophene carbon atoms of **4** were initially refined anisotropically, however, this led to unacceptable bond distances caused by the averaging of the positions of unique atoms with reflections on the mirror plane. Thus, the tetrahydrothiophene carbon atoms were refined isotropically with a restrained refinable bond distance. All other non-hydrogen atoms were refined with anisotropic displacement coefficients. Hydrogen atoms were treated as idealized contributions. All software and sources of the scattering factors are contained in either the SHELXTL (5.1) or the SHELXTL

PLUS (4.2) program libraries (G. Sheldrick, Siemens XRD, Madison, WI).

RESULTS

Organothiol adducts

Stable, easily isolated adducts were obtained upon treatment of titanium tetrachloride with two equivalents of cyclohexylthiol, cyclopentylthiol, or 2,3-butanedithiol in hexane at ambient temperature. Workup afforded spectroscopically pure yellow solids of $TiCl_4(C_6H_{11}SH)_2$ (**1**, 77%), $TiCl_4(C_5H_9SH)_2$ (**2**, 89%), and $TiCl_4(C_4H_8(SH)_2)$ (**3**, 87%), respectively (eq. (1)). Sublimation of these crude products (60°C, 0.1 mmHg) yielded analytically pure, moisture-sensitive yellow crystals of **1–3**. Complexes **1–3** were fully characterized by spectroscopic and analytical techniques. The X-ray crystal structure of **1** has been previously published [7]. Compound **3** exists as a 1 : 1 mixture containing syn- and anti-2,3-butanedithiol ligands. The mixture is evident in the NMR spectra, which reveal resonances for two similar 2,3-butanedithiol ligands. The infrared spectra showed sharp S—H stretches (**1**, $\nu_{SH} = 2492$ cm^{-1}; **2** $\nu_{SH} = 2520$, 2505 cm^{-1}; **3**, $\nu_{SH} = 2518$ cm^{-1}), at values slightly lower than the neat thiols, (e.g., cyclohexylthiol, 2557 cm^{-1}). We propose that the lower S—H stretches in **1–3** are due to S—H···X (X = S or Cl) hydrogen bonding [12].

$$TiCl_4 + 2\,RSH \xrightarrow{\text{hexane, 23 °C}} TiCl_4(HSR)_2 \quad (1)$$

1, R = cyclohexyl
2, R = cyclopentyl
3, 2 RSH = 2,3-butanedithiol

Reaction of titanium tetrachloride with low-boiling organothiols, such as 1-propanethiol (b.p. 67°C) and 2-propanethiol (b.p. 57°C), afforded adducts of the formula $TiCl_4(RSH)_2$. However, these adducts were exceptionally difficult to handle, due to their high volatility (estimated vapor pressures $\geqslant 10$ mmHg at 22°C). Use of hexane as solvent gave isolation difficulties, since evaporation of the solvent also led to loss of the desired complexes. It was found that the isopropylthiol and propanethiol adducts could be prepared by mixing titanium tetrachloride with 2 equivalents of the thiol at ambient temperature. Using this procedure, relatively pure samples were obtained, which were characterized by ^{1}H and $^{13}C\{^1H\}$ NMR spectroscopy. Despite the absence of a solvent, we were unable to purify $TiCl_4(n\text{PrSH})_2$ or $TiCl_4(i\text{PrSH})_2$ on the small scales (*ca.* 2 mmol) that were used. It is likely that the adducts readily dissociate to titanium tetrachloride and the respective thiols. The adducts were not explored further, since they posed no advantage over the more easily manipulated complexes **1–3**.

Organosulfides

Treatment of titanium tetrachloride with two equivalents of tetrahydrothiophene, pentamethylene sulfide, or dimethyl sulfide in hexane at ambient temperature, followed by evaporation of the solvent afforded spectroscopically pure orange solids of $TiCl_4(C_4H_8S)_2$ (**4**, 87%), $TiCl_4(C_5H_{10}S)_2$ (**5**, 97%), and $TiCl_4(C_2H_6S)_2$ (**6**, 98%), respectively (eq. (2)). Sublimation of these crude products (25–50°C, 0.1 mmHg) yielded analytically pure, moisture-sensitive orange crystals of **4–6**. Complexes **4–6** were fully characterized by spectroscopic and analytical techniques. The ^{1}H and $^{13}C\{^1H\}$ NMR spectra of **4–6** were particularly diagnostic of the adduct structures and showed downfield shifts relative to the free ligands. For example, **6** revealed resonances at δ 2.54 in the ^{1}H NMR spectrum and 25.00 ppm in the $^{13}C\{^1H\}$ NMR spectrum. The analogous values for free dimethyl sulfide were δ 2.04 and 17.81 ppm. The vapor pressures of **4–6** were estimated to be *ca.* 1–2 mmHg at 22°C, as determined by differential pressure measurements. Again, these vapor pressures may reflect equilibrium dissociation of the complex to thiol and titanium tetrachloride. These values are similar to that of **1**, which we have previously reported to be a single-source precursor to titanium disulfide films [7]. Complexes **4–6** have been previously reported, and our physical data generally agree with those of previous workers [9–11].

$$TiCl_4 + 2\,R_2S \xrightarrow{\text{hexane, 23 °C}} TiCl_4(R_2S)_2 \quad (2)$$

4, $R_2 = (CH_2)_4$
5, $R_2 = (CH_2)_5$
6, $R_2 = 2\,CH_3$

Organodisulfides

Treatment of titanium tetrachloride with dimethyl disulfide ($\geqslant 0.5$ equiv.) under conditions used to prepare **1–6** afforded $(TiCl_4)_2(CH_3SSCH_3)$ (**7**, 98%) as a yellow-brown powder upon workup (eq. (3)). NMR analysis of **7** revealed intact methyl groups with downfield shifts (^{1}H NMR δ 2.56, $^{13}C\{^1H\}$ NMR 23.20 ppm), relative to free methyl disulfide (^{1}H NMR δ 2.38, $^{13}C\{^1H\}$ NMR 21.94 ppm), which suggested an adduct structure. The microanalysis results for **7** were incompatible with a structure analogous to **1–6**, but rather implied a formulation with a 2 : 1 ratio between titanium tetrachloride and methyl disulfide. The molecular geometry of **7** was established by an X-ray structure determination (*vide infra*). Complex **7** was easily sublimed and possessed a vapor pressure similar

to **1–6**. Treatment of titanium tetrachloride with isopropyl disulfide or tert-butyl disulfide under conditions used to prepare **7** afforded complicated mixtures that we are still studying.

$$2\,TiCl_4 + CH_3SSCH_3 \xrightarrow{\text{hexane, 23 °C}} (TiCl_4)_2(CH_3SSCH_3) \quad (3)$$

7

Crystal structures of **4** *and* **7**

The crystal structures of **4** and **7** were determined in order to establish their nuclearities and molecular geometries. X-ray data were collected under the conditions summarized in Table 1. Bond lengths and bond angles are provided in Tables 2 and 3. Perspective views of **4** and **7** are shown in Figs 1 and 2.

Complex **4** crystallized as a distorted octahedral monomer with cis-tetrahydrothiophene ligands. The tetrahydrothiophene ligands were disordered; the disorder was treated as described in the experimental section. The titanium–chlorine bonds that were trans to sulfur atoms (Ti—Cl(1) 2.232(8) Å, Ti—Cl(3) 2.233(8) Å) were *ca.* 0.05 Å shorter than the chlorines that were mutually trans (Ti—Cl(2,2A) 2.280(4) Å). The shorter bond lengths of the titanium-chlorine bonds that are trans to sulfur can be understood by the weaker trans influence of sulfur, relative to chloride. The titanium–sulfur bond lengths were 2.626(7) Å (Ti—S(1)) and 2.625(7) Å (Ti—S(2)). The cis-chlorine–titanium–chlorine angles ranged from 97.0–98.9° (av. = 97.5°), while the chlorine–titanium–sulfur angles ranged from 81.1–90.1° (av. = 83.9°). The trans chlorine–titanium–chlorine angle (Cl(2)—Ti—Cl(2A)) was 158.0(2)°, which is a considerable deviation from the idealized 180° angle. The chlorine–titanium–sulfur angles were 171.3(3)° (Cl(1)—Ti—S(2)) and 171.0(3)° (Cl(3)—Ti—S(1)). The slightly extended angles associated with cis chlorine–titanium–chlorine can be attributed to steric crowding about the titanium center caused by the shorter titanium–chlorine bonds, relative to the titanium–sulfur bonds. Such distortions were compensated by chlorine–titanium–sulfur angles that were slightly less than 90°. The disorder in the tetrahydrothiophene ligands, while successfully modeled, led to large uncertainties in the bond lengths associated with the ligands.

Table 1. Experimental crystallographic data for **4** and **7**

	4	**7**
Chemical formula	$C_8H_{16}Cl_4S_2Ti$	$C_2H_6Cl_8S_2Ti_2$
Formula weight	366.0	473.6
Space group	*Pnma* (No. 62)	*P*1 (No. 1)
a (Å)	14.285(5)	6.403(2)
b (Å)	8.574(3)	7.224(4)
c (Å)	12.580(3)	9.410(3)
α (°)		110.66(3)
β (°)		101.48(2)
γ (°)		99.15(4)
V (Å^3)	1540.7(8)	386.5(7)
Z	4	1
T (K)	296	296
λ (Å)	0.71073	0.71073
$\rho_{calc.}$ (g cm^{-3})	1.578	2.035
μ (cm^{-1})	14.90	26.48
Trans. coeff.	—	0.538–0.492
$R(F)^a$ (%)	5.29	4.11
$R(wF)^a$ (%)	6.24	4.34

$^a R = (\Sigma||\Delta F|)/\Sigma|F_o|$; $wR = [(\Sigma w|\Delta F|^2)/\Sigma wF_o^2]^{1/2}$.

Complex **7** crystallized as a Ti_2Cl_8 unit with each sulfur of the dimethyl disulfide ligand bonded to a titanium atom. There were three distinct types of titanium–chlorine bonds present in **7**. The bridging chlorides (Cl(1), Cl(2)) were symmetrically bonded and showed titanium–chlorine bond lengths ranging from 2.450–2.482 Å (av. = 2.464 Å). The equatorial chlorides (Cl(3), Cl(4), Cl(6), Cl(7)) (all trans to bridging chlorides) exhibited titanium–chlorine bond lengths of 2.187–2.200 Å (av. = 2.194 Å). These bonds are *ca.* 0.09 Å shorter than the titanium–chlorine bond in **4** that is trans to a terminal chloride. The shorter equatorial titanium–chlorine bonds in **7** are the result of a diminished trans influence of a bridging chloride, relative to a terminal chloride. The third type of titanium–chlorine bond was represented by the chlorines trans to the sulfurs. These bond lengths were 2.190(3) Å (Ti(1)—Cl(5)) and 2.184(3) Å (Ti(2)—Cl(8)), and were not significantly different than the equatorial titanium–chlorine bond lengths. The geometry about each titanium exhibited substantial deviations from idealized octahedral geometry. The cis chlorine–titanium–chlorine angles ranged from 87.4–102.6°, with an average value of 95.1°. The angles associated with the bridging chlorides (Cl(1)—Ti(1)—Cl(2) 79.0(1)°, Cl(1)—Ti(2)—Cl(2) 78.8(1)°) were constrained to be considerably less than an idealized 90° by the Ti_2Cl_2 ring. The trans chlorine–titanium–chlorine angles ranged from 159.7–164.6° (av. = 161.8°). The data for the dimethyl disulfide ligand in **7** merit discussion. The sulfur–sulfur bond length was 2.052(3) Å, while the sulfur–carbon bond lengths were 1.784(5) Å (S(1)—C(1)) and 1.801(6) Å (S(2)—C(2)). The angles associated with the dimethyl disulfide ligand illustrate the geometrical distortions that are required to bind this ligand to the Ti_2Cl_8 moiety. The sulfurs were bent in toward the center of the Ti_2Cl_2 core. In addition, each sulfur was bent out of the plane containing Ti(1), Cl(5), Ti(2), and Cl(8) (i.e., S(1)—Ti(1)—Cl(1) 72.6(1)°, S(1)—Ti(1)—Cl(2) 86.2(1)°, S(1)—Ti(1)—Cl(3) 79.5(1)°, S(1)—Ti(1)—Cl(4) 91.8(1)°; S(2)—Ti(2)—Cl(1) 84.6(1)°, S(2)—Ti(2)—Cl(2) 73.1(1)°, S(2)—Ti(2)—Cl(6)

Table 2. Bond lengths (Å) and selected angles (°) for **4**

Ti—Cl(1)	2.232(8)	Ti—Cl(2)	2.280(4)
Ti—Cl(3)	2.233(8)	Ti—S(1)	2.626(7)
Ti—S(2)	2.625(7)	Ti—Cl(2A)	2.280(4)
S(1)—C(1)	1.823(18)	S(1)—C(1A)	1.823(18)
S(2)—C(3)	1.811(17)	S(2)—C(3A)	1.811(17)
C(1)—C(2)	1.549(31)	C(1)—C(2′A)	1.433(37)
C(2)—C(2′)	1.549(42)	C(2)—C(2A)	1.077(47)
C(2)—C(2′A)	0.739(42)	C(2′)-C(1A)	1.433(37)
C(2′)—C(2A)	0.739(42)	C(2′)—C(2′A)	1.723(69)
C(3)—C(4)	1.549(30)	C(3)—C(4′A)	1.449(38)
C(4)—C(4′)	1.549(44)	C(4)—C(4A)	1.107(51)
C(4)—C(4′A)	0.775(44)	C(4′)—C(3A)	1.449(38)
C(4′)—C(4A)	0.775(44)	C(4′)—C(4′A)	1.626(73)
Cl(1)—Ti—Cl(2)	97.0(2)	Cl(1)—Ti—Cl(3)	98.9(3)
Cl(2)—Ti—Cl(3)	97.3(2)	Cl(1)—Ti—S(1)	90.1(3)
Cl(2)—Ti—S(1)	81.5(1)	Cl(3)—Ti—S(1)	171.0(3)
Cl(1)—Ti—S(2)	171.3(3)	Cl(2)—Ti—S(2)	81.8(1)
Cl(3)—Ti—S(2)	89.8(3)	S(1)—Ti—S(2)	81.1(2)
Cl(1)—Ti—Cl(2A)	97.0(2)	Cl(2)—Ti—Cl(2A)	158.0(2)
Cl(3)—Ti—Cl(2A)	97.3(2)	S(1)—Ti—Cl(2A)	81.5(1)
S(2)—Ti—Cl(2A)	81.8(1)		

Table 3. Bond lengths (Å) and angles (°) for **7**

Ti(1)—S(1)	2.712(3)	Ti(1)—Cl(1)	2.459(3)
Ti(1)—Cl(2)	2.463(2)	Ti(1)—Cl(3)	2.200(2)
Ti(1)—Cl(4)	2.187(3)	Ti(1)—Cl(5)	2.190(3)
Ti(2)—S(2)	2.742(3)	Ti(2)—Cl(1)	2.482(3)
Ti(2)—Cl(2)	2.450(3)	Ti(2)—Cl(6)	2.193(3)
Ti(2)—Cl(7)	2.195(4)	Ti(2)—Cl(8)	2.184(3)
S(1)—S(2)	2.052(3)	S(1)—C(1)	1.784(5)
S(2)—C(2)	1.801(6)		
S(1)—Ti(1)—Cl(1)	72.6(1)	S(1)—Ti(1)—Cl(2)	86.2(1)
Cl(1)—Ti(1)—Ti(2)	79.0(1)	S(1)—Ti(1)—Cl(3)	79.5(1)
Cl(1)—Ti(1)—Cl(3)	91.1(1)	Cl(2)—Ti(1)—Cl(3)	164.6(1)
S(1)—Ti(1)—Cl(4)	91.8(1)	Cl(1)—Ti(1)—Cl(4)	160.1(1)
Cl(2)—Ti(1)—Cl(4)	87.9(1)	Cl(3)—Ti(1)—Cl(4)	98.3(1)
S(1)—Ti(1)—Cl(5)	165.5(1)	Cl(1)—Ti(1)—Cl(5)	93.0(1)
Cl(2)—Ti(1)—Cl(5)	92.7(1)	Cl(3)—Ti(1)—Cl(5)	99.6(1)
Cl(4)—Ti(1)—Cl(5)	102.6(1)	S(2)—Ti(2)—Cl(1)	84.6(1)
S(2)—Ti(2)—Cl(2)	73.1(1)	Cl(1)—Ti(2)—Cl(2)	78.8(1)
S(2)—Ti(2)—Cl(6)	91.0(1)	Cl(1)—Ti(2)—Cl(6)	87.4(1)
Cl(2)—Ti(2)—Cl(6)	159.7(1)	S(2)—Ti(2)—Cl(7)	79.5(1)
Cl(1)—Ti(2)—Cl(7)	163.0(1)	Cl(2)—Ti(2)—Cl(7)	90.7(1)
Cl(6)—Ti(2)—Cl(7)	98.9(1)	S(2)—Ti(2)—Cl(8)	166.8(1)
Cl(1)—Ti(2)—Cl(8)	93.5(1)	Cl(2)—Ti(2)—Cl(8)	93.7(1)
Cl(6)—Ti(2)—Cl(8)	102.0(1)	Cl(7)—Ti(2)—Cl(8)	100.5(1)
Ti(1)—S(1)—S(2)	103.9(1)	Ti(2)—S(2)—S(1)	103.9(1)
Ti(1)—Cl(1)—Ti(2)	99.6(1)	Ti(1)—Cl(2)—Ti(2)	100.4(1)
Ti(1)—S(1)—C(1)	109.2(2)	Ti(2)—S(2)—C(2)	110.4(2)
S(2)—S(1)—C(1)	102.3(2)	S(1)—S(2)—C(2)	103.4(2)

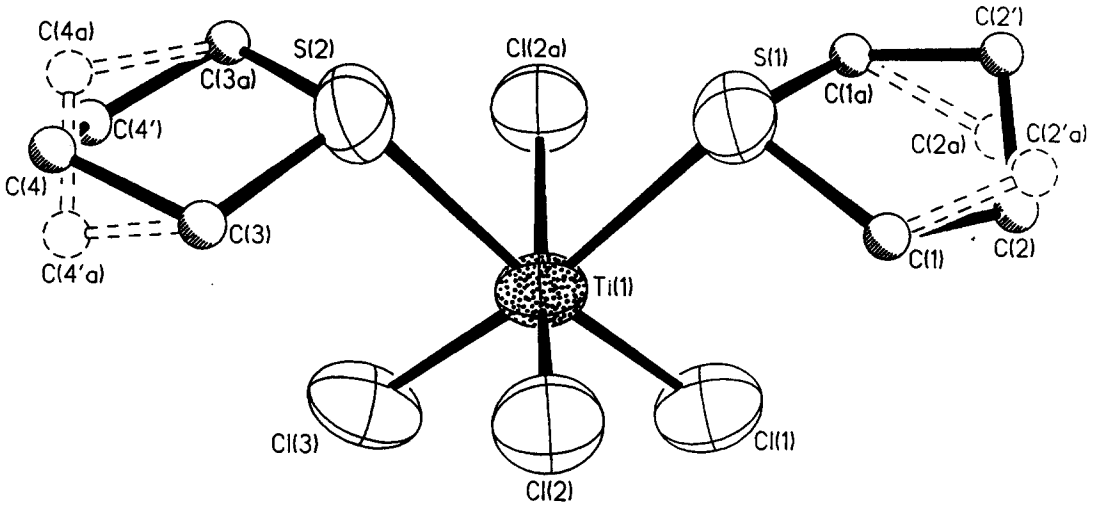

Fig. 1. Perspective view of **4** drawn with 35% probability ellipsoids.

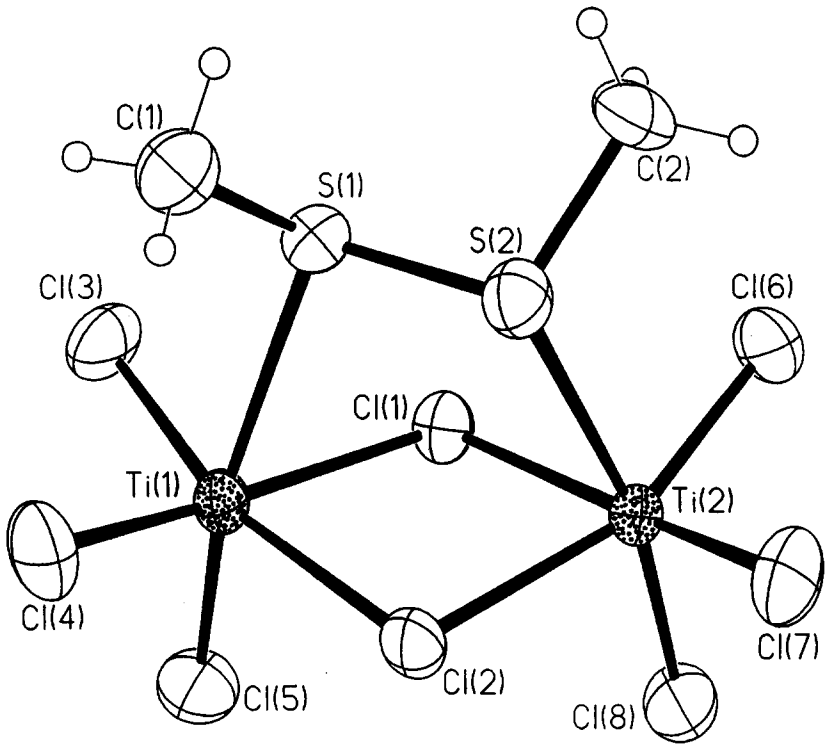

Fig. 2. Perspective view of **7** drawn with 35% probability ellipsoids.

91.0(1)°, S(2)—Ti(2)—Cl(7) 79.5(1)°). In effect, the dimethyl disulfide ligand is bonded to the Ti_2Cl_8 fragment with an approximate C_2 axis that runs through the center of the S(1)—S(2) bond and the center of the Ti_2Cl_2 ring, although such symmetry is not crystallographically imposed. The sum of the angles about each sulfur (S(1) 315.4°, S(2) 317.7°) is slightly less than that expected for pyramidal, trisubstituted sulfur with one lone pair (*ca* 328.5°).

Solution structures

We sought to determine if the solid state structures established for **4** and **7** persisted in solution. It is possible that these structures happen to be the most crystalline phases, and that different structures could be present in solution. Accordingly, variable temperature ^1H NMR spectra were recorded for **6** and **7**. With **6** in dichloromethane-d_2 the methyl singlet was

invariant at δ 2.51 between +20 and −80°C. At −80°C, a trace of dimethyl sulfide (δ 2.06, *ca.* 10% of total integration) was present. With **7** in dichloromethane-d_2, the methyl signal in the ^{1}H NMR spectrum moved steadily downfield from δ 2.52 at +20°C to δ 3.00 at −80°C. Between +20°C and −60°C, there was only one methyl singlet present. However, below −70°C a second minor methyl singlet appeared. At −80°C, the major species was at δ 3.00, the minor species appeared at δ 2.89, and the ratio between the two was 87 : 13. Free methyl disulfide (^{1}H NMR δ 2.38 at +20°C) was not observed at any temperature.

DISCUSSION

The motivation for the present study was to characterize complexes that might be involved in chemical vapor deposition processes. Furthermore, such compounds might serve as single-source precursors to titanium disulfide films. With thiols and sulfides, adducts are formed that are monomeric in the solid state by X-ray crystallography. The static chemical shift of the methyl groups in **6** suggests that there are not major changes in the coordination sphere of **6** in solution between +20 and −80°C. We propose that **6** is monomeric and 6-coordinate in solution, with a structure similar to that observed in the solid state. Based upon the easy formation of **1–6**, it is very likely that adducts of the formula $TiCl_4(HSR)_2$ and $TiCl_4(R_2S)_2$ form in the gas phase, at least in equilibrium with titanium tetrachloride and the organosulfur compounds, and are present in a CVD reaction employing titanium tetrachloride and these sulfur compounds.

Complexes **4** and **5** did not serve as single-source precursors to films under CVD conditions, while **6** and **7** gave titanium disulfide films at reactor temperatures between 400–600°C [10]. We suggest that the failure of **4** and **5** to function as precursors to titanium disulfide films can be attributed to kinetically slow β-hydrogen cleavage from the cyclic sulfur ligands due to the strained nature of such a transition state, relative to an acyclic sulfur ligand. We have previously noted that the atmospheric pressure CVD reaction of titanium tetrachloride with dimethyl sulfide or dimethyl disulfide fails to afford titanium disulfide films under conditions where tert-butythiol gives excellent coatings [6]. The presence of preformed titanium–sulfur bonds in **6** and **7** must provide a kinetically viable path for titanium disulfide film formation, while a similar path is inefficient in the two-component atmospheric pressure CVD process.

Adduct **7** adopts a very different structure than is found in **1–6**. The dinuclear structure appears to form because the disulfide ligand cannot bind strongly to the small titanium center in a bidentate fashion. Instead, the methyl disulfide coordinates to two faces of a Ti_2Cl_8 unit, leading to a bridging methyl disulfide ligand. The large chemical shift change observed upon cooling **7** from +20 to −80°C raises the possibility that there is a major change that is occurring in the coordination sphere in this temperature range. While the data do not require a change in structure, a possible structure change would be a rapid equilibrium between dinuclear **7** and a monomeric titanium tetrachloride adduct with an η^2-dimethyl disulfide ligand. Accordingly, **7** may simply be the most crystalline complex and may not be the major species in dichloromethane solution. Freezing point depression molecular weight measurements on **7** in cyclohexane and benzene designed to probe this point were inconclusive due to preciptation near the freezing points of these solvents.

Complex **7** functions as a single-source precursor to titanium disulfide films at reactor temperatures of 400–600°C [13]. Schleich has reported that the two-component CVD reaction of titanium tetrachloride with di-butyl disulfide affords titanium trisulfide films between 260–400°C, and titanium disulfide films above 400°C [4]. By contrast, di-tert-butyl sulfide gave titanium disulfide films above 260°C. It was proposed that di-butyl disulfide acts as a disulfido ion synthon, which leads to the sulfur-rich titanium phase as a kinetic product at low deposition temperatures. Our present data do not allow us to comment on Schleich's work in any detail. However, our results demonstrate that the interaction of organic sulfides and organic disulfides with titanium tetrachloride leads to different structure types. The formation of dinuclear adducts of organic disulfides may be a factor that leads to sulfur-rich phases at low temperatures. This could be a significant observation, given the current interest in the "design" of precursors to desired phases. We are continuing to explore the coordination chemistry of titanium tetrachloride with organosulfur compounds in the context of chemical vapor deposition and will report further studies in the near future.

Acknowledgements—We are grateful to the NSF (CHE-9123339 and CHE-9510712 to C.H.W.) for support of this research.

REFERENCES

1. For leading references to the use of titanium disulfide as cathodes in lithium batteries, see: Venkatasetty, H. V., ed, Lithium Battery Technology; Wiley-Interscience, New York, 1984; Kanehori, K.; Matsumoto, K.; Miyauchi, K. and Kudo, T., *Solid State Ionics*, 1983, **9/10**, 1445; Whittingham, M. S., *Prog. Solid State Chem.*, 1978, **12**, 41; Wilson, J. A. and Yoffe, A. D., *Adv. Phys.*, 1969, **18**, 193; Scrosati, B., *Electrochim. Acta*, 1981, **26**, 1559.
2. For leading references, see: Bill, R. C., *Wear*, 1985, **106**, 283; Newnham, J. and Singh, K., *Sci. Tech. Aerosp. Rep.*, 1977, **15**, Abstr. No. N77-32323; Zuev, A. M. and Klabakov, A. G., *Tr., Chelyab, Politekh. Inst.*, 1974, **152**, 127; *Chem.*

Abstr., 1977, **87,** 120191f; Hopkins, V. and Campbell, M., *Lubr. Eng.*, 1977, **33,** 252; McCommell, B. D., *Natl. Bur. Stand. (U.S.) Spec. Publ.*, 1976, **452,** 124.

3. CVD routes to titanium disulfide films: (a) Kanehori, K., Kirino, F., Miyauchi, K. and Kudo, T., *J. Electrochem. Soc.*, 1989, **136,** 1265; (b) Kikkawa, S., Miyazaki, M. and Koizumi, M., *J. Mater. Res.*, 1990, **5,** 2894; (c) Kanehori, K., Ito, Y., Kirino, F., Miyauchi, K. and Kudo, T., *Solid State Ionics*, 1986, **18/19**, 818; (d) Zehnder, D., Deshpandey, C., Dunn, B. and Bunshah, R. F., *Solid State Ionics*, 1986, **18/19**, 813; (e) Ogumi, Z., Uchimoto, Y. and Takehara, Z. I., *J. Power Sources*, 1989, **26,** 457; (f) Kanehori, Y., Ogumi, Z. and Takehara, Z., *GS News Tech. Rep.*, 1987, **46,** 21.
4. Chang, H. S. W. and Schleich, D. M., *J. Solid State Chem.*, 1992, **100,** 62.
5. For other routes to titanium disulfide films, see: Meunier, G., Dormoy, R. and Levasseur, A., *Mater. Sci. Eng., B*, 1989, **B3,** 19; Uchida, T., Fuji, Y. and Wakihara, M., *Proc. Electrochem. Soc.*, 1988, **88,** 401.
6. Winter, C. H., Lewkebandara, T. S. and Proscia, J. W., *Chem. Mater.*, 1992, **4,** 1144; Winter, C. H. and Lewkebandara, T. S., US Patents 5 112 650, 1992; 5 298 295, 1994; 5 409 735, 1995; 5 409 735, 1995.
7. Winter, C. H., Lewkebandara, T. S., Proscia, J. W. and Rheingold, A. L., *Inorg. Chem.*, 1993, **32,** 3807.
8. Thiol and hydrogen sulfide adducts: Demarçay, M. E., *Bull. Soc. Chim. Fr.*, 1873, **20,** 127; Biltz, W. and Keunecke, E., *Z. Anorg. Chem.*, 1925, **147,** 171; Ralston, A. W. and Wilkinson, J. A., *J. Am. Chem. Soc.*, 1928, **50,** 258; Ahuja, H. S., Jain, S. C. and Rivest, R., *J. Inorg. Nucl. Chem.*, 1968, **30,** 2459; Bosnea, L. and Fisel, S., *An. Stiint. Univ. "Al. I. Cuza" Iais, Sect.* 1c, 1974, **20,** 75; Bensalem, A. and Schleich, D. M., *Mat. Res. Bull.*, 1988, **23,** 857.
9. Adducts of tetrahydrothiophene and pentamethylene sulfide: Kharlamova, E. N., Guryanova, E. N. and Kharchenko, V. G., *Zh. Struk. Khim.*, 1971, **12,** 637; Goldshtein, I. P., Kharlamova, E. N. and Guryanova, E. N., *J. Gen. Chem. USSR*, 1968, **38,** 1925; Kharlamova, E. N. and Guryanova, E. N., *Zh. Struk. Khim.*, 1965, **6,** 859; Ahuja, H. S., Jain, S. C. and Rivest, R., *J. Inorg. Nucl. Chem.*, 1968, **30,** 2459; Hessett, B. and Perkins, P. G., *J. Chem. Soc.*, 1970, 3229.
10. Adducts of dimethyl sulfide: Valloton, M. and Herbach, A. E., *Helv. Chim. Acta*, 1975, **58,** 2272; Baker, K. and Fowles, G. W. A., *J. Less Common Metals*, 1965, **8,** 47; Turin, E., Nielson, R. M. and Merbach, A. E., *Inorg. Chim. Acta*, 1987, **134,** 67; Beattie, I. R. and Webster, M., *J. Chem. Soc.*, 1964, 3507; Westland, A. D. and Westland, L., *Can. J. Chem.*, 1965, **43,** 426.
11. For other organosulfur adducts of titanium tetrachloride, see: Clark, R. J. H. and Errington, W., *Inorg. Chem.*, 1966, **5,** 650; Wade, S. R. and Willey, G. R., *Inorg. Chim. Acta*, 1983, **72,** 201.
12. For a discussion of E—H···Cl—Ti hydrogen bonding, see: Winter, C. H., Sheridan, P. H. and Heeg, M. J., *Inorg. Chem.*, 1991, **30,** 1962.
13. McKarns, P. J., Lewkebandara, T. S., Proscia, J. W. and Winter, C. H., unpublished results, Wayne State University.

Pergamon

PII: S0277-5387(97)00273-8

Polyhedron Vol. 17, No. 1, pp. 11–16, 1998
© 1997 Elsevier Science Ltd
All rights reserved. Printed in Great Britain
0277-5387/98 $19.00+0.00

Structural and spectroscopic studies of cobalt(II) complexes incorporating the bidentate phosphine ligand $Ph_2PCH_2Si(CH_3)_2CH_2PPh_2$

Paul R. Meehan, Elmer C. Alyea,* Ram P. Shakya and George Ferguson

Department of Chemistry and Biochemistry, University of Guelph, Guelph, Ontario, Canada N1G 2W1

(Received 27 May 1997; accepted 23 June 1997)

Abstract—A series of cobalt(II) complexes of general formula $[CoX_2L^2]$ (X = Cl, Br, I, NO_3, ClO_4, NCS; $L^2 = Ph_2PCH_2Si(CH_3)_2CH_2PPh_2$) have been synthesised and characterised by electronic and infrared spectroscopy and by magnetic moment studies. The bidentate phosphine ligand is an analogue of 1,3-bis(diphenylphosphino)propane (dppp). X-ray analysis of the $[CoBr_2L^2]$ complex proves tetrahedral geometry at the metal centre with the bidentate phosphine exhibiting a bite angle of 101.54(6)°. A range of evidence supports the existence of tetrahedral geometry about the metal in all the complexes in both the solid state and solution. Electronic spectroscopy is diagnostic for the tetrahedral d^7 metal ion in each case, with the ν_2 and ν_3 transitions clearly visible. Calculations of D_q and B', the RACAH parameter, have been performed for each complex; the relative magnitudes of B' indicate that the metal-phosphorus bonds are of increased covalency in comparison with Co(dppp) analogues. Magnetic moment studies show values of μ_B in the range 4.4–4.9 B.M., as expected for tetrahedral cobalt(II). IR studies show that the nitrate and perchlorate ions in the respective complexes are bound in monodentate fashion, while the $[Co(NCS)_2(L^2)]$ complex exhibits N-bonded thiocyanate groups. © 1997 Elsevier Science Ltd

Keywords: cobalt II; bidentate phosphine; X-ray structure; spectroscopic studies.

Tertiary phosphine ligands form an extensive part of the known co-ordination chemistry of the transition metals [1]. Bidentate phosphine ligands comprise an integral part of this chemistry, with the ligand 1,2-bis(diphenylphosphino)ethane (dppe) perhaps the most widely studied. The bidentates offer greater stability than their monodentate equivalents, and influence control over the stereochemistry, co-ordination number and stoichiometry of their complexes [2]. There is interest [3] in observing the effects that varying the length of the backbone in $R_2P(CH_2)_nPR_2$ ligands has upon the stereochemistry of metal complexes. Transition metal complexes of the tertiary phosphines are also of interest as homogeneous catalysts; the nature of the complex can influence selectivity, reactivity and stability [4].

The incorporation of silicon into the backbone of phosphine ligands was first carried out in 1962 [5]. Alyea and co-workers [6] subsequently reported the preparation of the novel ligand 2,2-dimethyl-2-sila-1,3-bis(diphenylphosphino)propane, $Ph_2PCH_2Si(CH_3)_2CH_2PPh_2$, subsequently denoted L^2. This ligand is a cousin of the more renowned 1,3-bis(diphenylphosphino)propane (dppp), but the presence of the dimethylsilyl backbone confers several advantages over the dppp analogue: L^2 is highly soluble in organic solvents, and the dimethylsilyl group provides a sensitive NMR probe. The crystal structure of $[Ni(NO_3)_2L^2]$ was reported in 1987 [7]. The complex provided a rare example of *allogons*, where both square planar and tetrahedral forms occur for the same complex; the square planar form was structurally characterised.

Cobalt(II) combines with diphosphines in 1:1, 1:2 and, rarely, 1:1.5 stoichiometry [1]. Studies again revolve around dppe-type ligands, with pseudo-tetrahedral geometries reported for $[Co(dppm)X_2]$ [8] and $[Co(dppe)X_2]$ [9] (X = Cl, Br, I). Complexes with dppp, the analogue of L^2, are also known; the pseudo-

* Author to whom correspondence should be addressed.

tetrahedral [Co(dppp)(SPh)$_2$] [10] is a rare example of a crystallographically characterised four co-ordinate cobalt(II)-dppp complex. Complexes of general formula [Co(dppp)$_{1.5}$X$_2$] (X = CN, NCS) have also been reported [11]. These latter compounds were thought to exhibit a dimeric structure in which one of the dppp groups acted as a bidentate bridging ligand between the two cobalt centres.

The scope of the research reported here was to synthesise a range of complexes of general formula [CoX$_2$L^2] and investigate their co-ordination properties by structural, magnetic and spectroscopic (electronic, infrared) studies. Characterisation of these species would afford a direct comparison between L^2 and dppp complexes of cobalt(II) and also provide some insight into the different bonding properties of the two ligands. A further objective was to use spectroscopic techniques to determine the mode of co-ordination of the nitrate, perchlorate and thiocyanate ligands in the respective complexes.

EXPERIMENTAL

General comments

Ligand L^2 was prepared according to the literature method [6]. All complexes were prepared and handled under a nitrogen atmosphere using standard Schlenk techniques. The solvents used were reagent grade and were dried and distilled immediately prior to use. Elemental analyses were performed by M.H.W. Laboratories, Phoenix, Az. UV–vis spectra were recorded on CsI plates as Nujol mulls on a Cary-14 UV-visible spectrophotometer. Infrared spectra were recorded on a Perkin–Elmer 180 double beam spectrometer. Magnetic moment measurements were performed by the Evans method[12] on a Varian EM 360 NMR spectrometer.

X-ray crystallography

Diffraction-quality crystals of (**1**) were obtained by slow evaporation of a dichloromethane solution of the complex. The crystallographic data are summarised in Table 1. X-ray measurements were made on an Enraf–Nonius CAD4 diffractometer equipped with graphite-monochromated Mo-K_α radiation. Data were collected in the range $4 \leqslant 2\theta \leqslant 55°$ and corrected for Lorentz, polarisation and absorption effects. The structure was solved using the heavy-atom method and the NRCVAX [13] program system. Final refinement was performed with SHELXL-93 [14] using all F^2 data, with all non-H atoms allowed anisotropic motion and hydrogen atoms allowed for as riding atoms.

Table 1. Crystallographic data for [CoBr$_2$L^2] (**1**)

formula	$C_{28}H_{30}Br_2CoP_2Si$
fw	675.30
colour	green
space group	$P2_1/n$
a (Å)	9.4893(8)
b (Å)	18.457(2)
c (Å)	16.632(2)
β (deg)	90.122(8)
V (Å^3)	2912.9(5)
Z	4
T (°C)	20
λ (Mo-K_α Å)	0.70930
ρ_{calcd} (g cm^{-3})	1.540
μ (mm^{-1})	3.499
R^a	0.0531
R_w^a	0.0758

[a] Residuals calculated for reflections with $I > 2\sigma(I)$; $R = \Sigma\|\|F_o| - |F_c\|/\Sigma|F_o|$; $R_w = [\Sigma w(|F_o| - |F_c|)^2/\Sigma w|F_o|^2]^{1/2}$.

[CoX$_2$(Ph$_2$PCH$_2$Si(CH$_3$)$_2$CH$_2$PPh$_2$)] (X = Cl, Br, NO$_3$, ClO$_4$)

Addition of the ligand dissolved in dichloromethane to stirred solutions of the cobalt(II) salts in ethanol (60 cm^3) and dimethoxypropane (2 cm^3) in a 1 : 1 molar ratio produced the immediate deposition of blue to green coloured precipitates. After stirring for 4 h at room temperature the precipitates were filtered, washed with ethanol and dry ether and pumped dry overnight. Yields 60–75%. Anal.Calcd for $C_{28}H_{30}CoCl_2P_2Si$: 57.35; H, 5.16. Found: C, 57.43; H, 5.38. Anal. Calcd for $C_{28}H_{30}CoBr_2P_2Si$: C, 49.80; H, 4.48. Found: C, 49.96; H, 4.46. Anal. Calcd for $C_{28}H_{30}CoN_2O_6P_2Si$: C, 52.59; H, 4.73; N, 4.38. Found: C, 52.59; H, 5.08; N, 4.34. Anal. Calcd for $C_{28}H_{30}CoCl_2O_8P_2Si$: C, 47.07; H, 4.23. Found: C, 47.11; H, 4.39.

CAUTION! Perchlorate salts of metal complexes containing organic ligands are potentially explosive. Only small amounts of such complexes should be made, and should be handled with great care [15].

[CoI$_2$(Ph$_2$PCH$_2$Si(CH$_3$)$_2$CH$_2$PPh$_2$)]

To a solution of [CoCl$_2$(Ph$_2$PCH$_2$Si(CH$_3$)$_2$CH$_2$PPh$_2$)] (0.3 g, 0.5 mmol) in dichloromethane (120 cm^3), a solution of potassium iodide (0.35 g, 2.1 mmol) in hot ethanol (40 cm^3) was added. The solution turned purple immediately. After 3 h the green precipitate that appeared was filtered, washed with ethanol and pumped dry overnight. Yield 65%. Anal. Calcd for $C_{28}H_{30}CoI_2P_2Si$: C, 43.71; H, 3.93. Found: C, 43.78; H, 3.98.

[Co(NCS)$_2$(Ph$_2$PCH$_2$Si(CH$_3$)$_2$CH$_2$PPh$_2$)]

Equimolar amounts of an ethanolic solution of Co(NCS)$_2$ and a dichloromethane solution of the

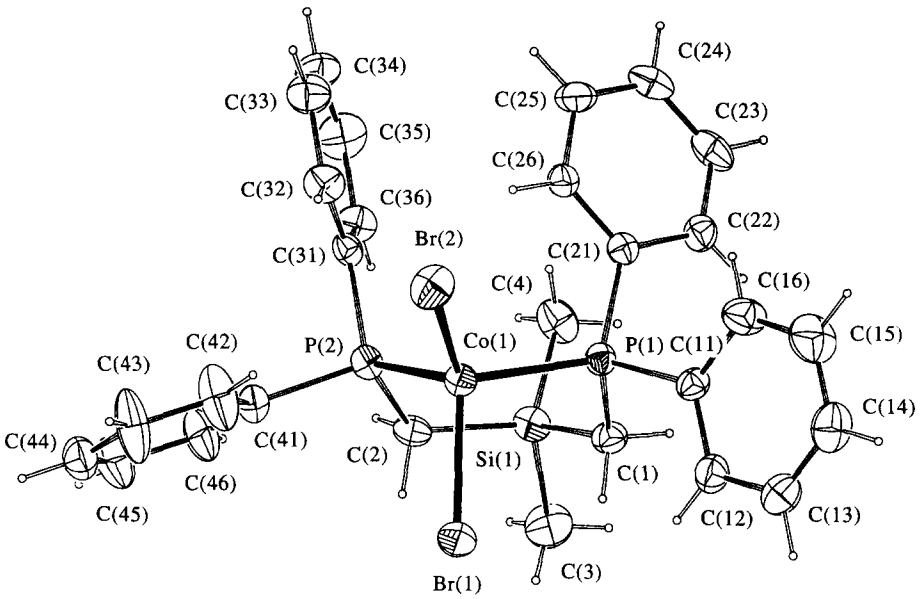

Fig. 1. ORTEP view of **1**. Thermal ellipsoids are drawn at the 30% probability level.

ligand were added together and stirred for 1 h. The resultant green precipitate was filtered, washed with ethanol and dry ether and dried *in vacuo* overnight. Yield 62%. Anal. Calcd for $C_{30}H_{30}CoN_2P_2S_2Si$: C, 57.05; H, 4.79; N, 4.43. Found: C, 57.21; H, 4.93; N, 4.50.

RESULTS AND DISCUSSION

Crystal structure of $[CoBr_2(Ph_2PCH_2Si(CH_3)_2CH_2PPh_2)]$ (**1**)

An ORTEP [16] view of the molecule appears in Fig. 1, and selected bond lengths and angles are given in Table 2. The metal centre is tetrahedral, bound to two bromine atoms [Co(1)—Br(1) 2.360(1), Co—Br(2) 2.347(1) Å] and the two phosphorus donor sites on the bidentate ligand. The Co—P distances [Co(1)—P(1) 2.344(2), Co(1)—P(2) 2.364(2) Å] compare closely with values noted in the two structurally characterised four co-ordinate Co-dppp complexes ($[CpCo(dppp)(SPh)]PF_6$ [17] Co—P 2.225, $[Co(dppp)(SPh)_2]$ [10] Co—P 2.346 Å). Angles around the metal centre range from 101.54(6) [P(1)—Co(1)—P(2)] to 117.54(4)° [Br(1)—Co(1)—B(2)]. The six membered chelate ring comprising Co(1), P(1), C(1), Si(1), C(2), P(2) adopts a chair conformation; it is noteworthy that the equivalent chelate ring in $[Ni(NO_3)_2L^2]$ [7] adopts a boat conformation. This difference is presumably due to the square planar metal centre in the nickel analogue. The chelate bite angle in (**1**) is 101.54(6)° [P(1)—Co(1)—P(2)]; this compares to much lower values observed in the dppp complexes, the enhanced value reflecting the incorporation of the larger silicon

Table 2. Selected bond distances (Å) and angles (°) for the crystal structure of $[CoBr_2L^2]$ (**1**)

Co(1)—Br(1)	2.360(1)	P(1)—C(11)	1.804(6)
Co(1)—Br(2)	2.347(1)	P(1)—C(21)	1.816(6)
Co(1)—P(1)	2.344(2)	P(2)—C(2)	1.821(5)
Co(1)—P(2)	2.364(2)	P(2)—C(31)	1.812(6)
P(1)—C(1)	1.823(5)	P(2)—C(41)	1.823(6)
Br(1)—Co(1)—Br(2)	117.54(4)	C(1)—Si(1)—C(3)	106.3(3)
Br(1)—Co(1)—P(1)	102.31(5)	C(1)—Si(1)—C(4)	111.3(3)
Br(1)—Co(1)—P(2)	101.93(5)	C(2)—Si(1)—C(3)	105.1(3)
Br(2)—Co(1)—P(1)	113.86(5)	C(2)—Si(1)—C(4)	114.0(3)
Br(2)—Co(1)—P(2)	117.30(5)	Co(1)—P(1)—C(11)	115.0(2)
P(1)—Co(1)—P(2)	101.54(6)	Co(1)—P(1)—C(21)	116.8(2)
Co(1)—P(1)—C(1)	107.1(2)	Co(1)—P(2)—C(31)	117.9(2)
Co(1)—P(2)—C(2)	107.9(2)	Co(1)—P(2)—C(41)	113.3(2)
C(1)—Si(1)—C(2)	111.0(3)		

atom into the ligand backbone. The C—Si—C angles in complex (**1**) range from 105.1(3) [C(2)—Si(1)—C(3)] to 114.0(3)° (C(2)—Si(1)—C(4)), with the C(1)—Si(1)—C(2) backbone at 111.0(3)°.

Electronic spectra

The electronic spectra of tetrahedral complexes of cobalt(II) show three electronic transitions from the $^4A_2$ ground state. ν_1 ($^4A_2 \rightarrow {}^4T_2$) occurs in the range 3000–5000 cm^{-1} and is rarely observed. ν_2 [$^4A_2 \rightarrow {}^4T_1(F)$] is usually a broad band which appears in the near IR region, while ν_3 [$^4A_2 \rightarrow {}^4T_1(P)$] is broad and intense, with noticeable fine structure. Unfortunately the broadness of these latter two bands renders their assignment somewhat arbitrary. However, electronic spectroscopy can be used to ascertain metal geometry: the structures of $[CoX_2(L)]$ (X = Cl, Br and L = dppe, dppp) and $[Co(dppe)_2I]I$ were identified as tetrahedral and pentaco-ordinate, respectively, on the basis of their electronic spectra [18a].

The electronic spectroscopic data for the cobalt(II) complexes are presented in Table 3. The solid state and solution UV–vis spectra are very similar: the spectra in the visible range for $CoCl_2L^2$ appear in Fig. 2. Bands corresponding to the ν_2 transition appear in the near-IR region; they are typically broad, with a degree of splitting observed. Dynamic Jahn–Teller effects in the excited states are almost certainly responsible for the energy spread. The bands arising from ν_3 appear in the range 13,000–20,000 cm^{-1}. The assignment of ν_2 and ν_3 allows calculation of ligand field strength Dq and the RACAH parameter B; for example, the chloride complex has average values of $\nu_2 = 7775$ cm^{-1} and $\nu_3 = 16{,}310$ cm^{-1}. These values are calculated using the method reported by Drago [18b]. B is a measure of electron–electron repulsion and has a lower value in complexes as compared with the free ion: it is hence denoted B′. Values for Dq and B′ also appear in Table 3.

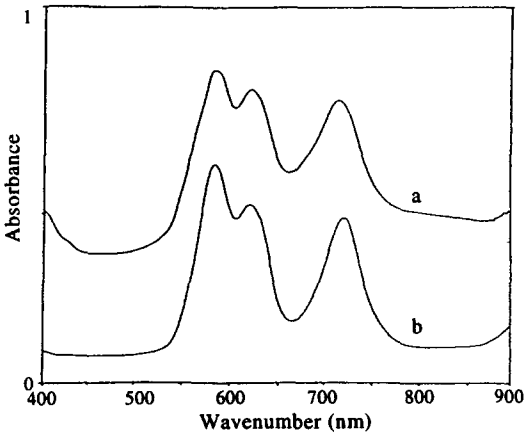

Fig. 2. UV–vis spectra of $[CoCl_2L^2]$: (a) solid state, (b) dichloromethane solution. The absorbance (*y*-axis) scale has arbitrary units.

On the basis of the Dq values calculated for the cobalt(II) complexes here, it is possible to assign the spectrochemical series as $I^- < Br^- < Cl^- \leqslant ClO_4^- < NO_3^- \leqslant NCS^-$. This is consistent with previously reported complexes [19,20]. Calculation of Dq for $[CoX_2(dppp)]$ (X = Cl, Br, I) using data given in Ref. [18a] resulted in slightly lower values than in the analogous L^2 systems here. Thus L^2 shows a slightly greater ligand field strength and a different bonding ability than dppp. It is also possible to determine that the thiocyanate ligands in $[Co(NCS)_2L^2]$ are N-bonded to the metal centre; if the ligand was S-bonded it would appear between Br^- and Cl^- in the spectrochemical series. B′ values for all the complexes are 60–73% of the free ion values, reflecting an appreciable orbital overlap. The intensities of the bands in the

Table 3. UV–vis data[a] for $[CoX_2L^2]$ complexes

X	UV–vis λ_{max}, nm (ε^b, M^{-1} cm^{-1})	D_q (cm^{-1})	B′[c] (cm^{-1})
Cl	598 (1160), 629 (960), 725 (850), 847 sh., 1205 (160), 1449 (200)	454	697[d]
Br	624 (1180), 666 (1130), 741 (970), 877 sh., 1266 (160), 1471 (170)	438	657
I	675 (1150), 714 (980), 763 (880), 847 sh., 1299 (150), 1493 (120)	432	586[d]
NO_3	598 (770), 629 (800), 730 (530), 862 sh., 1190 (150), 1408 (180)	464	680
ClO_4	600 (940), 629 (800), 730 (740), 1205 (170), 1449 (200)	455	695
NCS	575 (640), 625 (800), 1163 (220), 1449 (120)	466	713

[a] in CH_2Cl_2.
[b] extinction coefficient.
[c] RACAH parameter for Co^{2+} = 971 cm^{-1}.
[d] values of B′ for $[CoX_2(dppp)]$ 705 (Cl), 678 (I) cm^{-1} (calculated from data in Ref. [18]).

electronic spectra are due in large part to molecular orbital mixing i.e. covalency [9]. The extinction coefficients of the L^2 complexes are higher than those of analogous dppp systems, again reflecting increased covalency. Lower values of the RACAH parameter B′ for $[CoCl_2L^2]$ and $[CoI_2L^2]$ compared to their dppp analogues also suggests increased covalency in the Co—P bonds in the L^2 complexes.

Magnetic moment studies

Magnetic moments for the complexes were measured by the Evans method [12] and were corrected for ligand diamagnetism and temperature-independent paramagnetism (T.I.P.). The values, which appear in Table 4, fall in the range 4.4–4.9 μ_B and are similar to those for other pseudotetrahedral cobalt(II)–phosphine complexes [21]. The values are slightly higher for complexes of L^2 than the dppp analogues (μ_B = 4.43 (Cl), 4.47 (Br), 4.56 (I) B.M.], indicative of more regular tetrahedral geometry around the metal; this is a reflection of the larger chelate ring available in L^2. The data are also consistent with the $S = 3/2$ ground state with a significant orbital contribution to the magnetic moment (μ_{eff} = 3.87 B.M. (spin only)]. The magnetic moment order ($I^- > Br^- > Cl^- \geqslant NO_3^- > ClO_4^- > NCS^-$) is concurrent with the order established by Cotton [19] and Nicolini [22] for tetrahedral $[CoX_2(L)_2]$ (L = amine) complexes.

Infrared spectra

All the complexes display characteristic ligand bands [23]. The halide complexes each show characteristic Co–X stretching frequencies, with ν(Co—Cl) 320, ν(Co—Br) 270, ν(Co—I) 224 cm^{-1}. The presence of these bands is indicative of terminal Co-halide bonds [24]. Co—P stretches are assigned in the region 210–250 cm^{-1} and, although weak, their appearance is consistent with tetrahedral geometry. For the complex $[Co(NCS)_2L^2]$ the infrared spectrum confirms the presence of N-bonded thiocyanate; Bailey *et al.* [25] established IR patterns in M–NCS, M–SCN and M–NCS–M′ systems and concluded that for S-bonded thiocyanate, the characteristic IR stretch appeared at 2130–2160 cm^{-1}. The band at 2050 cm^{-1} in the complex here is concurrent with the N-bonded form. Signals at 790 [ν(CS)] and 485 [δ(NCS)] cm^{-1} provide additional confirmation.

Table 4. Magnetic data[a] for $[CoX_2L^2]$ complexes

X	χ_g[b] × 10^{-6} c.g.s.	χ_m[b] × 10^{-6} c.g.s.	μ_{eff}[d] (B.M.)
Cl	13.43	8693.3	4.6
Br	12.72	9430.7	4.8
I	11.43	9664.5	4.9
NO_3	12.04	8510.3	4.6
ClO_4	10.29	8189.2	4.5
NCS	10.99	7766.2	4.4

[a] in CH_2Cl_2 at 303 K.
[b] gram susceptibility.
[c] molar susceptibility, corrected for T.I.P. (500 × 10^{-6} c.g.s. units) and diamagnetism (L^2 correction = 262.1 × 10^{-6} c.g.s. units)
[d] $\mu \pm 0.1$ B.M.

Electronic spectroscopy and magnetic moment studies point to a tetrahedral geometry for $[Co(NO_3)_2L^2]$, with each nitrate ligand bound in monodentate fashion. The extent of splitting of the ν_3 band is often used to determine mono- or bidentate co-ordination of nitrate ions, with a separation of > 150 cm^{-1} implying a bidentate mode, and a corresponding value < 150 cm^{-1} pointing towards monodenticity. In this case bands at 1380 and 1280 cm^{-1} (ν_3) have a separation of 100 cm^{-1}: other bands at 1005 (ν_1), 830 (ν_2) and 750, 720 (ν_4) are consistent with monodentate NO_3^- groups. The previously-reported [7] $Ni(NO_3)_2$ complex of L^2 also shows monodentate nitrate, with a ν_3 splitting of 85 cm^{-1}.

The perchlorate complex $[Co(ClO_4)_2L^2]$ shows a split in the fundamental ν_3 (1100, 1030) and ν_4 (640, 605 cm^{-1}) modes, suggesting monodentate ClO_4^- of C_{3v} symmetry. Observation of bands for ν_2 (920) and ν_6 (440 cm^{-1}) verifies the monodentate nature of the perchlorate [26]. Tetrahedral perchlorate usually has four modes of vibration with only ν_3 and ν_4 IR active. However, monodentate co-ordination lowers the symmetry to C_{3v} and the extra modes thus appear.

CONCLUSIONS

The novel ditertiary phosphine ligand L^2, an analogue of dppp, readily forms 1:1 complexes with cobalt(II) salts (anions = Cl^-, Br^-, I^-, NO_3^-, ClO_4^-, NCS^-). The electronic and infrared spectroscopic and magnetic moment data indicate that Co^{II} has tetrahedral geometry in both the solid state and solution. The IR evidence shows that the nitrate and perchlorate anions are monodentate and that the thiocyanate group is N-bonded. The electronic spectral and magnetic data suggest that the Co—P bonds in

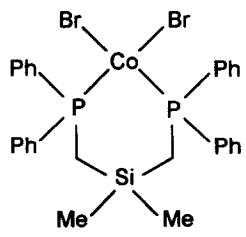

(1)
Scheme 1.

the L^2 complexes are of increased covalent character than those in corresponding dppp analogues, and that the L^2 ligand chelates better to the tetrahedral sites. Verification of the metal geometry and these deductions was obtained by the X-ray structural determination of the $[CoBr_2L^2]$ complex, in which the bidentate L^2 phosphine ligand exhibits a bite of 101.54(6)°.

Supplementary data—Tables of X-ray experimental details and crystallographic data, all atomic coordinates, anisotropic displacement parameters and bond distances and angles for the crystal structure of (**1**) (15 pages). Ordering information is given on any current masthead page.

Acknowledgements—E.C.A. and G.F. would like to thank NSERC (Canada) for research grants.

REFERENCES

1. McAuliffe, C. A. and Levason, W. *Phosphine, Arsine and Stibine Complexes of the Transition Elements*, Elsevier, Amsterdam (1979).
2. Meek, D. W. in *Homogeneous Catalysis with Metal Phosphine Complexes*, Pignolet, L. H. ed., Plenum Press, New York (1983).
3. (a) Barrow, M., Burgi, H. B., Johnson, D. K. and Venanzi, L. M. *J. Am. Chem. Soc.*, 1976, **98,** 2356; (b) Shaw, B. L. in *Catalytic Aspects of Metal Phosphine Complexes*, American Chemical Society, Washington, DC (1982).
4. Pignolet, L. H. *Homogeneous Catalysis with Metal Phosphine Complexes*, Alyea, E. C. and Meek, D. W. Eds, Plenum Press, New York (1983).
5. Niebergall, H. *Chem. Abst.*, 1962, **56,** 11622a.
6. Alyea, E. C., Fisher, K. J., Shakya, R. P. and Vougioukas, A. E. *Synth. React. Inorg. Met.-Org. Chem.*, 1988, **18,** 163.
7. Alyea, E. C., Ferguson, G., Ruhl, B. L. and Shakya, R. *Polyhedron*, 1987, **6,** 1223.
8. Chow, K. K. and McAuliffe, C. A. *Inorg. Chim. Acta*, 1975, **14,** 121.
9. Stalick, J. K., Corfield, P. W. R. and Meek, D. W. *Inorg. Chem.*, 1973, **12,** 1668.
10. Wei, G., Huang, M. H. Z. and Liu, H. *J. Chem. Soc., Dalton Trans.*, 1991, 3145.
11. Rigo, P., Bressan, M. and Turco, A. *Inorg. Chem.*, 1968, **7,** 1460.
12. Evans, D. F. *J. Chem. Soc.*, 1958, 2003.
13. Gabe, E. J., Le Page, Y., Charland, J.-P, Lee, F. L. and White, P. S. *J. Appl. Cryst.*, 1989, **22,** 384.
14. Sheldrick, G. M. *SHELXL*-93. Program for the refinement of crystal structures. University of Göttingen, Germany.
15. Cartwright, R. V., *Chem. Eng. News*, 1983, **61**(6), 4.
16. Johnson, C. K. *ORTEPII.* Report ORNL-5138. Oak Ridge National Laboratory, Tennessee.
17. Bao, Q.-B., Rheingold, A. L. and Brill, T. B. *Organometallics*, 1986, **5,** 2259.
18. (a) Horrocks Jr., W. deW., van Hecke, G. R. and Hall, D. deW. *Inorg. Chem.*, 1967, **6,** 694; (b) Drago, R. S. *Physical Methods In Chemistry*, p. 647, W. B. Saunders Co., Philadelphia (1977).
19. Cotton, F. A., Goodgame, D. M. L. and Goodgame, M. *J. Am. Chem. Soc.*, 1961, **83,** 4690.
20. Reed, C. A., Mashiko, T., Bentley, S. P., Castener, M. E., Scheidt, W. R., Spartalian, K. and Long, G. *J. Am. Chem. Soc.*, 1979, **101,** 2948.
21. Lever, A. B. P. *Inorganic Electronic Spectroscopy*, 2nd ed., Elsevier, Amsterdam (1984).
22. Nicolini, M., Pecile, C. and Turco, S. *Coord. Chem. Rev.*, 1966, **1,** 133.
23. Shakya, R. P., Ph.D. Thesis, University of Guelph, 1986.
24. Levason, W., McAuliffe, C. A. and Murray, S. G. *Inorg. Chim. Acta*, 1977, **24,** 63.
25. Bailey, R. A., Kozak, S. L., Michelsen, T. W. and Mills, W. L. *Coord. Chem. Rev.*, 1971, **6,** 407.
26. Souza, P., Gracia-Vazquez, J. A. and Masaguer, J. R. *Trans. Met. Chem.*, 1985, **10,** 410.

Pergamon

PII: S0277-5387(97)00271-4

Polyhedron Vol. 17, No. 1, pp. 17–26, 1998
© 1997 Elsevier Science Ltd
All rights reserved. Printed in Great Britain
0277-5387/98 $19.00+0.00

Tris(4-bromo-1*H*-pyrazol-1-yl)borato derivatives of first-row transition and group 12 and 14 metals. X-ray crystal structure of [HB(4-Brpz)$_3$]$_2$Cd. ^{113}Cd solution NMR study of bis[poly(pyrazolyl)borato]cadmium complexes

Giancarlo Gioia Lobbia,[a]* Bruna Bovio,[b]† Carlo Santini,[a] Patrizio Cecchi,[c] Claudio Pettinari[a] and Fabio Marchetti[a]

[a]Dipartimento di Scienze Chimiche, Università di Camerino, Via S. Agostino I, I-62032 Camerino, Italy

[b]Dipartimento di Chimica Generale, Università di Pavia, viale Taramelli 12, I-27100 Pavia, Italy

[c]Dipartimento di Agrobiologia ed Agrochimica, Università della Tuscia, Via S. C. De Lellis, I-01100 Viterbo, Italy

(Received 21 April 1997; accepted 23 June 1997)

Abstract—A series of metal complexes M[HB(4-Brpz)$_3$]$_2$ [HB(4-Brpz)$_3$ = hydridotris(4-bromo-1*H*-pyrazol-1-yl)borate and M = Mn, Fe, Co, Ni, Cu, Zn, Cd, Pb] were obtained from reaction of K[HB(4-Brpz)$_3$] and the appropriate metal salt in aqueous solution. These air-stable complexes are sparingly soluble in most common solvents; they have been investigated through elemental analysis, conductivity measurements, IR, UV–vis and, in the case of diamagnetic compounds, ^{1}H and ^{13}C NMR spectroscopy. The X-ray crystal structure of cadmium(II)bis[hydridotris(4-bromo-1*H*-pyrazol-1-yl)borate] has been resolved. Six-coordinate cadmium is present in a slightly distorted octahedron with the axes not linear [angles 176.8(3), 177.2(3) and 178.7(3)°]. The 'bite' of the ligand, i.e. N—Cd—N angle, lies in the range 81.6(2)–84.1(3)° (weighted average 82.4(4)°). The Cd—N distances vary from 2.298(8) to 2.329(8) Å (weighted average 2.317(5) Å). The geometry around the B atom is tetrahedral. The N—B—N angles range from 105.8(8) to 110.5(7)° (weighted average 108.5(7)°); the B—N bond distances vary from 1.53(2) to 1.62(1) Å (weighted average 1.58(1) Å). We report and discuss also the ^{113}Cd NMR solution data of several cadmium poly(pyrazol-1-yl)borates). © 1997 Elsevier Science Ltd

Keywords: pyrazolyl borates; group 12 and 14 complexes; cadmium; ^{113}Cd NMR; X-ray; boron.

Poly(pyrazol-1-yl)borates are a versatile class of uninegative nitrogen-donor ligands [1], which form several stable coordination compounds with transition and main-group metal ions [2]. These stable and flexible polydentate ligands are ideally suited for the synthesis of monomeric derivatives in which the coordination sphere about the metal atom can be carefully controlled. Several metal derivatives containing poly(pyrazol-1-yl)borates have been found to be excellent model compounds in the interpretation of the spectroscopic features of biological systems [3].

We have recently reported on the interaction between M^{II} transition metal ions and two anionic tridentate chelating donors, namely hydridotris(4-methylpyrazol-1-yl)borate {HB(4-Mepz)$_3$} and tetrakis(4-methylpyrazol-1-yl)borate {B(4-Mepz)$_4$} [4]. These ligands incorporate respectively three and four pyrazole rings with a methyl substituent in the 4-position which can display its electronic effect on the donor strength without any additional steric influence on the metal site, as has been observed in the case of 3- and 3,5-substituted poly(pyrazolyl)borates, currently employed by other researchers.

* Corresponding author.
† Corresponding author for the X-ray structure analysis.

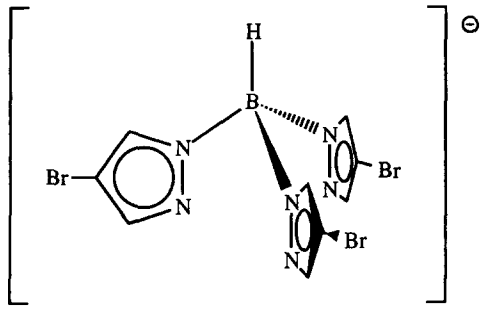

Fig. 1. Ligand used in this work.

It seemed interesting to replace an electron releasing group such as a methyl with an electron withdrawing one such as Br, to investigate the consequent net electronic effect on the chelating ability of the resulting ligand.

The present account details the synthesis and analytical and spectroscopic characterization of the anionic hydridotris(4-bromopyrazol-1-yl)borates {$HB(4\text{-}Brpz)_3$} (Fig. 1) and of its derivatives with first-row transition and post-transition M^{2+} metal ions.

We also report the X-ray crystal structure and the ^{113}Cd solution NMR characterization of the cadmium derivative $Cd[HB(4\text{-}Brpz)_3]_2$ together with a detailed comparison of the structural features of analogous cadmium compounds.

Comparison is made with the ^{113}Cd solution NMR data of several poly(pyrazolyl)borate cadmium complexes [4,5]. In fact the ^{113}Cd NMR spectroscopy, based on the fact that cadmium has two important NMR active isotopes with spins = 1/2, has been used as a 'spin spy' in the study of the properties of proteins containing zinc and other spectroscopically silent metals [6]. In the last few years Reger *et al.* have investigated the synthesis and ^{113}Cd NMR characterization of several $Cd[HB(Pz)_3]_2$ [7], $[HB(Pz)_3]CdL$ [8] and $[HB(Pz)_3]CdR$ [9] (where $HB(Pz)_3$ stands for tris (pyrazolyl)borates in general and L = N_3-, N_2-, O_2- and S_2-donors, and R = alkyl and aryl groups), containing CdN_6, CdN_5, CdN_4, CdN_3O_2, CdN_3S_2 and CdN_3C central cores. The present ^{113}Cd NMR investigation would be a further support of the actual knowledge of the rules governing ^{113}Cd NMR chemical shift in solution of this kind of complexes.

RESULTS AND DISCUSSION

Synthesis of the derivatives

Derivatives **1–8** were synthesized in a water solution by the metathetic reaction of $K[HB(4\text{-}Brpz)_3]$ with the appropriate metal salt in the ratio 2 : 1, as indicated in the following equation:

$$MX_2 + 2K[HB(4\text{-}Brpz)_3] \xrightarrow{H_2O} M[HB(4\text{-}Brpz)_3]_2 + 2KX \quad (1)$$

1–8

M = Mn, Co, Ni, Zn, Cd or Pb, X = Cl
M = Fe or Cu, $X_2 = SO_4$

All the complexes were isolated as micro crystalline air-stable solids. Analytical data or derivatives **1–8** are summarized in Table 1. Some of them are high-melt-

Table 1. Analytical data of compounds **1–8**

Compound[a]	No.	Color	Yield (%)	M.p. (°C)	Elemental analysis[b] C	H	N
$Mn[HB(4\text{-}Brpz)_3]_2$	**1**	colourless	88	320 dec[c]	22.8	1.4	16.5
$C_{18}H_{14}B_2N_{12}Mn$					(22.7)	(1.5)	(16.7)
$Fe[HB(4\text{-}Brpz)_3]_2$	**2**	purple	86	>320	22.5	1.4	17.8
$C_{18}H_{14}B_2N_{12}Fe$					(22.6)	(1.5)	(17.6)
$Co[HB(4\text{-}Brpz)_3]_2$	**3**	pink–yellow	84	>320	22.5	1.5	17.5
$C_{18}H_{14}B_2N_{12}Co$					(22.6)	(1.5)	(17.6)
$Ni[HB(4\text{-}Brpz)_3]_2$	**4**	lilac	84	>320	22.4	1.6	17.4
$C_{18}H_{14}B_2N_{12}Ni$					(22.6)	(1.5)	(17.6)
$Cu[HB(4\text{-}Brpz)_3]_2$	**5**	sky-blue	86	320 dec[c]	22.5	1.5	17.3
$C_{18}H_{14}B_2N_{12}Cu$					(22.5)	(1.5)	(17.5)
$Zn[HB(4\text{-}Brpz)_3]_2$	**6**	white	87	308–311	22.2	1.4	17.5
$C_{18}H_{14}B_2N_{12}Zn$					(22.4)	(1.5)	(17.4)
$Cd[HB(4\text{-}Brpz)_3]_2$	**7**	white	83	312–314	21.3	1.3	16.3
$C_{18}H_{14}B_2N_{12}Cd$					(21.4)	(1.4)	(16.6)
$Pb[HB(4\text{-}Brpz)_3]_2$	**8**	white	84	266–268	19.5	1.3	15.0
$C_{18}H_{14}B_2N_{12}Pb$					(19.5)	(1.3)	(15.2)

[a] $[HB(4\text{-}Brpz)_3]$ is hydridotris(4-bromopyrazol-1-yl)borate $C_9H_7BN_6$.
[b] Calculated values in parentheses.
[c] Decomposes without melting.

ing solids whereas some others gradually decompose on heating without melting. They are insoluble in water, alcohols and hydrocarbons, and moderately soluble in chlorinated solvents, DMSO, aromatic hydrocarbons and acetone, in which they are not electrolytes.

IR data

Selected infrared data of the spectra of derivatives **1–8** in the solid (Nujol mull) state, are shown in Table 2.

In all the compounds **1–8** a medium absorption in the range 2460–2480 cm^{-1}, due to ν(B—H) stretching, has been detected. This band is generally shifted to higher frequencies with respect to that of the potassium ligand salt K[HB(4-Brpz)$_3$], and appears as a single neat peak, whereas in the derivatives of {HB(4-Mepz)$_3$} it was always split into two components [4].

Besides the expected weak absorptions over 3000 cm^{-1}, assignable to heterocyclic ν(C—H) stretching, we have found the bands due to 'breathing' of the pyrazole rings at unusually high frequencies, in the range 1650–1700 cm^{-1}; the same bands in the case of {HB(pz)$_3$} and {HB(4-Mepz)$_3$} derivatives were found in the range 1550–1600 cm^{-1} [1,4]. This fact could be explained by a stronger polarization on the pseudo-double C—C and C—N pz bonds in M[HB(4-Brpz)$_3$]$_2$, caused by the presence of an electron withdrawing group such as Br in 4-position. The bands assignable to ν(B—N) vibrations are probably hidden under the typical strong absorptions of Nujol.

In the far-IR region two main groups of absorptions, likely due to various bending modes of vibration of the ligand skeleton, have been detected: the first

Table 2. Selected IR data (Nujol mull) of derivatives **1–8**

No.	Compound	ν(C—H)$_{az}$	ν(B—H)	1500–1700	>600
	K[HB(4-Brpz)$_3$]	3155m 3142w	2418m	1694m, 1682m 1661m, 1514m 1504m	464w, 448m, 425m 380w, 322m, 304m 280w, 256m, 226w 211w, 202w
1	Mn[HB(4-Brpz)$_3$]$_2$	3128m 3114m	2476m	1689m, 1678sh 1662m, 1515m 1506w	472m, 444w, 414m 336s, 306m, 289w 280w, 257sh, 245s 225w, 202s
2	Fe[HB(4-Brpz)$_3$]$_2$	3131m	2488m	1676m, 1654m 1636m, 1519m 1506w	488w, 474m, 428s 417m, 348m, 325w 315m, 304w, 290w 279m, 260m, 247w 227m, 211m
3	Co[HB(4-Brpz)$_3$]$_2$	3128m	2474m	1694m, 1654m 1515m	476m, 417m, 351m 322m, 295w, 265m 247w, 213m, 203m
4	Ni[HB(4-Brpz)$_3$]$_2$	3122m	2484m	1695s, 1654m 1515m	477m, 418m, 357m 326m, 301w, 275w 269m, 253w, 231m
5	Cu[HB(4-Brpz)$_3$]$_2$	3120m	2482m	1696m, 1663m 1636m, 1514m	478m, 416m, 364m 345m, 312m, 290w 282w, 262m, 245w 234m, 226w, 202m
6	Zn[HB(4-Brpz)$_3$]$_2$	3150m	2460w	1684m, 1652m 1634m, 1515m 1505m	478m, 457w, 439m 418m, 382m, 376m 313m, 300m, 247m 363w, 340m, 311w 303m, 278m, 254m 224m
7	Cd[HB(4-Brpz)$_3$]$_2$	3128m 3114m	2472m	1684m, 1661m 1516m	470m, 412m, 332m 304m, 290w, 247m 226m, 210w
8	Pb[HB(4-Brpz)$_3$]$_2$	3133w	2475sh 2456m	1695m, 1678m 1644m, 1635m 1510m	456s, 419w, 409w 399w, 355w, 341m 325m, 302w, 268w 254m, 247m, 224m 203m

between 480 and 400 cm^{-1} and the second between 300 and 200 cm^{-1}. Finally the medium or strong absorptions at *ca* 380–330 cm^{-1} could be tentatively assigned to ν(N—M) stretching frequencies modes [10].

UV–vis data

The UV–vis spectra of the potassium ligand salt and of derivatives **1–8** have been carried out in chloroform solution and the absorption maxima with their extinction coefficients are reported in Table 3.

In all cases the extinction coefficient of the band at 240 nm is approximately twice of that found for K[HB(4-Brpz)$_3$], in agreement with the 2 : 1 ligand to metal ratio found by elemental analyses (Table 1).

In all the spectra a broad and intense absorption was detected at *ca* 240 nm, which is due to the pyrazolyc intraligand transition [4,11]. This band is similar to that found in the spectra of {HB(4-Mepz)$_3$} derivatives [4], thus indicating that substitution of an electron releasing group (Me) with an electron withdrawing one (Br) doesn't give rise to appreciable electronic changes on the relative energy levels of HOMO and LUMO in pz chromophores of the ligand.

It is worth noting that the derivatives **1–8** are less soluble in chlorinated solvents with respect to analogues {HB(4-Mepz)$_3$} derivatives, and none of the expected *d–d* transition bands were detected at the concentration employed. Consequently a comparison of the crystal field stabilization energies between {HB(4-Brpz)$_3$}, {HB(4-Mepz)$_3$} [4] and {HBpz$_3$} [11] derivatives is impossible.

In the spectra of Fe, Co and Cu complexes, two additional bands at 270–290 and 310–340 nm were observed, which should be attributed to 'metal to ligands charge transfer' (MLCT) transitions, based on their relatively high extinction coefficient [11]. The MLCT absorption (ε = 11620) found at 336 nm in the spectrum of Fe[HB(4-Brpz)$_3$]$_2$ is particularly intense.

NMR data

The ^{1}H and ^{13}C NMR spectra have been performed in the case of diamagnetic zinc, cadmium and lead derivatives and the data are reported in Table 4. The choice of the deuterated solvent employed was dictated by the solubility of the derivatives, K[HB(4-Brpz)$_3$] being sufficiently soluble only in protic solvents such as water and methanol, whereas Zn[HB(4-Brpz)$_3$]$_2$ only in deuterated DMSO.

The presence of only one set of signals in both proton and carbon NMR spectra, over the temperature range 220–300 K indicates equivalence of the three pz rings and, as expected, the presence of ligands acting as tridentate not only in the solid state (see crystallographic section) but probably also in solution.

The 3- and 5-H resonances are downfield shifted upon coordination, those of Cd[HB(4-Brpz)$_3$]$_2$ being more deshielded with respect to those of Zn[HB(4-Brpz)$_3$]$_2$, in accordance with a likely stronger donation of the ligand in the former compound, and also with that observed in the other Zn and Cd poly(pyrazolyl)borates derivatives previously synthesized [4,5].

The C(3) and C(5) nuclei absorb at approximately the same frequencies observed in Zn[HB(4-Mepz)$_3$]$_2$ and Cd[HB(4-Mepz)$_3$]$_2$ [4], whereas C(4) resonance

Table 3. UV–vis data (in $CHCl_3$) of derivatives **1–8**

No.	Compound	Λ^a	ε^b	C^c	Assignment^d
	K[HB(4-Brpz)$_3$]	240	3480	5.7×10^{-4}	intraligand
1	Mn[HB(4-Brpz)$_3$]$_2$	242	8990	3.6×10^{-4}	intraligand
2	Fe[HB(4-Brpz)$_3$]$_2$	242	8980	4.6×10^{-4}	intraligand
		294sh	4640		MLCT
		336	11620		MLCT
3	Co[HB(4-Brpz)$_3$]$_2$	242	11420	3.2×10^{-4}	intraligand
		284sh	1390		MLCT
		310sh	720		MLCT
4	Ni[HB(4-Brpz)$_3$]$_2$	244	6690	5.1×10^{-4}	intraligand
5	Cu[HB(4-Brpz)$_3$]$_2$	242	9220	3.2×10^{-4}	intraligand
		268	1330		MLCT
		308	645		MLCT
6	Zn[HB(4-Brpz)$_3$]$_2$	240	11100	1.0×10^{-4}	intraligand
7	Cd[HB(4-Brpz)$_3$]$_2$	240	8600	0.8×10^{-4}	intraligand
8	Pb[HB(4-Brpz)$_3$]$_2$	242	15990	1.1×10^{-4}	intraligand

^{a} Λ in nm.
^{b} ε in $(mol/l)^{-1}$ cm^{-1}.
^{c} C in mol/l.
^{d} MLCT stands for 'Metal to Ligand Charge Transfer'.

Table 4. ^{1}H and ^{13}C NMR data (in $CDCl_3$) of derivatives **6–8**

No.	Compound	Solvent	H-3 or H-5 δ		C-3 or C-5 δ		C-4
	K[HB(4-Brpz)$_3$]	CD_3OH	7.59	7.30	142.8	136.6	93.9
		D_2O	7.64	7.32	144.7	138.2	95.6
6	Zn[HB(4-Brpz)$_3$]$_2$	DMSO	7.56	6.78	142.8	135.5	93.1
7	Cd[HB(4-Brpz)$_3$]$_2$	$CDCl_3$	7.75	7.34	141.2	137.0	93.5
8	Pb[HB(4-Brpz)$_3$]$_2$	$CDCl_3$	7.75	7.32	141.1	136.8	93.6

has been found in the range 93–96 ppm, upfield shifted of *ca* 20 ppm with respect to C(4) in {HB(4-Mepz)$_3$} analogues [4], due to the different electronic features of the 4-substituents Br and Me.

The X-ray crystal structure of Cd[HB(4-Brpz)$_3$]$_2$

The crystal structure of the title compound consists of discrete molecules. The representation of the molecule along the *b* axis with the numbering scheme drawn with the program ORTEP [12] is given in Fig. 2.

The molecule shows a virtual C_{3i} symmetry although it exhibits no real crystallographic symmetry and all atoms occupy general positions.

Since the differences among chemically equivalent interatomic distances or angles have only relative meaning, their average values are given in Table 5, whereas selected bond distances and angles in the coordination sphere are listed in Table 6.

The packing of the molecules in the crystal is ensured by intermolecular short approaches: Br(3)···C(5D) *i* 3.74(1) Å, where *i* means $1+x$, y, z; N(1E)···Br(1) *ii* 3.46(1), C(5C)···Br(5) *ii* 3.72(1), C(3E)···Br(1) *ii* 3.59(1), C(4E)···Br(1) *ii* 3.54(1), C(5E)···Br(1) *ii* 3.50 (1), Br(2)···C(4F) *ii* 3.58(1), Br(2)···C(5F) *ii* 3.56(1), Br(4)···C(4B) *ii* 3.70(1), Br(4)···C(5B) *ii* 3.47(1) Å, where *ii* means $3/2-x$, $1/2+y$, $1/2-z$.

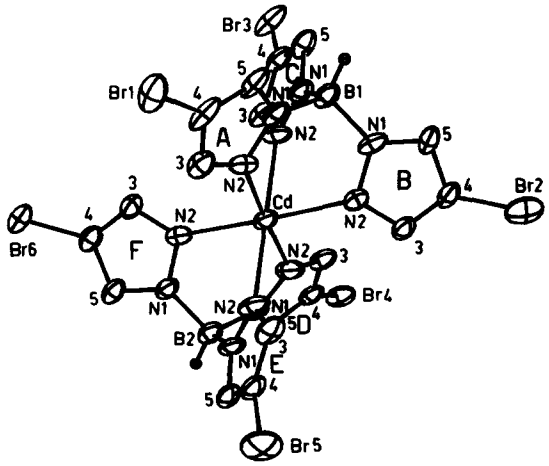

Fig. 2. ORTEP view of the derivative Cd[HB(4-Brpz)$_3$]$_2$.

Table 5. Average bond distances (Å) and angles (°) with their standard errors[a] of Cd[HB(4-Brpz)$_3$]$_2$

	N	X_m	σ_m	σ'_m
Cd—N	6	2.317	0.005	0.003
B—N	6	1.577	0.012	0.006
N(1)—N(2)	6	1.382	0.010	0.004
N(2)—C(3)	6	1.347	0.007	0.005
C(3)—C(4)	6	1.388	0.011	0.005
C(4)—C(5)	6	1.409	0.010	0.005
C(4)—Br	6	1.843	0.004	0.004
C(5)—N(1)	6	1.375	0.010	0.005
N(2)—Cd—N(2)[b]	6	82.4	0.4	0.1
N(2)—Cd—N(2')[c]	6	97.6	0.9	0.1
N(2)—Cd—N(2')[d]	3	177.6	0.6	0.2
Cd—N(2)—N(1)	6	118.5	0.7	0.2
Cd—N(2)—C(3)	6	134.6	0.8	0.2
N(2)—N(1)—C(5)	6	111.7	0.2	0.3
N(2)—N(1)—B	6	122.4	0.9	0.3
C(5)—N(1)—B	6	126.0	0.9	0.3
N(1)—N(2)—C(3)	6	106.1	0.4	0.3
N(2)—C(3)—C(4)	6	109.5	0.4	0.3
C(3)—C(4)—C(5)	6	108.2	0.2	0.3
C(3)—C(4)—Br	6	126.3	0.9	0.3
C(5)—C(4)—Br	6	125.6	1.0	0.3
C(4)—C(5)—N(1)	6	104.3	0.3	0.3
N(1)—B—N(1)	6	108.5	0.7	0.3

[a] All values were calculated according to A. Domenicano, A. Vaciago and C. A. Coulson, *Acta Cryst.*, 1975, **B31**, 221.
[b] *cis* intraligand.
[c] *cis* interligand.
[d] *trans* interligand.

The structure of Cd[HB(4-Brpz)$_3$]$_2$ is a distorted octahedron where the Cd—N distances vary from 2.298(8) to 2.329(8) Å with a weighted average of 2.317(5) Å, slightly shorter than the values found in other similar complexes given in Table 7. The crystal data, data collection and refinement of the structure are reported in Table 8.

The chelate rings restrain the intraligand N—Cd—N bond angles in the range 81.6(2)–84.1(3)°, with a weighted average 82.4(4)°, whereas the *cis* interligand N—Cd—N bond angles range from 95.2(3)

Table 6. Selected interatomic distances (Å) and bond angles (°) with e.s.d.'s in parentheses of $Cd[HB(4\text{-}Brpz)_3]_2$

Cd—N(2A)	2.298(8)	Cd—N(2D)	2.329(8)
Cd—N(2B)	2.312(8)	Cd—N(2E)	2.329(6)
Cd—N(2C)	2.312(6)	Cd—N(2F)	2.315(7)
N(2A)—Cd—N(2B)	82.3(3)	N(2B)—Cd—N(2F)	177.2(3)
N(2A)—Cd—N(2C)	82.4(3)	N(2C)—Cd—N(2D)	98.4(3)
N(2A)—Cd—N(2D)	178.7(3)	N(2C)—Cd—N(2E)	176.8(3)
N(2A)—Cd—N(2E)	95.2(3)	N(2C)—Cd—N(2F)	100.6(3)
N(2A)—Cd—N(2F)	96.6(3)	N(2D)—Cd—N(2E)	84.1(3)
N(2B)—Cd—N(2C)	81.8(3)	N(2D)—Cd—N(2F)	82.2(3)
N(2B)—Cd—N(2D)	98.8(3)	N(2E)—Cd—N(2F)	81.6(2)
N(2B)—Cd—N(2E)	95.9(3)		

Table 7. Comparison of relevant structural data of CdN_6 derivatives

Complex	Cd—N	Cd—N_{av} (Å)	N—Cd—N (bite)	N—Cd—N_{av} (bite) (deg.)	Ref.
A[a]	2.348(5)	2.35	82.7(1)	82.7	[7b]
B[b]	2.362(8), 2.308(8)	2.34	81.0(3), 82.3(3)	81.9	[7b]
	2.365(8)		82.3(3)		
C[c]	2.314(3), 2.387(3)	2.33	78.7(1), 84.8(1)	80.9	[7b]
	2.284(3)		79.1(1)		
D[d]	2.341(6), 2.282(5)	2.33	83.4(2), 78.9(2)	81.8	[7d]
	2.357(6), 2.355(6)		83.8(3), 83.5(2)		
	2.293(6), 2.371(6)		78.2(2), 83.2(2)		
E[e]	2.389(6), 2.415(6)	2.38	84.23(2), 85.57(2)	85.2	[7d]
	2.351(6)		85.76(2)		
F[f]	2.380(11), 2.411(10)	2.38	81.5(4), 81.5(4)	81.4	[7d]
	2.392(11), 2.313(11)		84.3(4), 80.6(4)		
	2.397(11), 2.369(10)		81.1(4), 79.6(4)		
G[g]	2.298(8), 2.312(8)	2.32	82.3(3), 82.4(3)	82.4	This
	2.312(6), 2.329(8)		81.8(3), 84.1(3)		work
	2.329(6), 2.315(7)		82.2(3), 81.6(2)		

[a] **A** is $Cd[HB(3,5\text{-}Me_2pz)_3]_2$.
[b] **B** is $Cd[B(3\text{-}Mepz)_4]_2$.
[c] **C** is $Cd[B(pz)_4]_2$.
[d] **D** is $Cd[HB(pz)_3]_2$.
[e] **E** is $Cd[HB(3\text{-}phpz)_3]_2$.
[f] **F** is $[B(pz)_4]Cd[HB(3\text{-}phpz)_3]$.
[g] **G** is $Cd[HB(4\text{-}Brpz)_3]_2$.

to 100.6(3)°, with weighted average 97.6(9)°. These angles are comparable with the corresponding angles 82.7(1) and 97.3(1)° found in $Cd[HB(3,5\text{-}Me_2pz)_3]_2$ [7b]. The *trans* interligand N—Cd—N bond angles are in the range 176.8(3)–178.7(3)°, with a weighted average 177.6(6)°. The weighted average intraligand N···N non-bonding distances for the donor atoms is 3.05(1) Å whereas the weighted average interligand N···N is 3.48(2) Å.

The planarity of the six pyrazole rings was derived from the least-squares planes. The probability that the ring is non-planar turned out to be: $P > 99\%$ for N(1B)—C(5B), N(1C)—C(5C), N(1D)—C(5D) and N(1F)—C(5F); $P = 26.5\%$ for N(1A)—C(5A) and $P = 98.7\%$ for N(1E)—C(5E). Maximum out of plane displacement (Å): C(5B) −0.029(9), C(3C) 0.025(11), C(5D) 0.024(10), C(5E) 0.016(11) and C(3F) −0.029(11). In the pyrzole rings, the rules about the pattern of values for the angles [13] apply: Cd—N(2)—C(3) > Cd—N(2)—N(1) (weighted average 134.6(8) > 118.5(7)°), N(2)—N(1)—C(5) > N(1)—N(2)—C(3) (weighted average 111.7(3) > 106.1(4)°), N(2)—C(3)—C(4) > C(4)—C(5)—N(1) (weighted average 109.5(4) > 104.3(3)°). A similar trend was observed in $[HB(pz)_3Cu(PPh_3)]$ [14] and in $Zn[HB(4\text{-}Mepz)_3]_2$ [4].

The geometry around the B atom is tetrahedral. The B—N bond distances vary from 1.53(2) to 1.62(1)

Å with weighted average 1.58(1) Å, longer than the values found in $Zn[HB(pz)_3]_2$, 1.541(3) [15] and in $Zn[HB(4\text{-}Mepz)_3]_2$, 1.547(6) Å [4]. The angles N—B—N range from 105.8(8) to 110.5(7)° with weighted average 108.5(7)°, comparable with the values found in $Zn[HB(pz)_3]_2$ 108.9(5)° [15] and in $Zn[HB(4\text{-}Mepz)_3]_2$ 108.7(7)° [4]. The B(1)···Cd and B(2)···Cd distances are 3.37(1) and 3.43(1) Å (weighted average 3.40(3) Å); the B(1)···Cd···B(2) angle is 177.8(3)°.

It is also of interest to compare the structural data of the coordination environment of the metal of $Zn[HB(pz)_3]_2$ (M—N_{av} 2.15 Å, N—M—N_{av} 85.6°) [15], $Zn[HB(3,5\text{-}Me_2pz)_3]_2$ (M—N_{av} 2.17 Å, N—M—N_{av} 86.4°) [16] and $Zn[HB(4\text{-}Mepz)_3]_2$ (M—N_{av} 2.14 Å, N—M—N_{av} 85.5°) [4] with those of homoleptic $Cd[HB(pz)_3]_2$ (M—N_{av} 2.33 Å, N—M—N_{av} 81.8°) [7d], $Cd[HB(3,5\text{-}Me_2pz)_3]_2$ (M—N_{av} 2.35 Å, N—M—N_{av} 82.7°) [7b] and our $Cd[HB(4\text{-}Brpz)_3]_2$ (M—N_{av} 2.32 Å, N—M—N_{av} 82.4°). All the structures are six-coordinate, but there is an average M—N bond distance increase of 0.18 Å together with an average N—M—N bond angle decrease of 3.53°, on going from zinc to cadmium derivatives, caused by the larger cadmium atom size, compared to that of the zinc atom [17].

The steric demand of the ligands determine the stability of complexes, in ligand competition and exchange [18]. It is interesting to calculate effective cone angles of ligands from the crystallographic structural data. For the $\{HB(4\text{-}Brpz)_3\}$ ligands, the cone vertex was centered on the cadmium atom and the middle of the Cd—N vectors was assumed to be the cone axes. The angle between the cone axes and the vector which touches the van der Waals radii of the hydrogen atoms closest to Cd (r = 1.17 Å) is: 100.5° for H(3A), 100.2° for H(3B) and 100.9° for H(3C) for one ligand and: 100.0° for H(3D), 98.6° for H(3E) and 100.0° for H(3F) for the other ligand. These angles correspond to a total average value θ: 201.0 and 199.1°, respectively. These angles are narrower than the corresponding angles 212.2° found in the complex $[HB(pz)_3Cu(PPh_3)]$ [14] and 208.0 and 212.0° found in $Zn[HB(4\text{-}Mepz)_3]_2$ [4]. The difference is attributable to the longer Cd—N bond distance 2.317(5) Å as compared with the corresponding Cu—N 2.076(6) [14] or Zn—N 2.135(15) Å [4] bond distances.

^{113}Cd *NMR data*

The ^{113}Cd NMR chemical shifts of various bis(polypyrazolyl)borate cadmium derivatives [4,5] have been recorded in $CDCl_3$ and acetone-d_6 solutions, at concentrations ranging from 0.5 to 1.0 mM, and are given in Table 9.

We have thought to employ both deuterated chloroform and acetone in order to compare the effects of the chemical shift caused by a non-polar solvent and a polar one, respectively. All the absorptions fall in

Table 8. Crystal data, data collection and refinement of the structure of $Cd[HB(4\text{-}Brpz)_3]_2$

Formula	$C_{18}H_{14}B_2N_{12}Br_6Cd$
Formula weight	1011.84
Space group	$P2_1/n$
Color	colorless
a (Å)	12.076(1)
b (Å)	14.29(1)
c (Å)	20.870(1)
β (°)	93.511(5)
V_c (Å^3)	3595(4)
Z	4
D_{calcd} (g cm^{-3})	1.87
Crystal size (mm)	0.98 × 0.28 × 0.24
μ (Cu-K_α) (cm^{-1})	140.2
Data collection instrument	Enraf–Nonius CAD4
Radiation (monochromated)	Cu-K_α (λ = 1.5418 Å)
T (K)	293
Scan mode	$\omega/2\theta$
Data collection range	$4° < 2\theta < 70°$
Stds (measured every 300 min)	30-5, 017, 413
No. of unique reflections measured	6761 ($h, k, \pm 1$)
No. of data with $F_o^2 > 3\sigma(F_o^2)$	4234
No. of parameter refined	352
R^a	0.047
$R_w{}^b$	0.050

[a] $R = (\Sigma||F_o| - k|F_c||)/\Sigma|F_o|$.
[b] $R_w = \{\Sigma_w(|F_o| - k|F_c|)^2/\Sigma w|F_o|^2\}^{1/2}$.

Table 9. ^{113}Cd NMR data

Compound	Acetone-d_6	$CDCl_3$	Ref.
$Cd[B(4\text{-}Mepz)_4]_2$	216.0	218.3	[4]
$Cd[B(3\text{-}Mepz)_4]_2$	—	202.5	[7b]
$Cd[B(pz)_4]_2$	—	221.1	[7b]
$Cd[HB(3,5\text{-}Me_2pz)_3]_2$	insoluble	201.9	[7b]
$Cd[HB(3\text{-}Mepz)_3]_2$	insoluble	200.0	[5]
$Cd[HB(pz)_3]_2$	196.4	198.3	[7b]
$Cd[HB(4\text{-}Mepz)_3]_2$	193.6	195.9	[4]
$Cd[HB(4\text{-}Brpz)_3]_2$	187.6	193.8	This work

the range typical for six-coordinate species [7,8,9] and, apart from a general increase in shielding (*ca* 2–6 ppm), which could be ascribed to a secondary effect such as dipolar interactions between solvent molecules and the B—H fragment in tris or with the free lone pair of N donor atom of the fourth pyrazole in tetrakis, the choice of acetone as solvent does not produce any other relevant effect on ^{113}Cd chemical shift for coordinatively saturated CdN_6 complexes.

The value of $Cd[B(4\text{-}Mepz)_4]_2$ (218.3 ppm) can be compared to those of $Cd[B(pz)_4]_2$ (221.1 ppm) [7b] and of $Cd[B(3\text{-}Mepz)_4]_2$ (202.5 ppm) [7b], the only other tetrakis cadmium derivatives till now known. It seems that the Me group in 4- and mainly in 3-position of the pyrazole rings produces a shielding with respect to the unsubstitute tetrakis:

$$\{B(3\text{-}Mepz)_4\} > \{B(4\text{-}Mepz)_4\} > \{B(pz)_4\}$$

In the case of tris(pyrazolyl)borate cadmium derivatives more ^{113}Cd data are available [7,8,9]. The following trend of shielding power for Tris (pyrazolyl)borate donors is found:

$$\{HB(4\text{-}Brpz)_3\} > \{HB(4\text{-}Mepz)_3\} > \{HB(pz)_3\}$$
$$> \{HB(3\text{-}Mepz)_3\} > \{HB(3,5\text{-}Me_2pz)_3\}$$

It is interesting to note that the chemical shift of cadmium complexes of $\{HB(4\text{-}Brpz)_3\}$, $\{HB(4\text{-}Mepz)_3\}$ and $\{HB(pz)_3\}$ ligands cannot be related to pK_a of the pyrazole moiety [19]. If we compare the ^{113}Cd NMR data of our derivatives with those reported in literature for analogous compounds it can be noted that in the case of derivatives containing donors having relatively small or no substituents in pz rings, a decrease in Cd—N_{av} bond distance is accompanied by an increase in shielding.

It has been argued by Reger [7d] that the ^{113}Cd shielding effect depends upon the coordination number and the geometry, primarily the Cd—N distances. In order to vary the M—N bond lengths it has been recently demonstrated [7,8,9] that the steric hindrance in 3-position plays a relevant role, while other electronic effects can also be introduced by changing the 5-position of the rings and/or going from a tris (pyrazolyl)borate to a tetrakis one.

With regard to ^{119}Sn NMR spectroscopy, the trends observed are easier to explain [20], whereas in the case of ^{113}Cd, at this stage of the research it is not clear why our ligand $\{HB(4\text{-}Brpz)_3\}$ is able to generate a higher shielding of Cd nucleus with respect to $\{HB(pz)_3\}$ and to $\{HB(4\text{-}Mepz)_3\}$, which differ by a H and a Me in 4-position, respectively. Additional X-ray structural data are necessary to further investigate the effect of substitution in 4-position upon ^{113}Cd NMR chemical shifts here discussed, and several studies are ongoing in our laboratory regarding this point on mixed donor atom combinations and also in presence of 4-substituted neutral bis- and tris (pyrazolyl)methanes [21], which are isoelectronic analogues of the anionic poly(pyrazolyl)borate donors.

EXPERIMENTAL

General laboratory equipment

Concentration was always carried out *in vacuo* (water aspirator). The samples were dried *in vacuo* till constant weight (20°C, *ca* 0.1 Torr). Carbon, hydrogen, and nitrogen analyses were carried out on a Fisons Instruments EA 1108 CHNS-O, while molecular weight determinations were performed by a Knauer membrane osmometer. Infrared spectra were recorded from 4000 to 250 cm^{-1} on a Perkin–Elmer 2000 System Series FTIR instrument. The electronic spectra were recorded in chloroform solution with an HP 8452A Diode Array Spectrophotometer. ^{1}H-, ^{13}C- and ^{113}Cd-NMR spectra were recorded on a Varian VXR-300 spectrometer operating at room temperature (299.94 MHz for ^{1}H, 75.05 MHz for ^{13}C and 66.55 MHz for ^{113}Cd). Some spectra were also recorded on a Varian Gemini-200 (200 MHz for ^{1}H, 50 MHz for ^{13}C). The chemical shift is reported in ppm from Me_4Si (^{1}H and ^{13}C, calibration from internal deuterium solvent lock) and $CdClO_4$ (^{113}Cd) values. The conductivity of the acetone solutions was measured with a Crison CDTM 522 conductimeter at room temperature.

Synthesis

Potassium[hydridotris(4-bromo-1H-pyrazol-1-yl)borato], *K[HB(4-Brpz)$_3$]*. A mixture of 4-Br-pyrazole (20 g, 0.136 mol) and KBH_4 (1.83 g, 0.034 mol) was heated gradually. Melting with a slight evolution of hydrogen occurred at *ca* 90°C. The mixture was finally heated at 170°C until the volution of 3 equiv. of hydrogen per KBH_4. The mixture was cooled to room temperature and xylene was added with vigorous stirring. The xylene solution was separated by filtration. This treatment was repeated several times to remove unreacted 4-Br-pyrazole. The remaining solid was washed with hexane–petroleum ether (1 : 1 *v/v*) to give a white crystalline solid, which was identified as K[HB(4-Brpz)$_3$] by elemental and spectral analyses. M.p.: 287–

289°C. Elemental analyses calcd for $C_9H_7BBr_3KN_6$: C, 22:1; H, 1.4; N, 17.2; found: C, 22.2; H, 1.5; N, 16.9.

Bis[hydridotris(4-bromo-1H-pyrazol-1-yl)borate] metal (II), **1–9**. These compounds were prepared by adding an aqueous solution (*ca* 50 cm^3) of 1 mmol of the appropriate metal salt to an aqueous solution (*ca* 50 cm^3) of potassium hydridotris(4-bromo-1*H*-pyrazol-1-yl)borate in a 1:2 molar ratio. The compounds **1–8** precipitated immediately: the complexes were filtered off, washed with diethyl ether, and dried *in vacuo*.

X-ray analysis

Suitable crystals of the complex $Cd[HB(4\text{-}Brpz)_3]_2$ were obtained by crystallization from dichloromethane/acetonitrile. A crystal of dimensions $0.24 \times 0.28 \times 0.98$ mm was used for data collection. Accurate unit-cell parameters were determined from a least-squares fit for 25 reflections measured on the Enraf–Nonius CAD4 diffractometer with graphite-monochromated Cu-K_α radiation of the Centro Grandi Strumenti dell'Università, Pavia, Italy.

The intensities of 6761 independent reflections in a complete quarter of the reflection sphere were collected by the $\omega/2\theta$ scan technique within the angular range $4 < 2\theta < 70°$. A total 4234 reflections having $I > 3\sigma(I)$ were regarded as observed and used in the structure analysis. The data were corrected for Lorentz-polarization effects and for absorption according to North *et al.* [22] with minimum and maximum absorption factors of 0.7150 and 0.9997. An approximate absolute scale factor and a mean thermal parameter of 6.54 $Å^2$ were determined by Wilson's method [23]. Crystal data, intensities data collection parameters and structure refinement results are summarized in Table 8.

Structure determination and refinement

The structure was solved by Patterson and Fourier methods. The positional parameters of the cadmium atom derived from the three-dimensional Patterson map and the isotropic thermal parameter, were refined in three cycles of least-squares refinement. A subsequent three dimensional difference Fourier synthesis revealed all the remaining non-hydrogen atoms. The full-matrix least-squares method refined the positional and first isotropic and later anisotropic thermal parameters. The positions of hydrogen atoms were calculated from the geometry of the compound and checked in a final difference Fourier map and not refined but included in the calculations in fixed positions, with the same isotropic thermal parameters of their bonded atoms.

The final R was 0.047 for the observed reflections. At all stages of the analysis the observed reflections were given unit weight, since the use of weights obtained from counting statistics did not lead to better results. The average shift/esd ratio in the final refinement cycle was 0.02 both in the positional and in the thermal parameters of the non-hydrogen atoms. The final difference Fourier map showed maximum and minimum $\Delta\rho$ values 0.674 and -0.349 e $Å^{-3}$.

All calculations were carried out with the Enraf–Nonius SDP crystallographic computing package [24] and with local programs.

Supplementary material—Tables of atomic positional parameters of non-hydrogen atoms and hydrogen atoms, table of anisotropic thermal parameters, tables of bond distances and bond angles involving non-hydrogen atoms and hydrogen atoms, table of planarity of molecular regions and a listing of observed and calculated structure factors (total of 40 pages).

Acknowledgements—We gratefully acknowledge the Universities of Camerino and of Pavia, and the Consiglio Nazionale delle Ricerche for financial support.

REFERENCES

1. (a) Trofimenko, S., *J. Am. Chem. Soc.*, 1966, **88,** 1842; (b) idem, ibidem, **89,** 1967, 3165, 3170, 6288.
2. (a) Trofimenko, S., *J. Prog. Inorg. Chem.*, 1986, **34,** 115; (b) Trofimenko, S., *Chem. Rev.*, 1993, **93,** 943.
3. (a) Gorrell, I. B., Looney, A. and Parkin, G., *J. Chem. Soc. Chem. Commun.*, 1990, 220; (b) Han, R., Gorrell, B., Looney, A. and Parkin, G., *J. Chem. Soc. Chem. Commun.*, 1991, 717; (c) Alfasser, R., Trofimenko, S., Looney, A., Parkin, G. and Vahrenkamp, H., *Inorg. Chem.*, 1991, **30,** 4098; (d) Looney, A., Parkin, G., Alfasser, R., Ruf, M. and Vahrenkamp, H., *Angew. Chem. Int. Ed. Engl.*, 1992, **31,** 92; (e) Han, R., Looney, A., McNeill, K., Parkin, G., Rheingold, A. L. and Haggerty, B. S., *J. Inorg. Biochem.*, 1993, **49,** 105; (f) Looney, A., Han, R., McNeill, K. and Parkin, G., *J. Am. Chem. Soc.*, 1993, **115,** 4690; (g) Looney, A., Saleh, A., Zhang, Y. and Parkin, G., *Inorg. Chem.*, 1994, **33,** 1158; (h) Kitajima, N., Hikichi, S., Tanaka, M. and Moro-oka, Y., *J. Am. Chem. Soc.*, 1993, **115,** 5496; (i) Han, R. and Parkin, G., *J. Am. Chem. Soc.*, 1991, **113,** 9707.
4. Gioia Lobbia, G., Bovio, B., Santini, C., Pettinari, C. and Marchetti, F., *Polyhedron*, 1996, **16,** 671.
5. Cecchi, P., Gioia Lobbia, G., Marchetti, F., Valle, G. and Calogero, S., *Polyhedron*, 1994, **13,** 2173.
6. Rodesiler, P. F., Griffith, E. A. H., Ellis, P. D. and Amma, E. L., *J. Chem. Soc. Chem. Commun.*, 1980, 492, an exhaustive list of references to ^{113}Cd NMR spectroscopy is contained herein.
7. (a) Reger, D. L., Mason, S. S., Takats, J., Zhang, X.-W., Rheingold, A. L. and Haggerty, B. S., *Inorg. Chem.*, 1993, **32,** 4345; (b) Reger, D. L., Mason, S. S., Rheingold, A. L. and Ostrander, R. L., *Inorg. Chem.*, 1993, **32,** 5216; (c) Lipton, A. S., Mason, S. S., Reger, D. L. and Ellis, P. D., *J. Am. Chem. Soc.*, 1994, **116,** 10,182; (d) Reger, D. L., Myers, S. M., Mason, S. S., Darensbourg, D.

J., Holtcamp, M. W., Reibenspies, J. H., Lipton, A. S. and Ellis, P. D., *J. Am. Chem. Soc.*, 1995, **117,** 10,998; (e) Reger, D. L., Mason, S. S. and Rheingold, A. L., *Inorg. Chim. Acta*, 1995, **240,** 669.

8. (a) Reger, D. L., Myers, S. M., Mason, S. S., Rheingold, A. L., Haggerty, B. S. and Ellis, P. D., *Inorg. Chem.*, 1995, **34,** 4996; (b) Reger, D. L., Collins, J. E., Myers, S. M., Rheingold, A. L. and Liable-Sands, L. M., *Inorg. Chem.*, 1996, **35,** 4904.
9. (a) Reger, D. L. and Mason, S. S., *Organometallics*, 1993, **12,** 2600; (b) Reger, D. L. and Mason, S. S., *Polyhedron*, 1994, **13,** 3059.
10. Oliver, J. D., Mullica, D. F., Hutchinson, B. B. and Milligan, W. O., *Inorg. Chem.*, 1980, **19,** 165.
11. Jesson, J. P., Trofimenko, S. and Eaton, D. R., *J. Am. Chem. Soc.*, 1967, **89,** 3148, 3158.
12. Johnson, C. K., ORTEP, Report ORNL-3793, Oak Ridge National Laboratory, Tennessee, U.S.A., 1965.
13. Bonati, F., *Gazz. Chim. Ital.*, 1989, **120,** 341; Bonati, F. and Bovio, B., *J. Crystallogr. Spectrosc. Res.*, 1990, **20,** 233.
14. Gioia Lobbia, G., Pettinari, C., Marchetti, F., Bovio, B. and Cecchi, P., *Polyhedron*, 1996, **15,** 881.
15. Nakata, K., Kawabata, S. and Ichikawa, K., *Acta Cryst.*, 1995, **C51,** 1092.
16. Looney, A., Han, R., Gorrell, I. B., Cornebise, M., Yoon, K., Parkin, G. and Rheingold, A. L., *Organometallics*, 1995, **14,** 274.
17. Shannon, R. D., *Acta Cryst.*, 1976, **A32,** 751.
18. Tolman, C. A., *Chem. Rev.*, 1977, **77,** 313.
19. Elguero, J., in *Pyrazoles and their Benzo Derivatives*, in *Comprehensive Heterocyclic Chemistry*, Vol. 5, part 4A, eds. in Chief A. R. Katritzky and C. V. Rees, ed. K. T. Potts. Pergamon Press, Oxford, 1984, p. 223.
20. (a) Gioia Lobbia, G., Valle, G., Calogero, S., Cecchi, P., Santini, C. and Marchetti, F., *J. Chem. Soc. Dalton Trans.*, 1996, 2475; (b) Calogero, S., Valle, G., Gioia Lobbia, G., Santini, C., Cecchi, P. and Stievano, L., *J. Organomet. Chem.*, 1996, **526,** 269.
21. (a) Pettinari, C., Santini, C., Leonesi, D. and Cecchi, P., *Polyhedron*, 1994, **13,** 1553; (b) Pettinari, C., Lorenzotti, A., Sclavi, G., Cingolani, A., Rivarola, E., Colapietro, M. and Cassetta, A., *J. Organomet Chem.*, 1995, **496,** 69; (c) Pettinari, C., Lorenzotti, A., Pellei, M. and Santini, C., *Polyhedron*, 1997, **16,** 3425.
22. North, A. C., Phillips, D. C. and Mathews, F. C., *Acta Cryst.*, 1968, **A24,** 3561.
23. Wilson, A. J. C., *Nature*, 1942, **150,** 152.
24. Frenz, B. A. and Associates Inc., College Station, RX 77840 and Enraf–Nonius, Delft, The Netherlands, 1985.

Pergamon

PII: S0277-5387(97)00263-5

Polyhedron Vol. 17, No. 1, pp. 27–34, 1998
© 1997 Elsevier Science Ltd
All rights reserved. Printed in Great Britain
0277-5387/98 $19.00+0.00

Structural and textural properties of the $NiO–Al_2O_3$ catalyst

E. Kiš,[a]* R. Marinković-Nedučin,[a] G. Lomić,[a] G. Bošković,[a] D. Ž. Obadović,[b] J. Kiurski[b] and P. Putanov[c]

[a]University of Novi Sad, Faculty of Technology, Yugoslavia

[b]University of Novi Sad, Faculty of Sciences, Institute of Physic, Yugoslavia

[c]The Serbian Academy of Sciences and Arts, Belgrade, Yugoslavia

(Received 1 November 1996; accepted 16 June 1997)

Abstract—Influence of nickel oxide loading (5; 10; 20 wt% Ni) and temperature of heat treatment (400, 700, 1100°C) on the structure, texture and reducibility of coprecipitated $NiO–Al_2O_3$ catalyst was investigated. X-ray diffraction (XRD), diffuse reflectance spectroscopy (DRS), low temperature nitrogen adsorption (LTNA) and hydrogen reduction confirmed significant changes in physico-chemical properties as the function of mentioned variables. The results showed that the interactions in coprecipitated $NiO–Al_2O_3$ system are intensive even at 400°C. At 700°C the observed interactions are accompanied by considerable changes in surface area, reducibility and the coordination of Ni(II), while at 1100°C treatment intensive structural and textural changes were registered. © 1997 Elsevier Science Ltd

Keywords: structure; Ni^{II} coordination; texture; reducibility; coprecipitation; nickel–alumina catalyst.

The behavior of $NiO–Al_2O_3$ catalysts is strongly dependent on the preparation method, as well as on pretreatment conditions. Different methods of $NiO–Al_2O_3$ system preparation include precipitation of Ni ions on Al_2O_3 support [1,2], coprecipitation of Ni and Al ions on Al_2O_3 [3], coprecipitation of Ni and Al ions [4,5,6], impregnation of appropriate form of alumina [4,7,8–10] by different Ni-precursor solutions; bulk fusion of nickel and aluminum salts [2], mechanical powder mixing [2] etc. The complete procedure of catalyst synthesis includes different subsequent steps of drying, dehydration, activation (calcination/reduction) and passivation. It has been shown that each step in this preparation sequence affects the performance of the obtained catalysts [7,9]. For nickel–alumina catalyst, obtained by wet impregnation with nitrate solution, Bartholomew and Farrauto [7] have shown that the calcination temperature, temperature and heating rate during reduction step, hydrogen space velocity during reduction, nickel loading and passivation procedures affect the surface area and the fraction of the reduced nickel. We do believe that these observations could be generalized for the other catalysts, prepared by different methods.

Catalyst component interactions, influenced by each of the steps in complex catalyst preparation procedure, have an additional affect on catalyst activity and selectivity. Tauster *et al.* [11] were first to report about these phenomena in the TiO_2 supported catalyst. They observed that hydrogen and carbon monoxide chemisorption on reduced transient metal oxides, deposited on titania support, decrease with the increase of reduction temperature. The phenomenon was explained by formation of metal–metal bonding between transient metal and either titanium atoms, or titanium cations, resulting in $TiPt_3$-type compounds on the catalyst surface. This type of interaction was later on signified as strong metal support interactions (SMSI). Metal support interactions were not studied in $NiO–Al_2O_3$ systems for quite a long time, perhaps since alumina is not a reducible oxide. However, Huang *et al.* [12] have revealed that in the system $NiO–Al_2O_3$ some kind of metal-support interactions apparently are present. In these systems SMSI are promoted by formation of nickel spinel $NiAl_2O_4$. A small amount of metallic nickel on $Ni^{2+}/NiAl_2O_4/Al_2O_3$ catalyst surface, detectable only by ESCA,

* Author to whom correspondence should be addressed.

does not adsorb hydrogen. Namely, some species of mobile $/Al_xO_y/_n$ aggregates, formed during the thermal disproportiation of $NiAl_2O_4$, prevent or hinder hydrogen adsorption. The surface of metallic nickel is partially covered by $/Al_xO_y/_n$ species. It has to be mentioned that the hydrogen adsorption on the catalyst surface is increased after catalyst pretreatment by CO and O_2, similar to the behavior of the transient metals supported on titania.

The considerable influence of the variety of subtle structural differences on catalyst properties could be an explanation why the supported nickel catalyzes such different processes, as steam reforming [13,14], methanation [9,15], oxidation [16–20], hydrogenolysis [21] and enantioselective processes [22].

The investigations on the effect of catalyst preparation procedure on structural, textural and other physico-chemical properties of the $NiO–Al_2O_3$ as catalyst precursor for different processes were performed. The results on the $NiO–Al_2O_3$ catalyst precursors prepared by coprecipitation method are presented in the paper. The following papers will consider the catalyst prepared by impregnation and mechanical powder mixing.

EXPERIMENTAL

Catalyst preparation

Catalyst precursors were coprecipitated from nitrate solution by NaOH (20 wt% solution, pH = 9.5, ambient temperature). The Ni/Al ratio in initial nitrate solutions was varied in order to obtain different Ni loading. The precipitates, matured for 24 hrs, were vacuum filtered and subsequently washed until free of nitrate. The air dried samples (105°C, 48 h) were ground in an agate mortar and the powders obtained were air dried again (105°C, 6 h). The nickel loading obtained in the dried samples was 5.1, 9.93 and 19.96 wt%, respectively. The samples were thermally treated at 400, 700 and 1100°C in a static air atmosphere for 6 h.

Sample characterization

Wet chemical analysis. The amount of nickel in the oxide form was determined by acidic extraction of nickel from the sample, followed by dimethylglyoxime precipitation [23,24].

Total surface area. The surface area was determined by dynamic low temperature nitrogen adsorption in helium as a carrier (Perkin–Elmer Shell, Sorptometer Model 212 D). The data were interpreted using the BET equation and an effective N_2 cross-sectional area of 16.2 nm^2.

Porosity. The total porosity (Q) was calculated from apparent (γ) and true (d) densities, $Q(\%) = (1-\gamma/d)\,100$, determined pycnometrically using mercury and benzene vapors as working fluids [25].

Pore size distribution. Pore size distribution was determined by mercury porosimetry (Carlo Erba, Series 1500), pressure range up to 1500 bars.

X-ray diffraction. Phase composition was determined by X-ray diffraction (XRD) (Philips PW 1050 diffractometer with Ni filter and Cu radiation). The average crystallite size (D) was calculated by Scherrer method (X-ray line broadening, $D = K\lambda/\beta\cos\theta$) with NaCl as an internal standard. The half-maximum line width (β) for NiO (111), NiO (200) and NiO (220) planes were applied. The constant K was approximated as 0.95 as previously published [18].

Diffuse reflectance spectroscopy. Diffuse reflectance spectra were registered in the range 10,000–45,000 cm^{-1} at room temperature. (Carl Zeiss Jena, SPM-2). The Kubelka–Munk function $F(R) = (1-R_\infty)^2/2R_\infty$ was applied in data interpretation.

Reducibility. The reducibility of the samples were analyzed by dynamic DSC method (Du Pont 1050) in dry hydrogen flow 25 cm^3/min, in the temperature range 20–450°C at heating rate 10°C/min.

Nomenclature of the samples

The following unified C–W–T nomenclature of the catalyst samples was used in the paper: C-designate the coprecipitation preparation method; *W*—nickel loading in wt%, *T*—temperature of the heat treatment (as example C-5-400 is sample prepared by coprecipitation, containing 5 wt% of Ni, thermally treated at 400°C).

RESULTS AND DISCUSSION

X-ray phase and crystallite size analysis

The phase composition of the coprecipitated samples is illustrated by the XRD patterns in Fig. 1. The broadened Bragg peaks observed for the samples heated at 400°C indicate the small particle sizes of crystalline phases. The presence of γ–Al_2O_3 is confirmed in all samples. Akimov *et al.* [26] claimed, based on phase composition and magnetic properties of similar materials prepared by coprecipitation using ammonia, that spinel formation is possible at temperatures as low as 400°C. Based on our results it is difficult to say anything about $NiAl_2O_4$ formation, since in the broadened XRD patterns, the signals of nickel spinel and γ–Al_2O_3, having very similar crystal lattices, overlapped. The color of the samples are bright gray, characteristic of a mixture of diluted nickel and alumina oxides. The d-spacing of the γ–Al_2O_3 was increased related to the ASTM data; for C-5-400 sample the experimental and reference ASTM values are as follows: 2.392/2.39 (311); 1.977/1.977 (400) and 1.406/1.395 (440). The increase of the d-spacing could be explained by NiO–γ-Al_2O_3 solid solution formation. Since the increase of d-spacing is not

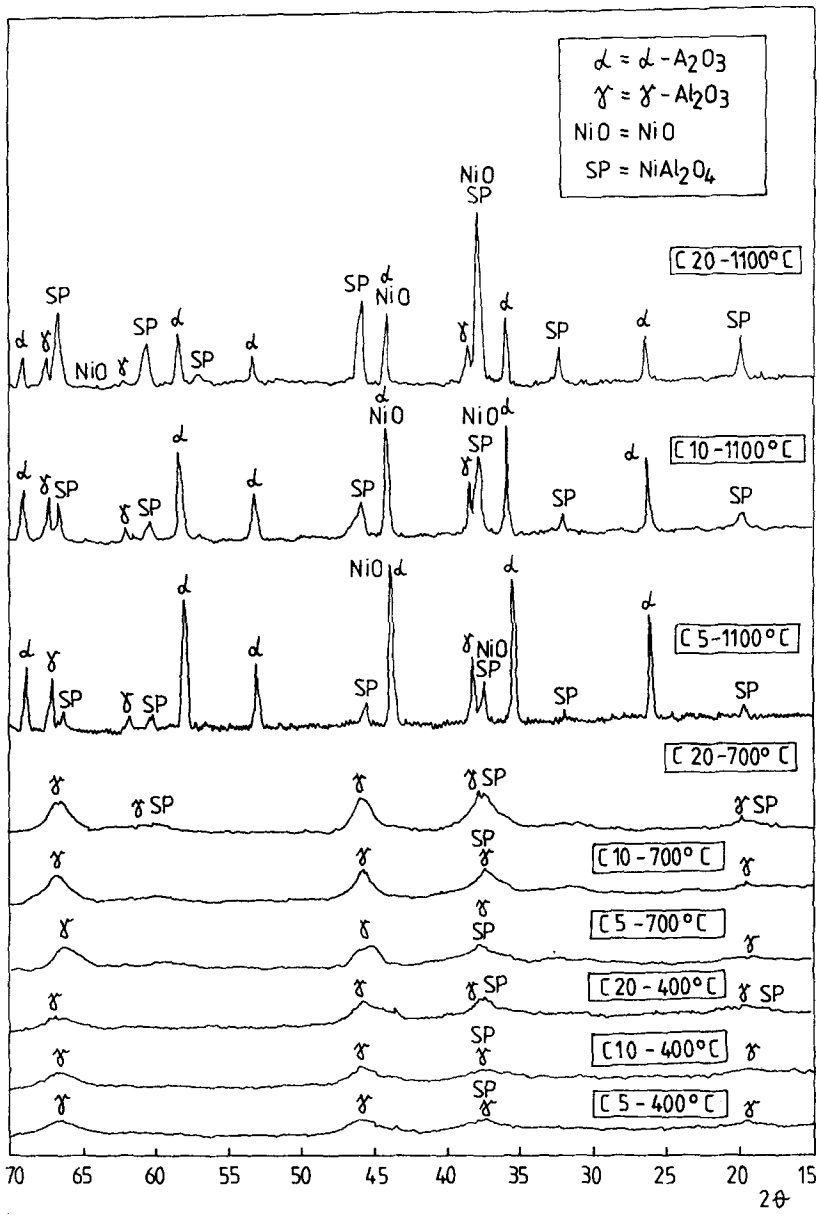

Fig. 1. XRD patterns of the coprecipitated samples.

linearly proportional to the NiO content, the effect of $NiAl_2O_4$ formation, its crystallinity and/or clustering of dopant ions within structures, i.e. regions of high or low concentrations, should be additionally considered. It could be concluded that in the coprecipitated $NiO–Al_2O_3$ system treated at 400°C, with up to 20 wt% of Ni, the components form a solid solution of $NiO–NiAl_2O_4$-γ-Al_2O_3.

The diffraction patterns of the samples treated at 700°C are similar to those obtained at lower temperature, the sharpening of the Bragg peaks indicating some higher crystallinity in the system. The increased d-spacing of the γ–Al_2O_3 in comparison to the ASTM data is also observed; for C-5-400 sample values are: 2.392/2.39 (311); 2.019/1.977 (400) and 1.413/1.395 (440). These results also suggest the formation of a solid solution NiO-$NiAl_2O_4$-γ-Al_2O_3 with previously mentioned additional effects.

In all samples treated at 1100°C, the diffraction lines for the following phases: NiO, $NiAl_2O_4$ γ- and α-Al_2O_3 were identified. The presence of γ-Al_2O_3 in the samples treated at so high temperatures suggests that the nickel oxide hinders the crystallization and phase transformations of alumina. However, since there is overlapping of main XRD signals of the presence phases, as illustrated in Table 1, the calculation of NiO crystallite size was not reliable.

For semi-quantitative estimation of $NiAl_2O_4$, for-

Table 1. XRD data of the nickel and aluminum compounds

Compound	2θ (°)	d (Å)	I/I (%)	*hkl*	ASTM
$NiAl_2O_4$	37.04	2.427	100	311	10-339
NiO	37.31	2.410	91	111	4-0835
η-Al_2O_3	37.47	2.400	60	311	4-0875
γ-Al_2O_3	37.63	2.390	80	311	10-425
NiO	43.33	2.088	100	200	4-0835*
α-Al_2O_3	43.39	2.013	65	113	10-173

med during the thermal treatment of the samples, the (440) plane ($2\theta = 65.69°$) is most suitable [27], showing the increase of spinel quantity by increased initial NiO content and treatment temperature (Fig. 1).

Reflectance spectra analysis

In Table 2 the reflection spectral bands of the samples depending on nickel content and temperature of heat treatment are presented.

Based on the data of energies of optical transitions cited in reference [28], the following points could be outlined:

(i) In all the samples a nickel spinel like phase is formed. The characteristic bands in the region of $^3T_1 \rightarrow {}^3T_1$ (*P*) at 16,000 cm^{-1} and $^3T_1 \rightarrow {}^1E$ at 13,350 cm^{-1} are present in the samples treated at 400 and 700°C.

(ii) The fact that the more intense band for the purely octahedral nickel is at 27,000 cm^{-1} [29] and for the tetrahedral nickel is at 16,000–17,000 cm^{-1} [30] suggests that the tetrahedral Ni^{II} is dominant in the spinel like phases, increasing with the nickel oxide content in the samples. Namely, the intensity ratio of the most intense octahedral band (27,000 cm^{-1}) and the most intense tetrahedral bands (16,000–17,000 cm^{-1}) indicate the distribution of the Ni^{II} ions among tetrahedral and octahedral sites.[31] Figure 2 shows the increased tetrahedral Ni^{II} content in the samples treated at 1100°C.

(iii) For the sample C-20-1100 a strong absorption is present above 30,000 cm^{-1}. Absorption in this region emerge if small amounts of free NiO [28] are present. The other two samples (C-5-1100 and C-10-1100) showed a weaker absorption band in the same region (Fig. 2), which is in accordance with the XRD results (Fig. 1).

(iv) The degree of occupancy of tetrahedral/octahedral sites, *i.e.* the degree of spinel inversion, depends on temperature of heat treatment. The intensity of the octahedral band, at 27,000 cm^{-1} in the sample treated at 1100°C is more pronounced than in the sample treated at 700°C (Fig. 3).

In the case of full inversion, Ni^{II} cations occupy the octahedral positions and the formula of inverse spinel can be written as $Al(NiAl)O_4$. Namely, in the spinel structure the oxygen ions are in a face-centered cubic lattice. The unit cell contains 32 oxygen ions, 64 tetrahedral holes, and 32 octahedral holes. In normal spinel, AB_2O_4, $8A^{2+}$ cations occupy 8 tetrahedral positions and $16B^{3+}$ cations 16 octahedral positions. In

Table 2. Electronic spectral data of Ni(II) in the coprecipitated catalyst

	ν (cm^{-1})								
	Sample			Sample			Sample		
Transition	C-5-400	C-5-700	C-5-1100	C-10-400	C-10-700	C-10-1100	C-20-400	C-20-700	C-20-1100
$^3A_{2g} \rightarrow {}^3T_{2g}$	10,000	10,200	10,200	10,600	10,600	10,600	10,400	10,600	10,200
$^3T_1 \rightarrow {}^1T_2$	—	—	—	—	—	—	—	—	—
$^3A_{2g} \rightarrow {}^1E_g$	—	—	—	—	—	—	—	—	13,600
$^3T_1 \rightarrow {}^1E$	—	15,800	15,800	—	15,800	15,800	15,400	15,800	—
$^3T_1 \rightarrow$ $^3T_1$ (P)	16,600	17,000	16,800	16,000	16,600	16,800	—	16,800	16,000
$^3A_{2g} \rightarrow {}^1T_{2g}$	24.600	25,600	24,200	24,400	23,500	23,500	23,000	—	—
$^3A_{2g} \rightarrow {}^3T_{1g}$	27,400	27,400	27,400	—	27,800	27,000	25,800	27,400	27,400
IL_1	35,000	34,400	34,400	34,400	34,000	34,000	33,600	33,800	34,600
IL_2	42,800	42,400	42,600	41,400	42,000	43,000	40,600	42,200	42,800
Symmetry	Oh+Td	Oh+Td	Oh+Td	Oh+Td	Oh+Td	Oh+Td	Oh+Td	Oh+Td	Oh+Td

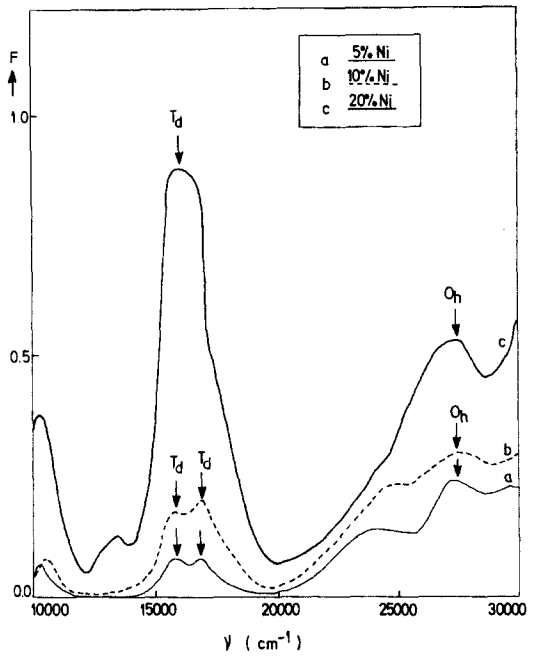

Fig. 2. Kubelka–Munk functions of coprecipitated samples with (a) 5, (b) 10 and (c) 20 wt% of nickel treated at 1100°C in air.

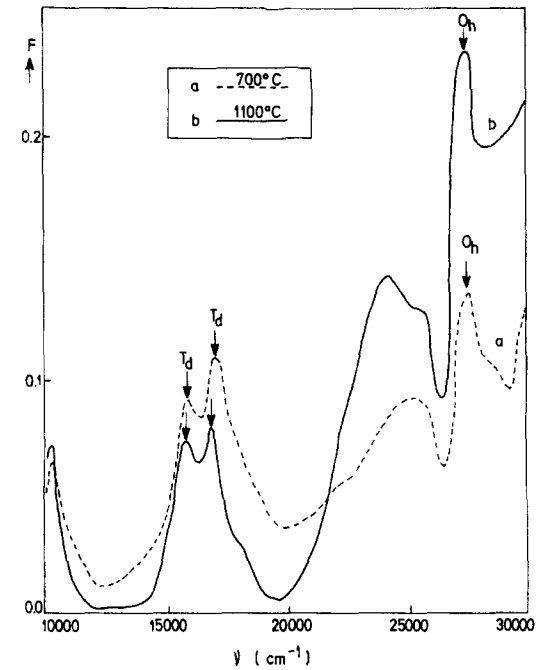

Fig. 3 Kubelka–Munk functions of coprecipitated samples with 10 wt% of nickel treated at (a) 700°C and (b) 1100°C.

inverse spinel $8B^{3+}$ cations occupy 8 tetrahedral positions, and $8B^{3+}$ and $8A^{2+}$ cations 16(8+8) octahedral positions [32].

Textural properties

Textural properties of the coprecipitated catalysts are presented in Table 3. The surface area of the catalyst is decreasing with the increased initial nickel oxide content in the samples and temperature of heat treatment.

It is interesting to note that the porosity of samples reach the maximal value at 700°C, when the surface area is about a half of the surface area of the respective samples treated at 400°C. That means that at the temperature as low as 700°C the surface area of the catalyst is not determined by sintering, but by polymorphic transformations of alumina and its interaction with nickel oxide. The surface area of the samples treated at 1100°C is about 40 times less than the surface area of the samples treated at 400°C. This dramatic drop of surface area is caused by sintering, followed by chemical interaction between NiO and Al_2O_3, i.e. by $NiAl_2O_4$ spinel formation, and alumina phase transformation to the stable α–Al_2O_3 form. The pore size distribution of some samples seems to be bimodal, but in these samples the main pore volume contribute to *ca* 80% of the total porosity. These dominant pores are characterized by lower radius values in the case of samples treated at 400°C and 700°C, and in samples treated at 1100°C with the higher radius values. The data of average pore radius r (Table 3), are calculated as $r = 2Q/\gamma S = 2V/S$, where Q is porosity; γ—apparent density; V—pore volume and S—surface area of the samples [33]. The average pore radii of the samples treated at 400 and 700°C are closer to the lower dominant pore radius, and in the samples treated at 1100°C to the higher dominant pore radius, experimentally determined by Hg-porosimeter.

Reducibility

According to the phase composition of the samples and reflectance spectra of Ni^{II}, the catalysts consists of nickel oxide partially dissolved in alumina and poorly ordered spinel. The ordering of the $NiAl_2O_4$ structure is improved when the temperature of heat treatment was raised. It is known that the coprecipitated catalysts are difficult to reduce, because of the high distribution of nickel oxide in alumina and therefore a good opportunity for interaction [34], as confirmed also by the present results. There are differences in reducibility between free nickel oxide and alumina supported nickel oxide even at higher nickel oxide loading because alumina dissolves in NiO, so NiO could not be considered as a free and independent component of the system [35]. Even the reduction of unsupported nickel oxide is rather difficult, demanding an induction period up to reduction temperature of 400°C [36]. However, kinetic studies of NiO reduction were carried out even at significantly lower temperatures, e.g. Frety *et al.* [37] studied the reducibility of NiO at 240°C.

Table 3. Textural properties of the coprecipitated catalyst

	Sample								
	C-5-400	C-5-700	C-5-1100	C-10-400	C-10-700	C-10-1100	C-20-400	C-20-700	C-20-1100
Surf.area (m^2/g)	44.52	211.6	13.8	428.2	186.3	12.0	320.4	114.4	6.9
Porosity (%)	55.1	75.5	59.2	40.4	57.9	52.1	46.9	69.1	57.2
Av. pore radius (nm)	4.1	13.0	73.2	2.3	8.8	73.1	3.4	15.8	120.8
Pore size distr. (nm)	8;80	7.5;140	65	9.5;50	12.5	9;60	8	8	7.5;75

The DSC curves of the synthesized catalyst samples in hydrogen flow are shown in Fig. 4. The exothermal effects of NiO reduction are registered in all catalyst samples, being shifted to significantly higher temperatures compared to the data obtained for similar systems by means of DTA (195–210°C) [38].

The reduction temperature of the samples with 5 and 10 wt% of nickel is higher at 700 than at 400°C pretreatment temperature. Such behavior is expected because of stronger interaction of NiO and Al_2O_3 and more intensive spinel formation of higher temperature. For the sample with 20 wt% of nickel the inverse trend is observed, indicating the presence of small amount of free NiO in the catalyst. This assumption is supported by the high spinel and proportionally low alumina content, visible from the XRD data, Fig. 1. The reduction temperature of all the samples treated at 1100°C is lower compared to those pretreated at

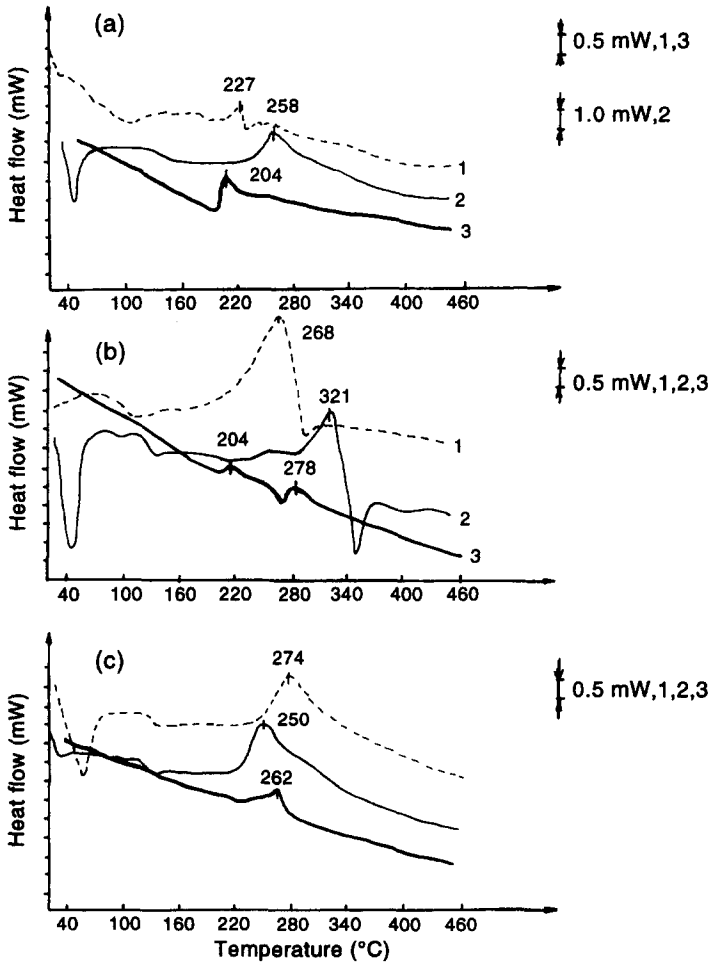

Fig. 4. DSC curves of coprecipitated NiO–Al_2O_3 samples, in hydrogen flow (20–25 cm^3/min) (a) 5; (b) 10; and (c) 20 wt% of nickel in the samples; pretreatment of samples at 400 (1); 700 (2); and 1100°C (3) in air.

lower temperatures, which could be explained by the presence of the small fraction of nickel oxide segregated during the spinel formation at high temperature [35]. The previous result is in accordance with the results of Chespokova *et al.* [38] who claim that the reducibility of NiO in binary and ternary systems is not determined by NiO content and chemical composition of nickel oxide containing phases, but by the inhomogeneity of the system.

CONCLUSIONS

It has been shown that in the $NiO–Al_2O_3$ coprecipitated catalysts metastable mixed oxides are formed. During the heat treatment of the catalysts, the strength and the degree of NiO and Al_2O_3 interaction is changing, depending on the treatment temperature. That is manifested by phase segregation, chemical interactions and polymorphic transformations of alumina support. Nickel oxide hinder the crystallization and phase transformations of alumina. Formation of surface spinel, $NiAl_2O_4$, was registered in all samples. The cation distribution is affected by the nickel content and the temperature of heat treatment. Both the nickel loading and the temperature of the heat pretreatment are the factors influencing the reducibility of the nickel in the catalyst. It seems, however, that the nickel loading, after reaching a critical temperature become the more significant factor in the formation of the tetrahedral coordinated nickel, Ni^{II}.

The surface area of the samples is regularly increasing with alumina content of the catalyst. The strong changes of textural properties of the coprecipitated $NiO–Al_2O_3$ catalyst at 700°C are caused by chemical interaction of catalyst components and by polymorphic transformation of alumina. The dramatic decrease of surface area at 1100°C is caused by intensive $NiAl_2O_4$ and α-Al_2O_3 formation and by sintering of oxide particles.

Acknowledgement—The authors would like to thank the Ministry of Science and Technology, Republic of Serbia, for financial support for this work.

REFERENCES

1. Mukherjee, D. K., Misra, J., Chowdhury, R. L. and Sen, S. P., *Proc. Indian Nat. Sci. Acad.*, 1975, **41,** 74.
2. Arora, B. R., Banerjee, R. K., Ganguli, N. C. and Sen, S. P., *Proc. Symp. Chemic. and Oil from Coal, (India)*, 1975, **21,** 203.
3. Banerjee, A. K., Misra, J., Mukherjee, D. K., Naidu, S. R. and Sen, S. P., *Technology (India)*, 1975, **12,** 44.
4. Dollimore, D. and Jones, T. E., *J. Appl. Chem. Biotechnol.*, 1973, **23,** 29.
5. Williams, A., Butler, G. A., and Hammonds, J., *J. Catal.*, 1972, **24,** 352.
6. Hakvoort, G., Proc. 12 Intern. Conf., *Science of Ceramics* (ed. P. Vincenzini) **12,** p. 81 (1983).
7. Bartholomew, C. H. and Farrauto, R. J., *J. Catal.*, 1976, **45,** 41.
8. Huang, Y.-J., Barrett, B. T. and Schwarz, J. A., *Appl. Catal.*, 1986, **24,** 241.
9. Huang, Y.-J. and Schwarz, J. A., *Appl. Catal.*, 1987, **30,** 239.
10. Huang, Y.-J. and Schwarz, J. A., *Appl. Catal*, 1987, **32,** 45.
11. Tauster, S. J., Fung, S. L. and Garten, R. L., *J. Am. Chem. Soc.*, 1978, **100,** 170.
12. Huang, Y.-J., Schwarz, J. A., Diehl, J. R. and Baltrus, J. P., *Appl. Catal.*, 1988, **37,** 229.
13. Rostrup-Nielsen, J. R., *Stem Reforming Catalysts*, Teknisk Forlag A/S, Copenhagen, (1975).
14. A. Al-Ubaid and E. E. Wolf., *Appl. Catal.*, 1988, **40,** 73.
15. Chen, B., Falconer, J. L., Bailey, K. M. and Sen, B., *Appl. Catal.*, 1990, **66,** 283.
16. Huszar, K., Racz, Gy. and Szekely, Gy., *Acta Chim. (Budapest)*, 1971, **70,** 287.
17. Racz, Gy. and Szekely, Gy., *Acta Chim.*, 1971, **70,** 301.
18. Gavalas, G. R., Phichitkul, C. and Voecks, G. E., *J. Catal.*, 1984, **88,** 54.
19. Gavalas, G. R., Phichitkul and Voecks, G. E., *J. Catal.*, 1984, **88,** 65.
20. El-Shobaky, G. A. and Al-Noaimi, A. N., *Appl. Catal.*, 1987, **29,** 235.
21. Nazimek, D. and Ryczkowski, J., *Appl. Catal.*, 1986, **26,** 47.
22. Nitta, Y., Kawabe, M. and Imanaka, T., *Appl. Catal.*, 1987, **30,** 141.
23. Kolthoff, I. M. and Sandell, E. B., Textbook of Quantitative Inorganic Analysis, Naučna knjiga, Beograd, 1968.
24. Vedrine, J. C., Hollingerand, G., Minh, O. T., *J. Phys. Chem.*, 1978, **82,** 1968.
25. Putanov, P., (Yugoslavia), 1969, **1,** 142.
26. Akimov, V. M., Slinkin, A. A., Kretalova, L. D., Rubinstein, A. M., IAN SSSR *Otd. Him. Nauk*, (Russian), 1960, **4,** 624.
27. Kis, E. E., Ph.D. Thesis, Faculty of Technology, Novi Sad, 1981.
28. Jacono, M. Lo., Schiavello, M. and Cimino, A., *J. Phys. Chem.*, 1971, **75,** 1044.
29. Low, W., *Phys. Rev.*, 1958, **109,** 256.
30. Schmitz Du Mont, D., Lule, A., Reinen, D., *Ber. Bunsenges. Phys. Chem.*, 1965, **69,** 76.
31. Jacono, M. Lo. and Schiavello, M., *Preparation of Catalysts I*, (eds B. Delmon, P. A., Jacobs and G. Poncelet) p. 473, Elsevier, Amsterdam p. 473 (1976).
32. Durrant, P. J., Durrant, B., *Introduction to Advanced Inorganic Chemistry*, (Second Edition), p. 388, Longman, London (1970).
33. Linsen, B. G., *Physical Chemical Aspects of Adsorbents and Catalysts*, p. 276, Academic Press, London and New York (1970).
34. Holm, V. C. F. and Clark, D., *J. Cat.*, 1968, **11,** 305.
35. Simonova, L. G., Dzisko, V. A., Borisova, M. S.,

Karakchiev, L. G. and Olenkova, L. P., *Kinetika i Kataliz* (Russian), 1973, **14,** 1566.
36. Rozhdestvenskii, V. P., Volgina, L. M. and Strokova, T. P., *Zhurnal Prikladnoi Himii* (Russian), 1967, **XL,** 705.
37. Frety, R., Tournayan, L., and Charcosset, H., *Annal. Chim.*, 1974, **9,** 341.
38. Chespokova, R. V., Bondareva, A. A., Astahov, N. N. and Zhivotenko, N. N., *Zhurnal Neorganiceskoi Himii* (Russian), 1982, **27,** 286.

Pergamon

PII: S0277-5387(97)00258-1

Polyhedron Vol. 17, No. 1, pp. 35–41, 1998
© 1997 Elsevier Science Ltd
All rights reserved. Printed in Great Britain
0277-5387/98 $19.00+0.00

Synthesis and characterization of double $MCoC_2$ and MFeCoS (M = Mo, W) tetrahedral cluster complexes bridged by various biscyclopentadienyl ligands

Li-Cheng Song*, Jin-Yu Shen, Xiang-Yang Wu and Qing-Mei Hu

Department of Chemistry, Nankai University, Tianjin 300071, P. R. China

(Received 7 May 1997; accepted 11 June 1997)

Abstract—The bridged double tetrahedral clusters $[RPhC_2MCo(CO)_5(\eta^5\text{-}C_5H_4)]_2[C(O)CH_2CH_2C(O)]$ (**1a** M = Mo, R = Ph; **1b** Mo, *p*-MeC_6H_4; **1c** Mo, *m*-$MeOC_6H_4$; **1d** W, Ph), $[Ph_2C_2MCo(CO)_5(\eta^5\text{-}C_5H_4)]_2[p\text{-}C(O)C_6H_4C(O)\text{-}p]$ (**2a** M = Mo; **2b** W) and $[Ph_2C_2MCo(CO)_5(\eta^5\text{-}C_5H_4)]_2[o\text{-}CH_2C_6H_4CH_2\text{-}o]$ (**4**) were synthesized from single tetrahedral clusters $RPhC_2Co_2(CO)_6$ and corresponding bridging intermediate reagents $[NaM(CO)_3(\eta^5\text{-}C_5H_4)]_2Z$ (Z = $C(O)CH_2CH_2C(O)$, *p*-$C(O)C_6H_4C(O)$-*p*, *o*-$CH_2C_6H_4CH_2$-*o*), whereas those clusters $[FeMCoS(CO)_8(\eta^5\text{-}C_5H_4)]_2[p\text{-}C(O)C_6H_4C(O)\text{-}p]$ (**3a** M = Mo; **3b** W), $[FeMCoS(CO)_8(\eta^5\text{-}C_5H_4)]_2[o\text{-}CH_2C_6H_4CH_2\text{-}o]$ (**5**) and $[FeMoCoS(CO)_8(\eta^5\text{-}C_5H_4)]_2[Me_2SiOSiMe_2]$ (**6**) were prepared by reactions of a single tetrahedral cluster $FeCo_2(CO)_9(\mu_3\text{-}S)$ with bridging intermediate reagents $[NaM(CO)_3(\eta^5\text{-}C_5H_4)]_2Z$ (Z = *p*-$C(O)C_6H_4C(O)$-*p*, *o*-$CH_2C_6H_4CH_2$-*o*) or $[LiMo(CO)_3(\eta^5\text{-}C_5H_4)]_2$ $[Me_2SiOSiMe_2]$, respectively. Further reactions of **3a–b** with reducing agent $NaBH_4$ gave corresponding bridged double clusters $[FeMCoS(CO)_8(\eta^5\text{-}C_5H_4)]_2[p\text{-}CH(OH)C_6H_4CH(OH)\text{-}p]$ (**8a** M = Mo; **8b** W), whereas **1a** reacted with $NaBH_4$ afforded $[Ph_2C_2MoCo(CO)_5(\eta^5\text{-}C_5H_4)]_2[CH(OH)CH_2CH_2CH(OH)]$ (**7**), which could be converted to its ether cluster derivative $[Ph_2C_2MoCo(CO)_5(\eta^5\text{-}C_5H_4)]_2[\alpha\text{-}CHCH_2CH_2CH\text{-}\alpha]$ (**9**). All the new clusters **1–9** have been characterized by elemental analysis, IR and ^1H NMR spectroscopy, whereas new terephthaloylbis(cyclopentadienylsodium) used to prepare intermediate reagents $[NaM(CO)_3(\eta^5\text{-}C_5H_4)]_2[p\text{-}C(O)C_6H_4C(O)\text{-}p]$ has been isolated and characterized by IR and ^1H NMR spectroscopy. © 1997 Elsevier Science Ltd

Keywords: double $CoMC_2$ (M = Mo, W) clusters; double FeMCoS clusters; bridging biscyclopentadienyl ligands; synthesis; characterization.

Since the mid-1970s transition metal cluster chemistry has enjoyed tremendous growth, largely due to the potential applications of transition metal cluster complexes in catalysis, as well as the novelty and diversity of their structures and reactions [1–5]. However, there are so far very few transition metal double cluster complexes containing bridging biscyclopentadienyl ligands [6] although numerous such dinuclear complexes have been well-documented in the literature [7–9].

In connection with our project aimed to develop the synthetic methodology for clusters [6,10–12], we initiated investigations on the isolobal displacement reactions of a series of isolobal reagents containing bridging biscyclopentadienyl ligands with tetrahedral Co_2C_2 and $FeCo_2S$ clusters, and on the functional transformation reactions of some isolobal displacement products, through which corresponding novel transition metal double cluster complexes were successfully synthesized. Herein we report the results concerning this study.

RESULTS AND DISCUSSION

We recently reported [6] the reaction of bridging biscyclopentadienyl transition metal reagents $[NaM(CO)_3(\eta^5\text{-}C_5H_4)]_2[C(O)CH_2CH_2C(O)]$ (M = Mo, W) with a tetrahedral cluster $FeCo_2(CO)_9$

* Author to whom correspondence should be addressed.

(μ_3-S). This is actually a new type of isolobal displacement reaction [13,14], which involves the double displacement of two d^9ML_3 isolobal fragments in two molecules of $FeCo_2(CO)_9(\mu_3\text{-}S)$ by two d^5ML_5 fragments derived from the bridging reagent. In order to show the generality of this new double isolobal displacement mode in the synthesis of bridged double cluster complexes, we carried out a series of reactions between various tetrahedral clusters and bridging bis[cyclopentadienyltricarbonylmolybdenum (or tungsten) sodium]. We found that the bridging biscyclopentadienyl intermediate reagents $[NaM(CO)_3(\eta^5\text{-}C_5H_4)]_2[C(O)CH_2CH_2C(O)]$ (M = Mo, W) prepared from 1,4-succinoyl bis(cyclopentadienylsodium) and $M(CO)_6$ reacted *in situ* with tetrahedral Co_2C_2 clusters in THF at reflux to give a series of double isolobal displacement products **1a–d,** as shown in Scheme 1.

Reagents $[NaM(CO)_3(\eta^5\text{-}C_5H_4)]_2[p\text{-}C(O)C_6H_4C(O)\text{-}p]$ (M = Mo, W) prepared from $M(CO)_6$ and terephthaloylbis(cyclopentadienylsodium) could also react *in situ* with cluster $Ph_2C_2Co_2(CO)_6$ or $FeCo_2(CO)_9(\mu_3\text{-}S)$ in THF at reflux to afford the bridged double clusters **2a–b** and **3a–b**. The terephthaloylbis(cyclopentadienylsodium) was prepared by reaction of sodium cyclopentadienide with dimethylterephthalate and isolated as a slightly air-sensitive and quite moisture-sensitive, yellow solid. The reactions mentioned above are shown in Scheme 2.

Other bridged double clusters could be similarly prepared by this type of double isolobal displacement reaction. For example, clusters **4** and **5** might be obtained by the reaction of $[NaMo(CO)_3(\eta^5\text{-}C_5H_4)]_2[o\text{-}CH_2C_6H_4CH_2\text{-}o]$ prepared from $Mo(CO)_6$ and $[Na(\eta^5\text{-}C_5H_4)]_2[o\text{-}CH_2C_6H_4CH_2\text{-}o]$ with $Ph_2C_2Co_2(CO)_2$ or $FeCo_2(CO)_9(\mu_3\text{-}S)$, whereas cluster **6** was prepared by reaction of $[LiMo(CO)_3(\eta^5\text{-}C_5H_4)]_2[Me_2SiOSiMe_2]$ derived from $M(CO)_6$ and $[Li(\eta^5\text{-}C_5H_4)]_2[Me_2SiOSiMe_2]$, with $FeCo_2(CO)_9(\mu_3\text{-}S)$, as shown in Scheme 3.

Interestingly, clusters **1a** and **3a–b** could be reduced under the action of $NaBH_4$ to give dihydroxyl double clusters **7** and **8a–b,** whereas **7** might be further converted to corresponding ether double cluster **9** by elimination of one molecule of water intramolecularly in the presence of Et_3OBF_4, as shown in Scheme 4.

The bridged double clusters **1–9** are all new and have been fully characterized by elemental analysis. IR and ^1H NMR spectroscopy. For example, the IR spectra for those double $MCoC_2$ clusters **1, 2, 4, 7** and **9** have four terminal carbonyl absorption bands at 2057–1926 cm^{-1}, whereas those for the double FeCoMS clusters **3, 5, 6** and **8** contain six to seven terminal carbonyl absorption bands in the range 2082–1852 cm^{-1}. The latter clusters, compared to the former, have more IR bands for the terminal carbonyls, which is obviously due to the more terminal carbonyls present in the latters' molecules. Additionally, the IR spectra of the clusters containing 1,4-succinoyl biscyclopentadienyl and *p*-bis(cyclopentadienylcarbonyl) benzene bridges, namely **1–3,** all have a medium absorption band at 1680–1647 cm^{-1}, characteristic of the ketonic groups, whereas those of the clusters with 1,4-biscyclopentadienyl-1,4-dihydroxylbutylene- and *p*-bis(cyclopentadienylhydroxylmethyl)benzene bridges, i.e. **7** and **8,** contain a broad band centered at about 3420 cm^{-1}, diagnostic of the hydroxyl groups. The ^1H NMR spectra of clusters **1–9** show the presence of their corresponding organic groups. For example, for the two substituted cyclopentadienyl rings the ^1H NMR spectra of clusters **4, 5** and **7** show one multiplet at about 4.9–5.6 ppm, whereas those of clusters **1–3, 6, 8** and **9** exhibit two sets of peaks at about 5.1–6.5 ppm. For clusters **1–3,** the downfield set of the peak has been assigned to H^2 and H^5, and the upfield assigned to H^3 and H^4, whereas for clusters **6, 8** and **9** the assignment of those protons is opposite. This is because the substituents on cyclopentadienyl rings for the formers, in contrast to those for the latters, are electron-withdrawing. In addition, the ^1H NMR spectra of **8a–b** have one broad peak centered at about 2.5 and 2.4 ppm, assigned to their hydroxyl groups. However, those two peaks disappeared when determining their ^1H NMR spectra in D_2O, due to D/H exchange. Finally, it should be pointed out that the terephthaloylbis(cyclopentadienylsodium) used in the synthesis, for example, of **2a–b** is new and has been

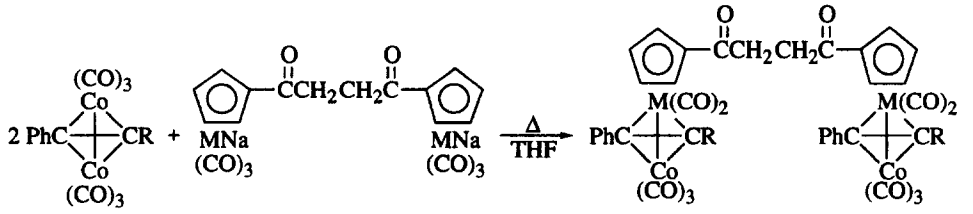

1a R = Ph M = Mo
1b R = p-MeC_6H_4 M = Mo
1c R = m-$MeOC_6H_4$ M = Mo
1d R = Ph M = W

Scheme 1.

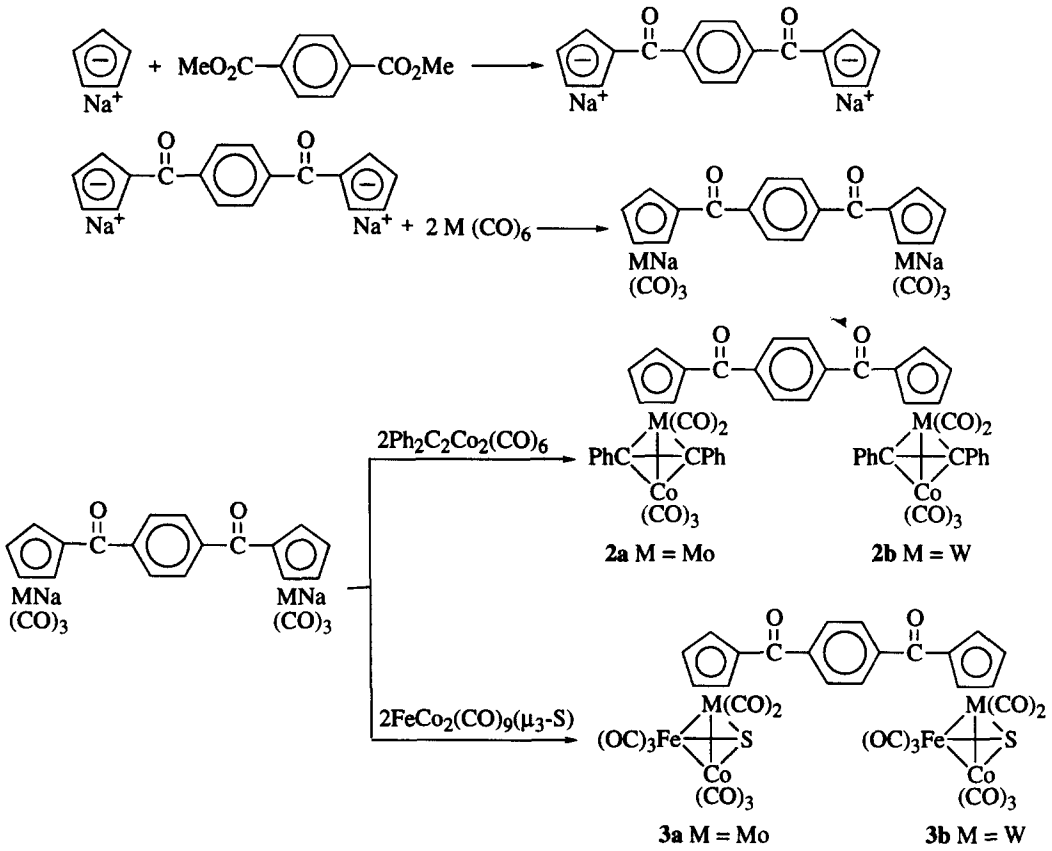

Scheme 2.

characterized by IR and ^{1}H NMR spectroscopy. The IR spectrum shows its ketonic carbonyl absorption band at 1636 cm^{-1}, and its ^{1}H NMR spectrum exhibits corresponding resonances for C_5H_4 and C_6H_4 groups, as well as two triplets in equal intensity assigned to four α-protons and four β-protons of THF. The terephthaloylbis(cyclopentadienylsodium), therefore, exists in a THF solvated form and could be best formulated as $C_{18}H_{12}O_2Na_2 \cdot C_4H_8O$ in terms of the integral value of corresponding signals.

EXPERIMENTAL

All reactions were carried out under prepurified tank nitrogen using standard Schlenk techniques. THF and diglyme were distilled from sodium-benzophenone ketyl under nitrogen. Column chromatography and TLC were carried out by using silica gel of 300–400 mesh and silica gel G (10–40 μm), respectively. $Mo(CO)_6$ and $W(CO)_6$ were purchased from Strem Chemicals Inc. $[NaC_5H_4C(O)CH_2]_2$ [9], o-$[NaC_5H_4CH_2]_2C_6H_4$/THF solution [15], $C_5H_5Si(Me_2)OSi(Me_2)C_5H_5$ [16], Et_3OBF_4 [17], $FeCo_2(CO)_9(\mu_3\text{-}S)$ [18], $Ph_2C_2Co_2(CO)_6$ [19], $Ph(p\text{-}MeC_6H_4)C_2Co_2(CO)_6$ [20], $Ph(m\text{-}MeOC_6H_4)C_2Co_2(CO)_6$ [20] were prepared according to literature methods. IR spectra were recorded on a NICOLET FT-IR 5DX infrared spectrometer; ^{1}H NMR spectra were recorded on a JEOL FX 90Q NMR spectrometer. C/H analyses and melting points were determined on a 240 C analyzer and a Yanaco micromelting point apparatus MP-500.

Preparation of **1a**

A 100 cm^3 three-necked flask fitted with a magnetic stir-bar, a rubber septum, and a reflux condenser topped with a nitrogen inlet tube was charged with 528 mg (2.0 mmol) of $Mo(CO)_6$, 258 mg (1.0 mmol) of $[NaC_5H_4C(O)CH_2]_2$ and 20 cm^3 of THF. The mixture was refluxed for 20 h. Upon cooling to room temperature, 928 mg (2.0 mmol) of $Ph_2C_2Co_2(CO)_6$ was added and the mixture stirred at reflux for 7 h. Solvent was removed under reduced pressure and the residue was extracted with CH_2Cl_2. The extracts were subjected to TLC using 2:1 CH_2Cl_2/petroleum ether as eluent. Several tiny bands with a major band developed. From the major band 285 mg (25%) of **1a** was obtained as a brown-yellow solid. M.p. 81–83°C. Found: C, 54.23; H, 3.13. Calc. for $C_{52}H_{32}Co_2Mo_2O_{12}$: C, 53.91; H, 2.78%. IR (KBr disk): $\nu_{C\equiv O}$, 2057 (s), 2009 (vs), 1983 (vs), 1942 (s); $\nu_{C=O}$ 1680

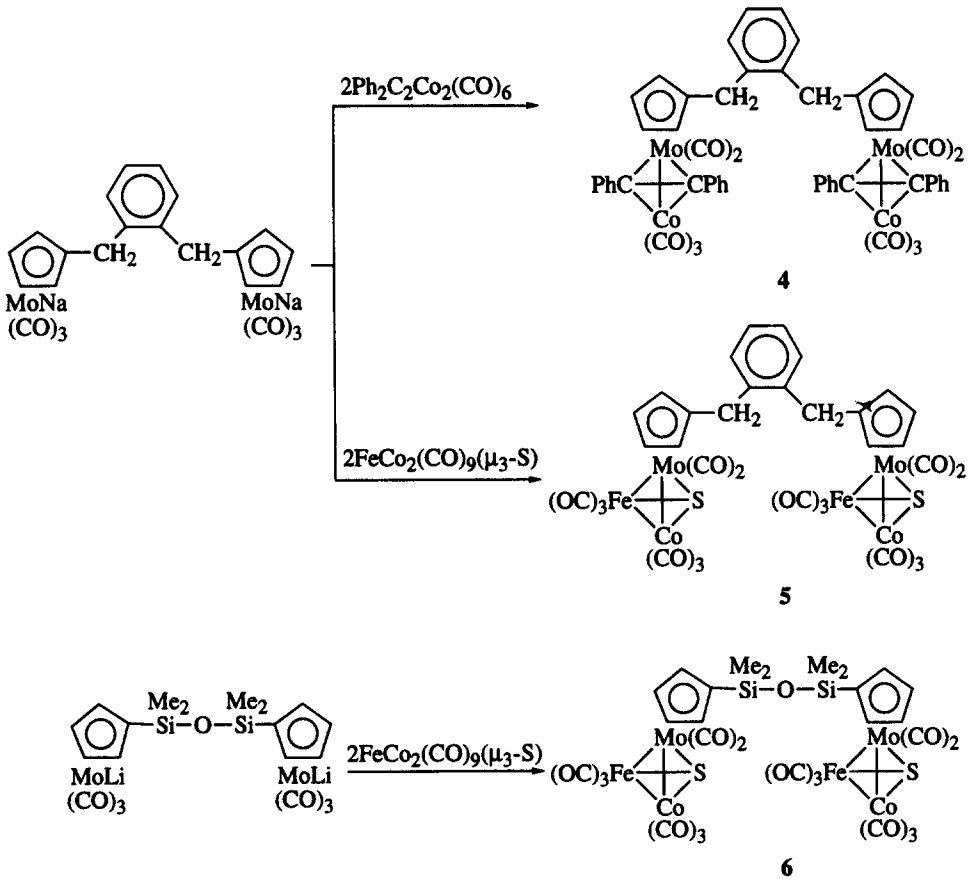

Scheme 3.

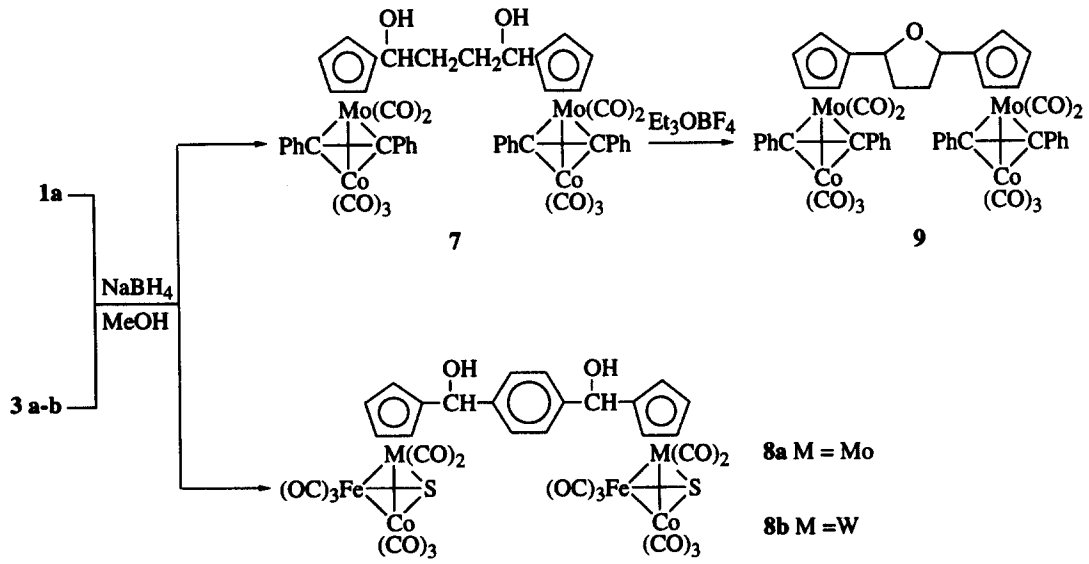

Scheme 4.

(m) cm^{-1}. ^1H NMR ($CDCl_3$, δ, ppm): 2.59 (s, 4H, CH_2CH_2), 5.46 (t, 4H, $2H^3$, $2H^4$), 5.88 (t, 4H, $2H^2$, $2H^5$), 7.31 (s, 20H, $4C_6H_5$).

Preparation of **1b**

The same procedure as that for **1a** was followed, but 956 mg (2.0 mmol) of Ph (p-MeC_6H_4)$C_2Co_2(CO)_6$ was used instead of $Ph_2C_2(CO)_6$ to give 185 mg (16%) of **1b** as a brown–yellow solid. M.p. 88–90°C. Found: C, 54.16; H, 3.17. Calc. for $C_{54}H_{36}Co_2Mo_2O_{12}$: C, 54.66; H, 3.06%. IR (KBr disk): $\nu_{C\equiv O}$, 2057 (s), 2008 (vs), 1983 (vs), 1942 (s); $\nu_{C=O}$ 1672 (m) cm^{-1}. ^1H NMR ($CDCl_3$, δ, ppm): 2.36 (s, 6H, $2CH_3$), 2.62 (s, 4H, CH_2CH_2), 5.54 (t, 4H, $2H^3$, $2H^4$), 5.94 (t, 4H, $2H^2$, $2H^5$), 7.08–7.64 (m, 18H, $2C_6H_5$, $2C_6H_4$).

Preparation of **1c**

The same procedure as that for **1a** was followed, but 988 mg (2.0 mmol) of Ph (*m*-MeO-C_6H_4)$C_2Co_2(CO)_6$ was used instead of $Ph_2C_2Co_2(CO)_6$ to give 130 mg (11%) of **1c** as a brown–yellow solid. M.p. 100–102°C. Found: C, 53.78; H, 3.08. Calc. for $C_{54}H_{36}Co_2Mo_2O_{14}$: C, 53.22; H, 2.98%. IR (KBr disk): $\nu_{C\equiv O}$, 2057 (s), 2008 (vs), 1983 (vs), 1942 (s); $\nu_{C=O}$ 1672 (m) cm^{-1}. ^1H NMR ($CDCl_3$, δ, ppm): 2.54 (s, 4H, CH_2CH_2), 3.76 (s, 6H, $2CH_3O$), 5.50 (t, 4H, $2H^3$, $2H^4$), 5.90 (t, 4H, $2H^2$, $2H^5$), 6.70–7.08 (m, 8H, $2C_6H_4$), 7.34 (s, 10H, $2C_6H_5$).

Preparation of **1d**

The 100 cm^3 flask described above was charged with 704 mg (2.0 mmol) of $W(CO)_6$, 258 mg (1.0 mmol) of $[NaC_5H_4C(O)CH_2]_2$ and 20 cm^3 of diglyme. The mixture was refluxed for 6 h. After removing diglyme 928 mg (2.0 mmol) of $Ph_2C_2Co_2(CO)_6$ and 20 cm^3 of THF was added and the mixture stirred at reflux for 7 h. The same workup as that for **1a** gave 345 mg (26%) of **1d** as a brown–yellow solid. M.p. 85–87°C. Found: C, 48.62; H, 2.52. Calc. for $C_{52}H_{32}Co_2O_{12}W_2$: C, 48.81; H, 2.42%. IR (KBr disk): $\nu_{C\equiv O}$, 2049 (s), 2008 (vs), 1983 (vs), 1934 (s); $\nu_{C=O}$ 1680 (m) cm^{-1}. ^1H NMR ($CDCl_3$, δ, ppm): 2.61 (s, 4H, CH_2CH_2), 5.61 (t, 4H, $2H^3$, $2H^4$), 5.89 (t, 4H, $2H^2$, $2H^5$), 7.31 (s, 20H, $4C_6H_5$).

Preparation of terephthaloylbis(cyclopentadienylsodium)

The 100 cm^3 flask described above was charged with 1.15 g (50 mmol) of sodium sand and 60 cm^3 of THF. The mixture was stirred and cooled by an ice-bath. To this suspension was slowly added 5.5 cm^3 (60 mmol) of freshly cracked cyclopentadiene and the mixture continued to be stirred at room temperature for 3 h. To this resulting pink solution of sodium cyclopentadienide was added 4.85 g (25 mmol) of dimethyl terephthalate and the mixture refluxed for 25 h. Solvent was removed at reduced pressure. The residue was carefully washed under nitrogen with 3×50 cm^3 of absolute ethyl ether and dried *in vacuo* to give 6.732 g (71%) of 1:1 THF solvated terephthaloylbis (cyclopentadienylsodium) p-$[NaC_5H_4C(O)]_2C_6H_4 \cdot$ THF as a yellow solid. M.p. 190°C (dec). IR (KBr disk): $\nu_{C=O}$, 1636 (s) cm^{-1}. ^1H NMR ($CDCl_3$, δ, ppm): 1.81 (t, $J = 6.5$ Hz, 4H, CH_2CH_2 of THF), 3.69 (t, $J = 6.5$ Hz, 4H, CH_2OCH_2 of THF), 6.28, 6.78 (br. s, 8H, $2C_5H_4$), 7.62 (s, 4H, C_6H_4).

Preparation of **2a**

The 100 cm^3 flask was charged with 700 mg (2.0 mmol) of p-$[NaC_5H_4C(O)]_2C_6H_4 \cdot$THF, 1.056 g (4.0 mmol) of $Mo(CO)_6$ and 30 cm^3 of THF. The mixture was refluxed for 15 h. Upon cooling to room temperature 1.856 g (4.0 mmol) of $Ph_2C_2Co_2(CO)_6$ was added and the mixture was refluxed for 7 h. Solvent was removed and the residue was subjected to TLC using 2:1 CH_2Cl_2/petroleum ether as eluent. Several tiny bands with a major band developed. The major yellow–brown band was collected to give 152 mg (8%) of **2a** as a red solid. M.p. 175–177°C. Found: C, 56.63; H, 2.69. Calc. for $C_{56}H_{32}Co_2Mo_2O_{12}$: C, 55.74; H, 2.67%. IR (KBr disk): $\nu_{C\equiv O}$, 2057 (s), 2008 (vs), 1983 (vs), 1950 (s); $\nu_{C=O}$ 1647 (m) cm^{-1}. ^1H NMR ($CDCl_3$, δ, ppm): 5.44 (br. s, 4H, $2H^3$, $2H^4$), 5.92 (br. s, 4H, $2H^2$, $2H^5$), 7.25 (s, 20H, $4C_6H_5$), 7.64–7.88 (m, 4H, C_6H_4).

Preparation of **2b**

The 100 cm^3 flask was charged with 352 mg (1.0 mmol) of p-$[NaC_5H_4C(O)]_2C_6H_4 \cdot$THF, 700 mg (2.0 mmol) of $W(CO)_6$ and 30 cm^3 of diglyme. The mixture was refluxed for 6 h. After removing diglyme under reduced pressure 928 mg (2.0 mmol) of $Ph_2C_2Co_2(CO)_6$ and 30 cm^3 of THF were added. The mixture was stirred at reflux for an additional 7 h. Solvent was removed at reduced pressure. The residue was extracted with CH_2Cl_2. The extracts were subjected to TLC using 2:1 CH_2Cl_2/petroleum ether as eluent. Several tiny bands with a major band developed. From the major band was obtained 142 mg (12%) of **2b** as a red solid. M.p. 163–165°C. Found: C, 48.59; H, 2.68. Calc. for $C_{56}H_{32}Co_2O_{12}W_2$: C, 48.66; H, 2.33%. IR (KBr disk): $\nu_{C\equiv O}$, 2049 (s), 2008 (vs), 1975 (vs), 1950 (s); $\nu_{C=O}$ 1655 (m) cm^{-1}. ^1H NMR ($CDCl_3$, δ, ppm): 5.52 (br. s, 4H, $2H^3$, $2H^4$), 6.00 (br. s, 4H, $2H^2$, $2H^5$), 7.29 (s, 20H, $4C_6H_5$), 7.78 (s, 4H, C_6H_4).

Preparation of **3a**

The 100 cm^3 flask was charged with 312 mg (1.0 mmol) of p-$[NaC_5H_4C(O)]_2C_6H_4 \cdot$THF, 528 mg (2.0

mmol) of $Mo(CO)_6$ and 30 cm^3 of THF. The mixture was refluxed for 15 h. Upon cooling to room temperature 932 mg (2.0 mmol) of $FeCo_2(CO)_9(\mu_3\text{-}S)$ was added and the mixture was stirred for 30 min at reflux. Solvent was removed under reduced pressure. The residue was extracted with CH_2Cl_2. The extracts were subjected to column chromatography. Several tiny bands with a major band developed using petroleum ether, 2 : 1 CH_2Cl_2/petroleum and CH_2Cl_2 as eluents successively. The major brown band was eluted with CH_2Cl_2 to give 150 mg (16%) of **3a** as a black powder. M.p. 125–127°C. Found: C, 34.33; H, 1.61. Calc. for $C_{34}H_{12}Co_2Fe_2Mo_2O_{18}S_2$: C, 34.20; H, 1.01%. IR (KBr disk): $\nu_{C\equiv O}$, 2082 (s), 2032 (vs), 2008 (vs), 1975 (s), 1934 (m), 1901 (m), 1852 (m); $\nu_{C=O}$ 1647 (m) cm^{-1}. ^1H NMR ($CDCl_3$, δ, ppm): 5.60–5.92 (m, 4H, $2H^3$, $2H^4$), 6.00–6.24 (m, 4H, $2H^2$, $2H^5$), 7.96 (br. s, 4H, C_6H_4).

Preparation of **3b**

The flask described above was charged with 352 mg (1.0 mmol) of p-$[NaC_5H_4C(O)]_2C_6H_4 \cdot THF$, 700 mg (2.0 mmol) of $W(CO)_6$ and 30 cm^3 of diglyme. The mixture was refluxed for 6 h. After removal of diglyme under reduced pressure 932 mg (2.0 mmol) of $FeCo_2(CO)_9(\mu_3\text{-}S)$ and 30 cm^3 of THF were added and the mixture was stirred at reflux for 30 min. Solvent was removed under reduced pressure. The residue was extracted with CH_2Cl_2. The extracts were first subjected to short column chromatography using 1 : 2 acetone/petroleum ether as eluent. From the major band 180 mg (16%) of **3b** was obtained as a black powder. M.p. 98–100°C. Found: C, 29.42; H, 0.57. Calc. for $C_{34}H_{12}Co_2Fe_2O_{18}S_2W_2$: C, 29.81; H, 0.88%. IR (KBr disk): $\nu_{C\equiv O}$, 2082 (s), 2032 (vs), 2008 (vs), 1983 (s), 1942 (m), 1909 (m), 1860 (m); $\nu_{C=O}$ 1647 (m) cm^{-1}. ^1H NMR ($CDCl_3$, δ, ppm): 5.92–6.18 (m, 4H, $2H^3$, $2H^4$), 6.20–6.42 (m, 4H, $2H^2$, $2H^5$), 7.91–8.18 (m, 4H, C_6H_4).

Preparation of **4**

The flask described above was charged with 660 mg (2.5 mmol) of $Mo(CO)_6$, 4.4 cm^3 (1.23 mmol) of o-$(NaC_5H_4CH_2)_2C_6H_4$/THF solution and 20 cm^3 of THF. The mixture was refluxed for 20 h. Upon cooling to room temperature 1.16 g (2.5 mmol) of $Ph_2C_2Co_2(CO)_6$ was added and the mixture was stirred for 30 min and at reflux for an additional 5 h. Solvent was removed under reduced pressure. The residue was extracted with CH_2Cl_2. The extracts were subjected to TLC using 1 : 5 CH_2Cl_2/petroleum ether as eluent. Several tiny bands with a major band developed. From the major band 300 mg (20%) of **4** was obtained as a brown–yellow solid. M.p. 75–77°C. Found: C, 57.28; H, 3.12. Calc. for $C_{56}H_{36}Co_2Mo_2O_{10}$: C, 57.07; H, 3.08%. IR (KBr disk): $\nu_{C\equiv O}$, 2049 (s), 1991 (vs), 1975 (vs), 1926 (s) cm^{-1}. ^1H NMR ($CDCl_3$, δ, ppm): 3.32 (s, 4H, $2CH_2$), 4.98–5.34 (m, 8H, $2C_5H_4$), 6.82–7.54 (m, 24H, C_6H_4, $4C_6H_5$).

Preparation of **5**

The flask was charged with 528 mg (2.0 mmol) of $Mo(CO)_6$, 3.6 cm^3 (1.0 mmol) of o-$(NaC_5H_4CH_2)_2C_6H_4$/THF solution and 20 cm^3 of THF. The mixture was refluxed for 20 h. Upon cooling to room temperature 916 mg (2.0 mmol) of $FeCo_2(CO)_9(\mu_3\text{-}S)$ was added and the mixture stirred at reflux for an additional 1 h. The same workup as that for **4** gave 160 mg (14%) of **5** as a black solid. M.p. 135–137°C. Found: C, 35.08; H, 1.34. Calc. for $C_{34}H_{16}Co_2Fe_2Mo_2O_{16}S_2$: C, 35.02; H, 1.38%. IR (KBr disk): $\nu_{C\equiv O}$, 2073 (s), 2036 (s), 2016 (vs), 2004 (vs), 1975 (s), 1948 (m), 1876 (m) cm^{-1}. ^1H NMR ($CDCl_3$, δ, ppm): 3.90 (s, 4H, $2CH_2$), 5.20–5.60 (m, 8H, $2C_5H_4$), 7.52 (s, 4H, C_6H_4).

Preparation of **6**

The flask was charged with 262 mg (1.0 mmol) of $C_5H_5Si(Me_2)OSi(Me_2)C_5H_5$ and 15 cm^3 of diglyme, and then 1.4 cm^3 (2.0 mmol) of n-BuLi/hexane solution was dropped into the flask under −50°C. The mixture was stirred for 0.5 h at room temperature. Then, 528 mg (2.0 mmol) of $Mo(CO)_6$ was added and the mixture stirred at reflux for 6 h. After removing diglyme under reduced pressure 20 cm^3 of THF and 916 mg (2.0 mmol) of $FeCo_2(CO)_9(\mu_3\text{-}S)$ were added and the mixture was refluxed for an additional 1 h. The same workup as that for **4** gave 230 mg (19%) of **6** as a brown oil. Found: C, 30.05; H, 2.05. Calc. for $C_{30}H_{20}Co_2Fe_2Mo_2O_{17}S_2Si_2$: C, 30.17; H, 1.69%. IR (KBr disk): $\nu_{C\equiv O}$, 2073 (s), 2035 (s), 2000 (vs), 1965 (vs), 1925 (s), 1893 (s) cm^{-1}. ^1H NMR ($CDCl_3$, δ, ppm): 0.32, 0.40 [s, s, 12H, J = 3.6 Hz, $2Si(CH_3)_2$], 5.36 (t, 4H, $2H^2$, $2H^5$), 5.56 (t, 4H, $2H^3$, $2H^4$).

Preparation of **7**

The 50 cm^3 flask was charged with 100 mg (0.086 mmol) of **1a**, 13 mg (0.34 mmol) of $NaBH_4$ and 5 cm^3 of MeOH. The mixture was stirred for 1 h at room temperature. The residue was extracted with CH_2Cl_2. The extracts were subjected to TLC using CH_2Cl_2 as eluent. Several tiny bands with a major band developed. From the major band was obtained 30 mg (30%) of **7** as a brown–yellow solid. M.p. 95–97°C. Found: C, 53.69; H, 3.09. Calc. for $C_{52}H_{36}Co_2Mo_2O_{12}$: C, 53.72; H, 3.12. IR (KBr disk): $\nu_{C\equiv O}$, 2049 (s), 2008 (vs), 1975 (vs), 1934 (s); ν_{OH} 3427 (m) cm^{-1}. ^1H NMR ($CDCl_3$, δ, ppm): 1.52–1.80 (m, 4H, CH_2CH_2), 1.96–2.28 (m, 2H, 2OH), 3.96–4.28 (m, 2H, 2CH), 5.08–5.48 (m, 8H, $2C_5H_4$), 7.00–7.74 (m, 20H, $4C_6H_5$).

Preparation of **8a**

The 50 cm^3 flask was charged with 100 mg (0.083 mmol) of **3a,** 11 mg (0.29 mmol) of $NaBH_4$ and 4 cm^3 of MeOH. The mixture was stirred at room temperature for 10 min. Solvent was removed under reduced pressure. The residue was extracted with CH_2Cl_2. The extracts were subjected to TLC using CH_2Cl_2 as eluent. From the major band was obtained 37 mg (37%) of **8a** as a black solid. M.p. 122–124°C. Found: C, 34.25; H, 2.09. Calc. for $C_{34}H_{16}Co_2Fe_2Mo_2O_{18}S_2$: C, 34.09; H, 1.35. IR (KBr disk): $\nu_{C\equiv O}$, 2073 (s), 2034 (s), 2024 (vs), 1998 (vs), 1975 (s), 1877 (m), ν_{OH} 3400 (m) cm^{-1}. ^1H NMR ($CDCl_3$, δ, ppm): 2.52 (br. s, 2H, 2OH), 5.16 (br. s, 4H, $2H^2$, $2H^5$), 5.28 (br. s, 2H, 2CH), 5.40–5.60 (m, 4H, $2H^3$, $2H^4$), 7.28 (s, 4H, C_6H_4).

Preparation of **8b**

The same procedure as that for **8a** was followed, but 150 mg (0.109 mmol) of **3b,** 16 mg (0.42 mmol) of $NaBH_4$ and 6 cm^3 of MeOH was used instead of those for **8a** to give 60 mg (40%) of **8b** as a black solid. M.p. 136–138°C. Found: C, 29.79; H, 1.40. Calc. for $C_{34}H_{16}Co_2Fe_2O_{18}S_2W_2$: C, 29.72; H, 1.17. IR (KBr disk): $\nu_{C\equiv O}$, 2073 (s), 2032 (vs), 2010 (vs), 1991 (vs), 1976 (s), 1893 (m), ν_{OH} 3420 (m) cm^{-1}. ^1H NMR ($CDCl_3$, δ, ppm): 2.40 (br. s, 2H, 2OH), 5.16 (br. s, 4H, $2H^2$, $2H^5$), 5.40 (br. s, 2H, 2CH), 5.48–5.68 (m, 4H, $2H^3$, $2H^4$), 7.32 (s, 4H, C_6H_4).

Preparation of **9**

The 50 cm^3 flask was charged with 75 mg (0.065 mmol) of **7,** 85 mg (0.45 mmol) of Et_3OBF_4 and 4 cm^3 of CH_2Cl_2. The mixture was refluxed for 10 min. Solvent was removed under reduced pressure. The residue was extracted with CH_2Cl_2. The extracts were subjected to TLC using 1 : 1 CH_2Cl_2/petroleum ether as eluent. From the major band was obtained 37 mg (51%) of **9** as a brown–yellow solid. M.p. 75–77°C. Found: C, 54.65; H, 2.85. Calc. for $C_{52}H_{34}Co_2Mo_2O_{11}$: C, 54.57; H, 2.99%. IR (KBr disk): $\nu_{C\equiv O}$, 2049 (s), 2008 (vs), 1983 (vs), 1934 (s) cm^{-1}. ^1H NMR ($CDCl_3$, δ, ppm): 1.60–2.40 (m, 4H, CH_2CH_2), 4.28–4.80 (m, 2H, CHCH), 5.22 (t, 4H, $2H^2$, $2H^5$), 5.32–5.52 (m, 4H, $2H^3$, $2H^4$), 7.32 (s, 20H, $4C_6H_5$).

Acknowledgements—We are grateful to the National Natural Science Foundation of China and State Key Laboratory of Structural Chemistry and Elemento-Organic Chemistry for financial support of this work.

REFERENCES

1. Roberts, D. A. and Geoffroy, G. L., in *Comprehensive Organometallic Chemistry*, Vol. 6, p. 763, G. Wilkinson, F. G. A. Stone, E. W. Abel, Eds, Pergamon Press, Oxford (1982).
2. Braunstein, P. and Rose, J., in *Comprehensive Organometallic Chemistry II*, Vol. 10, p. 351, E. W. Abel, F. G. A. Stone, G. Wilkinson, Eds, Pergamon Press, Oxford (1995).
3. Vahrenkamp, H., in *Transition Metal Chemistry-Current Problems of General, Biological and Catalytic Relevance*, p. 35, A. Müller, E. Diemann, Eds, Verlag Chemie, Weinheim (1981).
4. Johnson, B. F. G., *Transition Metal Cluster Compounds*, Wiley, Chichester (1980).
5. Shriver, D. F., Kaesz, H. D. and Adams, R. D., *The Chemistry of Metal Cluster Complexes*, VCH, Weinheim (1990).
6. Song, L.-C., Shen, J.-Y., Hu, Q.-M. and Huang, X.-Y., *Organometallics*, 1995, **14,** 98.
7. Heck, J., Kriebisch, K.-A. and Mellinghoff, H., *Chem. Ber.*, 1988, **121,** 1753.
8. Buzinkai, J. F. and Schrock, R. R., *Inorg. Chem.*, 1989, **28,** 2837.
9. Bitterwolf, T. E., *J. Organomet. Chem.*, 1990, **386,** 9.
10. Song, L.-C., Shen, J.-Y., Hu, Q.-M., Wang, R.-J. and Wang, H.-G., *Organometallics*, 1993, **12,** 408.
11. Song, L.-C., Shen, J.-Y., Hu, Q.-M., Han, B.-S., Wang, R.-J. and Wang, H.-G., *Inorg. Chim. Acta*, 1994, **219,** 93.
12. Song, L.-C., Wang, J.-Q. and Hu, Q.-M., *Polyhedron*, 1996, **15,** 4295.
13. Hoffman, R., *Angew. Chem., Int. Ed. Engl.*, 1982, **21,** 711.
14. Vahrenkamp, H., *Comments, Inorg. Chem.*, 1985, **4,** 253.
15. Chen, S.-S., Chen, Y.-X., Wang, J.-T., *Acta Chim. Sin.*, 1990, **48,** 298.
16. Curtis, M. D., D'Errico, J. J., Duffy, D. N., Epstein, P. S. and Bell, L. G., *Organometallics*, 1983, **2,** 1808.
17. Meerwein, H., *Org. Synth.*, 1966, **46,** 113.
18. Cowie, M., Dekock, R. L., Wagenmaker, T. R., Seyferth, D., Henderson, R. S. and Gallagher, M. K., *Organometallics*, 1989, **8,** 119.
19. Sternberg, H. W., Greenfield, H., Friedel, R. A., Wotiz, J., Markby, R. and Wender, I., *J. Am. Chem. Soc.*, 1954, **76,** 1457.
20. Song, L.-C., Wang, Z.-X. and Wang, J.-T., *Chem. J. Chin. Univ.*, 1987, **8,** 610.

Pergamon

PII: S0277-5387(97)00259-3

Polyhedron Vol. 17, No. 1, pp. 43–47, 1998
© 1997 Elsevier Science Ltd
All rights reserved. Printed in Great Britain
0277-5387/98 $19.00+0.00

Synthesis and structure of a dimeric hydroxo-bridged erbium(III) complex, di-μ-hydroxo-bis[(1,4,7,10,13,16-hexaazacyclooctadecane) erbium(III)] tetra(trifloromethanesulfonate)

Rui-Yao Wang,[a] Jian-Jun Zhao,[a] Tian-Zhu Jin,[a]* Guang-Xian Xu,[a] Zhong-Yuan Zhou[b] and Xiang-Ge Zhou[b]

[a] State Key Laboratory of Rare Earth Materials Chemistry and Applications, Peking University, Beijing 100871, P. R. China

[b] Chengdu Institute of Organic Chemistry, the Chinese Academy of Sciences, Chengdu 610041, P. R. China

(Received 22 April 1997; accepted 11 June 1997)

Abstract—The title complex was synthesized by the reaction of 1,4,7,10,13,16-hexaazacyclooctadecane (abbreviated as hexacyclen) with erbium(III) trifloromethanesulfonate in 1:1 (molar ratio) in acetonitrile under nitrogen. The crystal structure determination shows that the complex is dinuclear with two erbium ions bridged by two hydroxide ions. Each of the two metal ions is coordinated similarly by the two bridging hydroxide groups and six nitrogen atoms of a hexacyclen molecule, giving a coordination number eight and a slightly distorted dodecahedron geometry. The four trifloromethanesulfonate ions are not included in the coordination of the metal ions. © 1997 Elsevier Science Ltd

Keywords: erbium; 1,4,7,10,13,16-hexaazacyclooctadecane; crystal structure; lanthanide complex.

As the nitrogen analogue of 18-crown-6, the macrocycle 1,4,7,10,13,16-hexaazacyclooctadecane (abbreviated as hexacyclen) has been studied extensively for the stereochemistry of its complexes with transition metal ions like Co^{3+} and Ni^{2+} arising from the coordination of the ligand [1] as well as its great ability to form 1:1 or 1:2 complexes with many different metal ions [1–5]. But up to now, only six metal complexes [6–11] with M/L = 1:1 for Co^{3+}, Cr^{3+}, Hg^{2+}, UO_2^{2+} and two [4,5] with 2:1 for Pd^{2+} have been structurally determined by single-crystal X-ray diffraction methods. The structural information of these complexes indicated that the geometry of the six nitrogen atoms of the ligand around a central ion seems based on two factors: the favor coordination geometry of the metal ion and the radius of the metal ion. This is somewhat different from the results obtained from the molecular mechanics calculation [10].

* Author to whom correspondence should be addressed.

We are interested in the coordination chemistry of lanthanide complexes with aza-crown and have determined the crystal and molecular structures of [La(Me-cyclen)(OSO_2CF_3)(OH_2)(NCMe)] [12], [Nd(Me-cyclen)(NCMe)(OSO_2CF_3)$_3$] [13], and [Er(cyclen)(NCMe)(OSO_2CF_3)$_3$] [14]. As a further investigation, we synthesized and structurally characterized the title complex.

EXPERIMENTAL

Preparation

Anhydrous $Er(CF_3SO_3)_3$ [15] and hexacyclen [16] was synthesized using the literature procedures. Acetonitrile was distilled from P_2O_5 immediately before use.

The title complex was synthesized by the addition of 0.52 mmol (0.38 g) of $Er(CF_3SO_3)_3$ to a solution of 0.59 mmol (0.15 g) of hexacyclen in 12 cm^3 of acetonitrile under N_2. A light pink solid appeared after

heating the resulting suspension to reflux for 2 h. Then a small amount of acetonitrile was added gradually to the system until the solid dissolved. The solution was kept in a desiccator with P_2O_5 at room temperature. Light pink prism crystals suitable for X-ray determination were obtained after 2 weeks. IR (KBr): 3297 m, 1621 w, 1091 w, 575 w cm^{-1}. Anal. Calcd for $Er_2C_{28}H_{12}O_{14}S_4F_{12}$: C, 22.69; H, 4.22; N, 11.35. Found: C, 22.56; H, 4.02; N, 11.36%.

X-ray structure determination

A crystal with approximate dimensions $0.24 \times 0.34 \times 0.36$ mm was quickly mounted in a glass capillary. Diffraction measurements were performed on a Siemens P4 diffractometer with Mo-K_α radiation ($\lambda = 0.71073$ Å) and a graphite monochromator. A total of 8156 ($R_{int} = 2.02\%$) independent reflections were collected by ω scanning technique in the range $2.0 \leqslant 2\theta \leqslant 50.0°$ with scan speed 6.00°/min in ω. Three standard reflections were monitored every 97 reflections. Intensity data were corrected by the ψ-scan technique. The structure was solved by direct methods using Siemens SHELXTL P4/PC software and refined by full-matrix least-squares techniques using 6168 reflections with $F > 4.0\ \sigma(F)$ and refining 649 parameters. The hydrogen atoms, except the two on the bridging O atoms, were added in calculated positions and their positions refined isotropically. All non-hydrogen atoms were refined anisotropically. The final values for R, wR and GOF for observed data are given in Table 1 and for all data.

Table 1. Crystal data, details of data collection and refinement

Empirical formula	$Er_2C_{28}H_{62}N_{12}O_{14}S_4F_{12}$
Colour	Light pink
Crystal size (mm)	$0.24 \times 0.34 \times 0.36$
Crystal System	Triclinic
Space group	$P\bar{1}$
a(Å)	12.003(2)
b(Å)	12.335(2)
c(Å)	19.468(3)
α(°)	96.96(1)
β(°)	102.62(1)
γ(°)	109.98(1)
V(Å^3)	2582.4(7)
Z	2
M	1481.6
D_c (g/cm^3)	1.905
Absorption coefficient	3.500
F(000)	1468
λ(Å)(Mo-K_α)	0.71073
Monochromator	Graphite
2θ Range (°)	2.0–50.0
Scan type	ω
Scan speed (°/min)	Constant: 6.00 in ω
Standard reflections	3/97
Index range h; k; l	0–14; −13–12; −21–21
Reflections collected	8583
Independent reflections	8156 ($R_{int} = 2.02\%$)
Observed reflections	6168 ($F > 4.0\ \sigma(F)$)
Absorption correction	ψ scan
Quantity minimized	$\Sigma\omega(F_o - F_c)^2$
Hydrogen atoms	Riding model, fixed isotropic U
Weighting scheme	$w^{-1} = \sigma^2(F) + 0.0008F^2$
Number of parameter refined	649
Final R indices (obs. Data)	$R = 0.0417$, $wR = 0.0639$
R Indices (all data)	$R = 0.0562$, $wR = 0.0851$
Goodness-of-fit	1.95
Largest and mean Δ/σ	0.006, 0.002
Max., min. residual peak (e/Å^3)	0.97, −0.72

RESULTS AND DISCUSSION

Figure 1 shows the view of the molecular structure of the title complex. The complex is dinuclear with two erbium ions bridged by two hydroxide ions. Each of the two metal ions is coordinated by the two bridging OH^- ions and six nitrogen atoms of a ligand, giving a coordination number eight. The coordination geometries of the two erbium ions are similar and can be described as slightly distorted dodecahedrons (Fig. 2). The four $CF_3SO_3^-$ ions are not involved in the coordination of the metal ions. The examination of the distances between N(hexacyclen) and O($CF_3SO_3^-$), which are near or longer than 3.0 Å, reveals that there is no strong H-bond interaction between the $CF_3SO_3^-$ ions and the hexacyclen molecules. They interact with the complex species [(hexacyclen)Er(μ-OH)$_2$Er(hexacyclen)]$^{4+}$ through electrostatic forces and keep the molecule neutral (see Fig. 3).

Selected bond lengths and angles of the title complex are listed in Table 2. The coordination of the two erbium ions are similar though they are different crystallographically. The Er—O bond lengths average 2.264 Å with the Er(1)···Er(2) distance 3.802 Å. The two metal ions and the two bridging oxygen atoms form a planar four membered-ring with the mean deviation 0.0314 Å. This result agrees with those in complex species [Yb(paphy)$(H_2O)_3(\mu$-OH)]$_2^{4+}$ [17] and [Y(μ-OH)$(H_2O)_2$(Phen)$_2]_2^{4+}$ [18], where the M—O(μ-OH^-) bond distances averaged 2.225(3) and 2.20(1) Å for Y^{3+} and Yb^{3+}, and the separation of the two metal ions was 3.651(2) and 3.608(1) Å for Y^{3+} and Yb^{3+}. The Er—N bond lengths of the title complex range from 2.522(3) to 2.609(2) Å [average 2.552(3) Å] for Er(1) and from 2.504(3) to 2.588(2) Å [average 2.541(3) Å] for Er(2), indicating a slight difference on conformation of the two hexacyclen. Comparing with its cyclen analogue: [Er(cyclen)(NCMe)$(OSO_2)_3$] [14], where the Er—N bond lengths are between 2.460(5) and 2.51(1) Å with the mean value 2.48(2) Å, and Er—O($OSO_2CF_3^-$) bond lengths averaged 2.32(2) Å, we find that the title complex has longer Er—N distances and shorter Er—O distances.

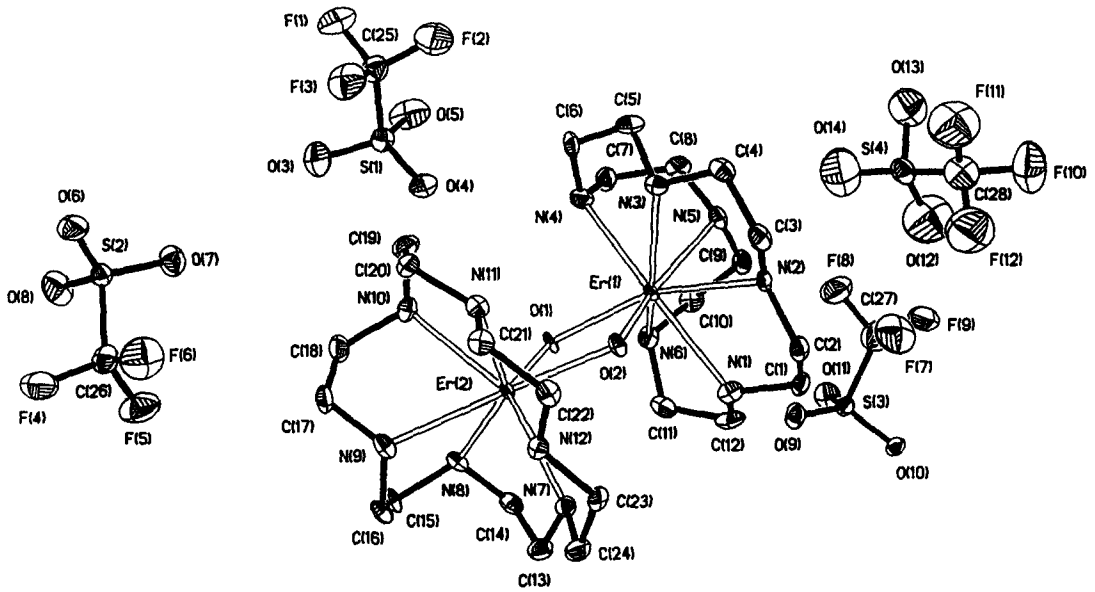

Fig. 1. ORTEP drawing of [(hexacyclen)Er(μ-OH)$_2$Er(hexacyclen)](CF$_3$SO$_3$)$_4$ with 50% probability ellipsoids.

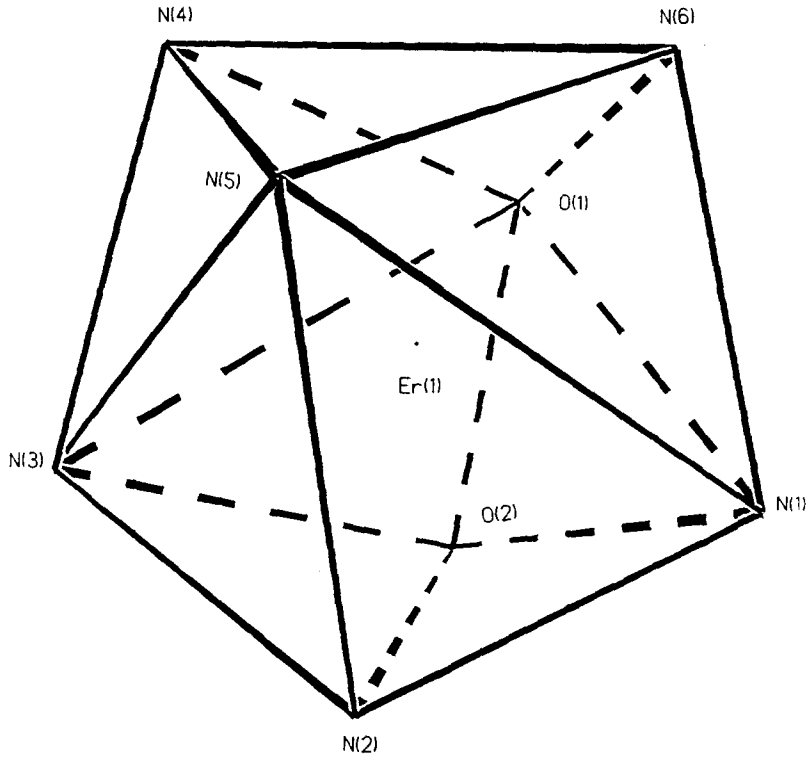

Fig. 2. Coordination polyhedron of Er^{3+} [Er(1) shown].

We owe this to the stronger coordination ability of hydroxide ions than that of trifloromethanesulfonate ions and the limited deformation ability of a hexacyclen molecule. The C—C bond lengths are normal, ranging from 1.463(4) to 1.535(3) Å. The C—N bond lengths vary from 1.443(4) to 1.533(3) Å, which agree with those in the complex species $[UO_2(hexacyclen)]^{2+}$ (1.41 ~ 1.56 Å) [11], *fac*-$[Co(hexacyclen)]^{3+}$ (1.48 ~ 1.51 Å) [8] and $[H_4(hexacyclen)]^{4+}$ (1.49 ~ 1.52 Å) [19], but apparently longer than those in neutral hexacyclen (1.45 ~ 1.47 Å) [18]. This indicates that the C—N bonds are weakened by the formation of N—M (M = positive ions) dative bonds.

The title complex contrasts markedly with its pre-

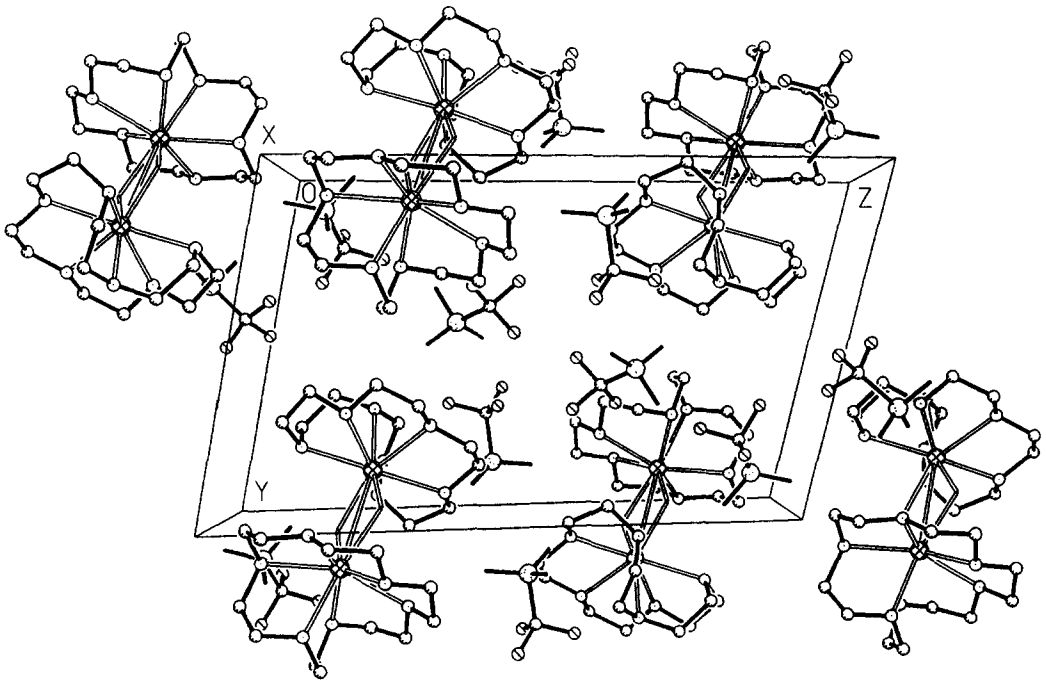

Fig. 3. Arrangement of [(hexacyclen)Er(μ-OH)$_2$Er(hexacyclen)](CF$_3$SO$_3$)$_4$ in unit cell.

Table 2. Selected bond lengths (Å) and angles (°)

Er(1)—O(1)	2.246(2)	Er(1)—O(2)	2.275(2)
Er(1)—N(1)	2.534(3)	Er(1)—N(2)	2.522(3)
Er(1)—N(3)	2.533(3)	Er(1)—N(4)	2.550(3)
Er(1)—N(5)	2.609(2)	Er(1)—N(6)	2.560(2)
Er(2)—O(1)	2.237(3)	Er(2)—O(2)	2.310(3)
Er(2)—N(7)	2.533(3)	Er(2)—N(8)	2.556(2)
Er(2)—N(9)	2.588(2)	Er(2)—N(10)	2.540(3)
Er(2)—N(11)	2.504(3)	Er(2)—N(12)	2.521(2)
Er(1)—O(1)—Er(2)	116.0(1)	Er(1)—O(2)—Er(2)	112.0(1)
O(1)—Er(1)—O(2)	66.1(1)	O(1)—Er(1)—N(1)	102.1(1)
O(1)—Er(1)—N(2)	145.6(1)	O(1)—Er(1)—N(3)	114.2(1)
O(1)—Er(1)—N(4)	78.4(1)	O(1)—Er(1)—N(5)	133.4(1)
O(1)—Er(1)—N(6)	77.3(1)	O(2)—Er(1)—N(1)	86.7(1)
O(2)—Er(1)—N(2)	80.4(1)	O(2)—Er(1)—N(3)	82.2(1)
O(2)—Er(1)—N(4)	118.1(1)	O(2)—Er(1)—N(5)	159.6(1)
O(2)—Er(1)—N(6)	129.5(1)	N(1)—Er(1)—N(2)	67.0(1)
N(1)—Er(1)—N(3)	133.2(1)	N(1)—Er(1)—N(4)	151.7(1)
N(1)—Er(1)—N(5)	93.4(1)	N(1)—Er(1)—N(6)	67.6(1)
N(2)—Er(1)—N(3)	66.4(1)	N(2)—Er(1)—N(4)	127.1(1)
N(2)—Er(1)—N(5)	80.9(1)	N(2)—Er(1)—N(6)	122.4(1)
N(3)—Er(1)—N(4)	68.0(1)	N(3)—Er(1)—N(5)	83.0(1)
N(3)—Er(1)—N(6)	146.7(1)	N(4)—Er(1)—N(5)	68.3(1)
N(4)—Er(1)—N(6)	85.2(1)	N(5)—Er(1)—N(6)	68.5(1)

viously reported analogues in two ways: first, in the geometry of the ligand arranged around metal ions, and secondly, in the presence of the bridging hydroxide groups. In the previously reported 1 : 1 complexes of hexacyclen, the six nitrogen atoms were arranged in octahedral symmetries for smaller metal ions like Co^{3+} and Cr^{3+} (where the M—N bond lengths are about 2.0 Å) [6–9], in a distorted trigonal prism for a medium ion Hg^{2+}(Hg—N, ~2.5 Å) [10] and in a hexagonal plane for a larger ion UO^{2+}(U—N, ~2.7 Å) [11]. Furthermore, a series of lanthanide complexes with the oxygen analogue of hexacyclen, 18-crown-6, have been structurally characterized with the ligand folding around the metal ions and the other species such as anions (Cl^- and NO_3^-) and solvent molecules (H_2O) coordinating to the metal ions from 'above' and

'below' the crown ether [20]. But completely different from the structures mentioned above, the title complex is eight coordinated with each of the two metal ions siting between a hexacyclen ligand and the two bridging hydroxide ions. Thus, the structure of the title complex is rather unusual. The presence of the bridging coordinated hydroxide ions is another feature of the complex. Although the presence of the complex species 'Ln(OH)-hexacyclen' in aqueous solution has been predicted by W. Szczepaniak *et al.* in 1988 [3], no structural information for such a species has been reported until now. And it is of interest to note that the title complex can form in an anhydrous system and the ligand can stabilize the complex. In a similar synthesis, we have obtained a monoaquo–lanthanum complex: [La(Me-cyclen)(NCMe)(OH_2)(OSO_2CF_3)$_3$] [12], where a water molecule is included in the coordination sphere and the lanthanum ion does not hydrolyze.

Acknowledgement—This work was supported by the Climbing Program, a National Key Project for Fundamental Research.

REFERENCES

1. Hay, R. W., Jeragh, B., Lincoln, S. F. and Searle, G. H., *Inorg. Nucl. Chem. Lett.*, 1978, **14,** 435.
2. Kodama, M., Kimura, E. and Yamagushi, S., *J. Chem. Soc., Dalton Trans.*, 1980, 2537.
3. Szczepaniak, W., Juskowiak, B. and Ciszewska, W., *Inorg. Chim. Acta*, 1988, **147,** 261.
4. McAuley, A., Whitcombe, T. W. and Zaworotko, M. J., *Inorg. Chem.*, 1991, **30,** 3513.
5. Bencini, A., Bianchi, A., Dapporto, P., Garcia-Espana, E., Micheloni, M., Paoletti, P. and Paoli, P., *J. Chem. Soc., Chem. Commun.*, 1990, 1382.
6. Yoshikawa, Y., Toriumi, K., Ito, T. and Yamatera, H., *Bull. Chem. Soc. Jpn.*, 1982, **55,** 1422.
7. Royer, D. J., Grant, G. J., Van der Derveer, D. G. and Castillo, M. J., *Inorg. Chem.*, 1982, **21,** 1902.
8. Searle, G. H. and Tiekink, E. R. T., *J. Coord. Chem.*, 1989, **20,** 229.
9. Chandrasekhar, S., Fortier, D. G. and McAuley, A., *Inorg. Chem.*, 1993, **32,** 1424.
10. Carrondo, M., Felix, V., Duarte, M. T. and Santos, A., *Polyhedron*, 1993, **12,** 931.
11. Nierlich, M., Sabattie, J.-M., Keller, N., Lance, M. and Vigner, J.-D., *Acta Cryst.*, 1994, **C50,** 52.
12. Wei, P.-R., Jin, T.-Z., Xu, G.-X. and Jin, Z.-S., *Chem. J. Chin. Univ.*, 1992, **13,** 437.
13. Wei, P.-R., Jin, T.-Z., Xu, G.-X. and Jin, Z.-S., *Acta Chim. Sinica*, 1992, **50,** 883.
14. Wang, X.-Q., Yang, W.-C., Jin, T.-Z., Xu, G.-X., Ma, Z.-S. and Shi, N.-C., *Acta Chim. Sinica*, 1996, **54,** 347.
15. Smith, P. H. and Raymond, K. N., *Inorg. Chem.*, 1985, **24,** 3469.
16. Lukyanenko, N. G., Basok, S. S. and Filonova, L. K., *J. Chem. Soc., Perkins Trans. I*, 1988, 3141.
17. Baraniak, E., Bruce, R. St. L., Freeman, H. C., Hair, N. J. and James, J., *Inorg. Chem.*, 1976, **15,** 2226.
18. Grillone, M. D., Benetollo, F. and Bombieri, G., *Polyhedron*, 1991, **10,** 2171.
19. Thuery, P., Keller, N., Lance, M., Vigner, J.-D. and Nierlich, M., *Acta Cryst.*, 1995, **C51,** 1407.
20. Rogers, R. D., Kurihara, L. K., Vess, E. J., *Inorg. Chem.*, 1987, **26,** 2360.

Pergamon

PII: S0277-5387(97)00257-X

Polyhedron Vol. 17, No. 1, pp. 49–53, 1998
© 1997 Elsevier Science Ltd
All rights reserved. Printed in Great Britain
0277-5387/98 $19.00+0.00

New solid state routes to lithium transition metal oxides *via* reactions with lithium oxide

Marco D. Aguas, Graham C. Coombe and Ivan P. Parkin*

Department of Chemistry, Christopher Ingold Laboratory, University College London, 20 Gordon Street, London, WC1H OAJ.

(Received 14 April 1997; accepted 11 June 1997)

Abstract—Thermolysis of a mixture of lithium oxide and transition metal halides MX_n (M = Ti, Zr, Hf, V, Nb, Ta, Mo, W, Fe, Mn) at 800°C for 2–12 h produces crystalline lithium transition metal oxides Li_2MO_3 (M = Ti, Zr, Hf, Mn), Li_3MO_4 (M = V, Nb, Ta), Li_2MnO_3 $Li_2Fe_3O_4$ and Li_2MO_4 (M = Mo, W). For M = Cr, Co, Ni, Cu and Zn the reaction produces the metal oxides Cr_2O_3, NiO, CuO, ZnO and Co_3O_4. The metal oxides and lithium metal oxides were characterised by X-ray powder diffraction. SEM/EDAX, FT-IR and magnetic moment measurements. © 1997 Elsevier Science Ltd

Keywords: lithium oxide; solid state metathesis.

Transition metal oxides have a wide variety of structural types and an extensive range of properties from dielectric insulators to superconductors [1]. Commercially, lithium transition metal oxides have been used as solid breeder materials for nuclear reactors (Li_2ZrO_3) [2], non linear optical materials ($LiNbO_3$) [3] and corrosion inhibitors ($LiCrO_2$) [4,5].

Transition metal oxides can be made by heating the metal nitrate or carbonate in air [6]. Other routes include hydrothermal synthesis, molecular precursor, sol–gel and self propagating high temperature synthesis for bulk materials; CVD and MBE routes for coatings [7]. These materials are probably the most important class of ceramics both for industrial usage and for academic interest. Lithium transition metal oxides are typically made by reaction of metal carbonates or the action of Li_2O on metal oxide at 1200°C.

Solid state metathesis (SSM) reactions have been used to prepare a wide range of metal nitrides, phosphides, arsenides, stibides, oxides, sulfides and selenides [8]. In these reactions a metal halide is reacted with a group Ia or IIa pnictide or chalcogenide Eq (1). The coproduced halide provides for up to 90% of the reaction enthalpy and insures a rapid exothermic reaction.

$$Na_3E + MCl_3 \rightarrow 3NaCl + ME \quad (1)$$

In a previous paper [9] we reported on the synthesis of metal oxides from reactions of lithium oxide and anhydrous metal halides in sealed glass ampoules under vacuum. In all cases metal oxides and lithium chloride were produced except for Nb and Ta where $LiNbO_3$ and $LiTaO_3$ were obtained. In this paper we detail the effect of carrying out SSM reactions in air and with different stoichiometries.

EXPERIMENTAL

All preparations were conducted in a Saffron scientific glove box under a nitrogen atmosphere. Thermal studies were obtained in open ceramic crucibles in a Lenton Thermal Designs tube furnace. Metal chlorides and lithium oxide were purchased from Aldrich Chemical Co and used as supplied. X-ray powder diffraction was obtained using a Siemens D5000 diffractometer using germanium monochromated Cu-$K_{\alpha 1}$ radiation (λ = 1.54056 Å). Patterns were indexed using the TREOR program. SEM and EDAX analysis were obtained on a Jeol JSM 820 instrument using Quantex 6.2 with quantum detector Kevex delta 4. FT-IR spectra were obtained as pressed KBr pellets on a Nicholet 205; magnetic moment measurements were obtained on a Johnson Matthey balance.

* Author to whom correspondence should be addressed.

Table 1. X-ray powder diffraction and magnetic moment data from the reactions of metal chlorides and lithium oxide in air

Initial metal halide	Colour of product	Phase identified	Observed lattice[a] parameters (Å)	Literature lattice [11] parameters (Å)	μ(Bm) obs	μ(Bm) calc.
$TiCl_3$	white	Li_2TiO_3	5.06 8.79 9.60	5.07 8.80 9.60	0	0
$ZrCl_4$	white	Li_2ZrO_3	5.43 9.06 5.44	5.43 9.03 5.42	0	0
$HfCl_4$	white	Li_2HfO_3	5.42 8.92 5.39	5.42 8.91 5.43	0	0
VCl_3	yellow	Li_3VO_4	6.46 10.97 5.22	6.46 11.04 5.20	0	0
$NbCl_5$	white	Li_3NbO_4	8.43	8.43	0	0
$TaCl_5$	white	Li_3TaO_4	8.48 14.91	8.50 14.91	0	0
$CrCl_3$	green	Cr_2O_3	$4.96\ 13.59^R$	4.95 13.63	3.82	3.87
$MoCl_3$	white	Li_2MoO_4	$14.33\ 9.58^H$	14.34 9.59	0	0
WCl_4	black	Li_2WO_4	$14.33\ 9.58^H$	14.36 9.60		
$MnCl_2$	red	Li_2MnO_3	4.93 8.53 9.63	4.93 8.53 9.60	4.04	3.87
$CoCl_2$	black	Co_3O_4	8.10	8.08		
$NiCl_2$	black	NiO	2.95 7.24	2.95 7.24		
$CuCl_2$	grey	CuO	4.93 3.43 5.13	4.68 3.43 5.13		
$ZnCl_2$	white	ZnO	$2.95\ 7.24^H$	2.95 7.24	0	0

[a] Observed XRD parameters were obtained to +/− 0.01 Å. The *a*, *b*, and *c* cell constants are given in order except for cubic cells where only one parameter is quoted and for hexagonal cells where the last number is the *c* constant. ^{R} = Rhombohedral, ^{T} = Tetragonal, ^{H} = Hexagonal.

Lithium transition metal oxide preparation (M = Ti, Zr, Hf, V, Nb, Ta, Mn, Fe)

Metal chlorides and lithium oxide (100–200 mg, 33–66 mmol) were combined such that the stoichiometric ratio of lithium to chloride was 1 : 1 (see Table 1). The reactants were ground together in a pestle and mortar and then sealed in an ampoule under nitrogen. The reaction mixture was opened in air and immediately placed in an open ceramic crucible at 300°C. The crucible was heated to 800°C for 12 h before allowing to cool to room temperature (*ca* 2 h). The product was triturated with water (2×50 cm^3) acetone (2×20 cm^3) and air dried. Products were analysed by power X-ray diffraction (Table 1). FT-IR, magnetic moment measurement and SEM/EDAX. Typical yields were in the range of 75–95%. Variation in reaction temperature (500 and 800°C) times (2 and 48 h) and reaction stoichiometries were explored for selected samples.

[Note the 1 : 1 stoichiometries of lithium to halide utilised above could not give rise to some of the phases and idealised equations (1–11) outlined below, too much lithium is required. In this case it is probable that some of the starting metal halide is evaporated during the course of the reaction. In a number of reactions excess over the 1 : 1 lithium to halide stoichiometry was tried, this gave the same lithium metal oxide product in a higher yield, this is commented upon below]

Caution. Metal halides and lithium oxide/metal halide reaction mixtures can undergo extremely exothermic reactions when heated and can produce a thermal flash. Reactions should be conducted in a fume cupboard behind a glass safety screen.

RESULTS AND DISCUSSION

Characterisation

Reaction of ground powders of Li_2O and anhydrous transition metal halides at 800°C for 12 h produces crystalline lithium transition metal oxides in good yield (*ca* 80%), Eqs (2)–(11).

$$TiCl_3 + 5/2Li_2O + 1/2O_2 \rightarrow Li_2TiO_3 + 3LiCl \quad (2)$$

$$MCl_4 + 3Li_2O \rightarrow Li_2MO_3 + 4LiCl \quad (M = Zr, Hf) \quad (3)$$

$$VCl_3 + 3Li_2O \rightarrow Li_3VO_4 + 3LiCl \quad (4)$$

$$MCl_5 + 4Li_2O \rightarrow Li_3MO_4 + 5LiCl \quad (M = Nb, Ta) \quad (5)$$

$$2CrCl_3 + 3Li_2O \rightarrow Cr_2O_3 + 6LiCl \quad (6)$$

$$MCl_4 + 3Li_2O \rightarrow Li_2MO_4 + 4LiCl \quad (M = Mo, W) \quad (7)$$

$$3FeCl_2 + 4Li_2O \rightarrow Li_2Fe_3O_4 + 6LiCl \quad (8)$$

$$MnCl_2 + 2Li_2O + 1/2O_2 \rightarrow Li_2MnO_3 + 2LiCl \quad (9)$$

$$3CoCl_2 + 3Li_2O + 1/2O_2 \rightarrow Co_3O_4 + 6LiCl \quad (10)$$

$$MCl_2 + Li_2O \rightarrow MO + 2LiCl \quad (M = Ni, Cu, Zn) \quad (11)$$

The products from the reactions were often fused coloured masses. Trituration with water and acetone removed the co-produced lithium chloride. The powders were characterised by X-ray powder diffraction

(Table 1). FT-IR, magnetic moment measurements, SEM and EDAX.

The SEM profile of the triturated powders revealed a variety of morphologies dependent on the sample from micron size crystallites with sharp angles and faces through to porous materials with a rounded structure. EDAX showed only the presence of transition metal, oxygen and some chlorine in the untriturated powders commensurate with the formation of lithium metal oxide and some lithium chloride (lithium is below the EDAX detection threshold). On trituration the EDAX peak for chloride disappeared leaving only peaks for metal and oxygen in the expected ratios.

The FT-IR spectra of the triturated lithium transition metal oxides and metal oxides were identical to authentic samples and typically showed a broad band centred at 650–450 cm^{-1} corresponding to a metal oxygen stretch. In no cases were other bands such as an O—H stretch observed. The magnetic moments (Table 1) of the paramagnetic materials were consistent with calculated spin only values.

The X-ray powder diffraction data for the lithium transition metal oxides and the metal oxides are summarised in Table 1. In general after a reaction time of 12 h at 800°C a crystalline material was formed, crystallite sizes varied from *ca* 300–1000 Å as assessed from the Scherrer equation [10]. In virtually all the reactions after trituration a single phase was identified by X-ray powder diffraction [11].

Scope of the reaction

Reaction of lithium oxides and anhydrous transition metal halides in air at 800°C for 2 h produces either metal oxide or lithium metal oxide. For early transition metals, lithium metal oxides were formed whilst for the latter transition metals no lithium incorporation was observed and metal oxides were produced. In the cases where metal oxides were produced, the metal was not oxidised in the reaction except for cobalt where Co_3O_4 was produced. In the cobalt case the oxidation is promoted by oxygen in the air because in sealed ampoule reactions CoO is produced. Reaction of the anhydrous chlorides of group IVa and Va with Li_2O at 800°C for 12 h produces only a single phase of material Li_2MO_3 (Fig. 1) and Li_3MO_4 respectively. In both cases the transition metal is in its maximum oxidation state. For the reactions of $TiCl_3$ and VCl_3 the metal has been oxidised in air. In comparable sealed ampoule reactions at 550°C the transition metal is not oxidised and little or no lithium incorporation is observed (except for $LiNbO_3$ and $LiTaO_3$) [9]. Reactions involving Mn and Fe chlorides with Li_2O in air show both oxidation of the metal and lithium incorporation. The reaction of $MoCl_5$ or $MoCl_3$ with Li_2O at 700°C produced Li_2MoO_4 (Fig. 2). Reducing the reaction temperature to 600°C produce a mixed phase of material in the case of $MoCl_3$; Li_2MoO_4 and Li_4MoO_5. The lithium incorporation in the lithium metal oxide could be increased by using more Li_2O.

Reaction pathway

The pathway followed in these reactions is difficult to determine. It could be a direct solid state metathesis reaction between Li_2O and metal halide. Alternatively the metal halide could decompose on heating in air to form a metal oxide that could then combine with the lithium oxide at the elevated temperatures to form lithium metal oxide. A number of reactions were followed to try and determine the reaction pathway.

Reaction of finely divided metal oxide and lithium oxide did not produce crystalline lithium metal oxide at 800°C after 8 h (M = Ti, Nb). Heating a mixture of LiCl with metal oxides or metal halides under similar conditions did not produce lithium metal oxides. Competitive reactions were investigated by reaction of a mixture of MCl_n and $M'O_x$ with Li_2O. This produced only $LiMO_p$ and no $LiM'O_p$. This indicates that the metathesis pathway is probably favoured.

Reducing the reaction time to 2 h for the reaction of Li_2O and MCl_n and lowering the temperature to 500°C did, in general, produce the same phases of material as the higher temperature reactions however the products were notably less crystalline.

It should be noted that in the majority of the reactions the amount of lithium oxide added was adjusted to remove all the lithium as lithium chloride. In the reactions carried out in a sealed ampoule no metal halide can escape during the course of the reaction and the degree of lithium incorporation is low or non existent. In the reactions carried out in air the metal halides which in some cases are relatively volatile can be partly lost from the reaction or evaporated (in the case of reactions that proceed with a thermal flash). This would mean that an excess of lithium oxide is available for combination and allows for the formation of lithium metal oxides. Indeed the most volatile metal halides studied ($NbCl_5$, $TaCl_5$) showed the greatest degree of lithium incorporation in the product.

Reaction of excess lithium oxide over the stoichiometric 1 : 1 lithium to chloride ratio was also studied. Once the preferred formula of the product had been determined from the stoichiometric reactions outlined above, excess lithium oxide was used in the reaction. These reactions proved to give a single phase of the required material in slightly higher isolated yields than the stoichiometric reactions. This observation supports the idea that some metal halide is lost by evaporation in the stoichiometric reactions. Notably no new or lithium rich phases were observed on increasing the amount of lithium oxide in the reaction, just improved yields.

The temperatures employed in this new route to lithium transition metal oxides are up to 500°C lower

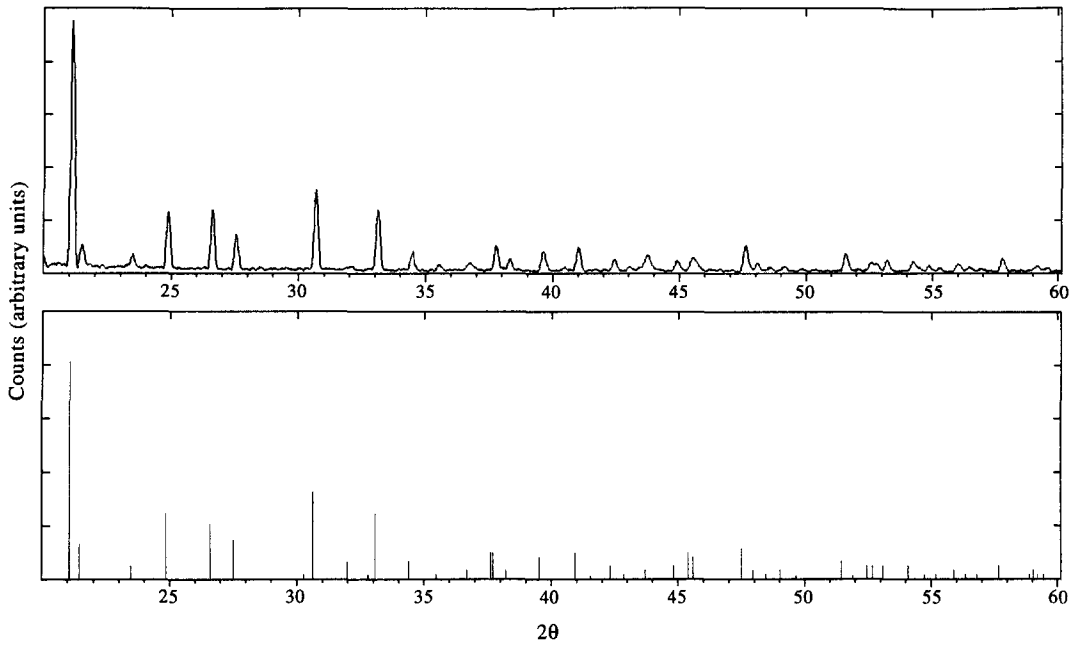

Fig. 1. Upper trace; pattern obtained from reaction of Li_2O and $HfCl_4$ in air at 800°C. Lower trace; stick pattern for Li_2HfO_3.

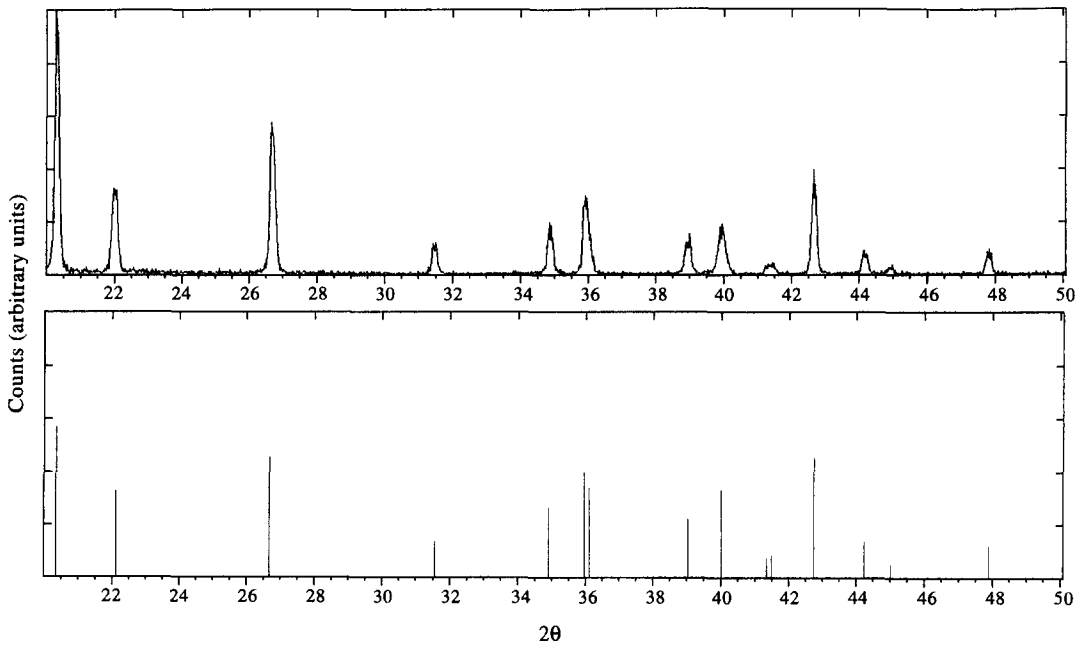

Fig. 2. Upper trace; pattern obtained from reaction of Li_2O and $MoCl_3$ in air at 800°C. Lower trace; stick pattern for Li_2MoO_4.

than conventional preparations from the oxides. The procedure is also relatively straightforward and does not involve the use of multiple heating and grinding stages or long annealing periods used in traditional methods. Compared to hydrothermal routes this method does not involve any prior wet chemistry stage. The new method is easy to duplicate, involves inexpensive apparatus and can be achieved without pelletising the reagents. The lower temperature and shorter times in these reactions is attributable to the ease in which the solid state diffusion barrier is overcome as the starting metal chlorides melt or partly decompose during the reaction, further the coproduced lithium halide provides a flux for the reactants.

The reaction may be proceeding *via* a solid state metatheses reaction. It should be noted that no unusual or novel phases of lithium metal oxides have been achieved using this route. It would be desirable to produce highly oxidised phases such as $Li_xNi_{1-x}O$ via this method, however all attempts to date have been unsuccessful.

CONCLUSIONS

Reaction of lithium oxide with anhydrous metal halides in air at 800°C provides a straightforward relatively high yield route to lithium metal oxides. The phases isolated are significantly different to sealed ampoule reactions of lithium oxide and anhydrous metal halides where metal oxides were produced. It is likely that the reaction occurs via solid state metathesis. The new reaction to form lithium metal oxides is at significantly lower furnace temperature than conventional methods possibly because a flux of lithium chloride is coproduced in the reaction.

Acknowledgements—The Royal Society and the University of London Central Research fund are thanked for equipment grants.

REFERENCES

1. Goodenough, J. B., Manthiran, A., Dia, Y. and Champion, A., *Super. Sci. Tech.*, 1990, **3,** 26.
2. Slagle, O. D., Hollenberg, G. W. and Baldwin, D. L., *J. Nuc. Mater.*, 1991, **179,** 831.
3. Collongues, R., *Jap. J. App. Phys*, 1993, **32,** 442.
4. Uesugi, U., *Radio Science*, 1982, **17,** 197; Arvidsson, G. and Laurell, F., *Thin Solid Films*, 1986, **136,** 29.
5. Vossen, J. P. T., Makkus, R. C. and Dewit, J. H. W., *J. Electrochem. Soc.*, 1996, **143,** 1.
6. Greenwood, N. N. and Earnshaw, E. A., *Chemistry of the Elements*, Pergamon Press, Oxford (1984).
7. Kim, Y. J., Gao, Y. and Chambers, S. A., *Surface Science*, 1997, **371,** 358; Nakamura, T.,, Inada, H. and Iiyama, M., *Jap. J. App. Phys.*, 1997, **36,** 90.
8. Parkin, I. P., *Chem. Rev.*, 1996, 199; Treece, R. E., Gillan, E. G. and Kaner, R. B., *Comments on Inorg. Chem.*, 1995, **16,** 313.
9. Hector, A. L. and Parkin, I. P., *Polyhedron*, 1993, **12,** 1855.
10. Klug, H. P. and Alexander, L. E., *X-ray Diffraction Procedure for Polycrystalline and Amorphous Materials*, 2nd Ed., Wiley, New York (1974).
11. PDF-2 data base, International centre for Diffraction data; Swartmore PA, 19081.

Pergamon

PII: S0277-5387(97)00254-4

Polyhedron Vol. 17, No. 1, pp. 55–62, 1998
© 1997 Elsevier Science Ltd
All rights reserved. Printed in Great Britain
0277-5387/98 $19.00+0.00

X-ray and NMR studies of a diammonium (nitrilotriacetato)dioxovanadate(V) complex

Man-Ho Lee,[a]* Nam Ho Heo[a] and Shigenobu Hayashi[b]

[a] Department of Industrial Chemistry, Kyungpook National University, Taegu 702–701, Korea

[b] National Institute of Materials and Chemical Research, Tsukuba, Ibaraki 305, Japan

(Received 7 April 1997; accepted 11 June 1997)

Abstract—A new vanadium(V) complex, diammonium (nitrilotriacetato)dioxovanadate(V) $(NH_4)_2$ [VO_2NTA], has been synthesized. The structure of the complex has been studied by solution and solid-state NMR spectroscopies as well as single crystal X-ray crystallography. It is confirmed from NMR studies that the octahedral geometry is retained in both solution and solid-state of the complex. The chemical exchange between glycinate rings *cis* to and *trans* to V=O bond in the complex has been observed in the solution ^{13}C NMR spectra at elevated temperatures. Large ^{51}V chemical shift anisotropy ($\Delta\delta_{aniso} = -800$ ppm) and quadrupole coupling ($e^2qQ/h = 8.80$ MHz) were observed in ^{51}V spectra of the solid complex. Distortion of octahedron also results in an increase of the electric field gradient at a V nucleus. The NMR spectra are discussed on the basis of the crystal structure. © 1997 Elsevier Science Ltd

Keywords: X-ray; NMR; nitrilotriacetate; vanadium(V) complex; dioxovanadate(V) complex; ^{51}V NMR.

With the recent discoveries of the first two naturally occurring vanadium-containing enzymes, the bromoperoxidase and nitrogenase, the coordination chemistry and reactivity of vanadium is receiving renewed attention [1]. Of the various ligands, many carboxylates are known to form anhydrides with vanadate in solution, if they have additional hydroxyl or amine groups available for chelation. Oxalate [2–4] gives the simple mono- and *bis*-oxalato octahedral complexes, presumably with *cis*-VO_2 species. Aminopolycarboxylate such as ethylenediaminetetraacetate (EDTA) also forms similar octahedral complex having *cis*-VO_2 species [5–8]. However, 2-hydroxycarboxylates such as lactate and glycerate etc., form a variety of derivatives, including simple esters and chelates having trigonal bipyramidal coordination, and two binuclear complexes with mixed coordination [3,9,10].

Not many crystal structures of the vanadium(V) complexes are known yet. The vanadium(V) complexes of oxalate [11,12] and EDTA [13,14], in which the anion has irregular octahedral geometry with two double-bonded oxygen atoms, are known to have a *cis*-VO_2 core from the X-ray diffraction studies.

In recent years, solid-state ^{51}V NMR spectroscopy has emerged as a powerful tool for studying the local environment of vanadium in vanadia based catalysts [15], metavanadates [16,17] and vanadium complexes [8]. However, the resulting ^{51}V magic-angle-spinning (MAS) spectra are not simple due to the simultaneous line-broadening effects arising from quadrupole and chemical shift anisotropy. The ^{51}V nucleus (spin $I = 7/2$, natural abundance 99.76%) has an electric quadrupole moment which interacts with the gradient of the intramolecular electric field. This interaction produces the so called quadrupole effects of the first and second order in ^{51}V NMR spectra [18]. The analysis of these effects allows one to measure the quadrupolar coupling constant, e^2qQ/h, and asymmetry parameter, η_Q. These parameters directly characterize the gradient of the electric field which is created at the ^{51}V nucleus by the surrounding atoms and thus can be related to distortions of the symmetry of the local environment of the V atom. As found recently, the principal components of the chemical shift tensor δ_1, δ_2 and δ_3 are also very sensitive to the type of local environment of ^{51}V nucleus [19].

In this paper we have prepared a new vanadium(V) complex, diammonium (nitrilotriacetato)dioxovanadate(V), and its structure has been studied by the

* Author to whom correspondence should be addressed.

solution (^{1}H, ^{13}C and ^{51}V) and solid-state (^{13}C and ^{51}V) NMR spectroscopies, for the purpose of studying the interactions of vanadium(V) with amino-polycarboxylate ligand. Also the NMR spectra were discussed on the basis of the X-ray structure of the complex.

EXPERIMENTAL

Materials

All reagent grade chemicals were used without further purification. Ammonium metavanadate (NH_4VO_3), nitrilotriacetic acid (H_3NTA), 25% ammonia water and D_2O were purchased from Aldrich Chemical Company.

Synthesis of the vanadium(V) complex

The reaction of NH_4VO_3 (0.02 mole, 2.34 g) with H_3NTA (0.02 mole, 3.82 g) and 25% ammonia water (0.02 mole, 1.3 cm^3) in 100 cm^3 of water produced a yellow solution, which was filtered after being stirred for 3 h. The solution was concentrated by passing a stream of dry air at room temperature for 2 days. The pale yellow crystals were formed and then filtered. The complex was recrystallized from water. The yield was 1.95 g (63.1%). The single crystals were obtained by evaporating slowly the aqueous solution of the complex. Chemical formula of the complex is $VN_3O_8C_6H_{14}$ on the basis of elemental analyses. Analytical data; calculated (%): C 23.46, H 4.59, N 13.68, found (%): C 23.34, H 4.68, N 13.83.

X-ray measurements

Preliminary experimentation and data collection for the X-ray crystal structure determination were performed on an Enraf–Nonius CAD4/Turbo diffractometer using Mo-K_α radiation ($\lambda = 0.71069$ Å). A small single crystal, $0.5 \times 0.5 \times 0.5$ mm, was cut from a larger one and glued to a glass fiber with an epoxy resin. Twenty-five reflections in diverse reciprocal space were centered by an automatic search program and used to obtain cell parameters. After the preliminary cell was confirmed, high-angle data ($2\theta > 20°$) were collected and 25 of these reflections were centered and used to obtain more accurate cell parameters. Unit cell parameters and the systematic absences indicated the monoclinic space group $P2_1/n$ (No. 14) [20] with $Z = 4$. Data were collected on this improved unit cell at ambient temperature up to $2\theta = 50°$. Data reduction including the corrections for Lorentz-polarization, decay and absorption were performed. The crystal structure was solved and refined with full-matrix least-squares by using MolEN, the Enraf–Nonius structure determination package, resulting in R_1 and R_w indices of 0.049 and 0.076, respectively, without hydrogen atoms. Other details of crystallographic data are summarized in Table 1. The selected bond distances and angles are tabulated in Table 2. The structure model was drawn using ORTEP, Oak Ridge Thermal Ellipsoid Plot Program [21].

Solution and solid-state NMR measurements

^{13}C and ^{51}V NMR spectra of samples in D_2O were recorded on a JEOL GSX-400 NMR spectrometer at 100.5 and 105 MHz, respectively, at 298 K. The solution ^{13}C spectra were measured with broad-band ^{1}H decoupling. ^{13}C spectra of solid samples (*ca* 0.2 g) were recorded on a Bruker MSL-300 spectrometer (75.47 MHz) with cross-polarization/magic-angle-spinning (CP/MAS) technique at ambient temperature. A spectral width of 29,411 Hz and an accumulation of 200 transients with an acquisition time of 0.85 s were used. The contact time was 2 ms and the delay between each scan was 5 s. Spinning (MAS and off-MAS) and static ^{51}V spectra of the powder samples were recorded at room temperature on a Bruker MSL-400 and an ASX-200 spectrometer at 105.25 and 52.64 MHz, respectively. The angle in the off-MAS measurements was chosen so that the intensities of the spinning sidebands caused by the satellite transitions were negligible. The spinning axis used in off-MAS was inclined at 53.9 and 53.7° to the magnetic field for MSL-400 and ASX-200, respectively. The spin rates for spinning spectra were between 8 and 12 kHz. The ordinary single pulse sequence with phase alternation was used

Table 1. X-ray crystallographic parameters

Formula	$VN_3O_8C_6H_{14}$
Formula wt	307.1
a (Å)	6.923 (1)
b (Å)	8.814 (2)
c (Å)	19.218 (11)
β (°)	91.60 (3)
V (Å^3)	1172.1 (7)
Z	4
d_{calc} (g cm^{-3})	1.714
Space group	$P2_1/n$
Temperature	ambient
Radiation (Å)	Mo-K_α (0.71073)
Lin. abs. Coeff. (cm^{-1})	8.5
Scan mode	θ–2θ
$2\theta_{max}$ (°)	50
No. of obsd. refl.	1874
No. of variables	164
R^a	0.049
$R_w{}^b$	0.076
Goodness of fit^c	2.60

[a] $R_1 = \Sigma||F_o| - |F_c||/\Sigma F_o$.

[b] $R_w = [\Sigma w(F_o - |F_c|)^2/\Sigma w F_o^2]^{1/2}$.

[c] Goodness of fit $= [\Sigma w(F_o - |F_c|)^2/\Sigma(m-s)]^{1/2}$, where m = number of observed data and s = number of variables.

Table 2. Selected bond distances (Å) and angles (°)[a]

V—O(1)	1.653(3)	V—O(2)	1.613(3)
V—O(3)	1.980(3)	V—O(4)	2.225(3)
V—O(5)	1.995(3)	V—N(1)	2.246(3)
O(1)—V—O(2)	107.1(2)	O(1)—V—O(3)	99.2(2)
O(1)—V—O(4)	85.3(1)	O(1)—V—O(5)	103.2(1)
O(1)—V—N—(1)	160.2(1)	O(2)—V—O—(3)	96.8(2)
O(2)—V—O(4)	167.6(1)	O(2)—V—O(5)	94.1(2)
O(2)—V—N—(1)	92.6(1)	O(3)—V—O(4)	81.8(1)
O(3)—V—O(5)	150.9(1)	O(3)—V—N(1)	77.6(1)
O(4)—V—O(5)	81.9(1)	O(4)—V—N(1)	75.0(1)
O(5)—V—N(1)	75.0(1)		

[a] Numbers in parentheses are the estimated standard deviations in the units of the least significant figure given for the corresponding parameters.

with and without ^1H high-power decoupling during signal acquisition. ^1H high-power decoupling had negligible effect on the line shape. ^1H decoupling power was 56 kW for both MSL-400 and ASX-200 spectrometers. Typical accumulation numbers were 800 for MAS and 1200 for static and off-MAS by MSL-400, and 2400 for MAS and off-MAS by ASX-200. The $\pi/2$ pulse width for solution was set at 6.0 μs. The pulth length used was 1.0 μs and the repetition time was 1.0 s. Recovery time after the pulse transmission was set at 5 μ s at 105.25 MHz. The detailed measuring conditions are described elsewhere [26]. ^{13}C and ^{51}V chemical shifts are referred to external TMS and $VOCl_3$, respectively.

Analysis of solid-state ^{51}V NMR spectra

The line shape of the spectra and the intensity of spinning side band (SSB) were analyzed using our own software written in Fortran and working on an NEC PC9801 series personal computer. The powder averaging procedure incorporates the two-dimensional interpolation and partitioning all directions presented by Alderman *et al.* [22] The intensity of SSB in MAS spectra produced by chemical shift anisotropy was calculated using the formula derived by Herzfeld and Berger [23]. Chemical shift anisotropy was estimated from the SSB intensity using a least squares fitting [24], in which the procedure was based on Fenzke *et al.* [25] The detailed procedure is described elsewhere [26].

RESULTS AND DISCUSSION

It is reported from the kinetic study that the VO_{2+}ion formed a 1:1 complex with NTA ($K_{VO_2NTA} = 10^{13.8}$ at 25°C) [27]. Nitrilotriacetate, containing a nitrogen and three oxygens, is considered to react with VO_{2+}ion as a tetradentate ligand. The synthesized vanadium-NTA complex is soluble in water and stable at room temperature. Its synthesis is readily accomplished in good yield (63.1%). Large single crystals were easily grown by slow evaporation of the aqueous solution and showed no evidence of twinning and other defects.

X-ray crystal structure

The solid-state structure of the complex is remarkably simple with four discrete $(NH_4)_2[VO_2NTA]$ units in a unit cell. There is no particular interaction between adjacent complexes in the unit cell and the geometry around the vanadium (V) ion appears to be distorted octahedron as shown in Fig. 1.

The anion $[VO_2NTA]^{2-}$ has a slightly irregular octahedral geometry in which two oxo ligands are *cis* to each other as shown in oxalate [11,12] and EDTA [13,14] complexes. These two oxygens have short V—O bonds (1.653 and 1.613 Å) which indicate strong multiple bond character. The O—V—O angle [107.1 (2)°] in the VO_2 moiety is larger than 90° that is the standard octahedral value. The small difference (0.040 Å) of V=O bonds observed in the unconstrained complex might be due to interactions with the

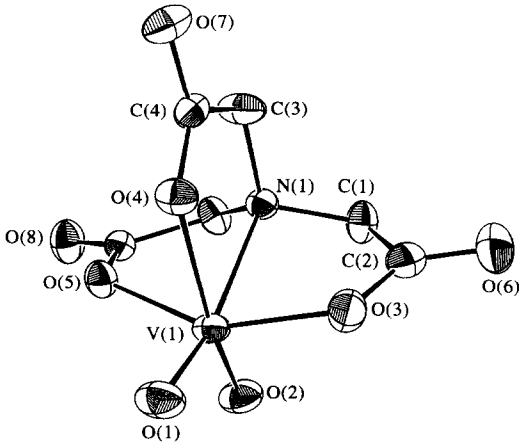

Fig. 1. ORTEP of $[VO_2NTA]^{2-}$ anion.

asymmetric environments. The average V=O bond length (1.633 Å) in the complex is shorter (1.648 Å) than that found in EDTA complex [14].

The remaining four coordination sites of vanadium atom are occupied by a nitrogen atom and three oxygen atoms of the NTA ligand, giving three five-membered glycinato rings in the complex. Three oxygen atoms of the NTA ligand in the complex fall into two groups depending on whether or not they are *trans* to a V=O bond. The *trans* V—O (glycinate) bond (2.225 Å) is significantly longer than the other bonds (1.980 and 1.995 Å), showing a good illustration of the structural *trans* effect. This lengthening (by an average 0.237 Å) and weakening of V—O bond which is *trans* to the oxo ligands can also be found in the crystal structure of vanadium(V)–oxalate complexes (by 0.23 Å) [11]. This weakening of the σ bond strength is reflected throughout the rest of the anion. The stronger of the inner C—O bonds are adjacent to the weaker of the V—O bonds. It is assumed that the hydrogen bonding to the vanadyl oxygen atoms occurs in the complex, also giving unsymmetric V=O bond lengths. The longer of the non-equivalent V=O bonds is the one which has the stronger hydrogen bonding to it.

The bond length of V—N is shorter in NTA complex (2.246 Å) than in EDTA complex (2.359 and 2.366 Å) [14], indicating stronger bond in NTA complex. A short V—N bond would give some reduction of strain within the glycinato rings in the complex. Since a difference of ~0.04 Å in V—O and V—N distance is predicted from consideration of the covalent radii of oxygen and nitrogen [13], the V—N bond is much stronger than the V—O(4) bond in the complex. It appears that the difference (0.021 Å) between the bond distances to nitrogen and carboxylate oxygen which is *trans* to V=O in the NTA complex is indicative of a low affinity of the VO_2^+ ion for carboxylate oxygen relative to amino nitrogen. Minor variations in length of the C=O bonds can also be attributed to hydrogen bonding with ammonium ions. The oxygens of C=O groups are the atoms most influenced by the environment of the anion.

Solution NMR spectroscopy

In the ^{13}C NMR spectrum of the complex in D_2O as shown in Fig. 2, there are two sets of glycinate group signals at room temperature: one set (65.03 and 179.72 ppm) is assigned to the glycinate *trans* to V=O and the other set (66.64 and 181.25 ppm) is assigned to the glycinate to *cis* to V=O. The assignment of ^{13}C peaks was based on the relative intensities of peaks and the chemical shifts in EDTA complex [8]. This indicates that the fast exchange between two types of the glycinate groups does not occur on NMR time scale at room temperature. But at elevated temperature the carboxylate group *trans* to the V=O bond will be easily broken and the chemical exchange between the glycinate groups *trans* to and *cis* to the V=O bond will occur faster, giving one set of glycinate signals, as shown in Fig. 3. Below the coalescence temperature (T_c) of 300 K, two sets of signals are observed in ^{13}C NMR spectrum. But at higher temperature the exchange rate increases and, thus, two sets of signals coalesce to give a set of signals. The process for the exchange might be a one-ended dissociation equilibration of the coordinated ligand, accompanied by a rotation and reclosure of the glycinate group. This phenomenon is also observed in the ^{13}C NMR spectrum of the $[VO_2\ (oxalate)_2]^{3-}$ anion [4], in which the exchange between two types of carboxylate groups *trans* and *cis* to V=O occurs at elevated temperature.

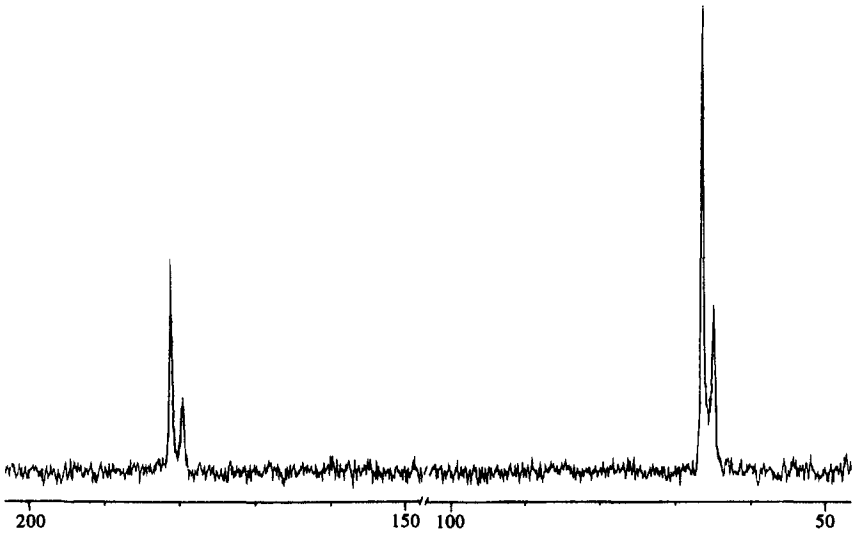

Fig. 2. ^{13}C NMR spectrum of $(NH_4)_2[VO_2NTA]$ in D_2O at ambient temperature.

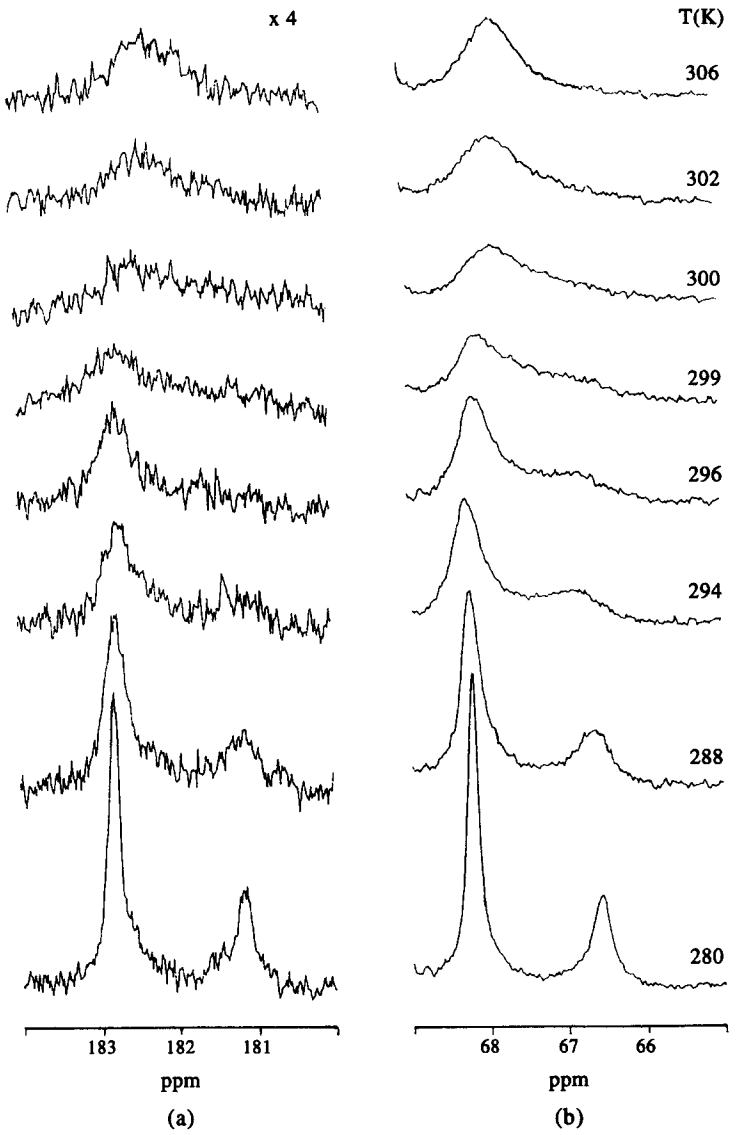

Fig. 3. (a) Methylene and (b) carboxylate regions of ^{13}C NMR spectrum of $(NH_4)_2[VO_2NTA]$ in D_2O at various temperatures.

The complex shows the ^{51}V peak at -504.3 ppm which falls in the range of octahedral coordination around vanadium atom [28]. The half-width (430 Hz) of ^{51}V peak is smaller than that (1000 Hz) of EDTA complex [8], due to increase of symmetry in the structure of NTA complex.

Solid-state NMR spectroscopy

The CP/MAS ^{13}C spectrum of the powder $(NH_4)_2[VO_2NTA]$ is shown in Fig. 4. There is only one CH_2 signal at 66.20 ppm, but two COO signals at 180.02 and 178.14 ppm indicating inequivalence of two COO groups. The broad line width of the CH_2 signal might be produced by residual dipolar coupling with the nearby ^{14}N, which disables the observation of the inequivalency of CH_2 groups. This result indicates that the chemical exchange between the two types of glycinate groups does not occur in the solid-state complex. These are consistent with X-ray diffraction results.

MAS ^{51}V spectrum of the powder $(NH_4)_2[VO_2NTA]$ is shown in Fig. 5(a). A large number of spinning sidebands are observed over a frequency range wider than 1.0 MHz. These sidebands originate mainly from the satellite transitions broadened by the first-order quadrupole interaction. Several stronger signals in the central position might be originated from the central transition. The large shielding anisotropy at high magnetic field (9.4 T) causes the MAS spectrum to be broken up into centerbands and an extensive set of the spinning side bands, which are spaced by integer multiples of the spinning frequency. We cannot separate the central transition from the satellite transitions due to the severe overlapping. Thus, we measured off-MAS ^{51}V spectrum, as shown

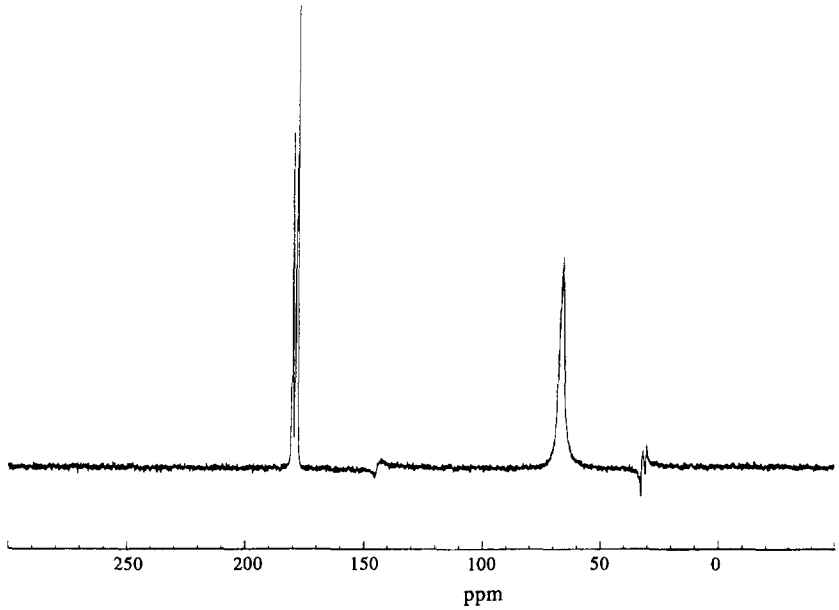

Fig. 4. CP/MAS ^{13}C NMR spectrum of the powder $(NH_4)_2[VO_2NTA]$.

in Fig. 5(b) to obtain only the signals from the central transitions [16]. These signals are ascribed to the central transition. The first-order quadrupole interaction does not work on the central transition ($+1/2 \leftrightarrow 1/2$), and therefore, the chemical shift anisotropy and the second-order quadrupole interaction influence the line shape and the chemical shift of ^{51}V signal. We analyzed the SSB intensities and line shapes of the off-MAS spectrum to obtain chemical shift anisotropy and the quadrupole coupling data, summarized in Table 3.

We have also measured the ^{51}V spectrum for a static sample as shown in Fig. 6. Static spectrum signals from the satellite transitions are not clearly observed and the line shape of the central transition is governed dominantly by chemical shift anisotropy. We have simulated the static spectrum to check and confirm

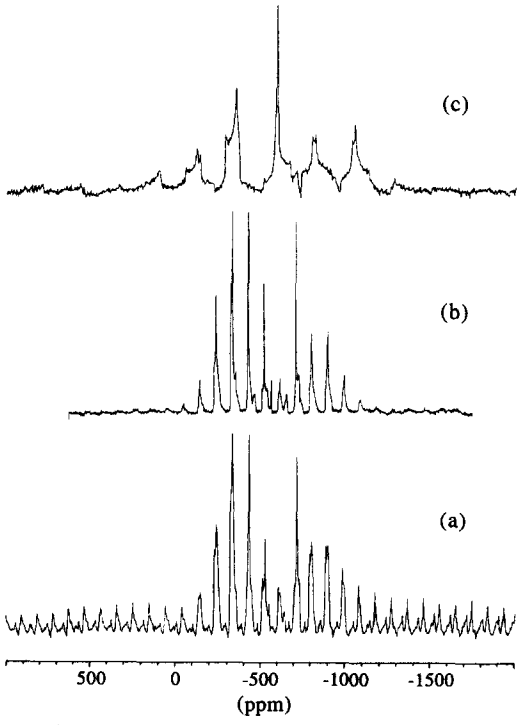

Fig. 5. ^{51}V NMR spectra of the powder $(NH_4)_2[VO_2NTA]$. (a) MAS and (b) off-MAS spectra measured at 105.25 MHz and (c) off-MAS spectra at 52.64 MHz. The spinning rates were (a, b) 10.00 kHz and (c) 12.00 kHz.

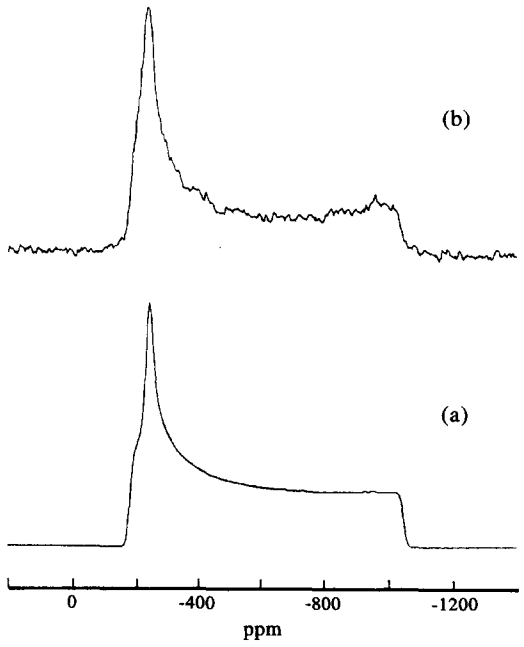

Fig. 6. (a) Calculated and (b) observed static ^{51}V NMR spectra of the powder $(NH_4)_2[VO_2NTA]$ at 105.25 MHz.

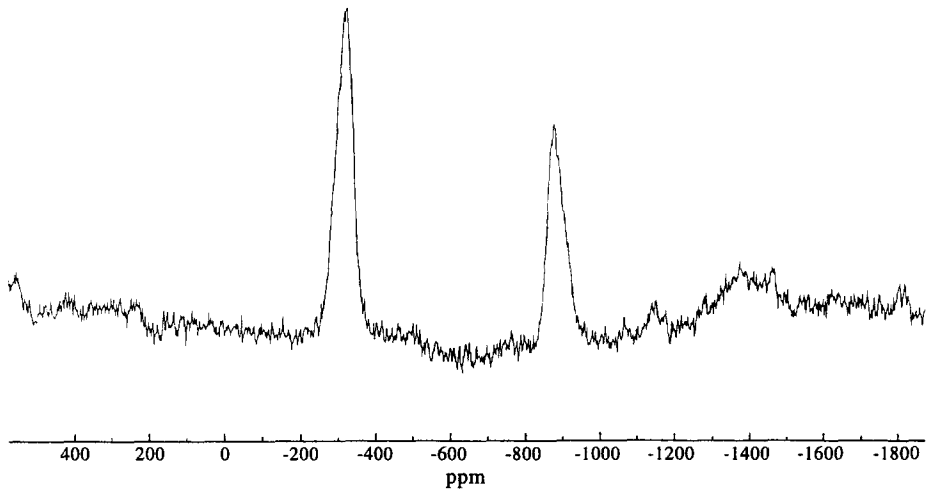

Fig. 7. Static ^{51}V NMR spectra of the single crystal $(NH_4)_2[VO_2NTA]$ at 105.25 MHz.

Table 3. Parameters[a] of chemical shift anisotropy and quadrupole coupling

δ_{iso} (ppm)	-507.0 ± 0.5
$\Delta\delta_{aniso}$ (ppm)	-800 ± 10
δ_1 (ppm)	-230 ± 10
δ_2 (ppm)	-250 ± 10
δ_3 (ppm)	-1040 ± 10
η_c	0.04 ± 0.02
QCC (MH_Z)	8.80 ± 0.05
η_Q	0.75 ± 0.02
α_C	$0 \pm 30°$
β_C	$0 \pm 2°$
γ_C	$0 \pm 30°$
$\delta_{solution}$ (ppm)	-504.3 ± 0.1

[a] Definitions of parameters are the same as in Ref. [26]. Reanalysis resulted in slightly different values from Ref. [26] for some parameters.

validity of the parameters obtained from analysis of the off-MAS spectrum. We obtained the large chemical shift anisotropy ($\Delta\delta_{aniso} = -800$ ppm) for ^{51}V atom. The components of the ^{51}V chemical shift tensor are very sensitive to the type of atoms in the first coordination sphere of the V atom. The isotropic chemical shift δ_{iso} of the powder complex, having five oxygens and a nitrogen is -507.0 ppm which is very close to the value obtained from solution measurement. The peak of the solid-state ^{51}V is essentially unshifted in frequency from the solution value except by outer-sphere interactions. The values of eulerian angles (α_C, β_C and γ_C) indicate that the principal axes of chemical shift tensor and quadrupole interaction tensor are almost the same.

Vanadium in a distorted octahedral environment gives spectra with the nearly axial symmetry of the chemical shift tensor (i.e. $\delta_1 \sim \delta_2 \neq \delta_3$), which reflects similar deshielding environments for both nitrogen and oxygen donor atoms. The stronger the distortion from a regular octahedron, the larger the value of $\Delta\delta$ is. Thus, for the vanadium complex, the anisotropy of the ^{51}V chemical shift is much more sensitive to the character of the local arrangement of donor atoms around the V atom, than the isotropic chemical shift δ_{iso} is. Distortion of the octahedron also results in an increase of the electric field gradient at the V nucleus, giving a large quadrupolar coupling constant (8.80 MHz). It seems to expect a correlation between $\Delta\delta$ and the quadrupolar coupling constant, e^2qQ/h, and the asymmetry parameter η_Q for metavanadates [15]. From the proximity of the ^{51}V chemical shifts in solution and solid-state complex, we speculate that the geometry in the solid-state might be retained in the solution. The static ^{51}V spectrum of a single crystal is shown in Fig. 7. Two distinguishable signals appeared, indicating two magnetically inequivalent but chemically identical vanadium sites. These sites are generated by the 2_1 symmetry operator within the unit cell [20].

Acknowledgement—One of us (M.-H.L.) wishes to thank Korea Research Foundation for the financial support through the Non-Directed Research Fund Program (1994).

REFERENCES

1. Chasteen, N. D., Ed. *Vanadium in Biological Systems*, Kluwer Academic Press, Dordrecht, Netherlands (1990).
2. Ehde, P. M., Andersson, I. and Pettersson, L., *Acta Chem. Scand. Ser. A*, 1986, **A40**, 489.
3. Tracey, A. S., Gresser, M. J. and Parkinson, K. M., *Inorg. Chem.*, 1987, **26**, 629.
4. Lee, M. -H. and Schaumburg, K., *Magn. Reson. Chem.*, 1991, **29**, 865.
5. Amos, L. W. and Sawyer, D. T., *Inorg. Chem.*, 1983, **11**, 2692.
6. Lee, M.-H. and T. S. O., *J. Korean Chem. Soc.*, 1983, **27**, 117.

7. Lee, M.-H., *Bull. Korean Chem. Soc.*, 1992, **13,** 22.
8. Lee, M.-H., and Hayashi, S., *Bull. Korean Chem. Soc.*, 1994, **15,** 685.
9. Calderia, M. M., Ramos, L. M., Oliveira, N. C. and Gil, V. M. S., *Can. J. Chem.*, 1987, **65,** 2434.
10. Lee, M.-H. and Kim, I.-W., *Bull. Korean Chem. Soc.*, 1993, **14,** 557.
11. Scheidt, W. R., Tsai, C. and Hoard, J. L., *J. Am. Chem. Soc.*, 1971, **93,** 3867.
12. Drew, R. E., Einstein, F. W. B. and Gransden, S. E., *Can. J. Chem.*, 1974, **52,** 2184.
13. Scheidt, W. R., Collins, D. M. and Hoard, J. L., *J. Am. Chem. Soc.*, 1971, **93,** 3873.
14. Scheidt, W. R., Countryman, R. and Hoard, J. L., *J. Am. Chem. Soc.*, 1971, **93,** 3878.
15. Lapina, O. B., Mastikhin, V. M., Shubin, A. A., Krasilnikov, V. N. and Zamaraev, K. I., *Prog. NMR Spectrosc.*, 1992, **24,** 457 and refs therin.
16. Oldfield, E., Kinsey, R. A., Montez, B., Ray, T. and Smith, K. A., *J. Chem. Soc. Chem. Commun.*, 1982, 254.
17. Hayashi, S. and Hayamizu, K., *Bull. Chem. Soc. Jpn.*, 1990, **63,** 961.
18. Rehder, D., *Bull. Magn. Reson.*, 1982, **4,** 33.
19. Eckert, H. and Wachs, I. E., *J. Phys. Chem.*, 1989, **93,** 6796.
20. Henry, N. F. M. and Lonsdale, K., Ed. *International Tables for X-Ray Crystallography*, Vol. I, Kynoch Press, Birmingham, England (1952).
21. Johnson, C. K., *ORTEP(II)*, Oak Ridge National Laboratory, Oak Ridge, Tenn. (1976).
22. Alderman, D. W., Solum, M. S., and Grant, D. M., *J. Chem. Phys.*, 1986, 4, 3717.
23. Herzfeld, J. and Berger, A. E., *J. Chem. Phys.*, 1980, **73,** 6021.
24. Hayashi, S. and Hayamizu, K., *Chem. Phys.*, 1991, **157,** 381.
25. Fenzke, D., Maess, B. and Pfeifer, H., *J. Magn. Reson.*, 1990, **88,** 172.
26. Hayashi, S., *Magn. Reson. Chem.*, 1996, **34,** 791.
27. Yamada, S., Nagase, J., Funahashi, S. and Tanaka, M., *J. Inorg. Nucl. Chem.*, 1976, **38,** 617.
28. Howarth, O. W., *Prog. NMR Spectrosc.*, 1990, **22,** 453.

Pergamon

PII: S0277-5387(97)00252-0

Polyhedron Vol. 17, No. 1, pp. 63–68, 1998
© 1997 Elsevier Science Ltd
All rights reserved. Printed in Great Britain
0277-5387/98 $19.00+0.00

Simple adducts of samarium and ytterbium diiodide: synthesis and molecular structures of $LnI_2(3,5\text{-lutidine})_4$ (Ln = Sm, Yb) and $YbI_2(4\text{-t-butylpyridine})_4$

Graham H. Maunder and Andrea Sella*

Christopher Ingold Laboratories, University College London, 20 Gordon Street, London WC1H 0AJ, U.K.

(Received 22 April 1997; accepted 9 June 1997)

Abstract—Reaction of LnI_2 (Ln = Sm, Yb) with substituted pyridines in THF gives good yields of the highly coloured complexes $[LnI_2(py)_4]$. The structures of complexes $[LnI_2(3,5\text{-lutidine})_4]$ (Sm, Yb) and $[YbI_2(4\text{-t-butylpyridine})_4]$ have been determined by X-ray crystallography and show simple octahedral coordination about the metal centre with *trans*-iodide ligands. © 1997 Elsevier Science Ltd

Keywords: lanthanide; crystal structure; pyridine; iodide; samarium; ytterbium.

The divalent iodides of ytterbium and samarium are increasingly used as one-electron reducing agents in organic synthesis in reactions which often have remarkably high stereoselectivity [1]. Indeed solutions of samarium iodide in THF have been available commercially for several years but are conveniently prepared by direct reaction of an excess of metal with diiodoethane [2]. From an inorganic point of view the iodides are among the most convenient starting materials for the exploration of the divalent state of these elements [3]. It came as something of a surprise to us to realize that the simple coordination chemistry of the iodides themselves remains essentially unexplored. Recent work by Yamanuchi has shown that the reducing power of the SmI_2 greatly increased upon addition of hexamethylphosphoramide, and that in some cases the chemoselectivity of the reactions are sometimes significantly altered [1]. Hou and Wakatsuki have recently reported the crystal structures of HMPA adducts of samarium and ytterbium and have suggested that the behaviour of HMPA may be unique [4]. In this note we report on our studies of the addition of pyridines to solutions of LnI_2 (Ln = Sm, Yb) and on the crystal structures of the 3,5-dimethylpyridine adducts of each.

*Author to whom all correspondence should be addressed.

RESULTS AND DISCUSSION

During one attempt to displace the coordinated THF from $[Tp^3\text{-}t\text{-Bu-5-MeSmI(THF)}_2]$ [5], a large excess of 3,5-lutidine (3,5-Me_2py) was added to a solution of this complex in toluene. Slow diffusion of 30/40 petrol into this solution gave black crystals (**1a**). IR spectroscopy of this product showed that it no longer contained a pyrazolylborate ligand. The ^{1}H NMR spectrum simply showed peaks due to the pyridine shifted slightly from their normal positions by the paramagnetic samarium centre.

The complex $[SmI_2(3,5\text{-}Me_2py)_4]$, **1a**, could also be prepared directly by reaction of SmI_2 in THF with an excess of 3,5-lutidine, and precipitates as black crystals upon diffusion of 30/40 petrol into this solution or by slow evaporation of THF.

$$SmI_2 + 4(3,5\text{-}Me_2py) \rightarrow [SmI_2(3,5\text{-}Me_2py)_4]$$

1a is very slightly soluble in benzene or toluene and gave broad ^{1}H NMR spectra. The corresponding ytterbium compound, $[YbI_2(3,5\text{-}Me_2py)_4]$ **2a**, was prepared similarly. The insolubility of **2a** precluded the recording of solution spectra. The ^{13}C CPMAS NMR spectrum however was sharp, consistent with the presence of the diamagnetic f^{14} ytterbium(II) ion. Attempts to prepare the corresponding complexes with pyridine gave deeply coloured, air-sensitive crys-

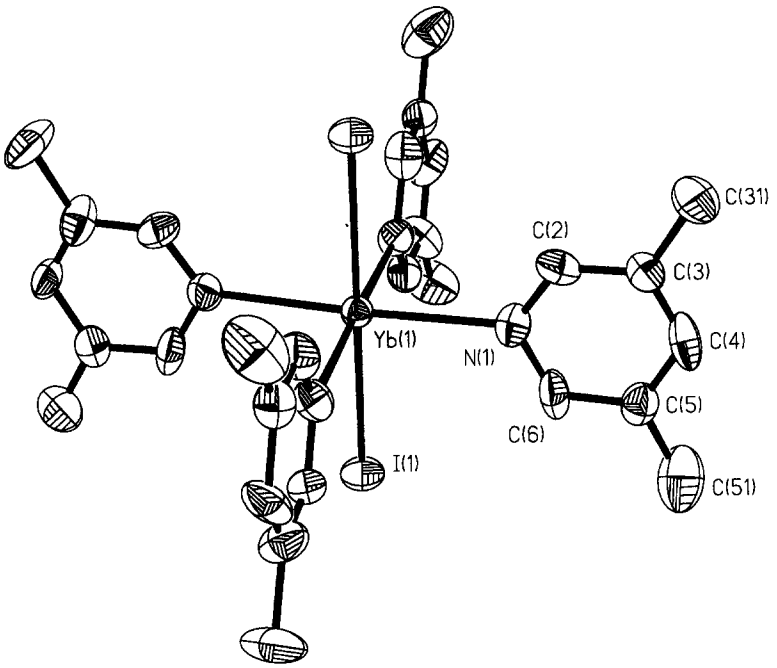

Fig. 1. ORTEP view of $YbI_2(C_7H_9N)_4$, **2a** (50% probability ellipsoids, H atoms are omitted for clarity).

talline solids which degraded rapidly when removed from the mother liquor, as a result of which consistent NMR spectra and elemental analyses were not obtained. In order to increase the solubility of the complex in non-polar solvents without however altering the steric demand of the pyridine, complexes were prepared with 4-*t*-butylpyridine. Addition of 4-*t*-butylpyridine to a solution of ytterbium diiodide in THF gave a dark purple solution from which crystals of **2b** were obtained upon addition of low boiling petroleum spirit. The elemental analyses of this complex was consistent with a stoichiometry of $[YbI_2(t\text{-}BuC_5H_4N)_5]$. Crystal structure determinations were therefore undertaken to compare the two coordination environments. The structures of **1a, 2a,** and **2b** were determined and to our surprise all three were found to be remarkably similar and will be discussed together.

Crystallographic studies

Crystals of **1a** and **2a** were obtained by slow diffusion of pentane into a tetrahydrofuran solution of the diiodide saturated with 3,5-lutidine yielding isomorphous crystals in the space group $I\bar{4}$. Each molecule has crystallographically imposed D_{4h} symmetry. The molecular structure of **2a** is shown in Fig. 1. The metal lies on the $\bar{4}$ site at the origin with the iodide ligands lying on the fourfold axis, and the plane of the pyridine ligands lying aligned parallel to that axis. **2b** crystallized from a similar mixture of solvents containing *t*-butylpyridine, in the space group $C2/c$. Thus only half the molecule is crystallographically unique. The data set collected for **1a** was of substantially lower quality than that of **2a** and only the heavy atoms could be refined anisotropically. For **2b** some unresolved disorder of the *t*-butyl groups somewhat reduces the reliability of the structure. The metal iodide distances are **1a** 3.221(1) Å (Ln = Sm), **2a** 3.132(1) Å and **2b** 3.120(2) Å (Ln = Yb), the differences being consistent with the contraction in ionic radius across the lanthanide series. For **1a** the distance is less than that in the six-coordinate compound $SmI_2(HMPA)_4$, 3.390(2) Å [4], as expected due to the rather large HMPA ligands. Furthermore the distance of **1a** is slightly shorter than for the two seven-coordinate complexes recently reported by Evans, $SmI_2(THF)(DME)_2$ [3.246(1) Å] and $[SmI_2(THF)_3(DME)]$, 3.233(1) Å [6], due to the reduced coordination number. A trivalent phosphine oxide complex $[Sm(OPMePh_2)_4I_2]I$ crystallized by Sen shows much shorter distances due to the smaller ion 3.077(1) Å [7]. For **2a** and **2b** the metal iodide distances are somewhat longer than in $YbI_2(THF)_4$ [3.103(1) Å] [8] suggesting the steric demand of the rigid pyridine groups to be intermediate between that of HMPA and the flexible THF group.

The metal nitrogen distances follow a similar pattern, **1a** 2.708(10) (Ln = Sm), **2a** 2.586(3) and **2b** 2.56(2) Å (Ln = Yb). Although few samarium pyridine complexes have been isolated, octahedral coordination has been found for the majority of tetrakis–pyridine divalent ytterbium derivatives, including borohydrides, thiolates, selenolates, which have been crystallographically characterized and show similar Yb—N bond distances $[Yb(BH_4)_2(C_5H_5N)_4]$ {av. 2.573(5)} [9], $[Yb(SePh)_2(C_5H_5N)_4]$ {av. 2.532(6) Å} [10], $[Yb(SPh)_2(C_5H_5N)_4]$ {av. 2.549(9) Å} [11].

Intriguingly the tellurolate analogue is seven-coordinate $[Yb(TePh)_2(C_5H_5N)_5]$, Yb—N = 2.61(1) Å [10]. Other divalent ytterbium complexes with pyridine ligands also exhibit similar Yb—N distances: $[Yb(C_5H_5N)_5(CH_3CN)_2]^{2+}$ 2.50(5) Å [12], $[Yb(\eta\text{-}C_5Me_5)_2(C_5H_5N)_2]$ 2.565(3) Å [13] $[(\eta^8\text{-}C_8H_8)Yb(C_5H_5N)_3]$ (av.) 2.58(2) Å [14].

DISCUSSION

All three compounds adopt a structural motif which is quite common and a range of six-coordinate compounds have been reported previously: $[Ti(C_5H_5N)_2I_2]I$ [15], [Co(3,5-dimethylpyridine)$_2I_2$] [16], $[Cu(C_5H_5N)_2I_2]$ [17], $[Ni(C_5H_5N)_2I_2]$ [18], $[Cd(C_5H_5N)_2I_2]$ [19], and [Sr(3,5-dimethylpyridine)$_2I_2$] [20]. The observation of six rather than seven coordination in the crystal structure of **2b** as had been expected from the elemental analysis suggests that a crystal unrepresentative of bulk of the material may have been chosen. Nevertheless, the observation of six-coordinate complexes for both **1** and **2,** as for the other lanthanide(II) iodides, regardless of ionic radius, goes some way towards accounting for the stereoselectivities observed for divalent lanthanide reagents. Although the reactivity of the divalent lanthanides is the result of one-electron transfer, the possibility of substrates binding to a stereochemically rigid six-coordinate metal coordination sphere should not be discounted.

The remarkable colour changes which occur upon coordination of pyridine are intriguing. Ytterbium diiodide is canary yellow both in THF solution and in the solid state with absorptions at 390, 342 and 307 nm which have been attributed previously to electronic transitions from the 4*f* and 5*d* orbitals and are very intense by virtue of being fully allowed [21]. The colour is virtually unaltered by substitution by other anionic ligands such as borohydride [22] or a single pyrazolylborate ligand [23]. Although the structure of these complexes is not known in solution it is reasonable to conclude that such ligands do not alter the energy of the *d*-orbitals significantly. In contrast, the recently prepared hydrocarbyl, alkoxide and amide complexes tend to be red, although the absorption spectra have not been reported, this may well arise from perturbation of the *d* levels by these strongly electron releasing groups. For all such compounds, addition of pyridine results in the appearance of a deep red/purple colour* which has been attributed by Brennan to metal to ligand charge transfer transitions. In the case of **1a** there is a strong absorption at 450 nm with a shoulder at 660 nm while in **2a** the corresponding bands are at 367 and 573 nm respectively, the shifts being consistent with the changes in reduction potential of the metal itself.

* $Yb(OR)_2(pyr)_n$ has been reported to be green.

EXPERIMENTAL

All preparations and manipulations were carried out using dry box techniques in an atmosphere of dinitrogen [24]. Oxygen-free nitrogen was purified by passage over columns containing 3 Å molecular sieves and MnO [25]. All solvents were pre-dried over 5 Å molecular sieves or sodium wire and distilled under nitrogen from appropriate drying agents {Na (toluene), K (benzene, tetrahydrofuran), Na/K alloy (petroleum ether b.p. 40–60°C, pentane, diethyl ether), CaH_2 (CH_2Cl_2)} before use. Pyridines were dried and distilled from calcium hydride before use. Ytterbium iodide was prepared from ytterbium metal (Aldrich) and ammonium iodide in liquid ammonia [26]. Samarium iodide was prepared from samarium metal and diiodoethane in THF [13].

Infrared spectra were recorded as KBr pellets or in $CDCl_3$ solution on a Nicolet 205 FTIR spectrometer. ^1H and ^{13}C spectra in solution were recorded on Varian XL-200 and VXR-400 spectrometers at 200 and 400 and 100.6 MHz, respectively. Spectra were calibrated using residual proton (^1H) and solvent resonances (^{13}C) respectively and chemical shifts are reported relative to tetramethylsilane. Elemental microanalyses were determined by Mr Alan Stones of the UCL Analytical Services.

Preparation of $[SmI_2(3,5\text{-}Me_2py)_4]$

$SmI_2 \cdot 1.65THF$ (0.098 g, 0.187 mmol) was dissolved in THF (5 cm^3) and 3,5-dimethylpyridine (3,5-Me_2py; *ca* 0.6 g, 5.6 mmol) was added dropwise to give a dark green solution. This was layered with 30/40 petrol (10 cm^3) and, after equilibration, black block-like crystals were deposited. Following removal of solvent, the product was washed with 30/40 petrol (3×2 cm^3) to leave 0.116 g (0.139 mmol, 74%) of $[SmI_2(3,5\text{-}Me_2py)_4]$.

Solid state CPMAS ^{13}C NMR: δ 147, 114 (aromatic C); 13 (Me); (all resonances were broad, *ca* 1000 Hz). UV–vis (KBr): 450 nm; 660 nm (br sh). Analysis (%) calc. for $SmC_{28}H_{36}N_4I_2$: C, 40.38; H, 4.36; N, 6.73. Found: C, 40.22; H, 4.44; N, 6.90.

Preparation of $[YbI_2(3,5\text{-}Me_2py)_4]$

$YbI_2 \cdot 1.7THF$ (0.162 g, 0.295 mmol) was dissolved in THF (5 cm^3). 3,5-Dimethylpyridine (*ca* 0.5 g, 4.7 mmol) was added dropwise giving an immediate colour change from pale yellow to dark red. The solution was layered with 30/40 petrol (10 cm^3) and left to equilibrate for several days. Large black block-like crystals were formed, which were washed with 30/40 petrol (3×2 ml). Yield: 0.164 g (0.192 mmol, 65%).

Table 1. Crystal data, structure solution and refinement for $SmI_2(C_7H_9N)_4$ **1a**, $YbI_2(C_7H_9N)_4$ **2a**, and $YbI_2(C_9H_{13}N)_4$ **2b**

Compound number	**1a**	**2a**	**2b**
Chemical formula	$C_{28}H_{36}I_2N_4Sm_1$	$C_{28}H_{36}I_2N_4Yb_1$	$C_{36}H_{52}N_4I_2Yb_1$
Molecular weight	832.83	855.47	967.69
T (K)	293	293	293
Crystal system, space group	Tetragonal $I\bar{4}$	Tetragonal $I\bar{4}$	Monoclinic $C2/c$
a (Å)	9.833(1)	9.711(1)	24.595(3)
b (Å)	9.833(1)	9.711(1)	10.258(3)
c (Å)	17.216(3)	17.124(6)	17.061(5)
α (°)	90	90	90
β (°)	90	90	107.74(3)
γ (°)	90	90	90
Volume	1665(1)	1615(1)	4100(1)
Z	2	2	4
Density (calc.)	1.66	1.64	1.55
Absorption coefficient μ (cm^{-1})	36.2	48.0	38.0
$F(000)$	800	816	2184
Reflections for cell refinement	29($15.1 \leqslant 2\theta \leqslant 29.2$)	25($19.3 \leqslant 2\theta \leqslant 33.9$)	26($20.8 \leqslant 2\theta \leqslant 30.0$)
Crystal colour	Black	Black	Black
Crystal size (mm)	$0.40 \times 0.25 \times 0.35$	$0.60 \times 0.35 \times 0.22$	$0.56 \times 0.46 \times 0.36$
Data collection method	ω–2θ	ω–2θ	ω
2θ range for data collection	5–50	5–50	5–50
Index ranges (maximum)	$0 \leqslant h \leqslant 12$, $0 \leqslant k \leqslant 12$, $0 \leqslant l \leqslant 21$	$0 \leqslant h \leqslant 13$, $0 \leqslant k \leqslant 13$, $-23 \leqslant l \leqslant 23$	$0 \leqslant h \leqslant 30$, $0 \leqslant k \leqslant 13$, $-21 \leqslant l \leqslant 21$
Reflections collected	1141	4129	3610
Independent reflections	848	1855	2662
R_{int}	0.0313	0.0316	0.0350
Observed reflections	558 [$I > 3\sigma(I)$]	1691 [$I > 3\sigma(I)$]	1906 [$I > 3\sigma(I)$]
Max and Min transmission	0.949, 0.692	1.000, 0.732	0.989, 0.695
Structure solution	Patterson	Direct methods	Direct methods
Refinement method (see text)	F	F	F
Weighting parameters	0.000423[a]	0.001958[a]	0.014517
Parameters	40	80	180
Final R indices (defined below)	0.0381[b]/0.0384[c]	0.00263[b]/0.0316[c]	0.0527[b]/0.0604[c]
Largest shift/esd in final refinement	0.017	0.177	0.088
Largest difference peak/hole	+0.573/−0.663	+1.44/−2.32	+0.936/−1.428

[a] $w^{-1} = \sigma(F^2) + w(F)^2$.
[b] $R = \{\Sigma| |F_o| - |F_c| |/\Sigma|F_o|\}$.
[c] $R_w = \{\Sigma[w(|F_o| - |F_c|)^2]/\Sigma[w|F_o|^2]\}^{1/2}$.

Table 2. Selected bond lengths (Å) and angles (°) for **1a** and **2a**

Sm(1)—I(1)	3.221(1)	Yb(1)—I(1)	3.132(1)
Sm(1)—N(1)	2.708(10)	Yb(1)—N(1)	2.586(3)
I(1)—Sm(1)—N(1)	87.2(5)	I(1)—Yb(1)—N(1A)	88.7(2)
I(1)—Sm(1)—I(1A)	180.0(1)	I(1)—Yb(1)—I(1A)	180.0(1)
I(1)—Sm(1)—N(1A)	92.8(5)	I(1)—Yb(1)—N(1)	91.3(2)
N(1)—Sm(1)—N(1A)	90.1(1)	N(1)—Yb(1)—N(1A)	90.0(1)
I(1)—Sm(1)—N(1B)	87.2(5)	I(1)—Yb(1)—N(1A)	88.7(2)
N(1)—Sm(1)–N(1B)	174.4(10)	N(1)—Yb(1)—N(1B)	177.4(4)

Table 3. Selected bond lengths (Å) and angles (°) for **2b**

Yb(1)—I(1)	3.120(2)
Yb(1)—N(1)	2.552(13)
Yb(1)—N(2)	2.563(10)
I(1)—Yb(1)—N(1)	88.3(2)
I(1)—Yb(1)—N(2)	89.3(2)
N(1)—Yb(1)—N(2)	86.8(4)
I(1)—Yb(1)—I(1A)	180.0(1)
N(1)—Yb(1)—I(1A)	91.7(2)
N(2)—Yb(1)—I(1A)	90.7(2)
N(1)—Yb(1)—N(1A)	180.0(1)
N(2)—Yb(1)—N(1A)	93.2(4)

Analysis (%) calc. for $YbC_{28}H_{36}N_4I_2$: C, 39.31; H, 4.24; N, 6.55; I, 29.67. Found: C, 39.15; H, 4.33; N, 6.84; I, 29.25. Solid state CPMAS ^{13}C NMR: δ 149.1, 137.8, 133.8 (aromatic C); 20.3 (Me). UV–vis (KBr): 367 nm; 573 nm.

Preparation of $SmI_2(py)_n$

$SmI_2 \cdot 1.65THF$ (0.200 g, 0.382 mmol) was dissolved in THF (20 cm^3) and pyridine (*ca* 0.60 g, 7.6 mmol) was added drop-wise, giving an immediate colour change from dark blue to dark green. The solution was layered with 30/40 petrol (20 cm^3) and left to equilibrate for several days. Large black crystals were formed which desolvated rapidly upon removing the solvent and washing with 30/40 petrol (3 × 2 ml). Yield: *ca* 0.25 g.

Preparation of $YbI_2(py)_n$

YbI_2 (0.400 g, 0.897 mmol) was dissolved in THF (20 cm^3) and Yb metal removed by vacuum filtration. Pyridine (py; *ca* 1.0 g, 13 mmol) was then added dropwise, giving an immediate colour change from pale yellow to dark red. The solution was layered with 30/40 petrol (20 cm^3) and left to equilibrate for several days. Large black crystals were formed which desolvated and turned dark brown/red on the surface upon removing the solvent and washing with 30/40 petrol (3 × 2 cm^3). Yield: 0.49 g.

Analysis (%) calc. for $YbC_{17}H_{17}N_{3.4}I_2$ ($YbI_2(py)_{3.4}$): C, 29.35; H, 2.46; N, 6.84. Found: C, 29.31; H, 2.56; N, 6.86.

Preparation of $[SmI_2(4\text{-}Bu^tpy)_4]$

$SmI_2 \cdot 1.65THF$ (0.212 g, 0.405 mmol) was dissolved in THF (5 cm^3) and *tert*-butylpyridine (*ca* 1.0 g, 7.4 mmol) was added. The dark green solution was layered with 30/40 petrol (10 cm^3) and, after equilibration, large black blocks were deposited which were washed with 30/40 petrol (3 × 2 cm^3). The surface of the crystals became opaque on standing. Yield: 0.225 g (0.238 mmol, 59%).

^1H NMR (C_6D_6): δ 4.36 (s, $w_{1/2}$ = 50 Hz, 8H, 2,6-H py); 2.90 (s, $w_{1/2}$ = 21 Hz, 8H, 3,5-H py); −0.27 (s, 36H, CMe_3). ^{13}C NMR (C_6D_6): δ 225.3 (d, $w_{1/2}$ = 16 Hz, 2-C py); 175.0 (s, 4-C py); 103.5 (d, 3-C py); 33.9 (q, CMe_3 py); 28.2 (s, CMe_3 py). UV–vis (toluene): 381 nm (ε = 700); 443 nm (ε = 700); 642 nm (ε = 500). Analysis (%) calc. for $SmC_{36}H_{52}N_4I_2$: C, 45.76; H, 5.55; N, 5.93. Found: C, 44.13; H, 5.28; N, 5.99.

Preparation of $[YbI_2(4\text{-}Bu^tpy)_4]$

YbI_2 (0.168 g, 0.385 mmol) was dissolved in THF (5 cm^3) and Yb metal removed by vacuum filtration. *tert*-Butylpyridine (*ca* 0.5 g, 3.7 mmol) was added dropwise, causing an immediate colour change from pale yellow to dark red. The solution was layered with 30/40 petrol (10 cm^3) and left to equilibrate for several days. Black crystals were formed which were washed with 30/40 petrol (3 × 2 cm^3) and dried under dynamic vacuum. Yield: 0.210 g (0.217 mmol, 56%). ^1H NMR (C_6D_6): δ 9.73 (s, $w_{1/2}$ = 17 Hz, 8H, 2,6-H py); 6.68 (s, $w_{1/2}$ = 14 Hz, 8H, 3,5-H py); 0.79 (s, 36H, CMe_3). ^{13}C NMR (C_6D_6): δ 161.3 (s, 4-C py); 151.2 (d, 2-C py); 121.1 (d, 3-C py); 34.5 (s, CMe_3 py); 30.0 (q, CMe py). UV–vis (toluene): 359 nm (ε = 800); 410 nm (ε = 800); 480 nm (ε = 700). Analysis (%) calc. for $YbC_{36}H_{52}N_4I_2$: C, 44.68; H, 5.42; N, 5.79. Found: C, 50.31; H, 5.92; N, 6.51.

X-ray crystallography

Data collection and processing for 1*a*, 2*a*, *and* 2*b*. All data were collected on a Nicolet R3mV four-circle diffractometer using graphite-monochromated Mo-K_α (λ = 0.71073 Å) radiation. Crystals were mounted in Lindemann glass capillaries in a nitrogen filled glovebox. Data were corrected for Lorenz polarization effects, and for absorption by a semi-empirical method based on ψ-scan data. The intensity of three check reflections measured every 97 reflections showed no decay over the course of the data collection.

Structure solution and refinement for 1*a*, 2*a*, *and* 2*b*. Crystallographic calculations were carried out with the SHELXTL PLUS suite of programmes on a MicroVAX II computer. The structures were solved by Patterson or Direct methods and developed by alternating cycles of full-matrix least squares refinement and difference Fourier techniques. For **2a**, all non-hydrogen atoms were refined anisotropically and hydrogen atoms were placed in calculated positions with one overall, refined, [U_{iso} = 0.08(2) Å^2]. For **1a**, the quality of the data set did not allow anisotropic refinement of any atom other than the samarium and iodine. Hydrogen atoms were placed in calculated positions as for **2a**. For **2b**, the *t*-butyl groups were found to be disordered and were therefore refined as

two sets of interpenetrating groups with the methyl to central carbon distance set to 1.55 ± 0.001 Å and the Me–Me distance set at 2.50 ± 0.01 Å. The occupancies of the pairs of groups were refined independently. Atomic coordinates, bond lengths and angles, and displacement parameters have been deposited with the Cambridge Crystallographic Data Centre (CCDC). See Information for Authors, Issue No. 1.

Acknowledgements—We are grateful to the Royal Society and the University of London Central Research Fund for support and to the EPSRC for a studentship to GHM. We are grateful to Dr G. Hogarth for access to his glove box and to Dr D. A. Tocher for assistance with the crystal structures and to Dr John Brennan for illuminating discussions.

REFERENCES

1. Molander, G. A., *Chem. Rev.*, 1992, **92,** 29; Imamoto, T., *Lanthanides in Organic Synthesis*, Academic Press, London, 1994.
2. Kagan, H. B., *J. Am. Chem. Soc.*, 1980, **102,** 2693.
3. Cloke, F. G. N., *Chem. Soc. Rev.*, 1993, 17.
4. Hou, Z. and Wakatsuki, Y., *J. Chem. Soc., Chem. Commun.*, 1994, 1205.
5. Maunder, G. H. and Sella, A., unpublished observations.
6. Evans, W. J., Gutersheim, T. S. and Ziller, J. W., *J. Am. Chem. Soc.*, 1995, **117,** 8999.
7. Sen, A., Chebolu, V. and Holt, E. M., *Inorg. Chim. Acta*, 1986, **118,** 87.
8. van den Hende, J. R., Hitchcock, P. B., Holmes, S. A., Lappert, M. F., Leung, W.-P., Mak, T. C. W. and Prashar, S., *J. Chem. Soc., Dalton Trans.*, 1995, 1427.
9. White, J. P., Deng, H. and Shore, S. G., *Inorg. Chem.*, 1991, **31,** 2337.
10. Brewer, M., Khasnis, D., Buretea, M., Berardini, M., Emge, T. J. and Brennan, J. G., *Inorg. Chem.*, 1994, **33,** 2743.
11. Lee, J., Brewer, M., Berardini, M. and Brennan, J. G., *Inorg. Chem.*, 1995, **34,** 3215.
12. White III, J. P., Deng, H., Boyd, E. P., Gallucci, J. and Shore, S. G., *Inorg. Chem.*, 1994, **33,** 1685.
13. Tilley, T. D., Andersen, R. A., Spencer, B. and Zalkin, A., *Inorg. Chem.*, 1982, **21,** 2647.
14. Wayda, A. L., Mukerji, I., Dye, J. L. and Rogers, R. D., *Organometallics*, 1987, **6,** 1328.
15. Troyanov, S. I., Mizo, G. N., Rybakov, V. B. and Budkina, K. V., *Koord. Khim*, 1990, **16,** 466.
16. Keniskas, J., Leskela, M., Kennessey, J., Werner, P. E. and Liptay, G., *Acta Chim. Scand.*, 1994, **48,** 951.
17. Durand, P. B. and Holt, E. M., *Acta Cryst. Sect. C*, 1995, **51,** 850.
18. Han, D. J., Bordner, J. and Schreiner, A. F., *Inorg. Chim. Acta*, 1973, **7,** 637.
19. Ito, M., Shibata, T. and Saito, Y., *Acta Cryst. Sect. C*, 1980, **40,** 2041.
20. Water, A. F. and White, A. H., *Austr. J. Chem.*, 1996, **49,** 35.
21. Namy, J. L., Girard, P., Kagan, H. B. and Caro, P. E., *New J. Chem.*, 1981, **5,** 479.
22. Karamallakis, H. and Sella, A., unpublished results.
23. Hasinoff, L., Takats, J. and Zhang, X. W., *J. Am. Chem. Soc.*, 1994, **116,** 8833.
24. McNally, S., and Cooper, N. J., in *Experimental Organometallic Chemistry: A Practicum in Synthesis and Characterization*, A. L. Wayda and M. Y. Darensbourg, eds. ACS Symposium Series v. 357, American Chemical Society, Washington, D.C. (1987).
25. Shriver, D. F. and Drezdzon, M. A., *The Manipulation of Air-Sensitive Compounds*, 2nd Edn., Wiley, New York (1986).
26. Boncella, J., Berg, D. J. and Andersen, R. A., *Inorg. Synth.*, 1991, **27,** 146.

Pergamon

PII: S0277-5387(97)00248-9

Polyhedron Vol. 17, No. 1, pp. 69–73, 1998
© 1997 Elsevier Science Ltd
All rights reserved. Printed in Great Britain
0277-5387/98 $19.00+0.00

Synthesis and characterization of bis(1,1,1,5,5,5,-hexafluoropentane-2,4-ionato) strontium and barium adducts with O- and N- ancillary ligands; crystal structure of $Sr(HFAC)_2 \cdot (BPY)_2$

Yingzhong shen,[a] Yi Pan,[a]* Gang Dong,[a] Xiangzhen Sun[a] and Xiaoying Huang[b]

[a] Department of Chemistry, Nanjing University, Nanjing 210093, P. R. China

[b] State Key Laboratory of Structure Chemistry, Fuzhou 250003, P. R. China

(Received 11 April 1997; accepted 9 June 1997)

Abstract—Complexes of $M(hfac)_2 \cdot Ln$ [M = Sr, n = 1, L = tetraglyme, db24c8; n = 2, L = bpy, phen; M = Ba, n = 1, L = tetraglyme, db24c8] have been prepared by *in situ* reactions of MX_2 (X = OH, OAc) with Hhfac in the presence of the ancillary ligands in aqueous ethanol in high yields and characterized by ^1H NMR, IR, mass spectrometry and elemental analysis. A molecular structure of the complex $Sr(hfac)_2 \cdot (bpy)_2$ has been determined by X-ray single crystal analysis. © 1997 Elsevier Science Ltd

Keywords: strontium; barium; MOCVD; β-diketones; bipyridine.

There has been considerable interest recently in the chemistry of alkaline–earth metal β-diketonates, mostly because of their potential application as MOCVD precursors in the epitaxy of metal oxide thin films [1–6]. It is found that fluorocarbon-based β-diketonates are among the best performing precursors in terms of their stability and volatility [7–9]. Coordination of the appropriate ancillary ligands due to the β-diketonates could increase their volatility [10–13]. The free ancillary ligands applied so far are mostly polyethers. Here, we hope to report two nitrogen donor ligands coordinated complexes $Sr(hfac)_2(bpy)_2$ and $Sr(hfac)_2(phen)_2$ (hfac = 1,1,1,5,5,5-hexafluoropentane-2,4-dinato; bpy = 2,2′-bipyridine-N,N′, phen = 1,10-phenanthroline-N^1,N^{10}).

Syntheses of the complexes $M(hfac)_2Ln$ were usually performed under anaerobic conditions. We [15] found that the preparation could be easily carried out in aqueous ethanol solution with the metallic hydroxides or acetates as the starting material. Whilst our work was proceeding, Malandrino *et al.* [4] reported a similar one-step procedure for $M(hfac)_2 \cdot$ tetraglyme (M = Ca, Sr, Ba). In this paper, we hope to present the detailed procedures of our preparation. Apart from the two nitrogen donor ligand coordinated adducts mentioned above, several polyether coordinated complexes $M(hfac)_2$(polyether) [M = Sr, Ba; polyether = tetraglyme, dibenzo-24-crown-8 (db24c8)] have also been prepared.

All complexes obtained have been characterized by ^1H NMR, IR, mass spectrometry and elemental analysis. $Sr(hfac)_2(bpy)_2$ has also been characterized by single crystal structure analysis.

EXPERIMENTAL

All reagents used were of commercial quality. Elemental analyses were performed on a Perkin–Elmer 240 elemental analysis instrument. ^1H NMR spectra were recorded on a Bruker AM-500 and JEOL PMX-60SI spectrometer with TMS as internal standard. IR spectra were obtained as KBr pellets on 5DX FT-2 spectrometer. Mass spectra were obtained on

* Author to whom correspondence should be addressed.

a VG ZAB-HS GC-MS spectrometer. Melting and boiling points are given without correction.

Preparation of Sr(hfac)$_2$ · tetraglyme

Hhfac (0.833 g, 4.0 mmol) was added dropwise to a stirred solution of $Sr(OH)_2 \cdot 8H_2O$ (0.532 g, 2.0 mmol) or $Sr(OAc)_2$ (0.411 g, 2.0 mmol) in aqueous ethanol solution (20 cm^3, 35% *aq.* EtOH) in 5 min. After stirring for 10 min, tetraglyme (0.444 g, 2.0 mmol) in ethanol (4 ml) was added dropwise. Stirring was continued for 20 min. The product as white powder was isolated by filtration dried *in vacuo* at 60°C for 3 h. The complex sublimed readily at 140–145°C/0.03 mmHg. Yield: 1.32 g (91.1%), mp: 137–139°C. Anal. Calc. for $C_{20}H_{24}O_9F_{12}Sr$: C, 33.18; H, 3.34. Found: C, 33.19; H, 3.34%. The ^{1}H NMR and IR data are in good agreement with those reported [6].

Preparation of Ba(hfac)$_2$ · tetraglyme

Prepared as described for Sr(hfac)$_2$ · tetraglyme from Hhfac (0.833 g, 4 mmol), $Ba(OH)_2 \cdot 8H_2O$ (0.631 g, 2.0 mmol) or $Ba(OAc)_2$ (0.511 g, 2.0 mmol) and *aq.* EtOH. Yield: 1.42 g (91.7%), m.p.: 147–150°C. The complex sublimed readily at 140–145°C/0.03 mm Hg. Anal. Calc. for $C_{20}H_{24}O_9F_{12}Ba$: C, 31.04; H, 3.13. Found: C, 31.37; H, 3.14%. The ^{1}H NMR and IR data are in good agreement with those reported [16].

Preparation of Sr(hfac)$_2$ · (bpy)$_2$

Hhfac (0.833 g, 4.0 mmol) was added dropwise, with stirring to a solution of $Sr(OH)_2 \cdot 8H_2O$ (0.532 g, 2.0 mmol) in aqueous ethanol solution (20 cm^3, 35% *aq.* EtOH). After stirring for 10 min, a solution of bpy (0.624 g, 4.0 mmol) in water (10 cm^3) was added. The resulting heavy turbid solution was filtered. The product obtained was recrystallized with ethanol and dried *in vacuo* at 60°C for 3 h. Yield: 1.50 g (92.1%). The complex sublimed at 165–170°C/0.10 mm Hg. Melting point: 179–181°C. Anal. Calc. for $C_{30}H_{18}N_{14}F_{12}O_4Sr$: C, 44.24; H, 2.23; N, 6.88. Found: C, 44.20; H, 2.14; N, 7.19%. IR data: 3400 (m), 3100 (w), 1691 (vs), 1605 (m), 1532 (m), 1484 (m), 1435 (m), 1320 (m), 1260 (s), 1139 (vs), 1084 (m), 1005 (m), 800 (m), 757 (m), 660 (m), 576 (m), 539 (m), 490 (w), 430 (w) cm^{-1}. ^{1}H NMR: 8.71 (d, 4H J = 4.3 Hz), 7.95 (t, 4H, J = 7.0 Hz), 7.45 (dd, 4H, J = 4.97, 7.03 Hz), 8.45 (d, 4H, J = 7.02), 5.66 (s, 2H) ppm. MS data: 295 (6.7%), 419 (3.4%), 107 (100%), 147 (15.6%), 157 (15.3%), 195 (22.9%), 451 (1.5%), 623 (1.3%), 815 (0.2%).

Preparation of Sr(hfac)$_2$ · (phen)$_2$

Prepared as described for Sr(hfac)$_2$ · (bpy)$_2$ from Hhfac (0.833 g, 4.0 mmol), $Sr(OH)_2 \cdot 8H_2O$ (0.532 g, 2.0 mmol) and phen (0.720 g, 4.0 mmol). The adduct was purified by recrystallization from ethanol. Yield: 1.54 g (89.3%). M.p. 269–271°C. Anal. Calc. for $C_{34}H_{18}N_{14}F_{12}O_4Sr$: C, 47.35; H, 2.10; N, 6.50. Found: C, 47.15; H, 2.13; N, 6.46%. IR data: 3400 (m), 1671 (vs), 1526 (s), 1423 (m), 1345 (w), 1260 (s), 1193 (s), 1139 (vs), 1084 (m), 45 (m), 860 (m), 848 (m), 836 (m), 794 (m), 733 (m), 666 (s), 582 (m), 527 (w). ^{1}H NMR: 9.20 (d, 2H, J = 4.3), 7.8 (dd, 2H, J = 8.33, 4.73), 8.53 (d, 2H, J = 8.39), 7.99 (s, 1H), 5.64 (s, 1H). MS data: 655 (6%), 475 (9.6%), 287 (12.5%), 217 (55.1%), 181 (67.4), 109 (32.8%), 91 (100%).

Preparation of Sr(hfac)$_2$ · db24c8

Prepared as described for Sr(hfac)$_2$ · (bpy)$_2$ from Hhfac (0.833 g, 4.0 mmol), $Sr(OH)_2 \cdot 8H_2O$ (0.532 g, 2.0 mmol) and dibenzo-24-crown-8 (0.897 g, 2.0 mmol in 10 ml ethanol). The adducts was recrystallized from ethanol. Yield: 1.67 g (87.9%). M.p.: 246–247°C. Anal. Calc. for $C_{34}H_{34}F_{12}O_{12}Sr$: C, 42.96; H, 361. Found: C, 42.72; H, 3.53. IR data: 2984 (w), 1669 (s), 1554 (s), 1527 (s), 1449 (m), 1461 (w), 1308 (w), 1259 (vs), 1204 (s), 1138 (vs), 1089 (m), 1050 (m), 947 (w), 788 (w), 775 (w), 662 (m), 575 (m) cm^{-1}. ^{1}H NMR: 6.83–7.13 (s, 8H), 5.67 (s, 2H), 3.73–4.33 (m, 16H). MS data: 743 (11.8%), 448 (32%), 208 (2.8%).

Synthesis of Ba(hfac)$_2$ · db24c8

Prepared as described for Sr(hfac)$_2$ · (bpy)$_2$ from Hhfac (0.833 g, 4.0 mmol), $Ba(OH)_2 \cdot 8H_2O$ (0.631 g, 2.0 mmol) and db24c8 (0.897 g, 2.0 mmol in 10 cm^3 ethanol). The adduct was recrystallized from ethanol. Yield: 1.80 g (90.0%). M.p. 246–247°C. Anal. Calc. for $C_{34}H_{34}F_{12}O_{12}Ba$: C, 40.82, H, 3.43. Found: C, 40-.06, H, 3.23. IR data: 2937 (w), 2894 (s), 1712 (m), 1669 (s), 1543 (s), 1499 (s), 1461 (m), 1253 (vs), 1198 (vs), 1133 (vs), 1045 (m), 947 (m), 783 (m), 755 (w), 662 (m) cm^{-1}. ^{1}H NMR: 6.83–7.16 (s, 8H), 5.6 (s, 2H), 3.84–4.5 (m, 16H). MS data: 792 (5.2%), 5.85 (0.2%), 448 (31.1%), 345 (2.1%).

X-ray determination of Sr(hfac)$_2$ · (bpy)$_2$

The crystal was obtained from ethanol. Crystallographic data are summarized in Table 1. The structure was solved by the direct methods using MITHRIL [17] and subsequent Fourier techniques. Hydrogens were added geometrically (before the final amendment). All calculations were performed using TEXSAN [18]. ORTEPII [9] was used to produce the figures and CAD-4 software [20] was used for data collection and cell refinement.

RESULTS AND DISCUSSION

Reactions of Hhfac with both $M(OAc)_2$ and $M(OH)_72$ (M = Sr and Ba) in the presence of the

Table 1. Crystal data for $Sr(hfac)_2 \cdot (bpy)_2$

Formula	$C_{30}H_{18}F_{12}N_4O_4Sr$
Space group	$C2/c$ (#15)
Crystal system	monoclinic
a (Å)	28.105 (2)
b (Å)	16.345 (2)
c (Å)	17.106 (3)
β (°)	121.926 (9)
V (Å^3)	6669 (2)
Z	8
Crystal dimension (mm)	$0.6 \times 0.38 \times 0.28$
Crystal colour	colourless
D(calc) (g/cm^{-3})	1.622
μ(Mo-K_α) (cm^{-1})	16.72
T (°C)	23
T(max)/T(min)	1.169
Data collection:	
Diffractometer	Enraf–Nonius CAD4
Monochromator	Graphite
Radiation	Mo-K_α
R_{int}	0.041
θ_{max} (°)	26
Index range (°)	$0 \leqslant h \leqslant 34$, $0 \leqslant k \leqslant 20$, $-21 \leqslant l \leqslant 21$
Scan speed (°/min)	5.49
Reflections collected	6903
Independent collections	6779
Independent reflections observed	3241
Standard reflections	3std/300 reflns
Variations in standards	2.2%
Refinement:	
R(F)	0.058
wR	0.060
S	1.38
No. of reflections used in refinement	3241
No. of parameters refined	541
$\Delta\rho_{max}$ (e Å^{-3})	0.55
$\Delta\rho_{min}$ (e Å^{-3}	−0.29
$(\Delta/\sigma)_{max}$	0.66

stoichiometric free ancillary ligands proceeded very smoothly in *aq.* ethanol. Complexes $M(hfac)_2 \cdot Ln$ (M = Sr, $n = 1$, L = tetraglyme, db24c8; $n = 2$, L = bpy, phen; M = Ba, $n = 1$, L = tetraglyme, db24c8) were isolated in nearly quantitative yields. As both the metallic salts and the ligands used were fairly soluble in *aq.* ethanol and the adducts formed were nearly insoluble, separation and purification procedures were simple. Intermediate $Sr(hfac)_2 \cdot nH_2O$ was also isolated and characterized by IR spectroscopy. Interaction of $Sr(hfac)_2 \cdot nH_2O$ with tetraglyme yielded the expected adduct $Sr(hfac)_2 \cdot$ tetraglyme. $Sr(hfac)_2 \cdot (bpy)_2$ could be sublimed easily. It is obvious that the adduct is much more volatile than $Sr(hfac)_2$ itself, although it is a little less volatile than $Sr(hfac)_2 \cdot$ tetraglyme. $Sr(hfac)_2 \cdot (bpy)_2$ could be a potential MO precursor for MOCVD application. Attempts to sublime the complex $Sr(hfac)_2 \cdot (phen)_2$ (over 175°C/0.1 mmHg) resulted in the dissociation of the adduct. The free ancillary ligand phen was collected on the cool-finger of the sublimator instead of the adduct.

All the products obtained gave satisfactory elemental analysis results. They have also been characterized by IR, ^{1}H NMR and mass spectroscopy respectively. The spectroscopic data of the compounds $Sr(hfac)_2 \cdot$ tetraglyme and $Ba(hfac)_2 \cdot$ tetraglyme are in very good agreement with those previously reported. The chemical shift of the protons on hfac in compound $Sr(hfac)_2 \cdot (bpy)_2$ moves ~0.2 ppm further upfield than those of the tetraglyme adduct. This demonstrates good electron donating nature of the nitrogens on bpy. A similar phenomenon was observed for the phen adduct. ^{1}H NMR data for $Sr(hfac)_2 \cdot$ db24c8 and $Ba(hfac)_2 \cdot$ db24c8 were similar to those of $Ba(hfac)_2 \cdot$ 18c6 [13]. In MS spectra, only fragments were observed for all the compounds obtained. For the complex $Sr(hfac)_2 \cdot (phen)_2$, clear fragments for

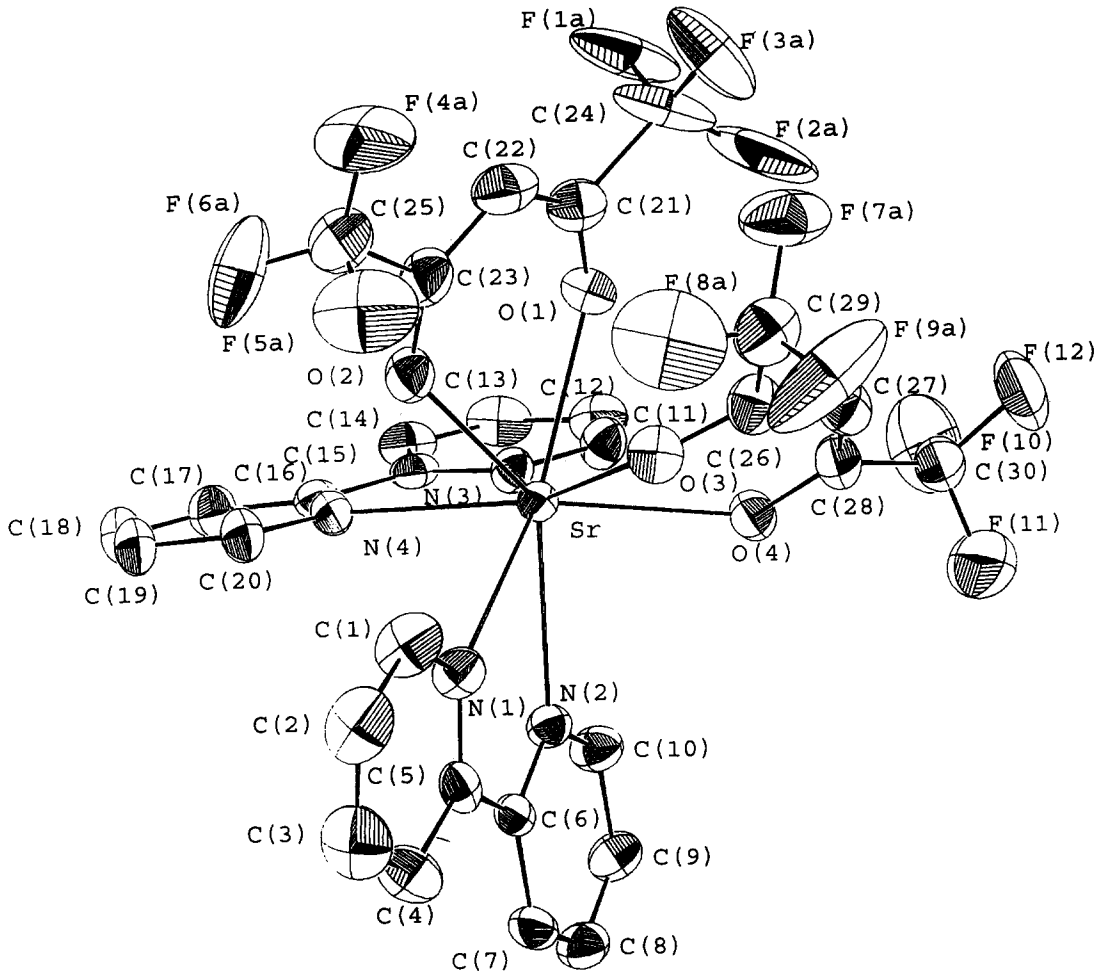

Fig. 1. Molecular structure of $Sr(hfac)_2 \cdot (bpy)_2$ showing the atom numbering scheme. Hydrogen atoms are omitted for clarity.

$Sr(hfac)(phen)_2$ (655, 6.0%) and $Sr(hfac)(phen)$ (475, 9.6%) were observed. It is quite interesting to note that peaks of $bpy+H^+$ (15.3%) and $phen+H^+$ (67.4%) are even more abundant then the free bpy (not observed) and phen (2.2%). For $Sr(hfac)_2 \cdot$ db24c8, the peak of $Sr(hfac) \cdot$ db24c8 (743, 11.8%) is visible. In IR spectra, the stretch vibration absorptions for the carbonyl groups of all compounds locate at almost the same region (about 1670 cm^{-1}).

The molecular structure of $Sr(hfac)_2 \cdot (bpy)_2$ is shown in Fig. 1 with selected bond lengths and angles listed in Table 2. In the structure, the center Sr atom is eight coordinated with two hfac moieties on one side and the two bpy ligands on the other. The location of the two hfacs and the two bpys could be described as *cis*. This is different from those in $Sr(Ph_2acac)_2 \cdot$ (tetraglyme) [21] and the analogous barium complexes $Ba(hfac)_2 \cdot$ (tetraglyme) [12,22] and $Ba(thd)_2 \cdot$ (tetraglyme) [3], where the two hfac moieties are positioned on either side of the polyether plane. The coordination geometry around the Sr center is better described as square antiprism. The Sr—O bond distances in $Sr(hfac)_2 \cdot (bpy)_2$ range from 2.529 (5) to 2.559 (5) Å (average 2.540 (5) Å) which are exactly the same as those in $Sr(Ph_2acac)_2 \cdot$ (tetraglyme) [2.500 (6)–2.564 (6), average 2540 (6)]. This implies a similar Sr—O bond strength between the compounds. The Sr—N bond lengths range from 2.703 (6) to 2.733 (5) Å, with an average 2.717 (6) Å. The much longer Sr—N bond distances compared to those of Sr—O in the compound, means that bonding between Sr and N is much weaker than that between Sr and O. The average bond angle of O—Sr—O in hfac is 69.7 (2)°, about 1° larger than those in $Sr(Ph_2acac)_2 \cdot$ (tetraglyme) [average 68.5 (2)°]. This could be attributed to the less steric hindrance of the bpy ligands. The dihedral angle between the two bpy planes is 85.25°. The obtuse angle (144.08°) between the two hfac planes, O(1)—C(21)—C(22)—C(23)—O(2) plane and O(3)—C(26)—C(27)—

Table 2.

Sr—O(1)	2.532(5)	N(2)—C(10)	1.32(1)
Sr—O(4)	2.541(5)	N(2)—C(6)	1.336(8)
Sr—O(3)	2.559(5)	N(3)—C(15)	1.34(1)
Sr—N(3)	2.703(6)	N(3)—C(11)	1.35(1)
Sr—N(4)	2.708(6)	N(4)—C(16)	1.33(1)
Sr—N(1)	2.723(6)	N(4)—C(20)	1.34(1)
Sr—N(2)	2.733(5)	C(1)—C(2)	1.34(2)
O(2)—Sr—O(1)	70.6(2)	O(2)—Sr—O(4)	135.4(2)
O(2)—Sr—O(3)	73.4(2)	O(2)—Sr—N(3)	114.7(2)
O(2)—Sr—N(4)	74.8(2)	O(2)—Sr—N(1)	82.3(2)
O(2)—Sr—N(2)	137.1(2)	O(1)—Sr—O(4)	79.4(2)
O(1)—Sr—O(3)	78.6(2)	O(1)—Sr—N(3)	75.6(2)
O(1)—Sr—N(4)	101.1(2)	O(1)—Sr—N(1)	149.1(2)
O(1)—Sr—N(2)	151.1(2)	O(4)—Sr—O(3)	68.8(2)
O(4)—Sr—N(3)	87.7(2)	O(4)—Sr—N(4)	144.9(2)
O(4)—Sr—N(1)	112.5(2)	O(4)—Sr—N(2)	81.0(1)
O(3)—Sr—N(3)	147.9(2)	O(3)—Sr—N(4)	146.2(2)
O(3)—Sr—N(1)	79.7(2)	O(3)—Sr—N(2)	113.3(2)
N(3)—Sr—N(4)	59.2(2)	N(3)—Sr—N(1)	131.0(2)
N(3)—Sr—N(2)	82.6(2)	N(4)—Sr—N(1)	85.2(2)
N(4)—Sr—N(2)	83.3(2)	N(1)—Sr—N(2)	59.2(2)

C(28)—O(4) plane, demonstrates the steric repulsion between the two ligands.

REFERENCES

1. Yamane, H., Kurosawa, H., Hirai, T., Iwasaki, H., Kobayashi, N. and Muto, Y., *Jpn. J. Appl. Phys.*, 1988, **27,** L1495.
2. Berry, A. D., Holm, R. T., Cukauskas, E. J., Fatemi, M., Gaskill, D. K., Kaplan, R. and Fox, W. B., *J. Cryst. Growth*, 1988, **92,** 344.
3. Zhang, J. M., Zhao, J., Marcy, H. O., Tonge, L. M., Wessels, B. W., Marks, T. J. and Kannewurf, C. R., *Appl. Phys. Lett.*, 1989, **54,** 1166.
4. Berry, A. D., Holm, R. T., Fatemi, M. and Gaskill, D. K., *J. Mater. Res.*, 1990, **5,** 1169.
5. Endo, K., Hayashida, S., Ishiai, J., Matruki, Y., Lkedo, L., Misawa, S. and Yoshida, S., *Jpn. J. Appl. Phys.*, 1990, **29,** L294.
6. Zhang, J. M., Wessels, B. W., Richeson, D. S., Marks, T. J., Degroot, D. C., Kannewurf, C. R., *J. Appl. Phys.*, 1991, **69,** 2743.
7. Sievers, R. E. and Sadlowski, J. E., *Science*, 1978, **201,** 217.
8. Tonge, L. M., Richeson, D. S., Marks, T. J., Zhao, J., Zhang, J. M., Wessels, B. W., Marcy, H. O. and Kannewurf, C. R., *Adv. Chem. Ser.*, 1990, **226,** 351.
9. Nemoto, M. and Yamanaka, M., *J. Mater. Res.*, 1990, **1,** 1.
10. Malandrino, G., Richeson, D. S., Marks, T. J., DeGroot, D. C. and Kannewurf, C. R., *Appl. Phys. Lett.*, 1991, **58,** 182.
11. Wills, L. A., Wessels, B. M., Richeson, D. S. and Marks, T. J., *Appl. Phys. Lett.*, 1992, **60,** 41.
12. Gardiner, R., Brown, D. W., Kirlin, P. S. and Rheingold, A. L., *Chem. Mater.*, 1991, **3,** 1053.
13. Norman, J. A. T. and Pez, G. P., *J. Chem. Soc., Chem. Commun.*, 1991, 971.
14. Malandrino, G., Castelli, F., Fragala, I. L., *Inorg. Chim. Acta*, 1994, **224,** 203.
15. Shen, Y. Z., Pan, Y., Lu, Z. B., Chen, J. X., Sun, X. Z., The Fourth National Symposium on MOCVD, Xian, China, 1995.
16. Timmer, K., Spee, K. I. M. A., Mackor, A., Meinema, H. A., Spek, L. and van der Sluis, P., *Inorg. Chim. Acta*, 1991, **190,** 109.
17. Gilmore, C. J., *MITHRIL. Computer Program for the Automatic Solution of Crystal Structure from X-ray Data.* Department of Chemistry, University of Glasgow, Scotland, 1983.
18. Molecular Structure Corporation., *TEXSAN. Single Crystal Structure Analysis Software. Version* 5.0, MSC, 3200 Research Forest Drive, The Woodlands TX 77381, USA, 1989.
19. Johnson, C. K., *ORTEP* II. Repot ORNL-5138. Oak Ridge National Laboratory, Tennessee, USA, 1976.
20. Enraf–Nonius, *CAD-4 Software.* Version 5. Enraf–Nonius, Delft, The Netherlands, 1989.
21. Drake, S. R., Miller, S. A. S., Hursthouse, M. B. and Abdul Malik, K. M., *Polyhedron*, 1993, **12,** 1621.
22. van der Sluis, P., Spek, A. L., Timmer, K. and Meinema, H. A., *Acta. Cryst.*, 1990, **C46,** 1741.

Pergamon

PII: S0277-5387(97)00250-7

Polyhedron Vol. 17, No. 1, pp. 75–79, 1998
© 1997 Elsevier Science Ltd
All rights reserved. Printed in Great Britain
0277-5387/98 $19.00+0.00

Self-assembly of copper and magnesium ions with L-glutamate: spectroscopic and structural properties of $[CuMg(L\text{-}GLUTAMATO)_2(H_2O)_3]\cdot 2H_2O$

Tongbu Lu,[a]* Xiaoyan Li,[a] Zongwan Mao,[a] Wenbin Qiu,[a] Liangnian Ji[a] and Kaibei Yu[b]

[a] Department of Chemistry, Zhongshan University, Guangzhou 510275, P.R. China

[b] Chengdu Center of Analysis and Measurement, Academia Sinica, Chengdu 610041 P.R. China

(Received 9 April 1997; accepted 9 June 1997)

Abstract—The mixed-metal complex of copper(II) and magnesium(II) ions with glutamate has been firstly synthesized by self-assembling, and characterized by elemental analyses, IR spectra and electronic spectra. The structure of the complex has been determined by single-crystal X-ray diffraction. The $[CuMg(L\text{-}glu)_2(H_2O)_3]\cdot 2H_2O$ (L-glu = L-glutamate) complex has a one-dimensional polymeric structure, in which Cu^{II} and Mg^{II} ions are bridged by glutamate. Each Cu atom exhibits distorted square pyramidal five-coordination, with two glutamate ions acting as a bidentate ligand through the amino N and the α-carboxylate O atoms in trans positions in the equatorial plane, forming two glycine-like rings, and with a water molecule in apical position. Each Mg atom is coordinated in a slightly distorted octahedral geometry by two γ-carboxylate O atoms from two glutamate ions and by four water molecules. The average Cu—O, Cu—N and Mg—O distances are 2.048(2), 1.979(3) and 2.084(2) Å, respectively. The coordination patterns of glutamate ion in different glutamate Cu^{II} complexes are also discussed. © 1997 Elsevier Science Ltd

Keywords: copper(II); magnesium(II); L-glutamate; structure.

Metal–glutamate complexes and their adducts with amine have been extensively investigated both in solution [1,2] and in solid state [3–6]. It is generally considered that chelation of the amino and α-carboxylate groups occurs readily, and much of the study of metal binding has been devoted to attempts to deduce whether the side chain carboxylate (γ-carboxylate) is also coordinated to the metal ion [1]. X-ray diffraction analysis has shown that the coordination patterns of glutamate in different glutamate Cu^{II} complexes are much different [3,5], in which the γ-carboxylates are coordinated or uncoordinated to the metal ions, forming polymeric or mononuclear complexes.

Although metal–glutamate chemistry has a very long history, all of the studies were only focused on the coordination behavior of monometallic salts with glutamate, the mixed-metal complexes, to our knowledge, have not been reported. The design and synthesis of polynuclear mixed-metal complexes have attracted much current attention. These compounds have been studied as metal enzyme models [7], as supramolecular devices [8], as magnetic materials [9], and as possible precursors production of high temperature superconductor [10]. Glutamate has three binding sites for metal ions [1], the amino N atom is bound to transitional metal ions first, while the α- and γ-carboxylate O atoms are bound to alkaline earth metal ions first. So mixed-metal complexes may be formed by self-assembling of glutamate with different metal ions. In this paper, we firstly report the synthesis and spectroscopic and structural investigations on the mixed-metal complex of copper and magnesium ions with L-glutamate. X-ray diffraction analysis shows that L-glutamate can be bound to Cu^{II} and Mg^{II} ions to form a polymeric compound in an extended-chain

* Author to whom correspondence should be addressed.

configuration, in which the glycinate and γ-carboxylate groups are coordinated selectively to Cu^{II} and Mg^{II} ions, respectively.

EXPERIMENTAL

All the reagents were commercially available and used without further purification. Carbon, nitrogen and hydrogen contents were determined using a Perkin–Elmer elemental analyser. The IR spectra were recorded in the 4000–400 cm^{-1} region using KBr pellets and a Nicolet 5DX spectrometer. A Shimadzu UV-240 spectrophotometer was used to obtain the electronic absorption spectra. Thermal analyses (TG and DTA) were performed on a Beijing PcT-2 thermobalance. The heating rate was 10°C min^{-1}.

Preparation of the complex

A mixed water solution (10 cm^3) of $CuCl_2 \cdot 2H_2O$ (0.341 g, 2 mmol) and $MgCl_2 \cdot 6H_2O$ (0.407 g, 2 mmol) was added to a water solution (10 cm^3) of glutamic acid (0.588 g, 4 mmol). The resulting solution was adjusted to pH ≈ 6 by very slow addition of 0.5 mol dm^{-3} aqueous NaOH. The mixture was stirred at room temperature for 24 h, then was evaporated to 10 cm^{-3} under heating. The blue precipitate was filtered, washed with water/alcohol (1 : 2) several times, and dried in a desiccator over P_4O_{10} for 3 days. Yield 70% (Found: C, 28.2; H, 4.3; N, 6.6. Calc. for $C_{10}H_{20}N_2O_{11}CuMg$: C, 27.8; H, 4.6; N, 6.5%).

Single crystals of the complex were obtained by dissolving the powdery solid complex in water, and leaving the solution in acetonitrile. After about 7 days, blue prismatic crystals suitable for X-ray analysis formed from the solution.

Crystallography

Crystal data. $C_{10}H_{24}N_2O_{13}CuMg$, $M = 467.96$, orthorhombic, space group $C222_1$, $a = 10.260(2)$, $b = 16.262(2)$, $c = 11.609(1)$ Å, $U = 1979.8(5)$ $Å^3$, $F(000) = 1052$, $Z = 8$, $D_C = 1.692$ g cm^{-3}, λ(Mo-K_α) = 0.71073 Å, $\mu = 1.213$ mm^{-1}.

Data collection. X-ray diffraction intensities were collected at 296 K from crystals of dimensions 0.58 × 0.42 × 0.20 mm on an R3M/E four circle X-ray diffractometer with graphite-monochromatized Mo-K_α radiation, by using the $\theta/2\theta$ scan technique. Negligible change in the intensities of three standards monitored during the data collection indicated no crystal decomposition. Some 2268 independent reflections were collected in the range $2.33 \leqslant \theta \leqslant 25.99°$ (h from 0 to 12, k from −1 to 20, l from −14 to 14). Of these, 1953 reflections with $I > 2\sigma$ (I) were used in the structure determination and refinement, $R_{int} = 0.0304$ after absorption correction (maximum and minimum transmission factors = 0.9421 and 0.7362). The intensities were corrected for Lorentz-polarization effects, and for empirical absorption.

Structure solution and refinement. The structure was solved using the Patterson heavy-atom method which revealed the positions of the Cu and Mg atoms. The remaining atoms were located in subsequent difference-Fourier synthesis and refined by full-matrix least-squares methods with anisotropic thermal factors. All the hydrogen atoms (except the hydrogen atoms of uncoordinated water molecules) were revealed by the difference-Fourier synthesis and refined with isotropic thermal factors. All calculations were performed by using the SHELXTL system of computer programs [11]. The final cycle of full-matrix least-squares refinement (F) was based on 1953 reflections [$I > 2\sigma$ (I)] and 183 variable parameters and converged with R and R' values of 0.0289 and 0.0327, respectively. The weighting scheme was $w = 1/[2\sigma^2(F_o)^2 + 0.0541P]$, where $P = [\max.(F_o^2, 0) + 2F_c^2]/3$. The maximum and minimum peaks on the final difference-Fourier map corresponded to 0.424 and −0.284 e $Å^{-3}$. Selected bond lengths and angles are listed in Table 1.

RESULTS AND DISCUSSION

Spectroscopic results

IR spectra. The results of the IR spectra show that the asymmetric and symmetric absorptions of the carboxylate groups shift from 1583 and 1421 cm^{-1} in the free glutamic acid ligand to 1546 and 1405 cm^{-1} in the complex, indicating that the carboxylate groups are coordinated to the metal ions [12]. The disappearance of the $\nu(NH_3^+)$ absorption of 3050 cm^{-1} in the free L-glutamic acid and the appearance of two absorptions of 3261 and 3332 cm^{-1} assigned to N—H stretching modes in the complex suggest the amino N atom is also coordinated to the metal ion [12]. Owing to the presence of extensive hydrogen bonding, it's difficult to distinguish between the bidentate coordination and the monodentate coordination of the carboxylate groups [13].

Thermal analyses. The ligand decomposes at 231°C, and continuous weight loss is detected up to 620°C, at this temperature the ligand decomposes completely. The thermal analytical result of $[CuMg(L\text{-glu})_2(H_2O)_3] \cdot 2H_2O$ shows that the two uncoordinated water molecules are lost below 100°C, while the three coordinated water molecules are lost in the 150 ~ 170°C temperature range. After the loss of water molecules, the complex decomposes exothermically at 331°C. After this other exothermic peaks and continuous weight loss are detected up to 800°C.

From the above thermal analytical results it can be found that the thermal decomposition temperature of the ligand (231°C) is much lower than that of the

Table 1. Selected bond lengths (Å) and bond angles (°) for the complex*

Cu—O(1)	1.950(2)	Cu—O(1A)[a]	1.950(2)
Cu—N	1.979(3)	Cu—N(OA)[a]	1.979(3)
Cu—O(5)	2.243(3)		
Mg—O(3)	2.084(2)	Mg—O(3B)[b]	2.084(2)
Mg—O(6)	2.082(3)	Mg—O(7)	2.066(3)
Mg—O(8)	2.093(2)	Mg—O(8B)[b]	2.093(2)
N—C(2)	1.473(4)	O(1)—C(1)	1.283(3)
O(2)—C(1)	1.239(4)	O(3)—C(5)	1.263(3)
O(4)—C(5)	1.268(4)	C(1)—C(2)	1.527(3)
C(2)—C(3)	1.532(5)	C(3)—C(4)	1.526(4)
C(4)—C(5)	1.507(4)		

O(1A)[a]—Cu—O(1)	177.2(2)	O(1A)[a]—Cu—N	95.05(10)
O(1)—Cu—N	84.50(10)	O(1A)[a]—Cu—N(OA)[a]	84.50(10)
O(1)—Cu—N(OA)[a]	95.05(10)	N—Cu—N(OA)[a]	161.3(2)
O(1A)[a]—Cu—O(5)	91.38(9)	O(1)—Cu—O(5)	91.38(9)
N—Cu—O(5)	99.33(10)	N(OA)[a]—Cu—O(5)	99.33(10)
O(7)—Mg—O(6)	180.0	O(7)—Mg—O(3B)[b]	91.56(8)
O(6)—Mg—O(3B)[b]	88.44(8)	O(7)—Mg—O(3)	91.56(8)
O(6)—Mg—O(3)	88.44(8)	O(3B)[b]—Mg—O(3)	176.9(2)
O(7)—Mg—O(8B)[b]	88.67(9)	O(6)—Mg—O(8B)[b]	91.33(9)
O(3B)[b]—Mg—O(8B)[b]	92.05(8)	O(3)—Mg—O(8B)[b]	88.02(8)
O(7)—Mg—O(8)	88.67(9)	O(6)—Mg—O(8)	91.33(9)
O(3B)[b]—Mg—O(8)	88.02(8)	O(3)—Mg—O(8)	92.05(8)
O(8B)[b]—Mg—O(8)	177.3(2)	C(2)—N—Cu	109.4(2)
C(1)—O(1)—Cu	114.9(2)	C(5)—O(3)—Mg	133.9(2)
O(2)—C(1)—O(1)	123.5(3)	O(2)—C(1)—C(2)	119.3(3)
O(1)—C(1)—C(2)	117.2(3)	N—C(2)—C(1)	109.9(3)
N—C(2)—C(3)	111.9(3)	C(1)—C(2)—C(3)	109.5(3)
C(4)—C(3)—C(2)	115.8(3)	C(5)—C(4)—C(3)	119.6(2)
O(3)—C(5)—O(4)	123.7(3)	O(3)—C(5)—C(4)	120.5(3)
O(4)—C(5)—C(4)	115.8(3)		

* Symmetry transformation used to generate equivalent atoms: [a] $-x+2, y, z+1/2$; [b] $-x+1, y, -z+1/2$

complex (331°C), indicating that the complex is more thermally stable than the ligand.

Electronic spectra. The electronic spectra of the complex was recorded at room temperature, and the maximum at 16023 cm^{-1}, is assigned to *d–d* transition. This data is similar to those of other square-pyramidal copper(II) complexes [13], indicating the coordination geometry of the Cu atom in the complex is a square pyramid. This result is consistent with that of X-ray diffraction analysis. The *d–d* band maximum in $[CuMg(L\text{-}glu)_2(H_2O)_3]\cdot 2H_2O$ with CuN_2O_3 chromophore, at lower energy than those of the $[Cu(L\text{-}glu)(o\text{-}phen)H_2O]\cdot 3H_2O$ (16530 cm^{-1}) and $[Cu(L\text{-}asp)(bpy)H_2O]\cdot 3H_2O$ (16390 cm^{-1}) complexes [5] with CuN_3O_2 chromophore, indicates that the crystal field stabilization energy in the former is smaller than those of the latter.

Description of the structure

Figure 1 shows the molecular structure of $[CuMg(L\text{-}glu)_2(H_2O)_3]\cdot 2H_2O$. Figure 2 illustrates the molecular packing arrangement in the unit cell. For the sake of comparison, a summary of structural parameters for the known L-glutamate Cu^{II} complexes is presented in Table 2.

The structure is made up of one-dimensional polymeric chains by self-assembling of Cu^{II} and Mg^{II} ions with L-glutamate, in which copper and magnesium ions are bridged by L-glutamate. The uncoordinated water molecules provide crystalline stability through a network of hydrogen-bonding interactions. Each Cu atom exhibits distorted square pyramidal five-coordination, with two glutamate ions acting as a bidentate ligand through the amino N and the α-carboxylate O atoms in *trans* positions in the equatorial plane, forming two five-membered glycine-like rings, and with a water molecule in apical position. This coordination pattern of L-glutamate has not been found in other Cu^{II}–glutamate complexes. Each Mg atom is coordinated in a slightly distorted octahedral geometry by two γ-carboxylate O atoms from two L-glutamate ions and by four water molecules. The Cu—N distance is 1.979(3) Å, which is the shortest in all the square pyramidal Cu^{II}–glutamate complexes (see Table 2). The Cu—O distances lie in the range 1.950(2)–

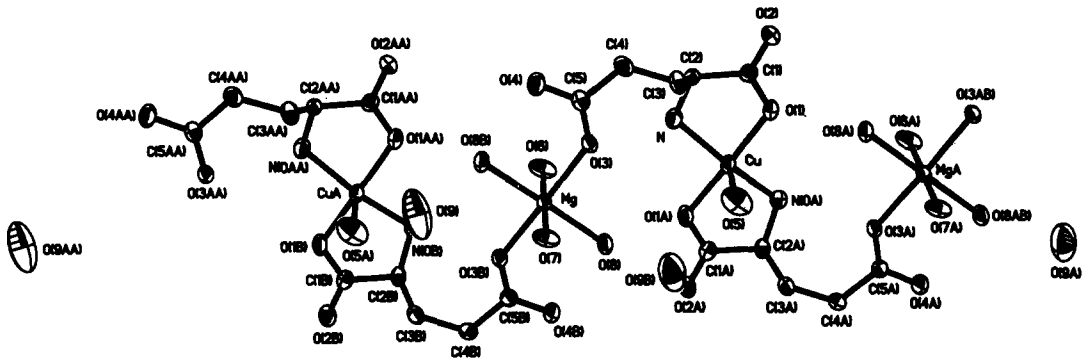

Fig. 1. The molecular structure of $[CuMg\ (L\text{-}glu)_2\ (H_2O)_3]\cdot 2H_2O$.

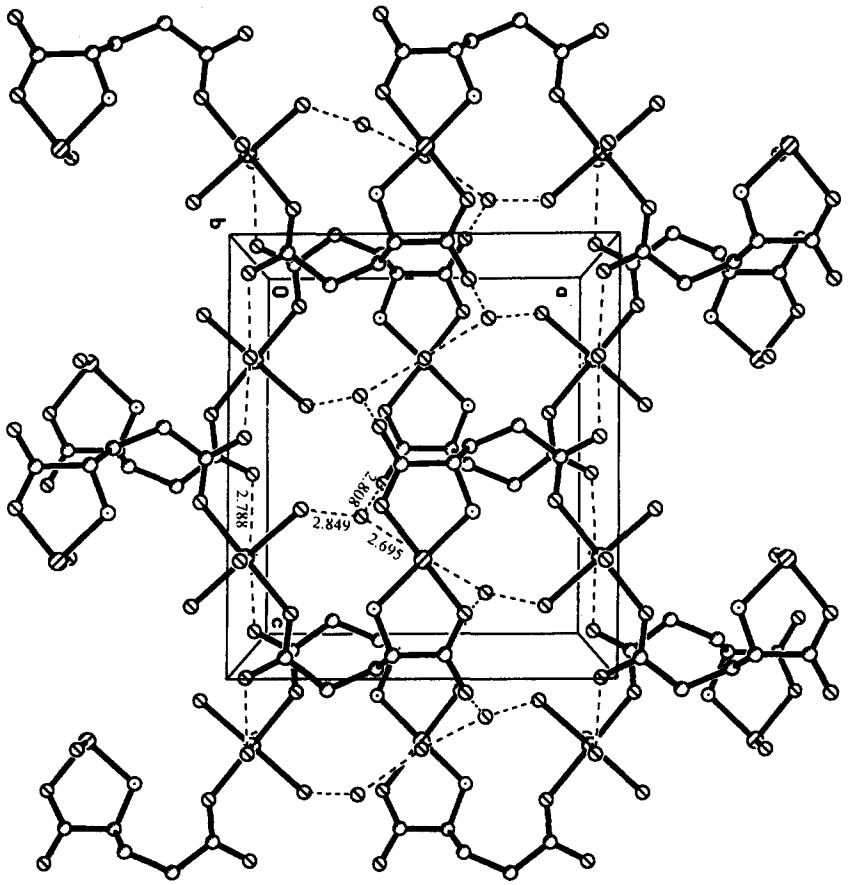

Fig. 2. The molecular packing arrangement in the unit cell. Hydrogen bonds are shown as dashed lines.

2.243(3) Å and averaged 2.048(2) Å. The rather longer Cu—O apical bond length of 2.243(3) Å is consistent with the values found in other Cu^{II}–glutamate complexes (Table 2). The six Mg-O distances lie in the range 2.066(3)–2.093(2) Å and averaged 2.084(2) Å.

It is interesting to make a comparison of the coordination patterns of L-glutamate in different Cu^{II}–glutamate complexes listed in Table 2. In [Cu(L-glu)(*o*-phen)$(H_2O)]\cdot 3H_2O$ complexes [5], L-glutamate acts as a simple bidentate ligand, giving rise to mononuclear complex. In [Cu(L-glu) (im)] [5] and [Cu(L-glu)(bpy)] [5] complexes, the L-glutamate binds one Cu^{II} ion through the glycinate ring and bridges a second Cu^{II} ion through the γ-carboxylate O atoms, forming one-dimensional polymeric chain structural complexes. In $[CuMg(L\text{-}glu)_2\ (H_2O)_3]\cdot 2H_2O$ complex, the L-glutamate bridges another different metal ion (Mg^{II}) through the γ-carboxylate O atom to form a mixed-metal complex. In [Cu(L-glu) $(H_2O)]\cdot H_2O$ complex, a third Cu^{II} ion is bridged through the α-carboxylate O atom, forming a two-dimensional polymeric network structural complex [3]. From the above comparison it can be found that the γ-carboxylate group of glutamate can be coor-

Table 2. Comparative structure parameters of the known L-glutamate Cu^{II} complexes

	[Cu(L-glu)(H_2O)]·H_2O	[Cu(L-glu)(im)]	[Cu(L-glu)(bpy)]	[Cu(L-glu)(*o*-phen)(H_2O)]·$3H_2O$	[CuMg(L-glu)$_2$$(H_2O)_3$]·$2H_2O$
Space group	$P2_12_12_1$	$P2_12_12_1$	$P2_12_12_1$	$P2_1$	$C222_1$
Z	4	4	8	4	8
Structure	2-D polymer	1-D polymer	1-D polymer	discrete molecules	1-D polymer
Coord. geometry	square pyramidal	square planar	square pyramidal	square pyramidal	square pyramidal
Amino acidate	O, N(gly ring)	O, N(gly ring)	O, N(gly ring)	O, N(gly ring)	O, N(gly ring)
Binding sites	O(α-carboxyl) O(γ-carboxyl)	O(γ-carboxyl)	O(γ-carboxyl)		O(γ-carboxyl)
Cu—O(gly ring) (Å)	1.967(4)	1.924(5)	1.943(9)	1.920(4)	1.950(2)
Cu—N(gly ring) (Å)	1.998(4)	1.989(6)	1.99(1)	2.011(6)	1.979(3)
Cu—O(apical) (Å)	2.299(4)		2.20(1)	2.258(7)	2.243(3)
Ref.	3	5	5	5	This work

dinated not only to the same metal ion but to the different metal ion, and the coordination patterns of L-glutamate are much different in different complexes.

Acknowledgements—This work was supported by the Guangdong Provincial Natural Science Foundation.

REFERENCES

1. Evans, C. A., Guevremont, R. and Rabenstein, D. L., *Met. Ions Biol. Syst.*, eds. H. Sigel, Marcel Dekker, Inc., New York and Basel, 1979, Vol. 9, Ch. 2, pp. 42–75 and ref therin.
2. Bottari, E., Festa, M. R. and Jasionowska, R., *Polyhedron*, 1989, **8,** 1019.
3. Gramaccioli, C. M. and Marsh, R. E., *Acta Cryst.*, 1966, **21,** 594.
4. Flook, R. J., Freeman, H. C. and Scudder, M. L., *Acta Cryst., Sect. B: Struct. Cryst. Cryst. Chem.*, 1977, **33,** 801.
5. Antolini, L., Marcotrigiano, G., Menabue, L., Pellacani, G. C., Saladini, M. and Sola, M., *Inorg. Chem.*, 1985, **24,** 3621.
6. Legendziewicz, J., Huskowska, E., Argay, G. Y. and Waskowska, A., *Inorg. Chim. Acta.*, 1984, **95,** 57.
7. Hay, R. W., *Bio-inorganic Chemistry*, John Wiley, New York, (1984); Z. W. Mao, M. Q. Chen, X. S. Tan, J. Liu and W. X. Tang, *Inorg. Chem.*, 1995, **34,** 2889.
8. Lehn, J.M., *Angew. Chem., Int. End. Engl.*, 1988, **27,** 89; Balzani, V. and Scandola, F., *Supramolecular Photochemistry*, Ellis Horwood, Chichester (1991).
9. Nakatani, K., Bergerat, P., Codiovi, E., Mathoniere, C., Pei, Y. and Kahn, O., *Inorg. Chem.*, 1991, **30,** 3977; Zhuang, Z. J., Matsumoto, N., Okawa, H. and Kida, S., *Chem. Lett.*, 1990, 87; Pei, Y., Journaux, Y., Kahn, O., Dei, A. and Gatteschi, D., *J. Chem. Soc., Chem. Commun*, 1986, 1300; Kahn, O., Galy, J., Journaux, Y., Jaudand, J. and Morgenstern-Badarau, I., *J. Am. Chem. Soc.*, 1982, **104,** 2165.
10. Sauer, N. N., Garcia, E., Salazar, K. V., Ryan, R. R. and Martin, J. A., *J. Am. Chem. Soc.*, 1990, **112,** 1524; Wang, S., Pang, Z. and Smith, D. L., *Inorg. Chem.*, 1993, **32,** 4992; Blake, A. J., Gould, R. O., Miline, P. E. Y., and R. E. Winpenny, *J. Chem. Soc., Chem. Commun.*, 1992, 522.
11. Sheldrick, G. M., SHELXTL (Revision 4.1), System of Computer Programs for X-ray Structure Determination, University of Cambridge, 1983.
12. Nakamoto, K., *Infrared and Raman Spectra of Inorganic and Coordination Compounds*, 3rd edn. John Wiley, New York (1978); Antolini, L., Marcotrigiano, G., Menabue, L., Pellacani, G. C. and Saladini, M., *Inorg. Chem.*, 1982, **21,** 2263.
13. Yokoi, H., Sai, M., Isobe, T., Oshawa, S., *Bull. Chem. Soc. Jpn.*, 1972, **45,** 2189; Simmons, C. J., Lundeen, M. and Seff, K., *Inorg. Chem.*, 1978, **17,** 1429; Dehand, J., Jordanow, J., Keck, F., Mosset, A., Bonnet, J. J. and Galy, J., *Inorg. Chem.*, 1979, **18,** 1543.

Pergamon

PII: S0277-5387(97)00249-0

Polyhedron Vol. 17, No. 1, pp. 81–84, 1998
© 1997 Elsevier Science Ltd
All rights reserved. Printed in Great Britain
0277-5387/98 $19.00+0.00

Synthesis, crystal structure and spectral properties of VO(acetylacetone benzoylhydrazone)(8-quinolinol)

Shi-Xiong Liu* and Shan Gao

Dept. of Chemistry, Fuzhou University, Fuzhou 350002, P.R. China

(Received 5 March 1997; accepted 9 June 1997)

Abstract—The title complex was prepared by the reaction of bis(acetylacetonato)oxovanadium(IV) benzoylhydrazine and 8-quinolinol in methanol and characterized by IR, Raman, UV spectra and cyclic voltammetry measurements. The vanadium atom has a distorted octahedral VO(ONO)(ON) coordination with a normal V=O bond [1.580(4)Å]. Two oxygen atoms and one nitrogen atom of the tridentate hydrazone ligand, and one oxygen atom of 8-quinolinol ligand are coordinated to a vanadium(V) atom, forming an equatorial plane, the axial positions being occupied by an oxo oxygen atom and a nitrogen atom of the 8-quinolinol ligand, respectively. The title complex is the first example of a six-coordinated VO^{3+} complex with acetylacetone benzoylhydrazone ligand. © 1997 Elsevier Science Ltd

Keywords: monooxovanadium complex; hydrazone complex; crystal structure; spectral properties.

There has been considerable interest in coordination chemistry and biochemistry of vanadium due to the discovery of haloperoxidases (V-PO) [1–3] and nitrogenase [4] in the past ten years. For example, the vanadium-dependent bromoperoxidase (V-BrPO) [5–7] not only catalyze the oxidation of halides by hydrogen peroxide and form a halogenated organic substrates, but also have some potential antifungal, antibacterial and antitumour properties [8]. EXAFS measurements on the enzyme containing vanadium(V) suggest that the catalytically active centre contains a mononuclear oxovanadium(V) coordinated by six oxygen/nitrogen atoms, and that neither a metal sulfide cluster nor a vanadoporphyrin is an appropriate description of the active site. Therefore it is more important to intensively study the relationship of the syntheses, structures and biological effects of the vanadium complexes.

In contrast to the common monooxovanadium(IV)(VO^{2+}) and dioxovanadium(V)(VO_2^+) compounds, little is known about the structures of VO^{3+} complexes [9,10]. On the other hand, most of hydrazone ligands are coordinated to the metal centre through their oxygen/nitrogen atoms and are similar to the coordination environments of the biological system. So far only a few kinds of the VO^{3+} compounds with hydrazone ligands are synthesized, in which the hydrazone ligands are only formed by the condensing hydrazine with salicylaldehyde [9,11,12] or benzoylacetone [9,10,13,14]. Here we describe the synthesis, structure and spectroscopic characterization of a novel VO^{3+} complex, VO(L)(hquin), where L and hquin are acetylacetone benzoylhydrazone and 8-quinolinol, respectively.

EXPERIMENTAL

Materials and measurements

The materials $VO(acac)_2$ (acac = acetylacetonate) was synthesized according to the literature [15]. Analytically pure dichloromethane was distilled over calcium hydride before use. All other analytical grade chemicals and solvents were purchased commercially and used without further purification.

IR spectra were recorded on a Nicolet Magna 750 Fourier transform IR spectrometer by use of KBr discs in the 400–4000 cm^{-1} range. Raman spectra were measured using a Nicolet Raman 910 Fourier transform laser Raman spectrometer in the 200–4000

* Author to whom correspondence should be addressed.

cm^{-1} range. UV–vis spectra were obtained on a Perkin–Elmer lambda 9 UV–vis–IR spectrometer in CH_2Cl_2 solution and in the 300–800 nm range. Cyclic voltammetry was performed on a BAS 100A electrochemical analyzer. A three-electrode system was employed with a platinum-head as the working electrode, an Ag/AgCl reference electrode and a platinum-wire auxiliary electrode, CH_2Cl_2 being the solvent, $(Et_4N)ClO_4$ (0.1 M) being the supporting electrolyte.

Synthesis of VO(L)(hquin)

Benzoylhydrazine (0.116 g, 1 mmol) dissolved in 15 cm^3 of methanol and was added dropwise to a methanol solution containing 0.263 (1 mmol) of $VO(acac)_2$ with stirring, and then the mixture was refluxed with stirring for 2 h. 10 cm^3 of mixed solution of methanol and 8-quinolinol was added to the above red–black solution. The reaction mixture was stirred for 30 min and filtered off. The red–black crystals of the title complex were formed upon slow evaporation of the filtrate for several days and collected under vacuum over P_4O_{10}.

X-ray structure determination

X-ray diffraction on a crystal with dimensions $0.35 \times 0.35 \times 0.20$ mm was obtained on a Rigaku AFC5R diffractometer with graphite-monochromated Mo-K_α radiation ($\lambda = 0.71069$ Å). Cell dimensions were refined using 25 reflections in the range $20 < 2\theta < 30°$. The reflection data were collected with ω–2θ mode in the range $2\theta < 50.1°$. The data were corrected for Lorentz effect, polarization effect and DIFABS correction.

The structure was solved by direct methods and refined by a full-matrix least-squares procedure. All non-hydrogen atoms were refined with anisotropic thermal parameters. All hydrogen atoms were located by combination of the difference Fourier map and HYDROGEN program and added to the structure factor calculation, but their positions were not refined. The final R and R_w values were 0.056 and 0.071, respectively. The maximum residual electron density peak in the final difference Fourier map was 417 e/nm^3 with no chemically significant features. The crystallographic data and the selected bond distances and angles are listed in Table 1 and 2, respectively.

Table 1. Crystallographic data for VO(L)(hquin)

Formula	$C_{21}H_{18}N_3O_4V$
Formula weight	427.33
Space group	$P2_1/c$
a (Å)	7.725(3)
b (Å)	14.152(6)
c (Å)	17.985(5)
β(°)	90.76(3)
V(Å^3)	1966(1)
Z	4
D_c (g.cm^{-3})	1.44
μ (cm^{-1})	5.18
Range of 2θ (°)	50.1
No. unique data	3644
No. observed data with $I > 3\sigma(I)$	2026
No. of variables	262
R	0.056
R_w	0.071

RESULTS AND DISCUSSION

Spectroscopic studies

The N—H and C=O absorptions of free tridentate L, and the O—H absorption of free Hhquin in the IR and Raman spectra are absent in the spectra of the title complex, showing that the tridentate ligand is in dinegative form of the type ($^-O\sim N\sim O^-$) [10] and the 8-quinolinol ligand is in monoanion form of the type ($^-O\sim N$). The strong absorption bands at 1603, 1453 cm^{-1} in the IR spectrum and at 1602, 1450 cm^{-1} in the Raman are related to the stretching vibration of unsaturated C=C and C=N linkage [16], and the C=N stretching vibration is displaced to a lower frequency [17,18]. The medium bands at 1319, 1267 cm^{-1} in IR and at 1321, 1263 cm^{-1} in Raman are attributed to the C—O (phenolic oxygen and alkoxidic oxygen) stretching frequencies, respectively [16], which display the shifts to higher frequency owing to the V—O bonds [10,17,18]. The IR band and Raman band due to ν(V=O) stretching vibration are observed at 955 cm^{-1} (m.s.) and 956 cm^{-1} (w.), respectively. This is within the usually observed range (950–990 cm^{-1}) for six-coordinate oxovanadium(V) complexes [9,10]. The stretching vibrations of bonds V—O and V—N have been observed at 497 cm^{-1}, 363 cm^{-1} (far-IR) and 500 cm^{-1}, 368 cm^{-1} (Raman).

The transition ($\lambda = 548$ nm) is considered as a charge transfer from a p_π orbital on the phenolato oxygen long-pair to the empty 3d-orbitals of vanadium atom. The other strong band ($\lambda = 331$ nm) is generally attributed to the alkoxo or the phenolate bound vanadium(V) species. It is consistent with the two LMCT transition ranges of 320–380 and 475–550 nm reported in some d^0 oxovanadium(V) complexes [9,17].

There is a quasi-reversible redox behavior corresponding to a V^V/V^{IV} couple in dichloromethane solution, as shown in Fig. 1. Its redox potential is at $E_{1/2} = -0.287$ V, which was calculated from the average of anodic $E_{pa} = -0.245$ V and cathodic $E_{pc} = -0.330$ V *vs* Ag/AgCl. The peak-to-peak separation (ΔE_p of coupled peaks D/E) is 85 mV at a rate of 200 mV s^{-1}, suggesting that the electrode process is an one-electron transformation [9,17]. Consequently,

Table 2. Selected bond distances (Å) and angles (°)

V(1)—O(4)	1.580(4)	O(1)—C(2)	1.302(6)	N(3)—C(13)	1.323(6)
V(1)—O(3)	1.842(4)	O(2)—C(6)	1.317(6)	N(3)—C(21)	1.362(7)
V(1)—O(1)	1.873(4)	O(3)—C(19)	1.338(6)	C(1)—C(2)	1.496(8)
V(1)—O(2)	1.912(4)	N(1)—C(4)	1.317(6)	C(2)—C(3)	1.344(8)
V(1)—N(1)	2.051(4)	N(1)—N(2)	1.389(6)	C(3)—C(4)	1.422(8)
V(1)—N(3)	2.335(5)	N(2)—C(6)	1.294(6)	C(6)—C(7)	1.474(7)

O(4)—V(1)—O(3)	98.7(2)	N(1)—V(1)—N(3)	86.1(2)
O(4)—V(1)—O(1)	98.7(2)	C(2)—O(1)—V(1)	132.8(4)
O(4)—V(1)—O(2)	100.9(2)	C(6)—O(2)—V(1)	118.0(3)
O(4)—V(1)—N(1)	99.8(2)	C(19)—O(3)—V(1)	123.9(3)
O(4)—V(1)—N(3)	174.0(2)	C(4)—N(1)—N(2)	115.3(4)
O(3)—V(1)—O(1)	103.0(2)	C(4)—N(1)—V(1)	127.9(4)
O(3)—V(1)—O(2)	90.4(2)	N(2)—N(1)—V(1)	116.7(3)
O(3)—V(1)—N(1)	158.5(2)	C(6)—N(2)—N(1)	108.3(4)
O(3)—V(1)—N(3)	75.6(2)	C(13)—N(3)—V(1)	135.4(4)
O(1)—V(1)—O(2)	154.3(2)	C(13)—N(3)—C(21)	117.0(5)
O(1)—V(1)—N(1)	84.9(2)	O(1)—C(2)—C(1)	114.7(5)
O(1)—V(1)—N(3)	81.2(2)	O(1)—C(2)—C(3)	122.7(5)
O(2)—V(1)—N(1)	75.4(2)	N(1)—C(4)—C(3)	121.0(5)
O(2)—V(1)—N(3)	81.0(2)	N(2)—C(6)—O(2)	121.5(5)

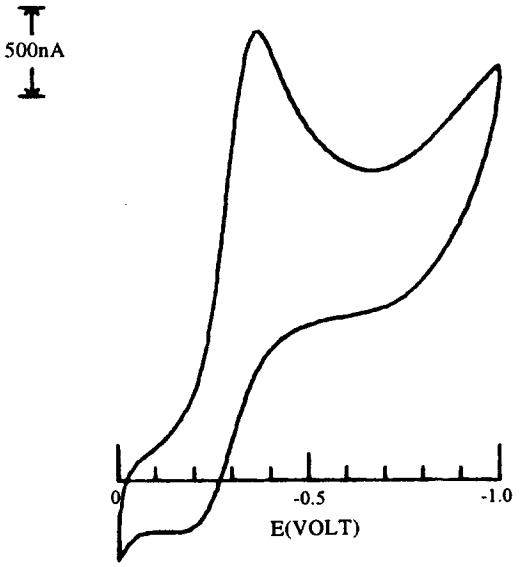

Fig. 1. Cyclic voltammogram of VOL(hquin) in dichloromethane.

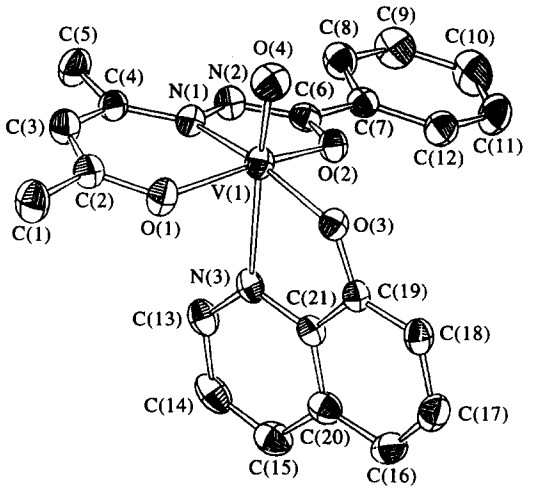

Fig. 2. Molecular structure of VOL(hquin) showing the atom numbering and 30% probability displacement ellipsoids.

the redox process may be expressed by the following equation:

$$[V^{V}O(L)(ON)] + e^{-} \rightleftarrows [V^{IV}O(L)(ON)]^{-}$$

Crystal structure studies

The molecular structure of the title complex is illustrated in Fig. 2. The vanadium atom is coordinated by four oxygen atoms and two nitrogen atoms to form a distorted octahedral O_4N_2 configuration, O(1), O(2) and N(1) from a fully deprotonated tridentate L; atoms O(3) and N(2) from a hquin, and atom O(4) from the vanadyl oxygen atom. The equatorial plane is defined by the atoms O(1), O(2), N(1) and O(3) with the mean deviation of 0.004 Å, vanadium atom is 0.312 Å out the plane and toward the oxo oxygen atom O(4). In most of the VO^{3+} complexes with hydrazone, vanadium atom has a square pyramidal coordination; only two six-coordinated VO^{3+} complexes are known [9,11]. To our knowledge, the title complex is the first example of a six-coordinated VO^{3+} complex with an acetylacetone benzoylhydrazone ligand.

The five-membered chelate ring of O(2), C(6), N(2), N(1) and V(1) is a good plane with a small mean derivation (0.003 Å), but the six-membered chelate

ring of O(1), C(2), C(3), C(4), N(1) and V(1) is non-planar.

The V(1)=O(4) distance of 1.580(4) Å is within the normal values in the structures of VO^{3+} complexes [9–14,19,20]. The bonds V(1)—O(1), V(1)—O(2), V(1)—O(3) and V(1)—N(1) in the equatorial plane are 1.873(4), 1.912(4), 1.842(4) and 2.051(4) Å, respectively. The bond length of V(1)—O(3) (phenolate) is significantly shorter than that of V(1)—O(1) and V(1)—O(2) in the fragment including V atom and tridentate ligand. The bond distance of V(1)—N(3) (2.333(5) Å) is relatively longer due to structural *trans* effect [21].

Supplementary material—Tables of the atomic coordinates, thermal parameters, non-essential bond distances and angles and positional parameters of hydrogen atoms are available from author S.-X. Liu.

Acknowledgements—The authors wish to thank Associate Professor Yu Zheng for the IR and Raman measurements and her valuable discussion.

REFERENCES

1. Vitler, H., *Phytochemistry*, 1984, **23,** 1387.
2. Plat, H., Krenn, B. E. and Wever, R., *Biochem. J*, 1987, **248,** 277.
3. Soedjak, H. S. and Butler, A., *Biochemistry*, 1990, **29,** 7974.
4. Hales, B. J., Case, E. E., Morningstar, J. E., Dzeda, M. F. and Mauterer, L. A., *Biochemistry*, 1986, **25,** 7251.
5. Arber, J. M., Dobson, B. R., Eady, R. R., Stevens, P., Hasnain, S. S., Garner, C. D. and Smith, B. E., *Nature*, 1987, **325,** 372.
6. Butler, A. and Carrano, C. J., *Coord. Chem. Rev.*, 1991, **109,** 61.
7. Rehder, D., *Angew. Chem. Int. Ed. Engl*, 1991, **30,** 148.
8. Butler, A. and Walker, J. V., *Chem. Rev.*, 1993, **93,** 1937.
9. Chakravarty, J., Dutta, S., Dey, A. and Chakravorty, A., *J. Chem. Soc., Dalton Trans.*, 1994, 557.
10. Wang, W., Zeng, F.-L., Wang, X and Tan, M.-Y., *Polyhedron*, 1996, **15,** 1699.
11. Bansse, W., Ludwig, E., Uhlemann, E., Weller, F., Dehnicke, K. and Herrmann, W., *Z. Anorg. Allg. Chem.*, 1992, **613,** 36.
12. Yan, S.-P., Wang, G.-L., Wang, H.-G. and Yao, X.-K., *Chin. J. of Struct. Chem.*, 1992, **11,** 47.
13. Diamantis, A. A., Frederiksen, J. M. and Salam, M. A., *Aust. J. Chem*, 1986, **39,** 1081.
14. Wang, W., Wang, X., Liu, H.-X. and Tan, M.-Y., *J. Coord. Chem.*, 1995, **36,** 49.
15. Rowe, R. A. and Jones, M. M., *Inorg. Synth.* 1957, **5,** 113.
16. Nakamota, K., Infrared and Raman Spectra of Inorganic and Coordination Compounds, 4th edn., John Wiley & Sons, New York (1986).
17. Asgedom, G., Sreedhara, A. and Rao, C. P., *Polyhedron*, 1995, **14,** 1873.
18. Zamian, J. R., Dockal, E. R., Castellano, G. and Oliva, G., *Polyhedron*, 1995, **14,** 2411.
19. Clague, M. J., Keder, N. L. and Butler, A., *Inorg. Chem.*, 1993, **32,** 4754.
20. (a) Mondal, S., Dutta, S. and Chakravorty, A., *J. Chem. Soc., Dalton Trans.*, 1995, 1115. (b) Mondal, S., Rath, S. P., Dutta, S. and Chakravorty, A., *J. Chem. Soc., Dalton Trans.*, 1996, 99.
21. Scheidt, W. R., *Inorg. Chem.*, 1973, **12,** 1758.

Pergamon

PII: S0277-5387(97)00253-2

Polyhedron Vol. 17, No. 1, pp. 85–91, 1998
© 1997 Elsevier Science Ltd
All rights reserved. Printed in Great Britain
0277-5387/98 $19.00+0.00

Mixed-metal copper(II) and lead(II) complexes due to μ- and μ_3-bridging alkoxo groups from 2-dimethylaminoethanol. Chains and layers in $[CuPbCl_2(Me_2NCH_2CH_2O)_2]_n \cdot n/2H_2O$ and $[CuPbI_2(Me_2NCH_2CH_2O)_2]_2$

Olga Yu. Vassilyeva,[a]* Larisa A. Kovbasyuk,[a] Volodymyr N. Kokozay,[a] Brian W. Skelton[b] and Wolfgang Linert[c]

[a] Department of Inorganic Chemistry, Kyiv Shevchenko University, Volodimirska st., 64, Kyiv 252033, Ukraine

[b] Department of Chemistry, University of Western Australia, Nedlands, Western Australia 6009, Australia

[c] Institute of Inorganic Chemistry, Vienna University of Technology, Getreidemarkt 9/153 A-1060 Vienna, Austria

(Received 20 February 1997; accepted 9 June 1997)

Abstract—A number of mixed-metal complexes of Cu^{II} and Pb^{II} containing 2-dimethylaminoethanol (HL) is reported. The compounds were identified and characterized by chemical analyses and IR investigations. The crystal structure of $[CuPbCl_2L_2]_n \cdot n/2H_2O$ and $[CuPbI_2L_2]_2$ were determined by X-ray crystallographic analysis. The metal complex motif of both compounds is a centrosymmetric tetranuclear dimer with square pyramidal coordination geometry around the Cu atom and highly distorted octahedral coordination to the Pb atom. The Cu and Pb atoms are bridged by alkoxide oxygens from L to form a $Pb_2Cu_2O_4$ core which displays a flattened chair conformation. In the chloride complex tetranuclear units are connected successively *via* μ-chloro bridging between two Pb sites forming polymeric chains. In the iodide complex the I atom bonded to the Pb atom bridges to Cu and Pb atoms of adjacent complex molecules to produce a layer parallel to the *bc* plane. © 1997 Elsevier Science Ltd

Keywords: mixed-metal complexes; crystal structure; coordination polymers.

The interest in mixed-metal complexes may be attributed to increased recognition of the importance of polynuclear centres in biological catalytic processes and the potential application of expected metal–metal interactions to synthetic systems possessing useful magnetic and electrochemical properties [1,2]. From a chemical point of view a major task is to achieve systems to keep the two metal ions not too distant from each other at the scale of the whole lattice. Many mixed-metal complexes have been synthesized to date as complexes of binucleating or polynucleating macrocycles through the design of appropriate macrocyclic ligands [1, 3]. A different approach can be the use of bridging ligands to bind two metal ions [4, 5]. Our previous work in the field of synthesis of coordination compounds from metal powders or metal oxides [6] prompted us to design a procedure for the synthesis of mixed-metal complexes. Our strategy consists of reacting a copper powder with lead salt in non-aqueous solution of 2-dimethylaminoethanol (HL):

$$Cu + PbX_2 + 2HL + 1/2O_2 \xrightarrow{Solv} CuPbX_2L_2 + H_2O$$

X–Cl, Br, I, SCN; Solv–dmf, dmso, CH_3CN, CH_3OH

The synthesis of metal complexes from metal powders is the fascinating and promising approach to provide complexes of unusual stoichiometry and

* Author to whom correspondence should be addressed.

structure [7–9]. We have used aminoalcohol to bridge unlike metal atoms, namely copper and lead, due to the attractive feature of these ligands to form polynuclear oxygen-bridged metal complexes [10–12]. The halide anion is also an effecting bridging ligand, which imposes few steric constraints upon the coordination geometry.

The merit of the procedure is one-pot synthesis under mild reaction conditions and short reaction time, good yield and its versatility. We can prepare predictable mixed-metal complexes by reacting different metal powders and metal salts in solutions of different aminoalcohols or other complexing agents. Here we describe the preparation and X-ray structure of $[CuPbCl_2L_2]_n \cdot n/2H_2O$ (**1**) and $[CuPbI_2L_2]_2$ (**2**).

EXPERIMENTAL

All chemicals were commercial products of reagent grade, used without further purification, all experiments were carried out in air. As is clear from Table 1, in the studied systems several types of complexes formed mainly depending on the ratio of initial reagents and the nature of solvent. Mixed-metal complexes $[CuPbI_2L_2dmso]_2 \cdot 2dmso$ and $[CuPbBr_2L_2dmso]_2$ have been crystallographically characterized and reported previously [13,14]. All the complexes were prepared by similar procedures as those for above mentioned complexes [13,14] and a typical procedure for **1** is given below.

Copper powder (0.63 g, 0.01 mol), $PbCl_2$ (2.78 g, 0.01 mol), dmso (15 cm^3) and 2-dimethylaminoethanol (2.0 cm^3, 0.02 mol) were heated to 60°C and stirred until total dissolution of Cu and $PbCl_2$ was observed (30–35 min). The resulting clear solution was allowed to stand at room temperature for 12 h after which blue crystals **1** separated from the solution. They were filtered, washed with dry isopropanol and finally dried *in vacuo* at room temperature; yield 4.29 g (81.2%).

All the compounds obtained are green or blue crystalline substances which are insoluble in water and sparingly soluble in common organic solvents. Elemental analyses were performed by the Institute of

Table 1. Compositions of obtained mixed-metal compounds

Systems	Analytical Results, %[a]						Assumed Composition
	Pb	Cu	X	C	H	N	
$PbCl_2$-Cu-HL-dmso	40.1 / 39.34	12.3 / 12.06	13.6 / 13.48	17.9 / 18.22	4.1 / 3.99	5.0 / 5.31	$[CuPbCl_2L_2]_n \cdot n/2H_2O$ (**1**)
$PbCl_2$-Cu-HL-CH_3CN	39.9 / 39.90	12.9 / 12.27	13.8 / 13.69	18.2 / 18.53	4.2 / 3.86	5.2 / 5.40	$CuPbCl_2L_2$
$PbCl_2$-2Cu-HL-dmf	29.7 / 29.38	17.3 / 18.02	14.6 / 15.08	20.5 / 20.44	4.3 / 4.26	5.7 / 5.97	$Cu_2PbCl_3L_3$
$PbBr_2$-Cu-HL-dmf	34.1 / 34.15	10.5 / 10.47	24.5 / 26.34	15.6 / 15.83	3.4 / 3.32	4.4 / 4.62	$CuPbBr_2L_2$
$PbBr_2$-Cu-HL-dmso	29.6 / 30.25	8.7 / 9.28	22.8 / 23.33	17.7 / 17.54	3.9 / 3.83	4.0 / 4.09	$[CuPbBr_2L_2dmso]_2$
PbI_2-Cu-HL-dmf	29.7 / 29.57	8.9 / 9.07	35.9 / 36.22	13.5 / 13.71	2.8 / 2.88	4.2 / 4.00	$[CuPbI_2L_2]_2$ (**2**)
PbI_2-2Cu-HL-dmf	22.6 / 22.05	13.1 / 13.52	28.4 / 27.01	18.6 / 20.43	4.2 / 4.29	5.4 / 5.96	$Cu_2PbI_2L_4$
$2PbI_2$-Cu-HL-CH_3OH	36.3 / 36.89	6.0 / 5.65	32.2 / 33.89	13.8 / 12.83	3.0 / 2.69	4.4 / 3.74	$CuPb_2I_3L_3$
PbI_2-Cu-HL-dmso	24.3 / 24.18	7.4 / 7.41	30.1 / 29.61	16.9 / 16.82	3.2 / 3.27	3.7 / 3.76	$[CuPbI_2L_2dmso]_2 \cdot 2dmso$
$Pb(SCN)_2$-Cu-HL-dmso	37.1 / 36.79	10.9 / 11.28	19.8 / 20.63	21.0 / 21.30	3.4 / 3.55	9.6 / 9.95	$CuPb(SCN)_2L_2$

[a]Numerator is found value; denominator is value calculated for marked formula.

Organic Chemistry, National Academy of Sciences of Ukraine microanalytical service.

Infrared spectra were recorded as KBr discs on a UR-10 spectrophotometer in the 4000–400 cm^{-1} region using conventional techniques.

$[CuPbCl_2L_2]_n \cdot n/2H_2O$ (**1**). 3630–3200 (br), 3010 (w), 2980 (sh), 2950 (m), 2910 (sh), 2870 (m), 2840 (sh), 2800 (m), 1640 (w), 1620 (sh), 1480 (m), 1470 (m), 1430 (w), 1380 (w), 1350 (w), 1280 (w), 1250 (w), 1190 (w), 1110 (w), 1070 (s), 1030 (m), 950 (m), 900 (m), 880 (m), 780 (m), 620 (m), 585 (w), 510 (w), 460 (w), 430 (w) cm^{-1}.

$CuPbCl_2L_2$. 3530 (br), 3450 (br), 3010 (w), 2970 (br), 2870 (s), 2850 (s), 2800 (m), 2750 (w), 1480 (s), 1460 (s), 1380 (w), 1350 (w), 1280 (w), 1250 (w), 1240 (w), 1180 (w), 1080 (s), 1060 (s), 1030 (m), 1010 (m), 950 (s), 900 (s), 780 (m), 625 (m), 600 (w), 500 (br), 470 (m), 435 (m) cm^{-1}.

$Cu_2PbCl_3L_3$. 3600–3300 (br), 3010 (w), 2980 (m), 2910 (s), 2870 (s), 2850 (s), 2800 (w), 1640 (br), 1470 (s), 1380 (w), 1350 (w), 1280 (w), 1260 (w), 1250 (w), 1180 (w), 1110 (w), 1070 (s), 1020 (m), 950 (s), 900 (s), 780 (m), 620 (m), 610 (m), 505 (m), 470 (br), 430 (sh) cm^{-1}.

$CuPbBr_2L_2$. 3600–3350 (br), 3010 (w), 2960 (sh), 2900 (sh), 2870 (s), 2840 (s), 2800 (m), 1460 (s), 1380 (w), 1350 (w), 1280 (w), 1250 (w), 1240 (w), 1180 (w), 1110 (w), 1060 (s), 1020 (m), 1010 (m), 950 (s), 900 (s), 780 (m), 625 (m), 600 (m), 510 (m), 475 (m), 435 (sh) cm^{-1}.

$[CuPbBr_2L_2dmso]_2$. 3600–3350 (br), 3010 (sh), 2980 (m), 2950 (w), 2900 (sh), 2870 (s), 2840 (sh), 2800 (m), 1630 (br), 1470 (m), 1460 (sh), 1420 (w), 1380 (w), 1350 (w), 1310 (w), 1280 (w), 1250 (w), 1190 (sh), 1180 (w), 1070 (s), 1020 (m), 1010 (m), 1000 (s), 950 (s), 900 (s), 780 (m), 620 (m), 600 (w), 510 (w), 470 (m), 430 (w) cm^{-1}.

$[CuPbI_2L_2]_2$ (**2**). 3600–3350 (br), 3000 (w), 2960 (m), 2900 (m), 2870 (s), 2840 (m), 2800 (w), 1650 (m), 1480 (w), 1460 (s), 1430 (w), 1380 (w), 1350 (w), 1280 (w), 1250 (w), 1240 (w), 1180 (w), 1100 (w), 1070 (m), 1050 (s), 1020 (m), 1010 (m), 950 (s), 900 (s), 780 (m), 625 (m), 600 (m), 510 (m), 475 (m), 435 (w) cm^{-1}.

$Cu_2PbI_2L_4$. 3600–3350 (br), 3000 (w), 2970 (w), 2940 (m), 2920 (m), 2870 (m), 2850 (m), 2810 (w), 1670 (s), 1460 (m), 1380 (m), 1350 (w), 1280 (w), 1250 (w), 1240 (w), 1180 (w), 1070 (s), 1030 (m), 1010 (m), 950 (s), 910 (m), 780 (m), 635 (m), 520 (v), 480 (m), 440 (w), 410 (w) cm^{-1}.

$CuPb_2I_3L_3$. 3600–3350 (br), 3000 (w), 2960 (w), 2900 (sh), 2860 (m), 2840 (m), 2800 (w), 1470 (sh), 1460 (s), 1430 (w), 1380 (w), 1350 (w), 1280 (w), 1250 (w), 1180 (w), 1100 (w), 1070 (sh), 1060 (s), 1030 (m), 1010 (sh), 950 (s), 900 (m), 780 (m), 600 (m), 625 (m), 510 (m), 470 (m), 335 (w) cm^{-1}.

$[CuPbI_2L_2dmso]_2 \cdot 2dmso$. 3600–3300 (br), 2970 (m), 2940 (sh), 2890 (sh), 2880 (m), 2840 (s), 2790 (m), 1630 (br), 1480 (m), 1460 (s), 1430 (m), 1410 (m), 1380 (w), 1350 (w), 1310 (w), 1280 (sh), 1270 (w), 1230 (w), 1180 (w), 1170 (w), 1100 (w), 1070 (m), 1050 (s), 1010 (s), 1000 (sh), 960 (m), 940 (m), 900 (m), 780 (m), 625 (m), 600 (w), 510 (m), 475 (m), 435 (w), 410 (m).

$CuPb(SCN)_2L_2$. 3600–3350 (br), 3000 (w), 2970 (m), 2950 (m), 2910 (sh), 2890 (m), 2860 (m), 2840 (m), 2790 (w), 2110 (vs), 2060 (vs), 1630 (br), 1460 (m), 1410 (w), 1380 (w), 1350 (w), 1280 (w), 1260 (w), 1180 (w), 1100 (w), 1060 (s), 1040 (sh), 1030 (m), 1010 (m), 950 (s), 890 (s), 820 (w), 780 (m), 625 (m), 610 (m), 595 (sh), 510 (m), 460 (s), 430 (m) cm^{-1}.

Crystal structure determination

Crystallographic measurements were made at 20°C using an Enraf–Nonius CAD-4 diffractometer operating in the $\omega/2\theta$ scan mode. The accurate unit cell parameters and the orientation matrix for data collection were obtained from least-squares refinement of the setting angles of 24 reflections in the range $13 < \theta < 15°$. The crystallographic data are summarized in Table 2. Correction for the Lorentz and polarization effects as well as an empirical absorption correction using DIFABS [20] for **1** and an analytical correction by the Gaussian method [21] for **2** [A*(min, max) = 2.57, 3.24] were applied.

The structures were solved by direct (**1**) and Patterson (**2**) methods followed by subsequent difference Fourier routines and refined by full matrix least squares on *F*. Anisotropic thermal parameters were assigned and refined for all non-hydrogen atoms in case of **2** and only for Pb, Cu and Cl atoms for **1**. All the hydrogen atoms in the structures were included in calculated positions, but not refined. Each hydrogen atom was assigned an isotropic thermal parameter of 1.25; 1.5 times that of attached C atom for CH_2 and CH_3 groups, respectively, (**1**) and fixed $B_{iso} = 5$ Å^2 (**2**). 'Solvent' in the structure **1** was modelled as oxygen of water molecule with population 0.5, hydrogen atoms were not included for the solvent molecule. The convergences were reached at the agreement factors listed in Table 2.

Selected bond distances and angles are given in Tables 3 and 4. Atomic coordinates, anisotropic displacement parameters, observed and calculated structure factors, the list of interatomic distances, bond angles and torsion angles are given in the supplementary material.

RESULTS AND DISCUSSION

In the IR spectra of the compound $CuPb(SCN)_2L_2$ only the very strong ν(CN) vibrations of the thiocyanate groups (2110 and 2060 cm^{-1}) coordinated in bridging mode and *via* the nitrogen atom can be identified easily [15]. The rather strong bands corresponding to $\nu(SO) = 1000$ and weak one corresponding to $\delta(H_2O) = 1620$ cm^{-1} vibrations of the coordinated dmso and water molecules of crys-

Table 2. Crystal data and summary of intensity data collection and refinement

Compound	**1**	**2**
Formula	$C_8H_{20}Cl_2CuN_2O_2Pb \cdot 1/2H_2$	$C_8H_{20}I_2CuN_2O_2Pb$
Formula weight	526.91	700.80
Crystal size (mm)	$0.31 \times 0.09 \times 0.08$	$0.25 \times 0.20 \times 0.15$
Colour	blue	dark-green
Habit	needle	prismatic
Crystal system	monoclinic	monoclinic
Space group	$P2_1/n$	$P2_1/c$
a (Å)	7.995(3)	12.485(1)
b (Å)	15.008(7)	8.490(1)
c (Å)	13.255(7)	15.494(4)
α (°)	90	90
β (°)	105.88(4)	93.68(2)
γ (°)	90	90
V (Å^3)	1529.8(2)	1639.0(8)
Z	4	4
D_{calcd} (g cm^{-3})	2.288	2.840
μ (Mo-K_α) (cm^{-1})	127.2	153.6
Radiation (Å)	Mo-K_α (0.71073)	Mo-K_α (0.71073)
F(000)	992	1260
$2\theta_{max}$ (°)	50	44
Unique data	2682	2110
Observed data $[I \geqslant 3\sigma(I)]$	1256	1740
R$[I \geqslant 3\sigma(I)]$	0.061	0.030
wR	0.064 $[\sigma^2(I) = \sigma^2(I)_{diff} + n\sigma^4(I)_{diff}$, $n = 4 \times 10^{-4}]$	0.041 $[w^{-1} = \sigma^2 F + 0.0016F^2]$
Goodness of fit	1.832	1.36
Software	XTAL3.4 [18]	SDP-PLUS [19]

tallization, respectively, were observed in the spectra of compounds $[CuPbBr_2L_2dmso]_2$, $[CuPbI_2L_2dmso]_2 \cdot 2dmso$ and **1** [16]. On coordination, changes in absorption frequencies of 2-dimethylaminoethanol occurred; namely, the strong mode found in spectra of the free ligand [17] at 1040 cm^{-1} shifts 20–30 cm^{-1}

Table 3. Selected bond lengths (Å) and angels (°) for **1**

Pb—Cl(1)	2.791(9)	Cu—Cl(2)	2.605(8)
Pb—O(1)	2.66(2)	Cu—O(1)	2.01(2)
Pb—O(2)	2.36(2)	Cu—O(2)	1.94(3)
Pb—Cl(2′)	3.120(9)	Cu—N(1)	2.08(3)
Pb—O(1′)	2.36(2)	Cu—N(2)	2.06(3)
Pb—Cl(1″)	3.12(1)		

Cl(1)—Pb—O(1)	148.8(4)	Cl(2)—Cu—O(1)	93.2(5)
Cl(1)—Pb—O(2)	87.6(7)	Cl(2)—Cu—O(2)	98.7(7)
Cl(1)—Pb—Cl(2′)	90.5(3)	Cl(2)—Cu—N(1)	98.9(7)
Cl(1)—Pb—O(1′)	91.4(4)	Cl(2)—Cu—N(2)	94.9(6)
Cl(1)—Pb—Cl(1″)	82.7(3)	O(1)—Cu—O(2)	81.4(8)
O(1)—Pb—O(2)	61.4(7)	O(1)—Cu—N(1)	84.9(9)
O(1)—Pb—Cl(2′)	115.7(4)	O(1)—Cu—N(2)	164.9(8)
O(1)—Pb—O(1′)	80.5(5)	O(2)—Cu—N(1)	158.2(9)
O(1)—Pb—Cl(1″)	97.6(4)	O(2)—Cu—N(2)	84.8(9)
O(2)—Pb—Cl(2′)	153.9(7)	N(1)—Cu—N(2)	106(1)
O(2)—Pb—O(1′)	79.3(7)	Cl(2′)—Pb—Cl(1′)	118.6(2)
O(2)—Pb—Cl(1″)	87.0(6)	O(1′)—Pb—Cl(1″)	165.3(4)
Cl(2′)—Pb—O(1′)	74.7(4)		

Symmetry operations: ′ 1 − x, 1 − y, 1 − z; ″ 2 − x, 1 − y, 1 − z.

Table 4. Selected bond lengths (Å) and angles (°) for **2**

Pb—I(1)	3.2381(8)	Cu—N(1)	2.068(8)
Pb—I(2)	3.1966(9)	Cu—N(2)	2.07(1)
Pb—O(1)	2.339(6)	Cu—O(1)	1.903(6)
Pb—O(2)	2.560(7)	Cu—O(2)	1.936(6)
Pb—O(2′)	2.551(7)		
I(1)—Pb—I(2)	91.57(2)	O(1)—Cu—O(2)	81.6(3)
I(1)—Pb—O(1)	90.1(1)	O(1)—Cu—N(1)	85.6(3)
I(1)—Pb—O(2)	151.5(1)	O(1)—Cu—N(2)	167.3(3)
I(2)—Pb—O(1)	89.1(2)	O(2)—Cu—N(1)	167.1(3)
I(2)—Pb—O(2)	85.8(2)	O(2)—Cu—N(2)	86.8(3)
O(1)—Pb—O(2)	61.4(2)	N(1)—Cu—N(2)	105.9(4)

Symmetry operation: ′ 1 − x, −y, −z.

to higher energy, the strong bands at 1270 and 1100 cm^{-1} are not observed and the intensive band near 900 cm^{-1} appears.

Complex **1** is a centrosymmetric dimer composed of two $CuPbCl_2L_2$ units linked by alkoxobridges of L groups (Fig. 1). The Pb atom is six-coordinate, being surrounded by three oxygen atoms, O(1), O(2) and O(1) $\{1-x, 1-y, 1-z\}$ from the three L groups and three chloride atoms, Cl(1), Cl(1) $\{2-x, 1-y, 1-z\}$ and Cl(2) $\{1-x, 1-y, 1-z\}$ with substantial departure from an ideal octahedral geometry. The coordination geometry around the Cu atom is distorted square pyramidal. The basal plane consists of two oxygen, O(1), O(2) and two nitrogen atoms, N(1) and N(2) from the two L groups while the axial coordination site is occupied by Cl(2) atom. The Cu and Pb atoms are bridged by an alkoxide oxygen O(2) from L resulting in Cu-Pb separation of 3.463(4) Å with Cu—O(2)—Pb angle 107.0(1.2)°. The alkoxide oxygen O(1) forms a bridge between three metal centres linking Cu and Pb to a centrosymmetric Pb′ $\{1-x, 1-y, 1-z\}$, resulting in Pb—Pb′ and Cu—Pb′ distances of 3.840(2) and 3.557(4) Å, respectively, with Cu—O(1)—Pb′ angle of 108.4(6)°. The Cu and Pb′ atoms are asymmetrically bridged by μ-Cl(2) atom. $Pb_2Cu_2O_4$ core displays a flattened chair conformation with the $PbCuO_2$ planes each folded by 70(1)° with respect to the strictly planar Pb_2O_2 plane.

The basic complex motifs are further extended through μ-Cl(1) bridging between two Pb sites to form doubly-bridged chains running along the *a* axis at $b = ca$ 0 and 0.5 (Fig. 1). These chains are considerably flattened staircase polymers with an angle between adjacent Pb_2O_2 and Pb_2Cl_2 planes of 32.6(2)°. The chains are in turn crosslinked *via* hydrogen bonds to the included water molecules (Fig. 2). The oxygen atom O(3) forms hydrogen bonds with Cl(2) and Cl(2)′ $\{-x, 1-y, -z\}$ atoms with distances of 3.25 and 3.21 Å, respectively, and O(3)···Cl(2)···O(3)′ $\{-x, 1-y, -z\}$ angle of 151(2)°.

The overall structure of complex **2** with square pyramidal coordination geometry around the Cu atom

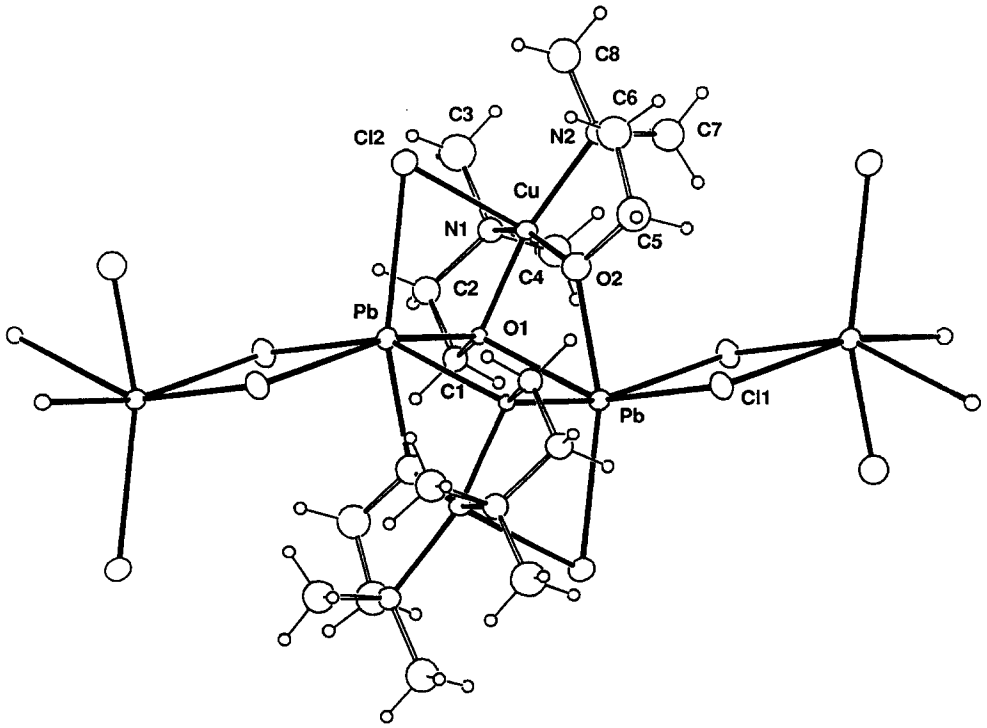

Fig. 1. Fragment of the polymeric chain present in the crystal structure of **1**.

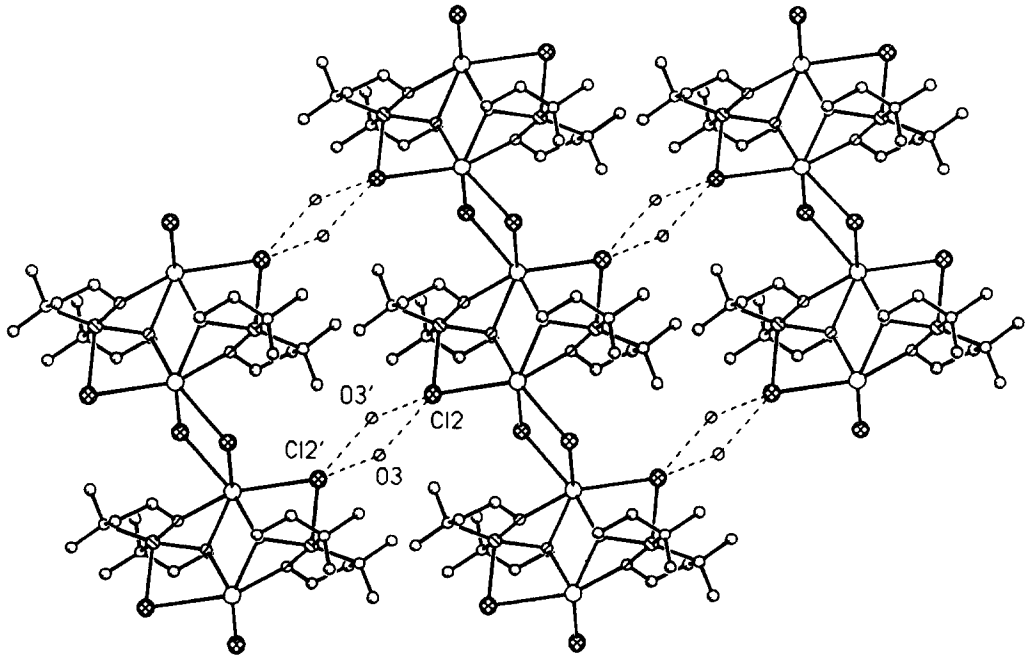

Fig. 2. Plan-view of part of the polymeric chains linked *via* hydrogen bonding to included water molecules in the crystal structure of **1** (hydrogen atoms are omitted for clarity, the additional interactions are shown as dashes).

and highly deformed octahedral coordination of the Pb atom resembles that of the compound **1** (Fig. 3). The copper and lead metal centres are bridged by alkoxide oxygens from L groups resulting in Cu—Pb, Cu—Pb′ $\{1-x, -y, -z\}$ separations of 3.343(1) and 3.753(1) Å, respectively with 103.5(2)° Cu—O(1)—Pb and 112.8(3)° Cu—O(2)—Pb′ angles. The I(1) atom bound to Pb bridges to Cu $\{x, -0.5-y, 0.5+z\}$ and Pb $\{1-x, -0.5+y, 0.5-z\}$ atoms of adjacent complex molecule (3.649(1), 3.5326(8) Å, respectively) to form a layer parallel to the *bc* plane (Fig. 4).

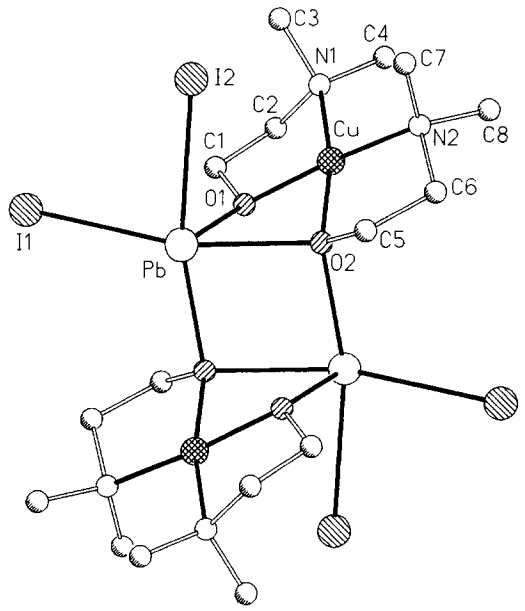

Fig. 3. The molecular structure of **2** (hydrogen atoms are omitted for clarity).

The 2-dimethylaminoethoxo groups in both compounds are structurally normal [22] [d(O—C) *ca* 1.42(1)–1.45(5), d(C—C) *ca* 1.47(2)–1.52(2), d(C—N) *ca* 1.48(2)–1.53(5), d[(N–C(terminal)] *ca* 1.43(2)–1.52(5) Å] and are coordinated to copper *via* oxygen and nitrogen atoms, forming five-membered puckered rings with the *gauche* configuration [the torsion N—C—C—O angles are *ca* 47(4)–53(1)°]. The oxygen atoms of the L groups are in μ- and μ_3-bridging positions.

From comparison of the structures of **1, 2** and ones reported previously [13,14] we can suppose that $Cu_2Pb_2L_4$ unit should be sufficiently rigid to retain the structural similarity in these complexes, and the compounds from Table 1 of composition $CuPbX_2L_2$ should contain the tetranuclear complexes with similar structures, with the $Pb_2Cu_2O_4$ core and the bridging halide or SCN groups.

Acknowledgements—X-ray data were collected and one of the structures was solved in part at the IUCr/ACA Summer Course in Crystallography, Pittsburgh, 1996. We thank the IUCr for financial support for O. Yu. V. to attend the Course.

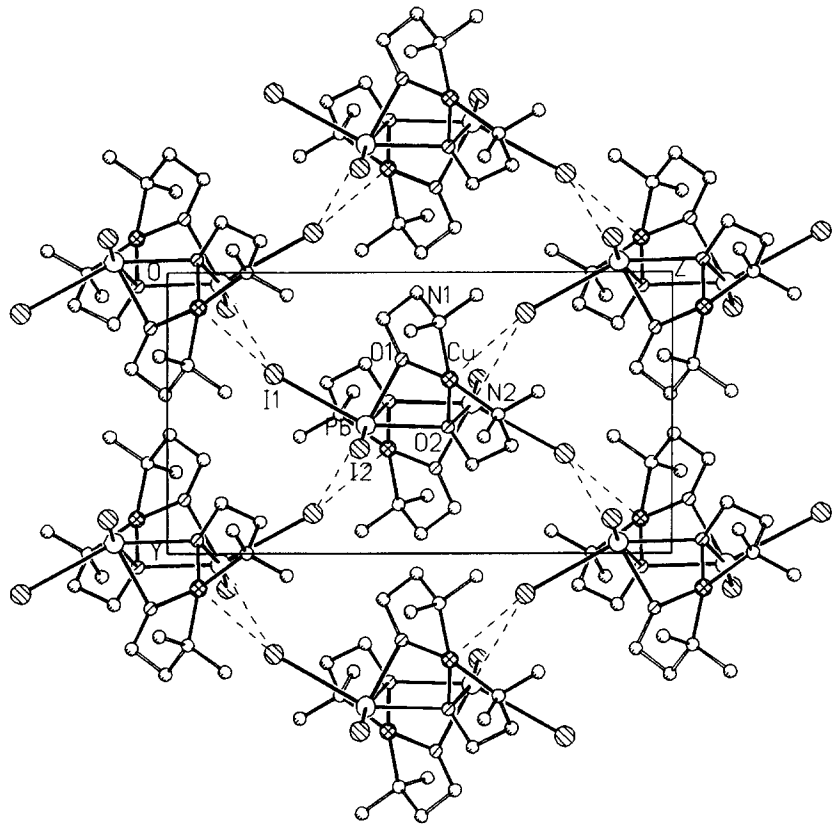

Fig. 4. Projection of part of the layer present in the crystal structure of **2** onto the *bc* plane (hydrogen atoms are omitted for clarity, the additional interactions are shown as dashes).

REFERENCES

1. Lehn, J.-M., *Angew. Chem. Int. Ed. Engl.*, 1988, **27,** 89.
2. Kahn, O., *Molecular Magnetism.* VCH Publishers, New York (1993).
3. Kaden, Th. A., in *Transition Metals in Supramolecular Chemistry*, ASIC 448, p. 211 eds. L. Fabbrizzi and A. Poggi, Kluwer Academic Publishers, Dordrecht (1994).
4. Stephan, D. W., *Coord. Chem. Rev.*, 1989, **95,** 41.
5. West, B. O., *Polyhedron*, 1993, **8,** 219.
6. Skopenko, V. V., Kokozay, V. N. and Pavlenko, V. A., *Ukr. Khim. Zh.* (*Russ. Ed.*), 1993, **59,** 485.
7. Godfrey, S. M., McAuliffe, C. A. and Pritchard, R. G., *J. Chem. Soc., Dalton Trans.*, 1993, 2875.
8. Garnovskii, A. D., Kharisov, B. I., Gojon-Zorrilla, G. and Garnovskii, D. A., *Russ. Chem. Rev.* (*Engl. Transl.*), 1995, **64,** 201.
9. Mashima, K., Nakayama, Yu., Shibahara, T., Fukumoto, H. and Nakamura, A., *Inorg. Chem.*, 1996, **35,** 93.
10. Smolander, K., *Annales Academiae Scientirum Finnicae*, Series A 1983, **2,** 1.
11. Kokozay, V. N. and Sienkiewicz, A., *Polyhedron*, 1993, **12,** 2421.
12. Sienkiewicz, A. and Kokozay, V. N., *Polyhedron*, 1994, **13,** 1439.
13. Vassilyeva, O. Yu., Kokozay, V. N., Zhukova, N. A. and Kovbasyuk, L. A., *Polyhedron*, 1997, **16,** 263.
14 Kovbasyuk, L. A., Vassilyeva, O. Yu., Kokozay, V. N. and Linert, W., *Z. Naturforsch*, 1997, **526,** 337.
15. Golub, A., Kohler, H., Skopenko, V. (Eds), *Chemistry of Pseudohalides.* Elsevier, Amsterdam (1986).
16. Nakamoto, K., *Infrared and Raman Spectra of Inorganic and Coordination Compounds*, 4th edn. Wiley–Interscience (1986).
17. The Aldrich Library of FT-IR Spectra, Aldrich Chem. Comp. Inc., USA (1985).
18. Hall, S. R., King, G. S. D. and Stewart, J. M., *XTAL*3.4. *User's Manual*, University of Western Australia, Lamb, Perth (1995).
19. Frenz, B. A., in *Computing in Crystallography* (Eds H. Schenk, R. Olthof-Haselkamp, H. van Koningsveld and G. C. Bussi), Delft University Press, Delft (1978).
20. Walker, N. and Stuart, D., *Acta Cryst.*, 1983, **A39,** 158.
21. Busing, W. R. and Levy, H. A., *Acta. Cryst.*, 1967, **22,** 457.
22. Wells, A. F., *Structural Inorganic Chemistry*, Clarendon Press, Oxford (1986).

Pergamon

PII: S0277-5387(97)00246-5

Polyhedron Vol. 17, No. 1, pp. 93–104, 1998
© 1997 Elsevier Science Ltd
All rights reserved. Printed in Great Britain
0277–5387/98 $19.00+0.00

13-Membered macrocycles and their complexometric properties: study of 7,11-bis(carboxymethyl)-1,4-dioxa-7,11-diazacyclotridecane

Sílvia Chaves[a,c], Ana Cerva[b] and Rita Delgado[b,c]*

[a]Centro de Química Estrutural, Av. Rovisco Pais, 1096 Lisboa codex, Portugal

[b]Instituto de Tecnologia Química e Biológica, Rua da Quinta Grande, 6, 2780 Oeiras, Portugal

[c]Instituto Superior Técnico, Av. Rovisco Pais, 1096 Lisboa codex, Portugal

(Received 29 April 1997; accepted 3 June 1997)

Abstract—The protonation constants of **L1** [7,11-bis(carboxymethyl)-1,4-dioxa-7,11-diazacyclotridecane] and the stability constants of complexes formed by this ligand with the alkaline-earth metal ions, the divalent first-row transition metal ions, Cd^{2+}, and Pb^{2+} were determined by potentiometric methods, at 25°C and ionic strength 0.10 M in tetramethylammonium nitrate. In general, the stability constant values for the complexes studied are lower than expected for a potential six-co-ordinate ligand with an N_2O_4 co-ordination sphere. The complexes of **L1** with metal ions, forming mainly electrostatic interactions (the alkaline–earth metal ions, Mn^{2+} and Pb^{2+}), have a sharp decrease of stability when compared with the corresponding complexes of 12-membered ligands, **L3** and **L4** [7,10-bis(carboxymethyl)-1,4-dioxa-7,10-diazacyclodecane and 4,10-bis(carboxymethyl)-1,7-dioxa-4,10-diazacyclododecane, respectively]. However, the Cu^{2+} and Ni^{2+} complexes of **L1** and **L4** have about the same values of stability constants. Hence, the 13-membered ligand is more selective for the divalent first-row transition metal ions than the 12-membered ones are. To explain these results we suggest that probably all the donor atoms of the ligands (**L1, L3** and **L4**) are involved on the co-ordination to the metal ions when mainly electrostatic interactions take place (also to the Co^{2+}, as spectroscopic measurements have revealed) but the distances and principally the orientation of the lone-pairs of electrons of **L1** are not in the better position for the co-ordination. Based on electronic and EPR spectroscopic measurements in solution and in magnetic moments of the complexes some explanations about the peculiarities of the Ni^{2+} and Cu^{2+} complexes of **L1** and **L4** were proposed. The Ni^{2+} complexes of both ligands exhibit tetragonally distorted octahedral geometry, but this metal ion seems to fit better in the cage formed by **L1** than that of **L4,** as indicated by the values of stability constants. Both ligands should adopt different arrangements around the metal ion, the distortion from the octahedron being more important for **[NiL4]** reflecting the loss in terms of crystal field stabilisation energy. However, the Cu^{2+} forms with **L1** a square pyramidal pentaco-ordinate complex while **L4** prefers a distorted octahedral arrangement. © 1997 Elsevier Science Ltd

Keywords: macrocycle; bis(carboxymethyl)-dioxa-diazacyclotridecane; stability constants; protonation constants; EPR copper complexes; Co^{2+}, Ni^{2+} and Cu^{2+} complexes.

The increase in size of the cavity of macrocycles carrying pendant N-methyl carboxylate arms, from 12- to 15-membered rings, causes a sharp decrease in stability of the metal complexes when the metal ion forms mainly electrostatic interactions, such as the alkaline–earth ions, Mn^{2+} or Pb^{2+} [1–4]. However, for the first-row transition divalent metal ions involved mainly in covalent interactions upon complexation, the situation is completely different; the increase of the number of atoms on the ring of the macrocycle does not significantly affect the stability of the complexes, specifically those of Co^{2+}, Ni^{2+} and Cu^{2+} [1–4]. Nevertheless, data in the literature are scarce to draw general conclusions. Only one series is completely studied, that of the N-tetracarboxymethylate

* Author to whom correspondence should be addressed.

tetraazamacrocylces, DOTA, TRITA and TETA [1,2] (*cf* Scheme 1) where the above conclusions were verified. The series of the N-tricarboxymethylate oxatriaza-macrocycles was undertaken [5–7], but data for the 13- and 14-membered ligands are not yet completely published. Another series of N-tricarboxymethyl tetraazamacrocycles containing a pyridine in the ring was also studied and the results published only for the 12-membered [3] and a 14-membered [8] ligands.

It is known that for the parent amines, the increase of the macrocyclic ring size may lead to an increase of the stability constants. For instance, for the tetraazamacrocycles, the peak in stability constants for the Ni^{2+} and Cu^{2+} complexes occurs for cyclam, the 14-membered ring [9,10]. The explanations are fully discussed [9,10].

Therefore, in order to have a complete knowledge of the effect of the increase of the ring size of these macrocycles results for the 13-membered ligands are

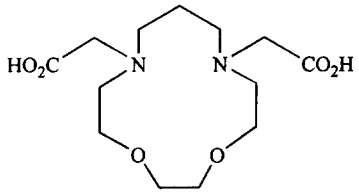

H_2L1

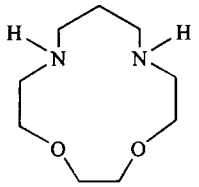

L2

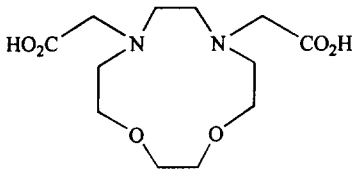

H_2L3

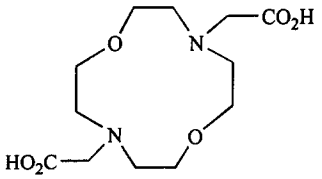

H_2L4

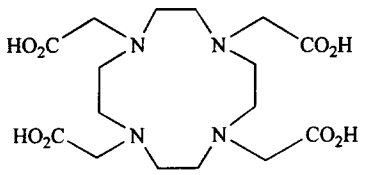

H_4DOTA

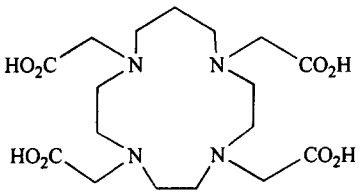

H_4TRITA

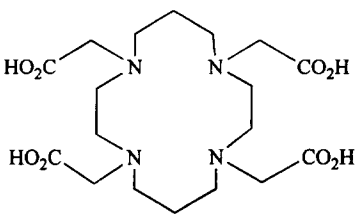

H_4TETA

Scheme 1.

needed but not available owing to difficulties of their synthesis. The yield of the cyclization step for the 13-membered ligands is low, using the procedures developed for the 12- and 14-membered compounds, and the last step, of introduction of the N-carboxymethyl groups, leads to mixtures hard to work up.

We decided to undertake the synthesis of the 13-membered N-carboxymethyl dioxadiaza macrocycle, **L1**, because two 12-membered compounds of this series were studied before, **L3** and **L4**. Although we knew that the stability constants of the complexes involving these ligands were relatively low [6], the preparation of **L1** was not hard and has made possible the comparison of the behaviour of the complexes of this ligand with the corresponding 12-membered ones and also the study of the effect of the replacement of two nitrogen by two oxygen atoms of the ring to compare with the tetraaza series, DOTA and TRITA.

The parent amine, **L2** (1,4-dioxa-7,11-diazacyclotridecane), has been previously synthesised [11–13] and its protonation and stability constants with some first-row transition divalent metal ions have been published [11,12]. **L1** has been obtained by Ewin and Hill [13] and the stability constants of its complexes with the alkaline–earth metal ions determined. However, the results are so different from ours that we decided to repeat the determinations for all of them and extend the study to the complexes of all the divalent first-row transition metal ions, and also Cd^{2+} and Pb^{2+}.

Note that completely deprotonated forms of the ligands are charged species but for simplicity the charges will generally be omitted in the text.

EXPERIMENTAL

Reagents

The commercial chemicals were of reagent grade and used without further purification. 1,2-Propanediamine (99%), 2,2′-ethylenedioxybis(ethanol) (98%), anhydrous disodium phosphate (99%) and mercury, p.a. were obtained from Merck, sodium hydride (20% in paraffin oil) and sodium lumps (99.5%) from Riedel, anhydrous sodium sulfate (99%) from Pronalab, chloroacetic acid and Amberlite IR-120 ion exchange resin standard grade in the Na^+ form (which was treated with 1.0 mol dm^{-3} hydrochloric acid before use) from BDH, and K_2H_2EDTA (dipotassium 1,2-diaminoethane-N,N,N′,N′-tetraacetate) from Fluka. N,N′-di-*p*-toluenesulfonyl-1,2-propanediamine and di-*p*-toluene-sulfonyl-2,2′-ethylenedioxybis(ethanol) were prepared as described before [14–16]. The organic solvents were purified by standard methods [17].

Synthesis and characterisation of the ligands

L2 was synthesised by the cyclization procedure of Richman and Atkins [18] with small modifications. In a typical experiment a solution of disodium salt of N,N′-di-*p*-toluenesulfonyl-1,2-propanediamine was prepared by the slow addition of sodium hydride (3 g), as a suspension in oil, in dry dimethylformamide (dmf) (62 cm^3) to a solution of N,N′-di-*p*-toluenesulfonyl-1,2-propanediamine (0.05 mol; 19.12 g) in dry dmf (250 cm^3), at room temperature and under nitrogen. After the evolution of hydrogen ceased the temperature of the solution was increased to 110–120°C and di-*p*-toluenesulfonyl-2,2′-ethylenedioxybis(ethanol) (0.05 mol; 22.91 g) in dmf (250 cm^3) was added, dropwise, under nitrogen over 5 h. The temperature and stirring was continued for another 3 h and left overnight at room temperature. Then the mixture was filtered off, the volume of the filtrate reduced by vacuum distillation and slowly poured into crushed ice. The white precipitate of the ditosylated cyclic amine (tosyl ≡ *p*-toluenesulfonyl) formed was filtered and washed several times with warm water (200 cm^3 at 75°C), then a solution of sodium hydroxide 2M (200 cm^3 at 75°C), finally with cold water several times and then recrystallized from toluene/n-hexane. Yield: 4.22 g (17%); m.p. 195–197°C; ^{1}H NMR ($CDCl_3$, TMS): δ 7.69 (d, 4H, tosyl groups), 7.32 (d, 4H, tosyl groups), 3.67 (t, 4H, —OCH_2—), 3.58 (s, 4H, —OCH_2CH_2O—), 3.22 (m, 8H, —NCH_2—), 2.43 (s, 6H, —CH_3) and 2.18 (q, 2H, —CH_2C$H_2$$CH_2$—) p.p.m.

The tosyl groups were removed under reductive alkaline conditions with a sodium amalgam in buffered methanol solution [6,19]. A mixture of the cyclic tritosylamine (2.02 mmol, 1.00 g), anhydrous disodium phosphate (17.5 mmol, 2.48 g) and 2% sodium amalgam (48 g) in dry methanol (20 cm^3) was stirred rapidly and heated to reflux for about 20 h, under nitrogen. After cooling to room temperature, the mercury was decanted from the slurry and the solution filtered off. The filtrate was concentrated almost to dryness, water was added (25 cm^3) and extracted four times with chloroform (25 cm^3). The organic layers were combined and dried over anhydrous sodium sulfate. The mixture was filtered off and the solvent removed *in vacuo* to obtain **L2** as a pale yellow oil. The oil was dissolved in chloroform (5 cm^3), 5 M hydrochloric acid (20 cm^3) was added slowly and then the solvent was removed. A white powder was formed when ethanol was added, corresponding to **L2**·2HCl. Yield: 0.265 g (≈50%); m.p. 220–222°C. ^{1}H NMR (D_2O, DSS; pD 4.08): δ 3.74 (t, 4H, —OCH_2—), 3.62 (s, 4H, —OCH_2CH_2O—), 3.27–3.21 (m, 8H, —NCH_2—), 2.08 (q, 2H, —CH_2C$H_2$$CH_2$—) p.p.m. ^{13}C NMR ($D_2O$, dioxane; pD 4.08): δ 69.76, 64.63, 45.16, 42.68, 21.26 p.p.m. Found: C, 37.88; H, 8.28; N, 9.58. Calc. for $C_9H_{22}N_2O_2Cl_2$1.25H_2O: C, 38.09; H, 8.64; N, 9.88%. (The microanalysis data were provided by the 'Laboratório de Análises Químicas', IST, Lisbon.)

The N-carboxymethylated ligand (**L1**) was synthesised by condensation of the parent dihydrochloridrated amine, **L2**·2HCl (1.92 mmol; 0.5 g)

with sodium chloroacetate (obtained by addition of 3 M NaOH solution to a concentrated aqueous chloroacetic acid, 4.02 mmol, 1.34 cm^3, at 5°C), in aqueous basic solution. The temperature was increased slowly during the reaction to a maximum of 65°C and the pH was kept below 10.5, by slow addition of 3 M NaOH. When the pH no longer changed, the reaction was considered completed (40 days); then the mixture was cooled and the pH adjusted to ≈ 1 with 5 M hydrochloric acid. Upon withdrawal of part of the solvent *in vacuo*, a precipitate of NaCl was formed and filtered off. The desired product was purified by chromatography using a cationic resin in the H^+ form (column 20.0 × 2.0 cm). The flow rate was kept at 1.0 $cm^3\ min^{-1}$. After washing with water (250 cm^3), the final product was eluted with a solution of 0.5 M ammonia. The pure product was isolated from the column fractions 15–21 (each fraction of 15 cm^3). The fractions were collected, the solvent evaporated and the white solid obtained was washed with ethanol and acetone. Yield: 55%; m.p. 151–153°C (decomp.); ^1H NMR (D_2O, DSS, pD = 5.03): δ 3.85 (t, 4H, —OCH_2—); 3.71 (s, 4H, —NC$H_2CO_2^-$); 3.63 (s, 4H, —OCH_2CH_2O—); 3.47 (t, 4H, —NCH_2—); 3.36 (t, 4H, —NCH_2—); 2.26 (q, 2H, —$CH_2CH_2CH_2$—) p.p.m. ^{13}C NMR (D_2O, dioxane; pD = 5.03): δ 169.77; 69.91; 64.66; 57.39; 53.66; 51.90; 18.33 p.p.m. Found: C, 39.52; H, 6.81; N, 10.93%. Calc. for $C_{13}H_{24}N_2O_6.1.2HNO_3.H_2O$ (after addition of HNO_3 to the product obtained by chromatography): C, 39.24; H, 6.84; N, 11.27%. The amount of HNO_3 in the final product was confirmed by titration with a standard solution of NaOH.

Potentiometric measurements

Reagents and solutions. Metal ion solutions were prepared at about 0.010 and 0.100 M from the nitrate salts of the metals, of analytical grade, with demineralized water (obtained by a Millipore/Milli-Q system) and were standardised by titration with K_2H_2EDTA. Carbonate-free solutions of the titrant, $(CH_3)_4NOH$, were prepared as described earlier [8]. Solutions were discarded when the percentage of carbonate was about 0.5% of the total amount of base.

Equipment and work conditions. The equipment used was described earlier [8]. All the experiments were monitored by computer. The temperature was kept at 25.0 ± 0.1°C; atmospheric CO_2 was excluded from the cell by passing purified N_2 across the top of the experimental solution. The ionic strength of the solutions was kept at 0.10 M with $(CH_3)_4NNO_3$.

Measurements. The hydrogen ion concentration, $[H^+]$, was determined by the measurement of the emf of the cell, $E = E'^0 + Q \log [H^+] + E_j$. E'^0 and Q were obtained by previous calibration, titrating a standard solution of known hydrogen-ion concentration at the same ionic strength, using the values of the acid range. The term pH is defined as $-\log [H^+]$. The liquid-junction potential, $E_j = j_H[H^+] + j_{OH}[OH^-]$, whose constants j_H and j_{OH} were determined by an acid/base titration of concentrated solutions [20], was found to be negligible in the experimental conditions used. The value of $K_W = ([H^+][OH^-])$, was determined from data obtained in the alkaline range of the calibration, considering E'^0 and Q valid for the entire pH range, and found equal to $10^{-13.77}\ M^2$.

The potentiometric equilibrium measurements were performed on 20 cm^3 of ligand solutions $\cong 2.50 \times 10^{-3}$ M, diluted to a final volume of 30 cm^3, first in the absence of metal ions and then in the presence of each metal ion for which the $C_M : C_L$ ratios were 1:1, 1:2 and in some cases 2:1. The emf values were taken after additions of 0.025 or 0.050 cm^3 increments of standard 0.0974 M $(CH_3)_4NOH$ solution, and after stabilisation in this direction, equilibrium was then approached from the other direction by adding standard 0.100 M nitric acid solution.

Stabilisation of the systems studied. The formation of complexes of **L1** with all the metal ions studied in this work was fairly rapid, as verified by the fast stabilisation of the emf of the solutions and potentiometric titrations could be performed by an automated technique. For the Co^{2+} and Ni^{2+} complexes (the slowest cases) the equilibrium was verified by a backtitration with a HNO_3 solution as titrant.

Calculation of equilibrium constants. Protonation constants:

$$K_i^H = \frac{[H_iL]}{[H_{i-1}L][H]}$$

were calculated by fitting the potentiometric data obtained for the free ligand to the SUPERQUAD program [21]. Stability constants of the various species formed in solution were obtained from the experimental data corresponding to the titration of solutions of different ratios of the ligand and metal ions, also with the aid of the SUPERQUAD program. The results were obtained in the form of overall stability constants or $\beta_{M_mH_hL_l}$ values:

$$\beta_{M_mH_hL_l} = \frac{[M_mH_hL_l]}{[M]^m[L]^l[H]^h}$$

Only mononuclear species, ML, MHL, $MH_{-1}L$ (being $\beta_{MH_{-1}L} = \beta_{MLOH} \times K_W$) were found. Differences, in log units, between the values β_{MHL} (or $\beta_{MH_{-1}L}$) and β_{ML} provide the stepwise protonation reaction constants. The errors quoted are the standard deviations of the overall stability constants given directly by the program. In the case of the stepwise constants the standard deviations were determined by the normal propagation rules and do not represent the total experimental errors. The protonation constants were obtained from ≈ 200 experimental points (6 titration curves) and stability constants for each metal ion from 75 to 150 experimental points (2–6 titration curves).

Spectroscopic studies

^{1}H NMR spectra were recorded with a Varian Unity 300 spectrometer at probe temperature. Solutions of the ligand for the measurements ($\approx$0.01 M) were made up in D_2O and the pD was adjusted by addition of DCl or CO_2-free KOD with a Crison 2001 instrument fitted with a combined Ingold microelectrode. The $-\log[D^+]$ was measured directly in the NMR tube, after the calibration of the microelectrode with buffered aqueous solutions. The final pD was calculated from pD = pH + 0.40 [22]. Sodium 3-(trimethylsilyl)-d_4-propionate (DSS) was used as an internal reference. ^{13}C NMR spectra were recorded with the same spectrometer and dioxane was used as internal reference. The metal complexes, for the determination of the magnetic moments, were prepared in H_2O by addition of the metal ion, in the form of nitrate salts, to an equivalent amount of the ligand and enough KOH to obtain the final pH, and after evaporation of water were taken in D_2O. Magnetic moments of the complexes were determined by the Evans method in solution [23] at room temperature.

Electronic spectra were performed with an electronic spectrophotometer, Perkin–Elmer, model Lambda 9 for UV–vis–near-IR, using aqueous solutions of the complexes prepared as indicated in the last paragraph, in 1 cm cells. The temperature of the solutions was kept at 25.0 $\pm$ 0.1°C using a thermostat Grant W6. The spectra were recorded in the range 250–1350 nm.

EPR spectra were recorded with a Bruker ESP 380 spectrometer equipped with a continuous-flow cryostat for liquid nitrogen, operating at X-band. The spectra of the Cu^{2+} complexes ($1.1–1.3 \times 10^{-3}$ M in 1.0 M $NaClO_4$) were recorded at 100 K. The computer simulation of the EPR spectrum of the complex was carried out with a program for a microcomputer [24].

RESULTS AND DISCUSSION

Synthesis

L2 has been synthesised by Hill *et al.* and Hancock *et al.* [11–13]. Rasshofer *et al.* have prepared the precursor **L2·2Ts** but it is not clear from the publication if the removal of the tosyl groups was tried [25]. **L1** was only synthesised before by Ewin and Hill [13]. However, the technique for the removal of the tosyl groups used by the last authors, and giving 89% yield, could not be reproduced neither by us nor by Hancock *et al.* [11,12]. These authors described an alternative method in basic conditions (sodium in isoamyl alcohol) which did not lead to the expected result in our case. Indeed, the critical step of the synthesis of **L2** is the withdrawal of the tosyl groups, because in acid conditions the breaking of ether linkage of the macrocyclic ring is faster than removal of the tosyl groups, so that at long reaction times there is a total degradation of the free amine formed, although some tosylated amine remains. The protonation of the oxygen atom seems to be the first step in the acid dissociation of the ether linkage, therefore intramolecular hydrogen bonds involving the ether oxygen atom do not favour this step [26]. We have preferred to remove the tosyl groups under reductive alkaline conditions by sodium amalgam in a buffered methanol as described earlier [6,19]. Even in these conditions our yield was only of about 50%.

Protonation

Table 1 summarises the protonation constants (K_i^H, in log units) for the ligand studied in the present work and also for some other ligands with the same number and type of donor atoms, for comparison. Also Table 1 refers to the only value of the protonation constant reported in the literature for **L1**. This ligand has four basic centres for which we could determine three protonation constants by potentiometric measurements. The last one is very low to be obtained by this technique. The ligand presents a high value for the first protonation constant and a fairly high value for the second one, which correspond to the protonation of the two nitrogen atoms of the ring. The other two constants correspond to the protonation of the two carboxylate groups and are low when compared with the value of acetic acid ($\log K = 4.8$) or, even, of that of some other polyacetatepolyaza macrocyclic ligands, such as DOTA [1]. These values can be explained by the presence of the positive charge of the nitrogen atoms already protonated and probably also by the simultaneous disruption of the hydrogen bonds in which these carboxylate groups are involved. The protonation of the two amines of the ring occurs before the protonation of the carboxylate ones, in spite of the short distance between the two charged nitrogen and the possible electrostatic repulsions between them. The same happens with **L3** and **L4**, although in **L4** the two nitrogen atoms are in opposite position in the macrocyclic ring, and in **L3** the distances between the two ammonium ions are shorter leading to the decrease of the second protonation constant of this ligand ($\log K_2 = 4.84$) [6]. So the second constant of **L1** has an intermediate value between that of **L3** and **L4**.

The 12 to 14-membered tetraaza macrocycles usually have two high values of protonation constants, corresponding to the protonation of two nitrogen atoms in opposite positions, two values of about 4 for the protonation of the carboxylate groups bound to non-protonated nitrogens, and finally protonation constants of about 2 or less corresponding to the protonation of the remaining carboxylate groups and nitrogen atoms of the ring [1]. This means that the repulsions within the macrocycle are strong enough and the protonation of a nitrogen contiguous to another already protonated only occurs at very low pH

Table 1. Protonation ($\log K_i^H$) constants of **L1** and similar ligands (**L2, L3, L4** and **EDDA**) for comparison. ($T = 25.0°C$; $I = 0.10$ M in $(Me)_4NNO_3$)

Ion	Equilibrium quotient	**L1**	**L2**[b]	**L3**[c]	**L4**[c]	**EDDA**[d]
H^+	[HL]/[H] [L]	9.91(1); 11.6[a]	10.36	10.54	9.532	9.61
	$[H_2L]/[HL]$ [H]	6.95(2)	6.62	4.84	7.46	6.55
	$[H_3L]/[H_2L]$ [H]	2.42(3)		1.0	2.11	2.36
	$[H_4L]/[H_3L]$ [H]	—				(1.3)
	$[H_2L]/[L]$ $[H]^2$	16.86	16.98	15.38	16.992	16.16
	$[H_3L]/[L]$ $[H]^3$	19.28		16.38	19.10	18.52

[a] $I = 0.1$ M $NaClO_4$, ref. [13].
[b] $I = 0.1$ M $NaNO_3$, refs [11] and [12].
[c] Ref. [6].
[d] $I = 0.10$ M, ref. [27].

values. This is not observed with the dioxadiaza macrocycles where the second nitrogen atom to be protonated is adjacent and consequently the charge concentration must be lower and the mobility of the macrocycle more important, making the protonation behaviour of this kind of macrocycles more similar to that of linear ligands [27], as shown in Table 1 for **L1** and EDDA (1,2-diaminoethane-N,N′-diacetic acid).

Complexation

The stability constants of **L1** with the alkaline–earth and divalent first-row transition metal ions are collected in Table 2, together with the constants for the complexes formed with some related ligands with the same metal ions taken from the literature. Only mononuclear species (1:1, metal to ligand ratio) were found for the complexes of **L1**. In most cases only ML and hydroxocomplexes (MLOH) species are formed, but protonated species (MHL) were also detected for the Fe^{2+}, Zn^{2+}, Cd^{2+} and Pb^{2+} systems. However, the hydroxocomplexes are always formed at high pH values ($\geqslant 10.3$). We have checked the possibility of formation of other species such as other protonated, MH_iL ($i \geqslant 2$) or dinuclear, but they do not seem to be formed under our conditions. The constants for the alkaline–earth metal ion complexes were determined before [13] but the difference from ours is very great, higher for the Mg^{2+} complex and lower for the others. Ewin and Hill [13] have made their measurements in a different medium ($NaClO_4$) but this does not explain the discrepancies as the ligand forms no complexes with Na^+. They determined the constants by a thermometric titrimetric method, $\log K_{ML}$, ΔH and ΔS being calculated simultaneously. We have before detected the same type of disagreement in other values from the same publication [13] for the complexes of other ligand [28] (higher stability constant for the Mg^{2+} complex and smaller ones for the other alkaline–earth metal ions) and we have also checked that the different media did not justify the discrepancies found.

The examination of Table 2 and Fig. 1 leads to the following conclusions: (1) The values of the stability constants of **L1** are lower than expected for a potential hexadentate ligand, specially for the complexes of the alkaline–earth metal ions, as shown when data of this ligand are compared with those of 12-membered macrocycles such as **L3** and **L4**, or even with linear hexadentate ligands with the same set of donor atoms [27,29]. (2) However, when stability constants of **L1** are compared with those of EDDA, a linear ligand with two amines and two carboxylate groups, it is possible to infer that the oxygen atoms of the ring of **L1** are involved on the co-ordination to the metal ions (at least one of them). (3) **L1** is more selective for the complexation of the divalent first-row transition metal ions than are the 12-membered ligands. (4) When the size of the ring of those N-acetate macrocyclic ligands increases from 12- to 13-membered, there is a significant fall in the values of the stability constants of the complexes formed mainly by electrostatic interactions, such as those of alkaline–earth metal ions, Mn^{2+} and Fe^{2+}. However, the stability of the Ni^{2+} and the Cu^{2+} complexes seems indifferent to the increase of the size of the cavity and the Zn^{2+} and Cd^{2+} complexes have an intermediate behaviour. The Co^{2+} and Pb^{2+} complexes are apparently anomalous, although the last complex behaves in the expected manner if compared with **L3**. (Note that **L1** and **L4** have the same overall basicity, but **L3** has a lower value (*cf* Table 1), so to have identical conditions concerning competition between protons and metal ions for the ligand, we shall compare the ability of our ligand to form complexes predominantly with that of **L4**.)

The same behaviour was found for the tetraazamacrocyclic ligand series, DOTA and TRITA (see Fig. 1). In spite of the stability constants of the complexes formed by those ligands being much higher than those studied in this work, the differences arising from the increase of the cavity (from 12 to 13-membered) are similar to those found in the present work. The determination of ΔH and ΔS of the complexes of

Table 2. Stability contants (log $K_{M_mH_hL_l}$) of complexes of **L1** and similar ligands **L2, L3, L4** and **EDDA** with some metal ions. (T = 25.0°C; I = 0.10 M in $(Me)_4NNO_3$)

Ion	Equilibrium quotient	L1	L2[b]	L3[c]	L4[c]	EDDA[d]
Mg^{2+}	[ML]/[M] [L]	2.38(9); 4.2[a]	—	4.79	5.62	4.3
	[ML]/[MLOH] [H]	10.9(1)	—	—	—	
Ca^{2+}	[ML]/[M] [L]	4.93(1); 3.5[a]	—	8.12	8.50	2.9
	[ML]/[MLOH] [H]	11.66 (4)	—	—	—	
Sr^{2+}	[ML]/[M] [L]	3.74(2); 2.6[a]	—	7.19	7.38	2.3
	[ML]/[MLOH] [H]	11.36 (3)	—	—	—	—
Ba^{2+}	[ML]/[M] [L]	3.37(3); 2.5[a]	—	6.68	6.652	1.2
	[ML]/[MLOH] [H]	11.24(3)	—	—	—	—
Mn^{2+}	[ML]/[M] [L]	8.03(2)	—	10.72	11.03	7.05
	[ML]/[MLOH] [H]	10.89(5)	—	—	—	—
Fe^{2+}	[ML]/[M] [L]	8.38(1)	—	11.52	11.86	8.63
	[MHL]/[ML] [H]	5.14(6)	—	—	—	—
	[ML]/[MLOH] [H]	pp	—	—	—	—
Co^{2+}	[ML]/[M] [L]	9.94(3)	—	12.89	13.126	11.23
	[ML]/[MLOH] [H]	(9.7)[e]	—	—	—	—
Ni^{2+}	[ML]/[M] [L]	12.94(1)	5.83	12.86	12.129	13.65
	[ML]/[MLOH] [H]	—	—	—	—	—
Cu^{2+}	[ML]/[M] [L]	16.08(3)	8.39	14.33	15.95	16.2
	[ML]/[MLOH] [H]	10.46(7)	—	—	—	—
Zn^{2+}	[ML]/[M] [L]	10.26(1)	4.89	12.52	12.277	11.1
	[MHL]/[ML] [H]	4.08(9)	—	—	—	—
Cd^{2+}	[ML]/[M] [L]	11.93(2)	5.40	13.58	14.09	9.1
	[MHL]/[ML] [H]	3.63(7)	—	—	—	—
	[ML]/[MLOH] [H]	10.98(9)	—	—	—	—
Pb^{2+}	[ML]/[M] [L]	11.56(1)	5.70	14.63	12.434	10.7
	[MHL]/[ML] [H]	3.58(6)	—	—	—	—
	[ML]/[MLOH] [H]	10.31(8)	—	—	—	—

[a] I = 0.1 M $NaClO_4$, ref. [13].
[b] I = 0.1 M $NaNO_3$, refs [11] and [12].
[c] Ref. [6].
[d] I = 0.10 M, refs [27] and [29].
[e] Value with less precision due to precipitation.

DOTA and TRITA [2] have revealed that for the complexes mainly formed by electrostatic interactions the difference is essentially due to the enthalpic variations, although a decrease in the entropic variations was also observed. The decrease of the values of ΔH with the increase of the size of the ring is probably due to the increase in the distances between the metal ions and the donor atoms and also a less favourable orientation of the lone-pair electrons of the donor atoms. However, the metal ions forming more covalent bonds, which are more strict for specific co-ordination geometries (Fe^{2+} to Zn^{2+}), probably select the donor atoms of the ligand in better position for the preferred geometry, some of them should not be used on the co-ordination [2].

An analogous explanation may also be advanced for the behaviour of the **L1** and **L4** complexes. Hence, probably all the donor atoms of both ligands are involved on the co-ordination to metal ions forming mainly electrostatic interactions but the distances and/or the orientation of the lone-pairs of electrons of the nitrogen and oxygen atoms of the ring of **L1** were not in the best position for the co-ordination to the metal ions. For the Cu^{2+} and Ni^{2+} ions, whose complexes have identical stability with both ligands, and the ligands have the right number of donor atoms to form six co-ordinate complexes, a different explanation is needed. To have more insight about the co-ordination sphere of the Co^{2+}, Ni^{2+} and Cu^{2+} complexes some spectroscopic measurements were performed.

Spectroscopic measurements

Spectroscopic UV–vis–near-IR data for Co^{2+}, Ni^{2+} and Cu^{2+} complexes of **L1** and **L4** and EPR parameters for the Cu^{2+} complexes of **L1, L2** and **L4**, in water solution, were collected in Tables 3 and 4.

The electronic spectrum of the [Co**L1**] exhibits a shoulder located at 304 nm, which is probably a charge transfer band, a multiple structured band in the visible region with shoulders at higher and lower energies and a large near-IR band at 1226 nm with a shoulder at 946 nm (*cf* Table 3). All the bands have very low intensities, which slightly increase between pH values

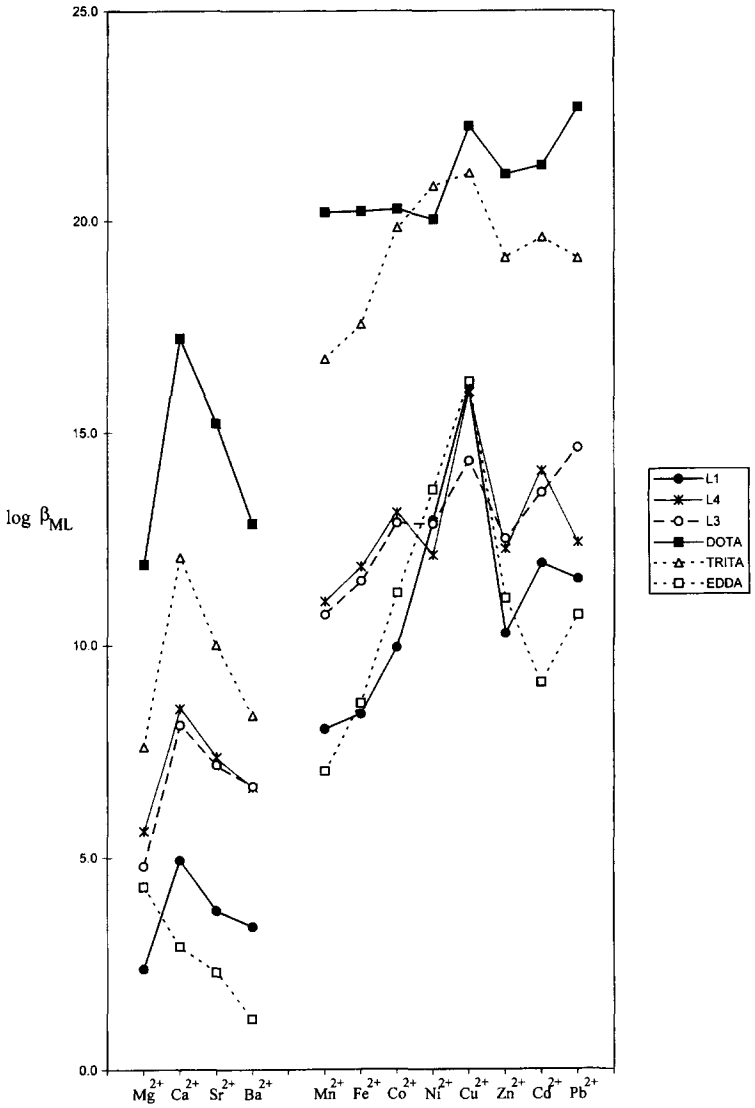

Fig. 1. Variation of the stability constants (log K_{ML}) of the metal complexes of **L1** (●), **L3** (○), **L4** (*), DOTA (■), TRITA (△) and EDDA (□) with the atomic number of the metal ion.

2.8 to about 7. This spectrum, together with the value of the magnetic moment, point to a six co-ordinate symmetry of a high-spin species [30–32]. It is known that six co-ordinate chromophores have in general low absorptions since all transitions are forbidden and magnetic susceptibility values between 5.0 and 5.4 BM [30]. Carlin [33] indicates lower values (4.7–5.2 BM). At high pH values (>9) two new bands appear (at 647 and 592 nm) and the band at about 900 nm moves to higher energy. Decreasing the pH the spectrum acquires the original form but loses intensity. Until pH values of about 8 are reached, the complex does not undergo degradation with time. The complex of the 12-membered ligand, [Co**L4**], exhibits a similar electronic spectrum but with less intense bands and a magnetic moment of 4.93 BM. Thus, in this case there is no ambiguity in its characterisation as a high-spin distorted octahedral complex. At high pH (>9) the spectrum presents new bands at 646 and 596 nm. These additional bands, appearing in both **L1** and **L4** Co^{2+} complexes, are probably related to the formation of hydroxocomplexes and subsequent degradation by dimeric species.

The electronic spectrum of the blue solution of [Ni**L1**] exhibits three main bands at 969, 575 and 356 nm, several shoulders and a small band at 798 nm (*cf* Table 3). This spectrum and the value of the magnetic momentum (3.21 BM) are characteristic of a tetragonally distorted octahedral symmetry. The ratio between the near-IR and the visible bands is 1.68, also characteristic of tetragonal nickel(II) [31]. The spectrum of a d^8 complex with octahedral symmetry shows three bands of low intensities corresponding to the three spin allowed transitions and the reduction of symmetry to a tetragonal leads to additional d-orbital splittings or band broadening [31–35]. The

Table 3. Spectroscopic UV–vis–near IR data for the Co^{2+}, Ni^{2+} and Cu^{2+} complexes of **L1**, **L2** and **L4** (T = 25.0°C)

Complex; colour	pH	UV–vis–near IR Absorption max/nm (ε_{molar}/dm^3 mol^{-1} cm^{-1})
[Co**L1**] (pink)	6.69	1226 (4.7); 946 (sh., 3.1); 612 (sh., 3.9); 534 (sh., 10.8); 512 (sh., 13.5); 492 (14.3); 462 (sh., 12.0); 304 (sh., 81.1)
	9.31	1224 (4.2); 912 (3.6); 647 (5.8); 592 (6.2); 492 (12.0); 462 (12.0); 314 (sh., 61.8)
[Ni**L1**] (blue)	5.94	1268 (sh., 7.0); 1186 (sh., 8.9); 1120 (sh., 11.1); 1064 (sh., 13.1); 969 (14.7); 798 (5.8); 664 (sh., 7.0); 575 (12.0); 392 (51.0); 356 (68.7); 304 (sh., 158.3); 286 (sh., 184.9); 276 (sh., 198.8)
[Cu**L1**] (turquoise)	6.83	900 (sh., 9.5); 720 (sh., 33.8); 630 (48.5); 268 (5.3×10^2)
$[Ni\mathbf{L2}(H_2O)_2]^{2+}$ [a]	—	1053; 760; 610; 373
$[Cu\mathbf{L2}(H_2O)_2]^{2+}$ (blue)	8.85	1056 (sh., 22.1); 880 (sh., 51.8); 667 (131.0); 296 (77.0)
[Co**L4**] (pink)	5.22	1164 (1.6); 1056 (1.5); 612 (1.5); 592 (1.8); 544 (sh., 6.4); 508 (8.4); 468 (sh., 6.0); 300 (52.6)
	9.14	1134 (1.0); 1060 (1.5); 918 (1.0); 646 (5.2); 596 (6.4); 544 (sh., 9.6); 512 (10.8); 468 (10.6); 300 (84.3)
[Ni**L4**] (green)	6.10	1249 (7.5); 1082 (6.7); 1025 (sh., 6.0); 928 (4.0); 760 (sh., 4.0); 690 (sh., 4.8); 625 (5.6); 420 (sh., 9.3); 388 (14.5); 296 (51.2)
[Cu**L4**] (blue)	4.31	936 (19.4); 685 (37.5); 272 (4.6×10^3)

[a] Ref. [12].

Table 4. Spectroscopic EPR data for the Cu^{2+} complexes of **L1**, **L2** and **L4** and other similar complexes

Complex	Visible band, nm (ε_{molar}/dm^3 mol^{-1} cm^{-1})	EPR ($A_i \times 10^4$ cm^{-1})						Ref.
		g_x	g_y	g_z	A_x	A_y	A_z	
[Cu**L1**]	630 (48.5)	2.045	2.073	2.251	5.4	16.6	187.81	This work
$[Cu\mathbf{L2}(ClO_4)]^+$	667 (131)	2.045	2.090	2.270	5.0	4.1	171.0	This work
[Cu**L4**]	685.2 (37.5)	2.055	2.080	2.284	1.0	0.9	168.7	This work
$[Cu(EDTA)]^{2-}$	735.3 (99)	2.071		2.295	—	—	166.0	49

electronic spectrum of the green [Ni**L4**] exhibits six broad but well defined bands at 1249, 1082, 928, 625, 388 and 296 nm with several shoulders, similar to that of five co-ordinate high spin derivatives [31,32,35–39]. The magnetic moment (3.42 BM) also falls in the range normally observed for high-spin five co-ordinate Ni^{2+} species [31,32,35,40]. However, the molar absorptivity of all the bands are too low for a square pyramidal or a trigonal bipyramidal symmetry and probably the most probable geometry of this complex is also a tetragonally distorted octahedral one.

The turquoise [Cu**L1**] exhibits a broad band in the visible region with two shoulders at lower energies, due to the copper *d–d* transitions, and an intense band in the ultraviolet region. The copper(II) complex of **L2** is blue showing an electronic spectrum similar to that of **L1** but shifted to lower energies and having more intense bands. The Cu^{2+} complex of **L4** is also blue but exhibits an electronic spectrum with two broad bands in the visible/near IR region and an intense band in the UV region (*cf* Table 3). The EPR spectra of the three Cu^{2+} complexes are shown in Fig. 2. All of them exhibit three well resolved lines of the four expected at low field, due to the interaction of the unpaired electron spin with the copper nucleus, and no superhyperfine splitting due to the coupling with the four nitrogen atoms of the macrocycle. The fourth copper line is completely overlapped by the high field part of the spectra. The simulation of the spectra [24] led to three different principal values of g, indicating that the Cu^{2+} ion in these complexes is in a rhombically-distorted ligand field. The hyperfine coupling constants and g values are compiled in Table 4.

Though electronic and EPR spectra of Cu^{2+} complexes are not specially good indicators of geometry [41], the comparison of spectra of complexes of the same series, such as those compiled in Table 4, allows some conclusions. The EPR spectra of the Cu^{2+} complexes of **L1**, **L2** and **L4** show $g_z > (g_x + g_y)/2$ and the lowest $g > 2.04$, typical of rhombic symmetry of the copper(II) ion with elongation of the axial bonds and a $d_{x^2-y^2}$ ground state. Elongated rhombic–octahedral, rhombic square-coplanar or distorted square-based

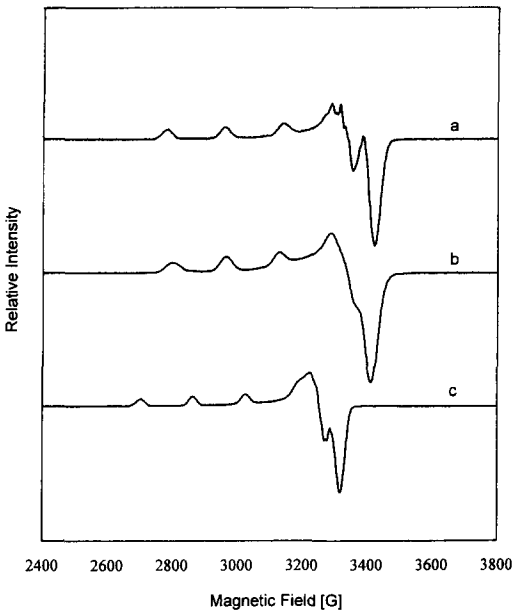

Fig. 2. EPR X-band spectra of the Cu^{2+} complexes of (a) **L1**, (b) **L2** and (c) **L4**, in 1.0 mol dm^{-3} $NaClO_4$, recorded at 100 K, microwave power of 2.4 mW, modulation amplitude of 1 mT. The frequency (ν) was of 9.61, 9.62 and 9.41 GHz for *a*, *b* and *c*, respectively.

pyramidal stereochemistries would be consistent with these data. Consequently it is possible to exclude a trigonal–bipyramidal geometry or a tetragonal structure involving compression of axial bonds [42,43].

The g values and hyperfine constants (A_i) may be related to the electronic transitions by the usual factors derived from the ligand field theory [44–46]. The strength of the axial donor and the displacement of the copper from the donor atoms plane. The g values increase and the A_z value decrease as the planar ligand field becomes weaker, or as the axial ligand field becomes stronger and this is accompanied by a red-shift of the *d–d* absorption bands in the electronic spectra [45–48]. This sequence, in principle, parallels the degree of distortion from a square-planar arrangement to a square pyramidal geometry, and then to an octahedral or tetragonal symmetry.

Data of Table 4 show that [Cu**L4**] and $[CuEDTA]^{2-}$ [49,50] have similar EPR parameters and analogous electronic spectra. It is known by X-ray diffraction analysis that $[CuEDTA]^{2-}$ [32,51] and [Cu**L4**] [52] exhibit octahedral structures. In the last complex the Cu^{2+} is in a very distorted octahedral environment, with the macrocycle in a folded conformation, the two nitrogen atoms and the two oxygen of the acetate groups forming the equatorial plane and the two oxygen atoms of the ring in axial positions (the O_{axial}—Cu—O_{axial} angle being 147.7°). However, [Cu**L1**] which presents lower g values, higher A_z and a blue-shift of the electronic spectra when compared with the $[CuEDTA]^{2-}$ or [Cu**L4**] spectra, can be considered penta co-ordinate with a square-pyramidal arrangement. This means that in this case one of the oxygen atoms (either from the macrocycle or from one of the acetate groups), is not co-ordinated to the copper ion or is located at a longer distance. The Cu^{2+} complex of **L2** showing a slight decrease of g values and a slight increase of A_z compared with those of [Cu**L4**] or $[CuEDTA]^{2-}$, probably is also penta-coordinate, but with a different coordination sphere. Probably the donor atoms of the macrocycle form the equatorial plane and one perchlorate ion occupies an axial position in a square pyramid, and so its data do not fit well in the analysed series.

CONCLUSION

The complexes of **L1** with metal ions forming mainly electrostatic interactions (the alkaline–earth metal ions, Mn^{2+} and Pb^{2+}) and also Co^{2+}, show a sharp decrease of stability when compared with the corresponding complexes of 12-membered ligands, **L3** and **L4**. However, the Cu^{2+} and Ni^{2+} complexes of **L1** and **L4** have about the same values of stability constants. To explain these results we propose that all the ligand donor atoms (**L1, L3** and **L4**) are involved in the co-ordination to metal ions which form mainly electrostatic interactions (and also to Co^{2+}, as spectroscopic measurements have revealed) but the distances, and specially the orientation of the lone-pairs of electrons, are not in the best position for the co-ordination to **L1**. Also for the Ni^{2+} complexes, all the donor atoms of the ligands are involved in the co-ordination to the metal, as shown by electronic spectroscopy in solution and the value of the magnetic moments of [Ni**L1**] and [Ni**L4**], both complexes exhibiting tetragonally distorted octahedral geometry. Therefore it seems that Ni^{2+} probably fits better in the cage formed by **L1** than that of **L4**, as indicated by the values of stability constants, both ligands probably adopting different arrangements around the metal ion. Additionally, the structure adopted by [Ni**L4**] would be similar to that of the Cu^{2+} one, for which the crystal X-ray structure [52] and preliminary molecular mechanics studies [53] have revealed a significant distortion (the O_{axial}—Cu—O_{axial} angle being about 150°, far from the 180° predicted for the octahedron) and so the loss in terms of crystal field stabilisation energy (CFSE) is very important (as the octahedral Ni^{2+} complexes are more favoured in CFSE than the other first row transition metal ions). The more plastic Cu^{2+} ion would adjust better to the different arrangement of the ligands and so with **L1** forms a pentacoordinate complex, while **L4** prefers an octahedral arrangement.

As mentioned earlier [6] the Ni^{2+} complex of **L4** presents a lower stability constant than the Co^{2+} one and therefore the complexes of the divalent first-row transition metal ions with **L4** do not obey the Irving–Williams series. This was tentatively interpreted [6] speculating a possible pentacoordination of the Ni^{2+} complex of **L4**, which is not favoured in terms of

CFSE [6,54]. However, this hypothesis was not proved in the present work. The Cu^{2+} complex of **L1** presents a slightly higher value of stability constant than that of **L4** because the copper ion is more stable (by crystal field stabilisation energy) when pentacoordinated (square-pyramidal or trigonal bipyramidal) [54] and the structure adopted by the complex of **L1** points to a square pyramidal one.

REFERENCES

1. Delgado, R. and Fraústo da Silva, J. J. R., *Talanta*, 1982, **29,** 815; Chaves, S., Delgado, R. and Fraústo da Silva, J. J. R., *Talanta*, 1992, **39,** 249.
2. Delgado, R., Fraústo da Silva, J. J. R. and Vaz, M. C. T. A., *Inorg. Chim. Acta*, 1984, **90,** 185.
3. Delgado, R., Quintino, S., Teixeira, M. and Zhang, A., *J. Chem. Soc., Dalton Trans.*, 1997, 55.
4. Izatt, R., Pawlak, K., Bradshaw, J. S. and Bruening, R. L., *Chem. Rev.*, 1995, **95,** 2592.
5. Amorim, M. T., Delgado, R., Fraústo da Silva, J. J. R., Vaz, M. C. T. A. and Vilhena, M. F., *Talanta*, 1988, **35,** 741.
6. Amorim, M. T. and Delgado, R., Fraústo da Silva, J. J. R., *Polyhedron*, 1992, **11,** 1891.
7. Chaves, S., Delgado, R., Duarte, M. T., Silva, J. A. L., Félix, V. and Carrondo, M. A. A. F. de C. T., *J. Chem. Soc., Dalton Trans.*, 1992, 2579.
8. Costa, J., Delgado, R., Figueira, M. C., Henriques, R. T. and Teixeira, M., *J. Chem. Soc., Dalton Trans.*, 1997, 65.
9. Bianchi, A., Micheloni, M. and Paoletti, P. *Coord. Chem. Rev.*, 1991, **110,** 17.
10. Hancock, R. D. and Martell, A. E., *Comments Inorg. Chem.*, 1988, **6,** 237.
11. Thöm, V. J. and Hancock, R. D., *Inorg. Chim. Acta*, 1985, **96,** L43.
12. Thöm, V. J., Shaikjee, M. S. and Hancock, R. D., *Inorg. Chem.*, 1986, **25,** 2992.
13. Ewin, G. and Hill, J. O., *J. Chem. Research (S)*, 1985, 334; *J. Chem. Research (M)*, 1985, 3501.
14. Koyama, H. and Yoshino, T., *Bull. Chem. Soc. Jpn.*, 1972, **45,** 481.
15. Dale, J. and Kristiansen, P. O., *Acta Chem. Scand.*, 1972, **26,** 1471.
16. Nelson, E. R., Maienthal, M., Lane, L. A. and Benderly, A. A., *J. Am. Chem. Soc.*, 1957, **79,** 3467.
17. Perrin, D. D. and Armarego, W. L. F., *Purification of Laboratory Chemicals*, 3rd edn, Pergamon, Oxford (1988).
18. Richman, J. E. and Atkins, T. J., *J. Am. Chem. Soc.*, 1974, **96,** 2268; Atkins, T. J., Richman, J. E. and Oettle, W. F., *Org. Synth.*, 1978, **58,** 86.
19. Trost, B. M., Arndt, H. C., Strege, P. E. and Verhoeven, T. R., *Tetrahedron Lett.*, 1976, 3477; Vriesema, B. K., Biter, J. and Kellogg, R. M., *J. Org. Chem.*, 1984, **49,** 110; Sessler, J. L., Sivert, J. W., Hugdahl, J. D. and Lynch, V., *Inorg. Chem.*, 1989, **28,** 1417.
20. Pehrsson, L., Ingman, F. and Johansson, A., *Talanta*, 1976, **23,** 769.
21. Gans, P., Sabatini, A. and Vacca, A., *J. Chem. Soc., Dalton Trans.*, 1985, 1195.
22. Delgado, R., Fraústo da Silva, J. J. R., Amorim, M. T. S., Cabral, M. F., Chaves, S. and Costa, J., *Anal. Chim. Acta*, 1991, **245,** 271.
23. Evans, D. F., *J. Chem. Soc.*, 1959, 2003.
24. Neese, F., Diploma Thesis, University of Konstanz (Germany), June 1993.
25. Rasshofer, W., Wehner, W. and Vögtle, F., *Liebigs Ann. Chem.*, 1976, 916.
26. Rasshofer, W. and Vögtle, F., *Liebigs Ann. Chem.*, 1977, 1340.
27. Smith, R. M., Martell, A. E. and Motekaitis, R. J., *Nist Critical Stability Constants of Metal Complexes Database*, U.S. Department of Commerce, Gaithersbug (1993).
28. Cabral, M. F., Costa, J., Delgado, R., Fraústo da Silva, J. J. R. and Vilhena, M. F., *Polyhedron*, 1990, **9,** 2847.
29. Pettit, L. D. and Powell, H. K. J., *IUPAC Stability Constants Database*, Academic Software, Timble (1993).
30. Bertini, I. and Luchinat, C., *Adv. Inorg. Biochem.*, 1984, **6,** 71.
31. Lever, A. B. P., *Inorganic Electronic Spectroscopy*, 2nd edn, Elsevier, Amsterdam (1984).
32. Averill, D. F., Legg, J. I. and Smith, D. L., *Inorg. Chem.*, 1972, **11,** 2344.
33. Carlin, R. L., *Trans. Met. Chem.*, 1965, **1,** 1.
34. Martin, L. Y., Sperati, C. R. and Busch, D. H., *J. Am. Chem. Soc.*, 1977, **99,** 2968.
35. Sacconi, L., Mani, F. and Bencini, A., in *Comprehensive Coordination Chemistry*, ed. by G. Wilkinson, R. D. Gillard and J. A. McCleverty, vol. V, pp. 1–347, Pergamon Press, (1987).
36. Bürki, S. and Kaden, T. A., *J. Chem. Soc., Dalton Trans.*, 1991, 805.
37. Ciampolini, M. and Nardi, N., *Inorg. Chem.*, 1966, **5,** 41; *ibid.*, 1967, **6,** 445.
38. Ciampolini, M., *Inorg. Chem.*, 1966, **5,** 35.
39. Renfrew, R. W., Jamison, R. S. and Weatherburn, D. C., *Inorg. Chem.*, 1979, **18,** 1584.
40. Smierciak, R., Passariello, J. and Blinn, E. L., *Inorg. Chem.*, 1977, **16,** 2646.
41. Hathaway, B. J., *Coord. Chem. Rev.*, 1983, **52,** 87.
42. Styka, M. C., Smierciak, R. C., Blinn, E. L., DeSimone, R. E. and Passarielo, J. V., *Inorg. Chem.*, 1978, **17,** 82.
43. Vänngard, T., in *Biological Application of Electron Spin Resonance*, ed. H. M. Swartz, J. R. Bolton and D. C. Borg, Wiley–Interscience, New York (1972).
44. Gersmann, H. R. and Swalen, J. D., *J. Chem. Phys.*, 1962, **36,** 3221.
45. Yokoi, H., Sai, M., Isobe, T. and Ohsawa, S., *Bull. Chem. Soc. Jpn.*, 1972, **45,** 2189.
46. Lau, P. W. and Lin, W. C., *J. Inorg. Nucl. Chem.*, 1975, **37,** 2389.
47. Addison, A. W., Carpenter, M. and Lau, L. K.-M. and Wicholas, M., *Inorg. Chem.*, 1978, **17,** 1545.
48. Maroney, M. J. and Rose, N. J., *Inorg. Chem.*, 1984, **23,** 2252.
49. Delgado, R., Fraústo da Silva, J. J. R. and Vaz, M. C. T. A., *Talanta*, 1986, **33,** 285.

50. Micera, G., Sanna, D., Dallocchio, R. and Dessi, A., *J. Coord. Chem.*, 1992, **25,** 265.
51. Stephens, F. S., *J. Chem. Soc.* (*A*), 1969, 1723.
52. Urbanczky-Lipkowska, Z., Krajewski, J. W., Gluzinski, P., Kolinski, R. A. and Bocelli, G., *J. Cryst. Spectrosc.*, 1988, **18,** 157.
53. Félix, V., personal communication.
54. Furlani, C., *Coord. Chem. Review*, 1968, **3,** 141.

Pergamon

PII: S0277-5387(97)00247-7

Polyhedron Vol. 17, No. 1, pp. 105–118, 1998
© 1997 Elsevier Science Ltd
All rights reserved. Printed in Great Britain
0277-5387/98 $19.00+0.00

Preparation and characterization of different two types of di-μ-oxo dimanganese(IV) complexes with tetradentate Schiff bases

Hitoshi Torayama, Tamao Nishide, Hideyuki Asada, Manabu Fujiwara and Takayuki Matsushita*

Department of Materials Chemistry, Faculty of Science and Technology, Ryukoku University, Seta, Otsu 520-21, Japan

(Received 22 April 1997; accepted 3 June 1997)

Abstract—Novel di-μ-oxo dimanganese(IV) complexes with a series of tetradentate Schiff base ligands have been prepared and characterized by spectroscopy, magnetic susceptibility, electrochemical measurements and X-ray crystallography. The di-μ-oxo dimanganese(IV) complexes, $[Mn^{IV}(\mu\text{-salophen})(\mu\text{-O})]$, **1** (salophen H_2 = *N*,*N*′-disalicylidene-1,2-diaminobenzene), $[Mn(\mu\text{-salen})(\mu\text{-O})]_2$, **2** (salen$H_2$ = *N*,*N*′-disalicylidene-1,2-diaminoethane), $[Mn(salen)(\mu\text{-O})]_2$, **3**, $[Mn(salipn)(\mu\text{-O})]_2$, **4** (salipn$H_2$ = *N*,*N*′-disalicylidene-1,2-diaminopropane) and $[Mn(salbn)(\mu\text{-O})]_2$, **5** (salbn$H_2$ = *N*,*N*′-disalicylidene-1,4-diaminobutane), have been found to be obtained by the reaction of the tetradentate Schiff base ligands and potassium permanganate ($KMnO_4$) in MeCN with stirring at room temperature. X-ray analysis revealed that these complexes are classified by two different types of di-μ-oxo manganese(IV) complexes in the coordination features of the ligands: one of them (**1** and **2**) has a structure in which salophen or salen ligands are coordinated to two manganese ions as a bridging bidentate ligand, whereas the other (**3, 4** and **5**) has a structure in which salen, salipn or salbn ligands are coordinated to each manganese ion as a tetradentate ligand. These types were characterized from their IR spectra around 650 cm^{-1}, UV–vis spectra and electrochemical properties. © 1997 Elsevier Science Ltd

Keywords: Photosystem II; oxygen-evolving center; di-μ-oxo dimanganese(IV) complexes; tetradentate Schiff base ligand; crystal structure.

Manganese plays an important role in biological redox systems, which is exemplified by the oxygen-evolving center of Photosystem II (PSII OEC) in green plants. The current understanding is that there are four manganese atoms per OEC, although their precise arrangement has not been determined unambiguously. EXAFS spectra of the OEC indicate that the catalytic site in the system consists of an oxo-manganese tetramer with two short Mn–Mn (2.7 Å) and two somewhat longer Mn–Mn (3.3 Å) distances [1–3]. During the water oxidation cycle these are of the (II), (III), and (IV) valence states. In order to understand its function, a number of oxomanganese cluster with various nuclearity, ligation, and number and type of oxo-bridges, have been prepared and studied [4–10]. In particular, there have been many reports on the preparation of structurally characterized di-μ-oxo dimanganese complexes, since the close Mn–Mn distance of OEC (2.7 Å) implies a strong interaction between the manganese atoms of the substructure consistent with a di-μ-oxo dimanganese core. All of the common stable higher oxidation states (i.e. III,III; III,IV; IV,IV) of manganese have been achieved in the di-μ-oxo dimanganese complexes. So far, the most of di-μ-oxo dimanganese(IV) complexes [11–22], such as $[Mn^{IV}(salpn)(\mu\text{-O})]_2$, **6** (salpn$H_2$ = *N*,*N*′-disalicylidene-1,3-diaminopropane) [11–13], have been prepared by the reaction of mononuclear manganese(II) or manganese(III) complexes with dioxygen, hydrogen peroxide, or other oxidants.

Recently, we have reported on the properties and molecular structures of di-μ-oxo dimanganese(IV) complexes, $[Mn^{IV}(\mu\text{-salophen})(\mu\text{-O})]_2$, **1** (salophen$H_2$ = *N*,*N*′-disalicylidene-1,2-diaminobenzene), $[Mn^{IV}(salbn)(\mu\text{-O})]_2$, **5** (salbn$H_2$ = *N*,*N*′-disalicylidene-1,4-diaminobutane) and $[Mn^{IV}(N\text{-R-X-sal})_2(\mu\text{-O})]_2$ (*N*-R-X-salH = *N*-alkyl-substituted-salicyli-

* Author to whom correspondence should be addressed.

deneamine) obtained by the reaction of $KMnO_4$ with these ligands in MeCN [23,24]. In this paper, we describe the preparation and the detailed properties of different two types of novel dinuclear manganese(IV) complexes with a di-μ-oxo structure.

EXPERIMENTAL

Preparation of tetradentate Schiff base ligands

The tetradentate Schiff base ligands used in this work, *N,N'*-disalicylidene-1,2-diaminobenzene (salophenH_2), *N,N'*-disalicylidene-1,2-diaminoethane (salenH_2), *N,N'*-disalicylidene-1,2-diaminopropane (salipnH_2), and *N,N'*-disalicylidene-1,4-diaminobutane (salbnH_2) were obtained by the condensation of salicylaldehyde and appropriate diamines in methanol. The products were recrystallized from methanol and dried *in vacuo*.

Preparation of di-μ-oxo dimanganese complexes

$[Mn^{IV}(\mu\text{-}salophen)(\mu\text{-O})]_2$, **1**. The manganese(IV) complex, $[Mn^{IV}(\mu\text{-salophen})(\mu\text{-O})]_2$, **1,** was prepared by the reaction of salophenH_2 (0.27 g, 1.0 mmol) and $KMnO_4$ (0.16 g, 1.0 mmol) in MeCN (400 cm^3) with stirring at room temperature. The solution color changed from purple to brown and was allowed to stand in the dark at room temperature. Two weeks later the resulting brownish black crystals were collected on a glass filter (yield 51%). IR spectrum on KBr pellets (cm^{-1}): 1608(vs), 1586(m), 1534(s), 1464(m), 1444(s), 1318(m), 1190(m), 1150(m), 755(m), 641(s), 632(m).

$[Mn^{IV}(\mu\text{-}salen)(\mu\text{-O})]_2$, **2** *and* $[Mn^{IV}(salen)(\mu\text{-O})]_2$, **3**. The reaction of salenH_2 and $KMnO_4$ yielded two types of di-μ-oxo dimanganese(IV) complexes. The manganese(IV) complex, $[Mn^{IV}(\mu\text{-salen})(\mu\text{-O})]_2$, **2** and $[Mn^{IV}(salen)(\mu\text{-O})]_2$, **3** were prepared by the reaction of salenH_2 (1.08 g, 4.0 mmol) and $KMnO_4$ (0.64 g, 2.0 mmol) in MeCN (200 cm^3) with stirring at room temperature. The solution color changed from purple to brown red and 24 h after a mixture of **2** and **3** precipitated as brown solids was collected on a glass filter and dried *in vacuo*. They were extracted with dichloromethane (CH_2Cl_2) (250 cm^3), and **3** was obtained with manganese oxide as the brown residue. The extract was reprecipitated by the addition of MeCN and the resulting brownish red micro crystals, **2,** were collected on a glass filter and dried *in vacuo*. They were recrystallized from CH_2Cl_2 and MeCN (yield 0.45 g, 30%). In addition, **3** was found to be obtainable preferentially by the reaction of the Schiff base (0.56 g, 2.0 mmol) and $KMnO_4$ (0.32 g, 2.0 mmol) in a mixed solvent of MeCN and H_2O (4 : 1) (200 cm^3) with stirring at room temperature. The solution color changed from purple to brown and was allowed to stand in the dark at room temperature. Two weeks later the resulting brownish black crystals, **3,** were collected on a glass filter (yield 70%). IR spectrum on KBr pellets (cm^{-1}) : complex **2** ; 1627(vs), 1600(s), 1543(m), 1468(m), 1449(s), 1298(s), 753(m), 634(s), 453(m). Complex **3**; 3435(m), 1632(vs), 1600(s), 1540(s), 1447(s), 1339(m), 1297(s), 757(m), 658(m), 648(m), 627(m), 604(s), 460(m).

$[Mn^{IV}(salipn)(\mu\text{-O})]_2$, **4**. The manganese(IV) complex, $[Mn^{IV}(salipn)(\mu\text{-O})]_2$, **4,** was prepared by the reaction of the Schiff base (0.56 g, 2.0 mmol) and $KMnO_4$ (0.32 g, 2.0 mmol) in MeCN (200 cm^3) with stirring at room temperature. The solution color changed from purple to brown and was allowed to stand in the dark place at room temperature. Two weeks later the resulting brownish black crystals were collected on a glass filter (yield 75%). A single crystal of **4** was obtained by recrystallization from methanol. This complex is considered to be one of isomers of $[Mn^{IV}(salipn)(\mu\text{-O})]_2$, because the salipn ligand has an asymmetric carbon atom on the bridging propylene group. Single crystals of $\mathbf{4}\cdot 2CH_3OH$ have been used for X-ray crystallographic characterization. IR spectrum on KBr pellets (cm^{-1}): 1628(vs), 1600(s), 1540(m), 1445(s), 1336(m), 1299(s), 760(m), 663(m), 638(m), 609(s), 454(m).

$[Mn^{IV}(salbn)(\mu\text{-O})]_2$, **5**. The manganese(IV) complex, $[Mn^{IV}(salbn)(\mu\text{-O})]_2$, **5,** was prepared by the reaction of salbnH_2 (0.59 g, 2.0 mmol) and $KMnO_4$ (0.32 g, 2.0 mmol) in MeCN (400 cm^3) with stirring at room temperature. The solution color changed from purple to brown and was allowed to stand in the dark at room temperature. After one week the resulting brownish black crystals were collected on a glass filter (yield 76%). IR spectrum on KBr pellets (cm^{-1}): 2955(m), 2925(m), 1622(vs), 1598(s), 1542(s), 1470(m), 1444(s), 1333(m), 1308(s), 1149(m), 756(s), 738(m), 650(m), 631(s), 619(s), 603(m).

Elemental analyses data for all of the complexes are given in Table 1.

Physical measurements

Elemental analyses were made on Yanaco Model CHN-CORDER MT-5. UV–vis and IR spectra were recorded on a Shimadzu Model UV-3100 spectrophotometer and Shimadzu Model IR-470 infrared spectrophotometer, respectively. Electrochemical studies were performed under argon, using a BAS Model CV-27 voltammograph equipped with a Graphtec Model WX 2400 XY recorder and a standard three-electrode assembly (glassy carbon working, Pt wire auxiliary, and Ag/AgCl MeCN 0.1 M *n*-Bu_4NClO_4, TBAP, reference electrode) with 0.1 M TBAP (*n*-Bu_4NClO_4) as the supporting electrolyte. All the redox potentials were corrected to the saturated calomel electrode (SCE). Magnetic susceptibility measurements were carried out by the Gouy method at room temperature. The temperature dependency of the magnetic susceptibilities was obtained by the Faraday method from 5 to 290 K, using a Tamagawa Faraday method magnetic balance.

Table 1. Elemental analyses of the complexes

Complex	Formula	Analyses[a] C (%)	H (%)	N (%)	Mn (%)
1·2MeCN	$Mn_2C_{44}H_{34}N_6O_6$	62.2 (62.0)	4.10 (4.02)	9.86 (9.86)	12.5 (12.9)
2·2MeCN	$Mn_2C_{36}H_{34}N_6O_6$	56.6 (57.2)	4.50 (4.53)	10.9 (11.1)	14.9 (14.5)
3·H_2O	$Mn_2C_{34}H_{32}N_4O_7$	55.6 (55.5)	4.37 (4.37)	8.18 (8.09)	15.5 (15.9)
4·2CH_3OH	$Mn_2C_{36}H_{40}N_4O_8$	56.2 (56.4)	5.23 (5.26)	7.29 (7.31)	13.8 (14.3)
5·2MeCN	$Mn_2C_{40}H_{42}N_6O_6$	58.8 (59.1)	5.29 (5.21)	10.2 (10.3)	13.4 (13.5)

[a] Required values in parentheses.

X-ray crystallography

Single crystals of **1**·2MeCN, **2**·2MeCN and **5**·2MeCN were obtained by one-step reaction of the Schiff bases and $KMnO_4$. On the other hand, single crystals **4**·2CH_3OH were obtained by recrystallization from CH_3OH. A crystal was mounted in a glass capillary and coated with silicone oil. All the data were collected on a Rigaku AFC7R four circle automated diffractometer with graphite monochromated Mo-K_α radiation ($\lambda = 0.71069$ Å) at room temperature. Unit-cell parameters were obtained from a least squares fit of 25 reflections, $8.0 < 2\theta < 15.9°$ for **1**·2MeCN, $6.5 < 2\theta < 21.8°$ for **2**·2MeCN, $8.0 < 2\theta < 14.6°$ for **4**·2CH_3OH and $8.2 < 2\theta < 15.3°$ for **5**·2MeCN. Three standard reflections were measured every 150 reflections; they showed no systematic decay throughout data collection. The data were corrected for Lorentz and polarization effects. All the calculations were carried out using the TEXSAN [25] crystallographic software package. The structure of **1**·2MeCN was solved using direct methods (MITHRIL84) [26] and expanded using Fourier techniques (DIRDIF) [27]. The structure of **2**·2MeCN was solved using heavy-atom Patterson methods (SAP191) [28] and expanded using Fourier techniques. The structures of **4**·2CH_3OH and **5**·2MeCN were solved using direct methods (SHELX86) [29] and expanded using Fourier techniques. These structures were refined by the full-matrix least-squares technique with anisotropic thermal parameters for all non-hydrogen atoms. Hydrogen atoms were introduced in calculated positions but not refined. Crystallographic data are summarized in Table 2.

Reagents

The reagents (salicylaldehyde and diamines) were obtained commercially and used without further purification. $KMnO_4$ was of the reagent grade (99.5%). MeCN was purified by distillation over P_4O_{10} twice and then distilled further before use. Other solvents were purified by usual method.

RESULTS AND DISCUSSION

Reactions of $KMnO_4$ with tetradentate Schiff base ligands

In acidic or basic aqueous solutions, a permanganate ion acts as a powerful oxidizing agent: its standard electrode potential being +1.51 or +0.50 V, respectively. We have found that $KMnO_4$ is soluble in dry acetonitrile (MeCN) and the solution is stable for about 24 h. The redox potential of $KMnO_4$ in MeCN was found to be −1.10 V (*vs* SCE), which can be assigned to the redox couple of $Mn^{VII}O_4^- \leftrightarrow Mn^{VI}O_4^{2-}$. This means that MnO_4^- is not so powerful oxidant in MeCN.

Figure 1 shows the absorption spectral changes of a MeCN solution of $KMnO_4$ caused by the addition of a MeCN solution of salbnH_2 in different molar ratios measured at room temperature. The intensity of characteristic absorption bands at 525, 545 and 570 nm for MnO_4^- ion decreased with addition of the salbnH_2 solution. The final absorption spectrum observed after 12 h exhibits a new broad absorption band around 500 nm, which can be assigned to LMCT transitions for Mn—O bonds of a di-μ-oxo dimanganese(IV) complex.

The dinuclear manganese(IV) complexes with a di-μ-oxo structure were prepared by the reaction of a series of tetradentate Schiff base ligands and $KMnO_4$ in MeCN with stirring at room temperature. This synthetic method has the advantage that high-valent manganese complexes can be obtained as crystals in 50–70% yields depending on the ligands by one-step reaction, in which MnO_4^- may be reduced with a part of the ligands.

Molecular structures of di-μ-oxo dimanganese complexes

From the X-ray crystallography, the complexes obtained by the reaction of $KMnO_4$ with tetradentate Schiff base ligands are found to be classified into two different types of di-μ-oxo dimanganese(IV) complex: one of them, **1** and **2**, is a bridging ligand, and the other, **4**, **5** and $[Mn^{IV}(salpn)(\mu\text{-}O)]_2$, **6**, is a dimer type.

Table 2. Crystallographic parameters for **1**, **2**, **4** and **5**

Compound	**1**·2MeCN	**2**·2MeCN	**4**·2CH$_3$OH	**5**·2MeCN
Chemical formula	$Mn_2C_{44}H_{34}N_6O_6$	$Mn_2C_{36}H_{34}N_6O_6$	$Mn_2C_{36}H_{40}N_4O_8$	$Mn_2C_{40}H_{42}N_6O_6$
Formula weight	851.65	756.58	766.61	812.68
Crystal color, habit	dark brown, prism	dark red, prism	brown, prism	dark brown, prism
Crystal size (mm)	0.30 × 0.10 × 0.07	0.15 × 0.05 × 0.08	0.20 × 0.20 × 0.15	0.45 × 0.30 × 0.35
a(Å)	8.937(2)	10.062(2)	9.821(1)	10.003(3)
b(Å)	12.382(2)	10.073(3)	17.579(4)	10.740(4)
c(Å)	17.736(2)	9.153(7)	9.843(2)	9.972(2)
α (°)	—	111.31(2)	—	95.24(2)
β (°)	95.98(1)	92.07(4)	94.92(1)	100.48(2)
γ (°)	—	94.03(3)	—	64.84(2)
V(Å^3)	1951.9(5)	860.2(6)	1692.9(5)	953.3(5)
Z	2	1	2	1
Crystal system	monoclinic	triclinic	monoclinic	triclinic
Space group	$P2_1/n$	$P\bar{1}$	$P2_1/a$	$P\bar{1}$
D_{calc}(g/cm^3)	1.451	1.460	1.504	1.415
$2\theta_{max}$(°)	55.0	55.0	55.0	55.0
Total data collected	4983	3290	4263	4623
Unique data	4693	3104	4040	4371
Obsd data ($I > 3\sigma(I)$)	2012	1553	1555	2799
R[a]	0.054	0.040	0.070	0.043
R_w[b]	0.048	0.038	0.078	0.034

[a] $R = \Sigma||F_o| - F_c||/\Sigma|F_o|$.
[b] $R_w = [\Sigma w(|F_o| - |F_c|)^2/\Sigma wF_o^2]^{1/2}$, $w = 4F_o^2/\sigma^2(F_o^2)$.

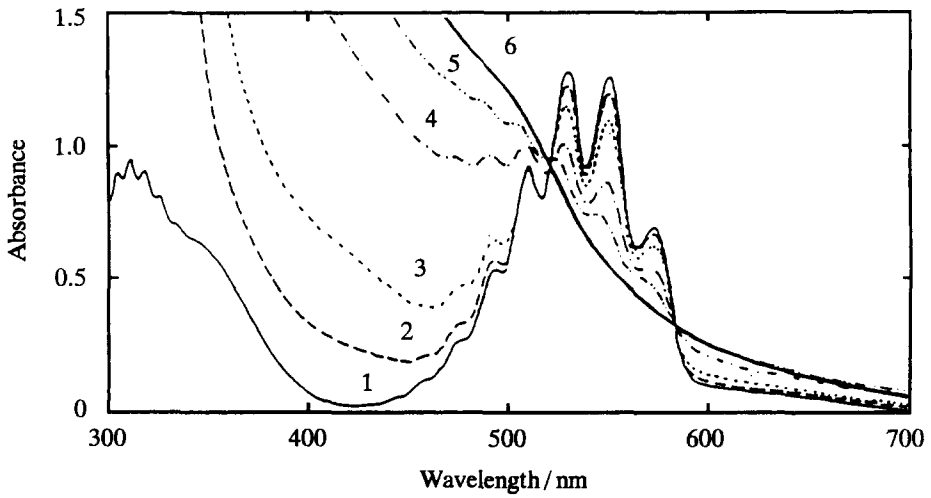

Fig. 1. Spectral changes of a MeCN solution of $KMnO_4$ (5×10^{-4} M) caused by the addition of a MeCN solution of salbnH_2. (1) No addition; (2) [salbnH_2]/[$KMnO_4$] = 1 (measured immediately after addition); (3) [salbnH_2]/[$KMnO_4$] = 2 (measured immediately after addition); (4) after allowing to stand the solution of (3) for 1 h; (5) after 3 h; (6) after 12 h. Cell length: 1.0 cm.

Although X-ray structural analysis of **3** has not yet been successful, the results of other physico-chemical measurements indicate that **3** belongs to the dimer type of di-μ-oxo manganese(IV) complex.

Bridging ligand type

The di-μ-oxo dimanganese(IV) complexes, [Mn^{IV}(μ-salophen)(μ-O)]$_2$, **1**, and [Mn^{IV}(μ-salen)(μ-O)]$_2$, **2**, adopt the unusual structure in which two tetradentate Schiff base ligands bridge two manganese atoms. The ORTEP plots of **1** and **2** are shown in Figs 2 and 3 and these selected bond distances and angles are listed in Tables 3 and 4, respectively. These structures consist of two Mn^{IV} centers bridged by two oxygen atoms to yield a planar Mn_2O_2 core. In the structures of **1** and **2** two salophen or salen ligands bridge two manganese atoms with a planar Mn_2O_2 core and bond *via* one phenolic oxygen atom and

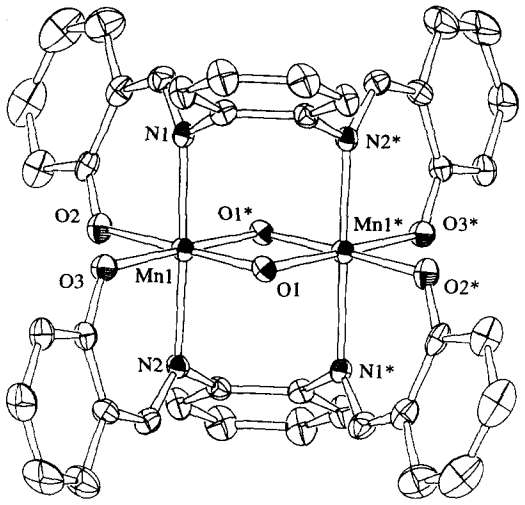

Fig. 2. Molecular structure of $[Mn^{IV}(\mu\text{-salophen})(\mu\text{-O})]_2$, **1**.

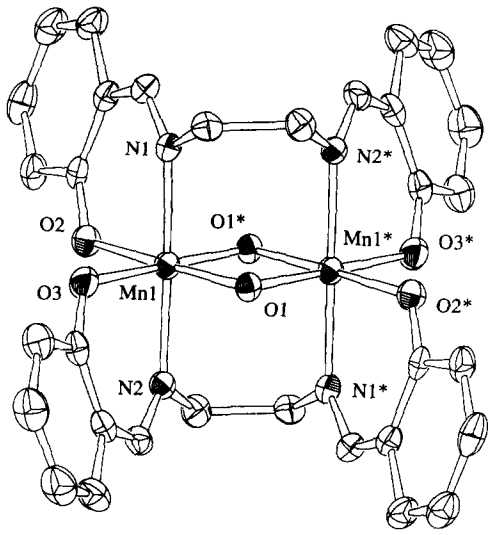

Fig. 3. Molecular structure of $[Mn^{IV}(\mu\text{-salen})(\mu\text{-O})]_2$, **2**.

one imine nitrogen atom to each manganese atom to complete the roughly octahedral coordination environment. The Mn–Mn separations of 2.718 (2) Å for **1** and 2.706 (2) Å for **2** are shorter than those reported for the $[Mn^{IV}(salpn)(\mu\text{-O})]_2$, **6** [2.728 (1) or 2.731 (2) Å] [12,13], and this may be caused by the existence of μ-salophen or μ-salen as a bridging ligand. As a stronger ligating atom, phenolic oxygen atoms of the ligands are oriented in the plane with the Mn_2O_2 core, and as a weaker ligating atom, imine nitrogen atoms are located to *cis* positions of the Mn_2O_2 core. The Mn—O (phenolate oxygen) and Mn—N (imine nitrogen) bond distances of **1** and **2** are almost regular: Mn—O, 1.934 (3) and 1.923 (4) Å for **1**, and 1.916 (4) and 1.926 (4) Å for **2**; Mn—N, 2.024 (5) and 2.015 (4) Å for **1**, and 2.002 (4) and 2.014 (4) Å for **2**.

As for complexes **1** and **2**, N—Mn—O angles formed by phenolic oxygen and imine nitrogen ligating atoms of these ligands and the manganese atom are close to a right angle [88.7 (2), 88.5 (2), 90.7 (2) and 90.2 (2)° for **1** and 90.4 (2), 90.6 (2), 88.3 (2) and 89.6 (2)° for **2**] and N—Mn—N angles are close to 180° [177.1 (2) for **1** and 177.7 (2)° for **2**]. Thus, there are few distortions around the manganese ions of **1** and **2**.

Recently, the bridging ligand type of the di-μ-oxo dimanganese(IV) complex, $[Mn^{IV}(\mu\text{-dbsalen})(\mu\text{-O})]_2$ ($dbsalenH_2$ = *N,N'*-di-3,5-dibromo-salicylidene-1,2-diaminoetane), has been prepared from the reaction of $dbsalenH_2$ and $Mn(ClO_4)_2 \cdot 6H_2O$ in air [30]. Its structure is very similar to those of the present complexes, with the Mn–Mn distance being 2.688 (1) Å.

Dimer type

The ORTEP plots of the dimer type of di-μ-oxo dimanganese(IV) complexes $[Mn^{IV}(salipn)(\mu\text{-O})]_2$, **4**, and $[Mn^{IV}(salbn)(\mu\text{-O})]_2$, **5**, are shown in Figs 4 and 5 and these selected bond distances and angles are listed in Tables 5 and 6, respectively. These structures

Table 3. Selected interatomic distances (Å) and angles (°) for **1**

Mn(1)—Mn(1*)	2.718(2)	Mn(1)—O(1)	1.811(4)
Mn(1)—O(1*)	1.822(3)	Mn(1)—O(2)	1.923(4)
Mn(1)—O(3)	1.934(3)	Mn(1)—N(1)	2.024(5)
Mn(1)—N(2)	2.015(4)		
Mn(1)—O(1)—Mn(1*)	96.9(2)	O(1)—Mn(1)—O(1*)	83.1(2)
O(1)—Mn(1)—O(2)	177.3(2)	O(1)—Mn(1)—O(3)	92.8(2)
O(1)—Mn(1)—N(1)	91.2(2)	O(1)—Mn(1)—N(2)	91.6(2)
O(1*)—Mn(1)—O(2)	94.2(2)	O(1*)—Mn(1)—O(3)	175.9(2)
O(1*)—Mn(1)—N(1)	88.7(2)	O(1*)—Mn(1)—N(2)	90.6(2)
O(2)—Mn(1)—O(3)	89.8(2)	O(2)—Mn(1)—N(1)	88.7(2)
O(2)—Mn(1)—N(2)	88.5(2)	O(3)—Mn(1)—N(1)	90.7(2)
O(3)—Mn(1)—N(2)	90.2(2)	N(1)—Mn(1)—N(2)	177.1(2)

Table 4. Selected interatomic distances (Å) and angles (°) for **2**

Mn(1)—Mn(1*)	2.706(2)	Mn(1)—O(1)	1.815(3)
Mn(1)—O(1*)	1.818(4)	Mn(1)—O(2)	1.916(4)
Mn(1)—O(3)	1.926(4)	Mn(1)—N(1)	2.002(4)
Mn(1)—N(2)	2.014(4)		
Mn(1)—O(1)—Mn(1*)	96.3(2)	O(1)—Mn(1)—O(1*)	83.7(2)
O(1)—Mn(1)—O(2)	175.9(2)	O(1)—Mn(1)—O(3)	92.8(2)
O(1)—Mn(1)—N(1)	89.8(2)	O(1)—Mn(1)—N(2)	89.5(2)
O(1*)—Mn(1)—O(2)	92.2(2)	O(1*)—Mn(1)—O(3)	176.4(2)
O(1*)—Mn(1)—N(1)	90.9(2)	O(1*)—Mn(1)—N(2)	91.2(2)
O(2)—Mn(1)—O(3)	91.4(2)	O(2)—Mn(1)—N(1)	90.4(2)
O(2)—Mn(1)—N(2)	90.6(2)	O(3)—Mn(1)—N(1)	88.3(2)
O(3)—Mn(1)—N(2)	89.6(2)	N(1)—Mn(1)—N(2)	177.7(2)

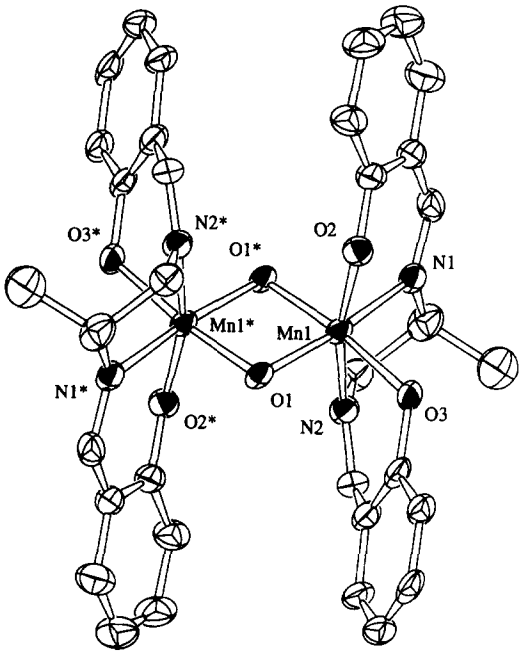

Fig. 4. Molecular structure of $[Mn^{IV}(salipn)(\mu\text{-}O)]_2$, **4**.

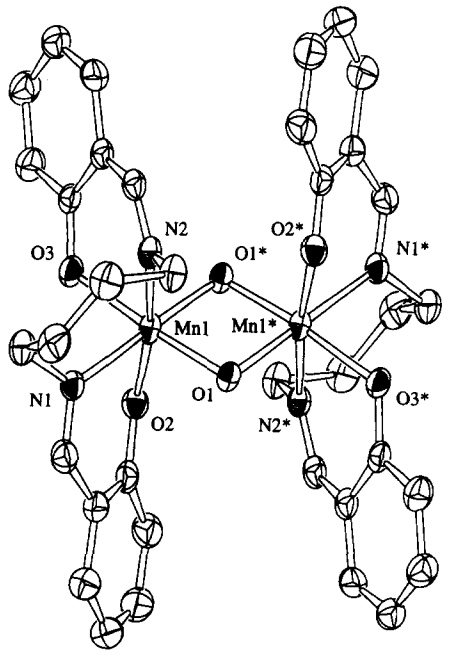

Fig. 5. Molecular structure of $[Mn^{IV}(salbn)(\mu\text{-}O)]_2$, **5**.

consist of two Mn^{IV} centers bridged by two oxygen atoms to yield a planar Mn_2O_2 core with a Mn–Mn separation of 2.733 (3) Å for **4** and 2.729 (1) Å for **5**. In the structures of **4** and **5**, the salipn or salbn ligand bonds *via* two phenolic oxygen atoms and two imine nitrogen atoms around each manganese atom to complete a roughly octahedral coordination environment similar to **6**. These complexes have one phenolic oxygen atom and one imine nitrogen atom at *trans* and *cis* positions to a bridging oxo group of Mn_2O_2 unit. A distinct lengthening of the Mn—O (phenolate oxygen) and Mn—N (imine nitrogen) bond distances *trans* to the Mn—O (oxo) bonds is observed: Mn—O, 1.931 (6) (*trans*) and 1.907 (7) (*cis*) Å for **4** and 1.940 (2) (*trans*) and 1.910 (3) (*cis*) Å for **5**; Mn—N, 2.056 (8) (*trans*) and 1.975 (8) (*cis*) Å for **4** and 2.069 (3) (*trans*) and 2.008 (3) (*cis*) Å for **5**. As the length of bridging diamines of the Schiff base ligands becomes short to the turn of 1,4-diaminobutane (salbn), 1,3-diaminopropane (salpn) and 1,2-diaminopropane (salipn), the bond angles of these complexes at around manganese ions N(1)—Mn—N(2), O(2)—Mn—N(2) and O(3)—Mn—N(1) deviate gradually from a right angle or 180°; N(1)—Mn—N(2), 86.0 (1) for **5**, 84.7 (2) for **6** and 78.6 (4)° for **4**; O(2)—Mn—N(2), 171.8 (1) for **5**, 169.7 (1) for **6** and 166.4 (4)° for **4**; O(3)—Mn—N(1), 90.2 (1) for **5**, 95.5 (1) for **6** [13] and 100.1 (3)° for **4**. On the other hand, the other bond angles of these complexes, O(2)—Mn—N(1), O(3)—Mn—N(2) and O(2)—Mn—O(3), are almost constant and close to a right angle.

Structural distortions of the dimer type complexes **4**, **5** and **6** are significant compared with the ligand bridging type complexes. The Schiff base ligands, salipn, salbn and salpn in the dimer type complexes should coordinate to the central manganese ion by

Table 5. Selected interatomic distances (Å) and angles (°) for **4**

Mn(1)—Mn(1*)	2.733(3)	Mn(1)—O(1)	1.804(6)
Mn(1)—O(1*)	1.828(6)	Mn(1)—O(2)	1.907(7)
Mn(1)—O(3)	1.931(6)	Mn(1)—N(1)	2.056(8)
Mn(1)—N(2)	1.975(8)		
Mn(1)—O(1)—Mn(1*)	97.6(3)	O(1)—Mn(1)—O(1*)	82.4(3)
O(1)—Mn(1)—O(2)	97.4(3)	O(1)—Mn(1)—O(3)	91.1(3)
O(1)—Mn(1)—N(1)	166.6(3)	O(1)—Mn(1)—N(2)	95.1(3)
O(1*)—Mn(1)—O(2)	95.6(3)	O(1*)—Mn(1)—O(3)	172.9(3)
O(1*)—Mn(1)—N(1)	86.0(3)	O(1*)—Mn(1)—N(2)	91.4(3)
O(2)—Mn(1)—O(3)	88.0(3)	O(2)—Mn(1)—N(1)	90.3(3)
O(2)—Mn(1)—N(2)	166.4(4)	O(3)—Mn(1)—N(1)	100.1(3)
O(3)—Mn(1)—N(2)	86.2(3)	N(1)—Mn(1)—N(2)	78.6(4)

Table 6. Selected interatomic distances (Å) and angles (°) for **5**

Mn(1)—Mn(1*)	2.729(1)	Mn(1)—O(1)	1.819(2)
Mn(1)—O(1*)	1.826(2)	Mn(1)—O(2)	1.910(3)
Mn(1)—O(3)	1.940(2)	Mn(1)—N(1)	2.069(3)
Mn(1)—N(2)	2.008(3)		
Mn(1)—O(1)—Mn(1*)	96.9(1)	O(1)—Mn(1)—O(1*)	83.1(1)
O(1)—Mn(1)—O(2)	93.5(1)	O(1)—Mn(1)—O(3)	175.2(1)
O(1)—Mn(1)—N(1)	94.3(1)	O(1)—Mn(1)—N(2)	90.8(1)
O(1*)—Mn(1)—O(2)	95.6(1)	O(1*)—Mn(1)—O(3)	92.3(1)
O(1*)—Mn(1)—N(1)	176.6(1)	O(1*)—Mn(1)—N(2)	91.8(1)
O(2)—Mn(1)—O(3)	88.1(1)	O(2)—Mn(1)—N(1)	86.8(1)
O(2)—Mn(1)—N(2)	171.8(1)	O(3)—Mn(1)—N(1)	90.2(1)
O(3)—Mn(1)—N(2)	88.1(1)	N(1)—Mn(1)—N(2)	86.0(1)

adjusting their configurations due to the rigidity of the Mn_2O_2 unit; in fact the angularity distortion of the plane constituted by Mn_2O_2 unit was not observed by changes in the type of these Schiff base ligands (Table 7).

The different coordination feature of the Schiff base ligands between the bridging ligand and the dimer types may arise mainly from the difference in their flexibility. However, there is possibility that two types of complexes are formed in solution, because the Schiff base ligands salenH_2 and salipnH_2 having the same length of bridging diamine group [i.e. 1,2-diaminoethane (salen) and 1,2-diaminopropane (salipn)] take different coordination feature.

IR spectra

It has been reported that IR spectra of the di-μ-oxo dimanganese(IV) complexes exhibit sharp absorption bands characteristic for a $\{Mn_2O_2\}$ core in the region 600–700 cm^{-1}, which can be assigned to stretching vibrations of Mn—O (oxo) bonds [31]. Figure 6 shows the IR spectra of the bridging ligand type complexes,

Table 7. Inter-metal distances (Å) and angles (°) of di-μ-oxo dimanganese(IV) complexes with Schiff base ligands

Complex	Mn—Mn	Mn—O_{oxo}—Mn	O_{oxo}—Mn—O_{oxo}	Ref
1	2.718(2)	96.9(2)	83.1(2)	this work
2	2.705(2)	96.2(2)	83.8(2)	this work
4	2.732(3)	97.6(3)	82.4(3)	this work
5	2.729(1)	96.9(1)	83.1(1)	this work
6	2.728(1)	97.2(1)	82.8(1)	[12]
$[Mn^{IV}(\mu\text{-dbsalen})(\mu\text{-O})]_2$	2.688(1)	96.7(2)	83.3(2)	[30]
$[Mn^{IV}(N\text{-Hx-sal})_2(\mu\text{-O})]_2$	2.780(2)	99.5(3)/99.9(3)	80.4(3)/80.2(3)	[24]

(*N*-Hx-salH = *N*-hexyl-salicylideneamine)

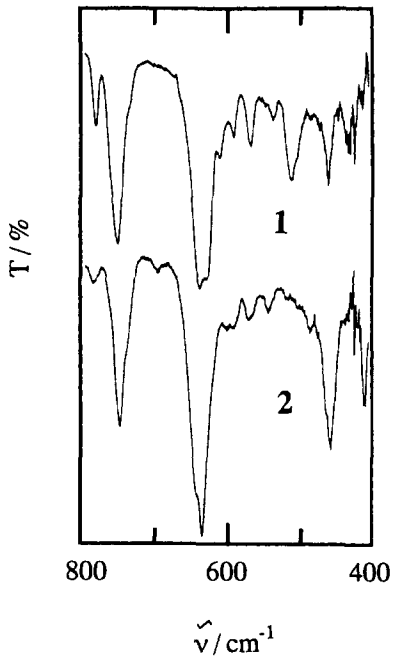

Fig. 6. IR spectra of the bridging ligand type di-μ-oxo dimanganese(IV) complexes, **1** and **2**.

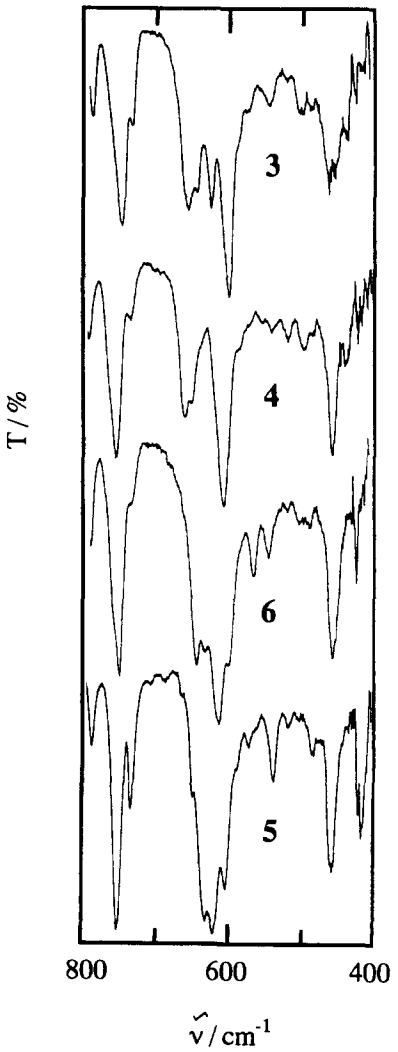

Fig. 7. IR spectra of the dimer type di-μ-oxo dimanganese(IV) complexes **3**–**6**.

1 and **2**, in this region which exhibit two intense bands at 641 and 632 cm^{-1} for **1** and at 642 and 634 cm^{-1} for **2**. On the other hand, the IR spectra of the dimer type complexes, **3**, **4**, **5** and **6**, exhibit a combination of three or four intense bands, 658, 648, 627 and 604 cm^{-1} for **3**, 660, 638 and 609 cm^{-1} for **4**, 650, 631, 619 and 603 cm^{-1} for **5**, and 648, 636, 618 and 604 cm^{-1} for **6**, as shown in Fig. 7. A clearly different spectral pattern is seen between the bridging ligand and dimer type complexes, nevertheless complexes **2** and **3** possess the same salen ligand. Such a difference may have arisen from the difference in the symmetry around the central manganese atoms: as shown in the structural determination of these complexes, the two *trans* positions of Mn—O (oxo) bonds in the bridging ligand type complexes are occupied by the phenolic oxygen atoms, whereas the corresponding *trans* positions in the dimer type complexes are occupied by the phenolic oxygen and imine nitrogen atoms. Moreover, different spectral features of these complexes are seen at around 1300 cm^{-1}, which can be assigned to the stretching vibrations due to the phenolic C—O bond. In this region, the spectra of the bridging ligand type (**1** and **2**) exhibit one intense band at 1318 cm^{-1} for **1** and at 1298 cm^{-1} for **2**, whereas those of the dimer type, (**3**, **4**, **5** and **6**) exhibit a medium intensity band additional to an intense band at 1339 and 1297 cm^{-1} for **3**, at 1336 and 1299 cm^{-1} for **4**, at 1333 and 1308 cm^{-1} for **5**, and at 1340 and 1298 cm^{-1} for **6**. This may arise from the fact that two phenolic oxygen atoms in these complexes are located each at *trans* and *cis* positions to the bridging oxo group of the Mn_2O_2 unit. These results indicate that both types can be distinguished by the IR spectra.

Electronic spectra

Figure 8 shows the electronic absorption spectra of the complexes, **1**, **2**, **4** and **5** in CH_2Cl_2. A general spectral feature exhibits two absorption bands around 410 and 480 nm with moderate intensity in the visible region and two or three absorption bands around 245, 270 and 360 nm with high intensity in the near- and ultra-violet region. All the numerical data are listed in Table 8. The former absorption bands can be assigned to the ligand to metal charge-transfer transitions from oxygen atoms of the oxo groups to manganese atoms, and the latter bands mainly to the transitions in the ligands themselves.

Although these absorption bands could not be assigned correctly, a clear difference in the UV spectra between the bridging ligand and dimer types of the di-

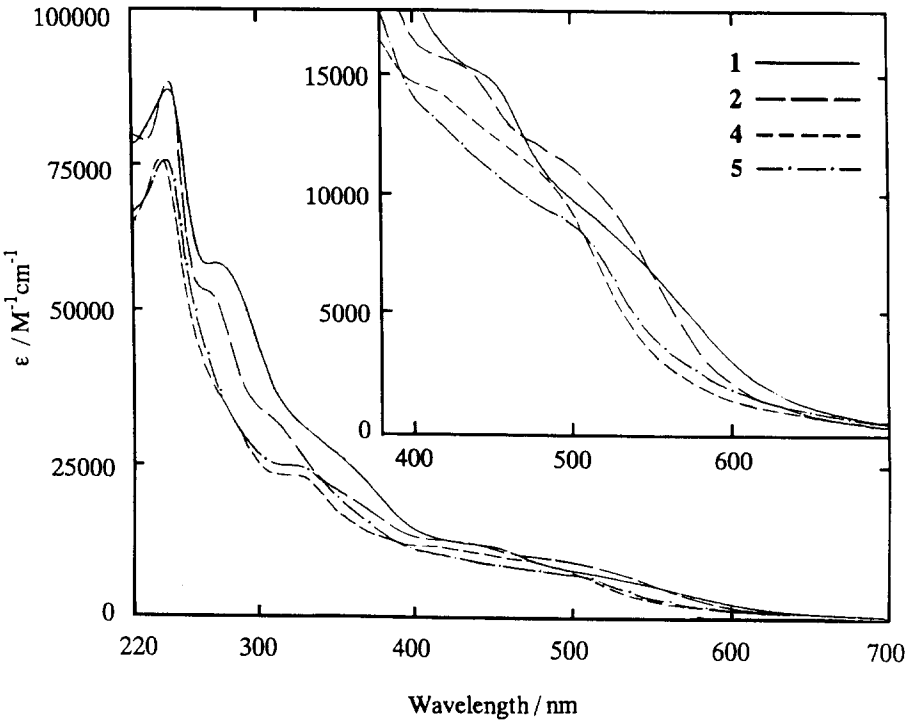

Fig. 8. Electronic absorption spectra of the complexes **1, 2, 4** and **5** in CH_2Cl_2.

Table 8. Absorption spectra and electrochemical data for the di-μ-oxo dimanganese(IV) complexes

Complex		λ_{max}[a] (nm)	($\varepsilon \times 10^{-3}$) ($dm^3mol^{-1}cm^{-1}$)		E_{cp}[b] V (*vs* SCE)	E_{ap}[b] V (*vs* SCE)	ΔE[c] (V)
1	244 (86.8)	274 (58.1)	351 (26.9)	446 (11.8)	−0.24	−0.10	0.14
	524 (6.72)						
2	244 (87.6)	268 (53.1)	309 (32.4)	360 (19.0)	−0.36	−0.23	0.13
	428 (12.2)	521 (7.62)					
3[b]	319 (24.6)	403 (12.1)	486 (7.56)		−0.47	−0.24	0.23
4	239 (75.0)	319 (23.2)	412 (11.5)	485 (8.38)	−0.51	−0.18	0.33
5	242 (75.4)	320 (24.6)	423 (9.97)	494 (7.19)	−0.46	−0.22	0.24

[a] Measured in CH_2Cl_2.
[b] Measured in DMSO.
[c] $E_{ap} - E_{cp}$.

μ-oxo dimanganese(IV) complexes is seen in Fig. 8: the spectra of the former type exhibit an additional absorption peak around 270 nm, which is lacked in the spectra of the latter type. These absorption spectral differences may be caused by the difference in hybridization of the ligand π orbital systems and manganese $d\pi$ orbitals. As mentioned in the above IR spectra, two coordinating types of the tetradentate Schiff base ligands are also found to be discriminative from the UV spectra.

Electrochemistry

Cyclic voltammograms (CV) of the di-μ-oxo dimanganese(IV) complexes **1–5** were measured in dimethyl sulfoxide (DMSO) over the potential range from +1.00 to −1.70 V. In a DMSO solution, all the complexes exhibit a pair of quasi-reversible reduction and oxidation (see Fig. 9 and Table 8). The reduction waves of **1** and **2** (−0.24 and −0.36 V *vs* SCE, respectively) are observed at slightly positive potentials com-

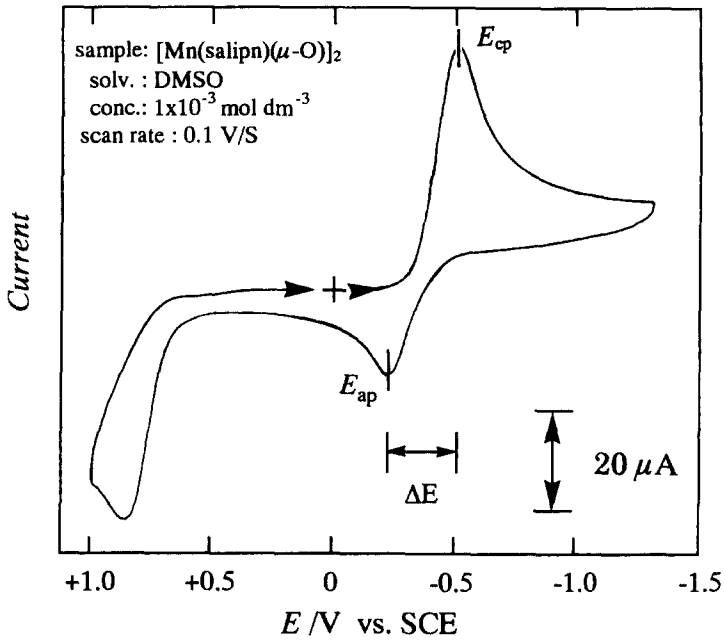

Fig. 9. Cyclic voltammogram (CV) of **4** in DMSO.

pared with those for **3**, **4** and **5** (−0.47, −0.51 and −0.46 V *vs* SCE, respectively). Controlled potential reduction of **5** in DMSO at −0.60 V showed that the reduction of the complex undergoes *via* a 2-electron electrode process, which means that $[Mn^{IV}O_2Mn^{IV}]^0$ is reduced to $[Mn^{III}O_2Mn^{III}]^{2-}$.

Magnetic properties

The magnetic susceptibilities were measured for complexes **1**, **2** and **5** in the temperature range 5–290 K and for the complexes **3** and **4** in the range 77–290 K by the Faraday method. The temperature-dependent effective magnetic moments for **1**, **2** and **5** per dimeric unit at 5, 77 and 290 K are calculated as follows: 0.86, 1.68 and 3.09 μ_B for **1**, 0.45, 1.29 and 2.98 μ_B for **2** and 0.75, 1.37 and 2.96 μ_B for **5**, respectively. And those for **3** and **4** per dimeric unit at 77 and 290 K are calculated as follows: 1.31 and 2.77 μ_B for **3** and 0.91 and 2.58 μ_B for **4**, respectively. These values indicate that an intramolecular antiferromagnetic interaction between the two manganese(IV) ions (d^3) exists in these complexes. The magnetic data obtained for **2** and **5** (Figs 10 and 11) were fitted by employing an expression derived from an isotropic spin-exchange Hamiltonian $H = -2JS_1 \cdot S_2$ ($S_1 = S_2 = 3/2$) and the Van Vleck equation. The magnetic data obtained for **1**, **3** and **4** (Figs 12 and 13) were fitted by the same method as the above, although these were used somewhat roughly approximation. The curve fitting leads to values of $J = -80$ cm^{-1}, $g = 1.78$, TIP $= 1.0 \times 10^{-3}$ and $P = 0.7\%$ for **2** and $J = -78$ cm^{-1}, $g = 1.71$, TIP $= 1.25 \times 10^{-3}$ and $P = 2.2\%$ for **5**, where TIP is the temperature-independent paramagnetism and P is the mole per cent of paramagnetic impurities assumed to be a mononuclear manganese(III) complex. The J values (g value) for **1**, **3** and **4** were −80 (1.85), −95 (1.71) and −88 cm^{-1} (1.87), respectively. These J values are comparable with those observed for the di-μ-oxo dimanganese(IV) having an ancillary ligand with both of O and N donating atoms, i.e. complex **6** [$J = -82$ cm^{-1} ($g = 1.79$)] [12] and $[Mn^{IV}(pic)_2(O)]_2$ [$J = -87$ cm^{-1} ($g = 1.83$)] (pic denotes a monoanion of picolinic acid) [14], and slightly lower than those ($J \approx -125$ cm^{-1}) for the di-μ-oxo dimanganese(IV) complexes having an ancillary ligand with all N donating atoms [15–17].

The temperature-dependent magnetic behavior for **1** is peculiar and will require further study: it did not fit and deviated at lower temperatures from the calculated values by applying the above mentioned equations. It can be ruled out that more paramagnetic impurities were included in the complex **1**, because the repeated measurements for it obtained from the different batch preparations also gave almost the same results. Figure 14 shows intermolecular close π–π stacking between the phenylene rings of *o*-phenylenediamine groups of salophen ligands of **1**, which are placed to form a parallel plane with separation by 3.40 Å (plane to plane distance). This distance is enough for π–π interaction between the phenylene rings [32–34]. Therefore, the temperature-dependent magnetic behavior for **1** may be caused by existence of intermolecular ferromagnetic interaction *via* the phenylene rings of *o*-phenylenediamine groups of salophen ligands. In this work, further experiments have not been carried out.

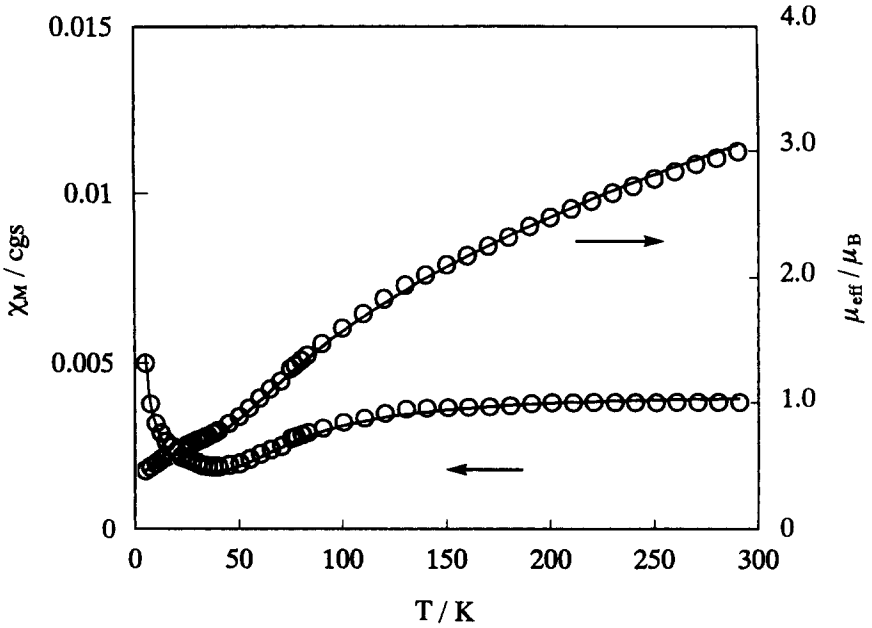

Fig. 10. Plots of molar susceptibility (left scale) and effective magnetic moment (right scale) per dimer *vs* temperature of a polycrystalline sample of complex **2**. Solid lines represent best fits of the data using the parameters described in the text.

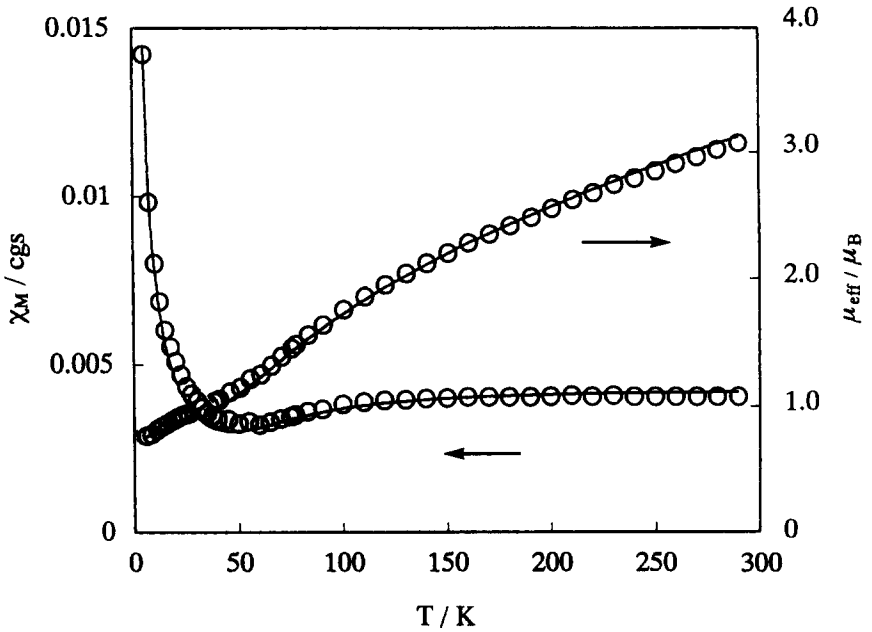

Fig. 11. Plots of molar susceptibility (left scale) and effective magnetic moment (right scale) per dimer *vs* temperature of a polycrystalline sample of complex **5**. Solid lines represent best fits of the data using the parameters described in the text.

CONCLUSION

Two different types of di-μ-oxo dimanganese(IV) complex have been found to be obtained by the one step reaction of $KMnO_4$ with tetradentate Schiff base ligands in MeCN. The bridging ligand type of di-μ-oxo dimanganese(IV) complexes, **1** and **2**, adopts the unusual structure in which two tetradentate Schiff base ligands bridge two manganese atoms. In contrast, the dimer type, **3**, **4** and **5**, has a structure in which salen, salipn or salbn ligands are coordinated to each manganese ion as a tetradentate ligand. In addition,

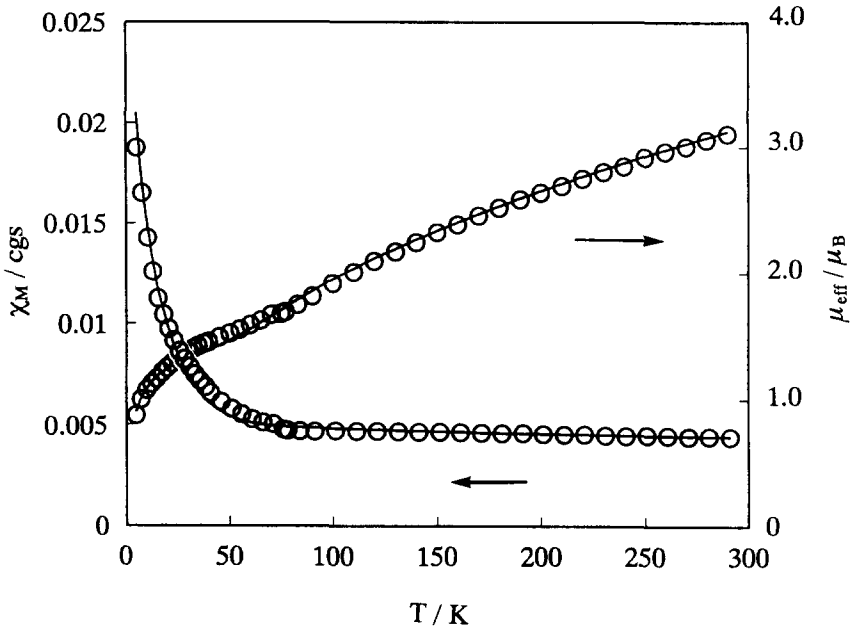

Fig. 12. Plots of molar susceptibility (left scale) and effective magnetic moment (right scale) per dimer *vs* temperature of a polycrystalline sample of complex **1**. Solid lines represent best fits of the data using the parameters described in the text.

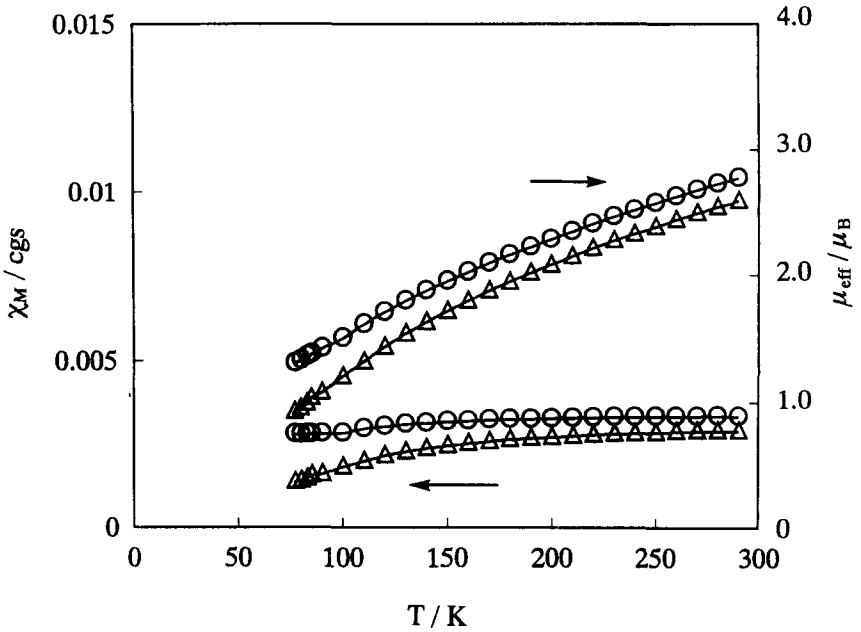

Fig. 13. Plots of molar susceptibility (left scale) and effective magnetic moment (right scale) per dimer *vs* temperature of polycrystalline samples of complexes **3** (○) and **4** (△).

these two types of di-μ-oxo dimanganese(IV) complexes, **2** and **3**, have been also obtained by the oxygenation of Mn^{II}(salen) with molecular oxygen, depending upon the organic solvents used [35]. Two such coordinating types of the Schiff base ligands are also found to be discriminative from the IR and UV spectra. The temperature-dependent effective magnetic moments of these complexes, with the exception of $[Mn^{IV}(\mu\text{-salophen})(\mu\text{-O})]_2$, **1**, indicate that an intramolecular antiferromagnetic interaction between the two manganese(IV) ions (d^3) exists in these complexes. A curious temperature-dependent mag-

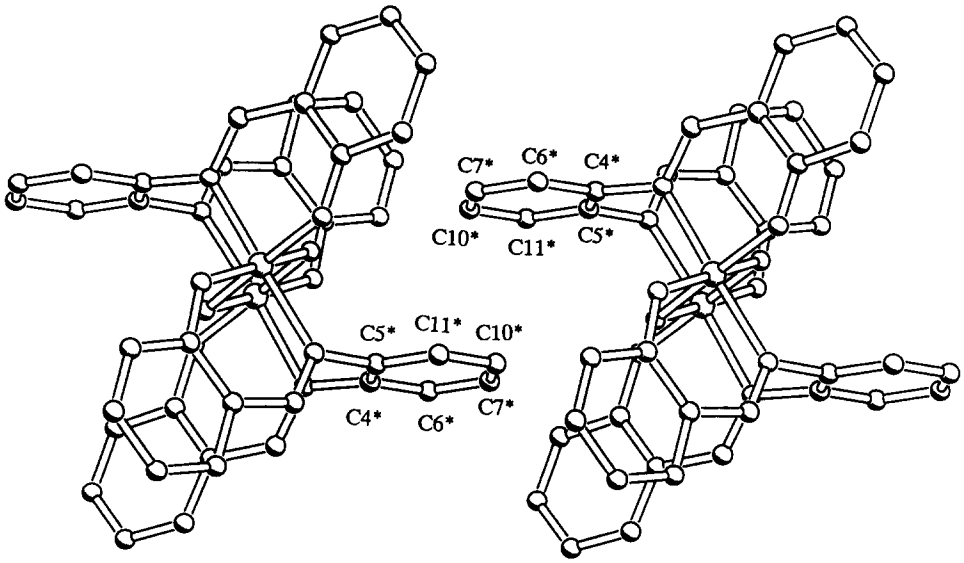

Fig. 14. A representation of intermolecular π–π stacking interaction of **1**.

netic behavior for **1** may be caused by existence of intermolecular ferromagnetic interaction *via* the phenylene rings of *o*-phenylenediamine groups of salophen ligands.

REFERENCES

1. Pecoraro, V. L., Ed., *Manganese Redox Enzymes*, VCH Publishers, New York (1992).
2. Yachandra, V. K., DeRose, V. J., Latimer, M. J., Mukerji, I., Sauer, K. and Klein, M. P., *Science*, 1993, **260,** 675.
3. Yachandra, V. K., Sauer, K. and Klein, M. P., *Chem. Rev.*, 1996, **96,** 2927.
4. Manchanda, R., Brudvig, G. W. and Crabtree, R. H., *Coord. Chem. Rev.*, 1995, **144,** 1.
5. Wieghardt, K., *Angew. Chem. Int. Ed. Engl.*, 1994, **33,** 725.
6. Wieghardt, K., *Angew. Chem. Int. Ed. Engl.*, 1989, **28,** 1153.
7. Gallo, E., Solari, E., Angelis, S. D., Floriani, C., Re, N., Chiesi-Villa, A. and Rizzoli, C., *J. Am. Chem. Soc.*, 1993, **115,** 9850.
8. Gultneh, Y., Ahvazi, B., Khan, A. R., Butcher, R. J. and Tuchagues, J. P., *Inorg. Chem.*, 1995, **34,** 3633.
9. Mikuriya, M., Hashimoto, Y. and Kawamori, A., *Chem. Lett.*, 1995, 1095.
10. Mikuriya, M., Yamato, Y. and Tokii, T., *Bull. Chem. Soc. Jpn.*, 1992, **65,** 2624.
11. Larson, E. J. and Pecoraro, V. L., *J. Am. Chem. Soc.*, 1991, **113,** 3810.
12. Gohodes, J. W. and Armstrong, W. H., *Inorg. Chem.*, 1992, **31,** 368.
13. Larson, E. J., Lah, M. S., Li, X., Bonadies, J. A. and Pecoraro, V. L., *Inorg. Chem.*, 1992, **31,** 373.
14. Libby, E., Webb, R. J., Streib, W. E., Folting, K., Huffman, J. C., Hendrickson, D. N. and Christou, G., *Inorg. Chem.*, 1989, **28,** 4037.
15. Stebler, M., Ludi, A. and Bürgi, H.-B., *Inorg. Chem.*, 1986, **25,** 4743.
16. Oki, A. R., Glerup, J. and Hodgson, D. J., *Inorg. Chem.*, 1990, **29,** 2435.
17. Goodson, P. A., Glerup, J., Hodgson, D. J., Michelsen, K. and Pedersen, E., *Inorg. Chem.*, 1990, **29,** 503.
18. Goodson, P. A., Glerup, J., Hodgson, D. J., Michelsen, K. and Weihe, H., *Inorg. Chem.*, 1991, **30,** 4909.
19. Pal, S. and Armstrong, W. H., *Inorg. Chem.*, 1992, **31,** 5417.
20. Sarneski, J. E., Didiuk, M., Thorp, H. H., Crabtree, R. H., Brudvig, G. W., Faller, J. W. and Schulte, G. K., *Inorg. Chem.*, 1991, **30,** 2833.
21. Pal, S., Chan, M. K. and Armstrong, W. H., *J. Am. Chem. Soc.*, 1992, **114,** 6398.
22. Pal, S., Olmstead, M. M. and Armstrong, W. H., *Inorg. Chem.*, 1995, **34,** 4708.
23. Torayama, H., Nishide, T., Asada, H., Fujiwara, M. and Matsushita, T., *Chem. Lett.*, 1996, 387.
24. Torayama, H., Asada, H., Fujiwara, M. and Matsushita, T., *Chem. Lett.*, 1996, 1067.
25. TEXSAN: Single Crystal Structure Analysis Package, Molecular Corporation (1985 & 1992).
26. Gilmore, C. J., MITHRLIL84 an integrated direct methods computer program. Univ. of Glasgow, Scotland, *J. Appl. Cryst.*, 1984, **17,** 42.
27. Beurskens, P. T., Admiraal, G., Beurskens, G., Bosman, W. P., de Gelder, R., Israel, R. and Smits, J. M. M. (1994). The DIRDIF program system, Technical Report of the Crystallography Laboratory, Univ. of Nijmegen, The Netherlands.
28. Fan, H., Structure Analysis Programs with Intelligent Control, Rigaku Corporation, Tokyo, Japan, 1991.
29. Sheldrick, G. M., SHELXS86 in *Crystallographic Computing* 3, p. 175 eds G. M. Sheldrick, C. Kruger and R. Goddard, Oxford University Press (1985).

30. Bermejo, M. R., Castineiras, A., Garicia-Monteagudo, J. C., Rey, M., Sousa, A., Watkinson, M., McAuliffe, C. A., Pritchard, R. G. and Beddoes, R. L., *J. Chem. Soc., Dalton Trans.*, 1996, 2935.
31. Matsushita, T., Spencer, L. and Sawyer, D. T., *Inorg. Chem.*, 1988, **27,** 1167.
32. Hartshorn, C. M. and Steel, P. J., *Inorg. Chem.*, 1996, **35,** 6902.
33. Mandal, S. K., Thompson, L. K., Newlands, M. J., Gabe, E. J. and Lee, F. L., *Inorg. Chem.*, 1990, **29,** 3556.
34. Torayama, H., Nishide, T., Asada, H., Fujiwara, M. and Matsushita, T., *Polyhedron*, in press.
35. Asada, H., Torayama, H., Fujiwara, M. and Matsushita, T., unpublished results.

Pergamon

PII: S0277-5387(97)00239-8

Polyhedron Vol. 17, No. 1, pp. 119–124, 1998
© 1997 Elsevier Science Ltd
All rights reserved. Printed in Great Britain
0277-5387/98 $19.00+0.00

Syntheses and Characterisation of Amino(pentafluorophenyl)boranes. Crystal Structure of $[(Me_3Si)_2NB(C_6F_5)_2]$

Jane R. Galsworthy,[a] Malcolm L. H. Green,[a]* V. Clifford Williams[a] and Alex N. Chernega[b]

[a] Inorganic Chemistry Laboratory, South Parks Road, Oxford, OX1 3QR, U.K.

[b] Chemical Crystallography Laboratory, 9 Parks Road, Oxford, OX1 3PD, U.K.

(Received 21 April 1997; accepted 2 June 1997)

Abstract—The chloroborane, $ClB(C_6F_5)_2$, has been investigated as a useful synthon for the preparation of a series of amino(pentafluorophenyl)boranes. The compounds $[(Me_3Si)_2NB(C_6F_5)_2]$, **1**, $[(Me_3Si)(H)NB(C_6F_5)_2]$, **2**, and $[HN\{B(C_6F_5)_2\}_2]$, **3**, have been synthesised and **1** has been characterised by X-ray crystallography.
© 1997 Elsevier Science Ltd

Keywords: aminoborane; Lewis acid; X-ray crystallography; ^{11}B NMR spectroscopy; N—B π-bonding; pentafluorophenyl.

The nature of the bonding in aminoborane compounds has been subjected to numerous investigations as these species are analogues of asymmetrically substituted alkenes [1]. In particular, numerous attempts to quantify the extent of N—B π-bonding in these compounds *via* ^1H, ^{11}B and ^{13}C NMR spectroscopic measurements [2] and X-ray diffraction studies have been reported [3]. Pentafluorophenyl rings have been utilised as a means of introducing strongly electron withdrawing groups into Lewis acids and hence increasing the electrophilicity of the acceptor atom [4]. Metal imido complexes may be readily prepared by the reaction of H_2NR, $HN(SiMe_3)R$ or $RN(SiMe_3)_2$, R = alkyl or aryl, with suitable transition metal complexes [5] and we hoped that these aminoboranes would behave in an analogous manner. Most complexes containing the M=NR unit display little reactivity associated with the imido moiety and we hoped to activate this functionality by synthesising $L_nM{=}NBR_2$ complexes from aminoborane compounds possessing the highly electrophilic $\{B(C_6F_5)_2\}$ unit. Herein we report the synthesis of a series of aminoboranes from the precursor $ClB(C_6F_5)_2$ and a preliminary exploration of their reactivities.

* Author to whom correspondence should be addressed.

RESULTS AND DISCUSSION

The reaction of equimolar amounts of $MN(SiMe_3)_2$, M = Na or K, and $ClB(C_6F_5)_2$ in toluene leads smoothly to the formation of a white solid characterised as $[(Me_3Si)_2NB(C_6F_5)_2]$, **1**. Cooling a concentrated pentane solution of the aminoborane produces large colourless crystals which were studied by X-ray crystallography. The molecular structure of **1** is shown in Fig. 1 and selected bond lengths and angles are given in Table 1. The analytical and spectroscopic data of compound **1** are unexceptional and are reported in Table 2.

The N—B bond length of 1.400(3) Å is at the shorter end of the range observed for N—B bonds in similar environments reflecting the strong electron

Table 1. Selected bond distances (Å) and angles (°) for compound **1**

B(1)—N(1)	1.400(3)	Si(1)—N(1)—Si(2)	118.92(9)
B(1)—C(1)	1.590(3)	Si(1)—N(1)—B(1)	120.4(1)
B(1)—C(7)	1.596(3)	Si(2)—N(1)—B(1)	120.6(1)
N(1)—Si(1)	1.790(2)	N(1)—B(1)—C(1)	122.6(2)
N(1)—Si(2)	1.783(2)	N(1)—B(1)—C(7)	122.6(2)
		C(1)—B(1)—C(7)	114.7(2)

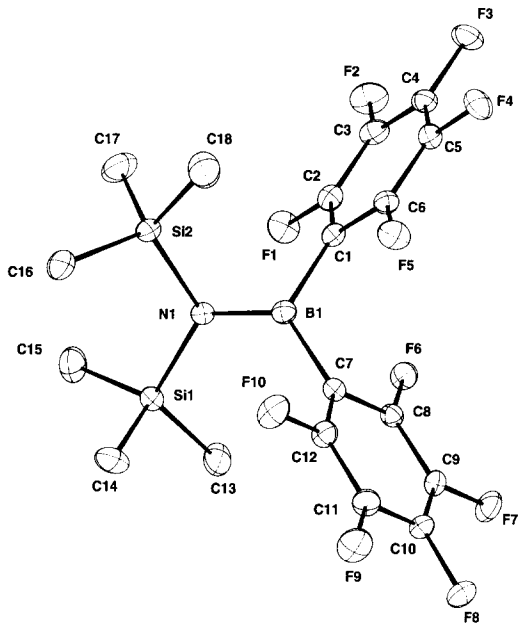

Fig. 1. Molecular structure of $[(Me_3Si)_2NB(C_6F_5)_2]$, **1**.

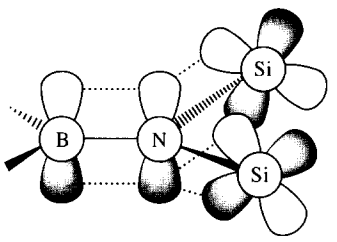

Fig. 2. Schematic representation of the extended π-bonding in compound **1**.

withdrawing capacity of the pentafluorophenyl rings; compare with 1.433(6) Å in $[^tBu(Me_3Si)NBPh_2]$, 1.430(3) Å in $[HN(BPh_2)_2]$, 1.435(3) Å in $[(Me)N(BPh_2)_2]$ and 1.439(3) Å in $[HN\{B(2,4,6\text{-trimethylphenyl})_2\}_2]$ [6]. The Si, N and B atoms in compound **1** are coplanar indicating some degree of delocalised π-bonding (Fig. 2). The bulkiness of the pentafluorophenyl rings preclude them from participating fully in this type of bonding and they adopt an orientation which strikes a compromise between maximum π-bonding and minimum steric repulsions, one in which the rings are separated by an interplanar angle of 89.1°. The interplanar angle, α, between the C_2B and NSi_2 planes is 34.0°. The closely related compound, $[^tBu(Me_3Si)NBPh_2]$, mentioned above [6], was synthesised in a similar fashion from the reaction of Ph_2BBr and $LiN^tBu(SiMe_3)$ and displays little structural variation from compound **1**. The molecule $[(F_3C)_2BNMe_2]$ has also been structurally characterised by electron diffraction and exhibits a B—N bond length of 1.425(18) Å [7]. The CF_3 group has similar σ acceptor properties to those of the C_6F_5 moiety but whilst the latter species is also able to function as a π donor the former is not.

In an attempt to prepare the mono(trimethylsilyl) analogue of **1**, $ClB(C_6F_5)_2$ was reacted with one equivalent of $HN(SiMe_3)_2$ in toluene. After heating at 70°C for 1.5 h, under slightly reduced pressure, the solvent was removed *in vacuo* and the product extracted with hexane. Concentration and cooling of this colourless solution to −78°C results in the formation of a white solid identified as having the empirical formula $[(Me_3Si)(H)NB(C_6F_5)_2]$. Characterising data for the compound is given in Table 2. The ^{11}B NMR spectrum of this compound in C_6D_6 reveals two signals in the ratio of approximately 4 : 1 (δ 38.2 ppm, **2**, and δ −2.8 ppm, **2′**, respectively). The minor signal is typical of a four co-ordinate boron environment indicating that in solution about 20% of the aminoborane exists as a dimer, **2′** (Fig. 3).This phenomenon has been frequently observed for $R_2NBR'_2$ compounds and, when R and R′ are alkyl or aryl substituents, the extent of dimerisation appears to be mainly dependent on the steric demands of the R groups [1,8]. No dimer formation is observed for compound **1** presumably due to increased steric crowding around the nitrogen centre in the *bis*(trimethylsilyl) derivative. If the nitrogen lone pair is involved in π bonding to silicon in both **1** and **2** then the presence of a single $SiMe_3$ substituent in **2** should, on purely electronic grounds, encourage dimerisation in the (*mono*)trimethylsilylated species.

Harsher reaction conditions (70°C in octane for 7 h) are required to synthesise $[HN\{B(C_6F_5)_2\}_2]$, **3**, from the reaction between $HN(SiMe_3)_2$ and 2 equiv. of $ClB(C_6F_5)_2$. Under the same conditions the reaction of equimolar amounts of $HN(SiMe_3)_2$ and $ClB(C_6F_5)_2$

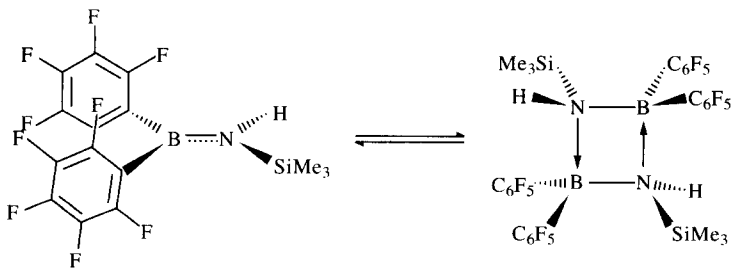

Fig. 3. Schematic representation of the monomer-dimer equilibrium occurring for compound **2**.

Table 2. Analytical and spectroscopic data for compounds **1**, **2** and **3**

Complex[a]	Spectroscopic data[b]
1 $[(Me_3Si)_2NB(C_6F_5)_2]$ C, 43.3 (42.8); H, 3.5 (3.6); B, 2.2 (2.2); N, 2.8 (2.8) Mass: *m/z* 506 [M^+], 491 [M^+—Me]	IR: 2986 m, 2910 w, 1650 s, 1519 vs, 1489 vs, 1388 vs, 1363 s, 1334 vs, 1303 vs, 1282 s, 1145 s, 1093 s, 976 s, 878 s, 791 s, 766 s, 731 w, 686 s, 657 w, 643 m, 626 m ^1H: −0.11 [s, CH_3] ^{13}C: 146.9 [d, *J* 400, C—F], 143.4 [d, *J* 419, C—F], 137.61 [d, *J* 425, C—F], 3.16 [s, CH_3] ^{11}B: 43.6 [br] ^{19}F: −137.08 [d, *J* 12.4, *ortho* F], −155.63 [*t*, *J* 11.3, *para* F], −166.19 [s, *meta* F]
2 '$[(Me_3Si)(H)NB(C_6F_5)_2]$ C, 41.4 (41.6); H, 2.3 (2.3); B, 2.5 (2.5); N, 3.2 (3.2) Mass: *m/z* 417 (M^+—Me)	IR: [d]3646 w, 3096 w, 2973 w, 1651 s, 1522 vs, 1475 vs, 1417 s, 1400 s, 1389 s, 1315 s, 1299 s, 1257 s, 1134 vs, 1092 vs, 973 vs, 940 m, 871 vs, 850 vs, 794 s, 760 m, 746 m, 718 m, 703 m, 683 m, 638 m, 627 m ^1H: 4.8 [1H, s(br), NH], −0.16 [9H, s, CH_3] ^{13}C: 151.2 [d, *J* 307, C—F], 142.9 [d, *J* 373, C—F], 137.8 [d, *J* 375, C—F], 0.3 [s, CH_3] ^{11}B: 38.2 [br] ^{19}F: −135.14 [dd, *J* 9.3, 5.4, *ortho* F], −138.87 [dd, *J* 14.7, 5.3, *ortho* F], −153.77 [t, *J* 11.3, *para* F], −159.50 [t, *J*, 12.4, *para* F], −164.31 [td, *J* 14.7, 6.2, *meta* F], −166.12 [td, *J* 14.4, 5.91, *meta* F]
2' $[(Me_3Si)(H)NB(C_6F_5)_2]_2$	^1H: 4.2 [1H, s(br), NH], −0.20 [9H, s, CH_3] ^{11}B: −2.8[br]
3 $[(H)N\{B(C_6F_5)_2\}_2]$ C, 41.2 (40.9); H, 0.2 (0.14); B, 2.8 (3.1), N 2.3 (2.0) Mass: *m/z* 360 (M^+—$B(C_6F_5)_2$), 529 ($H_3N\cdot B(C_6F_5)_3$), 512 ($B(C_6F_5)_3$)	IR: [d,e]3647 br (N—H) ^1H: 4.8 [1H, s(br), NH] ^{13}C: [f]139.72 [d, *J* 270.8, C—F], 132.13 [d, *J* 270.8, C—F], 129.04 [d, *J* 270.8, C—F], 107.9 [s(br), C—B]. ^{11}B: [f]−9.7 [br] ^{19}F: [f]−138.28 [dd, *J* 15.5, 4.5 Hz, *ortho* FC_6F_5], −159.04 [t, *J* 12.5 Hz, *para* F], −166.73 [td, *J* 15.5, 4.5 Hz, *meta* F]

[a] Analytical data given as found (calculated) in %. Mass spectra data given as: *m/z* [assignment].

[b] IR data (cm^{-1}) determined as KBr discs, selected stretches are reported; NMR data (C_6D_6, 298 K), unless otherwise stated, given as: chemical shift (δ) [relative intensity, multiplicity (*J* in Hz), assignment].

[c] **2'** denotes $[(Me_3SiN)(H)B(C_6F_5)_2]_2$, dimeric form of **2**, ≈20%, in C_6D_6 solution at 298 K.

[d] CsI disc.

[e] N—H stretch only, remaining stretches are almost identical to those of compound **2**.

[f] CD_2Cl_2.

also produces compound **3** but in slightly reduced yield. The aminoborane may be purified by crystallisation although unfortunately the crystals obtained were unsuitable for X-ray diffraction. The spectroscopic properties of compound **3** are unexceptional and described in Table 2. The molecular ion peak was not observed by mass spectroscopy although a peak was visible at 360 amu corresponding to $\{HNB(C_6F_5)_2\}$ presumably formed by loss of $\{B(C_6F_5)_2\}$ from the parent ion. Evidently decomposition occurs resulting in the observation of further peaks assignable to $B(C_6F_5)_3$ and $H_3N\cdot B(C_6F_5)_3$. The spectroscopic data of compound **3** is consistent with the structure described in Fig. 4.

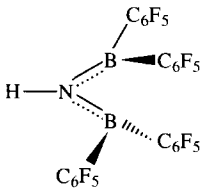

Fig. 4. Structural representation of compound **3**.

It is clear that the reaction of $ClB(C_6F_5)_2$ with $HN(SiMe_3)_2$ proceeds *via* elimination of $SiMe_3Cl$ in a stepwise fashion such that, after a reaction time of 1.5 h, compound **2** and one mole of $SiMe_3Cl$ has formed [9]. If the reaction is continued further, a second equivalent of $SiMe_3Cl$ is produced with concomitant for-

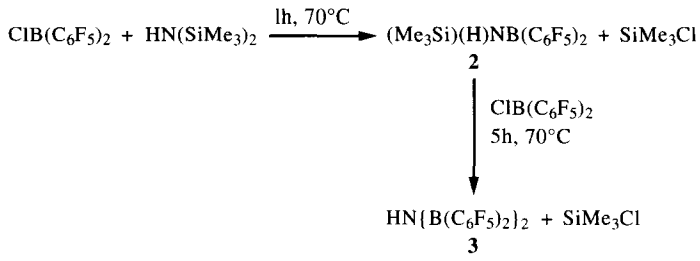

Stepwise formation of compound **3** from $ClB(C_6F_5)_2$ and $HN(SiMe_3)_2$.

mation of aminoborane **3**, eq. (1). Attempts to monitor the reaction *via in situ* ^{11}B and ^{1}H NMR spectroscopies in a sealed NMR tube were hindered by the observation that under such conditions the reaction reaches an equilibrium mixture of $SiMe_3Cl$, $ClB(C_6F_5)_2$, $HN(SiMe_3)_2$ and compound **2** and that the ^{11}B NMR spectroscopic resonances for $ClB(C_6F_5)_2$ and compound **2** are coincident. From integration of the ^{1}H NMR spectroscopic signals assigned to the $SiMe_3$ groups it appears that equilibrium is reached when approximately 80% of $HN(SiMe_3)_2$ has reacted to form compound **2**; the absence of a broad signal attributable to the amine proton in compound **3** indicates that **3** is formed from **2** only after complete consumption of $HN(SiMe_3)_2$.

Reactivity of compounds **1** *and* **2**

Compounds **1** and **2** were originally synthesised so as to obtain amines substituted with highly electrophilic $\{B(C_6F_5)_2\}$ units which would hopefully react with transition metal complexes to generate metal imido species with the general formula $L_xM{=}NB(C_6F_5)_2$. To date only one compound containing the $M{=}NBR_2$ moiety has been prepared; *cis,cis,trans*-$[W\{NB(mes)_2\}_2Cl_2(PMe_3)_2]$, mes = 1,3,5-trimethylphenyl, has been synthesised from the reaction of $[W(PMe_3)_4Cl_2]$ with N_3Bmes_2 and crystallography characterised [10]. However there are numerous examples of metal imido complexes which have been synthesised from the reaction of H_2NR, $RN(SiMe_3)_2$ or $HN(SiMe_3)R$, R = alkyl or aryl, with metal chlorides which is accompanied by HCl or HNR_3Cl formation [5].

To investigate the reactivity of compounds **1** and **2** we typically refluxed equimolar quantities of the aminoborane and metal chloride in CH_2Cl_2 for a few hours. None of the reactions were successful. For the complexes MCl_4, M = Zr, Hf, U, $[(\eta\text{-}^{i}PrC_5H_4)MoCl_4]$, $[(\eta\text{-}C_5Me_5)RhCl_2]_2$, $[(\eta\text{-}C_5H_5)NbCl_4]$, $[(\eta\text{-}C_5H_5)_2TiCl_2]$, $[(\eta\text{-}C_5Me_5)UCl_2]$, $[(\eta\text{-}C_5H_5)UCl_3]$ and $[UOCl_5]^-$ the starting materials could be recovered unchanged whilst reactions with $MoCl_5$ and $NbCl_5$ gave numerous uncharacterisable species. It is believed that formation of the M=NR unit proceeds *via* initial coordination of the nitrogen lone pair to the metal centre followed by elimination of either HCl or $SiMe_3Cl$. Based upon this premise the lack of reactivity of the nitrogen lone pair in aminoboranes **1** and **2** may be because it is either too sterically protected or electronically unavailable, the latter due to delocalised Si—N—B π-bonding. Attempts to generate the anion $[(SiMe_3)NB(C_6F_5)_2]^-$ by reaction of compound **1** with $^{n}Bu_4NF$ (as a THF solution containing 5% H_2O) resulted in the formation of $[^{n}Bu_4N][B(C_6F_5)_2F(OH)]$ (^{11}B NMR: 1.3 d, J_{BF} = 56 Hz) [11] whilst KF in the presence of 18-crown-6 failed to elicit any reaction. The reaction of compound **2** with $^{n}BuLi$ in pentane at $-78^{\circ}C$ resulted in the formation of a white solid however, as the reaction was gradually warmed to room temperature a small explosion occurred suggesting that LiC_6F_5, which is extremely thermally sensitive, may have been formed. Finally, to try and understand the failure of these aminoboranes to react with metal chlorides, we investigated the reaction of compound **2** with $[NMe_3 \cdot HCl]$. The formation of metal-imido species from the reaction of L_xMCl_y complexes with primary or secondary amines simultaneously generates HCl which may prevent the formation of the desired $[L_xM{=}N{-}B(C_6F_5)_2]$ species. Hydrogen chloride is observed to add across the N—B bond to form the Lewis acid adduct $(Me_3Si)NH_2 \cdot ClB(C_6F_5)_2$.

EXPERIMENTAL

Fourier-transform ^{1}H and ^{11}B NMR spectra were recorded on a Bruker AM 300 spectrometer at 300 and 96 MHz, respectively, ^{13}C NMR spectra were recorded on a Bruker AM 300 spectrometer at 75.5 MHz or Varian Unity plus 500 spectrometer at 125 MHz, ^{19}F NMR spectra were recorded similarly at 470 MHz: ^{1}H and ^{13}C shifts are reported with respect to δ 0 for $SiMe_4$, ^{11}B with respect to δ 0 for $BF_3 \cdot OEt_2$, ^{19}F with respect to δ 0 for $CFCl_3$; all downfield shifts are positive. Infrared spectra were recorded on either Mattson 'Polaris' Fourier–transform, Perkin–Elmer FT 1710 spectrophotometer, or Perkin–Elmer 457 grating spectrometers. Mass spectra were obtained on a Varian MSS instrument in this department or by Dr Ballantyne at the SERC facility at the University of Swansea on a Varian E 109 instrument. Microanalyses were obtained from the microanalytical department of this department.

All reactions were carried out under nitrogen using standard Schlenk techniques. Solvents were dried over suitable reagents and freshly distilled under N_2 before use. The compounds $[KN(SiMe_3)_2]$, $[NaN(SiMe_3)_2]$, $HN(SiMe_3)_2$, KF and 18-crown-6 were used as received (Aldrich), $^nBu_4NF$ was obtained as a THF solution (5% H_2O) (Aldrich) and used without further purification whilst $ClB(C_6F_5)_2$ [4c] was prepared as previously described.

Preparations

$[(Me_3Si)_2NB(C_6F_5)_2]$, **1**. $ClB(C_6F_5)_2$ (760 mg, 2.00 mmol) was dissolved in petroleum ether (b.p. 30–40°C) and slowly added at room temperature to a toluene solution of $NaN(SiMe_3)_2$ (370 mg, 2.02 mmol). The mixture was allowed to stir for 30 min and then pumped to dryness. The title compound was extracted from the residue using pentane leaving behind KCl as a white solid. Concentration of this solution and cooling to 5°C resulted in the formation of large colourless block shaped crystals of $[(Me_3Si)_2NB(C_6F_5)_2]$ (952 mg, 94% yield). Compound **1** sublimes at 75°C.

$[(Me_3Si)(H)NB(C_6F_5)_2]$, **2**. $ClB(C_6F_5)_2$ (760 mg, 2.00 mmol) was dissolved in toluene (30 cm^3) in a Rotaflo ampoule and $HN(SiMe_3)_2$ (0.42 cm^3, 2.00 mmol) added. The ampoule was sealed under slightly reduced pressure and heated at 70°C for 1.5 h. The solvent was removed *in vacuo* to leave a white solid. The product was extracted into pentane and the solution concentrated and cooled to −80°C. A white solid precipitated and, after removal of the supernatant liquid and drying *in vacuo*, $[(Me_3Si)(H)NB(C_6F_5)_2]$ was isolated (682 mg, 79% yield).

$[HN\{B(C_6F_5)_2\}_2]$, **3**. $ClB(C_6F_5)_2$ (760 mg, 2.00 mmol) was dissolved in octane (50 cm^3) in a Rotaflo ampoule and $HN(SiMe_3)_2$ (0.21 cm^3, 1.00 mmol) was added. The ampoule was closed and heated at 70°C for 7 h with regular removal of Me_3SiCl under reduced pressure. The solvent was removed *in vacuo* and the residual solid washed with hexanes. The product was extracted into toluene and the filtrate was concentrated and cooled to −80°C to give small white crystals of $[HN\{B(C_6F_5)_2\}_2]$ (282 mg, 40% yield).

Reaction of $[(Me_3Si)_2NB(C_6F_5)_2]$, **1**, *with* KF *and* 18-*crown*-6. $[(Me_3Si)_2NB(C_6F_5)_2]$ (134 mg, 0.265 mmol) was dissolved in toluene and slowly added to a toluene suspension of KF (30 mg, 0.52 mmol) and 18-crown-6 ether (70 mg, 0.265 mmol). The mixture was stirred at room temperature for 3.5 h and then the solvent removed *in vacuo*. Extraction with petroleum ether (b.p. 30°C–40°C) led to the recovery of unreacted aminoborane.

Reaction of $[(Me_3Si)_2NB(C_6F_5)_2]$, **1**, *with* $^nBu_4NF$. $[(Me_3Si)_2NB(C_6F_5)_2]$ (234 mg, 0.463 mmol) was dissolved in THF and a 1.0 M THF solution of $^nBu_4NF$ (0.47 ml, 0.47 mmol) was slowly added. The colourless solution was stirred at room temperature for 2 h. Solvent was removed *in vacuo* and the residue extracted into with petroleum ether (b.p. 30–40°C) to give the isolation of a white, non boron-containing solid: NMR (CD_2Cl_2, 298 K) ^1H (300 MHz) δ 3.5 (s); the residual solid is tentatively characterised as $[^nBu_4N][B(C_6F_5)_2F(OH)]$. ^{11}NMR ($CD_2Cl_2$, 298 K); ^{11}B (96 MHz) δ 1.3 (d, $J_{BF} = 56$ Hz).

Reaction of $[(Me_3Si)_2NB(C_6F_5)_2]$, **1**, *or* $[(Me_3Si)(H)NB(C_6F_5)_2]$, **2**, *with the metal chlorides*. MCl_4, M = Zr, Hf, U, $[(\eta\text{-}^iPrC_5H_4)MoCl_4]$, $[(\eta\text{-}C_5Me_5)RhCl_2]_2$, $[(\eta\text{-}C_5H_5)NBCl_4]$, $[(\eta\text{-}C_5H_5)_2TiCl_2]$, $[(\eta\text{-}C_5Me_5)UCl_2]$, $[(\eta\text{-}C_5H_5)UCl_3]$, $[UOCl_5]^-$, $MoCl_5$ *and* $NbCl_5$. Typically equimolar quantities of the aminoborane and metal chloride were refluxed in CH_2Cl_2 for a few hours. The reactions between $MoCl_5$ or $NbCl_5$ and compound **2** produced several products which could not be characterised. From all other reactions the starting reagents could be recovered unchanged.

Crystal structure determination of compound **1**

Experimental. Crystals of compound **1** were grown from pentane solutions at 278 K and dried *in vacuo*. A crystal was immersed in highly viscous perfluoropolyether to exclude oxygen and prevent solvent loss. It was then mounted on a glass fibre and plunged in a cold stream (150 K) nitrogen stream.

Crystal data. Compound **1**, $C_{18}H_{18}BF_{10}NSi_2$, $M = 505.31$ g mol^{-1}, monoclinic, $a = 11.054(4)$ Å, $b = 11.228(4)$ Å, $c = 18.619(3)$ Å, $\alpha = 105.77(2)°$, $V = 2224(1)$ Å^3, space group $P2_1/c$, $Z = 4$, $D_x = 1.51$ g cm^{-3}, $\mu = 23.12$ cm^{-1}, transparent prism, crystal dimensions $0.48 \times 0.51 \times 0.64$ mm^3.

Data collection and processing. The data for compound **1** was collected at 150 K on an Enraf-Nonius MACH3 diffractometer, ω–2θ scan mode with the ω scan width $= 0.66 + 0.25 \tan\theta$, ω scan speed 1.4–10.1° min^{-1}, graphite-monochromated Cu-K_α radiation ($\lambda = 1.5418$ Å). 4424 reflections were measured ($2 < \theta < 70°$, 0, h; 0, k; −1, l), 3978 unique (merging $R = 0.055$), giving 3844 with $I > 3\sigma(I)$. Neither significant crystal decay nor movement was noted.

Structure solution and refinement. The crystal structure was solved by direct methods and refined by the full-matrix least-squares method with all non-hydrogen atoms in anisotropic approximation (289 variables, observations/variables = 13.3). All hydrogen atoms were located in the difference Fourier maps and included in the final refinement with fixed positional and thermal parameters. Chebyshev weighting scheme [12] with parameters 31.90, 2.84 and 17.60 was applied. Corrections for Lorentz and polarisation effects but not for absorption were applied. Final R and R' values are 0.049 and 0.053. Minimum and maximum peaks in the final difference synthesis are −0.37 and 0.46 e Å^{-3}. All crystallographic calculations were carried out using the CRYSTALS program package on PC/AT −486 [13]. Neutral atom

scattering factors were taken from the usual sources [14]. Additional material is available from the Cambridge Crystallographic Data Centre.

CONCLUSION

The aminoboranes $[(Me_3Si)_2NB(C_6F_5)_2]$, **1**, $[(Me_3Si)(H)NB(C_6F_5)_2]$, **2**, and $[HN\{B(C_6F_5)_2\}_2]$, **3**, have been prepared and characterised. Compounds **1** and **2** fail to produce metal imido complexes when reacted with a variety of metal chloride complexes. This lack of reactivity may be caused by steric shielding of the nitrogen lone pair or reduced basicity due to strong Si_x—N—B π-bonding, $x = 2$ for compound **1**, 1 for compound **2**.

Acknowledgements—We thank the University of Oxford for a Violette and Samuel Glasstone Fellowship (J.R.G.), British Nuclear Fuels Limited (V.C.W.), and the E.P.S.R.C. for support of this work.

REFERENCES

1. Muetterties, E. L., The Chemistry of Boron and its Compounds, Wiley, 1967.
2. (a) Noth, H. and Vahrenkamp, H., *J. Organomet. Chem.*, 1968, **12,** 23; (b) Cragg, R. H. and Miller, T. J., *J. Organomet. Chem.*, 1981, **217,** 1.
3. Okada, K., Suzuki, R. and Oda, M., *J. Chem. Soc., Chem. Commun.*, 1995, 2069.
4. (a) Massey, A. G. and Park, A. J., *J. Organomet. Chem.*, 1964, **2,** 245; (b) Paetzold, P. and Truppat, R., *Chem. Ber.*, 1983, **116,** 1531; (c) Chambers, R. D. and Chivers, T., *J. Chem. Soc.*, 1965, 3933; (d) Parks, D. J., von H. Spence, R. E. and Piers, W. E., *Angew. Chem., Int. Ed. Eng.*, 1995, **34,** 809.
5. For a comprehensive review see Wigley, D. E., *Organoimido Complexes of the Transition Metals*, *Prog. Inorg. Chem.*, **42,** 239.
6. Mannig, D., Noth, H., Prigge, H., Rotsch, A.-R., Gopinanthan, S. and Wilson, J. W., *J. Organomet. Chem.*, 1986, **310,** 1.
7. Hausser-Wallis, R., Oberhammer, H., Burger, H. and Pawelke, G., *J. Chem. Soc., Dalton Trans.*, 1987, 1839.
8. (a) Noth, H., *Chem. Ber.*, 1971, **104,** 558; (b) Turner, H. S. and Warne, R. J., *J. Chem. Soc.*, 1965, 6421.
9. Jenne, H. and Niedenzu, K., *Inorg. Chem.*, 1964, **3,** 68.
10. Danopoulos, A. A., Redshaw, C., Vaniche, A., Wilkinson, G., Hussain-Bates, B. and Hursthouse, M. B., *Polyhedron*, 1993, **12,** 1061.
11. Noth, H. and Wrackmeyer, B., *NMR Spectroscopy of Boron Compounds*, Springer-Verlag Inc., Ed. P. Diehl, E. Fluck, R. Kosfeld, 1978, pp. 105, 378.
12. Prince, E., *Mathematical Techniques in Crystallography and Material Sciences*, Springer-Verlag Inc., New York (1982).
13. Watkins, D. J., Prout, C. K., Carruthers, J. R. and Betteridge, P. W., *CRYSTALS Issue* 10, Chemical Crystallography Laboratory, University of Oxford (1996).
14. *International Tables for Crystallography*, Vol. C, Kluwer Academic Publishers, Dordrecht (1992).

Pergamon

PII: S0277-5387(97)00236-6

Polyhedron Vol. 17, No. 1, pp. 125–129, 1998
© 1997 Elsevier Science Ltd
All rights reserved. Printed in Great Britain
0277-5387/98 $19.00+0.00

Kinetics of ligand replacement, in N-substituted ethylenediamine palladium(II) complexes

Matteo Cusumano*, Antonino Giannetto and Antonino Imbalzano

Dipartimento di Chimica Inorganica, Chimica Analitica e Chimica Fisica, University of Messina, 98100 Messina, Italy

(Received 11 April 1997; accepted 2 June 1997)

Abstract—The rate of substitution by ethylenediamine, of Cl^-, in the substrates $[Pd(R_2N(CH_2)_2NR_2)Cl_2]$ and of 2,2′-bipyridine (bpy), in the complexes $[Pd(bpy)(R_2N(CH_2)_2NR_2)](ClO_4)_2$ (R = H, methyl, ethyl or phenyl) have been studied, at 25°C, respectively in dimethylformamide and in water. In both processes the rate of reaction depends on the nature of the substituent R at nitrogen. While the kinetic data for neutral complexes can be accounted for simply in terms of electronic and steric properties of the ligands, the trend of the kinetic constants seem to be related to the capacity of the various complexes to form hydrogen bonding with water.
© 1997 Elsevier Science Ltd

Keywords: palladium(II) complexes; kinetics; ligand replacement; 2,2′-bipyridine; N-substituted ethylenediamine.

Dependence of the rate of reaction on electron density of the central metal is one of the essential features of the substitution reactions at square planar complexes [1]. In these processes, usually associative in character, decreasing electron density on the metal favours, in fact, the attack of the nucleophile, easing the formation of the activated complex so leading to increase in the rate of reaction. The capability of a ligand to exert its electron withdrawing or electron donating properties on the central metal, is therefore reflected on the rate of substitution of one of the coordinated ligands [2]. For a series of homologous complexes, differing only by the nature of the substituents at one of the ligands, the rate of displacement of a given ligand by a given nucleophile can be taken as a direct indication of the electron donating ability of the substituent.

In this investigation we have synthesised a series (Table 1) of neutral and dicationic palladium(II) complexes of the type $[Pd(RR'N(CH_2)_2NR''R''')Cl_2]$ and $[Pd(bpy)(RR'N(CH_2)_2NR''R''')](ClO_4)_2$ (bpy = 2,2′-bipyridyl; R = H, methyl, ethyl or phenyl) differing each other only be the nature of the substituents at the nitrogen atoms of ethylenediamine. Furthermore we have studied the rate of substitution of chloride, by ethylenediamine (en), in the neutral complexes, in dimethylformamide at 25°C, and the rate of substitution of bipy, by en, in the cationic complexes, in water at the same temperature. The kinetic parameters should give information on the electron donating properties of the substituents at ethylenediamine and, if charge is transmitted through the metal to the ancillary ligands, on the electron density of the coordinated ligands. This is particularly useful in the case of the cationic complexes since $[Pd(bpy)(H_2N(CH_2)_2NH_2)]^{2+}$ is known to interact [3] with DNA by intercalation. Variation of the rate of reaction in these complexes could give indications of the variations of electron density on bipyridine rings, useful to correlate the interactions of the various complexes with DNA.

EXPERIMENTAL

The chloro complexes $[Pd(RR'N(CH_2)_2NR''R''')Cl_2]$ were prepared following the procedure reported in the literature [4]. To this end, $K_2[PdCl_4]$ was heated with the appropriate substituted ethylenediamine in the presence of HCl. Experimental conditions such

*Author to whom correspondence should be addressed.

Table 1. List of complexes studied

	R	R′	R″	R‴
$[Pd(RR'N(CH_2)_2NR''R''')Cl_2]$	Me	Me	Me	H
	Me	H	Me	H
	Me	Me	H	H
	Me	Me	Me	Me
	Et	Et	Et	H
	Et	H	Et	H
	Et	Et	H	H
	Et	Et	Et	Et
	Φ	H	H	H
	Φ	H	Φ	H
$[Pd(bpy)(R,R'N(CH_2)_2NR'',R''')](ClO_4)_2$	H	H	H	H
	Me	H	H	H
	Me	H	Me	H
	Me	Me	H	H
	Et	H	H	H
	Et	H	Et	H
	Et	Et	H	H

as pH and reaction time were found to be strongly dependent on the particular ligand.

The complexes $[Pd(bpy)(RR'N(CH_2)_2NR''R''')](ClO_4)_2$ were prepared by treating the respective chlorocomplexes with silver perchorate in a ratio 1 : 2 in acetone and adding, after filtering off the formed silver chloride, to the resulting solution the stoichiometric amount of 2,2′-bipyridyl. The formed complexes, crystallized from acetone/methanol mixtures, were characterized by elemental analysis and NMR [5]. Ethylenediamine was distilled over potassium hydroxide pellets; N,N′-dimethylformamide was distilled over calcium sulfate and stored over molecular sieves. Other chemicals were of reagent grade.

The rates of reaction were followed either spectrophotometrically or conductometrically; a Perkin–Elmer Lambda 5 spectrophotometer and a Radiometer CDM3 conductivity bridge connected to a computer were used respectively. In all cases a large excess of ethylenediamine was used to provide pseudo-first-order conditions and to force the reaction to completion. Pseudo-first order rate constants k_{obsd} were obtained from non-linear least squares fit of the experimental spectrophotometric data to $A_t = A_\infty + (A_0 - A_\infty)\exp(-k_{obsd}t)$, where A_0, A_∞ and k_{obsd} were the parameters to be optimized (A_0 = absorbance after mixing of the reagents, A_∞ = absorbance at completion of reaction). An analogous equation using conductivity instead of absorbance was used to fit the experimental conductivity data. In both cases the k_{obsd} values were reproducible to better than ±5%. The k_{obsd} values are listed in Table 2.

Table 2. Observed rate constants k_{obsd} (s^{-1}) for reactions (1)–(3)

Complex	10^2 [en], (mol^{-1} dm^3)	0.5	1	2	3	4	5
$[Pd(MeHN(CH_2)_2NH_2)Cl_2]$	k_{obsd} (s^{-1})	0.104	0.170	0.347	0.540	0.680	0.869
$[Pd(Me_2N(CH_2)_2NH_2)Cl_2]$	k_{obsd} (s^{-1})	0.053	0.083	0.180	0.310	0.410	0.502
$[Pd(MeHN(CH_2)_2NHMe)Cl_2]$	k_{obsd} (s^{-1})	0.100	0.193	0.330	0.514	0.790	0.910
$[Pd(Me_2N(CH_2)_2NMe_2)Cl_2]$	k_{obsd} (s^{-1})	0.007	0.012	0.023	0.035	0.049	0.059
$[Pd(EtHN(CH_2)_2NH_2)Cl_2]$	k_{obsd} (s^{-1})	0.088	0.183	0.334	0.496	0.697	0.885
$[Pd(Et_2N(CH_2)_2NH_2)Cl_2]$	k_{obsd} (s^{-1})	0.085	0.132	0.280	0.430	0.570	0.746
$[Pd(EtHN(CH_2)_2NHEt)Cl_2]$	k_{obsd} (s^{-1})	0.052	0.105	0.220	0.320	0.416	0.520
$[Pd(Et_2N(CH_2)_2NEt_2)Cl_2]$	10^3 k_{obsd} (s^{-1})	0.350	0.700	1.40	2.10	2.80	3.60
$[Pd(ΦHN(CH_2)_2NHMe)Cl_2]$	k_{obsd} (s^{-1})	0.195	0.350	0.740	1.210	1.597	1.920
$[Pd(ΦHN(CH_2)_2NH_2)Cl_2]$	k_{obsd} (s^{-1})	0.181	0.460	0.827	1.29	1.68	2.14
$[Pd(bpy)(MeHN(CH_2)_2NH_2)]^{2+}$	10^2 k_{obsd} (s^{-1})	0.45	1.04	2.21	3.30	4.71	6.06
$[Pd(bpy)(Me_2N(CH_2)_2NH_2)]^{2+}$	10^3 k_{obsd} (s^{-1})	0.48	1.20	2.50	3.85	5.23	6.88
$[Pd(bpy)(MeHN(CH_2)_2NHMe)]^{2+}$	10 k_{obsd} (s^{-1})	0.27	0.63	1.30	2.00	2.80	3.50
$[Pd(bpy)(EtHN(CH_2)_2NH_2)]^{2+}$	10^2 k_{obsd} (s^{-1})	0.76	1.30	2.95	4.30	6.48	7.60
$[Pd(bpy)Et_2N(CH_2)_2NH_2)]^{2+}$	10^3 k_{obsd} (s^{-1})	0.72	1.32	2.55	4.13	5.57	6.80
$[Pd(bpy)(EtHN(CH_2)_2NHEt)]^{2+}$	10 k_{obsd} (s^{-1})	0.33	0.71	1.40	2.10	2.80	3.50

RESULTS AND DISCUSSION

Chloro complexes

The complexes $[Pd(RR'N(CH_2)_2NR''R''')Cl_2]$ react with ethylenediamine according to the reaction:

$$[Pd(RR'N(CH_2)_2NR''R''')Cl_2] + en \rightarrow [Pd(RR'N(CH_2)_2NR''R''')(en)]^{2+} + 2Cl^- \quad (1)$$

The kinetic course of this reaction in dimethylformamide has been followed by monitoring the increase in time of the conductivity. A 1 : 2 electrolyte is in fact formed starting from neutral reagents. Under pseudo-first-order conditions with respect to the complex the observed rate law is:

$$k_{obs} = k_2[en] \quad (2)$$

Ethylenediamine is a bidentate ligand, however the circumstance that the conductivity increase occurs in only one step, shows that ring closure is fast and the monitored kinetic process refers to the replacement of the first chloride coordinated to palladium. The absence of a k_1 term in the rate law indicates that the substitution process occurs essentially by direct attack of the nucleophile en on palladium. The k_2 values (Table 3) are dependent on the nature of the substituents at nitrogen of ethylenediamine and the extreme values of the series vary by over 500 times. In terms of reactivity the substrates can be divided into three sets (Fig. 1) (i) a first set of complexes, where ethylenediamine is partially substituted at nitrogen by aryl groups, which exhibit the highest reactivity; (ii) a second set of less reactive complexes including those substrates where ethylenediamine is partially replaced at nitrogen by alkyl groups, and finally (iii) a third set of substances, where ethylenediamine is totally substituted at nitrogen by alkyl groups, which shows the largest inertness toward substitution by en.

The presence of a substituent at a ligand coordinated to the central atom, even in a peripheral position, can influence to large extent the rate of substitution [2,6].

Table 3. Second order rate constants, k_2 ($dm^3\ mol^{-1}\ s^{-1}$) for reaction (1) in dimethylformamide at 25°C

Complex	k_2
$[Pd(MeHN(CH_2)_2NH_2)Cl_2]$	17.1(3)
$[Pd(Me_2N(CH_2)_2NH_2)Cl_2]$	10.4(3)
$[Pd(MeHN(CH_2)_2NHMe)Cl_2]$	19(1)
$[Pd(Me_2N(CH_2)_2NMe_2)Cl_2]$	1.18(3)
$[Pd(EtHN(CH_2)_2NH_2)Cl_2]$	17.5(4)
$[Pd(Et_2N(CH_2)_2NH_2)Cl_2]$	14.7(4)
$[Pd(EtHN(CH_2)_2NHEt)Cl_2]$	10.4(1)
$[Pd(Et_2N(CH_2)_2NEt_2)Cl_2]$	0.072(1)
$[Pd(\Phi HN(CH_2)_2NH_2)Cl_2]$	42.7(8)
$[Pd(\Phi HN(CH_2)_2NH\Phi)Cl_2]$	40(1)

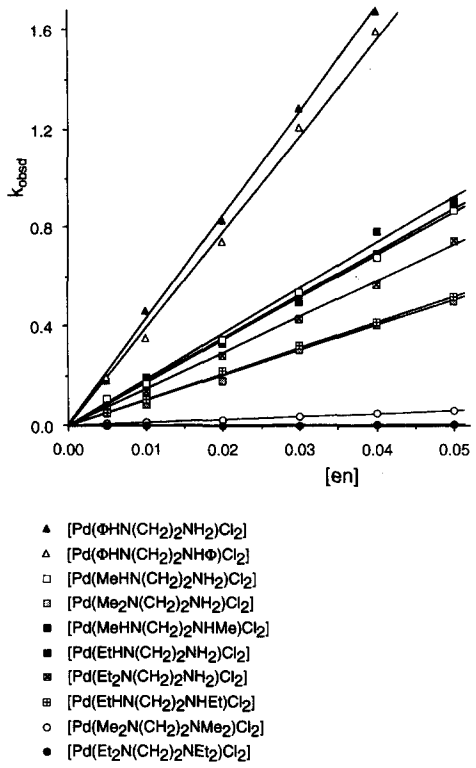

Fig. 1. Plot of k_{obs} against ethylenediamine concentration for reaction (1) in dimethylformamide at 25°C.

In the case of the complexes here studied only the aryl substituents are able to exert their strong electron withdrawing capacity on the reaction centre favouring the attack of ethylenediamine so leading to an increase in reaction rate with respect to the complexes with unsubstituted ethylenediamine. By contrast, the electrondonating properties of the alkyl substituents are not transmitted to palladium and the presence of one or two methyl or ethyl groups does not alter significantly the reactivity of this series of complexes. The drop in reaction rate of the tetraalkylsubstituted complexes, therefore, is not interpretable in terms of electronic effects but rather in terms of steric hindrance created by the presence of alkyl groups below and above the reaction centre. Steric hindrance plays a role also in the case of N-arylsubstituted ethylenediamine. The rate constant for reaction of $[Pd(H\Phi N(CH_2)_2N\Phi H)Cl_2]$, in fact, is not higher than that of the homologous monophenylsubstituted complex, as expected on the basis of the number of electron withdrawing substituents; the more effective shielding of the reaction centre by a second bulky phenyl in the first substrate can account for the relative reactivity of these to complexes.

Cationic complexes

All the complexes $[Pd(bpy)(R,R'N(CH_2)_2NR'', R''')](ClO_4)_2$ are very stable in aqueous solution in

which they behave as 1:2 electrolytes; the conductivity values in water, for 5×10^{-4} mol dm^{-3} solutions of the substrates, range in fact from 130 to 160 μS [7] and do not change in time. In addition the linear dependence of absorbance on concentration, in the range used for the experiments (2×10^{-5}–2×10^{-4} mol dm^{-3}), rules out self-association of the complexes. The absence of spectral variations in the UV spectra of the substances, on alkalinization of the solutions with OH^-, excludes also the presence of solvolytic equilibria with formation of aquospecies easily deprotonable by addition of base. The complexes react with ethylenediamine in water according to the reaction:

$$[Pd(bpy)(RR'N(CH_2)_2NR''R''')]^{2+} + en \rightarrow [Pd(RR'N(CH_2)_2NR''R''')(en)]^{2+} + bpy \quad (3)$$

The reaction is associated to large spectral variations in the UV–vis region (Fig. 2) and the reaction course can be easily monitored following the decrease in absorbance of the coordinated bipy ligand or the increase in absorbance of free bipyridine formed. Only one step of reaction can be observed and therefore ring closure of the bidentate ligand is fast. The term k'_2 in the rate law

$$k_{obs} = k'_2[en] \quad (4)$$

is, so, to refer to the replacement of the first nitrogen atom of bipyridine. The linear relation between k_{obs} and nucleophile concentration, also at very high values of (en), shows that the process is pH independent.

The k_2 values, reported in Table 4, show as well as for the analogous dichloro compounds, dependence on the nature of the substituents at nitrogen of ethylenediamine. However, the trend of the k_2 values for the two series of complexes are very different and for the cationic complexes the dependence of the rate constants on the nature of the group R,R'N-$(CH_2)_2$-NR''R''', is not straightforward. In fact, in contrast with the expected decrease in reactivity as a result of electron donor or steric properties of alkyl groups, the k_2 values increase on going from the complex with unsubstituted ethylenediamine to the complexes with alkylated ethylenediamine.

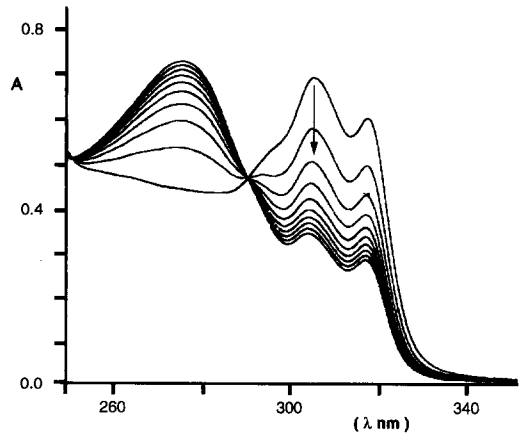

Fig. 2. Spectral variations in time on addition of en to a 5×10^{-5} mol dm^{-3} solution of $[Pd(bpy)(H_2N(CH_2)_2NH_2)]^{2+}$.

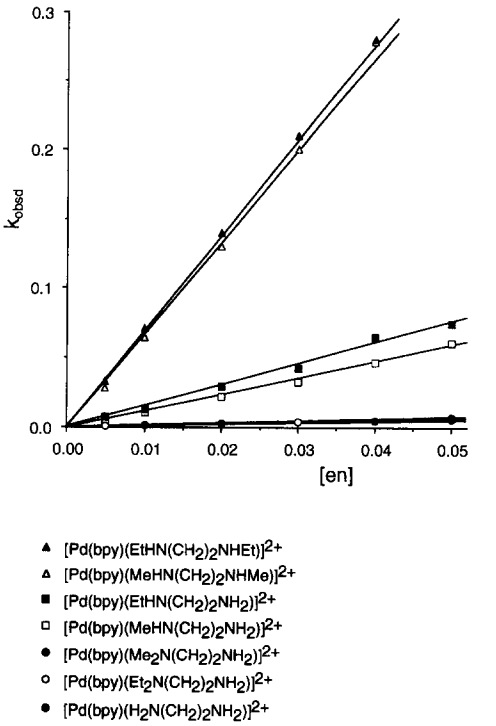

Fig. 3. Plot of k_{obs} against ethylenediamine concentration for reaction (3) in water at 25°C.

Table 4. Second order rate constants, k'_2 (dm^3 mol^{-1} s^{-1}) for reaction (4) in water at 25°C

Complex	k'_2
$[Pd(bpy)(H_2N(CH_2)_2NH_2)]^{2+}$	0.14[a]
$[Pd(bpy)(MeHN(CH_2)_2NH_2)]^{2+}$	1.24(3)
$[Pd(bpy)(Me_2N(CH_2)_2NH_2)]^{2+}$	0.14(1)
$[Pd(bpy)(MeHN(CH_2)_2NHMe)]^{2+}$	7.19(1)
$[Pd(bpy)(EtHN(CH_2)_2NH_2)]^{2+}$	1.58(6)
$[Pd(bpy)(Et_2H(CH_2)_2NH_2)]^{2+}$	0.14(1)
$[Pd(bpy)(EtHN(CH_2)_2NHEt)]^{2+}$	7.02(3)

[a] Value from ref. [8].

A possible explanation for the observed trend of k_2 values may lie in the nature of the solvent, i.e. water. It is well known that in substrates containing bipyridine the hydrogen atoms of groups coordinated to platinum(II) an palladium(II) are acidic [10]. For instance the pH of a 6×10^{-3} mol dm^{-3} solution of $[Pd(bpy)(H_2O)_2]^{2+}$, at $I = 0.1$ mol dm^{-3}, is 2.8 [10]. In the present studies deprotonation of amino groups

is conceivable and as a matter of fact a stable monoprotonated adduct of $[Pt(bpy)(H_2N(CH_2)_2NH_2)]I_2$ [11] has been reported. Therefore, in the cationic complexes here studied, strong hydrogen bonds between the acidic hydrogen atoms of the amino groups of en and the oxygen atom of water are expected to be present; thus complexes with a larger number of hydrogen atoms bound to nitrogen should be more stabilized by interaction with water. The passage from ground state to transition state, where both the interaction of palladium with the lone pair of a fifth ligand and the contemporary bond weakening with nitrogen atoms of bpy should reduce the acidity of the amino groups, leading to substantial desolvation. Therefore, the observed decrease in reactivity along the series of complexes, could be correlated to an increasing degree of desolvation on forming the activated complex. Accordingly the complex with unsubstituted ethylenediamine is the most inert one. The lower reactivity of the complexes $[Pd(bpy)(R,R'N(CH_2)_2NH_2]^{2+}$, where two alkyl groups are bound to the same nitrogen atom, may be simply due to steric reasons owing to the shielding of the reaction centre by these groups.

In conclusion, in both series of complexes electronic effects due to the presence of substituents at nitrogen of en play a minor role, while, in some cases, steric effects become dominant; the electron density on bipyridine rings should be almost unchanged along the series of cationic complexes.

Acknowledgement—Financial support from MURST and CNR is acknowledged.

REFERENCES

1. Basolo, F. and Pearson, R. G. in *Mechanisms of Inorganic Reactions*, 2nd Edition, Wiley, New York (1967); Cattalini, L. in *Inorganica Reaction Mechanisms*, Ed. J. O. Edwards, Wiley, New York (1970).
2. Tobe, M. L. in *Comprehensive Coordination Chemistry*, Ed. G. Wilkinson, R. D. Gillard and McCleverty, Vol. 1, pp. 315–318, Pergamon, Oxford (1987).
3. Nordén, B., *Inorg. Chim. Acta*, 1978, **30,** 83; Howe-Grant, M., Wu, K. C., Bauer, W. R. and Lippard, S. J., *Biochemistry*, 1976, **19,** 4339; Lippard, S. J., Bond, P. J., Wu, K. C. and Bauer, W. R., *Science* 1976, **194,** 726.
4. Drew, H. D. K., Pinkard, F. V. W. Preston, G. H. and Wardlaw, W., *J. Chem. Soc.*, 1932, 1895; Johnson, G. L. and Michelfield, T., *Inorganic Syntheses*, 1966, **VIII**, 242.
5. Erickson, L. E., *J. Am. Chem. Soc.*, 1969, **91,** 6284.
6. Cusumano, M., Guglielmo, G. and Ricevuto, V., *J. Chem. Soc., Dalton Trans.*, 1980, 2044; Cusumano, M., *Inorg. Chem.*, 1979, **18,** 3612.
7. Geary, W. D., *Coord. Chem. Rev.*, 1971, **7,** 81.
8. Cavasino, F. P., Sbriziolo, C., Turco Liveri, M. L. and Turco Liveri, V., *J. Chem. Soc., Faraday Trans.*, 1994, **90,** 311.
9. Anderegg, G. and Wanner, H., *Inorg. Chim. Acta*, 1977, **99,** 777.
10. Alibrandi, G., Cusumano, M., Giannetto, A. and Minniti, D., *J. Chem. Soc., Dalton Trans.*, 375, 1989.
11. Watt, W. G. and Upchurch, D. G., *J. Am. Chem. Soc.*, 1968, **90,** 914.

Pergamon

PII: S0277-5387(97)00240-4

Polyhedron Vol. 17, No. 1, pp. 131–143, 1998
© 1997 Elsevier Science Ltd
All rights reserved. Printed in Great Britain
0277-5387/98 $19.00+0.00

Synthesis and characterization of indium(III) complexes with tri- and pentadentate thiosemicarbazones. Crystal and molecular structure of $[InCl_2(HDAPTSC)] \cdot 2$ DMSO, $\{O[In(HDAPTSC)(OH)]_2\} \cdot 5$ MeOH, $[InCl_2(APTSC)(MeOH)]$, $[In(APTSC)_2]PF_6$ and $(H_2APTSC)][InCl(APTSC)(mnt)] \cdot 0.5\ H_2O$ ($H_2DAPTSC$ = 2,6-diacetylpyridine-bis(thiosemicarbazone), HAPTSC = 2-acetylpyridine-thiosemicarbazone, mnt^{2-} = 1,2-dicyanoethene-1,2-dithiolate)

Sonja Abram,[a] Cäcilia Maichle-Mössmer[a] and Ulrich Abram[b]*

[a]University of Tübingen, Institute of Inorganic Chemistry, Auf der Morgenstelle 18, D-72076 Tübingen, Germany

[b]Forschungszentrum Rossendorf, Institute of Radiochemistry, c/o Dresden University of Technology, Institute of Analytical Chemistry, D-01062 Dresden, Germany

(Received 8 April 1997; accepted 2 June 1997)

Abstract—The synthesis and characterization of novel indium(III) complexes with pyridine-thiosemicarbazone ligands are reported as well as ligand exchange reactions on the products. 2,6-Diacetylpyridine-bis(thiosemicarbazone), $C_5H_3N(C_3N_3SH_6)_2$ ($H_2DAPTSC$), and 2-acetylpyridine-thiosemicarbazone, $C_5H_4N(C_3N_3SH_6)$ (HAPTSC), were reacted with indium(III) halides and indium(III) nitrate, respectively, to give $[InX_2(HDAPTSC)]$, $\{O[In(HDAPTSC)(OH)]_2\}$, $[InX_2(APTSC)(MeOH)]$ and $[In(APTSC)_2]PF_6$. © 1997 Elsevier Science Ltd

Keywords: indium complexes; thiosemicarbazones; nitrogen donor liquids; mixed ligand complexes; X-ray structure.

Heterocyclic thiosemicarbazones, as well as their metal complexes, are currently under discussion because of their biological activity [1–8]. They are of interest due to their antibacterial [3], antineoplastic [4], antimalarial [5], and antivirial behaviour [6]. Relationship has been found between chelate formation in the complexes and *in vivo* activity [9–12]. This makes structural studies on complexes with tri-, tetra- and pentadentate thiosemicarbazone ligands interesting. Although there exists a number of studies dealing with complex formation properties of thiosemicarbazones [8,13], comparatively few structural reports are published. They deal with iron(II) [14], cobalt(III) [15], nickel(II) [16,17], copper(II) [17–19], palladium(II) [20], zinc(II) [21], tin(II) [22], tin(IV)

* Author to whom correspondence should be addressed.

[23] and bismuth(III) [24]. Indium complexes with this type of ligand have not yet been reported.

As part of our systematic studies on indium complexes with tri- and pentadentate ligands, we prepared novel In^{III} compounds by reaction of InX_3 (X = Cl, Br) with the potentially pentadentate thiosemicarbazone 2,6-diacetylpyridine-bis(thiosemicarbazone) (H_2DAPTSC) and its tridentate analogue 2-acetylpyridine-thiosemicarbazone (HAPTSC). Here we report the synthesis and characterization of $[InX_2(HDAPTSC)]$, $\{O[In(HDAPTSC))(OH)]_2\}$, $[InX_2(APTSC)(MeOH)]$ (X = Cl, Br) and $[In(APTSC)_2]^+(Y)^-$ (Y = BPh_4^-, BF_4^-, $F_3CSO_3^-$, PF_6^-) complexes and of the mixed-chelate complexes [In-

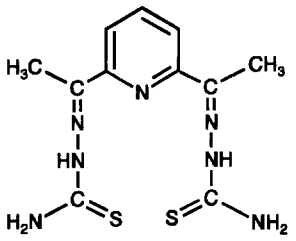

H_2DAPTSC

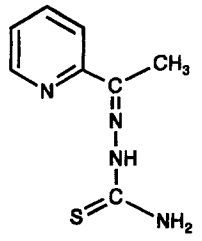

HAPTSC

$Cl(APTSC)(mnt)]^-$, $[InCl(APTSC)(Et_2dtc)]$ (mnt^{2-} = 1,2-dicyanoethene-1,2-dithiolate, Et_2dtc^- = diethyldithiocarbamate). The complexes $[InCl_2(HDAPTSC)]\cdot 2$ DMSO, $\{O[In(HDAPTSC)(OH)]_2\}\cdot 5$ MeOH, $[InCl_2(APTSC)(MeOH)]$, $[In(APTSC)_2]PF_6$ and $(H_2APTSC)[InCl(APTSC)(mnt)]\cdot 0.5\ H_2O$ have been characterized crystallographically.

EXPERIMENTAL

General considerations

Routine infrared spectra were recorded as KBr discs on a Bruker IFS 25. Mass spectra were recorded on a MAT TSQ-70 spectrometer (Finnigan). For the FAB measurements xenon was used as primary beam gas. The ion gun was operated at 8 kV and 100 μA (probe temperature 30°C); nitrobenzylalcohol was used as matrix. ^1H and ^{13}C NMR spectra were recorded on a Bruker DRX250 spectrometer in acetone-d_6 or dmso-d_6.

Elemental analyses for carbon, hydrogen, nitrogen, sulfur and chlorine were carried out by the Analytical Service Department of the University of Tübingen.

$InCl_3$ and $InBr_3$ were purchased from Fluka and Strem Chemicals, respectively. The thiosemicarbazones H_2DAPTSC, HAPTSC and HAPTSC $\cdot$HCl have been prepared according to previously published procedures [25,26]. Na_2mnt has been synthesized from NaCN and CS_2 following the route of Bähr and Schleitzer [27]. $NaEt_2dtc\cdot 3H_2O$, KPF_6, $NH_4(F_3CSO_3)$, $NaBF_4$ and $Na(BPh_4)$ were purchased from Merck. The chemicals were used without further purification. All operations were carried out in normal laboratory equipment under a normal atmosphere. Standard procedures have been used to dry solvents.

Syntheses

Dichloro[2,6 - *diacetylpyridine - bis*(*thiosemicarbazonato*)]*indium*(*III*), $[InCl_2(HDAPTSC)]$. H_2DAPTSC (77 mg, 0.25 mmol) was placed into a flask along with 50 cm^3 of methanol. The ligand nearly dissolved upon heating. $InCl_3$ (55 mg, 0.25 mmol) in 5 cm^3 of methanol was slowly added to the hot mixture. A clear yellow solution was formed immediately. After a few minutes a pale yellow solid began to precipitate. The reaction was completed after 30 min and after cooling to room temperature the nearly insoluble solid was isolated by filtration and washed with hot water and methanol (yield 70%). Anal. Calcd for $C_{11}H_{14}N_7S_2Cl_2In$: C, 26.74; H, 2.86; N, 19.84; S, 12.98; Cl, 14.35%; Found: C, 25.95; H, 2.65; N, 19.79; S, 12.88; Cl, 14.00%. IR: ν(NH) 3610(br), 3410(br), 3292(br), 3134 cm^{-1}, ν(C=N) 1609 cm^{-1}. FAB^+ MS: m/z = 422 ($[In(DAPTSC)]^+$).

Dibromo - [2,6 - *diacetylpyridine - bis*(*thiosemicarbazonato*)]*indium*(*III*), $[InBr_2(HDAPTSC)]$. The complex was prepared according to the procedure for the chloro analogue starting from $InBr_3$ and H_2DAPTSC. Yellow powder (yield 85%). Anal. Calcd for $C_{11}H_{14}N_7S_2Br_2In$: C, 22.66; H, 2.42; N, 16.82; S, 11.00%. Found: C, 22.92; H, 2.31; N, 17.08; S, 10.87%. IR: ν(NH) 3470m (br), 3320 (br), 3215m (br), 3149m cm^{-1}, ν(C=N) 1599 cm^{-1}. FAB^+ MS: m/z = 502/504 ($[InBr(HDAPTSC)]^+$), 422 ($[In(DAPTSC)]^+$).

μ_2 - *oxo* - *bis*{[2,6 - *diacetylpyridine - bis*(*thiosemicarbazonato*)](*hydroxo*)*indium*(*III*)}, $\{O[In(HDAPTSC)(OH)]_2\}$. H_2DAPTSC (77 mg, 0.25 mmol) was dissolved in about 50 cm^3 of hot methanol and $In(NO_3)_3\cdot 5\ H_2O$ in 5 cm^3 of methanol was slowly added. The mixture was heated under reflux for about 30 min. The colour of the reaction mixture turned to red-brown. The volume was reduced to about 20 cm^3 and stored overnight at ambient temperature. During this time pale yellow cubes deposited which were collected and washed with cold methanol. (Yield 65%). Anal. Calcd for $C_{22}H_{30}N_{14}S_4O_3In$: C, 29.48; H, 3.37; N, 21.87; S, 14.31%. Found: C, 30.01; H, 3.60; N, 21.78; S, 14.50%. IR: ν(NH, OH) 3450, 3310, 3245, 3144 cm^{-1}, ν(C=N) 1612 cm^{-1}. FAB^+ MS: m/z = 422 ($[In(DAPTSC)]^+$).

(2 - *Acetylpyridine - thiosemicarbazonato*)*dichloro*(*methanol*)*indium*(*III*), $[InCl_2(APTSC)(MeOH)]$. HAPTSC (48.5 mg, 0.25 mmol) was dissolved in 25 cm^3 of methanol and $InCl_3$ (55 mg, 0.25 mmol) in 5

cm^3 of methanol was slowly dropped into the solution. After heating on reflux for 30 min, the hot solvent was reduced to about 10 cm^3 and the mixture was placed in a refrigerator. Overnight yellow crystals deposited (yield 70%). Anal. Calcd for $C_9H_{13}N_4SOCl_2In$: C, 26.30; H, 3.19; N, 13.63; S, 7.80; Cl, 17.25%. Found: C, 25.79; H, 3.27; N, 13.59; S, 7.75; Cl, 17.01%. IR: ν(NH, OH) 3422, 3309, 3184, 3062 cm^{-1}, ν(C=N) 1601 cm^{-1}. FAB^+ MS: $m/z = 308$ ($[In(APTSC)]^+$), 343 ($[InCl(APTSC)]^+$), 378 ($[InCl_2(APTSC)]^+$). ^{1}H-NMR (dmso-d_6, 293 K): pyridine δ 8.93–7.91 (m, 4H); NH_2 δ 7.61 (s, 2H); CH_3(APTSC) δ 2.70 (s, 3H); CH_3 (methanol) δ 2.57 (s, 3H). ^{13}C-NMR (dmso-d_6, 293 K): C=S δ 175.3; C=N δ 148.6; pyridine δ 146.7, 146.3, 142.3, 126.1, 124.1; CH_3(APTSC) δ 13.8; CH_3 (methanol) δ 12.3.

(2 - *Acetylpyridin - thiosemicarbazonato)dibromo (methanol)indium(III)*, [$InBr_2$(APTSC)(MeOH)]. The complex was prepared following the procedure outlined for the chloro analogue. Yellow crystals (yield 65%). Anal. Calcd for $C_9H_{13}N_4SOBr_2In$: C, 21.62; H, 2.62; N, 11.21; S, 6.41%. Found: C, 21.91; H, 2.77; N, 11.35; S, 6.55%. IR: ν(NH) 3452, 3425, 3313, 3164 cm^{-1}, ν(C=N) 1593 cm^{-1}. FAB^+ MS: $m/z = 469$ ($[InBr_2(APTSC)]^+$), 387/389 ($[InBr(APTSC)^+$), 308 ($[In(APTSC)]^+$).

Bis(2 - *acetylpyridine - thiosemicarbazonato) indium(III) hexafluorophosphate*, [In(APTSC)$_2$]PF_6. $In(NO_3)_3 \cdot 5\ H_2O$ (98 mg, 0.25 mmol) was dissolved in 20 cm^3 of methanol, mixed with HAPTSC (122 mg, 0.625 mmol) in 20 cm^3 of methanol and heated under reflux for 30 min. After addition of NH_4PF_6 (50 mg, 0.3 mmol) yellow needles precipitated from the reaction mixture. More product could be obtained by reducing the solvent to half of its volume. Yellow crystals (yield 68%). Anal. Calcd for $C_{16}H_{18}N_8S_2PF_6In$: C, 29.74; H, 2.81; N, 17.34; S, 9.92%. Found: C, 29.72; H, 2.79; N, 16.98; S, 9.94%. IR: ν(NH) 3359, 3230, 3166 cm^{-1}, ν(C=N) 1602, 1579 cm^{-1}, ν(PF) 847 cm^{-1}. FAB^+ MS: $m/z = 501$ ($[In(APTSC)_2]^+$). ^{1}H NMR (acetone-d_6, 293 K): pyridine δ 8.33–7.37 (m, 4H); NH_2 δ 8.24 (s, 2H); CH_3 δ 2.09 (s, 3H). ^{13}C NMR (acetone-d_6, 293 K): C=S δ 175.8; C=N δ 148.9; pyridine δ 147.4, 146.8, 142.5, 127.2, 124.4; CH_3 δ 14.2.

Bis(2 - *acetylpyridine - thiosemicarbazonato) indium(III) tetraphenylborate*, [In(APTSC)$_2$]BPh_4. The compound was prepared following the route described for the PF_6^- salt from $In(NO_3)_3 \cdot 5\ H_2O$ (391 mg, 1 mmol), HAPTSC (485 mg, 2.5 mmol) and $Na(BPh_4)$ (342 mg, 1 mmol). Recrystallization from acetone/methanol gave yellow blocks (yield 80%). Anal. Calcd for $C_{40}H_{38}N_8S_2BIn$: C, 58.55; H, 4.67; N, 13.66; S, 7.82%. Found: C, 58.71; H, 4.39; N, 13.70; S, 7.85%. IR: ν(NH) 3405, 3281, 3167 cm^{-1}, ν(C=N) 1595 cm^{-1}. FAB^+ MS: $m/z = 501$ ($[In(APTSC)_2]^+$). ^{1}H NMR (acetone-d_6 293 K): aromatic protons δ 8.83–7.89 (m, 28H); NH_2 δ 8.63 (s 4H); CH_3 δ 2.42 (s, 6H). ^{13}C NMR (dmso-d_6, 293 K): C=S δ 178.4; C=N δ 147.4; pyridine δ 143.9, 142.7, 138.9, 124.8, 124.4; phenyl δ 143.3, 136.4, 126.2, 122.4; CH_3 δ 14.2.

Bis(2 - *acetylpyridine - thiosemicarbazonato) indium(III) tetrafluoroborate*, [In(APTSC)$_2$]BF_4. The compound was prepared from $In(NO_3)_3 \cdot 5\ H_2O$ (391 mg, 1 mmol), HAPTSC (485 mg, 2.5 mmol) and $NaBF_4$ (110 mg, 1 mmol) according to the procedure reported for the PF_6^- salt. No precipitate was formed spontaneously. The solution was halved in volume, placed in a refrigerator at 5°C and overnight yellow crystals of [In(APTSC)$_2$]BF_4 deposited which were isolated by filtration and recrystallized from boiling methanol. Yellow plates (yield 70%). Anal. Calcd for $C_{16}H_{18}N_8S_2BF_4In$: C, 32.68; H, 3.09; N, 19.05; S, 10.90%. Found: C, 33.01; H, 3.13; N, 19.01; S, 10.12%. IR: ν(NH) 3624, 3410, 3322, 3166 cm^{-1}, ν(C=N) 1599 cm^{-1}, ν(BF) 1082 cm^{-1}. FAB^+ MS: $m/z = 501$ ($[In(APTSC)_2]^+$). ^{1}H NMR (acetone-d_6, 293 K): pyridine δ 8.19–7.22 (m, 4H); NH_2 8.11 (s, 2H); CH_3 δ 1.95 (s, 3H). ^{13}C NMR (acetone-d_6 293 K): C=S δ 175.6; C=N δ 149.7; pyridine δ 148.1, 147.6, 143.3, 128.0, 125.2; CH_3 δ 15.0.

Bis(2 - *acetylpyridine - thiosemicarbazonato) indium(III) trifluormethylsulfonate*, [In(APTSC)$_2$](F_3CSO_3). The compound was prepared from $In(NO_3)_3 \cdot 5\ H_2O$ (391 mg, 1 mmol), HAPTSC (485 mg, 2.5 mmol) and $NH_4(F_3CSO_3)$ (167 mg, 1 mmol) as described for the tetrafluoroborate salt. Yellow crystals (yield 60%). Anal. Calcd for $C_{17}H_{18}N_8S_3O_3F_3In$: C, 31.39; H, 2.79; N, 17.23; S, 14.79%. Found: C, 31.18; H, 2.87; N, 16.92; S, 15.00%. IR: ν(NH) 3359, 3229, 3165 cm^{-1}, ν(C=N) 1601 cm^{-1}. FAB^+ MS: $m/z = 501$ ($[In(APTSC)_2]^+$). ^{1}H NMR (dmso-d_6, 293 K): pyridine δ 8.81–7.84 (m, 4H); NH_2 δ 8.59 (s, 2H); CH_3 δ 2.42 (s, 3H). ^{13}C NMR (dmso-d_6 293 K): C=S δ 178.7; C=N δ 148.2; pyridine δ 147.4, 143.4, 140.0, 124.9, 123.4; CH_3 (APTSC) δ 11.9.

(2 - *Acetylpyridine - thiosemicarbazonato)chloro (diethyldithiocarbamoto)indium(III)*, [InCl(APTSC) (Et_2dtc)]. [$InCl_2$(APTSC)(MeOH)] (103 mg, 0.25 mmol) was dissolved in 25 cm^3 of hot methanol and allowed to cool to room temperature. Na(Et_2dtc) $\cdot 3\ H_2O$ (37 mg, 0.25 mmol) in 5 cm^3 of methanol was slowly added under stirring to the cold solution. The mixture was stirred for another 30 min. Tiny yellow crystals formed upon slow evaporation of the solvent. Recrystallization from methanol gave yellow needles (yield 60%). Larger crystals could be obtained from slow diffusion of *n*-hexane into a CH_2Cl_2 solution of the complex. Anal. Calcd for $C_{13}H_{19}N_5S_3ClIn$: C, 31.75; H, 3.89; N, 14.24; S, 19.56; Cl, 7.21%. Found: C, 31.92; H, 3.80; N, 14.17; S, 20.01; Cl, 7.20. IR: ν(NH) 3420, 3350, 3270 cm^{-1}, ν(C=N) (APTSC) 1605 cm^{-1}. FAB^+MS: $m/z = 308$ ($[In(APTSC)]^+$), 343 ($[InCl(APTSC)]^+$), 456 ($[In(APTSC)(Et_2dtc))]^+$).

(2 - *Acetylpyridiniumthiosemicarbazone*)(2 - *acetylpyridine - thiosemicarbazonato)chloro*(1,2 - *dicyanoethene*-1,2-*dithiolato)indium(III)*, (H_2APTSC)[InCl (APTSC)(mnt)]. [$InCl_2$(APTSC)(MeOH)] (103 mg,

0.25 mmol) was dissolved in 25 cm^3 of hot methanol and allowed to cool to room temperature. Na_2mnt (46.5 mg, 0.25 mmol) in 10 cm^3 methanol was added dropwise. The clear solution was stirred at room temperature for 1 h and placed in a refrigerator. Overnight, a yellow precipitate was formed which was filtered off. The product was extracted with hot methanol leaving a small amount of an insoluble solid. The solvent was reduced to a volume of about 5 cm^3. Yellow plates of $(H_2APTSC)[InCl(APTSC)(mnt)]$ were formed upon standing overnight at ambient temperature (yield 25%). Anal. Calcd for $C_{20}H_{20}N_{10}S_4ClIn$: 35.38; H, 2.97; N, 20.63; S, 18.89; Cl, 5.22%. Found: C, 35.29; H, 2.80; N, 20.51; S, 18.88; Cl, 5.70%. IR: ν(NH) 3433, 3293, 3105 cm^{-1}, $\nu(C{\equiv}N)$ 2205 cm^{-1}, $\nu(C{=}N)$ 1617 cm^{-1}, $\nu(C{=}C)$ 1555 cm^{-1}, FAB^+ MS: $m/z = 308$ ($[In(APTSC)]^+$), 343 ($[InCl(APTSC)]^+$), 448 ($[In(APTSC)(mnt)]^+$). FAB^-MS: $m/z = 448$ ($[In(APTSC)(mnt)]^-$), 483 ($[InCl(APTSC)(mnt)]^-$). The compound was too insoluble to get NMR spectra of reasonable quality.

X-ray crystallography

$[InCl_2(HDAPTSC)] \cdot 2$ DMSO, $\{O[In(HDAPTSC)(OH)]_2\} \cdot 5$ MeOH, $[InCl_2(APTSC)(MeOH)]$, $[In(APTSC)_2]PF_6$ and $(H_2APTSC)[InCl(APTSC)(mnt)] \cdot 0.5\ H_2O$ were studied in detail by X-ray structure determinations. The structure determination on $[InCl(APTSC)(Et_2dtc)]$ could not be finished due to decomposition of the crystals during the measurement. Nevertheless, the obtained data allowed to derive the structure of the complex molecule. Therefore, the measurement will be briefly described (monoclinic, space group $P2_1/c$, $a = 18.527$, $b = 7.926$, $c = 13.314$ Å; $\beta = 103.13°$; $Z = 4$; 1937 reflections, 1496 unique reflections; 118 parameters, anisotropic refinement for In, Cl, S; $R_1 = 0.049$, $wR_2 = 0.129$). Crystal data and refinement parameters for the other X-ray measurements are summarized in Table 1. All measurements have been done on automated single-crystal CAD4 diffractometers (Enraf–Nonius) using Mo-K_α and Cu-K_α radiation, respectively, at 203(2)K. Absorption corrections (ψ scans) were applied when appropriate. Standard procedures have been used for data reduction (CAD4 software, HELENA/PLATON [28]), structure solution (SHELXS-86 [29]) and refinement (SHELXL-93 [30]). Anisotropic thermal parameters have been used in the refinement for all non-hydrogen atoms.

Single crystals of $[InCl_2(HDAPTSC)] \cdot 2$ DMSO were obtained by dissolving the only sparingly soluble compound in boiling DMSO, filtration of the hot solution and slow cooling (about 10°/h). The crystals contain two molecules of the solvent DMSO per complex molecule. One of the solvent molecules is disordered which has been considered in the calculation by refining two positions for the atom S(42) with an occupancy of 50 per cent. The hydrogen positions have been derived from the final Fourier map and refined.

Single crystals of $\{O[In(HDAPTSC)(OH)]_2\} \cdot 5$ MeOH have been obtained directly from the reaction mixture. The solvent molecules are highly disordered by occupying 'tube-like' vacancies which are formed by the staggered arrangement of the almost planar complex dimers. Therefore, only the atoms of the complex molecule have been refined anisotropically and the C and O atoms of the solvent which have 50% occupancy are considered with isotropic thermal parameters. The obtained model was checked by comparison with that obtained with the program SQUEEZE [28] which allows detection and evaluation of highly disordered solvent areas in crystal structure calculations. Approximately 70 e^- have been detected for our example and an 'artificial correction' by removing the disordered solvent molecules by SQUEEZE would lead to a final R_1 value of 0.056. The hydrogen atoms have been calculated for idealized positions and treated in the refinement with the 'riding model' option of SHELXL-93 [30]. The H atoms of the solvent molecules have been omitted.

Single crystals of $[InCl_2(APTSC)(MeOH)]$ of X-ray quality were obtained by slow cooling of a hot methanol solution of the complex. The hydrogen atoms H(12A), H(12B) and H(20) which might be important for the discussion of the structure have been derived from the Fourier map and refined. All other hydrogen atoms have been calculated for idealized positions using the 'riding model' option of SHELXL-93 [30].

Single crystals of $[In(APTSC)_2]PF_6$ were obtained by recrystallization from hot methanol. All hydrogen positions have been derived from the final Fourier map and refined.

Single crystals of $(H_2APTSC)[InCl(APTSC)(mnt)] \cdot 0.5\ H_2O$ were grown by slow evaporation of a methanol/water (5/1 v/v) solution of the compound. Hydrogen positions have been calculated and refined using the 'riding model' option except those on the nitrogen atoms which are of relevance for the discussion of the structure. They have been derived from the final Fourier map and refined freely. The H atoms of the solvent water have been omitted.

RESULTS AND DISCUSSION

The reaction of indium(III) chloride or indium(III) bromide with 2,6-diacetylpyridinebis(thiosemicarbazone) yields seven coordinate complexes according to eq. (1). The complexes are airstable. They are sparingly soluble in the most common solvents. Considerable amounts are only soluble in hot DMSO. Thus, single-crystals for an X-ray analysis could be

Table 1. X-ray structure data collection and refinement parameters

	$[InCl_2(HDAPTSC)] \cdot 2$ DMSO	$\{O[In(HDAPTSC)(OH)]_2\} \cdot 5$ MeOH	$[InCl_2(APTSC)(MeOH)]$	$[In(APTSC)_2]PF_6$	$(H_2APTSC)[InCl(APTSC)(mnt)] \cdot 0.5\ H_2O$
Crystal dimensions (mm^3)	$0.3 \times 0.05 \times 0.05$	$0.15 \times 0.15 \times 0.15$	$0.2 \times 0.2 \times 0.1$	$0.25 \times 0.1 \times 0.1$	$0.2 \times 0.15 \times 0.1$
Formula	$C_{15}H_{26}Cl_2N_7O_2S_4In$	$C_{27}H_{50}N_{14}O_8S_4In_2$	$C_9H_{13}Cl_2N_4OSIn$	$C_{16}H_{18}N_8S_2PF_6In$	$C_{20}H_{21}ClN_{10}O_{0.5}S_4In$
M	650.39	1056.53	411.01	646.29	757.10
Crystal system	orthorhombic	monoclinic	orthorhombic	monoclinic	monoclinic
Space group	*Pbca*	*C2/c*	*Pbca*	$P2_1/c$	$P2_1/c$
Unit cell (Å, °)	$a = 12.981(1)$	$a = 17.361(5)$	$a = 13.846(9)$	$a = 11.536(3)$	$a = 8.770(1)$
	$b = 19.241(1)$	$b = 19.570(2)$	$b = 13.021(9)$	$b = 13.457(1)$	$b = 12.912(1)$
	$c = 20.149(2)$	$c = 14.750(4)$	$c = 15.557(2)$	$c = 15.219(3)$	$c = 24.490(3)$
		$\beta = 118.33(1)$		$\beta = 97.41(1)$	$\beta = 98.10(1)$
V ($Å^3$)	5032.7(6)	4411(2)	2805(3)	2342.9(8)	2745.5(5)
Z	8	4	8	4	4
D_c ($g\ cm^{-3}$)	1.717	1.561	1.947	1.832	1.662
Radiation/(λ)	Cu-K_α (1.54184)	Mo-K_α (0.71073)	Cu-K_α (1.54184)	Mo-K_α (0.71073)	Cu-K_α (1.54184)
Linear absorption coefficient (mm^{-1})	12.803	1.292	18.329	1.326	11.649
Absorption correction	ψ-Scans	none	ψ-Scans	none	ψ-Scans
T_{min}	0.7712		0.7249		0.8449
T_{max}	0.9960		0.9983		0.9989
Measured Reflections	4338	4369	2626	5877	5289
Independent Reflections	3955	3886	2242	5112	4287
Independent Reflections [$I > 2\sigma(I)$]	2931	2728	1782	3281	3641
Refined Parameters	370	275	175	361	355
$R_1(F)/wR2$ (F^2)	0.039/0.086	0.069/0.1714	0.043/0.105	0.044/0.076	0.052/0.133
GoF	1.101	1.080	1.096	1.024	1.066

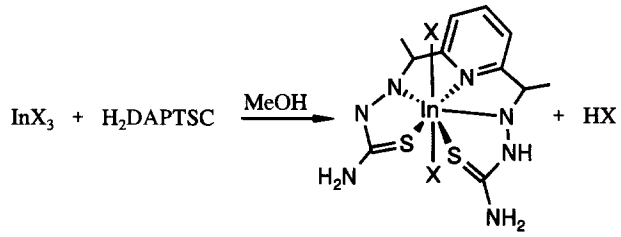

equ. (1)

obtained, however, their solubility was too low for NMR measurements. FAB mass spectra could be measured by mixing a hot saturated DMSO solution of the complexes with nitrobenzylalcohol immediately before the measurement. No evidence was found for the molecular ion. However, peaks due to the $[In(HDAPTSC)]^+$ fragment could be observed at $m/z = 422$ (about 20% B) in the spectra of both complexes. The IR spectra of the complexes suggest an only single deprotonation. This is confirmed by an X-ray structural study on $[InCl_2(HDAPTSC)]$. The compound crystallizes in monomeric units together with two equivalents of the solvent dimethylsulfoxide. An ORTEP [31] representation of the complex molecule is given in Fig. 1. Selected bond lengths and angles are summarized in Table 2. The coordination polyhedron of indium can be discussed as a distorted pentagonal bipyramid with the chloro ligands occupying the axial positions [Cl(1)—In—Cl(2) angle: 166.02(5)°]. The pentadentate thiosemicarbazone forms the equatorial coordination sphere. The atoms of this ligand and In are coplanar within 0.579(6) Å. Different bond lengths in the chelate rings confirm that the ligand is only deprotonated at N(10). Consequently, S(13) possesses 'thiolate character' and the S(13)–C(11) distance is longer by 0.063 Å than the distance S(20)—C(18). The bond lengths inside the 5-membered chelate rings support the conclusion drawn: the N(10)—C(11) and In—S(13) distances are shorter than the corresponding values in the protonated part of the molecule. The detection of H(17) in the final Fourier map confirms the conclusions of this discussion.

The same bonding situation is expected for $[InBr_2(HDAPTSC)]$. The IR spectrum is similar to that of the chloro analogue: ν(NH) frequencies can be detected at 3470, 3320, 3215 and 3149 cm^{-1}. Fragments due to $[InBr(HDAPTSC)]^+$ and $[In(HDAPTSC)]^+$ could be assigned in the FAB^+ mass spectrum of the compound at $m/z = 502/504$ ($^{79,81}Br$ isotopic pattern) and $m/z = 422$.

Despite the general reaction pattern of $H_2DAPTSC$ with indium(III) halides [eq. (1)] the reaction with $In(NO_3)_3 \cdot 5\ H_2O$ gives a μ-oxo-bridged dimer with angle deprotonated thiosemicarbazonato and terminal hydroxo ligands. The formation of an oxo-bridge is unexpected and can be understood by the absence of halide ligands. The dimeric unit is stable and does not undergo further hydrolysis when treated with water. An ORTEP [31] representation of the dimeric complex is given in Fig 2. Corresponding bond lengths and angles are summarized in Table 3. The μ-oxo ligand resides on a two-fold crystallographic axis. Despite the situation in the μ-oxo-

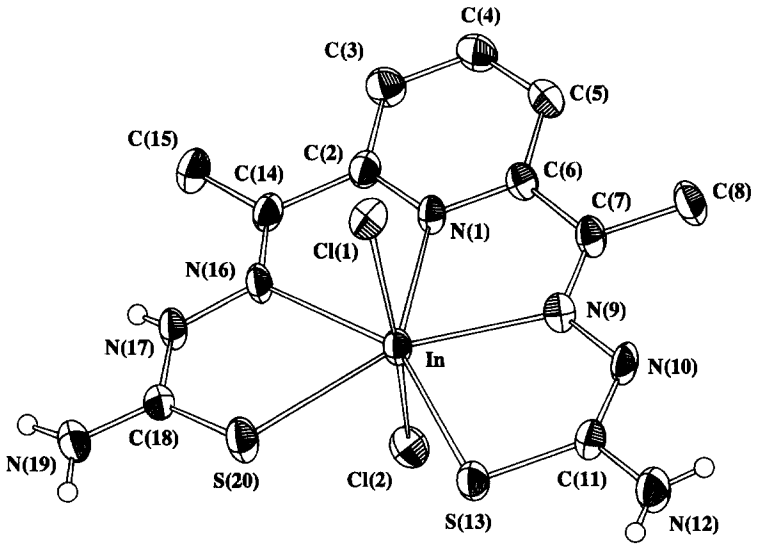

Fig. 1. ORTEP representation [31] of $[InCl_2(HDAPTSC)]$. Thermal ellipsoids represent 50% probability. H atoms at the carbon atoms have been omitted for clarity.

Table 2. Selected bond lengths (Å) and angles (°) for $[InCl_2(HDAPTSC)] \cdot 2$ DMSO

In—Cl(1)	2.497(2)	N(1)—C(2)	1.345(7)
In—Cl(2)	2.535(2)	N(1)—C(6)	1.347(7)
In—S(13)	2.572(2)	N(9)—C(7)	1.280(8)
In—S(20)	2.670(2)	N(10)—C(11)	1.322(8)
In—H(1)	2.330(5)	N(16)—N(17)	1.376(7)
In—N(9)	2.335(5)	N(16)—C(14)	1.281(8)
In—N(16)	2.458(5)	N(17)—C(18)	1.361(8)
S(13)—C(11)	1.743(6)	C(2)—C(14)	1.484(8)
S(20)—C(18)	1.680(6)	C(6)—C(7)	1.481(8)

Cl(1)—In—Cl(2)	166.02(5)	S(20)—In—N(16)	71.5(1)
Cl(1)—In—S(13)	101.07(5)	N(1)—In—N(9)	69.3(2)
Cl(1)—In—S(20)	89.43(5)	N(1)—In—N(16)	66.0(2)
Cl(1)—In—N(1)	83.3(1)	N(9)—In—N(16)	135.2(2)
Cl(1)—In—N(9)	90.3(1)	S(13)—C(11)—N(10)	127.2(4)
Cl(1)—In—N(16)	87.5(1)	S(20)—C(18)—N(17)	123.4(4)
Cl(2)—In—S(13)	92.91(5)	N(1)—C(2)—C(14)	116.4(5)
Cl(2)—In—S(20)	93.36(5)	N(1)—C(6)—C(7)	116.8(5)
Cl(2)—In—N(1)	85.4(1)	N(9)—N(10)—C(11)	115.5(5)
Cl(2)—In—N(9)	93.3(1)	N(9)—C(7)—C(6)	115.9(5)
Cl(2)—In—N(16)	80.4(1)	N(10)—N(9)—C(7)	115.9(5)
S(13)—In—S(20)	79.59(5)	N(16)—N(17)—C(18)	120.8(5)
S(13)—In—N(1)	143.3(1)	N(16)—C(14)—C(2)	114.3(5)
S(13)—In—N(9)	74.3(1)	N(17)—N(16)—C(14)	118.4(5)
S(13)—In—N(16)	149.7(1)	C(2)—N(1)—C(6)	120.5(5)
S(20)—In—N(1)	137.1(1)	C(11)—S(13)—In	99.1(2)
S(20)—In—N(9)	153.4(1)	C(18)—S(20)—In	102.6(2)

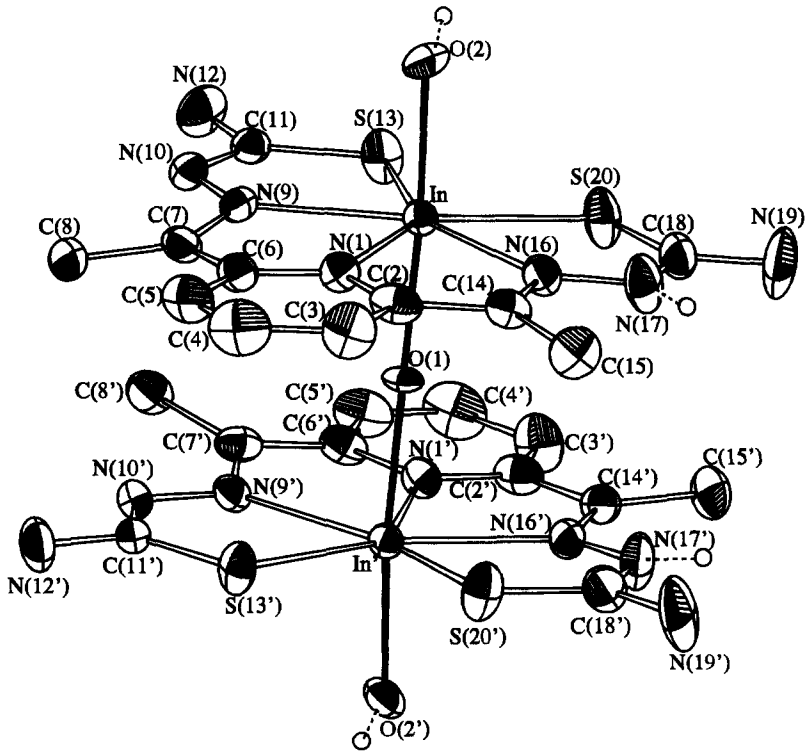

Fig. 2. ORTEP plot [31] of the $\{O[In(HDAPTSC)(OH)]_2\}$ dimer with thermal ellipsoids of 30% probability. H atoms at N(17) and O(2) are calculated for idealized positions and introduced to illustrate the bonding situation in the molecule.

Table 3. Selected bond lengths (Å) and angles (°) for $\{O[In(HDAPTSC)(OH)]_2 \cdot 5\,MeOH$

In—O(1)	2.0750(9)	N(1)—C(2)	1.35(1)
In—O(2)	2.170(7)	N(1)—C(6)	1.32(1)
In—S(13)	2.558(3)	N(9)—N(10)	1.38(1)
In—S(20)	2.595(3)	N(10)—C(11)	1.33(1)
In—N(1)	2.292(7)	N(16)—N(17)	1.34(1)
In—N(9)	2.357(8)	N(16)—C(14)	1.32(1)
In—N(16)	2.391(8)	N(17)—C(18)	1.34(2)
S(13)—C(11)	1.71(1)	C(2)—C(14)	1.47(2)
S(20)—C(18)	1.64(1)	C(6)—C(7)	1.49(2)

In—O(1)—In′	179.8(5)	S(20)—In—N(16)	71.6(2)
O(1)—In—O(2)	165.0(2)	N(1)—In—N(9)	69.0(3)
O(1)—In—S(13)	95.2(2)	N(1)—In—N(16)	68.4(3)
O(1)—In—S(20)	91.4(2)	N(9)—In—N(16)	137.5(3)
O(1)—In—N(1)	79.6(2)	S(13)—C(11)—N(10)	127.7(7)
O(1)—In—N(9)	86.4(3)	S(20)—C(18)—N(17)	123.9(8)
O(1)—In—N(16)	85.2(3)	N(1)—C(2)—C(14)	116.6(8)
O(2)—In—S(13)	98.1(2)	N(1)—C(6)—C(7)	116.5(8)
O(2)—In—S(20)	98.1(2)	N(9)—N(10)—C(11)	114.2(8)
O(2)—In—N(1)	85.7(3)	N(9)—C(7)—C(6)	114.9(9)
O(2)—In—N(9)	90.9(3)	N(10)—N(9)—C(7)	116.4(9)
O(2)—In—N(16)	86.9(3)	N(16)—N(17)—C(18)	119.4(9)
S(13)—In—S(20)	77.44(9)	N(16)—C(14)—C(2)	115.0(8)
S(13)—In—N(1)	142.1(2)	N(17)—N(16)—C(14)	118.9(8)
S(13)—In—N(9)	73.2(2)	C(6)—N(1)—C(2)	119.7(8)
S(13)—In—N(16)	149.1(2)	C(11)—S(13)—In	100.6(4)
S(20)—In—N(1)	139.6(2)	C(18)—S(20)—In	103.2(4)
S(20)—In—N(9)	150.2(2)		

bridged dimer $\{O[In(acetato\text{-}O)_2L]\}$ (L = 1,4,7-triazacyclononane-N,N′,N″) [32], where the oxo bridge is bent with an angle of 142°, the In—O(1)—In′ angle in $\{O[In(HDAPTSC)(OH)]_2\}$ is 179.8(5)°. The In—O bond lengths in the bridge are shorter by 0.1 Å than those to the terminal hydroxy groups. With this, they come close to the In—O distances in the solid state structure of In_2O_3 [33]. The chelating ligand is singly deprotonated as in $[InCl_2(HDAPTSC)]$. This has been checked by IR and mass spectra. A unequivocal verification by X-ray structural results cannot be given, since we were not able to locate all hydrogen atoms in the final Fourier map. However, the bond length differences in the sulfur-containing chelate rings suggest deprotonation of N(10).

tonation of the ligand is realized without addition of base. To obtain pure $[InBr_2(APTSC)(MeOH)]$ it is necessary to start from HAPTSC instead of from HAPTSC · HCl. The use of the hydrochloride works well with $InCl_3$, but causes halide exchange on the bromo complex and considerable amounts of $[InCl_2(APTSC)(MeOH)]$ are formed.

$[InCl_2(APTSC)(MeOH)]$ and its bromo analogue are yellow solids which are soluble in $CHCl_3$, CH_2Cl_2 and methanol. They are insoluble in hydrocarbons. The compounds are indefinitely stable in air as solids as well as in solution. The infrared spectral results obtained agree with the coordination of a deprotonated thiosemicarbazonato ligand. FAB^+ spectra show peaks at $m/z = 308$ which can easily be assigned

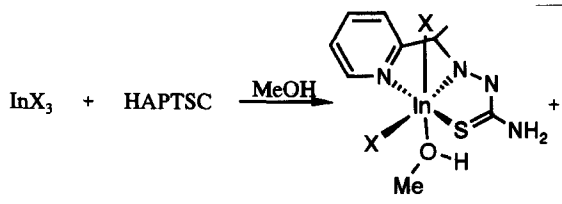

equ. (2)

The potentially tridentate ligand HAPTSC reacts with $InCl_3$ and $InBr_3$ in methanol under formation of six-coordinate species of the composition $[InX_2(APTSC)(MeOH)]$ according to eq. (2). Deprotonation of the ligand is realized without addition of base. To obtain pure $[InBr_2(APTSC)(MeOH)]$ it is necessary to start from HAPTSC instead of from HAPTSC · HCl. The use of the hydrochloride works well with $InCl_3$, but causes halide exchange on the bromo complex and considerable amounts of $[InCl_2(APTSC)(MeOH)]$ are formed.

$[InCl_2(APTSC)(MeOH)]$ and its bromo analogue are yellow solids which are soluble in $CHCl_3$, CH_2Cl_2 and methanol. They are insoluble in hydrocarbons. The compounds are indefinitely stable in air as solids as well as in solution. The infrared spectral results obtained agree with the coordination of a deprotonated thiosemicarbazonato ligand. FAB^+ spectra show peaks at $m/z = 308$ which can easily be assigned as $[In(APTSC)]^+$. Additionally, signals of less intensity due to the molecular ion and $[InX(APTSC)]^+$ can be observed. ^1H and ^{13}C NMR spectra confirm the formation of the product.

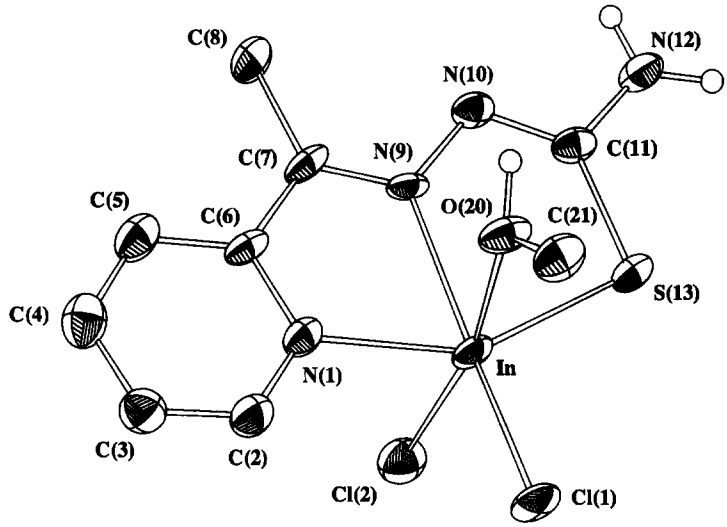

Fig. 3. ORTEP representation [31] of $[InCl_2(APTSC)(MeOH)]$ with thermal ellipsoids of 50% probability. H atoms at the carbon atoms have been omitted for clarity.

A crystal structure determination has been performed for $[InCl_2(APTSC)(MeOH)]$. The compound crystallizes as monomeric neutral molecules in an orthorhombic unit cell. Fig. 3 contains an ORTEP representation of the molecule. Selected bond lengths and angles are summarized in Table 4. The coordination polyhedron can best be described as a distorted octahedron. Deviations from the idealized symmetry result from the restricted bite angle of the tridentate ligand [N(1)—In—S(13): 150.9(2)°]. The chloro ligands are in *cis* arrangement and the In—Cl(1) bond length is shorter by 0.053 Å compared with the In—Cl(2) distance. The bonding situation in the In—N(9)—N(10)—C(11)—S(13) chelate ring is very similar to that in the 'deprotonated half' of $[InCl_2(HDAPTSC)]$ showing relatively short N(10)—C(11) [1.331(1) Å] and long C(11)—S(13) [1.744(7) Å] distances. The thiosemicarbazonato ligand is coplanar with In and Cl(1) within 0.541(3) Å. The methanol ligand is coordinated without deprotonation.

As a side-product of the reactions of $InCl_3$ or $InBr_3$ with HAPTSC, the cationic bis-chelate $[In(APTSC)_2]^+$ can be detected (e.g. by mass spectrometry). Small amounts of this complex can be isolated when excess HAPTSC is used. Reasonable amounts of $[In(APTSC)_2]^+$ can be prepared from $In(NO_3)_3 \cdot 5\ H_2O$ and HAPTSC. The bis-chelate can be precipitated with anions like PF_6^-, BF_4^-, $CF_3SO_3^-$ or BPh_4^-. A crystal structure determination has been done with $[In(APTSC)_2]PF_6$. The structure consists of discrete complex cations and PF_6^- anions. An ORTEP plot of $[In(APTSC)_2]^+$ is shown in Fig. 4. The corresponding bond lengths and angles are contained in

Table 4. Selected bond lengths (Å) and angles (°) for $[InCl_2(APTSC)(MeOH)]$

In—O(20)	2.363(6)	S(13)—C(11)	1.744(7)
In—Cl(1)	2.412(2)	N(1)—C(6)	1.359(9)
In—Cl(2)	2.465(3)	N(9)—N(10)	1.375(9)
In—S(13)	2.483(3)	N(10)—C(11)	1.33(1)
In—N(1)	2.233(7)	C(6)—C(7)	1.48(1)
In—N(9)	2.269(6)	C(7)—N(9)	1.30(1)
O(20)—In—Cl(1)	86.0(1)	Cl(2)—In—N(9)	95.5(2)
O(20)—In—Cl(2)	168.7(2)	S(13)—In—N(1)	150.9(2)
O(20)—In—S(13)	89.9(2)	S(13)—In—N(9)	78.3(2)
O(20)—In—N(1)	81.8(2)	N(1)—In—N(9)	72.6(2)
O(20)—In—N(9)	77.4(2)	S(13)—C(11)—N(10)	128.9(6)
Cl(1)—In—Cl(2)	100.02(7)	N(1)—C(6)—C(7)	117.2(7)
Cl(1)—In—S(13)	107.57(7)	N(9)—N(10)—C(11)	114.9(6)
Cl(1)—In—N(1)	99.7(2)	N(9)—C(7)—C(6)	115.9(6)
Cl(1)—In—N(9)	162.5(2)	N(10)—N(9)—C(7)	121.0(6)
Cl(2)—In—S(13)	97.28(7)	C(6)—N(1)—In	115.9(6)
Cl(2)—In—N(1)	87.8(2)	C(11)—S(13)—In	96.6(3)

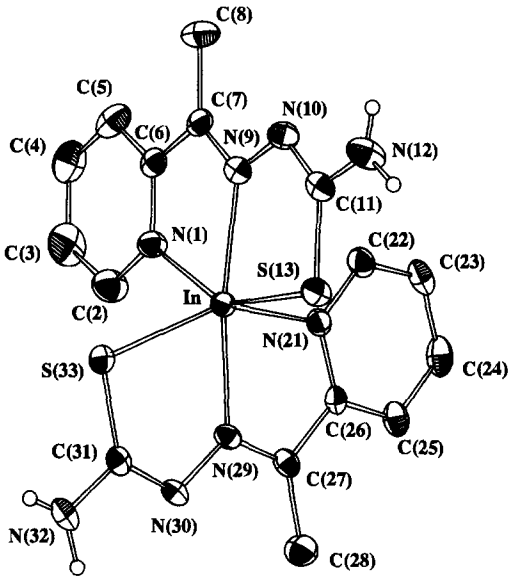

Fig. 4. ORTEP representation [31] of the cation $[In(APTSC)_2]^+$. Thermal ellipsoids represent 50% probability. H atoms at the carbon atoms have been omitted for clarity.

Table 5. The metal is six-coordinate with approximately planar tridentate ligands. While the bond distances and angles inside the thiosemicarbazone moiety are almost equal for both ligands, slightly different bond lengths have been observed for the In—S and In—N bonds. Similar differences have been found for a cationic cobalt(III) complex $[Co(L4M)_2]BF_4$ (L4M = 2-acetyl-^{4}N-methylthiosemicarbazonate) [15]. This is result is restricted to the solid state structure of the complex and should be assigned to crystal packing effects. ^{1}H and ^{13}C NMR spectra confirm equivalence for the two coordinated ligands in solution.

$[InCl_2(APTSC)(MeOH)]$ has been proved to be a good starting material for further ligand exchange reactions. This has been checked with bidentate sulfur-containing ligands. The reaction with sodium diethyldithiocarbamate, $NaEt_2dtc$, at room temperature yields the six-coordinate complex $[InCl(APTSC)(Et_2dtc)]$ (Fig. 5). The compound can be isolated as pale-yellow needles which are airstable and readily soluble in chloroform or dichloromethane. The FAB^+ mass spectrum shows an intense peak (80% B) at $m/z = 455$ which corresponds to a fragment of the composition $[In(ATPSC)(Et_2dtc)]^+$. The structure of the complex is confirmed by the IR and NMR results as well as by an X-ray structure determination. Since the data collection was interrupted after about 2000 reflections due to crystal decomposition, only In, Cl and S atoms could be refined anisotropically. Therefore, this crystal structure shall not be discussed in full detail. Nevertheless, main structural features could be derived and are contained in Fig. 5. The remaining chloro ligand is positioned *trans* to a sulfur atom of the dithiocarbamate and the coordination geometry of the metal significantly deviates from an idealized octahedron as a consequence of the bite angles of the chelating ligands (selected bond angles: N(1)—In—N(9) 72.1(5)°, N(1)—In—Cl 87.9(3)°, N(1)—In—S(13) 149.8(3)°,

Table 5. Selected bond lengths (Å) and angles (°) for $[In(APTSC)_2](PF_6)$

In—S(13)	2.519(1)	In—S(33)	2.505(1)
In—N(1)	2.283(4)	In—N(21)	2.297(4)
In—N(9)	2.230(4)	In—N(29)	2.250(4)
S(13)—C(11)	1.745(5)	S(33)—C(31)	1.749(5)
N(1)—C(6)	1.348(6)	N(21)—C(26)	1.346(6)
N(9)—N(10)	1.381(5)	N(29)—N(30)	1.369(5)
N(9)—C(7)	1.294(6)	N(29)—C(27)	1.294(6)
N(10)—C(11)	1.313(6)	N(30)—C(31)	1.312(6)
C(6)—C(7)	1.484(7)	C(26)—C(27)	1.473(7)

S(13)—In—S(33)	103.39(4)	N(10)—C(11)—S(13)	129.4(4)
S(13)—In—N(1)	149.61(11)	N(30)—C(31)—S(33)	129.5(4)
S(13)—In—N(9)	78.10(11)	N(10)—C(6)—C(5)	120.2(5)
S(13)—In—N(21)	94.77(11)	N(1)—C(6)—C(7)	116.5(4)
S(13)—In—N(29)	104.52(10)	N(9)—C(7)—C(6)	115.2(4)
S(33)—In—N(1)	91.02(11)	C(7)—N(9)—N(10)	117.1(4)
S(33)—In—N(9)	114.72(10)	N(21)—C(26)—C(27)	116.2(4)
S(33)—In—N(21)	146.98(10)	C(31)—N(30)—N(29)	114.4(4)
S(33)—In—N(29)	77.75(10)	C(27)—N(29)—N(30)	118.4(4)
N(1)—In—N(9)	71.56(14)	C(6)—N(1)—In	115.9(3)
N(1)—In—N(21)	86.66(14)	C(7)—N(9)—In	120.5(3)
N(1)—In—N(29)	104.63(14)	C(11)—S(13)—In	95.4(2)
N(9)—In—N(21)	95.74(13)	C(26)—N(21)—In	115.9(3)
N(9)—In—N(29)	166.62(14)	C(27)—N(29)—In	119.0(3)
N(21)—In—N(29)	71.06(13)	C(31)—S(33)—In	95.7(2)

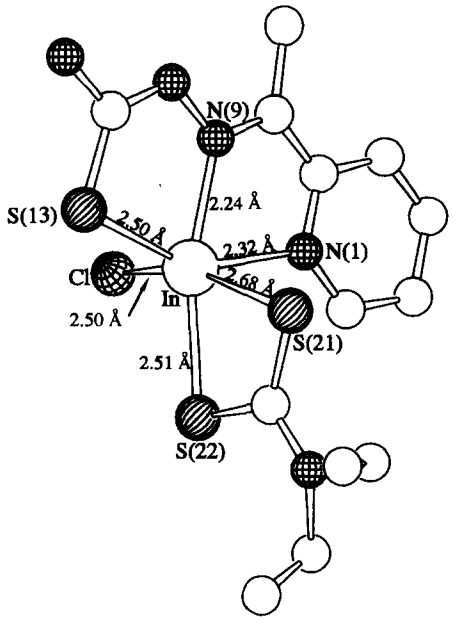

Fig. 5. SCHAKAL plot [35] of [InCl(APTSC)(Et_2dtc)] together with selected bond lengths.

N(1)—In—S(21) 85.4(3)°, N(1)—In—S(22) 96.7(3)°, N(9)—In—Cl 94.4(3)°, N(9)—In—S(13) 77.9(4)°, N(9)—In—S(21) 101.3(3)°, N(9)—In—S(22) 166.6°, S(13)—In—Cl 97.5(2)°, S(13)—In—S(21) 97.6(2)°, S(13)—In—S(22) 112.5(2)°, Cl—In—S(21) 160.1(2)°, Cl—In—S(22) 92.6(1)°, S(21)—In—S(22) 69.7(1)).

When excess of $NaEt_2$dtc is used, the ligand exchange does not stop at the mixed ligand complex stage but yields the well known tris-chelate [In(Et_2dtc)$_3$] according to eq. (3). Similar

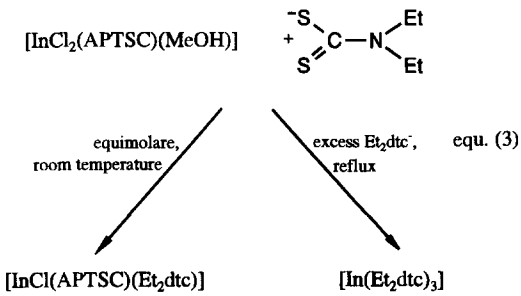

results have been found earlier for indium(III) complexes with 2-acetylpyridineoxime where the reaction with dithiocarbamates gives the [In(R_2dtc)$_3$] chelates in high yields [34].

A similar tendency can be discussed for the reaction of [$InCl_2$(APTSC)(MeOH)] with disodium 1,2-dicyanoethene -1,2-dithiolate, Na_2mnt, where in a first stage a ligand exchange 2 Cl^- *vs* mnt^{2-} takes place. Parallely, $APTSC^-$ is removed from the metal and the anion $[InCl(mnt)_2]^{2-}$ is formed. This complex can be detected mass spectrometrically using the negative ionization FAB technique. It can be isolated after addition of (Ph_4As)Cl to the methanolic reaction mixture. Formation of the tris-chelate $[In(mnt)_3]^{3-}$ could not be detected when Na_2mnt and [$InCl_2$(APTSC)(MeOH)] were reacted stoichiometrically. Without addition of a bulky cation $[InCl(mnt)_2]^{2-}$ remains in solution and upon slow evaporation of the solvent yellow crystals of (H_2APTSC)[InCl(APTSC)(mnt)] deposit. Considerable amounts of $[InCl(mnt)_2]^{2-}$ can be obtained from the oily residue after complete evaporation of the solvent and extraction with acetonic tetrabutylammonium or tetraphenylarsonium chloride solutions.

In the yellow crystals which precipitate directly from the mother liquor, the mixed ligand anion $[InCl(APTSC)(mnt)]^-$ crystallizes as H_2APTSC^+ salt together with a half molecule of solvent water. This composition has been confirmed by spectroscopic methods and X-ray crystallography. The thiosemicarbazonate coordinates in the same way as discussed above, as monoanionic, tridentate ligand. Figure 6 gives an ORTEP [31] representation of the ion pair. Selected bond lengths and angles are summarized in Table 6. The bonding situation inside the $APTSC^-$ skeleton of the complex anion is the same as found in [$InCl_2$(APTSC)(MeOH)] or $[In(APTSC)_2]^+$ with a relatively short N(10)—C(11) [1.325(9) Å] and a relatively long C(11)—S(13) [1.729(7) Å] distance suggesting an extended π-system inside the chelate ring. This contrasts the bonding mode in the H_2APTSC^+ counterion where an almost isolated C—S double bond can be found between C(41) and S(43) [1.675(7) Å] and the N(40)—C(41) distance of 1.371(8) Å has single bond character. Weak hydrogen bonds can be discussed between the chloro ligand and H(31) (distance: 2.402 Å) and H(42B) (2.565 Å) of the cation and H(12A) (2.688 Å) of the complex anion. These weak interactions between the ion pair might be responsible for the stereochemistry of the H_2APTSC^+ cation which prefers hydrogen bonds to the complex anion rather than an intramolecular hydrogen bridge between H(40) and S(43) which has been found for the related thiosemicarbazone 2'-[1-(2-pyridyl) ethylidene] - 3 - azabicyclo[3.2.2]nonane - 3 - carbthiohydrazide [34]. With this, the bonding situation of the cation in (H_2APTSC)[InCl(APTSC)(mnt)] compares with that in ($H_2APTSC)^+Cl^-$, the structure of which has been reported previously [26].

CONCLUSIONS

Indium(III) complexes with tri- and pentadentate thiosemicarbazones can be easily prepared from either indium(III) halides or $In(NO_3)_3 \cdot 5\ H_2O$. Halide ligands remain in the coordination sphere of the metal, whereas the reactions from indium nitrate yields cationic bis-chelates with tridentate ligands and neutral μ-oxobridged hydroxo species when pentadentate bis(thiosemicarbazones) are used. The symmetrical, pentadentate bis(thiosemicarbazone) H_2DAPTSC

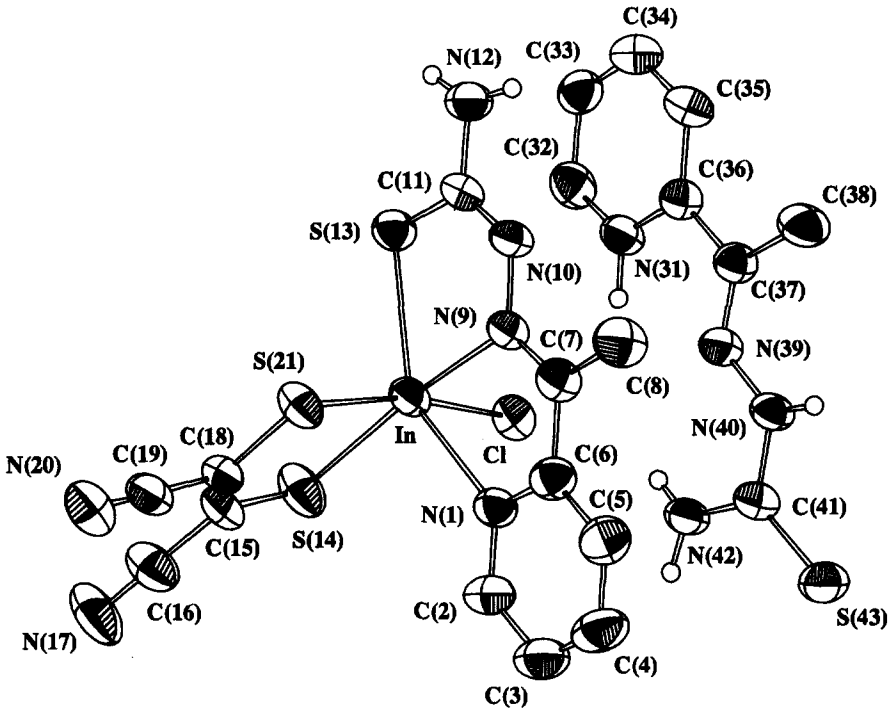

Fig. 6. ORTEP representation [31] of $(H_2APTSC)[InCl(APTSC)(mnt)]$ with thermal ellipsoids of 50% probability. H atoms at the carbon atoms have been omitted for clarity.

Table 6. Selected bond lengths (Å) and angles (°) for $(H_2APTSC)[InCl(APTSC)(mnt)] \cdot 0.5\ H_2O$

In—Cl	2.571(2)	C(6)—C(7)	1.477(9)
In—S(13)	2.529(2)	S(14)—C(15)	1.744(7)
In—S(14)	2.510(2)	S(21)—C(18)	1.723(6)
In—S(21)	2.561(2)	C(15)—C(18)	1.367(10)
In—N(1)	2.308(5)	S(43)—C(41)	1.672(7)
In—N(9)	2.286(5)	N(31)—C(36)	1.348(8)
S(13)—C(11)	1.729(6)	N(39)—N(40)	1.359(7)
N(1)—C(6)	1.345(9)	N(39)—C(37)	1.288(8)
N(9)—N(10)	1.367(7)	N(40)—C(41)	1.371(8)
N(9)—C(7)	1.301(8)	C(41)—N(42)	1.319(8)
N(10)—C(11)	1.328(8)	C(36)—C(37)	1.467(9)
Cl—H(31)	2.402	Cl—H(42B)	2.565
Cl—H(12A)′	2.688		

S(13)—In—Cl	91.51(6)	C(15)—C(18)—S(21)	127.5(5)
S(14)—In—Cl	86.62(6)	N(1)—C(6)—C(7)	117.2(6)
S(21)—In—Cl	170.15(5)	C(11)—N(10)—N(9)	113.9(5)
N(1)—In—Cl	84.00(14)	N(9)—C(7)—C(6)	116.1(6)
N(9)—In—Cl	97.18(14)	C(7)—N(9)—N(10)	117.8(5)
S(13)—In—S(14)	111.45(7)	N(10)—N(9)—In	122.6(4)
S(13)—In—S(21)	97.39(6)	C(6)—N(1)—In	116.2(4)
S(13)—In—N(1)	145.96(13)	C(7)—N(9)—In	119.3(4)
S(13)—In—N(9)	76.29(13)	C(11)—S(13)—In	96.8(2)
S(14)—In—S(21)	86.20(6)	C(15)—S(14)—In	100.0(2)
S(14)—In—N(1)	101.97(14)	C(18)—S(21)—In	99.1(2)
S(14)—In—N(9)	171.38(13)	S(43)—C(41)—N(40)	120.7(5)
S(21)—In—N(1)	90.90(14)	N(31)—C(36)—C(37)	117.1(5)
S(21)—In—N(9)	89.06(14)	N(39)—N(40)—C(41)	119.1(6)
N(1)—In—N(9)	70.9(2)	N(39)—C(37)—C(36)	114.8(6)
N(10)—C(11)—S(13)	129.4(4)	C(37)—N(39)—N(40)	120.7(5)
N(12)—C(11)—S(13)	116.3(5)	N(42)—C(41)—N(40)	116.0(6)
C(18)—C(15)—S(14)	127.0(5)	C(32)—N(31)—C(36)	123.3(6)

Symmetry code: (′) $-x, -0.5+y, 0.5-z$.

undergoes only a single deprotonation during the complex formation.

[InX_2(APTSC)(MeOH)] complexes are suitable starting materials for the synthesis of mixed-ligand indium(III) compounds when powerful chelating ligands as dialkyldithiocarbamates or maleonitrildithiolate are used. One halide and the methanol ligand are replaced when mild conditions are applied. Additional ligand exchange including the tridentate thiosemicarbazonate occurs when excess of the sulfur donor ligand and longer refluxing periods are applied.

The new compounds represent a novel class of indium(III) complexes which may possess interesting biological properties. Cell toxicity studies are presently under progress.

Acknowledgements—This work was supported by the Deutsche Forschungsgemeinschaft and the Fonds der Chemischen Industrie. We thank Professor J. Strähle (Tübingen) for his kind hospitility and for providing us with facilities. S.A. thanks the University of Tübingen for financial support.

REFERENCES

1. Scovill, J. P., Klayman, D. L. and Franchino, C. F., *J. Med. Chem.*, 1982, **25,** 1261.
2. Bhoon, Y. K., Scovill, J. P. and Klayman, D. L., *Indian J. Chem.*, 1983, **22A,** 267.
3. Dobek, A. S., Klayman, D. L., Dickson, E. T., Scovill, J. P. and Oster, C. N., *Arzneim. Forsch.*, 1983, **33,** 1583.
4. Klayman, D. L., Scovill, J. P., Mason, C. J., Bartosevich, J. F., Bruce, J. and Lin, A., *Arzneim. Forsch.*, 1983, **33,** 909.
5. Klayman, D. L., Scovill, J. P., Bartosevich, J. F. and Mason, C. L., *J. Med. Chem.*, 1979, **22,** 1367.
6. Shipman Jr., C., Smith, S. H., Drach, J. C. and Klayman, D. L., *Antiviral Res.*, 1986, **6,** 197.
7. French, F. A. and Blanz Jr., E., *J. Med. Chem.*, 1970, **13,** 1117.
8. West, D. X., Carlson, C. S., Galloway, C. P., Liberta, A. E. and Daniel, C. R., *Trans. Met. Chem.*, 1990, **15,** 43 and refs therein.
9. Levinson, W. E., *Antibiol. Chemother.*, 1980, **27,** 288.
10. Saryan, L. A., Mailer, K., Krishnamurti, C., Atholine, W. and Petering, D. H., *Biochem. Pharmacol.*, 1981, **30,** 1595.
11. Sartorelli, A. C., Agrawal, K. C., Tsiftsoglou, A. S. and Moore, E. C., *Adv. Enzyme Reg.*, 1977, **15,** 117.
12. Scovill, J. P., Klayman, D. L., Lambrose, C., Childs, G. E. and Notsch, J. D., *J. Med. Chem.*, 1984, **27,** 87.
13. Garg, B. S., Kurup, M. R. P., Jain, S. K. and Bhoon, Y. K., *Trans. Met. Chem.*, 1988, **13,** 247 and refs therein.
14. Dessy, G. and Fares, V., *Cryst. Struct. Comm.*, 1981, **10,** 1025.
15. Castineiras, A., West, D. X., Gebremedhim, H. and Romack, T. J., *Inorg. Chim. Acta*, 1994, **216,** 229.
16. West, D. X., Gebremedhim, H., Butcher, R. J., Jasinski, J. P. and Liberta, A. E., *Polyhedron*, 1993, **12,** 2489.
17. West, D. X., Scovill, J. P., Silverton, J. K. and Baroso, A., *Trans. Met. Chem.*, 1986, **11,** 123.
18. West, D. X., Gebremedhim, H., Butcher, R. J. and Jasinski, J. P., *Trans. Met. Chem.*, 1995, **20,** 84.
19. Butcher, R. J. and West, D. X., *Trans. Met. Chem.*, 1993, **18,** 449.
20. Kovala-Demertzi, D., Domopolous, A., Demertzis, M., Raptopoulou, C. P. and Terzis, A., *Polyhedron*, 1994, **13,** 1917.
21. Bino, A. and Cohen, N., *Inorg. Chim. Acta*, 1993, **210,** 11.
22. de Sousa, G. F., Filqueiras, C. A. L., Abras, A., Al-Juaid, S. S., Hitchcock, P. B. and Nixon, J. F., *Inorg. Chim. Acta*, 1994, **218,** 139.
23. Casas, J. S., Castineiras, A., Sanchez, A., Sordo, J., Vazques-Lopez, A., Rodriguez-Arguelles, M. C. and Russo, U., *Inorg. Chim. Acta*, 1994, **221,** 61.
24. Battaglia, L. P., Corradi, A. B., Pelizzi, C., Pelosi, G. and Tarasconi, P., *J. Chem., Soc. Dalton Trans.*, 1990, **385,** 3857.
25. Palenick, G. J., Wester, D. W., Rychlewska, U. and Palenik, R. C., *Inorg. Chem.*, 1976, **15,** 1814.
26. Abram, S. and Abram, U., *Acta Cryst.*, 1997, **C53,** 360.
27. Bähr, G. and Schleitzer, G., *Chem. Ber.*, 1957, **90,** 438.
28. Spek, A., HELENA, PLATON, SQUEEZE, A multi-purpose crystallographic tool, University of Utrecht, 1994.
29. Sheldrick, G. M., SHELXS-86, A program for solution of crystal structures, University of Göttingen, 1986.
30. Sheldrick, G. M., SHELXL-93, A program for the refinement of crystal structures, University of Göttingen, 1993.
31. Zsolnai, L., ZORTEP, A program for the representation of thermal ellipsoids, University of Heidelberg, 1994.
32. Wieghardt, K., Kleine-Boymann, M., Nuber, B. and Weiss, J., *Inorg. Chem.*, 1986, **25,** 1654.
33. (a) Christensen, A. N., Broch, N. C., Heidenstamm, O. V. and Nilson, A., *Acta Chem. Scand.*, 1967, **21,** 1046; (b) Marezio, U., *Acta Cryst.*, 1966, **20,** 723.
34. Daneshwar, N. N., Tavale, S. S. and Guru Row, T. N., *Acta Cryst.*, 1985, **C41,** 1188.
35. Keller, E., SCHAKAL, A program for the representation of crystal structures, University of Freiburg, 1992.

Pergamon

PII: S0277-5387(97)00251-9

Polyhedron Vol. 17, No. 1, pp. 145–147, 1998
© 1997 Elsevier Science Ltd
All rights reserved. Printed in Great Britain
0277-5387/98 $19.00+0.00

Synthesis, acid–basic and complexing properties of cyclene based cryptands

Ivan Zheltvay, Yurii Popkov, Sergey Shevchuk, Yurii Korovin* and Ninel Nazarenko

A. V. Bogatsky Physico-Chemical Institute of National Academy of Sciences of Ukraine, 86 Lustdorfskaya doroga, 270080 Odessa, Ukraine

(Received 24 February 1997; accepted 30 May 1997)

Abstract—The protonation of 1,4,7,10-tetraazabicyclododecane (L^2), 4,7-dioxa 1,10,13,16-tetraazabicyclo[8.8.2]eicosane (L^3) and 1,4,7,10,13,16-hexaazabicyclo[8.8.2]eicosane (L^7) was studied by potentiometric methods at 18°C and ionic strength of 0.1 ($NaClO_4$) in aqueous medium. In all instances, two buffer regions have been observed. The logarithms of the protonation constants were equal to 10.55, 9.50, 3.00 for L^2, 10.80, 9.95, 8.60, 3.30 for L^3 and 10.25, 9.00, 7.80, 5.70, 2.80, 1.20 for L^7. The stability constants for copper(II) complexes were determined. The methods of synthesis of cryptands L^3, L^7 are presented. © 1997 Elsevier Science Ltd

Keywords: cyclene; cryptands; protonation constants; copper complexes; stability constants; absorption spectra.

It is known that cryptands containing nitrogen atoms have three-dimensional macrocycles, the cavities of which can accommodate suitable cations [1–3] or anions [4]. These complexes are approximately ellipsoidal, the 'meridians' of which contain various heteroatoms.

In terms of the complexing ability of cryptands, the structures with hemispherical cavities are of interest. This situation occurs when one of the chains connecting the polar nitrogen atoms is considerably shorter than the others. The well-known representative of this class cryptands is 4,7,13,16-tetraoxa-1,10-diazabicyclo[8.8.2]eicosane (L^1), X-ray data [5] for which confirm a clamlike construction. The polyether links rotate with respect to the $>N(CH2)_2N<$ fragment and selectively bind alkaline–earth ions and there is a correlation between the angle of opening and stability of the corresponding cryptates [6,7]

In this work, we consider the complexing ability of structural analogues of L^1 containing links with donor nitrogen atoms instead of polyether chains. The synthesis of two new cryptands, 4,7-dioxa-1,10,13,16-tetraazabicyclo[8.8.2]eicosane (L^3) and 1,4,7,10,13,16-hexaazabicyclo[8.8.2]eicosane (L^7), that can be considered as bicyclic derivatives of cyclene, 1,4,7,10-tetraazabicyclododecane (L^2), is described. The latter relates to the class of cyclic tetraamines and forms stable complexes with copper(II) ions [8,9]. The scheme for the synthesis of cryptands and intermediates is shown in Scheme 1.

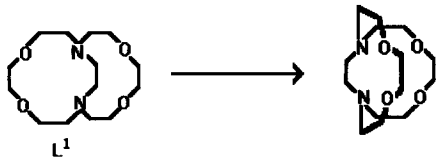

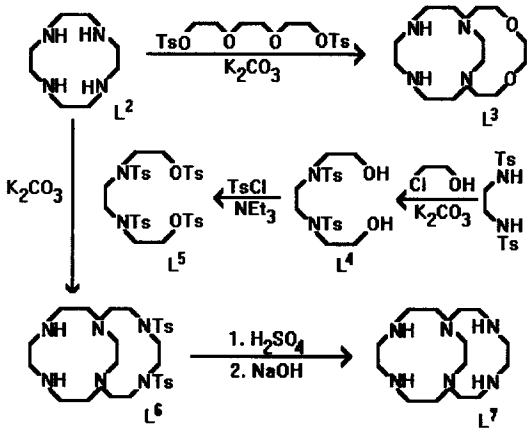

Scheme 1.

Alkylation of the cyclene by triethyleneglycol ditosylate in dry DMF, in the presence of K_2CO_3, leads to the formation of L^3. In analogous conditions, L^6 was prepared by a condensation of L^2 with N,N′-bis(2-hydroxyethyl)ethylenediamine tetratosylate L^5. After removing the tosyl fragments, the bicyclic hexaamine L^7 was obtained. The reagent L^5, required for this synthesis, was obtained from the initial ditosylate in two steps.

EXPERIMENTAL

1,4,7,10-tetraazacyclododecane (cyclene) (L^2) (Aldrich) was used as received.

Measurements

The control of the reaction course and purity of compounds synthesized was determined by TLC methods on Silufol UV-254 plates, the eluent was ethanol–acetonitrile–aqueous ammonia, 10:3:5. ^{1}H NMR spectra of $CDCl_3$ solutions of the compounds were recorded on a Bruker AM-250 spectrometer. Electronic spectra of the copper complex solutions were obtained on a Perkin–Elmer Lambda 9 spectrophotometer. Mass spectra were measured on a Varian MAT CH-112 spectrometer.

Protonation constants for the ligands and stability constants for the copper complexes were determined by pH-potentiometric titration methods at the temperature $T = 18°C$ and ionic strength $\mu = 0.1$ ($NaClO_4$). Titrant was 0.1 M $HClO_4$ aqueous solution. Measurements were performed on a OP0211/1 laboratory digital pH-meter (Radelkis, Budapest, Hungary).

Preparation of 4,7-*dioxa*-1,10,13,16-*tetraazabicyclo*[8.8.2]*eicosane* (L^3)

Ethyleneglycol ditosylate, 4.12 g (0.009 mole) dissolved in 50 cm^3 of DMF was slowly added to 80 m^3 of dry DMF containing 1,4,7,10-tetraazacyclododecane (L^2) (1.72 g, 0.01 mole) and 3.2 g of freshly prepared K_2CO_3, and the mixture was stood for 3 h 100°C. The reaction mixture was cooled, filtered and evaporated under reduced pressure. The oil-like residue was extracted by hot hexane, the solvent was removed by distillation, and the resulting light-yellow product was crystallized from pentane. Yield 0.84 g (32.8%), M.p. 109–111°C, ^{1}H NMR, 250 MHz (δ, ppm relative to TMS): 2.47–2.78 (22H, m, CH_2N, NH), 3.54–3.80 (8H, m, CH_2O). Found: C, 59.01; H, 10.43; N, 19.61. Calc. for $C_{14}H_{30}N_4O_2$: C, 58.74; H, 10.49; N, 19.58%.

Preparation of 1,4,7,10,13,16-*hexaazabicyclo*[8.8.2]*eicosane* (L^7)

5.92 g of compound L^5 was dissolved in 50 cm^3 of 96% H_2SO_4, heated to 110–115°C and stirred for 20 h. To a cooled reaction mixture, 200 cm^3 of ether was slowly added. The precipitate was filtered, dissolved in a minimal amount of water that saturated with granular KOH or NaOH. The resulting oil-like product was isolated by extraction with hot benzene. Yield 1.65 g (58%). ^{1}H NMR, 250 MHz (δ, ppm relative to TMS): 2.11–2.16 (4H, s, NH), 2.59–2.71 (28H, m, CH_2N). Found: C, 59.48; H, 11.43; N, 29.61. Calc. for $C_{14}H_{32}N_6$: C, 59.15; H, 11.27; N, 29.58%.

RESULTS AND DISCUSSION

The isolated cryptands are soluble in water and are strong bases. Their titration curves against perchloric acid consist of two buffer regions. Before a jump of pH, 3 and 4 equiv. of the acid are expended for a titration of L^3 and L^7, respectively. From the titration data, the formation curves were obtained as the functions of $n = f(pH)$, where n is average number of attached protons. Then the protonation constants (K_n) (the inverse values of acid dissociation constants) were calculated using established equations [10]. For comparison, the protonation constants for cyclene were determined under similar conditions and the values for the first two protonation constants are in good agreement with the literature data (Table 1). The log K_3 value is somewhat increased, but has the same order of magnitude as the log K_n value for synthesized cryptands corresponding to the last buffer region. These data correspond well with the accepted scheme for protonation of macrocyclic polyamines [11], according to which, the first proton is attached to one of the secondary amino groups, and the second forms a hydrogen bond, bridging between adjoining nitrogen atoms. Two such possibilities exist for cyclene and hexaamine L^7 and one for tetraamine L^3. In the presence of copper(II) ions, the titration curve of L^2 is in the acid region when 2 equiv. of acid are already added, while the copper complex of the cryptand L^3 is protonated easily on the first step. Competition between protons and the copper(II) ion for cryptand L^3 occurs in the range K_2–K_3 and is expressed by an equation:

$$Cu^{2+} + LH_3^{3+} \leftrightarrow CuLH^{3+} + 2H^+$$

The stability constant for the complex, $K_s = [CuLH^{3+}]/[Cu^{2+}][LH^+]$, can be calculated by a graphical method used for two basic ligands [13]. Comparing the values of the stability constants of complexes with L^2 and L^3 and taking into account the nearness of their spectral parameters in region of *d–d* transitions (Table 2), it can be supposed that both in cyclene and cryptand L^3 the copper(II) ions possess closed environments.

The resulting value of log $K = 19.8$, and a considerable hypsochromic shift for the band ($\lambda_{max} = 641$ nm) of *d–d* transition in electronic absorption spectrum allow us to propose that the nitrogen atoms of

Table 1. Ligand protonation constants [$\mu = 0.1$ ($NaClO_4$); $T = 18°C$]

Protonation step	log K_n[a]		
	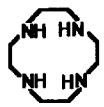	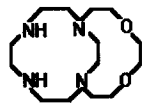	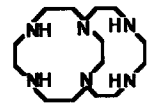
1	10.55 (10.6)[b]	10.80	10.25
2	9.50 (9.6)[b]	9.95	9.00
3	3.00 (1.15)[b]	8.60	7.80
4		3.30	5.70
5			2.80
6			<2

[a] Values were determined at confidential interval of ± 0.05.
[b] Data of Ref. [12].

Table 2. Stability constants and electronic spectra of copper complexes in the region of the *d–d* transitions

Complex	log K_s	λ_{max} (nm)	ε ($m^{-1} \cdot dm^3 \cdot cm^{-1}$)
$CuL_2(ClO_4)_2$	23.5 (24.8)[a]	592 (598)[a]	270 (257)[a]
$CuHL_3(ClO_4)_3$	21.2	594	287
$CuL_7(ClO_4)_2$	19.8	641	170

[a] Data of Ref. [8].

the secondary amino groups are involved in the copper coordination environment in the complex of **L**[7].

Acknowledgements—This work has been supported in part by the firm 'Double W' (Odessa, Ukraine, president: Dr Vladimir V. Goraschenko).

REFERENCES

1. Lehn, J.-M., *Acc. Chem. Res.*, 1978, **1,** 49.
2. Creaser, I. I., Geue, R. J., MacB. Harrowfield, J., Herlt, A. J., Sargeson, A. M., Snow, M. R. and Springbord, J., *J. Am. Chem. Soc.*, 1982, **104,** 6016.
3. Ciampolini, M., Micheloni, M., Orioli, P., Vizza, F., Mangani, S. and Zanobini, F., *Gazz. Chim. Ital.*, 1986, **116,** 189.
4. Reilly, S. D., Khalsa, G. R. K., Ford, D. K., Brainard, J. R., Hay, B. P. and Smith, P. H., *Inorg. Chem.*, 1995, **34,** 569.
5. Alfheim, T., Dale, J., Groth, P. and Krautwurst, K. D., *J. Chem. Soc., Chem. Commun.*, 1984, **22,** 1502.
6. Abou-Hamdan, A. and Lincoln, S. F., *Inorg. Chem.*, 1991, **30,** 462.
7. Lincoln, S. F. and Stephens, A. K. W., *Inorg. Chem.*, 1991, **30,** 3529.
8. Clay, R. M., McCormac, H., Micheloni, M. and Paoletti, P., *Inorg. Chem.*, 1982, **21,** 2494.
9. Hancock, R. D., Ngwenya, M. P., Evers, A., Wade, P. W., Boeyens, J. C. A. and Dobson, S. M., *Inorg. Chem.*, 1990, **29,** 264.
10. Beck, M., *Chemistry of Complex Equilibria*, van Nostrand Reinhold Comp., London, New York, Toronto, Melbourne (1970).
11. Yatsimirskii, K. B., Lampeka, Ya. D., *Physical Chemistry of Metal Complexes with Macrocyclic Ligands*, Naukova Dumka, Kiev (1985).
12. Martell, A. E., *Critical Stability Constants*, p. 5, Plenum Press, New York (1982).
13. Zheltvay, I. I. and Belevich, L. V., *Zh. Ukr. Khim.*, 1987, **53,** 123.
14. Dyatlova, N. M., Temkina, V. Ya., Kolpakova, I. D., *Complexones*, Khimiya, Moscow (1970).

Pergamon

PII: S0277-5387(97)00212-X

Polyhedron Vol. 17, No. 1, pp. 149–152, 1998
© 1997 Elsevier Science Ltd
All rights reserved. Printed in Great Britain
0277-5387/98 $19.00+0.00

Location of tin and charge balance in materials of composition $Fe_{3-x}Sn_xO_4$ ($x < 0.3$)

Frank J. Berry,[a]* Stephen J. Skinner,[a] Orn Helgason,[b] Robert Bilsborrow[c] and José F. Marco[d]

[a] Department of Chemistry, The Open University, Walton Hall, Milton Keynes MK7 6AA, U.K.

[b] Science Institute, University of Iceland, Dunhagi 3, IS 107 Reykavik, Iceland

[c] Daresbury Laboratory, Daresbury, Warrington WA4 4AD, U.K.

[d] Instituto de Quimica Fisica 'Rocasolano', Consejo Superior de Investigaciones Cientificas, c/Serrano 119, 28006 Madrid, Spain

(Received 10 March 1997; accepted 20 May 1997)

Abstract—Tin K-edge EXAFS show that low concentrations of tin in compounds of composition $Fe_{3-x}Sn_xO_4$ ($x < 0.3$) adopt the octahedral, as opposed to tetrahedral, sites of the inverse spinel structure. X-ray photoelectron spectroscopy shows that incorporation of tin is accompanied by the partial reduction of Fe^{3+} to Fe^{2+}.
© 1997 Elsevier Science Ltd

Keywords: tin-doped magnetite; doped ion oxides.

The iron oxide of composition Fe_3O_4 which is called magnetite adopts the inverse spinel structure in which Fe^{3+} occupies the tetrahedral sites whilst the octahedral sites are occupied by both Fe^{3+} and Fe^{2+}.

Iron–titanium oxides of composition $Fe_{3-x}Ti_xO_4$ have attracted interest because of their magnetic properties and the time–temperature-dependent phase transformations which they undergo [1]. Some initial studies of tin-doped Fe_3O_4 of composition $Fe_{3-x}Sn_xO_4$ described [2,3] the materials as ferrimagnets with the same inverse spinel structure as that observed in $Fe_{3-x}Ti_xO_4$. We have recently [4] prepared materials of composition $Fe_{3-x}Sn_xO_4$ ($x = 0.1$ and 0.2) by solid state reactions in sealed tubes. X-ray powder diffraction and ^{57}Fe- and ^{119}Sn-Mössbauer spectroscopy showed [4] the Curie temperature to be lower than that of Fe_3O_4 and related $Fe_{3-x}Ti_xO_4$ compounds. However, we were unable to identify whether tin in the Fe_3O_4 structure was located on the octahedral or tetrahedral sites of the spinel-related structure. We therefore report here on our study of the location of tin in $Fe_{3-x}Sn_xO_4$ and on the mechanism of charge balance.

* Author to whom correspondence should be addressed.

EXPERIMENTAL

Compounds of composition $Fe_{3-x}Sn_xO_4$ ($x < 0.3$) were prepared by heating stoichiometric quantities of powdered tin (IV) oxide, iron (III) oxide and metallic iron in sealed evacuated quartz ampoules at 900°C for 48 h and allowing the products to cool in the furnace.

Tin K-edge EXAFS measurements were performed at the Synchrotron Radiation Source at Daresbury Laboratory U.K. with an average current of 200 mA at 2 GeV. The data were collected in transmission geometry on Station 9.2 (5T wiggler) with 50% higher harmonic rejection. All data were recorded at 298 K. The raw data were background-subtracted using the Daresbury programme EXBACK and fitted using the non-linear least squares minimisation programme EXCURV92 which calculates the theoretical EXAFS function using the fast curved wave theory.

X-ray photoelectron spectra were recorded with a triple channeltron CLAM 2 analyser using Al-Kα radiation under an operating vacuum better than 1×10^{-8} m bar and a constant analyser transmission energy of 20 eV. The powdered samples were pressed on double sided adhesive conductive carbon tape. All binding energies were corrected to the C ls signal which was set at 284.6 eV.

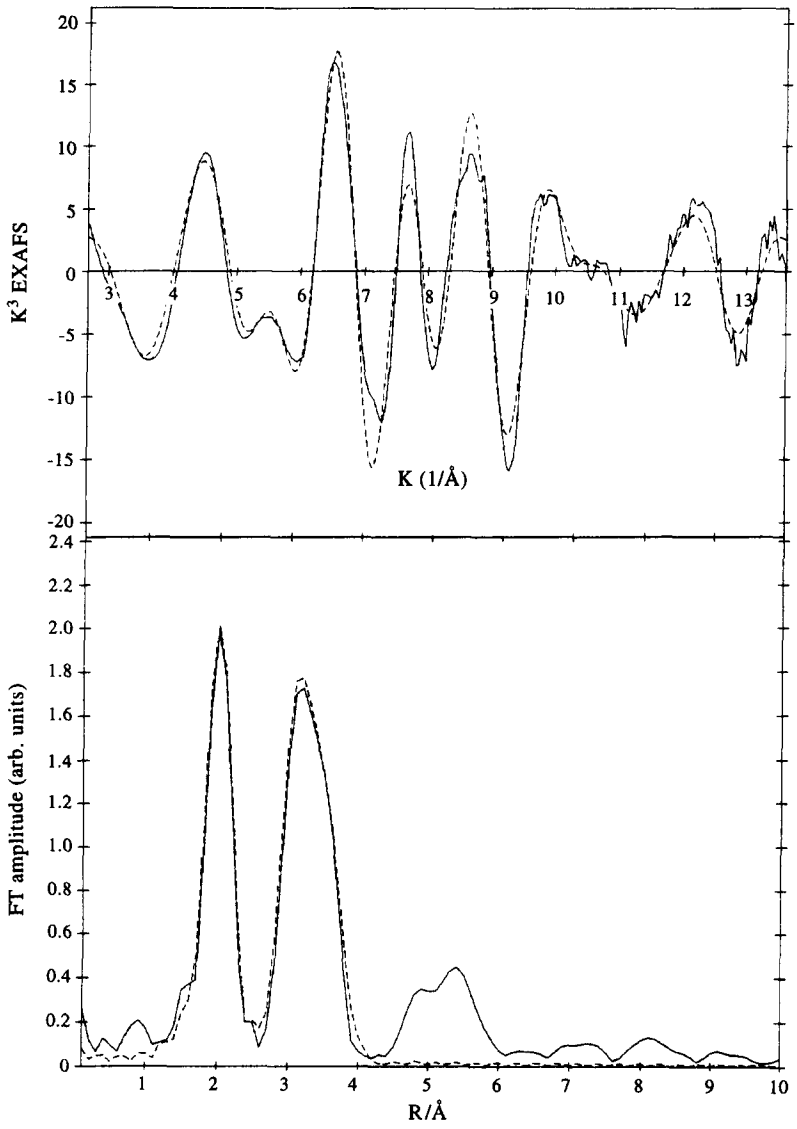

Fig. 1. Tin K-edge EXAFS and Fourier Transform recorded from $Fe_{2.9}Sn_{0.1}O_4$.

RESULTS AND DISCUSSION

X-ray powder diffraction showed the products to be monophasic. The compositions were confirmed by edx analysis. The tin K-edge EXAFS and its Fourier Transform recorded from the compound of composition $Fe_{2.9}Sn_{0.1}O_4$ are shown in Fig. 1. The data are collected in Table 1.

Table 1. Best fit parameters to tin K-edge EXAFS showing coordination around tin in $Fe_{2.9}Sn_{0.1}O_4$

Atom type	R (Å)	$2\sigma^2$ (Å^2)
6O	2.04(1)	0.007
6 Fe	3.07(1)	0.014
6 Fe	3.49(1)	0.016

The results show the tin to be coordinated by six oxygen atoms at 2.037 Å. The results demonstrate that the tin atoms in tin-doped Fe_3O_4 adopt the octahedral, as opposed to tetrahedral, sites in the inverse spinel structure. The tin-oxygen distance compares well with that observed in tin dioxide of 2.041 Å (as also determined here by tin K-edge EXAFS) which is consistent with data recorded by X-ray diffraction [5].

The Fe 2*p* X-ray photoelectron spectrum and the Fe $2p_{3/2}$ binding energy of 710.9 eV recorded from Fe_3O_4 (Fig. 2, Table 2) were similar to data reported in the literature [6,7]. The peaks in the Fe 2*p* X-ray photoelectron spectra recorded from $Fe_{2.9}Sn_{0.1}O_4$ and $Fe_{2.8}Sn_{0.2}O_4$ (Fig. 2) were broader than those observed in the spectrum recorded from Fe_3O_4 and the maxima of the Fe $2p_{3/2}$ envelopes were shifted to the lower energies of 710.4 eV and 710.0 eV respectively. A peak at 715.4 eV, which corresponds to the binding energy

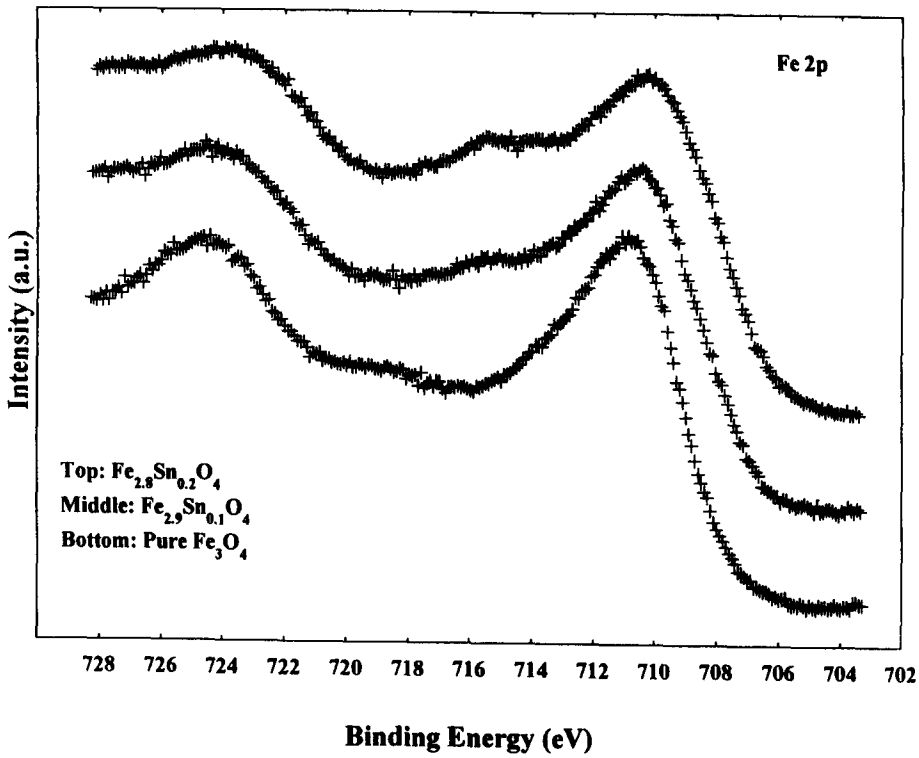

Fig. 2. Fe 2*p* X-ray photoelectron spectra recorded from Fe_3O_4, $Fe_{2.9}Sn_{0.1}O_4$ and $Fe_{2.8}Sn_{0.2}O_4$.

Table 2. Fe $2p_{3/2}$ binding energy values obtained from the compounds Fe_3O_4, $Fe_{2.9}Sn_{0.1}O_4$ and $Fe_{2.8}Sn_{0.2}O_4$

Compound	BE (eV)	I_{rel} (%)[a]	Assignment
Fe_3O_4	710.9	100	Fe^{3+}
$Fe_{2.9}Sn_{0.1}O_4$	709.2	43	Fe^{2+}
	710.7	57	Fe^{3+}
$Fe_{2.8}Sn_{0.2}O_4$	709.1	66	Fe^{2+}
	710.7	34	Fe^{3+}

[a]The relative intensity of the Fe^{2+} contribution includes the satellite contribution at the 714.0 eV.

of the Sn $2p_{3/2}$ core level, was also visible in both spectra. The Fe 2*p* spectrum recorded from $Fe_{2.8}Sn_{0.2}O_4$ suggested an additional structure at 714.0 eV which we associate with the presence of a Fe^{2+} satellite. The shifts to lower binding energy of the Fe $2p_{3/2}$ level, the increase in broadening of the Fe 2*p* peaks and the development of satellite structure are all indicative [7,8] of increasing Fe^{2+} content as increasing amounts of tin are incorporated within the Fe_3O_4 structure. This is more clearly demonstrated in Fig. 3 which shows the deconvolution of the Fe $2p_{3/2}$ peak. The single component in the Fe $2p_{3/2}$ peak of Fe_3O_4 at 710.9 eV is characteristic of Fe^{3+} and, although Fe_3O_4 contains both Fe^{2+} and Fe^{3+}, the

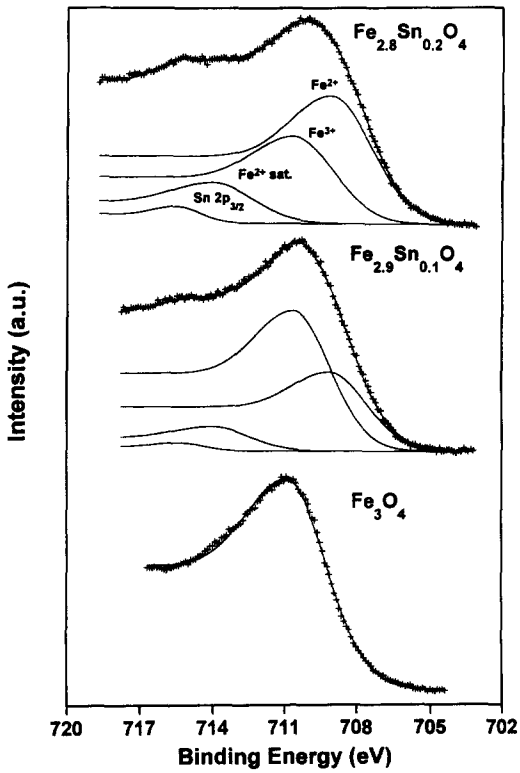

Fig. 3. Deconvolution of the Fe $2p_{3/2}$ X-ray photoelectron spectra recorded from Fe_3O_4, $Fe_{2.9}Sn_{0.1}O_4$ and $Fe_{2.8}Sn_{0.2}O_4$.

surface is usually oxidised such that only the Fe^{3+} contribution is observed in the X-ray photoelectron spectrum [9,10]. In contrast the Fe $2p_{3/2}$ peak in the spectra recorded from $Fe_{2.9}Sn_{0.1}O_4$ and $Fe_{2.8}Sn_{0.3}O_4$ were deconvoluted to four peaks. The peaks at 710.7 eV and 715.4 eV correspond to Fe^{3+} and the Sn $2p_{3/2}$ level respectively whilst the peak at 709.2 eV, together with the satellite at 714.0 eV, are characteristic [7,8] of Fe^{2+}.

The developing presence of Fe^{2+} as tin is incorporated within Fe_3O_4 was endorsed by the Fe 3*p* spectra (Fig. 4) which, with increasing tin content in the oxide, broaden and shift to lower energies. Deconvolution of the Fe 3*p* spectra showed a contribution at 56.2 eV characteristic [7] of Fe^{3+} together with a peak in the tin-containing materials at 54.3 eV characteristic [7] of Fe^{2+} which increased in intensity as the tin content increased (Table 3). The relative intensities obtained from the fit of the Fe 3*p* spectra agree well with those obtained from the fit of the Fe 2*p* spectra. The possible enrichment of the surface layers by either iron or tin was investigated using methods previously described [11,12] and by constructing calibration curves using standard compounds. The results gave no unequivocal evidence for the enrichment of the surface layers by either tin or iron.

Table 3. Fe 3*p* binding energy values obtained from the compounds Fe_3O_4, $Fe_{2.9}Sn_{0.1}O_4$ and $Fe_{2.8}Sn_{0.2}O_4$

Compound	BE (eV)	I_{rel} (%)	Assignment
Fe_3O_4	56.2	100	Fe^{3+}
$Fe_{2.9}Sn_{0.1}O_4$	54.3	47	Fe^{2+}
	56.2	53	Fe^{3+}
$Fe_{2.8}Sn_{0.2}O_4$	54.3	62	Fe^{2+}
	56.2	38	Fe^{3+}

Taken together the results show that the replacement of Fe^{3+} by Sn^{4+} in Fe_3O_4 is achieved by substitution on the octahedral sites of the inverse spinel structure and is accompanied by the partial reduction of Fe^{3+} to Fe^{2+}. It would seem that the lowering of the Curie temperature [4] of low tin-content tin-doped Fe_3O_4 as compared to that of Fe_3O_4 may therefore be associated with tin occupying the octahedral sites.

Acknowledgements—We thank the EPSRC for the award of a studentship (SS) and the provision of beamtime at Daresbury laboratory.

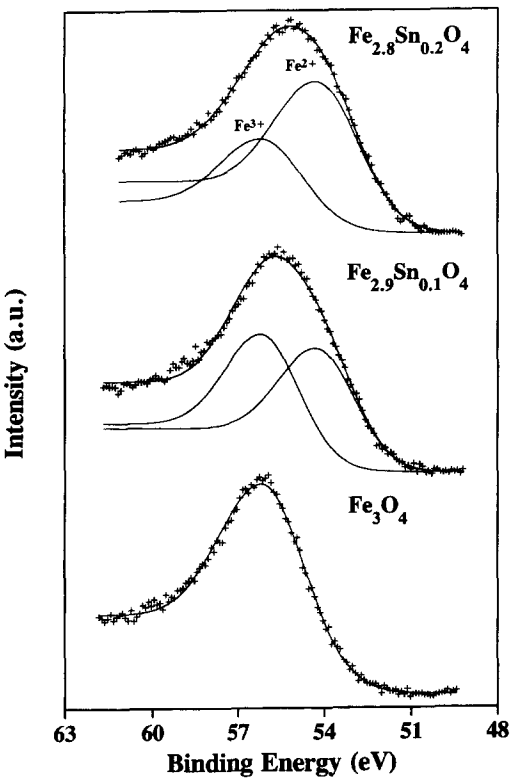

Fig. 4. Deconvolution of the Fe 3*p* X-ray photoelectron spectra recorded from Fe_3O_4, $Fe_{2.9}Sn_{0.1}O_4$ and $Fe_{2.8}Sn_{0.2}O_4$.

REFERENCES

1. Helgason, O., Gunnlaugsson, H. P., Steinflorsson, S. and Morup, S., *Hyperfine Interactions*, 1992, **70,** 981.
2. Djega-Mariadassou, C., Basile, F., Poix, P. and Michel, A., *Ann. Chim.*, 1973, **8,** 15.
3. Basile, F., Djega-Mariadossou, C. and Poix, P., *Mat. Res. Bull*, 1973, **8,** 619.
4. Berry, F. J., Helgason, O., Jonson, K. and Skinner, S. J., *J. Solid State Chem.*, 1996, **122,** 353.
5. Bauer, W. H. and Khan, A. A., *Acta Cryst.*, 1971, **B27,** 2133.
6. Welsh, I. D. and Sherwood, P. M. A., *Phys. Rev. B.*, 1989, **40,** 6386.
7. Kuivila, C. S., Butt, J. D. and Stair, P. C., *Appl. Surf. Sci.*, 1988, **32,** 99.
8. Allen, G. C., Tucker, P. M. and Wild, R. K., *Phil. Mag.*, 1982, **B46,** 411.
9. Allen, G. C., Curtis, M. T., Hooper, A. J. and Tucker, P. M., *J. Chem. Soc., Dalton Trans.*, 1974, 1525.
10. Choudhury, T., Saied, S. O., Sullivan, J. L. and Abbot, A. M., *J. Phys. D: Appl. Phys.*, 1989, **22,** 1185.
11. Wagner, C. D., Davis, L. E., Zeller, M. W., Taylor, J. A., Raymond, R. H. and Gale, L. H., *Surf. Interface Anal.*, 1981, **3,** 211.
12. Weng, L. T., Wereecke, G., Genet, M. J., Rouxhet, P. G., Stone-Masui, J. H., Bertrand, P. and Stone, W. E. E., *Surf. Interface Anal.*, 1993, **20,** 193.

Pergamon

PII: S0277-5387(97)00211-8

Polyhedron Vol. 17, No. 1, pp. 153–158, 1998
© 1997 Elsevier Science Ltd
All rights reserved. Printed in Great Britain
0277-5387/98 $19.00+0.00

Preparation and catalase-type activity of manganese(II) amino acid complexes

Michael Devereux,[a]* Maura Jackman,[a] Malachy McCann[b] and Michael Casey[b]

[a] Dublin Institute of Technology, Cathal Brugha Street, Dublin, Ireland

[b] Chemistry Department, St. Patrick's College, Maynooth, Co. Kildare, Ireland

(Received 21 January 1997; accepted 20 May 1997)

Abstract—Manganese(II) complexes of the amino acids L-leucine, glycine, L-valine, L-glutamine, L-threonine, L-tryptophan, L-phenylalanine, L-methionine, L-aspartic acid and L-glutamic acid have been prepared. The complexes have metal : acid ratios of 1 : 2. Spectroscopic, magnetic and physical data for the complexes are presented. All of the manganese complexes catalytically disproportionate hydrogen peroxide in the presence of imidazole. © 1997 Elsevier Science Ltd

Keywords: manganese(II) complexes; amino acid complexes.

Recently, a number of manganese containing non-haem catalases have been isolated and characterised [1–3], and these enzymes catalytically disproportionate hydrogen peroxide, a reaction which is important for cell detoxification. Evidence has accumulated that the active site of the pseudo-catalase isolated from *Lactobacillus plantrum* comprises two manganese ions per protein subunit [3], and currently intense efforts are being made to design and synthesise manganoenzyme mimetic complexes [4–12].

In this laboratory, previous efforts in this area have focused on the preparation, structural characterization and catalytic testing of manganese(II) carboxylates [13–18]. Herein we detail the preparation and properties of manganese(II) complexes of the amino acids L-leucine (L-leuH), glycine (glyH), L-valine (L-valH), L-glutamine (L-glnH), L-threonine (L-thrH), L-tryptophan (L-trpH), L-phenylalanine (L-pheH), L-methionine (L-metH), L-aspartic acid (L-aspH_2) and L-glutamic acid (L-gluH_2). The ability of the complexes to catalytically disproportionate hydrogen peroxide is also discussed.

RESULTS AND DISCUSSION

The complexes were synthesised using modifications of the methods previously published for the preparation of manganese(II) complexes of glycine, L-tryptophan and L-aspartic acid [19]. Synthetic routes to the manganese(II) amino acid derivatives are summarized in Scheme 1 (for complexes **1**–**8**) and Scheme 2 (for complexes **9** and **10**). The physical, analytical and IR spectral data for the complexes are given in Table 1. On the basis of microanalytical data the compounds were formulated as [Mn(L-leu)$_2$] (**1**), [Mn(gly)$_2$] (**2**), [Mn(L-val)$_2$]·1.5H_2O (**3**), [Mn(L-gln)$_2$] (**4**), [Mn(L-thr)$_2$]·H_2O (**5**), [Mn(L-phe)$_2$]·0.5 H_2O (**6**), [Mn(L-trp)$_2$]·H_2O (**7**), [Mn(L-met)$_2$]·

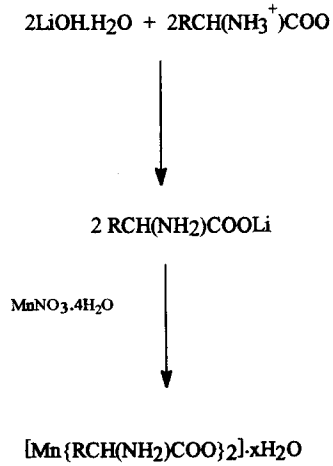

Scheme 1.

* Author to whom correspondence should be addressed.

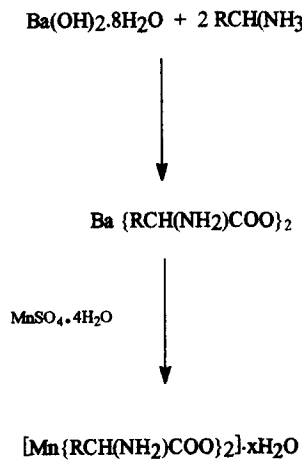

Scheme 2.

$0.5H_2O$ (**8**), $[Mn(L\text{-}aspH)_2]\cdot 3H_2O$ (**9**) and $[Mn(L\text{-}gluH)_2]\cdot 4H_2O$ (**10**), respectively.

The IR spectra of the complexes were compared with those of the free amino acids and a number of differences were noted. The characteristic bands for the amino acids and the important IR spectral bands that provide evidence for the structures of the complexes are listed in Table 2. The IR spectra of the amino acids contain broad, strong $—NH_3^+$ stretching bands in the region 3100 cm^{-1} which were replaced by several sharp bands (some of which were to higher frequencies) in the spectra of the manganese(II) complexes. Such changes are known to signify deprotonation and coordination of the $—NH_2$ groups [20]. Combination and overtone bands in the 2100 cm^{-1} region characteristic of $—NH_3^+$ groups were absent from the spectra of the complexes. Furthermore, the spectra of all of the complexes contained bands characteristic of species containing coordinated NH_2 functions [20]. In addition there were differences in the positions of the $\nu_{asym}(OCO)$ and $\nu_{sym}(OCO)$ stretching vibrations of the free acids and the complexes consistent with the coordination of the carboxyl groups (Table 2). The $\Delta(OCO)$ values for the complexes are all greater than the $\Delta(OCO)$ values found for the free amino acids (Table 2). Such increase in the value of $\Delta(OCO)$ values is indicative of monodentate coordination of the amino acidato carboxyl function [21].

Thus, from the IR data, one can deduce that the monovalent anions of the amino acids are coordinated to the metal as bidentate N,O-ligands (Fig. 1) [22]. With the exception of **5** and **8** the IR spectra of the complexes appear to posses only one Mn—N band (Table 2) which may suggest a *trans* coordination of the amino acid ligands [Fig. 1(a)] [21]. The spectra of **5** and **8** on the other hand each exhibit two possible Mn—N bands (Table 2) and thus it is possible that in these complexes the ligands are bound to the metals in a *cis*-configuration [Fig. 1(b)] [21].

The magnetic moment values for **1–10** (μ_{eff} = 5.6–6.0 B.M per Mn) are in the range expected for normal manganese(II) complexes, i.e. those lacking Mn—Mn interactions [23]. Whereas complexes **1, 6, 8–10** were found to be water soluble the others were insoluble in all common solvents suggesting that they may be polymeric in the solid state. All attempts to crystallise the soluble complexes from water were unsuccessful. Furthermore, the use of buffered solutions yielded either precipitated manganese dioxide (from basic solution) or crystals of the free amino acids (from acidic solution).

We have recently described the synthesis and structures of a series of manganese(II) carboxylate complexes, and demonstrated their ability to catalyse the disproportionation of H_2O_2 [13–18,24]. The reactivity of the present complexes as catalysts for peroxide disproportionation was investigated in the presence of the base imidazole. All of the amino acid complexes were found to be ineffective for the disproportionation of hydrogen peroxide in the absence of the added base. In the presence of added imidazole the complexes vigorously catalysed the breakdown of the peroxide. The results of these reactions are summarised in Tables 3 and 4. Examination of Table 4 shows that over the first minute of reaction complex **10** appears to be the most efficient catalyst with 2362 molecules of peroxide being disproportionated by one molecule of the complex. Complex **5** appears to be the least efficient catalyst over the first minute with one molecule of the compound knocking down 1302 molecules of the peroxide. It should be noted that the imidazole by itself causes only a very slight disproportionation of peroxide (Table 3). Such an enhancement in the rate of peroxide disproportionation in the presence of added base was also found to be the case for the manganese(II) carboxylate complexes previously synthesised in this laboratory [24]. Furthermore, similar effects have been reported previously by other workers [8,9,12,25]. It is significant that heterocyclic bases are known to be present in the vicinity of the active sites of manganoenzymes [26].

With the exception of $[Mn(\eta^1\eta^1\text{-nda})(phen)_2]\cdot EtOH\cdot H_2O$[15] ($ndaH_2$ = *cis*-5-norbornene-*endo*-2,3-dicarboxylic acid, and phen = 1,10-phenanthroline), the amino acid complexes **3, 4, 6, 7, 8** and **10** appear to be more efficient catalysts than the manganese(II) carboxylate complexes previously published by our group [13,14,16–18]. Furthermore, the performance of complexes **3, 4, 6, 7, 8** and **10** as catalysts for the disproportionation reaction appear to be superior to that of most of the binuclear manganese catalase mimetic complexes reported thus far.

EXPERIMENTAL

The amino acids were purchased from commercial sources and used without further purification. IR spectra (KBr discs) were recorded in the region 4000–400 cm^{-1} on a Nicolet Impact 400DST/IR spectrophotometer. Room temperature magnetic sus-

Table 1. Physical, analytical and IR spectral data for the manganese(II) amino acid complexes

Complex	Method	Yield %	Color	μ_{eff}	%C found	%C Calc.	%H found	%H Calc.	%N found	%N Calc.	IR data (cm^{-1})
1	1	94.5	white	5.96	45.8	45.5	7.9	8.3	8.7	8.8	3358, 3284, 2945, 2875, 1590, 1418, 1349, 1194, 1131, 1103, 1053, 997, 969, 857, 779, 703, 653, 571
2	1	92.5	pale brown	5.60	23.4	23.4	4.9	4.9	14.0	13.7	3346, 3282, 3198, 2607, 2129, 1560, 1424, 1342, 1195, 1110, 1068, 1039, 962, 899, 698, 599
3	1	84	pale brown	5.70	38.1	37.9	6.6	8.0	10.3	8.9	3430, 3149, 2882, 2628, 2108, 1602, 1595, 1510, 1461, 1381, 1328, 1271, 1180, 1138, 1110, 1054, 1018, 955, 899, 829, 780, 709
4	1	95.3	pale brown	5.90	35.2	35.5	5.3	5.8	16.1	16.1	3353, 3282, 1672, 1596, 1400, 1335, 1166, 1166, 1131, 1103, 1082, 1061, 1025, 984, 920, 892, 857, 814, 628, 579
5	1	80.3	pink	5.70	30.9	31.7	6.5	5.7	9.0	9.3	3390, 3378, 3282, 2959, 1603, 1574, 1400, 1349, 1138, 1054, 998, 941, 899, 843, 797, 599, 552
6	1	84	off-white	6.00	54.2	54.8	5.2	5.9	7.6	7.1	3358, 3272, 3029, 2938, 1596, 1503, 1408, 1328, 1096, 1054, 984, 920, 752, 702, 574, 548
7	1	69	off-white	5.69	54.4	54.6	4.6	5.5	12.2	11.6	3409, 3371, 3360, 3282, 2924, 1609, 1447, 1393, 1314, 1223, 1096, 1032, 984, 920, 808, 745, 660, 582, 516
8	1	89.5	off-white	5.70	33.5	33.1	5.9	6.4	8.5	7.7	3371. 3272, 2924, 1598, 1415, 1342, 1243, 1152, 1103, 1046, 984, 871, 787, 693, 599, 562, 528
9	2	64	white	5.97	24.9	25.6	4.8	5.4	7.1	7.5	3408, 3161, 1602, 1492, 1424, 1276, 1103, 660, 530
10	2	86	white	5.85	28.4	28.5	5.4	6.2	6.3	6.7	3408, 3112, 1584, 1417, 1342, 1089, 1007, 934, 874, 815, 779, 548

Table 2. Selected IR data (cm^{-1}) for the uncomplexed amino acids and manganese(II) complexes

Amino acid	Complex	$\nu(NH_2)$	$\nu(NH_3^+)$	$\nu_{asym}(OCO)$	$\nu_{sym}(OCO)$	$\Delta(OCO)^a$	$\nu(Mn—N)$
L-leuH			2113	1510	1400	110	
	(1)	3358, 3284		1590	1418	172	571
glyH			2113	1529	1418	111	
	(2)	3346, 3282, 3198		1560	1424	136	599
L-valH			2120	1510	1384	126	
	(3)	3430, 3149		1595	1381	214	599
L-glnH			2040	1584	1486	98	
	(4)	3380, 3403		1596	1400	196	579
L-thrH			2046	1603	1480	123	
	(5)	3309, 3272		1603	1400	203	599, 552
L-pheH			2156	1567	1412	155	
	(6)	3358, 3272		1596	1408	188	574
L-trpH			2076	1609	1412	197	
	(7)	3409, 3371, 3360		1609	1393	216	516
L-metH			2113	1588	1412	176	
	(8)	3371, 3272		1598	1415	183	562, 528
L-aspH$_2$			2101	1516	1430	86	
	(9)	3408, 3161		1602	1424	178	530
L-gluH$_2$			2076	1523	1430	93	
	(10)	3408, 3112		1584	1417	167	548

$^a\Delta(OCO) = \nu_{asym}(OCO) - \nu_{sym}(OCO)$

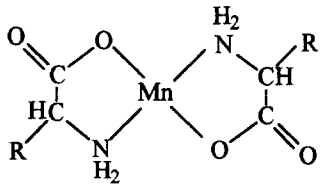

(a)

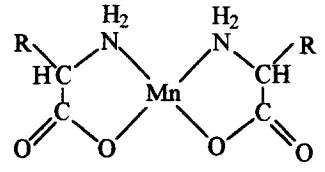

(b)

Fig. 1. Possible binding modes of the amino acid ligands in the bis(amino acid)manganese(II) complexes: (a) *trans*-configuration, (b) *cis*-configuration.

ceptibility measurements were made using a Johnson Matthey Magnetic Susceptibility Balance ($\mu_{eff} \pm 0.2$ B.M.) and $Hg[Co(SCN)_4]$ was used as a reference standard. Elemental analyses were carried out by the Microanalytical Laboratory, University College Cork, Ireland. The complexes were prepared using the methods described below.

Method 1

$LiOH \cdot H_2O$ (5.50 mmol) was dissolved in ethanol (70 cm^3) and any undissolved material was removed by gravimetric filtration. The amino acid (5.90 mmol) was then added to the filtrate and the solution was refluxed for 1.5 h. To the solution was added $Mn(NO_3)_2 \cdot 4H_2O$ (2.70 mmol) and refluxing was continued for a further 1.5 h. The resulting suspension was cooled to room temperature and the solid product was filtered off, washed with ethanol and air-dried at *ca* 25°C.

Method 2

To a solution of $Ba(OH)_2 \cdot 8H_2O$ (8.0 mmol) in water (90 cm^3) was added the amino acid (16 mmol) and the solution was stirred at room temperature for 2 h. The resulting solution was filtered and the supernatant was evaporated to *ca* 20 cm^3. To the supernatant was added ethanol (10 cm^3) to give a white suspension of the barium salt of the respective amino

Table 3. Time course of O_2 evolution in H_2O_2 disproportionation by the complexes (in the presence of added imidazole) at 25°C

Complex	Mass (mg)	Oxygen evolved (ml) and time (min) 1	2	5	10	15	20	30	40	50	60
(1)	10.1	609	707	818	930	988	1003	1028	1066	1098	1214
(2)	10.1	1071	1092	1133	1168	1188	1203	1221	—	—	—
(3)	9.8	640	742	886	942	980	1018	1074	1118	—	—
(4)	10.2	569	698	847	909	953	986	1038	1077	1110	—
(5)	9.9	506	601	729	800	855	888	946	933	1029	1058
(6)	10	430	523	687	808	898	932	990	1020	1061	1091
(7)	10.6	467	576	694	802	858	898	961	1017	1054	1083
(8)	10	540	670	814	945	992	1035	1099	1140	1159	—
(9)	10	620	785	925	1059	1128	1169	1222	1258	—	—
(10)	10	685	783	807	872	918	974	1004	1062	1105	1143
imidazole	50	4	12	29	35	—	—	—	—	—	—

Table 4. Molecules of H_2O_2 disproportionated by the complexes

Complex	Total No. of Molecules of H_2O_2 disproportionated by one molecule of complex	Molecules of H_2O_2 disproportionated during first min by one molecule of the complex
(1)	3210	1565
(2)	2028	1778
(3)	2951	1689
(4)	3091	1584
(5)	2720	1302
(6)	3519	1387
(7)	4024	1736
(8)	3436	1602
(9)	3861	1903
(10)	3939	2362

acid and this was concentrated to dryness. The solid was washed with ethanol and air-dried at *ca* 25°C.

To a solution of the amino acid barium salt (8 mmol) in water (60 cm^3) was added a solution of $MnSO_4 \cdot H_2O$ (8 mmol) in water (20 cm^3) and the resulting suspension was stirred, at room temperature, for 2 h. The solid was filtered off and the supernatant was evaporated to *ca* 25 cm^3. To the supernatant was added ethanol (10 cm^3) to give a suspension and this was concentrated to dryness, yielding a solid. The solid was washed with ethanol and air-dried at *ca* 25°C for several days.

Hydrogen peroxide disproportionation studies

To a solid sample (*ca* 10 mg) of the manganese complex was added aqueous H_2O_2 (35% w/w, 5 cm^3, 57 mmol). The mixture was stirred and thermostated at 25°C, and the evolved O_2 was measured volumetrically (volume $\pm$ 0.10 cm^3). In cases where imidazole (50 mg) was added this was introduced into the reaction vessel before the addition of H_2O_2.

Acknowledgements—M.D. thanks Noel O'Reilly (D.I.T.) for technical assistance, and M.J. acknowledges the S.R.D. funding scheme (D.I.T.) for financial assistance.

REFERENCES

1. Kono, Y. and Fridovich, I., *J. Biol. Chem.*, 1983, **258,** 6015.
2. Algood, G. S. and Perry, J. J., *J. Bacteriol.*, 1986, **168,** 563.
3. Barynin, V. V., Grebenko, A., *Dokl. Akad. Nauk. S. S. S. R.*, 1986, **286,** 461.
4. Sakiyama, H., Okawa, H. and Suzuki, M., *J. Chem. Soc., Dalton Trans.*, 1993, 3823.
5. Sakiyama, H., Okawa, H. and Suzuki, M., *J. Chem. Soc., Chem. Commun.*, 1993, 882.
6. Higuchi, C., Sakiyama, H., Okawa, H., Isobe, R.

and Fenton, D. E., *J. Chem. Soc., Dalton Trans.*, 1994, 1097.
7. Nagata, T., Ikawa, Y. and Maruyama, K., *J. Chem. Soc., Chem. Commun.*, 1994, 471.
8. Naruta, Y. and Maruyama, K., *J. Am. Chem. Soc.*, 1991, **113,** 3595.
9. Naruta, Y. and Sasayama, M., *J. Chem. Soc., Chem. Commun.*, 1994, 2667.
10. Bossek, U., Saher, M., Weghermuller, T. and Wieghardt, K., *J. Chem. Soc., Chem. Commun.*, 1992, 1780.
11. Larson, E. J. and Pecoraro, V. L., *J. Am. Chem. Soc.*, 1991, **113,** 7809.
12. Larson, E. J. and Pecoraro, V. L., *J. Am. Chem. Soc.*, 1991, **113,** 3810.
13. Casey, M. T., McCann, M., Devereux, M., Curran, M., Cardin, C., Convery, M., Quillet, V. and Harding, C., *J. Chem. Soc., Chem. Commun.*, 1994, 2643.
14. Devereux, M., McCann, M., Casey, M. T., Curran, M., Ferguson, G., Cardin, C., Convery, M. and Quillet, V., *J. Chem. Soc., Dalton Trans.*, 1995, 771.
15. Devereux, M., Curran, M., McCann, M., Casey, M. T. and McKee, V., *Polyhedron*, 1995, **14,** 2247.
16. Devereux, M., Curran, M., McCann, M., Casey, Rev. M. T. and McKee, V., *Polyhedron*, 1996, **15,** 2029.
17. McCann, M., Casey, Rev. M. T., Devereux, M., Curran, M., Cardin, C. and Todd, A., *Polyhedron*, 1996, **15,** 2117.
18. McCann, M., Casey, Rev. M. T., Devereux, M., Curran, M., Cardin, C. and McKee, V., *Polyhedron*, 1996, **15,** 2321.
19. Berezina, L. P., Pozigun, A. I. and Misyurenko, V. L., *Russ. J. Inorg. Chem.*, 1970, **15,** 1244.
20. Nakamoto, K., *Infrared and Raman Spectra of Inorganic and Coordination Compounds*, 3rd edn., Wiley, New York (1978).
21. Chow, S. T. and McAuliffe, C. A., *Prog. Inorg. Chem.*, 1975, **19,** 51.
22. Abdel-Rahman, L. H. and Battaglia, L. P., *Polyhedron*, 1996, **15,** 327.
23. Cotton, F. A. and Wilkinson, G. K., *Advanced Inorganic Chemistry*, p. 702, 5th edn., Wiley, New York (1988).
24. Devereux, M., McCann, M., Curran, M. and Casey, M., *Irish patent*, I. P. A. No. S940892.
25. Balasubramanian, P. N., Schmidt, E. S. and Bruice, T. C., *J. Am. Chem. Soc.*, 1987, **109,** 7865.
26. Larson, E. J. and Pecoraro, V. L., *Manganese Redox Enzymes*, ch. 1 and refs therein, Ed. V. L. Pecoraro, VCH, New York (1992).

Pergamon

PII: S0277-5387(97)00208-8

Polyhedron Vol. 17, No. 1, pp. 159–161, 1998
© 1997 Elsevier Science Ltd
All rights reserved. Printed in Great Britain
0277-5387/98 $19.00+0.00

Correlation between solid state and solution data in some substituted bis-1,10 phenanthroline cuprous complexes

Walter Zamudio*, Ruth Baraona and Marcelo Campos

* Facultad de Ciencias Físicas y Matenráticas, Universidad de Chile, Casilla 2777, Santiago, Chile

Facultad de Ciencias, Universidad de Chile, Casilla 653, Santiago, Chile

(Received 6 February 1997; accepted 15 May 1997)

Abstract—The values of the first formation constant are reported for some substituted bis(1,10-phenanthroline)Cu^{I} complexes in dimethylsulfoxide. The formation constant increases along the series 5 Cl phen < phen < 5,6 diCH_3 phen < 3,4,7,8 tetraCH_3 phen. A lineal correlation is found between formation constant or acidity constant of the substituted phenanthroline with the vibration frequency of the Cu—N bond. © 1997 Elsevier Science Ltd

Keywords: cuprous complexes; 1,10 phenanthroline; formation constant.

Some years ago we reported that the substituents on the coordinated ligand affects the rate of oxidation of the corresponding bis-(1,10-phenanthroline) copper(I) complexes.

The changes in the oxidation rates are attributed to the electronic effect of the substituents. Therefore, the methyl groups increases the oxidation rate whereas the chlorine group decreases the rate of the reaction in such a way that these effects can be correlated with the basicity of the complexing agent by using the Hammett linear free energy relationship [1].

The stepwise instability constants of bis(1,10-phenanthroline)Cu^{I} complex in dimethysulfoxide (DMSO) are so small, $-\log K_1 = 5.56$ and $-\log K_2 = 5.44$, at 23°C that the optical data can be used to obtain the first instability constant ($-\log K_1^* = 5.53$) omitting the second dissociation step [2]. Only the partial formation constants of bis(2,9-Dimethyl-1,10-phenanthroline)Cu^{I} complex has been reported in aqueous solution [3].

EXPERIMENTAL

Dimethylsulfoxide was purified and dried by standard methods and stored in a deoxigenated, dried, N_2 atmosphere. The purified DMSO contained H_2O of concentration in 10^{-2}–10^{-3} mol dm^3 range as found by using Karl–Fischer reagent. The substituted phenanthrolines were obtained from Aldrich Chem Co. All the cuprous complexes were prepared in an inert atmosphere by the technique described by Schilt and Taylor [4].

A Unicam SP8000 Spectrophotometer with a thermostatted cell compartment and quartz cell (1.0 cm) was used to measure the optical density at 23°C.

RESULTS AND DISCUSSION

Spectrophotometric determination

The dissociation of the substituted bis(1,10-phenanthroline)copper^{I} complex, $Cuph_2$, in solution may be represented by the following equations:

$$Cuph_2 \overset{K_1}{\rightleftharpoons} Cuph + ph \quad (1)$$

$$Cuph \overset{K_2}{\rightleftharpoons} Cu + ph \quad (2)$$

Where the solvent and the charge on the particles are omitted. Considering that K_2 value is very small it is possible to use the optical density data of the

* Author to whom all correspondence should be addressed.

Table 1. First formation constant of substituted bis-(1,10-phenanthroline)Cu^{I} complexes in dimethylsulfoxide at 23°C

	ε ($mol^{-1}\,dm^3\,cm^{-1}$)	λ nm	$10^6\,K_1^*$ ($mol\,dm^{-3}$)	$\log \beta_1^*$	ν(Cu—N)[a] (cm^{-1})
$Cu(5Clphen)_2^+$	6786	451	5.24	5.28	280
$Cu(1,10\text{-phen})_2^+$	7200[b]	445	2.95	5.53	288
$Cu(5,6DiMe\text{-phen})_2^+$	7636	450	1.25	5.9	301
$Cu(3,4,7,8\,tetraMephen))_2^+$	9056	436	0.66	6.18	306

[a] Asymmetric copper–nitrogen stretching vibrations reported in Ref. [5].
[b] Ref. [8].

$Cuph_2$ complex to calculate a K_1^* value omitting the second dissociation (2). Then $K_1 \sim K_1^*$.

$$K_1^* = \frac{[Cuph][ph]}{[Cuph_2]} \tag{3}$$

The analytical concentration of copper $[Cu]_A$, and substituted 1,10-phenanthroline, $[ph]_A$, are represented by eqs (4) and (5)

$$[Cu]_A = [Cuph_2] + [Cuph] \tag{4}$$

$$[ph]_A = [ph] + [Cuph] + 2[Cuph_2] \tag{5}$$

The equilibrium concentration necessary to calculate K_1^* with eq. (3) can be evaluated by using eqs 4, 5, 6 and 7.

$$\varepsilon_{Cuph2}[Cuph_2] = O.D. \tag{6}$$

$$[Cuph] = [ph] = [Cuph_2]_A - [Cuph_2] \tag{7}$$

Where ε_{Cuph_2} corresponds to the molar absorptivity of the $Cuph_2$ complex at λ (wavelength) in the visible spectral range and O.D. corresponds to the optical density.

Table 1 gives the average value of the first dissociation constant K_1^* (formation constant $\log \beta_1^* = -\log K_1^*$) at 23°C in dimethylsulfoxide of substituted bis(1,10-phenanthroline) cuprous complexes and its maximum molar absorptivity at λ.

Let us consider the dissolution process of a solid phase of the $Cuph_2ClO_{4(s)}$ complex, in a solvent S in several steps.

$$Cuph_2ClO_{4(S)} \xrightarrow{S} [S]Cuph_2ClO_4 \tag{8}$$

$$[S]Cuph_2ClO_4 \rightarrow [S]Cuph_2^+ + [S]ClO_4^- \tag{9}$$

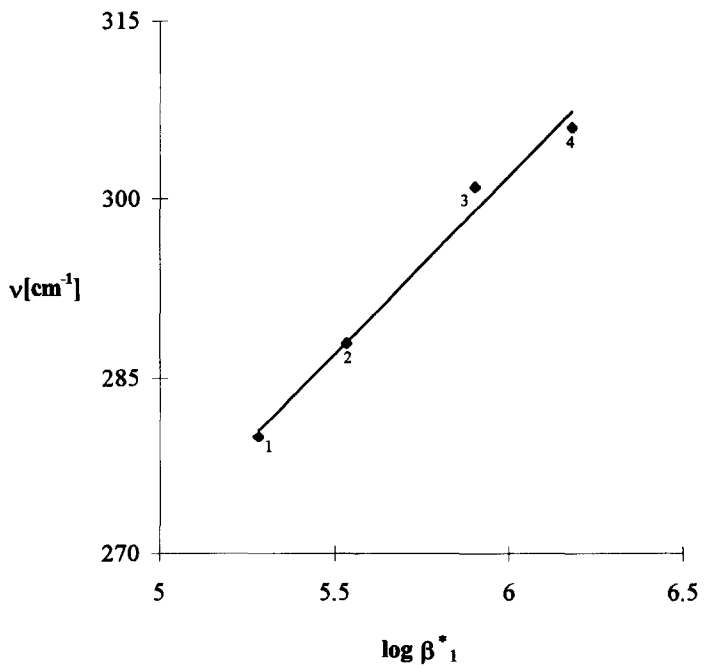

Fig. 1. Dependence of IR vibration frequency of the Cu—N bond on the log of the first formation constant β_1^* of the cuprous complexes obtained from substituted 1,10-phenanthroline. (1): 5 Cl phen; (2): phen; (3): 5,6 dimethylphen; (4): 3,4,7,8 tetramethylphen.

$$[S]Cuph_2^+ \overset{K_1}{\rightleftharpoons} [S]Cuph(S)^+ + [S]ph \qquad (10)$$

Where [S] corresponds to a solvent with a weak interaction with a neutral particle or with an ion, (S) correspond to a coordinated solvent molecule with the cuprous ion.

Reactions 8 and 9 correspond to a simple dissolution process but reaction 10 is concerned with a breaking Cu—N bond process and the formation of the Cu—S bond.

The strength of the Cu—N bond in the solid phase is related to the vibration frequency that changes to a ν' value owing to the solvation process of $Cuph_2^+$ ion complex in the solution. In a series of cuprous complexes obtained from a family of complexing agents like the substituted phenanthroline it is possible to assume similar perturbation value. We should expect therefore that for a greater Cu—N bond strength, related with ν, the dissociation constant to form $Cuph(S)^+$ ion complex should be smaller. It should be possible to find a correlation between ν and the dissociation constant if the free energy variation of reaction 10 is the greater one.

Figure 1 shows that there is a roughly lineal relationship between the I.R. vibration frequency of the Cu—N bond [5] and log β_1^*. A similar linear plot is found between ν and the acidity constants of the substituted, 1,10-phenanthroline [6] but the ν frequency of the cuprous complexes related to 4,7 dimethyl and 5-methyl phenanthroline, 282 and 284 cm^{-1}, respectively, does not follow this trend because they have lower frequencies than with the unsubstituted phenanthroline (288 cm^{-1}).

A more elegant approach can be designed with a Born–Haber cycle, but there is no available gas-phase reaction values to carry out the calculation.

Bond distance is the other magnitude that it is possible to obtain from the crystallographic data in the solid phase. In spite of the Cu—N distance in bis-(1,10-phenanthroline)Cu^I complex has been reported, 2.045 Å [7], our attempts to form X-ray quality crystals of the cuprous complexes with substituted phenanthrolines failed.

Acknowledgements—The authors thank the Research Commission of the University of Chile for financial support (DTI project 1966 and Fondecyt project 1950397).

REFERENCES

1. Arce, J., Spodine, E. and Zamudio, W., *J. Inorg. Nucl. Chem.*, 1976, **18,** 2029.
2. Zamudio, W. and García, A., *Trans. Met. Chem.*, 1986, **11,** 422.
3. Lei, Y. and Anson, F. C., *Inorg. Chem.*, 1995, **34,** 1083.
4. Schilt, A. and Taylor, A., *J. Inorg. Nucl. Chem.*, 1959, **9,** 211.
5. Campos, M., Clavijo, R., Mendizabal, F., Zamudio, W., Baraona, R. and Díaz, G., *Vib. Spectros.*, 1996, **12,** 37.
6. McBride, W. A., IUPAC. Chemical Data Lines No 17 Pergamon Press, Oxford, 1978.
7. Healy, P. C., Engelhardt, L. and White, A. H., *J. Chem. Soc. Dalton Trans*, 1985, 2541.
8. Zamudio, W. and Garcia, A., *Bol. Soc. Chil. Quím.*, 1992, **37,** 273.

Pergamon

PII: S0277-5387(97)00192-7

Polyhedron Vol. 17, No. 1, pp. 163–171, 1998
© 1997 Elsevier Science Ltd
All rights reserved. Printed in Great Britain
0277-5387/98 $19.00+0.00

Synthesis and characterization of some unique heterocyclic derivatives containing aluminium(III) atoms in different coordination states—4. Reaction of bis(β-diketonato) aluminium(III)-di-μ-isopropoxo-di-isopropoxo aluminium(III) with 8-hydroxyquinoline

Anita Dhammani, Rakesh Bohra* and Ram C. Mehrotra

Department of Chemistry, University of Rajasthan, Jaipur 302004, India

(Received 5 March 1997; accepted 14 May 1997)

Abstract—Reactions of bis(β-diketonato)aluminium(III)-di-μ-isoproxo-di-isopropoxo aluminium(III), $[(CH_3COCHCOR)_2Al(\mu\text{-}OPr^i)_2Al(OPr^i)_2]$ with 8-hydroxyquinoline, C_9H_6NOH in 1 : 1 and 1 : 2 molar ratios, have resulted in the synthesis of $[(CH_3COCHCOR)_2Al(\mu\text{-}OPr^i)_2Al(ONC_9H_6)(OPr^i)]$ and $[(CH_3COCHCOR)_2Al(\mu\text{-}OPr^i)_2Al(ONC_9H_6)_2]$, respectively. These are soluble in a variety of organic solvents (e.g. benzene, chloroform and dimethylsulfoxide), except $[(CH_3COCHCOCH_3)_2Al(\mu\text{-}OPr^i)_2Al(ONC_9H_6)_2]$ and $[(CH_3COCHCOOC_2H_5)_2Al(\mu\text{-}OPr^i)_2Al(ONC_9H_6)_2]$, which are insoluble in benzene but soluble in chloroform and dimethylsulfoxide. These derivatives show dinuclear behaviour in chloroform. Plausible structures have been proposed on the basis of elemental analyses, molecular weight measurements, IR and NMR (^1H, ^{13}C and ^{27}Al) spectral studies. ^{27}Al NMR spectra show the presence of six and four/five coordinated aluminium sites.
© 1997 Elsevier Science Ltd

Keywords: heterocyclic derivatives; bis(β-diketonato)aluminium(III)-di-μ-isopropoxo-di-isopropoxo aluminium(III); aluminium(III)isopropoxide; 8-hydroxyquinoline; ^{27}Al NMR spectra; coordination states.

8-Hydroxyquinoline behaves as a strong bidentate chelating ligand with aluminium(III) [1–3] in its compounds.

In continuation with our interest in the reactivity of $[(CH_3COCHCOR)_2Al(\mu\text{-}OPr^i)_2\ Al(OPr^i)_2]$ derivatives with various ligands containing hard [4,5] or/and soft [6] donor atoms, the present work deals with the reaction of $[(CH_3COCHCOR)_2Al(\mu\text{-}OPr^i)_2Al(OPr^i)_2]$ with C_9H_6NOH in 1 : 1 and 1 : 2 molar ratios.

RESULTS AND DISCUSSIONS

The reactions of $[Al(CH_3COCHCOR)(OPr^i)_2]_2$ with 8-hydroxyquinoline in 1 : 1 and 1 : 2 molar ratios in refluxing benzene, can be represented by the following equation:

$$[Al(CH_3COCHCOR)(OPr^i)_2]_2 + xC_9H_6NOH \xrightarrow[\text{Reflux}]{\text{Benzene}}$$

$$[(CH_3COCHCOR)_2Al(\mu\text{-}OPr^i)_2$$

$$Al(ONC_9H_6)_x(OPr^i)_{2-x}] + xPr^iOH\uparrow$$

($x = 1$ or 2 and R = $-CH_3$, $-C_6H_5$ and $-OC_2H_5$)

These reactions are facile and pushed to completion by fractionating out azeotropically the liberated isopropanol which was estimated. The analytical data of these complexes support the stoichiometry assigned to these compounds. All these derivatives are hygroscopic, bright yellow solids, soluble in a variety of organic solvents (e.g. benzene, chloroform and dimethylsulfoxide), except $[(CH_3COCHCOCH_3)_2 Al(\mu\text{-}OPr^i)_2\ Al(ONC_9H_6)_2]$ and $[(CH_3COCHCOOC_2$

* Author to whom correspondence should be addressed.

$H_5)_2Al(\mu\text{-}OPr^i)_2$ $Al(ONC_9H_6)_2]$, which are insoluble in benzene but soluble in chloroform and dimethylsulfoxide. These derivatives show dinuclear behaviour in chloroform and can be recrystallised unchanged from dichloromethane and n-hexane mixture.

IR spectra

The tentative assignments of some of the important bands have been made and are recorded in Table 1.

The broad stretching vibration at $\sim 3242\ cm^{-1}$ due to —O—H group of the free 8-hydroxyquinoline ligand was found to be absent in all these derivatives, suggesting the formation of Al—O bond with the 8-hydroxyquinolinate moiety. The single peak observed at $1586\ cm^{-1}$ in the free 8-hydroxquinoline due to ν(C=C)/ν(C=N) vibrations is found to split into two sharp peaks in the regions 1600–1605 and 1565–1598 cm^{-1} in all these derivatives, probably as a result of augmentation [2] of the ν(C=N) which was previously hidden in the ring C=C vibration. This appears to suggest that the lone pair on nitrogen is also involved in the formation of a coordinate bond with aluminium(III), leading to a reduction in the double bond character of the C=N bond and appearance of two sharp peaks as compared to the free ligand. Thus it may be assumed that the 8-hydroxyquinolinate moiety, in all these complexes is behaving as a bidentate chelating ligand.

The shifting of ν(C···O) of β-diketonate moiety towards lower wave numbers (at 1530–1540 cm^{-1}) as compared to the free ligand and the presence of a strong band at 1500–1505 cm^{-1} due to C···C stretching vibrations, appear to indicate bidentate quasi-aromatic nature of β-diketonate moiety [7].

The C—O stretching vibrations of the bridging isopropoxy groups were observed in region 1000–1009 cm^{-1}. The weak absorption at 750–759 cm^{-1} may be ascribed [8] to Al—O—Al stretching vibrations. Bands in the lower region 700–450 cm^{-1} may be arising [8] due to Al—O and Al—N stretching vibrations.

^{1}H *NMR spectra*

Characteristic chemical shifts of these derivatives are given in Table 2. The signal due to hydroxy proton of the free 8-hydroxyquinoline (QOH) ligand at δ 8.45 ppm (Table 2) is found to be absent in all these complexes, indicating the formation of Al—O bond by deprotonation of the 8-hydroxquinoline ligand.

The signal due to CH(2) ring proton at δ 8.30 ppm in the spectra of 8-hydroxyquinoline undergoes an upfield shift at δ 8.18–8.30 ppm in these complexes, suggesting coordination of nitrogen to aluminium. The doublet at δ 8.92 ppm in the spectra of free QOH ligand undergoes an upfield shift at δ 8.64–8.81 ppm.

The methyl and methine signals of the bridging isopropoxy group present in the derivative, $[(CH_3CO\text{-}CHCOR)_2Al(\mu\text{-}OPr^i)_2Al(ONC_9H_6)_2]$ appear at δ 1.18–1.21 and δ 4.05–4.09 ppm, respectively. In the case of $[(CH_3COCHCOR)_2Al(\mu\text{-}OPr^i)_2Al(ONC_9H_6)(OPr^i)]$ the methine protons of the terminal and the bridging isopropoxy groups were observed at δ 3.53–4.02 and δ 4.02–4.51 ppm, respectively, while the corresponding methyl protons appeared in the region δ 1.18–1.21 ppm (Table 2).

The methyl and methine signals of the β-diketonate moiety appear at δ 1.88–2.15 and δ 4.92–6.30 ppm, respectively, in all these complexes. The methylene protons of the ethylacetylacetate moiety appeared in the range δ 3.92–3.98 ppm and the aromatic protons of the benzoylacetone moiety are observed in the region δ 6.93–7.69 ppm.

^{13}C *NMR spectra*

The ^{13}C NMR chemical shifts of these compounds and the free QOH ligand were recorded in chloroform at ambient temperature (Table 3).

In all these complexes, both the C(8) and C(9) carbons of the 8-hydroxyquinoline moiety are slightly shifted as compared to the corresponding signals present in the free QOH ligand. The other aromatic carbons of the QOH and benzoylacetone moieties were observed in the range δ 110.40–138.99 ppm.

Methyl carbons of the terminal and bridging isopropoxy groups are observed at δ 24.92–25.13 and δ 25.52–26.02 ppm, respectively. While the methine carbons of the terminal and bridging isopropoxy groups are observed at δ 59.70–63.66 and δ 63.71–64.74 ppm, respectively. In the case of $[(CH_3CO\text{-}CHCOR)_2Al(\mu\text{-}OPr^i)_2Al(ONC_9H_6)_2]$, only a single peak at δ 25.34–26.00 and δ 63.55–65.01 ppm, corresponding to the methyl and methine carbons of the bridging isopropoxy groups have been observed.

The carbonyl carbons of the β-diketonate moiety appear at δ 183.62–193.40 ppm, while that of ester group, at δ 170.58–174.60 ppm. The methyl and methine carbons of the β-diketonate moiety have been observed at δ 24.24–27.36 and δ 85.22–100.71 ppm, respectively. The methyl and methylene carbons of $—OCH_2CH_3$ group of the ethylacetylacetate moiety are observed at δ 14.30–14.41 and δ 60.79–60.81 ppm, respectively.

^{27}Al *NMR spectra*

The ^{27}Al NMR spectrum of $[(CH_3COCHCO\ CH_3)_2Al(\mu\text{-}OPr^i)_2Al(ONC_9H_6)(OPr^i)]$ at 23.79 MHz in benzene (25°C) exhibits an unresolved signal at δ 0.79 ppm. No further resolution of this signal could be observed even after varying the temperature.

Since the chemical shift value depends on the field strength, ^{27}Al NMR spectra of some of these representative derivatives have been recorded at 78.16 MHz in toluene (Table 4). The ^{27}Al NMR spectra of $[(CH_3COCHCOR)_2Al(\mu\text{-}OPr^i)_2Al(ONC_9H_6)(OPr^i)]$

Table 1. IR spectral data (cm^{-1}) of $[(CH_3COCHCOR)_2Al(\mu\text{-}OPr^i)_2Al(ONC_9H_6)(OPr^i)]$ and $[(CH_3COCHCOR)_2Al(\mu\text{-}OPr^i)_2Al(ONC_9H_6)_2]$

S. No.	Compound	β-Diketonate moiety		Isopropoxy group	8-Hydroxyquinolinate moiety			
		ν(C···O)	ν(C···C)	ν(C—O)	ν(O—H)	ν(C···C)/ν(C···N)	ν(Ar—O)	ν(Al—O—Al)
1	Ligand C_9H_6NOH	—	—	—	3242br	1586s	1090m	—
2	$[(CH_3COCHCOCH_3)_2Al(\mu\text{-}OPr^i)_2Al(ONC_9H_6)(OPr^i)]$	1540s	1505s	1000m	—	1605s/1579s	1125m	755w
3	$[(CH_3COCHCOCH_3)_2Al(\mu\text{-}OPr^i)_2Al(ONC_9H_6)_2]$	1538s	1504s	1005m	—	1603s/1598s	1122m	755w
4	$[(CH_3COCHCOC_6H_5)_2Al(\mu\text{-}OPr^i)_2Al(ONC_9H_6)(OPr^i)]$	1530s	1502s	1000m	—	1600s/1565s	1123m	750w
5	$[(CH_3COCHCOC_6H_5)_2Al(\mu\text{-}OPr^i)_2Al(ONC_9H_6)_2]$	1540s	1500s	1005m	—	1600s/1570s	1130m	756w
6	$[(CH_3COCHCOOC_2H_5)_2Al(\mu\text{-}OPr^i)_2Al(ONC_9H_6)(OPr^i)]$	1532s	1500s	1006m	—	1602s/1570s	1123m	759w
7	$[(CH_3COCHCOOC_2H_5)_2Al(\mu\text{-}OPr^i)_2Al(ONC_9H_6)_2]$	1536s	1500s	1009m	—	1600s/1578s	1123m	751w

s = strong, m = medium, w = weak.

Table 2. ^{1}H NMR spectral data (δ ppm) of $[(CH_3COCHCOR)_2Al(\mu\text{-}OPr^i)_2Al(ONC_9H_6)(OPr^i)]$ and $[(CH_3COCHCOR)_2Al(\mu\text{-}OPr^i)_2Al(ONC_9H_6)_2]$

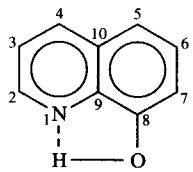

Compound[a]	β-Diketonate moiety				Isopropoxy group					
	—CH_3 att. to —OCH_2—	—CH_3	—OCH_2—	—CH<	—CH_3	—OCH<	CH(2)	—O—H	CH(7)	Other aromatic protons
1	—	—	—	—	—	—	8.30, d(1H)	8.45, br(1H)	8.92, d(1H)	7.24–7.69, m(4H)
2	—	2.01, s(12H)	—	5.52, s(2H)	1.18, d(18H)	3.53; 4.02, m(3H)	8.26, d(1H)	—	8.67, d(1H)	6.93–7.64 m(4H)
3	—	2.01, s(12H)	—	5.57, s(2H)	1.21, d(12H)	4.05, m(2H)	8.18, d(2H)	—	8.72, d(2H)	7.06–7.68, m(8H)
4	—	2.15, s(6H)	—	6.30, s(2H)	1.21, d(18H)	4.02; 4.51, m(3H)	8.25, d(1H)	—	8.81, d(1H)	7.06–7.69, m(16H)
5	—	2.14, s(6H)	—	6.30, s(2H)	1.18, d(12H)	4.05, m(2H)	8.27, d(2H)	—	8.81, d(2H)	7.06–8.05, m(20H)
6	1.32, u(6H)	1.83, s(6H)	3.98, u(4H)	4.92, s(2H)	1.21, d(18H)	3.89; 4.07, m(3H)	8.30, d(1H)	—	8.72, d(1H)	6.93–7.64, m(4H)
7	1.30, u(6H)	1.88, s(6H)	3.92, u(4H)	4.96, s(2H)	1.18, d(12H)	4.09, m(2H)	8.18, d(2H)	—	8.64, d(2H)	7.20–7.69, m(8H)

[a] Compound numbers as in Table 1.

s = singlet, d = doublet, m = multiplet, br = broad, u = unresolved.

Table 3. ^{13}C NMR spectral data (δ ppm) of $[(CH_3COCHCOR)_2Al(\mu\text{-}OPr^i)_2Al(ONC_9H_6)(OPr^i)]$ and $[(CH_3COCHCOR)_2Al(\mu\text{-}OPr^i)_2Al(ONC_9H_6)_2]$

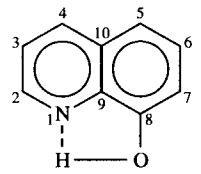

Compound[a]	β-Diketonate moiety					Isopropoxy group		C(9)	C(8)	Other aromatic carbons of $C_9H_6NOH/-C_6H_5$
	$-CH_3$ att. to $-OCH_2-$	$-CH_3$	$-OCH_2-$	$-CH<$	$>C\cdots O$	$-CH_3$	$-CH<$			
1	—	—	—	—	—	—	—	147.79	152.34	110.46, 117.78, 121.46, 126.58, 127.47, 135.98, 137.86
2	—	24.24	—	100.34	192.51	25.13, 26.02	61.18, 64.74	143.88	158.99	110.54, 117.70, 121.21, 128.30, 129.21, 130.54, 138.54
3	—	24.36	—	100.71	192.50	26.00	64.69	143.72	158.92	110.40, 117.80, 121.32, 128.20, 129.26, 130.56, 138.50
4	—	27.36	—	97.68	183.62, 193.40	24.92, 25.52	59.70, 63.71	143.91	159.89	110.70, 117.85, 121.21, 127.20, 127.80, 128.40, 129.27, 130.59, 130.94, 137.23, 138.63
5	—	27.20	—	97.62	183.63, 193.35	25.34	63.55	143.82	159.79	110.73, 117.74, 121.07, 127.25, 127.80, 128.22, 129.29, 130.58, 130.79, 137.20, 138.68
6	14.30	26.27	60.79	85.43	174.60, 187.34	24.68, 25.52	63.66, 64.20	143.91	158.91	110.73, 117.72, 121.07, 128.22, 129.19, 130.50, 138.58
7	14.41	26.29	60.81	86.22	170.58, 187.21	25.50	65.01	143.88	159.88	112.32, 117.69, 121.32, 128.31, 129.21, 130.99, 138.99

[a] Compound numbers same as in Table 1.

Table 4. ^{27}Al NMR spectral data (δ ppm) at 78.16 MHz of $[(CH_3COCHCOR)_2Al(\mu\text{-}OPr^i)_2Al(ONC_9H_6)(OPr^i)]$ and $[(CH_3COCHCOR)_2Al(\mu\text{-}OPr^i)_2Al(ONC_9H_6)_2]$

S. No.	Compound	Shift (δ)	Coordination number
1	$[(CH_3COCHCOCH_3)_2Al(\mu\text{-}OPr^i)_2Al(ONC_9H_6)(OPr^i)]$	+0.812	Hexa-coordinated
		+11.221	Penta-coordinated
2	$[(CH_3COCHCOCH_3)_2Al(\mu\text{-}OPr^i)_2Al(ONC_9H_6)_2]$	+0.787	Hexa-coordinated
		+11.421	Penta-coordinated
		+21.230	Tetra-coordinated
3	$[(CH_3COCHCOC_6H_5)_2Al(\mu\text{-}OPr^i)_2Al(ONC_9H_6)(OPr^i)]$	+2.724	Hexa-coordinated
		+12.683	Penta-coordinated
4	$[(CH_3COCHCOC_6H_5)_2Al(\mu\text{-}OPr^i)_2Al(ONC_9H_6)_2]$	+2.724	Hexa-coordinated
		+12.732	Penta-coordinated
		+21.055	Tetra-coordinated

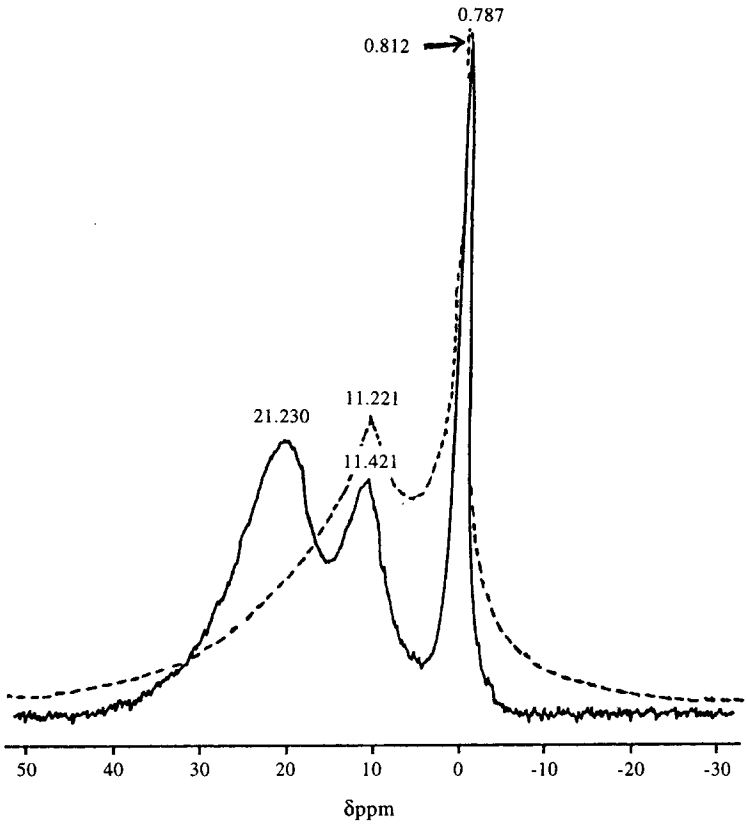

Fig. 1. ^{27}Al NMR spectra of $[(CH_3COCHCOCH_3)_2Al(\mu\text{-}OPr^i)_2Al(ONC_9H_6)(OPr^i)]$ (dotted line); $[(CH_3COCHCOCH_3)_2Al(\mu\text{-}OPr^i)_2Al(ONC_9H_6)_2]$ (dark line).

(R = —CH_3 and —C_6H_5) at 78.16 MHz exhibit two signals in the ranges at δ +0.812 to +2.724 and δ +11.221 to +12.683 ppm corresponding to six- and five-coordinated aluminium(III) atoms.

It is interesting to point out here that the ^{27}Al NMR spectra of $[(CH_3COCHCOR)_2Al(\mu\text{-}OPr^i)_2Al(ONC_9H_6)_2]$ (R = —CH_3 and —C_6H_5) at 78.16 MHz exhibit three signals in the ranges δ +0.787 to +2.724, δ +11.421 to +12.732 and δ +21.230 to +21.055 ppm, corresponding to six-, five- and four-coordinated aluminium(III) atoms.

The ^{27}Al NMR spectra of the two representative derivatives, $[(CH_3COCHCOCH_3)_2Al(\mu\text{-}OPr^i)_2Al(ONC_9H_6)(OPr^i)]$ and $[(CH_3COCHCOCH_3)_2Al(\mu\text{-}OPr^i)_2Al(ONC_9H_6)_2]$ have been shown in Fig. 1.

Although the actual structures can be established only after X-ray analysis, yet the available physicochemical data suggest that following unique structure for $[(CH_3COCHCOR)_2Al(\mu\text{-}OPr^i)_2Al(ONC_9H_6)(OPr^i)]$ derivatives, in which coordination around aluminium(III) atoms is six and five (Fig. 2).

Although, a number of references are available in

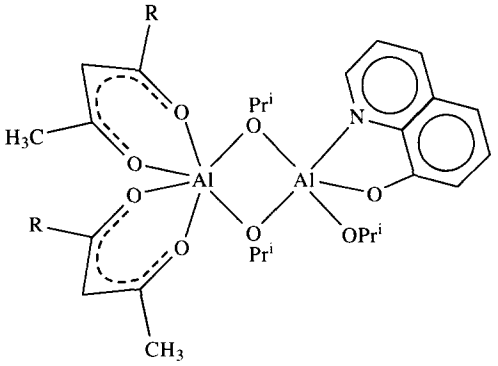

Fig. 2. Structure of $[(CH_3COCHCOR)_2Al(\mu\text{-}OPr^i)_2Al(ONC_9H_6)(OPr^i)]$ (R = —CH_3, —C_6H_5 and —OC_2H_5).

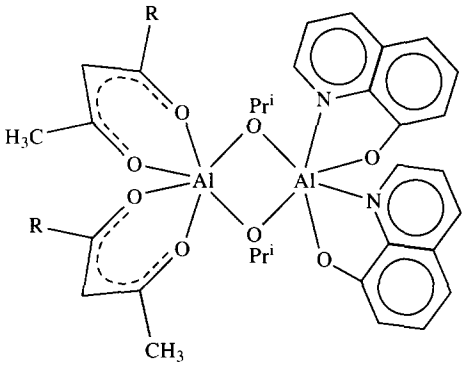

Fig. 3. Expected structure of $[(CH_3COCHCOR)_2Al\ (\mu\text{-}OPr^i)_2\ Al(ONC_9H_6)_2]$ (R = —CH_3, —C_6H_5 and —OC_2H_5).

the literature dealing with comparatively less stable penta-coordination around aluminium(III) atom, yet the above derivative, of the type $[(CH_3CO\text{-}CHCOR)_2Al(\mu\text{-}OPr^i)_2Al(ONC_9H_6)(OPr^i)]$ appears to be unique containing both hexa- and penta-coordination around aluminium(III) atoms, similar to that reported [9] for the anion, $[Al_3(OCH_2\ CH_2O)_5(OCH_2CH_2OH)_2]^{-3}$.

The structure of the corresponding 1 : 2 derivatives of the type $[(CH_3COCHCOR)_2Al(\mu\text{-}OPr^i)_2Al\ (ONC_9H_6)_2]$ is also unique. From the available physico-chemical data, excluding ^{27}Al NMR spectral studies, one would expect structure containing two hexa-coordinated aluminium(III) atoms (Fig. 3).

If the above structure is assumed for these derivatives then the ^{27}Al NMR spectra should exhibit two close peaks in octahedral range corresponding to two octahedrally coordinated aluminium(III) atoms. However, the presence of three ^{27}Al NMR signals corresponding to hexa-, penta- and tetra-coordinated aluminium(III) atoms may suggest an equilibrium of the following type (Fig. 4). This equilibrium is obviously not observed in the ^1H and ^{13}C NMR spectra of these derivatives due to differences in the timescales of these and the ^{27}Al NMR experiments carried out during the course of these investigations.

The above structures can be explained by steric hindrance around aluminium(III) atom due to the presence of two QOH moiety, which do not permit the coordination of both the nitrogen atoms simultaneously, thus resulting in the unusual five-coordination around aluminium(III), rather than stable six-coordination. In view of these interesting inferences, efforts were made to record the X-ray crystal structures of the different derivatives, but unfortunately substained efforts to obtain good quality crystals have not been successful.

EXPERIMENTAL

All the solvents used during the present investigation were of reagent grade and were made anhydrous by standard methods. Aluminium isopropoxide was prepared as described by Mehrotra [10]. Benzoylacetone, acetylacetone and ethylacetylacetate were distilled before use, while 8-hydroxyquinoline was purified by crystallization from diethylether. Isopropanol was estimated [11] by oxidation with normal $K_2Cr_2O_7$ solution in 12.5% H_2SO_4. Isopropoxy groups in the products were estimated by hydrolysing them and collecting the liberated isopropanol azeotropically with benzene. Aluminium was estimated gravimetrically as the oxinate.

Infrared spectra were recorded as Nujol mulls on a Perkin–Elmer 577 spectrophotometer in the range 4000–200 cm^{-1}. ^1H NMR spectra were recorded on a Jeol FX 90Q spectrometer in $CDCl_3$ using TMS as an internal reference. ^{13}C NMR spectral studies have been carried out in chloroform at 22.49 MHz using D_2O locks. ^{27}Al NMR spectral studies have been carried out in benzene/chloroform on a Jeol FX 90Q MHz at 23.79 MHz, using aluminium nitrate as standard reference. Some ^{27}Al NMR spectra were recorded on a varian 300 MHz at 78.16 MHz in toluene. Molecular weight measurements were carried out on a Knauer Vapour Pressure Osmometer in chloroform at 45°C temperature.

$[Al(CH_3COCHCOR)(OPr^i)_2]_2$ was prepared as reported earlier [4–6,12]. All the present mixed ligand aluminium(III) complexes were synthesized by a similar route and hence, synthesis of only one representative compound is described below.

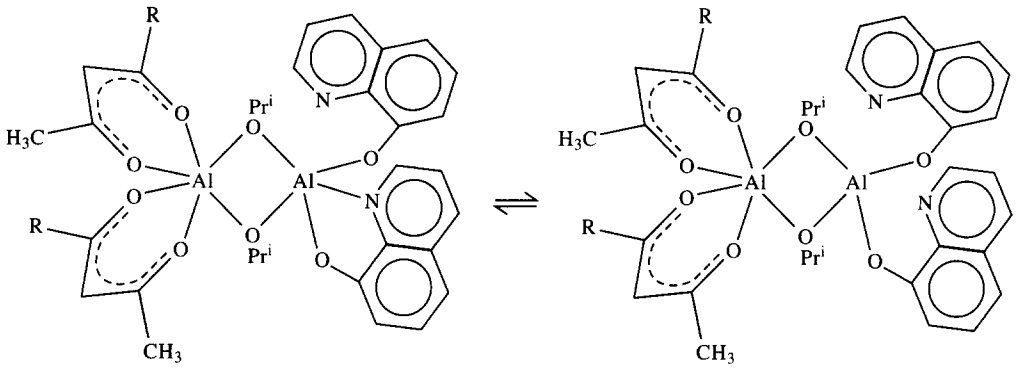

Fig. 4. Interconversion between penta- and tetra-coordination states of aluminium.

Table 5. Synthetic and analytical data of $[(CH_3COCHCOR)_2Al(\mu\text{-}OPr^i)_2Al(ONC_9H_6)(OPr^i)]$ and $[(CH_3COCHCOR)_2Al(\mu\text{-}OPr^i)_2Al(ONC_9H_6)_2]$

Reactants (g) a	b						
$[Al(CH_3COCHCOR)(OPr^i)_2]_2$	C_9H_6NOH	Molar ratio	Pr-OH (g) liberated (calcd.)	Compound[a]	Analysis % found (calcd.) Al	—OPr^i	Mol. wt found (calcd.)
1. R = —CH_3 4.68	1.39	1:1	0.56 (0.58)	2	9.39 (9.41)	30.48 (30.91)	587 (579)
2. R = —CH_3 3.35	1.99	1:2	0.80 (0.83)	3	8.06 (8.19)	17.42 (17.94)	642 (659)
3. R = —C_6H_5 3.59	0.85	1:1	0.34 (0.35)	4	7.69 (7.73)	25.10 (25.40)	686 (698)
4. R = —C_6H_5 3.15	1.49	1:2	0.61 (0.62)	5	6.82 (6.89)	14.70 (15.09)	763 (783)
5. R = —OC_2H_5 4.44	1.18	1:1	0.48 (0.49)	6	8.49 (8.52)	27.35 (27.97)	648 (634)
6. R = —OC_2H_5 530	2.81	1:2	0.84 (0.86)	7	7.49 (7.51)	16.13 (16.44)	700 (719)

[a] Compound numbers as in Table 1.

Reaction of $[Al(CH_3COCHCOCH_3)(OPr^i)_2]_2$ *with* C_9H_6NOH *in* 1 : 1 *molar ratio: synthesis of* $[(CH_3COCHCOCH_3)_2Al(\mu\text{-}OPr^i)_2Al(ONC_9H_6)(OPr^i)]$

8-Hydroxyquinoline (1.39 g, 9.58 mmol) was added in benzene solution (~70 ml) of $[Al(CH_3COCHCOR)(OPr^i)_2]_2$ (4.68 g, 9.58 mmol) and was refluxed on a fractionating column for about 3 h. The isopropanol in the reaction was fractionated out azeotropically with benzene. Progress as well as the completion of the reaction was checked by the estimation of isopropanol in azeotrope by oxidimetric method [11]. The product was found to be soluble in benzene. After stripping off the solvent under reduced pressure, a bright yellow coloured solid was obtained in good yield, which was purified by recrystallization from a mixture of dichloromethane and *n*-hexane.

Details of synthesis of other derivatives and the analytical data have been summarized in Table 5.

Acknowledgement—One of us (A.D.) thanks the C.S.I.R., New Delhi for the award of Senior Research Fellowship and R.S.I.C., Bombay for obtaining ^{27}Al NMR spectral data of some of the samples.

REFERENCES

1. Vevere, I., Maijs, L. and Reikstina, D., *Latv. PSR Zinat. Akad. Vestis Khim. Ser.*, 1970, 405; *Chemical Abstracts*, 1971, **74,** 27607 t.
2. Sonsale, A. Y., Gopinathan, S. and Gopinathan, C., *Indian J. Chem.*, 1976, **14A,** 408.
3. Kushi, Y. and Fernando, Q., *J. Am. Chem. Soc.*, 1970, **92,** 91.
4. Dhammani, A., Bohra, R. and Mehrotra, R. C., *Polyhedron*, 1995, **14,** 733.
5. Dhammani, A., Bohra, R. and Mehrotra, R. C., *Main Group Met. Chem.*, 1995, **18,** 687.
6. Dhammani, A., Bohra, R. and Mehrotra, R. C., *Polyhedron*, 1996, **15,** 733.
7. Jain, R., Rai, A. K. and Mehrotra, R. C., *Inorg. Chim. Acta*, 1987, **126,** 99.

8. Singh, A., Rai, A. K. and Mehrotra, R. C., *Indian J. Chem.*, 1973, **11,** 478.
9. Gainsford, G. J., Kemmitt, T. and Milestone, N. B., *Inorg. Chem.*, 1995, **34,** 5244.
10. Mehrotra, R. C., *J. Indian Chem. Soc.*, 1953, **30,** 585.
11. Bradley, D. C., Halim, F. M. A. and Wardlaw, W., *J. Chem. Soc.*, 1950, 3450.
12. Wengrovius, J. H., Garbauskas, M. F., Williams, E. A., Going, R. C., Donahue, P. E. and Smith, J. F., *J. Am. Chem. Soc.*, 1986, **108,** 982.

Pergamon

PII: S0277-5387(97)00209-X

Polyhedron Vol. 17, No. 1, pp. 173–178, 1998
© 1997 Elsevier Science Ltd
All rights reserved. Printed in Great Britain
0277-5387/98 $19.00+0.00

Redox chemistry of copper acetate binuclear complexes in acetic acid–methanol mixture as solvent

I. Toledo, M. Arancibia, C. Andrade and I. Crivelli*

Facultad de Ciencias, Universidad de Chile, Casilla 653, Santiago, Chile

(Received 17 February 1997; accepted 14 May 1997)

Abstract—The redox chemistry of the photochemically generated bioinorganic model $(CH_3COO)_2Cu^{II}Cu^{I}(OOCCH_3)_2$ and the parent species $(CH_3COO)_2Cu^{II}Cu^{II}(OOCCH_3)_2$ (complex **I**) are reported. The purpose is to achieve a more complete physicochemical characterization of the acetate binuclear copper complex and consequently a closer evaluation of its behaviour as a model of type III Cu sites in cuproproteins. Complex I may be sequentially reduced (broad not resolved peaks around −0.2 and −0.4 V) and reoxidized (peaks at 0.16 and 0.36 V), but in competition with a thermal disproportionation to Cu^{II} and Cu^0. Controlled potential electrolysis (CPE) at −0.4 V measures quantitatively the overall reduction process including disproportionation and involves four electrons per mole of initial complex **I**. Structural changes seem to play a role in the oxidation–reduction processes as suggested by $ip/\sqrt{v}$ *vs* v studies (Nicholson and Shain's criteria), and they make the processes irreversible. The mixed-valence Cu^{II}–Cu^{I} species could not be produced by CPE at any voltage before the second reduction peak; however, its electrochemical generation by pulses at −0.4 V render direct experimental evidence that the reduction process is sequential. The voltammograms of the Cu^{II}–Cu^{I} species generated photochemically are more complicated: the reduction and oxidation peaks are centered at −0.2 and 0.0 V, respectively. The species Cu^{II}–Cu^{II} originated from the oxidation of this mixed valence complex, called as complex **II**, shows similarities and differences with complex **I**. The results are discussed in relation to the structure stability and to the copper interactions in the binuclear species considered as models for the copper protein centers. © 1997 Elsevier Science Ltd

Keywords: copper binuclear; copper mixed-valence; copper acetate; copper electrochemistry; copper proteins model; copper redox chemistry.

The absorption spectra of the prototype dimeric copper species $(CH_3COO)_2Cu^{II}Cu^{II}(OOCCH_3)_2$ and the interaction between the copper centers in it have been studied for several years [1], however, only recently have the magnetic properties of the copper acetate bridged pyrazine dimer been properly understood and the observed 'dimer band' assigned as a *z*-polarized A_{1g}–A_{2g} acetate ligand-to-metal charge transfer [2].

Recently, we reported [3] an electron transfer study in the mixed-valence $(CH_3COO)_2Cu^{II}Cu^{I}(OOCCH_3)_2$, species |MV|, generated by UV irradiation of the Cu^{II}–Cu^{II} precursor species in acetic acid-methanol mixtures. The Cu^{II}–Cu^{II} species shows antiferromagnetic coupling [2] and the MV species shows a weak interaction between the metallic centers (class II in the Robin and Day classification [4]). The results also indicate that the symmetry of the Cu^{II} and Cu^{I} sites is similar. Otherwise, the MV complex has some characteristics in common with type III copper observed in copper oxidases in the MV state [3]. It appears interesting to determine the feasibility of generating the MV species electrochemically, since this fact thermodynamically means that the overall redox process Cu^{II}–$Cu^{II} \rightarrow Cu^{I}$–$Cu^{I}$ proceeds through sequential one electron steps and also from the kinetic point of view this fact means a certain stability of the electrochemically generated Cu^{II}–Cu^{I} (and Cu^{I}–Cu^{I}) complex [5].

The thermodynamic stability of the MV species may be appreciated from the peak-to-peak separation, ΔE_p, on a cyclic voltammogram for the sequential reduction of binuclear Cu^{II}–Cu^{II} to binuclear Cu^{I}–Cu^{I}. In the absence of major structural changes, i.e.,

* Author to whom correspondence should be addressed.

changes in coordination number, bond making and breaking, and severe changes in coordination geometry associated with the redox process, ΔE_p reflects the interaction between the metal centers, the magnetic superexchange effects between them, and the electron delocalization in the MV state [6a,b]. A combination of factors, including structural changes, will determine if the overall two-electron reduction of the binuclear Cu^{II} species will consist of a simultaneous two- electron or two one-electron steps, at the same or different potential [7]. Considering the system as a bioinorganic model, it seems also important to know were the redox changes take place (positive or negative potentials).

In this paper we report studies of the redox behaviour of both the Cu^{II}–Cu^{II} and the mixed-valence species photochemically generated in order to achieve a more complete physicochemical characterization of the acetate binuclear copper complex and consequently a closer evaluation of its behaviour as a model of type III—Cu sites.

EXPERIMENTAL

Materials

$(CH_3COO)_2Cu \cdot H_2O$ p.a. Merck was used without further purification. Glacial acetic acid (AcOH) 100% p.a. Merck and methanol (MeOH) (Merck–Uvasol spectroscopic grade) were used directly. Solutions of the cupric acetate dimer $(CH_3COO)_4Cu_2$ were prepared by dissolving $(CH_3COO)_2Cu \cdot H_2O$ in 95/5% (vol./vol.) MeOH/AcOH mixtures to obtain solutions approximately 6×10^{-3} mol dm^{-3} in copper(II). Tetrabutylammonium tetrafluoroborate ($TBABF_4$) was purchased from Aldrich Chemical Co. The violet mixed-valence compound (MV) was generated *in situ* as indicated in reference [3]. Argon or N_2 gas was used to provide an inert atmosphere.

Electrochemistry

The controlled-potential electrolysis (CPE) and cyclic voltammetry (CV) measurements were recorded with a PAR 173 potentiostat-galvanostat coupled to a PAR 176 current-detection module. For the cyclic voltammetry experiments, a PAR 175 universal programmer was also used. A Watanabe WX 4301 X-Y recorder was used for i versus V plots. A three-electrode system, with SCE as reference, was used for both CPE and CV experiments. In the last case, a platinum wire was used as working electrode and a platinum coil as auxiliary electrode. For the CPE measurements, a platinum mesh and coiled platinum wire were used as working and auxiliary electrodes, respectively. ($TBABF_4$) 0.1 M was used as supporting electrolyte. The concentration of the complex under study was 1.5×10^{-3} M.

RESULTS

Electrochemistry of $(CH_3COO)_2Cu^{II}Cu^{II}(OOCCH_3)_2$ *(complex* **I**)

The cyclic voltammogram of the $(CH_3COO)_2Cu^{II}Cu^{II}(OOCCH_3)_2$ solution is shown in Fig. 1. It shows two broad reduction peaks, one from +0.2 to −0.2 (A) V and a second one centered at −0.4 (B) V. Two oxidation peaks appear at −0.16 (C) and 0.36 (D) V by reversing the potential sweep after the reduction processes have occurred. Figs 2 and 3 shows the relationship between the oxidation and reduction reactions, i.e. between (A) and (D), and (B) and (C), (E) peaks. The sharp peak around 0 V provides evidence for a metal (Cu^0) deposit on the Pt electrode surface and the small shoulder around 0.2 V, observed in the CV of the Cu^{II} salts, evidences the presence of Cu^{II} ions in solution. Both species Cu^0 and Cu^{II} ions result from a disproportionation process. The disproportionation does not take place at potentials below −0.4 V (Figs 2 and 3) although there is a dependence on the scan speed (Fig. 5) indicating the presence of a kinetic factor. Figure 4 and Fig. 5 show the CV study of the redox processes as a function of the scan speed. Analysis of the *ip vs* $\sqrt{v}$ data shows that the processes are diffusion controlled (not shown). Figures 6 and 7 show the Nicholson and Shain diagrams [8].

CPE at −0.4 V results in an uncoloured solution after the overall passage of four electrons per mole of complex and Cu^0 deposition on the platinum working electrode is verified.

Electrochemical generation of $(CH_3COO)_2Cu^{II}Cu^{I}(OOCCH_3)_2$

The mixed-valence species could not be generated by CPE at any voltage in the range of the first

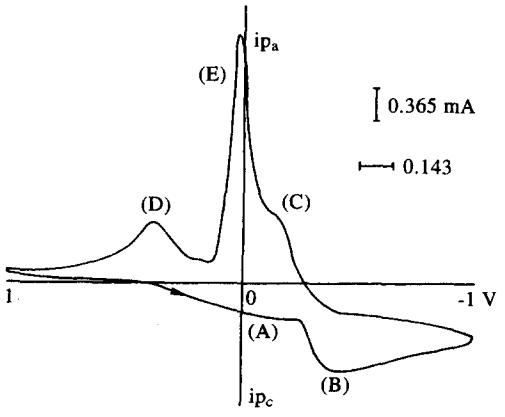

Fig. 1. Cyclic voltammogram of a 1.5×10^{-3} M degassed solution of cupric acetate dimer inn 0.1 M $TBABF_4$ 95/5% (vol/vol) MeOH/AcOH mixture as solvent. Scan rate 200 mV/s^{-1}. Saturated calomel electrode as reference; platinum wire and platinum coil as working and auxiliary electrodes, respectively.

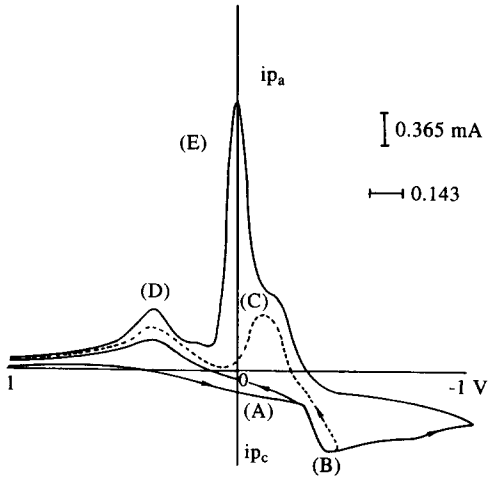

Fig. 2. Relationship between the reduction (A) and oxidation (D) peaks in the cyclic voltammogram of a 1.5×10^{-3} M degassed solution of cupric acetate dimer in 0.1 M $TBABF_4$ 95/5% (vol/vol) MeOH/AcOH mixture as solvent. Same conditions as Fig. 1. Peak (E) is related to Cu^0 deposit on the working electrode.

reduction zone, but when short pulses of current were applied at −0.4 V the original green solution turns to a blue–violet color, presumably the mixed-valence species. The concentration of the generated blue–violet species may be increased only to a maximum value since after several pulses (4–6) the blue–violet color began to decrease.

Due to the low concentration of the blue–violet species, the differential spectra did not allow the determination of the visible and near IR band maxima that are characteristic of the MV species [3]. If oxygen diffuses into the solution the violet colour changes to the original green of the Cu^{II}–Cu^{II} dimeric complex.

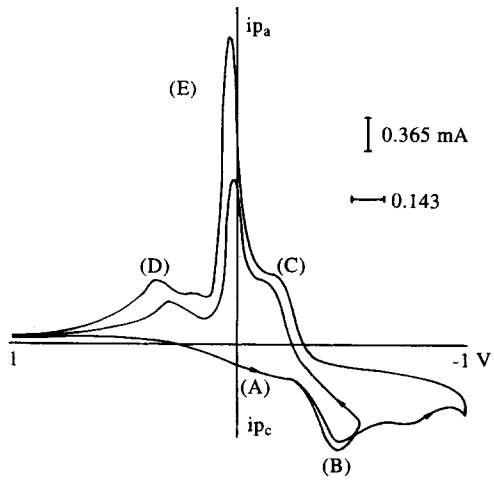

Fig. 3. Same as Fig. 2, but for (B) and (C), (E) peaks.

Electrochemistry study of the MV complex generated photochemically

Figure 8 shows the CV of the MV species starting from a small negative potential toward reduction and oxidation and Fig. 9 from a small positive potential also toward reduction and oxidation. The reduction processes (approximately at −0.1 and −0.3 V) are diffusion controlled as indicated from the ip *vs* $\sqrt{v}$ function (not shown). The analysis of the $ip/\sqrt{v}$ *vs* v study starting from the oxidized species, i.e. from +1 V, is shown in Fig. 10 which is similar to Fig. 6a.

DISCUSSION

The electrochemical results for the $(CH_3COO)_2Cu^{II}Cu^{II}(OOCCH_3)_2$ complex in AcOH/MeOH mixture (Figs 1, 2 and 3) show that it is sequentially reduced to the $(CH_3COO)_2Cu^{I}Cu^{I}(OOCCH_3)_2$ species which may be reoxidized, also sequentially, but in competition with the thermal disproportionation to Cu^0 (s) and Cu^{II} ions. In fact, this may be seen in Fig. 2 from a comparison of the extended range and dotted voltammograms and from Fig. 6a in which the dependence of $ip/\sqrt{v}$ *vs* v indicates that the reduction process at −0.4 V is followed by an irreversible catalytic reaction, i.e.

$$Cu^{II}\text{–}Cu^{II} + 2e \leftrightarrow Cu^{I}\text{–}Cu^{I} \quad (1)$$

$$Cu^{I}\text{–}Cu^{I} \rightarrow Cu^0 + Cu^{II} \quad (2)$$

The CPE at −0.4 V is a quantitative measure of the overall reduction process including the disproportionation reaction, since it involves four electrons per mole of initial binuclear Cu(II) complex. If the CV scan range is reduced from (+1.0, −1.0) V to (+1.0, −0.4) V (Fig. 3 and Fig. 5) and depending on the scan rate, the dismutation process may not be detected during the electrode process. Consequently, the $ip/\sqrt{v}$ *vs* v plot (Fig. 6b) is different and in light of the ip_a/ip_c *vs* v dependence (Fig. 6c), it shows that the reduction process is in this case followed by an irreversible reaction. Since the Cu^{I}–Cu^{I} species may be sequentially oxidized, as may be seen in the voltammograms, this irreversible reaction should not be associated with a destructive process of the species. Furthermore, taking in account that a comparison of the solid X-ray data for Cu^{II} acetate [9a] and Cu^{I} acetate [9b] suggests only a small axial distortion expected for Cu^{I} as compared to Cu^{II} sites, it is possible that this irreversible process may be associated with a structural change. Similarly, the electrochemical irreversibility of the first couple (Fig. 2) may also be associated with a structural change. In this case, the Nicholson and Shain criteria for two reduction processes (A and B) coupled with a 'chemical reaction' [8b], indicate that Fig. 6b is in agreement with the R–R case, that is two sequential one-electron reduction processes both of which are reversible.

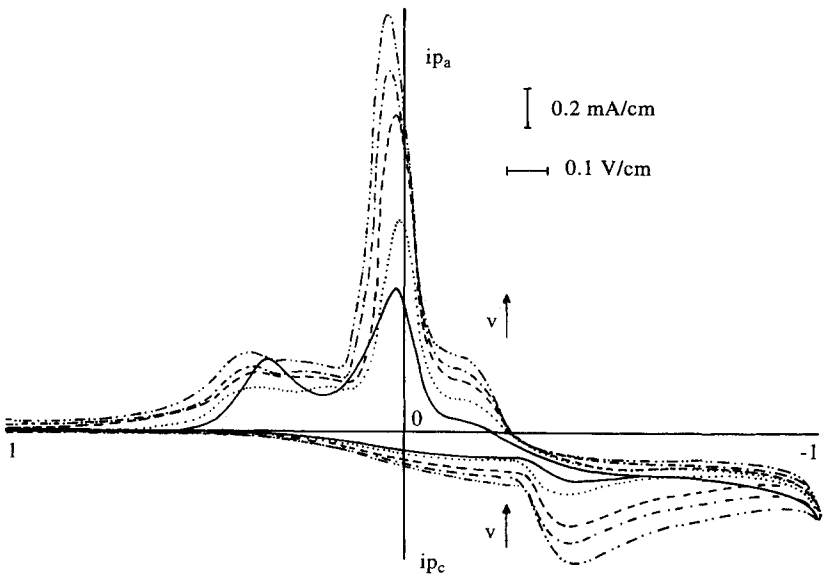

Fig. 4. Cyclic voltammogram of a 1.5×10^{-3} M degassed solution of cupric acetate dimer in 0.1 M $TBABF_4$ 95/5% (vol/vol) MeOH/AcOH solvent mixture as a function of the scan rate: scan range +1 to −1 V. v: 10(–), 25(...), 50(– – –), 75(– · – · –), 100(– · · – · ·) m Vs^{-1}. Same conditions as Fig. 1.

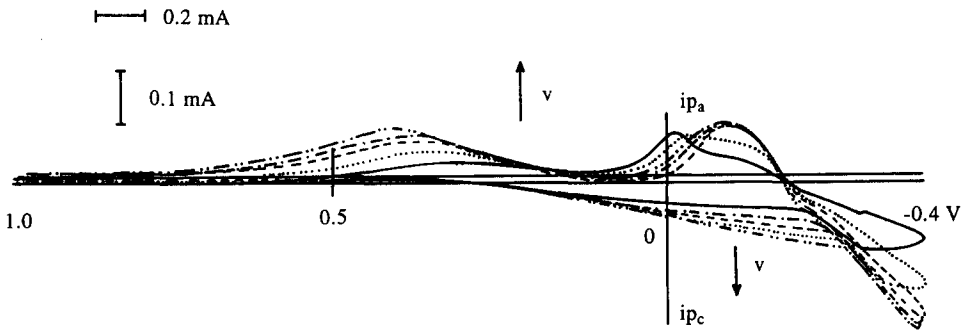

Fig. 5. Same as Fig. 4 but in restricted potential range +1 to −0.4 V. v: 10(–), 25(...), 50(– – –), 75(– · – · –), 100(– · · – · ·).

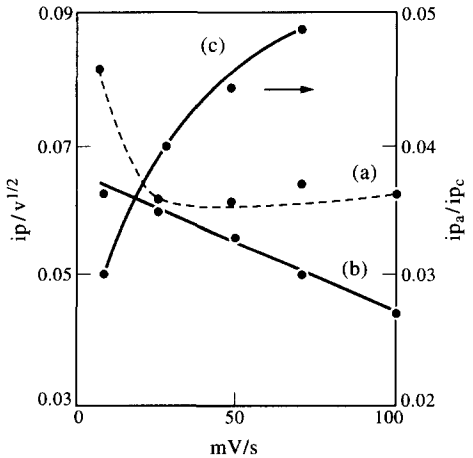

Fig. 6. Plot of the current function $ip/\sqrt{v}$ as a function of the scan rate for the electrode process at −0.4 V (a) extended range (see Fig. 3 (a), (b)) restricted range (see Fig. 3 (b), (c)) *ipa/ipc vs v* restricted range.

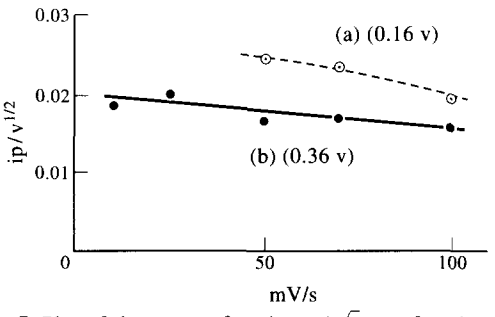

Fig. 7. Plot of the current function $ip/\sqrt{v}$ as a function of the scan rate for the electrode process at −0.16 V and +0.36 V in restricted range (see Fig. 3).

Unfortunately, the presence of the competitive disproportionation process, after the second reduction and before the first oxidation peaks, complicates the results and prevents us from analyzing the four peak behaviour (two red., two oxid.) as a whole for the R–R case. Nevertheless, the diagrams of Fig. 7, for each

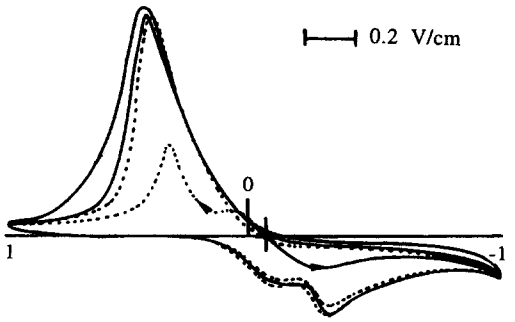

Fig. 8. Cyclic voltammogram of a 1.5×10^{-3} M degassed solution of $(CH_3COO)_2Cu^{II}Cu^{I}(OOCCH_3)_2(MV)$ species generated *in situ* as indicated in ref. [3], in 0.1 M $TBABF_4$ 95/5% (vol/vol) MeOH/AcOH mixture as solvent, starting from a small negative potential toward reduction and oxidation.

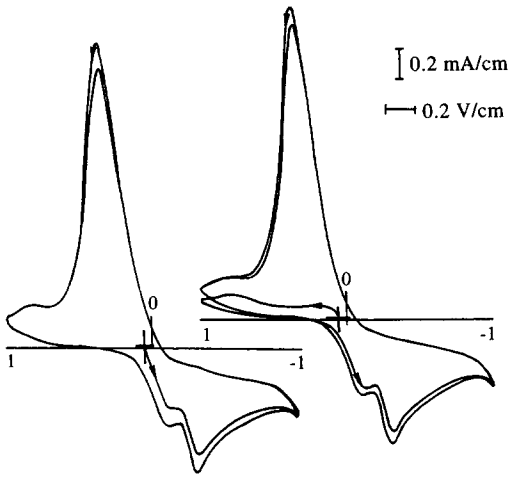

Fig. 9. Same as Fig. 8 but starting from a small positive potential.

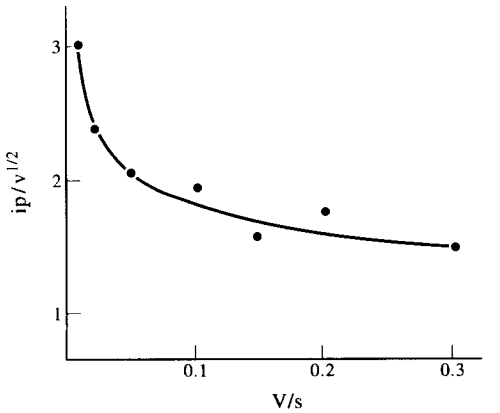

Fig. 10. Plot of the current function $ip/\sqrt{v}$ as a function of the scan rate for the electrode process at -0.30 V for the Cu^{II}–Cu^{II} species (complex **II**) generated from the MV species solution of Fig. 8.

process at -0.16 and 0.36 V in the oxidation direction, show that both processes are preceded by an irreversible reaction. These irreversible reactions may be considered as structural changes since they are congruent with the structural framework requirements of the Cu^{II} and Cu^{I} sites and with the change observed in the reduction direction.

Direct experimental evidence that the reduction process of the Cu^{II}–Cu^{II} complex is a sequential electrode reduction, and not a simultaneous two-electron reaction, is given by the fact that the mixed-valence complex may be generated at -0.4 V as indicated in the experimental section. It may be suggested that, the MV species can be generated by short pulses and not by CPE, due to the fact that after being produced by the pulse, the MV species diffuses away from the electrode surface, so when the next pulse is applied the Cu^{II}–Cu^{II} species is preferentially reduced. However, after several pulses the concentration distribution of both species, (MV and Cu^{II}–Cu^{II}) around the electrode becomes similar and the probability of reduction of the MV increases; therefore, the next pulse may reduce both species allowing the MV species to be formed only in a small amount. It must be mentioned that, although the MV species is involved in a disproportionation equilibrium in which *Kc* may be estimated to be on the order of 10^3 at room temperature [10], we think this equilibrium is not a factor in the decrease of the MV concentration after several pulses.

Therefore, the electrochemical behaviour of the $(CH_3COO)_2Cu^{II}Cu^{II}(OOCCH_3)_2$ complex may be summarized as:

$$Cu^{II}\text{–}Cu^{II} + 1e \leftrightarrow Cu^{II}\text{–}Cu^{I} \quad -0.2\,V \qquad (3)$$

$$2\,Cu^{II}\text{–}Cu^{I} \leftrightarrow Cu^{II}\text{–}Cu^{II} + Cu^{I}\text{–}Cu^{I} \qquad (4)$$

$$Cu^{II}\text{–}Cu^{I} \rightarrow [Cu^{II}\text{–}Cu^{I}]\ (d) \qquad (5)$$

$$[Cu^{II}\text{–}Cu^{I}](d) + 1e \leftrightarrow Cu^{I}\text{-}Cu^{I} \quad -0.4\,V \qquad (6)$$

$$Cu^{I}\text{–}Cu^{I} \rightarrow [Cu^{I}\text{–}Cu^{I}]\ (d) \qquad (7)$$

$$Cu^{I}\text{–}Cu^{I} \rightarrow Cu^{0} + Cu^{II} \qquad (8)$$

(d) = structural change

which indicates that the global electrochemical reduction process appears as irreversible, in which the structural changes play an important role. In relation with the electrochemical behaviour of the MV complex generated photochemically, the analysis of the cyclic voltammograms is more complex. The reduction peak is broad and centered at ~ 0.2 V (Fig. 8). When the potential sweep is reversed after reduction, a large and broad oxidation peak appears around 0.4 V. In a second cycle two overlapping reduction peaks are observed at -0.1 and -0.3 V, respectively, associated with the reduction of the Cu^{II}–Cu^{II} species just generated (complex **II**).

Otherwise, Figs 8 and 9 show that the voltammograms are highly dependent on the starting

voltage and it may be seen also that the oxidation potential of the MV complex seems to be around 0 V. The broad and large oxidation peak envelopes the 0.2 V peak associated with the Cu(II) ions and the peak related to the Cu^0 metal deposit on the platinum electrode surface. In fact, when the $ip/\sqrt{v}$ *vs* v dependence on the scan speed is studied starting from the completely oxidized species (complex **II**) i.e., starting from +1 V, the Nicholson and Shain criteria indicate that the electrochemical process at the second reduction peak is similar to the reduction process in the parent, non-irradiated Cu^{II}–Cu^{II} complex (complex **I**) (Fig. 6a and Fig. 10). This similarity shows that the overall process is also similar (i.e., reduction followed by a disproportionation process), generating a Cu^0 deposit and Cu^{II} ions in solution. Although complex **II** (Cu^{II}–Cu^{II} species obtained by electrochemical oxidation of the MV species generated photochemically) exhibits an overall behavior similar to that of the Cu^{II}–Cu^{II} species studied in the first part of this paper (complex **I**), some differences are apparent. In fact, although the overlapping makes it difficult to know the real value of the reduction potentials, they appear different: complex **II** shows less negative values and more resolved peaks than complex **I**. In addition, the disproportionation reaction seems competitive at higher rates for complex **II** than for complex **I** (Figs 6a and 10). It is possible to speculate that these differences may be related to a more appropriate structural framework toward reduction in complex **II** and to a greater interaction between the coppers derived from a shorter Cu–Cu distance; both facts may be associated with the structure of the complex **II** precursor species and with the observation that the structural changes have measurable kinetic rate evidenced by the Nicholson and Shain diagrams.

In summary, the results of this work reveal:

(a) A violet mixed-valence species Cu^{II}–Cu^{I} may be generated electrochemically from the Cu^{II}–Cu^{II} complex. The species is thermodynamically and kinetically stable in the absence of oxygen, at least for 4 h. Oxygen oxidizes the MV species to the original green Cu^{II}–Cu^{II} complex. Considering that the mixed-valence species may be a good bioinorganic model for copper type III in multicopper oxidases, as shown in refs [3] and [11], it is particularly interesting that a similar species may be generated from the binuclear Cu^{II}–Cu^{II} complex which can be sequentially reduced.

(b) Nicholson and Shain criteria indicate that there are 'thermal reactions' coupled to the electrochemical processes making the overall process irreversible. The coupled thermal process related to the Cu^{II}–Cu^{II} → Cu^{I}–Cu^{II} → Cu^{I}–Cu^{I} redox reactions are considered to be structural distortions according to the different symmetry sites preferred for Cu^{II} and Cu^{I} centers. It is very important to note that these results are in agreement with the fact that a comparison of the solid state X-ray data for Cu^{II} acetate and Cu^{I} acetate suggests only a small axial distortion expected for the Cu(I) site as compared to Cu^{II} and with the similarity of the symmetry of both metal sites signalled for the UV–vis–NIR spectroscopic studies of ref. [3].

(c) Associated with the Cu^{I}–Cu^{I} species there is also a disproportionation process which is kinetically in competition with the electrochemical reoxidation. This irreversible reaction may be seen from the Nicholson and Shain criteria applied to the extended range voltammogram and also from the Cu^0 deposition on the platinum working electrode in the electrolysis experiments.

(d) The mixed-valence species generated photochemically may be reduced to Cu^{I}–Cu^{I} and oxidized to Cu^{II}–Cu^{II} at less negative and less positive potentials, respectively, in comparison with the species generated electrochemically. Furthermore, the Cu^{II}–Cu^{II} (complex **II**) species resulting from the oxidation of the MV species photochemically generated shows a less negative reduction potential with better resolved peaks, and the resulting Cu^{I}–Cu^{I} species disproportionates to Cu^0 and Cu^{II} ions at a faster rate than the Cu^{I}–Cu^{I} species resulting from reduction of complex **I**.

Although the structural factors may not be the only ones, it is possible to suggest that a shorter Cu–Cu distance in the MV generated photochemically is responsible for the different electrochemical behaviour of this MV complex and species derived from it.

Acknowledgements—This work was supported by the Universidad de Chile (grant Q-3066/9223) and Fondecyt (grant 0831-92).

REFERENCES

1. Hansen, A. E. and Balhausen, C. J., *Trans. Faraday. Soc.*, 1965, **61,** 631.
2. Ross, P. K., Allendorf, M. D. and Solomon, E. I., *J. Am. Chem. Soc.*, 1989, **111,** 4009.
3. Crivelli, I. G. and Andrade, C. G., *Inorg. Chim. Acta*, 1993, **203,** 115 and refs therein.
4. Robin, M. B. and Day, P., *Adv. Inorg. Chem. Radiochem.*, 1967, **10,** 802.
5. Zanello, P., Tamburini, S., Vigato, P. and Mazzochin, G., *Coord. Chem. Rev.*, 1987, **77,** 165.
6. (a) Gagné, R. and Spiro, C., *J. Am. Chem. Soc.*, 1980, **102,** 1443. (b) Gagné, R., Spiro, C., Smith, T. J., Hamam, C. A., Thies, W. R. and Shienko, A. K., *J. Am. Chem. Soc.*, 1981, **103,** 4073.
7. Fenton, D. E. and Linvedt, R. L., *J. Am. Chem. Soc.*, 1978, **100,** 6367.
8. (a) Nicholson, R. and Shain, I., *Anal. Chem.*, 1964, **36,** 706. (b) ibid, 1965, **37,** 178.
9. (a) Rao, V. M. and Monahar, H., *Inorg. Chem. Acta*, 1979, **34,** L213. (b) Mounts, R., Ogura, T. and Fernando, Q., *Inorg. Chem.*, 1974, **13,** 802.
10. Loeb, B., Andrade, C., Francois, A. and Crivelli, I., in preparation.
11. Loeb, B., Crivelli, I. and Andrade, C., *Inorg. Chim. Acta*, 1995, **231,** 21.

Pergamon

PII: S0277-5387(97)00210-6

Polyhedron Vol. 17, No. 1, pp. 179–184, 1998
© 1997 Elsevier Science Ltd
All rights reserved. Printed in Great Britain
0277-5387/98 $19.00+0.00

New multiply-bonded dimetal compounds containing bridging 1,3,4,6,7,8-hexahydro-2H-pyrimido[1,2-a]pyrimidinato groups—I. The V_2^{4+}, Cr_2^{4+} and Mo_2^{4+} compounds and some salts of the protonated ligand

F. Albert Cotton* and Daren J. Timmons

Department of Chemistry and Laboratory for Molecular Structure and Bonding, Texas A & M University, College Station, TX 77843-3255, U.S.A.

(Received 10 March 1997; accepted 12 May 1997)

Abstract—The reactions of Lihpp with vanadium(II) chloride, chromium(II) chloride and tetrakis(trifluoroacetato)dimolybdenum produce the dinuclear tetrabridged compounds $V_2(hpp)_4$, **1**, $Cr_2(hpp)_4$, **2**, and $Mo_2(hpp)_4$, **3**. Compound **1** crystallizes as red blocks in the space group $P\bar{1}$ with unit cell dimensions, $a = 8.489(2)$, $b = 9.709(2)$, $c = 9.835(2)$ Å, $\alpha = 89.98(3)$, $\beta = 73.04(3)$ and $\gamma = 79.29(3)°$. This compound contains the shortest known vanadium to vanadium bond, 1.932(1) Å. Compound **2** crystallizes as orange blocks in the space group $P\bar{1}$ with unit cell dimensions, $a = 8.488(2)$, $b = 9.687(2)$, $c = 9.747(2)$ Å, $\alpha = 90.89(3)$, $\beta = 100.86(3)$ and $\gamma = 106.42(3)°$. This compound contains a 'supershort' chromium to chromium bond, 1.8517(7) Å. Compound **3** crystallizes as red blocks in the space group $P\bar{1}$ with unit cell dimensions, $a = 8.455(2)$, $b = 9.702(2)$, $c = 10.094(2)$, $\alpha = 88.84(3)$, $\beta = 72.01(3)$ and $\gamma = 79.89(3)°$ and has a short molybdenum to molybdenum bond distance of 2.067(1). Both **2** and **3** have M—M bonds distances shorter than most analogous compounds containing nitrogen donor atom bridges. The basicity of Hhpp is also evidenced by the formation of the cation $[H_2hpp]^+$ upon reaction with trifluoroacetic acid and acetic acid. $[H_2hpp][O_2CCF_3]$, **4**, crystallizes as colorless needles in the space group $P2_1/c$ with cell dimensions, $a = 7.431(2)$, $b = 13.243(2)$, $c = 11.741(2)$, $\beta = 96.50(3)°$. $[H_2hpp][O_2CCH_3]$, **5**, crystallizes as colorless needles in the space group $P2_1/n$ with cell dimensions, $a = 7.888(2)$, $b = 11.182(2)$, $c = 11.902(2)$, $\beta = 91.91(3)°$. © 1997 Elsevier Science Ltd

Keywords: metal–metal bond; divanadium; dichromium; dimolybdenum; supershort; bridging ligand.

The usefulness of bridging ligands of the general type **I** for stabilizing multiply bonded (as well as singly bonded) dimetal units, M_2^{n+}, has been long recognized [1]. Some of the first [e.g., $Mo_2(O_2CCH_3)_4$] although not the first (i.e., $Re_2Cl_8^{2-}$) multiply bonded M_2 complexes to be recognized have the carboxylate anion as the bridging ligand.

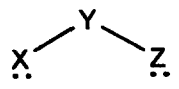

I

Scheme 1.

More recently, it was recognized that the amidinate anions, especially the formamidinate anions, [PhN-C(H)NPh]$^-$ and [(*p*-tol)NC(H)N(*p*-tol)]$^-$ are especially useful. Indeed, at present, there is a greater variety of M_2^{n+} units stabilized by these ligands than by any others [1]. However, even more recently, it has been found that the formamidinates have a major problem, in that they are cleaved under certain reaction conditions into ArN and ArNC fragments [2]. Thus, products containing these fragments rather than the intact ArNC(H)NAr$^-$ ligand are obtained.

These disappointing (although interesting) results posed the challenge of finding, if possible, a ligand having the essential desirable features of the amidinato anions (especially their high basicity) while at

* Author to whom correspondence should be addressed.

the same time showing promise of displaying greater resistance to cleavage. Bicyclic systems in which the likelihood of the two nitrogen atoms being separated naturally came to mind. The 1,8-naphthyridine type, **II,** is not exactly suitable since it is neutral, whereas an anionic system is preferable. Another, and more attractive candidate is the 7-azaindole anion, **III**. In fact this has been looked into before [3], and it was recognized that this has two disadvantages. The major one is that the preferred N—M bond directions diverge thus biasing this ligand against short M—M distances, and the minor one in that there tends to be orientational disorder of the ligands because of the steric similarity of the 5- and 6-membered rings.

The bicyclic system **IV,** or something similar, then came to mind but this has the practical disadvantages that it is neither commercially available nor simple to prepare. However, the similar compound, **V,** 1,3,4,6,7,8-hexahydro-2H-pyrimido[1,2-a]pyrimidine, which is conveniently represented by Hhpp is available commercially at a reasonable price.

Some minds do tend to run in the same channels and we were anticipated in the use of the hpp^- ligand by Bear *et al.* [4], who recently reported the first $M_2(hpp)_4$ species, $Ru_2(hpp)_4Cl_2$. However, our interest in finding the most robust possible $RNC(\dot{R})NR^-$ type ligand for purposes of our own was whetted further by Bear's success and we have undertaken a broad exploration of the capabilities of the hpp^- for promoting the stability of M_2^{n+} units.

We chose to begin with Mo_2^{4+}, Cr_2^{4+}, and V_2^{4+} because (a) Mo_2^{4+} offers the largest group of M_2L_4 species with which to make comparisons, (b) Cr_2^{4+} forms the shortest known metal–metal bonds, and (c) V_2^{4+} has so far been obtained only twice, in the compounds $V_2(DtolF)_4$ [5] and $V_2(DCyF)_4$ [5] and it was considered desirable to enlarge the group. We report here the preparation and characterization of the three compounds $Mo_2(hpp)_4$, $Cr_2(hpp)_4$ and $V_2(hpp)_4$ as well as two compounds, $[H_2hpp][CF_3CO_2]$ and $[H_2hpp][CH_3CO_2]$ that turned up unexpectedly.

EXPERIMENTAL

$VCl_3(THF)_3$ [7] and $Mo_2(O_2CCF_3)_4$ [8] were prepared according to literature procedures. Hhpp was obtained from Aldrich Co. and further purified by vacuum sublimation. Li[hpp] was prepared *in situ* at room temperature by deprotonation of Hhpp with one equivalent of MeLi. All other reagents, including 1.0 M MeLi in THF/cumene and 1.0 M $NaHBEt_3$ in toluene, were obtained from commercial sources and used without further purification. All solvents were freshly distilled from sodium/potassium benzophenone. All manipulations were carried out in either an argon atmosphere dry box, or in dry nitrogen using standard Schlenk techniques. ^{1}H-NMR studies were performed on a Varian XL-200 spectrometer; IR spectra were recorded on a Perkin–Elmer 16PC FT-IR spectrophotometer as KBr pellets. UV–vis spectra were recorded on a Cary-17D spectrometer.

Preparation of $V_2(hpp)_4$, **1**

$VCl_3(THF)_3$ (0.75 g, 2.0 mmole) was reduced by one equivalent of $NaHBEt_3$ in 25 cm^3 THF at $-78°C$ resulting in a deep purple solution. A cold ($-78°C$) solution of Li[hpp] (4.0 mmole) in 15 cm^3 THF was then added and the solution was allowed to warm to room temperature while stirred. An additional 30 min of stirring resulted in a brown solution. The solvent was removed under vacuum, and the dried brown powder was extracted with 30 cm^3 warm toluene, and the extract was filtered through Celite®. The toluene was then removed under vacuum allowing isolation of a brown powder in 62% yield. Crystallization by slow diffusion of a layer of hexanes into a toluene

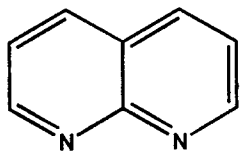

II

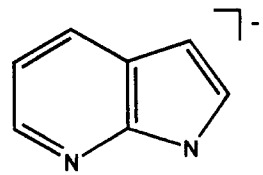

III

Scheme 2.

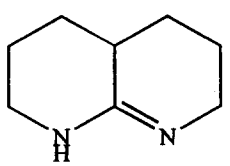

IV

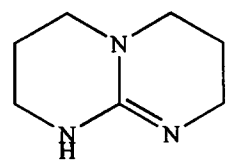

V

Scheme 3.

solution of **1** yielded orange/brown, block-shaped crystals in a few days.

^{1}H NMR (C_6D_6, 25°C) $\delta = 2.016$ (quin), 3.063 (trip), 3.160 (trip). UV–vis (THF): λ_{max} [nm] = 280. IR (KBr, cm^{-1}): 2932, 2856, 1636, 1522, 1441, 1380, 1319, 1262, 1197, 1023, 802.

Preparation of $Cr_2(hpp)_4$, **2**

A solution of Li[hpp] (4.0 mmole) in 10 cm^3 THF cooled in a dry ice/ethanol bath was transferred via cannula into a grey 10 cm^3 THF suspension containing 0.2 g (1.63 mmole) of anhydrous $CrCl_2$ at −78°C. The reaction mixture turned brown immediately, but gradually became yellow. The reaction was allowed to warm to room temperature, and a yellow-orange solid that precipitated was collected on a frit and dried *in vacuo* to yield 0.46 g (0.7 mmole); 43%. Crystals were grown from an orange solution in benzene layered with hexanes at room temperature.

^{1}H NMR (C_6D_6, ppm): 2.0 (quin, CH_2), 3.0 (t, CH_2), 3.32 (t, CH_2). UV–vis (benzene): λ_{max} (nm) = 430. IR (KBr, cm^{-1}): 2933, 2843, 1617, 1560, 1525, 1447, 1385, 1316, 1197, 1082, 804.

Preparation of $Mo_2(hpp)_4$, **3**

A solution of Li[hpp] (1.0 mmole) prepared in 5 cm^3 toluene was added to a yellow solution of $Mo_2(O_2CCF_3)_4$ (0.155 g, 0.24 mmole) in 10 cm^3 toluene. The resulting dark red solution was stirred for 45 min, filtered into a Schlenk tube, and layered with hexanes. Red crystals of **3** were observed within 1 day. The crystalline yield was 22% but more of **3** could be obtained by reduction of the mother liquor.

^{1}H NMR (C_6D_6, ppm): 1.95 (quin, CH_2), 2.95 (t, CH_2), 3.61 (t, CH_2). UV–vis (THF): λ_{max} (nm) = 460, 365, 335. IR (KBr, cm^{-1}): 2962, 2869, 1636, 1420, 1262, 1098, 1045, 804.

Preparation of $[H_2hpp][O_2CCF_3]$, **4**

Hhpp (0.28 g, 2.0 mmole) was dissolved in 10 cm^3 toluene. Upon addition of 2 mmole trifluoroacetic acid, a white solid, **4**, precipitated. The toluene was removed *in vacuo*. **4** was isolated in nearly quantitative yield and recrystallized by the cooling of a saturated solution in acetone.

^{1}H NMR (D_2O, ppm): 1.74 (quin, CH_2), 3.02 (t, CH_2), 3.08 (t, CH_2). IR (KBr, cm^{-1}): 1684, 1653, 1559, 1420, 1325, 1199, 1122, 799, 720.

Preparation of $[H_2hpp][O_2CCH_3]$, **5**

Hhpp (0.14 g, 1.0 mmole) was dissolved in 5 cm^3 toluene. Upon addition of 1 mmole acetic acid, a white solid, **5**, precipitated. The toluene was removed *in vacuo*. **5** was isolated in nearly quantitative yield and recrystallized by the cooling of a saturated solution in acetone.

^{1}H NMR (D_2O, ppm): 1.71 (s, CH_3), 1.73 (quin, CH_2), 3.02 (t, CH_2), 3.09 (t, CH_2). IR (KBr, cm^{-1}): 2976, 1656, 1569, 1412, 1322, 1293, 1262, 1207, 1068, 1020, 925, 832, 709, 461.

Crystallographic studies

In each case, a crystal was mounted on the tip of a quartz fiber and cooled to −60°C under a nitrogen stream on the diffractometer. All data were collected on a Nonius FAST area-detector system. Unit cell dimensions were obtained for each by indexing between 153 and 250 strong reflections in 2θ ranges of approximately 10.4–41.6°. Axial lengths and Laue symmetry were confirmed from axial images. Details of the use of the FAST in our laboratory have been described elsewhere [9]. These highly redundant data sets were corrected for Lorentz and polarization effects. The absorption correction, only done on **2**, was based on fitting a function to the empirical transmission surface as sampled by multiple equivalent measurements [10].

In each case the structure was solved either by direct methods or a Patterson map and refined using the SHELXTL programs [11]. All non-hydrogen atoms were refined with anisotropic displacement parameters. The amine hydrogen atoms in **4** and **5** were found in the difference map and refined with light restrictions; all other hydrogen atoms in the five complexes were placed in calculated positions and refined constrained to their parent atoms.

Crystallographic parameters are summarized in Tables 1, 2 and 3.

RESULTS AND DISCUSSION

The synthesis of **1**, by the low temperature addition of Li[hpp] in THF to vanadium (II) chloride in THF, followed a previously reported procedure [5] with few variations. The product was separated from LiCl by extraction of the dried reaction mixture with toluene and filtration through Celite®.

The analogous chromium complex, **2**, was readily prepared by the addition of Li[hpp] in THF to a suspension of cold anhydrous chromium(II) chloride in THF. The LiCl stayed in solution while the desired product precipitated. ^{1}H NMR of the yellow powder and of the orange powder isolated from the benzene extract gave identical spectra. $Cr_2(hpp)_4$ is diamagnetic (by NMR). The THF and benzene solutions are extremely air and moisture sensitive and turn green upon exposure. The powder of **2** is also very sensitive, and the crystals are stable for only a couple of minutes in air. The reflux of $Cr(CO)_6$ and Hhpp in a high boiling solvent can also be used to prepare **2**, but the reaction is more difficult to control.

The synthesis of **3** was quite straightforward once

Table 1. Crystallographic parameters for $V_2(hpp)_4$, **1**, $Cr_2(hpp)_4$, **2**, $Mo_2(hpp)_4$, **3**, $[H_2hpp][O_2CCF_3]$, **4**, and $[H_2hpp][O_2CCH_3]$, **5**

	1	**2**	**3**	**4**	**5**
Formula	$C_{28}H_{48}N_{12}V_2$	$C_{28}H_{48}N_{12}Cr_2$	$C_{28}H_{48}N_{12}Mo_2$	$C_9H_{14}F_3N_3O_2$	$C_9H_{17}N_3O_2$
Fw	654.66	656.78	744.66	251.22	199.25
Space group	$P\bar{1}$	$P\bar{1}$	$P\bar{1}$	$P2_1/c$	$P2_1/n$
a (Å)	8.489(2)	8.488(2)	8.455(2)	7.431(2)	7.888(2)
b (Å)	9.709(2)	9.687(2)	9.702(2)	13.243(3)	11.182(2)
c (Å)	9.835(2)	9.747(2)	10.094(2)	11.741(2)	11.902(2)
α (°)	89.98(3)	90.89(3)	88.84(3)	90	90
β (°)	73.04(3)	100.86(3)	72.01(3)	96.50(3)	91.91(3)
γ (°)	79.27(3)	106.42(3)	79.89(3)	90	90
V (Å^3)	760.5(3)	752.9(3)	774.8(3)	1148.0(4)	1049.2(4)
Z	1	1	1	4	4
d_{calc} (g cm^3)	1.429	1.449	1.596	1.454	1.033
μ (mm^{-1})	0.656	0.763	0.850	0.136	0.075
radiation			Mo-Kα (λ_α = 0.71073 Å)		
T (K)			213(2)		
$R1$,[a] $wR2$[b]	0.038, 0.104	0.041, 0.107	0.053, 0.119	0.129, 0.215	0.065, 0.139
Weight parameters[b]	0.0643, 0.7732	0.0658, 0.5053	0.0309, 6.941	0.000, 5.5960	0.0563, 1.1184

[a] $R1 = \Sigma(|F_o|-|F_c|)/\Sigma|F_o|$.
[b] $wR2 = [\Sigma w[(F_o^2-F_c^2)^2/\Sigma[w(F_o^2)^2]]^{1/2}$; $w = 1/[\sigma^2(F_o^2)+(aP)^2+bP]$, $P = [\max(F_o^2 \text{ or } 0)+2(F_c^2)]/3$

Table 2. Selected bond lengths (Å) and angles (°) for $M_2(hpp)_4$

	M = V, **1**	M = Cr, **2**	M = Mo, **3**
M(1)—M(1)′	1.932(1)	1.8517(7)	2.067(1)
M(1)—N(11)	2.061(4)	2.041(2)	2.159(6)
M(1)—N(12)′	2.058(4)	2.038(2)	2.167(6)
M(1)—N(21)	2.070(3)	2.032(2)	2.151(6)
M(1)—N(22)′	2.076(3)	2.037(2)	2.150(5)
M(1)′—M(1)—N(11)	94.31(8)	95.44(7)	92.3(2)
M(1)′—M(1)—N(12)′	95.29(9)	95.85(7)	93.1(2)
N(21)—M(1)—N(11)	89.3(1)	89.58(9)	90.2(2)
N(21)—M(1)—N(12)′	89.2(1)	89.34(9)	89.5(2)
M(12)′—M(1)—N(11)	170.3(1)	168.70(8)	174.6(2)
N(11)—C(17)—N(12)	115.3(4)	116.2(2)	118.1(6)
N(22)—C(27)—N(21)	116.0(3)	116.6(2)	117.1(6)

[a] Primed atoms are generated by an inversion center.

Table 3. Selected bond lengths (Å) and angles (°) for $[H_2hpp][O_2CCF_3]$, **4**, and $[H_2hpp][O_2CCH_3]$, **5**

	4	**5**
N(11)—C(17)	1.342(9)	1.335(4)
N(12)—C(17)	1.33(1)	1.331(4)
N(13)—C(17)	1.335(9)	1.330(4)
N(12)—C(17)—N(11)	118.4(7)	117.3(3)

the appropriate molybdenum source was used. The addition of Li[hpp] in toluene to $Mo_2(O_2CCF_3)_4$ in toluene resulted in a red solution of **3**. The red solution was filtered through Celite® to remove the LiO_2CCF_3.

Two of the three metal complexes, $V_2(hpp)_4$ and $Mo_2(hpp)_4$, are crystallographically isotypic but the packing of the molecules in $Cr_2(hpp)_4$ does not conform to the same pattern. It is possible to choose a unit cell for $Cr_2(hpp)_4$ that more closely resembles those for the other two compounds, but then the frac-

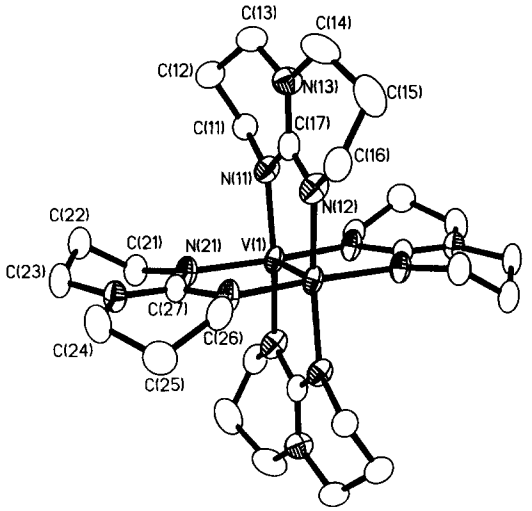

Fig. 1. Molecular Structure of $V_2(hpp)_4$, **1**, with ellipsoids at the 50% probability level. Hydrogen atoms have been omitted for clarity.

tional coordinates of the atoms do not correspond. It is surprising that this occurs, but it does not mean anything from a chemical point of view. Because each $M_2(hpp)_4$ molecule lies on an inversion center and the M—M—N—C—N rings are essentially planar (no atom deviates by more than 0.005 Å), each molecule has an eclipsed conformation. Figures 1 and 2 show views of two of the molecules. The three structures are all so similar that this should suffice for all.

In all three metal complexes the M—M bond lengths are remarkably short. $V_2(hpp)_4$ contains the shortest V—V bond known (1.932 (1) Å). Two other vanadium paddlewheel complexes exist: $V_2(DTolF)_4$ [5] (1.978 (2) Å); $V_2(CyNC(H)NCy)_4$ [6] (1.968 (2) Å). The M—M bonds in $Cr_2(hpp)_4$ and $Mo_2(hpp)_4$ are not the shortest known, but they are shorter than those in most similar complexes containing nitrogen-donor atom bridges. The Cr—Cr bond distance in $Cr_2(hpp)_4$ is shorter than in the two known formamidinato complexes [6,12] and the triazenato complex [13], but not as short as that in Cr_2(dimethybenzamidinate)$_4$ [14] (1.843 Å). The corresponding molybdenum analogs [13,15,16] all contain longer Mo—Mo bonds than in $Mo_2(hpp)_4$.

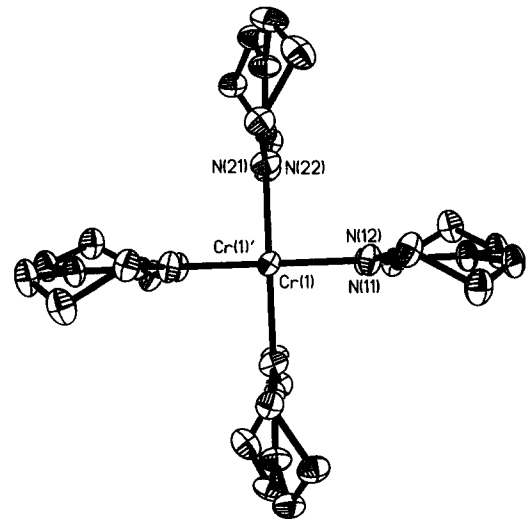

Fig. 2. Molecular Structure of $Cr_2(hpp)_4$, **2**, along the metal-to-metal bond axis. Hydrogen atoms have been omitted for clarity.

The hpp ligands are all puckered. The average C_{17}—N distance is 1.35(2) Å, which is consistent with partial double bond character in these bonds. The C_{17} and three nitrogen atoms can be regarded as sp^2 hybridized with some of their electrons occupying $p\pi$ molecular orbitals. This leads to planarity, or near planarity, in the central part of the ligand, but the two sets of three CH_2 groups need not, and do not, all lie in this plane. In each of the $M_2(hpp)_4$ compounds the conformation of each ligand is such that in one ring the central CH_2 group deviates in one direction and in the other ring the corresponding CH_2 group deviates in the opposite direction.

In all three of our $M_2(hpp)_4$ molecules we found that the puckered ligand rings were well ordered. This is in contrast to the disorder found by Bear *et al.* in their $Ru_2(hpp)_4Cl_2$ compound. We were pleased to see that the problem of refining disordered ligands need not arise in all cases.

While the high basicity of the hpp^- anion is one of its attractive features, the Hhpp molecule itself also has high basicity. This follows from the fact that it is a derivative of the extremely basic prototype guanidine, $(H_2N)_2C{=}NH$. Hhpp is therefore easily protonated to form the H_2hpp^+ ion, and this happens whenever it is used in an acid medium [17]. Having encountered this behavior several times by accident, we decided to prepare two such compounds deliberately and determine the structure of the H_2hpp^+ ion.

Turning now to the conformation of the H_2hpp^+ cation in compounds **4** and **5**, we note that these too are puckered, but in such a way, as shown in Fig. 3, that the two most deviant atoms, one in each ring, go in the same direction out of the mean plane. There is some disorder at C_{12} in **5** and at both C_{12} and C_{15} in **4**.

In conclusion, it can be said that the work reported here as well as that of Bear *et al.* on $Ru_2(hpp)_4Cl_2$ shows that the hpp^- ligand has the same general character as the amidinato anions and hence the same capacity to stabilize dimetal units in paddle wheel molecules. In view of the more connected internal structure of the hpp-ligand it is reasonable to expect it to be more robust and resistant to the fragmentation processes that have so often frustrated attempts to employ the amidinato ligands in conjunction with very highly reactive M_2^{n+} such as Nb_2^{4+} and Ta_2^{4+}.

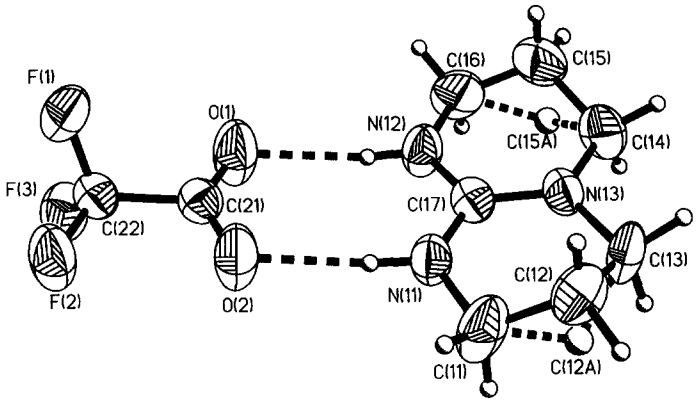

Fig. 3. Molecular Structure of $[H_2hpp][CF_3CO_2]$, **4,** with ellipsoids at the 50% probability level. C(12) and C(15) are disordered over two positions.

Acknowledgements—We thank the National Science Foundation for financial support. We also thank Prof. C. A. Murillo, Dr L. M. Daniels, Dr J. H. Matonic and Dr A. Yokochi for helpful discussion.

REFERENCES

1. Cotton, F. A. and Walton, R. A., *Multiple Bonds between Metal Atoms*, 2nd ed. Oxford University Press: New York (1993).
2. Cotton, F. A., Daniels, L. M., Matonic, J. H., Murillo, C. A. and Wang, X., *Polyhedron*, 1997, **16,** 1177.
3. Cotton, F. A., Falvello, L. R. and Wang, W., *Inorg. Chim. Acta*, 1997, **261,** 772.
4. Bear, J. L., Li, Y., Han, B. and Kadish, K. M., *Inorg. Chem.*, 1996, **35,** 1395.
5. Cotton, F. A., Daniels, L. M. and Murillo, C. A., *Angew. Chem. Int. Ed. Engl.*, 1992, **31,** 737.
6. Hao, S., Berno, P., Minhas, R. K. and Gambarotta, S., *Inorg. Chim. Acta.*, 1996, **244,** 37.
7. Manzer, L., *Inorg. Synth.*, 1982, **21,** 135.
8. Cotton, F. A. and Norman, Jr, J. G., *J. Coord. Chem.*, 1971, **1,** 161.
9. Bryan, J. C., Cotton, F. A., Daniels, L. M., Haefner, S. C. and Sattelberger, A. P., *Inorg. Chem.*, 1995, **34,** 1875.
10. Blessing, R. H., *Acta Cryst.*, 1995, **A51,** 33.
11. SHELXTL V.5, Siemens Industrial Automation, Madison, WI, 1990.
12. Cotton, F. A. and Ren, T. J., *J. Am. Chem. Soc.*, 1992, **114,** 2237.
13. Cotton, F. A., Rice, G. W. and Sekutowski, J. C., *Inorg. Chem.*, 1979, **18,** 1143.
14. Bino, A., Cotton, F. A. and Kaim, W., *Inorg. Chem.*, 1979, **18,** 3566.
15. Cotton, F. A., Inglis, T., Kilner, M. and Webb, T. R., *Inorg. Chem.*, 1975, **14,** 2023.
16. Cotton, F. A., Feng, X. and Matusz, M., *Inorg. Chem.*, 1989, **28,** 594.
17. Schroeder, G., Boguslawa, L., Jarczewski, A., Nowak-Wydra, B. and Brzezinski, B., *J. Mol. Str.*, 1995, **344,** 77.

Pergamon

PII: S0277-5387(97)00196-4

Polyhedron Vol. 17, No. 1, pp. 185–192, 1998
© 1997 Elsevier Science Ltd
All rights reserved. Printed in Great Britain
0277-5387/98 $19.00+0.00

Palladium complexes of unsaturated secondary aziridines. Crystal structure of *trans*-dichlorobis(2,2-dimethyl-3-phenyl-3-allylaziridine)palladium(II)

Ridha Ben Cheikh,[a]* Refaat Chaabouni,[a] Michel C. Bonnet[b]* and Françoise Dahan[c]

[a] Ecole Nationale d'Ingénieurs de Tunis, BP 37, 1002 Tunis Bélvédère, Tunisia

[b] Institut de Recherches sur la Catalyse, CNRS, 2 Avenue A. Einstein, 69626 Villeurbanne Cedex, France

[c] Laboratoire de Chimie de Coordination du CNRS, 205 Route de Narbonne, 31077 Toulouse Cedex, France

(Received 25 February 1997; accepted 12 May 1997)

Abstract—Six secondary aziridines (Az) bearing unsaturated vinylic or allylic groups on one of the carbon atoms of the ring have been reacted with palladium compounds. Complexes of general formula $PdCl_2(Az)_2$ have been isolated and spectroscopically characterized for fully substituted aziridines. The crystal structure of the complex of allylaziridine has been determined, showing the *trans*-arrangement of the ligands around the palladium center. © 1997 Elsevier Science Ltd

Keywords: complex; palladium; aziridine; allyl; vinyl; X-ray structure.

Hybrid ligands exhibiting two different coordination sites have been widely studied and have found numerous applications in coordination chemistry and in homogeneous catalysis, as proved by the industrial SHOP process of oligomerization of ethylene to linear α-olefins [1]. We continue to be interested in the chemistry of hybrid ligands containing one nitrogen site and either phosphorus or carbon–carbon double bond as second coordination site. The first case is illustrated by synthesis of transition-metal complexes of cyclic aminophosphonites arising from the P—N bond cleavage of bicyclic phosphoranes [2] and their applications in homogeneous hydroformylation, oligomerization and teleomerization of alkenes and dienes. The second series of hybrid ligands is confined to secondary aziridines (abbreviated Az) bearing an unsaturated substituent on one of the carbon atoms of the ring. We have recently described the synthesis of rhodium complexes with 2,2-dimethyl-3-phenyl-3-allylaziridine **1**. The X-ray crystal structure of the carbonyl complex Rh(CO)(Az)Cl (Az = **1**) has proved that **1** is simultaneously bound to the metal by the double bond of the allyl substituent and by the nitrogen atom in a chelating mode [3]. This species is active for the hydroformylation of styrene and is recovered unchanged after reaction. The complex is very stable and the double bond of the allyl group is not activated by coordination to rhodium. Then, it should be interesting to change the metal in order to make the double bond reactive and to transform the starting aziridine. Thus, we have devoted the present paper to a study of the reactions between some palladium complexes with the unsaturated aziridines described in Scheme 1.

The literature concerning the reactions between palladium and aziridines is limited and can be divided in two groups: aziridine as a ligand or stoichiometric reagent in palladium complexes or as a substrate in reactions catalysed by palladium compounds. Since the pioneering work of Jackson *et al.* [4] on the synthesis of $PdCl_2(Az)_2$ (Az = ethylenimine), Porta *et al.* [5] have synthesized aziridine ligands by reacting the complex $PdCl_2(coe)_2$ (coe = cyclooctene) with phenyl

* Author to whom correspondence should be addressed.

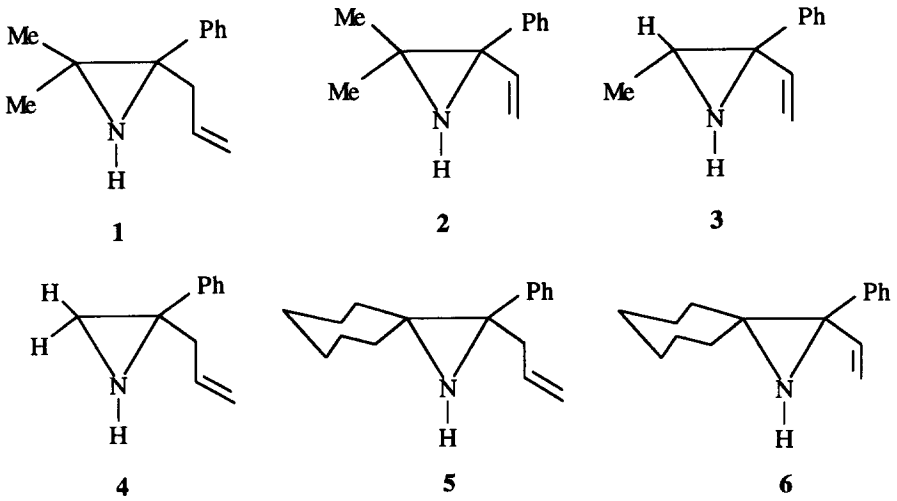

Scheme 1.

azide and have obtained a *trans*-$PdCl_2(Az)_2$ species. Bertani *et al.* [6] proved the formation of carbene complexes from ethylenimine and isocyanide palladium complexes. Tanner [7] described the use of chelating bis-aziridines in palladium complexes and their use in various catalytic reactions. Very recently, Beck *et al.* [8] studied the chelating behavior of L-aziridine-2-carboxylate with various transition metals. Most of the catalytic reactions described in the literature are devoted to the ring expansion of the aziridine by insertion in the C—N bond of either carbon monoxide [9], heteroallenes [10], or C—C double bond [11] giving rise to four and five-membered heterocycles. Other reactions are represented by isomerization [12], formation of unsaturated amines by aziridine ring opening [13] and catalytic hydrogenation [14].

RESULTS AND DISCUSSION

The allyl and vinylaziridines **1–4** have already been described and were prepared according to the published methods [15]. The hitherto unknown spiro aziridines **5** and **6** have been synthesised by the action of respectively allyl and vinyl magnesium bromide on cyclohexyl-2-spiro-3-phenyl azirine [16] following the method described by Chaabouni *et al.* [15] and have been fully characterized.

Reaction of aziridines **1–6** does not give any defined product with Pd(dibenzylideneacetone)$_2$, $Pd(PPh_3)_4$, $PdCl_2$ or $PdCl_2(PPh_3)_2$. Two equivalents of **1–6** react with 1 equiv. of $PdCl_2(PhCN)_2$ or $PdCl_2$(cod), but only the tetrasubstituted compounds **1**, **2**, **5** and **6** give a well defined complex of formula $PdCl_2(Az)_2$ in good yields (Scheme 2).

The non-fully substituted aziridines **3** and **4** are not stable enough in the presence of the palladium salt. Indeed, the aziridine **3** gives the corresponding complex **9**, but in only moderate yield (55%), while the aziridine **4** undergoes decomposition and polymerization under the reaction conditions. Therefore, the degree of substitution of the starting aziridine strongly influences its coordinating properties.

The infrared NH stretching band of aziridine in the complexes $PdCl_2(Az)_2$ are slightly shifted towards low frequencies as expected for a coordinated NH group (Table 1). On the contrary, the C=C stretching bands are practically unchanged, in accordance with a free double bond.

NMR spectra of the complexes are described in the Experimental section and the discussion will be focused on complex **7** with the aziridine **1**. The main feature of the ^1H NMR spectrum is a significant deshielding of most of the peaks, compared to those of the corresponding free aziridine. Simultaneously, the protons of the methyl groups give rise to two singlets of unequal intensity. All the signals in the $^{13}C\{^1H\}$ NMR spectrum, but those of the methylene group of the allylic substituent are split. Such a splitting may originate from several reasons. First, both aziridine ligands are not strictly symmetrical around palladium. However, in this case, the magnitude of the splitting would be much smaller than that observed, particularly for the most shielded methyl group ($\Delta\delta$ = 0.08 ppm for aziridine **1**). A second possibility is the presence of both *cis*- and *trans*-isomers, but that would give rise to two distinct peaks for the NH signal. Finally, the existence of two asymmetric centres for the aziridine ligands in the complex can induce the formation of a mixture of two diastereomeric complexes (R,R) and (R,S). This last hypothesis has been confirmed for complex **7** $PdCl_2(Az)_2$ with Az = **1** by means of an X-ray crystal structure analysis. Single crystals of **7** were grown by slow evaporation of 0.5 g of the complex dissolved in a hot mixture of 25% THF/75% petroleum ether *v/v* and contained 5% THF. The diastereomeric species isolated in the crystalline form has the (R,R) configuration. The structure consists of two slightly different molecules ligated by hydrogen bonds between hydrogen atom of the

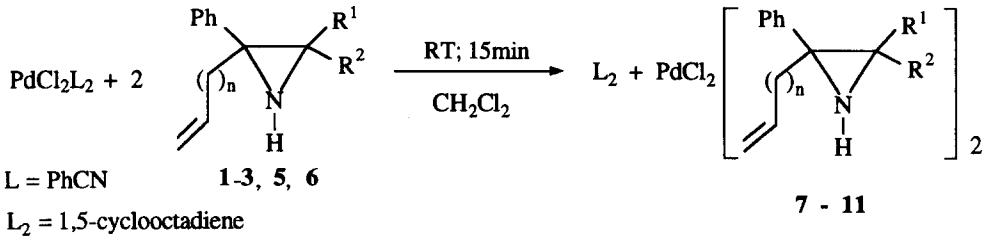

Scheme 2.

Table 1. Infrared data of aziridines **1–6** and their complexes in $CHCl_3$ (cm^{-1})

Aziridine	Band	Free	Pd-bound
1	N—H	3250	3185
	C=C	1645	1645
2	N—H	3290	3160
	C=C	1630	1625
3	N—H	3300	3130
	C=C	1650	1610
4	N—H	3300	—
	C=C	1640	—
5	N—H	3270	3200
	C=C	1640	1640
6	N—H	3280	3200
	C=C	1620	1625

NH groups of **1** in the molecule **A** and chlorine atoms of the other molecule **B**, as shown in Table 2 and Fig. 1. The N(A)···Cl(B) and N(B)···Cl(A) distances (3.36 Å) between two adjacent molecules indicate the existence of weak hydrogen bonding, ensuring the crystalline cohesion.

Figure 2 shows a perspective view of one molecule of complex **7** and clearly indicates that the aziridine ligands are bound to palladium in a monodentate mode, by their nitrogen atom and that they are located in *trans* position. This structure is very close of that observed by Hassner *et al.* [17] for a *trans*-$PdCl_2$(2-*p*-tolyl-azirine)$_2$. Some selected distances and bond angles are gathered in Table 3.

The coordination polyhedron around palladium is roughly square planar, as proved by Cl—Pd—N angles ranging from 88.0(1) to 92.6(1)° and a mean value of N—Pd—N equal to 169.7° and of Cl—Pd—Cl to 176°. The mean Pd—Cl (2.305 Å) and Pd—N bonds (2.034 Å) fall in the range generally observed [18], 2.326(43) Å and 2.04(36) Å, respectively. The projection of the molecule clearly demonstrates that the absolute configuration of C(1) and C(14) atoms is (R*,R*).

The bond lengths inside the aziridine ring (C(1)—N = 1.498 Å; C(2)—N = 1.495 Å; C(1)—C(2) = 1.501 Å) are very similar to those observed in Rh(Az)(CO)Cl (C(1)—N = C(2)—N = 1.499 Å; C(1)—C(2) = 1.498 Å). In contrast, the C=C bond length of the allylic substituent (C(19)—C(20) = 1.256 Å) is shorter than in the rhodium complex in which the double bond is coordinated (1.388 Å), and close to the value generally found for a free C=C double bond (1.299 Å) [18].

The chemistry of such complexes has been detailed for the allylaziridine complex, with the main objective being to synthesize a complex in which both nitrogen atom and C=C double bond are bound to the palladium in a chelating or bridging mode. Such a π-coordinated double bond might be activated and manifest enhanced reactivity. The reaction of only one equivalent of aziridine per PdL_2Cl_2 [L_2 = cod, $(PhCN)_2$] might give the expected Pd[κ^2-

Table 2. Hydrogen bonds (Å) and angles (°) in complex **7**: *cis*-dichlorobis(2,2-dimethyl-3-phenyl-3-allylaziridine) palladium(II)

N(1A)···Cl(1B)	3.370(4)	N(1B)···Cl(1A)	3.317(4)
N(1A)—H(N1A)	0.90(6)	N(1B)—H(N1B)	0.89(4)
H(N1A)···Cl(1B)	2.49(5)	H(N1B)···Cl(1A)	2.52(6)
N(1A)—H(N1A)···Cl(1B)	165(6)	N(1B)—H(N1B)···Cl(1A)	149(5)
N(2A)···Cl(2B)	3.421(4)	N(2B)···Cl(2A)	3.327(4)
N(2A)—H(N2A)	0.89(5)	N(2B)—H(N2B)	0.89(6)
H(N2A)···Cl(2B)	2.63(6)	H(N2B)···Cl(2A)	2.44(5)
N(2A)—H(N2A)···Cl(2B)	147(6)	N(2B)—H(N2B)···Cl(2A)	170(6)

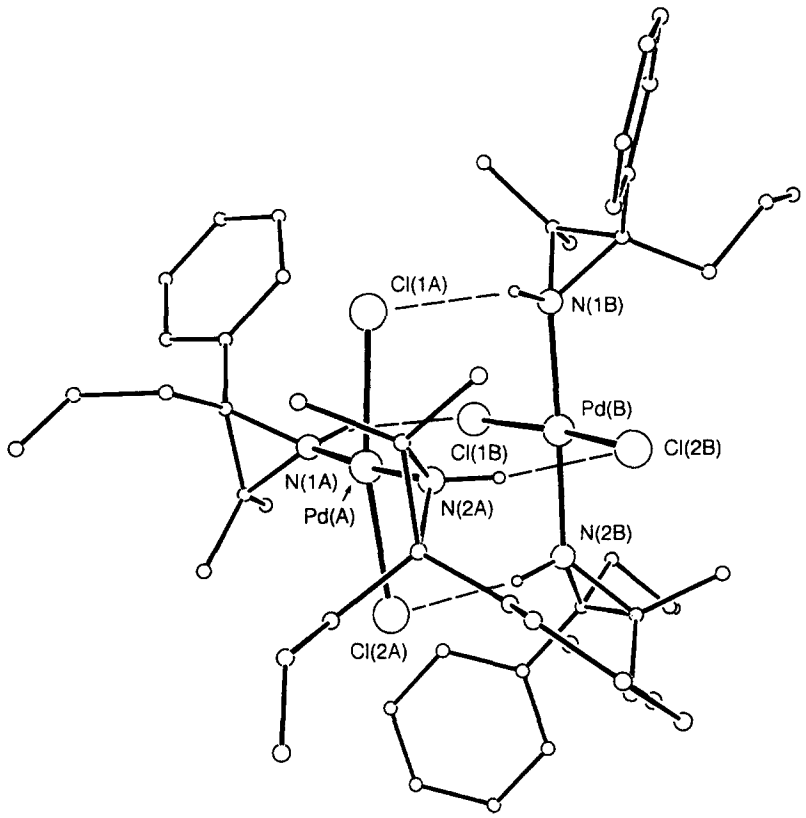

Fig. 1. Perspective view of two molecules of complex **7** illustrating the intermolecular hydrogen bond interactions.

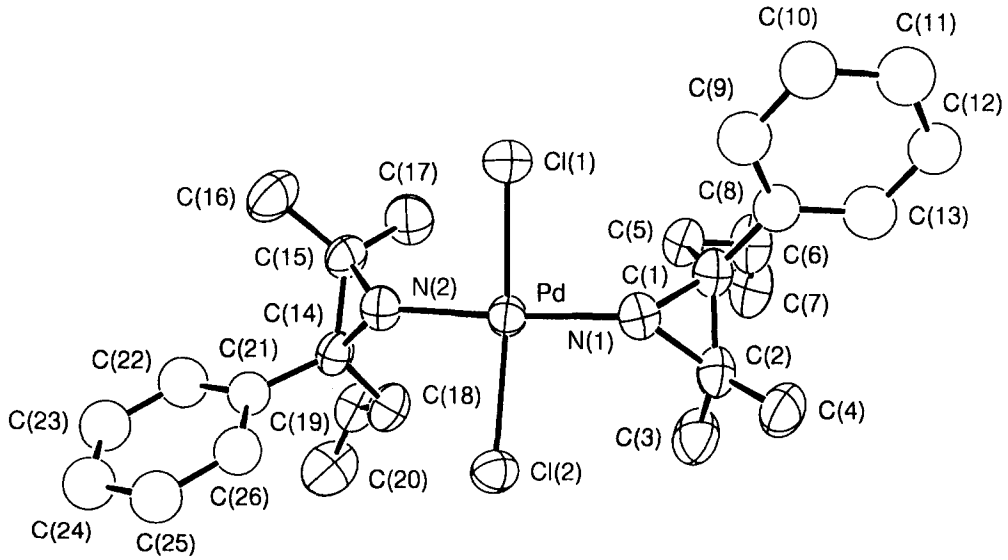

Fig. 2. ORTEP representation of molecule of complex **7**.

N,C=C)Az]Cl_2 species, but actually gives only an equimolar mixture of the starting material and the disubstituted complex $PdAz_2Cl_2$. Another possibility lies in the methatetical exchange of chloro ligands of the pre-formed $Pd(Az)_2Cl_2$ by non-coordinating anions, like tetrafluoroborate or hexafluorophosphate by means of the silver or thallium salt, giving rise to a cationic complex **12** (Scheme 3).

A third way going through the preliminary formation of a cationic complex and further addition of

Table 3. Selected bond lengths (Å) and angles (°) in molecules A and B of complex **7**

	Molecule **A**	Molecule **B**
Palladium environment		
Pd—Cl(1)	2.301(1)	2.302(2)
Pd—Cl(2)	2.303(1)	2.313(2)
Pd—N(1)	2.037(4)	2.039(4)
Pd—N(2)	2.028(4)	2.033(3)
Cl(1)—Pd—Cl(2)	169.19(4)	170.73(4)
Cl(1)—Pd—N(1)	88.6(1)	92.6(1)
Cl(1)—Pd—N(2)	88.0(1)	89.7(1)
Cl(2)—Pd—N(1)	93.0(1)	88.1(1)
Cl(2)—Pd—N(2)	90.1(1)	89.0(1)
N(1)—Pd—N(2)	176.6(2)	175.5(2)
Ligand		
N(1)—C(1)	1.494(6)	1.502(6)
C(1)—C(2)	1.506(7)	1.497(8)
C(2)—N(1)	1.502(6)	1.487(7)
C(1)—C(5)	1.524(7)	1.505(8)
C(1)—C(8)	1.505(8)	1.500(8)
C(5)—C(6)	1.474(9)	1.490(10)
C(6)—C(7)	1.269(11)	1.201(16)
C(14)—C(15)	1.508(6)	1.507(7)
C(15)—N(2)	1.499(6)	1.482(6)
C(14)—C(18)	1.521(7)	1.512(8)
C(14)—C(21)	1.494(7)	1.501(7)
C(18)—C(19)	1.507(9)	1.516(8)
C(19)—C(20)	1.263(12)	1.252(12)
Pd—N(1)—C(1)	127.0(3)	127.6(3)
Pd—N(1)—C(2)	132.2(3)	133.5(3)
C(1)—N(1)—C(2)	60.4(3)	60.1(3)
Pd—N(2)—C(14)	131.6(3)	134.0(3)
Pd—N(2)—C(15)	128.1(3)	129.1(3)
C(14)—N(2)—C(15)	60.4(3)	60.7(3)
N(1)—C(1)—C(2)	60.1(3)	59.4(3)
N(1)—C(2)—C(1)	59.5(3)	60.4(3)
C(1)—C(5)—C(6)	113.7(5)	114.0(5)
C(5)—C(6)—C(7)	126.2(8)	132.4(9)
N(2)—C(14)—C(15)	59.8(3)	59.1(3)
N(2)—C(15)—C(14)	59.7(3)	60.3(3)
C(14)—C(18)—C(19)	112.3(4)	112.5(5)
C(18)—C(19)—C(20)	125.8(7)	128.0(8)

Estimated standard deviations in the least significant digit are given in parentheses.

aziridine does not work either. Finally, addition of triphenylphosphine on the $Pd(Az)_2Cl_2$ species with various PPh_3/Pd ratios only induces the substitution of the aziridine ligand by the phosphorus ligand without any formation of mixed complexes containing both types of ligand. Only $Pd(PPh_3)_2Cl_2$ is detected in the reaction mixture beside the starting complex. This observation is in agreement with the fact that neither $Pd(PPh_3)_4$ nor $Pd(PPh_3)_2Cl_2$ reacts with aziridine. Such behavior is very similar to that observed with cyclic aminophosphonite ligands, for which rhodium complexes always exhibit bidentate κ^2-P, N chelation, whereas palladium prefers the monodentate κ^1-P mode in most of the characterized complexes [2].

EXPERIMENTAL

All manipulations were performed under argon atmosphere. All solvents were dried by standard methods and distilled before use. The starting allyl and vinylaziridines **1–4**, palladium complexes $PdCl_2(PhCN)_2$ and $PdCl_2(cod)$ were prepared according to literature methods [15,16].

Spectroscopic measurements were performed with the following equipment. IR: Perkin–Elmer 597 and FT-IR 1725 X (Nujol mull or film between KBr plates or in solution). NMR: Bruker AC 200 (^1H, 200.13 MHz; ^{13}C, 50.32 MHz, TMS as external standard; ^{31}P, 81.01 MHz, H_3PO_4 85% in D_2O as external/internal standard, in a coaxial capillary tube).

Elemental analyses were obtained from the Service d'Analyse du Laboratoire de Chimie de Coordination du CNRS in Toulouse and the Service Central d'Analyse du CNRS in Solaize.

Syntheses of new aziridines **5** *and* **6**

The cyclohexyl-2-spiro-3-phenyl-3-allyl aziridine **5** was prepared by the action of 30 mmol of magnesium allyl bromide in THF with 15 mmol of cyclohexyl-2-spiro-3-phenyl azirine according to the method described by the literature [15]. The crude was distilled *in vacuo* leading to **5** with 85% yield. Anal. $C_{16}H_{21}N$

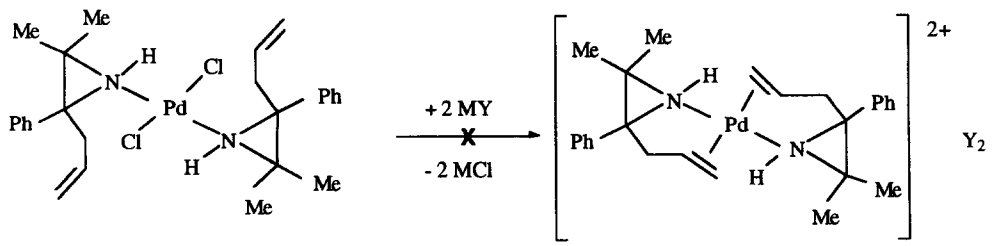

7 **12**

Scheme 3.

(277) Calc.: C, 84.54; H, 9.30; N, 6.16 Found: C, 84.95; H, 9.34; N, 5.93 NMR ($CDCl_3$): δ (^1H): 1.40–2.10 (m, 11H); 2.29–2.95 (m, 2H); 4.83–4.92 (m, 2H); 5.55–5.71 (m, 1H); 7.2–7.9 (m, 5H Ph).

δ (^{13}C): 24.23 (t); 25.13 (t); 25.52 (t); 31.74 (t); 33.76 (t); 40.06 (t); 46.18 (s); 51.05 (s); 116.61 (t); 126.07 (d, Ph); 127.46 (d, Ph); 127.88 (d, Ph); 128.63 (d, Ph); 134.19 (d); 141.29 (s, Ph).

The cyclohexyl-2-spiro-3-phenyl-3-vinyl aziridine **6** was prepared in the same manner as **5** and purified by silica gel column chromatography using a mixture of 50% ether-50% petroleum ether as eluent and leading to 6H with 50% yield. NMR ($CDCl_3$): δ (^1H): 1.01–1.70 (m, 11H); 4.94 (dd, 1H, $J = 20$ Hz, $J' = 2$ Hz); 5.15 (dd, 1H, $J = 12$ Hz, $J' = 2$ Hz); 6.16 (dd, 1H, $J = 18$ Hz, $J' = 7$ Hz); 7.2–7.4 (m, 5H Ph).

δ (^{13}C): 24.37 (t); 25.42 (t); 25.66 (t); 31.83 (t); 33.24 (t); 48.45 (s); 53.11 (s); 116.55 (t); 126.52 (d, Ph); 127.90 (d, Ph); 128.42 (d, Ph); 138.89 (d); 139.79 (s, Ph).

Syntheses of palladium complexes **7–11**

The dichlorobis(2,2-dimethyl-3-phenyl-3-allyl-aziridine)$_2$palladium(II) **7** was prepared by dropwise addition of a solution of 385 mg of aziridine **1** (2.06 mmol) in CH_2Cl_2 (5 cm^3) to a solution of 500 mg of $PdCl_2(PhCN)_2$ (1.03 mmol)] in the same solvent (10 cm^3). After stirring for 15 min and having removed 75% of the solvent *in vacuo*, the addition of 5 cm^3 of petroleum ether caused the immediate precipitation of a yellow solid. The precipitate was filtered off, washed with petroleum ether and crystallised from a mixture of 50% ether and 50% petroleum ether leading to 540 mg (95% yield) of complex **7**. The same complex **7** was also obtained from $PdCl_2$(cod): a solution of 419 mg of **1** (2.24 mmol)] in toluene (15 cm^3) was added dropwise to a solution of 320 mg of $PdCl_2$(cod) (1.12 mmol)] in the same solvent (5 cm^3). The colour turned yellow. After 4 h of stirring, the solution was evacuated to dryness and the crude was then dissolved in 5 cm^3 of hexane and maintained for a night in the freezer. A precipitate appeared which was filtered off, leading to 605 mg (97% yield) of **7**. Anal. $C_{26}H_{34}N_2PdCl_2$ (551.30) Calc.: C, 56.59; H, 6.21; N, 5.1 Found: C, 56.88; H, 6.33; N, 5.9. NMR ($CDCl_3$): δ (^1H): 1.20 and 1.33 (s, 3H); 1.86 (s, 3H); 3.18 (m, 2H); 3.92 (s broad, NH); 4.75–5.16 (m, 2H); 5.5–6.06 (m, 1H); 7.1–7.6 (m, 5H Ph).

δ (^{13}C): 21.70 and 21.95 (q); 25.18 and 25.41 (q); 42.71 and 43.16 (t); 46.12 and 46.41 (s); 54.17 and 54.43 (s); 118.43 (t); 127.35 and 127.70 (d, Ph); 127.85 (d, Ph); 128.17 and 128.39 (d, Ph); 129.11 and 129.39 (d, Ph); 133.25 and 133.35 (d); 137.72 and 138.07 (s, Ph).

Complexes **8–11** were synthesized by the first method used for complex **7**.

Dichlorobis(2,2-dimethyl-3-phenyl-3-vinylaziridine)$_2$ palladium(II), **8** (*yield*: 98%). Anal. $C_{24}H_{30}N_2PdCl_2$ (527.30) Calc.: C, 55.06; H, 5.77; N, 5.35; Cl, 13.55; Pd, 20.33 Found: C, 55.09; H, 6.03; N, 5.23; Cl, 13.87; Pd, 20.27. NMR ($CDCl_3$): δ (^1H): 1.25 and 1.33 (s, 3H); 1.84 and 1.86 (s, 3H); 4.06 and 4.39 (s broad, NH); 4.78 and 4.84 (2d, 1H, $J = 16$ Hz, $J' = 17$ Hz); 5.35 and 5.39 (2d, 1H, $J = 10.3$ Hz, $J' = 10.5$ Hz); 6.77 (dd, 1H, $^3J = 18$ Hz, $^3J' = 11$ Hz); 7.22–7.59 (m, 5H, Ph).

δ (^{13}C): 23.29 (q); 25.27 and 25.35 (q); 47.96 and 48.08 (s); 55.24 and 55.34 (s); 118.85 and 119.08 (t); 127.64 (d, Ph); 127.70 and 127.88 (d, Ph); 129.68 (d, Ph); 129.94 (d, Ph); 135.93 and 136.18 (s, Ph); 138.92 and 139.20 (d).

Dichlorobis(2-methyl-3-phenyl-3-vinylaziridine)$_2$ palladium(II), **9** (*yield*: 55%). NMR ($CDCl_3$): δ (^1H): 1.10 (d, 3H, $J = 7$ Hz); 1.67 (s, broad 1H, NH); 3.47 (q, 1H, $J = 7$ Hz); 4.97 (d, 1H, $J = 17$ Hz); 5.5 (d, 1H, $J = 11$ Hz); 6.76 (dd, 1H, $J = 17$ Hz, $J' = 11$ Hz); 7.3–7.9 (m, 5H, Ph).

δ (^{13}C): 15.47 and 15.50 (q); 42.76 and 42.87 (d); 53.59 and 53.64 (s); 119.38 and 119.46 (t); 128.48 and 128.51 (d, Ph); 128.57 and 128.76 (d, Ph); 129.14 (d, Ph); 129.50 (d, Ph); 132.12 and 132.82 (d, Ph); 137.75 and 137.82 (s, Ph); 140.32 and 140.43 (d).

Dichlorobis(cyclohexyl-2-spiro-3-phenyl-3-allylazi ridine)$_2$palladium(II), **10** (*yield*: 97%). Anal. $C_{32}H_{42}N_2PdCl_2$ (632.0) Calc.: C, 60.81; H, 6.70; N, 4.43. Found: C, 60.83; H, 7.26; N, 4.41. NMR ($CDCl_3$): δ (^1H): 1.40–1.80 (m, 10H); 2.10–2.50 (m, 2H); 2.80–3.20 (1H, NH); 4.80–5.10 (m, 2H); 5.50–6.01 (m, 1H); 7.20–7.30 (m, 5H Ph).

δ (^{13}C): 24.37 and 24.45 (t); 25.21 and 25.58 (t); 29.41 and 29.55 (t); 33.65 and 34.50 (t); 39.40 and 39.80 (t); 42.46 and 42.91 (t); 51.38 and 51.66 (s); 56.42 and 56.82 (s); 118.14 and 118.25 (t); 126.62 and 126.88 (d, Ph); 127.30 and 127.42 (d, Ph); 127.81 (d, Ph); 128.11 and 128.28 (d, Ph); 133.35 and 133.79 (d); 137.68 and 138.01 (s, Ph).

Dichloro(cyclohexyl-2-spiro-3-phenyl-3-vinylaziridine)$_2$palladium(II), **11** (*yield*: 95%). NMR ($CDCl_3$): δ (^1H): 0.70–2.20 (m, 10H); 2.30–2.60 (m, 1H); 4.90 (dd, 1H, $J = 20$ Hz, $J' = 4$ Hz); 5.35 (dd, 1H, $J = 14$ Hz, $J' = 2$ Hz); 6.05–6.90 (m, 1H); 7.0–7.7 (m, 5H Ph).

δ (^{13}C): 21.39 and 21.41 (t); 24.07 and 24.31 (t); 29.57 and 29.60 (t); 34.32 and 34.56 (t); 36.92 (t); 41.66 (s); 53.25 (s); 119.52 and 120.08 (t); 127.67 and 127.76 (d, Ph); 127.93 and 128.15 (d, Ph); 128.34 (d, Ph); 128.59 (d, Ph); 132.01 and 132.6 (d, Ph); 136.79 and 136.87 (d); 139.01 (s, Ph)

X-ray diffraction study of complex **7**

Suitable monocrystals of **7** were grown by slow evaporation of a solution of 0.5 g of **7** in a THF 25/petroleum ether 75 mixture and contained 5% of THF: $[C_{26}H_{34}N_2Cl_2Pd]$ 5% THF. X-ray diffraction measurements are summarized in Table 4.

The treatment of intensity data uses the following

Table 4. Crystal data, experimental details of the X-ray diffraction study

Crystal Parameters at 20°C from a least-squares fit of the setting angles of 25 reflections with $12.1° < \theta < 16.6°$

Chem. Formula:	$C_{26.2}OH_{34.40}Cl_2N_2O_{0.05}Pd$
Fw = 555.46	$\lambda = 0.71073$ Å
Crystal habit	red parallelepiped
Crystal dimensions	$0.50 \times 0.45 \times 0.30$ mm
Crystal system	Monoclinic
Absences:	hkl, $h+k+l = 2n+1$, $h0\,1$, $h,l = 2n+1$
Space Group: I2/a (No. 15)	$a = 19.909(2)$ Å
$b = 24.857(3)$ Å	$c = 23.237(3)$ Å, $\beta = 102.990(9)°$
$Z = 16$	$V = 11205(2)$ Å^3
$\rho_{calc} = 1.317$ g.cm^{-3}	$\mu = 0.868$ mm^{-1}, $F(000) = 4576$

Measurement of intensity data

Instrument: Enraf–Nonius CAD4	Scan speed: 1.10–8.24°/min
Radiation: Mo-Kα	($\lambda = 0.71073$ Å) graphite monochromated
Max 2θ 47°	(h 0.21 k 0.27 l −26.26)
Detector window	Height 4.0 nm
Standard	Intensity 3 refl. every 2 h
Width 4.0 mm	Orientation 3 refl. every 400 data refl.
Scan mode ω–2θ	Take-off angle 4.0°
Scan range $(0.80+0.35\tan\theta)°$	No. of refl. collected 7817

procedure: Reduction to F_O^2 and $\sigma(F_O^2)$, corrections for backgrounds, attenuator and LP in the usual manner [19]. No significant standards variation (±0.9%). Empirical absorption corrections [20] ($T_{min} = 0.9621$, $T_{max} = 0.9998$). All measured reflections were unique and used. No. of observed data [$F_O^2 > 2\sigma(F_O^2)$]: 5818.

Structure solution and refinement use direct methods using SHELXS-86 [21]. Full-matrix least-squares refinement using SHELXL-93 [22]. Two independent molecules in the asymmetric unit and one solvent molecule (i.e. THF, O atom in special position refined with an occupancy factor of 0.10 and 2 C atoms with an occupancy factor of 0.20). All non-H atoms anisotropic, except those of phenyl rings and of solvent molecule which were refined isotropically. H atoms bonded to C atoms were introduced in calculations in idealized geometry [d(C—H) = 0.97 Å]. H atoms bonded to N atoms were allowed to vary. All hydrogen thermal parameters were isotropic and kept fixed in final refinement cycles. Scattering factors were taken from 'International Tables for X-ray Crystallography' [23]. Refinement on F_O^2 for all reflections (7817). Weighted R-factors wR and goodnesses of fit S are based on F_O^2, conventional R-factors R are based on F_O, with F_O set to zero for negative F_O^2. Last refinement cycle: wR(all) = 0.1009, R(all) = 0.0632, wR(obs) = 0.0866, R(obs) = 0.0364 with 5818 obs. reflections > $4\sigma(F_O)$, 461 variable parameters, $w = [\sigma^2(F_O^2) + (0.0457\ P)^2 + 40.5368\ P]^{-1}$ where $P = (F_O^2 + 2F_O^2)/3$, S(all) = 1.026, S(obs) = 1.031, max. shift/esd = 0.056, mean shift/esd = 0.002, max. and min. residual peaks of 0.502 and 0.519 e/Å^3.

Acknowledgements—The authors are grateful to the CNRS for support and to Dr I. Tkatchenko and D. Ballivet-Tkatchenko for fruitful discussions.

REFERENCES

1. Bauer, R. S., Chung, H., Glockner, P. W. and Keim, W., *US Patent* 3,644,563 (1972).
2. Agbossou, S., Bonnet, M. C., Dahan, F. and Tkatchenko, I., *Acta Crystallogr., Sect. C*, 1989, **45C,** 1149, and refs therein.
3. Ben Cheikh, R., Bonnet, M. C., Chaabouni, R. and Dahan, F., *J. Organomet. Chem.*, 1992, **438,** 217.
4. Jackson, T. B. and Edwards, J. O., *Inorg. Chem.*, 1962, **1,** 398.
5. Porta, F., Pizzotti, M., La Monica, G., Finessi, L. A., Cenini, S., Bellon, P. L. and Demartin, F., *J. Chem. Soc., Dalton Trans.*, 1984, 2409.
6. Belluco, U., Michelin, R. A., Ros, R., Bertani, R., Facchin, G., Mozzon, M. and Zanotto, L., *Inorg. Chim. Acta*, 1992, **198–200**, 883 and refs therein.
7. Tanner, D., Andersson, P. G., Harden, A. and Somfai, P., *Tetrahedron Lett.* 1994, **35,** 4631; Andersson, P. G., Harden, A., Tanner, D. and Norrby, P.-O., *Chem. Eur. J.*, 1994, **1,** 12; Tanner, D., Harden, A., Johansson, F., Wyatt, P. and Andersson, P. G., *Acta Chem. Scand.*, 1996, **50,** 361.
8. Hauck, T., Sünkel, K. and Beck, W., *Inorg. Chim. Acta*, 1995, **235,** 391.
9. Spears, G. W., Nakanishi, K. and Ohfune, Y., *Synlett*, 1991, 91; Tanner, D. and Somfai, P., *Bioinorg. Medic. Chem. Lett.*, 1993, **3,** 2415; Khumtaveeporn, K. and Alper, H., *Acc. Chem. Res.*, 1995, **28,** 414, and refs therein.
10. Baeg, J.-O., Bensimon, C. and Alper, H., *J. Am. Chem. Soc.*, 1995, **117,** 4700 and refs therein.
11. Fugami, K., Morizawa, Y., Oshima, K. and Nozaki, H., *Tetrahedron*, 1985, **26,** 857; Fugami, K., Miura, K., Morizawa, Y., Oshima, K., Utimoto, K. and Nozaki, H., *Tetrahedron*, 1989, **45,** 3089.
12. Mimura, N., Ibuka, T., Akaji, M., Miwa, Y., Taga, T., Nakai, K., Tamamura, H., Fujii, N. and Yamamoto, Y., *Chem. Commun.*, 1996, 351.
13. Satake, A., Shimizu, I. and Yamamoto, A., *Synlett.*, 1995, 64.
14. Lim, Y. and Lee, W. K., *Tetrahedron Lett.*, 1995, **36,** 8431.
15. Chaabouni, R., Laurent, A. and Marquet, B., *Tetrahedron*, 1980, **36,** 877.
16. Sato, S., *Bull. Chem. Soc. Jpn*, 1967, **6,** 1440.
17. Hassner, A., Bunnell, C. A. and Haltiwanger, K., *J. Org. Chem.*, 1978, **43,** 57.

18. Orpen, A. G., Brammer, L., Allen, F. H., Kennard, O., Watson, D. G. and Taylor, R., *J. Chem. Soc., Dalton Trans.*, 1989, S1 17. *CRC Handbook of Chemistry and Physics*, p. **9**–4, 75th Ed., CRC Press Boca Raton, U.S.A. (1994).
19. Fair, C. K., *MolEN. Structure Solution Procedures*, Enraf–Nonius, Delft, Holland, 1990.
20. North, A. C. T., Phillips, D. C. and Matthews, F. S., *Acta Crystallogr., Sect. A*, 1968, **A21,** 351.
21. Sheldrick, G. M., *SHELXS*-86. *Program for Crystal Structure Solution*, Univ. of Göttingen, Göttingen, FRG, 1986.
22. Sheldrick, G. M., *SHELXL*-93. *Program for the Refinement of Crystal Structures from Diffraction Data*. Univ. of Göttingen, Göttingen, FRG, 1993.
23. *International Tables for Crystallography*, Tables 4.2.6.8 and 6.1.1.4., Vol. C, Kluwer Academic Publishers, Dordrecht, The Netherlands (1992).

Pergamon

PII: S0277-5387(97)00237-4

Polyhedron Vol. 17, No. 1, pp. 193–197, 1998
© 1997 Elsevier Science Ltd
All rights reserved. Printed in Great Britain
0277-5387/98 $19.00+0.00

Characterization of a novel $[Sm(HMPA)_4I_2]I$ complex by positive ion fast atom bombardment and high resolution mass spectrometry

A. Cabrera,[a]* M. Salmón,[a] N. Rosas,[a] J. Pérez-Flores,[a] L. Velasco,[a]* G. Espinosa-Pérez[a] and J. L. Arias[b]

[a] Instituto de Química UNAM Circuito Exterior Coyoacán 04510 México D.F.

[b] Facultad de Estudios Superiores Cuautitlán UNAM Cuautitlán Izcalli, Estado de México, México

(Received 24 January 1997; accepted 12 May 1997)

Abstract—A positive-ion Fast Atom Bombardment (FAB) study was performed to determine the structure of samarium(III) triiodine complex (**I**). Collision Induced Dissociation (CID) and High Resolution Mass Spectrometry were used to establish the fragmentation pattern of the $C_{24}H_{72}O_4N_{12}P_4I_3Sm$ compound. The structure of (**I**) was confirmed by X-ray analysis. © 1997 Elsevier Science Ltd

Keywords: samarium complex; mass spectrometry; fast atom bombardment; collision induced dissociation; α,β-unsaturated ketones.

Samarium diiodide, a unique one-electron transfer reagent first introduced by Kagan and coworkers [1] has become the focus of growing interest in organic chemistry [2], mainly because in some processes [3] the reactions can be strongly accelerated with the addition of hexamethyl phosphoramide (HMPA) ligand $[(CH_3)_2N]_3PO$. As a part of our research program, we studied the behavior of SmI_2/HMPA system in the reductive coupling of α,β-unsaturated ketones. At the end point of the named reaction, we were able to isolate two crystalline coordination compounds as by-products highly sensitive to moisture; both ionic solids were non volatile compounds to give the conventional mass spectra, however one of them, using Fast Atom Bombardment technique (FAB) afforded an excellent spectrum. In this contribution the structure of the compound (**I**) is suggested based on the use of collisional induced dissociation (CID) [4,5] and high resolution mass spectrometry. The structure of **I** was finally confirmed by the X-ray diffraction study [6].

* Authors to whom correspondence should be addressed.

RESULTS AND DISCUSSION

The main fragmentation pathway of $[Sm(HMPA)_4I_2]I$ (**I**) has been investigated with the aid of high resolution data, the highest peak observed (a) at *m/z* 1122 is proposed for this process (Scheme 1) and Figs 1–2, where the CID spectra is represented. The elemental composition for (a) was found to be $C_{24}H_{72}O_4N_{12}P_4I_2Sm$ (Table 1) (1122.2037 observed) which suggests that the I^- ion was lost from the molecular ion (*m/z* 1249); the M—I^- fragmentation is supported by the *m/z* 127 (I^-) fragment observed in negative ion (FAB) mass spectra of compound (**I**) and also because the elemental analysis of the named complex $[C_{24}H_{72}O_4N_{12}P_4I_2]^+I^-$ affords 30.66% of Iodine (found) and 30.50% (calc.). Other primary fragmentations observed in the mass spectra of (**I**) are due to the loss of HMPA ligands yielding the species (b) at *m/z* 943 $C_{18}H_{54}O_3N_9P_3I_2Sm$ (943.0867), (c) at *m/z* 764 $C_{12}H_{36}O_2N_6P_2I_2Sm$ (763.9619) and (d) at *m/z* 585 $C_6H_{18}ON_3PI_2Sm$ (584.8469), this last peak gives (e) for expulsion of I^- radical with *m/z* 458 $C_6H_{18}ON_3$ PISm (457.9421). A secondary fragmentation of ion

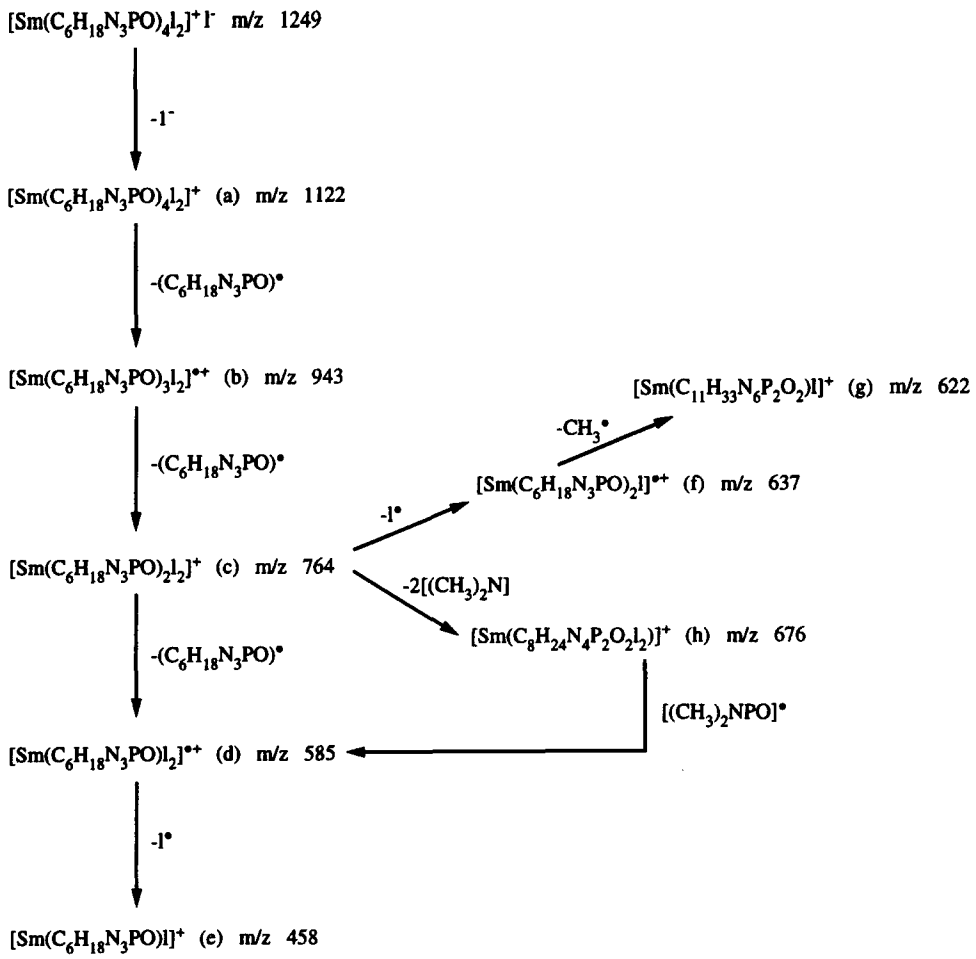

Scheme 1.

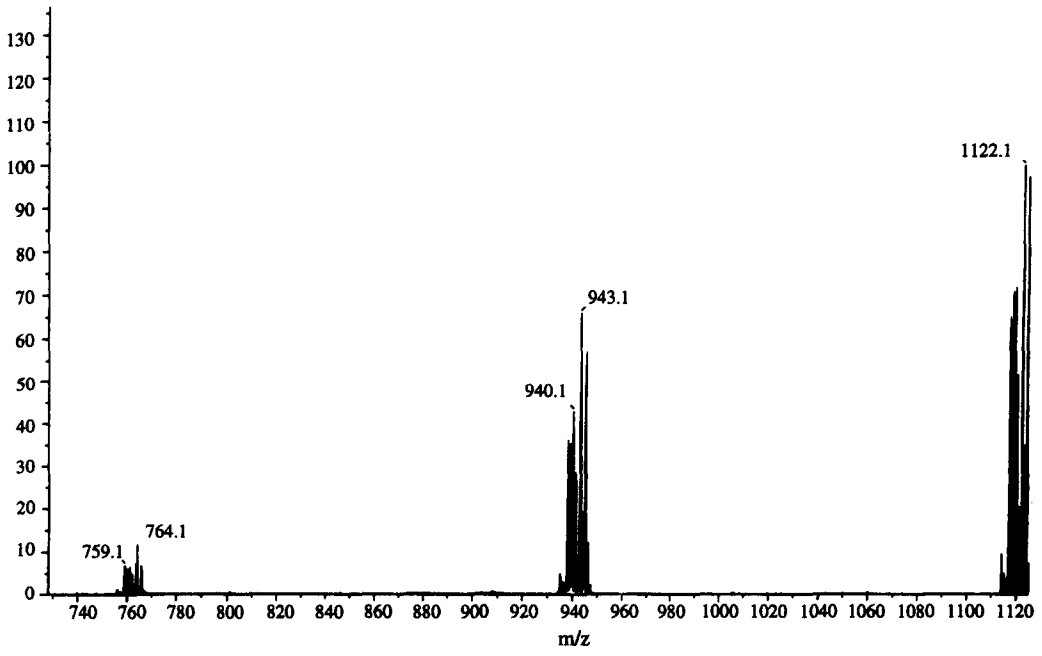

Fig. 1. Linked scan at constant (B/E) spectra of fragment (a).

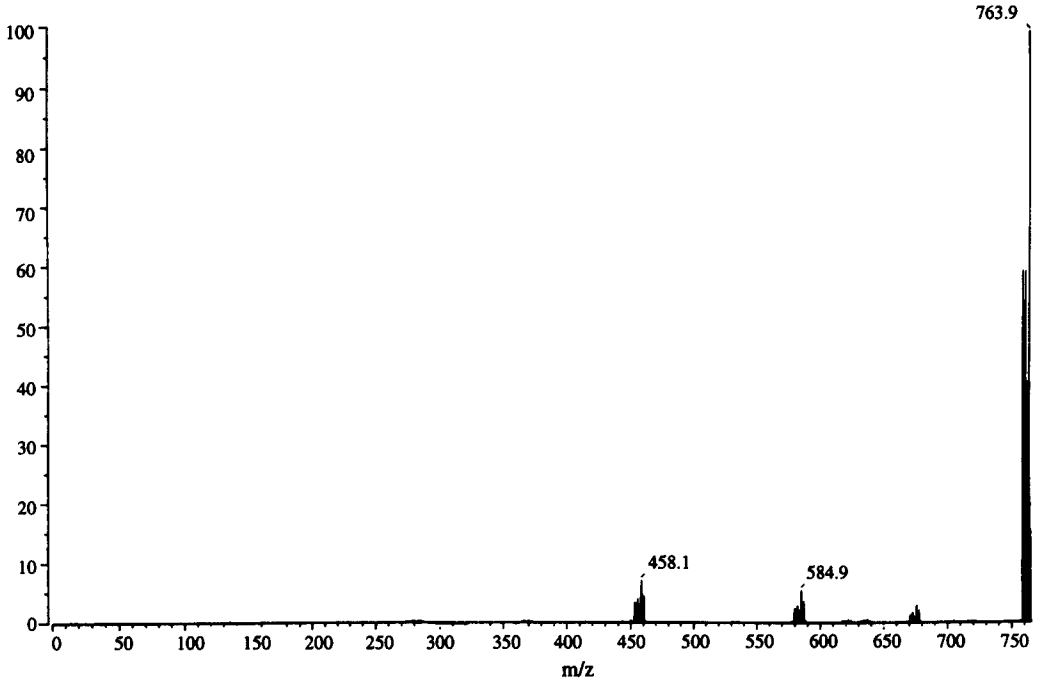

Fig. 2. Linked scan at constant (B/E) spectra of fragment (c).

Table 1. Elemental composition of ions produced by FAB

Fragment	Composition	*m/z* Observed	*m/z* Estimated	Error (ppm)
a	$C_{24}H_{72}O_4N_{12}P_4I_2Sm$	1122.2037	1122.2045	+0.7
b	$C_{18}H_{54}O_3N_9P_3I_2Sm$	943.0867	943.0849	+1.9
c	$C_{12}H_{36}O_2N_6P_2I_2Sm$	763.9619	763.9662	−5.6
h	$C_8H_{24}O_2N_4P_2I_2Sm$	675.8683	675.8661	+3.2
f	$C_{12}H_{36}O_2N_6P_2ISm$	637.0623	637.0617	+0.9
g	$C_{11}H_{33}O_2N_6P_2ISm$	622.0388	622.0382	+0.9
d	$C_6H_{18}ON_3PI_2Sm$	584.8469	584.8774	−0.9
e	$C_6H_{18}ON_3PISm$	457.9421	457.9430	−1.9

(c) gives the (f), (g) and (h) fragments. The elemental composition $C_{12}H_{36}O_2N_6P_2ISm$ (637.0623) for (f), $C_{11}H_{33}O_2N_6P_2ISm$ (622.0388) for (g) and $C_8H_{24}O_2N_4P_2I_2Sm$ (675.8683) for (h) are in agreement with the proposed pattern shown in scheme 1. The structure of samarium complex (**I**) determined by X-ray diffraction and shown in Figs. 3 and 4 agrees with the mass spectrometry study reported here.

EXPERIMENTAL

The FAB mass spectra were obtained with a Jeol SX 102 Double-Focusing mass spectrometer with reverse geometry using a 6 Kv Xenon Beam (10 mA); *m*-Nitrobenzyl alcohol was used as matrix for recording the mass spectra, the samples were dissolved in acetone. The FAB desorbed ions were accelerated to 10 KeV. The range of the mass measurement was set so as to cover at least two standard peaks which encompassed the sample peak. The mass calibration was carried out by interpolation of two signals observed in the spectrum of polyethyleneglycol 1500 (1207.7261 and 1251.7524). The mass resolution and scanning speed used were 10,000 and 120 s/decade, respectively. The accurate mass was given as the mean value of the masses observed 5–10 scans of mass spectra and determined from mass centroids of $[M+H]^+$ peaks. Elemental compositions for the accurate mass were calculated within an error of 10 ppm by using the program installed in the above system. The CID spectra were recorded with the same instrument using the constant B/E linked scan-technique. The Helium pressure in the first field-free region collision cell was adjusted until the main beam signal was reduced 50%. Each B/E scan spectrum reported here is the average of 5–10 scans. The general procedure used for the reductive coupling reaction was reported previously [7,8]. The two sensitive samarium complexes $[Sm(HMPA)_4I_2]I$ (**I**) and $[Sm(HMPA)_3(H_2O)]I_3$ [8],

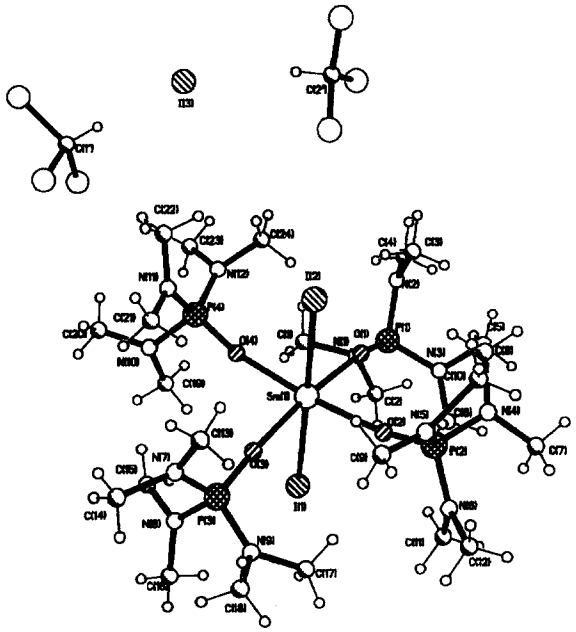

Fig. 3. View of molecules **1** and the atomic numbering. Select bond lengths (Å) and bond angle (°). Sm(1)—I(1): 3.118 (3), Sm(1)—I(2): 3.146 (3) Sm(1)—O(1): 2.299 (21), Sm(1)—O(2): 2.301 (20), Sm(1)—O(3): 2.270 (22), Sm(1)—O(4): 2.257 (20), I(1)—Sm(1)—I(2): 178.5 (1), I(1)—Sm(1)—O(1): 87.5 (5), I(2)—Sm(1)—O(1): 93.8 (5), I(1)—Sm(1)—O(2): 93.3 (5), I(2)—Sm(1)—O(2): 87.2 (5), I(1)—Sm(1)—O(3): 85.9 (6), I(2)—Sm(1)—O(3): 92.8 (6), I(1)—Sm(1)—O(4): 93.3 (5), I(2)—Sm(1)—O(4): 86.2 (5), O(1)—Sm(1)—O(2): 87.2 (7), O(1)—Sm(1)—O(3): 172.9 (8), O(2)—Sm(1)—O(3): 90.5 (8), O(1)—Sm(1)—O(4): 91.9 (7), O(2)—Sm(1)—O(4): 173.3 (7), O(3)—Sm(1)—O(4): 91.2 (7).

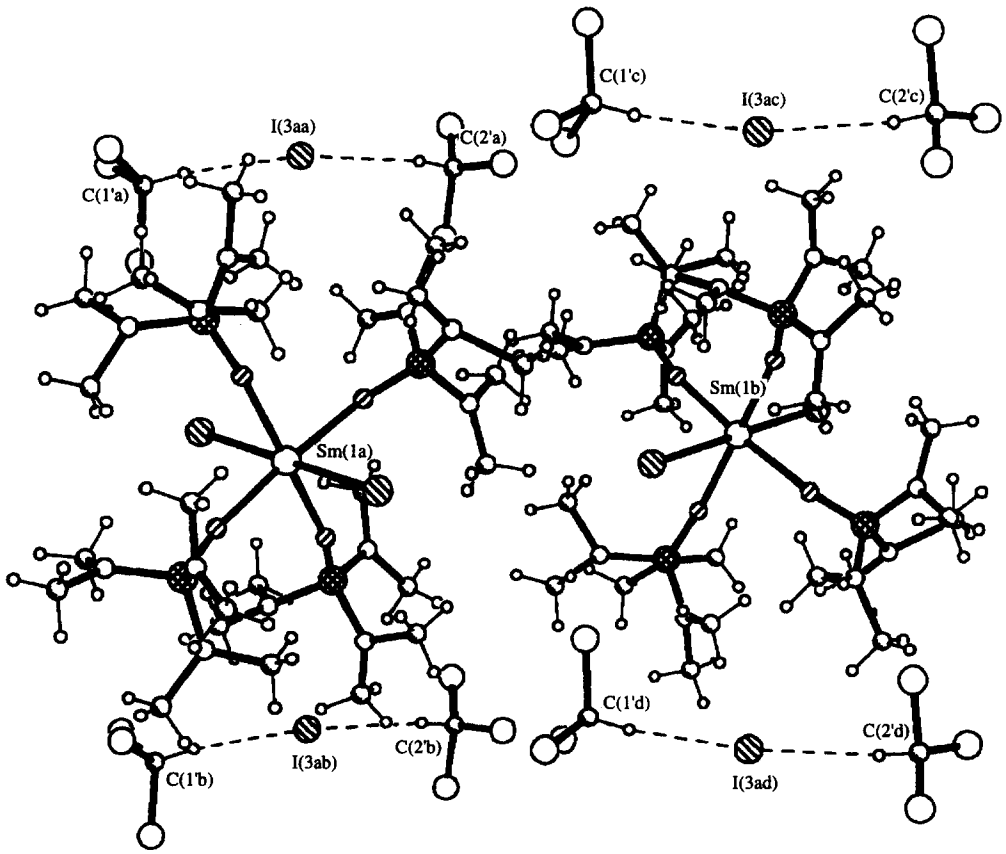

Fig. 4. The crystal packing arrangement of the Sm^{III} complex. $Cl_2C(2')$—H, $I^-(3)$ hydrogen bond: C(donor)—H and H···I(3): 0.96(0) Å and 3.04(4) Å. $Cl_3C(1')$—H, $I^-(3)$ hydrogen bond: C(donor)—H and H···I(3): 0.96(0) Å and 2.69(5) Å. C(donor)···I(3): 3.99(4) and 3.64(5) Å, respectively. The angle C(donor)—H···I(3): 170.6(6) and 172(1)°, respectively.

were isolated as by products from the α,β-insaturated ketones [9] cyclodimerization reaction promoted with SmI_2/HMPA system.

CONCLUSION

The structure of compound (**I**) was suggested based on the use of some soft ionization mass spectrometric techniques. The X-ray data was used to confirm the FAB-CID study.

REFERENCES

1. Girard, P., Namy, J. L. and Kagan, H. B., *J. Am. Chem. Soc.*, 1980, **102,** 2693.
2. See for example (a) Kagan, H. B. and Namy, J. L., *Tetrahedron*, 1986, **42,** 6573; (b) Soderquist, J. A. *Aldrichim Acta*, 1991, **24,** 15; (c) Kagan New, H. B. *J. Chem.*, 1990, **14,** 453; (d) Molander, G. *Chem. Rev.*, 1992, **92,** 29.
3. (a) Handa, Y., Inanaga, J. and Yamaguchi, M., *Chem. Commun.*, 1989, 298; (b) Inanaga; J., Handa, Y., Tabuchi, T., Otsubo, J., Yamaguchi, M. and Hanamoto, T. *Tetrahedron Lett.*, 1992, **32,** 6557.
4. The use of a collision gas to enhance fragmentation is referred to as collision-induced dissociation (CID). It is usually employed in conjunction with one of the metastable or linked scanning techniques. It is possible to distinguish the fragments formed as a result of the collision process from those that would have been formed in any case unimolecular dissociation of precursor ions.
5. Grahams Cooks, R., *J. Mass Spectrum.*, 1995, **30,** 1215.
6. Crystallographic data for $[SmI_2(HMPA)_4]I \cdot (CHCl_3)_2$: The yellow crystals of **1,** were grown from $HCCl_3$. FW = 1486.6, orthorhombic space group Pca21, $a = 21.855(4)$, $b = 13.534(2)$, $c = 20.362(6)$, $V = 6023(2)$, $D_c = 1.639$ g cm^{-3}, $Z = 4$, $F(000) = 2916$, μ(Mo-K_α) = 2.9 mm^{-1}. Final R = 7.95% (285 parameters), $R_w = 8.13\%$ for 3452 observed reflections with $F \geqslant 3\sigma F$ in the range $3.0 \leqslant \theta \leqslant 50°$. $T = 243$ K. Intensities were corrected for background, Lorentz and polarization effects. The structure was solved by direct methods and refined by full-matrix least-squares with anisotropic temperature factor for the Samarium, Iodine, Oxygen and Phosphorus atoms. The hydrogen atoms were included at idealized positions, all hydrogens with a fixed temperature factor $U = 0.08$ Å^2. The view of molecule **I** and the atomic numbering in Fig. 3, shown the Sm^{III} ion coordinated in *trans* position with two Iodine atoms and in coplanar position with four HMPA groups via the oxygen atoms. One I^- anion is located in the outer-sphere, with no bond to the central samarium atom showing interactions with two chloroform molecules via hydrogen bonds. In the unit cell the Sm^{III}-complex is confined between two layers of the solvent molecules (Fig. 4).
7. Cabrera, A. and Alper, H., *Tetrahedron Lett.*, 1992, **33,** 5007.
8. Cabrera, A., Rosas, N., Alvarez, C., Sharma, P., Toscano, A., Salmón, M. and Arias, J. L. *Polyhedron*, 1996, **15,** 2971.
9. The cyclodimerization of linear and aromatic α,β-insaturated ketones is actually under study.

Pergamon

PII: S0277-5387(97)00191-5

Polyhedron Vol. 17, No. 1, pp. 199–206, 1998
© 1997 Elsevier Science Ltd
All rights reserved. Printed in Great Britain
0277-5387/98 $19.00+0.00

Synthesis and characterization of nickel(II), zinc(II), copper(II), cobalt(II) and cobalt(III) complexes of α-dicarbonylbis(aroylhydrazone)

Laila El-Sayed, Magdi F. Iskander*, Nahed M. Hawash and Salah S. Massoud*

Department of Chemistry, Faculty of Science, Alexandria University, P.O. Box 426, Ibrahimia, Alexandria 21321, Egypt

(Received 3 December 1996; accepted 12 May 1997)

Abstract—A variety of α-dicarbonylbis(aroylhydrazone) H_2L (**1**) ligands were synthesized and used to synthesize complexes formulated as $NiL \cdot nH_2O$, $Zn_2L_2 \cdot nH_2O$, CuL, $CoL \cdot nH_2O$ and $Na[CoL(NO_2)_2]$, where L refers to the dinegative anion of α-dicarbonylbis(aroylhydrazone) ligand. These complexes were investigated by elemental analyses, IR and UV–vis spectra and, for zinc(II), $Na[CoL(NO_2)_2]$ and the anhydrous NiL complexes, ^1H NMR spectra were measured in order to elucidate their structures. Other octahedral complexes such as $Ni(H_2L)_2(OAc)_2$ and $Co(HL)_3 \cdot nH_2O$ were isolated and characterized. Different modes of coordination were assigned to the ligand **1** and its anions in the isolated complexes; dinegative tetradentate, mononegative bidentate and neutral bidentate. © 1997 Elsevier Science Ltd

Keywords: Schiff bases; nickel(II) complexes; zinc(II) complexes; copper(II) complexes; cobalt(II) complexes; cobalt(III) complexes; α-dicarbonylbis(aroylhydrazone).

It has long been known that condensation of α-dicarbonyl compounds with aroylhydrazines affords the corresponding α-dicarbonylbis(aroylhydrazone) [1,2] compounds, H_2L (**1**). Due to the ability of these compounds to form coloured products with various metal ions, they have been used as analytical reagents [3–7].

Most of the information about the reactivity of α-dicarbonylbis(aroylhydrazone), (**1**), focused on their reactions with different oxidizing agents such as potassium ferricyanide [8], silver oxide [9], iodine [10], a mixture of mercuric oxide and iodine [9,10] and nickel peroxide [11]. The products of these reactions were found to vary considerably with the nature of the oxidizing agents [8–11].

Compounds **1** provide potentially tetradentate ligands with NNOO donor atoms which can form stable chelates with metal ions. In fact, the first metal complex of this type of ligands was [diacetylbis(benzoylhydrazone)(-2)]nickel(II) (**2**: $R = R' = CH_3$, $R'' = C_6H_5$; $M = Ni^{2+}$) [12] where it has been shown that the central nickel ion is in a distorted square–planar arrangement with the coordination of the two oxygen atoms in *cis*-configuration [13]. The following study was undertaken in order to shed the light on the chelating properties of α-dicarbonylbis(aroylhydrazone) compounds.

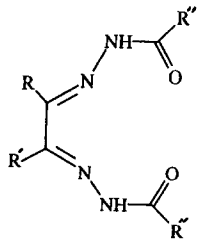

[1]

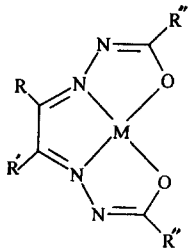

[2]

* Authors to whom correspondence should be addressed.

EXPERIMENTAL

Preparation of compounds

Organic ligands. Aroylhydrazones were generally prepared by the reaction of α-dicarbonyl compounds (glyoxal, phenylglyoxal, phenylmethylglyoxal, diacetyl, benzil) with two equimolar amounts of aroylhydrazine in an ethanol–water mixture (2 : 1). A few drops of conc. HCl or HOAc were added and the reaction mixture was refluxed for *ca* 30 min. The product was filtered and washed with ethanol-water mixture (1 : 1) and air dried (yield : 60–80%).

Metal complexes

Nickel(II) complexes. NiL : a hot suspension of α-dicarbonylbis(aroylhydrazone) (20 mmol) and KOH (20 mmol) in MeOH (30 cm^3) was treated with a hot solution of $Ni(OAc)_2 \cdot 4H_2O$ (10 mmol/20 cm^3 of MeOH). The reaction mixture was refluxed with stirring for 2 h. The precipitate was collected by filtration, recrystallized from chloroform or benzene and then dried *in vacuo* (yield : 60–75%). Crystallization of the pale green complex, $NiL \cdot 4H_2O$ derived from glyoxalbis(benzoylhydrazone) afforded the anhydrous form. With benzilbis(benzoylhydrazone), a grey–green precipitate insoluble in MeOH was obtained. Also, a dark green precipitate was obtained when the reaction was performed in DMSO. This was recrystallized from benzene.

$Ni(H_2L)_2(OAc)_2$ {$H_2L \equiv$ **1**: R = R′ = R″ = C_6H_5}. This complex was prepared by treating a hot solution of 10 mmol of benzilbis(benzoylhydrazone), dissolved in DMSO (20 cm^3) with a hot solution of $Ni(OAc)_2 \cdot 4H_2O$ (10 mmol) in MeOH (20 cm^3) and the reaction mixture was then refluxed for 1 h. The isolated pale yellow complex was crystallized from benzene–methanol solution (yield : 50% ; m.p. 70°C).

Copper(II) complexes. $CuL \cdot nH_2O$ (n = 0, 1/2, 1): these complexes were prepared in a similar manner to that described above for NiL complexes (yield : 40–60%) using excess NaOAc. In case of glyoxalbis(benzoylhydrazone), 2 equiv. of KOH were added instead of NaOAc.

$Cu(H_2L)_2X_2$ {$H_2L \equiv$ **1**: R = R′ = H, R″ = C_6H_5, p-$CH_3 \cdot C_6H_4$; X = OAc^-, Cl^-}. A hot methanolic solution of 10 mmol of $CuCl_2$ or $Cu(OAc)_2 \cdot 2H_2O$ and excess NaOAc was added dropwise to a hot suspension of glyoxalbis(aroylhydrazone) (20 mmol) in MeOH (20 cm^3). The reaction mixture was then refluxed with constant stirring for 4 h, after which the corresponding dichloro or diacetato complex was filtered off, washed with boiling methanol and dried *in vacuo*.

Zinc(II) complexes. $ZnL \cdot nH_2O$: these were prepared following procedures similar to those described for the corresponding NiL complexes. Shiny yellow complexes were isolated when solutions were reduced to small volumes (yield : 40–60%).

Cobalt(II) complexes. $CoL \cdot nH_2O$: an ethanolic solution of $CoCl_2 \cdot 6H_2O$ or $Co(OAc)_2 \cdot 4H_2O$ (10 mmol) was added to a hot suspension of 10 mmol of α-dicarbonylbis(aroylhydrazone) and KOH (20 mmol). The reaction mixture was refluxed for 30 min and volume was reduced by evaporation. The isolated brick-red complex was recrystallized from chloroform and dried *in vacuo* over P_4O_{10} (yield : 70–80%).

Cobalt(III) complexes. $Na[CoL(NO_2)_2] \cdot nH_2O$ (n = 0, 1/2, 1) : a hot ethanolic (40 cm^3) suspension of 20 mmol of the α-dicarbonylbis(aroylhydrazone) was treated dropwise with a hot solution of $Na_3[Co(NO_2)_6]$ (20 mmol), dissolved in H_2O (10 cm^3). The resulting solution which turned red was filtered while hot and evaporated to a small volume. The crude precipitate which was separated upon standing at room temperature was filtered off and recrystallized from absolute ethanol (yield : 40–50%). In case of benzilbis(benzoylhydrazone), crystallization of the crude product from chloroform afforded two complexes ; $Na[CoL(NO_2)_2]$ as an insoluble compound and $Co(HL)_3 \cdot 3H_2O$. The latter was obtained by evaporating the filtrate till crystallization.

Physical measurements

The IR spectra were recorded with a Perkin–Elmer 1430 ratio recording infrared spectrophotometer. Solid samples were examined between KBr plates. UV–vis spectra of the complexes were obtained with a Perkin–Elmer Lambda 4B spectrophotometer using 2 mm and/or 10 mm quartz cells. ^1H NMR spectra were recorded with a Varian 90 MHz spectrometer using TMS as an internal reference. The metal contents in the synthesized complexes were determined by the standard literature methods. The elemental analyses were performed at the Micro analytical Laboratory at Kuwait University, Kuwait and at Darmstadt University, Germany.

RESULTS AND DISCUSSION

Synthesis of the complexes

The reaction of α-dicarbonylbis(aroylhydrazone) (**1** ≡ H_2L) with $Ni(OAc)_2$ in presence of potassium hydroxide in methanol resulted in the formation of green neutral mono ligand complexes, NiL where L refers to the dinegative anion (**2**: R = R′ = CH_3, R″ = C_6H_5, *p*-$CH_3 \cdot C_6H_4$, *p*-$Cl \cdot C_6H_4$; R = CH_3, R′ = R″ = C_6H_5). With glyoxalbis(benzoylhydrazone) (**1**: R = R′ = H, R″ = C_6H_5), the isolated complex, $NiL \cdot 4H_2O$ undergoes dehydration to produce the anhydrous red species. In DMSO and MeOH, the reaction of $Ni(OAc)_2$ with benzilbis(benzoylhydrazone) (**1**: R = R′ = R″ = C_6H_5)

yielded dark and grey green complexes, respectively of stoichiometric composition NiL. The former complex has the same characteristic features as those reported for the above monomeric species, whereas the grey green complex was found to be insoluble in most common organic solvents; a property which may suggest a polymeric structure. When the reaction was conducted in DMSO–MeOH mixture (1 : 1), a yellow compound of the formula $Ni(H_2L)_2(OAc)_2$ was obtained.

In methanol the reaction of copper(II) acetate or chloride with α-dicarbonylbis(aroylhydrazone) in presence of excess NaOAc gave complexes of the general formula $CuL \cdot nH_2O$ ($n = 0$, 1/2, 1). The glyoxal derivatives were only isolated when KOH was used instead of NaOAc, however when the latter was used in excess $Cu(H_2L)_2(OAc)_2$ complexes were obtained. Similarly the corresponding $Cu(H_2L)_2Cl_2$ were isolated when the reactions were carried out using $CuCl_2 \cdot 2H_2O$ and in absence of a base.

Hydrated zinc(II) and cobalt(II) complexes of the general formula $ML \cdot nH_2O$ were isolated from reactions of **1** with zinc(II) or cobalt(II) acetate in presence of KOH. Also, reaction of **1** with $Na_3[Co(NO_2)_6]$ in aqueous ethanol afforded $Na[Co^{III}L(NO_2)_2]$ complexes. With benzilbis(benzoylhydrazone), besides the expected dinitro compound, the tris complex $Co(HL)_3 \cdot 3H_2O$ was isolated.

The purity of the synthesized complexes were checked by elemental analyses (Table 1).

Table 1. Elemental analyses of metal complexes derived from α-dicarbonylbis(aroylhydrazone) (**1**)

Complex	R	R′	R″	%C Calc. (Found)	%H Calc. (Found)	%N Calc. (Found)	%M Calc. (Found)
Nickel(II) complexes							
NiL	H	H	C_6H_5				16.7 (16.0)
NiL	CH_3	CH_3	C_6H_5	57.0 (57.2)	4.3 (4.4)	14.8 (15.0)	15.3 (15.5)
NiL	CH_3	CH_3	p-$CH_3 \cdot C_6H_4$	59.0 (58.9)	5.0 (5.0)	13.8 (13.8)	14.4 (13.4)
NiL	CH_3	CH_3	p-$Cl \cdot C_6H_4$	48.2 (48.3)	3.2 (3.3)	12.5 (12.3)	13.1 (12.2)
NiL	CH_3	C_6H_5	C_6H_5				13.3 (12.9)
NiL[a]	C_6H_5	C_6H_5	C_6H_5	66.8 (66.6)	4.0 (3.8)	11.1 (11.2)	11.7 (11.9)
$Ni(H_2L)(OAc)_2$	C_6H_5	C_6H_5	C_6H_5				5.5 (5.5)
Copper(II) complexes							
CuL	CH_3	CH_3	C_6H_5	66.2 (66.3)	4.0 (4.0)	11.0 (11.5)	16.6 (16.3)
$CuL \cdot H_2O$	CH_3	CH_3	p-$CH_3 \cdot C_6H_4$	55.9 (56.4)	5.2 (4.9)	13.0 (13.2)	14.8 (15.0)
CuL	CH_3	C_6H_5	C_6H_5	61.9 (62.1)	4.1 (4.2)	12.6 (12.3)	14.2 (14.2)
$CuL \cdot 1/2H_2O$	C_6H_5	C_6H_5	C_6H_5	65.0 (66.1)	4.1 (4.5)	10.8 (10.6)	12.3 (12.5)
CuL	H	H	C_6H_5				17.9 (17.3)
$Cu(H_2L)Cl_2$	H	H	C_6H_5	56.3 (56.8)	4.2 (4.4)	14.6 (15.0)	14.8 (14.0)
$Cu(H_2L)Cl_2$	H	H	p-$CH_3 \cdot C_6H_4$				13.9 (14.2)
$Cu(H_2L)(OAc)_2$	H	H	p-$CH_3 \cdot C_6H_4$	56. (56.5)	4.2 (4.1)	14.6 (14.2)	12.9 (13.1)
Zinc(II) complexes							
$ZnL \cdot 5/2H_2O$	CH_3	CH_3	C_6H_5	50.2 (50.0)	4.9 (4.5)	13.0 (12.9)	15.2 (15.5)
$ZnL \cdot 3/2H_2O$	CH_3	CH_3	p-$CH_3 \cdot C_6H_4$	54.5 (54.8)	5.3 (5.2)	12.7 (12.8)	14.8 (15.0)
$ZnL \cdot 2H_2O$	CH_3	CH_3	p-$Cl \cdot C_6H_4$	44.7 (44.2)	3.8 (3.5)	11.6 (11.4)	13.5 (14.1)
$ZnL \cdot 3H_2O$	CH_3	C_6H_5	C_6H_5	55.1 (55.2)	4.8 (4.5)	11.2 (11.0)	13.0 (14.4)
Cobalt(II) complexes							
$CoL \cdot 5H_2O$	H	H	C_6H_5	43.6 (44.0)	5.0 (5.0)	12.7 (12.4)	13.9 (13.6)
$CoL \cdot 2H_2O$	CH_3	CH_3	C_6H_5	52.1 (52.6)	4.9 (4.4)	13.5 (13.2)	14.2 (14.3)
$CoL \cdot 2H_2O$	C_6H_5	C_6H_5	C_6H_5	62.3 (65.6)	4.5 (4.6)	10.4 (10.8)	10.9 (10.7)
$CoL \cdot 2H_2O$	CH_3	CH_3	p-$Cl \cdot C_6H_4$	44.6 (44.3)	3.8 (3.4)	11.6 (11.5)	12.2 (12.4)
$CoL \cdot 4H_2O$	CH_3	C_6H_5	C_6H_5				11.4 (11.5)
Cobalt(III) complexes							
$Na[CoL(NO_2)_2]$[b]	CH_3	C_6H_5	C_6H_5	43.0 (42.9)	3.4 (3.4)	16.8 (16.8)	11.7 (11.8)
$Na[CoL(NO_2)_2]$[c]	CH_3	C_6H_5	C_6H_5	48.1 (48.5)	3.5 (4.0)	14.6 (13.5)	10.3 (10.0)
$Na[CoL(NO_2)_2]$	C_6H_5	C_6H_5	C_6H_5	54.4 (54.6)	3.3 (3.4)	13.6 (13.4)	9.5 (9.8)
$Co(HL)_3 \cdot 3H_2O$	C_6H_5	C_6H_5	C_6H_5	69.7 (69.7)	4.8 (4.9)	12.6 (11.3)	4.1 (3.7)

[a] The dark green complex.
[b] Isolated as hemihydrate.
[c] Isolated as monohydrate.

IR spectra

α-Dicarbonylbis(aroylhydrazone) compounds and their complexes are similar to those of aroylhydrazones derived from monocarbonyl compounds, both can exist in the keto or enol forms depending on the pH of solution [14–17]. The ligands under investigation, **1** display different modes of chelation with divalent metal ions [12,18–22].

The infrared spectra of ligands **1** exhibit absorption bands characteristic for aroylhydrazone residue, CONH—N=C [17,23,24]. The IR data are listed in Table 2. In general the complexes $ML \cdot nH_2O$ and $Na[CoL(NO_2)_2]$ lack absorption bands due to ν(N—H), amide I ν(C=O) and amide II; instead they display a very intense band at 1600–1580 cm^{-1}, attributable to ν(C=N—N=C). This finding clearly indicates the deprotonation of the two amide residues and may suggest the coordination of the hydrazone ligand *via* the two azomethine nitrogens and the two ionized enolic oxygens in a fashion similar to that described by structure **2**.

The IR spectra of the complexes $M(H_2L)_2X_2$ (M = Ni, X = OAc, R = R′ = C_6H_5, R″ = C_6H_5; M = Cu, X = Cl, OAc, R = R′ = H, R″ = C_6H_5; *p*-$CH_3 \cdot C_6H_4$) show ν(N—H), amide I ν(C=O) and amide II bands at almost the same positions as those found in their parent free ligands, indicating that the two carbonyl groups remain uncoordinated. The lower frequency shift observed for the ν(C=N) stret-

Table 2. Selected infrared spectral bands (cm^{-1}) for α-dicarbonylbis(aroylhydrazone) ligands, **1** and their corresponding metal complexes

Complex	R	R′	R″	ν(N—H)	Amide I ν(C=O)	ν(C=N)+ν(C=C) or ν(C=N—N=C)	Amide II [δ(N—H)+ ν(C—N)]	Amide III ν(C—O)
H_2L	H	H	C_6H_5	3210	1651	1579	1538	1311, 1274
NiL	H	H	C_6H_5			1593	1544	1371, 1296
$CoL \cdot 5H_2O$	H	H	C_6H_5			1584	1532	1373, 1292
H_2L	CH_3	CH_3	C_6H_5	3206, 3173	1655	1598, 1574	1528	1365, 1282
NiL	CH_3	CH_3	C_6H_5			1585	1549	1394, 1296
CuL	CH_3	CH_3	C_6H_5			1585	1515	1370, 1282
$CoL \cdot 2H_2O$	CH_3	CH_3	C_6H_5			1596	1543	1376, 1295
$ZnL \cdot 5/2H_2O$	CH_3	CH_3	C_6H_5			1583	1545	1365, 1295
$Na[CoL(NO_2)_2]1/2H_2O$	CH_3	CH_3	C_6H_5			1596	1548	1309
H_2L	CH_3	CH_3	*p*-$CH_3 \cdot C_6H_4$	3289	1654	1608	1523	1370, 1269
NiL	CH_3	CH_3	*p*-$CH_3 \cdot C_6H_4$			1581	1510	1380, 1292
$CuL \cdot H_2O$	CH_3	CH_3	*p*-$CH_3 \cdot C_6H_4$			1577	1552	1362, 1281
$ZnL \cdot 3/2H_2O$	CH_3	CH_3	*p*-$CH_3 \cdot C_6H_4$			1578	1546	1365, 1293
H_2L	CH_3	CH_3	*p*-Cl·C_6H_4	3219	1657	1591	1528	1286, 1268
NiL	CH_3	CH_3	*p*-Cl·C_6H_4			1581	1532	1309, 1285
$CoL \cdot 2H_2O$	CH_3	CH_3	*p*-Cl·C_6H_4			1577	1545	1291, 1277
$ZnL \cdot 2H_2O$	CH_3	CH_3	*p*-Cl·C_6H_4			1578	1547	1307, 1289
H_2L	CH_3	C_6H_5	C_6H_5	3283, 3182	1641	1596	1571	1353
NiL	CH_3	C_6H_5	C_6H_5			1599	1530	1322, 1271
CuL	CH_3	C_6H_5	C_6H_5			1586	1544	1331, 1298
$CoL \cdot 4H_2O$	CH_3	C_6H_5	C_6H_5			1585	1528	1325, 1294
$ZnL \cdot 3H_2O$	CH_3	C_6H_5	C_6H_5			1583	1532	1321, 1291
$Na[CoL(NO_2)_2H_2O$ H_2O	CH_3	C_6H_5	C_6H_5			1582	1480	1319, 1253
H_2L	C_6H_5	C_6H_5	C_6H_5	3231	1672	1580	1526	1260
NiL	C_6H_5	C_6H_5	C_6H_5			1599	1533	1292, 1268
$CuL \cdot 1/2H_2O$	C_6H_5	C_6H_5	C_6H_5			1585	1561	1302, 1253
$CoL \cdot H_2O$	C_6H_5	C_6H_5	C_6H_5			1585	1547	1299, 1257
$Na[CoL(NO_2)_2]$	C_6H_5	C_6H_5	C_6H_5			1584	1548	1298, 1258
$Co(HL)_3 \cdot 3H_2O$	C_6H_5	C_6H_5	C_6H_5	3230	1671	1575	1525	1260

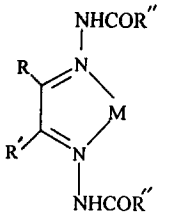

[3]

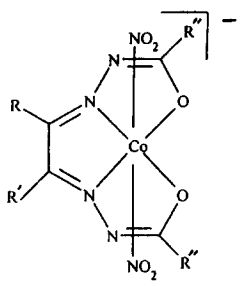

[4]

ching vibration confirms the NN bidentate nature of the hydrazone molecule; chelation mode **3**.

The N-bonded nature for NO_2^- in $Na[CoL(NO)_2]$ was confirmed by the presence of strong absorption bands in the 1430–1420 and 1320–1300 cm^{-1} regions, attributed to $\nu_a(NO_2)$ and $\nu_s(NO_2)$ stretching vibrations, respectively [25]. The presence of a single band for each type of vibration is in agreement with the *trans* geometry [26] expected in these complexes (**4**).

The IR spectrum of tris[benzilbis(benzoylhydrazonato)(-1)]cobalt(III) trihydrate, $Co(HL)_3 \cdot 3H_2O$ displayed a series of bands at 3230, 1671 and 1525 cm^{-1} due to ν(N—H), amide I ν(C=O) and amide II, respectively; same positions as those observed in the parent organic ligand (Table 2). Also, the spectrum exhibits a new intense band at 1575 cm^{-1} attributable to ν(C=N—N=C) of the deprotonated ligand. These results clearly indicate that the hydrazone molecule is acting as a mononegative NO bidentate where half of the ligand is uncoordinated and exists in the keto form and the second half is binding to Co^{III} through the azomethine nitrogen and the enolic group. Thus, the following mode of chelation can be proposed for $Co(HL)_3 \cdot 3H_2O$ complex.

^{1}H *NMR spectra*

The ^{1}H NMR spectral data for diacetyl- and methylphenylglyoxalbis(benzoylhydrazone) molecules and their diamagnetic zinc(II), nickel(II) ($ML \cdot nH_2O$) and cobalt(III) ($Na[CoL(NO_2)_2]$) complexes are summarized in Table 3. The spectrum of **1** (R = R′ = CH_3, R″ = C_6H_5) shows two equivalent signals at 10.60 and 2.32 ppm due to N—H and the two equivalent CH_3 protons, respectively and two multiplets centered at 7.77 and 7.46 ppm attributable to the two aromatic protons. The spectrum of methylphenylglyoxalbis(benzoylhydrazone) (**1**: R = CH_3, R′ = R″ = C_6H_5) gave the resonances expected for the two phenyl groups, also it displays two proton signals for each methyl (2.13 and 2.33 ppm) and the N—H protons (11.03 and 10.67 ppm). These signals can be rationalized by considering the following two isomers: rotomeric species **6** and **7** in solutions.

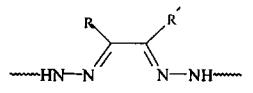

[6]

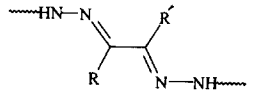

[7]

The complexes $ML \cdot nH_2O$ (M = Zn^{II}, Ni^{II}) and $Na[CoL(NO_2)_2]$ derived from the diacetyl and methylphenylglyoxal display spectra comparable to those of their parents, except the lack of the N—H signals. The ^{1}H NMR signals of the aromatic and methyl groups in $ML \cdot nH_2O$ complexes show clear upfield shifts relative to those observed in the free ligands. This may result from the increased electron densities; delocalization of the two negative charges all over the highly conjugated bis-hydrazone residues as well as the back donation from the occupied metal ion orbitals to the unoccupied π^* ligand orbitals (M → L). In [methylphenylglyoxalbis(benzoylhydrazonato)(-2)]zinc(II) complex, the CH_3 protons appear as a doublet at 1.37 and 1.43 ppm. The nonequivalency of the two methyl groups can be interpreted by assuming the existence of the two dimeric structures **8** and **9**, where the methyl and phenyl groups are oriented differently with respect to the plane formed by Zn^{2+} ions and the two oxygen bridges. For [diacetylbis(benzoylhydrazonato)(-2)]zinc(II) complex, all the CH_3 protons are equivalent and hence only one dimeric isomer would be predicted.

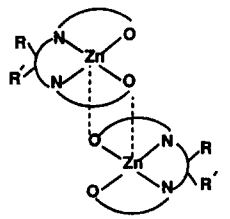

[8]

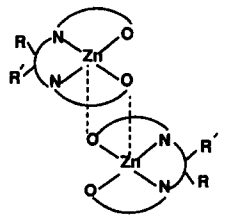

[9]

The ^{1}H NMR spectra of cobalt(III) complexes, $Na[CoL(NO_2)_2]$ derived from diacetyl- and methylphenylglyoxalbis(benzoylhydrazone) exhibit the methyl and aromatic protons at low fields; only σ-interaction is taking place in these complexes.

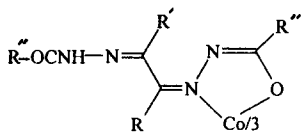

[5]

Electronic spectra

The visible spectral data for the complexes under investigation are listed in Table 4. The electronic spec-

Table 3. ^{1}H NMR chemical shifts, δ (ppm) of diacetyl- and methylphenylglyoxalbis(benzoylhydrazone) and their corresponding metal complexes

Compound	R	R′	R″	Solvent	—CH_3	δ(no. of protons) aromatic	N—H
H_2L	CH_3	CH_3	C_6H_5	d^6-DMSO	2.23 (6)	7.46 (6) 7.77 (4)	10.1 (2)
NiL	CH_3	CH_3	C_6H_5	$CDCl_3$	1.87 (6)	7.26 (6) 7.87 (4)	
$ZnL \cdot 5/2H_2O$	CH_3	CH_3	C_6H_5	$CDCl_3$	1.43 (6)	7.03 (6) 7.65 (4)	
$Na[CoL(NO_2)_2] \cdot 1/2\ H_2O$	CH_3	CH_3	C_6H_5	d^6-DMSO	2.39 (6)	7.30 (6) 7.89 (4)	
H_2L	CH_3	C_6H_5	C_6H_5	d^6-DMSO	2.13 (3) 2.33 (3)	7.43 (13) 7.90 (2)	10.67 (1) 11.03 (1)
NiL	CH_3	C_6H_5	C_6H_5	$CDCl_3$	1.93 (3)	7.23 (10) 7.80 (5)	
$ZnL \cdot 3H_2O$	CH_3	C_6H_5	C_6H_5	$CDCl_3$	1.37 (3) 1.43 (3)	7.03 (10) 7.70 (5)	
$Na[CoL(NO_2)_2] \cdot H_2O$	CH_3	C_6H_3	C_6H_5	d^6-DMSO	2.47 (3)	7.40 (11) 7.87 (4)	

tra of the $ZnL \cdot nH_2O$ complexes exhibit a series of bands at *ca* 300 and 400 nm, due to π–π^* transitions in the highly conjugated dinegative anion, L^{2-}. The bands at *ca* 450 nm are most probably due to MLCT transitions.

The band maxima detected at 430–470 nm in the CuL chelates are quite similar to those found in square planar CuN_2O_2 complexes, and most probably due to LMCT transitions [27]. Moreover, the spectra exhibit an absorption band or a shoulder in the 500 nm region due to MLCT band. The *d*–*d* transitions which were detected as a broad band or a shoulder in the 650–730 nm region ($\varepsilon = 120\ M^{-1}\ cm^{-1}$) result from the two energetically close $^2A_{1g} \leftarrow {}^2B_{1g}$ and $^2B_{2g} \leftarrow {}^2B_{1g}$ transitions [27]. In cobalt(II) complexes, $CoL \cdot nH_2O$, the expected weak *d*–*d* transition in the octahedral environment is obscured by the intense LMCT band.

The spectra of the cobalt(III) complexes of $Na[CoL(NO_2)_2]$ (Table 4) clearly reveal the presence of three maxima in the visible region located at 465, 529, 575 nm and 464, 548, 598 nm for diacetyl and for methylphenylglyoxal derivatives, respectively. These bands can be assigned for $^1T_{2g} \leftarrow {}^1A_{1g}$, $^1A_{2g} \leftarrow {}^1A_{1g}$ and $^1E_g \leftarrow {}^1A_{1g}$ transitions, respectively as would be predicted in d^6 low-spin *trans*-octahedral species [27,28]. The splitting of the low energy band is not clearly pronounced due to the small difference in ligand field strengths between the axial NO_2^- and the planar N_2O_2 coordinating sites. The relative strong intensity of the three observed bands presumably results from the contribution of the MLCT transition. The electronic spectra for $Na[CoL(NO_2)_2]$ chelates are illustrated in Fig. 1.

The visible spectra of the nickel(II) complexes, NiL in chloroform display several bands as depicted in Fig. 1. The band located around 525 nm is most probably due to a LMCT transition. The three intense bands detected at the wavelength region 640–810 nm (Table 4) can be attributed to the different d(M) → π^*(L) transitions (MLCT) rather than *d*–*d* transitions. This assignment is based on the fact that Ni^{2+} ion is located at the center of a delocalized π-bond of three conjugated chelate rings. Thus, the extended conjugation as well as the *p*–π interaction in these complexes tend to decrease the energy difference between the unoccupied ligand π^* orbitals (LUMO) and the occupied metal *d*-orbitals (HOMO).

In conclusion, α-dicarbonylbis(aroylhydrazone) compounds provide ligands with great tendency to bind different metal ions in planar arrangements as a result of the high delocalization of dinegative charge of the anion.

Table 4. The visible spectral data[a] of metal chelates derived from α-dicarbonylbis(aroylhydrazone) (**1**) ligands

Complex	R	R′	R″	λ_{max} (log ε), nm (mol dm^{-3} cm^{-1})
Nickel(II) chelates[b]				
NiL	CH_3	CH_3	C_6H_5	391(4.19), 512(sh), 567(sh), 635(sh), 686(3.07), 756(2.85)
NiL	CH_3	CH_3	p-$CH_3 \cdot C_6H_4$	397(4.34), 510(sh), 566(sh), 644(sh), 683(3.19), 752(2.98)
NiL	CH_3	CH_3	p-$Cl \cdot C_6H_4$	392(4.30), 516(sh), 575(sh), 643(sh), 687(3.16), 757(2.94)
NiL	CH_3	C_6H_5	C_6H_5	400(4.17), 524(sh), 584(sh), 657(sh), 713(3.07), 787(2.86)
NiI	C_6H_5	C_6H_5	C_6H_5	388(4.24), 539(sh), 602(sh), 672(2.92), 731(3.01), 810(2.81)
Copper(II) chelates[c]				
CuL	CH_3	CH_3	C_6H_5	403(3.92), 432(sh), 497(3.37), 728(sh)
$CuL \cdot H_2O$	CH_3	CH_3	p-$CH_3 \cdot C_6H_4$	458(sh), 496(4.01), 645(sh)
CuL[d]	CH_3	C_6H_5	C_6H_5	497(sh), 507, 650(sh)
$CuL \cdot 1/2H_2O$	C_6H_5	C_6H_5	C_6H_5	387(4.16), 436(sh), 571(sh), 734(sh)
Zinc(II) chelates[c]				
$ZnL \cdot 5/2H_2O$	CH_3	CH_3	C_6H_5	403(4.04), 450(3.87), 464(sh)
$ZnL \cdot 3/2H_2O$	CH_3	CH_3	p-$CH_3 \cdot C_6H_4$	404(4.01), 443(3.87), 462(sh)
$ZnL \cdot 2H_2O$	CH_3	CH_3	p-$Cl \cdot C_6H_4$	403(4.07), 450(3.89), 466(sh)
$ZnL \cdot 3H_2O$	CH_3	C_6H_5	C_6H_5	413(4.05), 449(sh), 466(3.98)
Cobalt(II) chelates[b]				
$CoL \cdot 2H_2O$	CH_3	CH_3	C_6H_5	395(sh), 423(sh), 435(3.58)
$CoL \cdot 2H_2O$	CH_3	CH_3	p-$Cl \cdot C_6H_5$	405(4.09), 439(sh), 477(3.75)
$CoL \cdot 4H_2O$	CH_3	C_6H_5	C_6H_5	412(3.92), 442(sh), 471(sh)
Cobalt(III) chelates[c]				
$Na[CoL(NO_2)_2] \cdot 1/2H_2O$	CH_3	CH_3	C_6H_5	465(3.55), 529(3.44), 575(3.34)
$Na[CoL(NO_2)_2] \cdot H_2O$	CH_3	C_6H_5	C_6H_5	464(sh), 548(3.37), 598(3.24)

[a] sh = shoulder.
[b] In chloroform.
[c] In benzene.
[d] Saturated solution.
[e] In ethanol.

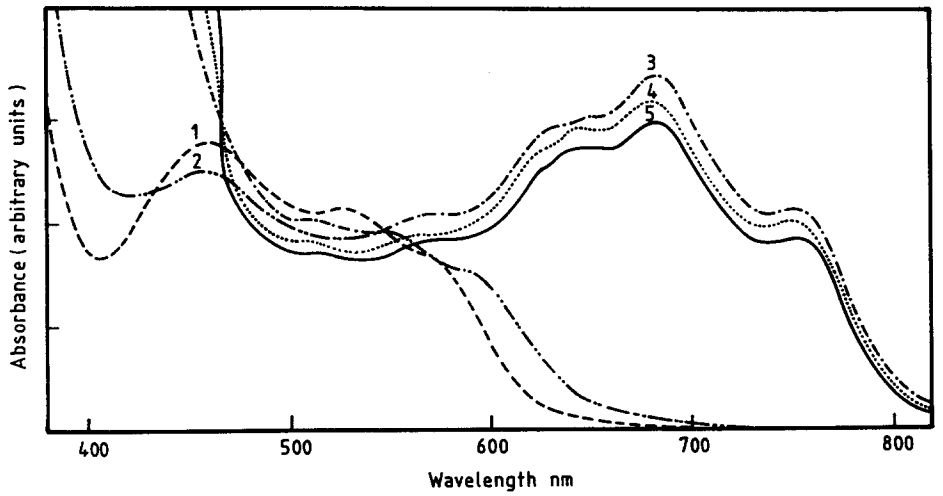

Fig. 1. The visible spectra of $Na[CoL(NO_2)_2]$ in ethanol and NiL complexes in chloroform: (1)———, $Na[CoL(NO_2)_2]$ (**4**: R = CH_3, R′ = R″ = C_6H_5); (2) ———, $Na[CoL(NO_2)_2]$ (**4**: R = R′ = CH_3, R″ = C_6H_5); (3) ———, NiL (**2**: R = R′ = CH_3, R″ = C_6H_5); (4)·····, NiL (**2**: R = R′ = CH_3, R″ = p-$CH_3 \cdot C_6H_4$); (5) ——, NiL (**2**: R = R′ = CH_3, R″ = p-$Cl \cdot C_6H_4$).

REFERENCES

1. Von Pechmann, H. and Bauer, W., *Ber. Dtsch. Chem. Ges.*, 1909, **42,** 659.
2. Curtis, T. and Strove, G., *J. Prakt. Chem.* [2], 1884, **50,** 295.
3. Silva, M. and Valcarecel, M., *The Analyst*, 1980, **105,** 1248.
4. Silva, M., Gallego, M. and Valcarecel, M., *Talanta*, 1980, **27,** 615.
5. Lever, M., *Anal. Chim. Acta*, 1973, **65,** 311.
6. Lever, M., *Anal. Biochem.*, 1972, **47,** 273.
7. Irving, H. M. N. H. and Al-Niami, N. S., *J. Inorg. Nucl. Chem.*, 1965, **27,** 213.
8. Curtin, D. Y. and Alexandrou, N. E., *Tetrahedron*, 1963, **19,** 1697.
9. Alexandrou, N. E., *Tetrahedron*, 1966, **22,** 1309.
10. Stolle, R., *Ber. Dtsch. Chem. Ges.*, 1926, **59,** 1743.
11. Balachandran, K. S. and George, M. V., *Tetrahedron*, 1973, **29,** 2119.
12. Sacconi, L., *Z. Anorg. Chem.*, 1954, **275,** 249.
13. Yusupov, V. G., Tosher, M. T., Aleksandrov, G. G., Parpiev, N. A., Karimov, M. M., Dustov, K. H. and Sharopov, A. U., *Koord. Khim.*, 1988, **14(7)**, 985.
14. Massoud, S. S., Labib, L. and Iskander, M. F., *Polyhedron*, 1994, **13,** 517.
15. Iskander, M. F. and Saddeck, S., *Inorg. Chim. Acta*, 1977, **22,** 141.
16. Iskander, M. F., El-Sayed, L. and Lasheen, M. A., *Inorg. Chim. Acta*, 1976, **16,** 147.
17. Iskander, M. F. and El-Sayed, L., *J. Inorg. Nucl. Chem.*, 1971, **33,** 435.
18. Sacconi, L., Lombardo, G. and Paoletti, P., *J. Am. Chem. Soc.*, 1958, **80,** 848.
19. Cefau, R., Maggio, F., Pellerito, L. and Romano, V., *Inorg. Nucl. Chem. Lett.*, 1974, **10,** 529.
20. Cusumano, M., *J. Chem. Soc., Dalton Trans.*, 1980, 2456.
21. Dakternieks, D., Orlandini, A. and Sacconi, L., *Inorg. Chim. Acta*, 1978, **29,** L205.
22. Lindoy, L. F. and Livingstone, S. E., *Coord. Chem. Rev.*, 1967, **2,** 173.
23. Nonoyama, M. and Sugimoto, *Inorg. Chim. Acta*, 1979, **35,** 131.
24. Dimono, P., Musatti, A-M., Nardell, M. and Pelizzi, C., *J. Chem. Soc., Dalton Trans.*, 1975, 295.
25. Nakamoto, K., Fujita, J. and Murata, H., *J. Am. Chem. Soc.*, 1958, **80,** 4817.
26. Nakamoto, K., *Infrared and Raman Spectra of Inorganic and Coordination Compounds*, p. 228, 4th ed. John Wiley & Sons, New York (1986).
27. Lever, A. B. P., *Inorganic Electronic Spectroscopy*, pp. 473–490, pp. 570–571, 2nd ed. Elsevier, New York (1984).
28. Basolo, F., Ballhausen, C. J. and Bjerrum, J., *Acta Chem. Scand.*, 1955, **9,** 810.

Pergamon

PII: S0277-5387(97)00255-6

Polyhedron Vol. 17, No. 1, pp. 207–209, 1998
© 1997 Elsevier Science Ltd
All rights reserved. Printed in Great Britain
0277-5387/98 $19.00+0.00

COMMUNICATION

Unexpected coordination behavior of dinucleating ligand: infinite zigzag chain of alternating sodium(I) and dinuclear-zinc(II) units

Masahiro Mikuriya* and Sumiko Tashima

Department of Chemistry, School of Science, Kwansei Gakuin University, Uegahara, Nishinomiya 662, Japan

(Received 21 May 1997; accepted 9 June 1997)

Abstract—A zinc(II) complex, $[Zn_4Na_2L_2(CH_3COO)_4CH_3CN]_n \cdot 2nCH_3CN \cdot 2nH_2O$ (H_3L = 2,6-bis(saliclylideneaminomethyl)-4-methylphenol), has been isolated and characterized by X-ray crystallography, which reveals a unique zigzag-chain structure consisting of dinuclear $Zn_2L(CH_3COO)_2$ units and sodium ions.
© 1997 Elsevier Science Ltd

Keywords: sodium(I); zinc(II); Schiff-base; dinucleating ligand; sodium(I)–zinc(II) complex; crystal structure.

There has been much interest in the synthesis of polynuclear metal complexes because of their structural variety and novelty. An interesting approach to design of such compounds is to assemble dinuclear metal units into polynuclear molecules. Schiff-bases as dinucleating ligands are known to give dinuclear units for *d*-block metal ions [1]. One of these dinucleating ligands, 2,6-bis(saliclylideneaminomethyl)-4-methylphenol (H_3L) which has two terminal phenoxo-oxygen atoms in addition to the central phenoxo-oxygen atom as the bridging group, has potential to form polynuclear compounds on deprotonation to L^{3-} (Fig. 1). We recently described synthesis of dinuclear (**I**) [2], tetranuclear (**II**) [3,4], and pentanuclear (**III**) [5] complexes which are formed by the use of the L^{3-} ligand (Fig. 2). In the case of the tetranuclear complexes [3,4], two dinuclear units (**I**) are associated

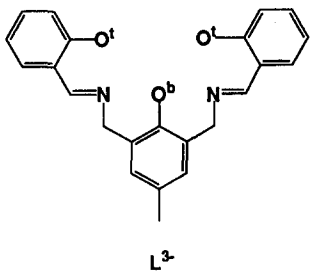

Fig. 1. The L^{3-} ligand (O^t: terminal phenoxo-oxygen atom; O^b: central bridging phenoxo-oxygen atom).

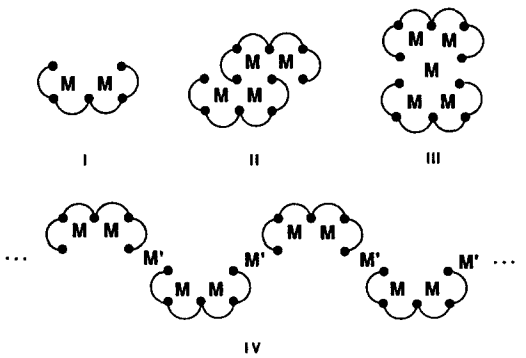

Fig. 2. Polynuclear metal complexes with the L^{3-} ligands.

* Author to whom correspondence should be addressed.

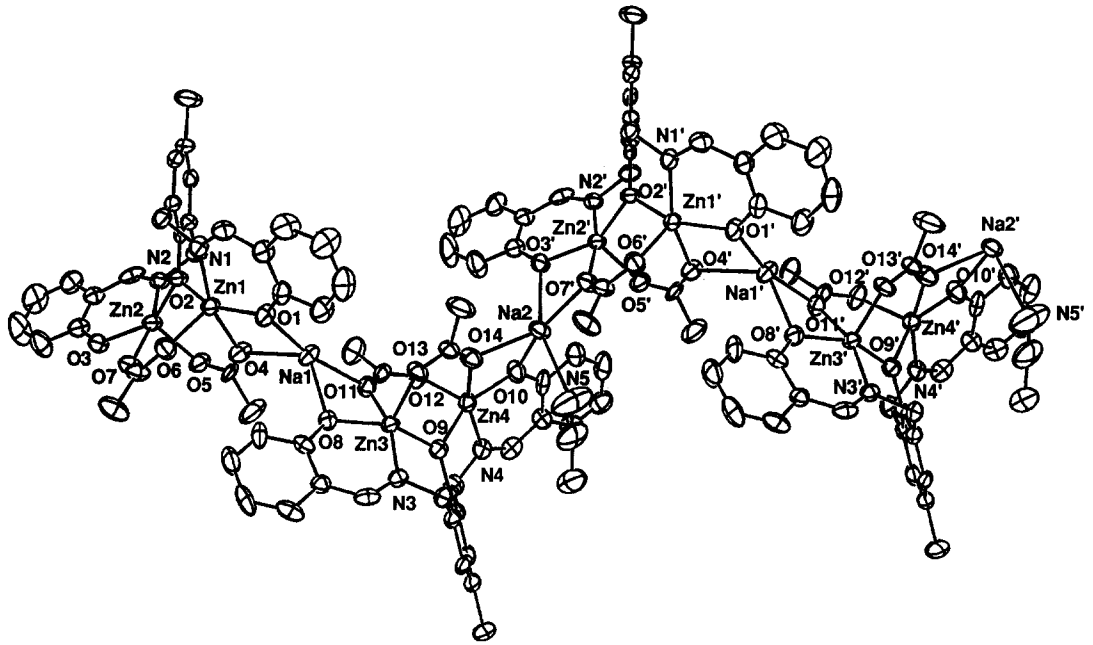

Fig. 3. Perspective view of chain structure of **1**. Selected bond distances (l/Å) and angles (ϕ/°): Zn(1)—O(1) 1.985(10), Zn(1)—O(2) 2.024(9), Zn(1)—O(4) 2.172(10), Zn(1)—O(6) 1.985(10), Zn(1)—N(1) 2.090(13), Zn(2)—O(2) 1.990(10), Zn(2)—O(3) 2.008(10), Zn(2)—O(5) 1.996(11), Zn(2)—O(7) 2.175(9), Zn(2)—N(2) 2.076(10), Zn(3)—O(8) 1.996(10), Zn(3)—O(9) 2.019(9), Zn(3)—O(11) 2.158(9), Zn(3)—O(13) 1.998(10), Zn(3)—N(3) 2.068(10), Zn(4)—O(9) 2.037(9), Zn(4)—O(10) 1.988(11), Zn(4)—O(12) 1.998(11), Zn(4)—O(14) 2.167(11), Zn(4)—N(4) 2.088(12), Na(1)—O(1) 2.301(12), Na(1)—O(4) 2.377(13), Na(1)—O(8) 2.316(11), Na(1)—O(11) 2.343(12), Na(2)—O(3′) 2.317(11), Na(2)—O(7′) 2.434(12), Na(2)—O(10) 2.331(13), Na(2)—O(14) 2.415(13), Na(2)—N(5) 2.495(23); Zn(1)—O(2)—Zn(2) 111.9(4), Zn(1)—O(1)—Na(1) 105.9(4), Zn(1)—O(4)—Na(1) 97.6(4), Zn(3)—O(9)—Zn(4) 111.0(5), Zn(3)—O(8)—Na(1) 100.9(4), Zn(3)—O(11)—Na(1) 95.4(4), Zn(4)—O(10)—Na(2) 105.2(5), Zn(4)—O(14)—Na(2) 97.1(4). Primes refer to the equivalent positions ($x-1$, y, z).

to form the tetranuclear molecules (**II**) by the bridging of the terminal phenoxo-oxygen atoms of L^{3-}. In the course of this study, we have isolated a novel polynuclear complex which has a chain structure (**IV**). Although successful chain formation has been accomplished for metal carboxylate dimers [6], there appears to be no examples using dinuclear units other than metal carboxylates for one-dimensional array. Herein we report an intriguing method using the dinucleating ligand to obtain a new class of chain compound.

Treatment of H_3L (0.04 mmol) with zinc(II) acetate dihydrate (0.11 mmol) and sodium perchlorate (0.14 mmol) in acetonitrile (6.5 cm^3) containing three drops of triethylamine and two drops of *N,N*-dimethylacetamide resulted in deposition of pale yellow crystals (**1**). An X-ray crystallographic study revealed that the compound is composed of a chain of the Schiff-base ligands L^{3-}, each of which binds two zinc (II) atoms, bound to sodium ions to give a ZnZnNa-zigzag chain (Fig. 3).‡ The asymmetric unit contains two crystallographically different dinuclear zinc(II) units and sodium ions, $[Zn_4Na_2L_2(CH_3COO)_4 CH_3CN]$. Each dinucleating ligand L^{3-} is octadentate and the central phenoxo oxygen [O(2), O(9)] acts as the bridging atom binding two zinc atoms. The distances are 3.325(2) and 3.343(2) Å for Zn(1)–Zn(2) and Zn(3)–Zn(4), respectively. Two acetate ions are incorporated in each dinuclear units as two exogenous *syn–syn* bridges. Each zinc atom adopts a distorted trigonal–bipyramidal coordination geometry with Zn–O distances in the range 1.985(10)–2.037(9) Å for the equatorial bonds [Zn(1)—O(1), Zn(1)—O(2), Zn(1)—O(6); Zn(2)—O(2), Zn(2)—O(3), Zn(2)—O(5); Zn(3)—O(8), Zn(3)—O(9), Zn(3)—O(13); Zn(4)—O(9), Zn(4)—O(10), Zn(4)—O(12)] and 2.158(9)–2.175(9) and 2.068–2.090(13) Å for the axial oxygen [O(4), O(7), O(11), O(14)] and nitrogen [N(1), N(2), N(3), N(4)] atoms, respectively. The two terminal phenoxo oxygens [O(1), O(3); O(8), O(10)] of each dinucleating ligand L^{3-} act as bridging groups being further coordinated to sodium ions [Na(1),

‡ Crystallographic data: **1**; $C_{60}H_{63}N_7Na_2O_{16}Zn_4$, F.w. = 1445.67, triclinic, space group $P\bar{1}$, a = 14.533(6), b = 20.487(6), c = 12.108(7) Å, α = 100.34(2), β = 92.95(3), γ = 89.55(3)°, V = 3542(3) Å^3, Z = 2, D_m = 1.43, D_c = 1.36 g cm^{-3}, μ(Mo-K_α) = 14.46 cm^{-1}, 10,050 reflections measured ($2\theta_{max}$ = 48°), 5450 [$I \geqslant 3\sigma(I)$] used in the refinement, R = 0.065, R_w = 0.097. Intensity data were collected on an Enraf–Nonius CAD4 diffractometer using graphite-monochromated Mo-K_α radiation. All the structures were solved by the direct method and refined by the full-matrix least-squares method using a MolEN program package.

Na(2)] with one of the exogenous acetate bridges in a monatomic bridging; the intermetallic separations are Zn(1)—Na(1) 3.425(7), Zn(3)—Na(1) 3.331(7), Zn(4)—Na(2) 3.438(7), and Zn(2′)—Na(2) 3.349(7) Å. One of the most interesting findings in **1** is the combination of *syn–syn* and monatomic bridging of the acetate ions. Such an η^3 behavior is seldom observed in metal carboxylates [7]. The IR spectrum exhibits absorptions indicative of the bridging nature of the acetate groups [$\nu_{asym}(CO_2^-)$ 1591s, $\nu_{sym}(CO_2^-)$ 1434s cm^{-1}] [8]. In the asymmetric unit, an acetonitrile molecule is coordinated to one [Na(2)] of the two sodium ions. Thus the coordination geometries of the sodium ions are distorted tetrahedral and trigonal bipyramidal for Na(1) and Na(2), respectively. The Na—O distances are in the range 2.301(11)–2.434(12) Å and the Na—N [Na(2)—N(5)] distance is 2.495(23) Å. Within a crystal, the heterometal asymmetric units are united to form an infinite zigzag chain along the *a* axis. To our knowledge, this is the first example of polymeric assembling by dinucleating ligands.

The Na ions play a vital structural role in that all the terminal phenoxo groups of the dinucleating ligands interact with these ions. The present result emphasizes the importance of the use of bridging properties of the terminal groups of the dinucleating ligands as part of the design strategy for creating new polynuclear complexes.

Acknowledgements—The work was supported in part by a Grant-in-Aid for Scientific Research (No. 08404046) from the Ministry of Education, Science, Sports and Culture of Japan.

REFERENCES

1. Okawa, H. and Kida, S., *Bull. Chem. Soc. Jpn.*, 1972, **45,** 1759.
2. Mikuriya, M. and Fukuya, M., *Bull. Chem. Soc. Jpn.*, 1996, **69,** 679.
3. Mikuriya, M., Nakadera, K., Kotera, T., Tokii, T. and Mori, W., *Bull. Chem. Soc. Jpn.*, 1995, **68,** 3077.
4. Mikuriya, M., Nakadera, K. and Kotera, T., *Bull. Chem. Soc. Jpn.*, 1996, **69,** 399.
5. Mikuriya, M. and Nakadera, K., *Chem. Lett.*, 1995, 213.
6 (a) Cotton, F. A. and Felthouse, T. R., *Inorg. Chem.*, 1980, **19,** 328; (b) Cotton, F. A. and Felthouse, T. R., *Inorg. Chem.*, 1981, **20,** 600; (c) Handa, M., Takata, A., Nakao, T., Kasuga, K., Mikuriya, M. and Kotera, T., *Chem. Lett.*, 1992, 2085; (d) Mikuriya, M., Nukada, R., Morishita, H. and Handa, M., *Chem. Lett.*, 1995, 617; (e) Handa, M., Mikuriya, M., Kotera, T., Yamada, K., Nakao, T., Matsumoto, H. and Kasuga, K., *Bull. Chem. Soc. Jpn.*, 1995, **68,** 2567; (f) Handa, M., Mikuriya, M., Sato, Y., Kotera, T., Nukada, R., Yoshioka, D. and Kasuga, K. *Bull. Chem. Soc. Jpn.*, 1996, **69,** 3483.
7. Drew, M. G. B., Edwards, D. A. and Richards, R., *J. Chem. Soc., Chem. Commun.*, 1973, 124.
8. Nakamoto, K., *Infrared and Raman Spectra of Inorganic and Coordination Compounds*, 4th ed. p. 230. Wiley Interscience, New York (1986).

Pergamon

PII: S0277-5387(97)00384-7

Polyhedron Vol. 17, No. 2–3, pp. 211–220, 1998
© 1997 Elsevier Science Ltd
All rights reserved. Printed in Great Britain
0277-5387/98 $19.00+0.00

Coordination chemistry of mixed pyridine-phenol ligands; mononuclear palladium(II) and dinuclear copper(II) complexes of derivatives of bidentate *N,O*-chelating ligands based on 2-(2-hydroxyphenyl)pyridine

Carl A. Otter, David A. Bardwell, Samantha M. Couchman, John C. Jeffery, John P. Maher and Michael D. Ward*

School of Chemistry, University of Bristol, Cantock's Close, Bristol BS8 1TS, U.K.

(Received 4 August 1997; accepted 18 September 1997)

Abstract—The new ligands 2-(2-hydroxyphenyl)-4-'butyl-pyridine (HL^1), 2-(2-hydroxyphenyl)-6-methyl-pyridine (HL^2) and 2-(2-hydroxyphenyl)-6-[(2-phenyl)ethyl]pyridine (HL^3) were prepared. They are all substituted derivatives of the simple *N,O*-bidentate chelating ligand 2-(2-hydroxyphenyl)pyridine. HL^1 is solubilised derivative bearing a 'Bu substituent in a position which will not sterically interfere with metal-ion coordination; HL^2 and HL^3 contain substituents at C^6 of the pyridyl ring, adjacent to the N atom, which will therefore sterically hinder metal-ion coordination. The complexes $[PdL_2]$ (L = L^1, L^2 and L^3) were prepared and structurally characterised to determine the effects (if any) of the substituents on the structures of the metal complexes. All are four-coordinate complexes with square planar coordination geometry about the Pd(II) ion, but the sterically hindered ligands L^2 and L^3 have to adopt a different conformation from L^1 to allow planar coordination, resulting in "bowl-like" structures. $[Cu_2(L^1)_4]$ was also prepared and found to be a phenolate-bridged dinuclear complex in the solid state, both by X-ray crystallography and EPR measurements. In solution, however, it dissociates to give $[Cu(L^1)_2]$ monomeric units. Cu(II) complexes of L^2 and L^3 could not be isolated. © 1997 Elsevier Science Ltd

Keywords: copper; palladium; crystal structures.

As part of our continuing study on the synthesis and coordination chemistry of mixed-donor polydentate ligands [1–5], we describe here some derivatives of the simple bidentate ligand 2-(2-hydroxyphenyl)pyridine HL, an *N,O*-donor chelate. Remarkably little coordination chemistry of this simple ligand was described until recently, despite its appeal as a hydrolytically stable structural and electronic analogue of salicylaldimines, because it was difficult to prepare; prior to our work the sole structurally characterised complexes were $[PdL_2]$ and $[CoL_3]$ [6]. We recently developed [4] a simple, high-yield synthesis of HL and subsequently described the crystal structures, electrochemical and spectroscopic properties of a series of ruthenium (II and III) and chromium(III) complexes [4,5].

In this paper we describe the preparation of three new substituted derivatives of HL. Ligand HL^1, containing a tertiary-butyl substituent at the C^4 position of the pyridyl ring, is a soluble analogue of HL which was prepared to facilitate characterisation of those complexes of HL which were only poorly soluble. Ligands HL^2 and HL^3 contain substituents at the C^6 position of the pyridyl ring, which are intended to provide steric hindrance to square-planar or octahedral coordination. Ligands which can impose an irregular geometry on metal ions may provide the basis for selective extraction of metal ions other than Cu(II) from a mixture [7] and we were therefore interested to see the extent to which addition of bulky substituents at the C^6 positions of these ligands would result in distortions away from regular coordination geometries.

The preparations and crystal structures of the three

* Author to whom correspondence should be addressed.

mononuclear Pd(II) complexes $[Pd(L^1)_2]$, $[Pd(L^2)_2]$ and $[Pd(L^3)_2]$, and the dinuclear Cu(II) complex $[Cu_2(L^1)_4]$, are described in this paper.

EXPERIMENTAL

Preparation of 2-(2-methoxyphenyl)-4-^{t}butyl-pyridine (MeL^1)

A solution containing 2-lithioanisole was prepared by adding lithium pieces (388 mg, 56 mmol) to 2-bromoanisole (6.89 g, 37 mmol) in dry ether (50 cm^3) under N_2, and stirring the mixture at room temperature for 2 h. This solution was added to a solution of 4-tert-butylpyridine (4.99 g, 37 mmol) in dry toluene (40 cm^3), and the resultant mixture was stirred at 50°C under N_2 for 48 h. The solvents were removed under reduced pressure, and the residue was dissolved in acetone (50 cm^3). A saturated solution of $KMnO_4$ in acetone (3×100 cm^3) was added to oxidise the dihydropyridine, and the MnO_2 was removed by filtration through Celite. Evaporation of the acetone afforded a brown oil which was purified by column chromatography on alumina, using CH_2Cl_2 as the eluent to give a yellow oil. Yield: 1.27 g (14%). EIMS: $m/z = 241$ (M^+), 196 (M^+—^{t}Bu), 136 (M^+—C_7H_8O). Anal. Found C, 79.1; H, 8.0; N, 6.0%. Required for $C_{16}H_{19}NO$: C, 79.3; H, 7.5; N, 6.2%. See Table 1 for ^{1}H NMR data.

Preparation of 2-(2-hydroxyphenyl)-4-^{t}butyl-pyridine (HL^1)

This was prepared by demethylation of the precursor MeL^1 (1.20 g, 5 mmol) using molten pyridinium chloride at 190°C for 1.75 h according to the published method [8]. The mixture was allowed to cool, water (50 cm^3) was added and the dark red solution was neutralised using aqueous KOH. The resulting precipitate was extracted into CH_2Cl_2 and purified further on silica using CH_2Cl_2 as the eluent to give a yellow solid. Yield: 0.50 g (45%). EIMS: $m/z = 227$ (M^+). Anal. Found C, 78.8; H, 7.1; N 5.9. Required for $C_{15}H_{17}NO$: C, 79.6; H, 7.1; N, 6.2. See Table 1 for ^{1}H NMR data.

Preparation of 2-bromo-6-methylpyridine

This preparation is based on a published method [9]. To a three necked flask fitted with a mechanical stirrer, a low temperature thermometer, and containing 45% HBr (60 cm^3), 2-amino-6-picoline (17.5 g, 0.16 mol) was carefully added. The mixture was cooled to −40°C and bromine (24 cm^3, 0.47 mol) was added dropwise with vigorous stirring. A solution of sodium nitrite (27.5 g, 0.40 mol) in water (60 cm^3) was then added dropwise to the orange perbromide, whilst maintaining the temperature below −10°C. A solution of sodium hydroxide (60 g, 1.5 mol) in water (60 cm^3) was added slowly, maintaining the temperature

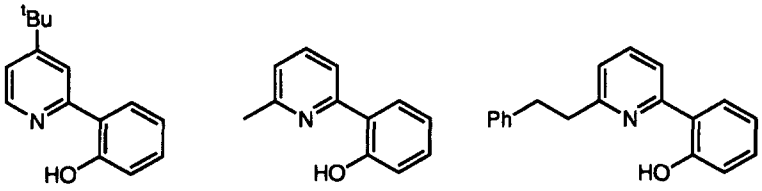

Table 1. ^{1}H NMR spectral data for the new ligands and their methylated precursors ($CDCl_3$, 300 MHz, 293 K)[a]

	Pyridyl protons	Phenyl protons	Other protons
MeL^1	8.60 (dd), 7.79 (d), 7.72 (dd)	7.37 (ddd), 7.21 (dd), 7.07 (td), 7.01 (dd)	3.86 (3H, OMe)
HL^1	8.42 (dd), 7.91 (d), 7.84 (dd)	7.30 (td), 7.26 (dd), 7.02 (dd), 6.92 (td)	*b*
MeL^2	7.73 (dd), 7.56 (2H, m)	7.37 (ddd), 7.21 (dd), 7.07 (td), 7.01 (dd)	3.80 (3H, OMe); 2.60 (3H, Me)
HL^2	7.79 (dd), 7.71 (2H, m)	7.29 (td), 7.08 (t), 7.02 (dd), 6.89 (td)	14.79 (1H, OH)
MeL^3	7.76 (dd), 7.63 (2H, m)	7.38 (td), 7.18–7.30 (5H, m), 7.09 (td), 7.02 (2H, m)	3.86 (3H, OMe); 3.1–3.2 (4H, CH_2CH_2)
HL^3	7.80 (dd), 7.74 (2H, m)	7.25–7.35 (3H, m), 7.15–7.22 (3H, m), 7.06 (dd), 7.02 (dd), 6.92 (td)	3.1–3.2 (4H, CH_2CH_2)[b]

[a] All signals correspond to one proton unless stated otherwise.
[b] Hydroxyl proton not visible.

below 0°C. After warming up to room temperature, the mixture was extracted with ether (2×100 cm^3) and the product purified using column chromatography on silica with CH_2Cl_2 as the eluent. Yield 18.5 g (67%). EIMS: $m/z = 171$ (M^+) (based on ^{79}Br). Anal. Found C, 42.0; H, 3.7; N, 7.7%. Required for C_6H_6NBr: C, 42.1; H, 3.5; N, 8.2%.

Preparation of 2-(2-methoxyphenyl)-6-methylpyridine (MeL^2)

To an ice-cold mixture of $Ni(dppe)Cl_2$ (0.53 g, 1 mmol) and 2-bromo-6-methylpyridine (5.68 g, 33 mmol) in dry THF (50 cm^3) under N_2, a solution of the Grignard reagent prepared from 2-bromoanisole (9.26 g, 50 mmol) and magnesium turnings (1.2 g, 50 mmol) in THF (50 cm^3) was added. The mixture was allowed to warm up slowly to room temperature, and then stirred under N_2 for 24 h. The reaction was quenched with water (50 cm^3), and the solvents were removed under reduced pressure. The remaining oil was purified by column chromatography on alumina with CH_2Cl_2/MeOH (98:2) as the eluent to give a straw-coloured oil. Yield: 4.22 g (71%). EIMS: $m/z = 199$ (M^+), 169 (M^+—OMe). Anal. Found C, 78.0; H, 6.4; N, 7.1%. Required for $C_{13}H_{13}NO$: C, 78.4; H, 6.6; N, 7.0%. See Table 1 for ^{1}H NMR data.

Preparation of 2-(2-hydroxyphenyl)-6-methylpyridine (HL^2)

This was prepared by demethylation of the precursor MeL^2 (0.82 g, 4 mmol) using molten pyridinium chloride at 190°C for 1.75 h according to the published method [8]. After allowing the mixture to cool to room temperature, water (50 cm^3) was added and the resultant dark red solution was neutralised using aqueous KOH. The resulting precipitate was extracted into CH_2Cl_2, and purified on silica using CH_2Cl_2 as the eluent to give HL^2 as a yellow solid. Yield: 0.52 g (70%). EIMS: $m/z = 185$ (M^+). Anal. Found C, 77.7; H, 5.8; N 7.4%. Required for $C_{12}H_{11}O$: C, 77.8; H, 6.0; N, 7.6%. See Table 1 for ^{1}H NMR data.

Preparation of 2-bromo-6-[(2-phenyl)ethyl]-pyridine

This preparation is based on a published method for alkylation of the methyl group of 2-bromo-6-methylpyridine [10]. A solution containing lithium diisopropylamide (LDA; 40 mmol) was prepared by mixing diisopropylamine (4.05 g, 40 mmol) and *n*-butyllithium (26.6 cm^3 of a 1.5 M solution in hexanes, 40 mmol) at −78°C under N_2 and then allowing the mixture to warm up to 0°C. The solution was cooled back to −78°C, and a solution of 2-bromo-6-methylpyridine (6.23 g, 36 mmol) in dry THF (20 cm^3, precooled to −10°C) was added and the mixture stirred at −78°C for 0.5 h. Benzyl bromide (6.84 g, 40 mmol) was added, and the mixture was allowed to warm up to room temperature and stirred for 24 h. Removal of the THF afforded a dark brown residue which was dissolved in ether and washed with aqueous NaOH. The organic layer was purified by column chromatography on flash silica using CH_2Cl_2/hexane (2:1, v/v) as the eluent, to give a pale yellow oil which slowly crystallised on standing. Yield: 6.17 g (66%). EIMS: $m/z = 261$ (M^+), 185 (M^+—C_6H_5), 171 (M^+—C_7H_8) (all based on ^{79}Br). Anal. Found C, 58.7; H, 4.7; N, 5.6%. Required for $C_{13}H_{12}NBr$: C, 59.8; H, 4.6; N, 5.4%.

Preparation of 2-(2-methoxyphenyl)-6-[(2-phenyl) ethyl]pyridine (MeL^3)

To an ice cold mixture of $Ni(dppe)Cl_2$ (0.53 g, 1 mmol) and 2-bromo-6-[(2-phenyl)ethyl]pyridine (5.0 g, 19 mmol) in dry THF (50 cm^3), a solution of the Grignard reagent prepared from 2-bromoanisole (4.30 g, 23 mmol) and magnesium turnings (0.55 g, 23 mmol) in THF (50 cm^3) was added. The mixture was allowed to warm up slowly to room temperature, and was then stirred under N_2 for 24 h. The reaction was quenched with water (50 ml), and the solvents were removed under reduced pressure. The remaining oil was purified using column chromatography on alumina with CH_2Cl_2/MeOH (98:2) as the eluent to give a straw-coloured oil. Yield: 1.27 g (23%). EIMS: $m/z = 289$ (M^+), 258 (M^+—OMe), 212 (M^+—C_6H_5). Anal. Found C, 82.6; H, 6.7; N, 4.7%. Required for $C_{20}H_{19}NO$: C, 82.8; H, 6.9; N, 4.8%. See Table 1 for ^{1}H NMR data.

Preparation of 2-(2-hydroxyphenyl)-6-[(2-phenyl) ethyl]pyridine (HL^3)

This was prepared by demethylation of the precursor MeL^3 (1.00 g, 3.5 mmol) using molten pyridinium chloride at 190°C for 1.75 h according to the published method [8]. The mixture was allowed to cool, water (50 cm^3) was added and the dark red solution was neutralised using aqueous KOH. The resulting precipitate was extracted into CH_2Cl_2 and purified further on silica using CH_2Cl_2 as the eluent to give a yellow crystalline solid. Yield: 0.56 g (59%). EIMS: $m/z = 274$ (M^+). Anal. Found, 82.6; H, 6.7; N, 4.7%. Required for $C_{19}H_{17}NO$: C, 82.8; H, 6.9; N, 4.8%. See Table 1 for ^{1}H NMR data.

Preparation of complexes with Pd(II) and Cu(II)

The complexes $[Pd(L^1)_2]$, $[Pd(L^2)_2]$ and $[Pd(L^3)_2]$, and $[Cu_2(L^1)_4]$ were all prepared by reaction of the appropriate metal acetate (1 equivalent) with the appropriate ligand (2 equivalents) in MeOH at reflux for 30 min. The typical reaction scale was 0.5 mmol

of metal and 1 mmol of ligand in 20 cm^3 of solvent. After evaporation of the solvent *in vacuo*, the residue was recrystallised from CH_2Cl_2/hexane by layering the hexane onto a concentrated solution of the crude complex in CH_2Cl_2 and slowly allowing the layers to mix. This afforded a crop of X-ray quality crystals in every case. The crude yields were near-quantitative; the yields of crystalline material were much lower (10–40%) but not optimised. FAB mass spectral data (3-nitrobenzylalcohol matrix) were as follows: $[Pd(L^1)_2]$, $m/z = 558$ (M^+); $[Pd(L^2)_2]$, $m/z = 474$ (M^+); $[Pd(L^3)_2]$, $m/z = 655$ (M^+) and 381 $\{Pd(L^3)\}$; $[Cu_2(L^1)_4]$, $m/z = 804$ $\{Cu_2(L^1)_3\}$, 579 $\{Cu_2(L^1)_2\}$, 516 $\{Cu(L^1)_2\}$ and 289 $\{Cu(L^1)\}$. Satisfactory elemental analytical data were obtained for each complex.

X-ray crystallography

Suitable crystals were coated with paraffin oil, mounted on a brass pin, and quickly transferred to the diffractometer under a stream of cold N_2. Data were collected using a Siemens SMART three-circle diffractometer with a CCD area detector (173 K, graphite-monochromatised Mo—K_α X-radiation, $\lambda = 0.71073$ Å); a full description of the general experimental method has been given elsewhere [11]. Data were collected for Lorentz/polarisation effects, and for absorption effects by an empirical method based on multiple measurements of equivalent data. Details of the crystal parameters, data collection and refinement are in Table 2, and bond lengths and angles are in Tables 3 and 4. The structures were solved by conventional direct or heavy-atom methods, and refined by the full-matrix least-squares method on all F^2 data, using the SHELX suite of programs [12] on a Silicon Graphics Indy computer. All non-hydrogen atoms were refined anisotropically; hydrogen atoms were included in calculated positions and refined with isotropic thermal parameters.

RESULTS AND DISCUSSION

Ligand syntheses

Preparation of the 2-(2-hydroxyphenyl)pyridine core of HL^2 follows the previously-published method used for HL; viz. Ni(dppe)Cl_2-catalysed coupling of the Grignard reagent 2-$MeOC_6H_4$–MgBr with a substituted 2-bromopyridine [4] (in this case 2-bromo-6-methyl-pyridine which is readily prepared from the commercially available 2-amino-6-methyl-pyridine) to give the protected MeL^2, followed by deme-

Table 2. Crystallographic data for the four new complexes

Complex	$[Pd(L^1)_2]$	$[Pd(L^2)_2]$	$[Pd(L^3)_2]$	$[Cu_2(L^1)_4]$
Formula	$C_{30}H_{32}N_2O_2Pd$	$C_{24}H_{20}N_2O_2Pd$	$C_{38}H_{32}N_2O_2Pd$	$C_{60}H_{64}Cu_2N_4O_4$
M	558.98	474.82	655.06	1032.24
System, space group	Monoclinic, $P2_1/c$	Triclinic, $P\bar{1}$	Monoclinic, $P2_1/n$	Monoclinic, $P2_1/c$
a/Å	12.127(2)	9.657(3)	8.875(2)	9.762(2)
b/Å	11.932(2)	10.398(4)	12.093(2)	15.523(3)
c/Å	8.9543(12)	10.598(4)	27.719(5)	17.038(4)
α/°	90	77.16(3)	90	90
β/°	93.514(13)	84.58(3)	99.10(2)	95.02(2)
γ/°	90	65.33(3)	90	90
U/Å^3	1293.2(3)	942.9(5)	2937.3(9)	2571.9(9)
Z	2	2	4	2
D_c/g cm^{-3}	1.435	1.672	1.481	1.333
μ/mm^{-1}	0.747	1.008	0.670	0.879
$F(000)$	576	480	1344	1084
T/K	173	173	173	173
Crystal size/mm^3	0.1 × 0.4 × 0.5	0.6 × 0.3 × 0.25	0.5 × 0.15 × 0.15	0.4 × 0.4 × 0.5
2θ	3–55	5–50	3–50	5–50
Reflections collected (total, independent, R_{int})	8026, 2936, 0.0193	4450, 3190, 0.0233	14,624, 5161, 0.556	12,037, 4499, 0.0278
Data, restraints, parameters	2936, 0, 170	3189, 0, 264	5161, 0, 388	4496, 0, 353
Weighting factors (a, b)[a]	0.0339, 0	0.0308, 1.7641	0.0621, 0	0.0279, 2.5201
Final R_1, wR_2[a,b]	0.0200, 0.0565	0.0261, 0.0700	0.0574, 0.1322	0.0317, 0.0806
Largest peak, hole/e Å^{-3}	+0.574, −0.516	+1.061, −0.760	+1.640, −1.233	+0.312, −0.348

[a] $wR_2 = [\Sigma[w(F_o^2 - F_c^2)^2]/\Sigma w(F_o^2)^2]^{1/2}$ where $w^{-1} = [\sigma^2(F_o^2) + (aP)^2 + bP]$ and $P = [\max(F_o^2, 0) + 2F_c^2]/3$.

[b] Structure was refined on F_o^2 using all data; the value of R_1 is given for comparison with refinements based on F_o with a threshold of $F \geqslant 4\sigma(F)$.

Table 3. Selected bond lengths (Å) and angles (°) for the three Pd(II) complexes

$[Pd(L^1)_2]^a$		$[Pd(L^2)_2]$		$[Pd(L^3)_2]$	
Pd(1)—O(20)	1.9662(12)	Pd—O(21)	2.017(2)	Pd(1)—O(10)	2.000(3)
Pd(1)—N(11)	2.0236(14)	Pd—O(41)	2.007(2)	Pd(1)—O(40)	2.011(3)
		Pd—N(11)	2.036(2)	Pd(1)—N(21)	2.034(4)
		Pd—N(31)	2.034(2)	Pd(1)—N(51)	2.047(4)
O(20)—Pd(1)—O(20A)	180	O(41)—Pd—O(21)	176.01(7)	O(10)—Pd(1)—O(40)	179.79(12)
N(11)—Pd—N(11A)	180	N(31)—Pd—N(11)	177.66(8)	N(21)—Pd(1)—N(51)	171.7(2)
O(20)—Pd(1)—N(11A)	91.01(5)	O(41)—Pd—N(31)	86.31(9)	O(10)—Pd(1)—N(21)	86.70(14)
O(20)—Pd(1)—N(11)	88.99(5)	O(21)—Pd—N(31)	93.84(9)	O(40)—Pd(1)—N(21)	93.51(13)
		O(41)—Pd—N(11)	94.34(9)	O(10)—Pd(1)—N(51)	94.41(14)
		O(21)—Pd—N(11)	85.35(9)	O(40)—Pd(1)—N(51)	85.38(14)

[a] Complex is centrosymmetric.

Table 4. Selected bond lengths (Å) and angles (°) for $[Cu_2(L^1)_4]$

Cu(1)—O(10)	1.889(2)	Cu(1)—N(51)	2.050(2)
Cu(1)—O(40)	1.9147(14)	Cu(1)—O(40A)	2.193(2)
Cu(1)—N(21)	2.028(2)		
O(10)—Cu(1)—O(40)	168.75(6)	O(10)—Cu(1)—N(21)	90.01(7)
O(40)—Cu(1)—N(21)	94.52(7)	O(10)—Cu(1)—N(51)	94.44(7)
O(40)—Cu(1)—N(51)	87.85(7)	N(21)—Cu(1)—N(51)	144.42(7)
O(10)—Cu(1)—O(40A)	91.60(6)	O(40)—Cu(1)—O(40A)	77.19(6)
N(21)—Cu(1)—O(40A)	109.53(7)	N(51)—Cu(1)—O(40A)	105.61(6)

thylation of the methoxy group with molten pyridinium chloride. HL^3 was likewise prepared from the cross-coupling of 2-bromo-6-[(2-phenyl)ethyl] pyridine (readily prepared by alkylation of deprotonated 2-bromo-6-methyl-pyridine with benzyl bromide) and 2-$MeOC_6H_4$–MgBr, followed by demethylation of the methoxy group. Ligand HL^1 in contrast was prepared by this route, as the required 2-bromo-4-*tert*-butyl-pyridine is not easily available. Instead, it was prepared by the direct reaction of the lithium reagent 2-$MeOC_6H_4Li$ with 4-*tert*-butyl-pyridine to give MeL^1, followed by demethylation. This is a low-yield reaction but allows preparation of reasonable quantities of HL^1 if done on a large scale, and would doubtless also be effective as route preparing the parent ligand HL. The identities of all three new ligands were confirmed by mass spectrometry and ^1H NMR spectroscopy, as well as the crystal structures of their complexes.

Syntheses and structures of $[Pd(L^1)_2]$, $[Pd(L^2)_2]$ *and* $[Pd(L^3)_2]$

We were interested in the Pd(II) complexes of these ligands to see if the various ligand substituents were capable of imposing a distorted coordination geometry on a metal ion that has a very pronounced stereoelectronic preference for regular square-planar geometry. Reaction of each ligand with 0.5 equivalents of palladium(II) acetate afforded neutral, CH_2Cl_2-soluble complexes for which analytical data in each case indicated a 1 : 2 metal : ligand ratio. All three of these were crystallographically characterised and the structures are in Figs 1, 2 and 3.

$[Pd(L^1)_2]$ (Fig. 1) is mononuclear and centrosymmetric, and the coordination geometry is a near-perfect square plane with a *trans* N_2O_2 donor set and unremarkable bond lengths. The ligands each have an angle of 35° between the pyridyl and phenolate rings, and the ligands are disposed such that the phenyl rings are directed towards opposite faces of the PdN_2O_2 plane for steric reasons. This structure is similar to that of $[PdL_2]$ [6]. This arrangement of ligands could not tolerate the addition of bulky substituents to the pyridyl C^6 position, as these substituents would be directed towards the phenyl ring of the alternate ligand, one on each side of the PdN_2O_2 plane.

The structure of $[Pd(L^2)_2]$ (Fig. 2) shows how the ligand conformation has changed to alleviate unfavourable steric effects involving the methyl groups, whilst still allowing the metal centre to retain a regular square-planar geometry. The ligands are

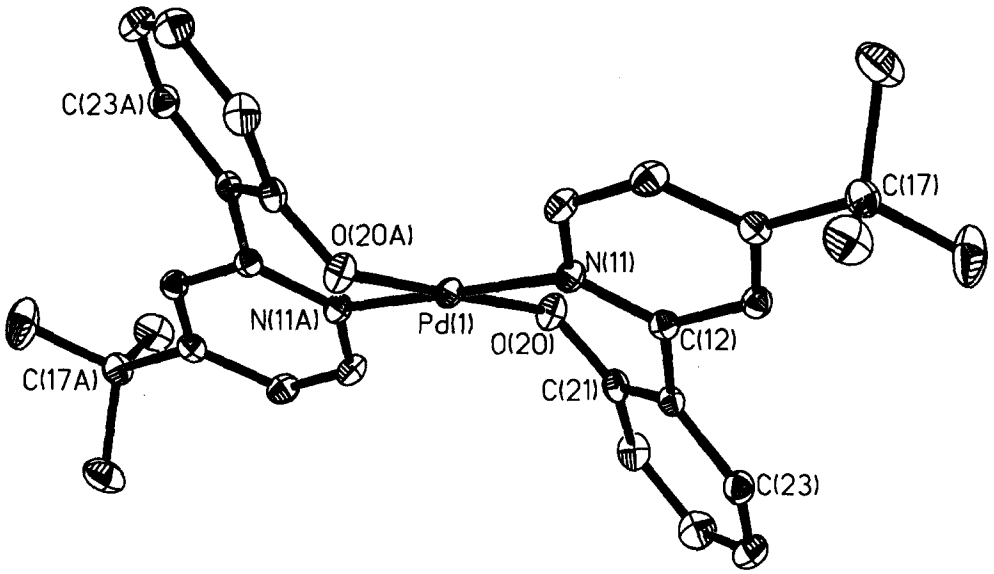

Fig. 1. Crystal structure of $[Pd(L^1)_2]$ (thermal ellipsoids at 40% probability level).

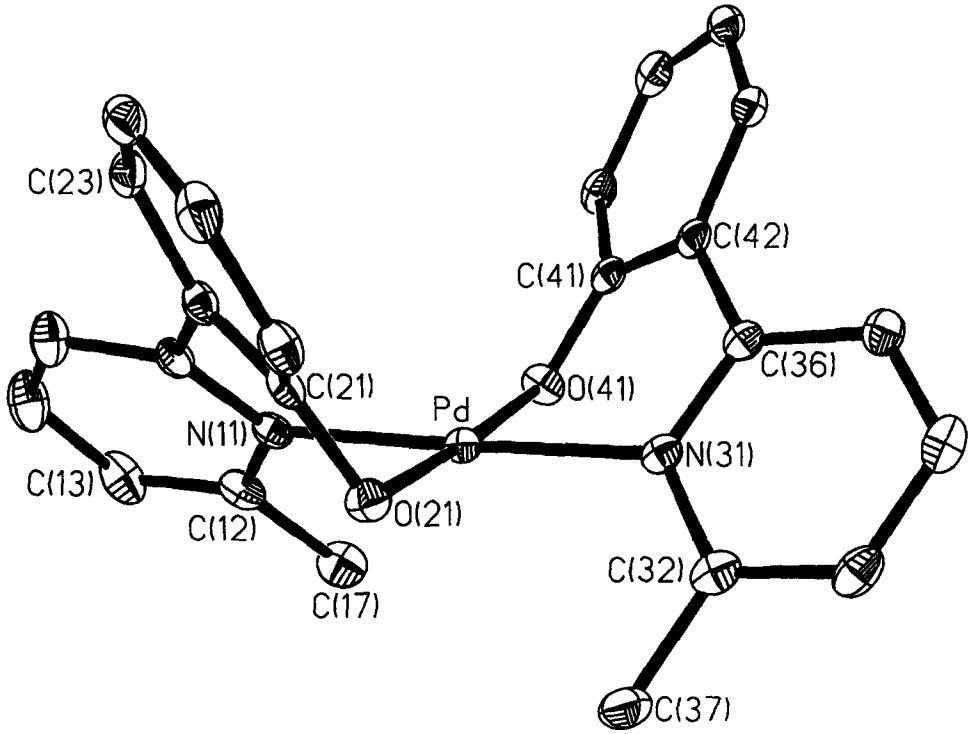

Fig. 2. Crystal structure of $[Pd(L^2)_2]$ (thermal ellipsoids at 40% probability level).

now disposed such that both phenyl rings are directed towards the same face of the *trans*-PdN_2O_2 plane, with both methyl groups directed to the opposite face. The dihedral angles between the mean planes of the aromatic rings within each ligand are 39.6° between rings 1 and 2, and 33.5° between rings 3 and 4, where the ring number is given by the first digit of the crystallographic atom numbering scheme [e.g., ring N(21) to C(26) is ring 2]. All of the metal-ligand bond distances are fractionally longer in $[Pd(L^2)_2]$ than in $[Pd(L^1)_2]$, by about 0.01 Å, which is about five standard deviations and therefore just significant.

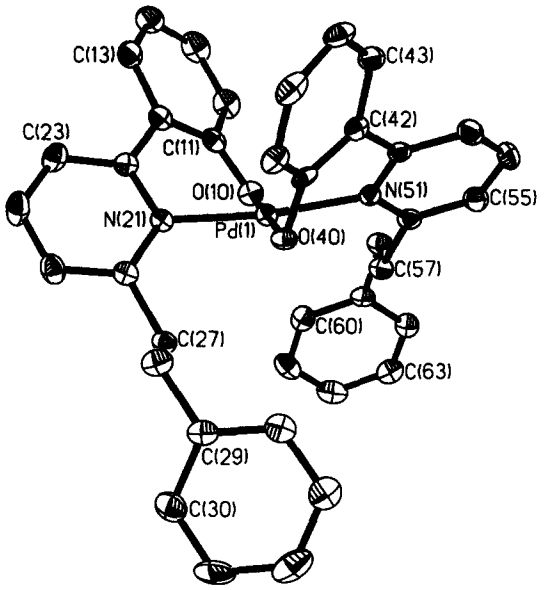

Fig. 3. Crystal structure of $[Pd(L^3)_2]$ (thermal ellipsoids at 40% probability level).

In $[Pd(L^3)_2]$ (Fig. 3) the same type of behaviour is observed. The two CH_2CH_2Ph substituents pendant from the C^6 position of the pyridyl rings are directed to one face of the *trans*-PdN_2O_2 plane, and the two phenyl rings lie on the other side. The disposition of the pyridine/phenol fragments of each ligand are very similar to that observed in $[Pd(L^2)_2]$, which allows relief of all unfavourable steric effects whilst maintaining the planar geometry about the metal centre. The dihedral angles between the mean planes of the aromatic rings within each ligand are 34.8° between rings 1 and 2, and 37.0° between rings 3 and 4. The Pd—O and Pd—N bond lengths are not significantly different from those of $[Pd(L^2)_2]$.

An interesting feature of the latter two structures is that the non-planar conformation of the ligands results in the formation of cavities enclosed by ligand fragments on either face of the metal coordination plane. In both $[Pd(L^2)_2]$ and $[Pd(L^3)_2]$ the two phenyl groups form the base of a bowl-like cavity on one face of the complex. Addition of more substituents to the C^4 positions of the phenyl rings, which should be synthetically straightforward, could extend the bowl and form a "calixarene-like" cavity which could protect/enclose guest species such as solvent molecules or axial ligands. On the other face of the complex, the CH_2CH_2Ph substituents of $[Pd(L^3)_2]$ perform the same function, forming a protective cavity around the space directly "under" the metal centre to which an axial ligand would coordinate. By attachment of suitable "upwardly-directed" substituents at the phenyl C^4 positions, and/or "downwardly-directed" substituents to the pyridyl C^6 position, complexes may be formed which can bind a guest molecule within the protective cavity adjacent to a (coordinatively unsaturated) metal centre, with interesting implications for catalysis. Investigations along these lines are in progress. We note, however, that our original aim of preventing the adoption of a regular square planar geometry about the metal centre was unsuccessful because of the flexibility of the ligands.

Syntheses and structure of $[Cu_2(L^1)_4]$

The Cu(II) complex $[CuL_2]$ was described earlier by Ganis *et al.* but not characterised except by elemental analysis [6]. In view of the tendency of phenolate-containing ligands to form phenolate-bridged dimeric complexes with Cu(II) [3], we were interested to re-investigate $[CuL_2]$. However crystallographic (and spectroscopic) characterisation of $[CuL_2]$ was prevented by its poor solubility, so we instead prepared the Cu(II) complex of the more soluble ligand HL^1. A material analysing as $Cu(L^1)_2$ was easily prepared, and gave X-ray quality crystals from CH_2Cl_2/hexane.

The crystal structure (Figs 4 and 5) shows this complex to be in fact the phenolate-bridged dimer $[Cu_2(L^1)_4]$. The complex is centrosymmetric. Each Cu(II) ion is in an irregular 5-coordinate N_2O_3 geometry, arising from two bidentate ligands $[L^1]^-$ and an additional (bridging) phenolate from a ligand associated with the other metal. The geometry is approximately square-pyramidal, with the basal plane containing N(21), O(10), O(40) and N(51) within each $Cu(L^1)_2$ monomeric unit. The metal atom is situated 0.219 Å out of the mean plane of these four donor atoms, displaced towards to the two oxygen donors. The axial site is used for the bridging interaction to O(40A) associated with the other metal centre. The

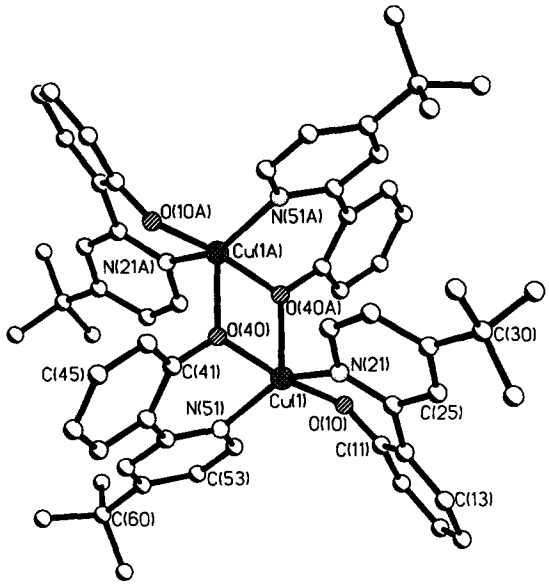

Fig. 4. Crystal structure of $[Cu_2(L^1)_4]$.

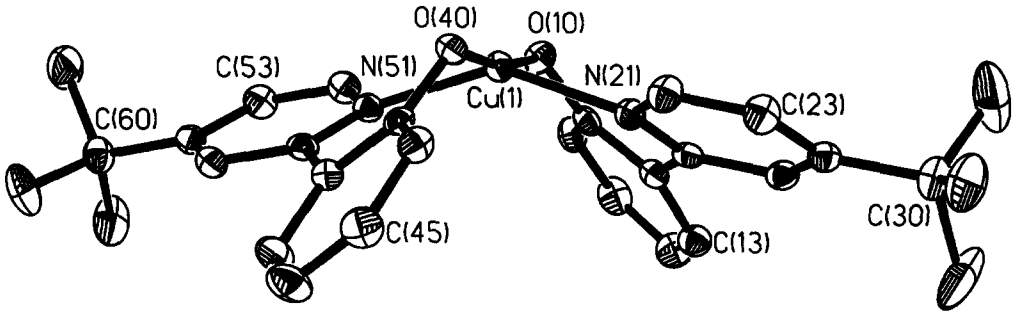

Fig. 5. Crystal structure of the monomer unit of $[Cu_2(L^1)_4]$ (thermal ellipsoids at 40% probability level).

axial metal–ligand bond distance at 2.193(2) Å is significantly longer than the four equatorial ones due to the expected Jahn–Teller distortion. As usual, there is a substantial twist between the mean planes of the pyridyl and phenolate rings within each ligand because of the steric constraints of the six-membered chelate rings: the dihedral angles are 28.8° between rings 1 and 2, and 29.5° between rings 4 and 5. The Cu···Cu separation is 3.215 Å.

EPR spectroscopic studies on this complex gave some interesting information on its solution structure (Fig. 6). A room-temperature spectrum of the powdered microcrystalline material is poorly resolved [Fig. 6(a)], but has the appropriate number of features for a triplet species [2] including a half-field transition at 1580 G ($g = 4.44$), which confirms the presence of the dimer that was apparent from the crystal structure. Figures 6(b) and 6(c) show the spectra of $[Cu_2(L^1)_4]$ dissolved in CH_2Cl_2/thf (2:1, v/v) at room temperature and at 77 K respectively. These spectra in contrast are entirely characteristic of isolated, mononuclear Cu(II) centres with a basically planar structure and the unpaired electron in the $d(x^2-y^2)$ orbital. The axial bridging interactions of $[Cu_2(L^1)_4]$ therefore break in solution to give mononuclear $[Cu(L^1)_2]$ fragments. The spectral parameters are as follows: room temperature; $g_{iso} = 2.114$, $A_{iso} = 70$ G: 77 K; $g_{\parallel} = 2.257$, $g_{\perp} = 2.046$, $A_{\parallel} = 171$ G. Also apparent in the room temperature spectrum is superhyperfine coupling to the N atoms, which can be seen clearly on the highest-field component of the signal and is also just apparent on the adjacent component. Differentiation of the signal [Fig. 6(d)] shows this superhyperfine coupling much more clearly, and a 1:2:3:2:1 quintet is apparent with $A_N = 13$ G, consistent with coupling to two equivalent nitrogen atoms, which is what we would expect in the $[Cu(L^1)_2]$ monomer assuming a high-symmetry (probably planar) structure.

The 77 K frozen glass spectrum showed no evidence for the half-field signal that would be expected if the dimeric structure were retained in solution [2,3]. It is

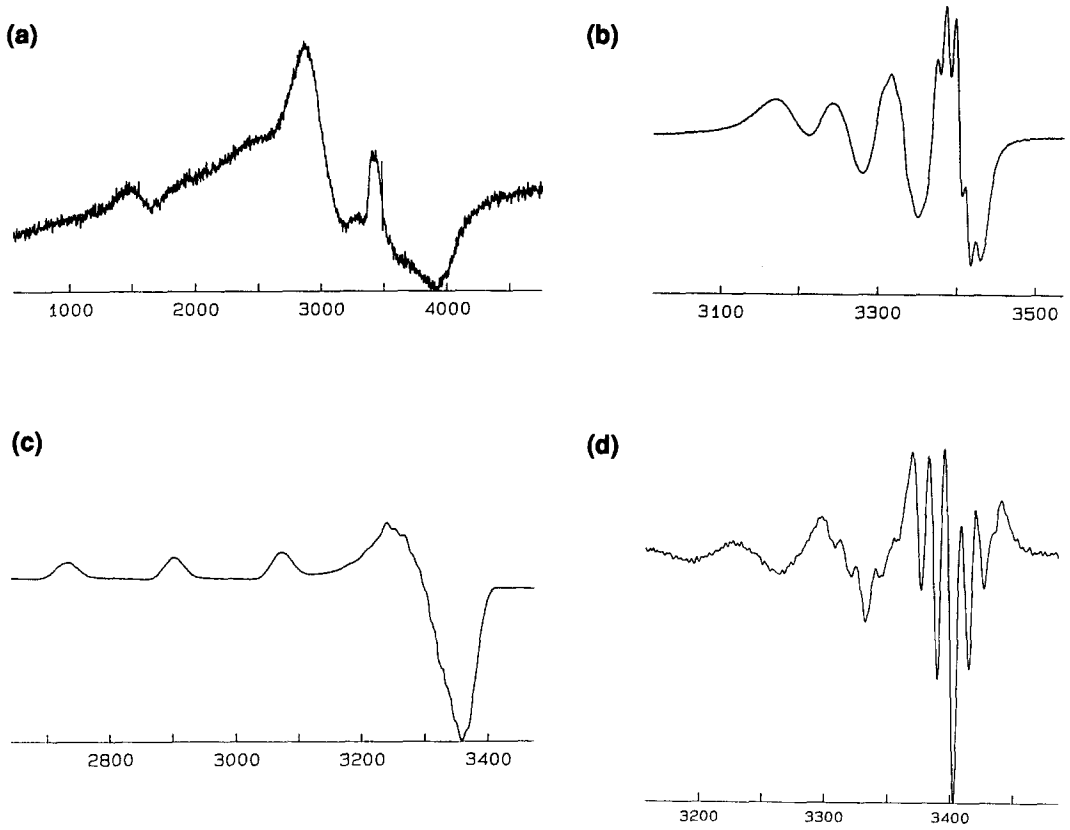

Fig. 6. X-band EPR spectra of $[Cu_2(L^1)_4]$: (a) microcrystalline powdered solid at room temperature; (b) CH_2Cl_2/thf solution at room temperature; (c) CH_2Cl_2/thf frozen glass at 77 K; (d) derivative of (b) emphasising the superhyperfine nitrogen coupling (1 : 2 : 3 : 2 : 1 quintet). Units on the x-axes are Gauss in every case.

perhaps surprising that the dimer is cleaved so easily. In a related dimeric Cu(II) complex with much weaker phenolate bridges [Cu—O(axial) $\approx$ 2.4 Å] the dimeric structure was largely retained in CH_2Cl_2/dmf solution, and addition of pyridine was required to break up the dimer. In this case, however, there was crystallographic evidence for aromatic π-stacking between the aromatic ligands of two near-planar monomeric units, and it may be that this aided association in solution. In $[Cu_2(L^1)_4]$ by contrast there is no evidence for strong inter-component π-stacking interactions, and the dimer dissociates more readily despite the stronger Cu—O(axial) bonds.

Attempts to prepare Cu(II) complexes with the more sterically hindering ligands HL^2 and HL^3 were unsuccessful. Although reaction of the ligand with $Cu(OAc)_2 \cdot 2H_2O$ in methanol immediately afforded a dark green solution similar in colour to solutions of $[Cu_2(L^1)_4]$, these decomposed on concentration and recrystallisation. It appears that the addition of bulky substituents at the pyridyl C^6 position is sufficient to destabilise the planar Cu(II) complexes even though planar Pd(II) complexes could be prepared with the same ligands.

Acknowledgements—We thank the EPSRC and Zeneca Specialities for a CASE award (to CAO) and the EPSRC for grants to purchase the EPR spectrometer and the diffractometer.

REFERENCES

1. Bardwell, D. A., Jeffery, J. C. and Ward, M. D., *J. Chem. Soc., Dalton Trans.*, 1995, 3071; Bardwell, D. A., Jeffery, J. C. and Ward, M. D., *Inorg. Chim. Acta*, 1996, **241**, 125; Cargill Thompson, A. M. W., Bardwell, D. A., Jeffery, J. C., Rees, L. H. and Ward, M. D., *J. Chem. Soc., Dalton Trans.*, 1997, 721; Cargill Thompson, A. M. W., Batten, S. R., Jeffery, J. C., Rees, L. H. and Ward, M. D., *Aust. J. Chem.*, 1997, **50**, 109 and refs. therein.
2. Maher, J. P., Rieger, P. H., Thornton, P. and Ward, M. D., *J. Chem. Soc., Dalton Trans.*, 1992, 3353; Jeffery, J. C., Schatz, E. and Ward, M. D., *J. Chem. Soc., Dalton Trans.*, 1992, 1921; Holligan, B. M., Jeffery, J. C. and Ward, M. D., *J. Chem. Soc., Dalton Trans.*, 1992, 3337.
3. Jeffery, J. C., Maher, J. P., Otter, C. A., Thornton,

P. and Ward, M. D., *J. Chem. Soc., Dalton Trans.*, 1995, 819.
4. Holligan, B. M., Jeffery, J. C., Norgett, M. K., Schatz, E. and Ward, M. D., *J. Chem. Soc., Dalton Trans.*, 1992, 3345.
5. Bardwell, D. A., Black, D., Jeffery, J. C., Schatz, E. and Ward, M. D., *J. Chem. Soc., Dalton Trans.*, 1993, 2321.
6. Ganis, P., Saporito, A., Vitagliano, A. and Valle, G., *Inorg. Chim. Acta*, 1988, **142,** 75.
7. Lindoy, L. F., in *'Synthesis of Macrocycles; the Design of Selective Complexation Agents'* (Eds. R. M. Izatt and J. J. Christensen), Wiley, New York, 1987 (Ch. 2).
8. Dietrich-Buchecker, C. and Sauvage, J.-P., *Tetrahedron*, 1990, **46,** 503.
9. Case, F. H. and Kasper, T. J., *J. Am. Chem. Soc.*, 1956, **78,** 5842.
10. Davies, S. G. and Shipton, M. R., *J. Chem. Soc., Perkin Trans.* 1, 1991, 501.
11. Jones, P. L., Amoroso, A. J., Jeffery, J. C., McCleverty, J. A., Psillakis, E., Rees, L. H. and Ward, M. D., *Inorg. Chem.*, 1997, **36,** 10.
12. SHELXTL 5.03 program system; Siemens Analytical X-ray Instruments, Madison, WI, U.S.A., 1995.

Pergamon

PII: S0277-5387(97)00342-2

Polyhedron Vol. 17, No. 2-3, pp. 221-229, 1998
© 1997 Elsevier Science Ltd
All rights reserved. Printed in Great Britain
0277-5387/98 $19.00+0.00

Platinum(II) thiosalicylate and related complexes as ligands towards mercury(II) halides; X-ray crystal structure of the tetrametallic complex $\{[Pt(SC_6H_4CO_2)(PPh_3)_2] \cdot HgI_2\}_2$

Louise J. McCaffrey, William Henderson* and Brian K. Nicholson

Department of Chemistry, University of Waikato, Private Bag 3105, Hamilton, New Zealand

(Received 3 June 1997; accepted 8 August 1997)

Abstract—The platinum(II) thiosalicylate complex $[Pt(SC_6H_4CO_2)(PPh_3)_2]$ **1a** reacts with HgI_2 to form a tetrametallic complex comprising an $IHg(\mu\text{-}I)_2HgI$ central core with the thiolate sulphur of **1a** coordinated to each mercury centre, completing a distorted tetrahedral coordination environment. Overall, the structural features of the complex, determined by an X-ray diffraction study, are similar to the parent thiosalicylate complex **1a**, but with an increased fold angle (59° compared to 46°) of the thiosalicylate ligand relative to the platinum coordination plane. Reactions of related five-membered ring thiolate complexes $[Pt(SCHRCO_2)(PPh_3)_2]$ (R=H or Me) and of **1a** with a range of metal cations were investigated using ^{31}P NMR spectroscopy. Changes in the $^1J(PtP)$ coupling constants are discussed in terms of coordination to the various metal halide moieties. Reactions of the organomercury(II) thiosalicylate complex Thiomersal ($EtHgSC_6H_4CO_2Na$) with *cis*-$[PtCl_2(PPh_3)_2]$, or *cis*-$[MCl_2(dppe)]$ (M=Ni or Pd) leads to complete transfer of the thiosalicylate ligand from the mercury, and isolation of the previously reported thiosalicylate complexes $[Pt(SC_6H_4CO_2)(PPh_3)_2]$ and $[M(SC_6H_4CO_2)(dppe)]$ (M=Ni, Pd) in high yields. © 1997 Elsevier Science Ltd

Keywords: platinum; mercury; thiolate; thiosalicylate; crystal structure.

Thiosalicylic acid **I** is an interesting heterodifunctional ligand capable of coordinating to both hard and soft metal centres in a variety of bonding modes [1]. In a recent paper [2] we reported the syntheses of a range of platinum(II) **1**, palladium(II) **2** and nickel(II) **3** metallacyclic complexes containing thiosalicylate dianions, together with some related complexes **4** derived from thioglycollic and 2-mercaptopropionic acids. X-ray crystal structure determinations on the platinum and nickel thiosalicylate derivatives $[Pt(SC_6H_4CO_2)(PPh_3)_2]$ **1a** and $[Ni(SC_6H_4CO_2)(dppp)]$ **3a** [dppp = 1,3-bis(diphenylphosphino)propane] revealed different bonding arrangements of the thiosalicylate ligand towards the two metal ions. These differences were tentatively ascribed to the effects of metals of different sizes coordinated by a relatively inflexible ligand. Metal thiolate complexes are well known to possess ligand properties towards other metal centres [3] and we have previously shown that the five-membered ring thiolate complex **5** coordinates to mercury(II) halides to form tetrametallic complexes consisting of an $XHg(\mu\text{-}X)_2HgX$ core, with each mercury atom ligated by the sulphur atom of a platinum–thiolate complex, i.e. **6a** [4]. The bis(thiosalicylato) mercury(II) complex $[Hg(tsalH)_2]$ (containing S-bonded thiosalicylate monoanions) is known to be able to complex other metal ions, such as Zn^{2+}, Cd^{2+} and Pb^{2+} [5]. Metal–thiosalicylate complexes are known to display a range of coordination geometries [1] and thus it was of interest to investigate whether coordination of the sulphur

* Author to whom correspondence should be addressed. Fax: 0064-7-838-4219; E-mail: w.henderson@waikato.ac.nz.

atom of **1a** would influence the geometry of the platinum–thiosalicylate moiety.

In this contribution we report that the platinum–thiosalicylate complex **1a,** together with the related cyclic thiolate complexes **4,** have analogous ligand properties towards mercury(II) halides. We also report that the thiosalicylate ligand is completely transferred from the organomercury complex $EtHgSC_6H_4CO_2Na$ to platinum(II), palladium(II) and nickel(II) centres.

RESULTS AND DISCUSSION

Synthesis and X-ray crystal structure

Reactions of the platinum(II) cyclic thiolate complexes **1a, 4a** and **4b** with excess solid $HgBr_2$ or HgI_2 were carried out in dichloromethane solution. Addition of the mercury salt followed by shaking typically resulted in a lightening of the solution (for $HgBr_2$), or little change (for HgI_2), though when smaller quantities of the mercury salt were used, dissolution was observed. In general, crystalline products **6b–6e** were obtained by slow diffusion of diethyl ether into the solution (after removal of excess HgX_2). However, the mercaptopropionate–HgI_2 complex did not crystallise well, though it was analytically pure. The attempted synthesis of a comparable HgI_2 complex of the cyclo-octa-1,5-diene (COD) complex $[Pt(SC_6H_4CO_2)(COD)]$ led only to the crystallisation of the pure platinum starting complex, as shown by elemental microanalytical data.

In order to unambiguously confirm the structure of one derivative (which was considered important given

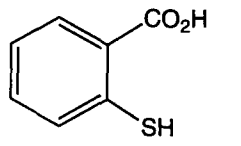

I

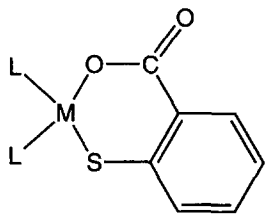

1; M = Pt
1a; L = PPh_3

2; M = Pd
2a; L-L = $Ph_2PCH_2CH_2CH_2PPh_2$

3; M = Ni
3a; L-L = $Ph_2PCH_2CH_2CH_2PPh_2$

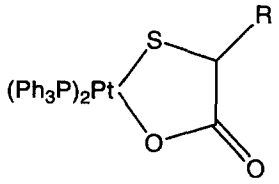

4a; R = H
4b; R = Me

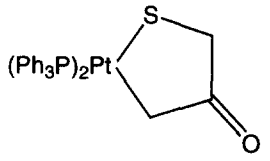

5

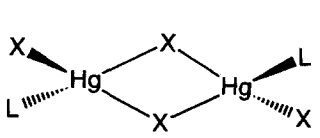

6a; L = **5**; X = Br
6b; L = **1a**; X = I
6c; L = **4a**; X = I
6d; L = **4b**; X = I
6e; L = **4a**; X = Br
6f; L = **1a**; X = Cl

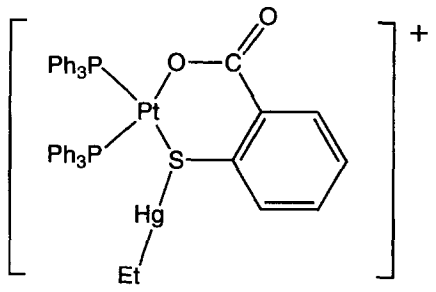

7

the known structural complexity of the coordination chemistry of mercury(II) halides with neutral donor ligands [6]) a single-crystal X-ray diffraction study was carried out on the HgI_2 complex **6b**. Since excess mercury halide was used, and complexes of the type $LHgX_2$ are known to commonly have dimeric structures [6] it is likely that the range of related HgX_2 (X=Cl, Br, I) complexes **6** have similar structures.

The structure of **6b** comprises a centrosymmetric dimer with a near-rectangular $Hg_2(\mu\text{-}I)_2$ core. The Hg is further coordinated to a terminal I ligand and to the S atom of a $[Pt(SC_6H_4CO_2)(PPh_3)_2]$ molecule. It is related to a range of other $[L(I)Hg(\mu\text{-}I)]_2$ dimers, and three structures have been reported where L is a sulphur donor ligand [7]. Additionally we have previously reported the structure of the related $HgBr_2$ adduct **6a** [4].

The coordination about the Hg atom is distorted tetrahedral, with angles subtended at Hg ranging from 87° to 125°. The iodo-bridge is strongly unsymmetrical with Hg—I distances of 2.7139(5) and 3.2870(5) Å; both of these are longer than the bond to the terminal iodo ligand [2.6667(5) Å]. The large iodo bridge results in an essentially rectangular motif, with I—Hg—I and Hg—I—Hg angles of 87.76(1) and 92.24(1)° respectively. These features are in accord with those in other examples [7].

The attachment of the sulphur atom to the Hg atom has only a small effect on the geometry of the platinum-complex part of the molecule, in comparison with the free species **1a**. The Pt(1)—S(1)—C(7) angle in the mercury adduct is 99.2(2)°, from 103.8(2)° in **1a**, but the Pt—S and S—C distances show negligible change. There is an apparent change in the Pt—O(1)—C(1) angle from 135.8(4) to 126.0(3)°, with a decrease in the Pt—O(1) distance from 2.109(3) to 2.076(3) Å in the adduct, but the significance of this must remain tentative in view of the suspicion that the parameters involving O(1) may be unreliable in the free complex [2]. The S—Pt—O(1) angle and the P(1)—Pt—P(2) angles show no chemically significant differences on attachment to the mercury atom.

The coordination about the platinum atom is essentially planar, with a small twist defined by the dihedral angle of 8.2° between the P(1)—Pt—P(2) and S(1)—Pt—O(1) planes. The CO_2 group of the thios-

Table 1. Selected bond lengths [Å] and angles [°] for complex **6b**

Pt(1)—O(1)	2.076(3)	Pt(1)—P(2)	2.2411(13)
Pt(1)—P(1)	2.2971(14)	Pt(1)—S(1)	2.3159(14)
Hg(1)—S(1)	2.5694(15)	Hg(1)—I(2)	2.6667(5)
Hg(1)—I(1)	2.7139(5)	Hg(1)—I(1)#1	3.2870(5)
I(1)—Hg(1)#1	3.2870(5)	S(1)—C(7)	1.789(6)
P(1)—C(31)	1.809(6)	P(1)—C(11)	1.812(5)
P(2)—C(41)	1.805(6)	P(2)—C(51)	1.815(5)
P(2)—C(61)	1.833(6)	O(1)—C(1)	1.304(7)
O(2)—C(1)	1.229(7)	C(1)—C(2)	1.510(8)
C(2)—C(3)	1.398(8)	C(2)—C(7)	1.406(8)
C(3)—C(4)	1.371(10)	C(4)—C(5)	1.395(12)
C(5)—C(6)	1.368(10)	C(6)—C(7)	1.379(9)
O(1)—Pt(1)—P(2)	176.01(11)	O(1)—Pt(1)—P(1)	81.89(12)
P(2)—Pt(1)—P(1)	98.55(5)	O(1)—Pt(1)—S(1)	85.65(12)
P(2)—Pt(1)—S(1)	94.42(5)	P(1)—Pt(1)—S(1)	165.36(5)
S(1)—Hg(1)—I(2)	106.91(3)	S(1)—Hg(1)—I(1)	124.85(3)
I(2)—Hg(1)—I(1)	125.800(18)	S(1)—Hg(1)—I(1)#1	94.99(3)
I(2)—Hg(1)—I(1)#1	103.898(17)	I(1)—Hg(1)—I(1)#1	87.757(14)
Hg(1)—I(1)—Hg(1)#1	92.244(14)	C(7)—S(1)—Pt(1)	99.2(2)
C(7)—S(1)—Hg(1)	105.78(18)	Pt(1)—S(1)—Hg(1)	96.51(5)
C(31)—P(1)—C(11)	106.0(3)	C(31)—P(1)—C(21)	102.0(3)
C(11)—P(1)—C(21)	105.6(3)	C(31)—P(1)—Pt(1)	115.69(19)
C(11)—P(1)—Pt(1)	102.83(18)	C(21)—P(1)—Pt(1)	123.32(18)
C(41)—P(2)—C(51)	111.4(3)	C(41)—P(2)—C(61)	101.4(3)
C(51)—P(2)—C(61)	102.5(3)	C(41)—P(2)—Pt(1)	111.98(19)
C(51)—P(2)—Pt(1)	112.46(17)	C(61)—P(2)—Pt(1)	116.17(18)
C(1)—O(1)—Pt(1)	126.0(3)	O(2)—C(1)—O(1)	121.1(5)
O(2)—C(1)—C(2)	119.1(5)	O(1)—C(1)—C(2)	119.8(5)
C(3)—C(2)—C(7)	118.4(5)	C(3)—C(2)—C(1)	116.5(5)
C(7)—C(2)—C(1)	125.0(5)	C(4)—C(3)—C(2)	121.6(7)
C(3)—C(4)—C(5)	119.7(7)	C(6)—C(5)—C(4)	119.1(7)
C(5)—C(6)—C(7)	122.3(7)	C(6)—C(7)—C(2)	119.0(6)
C(6)—C(7)—S(1)	115.3(5)	C(2)—C(7)—S(1)	125.7(4)

alicylate ligand is twisted so that O(1) and O(2) are displaced by ca 0.3 Å from the plane of the rest of the ligand. Somewhat unexpectedly, it was found that the thiosalicylate ligand plane of **1a** was inclined at an angle of 46° to the platinum coordination plane. This feature is maintained in the mercury adduct **6b,** with the corresponding angle increased to 59°. This is not an essential requirement to accommodate the Hg atom at the S, since the corresponding $HgBr_2$ adduct **6a** forms by coordination from the S atom in a complex in which the chelating ligand lies essentially within the coordination plane.

NMR spectroscopy and electrospray mass spectrometry

Reactivity of the platinum–thiolate complexes towards mercury(II) halides, and other metal centres, can be conveniently monitored using ^{31}P NMR spectroscopy; chemical shift and coupling constant data are summarised in Table 2. For example, after addition of an excess of solid HgI_2, $HgBr_2$ or $HgCl_2$ to a $CDCl_3$ solution of **1a,** the ^{31}P-$\{^1H\}$ NMR spectra showed overall similar features to the starting complex (*viz* an AB spin system with ^{195}Pt satellites), but with the chemical shifts of all triphenylphosphines shifted to lower δ by about 3–4 ppm; no ^{199}Hg-^{31}P coupling could be ascertained in any of the complexes. The $^1J(PtP)$ coupling constant for the PPh_3 ligand *trans* to the thiolate increases from 2884 Hz in **1a** to 3073, 3112, 3156 Hz on addition of HgI_2, $HgBr_2$ or $HgCl_2$ respectively. These are similar to those observed previously [4] and are consistent with the reduction in the *trans* influence of the thiolate ligand upon coordination to mercury(II). There is a concomitant decrease in the magnitude of $^1J(PtP)$ for the phosphine *trans* to the carboxylate upon coordination of the sulphur atom. The decreasing electron-withdrawing nature in the series $HgCl_2 > HgBr_2 > HgI_2$ influences the strength of interaction; the more electrophilic $HgCl_2$ effects a greater interaction with the Pt—S group, strengthening the *trans* Pt—P bond, increasing its coupling constant. Correspondingly, the $^1J(PtP)$ coupling constant for the phosphine *trans* to oxygen (i.e. *cis* to the thiolate) decreases from the starting complex (3899 Hz) to the $HgBr_2$ complex (3842 Hz), and even further for the $HgCl_2$ complex (3808 Hz).

The trends in $^1J(PtP)$ values are also extended further to the HgI_2 complexes of **1a, 4a** and **4b**. It is interesting for this series of complexes to compare the magnitude of change in $^1J(PtP)$ values for both triphenylphosphines, upon complex formation with HgI_2. Upon addition of HgI_2 to **1a,** the value of $^1J(PtP)$ for the phosphine *trans* to thiolate increases by 182 Hz, while that for the phosphine *trans* to carboxylate decreases by 88 Hz. For **4a** and **4b** upon addition of HgI_2, the $^1J(PtP)$ values for the phosphines *trans* to thiolate increase by 278 and 304 Hz respectively, while the values of $^1J(PtP)$ for the phosphines *trans* to carboxylate decrease by 151 and 159 Hz respectively. Thus, the changes upon coordination for **4a** and **4b** are almost twice those for **1a,** suggesting a much stronger interaction of the HgI_2 moiety with complexes **4**. This

Table 2. A comparison of ^{31}P NMR spectroscopic data, recorded in $CDCl_3$ solution, for the platinum–thiolate complexes[a] and their HgX_2 adducts, isolated by crystallisation, or generated *in situ*[b]

		PPh_3 *trans* S		PPh_3 *trans* O		
Complex	Added MX_2[c]	δ/ppm	$^1J(PtP)$/Hz	δ/ppm	$^1J(PtP)$/Hz	$^2J(PP)$/Hz
1a	—	24.5	2884	10.2	3899	22
1a	$HgCl_2$	21.0	3156	6.5	3808	21
1a	$HgBr_2$	21.2	3112	7.0	3842	22
1a	HgI_2	21.4	3073	7.6	3807	22
6b	—	23.2	3055	7.8	3811	22
1a	CdI_2	24.3	2893	9.9	3912	22
1a	$CdCl_2$	24.5	2884	10.1	3905	22
1a	$PdCl_2$	24.5	2887	10.1	3903	22
4a	—	22.1	2868	12.1	3766	22
6c	—	19.4	3146	8.4	3615	23
4b	—	22.2	2849	12.5	3790	22
6d	—	19.2	3153	8.3	3631	23

[a] NMR spectroscopic properties for the starting thiolate complexes **1** and **4** are from Ref. [2].

[b] Data are also included for other metal centres where little or no interaction is considered to occur, evidenced by no change in the ^{31}P chemical shifts or coupling constants. Experiments were carried out by dissolving the platinum complex in $CDCl_3$, adding the solid metal salt (where appropriate), briefly shaking, and then recording the ^{31}P NMR spectrum.

[c] Addition of $ZnBr_2$ produced a mixture of products, including *cis*-$[PtBr_2(PPh_3)_2]$.

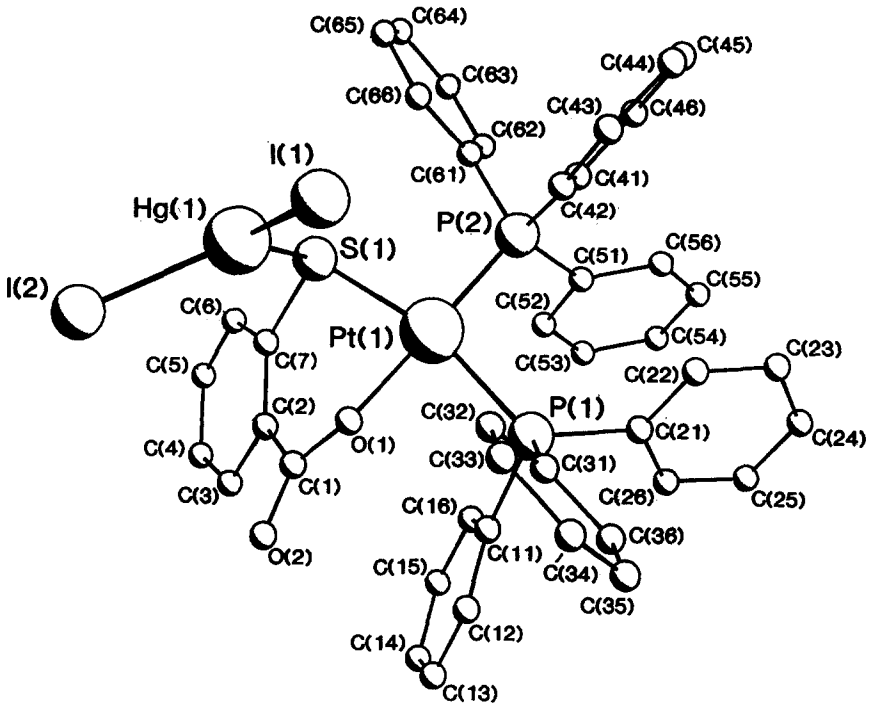

Fig. 1. Molecular structure of the unique half of complex **6b** showing the atom numbering scheme.

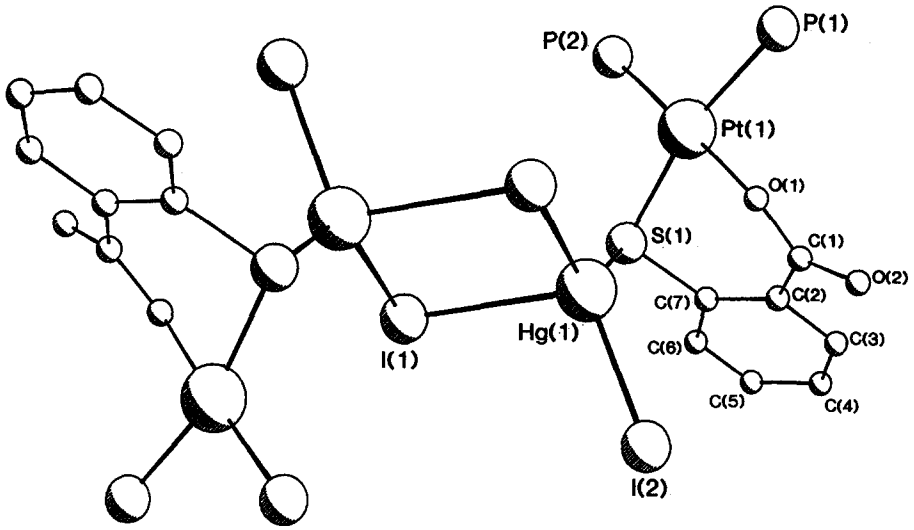

Fig. 2. Diagram showing the central core unit of complex **6b**; all hydrogen and triphenylphosphine carbon atoms have been omitted for clarity.

is not unexpected, since the *ortho*-phenyl hydrogen of the thiosalicylate group is likely to experience a steric interaction with a metal centre coordinated to the sulphur atom.

It is worth noting that a small amount of *cis*-$[PtCl_2(PPh_3)_2]$ is formed as a by-product along with **6f** in the reaction of **1a** with $HgCl_2$, identified by ^{31}P NMR spectroscopy. Upon allowing the solution to stand overnight with excess $HgCl_2$, no additional *cis*-$[PtCl_2(PPh_3)_2]$ was formed. No $[PtBr_2(PPh_3)_2]$ or

$[PtI_2(PPh_3)_2]$ complexes were detected by NMR in the reactions with $HgBr_2$ or HgI_2, presumably due to the less electrophilic nature of these metal centres.

Reaction of **1a** with $Hg(SCN)_2$ produces a rather complex mixture of products, identified by ^{31}P NMR, possibly in part as a result of thiocyanate transfer from mercury to platinum. Similarly, a mixture of products was observed with added $ZnBr_2$, though *cis*-$[PtBr_2(PPh_3)_2]$ could be identified from its ^{31}P-$\{^1H\}$ NMR spectrum. There appeared to be no interaction between **1a** and either $CdCl_2$, CdI_2 or $PdCl_2$, by ^{31}P NMR spectroscopy.

Electrospray mass spectrometry (ESMS) has also been evaluated as a potential technique for characterisation of the complexes formed between the cyclic platinum–thiolate complexes and mercury(II) ions, particularly in light of the NMR results described above. One of the principal attractions of the ESMS technique is that it allows the direct analysis of species in solution [8]. We have previously used ESMS to characterise the neutral thiosalicylate complexes **1–3** [2]. However, when crystals of the HgI_2 adduct **6b** were analysed in MeCN—H_2O solution, no Pt—Hg adducts could be observed. Instead, the spectrum indicated that the complex had completely dissociated, with the starting complex $[\mathbf{1a}+H]^+$ being the base peak at *m/z* 872, as observed for the pure complex **1a**. Identical results were observed for the complex **6d**. Complexes of mercury(II) halides with thioether ligands would be expected to relatively labile in solution [6], although a thiolate-bridged structure might be expected to be less labile.

Addition of a small quantity of NaCl to the ESMS solution of **6b** in MeCN—H_2O solution yielded the species HgI_3^- (*m/z* 583), HgI_2Cl^- (*m/z* 491) and $HgICl_2^-$ (*m/z* 399) in the negative ion ESMS spectrum; no adducts of the parent thiosalicylate complex **1a** with mercury species were detected.

Thiosalicylate transfer reactions with Thiomersal ($EtHgSC_6H_4CO_2Na$)

Following the successful reactions between the platinum–thiosalicylate complex **1a** and HgX_2, we wished to investigate whether the organomercury complex Thiomersal (Merthiolate, sodium ethylmercurithiosalicylate), which contains a monodentate thiosalicylate ligand, could be used as a ligand towards platinum(II) centres. This was considered as a possible alternative route to other types of platinum–mercury thiosalicylate-bridged complexes. Thiomersal is of interest since it has biological activity and has been used as an antiseptic [9].

The reaction of *cis*-$[PtCl_2(PPh_3)_2]$ with one mole equivalent of Thiomersal in hot methanol yields the platinum–thiosalicylate complex **1a** *via* a thiolate-transfer reaction, eqn (1). In this case, the thiolate ligand is completely transferred from mercury(II) to platinum(II), and thus EtHgCl and NaCl are the presumed byproducts, though no attempt was made to confirm these;

$$cis\text{-}[PtCl_2(PPh_3)_2] + EtHgSC_6H_4CO_2Na \rightarrow [Pt(SC_6H_4CO_2)(PPh_3)_2] \quad \mathbf{1a}$$

Eq. 1 $(+EtHgCl+NaCl)$

Analogous reactions also proceeded readily when $[PdCl_2(dppe)]$ [dppe = 1,2-bis(diphenylphosphino) ethane] or $[NiCl_2(dppe)]$ were reacted with Thiomersal, also in methanolic solution, giving the previously reported [2] thiosalicyate complexes $[M(SC_6H_4CO_2)(dppe)]$ (M=Ni, Pd). In methanol solvent, there is a vary rapid colour change to that of the product. However, the reaction of *cis*-$[PtCl_2(PPh_3)_2]$ with Thiomersal can be slowed down by carrying it out in $CDCl_3$, so that the course of the reaction can be followed by ^{31}P NMR spectroscopy. The reaction proceeds smoothly, with consumption of the starting *cis*-$[PtCl_2(PPh_3)_2]$ complex with a concomitant increase in intensity of resonances due to the thiosalicylate product **1a**. Only one very minor additional peak was present, and since $^1J(PtP)$ data could not be discerned, it is not possible to comment upon the identity of this species. Any possible intermediates formed in the reaction, such as **7**, containing Pt—S—Hg thiosalicylate-bridged species clearly do not reach significant concentrations under these conditions.

In a separate experiment, the reaction was monitored by positive-ion ESMS. An equimolar mixture of *cis*-$[PtCl_2(PPh_3)_2]$ and Thiomersal was analysed several minutes after mixing in 1 : 1 MeCN—H_2O. The spectrum showed the platinum–thiosalicylate complex $[\mathbf{1a}+H]^+$ at *m/z* 872 as the predominant ion together with a small ion at *m/z* 894, assigned as the sodium adduct $[\mathbf{1a}+Na]^+$; this ion is not unexpected, since Thiomersal is a sodium carboxylate salt. Addition of alkali metal salts to pure samples of **1a** also yielded $[M+cation]^+$ ions in the ESMS spectra [2]. The ion $[(\mathbf{1a})_2+H]^+$ was also observed at *m/z* 1744, as observed previously for **1a** [2]. A very weak ion at around *m/z* 1100 can be tentatively assigned as the species $[(Ph_3P)_2Pt(SC_6H_4CO_2)+EtHg]^+$. This complex, for which **7** is a likely structure, is a plausible intermediate in the thiosalicylate transfer reaction. However, an isotope pattern could not be obtained for this ion, and so its assignment remains tentative. The ESMS results therefore parallel the NMR results by showing no significant intermediates. The absence of the ions $[PtCl(PPh_3)_2]^+$ and $[PtCl(MeCN)(PPh_3)_2]^+$ which are observed for *cis*-$[PtCl_2(PPh_3)_2]$ in MeCN—H_2O solutions also confirms the rapid conversion of *cis*-$[PtCl_2(PPh_3)_2]$ into **1a** [10]. No platinum-containing intermediates were observed when the *cis*-$[PtCl_2(PPh_3)_2]$/Thiomersal reaction mixture was analysed in negative-ion mode.

Thiolate transfer reactions have been documented in the literature, generally transferring the thiolate

ligand from a harder metal centre to a softer one, which provides a driving force for the reaction [11]. Despite the very strong affinity of mercury for thiolate ("mercaptan") ligands, it is evident that the formation of the chelating thiosalicylate complexes, possibly assisted by precipitation of NaCl, is the major driving force in this exchange reaction. The tendency for mercury(II) thiolate complexes to adopt low coordination numbers, in many cases typified by linear two-coordination, is also likely to bear a major influence [12].

EXPERIMENTAL

General experimental procedures have been described previously [2]. All complexes described in this work are air-stable, and reactions were carried out without regard for the exclusion of air. Diethyl ether and petroleum spirits (bp 40–60°C) were LR grade, while dichloromethane was distilled from CaH_2 prior to use. Standardless EDAX analyses were obtained on a Hitachi S4000 scanning electron microscope.

The following compounds were used as supplied from BDH: red mercury(II) iodide, mercury(II) bromide, mercury(II) chloride, cadmium iodide, cadmium chloride and zinc bromide. The complexes $[Pt(SC_6H_4CO_2)(PPh_3)_2]$ **1a**, $[Pt(SCH_2CO_2)(PPh_3)_2]$ **4a** and $[Pt(SCHMeCO_2)(PPh_3)_2]$ **4b** were prepared as described previously [2]. $[PdCl_2(dppe)]$ was prepared by ligand substitution of the COD ligand of $[PdCl_2(COD)]$ [13] with 1 mole equivalent of dppe in CH_2Cl_2. $[NiCl_2(dppe)]$ was prepared by the literature procedure [14].

Synthesis of the thiolate-bridged platinum–mercury complexes **6**. *General method*

To a solution of the platinum complex (ca 100 mg) in dichloromethane (ca 2 cm^3) was added an excess of the solid mercury(II) halide, and the mixture briefly shaken. After allowing the excess mercury salt to settle, the supernatant was removed by a Pasteur pipette and transferred to a glass vial. Vapour diffusion of diethyl ether into the solution yielded a crystalline or microcrystalline product in most cases, which was dried *in vacuo* for 24 h.

$\{[Pt(SC_6H_4CO_2)(PPh_3)_2]\cdot HgI_2\}_2$

The platinum complex **1a**. 0.33MeOH (82 mg, 0.093 mmol) and HgI_2 (190 mg, 0.418 mmol) gave bright yellow crystals of **6b** (122 mg, 99%), m.p. 198–203°C (decomp.). Despite several attempts, satisfactory elemental analytical data could not be obtained for this compound. Found: C, 35.9; H, 2.1; N, 0.0. $C_{43}H_{34}O_2P_2PtSHgI_2$ requires C, 38.9; H, 2.6; N, 0.0%.

The presence of Pt, Hg and I were confirmed using EDAX analysis.

$\{[Pt(SCH_2CO_2)(PPh)_2]\cdot HgI_2\}_2$

The platinum complex **4a** (75 mg, 0.093 mmol) and HgI_2 (170 mg, 0.374 mmol) gave light yellow microcrystals of **6c** (94 mg, 80%), m.p. 207–209°C (decomp.). Found: C, 36.4; H, 2.4; N, 0.0. $C_{38}H_{32}O_2P_2PtSHgI_2$ requires C, 36.1; H, 2.6; N, 0.0%.

$\{[Pt(SCHMeCO_2)(PPh_3)_2]\cdot HgI_2\}_2$

The platinum complex **4b** (79 mg, 0.096 mmol) and HgI_2 (224 mg, 0.493 mmol) gave a pale yellow solid of **6d** (59 mg, 48%), m.p. 204–208°C (decomp.). Found: C, 36.8; H, 2.4; N, 0.0. $C_{39}H_{34}O_2P_2PtSHgI_2$ requires C, 36.6; H, 2.7; N, 0.0%.

Attempted synthesis of $\{[Pt(SC_6H_4CO_2)COD]\cdot HgI_2\}_2$

The platinum complex $[Pt(SC_6H_4CO_2)(COD)]$ and excess HgI_2 gave bright yellow crystals, which were found to be the unreacted platinum complex, by elemental analysis: Found: C, 39.6; H, 3.4. $C_{15}H_{16}O_2PtS$ requires C, 39.6; H, 3.5%.

Thiolate exchange reaction between cis-$[PtCl_2(PPh_3)_2]$ *and* $EtHgSC_6H_4CO_2Na$

A suspension of *cis*-$[PtCl_2(PPh_3)_2]$ (391 mg, 0.495 mmol) and Thiomersal (200 mg, 0.494 mmol) in methanol (25 cm^3) was refluxed for 2 h; the mixture turned bright yellow over the course of several minutes. Water (50 cm^3) was added, and the resulting yellow precipitate filtered, washed with water and diethyl ether, and dried *in vacuo*. Yield 378 mg (88%). The product was identified as **1a** by ^{31}P-$\{^1H\}$ NMR spectroscopy.

Thiolate exchange reaction between $[PdCl_2(dppe)]$ *and* $EtHgSC_6H_4CO_2Na$

A suspension of $[PdCl_2(dppe)]$ (109 mg, 0.189 mmol) and Thiomersal (77 mg, 0.189 mmol) was refluxed in methanol (20 cm^3) for 20 min, to give an orange suspension. Water (60 cm^3) was added, the product filtered, washed with water (10 cm^3) and ether (10 cm^3) and dried under vacuum to give 88 mg (71%) of **2a**, identified by ^{31}P-$\{^1H\}$ NMR spectroscopy.

Thiolate exchange reaction between $[NiCl_2(dppe)]$ *and* $EtHgSC_6H_4CO_2Na$

A suspension of $[NiCl_2(dppe)]$ (77 mg, 0.146 mmol) and Thiomersal (59 mg, 0.146 mmol) was refluxed in

methanol (10 cm^3) for 30 min, to give a red-orange solution/suspension. Water (50 cm^3) was added, the product filtered, washed with water (10 cm^3) and ether (10 cm^3) and dried under vacuum to give 60 mg (68%) of [Ni($SC_6H_4CO_2$)(dppe)], identified by ^{31}P-{^1H} NMR spectroscopy.

Crystal structure determination of {[$Pt(SC_6H_4CO_2)(PPh_3)_2$]·HgI_2}$_2$ **6b**.

Bright yellow crystals of **6b** were obtained from the slow diffusion of ether into a CH_2Cl_2 solution. The unit cell dimensions and intensity data were obtained on a Siemens SMART diffractometer. The data collection nominally covered over a hemisphere of reciprocal space, by a combination of three sets of exposures; each set had a different ϕ angle for the crystal and each exposure 0.3° in ω. The crystal to detector distance was 5.0 cm. The data set was corrected empirically for absorption using SADABS [15].

Crystal data and refinement for **6b**

$C_{43}H_{34}HgI_2O_2P_2PtS$. 0.5 $(C_2H_5)_2O$, M_r 1363.24, triclinic, space group $P\bar{1}$, $a = 12.4725(2)$, $b = 12.6573(2)$, $c = 14.9196(1)$ Å, $\alpha = 79.420(1)$, $\beta = 70.357(1)$, $\gamma = 82.106(1)°$, U 2173.27(5) $Å^3$. $D_{calc} = 2.083$ g cm^{-3}, $Z = 2$, $F(000)$ 1278, μ(Mo–K_α) = 8.323 mm^{-1}. Crystal size 0.52 × 0.32 × 0.24 mm. A total of 21,943 reflections were collected at 203(2) K in the range $1.5° < \theta < 28.2°$, corresponding to 9691 unique data ($R_{int} = 0.0368$), $T_{max,min}$ 0.2633, 0.1342.

The structure was solved by automatic interpretation of a Patterson map and developed routinely. In a penultimate difference map an Et_2O of crystallisation, disordered across an inversion centre, was revealed. In the final cycles of least-squares refinement based on F^2 against all data, all non-hydrogen atoms were treated anisotropically and hydrogen atoms (other than those of the disordered solvent) were included in their calculated positions. The refinement converged with $R_1 = 0.0387$ [for 6817 data with $I > 2\sigma(I)$], $R_1 = 0.0437$, $wR_2 = 0.1033$, GoF 1.079 (all data). The largest features in a final difference map were +2.707/−3.634 e $Å^{-3}$ adjacent to heavy metal atoms. The SHELX-96 package [16] was used for all calculations.

Complete lists of atomic coordinates, bond parameters and tables of thermal parameters and hydrogen atom coordinates have been deposited at the Cambridge Crystallographic Data Centre (CCDC), and are available from the authors on request.

Acknowledgements—The University of Waikato and the New Zealand Lottery Grants Board are acknowledged for financial support of this work. We thank Assoc. Prof. C. E. F. Rickard and Dr L. J. Baker (University of Auckland) for collection of the X-ray data set, and Johnson-Matthey plc for a generous loan of platinum metal salts. Alf Harris (Waikato Microscope Unit) is thanked for EDAX measurements.

REFERENCES

1. Mitra, S., Biswas, H. and Bandyopadhyay, P., *Polyhedron*, 1997, **16,** 447; Schneider, W., Bauer, A. and Schmidbaur, H., *Organometallics*, 1996, **15,** 5445; Sladek, A., Schneider, W., Angermaier, K., Bauer, A. and Schmidbaur, H., *Z. Naturforsch.*, 1996, **51b,** 765; Li-Kao, J., Gonzalez, O., Mariezcurrena, R., Baggio, R., Garland, M. T. and Carrillo, D., *Acta Crystallogr. Sect. C*, 1995, **51,** 2486; Li-Kao, J., Gonzalez, O., Baggio, R. F., Garland, M. T. and Carillo, D., *Acta Crystallogr., Sect. C*, 1995, **51,** 575; Bashkin, J. S., Huffman, J. C. and Christou, G., *J. Am. Chem. Soc.*, 1986, **108,** 5038; Bodini, M. E. and Del Valle, M. A., *Polyhedron*, 1990, **9,** 1181; Hegetschweiler, K., Keller, T., Baumle, M., Rihs, G. and Schneider, W., *Inorg. Chem.*, 1991, **30,** 4342; Depree, C. V., Main, L., Nicholson, B. K. and Roberts, K., *J. Organomet. Chem.*, 1996, **517,** 201; Ainscough, E. W., Brodie, A. M., Coll, R. K., Mair, A. J. A. and Waters, J. M., *J. Organomet. Chem.*, 1996, **509,** 259; Kumar, L., Puthraya, K. H. and Srivastava, T. S., *Inorg. Chim. Acta*, 1984, **86,** 173.
2. McCaffrey, L. J., Henderson, W., Nicholson, B. K., Mackay, J. E. and Dinger, M. B., *J. Chem. Soc., Dalton Trans.*, 1997, 2577.
3. See for example: Fujita, K., Ikeda, M., Kondo, T. and Mitsudo, T., *Chem. Lett.*, 1997, 57; Ara, I., Delgado, E., Forniés, J., Hernández, E., Lalinde, E., Mansilla, N. and Moreno, M. T., *J. Chem. Soc., Dalton Trans.*, 1996, 3201; Amador, U., Delgado, E., Forniés, J., Hernández, E., Lalinde, E. and Moreno, M. T., *Inorg. Chem.*, 1995, **34,** 5279; Davidson, J. L., McIntosh, C. H., Leverd, P. C., Lindsell, W. E. and Simpson, N. J., *J. Chem. Soc., Dalton Trans.*, 1994, 2423; Huang, Y., Drake, R. J. and Stephan, D. W., *Inorg. Chem.*, 1993, **32,** 3022; Mitchell, K. A., Streveler, K. C. and Jensen, C. M., *Inorg. Chem.*, 1993, **32,** 2608; Chojnacki, S. S., Hsaio, Y.-M., Darensbourg, M. Y. and Reibenspies, J. H., *Inorg. Chem.*, 1993, **32,** 3573; Blower, P. J. and Dilworth, J. R., *Coord. Chem. Rev.*, 1987, **76,** 121; Roundhill, D. M., *Inorg. Chem.*, 1980, **19,** 557.
4. Henderson, W., Nicholson, B. K. and Kemmitt, R. D. W., *J. Chem. Soc., Dalton Trans.*, 1994, 2489.
5. Alsaadi, B. M. and Sandström, M., *Acta Chem. Scand.*, 1982, **A36,** 509.
6. Dean, P. A. W., *Prog. Inorg. Chem.*, 1978, **24,** 109.
7. Hiller, W., Castineiras, A., Arquero, A. and Masaguer, J. R., *Acta Cryst.*, 1986, **C42,** 151; Castineiras, A., Arquero, A., Masaguer, J. R., Martinez-Carrera, S. and Garcia-Blanco, S., *Z. Anorg. Allg. Chem.*, 1986, **539,** 219; van Enckevort, W. J. P., Beurskens, P. T., Menger, E. M. and Boasman, W. P., *Cryst. Struct. Commun.*, 1977, **6,** 417.
8. Hop, C. E. C. A. and Bakhtiar, R., *J. Chem. Educ.*, 1996, **73,** A162; Colton, R., D'Agostino,

A. and Traeger, J. C., *Mass Spectrom. Rev.*, 1995, **14,** 79.
9. Kirk-Othmer Encyclopaedia of Chemical Technology, John Wiley & Sons, New York, 3rd Edition, Vol. 15, pp. 157–171.
10. Henderson, W. and Evans, C., unpublished results.
11. Osakada, K., Kawaguchi, Y. and Yamamoto, T., *Organometallics*, 1995, **14,** 4542; Shi, J.-C., Wen, T.-B., Zheng, Y., Zhong, S.-J., Wu, D.-X., Liu, Q.-T., Kang, B.-S., Wu, B.-M. and Mak, T. C. W., *Polyhedron*, 1997, **16,** 369.
12. Dance, I. G., *Polyhedron*, 1986, **5,** 1037; Wardell, J. L. in *Comprehensive Organometallic Chemistry*, ed. G. Wilkinson, Pergamon, 1982, Ch. 17.
13. Drew, D. and Doyle, J. R., *Inorg. Synth.*, 1972, **13,** 52.
14. Booth, G. and Chatt, J., *J. Chem. Soc.*, 1965, 3238.
15. Blessing, R. H., *Acta Cryst.*, 1995, **A51,** 33.
16. Sheldrick, G. M., SHELX-96, University of Göttingen, 1996.

Pergamon

PII: S0277-5387(97)00329-X

Polyhedron Vol. 17, No. 2–3, pp. 231–233, 1998
© 1997 Elsevier Science Ltd
All rights reserved. Printed in Great Britain
0277-5387/98 $19.00+0.00

Synthesis and crystal structure of a polyheteronuclear complex, $[Co(III)(Hdmg)_2(NH_3)_2Cu(II)Cl_3]$

Duanjun Xu,[a]* Jianming Gu,[b] Liang Xu,[a] Keli Liang[a] and Yuanzhi Xu[a]

[a] Department of Chemistry, Zhejiang University, Hangzhou, P.R. China

[b] Central Laboratory, Hangzhou University, Hangzhou, P.R. China

(Received 19 November 1996; accepted 1 August 1997)

Abstract—The title complex has been prepared by the reaction of $[Co(Hdmg)_2(NH_3)_2]Cl$ with $CuCl_2$ in HCl solution (where Hdmg = dimethylglyoxime monoanion) and its crystal structure has been determined by X-ray diffraction. The Co(III) and Cu(II) atoms lie on different two-fold axes. The coordination geometries around the Co(III) and Cu(II) atoms are octahedral and distorted trigonal bipyramidal, respectively. The Hdmg chelates Co(III) and bridges to the Cu(II) atoms to form a polyheteronuclear helical structure along the *c* axis. Based on the structure the IR spectrum of the complex is discussed. © 1997 Elsevier Science Ltd

Keywords: polynuclear complex; dimethylglyoximato complex; Co(III)–Cu(II) complex; crystal structure; helical structure.

Dimethylglyoxime normally behaves as a monoanionic chelate ligand (Hdmg) to form mononuclear complexes. The loss of both protons is unusual but is known—as in multinuclear bridging complexes, several such structures have been reported [1,2]. In each complex, the doubly deprotonated dimethylglyoxime chelates a metal atom, with both terminal oxime O atoms coordinating to adjacent metal atoms to form the multinuclear structure. During preparation of complexes bridged by dimethylglyoxime we have obtained a novel complex, in which the dimethylglyoxime behaves as a monoanionic chelate ligand and bridges to the adjacent metal atom, through the oxime O atom to form a novel polyheteronuclear helical structure.

EXPERIMENTAL

Synthesis

0.588 g (2 mmol) of $CoCl_2 \cdot 6H_2O$ and 0.464 g (4 mmol) of H_2dmg were dissolved in 20 cm^3 of a hot 95% ethanol solution, and 1.0 cm^3 of NH_4OH solution was added producing a yellow precipitate. Following the addition of 0.5 cm^3 of H_2O_2 solution to the solution the precipitate changes colour to dark yellow. After stirring for 0.5 h and standing overnight, the precipitate of $[Co(Hdmg)_2(NH_3)_2]Cl$ was filtered and washed with ethanol and ether.

0.100 g (0.28 mmol) of $[Co(Hdmg)_2(NH_3)_2]Cl$ and 0.038 g (0.28 mmol) of $CuCl_2$ were dissolved in a dilute HCl solution (pH = 1) at room temperature. After stirring 10 min and standing for two weeks, dark-red single crystals were obtained.

Elemental analysis

C, H and N were analyzed using a Carlo Erba 1160 Elemental Analyzer. Found: C 9.7, H 2.6, N 11.4; Calc. for $C_8H_{20}O_4N_6Cl_3CoCu$: C 9.8, H 2.6, N 11.4%.

Infrared spectra

The IR spectra were recorded with a Perkin-Elmer 683 spectrophotometer (4000–400 cm^{-1}) on a powdered sample spread on a KBr plate and a Nicolet FTIR 170sx spectrophotometer (500–100 cm^{-1}) employing CsI pellets.

* Author to whom correspondence should be addressed.

Crystal structure determination

Diffraction intensity data were collected on a Nonius-CAD4 diffractometer with graphite-monochromatized Mo–K_α radiation.

Up to 2θ value of 52° a total of 1933 independent reflections was collected, of which 844 observed reflections [$I > 3\sigma(I)$] were used for structure refinement. Lp correction and empirical absorption correction were applied.

The structure was solved by Patterson methods followed by Fourier syntheses. The structure refinement was carried out by full-matrix least-squares. H atoms were located in a difference Fourier map. Anisotropic refinement including all the non-H atoms converged to agreement factors $R = 0.052$ and $Rw = 0.058$, where $w = 1/\sigma^2(F)$. Atomic scattering factors were taken from *International Tables for X-ray Crystallography* [3]. All calculations were performed on a Micro Vax-II 3100 computer using TEXSAN software package [4].

Crystal data. $C_8H_{20}O_4N_6Cl_3CoCu$, $Mr = 492.7$, orthorhombic, $C222_1$, $a = 11.828(2)$, $b = 12.787(2)$, $c = 11.275(4)$ Å, $V = 1705.3(8)$ Å^3, $Z = 4$, $D_x = 1.92$ g cm^{-3}, F(000) = 996, μ(Mo–K_α) = 2.80 mm^{-1}, No. of variables = 107, $(\Delta/\sigma)_{max} = 0.01$, $(\Delta\rho)_{max} = 0.68$ e Å^{-3}.

RESULTS AND DISCUSSION

Crystal structure

The molecular structure of the title complex is illustrated in Fig. 1 with the numbering system. The selected bond distances and angles are presented in Table 1. In the crystal the Co(III) and Cu(II) atoms lie on different two-fold axes. The Hdmg ligands, related to each other by a two-fold axis, chelate to a Co(III) atom with an average Co–N distance of 1.903 Å. Two NH_3 molecules, lying on the two-fold axis, coordinate to the Co(III) atom with Co–N distances of 1.983 and 1.961 Å, respectively to complete an octahedral coordination around the Co(III) atom. Coordination distances between Co(III) and N atoms agree well with those in diammine-bis(dimethylglyoximato) cobalt(III) perchlorate and fluoroborate [5]. Each Hdmg ligand is coplanar with the Co(III) atom, but the dihedral angle of 7° between the least-squares planes of the Hdmg ligands shows an umbrella-like configuration around the Co(III) atom as reported previously [1]. The remarkable structural feature of the present complex is that each dimethylglyoxime loses only one oxime proton from the oxime O atom which coordinates to the adjacent Cu(II) atom to form a helical polyheteronuclear molecule along the *c* axis as illustrated in Fig. 2. It is interesting that the oxime O atom which has not lost its H atom does not coordinate to the Cu(II) atom and the H-bonding between Hdmg ligands, which is always found in *trans*-bis(dimethylglyoximato) complexes, does not exist in the present structure. The coordination geometry around the pentacoordinated Cu(II) atom is distorted trigonal bipyramidal. One Cl(1) atom, lying on a two-fold axis, and two oxime O atoms [O(1) and O(1)a], related by the two-fold axis, form the equatorial plane with a Cu(II) atom, while two Cl(2) atoms related by a two-fold axis occupy the apical sites. Both the Cl(2)—Cu—Cl(2)a bond angle of 161.04(5)° and Cl(1)—Cu—Cl(2) bond angle of 99.48(5)° indicate distortion of the trigonal bipyramid. The Cu–Cl(1) distance of 2.191(2) Å in the equatorial plane is slightly shorter than the Cu–Cl(2) distance of 2.236(2) Å in the apical direction. The Cu–O(1) distance of 2.298(5) Å is in agreement with 2.301(3) Å found in a dimer complex $[Cu(Hdmg)_2]_2$ [6]. The coordinated NH_3 molecules [N(4)] fill in the hole of the helical structure. The distance of 3.072 Å suggests the H-bonding between N(4) and Cl(2) atoms, which is considered to be the factor stabilizing the helical structure and to be the reason resulting in distortion of the trigonal bipyramid around the Cu(II) atom.

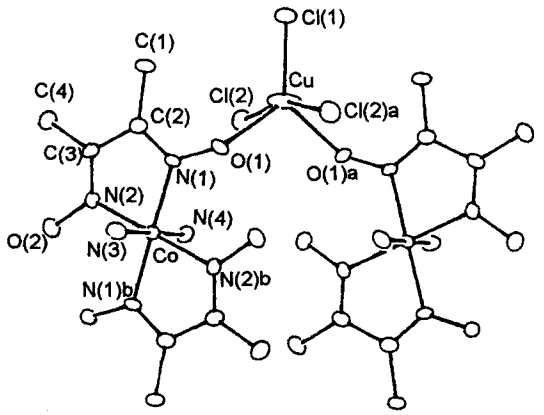

Fig. 1. ORTEP drawing of the title complex with 30% probability thermal ellipsoids, H atoms are omitted for clarity.

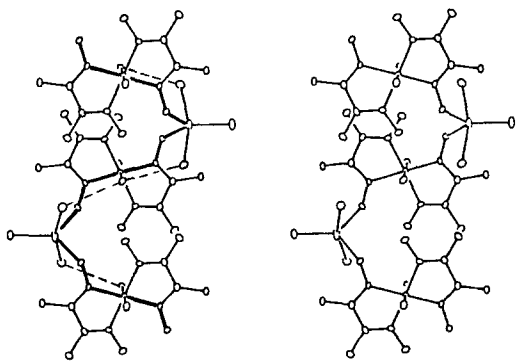

Fig. 2. Stereoview of the helix structure of the title complex, the hydrogen bonding stabilizing the structure being drawn by the dashed line.

Table 1. Selected bond distances (Å) and angles (°) with e.s.d's in parentheses for $Co(III)(Hdmg)_2(NH_3)_2Cu(II)Cl_3$

Cu—Cl(1)	2.191(2)	Cu—Cl(2)	2.236(2)
Cu—O(1)	2.298(5)	Co—N(1)	1.892(4)
Co—N(2)	1.914(4)	Co—N(3)	1.983(6)
Co—N(4)	1.961(6)	O(1)—N(1)	1.327(6)
O(2)—N(2)	1.354(6)	N(1)—C(2)	1.311(7)
N(2)—C(3)	1.269(7)	C(1)—C(2)	1.507(7)
C(2)—C(3)	1.466(8)	C(3)—C(4)	1.472(8)
Cl(1)—Cu—Cl(2)	99.48(5)	Cl(2)—Cu—Cl(2)[a]	161.04(5)
Cl(1)—Cu—O(1)	123.0(1)	Cl(2)—Cu—O(1)	81.1(1)
Cl(2)—Cu—O(1)[a]	88.6(1)	O(1)—Cu—O(1)[a]	114.0(1)
N(1)—Co—N(1)[b]	179.1(3)	N(1)—Co—N(2)	80.9(2)
N(1)—Co—N(2)[b]	99.1(2)	N(1)—Co—N(3)	90.5(2)
N(1)—Co—N(4)	89.6(2)	N(2)—Co—N(2)[b]	178.6(3)
N(2)—Co—N(3)	89.3(2)	N(2)—Co—N(4)	90.7(2)
Cu—O(1)—N(1)	127.0(4)	Co—N(1)—O(1)	121.5(4)
Co—N(1)—C(2)	115.9(4)	O(1)—N(1)—C(2)	122.6(5)
Co—N(2)—O(2)	122.3(3)	Co—N(2)—C(3)	117.3(4)
O(2)—N(2)—C(3)	120.3(5)	N(1)—C(2)—C(1)	123.7(5)
N(1)—C(2)—C(3)	113.3(5)	C(1)—C(2)—C(3)	123.0(5)
N(2)—C(3)—C(2)	112.5(5)	N(2)—C(3)—C(4)	123.6(6)
C(2)—C(3)—C(4)	123.9(5)		

Symmetry code: [a] $x, 2-y, 1-z$; [b] $1-x, y, 0.5-z$.

Infrared spectrum

The stretching vibrations of NH_3 are observed at 3225 and 3167 cm^{-1}, which is significantly lower than that found in the free NH_3 molecule and agrees well with that in $[Co(III)(NH_3)_6]Cl_3$ [7]; this frequency shift is considered to be due to coordination of the NH_3 molecule and H-bonding between Cl(2) and N(4) atoms. Rutherfold *et al.* assigned the band at 510 cm^{-1} to ν[Co—H(Hdmg)] for [Co(Hdmg)$_2$(py)Cl] based on isotopic labeling with ^{15}N [8], therefore the band at 509 cm^{-1} observed in the title complex is reasonably assigned to ν[Co—N(Hdmg)]. The bands at 463 and 440 cm^{-1} are assigned to ν(Co—NH_3), which are in agreement with that reported for other ammine cobalt(III) complexes [7]. The band at 302 cm^{-1} is assigned to ν(Cu—Cl), which is higher than the 268 cm^{-1} found in the trigonal bipyramidal structure of $[CuCl_5]^{3-}$ [9]. The band at 350 cm^{-1} is tentatively assigned to ν(Cu—O), which is consistent with the value of 340–360 cm^{-1} reported for ν(M—O) in nitrato complexes [10].

Acknowledgements—This project was supported by the Natural Science Foundation of Zhejiang Province and the National Natural Science Foundation of China.

REFERENCES

1. Xu, D., Lei, L., Cheng, C. and Xu, Y., *Acta Cryst.*, 1990, **C46,** 1447.
2. Kohler, U., Hausen, H. D. and Weidlein, J., *J. Organomet. Chem.*, 1984, **272,** 337.
3. *International Tables for X-ray Crystallography.* Vol. IV, Kynoch Press, Birmingham, 1974. (Present distributor Kluwer Academic Publishers, Dordrecht.)
4. Molecular Structure Corporation. TEXSAN. TEXRAY Structure Analysis Package. MSC, 3200 Research Forest Drive, The Woodlands, TX 77381, U.S.A., 1989.
5. Xu, L., Xu, D., Xu, Y. and Gu, J., *Acta Cryst.*, 1996, **C52,** 1119.
6. Vaciago, A. and Zambonelli, L., *J. Chem. Soc. A*, 1970, 218.
7. Nakamoto, K., *Infrared and Raman Spectra of Inorganic and Coordination Compounds*, 4th edn. Wiley, New York, 1986.
8. Rutherford, P. E. and Thornton, D. A., *Spectrochim. Acta*, 1979, **35A,** 711.
9. Long, T. V., Herlinger, A. W., Epstein, E. F. and Bernal, I., *Inorg. Chem.*, 1970, **9,** 459.
10. Cleare, M. J. and Griffith, W. P., *J. Chem. Soc. A.*, 1967, 1144.

Pergamon

PII: S0277-5387(97)00331-8

Polyhedron Vol. 17, No. 2-3, pp. 235-242, 1998
© 1997 Elsevier Science Ltd
All rights reserved. Printed in Great Britain
0277-5387/98 $19.00+0.00

Solvent and structural effects on catalase-like function of binuclear manganese(II) compounds with μ-phenoxide bridge

Yumiko Sasaki,[a] Tetsuya Akamatsu,[a] Kazuyoshi Tsuchiya,[a] Shigeru Ohba,[b] Masatomi Sakamoto,[a] and Yuzo Nishida[a]*

[a]Department of Chemistry, Faculty of Science, Yamagata University, Yamagata 990, Japan

[b]Department of Chemistry, Faculty of Science, and Technology, Keio University, Yokohama 223, Japan

(Received 27 May 1997; accepted 29 July 1997)

Abstract—The structures and ESR spectral properties of binuclear manganese(II) compounds which functionally mimic the bacterial dimanganese catalase enzyme have been developed. These compounds are formulated as $[(L^1)Mn_2X_2]Y$(X=Cl, Br, CH_3COO, C_6H_5COO, $(C_6H_5)_2HCCOO$; Y=ClO_4, PF_6), $[(L^2)Mn_2X_3]$ (X=Cl, Br), and $[(L^2)Mn_2(benzoate)_2$ (NCS)], where $H(L^1)$=2,6-bis[bis(2-pyridylmethyl)aminomethyl]-4-methyl-phenol and $H(L^2)$=2,6-bis[N-(2-dimethylamino)ethyl]iminomethyl]-4-methyl-phenol. An X-ray diffraction structure determination of $[(L^1)Mn_2Cl_2(CH_3OH)_2]PF_6$ confirmed the anticipated N_6O septadentate coordination of the (L^1)-ligand, binuclear manganese(II) complex with μ-phenoxide, and two halogenide ions and two methanol molecules. In the crystal of $[(L^2)Mn_2Cl_3]CH_3CN$, there exists tetranuclear manganese(II) complex having center of symmetry. The terminal and central manganese(II) ions are bridged by phenoxide oxygen and a chloride ion (Mn···Mn = 3.440(1) Å), and two central atoms are bridged by two chloride ions with Mn···Mn distance of 3.804(1) Å. In acetonitrile solution, catalase-like function of the manganese(II) compounds with $H(L^1)$-ligand are found to be highly dependent the anions coordinating the Mn(II) ion; the activity of the X=Cl complex is much higher than those of the acetate and benzoate. On the other hand, the activity of $[(L^2)Mn_2Cl_3]$ is slightly lower than that of the $[(L^2)Mn_2(benzoate)_2(NCS)]$, where two manganese ions are bridged by benzoate anion. The Mn(II/III) complex of $H(L^1)$, $[(L^1)Mn_2(CH_3COO)_2]^{2+}$ exhibits much higher activity than that of the corresponding Mn(II/III) complex, $[(L^1)Mn_2(CH_3COO)_2]^+$. In dimethylformamide(dmf) solutions, an induction period (at least 30 minutes) is necessary before vigorous evolution of oxygen gas occurs for both the Mn(II) complexes with (L^1) and (L^2), however, some binuclear Mn_2(II/III) and Mn_2(III/III) complexes exhibited high catalase-like function in dmf. The latter fact may give a reasonable explanation for the fact that the manganese cluster in S_2-state of the Photosystem II shows a high catalase-like function instead of the negligible action in the S_1-state. Based on these facts, it is concluded that the most important factor to control the catalase-like function of binuclear Mn(II) complex should be the oxidizable nature of the Mn(II) ion to a higher oxidation state, and the unusual behavior in dmf solution was accounted for on the assumption that dmf molecule may contribute to the activation of peroxide ion through interaction with an Mn(II)-peroxide adduct, leading to oxidation of the Mn(II) ion. © 1997 Elsevier Science Ltd

Keywords: catalase-like-function; binuclear Mn(II) complex; crystal structure; μ-phenoxide bridge; solvent effect; dimethylformamide.

Some bacterial catalases found in *thermophilic* [1] or *lactaterich* [2] possess a rare dimanganese active site, in contrast to more widely distributed monoheme cofactor of iron catalase. Catalysis appears to involve both Mn ions that are located within 3.6 Å to one another [3]. Spectroscopic studies of the dimanganese catalase have revealed a picture implicating two of the four accessible oxidation states, a "reduced Mn_2(II/III) state" and "oxidized Mn_2(III/III)" in the catalase mechanism (see Scheme I) [4,5]. In 1982, Nishida and co-workers reported that some binuclear

* Author to whom correspondence should be addressed.

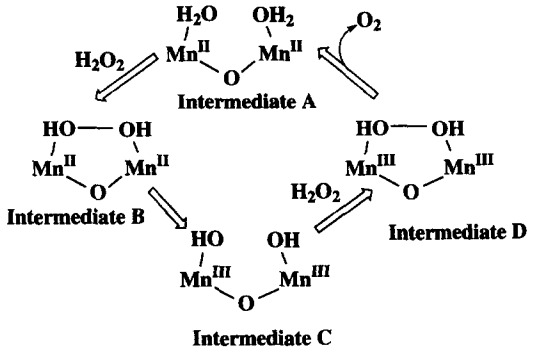

Scheme I.

manganese(III) complexes with μ-alkoxo bridge exhibit high catalase-like function instead of the negligible activity of the corresponding monomeric compounds [6]. Thus, the process assumed in Scheme I is consistent with Nishida's results, however, formation of an Mn(II) state from the Mn(III) state by the hydrogen peroxide (from Intermediate D to Intermediate A) is not confirmed in these model systems. Interestingly, it is well known that manganese cluster in the Photosystem II also exhibits a catalase-like function [7,8]. It vigorously disproportionates the added hydrogen peroxide in the dark following the formation of the S_2-state by a single flash [9]. These facts suggest that study on the catalase-like function of the dimeric manganese compounds should be very important in elucidating the function of manganese ions in the enzymes [10].

Very recently, Okawa *et al.* [11] investigated the catalase-like function of the binuclear Mn(II) complex, $[(L^2)Mn_2(benzoate)_2(NCS)]$ (for (L^2), see the figure below) in dmf(dimethylformamide) solution, and observed the formation of Mn(IV)=O species in the solution, and proposed that this Mn(IV)=O species is an active species for catalase-like function of the compound. However, we cannot detect the formation of an Mn(IV)=O species in the acetonitrile solution of the complex even at lower temperature (−20°C). Probably, this may be due to unstability of the Mn(IV)-species in acetonitrile solution or alternatively may indicate that formation of an Mn(IV)=O species is not related with the catalase-like function of the compound, because both manganese(II) compounds with (L^2)-ligand, $[(L^2)Mn_2Cl_3]$ and $[(L^2)Mn_2(benzoate)_2(NCS)]$, exhibit high catalase-like function in acetonitrile solution. In this study we have investigated the catalase-functions of several binuclear manganese(II) complexes with (L^1) and (L^2) in order to clarify the origin of the different behavior in the acetonitrile and dmf solvents, especially the role of dmf molecule for decomposition of hydrogen peroxide by the manganese(II) compounds.

EXPERIMENTAL

Materials

The manganese compounds, $[(L^1)Mn_2X_2]Y_2$ (X=Cl, Br, CH_3COO, C_6H_5COO, Y=ClO_4, PF_6), $[(L^2)Mn_2X_3]$(X=Cl, Br), and $[(L^2)Mn_2X_2]Y$ (X=CH_3COO, C_6H_5COO; Y=NCS, ClO_4) were prepared according to the published methods [12–14], chemical structures of $H(L^1)$ and (L^2) being illustrated below. Hydrogen peroxide (30% in aqueous solution) was titrated by the use of Titanium sulfate [15]. All other chemicals are obtained commercially and used as received.

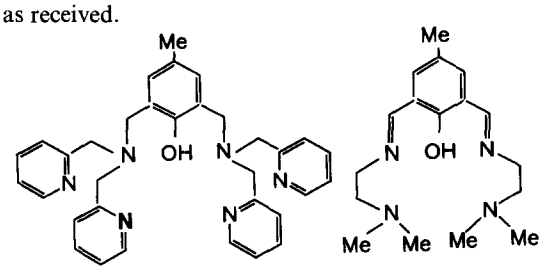

$H(L^1)$ $H(L^2)$

Crystal structure determination. The crystals of the compounds $[(L^1)Mn_2Cl_2(CH_3OH)_2]PF_6$ and $[(L^2)Mn_2Cl_3]CH_3CN$ were grown from a reaction mixture, and the single crystals of the compounds were mounted on a Rigaku AFC-5 four-circle diffractometer at Keio University for data collection. The crystal data are listed in Table 1. X-ray diffraction intensities were measured using Mo Kα radiation on a Rigaku four-circle diffractometer AFC-5 at Keio University. Absorption was corrected by a numerical method. Structure analysis was carried out using CRYSTAN-GM software version 6.3 on a SUN PARK10 workstation at Keio University [16]. The structures were solved by Direct methods, and refined by full-matrix least-squares. A full report of the experimental and refinement procedure, and the atomic coordinates are available as Supplementary data.

Catalase-like function. All reactions were performed at 25°C in a 10 cm^3 reactor containing a stirring bar under air. The flask containing a manganese complex (10 m mole) solution (5 cm^3) was closed with a rubber septum. Hydrogen peroxide solution (1 cm^3, commercial 30% aqueous solution was diluted to 1 M solution by solvent) was injected through the septum with a syringe. The reactor was connected to a graduated burette filled with water and dioxygen evolved was measured at an appropriate time by volumetry. In the case of MnO_2 as a catalyst, ca. 16 cm^3 of dioxygen evolved under our experimental conditions.

Physical measurements

x-band ESR spectra were obtained with a JEOL ESR apparatus model RE-2X spectrometer at 77 K.

Table 1. Crystallographic data of the Mn(II) compounds

Compound	$[(L^1)Mn_2Cl_2(CH_3OH)_2]PF_6$	$[(L^2)Mn_2Cl_3]\cdot CH_3CN$
Formula	$C_{35}H_{35}Cl_2Mn_2N_6O_3\cdot PF_6$	$C_{17}H_{27}Cl_3Mn_2N_4O\cdot C_2H_3N$
M	913.45	560.72
Crystal system	Monoclinic	Triclinic
Space group	$P2_1/n$	$P\bar{1}$
a/Å	10.275(1)	11.642(2)
b/Å	26.167(4)	11.915(2)
c/Å	15.324(2)	10.781(1)
$\alpha/^\circ$	90	114.39(1)
$\beta/^\circ$	99.48(1)	97.69(1)
$\gamma/^\circ$	90	104.82(1)
V/Å^3	4063.8(9)	1267.1(4)
Z	4	2
Dc/gcm^{-3}	1.493	1.470
2θ (Mo K α)$_{max}/^\circ$	45	55
Observed reflections (Fo > 3σ)	3165	4690
R	0.0652	0.0432
wR	0.0621	0.0450

Absorption spectra were measured with a Shimadzu Spectrophotometer model UV-2200 at 298 K.

RESULTS AND DISCUSSION

Crystallography

Two compounds, $[(L^1)Mn_2X_2(CH_3OH)_2]PF_6$ (X=Cl and X=Br) are isostructural. An ORTEP view of $[(L^1)Mn_2Cl_2(CH_3OH)_2]^+$ is shown in Figure 1, and the selected bond distances and angles are listed in Table 2. The solid state structure consists of discrete dimanganese(II) complex solution cation, and hexafluorophosphate anion. The binuclear manganese complex has a chemical twofold axis passing through C(42) and O(12) atoms, and two Mn coordination spheres are rotated relative to the bridging O—Mn bonds. Two manganese atoms within the complex exhibit a similar coordination number and geometries, and are six-coordinate and have an N_3O_2Cl distorted octahedral geometry. Two pyridine moieties and a tertiary amine from one-half of the heptadentate ligand (L^1) are coordinated to Mn1, and an analogous set of three nitrogen from the remaining half of the ligand are coordinated to Mn2. Two manganese atoms are bridged by the (L^1) phenoxy functional group, O(12). The coordinated methanol molecules form hydrogen bonds with the coordinated chloride ions to make a weak bridge. The average Mn1-N(pyridine) and Mn2-N(pyridine) distances are 2.272(7) and 2.265(7) Å, while the Mn1-N(amine) and Mn2-N(amine) distances are longer at 2.321(6) and 2.326(6) Å, respectively. The μ-phenoxo O12 atom forms a symmetrical bridge between Mn1 and Mn2 with observed distance of 2.169(5) and 2.170(5) Å, respectively. The Mn1—Mn2 separation of 3.923(2) Å and Mn1—O12—Mn2 angle of 129.3(3)° are different from those observed in related binuclear complexes containing another bridging group such as carboxylate [17]. The Mn1—O13 and Mn2—O14 methanol bonds are 2.210(7) and 2.237(6) Å are in good agreement with those observed in analogous compounds [5].

Table 2. Selected geometric data (Å, °) of $[(L^1)Mn_2Cl_2(CH_3OH)_2]PF_6$

Mn1—Mn2	3.923(2)	Mn2—Cl4	2.452(3)
Mn1—Cl3	2.427(3)	Mn2—O12	2.170(5)
Mn1—O12	2.169(5)	Mn2—O14	2.237(6)
Mn1—O13	2.210(7)	Mn2—N18	2.326(6)
Mn1—N15	2.321(6)	Mn2—N19	2.292(7)
Mn1—N16	2.302(7)	Mn2—N20	2.237(7)
Mn1—N17	2.241(7)	O13···Cl4	3.076(7)
Mn1—O12—Mn2	129.3(3)	O14···Cl3	3.058(6)

The ORTEP drawing of $[(L^2)Mn_2Cl_3]$ is shown in Figure 2, and the selected bond distances and angles are listed in Table 3. In the solid state, there is a tetranuclear manganese unit possessing a inversion center; the tetranuclear Mn_4 unit is a zig-zag chain, rather than a closed cluster. Mn1 is six-coordinate, having an N_2OCl_3 distorted octahedral geometry. The Mn(1) and Mn(1′) atoms are bridged by Cl(4) and Cl(4′) atoms with Mn—Cl distances 2.511(1) and 2.584(1) Å. Mn2 is five-coordinate with N_2OCl_2 coordination sphere, where basal plane is consisted of O(6), Cl(3), N(10), and N(9); Cl(5) being at the apical position of tetragonal pyramid. The Mn(1) and Mn(2) atoms are bridged by the ligand phenoxy oxygen atom O(6) and chloride ion Cl(3). The μ-phenoxo O(6) atom forms a symmetrical bridge between Mn(1) and Mn(2) with observed distances of 2.131(2) and

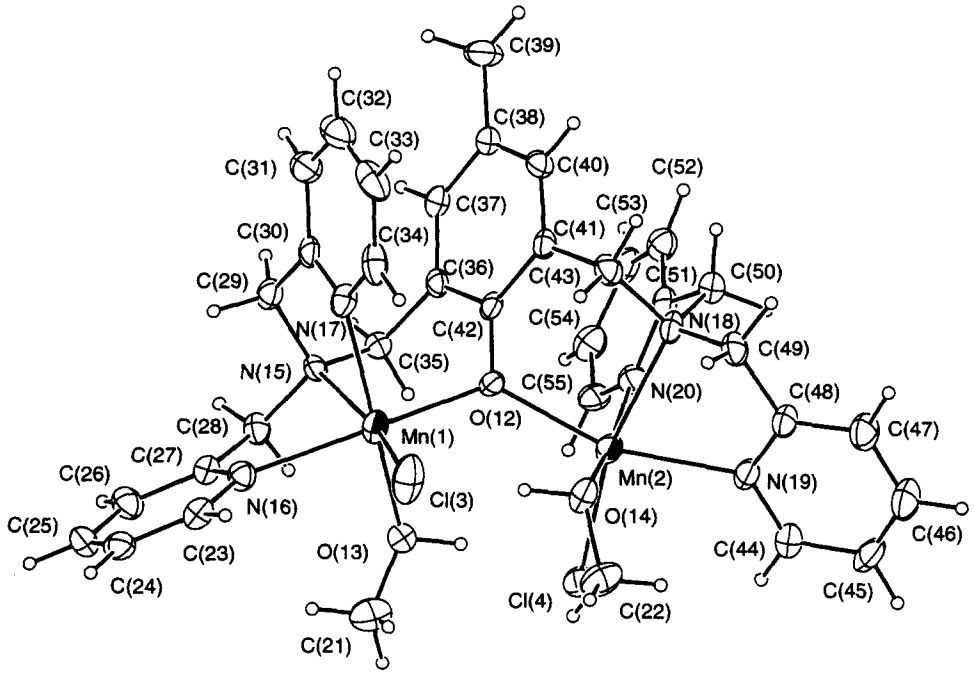

Fig. 1. ORTEP drawing of $[(L^1)Mn_2Cl_2(CH_3OH)_2]^+$.

2.095(2) Å, respectively. The Mn(1)···Mn(2) separation of 3.440(1) Å and Mn(1)—O(6)—Mn(2) angle 109.0(1)°.

Catalase-like function: in acetonitrile solution. The time course of O_2 evolution by the manganese(II) compounds are illustrated in Figure 3. As shown in Figure 3, the activity of $[(L^1)Mn_2Cl_2(CH_3OH)_2]^+$ in acetonitrile is much higher than those of the corresponding acetate and benzoate derivatives. When an acetonitrile solution of hydrogen peroxide was added to an acetonitrile solution of the X=Cl or Br compound, the colorless solution turned to dark brown immediately (see Figure 4), and the drastic change was also observed in the ESR spectra (see also Figure 5). In the ESR spectrum of the brown solution, a "16-line ESR signal" [18] is observed, indicating that a binuclear Mn_2(III/IV) species may exist in the solution. Little change was observed in the ESR spectra of the acetate compound upon the addition of hydrogen peroxide (data not shown). These are implying that the oxidation of Mn(II) ion by hydrogen peroxide is closely related with the appearance of catalase-like function of the (L^1)-compounds.

Interestingly, no remarkable change in ESR and absorption spectral features was observed for the $[(L^2)Mn_2Cl_3]$ and $[(L^2)Mn_2(benzoate)_2(NCS)]$ complexes upon addition of hydrogen peroxide, despite their high activity for catalase-like function (see Figure 3). It should be noted here that the present results are quite different from that reported by Okawa *et al.*, who reported the formation of an Mn(IV)=O species in the dmf solution of the $[(L^2)Mn_2(benzoate)_2(NCS)]$ [11]. This may be due to unstability of an Mn(III) state of the (L^2)-complex in acetonitrile solution.

Table 3. Selected geometric data (Å, °) of $[(L^2)Mn_2Cl_3]\cdot CH_3CN$

Mn1—Mn1^i	3.804(1)	Mn1—N8	2.229(2)
Mn1—Mn2	3.440(1)	Mn2—Cl13	2.441(1)
Mn1—Cl3	2.637(1)	Mn2—Cl5	2.353(1)
Mn1—Cl4	2.511(1)	Mn2—O6	2.095(2)
Mn1—Cl4^i	2.584(1)	Mn2—N9	2.225(2)
Mn1—O6	2.131(2)	Mn2—N10	2.259(2)
Mn1—N7	2.323(2)		
Mn1—Cl3—Mn2	85.2(1)	Mn1—O6—Mn2	109.0(1)
Mn1—Cl4—Mn1^i	96.6(1)		

Symmetry codes: (i) $1-x$, $1-y$, $1-z$.

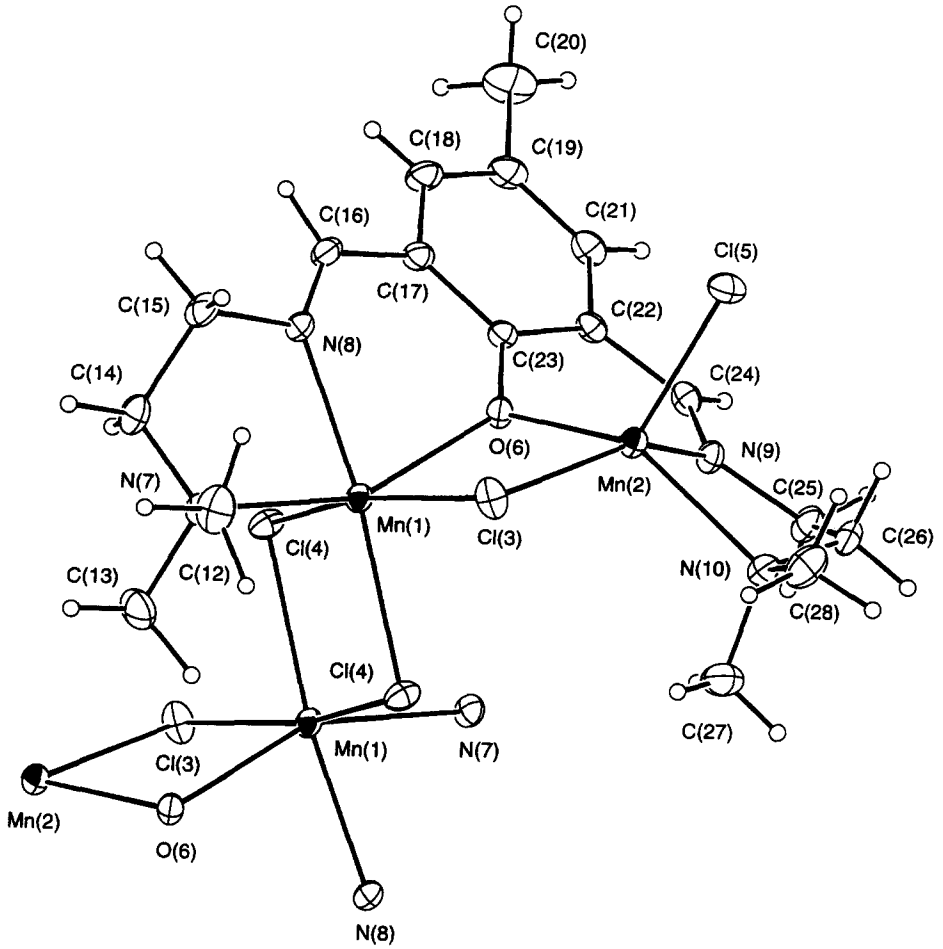

Fig. 2. ORTEP drawing of $[(L^2)Mn_2Cl_3]$.

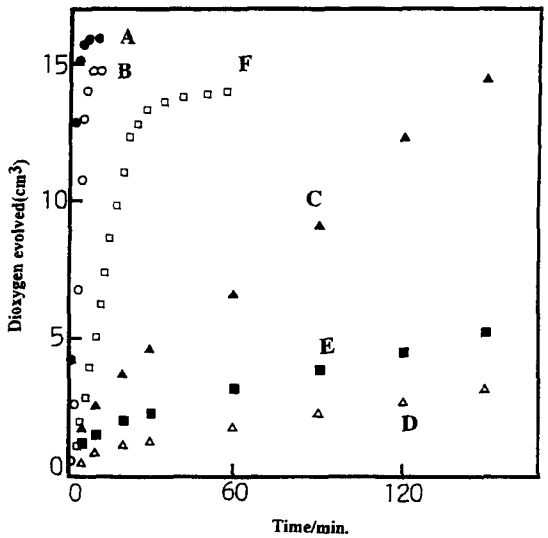

Fig. 3. Dioxygen evolution catalyzed by Mn(II) complexes (in acetonitrile, 25°C). (A) $[(L^1)Mn_2Cl_2(CH_3OH)_2]PF6$. (B) $[(L^2)Mn_2(benzoate)_2(NCS)]$. (C) $[(L^1)Mn_2(acetate)_2]ClO_4$. (D) $[(L^1)Mn_2(diphenylacetate)_2]ClO_4$. (E) $[(L^1)Mn_2(benzoate)_2]ClO_4$. (F) $[(L^2)Mn_2Cl_3]$.

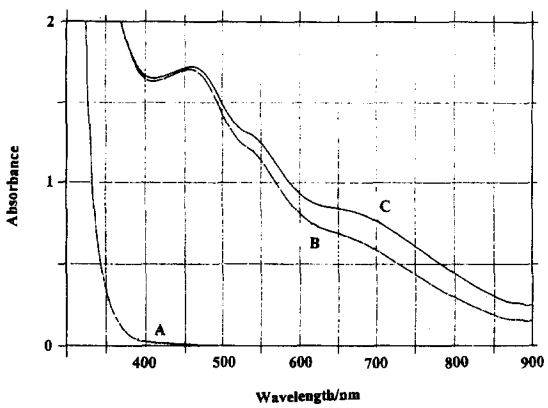

Fig. 4. Absorption spectra of $[(L^1)Mn_2Cl_2(CH_3OH)_2]PF_6([Mn^{2+}] = 2 \times 10^{-3}$ mol dm^{-3}). (A) In acetonitrile. (B) To 5 ml of the A-solution was added 1 ml H_2O_2-solution (acetonitrile, 0.5 mol dm^{-3} solution), and measured immediately after addition. (C) Measured at 15 minutes after addition of H_2O_2.

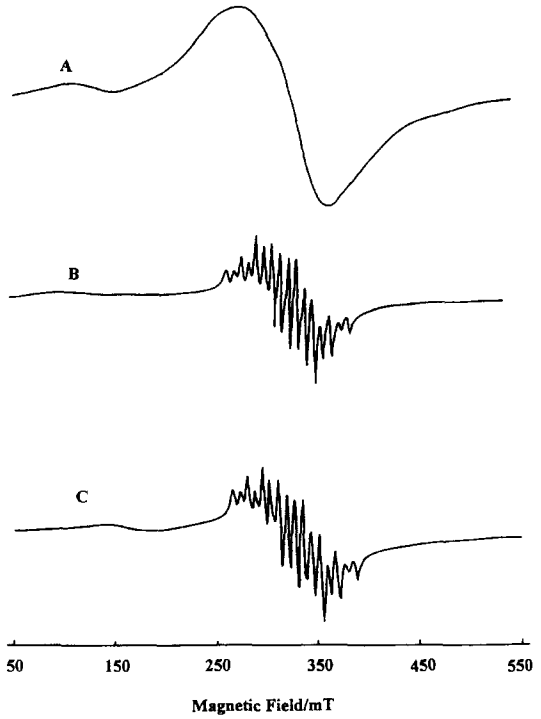

Fig. 5. ESR spectra (in acetonitrile, X-band, 77 K). (A) $[(L^1)Mn_2Cl_2(CH_3OH)_2]PF_6$. (B) Solution C in Figure 4. (C) $[(L^1)Mn_2(acetate)_2](PF_6)_2$ and H_2O_2 (measured at 15 minutes after addition of H_2O_2; experimental conditions are the same as those described for the corresponding $[(L^1)Mn_2Cl_2(CH_3OH)_2]PF_6$ complex).

The first dinuclear manganese complex to be reported that catalytically disproportionates H_2O_2 was that of Nishida and co-workers in 1982 [6]. This functional model contained two manganese(III) ions bridged by alkoxy group; in this paper they proposed the importance of coordination of a peroxide ion to two manganese(III) ions, forming a $(\mu\text{-}\eta^1:\eta^1)$-coordination mode (see the Intermediate D in Scheme I). This situation may make two-electron transfer between peroxide ion and manganese ions to be more facile. This consideration has been applied to several other systems; for example, Dismukes *et al.* explained the high catalase-like activity of manganese(II) complex with N,N,N′,N′-tetrakis(2-methylene-benzimidazolyl)-1,3-diaminopropane-2 on this consideration [4,5]. As shown in the present study, it is general that the binuclear manganese(II) complexes are active for decomposition of hydrogen peroxide in acetonitrile solutions. In the case of $[(L^1)Mn_2Cl_2(CH_3OH)_2]^+$, Mn···Mn distance is nearly 4 Å, indicating that Mn···Mn distance in this complex may be flexible in the solution, leading to facile formation of a peroxide adduct with $\mu\text{-}\eta^1:\eta^1$-coordination mode (see Intermediate B in Scheme I). The formation of a peroxide adduct with $(\mu\text{-}\eta^1:\eta^1)$-coordination mode may be less favorable for the acetate-bridged compound, because the acetate is chelated to manganese ions. This will explain the lower activities of the acetate and benzoate compounds, as shown in Figure 3. The high activity observed for the $[(L^2)Mn_2(benzoate)_2(NCS)]$ complex seems to be noteworthy, because in this complex benzoate is chelated to two manganese(II) ions, similar to that in the (L^1)-complex. The geometrical environment around the two manganese(II) ions in this complex are not identical (one, six-coordinate, and another one, five-coordinate), and this situation is very similar to that of the chloride-derivative $[(L^2)Mn_2Cl_3]$; the latter complex also contains a five-coordinate Mn(II) species. These are indicating that facile coordinating of peroxide ion to a manganese(II) ion, in this case five-coordinate Mn(II) ion, is closely related with high catalase-like function of the compound.

It should be noted that the bis(μ-acetato)Mn(II/III) binuclear complex with (L^1) [17] exhibits much higher catalase-like function than that of the μ-acetato Mn_2(II/II) complex (see trace (D) in Figure 7) [12]. This is demonstrating that the presence of an Mn(III) state induces high activity for decomposition of hydrogen peroxide. Above discussion may give a reasonable elucidation for the fact that high catalase-like function is observed in the S_2-state of the Photosystem II instead of the negligible effect observed in the S_1-state. Above discussion may be consistent with the fact that several binuclear manganese(III) complexes always show high catalase-like function, as observed at first by Nishida *et al.* [6], and also by the complex with H_3(L-5-sal) [19] (see the trace (E) in Figure 7) shown below:

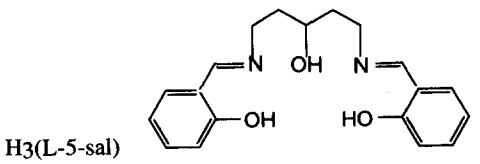

H3(L-5-sal)

Catalase-like function in dmf solution. As shown in Figure 6, the induction time (at least 30 minutes) is necessary before vigorous evolution (indicated by an arrow in Figure 6, trace A) of oxygen occurs in the dmf and dimethylacetamide solutions containing $[(L^1)Mn_2Cl_2(CH_3OH)_2]^+$ (see traces A and B) and also in the solution of $[(L^2)Mn_2(benzoato)_2(NCS)]$ [11]. These are quite different from those observed in the acetonitrile solutions. In the cases of the dmf solution, it seems likely that dmf molecules coordinate to a metal ion (see Scheme II (A)), and this may prevent the approach of hydrogen peroxide to a metal

Scheme II

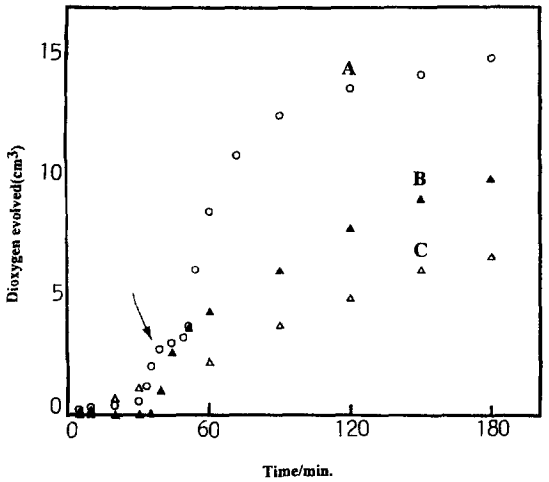

Fig. 6. Dioxygen evolution catalyzed by $[(L^1)Mn_2Cl_2(CH_3OH)_2]PF_6$. (A) In dimethylformamide (dmf). (B) In dimethylacetamide. (C) In dimethylsulfoxide.

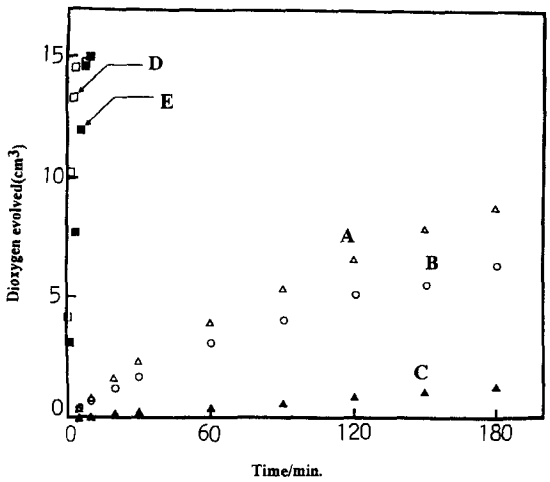

Fig. 7. Dioxygen evolution catalyzed by manganese compounds. (A) $[(L^1)Mn_2(acetate)_2]ClO_4$ in dimethylformamide. (B) $[(L^1)Mn_2(acetate)_2]ClO_4$ in dimethylacetamide. (C) $[(L^1)Mn_2(acetate)_2]ClO_4$ in dimethylsulfoxide. (D) $[(L^1)Mn_2(acetate)_2](PF_6)_2$ in acetonitrile. (E) $[Mn_2(L\text{-}5\text{-}sal)(acetate)(CH_3OH)]ClO_4$ in acetonitrile.

ion, leading to the lower activity of the compounds for decomposition of hydrogen peroxide. These may explain the presence of induction period before oxygen evolution as described above.

Upon the addition of hydrogen peroxide in the dmf solution of the Mn(II) compounds, formation of mono(dmf)-mono(peroxide) species (see Scheme II (B)) and (μ-η^1 : η^1) peroxide adduct (Intermediate B in Scheme I) may increase gradually. Formation of the intermediate B may lead to the same results as described for the acetonitrile solution, however, this may be inconsistent with the fact that an Mn(IV)=O formation is detected only in the dmf solution of $[(L^2)Mn_2(benzoate)_2(NCS)]$. Very recently, we have observed that dmf (and also dimethylacetoamide) molecule can activate peroxide ion in the presence of nickel(II) or cobalt(II)-acetylacetonate compounds through the intermediate formation of cis-mono(dmf)mono(peroxide)nickel(II) species [20], and this has been explained in the same manner to that proposed for activation of dioxygen molecule in the presence of an aliphatic aldehyde and nickel(II)-acetylacetonate [21]. Above discussion may be rationalized because dmf molecule is very similar to aldehydes on the structural and electronical points of view. We already reported that the peroxide ion in the intermediate (B) in Scheme II exhibits high electrophilicity, tending to bind with an organic moiety through electronic interaction [22]. Thus, it seems quite reasonable to assume that activation of peroxide ion in the mono(dmf)-mono(peroxide) Mn(II) species occurs through electronic interaction between them (see the figure below), and this will promote heterolytic cleavage of the peroxide adduct, leading to formation of an Mn(II)—O(atomic) and OH^- [23]; the former species may be alternatively written as an Mn(IV)=O. The sudden evolution of oxygen gas after the induction time in dmf solutions observed in both the (L^1)- and (L^2)-compounds should be elucidated in terms of the discussion that formation of an Mn(IV)=O species promoted by dmf molecule is a trigger for decomposition of hydrogen peroxide in these systems. Our model can well explain the reason why Mn(IV)=O species is detected only in the dmf solution, and may give a reasonable elucidation for formation of formic acid in the dmf solution containing a binuclear copper complex [24].

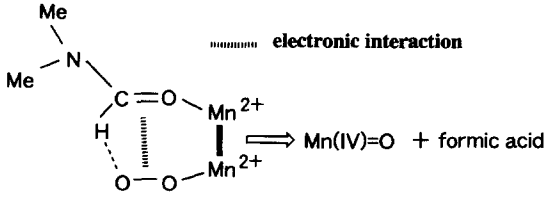

Based on the discussion described above, it should be recommended that dmf molecule should not be used as a solvent when oxygen or peroxide ion plays an important role in the reaction, and the results reported in this solvent hitherto must be re-evaluated.

REFERENCES

1. Khangulov, S. V., Barynin, V. V. and Barynina, S. V. A., *Biochim. Biophys. Acta*, 1990, **1020**, 25.
2. Waldo, G. S., Yu, S. and Hahn, *J. E. P.*, J. Am. Chem. Soc., 1992, **114**, 5869.
3. Barynin, V. V., Vagin, A. A., Melik-Adamyan, W. R., Grebenko, A. I., Khanguluv, S. V., Popov, A. N., Andrianova, M. E. and Vainshtein, B. K., *Dokl. Akad. Nauk. SSSR*, 1986, **288**, 877 (Russ).

4. Pessiki, P. J. and Dismukes, G. C., *J. Am. Chem. Soc.*, 1994, **116,** 898.
5. Pessiki, P. J., Khanguluv, S. V., Ho, D. M. and Dismukes, G. C., *J. Am. Chem. Soc.*, 1994, **116,** 891.
6. Oishi, N., Nishida, Y. and Kida, S., *Chem. Lett.*, 1982, 409.
7. Debus, R. J., *Biochim. Biophys. Acta*, 1992, **1102,** 269.
8. Velthuys, B. and Kok, B., *Biochim. Biophys. Acta*, 1978, **502,** 211; Mano, J., Takahashi, M.-A. and Asada, K., *Biochemistry*, 1987, **26,** 2495; Frasch, W. D. and Mei, R., *Biochim. Biophys. Acta*, 1987, **891,** 8.
9. Khabnuluv, S. V., Goldfeld, M. G., Gerasimenko, V. V., Andreeva, N. E., Barynin, V. V. and Grebenko, A. I., *J. Inorg. Biochem.*, 1990, **40,** 279.
10. Ruttinger, W. and Dismukes, G. C., *Chem. Rev.*, 1997, **97,** 1.
11. Sakiyama, H., Okawa, H. and Isobe, R., *J. Chem. Soc., Chem. Commun.*, **1993**, 882; Sakiyama, H., Okawa, H. and Suzuki, M., ibid., 1993, 3823.
12. Nishida, Y. and Nasu, M., *Inorg. Chim. Acta*, 1990, **190,** 1.
13. Suzuki, M., Murata, S., Uehara, A. and Kida, S., *Chem. Lett.*, 1987, 281.
14. Sakiyama, H., Tamaki, H., Kodera, M., Matsumoto, N. and Okawa, H., *J. Chem. Soc., Dalton Trans.*, 1993, 591.
15. Pobiner, H., *Anal. Chem.*, 1961, **33,** 1423.
16. List of atomic coordinates, displacement parameters, structural factors and complete geometry have been deposited with the IUCr (reference: PRINTCIF). References: Coppens, P., Leiserowitz, L. and Rabinovich, D., *Acta Cryst.*, 1965, **18,** 1035; Edwards, C., Gilmore, C. J., Mackay, S. and Stewart, N., 1996, CRYSTAN-GM. Version 6.3. Rigaku Coorporation (1993). AFC/MSC Diffractometer Control System.
17. Diril, K., Chang, H., Zhang, X., Larsen, S., Potenza, J. A., Pierpoint, C. G., Schugar, H. J., Isied, S. S. and Hendrickson, D. N., *J. Am. Chem. Soc.*, 1987, **109,** 6207.
18. Renger, G., *Angew. Chem. Int. Ed. Eng.*, 1987, **26,** 643.
19. Nishida, Y., Oshino, N. and Tokii, T., *Z. Naturforsch.*, 1988, **43B,** 472.
20. Sasaki, Y., Suzuki, M. and Nishida, Y., submitted.
21. Nishida, Y., Tanaka, N. and Okazaki, M., *Polyhedron*, 1994, **13,** 2245.
22. Ito, S., Okuno, T., Matsuhsima, H., Tokii, T. and Nishida, Y., *J. Chem. Soc., Dalton Trans.*, 1996, 4479.
23. Bash, R. B., Owensby, A. L., Gonzales, C. and Schlegel, H. B., *J. Am. Chem. Soc.*, 1991, **113,** 6001; Schroder, D., Schalley, C. A., Goldberg, N. and Schwarz, H., *Chem. Eur. J.*, 1996, **2,** 1235.
24. Murphy, N. N., Mahroof-Tahir, M. and Karlin, K. D., *J. Am. Chem. Soc.*, 1993, **115,** 10404.

Pergamon

PII: S0277-5387(97)00333-1

Polyhedron Vol. 17, No. 2–3, pp. 243–253, 1998
© 1997 Elsevier Science Ltd
All rights reserved. Printed in Great Britain
0277-5387/98 $19.00+0.00

Silver(I)-2,2′:6′,2″-terpyridine complexes: X-ray structures of $[\{Ag(tpy)(MeCN)\}_2][PF_6]_2$ and $[Ag(dptpy)(MeCN)][BF_4]\cdot MeCN$ (tpy = 2,2′:6′,2″-terpyridine; dptpy = 6,6″-diphenyl-2,2′:6′,2″-terpyridine)

Edwin C. Constable,[a]* Andrew J. Edwards,[b] Geoffrey R. Haire,[b] Michael J. Hannon[b] and Paul R. Raithby[b]

[a] Institut für Anorganische Chemie, Spitalstrasse 51, CH-4056 Basel, Switzerland

[b] Department of Chemistry, University of Cambridge, Lensfield Road, Cambridge CB2 1EW, U.K.

(Received 2 July 1997; accepted 28 July 1997)

Abstract—The coordination of silver(I) acetate with 2,2′:6′,2″-terpyridine (tpy) and 6,6″-diphenyl-2,2′:6′,2″-terpyridine (dptpy) has been investigated. In contrast to the behaviour with copper(I), no dinuclear double-helical species have been unambiguously isolated although there is evidence that double-helical $[Ag_2L_2]^{2+}$ complexes exist in weakly-coordinating solvents. In the case of 2,2′:6′,2″-terpyridine, a species containing a square-planar $[Ag(tpy)(MeCN)]^+$ caton has been isolated and structurally characterised whilst with 6,6″-diphenyl-2,2′:6′,2″-terpyridine a related but very distorted $[Ag(dptpy)(MeCN)]^+$ species has been structurally characterised. © 1997 Elsevier Science Ltd

Keywords: silver(I) complexes; oligopyridines; supramolecular chemistry; helicates; crystal structures; 2,2′:6′,2″-terpyridine.

We have long been interested in understanding the interplay between metal ions and ligands that controls the assembly of metallosupramolecules [1,2]. In particular, we have tried fully to comprehend the factors leading to the self-assembly of helical systems involving oligopyridines [3]. As a prototype system it has been demonstrated that simple 2,2′:6′,2″-terpyridines give rise to double-helical $[Cu_2L_2]^{2+}$ complexes upon reaction with copper(I) [4–6]. Recently, we have extended these studies to the control of the right-handed or left-handed chirality of the helix by the use of chiral oligopyridines [6–8] and have shown that enantiomerically pure chiral 2,2′:6′,2″-terpyridines lead to enantiomeric excesses of the *P* or *M* double helicates upon reaction with copper(I) [6]. The enantiomeric excesses observed were modest (75%) and we considered a number of approaches to improve them. We adopted three principal strategies: (i) variation of the metal ion (ii) increasing the number of donor atoms and (iii) increasing the amount of chiral information contained within the chiral ligand. In this paper we consider strategy (i) and report the behaviour of 2,2′:6′,2″-terpyridine (tpy) and 6,6″-diphenyl-2,2′:6′,2″-terpyridine (dptpy) with silver(I).

* Author to whom correspondence should be addressed. Tel: +41 61 267 1001; Fax: +41 61 267 1015; E-mail: constable@ubaclu.unibas.ch

EXPERIMENTAL

Infra-red spectra were recorded in compressed KBr discs on Perkin-Elmer 983 or Philips PU9624 Fourier-transform spectrophotometers, electronic spectra on a PU8730 spectrophotometer and ^1H NMR spectra on Bruker WM-250 or AM-400 spectrometers. Fast

atom bombardment (FAB) spectra were recorded on a Kratos MS-50 spectrometer; the sample was loaded using acetonitrile as solvent, and 3-nitrobenzyl alcohol as supporting matrix, 2,6-Bis(3-dimethylamino-1-oxopropyl)pyridine dichloride and *N*-(2-phenyl-2-oxoethyl)pyridinium iodide were prepared by the literature methods [9].

N-(2-phenyl-2-oxoethyl)pyridinium iodide

A mixture of iodine (25.38 g, 0.1 mol) and dry pyridine (100 cm^3) was warmed until the iodine had dissolved, after which acetophenone (12.0 g, 0.1 mol) was added and the mixture heated to reflux for 6 h. The reaction mixture was then cooled, the solid product filtered off, and recrystallised from ethanol to give cream crystals of *N*-(2-phenyl-2-oxoethyl)pyridinium iodide (16.3 g, 50%). Mp. 190–192°C. IR 3049 w, 2875 w, 2828 m, 1697 s, 1578 w, 1468 s, 1385 w, 1352 w, 1213 m, 1058 w, 997 m, 755 m, and 688 m cm^{-1}. MS (+ve FAB): *m/z* 199 {M-I}. Found: C. 47.8, H, 3.7; N, 4.3. Calc. for $C_{13}H_{12}INO$: C, 48.0; H, 3.7; N, 4.3%.

6,6″-Diphenyl-2,2′:6′,2″-terpyridine, dptpy

A mixture of ammonium acetate (2.8 g, 0.04 mol) and *N*-(2-phenyl-2-oxoethyl)pyridinium iodide (1.1 g, 3.4 mmol) were dissolved in methanol (20 cm^3) and the solution brought to reflux. 2,6-Bis(3-dimethylamino-l-oxopropyl)pyridine dichloride (0.5 g, 1.4 mmol) was added and the mixture refluxed for 12 h after which it was cooled and the resultant grey solid filtered off. Recrystallisation from ethanol gave dptpy as a pale cream solid (0.43 g, 80%). Mp. 206–206.5°C. IR 1567 s, 1431 m, 1268 w, 1076 w, 805 m, 762 s, and 695 m cm^{-1}. MS (+ve FAB): *m/z* 386 {M}. Found: C, 84.1; H, 5.0; N, 10.9. Calc. for $C_{27}H_{19}N_3$: C, 83.9; H, 5.0; N, 11.0%. ^1H NMR ($CDCl_3$): δ 7.42–7.60 (6H, m, H^m, H^p), 7.81 (2H, dd, *J* 0.9, 7.8 Hz, H^5), 7.95 (2H, t, *J* 7.8 Hz, H^4), 8.02 (1H, t, *J* 7.8 Hz, $H^{4'}$), 8.20 (4H, m, H^o), 8.63 (2H, dd, *J* 0.9, 7.8 Hz, H^3), 8.71 (2H, dd, *J* 7.8 Hz, $H^{3'}$).

$[Ag_2(tpy)_2][PF_6]_2$

A solution of tpy (0.030 g, 0.13 mmol) and Ag(OAc) (0.022 g, 0.13 mmol) was heated under reflux in methanol (5 cm^3) for 3 h. The pale yellow solution was filtered through cotton wool and then treated with excess methanolic $[NH_4][PF_6]$ to yield a white precipitate of $\{Ag(tpy)(PF_6)\}$ which filtered off and dried under reduced pressure (0.048 g, 77%). IR: 1591 m, 1580 m, 1563 m, 1479 w, 1471 w, 1449 m, 1423 m, 1401 w, 1312 w, 1287 w, 1248 w, 1188 w, 1168 w, 1104 w, 1095 w, 1076 w, 1041 w, 1025 w, 1005 w, 844 vs, 773 s, 762 s, 653 w, 630 w, and 559 s cm^{-1}. MS (+ve FAB): *m/z* 827 $\{Ag_2(tpy)_2(PF_6)\}$, 573 $\{Ag(tpy)_2\}$, 448 $\{Ag_2(tpy)\}$, 340 $\{Ag(tpy)\}$. Found: C, 37.0; H, 2.4; N, 8.8. Calc. for $C_{17}H_{14}AgF_6N_4P$: C, 37.0; H, 2.3; N, 8.6%.

$[Ag_2(tpy)_2][BF_4]_2$

This compound was prepared in a similar manner to $[Ag_2(tpy)_2][PF_6]_2$ but using $[NH_4][BF_4]$ to precipitate the product which was obtained as a white precipitate (0.044 g, 80%). IR: 1582 m, 1563 s, 1455 m, 1423 s, 1084 vs, 762 cm^{-1}. MS (+ve FAB): *m/z* 770 $\{Ag_2(tpy)_2(BF_4)\}$, 573 $\{Ag(tpy)_2\}$, 448 $\{Ag_2(tpy)\}$, 340 $\{Ag(tpy)\}$. Found: C, 42.2; H, 2.8; N, 9.6%. Calc. for $[Ag_2(tpy)_2][BF_4]_2$: C, 42.1; (H, 2.6; N, 9.8%).

$[Ag_2(tpy)_2(MeCN)_2][PF_6]_2$

Recrystallisation of $[Ag_2(tpy)_2][PF_6]_2$ from acetonitrile by the diffusion of diethyl ether vapour into the solution afforded colourless crystals of the salt $[Ag_2(tpy)_2(MeCN)_2][PF_6]_2$. IR: 1592 m, 1580 m, 1563 m, 1478 w, 1450 m, 1423 m, 1401 w, 1385 w, 1312 w, 1249 w, 1188 w, 1168 w, 1104 w, 1077 w, 1012 w, 845 vs, 796 m, 773 s, 653 m, 630 w, and 558 s cm^{-1}. MS (+ve FAB): *m/z* 827 $\{Ag_2(tpy)_2(PF_6)\}$, 573 $\{Ag(tpy)_2\}$, 340 $\{Ag(tpy)\}$. Found: C, 38.3; H, 2.8; N, 10.4. Calc. for $C_{34}H_{28}Ag_2F_{12}N_8P_2 \cdot 0.5\ H_2O$: C, 38.1; H, 2.8; N, 10.4%.

$[Ag(dptpy)][BF_4]$

A solution of $[Ag(MeCN)_4][BF_4]$ (0.2 g, 0.56 mmol) and dptpy (0.22 g, 0.56 mmol) were stirred in methanol (15 cm^3) for 3 h, after which period the pale yellow precipitate was filtered off and dried. IR: 3086 w, 1590 m, 1465 m, 1444 s, 1283 w, 1242 m, 1186 w, 1055 s, 809 s, 763 s, 705 m, and 655 w cm^{-1}. MS (+ve FAB): *m/z* 1074 $\{Ag_2(dptpy)_2(BF_4)\}$, 986 $\{Ag_2(dptpy)_2\}$, 879 $\{Ag(dptpy)_2\}$, 600 $\{Ag_2(dptpy)\}$, 492 $\{Ag(dptpy)\}$. Found: C, 55.9; H, 3.3; N, 7.25. Calc. For $C_{54}H_{38}N_6Ag_2B_2F_8$: C, 55.5; (H, 3.25; N, 7.75%). Recrystallisation from acetonitrile by the diffusion of diethyl ether vapour into the solution gave colourless crystals of $[Ag(dptpy)(MeCN)][BF_4]$.

X-ray crystallography of $[Ag_2(tpy)_2(MeCN)_2][PF_6]_2$ **(1)** *and* $[Ag(dptpy)(MeCN)][BF_4]$ **(2)**

Crystallographic measurements were made on a Rigaku AFC7 (**2**) or a Stoe four circle diffractometer (**1**) using Mo–K_α radiation ($\lambda = 0.71073$ Å) by standard procedures. The data were corrected for Lorrentz and polarization effects and also for absorption (semi-empirical). The structures were solved by direct methods (SHELXTL-PLUS for **1**) [10] and refined on F^2 by full-matrix least-squares (SHELXL93) [11]. The non-hydrogen atoms were refined anisotropically and

hydrogen atoms were included in calculated positions (riding model). Final wR (on F^2) and R (on F) were 0.0687 and 0.2007 or 481 parameters and all 4224 data for **1** and 0.1102 and 0.1485 for 381 parameters and all 2378 data for **2**. The corresponding R values for data with $I > 2\sigma(I)$ were 0.0547 and 0.1603 for **1** and 0.0554 and 0.1158 for **2**. Sources of atomic scattering factors are as in Ref. [10]. The diagrams were drawn with ORTEP3 [12]. The crystal data and data collection and structure refinement parameters are summarized in Table 1. Selected bond lengths and angles for the two structures are presented in Table 2. Final atom coordinates, displacement coefficients, and a full list of bond lengths and angles have been deposited with the Editor as supplementary material.

RESULTS AND DISCUSSION

Silver(I)-2,2′ : 6′,2″-terpyridine complexes

Although tpy usually functions as a chelating terdentate ligand this bonding mode is not possible with metal ions which have a tendency towards four-coordinate tetrahedral coordination. In these circumstances, it is possible to anticipate double-helical structures in which two quasi-four-coordinate metal centres are coupled by a bridging nitrogen of the central pyridine ring (Scheme 1). Such structures are formed with copper(I) [4–6] although we were always aware of the possibility of reaction with a good donor to give a square-planar species in which the tpy behaved in the expected terdentate manner (Scheme 1). Other low-charged metal ions with no electronically imposed preference for a particular geometry such as silver(I) were expected to behave in a similar manner to copper(I) as we have shown in the case of 2,2′ : 6′,2″-quaterpyridine ligands [13,14].

Although a number of reports of silver(I)–2,2′ : 6′,2″-terpyridine complexes have appeared [15–20], structural data is sparse [19,20] and no evidence for a dinuclear double-helical species has been presented. Of most relevance is a compound of stoichiometry $Ag_4(MeCN)(tpy)_5(ClO_4)_4$ isolated from a 1 : 1 reaction of tpy with silver(I) perchlorate which contains a helical, but not double helical,

Table 1. Crystal data for $[\{Ag(tpy)(MeCN)\}_2][PF_6]_2$ (**1**) and $[Ag(dptpy)(MeCN)][BF_4] \cdot MeCN$ (**2**)

	1	**2**
Formula	$C_{34}H_{28}Ag_2F_{12}N_8P_2$	$C_{31}H_{25}N_5AgBF_4$
Molecular weight	1054.32	662.24
Temperature (K)	153(2)	290(2)
Wavelength (Å)	0.71073	0.71073
Crystal system	Monoclinic	Monoclinic
Spacegroup	$P2(1)/c$	$P2(1)/c$
a (Å)	7.2390(10)	15.359(6)
b (Å)	25.172(5)	18.594(7)
c (Å)	20.984(4)	10.289(5)
β (°)	95.79(3)	101.78(3)
Volume (Å^3)	3804.2(12)	2876.5(21)
Z	4	4
$F(000)$	2080	1336
Density (g cm^{-3})	1.841	1.529
μ (mm^{-1})	1.212	0.757
Exptl. absorpt. correction type	Semi-empirical	Semi-empirical
Exptl. absorpt. correction T_{min}	0.457	0.877
Exptl. absorpt. correction T_{min}	0.788	1.000
Crystal type	Colourless block	Colourless block
Crystal size (mm)	$0.19 \times 0.21 \times 0.34$	$0.27 \times 0.27 \times 0.30$
θ min/max (°)	3.60/22.50	2.58/22.55
Index ranges	$-7 < h < 6, 0 < k < 27, 0 < l < 22$	$-3 < h < 16, -20 < k < 4, -11 < l < 10$
No. of measured reflections	5032	4057
No. of independent reflections	4893	3767
No. of reflns in refinement	4224 ($(I) > 2\sigma(I)$)	2378 ($(I) > 2\sigma(I)$)
No. of variables	481	381
Final $R1$ (obs)	0.0547	0.0554
Final $wR2$ (obs)	0.1603	0.1158
Last max/min in Difference map (e Å^{-3})	1.640/−1.137	0.549/−0.609

For **1** a weighting scheme of $w = 1/[\sigma^2(F_0^2) + (0.1342P)^2 + 20.1008P]$ was used whilst for **2** a $w = 1/[\sigma^2(F_0^2) + (0.0664P)^2 + 1.7012P]$. In both cases, $P = (F_0^2 + 2F_c^2)/3$.

Table 2. Selected bond lengths (Å) and bond angles (°) for $[\{Ag(tpy)(MeCN)\}_2][PF_6]_2$ (**1**) and $[Ag(dptpy)(MeCN)][BF_4] \cdot MeCN$ (**2**)

1			
Ag(1)—N(1)	2.222(8)	Ag(1)—N(21)	2.392(6)
Ag(1)—N(11)	2.401(7)	Ag(1)—N(31)	2.415(7)
Ag(1)—Ag(2)	3.1698(12)	Ag(2)—N(2)	2.211(9)
Ag(2)—N(51)	2.377(6)	Ag(2)—N(41)	2.389(8)
Ag(2)—N(61)	2.443(7)		
N(1)—Ag(1)—N(21)	164.9(3)	N(1)—Ag(1)—N(11)	117.6(3)
N(21)—Ag(1)—N(11)	68.7(2)	N(1)—Ag(1)—N(31)	103.9(3)
N(21)—Ag(1)—N(31)	68.1(2)	N(11)—Ag(1)—N(31)	136.8(2)
N(1)—Ag(1)—Ag(2)	120.3(2)	N(21)—Ag(1)—Ag(2)	71.5(2)
N(11)—Ag(1)—Ag(2)	91.1(2)	N(31)—Ag(1)—Ag(2)	77.1(2)
N(2)—Ag(2)—N(51)	169.8(3)	N(2)—Ag(2)—N(41)	115.5(3)
N(51)—Ag(2)—N(41)	68.9(2)	N(2)—Ag(2)—N(61)	107.0(3)
N(51)—Ag(2)—N(61)	68.7(2)	N(41)—Ag(2)—N(61)	137.4(2)
N(2)—Ag(2)—Ag(1)	101.5(2)	N(51)—Ag(2)—Ag(1)	84.6(2)
N(41)—Ag(2)—Ag(1)	110.9(2)	N(61)—Ag(2)—Ag(1)	61.2(2)
2			
Ag(1)—N(1)	2.174(8)	Ag(1)—N(31)	2.310(6)
Ag(1)—N(21)	2.435(6)	Ag(1)—N(41)	2.467(6)
N(1)—Ag(1)—N(31)	162.5(2)	N(1)—Ag(1)—N(21)	112.3(2)
N(31)—Ag(1)—N(21)	69.6(2)	N(1)—Ag(1)—N(41)	112.2(2)
N(31)—Ag(1)—N(41)	69.2(2)	N(21)—Ag(1)—N(41)	135.4(2)

$[Ag_3(tpy)_4]^{3+}$ unit in which two of the tpy ligands are bridging [19].

Ligand synthesis

We have previously shown that copper(I) complexes with 2,2′:6′,2″-terpyridines were stabilised by the introduction of sterically demanding substituents into the 6- and 6″-positions [5]. Accordingly, we have made parallel studies with tpy itself and with 6,6″-diphenyl-2,2′:6′,2″-terpyridine (dptpy) prepared by a Kröhnke type synthesis (Scheme 2). The key step involves the reaction of the bis(Mannich) salt of 2,6-diacetylpyridine with an acetophenone enolate equivalent in the presence of an excess of ammonium acetate. The new ligand was obtained in 80% yield as a pale buff solid. Characterisation data for dptpy are presented in the experimental section.

Coordination behaviour of silver(I) with tpy and dptpy

The reaction of one equivalent of silver acetate with one equivalent of tpy in methanol gave a colourless solution from which colourless microcrystalline solids were obtained upon the addition of $[NH_4][PF_6]$ or $[NH_4][BF_4]$. An analogous colourless solid was obtained from the reaction of $[Ag(MeCN)_4][BF_4]$ with dptpy in methanol. Microanalysis of these solids indicated a formulation $\{AgLX\}$ (L = tpy or tptpy; X = BF_4 or PF_6) to be appropriate. In no case, was evidence found for a coordinated solvent molecule. Assuming that the weakly coordinating anions are not directly coordinated to the metal centre, a mononuclear formulation of these materials would imply a three-coordinate silver(I) centre. Whilst three-coordinate silver(I) is relatively common, it is not likely to occur with the T-shaped donor set of the chelating tpy or dptpy ligands. Accordingly, we wish to propose that these initially formed materials are double-helical $[Ag_2L_2]^{2+}$ species with bridging tpy or dptpy ligands analogous to the previously reported copper(I) species.

Support for this proposal comes from the observation of intense peaks with the correct isotopomer distributions for $\{Ag_2L_2X\}^+$. In order to further elucidate the structures of these complexes we have made repeated attempts to obtain X-ray quality crystals from weakly coordinating solvents such as acetone, but have had no success to date. The materials obtained from acetonitrile solution will be discussed later.

Solutions of the complexes $\{Ag(tpy)X\}$ (X = BF_4 or PF_6) in any given solvent were identical, but showed a considerable solvent dependence (Table 3). All spectra were fully assigned by COSY methods and a representative example in CD_3SOCD_3 solution is presented in Fig. 1. The spectra in CD_3COCD_3 were broadened and varied with time. All of these data

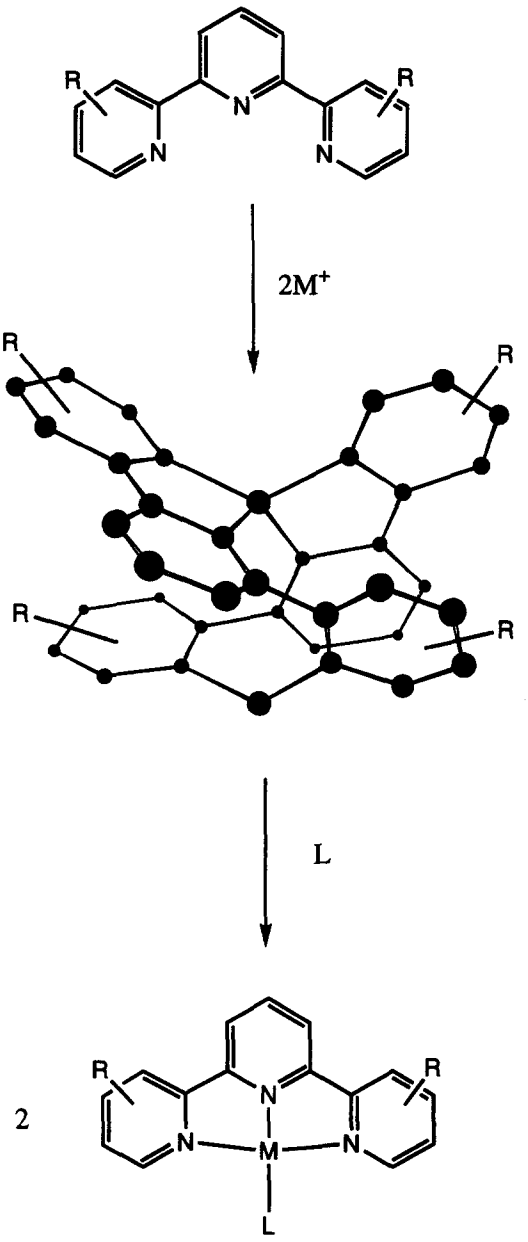

Scheme 1.

are compatible with an initially formed double-helical species reacting with solvent to give a mononuclear $[Ag(tpy)(S)]^+$ solvent species. We had hoped that the introduction of the phenyl substituents in the dptpy ligand would result in the formation of more stable double-helical species. However, a similar pattern of solvent dependence was observed. This is in contrast to the behaviour of copper(I) with dptpy which gives double-helical dinuclear $[Cu_2(dptpy)_2]^{2+}$ species which are soluble in a range of solvents. There are sufficient similarities between the spectra of acetone solutions of the copper(I) and silver(I) complexes of dptpy (Fig. 2) to propose that similar solution species are present in each case. In conclusion, we suggest that both tpy and dptpy react with silver(I) salts to give double-helical dinuclear species, but that these compounds are substantially less stable with respect to solvation and the formation of mononuclear complexes than the copper(I) analogues.

In the course of numerous attempts to obtain X-ray quality crystals of these materials we noted that the solids obtained from acetonitrile solutions consistently had a stoichiometry {Ag(tpy)(MeCN)X} or {Ag(dptpy)(MeCN)X} and also observed that these materials exhibited identical ^1H NMR spectra to solutions of the original compounds to CD_3CN. X-ray quality crystals of the acetonitrile solvates with both ligands have been obtained and show interesting differences.

X-ray structure of $[\{Ag(tpy)(MeCN)\}_2][PF_6]_2$

The X-ray structural analysis of this complex revealed a number of interesting features. First of all, the expected square-planar $[Ag(tpy)(MeCN)]^+$ unit was present. However, a dinuclear $[\{Ag(tpy)(MeCN)\}_2]^{2+}$ cation is present with a short silver–silver contact of 3.1698(12) Å (Fig. 3). This short contact is a common feature of silver complexes containing planar macrocyclic units [21] and is also found in disilver double-helicates [13,14]. Interestingly, the $[Ag(tpy)(MeCN)]^+$ cation is also present in the lattice of $Ag_4(MeCN)(tpy)_5(ClO_4)_4$ [19], but in this case, although short Ag···Ag contacts are present within the trinuclear $Ag_3(tpy)_4$ unit, no short contacts to the $[Ag(tpy)(MeCN)]^+$ cation are observed, which shows 4.728 Å and 5.332 Å distances to the closest silver atoms of two trinuclear units. The $[Ag(tpy)(MeCN)]^+$ cation within our structure exhibits significantly longer silver–nitrogen interactions with the acetonitrile ligands (2.211(9), 2.222(8) Å) and the central ring of the tpy (2.392(6), 2.377(6) Å) than in $Ag_4(MeCN)(tpy)_5(ClO_4)_4$, which presumably represents the increased electron density at silver as a result of the silver–silver interaction. The cations are very close to square-planar about each silver centre, with the sum of angles about the two independent silver atoms totalling 358.5 and 360.1°. Within the dinuclear unit, the N_4Ag planes are twisted about the Ag···Ag axis to give a 137.27° angle between the two acetonitrile ligands (Figure 4a). The acetonitrile ligands are significantly non-linear. The consequence of the short silver–silver contact and the twisting of the two AgN_4 planes is a near perfect stacking between terminal rings of the two tpy ligands within the dinuclear unit. The individual tpy units are not exactly planar and exhibit dihedral angles between the terminal rings and the central ring in the range 11.7–18.5°.

However, the dinuclear units are further arranged in stacks within the lattice giving a zig-zag chain of alternating short (3.1698(12) Å) and long (5.223 Å)

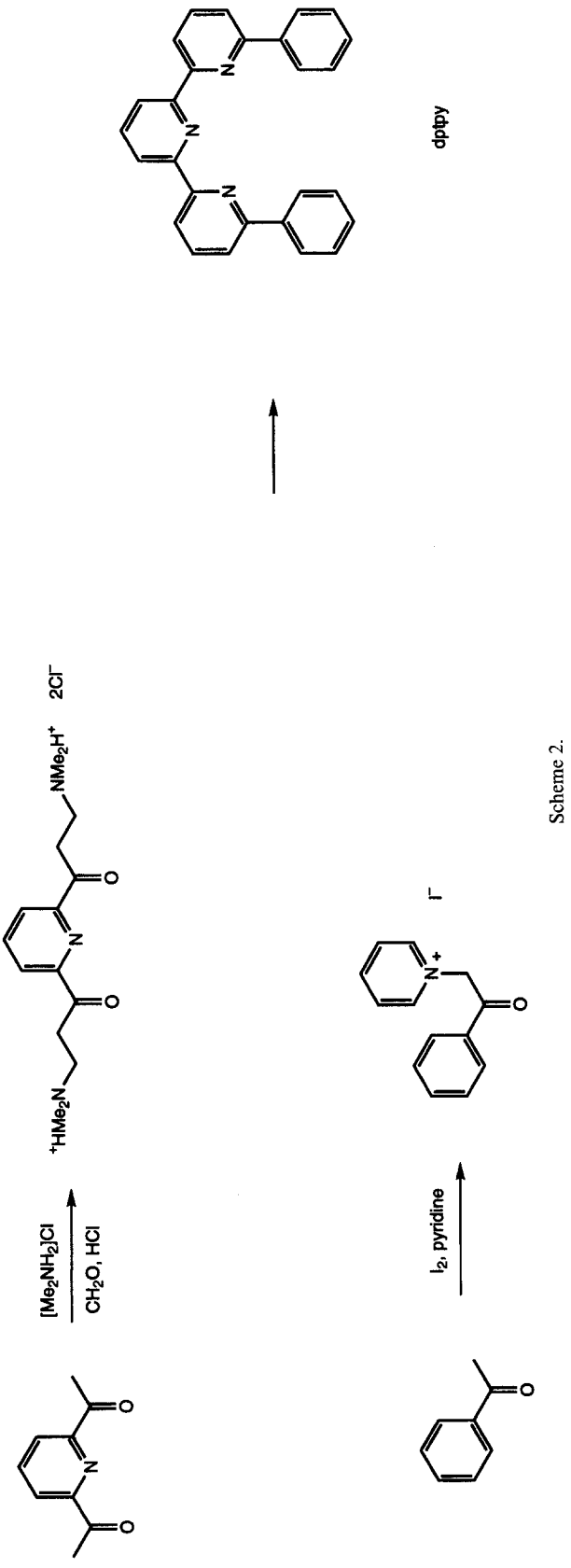

Scheme 2.

Table 3. ^{1}H NMR spectroscopic data for silver(I) and copper(I) complexes of tpy and tptpy

Complex	Solvent	H^3	H^4	H^5	H^6	$H^{3'}$	$H^{4'}$	H^o	H^m	H^p
Ag(tpy)X	CD_3CN	8.15–8.30	8.03	7.51	8.49	8.15–8.30	8.15–8.30			
Ag(tpy)X	CD_3SOCD_3	8.53	8.11	7.62	8.68	8.54	8.29			
Ag(tpy)X	CD_3OD	8.25–8.41	8.05	7.46	8.25–8.41	8.25–8.41	8.25–8.41			
Ag(tpy)X	CD_3COCD_3	8.40–8.53	8.17	7.46	8.30	8.40–8.53	8.40–8.53			
[{Ag(tpy)(MeCN)}$_2$][PF_6]$_2$	CD_3CN	8.15–8.30	8.03	7.51	8.49	8.15–8.30	8.15–8.30			
Ag(dptpy)X	CD_3COCD_3	8.28	8.20	7.86	—	8.30	8.19	7.63	7.25	7.25
[Cu_2(dptpy)$_2$][BF_4]$_2$	CD_3COCD_3	8.28	8.25	7.79	—	8.07	8.07	7.71	7.13	7.13

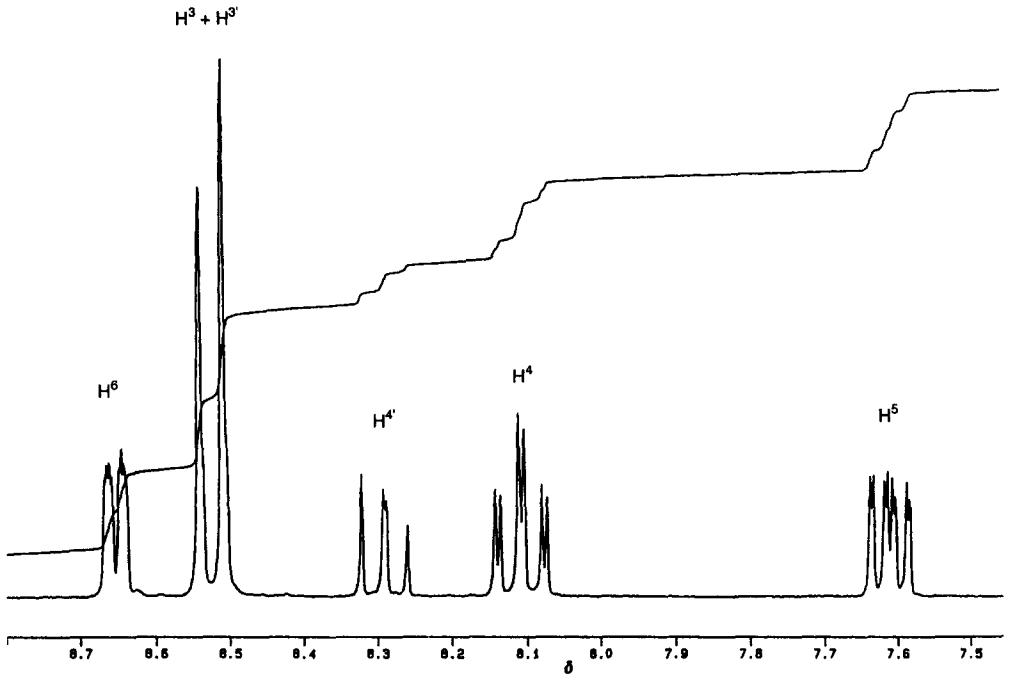

Fig. 1. 250 MHz ^{1}H NMR spectrum of a CD_3SOCD_3 solution of [Ag(tpy)(CD_3SOCD_3)][PF_6].

contacts (Figure 4b). Finally, these stacks are arranged in the crystal lattice with channels containing the hexafluorophosphate counterions lying between them (Figure 4c). There are no cation–anion interactions below 3.0 Å and no short Ag···F contacts below 4.0 Å

X-ray structures of [Ag(dptpy)(MeCN)][BF_4] · MeCN

The solid state structure of this complex differs significantly from that of the analogue with a tpy ligand. The gross structural feature of an approximately square-planar cation is retained, with the sum of angles about the silver totalling 363° (Fig. 5). There are no short silver–silver contacts and the closest contact between adjacent silver atoms is 5.656 Å. This distance is too great to allow any stacking between the aromatic rings of the ligands. The distortion from a square-planar arrangement is quite marked with the donors lying up to 0.36 Å from the least squares plane describing Ag(1), N(1), N(21), N(31) and N(41). The overall effect is to place both of the phenyl substituents above this plane and to bend the acetonitrile ligand below it. In effect, the two phenyl groups create a pocket for the acetonitrile ligand (Fig. 6). The additional steric interactions between the phenyl substituents and the acetonitrile lead to significant changes in the coordination around the silver. The bonds between the silver and the terminal pyridine rings are

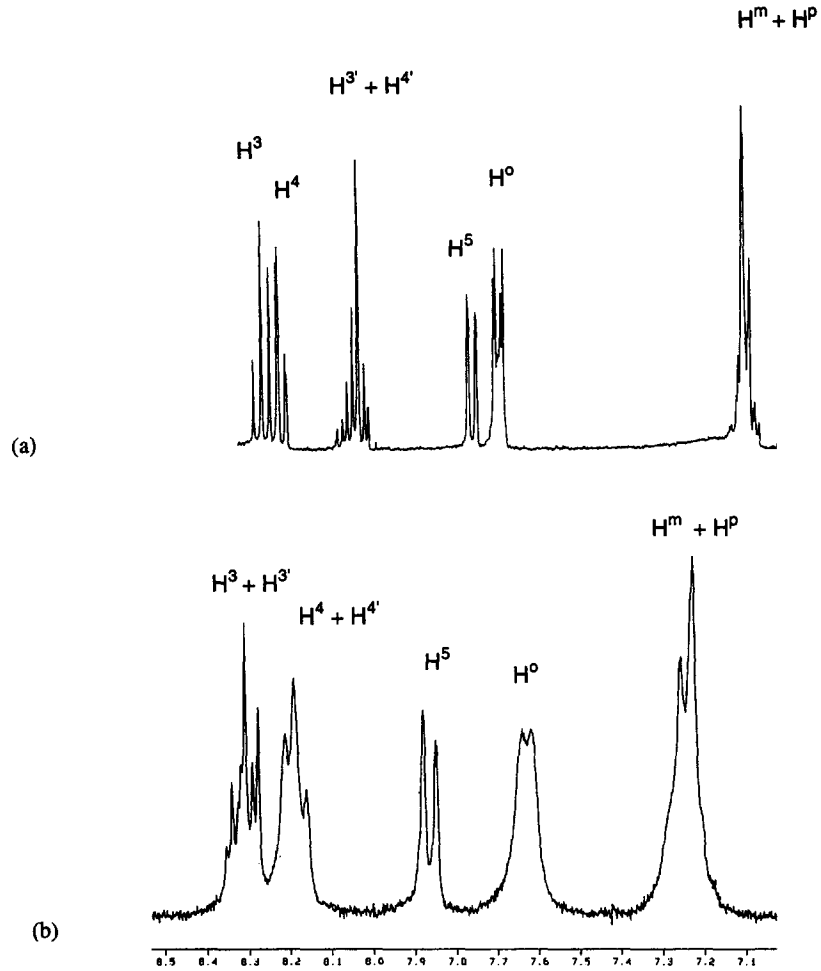

Fig. 2. 250 MHz ^{1}H NMR spectra of CD_3COCD_3 solutions of (a) $[Cu_2(dptpy)_2][BF_4]_2$ and (b) $[Ag_2(dptpy)_2][BF_4]_2$.

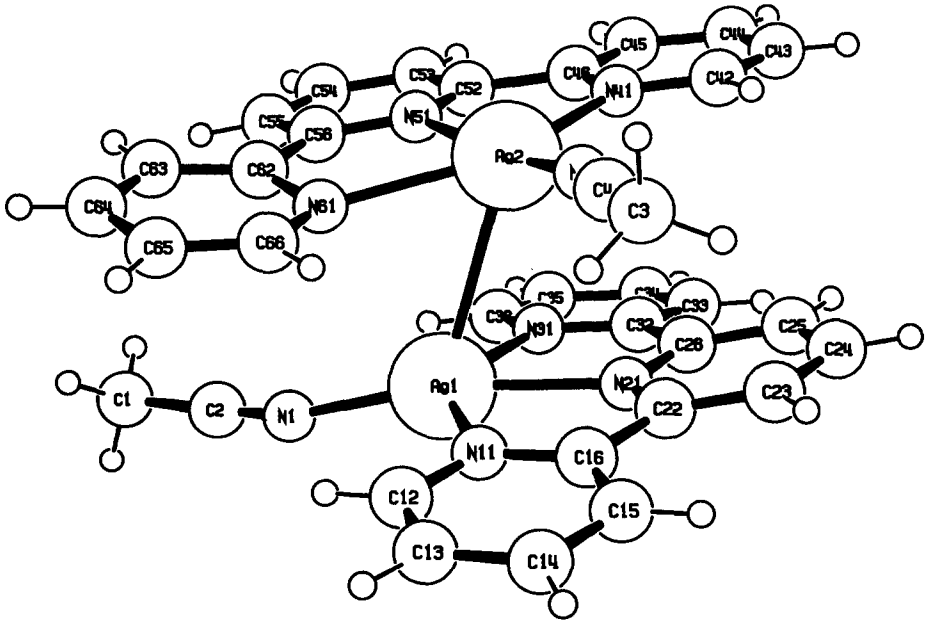

Fig. 3. Structure of the $[\{Ag(tpy)(MeCN)\}_2]^{2+}$ cation present in $[\{Ag(tpy)(MeCN)\}_2][PF_6]_2$ showing the numbering scheme adopted.

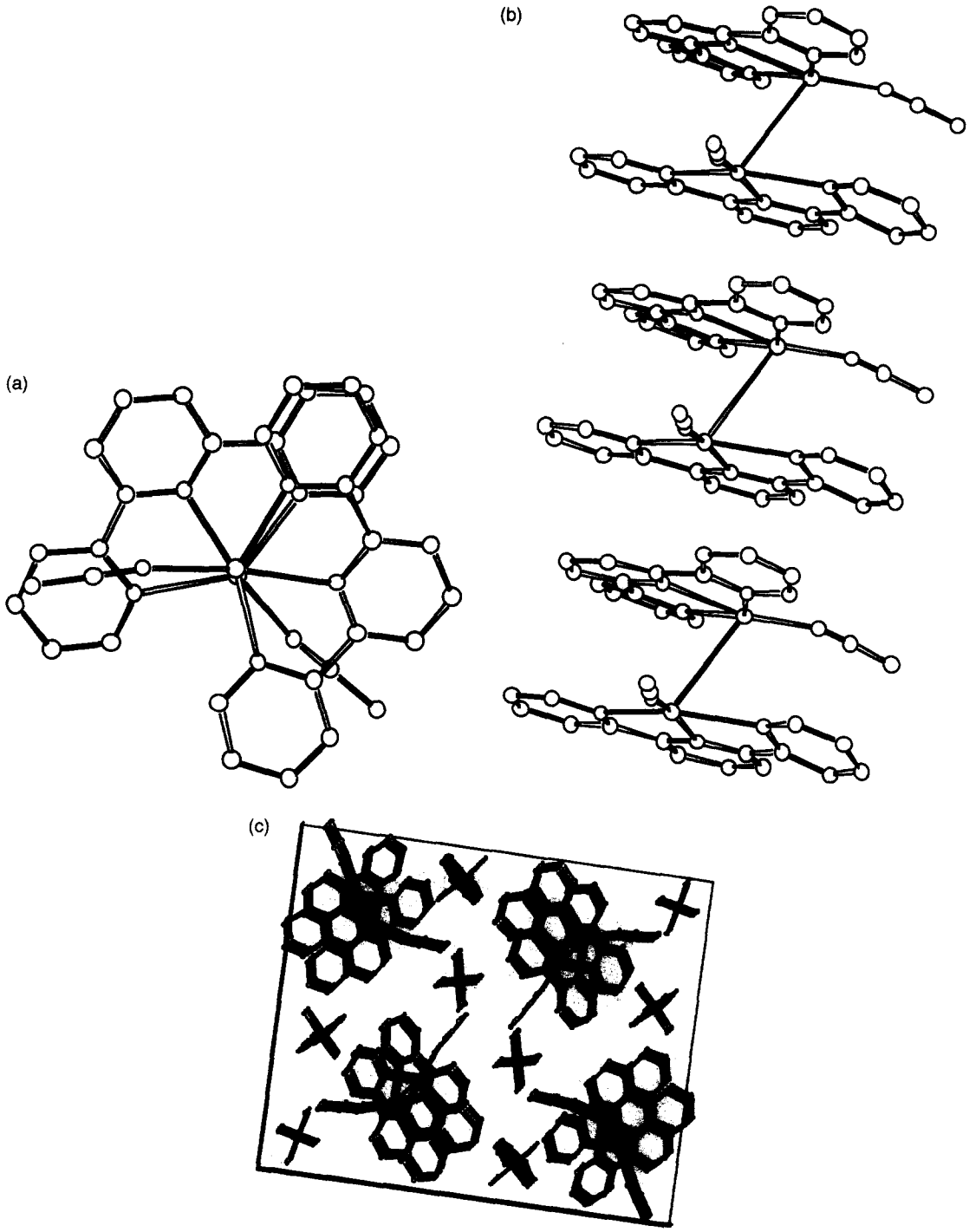

Fig. 4. (a) Structure of the $[\{Ag(tpy)(MeCN)\}_2]^{2+}$ cation present in $[\{Ag(tpy)(MeCN)\}_2][PF_6]_2$ emphasising the stacking of the two tpy ligands. (b) The arrangement of the $[\{Ag(tpy)(MeCN)\}_2]^{2+}$ cations in the lattice showing the alternating long and short silver–silver contacts. (c) Crystal packing within $[\{Ag(tpy)(MeCN)\}_2][PF_6]_2$ showing the stacking of the cations and the placing of the anions in the channels between these stacks.

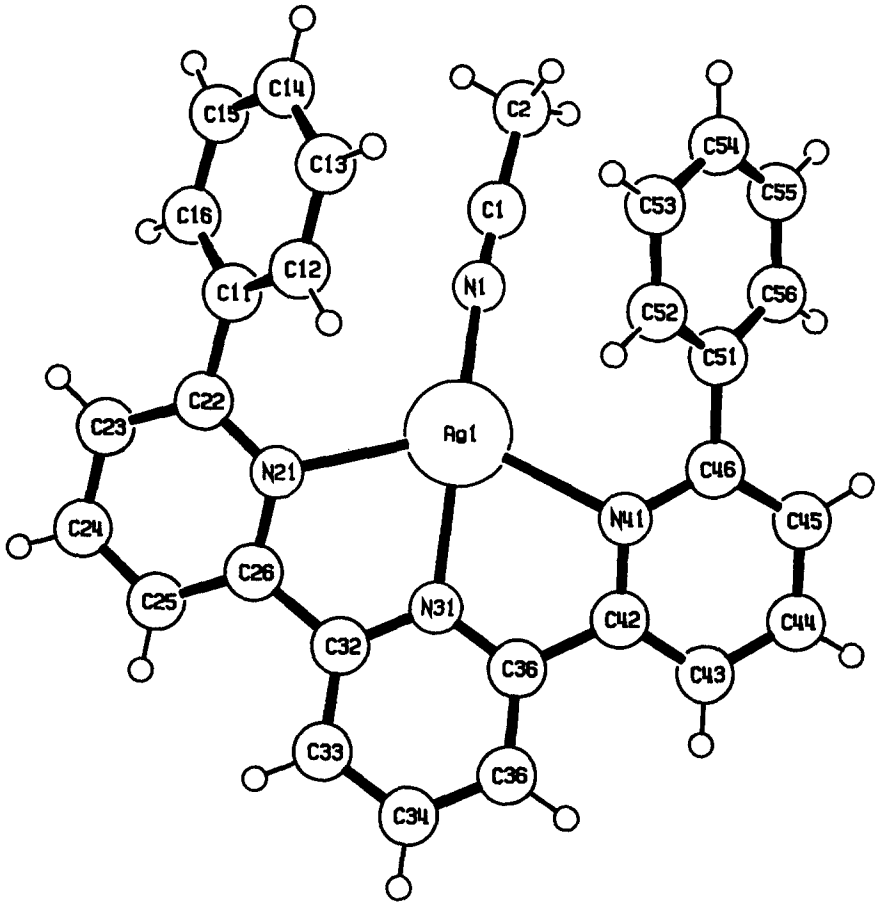

Fig. 5. Structure of the $[\{Ag(dptpy)(MeCN)\}_2]^{2+}$ cation present in $[Ag(dptpy)(MeCN)][BF_4] \cdot MeCN$ showing the numbering scheme adopted.

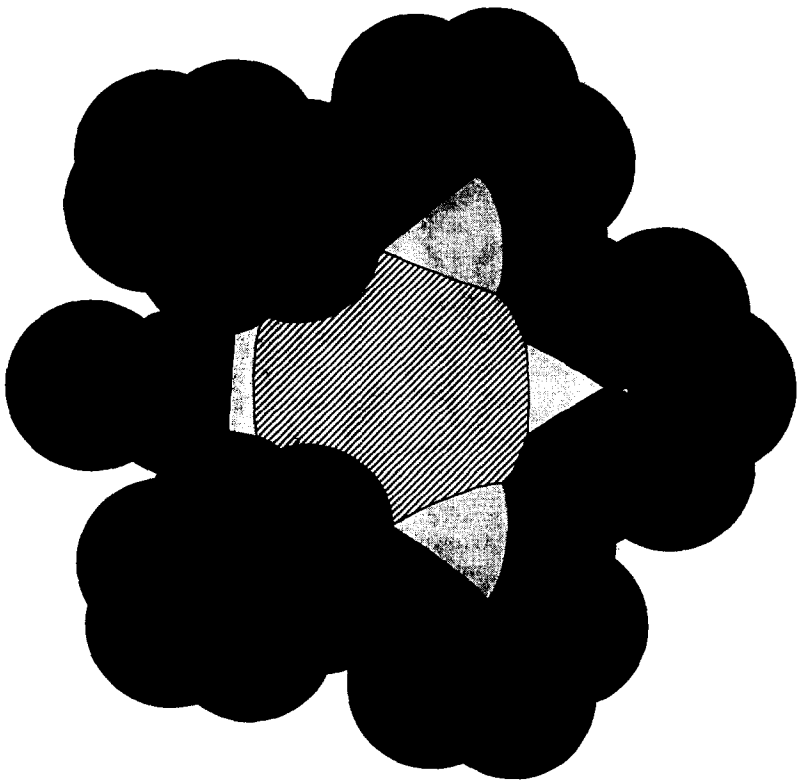

Fig. 6. Structure of the $[\{Ag(tpy)(MeCN)\}_2]^{2+}$ cation emphasising the arrangement of the phenyl substituents and the acetonitrile ligand.

considerably longer, and the bonds to the acetonitrile and the central pyridine ring shorter, than those in the $[Ag(tpy)(MeCN)]^+$ cation.

CONCLUSIONS

We have found some evidence for the formation of dinuclear (presumably double-helical) complexes between silver(I) and 2,2′ : 6′,2″-terpyridines in weakly coordinating solvents. However, we have also shown that under conditions in which the corresponding copper(I) double helicates are stable (acetonitrile solution), the silver complexes are solvolysed to give mononuclear species. In the light of these observations, we have decided that our original strategy (i) for increasing enantiomeric excesses of helicates involving chiral ligands is flawed and we will concentrate upon strategies (ii) and (iii).

Acknowledgements—We gratefully acknowledge the EPSRC, Johnson Matthey plc and the Schweizerischer Nationalfonds zur Förderung der Wissenenschaftlichen Forschung for financial support.

REFERENCES

1. Constable, E. C., *Prog. Inorg. Chem.*, 1994, **42,** 67.
2. Constable, E. C., *Tetrahedron*, 1992, **48,** 10013.
3. Constable, E. C. in *Comprehensive Supramolecular Chemistry*, Vol. 9, ed. J.-M. Lehn. Pergamon, Oxford, 1996, p. 213.
4. Potts, K. T., Keshavarzk, M., Tham, F. S., Abruna, H. D. and Arana, C., *Inorg. Chem.*, 1993, **32,** 4450.
5. Constable, E. C., Edwards, A. J., Hannon, M. J. and Raithby, P. R., *J. Chem. Soc., Chem. Commun.*, 1994, 1991.
6. Constable, E. C., Kulke, T., Neuburger, M. and Zehnder, M., *Chem. Commun.*, 1997, 489.
7. Constable, E. C., Kulke, T., Neuburger, M. and Zehnder, M., *New J. Chem.*, 1997, **21,** 633.
8. Constable, E. C., Kulke, T., Neuburger, M. and Zehnder, M., *New J. Chem.*, 1997, **21,** 1091.
9. Kröhnke, F., *Synthesis*, 1976, 1.
10. Scheldrick, G. M., SHELXTL-PLUS. *Program Package for X-ray Structure Determination.* Siemens Analytical Instruments Inc., Karlsruhe (1990).
11. Sheldrick, G. M., SHELXL93. *Program for Crystal Structure Analysis.* University of Göttingen, Germany (1993).
12. Ortep-3 for Window: Farrugia L. J., *J. Appl. Cryst.*, in press.
13. Constable, E. C., Hannon, M. J., Martin, A., Raithby, P. R. and Tocher, D. A., *Polyhedron*, 1992, **11,** 2967.
14. Constable, E. C., Elder, S. M., Hannon, M. J., Martin, A., Raithby, P. R. and Tocher, D. A., *J. Chem. Soc., Dalton Trans.*, 1996, 2423.
15. Morgan, G. T. and Burstall, F. H., *J. Chem. Soc.*, 1937. 1649.
16. Harris, C. M. and Lockyer, T. N., *Aust. J. Chem.*, 1970, **23,** 1125.
17. Ignaczak, M., Grzejdziak, A. and Degen-Piotrowska, E., *Monatsh. Chem.*, 1989, **120,** 515.
18. Ignaczak, M., Grzejdziak, A. and Olejniczak, B., *Monatsh. Chem.*, 1989, **120,** 529.
19. bin Silong, S., Kildea, J. D., Patalinghug, W. C., Skelton, B. W. and White, A. H., *Aust. J. Chem.*, 1994, **47,** 1545.
20. Ainscough, E. W., Brodie, A. M., Ingham, S. L. and Waters, J. M., *J. Chem. Soc., Dalton Trans.*, 1994, 215.
21. Constable, E. C., Khan, M. S., Liptrot, M. C., Lewis, J. and Raithby, P. R., *Inorg. Chim. Acta.*, 1991, **179,** 239.

Pergamon

PII: S0277-5387(97)00332-X

Polyhedron Vol. 17, No. 2–3, pp. 255–260, 1998
© 1997 Elsevier Science Ltd
All rights reserved. Printed in Great Britain
0277-5387/98 $19.00+0.00

Complexes of copper(II) carboxylates with 2-aminoethanol - syntheses, characterization and fungicidal activity; crystal structure of $Cu(O_2CC_8H_{17})_2(NH_2C_2H_4OH)_2$

Marko Petrič,[a]* Franc Pohleven,[a] Iztok Turel,[b] Primož Šegedin,[b] Andrew J. P. White[c] and David J. Williams[c]

[a] Department of Wood Science and Technology, Biotechnical Faculty, University of Ljubljana, Rožna dolina, C. VIII/34, 1000 Ljubljana, Slovenia

[b] Faculty of Chemistry and Chemical Technology, University of Ljubljana, Aškerčeva 5, POB 537, 1000 Ljubljana, Slovenia

[c] Department of Chemistry, Imperial College of Science, Technology and Medicine, South Kensington, London SW7 2AY, U.K.

(Received 14 April 1997; accepted 24 July 1997)

Abstract—Complexes of copper(II) octanoate, nonanoate and decanoate with 2-aminoethanol (ethanolamine) have been synthesized and characterized. The crystal structure of $Cu(O_2CC_8H_{17})_2(NH_2C_2H_4OH)_2$ consists of mononuclear units with pairs of amino nitrogen atoms and deprotonated nonanoato oxygen atoms forming a square coordination plane around the central copper. The hydroxyl oxygen atoms from the 2-aminoethanol ligands are positioned axially with respect to the coordination plane. Results of screening for fungicidal activity against the wood-rotting fungus *Trametes versicolor* (L. ex Fr.) Pilat show that the complexes totally inhibit fungal growth at a concentration of 1.0×10^{-3} mol/l but only partially at a concentration of 5.0×10^{-4} mol/l.
© 1997 Elsevier Science Ltd

Keywords: copper(II) carboxylates; 2-aminoethanol; octanoate; nonanoate; decanoate.

A large number of copper(II) carboxylates and their complexes, especially with nitrogen donor ligands, have been studied extensively and the results published in several monographs and reviews [1–7]. Our interest in copper(II) complexes of saturated carboxylic acids originates from their use as wood preservatives [8–10]. Copper(II) carboxylates of higher fatty acids are not soluble in water, though they are soluble in aqueous ammonia or other amine solutions. The aim of our work was to synthesize and characterize some complexes of copper(II) carboxylates with 2-aminoethanol and to examine their fungicidal activity.

* Author to whom correspondence should be addressed.

EXPERIMENTAL

Preparation of the complexes

The starting copper(II) octanoate, nonanoate and decanoate species were synthesized as described earlier [11]. To make the 2-aminoethanol adducts, 2.00 g of the copper complex (2.86 mmol of octanoate, 2.65 mmol of nonanoate or 2.46 mmol of decanoate) was dissolved in 30 cm^3 of boiling acetone (40 cm^3 for the decanoate species) with stirring and 2-aminoethanol added (0.69 cm^3, 0.64 cm^3 or 0.59 cm^3 which is 11.4, 10.6 or 9.9 mmol, respectively) to give 4:1 amine:carboxylate molar ratios in each case. Subsequent cooling resulted in the precipitation of blue solids.

These products were recrystallized from hot acetonitrile with yields in the range 78–87%.

Blue platy needles of $Cu(O_2CC_8H_{17})_2(NH_2C_2H_4OH)_2$ suitable for X-ray crystallographic analysis were obtained by dissolving 0.06 g of the compound in 20 cm^3 of acetonitrile, heating to boiling, filtering and slowly cooling to room temperature.

Physical measurements

Vibrational spectra in the region 4000–220 cm^{-1} were obtained using a Perkin-Elmer FT-IR 1720 X spectrophotometer using Nujol and poly(chlorotrifluoroethylene) oil suspension techniques. Room-temperature magnetic susceptibility measurements of powdered samples were performed with a Sherwood Scientific MSB-1 balance using $HgCo(NCS)_4$ as a calibrant. EPR spectra of the powders were recorded on a Bruker ESP-300 X-band spectrometer at room temperature and at 150 K.

Elemental analysis

$Cu(O_2CC_7H_{15})_2(NH_2C_2H_4OH)_2$; found (calc.): Cu 13.2 (13.5), C 49.8 (50.9), H 9.5 (9.3), N 6.0 (5.9)%. $Cu(O_2CC_8H_{17})_2(NH_2C_2H_4OH)_2$; Cu 12.4 (12.7), C 53.1 (52.8), H 9.6 (9.6), N 5.9 (5.6)%. $Cu(O_2CC_9H_{19})_2(NH_2C_2H_4OH)_2$; Cu 12.0 (12.0), C 53.7 (54.6), H 10.3 (9.9), N 5.4 (5.3)%.

Crystal data for bis(2-aminoethanol)di(nonanoato) copper(II)

$C_{22}H_{48}N_2O_6Cu$, $M = 500.2$, monoclinic, space group $P2_1/c$, $a = 18.015(2)$, $b = 4.908(1)$, $c = 15.898(3)$ Å, $\beta = 102.25(1)°$, $V = 1373.7(4)$ Å^3, $Z = 2$ (the molecule has crystallographic C_i symmetry), $D_c = 1.209$ g cm^{-3}, $\mu(Cu\text{–}K_\alpha) = 14.1$ cm^{-1}, $F(000) = 542$. A blue platy needle of dimensions $0.50 \times 0.20 \times 0.03$ mm was used. Data were measured on a Siemens P4/PC diffractometer with Cu–K_α radiation (graphite monochromator) using ω-scans. 2172 independent reflections were measured ($2\theta \leqslant 124°$) of which 1921 had $|F_0| > 4\sigma(|F_0|)$ and were considered to be observed. The data were corrected for Lorentz and polarization factors, but not for absorption. The structure was solved by direct methods and all the non-hydrogen atoms were refined anisotropically. The amino and hydroxyl hydrogen atoms were located from a ΔF map and refined isotropically subject to a distance constraint (0.90 Å). The positions of the remaining hydrogen atoms were idealized, assigned isotropic thermal parameters, $U(H) = 1.2U_{eq}(C)$ [$U(H) = 1.5U_{eq}(C\text{–}Me)$], and allowed to ride on their parent atoms. Refinement was by full-matrix least-squares based on F^2 to give $R_1 = 0.051$, $wR_2 = 0.140$ for the observed data and 155 parameters. The maximum and minimum residual electron densities in the final ΔF map were 0.54 and -0.70 eÅ^{-3} respectively. The mean and maximum shift/error ratios in the final refinement cycle were 0.000 and 0.000 respectively. Computations were carried out using the SHELXTL PC program system [12]. Additional material available from the Cambridge Crystallographic Data Center comprises H-atom coordinates, thermal parameters and remaining bond lengths and angles.

Screening of the compounds for fungicidal activity

0.1 cm^3 of solutions of the studied compounds in dimethyl sulfoxide (DMSO) were added to 10 cm^3 of sterilized cooling potato dextrose agar (PDA, Difco). Final concentrations of the tested substances in the growth medium were 1.0×10^{-3}, 5.0×10^{-4}, 2.5×10^{-4} and 1×10^{-4} mol/l. The solidified growth medium was inoculated by approximately 0.5 cm^2 pieces of mycelium of wood-decay fungus *Trametes versicolor* (L. ex Fr.) Pilat (ZIM, L053) [13]. Nine tubes with the inoculated medium were used for each substance. The tubes were then put into the growth chamber at 25°C. The fungal growth was estimated visually and compared with growth on the control medium without chemicals and on PDA containing 1 vol% of DMSO.

RESULTS AND DISCUSSION

Crystal and molecular structure of $Cu(O_2CC_8H_{17})_2(NH_2C_2H_4OH)_2$

The X-ray analysis of the product of the reaction between copper(II) nonanoate and 2-aminoethanol in acetone reveals the formation of a C_i symmetric square planar copper complex (Fig. 1). Selected bond lengths and angles are presented in Table 1. The nonanoic acid coordinates via the deprotonated oxygen atom [Cu—O(1) 2.009(2) Å] whilst the 2-aminoethanol is bound via the amino nitrogen atom [Cu—N(10) 1.999(3) Å]; the *cis* angles at copper are 89.8(1) [N(10)—Cu—O(1′)] and 90.3(1)° [N(10)—Cu—O(1)]. The 2-aminoethanol ligands have a *gauche* geometry about the C—C bond, being folded such that the terminal hydroxyl oxygen atoms are positioned axially with respect to the coordination plane, thereby filling the vacant octahedral sites at copper [Cu···O(13) 2.477(2) Å]. The O···Cu vector is inclined by ca 78° to the coordination plane. Examples of 2-aminoethanol behaving as a "bidentate" ligand to copper in this fashion are rare. Indeed, there is only one prior example of a crystal structure where an analogous octahedral geometry is observed [14], but this structure is of poor accuracy.

This secondary coordination results in the hydroxyl hydrogen atoms of the 2-aminoethanol ligands being directed towards the carbonyl oxygen atoms of the nonanoic acid moieties (the aliphatic chains of which

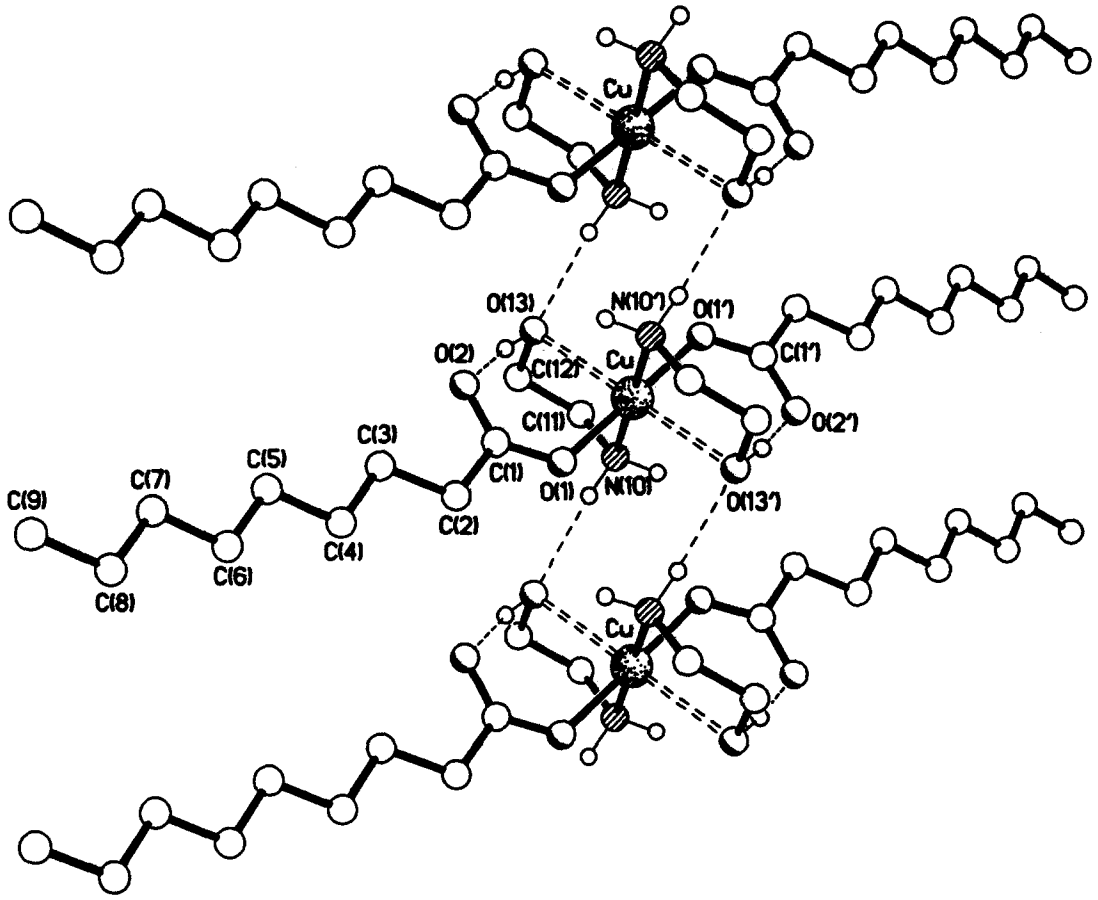

Fig. 1. Lattice translated $Cu(O_2CC_8H_{17})_2(NH_2C_2H_4OH)_2$ molecules showing the intermolecular N—H · · · O hydrogen bonds.

Table 1. Selected bond lengths (Å) and angles (°) with estimated standard deviations in parentheses

Cu—N(10)	1.999(3)	Cu—O(1)	2.009(2)
Cu—O(13)	2.477(2)	O(1)—C(1)	1.276(3)
C(1)—O(2)	1.233(4)	N(10)—C(11)	1.469(4)
C(11)—C(12)	1.475(5)	C(12)—O(13)	1.423(4)
N(10′)—Cu—N(10)	180.0	N(10)—Cu—O(1′)	89.75(10)
N(10)—Cu—O(1)	90.25(10)	O(1)—Cu—O(1′)	180.0
N(10)—Cu—O(13′)	101.68(9)	O(1)—Cu—O(13′)	88.22(7)
N(10)—Cu—O(13)	78.32(9)	O(1)—Cu—O(13)	91.78(7)
O(13)—Cu—O(13′)	180.0	C(1)—O(1)—Cu	125.1(2)
O(2)—C(1)—O(1)	125.1(3)	C(11)—N(10)—Cu	111.5(2)
N(10)—C(11)—C(12)	111.1(3)	O(13)—C(12)—C(11)	111.8(3)
C(12)—O(13)—Cu	101.4(2)		

have a near planar, extended all *anti* geometry), forming pairs of strong, intramolecular O—H · · · O hydrogen bonds [O · · · O 2.61, H · · · O 1.72 Å; O—H · · · O 169°].

Adjacent complexes are linked via pairs of N—H · · · O hydrogen bonds between one of the amino N—H hydrogen atoms in one molecule and the hydroxyl oxygen atom of the 2-aminoethanol ligand of a lattice translated counterpart [N · · · O 2.99, H · · · O 2.10 Å; N—H · · · O 167°] (Fig. 1). This pat-

tern of hydrogen bonding results in the aliphatic residues being aligned parallel to each other to form a sheet-like array. Adjacent sheets are oriented such that these aliphatic chains interleave head-to-tail to form a close-packed array, as shown in Fig. 2. The overall superstructure is thus dominated by alternating hydrophobic and hydrophillic regions.

Magnetic and spectroscopic data

The effective magnetic moments of the 2-aminoethanol adducts (Table 2) lie above the spin-only value of 1.73 BM, in the range between 1.92–1.97 BM, and are consistent with the presence of one unpaired electron in a mononuclear copper(II) complex [15]. These results were confirmed by EPR measurements of powder samples at room temperature and at 150 K (Table 2). The spectra are typical for axial symmetry and indicate a $d_{x^2-y^2}$ ground state ($g_\parallel > g_\perp > 2.0$) [15]. The value of $G = (g_\parallel - 2)/(g_\perp - 2)$ equals approximately 4.5 for all three compounds and signifies low exchange coupling [16].

IR spectra of all three copper(II) carboxylates are very similar, being noticeably different only in the region between 1350 and 1000 cm^{-1}, where the CH_2 "wagging" of long hydrocarbon chains exhibit a series of sharp regularly spaced bands. It is known that complexity of the spectra in this region increases with increasing chain length [17,18]. Between 3630 and 3150 cm^{-1} four bands were observed in each case, resulting from 2-aminoethanol O—H and N—H stretches. The shift of the N—H stretches toward lower wave numbers, compared to those of primary amines in the gas phase or in dilute solutions, can be explained by hydrogen bonding [19–21]. The band at 1600 cm^{-1}, present in the spectra of all three compounds, was assigned to the NH_2 asymmetric deformation and the bands at 1071 and 1032 cm^{-1} to the NH_2 symmetric deformation mode. Bands due to vibrations in the aliphatic chains of the carboxylato ligands are at the expected wavelengths, as assigned by Strommen and coworkers [18]. The broad and strong $\nu_{as}(COO)$ band is located at 1556–1560 cm^{-1} and the split band, tentatively assigned to the symmetric carboxylate stretch, $\nu_s(COO)$, occurs at 1408–1412 cm^{-1}. The separation, Δ, between these two bands is only 144–152 cm^{-1}, which is unexpectedly small for unidentate carboxylate ligands. It is even smaller than the difference of 171–177 cm^{-1} observed for the bridging bidentate carboxylate arrangement in copper(II) octanoate, nonanoate and decanoate [11]. The small magnitude

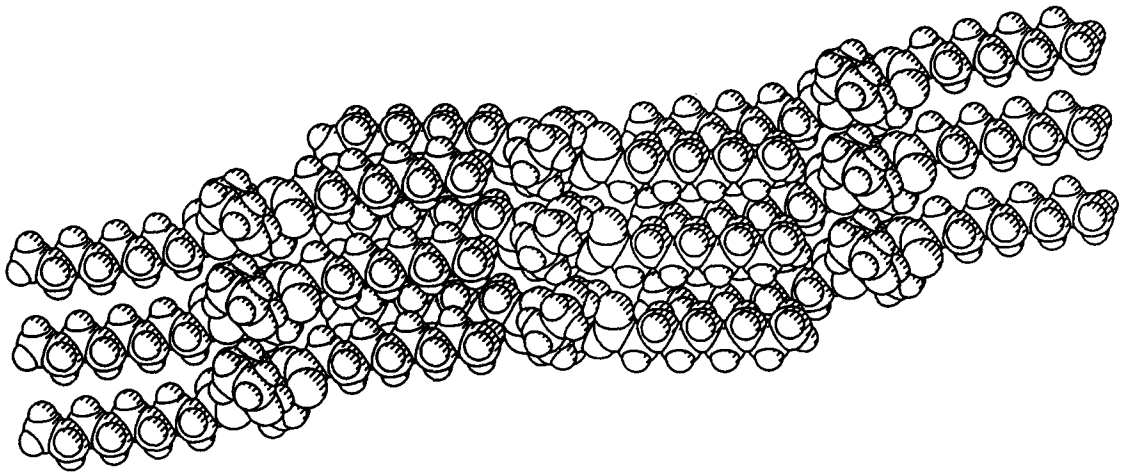

Fig. 2. Space-filling representation of the interleaved aliphatic chains showing the hydrophobic and hydrophilic domains.

Table 2. Magnetic moments and EPR parameters of copper(II) carboxylato–2-aminoethanol complexes

Compound	Room temperature μ_{eff} (BM)	Room temperature $g_\parallel$	Room temperature $g_\perp$	Room temperature G^a	T = 150 K $g_\parallel$	T = 150 K $g_\perp$	T = 150 K G^a
$Cu(O_2CC_7H_{15})_2(NH_2C_2H_4OH)_2$	1.92	2.296	2.067	4.4	2.297	2.066	4.5
$Cu(O_2CC_8H_{17})_2(NH_2C_2H_4OH)_2$	1.97	2.294	2.065	4.5	2.296	2.066	4.5
$Cu(O_2CC_9H_{19})_2(NH_2C_2H_4OH)_2$	1.93	2.294	2.065	4.5	2.297	2.066	4.5

[a] $G = (g_\parallel - 2)/(g_\perp - 2)$

Table 3. Fungicidal activity of copper(II) carboxylates and their complexes with 2-aminoethanol

Compound	Average values of estimates for fungal growth retardation, 7 days after inoculation[a]			
	1.0×10^{-3} mol/l	5.0×10^{-4} mol/l	2.5×10^{-4} mol/l	1.0×10^{-4} mol/l
None (control)	1	1	1	1
Dimethyl sulfoxide[b]	2	2	2	2
2-Aminoethanol	2	2	2	2
$Cu_2(O_2CC_7H_{15})_4$	5	5	5	2
$Cu_2(O_2CC_8H_{17})_4$	5	5	5	2
$Cu(O_2CC_9H_{19})_4$	5	5	5	2
$Cu(O_2CC_7H_{15})_2(NH_2C_2H_4OH)_2$	5	2	ND	2
$Cu(O_2CC_8H_{17})_2(NH_2C_2H_4OH)_2$	5	2	ND	2
$Cu(O_2CC_9H_{19})_2(NH_2C_2H_4OH)_2$	5	2	ND	2

[a] Fungicidal activity was estimated with fungal growth retardation, labelled by the following visually determined marks: 1, normal growth, no retardation; 2, slightly visible signs of retardation; 3, significant retardation; 4, retardation is very strong; 5, no fungal growth.

[b] Concentration of dimethyl sulfoxide in the growth medium was in all cases the same i.e. 1% by volume.

ND = Not determined.

of this separation in these 2-aminoethanol complexes can be attributed to strong intramolecular hydrogen bonding between the carbonyl oxygen atoms of the carboxylic acid ligands and hydroxyl hydrogen atoms of the 2-aminoethanol units (as already shown, the O···O distance in the nonanoato complex is only 2.61 Å). In the nickel complex $Ni(O_2CCH_3)_2(H_2O)_4$, which contains monodentate acetates, the low Δ value of 107 cm^{-1} has been attributed to hydrogen bonding of the uncoordinated carboxylate oxygen atom compensating for the asymmetry produced by the monodentate coordination [22].

The magnetic and spectroscopic data are very similar for all three complexes, strongly supporting our conclusion that they are of the same type as the structurally characterized bis(2-aminoethanol)di(nonanoato)copper(II) species.

Fungicidal activity

Results of screening for fungicidal activity against the wood-rotting fungus *Trametes versicolor* (L. ex Fr.) Pilat are presented in Table 3. The 2-aminoethanol complexes totally inhibit fungal growth at a concentration of 1.0×10^{-3} mol/l but only partially at a concentration of 5.0×10^{-4} mol/l. Fungicidal activity slightly increases with the chain length. The fungicidity of the complexes at 1.0×10^{-4} mol/l as well as the activity of 2-aminoethanol itself could not be determined due to the slight fungitoxic effect of the DMSO solvent, which masks any possible biological activity of other substances at low concentrations.

In order to evaluate the influence of 2-aminoethanol on the fungicidal activity of the studied complexes, a comparison with the activity of copper(II) octanoate, nonanoate and decanoate was performed. At the same Cu(II) concentration of 5.0×10^{-4} mol/l [concentration of binuclear $Cu_2(O_2CR)_4$ is 2.5×10^{-4} mol/l and 5.0×10^{-4} mol/l of mononuclear $Cu(O_2CR)_2(NH_2C_2H_4OH)_2$], the 2-aminoethanol complexes exhibit weaker fungicidal activity. It is well known that fungi require nitrogen for their growth [23] and we believe that the enhanced nitrogen content in the growth medium, originating from 2-aminoethanol, increases the activity of *Trametes versicolor* and its growth rate.

Indeed, Ruddick and Xie [24] showed that enrichment of nitrogen in ammoniacal-copper preservative treated wood enhances wood decay by brown rot fungi, e.g. *Postia placenta* and *Gloeophyllum trabeum*. In contrast to our results, they did not observe utilization of enhanced nitrogen by the white rot fungus *Trametes versicolor*. However, it has to be taken into account that Ruddick and Xie made their experiments with the preserved wood, whilst we were using a much more simple system—that of a solution of the preservatives in PDA growth medium.

Acknowledgements—This work was supported by the grant No. Z4-7063-0491-95 of The Ministry of Science and Technology of Republic of Slovenia. EPR spectra were recorded in the EPR center at the "Jožef Stefan" Institute in Ljubljana.

REFERENCES

1. Mehrotra, R. C. and Bohra, R., *Metal Carboxylates*, Academic Press, London (1983).
2. Oldham, C., *Progr. Inorg. Chem.*, 1968, **10**, 223.
3. Doedens, R. J., *Progr. Inorg. Chem.*, 1976, **21**, 209.
4. Melnik, M., *Coord. Chem. Rev.*, 1981, **36**, 1.
5. Melnik, M., *Coord. Chem. Rev.*, 1982, **42**, 259.

6. Kato, M. and Muto, Y., *Coord. Chem. Rev.*, 1988, **92,** 45.
7. Sundberg, M. R., Uggla, R. and Melnik, M., *Polyhedron*, 1996, **15,** 1157.
8. Richardson, B. A., *Wood Preservation, Second edition*, E & FN Spon, an imprint of Chapman & Hall, London, 1993.
9. Pohleven, F., Šentjurc, M., Petrič, M. and Dagarin, F., *Holzforschung*, 1994, **48,** 371.
10. Pohleven, F. and Petrič, M., *Internat. Res. Group on Wood Preserv.*, 1996, Document No.: IRG/WP 96-30109.
11. Petrič, M., Leban, I. and Šegedin, P., *Polyhedron*, 1995, **14,** 983.
12. SHELXTL PC version 5.03, Siemens Analytical X-Ray Instruments, Inc., Madison, WI, 1994.
13. ZIM : zbirka industrijskih mikroorganizmov Ljubljana. Katalog biokultur (=Slovenian Collection of Industrial Microorganisms Ljubljana. Catalogue of Strains), 1st Edition. Biotechnical Faculty, Ljubljana, Slovenia, 1995.
14. Amirov, G. T., Abdullaev, G. K. and Mamedov, H. S., *Zh. Strukt. Khim.*, 1975, **16,** 499.
15. Hathaway, B. J. and Billing, D. E., *Coord. Chem. Rev.*, 1970, **5,** 143.
16. Hathaway, B. J. and Tomlinson, A. A. G., *Coord. Chem. Rev.*, 1970, **5,** 1.
17. Meiklejohn, R. A., Meyer, R. J., Aronovic, S. M., Schuette, H. A. and Meloch, V. W., *Anal. Chem.*, 1957, **29,** 329.
18. Strommen, D. P., Giroud-Godquin, A. M., Maldivi, P., Marchon, J. C. and Marchon, B., *Liq. Cryst.*, 1987, **2,** 689.
19. Sundberg, M. R. and Klinga, M., *Inorg. Chim. Acta*, 1985, **105,** 115.
20. Sundberg, M. R. and Sillanpää, R., *Acta Chem. Scand.*, 1992, **46,** 34.
21. Sundberg, M. R., Klinga, M. and Uggla, R., *Inorg. Chim. Acta.*, 1994, **216,** 57.
22. Catterick, J. and Thornton, P., *Adv. Inorg. Chem. Radiochem.*, 1977, **20,** 291.
23. Zabel, R. A. and Morrell, J. J., *Wood Microbiology. Decay and Its Prevention*, pp. 108–110. Academic Press, Inc., San Diego, CA, 1992.
24. Ruddick, J. N. R. and Xie, C., *Mater. Org.*, 1995, **29,** 93.

Pergamon

PII: S0277-5387(97)00327-6

Polyhedron Vol. 17, No. 2–3, pp. 261–265, 1998
© 1997 Elsevier Science Ltd
All rights reserved. Printed in Great Britain
0277-5387/98 $19.00+0.00

Reactivity of bimetallic dibridged complexes $Cp_2Ta(H)(\mu\text{-}H)(\mu\text{-}PMe_2)M'(CO)_4$ (M′ = Cr, Mo, W) toward two-electron donor ligands L (L = PR_3, $Me_2P(CH_2)_nPMe_2$). Synthesis of linear trinuclear chain complexes $Cp_2Ta(H)_2(\mu\text{-}PMe_2)M'(CO)_4(Me_2P(CH_2)_2PMe_2)Cr(CO)_5$ (M′ = Mo, W)

Gilles Boni and Claude Moïse*

Laboratoire de Synthèse et d'Electrosynthèse Organométalliques (UMR 5632), Université de Bourgogne, Faculté des Sciences, 6 Boulevard Gabriel, 21000 Dijon, France

(Received 15 May 1997; accepted 21 July 1997)

Abstract—The reaction of the heterobimetallic phosphido- and hydrido-bridged complexes $Cp_2TaH(\mu\text{-}H)(\mu\text{-}PMe_2)M'(CO)_4$ (M′ = Cr, Mo, W) (**1–3**) with phosphines (L = PPh_2Me, PMe_2Ph) or diphosphines (L = dmpm, dmpe) leads to $Cp_2Ta(H)_2(\mu\text{-}PMe_2)M'(CO)_4(L)$ (**1a, 1b, c, d–3b, c, d**) with L regiospecifically coordinated to M′. Except for L = PPh_2Me, the reaction is stereospecific, since a cis arrangement (with respect to the PMe_2 bridge) on the M′ site is obtained. The new compounds $Cp_2Ta(H)_2(\mu\text{-}PMe_2)M'(CO)_4(Me_2P(CH_2)_2PMe_2)$ (M′ = Mo, W) are able to bind $[Cr(CO)_5]$ fragments affording the linear trinuclear chain compounds $Cp_2Ta(H)_2(\mu\text{-}PMe_2)M'(CO)_4(Me_2P(CH_2)_2PMe_2)(Cr(CO)_5)$ (**4, 5**). All new complexes have been fully characterized by NMR and IR spectroscopy, and by their elemental analyses. © 1997 Elsevier Science Ltd

Keywords: tantalum; phosphines; diphosphines; dibridged complexes; polynuclear species.

Considerable interest has focused on the synthesis and chemistry of binuclear complexes containing two different transition metals. In particular, the chemistry of heterometallic compounds stabilized by bridging phosphido groups continues to attract great interest [1–8]. In the course of our works on these systems we have recently described new synthetic routes to μ-PR_2 μ-CO [9–12] and μ-PR_2 μ-H [13,14] dibridged complexes involving group 5 metallophosphines as precursors. These metallophosphines are easily synthesized starting from chlorophosphines and d^2 monohydrido complexes $Cp_2M(H)(L)$ [15–19] or d^0 three hydrido complexes Cp_2MH_3 [13,20,21].

Addition reactions between μ-phosphido μ-carbonyl complexes and phosphines or isonitriles have been studied [10,11]. Described herein is the reactivity of μ-phosphido, μ-hydrido dibridged complexes toward Lewis bases. A synthetic route to linear heterotrinuclear complexes is also presented.

EXPERIMENTAL

All reactions were carried out under an argon atmosphere with use of standard Schlenk techniques. The solvents and eluents were dried and distilled under argon from sodium and benzophenone immediately before use. $Cp_2TaH(\mu\text{-}H)(\mu\text{-}PMe_2)M'(CO)_4$ (M′ = Cr, Mo, W) (**1–3**) were synthesised as previously described [13,14]. $Cr(CO)_5(THF)$ was prepared according to literature procedures [22]. PPh_2Me, PMe_2Ph, dmpm and dmpe (Strem) have been used as received.

* Author to whom correspondence should be addressed.

Elemental analyses (C, H) were performed by the "Service Central d'Analyse du CNRS" (Gif-sur-Yvette, France). Infrared spectra were recorded on a Nicolet 205 IR-FT. ^1H and ^{31}P NMR spectra were recorded on a Bruker AC 200 spectrometer; chemical shifts are given in ppm relative to Me_4Si (^1H) or (external) H_3PO_4 (^{31}P).

Synthesis of $Cp_2Ta(H)_2(\mu\text{-}PMe_2)M'(CO)_4(L)$ (M' = Cr, Mo, W; L = *phosphine, diphosphine*)

To a THF solution (40 mL) of $Cp_2Ta(H)(\mu\text{-}H)(\mu\text{-}PMe_2)M'(CO)_4$ (0.5 mmol) was added one equivalent of the Lewis base L. The reaction mixture was heated at 45°C for 2 h. The solvent was removed, and the product was washed with 3 × 20 mL of pentane and dried under vacuum. The analytical samples were obtained by recrystallization from acetone as yellow solids. Yields 75–80%.

$Cp_2Ta(H)_2(\mu\text{-}PMe_2)Cr(CO)_4(PPh_2Me)$ (**1a**). cis isomer (70%) ^{1}H NMR (CD_3COCD_3) δ 5.50 (broad signal, Cp), 1.90 (d, J = 7.8 Hz, Me), 1.37 (d, J = 4.9 Hz, Me), 0.64 (d, $J_{P\text{-}H}$ = 55.1 Hz, H), 7.29–7.74 (m, Ph). ^{31}P {^1H} NMR (CD_3COCD_3) δ 38.5 (d, J = 30.1 Hz, PPh_2Me), −88.1 (d, J = 30.1 Hz, PMe_2). trans isomer (30%) ^{1}H NMR (CD_3COCD_3) δ 5.55 (broad signal, Cp), 1.98 (d, J = 6.3 Hz, Me), 1.68 (d, J = 5.4 Hz, Me), 0.73 (d, $J_{P\text{-}H}$ = 57.1 Hz, H); 7.29–7.74 (m, Ph). ^{31}P {^1H}NMR (CD_3COCD_3) δ 59.8 (d, J = 25.1 Hz, PPh_2Me), −68.2 (d, J = 25.1 Hz, PMe_2). IR for the mixture (THF): ν(CO) 1984 (m), 1883 (s), 1870 (s) 1854 (vs) cm^{-1}. Found: C, 47.44; H, 4.32. Calc. for $C_{29}H_{31}TaCrP_2O_4$: C, 47.17; H, 4.23%.

$Cp_2Ta(H)_2(\mu\text{-}PMe_2)Cr(CO)_4(PMe_2Ph)$ (**1b**). cis isomer ^{1}H NMR (CD_3COCD_3) δ 5.44 (s, Cp), 1.73 (d, J = 6.5 Hz, Me), 1.35 (d, J = 5.0 Hz, Me), 0.50 (d, $J_{P\text{-}H}$ = 56.0 Hz, H), 7.40–7.60 (m, Ph). ^{31}P {^1H} NMR (CD_3COCD_3) δ 22.0 (d, J = 30.5 Hz, PMe_2Ph), −86.9 (d, J = 30.5 Hz, PMe_2). IR (THF): ν(CO) 1984 (w), 1878 (s), 1868 (vs), 1851 (vs) cm^{-1}. Found: C, 42.83; H, 4.37. Calc. for $C_{24}H_{29}CrO_4P_2Ta$: C, 42.62; H, 4.32%.

$Cp_2Ta(H)_2(\mu\text{-}PMe_2)Mo(CO)_4(PMe_2Ph)$ (**2b**). cis isomer ^{1}H NMR (CD_3COCD_3) δ 5.44 (s, Cp), 1.78 (d, J = 5.9 Hz, Me), 1.44 (d, J = 3.9 Hz, Me), 0.31 (d, $J_{P\text{-}H}$ = 56.1 Hz, H), 7.32–7.76 (m, Ph). ^{31}P {^1H} NMR (CD_3COCD_3) δ 0.1 (d, J = 25.1 Hz, PMe_2Ph), −104.7 (d, J = 25.1 Hz, PMe_2). IR (THF): ν(CO) 1999 (w), 1887 (s), 1879 (vs), 1849 (vs) cm^{-1}. Found: C, 39.51; H, 3.98. Calc. for $C_{24}H_{29}MoO_4P_2Ta$: C, 40.02; H, 4.06%.

$Cp_2Ta(H)_2(\mu\text{-}PMe_2)W(CO)_4(PMe_2Ph)$ (**3b**). cis isomer ^{1}H NMR (CD_3COCD_3) δ 5.46 (d, J = 0.5 Hz, Cp), 1.93 (d, J = 6.8 Hz, Me), 1.57 (d, J = 5.0 Hz, Me), 0.59 (d, $J_{P\text{-}H}$ = 56.6 Hz, H), 7.41–7.74 (m, Ph). ^{31}P {^1H} NMR (CD_3COCD_3) δ −19.8 (d, J = 20.1 Hz, PMe_2Ph), −127.3 (d, J = 20.1 Hz, PMe_2). IR (THF): ν(CO) 1994 (w), 1880 (s), 1869 (vs), 1844 (vs) cm^{-1}. Found: C, 35.81; H, 3.73. Calc. for $C_{24}H_{29}O_4P_2TaW$: C, 35.67; H, 3.62%.

$Cp_2Ta(H)_2(\mu\text{-}PMe_2)Cr(CO)_4(dmpm)$ (**1c**). cis isomer ^{1}H NMR (CD_3COCD_3) δ 5.56 (s, Cp), 1.90 (dd, J = 4.9 Hz, J = 2.9 Hz, CH_2), 1.56 (d, J = 5.0 Hz, Me), 1.53 (d, J = 6.2 Hz, Me), 1.15 (d, J = 3.8 Hz, Me), 0.58 (d, $J_{P\text{-}H}$ = 55 Hz, H). ^{31}P {^1H} NMR (CD_3COCD_3) δ −86.4 (d, J = 25 Hz, μ-PMe_2), 20.9 (t, J = 25 Hz, Cr-PMe_2), −56.4 (d, J = 25 Hz, CH_2-PMe_2). IR (THF): ν(CO) 1982 (m), 1877 (s), 1866 (vs), 1846 (vs) cm^{-1}. Found: C, 37.82; H, 4.89. Calc. for $C_{21}H_{32}CrO_4P_3Ta$: C, 37.40; H, 4.78%.

$Cp_2Ta(H)_2(\mu\text{-}PMe_2)Mo(CO)_4(dmpm)$ (**2c**). cis isomer ^{1}H NMR (CD_3COCD_3) δ 5.53 (s, Cp), 1.93 (dd, J = 4.7 Hz, J = 2.9 Hz, CH_2), 1.63 (d, J = 4.5 Hz, Me), 1.56 (d, J = 6.0 Hz, Me), 1.15 (d, J = 3.6 Hz, Me), 0.36 (d, $J_{P\text{-}H}$ = 56 Hz, H). ^{31}P {^1H} NMR (CD_3COCD_3) δ −103.1 (d, J = 25 Hz, μ-PMe_2), −3.4 (dd, J = 39 Hz, J = 25 Hz, Mo-PMe_2), −56.3 (d, J = 39 Hz, CH_2-PMe_2). IR (THF): ν(CO) 1998 (m), 1888 (s), 1876 (vs), 1849 (s) cm^{-1}. Found: C, 35.56; H, 4.45. Calc. for $C_{21}H_{32}MoO_4P_3Ta$: C, 35.12; H, 4.49%.

$Cp_2Ta(H)_2(\mu\text{-}PMe_2)W(CO)_4(dmpm)$ (**3c**). cis isomer ^{1}H NMR (CD_3COCD_3) δ 5.56 (s, Cp), 2.03 (dd, J = 5.5 Hz, J = 2.8 Hz, CH_2), 1.78 (d, J = 5.2 Hz, Me), 1.69 (d, J = 6.7 Hz, Me), 1.16 (d, J = 3.6 Hz, Me), 0.64 (d, $J_{P\text{-}H}$ = 56 Hz, H). ^{31}P {^1H} NMR (CD_3COCD_3) δ −126.0 (d, J = 21 Hz, μ-PMe_2), −23.9 (dd, J = 38 Hz, J = 21 Hz, $J_{P\text{-}W}$ = 110 Hz, W-PMe_2) −56.2 (d, J = 38 Hz, CH_2-PMe_2). IR (THF): ν(CO) 1993 (m), 1881 (s), 1866 (vs), 1844 (s) cm^{-1}. Found: C, 32.13; H, 4.15. Calc. for $C_{21}H_{32}WO_4P_3Ta$: C, 31.29; H, 4.00%.

$Cp_2Ta(H)_2(\mu\text{-}PMe_2)Cr(CO)_4(dmpe)$ (**1d**). cis isomer ^{1}H NMR (CD_3COCD_3) δ 5.56 (s, Cp), 1.56 (d, J = 4.3 Hz, Me), 1.42 (d, J = 6.6 Hz, Me), 1.04 (d, J = 2.5 Hz, Me), 0.64 (d, $J_{P\text{-}H}$ = 56 Hz, H), 1.75–1.92 (m, CH_2). ^{31}P {^1H} NMR (CD_3COCD_3) δ −86.3 (d, J = 26 Hz, μ-PMe_2), 21.2 (t, J = 26 Hz, Cr-PMe_2), −44.3 (d, J = 26 Hz, CH_2-PMe_2). IR (THF): ν(CO) 1981 (m), 1883 (s), 1867 (s), 1847 (vs) cm^{-1}. Found: C, 37.16; H, 4.35. Calc. for $C_{22}H_{34}CrO_4P_3Ta$: C, 38.39; H, 4.98%.

$Cp_2Ta(H)_2(\mu\text{-}PMe_2)Mo(CO)_4(dmpe)$ (**2d**). cis isomer ^{1}H NMR (CD_3COCD_3) δ 5.54 (s, Cp), 1.62 (d, J = 4.5 Hz, Me), 1.47 (d, J = 6.0 Hz, Me), 1.04 (d, J = 2.5 Hz, Me), 0.38 (d, $J_{P\text{-}H}$ = 56 Hz, H), 1.65–1.91 (m, CH_2). ^{31}P {^1H} NMR (CD_3COCD_3) δ −103.3 (d, J = 24 Hz, μ-PMe_2), −1.3 (t, J = 24 Hz, Mo-PMe_2), −44.3 (d, J = 24 Hz, CH_2-PMe_2). IR (THF): ν(CO) 1998 (m), 1888 (s), 1876 (vs), 1849 (vs) cm^{-1}. Found: C, 36.29; H, 4.31. Calc. for $C_{22}H_{34}MoO_4P_3Ta$: C, 36.08; H, 4.68%.

$Cp_2Ta(H)_2(\mu\text{-}PMe_2)W(CO)_4(dmpe)$ (**3d**). cis isomer ^{1}H NMR (CD_3COCD_3) δ 5.56 (s, Cp), 1.78 (d, J = 4.9 Hz, Me), 1.61 (d, J = 6.8 Hz, Me), 1.04 (d, J = 2.7 Hz, Me), 0.64 (d, $J_{P\text{-}H}$ = 56 Hz, H), 1.85–1.98 (m, CH_2). ^{31}P {^1H} NMR (CD_3COCD_3) δ −126.4 (d, J = 25 Hz, $J_{P\text{-}W}$ = 178 Hz, μ-PMe_2), −20.9 (t, J = 25 Hz, $J_{P\text{-}W}$ = 218 Hz, W-PMe_2), −44.4 (d, J = 25 Hz, CH_2-PMe_2). IR (THF): ν(CO) 1993 (m), 1881 (s),

1866 (vs), 1844 (s) cm^{-1}. Found: C, 32.26; H, 3.52. Calc. For $C_{22}H_{34}O_4P_3TaW$: C, 32.22; H, 4.18%.

Synthesis of $Cp_2Ta(H_2)(\mu\text{-}PMe_2)M'(CO)_4(dmpe)Cr(CO)_5$ (M' = Mo, W)

To a THF solution (30 mL) of $Cp_2Ta(H)_2(\mu\text{-}PMe_2)M'(CO)_4(dmpe)$ (0.5 mmol) was added one equivalent of $Cr(CO)_5(THF)$. The reaction mixture was stirred for 20 min at room temperature (the reaction was monitored by IR spectroscopy). The solvent was removed, and the product was washed with 3 × 20 mL of pentane and dried under vacuum affording an orange product. The analytical samples were obtained by recrystallization from acetone—yields 65–70%.

$Cp_2Ta(H_2)(\mu\text{-}PMe_2)Mo(CO)_4(dmpe)(Cr(CO)_5)$ (**4**). ^1H NMR (CD_3COCD_3) δ 5.54 (s, Cp), 1.64 (d, J = 5.1 Hz, Me), 1.63 (d, J = 7.8 Hz, Me), 1.54 (d, J = 6.0 Hz, Me), 0.40 (d, $J_{P\text{-}H}$ = 56 Hz, H), 2.07–2.30 (m, CH_2). ^{31}P $\{^1H\}$ NMR (CD_3COCD_3) δ −103.7 (d, J = 25 Hz, μ-PMe_2), 0.8 (t, J = 25 Hz, Mo-PMe_2), 21.2 (d, J = 25 Hz, PMe_2-Cr). IR (THF): ν(CO) 2060 (m), 1999 (m), 1936 (vs), 1891 (s), 1877 (s), 1847 (s) cm^{-1}. Found: C, 35.52; H, 3.87. Calc. for $C_{27}H_{34}CrMoO_9P_3Ta$: C, 35.08; H, 3.71%.

$Cp_2Ta(H_2)(\mu\text{-}PMe_2)W(CO)_4(dmpe)(Cr(CO)_5)$ (**5**). ^1H NMR (CD_3COCD_3) δ 5.56 (s, Cp), 1.79 (d, J = 5.0 Hz, Me), 1.67 (d, J = 6.8 Hz, Me), 1.63 (d, J = 7.8 Hz, Me), 0.66 (d, $J_{P\text{-}H}$ = 56 Hz, H), 2.03–2.36 (m, CH_2). ^{31}P $\{^1H\}$ NMR (CD_3COCD_3) δ −126.8 (d, J = 25 Hz, $J_{P\text{-}W}$ = 176 Hz, μ-PMe_2), 14.2 (t, J = 25 Hz, W-PMe_2), 21.0 (d, J = 25 Hz, PMe_2-Cr). IR (THF): ν(CO) 2060 (m), 1994 (m), 1935 (vs), 1883 (s), 1868 (s), 1842 (s) cm^{-1}. Found: C, 32.29; H, 3.59. Calc. for $C_{27}H_{34}CrO_9P_3TaW$: C, 32.04; H, 3.39%.

RESULTS AND DISCUSSION

Synthesis of dibridged complexes **1–3**

The trihydride Cp_2TaH_3 easily reacts with PMe_2Cl in toluene at room temperature affording the phosphine salt $[Cp_2Ta(H_2)(PMe_2H)]^+Cl^-$ which is deprotonated in aqueous KOH. The resulting metallophosphine $Cp_2Ta(H)(PMe_2H)$ is able to bind metal tetracarbonyl fragments $M'(CO)_4L_2$ (M' = Cr; L_2 = NBD—M' = Mo, W; L = piperidine) leading to the μ-phosphido μ-hydrido dibridged complexes **1–3** (Scheme 1) [13,14].

"Open" structures (**1a, 1b,c,d–3b,c,d**)

The dibridged μ-phosphido μ-hydrido complexes $Cp_2TaH(\mu\text{-}H)(\mu\text{-}PMe_2)M'(CO)_4$ (M' = Cr, Mo, W) (**1–3**) react at 45°C for 2 h with phosphines or diphosphines L (L = PMe_2Ph, PPh_2Me, $Me_2P(CH_2)PMe_2$ (dmpm) or $Me_2P(CH_2)_2PMe_2$ (dmpe)), in THF solution, leading to "open" structures $Cp_2Ta(H)(\mu\text{-}PMe_2)M'(CO)_4(L)$ (**1a, 1b,c,d–3b,c,d**) (Scheme 2). Experimental details and spectroscopic data for all complexes are given in the Experimental section.

The addition of L is regiospecific and can lead to cis or trans arrangements at the M' site. Bonding of phosphines or diphosphines to M' rather than to the tantalum site is clearly evidenced by the hydride resonance signal which appears as a single doublet (2H) in the range 0.30–0.70 ppm. When opposed to PPh_2Me complex **1** leads to a mixture of cis and trans "open" structures **1a** with a slight excess of the cis isomers (70%). In contrast, stereospecific addition in the cis position is observed with PMe_2Ph, dmpm and dmpe, whatever the nature of M'. It is worth noting that no addition reaction occurs with the bulky PPh_3. These results illustrate the dependence of the coordination site on the bulk of incoming ligands [23,24] and are in accordance with our previous studies concerning the dibridged μ-PR_2 μ-CO complexes [10,11].

Complexes **1b,c,d–3b,c,d** show four ν(CO) stretching vibrations indicating the cis position of the two phosphorus atoms around the M' metal. The ^1H NMR data are able to provide information on the selectivity of the addition at the M' site but cannot show whether a cis or a trans configuration arrangement is formed. However, for **1a**, a decisive con-

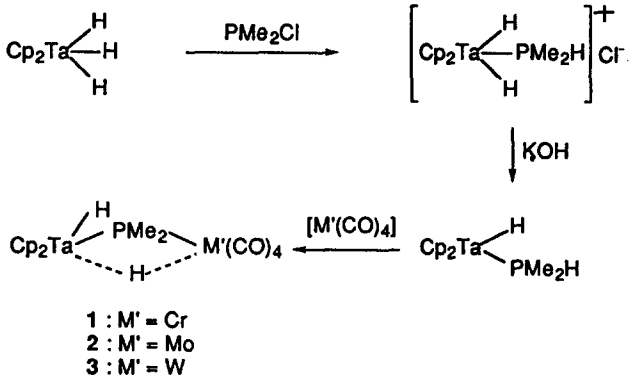

1 : M' = Cr
2 : M' = Mo
3 : M' = W

Scheme 1.

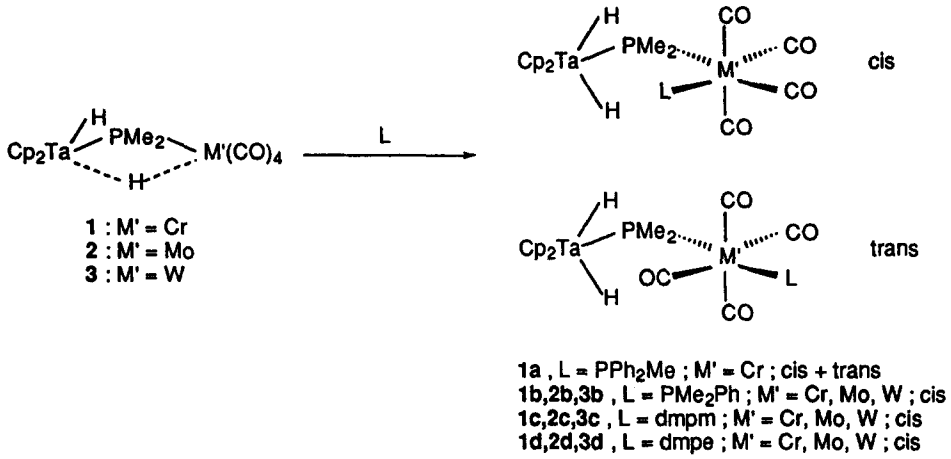

1 : M' = Cr
2 : M' = Mo
3 : M' = W

1a , L = PPh_2Me ; M' = Cr ; cis + trans
1b,2b,3b , L = PMe_2Ph ; M' = Cr, Mo, W ; cis
1c,2c,3c , L = dmpm ; M' = Cr, Mo, W ; cis
1d,2d,3d , L = dmpe ; M' = Cr, Mo, W ; cis

Scheme 2.

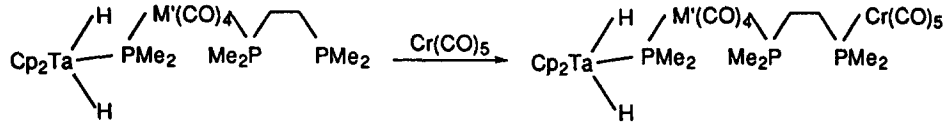

2d,3d , M' = Mo, W

4,5 , M' = Mo, W

Scheme 3.

figurationnal assignment is available from ^{31}P NMR chemical shifts since a trans configuration involves a systematic deshielding of the two phosphorus resonances ($\Delta\delta \approx 20$ ppm for **1a**) [25,26]. The ^{31}P NMR spectra reveals dramatic effects upon the breaking of the hydrido bridge: the μ-PMe_2 ^{31}P resonance is shifted upfield ($\Delta\delta \approx -120$ to -140 ppm) with respect to the parent complexes **1–3**, indicating the large increase of the Ta-PMe_2-M′ angle [27]. With dmpm or dmpe, the ^{31}P NMR data confirm the presence of a dangling phosphorus atom since two distinct resonances are observed: a downfield doublet assigned to the metal-bonded phosphorus atom, and a more shielded signal for the uncoordinated PMe_2 group whose chemical shift is very close to that of the free phosphine.

Linear trinuclear chain compounds (**4,5**)

Treatment of complexes $Cp_2Ta(H)_2(\mu\text{-}PMe_2)M'(CO)_4$(dmpe) (M′ = Mo, W) (**2c, 3c**) with $Cr(CO)_5$(THF), at room temperature, afford the expected trinuclear chain compounds **4** and **5** (Scheme 3). Structures of **4** and **5** are established from their spectra. In particular, the ^{31}P NMR data are very informative: the doublet resonance of the terminal PMe_2 is shifted downfield upon coordination of the fragment $[Cr(CO)_5]$ ($\Delta\delta \approx 65$ ppm).

An unexpected behaviour is observed with dmpm derivatives (**2d, 3d**) since no trimetallic structure is formed when opposed to $Cr(CO)_5$(THF). Both steric and electronic considerations can be advanced to account for the lack of reactivity of these complexes. A critical distance between the two phosphorus coordination sites should be required for minimizing the severe steric hindrance of the two metal carbonyl entities. In addition, as previously reported by Angelici *et al.* [28,29] monocomplexation by a Lewis acid organometallic fragment on a bidentate phosphine could greatly affect the basicity of the pendant phosphorus atom.

In conclusion, addition of Lewis bases to μ-phosphido μ-hydrido dibridged complexes (**1, 2, 3**) is regiospecific on the metal M′ and leads to a cis arrangement with respect to the phosphido bridge—except for the bulky PPh_2Me. The free phosphorus of the "open" structure $Cp_2Ta(H)_2(\mu\text{-}PMe_2)M'(CO)_4$(dmpe) (M′ = Mo, W) (**2c, 3c**) binds the metal carbonyl fragment $[Cr(CO)_5]$ to form new linear trimetallic complexes.

REFERENCES

1. Barré, C., Boudot, P., Kubicki, M. M. and Moïse, C., *Inorg. Chem.*, 1995, **34,** 284.
2. Barré, C., Kubicki, M. M., Leblanc, J. C. and Moïse, C., *Inorg. Chem.*, 1990, **29,** 5244.

3. Vaughan, G. A., Hillhouse, G. L. and Rheingold, A. L., *Organometallics*, 1989, **8,** 1760.
4. Kubicki, M. M., Kergoat, R., Cariou, M., Guerchais, J. E. and L'Haridon, P., *J. Organomet. Chem.*, 1987, **322,** 357.
5. Baker, R. T., Tulip, T. H. and Wreford, S. S., *Inorg. Chem.*, 1985, **24,** 1379.
6. Targos, T. S., Rosen, R. P., Whittle, R. R. and Geoffroy, G. L., *Inorg. Chem.*, 1985, **24,** 1375.
7. Wade, S. R., Wallbridge, M. G. H. and Willey, J. R., *J. Chem. Soc. Dalton Trans.*, 1983, 2555.
8. Baker, R. T., Whitney, J. F. and Wreford, S. S., *Organometallics*, 1983, **2,** 1049.
9. Oudet, P., Kubicki, M. M. and Moïse, C., *Organometallics*, 1994, **13,** 4278.
10. Boni, G., Sauvageot, P. and Moïse, C., *J. Organomet. Chem.*, 1995, **489,** C32.
11. Boni, G., Sauvageot, P., Marpeaux, E. and Moïse, C., *Organometallics*, 1995, **14,** 5652.
12. Oudet, P., Perrey, D., Bonnet, G., Moïse, C. and Kubicki, M. M., *Inorg. Chim. Acta*, 1995, **237,** 79.
13. Bonnet, G., Lavastre, O., Boni, G., Leblanc, J. C. and Moïse, C., *C. R. Acad. Sci. Paris*, Série II, 1994, **319,** 1293.
14. Lavastre, O., Bonnet, G., Boni, G., Kubicki, M. M. and Moïse, C., *J. Organomet. Chem.*, In press.
15. Lavastre, O., Bonnet, G., Leblanc, J. C. and Moïse, C., *Polyhedron*, 1995, **14,** 307.
16. Boni, G., Kubicki, M. M. and Moïse, C., *Bull. Soc. Chim. Fr.*, 1994, **131,** 895.
17. Challet, S., Lavastre, O., Moïse, C., Leblanc, J. C. and Nuber, B., *New J. Chem.*, 1994, **18,** 1155.
18. Bonnet, G., Kubicki, M. M., Moïse, C., Lazzaroni, R., Salvadori, P. and Vitulli, G., *Organometallics*, 1992, **11,** 964.
19. Bonnet, G., Lavastre, O., Leblanc, J. C. and Moïse, C., *New J. Chem.*, 1988, **12,** 551.
20. Nikonov, G. I., Lemenovskii, D. A. and Lorberth, J., *Organometallics*, 1994, **13,** 3127.
21. Nikonov, G. I., Kuzmina, L. G., Mountford, P. and Lemenovskii, D. A., *Organometallics*, 1995, **14,** 3588.
22. Strohmeier, W. and Mueller, F. J., *Chem. Ber.*, 1969, **102,** 3608.
23. Brown, T. L., *Inorg. Chem.*, 1992, **31,** 1286.
24. Tolman, C. A., *Chem. Rev.*, 1977, **77,** 313.
25. Kubicki, M. M., Le Gall, J. F., Kergoat, R. and Gomes De Lima, L. C., *Can. J. Chem.*, 1987, **65,** 1292.
26. Jameson, C. J. and Gutowsky, H. S., *J. Chem. Phys.*, 1964, **40,** 1914.
27. Carty, A. J., MacLaughlin, S. A. and Nucciarone, D., *Methods in Stereochemical Analysis*, ed. A. P. Marchand. VCH, Deerfield Beach, FL, 1987, p. 559.
28. Sowa, J. R. and Angelici, R. J., *Inorg. Chem.*, 1991, **30,** 3534.
29. Rottink, M. K. and Angelici, R. J., *Inorg. Chem.*, 1993, **32,** 2421.

Pergamon

PII: S0277-5387(97)00326-4

Polyhedron Vol. 17, No. 2–3, pp. 267–274, 1998
© 1997 Elsevier Science Ltd
All rights reserved. Printed in Great Britain
0277-5387/98 $19.00+0.00

A ^{1}H and ^{195}Pt NMR study of the protonation mediated interconversion of mono- (*S*) *versus* bidentate (*S,O*) co-ordination of Pt(II) by *N*-acyl-*N'*,*N'*-dialkylthioureas

Klaus R. Koch*, Tarron Grimmbacher and Cheryl Sacht

Department of Chemistry, University of Cape Town, P Bag Rondebosch, Cape Town 7700, South Africa

(Received 27 February 1997; accepted 21 July 1997)

Abstract—Treatment of *cis*-[Pt(L-*S,O*)$_2$] in $CDCl_3$ solution, directly in an NMR tube with concentrated mineral acid HX and/or HY (X = Cl^-, Y = Br^-), leads to the reversible protonation of the co-ordinated ligand of these complexes across the aqueous-organic phase boundary; these processes have been followed by means of ^{195}Pt and ^{1}H NMR. Treatment with HCl yields a mixture of *cis*- and *trans*-[Pt(HL-*S*)$_2$Cl$_2$] species, in addition to the partially-ring-opened [Pt(L^n-*S,O*)(HL^n-*S*)Cl] complex in solution, the *cis*-[Pt(HL-*S*)$_2$Cl$_2$] complex predominating in solution at steady-state. These species are rapidly and reversibly converted back to only the *cis*-[Pt(L-*S,O*)$_2$] complex on washing of the $CDCl_3$ solution with aqueous ammonia. Similar observations pertain to protonation by HBr, yielding the corresponding bromo complexes; treatment of *cis*-[Pt(L-*S,O*)$_2$] in $CDCl_3$ with a mixture of HCl and HBr, leads to the formation of mixed-halide species of *cis*- and *trans*-[Pt(HL-*S*)$_2$XY] in addition to the [Pt(HL-*S*)$_2$X$_2$] and [Pt(HL-*S*)$_2$Y$_2$] as well as the partially-ring-opened [Pt(L^n-*S,O*)(HL^n-*S*)X/Y] complexes in solution, which revert to *cis*-[Pt(L-*S,O*)$_2$] on treatment with aqueous base. These observations clearly have important consequences in the use of *N*-acyl-*N'N'*-dialkylthioureas for the solvent extraction of the platinum metals. © 1997 Elsevier Science Ltd

Keywords: *N*-benzoyl-*N'*,*N'*-dialkylthiourea; platinum(II) complexes; ^{195}Pt NMR; isomerism; protonation.

The ligands *N*-acyl-*N'*-alkyl- (**H$_2$L**) and *N*-acyl-*N'*,*N'*-dialkylthioureas (**HL**) have attracted attention in view of their selective co-ordination particularly of the 'softer' 2nd and 3rd row transition metals. In this context the pioneering work of Beyer *et al.* should be mentioned, in view of the use of *N*-acylthiourea ligands for the solvent extraction of transition metal ions [1]. The selective co-ordination of these ligands to the platinum group metals (PGMs) is particularly noteworthy as this allows for the efficient extraction and pre-concentration of the PGMs [2], as well as the analytical separation of traces of these metals by chromatographic means, notably HPTLC [3].

We have become interested in targeted ligand design incorporating the *N*-acylthiourea functional group as central motif, exploiting the ease of synthesis of these types of molecules to prepare a variety of new ligands with potential applications in the extractive metallurgy of the platinum metals. Consequently we have studied the deceptively simple co-ordination of ligands of type (**H$_2$L**) and (**HL**) to Pt(II), finding the binding of **H$_2$L** to be controlled by an intramolecular H-bond, resulting in essentially monodentate co-ordination of the ligand through the S-atom, yielding mixtures of *cis*- and *trans*-[Pt(H$_2$L-*S*)$_2$Cl$_2$] complexes [4]. By contrast, ligands of type **HL** react with $PtCl_4^{2-}$ in a neutral aqueous solution to form predominantly *cis*-[Pt(L-*S,O*)$_2$] complexes [5]. Recent studies by Sadler *et al.* on the co-ordination of L-methionine to $PtCl_4^{2-}$, have shown an interesting example of the reversible interconversion of bidentate *N,S* to monodentate *S* co-ordination of L-methionine to Pt(II), depending on the solution pH [6]. This work, as well as the negative effects of the presence of mineral acids which we observed on the attempted chromatographic separation of the platinum metals using *N*-acyl-*N'*,*N'*-dialkylthioureas as selective ligands, have prompted us to undertake an investigation of the effect of protonation of the *S,O*-bound *N*-benzoyl-*N'*,*N'*-dial-

* Author to whom correspondence should be addressed.

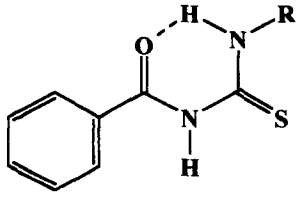

H_2L

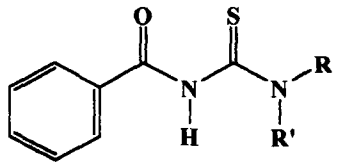

HL

kylthiourea ligand in complexes such as *cis*-[Pt(L-*S*,*O*)$_2$], with a view to establishing the nature of the resulting species in solution.

We show here that protonation of the co-ordinated ligand in *cis*-[Pt(L-*S*,*O*)$_2$] complexes in chloroform solution, with HCl or HBr, leads to the reversible opening of the 6-membered *S*-*O* chelate ring, with concomitant co-ordination of the Cl^- and/or Br^- ion to the Pt(II) atom, resulting in the *O*-donor atom of the **HL** ligand being pendant. In this contribution, we shall focus on the platinum complexes with the ligands *N*-benzoyl-*N'*,*N'*-di(*n*-butyl)thiourea (**HL**^{1}), *N*-(4Br-phenyl)-*N'*,*N'*-di(*n*-butyl)thiourea (**HL**^{2}), and *N*-(4NO_2-phenyl)-*N'*,*N'*-di(*n*-butyl)thiourea (**HL**^{3}) only.

EXPERIMENTAL

Preparation of ligands and cis-[Pt(L^1-*S*,*O*)$_2$] *complexes*

All ligands (**HL**^{1})–(**HL**^{3}) were prepared as previously described [5], and were satisfactorily characterized by means of C, H and N elemental analysis, and mass spectroscopy, as well as ^{1}H and ^{13}C NMR spectroscopy. The neutral complexes *cis*-[Pt(L^1-*S*,*O*)$_2$] (**I**), *cis*-[Pt(L^2-*S*,*O*)$_2$] (**II**) and *cis*-[Pt(L^3-*S*,*O*)$_2$] (**III**) were also prepared and characterized as previously described [5,7].

Preparation of bis(N-benzoyl-N'-propylthiourea)dichloroplatinum(II)

This complex was prepared and fully characterized as described previously, $C_{22}H_{28}Cl_2N_4O_2PtS_2$ requires C, 37.19; H, 3.97; N, 7.88%; Found C, 37.16; H, 4.0; N, 7.90% [4].

Preparation of bis(N-benzoyl-N'-propylthiourea)dibromoplatinum(II)

This complex was prepared by the same procedure as the corresponding *dichloro* complex, except that the $PtCl_4^{2-}$ was converted *in situ* to the corresponding $PtBr_4^{2-}$ by treatment with excess NaBr and 0.1 M HBr, prior to ligand addition. The complex was recrystallized from a chloroform–ethanol mixture, resulting in orange crystals in *ca* 75% yield, which are clearly a mixture of the *cis*- and *trans*-[Pt(H_2L-*S*)$_2$$Br_2$] complexes, as shown by the two distinct melting points at 162–164 and 174–178°C. (This isomerization is confirmed by the NMR spectra shown in Table 1 below.) $C_{22}H_{28}Br_2N_4O_2PtS_2$ requires C, 33.05; H, 3.53; N, 7.01%; Found C, 33.3; H, 3.53; N, 6.95%.

NMR spectroscopy

^{1}H and ^{195}Pt NMR spectra were recorded in 5 mm tubes in $CDCl_3$ solution, using a Varian UNITY-400 spectrometer operating at 400 and 85.8 MHz respectively (^{1}H, spectra at 25°C and ^{195}Pt at 30°C). The ^{195}Pt NMR spectra were recorded using 100 kHz spectral widths with 20 μs pulses ($\sim$90°) with 0.5 s pulse delay, since the T_1 of the ^{195}Pt nucleus was $<$0.1 s; between 2048 and 16,000 pulses gave excellent spectra for typical concentrations of the complex between 40–80 mg ml^{-1}. All ^{195}Pt shifts are quoted relative to external H_2PtCl_6 (500 mg ml^{-1} in 30% v/v D_2O/1 M HCl) at 30°C and are estimated to be accurate to $\pm$4 ppm.

Protonation experiments

Aliquots of 100 μL concentrated mineral acid (HX; X = Cl^-, Br^-) were directly added to the NMR tube containing 0.6 mL pale yellow solutions of *cis*-[Pt(L''-*S*,*O*)$_2$] complex in $CDCl_3$. After vigorous shaking the phases were allowed to separate, which was complete after *ca* 5 min; where necessary, the distinctly darker yellow/orange organic phase was filtered through microfibre glass-wool, resulting in a clear solution, prior to NMR spectroscopy. After spectral acquisition, the mineral acid was removed, the $CDCl_3$ solution washed with water and/or ammonia solution, filtered and followed by re-acquisition of the spectrum.

RESULTS AND DISCUSSION

The ^{195}Pt spectra of the uncharged complexes *cis*-[Pt(L''-*S*,*O*)$_2$], **I**–**III** in $CDCl_3$ solution, show only a single, relatively sharp, resonance at $\delta(^{195}Pt) = -2727$, -2719 and -2688 ppm respectively. The corresponding ^{1}H NMR spectra are all

Table 1. ^{195}Pt NMR assignments of complex species in $CDCl_3$ at 30°C. All shifts are estimated correct to ±4 ppm

Complexes	^{195}Pt chemical shift/ppm								
	cis-[Pt(L-*S*,*O*)$_2$]	*cis*-[Pt(L-*S*,*O*)(HL-*S*)X]		*cis*[Pt(L-*S*)$_2$X$_2$/Y$_2$]			*trans*[Pt(L-*S*)$_2$X$_2$/Y$_2$]		
		X = Cl	X = Br	X = Cl	XY[a]	Y = Br	X = Cl	XY[a]	Y = Br
I	−2727	−2968	n.o.[b]	−3218	—	−3630	−3034	—	−3609
II	−2719	−2959	−3104	−3212	−3407	−3624	−3029	−3311	−3606
III	−2688	−2938	−3085	−3213	−3413	−3626	−3029	−3315	−3605
cis/*trans*-[Pt(H$_2$L-*S*)$_2$Cl$_2$][c]	—	—	—	−3219	—	—	−3040	—	—
cis/*trans*-[Pt(H$_2$L-*S*)$_2$Br$_2$][d]	—	—	—	—	—	−3697	—	—	−3678

[a] Assignment of *cis* and *trans* shifts based on the observation that *cis* isomer resonances are *usually* upfield w.r.t. *trans*.
[b] Not observed.
[c] Shifts of authentic *cis*- and *trans*-bis(*N*-benzoyl-*N'*-propylthioureato)dichloroplatinum(II); ref. 4.
[d] Shifts of an authentic mixture of *cis*- and *trans*-bis(*N*-benzoyl-*N'*-propylthioureato)dibromoplatinum(II)

consistent with only a single unprotonated complex species in solution, as confirmed by the *absence* of the characteristic amido N–H resonance in the 10–12 ppm range; the full, detailed ^{1}H assignments are trivial and will not be given here.

Addition of 100 μL *conc.* HCl directly to the NMR tube containing **I** in $CDCl_3$ as described in the experimental section, yields a ^{1}H spectrum (acquired within 10 min of adding the HCl) showing the presence of at least three species, characterized by N–H resonances at 10.79 (6.6%), 11.14 (83.7%) and 11.27 (9.6%) ppm (relative intensities given in parentheses). These N–H resonances clearly indicate the protonation of the coordinated ligands by some HCl partitioned into the $CDCl_3$ phase. The corresponding ^{195}Pt spectrum of this solution (obtained within an acquisition time of *ca* 3 h) consists of only two ^{195}Pt resonances at $\delta = -3034$ (rel. int. 22%) and −3218 ppm (78%). After 4 h, the corresponding ^{1}H spectrum also shows only two resonances at 10.79 (10%) and 11.14 (90%) ppm, while the ^{195}Pt spectrum of this solution remains essentially unchanged. Thus the transient appearance of the ^{1}H resonance at 11.27 ppm, suggests a time dependent process in solution, which appears only to reach a steady-state after several hours.

The time dependence of these processes are well illustrated by the ^{1}H NMR spectra acquired as a function of time as a solution of **I** in $CDCl_3$ which has been treated with 50% *diluted* HCl (1+1, *conc.* HCl+water, v/v) as shown in Fig. 1(a). These spectra show the initial appearance of only two N–H resonances at 11.27 and 11.14 ppm, both of which slowly grow in intensity at differing relative rates over a 5 h period. Some 3.5 h after the addition of the 50% HCl, a new peak at 10.79 ppm appears in the spectrum, growing in intensity. Removal of the 50% HCl after *ca* 5 h and substitution by 100 μL *conc.* HCl, followed by spectral acquisition in the same way as before, leads to ^{1}H spectra as illustrated in Fig. 1(b). Evidently the resonance at 11.27 ppm disappears relatively rapidly, while the peaks at 11.14 and 10.79 ppm continue to grow in intensity reaching steady-state after *ca* 10 h; the ^{1}H spectral acquisition was arbitrarily terminated after *ca* 11 h. The ^{195}Pt NMR spectrum of this solution acquired immediately after this time shows only two resonances at $\delta(^{195}Pt) = -3034$ and −3218 ppm corresponding exactly to the case described above, in which *conc.* HCl was used from the start. After *ca* 24 h re-acquisition of both ^{1}H and ^{195}Pt NMR spectra confirm that only these two complex species exist in solution at steady-state.

In general, the appearance of the ^{195}Pt and ^{1}H NMR spectra for **II** and **III** obtained after addition of the *conc.* HCl show similar trends as illustrated for **I**, although the actual time-resonance intensity dependencies are somewhat different for each case. Significantly by sampling the ^{195}Pt NMR spectrum at the appropriate times after treatment with *conc.* HCl, it becomes possible to detect at least *four* species in solution, as illustrated for the protonation of **III**, for which we obtain a ^{195}Pt spectrum consisting of four peaks at −2688 (9%), −2938 (53%), −3029 (3%) and −3213 (33%) ppm, 4 h after addition of HCl to the NMR tube. After 24 h standing, followed by re-acquisition of the ^{195}Pt spectrum for the same solution the resulting spectrum shows resonances only at −2938 (30%), −3029 (2%) and −3213 (68%) ppm, the peak at −2688 ppm, corresponding to the starting *cis*-[Pt(L^{3}-*S*,*O*)$_2$] having disappeared; after 48 h the ^{195}Pt spectrum at steady state shows the same peaks at −2938 (17%), −3029 (9%) and −3213 (74%) ppm respectively with different relative intensities, Fig. 2. Evidently the species with $\delta(^{195}Pt) = -2938$ ppm is slowly converting into the species at −3029 and −3213 ppm. Similar observations can be made for the complexes **I** and **II**, where the ^{195}Pt resonance at

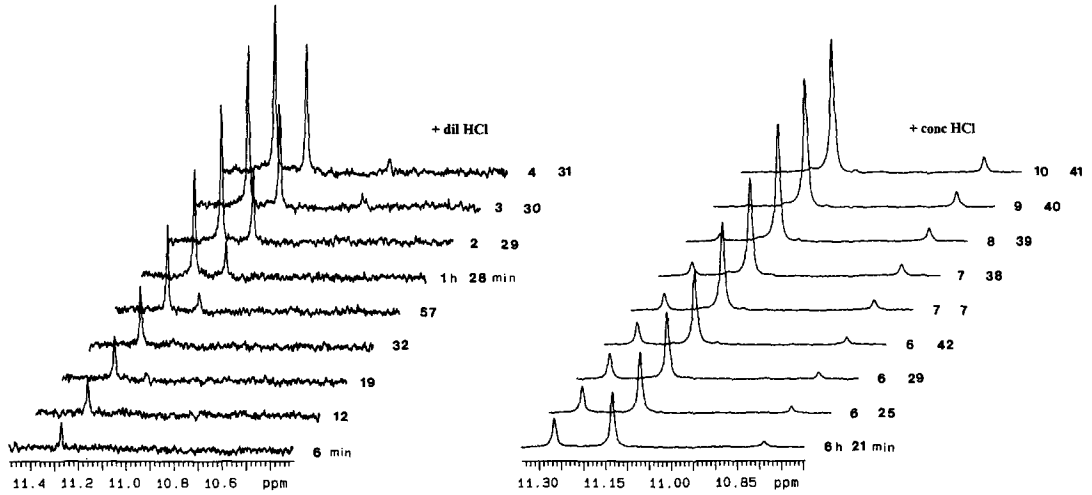

Fig. 1. (a) Partial ^{1}H NMR spectra of *cis*-[Pt(L^1-*S*,*O*)$_2$] in $CDCl_3$ acquired as a function of time after addition of dilute HCl (50% v/v *conc.* HCl+H_2O (acid addition at $t = 0$ min)). (b) solution (a) to which *conc.* HCl has been added after *ca* 6 h 4 min after removal of dilute HCl.

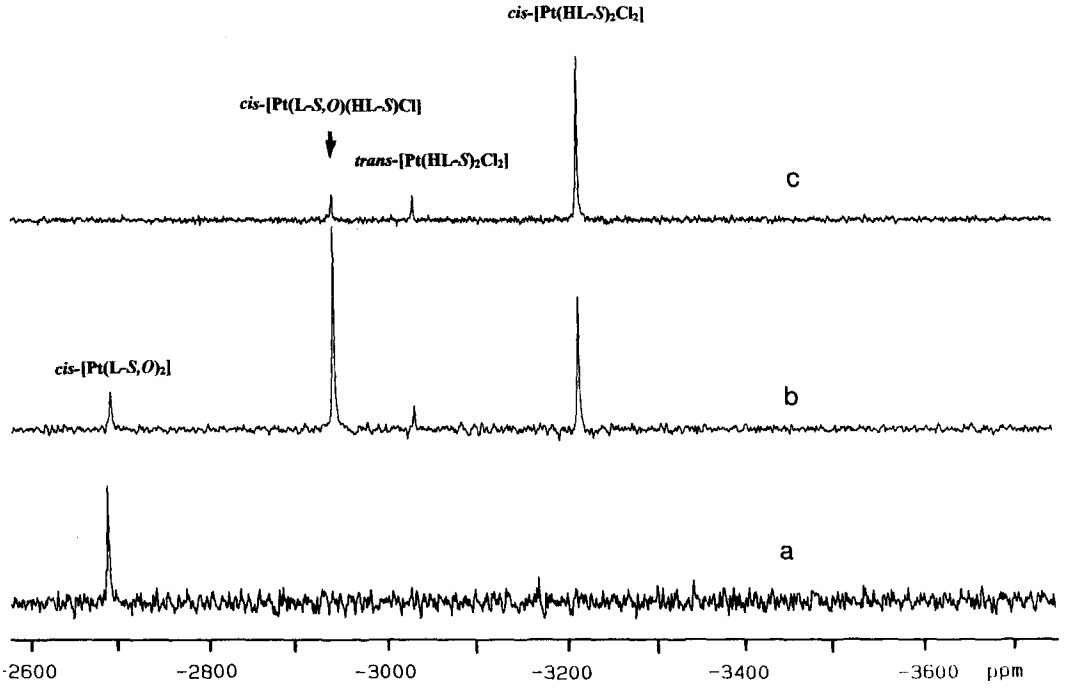

Fig. 2. ^{195}Pt NMR spectrum of (a) *cis*-[Pt(L^3-*S*,*O*)$_2$] in $CDCl_3$ after an acquisition time *ca* 30 min. (b) solution (a) to which *conc.* HCl has been added after *ca* 4 h acquisition time; (c) solution (b) after 48 h standing at room temperature followed by re-acquisition.

−2938 ppm for **III**, corresponds to similar peaks at −2968 and −2959 ppm for complexes **I** and **II**, respectively.

Removal of the excess mineral acid directly from the NMR tube containing the $CDCl_3$ solutions of complexes **I, II** and **III**, followed by *in situ* washing of the $CDCl_3$ phase with a small volume of 5 M ammonia, results in ^{195}Pt and ^{1}H spectra which are identical to those of the pure uncharged *cis*-[Pt(L^n-*S*,*O*)$_2$] complexes, there being no spectroscopic evidence for any other complex species in solution. It is significant to note that the ^{1}H spectra recorded immediately after washing with the ammonia solution are indistinguishable from those of the pure *cis*-[Pt(L^n-

$S,O)_2$] complexes, *within the time needed to record the* ^{1}H *spectrum* (*ca* 10 min). Evidently the effect of deprotonation of the various complex species in solution is qualitatively much more rapidly reversible, relative to the much slower changes induced by protonation with concentrated or diluted HCl.

Consideration of the ^{195}Pt and ^{1}H NMR spectra obtained by addition of HCl to $CDCl_3$ solutions of **I–III,** together with the well known sensitivity of the ^{195}Pt chemical shifts to changes in the co-ordination sphere of the metal [8], suggest that protonation of the bound ligand in the presence of co-ordinating Cl^- anions, leads to ring opening of the *S,O*-chelate such that the *N*-acyl-*N'N'*-dialkylthiourea ligand remains bound to Pt through the S-atom only. The O-atom of the ligand is thus displaced from the co-ordination sphere of the Pt(II) atom, the amido moiety of the S-atom bound ligand becoming pendant. Convincing support for this assignment is obtained from the ^{195}Pt spectrum of an *authentic* mixture of *cis-* and *trans*-bis(*N*-benzoyl-*N'*-propylthioureato)dichloroplatinum(II) in $CDCl_3$, which shows only ^{195}Pt resonances at -3219 and -3040 ppm respectively. The resonance at -3219 ppm has been shown to be due to the *cis*-bis(*N*-benzoyl-*N'*-propylthioureato)dichloroplatinum(II) complex, which has been characterized by means of x-ray crystallography [4]. Hence in the case of the protonation of **I–III** with HCl, we assign the resonances at *ca* -3220 ppm to the *cis*-[Pt(HL^n-*S*)$_2$Cl$_2$] complexes, while the smaller peaks which develop over time at *ca* -3030 ppm correspond to the *trans* isomers, which result from the isomerization of the *cis* species. Moreover, these assignments are consistent with the generally observed trend that, for complexes of type [PtA_2X_2], the *cis* isomer is usually more shielded by typically 200–500 ppm for X = Cl^-, depending on the nature of the donor atom of the ligand A [8]. Our assignment of the ^{195}Pt peak at *ca* -3029 ppm (corresponding to the 10.79 ppm ^{1}H peak, which is ultimately present in all concentrated acid treated solutions of **I–III**), to the *trans*-[Pt(HL^n-*S*)$_2$Cl$_2$] isomer, is also consistent with the work of Castan *et al.* who reported similar ^{195}Pt shift trends for simple *cis*/*trans*-[PtL_2X_2] complexes in DMSO-d_6 solution (where L = unsubstituted monodentate, S-atom bound thiourea and X = Cl^- and Br^-) [9].

Treatment of solutions of **I–III** in $CDCl_3$ with *conc.* HBr gives rise to quite different ^{195}Pt spectra, as may be anticipated by replacement of the co-ordinated Cl^- ion by a Br^- ion. This is illustrated for the case of **I,** for which a ^{195}Pt NMR spectrum consisting of only two resonances at -3609 (29%) and -3630 (71%) ppm, is obtained at steady-state, after treatment with HBr. The corresponding ^{1}H spectrum shows only two species with N–H resonances at 10.48 (28%) and 10.72 (72%) ppm respectively. Re-acquisition of the ^{195}Pt NMR spectrum after keeping the solution at room temperature for 24 h results in an identical spectrum; a careful search for any other ^{195}Pt resonances both ± 2500 ppm upfield and downfield of these shifts shows no additional resonances. Very similar ^{195}Pt spectra are obtained for complexes **II** and **III,** for which the corresponding ^{195}Pt peaks occur at -3606, -3624, and -3605, -3626 ppm respectively. These resonances are thus assigned to the *trans*-[Pt(HL^n-*S*)$_2$Br$_2$] and *cis*-[Pt(HL^n-*S*)$_2$Br$_2$] complexes respectively, where the much smaller shift differences between the bromo as compared with the chloro complexes is consistent with the generally observed trends for related complexes [8]. Final confirmation of these assignments is obtained from the comparison of the chemical shifts of an authentic mixture of *trans-* and *cis*-[Pt(H_2L-*S*)$_2$Br$_2$] (H_2L = *N*-benzoyl-*N'*-propylthiourea) in $CDCl_3$. The ^{195}Pt NMR spectrum of this mixture shows resonances at -3678 and -3697 ppm (Table 1), in which the resonance at a slightly higher field is assigned to the *cis* complex; the corresponding amido N–H resonances for *cis*-[Pt(H_2L-*S*)$_2$Br$_2$] appear at 11.49 and that for the *trans* complex at 11.31 ppm in the ^{1}H NMR spectrum respectively [10].

Removal of the excess HBr from the NMR tube containing complexes **I–III,** followed by washing of the $CDCl_3$ solution with 5 M aqueous ammonia solution, results again in single resonance ^{195}Pt NMR spectra, identical to those of the pure complexes **I–III.** These observations convincingly demonstrate the reversible, *S,O*-chelate ring opening on protonation of the amido-N atom of the co-ordinated ligand, with concomitant halide ion co-ordination to Pt(II).

Very interesting ^{195}Pt spectra are obtained when solutions of *cis*-[Pt(L^n-*S,O*)$_2$] are treated with mixtures of *conc.* HCl and HBr. As may be reasonably expected, if the above assignments are correct, it should be possible to observe in solution under appropriate conditions, the mixed-halide complexes of type [Pt(HL^n-*S*)$_2$XY], in addition to species such as [Pt(HL^n-*S*)$_2$X$_2$] and [Pt(HL^n-*S*)$_2$Y$_2$] (where X = Cl^-; Y = Br^-). This expectation is confirmed as shown in Fig. 3, for the complex **II** in $CDCl_3$ treated with 100 μL of a mixture of *conc.* HCl + HBr (0.7 + 0.3 v/v); the resulting ^{195}Pt spectrum consists of nine well defined resonances in the -2700 to -3700 ppm range. Apart from the residual peak at -2719 ppm, which is clearly due to a small amount of unchanged **II,** six of the remaining eight resonances may consistently be assigned to the four possible mononuclear, *cis-* and *trans*-dichloro- and dibromo-complexes, together with the two possible *cis-* and *trans*-[Pt(HL^2-*S*)$_2$XY] mixed-halide complexes (Table 1). The relative proportions of HCl to HBr in the acid mixture used in these experiments, determine the distribution of complex species as obtained in the ^{195}Pt spectra, so that if HBr is present in excess, the resulting spectrum resembles that obtained with pure HBr only. This is understandable in terms of the greater binding affinity of the Br^- ion to the Pt(II) atom with respect to that of the Cl^- anion. In general the ^{1}H NMR spectra are consistent with these assignments, although these become rather complicated due to extensive peak

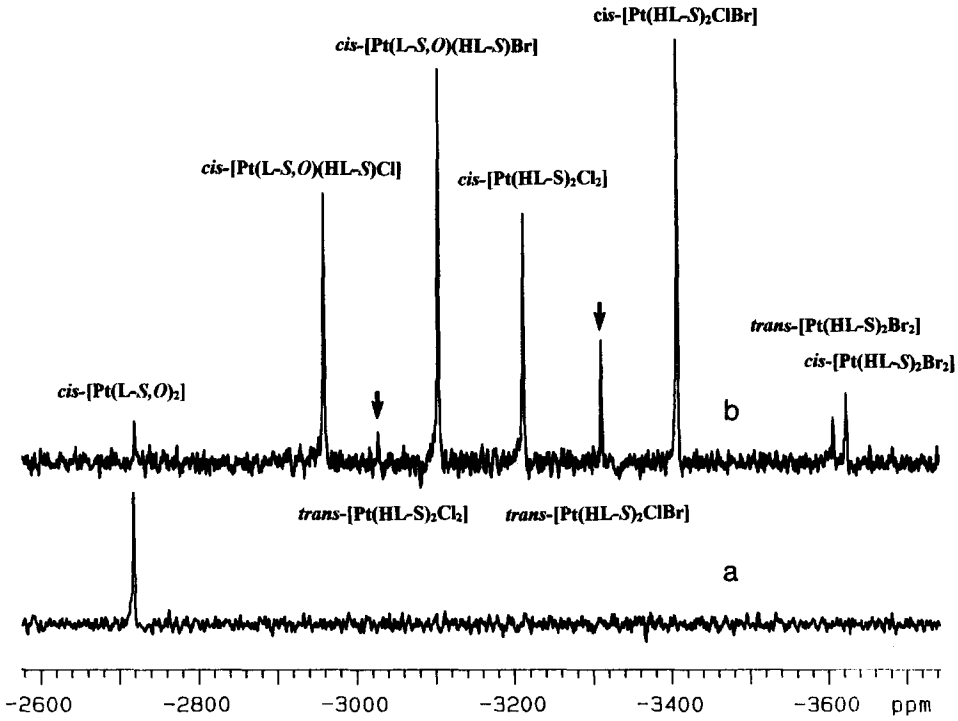

Fig. 3. ^{195}Pt NMR spectrum of (a) a fresh solution of *cis*-[Pt(L^2-*S*,*O*)$_2$] in $CDCl_3$; (b) after addition of a mixture of *conc* HCl + HBr (see text) followed by a 12 h spectral acquisition time.

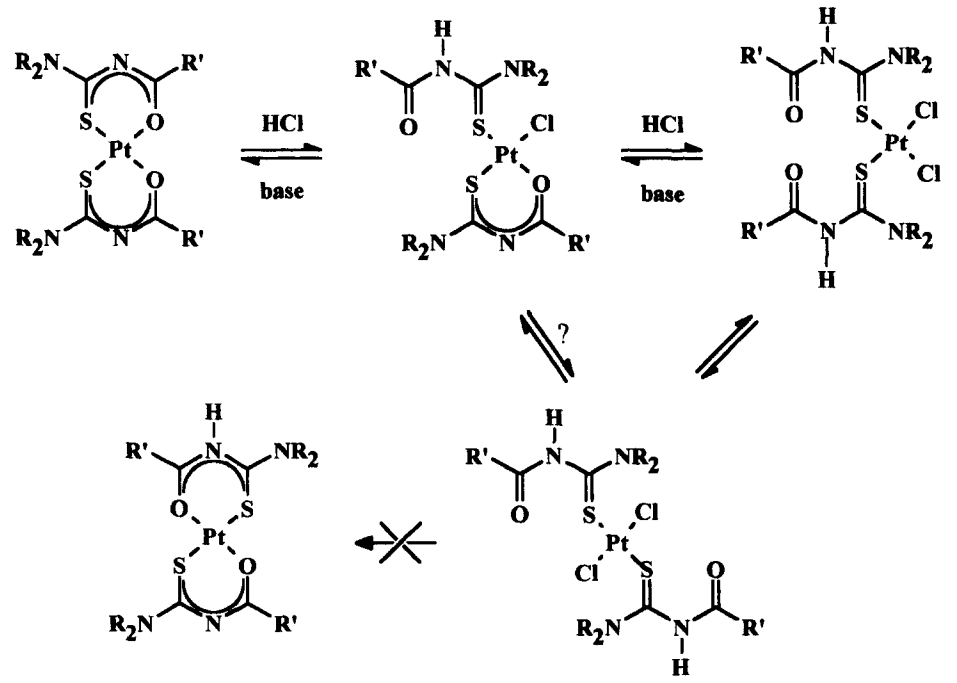

Fig. 4. Schematic representation of the effects of addition of *conc.* HCl to solutions of *cis*-[Pt(L^n-*S*,*O*)$_2$] complexes (n = 1-3) in $CDCl_3$.

overlap. Remarkably, on washing the mixed-acid treated solution of **II** in $CDCl_3$ with 5 M ammonia solution, one again obtains only the simple single line ^{195}Pt spectrum (−2719 ppm) of the parent *cis*-[Pt(L^2-*S*,*O*)$_2$] complex. Similar spectra are obtained for complexes **I** and **III**.

Finally, the two ^{195}Pt resonances at −2959 and −3104 ppm in the spectrum of **II** treated with the mixture of HCl and HBr, shown in Fig. 3(b) are assigned to the partially-ring-opened complex *cis*-[Pt(L^2-*S*,*O*)[HL^2-*S*)Cl] and *cis*-[Pt(L^2-*S*,*O*)(HL^2-*S*)Br] respectively. The ^{195}Pt peak at −2959 ppm (assigned to *cis*-[Pt(L^2-*S*,*O*)(HL^2-*S*)Cl]) corresponds to similar ^{195}Pt resonances in the range −2938 to −2968 ppm, which appear in the spectra of $CDCl_3$ solutions on treatment of **I–III** with only HCl, as described above. In the case of the HCl treated solutions of **I–III**, these ^{195}Pt resonances show a more marked time dependence, and correspond to the species giving rise to a peak at *ca* 11.27 ppm in the ^{1}H spectrum shortly after the addition of HCl to the fresh solutions of **I–III**, (Fig. 1(a)). In any event, the ^{195}Pt resonances in the −2938 to −2968 ppm range are assigned to the partially-ring-opened *cis*-[Pt(L″-*S*,*O*)(HL″-*S*)Cl] complexes. Evidently these *cis*-[Pt(L″-*S*,*O*)(HL″-*S*)Cl] complexes are relatively reactive, since in the presence of excess *conc.* HCl, this species eventually disappears fairly rapidly from the spectrum, it clearly becoming protonated to yield the *cis*-[Pt(HL″-*S*)$_2$Cl$_2$] complex, which in turn, isomerizes slowly to the *trans* isomer. Table 1 summarizes the full ^{195}Pt assignments for all complexes in this study.

There are two interesting aspects of the chemistry of this system, (i) the apparently rapid chelate ring closure of the *S*,*O*-chelate ring following de-protonation of the *S*-atom co-ordinated ligand and (ii) the fact that no evidence for the formation of a *trans*-[Pt(L″-*S*,*O*)$_2$] complex could be found despite several attempts to do so.

In respect to the first-mentioned observation, it is clear that de-protonation of a pendant *S*-atom co-ordinated ligand results in the carbonyl donor atom of the amido moiety becoming substantially more nucleophilic toward the Pt(II) atom, presumably as a result of the conversion of the carbonyl to a more highly charged O^- tautomeric form. The more nucleophilic pendant O^- donor atom of the co-ordinated ligand is likely to be held in a sterically favourable position within the co-ordination sphere of the Pt(II) atom, resulting in rapid closure of the *S*,*O*-chelate ring followed by concomitant expulsion of the halide ion from the co-ordination sphere of the metal ion. We envisage a concerted process taking place *via* a 5-co-ordinate trigonal–bipyramidal transition state, consistent with the generally observed associative nature of substitution reactions in square planar d^8 metals ions. As regards the second point, and particularly in view of our recent characterization of the first example of *trans*-bis(*N*,*N*-di-*n*-butyl-*N*′-naphthoylthioureato)platinum(II) [11], it is indeed interesting and somewhat surprising that no *trans*-[Pt(L″-*S*,*O*)$_2$] complex appears to be formed for the *N*-benzoyl substituted ligands studied in this work. This despite the demonstrated existence of *trans*-[Pt(HL″-*S*)$_2$XY], *trans*-[Pt(HL″-*S*)$_2$X$_2$] and *trans*-[Pt(HL″-*S*)$_2$Y$_2$] complexes (X = Cl^-; Y = Br^-) in solution prior to washing the $CDCl_3$ solution with ammonia; it is not unreasonable to expect ring closure to yield at least some *trans*-[Pt(L″-*S*,*O*)$_2$] complex. Evidently de-protonation of the ligand results in any *trans S*-co-ordinated species undergoing rapid isomerism during, or prior to, the *S*,*O*-chelate ring closure within the time scale of the NMR spectroscopic experiment, so yielding exclusively the thermodynamically favoured *cis*-[Pt(L″-*S*,*O*)$_2$] complexes. It is tempting to speculate that for the case of *trans*-bis(*N*,*N*-di-*n*-butyl-*N*′-naphthoylthioureato)platinum(II) [11], the steric demands of the *N*-naphthoyl moiety may play a role, particularly in view of a postulated 5-co-ordinate transition state, in which steric crowding may well lead to some *trans*-[Pt(L-*S*,*O*)$_2$] being formed. Finally the possibility of a photochemically induced *cis*/*trans* isomerism of the [Pt(L-*S*,*O*)$_2$] species cannot be ruled out at this stage, in view of experimental evidence for such isomerization in related systems [12]. Studies aimed at elucidating these questions are underway.

In conclusion, it is clear from this multinuclear NMR study, that treatment of complexes **I–III** in $CDCl_3$ with aqueous HCl results in reversible protonation with concomitant halide ion co-ordination across the phase boundary, the extent of which, and the rates of formation of the various species in the $CDCl_3$ solution, depends on the *effective* HCl concentration in the $CDCl_3$ phase. In view of the two phase nature of these protonation experiments, as well as the variable ^{1}H and ^{195}Pt spectral acquisition times, it is not meaningful to quantitatively estimate relative rates for the observed species formation on protonation; nevertheless our study shows qualitatively that the relative rates of protonation induced halide ion co-ordination of complexes **I–III** in $CDCl_3$ are substantially slower than the de-protonation induced *S*,*O*-chelate formation in these Pt(II) complexes. Moreover, subsequent washing of previously acid treated solutions of **I–III** with 5 M ammonia, results in the formation of exclusively the *cis*-[Pt(L″-*S*,*O*)$_2$] complexes. This implies that relatively rapid isomerization of any *trans*-[Pt(HL″-*S*)$_2$Cl$_2$] must occur on de-protonation and/or ring closure. These observations are summarized in a diagram for the addition of *conc.* HCl to solutions of *cis*-[Pt(L″-*S*,*O*)$_2$] in Fig. 4.

Such processes clearly have profound synthetic and mechanistic implications in the practical utilization of these ligands for the potential solvent extraction [2], and/or chromatographic separations [3] of the PGMs.

Acknowledgements—Financial assistance from the University of Cape Town and the Foundation for Research Development (fellowship to C.S. and bursary to T.G.) is

gratefully acknowledged. We thank Johnson Matthey for the loan of platinum salts.

REFERENCES

1. Mühl, P., Gloe, K., Dietze, F., Hoyer, E. and Beyer, L., *Z. Chem.*, 1986, **2**(1), 81.
2. Vest, P., Schuster, M. and König, K.-H., *Fresenius' Z. Anal. Chem.*, 1989, **335,** 759.
3. Schuster, M., *Fresenius' Z. Anal. Chem.*, 1992, **342,** 791.
4. Bourne, S. and Koch, K. R., *J. Chem. Soc., Dalton Trans.*, 1993, 2071.
5. Irving, A., Koch, K. R. and Matoetoe, M., *Inorg. Chim. Acta*, 1993, **206,** 193.
6. Norman, R. E., Ranford, J. D. and Sadler, P. J., *Inorg. Chem.*, 1992, **31,** 877.
7. Koch, K. R. and Matoetoe, M., *Magn. Reson. in Chem.*, 1991, **29,** 1158.
8. Pregosin, P. S., *Coord. Chem. Rev.*, 1982, **44,** 247.
9. Bret, J.-M., Castan, P., Commenges, G. and Laurent, J.-P., *Polyhedron*, 1983, **2,** 901.
10. Wang, Y., M.Sc. dissertation, University of Cape Town, 1997, unpublished results.
11. Koch, K. R., du Toit, J., Caira, M. R. and Sacht, C., *J. Chem. Soc., Dalton Trans.*, 1994, 785.
12. Scandola, Traverso, O., Balzani, V., Zucchini, G. L. and Carassiti, V., *Inorg. Chim. Acta*, 1967, **1,** 76.

Pergamon

PII: S0277-5387(97)00319-7

Polyhedron Vol. 17, No. 2-3, pp. 275-279, 1998
© 1997 Elsevier Science Ltd
All rights reserved. Printed in Great Britain
0277-5387/98 $19.00+0.00

Correlation of ^{95}Mo NMR chemical shifts, electronic absorption bands, and solvent donor numbers for some dimeric $Mo_2(O_2CR)_4L_2$ solvent adducts

Elmer C. Alyea* and José Campo

Department of Chemistry and Biochemistry, University of Guelph, Guelph, Ontario, Canada N1G 2W1

(Received 2 June 1997; accepted 15 July 1997)

Abstract—The ^{95}Mo NMR chemical shifts are reported for two series of solvent adducts of the dimeric molybdenum(II) complexes $Mo_2(O_2CR)_4L_2$ (R = CF_3, Bu^t; L = solvent). The large deshielding effect (over 450 ppm for the R = CF_3 series as the solvent changes from chloroform to hexamethylphosphoramide) correlates well with the donor number of the solvent. The lowest energy electronic absorption band corresponding to the δ–δ^* transition also moves to longer wavelength with the more strongly coordinating solvents, which is consistent with weakening of the Mo≡Mo quadruple bond and the dominance of the ΔE parameter in the paramagnetic term which controls the magnitude of $\delta(^{95}Mo)$. © 1997 Elsevier Science Ltd

Keywords: tetrakis-μ-carboxylatomolybdenum(II) complexes; correlations of ^{95}Mo NMR and visible spectral data; donor numbers.

The structural diversity and chemical reactivity of dinuclear complexes with strong multiple metal-to-metal bonds have attracted attention for many years [1]. Interest has focused on the nature of the metal–metal bond, synthetic strategies for producing the dinuclear units, and their potential catalytic activity for carbonylation and hydrogenation reactions [1,2].

Development of the chemistry of compounds containing the $[Mo_2]^{4+}$ core has often involved carboxylate ligands, as reflected by recent papers [3]. Extensive attention has been paid these dinuclear tetracarboxylate complexes containing $\sigma^2\pi^4\sigma^2$ Mo—Mo quadruple bonds because of their interesting structural and spectroscopic properties. However, few characterization studies of such species by ^{95}Mo NMR spectroscopy are known.

Previous ^{95}Mo NMR studies have shown that increased bond order in multiple bonded dimolybdenum species causes greatly deshielded chemical shifts, with the $\delta(^{95}Mo)$ values of ca 4000 ppm for the quadruply bonded $Mo_2(O_2CR)_4$ complexes [4] representing the lowest shielding reported for any molybdenum compound [5]. In contrast, the normal range for mononuclear Mo(II) species is between +70 and −2100 ppm [4b,6], though some nitrosyl species of the type $[Mo\{HB(Me_2pz)_3\}(NO)X_2]$ extend the range to nearly +2300 ppm [7]. Other quadruply bonded dinuclear compounds with phosphorus and halide ligands show $\delta(^{95}Mo)$ values which are several hundred ppm upfield (i.e. more shielded) compared to the carboxylates [5]. The earlier preliminary observations [4] that more polar solvents caused the molybdenum nucleus to be deshielded [e.g. by 325 ppm for $Mo_2(O_2CCF_3)_4$ in pyridine compared to $CDCl_3$] suggested that $\delta(^{95}Mo)$ values could serve as a very sensitive probe of the interaction of the dinuclear unit with weakly bound ligands. In this paper we have documented the influence of a range of different solvents on the ^{95}Mo NMR chemical shift for two tetrakis-μ-carboxylatodimolybdenum(II) complexes. The two derivatives, with R = CF_3 or Bu^t-substituents, were chosen because of the difference in electronegativity of the substituents, their stability and (especially, to reduce spectral accumulation times) their solubility. Correlations were examined between

* Author to whom correspondence should be addressed.

$\delta(^{95}Mo)$ values, donor numbers (DN) of the solvents, and the lowest energy electronic absorption band (λ_{max}).

EXPERIMENTAL

$[Mo_2(O_2CR)_4]$ (R = CF_3, *t*-Bu) were isolated by procedures described in the literature [8]. Dried and degassed solvents were used and the reactions were carried out under a dry oxygen-free dinitrogen atmosphere. Two new dinuclear carboxylates were prepared as follows.

$[Mo_2(O_2CC_6H_4N(CH_3)_2\text{-}p)_4]\cdot H_2O$

$Mo(CO)_6$ (2 g) and $p\text{-}HO_2CC_6H_4N(CH_3)_2$ (2.5 g) were mixed and diglyme (35 cm^3) was added. The mixture was stirred at reflux temperature for 3.5 h, during which a yellow–green precipitate formed. After cooling to room temperature, the solid was collected by filtration and washed with diethylether. The green solid was dried *in vacuo* at 70°C for 4 h. Found: C, 49.09; H, 4.56; N, 6.06. Calc.: C, 49.87; H, 4.88; N, 6.46. IR (in KBr): ν_{asym}, 1570 cm^{-1}, ν_{sym}, 1468 cm^{-1}. UV-vis (solid state): 310, 360 (sh), 800 nm. ^1H NMR ($CDCl_3$): 3.06 s; 6.66 d, 7.97 d (J = 9 Hz).

$[Mo_2(O_2CC_6H_4CF_3\text{-}p)_4]$

$Mo(CO)_6$ (0.66 g) and $HO_2CC_6H_4CF_3$ (0.95 g) were mixed and dichlorobenzene (30 cm^3) was added. After stirring the solution at reflux temperature for 2 h, the yellow–orange precipitate that had formed was collected at room temperature by filtration. The product was washed with diethylether and dried *in vacuo*. Found: C, 40.08; H, 1.86. Calc.: C, 40.52; H, 1.70. IR (in KBr): ν_{asym} (CO_2), 1502 cm^{-1}, ν_{asym} (CO_2), 1408 cm^{-1}. UV–vis (solid state): 275, 340 (sh), 385 (sh), 470, 770 nm. ^1H NMR ($CDCl_3$): 7.76 d, 8.23 d (*J* = 8 Hz).

The ^{95}Mo NMR spectra were acquired on a Varian Unity-400 spectrometer operating at 26.06 MHz in the FT mode at ambient temperature. Chemical shifts are relative to external aqueous 2M Na_2MoO_4 (at pH 11). Samples were freshly prepared just prior to ^{95}Mo NMR analysis. Typically, $[Mo_2(O_2CR)_4]$ (0.75 mmol) was dissolved in the appropriate solvent (2.5 cm^3) in a 10 mm NMR tube under a dinitrogen atmosphere. The UV–vis spectra were recorded in the 200–900 nm region for solutions of 10^{-3} M or less concentration in 1 cm silica cuvettes. Linear regression analyses were performed using Microcal Origin 4.1 with the confidence level being set at 0.99 in obtaining correlation coefficients.

RESULTS AND DISCUSSION

Tetrakis-μ-carboxylatodimolybdenum(II) compounds are well known to form $Mo_2(O_2CR)_4L_2$ complexes with Lewis bases [1,9]. Spectroscopic and structural data indicate that two main isomers are possible (Fig. 1); several other less symmetrical isomers than those depicted are also possible at least for phosphine ligands [9]. The common axial diadducts, type *a*, consist of four carboxylate groups bridging the Mo_2^{4+} unit, while the L donor ligands occupy the axial positions with a variable coordinating strength. The other main isomer, type *b*, has two monodentate and two bridging carboxylate groups, with the L donor ligands occupying an equatorial position on each molybdenum atom. In the present study involving donor solvents of variable coordinating strength, as reflected by their donor number, the $Mo_2(O_2CR)_4L_2$ (R = CF_3, Bu^t) diadducts are all expected to be type *a*, as already established by X-ray structural determinations for L = diethylene glycol dimethyl ether and pyridine [1,9]. However, two ^{95}Mo resonances were observed for the R = CF_3, L = N,N-dimethylacetamide (DMA) derivative, and thus we suggest the presence of an equatorial isomer (type *b*) also in that case. Whilst the two ^{95}Mo signals are separated by 73 ppm, it is noteworthy that neither IR nor UV–vis spectroscopy could be expected to definitively identify the existence of both isomers. The sensitivity of the ^{95}Mo chemical shift to the molybdenum environment results in $\delta(^{95}Mo)$ changing from 3920 to 4333 ppm as the solvent changes from nitrobenzene to hexamethylphosphoramide (HMPA), respectively, for the R = CF_3 series. At the same time, the electronic absorption band in the visible region (λ_{max}) increases from 421 nm to 501 ppm for the same solvents. Table 1 summarizes the $\delta(^{95}Mo)$ and λ_{max} values for 14 solvents for the R = CF_3 series and six solvents for the R = Bu^t series, listed according to the increasing magnitude of the solvent donor number (DN).

The paramagnetic shielding term which dominates in the Ramsey expression [eqn (1)] for quadrupolar nuclei such as ^{95}Mo (I = 5/2, natural abundance

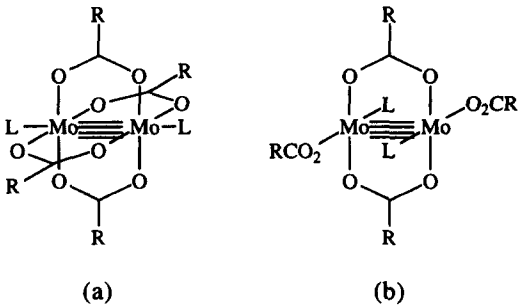

Fig. 1. Two main isomer types for $Mo_2(O_2CR)_4L_2$ complexes: type *a*, axial and type *b*, equatorial.

Table 1. Donor number, ^{95}Mo NMR chemical shift and wavelength data

No.	Solvent	Donor number	$Mo_2(O_2CCF_3)_4L_2$		$Mo_2(O_2CBu^t)_4L_2$	
			$\delta(^{95}Mo)$, ppm[a]	λ_{max}, nm	$\delta(^{95}Mo)$, ppm[a]	λ_{max}, nm
1	Nitrobenzene	4.4	3920 (750)	421	—	—
2	Benzonitrile	11.9	3984 (1000)	425	—	—
3	Acetonitrile	14.1	4029 (320)[b]	425	3599 (600)	420
4	Propionitrile	16.1	4019 (410)	427	—	—
5	Acetone	17.0	4023 (325)	429	3626 (600)	425
6	Ethanol	19.0	4125 (290)	433.5	—	—
7	Diethyl ether	19.2	3999 (220)	436.5	—	—
8	THF	20.0	4021 (480)[b]	435	3656 (1040)[b]	434[b]
9	DMF	24.0	4144 (640)[b]	442	3696 (1130)[b]	437
10	DMA	27.3	4129 (475)[c]	438	—	—
11	DMSO	29.8	4187 (180)	472.5	3773 (1000)	439
12	py	33.1	4199 (320)[b]	504[b]	3818 (760)	450
13	HMPA	38.8	4333 (700)	501	—	—

[a] Values in parentheses are half-widths of the signal.
[b] Data taken from Ref. [4].
[c] A peak at 4056 (650) ppm is assigned to the presence of a type *b* diadduct.

15.7%) can be expressed in a simplified form [eqn (2)] which is useful

$$\delta = \delta_{dia} + \delta_{para} \quad (1)$$

$$\delta_{para} = K\Delta E^{-1} < r^{-3} >_{4d} k^2 \quad (2)$$

for comparisons of complexes of the same symmetry. The spectrochemical parameter, ΔE, which is the HOMO–LUMO gap for paramagnetic circulations in the magnetic field corresponds to the ligand field splitting, the *d–d* excitations being magnetic dipole allowed. It is acknowledged that a summation over two or more ΔE terms may be required for low symmetries, but regardless, large excitation energies (such as normally due to strong ligand σ-bonding in mononuclear complexes) will lead to shielding. The radial term, $\langle r^{-3} \rangle_{4d}$, which is the inverse cube of the valence *d*-electron radius, and the covalency factor, k^2, which reflects the amount of covalent bonding, together constitute a nephelauxetic dependency for δ_{para}. Its magnitude will be low, giving greater shielding, the farther the paramagnetic circulation is from the resonant nucleus. Either the spectrochemical or nephelauxetic components of the δ_{para} expression can be dominant, as well documented [5,10].

As noted by previous works, the $\delta(^{95}Mo)$ values for the $Mo_2(O_2CR)_4L_2$ complexes constitute the most deshielded ones known [4,5]. Such high frequencies for these quadruply bonded species must be related to the existence of small ΔE excitation energies and considerable charge asymmetry in the valence shell (which would also explain the significant line broadening that occurs, as discussed below). The larger deshielding that occurs for the R = CF_3 complexes relative to the R = Bu^t complexes (ca 400 ppm) can be attributed to the large increase in acid strength of the carboxylic acid with the electronegative substituent. In other words, the weakly basic $CF_3CO_2^-$ anion induces smaller ΔE splittings, as indicated by the larger λ values (Table 1). Surprisingly, X-ray crystallography does not detect any influence on the interaction between the Mo atoms since the quadruple bond is identical (2.090(4) Å) for the free R = CF_3 derivative and the R = Bu^t complex [2.088(1) Å]. This constancy of the Mo≡Mo bond distance is an established feature in $Mo_2(O_2CR)_4$ complexes [1].

In the diadducts, the Mo atoms might be expected to be more shielded as the solvent ligands become more strongly coordinated, since greater σ donor ability increases ΔE in mononuclear complexes. However, the $\delta(^{95}Mo)$ values move to higher frequency in both series of diadducts as the donor number (DN) of the solvents increases. As a measure of the basicity or donor ability of a solvent, DN is defined [11] as the negative enthalpy of reaction of a base with the Lewis acid antimony pentachloride, i.e.

$$B + SbCl_5 \rightarrow B \rightarrow SbCl_5\,;\, DN \equiv -\Delta H, \quad (3)$$

Good linear correlations between $\delta(^{95}Mo)$ and DN are observed for both series ($r = 0.94$ for R = CF_3, with the plot shown in Fig. 2; $r = 0.95$ for R = Bu^t). Similarly, the lowest energy electronic absorption moves to longer wavelength, though the correlation of either $\delta(^{95}Mo)$ or DN and λ_{max} is only moderately good [e.g., $r = 0.86$ between $\delta(^{95}Mo)$ and λ_{max} for the R = CF_3 series]. The correlation coefficient becomes 0.90 if point 12 is not included, for the plot shown in Fig. 3. Coordination of solvents of better donor ability apparently induces a reduction in the orbital overlap between the molybdenum atoms, resulting in a smaller ΔE (or a further splitting of energy levels). Com-

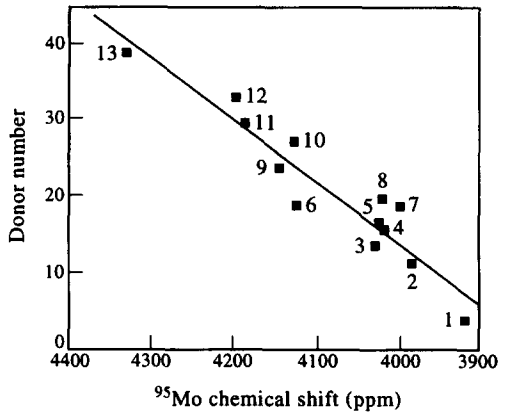

Fig. 2. The correlation of donor number and ^{95}Mo chemical shift (in ppm) for the $Mo_2(O_2CCF_3)_4L_2$ series.

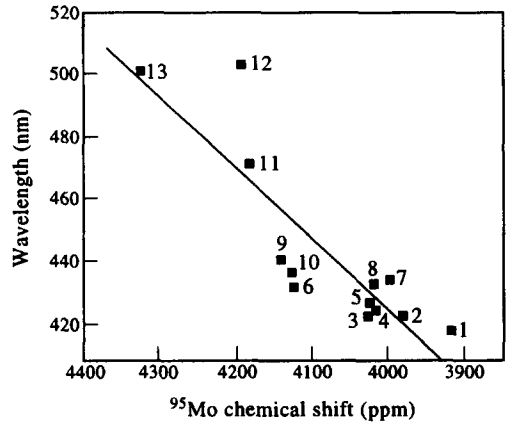

Fig. 3. The correlation of wavelength and ^{95}Mo chemical shift (in ppm) for the $Mo_2(O_2CCF_3)_4L_2$ series.

mensurate with these observations, the Mo≡Mo quadruple bond might be expected to increase in length within the diadducts as the solvent DN increases, but X-ray structural data are not yet available to verify this prediction. Further confirmation of the longer bond being expected for diaxial solvent coordination comes from the observation [12] of Raman Mo≡Mo stretching frequencies at 367 cm^{-1} for $Mo_2(O_2CCF_3)_4(py)_2$ vs 397 cm^{-1} for $Mo_2(O_2CCF_3)_4$, and at 363 cm^{-1} for $Mo_2(O_2CCH_3)_4(py)_2$, vs 404 cm^{-1} for $Mo_2(O_2CCH_3)_4$.

The linewidths observed for the ^{95}Mo spectral bands are significantly larger than those reported for complexes of higher symmetry, ranging from 180 to 1000 Hz for the R = CF_3 series (Table 1). Undoubtedly, the lower symmetry of these diaxial adducts leads to asymmetry in the electric field gradient, a primary factor in line broadening. Other factors such as solvent viscosity and correlation time may also be contributing to the observed large line widths. Nevertheless we note that the lowest linewidths, 180 Hz for the R = CF_3 series diadduct with DMSO, occurs for a viscous solvent (2.00 cp for DMSO). The strong DMSO coordination, and resultant expected short Mo—O (DMSO) bond, must lead to a higher charge symmetry in the Mo valence shell. The influence of correlation time in enlarging the line width can be seen as the coordinating ligand becomes larger (e.g. benzonitrile vs acetonitrile, and the R = Bu^t complexes vs the R = CF_3 ones).

The electronic spectra of tetrakis-μ-alkylcarboxylato-dimolybdenum complexes are well documented in the literature [1]. In general, representative bands occur near 230 nm ($\varepsilon \sim 4000$), 300 nm ($\varepsilon \sim 8000$) and 430 nm ($\varepsilon \sim 60\ cm^{-1}\ M^{-1}$). The origin of the weak, lowest energy band has been the subject of considerable controversy [1,13,14]. However, Martin *et al.* [15] and others later concluded that the lowest energy electronic excitation for such tetrakis (μ-carboxylate) complexes was an electric-dipole-allowed transition and thus should be the $\delta \rightarrow \delta^*$ transition. Much recent literature for the entire d^4–d^4 $M_2(O_2CR)_4$ (M = Cr, Mo, W) series concurs with this assignment [1,3]. Under a D_{4h} symmetry for these dimeric compounds, this characteristic $\delta \rightarrow \delta^*$ transition is denoted as ($^1A_{1g} \rightarrow {}^1A_{2u}$).

In both series of complexes (Table 1), the longest wavelength visible absorption band moves to longer wavelengths with better coordinating solvents. An earlier study of the axially coordinated adducts of $Mo_2(O_2CC_6H_5)_4$ noted only a very qualitative relationship between solvent donor character and the magnitude of the spectral shift [16]. The correlation in our case between λ_{max} and donor number is only moderately good ($r = 0.89$ for the R = CF_3 series) but nevertheless the trend is consistent with the observation that solvents with greater donor ability induce smaller $\delta \rightarrow \delta^*$ transitions which lead to larger δ_{para} values in the simplified Ramsay expression [eqn (2)], and thus more deshielded $\delta(^{95}Mo)$ values. A correlation between $\delta(^{95}Mo)$ and ΔE, as given by observed visible absorption bands, has already been noted for both Mo^0 and Mo^{VI} complexes [17]. Very recently, confirmation of the correlation was affirmed for both dimeric Mo^V complexes and mononuclear $Mo(CO)_4L_2$ complexes [18]. The same trend in the present Mo^{II} dimers suggest that although other factors cannot necessarily be assumed to be constant for the series under study, the ΔE term is nevertheless the dominant one affecting the δ_{para} magnitude. Our attempt to extend the $\delta(^{95}Mo)$ and ΔE correlation to new $Mo_2(O_2CR)_4$ species (R = $C_6H_4N(CH_3)_2$-*p* and R = $C_6H_4CF_3$-*p*) having very low wavelength absorptions was not successful; the low solubility of these two complexes precluded the observation of a ^{95}Mo NMR resonance, even after overnight accumulations at elevated temperatures.

Acknowledgements—ECA thanks NSERC Canada for a research grant and JAC thanks the Ministerio de Educación y Ciencia (Spain) for a postdoctoral fellowship.

REFERENCES

1. Cotton, F. A. and Walton, R. A., *Multiple Bonds Between Metal Atoms*, Oxford University Press, New York (1993).
2. Legzdins, P., Rempel, G. L. and Wilkinson, G., *J. Chem. Soc., Chem. Commun.*, 1969, 825; Legzdins, P., Mitchell, R. W., Rempel, G. L., Ruddick, J. D. and Wilkinson, G., *J. Chem. Soc. A*, 1970, 3322.
3. Cotton, F. A., Eglin, J. L. and Wiesinger, K. J., *Inorg. Chimica Acta*, 1992, **195,** 11; Guinan, P., McCann, M. and Ryan, H., *Polyhedron*, 1992, **11,** 205; McCann, M., Carvill, A., Guinan, P., Higgins, P., Campbell, J., Ryan, H. and Walsh, M., *Polyhedron*, 1991, **10,** 2273; Kerby, M. C., Eichhorn, B. W., Doviken, L. and Vollhardt, K. P. C., *Inorg. Chem.*, 1991, **30,** 156; Cayton, R. H., Chisholm, M. H., Huffman, J. C. and Lobkovsky, E. B., *J. Am. Chem. Soc.*, 1991, **113,** 8709.
4. Shehan, B. P., Kony, M., Brownlee, R. T. C., O'Connor, M. J. and Wedd, A. G., *J. Magn. Reson.*, 1985, **63,** 343; Grieves, R. A. and Mason, J., *Polyhedron*, 1986, **5,** 415.
5. Minelli, M., Enemark, J. H., Brownlee, R. T. C., O'Connor, M. J. and Wedd, A. G., *Coord. Chem. Rev.*, 1985, **68,** 169; Malito, J., *Ann. Rep. NMR Spectros.*, 1997, **33,** 151.
6. Minelli, M., Bell, A., Enemark, J. H. and Walton, R. A., *J. Organomet. Chem.*, 1985, **284,** 25.
7. Young, C. G., Minelli, M., Enemark, J. H., Hussain, W., Jones, C. J. and McCleverty, J. A., *J. Chem. Soc., Dalton Trans.*, 1987, 619.
8. Cotton, F. A. and Norman, J. G., *J. Coord. Chem.*, 1971, **1,** 161; Cotton, F. A., Extine, M. and Gage, L. D., *Inorg. Chem.*, 1978, **17,** 172.
9. Girolami, G. S., Mainz, V. V. and Anderson, R. A., *Inorg. Chem.*, 1980, **19,** 805; Cotton, F. A., and Wilkinson, G., eds, *Advanced Inorganic Chemistry*, 5th ed., p. 1089, J. Wiley and Sons, New York, 1988.
10. Mason, J., ed., *Multinuclear NMR*, Plenum Press, New York (1987).
11. Gutmann, V., *Coord. Chem. Rev.*, 1976, **18,** 225.
12. Cotton, F. A. and Norman, J. G. Jr., *J. Am. Chem. Soc.*, 1992, **94,** 5097.
13. Cotton, F. A., Martin, D. S., Webb, T. R. and Peters, P. J., *Inorg. Chem.*, 1976, **15,** 1199.
14. Trogler, W. S., Solomons, E. I., Trajber, I., Ballhausen, C. J. and Gray, H. B., *Inorg. Chem.*, 1977, **16,** 828.
15. Martin, D. S., Newman, R. A. and Fanwick, P. E., *Inorg. Chem.*, 1982, **21,** 3400.
16. San Filippo, J. Jr. and Sniadoch, H. J., *Inorg. Chem.*, 1976, **15,** 2209.
17. Gray, G. M. and Kraihanzel, C. S., *Inorg. Chem.*, 1983, **22,** 2259; Alyea, E. C. and Topich, J., *Inorg. Chim. Acta*, 1982, **65,** L95.
18. Ackermann, M., Fairbrother, W. G., Amin, N. S., Deodene, C. J., Lamborg, C. M. and Martin, P. T., *J. Organomet. Chem.*, 1996, **523,** 145; Wong, T. C., Huang, Q., Zhu, N. and Wu, X., *Polyhedron*, 1997, **16,** 2987.

Pergamon

PII: S0277-5387(97)00301-X

Polyhedron Vol. 17, No. 2-3, pp. 281-287, 1998
© 1997 Elsevier Science Ltd
All rights reserved. Printed in Great Britain
0277-5387/98 $19.00+0.00

New binucleating Schiff base Ni^{II} and Cu^{II} complexes—synthesis, spectral properties and crystal structure

Ewa M. Opozda,[a] Ewa Śledziewska,[b]* Wiesław Łasocha,[b] Kees Goubitz[c] and Henk Schenk[c]

[a]Institute of Chemistry, Pedagogical University, 25-020 Kielce, Poland

[b]Faculty of Chemistry, Jagiellonian University, 30-060 Kraków, Poland

[c]Laboratory for Crystallography, University of Amsterdam, 1018 WV Amsterdam, The Netherlands

(Received 5 September 1996; accepted 10 July 1997)

Abstract—Four novel oxamide type ligands have been obtained by reaction of "half units" **1–4** and oxalyl chloride. They were used to prepare corresponding related binuclear Cu^{II} and Ni^{II} complexes. The products obtained were characterized by elemental analysis, MS, IR and NMR spectra and X-ray single crystal analysis.
© 1997 Elsevier Science Ltd

Keywords: binuclear complexes; nickel and copper complexes; Schiff base; synthesis; NMR spectra; X-ray crystal structure.

There is increasing interest in binuclear complexes, which contain ligand structures capable of holding two metal centres in close proximity. These polymetallic systems are attractive as synthetic models of metallo biomolecules. Among the known polynucleating ligands, particular attention has recently been paid to oxalic acid derivatives due to their wide range of possibilities [1]. Our work described herein has concentrated on developing new binuclear complexes from more easily prepared tridentate precursors such as condensation products of the carbonyl function with only one amino group of a diamine ("half-units") **1–4**. The monocondensation products have received increasing attention due to interesting structural properties of their metal chelates [2] and also due to their application as intermediates in the synthesis of unsymmetrical multidentate Schiff base ligands [3] or heterocyclic compounds [4]. Recently Costes *et al.* have described the syntheses and characterization of new oxamido bridging Schiff bases from a monocondensation product and diethyl oxalate [5].

Experimental

Materials and physical measurements

All materials were reagent grade and were used without further purification, except for solvents which were dried by standard methods. The starting benzoylacetaldehyde, p-nitrobenzoylacetaldehyde and 3-ethoxyvinylidene-2,4-pentanedione were prepared by literature procedures [12, 13]. Compound **1** was prepared following a modified procedure of Cutler *et al.*

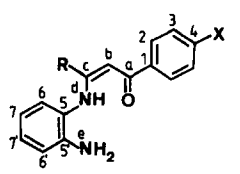

1: R = CH_3; X = H

2: R = H; X = H

3: R = H; X = NO_2

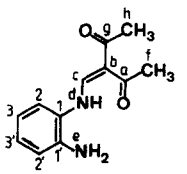

4

*Author to whom correspondence should be addressed.

[6b]. All melting points are uncorrected. IR spectra were measured as KBr discs using a Specord M-50 (Carl Zeiss Jena) spectrometer over the range 200–4000 cm^{-1}, ^1H and ^{13}C NMR spectra were taken on a Bruker AMX-500 NMR spectrometer in $CDCl_3$ with TMS as an internal standard. Mass spectra were recorded on a LKB 2091 mass spectrometer at 15 and 75 eV ionization potentials.

X-ray structure analysis

$C_{34}H_{26}N_4O_4Cu_2$, Mr = 681.7, monoclinic $P2_1/c$, $a = 6.5137(4)$, $b = 8.0053(6)$, $c = 27.182(2)$ Å, $\beta = 90.382(4)°$, $V = 1417.3$ Å^3, $Z = 2$, $D_x = 1.6$ g cm^{-3}, $\lambda = 1.5418$ Å. A crystal with approximate dimensions $0.05 \times 0.10 \times 0.40$ mm was used for data collection on an Enraf-Nonius CAD-4 diffractometer with graphite-monochromated Cu K_α radiation and ω-2θ scan. A total of 2662 unique reflections was measured within the range $-7 \leq h \leq 0$, $0 \leq k \leq 9$, $-31 \leq l \leq 31$. Of these reflections 1910 were above the significance level of 2.5 s(I). The range of $(\sin\theta)/\lambda$ was 0.037–0.609 Å^{-1} ($2.3 < \theta < 69.8°$). Two reference reflections (200 and 012) were measured hourly and showed no decrease during the 42 h collecting time. Unit cell parameters were refined by a least-squares fitting procedure using 23 reflections with $39.9 < \theta < 44.8°$. Data were corrected for Lorentz and polarization factors. Absorption correction was performed with the program ABSCAL [15] using Ψ-scans of the 200 reflection, with coefficients in the range 1.02–1.74.

The structure was solved both by the PATT option of SHELXS 86 [16] and PATTY option of DIRDIF 94 [17] programs system. Initial positions of hydrogen atoms were calculated. Full-matrix least-squares refinement on F, anisotropic for the non-hydrogen atoms and isotropic for hydrogen atoms, restraining the latter in such a way that the distance to their carrier remained constant at approximately 1.0 Å, converged to $R = 0.056$, $R_w = 0.054$, $(\Delta/\sigma)_{max} = 0.32$, $S = 0.854$). A weighting scheme $w = [3.0 + 0.1*(\sigma(F_o))^2 + 0.001/(\sigma(F_o))]^{-1}$ was used. The secondary isotropic extinction coefficient [18] refined to Ext = 0.009(2). A final difference Fourier map revealed a residual electron density between −0.8 and 0.5 e Å^{-3}. Scattering factors were taken from Cromer and Mann [19]. The anomalous scattering of Cu was taken into account. All calculations were performed with XTAL [20], unless stated otherwise.

Preparation of the compounds.

Preparation of 1-*phenyl*-3-[*N*-(2′-*aminophenyl*)*amino*]-2-*propen*-1-*one* (**2**). Compound (**2**) was synthesized in a manner similar to the procedure described in the literature [7]. Benzoylacetaldehyde (5 g, 0.34 mol) was dissolved in methanol (30 cm^3) and added with stirring to a solution of 1,2-diaminobenzene (3.6 g, 0.34 mol) in methanol (15 cm^3) at room temperature. The separated solid was filtered off and recrystallized from *n*-propanol to give a yellow solid **2** (2.53 g, yield 31.2%). M.p. 158–160°C. Found: C, 75.2, H: 5.4; N: 11.5. Calc. for $C_{15}H_{14}N_2O$: C, 75.6; H, 5.9; N, 11.8%. MS[(*m*/*z*) ab.%]: 238 (M^+), 50; 219 (M^+–18), 15; 119 ($H_2NC_6H_4NH^+$), 100; 105 ($C_6H_5CO^+$), 30. IR(KBr): 3376br w, 3328w, 1640s, 1620s, 1600 m, 1580m, 1544m cm^{-1}. δ_H ($CDCl_3$) 12.49, [1H, *br d*, $J(H^dH^c)$ 11.5 Hz, N*H*^{d}], 6.81–8.40 [10H, *m*, C*H*$_{phen}$ + C*H*^{c}], 6.04 [1H, *d*, $J(H^bH^c)$ 7.5 Hz, C*H*^{b}], 4.25 [2H, *br s*, N*H*^{e}]. δ_C($CDCl_3$) 191.18 [C^a], 147.27 [C^c], 137.17 and 139.25 [C^1 and C$^{5'}$], 132.15, 131.50, 128.47, 127.53, 127.27 and 125.25 [C^2, C^3, C^4, C^5, C^7 and C$^{7'}$], 119.91 [C^6], 117.72 [C$^{6'}$], 95.47 [C^b].

Preparation of 1-(4′-*nitrophenyl*)-3-[*N*-(2′-*aminophenyl*)*amino*]-2-*propen*-1-*one*(**3**). The compound **3** was prepared from the reaction of stoichiometric amounts of p-nitrobenzoylacetaldehyde (5 g, 0.026 mol) and 1,2-diaminobenzene (1.9 g, 0.026 mol), as described in the literature [7]. Yield 3.35 g (54%). M.p. 171° (Lit. [7] 170–171°C). MS [(*m*/*z*) ab.%]: 238 (M^+), 45; 265 (M^+–18), 21; 150 ($NO_2C_6H_4CO^+$), 37; 119 ($H_2NC_6H_4NH^+$), 100; 104 ($C_6H_4CO^+$), 26. IR (KBr): 3375w, 3330w, 1640m, 1624s, 1600m, 1544m cm^{-1}. δ_H ($CDCl_3$) 12.29 [1H, *d*, $J(H^dH^c)$ 11.5 Hz, N*H*^{d}], 8.29 [2H, *d*, $J(H^3H^2)$ 8.5 Hz, C*H*$^3_{phen}$], 8.07 [2H, *d*, $J(H^2H^3)$ 8.5 Hz, C*H*$^2_{phen}$], 7.57 [1H, *dd*, $J(H^cH^d)$ 11.5 Hz, $J(H^cH^b)$ 7.5 Hz, C*H*^{c}], 7.11 [1H, *d*, $J(H^6H^7)$ 8.0 Hz, C*H*$^6_{phen}$], 7.03 [1H, *d*, $J(H^{6'}H^{7'})$ 8.0 Hz, C*H*$^{6'}_{phen}$], 6.83–6.88 [2H, *m*, C*H*$^{7,7'}_{phen}$], 6.07 [1H, *d*, $J(H^bH^c)$ 7.5 Hz, C*H*^{b}], 3.77 [2H, *br s*, N*H*^{e}]. δ_C($CDCl_3$) 187.99 [C^a], 149.72 [C^4], 148.72 [C^c], 144.53 [C^1], 137,32[C$^{5'}$], 128.42 and 128.17 [C^2, C$^{2'}$], 126.06 [C^5], 123.67, 120.14, 119.28 and 118.12 [C^3, C$^{3'}$, C^7 and C$^{7'}$], 119.28 [C^6], 117.56 [C$^{6'}$], 93.80 [C^b].

Preparation of 3-*acetylo*-4-[*N*-(2′-*aminophenyl*) *amino*]-3-*penten*-2-*one* (**4**). A solution of 3-ethoxy-vinylidene-2,4-pentanedione (3.0 g, 0.021 mol) in ethanol (50 cm^3), was added dropwise to 1,2-diaminobenzene (2.67 g, 0.021 mol) in ethanol (50 cm^3). The mixture was stirred at room temperature for 1 h. The light yellow solid was collected by filtration and was recrystallized from ethanol (3.9 g, yield 86%). M .p.: 159–160°C. Found: C, 66.1; H, 6.4; N, 12.6. Calc. for $C_{12}H_{14}N_2O_2$: C, 66.0; H, 6.5; N, 12.8%. IR (KBr): 1664m, 1624s, 1604s, 1576s, 1568s cm^{-1}. δ_H ($CDCl_3$) 12.66 [1H, *d*, $J(H^dH^c)$ 12.5 Hz, N*H*^{d}], 8.15 [1H, *d*, $J(H^cH^d)$ 12.5 Hz, C*H*^{c}], 7.11 and 7.09 [1H, *d*, $J(H^2H^3)$ 8.0 Hz; 1H, *d*, $J(H^{2'}H^{3'})$ 8.0 Hz, C*H*$^{2,2'}_{phen}$], 6.88–6.82 [2H, *m*, C*H*$^{3,3'}_{phen}$], 3.79 [2H, *s*, N*H*^{e}], 2.57 [3H, *s*, C*H*^{f}], 2.37 and 2.35 [3H, *s*; 3H, *s*; C*H*^{h}]; δ_C ($CDCl_3$) 201.18 and 194.72 [C^a and C^g], 154.54 [C^c], 138.52, 127.37, 127.05, 119.74, 119.54 and 117.38 [C^1, C$^{1'}$, C^2, C$^{2'}$, C^3 and C$^{3'}$], 113.4 [C^b], 31.90 and 27.28 [C^h and C^f].

Preparation of 1,16-*diphenyl*-3,14-*dimethyl*-5,6:11, 12-*dibenzo*-4,7,10,13-*tetraazaheksadeca*-2,14-2,14-*dien*-1,8,9,16-*tetraone* (**5**). A solution of 0.63 g (0.0185 mol) of oxalyl chloride in anhydrous benzene was

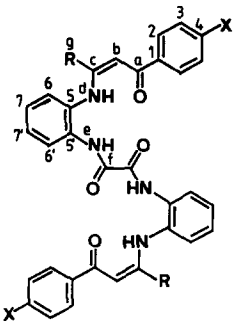

5: R = CH_3; X = H

6: R = H; X = H

7: R = H; X = NO_2

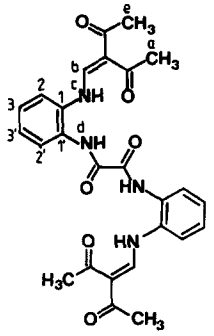

8

added dropwise to the vigorously stirred and cooled solution containing 2.5 g (0.037 mol) of monocondensation product **1** and 7.5 g (0.037 mol) of triethylamine in anhydrous benzene (150 cm^3). After addition was complete the mixture was stirred at room temperature for 3 h. The yellow precipitate was filtered off, suspended in saturated sodium hydrogen carbonate (200 cm^3) and stirred. The solid was collected by filtration, washed with water and dried *in vacuo*. Recrystallisation of the product from a large volume of chloroform gave a colourless solid **5**. Yield 0.8 g (45%). Found: C, 73.4; H, 6.2; N, 9.8. Calc. for $C_{34}H_{30}N_4O_4$; C, 73,1; H, 5.4; N, 10.0%. IR (KBr): 3500–3050br w, 1688s, 1605s, 1584s, 1564m, 1548m. δ_H ($CDCl_3$) 12.67 [2H, *br s*, N*H*^{d}], 9.40 [2H, *br, s*, N*H*^{e}], 7.34–8.41 [18H, *m*, C*H*$_{phen}$], 6.05 [2H, *s*, C*H*^{b}], 2.53 [6H, *s*, C*H*^{g}].

Preparation of 1,16-*diphenyl*-5,6:11,12-*dibenzo*-4,7,10,13-*tetraazaheksadeca*-2,14-*diene*-1,8,9,16-*tetraone* (**6**). Compound **6** was synthesized from monocondensation product **2** (2.0 g, 0.008 mol), oxalyl chloride (0.51 g, 0.004 mol) and triethylamine (0.81 g, 0.008 mol) according to the procedure described for **5** to give 0.71 g (32%) of a colourless solid. M.p.: 196–198°C. Found: C, 72.7: H, 5.1: N, 10.6. Calc. for $C_{32}H_{26}N_4O_4$: C, 72.4; H, 4.9: N, 10.6%. IR (KBr): 3350 w, 3289 m, 3150 w, 1672 s, 1632 s, 1592 m, 1552 m cm^{-1}. δ_H ($CDCl_3$) 12.16 [2H, *d*, J(H^{d}H^e) 11.5 Hz, N*H*^{d}], 9.57 [2H, *s*, N*H*^{e}], 7.89 and 7.82 [2H, *d*, J(H^{2}H^3) 7.5 Hz; 2H, *d*, J(H$^{2'}$H$^{3'}$) 7.5 Hz; C*H*$^{2,2'}_{phen}$], 7.55–7.15 [10H, *m*, C*H*$_{phen}$+C*H*^{e}], 6.08 [2H, *d*, J(H^{b}H^e) 7.5 Hz, C*H*^{b}]. δ_C ($CDCl_3$) 191.23 [C^a], 158.41 [C^f], 146.22 [C^e], 139.04 and 134.63 [C^1 and C$^{5'}$], 131.59 [C^4], 128.31, 127.74, 127.53, 126.15, 125.25, 124.71, 118.26 [C^2, C^3, C^5, C^6, C$^{6'}$, C^7 and C$^{7'}$], 95.38 [C^b].

Preparation of 1,16-*di*(4′-*nitrophenyl*)-5,6:11,12-*dibenzo*-4,7,10,13-*tetgraazaheksadeca*-2,14-*diene*-1,8,9,16-*tetraone* (**7**). Compound **7** was prepared from monocondensation product **3** (2.0 g, 0.007 mol), oxalyl chloride (0.44 g, 0.004 mol) and triethylamine (0.71 g, 0.007 mol) by a similar method to that described for **5** to give 5.09 g (41%) yellow solid. M.p.: 248°C. Found: C, 58.6; H, 3.6;N, 12.8. Calc. for $C_{32}H_{24}N_6O_8$: C, 61.9; H, 3.9; N, 13.5%. IR (KBr): 3270 s, 1750 s, 1630 s, 1580 m. Compound **7** is insoluble in most common organic solvents.

Preparation of 3,16-*diacetyl*-6,7:12,13-*dibenzo*-5,8,11,14-*tetraazaoctadeca*-2,9,10,17-*tetraone* (**8**). Compound **8** was obtained from monocondensation product **4** (2.0 g, 0.009 mol), oxalyl chloride (0.57 g, 0.005 mol) and triethylamine (0.91 g, 0.009 mol) by a similar method to that described for **5** to give 1.24 g (59%) of a light yellow solid. M.p. 267°C (decomp.). Found: C, 68.4; H, 5.8; N, 12.4. Calc. for $C_{26}H_{26}N_4O_4$: C, 68.1; H, 5.7; N, 12.2%. IR (KBr): 3100s 1680s, 1676s, 1624s, 1585s cm^{-1}. δ_H ($CDCl_3$) 12.73 [2H, *br*, *d*, J(H^{c}H^b) 12.5 Hz, N*H*^{c}], 9.43 [2 H, s, N*H*^{d}], 8.11 [2 H, *d*, J(H^{b}H^c) 12.5 Hz, C*H*^{b}], 7.73–7.71 [2 H, *m*, C*H*$^{2,2'}_{phen}$], 7.42–7.39 [4 H, *m*, C*H*$^{3,3'}_{phen}$], 2.53 and 2.37 [6 H, *s*, 6H, *s*, C*H*^{e}], 2.18 [12 H, *s*, C*H*^{a}].

General preparation of the complexes (**9–16**)

A solution of 0.01 mol of nickel(II) acetate tetrahydrate or solution of 0.01 mol of copper acetate monohydrate in DMF (20 cm^3) was added to a suspension of 0.01 mol of the corresponding ligand **5–8** in DMF (50 cm^3). The reaction mixture was heated under reflux for 1 h with stirring. After cooling a brown crystalline product was filtered off, washed with hot water and dried *in vacuo* for several hours. Average yield: 95–98%.

Complex **9**: Brown solid. M.p.: > 300°C. Found: C, 60.3; H, 4.3; N, 8.3. Calc. for $C_{34}H_{26}N_4O_4Ni_2$: C,

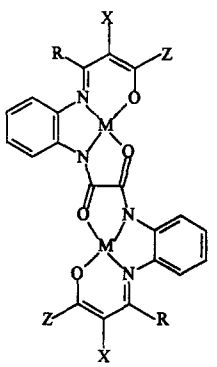

9: M = Ni(II); R = CH_3; Z = C_6H_5; X = H

10: M = Cu(II); R = CH_3; Z = C_6H_5; X = H

11: M = Ni(II); R = H; Z = C_6H_5; X = H

12: M = Cu(II); R = H; Z = C_6H_5; X = H

13: M = Ni(II); R = H; Z = p-$NO_2C_6H_4$; X = H

14: M = Cu(II); R = H; Z = p-$NO_2C_6H_4$; X = H

15: M = Ni(II); R = H; Z = CH_3; X = CH_3CO

16: M = Cu(II); R = H; Z = CH_3; X = CH_3CO

60.7; H, 3.9; N, 8.3%. IR (KBr): 1630 s, 1576 w, 1552 m, 1520 w, 1505 m.

Complex **10**: Dark purple solid. M.p.: > 300°C. Found: C, 59.7; H, 4.1; N, 8.6. Calc. for $C_{34}H_{26}N_4O_4Cu_2$: C, 59.9; H, 3.8; N, 8.2%. IR (KBr): 1625 s, 1608 s, 1552 m.

Complex **11**: Yellow-brown solid. M.p.: > 300°C. Found: C, 58.4; H, 3.7; N, 8.7. Calc. for $C_{32}H_{22}N_4O_4Ni_2$: C, 58.8; H, 3.4; N, 8.6% IR (KBr): 1632 s, 1584 w, 1560 m, 1512 m.

Complex **12**: Brown solid. M.p.: > 300°C. Found: C, 59.1; H, 3.3; N, 8.6. Calc. for $C_{32}H_{22}N_4O_4Cu_2$: C, 59.7; H, 3.4; N, 8.7%. IR (KBr): 1624 s, 1610 s, 1584 m.

Complex **13**: Brown solid. M.p.: > 300°C. Found: C, 51.0; H, 2.1; N, 11.4. Calc. for $C_{32}H_{20}N_6O_8Ni_2$: C, 52.4; H, 2.8; N, 11.4%. IR (KBr): 1604 s, 1572 s, 1516 s.

Complex **14**: Red-brown solid. M.p.: > 300°C. Found: C, 51.5; H, 2.8; N, 11.5. Calc. for $C_{32}H_{20}N_6O_8Cu_2$: C, 51.7; H, 2.7; N, 11.3%. IR (KBr): 1604 s, 1572 s, 1516 s.

Complex **15**: Red-brown solid. M.p.: > 300°C. Found: C, 57.2; H, 4.3; N, 10.2. Calc. for $C_{26}H_{22}N_4O_4Ni_2$: C, 57.8; H, 4.1; N, 10.4%. IR (KBr): 1632 s, 1625 s, 1592 m, 1568 s cm^{-1}.

Complex **16**: Grey green solid. M.p.: > 300°C. Found: C, 56.4; H, 4.0; N, 10.3. Calc. for $C_{26}H_{22}N_4O_4Cu_2$: C, 56.8; H, 4.0; N, 10.2%. IR (KBr): 1650 m, 1620 s, 1595 m, 1568 m.

RESULTS AND DISCUSSION

The monocondensation products **1–4** are readily obtained by reactions of equimolar amounts of 1,2-diaminobenzene and 1,3-dicarbonyl compounds such as benzoylacetone, benzoylacetaldehyde, p-nitrobenzoylacetaldehyde and 3-ethoxyvinylidene-2,4-pentanedione. Synthesis of compounds **1** and **3** was described earlier [6, 7], but in the case of compound **3** only elemental analyses were reported [7]. The "half units" **2–4** were characterized by IR, mass, ^1H and ^{13}C NMR spectroscopy. On the basis of our spectral investigations we have found that compounds **2**, **3** and **4** exist as enaminone tautomers rather than as imine-enol or iminone [8]. In the IR spectra a group of strong bands resulting from C=O, C=N, and C=C stretching vibrations are present in the *ca.* 1640–1540 cm^{-1} region. The MS data were suitable for structure proof of "half units" type compounds **2** and **3**. The mass spectra give the peak of low abundance corresponding to the molecular ion. For the compounds **2** and **3** the intense peak at 105 *m/z* (**2**) or 104 *m/z* (**3**) confirms the fact that the condensation takes place on the carbonyl of the formyl group. For compounds **2**, **3** and **4** in the ^1H NMR spectra the low-field proton signal appears as a one proton doublet with coupling constant *J ca.* 11.5–12.5 Hz. This large value of the coupling constant is typical for *trans* coupling in H—C=N—H systems [9]. On the basis of detailed analysis of NMR spectra (three singlets of methyl groups) it was possible to assume that the compound **4** may exist at room temperature as a mixture of two rotamers **A** and **B**.

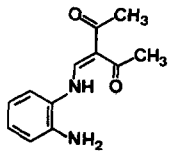

A

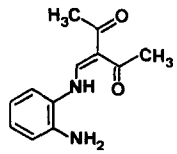

B

We have found that only in the case of the reaction of monocondensates **1–4** with oxalyl chloride, when the molar ratio of reagents was 2:1, could binucledating ligands **5–8** of the oxamido type be obtained. No such products have been isolated from the related reactions involving diethyl oxalate. The reactions leading to compounds **5–8** were carried out in the presence of triethylamine at room temperature according to the modified procedure of Amerago and Willette [10]. These oxamido ligands were characterised by elemental analyses and spectral methods, but ^1H and ^{13}C NMR spectra of ligand **7** and ^{13}C NMR spectra of ligands **5** and **8** could not be obtained by reason of their low solubility. Attempts to use mass spectra were unsuccessful because of decomposition of the compounds **5–8**. The IR spectra of the four ligands are very similar. In the case of compounds **6** and **8** we have observed the same effect of coupling H—C=N—H protons (as in the case of monocondensates **2–4**) and possibility of two rotamers of ligand **8**.

Binuclear complexes of Cu^{II} and Ni^{II} (**9–12**) with Schiff bases have been prepared by the reactions of ligands **5–8** with copper(II) acetate or nickel(II) acetate. These were characterised by combination of microanalyses and IR spectroscopy. ^1H and ^{13}C NMR spectra of the complexes of Ni^{II} (**8**, **11**, **13** and **15**) could not be obtained because of poor solubility. IR spectra of these complexes in comparison with the IR spectra of the ligands have shown the difference in the amine and carbonyl regions. In the IR spectra of complexes **9–16** no absorption is observed in the 3500–3000 cm^{-1} in accord with deprotonation of all NH enamine and amide groups upon complexation. The strong absorption at *ca.* 1750–1605 cm^{-1} assigned to the uncomplexed carbonyl groups, for coordinated ones is observed at *ca.* 1632–1604 cm^{-1} in accordance with earlier observations of similar complexes [11].

Structural studies

The X-ray crystal structure of the binuclear complex Cu^{II} (**10**) was determined. Figure 1 shows an

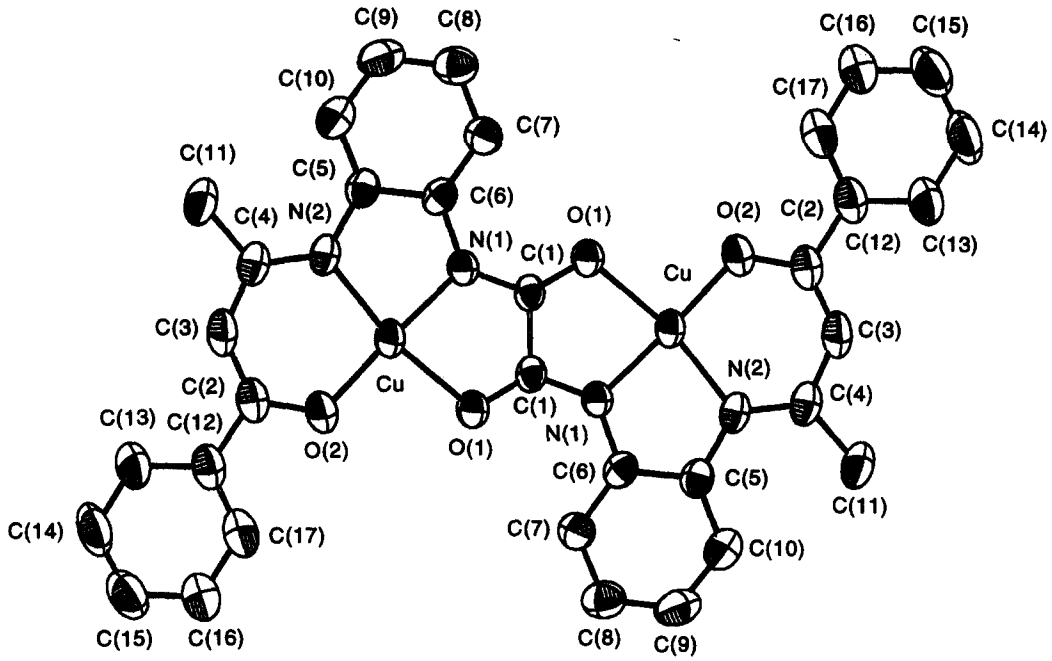

Fig. 1. ORTEP plot of **10** showing the atom numbering scheme.

Table 1. Interatomic distances (Å) for non-hydrogen atoms, with e.s.d. in parentheses, for complex **10**

Cu—N(1)	1.897(4)	C(5)—C(10)	1.390(8)
Cu—N(1)	1.960(4)	C(5)—N(2)	1.417(7)
Cu—N(2)	2.032(4)	C(6)—C(7)	1.389(7)
Cu—O(1)	1.863(4)	C(6)—N(1)	1.380(6)
Cu—O(2)	1.502(7)	C(7)—C(8)	1.381(8)
C(1)—C(1)[a]	1.266(6)	C(8)—C(9)	1.39(1)
C(1)[a]—N(1)	1.323(6)	C(9)—C(10)	1.38(1)
C(2)—C(3)	1.371(9)	C(12)—C(13)	1.40(1)
C(2)—C(12)	1.484(8)	C(12)—C(17)	1.36(1)
C(2)—O(2)	1.306(7)	C(13)—C(14)	1.38(1)
C(3)—C(4)	1.401(8)	C(14)—C(15)	1.36(1)
C(4)—C(11)	1.501(9)	C(15)—C(16)	1.37(1)
C(4)—N(2)	1.344(7)	C(16)—C(17)	1.39(1)
C(5)—C(6)	1.436(7)		

[a]Atoms related by symmetry operation $-x, -y, 1-z$.

ORTEP [14] plot of the title compound and the atom numbering scheme. Tables 1 and 2 list selected bond distances and angles for non-hydrogen atoms. The compound consists of discrete binuclear centrosymmetric $C_{34}H_{26}N_4O_4Cu_2$ units. There are two Cu atoms and four phenyl rings in each unit related by a symmetry centre. Each copper atom is surrounded by two nitrogen and two oxygen atoms. The oxygen and nitrogen ligands are *cis* coordinated to the metal. The whole molecule, including phenyl rings, is nearly planar. The dihedral angles between planes of phenyl rings formed by atoms C(12)—C(17), C(5)—C(10) and the least-squares plane of the main ring of the molecule (defined by C(1)—C(6), N(1), N(2), O(1), O(2) are 8.6(2) and 4.3(1)°, respectively. The Cu atoms are shifted from the least-squares plane of the molecule by 0.055(2) ≤ Å.

The Cu—Cu distance within the same molecule is 5.254 (8) Å, while the shortest intermolecular Cu—Cu distance is 5.66(5) Å. Within phenyl rings the bond lengths and angles are in good agreement with the corresponding values found in the literature.

From the molecular packing it is observed that no intermolecular contacts in this structure for different

Table 2. Bond angles (°) of the non-hydrogen atoms for complex **10** with standard deviations in parentheses

N(1)—Cu—N(2)	84.2(2)
N(1)—Cu—O(1)	83.7(2)
N(1)—Cu—O(2)	175.6(2)
N(2)—CU—O(1)	167.4(2)
N(2)—Cu—O(2)	99.2(2)
O(1)—Cu—O(2)	92.7(2)
C(1)[a]—C(1)—O(1)	120.1(4)
C(1)—C(1)[a]—N(1)	111.4(4)
C(3)—C(2)—C(12)	122.0(6)
C(3)—C(2)—O(2)	124.3(5)
C(12)—C(2)—O(2)	113.7(5)
C(2)—C(3)—C(4)	130.9(6)
C(3)—C(4)—C(11)	114.9(6)
C(3)—C(4)—N(2)	121.6(5)
C(11)—C(4)—N(2)	123.5(5)
C(6)—C(5)—C(10)	116.3(5)
C(6)—C(5)—N(2)	114.2(4)
C(10)—C(5)—N(2)	129.6(5)
C(5)—C(6)—C(7)	120.3(5)
C(5)—C(6)—N(1)	114.4(4)
C(7)—C(6)—N(1)	125.3(5)
C(6)—C(7)—C(8)	121.8(5)
C(7)—C(8)—C(9)	118.0(6)
C(8)—C(9)—C(10)	121.3(6)
C(5)—C(10)—C(9)	122.3(6)
C(2)—C(12)—C(13)	122.6(6)
C(2)—C(12)—C(17)	120.4(6)
C(13)—C(12)—C(17)	116.9(6)
C(12)—C(13)—C(14)	120.4(7)
C(13)—C(14)—C(15)	121.5(8)
C(14)—C(15)—C(16)	119.1(7)
C(15)—C(16)—C(17)	119.4(9)
C(12)—C(17)—C(16)	122.6(8)
Cu—N(1)—C(1)[a]	115.9(3)
Cu—N(1)—C(6)	115.3(3)
C(1)[a]—N(1)—C(6)	128.8(4)
Cu—N(2)—C(4)	120.8(4)
Cu—N(2)—C(5)	111.9(3)
C(4)—N(2)—C(5)	127.3(5)
Cu—O(1)—C(1)	108.8(3)
Cu—O(2)—C(2)	123.0(4)

[a]Atoms related by symmetry operation $-x, -y, 1-z$.

types of atoms are less than the sum of the corresponding van der Waals radii. This suggests that there are no forces other than van der Waals interactions stabilizing the structure.

Acknowledgement—The authors are grateful to Dr Anna Kolasa (Jagiellonian University, Kraków, Poland) for valuable discussion.

RERFERENCES

1. (a) Ojima, H. and Nonoyama, K., *Z. Anorg. Allg. Chem.*, 1972, **389,** 75; (b) Hall, G. R., Duggan, D. M. and Hendrickson, D. N., *Inorg. Chem.*, 1975, **14,** 1956; (c) Felthouse, T. R. and Laskowski, E. J., *Inorg. Chem.*, 1977, **16,** 1077; (d) McGregor, K. T. and Soos, Z. G., *Inorg. Chem.*, 1976, **15,** 2159; (e) Gleizer, A., Maury, F. and Gay, J., *Inorg. Chem.*, 1980, **19,** 2074; (f) Pei, Y., Verdaguer, M., Khan, O., Sletten, J. and Renard, J.-P., *Inorg. Chem.*, 1987, **26,** 138; (g) Pei, Y., Khan, O., Sletten, J., Renard, J.-P., Georges, R., Gianduzzo, J. C., Curely, J. and Xu, Q., *Inorg. Chem.*, 1988, **27,** 47.
2. (a) Gardner, A. P., Gatehouse, B. M., and White, J. C. B., *Acta Cryst., Sect B*, 1971, **27,** 1505; (b) Benson, T. H., Bilton, M. S. and Gill, N. S., *Aust. J. Chem.*, 1977, **30,** 261; (c) Kwiatkowski, E., Kwiatkowski, M., Olechnowicz, A. Ho, D. M. and Deutsch, E., *Inorg. Chim. Acta*, 1989, **158,** 37.
3. (a) Bett, G., Fenton, D. E. and Tate, J. R., *Inorg. Chim. Acta*, 1981, **54,** L101; (b) Costes, J.-P. and Cros, G., *C. R. Acad. Sci., Ser. 2,* 1982, **294,** 173; Kwiatkowski, E. and Kwiatkowski, M., *Inorg. Chim. Acta*, 1984, **82,** 101; (d) Costes, J.-P., Cros, G. and Laurent, J.-P., *Inorg. Chim. Acta*, 1985, **97,** 211; (e) Kwiatkowski, E. and Kwiatkowski, M., *Inorg. Chim. Acta*, 1984, **82,** 101; (f) Kwiatkowski, M., Kwiatkowski, M., Olechnowicz, A., Bandoli, G. and Dolmella, A., *Inorg. Chim. Acta*, 1992, **201,** 177; (g) Kwiatkowski M. and Bandoli, G., *J. Chem. Soc., Dalton Trans.*, 1992, 379; (h) Kwiatkowski, M., Kwiatkowski, E., Olechnowicz, A., Kościuszko-Panek, B. and Ho, D. M., *Polish J. Chem.*, 1994, **68,** 85.
4. Latif, N., Mishriky, N. and Assad, F. M., *Recl. Trav. Chim. Pays-Bas*, 1983, **102,** 73.
5. Costes, J.-P., Dahan, F. and Laurent, J.-P., *J. Chem. Soc., Dalton Trans.*, 1989, 1017.
6. (a) Sulca, M., Strakov, A. Ya. and Hirsbergs, J., *Latv. PSR Zinat. Akad. Vestis, Khim. Ser.*, 1971, 186; (b) Culter, A. R., Alleyne, C. S. and Dolphin, D., *Inorg. Chem.*, 1985, **24,** 2282.
7. Weissenfels, M., Kache, R. and Krauter, W., *J. Prakt. Chem.*, 1967, **35,** 166.
8. Brown, N. M. D. and Nonhebel, D. C., *Tetrahedron*, 1968, **24,** 5655.
9. (a) Forsen, S. and Nilsson, M., *Arkiv. Kemi*, 1962, **19,** 569; (b) Cameron, J. H. and McCullough, K. J., *J. Chem. Soc., Dalton Trans.* 1990, 935; (c) Kwiatkowski, M., Kwiakowski, E., Olechnowicz, A. Ho, D. M. and Deutsch E., *J. Chem. Soc., Dalton Trans.*, 1990, 2497.
10. Armarego, W. L. F. and Willette, R. E., *J. Chem. Soc.*, 1965, 1258.
11. (a) Mashuta, M. S., Doman, T. N., Pierce, W. and Buchanan, R. M., *Inorg. Chim. Acta*, 1988, **145,** 2; (b) Ueno, K. and Martell, A. E., *J. Phys. Chem.*, 1955, **59,** 998.
12. (a) Claisen L., *Liebigs Ann. Chem.*, 1897, **297,** 1; (b) Hesse, G., in *Methoden der organishe Chemie*, ed. Hauben-Weyl, Vol. VI/1d, Verlag, Stuttgart, 1978, p. 40–41.
13. Riley D. P. and Busch, D. H., *Inorg. Synth.*, 1978, **18,** 36.
14. Johnson, C. K., ORTEP, Report ORNL-3794, Oak Ridge National Laboratory, Oak Ridge, Tennessee, 1965.
15. Watenpaugh K. and Stewart, J., ABSCAL,

XTAL3.2 Reference Manual, ed. Hall, S. R., Flack, H. D. and Stewart, J. M., University of Western Australia, Geneva and Maryland, Lamb: Perth, 1992.
16. Sheldrick, G. M., *SHELXS 86, Program for the Solution of the Crystal Structures*, University of Goettingen, Germany, 1986.
17. Beurskens, P. T., Admiraal, G., Beurskens, G., Bosman, W. P., Geldeer, R., Israel, R. and Smita, J. M. M., *The DIRDIF-94 Program System.* Crystallography Laboratory, Unversity of Nijmegen, The Netherlands, 1994.
18. (a) Zachariasen, W. H., *Acta Cryst*, 1967, **A23,** 558; (b) Ahmed, F. R., Hall, S. R. and Huber, C. P., in *The Inclusion of Secondary Extinction in Least-Squares Refinement of Crystal Structures. Crystallographic Computing*, ed. Larson, A. C., Munksgaard, Copenhagen, 1969, p. 291–294.
19. (a) Cromer, D. T. and Mann, J. B., *Acta Cryst.*, 1968, **A24,** 321; (b) Cromer, D. T. and Waber, J. T., *International Tables for X-Ray Crystallography*, ed. Ibers, J. A. and Hamilton, W. C., Vol. IV, Kynoch Press, Birmingham, 1974, p. 55.
20. Hall, S. R., King, G. S. D. and Stewart, J. M., *Eds. XTAL 3.4 User's Manual.* University of Western Australia: Lamb, Perth, 1995.

Pergamon

PII: S0277-5387(97)00305-7

Polyhedron Vol. 17, No. 2–3, pp. 289–293, 1998
© 1997 Elsevier Science Ltd
All rights reserved. Printed in Great Britain
0277-5387/98 $19.00+0.00

A new tetraazamacrocycle functionalized with four pendant pyridyl groups: synthesis and crystal structure of the nickel(II) complex of 1,4,7,10-tetrakis(2-pyridylmethyl)-1,4,7,10-tetraazacyclododecane(L), $[NiL]^{2+}$

Xian-He Bu,[a] Xi-Chuan Cao,[a] Wei Chen,[a] Ruo-Hua Zhang[a]* and Clifford Thomas[b]

[a] Department of Chemistry, Nakai University Tianjin 300071, P.R. China

[b] Department of Chemistry, St. Andrews University, Fife, U.K.

(Received 11 March 1997; accepted 9 July 1997)

Abstract—The title complex, $[NiL](ClO_4)_2$ was synthesized by the reaction of nickel(II) perchlorate and the new macrocycle ligand, 1,4,7,10-tetrakis(2-pyridylmethyl)-1,4,7,10-tetraazacyclododecane (L) in ethanol solution. The crystal and molecular structure of this complex has been determined by single-crystal X-ray diffraction. The complex consists of $[NiL]^{2+}$ cation and two perchlorate anions. Within the $[NiL]^{2+}$ cation, the potential octadentate ligand is using its 4 nitrogen atoms of the macrocycle and 2 pyridine nitrogens to coordinate with the central nickel(II), while the other two pyridine nitrogens remained uncoordinated. The central nickel(II) ion is in a distorted-octahedral coordination environment and in high-spin state. © 1997 Elsevier Science Ltd

Keywords: nickel(II) complex; crystal structure; synthesis; 1,4,7,10-tetrakis(2-pyridylmethyl)-1,4,7,10-tetraazacyclododecane.

The coordination properties toward metal ions of macrocycles bearing pendant donor groups from the macrocycle skeleton have recently attracted much interest, mainly as the study of such systems may provide a basis for a better understanding of the metal environment in some metalloenzymes and metalloproteins [1,2]. Recently some reports have indicated that functionalized macrocycles containing pendant arms can form stable complexes with transition metals and exhibit functional properties. These types of macrocycles can bond to metals ion forming 1 : 1 or 1 : 2 molar ratio complex [2–5].

We report herein the functionalization of 1,4,7,10-tetraazacyclododecane (cyclen) with four pyridine groups connected to the macrocycle through methylene chains. This potential octadentate ligand, 1,4,7,10-tetrakis(2-pyridylmethyl)-1,4,7,10-tetraazacyclododecane (L), can form binuclear complexes with large metal ions (e.g. lanthanide ions) and mononuclear complexes with smaller metal ions (e.g., copper(II) and nickel(II) ions). In this paper, we describe the synthesis and characterization of the new ligand L and the crystal and molecular structure of its Ni(II) complex.

* Author to whom correspondence should be addressed.

EXPERIMENTAL

Materials

1,4,7,10-tetraazacyclododecane (cyclen) was prepared according to the literature method [6]. 2-(Chloromethyl)pyridine hydrochloride was obtained from Aldrich Co. Inc. and used without further purification. Other chemicals were of analytical grade.

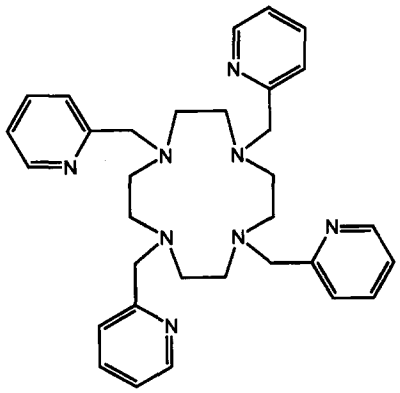

L

All the solvents were purified by standard procedures prior to use.

Physical measurements

IR spectra were recorded on a FT-IR 5DX (Nicolet) spectrophotometer using KBr discs. Proton NMR spectra were recorded on a Bruker AC-P 200 spectrometer (200 MHz, at 25°C, in $CDCl_3$ solution, with tetramethylsilane as the internal reference). EI-mass spectra (MS) were measured on a VG ZAB-HS instrument. Electronic absorption spectra were obtained by using a Shimadzu UV-240 spectrophotometer. Elemental analysis was performed on a P-E 240C analyzer. Magnetic susceptibility was measured on a Faraday balance at room temperature and the calibration was made with Mohr's salt. Effective magnetic moment was calculated by the equation $\mu_{eff} = 2.828(X_m T)^{1/2}$, where X_m is the magnetic susceptibility corrected for diamagnetism of the constituting atoms using Pascal's constants.

Synthesis of 1,4,7,10-*tetrakis*(2-*pyridylmethyl*)-1,4,7,10-*tetraazacyclododecane* (*L*)

To a solution of 1,4,7,10-tetraazacyclododecane (0.5 g, 2.9 mmol) in dichloromethane (30 cm^3) was added a solution of NaOH (0.93 g, 23.2 mmol) in water (25 cm^3). This two-phase mixture was stirred for *ca.* 30 min. Then, a solution of 2-(chloromethyl)pyridine hydrochloride (2.0 g, 12.6 mmol) in dichloromethane (15 cm^3) was added dropwise to the mixture over a period of *ca.* 1 h. The stirring was continued at *ca.* 30°C for one day and the organic layer was then separated. The aqueous layer was extracted with chloroform (5×50 cm^3), and the combined organic layers were evaporated to give a residue which was purified by column chromatography on silica gel (eluent: CH_2Cl_2 : Acetone = 98 : 2 ~ 10). The final product was obtained by recrystallization from $C_2H_5OH \sim (C_2H_5)_2O$ as colourless needles. Yield 1.24 g (80%), m.p. 159–161°C. EI-MS (*m*/*z* peak): 536 (Mr = 536.72). ^1H NMR (200 MHz, $CDCl_3$) δ 2.61 (broad peak, 16H, CH_2—CH_2), 3.37 (broad peak, 8H, N—CH_2—Py), 6.94 (t, 4H, Py), 7.09 (d, 4H, Py), 7.37 (t, 4H, Py), 7.58 (t, 4H, Py). Calc. for $C_{32}H_{40}N_8$: C, 71.61; H, 7.51; N, 20.88. Found: C, 71.52; H, 7.24; N, 20.77%. IR (KBr pellet, cm^{-1}): 2813 (C—H), 1631, 1592 (Py ring), 1095 (C—N). UV-vis (in CH_3OH) [λ_{max} nm (ε: 1 mol cm^{-1})]: 204 (2.13×10^4), 260 (0.94×10^4).

Preparation of [NiL] $(ClO_4)_2$

The violet single crystal of the title complex suitable for X-ray analysis was obtained by mixing a 1 : 1 molar ratio of $Ni(ClO_4)_2 \cdot 6H_2O$ (40 mg, 0.11 mmol) and L (60 mg, 0.11 mmol) in ethanol solution (10 cm^3) under reflux for *ca* 30 min. The reaction mixture was filtered and the beautiful violet crystal was obtained from the slow evaporation of the solvent. Yield: 44 mg (50%). IR (KBr pellet): 3483, 3070, 2870, 2013, 1608, 1571, 1593, 1475, 1436, 1352, 1308, 1090 (broad and strong), 1015, 968, 772, 622 cm^{-1}. Calc. for $C_{32}H_{40}N_8Cl_2O_8Ni$: C, 48.39; H, 5.08; N, 14.11. Found: C, 48.60; H, 5.32; N, 13.82%.

Warning! The perchlorate compounds are potentially explosive and should be handled carefully.

Crystallographic studies

A crystal (approximately $0.2 \times 0.3 \times 0.4$ mm) of complex [NiL] $\cdot (ClO_4)_2$ was mounted on an Enraf-Nonius CAD-4 diffractometer equipped with a graphite crystal monochromator situated in the incident beam for data collection. The determination of unit cell and the data collection were performed with Mo-K_α radiation ($\lambda = 0.71073$ Å). Unit cell dimensions were obtained by least-square refinements using 25 reflections in the range of $9.91° < \theta < 12.24°$. The intensities of reflections were measured at the $\omega/2\theta$ scan mode in the range of $2° < \theta < 23°$ at room temperature. A total of 4230 independent reflections were collected, in which 2396 reflections with $I \geqslant 3\sigma(I)$ were considered to be observed and used in the succeeding refinement. The structure was solved by SHELXS-86 method. Ni atom was located from an *E*-map. The other non-hydrogen atoms were determined with successive differential Fourier synthesis. The positions of hydrogen atoms were treated theoretically as riding on their relative atoms and refined isotropically. The final refinement by full matrix least-squares method with anisotropic thermal parameters for non-hydrogen atoms was converged with unweighted and weighted (unit weights for all observed reflections) agreement factors of 0.066 and 0.078. The highest peak on the final difference Fourier map had a height of 0.76 $eÅ^3$.

All the calculations were performed on a PDP11/44 computer, using SDP-PLUS, SHELXS-86 and

Table 1. Crystallographic data for $[NiL]^{2+}$

Formula	$C_{32}H_{40}N_8Cl_2O_8Ni$
Mr	794.34
Crystal colour	violet
Cryst. dimensions (mm)	$0.2 \times 0.3 \times 0.4$
Crystal system	monoclinic
Space group	$P2_1/c$
a (Å)	18.222(4)
b (Å)	9.446(2)
c (Å)	19.955(2)
β (°)	92.42(1)
V (Å^3)	3431.7(11)
Z	4
D_c (g cm^{-3})	1.537
μ (cm^{-1})	7.85
F (000)	1656
T (K)	299
Radiation	Mo-K_α
λ (Å)	0.71073
Scan mode	$\omega/2\theta$
θ_{max} (°)	23
Scan speed (°/min)	0.92–5.49
No. of measured reflections	5264
No. of independent reflections	4230
No. of observed reflections ($I \geqslant 3\sigma(I)$)	2396
R	0.066
R_w	0.078
$(\Delta/\sigma)_{max}$	0.81
S	1.10
Max. residual peak (e/Å^3)	0.76

SHELXL-93 program systems. The crystallographic data are summarized in Table 1.

RESULTS AND DISCUSSION

Synthesis of ligand and preparation of the complex

The synthesis of L can be carried out easily in water-dichloromethane two-phase solution by the reaction of cyclen with an excessive amount of 2-(chloromethyl)pyridine hydrochloride, and then extracted by chloroform and further purified by column chromatography and recrystallization from ethanol/ether in high yield. All the analytical data are in good agreement with the theoretical requirements of the ligand.

The complex was prepared by the reaction of hydrated nickel perchlorate and L in 1 : 1 molar ratio in ethanol solution in good yield. The violet crystalline compound is soluble in water and DMF, and is slightly soluble in ethanol and methanol.

General characterization of the complex

The ligand L shows strong IR bands at 1631 and 1592 cm^{-1} attributable to ν(py ring) stretching vibrations. There are two vibration bands in the IR spectrum of the complex assigning to the vibrations coordinated ($\sim$1608 and $\sim$1575 cm^{-1}). In addition, strong peaks of the vibrations of free perchlorate at $\sim$1090 and $\sim$622 cm^{-1} appeared in the IR spectrum of the complex.

The effective magnetic moment of the Ni^{II} complex is determined to be 3.12 B.M. (at room temperature), which indicates that the complex is octahedral and the central nickel(II) atom is in high spin state in nature [7]. Electronic spectrum of the complex in methanol solution shows strong absorption bands at 208 nm ($\varepsilon = 2.48 \times 10^4$ l mol^{-1} cm^{-1}) and 260 nm ($\varepsilon = 1.66 \times 10^4$ l mol^{-1} cm^{-1}), which can be assigned to the intra-ligand transitions. The spectra of the pseudo-octahedral nickel(II) complexes retain the simple form found in O_h symmetry showing validity of average environment rule [8]. The UV-vis spectra of nickel(II) complex in DMF solution gave three bands at 11364, 18315 and 26455 cm^{-1}, which corresponds to the transitions $^3A_{2g} \rightarrow {}^3T_{2g}(F)$, $^3T_{1g}(F)$ and $^3T_{1g}(P)$, respectively. The value of B (711.5 cm^{-1}), the Racah parameter, was calculated using the diagonal sum rule [8]. The calculated value of $\beta = B_{complex}/B_{free\,ion} = 0.691$ shows strong covalent bonding of nickel in the complex.

Crystal and molecular structure

The labelling scheme of the $[NiL]^{2+}$ cation is shown in Fig. 1 and the selected bond lengths and angles are presented in Table 2.

The structure consists of a discrete monomeric $[NiL]^{2+}$ cation and two uncoordinated perchlorate anions. The nickel(II) centre is six-coordinated [with N(1), N(2), N(3), N(4), N(11) and N(13)] and adopts a distorted-octahedral geometry. Only two of the four pyridine donor pendants in nonadjacent-positions interacting with the central nickel(II) and the other two pendant pyridines remaining uncoordinated. The four amine nitrogens span two contiguous faces of the distorted octahedron about the nickel atom, and the pyridine nitrogens occupy the remaining pair of *cis* positions in the coordination polyhedron.

The main deviations from the idealized geometry, possibly imposed by geometric requirements of the ligand, are due to (1) incomplete folding of the 12-membered macrocycle ring, revealed by the 105.3(3)° N(1)—Ni(1)—N(3) angle, larger than the expected 90° angle for the idealized geometry and (2) the inability of the nitrogen atoms of the macrocycle bearing pendant groups to reach *trans* positions in the coordination sphere. As a consequence of the latter constraint, the N(2)—Ni(1)—N(4) angle [153.7(3)°] is smaller than the expected 180° for the octahedral coordination geometry and all donor atoms of the macrocycle are forced to lie on one side of the nickel atom.

The macrocycle takes a *trans-I* configuration in which all the lone pairs in the four basal nitrogens are

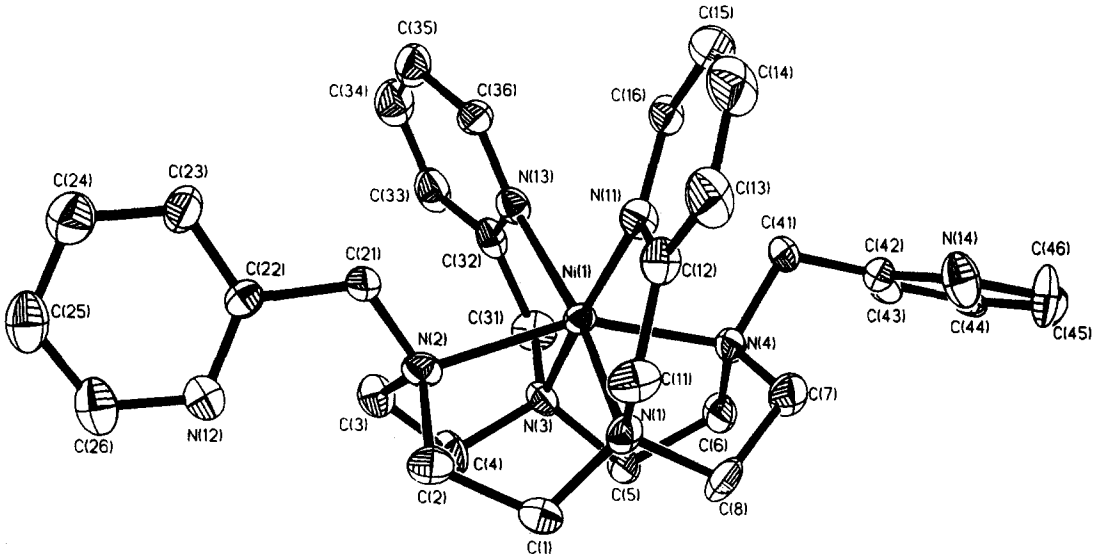

Fig. 1.

Table 2. Selected bond distances (Å) and angles (°)

Ni(1)—N(1)	2.120(8)	Ni(1)—N(2)	2.249(8)
Ni(1)—N(3)	2.102(8)	Ni(1)—N(4)	2.210(8)
Ni(1)—N(11)	2.066(8)	Ni(1)—N(13)	2.148(8)
N(1)—C(1)	1.498(15)	N(1)—C(8)	1.466(14)
N(1)—C(11)	1.482(14)	N(2)—C(2)	1.528(13)
N(2)—C(3)	1.489(13)	N(2)—C(21)	1.488(12)
N(3)—C(4)	1.482(14)	N(3)—C(5)	1.501(12)
N(3)—C(31)	1.500(13)	N(4)—C(6)	1.504(13)
N(4)—C(7)	1.491(14)	N(4)—C(41)	1.520(14)
N(1)—Ni(1)—N(2)	80.6(3)	N(1)—Ni(1)—N(3)	105.3(3)
N(2)—Ni(1)—N(3)	82.6(3)	N(1)—Ni(1)—N(4)	82.8(3)
N(2)—Ni(1)—N(4)	153.7(3)	N(3)—Ni(1)—N(4)	82.2(3)
N(1)—Ni(1)—N(11)	80.8(3)	N(2)—Ni(1)—N(11)	107.4(3)
N(3)—Ni(1)—N(11)	169.2(3)	N(4)—Ni(1)—N(11)	89.8(3)
N(1)—Ni(1)—N(13)	168.6(3)	N(2)—Ni(1)—N(13)	89.8(3)
N(3)—Ni(1)—N(13)	79.5(3)	N(4)—Ni(1)—N(13)	108.3(3)
N(11)—Ni(1)—N(13)	96.2(3)		

oriented to the same side of the macrocycle plane [9]. The macrocyclic ring folds to coordinate to the metal ion, thereby relieving steric strain within the macrocycle and minimizing repulsion among the coordinated pyridine groups.

The averaged Ni—N distances of the six Ni—N bonds are 2.166(8) Å, being typical Ni—N distance for the high spin nickel(II) in octahedral environment. This is in agreement with the effective magnetic moment of the complex. The bond distances of Ni(1)—N(1) and Ni(1)—N(3) are slightly shorter than those of Ni(1)—N(2) and Ni(1)—N(4), indicating weaker coordination of the macrocycle nitrogens connected to the uncoordinated methylpyridines than those connected to the coordinated methylpyridines, possibly for relieving steric strain within the macrocycle and minimizing repulsion among the coordinated pyridylmethyl groups. All sets of distances are in the ranges of values found for nickel complexes formed by other macrocycles [1,10].

The nickel atom is constrained to lie on the least-squares plane, defined by the atoms N(1), N(3), N(11), N(13) but is high above the mean plane formed by the four basal macrocycle nitrogens N(1), N(2), N(3) and N(4) by *ca* 0.9 Å, which in turn lie in pairs at 0.39 Å on opposite sides of that plane. While in the nickel(II) complex of Me_4-12aneN$_4$ [11], the nickel (II) ion extruded from the four basal macrocycle plane only by 0.29 Å. This great difference may arise from the fact that the nickel atom rises out of the basal plane to accept the strong coordination of the pendant pyridines in our complex.

Acknowledgements—This work was financially supported by the National Natural Science Foundation of China (NSFC) and the Natural Science Foundation of Tianjin, China.

REFERENCES

1. Alexandra, V., *Chem. Rev.*, 1955, **95,** 273.
2. Norante, G. M., Vaira, M. D., Mani, F., Mazzi, S. and Stoppioni, P., *Inorg. Chem.*, 1990, **29,** 2822.
3. Che, C.-M., Tang, W.-T. and Mak, T. C. W., *J. Chem. Soc., Dalton Trans.*, 1988, 2879.
4. Alcock, N. W., Balakrisknan, K. P. and Moore, P., *J. Chem. Soc., Dalton Trans.*, 1986, 1743.
5. Vaira, M. D., Mani, F., Nardi, N., Stoppioni, P. and Vacca, R., *J. Chem. Soc., Dalton Trans.*, 1996, 2679.
6. Richman, J. E. and Alkins, T. J., *J. Amer. Chem. Soc.*, 1974, **96,** 2268.
7. Lever, A. B. P. and Orden, D., *J. Chem. Soc.*, (*A*), 1967, 2041.
8. Bostrup, O. and Jørgensen, C. K., *Acta Chem. Scand.*, 1975, **11,** 1223.
9. Thom, V. J., Fox, C. C., Booyens, J. C. A. and Hancock, R. D., *J. Am. Chem. Soc.*, 1984, **106,** 5947.
10. Wieghardt, K., Schoffmann, E., Nuber, B. and Weiss, J., *Inorg. Chem.*, 1986, **25,** 4877.
11. Coates, J. H., Hadi, D. M. M. A., Hambley, T. W., Lincoln, S. F. and Rogers, J. R., *Cryst. Struct. Commun.*, 1982, **11,** 815.

Pergamon

PII: S0277-5387(97)00302-1

Polyhedron Vol. 17, No. 2–3, pp. 295–298, 1998
© 1997 Elsevier Science Ltd
All rights reserved. Printed in Great Britain
0277-5387/98 $19.00+0.00

Gold complexes with 2-selenoxo-1,3-dithiole-4,5-dithiolato

Elena Cerrada, Mariano Laguna* and Pedro A. Sorolla

Departamento de Química Inorgánica, Instituto de Ciencia de Materiales de Aragón, Universidad de Zaragoza-C.S.I.C., 50009 Zaragoza, Spain

(Received 9 June 1997; accepted 7 July 1997)

Abstract—The reaction of Na_2dmise (dmise = 2-selenoxo-1,3-dithiole-4,5-dithiolate) with [AuClL] in 1:2 molar ratio affords $[Au_2(dmise)L_2]$ (L = PR_3 or CH_2PPh_3) but in 1:1 ratio in the presence of (NBu_4) Br gives $(NBu_4)[Au(dmise)L]$. The PPh_2Me dinuclear derivative further reacts with $[Au(OClO_3)(PPh_2Me)]$ to give $[Au_3(dmise)(PPh_2Me_3)_3]ClO_4$. The reaction with $[Au_2(P\text{-}P)Cl_2]$ renders $[Au_2(P\text{-}P)(dmise)]_n$ with different nuclearity depending on the diphosphine used (P-P = dppe, $n = 1$; dppm, $n = 2$). Anionic derivatives $(PPN)_2[Au_2(dmise)(C_6F_5)_2]$ and $(PPN)[Au(dmise)_2]$ are obtained by reaction with the corresponding halo-anionic gold complexes. © 1997 Elsevier Science Ltd

Keywords: gold; dithiolate; dmise; phosphine; ylide.

The ligands dmit (2-thioxo-1,3-dithiole-4,5-dithiolate), dmise (2-selenoxo-1,3-dithiole-4,5-dithiolate) and analogues have been shown a considerable interest as versatile building blocks of conducting materials [1–6]. Since several examples of $M(dmit)_2$ salts with intramolecular S···S interactions *via* terminal thioxo group have been found [7], a selenoxo group is expected to increase these terminal contacts owing to the more diffuse and spatially extended orbitals of selenium compared with sulphur. Few studies on dmise ligand have been reported to date, in particular $[M(dmise)_2]^{n-}$ (M = Ni, Pd n = 1–2) [5,8] derivatives and only two of them have shown a metallic behaviour [1,9].

In this paper we report a study of co-ordination properties of dmise ligand with gold derivatives leading to complexes in which the dmise is acting as bidentate chelate {$(NBu_4)[Au(dmise)L]$ and $(PPN)[Au(dmise)_2]$} among others with novel coordination modes as bridge μ_2 {$[Au_2(dmise)L_2]$ (L = phosphine), $[Au_2(dmise)(L\text{-}L)]_n$ (L-L = dppm, dppe) or $(PPN)_2[Au_2(dmise)(C_6F_5)_2]$} and μ_3 {$[Au_3(dmise)L_3]ClO_4$}.

EXPERIMENTAL

General procedures

Infrared spectra were recorded on a Perkin Elmer 883 spectrophotometer, over the range 4000–200 cm^{-1}, by using Nujol mulls between polyethylene sheets, ^1H and ^{31}P NMR spectra on a Varian UNITY 300 in $CDCl_3$ solutions; chemical shifts are quoted relative to $SiMe_4$ (^1H) and H_3PO_4 (external ^{31}P). The C, H, N and S analyses were performed with a Perkin Elmer 2400 microanalyser. Conductivities were measured in acetone with a Philips PW 9509 apparatus. Mass spectra were recorded on a VG Autospec, by liquid secondary ion mass spectrometry (LSIMS + or −) using nitrobenzylalcohol as matrix. The yields C, H, N and S analyses and $^{31}P\{^1H\}$ and some ^1H NMR data are listed in Table 1.

Starting materials

4,5-Bis(benzoylthio)-1,3-dithiole-2-selenone [1,8(c)] $[AuCl(PR_3)]$ [15], $[AuCl(CH_2PR_3)]$ [16], $Q[Au(C_6F_5)X]$ [15], $[Au_2(\mu\text{-dppm})Cl_2]$ [17] and $[Au_2(\mu\text{-dppe})Cl_2]$ [17] were obtained according to the literature procedures.

* Author to whom correspondence should be addressed.

Table 1. Analytical and spectroscopic data for complexes **1–12**

Complex	Yield (%)	Analysis: found (calc.) (%) C	H	S	N	^{31}P NMR (ppm)	^{1}H NMR δ_{Me} (J_{P-H})
1 $[Au_2(dmise)(PPh_3)_2]$	65	39.65 (40.3)	2.4 (2.6)	11.6 (11.1)	—	36 (s)	—
2 $[Au_2(dmise)(P(p\text{-}C_6H_4OMe)_3)_2]$	68	39.8 (40.35)	2.7 (3.1)	8.85 (9.5)	—	35 (s)	2.3 (s)
3 $[Au_2(dmise)(PPh_2Me)_2]$	65	33.5 (33.5)	1.9 (2.4)	13.0 (12.4)	—	20 (s)	2.07 (d, 10.2 Hz)
4 $[Au_2(dmise)(PMe_3)_2]$	60	14.4 (13.7)	2.5 (2.3)	17.3 (16.3)	—	−8.6 (s)	1.6 (d, 11.2 Hz)
5 $[Au_2(dmise)(CH_2PPh_3)_2]$	65	41.8 (41.4)	3.15 (2.85)	11.5 (10.8)	—	31 (s)	1.9 (d, 12.2 Hz)
6 $[Au_3(dmise)(PPh_2Me)_3]ClO_4$	60	32.2 (32.9)	2.0 (2.5)	9.2 (8.3)	—	18.2 (s, br)[a]	2.11 (d, 10.2 Hz)
7 $[Au_2(dmise)(dppe)]$	62	33.8 (33.6)	1.9 (2.3)	10.9 (12.4)	—	32.7 (s)	3.45 (s)
8 $[Au_4(dmise)_2(dppm)_2]$	63	32.55 (32.9)	2.1 (2.15)	13.0 (12.5)	—	37.5 (dd) 24.1 (dd)	4.15 (m), 4.35 (m)
9 $(NBu_4)[Au(dmise)(PPh_3)]$	60	46.6 (47.0)	5.05 (5.4)	14.4 (13.6)	1.2 (1.5)	42.5 (s)	—
10 $(NBu_4)[Au(dmise)(PPh_2Me)]$	65	42.95 (43.5)	5.0 (5.5)	15.0 (14.5)	1.3 (1.6)	23.5 (s)	2.1 (d, 8.5 Hz)
11 $(PPN)_2]Au_2(dmise)(C_6F_5)_2]$	70	50.5 (51.0)	3.1 (2.45)	6.7 (6.3)	1.1 (1.35)	—	—
12 $PPN[Au(dmise)_2]$	90	41.8 (41.3)	2.3 (2.4)	22.0 (21.05)	1.3 (1.15)	—	—

[a] At −60°C: 17.6 (s) and 19.3 (s).

Preparation of $[Au_2(dmise)(L)_2]$ [L = PPh_3 (**1**), P(p-$C_6H_4OMe)_3$ (**2**), PPh_2Me (**3**), PMe_3 (**4**), CH_2PPh_3 (**5**)].

Sodium metal (9 mg, 0.4 mmol) and 4,5-bis(benzoylthio)-1,3-dithiole-2-selenone (68 mg, 0.15 mmol) were dissolved under nitrogen atmosphere in methanol (20 cm^3) to give a dark red solution of Na_2dmise, to which was added $AuCl(PPh_3)$ (148 mg, 0.3 mmol), $AuCl(P(p\text{-}C_6H_4OMe)_3)$ (175 mg, 0.3 mmol), $AuCl(PPh_2Me)$ (129 mg, 0.3 mmol), $AuCl(PMe_3)$ (93 mg, 0.3 mmol) or $AuCl(CH_2PPh_3)$ (152 mg, 0.3 mmol). Immediately different colour solid complexes (**1–5**) precipitated: dark yellow (**1, 4**), brown (**2, 3**) and orange (**5**), which were collected by filtration, washed with methanol and dried *in vacuo*.

Preparation of $[Au_3(dmise)(PPh_2Me)_3]ClO_4$ (**6**)

To a dichloromethane solution of $[AuCl(PPh_2Me)]$ (43 mg, 0.1 mmol) was added $AgClO_4$ (20 mg, 0.1 mmol). After stirring for 1 h the suspension was filtered through 1 cm of Celite, $[Au_2(dmise)(PPh_2Me)_2]$ (104 mg, 0.1 mmol) was added to the resulting solution. After stirring for 3 h the solution was concentrated by evaporation and the addition of diethyl ether led to precipitation of a dark garnet solid which was filtered off and dried *in vacuo*.

Preparation of $[Au_2(dmise)(L\text{-}L)]_n$ [$n = 1$, L-L = dppe (**7**), $n = 2$, L-L = dppm (**8**)]

To a methanolic solution (20 cm^3) with sodium metal and 4,5-bis(benzoylthio)-1,3-dithiole-2-selenone (68 mg, 0.15 mmol) under dinitrogen, was added $[Au_2(\mu\text{-dppe})Cl_2]$ (129 mg, 0.15 mmol) or $[Au_2(\mu\text{-dppm})Cl_2]$ (127 mg, 0.15 mmol). The solutions turn brown. After 1 h of stirring, the solutions were concentrated to dryness. Addition of acetone (20 cm^3) gave white solids corresponding to NaCl, which were filtered through 1 cm of Celite. Partial evaporation of the resulting solutions and addition of diethyl ether led to the precipitation of light brown solids which were filtered off and dried *in vacuo*.

Preparation of $NBu_4[Au(dmise)L]$ [L = PPh_3 (**9**), PPh_2Me (**10**)]

4,5-Bis-(benzoylthio)-1,3-dithiole-2-selenone (68 mg, 0.15 mmol) was dissolved under nitrogen atmosphere in a methanol (20 cm^3) solution containing sodium metal (9 mg, 0.4 mmol). A dichloromethane (5 cm^3) solution of $AuCl(PPh_3)$ (75 mg, 0.15 mmol) or $AuCl(PPh_2Me)$ (64 mg, 0.15 mmol) was added followed by a dichloromethane (5 cm^3) solution of NBu_4Br (48 mg, 0.15 mmol) with stirring. The solu-

tions turned red. After stirring for 12 h the solutions were evaporated to remove all the solvent, and acetone (15 cm^3) was added affording a white solid corresponding to NaCl, which was filtered off. The solutions were concentrated to 5 cm^3. Addition of diethyl ether precipitated garnet solid, which was filtered off.

Preparation of $(PPN)_2[Au_2(dmise)(C_6F_5)_2]$ **(11)**

Sodium metal (9 mg, 0.4 mmol) and 4,5-bis(benzoylthio)-1,3-dithiole-2-selenone (68 mg, 0.15 mmol) were dissolved under nitrogen atmosphere in methanol (20 cm^3) to give a dark red solution, to which was added PPN[Au(C_6F_5)Cl] (222 mg, 0.3 mmol). Immediately pink solid precipitated, which was collected by filtration, washed with methanol and dried *in vacuo*.

Preparation of PPN[Au(dmise)$_2$] **(12)**

Sodium metal (9 mg, 0.4 mmol) and 4,5-bis(benzoylthio)-1,3-dithiole-2-selenone (90 mg, 0.2 mmol) were dissolved under nitrogen atmosphere in methanol (20 cm^3) to give a dark red solution, to which was added PPN[$AuBr_4$] (105 mg, 0.1 mmol). A garnet solid precipitated which was collected by filtration, washed with methanol and dried *in vacuo*.

RESULTS AND DISCUSSION

The synthesis of complexes with dmit and analogues ligands with other calcogen atoms reported to date have been carried out starting from the COPh protected derivatives. In our case, the reaction of methanolic solutions of dmise$(COPh)_2$ in the presence of sodium to give Na_2dmise with chlorogold(I) complexes [AuClL] (L = phosphine or ylide) in 1 : 2 molar ratio, leads to dinuclear compounds where the dmise ligand acts as a bridge between the metallic centres, in a similar way to those reported by us for dmit derivatives [10] (See Scheme 1, i).

Complexes with the general formula [Au_2(dmise)L_2] (L = PPh_3 **1**, $P(p\text{-}C_6H_4OMe)_3$ **2**, PPh_2Me **3**, PMe_3 **4**, CH_2PPh_3 **5**) can be isolated as air- and moisture-stable solids at room temperature. Their spectroscopic properties are in agreement with its formulation: one singlet in $^{31}P\{^1H\}$ NMR very close to the values observed in the analogues of dmit, since the selenoxo group is too far to affect these signals. Their IR spectra show a band at *ca* 950 cm^{-1} due to ν(C=Se) vibration [11] and a band at 580 cm^{-1} assignable to ν(Au—C_{ylide}) [12]. The mass spectra (LSIMS+) show the parent peak M^+ at m/z (%): 1161 (15) **1**, 1341 (9) **2**, 1037 (15) **3**, 789 (20) **4**, with the expected isotopic distribution which in this case are illustrative because of the presence of six isotopes of selenium. As occurred for the dmit derivatives there

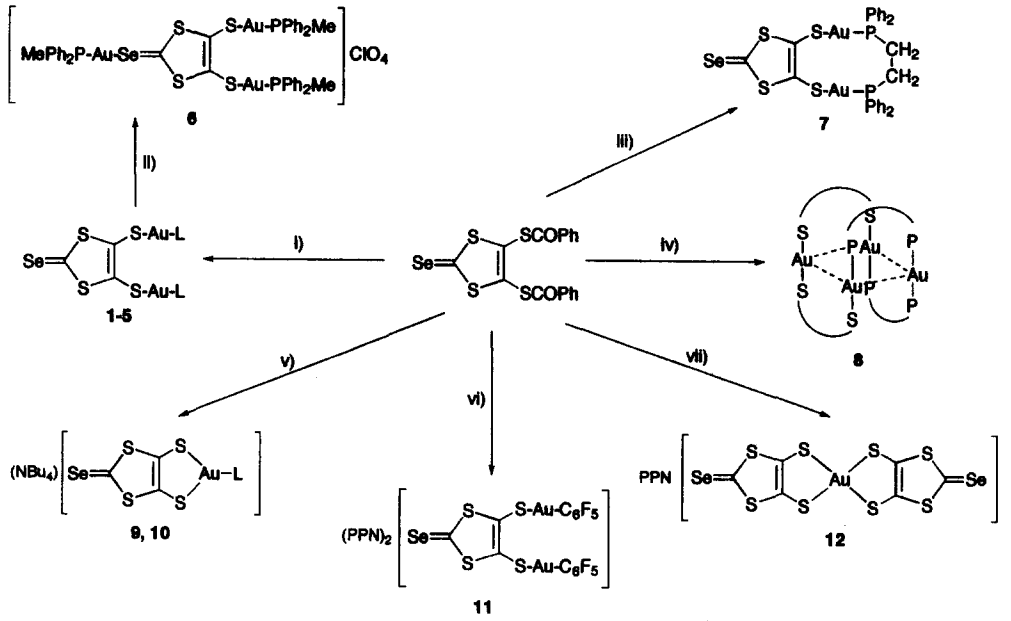

I) 2 [AuClL], II) [$AuOClO_3PPh_2Me$], III) [$Au_2(\mu$-dppe)Cl_2] IV) [$Au_2(\mu$-dppm)Cl_2], V) [AuClL] + NBu_4Br, VI) 2 PPN[Au(C_6F_5)Cl], VII) 1/2 PPN[$AuBr_4$]

Scheme 1.

are signals due to $[M+AuL]^+$ ion at *m/z* (%): 1620 (10) **1**, 1890 (6) **2**, 1434 (5) **3**, 1062 (30) **4**. The corresponding trinuclear complex in the case of L = PPh_2Me **6** can be achieved by a reaction of the dinuclear one **2** and a fresh solution of [Au($OClO_3$)(PPh_2Me)] (ii). Its ^1H NMR spectrum shows a doublet at 2.11 ppm [$^2J_{H-P} = 10.2$ Hz] and the $^{13}P\{^1H\}$ NMR at room temperature shows a broad signal, which is resolved in two singlets of relative intensity 2 : 1 at −60°C. This complex shows conductivity in acetone solution (5×10^{-4} M) characteristic of a 1 : 1 electrolyte [13] and the mass spectrum shows the parent ion at *m/z* (%) 1899 (16). According to the data for **1–6** complexes, we can postulate similar structures to those reported for dmit ligand, with the dmise ligand acting as μ_2 and μ_3 bridge.

Similar reaction with bisphosphine gold complexes (iii and iv) give different results depending on the phosphine. So, when dppe (1,2-bis(diphenylphosphine)ethane) is used, complex [Au_2(dmise)(dppe)] **7** can be isolated, but with dppm (1,2-bis(diphenylphosphine) methane) [Au_2(dmise)(dppm)]$_2$ **8** is obtained instead. The $^{31}P\{^1H\}$ NMR for **7** consists on a singlet centred at 32.7 ppm in accordance with the proposed formulation and complex **8** shows an AA′XX′ system: $\delta_A = 37.7$ ppm, $\delta_X = 24.1$ ppm, $^2J_{AA'} = 81$ Hz, $^2J_{AX} = {}^2J_{A'X} = 46.4$ Hz. These data are very close to those reported to the dmit derivatives pointing out similar structures for dmit and dmise compounds [10,14] (see Scheme 1).

When the reaction i with [AuClL] is made in 1 : 1 molar ratio and after addition of NBu_4Br (v) anionic NBu_4[Au(dmise)L] (L = PPh_3 **9**, PPh_2Me **10**) are obtained. Complexes **9** and **10** behave as 1 : 1 electrolytes in acetone solution in accordance with their formulation. Their $^{31}P\{^1H\}$ NMR spectra show singlets displaced down field with respect to the dinuclear compounds **1** and **3** (Table 1) and in a similar δ to those reported for the corresponding tricoordinated dmit complexes [10].

Other anionic gold dmise complexes can be obtained starting from anionic halo gold derivatives such as PPN[Au(C_6F_5)Cl] and PPN[$AuBr_4$] and reacting with a solution of Na_2dmise in 1 : 2 and 2 : 1 molar ratio, respectively (vi and vii). The corresponding complexes (PPN)$_2$[Au_2(dmise)(C_6F_5)$_2$] **11** and (PPN)[Au(dmise)$_2$] **12** are isolated as pink and garnet coloured solids and only **11** is soluble enough in acetone showing a Λ_M value characteristic of 2 : 1 electrolyte. The ^{19}F NMR spectrum of **11** shows three signals: −115.1 (m, F_o), −163.4 (t, F_p), −164.5 (m, F_m) in accordance with two equivalents C_6F_5 groups. Both complexes show in the mass spectra (LSIMS−) signals corresponding to the parent anion [**11**−2PPN]$^-$, [**11**−PPN]$^-$, [**12**−PPN]$^-$ at *m/z* (%): 972 (10), 1510 (4) and 684 (8) respectively. It is noteworthy that the mass spectra of complex **11** shows other ion-molecule association as [**11**+Au(C_6F_5)−2PPN]$^-$ and [**11**+Au(C_6F_5)−PPN]$^-$ at *m/z* (%): 1336 (6) and 1874 (4).

REFERENCES

1. Cornelissen, J. P., Pomarède, B., Spek, A. L., Reefman, D., Haasnoot, J. G. and Reedijk, J., *Inorg. Chem.*, 1993, **32,** 3720.
2. Cornelissen, J. P., Reefman, D., Haasnoot, J. G., Spek, A. L. and Reedijk, J., *Recl. Trav. Chim. Pays-Bas*, 1991, **110,** 345.
3. Faulmann, C., Legros, J.-P., Cassoux, P., Cornelissen, J. P., Brossard, L., Inokuchi, M., Tajima, H. and Tokumoto, M., *J. Chem. Soc., Dalton Trans.*, 1994, 249.
4. Olk, R.-M., Kirmse, R., Hoyer, E., Faulmann, C. and Cassoux, P., *Z. Anorg. Allg. Chem.*, 1994, **620,** 90.
5. Olk, R.-M., Olk, B., Rocholf, J., Reinold, J., Sieler, J., Trübenbach, K., Kirmse, R. and Hoyer, E., *Z. Anorg. Allg. Chem.*, 1992, **609,** 103.
6. Olk, R.-M., Semmelmann, C., Kirmse, R., Köhler, K., Hoyer, E. and Olk, B., *Z. Anorg. Allg. Chem.*, 1990, **581,** 59.
7. Kato, R., Kobayashi, H., Kim, H., Kobayashi, A., Sasaki, Y., Mori, T. and Inouchi, H., *Chem. Lett.*, 1988, 865.
8. (a) Olk, R.-M., Olk, B., Rocholf, J. and Hoyer, E., *Z. Chem.*, 1990, **30,** 445; (b) Kato, R., Kobayashi, H. and Kobayashi, A., *Synth. Met.*, 1991, **42,** 2495; (c) Khodorkvskii, V. Y., Kreicberga, J., Balodis, K. A. and Neiland, O. Y., *Isv. Akad. Nauk, Latv. SSR, Ser. Khim.*, 1988, 120.
9. Naito, T., Sato, A., Kawano, K., Tateno, A., Kobayashi, H. and Kobayashi, A., *J. Chem. Soc., Chem. Commun.*, 1995, 351.
10. Cerrada, E., Jones, P. G., Laguna, A. and Laguna, M., *Inorg. Chem.*, 1996, **35,** 2995.
11. Gayathri Devi, K. R., Sathyanarayama, D. N. and Engler, E. M., *J. Mol. Struct.*, 1981, **71,** 1.
12. Schmidbaur, H. and Franke, R., *Inorg. Chim. Acta*, 1975, **13,** 185.
13. Geary, G., *Coord. Chem. Rev.*, 1971, **7,** 81.
14. Cerrada, E., Laguna, A., Laguna, M. and Jones, P. G., *J. Chem. Soc., Dalton Trans.*, 1994, 1325.
15. Usón, R. and Laguna, A., *Organomet. Synth.*, 1985, **3,** 325.
16. Usón, R., Laguna, A., Laguna, M., Usón, A. and Gimeno, M. C., *Inorg. Chim. Acta*, 1986, **114,** 91.
17. Schmidbaur, H., Wohleben, A., Wagner, F., Orana, O. and Huttner, G., *Chem. Ber.*, 1977, **110,** 1748.

Pergamon

PII: S0277-5387(97)00312-4

Polyhedron Vol. 17, No. 2–3, pp. 299–304, 1998
© 1997 Elsevier Science Ltd
All rights reserved. Printed in Great Britain
0277-5387/98 $19.00+0.00

The reactivity of zirconium acetylacetonate with phenols

William J. Evans,* Mohammad A. Ansari and Joseph W. Ziller

Department of Chemistry, University of California, Irvine, CA 92697-2025, U.S.A.

(Received 2 June 1997; accepted 7 July 1997)

Abstract—Although zirconium acetylacetonate, $Zr[CH_3C(O)CHC(O)CH_3]_4$, **1**, does not react with phenol, 4-methylphenol, or 2,6-dimethylphenol at reflux temperature in toluene or THF, it does react with *p*-nitrophenol in THF at room temperature to form $(acac)_3Zr(OC_6H_4NO_2\text{-}4)$, **2**, in 70% yield. **1** also reacts with 1,4-dihydroxybenzene to form bimetallic $[(acac)_3Zr]_2(\mu OC_6H_4O\text{-}4)$, **3**, in 90% yield. **2** crystallizes from THF to form a capped trigonal prismatic geometry around zirconium with the aryloxide ligand in the capping position. **3** crystallizes from THF/C_6H_6 to form a structure similar to that of **2** except that the aryloxide ligand occupies a trigonal prismatic vertex in the square face which is capped. © 1997 Elsevier Science Ltd

Keywords: zirconium; aryloxide; acetylacetonate; bimetallic.

Metal alkoxide and aryloxide complexes are desirable precursors for the preparation of metal-containing ceramics since they can be decomposed at a relatively low temperature with the formation of volatile organic byproducts which are not incorporated in the final product [1]. Although an extensive alkoxide and aryloxide chemistry has been developed for many of the early transition metals and the *f* elements [2], the chemistry of zirconium complexes is less extensive despite the fact that zirconium is an important component in a variety of practical ceramic devices [3]. The number of fully characterized zirconium inorganic aryloxide complexes is particularly small [4].

In efforts to extend the range of known zirconium aryloxide complexes and to examine the utility of zirconium acetylacetonate, $Zr(acac)_4$, **1** [acac = $CH_3C(O)CHC(O)CH_3$], as a precursor, we have examined the reactivity of **1** with various phenols. Zirconium acetylacetonate is an attractive starting material since it is a relatively inexpensive, alkane and arene soluble, water-free compound which has ligands which stabilize by chelation. In addition, the acetylacetonate ligands have the potential to bridge to form polyzirconium complexes, a class of compounds for which there are not many examples [5]. Although zirconium acetylacetonate does not readily react with simple phenols, we have found that by increasing the acidity of the phenol fully characterizable zirconium aryloxide acetylacetonate derivatives can be obtained from **1**.

EXPERIMENTAL

The chemistry described below was performed under nitrogen with rigorous exclusion of air and water using Schlenk, vacuum line, and glovebox techniques. Solvents were purified as previously described [6]. NMR spectra were recorded on a General Electric QE 300 spectrometer at 25°C. Elemental analyses were determined on a Carlo Erba EA 108 intrument or performed by Analytische Laboratorien, Gummersbach, Germany. 2,6-Dimethylphenol, 4-methylphenol, and 4-nitrophenol were obtained from Aldrich and sublimed before use. $Zr(acac)_4$ was obtained from Aldrich.

Synthesis of $Zr(acac)_3(OC_6H_4NO_2\text{-}4)$, **2**

In the glovebox, colorless $Zr(acac)_4$ (487 mg, 1.0 mmol) was added to 4-nitrophenol (140 mg, 1.0 mmol) in 10 cm^3 of THF and stirred for 2 days. Removal of solvent by rotary evaporation gave a yellow powder which was washed with hexanes and recrystallized from THF/benzene to form **2** (385 mg, 73%). The complex is only slightly soluble in toluene. Anal. calcd for $C_{21}H_{25}NO_9Zr$: C, 47.89; H, 4.78; N, 2.65; Zr, 17.32. Found: C, 47.68; H, 4.63; N, 2.65; Zr, 17.55. IR (Nujol): 1580 s, 1560 m, 1525 s, 1495 s, 1420 w, 1385 w, 1360 s, 1315 s, 1295 m, 1160 w, 1122 m, 1030 m, 1025 m, 944 w, 875 s, 862 w, 665 w cm^{-1}. ^1H NMR (C_6D_6):

8.10 (d, 2H, $C_6H_4NO_2$), 6.80 (d, 2H, $C_6H_4NO_2$), 5.24 (s, 3H, $CH_3COCHCOCH_3$), 1.68 (18 H, CH_3CO $CHCOCH_3$). ^{13}C NMR (C_6D_6): 190.8 (CH_3CO $CHCOCH_3$), 126.0 ($C_6H_4NO_2$), 119.6, ($C_6H_4NO_2$), 104.3 ($CH_3COCHCOCH_3$), 26.7 ($CH_3COCHCO$ CH_3).

X-ray data collection, structure determination, and refinement for $(acac)_3Zr(OC_6H_4NO_2\text{-}4)$, **2**

A pale yellow crystal of approximate dimensions $0.15 \times 0.30 \times 0.30$ mm was mounted on a glass fiber and transferred to a Siemens P4 rotating anode diffractometer. The determination of Laue symmetry, crystal class, unit cell parameters, and the crystal's orientation matrix were carried out according to standard procedures [7]. Intensity data were collected at 158 K using a $2\theta/\omega$ scan technique with Mo-$K\alpha$ radiation. The raw data were processed with a local version of CARESS [8] which employs a modified version of the Lehman–Larsen algorithm to obtain intensities and standard deviations from the measured 96-step peak profiles. Subsequent calculations were carried out using the SHELXL program [9]. All 2933 data were corrected for Lorentz and polarization effects and were placed on an approximately absolute scale. The diffraction symmetry was *mmm* and the systematic absences are consistent with the noncentrosymmetric space group $P2_12_12_1$. The analytical scattering factors for neutral atoms were used throughout the analysis [10]. The structure was solved by direct methods and refined on F^2 by full matrix least-squares techniques. Hydrogen atoms were included using a riding model. At convergence, $wR2 = 0.0770$ and GOF = 1.104 for 296 variables refined against all 2993 unique data [as a comparison for refinement on F, $R1 = 0.0279$ for those 2650 data with $F > 4.0\sigma(F)$]. The absolute structure was assigned by refinement of the Flack parameter [11]. Details are in Table 1.

Synthesis of $[(acac)_3Zr]_2(OC_6H_4O\text{-}4)$, **3**

In the glovebox, addition of a solution of 1,4-$(HO)_2C_6H_4$ (55 mg, 0.5 mmol) in 5 cm^3 of THF to a solution of $Zr(acac)_4$ (487 mg, 1.0 mmol) in 10 mL of THF causes an immediate color change from colorless to yellow. After stirring overnight the product was isolated as a light yellow powder by centrifugation and washing with hexanes (410 mg, 90%). The complex is only slightly soluble in toluene and THF and was crystallized from hot toluene. Anal. calcd for $C_{36}H_{46}O_{14}Zr_2$: C, 48.84; H, 5.24; Zr, 20.60. Found: C, 49.03; H, 5.07; Zr, 20.40. IR (Nujol): 1580 m, 1530 s, 1495 m, 1360 w, 1280 m, 1240 s, 1020 s, 935 m, 850 m, 832 m, 810 w, 775 w, 760 w, 665 m cm^{-1}. ^1H NMR (C_6D_6): 6.98 (s, 4H, C_6H_4), 5.28 (s, 6H, CH_3CO-$CHCOCH_3$), 1.74 (36 H, $CH_3COCHCOCH_3$).

X-ray data collection, structure determination, and refinement for $[(acac)_3Zr]_2(\mu\text{-}OC_6H_4O\text{-}4)$, **3**

A colorless crystal of approximate dimensions $0.34 \times 0.40 \times 0.47$ mm was mounted on a glass fiber and transferred to the Siemens P4 diffractometer and handled as described above for **2**. There were no systematic absences nor any diffraction symmetry other than the Friedel condition. The centrosymmetric triclinic space group $P\bar{1}$ was assigned and later determined to be correct. The structure was solved as described for **2**. Hydrogen atoms were located from a series of difference-Fourier maps and refined isotropically. The molecule is located about an inversion center. There is one molecule of benzene solvent present per formula unit. At convergence, $wR2 = 0.0548$ and GOF = 1.055 for 366 variables refined against all 2790 unique data [as a comparison for refinement on F, $R1 = 0.0219$ for those 2537 data with $F > 4.0\sigma(F)$].

RESULTS AND DISCUSSION

The complex $(acac)_3Zr(OC_6H_4NO_2\text{-}4)$, **2**

$Zr(acac)_4$, **1**, reacts with 1 equiv. of $HOC_6H_4NO_2$-4 ($pK_a = 7.16$) in THF according to equation 1 to give the pale yellow complex, **2**

$$\underset{\mathbf{1}}{Zr(acac)_4} + HOC_6H_4NO_2\text{-}4 \xrightarrow{THF} \underset{\mathbf{2}}{(acac)_3Zr(OC_6H_4NO_2\text{-}4)} + Hacac. \quad (1)$$

Attempts to use $Zr(acac)_4$ as a precursor to aryloxide derivatives of phenol ($pK_a = 10$), 4-methylphenol ($pK_a = 10.26$), and 2,6-dimethylphenol ($pK_a = 10.65$) were unsuccessful in both refluxing THF and toluene. This reactivity is consistent with the pK_a of acetylacetone which is 9.0.

The ^1H NMR spectrum of **2** indicated the presence of a single type of $CH_3COCHCOCH_3$ ligand with chemical shifts only slightly different from the starting material and a 3:1 acac:aryloxide ratio. Complex **2** crystallizes readily from THF/benzene at ambient temperature in >70% yield and an X-ray diffraction study was carried out to definitively characterize it as the neutral monometallic complex $(acac)_3Zr(OC_6H_4NO_2\text{-}4)$, Fig. 1.

Complex **2** contains a heptacoordinate zirconium center attached to three bidentate acetylacetonate ligands and a nitrophenoxide ligand through the phenolic oxygen. The closest examples to **2** in the literature are the mixed ligand complexes $Zr(acac)_3Cl$ [12] and $Zr(acac)_3NO_3$ [13]. Important bond lengths and distances are given in Table 2.

The coordination geometry around zirconium in complex **2**, Fig. 2, is best described as a distorted square-face-capped trigonal prism with the O(7) nitrophenoxide oxygen in the capping position. The

Table 1. Crystallographic data for $(acac)_3Zr(OC_6H_4NO_2\text{-}4)$, **2**, and $[(acac)_3Zr]_2(\mu\text{-}OC_6H_4O\text{-}4)$, **3**

Compound	**2**	**3**
Formula	$C_{21}H_{25}NO_9Zr$	$C_{36}H_{46}O_{14}Zr_2 \cdot C_6H_6$
Formula weight	526.64	963.28
Space group	$P2_12_12_1$	$P\bar{1}$
a (Å)	8.0250(9)	7.882(4)
b (Å)	12.6975(10)	11.642(3)
c (Å)	21.956(2)	12.436(4)
α (°)		102.34(2)
β (°)		91.23(3)
γ (°)		105.33(3)
V (Å^3)	2237.2(4)	1070.3(7)
Z	4	1
D_{calc} (g cm^{-3})	1.564	1.493
Radiation (1)	0.7107	0.71073
Abs. coefficient (mm^{-1})	0.543	0.552
$R1$, $[I > 2\sigma(I)]$	0.0279	0.0219
$wR2$, all data	0.0770	0.0548
GOF on F^2	1.104	1.055

$R1 = \Sigma||Fo|-|F_c||\Sigma|Fo|$; $wR2 = [\Sigma[w(Fo^2-Fc^2)^2]/\Sigma(w(Fo^2)^2]]^{1/2}$.

closely-related capped-octahedral geometry is not as good a description since there are no O—Zr—O angles close to the 180° expected of trans ligands in an octahedron. The largest O—Zr—O angle is 157.10(11)°.

The irregularity of the structure can be seen from

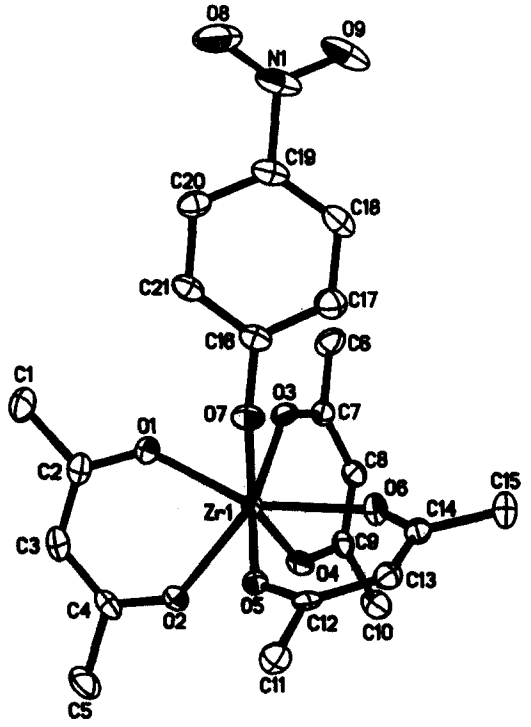

Fig. 1. Structure of $(acac)_3Zr(OC_6H_4NO_2\text{-}4)$, **2**. The thermal ellipsoid plot is shown at the 50% probability level.

Table 2. Important angles (°) and distances (Å) for $(acac)_3Zr(OC_6H_4NO_2\text{-}4)$, **2**, and $[(acac)_3Zr]_2(\mu\text{-}OC_6H_4O\text{-}4)$, **3**

	2	**3**
Zr(1)—O(1)	2.139(3)	2.142(2)
Zr(1)—O(2)	2.168(3)	2.158(2)
Zr(1)—O(3)	2.154(3)	2.198(2)
Zr(1)—O(4)	2.120(3)	2.146(2)
Zr(1)—O(5)	2.106(3)	2.152(2)
Zr(1)—O(6)	2.195(3)	2.179(2)
Zr(1)—O(7)	2.045(3)	1.977(2)
O(1)—Zr(1)—O(2)	75.14(11)	77.85(7)
O(1)—Zr(1)—O(3)	77.03(11)	75.78(7)
O(1)—Zr(1)—O(4)	113.09(12)	152.40(7)
O(1)—Zr(1)—O(5)	117.54(11)	126.64(7)
O(1)—Zr(1)—O(6)	154.83(11)	73.35(7)
O(1)—Zr(1)—O(7)	79.66(12)	97.85(7)
O(2)—Zr(1)—O(3)	128.61(11)	77.26(7)
O(2)—Zr(1)—O(4)	74.71(11)	91.24(7)
O(2)—Zr(1)—O(5)	73.95(11)	80.08(7)
O(2)—Zr(1)—O(6)	129.91(10)	117.17(7)
O(2)—Zr(1)—O(7)	131.35(11)	160.22(7)
O(3)—Zr(1)—O(4)	77.84(10)	77.12(7)
O(3)—Zr(1)—O(5)	157.19(11)	143.32(7)
O(3)—Zr(1)—O(6)	83.06(10)	141.54(7)
O(3)—Zr(1)—O(7)	83.50(11)	82.97(7)
O(4)—Zr(1)—O(5)	108.96(10)	74.93(7)
O(4)—Zr(1)—O(6)	76.89(11)	133.45(7)
O(4)—Zr(1)—O(7)	153.92(11)	83.85(7)
O(5)—Zr(1)—O(6)	77.54(11)	74.87(7)
O(5)—Zr(1)—O(7)	82.18(10)	116.73(7)
O(6)—Zr(1)—O(7)	82.96(11)	79.13(7)

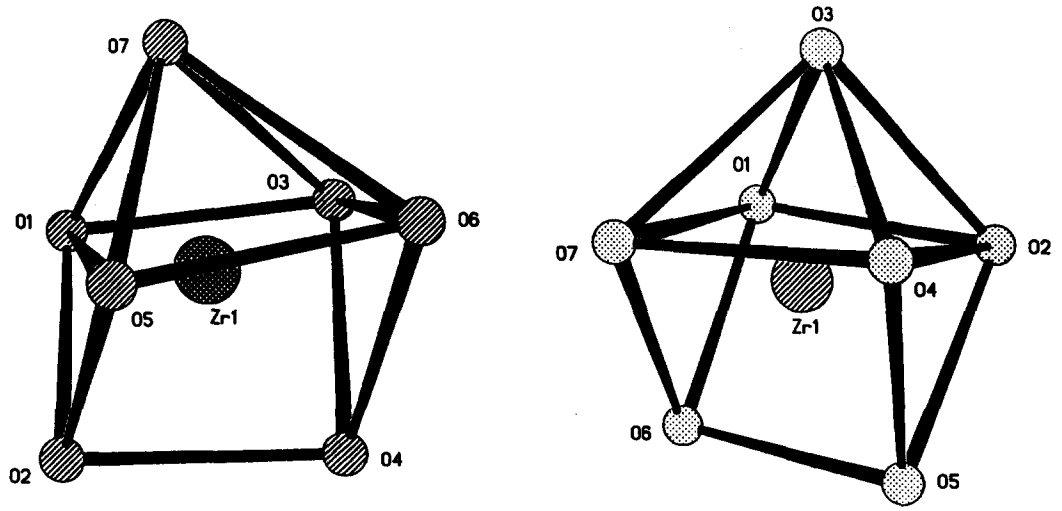

Fig. 2. Capped trigonal prismatic coordination spheres of zirconium in $(acac)_3Zr(OC_6H_4NO_2\text{-}4)$, **2**, left, and $[(acac)_3Zr]_2(\mu\text{-}OC_6H_4O\text{-}4)$, **3**, right.

the unequal 131.35(11)° O(7)—Zr—(O2) and 153.92(11)° O(7)—Zr—O(4) angles which would be equivalent in an idealized capped trigonal prism. The oxygen atoms comprising the three square faces of the prism are coplanar to within 0.12 Å for O(1,2,3,4), 0.15 Å for O(2,4,5,6), and 0.30 Å for O(1,3,5,6). The zirconium atom lies 0.03 Å below this latter plane and is 0.41 Å from the centroid of the oxygen atoms. The four O(7)—Zr—O(1,3,5,6) angles involving the capping O(7) position and the square face which it caps fall in the narrow range of 79.66(12) to 83.50(11)°. The O—Zr—O bite angles for the acetylacetonate ligands vary from only 75.14(11) to 77.84(10)°. The analogous angles in $Zr(acac)_4$ are 75.1(1) and 74.6(1)°.

The Zr—O(acac) distances involving the oxygens in the trigonal prism have a narrow 2.106(3) to 2.195(3) Å range and the 2.15(3) Å average Zr—O(acac) distance can be compared with the 2.188(6) and 2.141(4) Å averages in eight coordinate $Zr(acac)_4$ [14] and $Zr(acac)_3NO_3$ [13], respectively. The 2.045(3) Å Zr—O(nitrophenoxide) length is the shortest Zr—O distance in the structure and is similar to the 2.030(6) and 2.047(7) Å lengths reported for $Zr(OC_6H_3Bu^t_2\text{-}2,6)_2(=NPh)$ (4-pyrrolidinopyridine)$_2$ [4h]. The nitro group is too distant from the metal center of any neighboring molecule to have an interaction.

The complex $[(acac)_3Zr]_2(\mu\text{-}OC_6H_4O\text{-}4)$, **3**

Since the reaction of $Zr(acac)_4$ with $HOC_6H_4NO_2\text{-}4$ did not lead to a bridged structure through either the acetylacetonate or the nitrophenoxide ligands, reactions with a precursor more likely to form bridged structures, $HOC_6H_4OH\text{-}4$, were examined. The reaction of 2 equiv. of $Zr(acac)_4$ with 1 equiv. of $HOC_6H_4OH\text{-}4$ in THF formed **3** as a yellow powder in 80% yield according to reaction (2)

$$\underset{\mathbf{1}}{2Zr(acac)_4} + HOC_6H_4OH\text{-}4 \xrightarrow{THF} \underset{\mathbf{3}}{[Zr(acac)_3]_2(\mu\text{-}OC_6H_4O\text{-}4)} + 2Hacac \quad (2)$$

The ^1H NMR spectrum of **3** indicated the presence of both aryloxide and acetylacetonate ligands in a 1:6 ratio, but it was not structurally definitive. X-ray diffraction revealed the existence of a bimetallic complex as shown in Fig. 3.

Complex **3** crystallizes as a centrosymmetric dimer. Like **2**, it has seven coordinate zirconium centers which have distorted square-face-capped trigonal prismatic geometries, Fig. 2. In this case, however, oxygen donor atom, O(7), of the aryloxide ligand is in a prismatic rather than a capping position. As shown in Table 2, the metrical parameters in the two complexes are similar despite the different location of the aryloxide ligand. Since there are no O—Zr—O angles greater than 161°, again a capped-octahedral structure is ruled out. The four O(3)—Zr—O(1,2,4,7) angles fall in a narrow 75.78(7)–82.97(7)° range and the three planes of four oxygen atoms are coplanar to 0.09 Å (1,2,5,6), 0.12 Å (4,5,6,7) and 0.07 Å (1,2,4,7). The zirconium lies 0.43 Å below the O(1,2,4,7) plane and is 0.44 Å from the centroid of the oxygen atoms. The capped trigonal prism is somewhat more regular than in **2**. For example, the 143.32(7)° O(3)—Zr—O(5) and 141.54(7)° O(3)—Zr—O(6) angles involving the capping oxygen are quite similar. The Zr—O(acac) distances average 2.16(4) Å with a 2.142(2)–2.198(2) Å range similar to that in **2**. The acetylacetonate oxygen in the unique capping position, O(3), has the longest Zr—O distance, but it is

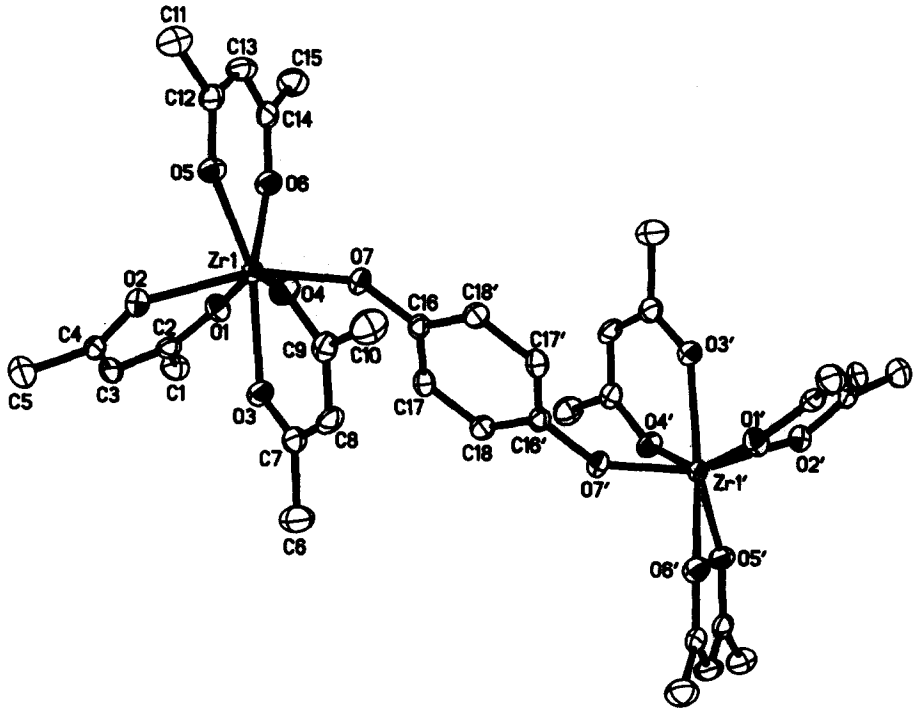

Fig. 3. Structure of $[(acac)_3Zr]_2(\mu\text{-}OC_6H_4O\text{-}4)$, **3**. The thermal ellipsoid plot is shown at the 50% probability level.

not unusually long. Neither does this acetylacetonate have an unusual O—Zr—O bite angle: the 74.87(7)–77.85(7)° range for all of the acac ligands is normal. The 1.977(2) Å Zr—O(aryloxide) length, Zr—O(7), is the shortest Zr—O distance as in **2**.

CONCLUSIONS

The reactivity of zirconium acetylacetonate with phenols can be correlated with the acidity of the phenol. Phenols with $pK_a < 9.0$ substitute one acetylacetonate ligand and readily form $Zr(acac)_3(OAr)$ complexes. 1,4-Dihydroxybenzene provides a method to generate bimetallic aryloxide acetylacetonate zirconium complexes.

Acknowledgments—For support of this research, we thank the Division of Chemical Sciences of the Office of Basic Energy Sciences of the Department of Energy and the Phillips Laboratory Propulsion Directorate of Edwards Air Force Base. Helpful discussions with Dr J. Lichtenhan are gratefully acknowledged.

REFERENCES

1. Bradley, D. C. *Polyhedron*, 1994, **13,** 1111; Bradley, D. C. *Chem. Rev.* 1989, **89,** 1317; Hubert-Pfalzgraf, L. G. *New J. Chem.* 1995, **19,** 727; Caulton, K. G. and Hubert-Pfalzgraf, L. G. *Chem. Rev.* 1990, **90,** 969; Saka, S. *Am. Ceram. Soc. Bull.* 1985, **64,** 1463.
2. Only some leading references can be given: Bradley, D. C., Mehrotra, R. C. and Gauer, D. P. *Metal Alkoxides*. Academic Press: London (1978); Mehrotra, R. C., Singh, A. and Tripathi, U. M. *Chem. Rev.* 1991, **91,** 1287; Bradley, D. C., Chudzynska, H., Hursthouse, M. B. and Motevalli, M. *Polyhedron*, 1994, **10,** 7; Clark, D. L., Hollis, R. V., Scott, B. L. and Watkin, J. G. *Inorg. Chem.* 1996, **34,** 667; Lappert, M. F., Singh, A. and Smith, R. G. *Inorg. Synth.* 1990, **27,** 164; Coan, P. S., McGeary, M. J., Lobkovsky, E. B. and Caulton, K. G. *Inorg. Chem.* 1991, **30,** 3570; Hermann, W. A., Anwander, R. and Scherer, W. *Chem. Ber.* 1993, **126,** 1533. Deacon, G. B., Gatehouse, B. M., Shen, Q. and Ward, G. N. *Polyhedron* 1993, **12,** 1289; Sen, A., Stecher, H. A. and Rheingold, A. *Inorg. Chem.* 1992, **31,** 473; Schumann, H., Kociok-Köhn, G. and Loebel, J. *Z. Anorg. Chem.* 1990, **581,** 69; Daniele, S., Hubert-Pfalzgraf, L. G. and Daran, J. C. *Polyhedron* 1996, **15,** 1063; Edelmann, F. T., Steiner, A., Stalke, D., Gilje, J. W., Jagner, S. and Hakansson, M. *Polyhedron* 1994, **13,** 539; Evans, W. J., Golden, R. E. and Ziller, J. W. *Inorg. Chem.* 1993, **32,** 3041.
3. Elvers, B. and Hawkins, S. in *Ullmann's Encyclopedia of Industrial Chemistry*, 5th Ed. 1985, **A28,** 557; Boyle, T. J. and Schwartz, R. W. *Comments Inorg. Chem.* 1994, **16,** 243; Buchanan, R. C. in *Ceramic Materials for Electronics*, Marcel

Dekker, New York (1991), PLZT Electrooptic Ceramics and Devices; Heartling, G. H. in *Industrial Applications of Rare Earth Elements*, ed. K. A. Gschneider, Jr., *ACS Symp. Ser.* 1980, **164,** 265; Mazdiyasni, K. S., Lynch, C. J. and Smith II, J. S. *J. Am. Ceram. Soc.* 1967, **50,** 532.

4. From a search of the Cambridge Data Base excluding organometallic structures: (a) Latesky, S., McMullen, A. K., Rothwell, I. P. and Huffman, J. C. *Organometallics* 1985, **4,** 902; (b) McMullen, A. K., Rothwell, I. P. and Huffman, J. C. *J. Am. Chem. Soc.* 1985, **107,** 1072; (c) Latesky, S. L., McMullen, A. K., Niccolai, G. P., Rothwell, I. P. and Huffman, J. C. *Organometallics* 1985, **4,** 1896; (d) Fanwick, P. E., Kobriger, L. M., McMullen, A. K. and Rothwell, I. P. *J. Am. Chem. Soc.* 1986, **108,** 8095; (e) Chamberlain, L. R., Durfee, L. D., Fanwick, P. E., Kobriger, L. M., Latesky, S. L., McMullen, A. K., Steffey, B. D., Rothwell, I. P., Folting, K. and Huffman, J. C. *J. Am. Chem. Soc.* 1987, **109,** 6068; (f) Kresinski, R. A., Hanmor, T. A., Isam, L., Jones, C. J. and McCleverty, J. A. *Polyhedron* 1989, **8,** 845; (g) Zambrano, C. H., McMullen, A. K., Kobriger, L. M., Fanwick, P. E. and Rothwell, I. P. *J. Am. Chem. Soc.* 1990, **112,** 6565; (h) Profilet, R. D., Zambrano, C. H., Fanwick, P. E., Nash, J. J. and Rothwell, I. P. *Inorg. Chem.* 1990, **29,** 4362; (i) Kresinski, R. A., Isam, L., Hamor, T. A., Jones, C. J. and McCleverty, J. A. *J. Chem. Soc., Dalton Trans.* 1991, 1835; (j) Kresinski, R. A., Hamor, T. A., Jones, C. J. and McCleverty, J. A. *J. Chem. Soc., Dalton Trans.* 1991, 603; (k) Zambrano, C. H., Profilet, R. D., Hill, J. E., Fanwick, P. E. and Rothwell, I. P. *Polyhedron* 1993, **12,** 689; (l) Yasuda, H., Nakayama, Y., Takei, K., Nakamura, A., Kai, Y. and Kanehisa, N. *J. Organomet. Chem.* 1994, **473,** 105.
5. Coucouvanis, D., Lester, R. K., Kanatzidis, M. G. and Kessissoglou, D. P. *J. Am. Chem. Soc.* 1985, **107,** 8279; Evans, W. J., Ansari, M. A. and Ziller, J. W., *Polyhedron* (in press).
6. Evans, W. J., Chamberlain, L. R., Ulibarri, T. A. and Ziller, J. W. *J. Am. Chem. Soc.* 1988, **110,** 6423.
7. XSCANS Software Users Guide, Version 2.1, Siemens Industrial Automation, Inc., Madison, WI, 1994.
8. Broach, R. W. Argonne National Laboratory, Argonne, IL, 1978.
9. Sheldrick, G. M. Siemens Analytical X-Ray Instruments, Inc., Madison, WI, 1994.
10. *International Tables for X-Ray Crystallography*, Vol. C., Kluwer Academic Publishers, Dordrecht (1992).
11. Flack, H. D. *Acta Cryst.* 1983, **A39,** 876.
12. Von Dreele, R. B., Stezowski, J. J. and Fay, R. C. *J. Am. Chem. Soc.* 1971, **93,** 2887.
13. Muller, E. G., Day, V. W. and Fay, R. C. *J. Am. Chem. Soc.* 1976, **98,** 2165.
14. Clegg, W. *Acta Cryst.* 1987, **C43,** 789; Silverton, J. V. and Hoard, J. L. *Inorg. Chem.* 1963, **2,** 243.

Pergamon

PII: S0277-5387(97)00303-3

Polyhedron Vol. 17, No. 2-3, pp. 305-312, 1998
© 1997 Elsevier Science Ltd
All rights reserved. Printed in Great Britain
0277-5387/98 $19.00+0.00

Crystal structure and vibrational characterization of the reaction products of *N*-methylthiazolidine-2(3H)-selone (1) and *N*-methylbenzothiazole-2(3H)-selone (2) with Br_2

Francesco A. Devillanova,[a]* Paola Deplano,[a] Francesco Isaia,[a] Vito Lippolis,[a] Maria Laura Mercuri,[a] Silvia Piludu,[a] Gaetano Verani[a] and Francesco Demartin[b]

[a] Dipartimento di Chimica e Tecnologie Inorganiche e Metallorganiche, Universita' di Cagliari, via Ospedale 72, I-09124 Cagliari, Italy

[b] Dipartimento di Chimica Strutturale e Stereochimica Inorganica e Centro CNR, Universita' di Milano, via G. Venezian 21, I-20133 Milano, Italy

(Received 30 May 1997; accepted 7 July 1997)

Abstract—The products obtained by reacting the title selenium donors, **1** and **2**, with molecular dibromine, both in 1 : 1 and 1 : 2 **1**(**2**)/Br_2 molar ratios in CH_2Cl_2 solution, are described. Depending on the molar ratio of the reagents, **1** gives two different products having stoichiometries **1** · Br_2 (**I**) and $C_8H_{14}Br_8N_2S_2Se$ (**II**). Compound **II**, characterised by X-ray diffraction on a single crystal, is an ionic compound having formula $(C_4H_7BrNS)_2[SeBr_6]$. Thus, the reaction occurs through C=Se bond breaking and formation of the *N*-methyl-2-bromothiazolidinium cation and oxidation of the selenium atom to a hexabromo selenate(2-) anion. In the corresponding reaction with **2**, the same compound of stoichiometry **2** · Br_2 (**III**) is obtained in both molar ratios. The X-ray diffractometric analysis on a single crystal of **III** shows that it is a hypervalent Se-compound, $C_8H_7Br_2NSSe$, bearing the Br—Se—Br linear group. FT-IR and FT-Raman spectra are in accordance with structural results for **II** and **III** and help to characterise **I**. © 1997 Elsevier Science Ltd

Keywords: *N*-methylthiazolidine-2(3H)-selone; *N*-methylbenzothiazole-2(3H)-selone; hypervalent selenium compounds with bromine; hexabromoselenate(2-); X-ray structures.

We are extensively investigating the donor/acceptor reactions between heterocycles containing the thionic and selonic groups and dihalogens or interhalogens. We have found that, besides the donor/acceptor adducts, a large variety of products can be obtained and that X-ray crystal structure determination plays a crucial role in their characterisation. As an example of the above, Scheme 1 summarizes the case of the reaction of the donors *N*-methyl-1,3-thiazolidine-2(3H)-selone (**1**) and *N*-methylbenzothiazole-2(3H)-selone (**2**) with the acceptors I_2 and IBr [1]. An analogous variety of products has also been found with other selenium donors [2–8]. As a development of our research in this field, we here report the results obtained by reacting **1** and **2** with molecular dibromine in CH_2Cl_2 solution (also collected in Scheme 1). Whatever the reagent molar ratio, **2** gives the hypervalent compound $C_8H_7Br_2NSSe$ (**III**), which bears the Br—Se—Br linear group. **1** gives the hypervalent compound $C_4H_7Br_2NSSe$ (**I**) when the reaction is carried out in 1 : 1 **1**/Br_2 molar ratio while by using the 1 : 2 or lower reagent molar ratios, ionic compound $2[C_4H_7BrNS]^+ [SeBr_6]^{2-}$ (**II**) is obtained.

EXPERIMENTAL

Materials

N-methyl-1,3-thiazolidine-2(3H)-selone (**1**) was synthesized according to the procedure report in [9]. *N*-methylbenzothiazole-2(3H)-selone (**2**) and dibro-

* Author to whom correspondence should be addressed. E-mail address: DEVILLA@VAXCA1.UNICA.IT

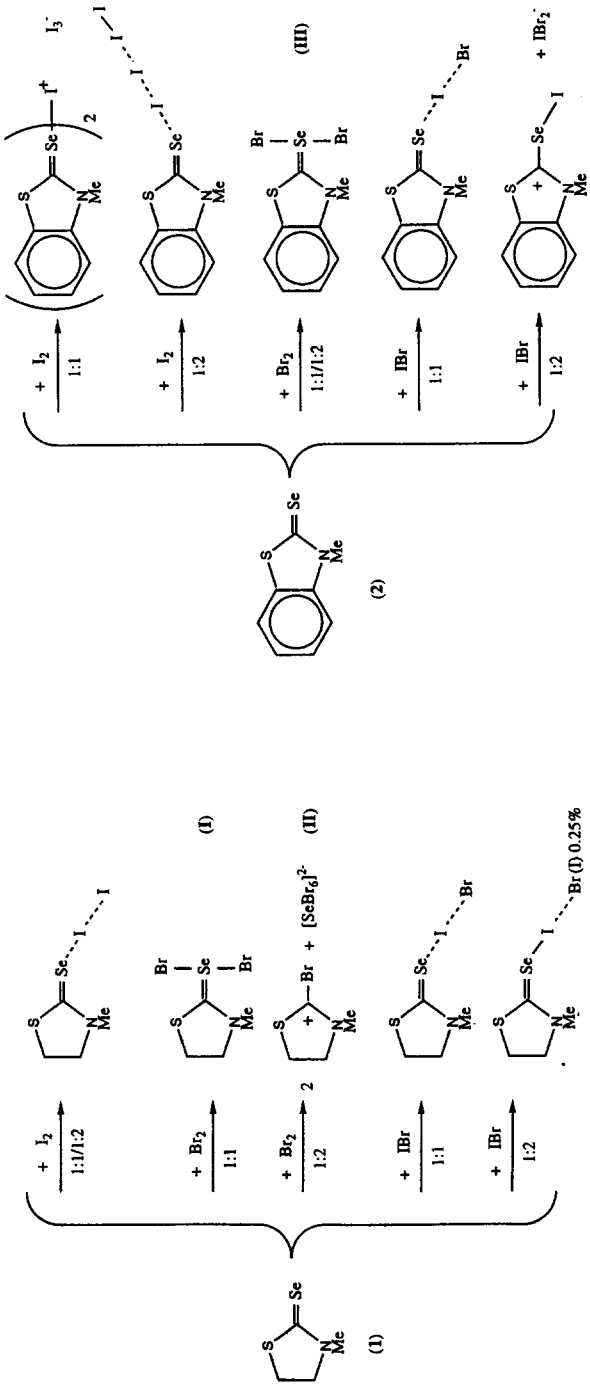

Scheme 1. All the compounds obtained by reacting **1** and **2** with I_2, Br_2 and IBr (1 : 1 and 1 : 2 molar ratios) in CH_2Cl_2 solutions.

mine were purchased from Aldrich and used without further purification.

N-methyl-1,3-thiazolidine-2-ylium dibromo selenanide (**I**). This compound was obtained as yellow-orange microcrystals by evaporating a dichloromethane solution of *N*-methyl-1,3-thiazolidine-2(3H)-selone (**1**) (0.05 g, 2.8×10^{-4} moles) and bromine (2.8×10^{-4} moles) in air at room temperature (yield 94%). m.p. 115–117°C; Found (Calc. for $C_4H_7Br_2NSSe$): C, 14.38 (14.13); H, 2.09 (2.08); N, 4.18 (4.12); S, 9.46 (9.43)%.

N-methyl-2-bromothiazolidinium hexabromoselenate(2-) (**II**). **II** was obtained as yellow-orange crystals by evaporating a dichloromethane solution of *N*-methyl-1,3-thiazolidine-2(3H)-selone (**1**) (0.05 g, 2.8×10^{-4} moles) and bromine (5.6×10^{-4} moles) in air at room temperature. m.p. 129–135°C; Found (Calc. for $C_8H_{14}Br_8N_2S_2Se$): C, 10.32 (10.44); H, 1.43 (1.53); N, 2.97 (3.04); S, 6.75 (6.97); Se, 8.60 (8.58)%. After ascertaining the stoichiometry, subsequent preparations were repeated using bromine amounts corresponding to 1:2.5 molar ratio (yield 60%).

N-methylbenzothiazole-2-ylium dibromo selenanide (**III**). This compound was quantitatively obtained as red-black crystals by evaporating a dichloromethane solution of *N*-methylbenzothiazole-2(3H)-selone (**2**) (0.05 g, 2.2×10^{-4} moles) and bromine (2.2×10^{-4} moles) in air at room temperature. m.p. 219–220°C; Found (Calc. for $C_8H_7Br_2NSSe$): C, 24.50 (24.77); H, 1.91 (1.82); N, 3.55 (3.61); S, 8.05 (8.26)%. The same compound was obtained using double the amount of dibromine.

FT-Raman and FT-IR spectra

The FT Raman spectra were recorded by means of a Bruker FRS 100 Fourier Transform Raman Spectrometer, operating with a diode-pumped Nd:YAG exciting laser emitting at a 1064 nm wavelength and having a power impinging on the sample tunable up to 350 mW. The detection of the signal was made with an Indium-Gallium-Arsenide detector operating at room temperature; all spectra were recorded at a 4 cm^{-1} resolution, down to about a Raman shift of 50 cm^{-1}. The solid samples were packed into a suitable cell and fitted into the compartment designed to use a 180° scattering geometry. No sample decomposition was observed during the experiments. The infrared spectra were recorded by means of a Bruker IFS66 Fourier Transform Infrared Spectrometer on polyethylene pellets in the 500–80 cm^{-1} range.

X-ray crystal structure determination

Details of the data collection and refinement of the structures are reported in Table 1 [10]. Crystals of compounds **II** and **III** were mounted on a glass fiber in a random orientation. Preliminary examination and data collection were performed with graphite monochromatized Mo-K_α radiation (0.71073 Å) on an Enraf-Nonius CAD4 computer controlled kappa axis diffractometer. Cell constants and an orientation matrix for data collection were obtained from least-squares refinement, using the setting angles of 25 reflections. The data were collected at room temperature using a variable scan rate (2 to 20° min in omega). Three representative reflections were measured every hour to check the stability of the crystals under X-ray exposure; these measurements revealed a decay of the scattering power of the crystal which amounts to about 8 and 7% (on F_o) for **II** and **III**, respectively. Lorentz, polarization and a linear correction for decay were applied to the intensities. An empirical absorption correction, performed as described in [11], was also applied to the data. Both structures were solved using direct methods (MULTAN) and difference Fourier syntheses, and were refined in full-matrix least-squares, the function minimized being $\Sigma w(|F_o| - |F_c|)^2$. All the hydrogen atoms were seen in a difference map and introduced in the structure model at idealized positions (C—H 0.95 Å) and not refined. Scattering factors were taken from Cromer and Waber [12]. Anomalous dispersion effects were included in F_c; the values for $\delta f'$ and $\delta f''$ were those of Cromer [13]. All calculations were performed on an 80486/33 computer using Personal SDP software [14]. Selected interatomic distances and angles are shown in Table 2.

RESULTS AND DISCUSSION

As summarized in Scheme 1, the variety of products, obtained by reacting *N*-methyl-1,3-thiazolidine-2(3H)-selone (**1**) and *N*-methylbenzothiazole-2(3H)-selone (**2**) with molecular diiodine and iodinebromine in CH_2Cl_2 solution, is further increased by using the molecular dibromine as acceptor. In fact, while with a 1:1 reagent molar ratio, both **1** and **2** yield compounds having $\mathbf{1} \cdot Br_2$ (**I**) and $\mathbf{2} \cdot Br_2$ (**III**) stoichiometry, with a 1:2 reagent molar ratio, the isolated products are very different. **2** gives the same compound **III**, and **1** produces the ionic compound **II**. **I** and **III** are hypervalent selenium compounds, bearing the Br—Se—Br linear group (see later) and **II** is the unusual compound *N*-methyl-2-bromothiazolidinium hexabromoselenate(2-), in which the C=Se double bond of **1** has been broken [15] with oxidation of the selenium atom to $[SeBr_6]^{2-}$ and formation of $[C_4H_7BrNS]^+$ cations. **I**, **III** and the $[C_4H_7BrNS]^+$ cation may be regarded as adducts of the nucleophilic carbene ligands thiazolin-2-ylidene (C_4H_7NS) and benzothiazol-2-ylidene (C_8H_7NS) with the acceptors $SeBr_2$ (**I** and **III**) and Br^+ (**II**).

Crystal structure of N-methyl-2-bromothiazolidinium hexabromoselenate(2-) (**II**)

A projection of the crystal structure of **II**, seen almost along [010] is shown in Fig. 1. The unit cell

Table 1. Crystallographic data

Compound	II	III
Formula	$C_8H_{14}Br_8N_2S_2Se$	$C_{16}H_{14}Br_4N_2S_2Se_2 \cdot 0.5\ CH_2Cl_2$
f.w. (amu)	920.57	818.46
Space Group	$C2/c$ (no. 15)	$P2_1/c$ (no. 14)
a (Å)	16.819 (6)	12.571 (5)
b (Å)	11.389 (3)	13.722 (7)
c (Å)	12.434 (4)	14.221 (4)
α (°)	90	90
β (°)	113.09 (3)	90.74 (3)
γ (°)	90	90
V (Å^3)	2191 (1)	2453 (2)
Z	4	4
D_{calc} (g cm^{-3})	2.791	2.216
μ (Mo-K_α) (cm^{-1})	163.3	97.2
Final R and R_w indices[a]	0.044, 0.053	0.034, 0.034

[a] $R = [\Sigma(F_o - k|F_c|)/\Sigma F_o]$; $R_w = [\Sigma w(F_o - k|F_c|)^2/\Sigma w F_o^2]^{1/2}$; GOF $= [\Sigma w(F_o - k|F_c|)^2/(N_{observations} - N_{variables})]^{1/2}$.

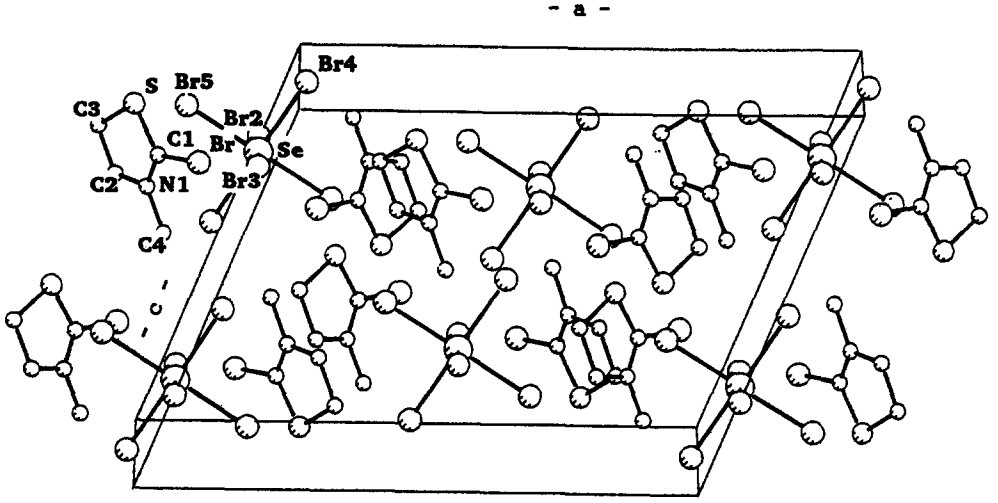

Fig. 1. Crystal packing of II.

contains eight $C_4H_7BrNS^+$ cations in general position and four $SeBr_6^{2-}$ anions located on crystallographic two-fold axes. The $C_4H_7BrNS^+$ cations are essentially planar; their geometry can be compared with that of the *N*-methyl-1,3-thiazolidine-2(3H)-selone molecule in the adducts with I_2 or IBr [1]. The effects on bond distances and angles of the pentaatomic ring, due to replacement of a Se atom with a bromine atom and also to the presence of a delocalized positive charge are not appreciable, because of the high e.s.d.s observed in all these compounds. However, a regular trend in the shortenings of the S—C(1) and N(1)—C(1) bond distances can be seen as well as in the opening of the S—C(1)—N(1) angle on increasing the positive charge on the ring passing from **I** · I_2 to **1** · IBr [1] and to the $C_4H_7BrNS^+$ cation. The higher value of the N—C—N angle in 1,3-dimesitylimidazolinium chloride with respect to that observed in 1,3-dimesitylimidazolin-2-ylidene has been recently pointed out by Arduengo *et al.* [16] as one of the noteworthy differences in the pentaatomic ring structure between the two compounds. For the stabilization of **I** (hypervalent Se-compound) and of the cation in **II** (formally an adduct of the thiazolin-2-ylidene with Br^+) it is evident that the delocalization of the positive charge on the whole pentaatomic ring, as occurs for **III**, is not necessary. Also for the dications bearing the —Se—Se— bridge, recently reported by us [8], the delocalization of the positive charge on the whole ring is not strictly necessary to their stability, as proved by the isolation of such dications starting from 1,3-dimethyl-4-imidazoline-2-selone and 1,3-dimethylimidazolidine-2-selone.

The $SeBr_6^{2-}$ anion does not have the distorted octa-

Table 2. Selected interatomic distances (Å) and angles (°)

Compound **II**			
Se—Br(2)	2.616(2)	Br(2)—Se—Br(3)	180.00(0)
Se—Br(3)	2.532(2)	Br(2)—Se—Br(4)	90.21(4)
Se—Br(4)	2.570(1)	Br(2)—Se—Br(5)	90.47(4)
Se—Br(4)[a]	2.570(1)	Br(3)—Se—Br(4)	89.79(4)
Se—Br(5)	2.568(1)	Br(3)—Se—Br(5)	89.53(4)
Se—Br(5)[a]	2.568(1)	Br(4)—Se—Br(4)[a]	179.59(7)
		Br(4)—Se—Br(5)	90.84(3)
		Br(4)—Se—Br(5)[a]	89.15(3)
		Br(5)—Se—Br(5)[a]	179.07(7)
Br—C(1)	1.849(9)	N(1)—C(2)	1.449(11)
S—C(1)	1.694(10)	N(1)—C(4)	1.475(11)
S—C(3)	1.798(9)	C(2)—C(3)	1.546(11)
N(1)—C(1)	1.273(10)		
C(1)—S—C(3)	92.1(4)	Br—C(1)—N(1)	123.1(7)
C(1)—N(1)—C(2)	115.6(8)	S—C(1)—N(1)	116.9(7)
C(1)—N(1)—C(4)	127.7(9)	N(1)—C(2)—C(3)	108.4(8)
C(2)—N(1)—C(4)	116.7(8)	S—C(3)—C(2)	105.8(6)
Br—C(1)—S	120.1(5)		
Compound **III**			
Br(11)—Se(11)	2.564(2)	Br(21)—Se(21)	2.510(2)
Br(12)—Se(11)	2.571(2)	Br(22)—Se(21)	2.612(2)
Se(11)—C(17)	1.916(10)	Se(21)—C(27)	1.908(10)
S(11)—C(16)	1.727(10)	S(21)—C(26)	1.734(10)
S(11)—C(17)	1.687(10)	S(21)—C(27)	1.701(10)
N(11)—C(11)	1.420(12)	N(21)—C(21)	1.392(12)
N(11)—C(17)	1.303(11)	N(21)—C(27)	1.309(12)
N(11)—C(18)	1.453(12)	N(21)—C(28)	1.442(13)
C(11)—C(12)	1.404(13)	C(21)—C(22)	1.394(14)
C(11)—C(16)	1.358(13)	C(21)—C(26)	1.350(14)
C(12)—C(13)	1.377(15)	C(22)—C(23)	1.385(15)
C(13)—C(14)	1.367(16)	C(23)—C(24)	1.363(16)
C(14)—C(15)	1.409(15)	C(24)—C(25)	1.365(15)
C(15)—C(16)	1.422(14)	C(25)—C(26)	1.406(14)
Br(11)—Se(11)—Br(12)	173.6(1)	Br(21)—Se(21)—Br(22)	175.1(1)
Br(11)—Se(11)—C(17)	86.5(3)	Br(21)—Se(21)—C(27)	86.2(3)
Br(12)—Se(11)—C(17)	87.2(3)	Br(22)—Se(21)—C(27)	88.9(3)
Se(11)···Br(22)	3.492(2)	Se(21)···Br(11)	3.503(2)

Symmetry code: $a = -x, y, 1/2-z$.

hedral geometry expected for AX_6E molecules on the basis of the VSEPR theory [17] the bond angles are very close to the ideal values of 90 and 180°, and only a slight asymmetry can be appreciated in the Se—Br distances, ranging from 2.532(2) to 2.616(2) Å, probably due to packing effects. Their average value (2.570 Å) is very close to that observed in K_2SeBr_6 [2.575(2) Å] [18]. These features, also common to other isoelectronic anions such as TeX_6^{2-} and $SbBr_6^{3-}$, have been explained assuming that on increasing the size of the central atom the lone pair is drawn inwards toward the core and spread around it, and consequently the bond pairs move further from the central nucleus [17]. In fact the Se—Br distances are considerably longer than the sum of the covalent radii (*ca.* 2.31 Å).

Crystal structure of N-methylbenzothiazole-2-ylium dibromo selenanide (**III**)

The crystal packing of compound **III** is shown in Fig. 2. The content of the unit cell consists of four pairs of $C_8H_7Br_2NSSe$ molecules and two dichloromethane molecules, the latter being disordered about crystallographic inversion centers. Each $C_8H_7Br_2NSSe$ molecule contains an almost linear Br—Se—Br moi-

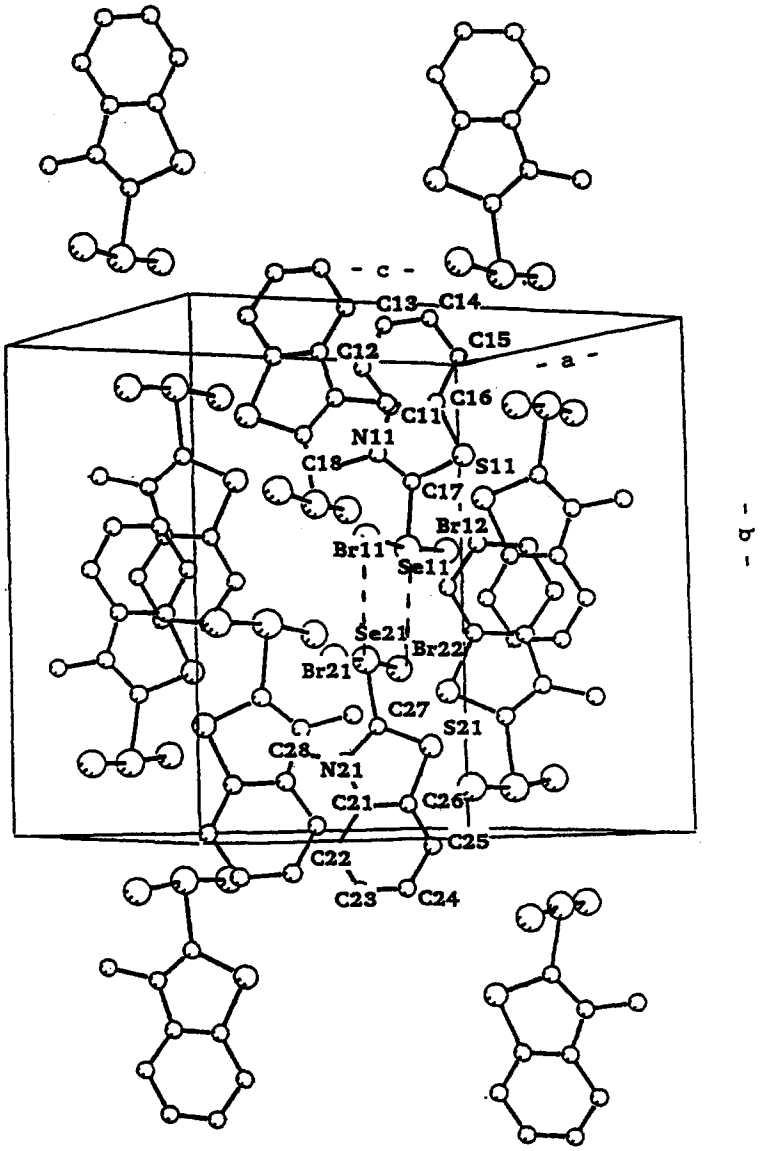

Fig. 2. Crystal packing of **III**.

ety [Br—Se—Br angles are 173.6(1) and 175.1(1)°, respectively], which is roughly perpendicular to the plane of the benzothiazole molecule [the Br—Se—C—S torsion angles are 102.4(6) and 92.0(6)° for the two molecules, respectively]. Within the pentaatomic ring, the S(11)—C(17)—N(11) and S(21)—C(27)—N(21) angles [average value of the two independent molecules is 113.6(7) Å] are somewhat closed compared with the derivatives of **1** (**1**·I_2 and **1**·IBr) [1] and with the $C_4H_7BrNS^+$ cation, according to shorter C(11)—C(16) and C(21)—C(26) bonds [average value 1.354(14) Å] relative to C(2)—C(3) values, 1.546(11), 1.522(18) and 1.449 (15) Å in **II**, **1**·IBr [1] and **1**·I_2 [1] respectively. The two independent molecules interact to form a dimeric unit through the Se and Br interactions (the Se(11)···Br(22) and Se(21)···Br(11) contacts are 3.492(2) and 3.503(2) Å respectively). In spite of being about 1 Å longer than the distances corresponding to Se—Br bonds (average value 2.564 Å), these secondary interactions are significantly shorter than the sum of the van der Waals radii of Se and Br, and allow the charge density on the Se atom to be further delocalized. In this way, the T-shape arrangement about the Se atoms could be considered almost square planar.

FT-IR and FT-Raman spectra of **II** are reported in Fig. 3. The simpleness of the Raman spectrum of **II** agrees well with a high symmetry of the octahedral structure of the $[SeBr_6]^{2-}$ ion in accordance with X-ray results. The Raman bands at 168 (ν_1) [19], 152 (ν_2) and 93 (ν_5) cm^{-1} agree well with the values reported for the $[SeBr_6]^{2-}$ and $[TeBr_6]^{2-}$ ions in O_h symmetry [20]. The IR spectrum contains an intense absorption

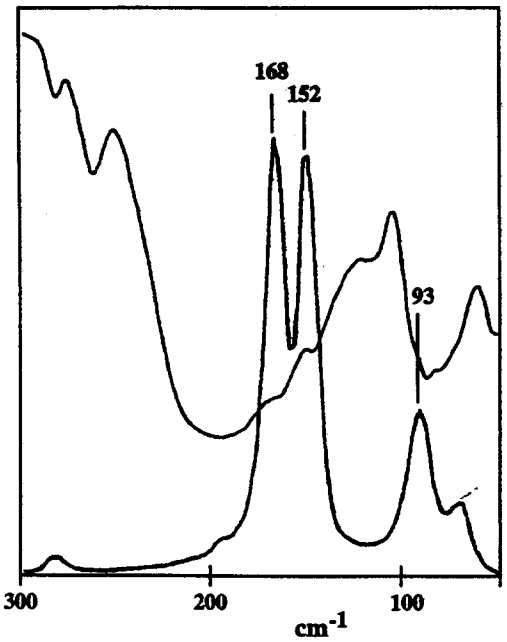

Fig. 3. FT-IR and FT-Raman spectra of II.

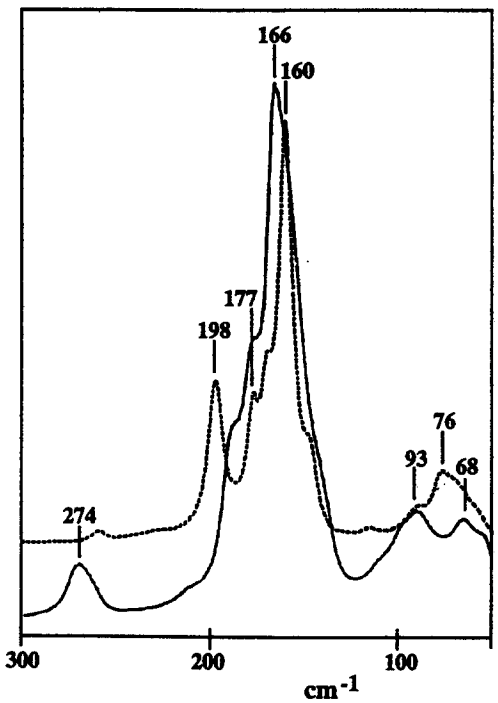

Fig. 4. Superimposed FT-Raman spectra of I (full line) and III (dotted line).

centred at 199 (ν_3) cm^{-1} and extending from 140 to 240 cm^{-1} with shoulders at 149 and 167 cm^{-1}, close to the Raman values.

The superimposed FT-Raman spectra of **I** and **III** are reported in Fig. 4; the similarity of the spectra indicates that **I**, like **III**, is a compound bearing the Br—Se—Br group. They show the most intense peak, which is attributable to the symmetric stretching of the Br—Se—Br group, at 166 and 160 cm^{-1} for **I** and **III** respectively. According to selection rules, the antisymmetric stretching vibration and the deforming of the Br—Se—Br group appear with high intensity in the infrared spectrum of **I** (not reported here) and fall at 184 (broad band) and 149 cm^{-1} respectively. At these frequencies, shoulders appear in its Raman spectrum. For **III**, the infrared spectrum shows an unresolved band envelops centred at about 170 cm^{-1} (ranging from 140 to 210 cm^{-1}), so that the frequencies of the antisymmetric stretching vibration and of the deforming cannot be assigned; however, the medium-weak peak at 198 cm^{-1} and the shoulder at about 150 cm^{-1}, present in the Raman spectrum of **III** (see Fig. 4), could be attributed to the antisymmetric stretching vibration and the deforming respectively, on the basis of the similarity with **I**.

Acknowledgements—We thank the Regione Autonoma della Sardegna and MURST for support in this research.

REFERENCES

1. Cristiani, F., Demartin, F., Devillanova, F. A., Isaia, F., Lippolis, V. and Verani, G., *Inorg. Chem.*, 1994, **33**, 6315.
2. Herbstein, F. H. and Schwotzer, W., *J. Am. Chem. Soc.*, 1984, **106**, 2367; *Angew. Chem. Int. Ed. Engl.*, 1982, **21**, 219.
3. Schweikert, W. W. and Meyers, E. A., *J. Phys. Chem.*, 1968, **72**, 1561.
4. Bransford, J. W. and Meyers, E. A., *Cryst. Struct. Comm.*, 1978, **7**, 697.
5. (a) Demartin, F., Deplano, P., Devillanova, F. A., Isaia, F., Lippolis, V. and Verani, G., *Inorg. Chem.*, 1993, **32**, 3694; (b) Bigoli, F., Pellinghelli, A. M., Deplano, P., Devillanova, F. A., Lippolis, V., Mercuri, L. and Trogu, E. F., *Gazz. Chim. It.*, 1994, **124**, 445.
6. (a) Freeman, F., Ziller, J. W., Po, H. N. and Keindl, M. C., *J. Am. Chem. Soc.*, 1988, **110**, 2376; (b) Arduengo, A. J. and Burgess, E. M., *J. Am. Chem. Soc.*, 1977, **99**, 2376; (c) Hayward, G. C. and Hendra, P. J., *J. Chem. Soc. A*, 1969, 1760; (d) Lin, G. H.-Y. and Hope, H., *Acta Cryst.*, 1972, **B28**, 643; Lin, G. H.-Y. and Hope, H., *Chem. Commun.*, 1970, 169; (e) du Mont, W. W., Kubiniok, S., Peters, S. and Von Schnering, H. G., *Angew. Chem. Int. Ed. Engl.*, 1987, **26**, 780; (f) du Mont, W. W., *Main Group Chem. News*, 1994, **2**, 18.
7. Demartin, F., Devillanova, F. A., Isaia, F., Lippolis, V. and Verani, G., *Inorg. Chim. Acta*, 1997, **255**, 203.
8. Bigoli, F., Demartin, F., Deplano, P., Devillanova, F. A., Isaia, F., Lippolis, V., Mercuri, M. L., Pellinghelli, A. M. and Trogu, E. F., *Inorg. Chem.*, 1996, **35**, 3194.
9. Cristiani, F., Devillanova, F. A. and Verani, G., *J. Chem. Soc., Perkin Trans. II*, 1977, 324.
10. Crystallographic data (excluding structure factors) for the structures reported in this paper have

been deposited with the Cambridge Crystallographic Data Centre. Deposition number 100 344.
11. Demartin, F., Gramaccioli, C. M. and Pilati, T., *Acta Crystallogr.*, 1992, **C48**, 1.
12. Cromer, D. T. and Waber, J. T., *International Tables for X-ray Crystallography*, The Kynoch Press, Birmingham, England, 1974, Table 2.2B.
13. Cromer, D. T., *International Tables for X-ray Crystallography*, Vol. IV, The Kynoch Press, Birmingham, England, 1974, Table 2.3.1.
14. Frenz, B., *Computers in Physics*, 2, No. 3, May/June, 1988, 42–48; Frenz, B., *Crystallographic Computing* 5, Oxford University Press, 1991, Ch. 11, pp. 126–135.
15. Recently the breaking of the C=Se bond of **2** has been carried out by electrochemical oxidation; in fact, we have synthesized the compound tetrakis(*N*-methylbenzothiazole-2(3H)-selone) selenium(2+) tetrafluoroborate, in which a formally Se^{2+} is coordinated by four neutral molecules of **2** to give an uncommon dication containing a non-cyclic square-planar Se_5 framework. Adamo, C., Demartin, F., Deplano, P., Devillanova, F. A., Isaia, F., Lelj, F., Lippolis, V., Lukes, P. and Mercuri, M. L., *J. Chem. Soc., Chem. Commun.*, 1996, 873.
16. Arduengo, A. J., Goerlich, J. R. and Marshall, J. W., *J. Am. Chem. Soc.*, 1995, **117**, 11027.
17. Gillespie, R. J. and Hargittai, I., *The VSEPR Model of Molecular Geometry*, Allyn & Bacon, Boston, 1991.
18. Abriel, W. and White, M. A., *J. Chem. Phys.*, 1990, **93**, 8321.
19. The labels of the vibrations are those reported by Nakamoto. Nakamoto, K., *Infrared and Raman Spectra of Inorganic and Coordination Compounds*, 4th Edn., Wiley, New York, 1986.
20. Baker, L.-J., Richard, C. E. F. and Taylor, M. J., *Polyhedron*, 1995, **14**, 401.

Pergamon

PII: S0277-5387(97)00306-9

Polyhedron Vol. 17, No. 2-3, pp. 313-318, 1998
© 1997 Elsevier Science Ltd
All rights reserved. Printed in Great Britain
0277-5387/98 $19.00+0.00

Electrochemical behaviour of $[Ru(4,4'\text{-}Me_2bpy)_2(PPh_3)(H_2O)](ClO_4)_2$ in homogeneous solution and incorporated into a carbon paste electrode. Application to oxidations of benzylic compounds

Eder C. Lima, Paula G. Fenga, José R. Romero and Wagner F. De Giovani*

Departamento de Química, Faculdade de Filosofia Ciências e Letras de Ribeirão Preto, Universidade de São Paulo, 14040-901-Ribeirão Preto-SP, Brazil

(Received 22 March 1997; accepted 3 July 1997)

Abstract—The complex $[Ru(4,4'\text{-}Me_2bpy)_2(PPh_3)(H_2O)](ClO_4)_2$ has been synthesized and characterized by elemental analysis, spectroscopic and electrochemical methods. $E_{1/2}$ *vs* pH studies are consistent with one-electron, one-proton transfer; at higher pH the potentials become pH independent. The catalytic activity of the complex has been investigated at pH 6.5 in the homogeneous electrooxidation of benzylic compounds. The reactivity was found to decrease in the order 1-phenylethanol ≫ phthalic alcohol > benzyl alcohol > 4-methylbenzyl alcohol > ethylbenzene > toluene. Carbon paste electrode (CPE) containing the complex has shown catalytic activity in oxidations of alcohols. Benzyl alcohol oxidation by CPE is first order on substrate concentration and for low concentrations is controlled by the diffusion rate of the substrate from solution.
© 1997 Elsevier Science Ltd

Keywords: ruthenium aquacomplex; electrocatalysis; electrooxidation; carbon paste electrode; alcohols; benzylic compounds.

The chemistry of ruthenium-aqua/ruthenium-oxo complexes system has received much attention due, in part, to the potential applications of these complexes as oxidation catalysts [1–14]. The chemistry and use as oxidants of oxo ruthenium complexes containing polypyridyl and tertiary phosphine ligands have been recently studied [5,12].

Electrocatalysis with chemically modified electrode surfaces has been a research topic of large interest [15,16]. Electrooxidations of alcohols using modified electrodes by polypyrrole films containing ruthenium complexes have been reported recently [17–19]. Carbon paste electrodes into which mediators have been admixed have also been used as electrocatalysts [20,21].

We report here the synthesis of $[Ru(4,4'\text{-}Me_2bpy)_2(PPh_3)(H_2O)](ClO_4)_2$ (**1**) ($4,4'\text{-}Me_2bpy$ = 4,4′-dimethyl-2,2′-bipyridine). We have studied the electrochemical and spectrochemical properties of (**1**) in solution and we describe its use in oxidation of benzylic compounds. The oxo-aqua ligands provide for rapid proton transfer concomitant with electron transfer permitting the accessibility of several oxidation states *via* gain or loss of protons. The interest in phosphine-ruthenium(IV)-oxo complex lies in its ability to act as a two-electron, two-proton redox agent which is selective due to the electronic, steric and hydrophobic versatility of the phosphine ligand [5]. In addition, the complex was admixed with carbon powder and mineral oil to form the modified carbon paste electrode. In the Ru^{IV} state, the electrode electrocatalyzes the oxidation of alcohols.

EXPERIMENTAL

Materials

Water was distilled twice from alkaline potassium permanganate. $RuCl_3 \cdot 3H_2O$, 4,4′-dimethyl-2,2′-bipyridine, PPh_3 and mineral oil were obtained from Aldrich Chemical Co. Carbon powder was purchased

* Author to whom correspondence should be addressed. Fax: 55-16-6338151. E-mail: wfdgiova@usp.br

from Bioanalytical Systems (CF-1010). 4-methylbenzyl alcohol [22(a)], 1-phenylethanol [22(b)] and phthalic alcohol [22(b)] were prepared according to literature procedures. All other reagents and solvents were of reagent quality and were used without further purification.

Measurements

UV-vis spectra were obtained in quartz cells by using a 8452A Hewlett-Packard spectrophotometer. Electrochemical experiments were carried out with a PAR model 273A Potentiostat/Galvanostat. Cyclic voltammetric experiments were conducted in a one-compartment cell using glassy carbon, carbon paste or platinum working electrodes, a platinum wire auxiliary electrode and a saturated calomel reference electrode (SCE). The $E_{1/2}$ values for reversible couples were calculated from half the difference between E_p values for the cathodic and anodic waves. The bulky electrolyses experiments were performed in a two-compartment cylindrical cell, at 25 ± 1°C, using a platinum gauze working electrode, a platinum plate auxiliary electrode and a SCE. The electrolyses were performed at a fixed applied potential of +0.90 V which is sufficient to generate the $Ru^{IV}{=}O^{2+}$ oxidant from the corresponding $Ru^{II}{-}OH_2^{2+}$ complex. The products of the electrolyses were extracted with diethyl ether and identified by conventional methods. The pH values of aqueous solutions were buffered at an ionic strength of 0.20 mol l^{-1} by HNO_3 and $NaNO_3$ (pH 1.0–2.6), potassium hydrogen phthalate, HNO_3 and $NaNO_3$ (pH 3.1–3.8), potassium hydrogen phthalate, NaOH and $NaNO_3$ (pH 4.4–5.2), Na_2HPO_4 and NaH_2PO_4 (pH 5.6–8.0), $Na_2B_4O_7 \cdot 10\ H_2O$ and $NaNO_3$ (pH 8.8) and $Na_2B_4O_7 \cdot 10\ H_2O$ and NaOH (pH 10.1). ^1H NMR spectra were obtained with a Brucker AC-80 spectrometer. GL chromatograms were recorded with Intralab 300 gas chromatograph. IR spectra were registered on a 1600 FT Perkin-Elmer spectrophotometer. Mass spectra were obtained with a Hewlett-Packard Gas Chromatograph/MS System 5988A.

Syntheses of the complex

$[Ru(4,4'\text{-}Me_2bpy)_2(PPh_3)(H_2O)](ClO_4)_2$ [23] (**1**) as well its precursors *cis*-$[Ru(4,4'\text{-}Me_2bpy)_2Cl_2] \cdot 2H_2O$ [24] (**2**) and $[Ru(4,4'\text{-}Me_2bpy)_2(PPh_3)Cl](PF_6)_2$ [23,25] (**3**) were prepared by procedures described for related complexes. The preparation of (**1**) was performed in a mixture of 3:2 ethanol:water; the reaction for (**2**) was conducted in ethylene glycol, and for (**3**), in 4:1 ethanol:water. Yield of (**1**) in the last step: 86%. Found: C, 53.5; H, 4.2; N, 5.4. Calc. for $C_{42}H_{41}N_4Cl_2O_9PRu$: C, 53.2; H, 4.4; N, 5.9%.

Carbon paste electrodes

Carbon paste electrodes containing 60:40% by weight of carbon powder and mineral oil were used for cyclic voltammetric studies. The modified electrodes contained 88:12% by weight of paste and complex. The carbon paste holder was constructed of a thick walled Teflon tube with 0.3 cm i.d. A copper sleeve equipped with a copper wire plunger was mounted at the top of the Teflon tube. By rotating the sleeve, the plunger could be made to extrude a used paste layer which was sliced off to form a fresh paste surface.

RESULTS AND DISCUSSION

Spectroscopic and redox properties of $[Ru(4,4'\text{-}Me_2bpy)_2(PPh_3)H_2O)](ClO_4)_2$ *in solution*

Figure 1 shows the absorption spectrum of the complex $[Ru(4,4'\text{-}Me_2bpy)_2(PPh_3)(H_2O)]^{2+}$ (**1**) in aqueous solution. Table 1 shows spectroscopic and redox data for the synthesized complexes. The bands in the UV region are assignable to ligands $\pi \rightarrow \pi^*$ excitations; the bands in the visible region can be attributed to metal to ligands transitions. When an aqueous solution of (**1**) is submitted to a potential of +0.90 V one can observe the disappearance of the band at 432 nm, since the species $Ru^{IV}{=}O^{2+}$ is practically transparent in the visible region; the same

Table 1. $E_{1/2}$ potentials and UV-vis spectral data for the complexes

Complexes	$E_{1/2}$(V) $Ru^{III/II}$	$Ru^{IV/III}$	λ_{max}, nm ($\varepsilon_{max} \times 10^3$, mol^{-1} l cm^{-1})
$[Ru(4,4'\text{-}Me_2bpy)_2Cl_2]$	+0.22[a]		380 (8.5), 558 (5.9)[b]
$[Ru(4,4'\text{-}Me_2bpy)_2(PPh_3)Cl]^{2+}$	+0.86[c]		292 (33), 330 (7.6), 460 (6.7)[b]
$[Ru(4,4'\text{-}Me_2bpy)_2(PPh_3)(H_2O)]^{2+}$	+0.89	+1.21[d]	222 (34), 288 (3.3), 432 (6.3)[e]
	+0.53	+0.75[e]	

[a] MeCN + 0.1 mol l^{-1} TBAP; glassy carbon working electrode; v = 100 mV s^{-1}.
[b] CH_2Cl_2.
[c] Same condition as [a], v = 200 mV s^{-1}.
[d] CH_2Cl_2 + 0.1 mol l^{-1}; platinum working electrode; v = 50 mV s^{-1}.
[e] pH 6.5 in 8:2 aqueous phosphate buffer (μ = 0.2 mol l^{-1}): tert-butyl alcohol.

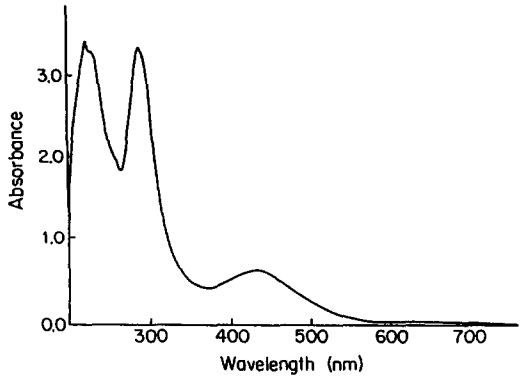

Fig. 1. UV-vis spectrum of 1.0×10^{-4} mol l^{-1} $[Ru(4,4'\text{-}Me_2bpy)_2(PPh_3)(H_2O)]^{2+}$ in 8:2 phosphate buffer solution (μ = 0.20 mol l^{-1}): tert-butyl alcohol, pH 6.5.

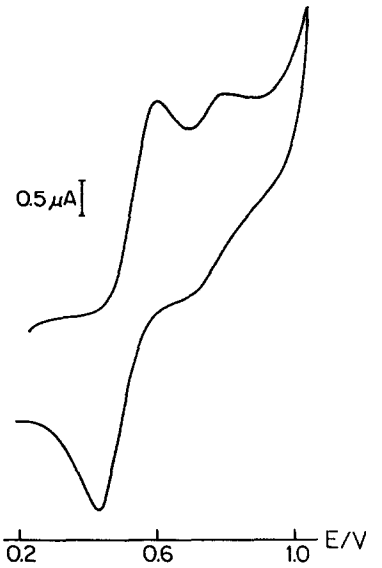

Fig. 2. Cyclic voltammogram of 1.0×10^{-3} mol l^{-1} $[Ru(4,4'\text{-}Me_2bpy)_2(PPh_3)(H_2O)]^{2+}$ in 8:2 phosphate buffer solution (μ = 0.20 mol l^{-1}): tert-butyl alcohol, pH 6.5; glassy carbon working electrode (diameter 3 mm); v = 10 mV s^{-1}.

observation occurs when (**1**) is oxidized stoichiometrically by Ce^{4+}. When the oxidized solution is reduced electrochemically at +0.1 V, the band at 432 nm is regenerated but a low broad band at 650 nm appears. This band can be due to the formation of Ru^{III}—O—Ru^{III} dimer [26] (eq. (1)) which is formed as consequence of rapid coproportionation reaction (eq. (2)).

$$2[(4,4'\text{-}Me_2bpy)_2(PPh_3)Ru^{III}\text{—}OH]^{2+} \leftrightarrows [\{(4,4'\text{-}Me_2bpy)_2(PPh_3)Ru^{III}\}_2O]^{4+} \quad (1)$$

$$[(4,4'\text{-}Me_2bpy)_2(PPh_3)Ru^{III}\text{—}OH_2]^{2+} + [(4,4'\text{-}Me_2bpy)_2(PPh)Ru^{IV}O]^{2+} \rightarrow 2[(4,4'\text{-}Me_2bpy)_2(PPh)Ru\text{—}OH]^{2+} \quad (2)$$

Cyclic voltammogram of (**1**) in aqueous solution (Fig. 2) shows two reversible redox waves corresponding to the $Ru^{III/II}$ and $Ru^{IV/III}$ couples, according to Scheme 1:

$$(4,4'\text{-}Me_2bpy)_2(PPh_3)Ru^{II}\text{—}OH_2^{2+} \underset{+e,+H^+}{\overset{-e,-H^+}{\rightleftarrows}} (4,4'\text{-}Me_2bpy)_2(PPh_3)Ru^{III}\text{—}OH^{2+} \underset{+e,+H^+}{\overset{-e,-H^+}{\rightleftarrows}} (4,4'\text{-}Me_2bpy)_2(PPh_3)Ru^{IV}{=}O^{2+}$$

Scheme 1.

The observed potentials in methylene chloride are higher than those obtained in aqueous solution. The separation between the two couples (320 mV) is larger than in water (220 mV). This behavior can be due to a very slow deprotonation kinetic of the first oxidized species.

The potentials for the $Ru^{III/II}$ couple vary with the pH of the solution, resulting in the $E_{1/2}$ *vs* pH variations shown in Fig. 3. Within the 7.8 > pH > 2.0 region, the potentials form a straight line, with slope (−0.064) very close to Nernstian prediction of −0.059 V/pH unit, indicative of one-electron oxidation accompanied by the dissociation of one proton (first step in Scheme 1). At pH > 7.8, the potentials become pH independent indicating that, in this region, $[Ru^{II}(4,4'\text{-}Me_2bpy)_2(PPh)(OH)]^+$ is the dominant species, and the couple becomes

$$(4,4'\text{-}Me_2bpy)_2(PPh_3)Ru^{II}\text{—}OH^+ \underset{+e}{\overset{-e}{\rightleftarrows}} (4,4'\text{-}Me_2bpy)_2(PPh_3)Ru^{III}\text{—}OH^{2+}$$

The $Ru^{IV/III}$ couple is not well-behaved in the studied pH range.

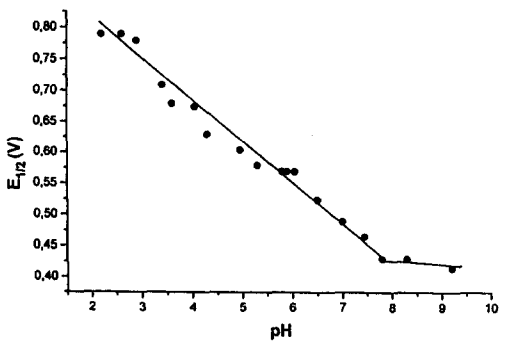

Fig. 3. Plot of $E_{1/2}$ *vs* pH for the $Ru^{III/II}$ redox couple of $[Ru(4,4'\text{-}Me_2bpy)_2(PPh_3)(H_2O)]^{2+}$; glassy carbon working electrode.

Table 2. Electrocatalytic oxidation of benzylic compounds by $[Ru(4,4'\text{-}Me_2bpy)_2(PPh_3)(OH_2)]^{2+}$[a]

Substrate[b]	Product	% yield[c]	Oxidative coulombs passed	Reaction time (h)
Benzyl alcohol	Benzaldehyde	78	252	22
4-Methylbenzyl alcohol	4-Methylbenzaldehyde	76	273	21
1-Phenylethanol	Acetophenone	81	286	16
Phthalic alcohol	Phthalic aldehyde	42	462	21
	Phthalide	35		
Ethylbenzene	Acetophenone	69	293	22
Toluene	Benzaldehyde	30	241	22

[a] In 25 cm^3 8:2 phosphate buffer ($\mu = 0.20$ mol l^{-1}): tert-butyl alcohol, pH 6.5. Catalyst concentration: 2.0 mmol l^{-1}.

[b] Substrate concentration: 50.0 mmol l^{-1}.

[c] Based on total coulombs passed.

Electrocatalytic oxidations of benzylic compounds in homogeneous solution

In the presence of excess of benzyl alcohol (25 times), the cyclic voltammogram of (**1**) shows a great enhancement of the oxidation current peaks and a decreasing of the reduction peaks upon potential scan reversal (Fig. 4). This is indicative of catalytic activity.

Table 2 shows the results obtained in electrooxidations of benzyl alcohol, 4-methylbenzyl alcohol, 1-phenylethanol, phthalic alcohol, ethylbenzene and toluene. The efficiency of current by time unit relationship can give a reactivity order for the electrooxidations: 1-phenylethanol ≫ phthalic alcohol > benzyl alcohol > 4-methylbenzyl alcohol > ethylbenzene > toluene. The proposed mechanism for oxidations using ruthenium oxo complexes suggests the formation, in the transition state, of an electron-deficient carbon [27]. A substituting group can decrease the reaction activation energy, inducing a delocalization of the positive charge by hyperconjugation, inductive or resonance effects. In this way, the secondary 1-phenylethanol is the more reactive due to the methyl group bound to the benzylic carbon. The primary benzylic diol, phthalic alcohol, is more reactive than the benzylic monoalcohols as expected. Benzyl alcohol has unexpected higher reactivity than 4-methylbenzyl alcohol; although the difference in reactivity between 4-methylbenzyl alcohol and benzyl alcohol was not pronounced, higher reactivity was expected for the former due to the presence of the methyl group; we have observed that 4-methoxylbenzyl alcohol is more reactive than benzyl alcohol when $Ru(trpy)(bpy)O^{2+}$ (trpy = 2,2′:6′,2″-terpyridine) was used [7]: methoxyl group is a strong π donor and methyl group is a weak σ donor. Ethylbenzene is more reactive than toluene, due to the methyl group in the α position relative to the benzylic carbon, which contributes to the positive charge delocalization by hyperconjugation or inductive effect.

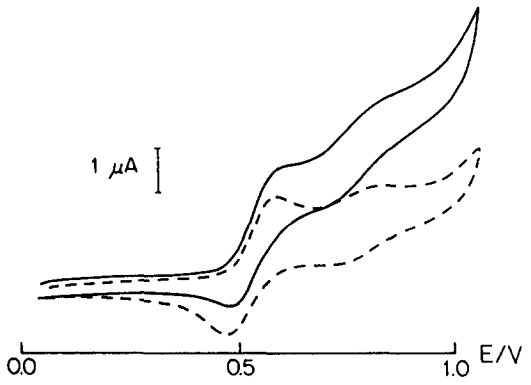

Fig. 4. Cyclic voltammograms at glassy carbon electrode (diameter 3 mm) of 1.0×10^{-3} mol l^{-1} $[Ru(4,4'\text{-}Me_2bpy)_2(PPh_3)(H_2O)]^{2+}$ in 8:2 phosphate buffer solution ($\mu = 0.20$ mol l^{-1}): tert-butyl alcohol, pH 6.5 in absence (---) and presence (——) of 25×10^{-3} mol l^{-1} benzyl alcohol.

It is worth noting the importance of the results from the point of view of synthesis: benzyl alcohol, 4-methylbenzyl alcohol yield the corresponding aldehydes exclusively (electrooxidations using $Ru(trpy)(bpy)(OH_2)^{2+}$ yielded carboxylic acids [7,28]), in the case of 4-methylbenzyl alcohol it should be noted that the methyl group was not oxidized as occurs when $Ru(trpy)(bpy)(OH_2)^{2+}$ was used [28]. In the oxidation of phthalic alcohol similar yields of phthalic aldehyde and phthalide were obtained, the latter being obtained from the formation of a hemiketal intermediate. The oxidation of toluene to benzaldehyde is another result to be noted; using $Ru(trpy)(bpy)(OH_2)^{2+}$ the product was benzoic acid [28]. The oxidation of ethylbenzene yielding acetophenone is very interesting, because alkylaromatics are mostly oxidized to benzoic acids [29]. These results demonstrate that the phosphine-ruthenium(IV)-oxo complex is a mild oxidant, which is advantageous since more powerful oxidants usually cause undesirable side reactions.

Electrocatalysis of alcohols with carbon paste electrode containing complex (**1**) (*CPE*)

The cyclic voltammogram of CPE in 8 : 2 phosphate buffer: tert-butyl alcohol, pH 6.5 shows only the reversible wave for the Ru^{IV}/Ru^{III} couple at +0.75 V while the redox wave for the Ru^{III}/Ru^{II} couple observed in solution is kinetically hindered in the carbon paste.

The cyclic voltammetric behavior of CPG in pH 6.8 phosphate buffer in the presence of benzyl alcohol, phthalic alcohol and cyclohexanol shows pronounced enhancement of the anodic currents corresponding to Ru^{IV}/Ru^{III} couple. There were no reduction peaks upon reversal scan direction, which are typical for electrocatalytic processes. The recorded oxidation peak decreased upon potential cycling between 0.0 and +1.0 V. Therefore, each quantitative experiment was performed at a new surface, freshly extruded from the holder. The peak height reproducibility at a fresh carbon paste electrode was 5% (standard deviation of 5 independent measurements). The observed reactivity order is benzyl alcohol > phthalic alcohol > cyclohexanol. The higher reactivity of the primary benzylic alcohol related to the secondary one was also observed in homogeneous catalysis by using $Ru(trpy)(bpy)(H_2O)^{2+}$ [7,8]. The high reactivity of benzyl alcohol can be due to its higher permeability into the active surface of the carbon paste electrode. For quantitative evaluation of the electrocatalysis surface, the dependence of the peak height on the benzyl alcohol bulky concentration and on the potential scan rate were studied. The respective results are presented in Figs 5 and 6. The peak height was linearly dependent (Fig. 5) (correlation coefficient 0.986) with plot intercept close to zero, on the concentration of benzyl alcohol indicating that the electrocatalysis is first-order in this benzyl alcohol concentration range. The dependence of the peak height on the square root of the potential scan rate (Fig. 6) was studied in pH 6.8 phosphate buffer solution for five different concentrations of benzyl alcohol in the range of v from 10 mV s^{-1} to 200 mV s^{-1}; the straight lines have a correlation coefficient close to 1.0 and for concentrations of 15, 25 and 35 mmol l^{-1} have plot intercept very close to zero. One can say that, for low concentrations, the behavior is characteristic for surface electrocatalysis with a catalyst confined to the electrode surface under diffusion rate control of the substrate from solution.

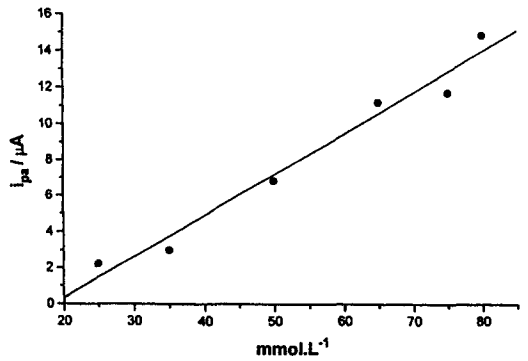

Fig. 5. Plot of the oxidation peak currents of CPE in pH 6.8 phosphate buffer solution (μ = 0.20 mol l^{-1}) against benzyl alcohol concentration.

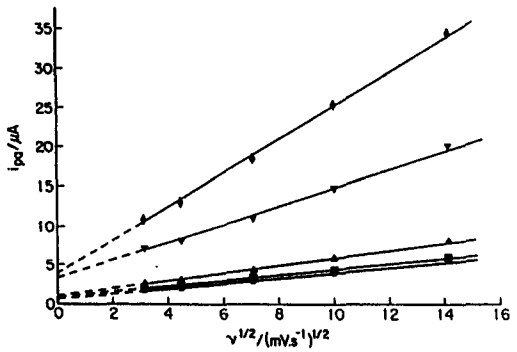

Fig. 6. Plot of the oxidation peak currents of CPE in pH 6.8 phosphate buffer solution (μ = 0.20 mol l^{-1}) against square root of the potential scan rate for different benzyl alcohol concentrations: (●) 15 mmol l^{-1}; (■) 25 mmol l^{-1}; (▲) 35 mmol l^{-1}; (▼) 50 mmol l^{-1}; (◆) 65 mmol l^{-1}.

One can conclude that $[Ru(4,4'\text{-}Me_2bpy)_2(PPh_3)(H_2O)]^{2+}$ is useful in selective oxidations of benzylic compounds and that the preparation of the carbon paste electrode is simple and straightforward and the characteristic of the mediator is fully preserved upon transfer from solution to the immobilized state.

Acknowledgements—We are grateful to FAPESP and CNPq for financial support.

REFERENCES

1. Moyer, B. A., Thompson, M. S. and Meyer, T. J., *J. Am. Chem. Soc.*, 1980, **102,** 2310.
2. Meyer, T. J., *J. Electrochem. Soc.*, 1984, **131,** 221C.
3. Thompson, M. S., De Giovani, W. F., Moyer, B. A. and Meyer, T. J., *J. Org. Chem.*, 1984, **25,** 4972.
4. Madurro, J. M., Chiericato, G., Jr, De Giovani, W. F. and Romero, J. R., *Tetrahedron Lett.*, 1988, 765.
5. Marmion, M. E. and Takeuchi, K. J., *J. Chem. Soc., Dalton Trans.*, 1988, 2385.
6. Campos, J. L., De Giovani, W. F. and Romero, J. R., *Synthesis*, 1990, 597.
7. Navarro, M., De Giovani, W. F. and Romero, J. R., *Synth. Commun.*, 1990, **20,** 399.
8. Navarro, M., De Giovani, W. F. and Romero, J. R., *Tetrahedron*, 1991, **47,** 851.
9. Oliveira, S. M., De Giovani, W. F., Romero, J. R. and Miller, J., *J. Braz. Chem. Soc.*, 1992, **3,** 70.

10. Li, C. K., Che, C. M., Tong, W. F. and Lai, T. F., *J. Chem. Soc., Dalton Trans.*, 1992, 813.
11. Che, C. M., Tang, W. T., Lee, W. O., Wong, K. Y. and Lau, T. C., *J. Chem. Soc., Dalton Trans.*, 1992, 1551.
12. Muller, J. G., Acquaye, J. H. and Takeuchi, K. J., *Inorg. Chem.*, 1992, **31,** 4552.
13. Dovletoglou, A. and Meyer, T. J., *J. Am. Chem. Soc.*, 1994, **116,** 215.
14. Navarro, M., Galembeck, S. E., Romero, J. R. and De Giovani, W. F., *Polyhedron*, 1996, **15,** 1531.
15. Abruña, H. D., *Coord. Chem. Rev.*, 1988, **86,** 135.
16. Merz, A., *Topics Curr. Chem.*, 1990, **152,** 49.
17. De Giovani, W. F. and Deronzier, A., *J. Electroanal. Chem.*, 1992, **337,** 285.
18. De Giovani, W. F. and Deronzier, A., *J. Chem. Soc., Chem. Commun.*, 1992, 1461.
19. Sauthier, M. N. C. D., Deronzier, A., LeBozec, H. and Navarro, M., *J. Electroanal. Chem.*, 1996, **410,** 21.
20. Kutner, W., Meyer, T. J. and Murray, R. W., *J. Electroanal. Chem.*, 1985, **195,** 375.
21. Kutner, W., *J. Electroanal. Chem.*, 1989, **259,** 99.
22. (a) Fieser, L. F. and Fieser, M., *Reagents for Organic Synthesis*, Vol. 1, John Wiley & Sons, New York, 1967, p. 584; (b) *ibid*, p. 883.
23. Marmion, M. E. and Takeuchi, K. J., *J. Am. Chem. Soc.*, 1988, **110,** 1472.
24. Collin, J. P. and Sauvage, J. P., *Inorg. Chem.*, 1986, **25,** 135.
25. Sullivan, B. P., Salmon, D. J. and Meyer, T. J., *Inorg. Chem.*, 1978, **17,** 3334.
26. Doppelt, P. and Meyer, T. J., *Inorg. Chem.*, 1987, **26,** 2027.
27. Thompson, M. S. and Meyer, T. J., *J. Am. Chem. Soc.*, 1982, **104,** 4106.
28. Carrijo, R. and Romero, J. R., *Synth. Commun.*, 1994, **24,** 433.
29. House, H. O., *Modern Synthetic Reactions*, The Benjamin/Cummings Publ. Co., Menlo Park, 1972.

Pergamon

PII: S0277-5387(97)00299-4

Polyhedron Vol. 17, No. 2-3, pp. 319-324, 1998
© 1997 Elsevier Science Ltd
All rights reserved. Printed in Great Britain
0277-5387/98 $19.00+0.00

The synthesis and characterization of copper(II) complexes of a novel binucleating tetraoxime ligand

Serdar Karaböcek[a]* and Nevin Karaböcek[b]

Departments of [a]Chemistry and [b]Science Education, Karadeniz Technical University, Trabzon, Turkey

(Received 23 April 1977; accepted 2 July 1997)

Abstract—6,6′-Methylenebis-[1,11-di(hydroximino)2,3:9,10-dibenzo-4,8-dioxaundecane], (H_4L) **4** was prepared by the reaction of 6,6′-methylenebis-(5′-on-3′,4′-benzo-2′-oxapentyl)-1,11-dion-2,3:9,10-dibenzo-4,8-dioxaundecane, **3** with hydroxylamine hydrochloride. Di- and tetranuclear copper(I) and (II) complexes with a bistetradentate ligand, (LH_4) have been prepared and identified by a combination of elemental analysis, ^{13}C, ^1H-NMR, mass spectra, magnetic moments, IR, UV/Vis, and ESR spectral studies. A geometric optimization of the synthesized ligand **4** was made by the method of molecular mechanics (MM2) in order to establish a stable conformation. The total energy for these conformations are calculated to be 10.94 and 9.49 kcal/mol.
© 1997 Elsevier Science Ltd

Keywords: tetraoxime; bistetradentate ligand; dinuclear; tetranuclear.

In recent years, binucleating macrocyclic or acyclic compounds have been extensively studied since these structural units are thought to be involved in a variety of biochemical and industrial processes [1–3]. The study of the exchange interaction between metal centers through extended bridges has been one of the most active research fields in magnetism [4–6]. The fundamental understanding of the factors that govern the magnetic properties, the design of new materials which can fulfil specific tasks and the biological relevance of the exchange-coupled polynuclear systems are at the origin of the increasing interest in this phenomenon.

Many reports are available for the preparation and properties of model copper complexes which mimic copper-containing metalloproteins such as hemocyanine and tyrosinase. Two noticeable properties of copper proteins are an intense absorption band [7–9] near 600 nm and relatively high copper(II)/copper(I) reduction potentials [8–10]. Particular attention was focused on their correlation with the active site of metalloenzymes and metalloproteins containing dinuclear metallocenters in order to elucidate the factors that determine the reversible binding and activation of O_2 in various natural oxygen transport systems and mono- and dioxygenases and to mimic their activity [7–9]. A number of dinuclear complexes containing linear ligand systems have been prepared and examined for oxygen uptake [10–12]. Such metal complexes have been prepared by using an acyclic ligand containing a bi-coordination site which can link one metal ion in the inner N_2O_2 [13–16].

In the present study, a binucleating tetraoxime ligand was prepared. This ligating system provide an additional active site besides conferring on the copper(II) ion within a square-planar N_2O_2 environment (Fig. 1).

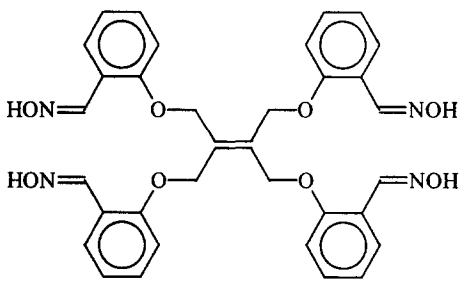

Fig. 1. Proposed structure of the ligand (**4**).

*Author to whom correspondence should be addressed.

EXPERIMENTAL

Tetrabromomethylethylene **2**, was prepared by a reported procedure [17]. ^{1}H-NMR spectra were recorded on a Bruker 200-MHz spectrometer. Mass spectra [FAB(positive)-MS] were measured on a VG AutoSpec provided by GV Analytical Instruments. C, H, N were analyzed microanalytically on a Hewlett Packard 85 CHN analyzer. Copper was estimated spectrophotometrically on a Hitachi 180-80 atomic absorption spectrometer. Electronic spectra were obtained on a ATI Unicam UV2 Model UV-Vis spectrophotometer. ESR measurements were made with a Varian model 109C E-line X-band spectrometer fitted with a quartz Dewar for measurements at liquid nitrogen temperature, IR spectra were recorded on a Matson 1000 Model FTIR spectrophotometer as KBr pellets. Room temperature magnetic susceptibility measurements were done on a PAR model 155 vibrating sample magnetometer. TLC was done on Merck Kieselgel 60-HF_{254} precoated aluminium plates. Conformational analysis was made by using the Allinger's MM2 method.

6,6′-*methylenebis*-(5′-*on*-3′,4′-*benzo*-2′-*oxapentyl*)-1,11-*dione*-2,3:9,10-*dibenzo*-4,8-*dioxaundecane*, (3)

Freshly prepared potassium 2-formylphenolate 6.4 g (40 mmol) and tetrabromomethylethylene **2**, (4 g, 10 mmol) were refluxed for 4 h in dimethylformamide (DMF) (50 cm^3). The solution was then poured onto ice-water (200 cm^3) and the solid product filtered off and recrystallised from acetone with decolourising charcoal. The compound **3**, m.p. 160°C, was isolated in 72% yield; IR (KBr disc.)/cm^{-1} 1690 (C=O) and 1234 (C—O); ^{1}H-NMR($CDCl_3$)/ppm δ: 10.20 (s, 4H, CHO), 6.80–7.95 (m, 16H, aryl) and 5.10 (s, 8H, OCH_2) MS (ei.) m/z = 564. Found: C, 73.8; H, 5.2. Calc. for $C_{34}H_{28}O_8$: C, 73.7; H, 5.0%.

6,6′-*methylenebis*-[1,11-*di*(*hydroximino*)2,3:9,10-*dibenzo*-4,8-*dioxaundecane*], (4)

A solution of tetraldehyde **3**, (5.54 g, 10 mmol) and hydroxylamine hydrochloride (5.5 g, 80 mmol) in pyridine (100 cm^3) was stirred at room temperature for 48 h. The mixture was then poured into ice-cold water (300 cm^3). The resulting precipitate was collected, washed successively with ice-cold water and diethyl ether, and dried *in vacuo* over P_2O_5. Recrystallization from a mixture of DMSO and MeOH (7:1) gave **4** as a colourless microcrystalline solid in 85% yield; m.p. 208–210°C; IR, (KBr disc)/cm^{-1} 1600 (C=N), 3200 (=N—O—H) and 1230 (C—O); ^{1}H-NMR ($CDCl_3$)/ppm δ: 12.15 (s, 4H, =N—OH) 9.80 (s, 4H, N=CH), 6.95–8.15 (m, 16H, aryl) and 5.45 (s, 8H, OCH_2) MS (FAB-positive) m/z = 624. Found: C, 66.3; H, 5.3; N, 9.1. Calc. for $C_{34}H_{32}N_4O_8$: C, 66.4; H, 5.2; N, 9.1%.

Preparation of $[Cu_2(LH_2)(ClO_4)_2 \cdot (H_2O)_2]$, (5)

A solution of $Cu(ClO_4)_2 \cdot 6H_2O$ (2 mmol, 741 mg) in dried acetone was added to the ligand (1 mmol, 624 mg) suspended in 30 cm^3 of acetone, and the mixture was refluxed with stirring for 12 h. A green-brown product was filtered off, washed with acetone and Et_2O and dried over P_4O_{10}. Found: C, 41.3; H, 3.5; N, 5.6; Cu, 13.0. Calc. for $C_{34}H_{34}N_4O_{18}Cl_2Cu_2$: C, 41.5; H, 3.5; N, 5.7; Cu, 12.9%.

Preparation of $[Cu_4(L)(ClO_4)_2(H_2O)_2L'_2] \cdot (ClO_4)_2$, (6)

L′:1,10-*phenanthroline*

Dinuclear copper complex (0.5 mmol, 490 mg) was mixed with triethylamine (1 mmol) by stirring for 0.5 h and then the solution in acetone (30 cm^3) was added to a 20 cm^3 solution of $Cu(ClO_4)_2 \cdot 6H_2O$ (1 mmol, 370 mg) and then subsequently to a solution of 1,10-phenanthroline (1 mmol, 180 mg) in 10 cm^3 acetone, and the mixture was refluxed for 8 h. The blue product was filtered off, washed with EtOH and Et_2O and dried over P_4O_{10}. Moreover, oxidation of the tetranuclear copper(I) complex in DMF with H_2O_2 gave the copper(II) complexes of tetraoxime. Found: C, 41.8; H, 3.0; N, 6.6; Cu, 15.3. Calc. for $C_{44}H_{48}N_8O_{26}Cl_4Cu_4$: C, 41.8, 2.9; N, 6.7; Cu, 15.2%.

RESULTS AND DISCUSSION

6,6′-Methylenebis-[1,11-di(hydroximino)2,3:9,10-dibenzo-4,8-dioxaundecane], (**4**) was prepared by the reaction of 6,6′-methylenebis-(5′-on-3′,4′-benzo-2′-oxapentyl)-1,11-dione-2,3:9,10-dibenzo-4,8-dioxaundecane (**3**), with hydroxylamine hydrochloride (Scheme 1). The structures of the tetraoxime (**4**), and tetraaldehyde (**3**), which is a precursor of the tetraoxime, were identified by a combination of elemental analysis, ^{1}H-NMR, IR and mass spectroscopy and their conformational analysis were made by molecular mechanics (MM2). The mass (FAB-positive) of (**4**) exhibits a strong parent ion at m/z 625 $[M+1]^+$, which indicates formation of the 13-membered acyclic bis-dioxime (**4**). ^{1}H-NMR spectrum of this compound in DMSO-d_6 clearly demonstrates the presence of a four =N—OH environment. The singlets at δ = 9.80 and 12.15 at ppm correspond to the =N—OH and N=CH proton resonances, respectively. In 12.15 ppm, the singlet disappears on deuterium exchange. In addition to 10.20 at ppm band, a singlet belonging to tetraldehyde protons of (**3**) disappears after the added reaction of hydroxylamine. A singlet chemical shift for the hydroximino protons indicates that oxime groups are in the tetraoxime [18–20] (**4**). In the IR spectrum of (**4**), the O—H stretching vibration is observed at 3200 cm^{-1}. The azomethine (C=N) stretching vibration is located at 1600 cm^{-1}. The

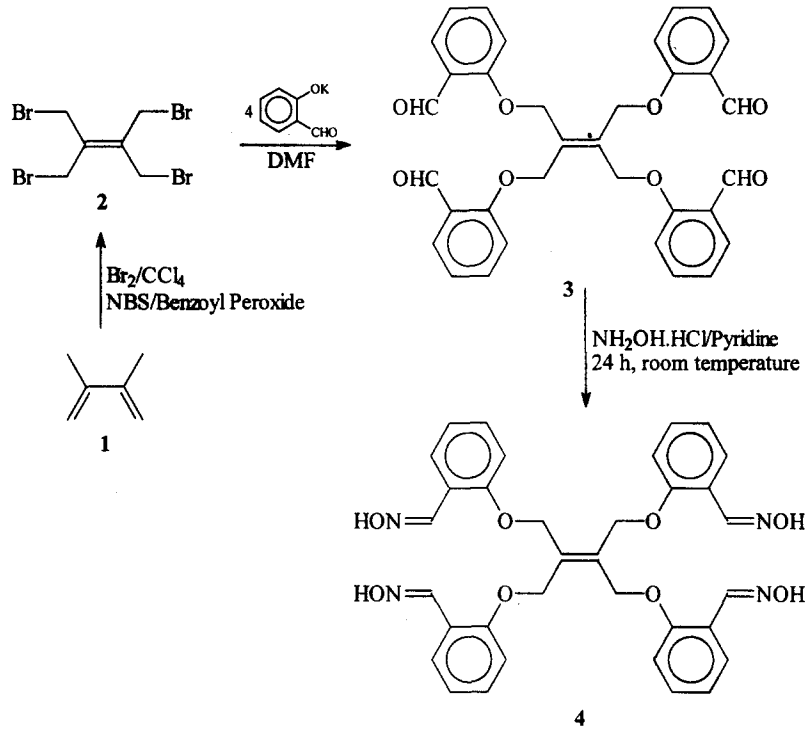

Scheme 1.

strong sharp band at 1230 cm^{-1} doublet was due to the N—O and C—O stretching vibrations [20].

A geometric optimization of the synthesized ligand, (**4**) was made by the method of molecular mechanics [21] (MM2) in order to establish a stable conformation and the data were compared with the experimental observations. The data for the two most stable conformations are listed in Table 1. These two conformations are given in Fig. 2. The total energy for one of these conformations is calculated to be 10.94 kcal/mol (Fig. 2(A)) and that of the other is 9.49 kcal/mol (Fig. 2(B)). Analysis of total energies for both of the conformations has shown that the energies are primarily due to especially the angle bending and van der Waals interactions (Table 1). All of the data obtained from the spectral and molecular mechanics (MM2) studies support the structural properties of the ligand.

X-Band ESR studies of copper(II) complexes were obtained in DMSO. The spectra reveal the presence of less than four components. The broadening of the $g_\perp$ line and splitting is due to the overlap of $g_\parallel$ and $g_\perp$ components, further indicating a lowered site simetry [22–24]. The $g_\parallel$ is 2.23 as observed in dinuclear complexes (Table 2). A clear five-line pattern emerges on the $g_\parallel$ component with ≈ 14.5 G. Thus, the ESR data supports the binding of the tetradentate ligand with two N and two O donor sites to the copper(II) ion, providing a square planar geometry, the other axial sites being occupied by chlorate anion and water molecule [25]. Figure 3 shows the ESR spectra of the $[Cu_2(LH_2)(ClO_4)_2 \cdot (H_2O)_2]$ complex in frozen DMSO. The value of the coupling constant evaluated from the peaks is *ca.* 118 G. This value is nearly half of that found for the present mononuclear complexes (Table 2). This situation could arise when four equivalent copper(II) ions are coupled *via* an exchange inter-

Table 1. Energies of the most stable two conformations of the ligand (H_4L, Fig. 2) from the MM2 force field calculations (energies in kcal/mol)

Conformation	Total	Bond	Angle	Torsional (dihedral)	van der Waals	Stretch-bend	Electrostatic
A	10.94	2.83	10.46	−28.94	26.17	0.090	0.33
B	9.49	2.62	9.82	−27.64	24.65	0.037	−0.009

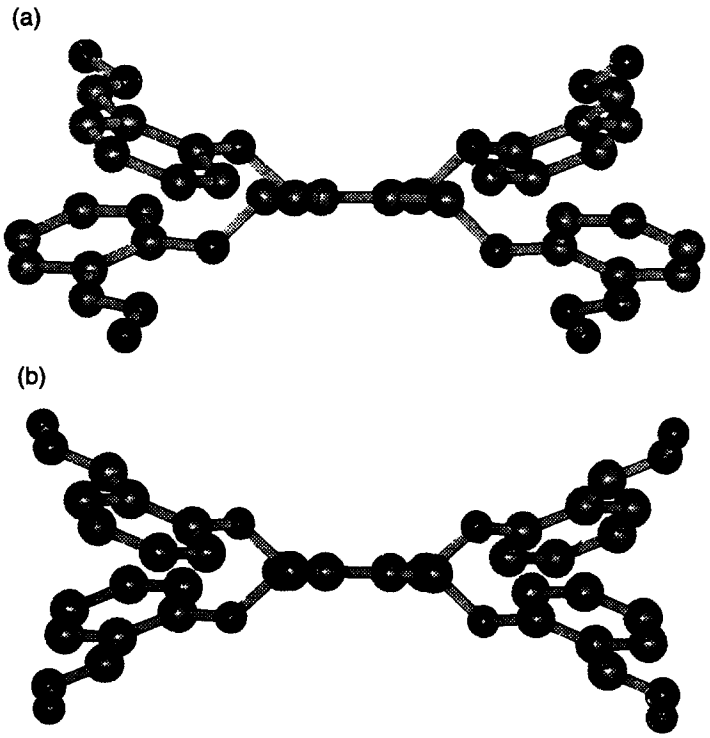

Fig. 2. Calculated (MM2) conformation for compound (**4**). (Total strain energy (a) 10.94, and (b) 9.49 kcal/mol).

Table 2. X-Band ESR, electronic spectra and magnetic moment data of H_4L and its copper(II) complexes

Compound		Sol.[a] λ_{max} (nm)	μ_{eff}/atom (B.M.)	$g_\parallel$	$g_\perp$	$A_\parallel$	$g_\parallel/A_\parallel$	$g_\perp$ splitting
Tetraoxime, H_4L	(**4**)	375 255 325						
$[Cu_2(LH_2)(ClO_4)_2 \cdot (H_2O)_2]$	(**5**)	628 450 380	1.80	2.23	1.98	200.00	110	114
$[Cu_4(L)(ClO_4)_2(H_2O)_2L'_2] \cdot (ClO_4)_2$	(**6**)	437 375	1.46					

[a] All spectra were taken in DMSO.

action, in a tetranuclear complex. The room temperature solid state magnetic moment data of the copper(II) complexes are listed in Table 2. Dinuclear copper(II) complex showed normal magnetic moment. The tetranuclear complex shows μ_{eff} value of 1.46 B.M., indicating an exchange coupled tetrameric complex, a structure also supported by ESR study [13, 22, 33].

The ligand was dissolved in DMF and shows characteristic UV-Vis spectra of the oxime group. The absorption bands are given in Table 2. The electronic spectra of all complexes measured in DMF showed intense absorptions around 400 nm which are assigned to charge-transfer transition from the $p\pi$ orbitals of the donor atoms to the d orbitals of the metal (Table 2). In the dinuclear-copper(II) complex, d–d transition base observed at 628 nm. The energy of the d–d transition suggests a distorted octahedral copper(II) complex [26].

Infrared spectra of complexes **5** and **6** have been compared with that of similar structures in order to establish the coordination modes of the oxime ligand

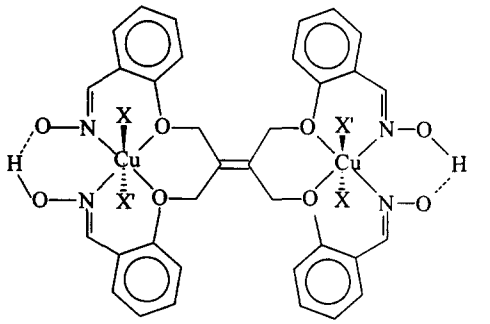

(5)

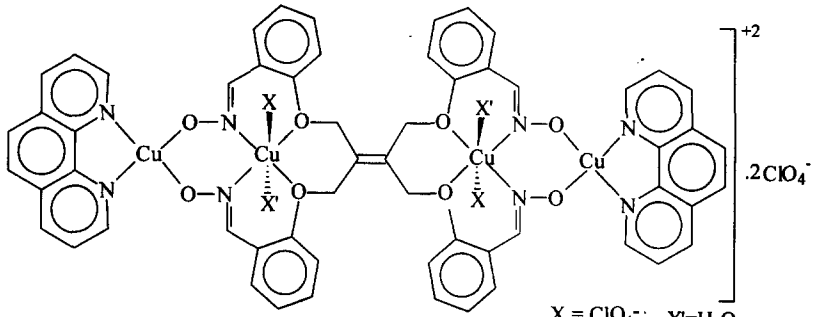

(6)

Fig. 3. Proposed structures of copper(II) complexes (**5**) dinuclear, (**6**) tetranuclear.

in complexes **5** and **6**. The more relevant OH, C=N and N—O absorption bands are listed in Table 3. In general, the complexes exhibited very similar IR features. This is indirect evidence that the complexes are of similar structures. In the IR spectra of these complexes (OH) stretching vibrations have disappeared and there is no distinct shift in (C=N) stretches after complex formation. The absence of O—H stretching vibrations for the free ligand indicates the formation of a hydrogen bridge between tetraoxime oxygen atoms [27].

IR data confirms the binding of the copper(II) by O and N donor groups of the present ligand and supports the tentative structure of the complexes (Fig. 1). The sharp intensity bands in the 1600 cm^{-1} region of **4** were assigned to C=N stretching vibrations. The

Table 3. Observed frequencies and proposed mode of assignments for the ligand and the complexes

Compound	(O—H)	(C=N)	(N—O)	(C—N)	(ClO_4)	(Cu—N)	(Cu—O)	(O—H···O)
Tetraoxime, H_4L (**4**)	3184	1600	1230	1491	—	—	—	
$[Cu_2(LH_2)(ClO_4)_2 \cdot (H_2O)_2]$ (**5**)	3446br	1598	1225	1495	1103 1006 621	438	375	1684
$[Cu_4(L)(ClO_4)_2(H_2O)_2L_2'] \cdot (ClO_4)_2$ (**6**)	3464br	1600	1225	1495	1114 628	428	350	

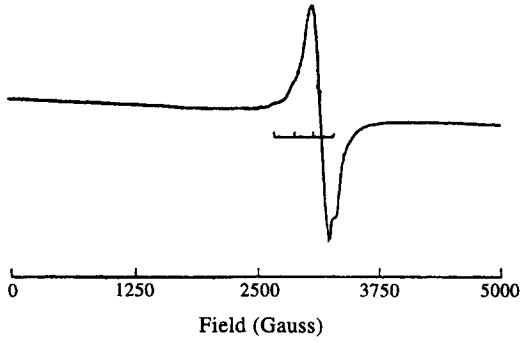

Fig. 4. ESR spectra of frozen DMSO solution of $[Cu_2(LH_2)(ClO_4)_2 \cdot (H_2O)_2]$.

N—O stretching vibrations for the complex shift to upfield suggesting that the oxime groups are nitrogen coordinated.

As a conclusion, in the complex **5**, both copper atoms are in a slightly distorted octahedral environment formed by the two oxime-nitrogen atoms and two phenolate-oxygen atoms from the tetraoxime ligand. Moreover, one perchlorate anion and one water molecule are arranged in axial positions. The small distortion from planar toward tetrahedral stereochemistry around the copper atoms of these four donor sets of atoms within tetraoxime ligand is characterized by a twisting angle as calculated by molecular mechanics (MM2) minimization. In complex **6**, four copper-containing fragments, Cu_2L and $Cu_2(Phen)_2$ are joined through the 1,10-phenantroline-nitrogen atoms to form a tetrameric compound. Since the ligand is a very symmetrical molecule, shifts in IR absorption bands are very slight. However, in compound **5**, the bands belonging to OH groups at 3184 cm^{-1} disappear, and a band at 1684 cm^{-1} belonging to O···H—O appears upon complexation, whereas in compound **6**, the O···H—O band at 1684 cm^{-1} disappears. The results are all in good agreement with the proposed structures for the obtained complexes. Moreover, all of the data obtained from the spectral studies support the structural properties of the complexes (Fig. 4).

Acknowledgements—This work was supported by The Research Fund of Karadeniz Technical University. The authors thank Dr Saadettin Güner of Karadeniz Technical University.

REFERENCES

1. Lehn, J. M., *Angew. Chem., Int. Engl.*, 1988, **27,** 89.
2. Vigato, P. A., Tamburini, S. and Fenton, D. E., *Coord. Chem. Rev.*, 1990, **106,** 25.
3. McKenzie, C. J. and Robson, R. J., *J. Chem. Soc., Chem. Commun.*, 1988, 112.
4. Willett, R. D., Gatteschi, D. and Kahn, O., eds, *Magneto-Structural Correlations in Exchange Coupled Systems*, NATO ASI Series, Vol. 140, Reidel, Dordrecht, 1985.
5. Delhaes, P. and Derillon, M., eds, *Organic and Inorganic Low-Dimensional Crystalline Materials*, NATO ASI Series, Vol. 168, Plenum, New York, 1987.
6. Gatteschi, D., Kahn, O., Miller, J. S. and Palacio, F., eds, *Magnetic Molecular Materials*, NATO ASI Series, Vol. 198, Kluwer, Dordrecht, 1987.
7. Malkin, R., in *Inorganic Biochemistry*, G. L. Eichhorn, ed., Elsevier, New York, 1973, p. 689.
8. Fee, J. A., *Struct. Bond.*, 1975, **23,** 1.
9. Malkin, R. and Malmstrom, B. G., *Adv. Enzymol.*, 1970, **33,** 177.
10. Sailasuta, N., Anson, F. C. and Gray, H. B., *J. Am. Chem. Soc.*, 1979, **101,** 455.
11. Karlin, K. D. and Zubieta, J., *Copper Coordination Chemistry and Biochemistry: Biochemical and Inorganic Perspectives*, Adenine Press, Guilderland, NY, 1983.
12. Fenton, D. E., Casellato, U., Vigato, P. A. and Vidali, M., *Inorg. Chim. Acta*, 1984, **95,** 187.
13. Luneau, D., Oshio, H., Okawa, H., Koikawa, M. and Kida, S., *Bull. Chem. Soc. Jpn*, 1990, **63,** 2212.
14. Kitajima, N. and Morooka, Y., *Chem. Rev.*, 1994, **94,** 737.
15. Tsumaki, T., *Bull. Chem. Soc. Jpn*, 1938, **13,** 2525.
16. Casella, L. and Rigoni, L., *J. Chem. Soc., Chem. Commun.*, 1985, 1668.
17. Cope, A. C. and Kagan, F., *J. Am. Chem. Soc.*, 1958, **80,** 5499.
18. Gök, Y. and Kantekin, H., *Chem. Ber.*, 1990, **123,** 1479.
19. Pedersen, S. B. and Larsen, E., *Acta Chem. Scand.*, 1973, **27,** 3291.
20. Daniel, A. and Pavia, A. A., *Tetrahedron Lett.*, 1967, **13,** 114.
21. Allinger, N. L., *J. Am. Chem. Soc.*, 1977, **99,** 8127.
22. Sharma, Y. S., Pandey, H. N. and Mathur, P., *Polyhedron*, 1994, **22,** 3111.
23. Karaböcek, S. and Karaböcek, N., *Polyhedron*, 1997, **16,** 1771.
24. Ito, N., Phillips, S. E. W., Stevens, C., Ogel, Z. B., McPherron, M. Y., Keen, T. N., Yadav, K. S. and Knowles, P. F., *Nature*, 1991, **350,** 87.
25. Ito, N., Philips, S. E. W., Stevens, C., Ogel, Z. B., Mepherron, M. Y., Keen, T. N., Yadav, K. D. S. and Knowles, P. F., *J. Inorg. Biochem.*, 1991, **43,** 165.
26. Gül, A., Okur, A. I., Cihan, A., Tan, N. and Bekaroglu, Ö, *Synt. React. Inorg., Met.-Org. Chem.*, 1986, **16,** 871.
27. Ramanujam, V. V. and Alexander, V., *Inorg. Chim. Acta*, 1987, **26,** 3124.

Pergamon

PII: S0277-5387(97)00308-2

Polyhedron Vol. 17, No. 2-3, pp. 325-330, 1998
© 1997 Elsevier Science Ltd
All rights reserved. Printed in Great Britain
0277-5387/98 $19.00+0.00

Syntheses, solubilities and oxygen absorption properties of new cobalt(II) Schiff-base complexes

Sangsook Park, V. K. Mathur,* and Roy P. Planalp*

Departments of Chemical Engineering and Chemistry, University of New Hampshire, Durham, New Hampshire, 03824, U.S.A.

(Received 25 November 1996; accepted 30 June 1997)

Abstract—The syntheses, solubilities and oxygen absorption properties of cobalt(II) complexes of *N,N'*-bis(salicylidene)-2,2'-dimethyl-1,3-propanediimine ligand derivatives, termed CoSaldmpr, are reported. These are homologs of the well-known *N,N'*-bis(salicylidene)ethylenediiminocobalt(II) (CoSalen) complexes, in which a 2,2-dimethyl-1,3-propanediimino bridging group replaces the ethylenediimino bridging group of CoSalen. Solubility data and limited oxygen-carrying properties of the complexes in 1-methyl-2-pyrrolidinone (NMP) solution, either alone or in the presence of 2-cyanopyridine (2 M) as an axial base, are reported. Oxygen transport of the solutions is tested with a flow system and a thermal swing process with O_2 absorption conditions of 37°C and desorption conditions of 100–180°C. The two CoSaldmpr complexes that are tested have higher solubilities and oxygen affinities than the CoSalen homologs. In NMP solution with 2 M 2-cyanopyridine axial base, loading of Co(3-methoxy-Saldmpr), measured in (g O_2/g solution) remains about 35% higher than Co(3-methoxy-Salen) for at least four absorption/desorption cycles. © 1997 Elsevier Science Ltd

Keywords: cobalt(II) Schiff-base complexes; oxygen complexes; oxygen carriers; oxygen separation; thermal swing absorption.

Synthetic dioxygen carriers [1] have attracted much attention since the initial reports concerning the cobalt Schiff-base complex *N,N'*-bis(salicylidene)ethylenediiminocobalt(II) (CoSalen) [2]. Numerous reports of systems for the separation of oxygen from air using complexes of the cobalt bis(salicylidene) family have appeared. Among these are solution-phase [3], solid-phase [4] and liquid-membrane systems [5]. The need for methods for separation of oxygen which are less energy-intensive than the cryogenic process of distillation of liquid air is clear. The use of a thermal swing process in which oxygen carriers which absorb oxygen from air at ambient temperature, followed by desorption at elevated temperature, may provide oxygen-enriched combustion air to a furnace [6]. This application would be energy-efficient in that waste heat from the furnace may be used to accomplish the desorption of oxygen. The key problem with these systems has been the stability of the complexes to oxidative degradation over repeated oxygen separation cycles at room temperature and above [7]. An additional practical requirement of the solution-phase and liquid-membrane systems is high solubility of the carriers in polar organic solvents, which will maximize the amount of oxygen carried per mass of solution or area of membrane.

This paper describes our studies of effect of carrier structure on solubility, oxygen affinity and stability. We have previously described the development of a thermal swing absorption oxygen carrying system which can be run continuously for many cycles that uses known Co^{II} Schiff-base oxygen carriers [8]. Previous studies have indicated that addition of electron-donating groups such as alkoxy to carriers can increase oxygen affinity, with some quantitative affinity data available [2(c)]. Further, steric effects in the immediate environment about cobalt [9] can be expected to increase stability of the carriers through preventing μ-peroxo dimer formation, but in only one study have hindered-bridge salicylidene (diimino) carriers been prepared and quantitatively tested for oxy-

* Authors to whom correspondence should be addressed.

gen absorption [10]. To increase oxygen carrier performance, we pursued the strategies of addition of steric hindrance and electron-donating groups, and of increasing carrier solubility. We report the preparation of new carriers employing the Schiff-base ligand *N,N'*-bis(salicylidene)-2,2'-dimethyl-1,3-propanediimine [11] (Saldmpr, Chart 1) in place of ethylenediiminosalicylidene (Salen), and the addition of alkoxy groups to the salicylidene phenyl rings of Saldmpr. The solubility in 1-methyl-2-pyrrolidinone (NMP) and the stability to several cycles of oxygen absorption and desorption of Saldmpr carriers relative to Salen carriers is reported.

Chart 1

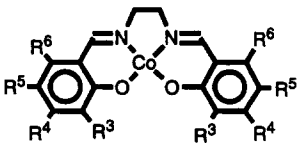

CoSalen (1): $R^3 = R^4 = R^5 = R^6 = H$
3-MeOCoSalen (2): $R^3 = CH_3O$; $R^6 = R^4 = R^5 = H$
3-EtOCoSalen (3): $R^3 = C_2H_5O$; $R^6 = R^4 = R^5 = H$
4-MeOCoSalen (4): $R^4 = CH_3O$; $R^3 = R^5 = R^6 = H$
4,6-$(MeO)_2$CoSalen (5): $R^4 = R^6 = CH_3O$; $R^3 = R^5 = H$

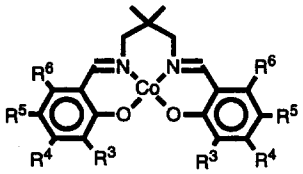

CoSaldmpr (6): $R^3 = R^4 = R^5 = R^6 = H$
3-MeOCoSaldmpr (7): $R^3 = CH_3O$; $R^6 = R^4 = R^5 = H$
3-EtOCoSaldmpr (8): $R^3 = C_2H_5O$; $R^6 = R^4 = R^5 = H$
4-MeOCoSaldmpr (9): $R^4 = CH_3O$; $R^3 = R^5 = R^6 = H$
4,6-$(MeO)_2$CoSaldmpr (10): $R^4 = R^6 = CH_3O$; $R^3 = R^5 = H$

EXPERIMENTAL

General

All operations were conducted using Schlenk technique [12]. Chemicals were purchased from Aldrich, except for 3-ethoxysalicylaldehyde which was purchased from Pfaltz and Bauer. Salicylaldehyde was vacuum distilled. The CoSalen ligand and complex derivatives were prepared as previously reported [13]. Proton NMR spectra were measured on a Bruker 360 MHz NMR spectrometer. Mass spectra were measured on a Hewlett Packard 5890 GC/MS spectrometer. Elemental analyses were carried out by the University of New Hampshire Instrumentation Center using a Perkin-Elmer Series II 2400 analyzer.

Oxygen absorption and desorption measurements

The measurement system, as previously described [8], is shown in Fig. 1. Air (A) was passed through a needle valve and a calibrated Hastings mass-flow meter (B) to establish and measure the air flow rate. The air was bubbled through the reactor (D) where absorption and desorption take place. Each absorption/desorption cycle requires about 1.5 h. The effluent of the reactor was passed through an Infrared Industries IR-2200 Oxygen Analyzer (E) and then exhausted into a hood. A bypass line (C) around the reactor allowed for calibration and check of the analyzer. The reactor consists of an outer metal jacket around a glass reaction vessel fitted with a rubber stopper through which the gas inlet, gas outlet, thermometer and thermocouple were passed. The reactor was alternately cooled in each absorption cycle and heated in each desorption cycle. The gas inlet consisted of a glass line with a fritted glass termination attached to promote contact of the gas with the liquid.

The data from the oxygen analyzer, mass flow meter, and thermocouple were collected using an IBM PC/XT with the labtech/Notebook data acquisition system. The amount of oxygen absorbed and desorbed was calculated by integrating the product of the oxygen concentration and flow rate over the cycle.

N,N' - Bis(salicylidene) - 2,2 - dimethyl - 1,3 - propane - diimine

This is a modification of [11]. 2,2-Dimethyl-1,3-propanediamine (2.4 cm^3, 20 mmol) was added to a boiling solution of salicylaldehyde (4.3 cm^3, 40 mmol) in 50 cm^3 of ethanol, causing a color change from colorless to yellow. About one-third of the solvent was removed under reduced pressure, initiating the formation of yellow crystals. When crystal formation ended, the product was filtered and dried *in vacuo* (5.2 g, 83%). Mp: 96–97.5°C. Found: C, 73.51; H, 7.04; N, 8.96. Calc. for $C_{19}H_{22}N_2O_2$: C, 73.55; H, 7.10; N, 9.03%. ^1H NMR ($CDCl_3$, 25°C): δ 1.05 (s, 3 H, CH_3), 3.47 (s, 2 H,—CH_2), 6.84–7.52 (m, 4 H, C_6H_4), 8.32 (s, 1 H, C*H*), 11.26 (s, 1 H, O*H*). MS (EI, 70 eV): 310 amu (M^+).

N,N' - Bis(salicylidene) - 2,2 - dimethyl - 1,3 - propane - diiminocobalt(II) hemihydrate (6)

A mixture of bis(salicylidene)ethylenediimine (5.15 g, 16.6 mmol), sodium acetate (0.050 g, 0.61 mmol), 1.07 M NaOH (31.0 cm^3, 33.2 mmol), distilled water (30 cm^3) and ethanol (60 cm^3) was warmed to 70°C to dissolve the ligand. Aqueous cobalt chloride (3.95 g in 20 cm^3 H_2O, 16.6 mmol) at 50°C was added to the solution. The brown powder (5.4 g, 89% yield) was separated by filtration and dried at 110°C under reduced pressure for 3 h. Mp: 312–315°C (dec). Found: C, 60.72; H, 5.38; N, 7.48. Calc. for $C_{19}H_{20}N_2O_2Co \cdot 0.5\ H_2O$: C, 60.64; H, 5.62; N, 7.44%. MS (EI, 70 eV): 367 amu (M^+).

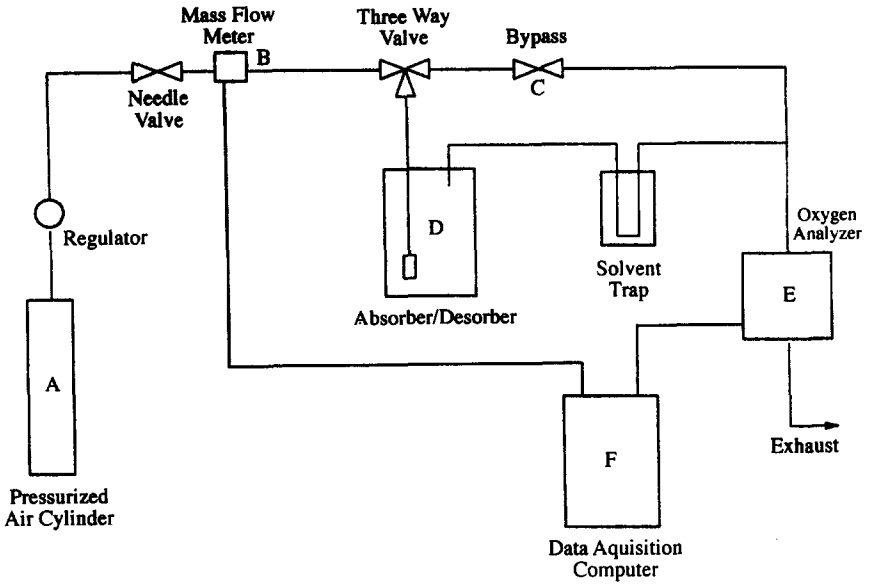

Fig. 1. Oxygen Absorption and Desorption Measurement System.

N,N' - Bis(3 - methoxysalicylidene) - 2,2 - dimethyl - 1,3 - propanediimine

2,2-Dimethyl-1,3-propanediamine (1.4 cm^3, 12 mmol) was added to a boiling solution of 3-methoxysalicylaldehyde (3.5 g, 23 mmol) in 30 cm^3, of ethanol, causing a color change from colorless to yellow. About one-third of the ethanol was removed under reduced pressure, leading to formation of a yellow precipitate. The precipitate was separated by filtration, dried under reduced pressure, and recrystallized from toluene/hexane (30 cm^3: 20 cm^3) at −5°C, giving yellow crystals (3.2 g, 75%). Mp: 113–114°C. Found: C, 68.10; H, 7.19; N, 7.44. Calc. for $C_{21}H_{26}N_2O_4$: C, 68.11; H, 7.03; N, 7.57%. ^1H NMR ($CDCl_3$, 25°C): δ 1.06 (s, 3 H, CH_3), 3.48 (s, 2 H, —CH_2), 3.89 (s, 3 H, OCH_3), 6.76–6.92 (m, 3 H, C_6H_3), 8.34 (s, 1 H, C*H*), 10.68 (s, 1 H, O*H*). MS (EI, 70 eV): 370 amu (M^+).

N,N' - Bis(3 - ethoxysalicylidene) - 2,2 - dimethyl - 1,3 - propanediimine

2,2-Dimethyl-1,3-propanediamine (3.6 cm^3, 30 mmol) was added to a boiling solution of 3-methoxy salicylaldehyde (10.0 g, 60.2 mmol) in 50 cm^3 of ethanol, causing a color change from colorless to yellow. The solution volume was reduced to 15 cm^3 giving a yellow precipitate which was separated by filtration, dried under reduced pressure, and recrystallized from toluene/hexane (1:1 75 v/v) to give yellow crystals (7.8 g, 65%). Mp: 96–98°C. Found: C, 69.22; H, 7.68; N, 6.95. Calc. for $C_{23}H_{30}N_2O_4$: C, 69.35; H, 7.54; N, 7.04%. ^1H NMR ($CDCl_3$, 25°C): δ 1.05 (s, 3 H, CH_3), 1.48–1.50 (t, 3 H, CH_3), 3.47 (s, 2 H, —CH_2), 4.07–4.13 (q, 2 H, OCH_2), 6.75–6.91 (m, 3 H, C_6H_3), 8.30 (s, 1 H, C*H*), 10.79 (s, H, O*H*), MS (EI, 70 eV): 398 amu (M^+).

N,N' - Bis(3 - methoxysalicylidene) - 2,2 - dimethyl - 1,3 - propanediiminocobalt(II) (**7**)

This complex was prepared as for **6** using 3.0 g (8.0 mmol) of the corresponding Schiff base, 15 cm^3 of aqueous sodium hydroxide (1.07 M, 16 mmol), 0.026 g (0.31 mmol) of sodium acetate, 15 cm^3 water, 30 cm^3 ethanol, and 2.0 g (8.0 mmol) cobalt chloride (solution in 10 cm^3 H_2O). A brown powder was obtained (2.9 g, 85% yield). Mp: 299°C (dec). Found: C, 58.46; H, 5.74; N, 6.52. Calc. for $C_{21}H_{24}N_2O_4Co$: C, 59.02; H, 5.62; N, 6.56%. MS (EI, 70 eV): 427 amu (M^+).

N,N' - Bis(3 - ethoxysalicylidene) - 2,2 - dimethyl - 1,3 - propanediiminocobalt(II) hemihydrate (**8**)

This complex was prepared as for **6** using 7.76 g (19.5 mmol) of the corresponding Schiff base, 35.5 cm^3 of aqueous sodium hydroxide (1.07 M, 39.0 mmol), 0.059 g (0.72 mmol) of sodium acetate, 40 cm^3 water, 80 cm^3 ethanol, and 4.64 g (19.5 mmol) cobalt chloride (solution in 30 cm^3 H_2O). A brown powder was obtained (7.1 g, 80%). Mp: 252°C (dec). Found: C, 59.98; H, 6.21; N, 6.01. Calc. for $C_{23}H_{28}N_2O_4Co \cdot 0.5\ H_2O$: C, 59.48; H, 6.29; N, 6.03%. MS (EI, 70 eV): 455 amu (M^+).

N,N′-Bis(4-methoxysalicylidene)-2,2-dimethyl-1,3-propanediimine

2,2-Dimethyl-1,3-propanediamine (4.4 cm^3, 35 mmol) was added to a boiling solution of 4-methoxysalicylaldehyde (10.7 g, 70.4 mmol) in 40 cm^3 of ethanol, causing a color change from colorless to yellow. About 30 cm^3 of solvent was removed under reduced pressure, initiating the formation of yellow crystals. When crystal formation ended, the product was filtered, dried *in vacuo*, and recrystallized from toluene/hexane (2/3 v/v) giving yellow crystals (8.5 g, 65%). Mp: 96–99°C. Found: C, 67.46: H, 7.10; N, 7.47. Calc. for $C_{21}H_{26}N_2O_4$: C, 68.11; H, 7.02; N, 7.57%. ^1H NMR ($CDCl_3$, 25°C): δ 1.05 (s, 3 H, CH_3), 3.39 (s, 2 H, —CH_2), 3.79 (s, 3 H, OCH_3), 6.36–6.45 (m, 3 H, C_6H_3), 8.34 (s, 1 H, C*H*), 13.20 (s, 1 H, O*H*). MS (EI, 70 eV): 370 amu (M^+).

N,N′-Bis(4-methoxysalicylidene)-2,2-dimethyl-1,3-propanediiminocobalt(II) hemihydrate (**9**)

This complex was prepared as for **6** using 7.85 g (21.2 mmol) of the corresponding Schiff base, 38.5 cm^3 of aqueous sodium hydroxide (1.07 M, 42.4 mmol), 0.064 g (0.78 mmol) of sodium acetate, 40 cm^3 water, 100 cm^3 ethanol, and 5.05 g (21.2 mmol) cobalt chloride (solution in 30 cm^3 H_2O). A brown powder was obtained (7.97 g, 88%). Mp: 180–190°C (dec). Found: C, 58.10; H, 5.84; N, 6.58. Calc. for $C_{21}H_{24}N_2O_4Co \cdot 0.5\ H_2O$: C, 57.80; H, 5.77; N, 6.42%. MS (EI, 70 eV): 427 amu (M^+).

N,N′-Bis(4,6-dimethoxysalicylidene)-2,2-dimethyl-1,3-propanediimine

2,2-Dimethyl-1,3-propanediamine (2.6 cm^3, 11 mmol) was added to a boiling solution of 4,6-dimethoxysalicylaldehyde (8.0 g, 22 mmol) in 50 cm^3 of ethanol, causing a color change from colorless to yellow. After 30 min, all volatile material was removed under reduced pressure and the resulting solid was washed by stirring in hexane (85 cm^3) for 12 h. The resulting yellow powder (2.9 g, 62%) was dried under reduced pressure. Mp: 116–118°C. Found: C, 64.59; H, 7.44; N, 6.54. Calc. for $C_{23}H_{30}N_2O_6$: C, 64.19; H, 6.98; N, 6.51%. ^1H NMR ($CDCl_3$, 25°C): δ 1.06 (s, 3 H, CH_3), 3.34 (s, 2 H, —CH_2), 3.75 (s, 3 H, OCH_3), 3.76 (s, 3 H, OCH_3), 5.64–5.91 (m, 2 H, C_6H_2), 8.34 (s, 1 H, C*H*), 10.23 (s, 1 H, O*H*). MS (EI, 70 eV): 430 amu (M^+).

N,N′-Bis(4,6-dimethoxysalicylidene)-2,2-dimethyl-1,3-propanediiminocobalt(II) hemihydrate (**10**)

This complex was prepared as for **6** using 5.88 g (13.6 mmol) of the corresponding Schiff base, 25.0 cm^3 of aqueous sodium hydroxide (1.07 M, 27.2 mmol), 0.041 g (0.50 mmol) of sodium acetate, 75 cm^3 water, 45 cm^3 ethanol, and 3.24 g (13.6 mmol) cobalt chloride (solution in 20 cm^3 H_2O). A brown powder was obtained (5.50 g, 83%). Mp: 282°C (dec). Found: C, 55.53; H, 5.76; N, 5.34. Calc. for $C_{23}H_{28}N_2O_6Co \cdot 0.5\ H_2O$: C, 55.65 H, 5.89; N, 5.64%. MS (EI, 70 eV): 487 amu (M^+).

RESULTS AND DISCUSSION

Synthesis and characterization

The cobalt(II) Schiff-base complexes (see Chart 1) were prepared by known synthetic methods in a two-step process. Schiff-base ligands were prepared in the first step by condensing salicylaldehyde with a diamine. In aqueous ethanol, these were then reacted with cobalt(II) chloride in presence of a trace of sodium acetate (forming cobalt(II) acetato complexes which are more soluble in alcohol than cobalt chloro compounds) and 2 molar equivalents of aqueous sodium hydroxide. All compounds were characterized by elemental analysis, melting point, and mass spectroscopy. Ligands were also characterized by ^1H NMR spectroscopy.

Solution formulations

Solubility of carrier or carrier–axial base complex is an important parameter in the total oxygen capacity of solutions because more concentrated carrier solutions will have higher capacity, as long as degradation is not induced or accelerated by higher carrier concentrations. Solubilities of the complexes in NMP are given in Table 1. These data indicate that metal complex solubilities increase with the number of alkoxy groups substituted on the phenyl ring of the ligands and with length of the alkoxy group chain. Further, a Saldmpr complex has greater solubility than the

Table 1. Solubilities of cobalt Schiff-Base complexes in 1-methyl-2-pyrrolidinone solvent at 25°C

Complex	Solubility (M)
CoSalen	0.09
3-MeOCoSalen	0.10
3-EtOCoSalen	0.20
4-MeOCoSalen	0.15
4,6-$(MeO)_2$CoSalen	0.30
CoSaldmpr	0.15
3-MeOCoSaldmpr	0.20
3-EtOCoSaldmpr	0.25
4-MeOCoSaldmpr	0.20
4,6-$(MeO)_2$CoSaldmpr	0.35

corresponding Salen complex, as expected due to the addition of methyl groups to the diimino bridging group. Recently, complexes of Saldmpr with metals, including, In^{III} and Re^{V}, have been reported [14].

Oxygen-carrying properties

Results of oxygen capacity studies of solutions of carriers **1**, **2**, **6**, and **7** are reported in Table 2. An additional five cycles of absorption and desorption were conducted 24 h after the data in Table 2 were obtained. There is no sign of carrier degradation, as judged by use of GC/MS to monitor the gas stream exiting the carrier solution for CO_2 and H_2O. Preliminary results indicate some loss of O_2 binding and formation of CO_2 after 20 cycles. The average carrier loading gives an indication of the carrier affinity for oxygen. At this point we are only describing this affinity empirically, as we do not have mechanistic oxygen complexation information, such as whether the oxygen binding species is a 2 : 1 or 1 : 1 complex of carrier to dioxygen [2(c)]. The presence of 2-cyanopyridine axial base clearly increases oxygen affinity, as seen from the affinity data for solutions of CoSalen and 3-MeOCoSalen. This may be ascribed to the electron-donating nature of the base which strengthens the cobalt-dioxygen interaction.

The 3-methoxy ring-substitution of the CoSaldmpr carrier leads to a greater than twofold increase in carrier loading. Surprisingly, under these conditions, 3-methoxy ring substitution of Cosalen has no effect on loading. Clearly, further oxygen absorption tests, including those of **8–10**, may clarify the substitution effects and the structure effects on oxygen affinity and determine the extent of influence of the 2,2-dimethyl-1,3-propanediimino bridging group on the stability of the carriers. Additionally, the amount of oxygen absorbed by the solutions as a function of oxygen partial pressure will provide an indication of the

Table 2. Oxygen absorption capacities of cobalt Schiff-base oxygen carriers in 1-methyl-2-pyrrolidinone solution at 37°C

Carrier	Carrier conc ($\times 10^{-2}$ M)	Axial base and conc (M)	Desorption temperature (°C)	Cycle number	Oxygen capacity ($\times 10^{-4}$ [g O_2/g soln])	Carrier loading (%)	Average carrier loading (%)[a]
CoSalen (**1**)	9.00	none	100	1	2.60	9.32	9.28 ± 2.2
				2	3.10	11.1	
				3	2.00	7.17	
				4	2.67	9.57	
CoSalen (**1**)	9.00	2-CNpy,[b] 2	180	1	3.52	12.5	14.0 ± 2.1
				2	4.55	16.1	
				3	3.85	13.7	
				4	3.80	13.5	
3-MeOCoSalen (**2**)	10.0	none	170	1	2.67	8.60	8.79 ± 1.7[c]
				2	2.79	9.00	
				3	—	—	
				4	—	—	
3-MeOCoSalen (**2**)	10.0	2-CNpy, 2	180	1	5.14	16.5	15.5 ± 0.92
				2	4.75	15.2	
				3	4.70	15.1	
				4	4.73	15.2	
CoSaldmpr (**6**)	15.0	2-CNpy, 2	180	1	4.83	10.3	9.51 ± 1.4
				2	4.79	10.2	
				3	3.85	8.22	
				4	4.36	9.30	
3-MeOCoSaldmpr (**7**)	10.0	2-CNpy, 2	180	1	6.43	20.6	21.8 ± 1.2
				2	6.87	22.0	
				3	6.97	22.3	
				4	6.99	22.4	

[a] (Mol O_2 carried/mol O_2 carrier complex) × 100%, given as "mean ± 95% confidence limit $N = 4$."
[b] 2-cyanopyridine.
[c] $N = 2$.

nature of oxygen-carrying species, i.e., 1 : 1, 2 : 1, or both.

Acknowledgements—We acknowledge the support of the DOE Office of Industrial Programs, Washington, D.C. We thank Mr Ramesh Jain for helpful discussions. We also thank Mr John David for oxygen absorption measurements.

REFERENCES

1. Jones, R. D., Summerville, D. A. and Basolo, F., *Chem. Rev.*, 1979, **79,** 139.
2. (a) Tsumaki, T., *Bull. Chem. Soc. Jpn*, 1938, **13,** 252; (b) Wilmarth, W. K., Aranoff, S. and Calvin, M., *J. Am. Chem. Soc.*, 1946, **68,** 2263; (c) Chen, D., Martell, A. E. and Sun, Y., *Inorg. Chem.*, 1989, **28,** 2647.
3. Roman, I. C., U.S. Patent 4,451,270, 29 May 1984.
4. Adduci, A. J., *Chemtech*, 1976, **6,** 575.
5. Norman, J. A. T., Pez, G. P. and Roberts, D. A., In *Oxygen Complexes and Oxygen Activation by Transition Metals*, eds. A. E. Martell and D. T. Sawyer, Plenum, New York, 1988, pp 107.
6. Kobayashi, H., *Oxygen Enriched Combustion System Performance Study*, vol 1, Union Carbide Corp., March 1987.
7. Niederhoffer, E. C., Timmons, J. H. and Martell, A. E., *Chem. Rev.*, 1984, **84,** 137.
8. Park, S., McLarnon, C., Mathur, V. K., Tomellini, S. A. and Planalp, R. P., *Prepr. Pap. Am. Chem. Soc., Div. Fuel Chem.*, 1991, **36,** 1361.
9. Calligaris, M., Nardin, G. and Randaccio, L., *J. Chem. Soc., Dalton Trans.*, 1973, 419.
10. Friesen, D. T., Miller, W. K., Johnson, B. M. and Edlund, D. J. US Pat. 5,266,283, 30 November 1993.
11. Pillai, M. R. A., John, C. S., Lo, J. M. and Troutner, D. E., *Appl. Radiat. Isot.*, 1990, **41,** 557.
12. Shriver, D. F., *The Manipulation of Air-Sensitive Compounds*, Wiley, New York, 1992.
13. (a) Bailes, R. H. and Calvin, M., *J. Am. Chem. Soc.*, 1947, **69,** 1886; (b) Diehl, H. and Hach, C. C., *Inorg. Syn.*, 1950, **3,** 196; (c) Martell, A. E., Belford, R. L. and Calvin, M., *J. Inorg. Nucl. Chem.*, 1958, **5,** 170; (d) Nishida, Y. and Kida, S., *Chem. Lett.*, 1973, 57.
14. (a) Lin, C. H., *Synth. React. Inorg. Met.-Org. Chem.*, 1993, **23,** 1097; (b) Herrmann, W. A., Rauch, M. U. and Roesky, P. W., *J. Organomet. Chem.*, 1996, **511,** 299; (c) Hughes, D. L., Kleinkes, U., Leigh, G. J., Maiwald, M., Sanders, J. R., Sudbrake, C. and Weisner, J., *J. Chem. Soc., Dalton Trans.*, 1993, 3093.

Pergamon

PII: S0277-5387(97)00295-7

Polyhedron Vol. 17, No. 2–3, pp. 331–339, 1998
© 1997 Elsevier Science Ltd
All rights reserved. Printed in Great Britain
0277-5387/98 $19.00+0.00

A novel network of bis(2-mercapto-3-pyridinol)oxovanadium(IV) based on hydrogen-bond interactions: synthesis, structure and EPR spectroscopic properties

Ting-Bin Wen,* Ji-Cheng Shi, Xin Huang, Zhong-Ning Chen,† Qiu-Tian Liu and Bei-Sheng Kang*†

State Key Laboratory of Structural Chemistry and Fujian Institute of Research on the Structure of Matter, Chinese Academy of Sciences, Fuzhou, Fujian 350002, P.R. China

(Received 17 April 1997; accepted 27 June 1997)

Abstract—Reaction of VCl_3 with 2-mercapto-3-pyridinol (H_2mpp) in the presence of CH_3ONa yields $(VO(Hmpp)_2 \cdot CH_3CN$ (**1**). The coordination geometry around the vanadium is square pyramidal, with a V=O double bond of 1.602(6) Å and average V—S and V—O distances of 2.392 and 1.943 Å, respectively. The mpp ligands behave as the thione tautomer with the N atoms prontonated rather than the thiol alternative form. The intermolecular hydrogen bonding interactions between the protonated N atoms and the terminal O or the coordinated O atoms of mpp ligands result in an infinite two-dimensional network of $VO(Hmpp)_2$. Complex (**1**) has been characterized by infrared, and EPR spectroscopic studies. © 1997 Elsevier Science Ltd

Keywords: 2-mercapto-3-pyridinol; oxovanadium complex; thione; hydrogen bonding; network.

Vanadium thiolate chemistry has drawn our attention for several reasons. Some of the impetus has derived from the relevance of this area to industrial petroleum refining. Certain crude oils contain large amounts of soluble vanadyl (VO^{2+}) impurities categorized into two types according to their ligands [1], the vanadyl petroporphyrins, which have been well studied and characterized [2]; and the vanadyl non-porphyrins whose ligand environment is thought to contain S, N, and/or O donor atoms [3]. These vanadyl impurities result in formation of insoluble vanadium sulfide deposits which poison the catalyst (e.g. Mo/Co/S on alumina) during hydrodesulfurization (HDS) [4–8]. This has stimulated interest both in the identification of the crude oil impurities and in the mechanism of their subsequent conversion to vanadium sulfide. Further motivation has come from the recently discovered roles of vanadium in biological systems [9], including the vanadium nitrogenase [10], in which the vanadium is bounded to S and probably also to O and or N atoms simultaneously. In addition, another driving force for our investigation of vanadium thiolate chemistry is our current interest in construction of transition-metal cluster complexes from simple thiolate containing building blocks [11].

Over the last few years, we have engaged in developing the thiolate chemistry of vanadium, concentrating on a ligand system with mixed sulfur and oxygen donors at 1,2-positions. Vanadium complexes with ligands that provide S and O donors simultaneously are not so well explored as compared to independent oxo-vanadium or thio-vanadium complexes. Oxovanadium(IV) mercaptocarboxylate has been investigated in aqueous solution [12], while bis(2-mercaptopyridine N-oxide) oxovanadium(IV) has recently been structurally characterized [13]. Our efforts along these lines with the ligand 2-mercaptophenolate (mp^{2-}, $C_6H_4OS^{2-}$) afforded already the trinuclear complex $[V_3(mp)_6]^-$ [14], and the dimeric complexes $[V(mp)_3NaLL']_2^{2-}$ (L, L′ = solvent) [15] and $[\{V(mp)_3\}_2Na]^{3-}$ [16]. In related works, Klich [17] reported a series of mononuclear vanadium(IV) complexes $[VO(mp)_2]^{2-}$, $[V(mp)_3]^{2-}$

* Authors to whom correspondence should be addressed.
† Present address: Department of Chemistry, Zhongshan University, Guangzhou, Guangdong 510275, P.R. China.

and $[V(mmp)_3]^{2-}$ (H_2mmp = 2-mercapto-4-methylphenol). We now set out to further explore the chemistry of vanadium with the ligand 2-mercapto-3-pyridinol (H_2mpp, C_5H_5NOS) and obtain a product which is simultaneously self-assembled via coordinate- and hydrogen-bond formation.

Molecular self-assembly through hydrogen bonding has become a hot topic in crystal engineering recently [18]. In particular, the aggregation of transition-metal containing building blocks based on hydrogen bonding interaction is very important, because the incorporation of transition-metal ions into such systems introduces magnetic, optical and conductive properties characteristic of these ions into materials with potential for nonlinear optical, conducting and ferromagnetic properties [18,19]. We report herein the synthesis and crystal structure of $[VO(Hmpp)_2]\cdot CH_3CN$ (1), a novel self-assembly network of bis(2-mercapto-3-pyridinol)oxovanadium(IV) based on hydrogen bonding interactions, together with the IR and EPR spectroscopic data.

EXPERIMENTAL

All operations were carried out under an atmosphere of dinitrogen using conventional Schlenk techniques. All solvents were dried over molecular sieves and degassed before use. VCl_3 (Aldrich) and 2-mercapto-3-pyridinol (H_2mpp) (Aldrich) were used as received.

Infrared spectra were obtained as KBr pellet on a Bio-Rad FTS-40 spectrophotometer over the range 4000–200 cm^{-1}. Magnetic moment was measured at room temperature (298 K) on a model CF-1 superconducting extracting sample magnetometer at the magnetic field of 5.0 T with the powder sample kept in a capsule. EPR spectra were recorded on a Bruker ER-420 spectrometer at the X-Band frequency. Elemental analyses were carried out by the Analytical Chemistry Group of this Institute.

Synthesis of $[VO(Hmpp)_2]\cdot CH_3CN$ (1)

The mixture of H_2mpp (0.53 g, 4.2 mmol) and CH_3ONa (0.30 g, 5.6 mmol) in 20 cm^3 of EtOH was added to a stirred solution of VCl_3 (0.22 g, 1.4 mmol) in EtOH (15 cm^3). The reacting solution rapidly turned red–purple then converted to red–brown. After 2 h of stirring, the resultant solution was filtered and the filtrate stored at 4°C for several days to give the dark-purple microcrystalline product which was collected by filtration and dried *in vacuo*. Recrystallization from $EtOH/CH_3CN$ (1:1) gave (1) as prismatic crystals, yield 0.13 g (26%, based on VCl_3). The same procedure in the presence of Et_4NCl ($Et_4NCl:VCl_3$ ratio of 2:1) afforded the same products. Anal. Calcd for $C_{12}H_{11}N_3O_3S_2V$ (%): C, 40.00; H, 3.08; N, 11.66; S, 18.13; V, 14.14. Found: C, 40.49; H, 2.86; N, 11.92; S, 17.78; V, 13.82. IR (KBr): 3187(m), 3014(m), 2984(m), 2869(m), 2613(w), 2100(w), 1594(s), 1576(m), 1503(s), 1447(s), 1338(m), 1291(s), 1192(s), 1161(w), 1129(s), 1104(w), 1050(s), 937(s), 854(s), 787(s), 720(m), 698(s), 620(s), 575(w), 448(m), 390(s), 349(m) cm^{-1}.

Crystal data, structure determination and refinement

Crystallographic data for (1) are summarized in Table 1. Diffraction data were collected on an Enraf-Nonius CAD 4 diffractometer with Mo-$K\alpha$ radiation (λ = 0.71073 Å) and graphite monochromator using ω–2θ scan mode. The intensities of three standard reflections were measured every 120 min, indicating a total loss in intensity of 3.0%. The reflections were corrected for anisotropic decay and Lorentz-polarization effects. Intensity of equivalent reflections were averaged (R_{int} = 3.5%). The structure was solved by direct methods on a COMPAQ PL4/50 computer with the MolEN/PC program package [20] and refined by full matrix least-squares procedures with anisotropic thermal parameters for all the non-hydrogen atoms. The hydrogen atoms were visible in a difference Fourier map phased on the non-hydrogen atoms. The two hydrogen atoms [H(1A) and H(2A)] attached to the N atoms of the Hmpp ligands were

Table 1. Crystallographic data for compound (1)

Empirical formula	$C_{12}H_{11}N_3O_3S_2V$
Molecular weight	360.31
Crystal color, size (mm)	dark purple, $0.20\times0.20\times0.22$
Temperature (K)	296(1)
Crystal system	monoclinic
Space group	$P2_1/n$ (no. 14)
a (Å)	7.193(3)
b (Å)	21.416(7)
c (Å)	10.962(4)
β (°)	109.12(4)
V (Å^3)	1521.1
Z	4
D_{calc} (g cm^{-3})	1.57
μ (Mo-$K\alpha$) (cm^{-1})	9.1
2θ range (°)	2–48
$F(000)$	732
No. of reflections measured	2682
No. of independent reflections	2472
No. of observed reflections ($I>1.5\sigma(I)$)	1445
No. of parameters refined	190
R^a	0.066
$R_w{}^b$	0.064
Weight scheme	$4F_o^2/\sigma^2(F_o^2)$
Goodness of fit	1.16
Max. shift in final cycle	0.00
Final $\Delta\rho_{max}$ (e Å^{-3})	0.45

[a] $R = \Sigma(|F_o|-|F_c|)/\Sigma|F_o|$.
[b] $R_w = [\Sigma w(|F_o|-|F_c|)^2/\Sigma w|F_o|^2]^{1/2}$.

located from the difference Fourier synthesis and the remaining ones were placed in an ideal position with C—H = 0.95 Å. All hydrogen atoms were added to the structure factor calculations but not refined.

RESULTS AND DISCUSSION

Synthesis

Our work with the H_2mpp ligand was an extension to earlier studies [14,15] employing H_2mp. The latter ligand had been shown to react with VCl_3 in alchol to yield purple solutions containing the $[V(mp)_3]^{2-}$ fragments, which further coordinate to the metal ions present in the solution to form polynuclear complexes such as $[V_3(mp)_6]^-$ and $[V(mp)_3NaLL']_2^{2-}$ (L, L′ = solvent). We decide to investigate similar reaction with H_2mpp, which possesses the same ring size and donors as H_2mp. Initial reaction was employed with a mixture comprising VCl_3, H_2mpp, CH_3ONa and Et_4NCl in a 1:3:6:2 molar ratio in EtOH, but this was fruitless. Consequently, we adjusted the reaction stoichiometry in a VCl_3:H_2mpp:CH_3ONa ratio of 1:3:4 in the presence or absence of Et_4NCl. No likely species corresponding to $[V(mp)_3]^{2-}$ was obtained, except the oxovanadium(IV) complex (**1**). The source of the terminal oxygen is most probably adventitious O-containing impurities (H_2O or O_2) in the solvents of N_2 atmosphere.

As an offshoot of our interest in transition-metal 1,2-bidentate thiolates as building blocks and their construction into cluster complexes, we have previously reported [11] that oxometal complexes $M(O)L_2$ (L = bidentate sulfur-containing ligand) can function as building blocks. For example, in the reaction of $MoOCl_3(THF)_2$ with mp^{2-} [21], the building block $Mo(O)(mp)_2$ was presumably formed, two of which then condensed with the elimination of one ligand to give complex $[\{MoO(mp)\}_2(\mu\text{-mp})(\mu\text{-OR})]^-$ (R = Me [21a] or Et [21b]) or $[\{MoO(mp)\}_2(\mu\text{-mp})(\mu\text{-O})Na(EtOH)_2]_2^{2-}$ [21b, c] as shown in eqn (1).

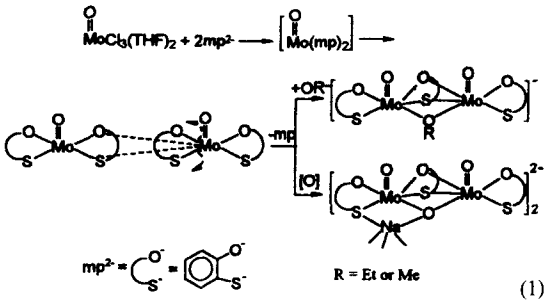

(1)

For the recently documented complex $V_2O_2(pyt)_4$ (Hpyt = pyridine-2-thiolate) [22,23], the moiety $VO(pyt)_2$ can be visualized as the building block, two of which bridged through the sulfur donor atoms to form the binuclear complex [eqn (2)]. Dissociation of this complex to mononuclear $VO(pyt)_2$ species in solution has been shown by EPR studies [23].

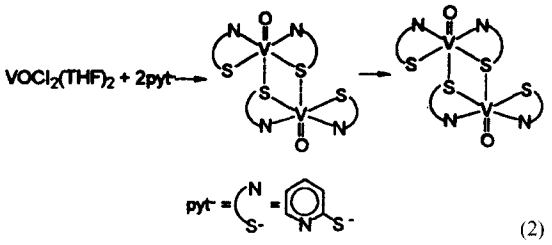

(2)

The anions $[VO(edt)_2]^{2-}$ [24] (edt^{2-} = ethane-1,2-dithiolato) and $[VO(mp)_2]^{2-}$ [17] have been known to further coordinate to the Na^+ ions present in the solutions to form dimeric complexes as depicted in the eqns (3) and (4), respectively.

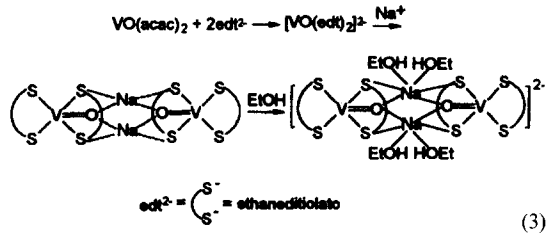

(3)

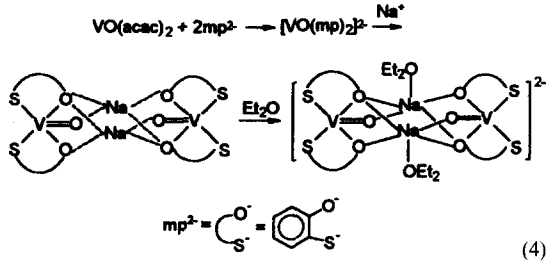

(4)

In this regards, the $VO(Hmpp)_2$ moiety has attracted our interest as a potential building block of which the reactivity is still under investigation.

Structure description

The acetonitrile solvent molecule is well separated from the metal and will not be further discussed. The structure of $VO(Hmpp)_2$ is shown in Fig. 1. Selected bond lengths and bond angles are given in Table 2 in which C(11), C(12) and N(3) represent the acetonitrile solvent molecule.

The geometry of $VO(Hmpp)_2$ can be described as a square pyramid in which the V atom is coordinated to a terminal O atom and two Hmpp ligands through the O and S atoms in the basal positions, each forming

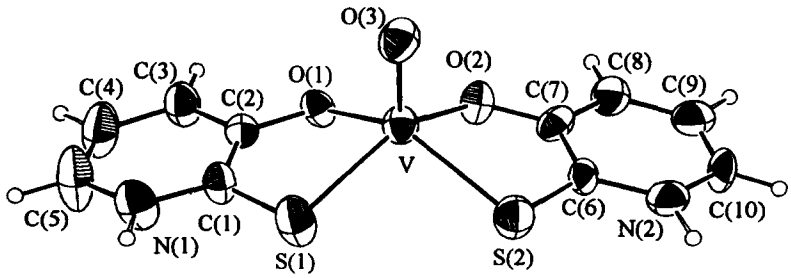

Fig. 1. ORTEP structure of $VO(Hmpp)_2$. Thermal ellipsoids are drawn in 50% probability.

Table 2. Selected bond lengths (Å) and bond angles (°) for (**1**)

V—S(1)	2.389(3)	N(2)—C(10)	1.34(1)
V—S(2)	2.396(3)	C(1)—C(2)	1.40(1)
V—O(1)	1.936(5)	C(2)—C(3)	1.38(2)
V—O(2)	1.950(6)	C(3)—C(4)	1.39(1)
V—O(3)	1.602(6)	C(4)—C(5)	1.35(1)
S(1)—C(1)	1.699(9)	C(6)—C(7)	1.43(1)
S(2)—C(6)	1.699(9)	C(7)—C(8)	1.36(1)
O(1)—C(2)	1.325(9)	C(8)—C(9)	1.39(1)
O(2)—C(7)	1.320(9)	C(9)—C(10)	1.35(1)
N(1)—C(1)	1.33(2)	N(3)—C(11)	1.12(1)
N(1)—C(5)	1.36(1)	C(11)—C(12)	1.41(2)
N(2)—C(6)	1.37(1)		
S(1)—V—S(2)	88.9(1)	N(1)—C(1)—C(2)	117.4(8)
S(1)—V—O(1)	83.8(2)	O(1)—C(2)—C(1)	119.0(7)
S(1)—V—O(2)	146.1(2)	O(1)—C(2)—C(3)	121.8(8)
S(1)—V—O(3)	106.6(2)	C(1)—C(2)—C(3)	119.3(9)
S(2)—V—O(1)	144.7(2)	C(2)—C(3)—C(4)	120.0(9)
S(2)—V—O(2)	83.9(2)	C(3)—C(4)—C(5)	120.1(9)
S(2)—V—O(3)	109.1(2)	N(1)—C(5)—C(4)	118.3(9)
O(1)—V—O(2)	83.2(2)	S(2)—C(6)—N(2)	122.3(7)
O(1)—V—O(3)	106.1(3)	S(2)—C(6)—C(7)	121.5(7)
O(2)—V—O(3)	107.0(3)	N(2)—C(6)—C(7)	116.1(8)
V—S(1)—C(1)	94.0(3)	O(2)—C(7)—C(6)	116.9(8)
V—S(2)—C(6)	93.7(3)	O(2)—C(7)—C(8)	124.3(8)
V—O(1)—C(2)	120.0(5)	C(6)—C(7)—C(8)	118.8(8)
V—O(2)—C(7)	121.5(5)	C(7)—C(8)—C(9)	121.8(9)
C(1)—N(1)—C(5)	124.9(8)	C(8)—C(9)—C(10)	119.0(1)
C(6)—N(2)—C(10)	124.6(9)	N(2)—C(10)—C(9)	119.7(9)
S(1)—C(1)—N(1)	122.5(8)	N(3)—C(11)—C(12)	176.0(1)
S(1)—C(1)—C(2)	120.0(7)		

two five-membered chelate rings V–O–C–C–S in a *cis* configuration. The whole molecule thus exhibits *pseudo-*C_s symmetry with the σ plane passing through the apical V—O(3) bond and bisecting the O(1)···O(2) and S(1)···S(2) vectors. The same *cis* configuration is found in other oxovanadium(IV) complexes [13,17,25] with an O_2S_2 donor set in the basal plane. Structural features of (1) are compared in Table 3 with related oxovanadium complexes possessing O_2S_2, N_2S_2, S_4 and N_2O_2 donor sets.

The vanadium atom is displaced 0.636 Å towards the oxo ligand above the O_2S_2 least-squares plane [the maximum deviation from which is 0.013 Å for O(1)]. This value is almost identical to the corresponding displacement in $VO(mpo)_2$ (0.642 Å) and $[VO(mp)_2]^{2-}$ (0.638 Å), but is longer by 0.03 Å than that in VO(tsalen) (tsalen = N,N′-ethylene-bis(thiosalicylideneaminato), 0.608 Å) and shorter by 0.03 Å than that in $[VO(edt)_2]^{2-}$ (0.668 Å) (see Table 3). This difference is probably subject to the change of flexibility of the ligands [13b]. The former three complexes display similar values of this distance due to

Table 3. Comparison of structural parameters of (1) and related compounds (Å)

Complex	Donor set	V=O	Distance of V to basal place	V—O (basal plane)	V—S (basal plane)	Ref.
$VO(Hmpp)_2$	$(OS)_2$	1.602(6)	0.636	1.943(5)	2.392(3)	This work
$VO(mpo)_2$[a]	$(OS)_2$	1.593(3)	0.642	1.956(3)	2.374(2)	[13]
$[VO(mp)_2]^{2-}$[a]	$(OS)_2$	1.611(5)	0.638	1.959(4)	2.365(2)	[17]
$VO[SSi(OBu^n)_3]_2$	$(OS)_2$	1.642(13)		2.106(13)	2.333(6)	[25]
VO(tsalen)[a]	(N_2S_2)	1.598(6)	0.608		2.346(3)	[26]
$[VO(edt)_2]^{2-}$[a]	$(SS)_2$	1.625(2)	0.668		2.378(1)	[27]
VO(salphen)[a]	(O_2N_2)	1.589(3)		1.927(2)		[28]

[a] mpo = 2-mercaptopyridine N-oxido, $C_5H_4NOS^-$; mp = 2-mercaptophenolato, $C_6H_4OS^{2-}$; tsalen = N,N′-ethylene-bis(thiosalicylideneaminato); edt = ethane-1,2-dithiolato; salphen = N,N′-disalicylidene-*o*-phenylenediaminato.

the similar flexibility of the ligands mpp, mpo and mp. In VO(tsalen), the less rigidity of the ligand (as compared to mpp, mpo and mp) provides a more flattened pyramid, while the anion $[VO(edt)_2]^{2-}$, with a more flexible aliphatic dithiolate gives rise to a more pronounced pyramid geometry. The V—O(3) bond is tilted slightly relative to the normal to the basal plane, with which it makes an angle of 3.6°. The V—O(3) bond length of 1.602(6) Å is close to the average distance of 1.598 Å found by Mayer [29] for a substantial number of oxovanadium(IV) complexes, consistent with the presence of a V=O double bond. It is likewise within the reported range of the related complexes (1.589–1.642 Å, Table 3). The V—S bonds in the basal plane average to 2.392 Å, which is slightly longer than that in $VO[(SSi(OC_4H_9)_3]_2$ (av. 2.333 Å) and is comparable to those in other related oxovanadium(IV) complexes (Table 3). This value is also comparable to the average V—S distances observed in the *tris*-chelated vanadium(IV) complexes $[V(mmp)_3]^{2-}$ (av. 2.363 Å, mmp = 2-mercapto-4-methylphenolato) [17], $[V(mp)_3NaLL']_2^{2-}$ (av. 2.369 Å) [15] and $[\{V(mp)_3\}_2Na]^{3-}$ (av. 2.367 Å) [16]. The basal V—O bonds averaging 1.943 Å are somewhat shorter than those in $VO[SSi(OC_4H_9)_3]_2$ (av. 2.106 Å), but close to those in other complexes containing similar donor sets (Table 3).

The organic ligands are essentially coplanar, respectively, with maximum deviations observed for C(4) (0.020 Å) and C(6) (0.022 Å), respectively. The two five-membered chelate rings V–O–C–C–S are folded about the O–S vector, showing an envelope configuration. The ligand planes bend toward the apical O and make angles of 15.9(5)° and 13.9(4)° with the O(1)—V—S(1) and O—(2)—V—S(2) planes, respectively (Fig. 1). This folding of the ligand planes has also been observed in $VO(mpo)_2$ [13] and $[VO(mp)_2]^{2-}$ [17]. The mean chelate V—O—C angle of 120.8° suggests that the O donor atoms are sp^2 hybridized, while the mean value of the V—S—C angles of 93.9° shows the bonding orbitals of the S donor atoms are predominantly of *p* character.

It has been shown that the N-heteroaromatic mercapto ligand exists in two tautomeric forms (thiol or thione) and has been established that the thione form is the predominant one [23,30–33]. Again, as was the case for the free ligand 2-mercaptopyridine (Hpyt) [23] and 2-mercaptopyridine N-oxide (Hmpo) [33], the H_2mpp molecule exists as a tautomeric equilibrium between the thiol (A) and thione (B) forms shown.

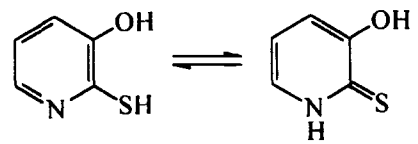

A B

The C—S bond lengths in (1), averaging to 1.699(1) Å, are significantly shorter than the normal covalent distance (1.81 Å) [34] for a single bond and considerably shorter than the C—S bonds values of aryl thiolates observed in the bdt (benzenedithiolate, av. 1.76 Å), tdt (toluene-3, 4-dithiolate, av. 1.79 Å) or mp (av. 1.75 Å) ligated complexes that contain delocalization of $p\pi$-electrons in the chelate rings [11]. In fact, the rather short C—S distances approach the C=S distance in thiourea [35] [1.720(9) Å] and its derivatives [1.67(2)–1.73(1) Å] [36]. Similar results have been found in the mpo ligated complexes (C—S average to 1.71 Å), in which the C—S bonds show double bond character due to the predominant thione contribution of the mpo ligand [11,37]. In this regard, the mpp ligands should exist in the thione tautomer (B) instead of the thiol alternative form (A) in complex (1). Further support for this conclusion comes from the facts as follows: (i) for all pyridine derivatives, the C—N—C angle in the rings is sensitive to the protonation (or nonprotonation) of the N atom, protonated (or nonprotonated) N atoms possess angles larger (or smaller) than 120°, respectively [23,32,38]. In this case, the C—N—C angles of the

mpp ligands are 124.9(8) and 124.6(9)°, respectively, consistent with the protonated form (B). (ii) The hydrogen atoms attached to the N atoms can be located in a difference Fourier map phased on the nonhydrogen atoms. (iii) The six-membered pyridinyl rings show varied C—C bond lengths expected for the thione form (B) rather than equivalent ones expected for the thiol form (A) which is aromatic.

The X-ray analysis of (1) shows that the intermolecular contacts of N(2)···O(3′) (2.843 Å) and N(1)···O(2″) (2.950 Å) are in the normal hydrogen-bonding interaction range for N—H···O [39] (Symmetry code: $' = x-1,\ y,\ z$; $'' = x-1/2,\ y-1/2,\ -z-1/2$). The crystal packing is mainly determined by a network of these two hydrogen bonds (Fig. 2).

As can be seen from Fig. 2, the parallel $VO(Hmpp)_2$ moieties related by the symmetry operation $(x-1, y, z)$ are linked to each other *via* N(2)—H(2A)···O(3′) hydrogen bonds to form staircase-like tapes. Further cross-linking between adjacent tapes related by the operation $(x-1/2,\ y-1/2,\ -z-1/2)$ *via* N(1)—H(1A)···O(2″) hydrogen bonds result in a novel infinite two-dimensional network along the *ac* plane (Fig. 3).

Spectroscopic studies

The IR spectrum (KBr pellet) of (**1**) shows strong V=O stretching at 937 cm^{-1}. The relatively low value at the lower end in the range 935–1035 cm^{-1} as reported for a large set of oxovanadium complexes [40] is consistent with the rather long V=O bond (1.602 Å as compared to 1.56–1.60 Å for most square pyramid vanadyl(IV) complexes) [17,24]. It is almost identical to that in $[VO(mp)_2]^{2-}$ (940 cm^{-1}) [17], but is substantially lower than those in VO(salphen) (984 cm^{-1}) [28], $VO(mpo)_2$ (984 cm^{-1}) [13b] and VO(t-salen) (975 cm^{-1}) [26], but slightly higher than that in $[VO(edt)_2]^{2-}$ (930 cm^{-1} for the Me_4N^+ cation and 909 cm^{-1} for the Ph_4P^+ cation) [24], in accord with the trends in V=O bond lengths (Table 3). The characteristic metal-ligand absorptions at 448 [ν(V—O)], 390 [$\nu(V—S)_{as}$] and 349 [$\nu(V—S)_s$] cm^{-1} agree well with those reported for $VO(mpo)_2$ [13b]. The doublet appeared at 1129 and 1104 cm^{-1} is assigned to the C—S stretch, consistent with the double bond character [30,31,33a,37]. Only one absorption at 3187 cm^{-1} is assignable to the ν (N—H) stretch [31], indicating that there are hydrogen bonding interactions concerning all N—H groups of $VO(Hmpp)_2$ moieties.

The room temperature magnetic moment of 1.69 μ_B of solid (1) is consistent with the spin-only value of 1.73 μ_B expected for a vanadium(IV) complex (d^1, $S = 1/2$).

The powder EPR spectra of (1) both at room temperature and at 77 K show only one broad signal with g_0 values of 1.978 and 1.980, respectively. In DMF solution at room temperature, the EPR spectrum displays the characteristic eight-line pattern of vanadium (^{51}V, $I = 7/2$) (see Fig. 4a), with isotropic g_0 and hyperfine coupling parameter A_0 values of 1.981 and 81.0×10^{-4} cm^{-1}, respectively (Table 4). The spectrum recorded for the frozen solution at 77 K is more informative (Fig. 4b). The corresponding g and A values are given in Table 4, together with EPR data for complexes with related donor sets.

The anisotropic g and A values of (**1**) are typical for square-pyramidal oxovanadium(IV) complexes having the unpaired electron largely in a d_{xy} orbital (for the ligands along x and y) [17,44,45]. As can be

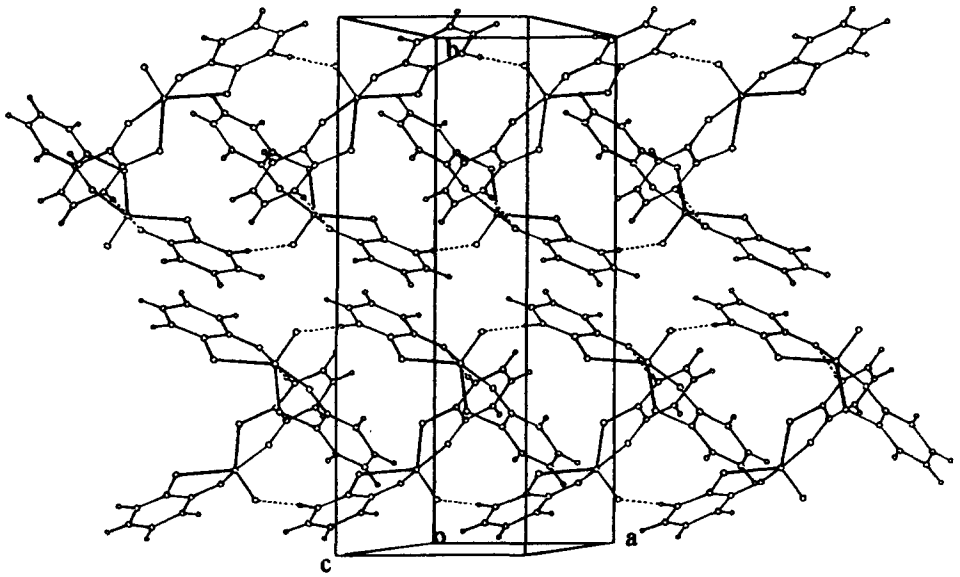

Fig. 2. Stereoview of the packing diagram of the $VO(Hmpp)_2$ moieties. The CH_3CN solvent molecules are omitted for clarity.

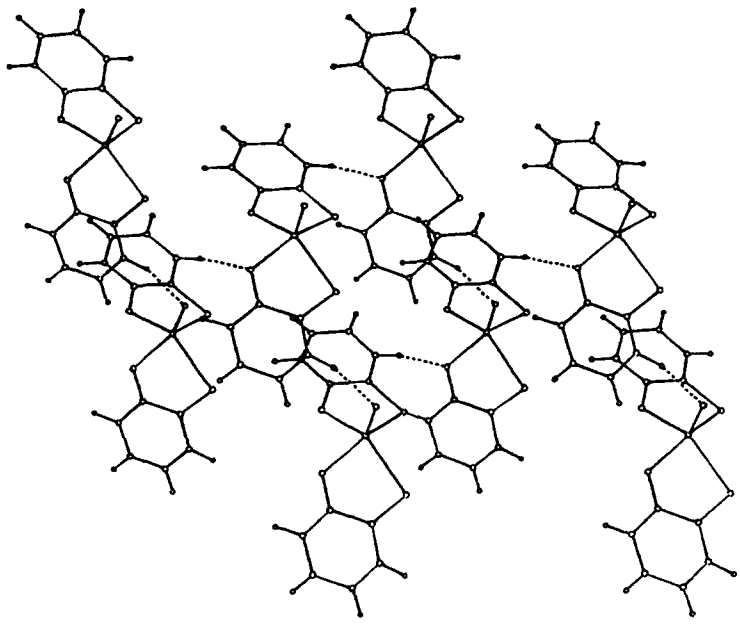

Fig. 3. Part of the hydrogen-bonded network formed by $VO(Hmpp)_2$. The additional hydrogen-bond parameters: distances, N(1)—H(1A), 0.859; H(1A)···O(2″), 2.131; N(2)—H(2A), 0.943; H(2A)···O(3′), 1.931Å; angles, N(1)—H(1A)···O(2″), 159.1; N(2)—H(2A)···O(3′), 161.8°.

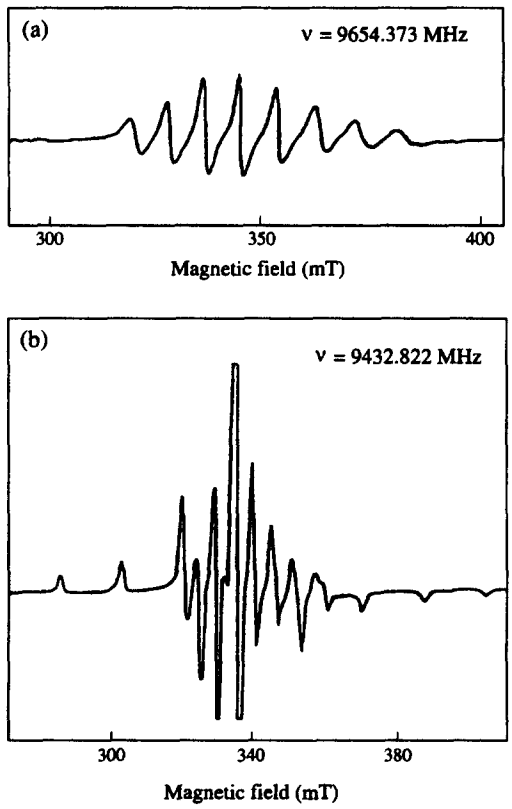

Fig. 4. EPR spectra of (1) in DMF solution: (a) at ambient temperature; (b) at 77 K (frozen solution).

Table 4. EPR parameters of (1) and related oxovanadium(IV) complexes

Complex	Donor set	Solvent	A_0^b		g_z	$g_{x,y}$	A_z	$A_{x,y}$	Ref.
			g_0^b	10^{-4} cm^{-1}			10^{-4} cm^{-1}	10^{-4} cm^{-1}	
			298 K		77 K				
(1) $VO(Hmpp)_2$	$(OS)_2$	DMF	1.981	80.9	1.963	1.996	150.6	51.4	This work
$[VO(mp)_2]^{2-}$	$(OS)_2$	MeCN	1.985	81	1.975	2.003[c]	150	40	[17]
$[VO(edt)_2]^{2-}$	$(SS)_2$	DMF	1.981	71.6	1.976	1.977[c]	133.8	39.7	[27]
$[VO(mnt)_2]^{2-a}$	$(SS)_2$	$CHCl_3$	1.984	71.6	1.973[d]	1.986[d]	135[d]	43[d]	[41]
$[VO(dmit)_2]^{2-a}$	$(SS)_2$	MeCN	1.990	77.1					[42]
VO(tsalen)	(N_2S_2)	DMF			1.978	1.986	148	51	[26]
VO(salen)[a]	(N_2O_2)	DMF			1.951	1.985	159	59	[43]
$[VO(cat)_2]^{2-a}$	$(OO)_2$	H_2O	1.975	82	1.947	1.981	154	50	[44]

[a] mnt = maleonitriledithiolene; dmit = 2-thioxo-1,3-dithiole-4,5-dithiolato; salen = N,N′-ethylene-bis(salicylideneaminato); cat = catecholato.

[b] g_0 and A_0 at ambient temperature in solution.

[c] Small rhombicity in $g_{x,y}$.

[d] 1 : 1 $CHCl_2$/DMF solvent.

seen in Table IV, such complexes exhibit $A_z > A_{x,y}$ and $g_z < g_{x,y}$.

CONCLUSIONS

Complex (1) has confirmed that 2-mercapto-3-pyridinol can coordinate to metal ions in its thione form. In particular, the thione form Hmpp ligand in (1) fulfils its bifunctional role by generating a network of transition-metal building block by a combination of coordinate- and hydrogen-bond formation. This work provides a new direction in the designed synthesis of supramolecular system containing transition-metal ions.

Supplementary material

List of observed and calculated structure factors, fractional atomic coordinates and anisotropic thermal parameters for non-hydrogen atoms, and hydrogen atoms parameters as well as complete bond distances and angles are available from the authors upon request.

Acknowledgments—We greatly appreciate the National Key Project for Fundamental Research, the NNSF of China and the Fund for Analysis & Measurement of Beijing Zhongguancun Associate Center for financial support.

REFERENCES

1. Yen, T. F., *The Role of Trace Metals in Petroleum*, Ch. 1, Ann Arbor Science, Ann Arbor, Michigan (1975).
2. Psundararaman, P., *Anal. Chem.*, 1986, **57,** 2204.
3. Reynords, J. G., Gallegos, E. J., Fish, R. H., Komlenic, J. J., *Energy Fuels*, 1987, **1,** 36.
4. Silbernagel, B. G., *J. Catal.*, 1979, **56,** 315.
5. Rose-Brussin, M. and Moranta, D., *Appl. Catal.*, 1984, **11,** 85.
6. Mitchell, P. C. H., Scott, C. F., Bonnelle, J. P. and Grimblot, J. G., *J. Chem. Soc., Faraday Trans. I*, 1985, **81,** 1047.
7. Money, J. K., Huffman, J. C. and Ghristou, G., *Inorg. Chem.*, 1988, **27,** 507.
8. Dean, N. S., Bartley, S. L., Streib, W. E., Lobkovsky, E. B. and Christou, G., *Inorg. Chem.*, 1995, **34,** 1608.
9. Rehder, D., *Angew. Chem. Int. Ed. Engl.*, 1991, **30,** 148.
10. Hales, B. J., Case, E. E., Morningstar, J. E., Dzeda, M. F. and Mauterer, L. A., *Biochemistry*, 1986, **25,** 7251.
11. Kang, B. S., Hong, M. C., Wen, T. B., Liu, H. Q. and Lu, J. X., *J. Cluster Science*, 1995, **6,** 379.
12. Kiss, T., Buglyo, P., Micera, G., Dessi, A. and Sanna, D., *J. Chem. Soc., Dalton Trans.*, 1993, **12,** 1849.
13. (a) Higes-Rolando, F. J., Perez-Florindo, A., Vanlenzuela-Calahorro, C., Martin-Ramos, J. D. and Romero-Garzon, J., *Acta Cryst. Sect. C*, 1994, **50,** 1049; (b) Tsagkalidis, W., Rodewald, D., Rehder, D. and Vergopoulos, V., *Inorg. Chim. Acta*, 1994, **219,** 213.
14. Kang, B. S., Weng, L. H., Liu, H. Q., Wu, D. X., Huang, L. R., Lu, C. Z., Cai, J. H., Chen, X. T. and Lu, J. X., *Inorg. Chem.*, 1990, **29,** 4873.
15. Weng, L. H., Kang, B. S., Chen, X. T., Hong, M. C., Lei, X. J., Hu, Y. H. andLiu, H. Q., *Chin. J. Chem.*, 1993, **11,** 30.
16. Wen, T. B., Xu, Y. J., Shi, J. C., Deng, Y. H., Chen, C. N., Liu, Q. T. and Kang, B. S., *Chin. J. Struct. Chem.*, 1995, **14,** 151.
17. Klich, P. R., Daniher, A. T., Challen, P. R. and

McConvill, D. B., Youngs, W. J., *Inorg. Chem.*, 1996, **35,** 347.
18. Burrows, A. D., Chan, C.-W., Chowdhry, M. M., McGrady, J. E. and Mingos, D. M. P., *Chem. Soc. Rev.*, 1995, 329 and refs therein.
19. Chowdhry, M. M., Mingos, D. M. P., White, A. J. P. and Williams, D. J., *J. Chem. Soc., Chem. Commun.*, 1996, 899.
20. MolEN, An Interactive Structure Solution Procedure, Enraf-Nonius Delft, The Netherlands (1990).
21. (a) Hu, Y. H., Kang, B. S., Chen, X. T., Huang, L. R., Weng, L. H. and Xu, Y. J., *Chin. J. Chem.*, 1993, **11,** 137; (b) Kang, B. S., Hu, Y. H., Weng, L. H., Wu, D. X., Chen, X. T. and Xu, Y. J., *Inorg. Biochem.*, 1992, **46,** 231; (c) Weng, L. H., Chen, X. T., Hu, Y. H. and Kang, B. S., *Chin. Chem. Lett.*, 1991, **2,** 315.
22. Reynolds, J. G., Sendlinger, S. C., Murray, A. M., Huffman, J. C. and Christou, G., *Angew. Chem. Int. Ed. Engl.*, 1992, **31,** 1253.
23. Reynolds, J. G., Sendlinger, S. C., Murray, A. M., Huffman, J. C. and Christou, G., *Inorg. Chem.*, 1995, **34,** 5745.
24. Money, J. K., Huffman, J. C. and Christou, G., *Inorg. Chem.*, 1985, **24,** 3297.
25. Preuss, F., Steidel, M. and Exner, R., *Z. Naturforsch B*, 1990, **45,** 1618.
26. Dutton, J. C., Fallon, G. D. and Murray, K. S., *Inorg. Chem.*, 1988, **27,** 34.
27. Money, J. K., Folting, K., Huffman, J. C., Collison, D., Temperley, J., Mabbs, F. E. and Christou, G., *Inorg. Chem.*, 1986, **25,** 4583.
28. Wang, X., Zhang, X. M. and Liu, H. X., *Polyhedron*, 1995, **14,** 293.
29. Mayer, J. M., *Inorg. Chem.*, 1988, **27,** 3899.
30. Jones, R. A. and Katritsky, A. R., *J. Chem. Soc.*, 1960, 2937.
31. Spinner, E., *J. Chem. Soc.*, 1960, 1237.
32. Ohons, U., Guth, H., Kutoglu, A. and Scheringer, C., *Acta Cryst. B*, 1982, **38,** 831.
33. (a) Robinson, M. R., *J. Inorg. Nucl. Chem.*, 1964, **26,** 1277; (b) West, D. X. and Frank, C. A., *J. Inorg. Nucl. Chem.*, 1979, **41,** 49; (c) Davidson, J. K., Preston, P. N. and Russo, M. V., *J. Chem. Soc., Dalton Trans.*, 1983, 783.
34. (a) Lydon, J. D., Elder, R. C. and Deutsch, E., *Inorg. Chem.*, 1982, **21,** 3186; (b) Mahadevan, C. J., *J. Cryst. Spectros. Res.*, 1986, **16,** 347.
35. Truter, M. R., *Acta Cryst.*, 1967, **22,** 556.
36. (a) Lopez-Castra, A. and Truter, M. R., *J. Chem. Soc.*, 1963, 1309; (b) Weininger, M. S., O'Connor, J. E. and Amma, E. L., *ibid.*, 1969, **8,** 424.
37. Chen, X. T., Hu, Y. H., Wu, D. X., Weng, L. H. and Kang, B. S., *Polyhedron*, 1991, **10,** 2651.
38. Kvick, A. and Booles, S. S., *Acta Cryst. B*, 1972, **28,** 3405.
39. (a) Vinogradov, S. N. and Linnell, R. H., *Hydrogen Bonding*, Van Nostrand Reinhold Company, New York (1971); (b) Wells, A. F., *Structural Inorganic Chemistry*, 4th ed., Oxford University Press, Oxford (1975).
40. (a) Selbin, J., *Chem. Rev.*, 1965, **65,** 153; (b) Selbin, J., *Coord. Chem. Rev.*, 1966, **1,** 293.
41. Atherton, N. M. and Winscom, C. J., *Inorg. Chem.*, 1973, **12,** 383.
42. Matsubayashi, G., Akiba, K. and Tanaka, T., *Inorg. Chem.*, 1988, **27,** 4744.
43. Bonadies, J. A. and Carrano, C. J., *J. Am. Chem. Soc.*, 1986, **108,** 4088.
44. Branca, M., Micera, G., Dessi, A., Dana, D. and Raymond, K. N., *Inorg. Chem.*, 1990, **29,** 1586.
45. Chasteen, N. D., In *Biological Magnetic Resonance*; L. J. Berliner, J. Reuben, Eds, Plenum Press, New York (1981) Vol. 3, Ch. 2 and refs cited therein.

Pergamon

PII: S0277-5387(97)00297-0

Polyhedron Vol. 17, No. 2–3, pp. 341–349, 1998
© 1997 Elsevier Science Ltd
All rights reserved. Printed in Great Britain
0277-5387/98 $19.00+0.00

The formation, characterisation and structures of *closo*-12-vertex dirhodathiaboranes containing rhodium(II) centres

Kerry J. Adams, Thomas D. McGrath,[a] and Alan J. Welch[b]*

Department of Chemistry, University of Edinburgh, West Mains Road, Edinburgh EH9 3JJ, U.K.

(Received 4 March 1997; accepted 27 June 1997)

Abstract—Reaction of Cs[6-*arachno*-SB_9H_{12}] with $[RhCl(CO)(PPh_3)_2]$ yields the known complex [8-CO-8,8-$(Ph_3P)_2$-8,7-*nido*-$RhSB_9H_{10}$], **1**. In contrast, treatment of the same thiaborane with $[RhCl(CO)(PPh_3)]_2$ affords a number of 12-vertex dirhodathiaboranes of the type [2,3-$(CO)_2$-$\mu_{2,3}$-CO-2,3-$(PPh_3)_2$-7-X-2,3,1-*closo*-$Rh_2SB_9H_8$] in modest yields. For X = H, **3a**, and X = Cl, **4**, single crystal X-ray diffraction studies are reported; crystals of **3a** contain the compound with X = OH, **3b**, in approximately 28% occupancy. © 1997 Elsevier Science Ltd

Keywords: borane; thiaborane; rhodium; phosphine; carbonyl; crystal structure.

Among the heteroatomic derivatives of the binary boranes, by far the most extensively studied are the carbaboranes [1] and their metal complexes [2]. Recently, however, the chemistry of other polyhedral hetero(metalla)boranes has seen greater development [3], in which arguably the most common non-carbon heteroatom has been sulfur. As a result a range of sulfur-containing heteroborane polyhedra is now known which encompasses diverse examples of intermediate- and larger-sized heterothiaboranes [4], metallathiaboranes [5] and metalladithiaboranes [6], and even 'macropolyhedral' dithiaboranes [7].

As part of our continuing synthetic and structural studies [8,9], of these and other larger metallaheteroboranes, we have investigated the reaction of Cs[6-*arachno*-SB_9H_{12}] with the complexes $[RhCl(CO)(PPh_3)_2]$ and $[RhCl(CO)(PPh_3)]_2$, and have obtained from the latter an unexpected series of dimetallic thiaborane-containing products.

* Author to whom correspondence should be addressed.
[a] Present address: School of Chemistry, University of Leeds, Leeds LS2 9JT, U.K.
[b] Present address: Department of Chemisty, Heriot Watt University, Edinburgh EH14 4AS, U.K.

EXPERIMENTAL

Synthesis and characterization

All reactions were carried out under an atmosphere of dry, oxygen-free dinitrogen using standard Schlenk line techniques, with some subsequent manipulation in air. Solvents were freshly distilled from appropriate drying agents and degassed immediately prior to use. Preparative thin-layer chromatography employed Kieselgel 60 F_{254} plates (Merck), pre-washed in the appropriate solvents. NMR spectra were recorded from $CDCl_3$ solutions at 298 K. The starting materials Cs[6-*arachno*-SB_9H_{12}] [10], $[RhCl(CO)_2]_2$ [11] and $[RhCl(CO)(PPh_3)_2]$ [12] were prepared as described.

Reaction of Cs[6-*arachno*-SB_9H_{12}] *with* $[RhCl(CO)(PPh_3)_2]$. *Preparation of* [8-CO-8,8-$(Ph_3P)_2$-8,7-*nido*-$RhSB_9H_{10}$], **1**

To a frozen (77 K) solution of $[RhCl(CO)(PPh_3)_2]$ (130 mg, 0.19 mmol) in CH_2Cl_2 (15 cm^3) was added solid Cs[6-*arachno*-SB_9H_{12}] (55 mg, 0.20 mmol). The mixture was allowed to warm to room temperature with stirring, and consumption of the starting Rh

complex was monitored by IR spectroscopy. After ca 18 h, the reaction mixture was evaporated at reduced pressure. The only thiaborane-containing product (identified by $^{31}P-\{^1H\}$ and $^{11}B-\{^1H\}$ NMR and infrared spectroscopy) was the known [13] compound [8-CO-8,8-$(Ph_3P)_2$-8,7-*nido*-$RhSB_9H_{10}$], **1**.

Reaction of $Cs[6\text{-}arachno\text{-}SB_9H_{12}]$ *with* $[RhCl(CO)(PPh_3)]_2$

Preparation of compounds **2–4**. $[RhCl(CO)(PPh_3)]_2$ [14] was formed *in situ* from $[RhCl(CO)_2]_2$ (100 mg, 0.257 mmol) and PPh_3 (134 mg, 0.511 mmol) in benzene (10 cm^3). This solution of $[RhCl(CO)(PPh_3)]_2$ was frozen to 77 K and solid $Cs[6\text{-}arachno\text{-}SB_9H_{12}]$ (141 mg, 0.514 mmol) added; the mixture was allowed to warm to room temperature and stirred for ca 3 h. During the course of the reaction gas evolution was apparent; the yellow solution became more intensely orange and an apparently yellow solid was deposited. The mixture was filtered and the orange filtrate evaporated at reduced pressure to yield an orange–brown solid. (Infrared spectroscopic analysis of the solid removed by filtration showed a broad absorption in the B—H stretching region, suggesting that this solid is largely residual $Cs[SB_9H_{12}]$ or its decomposition products, in addition to CsCl.)

The orange—brown residue was dissolved in a small amount (ca 5 cm^3) of CH_2Cl_2 and applied to chromatographic plates; repeated preparative thin layer chromatography (CH_2Cl_2/*i*-hexane, 3:2) gave bands as follows:

1. Brown: R_f 0.6, (very small amount, < 1 mg). IR (CH_2Cl_2): ν_{max}(BH) 2528 (m, br); ν_{max}(CO) 2027 (s, br), 1868 (vw, br) cm^{-1} (compound **2** was not further pursued).
2. Orange: R_f 0.5, (37 mg) (compounds **3a, 3b** and **3c**).
3. Red: R_f 0.4, (33 mg) (compound **4**).

Bands 2 and 3 yielded three identifiable metallathiaboranes, namely compounds **3a** and **3b,** and compound **4** respectively, which were characterised as described in the two following sections.

Characterisation of $[2,3\text{-}(CO)_2\text{-}\mu_{2,3}\text{-}CO\text{-}2,3\text{-}(PPh_3)_2\text{-}2,3,1\text{-}closo\text{-}Rh_2SB_9H_9]$ **3a** *and partial characterisation of* $[2,3\text{-}(CO)_2\text{-}\mu_{2,3}\text{-}CO\text{-}7\text{-}OH\text{-}2,3\text{-}(PPh_3)_2\text{-}2,3,1\text{-}closo\text{-}Rh_2SB_9H_8]$ **3b**

Band 2, upon repeated crystallisation (slow mutual diffusion of *i*-hexane and a CH_2Cl_2 solution at −30°C), afforded mainly red–orange *rods* which were very unstable with respect to solvent loss upon removal from the mother liquor; seven red–orange *crystals*, and a larger number of yellow *blocks* were also obtained. A single-crystal X-ray diffraction study (*vide infra*) of one of the second kind of red–orange crystals identified this as primarily $[cis\text{-}2,3\text{-}(CO)_2\text{-}\mu_{2,3}\text{-}CO\text{-}2,3\text{-}(PPh_3)_2\text{-}2,3,1\text{-}closo\text{-}Rh_2SB_9H_9]$, **3a,** and a fraction as the 7-OH derivative **3b**. The yellow crystals, **3c,** are as yet unidentified. However, there is very close similarity in the infrared and ^{31}P NMR spectra of all three crystal types obtained from band 2, and this strongly suggests them simply to be polymorphs of **3a**. (Moreover, microanalytical data are also consistent with compound **3b** being present in only small amounts overall.) Taking the bulk of band 2, therefore, to be of formulation $[(CO)_3(PPh_3)_2Rh_2SB_9H_9]$: combined yield (as crystals) of band 2: 27 mg, 0.030 mmol, 5.8% based on {Rh}.

Anal. Found: C, 49.40; H, 4.09 %. Calcd for $C_{39}H_{39}B_9O_3P_2Rh_2S$: C, 49.16; H, 4.13%. IR (CH_2Cl_2): ν_{max}(BH) 2529 (m, br); ν_{max}(CO) 2031 (s), 1863 (m, br) cm^{-1}. Cluster NMR data for **3a,** in the order $\delta(^{11}B)$ [$\delta(^1H)$] relative ^{11}B integral: +10.3 [+3.5] 1B, +6.2(br) [+3.0 (2H), +2.7 (2H), +2.6 (1H)] 5B, −3.2 [+2.4] 2B, −32.9 [+1.0] 1B. In addition: $\delta(^1H)$ +7.20 to +7.41 (m, C_6H_5); $\delta(^{31}P)$ +23.2 [d, $^1J(^{31}P\text{-}^{103}Rh)$ ca 110 Hz]. We tentatively assign an additional broad ^{11}B singlet resonance, at $\delta(^{11}B)$ ca +19, to the 7-OH substituted position in **3b**; other ^{11}B resonances due to **3b** appear to coincide with those of **3a,** as do the ^{31}P resonances of the two species.

Characterisation of $[2,3\text{-}(CO)_2\text{-}\mu_{2,3}\text{-}CO\text{-}7\text{-}Cl\text{-}2,3\text{-}(PPh_3)_2\text{-}2,3,1\text{-}closo\text{-}Rh_2SB_9H_8]$ **4**

The compound **4,** obtained as band 3 above, was fully characterised spectroscopically (*vide infra*) and was unambiguously identified as $[cis\text{-}2,3\text{-}(CO)_2\text{-}\mu_{2,3}\text{-}CO\text{-}7\text{-}Cl\text{-}2,3\text{-}(PPh_3)_2\text{-}2,3,1\text{-}closo\text{-}Rh_2SB_9H_8]$, by the single crystal X-ray diffraction study reported later. Yield (as crystals): 29 mg, 0.029 mmol, 5.7% based on {Rh}.

Anal. Found: C, 44.30; H, 3.11%. Calcd for $C_{39}H_{38}B_9ClO_3P_2Rh_2S$: C, 47.45; 3.88%. IR ($CH_2Cl_2$):

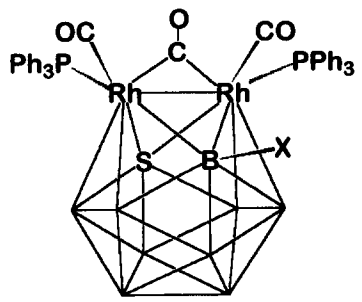

	X
3a	H
3b	OH
4	Cl

ν_{max}(BH) 2535 (m, br); ν_{max}(CO) 2064 (s), 1880 (m, br) cm^{-1}. Cluster NMR data for **4**, in the order $\delta(^{11}B)$ [$\delta(^{1}H)$] relative ^{11}B integral: +23.9 [−] 1B [B(7)], +11.2 [+4.44] 2B, +6.2 [+4.27] 2B, +0.9 [+2.48] 2B, −3.5 [+2.80] 2B, −35.6 [+0.61] 1B. In addition: $\delta(^{1}H)$ +7.26 to +7.48 (m, C_6H_5); $\delta(^{31}P)$ +22.6 [d, br, $^{1}J(^{31}P\text{-}^{103}Rh)$ ca 88 Hz].

Crystallisation of compound **4** (slow mutual diffusion of *i*-hexane and a concentrated CH_2Cl_2 solution at −30°C) afforded several well-formed dark red *blocks*, one of which was the subject of analysis by a single crystal X-ray diffraction experiment, as described below.

Crystallographic studies

Crystal data, and details of data collection and structure refinement, for compounds **3a/b** and **4** are listed in Table 1. Reflection data were measured at 293(2) K on an Enraf-Nonius CAD4 automatic four-circle diffractometer operating in the ω–2θ scan mode using graphite-monochromated Mo-K_α X-radiation, $\bar{\lambda} = 0.71073$ Å. Cell parameters and orientation matrices were determined from the setting angles of 25 accurately-measured reflections. Both data sets were corrected [15] for Lorentz and polarisation effects and, following isotropic convergence, benefited from an empirical absorption correction [16]. During data collection, some slight crystal decay (ca 2% for **3a/b**; ca 4% for **4**) was revealed by monitoring the intensity of two standard reflections measured after every 500 data; the data sets were corrected [15] to allow for this. In the latter stages of refinement, data were weighted according to $w^{-1} = [\sigma^2(F_o^2) + g_1^2P^2 + g_2P]$ where $P = (F_o^2 + 2F_c^2)/3$. Fractional atomic co-ordinates, full lists of bond distances and interbond angles and anisotropic thermal parameters have been deposited as supplementary data. Molecular geometry figures were drawn using SHELXTL-PC [17].

[2,3-$(CO)_2$-$\mu_{2,3}$-CO-2,3-$(PPh_3)_2$-7-X-2,3,1-*closo*-$Rh_2SB_9H_8$] (X = H/OH), **3a/b**. An irregular red–orange *block* of approximate dimensions 0.5 × 0.3 × 0.2 mm was selected for data collection.

Table 1. Crystallographic data and details of data collection and structure refinement for crystals of compounds **3a/b** and **4**

Compound	**3a/b**	**4**
Formula	$C_{39}H_{39}B_9O_3P_2Rh_2S$[a]	$C_{39}H_{38}B_9ClO_3P_2Rh_2S$
M_r	952.81[a]	987.29
System	orthorhombic	triclinic
Space group	$P2_12_12_1$	$P\bar{1}$
a/Å	10.802(2)	11.137(6)
b/Å	19.036(7)	13.558(7)
c/Å	20.631(4)	16.688(4)
α/°	90	108.44(3)
β/°	90	97.66(5)
γ/°	90	110.96(5)
U/Å^2	4242.3(19)	2144.1(17)
Z	4	2
D_c/M gm^{-3}	1.492[a]	1.532
μ/mm^{-1}	0.939[a]	0.979
F(000)	1912[a]	988
$\theta_{orientation}$/°	10–11	11–11.5
$\theta_{data\ collection}$/°	1.46–24.97	1.34–24.97
Period/h	192	228
h, k, l ranges	−12–12, 0–22, 0–24	0–13, −16–15, −19–19
Data measured	8151	7953
Unique data	7451	7526
R_{int}	0.0278	0.0096
T_{min}, T_{max}	0.905, 1.084	0.846, 1.156
Observed data [$F_o > 4\sigma(F_o)$]	5742	6384
R_1 [observed data]	0.0457	0.0270
R_1 [all data]	0.0830	0.0385
wR_2 [all data]	0.0959	0.0682
S	1.047	1.048
g_1, g_2	0.0444, 0	0.0371, 1.1485
Variables	444	467
Max., min. residue/eÅ^{-3}	0.427, −0.348	0.432, −0.559

[a] for **3a** only (i.e., ignores partial OH substituent)

The positions of the two rhodia were obtained by direct methods (*SHELXS*-86 [18]), whilst the B, C, O, P and S atoms were located in subsequent difference Fourier maps (*SHELXL*-93 [19]). Although most of the cage H atoms could also be located by this method, they would not subsequently satisfactorily refine with independent positions and so were set riding in idealised positions 1.10 Å from the corresponding B atom with isotropic thermal parameters equal to 1.2 times the equivalent isotropic thermal parameter of the parent B atom. The six phenyl rings were constrained to be planar, rigid hexagons (C—C 1.39 Å), with the attached H atoms in calculated positions (C—H 0.93 Å) and having isotropic thermal parameters equal to 1.2 times the equivalent isotropic thermal parameter of the corresponding C atom. This model (with all nine B atoms bearing only terminal H atoms) was refined towards isotropic convergence, at which point it became clear that a substantial residual electron density peak (ca 2 $eÅ^{-3}$) was located ca 1.3 Å from B(7). This was assigned as a (partial) terminal hydroxyl substituent on the basis of a reasonable B—X distance; both the OH group and the terminal H atom attached to B(7) were included with (refining) complementary occupancy. The O—H distance was constrained at 0.82 Å, and the B(7)—O—H angle was constrained to be tetrahedral, with free rotation about the B—O bond allowed such that the H atom was located at the position of maximum electron density (determined *via* structure factor calculation [19]). The H atom bound to B(7) was not further positionally refined once the partial OH group had been included in the model. At convergence the hydroxyl group had 0.28(2) fractional occupancy; no further attempt to model the disorder was deemed necessary. Refinement throughout was on F^2 using full-matrix least-squares methods (*SHELXL*-93), converging without difficulty and with no significant residual electron density. The Flack absolute structure parameter × was calculated to be 0.01(4), confirming the absolute configuration to be that chosen [20].

[2,3-$(CO)_2$-$\mu_{2,3}$-CO-7-Cl-2,3-$(PPh_3)_2$-2,3,1-*closo*-$Rh_2SB_9H_8$], **4**. A well-formed dark red *block* of approximate dimensions 0.45 × 0.25 × 0.15 mm was chosen for data collection. The positions of the two rhodium atoms were determined by inspection of the Patterson synthesis (*SHELX*-76 [21]); those of the B, C, O, P, S, Cl and cage H atoms were obtained by difference Fourier syntheses (*SHELXL*-93 [19]). The Cl atom was identified as such by comparison of its peak height in a difference map to that of a well-defined C atom, and is justified by its successful refinement, the reasonable B—Cl distance, and its chemical sense. The structure was refined by full-matrix least-squares on F^2 using *SHELXL*-93. Phenyl rings were treated as in **3a/b** above. Cage H atoms were successfully allowed positional refinement, and were assigned a common isotropic thermal parameter, $U_H = 0.062(4)$ $Å^2$ at convergence. All non-H atoms were permitted anisotropic refinement following the absorption correction. The model very readily converged and there are no significant residual peaks in the final difference Fourier map.

DISCUSSION

The reaction of [RhCl(CO)$(PPh_3)_2$] with Cs[6-*arachno*-SB_9H_{12}] in dichloromethane affords the known [13] eleven-vertex *tris*(ligand)-rhodathiaborane [8-CO-8,8-$(Ph_3P)_2$-8,7-*nido*-$RhSB_9H_{10}$], **1**, whose identity was established by ^{31}P-{^1H} and ^{11}B-{^1H} NMR and infrared spectroscopy. This complex was previously prepared by the addition of CO to [8,8-$(Ph_3P)_2$-8,7-*nido*-$RhSB_9H_{10}$] in benzene.

In contrast, the reaction between the dimer [RhCl(CO)(PPh_3)]$_2$ and the same thiaborane is far less straightforward. The Rh reagent [14] was prepared *in situ* from [RhCl$(CO)_2$]$_2$ and one molar equivalent (per Rh) of PPh_3, and the solid thiaborane salt added directly to this solution. During the reaction, considerable effervescence was noted: the stoichiometry of the products is consistent with evolution of H_2. Preparative thin layer chromatography of the filtered and concentrated reaction mixture revealed three distinct bands (see Experimental).

The first of these bands, designated compound **2**, was recovered in only very small quantity, readily decomposed and ultimately defied detailed characterisation. Nevertheless, given the identities of the other products, and the detection of (probable) terminal- and bridging-CO infrared bands in addition to BH stretching vibrations, we reasonably propose that **2** is related to the more well-defined compounds **3a**, **3b** and **4** below.

The second 'band' obtained by chromatography in fact consists of *at least* two compounds which proved too similar to be separated by this technique: repeated fractional crystallisation afforded three types of crystal which we believe (on the basis of ^{31}P-{^1H} NMR and infrared spectroscopy and microanalytical data) to be polymorphs containing largely a single compound. A single-crystal X-ray diffraction study (see below) showed one of these crystals to consist largely of [2,3-$(CO)_2$-$\mu_{2,3}$-CO-2,3-$(PPh_3)_2$-2,3,1-*closo*-$Rh_2SB_9H_9$], **3a**: this crystal was found to contain in addition the 7-hydroxyl analogue, **3b** in fractional occupancy (ca 28%). The two other crystal forms were never of adequate quality for a full X-ray diffraction structure determination.* [Formation of **3b**, pre-

* On a single occasion we succeeded in determining tentative unit cell parameters for a crystal of the form designated **3c** during a diffractometer random peak search: the cell volume so obtained was consistent with **3c** being *at least* related to **3a** and **3b** (primitive monoclinic, $Z = 4$, $U \approx 4300$ $Å^2$). In this context, we note also the possibility that there may exist an isomer of **3a** in which the Rh-bound triphenylphosphine (and terminal carbonyl) ligands are mutually *transoid*.

sumably from **3a**, conceivably occurs by reaction with silica (and/or atmospheric H_2O/O_2) during work-up.] The third band isolated by chromatography was solely the 7-Cl-substituted relative of compounds **3a** and **3b**, that is, [2,3-$(CO)_2$-$\mu_{2,3}$-CO-2,3-$(PPh_3)_2$-7-Cl-2,3,1-*closo*-$Rh_2SB_9H_8$], **4**, which was also studied by a single-crystal X-ray diffraction analysis, as discussed later. ^{11}B, ^1H and ^{31}P NMR spectra for **3a** and **4** are consistent with their crystallographically-determined structures. Six resonances occur in their ^{11}B-{^1H} NMR spectra in respective ratios (high → low frequency) of 1:2:2:1:2:1. Each of these signals becomes a doublet upon retention of proton coupling, save for the highest frequency resonance in the spectrum of **4** which is, therefore, assigned to the chloro-substituted vertex B(7). For both **3a** and **4**, the ^{31}P-{^1H} NMR spectra consist of a single ^{103}Rh-coupled doublet, as expected. Surprisingly, microanalytical results from crystals of **4** always differed significantly from expected values: we are unable fully to account for this (poor combustion may be suggested), given that microanalysis of the closely-related species **3** apparently gives good agreement with calculated figures.

X-ray diffraction studies of single crystals of compounds **3a** and **4**, to which the above spectroscopic studies are complementary, provided unequivocal identification of these species. Figure 1 shows a perspective view of **4**, whilst in Fig. 2 a view of the 'central' cluster and Rh environments in **3a** is presented. Selected interatomic distances and interbond angles for **3a/b** and **4** are listed in Table 2.

Compounds **3a** (and **3b**) and **4** are based on a distorted icosahedral 2,3,1-*closo*-Rh_2SB_9 cluster with approximate C_s molecular symmetry (ignoring the orientations of the pendant phenyl groups), fully consistent with their ^{11}B NMR spectra. In both clusters, a sulfur and two rhodium atoms are mutually adjacent at a triangular face. The unique boron atom, B(7), which is bound to both rhodia, has undergone substitution in **3b** and in **4**, whereby the *exo*-terminal H atom present in the unsubstituted parent **3a** has been replaced by -OH and -Cl substituents respectively. The B(7)—X distances determined here [B(7)—O in

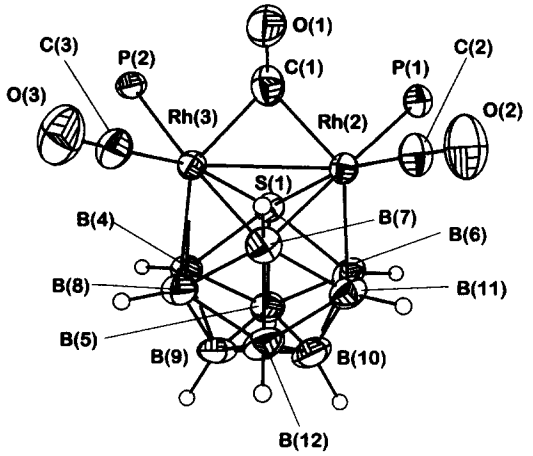

Fig. 2. View of the central Rh_2SB_9 cluster and the rhodium co-ordination environments in **3a**, drawn with the same conventions as in Fig. 1. The phenyl rings C(1*ni*) and C(2*ni*) (n = 1–3; i = 1–6, numbered cyclically) are bound to P(1) and P(2) respectively. Compound **3b**, which has a terminal hydroxyl substituent [O—H(70)] rather than an H atom bound to B(7), is present in 28(2)% occupancy in the crystal of **3a**.

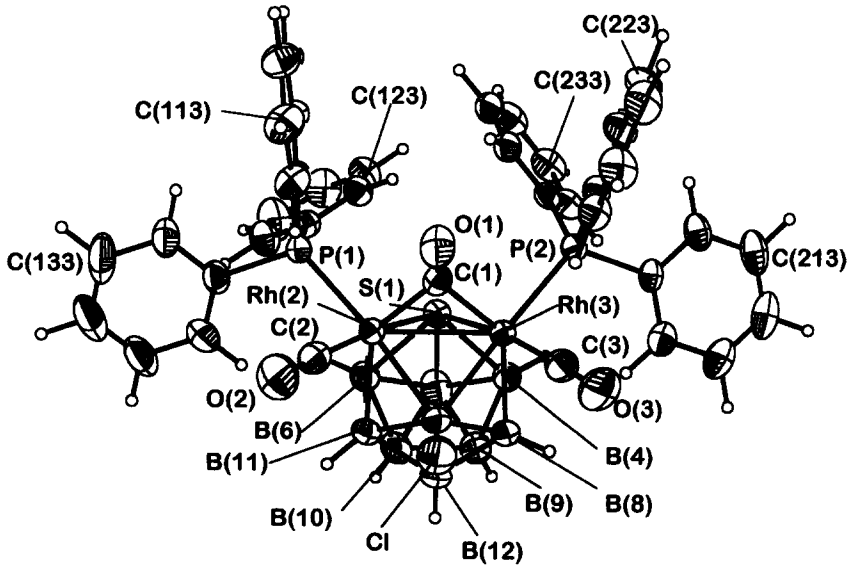

Fig. 1. Perspective view of **4** showing 50% probability ellipsoids. H atoms have artificial radii for clarity. H atoms bear the same numerical label as the heavy atom to which they are bound; phenyl rings are numbered cyclically.

Table 2. Selected interatomic distances (Å) and interbond angles (°) for **3a/b** and **4**

	3a/b	**4**
S(1)—Rh(2)	2.447(2)	2.4187(11)
S(1)—Rh(3)	2.433(2)	2.452(3)
S(1)—B(4)	2.066(8)	2.071(4)
S(1)—B(5)	1.981(9)	1.996(4)
S(1)—B(6)	2.096(9)	2.108(4)
Rh(2)—Rh(3)	2.7409(10)	2.749(2)
Rh(2)—B(6)	2.323(8)	2.313(4)
Rh(2)—B(7)	2.302(9)	2.305(4)
Rh(2)—B(11)	2.256(7)	2.263(4)
Rh(2)—P(1)	2.393(2)	2.377(2)
Rh(2)—C(1)	2.072(8)	2.111(3)
Rh(2)—C(2)	1.840(8)	1.856(4)
Rh(3)—B(4)	2.330(8)	2.336(4)
Rh(3)—B(7)	2.311(9)	2.308(4)
Rh(3)—B(8)	2.273(8)	2.265(4)
Rh(3)—P(2)	2.373(2)	2.3747(14)
Rh(3)—C(1)	2.066(7)	2.117(3)
Rh(3)—C(3)	1.828(8)	1.850(4)
B(7)—X	1.31(3)[a]	1.837(4)[b]
C(1)—O(1)	1.178(8)	1.145(3)
C(2)—O(2)	1.137(8)	1.136(4)
C(3)—O(3)	1.154(9)	1.136(4)
Rh(2)—S(1)—Rh(3)	68.34(5)	68.72(5)
Rh(2)—S(1)—B(6)	60.9(2)	60.99(11)
Rh(3)—S(1)—B(4)	61.8(2)	61.50(12)
B(4)—S(1)—B(5)	54.7(3)	54.5(2)
B(5)—S(1)—B(6)	55.0(3)	54.5(2)
S(1)—Rh(2)—Rh(3)	55.60(5)	56.21(6)
S(1)—Rh(2)—B(6)	52.1(2)	52.86(10)
S(1)—Rh(2)—P(1)	95.48(6)	95.65(6)
S(1)—Rh(2)—C(1)	95.1(2)	91.51(9)
S(1)—Rh(2)—C(2)	168.5(2)	171.17(11)
Rh(3)—Rh(2)—B(7)	53.7(2)	53.48(10)
Rh(3)—Rh(2)—P(1)	127.34(5)	131.85(5)
Rh(3)—Rh(2)—C(1)	48.4(2)	49.53(9)
Rh(3)—Rh(2)—C(2)	128.1(2)	126.26(12)
B(6)—Rh(2)—B(11)	45.7(3)	45.7(2)
B(6)—Rh(2)—P(1)	98.2(2)	94.33(12)
B(6)—Rh(2)—C(1)	143.0(3)	142.71(12)
B(6)—Rh(2)—C(2)	117.0(3)	118.9(2)
B(7)—Rh(2)—B(11)	47.5(3)	47.81(14)
B(7)—Rh(2)—P(1)	178.6(2)	173.60(9)
B(7)—Rh(2)—C(1)	79.4(3)	85.73(14)
B(7)—Rh(2)—C(2)	90.4(3)	90.54(14)
B(11)—Rh(2)—P(1)	131.1(2)	125.85(11)
B(11)—Rh(2)—C(1)	126.7(3)	133.53(13)
B(11)—Rh(2)—C(2)	84.0(3)	85.5(2)
P(1)—Rh(2)—C(1)	102.0(2)	100.60(11)
P(1)—Rh(2)—C(2)	89.4(2)	87.85(11)
C(1)—Rh(2)—C(2)	94.0(3)	95.82(14)
S(1)—Rh(3)—Rh(2)	56.06(4)	55.07(5)
S(1)—Rh(3)—B(4)	51.4(2)	51.20(10)
S(1)—Rh(3)—P(2)	96.59(6)	96.66(5)
S(1)—Rh(3)—C(1)	95.7(2)	90.48(9)
S(1)—Rh(3)—C(3)	167.9(3)	167.33(11)
Rh(2)—Rh(3)—B(7)	53.4(2)	53.38(9)
Rh(2)—Rh(3)—P(2)	123.87(5)	128.87(4)
Rh(2)—Rh(3)—C(1)	48.6(2)	49.36(9)
Rh(2)—Rh(3)—C(3)	129.3(2)	128.93(11)
B(4)—Rh(3)—B(8)	45.4(3)	45.9(2)
B(4)—Rh(3)—P(2)	103.4(2)	98.26(10)
B(4)—Rh(3)—C(1)	142.9(3)	140.14(13)
B(4)—Rh(3)—C(3)	116.8(3)	116.7(2)
B(7)—Rh(3)—B(8)	48.2(3)	47.86(13)
B(7)—Rh(3)—P(2)	175.5(2)	177.65(9)
B(7)—Rh(3)—C(1)	79.3(3)	85.53(12)
B(7)—Rh(3)—C(3)	91.5(3)	90.15(14)
B(8)—Rh(3)—P(2)	136.3(2)	130.00(10)
B(8)—Rh(3)—C(1)	127.3(3)	133.38(13)
B(8)—Rh(3)—C(3)	84.4(3)	83.0(2)
P(2)—Rh(3)—C(1)	96.2(2)	96.61(9)
P(2)—Rh(3)—C(3)	88.2(2)	88.52(11)
C(1)—Rh(3)—C(3)	94.8(3)	100.43(14)
S(1)—B(4)—Rh(3)	66.9(2)	67.30(12)
S(1)—B(6)—Rh(2)	67.0(2)	66.15(11)
Rh(2)—B(7)—Rh(3)	72.9(3)	73.15(11)
Rh(2)—C(1)—Rh(3)	82.9(3)	81.11(11)
Rh(2)—C(1)—O(1)	137.4(6)	139.4(2)
Rh(3)—C(1)—O(1)	136.3(6)	138.8(2)
Rh(2)—C(2)—O(2)	178.4(7)	178.4(3)
Rh(3)—C(3)—O(3)	177.1(7)	177.1(3)
Rh(2)—B(7)—X	119.0(14)[a]	114.6(2)[b]
Rh(3)—B(7)—X	112.7(13)[a]	113.3(2)[b]
B(8)—B(7)—X	113.7(14)[a]	118.4(2)[b]
B(11)—B(7)—X	112.0(13)[a]	118.9(2)[b]
B(12)—B(7)—X	111.3(4)[a]	114.3(2)[b]

[a] X = O.

[b] X = Cl.

Cluster B—B distance ranges: **3a/b**, 1.735(11) to 1.885(12)Å; **4**, 1.742(5) to 1.883(5)Å

Other cluster acute angles: B—B—B ranges: **3a/b**, 57.0(5)–65.2(5)°; **4**, 57.0(2)–65.0(2)°.

Rh—B—B ranges: **3a/b**, 64.9(4)–69.2(4)°; **4**, 64.9(2)–69.1(2)°.

S—B—B ranges: **3a/b**, 59.4(4)–65.6(4)°; **4**, 59.7(2)–65.8(2)°.

3b is 1.31(3) Å; B(7)—Cl in **4** is 1.837(4) Å] are well within the expected [22] ranges for bonds to such atoms attached to borane polyhedra (ca 1.23–1.63 Å for B—OR; ca 1.73–1.92 Å for B—Cl). Compound **3b** constitutes one of the few examples of an (albeit partially) structurally-characterised borane derivative bearing a terminal hydroxy group, rather than the relatively common alkoxy substituent. Previously reported B—OH distances are in the range 1.35(1)–1.628(19) Å; the relative shortness of the B—OH separation determined here for **3b** is *perhaps* an artefact of the crystallographic disorder.

The remainder of the thiaborane polyhedral fragment is substantially regular, and the ranges of Rh—B [**3a/b**: 2.256(7)–2.330(8) Å; **4**: 2.263(4)–2.336(4) Å], S—B [**3a/b**: 1.981(9)–2.096(9) Å; **4**: 1.996(4)–2.108(4) Å] and B—B [**3a/b**: 1.735(11)–1.885(12) Å; **4**: 1.742(5)–1.883(5) Å] distances are typical of such

metallaheteroboranes. There are, nevertheless, some significant deviations from ideal mirror symmetry within both clusters. This is evidenced by, for example, the environment of S(1): this atom is somewhat asymmetrically disposed with respect to a notional molecular mirror plane so that in **4** S(1) is 2.4187(11) Å from Rh(2), but 2.452(3) Å from the chemically equivalent Rh(3); a similar situation exists in **3a/b**.

Each rhodium vertex has a co-ordination environment resembling a distorted octahedron in which a conical $\{(CO)(\mu\text{-}CO)(PPh_3)Rh\}$ fragment is η^5-bonded to the $RhSB_3$ 'ligating face' of a $\{nido\text{-}RhSB_9\}$ polyhedron. The two terminal CO ligands, and likewise the two triphenylphosphine groups, are mutually *cisoid* in both **3a/b** and **4**; the Rh—Rh connectivity is (essentially) symmetrically bridged by one further carbonyl ligand in both cases. The rhodium-to-phosphorus bonding in both structures is unremarkable; and similarly the terminal CO functions are bound to Rh in a typical fashion and are essentially linear at carbon. The Rh(2)—Rh(3) internuclear distance is 2.7409(10) in **3a/b** and 2.749(2) Å in **4**; these are comparable to the length of the same vector in related compounds: For example, in **5** (see Table 3 below), the Rh—Rh separation is 2.6307(9) Å [23], whereas in **6** the unbridged (and perhaps, therefore, less restricted) Rh—Rh connectivity is longer, at 2.778(1) Å [24]. A steric contribution to this distance arising from the presence (and proximity) of bulky, mutually *cis* PPh_3 groups, might also be invoked in the present compounds. Both terminal CO ligands lie approximately *trans* to the cluster sulfur vertex in **3a/b** and in **4**. This is most likely a consequence of the greater basicity of the phosphines than of the carbonyl ligands, and we note that in the compound [8-CO-8-(dppm)-8,7-*nido*-$RhSB_9H_{10}$] [dppm = *bis*-(diphenylphosphino)methane], the CO ligand again is found to lie *trans* to sulfur [9]. (See refs [23–30].)

One possible consequence of this rather large metal vertex separation in **3a/b** and **4** is relatively long distances to the bridging carbonyl moiety. This is particularly so in compound **4** where C(1) is distant 2.111(3) Å from Rh(2) and 2.117(3) Å from Rh(3); the equivalent parameters in **3a/b** are 2.072(8) Å and 2.066(7) Å, respectively. The longer Rh—C(1) distances in **4** result in relatively poor overlap between Rh *d* hybrid orbitals and carbonyl σ- and π-type orbitals, so that in **4** C(1)—O(1) [1.145(3) Å] is relatively short for a μ-CO function, compared to the same separation, 1.178(8) Å, in **3a/b**. To our knowledge, the only other examples of a $\{M\cdots M\}$-bridging carbonyl function in comparable clusters are the isomeric pair of dicobalt compounds $[(CO)_5Co_2B_{10}H_8(SEt_2)_2]$ **15** and **16** [31]. In these, the much shorter intermetal separation (ca 2.49 Å) and the presence of first-row metal centres combine to afford much better orbital

Table 3. Composition of selected related species of formulation $\{7\text{-X-2,3,1-}closo\text{-}M_2EB_9\}$[a]

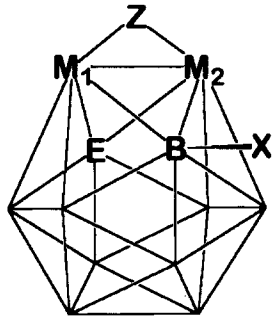

	M_1	M_2	E	X	Z	Ref.
5[b]	$(Ph_3P)(Ph_2P\text{-}C_6H_4\text{-}o\text{-})Rh$[c]	$(Cl)(Ph_3P)Rh$	S	$o\text{-}C_6H_4$[c]	Cl	[23]
6[b]	$(\eta^5\text{-}C_5Me_5)Rh$	$(\eta^5\text{-}C_5Me_5)Rh$	S	Cl	—	[24]
7	$(\eta^5\text{-}C_5H_5)Co$	$(\eta^5\text{-}C_5H_5)Co$	S	H	—	[25]
8[b]	$(\eta^5\text{-}C_5H_5)Co$	$(\eta^5\text{-}C_5H_5)Co$	S	I	—	[25]
9	$(\eta^5\text{-}C_5Me_5)Ir$	$(\eta^5\text{-}C_5Me_5)Ir$	S	Cl	—	[26]
10	$(\eta^6\text{-}p\text{-cym})Ru$	$(\eta^6\text{-}p\text{-cym})Ru$	S	H	—	[27]
11	$(\eta^6\text{-}p\text{-cym})Ru$	$(\eta^6\text{-}p\text{-cym})Ru$	S	Cl	—	[27]
12[b]	$(\eta^5\text{-}C_5H_5)Co$	$(\eta^5\text{-}C_5H_5)Co$	C	H	—	[28]
13	$(\eta^5\text{-}C_5H_5)Co$	$(\eta^5\text{-}C_5H_5)Co$	Se	H	—	[29]
14	$(\eta^5\text{-}C_5Me_5)Rh$	$(\eta^5\text{-}C_5Me_5)Rh$	P—Ph	Cl?	—	[30]

[a] *p*-cym = C_6H_4-Me-1-^{i}Pr-4.

[b] Characterised crystallographically.

[c] One Ph ring of a Rh-bound (formerly) Ph_3P ligand is *ortho*-cycloboronated to B(7).

overlap to the bridging carbonyl ligand, with bridging C—O distances (ca 1.18 Å) much closer to that found in **3a/b**.

Twelve-vertex complexes of formulation {2,3,1-*closo*-M_2SB_9} are not without precedent (*cf* Table 3), and the observation of B(7) substitution by a nucleophile is a common feature. The conversion of **7** to **8** has been demonstrated [25] by treatment of the former with I_2 at 250°C, in contrast to our (tentative) observation of the facile conversion of **3a** to **3b** during work-up under ambient laboratory conditions. In general, however, both substituted and non-substituted species have previously been isolated from the same reaction mixtures, and the two above observations tend to suggest that the *closo*-12-vertex Rh_2SB_9 polyhedron may be formed *prior to* B(7) substitution.

The anionic 1-carba- relative (**12**) [28] of **7** and (tentatively) the 1-selena- analogue (**13**) [29] of **7** have also been reported, although in the latter compound relative positions of vertices were not established; compound(s) **14**, 1-phenyl-1-phospha- relative(s) of compound **6** have also been identified [30]. An isomer of compound **7**, in which the cluster was proposed to have a 2,4,1-Co_2SB_9 architecture, has also been described [32]. We have formed **3** and **4** in a mild reaction at ambient conditions, whereas such compounds have previously been reported largely from reactions at elevated temperature or under 'metal vapour synthesis' conditions. Moreover, we note that the present compounds are, to our knowledge, the first examples of such dirhodathiaboranes where both metal vertices are formally in the +2 oxidation state. {The Rh(2)—C(1)—Rh(3) angles [82.9(3)° in **3a/b** and 81.11(11)° in **4**] and the μ-(CO) stretching frequencies (ca 1863 and 1880 cm^{-1}, respectively) identify the bridging carbonyl ligands as (CO) rather than $(CO)^{2-}$ [33].} Clearly the two unpaired electrons from the two isolated, formally Rh(II) fragments must in these compounds be paired in the cluster *molecular* orbital scheme: the easy observation of NMR spectra is consistent with diamagnetism.

We had anticipated that the reaction which led to the formation of compounds **2–4** might yield the species [8-CO-8-PPh_3-8,7-*nido*-$RhSB_9H_{10}$], an analogue of the 'non-Wadian' compound [8,8-$(PPh_3)_2$-8,7-*nido*-$RhSB_9H_{10}$] [23]. A novel Rh co-ordination environment (involving the phosphine-bound phenyl groups) has been proposed [8] to account for the failure of the latter rhodathiaborane to adopt the predicted [34] *closo* cluster geometry. However, if one PPh_3 ligand in the latter complex is replaced by CO the possibility of such co-ordination is severely limited, and the above (hypothetical) [*nido*-$(CO)(PPh_3)RhSB_9H_{10}$] complex would be required to 'close up'. It appears that such a scenario may be compromised by the need to accommodate an 'additional' (formerly bridging) H atom within the closed cluster, and the intermediate reacts by 'scavenging' a further metal vertex and appropriate ligands, with the ultimate result that the observed *closo*-12-vertex products are formed. In related systems where this 'additional' H atom has, in effect, been removed either by deprotonation [35], or by formal replacement of a $\{BH_2\}$ vertex by $\{B—PR_3\}$ [13], a *closo*-11-vertex {1,2-$RhSB_9$} cluster is obtained as expected. Perhaps surprisingly, we have thus far been unable significantly to alter the yields of compounds **3** and **4** by adjustment of reactant stoichiometry or reaction conditions.

As has already been noted, and Table 3 further suggests, compounds of this kind appear rather susceptible to nucleophilic substitution at that cluster boron atom [B(7)] which is adjacent to both metal vertices. There is considerable current interest [36] in the formation of *B*-substituted heteroboranes for a number of purposes. The ease of formation of compounds such as **3** and **4** leads us to consider them as candidates for further boron atom functionalisation: this work will be the subject of future contributions.

Acknowledgements—We thank the EPSRC for support (K.J.A., T.D.M.) and the Callery Chemical Company for a generous gift of decaborane. We acknowledge use of the EPSRC-funded Chemical Database Service at Daresbury.

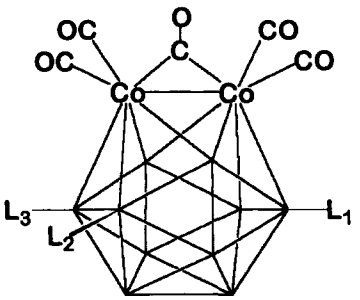

	L_1	L_2	L_3
15	Et_2S	Et_2S	H
16	Et_2S	H	Et_2S

REFERENCES

1. (a) Grimes, R. N., *Carboranes*, Academic Press, New York (1971); (b) Onak, T., in *Comprehensive Organometallic Chemistry*, Wilkinson, G., Stone, F. G. A. and Abel E., (eds), Pergamon Press, Elmsford, New York (1982). Volume I, Chapter 5.4, p. 543; (c) Bregadze, V. I., *Chem. Rev.*, 1992, **92**, 209; (d) Štíbr, B. *Chem. Rev.*, 1992, **92**, 225; (e) Onak, T., in *Comprehensive Organometallic Chemistry II*, Abel, E., Stone, F. G. A., and Wilkinson G., (eds-in-chief), Pergamon Press, Elmsford, New York (1995). Volume 1 (ed. C. E. Housecroft), Chapter 6, p. 217.
2. (a) Grimes, R. N., in ref. [1(b)], Chapter 5.5, p. 459; (b) Saxena, A. K. and Hosmane, N. S.,

Chem. Rev., 1993, **93,** 1081; (c) Grimes, R. N., in ref. 1(e), Chapter 9, p. 373.
3. (a) *Current Topics in the Chemistry of Boron*, ed. Kabalka, G. W., Royal Society of Chemistry, Cambridge and London, 1994; (b) *Advances in Boron Chemistry*, ed. Siebert, W., Royal Society of Chemistry, Cambridge and London, 1997; (c) Todd, L. J., in ref. [1(e)], Chapter 7, p. 257.
4. Jelínek, T., Kennedy, J. D. and Štíbr, B., *J. Chem. Soc., Chem. Commun.*, 1993, 1628.
5. Kang, S. O., Carroll, P. J. and Sneddon, L. G., *Organometallics*, 1988, **7,** 772.
6. Kang, S. O., and Sneddon, L. G., *Inorg. Chem.*, 1988, **27,** 3769.
7. Jelínek, T., Kennedy, J. D. and Štíbr, B., *J. Chem. Soc., Chem. Commun.*, 1994, 1415.
8. See, for example, Adams, K. J., McGrath, T. D. and Welch, A. J., *Acta Cryst.*, 1995, **C51,** 401.
9. Adams, K. J., McGrath, T. D., Rosair, G. M., Weller, A. S. and Welch, A. J., *J. Organomet. Chem.* (in press).
10. Rudolph, R. W., and Pretzer, W. R., *Inorg. Synth.*, 1983, **22,** 226.
11. McCleverty, J. A. and Wilkinson, G., *Inorg. Synth.*, 1966, **8,** 211.
12. McCleverty, J. A. and Wilkinson, G., *Inorg. Synth.*, 1966, **8,** 214.
13. Coughlan, S., Spalding, T. R., Ferguson, G., Gallagher, J. F., Lough, A. J., Fontaine, X. L. R., Kennedy, J. D. and Štíbr, B., *J. Chem. Soc., Dalton Trans.*, 1992, 2865.
14. Steele, D. F. and Stephenson, T. A., *J. Chem. Soc., Dalton Trans.*, 1972, 2161.
15. *CADABS*. Program for data reduction. Gould, R. O. and Smith, D. E., University of Edinburgh, (1986).
16. Walker, N. and Stuart, D., *Acta Cryst.*, 1983, **A39,** 158.
17. *SHELXTL-PC* version 4.2. G. M. Sheldrick. University of Göttingen, Germany. Seimens Analytical X-ray Instrumentation, Inc., Madison, Wisconsin, U.S.A. (1990).
18. Sheldrick, G. M., *SHELXS*-86. Program for crystal structure solution. University of Göttingen, Germany (1986).
19. Sheldrick, G. M., *SHELXL*-93. Program for crystal structure refinement. University of Göttingen, Germany (1993).
20. Flack, H. D., *Acta Cryst.*, 1983, **A39,** 876.
21. Sheldrick, G. M., *SHELX*-76. Program for crystal structure determination. University of Cambridge, UK (1976).
22. *The United Kingdom Chemical Database Service*. Fletcher, D. A., McMeeking, R. F. and Parkin, D. J., *J. Chem. Inf. Comput. Sci.*, 1996, **36,** 746.
23. Ferguson, G., Jennings, M. C., Lough, A. J., Coughlan, S., Spalding, T. R., Kennedy, J. D., Fontaine, X. L. R. and Štíbr, B., *J. Chem. Soc., Chem. Commun.*, 1990, 891.
24. Ferguson, G., Hawthorne, M. F., Kaitner, B. and Lalor, F. J., *Acta Cryst.*, 1984, **C40,** 1707.
25. Kang, S. O., Carroll, P. J. and Sneddon, L. G., *Inorg. Chem.*, 1989, **28,** 961.
26. Nestor, K., Fontaine, X. L. R., Greenwood, N. N., Kennedy, J. D. and Thornton-Pett, M., *J. Chem. Soc., Dalton Trans.*, 1991, 2657.
27. Bown, M., Fontaine, X. L. R., Greenwood, N. N. and Kennedy, J. D., *Z. Anorg. Allg. Chem.*, 1991, **602,** 17.
28. Šubrtová, V., Línek, A., Novák, C., Petrícek, V. and Jecný, J., *Acta. Cryst.*, 1977, **B33,** 3843.
29. Friesen, G. D., Barriola, A., Daluga, P., Ragatz, P., Huffman, J. C. and Todd, L. J., *Inorg. Chem.*, 1980, **19,** 458.
30. Bunkhall, S. R., Fontaine, X. L. R., Greenwood, N. N., Kennedy, J. D. and Thornton-Pett, M., *J. Chem. Soc., Dalton Trans.*, 1990, 73.
31. Schubert, D. M., Knobler, C. B., Wegner, P. A. and Hawthorne, M. F., *J. Am. Chem. Soc.*, 1988, **110,** 5219.
32. Plzák, Z., Plešek, J. and Štíbr, B., *J. Chromatogr.*, 1979, **168,** 280.
33. See, for example, Brown, M. P., Keith, A. N., Manojlovic-Muir, Lj., Muir, K. W., Puddephatt, R. J. and Sneddon, K. R., *Inorg. Chim. Acta*, 1979, **34,** L223.
34. Wade, K., *Adv. Inorg. Chem. Radiochem.*, 1976, **18,** 1.
35. Adams, K. J., McGrath, T. D., Thomas, Rh. Ll., Weller, A. S. and Welch, A. J., *J. Organomet. Chem.*, 1997, **527,** 283.
36. See, for example, Li, J. and Jones, M., Jr., *J. Am. Chem. Soc.*, 1992, **114,** 1094; Jang, W., Hartwell, D. E., Mortimer, M. D., Knobler, C. B. and Hawthorne, M. F., *Inorg. Chem.*, 1996, **35,** 4355; Mortimer, M. D., Knobler, C. B. and Hawthorne, M. F., *Inorg. Chem.*, 1996, **35,** 5750; Curtis, M. A., Sabat, M. and Grimes, R. N., *Inorg. Chem.*, 1996, **35,** 6703.

Pergamon

PII: S0277-5387(97)00285-4

Polyhedron Vol. 17, No. 2–3, pp. 351–355, 1998
© 1997 Elsevier Science Ltd
All rights reserved. Printed in Great Britain
0277-5387/98 $19.00+0.00

Synthesis and structure of (*P,P*-diphenylphosphino)methyl lithium-tetrahydrofuran

Dirk Steinborn,* Olaf Neumann, Horst Weichmann, Frank W. Heinemann and Jens-Peter Wagner

Institut für Anorganische Chemie der Martin-Luther-Universität Halle-Wittenberg, Kurt-Mothes-Str. 2, D-06120 Halle (Saale), Germany

(Received 30 April 1997; accepted 25 June, 1997)

Abstract—$Bu_3SnCH_2PPh_2$, prepared by reaction of Bu_3SnCH_2I with $NaPPh_2$ in liquid ammonia and by reaction of Bu_3SnCl with $LiCH_2PPh_2$/tmeda, reacts with BuLi in hexane as solvent in the presence of a small amount of THF to give $[\{Li(CH_2PPh_2)(thf)\}_\infty]$ (**4**). An X-ray structure analysis revealed that the (*P,P*-diphenylphosphino)methyl ligands are arranged in a μ_3-1:$2\kappa^2C$:$3\kappa P$ fashion. Thus, compound **4** exhibits a polymeric ladder-like structure in which six-membered $Li_2C_2P_2$ rings with a chair conformation and planar four-membered Li_2C_2 rings are arranged alternately. The interplanar angle between the Li_2C_2 rings and the planar Li_2C_2 units belonging to the neighbored six-membered rings amounts to 145.0(4)°. The Li—C bonds within the six-membered rings are shorter than those within the four-membered rings [2.21(1) *vs* 2.39(1) Å]. The distorted tetrahedral donor set of Li is made up by one phosphorus, one oxygen (tetrahydrofuran) and two methylene carbon atoms. © 1997 Elsevier Science Ltd

Keywords: phosphinomethyl lithium; functionalized methyl lithium compounds; tin–lithium transmetallation; crystal structure.

Structures of functionalized methyl lithium compounds of the type $LiCH_2YR_n$ with Lewis-basic heteroatoms Y are strongly dependent (i) on the nature of the heteroatom Y, (ii) on the type of the substituents R (alkyl, aryl) and (iii) on co-ligands which might be present. To date there have been found two common structural types: $[Li_2(CH_2SPh)_2(tmeda)_2]$ (**1a**) [1], $[Li_2(CH_2PMe_2)_2(tmeda)_2]$ (**2a**) [2], $[Li_2(CH_2PPhMe)_2(tmeda)_2]$ (**2b**) [2], $[Li_2(CH_2PPhMe)_2(sparteine)_2]$ (**2c**) [2], and $[Li_2(CH_2PPh_2)_2(tmeda)_2]$ (**2d**) [3] crystallize as dimers with six-membered rings $[Li_2C_2Y_2]$ in which the heteroatom Y is coordinated to lithium (type **A**). $[Li_2(CH_2SMe)_2(tmeda)_2]$ (**1b**) [1], $[Li_2(CH_2SPh)_2(thf)_4]$ (**1c**) [4], and $[Li_2(CH_2NPh_2)_2(thf)_3]$ (**3a**) [5] are dimeric complexes with four-membered rings $[Li_2C_2]$ in which the heteroatom is not coordinated to lithium (type **B**). $[\{Li(CH_2SMe)(thf)\}_\infty]$ (**1d**) [4] is the only example where the six-membered $Li_2C_2Y_2$ and the four-membered Li_2C_2 rings are arranged alternately giving a polymeric ladder-like structure. Furthermore, there is one example of a tetrameric structure, namely $[Li_4(CH_2NC_5H_{10})_4(thf)_2]$ (**3b**) [5].

Comparing **1a** with **1c** and **1b** with **1d**, it can be seen that the structures are strongly influenced by co-ligands. As far as structures of (phosphino)methyl lithium complexes are concerned, there have been reported only those with chelating N,N donors as co-ligands (**2a–d**). Thus, we were interested to synthesize the (*P,P*-diphenylphosphino)methyl lithium tetrahydrofuran adduct and to determine its structure. Of special interest is a comparison of the title compound with the special features observed in the structure of the corresponding amino derivative **3a** having a three

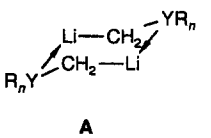

A

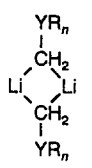

B

* Author to whom correspondence should be addressed.

coordinated lithium and an approximately planar environment of nitrogen [5].

RESULTS AND DISCUSSION

$Bu_3SnCH_2PPh_2$(Bu = *n*Bu) was prepared (i) by reaction of Bu_3SnCH_2I with $NaPPh_2$ in liquid ammonia and (ii) by reaction of Bu_3SnCl with $LiCH_2PPh_2$/tmeda, *cf.* Scheme 1.

The identity of $Bu_3SnCH_2PPh_2$ was established by microanalysis, NMR (^1H, ^{13}C, ^{31}P, ^{119}Sn) and mass spectroscopy. $Bu_3SnCH_2PPh_2$ react with BuLi in hexane as solvent in the presence of a small amount (*ca* 4 vol-%) of THF to give $[\{Li(CH_2PPh_2)(thf)\}_\infty]$ (**4**) as pale yellow precipitate [eq. (2)]. Without being added THF, the transmetallation reaction proceeds, too, but $LiCH_2PPh_2$ remains in solution.

Complex **4** is very sensitive to air and moisture. It is highly soluble in THF, sparingly soluble in ether and benzene and unsoluble in aliphatic hydrocarbons. **4** starts to decompose at 150°C and its identity was established by NMR spectroscopy. The methylene carbon and hydrogen atoms resonate at relatively high field [$\delta(^{13}C) = 2.0$ ppm, $\delta(^1H) = -0.39$ ppm] and exhibit typical coupling to phosphorus [$^1J(^{31}P,^{13}C) = 46.2$ Hz, $^2J(^{31}P,^1H) = 3.5$ Hz]. These values are the same as those of the TMEDA adduct **2d** [$\delta(^{13}C) = 2.2$ ppm, $\delta(^1H) = -0.37$ ppm, $^1J(^{31}P,^{13}C) = 46.2$ Hz, $^2J(^{31}P,^1H) = 3.4$ Hz] [3b]. The ^{31}P chemical shift amounts to 8.1 ppm. The corresponding value for **2d** is −1.9 ppm [3b].

The recrystallization of **4** from pentane/THF affords crystals suitable for X-ray investigations. A drawing of the solid state structure of complex **4** giving the atom numbering scheme is shown in Fig. 1. Selected bond lengths and bond angles are listed in Table 1. Compound **4** exhibits a polymeric structure in which six-membered $Li_2C_2P_2$ rings and planar four-membered Li_2C_2 rings are arranged alternately. Thus, the coordination of the organo ligands has to be designated as μ_3-(*P*,*P*-diphenylphosphino)methyl-$1{:}2\kappa^2C{:}3\kappa P$. The midpoints of the four- and six-membered rings are crystallographically imposed inversion centers. $[\{Li(CH_2SMe)(thf)\}_\infty]$ (**1d**) exhibits an analogous structure [4].

The Li—C distances in the six-membered $Li_2C_2P_2$ rings [Li(1)—C(1) 2.21(1) Å] are a little bit longer than those in the dimeric TMEDA complexes **2** [2.12(1)–2.174(4) Å], see Table 2. The distances between neighbored lithium and phosphorus [Li(1)—P(1′) 2.70(1) Å] correspond to those in the TMEDA adduct **2d** [2.686(5) Å] and in the other complexes **2a–2c** (*cf.* Table 2). In $[\{Li[o,o'\text{-}(Me_2PCH_2)_2C_6H_3]\}_2]$, a *P*-functionalized phenyllithium complex with a five membered Li—C—C—C—P ring, the Li—P distances range from 2.513(4) to 2.668(3)° [6].

As in the complexes **2a–2d,** the P—CH_2 distance [P(1)—C(1) 1.774(7) Å] is substantially shorter than the P—C_{Ph} distances [P(1)—C(2) 1.856(6) Å, P(1)—C(8) 1.861(6) Å] in spite of the smaller covalent radii of sp^2 hybridized carbons in comparison with sp^3 hybridized ones [7]. It seems likely that this in part arises from a stabilizing influence of phosphorus by polarization.

The torsion angles (absolute values) of the six-membered ring [P(1)—C(1)—Li(1)—P(1′) 54.58(5)°, C(1)—Li(1)—P(1′)—C(1′) 63.34(6)°, Li(1)—C(1)—P(1)—Li(1′) 57.63(5)°] indicate some deviations from the 'ideal' chair conformation (60°). A chair conformation was found in the dimeric TMEDA adducts **2a** and **2d,** whereas the phenylmethyl derivatives **2b** and **2c** exhibit six-membered rings with a boat conformation. The 'through space' Li(1)···P(1) distance within the six-membered rings of **4** amounts to 3.10(1) Å indicating a more compact ring structure than those of all other derivatives **2a–d** (3.16–3.45 Å), see Table 2.

The six-membered rings $Li_2C_2P_2$ are connected *via* Li—C bonds that form four-membered rings Li_2C_2. These Li—C bonds [Li(1)—C(1′) 2.39(1) Å] are much longer than those within the $Li_2C_2P_2$ rings [Li(1)—C(1) 2.21(1) Å]. They are also longer than those in other organo lithium compounds with Li_2C_2 rings (average: 2.29 Å for sp^3-hybridized carbon atoms [8]). The torsion angles P(1)—C(1)—Li(1)—C(1′) 177.6(5)° and P(1′)—Li(1)—C(1)—Li(1′) 123.0(6)° reveal that two of the four phosphorus atoms which are neighbored to the four-membered Li_2C_2 rings are lying in the planes of these rings.

The interplanar angle between the planar Li_2C_2 rings and the planar Li_2C_2 units that are parts of the neighboring six-membered rings amounts to 145.0(4)°. Thus, a ladder-like structure is obtained. The comparison with the corresponding angle in **1c** (114.7°) [4] reveals that the 'ladder' of structure **4** is more flat than those of **1c**.

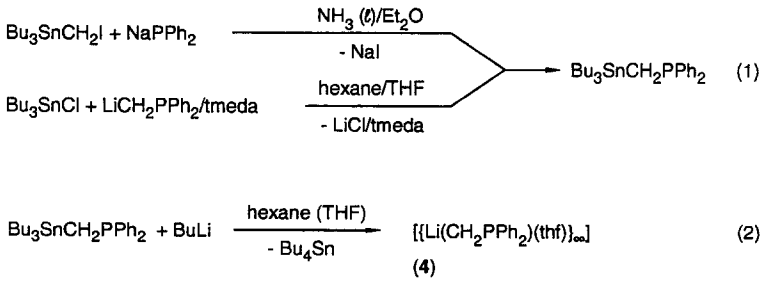

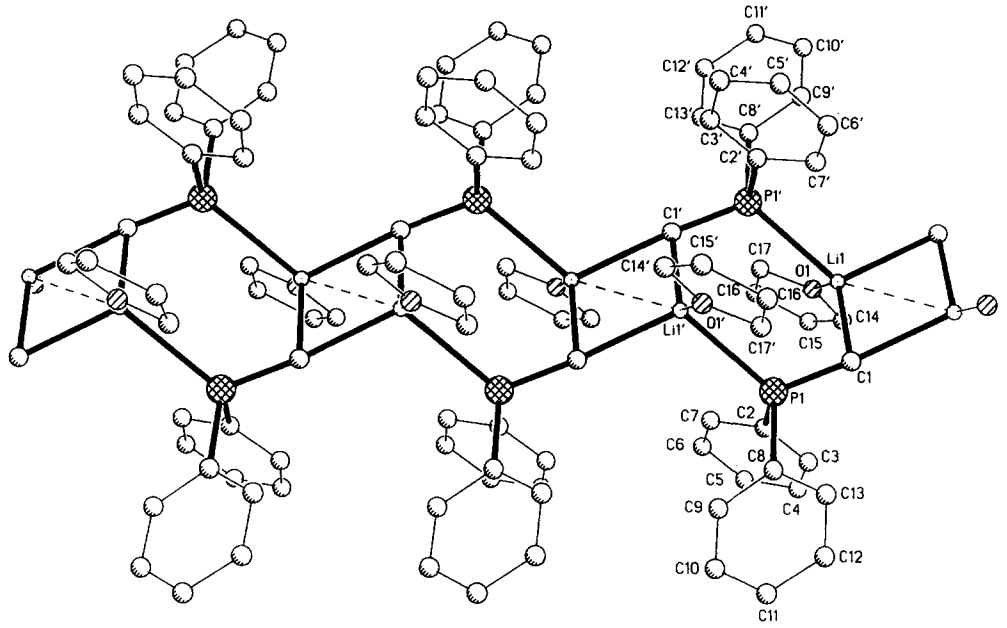

Fig. 1. Drawing of the structure of $[\{Li(CH_2PPh_2)(thf)\}_\infty]$ (**4**). Hydrogen atoms are omitted for clarity.

Table 1. Selected bond lengths (Å) and angles (°) for **4**

P(1)—C(1)	1.774(7)	P(1)—C(2)	1.856(6)
P(1)—C(8)	1.861(6)	Li(1)—C(1)	2.21(1)
Li(1)—C(1')(#2)[a]	2.39(1)	O(1)—Li(1)	2.01(1)
P(1)—Li(1')(#1)	2.70(1)	P(1)—Li(1)[b]	3.10(1)
Li(1)—Li(1)(#2)	2.80(2)		
C(1)—P(1)—C(2)	104.5(3)	C(1)—P(1)—C(8)	109.9(3)
C(2)—P(1)—C(8)	95.5(3)	C(1)—P(1)—Li(1')(#1)	116.7(3)
C(2)—P(1)—Li(1')(#1)	116.4(3)	C(8)—P(1)—Li(1')(#1)	111.7(3)
C(1)—P(1)—Li(1)	44.3(3)	O(1)—Li(1)—P(1')(#1)	97.4(5)
C(1)—Li(1)—P(1')(#1)	112.2(5)	C(1')(#2)—Li(1)—P(1')(#1)	112.8(5)
C(1)—Li(1)—C(1')(#2)	105.2(5)	O(1)—Li(1)—C(1)	126.2(6)
O(1)—Li(1)—C(1')(#2)	102.8(5)	C(1)—Li(1)—P(1)	34.1(2)
O(1)—Li(1)—P(1)	106.7(5)	P(1')(#1)—Li(1)—P(1)	90.7(3)
P(1)—C(1)—Li(1)	101.6(4)	P(1)—C(1)—Li(1')(#2)	175.7(5)
Li(1)—C(1)—Li(1')(#2)	74.8(5)	C(17)—O(1)—Li(1)	125.3(6)
C(14)—O(1)—Li(1)	127.2(6)		

[a] Symmetry transformations used to generate equivalent atoms: #1: $-x, -y+2, -z+1$; #2: $-x+1, -y+2, -z+1$.
[b] 'Through space' distance.

The coordination sphere of lithium is completed by tetrahydrofuran. Thus, the coordination of Li is distorted tetrahedrally provided the Li(1)···P(1) contacts are not considered.

In a marked contrast to **4**, the benzyl substituted complex $[Li(CHPhPPh_2 \times (OEt_2)_2]$ adopts a monomeric solid state structure [9] demonstrating the great variability of structures of $LiCH_2PPh_2$ in dependence not only on co-ligands but also on substituents of the methylene carbon.

In the same way as for **4**, (*P,P*-phenylmethylphosphino)methyl lithium, $LiCH_2PPhMe$, could be prepared in 50% yield from the reaction of Bu_3SnCH_2PPhMe with BuLi in *n*-hexane as solvent. To date such transmetallation reactions have been used to prepare other compounds $LiCH_2YR_n$ with nitrogen ($YR_n = NR_2$) [5,10,11,12] oxygen ($YR_n = OR$) [10,13] and sulfur ($YR_n = SR$) [4,10] as Lewis-basic heteroatoms Y but not with phosphorus. The phosphinomethyl lithium compounds are obtained with a high purity free of N,N chelating ligands *via* this transmetallation reaction that seems to be superior to the metallation of methylphosphines with BuLi/tmeda [2,3,14,15] or 'BuLi [16,17,18,19]

Table 2. Selected bond lengths (Å) and angles (°) in complexes $[Li_2(CH_2PRR')_2(L)_2]$ with six-membered rings $[Li_2C_2P_2]$

R/R′ L	Ph/Ph thf (**4**)[a]	Ph/Ph tmeda (**2d**) [3]	Me/Me tmeda (**2a**) [2]	Ph/Me tmeda (**2b**) [2]	Ph/Me sparteine (**2c**) [2]
Ring conformation	chair	chair	chair	boat	boat
Li—CH_2	2.21(1)	2.174(6)	2.150(8)/2.141(6)	2.15(1)/2.12(1)	2.21(3)/2.18(3)
P—CH_2	1.774(7)	1.752(3)	1.751(3)/1.754(5)	1.730(8)/1.755(7)	1.77(1)/1.78(1)
P—CRR′	1.856(6)/1.861(6)	1.836(3)/1.872(3)	1.825(5)–1.853(5)	1.836(8)–1.857(9)	1.83(1)–1.87(2)
Li—P	2.70(1)	2.686(5)	2.593(7)/2.615(6)	2.67(1)/2.61(1)	2.74(2)/2.70(2)
Li···P[b]	3.10(1)	3.28[c]	3.23/3.26	3.16/3.17	3.32/3.45

[a] This work.
[b] 'Through space' distance.
[c] Calculated with data given in lit. [3c].

where dimetallation might occur [14,18] and the separation from the starting phosphine might be difficult [17].

EXPERIMENTAL

General comments

All reactions and manipulations were carried out under purified argon using standard Schlenk techniques. *n*-Hexane, *n*-pentane and THF-d_8 were dried with $LiAlH_4$. THF and diethyl ether were distilled from sodium benzophenone ketyl. NMR spectra were recorded on Varian Gemini 300 or Varian Unity 500 NMR spectrometers using the protio impurities and the ^{13}C resonances of the deuterated solvents as references for ^1H and ^{13}C NMR spectroscopy, respectively. The chemical shift $\delta(^7Li)$ is reported relative to a solution of LiCl in THF-d_8 (external). Microanalyses (C, H) were obtained from the microanalytical laboratory of the Department of Chemistry.

Synthesis of $Bu_3SnCH_2PPh_2$

(*i*). To $NaPPh_2$ (0.1 mol) in liquid ammonia (300 cm^3) and diethyl ether (50 cm^3) [prepared from PPh_3 (26.2 g, 0.1 mol) and Na (4.6 g, 0.2 mol) [20]], Bu_3SnCH_2I [21] (43.1 g, 0.1 mol) in diethyl ether (50 cm^3) was added dropwise at −50°C. After evaporating ammonia and removing the solvents *in vacuo* 300–400 cm^3 diethyl ether were added. The precipitate (NaI) was filtered off, the solvents were distilled off *in vacuo* and the residue was fractionated (b.p. 165–174°C at 0.01 torr). Yield 21.3 g (45%).

(*ii*). To $LiCH_2PPh_2$/tmeda (0.25 mol) in hexane (250 cm^3) [prepared by metallation of PPh_2Me (50.0 g, 0.25 mol) with BuLi/tmeda (0.25 mol, 1.6 M in hexane) [14, 22]] Bu_3SnCl (80.6 g, 0.25 mol) in THF (200 cm^3) was added dropwise at 0°C. After stirring for 2 h at room temperature, water (250 cm^3) was added at 0°C. The reaction mixture was neutralized with an aqueous solution of NH_4Cl. The separated aqueous layer was washed twice with ether and the combined organic layers were dried (Na_2SO_4). The solvents were distilled off and the residue was fractionated (b.p. 170–180°C at 0.01 torr). Yield 71.0 g (60%). Anal. Calcd: C, 61.42; H, 8.03. Found: C, 62.08; H, 7.90. ^1H NMR (500 MHz, $CDCl_3$): δ 0.8 (t, 6H, $CH_3CH_2CH_2CH_2$), 1.40–1.46 (m, 6H, $CH_3CH_2CH_2CH_2CH_2$), 1.31 (se, 6H, $CH_3CH_2CH_2CH_2$), 0.93 (t, 9H, $CH_3CH_2CH_2CH_2$), 1.49 (s, 2H, CH_2P), 7.52 (m, 4H, *o*-H), 7.28–7.38 (m, 6H, *m*, *p*-H). ^{13}C NMR (125 MHz, $CDCl_3$): δ 9.91 [dd, $^1J(^{119}Sn,C)$ = 325.1 Hz, $^3J(P,C)$ = 4.0 Hz, $CH_3CH_2CH_2CH_2$], 28.9 [d, $^2J(^{119}Sn,C)$ = 20.0 Hz, $CH_3CH_2CH_2CH_2$], 27.2 [d, $^3J(^{119}Sn,C)$ = 58.8 Hz, $CH_3CH_2CH_2CH_2$], 13.6 (s, $CH_3CH_2CH_2CH_2$), 5.2 [dd, $^1J(^{119}Sn,C)$ = 209.4 Hz, $^1J(P,C)$ = 33.8 Hz, CH_2P], 142.5 [dd, $^3J(^{119}Sn,C)$ = 23.8 Hz, $^1J(P,C)$ = 14.9 Hz, *i*-C], 132.2 [d, $^2J(P,C)$ = 19.0 Hz, *o*-C], 128.08 (s, *m*-C), 128.13 (s, *p*-C). ^{31}P NMR (32 MHz, $CDCl_3$): δ −17.6 [s+d, $^2J(^{119}Sn,P)$ = 76.0 Hz]. ^{119}Sn NMR (30 MHz, $CDCl_3$): δ −10.2 [d, $^2J(^{119}Sn, P)$ = 77.2 Hz]. MS (70 eV, EI): *m/e* 434 (12%, $Bu_2SnCH_2PPh_2+H$), 377 (4%, $BuSnCH_2PPh_2+H$), 321 (75%, $SnCH_2PPh_2+2H$), 255 (11%, BuSnPh+H), 197 (49%, SnPh), 177 (20%, BuSn), 121 (100%, CH_2PPh-H), 120 (17%, Sn), 77 (13%, Ph).

Synthesis of $[\{Li(CH_2PPh_2)(thf)\}_\infty]$ (**4**)

To $Bu_3SnCH_2PPh_2$ (20.0 g, 42 mmol) in hexane (100 cm^3) and THF (4 cm^3) a solution of BuLi in hexane (50 mmol, 1.5 M) was added dropwise at 0°C. After stirring for 30 min at room temperature the precipitate was filtered off, washed with hexane (2 × 30 cm^3) and dried *in vacuo*. Yield 10.8 g (92%). ^1H NMR (200 MHz, THF-d_8): δ −0.39 [d, 2H, CH_2; $^2J(P,H)$ = 3.5 Hz], 6.83–6.95 (m, 2H, *p*-H), 6.96–7.04 (m, 4H, *m*-H), 7.41–7.49 (m, 4H, *o*-H). ^{13}C NMR (50 MHz, THF-d_8): δ 2.0 [d, CH_2; $^1J(P,C)$ = 46.2 Hz], 125.0 (s, *p*-C), 127.1 [d, *m*-C, $^3J(P,C)$ = 4.6 Hz], 132.3

[d, *o*-C, ^2J(P,C) = 17.0 Hz], 155.3 [d, *i*-C, ^1J(P,C) = 23.9 Hz]. ^{31}P NMR (81 MHz, THF-d_8): δ 8.13 (s). ^{7}Li NMR (194 MHz, THF-d_8): δ 0.52 (s). (Due to partial hydrolysis a small amount of PPh_2Me was detected in the spectra.)

X-ray structure determination of **4**

A suitable single crystal ($0.24 \times 0.16 \times 0.08$ mm^3) was obtained from pentane/THF solution at -35°C. X-ray measurement was performed on a Stoe STADI 4 diffractometer with Mo-K_α radiation ($\lambda = 0.71073$ Å, graphite monochromator) at 210(2) K. Due to the very weak diffracting power of the small crystal used data were collected only up to $2\theta = 40.0$°. The structure was solved by direct methods with SHELXS86 [23] and refined using full-matrix least-squares procedures on F^2 (SHELXL93) [24]. Non-hydrogen atoms were refined with anisotropic thermal parameters. The hydrogen atoms were geometrically positioned with fixed isotropic displacement parameters being 1.2 times the values of the equivalent isotropic displacement parameters of the carrying carbon atoms. Crystal data, details of data collection, structure solution and refinement are summarized in Table 3. Complete tables of the atomic coordinates, H atom parameters, bond distances, bond angles and anisotropic thermal parameters have been deposited with the Editor as supplementary material.

Table 3. Crystal data and structure refinement for **4**

Empirical formula	$C_{17}H_{20}LiOP$
Fw	278.24
Crystal system	monoclinic
Space group	$P2_1/n$
a, *b*, *c* (Å)	5.824(1), 17.001(3), 15.736(3)
α, β, γ (°)	90, 95.71(3), 90
V (Å^3)	1550.4(5)
Z	4
D_{calcd} (g cm^{-3})	1.192
μ(Mo-K_α) (mm^{-1})	0.168
F(000)	592
Scan range (°)	$1.77 < \theta < 20.00$
Index ranges	$-5 \leqslant h \leqslant 5$, $-16 \leqslant k \leqslant 16$, $-15 \leqslant l \leqslant 15$
Reflections collected	2901
Independent reflections	1460 ($R_{int} = 0.1118$)
Observed reflections [$I > 2\sigma(I)$]	716
Parameters refined	187
Goodness-of-fit on F^2	1.004
Weighting scheme	$w = 1/[\sigma^2(F_0^2) + (0.0343P)^2]$ $P = (F_0^2 + 2F_c^2)/3$
Final *R* indices [$I > 2\sigma(I)$]	$R1 = 0.0565$, $wR2 = 0.0857$
R indices (all data)	$R1 = 0.1675$, $wR2 = 0.1148$
Largest diff. peak and hole (e Å^{-3})	0.213 and -0.212

Acknowledgment—We are grateful to Deutsche Forschungsgemeinschaft and Fonds der Chemischen Industrie for financial support.

REFERENCES

1. Amstutz, R., Laube, T., Schweizer, W. B., Seebach, D. and Dunitz, J. D., *Helv. Chim. Acta*, 1984, **67,** 224.
2. Byrne, L. T., Engelhardt, L. M., Jacobsen, G. E., Leung, W.-P., Papasergio, R. I., Raston, C. L., Skelton, B. W., Twiss, P. and White, A. H., *J. Chem. Soc., Dalton Trans.*, 1989, **105.**
3. (a) Blaurock, S., Kühl, O. and Hey-Hawkins, E., *Organometallics*, 1997, **16,** 807; (b) Fraenkel, G., Winchester, W. R. and Williard, P. G., *Organometallics*, 1989, **8,** 2308; (c) Cambridge Structural Database (CSD), Cambridge Crystallographic Centre, University Chemical Laboratory, Cambridge, England.
4. Becke, F., Heinemann, F. W. and Steinborn, D., *Organometallics*, 1997, **16,** 2736.
5. Becke, F., Steinborn, D., Heinemann, F. W., Rüffer, T., Wiegeleben, P., Boese, R. and Bläser, D., *J. Organomet. Chem.*, submitted.
6. Pape, A., Lutz, M. and Müller, G., *Angew. Chem.*, 1994, **106,** 2375.
7. Huheey, J. E., Keiter, E. A. and Keiter, R. L., *Inorganic Chemistry, Principles of Structure and Reactivity*, 4th ed.; Harper Collins College Publ., New York (1993).
8. Setzer, W. N. and v. Ragué Schleyer, P., *Adv. Organomet. Chem.*, 1985, **24,** 353.
9. Decken, A. and Cowley, A. H., *J. Organomet. Chem.*, 1996, **509,** 135.
10. Peterson, D. J., *Organomet. Chem. Rev. A*, 1972, **7,** 295.
11. Peterson, D. J., *J. Am. Chem. Soc.*, 1971, **93,** 4027.
12. Steinborn, D., Becke, F. and Boese, R., *Inorg. Chem.*, 1995, **34,** 2625.
13. Schöllkopf, U. in E. Müller (ed.), *Methoden der Organischen Chemie* (*Houben-Weyl*), Vol. XIII/1, p. 87. Thieme Verlag, Stuttgart (1970).
14. Peterson, D. J., *J. Organomet. Chem.*, 1967, **8,** 199.
15. Rausch, M. D. and Ciappenelli, D. J., *J. Organomet. Chem.*, 1967, **10,** 127.
16. Peterson, D. J. and Hays, H. R., *Organomet. Chem. Rev. A*, 1965, **30,** 1939.
17. Karsch, H. H. and Schmidbaur, H., *Z. Naturforsch.*, 1977, **32b,** 762.
18. Peterson, D. J. and Collins, J. H., *Organomet. Chem. Rev. A*, 1966, **31,** 2373.
19. Karsch, H. H., *Z. Naturforsch.*, 1979, **34b,** 1178.
20. Gee, W., Shaw, R. A. and Smith, B. C., *Inorg. Synthesis*, 1967, **9,** 19.
21. Seyferth, D. and Andrews, S. B., *J. Organomet. Chem.*, 1971, **30,** 151.
22. Schore, N. E., Benner, L. S. and LaBelle, B. E., *Inorg. Chem.*, 1981, **20,** 3200.
23. Sheldrick, G. M., SHELXS-86, *Program for the Solution of Crystal Structures*, University of Göttingen, Germany, 1986; Sheldrick, G. M., *Acta Cryst. Sect. A*, 1990, **46,** 467.
24. Sheldrick, G. M., *SHELXL-93, Program for the Refinement of Crystal Structures*, University of Göttingen, Germany, 1993.

Pergamon

PII: S0277-5387(97)00274-X

Polyhedron Vol. 17, No. 2–3, pp. 357–366, 1998
© 1997 Elsevier Science Ltd
All rights reserved. Printed in Great Britain
0277–5387/98 $19.00+0.00

Electrochemical characterization of a series of substituted Dawson type tungstophosphates $\alpha[P_2W_{18-x}Mo_zV_yO_{62}]^{n-}$ $(x = y+z; n = 6+y)$

J. B. Tommasino,[a]* R. Contant,[b] J. P. Michaut[c] and J. Roncin[c]

[a] Laboratoire de Chimie Analytique, LICAS, EA1890, Université de Lyon I, ESCPE bat 308, 43 Bd du 11 Novembre 1918, 69622 Villeurbanne Cedex, France

[b] Laboratoire de Chimie des Métaux de Transition, URA 419 CNRS, Université de Paris VI, 4 Place Jussieu, 75252 Paris cedex 05, France

[c] Laboratoire de Physico-Chimie des Rayonnements, URA 75, CNRS, Université de Paris XI, Bat 330, 91 405 Orsay Cedex, France

(Received 7 April 1997; accepted 23 June 1997)

Abstract—The electrochemical study of heteropolyanions $\alpha[P_2W_{18-x}Mo_zV_yO_{62}]^{n-}$ $(x = y+z; n = 6+y)$ have been performed in various acidic media. The analysis of the voltammograms of monosubstituted compounds is described and the reduction sites are identified. These observations are extended to the polysubstituted compounds. The electrochemical results are correlated with an ESR study performed at room temperature: the ESR spectra indicate that the unpaired electron is localised around Mo or V atoms in the monosubstituted compounds. In the other compounds, ESR spectra show that electron delocalization occurs when the paramagnetic Mo^{V} ion is surrounded by other Mo^{VI} ions. The number of atoms of Mo or V substituted and their position are discussed versus their redox properties. © 1997 Elsevier Science Ltd

Keywords: molybdotungstophosphates; vanadotungstophosphates; Dawson structure; cyclic voltammetry; ESR; electrochemistry.

The very high number of papers reporting on the heteropolyanions (HPa) is certainly due, on the one hand, to the interesting properties that these compounds exhibit in heterogeneous and homogeneous catalysis [1–3], but also, on the other hand, to the fact that their synthesis is quite recent [4–9]. Concerning their catalytic activities, the position, the nature and the number of substituted atoms can play a very important part. Indeed, according to compounds used in a reaction, several questions appear: which is the determining step in the reaction and what is the function of substituted atoms of Mo or V in the catalytic properties? What is the importance of the localisation or the delocalisation of the electron in one electron reduced species?

Many works on this last subject have been described [10–15], in particular for the Keggin structure. ESR studies show that the single electron added on the monosubstituted compounds is trapped in the site occupied by the substituted metals Mo or V [12–13]. Moreover, Nadjo and co-workers have studied various aspects of their electrochemical properties [16–21]. From this point of view, we amplify here our knowledge on a new series of molybdo and vanadotungstophosphate $\alpha[P_2W_{18-x}Mo_zV_yO_{62}]^{n-}$ $(x = y+z; n = 6+y)$ with the Dawson structure. The synthesis of this series of compounds with a good purity is recent and only few electrochemical studies are related [4,9]. For clarity, we have represented in Fig. 1 the idealized structure for $\alpha[P_2W_{18}O_{62}]^{6-}$ and its substitution derivatives. The structures have three edges shared MO_6 octahedra in polar position and 12 shared MO_6 octahedra in equatorial position (M = W, Mo or V). The grey MO_6 group contains a central Mo atom substituted whereas the black MO_6 groups enclose a central V atom.

We attempted in this work to correlate the structure of the mixed heteropolyanion compounds with their redox properties. We report in this paper the elec-

* Author to whom correspondence should be addressed.

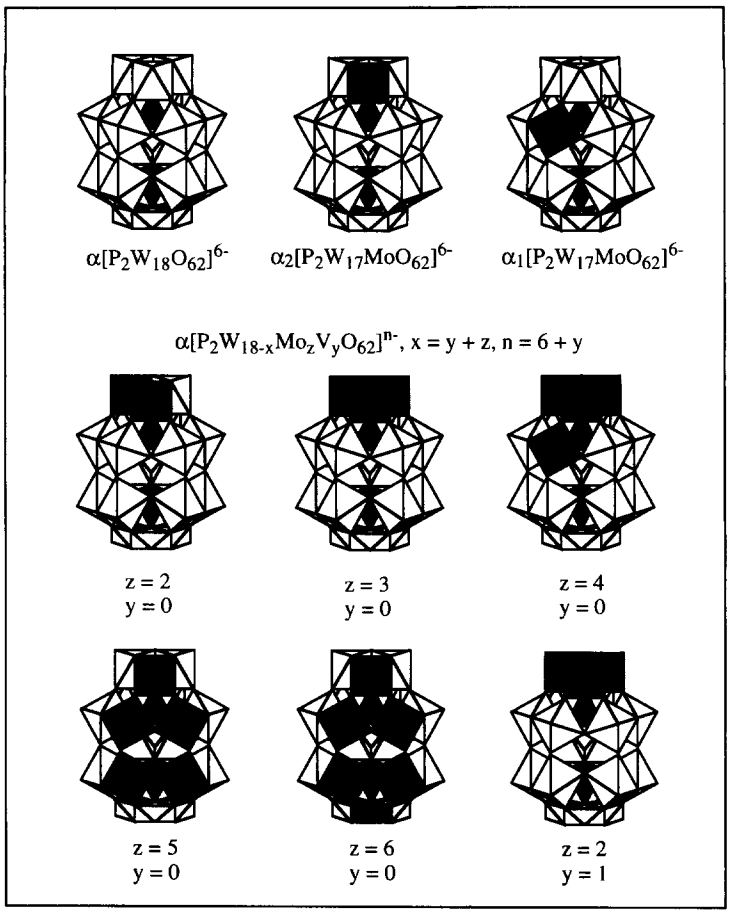

Fig. 1. Structure of $\alpha[P_2W_{18-x}Mo_zV_yO_{62}]^{n-}$ $(x = y+z; n = 6+y)$.

trochemical behavior of a series of molybdo-vanadotungstophosphate compounds $\alpha[P_2W_{18-x}Mo_zV_yO_{62}]^{n-}$ $(x = y+z; n = 6+y)$ in acidic solution. The influence of pH is described. An ESR study on the one- and two-electron-reduced compounds is also reported. The number of atoms of Mo or V substituted and their position are discussed versus their redox properties.

EXPERIMENTAL

Solution

Heteropoly-compounds were prepared by R. Contant laboratory [4,5,7]. Pure water was used throughout. It was obtained by de-ionisation and subsequent passing through a Millipore Q water purification set. The chloridic acid was used by dilution of a commercial solution (Prolabo, Titrinorm).

UV-visible

UV-vis spectroscopic measurements were conducted with a Perkin–Elmer spectrophotometer (1 or 2 mm cells were used).

ESR measurements

All the measurements were performed at room temperature using a 2000 Bruker ESR spectrometer equipped with an NMR gaussmeter and a 5340 A Hewlett-Packard frequency counter.

Electrochemical measurements

Cyclic voltammograms were obtained with a homemade potentiostat equipped with EGG Model 175 pilot. Data were recorded on a X-Y Sefram TGM 164. The cell used has a single compartment with a standard three-electrode configuration. The reference electrode consisted of a saturated calomel electrode (SCE) for aqueous media The counter electrode was a platinum wire. The working electrode was a glassy carbon (GC) disc (Carbone Lorraine). For each new electrode, the polishing procedure, using diamond paste (DP Diamond-Struers) of decreasing grain size, was as follows: 15 min polishing with a grain size of 6 μm, then 15 min with 3 μm grain size and finally, 30 min with 1 μm grain size. Before each experiment, the electrode was polished to a mirror finish according to

this procedure. The solutions were degassed with argon U and kept under this gas during the experiments. In HCl 2.2 N, two electrochemical studies have been carried out in the same solutions containing HPa. A first electrochemical analysis is performed on the solution recently prepared. These solutions have been kept out of light for one month. The cyclic voltammetry after one month carried out on these solutions presented a similar pattern which proves a surprising stability of these compounds at pH < 1.

We note that the peak potential E_p may be affected by uncompensated solution resistance. In our experimental conditions (cell, HCl 2.2 N, 20 mV/s), the uncompensated resistance has been estimated by the interrupt method [22(a)]: $R < 30\ \Omega$. In fact, with the peak intensity I_p measured, the iR drop is very weak and it has no influence on the value of peak potential (for instance, when $I_p = 20\ \mu A$ and $R = 30\ \Omega$, the iR drop is less than 1 mV).

Preparation of one-electron reduced species

Experimental conditions given in Table 3 have been carried out, in particular for $\alpha[P_2W_{18-x}Mo_xO_{62}]^{7-}$ with $x = 2$, 3 and 4, in order to obtain an efficient separation from the bielectronic wave to two monoelectronic waves, also allowing the preparation of one-electron-reduced species. For $\alpha[P_2W_{14}Mo_4O_{62}]^{6-}$, the voltammogram in these conditions (Table 3) shows a shoulder for the first monoelectronic wave and the value of imposed potential for electrolysis has been chosen on the voltammogram right at the start of the first reduction.

Electrochemical behaviour of $\alpha[P_2W_{18-x}Mo_xO_{62}]^{6-}$ *with* $x = 2$ *to* 6 *in* HCl 2.2 N

The voltammogram in HCl 2.2 N of $\alpha[P_2W_{16}Mo_2O_{62}]^{6-}$ shows two reduction peaks close to each other at $E_{p_1} \approx 0.230$ V (small shoulder) and $E_p = 0.155$ (Table 2, Fig. 4 presents only the cyclic voltammetry of these HPa described here in HCl 1 N and 6 N for more clarity). These two processes present the pattern of the reversible system when the potential scan rate changes between 10 and 200 mV/s. UV-visible spectroscopy is characterized by two absorption bands at 204 nm and 290 nm (shoulder). The exhaustive electrolysis of the solution at constant potential on the second wave ($E_i = 0.05$ V/SCE) confirms a two-electron reduction (Table 2) corresponding to two closely separated one-electron steps described in cyclic voltammetry: the initial yellow solution leads to a blue solution characteristic of the reduced form.

In the same conditions, the voltammogram of $\alpha[P_2W_{15}Mo_3O_{62}]^{6-}$ shows a reversible two-electron step at $E_{p_1} = 0.220$ V followed by a reversible one-electron step at $E_{p_2} = -0.06$ V (Table 2, the peak ratio for these two processes is equal to 1). The exhaustive electrolysis at constant potential on the second wave ($E_i = -0.100$ V) gives three electrons per mole: the final blue solution is characterised by two new bands in UV-visible spectroscopy at 550 and 740 nm. This coulometry result confirms that overall processes include apparently direct three electron transfer, two electron transfer in the first wave followed by a monoelectronic reduction in the second wave (we note that the exhaustive coulometry carried out in HCl 0.1 N on the first wave gave $n_{app} = 2$, see below in the pH influence section).

Likewise, for $\alpha[P_2W_{14}Mo_4O_{62}]^{6-}$ and $\alpha[P_2W_{13}Mo_5O_{62}]^{6-}$, the voltammograms present the pattern of a reversible system and the electrochemical results are in Table 2. Finally, the voltammogram obtained with $\alpha[P_2W_{12}Mo_6O_{62}]^{6-}$ has three reversible bielectronic steps at $E_{p_1} = 0.520$ V, $E_{p_2} = -0.020$ V and $E_{p_3} = -0.115$ V (for each process, the peak ratio is equal to 1). The exhaustive electrolysis performed on the first wave ($E_i = 0.20$ V) confirm two-electron reduction: the UV-visible spectrum of the final intense blue solution shows two absorption bands at 540 and 720 nm. From the comparison of the peak current of the first reduction versus the others shows that the second and the third waves are also bielectronic.

RESULTS AND DISCUSSION

Electrochemical behaviour

The monosubstituted compounds. Among the Dawson anions described here, the electrochemical behaviour of the monosubstituted molybdo-tungstophosphate is chosen as a representative example. Figure 2 shows a typical voltammogram at 20 mV/s of $\alpha_2[P_2W_{17}MoO_{62}]^{6-}$ in HCl 2.2 N at GC disc electrode. It is characterised by a reduction peak at 0.21 V followed by several reduction processes at negative potentials. The reduction processes are reversible whatever the HCl concentration (2.2 N to 0.1 N). The first reduction peak current I_p is proportional to the square root of the potential scan rate restricted from 0.02 V/s to 0.1 V/s and to the heteropolyanion concentration ($10^{-4}\ M \leqslant C \leqslant 10^{-3}\ M$). Under stationary conditions at a RDE, the diffusion current of the first reduction obeys the Levich law [22(b)] as for a diffusion-controlled process: The current I_D is linearly related to the square root of the rotation speed. UV-visible spectrum before electrolysis is characterised by two absorption bands at 204 nm and 295 nm (shoulder). Exhaustive electrolysis at constant potential $E_i = 0.0$ V confirms a monoelectronic reduction (the initial yellow solution leads to a blue solution after bulk electrolysis). The ESR spectrum of the resulting blue solution recorded at room temperature shows a signal at $g = 1.93$ corresponding to Mo^V ion (see below, Table 3 and Fig. 3). The UV-visible spectrum recorded after electrolysis shows two new bands at 492 nm and 735 nm. The oxidation of this blue

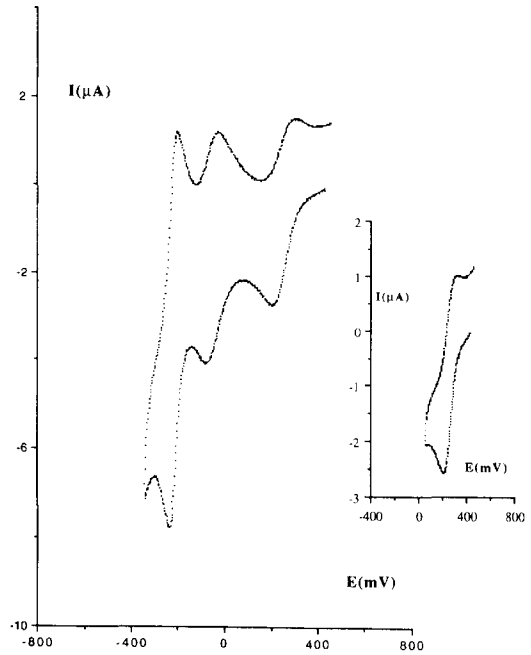

Fig. 2. Cyclic voltammetry of $\alpha_2[P_2W_{17}MoO_{62}]^{6-}$ $C \sim 10^{-3}$ M in HCl 2.2 N at a GC electrode (3 mm), scan rate 20 mV/s, potential in V *vs* SCE.

solution gives the initial species. All these results clearly correspond to a first monoelectronic reduction with a diffusion-controlled process without chemical complication. In comparison with the peak potentials of $\alpha[P_2W_{18}O_{62}]^{6-}$ in the same media, we can ascribe this first reduction peak to the monoelectronic reduction of molybdenum in the Dawson structure: the peak potential of the first reduction wave appears at $E_{p_1} = 0.00$ V for $\alpha[P_2W_{18}O_{62}]^{6-}$ and at $E_{p_1} = 0.21$ V for $\alpha_2[P_2W_{17}MoO_{62}]^{6-}$ (Table 1). The other reduction processes can be assigned to the reduction of the tungsten in the same structure. We deduce the same behaviour for the monovanado and the monomolybdotungstophosphates: the first reduction peak is more positive for these compounds than for $\alpha[P_2W_{18}O_{62}]^{6-}$. Table 1 summarizes the electrochemical results obtained for overall molybdo and vanado tungstophosphates in HCl 2.2 N.

Moreover, for the monosubstituted compounds, we observe that, on one hand, for two isomers α_1 and α_2, the substituted atoms on the belt of the structure (α_1) are more easily reduced than the substituted atoms on the cap of the structure (α_2), and, on the other hand, the first reduction peak potential of mono-

Table 1. Cyclic voltammetry of monomolybdo and monovanado tungstophosphate

	Peak potential (mV)								
Compounds without substituted atoms	E_{p_1}	ΔE_p	n_{app}	E_{p_2}	ΔE_p	n_{app}	Coulometry	Electron numbers/mole	
$\alpha[P_2W_{18}O_{62}]^{6-}$	0^{sh}	55	1	−130	60	1	$E_i = -0.20$ V	(2)	
	E_{p_1}	ΔE_p	n_{app}	E_{p_2}	ΔE_p	n_{app}	E_{p_3}	ΔE_p	n_{app}	Coulometry	Electron numbers/mole
Compounds with substituted atoms											
$\alpha_1[P_2W_{17}MoO_{62}]^{6-}$	**370**	**60**	**1**	−20	55	1	−345	40	2		
$\alpha_2[P_2W_{17}MoO_{62}]^{6-}$	**210**	**60**	**1**	−120	60	1	−270	30	2	$E_i = 0.00$ V	(1)
$\alpha_1[P_2W_{17}VO_{62}]^{7-}$	*490*	*70*	*1*	-120^{sh}		1	−230	30	2	$E_i = 0.30$ V	(1)
$\alpha_2[P_2W_{17}VO_{62}]^{7-}$	*430*	*70*	*1*	-55^{sh}		2	−120		2	$E_i = 0.20$ V	(1)

(10^{-3} M > C > 10^{-4} M) in HCl 2.2 N at GC electrode (ϕ = 3 mm)/SCE, v = 20 mV/s; n_{app} = integer value of apparent electron numbers calculated versus the first peak intensity of $\alpha_2[P_2W_{17}MoO_{62}]^{6-}$ (normalized *vs* the HPa concentration).

In bold: reduction ascribed to the Mo atoms; in italics: reduction assigned to the V atoms. Sh = shoulder.

vanadotungstophosphate is more positive than the first peak potential of monomolybdotungstophosphates (Table 1).

The generalization of this analysis for the monosubstituted compounds studied here ($\alpha_2[P_2W_{17}MoO_{62}]^{6-}$, $\alpha_1[P_2W_{17}MoO_{62}]^{6-}$, $\alpha_2[P_2W_{17}VO_{62}]^{7-}$ and $\alpha_2[P_2W_{17}VO_{62}]^{7-}$) shows that:

—For a same position, α_1 or α_2 respectively, the V atom is easier to reduce than Mo atom.

—For a same metal substituted, Mo or V, the metal in equatorial position α_1 is more easily reduced than the metal in polar position α_2.

If we take into account these observations and the location of the peak potential, the voltammogram of $\alpha[P_2W_{15}VMo_2O_{62}]^{7-}$ in the same conditions shows a first monoelectronic peak reduction at 0.48 V corresponding to the V atom followed by a bielectronic peak reduction at 0.145 V assigned to the Mo atoms (see Table 2). For this last compound, all V and Mo atoms are on the cap of the Dawson structure. The comparison of peak potentials emphasizes again that the V atom is easier to reduce than the Mo atom in this structure.

The polysubstituted compounds. According to this statement, the first redox processes of molybdo tungstophosphate described here in HCl should be ascribed to the reduction of molybdenum atoms in the structure. We attempted to extend this analysis to polysubstituted compounds. Table 2 summarizes the electrochemical results of the molybdotungstophosphate $\alpha[P_2W_{18-x}Mo_zV_yO_{62}]^{n-}$ ($x = y+z$; $n = 6+y$) with $z > 1$ in HCl 2.2 N. The electrochemical behaviour of these compounds is described in the Experimental section.

Among this electrochemical characterization, the apparent electron number of the first reduction steps seems consistent with the number of Mo atoms substituted: for $\alpha[P_2W_{16}Mo_2O_{62}]^{6-}$ a bielectronic wave, for $\alpha[P_2W_{15}Mo_3O_{62}]^{6-}$, a bielectronic wave followed by a monoelectronic reduction and finally, three two-electron steps for $\alpha[P_2W_{12}Mo_6O_{62}]^{6-}$. Moreover, the analysis of the redox potential versus $\alpha[P_2W_{18}O_{62}]^{6-}$ appears without ambiguity for the bisubstituted compound: the first peak potential $E_{p_1} = 250$ mV and $E_{p_2} = 155$ mV for $\alpha[P_2W_{16}Mo_2O_{62}]^{6-}$ are more positive than for $\alpha[P_2W_{18}O_{62}]^{6-}$ with $E_{p_1} = 0$ V. Unfortunately, the location of peak potential in comparison with the peak potentials of $\alpha[P_2W_{18}O_{62}]^{6-}$ in the same media doesn't allow us to confirm this hypothesis when the number of Mo substituted is above 3 (see Table 2): the peak potential becomes more negative than for $\alpha[P_2W_{18}O_{62}]^{6-}$.

ESR

In order to determine if the electron in the reduced species is localised on the molybdenum or vanadium site, we have carried out an ESR study at room temperature. The ESR parameters of molybdo tungstophosphate reduced obtained in HCl are listed in Table 3. We have chosen to report in Fig. 3 the representative example ESR spectra of reduced molybdo and vanado tungstophosphate in HCl at room temperature.

Molybdotungstophosphates. For the one-electron reduced monomolybdo-tungsto-phosphate, the ESR spectra carried out in HCl 1 N at room temperature show a typical characteristic of Mo^V ion: a strong central line due to the 75% abundant ^{96}Mo isotope ($I = 0$) while the weak line arises from the hyperfine coupling with the ^{97}Mo and ^{95}Mo isotope ($I = 1/2$). We cannot distinguish on the spectrum these two isotopes alone because, they have almost the same nuclear magnetic moment [12]. The behaviour illustrated by Fig. 3 clearly establishes that an unpaired electron is localised around the Mo atom at room temperature. These results seem to be in fair agreement with our electrochemical analysis (the first mono-

Table 2. Cyclic voltammetry of molybdo and vanado tungstophosphate

	Peak potential (mV)										
	E_{p_1}	ΔE_p	n_{app}	E_{p_2}	ΔE_p	n_{app}	E_{p_3}	ΔE_p	n_{app}	Coulometry	Electron numbers/mole
Compounds with substituted atoms											
$\alpha[P_2W_{16}Mo_2O_{62}]^{6-}$	**250^{sh}**			**155**			−260	30	2	$E_i = 0.05$ V	(2)
$\alpha[P_2W_{15}Mo_3O_{62}]^{6-}$	**220**	**60**	**2**	−60	60	1				$E_i = -0.10$ V	(3)
$\alpha[P_2W_{14}Mo_4O_{62}]^{6-}$	**530**	**40**	**2**	−155	30	2					
$\alpha[P_2W_{13}Mo_5O_{62}]^{6-}$	**530**	**30**	**2**	−60	30	2	−150^{sh}		2		
$\alpha[P_2W_{12}Mo_6O_{62}]^{6-}$	**520**	**30**	**2**	−20	30	2	−115	30	2	$E_i = 0.30$ V	(2)
$\alpha[P_2W_{15}VMo_2O_{62}]^{7-}$	*480*	*60*	*1*	**145**	**30**	**2**	−235	30	2	$E_i = 0.39$ V	(1)
$\alpha[P_2W_{13}VMo_4O_{62}]^{7-a}$	500^{Sh}			370			−195	30	2	$E_i = 0.20$ V	(2)

(10^{-3} M > C > 10^{-4} M) in HCl 2.2 N at GC electrode (ϕ = 3 mm)/SCE, v = 20 mV/s, n_{app} = integer value of apparent electron numbers calculated versus the first peak intensity of $\alpha_2[P_2W_{17}MoO_{62}]^{6-}$ (normalized *vs* the C_{HPa}).

[a] HCl 1 N.

In bold: reduction ascribed to the Mo atoms; in italics: reduction assigned to the V atoms; Sh = shoulder.

Table 3. ESR parameters of the reduced species at room temperature characteristics of Mo^{V}

Compounds	Media	g_{iso}	ΔH_{pp} (Gauss)
$\alpha_1[P_2W_{17}MoO_{62}]^{7-}$	HCl 1 N	1.914	22
$\alpha_2[P_2W_{17}MoO_{62}]^{7-}$	HCl 1 N	1.930	30
$\alpha[P_2W_{16}Mo_2O_{62}]^{7-}$	HCl 0.1 N	1.934	75
$\alpha[P_2W_{15}Mo_3O_{62}]^{7-}$	HCl 0.1 N	1.937	110
$\alpha[P_2W_{15}Mo_3O_{62}]^{9-}$	HCl 1 N	1.922	30
$\alpha[P_2W_{14}Mo_4O_{62}]^{7-}$	HCl 0.3 N/KCl 0.27 M	1.940	85
$\alpha[P_2W_{15}Mo_2VO_{62}]^{8-}$	HCl 1 N	2.017[a]	47[a]

ΔH_{pp} = the measured peak to peak ESR line width ; g_{iso} = isotropic g value.
[a] ESR parameters characteristic of V^{IV}.

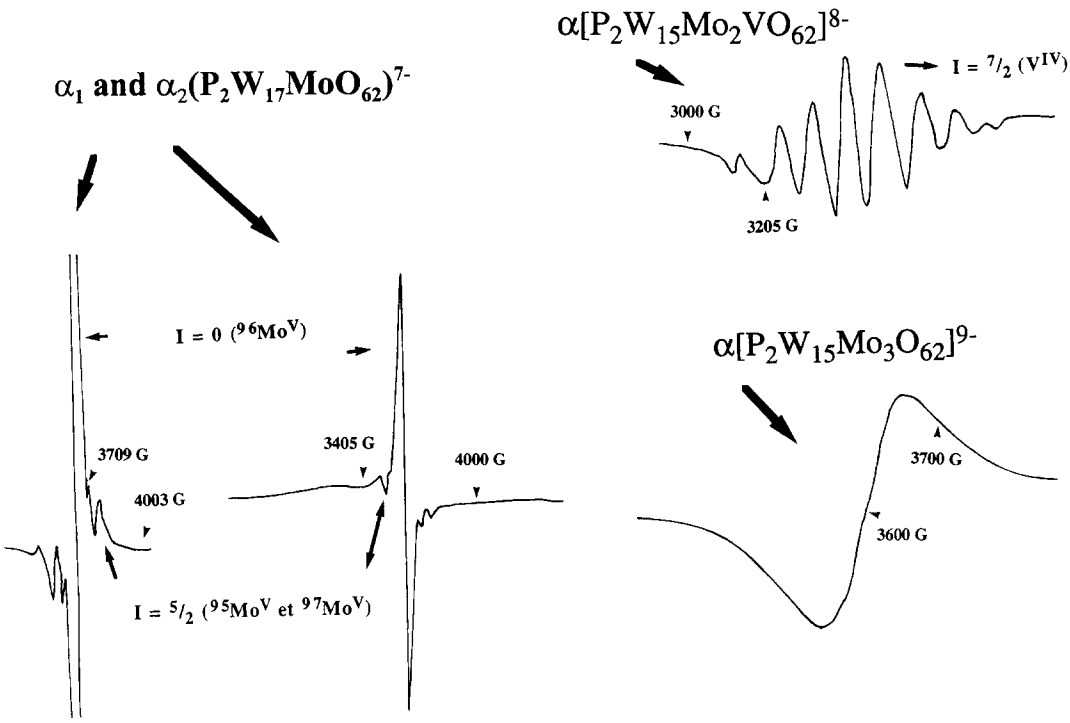

Fig. 3. ESR spectra of substituted tungstophosphates recorded at room temperature in HCl (see Experimental section).

electronic reduction is ascribed to the Mo atom) and so, with the results of Sanchez *et al.* for the mono-substituted polyanions with the Keggin structure [12,14], who concluded that the unpaired electron is trapped on a single Mo atom.

For the other reduced $\alpha[P_2W_{18-x}Mo_xO_{62}]^{7-}$ compounds ($1 < x < 5$, Table 3), the ESR spectra showed the same behaviour with a weak variation of the g_{iso} parameter. In fact, these spectra are characterised by a large strong central line due to the ^{96}Mo isotope without hyperfine coupling. The two-electron-reduced substituted compounds from two to six Mo substituted atoms exhibit no ESR signal as expected.

The broadening of the ESR spectra indicates that electron delocalization occurs when the paramagnetic Mo^{V} ion is surrounded by other Mo^{VI} ions [12,14]. This is due to electron hopping between metal sites. Such behaviour is typical of class II mixed valence compounds [23]. The analysis of the ΔHpp values for the one reduced $\alpha[P_2W_{18-x}Mo_xO_{62}]^{7-}$ ($O < x < 4$) compound substituted in polar corner-shared site shows clearly a linear variation of the line width ΔHpp versus the substitution number of molybdenum atoms. We first note that the ΔHpp value is of 30 G for $\alpha_2[P_2W_{17}MoO_{62}]^{7-}$ which corresponds to a localised electron around the Mo site. Then, we obtained 75 G for $\alpha[P_2W_{16}Mo_2O_{62}]^{7-}$, and 110 G for $\alpha[P_2W_{15}Mo_3O_{62}]^{7-}$. Moreover, the spectra of

$\alpha[P_2W_{15}Mo_3O_{62}]^{9-}$ and $\alpha_2[P_2W_{16}MoO_{62}]^{7-}$ have identical characteristics with a $\Delta Hpp = 30$ G by contrast with $\alpha[P_2W_{15}Mo_3O_{62}]^{7-}$ and $\alpha[P_2W_{15}Mo_3O_{62}]^{9-}$ (see Table 3). So, the increase of the line width versus the substitution number of molybdenum atoms may indicate an intramolecular electron transfer (hopping) at this temperature between the neighbouring Mo atoms: as expected, the one-electron reduced bi- and tri-molybdotungstophosphate are mixed valence compounds. These observations are consistent with the work of Kozik *et al.* [11,24].

For the three-reduced trimolybdotungstophosphate, if we consider the ΔHpp value, we can suggest that the three Mo sites are occupied by the three electrons with the same spin density repartition respectively, in which two electrons are paired and one electron is unpaired. Indeed, the ΔHpp value of 30 G recall the one-electron-reduced monosubstituted molybdotungstophosphate corresponding to an unpaired electron localised around the Mo atom. Investigations of the spectra at low temperature of the reduced $\alpha[P_2W_{15}Mo_3O_{62}]^{9-}$ must be carried out to validate this last interpretation.

So, we obtain for $\alpha[P_2W_{14}Mo_4O_{62}]^{7-}$ a ΔHpp intermediate value. We can suggest in a first approximation, that the added electron is delocalized over the four sites of molybdenum, including one equatorial corner-shared Mo site and three polar corner-shared Mo sites. The fact that the added electron remains favourably in the belt of the Dawson structure could generate a repartition of spin density different between the Mo in a polar site and the Mo in an equatorial site. This leads to the decrease of the ΔHpp parameter versus the ΔHpp of the $[P_2W_{15}Mo_3O_{62}]^{7-}$.

The spectroscopic results for $\alpha[P_2W_{16}Mo_2O_{62}]^{7-}$ and $\alpha[P_2W_{15}Mo_3O_{62}]^{7-}$ have shown that the two added electrons are delocalized over Mo atoms only. Indeed, the electron cannot be delocalized on the neighbouring tungsten atoms because the tungsten orbitals are higher in energy than the molybdenum orbitals [12]. From our spectroscopic results, a hopping of an unpaired electron between Mo^{V} and Mo^{VI} ion can be expected. This phenomenon is characterised by the variation of line width ΔHpp. An electron hopping between two sites can be thermally activated through the vibrations of the molecular compound. The thermal activation energy, however, is quite difficult to measure. It was already stressed that this value of thermal activation energy could be deduced from a careful analysis of the temperature dependence of the ESR line width [12,14]. The work on this interesting point of view is in progress.

Vanadomolybdotungstophosphate. The ESR spectra of $\alpha[P_2W_{15}Mo_2VO_{62}]^{8-}$ in HCl 1 N are given in Fig. 3. The room temperature spectrum shows the expected hyperfine interaction with the $^{51}V^{IV}$ nucleus (99.75%, $I = 7/2$). The g and ΔHpp parameters are listed in Table 3. This behaviour is characteristic of an unpaired electron localised around a vanadium atom. This result seems to be in agreement with the ESR study carried out on $\alpha[P_2W_{18-y}V_yO_{62}]^{(7+y)-}$ $(0 < y < 4)$ by Halmaker *et al.* [25]. But here, it seems that the energy barrier between the occupied orbital by the unpaired electron (around the vanadium site) and the Mo orbitals is high enough and doesn't allow, at room temperature, the delocalization of this single electron on the neighbouring sites of molybdenum. The peak potential analysis of $\alpha[P_2W_{15}Mo_2VO_{62}]^{7-}$, in comparison with the monosubstituted vanado and molybdotungstophosphate, leads to a similar conclusion: the first monoelectronic wave can be assigned to the reduction of the vanadium atom while the second bielectronic wave less positive is ascribed to the reduction of two molybdenum atoms (Table 1). A particular effect must be considered here: the electrochemistry of $\alpha[P_2W_{16}Mo_2O_{62}]^{6-}$ in HCl 2.2 N shows two closely one-electron steps (practically a bielectronic wave) with a shoulder whereas for $\alpha[P_2W_{15}Mo_2VO_{62}]^{7-}$ in the same conditions, the bielectronic wave corresponding to the Mo reduction is broad with a $\Delta E_p = 30$ mV. The comparison of NMR spectra of $\alpha[P_2W_{17}O_{62}]^{10-}$ and $\alpha[P_2W_{17}VO_{62}]^{7-}$ carried out by Kozik *et al.* [24] has shown that the two cap W's adjacent to the V and the two belt W's adjacent to the V in $\alpha[P_2W_{17}VO_{62}]^{7-}$ are perturbed: their lines are missing in the $\alpha[P_2W_{17}VO_{62}]^{7-}$ spectrum. The same trend was encountered in our electrochemical study except that the two cap atoms adjacent are the molybdenum atoms. The substitution of W by V on the top of the structure changes the redox properties of the molybdenum. The location of catholic peak potential of reduction of molybdenum seems less positive for the $\alpha[P_2W_{15}Mo_2VO_{62}]^{7-}$ compound than for the bisubstituted compound $\alpha[P_2W_{16}Mo_2O_{62}]^{6-}$.

Both electrochemical and spectroscopic results show clearly that the first redox processes correspond to the reduction of vanadium and/or of molybdenum in the Dawson structure. These conclusions are consistent with the spectroscopic results already described on similar compounds having Dawson or Keggin structure. Thus, the redox and acidic properties of these compounds in water are largely affected by the nature and the number of the substituted atom.

Influence of pH on the redox properties

As a general rule, the increasing pH modifies the redox properties of the HPa (Heteropolyanions) studied here. For the monosubstituted species α_1, $\alpha_2[P_2W_{17}MoO_{62}]^{6-}$ and α_1, $\alpha_2[P_2W_{17}VO_{62}]^{6-}$, the HCl concentration variation from 0.1 N to 2.2 N leads to the increase of the half-wave potential $E_{1/2}$ (defined by $E_{1/2} = E_p + \Delta E_p/2$). The general pattern of the voltammogram remains unchanged.

The bi- and tri-molybdotungstophosphate. The main electrochemical study in the function of pH has been carried out on $\alpha[P_2W_{16}Mo_2O_{62}]^{6-}$ and $\alpha[P_2W_{15}Mo_3O_{62}]^{6-}$ because all the substituted atoms

are on the cap of the structure allowing a better comparison (see Fig. 1). In this case, we observe a particular phenomenon. The present study is restricted to the first two waves. Figure 4(A) and (B) summarize the evolution of the cyclic voltammetric pattern observed in HPa solution with the hydrochloric concentration varying from 1 N to 6 N. The potential location of these first waves obtained in our experiments are gathered in Table 4.

$\alpha[P_2W_{16}Mo_2O_{62}]^{6-}$. The voltammogram of $\alpha[P_2W_{16}Mo_2O_{62}]^{6-}$ in HCl 0.1 M (not represented here) is characterized by two monoelectronic steps. At this pH value, the first wave is a shoulder of the second wave ($E_{p_1} = 170$ mV; $E_{p_2} = 40$ mV). Controlled-potential coulometry experiments carried out on the second wave gave a blue solution and an n_{app} value of 2. As expected for such diamagnetic compounds, no ESR signal was observed at room temperature. These results confirm two successive monoelectronic steps in this media. Then, with increasing HCl concentration, all the waves are displaced in the positive direction. From 0.1 N to 2.2 N, the second wave moves more quickly than the first wave. At 2.2 N, the first wave becomes a small shoulder. In 4 N hydrochloric acid, the voltammogram shows a reversible two-electron wave. At this HCl concentration, the two first waves are practically merged for a potential sweep rate of 20 mV/s. Now, this new wave is more higher than the monoelectronic wave and the $\Delta E_p = 100$ mV. In gradually more acid concentration, the composite first wave grows and the ΔE_p value decreases. The reduction peak potential becomes less negative. At 6 N HCl, the composite wave is broad with a $\Delta E_p = 70$ mV (Fig. 4(A)). When the HCl concentration is more than 6 N, the voltammogram is characterised by a very weak peak current. For instance, in HCl 7 N and with the same HPa concentration, the peak current decreases to 80% of that in HCl 6 N, but the voltammogram is basically similar. The weak stability of HPa in this strong acid media doesn't allow our study to go further.

$\alpha[P_2W_{16}Mo_3O_{62}]^{6-}$. We observe the same evolution for $\alpha[P_2W_{16}Mo_3O_{62}]^{6-}$. In this case, we obtain already a two-electron wave in HCl 1 N with a $\Delta E_p = 90$ mV

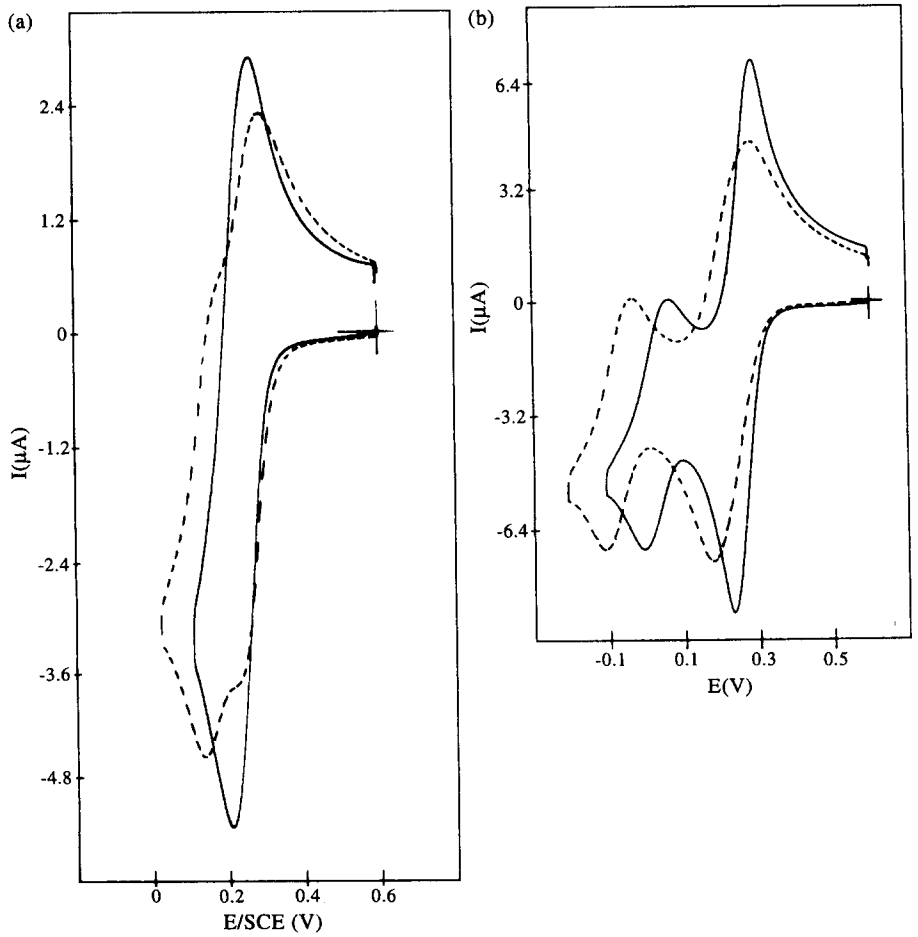

Fig. 4. Cyclic voltammetry of HPa, $C \sim 6.10^{-4}$ M, at a GC electrode (3 mm), scan rate 20 mV/s, potential in V *vs* SCE; (——) in HCl 6 N, (– – –) in HCl 1 N; (A): $\alpha[P_2W_{16}Mo_2O_{62}]^{6-}$; (B): $\alpha[P_2W_{15}Mo_3O_{62}]^{6-}$

Table 4. Cyclic voltammetry of molybdotungstophosphate

	Peak potential (mV)									
	$\alpha[P_2W_{18}O_{62}]^{6-}$				$\alpha[P_2W_{16}Mo_2O_{62}]^{6-}$				$\alpha[P_2W_{15}Mo_3O_{62}]^{6-}$	
	E_1	ΔE_1	E_2	ΔE_2	E_1	ΔE_1	E_2	ΔE_2	E_1	ΔE_1
HCl concentration:									Bielectronic wave	
1 N	5	55	−135	50	≈230^{sh}	55	125	≈30^{sh}	180	90
2.2 N					≈220^{sh}	45	155	≈30^{sh}	220	60
					Bielectronic wave					
					E_1	ΔE_1				
3.9 N					170	100			225	55
4 N	≈5		≈−90							
4.5 N									225	50
	Bielectronic wave									
	E_1	ΔE_1								
6 N	65	100			205	70			240	35
12.4 N	5	30								

(10^{-3} M > C > 10^{-4} M) in different concentrations of HCl on a GC electrode (ϕ = 3 mm)/SCE, v = 20 mV/s. Sh: shoulder; the peak potentials are given without considering the liquid junction potential. For $\alpha[P_2W_{18}O_{62}]^{6-}$ [18].

at a potential sweep rate of 20 mV/s (Fig. 4(B)): here, the two monoelectronic waves are already merged. Indeed, controlled potential coulometry carried out in these conditions on this wave gave a blue solution and an $n_{app} = 2$. No ESR signal was observed at room temperature on this blue solution. From HCl 1 N to HCl 4.5 N, the first wave grows higher and higher. The wave width characterised by the ΔE_p value decreases. The reduction peak potential becomes less negative. At HCl 4.5 N, this composite wave is broad with ΔE_p = 50 mV at 20 mV/s. At HCl 6 N, the ΔE_p value is equal to 35 mV, showing the characteristics of a bielectronic wave.

In contrast, decreasing the HCl concentration to 0.1 N leads to the beginning of separation into two waves: the voltammogram exhibits a small shoulder. We noted that the peak potential locations are slightly more positive for $\alpha[P_2W_{15}Mo_3O_{62}]^{6-}$ than for $\alpha[P_2W_{16}Mo_2O_{62}]^{6-}$. The main trends upon varying the hydrochloric acid for $\alpha[P_2W_{15}Mo_3O_{62}]^{6-}$ are summarized in Fig. 4(B).

Some general features emerge from the changing of cyclic voltammetric waves of $\alpha[P_2W_{15}Mo_3O_{62}]^{6-}$ and $\alpha[P_2W_{16}Mo_2O_{62}]^{6-}$. It must be emphasized that the electrochemical behaviour is strongly affected by the viscosity of the media. Therefore, the change of viscosity from acidic medium to another modifies the liquid junction potential. The variation of liquid junction affects the location of peak potential. In contrast, the anodic to cathodic peak separation remains constant throughout. In order to determinate this influence on peak potential location, we have calculated, as a first approximation, its value using the Henderson equation [27] for the electrolyte junction HCl/KCl with a saturated calomel electrode (3.5 M KCl). The mobility of H^+, K^+ and Cl^- in water are taken from literature [27]. We have considered here the variation of junction potential ΔE_j when the acid concentration goes from 0.1 N to 6 N. In this case, the value ΔE_j = 25 mV: the junction potential goes from +3 mV to −22 mV. This value shows that (i) increasing acid concentration decreases the junction potential slowly. This weak value of the junction potential obtained in the calculation with the Henderson equation can be explained by the fact that, on the one hand, the same anion Cl^- is included in the two media of the junction, HCl/KCl, and, on the other hand, the K^+ mobility is almost identical to Cl^- mobility. (ii) The working electrode appeared more negative than it really was.

A similar study with $\alpha[P_2W_{18}O_{62}]^{6-}$ in different acidic media showed the same trend [18]. The observed peak potentials in increasing acid media should be more positive than those obtained. So, the variation of the peak potential obtained in our experiments with $\alpha[P_2W_{18-x}Mo_xO_{62}]^{6-}$ seems consistent with the pH variation. For more accurate determinations, complementary experimental work is obviously needed to explain completely the quantitative variation observed. Nevertheless, the shift of some reduction peak in water allows a qualitative approach. Then, we can suggest that the evolution of the voltammetric pattern for this HPa seems to be dominated largely by acid-base properties of the reduced species. If we consider the following discussion is restricted mainly to the mechanism of formation of two electron waves, we can affirm that the bielectronic process of $\alpha[P_2W_{15}Mo_3O_{62}]^{6-}$ appears for weaker HCl concentrations than for $\alpha[P_2W_{16}Mo_2O_{62}]^{6-}$. The main point is that in water solutions the second wave of this HPa shifts to positive potential more quickly than the first wave with the increasing acid concentration (first wave remaining almost unchanged). Among our

experiments, complete merging of the waves is obtained in less acidic medium for $\alpha[P_2W_{15}Mo_3O_{62}]^{6-}$ than for $\alpha[P_2W_{16}Mo_2O_{62}]^{6-}$, which could indicate a more basic two-reduction trisubstituted species. This trend was already encountered in the case of $\alpha[P_2W_{18}O_{62}]^{6-}$ and $PW_{12}O_{40}^{5-}$ for stronger HCl concentrations [18]. Table 4 gives the results already published by Nadjo and co-workers. For the same HCl concentration, the ΔE_p value is smaller for $\alpha[P_2W_{15}Mo_3O_{62}]^{6-}$ than for $\alpha[P_2W_{16}Mo_2O_{62}]^{6-}$ and for $\alpha[P_2W_{18}O_{62}]^{6-}$. From experiments in HCl, it appears that the basicity of the reduced form of HPa follows the sequence $\alpha[P_2W_{15}Mo_3O_{62}]^{6-} > \alpha[P_2W_{16}Mo_2O_{62}]^{6-} > \alpha[P_2W_{18}O_{62}]^{6-}$. From this basicity scale, the molybdenum atom in the structure seems to have an important part. NMR and ESR studies [24–26,28,29] (see previously) on these reduced compounds have shown that the electrons are delocalised on the molybdenum site. If we take into account the spectroscopic results concerning the reduced species, it seems that the basic strength increases with the Mo substitution in the Dawson structure. Concerning the mechanism, these results in water solution can be explained with a qualitative approach, on the basis of the protonation of the reduced species. This statement is analogous to the reduction of an aromatic compound [30]: cascade of electron transfer and protonation sequence. An analogue phenomenon with this HPa in acidic medium can be considered: a reaction mechanism in which the electron transfer is followed by a protonation leading to an apparently two-electron transfer. In our experiments, the merged wave is linked to the pH and to the basicity properties of the reduced forms. In this case, the mechanism proposed is coherent at strong acidic media.

Acknowledgements—This work was supported by the CNRS (URA 1383, 419 and 75). Sincere thanks are addressed to Dr L. Nadjo (University Paris XI) for helpful advice.

REFERENCES

1. Pope, M. T., *Heteropoly and isopoly oxometallates, Inorganic Chemistry Concept*. Spring Verlag, Berlin, 1983.
2. Yamase, T., *Polyhedron*, 1986, **5,** 79; Farneth, W. E., Staley, R. H., Domaille, P. J. and Foster, P., *J. Am. Chem. Soc.*, 1987, **109,** 4018; Pope, M. T. and Muller, A., *Angew. Chem. Int. ed. Engl.*, 1991, **30,** 34; Misono, M., *Catal. Rev.*, 1987, 29; Jansen, R. J. J., *Recueil des travaux Chimiques des Pays Bas*, 1994, **113,** 3.
3. Dong, S. and Liu, M., *J. Elec. Chem.*, 1994, **372,** 95.
4. Abessi, M., Contant, R., Thouvenot, R. and Hervé, G., *Inorg. Chem.*, 1991, **30,** 1695.
5. Contant, R. and Cabrini, J. P., *J. Chem. Res.*, 1977, **222,** 2601.
6. Papaconstantinou, E. and Pope, M. T., *Inorg. Chem.*, 1991, **30,** 1695; *Inorg. Chem.*, 1967, **6,** 1152.
7. Contant, R. and Cabrini, J. P., *J. Inorg. Nucl. Chem.*, 1981, **43,** 1525.
8. Contant, R. and Thouvenot, R., *Can. J. Chem.*, 1991, **69.**
9. Cabrini, J. P., Thesis, University Paris VI, 1982.
10. Chauveau, F., *Bull. Soc. Chim. Fr.*, 1986, **2**; Smith, D. P., So, A., Bender, J. and Pope, M. T., *Inorg. Chem.*, 1973, **12,** 3.
11. Kozik, M., Casan-Pastor, N., Hammer, C. F. and Baker, L. C. W., *J. Amer. Chem. soc.*, 1988, **110,** 7697.
12. Sanchez, C., Livage, J., Launay, J. P., Fournier, M. and Jeannin, Y., *J. Amer. Chem. Soc.*, 1982, **104,** 3194.
13. Launay, J. P., Fournier, M., Sanchez, C., Livage, J. and Pope, M. T., *Inorg. Nucl. Chem. Lett.*, 1980, **16,** 257.
14. Sanchez, C., Livage, J., Launay, J. P. and Fournier, M., *J. Amer. Chem. Soc.*, 1983, **105,** 6817.
15. Kazansky, L. P., *Ser. Khim.*, 1978, **2,** 274; *Koord. Khim.*, 1976, **2,** 719.
16. Essadi, K., Keita, B. and Nadjo, L., *J. Electroanal. Chem.*, 1994, **367,** 275.
17. Keita, B., Essadi, K., Nadjo, L. and Desmadril, M., *Chem. Phys. Lett.*, 1995, **237,** 411.
18. Keita, B. and Nadjo, L., *J. Electroanal. Chem.*, 1987, **47,** 284; *J. Electroanal. Chem.*, 1987, **227,** 77.
19. Keita, B. and Nadjo, L., *Mat. Chem. and Phys.*, 1989, **22,** 77.
20. Keita, B., Lucas, T. and Nadjo, L., *J. Electroanal. Chem.*, 1986, **208,** 343.
21. Keita, B., Bouaziz, D. and Nadjo, L., *J. Electroanal. Chem.*, 1988, **135,** 87.
22. (a) Tommasino, J. B., PhD thesis, Université de Toulouse III (1992); Cassoux, P., David, C., Dartiguepeyron, R., de Montauzon, D., Tommasino, J. B. and Fabre, P. L., *Actualité Chimique*, January 1994, p. 49. (b) Bard, A. J. and Faulkner, L. R., *Electrochemical Methods*, J. Wiley & Sons, New York, 1980.
23. Hush, N. S., *Mixed Valence Compounds*, ed. D. B. Brown, D. Reidel, Dordrecht, 1980.
24. Kozik, M., Hammer, C. F. and Baker, L. C. W., *J. Amer. Chem. Soc.*, 1986, **108,** 7627; *J. Amer. Chem. Soc.*, 1986, **108,** 2748; *J. Amer. Chem. Soc.*, 1990, **112,** 7604.
25. Halmaker, S. P., Leparulo, M. A. and Pope, M. T., *J. Amer. Chem. Soc.*, 1983, **105,** 4286.
26. Acerete, R., Hammer, C. F. and Baker, L. C. W., *J. Amer. Chem. Soc.*, 1982, **104,** 5384.
27. Tremillion, B., *Electrochimie analytique et réactions en solution, Tome* 1, Edition Masson, Paris, 1993.
28. Acerete, R., Halmaker, S., Hammer, C. F., Baker, L. C. W. and Pope, M. T., *J. Chem. Soc., Chem. Comm.*, 1979, 777.
29. Kazansky, L. P. and Fedolov, M. F., *J. Chem. Soc., Chem. Comm.*, 1980, 644.
30. Amatore, C., *Organic Electrochemistry*, ed H. Hund and M. M. Baizer, M. Dekker Inc., New York, 1991.

Pergamon

PII: S0277-5387(97)00294-5

Polyhedron Vol. 17, No. 2–3, pp. 367–372, 1998
© 1997 Elsevier Science Ltd
All rights reserved. Printed in Great Britain
0277-5387/98 $19.00+0.00

Synthesis and X-ray crystal structures of tetra-alkyl diphosphine complexes of silver(I), $[Ag_2\{Bu^t_2P(CH_2)_3PBu^t_2\}_2][BF_4]_2 \cdot 2CH_2Cl_2$ and $[Ag_2\{Bu^t_2P(CH_2)_2PBu^t_2\}(H_2O)_2][BF_4]_2$

Simon P. Crabtree, Andrei S. Batsanov, Judith A. K. Howard and Melvyn Kilner*

Department of Chemistry, University of Durham, South Road, Durham, DH1 3LE, U.K.

(Received 24 April 1997; accepted 20 June 1997)

Abstract—The title complexes $[Ag_2(dbpp)_2](BF_4)_2$ (**1**) and $[Ag_2(dbpe)(H_2O)_2](BF_4)_2$ (**2**), obtained as unexpected by-products while using $AgBF_4$ to eliminate Cl^- from rhodium complexes, were isolated and characterised by single-crystal X-ray diffraction. **1** was also prepared directly. The Ag atoms are bridged by two (**1**) or one (**2**) diphosphine ligands and have a linear P, P or P, H_2O coordination. According to the $^{31}P\{^1H\}$ spectra, the cation of **1** retains this structure in solution. Weak Ag···F interactions with anions (in **2** 'supported' by OH···F hydrogen bonds) form two additional interaction bridges in **1** or link the Ag atoms in a *catena*-fashion in **2** and complement the Ag^I coordination to a trigonal–bipyramidal arrangement (with one equatorial site void). © 1997 Elsevier Science Ltd

Keywords: crystal structure; phosphines; secondary coordination; silver(I) complex; water coordination.

Diphosphines $R_2P(CH_2)_nPR_2$ (L) have a well-known ability to form relatively stable $M[P(CH_2)_nP]_2M$ ring frameworks which show interesting reactivity and catalytic properties [1]. The silver(I) ion, readily bonding with phosphines and prone for linear coordination, seems particularly suited to form such structures. Indeed, a variety of complexes with the $[Ag_2L_2]^{2+}$ core was prepared from diphosphines with $n = 1$, bis-diphenylphosphinomethane (dppm) and bis-dimethylphosphinomethane (dmpm) [1–6]. In the crystals of the compounds, counterions such as nitrate [1,2], acetate [3], hexafluoro-2,5-pentanedionate [4] and bromide [5] coordinate silver atoms at equatorial sites (sometimes giving rise to cores of higher nuclearity), while a poorer nucleophile PF_6^- only forms weak electrostatic Ag···F interactions [6]. Similar systems with $n > 1$ are studied much less, in spite of the fact that the stability of the $[Ag_2L_2]^{2+}$ ring increases with n, following the trend of the corresponding complexes with diamines [7] and due probably to the increase of nucleophilicity on the phosphorus atoms and the simultaneous decrease of the steric strain in the metallacycle. On the other hand, the stability of chelating coordination of diphosphines increases in the same succession, so that while dppm forms only di- or polynuclear complexes, bis(diphenylphosphino)-ethane (dppe) and -propane (dppp) yield mononuclear ones as well [7]. It is noteworthy that the only two complexes with $n = 2$ (L = dppe and bis(dimethylphosphino)ethane) characterised crystallographically [8], both present a peculiar $[Ag_2L_4]^{2+}$ core with two diphosphines bridging and two others chelating. For $n = 3$ only one X-ray structure, of $Ag_2(dppp)_2(NO_3)_2$, has been reported so far [9], while a series of stable $[Ag_2L_2]^{2+}$ ring cations, obtained by the reaction of $AgClO_4$ with L = dppm, dppe, and dppp in DMSO, has been characterised by NMR spectroscopy [7].

The present study was initiated by an accidental synthesis of a novel silver diphosphine complex $[Ag_2(dbpp)_2](BF_4)_2 \cdot 2CH_2Cl_2$ (**1**, dbpp = $Bu^t_2P(CH_2)_3PBu^t_2$) in the course of our work [10] aimed at the preparation of (diphosphine)rhodium complexes. Silver(I) salts are commonly used to remove halide ions from a transition metal atom, thus creating vacant coordination sites for the introduction of new

* Author to whom correspondence should be addressed.

ligands; earlier we used this procedure [10] to convert $[Rh_2Cl_2(C_2H_4)_4]$ into $[Rh_2Cl_2(dialkene)_2]$, then to $[Rh(dialkene)_2]^+$, prior to reaction with diphosphines L to form $[RhL(C_7H_8)]BF_4$. complexes. When we used dbpp in the above mentioned sequence of reactions, **1** was isolated, obviously due to the tendency of silver(I) to remain in solution and to carry through in the purification stages of the reaction.

Subsequently we synthesised **1** directly, from $AgBF_4$ and dbpp in a diethylether/dichloromethane solvent. An attempt to prepare a corresponding complex with $Bu^t_2P(CH_2)_2PBu^t_2$ (dbpe) by following the same route yielded instead a complex $[Ag_2(dbpe)(H_2O)_2](BF_4)_2$ (**2**) with a *single* diphosphine bridge. Herein we report the syntheses and structures of **1** and **2**.

RESULTS AND DISCUSSION

The synthesis of **1** proves that a range of complexes may be obtained directly from the treatment of silver (I) tetrafluoroborate with alkyl diphosphines L in the same way as for aryl diphosphines [1,4]. **1** is colourless, as expected for a silver(I) complex containing an alkylphosphine and a BF_4^- counterion, and is unusually light-, air- and moisture-stable. It can be exposed to the atmosphere without deterioration, and produces light- and air-stable solutions in polar solvents, including chloroform and THF. This stability against reduction to silver(0) was also demonstrated by cyclic voltammetry (1.0 V with respect to Ag/Ag^+).

Since the free bis(di-*tert*-butylphosphino)propane itself is both air- and light-sensitive, **1** may be useful in synthesis as a means of introducing this diphosphine into other complexes, *viz.*

$$2[M]\text{-}Cl + [Ag_2L_2]^{2+} \rightarrow 2[ML]^+ + 2AgCl.$$

We tried to transfer the diphosphine to $[MoCp(CO)_3Cl]$ and $[Mn(CO)_5Cl]$ in this way, to form respectively $[MoCp(CO)_2L_2]^+$ and $[Mn(CO)_5L_2]^+$. The attempts were unsuccessful under a variety of temperature and solution conditions, **1** being very robust and inactive. This is another indication of particular stability of a 12-membered $Ag(XCH_2CH_2CH_2X)_2Ag$ metallacycle towards dissociation, observed earlier for diamine (X = N) and dppp (X = P) bridging ligands (see above).

In the crystal structure of **1** (Fig. 1, Table 1) the asymmetric unit comprises half of the bis(diphosphine)disilver cation (located at an inversion centre), a tetrafluoroborate anion and a disordered CH_2Cl_2 molecule. The silver atom has, in the first instance, a linear coordination with two phosphorus atoms. The Ag···Ag distance of 5.260(2) Å is substantially longer than in the analogous complexes with $n = 1$ (3.04–3.20 Å) [1–6] but surprisingly less than in those with $n = 2$ (5.95–6.25 Å) [8], probably because the trimethylene chain in **1** acquires a compact trans-planar conformation [with the torsion angles around the C(1)—C(2) and C(2)—C(3) of 177.6(3) and 177.8(3)°], while no such favourable conformation is possible for an even-membered chain. It is well known that in Ag_2L_2 cores with $n = 1$ the metal–metal distance is relatively constant (indeed it is similar for

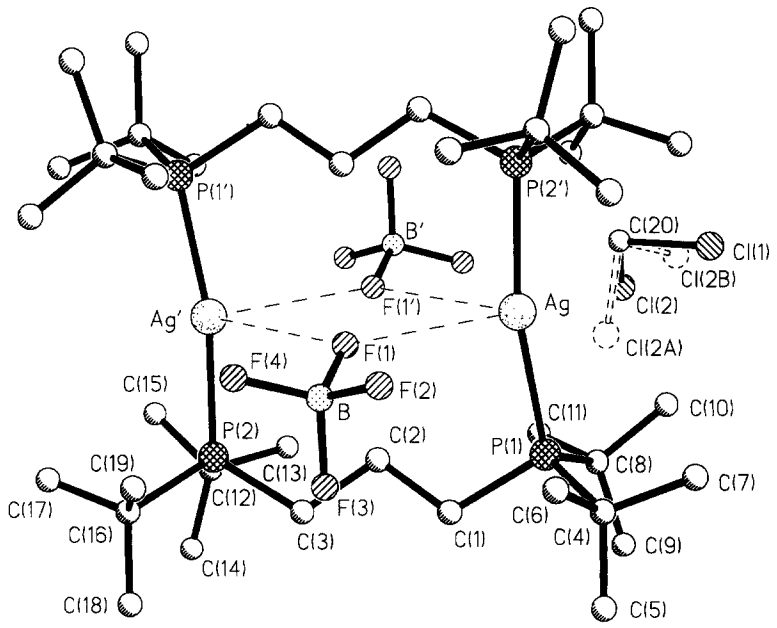

Fig. 1. X-ray molecular structure of **1**, showing the disorder of the solvate CH_2Cl_2 molecule. Atoms, symmetrically related *via* the inversion centre, are primed; hydrogen atoms are omitted.

Table 1. Selected bond distances (Å) and angles (°) in the structure of **1**

Ag—P(1)	2.406(1)	Ag—P(2′)	2.406(1)
Ag···F(1)	3.218(4)	Ag···F(1′)	3.795(4)
P(1)—C(1)	1.836(4)	P(2)—C(3)	1.839(4)
P(1)—C(4)	1.877(4)	P(2)—C(12)	1.879(4)
P(1)—C(8)	1.880(5)	P(2)—C(16)	1.876(4)
B—F(1)	1.376(7)	B—F(2)	1.373(7)
B—F(3)	1.402(7)	B—F(4)	1.360(6)
P(1)—Ag—P(2′)	169.49(4)	F(1)—Ag—F(1′)	83.1(1)
P(1)—Ag—F(1)	95.5(1)	P(2′)—Ag—F(1)	93.5(1)
P(1)—Ag—F(1′)	96.2(1)	P(2′)—Ag—F(1′)	90.3(1)
C(1)—P(1)—C(4)	104.1(2)	C(3)—P(2)—C(12)	106.2(2)
C(1)—P(1)—C(8)	106.4(2)	C(3)—P(2)—C(16)	102.7(2)
C(4)—P(1)—C(8)	112.9(2)	C(12)—P(2)—C(16)	113.0(2)
C(1)—P(1)—Ag	110.9(1)	C(3)—P(2)—Ag′	116.0(1)
C(4)—P(1)—Ag	111.4(2)	C(12)—P(2)—Ag′	109.6(2)
C(8)—P(1)—Ag	110.9(2)	C(16)—P(2)—Ag′	109.3(1)

different metals, irrespectively of whether any direct metal–metal bonding is present or not, the peculiarity largely responsible for the catalytic properties of such complexes) [1] and anions, whether coordinated or weakly interacting with silver, are situated on the outer side of the dimetallic core. On the contrary, in **1** the F(1) atom of the anion is in a pseudo-bridging position between the silver atoms, with the distances Ag···F(1) 3.218(4) and Ag′···F(1) 3.795(4)Å; the former can be regarded as a weak electrostatic interaction and the latter as a mere intermolecular contact. The Ag—F distances for coordinated BF_4^- are usually much longer than the sum of ionic radii (2.31 Å) [11], reflecting poor nucleophilic properties of this ligand, e.g. 2.82 Å in $(Ph_3P)_3AgBF_4$ [12], although this distance decreases to 2.47–2.49 Å in the presence of π-acceptor η-ligands [13]. A similar contact with PF_6^- anion (Ag···F 2.99 Å) exists in $[Ag_2(dmpm)_2](PF_6)_2$ (**3**) [6]. Nevertheless, this interaction causes a noticeable distortion of the linear coordination of the silver atoms (PAgP angle of 169.5(4)° in **1**, cf. 174.3° in **3**), the latter bending towards the centre of the cation. In $[Ag_2(dppp)_2](NO_3)_2$ (**4**) the nitrato anion has a similar pseudo-bridging function [10] (Ag···O 2.58 and 2.98 Å), reducing the Ag···Ag distance to 4.661 Å and the PAgP angle to 152.2°. The Ag—P bond distances of 2.406(1) Å in **1** exceed appreciably those in **3** [2.384(3) Å] wherein the silver coordination is the closest to purely linear but the substituents at the phosphorus atoms are less bulky. In other silver diphosphine complexes the Ag—P distances range from 2.41 to 2.46 Å.

The $^{31}P\{^1H\}$ NMR spectrum indicates that the cation of **1** retains its structure in solution. the ^{107}Ag–^{31}P coupling constant of 467 Hz is typical for two-coordinate silver bonded to phosphorus [1] and close to the estimated value of 452 Hz, based solely on *s*-orbital contributions to the coupling [14]. The data also agrees with that for silver monophosphine complexes [15], in which the Ag—P coupling constant tends to increase with the decrease of the Ag—P distance and with the increase of both the P—Ag—P angle and the nucleophilicity of the 'coordinating cation'. However, the lack of complementary ^{31}P NMR and crystallographic data for disilver-bis(diphosphine) ring systems makes any comparisons qualitative rather than quantitative.

The formation of **2** was the result of moisture contamination from an unknown source, probably due to an adventitious hydration of the $AgBF_4$ salt used, although a commercial sample was opened and handed in a dry-box, and Schlenk tube techniques were used throughout the synthesis and crystallisation. Complex **2** could not be synthesised intentionally by introducing controlled amounts of water into the $AgBF_4$/dbpe reaction, although many attempts were made.

The crystal structure of **2** contains $[(H_2O)Ag(dbpe)Ag(OH_2)]^{2+}$ cations with a crystallographic C_i symmetry and a trans-planar conformation of the dbpe bridge (Fig. 2, Table 2). Similar bridging function of dppe in disilver complexes is common [7,16], but to the best of our knowledge, **2** is the first complex containing a di-coordinated silver(I) atom with both phosphorus and oxygen ligands bonded simultaneously. The Ag—P distance in **2** is by 0.06 Å shorter than in **1**, reflecting the lower *trans*-influence of the aqua-ligand. The distorted linear coordination of the silver atoms within the cation is completed to a trigonal–bipyramidal arrangement (with one equatorial site vacant) by secondary interactions with two fluorine atoms of different tetrafluoroborate anions, related *via* a crystallographic glide plane *n*. Both anions are simultaneously engaged (by other fluorine atoms) in hydrogen bonds with the aqua-ligand. Such 'supported' secondary $[BF_4\cdots M]$ interactions have been observed earlier in Cu^{II} complexes [17], but not in linear Ag^I ones.

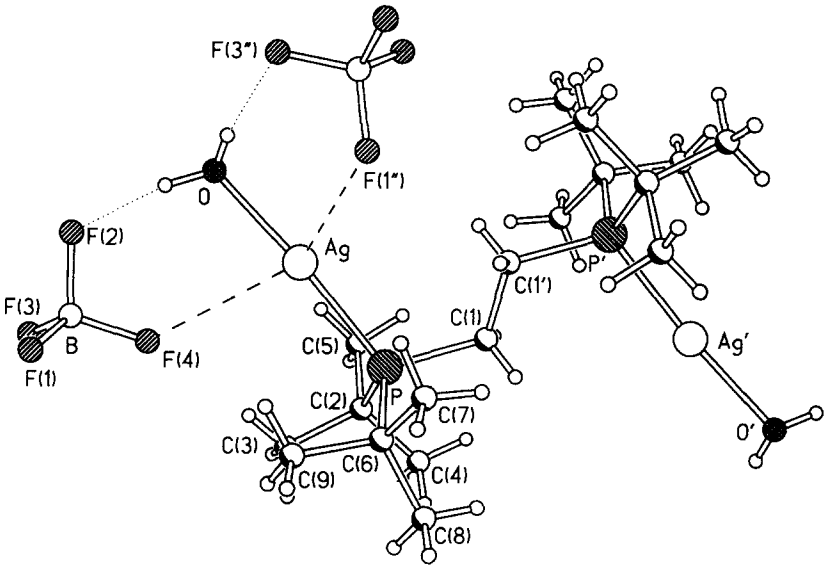

Fig. 2. X-ray molecular structure of **2**, showing the additional coordination of one silver atom, supported by hydrogen bonds. Primed atoms are symmetrically related via the inversion centre, double-primed *via* the *n* glide plane.

Table 2. Selected bond distances (Å) and angles(°) in the structure of **2**

Ag—P	2.347(1)	Ag—O	2.177(3)
Ag···F(1")	2.834(3)	Ag···F(4)	2.947(3)
P—C(1)	1.852(4)	P—C(2)	1.872(4)
P—C(6)	1.868(4)		
B—F(1)	1.375(5)	B—F(4)	1.370(5)
B—F(2)	1.394(5)	B—F(3)	1.397(5)
O···F(2)	2.730(4)	O···F(3")	2.689(4)
P—Ag—O	169.8(1)	F(1)—Ag—F(4)	122.9(1)
P—Ag—F(1)	108.96(6)	P—Ag—F(4)	102.83(5)
O—Ag—F(1")	80.3(1)	O—Ag—F(4)	74.5(1)
Ag—P—C(1)	114.5(1)	C(1)—P—C(2)	104.1(2)
Ag—P—C(2)	108.4(1)	C(1)—P—C(6)	105.6(2)
Ag—P—C(6)	109.8(1)	C(2)—P—C(6)	114.5(2)

EXPERIMENTAL

Silver(I) tetrafluoroborate was purchased from Aldrich Chemicals and used without further purification. The diphosphines were synthesised and purified by published methods [18]. Solvents were purified by standard procedures, stored under nitrogen and used under a nitrogen atmosphere. ^1H (400 MHz), $^{31}P\{^1H\}$ (161 MHz) and $^{13}C\{^1H\}$ (100 MHz) NMR spectra were recorded using a Varian 400 spectrometer, spectra being obtained in $CDCl_3$ solution. Chemical shifts are given relative to [$SiMe_4$] (external reference for ^1H and ^{13}C, measurements) and 85% aqueous H_3PO_4 (external reference for ^{31}P measurements). Carbon, hydrogen and nitrogen analyses were performed using a CE 440 elemental analyser. Cyclic voltammetry was undertaken in cyanomethane and dichloromethane solutions (ca 10^{-3} mol dm^{-3}) using a Bioanalytical System (type CV-1B) potential wave generator with a Ag/Ag^+ couple as a reference electrode and tetrabutylammonium tetrafluoroborate as the supporting electrolyte. Mass spectra were recorded using a VG analytical 707E spectrometer. Fast atom bombardment using xenon was used on the complexes in a nitrobenzylalcohol matrix.

Isolation of $[Ag_2\{Bu^t_2P(CH_2)_3PBu^t_2\}_2](BF_4)_2 \cdot 2CH_2Cl_2$, **1**

$[Rh(C_2H_4)_2Cl]_2$ (0.7 g, 1.78 mmol) was stirred in suspension in CH_2Cl_2 (30 cm^3) and cooled in an ice-bath. A solution of norbornadiene (0.79 g, 8.6 mmol) in CH_2Cl_2 (15 cm^3) was added to the slurry, causing the mixture to turn deep red–brown and evolve ethene. After 30 min, addition of excess $AgBF_4$ (1.00 g, 5.14 mmol) produced a colourless solid (AgCl) suspended in a deep red solution of $[Rh(C_7H_8)_2](BF_4)$. After a further 45 min stirring at room temperature, the solution was filtered and dbpp (0.43 g, 1.28 mmol) in CH_2Cl_2 (6 cm^3) added slowly over 10 min. An immediate colour change from red to orange was accompanied by precipitation of [Rh(dbpp)(C_7H_8)](BF_4), which was recrystallised from a THF/pentane mixture. Found: C, 50.51; H, 8.24. $C_{26}H_{50}BF_4P_2Rh$ requires C, 50.83; H, 8.20%. M.s. (FAB+ve ion): m/z 527.4 (M^+, 12.7%). Full spectroscopic characterisation will be reported elsewhere.

The mother liquor, on reduction to small volume and cooling to −20°, yielded a small number of colourless crystals of **1**, suitable for X-ray crystallography.

Isolation of $[Ag_2\{Bu^t_2P(CH_2)_2PBu^t_2\}(H_2O)_2](BF_4)_2$, **2**

The method described above was used to synthesise $[Rh\{Bu^t_2P(CH_2)_2PBu^t_2\}(C_7H_8)](BF_4)$ (to be reported elsewhere), except that dbpe (0.41 g, 1.28 mmol) was used in place of dbpp. The mother liquor, following the removal of the precipitated rhodium complex, when reduced in volume and cooled to −20°, yielded colourless, light-sensitive crystals of **2**, suitable for an X-ray crystallography, but insufficient in quantity for spectroscopic and other studies. Subsequent attempts to synthesise the same complex from $AgBF_4$ and the diphosphine failed. The ^{31}P NMR spectra of reaction solutions indicated the presence of several products in solution, none of which could be assigned with confidence.

Direct synthesis of **1**

Dbpp (0.42 g, 1.27 mmol) was dissolved in diethyl-ether (4 cm^3) and the solution added by cannular to a stirred suspension of $AgBF_4$ (0.25 g, 1.27 mmol) in dichloromethane (200 cm^3). The mixture was then stirred in the dark for 2 h. At the end of this period, the beige silver salt had reacted and a solution formed. The solvent volume was reduced *in vacuo* to *ca* 50 cm^3 the solution filtered, and the volume further reduced to *ca* 15 cm^3. Slow addition of hexane caused the precipitation of colourless crystals of **1**, which were removed by filtration. Cooling the filtrate to −15°C produced a second crop of crystals, shown to be identical to the first crop by spectroscopic methods. Yield: 0.50 g (75%). Found: C, 39.27; H, 7.33. $C_{40}H_{88}Ag_2B_2Cl_4F_8P_4$ requires C, 39.30; H, 7.26%. NMR ($CDCl_3$): ^1H; δ 5.30 (s), 1.88 (br m, 4H, PCH_2), 1.27 (t, 36H, $J_{P\text{-}H}$ 7.2 Hz), 1.18 (s, 2H, PCH_2CH_2): $^{13}C\{^1H\}$; δ 53.43 (s, CH_2Cl_2), 29.83 (s, PC-CH_3), 31.41 (m, P*C*-CH_3), 33.84 (m, PCH_2), 22.05 (m, PCH_2CH_2); ^{31}P δ 57.83 ppm [d, $J(^{107}Ag\text{-}P)$ 467 Hz, $J(^{109}Ag\text{-}P)$ 539 Hz]. FAB Mass Spectrum (nitrobenzyl alcohol matrix): −ve ion *m/z* [100%, BF_4^-]; +ve ion *m/z* 821.4 [3%, $(M—Bu^t)^+$], 439.3 [100%, $^{107}Ag(dbpe)^+$], 565.2 [20%, $(^{107}Ag_2C_{16}H_{36}P_4)^+$], 57.0 [52%, $(C_4H_9)^+$].

Crystal structure determination

X-ray single crystal diffraction experiment for **1** was performed on a Rigaku AFC6S 4-circle diffractometer (ω scan mode with Lehmann–Larsen profile analysis), for **2** on a Siemens SMART 3-circle diffractometer with a CCD area detector, both at $T = 150$ K (Cryostream open-flow N_2 gas cooling device), using graphite-monochromated Mo–K_α radiation, $\bar{\lambda} = 0.71073$ Å. The structures were solved by direct methods and refined by full-matrix least squares (non-H atoms with anisotropic displacement parameters, H atoms in **1**

Table 3. Crystal data for compounds **1** and **2**

	(1)	(2)
Formula	$C_{38}H_{84}Ag_2P_4^{2+}(BF_4^-)_2 \cdot 2CH_2Cl_2$	$C_{18}H_{44}Ag_2O_2P_2^{2+}(BF_4^-)_2$
Formula weight	1224.1	743.8
Colour; habit	Colourless prism	Colourless prism
Crystal size, mm	0.1 × 0.3 × 0.3	0.07 × 0.4 × 0.4
Crystal system	Triclinic	Monoclinic
Space group	$P\bar{1}$ (No. 2)	$P2_1/n$ (No. 14)
a (Å)	11.476(3)	7.829(1)
b (Å)	11.559(3)	16.134(2)
c (Å)	12.485(3)	12.035(2)
α (°)	67.49(2)	90
β (°)	82.37(2)	103.95(1)
γ (°)	65.71(2)	90
V (Å^3)	1393.9(6)	1475.3(5)
Setting reflections, θ (°)	25, 10–15	308, 4–23
Z	1	2
D_x, (g cm^{-3})	1.46	1.68
μ (cm^{-1})	10.6	15.0
Max. 2θ (°)	50	51.5
Data total, unique, R(int)	5169, 4902, 0.023	6107, 2513, 0.041[a]
Data observed, $I > 2\sigma(I)$	3878	2313
Number of variables	291	242
$R(F$, obs. data)	0.044	0.033
$wR(F^2$, all data)	0.095	0.086
Goodness-of-fit	1.01	1.10
max./min. $\Delta\rho$ (eÅ^{-3})	1.14[b], −0.83	0.38, −0.73

[a] 0.074 before absorption correction.

[b] Near the disordered Cl(2), elsewhere <0.4 eÅ^{-3}.

were treated as 'riding', in **2** were refined isotropically) against F^2 of all data, using SHELXTL [19]. For **1** the absorption was negligible (6% variation of a ψ-curve); for **2** an integration absorption correction [20] was applied (6 faces indexed, min./max. transmission 0.515/0.901). In **1** one chlorine atom of the CH_2Cl_2 molecule exhibits disorder, which was approximated by a major site Cl(2) with 86% occupancy and two minor ones, Cl(2A) and Cl(2B), with 7% occupancies (refined in isotropic approximation). Crystal data and other experimental details are listed in Table 3; atomic co-ordinates and thermal parameters, full lists of bond lengths and angles have been deposited at the Cambridge Crystallographic Data Centre.

Acknowledgements—We wish to thank Leverhulme Trust for financial support (to A.S.B.) and EPSRC for a CASE studentship (to S.P.C.) and ICI Acrylics plc for sponsoring the award. Our thanks are extended to Dr R.L. Tooze, the industrial supervisor, for his help and guidance, and to Dr J.M. Rawson for the cyclic voltammetry measurements.

REFERENCES

1. Ho, D. M. and Bau, R., *Inorg. Chem.*, 1983, **22,** 4073.
2. Tiekink, E. R. T., *Acta Cryst. Sect. C*, 1990, **46,** 235.
3. Soh, P. N., Zhou, Z.-Y., Mak, T. C. W. and Hor, T. S. A., *Inorg. Chem.*, 1995, **34,** 520.
4. Zheng, Y., Dryden, N. H., Vittel, J. J. and Puddephatt, R. J., *Can. J. Chem.*, 1994, **72,** 1605.
5. Perreault, D., Drouin, M., Michel, A., Miskowski, V. M., Schaefer, W. P. and Harvey, P. D., *Inorg. Chem.*, 1992, **31,** 695.
6. Karsch, H. H. and Shubert, U., *Z. Naturforsch. B.*, 1982, **37,** 186.
7. Di Bernardo, P., Dolcetti, G., Portanova, R., Tolazzi, M., Tomat, G. and Zanonato, P., *Inorg. Chem.*, 1990, **29,** 2859.
8. (a) Saboonchian, V., Wilkinson, G., Hussain-Bates, B. and Hursthouse, M. B., *Polyhedron*, 1991, **10,** 737; (b) Yang, H., Zheng, L., Xu, Y. and Zhang, Q., *Wuji Huaxue Xuebao*, 1992, **8,** 65–1; Cambridge Crystallographic Data Centre (CCDC) reference code JUVRAT.
9. Tiekink, E. R. T., *Acta Cryst. Sect C*, 1990, **46,** 1933.
10. Crabtree, S. P. and Kilner, M., unpublished results.
11. Shannon, R. D. and Prewitt, C. T., *Acta Cryst. Sect. B*, 1969, **25,** 925.
12. Camalli, M. and Caruso, F., *Inorg. Chim. Acta*, 1987, **127,** 209.
13. (a) Lang, H., Kohler, K. and Schiemenz, B., *J. Organomet. Chem.*, 1995, **495,** 135; (b) Batsanov, A. S., Crabtree, S. P., Howard, J. A. K., Lehmann, C. W. and Kilner, M., *J. Organomet. Chem.*, 1997, in press.
14. Camalli, M. and Caruso, F., *Inorg. Chim. Acta*, 1988, **144,** 205.
15. Barrow, M., Bürgi, H.-B., Camalli, M., Caruso, F., Fischer, E., Venanzi, L. M. and Zambonelli, L., *Inorg. Chem.*, 1983, **22,** 2356.
16. (a) Fornies, J., Lalinde, E., Martinez, F., Moreno, M. T. and Welch, A.. J., *J. Organomet. Chem.*, 1993, **455,** 271; (b) Yang, H.-H., Zheng, L. S., Zhang, Y., Zhang, P. and Zhang, Q.-E., *Jiegou Huaxue*, 1990, **9,** 137, CCDC ref. code KESLAV; (c) Huang, M., Zhang, P., Zhang, Y., Yang, H. and Zheng, L., *Wuli Huaxue Xuebao*, 1991, **7,** 694, CCDC ref. code PANDOX.
17. Batsanov, A. S., Hubberstey, P. and Russell, C. E., *J. Chem. Soc., Dalton Trans.*, 1994, 3189.
18. Perrin, D. D. and Armarego, W. L. F., *Purification of Laboratory Chemicals*, 3rd ed., Pergamon, Oxford (1988).
19. Sheldrick, G. M., SHELXTL, Version 5. Siemens Analytical X-Ray Instruments Inc., Madison, WI, U.S.A. (1995).
20. Coppens, P., Leiserowitz, L. and Rabinovich, D., *Acta Cryst.*, 1965, **18,** 1035.

Pergamon

PII: S0277-5387(97)00279-9

Polyhedron Vol. 17, No. 2–3, pp. 373–379, 1998
© 1997 Elsevier Science Ltd
All rights reserved. Printed in Great Britain
0277–5387/98 $19.00+0.00

Crystal structures of a series of Co^{II}, Cu^{II} and Zn^{II} complexes of 4′-(3,4-dihydroxyphenyl)-2,2′:6′,2″-terpyridine and 4′-(3,4-dimethoxyphenyl)-2,2′:6′,2″-terpyridine

Brenda Whittle, Emily L. Horwood, Leigh H. Rees, Stuart R. Batten, John C. Jeffery and Michael D. Ward*

School of Chemistry, University of Bristol, Cantock's Close, Bristol, BS8 1TS, U.K.

(Received 7 May 1997; accepted 9 June 1997)

Abstract—The crystal structures of the bis(terpyridyl)-metal(II) complexes $[Co(L^1)_2][PF_6]_2 \cdot 2.5MeCN$, $[Co(L^2)_2][PF_6]_2 \cdot 3dmf$, $[Cu(L^2)_2][PF_6]_2 \cdot MeCN$, $[Zn(L^1)_2][PF_6]_2 \cdot 2.5MeCN$, and $[Zn(L^2)_2][NO_3]_2 \cdot 3dmf$ are reported, where L^1 is 4′-(3,4-dihydroxyphenyl)-2,2′:6′,2″-terpyridine and L^2 is 4′-(3,4-dimethoxyphenyl)-2,2′:6′,2″-terpyridine. The two Co^{II} complexes and the Cu^{II} complex all show elongation along one axis in addition to the normal tetragonal compression imposed by terpyridyl chelates; this is ascribed to the Jahn–Teller effect, in the case of the Co^{II} complexes arising from the presence of a significant proportion of the low-spin state being present at the temperature used for the structural determination (173 K). The Zn^{II} complexes are the first structurally characterised bis(terpyridyl)-Zn^{II} compounds. These do not show the elongation along one axis that was apparent in the Co^{II} and Cu^{II} structures. The relatively small bite angles for the terpyridyl chelates (ca. 150°, compared to ca. 160° for the first three complexes), results in a greater distortion away from regular octahedral geometry, reflecting the absence of stereoelectronic requirements for Zn^{II} compared to Co^{II} and Co^{II}. © 1997 Elsevier Science Ltd

Keywords: terpyridyl; complexes; crystal structures.

We describe in this paper a series of crystal structures of complexes of Co^{II}, Cu^{II} and Zn^{II} with the two substituted terpyridine ligands 4′-(3,4-dihydroxyphenyl)-2,2′:6′,2″-terpyridine (L^1) and 4′-(3,4-dimethoxyphenyl)-2,2′:6′,2″-terpyridine (L^2). These complexes are: $[Co(L^1)_2][PF_6]_2 \cdot 2.5MeCN$; $[Co(L^2)_2][PF_6]_2 \cdot 3dmf$; $[Cu(L^2)_2][PF_6]_2 \cdot MeCN$; $[Zn(L^1)_2][PF_6]_2 \cdot 2.5MeCN$; and $[Zn(L^2)_2][NO_3]_2 \cdot 3dmf$. We have previously prepared ruthenium(II) complexes of L^1 and L^2, and used L^1 as a bridging ligand for the preparation of polynuclear complexes in which the terpyridyl site was coordinated to a ruthenium(II) core and the pendant deprotonated catechol site was coordinated to a variety of other metals [1]. We were interested to see if complexes of these ligands with first-row transition metals would also form oligonuclear species in the same way, and have found generally that simple mononuclear complexes with an $\{M(terpy)_2\}^{+}$-type core result.

Despite the large number of crystal structures of first-row transition metal complexes containing terpyridine ligands, the majority of these are of the type $[M(terpy)L_n]^{m+}$ with one terpyridine ligand and usually two or three monodentate ligands completing the coordination sphere. Crystal structures of homoleptic complexes of terpyridine and its substituted derivatives are relatively rare for first-row metals, especially considering the vast number of such ligands that are known, and a search (January 1997) of the Cambridge Structural Database found just 17 examples, all of which are confined to the later elements (Cr–Cu). Complexes of Co^{II} are the commonest (six examples) [2] because of the interest in the spin-crossover properties of $[Co(terpy)_2]^{2+}$ derivatives, which are sensitive to small changes in the crystalline lattice such as type of counter-ion and degree of solvation. There are also crystal structures of homoleptic bis-terpyridyl com-

* Author to whom correspondence should be addressed.

Table 1. Analytical and mass spectroscopic data for the new complexes

Complex	Elemental analyses (%)[a] C	H	N	FAB mass spectra (*m/z*) M—PF_6	M—$2PF_6$
$[Co(L^1)_2][PF_6]_2$	48.4 (48.9)	3.1 (2.9)	8.2 (8.1)	886	741
$[Co(L^2)_2][PF_6]_2$	50.8 (50.8)	3.6 (3.5)	7.8 (7.7)	942	797
$[Cu(L^2)_2][PF_6]_2$	50.5 (50.6)	3.6 (3.5)	7.9 (7.7)	946	801
$[Zn(L^1)_2][PF_6]_2$	47.8 (48.6)	3.1 (2.9)	7.7 (8.1)	891	746
$[Zn(L^2)_2][NO_3]_2 \cdot MeCN$[b]	51.1 (50.8)	3.9 (3.7)	8.7 (8.6)	947	802

[a] Expected values in parentheses.
[b] Sample for analysis recrystallised from MeCN/ether.

plexes of Co^{III} (one example) [3], Cr^{III} (one example) [4], Mn^{II} (one example) [5], Fe^{II} (two examples) [6], Ni^{II} (three examples) [7], and Cu^{II} (three examples) [8]. Surprisingly, there are no crystal structures of $[Zn(terpy)_2]^{2+}$ or its substituted derivatives, and the two Zn^{II} structures reported here are therefore the first of their type.

EXPERIMENTAL

Ligands L^1 and L^2 were prepared as described previously [1]. Complexes were prepared by adding a solution of the appropriate ligand (0.4 mmol) in H_2O/MeOH (1 : 2, 30 cm^3) to a solution of the appropriate metal salt (sulphate, chloride or nitrate) (0.2 mmol) in water (5 cm^3). After stirring for 1 h, excess aqueous KPF_6 was added to precipitate the complexes which were filtered off and dried *in vacuo*. Recrystallisation by diffusion of ether vapour into concentrated MeCN or dmf solutions of the complexes afforded X-ray quality crystals in all cases except $[Zn(L^2)_2][PF_6]_2$, which was therefore converted to its nitrate salt by anion metathesis; recrystallisation of $[Zn(L^2)_2][NO_3]_2$ from dmf/ether then afforded X-ray quality crystals. All complexes gave elemental analyses and fast-atom bombardment mass spectra in accord with their formulations (Table 1).

Crystals for X-ray analysis were mounted on glass fibres on a Siemens SMART diffractometer. A detailed description of the methods used for establishing unit cell parameters, and collecting, integrating and merging the data, has been published elsewhere [9]. Details of crystal parameters, data collection and refinement are summarised in Table 2. The structures were solved by conventional direct methods and refined by the full-matrix least-squares method on all F^2 data with the SHELXTL 5.03 package using a Silicon Graphics Indy computer. All non-hydrogen atoms were refined anisotropically; hydrogen atoms were included in calculated positions and refined with isotropic thermal parameters.

In $[Co(L^1)_2][PF_6]_2 \cdot 2.5MeCN$ the half molecule of MeCN is disordered over an inversion centre; the other two MeCN molecules are well defined. One of the peripheral hydroxyl groups is disordered between the C^3 and C^5 sites of the phenyl ring, appearing as O(47) [attached to C(43); 0.78 site occupancy] and O(49) [attached to C(45); 0.22 site occupancy]. Only the major component is shown in Fig. 1. $[Zn(L^1)_2][PF_6]_2 \cdot 2.5MeCN$ has very similar unit cell

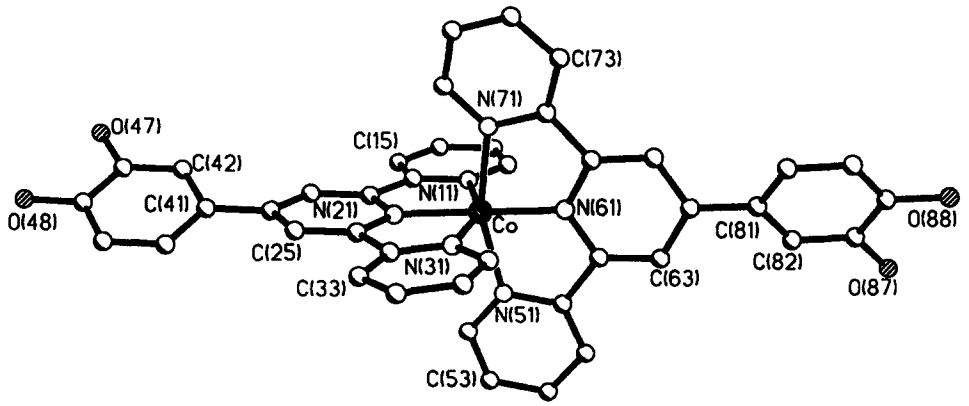

Fig. 1. Structure of the complex cation of $[Co(L^1)_2][PF_6]_2 \cdot 2.5MeCN$.

Table 2. Crystallographic data for the five new complexes

Complex	$[Co(L^1)_2][PF_6]_2 \cdot 2.5MeCN$	$[Co(L^2)_2][PF_6]_2 \cdot 3dmf$	$[Cu(L^2)_2][PF_6]_2 \cdot MeCN$	$[Zn(L^1)_2][PF_6]_2 \cdot 2.5MeCN$	$[Zn(L^2)_2](NO_3)_2 \cdot 3dmf$
Formula	$C_{47}H_{37.5}CoF_{12}N_{8.5}O_4P_2$	$C_{55}H_{59}CoF_{12}N_9O_7P_2$	$C_{48}H_{41}CuF_{12}N_7O_4P_2$	$C_{47}H_{36}F_{12}N_{8.5}O_4P_2Zn$	$C_{55}H_{59}N_{11}O_{13}Zn$
M	1134.23	1306.98	1133.36	1139.15	1147.50
System, space group	Triclinic, $P\bar{1}$	Triclinic, $P\bar{1}$	Triclinic, $P\bar{1}$	Triclinic, $P\bar{1}$	Triclinic, $P\bar{1}$
a (Å)	8.663(2)	9.9203(13)	9.8443(13)	8.710(2)	9.874(2)
b (Å)	9.081(2)	15.787(3)	12.420(2)	9.033(2)	13.829(3)
c (Å)	30.484(5)	19.441(5)	20.340(4)	30.878(7)	20.816(5)
α (°)	98.51(2)	92.203(13)	92.866(8)	97.90(3)	94.25(3)
β (°)	94.99(2)	93.901(14)	92.48(2)	95.79(2)	92.60(3)
γ (°)	94.661(13)	107.91(2)	106.927(10)	95.03(2)	106.93(2)
U (Å^3)	2352.0(7)	2884.8(10)	2371.8(7)	2381.3(8)	2705.1(11)
Z	2	2	2	2	2
D_c (g cm^{-3})	1.602	1.505	1.587	1.589	1.409
μ (mm^{-1})	0.536	0.452	0.629	0.685	0.530
F (000)	1152	1346	1154	1155	1200
T (K)	173(2)	173(2)	173(2)	173(2)	293(2)
Crystal size (mm^3)	$0.48 \times 0.20 \times 0.15$	$0.6 \times 0.3 \times 0.2$	$0.6 \times 0.2 \times 0.1$	$0.20 \times 0.15 \times 0.15$	$0.45 \times 0.30 \times 0.05$
2θ range (°)	5–50	5–50	5–50	5–50	5–50
Reflections collected (total, independent, R_{int})	11320, 8029, 0.020	13551, 9671, 0.037	11425, 8080, 0.021	11181, 7967, 0.023	12895, 9144, 0.042
Data, restraints, parameters	8029, 0, 693	9668, 75, 822	8075, 0, 698	7967, 0, 699	9136, 0, 721
Final R_1, wR_2[a,b]	0.055, 0.150	0.054, 0.133	0.035, 0.084	0.053, 0.146	0.073, 0.167
Weighting factors (a, b)[b]	0.0806, 1.0178	0.0238, 5.7420	0.0082, 3.0592	0.0797, 0.6201	0.0179, 11.5082
Largest peak, hole (e Å^{-3})	+0.935, −0.501	+0.814, −0.388	+0.379, −0.346	+0.712, −0.703	+0.692, −0.502

[a] Structure was refined on F_o^2 using all data; the value of R_1 is given for comparison with refinements based on F_o with a threshold of $F \geq 4\sigma(F)$.
[b] $wR_2 = [\Sigma[w(F_o^2 - F_c^2)^2]/\Sigma w(F_o^2)^2]^{1/2}$ where $w^{-1} = [\sigma^2(F_o^2) + (aP)^2 + bP]$ and $P = [\max(F_o^2, 0) + 2F_c^2]/3$.

parameters, the same disordered half-solvent molecule over an inversion centre, and the same disorder in the position of one of the hydroxyl groups between the C^3 and C^5 positions of the phenyl ring (site occupancies 0.76 and 0.24).

In $[Co(L^2)_2][PF_6]_2 \cdot 3dmf$ the complex cation, one of the anions, and all three solvent molecules are well ordered; the other hexafluorophosphate ion is disordered over two orientations such that the P(1), F(13) and F(15) are in fixed positions but the other four F atoms have two possible sites. The two components were successfully separated. The structure determinations of $[Cu(L^2)_2][PF_6]_2 \cdot MeCN$ and $[Zn(L^2)_2](NO_3)_2 \cdot 3dmf$ presented no problems of disorder.

RESULTS AND DISCUSSION

Cobalt complexes

The structure of the cation of $[Co(L^1)_2][PF_6]_2 \cdot 2.5MeCN$ is in Fig. 1; that of $[Co(L^2)_2][PF_6]_2 \cdot 3dmf$ is similar and not shown (the numbering scheme for the pyridyl rings is the same). Selected bond lengths and angles are in Table 3. The two structures have several features which are of significance. In both cases the Co—N bond lengths to the central rings of the terpyridine ligands [N(21) and N(61), 1.87–1.94 Å] are the shortest, which is a common steric consequence of the inability of the terminal pyridyl rings to bend around enough to achieve ideal octahedral coordination geometry at the metal centre [10]. Apart from this, the Co—N bond lengths to the terminal two pyridyl rings of one ligand [N(11) and N(31), ca. 2.15 Å] are markedly longer than the Co—N distances to the terminal pyridyl rings of the other ligand [N(51) and N(71), 1.99–2.05 Å]. Thus the N(11)—Co—N(31) axis is elongated with respect to the N(51)—Co—N(71) axis in each case, which is reflected in the separations between the *trans* pairs of pyridine ligands: in $[Co(L^2)_2][PF_6]_2$ for example, the N(11)···N(31) separation is 4.22 Å whereas the N(51)···N(71) separation is 3.94 Å, and the N(21)···N(61) separation—which would be expected to be the shortest—is 3.79 Å.

The geometry of $[Co(terpy)_2]^{2+}$ and its derivatives is sensitive to the spin-state of the Co^{II} centre, which is in turn sensitive to subtle lattice forces and therefore depends on the nature of the counter-ion and presence or absence of lattice solvent molecules. There is a clear relationship between the spin-state of the complex and the Co—N bond lengths [2]. Principally, the central Co—N bonds lengthen from ca. 1.9 Å to ca. 2.1 Å as the complex changes from predominantly low-spin to predominantly high-spin. The change in the terminal Co—N bond distances is less marked but still in the same sense, with the bonds lengthening by about 0.07 Å between predominantly low-spin and predominantly high-spin complexes [2]. In both $[Co(L^1)_2][PF_6]_2 \cdot 2.5MeCN$ and $[Co(L^2)_2][PF_6]_2 \cdot 3dmf$ therefore the values of the central Co—N bond lengths (values 1.904 and 1.942 Å for the former; 1.922 and 1.866 Å

Table 3. Selected bond lengths (Å) and angles (°) for $[Co(L^1)_2][PF_6]_2 \cdot 2.5MeCN$ and $[Co(L^2)_2][PF_6]_2 \cdot 3dmf$

$[Co(L^1)_2][PF_6]_2 \cdot 2.5MeCN$		$[Co(L^2)_2][PF_6]_2 \cdot 3dmf$	
Co—N(61)	1.904(3)	Co(1)—N(61)	1.866(3)
Co—N(21)	1.942(3)	Co(1)—N(21)	1.922(3)
Co—N(71)	2.041(3)	Co(1)—N(51)	1.993(3)
Co—N(51)	2.051(3)	Co(1)—N(71)	1.993(3)
Co—N(31)	2.148(3)	Co(1)—N(11)	2.147(3)
Co—N(11)	2.152(3)	Co(1)—N(31)	2.150(3)
N(61)—Co—N(21)	176.90(12)	N(61)—Co(1)—N(21)	179.11(12)
N(61)—Co—N(71)	80.14(12)	N(61)—Co(1)—N(51)	81.42(11)
N(21)—Co—N(71)	98.99(12)	N(21)—Co(1)—N(51)	99.43(11)
N(61)—Co—N(51)	79.49(12)	N(61)—Co(1)—N(71)	81.13(11)
N(21)—Co—N(51)	101.37(12)	N(21)—Co(1)—N(71)	98.00(11)
N(71)—Co—N(51)	159.63(12)	N(51)—Co(1)—N(71)	162.28(11)
N(61)—Co—N(31)	98.49(11)	N(61)—Co(1)—N(11)	100.72(11)
N(21)—Co—N(31)	78.50(11)	N(21)—Co(1)—N(11)	79.10(11)
N(71)—Co—N(31)	88.52(11)	N(51)—Co(1)—N(11)	88.57(11)
N(51)—Co—N(31)	94.73(11)	N(71)—Co(1)—N(11)	91.63(11)
N(61)—Co—N(11)	105.04(12)	N(61)—Co(1)—N(31)	101.62(11)
N(21)—Co—N(11)	77.96(11)	N(21)—Co(1)—N(31)	78.57(11)
N(71)—Co—N(11)	93.69(11)	N(51)—Co(1)—N(31)	94.74(11)
N(51)—Co—N(11)	91.31(11)	N(71)—Co(1)—N(31)	91.79(11)
N(31)—Co—N(11)	156.41(11)	N(11)—Co(1)—N(31)	157.66(10)

for the latter) are indicative of predominantly low-spin behaviour; the shortest previously-reported Co—N (central) distance was 1.88 Å in $[Co(terpy)_2]Br_2 \cdot [FS]3H_2O$, whose magnetic moment (2.9 BM) indicates a majority of low-spin character.

In a low-spin d^7 configuration and octahedral geometry, Jahn–Teller distortion would be expected, which could manifest itself either as a lengthening along the z-axis [as is common in Cu^{II}], or a lengthening along the x and y axes (i.e. relative compression along the z-axis). Since the steric limitations of terpyridyl chelates mean that all bis-terpyridyl complexes are necessarily compressed along one axis, then additional Jahn–Teller distortion is unnecessary. If we call the shortest axis (containing the two central pyridyl donors) the z-axis, their greater proximity to the metal ion means that the $d(z^2)$ orbital is necessarily higher in energy than $d(x^2-y^2)$, which would lift the orbital degeneracy of the low-spin d^7 configuration; thus the Jahn–Teller distortion matches the distortion imposed naturally by the ligand. This appears to be the situation in all bis(terpyridyl)-Co^{II} complexes structurally characterised so far, with the two Co—N(terminal) axes being more or less equivalent, resulting in a roughly square xy plane. These two new complexes, however, have a marked tetragonal elongation along one Co—N(terminal) axis in addition to the compression along the Co—N(central) axis, as mentioned above. If this elongation is arising from a Jahn–Teller effect then it is the first example of this type of structural distortion observed for bis(terpyridyl)-Co^{II} complexes, and may reflect the fact that the Co^{II} ions in both structures are predominantly low-spin [cf. the Co—N(central) bond lengths] so that Jahn–Teller effects are particularly apparent. This may arise from the low temperature used for the structural determinations (173 K). Unfortunately both sets of crystals lose solvent rapidly when removed from the mother liquor, which will result in a major change in the crystalline environment and will therefore perturb the spin state of the Co^{II} ions. It is not therefore possible to relate magnetic susceptibility measurements to the crystal structures.

The pendant substituted phenyl rings are in each case twisted away from coplanarity with the adjacent terpyridyl unit. In biphenyl-type groups, the competition between electronic effects (greater delocalisation can occur in a coplanar configuration) and steric effects (a dihedral twist between the two rings minimises steric interference between the H^2 and $H^{2'}$ protons of a biphenyl unit) typically results in a dihedral twist of 30–40° in the gas phase, although in the solid state this is subject to influence from crystal packing effects [11]. In $[Co(L^1)_2][PF_6]_2 \cdot 2.5MeCN$ the dihedral angles are 23.6° and 26.9°, involving phenyl rings C(41)—C(46) and C(81)—C(86) respectively, which is not much smaller than the typical values. In $[Co(L^2)_2][PF_6]_2 \cdot 3dmf$, however, the twists are much smaller at 8.1° and 6.4° respectively.

The peripheral hydroxyl groups of In $[Co(L^1)_2][PF_6]_2 \cdot 2.5MeCN$ are involved in hydrogen-bonding interactions with lattice solvent molecules and counter-ions. The OH group of O(47) is involved in a O—H···N hydrogen-bond to N(123) of a lattice MeCN, with the non-bonded O···N separation being 2.68 Å; likewise the O—H···F interaction involving O(48) and F(24) has a non-bonded O···F separation of 2.88 Å, and the O—H···N interaction involving O(87) and N(231) (of acetonitrile) has a non-bonded O···F separation of 2.67 Å. All of these separations are consistent with reasonably strong hydrogen-bonds [12]. In $[Co(L^2)_2][PF_6]_2 \cdot 3dmf$ in contrast there are no such strong hydrogen-bonds in the lattice.

Copper complex

The structure of the complex cation of $[Cu(L^2)_2][PF_6]_2 \cdot MeCN$ is shown in Fig. 2; selected bond lengths and angles are in Table 4. As we would expect, the Cu—N bonds to the central pyridyl ring of each ligand [N(21) and N(61); Cu—N distances 1.936 and 1.996 Å respectively] are the shortest for the steric reasons described above. It is comparison of the other two axes which is of more interest, and it is clear from Table 4 that the terminal rings of one ligand

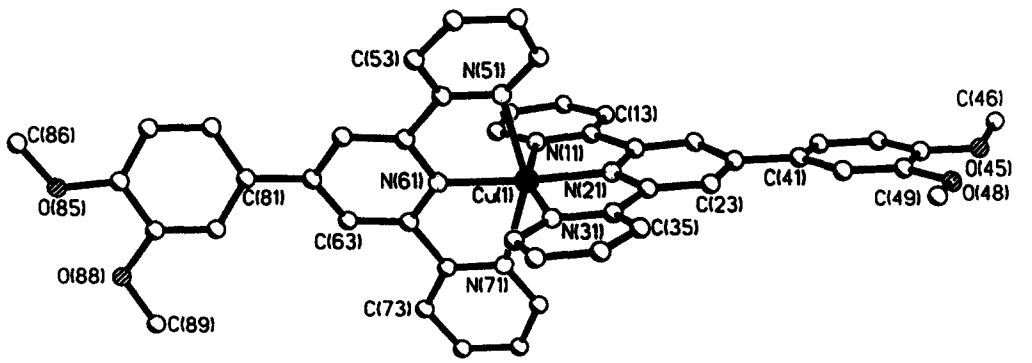

Fig. 2. Structure of the complex cation of $[Cu(L^2)_2][PF_6]_2 \cdot MeCN$.

Table 4. Selected bond lengths (Å) and angles (°) for $[Cu(L^2)_2][PF_6]_2 \cdot MeCN$

Cu—N(61)	1.996(2)		
Cu—N(21)	1.936(2)		
Cu—N(71)	2.261(2)		
Cu—N(51)	2.334(3)		
Cu—N(31)	2.085(2)		
Cu—N(11)	2.102(3)		
N(61)—Cu—N(21)	175.31(8)		
N(61)—Cu—N(71)	76.55(8)		
N(21)—Cu—N(71)	107.86(8)		
N(61)—Cu—N(51)	76.15(7)		
N(21)—Cu—N(51)	99.65(8)		
N(71)—Cu—N(51)	151.85(7)		
N(61)—Cu—N(31)	102.02(8)		
N(21)—Cu—N(31)	79.26(8)		
N(71)—Cu—N(31)	96.92(8)		
N(51)—Cu—N(31)	82.19(8)		
N(61)—Cu—N(11)	99.38(8)		
N(21)—Cu—N(11)	79.34(8)		
N(71)—Cu—N(11)	88.70(8)		
N(51)—Cu—N(11)	102.38(8)		
N(31)—Cu—N(11)	158.58(8)		

[N(51) and N(71); Cu—N distances 2.334 and 2.261 Å respectively] are much further from the metal than are those of the other ligand [N(11) and N(31); Cu—N distances 2.102 and 2.085 Å respectively]. This is reflected in a smaller bite angle for the more remote ligand (151.9° instead of 158.6°). There is therefore a very clear Jahn–Teller elongation along the N(51)—Cu—N(71) axis in addition to the compression along the N(2)—Cu—N(61) axis. This is entirely typical of six-coordinate Cu^{II} complexes and is similar to the distortions observed in the cobalt(II) complexes above. In these respects this structure is similar to those of other bis(terpyridyl)-Cu^{II} complexes [8]. The dihedral angles between the central pyridyl and pendant phenyl rings are 8.1° and 20.2° [at pyridyl rings N(21)–C(26) and N(61)–C(66) respectively].

Zinc complexes

As far as we know there are—surprisingly—no published crystal structures of bis(terpyridyl)-zinc(II) complexes; although $[Zn(terpy)_2]^{2+}$ complexes have been prepared, the crystal structures are confined to 1 : 1 complexes such as $[Zn(terpy)Cl_2]$. The structural parameters of the complex cations of $[Zn(L^1)_2][PF_6]_2 \cdot 2.5MeCN$ and $[Zn(L^2)_2](NO_3)_2 \cdot 3dmf$ are summarised in Table 5. Pictures are not given due to the similarity of these structures to those of the Co^{II} and Cu^{II} complexes already depicted; the numbering scheme is the same as that used for the other structures, with N(21) and N(61) [or N(121) and N(161)] being the central pyridyl rings of each ligand. There are several points to notice. Firstly, the Zn—pyridyl dis-

Table 5. Selected bond lengths (Å) and angles (°) for $[Zn(L^1)_2][PF_6]_2 \cdot 2.5MeCN$ and $[Zn(L^2)_2](NO_3)_2 \cdot 3dmf$

$[Zn(L^1)_2][PF_6]_2 \cdot 2.5MeCN$			$[Zn(L^2)_2](NO_3)_2 \cdot 3dmf$	
Zn—N(11)	2.175(3)		Zn(1)—N(111)	2.163(4)
Zn—N(21)	2.073(3)		Zn(1)—N(121)	2.074(4)
Zn—N(31)	2.181(3)		Zn(1)—N(131)	2.221(4)
Zn—N(51)	2.164(3)		Zn(1)—N(151)	2.179(4)
Zn—N(61)	2.074(3)		Zn(1)—N(161)	2.105(4)
Zn—N(71)	2.225(3)		Zn(1)—N(171)	2.194(4)
N(61)—Zn—N(21)	173.16(12)		N(161)—Zn(1)—N(121)	176.7(2)
N(61)—Zn—N(71)	74.99(12)		N(161)—Zn(1)—N(171)	75.0(2)
N(21)—Zn—N(71)	98.20(12)		N(121)—Zn(1)—N(171)	102.8(2)
N(61)—Zn—N(51)	75.79(12)		N(161)—Zn(1)—N(151)	74.8(2)
N(21)—Zn—N(51)	110.99(12)		N(121)—Zn(1)—N(151)	107.3(2)
N(71)—Zn—N(51)	150.65(12)		N(171)—Zn(1)—N(151)	149.7(2)
N(61)—Zn—N(31)	103.16(12)		N(161)—Zn(1)—N(131)	102.6(2)
N(21)—Zn—N(31)	75.75(12)		N(121)—Zn(1)—N(131)	74.9(2)
N(71)—Zn—N(31)	88.81(12)		N(171)—Zn(1)—N(131)	94.1(2)
N(51)—Zn—N(31)	95.23(12)		N(151)—Zn(1)—N(131)	91.1(2)
N(61)—Zn—N(11)	105.50(12)		N(161)—Zn(1)—N(111)	106.7(2)
N(21)—Zn—N(11)	75.46(12)		N(121)—Zn(1)—N(111)	75.8(2)
N(71)—Zn—N(11)	95.81(12)		N(171)—Zn(1)—N(111)	93.6(2)
N(51)—Zn—N(11)	94.46(11)		N(151)—Zn(1)—N(111)	96.3(2)
N(31)—Zn—N(11)	151.20(12)		N(131)—Zn(1)—N(111)	150.7(2)

tances are on average longer than the Co—pyridyl distances, and are also rather longer than those four Cu—N distances which do not suffer from additional Jahn–Teller elongation. This is a natural consequence of the increased occupancy of the antibonding $d(z^2)$ and $d(x^2-y^2)$ orbitals. Secondly, we see again the usual compression of the two Zn—N(central) bonds (2.074 and 2.105 Å) compared to the four Zn—N(terminal) bonds (2.16–2.23 Å). Thirdly, there is no obvious elongation along one of the Zn—N(terminal) axes. The average Zn—N distances in these directions (Table 5) differ by less than two standard deviations and are therefore equivalent within the limits of accuracy of the structure determination. This is in marked contrast to the two Co^{II} structures and the Cu^{II} structure, which all show evidence for elongation along one axis due to the Jahn–Teller effect and/or hydrogen-bonding interactions within the lattice. Fourthly, the absence of any stereoelectronic requirements for regular octahedral or tetragonal geometry is reflected in the bite angles of the coordinated terpyridyl fragments, which are all ca. 150° in the Zn^{II} complexes compared to 156–162° for the Co^{II} and Cu^{II} complexes [with the single exception of the ligand in the Cu^{II} complex which has an unusually low bite angle due to the Jahn–Teller elongation].

In $[Zn(L^1)_2][PF_6]_2 \cdot 2.5MeCN$ the dihedral angles between the pendant phenyl rings and the pyridyl rings to which they are attached are 27.6° and 25.3°; in $[Zn(L^2)_2](NO_3)_2 \cdot 3dmf$ these values are 2.5° and 19.1° respectively. This is the same pattern that was observed for the Co^{II} complexes, with the phenyl rings of L^1 more twisted away from the terpyridyl group than the phenyl rings of L^2. It is not possible to separate the different contributions to this that may arise from intermolecular (crystal packing, hydrogen-bonding) and intramolecular (electronic delocalisation) effects.

As with its isostructural Co^{II} analogue, $[Zn(L^1)_2][PF_6]_2 \cdot 2.5MeCN$ has hydrogen-bonding interactions in the lattice between the hydroxyl groups as donors, and solvent molecules or anions as acceptors. The most significant of these are O–H···N interactions between O(47)/N(132) (non-bonded O···N distance 2.71 Å) and between O(87)/N(113) (non-bonded O···N distance 2.80 Å).

Acknowledgements—We thank the EPSRC for financial support.

REFERENCES

1. Whittle, B., Everest, N. S., Howard, C. and Ward, M. D., *Inorg. Chem.*, 1995, **34,** 2025.
2. Henke, W. and Kremer, S., *Inorg. Chim. Acta*, 1982, **65,** L115; Figgis, B. N., Kucharski, E. S. and White, A. H., *Aust. J. Chem.*, 1983, **36,** 1527; Figgis, B. N., Kucharski, E. S. and White, A. H., *Aust. J. Chem.*, 1983, **36,** 1537; Takusagawa, F., Yohannes, P. G. and Mertes, K. B., *Inorg. Chim. Acta*, 1986, **114,** 165; Raston, C. L. and White, A. H., *J. Chem. Soc., Dalton Trans.*, 1976, 7; Maslen, E. N., Raston, C. L. and White, A. H., *J. Chem. Soc., Dalton Trans.*, 1974, 1803.
3. Figgis, B. N., Kucharski, E. S. and White, A. H., *Aust. J. Chem.*, 1983, **36,** 1563.
4. Wickramasinghe, W. A., Bird, P. H. and Serpone, N. *Inorg. Chem.*, 1982, **21,** 2694.
5. Bhula, R. and Weatherburn, D. C., *Aust. J. Chem.*, 1991, **44,** 303.
6. Baker, A. T. and Goodwin, H. A., *Aust. J. Chem.*, 1985, **38,** 207; Lainé, P., Gourdon, A. and Launay, J.-P., *Inorg. Chem.*, 1995, **34,** 5156.
7. Baker, A. T., Craig, D. C. and Rae, A. D., *Aust. J. Chem.*, 1995, **48,** 1373; Constable, E. C., Lewis, J., Liptrot, M. C. and Raithby, P. R., *Inorg. Chim. Acta*, 1990, **178,** 47; Arriortua, M. I., Rojo, T., Amigo, J. M., Germain, G. and Declerq, J. P., *Bull. Soc. Chim. Belg.*, 1982, **91,** 337.
8. Arriortua, M. I., Rojo, T., Amigo, J. M., Germain, G. and Declerq, J. P., *Acta Cryst.*, 1982, **38,** 1323; Folgado, J.-V., Henke, W., Allman, R., Stratemeier, H., Beltran-Porter, D., Rojo, T. and Reinen, D., *Inorg. Chem.*, 1990, **29,** 2035; Allman, R., Henke, W. and Reinen, D., *Inorg. Chem.*, 1978, **17,** 378.
9. Jones, P. L., Amoroso, A. J., Jeffery, J. C., McCleverty, J. A., Psillakis, E., Rees, L. H. and Ward, M. D., *Inorg. Chem.*, 1997, **36,** 10.
10. Constable, E. C., *Adv. Inorg. Chem. Radiochem.*, 1986, **30,** 69.
11. Eaton, V. J. and Steele, D., *J. Chem. Soc., Faraday Trans.* 2, 1973, 1601; Brock, C. P. and Minton, R. P., *J. Am. Chem. Soc.*, 1989, **111,** 4586.
12. Novak, A., *Struct. Bonding (Berlin)*, 1974, **18,** 177.

Pergamon

PII: S0277-5387(97)00284-2

Polyhedron Vol. 17, No. 2-3, pp. 381-389, 1998
© 1997 Elsevier Science Ltd
All rights reserved. Printed in Great Britain
0277-5387/98 $19.00+0.00

Synthesis of transition metal complexes with heteroazomethinic ligands: a comparison of traditional and electrochemical methods

B. I. Kharisov,[a]* L. M. Blanco,[a] A. D. Garnovskii,[b] A. S. Burlov,[b] L. I. Kuznetsova,[b] L. V. Korovina,[b] D. A. Garnovskii[b] and T. Dieck[c]

[a] Facultad de Ciencias Químicas, Universidad Autónoma de Nuevo León, Apdo. Postal 18-F, Ciudad Universitaria, 66450, San Nicholás de los Garza, Nuevo León, México

[b] Institute of Physical and Organic Chemistry, Rostov State University, 194/2, Stachki pr., Rostov-on-Don, 344090, Russia

[c] Departamento de Química, Instituto Tecnológico y de Estudios Superiores de Monterrey, Ave. E. Garza Sada Sur, 2501, C.P. 64849, Monterrey, Nuevo León, México

(Received 5 March 1997; accepted 29 May 1997)

Abstract—Transition metal complexes (M = Cu, Ni, Co, Pd, Zn and Cd) containing azomethinic ligands have been synthesized by conventional chemical methods and by direct electrochemical dissolution of the sacrificial metal anode. The resulting complexes were characterized by elemental analysis, IR and EPR-spectra and magnetochemical data. The influence of the type of metal, the peculiarities of the ligand structure and the methods of synthesis of metal chelates on their physico-chemical properties and structure are examined. © 1997 Elsevier Science Ltd

Keywords: electrochemical synthesis; heteroazomethinic ligands; transition metals.

Transition metal complexes with azomethinic ligand systems have been intensively studied in the last 30 years. The main research results have been reported in a series of articles and reviews [1–11]. The following azomethinic ligands, **I**,

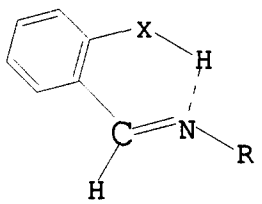

I

where:
X = NTs, O, S, Se, Ts; Ts = $-SO_2C_6H_4CH_3$-*p*
R = H, Alk, Ar, Het (heteroatoms), OH, $(CH_2)_nOH$ (n = 2,3); NR^1R^2, R^1 = H, R^2 = Alk, Ar;
$R^1 = R^2$ = Alk, Ar

present the peculiarity of produce different types of metal complexes starting from the same ligand [6,8,10] as a consequence of the presence of an inner-molecular hydrogen bond, of the tautomeric equilibrium between the keto–enol (thion–thiol) and imino–amine forms, and of the molecular spatial configuration, **I** and **III**.

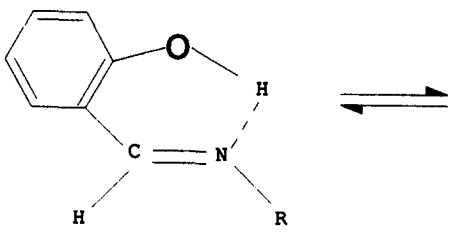

II

* Author to whom correspondence should be addressed.

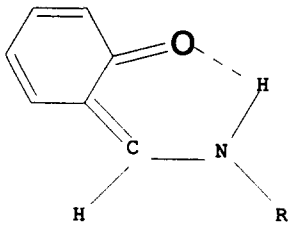

III

These structures [7,9,10] lead to the formation of two types of coordination compounds **IV** or **V**; the type **IV** are adducts (molecular complexes) with a conserved ligand system and **V** are chelates with a deprotonated azomethinic molecule having inner-chelate bonds [9,10]. The possibility of obtaining an adduct or a chelate depends on the nature of the metal and anion as well as the synthetic conditions

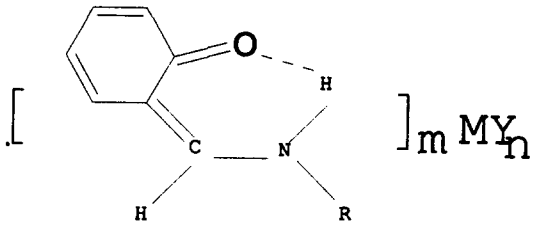

IV

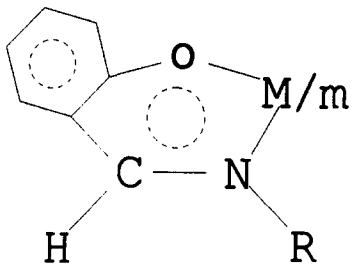

V

where:
Y = Hal, NO_3, NCO, NCS; n = 2–5; m = 1–3

The use of these ligands permits one to carry out a selective synthesis due to the possibilities of modifying the structural details of the ligands (e.g., control of tautomeric equilibrium, nature of donor atoms, character of aldehyde and amine fragments, the total number of atoms in the chelate rings and the number of N-atoms) [9–10].

In this work transition metal complexes (M = Cu, Ni, Co, Pd, Zn and Cd) have been obtained from the Schiff bases by conventional methods and by direct electrochemical dissolution of the sacrificial metal anode (Cu, Ni) in non-aqueous solvents containing the corresponding azomethinic ligands. The main advantage of electrochemical syntheses is that the reaction takes place in one step with high yields and in a short time [12–14].

EXPERIMENTAL

Synthesis of Schiff bases

The synthesis of the Schiff bases was carried out according to an established procedure [15]. In this work we describe the synthesis of two, **VI** and **VII**; the other ones have been prepared similarly.

1-Methylbenzimidazole-2-aldehyde-2′-mercaptophenylimine. A toluene solution (50 cm^3) containing 1.25 g (0.01 mol) of *o*-aminthiophenol was added to the toluene solution (50 cm^3) containing 1.6 g (0.01 mol) of 1-methyl-2-formylbenzimidazole and was heated at full reflux. After the reaction finished the toluene was distilled off in a rotation evaporator and 50 cm^3 of boiling methanol were added to the reaction mixture. After cooling, a slightly yellow product was isolated, filtered, and recrystallized from methanol (m.p. 220°C).

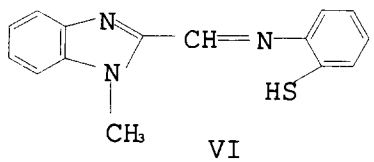

VI

1-Methylbenzimidazole-2-aldehyde-2′-o-tosylaminphenylimine. The synthesis was carried out according to the above method; recrystallization was made from dioxane (m.p. 200–203°C).

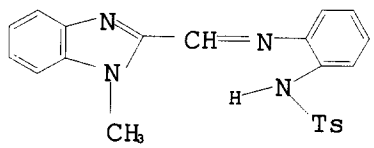

VII

Ts = $-SO_2-C_6H_4-CH_3$

The data about the azomethinic ligands VI and VII are presented in Table 1.

Synthesis of transition metal complexes

Synthesis by the conventional chemical methods. The syntheses have been carried out according to ref. [16]. The ligands and their corresponding metal acetates (molar ratios 1 : 1 or 1 : 2) were dissolved in methanol (acetone in the case of Pd) and then heated in a water bath for 1 h. The solids formed were filtered, purified three times with 5 cm^3 of methanol and dried *in vacuo* 150°C.

The reaction yields were in the range 75–80%. The elemental analyses and the physico-chemical properties of the complexes are presented in Table 1.

Table 1. Analytical and related data for metal chelates obtained

No	L, X	M	Composition	Formula	Elemental analysis data, % (found/calculated) C	H	N	S	M	Colour	M.P. (°C)	μ_{eff} B.M.
1	VI, S	H	HL	$C_{15}H_{13}N_3S$	67.33	4.66	14.97	11.85	—	Slight.	220	—
					67.41	4.87	15.73	11.99		yellow		
2	VI, S	Cu	$CuL_2 \cdot 3H_2O$	$C_{30}H_{30}N_6O_3S_2Cu$	55.37	4.48	11.69	8.99	9.14	Brown	180	2.07
					55.42	4.62	12.93	9.85	9.85			
3	VI, S	Ni	$NiLAc \cdot H_2O$	$C_{17}H_{17}N_3O_3SNi$	49.77	4.19	10.36	7.85	14.28	Brown	260	2.52
					50.78	4.23	10.46	7.97	14.62			
4	VI, S	Co	$CoL_2 \cdot 2H_2O$	$C_{30}H_{28}N_6O_2S_2Co$	57.00	4.07	12.75	9.88	9.27	Green	290	—
					57.42	4.46	13.40	10.21	9.40	-obsc.		
5	VI, S	Zn	$ZnLAc \cdot H_2O$	$C_{17}H_{17}N_3O_3SZn$	49.87	3.80	10.18	7.73	15.84	Red-	205	Diam.
					49.95	4.16	10.28	7.84	16.01	blood		
6	VI, S	Cd	CdLAc	$C_{17}H_{15}N_3O_2SCd$	46.31	3.18	9.47	7.15	25.11	Red	250	Diam.
					46.64	3.43	9.60	7.32	25.70			
7	VI, S	Pd	$PdLAc \cdot MeOH$	$C_{18}H_{19}N_3O_3SPd$	46.32	3.65	8.89	6.78	22.89	Black	280	Diam.
					46.61	4.10	9.06	6.90	22.96			
8	VII, NTs	H	HL	$C_{22}H_{20}N_4O_2S$	64.94	4.60	13.58	7.84	—	White	201	—
					65.45	4.95	13.86	7.92				
9	VII, NTs	Cu	CuLAc	$C_{24}H_{22}N_4O_4SCu$	54.69	4.06	10.15	5.98	13.03	Brown	250	1.75
					54.80	4.22	10.66	6.09	12.08			
10	VII, NTs	Ni	$NiLAc \cdot H_2O$	$C_{24}H_{24}N_4O_5SNi$	53.24	4.12	10.12	5.71	10.71	Red-	315	3.67
					53.46	4.46	10.39	5.94	10.90	bright		
11	VII, NTs	Co	$CoL_2 \cdot 2.5H_2O$	$C_{44}H_{43}N_8O_{6.5}S_2Co$	57.76	4.30	12.26	6.90	6.31	Brown	285	—
					58.03	4.73	12.31	7.03	6.48			
12	VII, NTs	Zn	$ZnL_2 \cdot H_2O$	$C_{44}H_{40}N_8O_5S_2Zn$	59.18	4.43	12.42	6.81	7.16	Red-	250	Diam.
					59.37	4.50	12.59	7.20	7.35	orange		
13	VII, NTs	Cd	$CdL_2 \cdot H_2O$	$C_{44}H_{40}N_8O_5S_2Cd$	55.99	4.06	11.75	6.47	11.46	Red–	315	Diam.
					56.39	4.27	11.96	6.83	12.00	orange		
14	VII, NTs	Pd	$PdLAc \cdot 2H_2O$	$C_{24}H_{26}N_4O_6SPd$	47.02	4.06	9.15	5.12	17.24	Black	350	Diam.
					47.65	4.30	9.27	5.29	17.60			
15	VII, NTs	Cu[a]	$CuL \cdot 2H_2O$	$C_{22}H_{23}N_4O_4SCu$	52.71	4.64	11.30	6.20	13.50	Brown	>250	2.24
					52.52	4.57	11.14	6.37	12.64			
16	VII, NTs	Ni[a]	$NiL_2 \cdot 2.5H_2O$	$C_{44}H_{43}N_8O_{6.5}S_2Ni$	57.89	4.39	12.20	6.98	6.26	Red	252	3.40
					58.04	4.73	12.31	7.04	6.45			
17	XIV, $R = C_2H_5$	Cu	$CuLAc \cdot H_2O$	$C_{25}H_{26}N_4O_5SCu$	53.74	4.20	9.48	5.41	11.21	Brown	241	2.01
					53.81	4.66	10.04	5.74	11.40			
18	XIV, $R = CH_3$	Cu[a]	$CuL \cdot 2H_2O$	$C_{22}H_{23}N_4O_4SCu$	52.33	4.36	10.80	6.15	12.36	Brown	267	2.02
					52.43	4.58	11.14	6.37	12.65			
19	XIV, $R = CH_3$	Ni[a]	NiL_2	$C_{44}H_{38}N_8O_4S_2Ni$	60.88	4.02	12.76	7.23	6.72	Brown	240	2.75
					61.06	4.39	12.95	7.40	6.79			
20	XV, R = H	Cu[a]	$CuL \cdot H_2O$	$C_{14}H_{12}N_3O_2Cu$	52.77	3.39	13.10	—	19.14	Yellow–	213	1.29
					52.91	3.78	13.23		20.01	brown		
21	XVI	Cu[a]	CuL_2	$C_{40}H_{34}N_4O_4S_2Cu$	62.93	4.15	7.17	8.27	7.98	Purple	278	1.96
					63.03	4.46	7.35	8.40	8.34			
22	XVI	Ni[a]	NiL_2	$C_{40}H_{34}N_4O_4S_2Ni$	62.99	4.21	7.25	8.32	7.60	Yellow–	218	3.52
					63.43	4.49	7.40	8.46	7.76	green		
23	XVII	Cu[a]	$CuL_2 \cdot 3H_2O$	$C_{36}H_{32}N_8O_5Cu$	59.47	4.12	15.40	—	8.61	Brown	247	2.20
					60.04	4.45	15.57		8.83			

[a] Obtained electrochemically.

Direct electrochemical synthesis of copper and nickel chelates

The complexes of Schiff bases have been obtained electrochemically. The electrosynthesis processes were carried out by anodic dissolution of metals in acetonitrile or methanol solutions of the corresponding ligands, according to the recommendations described by D. Tuck [12], M. Chakravorty *et al.* [13] and A. Sousa *et al.* [17–25] in the synthesis of similar complexes.

The cell consisted of a tall-form beaker, and the

solution phase contained the appropriate ligand (1–2 g) dissolved in acetonitrile, or in methanol containing tetrabutylammonium bromide or sodium chloride (0.1 N). The anode (sacrificial metal in each case) was supported on a platinum wire and a platinum sheet formed the cathode. All experiments were conducted at room temperature in an atmosphere of dry nitrogen, which was bubbled through the cell. The voltage was regulated to obtain an initial current of 20 mA. In each case the electrolysis was conducted for a period of 2–2.5 h, after which the anode was washed, dried and weighed in order to obtain the electrochemical efficiency. The complexes formed were filtered, washed with methanol or acetonitrile and dried in air. The experimental conditions are presented in Table 2. The yields of the final products were 85–96%.

In the case of copper complexes some of the product was occasionally formed on the surface of the anode (3 × 2 cm), which led to an increase of the voltage. To avoid this, we applied a combination of electrolysis with a simultaneous treatment by ultrasound. This stabilized the voltage because of a faster elimination of the complex formed on the anode surface [26]. The quantitative results of the study of electrosynthesis of some transition metal complexes with nitrogen-containing ligands using the combination of electrolysis and ultrasound, will be communicated later.

RESULTS AND DISCUSSION

As mentioned in the Introduction, the Schiff bases have many possibilities of modifying the structural and physico-chemical properties of their metal complexes [7,9,10]. The objective of this work is to compare the properties of metal chelates obtained in different synthetic conditions. We have obtained the complexes of Ni, Co, Zn, Cd, Pd, Cu with the ligands **VI** and **VII** by the conventional synthetic methods.

According to elemental analyses shown in Table 1, the Co, Zn, and Cd complexes of **II** have the composition $ML_2 \cdot nH_2O$ ($n = 1, 2.5$). However, the complexes of Cu, Ni and Pd with **VII** have the composition $MLAc \cdot nH_2O$ ($n = 0, 1, 2$).

Comparison of the IR-spectra (Table 3) for 1-methylbenzimidazole-2-aldehyde-2′-*o*-tosylaminphenylimine (**VII**) and the complexes 9, 11–14, 16, confirms the chelate structure of the metal complexes. Specifically, a decrease in the frequency of the azomethinic bond ν(C=N) from 1620 cm^{-1} by 27–40 cm^{-1} is observed, and the deprotonation of tosylamino group is confirmed by the disappearance of the band of the valency oscillations of the ν(NH) group in 3153 cm^{-1} in the spectra of these complexes.

It is known [27] that on coordination of the $NHSO_2$ group, a decrease of the frequencies ν_s and ν_{as} of the SO_2 group takes place between 1160 and 1353 cm^{-1}. Comparing the IR-spectra of the ligand **VII** and its chelates, we observed the shift of $\nu(SO_2)$ in the chelates, indicating the coordination of tosyl oxygens.

The ligands are tridentates, so a possibility of participation of the N-atom of heterocycle in the coordination with the metal is not excluded; it should be accompanied by the shift in the position of the absorption bands of the benzimidazole cycle in the ranges of 1630–1600 and 1580–1550 cm^{-1}. As it was observed in the IR-spectra of the obtained complexes, the absorption bands of the heterocycle have small shifts in comparison to their positions in the ligands. These shifts could not be attributed to an additional coordination [28].

The presence of water molecules in the coordination sphere is confirmed by the characteristic frequencies in the range of 3480–3300 cm^{-1}.

The elemental analysis for the metal complexes **2**–**7** (Table 1) with 1-methylbenzimidazole-2-aldehyde-2′-mercaphtophenylimine **VI** and also for the ligand **VII**, revealed the compositions $ML_2 \cdot nH_2O$ and $MLAc \cdot nH_2O$ ($n = 0$–3). The interpretation of their IR-spectra is difficult, because of the absence of both

Table 2. Experimental conditions for the electrosynthesis of metal chelates

No. compound	Metal	Initial voltage (V[a])	Time of electrolysis (h)	Metal dissolved (g)	Yield (g/%)
15	Cu	55	2	0.092	0.64/95
16	Ni	62	3	0.048	0.72/96
18	Cu	85	1.2	0.051	0.40/96
19	Ni	71	3	0.065	0.82/85
20	Cu	48	2	0.093	0.44/94
21	Cu	58	2	0.045	0.52/96
22	Ni	46	3	0.062	0.75/94
23	Cu	65	2	0.047	0.50/92

[a] To produce a current of 20 mA.

the sulphyrdril and the azomethinic absorption bands in their spectra due to the following equilibrium:

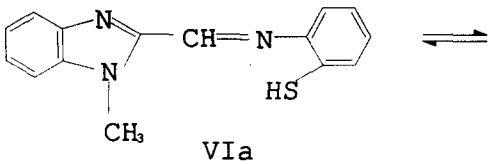

VIa

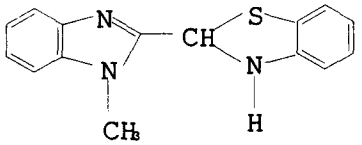

VIb

According to [29], it is possible to conclude that coordination of the ligand **VI** takes place only when it is in the azomethinic form. The frequency 1630 cm^{-1} was attributed to the ν(C=N) for the ligand **VI** with the group SCH_3 (instead of SH). In some cases (**3, 5, 6** and **7**) the acetate group is conserved.

Based on the discussed results, it is possible to assign the complexes the following formulae **VII** and **IX**:

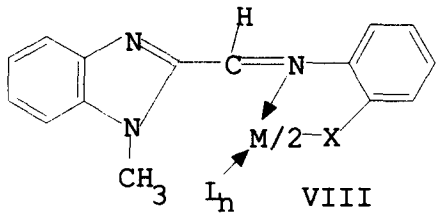

VIII

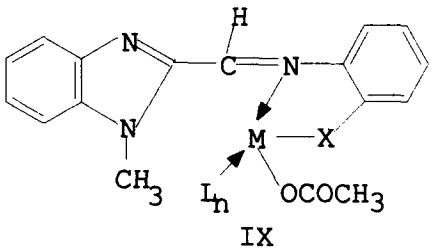

IX

L = H_2O, MeOH; n = 0–3.

The presence of 5-member chelate rings is confirmed by the agreement between our data and that reported in the reviews [9,10,27] and papers [30,31]. Also, these chelates formed initially from the ligand precursors **VI** and **VII** could contain two 5-member metal chelate rings, due to additional coordination of the nitrogen atom of benzimidazole ring to metal:

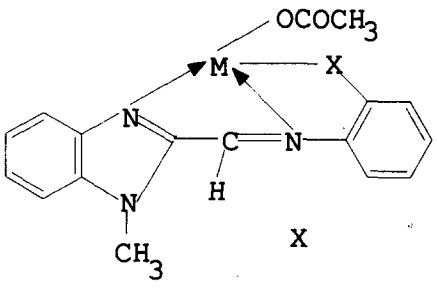

X

The existence of this type of structure has been confirmed [32] by the X-ray diffraction method for the palladium complex, **VI**.

In order to obtain metal complexes with the systems **VI** and **VII** without anions, we tried to electrosynthesize the compounds starting from zero-valent copper and nickel. However, it was impossible to isolate complexes of these metals with **VI** because of the considerable decomposition of this azomethinic compound under the conditions of electrolysis. The nickel and copper complexes 15 and 16 have been isolated as a result of electrosynthesis starting from the more stable VII. According to the elemental analyses, the complexes have a composition $ML_n \cdot mH_2O$ (n = 1, 2; m = 2, 2.5).

In order to compare the physico-chemical properties and the structure of copper complexes, obtained by the conventional chemical methods, 2(LH = VI, X = S) and 9 (LH = VII, X = NTs) (Table 1), against the electrochemical procedure 15 (LH = VII, X = NTs), we have measured their EPR spectra at X-band frequency in DMF at 77 K. As seen in the EPR spectrum of complex 2, $g_{\parallel} > g_{\perp} > 2.0023$ ($g_{\parallel}$ = 2.215, $g_{\perp}$ = 2.046, $A_{\parallel}$ = 165.2 G), which indicates a $d_{x^2-y^2}$ ground state. The isotropic spectrum (298 K) of this complex has well resolved lines, which can be attributed to the interaction of electron spin with the nuclear spin of Cu^{II} (I = 3/2) A_{Cu}(iso) = 61.2 G, g(iso) = 2.102. In the case of the complexes 9 and 15, the hyperfine features at 298 and 77 K were not seen in the solution and powder spectra. The EPR spectra of these complexes measured in frozen solutions (77 K) and in polycrystalline powders showed no resolved broad ΔM = 1 ($\approx$3200 G) and weak ΔM = 2 ($\approx$1600 G) absorptions. The appearance of the ΔM = 2 signals indicates that dinuclear structures exist even in solution. This fact could be related to the presence of dinuclear structures XII sufficiently stable for this complex, in which a magnetic exchange between

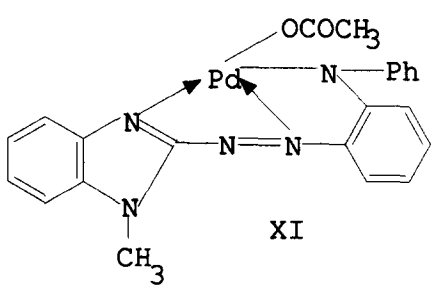

XI

copper atoms occurs probably through acetate groups:

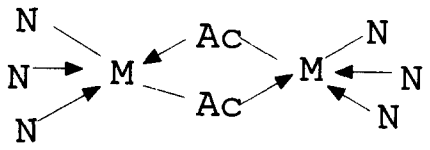

XII

This conclusion is also confirmed by the magnetochemical data as it is shown in Table 4. The magnetic susceptibility at different temperatures also shows the presence of a weak antiferromagnetic interaction between the copper atoms. An analogous result was obtained for the chelate 15 (LH = **VII**, X = NTs, by electrosynthesis). The data from the magnetochemical studies show a small antiferromagnetic change, which, in our opinion, could be attributed to the presence of OH-groups in the dinuclear structures $(CuL)_2$ **XIII**:

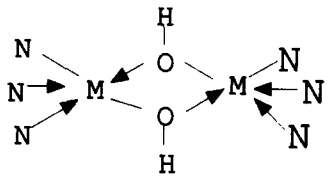

XIII

It is worth mentioning that nickel chelate 16 with the ligand VII (X = NTs, by electrosynthesis) $NiL_2 \cdot 2.5H_2O$, has a weak antiferromagnetic effect between nickel atoms (Table 4). Perhaps in this case the change is carried out through the conjugated system containing an heterofragment. An additional intermolecular coordination of nitrogen atoms takes place with the formation of the coordination kernel NiN_6.

We have described above the complexes of types **VII–X,** containing 5-member metal cycles. In order to study the influence of a number of atoms in the cycle and that of the method of synthesis on the character of the obtained complexes, we have prepared the chelates on the basis of the azomethinic compounds **XIV** and **XV,** containing 6-member cycles with intermolecular hydrogen bonds, i.e., derivatives of 2-tosylaminobenzal-2′-aminobenzimidazole **XIV** and salicylal-2-aminobenzimidazole **XV**.

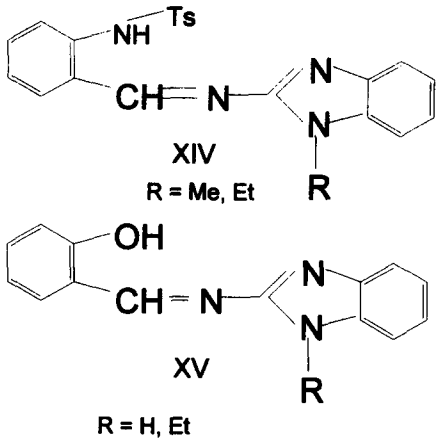

XIV

R = Me, Et

XV

R = H, Et

Table 3. IR spectral data of synthesized complexes

Ligand No.	Metal	ν(C=N), cm^{-1}	ν(NH), ν(OH), cm^{-1}	$\nu_{as}(SO_2)$, cm^{-1}	$\nu_s(SO_2)$, cm^{-1}
VI	H	1630 s			
	Cu	1606 w	3420, 3506 wide		
	Ni	1606 w	3488 wide		
	Co	1606 m	3393 wide		
	Zn	1613 m	3363 wide		
	Cd	1580 w	3433 wide		
	Pd	1606 w	3433 wide		
VII	H	1620 v.s.	3153 wide, 3080 m	1353 v.s.	1166 v.s.
	Cu	1593 w, 1586 s	3326 wide	1313 v.s.	1140 v.s.
	Ni	1588 s	3446 wide	1306 s	1126 s
	Co	1580 m	3326 wide	1300 s	1126 s
	Zn	1586 m	3476 w, wide	1300 s	1126 v.s.
	Cd	1580 m	3446 w, wide	1300 s	1126 v.s.
	Pd	1593 m, 1620 m	3440 w, wide	1320 m	1140 m
	Ni[a]	1586 m	3440 wide	1306 s	1126 m
XVI	H	1621 s	3150 w	1342 v.s.	1160 v.s.
	Cu	1612 s		1298 s	1135 v.s.
	Ni	1608 m		1300 m	1128 s

[a] Complex electrochemically obtained.

Table 4. Magnetic properties of chelates obtained

No.	M	T, K	μ_{eff} B.M.
2	Cu	306	2.07
	VI	286	2.04
	X = S	236	2.05
		218	2.04
		189	1.91
		166	1.99
		139	1.99
		122,5	1.93
		105	1.98
		82	1.97
16	Ni[a]	301	3.40
	VII	291	3.35
	X = NTs	235	3.24
		212	3.25
		190	3.19
		160	3.12
		131	3.06
		106	2.99
		82	3.04
9	Cu	297	1.75
	Lig. VII	286	1.72
	X = NTs	267	1.70
		219	1.69
		203	1.65
		180	1.65
		155	1.64
		138	1.62
		105	1.58
		82	1.64
18	Cu[a]	299	2.02
	XIV	284	1.96
	$R = CH_3$	217	1.78
		178	1.69
		131	1.55
		106	1.47
		82	1.39
15	Cu[a]	300	2.24
	Lig VII	285	2.20
	X = NTs	251	2.15
		237	2.12
		211	2.07
		185	2.02
		162	1.96
		140	1.89
		116	1.89
		82	1.77
20	Cu[a]	302	1.29
	XV	289	1.27
		253	1.22
		236	1.28
		213	1.24
		190	1.24
		160	1.27
		104	1.29
		82	1.25

[a] Complexes electrochemically obtained.

The chelate **17** $CuLAc \cdot H_2O$ was prepared (Table 1) following the conventional chemical synthesis, i.e. by the interaction between copper acetate and the ligand **XIV**, ($R = C_2H_5$.). The electrosynthesis with the ligands XIV and XV led to the formation of the chelates **18–20** (Table 1).

According to the IR spectra, the obtained complexes have structures of the chelate type. These spectra show a decrease of the frequency ν(C=N) 1630 cm^{-1} by 10–15 cm^{-1} and the disappearance of ν(N—H) at 3150 cm^{-1}. The saturation of the coordination sphere of copper is carried out at the expense of the deprotonization of *o*-tosyl-amino-(**17–19**) or *o*-hydroxo-(**20**) groups, coupled with the preservation of acetate anions (chemical method, **17**) or OH-groups (by electrosynthesis, **18, 20**). The magnetochemical study of the copper complexes **17** and **18** shows that the weak antiferromagnetic interaction takes place in these chelates, independent of the method of synthesis, chemical or electrochemical (Table 4). This fact could be connected with the formation of dimer structures stabilized at 77 K in the frozen solution, where spin–spin exchange is carried out through aceto- or OH-groups in the complexes, obtained chemically and electrochemically, respectively.

It is interesting to note that the copper complexes **18** (LH = **XIV**, $R = CH_3$) and **20** (LH = XV, R = H), obtained in the same electrochemical conditions and having the same composition $CuL \cdot nH_2O$, but different types of coordination kernels CuN_2O (LH = **XIV**) and $CuNO_2$ (LH = **XV**), have different magnetic properties. The substitution of tosylamino-group in LH = **XIV** by *o*-OH-group in LH = **XV** (R = H) leads to the formation of monomer complex **20** $CuL \cdot H_2O$ (LH = **XV**), where copper probably exists in a mixed-valent state: Cu^{I}, Cu^{II}, as it was confirmed by magnetochemical data (Table 4). The magnitude of the effective magnetic moment μ_{eff} for the complex 20 decreases (1.29 B.M.) at room temperature and does not change in the interval of 302–82 K.

The nickel chelate, 19, NiL_2 (LH = **XIV**, $R = CH_3$), obtained electrochemically, has a $\mu_{eff} = 2.75$ B.M., which is evidently related to the tetrahedral (instead of square planar) coordination environment of the metal.

In addition, we have obtained electrochemically the chelates of copper **21** and nickel **22** with the Schiff base system containing *o*-tosylamino-group, but without a heterocyclic fragment (LH = XVI):

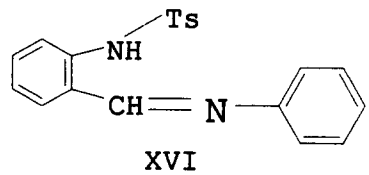

XVI

According to elemental analysis data and IR spectra (Tables 1 and 3), these compounds have the com-

position and structure which are typical [27] for metal chelates: ML_2 (LH = XVI). The EPR spectra data for the complex **21** at 77 K correspond to the data of an analogous complex obtained by the usual chemical method [28].

The electrosynthesis using a copper anode and the ligand **XVII** led to the formation of the complex ML_2, 23. The chelate structure was studied by IR spectra and magnetochemical data, $\mu_{eff} = 2.2$ B.M. at 273 K (Table 1). These results are in agreement with the data for the analogous complex obtained earlier [28] by the chemical method. It can then be concluded that the structure and the properties of these kind of complexes are independent from the method of synthesis used to obtain them.

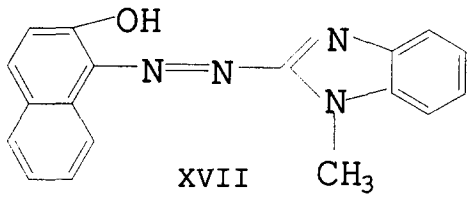

XVII

CONCLUSIONS

The substitution of conventional chemical methods by electrochemical methods of synthesis permits us to obtain complexes of azomethinic ligands and azo-compounds which have different compositions and stereochemistry.

The main advantages of electrosynthesis are the high yields (80–96%) and the absence of anions which are frequently present in the chelates of tridentate heteroarene ligands [32]. These results are especially interesting since they show the possibility of wider application of electrosynthesis [12–14] in the modern coordination chemistry.

Acknowledgements—The authors are grateful to Dr J. M. Barbarín Castillo (Dept of Chemistry, UANL, Monterrey, México), who worked on the revision of the manuscript.

REFERENCES

1. Holm, R. H., Everett, G. W. and Chakravorty, A., *Prog. Inorg. Chem.*, 1966, **7,** 83.
2. Holm, R. H. and O'Connor, M. J., *Prof. Inorg. Chem.*, 1971, **14,** 214.
3. Hobday, M. D. and Smith, T. D., *Coord. Chem. Rev.*, 1973, **9,** 311.
4. Panova, G. V., Vikulova, N. K. and Potapov, V. M., *Usp. Khim.*, 1980, **49,** 1234.
5. Yamada, S. and Takeudi, T., *Coord. Chem. Rev.*, 1982, **43,** 187.
6. Calligaris, M. and Randaccio, L., in *Comprehensive Coordination Chemistry*, G. Wilkinson (Ed.), Vol. 2, p. 715, Pergamon Press, Oxford (1987).
7. Garnovskii, A. D., *Koord. Khim.*, 1992, **18,** 675.
8. Costamagna, J., Vargas, V., Latorre, R., Alvarado, A. and Mena, G., *Coord. Chem. Rev.*, 1992, **119,** 67.
9. Garnovskii, A. D., *Russ. J. Coord. Chem.*, 1993, **19,** 368.
10. Garnovskii, A. D., Nivorozhkin, A. L. and Minkin, V. J., *Coord. Chem. Rev.*, 1993, **126,** 1.
11. Nivorozhkin, A. L., Uraev, A. I. and Garnovskii, A. D., *Russ. Khim. Zhurn. (Zhurn. Russ. Khim. Obshchestva im. D. I. Mendeleeva)*, 1996, **40,** 19.
12. (a) Tuck, D. G., *Pure Appl. Chem.*, 1979, **51,** 2005; (b) Tuck, O. G., *Molecular Electrochemistry of Inorganic, Bioinorganic and Organometallic Compounds*, p. 15. Kluwer Acad. Publishers, Dordrecht (1993).
13. Chakravorty, M. C. and Subrahmanyam, G. V. B., *Coord. Chem. Rev.*, 1994, **135/136,** 65.
14. Garnovskii, A. D., Kharisov, B. I., Gójon-Zorrilla, G. and Garnovskii, D. A., *Russ. Chem. Rev.*, 1995, **64,** 201.
15. Pozharskii, A. F., Anisimova, V. A. and Tsupak, E. B., *Practical Works on Heterocycle Chemistry*, Rostov University, Rostov-on-Don (1988).
16. Garnovskii, A. D., Kogan, V. A., Osipov, O. A., Kochin, S. G., Kuznetsova, L. Y. and Mitina, G. K., *Zh. Neorg. Khim.*, 1970, **15,** 2010.
17. Atherton, N. M., Fenton, D. E., Hewson, G. J., McLean, C. H., Bastida, R., Romero, J., Sousa, A. and Castellanos, E. E., *J. Chem. Soc., Dalton Trans.*, 1988, 1059.
18. Castro, J., Castiñeiras, A., Durán, M., García-Vázquez, J. A., Macías, A., Romero, J. and Sousa, A., *Z. Anorg. Allg. Chem.*, 1990, **586,** 203.
19. Bastida, R., Lage, T., Parrado, C., Rodríguez, T., Sousa, A. and Fenton, D. E., *J. Chem. Soc., Dalton Trans.*, 1990, 2101.
20. Bastida, R., González, S., Rodríguez, T., Sousa, A. and Fenton, D. E., *J. Chem. Soc., Dalton Trans.*, 1990, 3643.
21. Labisbal, E., De Blas, A., García-Vázquez, J. A., Romero, J., Durán, M. L., Sousa, A., Bailey, N. A., Fenton, D. E., Leeson, F. B. and Parish, R. V., *Polyhedron*, 1992, **11,** 227.
22. Bastida, R., De Blas, A., Fenton, D. E., Rial, C., Rodríguez, T. and Sousa, A., *J. Chem. Soc., Dalton Trans.*, 1993, 265.
23. Labisbal, E., Romero, J., García-Vázquez, J. A., Gómez, C. and Sousa, A., *Polyhedron*, 1994, **13,** 1735.
24. Labisbal, E., García-Vázquez, J. A., Romero, J., Picos, S., Sousa, A., Castiñeiras, A. and Machle-Mössmer, C., *Polyhedron*, 1995, **14,** 633.
25. Garnovskii, D. A., Sousa, A., Sigeikin, S. G., Vasil'chenko, I. S., Kurbatov, V. P. and Garnovskii, A. D., *Zh. Obshch. Khim.*, 1996, **66,** 147.
26. Kharisov, B. I., Gójon-Zorrilla, G., Blanco, L. M., Montoya, F. C., Burlov, A. S., Garnovskii, D. A., Vasil'chenko, I. S., Bren', V. A. and Garnovskii, A. D., *Koord. Khim.*, **6,** 132, 1992 (Abstracts of XVIII Chugaev Conference of Coordination Chemistry).
27. Garnovskii, A. D., Alekseenko, V. A., Burlov, A. S. and Nedzvetskii, V. S., *Zh. Neorg. Khim.*, 1991, **36,** 1011.

28. Alekseenko, V. A., Burlov, A. S., Divaeva, L. N., Garnovskii, A. D. and Nedzvetskii, V. S., *Zh. Neorg. Khim.*, 1988, **33,** 2307.
29. Garnovskii, A. D., Kogan, V. A., Osipov, O. A., Kochin, S. G., Kuznetsova, L. Y. and Mitina, G. K., *Zh. Obshch. Khim.*, 1971, **41,** 1370.
30. Garnovskii, A. D., Antsyshkina, A. S., Uraev, G. G. and Porai-Koshitz, M. A., *Zh. Neorg. Zhim.*, 1995, **40,** 1977.
31. Ergan, F., Ülkü, D., Angin, N., Güe-Oztas, S. and Tüzün, M., *Acta. Cryst.*, 1996, **C52,** 1141.
32. Garnovskii, A. D., Burlov, A. S., Antsyshkina, A. S. and Divaeva, L. N., *Zh. Neorg. Khim.*, 1996, **41,** 90.

Pergamon

PII: S0277-5387(97)00185-X

Polyhedron Vol. 17, No. 2-3, pp. 391-395, 1998
© 1997 Elsevier Science Ltd
All rights reserved. Printed in Great Britain
0277-5387/98 $19.00+0.00

COMMUNICATION

A barium–sulfur–phosphorous–nitrogen ring system: synthesis and crystal structure of $Ba[(SP(Ph)_2)_2N]_2 \cdot 2$ DME

Gertrud Kräuter, Sundeep K. Sunny and William S. Rees, Jr

School of Chemistry and Biochemistry and School of Materials Science and Engineering and Molecular Design Institute, Georgia Institute of Technology, Atlanta, GA 30332-0400, U.S.A.

(Received 4 April 1997; accepted 6 April 1997)

Abstract—The initial structural characterization of a barium–sulfur covalent interaction is reported. © 1997 Elsevier Science Ltd

Keywords: barium; thiolate; ring compound; structural characterization; dithioimidodiphosphinate.

Much effort has been focused on the topic of late Group 2 element *bis*(β-diketonate) compounds in recent years [1–3]. This is driven, to a great extent, by the potential of such species to serve as precursors for the growth of superconducting metal oxide thin films. Although β-diketonate ligands have served exceptionally as carriers for numerous metals, the large size/charge ratio for Ba^{2+} presents unique challenges for the chemist. For example, the highly sterically demanding $tmhd^-$-ligand (Htmhd: 2,2,6,6-tetramethyl-3,5-heptanedione) forms a tetrameric barium compound in the solid state [4]. In a search for possible alternates more suited to the particular difficulties of Ba^{2+}, we turned to other monoanionic bidentate ligands. Such a moiety $(SP(Ph)_2NP(Ph)_2S)^-$ has been used previously as a ligand for several transition metals [5–13] and a few main group elements including K^+ [14–15], Sn^{4+} [16], Bi^{3+} [17–19] and Te^{2+} [20].

Organometallic barium compounds have been known for over half a century [21–23]. Recently, they were joined by other classes of reagents which have been examined for use as precursors for barium-containing ceramic materials. They include barium alkoxides [24–28], -β-diketonates, [1–4,29,30] and -amides [31]. Examples of barium compounds containing less-traditional Ba—E bonds are rare. Included among them are $Ba(SiPh_3)_2$ [32], $[Ba(P(SiMe_3)_2)_2(THF)_2]_n$ [33], $Ba(P(SiME_3)_2)_2 \cdot 4$ THF [34] and $[Ba(TeSi(SiMe_3)_3)_2(pyridine)_5]$ [35]. Barium species containing Ba—S interactions have not been studied in detail. Barium is known to form complexes with dithiocarboxyllic acids [36], however, these compounds have a highly ionic character. Additionally, $Ba(SCN)_2$ [37] and examples of $R_2C{=}S \rightarrow Ba$ [38] and $R_2S \rightarrow Ba$ [39] have been characterized in the solid state. The initial characterization of a barium *bis* (thiolate) compound recently has been completed [40]. As one component of our efforts to prepare barium compounds containing Ba—S interactions, we have turned our attention to the tetraphenyldithioimidodiphosphinate ligand, $[SP(Ph)_2NP(Ph)_2S]^-$ [14]. This anion is available readily by the deprotonation of $HN(SP(Ph)_2)_2$ [41] (Eq. 1), and has the negative charge delocalized throughout the SPNPS-moiety, similar to the delocalization which occurs in β-diketonate ligands. Like β-diketonates, the

$[SP(Ph)_2NP(Ph)_2S]^-$ anion (**2**) interacts with metal centers in a chelating fashion. Barium metal reacts with $SP(Ph)_2NHP(Ph)_2S$ in the presence of gaseous NH_3 to form compound **3** (Eq. 2).

$$\underset{\mathbf{1}}{(SP(Ph)_2)_2NH} \xrightarrow[-H^+]{Base} \underset{\mathbf{2}}{[SP(Ph)_2NP(Ph)_2S]^-} \quad (1)$$

$$\mathbf{1} + Ba^\circ \xrightarrow[NH_3(g),R.T.]{THF} \underset{\mathbf{3}}{Ba[(SP(Ph)_2)_2N]_2 \cdot (THF)_n}$$

$$\xrightarrow{DME} \underset{\mathbf{4}}{Ba[(SP(Ph)_2)_2N]_2 \cdot 2\,DME} \quad (2)$$

Upon recrystallization from 1,2-dimethoxyethane (DME), the DME adduct **4** is obtained. Compounds **3** and **4** are highly soluble in organic solvents and show no sensitivity towards oxygen or water. The crystal structure of **4** has been determined by single crystal X-ray diffraction [42]. Compound **4** crystallizes as a discrete monomer in the space group Cc (Fig. 1). Both dithioimidodiphosphinato ligands interact with the metal center in a bidentate fashion resulting in the formation of two six-membered BaS_2P_2N rings with the barium atom at the *conjuncto* position. The four Ba—S interatomic distances are not equivalent, ranging from 321.07(24) pm [Ba-S(4)] to 327.0(3) pm [Ba-S(3)]. It is noteworthy that a trend is absent between the characterized derivatives of ligand **2** with *p*-block elements. For instance, non-equivalent M—S interatomic distances also are observed in the complex $Bi[(SP(Ph)_2)_2N]_3$ [18], which displays two sets of short and two sets of long Bi—S interactions. However, in the tin complex $Me_2Sn[(Sp(Ph)_2)_2N]_2$ the four Sn—S interatomic distances are equivalent [16].

The P—S interatomic distances observed for compound **4**, on average, are longer (198.5 pm compared to 194.3 pm) and the P—N interatomic distances are shorter (157.7 pm compared to 167.8 pm) when compared with the analogous data observed for compound **1** [43], indicating that the π-electrons in compound **4** are delocalized throughout the BaS_2P_2N moieties. There exists, to our knowledge, no similar parameters with which to compare Ba—S interatomic distances. Since this report is the first solid state characterization of such an interaction, comparison with ionic interactions observed in BaS (316 pm [44]) and the sum of the radii (Ba: 142 pm; S: 184 pm; sum: 326 pm) [45] is warranted [37–39]. The coordination sphere of the barium atom is completed by the oxygen atoms of two DME ligands, which form a belt around the central metal. The dihedral angle between the planes of BaS_2 units is 7.04°, while that between the planes of BaO_2 units is 5.80°. The BaS_2 to BaO_2 planes each are nearly perpendicular (range 86.28–96.86°, average of 91.62°). Thus, the overall geometry at the eight-coordinate metal center is pseudocubic. This closely approximates that observed for $[Ba(tmhd)_2 \cdot 2\ NH_3]_2$ [30], another highly symmetric molecule. The Ba—O interatomic distances observed for compound **4**, 272.4(7)–286.1(8) pm, fall within the range reported for $R_2O \rightarrow Ba$ interactions, although somewhat at the low end of the previous data, (278–282 [46], 283 [47], 281–289 [48], 286–296 [49]. The data for compound **4** are significantly longer than that found for RO^- interactions with barium (238–242 [50], 241 [46]).

The IR spectrum of **4** shows the expected differences when compared to the IR spectrum of the protonated ligand **1**. The asymmetrical P⟷N⟷P stretch is found at 1248 cm^{-1} in **4**, compared to 1217 and 1250 cm^{-1} observed for the tin complexes $Me_2Sn[(SP(Ph)_2)_2N]_2$ and $Me_3Sn[(SP(Ph)_2)N]$, respectively [16]. The protonated ligand displays a strong band at 652 cm^{-1}, which is characteristic for a P=S double bond [37]. These bands are replaced in **4** by a strong vibration at 574 cm^{-1}, attributed to delocalized P⟷S stretching.

The $^{31}P\{^1H\}$ NMR chemical shift observed for compound **4** (57.6 ppm) may be compared to that recorded for compound **1** (57.5 ppm).

In conclusion, the initial structural characterization of a barium–sulfur interaction within a ring system has been reported.

Acknowledgements—This work was supported by the Deutsch Forschungsgemeinschaft (posdoctoral fellowship to G. K.) and the US Office of Naval Research. Dr D. G. Van Derveer assisted with crystallography, Ms D. Moreno confirmed the ^{31}P NMR data and Dr H. Luten aided with the preparation of Figure 1.

Experimental Procedure

1: Synthesis according to ref. [51].

3: 7.20 g (16.0 mmol) of compound **1** was added to 1.21 g (8.8 mmol) of barium metal in 100 ml of THF. A strong stream of dry NH_3 gas was bubbled through the reaction mixture. After 30 min, the flow of NH_3 gas was stopped and the mixture was stirred overnight at ambient temperature. The majority of the elemental barium had been consumed by this time. The mixture was filtered and the THF was removed under vacuum. Compound **3** remained as a colorless crystalline material. Yield: 8.5 g (96.5% with respect to compound **1**).

4: 1 g of compound **3** was dissolved in 20 ml of hot DME. After 24 h at 5°C, compound **4** was isolated in quantitative yield. It is a molecular species in $CDCl_3$ solution; however, it thermally decomposes upon attempted sublimation at 10^{-5} mm Hg. M.p.: 150°C (decomp. 195°C); ^1H NMR (300 MHz, $CDCl_3$): δ = 3.27 (s, 12H, OCH_3), 3.40 (s, 8H, CH_2), 7.10–7.77 (m, 40H, aryl-H); IR (cm^{-1}, KBr pellet): 3053m, 2933m, 1446s, 1248s, 1117s, 715s, 751m, 715s, 696s, 603m, 574s, 513m.

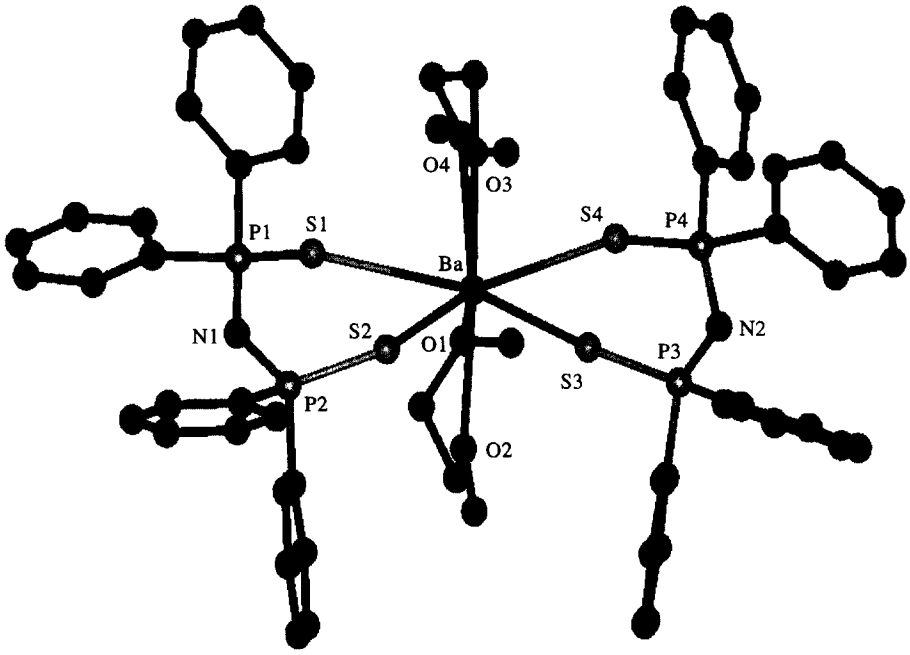

Fig. 1. Biosym representation of the solid state structure of $Ba[(SP(Ph)_2)_2N]_2 \cdot 2$ DME, as determined by a single crystal X-ray diffraction examination. Color code: Ba—purple, S—yellow, O—red, N—blue, P—pink, C—green.

REFERENCES

1. Sievers, R. E., Turnipseed, S. B., Huang, L. and Lagalante, A. F. *Coord. Chem. Rev.*, 1993, **128,** 285.
2. Rees, W. S., Jr. and Barron, A. R., *Materials Science Forum*, 1993, **137–139,** 473.
3. Barron, A. R. and Rees, W. S., Jr., *Adv. Matls. Opt. Elect.*, 1993, **2,** 271.
4. Drozdov, A. A. and Trojanov, S. I., *Polyhedron*, 1992, **11,** 2877.
5. Siiman, O., Wrighton, M. and Gray, H. B., *J. Coord. Chem.*, 1972, **2,** 159.
6. Siiman, O. and Gray, H. B., *Inorg. Chem.*, 1974, **13,** 1185.
7. Siiman, O., *Inorg. Chem.*, 1981, **20,** 2285.
8. Davidon, A. and Switkes, E., *Inorg. Chem.*, 1971, **10,** 837.
9. Czernuszewicz, R., Maslowsky, E. and Nakamoto, K., *Inorg. Chim. Acta*, 1980, **40,** 199.
10. Siiman, O., Huber, C. P. and Post, M. L., *Inorg. Chim. Acta*, 1977, **25,** L11.
11. Bereman, R. D., Wang, F. T., Nadjdzionek, J. and Braitsch, D. M., *J. Am. Chem. Soc.*, 1976, **98,** 7266.
12. Uson, R., Laguna, A. and Concepcion Gimeno, M., *J. Chem. Soc., Dalton Trans.*, 1989, 1883.
13. Laguna, A., Laguna, M., Rojo, A. and Fraile, M. N., *J. Organomet. Chem.*, 1986, **315,** 269.
14. Cea-Olivares, R. and Nöth, H., *Z. Naturforsch*, 1987, **42B,** 1507.
15. Slawin, A. M. Z., Ward, J., Williams, D. J. and Wollins, J. D., *J. Chem. Soc. Chem. Commun.*, 1994, 421.
16. Haiduc, I., Silvestru, C., Roesky, H. W., Schimidt, H.-G. and Noltemeyer, M., *Polyhedron*, 1993, **12,** 69.
17. Williams, D. J., *Inorg. Nucl. Chem. Lett.*, 1980, **16,** 189.
18. Williams, D. J., Quicksall, C. O. and Barkigia, K. M., *Inorg. Chem.*, 1982, **21,** 2097.
19. Williams, D. J., Travis, J. B. and Bergbauer, K. L., *J. Coord, Chem.*, 1987, **16,** 315.
20. Bjornevag, S., Husbye, S. and Maartmann-Moe, K., *Acta Chem. Scand.*, 1982, **A36,** 195.
21. Gilman, H. and Woods, L. A., *J. Am. Chem. Soc.*, 1943, **67,** 520.
22. Lindsell, W. E., in *Comprehensive Organomentallic Chemistry*, *Vol.* 1, pp. 223–252 (eds G. Wilkinson, F. G. A. Stone), Pergamon Press, Oxford (1982).
23. Hanusa, T. P., *Polyhedron*, 1990, **9,** 1345.
24. Lutz, H. Z., *Z. Anorg. Allg. Chem.*, 1968, **56,** 132.
25. Caulton, K. G., Chisholm, M. H., Drake, S. R. and Folting, K., *J. Chem. Soc., Chem. Commun.*, 1990, 1349.
26. Caulton, K. G., Chisholm, M. H., Drake, S. R. and Huffman, J. C., *J. Chem. Soc., Chem. Commun.*, 1990, 1498.
27. Miele, P., Foulon, J.-D., Hovnanian, M. and Cot, L., *Polyhedron*, 1993, **12,** 267.
28. Moreno, D. and Rees, W. S., Jr., *J. Chem. Soc., Chem. Commun.*, 1991, 1759.
29. Caballero, C. R., Hesse, W. and Rees, W. S., Jr., *Angew. Chem., Int. Ed.*, 1992, **31,** 735.
30 Rees, W. S., Jr., Carris, M. W. and Hesse, W., *Inorg. Chem.*, 1991, **30,** 4479.
31. Hanusa, T. P., *Chem. Rev.*, 1993, **93,** 1023.
32. Wiberg, E., Stecher, O., Andrascheck, H. J., Kreuzbichler, L. and Staude, E., *Angew. Chem.*, 1963, **75,** 516; *Angew. Chem., Int. Ed. Engl.*, 1963, **2,** 507.
33. Drake, S. R., Hall, P. and Lincoln, R., *Polyhedron*, 1993, **12,** 2307.
34. Westerhausen, M. and Schwarz, W., *J. Organomet. Chem.*, 1993, **463,** 51.
35. Gindelberger, D. E. and Arnold, J., *Inorg. Chem.*, 1994, **33,** 6293.
36. Coucouvanis, D. in *Progress in Inorganic Chemistry*, *Vol.* 11, p. 242 (ed. S. J. Lippard), Interscience, New York (1970).
37. Higenfeld, R., Hirayama, F., Bhagwat, V., Saenger, W., Weber, G., Sheldrick, G. M., Sieger, H. and Vögtle, F., *Israel J. Chem.*, 1984, **24,** 307.
38. Banbury, F. A., Davidson, M. G., Martin, A., Raithby, P. R., Snaith, R., Verhorevoort, K. L. and Wright, D. S., *J. Chem. Soc., Chem. Commun.*, 1992, 1152.
39. Weber, G., *Inorg. Chim. Acta.*, 1982, **58,** 27.
40. Rees, W. S., Jr. and Kraeuter, G., *Main Group Chemistry*, 1997, **2,** 9.
41. Schmidpeter, A. and Groeger, H., *Z. Anorg. Allg. Chem.*, 1966, **345,** 106.
42. Crystal Data for **4**: crystals from DME, crystal dimensions: $0.46 \times 0.34 \times 0.22$ mm, monoclinic, space group: *Cc*, $Z = 4$, $a = 31.063$ (12), $b = 10.857$ (4), $c = 17.168$ (5) Å, $\beta = 93.58$ (3)°, $V = 5778.63$ Å^3, $\rho = 1.396$ g cm^{-3}, 2θ (max) = 50.0°, no. of reflections measured: 5203, no. of unique reflections: 5203, no. of significant reflections ($I > 2.5\sigma$): 4307, Syntex Diffractometer, $R = 0.038$, $R_w = 0.049$ (significant reflections).
43. Nöth, H., *Z. Naturforsch.*, 1982, **37B,** 149.
44. *Gmelins Handbuch der Anorganischen Chemie*, 8th Ed., pp. 404–406 VCH, Weinheim (1960).
45. Greenwood, N. N. and Earnshaw, A., *Chemistry of the Elements*, p. 1221782 Pergamon Press, Oxford.
46. Drake, S. R., Strieb, W. E., Folting, K., Chisholm, M. H. and Caulton, K. G., *Inorg. Chem.*, 1992, **31,** 3205.
47. Rossetto, G., Polo, A., Benetollo, F., Porchia, M. and Zanella, P., *Polyhedron*, 1992, **11,** 979.
48. van der Suis, P. and Spek, A. L., *Acta Cryst.*, 1990, **C46,** 1741.
49. Drake, S. R., Miller, S. A. A., Hursthouse, M. B. and Malik, K. M. A., *Polyhedron*, 1993, **12,** 1621.
50. Tesh, K. F., Hanusa, T. P., Huffman, J. C. and Huffman, C. J., *Inorg. Chem.*, 1992, **31,** 5572.
51. Wang, F. T., Najdzionek, J., Leneker, K. L. and Wasserman, H., *Synth. React. Inorg. Met.-Org. Chem.*, 1978, **8,** 119.

Pergamon

PII: S0277-5387(97)00398-7

Polyhedron Vol. 17, No. 2-3, p. 397, 1998
© 1997 Elsevier Science Ltd
All rights reserved. Printed in Great Britain
0277-5387/98 $19.00+0.00

BOOK REVIEW

Chemistry of Precious Metals, S.A. Cotton, Blackie Academic and Professional, London,1997. £99.00

As the author acknowledges in the Introduction, this book is the linear descendent of Cotton and Hart's "*The Heavy Transition Elements*" that was familiar to many students and lecturers over the past two decades. This book restricts its coverage to the elements Ru, Os, Rh, Ir, Pd, Pt, Ag and Au—the platinum elements. Now excluded are the early transition elements and the lanthanoids and actinoids, although the chemistry of the latter groups are discussed in the author's excellent "*Lanthanides and Actinides*" (Macmillan, Basingstoke, 1991).

What you get for your money are 374 pages discussing the chemistry of the platinum elements. The format is highly reminiscent of "*The Heavy Transition Elements*" and I personally find it a little untidy and cluttered in places (see, for example, Figure 2.88). The basic premise leads to a book that you will either love or hate—the assumption is that chemistry ultimately depends upon a knowledge of facts, and facts are what you get aplenty. Personally, I find this a valid and good approach, but fear that it will endear the book rather to the lecturer searching for a convenient source of material than to the student. This is not a book that presents general trends and explanations in a pre-packaged and easily digestible form. As an example, I am not certain that a student would come away from this book with an appreciation of the common cause for square-planar coordination geometries with gold(I), platinum(II) and iridium(III). The book is reasonably up-to-date and references provide a convenient entry into the primary and secondary literature. Of course, in rapidly developing fields, such as platinum antitumor species, the book is already somewhat behind the times.

The book consists of four chapters, one each devoted to the heavier congeners of groups 8, 9, 10 and 11 together with 33 pages of references and an index. In general, the organometallic chemistry of these elements with π-bonding ligands is not covered, although -bonded organometallics are treated. I fully appreciate and understand this choice, but I wonder how much it can be justified within the, already limited, scope of the book and its relatively high price. Factual errors are few, but in general the literature is reveiewed in an encyclopedic rather than a critical manner. There are a number of results reported which are certainly not fully and uncritically accepted.

Accepting that the devil is in the detail, there are a number of points which should be brought to the potential reader's attention. The author is rather inconsistent in the use of square brackets to denote complex species. As a typical example, on page 20 we encounter the two complexes $K_2OsO_4(OH)_2$ and $K_2[OsO_2(OH)_4]$. I would hope that future editions would remedy this deficiency, since it can prove very confusing to the student. A similar cavalier attitude exists with respect to charges—compound (a) in Figure 3.97 most certainly is not a platinum(III) complex, the dianion is. I realise that nomenclature is a dangerous topic, but I feel strongly that books such as this should adopt IUPAC nomenclature where it is appropriate or realistic. This is most certainly not the case in this text; sulfur compounds are presented throughout with the -ph- spelling, ligand names are imprecise and non-systematic (terpyridyl, bipyridyl), bidentate is used rather than didentate.

Overall, my impression of the book is favorable. It is strong in an area in which Greenwood and Earnshaw is both somewhat weak and dated. The basic material is presented with few serious factual errors, although the appearance and "feel" might have benefited from additional technical editing. I certainly will be using this book as a source of material for lecture courses. The author states in the preface that the book is probably aimed at teachers rather than students, and this is certain to be the case. I feel that this is a pity, because there is a need for students to be equipped with a certain level of raw, indigestible facts.

Finally, I feel duty bound to comment on the price of this text. At about 25 pence per page this book is expensive. With a new, and undoubtedly cheaper, edition of Cotton and Wilkinson imminent, the budgetary questions that will be raised by ever more pressed library committees will be hard to answer.

Edwin C. Constable

Pergamon

Polyhedron Vol. 17, No. 2–3, p. 399, 1998
Elsevier Science Ltd. Printed in Great Britain

CORRIGENDUM

pH-Independent decomposition reactions of L-ascorbic acid in aqueous metal solutions—I. Formation and structures of Co^{II} and Gd^{III} oxalates. C. Ünaleroğlu, B. Zümreoğlu-Karan, Y. Zencir and T. Hökelek (*Polyhedron*, Vol. 16, No. 13, pp. 2155–2161 (1997)).

Page 2156, Paragraph 2, line 7: $Co(NO_3)_3 . 6H_2O$ should read $Co(NO_3)_2 . 6H_2O$.

Page 2157, Table 2, column 5, row 4: $Gd_2(C_2O_4) . 6H_4O$ should read $Gd_2(C_2O_4)_3 . 6H_2O$.

Page 2160, Table 5, columns 2, 3, 4, rows 4, 4: The intensities of the vibrations should be corrected as

2934 vw	2934 vw	2928 w
2864 vw	2864 vw	2851 vw

Pergamon

PII: S0277-5387(97)00388-4

Polyhedron Vol. 17, No. 4, pp. 399–403, 1998
© 1998 Elsevier Science Ltd
All rights reserved. Printed in Great Britain
0277-5387/98 $19.00+0.00

Kinetics of chelate formation between Pd^{II} and S-carboxymethyl-L-cysteine

V. M. Vasić,* M. S. Tošić,[a] T. Jovanović,[b] Lj. S. Vujisić,[a] and J. M. Nedeljković[a]

[a]Vinča Institute of Nuclear Sciences, 11001 Belgrade, P.O. Box 522, Yugoslavia

[b]Institute of Inorganic Chemistry, Faculty of Pharmacy, 11000 Belgrade, Yugoslavia

(Received 1 July 1997; accepted 18 September 1997)

Abstract—The kinetics of the complex formation between S-carboxymethyl-L-cysteine and palladium(II) was studied by using stopped-flow technique in the acidity range from pH 1 to 4 at 25°C. The reaction rate of the formation of 1 : 1 chelate species is strongly affected by the acidity. The reaction mechanism consisting of five parallel paths which involve Pd^{2+} and $PdOH^+$, as well as LH^-, LH_2 and LH_3^+ ligand species was proposed. Fairly good agreement between the computed and experimentally determined rate constants was found. The equilibrium constants of the complex formation were determined. © 1998 Elsevier Science Ltd. All rights reserved

Keywords: S-carboxymethyl-L-cysteine; palladium(II); stopped-flow; complex formation.

S-carboxymethyl-L-cysteine ($SCMCH_2$) belongs to a group of naturally occurring amino acid containing thioether group [1,2]. In spite of its biological importance as an intermediate in cystamine formation, $SCMCH_2$ is an effective antiseborrheic and antiacne agent and can be used as an antidote for treatment of some poisoning [1]. $SCMCH_2$ has three coordination sites and its reaction with Pd^{II} in the presence of micelles has been used as a model system in order to better understand interaction between metal ions and proteins on the surface of a biomembrane [3,4]. $SCMCH_2$ forms different complex species with metal ions such as Cu^{II}, Ni^{II} and Zn^{II} [5,6], in which the ligand chelate to the metal ion via the amino and carboxylate groups of the α-amino acid residue. The coordination of sulfur atom to the metal ion is also suggested [5,6].

Recently, the spectrophotometric method for determination of $SCMCH_2$ by using palladium(II) chloride ($PdCl_2$) have been developed [7], and the mechanism of this reaction was examined [8]. It was found that ligand attacks all $Pd(H_2O)_{4-n}Cl_n$ species ($n = 2$–4), the reaction rate being strongly dependent on Cl^- and pH.

The aim of this work was the investigation of the reaction mechanism between Pd^{2+} and $SCMCH_2$. Basically, both the free metal ion and the monohydroxy species are labile toward substitution with ligand, and different reaction pairs could be kinetically distinguished.

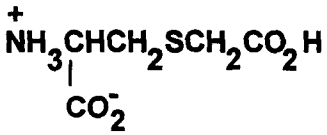

$SCMCH_2$ (1.99<pH<3.33)

EXPERIMENTAL

All reagents were commercial products of the highest purity available. A freshly prepared 2×10^{-3} M $SCMCH_2$ (ICN, Galenika) aqueous stock solution was used; more dilute solutions were obtained by appropriate dilution with water. The standard solution of 1×10^{-3} M Pd^{2+} was prepared as described elsewhere [9]. The acidity of the solutions were adjusted by the addition of Britton–Robinson buffer solutions. The pH of the solutions were measured by a Beckman Expandometric pH meter. The ionic

* Author to whom correspondence should be addressed.

strength was kept constant by the addition of $NaClO_4$ (I = 1.0).

The absorption spectra of the solutions were recorded on a Perkin-Elmer Lambda 5 UV–VIS spectrophotometer. For the stopped-flow experiments, the universal rapid kinetic accessory HI-TECH model SFA 12 was fitted to a spectrophotometer. The rate of the complex formation was allowed by monitoring the increase of the absorbance at 258 nm. The measurements were carried out under pseudo-first-order conditions. Values of k_{obs} were determined by fitting the experimental trace (A vs t) to the function $(A_e-A)/(A_e-A_o) = \exp(-k_{obs}t)$ (A_o and A_e are the initial and final absorbancies, respectively) by using a computer program based on the last square method. All kinetic measurements were reproducible within limits of error of $\pm 5\%$. The quoted values are the average of at least five runs under identical experimental conditions. All reported rate constants were determined at 25 ± 0.1°C.

RESULTS AND DISCUSSION

Absorption spectra and equilibra of the Pd^{II}-$SCMCH_2$ *complex*

The complex formation between Pd^{II} and $SCMCH_2$ was investigated in the pH range from 1 to 4. The absorption spectra of the solutions containing equal concentrations of Pd^{II} and $SCMCH_2$ at different acidities are shown in Fig. 1. The Pd^{II}-$SCMCH_2$ complex has the absorption maximum at 258 nm and the shoulder at 330 nm. For comparison, absorption spectra of the reacting species (Pd^{II} and $SCMCH_2$) are also given in Fig. 1.

The stoichiometry of the complex (Pd^{II}: $SCMCH_2$ = 1 : 1) was determined at different acidities (pH 1.10, 2.05 and 3.60) by continuous variation of the ratio between initial concentrations of Pd^{II} and $SCMCH_2$. Also, the absorption spectra at the constant $Pd^{II}/SCMCH_2$ ratio were followed as a function of the acidity. The absorption spectra indicated, that the metal chelate structure was not affected by the change in acidity. The slight shifts of the position and intensities of the absorption maximum are most likely due to the presence of different ionic forms of the ligand bound in the complex ($pK_{a3} = 1.99$, $pK_{a2} = 3.33$) [6]. In the acidity range close to pH 3.33 the dissociation of —COOH group in cysteine residue takes place, and most likely induces changes in absorption spectra. The extent of the changes in the absorption spectra is small and does not allow spectrophotometric determinations of equilibria constants.

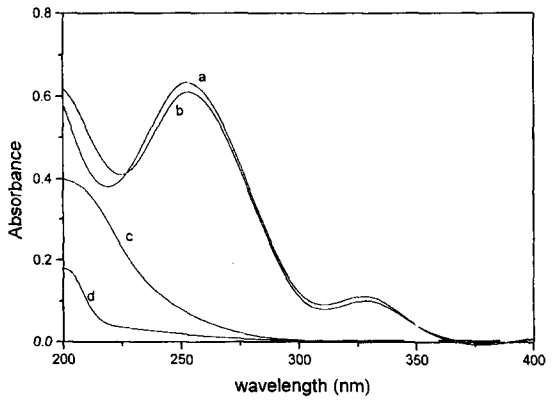

Fig. 1. Absorption spectra of solution containing equal concentrations of Pd^{II} and $SCMCH_2$ (5×10^{-5} M) at different acidities: (a) pH 1.1; (b) pH 2.3. Absorption spectra of solutions containing: (c) 5×10^{-5} M Pd^{II} at pH 1.1, and (d) 2×10^{-5} M $SCMCH_2$.

The equilibrium between the reactants and the complex is pH dependent. Under our experimental conditions, the hydrogen ion concentration is sufficiently high and its changes during the complex formation are negligible, so the equilibrium can be expressed as follows:

$$Pd_f + L_f \rightleftarrows \text{complex} \quad (1)$$

Further in the text $SCMCH_2$ should be denoted as LH_2. The pH dependent apparent formation constant (K_{app}) is defined as the total complex concentration divided by the product of concentrations of the total free Pd^{II} (Pd_f), and total free ligand (L_f):

$$K_{app} = \frac{[\text{complex}]_{tot}}{[Pd_f][L_f]} \quad (2)$$

Pd_f and L_f are given by eqns (3) and (4):

$$[L_f] = LH_3^+ + LH_2 + LH^- = \alpha[LH^-] \quad (3)$$

$$[Pd_f] = Pd^{2+} + Pd(OH)^+ = \beta[Pd^{2+}] \quad (4)$$

where $\alpha = 1 + [H^+]/K_{a2} + [H^+]^2/(K_{a2}K_{a3})$ and $\beta = 1 + K_h/[H^+]$. K_h, K_{a2} and K_{a3} are the equilibria constants of the following reactions:

$$LH_n^{(n-2)+} \overset{K_{an}}{\rightleftarrows} LH_{(n-1)}^{(n-3)+} + H^+ \quad (n = 1\text{–}3) \quad (5)$$

$$Pd^{2+} + H_2O \overset{K_h}{\rightleftarrows} Pd(OH)^+ + H^+ \quad (6)$$

α and β were calculated using the literature data: $pK_h = 2.12$ [10], $pK_{a2} = 3.33$ and $pK_{a3} = 1.91$ [6].

According to the absorption spectra of complex at different acidities, it is clear that two different complex species can be formed in the pH range from 1 to 4. The equilibrium constants are presented by eqns (7) and (8):

$$Pd^{2+} + LH_2 \overset{K''_{eq}}{\rightleftarrows} PdLH^+ + H^+ \quad (7)$$

$$Pd^{2+} + LH \overset{K'_{eq}}{\rightleftarrows} PdL + H^+ \quad (8)$$

The pH dependent apparent formation constant can be derived by appropriate manipulation of eqns (2)–(8):

Table 1. Experimental rate constant (k_{obs}) of complex formation between $SCMCH_2$ and Pd^{II} (2×10^{-5} M) as a function of the $SCMCH_2$ concentration at different acidities

$[L_f] \times 10^5$ (M)	k_{obs} (s^{-1})						
pH	3	5	7	10	15	20	30
1.00	0.185	0.204	0.211	0.234	0.260	0.283	0.358
1.50	0.182	0.211	0.221	0.239	0.290	0.319	0.406
2.10	0.166	0.188	0.227	0.267	0.337	0.423	0.559
2.25	0.167	0.197	0.245	0.294	0.381	0.483	0.670
2.58	0.168	0.241	0.279	0.363	0.471	0.582	0.891
3.00	0.214	0.264	0.313	0.404	0.531	0.662	0.940
3.38	0.220	0.287	0.341	0.425	0.580	0.736	0.997
4.00	0.231	0.295	0.340	0.430	0.562	0.710	0.991

$$K_{app} = \frac{K'_{eq} + \frac{K''_{eq}}{K_{a2}}[H^+]}{\alpha\beta[H^+]} \qquad (9)$$

The values of pH dependent apparent formation constant (K_{app}) were determined from kinetic measurements. Kinetics of the complex formation were investigated at different acidities ($1 < pH < 4$) under pseudo-first-order conditions (excess of ligand). Kinetic measurements in the presence of excess of Pd^{II} were not performed, because of overlapping between absorption spectra of complex and Pd^{II}. Under pseudo-first-order conditions the experimentally determined rate constant (k_{obs}) followed the simple rate expression:

$$k_{obs} = k_f[L_f] + k_r \qquad (10)$$

where k_f and k_r are the forward and reverse pH dependent rate constants, respectively. The collected values of k_{obs} as a function of L_f at constant acidity (see Table 1) indicated the presence of a measurable reverse reaction in the investigated range of acidity. The values of k_f and k_r, as well as formation constant ($K_{app} = k_f/k_r$) were determined at different pH from the plots of k_{obs} vs L_f (see Table 2). The values of K_{app} in the pH range from 2 to 4 (six points) were used to estimate K'_{eq} and K''_{eq}. The plot of $\alpha\beta[H^+]K_{app}$ vs $[H^+]$ (see eqn (9)) is shown in Fig. 2. A straight line with non-zero intercept indicated that both $[PdLH]^+$ and $[PdL]$ complex species are formed under these experimental conditions. The values of $K'_{eq} = (66 \pm 4)$ M^{-1} and $K''_{eq} = (2.7 \pm 0.1) \times 10^2$ M^{-1} were determined from the intercept and the slope, respectively.

Table 2. Forward (k_f) and reverse (k_r) rate constants as well as apparent formation constant ($K_{app} = k_f/k_r$) for the reaction between Pd^{II} and $SCMCH_2$ at different acidities

pH	k_f ($M^{-1} s^{-1}$)	k_r (s^{-1})	$K_{app} \times 10^4$ (M^{-1})
1.00	690	0.17	0.41
1.50	818	0.16	0.51
2.10	1480	0.12	1.23
2.25	1840	0.11	1.67
2.58	2340	0.12	1.95
3.00	2680	0.13	2.06
3.38	3000	0.13	2.31
4.00	2800	0.15	1.87

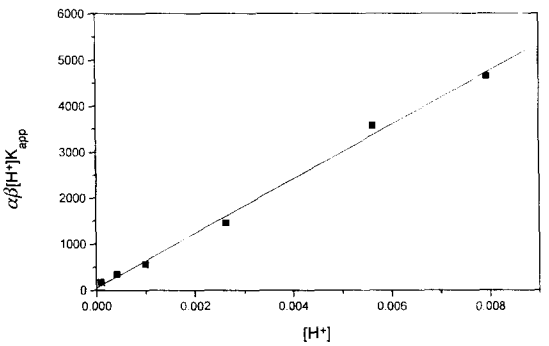

Fig. 2. The plot of $\alpha\beta[H^+]K_{app}$ vs $[H^+]$.

Mechanism of the complex formation

The results presented in Table 2 show significant increase of k_f with the decrease of acidity, while changes of k_r are negligible. This behaviour indicates that two different reacting species of Pd^{II} (Pd^{2+} and $PdOH^+$) are involved in the forward reaction. Also, in the pH range from 1 to 4 three acid-base forms of ligand are present. A reaction scheme which is compatible with pH dependence of k_f is given by reactions (11)–(15). Assumption was made that the reactions (5) and (6) are faster compared to the substitution by ligand, and consequently that the equilibrium between $Pd(OH)_i^{(2-i)^+}$, ($i = 0, 1$) was maintained throughout the kinetic run [10].

$$LH^- + PdOH + \underset{k_{-I}}{\overset{k_I}{\rightleftharpoons}} PdL + H_2O \quad (11)$$

$$K_{a_2} \uparrow\downarrow$$

$$LH_2 + PdOH^+ \underset{k_{-II}}{\overset{k_{II}}{\rightleftharpoons}} PdLH^+ + H_2O \quad (12)$$

$$K_h \uparrow\downarrow$$

$$LH_2 + Pd^{2+} \underset{k_{-III}}{\overset{k_{III}}{\rightleftharpoons}} PdLH^+ + H^+ \quad (13)$$

$$K_{a_3} \uparrow\downarrow$$

$$LH_3^+ + Pd^{2+} \underset{k_{-IV}}{\overset{k_{IV}}{\rightleftharpoons}} PdLH^+ + 2H^+ \quad (14)$$

$$LH_3^+ + PdOH^+ \underset{k_{-V}}{\overset{k_V}{\rightleftharpoons}} PdLH^+ + H^+ \quad (15)$$

Under our experimental conditions, the following rate low can be obtained for the proposed reaction mechanism:

$$\frac{[\text{dcomplex}]}{dt} = \frac{k_1 + k_2[H^+] + k_3[H^+]^2 + k_4[H^+]^3}{\alpha\beta[H^+]} \times \left[\frac{\alpha\beta[H^+]^2}{K'_{eq}} + L_f\left(1 + \frac{K'_{eq}K_{a2}}{K''_{eq}}\frac{1}{[H^+]}\right)\right] \times ([PdLH]_{eq} - [PdLH]) \quad (16)$$

It can be easily shown that under above mentioned experimental conditions pH dependence of k_f can be described as follows:

$$k_f = \frac{k_1 + k_2[H^+] + k_3[H^+]^2 + k_4[H^+]^3}{\alpha\beta[H^+]} \times \left(1 + \frac{K'_{eq}}{K''_{eq}}\frac{K_{a2}}{[H^+]}\right) \quad (17)$$

where $k_1 = k_I K_h$, $k_2 = k_{II}K_h/K_{a2}$, $k_3 = k_{III}/K_{a2} + k_V K_h/(K_{a2}K_{a3})$ and $k_4 = k_{IV}/(K_{a2}/K_{a3})$.

The experimentally determined pH dependence of k_f is shown by the points in Fig. 3. The best fit to eqn (17) was obtained by using k_{1-4} as a variable parameter. The agreement between experimentally determined and calculated values of k_f (see Fig. 3) was obtained for the following set of k_{1-4}: $k_1 = (20 \pm 5)$ M^{-1} s^{-1}, $k_2 = (5.81 \pm 0.18) \times 10^4$ M^{-1} s^{-1}, $k_3 = (2.12 \pm 0.07) \times 10^6$ M^{-1} s^{-1} and $k_4 = (1.19 \pm 0.06) \times 10^8$ M^{-1} s^{-1}.

It is clear that knowing values of k_1, k_2 and k_4 individual rate constants k_I, k_{II} and k_{IV} can be easily determined (see Table 3). The parameter k_3 gives the sum of contributions of path III and V. The individual rate constants k_{III} and k_V were estimated assuming that one of two rate constants is equal zero, and vice versa. The obtained values are the upper limit of individual rate constants, and they are also presented in Table 3.

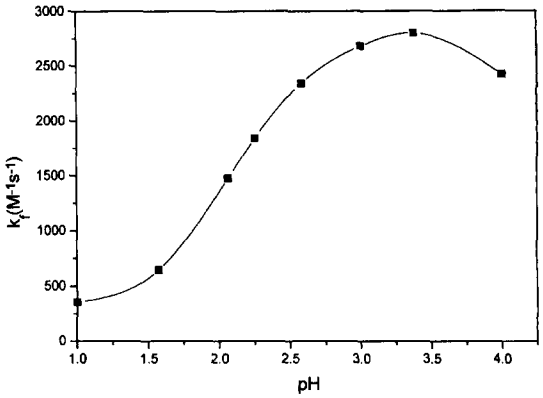

Fig. 3. pH profile of the forward rate constant (k_f) for the formation of the Pd^{II}-$SCMCH_2$ complex. The points were experimentally obtained, while the curve was calculated from eqn 17.

Table 3. Individual rate constants for different reaction paths in the Pd^{II}-$SCMCH_2$ system

Reaction path	Metal ion	Ligand	$k_{I-V} \times 10^{-2}$ (M^{-1} s^{-1})
I	$Pd(OH)^+$	LH^-	26
II	$Pd(OH)^+$	LH_2	35
III*	Pd^{2+}	LH_2	10
IV	Pd^{2+}	LH_3^+	6
V†	$Pd(OH)^+$	LH_3^+	0.09

* k_{III} was obtained by assuming that the rate of path V is negligible small.

† k_V was obtained by assuming that the rate of path III is negligible small.

The literature data suggest that an associative interchange mechanism takes place in substitution reaction of square planar hydrated Pd^{II} cation. The substitution rate is influenced by the nature of the entering ligand and a leaving ligand effect. The results presented in Table 3 show that $PdOH^+$ reacts faster with LH^- and LH_2 compared with Pd^{2+}. The enhanced reactivity of hydrolyzed species is a common feature of metal ions such as Ga^{III}, Al^{III} and Fe^{III} [11,12]. This could be explained in view of the labilising effect of OH^- on the remaining water molecules in the inner coordination sphere. From the comparison with previous results [8], it can be concluded that all ionic forms of $SCMCH_2$ react more rapidly with Pd^{2+} and $PdOH^+$ species than with $Pd(H_2O)_{4-n}Cl_n$ ($n = 1$–4), because the water can be more quickly replaced by attacking ligand than Cl^- ion.

Acknowledgement—This work was partially supported by the Ministry of Science and Technology of the Republic of Serbia.

REFERENCES

1. Meister, A., *Biochemistry of the Amino Acids*, 2nd edn. Academic Press, New York, 1965.
2. Kodoma, H., Ohmari, M., Suzuki, M. and Mizuhara, S., *Physiol. Chem. Phys.*, 1970, **2,** 287.
3. Vasić, V. M., Tošić, M. S. and Nedeljković, J. M., *J. Phys. Org. Chem.*, 1996, **9,** 398.
4. Tošić, M. S., Vasić, V. M., Nedeljković, J. M. and Ilić, L. A., *Polyhedron*, 1997, **16,** 1157.
5. Nakon, R., Beadle, E. M. and Angelici, J., *J. Am. Chem. Soc.*, 1974, **93,** 719.
6. Cromer-Morin, M. and Schraff, J. P., *Analyt. Chim. Acta*, 1979, **104,** 299.
7. Jovanović, T. S., Stanković, V. and Korićanac, Z., 51st International Congress of F.P.I., Book of abstracts, F.I.P., Washington, 1991, p. 111.
8. Nedeljković, J. M., Vasić, V. M., Vuković, V. V. and Jovanović, T. S., *J. Pharm. Biomed. Analysis*, 1995, **13,** 471.
9. Vasić, V. M. and Muk, A. A., *Polyhedron*, 1992, **11,** 1597.
10. Coe, J. S. and Rispoli, P. L., *J. Chem. Soc., Dalton Trans.*, 1976, 2215.
11. Perimutter-Hayman, B., Secco, F., Tapuhi, L. and Venturini, M., *J. Chem. Soc., Dalton Trans.*, 1980, 1124.
12. Mentasti, E., Secco, F. and Venturini, M., *Inorg. Chem.*, 1982, **21,** 602.

Pergamon

PII: S0277-5387(97)00389-6

Polyhedron Vol. 17, No. 4, pp. 405–412, 1998
© 1998 Elsevier Science Ltd
All rights reserved. Printed in Great Britain
0277-5387/98 $19.00+0.00

Lower-rim ferrocenyl substituted calixarenes: new electrochemical sensors for anions

Philip A. Gale,[a] Zheng Chen,[a] Michael G. B. Drew,[b] and Jennifer A. Heath[a] and Paul D. Beer[a]*

[a]Inorganic Chemistry Laboratory, University of Oxford, South Parks Road, Oxford, OX1 3QR, U.K.

[b]Department of Chemistry, University of Reading, Whiteknights, Reading RG2 6AD, U.K.

(Received 23 July 1997; accepted 16 September 1997)

Abstract—New ferrocene substituted calix[4 and 5]arenes have been prepared and the crystal structure of a lower-rim substituted bis ferrocene calix[4]arene (**7**) has been elucidated. The respective ferrocene/ferrocenium redox-couples of compounds **6** (a calix[4]arene tetra ferrocene amide) and **8** (a calix[5]arene pentaferrocene amide) are shown to be significantly cathodically perturbed in the presence of anions by up to 160 mV in the presence of dihydrogen phosphate. © 1998 Elsevier Science Ltd. All rights reserved

Keywords: sensors; ferrocene; calixarene; anion binding; amide; electrochemistry.

Anions are ubiquitous in biological systems [1]. Many proteins contain inorganic phosphate or sulfate anions coordinated via hydrogen bonds from water, amino-acid residues or amide bonds [2]. Additionally excess phosphate pollutants in the environment cause eutrophication of rivers and inland waterways [3], whereas nitrate pollutants and their metabolites are believed to be carcinogenic [4]. There is therefore great interest in the synthesis of receptor species containing hydrogen bond donor arrays [5,6], Lewis acid centres [7] or positive charges [8,9] as sequestering agents or sensors for anions. Early work by ourselves [10–13] and others [14,15] established that amide N—H groups in acyclic synthetic receptor molecules can coordinate anions. As part of this work we demonstrated that the calix[4]arene **1**, which contains a lower-rim ferrocene amide bridge is capable of electrochemically detecting the presence of anions *via* perturbations of the ferrocene/ferrocenium redox couple [16].

As a further extension to this work we decided to synthesise a series of calixarenes containing multiple amidoferrocenyl residues at the lower rim and study these systems as potential amperometric sensors for anions.

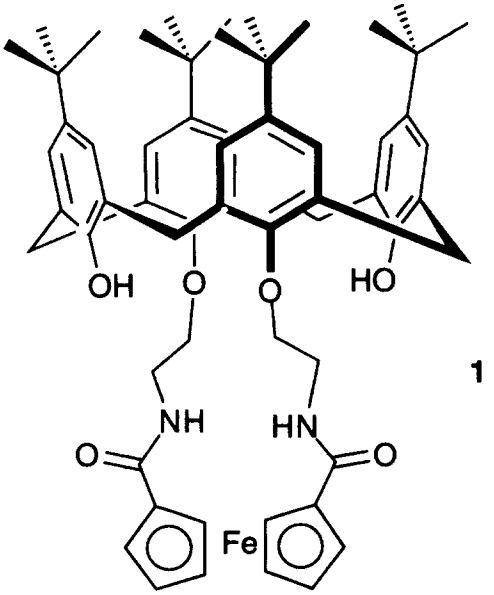

1

RESULTS AND DISCUSSION

Syntheses

p-tert-Butycalix[4]arene tetra (acid chloride) **2**, *p-tert*-butycalix[4]arene bis (acid chloride) **3**, *p-tert*-

* Author to whom correspondence should be addressed.

butycalix[5]arene penta (acid chloride) **4** [17,18] and ferrocenemethylamine **5** [19] were synthesised *via* literature procedures. An analogous synthetic procedure was employed in the preparation of each of the new calixarene–ferrocene conjugate compounds. Typically, the calixarene acid chloride was dissolved in dry dichloromethane, a 25% excess of ferrocenemethylamine **5** and triethylamine added, and the reaction mixture stirred under nitrogen overnight, in darkness. After washing with water, drying over magnesium sulfate and removal of solvent *in vacuo*, a pale brown solid was generally produced. This was purified by column chromatography (silica support) using dichloromethane/methanol as eluent affording the *p-tert*-butycalix[4]arene tetra amidoferrocene **6** in 21% yield, the *p-tert*-butylcalix[4]arene bis amidoferrocene **7** in 29% yield and the *p-tert*-butycalix[4]arene bis amidoferrocene **8** in 16% yield (Scheme 1). The moderate yields of these reactions may be due to the incomplete reaction of the calixarene acid chlorides with ferrocenemethylamine (due to steric interactions), leading to incomplete substitution of ferrocene at the lower rim of the calixarene.

Crystallography

Diffraction quality single crystals of **7** were grown from a dichloromethane/methanol solvent mixture. The structure confirms that **7** adopts the cone conformation in the solid state (Fig. 1) with two ferrocene groups appended at the lower rim. The calixarene has usual C_2 distortion with the angles between the plane of the four methylene groups and the four phenyl rings being 44.2, 66.0, 52.9 and 70.6°, respectively. As can be seen in the figure, there is a dichloromethane molecule encapsulated within the cavity. Crystal data is given in Table 1.

Anion coordination studies: NMR titrations

^{1}H NMR titrations were carried out in dichloromethane-d_2 solutions of compounds **6, 7** and **8**. In a typical titration, 5×10^{-6} mol of receptor was dissolved in 0.5 ml dichloromethane-d_2 and equivalents of the anion added as n-$Bu_4N^+X^-$ ($X^- = Cl^-$, HSO_4^- or $H_2PO_4^-$) in dichloromethane-d_2 (0.1 mol dm^{-3}) solution. The shifts of resonances of protons involved in anion coordination were then recorded and plotted as a function of the amount of anion added. Disappointingly, in the case of **7**, no significant shifts, i.e. greater than 0.01 ppm, were observed indicating that there is little interaction between this molecule and the anionic species. Partial substitution reduces the number of amide hydrogen bond donor sites at the lower rim of **7** compared to **6** and **8**, and this may be the cause for the poor anion coordination ability of this ligand. Another possibility is that in solution, the phenolic OH groups are hydrogen bonded to the amide functionalities via either OH···O=C or HO···H—N hydrogen bonds so blocking the potential coordinating sites. This is reflected in the chemical shift of the amide resonance in the ^{1}H NMR spectrum of **7** which occurs at 8.74 ppm (i.e. it is deshielded relative to the amide protons of **6** and **8** which resonate at 7.57 and 7.42 ppm, respectively). The tetra- and penta- substituted derivatives, however, display significant downfield shifts of the amide NH proton (approximately 0.1 ppm) in the presence of anions (Figs 2 and 3). This indicates that the amide NH protons are coordinating to the added anions. Titrations with compounds **6** or **8** with chloride anions produced titration curves which could be fitted to a 1 : 1 calixarene/anion stoichiometric model. Stability constants were determined with the EQNMR computer program [20] and are shown in Table 2. Compound **6** forms a more stable complex with chloride (55 M^{-1}) than does compound **8** (15 M^{-1}). This may be due to a spacial fit effect, with chloride coordinating to the amide moieties of **6** more efficiently than to those of the calix[5]arene **8**. An adequate fit could not be obtained for the titrations of **6** and **8** against hydrogen sulfate and dihydrogen phosphate to models consistent with 1 : 1 receptor/anion stoichiometries. This may be due to the formation of complexes of other stoichiometries, or aggregation of the anions in the relatively non-polar dichloromethane solvent. Unfortunately, precipitation problems were encountered during the titration studies upon addition of higher concentrations of anions. This precluded the limiting chemical shifts of the anion complexes in these experiments from being found.

Anion coordination studies: electrochemistry

The electrochemical properties of **6, 7** and **8** were investigated using cyclic voltammetry [21] in a dichloromethane/acetonitrile (35 : 65 v/v) solvent mixture, with $(n\text{-Bu})_4NBF_4$ as the supporting electrolyte. The working electrode used was a 5 mm glassy carbon disk and the counter electrode consisted of a platinum mesh. A Ag/Ag^+ electrode was used as reference (+ 330 mV vs S.C.E.). Argon gas saturated with dichloromethane was continually bubbled through the cell to de-oxygenate the solution. It must be noted that in all cases electrochemical experimentation proved difficult with many precipitation and solubility problems encountered, as well as frequent adsorption of the oxidised species onto the electrode in the presence of anions. Each of the ligands exhibited a single quasi-reversible oxidation wave in the region 0.12 to 0.20 V (vs Ag/Ag^+) (Table 2, Fig. 4) suggesting the ferrocene moieties are behaving independently of one another and are therefore being oxidised at the same potential.

Thin layer coulometry was used to confirm that **6, 7,** and **8** are undergoing four, two and five electron oxidations, respectively. In each case, the number of electrons transferred to the compound in question was found to be approximately equal to the number of ferrocene subunits present.

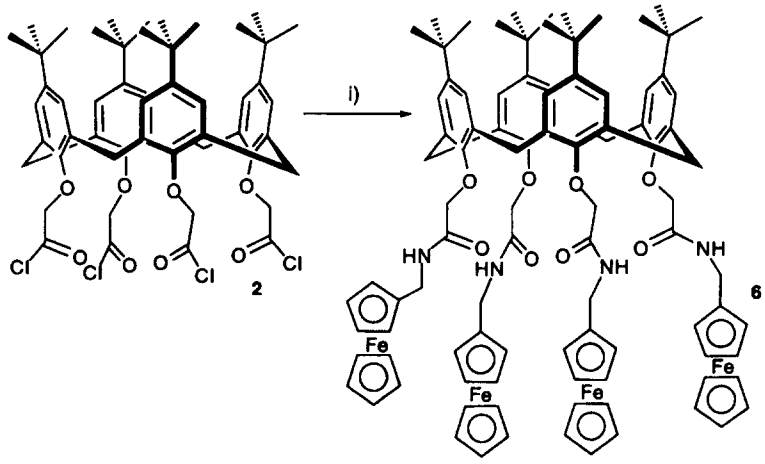

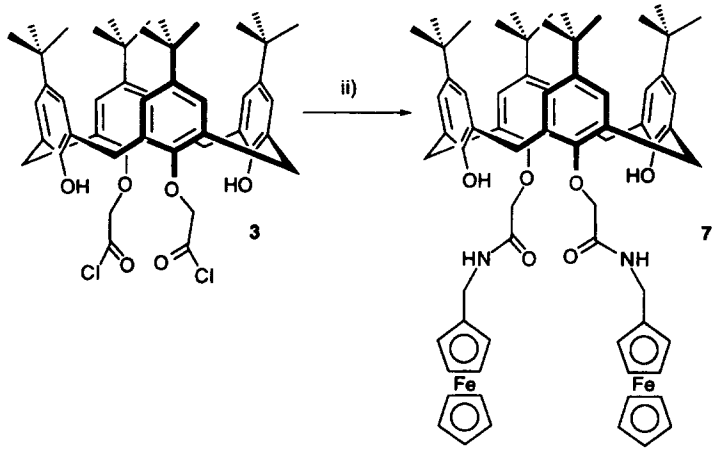

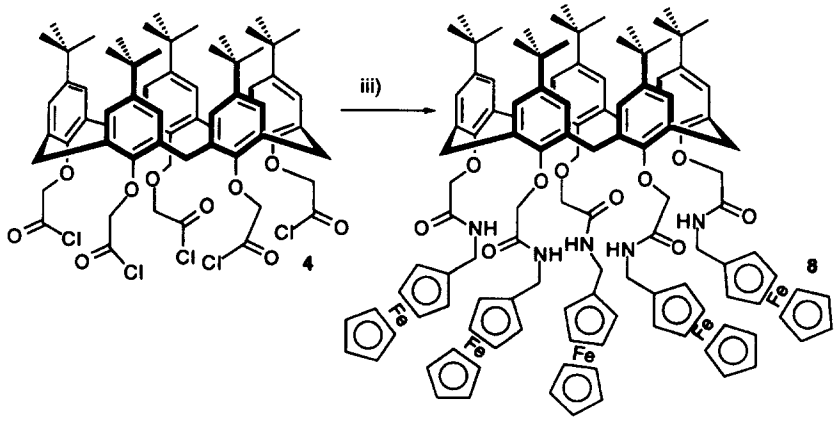

i) 5.0 $FcCH_2NH_2$, 5.0 Et_3N / CH_2Cl_2
ii) 2.5 $FcCH_2NH_2$, 2.5 Et_3N / CH_2Cl_2
iii) 6.0 $FcCH_2NH_2$, 6.0 Et_3N /CH_2Cl_2

Scheme 1.

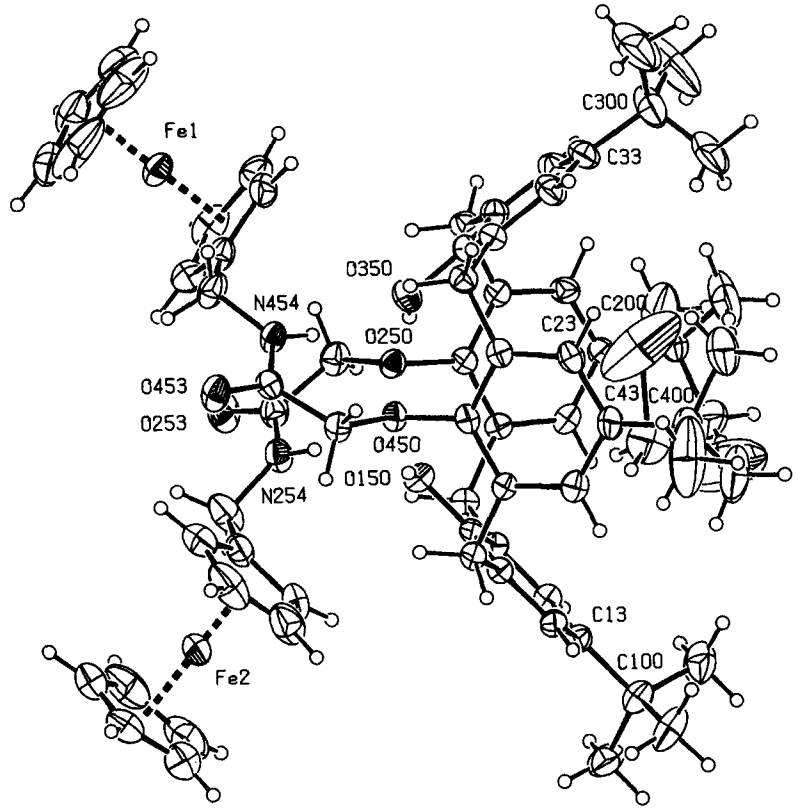

Fig. 1. The structure of **7**, with thermal ellipsoids drawn at the 30% probability level. Hydrogen atoms are included as small circles of arbitrary small radius. Intramolecular hydrogen bonds (not shown) are formed between the amide nitrogen atoms and the phenolic OH groups {N(254)···O(150) 2.98 Å, N(454)···O(350) 2.94 Å}.

Cyclic voltammograms were also recorded after progressive addition of stoichiometric equivalents of anionic guests as 0.1 M solutions of $(n\text{-}Bu_4N)H_2PO_4$, $(n\text{-}Bu_4N)HSO_4$ and $(n\text{-}Bu_4N)Cl$ in CH_2Cl_2/CH_3CN (35:65 v/v) to the electrochemical solutions of **6**, **7** and **8** (1×10^{-3} M) in CH_2Cl_2/CH_3CN (35:65 v/v), and the results are summarised in Table 3.

The addition of anions to electrochemical solutions of **6** and **8** produced cathodic shifts of the ferrocene/ferrocenium redox couple with the relative magnitudes following the order $H_2PO_4^- > Cl^- > HSO_4^-$. The most significant results were observed with compounds **6** and **8** with $H_2PO_4^-$ anions, Fig. 5. Similar results were observed with compound **1** [16].

The addition of dihydrogen phosphate anions causes a 160 mV cathodic shift in the ferrocene/ferrocenium redox couple. This large cathodic shift indicates a strong stabilisation of the oxidised forms of **6** and **8**, in the presence of dihydrogen phosphate. This may be due to dihydrogen phosphate coordination to the amide moieties of the calixarene, a consequence of suitable cavity size as defined by the pendant ferrocene amide groups. This places the anion in close proximity to the ferrocene/ferrocenium moieties, so perturbing the redox potential of these groups. No analogous result was observed with **7** (in agreement with the prior ^1H NMR titration studies).

Conclusions

In conclusion the redox-active ferroceneamide derivatised calix[4,5]arenes (**6**) and (**8**) have been shown to bind and electrochemically detect anions. The stability constants of **6** and **8** with chloride anions have been determined and found to be 55 M^{-1} and 15 M^{-1}, respectively. Compounds **6** and **8** electrochemically recognise Cl^-, HSO_4^- and $H_2PO_4^-$ anions with $H_2PO_4^-$ producing the largest shift of the ferrocene/ferrocenium redox couple (160 mV).

EXPERIMENTAL

General methods

All elemental analyses were carried out by the Inorganic Chemistry Laboratory Microanalysis Service. NMR spectra were recorded on a Bruker AM300 NMR spectrometer. Infrared spectra were recorded

Table 1. Crystal data and structure refinement for 7

Empirical formula	$C_{73}H_{92}Cl_2Fe_2N_2O_8$
Formula weight	1308.09
Temperature	293(2) K
Wavelength	0.71070 Å
Crystal system	Triclinic
Space group	$P\bar{1}$
Unit cell dimensions	$a = 13.772(10)$ Å
	$b = 16.550(10)$ Å
	$c = 17.097(10)$ Å
	$a = 66.883(1)^\circ$
	$b = 85.546(1)^\circ$
	$\gamma = 77.413(1)^\circ$
Volume	3498(4) Å^3
Z	2
Density (calculated)	1.242 Mg/m^3
Absorption coefficient	0.55 mm^{-1}
Crystal size	0.3 × 0.3 × 0.25 mm
Theta range for data collection	2.22 to 24.98°
Index ranges	$0 <= h <= 14$,
	$-18 <= k <= 19$,
	$-20 <= l <= 20$
Independent reflections	10,808
Refinement method	Full-matrix least-squares on F^2
Data/parameters	10,808/805
Goodness-of-fit on F^2	0.831
Final R indices [$I > 2\sigma(I)$]	$R1 = 0.075$, $wR2 = 0.232$
R indices (all data)	$R1 = 0.112$, $wR2 = 0.304$
Largest diff. peak and hole	1.006 and −1.396 e.Å^{-3}

$R_1 = \Sigma||F_o| - |F_c||/\Sigma|F_o|$ $wR_2 = [\Sigma w(F_o^2 - F_c^2)/\Sigma w(F_o)^2]^{1/2}$.

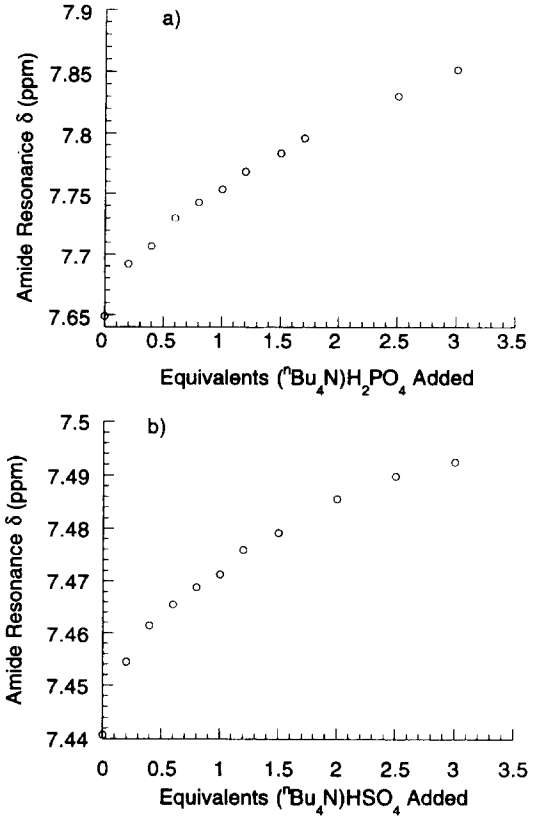

Fig. 2. NMR titrations (CD_2Cl_2) (a) **6** with (n-Bu_4N)H_2PO_4 and (b) **8** with n-Bu_4NHSO_4.

on a Mattson "Polaris" and Perkin Elmer "1710" Infrared Fourier Transform Spectrometers. Electrochemical experiments were conducted on a Princeton Applied Research Potentiostat/Galvanostat Model 273. Fast atom bombardment (FAB) mass spectra were carried out at the University of Wales, Swansea by the SERC/EPSRC Mass Spectrometry Service. Melting points were recorded in open capillaries on a Gallenkamp melting point apparatus and are uncorrected.

Synthesis of p-tert-butycalix[4]arenetetraferrocene-amide (**6**)

Ferrocenemethylamine (0.61 g, 2.84 mmol) was dissolved in dry CH_2Cl_2 (30 ml) and added to *p-tert*-butycalix[4]arene bis (acid chloride) (0.56 mmol). Et_3N (0.29 g, 2.87 mmol) was then added and the reaction mixture stirred under nitrogen overnight. After washing with water (4 × 25 ml), the organic layer was dried over magnesium sulfate. The solvent was then removed under reduced pressure to give a pale brown solid which was purified by column chromatography on silica gel, gradient eluting with CH_2Cl_2/MeOH (gradient elution: concentration of methanol from 0% to 5%). The product was collected, reduced *in vacuo* and then precipitated as a yellow powder from a dichloromethane/methanol solvent mixture as a yellow powder (0.2 g, 21%). ^{1}H NMR ($CDCl_3$, 300 MHz) δ: 1.05 (s, 36H, $C(CH_3)_3$), 3.12 (d, ^2J = 12.5 Hz, 4H, $ArCH_2Ar$: H_{eq}), 4.11 (m, 8H, FcH), 4.16 (s, 20H, FcH), 4.25 (m, 8H, FcH), 4.32 (d, 8H, —$NHCH_2Fc$) and (d, 4H, $ArCH_2Ar$: H_{ax}) coincident, 4.36 (s, 8H, OCH_2), 5.31 (CH_2Cl_2), 6.72 (s, 8H, ArH), 7.57 (t, 4H, NH). ^{13}C NMR/DEPT ($CDCl_3$, 75.42 MHz) δ: 31.33 ($(CH_3)_3C$), 31.49 ($ArCH_2Ar$), 33.66 ($C(CH_3)_3$), 38.70 (—$OCH_2C(O)$—), (68.07, 68.62, 68.63, (FcH)), 74.65 ($NHCH_2Fc$), 84.93 (Fc), 125.76 (ArH), (132.72, 145.71, 152.77 (Ar)), 169.02 (C=O). Microanalysis Calc. for $C_{96}H_{108}O_8N_4Fe_4 \cdot 1/3(CH_2Cl_2)$ C, 68.16; H, 6.45; N, 3.30. Found: C, 68.52; H, 6.53; N, 3.48. FAB MS: MNa^+@1693. Infared Data (KBr Disc) 1662 cm^{-1} (carbonyl stretch) m.p. 255°C.

Synthesis of p-tert-butycalix[4]arenebisferrocene-amide (7)

Ferrocenemethylamine (0.29 g, 1.35 mmol) and Et_3N (0.14 g, 1.38 mmol) were dissolved in dry dichloromethane (25 ml) and added to a round bottomed

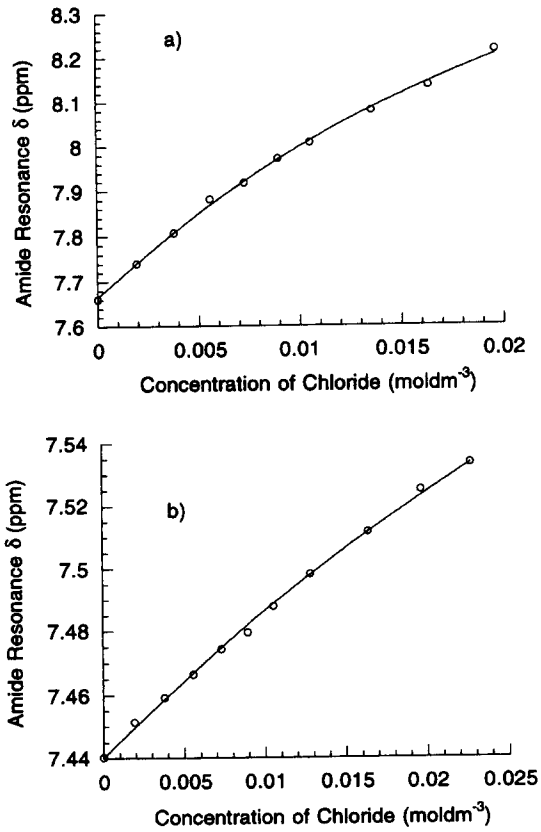

Fig. 3. NMR titrations (CD_2Cl_2) (a) **6** with Cl^- and (b) **8** with Cl^-.

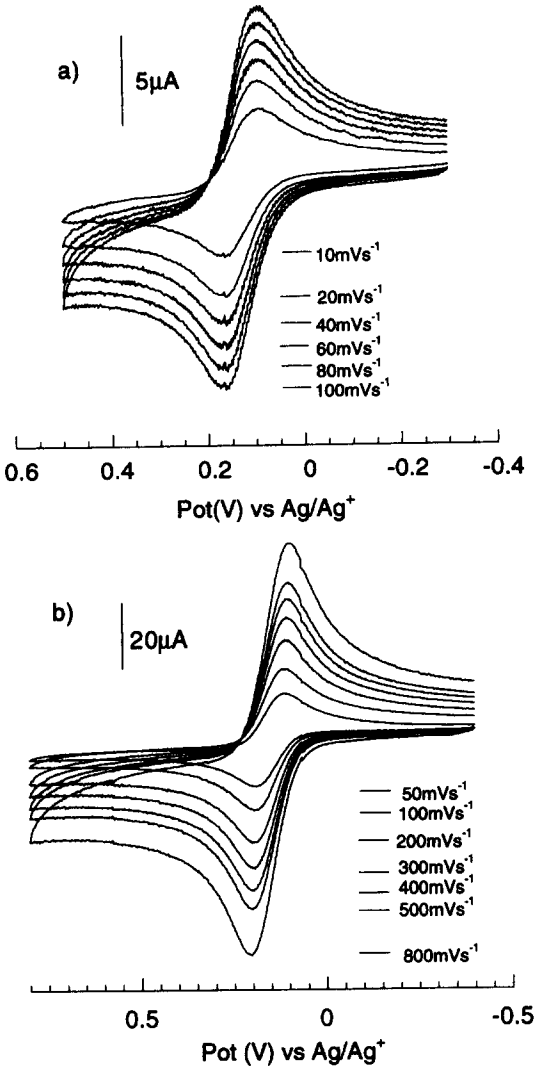

Fig. 4. Quasi-reversible cyclic voltammograms of (a) (**6**) and (b) (**7**) recorded at 1.0×10^{-3} mol dm^{-3} (ligand). Glassy carbon working electrode, Ag^+/Ag reference electrode (+330 mV vs S.C.E.). Recorded in CH_2Cl_2/CH_3CN (35:65 v/v).

Table 2. Stability constants obtained by ^1H NMR titrations with chloride in dichloromethane-d_2 (maximum error ± 20%)

Ligand	Stability constant (M^{-1})
6	55
8	15

flask containing *p-tert*-butylcalix[4]arene bis (acid chloride) (0.54 mmol). The reaction mixture was then left stirring under nitrogen, in the dark, for twenty hours to give a deep red solution. This was washed with water (4 × 25 ml), and the solvent removed *in vacuo* to give orange/red crystals. Purification by column chromatography on silica, gradient eluting with dichloromethane/methanol (gradient elution: concentration of methanol from 0% to 5%). The product was collected, reduced *in vacuo* to give orange/yellow crystals (0.18 g, 29%). ^1H NMR ($CDCl_3$, 300 MHz) δ: 0.95 (s, 18H, $(CH_3)_3C$), 1.26 (s, 18H, $(CH_3)_3C$), 3.27 (d, ^2J = 13.3 Hz, 4H, $ArCH_2Ar:H_{eq}$), 3.87 (d, ^2J = 13.3 Hz, 4H, $ArCH_2Ar:H_{ax}$), 4.10 (s, 4H, FcH), 4.13 (m, 4H, FcH), 4.15 (m, 4H, FcH), 4.28 (d, 4H, $NHCH_2Fc$), 4.38 (s, 4H, $(OCH_2C(O))$), 5.31 (CH_2Cl_2), 6.78 (s, 4H, ArH), 6.99 (s, 4H, ArH), 8.74 (t, 2H, NH). ^{13}C NMR/DEPT ($CDCl_3$, 75.42 MHz) δ: 30.90 ($(CH_3)_3C$), 31.83 ($(CH_3)_3C$), 31.88 ($ArCH_2Ar$), 33.89 ($(CH_3)_3C$), 34.20 ($(CH_3)_3C$), 39.91 (OCH_2), [68.34, 68.89, 69.56 (FcH)], 74.77 ($NHCH_2Fc$), 82.47 (Fc), 125.32 (ArH), 126.00 (ArH), [126.73, 132.10, 142.71, 148.21, 149.23 (Ar)], 167.76 (C=O). Microanalysis: Calc. for $C_{70}H_{82}O_6N_2Fe_2 \cdot 1/3(CH_2Cl_2)$ C, 71.14; H, 7.02; N, 2.36. Found: C, 71.88; H, 7.18; N, 2.48. FAB MS: M^+@1158; MNa^+@1181. Infared Data (KBr Disk): 1681 cm^{-1} (carbonyl stretch). m.p. 245°C (dec).

Table 3. Maximum cathodic shifts in the presence of excess anions

	Ligand 6	7	8
$E_{1/2}$/V(vs Ag/Ag^+)	0.1242	0.1892	0.1318
$\Delta(Cl^-)$/mV	15	<5	20
ΔE (HSO_4^-)/mV	15	<5	20
ΔE ($H_2PO_4^-$)/mV	160	<5	160

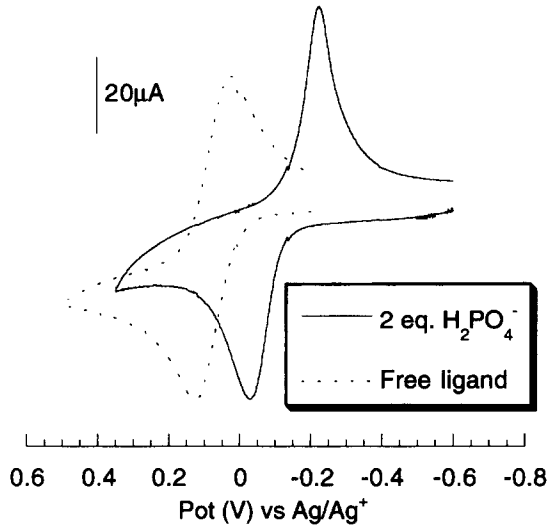

Fig. 5. Cyclic voltammograms of compound **6** in the absence and presence of two equivalents of dihydrogen phosphate in 35% CH_2Cl_2/CH_3CN. Scan rate 100 mV s^{-1}, glassy carbon working electrode, Ag^+/Ag reference electrode (+330 mV vs S.C.E.). Recorded in CH_2Cl_2/CH_3CN (35 : 65 v/v).

Synthesis of p-tert-butylcalix[5]arenepentaferroceneamide (**8**)

Ferrocenemethylamine (0.60 g, 2.79 mmol), triethylamine (0.28 g, 2.77 mmol) and *p-tert*-butycalix[5]arene penta (acid chloride) (4.7 mmol) were dissolved in dry dichloromethane (30 ml) and the reaction mixture stirred for eighteen hours. After washing with water, the product was dried over magnesium sulfate and the solvent removed under reduced pressure to give brown/orange crystals. These were purified by column chromatography on silica gel, gradient eluting with dichloromethane/methanol. The product was collected, reduced *in vacuo*, and then precipitated as a yellow powder (0.16 g, 16%) from a dichloromethane/methanol mixture (gradient elution: concentration of methanol from 0% to 5%). ^{1}H NMR ($CDCl_3$, 300 MHz) δ: 1.02 (s, 45H, $(CH_3)_3C$), 3.31 (d, 5H, J = 14.0 Hz, $ArCH_2Ar$: H_{eq}), 4.12 (s, 10H, OCH_2), 4.17 (s, 25H, FcH), 4.24 (m, 10H, FcH), 4.26 (m, 10H, FcH), 4.27 (d, 10H, —NHCH_2), 4.47 (d, 5H, J = 14.0 Hz, $ArCH_2Ar$: H_{ax}), 6.88 (s, 10H, ArH), 7.42 (t, 5H, NH). ^{13}C NMR ($CDCl_3$, 75.42 MHz) δ: 30.02 ($ArCH_2Ar$), 31.30 ($(CH_3)_3C$), 34.05 ($(CH_3)_3C$), 38.83 (OCH_2CO), [68.14, 68.59, 68.73 (FcH)], 72.93 ($NHCH_2$), 84.93 (Fc), [126.35, 132.62, 146.11, 151.15 (Ar)], 169.01 (C=O). Microanalysis: calc. for $C_{120}H_{135}O_{10}N_5Fe_5$: C, 69.07; H, 6.52; N, 3.36 Found: C, 69.41; H, 6.75; N, 3.33. FAB MS: MH^+@2087, MNa^+@2109. Infared Data (KBr Disk): 1672 cm^{-1} (carbonyl stretch). m.p. 295°C (dec).

Crystallography

Single crystal X-ray analysis of **7** was conducted using MoKα radiation with the MARresearch Image Plate System. The crystal was positioned at 75 mm from the X-ray source. 90 frames were measured at 2° intervals with a counting time of 2 mins. Data analysis was carried out with the XDS program [22]. The structure was solved using direct methods with the Shelx86 program [23]. Apart from the substituted calixarene, there were several solvent molecules and two methanol and one dichloromethane molecules were located, though there were indications of other disordered solvent molecules. The non-hydrogen atoms were refined with anisotropic thermal parameters apart from the carbon and oxygen atoms in the solvent. All hydrogen atoms were included in calculated positions apart from those in the solvent molecules. The structure was then refined using Shelx [24], R-factors are given in Table 1. All calculations were carried out on a Silicon Graphics R4000 Workstation at the University of Reading.

Acknowledgements—We thank the EPSRC for a studentship (PAG) and the EPSRC together with the University of Reading for the provision of the image plate diffractometer.

REFERENCES

1. Stryer, L., *Biochemistry*, 4th edn ed. W. H. Freeman and Co., New York, 1988.
2. Chakrabarti, P., *J. Mol. Biol.*, 1993, **234**, 463–482.
3. Moss, B., *Chem. and Ind.*, 1996, 407.
4. Glidewell, C., *Chem. Br.*, 1990, **26**, No. 2, 137.
5. Gale, P. A., Sessler, J. L., Král, V. and Lynch, V., *J. Am. Chem. Soc.*, 1996, **118**, 5140.
6. Gale, P. A., Sessler, J. L., Allen, W. E., Tvermoes, N. A. and Lynch, V., *Chem. Commun.*, 1997, 665.
7. Beer, P. D., *Chem. Commun.*, 1996, 689.
8. Sessler, J. L., Cyr, M. J., Lynch, V., McGhee, E. and Ibers, J. A., *J. Am. Chem. Soc.*, 1990, **112**, 2810.
9. Sessler, J. L., Cyr, M., Furuta, H., Král, V., Mody, T., Morishima, T., Shionoya, M. and Weghorn, S. J., *Pure and Appl. Chem.*, 1993, **65**, 393.
10. Beer, P. D., Hesek, D., Hodacova, J. and Stokes, S. E., *J. Chem. Soc. Chem. Commun.*, 1992, 270.
11. Beer, P. D., Hazlewood, C., Hesek, D., Hoda-

cova, J. and Stokes, S. E., *J. Chem. Soc. Dalton Trans.*, 1993, 1327.
12. Beer, P. D., Drew, M. G. B., Hazlewood, C., Hesek, D. and Stokes, S. E., *J. Chem. Soc. Chem. Commun.*, 1993, 229.
13. Beer, P. D., Drew, M. G. B., Hazlewood, C., Hesek, D., Hodacova, J. and Stokes, S. E., *J. Chem. Soc. Chem. Commun.*, 1993, 229.
14. Pascal, R. A., Spergel, J. and van Engen, D. V., *Tetrahedron Lett.*, 1986, **27,** 4099.
15. Valiyaveettil, S., Engbersen, J. F. J., Verboom, W. and Reinhoudt, D. N., *Angew. Chem. Int. Ed. Engl.*, 1993, **32,** 900.
16. Beer, P. D., Chen, Z., Goulden, A. J., Graydon, A., Stokes, S. E. and Wear, T., *J. Chem. Soc. Chem. Commun.*, 1993, 1834.
17. McKervey, M. A., Seward, E. M., Ferguson, G., Ruhl, B. and Harris, S. J., *J. Chem. Soc. Chem. Commun.*, 1985, 388.
18. Arnaud-Neu, F., Schwing-Weill, M. J., Ziat, K., Cremin, S., Harris, S. J. and McKervey, M. A., *New. J. Chem.*, 1991, **15,** 33.
19. Spencer, P., Polyaza redox-active acyclic and macrocyclic compounds designed to bind cations and anions, D.Phil. thesis, University of Oxford, 1994.
20. Hynes, M. J., *J. Chem. Soc., Dalton Trans.*, 1993, 311.
21. *Instrumental Methods in Electrochemistry*, Southampton Electrochemistry Group, Ellis Horwood Limited, University of Southampton, 1990.
22. Kabsch, W., *J. Appl. Cryst.*, 1988, **21,** 916.
23. Sheldrick, G. M., *Acta Cryst.*, 1990, **A46,** 467.
24. Sheldrick, G. M., Pers. comm., 1993.

Pergamon

PII: S0277-5387(97)00387-2

Polyhedron Vol. 17, No. 4, pp. 413–420, 1998
© 1998 Elsevier Science Ltd
All rights reserved. Printed in Great Britain
0277-5387/98 $19.00+0.00

A study on the reactivity of cobalt, copper and zinc complexes of 2-methylpyridine-*N*-oxide towards sulfur dioxide†

M. Fondo,[a] M. R. Bermejo,*[a] A. Sousa,*[a] J. Sanmartín,[a] M. I. Fernández[a] and C. A. McAuliffe*[b]

[a]Departamento de Química Inorgánica, Facultade de Química, Universidade de Santiago de Compostela, Santiago de Compostela, Galicia, E-15706 Spain

[b]Department of Chemistry, University of Manchester, Institute of Science and Technology, P.O. Box 88, Manchester M60 1QD, U.K.

(Received 18 June 1996; accepted 16 September 1997)

Abstract—A series of complexes of general formula $M(2\text{-}PyCO)_nX_2(H_2O)_m$ (M = Co, Cu, Zn; 2-PyCO = 2-methylpyridine-*N*-oxide, n = 1–2, X = Cl, Br, I and NO_3 and m = 0–1) has been prepared and characterised. The reactivity of these complexes with sulfur dioxide has been investigated in the solid state and in toluene slurries at room temperature. The effect of temperature on the ability of these complexes to fix SO_2 has been studied by thermogravimetrical analysis (TGA); the temperature range of study depending critically on the melting point of the initial precursors. The same technique has been used to study the reversibility of the reaction with sulfur dioxide.

The amount of sulfur dioxide fixed is dependent on the metal, the anion, the medium of the reaction and the temperature. In general, an increase in temperature results in a decrease in the reactivity of the metal precursors with SO_2 but the complexes of copper halides show that an increase in temperature favours the reaction. This is quite interesting behaviour not previously reported. © 1998 Elsevier Science Ltd. All rights reserved

Keywords: Metals; complexes; sulfur dioxide; 2-methylpyridine-*N*-oxide; fixation; reactivity.

Sulfur dioxide is an insidious pollutant, and the main cause of acid rain. There are many methods used in industry to try to remove SO_2 from gas streams but all are relatively expensive and generate large quantities of residues. For this reason it has become necessary to search for new methods to solve the environmental problems caused by the emission of sulfur dioxide to the atmosphere. The growing magnitude of these problems, combined with the academic interest in sulfur dioxide as a ligand, due to its numerous coordination modes [1–3], has resulted in recent developments in the chemistry of SO_2 with transition metal complexes.

We have focused our attention on the reactivities of the first row transition metal complexes [4–9] with SO_2, as a means of providing a better understanding of its chemistry and to find a cheap metal-fixing precursor which could have industrial applications. As an extension of our previous paper [9a] where we have studied the reactivity of the complexes $Mn(2\text{-}PyCO)_nX_2(H_2O)_m$ with SO_2, we now report the syntheses and characterisation of mono- and bis-ligand complexes of 2-methylpyridine-*N*-oxide with cobalt, copper and zinc halides and nitrates and their reactivity with SO_2 in the solid state and in toluene slurries.

EXPERIMENTAL

Synthesis of the metal precursors

The complexes $M(2\text{-}PyCO)_nX_2(H_2O)_m$ were synthesised in absolute ethanol, using the commercial

* Authors to whom correspondence should be addressed.

† Dedicated to the Royal University of Santiago de Compostela in the year of its fifth century.

metal salts $CoCl_2 \cdot 6H_2O$, $CoBr_2 \cdot xH_2O$, CoI_2, $Co(NO_3)_2 \cdot 6H_2O$, $CuCl_2$, $CuBr_2$, $Cu(NO_3)_2 \cdot 3H_2O$, $ZnCl_2$, $ZnBr_2$, ZnI_2, $Zn(NO_3)_2 \cdot 6H_2O$ and the ligand 2-methylpyridine-*N*-oxide without further purification. The syntheses were performed following a method previously described [10,11] consisting of mixing the salt and the ligands in stoichiometric ratios and stirring them in ethanol at room temperature for 24 h. The isolated solids were washed with diethyl ether and dried in air. $Zn(2\text{-}PyCO)_2(NO_3)_2$ was isolated as an oil that was transformed into a powder after trituration with diethyl ether.

It must be pointed out that for most of the salts, the 1 : 2 adducts were isolated regardless of the metal : ligand ratio. $CoCl_2$ only yields the 1 : 1 adduct when it is stirred with the ligand in 1 : 2 or 1 : 4 ratios (Table 1).

Reactions with sulfur dioxide

(*i*) *Solid state at room temperature.* The SO_2-adducts were synthesised by the method previously described [9] that essentially consists of monitoring the changes in mass of a sample (0.1–0.3 g) of the complex, contained in a Rotaflo tube, when it is exposed to a sulfur dioxide stream for several days until a constant mass is achieved (ca. one week).

(*ii*) *Toluene slurries.* The method employed has been previously reported [9]. The suspension of the metal precursor in dry distilled toluene (Na, benzophenone) was saturated with sulfur dioxide until no changes in colour and/or aspect occurred (*ca.* one week). The compounds were isolated by standard Schlenk techniques and dried in a stream of argon. Full details of the synthesis have been previously described [7a].

(*iii*) *Solid state at high temperature.* The absorption of sulfur dioxide at high temperature was studied using a thermogravimetric balance CAHN Instruments TG131. The programmed scheme, already reported [9], results in an increase in temperature of the sample until its melting point is reached whilst a gas flow of 50 $cm^3\ min^{-1}$ is maintained. The uptake of SO_2 is monitored for samples (0.04–0.08 g) using a series of temperature/partial pressure programmes.

(*iv*) *High temperature SO_2 desorption.* The studies on the lability of the coordinated sulfur dioxide were performed in the same thermogravimetric balance. The sample (0.02–0.5) was heated to the melting point of the complex and maintained under a nitrogen stream for 12–24 h or alternatively heated in a Rotaflo tube to the melting point under reduced pressure for 4 h. The resultant complexes were analysed by the USC and UMIST Microanalytical Services. Infrared spectra were obtained as KBr pellets using a Bruker IFS 66 V spectrophotometer in the 2000–500 cm^{-1} range.

RESULTS AND DISCUSSION

Metal precursors

The syntheses of the metal precursors described here follows the method previously described [10,11]. All the compounds prepared are air stable but are hygroscopic, changing colour when they are stored in moist air. Some structural aspects of the compounds have been previously discussed [12–19].

Reactions with sulfur dioxide

The reactivities of the metal precursors with sulfur dioxide have been studied by methods previously described in the solid state (Tables 2 and 3) and in toluene slurries (Tables 4 and 5) at room temperature and in the solid state at high temperature [9] (Table 7). The medium and the conditions of the reaction

Table 1. Elemental analyses of the metal precursors

Metal precursor	Colour	mp (°C)	ν(NO)/δ(NO)[a]	$\nu(NO_3)$[a]	%C[b]	%H[b]	%N[b]
$Co(2\text{-}PyCO)Cl_2(H_2O)$	violet	252	1190/843		28.2 (28.0)	3.2 (3.5)	5.6 (5.4)
$Co(2\text{-}PyCO)_2Br_2$	blue	149	1198/843		32.9 (32.9)	2.9 (3.0)	6.6 (6.4)
$Co(2\text{-}PyCO)_2I_2(H_2O)$	green	133	1200/845		25.7 (25.5)	2.7 (2.9)	5.2 (5.1)
$Co(2\text{-}PyCO)_2(NO_3)_2$	violet	105	1200/848	1300, 820	35.6 (35.9)	4.0 (3.5)	14.2 (13.9)
$Cu(2\text{-}PyCO)_2Cl_2$	green	138	1197/845		40.8 (40.8)	4.1 (3.9)	7.8 (7.9)
$Cu(2\text{-}PyCO)_2Br_2(H_2O)_3$	brown	105	1202/848		29.1 (29.0)	3.8 (4.0)	5.6 (5.6)
$Cu(2\text{-}PyCO)_2(NO_3)_2$	blue	152	1199/847	1281, 802	35.3 (35.5)	3.5 (3.4)	13.9 (13.8)
$Zn(2\text{-}PyCO)_2Cl_2$	white	134	1203/845		40.3 (40.6)	3.7 (3.9)	8.0 (7.9)
$Zn(2\text{-}PyCO)_2Br_2$	white	135	1203/843		32.3 (32.5)	3.0 (3.1)	6.6 (6.3)
$Zn(2\text{-}PyCO)_2I_2$	yellow	123	1204/845		26.7 (26.8)	2.5 (2.6)	5.5 (5.2)
$Zn(2\text{-}Py(CO)_2(NO_3)_2(H_2O)$	white	88	1205/847	1312, 818	33.5 (33.8)	3.7 (3.7)	13.4 (13.1)

[a] All the spectra have been obtained as KBr discs.
[b] Calculated values in parentheses.

Table 2. Elemental analyses of the adducts formed after interaction of the metal precursors with SO_2 in the solid state at room temperature

Metal precursor	Resultant adduct	%C[a]	%H[a]	%N[a]	%S[a]
$Co(2\text{-}PyCO)Cl_2(H_2O)$	No reaction				
$Co(2\text{-}PyCO)_2Br_2$	No reaction				
$Co(2\text{-}PyCO)_2I_2(H_2O)$	$Co(2\text{-}PyCO)_2I_2(SO_2)_{0.25}(H_2O)_2$	24.3 (24.7)	2.8 (2.7)	4.7 (4.8)	1.0 (1.4)
$Co(2\text{-}PyCO)_2(NO_3)_2$	$Co(2\text{-}PyCO)_2SO_4(SO_2)(H_2O)_2$	29.9 (30.4)	3.8 (3.4)	5.6 (5.4)	13.4 (13.5)
$Cu(2\text{-}PyCO)_2Cl_2$	$Cu(2\text{-}PyCO)_2Cl_2(SO_2)_{0.25}(H_2O)$	37.7 (37.2)	4.2 (4.1)	7.5 (7.2)	2.1 (2.1)
$Cu(2\text{-}PyCO)_2Br_2(H_2O)_3$	$Cu(2\text{-}PyCO)_2Br_2(SO_2)_{0.66}(H_2O)_3$	26.7 (26.7)	2.7 (3.7)	5.1 (5.2)	3.9 (4.0)
$Cu(2\text{-}PyCO)_2(NO_3)_2$	$Cu(2\text{-}PyCO)_2SO_4(SO_2)_{1.75}(H_2O)_3$	26.8 (26.5)	3.6 (3.7)	5.3 (5.1)	16.2 (16.1)
$Zn(2\text{-}PyCO)_2Cl_2$	No reaction				
$Zn(2\text{-}PyCO)_2Br_2$	No reaction				
$Zn(2\text{-}PyCO)_2I_2$	No reaction				
$Zn(2\text{-}PyCO)_2(NO_3)_2(H_2O)$	$Zn(2\text{-}PyCO)_2SO_4(SO_2)_{1.75}(H_2O)_2$	26.8 (27.3)	3.7 (3.4)	5.5 (5.3)	16.3 (16.7)

[a] Calculated values in parentheses.

Table 3. Some physical properties of the adducts formed after interaction of the metal precursors with SO_2 in the solid state at room temperature

Adduct	Colour	Aspect	$\nu(NO)/\delta(NO)$[b]	$\nu(SO_2)$[b]	$\nu(SO_4)$[b]
$Co(2\text{-}PyCO)_2I_2(SO_2)_{0.25}(H_2O)_2$	green	powder	1200/845		
$Co(2\text{-}PyCO)_2SO_4(SO_2)(H_2O)_2$	pink	powder	1200/830	1095	880, 630
$Cu(2\text{-}PyCO)_2Cl_2(SO_2)_{0.25}(H_2O)$	green	powder	1198/845		
$Cu(2\text{-}PyCO)_2Br_2(SO_2)_{0.66}(H_2O)_3$	brown	powder	1200/843	1113	
$Cu(2\text{-}PyCO)_2SO_4(SO_2)_{1.75}(H_2O)_3$	green	powder	1198/839	1310	642, 625, 588
$Zn(2\text{-}PyCO)_2SO_4(SO_2)_{1.75}(H_2O)_2$	yellow	powder	1201/845	1080	880

[b] All the spectra have been performed as KBr discs.

Table 4. Elemental analyses of the adducts resulting from the interaction of the metal precursors with SO_2 in toluene slurries

Metal precursor	Resultant adduct	%C[a]	%H[a]	%N[a]	%S[a]
$Co(2\text{-}PyCO)Cl_2(H_2O)$	No reaction				
$Co(2\text{-}PyCO)_2Br_2$	No reaction				
$Co(2\text{-}PyCO)_2I_2(H_2O)$	No reaction				
$Co(2\text{-}PyCO)_2(NO_3)_2$	$Co(2\text{-}PyCO)SO_4(SO_2)_{0.25}$	25.9 (25.7)	2.3 (2.5)	4.9 (5.0)	14.6 (14.3)
$Cu(2\text{-}PyCO)_2Cl_2$	$Cu(2\text{-}PyCO)_2Cl_2(SO_2)_{0.66}(H_2O)_2$	33.5 (33.4)	4.1 (4.1)	6.5 (6.4)	4.6 (4.9)
$Cu(2\text{-}PyCO)_2Br_2(H_2O)_3$	$Cu(2\text{-}PyCO)_2Br_2(SO_2)(H_2O)_3$	25.4 (25.7)	3.3 (3.5)	4.9 (5.0)	5.5 (5.7)
$Cu(2\text{-}PyCO)_2(NO_3)_2$	$Cu(2\text{-}PyCO)SO_4(SO_2)_{0.5}$	24.1 (23.9)	2.5 (2.3)	4.7 (4.7)	15.9 (16.0)
$Zn(2\text{-}PyCO)_2Cl_2$	No reaction				
$Zn(2\text{-}PyCO)_2Br_2$	No reaction				
$Zn(2\text{-}PyCO)_2I_2$	No reaction				
$Zn(2\text{-}PyCO)_2(NO_3)_2(H_2O)$	$Zn(2\text{-}PyCO)SO_4(SO_2)$	22.2 (21.5)	2.0 (2.1)	4.3 (4.2)	19.3 (19.1)

[a] Calculated values in parentheses.

Table 5. Some physical properties of the adducts resulting from the interaction of the metal precursors with SO_2 in toluene slurries

Found adduct	Colour	Aspect	$\nu(NO)/\delta(NO)$[b]	$\nu(SO_2)$[b]	$\nu(SO_4)$[b]
$Co(2\text{-}PyCO)SO_4(SO_2)_{0.25}$	pink	powder	1200/845	1080	885
$Cu(2\text{-}PyCO)_2Cl_2(SO_2)_{0.66}(H_2O)_2$	green	powder	1189/845	1281, 1164, 1118751, 617	
$Cu(2\text{-}PyCO)_2Br_2(SO_2)(H_2O)_3$	brown	pasty	1198/843	1240	
$Cu(2\text{-}PyCO)SO_4(SO_2)_{0.5}$	black	oil	1200/851	1069	885, 573
$Zn(2\text{-}PyCO)SO_4(SO_2)$	black	oil	1200/850	1250	870

[b] All the spectra have been obtained as KBr discs.

Table 6. Elemental analyses of the complexes after SO_2-desorption studies

SO_2-adduct	T (°C)	Time	Complex after desorption	%C[a]	%H[a]	%N[a]	%S[a]
$Co(2\text{-}PyCO)_2I_2(SO_2)_{0.25}(H_2O)_2$	90	4 h	$Co(2\text{-}PyCO)_2I_2(SO_2)_{0.25}$	24.4 (24.7)	2.6 (2.7)	4.5 (4.8)	1.5 (1.4)
$Co(2\text{-}PyCO)SO_4(SO_2)_{0.25}$	90	4 h	$Co(2\text{-}PyCO)SO_4(SO_2)_{0.25}$	25.3 (25.7)	2.7 (2.5)	4.7 (5.0)	14.8 (14.3)
$Cu(2\text{-}PyCO)_2Cl_2(SO_2)_{0.25}(H_2O)$	90	4 h	$Cu(2\text{-}PyCO)_2Cl_2(H_2O)$	38.6 (38.8)	3.9 (4.3)	7.1 (7.5)	
$Cu(2\text{-}PyCO)_2Cl_2(SO_2)_{0.66}(H_2O)_2$	90	4 h	$Cu(2\text{-}PyCO)_{1.5}Cl_2(SO_2)_{0.5}(H_2O)_2$	30.0 (29.5)	3.8 (4.0)	5.7 (5.7)	3.9 (4.4)
$Cu(2\text{-}PyCO)_2Br_2(SO_2)_{0.66}(H_2O)_3$	90	4 h	$Cu(2\text{-}PyCO)_{1.5}Br(SO_2)_{0.5}(H_2O)_2$	23.8 (23.7)	3.2 (3.2)	4.6 (4.6)	3.2 (3.5)
$Cu(2\text{-}PyCO)_2SO_4(SO_2)_{1.75}(H_2O)_3$	106	24 h	$Cu(2\text{-}PyCO)SO_4(SO_2)_{0.5}(H_2O)$	22.9 (22.6)	2.6 (2.8)	4.4 (4.4)	15.6 (15.1)
$Cu(2\text{-}PyCO)_2Br_2(SO_2)(H_2O)_3$	100	21 h	$Cu(2\text{-}PyCO)_2Br_2(SO_2)(H_2O)_2$	26.7 (26.6)	3.1 (3.3)	5.2 (5.2)	5.2 (5.9)
$Cu(2\text{-}PyCO)SO_4(SO_2)_{0.5}$	80	4 h	$Cu(2\text{-}PyCO)SO_4(SO_2)_{0.5}$	22.8 (23.9)	3.9 (2.3)	4.6 (4.6)	16.2 (16.0)
$Zn(2\text{-}PyCO)_2SO_4(SO_2)_{1.75}(H_2O)_3$	90	24 h	$Zn(2\text{-}PyCO)SO_4(SO_2)_{0.5}(H_2O)$	22.3 (22.5)	3.0 (2.8)	4.5 (4.4)	14.9 (14.9)

[a] Calculcated values in parentheses.

Table 7. Elemental analyses of the adducts resulting from interaction of the metal precursors with SO_2 in the solid state in the temperature range presented

Metal precursor	T (°C)	Time	Resultant adduct	%C[a]	%H[a]	%N[a]	%S[a]
$Co(2\text{-}PyCO)Cl_2(H_2O)$	240–30	5 h 30 min.	No reaction				
$Co(2\text{-}PyCO)_2Br_2$	125–30	3 h 20 min.	No reaction				
$Co(2\text{-}PyCO)_2I_2(H_2O)$	120–30	3 h 20 min.	No reaction				
$Co(2\text{-}PyCO)_2(NO_3)_2$	90–30	3 h 50 min.	$Co(2\text{-}PyCO)SO_4$	28.1 (27.2)	4.0 (2.7)	6.1 (5.3)	12.1 (12.1)
$Cu(2\text{-}PyCO)_2Cl_2$	150–30	3 h 50 min.	$Cu(2\text{-}PyCO)_2Cl_2(SO_2)$	32.8 (34.6)	3.7 (3.4)	6.3 (6.7)	7.6 (7.7)
$Cu(2\text{-}PyCO)_2Br_2(H_2O)_3$	125–30	3 h 20 min.	$Cu(2\text{-}PyCO)_2Br_2(SO_2)_{0.75}$	29.2 (29.40)	3.3 (2.9)	5.6 (5.7)	4.5 (4.9)
$Cu(2\text{-}PyCO)_2(NO_3)_2$	150–30	7 h 40 min.	$Cu(2\text{-}PyCO)_2SO_4(SO_2)(H_2O)_2$	28.7 (30.1)	4.0 (3.8)	5.6 (5.9)	13.7 (13.3)
$Zn(2\text{-}PyCO)_2Cl_2$	125–30	3 h 20 min.	No reaction				
$Zn(2\text{-}PyCO)_2Br_2$	125–30	3 h	20 min.	No reaction			
$Zn(2\text{-}PyCO)_2I_2$	87–30	3 h 20 min.	No reaction				
$Zn(2\text{-}PyCO)_2(NO_3)_2(H_2O)$	83–30	7 h 30 min.	$Zn(2\text{-}PyCO)SO_4$	26.8 (26.6)	3.3 (2.6)	5.1 (5.2)	12.0 (11.8)

[a] Calculated values in parentheses.

seem to play an important role in the ability of the compounds to react with SO_2, as different adducts are obtained from the same metal precursor in the solid state at room temperature (Table 2), at high temperature (Table 7) and in toluene slurries at room temperature (Table 4).

Reactions with sulfur dioxide at room temperature

The adducts obtained from the solid state and from toluene slurries are quite different but they show some common features.

The halide derivatives of cobalt and zinc do not react with SO_2 in any of the media. Only the iodide derivatives can fix 0.25 moles of SO_2 per mole of complex in the solid state but no binding is observed in toluene slurries. This SO_2 is linked to the precursor in an irreversible manner as it is not lost upon prolonged heating at reduced pressure (Table 6). The same kind of interaction is present in the compound $Co(2\text{-}PyCO)SO_4(SO_2)_{0.25}$ that retains 0.25 moles of SO_2 when it is heated at 90°C for 4 h at reduced pressure. However, $Cu(2\text{-}PyCO)_2Cl_2(SO_2)_{0.25}(H_2O)$ loses sulfur dioxide after desorption studies. This lability and the absence in the IR spectrum of new bands associated to S—O stretches (Table 3) allow us to propose a physical rather than chemical interaction of the SO_2 present in this compound. The same kind of interaction is to be expected for the 0.25 moles of SO_2 present in the adducts $Cu(2PyCO)_2SO_4(SO_2)_{1.75}(H_2O)_3$ and $Zn(2PyCO)_2SO_4(SO_2)_{1.75}(H_2O)_2$.

For all of the nitrate derivatives it was observed that the replacement of the nitrate group by a sulfate group occurs. This sulfate group probably comes from the oxidation of one molecule of SO_2, perhaps at the expense of the reduction of the nitrate group to nitrogen oxides, in agreement with previous results [8–9]. The presence of the sulfate groups is confirmed by new IR bands in the ranges 885–870 and 642–588 cm^{-1}. Such bands are characteristic of the sulfate group acting as a bidentate chelate [20], as is expected for a sulfate group resulting from a sulfur dioxide oxidation process [2,21]. The ν(NO) and δ(NO) for the 2-methylpyridine-*N*-oxide in the new adducts were assigned in the ranges 1201–1198 and 841–830 cm^{-1}, respectively, and are not significantly different from those of the metal precursors.

Reactions with sulfur dioxide in the solid state at room temperature

Although there are many binding modes established [3] for SO_2 (η^1-S pyramidal, η^1-S planar, η^1-O, η^2-S,O bridge, ligand bound or insertion) some of them have a low probability of existence in the complexes studied here. The η^1-S pyramidal coordination mode is quite unusual in first row transition metal complexes, but very common in the adducts of second and third row transition metals [3]. The η^1-O coordination mode has not been found for transition metals [22–23]. Consequently, the η^1-S pyramidal and η^1-O binding modes are quite improbable for the first row complexes studied here.

IR spectra

Although Kubas [3] has tried to correlate the S—O stretching frequencies with the coordination mode of the sulfur dioxide in adducts of SO_2. IR spectroscopy alone is not able to establish the binding mode. A good complement to this technique is the study of the reversibility of the reaction.

All the nitrate derivatives absorb one mole of SO_2 that is oxidised to sulfate and replaces the nitrate group as was discussed. However, all of them can fix an additional quantity of sulfur dioxide (1–1.75 moles) the IR spectra show new bands in the regions 1095–1080 and 1310 cm^{-1}. These bands are not possible for the η^2-S,O and η^1-O and S-bridge binding modes; furthermore the η^1-S pyramidal coordination mode is quite improbable (see above) and insertion is not possible as there are no metal–carbon or metal–halide bonds. So the compounds can only represent either a η^1-S planar or ligand bound binding modes. IR spectroscopy does not distinguish between these coordination modes but the studies on the reversibility of the reaction allow us to discern between them.

A different binding mode seems to be present in $Cu(2\text{-}PyCO)_2Br_2(SO_2)_{0.66}$, which has an IR band at 1113 cm^{-1}. This information alone is not enough to establish the coordination mode for the SO_2 but the similarity with other well characterised compounds [24] allows us to propose a trinuclear structure with the SO_2 acting as a bridge.

Desorption studies

The desorption studies are very useful, in combination with IR spectroscopy and analogy with other well characterised complexes, to determine the possible binding mode of sulfur dioxide in SO_2-adducts. In general, only when the SO_2 presents a η^1-S pyramidal or ligand bound mode is it labile in contrast with the η^1-S planar or S-bridge coordination modes [3].

Most of the adducts link at least one part of the sulfur dioxide in a reversible way but many of them present more than one binding mode and part of the SO_2 is retained in the adduct upon an increase in temperature.

The only compound that fixes all the sulfur dioxide irreversibly is $Co(2\text{-}PyCO)_2I_2(SO_2)_{0.25}(H_2O)_2$ (Table 6). This fact indicates that the SO_2 is no simply physically absorbed or housed within cage-like structures, so the interaction should be chemical, as previously proposed. $Cu(2\text{-}PyCO)_2Cl_2(SO_2)_{0.25}(H_2O)$ loses sulfur dioxide when it is heated (Table 6). This behaviour is

in accord with the proposed physical absorption of the SO_2.

All of the sulfate derivatives, obtained from the nitrate precursors by oxidation of one mole of SO_2, fix an additional quantity of SO_2, part of it in a reversible way. $Zn(2\text{-}PyCO)_2SO_4(SO_2)_{1.75}(H_2O)_2$ seems to bind the SO_2 in many ways. This adduct loses 1.25 moles of sulfur dioxide upon an increase in temperature (see Table 6). Perhaps 0.25 moles are physically absorbed while 1 mole is labile and the IR band at 1080 cm^{-1}, seems to suggest that it is ligand bound. The irreversibility of the reaction suggests that the 0.5 moles of SO_2 that remain in the adduct is in the form of S-bridge.

The same binding modes can be proposed for $Cu(2\text{-}PyCO)_2SO_4(SO_2)_{1.75}(H_2O)_3$, which loses 1.25 moles of SO_2 when it is heated (Table 6), and the presence of an IR band at 1310 cm^{-1} is in accord with the $\nu_{as}(SO)$ for a molecule of SO_2 binding in a ligand bound mode. In the case of $Co(2\text{-}PyCO)_2SO_4(SO_2)(H_2O)_2$, a band at 1095 cm^{-1} suggests again a ligand bound mode for the coordinated sulfur dioxide.

The desorption of $Cu(2\text{-}PyCO)_2Br_2(SO_2)_{0.66}(H_2O)_3$, shows that part of the sulfur dioxide is lost, giving a compound with elemental analysis corresponding to the empirical formula $Cu(2\text{-}PyCO)_{1.5}Br_2(SO_2)_{0.5}(H_2O)_2$. This result shows that the SO_2 is partially lost and it differs from the behaviour found for other adducts of stoichiometry 1 : 0.66, that fix all the sulfur dioxide in an irreversible way [24]. The desorption studies and the IR data do not correspond with any of the binding modes previously described and it appears that more than one binding mode is present in this adduct.

Reactions with sulfur dioxide in toluene slurries

Most of the precursors lose one mole of 2-methylpyridine-*N*-oxide when they react with sulfur dioxide in toluene slurries. This fact has been previously observed by Schenk and Conway [25,26] indicating that there is a substitution of sulfur dioxide for the ligand.

Infrared spectra

All the SO_2-adducts exhibit new bands between 2000–500 cm^{-1} assignable to S—O vibrations.

The nitrate derivatives fix SO_2 replacing the nitrate group by a new sulfate ligand. The $Co(2\text{-}PyCO)SO_4(SO_2)_{0.25}$ presents a band at 1080 cm^{-1}. This IR band seems to indicate a chemical rather than a physical interaction for the 0.25 moles of SO_2.

$Cu(2\text{-}PyCO)SO_4(SO_2)_{0.5}$ has a band at 1069 cm^{-1} associated with the 0.5 moles of SO_2. The frequency of this band is in accordance with a S-bridge binding mode for the sulfur dioxide [27].

The $Zn(2\text{-}PyCO)SO_4(SO_2)$ shows a very strong band at 1250 cm^{-1}. This value, and the fact that one molecule of 2-methylpyridine-*N*-oxide is replaced, suggests a η^1-*S* planar coordination mode for the SO_2, in accordance with the results previously found by Schenk and Conway [25,26].

The comparison of the IR spectrum of $Cu(2\text{-}PyCO)_2Br_2(SO_2)(H_2O)_3$, which has a band at 1240 cm^{-1}, with the IR spectrum of $Zn(2\text{-}PyCO)SO_4(SO_2)$, shows that the sulfur dioxide is also binding in a η^1-S planar mode in this compound.

Desorption studies

Most of the metal precursors link the sulfur dioxide in an irreversible way. This clearly demonstrates that the behaviour of the precursors towards sulfur dioxide is different in the solid state and toluene slurries.

$Co(2\text{-}PyCO)SO_4(SO_2)_{0.25}$ does not lose the sulfur dioxide when it is heated and this behaviour is similar to that found for $Co(2\text{-}MePyO)_2I_2(SO_2)_{0.25}(H_2O)_2$, obtained in the solid state. So the irreversibility of the reaction indicates that the sulfur dioxide is chemically absorbed but the data are not enough to predict the binding mode.

In $Cu(2\text{-}PyCO)_2Br_2(SO_2)(H_2O)_2$ and $Cu(2\text{-}PyCO)SO_4(SO_2)_{0.5}$ the sulfur dioxide is fixed irreversibly. This behaviour reinforces the η^1-S planar and S-bridge binding modes proposed on the basis of the IR bands.

Different behaviour is shown by $Cu(2\text{-}PyCO)_2Cl_2(SO_2)_{0.66}(H_2O)_2$, that only fixes one part of the SO_2 in an irreversible way (Table 6). The band at 1281 cm^{-1} is absent from the IR spectrum of the compound obtained after desorption. This suggests that part of the sulfur dioxide is present in the ligand bound mode. These desorption studies, in conjunction with the IR spectrum indicate that the binding mode in this compound must be the same as that present in the adduct $Cu(2\text{-}PyCO)_2Br_2(SO_2)_{0.66}(H_2O)_3$, obtained from the solid state.

Reactions with sulfur dioxide at high temperature

The interaction of the precursors with sulfur dioxide at high temperature has been performed in a thermogravimetric balance TG-131 CAHN. These thermogravimetric analyses are particularly useful because it is possible to study the thermal stability of the metal precursor and the optimum temperature range over which SO_2-absorption occurs. It must be pointed out that only the nitrate and the halide derivatives of copper react with SO_2 at a temperature higher than the room temperature. All the halide derivatives of cobalt and zinc show similar behaviour and they do not react at higher temperatures (Fig. 1).

The behaviour of the chloride and bromide derivatives of copper is quite interesting. $Cu(2\text{-}PyCO)_2Cl_2$ can fix one mole of SO_2 when it is exposed to a sulfur dioxide stream in the 150–30°C temperature range for 3h 10 min (Fig. 2) but only 0.25 moles when it is maintained in contact with sulfur dioxide for one week

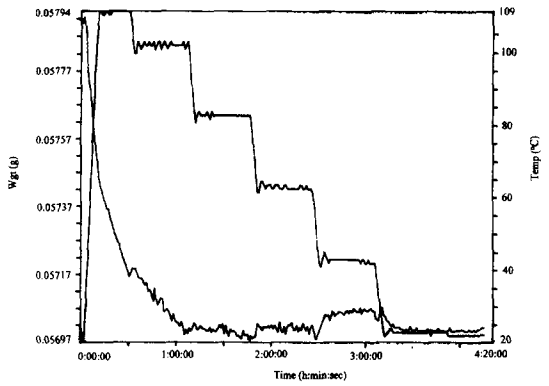

Fig. 1. Absorption thermogram for $Co(2\text{-}MePyO)_2I_2(H_2O)$. ♣ represents the temperature and ◆ the curve of the variation of mass vs the temperature and the time.

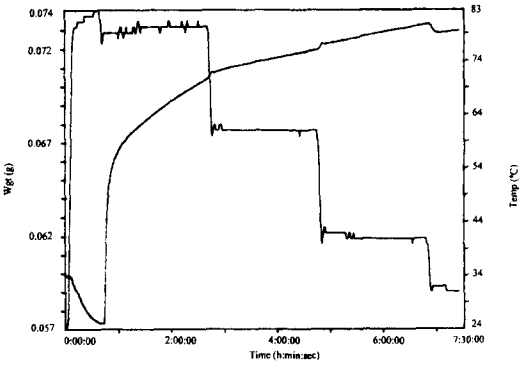

Fig. 3. Absorption thermogram for the $Zn(2\text{-}MePyO)_2(NO_3)_2(H_2O)$. ♣ represents the temperature and ◆ the curve of the variation of mass vs the temperature and the time.

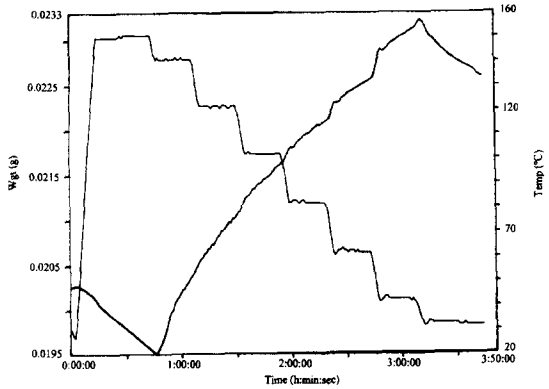

Fig. 2. Absorption thermogram for $Cu(2\text{-}MePyO)_2Cl_2$. ♣ represents the temperature and ◆ the curve of the variation of mass vs the temperature and the time.

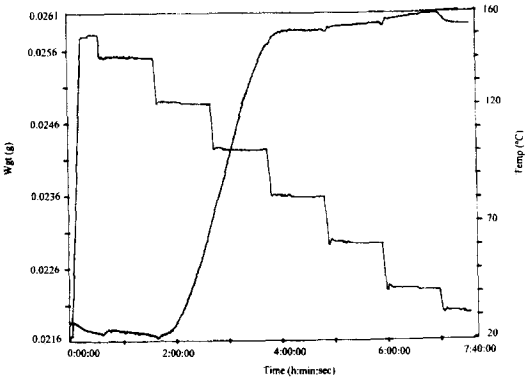

Fig. 4. Absorption thermogram for the $Cu(2\text{-}MePyO)_2(NO_3)_2$. ♣ represents the temperature and ◆ the curve of the variation of mass vs the temperature and the time.

at room temperature. In the same way $Cu(2\text{-}PyCO)_2Br_2(H_2O)_3$ retains 0.75 moles of sulfur dioxide per mole of precursor in the 120–30°C temperature range but only 0.66 moles at room temperature. This fact is quite important as it implies that the increased temperature favours the reaction, in contrast with the behaviour observed for other metal precursor [8,9].

The nitrate derivatives of cobalt and zinc show similar behaviour. One mole of 2-methylpyridine-*N*-oxide is displaced by a mole of SO_2 which is oxidized to sulfate. This reaction occurs at the maximum temperature permitted by the melting point of the precursor and the generated adduct cannot bind more sulfur dioxide even when the temperature is decreased to 30°C (Fig. 3).

$Cu(2\text{-}PyCO)_2(NO_3)_2$ seems to be more stable towards increasing temperature as it does not lose ligand at a temperature lower than 150°C. However, the compound is unreactive towards SO_2 at a temperature higher than 120°C. Between 120–100°C, the metal precursor binds two moles of sulfur dioxide, one of which is oxidised to sulfate. The compound is saturated at the temperature of 100°C and cannot fix any more sulfur dioxide even when the temperature is decreased to 30°C (Fig. 4).

As a result of this study we can say that the copper derivatives are more thermally stable and show more ability to bind sulfur dioxide at higher temperatures than the cobalt and zinc analogues. Furthermore the reactivity of the halide derivatives of copper is favoured by an increase in temperature.

REFERENCES

1. Mingos, D. M. P., *Trans. Met. Chem.*, 1978, **3**, 1.
2. Schenk, W. A., *Angew. Chem., Int. Ed. Engl.*, 1987, **28**, 98.
3. (a) Kubas, G. J., *Inorg. Chem.*, 1979, **18**, 182 and references therein; (b) Ryan, R. R., Kubas, G. J., Moody, D. C. and Eller, P. G., *Structure and Bonding*, 1981, **46**, 48.
4. (a) Gott, J. A., Fawcett, J., McAuliffe, C. A. and Rusell, D. R., *J. Chem. Soc., Chem. Commun.*,

1984, 1283; (b) McAuliffe, C. A., Beagley, B., Gott, G. A., MacKie, A. G., MacRory, P. P. and Pritchard, R. G., *Angew. Chem. Int. Ed. Engl.*, 1987, **26**, 264; (c) Beagley, B., El-Sayrafi, O., Gott, G. A., Kelly, D. G., McAuliffe, C. A., MacKie, A. G., MacRory, P. P. and Pritchard, R. G., *J. Chem. Soc., Dalton Trans.*, 1988, 1095.

5. (a) Al-Farham, K., Beagley, B., Sayrafi, O., Gott, G. A., McAuliffe, C. A., MacRory, P. P. and Pritchard, R. G., *J. Chem. Soc., Dalton Trans.*, 1990, 1243; (b) Beagley, B., Dyer, G., McAuliffe, C. A., MacRory, P. P. and Pritchard, R. G., *J. Chem. Soc., Chem. Commun.*, 1991, 965; (c) Banda, S. F., McAuliffe, C. A. and Matear, P. P., *Inorg. Chim. Acta*, 1992, **193**, 197; (d) Abbas, S., Beagley, B., Godfrey, S. M., Kelly, D. G., McAuliffe, C. A. and Pritchard, R. G., *J. Chem. Soc., Dalton Trans.*, 1992, 1915.
6. (a) Godfrey, S. M., Kelly, D. G. and McAuliffe, C. A., *J. Chem. Soc., Dalton Trans.*, 1992, 1305; (b) Banda, S. F., El-Sayrafi, O., McAuliffe, C. A. and Matear, P. P., *Inorg. Chim. Acta*, 1992, **194**, 227.
7. (a) Beagley, B., Kelly, D. G., MacRory, P. P., McAuliffe, C. A. and Pritchard, R. G., *J. Chem. Soc., Dalton Trans.*, 1990, 2657; (b) Godfrey, S. M., McAuliffe, C. A., Ranger, G. C. and Kelly, D. G., *J. Chem. Soc., Dalton Trans.*, 1993, 2809; (c) Godfrey, S. M., Kelly D. G., McAuliffe, C. A. and Pritchard, R. G., *J. Chem. Soc., Dalton Trans.*, 1995, 1095.
8. (a) Sanmartín J., Bermejo, M. R., Sousa, A., Fondo, M., McAuliffe, C. A. and Gómez-Forneas, E., *Inorg. Chim. Acta*, 1997, **225**, 269; (b) Sanmartín, J., Bermejo, M. R., Sousa, A., Fondo, M., McAuliffe, C. A. and Gómez-Forneas, E., *Acta Chem. Scand.*, 1997, **51**, 59; (c) Sanmartín, J., Bermejo, M. R., Sousa, A., Fondo, M., McAuliffe, C. A. and Gómez-Forneas, E., *Synth. and React. in Inorg. and Metal-Org. Chem.*, 1997, **27**, 1009.
9. (a) Fondo, M., Bermejo, M. R., Sousa, A., Sanmartín, J., McAuliffe, C. A. and Gómez-Forneas, E., *Polyhedron*, 1996, **15**, 3881; (b) Fondo, M., Bermejo, M. R., Sousa, A., Sanmartín, J., McAuliffe, C. A. and Fernández, M. I., *Polyhedron*, 1996, **15**, 4479.
10. Kidd, M. R., Sager, R. S. and Watson, W. H., *Inorg. Chem.*, 1967, **6**, 946.
11. Brown, D. H., Kenyon, D. and Sharp, D. W., *J. Chem. Soc.* (A), 1969, 1474.
12. Garvey, R. G., Nelson, J. H. and Ragsdale, R. O., *Coord. Chem. Rev.*, 1968, **3**, 375 and references herein.
13. Karayannis, N. M., Pytlewski, L. L. and Mikulski, C. M., *Coord. Chem. Rev.*, 1973, **11**, 93 and references therein.
14. Watson, W. H., *Inorg. Chem.*, 1969, **8**, 1879.
15. (a) Ramaswamy, H. N. and Jonassen, H. B., *J. Inorg. Nucl. Chem.*, 1965, **27**, 740; (b) Ramaswamy, H. N. and Jonassen, H. B., *Inorg. Chem.*, 1965, **4**, 1595.
16. Quagliano, J. V., Fujita, J., Franz, G., Phillips, D. J., Walsmsley, J. A. and Tayree, S. Y., *J. Am. Chem. Soc.*, 1961, **83**, 3770.
17. Issleib, K. and Kreibich, A., *Z. Anorg. Allg. Chem.*, 1961, **313**, 338.
18. Carlin, R. L. and Baker, M. J., *J. Chem. Soc.*, London, 1964, 5008.
19. Karayannis, N. M., Sonsino, S. D., Mikulski, C. M., Strocko, M. J., Pytlewski, L. L. and Labes, M. M., *Inorg. Chim. Acta*, 1970, **4**, 141.
20. Horn, R. W., Weisberger, E. and Collman, J. P., *Inorg. Chem.*, 1970, **9**, 2367.
21. Kubas, G. J., *Acc. Chem. Res.*, 1994, **27**, 183.
22. Hoppenheirt, R., Isenberg, W. and Mews, R., *Z. Naturfosch.*, 1982, **37b**, 1116.
23. Moore, J. W., Buird, H. W. and Miller, M. B., *J. Am. Chem. Soc.*, 1968, **90**, 1358.
24. Barratt, D. S., Benson, C. G., Gott, G. A., McAuliffe, C. A. and Tanner, P., *J. Chem. Soc., Dalton Trans.*, 1985, 2661.
25. Burschka, V. C., Bauman, F. E. and Schenk, W. A., *Z. Anorg. Allg. Chem.*, 1983, **502**, 191.
26. Conway, P., Grant, S. M., Manning, A. R. and Stephens, F. S., *Inorg. Chem.*, 1983, **22**, 3714.
27. Hill, W. E., Horley, S. D., Paul, D. K. and Newberry, V. F., *Inorg. Chem.*, 1985, **24**, 4429.

Pergamon

PII: S0277-5387(97)00377-X

Polyhedron Vol. 17, No. 4, pp. 421–428, 1998
© 1998 Elsevier Science Ltd
All rights reserved. Printed in Great Britain
0277-5387/98 $19.00+0.00

The synthesis, properties and structures of the tetraphenyl-arsonium salts of $[V_2O_3(NO_3)_2X_4]^{2-}$, X = Cl or NO_3

Stephen Arrowsmith, Michael F. A. Dove,* Norman Logan and Andrei Batsanov†

Department of Chemistry, University of Nottingham, Nottingham, NG7 2RD, U.K.

(Received 4 June 1997; accepted 10 September 1997)

Abstract—The complexes $[Ph_4As]_2[V_2O_3(NO_3)_6]$, **1** and $[Ph_4As]_2[V_2O_3Cl_4(NO_3)_2]$, **2**, crystallise from solution in the reaction of tetraphenylarsonium nitrate with $VO(NO_3)_3$ and $VOCl_3$, respectively. The compounds were characterised by their IR and Raman spectra and single crystal X-ray analysis. Compound **1** crystallises in the triclinic space group $P\bar{1}$, $a = 9.580(1)$, $b = 10.782(2)$, $c = 13.631(2)$ Å, $Z = 1$ and $R = 0.059$, whilst **2** crystallises in the monoclinic space group $P2_1/c$, $a = 10.176(1)$, $b = 17.691(2)$, $c = 13.955(2)$, $Z = 2$ and $R = 0.034$. The crystal structures show that the dianions are related, the vanadium atoms in both species possess distorted octahedral symmetry, this being achieved by one terminal and one bridging oxygen atom, one bidentate nitrate group and four other monodentate ligands. An unusual feature of **1** is the presence of both monodentate and bidentate modes of nitrate coordination whilst **2** is the first example of a mixed halonitrato species of vanadium(V) to be isolated. © 1998 Elsevier Science Ltd. All rights reserved

Keywords: tetraphenyl-arsonium salts; monodentate; bidentate; halonitrato.

Although the aqueous chemistry of vanadium(V) has been extensively studied [1] few examples of anhydrous nitrates of vanadium(V) are known; only trinitratooxovanadium(V) [2], nitratodioxovanadium (V) [3], the acetonitrile adduct of trinitratooxovanadium(V) [4] and the tetravanadium(V) crown anion, $[V_4O_8(CH_3CO_2)_4(NO_3)]^{-1}$ [5], have been reported, the latter two examples being the only species to have been studied crystallographically.

Trinitratooxovanadium(V), a viscous yellow liquid, was the first reported anhydrous nitrate of vanadium(V) [2]. The vanadium atom is believed on the basis of spectroscopic evidence to be seven coordinate, all nitrate groups coordinating in a bidentate manner. This was followed by the isolation of its monoacetonitrile adduct by Sutton and co-workers [4] in which vanadium is coordinated by oxygen, two bidentate and one monodentate nitrates and a nitrile ligand. Examples of complexes containing both monodentate and bidentate modes of nitrate coordination are rare [4,6,7]: X-ray diffraction analysis of compound **1** has demonstrated it to be a new example of such a complex [8]. Nitratodioxovanadium(V) was reported by Panontin *et al.* [3]; the species was only poorly characterised and may not be stable at ambient temperature. Several other nitrato and mixed halonitrato species have been characterised only in solution by NMR spectroscopy [9–11]: one of these, $V_2O_3(NO_3)_4$, is a dimeric species and is thus related to the two new dianions which have now been characterised for the first time.

RESULTS AND DISCUSSION

Syntheses of $[Ph_4As]_2[V_2O_3(NO_3)_6]$ **1** *and* $[Ph_4As][V_2O_3Cl_4(NO_3)_2]$ **2**

The reaction of trinitratooxovanadium(V) with tetraphenylarsonium nitrate in acetonitrile generates the vanadium(V) compound **1**, according to eqn (1).

* Author to whom correspondence should be addressed.
† Department of Chemistry, University of Durham, Durham, DH1 3LE, U.K.

$$2VO(NO_3)_3 + 2Ph_4AsNO_3 \rightarrow [Ph_4As]_2[V_2O_3(NO_3)_6] + N_2O_5 \quad (1)$$
$$\downarrow$$
$$N_2O_4 + \tfrac{1}{2}O_2$$

The reaction was carried out under rigorously anhydrous conditions owing to the extreme moisture-sensitive nature of the $VO(NO_3)_3$ starting material. A colour change from yellow to orange is observed on reaction and an atmosphere of brown NO_2 gas is observed above the reaction solution (presumably derived from the decomposition of N_2O_5). When the orange solution was gradually diluted with $CFCl_3$, by vapour phase diffusion, orange plate-shaped crystals of **1** were formed.

The analogous reaction of $VOCl_3$ yields two vanadium(V) compounds, eqn (2). The reaction solution, initially dark red owing to the presence of the $VOCl_3 \cdot 2MeCN$ adduct [17], was concentrated and then diluted with $CFCl_3$ by slow vapour phase diffusion. The solution

$$3VOCl_3 + 5Ph_4AsNO_3 \rightarrow 3[Ph_4As][VO_2Cl_2] + [Ph_4As]_2[V_2O_3Cl_4(NO_3)_2] + 2NO_2Cl + NOCl + Cl_2 \quad (2)$$

gradually decolourised and block shaped crystals of two different colours were produced, the major component being yellow and the minor purple. The yellow crystals were identified as $[Ph_4As][VO_2Cl_2]$, a species first isolated by Dehnicke [14], and the purple crystals were characterised as compound **2**.

Crystal structures of compounds **1** *and* **2**

Table 1 lists selected bond lengths and angles for the anion in compound **1**. The structure of **1** comprises dimeric $[(NO_3)_3(O)VOV(O)(NO_3)_3]^{2-}$ anions possessing crystallographic C_i symmetry, see Fig. 1, and tetrahedral Ph_4As^+ cations in general positions. Each vanadium atom is six coordinate and the approximately octahedral coordination is achieved by one monodentate and two bidentate nitrate groups, one terminal and one bridging oxo ligand. The latter, O(2), is disordered with equal probability over two positions related via the inversion centre. The reason for this disorder is not clear, there being no obvious chemical basis for this behaviour. It may be an artefact of the constraints induced by crystal symmetry requirements. This disorder is probably responsible for the enhanced thermal motions of other atoms in the anion especially those in the coordination sphere of vanadium.

The small bite of the bidentate nitrate group, O(31)—V—O(32) bond angle, 57.5°, gives rise to a distorted six-fold coordination around vanadium. This characteristic of bidentate nitrate coordination has been well documented [12], and other examples of distorted octahedral coordination can be observed in $[NO^+]_2[Cr(NO_3)_5]$ [6] and $[Ph_4As]_2[Ni(NO_3)_4]$ [6]. A further characteristic of bidentate nitrate is its ability to coordinate either in a symmetrical or an unsymmetrical fashion; the latter is said to occur [12] when there is a small but real difference, 0.2–0.7 Å, between the distances of the metal atom from the two coordinated oxygens of the nitrate group: in **1** the difference between the V—O distances is 0.35 Å and is thought to arise from the strong *trans* effect exerted on the V—O(32) bond by the terminal oxygen atom O(1).

The N—O bond lengths present in both the monodentate and bidentate nitrate groups are consistent with reported literature values [12]. The terminal V—O bond length of 1.555 Å is consistent with those observed in $VO(NO_3)_3 \cdot MeCN$ [4], $[Ph_4As][VOCl_4]$ [13], and $[Ph_3PMe][VO_2Cl_2]$ [14]. The bridging V—O bond lengths, of approximately 1.8 Å, are comparable to those observed in the tetranuclear vanadium species $[Ph_4As][V_4O_8(CH_3CO_2)_4(NO_3)]$ [5] and $[n\text{-}Bu_4N][V_4O_6F(PhPO_3)_4]$ [15].

Table 2 lists selected bond lengths and angles for the anion in compound **2**. The structure consists of an ionic lattice of tetraphenylarsonium cations and binuclear vanadium anions, $[(NO_3)Cl_2(O)VOV(O)Cl_2(NO_3)]$, Fig. 2. The anions possess crystallographic symmetry C_i. As in **1** the coordination sphere of each vanadium atom is severely distorted from octahedral being coordinated by two chlorides, one terminal and one bridging oxygen atom and one bidentate nitrate group. The bite of the bidentate nitrate group, O(11)—V—O(12) bond angle, 56.7°, is similar to that in **1**. The bidentate nitrate group coordinates in an unsymmetrical fashion, the V—O(11) and V—O(12) bond lengths differing by 0.32 Å; this is attributable to the *trans* effect of atom O(1) on the V—O(12) bond. The bridging oxygen atom O(2) is disordered with equal probability over two positions related via the inversion centre.

The V—Cl bond lengths in the anion, 2.27 and 2.29 Å, are comparable with those observed in $[Ph_4As][VOCl_4]$ [13] and $[Ph_3PMe][VO_2Cl_2]$ [14]. The terminal and bridging oxygen bond lengths together with those of the bidentate nitrate group are also fully consistent with literature examples [4,5,12–15]. An interesting feature of **2** is the presence within the coordination sphere of each vanadium atom of both chloride and nitrate as ligands. Chloride, a soft base, and nitrate, a harder base, are rarely observed together as ligands on a given metal. Vanadium(V) is considered a hard acid owing to its high oxidation state, small size and high positive charge density but may be stabilised by ligands such as O, F, Cl and NO_3. To our knowledge compound **2** is the first mixed chloronitrato species of vanadium(V) and, in the wider context, represents the first mixed halonitrato species of vanadium(V) to be isolated.

Table 1. Selected bond lengths (Å) and bond angles (°) for the $[V_2O_3(NO_3)_6]^{2-}$ anion in compound **1**

V—O(1)	1.555(6)	O(12)—N(1)—O(13)	120.6(10)
V—O(2)	1.82(2)	O(12)—N(1)—O(11)	119.9(10)
V—O(2′)	1.78(2)	O(13)—N(1)—O(11)	119.4(10)
V—O(11)	1.983(6)	O(22)—N(2)—O(23)	123.2(11)
V—O(21)	1.915(5)	O(22)—N(2)—O(21)	116.7(10)
V—O(31)	2.007(5)	O(23)—N(2)—O(21)	115.0(10)
V—O(32)	2.360(6)	O(31)—N(3)—O(32)	115.1(8)
N(1)—O(11)	1.275(8)	O(31)—N(3)—O(33)	120.2(9)
N(1)—O(12)	1.222(9)	O(32)—N(3)—O(33)	124.7(9)
N(1)—O(13)	1.162(9)		
N(3)—O(31)	1.279(7)	O(2′)—V—O(31)	142.1(4)
N(3)—O(32)	1.235(8)	O(31)—V—O(21)	85.4(2)
N(3)—O(33)	1.223(8)	O(2′)—V—O(21)	85.2(6)
V—O(2)—V′	149.4(7)	O(1)—V—O(11)	104.0(3)
V—O(11)—N(1)	127.8(7)	O(2)—V—O(11)	90.6(7)
V—O(11)—N(1)	128.8(6)	O(1)—V—O(31)	96.2(3)
V—O(31)—N(3)	101.5(5)	O(2)—V—O(31)	172.6(5)
V—O(32)—N(3)	85.9(5)	O(11)—V—O(31)	86.5(2)
O(1)—V—O(2′)	121.7(5)	O(2′)—V—O(32)	84.7(4)
O(1)—V—O(2)	91.2(5)	O(21)—V—O(32)	77.1(2)
O(31)—V—O(32)	57.5(2)	O(1)—V—O(32)	153.6(3)
O(2)—V—O(32)	115.2(4)	O(11)—V—O(32)	76.6(2)
O(11)—V—O(21)	152.8(3)	O(1)—V—O(21)	102.7(3)
O(2)—V—O(21)	94.1(6)	O(2′)—V—O(11)	85.3(7)

Primed atoms are symetry related by the inversion centre.

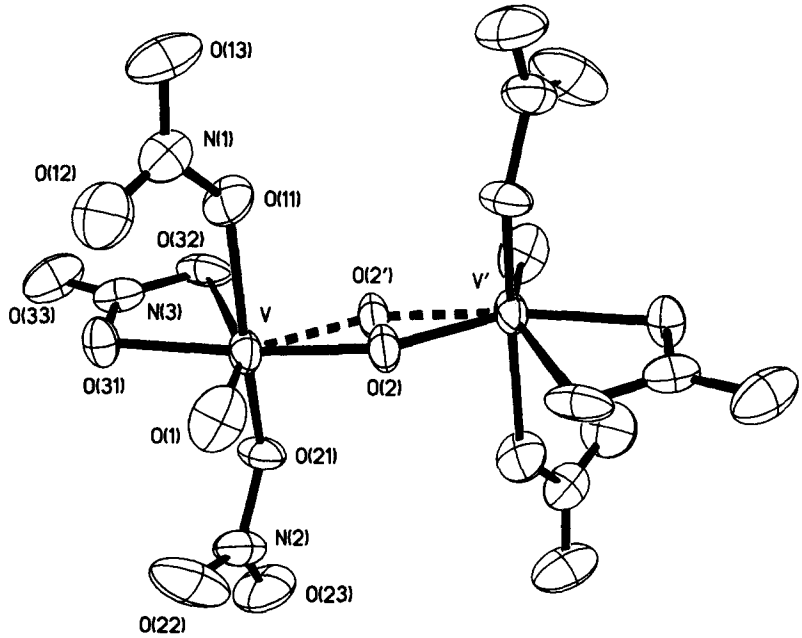

Fig. 1. The $[V_2O_3(NO_3)_6]^{2-}$ anion in the lattice of the tetraphenylarsonium salt **1**. Primed atoms and unmarked atoms in one half of the anion are related by the inversion centre to those in the other half. Thermal ellipsoids are at the 20% level.

Table 2. Selected bond lengths (Å) and bong angles (°) for the $[V_2O_3Cl_4(NO_3)_2]^{2-}$ anion in compound **2**

V—O(1)	1.566(4)	O(11)—N(1)—O(13)	120.4(5)
V—O(2)	1.70(6)	O(12)—N(1)—O(13)	125.8(5)
V—O(2′)	1.83(5)	O(11)—N(1)—O(12)	113.8(4)
V—Cl(1)	2.291(2)	O(11)—V—O(12)	56.7(1)
V—Cl(2)	2.272(2)	Cl(1)—V—Cl(2)	162.6(7)
V—O(11)	2.063(3)	Cl(1)—V—O(1)	96.6(2)
V—O(12)	2.381(4)	Cl(2)—V—O(1)	97.8(2)
N(1)—O(11)	1.300(5)	Cl(1)—V—O(2)	98.2(17)
N(1)—O(12)	1.240(6)	Cl(2)—V—O(2)	88.7(20)
N(1)—O(13)	1.197(5)	Cl(1)—V—O(2′)	89.1(16)
V—O(2)—V′	165.9(20)	Cl(2)—V—O(2′)	94.3(19)
V—O(11)—N(1)	101.4(3)	Cl(1)—V—O(11)	85.5(1)
V—O(12)—N(1)	88.0(3)	Cl(2)—V—O(11)	83.2(1)
O(1)—V—O(2)	100.4(15)	Cl(1)—V—O(12)	81.1(1)
O(1)—V—O(2′)	112.3(15)	Cl(2)—V—O(12)	81.7(1)
O(1)—V—Cl(1)	96.6(2)	O(2)—V—O(11)	161.6(18)
O(1)—V—Cl(2)	97.8(2)	O(2′)—V—O(11)	150.6(15)
O(1)—V—O(11)	97.0(2)	O(2)—V—O(12)	105.9(15)
O(1)—V—O(12)	153.7(2)	O(2′)—V—O(12)	93.9(15)

Primed atoms are symmetry related by the inversion centre.

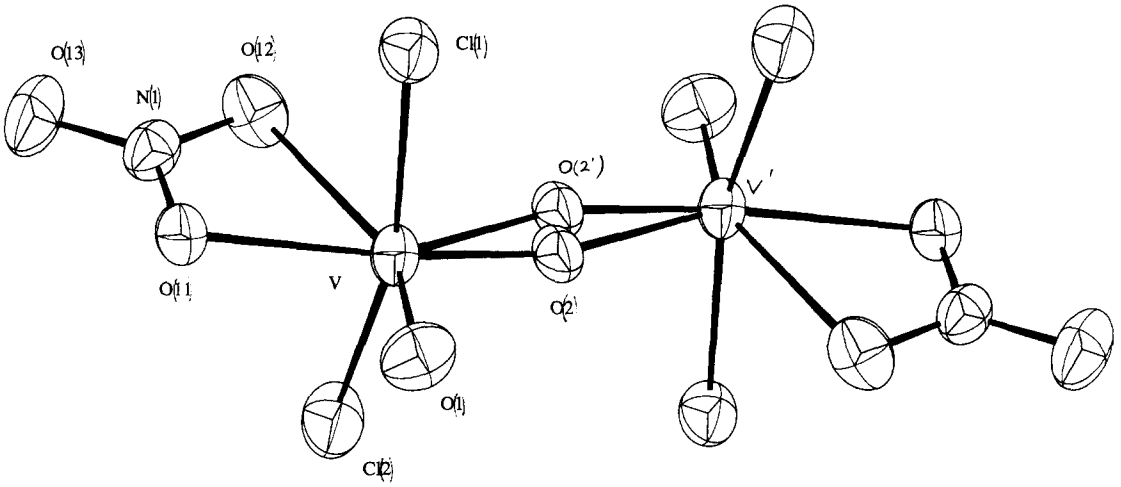

Fig. 2. The $[V_2O_3Cl_4(NO_3)_2]^{2-}$ anion in the lattice of the tetraphenylarsonium salt **2**. Primed atoms and unmarked atoms in one half of the anion are related by the inversion centre to those in the other half. Thermal ellipsoids are at the 30% level.

Infrared and Raman spectra of **1** *and* **2**

The infrared and Raman spectral bands of these compounds in the solid state, together with proposed assignments, are listed in Tables 3 and 4. Bands arising from the tetraphenylarsonium cation have been omitted and vibrational mixing and coupling effects are not discussed. No Raman polarisation data could be collected on either compound owing to their rapid decomposition in solution in acetonitrile. The presence of one bidentate and two crystallographically inequivalent monodentate nitrate ligands in the anion $[V_2O_3(NO_3)_6]^{2-}$ increases the complexity of its vibrational spectrum and assignment of the Raman bands arising from the vibrations of the unsymmetrically bidentate nitrate ligands on the basis of polarisation and band intensity criteria [12] is not applicable here.

In the 1500–1600 cm^{-1} region the antisymmetric stretch of the monodentate nitrate ligand, $\nu_{as}(NO_2)$, is assigned at a higher wave number than the terminal N=O stretch, ν(NO), of the unsymmetrically bidentate nitrate groups in both compounds. In the 1200 to 1300 cm^{-1} region the more intense band, appearing

Table 3. Infrared and Raman data (cm^{-1}) for the $[V_2O_3(NO_3)_6]^{2-}$ anion in compound **1**

Infrared	Raman	Assignment	
1589 w[a]	1563 m	$\nu_{as}(NO_2)$	mono
1546 s	1547 w	$\nu_{as}(NO_2)$	mono
1529 s	1536 w	$\nu(NO)$	bi
—	1287 m	$\nu_s(NO_2)$	mono
1265 vs	1265 w	$\nu_{as}(NO_2)$	bi
1010 w	1012 s	$\nu(NO)$	mono
958 w	962 w	$\nu(V{=}O)$	
930 m, br	925 w	$\nu_s(NO_2)$	bi
792 m	—	$\delta_s(NO_2)$	mono
[b]	765 w	$\delta_{as}(NO_2)$	and
[b]	746 w	$\pi(NO_3)$	bi
709 m	704 vw	$\nu_{as}(VOV)$	
—	494 m, br	$\nu_s(VOV)$	
[c]	346 m, vbr	See text	

[a] Possibly overtone of 792 cm^{-1}.
[b] Obscured by cation.
[c] Bands below 400 cm^{-1} not observed (AgCl windows).
mono, monodentate nitrate ligand.
bi, bidentate nitrate ligand.

Table 4. Infrared and Raman data (cm^{-1}) for the $[V_2O_3Cl_4(NO_3)_2]^{2-}$ anion in compound **2**

Infrared	Raman	Assignment
1513 m	1516 w	$\nu(NO)$
1282 m	1284 w	$\nu_{as}(NO_2)$
960 w	—	$\nu(V{=}O)$
925 vw, sh	926 vw	$\nu_s(NO_2)$
777 m	756 w	$\delta_s(NO_2)$
[a]	720 w	$\delta_{as}(NO_2)$
[a]	702 w	$\pi(NO_3)$ + $\nu_{as}(VOV)$
[a]	473 s	$\nu_{as}(VCl_2)$
[a]	319 vs	$\delta(OVCl)$

[a] Obscured by cation.
[b] bands below 400 cm^{-1} not observed (AgCl window cut-off).

at 1287 cm^{-1} in the Raman effect, is assigned to $\nu_s(NO_2)$ of the monodentate ligands. The lower intensity band, appearing at 1265 cm^{-1}, is assigned to $\nu_{as}(NO_2)$ of the bidentate ligand. Not only are the bonds giving rise to the vibrations in question, shorter for the monodentate nitrate ligands, adding weight to their assignment at higher frequency but, as the stretching mode of the monodentate nitrate group in this region is symmetric, it would be expected to give rise to a band of greater intensity in the Raman effect than the antisymmetric stretch of the bidentate nitrate ligand. The Raman band at 1287 cm^{-1} is not evident in the infrared, but the infrared band at 1265 cm^{-1} is very intense, supporting its assignment as an antisymmetric stretch.

The band appearing at 1012 cm^{-1} in the Raman spectrum is assigned to $\nu(NO)$ of the monodentate nitrate group, as this band is absent from the spectra of the anion $[V_2O_3Cl_4(NO_3)_2]^{2-}$ (Table 4). The high intensity of this band is also consistent with the intensity criterion for monodentate nitrate coordination [12]. The band occurring at 962 cm^{-1} in the Raman spectrum (958 cm^{-1}, i.r.) is assigned as $\nu(V{=}O)$, consistent with a similar infrared band observed for the chloronitrato-dimer $[V_2O_3Cl_4(NO_3)_2]^{2-}$ and with reported values for species such as $[VOCl_4]^-$ [13] and $[VO_2Cl_2]^-$ [14]. The band at ca 925 cm^{-1} in the vibrational spectra of both dimers is assigned to $\nu_s(NO_2)$ of bidentate nitrate.

A variety of low intensity bands is present in the 700 to 800 cm^{-1} region of the Raman spectrum, although some of these are obscured in the infrared owing to overlap with more intense cation bands. $\delta_s(NO_2)$, $\delta_{as}(NO_2)$ and $\pi(NO_3)$ modes for both monodentate and bidentate nitrate groups are expected in this region as well as $\nu_{as}(VOV)$ [16]. With so many possibilities, no firm assignments have been attempted.

The rather broad band at 494 cm^{-1} is assigned to $\nu_s(VOV)$ [16]. This feature is probably obscured in the Raman spectrum of $[V_2O_3Cl_4(NO_3)_2]^{2-}$ (Table 4) by the more intense $\nu_s(VCl_2)$ so no direct comparison with the latter anion can be made. A very broad feature centred around 346 cm^{-1} (Raman), which appears to consist of a number of overlapping bands, and bands occurring at even lower wave numbers are attributable to vibrational modes such as V—O stretches associated with both mono- and bidentate nitrate groups and deformations of terminal V=O and bridging V—O—V bonds. Vibrational coupling of these low frequency modes will further complicate this region.

Nitrate band assignments for compound **2** (Table 4) are simplified since there is only one unsymmetrically bidentate group. The infrared band at 960 cm^{-1} is assigned to $\nu(V{=}O)$ on similar grounds to those given for compound **1**. The reason for the absence of this band from the Raman spectrum is unclear. The same observations as were made on the 700–800 cm^{-1} region for compound **1** also apply here.

The intense Raman bands at 473 and 319 cm^{-1} are assigned to $\nu_s(VCl_2)$ and $\delta(OVCl)$, respectively. Similar bands can be observed in the spectra of $[VOCl_4]^-$ [13] and $[VO_2Cl_2]^-$ [14]. The $\nu_s(VCl_2)$ band is somewhat broad and may overlap the corresponding antisymmetric mode. A further vibrational mode which may possibly contribute to the broadness of this band is $\nu_s(VOV)$, which is reported [16] to occur in the 500 cm^{-1} region (cf. the band at 494 cm^{-1} in the Raman spectrum of compound **1**). A number of weak bands is observed below 400 cm^{-1}: the comments given for similar bands of compound **1** apply here.

Nuclear magnetic resonance studies of **1** *and* **2**

Compounds **1** and **2** were studied in solution by ^{51}V NMR; rapid decomposition was observed in acetonitrile solution for both species resulting in the production of multiple resonances. In both instances, over a period of hours one resonance grows in intensity at the expense of all the others. For compound **1** the singlet finally observed occurred at −543 ppm, close to the resonance first observed by Hibbert [10], who assigned it to the monomeric vanadium(V) oxonitrato species, $[VO_2(NO_3)_2]^-$. For **2** the resonance finally observed occurred at −364 ppm close to that reported by Dehnicke [14], who assigned it to the dichlorodioxovanadate(V) anion, $[VO_2Cl_2]^-$. The stability of both compounds **1** and **2** appears to be confined to the solid state, each appearing to be the most favoured crystalline form to be generated from a complex mixture under favourable conditions.

EXPERIMENTAL

Reagents

Yellow trinitratooxovanadium(V) was prepared by the reaction of V_2O_5 with N_2O_5 using a published method [2]; the purity of the product was determined by titration with potassium manganate(VII) (for vanadium after reduction to V(IV)) and by a Kjeldahl determination for nitrogen. Trichlorooxovanadium(V) (Aldrich, 99%) was purified by distillation. Tetraphenylarsonium nitrate was produced in quantitative yield by the decomposition of $Ph_4AsCl \cdot HCl \cdot 2H_2O$ *in vacuo* at 423 K, followed by a heterogeneous reaction with excess liquid N_2O_4. Dinitrogen tetroxide (British Oxygen Co. Ltd, >99%) was purified by vapour phase distillation through molecular sieve (grade 3A, Aldrich) to reduce the water content to 0.02 wt% as determined by ^1H FT NMR spectrometry [18]. Recrystallisation of the tetraphenylarsonium nitrate from ethanol (AR grade)/ether (AR grade) then drying *in vacuo* at 423 K yielded the pure product. Acetonitrile (99%, Aldrich) was dried over molecular sieve (grade 4A), refluxed with calcium hydride and fractionated before use. Fluorotrichloromethane (99+%, Aldrich) was dried over molecular sieve (grade 3A) and distilled.

Spectroscopic measurements

Infrared spectra were recorded on a Nicolet 205 FT-IR spectrometer with samples as nujol mulls placed between AgCl windows, KBr was not used to avoid halide-nitrate exchange between window and compound. Raman spectra were recorded on a Perkin-Elmer System 2000 NIR FT-Raman spectrometer with samples contained in sealed glass capillaries under an inert nitrogen atmosphere. NMR spectra were recorded on a Bruker WM250 spectrometer at 65.79 MHz for ^{51}V; trichlorooxovanadium(V) was used as the external standard.

Preparation of $[Ph_4As]_2[V_2O_3(NO_3)_6]$ **1**

To a solution of trinitratooxovanadium(V) (0.504 g, 0.002 mol) in acetonitrile (1.502g, 0.037 mol) was added tetraphenylarsonium nitrate (0.902 g, 0.002 mol) in acetonitrile (9.598 g, 0.234 mol). An immediate colour change from yellow to orange was observed. The reaction solution was then reduced to low volume by removal of solvent *in vacuo*. Gradual addition of $CFCl_3$ by vapour phase diffusion yielded orange crystals of **1**. Yield: 0.970g (75%) (Found: C, 44.4; H, 3.1; N, 6.2. $C_{48}H_{40}As_2N_6O_{21}V_2$ Requires: C, 44.7; H, 3.1; N, 6.5%).

Preparation of $[Ph_4As]_2[V_2O_3Cl_4(NO_3)_2]$ **2**

To a solution of trichlorooxovanadium(V) (0.450 g, 0.0026 mol) in acetonitrile (2.656 g, 0.065 mol) was added tetraphenylarsonium nitrate (1.114 g, 0.0025 mol) in acetonitrile (6.056 g, 0.1475 mol). The reaction solution was then reduced in volume by removal of solvent *in vacuo*. Gradual addition of $CFCl_3$ by vapour phase diffusion yielded yellow crystals of $[Ph_4As][VO_2Cl_2]$, Yield: 0.672g (80%) (Found: C, 53.7; H, 3.7; Cl, 13.7. $C_{24}H_{20}AsCl_2O_2V$ Requires: C, 53.6; H, 3.6; Cl, 13.2%) and purple crystals of **2**. Yield 0.135g (22%) (Found: C, 49.0; H, 3.36; Cl, 11.9; N, 2.15. $C_{48}H_{40}As_2Cl_4N_2O_9$ Requires: C, 48.7; H, 3.4; Cl, 12.0; N, 2.4 %).

X-Ray crystallography—data collection and processing

Crystal data and experimental details of the samples are given in Table 5.

Compound **1**. Intensities were collected using a Rigaku AFC6S 4-circle diffractometer at 293 K using graphite monochromated Mo–K_α radiation ($\lambda = 0.71073$ Å). The crystal was sealed in a glass capillary, crystal dimensions being $0.54 \times 0.30 \times 0.13$ mm. The cell parameters were obtained from 24 reflections $13.3 < \theta < 16.0°$. The intensities of three standard reflections, monitored every 150 intensity scans remained unchanged with only statistical fluctuations, 5360 reflections of which 4551 were unique ($R_{int} = 0.017$), were measured by ω scans $2\theta \leqslant 50°$. An analytical absorption correction [19] was applied giving $T_{max} = 0.749$, $T_{min} = 0.611$, in good agreement with T_{max}: T_{min} ratio of 0.794, estimated from 108 ψ-scans of three reflections. The structure was solved by direct methods (SHELX) [20], 361 variables being refined in a full-matrix least-squares calculation against F^2 of all data employing a two term Chebyshev weighting scheme using SHELXL-93 [21]. The final $wR(F^2)$ for all data being 0.129, $R(F)$ for 2753 data

Table 5. Crystal data[a] and structure refinement for compounds **1** and **2**

	Compound **1**	Compound **2**
Empirical Formula	$C_{48}H_{40}As_2N_6O_{21}V_2$	$C_{48}H_{40}As_2Cl_4N_2O_9V_2$
M	1288.58	1182.39
Crystal system	triclinic	monoclinic
Space group	$P\bar{1}$	$P2_1/c$
Z	1	2
a Å	9.580(1)	10.176(1)
b Å	10.782(2)	17.691(2)
c Å	13.631(2)	13.955(2)
α °	92.15(1)	90
β °	107.10(1)	99.85
γ °	96.97(1)	90
U Å^3	1331.8(3)	2475.2(5)
D_c g cm^{-3}	1.607	1.587
μ cm^{-1}	16.7	19.6
$F(000)$	650	1188
Crystal size mm	0.54 × 0.30 × 0.13	0.25 × 0.39 × 0.38
θ range °	13.3–16.0	2–25
Reflections collected	5360	5654
Independent reflections	4551	3832
R_{int}	0.017	0.031
Range hkl	−11–11, −6–12, −16–14	−1–12, −1–21, −16–16
Data parameters	4551/361	3832/307
Final R indices (all data)		
R	0.059	0.034
wR	0.129	0.070
Max., min. electron density/e Å^{-3}	0.65, −0.43	0.53, −0.37

[a] Details in common: T = 298 K, λ(Mo-K_α) = 0.71073 Å.

being 0.059 with $F^2 > 2\sigma(F^2)$, $\Delta\rho_{max} = 0.65$, $\Delta\rho_{min} = -0.43$ e Å^{-3}.

Compound **2**. Intensities were collected using an Enraf Nonius CAD4 4-circle diffractometer at 293 K using graphite monochromated Mo–K_α radiation (λ = 0.71073 Å), the crystal was sealed in a glass capillary, crystal dimensions being 0.25 × 0.39 × 0.38 mm. The cell parameters were obtained from 25 reflections $10.2 < \theta < 14.1°$. The intensities of three standard reflections, monitored every two hours showed no evidence of crystal decay. 5654 reflections of which 3832 were unique (R_{int} = 0.031), were measured by ω scans $2\theta \leqslant 50°$. An absorption correction following the DIFABS [22] procedure was applied, T_{min} and T_{max} being 0.0859 and 1.066 respectively. The structure was solved by direct methods (SIR92) [23], 307 variables were refined in a full-matrix least squares calculation using CRYSTALS [24] to $wR(F^2) = 0.070$ for all data. $R(F)$ For 2730 data being 0.034, with $F^2 > 3\sigma(F^2)$, $\Delta\rho_{max} = 0.53$, $\Delta\rho_{min} = -0.37$ e Å^{-3}.

Full atomic coordinates, bond lengths, bond angles and thermal parameters for compounds **1** and **2** [8] may be obtained from the Cambridge Crystallographic Data Centre.

Acknowledgements—Grateful thanks to J. A. K. Howard for the use of the crystallographic data collection and computing facilities at the University of Durham and to C. H. Schwalbe for the crystallographic data collected at the Joint Crystallography Unit of the Universities of Aston and Birmingham for compounds **1** and **2**, respectively.

REFERENCES

1. Pope, M. T. and Dale, B. W., *Chem. Soc. Quart Rev.*, 1968, **22,** 527.
2. Schmeisser, M., *Angew. Chem.*, 1955, **67,** 493.
3. Panontin, J. A., Fischer, A. K. and Heintz, E. A., *J. Chem. Soc., Dalton Trans.*, 1960, **14,** 145.
4. Einstein, F. W. B., Enwall, E., Morris, D. M. and Sutton, D., *Inorg. Chem.*, 1971, **10,** 678.
5. Arrowsmith, S., Dove, M. F. A., Logan, N. and Antipin, M. Y., *J. Chem. Soc., Chem. Commun.*, 1995, 627.
6. Addison, C. C., *Chem. Rev.*, 1980, **80,** 21.
7. Addison, C. C., Greenwood, A. J., Haley, M. J. and Logan, N., *J. Chem. Soc., Chem. Commun.*, 1978, 580.
8. Arrowsmith, S., Dove, M. F. A., Gibbons, M. N., Logan, N. and Batsanov, A., *J. Chem. Soc., Chem. Commun.*, 1995, 1733.
9. Hibbert, R. C., *J. Chem. Soc., Chem. Commun.*, 1985, 317.

10. Hibbert, R. C., *J. Chem. Soc., Dalton Trans.*, 1986, 751.
11. Hibbert, R. C., Logan, N. and Howarth, O. W., *J. Chem. Soc., Dalton Trans.*, 1986, 369.
12. Addison, C. C., Logan, N., Wallwork, S. C. and Garner, C. D., *Chem. Soc. Quart Rev.*, 1971, **25,** 289.
13. Beindorf, G., Strähle, J., Liebelt, W. and Dehnicke, K., *Z. Naturforsch.*, 1980, **35b,** 522.
14. Fenske, D., Shihada, A. F., Schwab, H. and Dehnicke, K., *Z. Anorg. Allg. Chem.*, 1980, **471,** 140.
15. Chen, Q. and Zubieta, J., *J. Chem. Soc., Chem. Commun.*, 1994, 2663.
16. Madic, C., Begun, G. M., Hahn, R. L., Lunay, J. P. and Thiessen, W., *Inorg. Chem.*, 1984, **23,** 470.
17. Funk, H., Weiss, W. and Zeising, M., *Z. Anorg. Allg. Chem.*, 1958, **296,** 36.
18. Dove, M. F. A., Logan, N. and Wood, S. A., *AIAA/SAE/ASME/ASEE 29th Jt. Propulsion Conf.* 1993, paper 93-02039.
19. de Meulenaer, J. and Tompa, H., *Acta Crystallogr., Sect. A.*, 1965, **19,** 1014.
20. Sheldrick, G. M., *Acta Crystallogr., Sect. A.*, 1990, **46,** 467.
21. Sheldrick, G. M., SHELXL-93, Program for the Refinement of Crystal Structures, University of Göttingen, Germany, 1993.
22. Walker, N. and Stuart, D., *Acta Crystallogr., Sect. A.*, 1983, **39,** 158.
23. Altmare, A. Cascarano, G. Giacovazzo, C. and Guagliardi, A., *J. Appl. Crystallogr.*, 1993, **26,** 343.
24. Watkin, D. J., Carruthers, J. R. and Betteridge, D. W., *CRYSTALS User's Guide* Chemical Crystallography Lab., Oxford, U.K., 1985.

Pergamon

PII: S0277-5387(97)00381-1

Polyhedron Vol. 17, No. 4, pp. 429–432, 1998
© 1998 Elsevier Science Ltd
All rights reserved. Printed in Great Britain
0277 5387/98 $19.00+0.00

Synthesis and characterization of mixed-ligand 1,3-dithiole-2-thione-4,5-dithiolate and 1,10-phenanthroline complexes of lanthanide chloride and their iodinated materials

Yu Tang, Xinmin Gan, Minyu Tan,* Xueqin Zheng

Department of Chemistry, Lanzhou University, Lanzhou 730000, P.R. China

(Received 15 July 1997; accepted 5 September 1997)

Abstract—The lanthanide complexes of general formula $K_2[Ln(dmit)(phen)_2Cl_3]\cdot 6H_2O$ (Ln = La, Nd, Sm, Gd, Er, Y; $dmit^{2-}$ = 1,3-dithiole-2-thione-4, 5-dithiolate anion; phen = 1,10-phenanthroline) have been prepared and characterized by means of elemental anlaysis, IR spectra, electronic spectra and conductivity measurements. These complexes behave as insulators at 25°C as compacted pellets. On doping iodine into the complexes, they have been partially oxidized to afford $K_2[Ln(dmit)(phen)_2Cl_3]\cdot Ix$ (Ln = La, $x = 3.5$; Ln = Er, $x = 3.0$), whose electrical conductivities are raised to the range of semi-conductors. The nature of the iodine species in these solids is determined by UV–visible and resonance Raman spectroscopies. © 1998 Elsevier Science Ltd. All rights reserved

Keywords: Lanthanide; $dmit^{2-}$; phen.

Considerable effort has been devoted to the preparation and study of conducting molecular solids and, in particular, the development of "molecular metals" and superconductors. Among the materials of interest in this connection, $[M(dmit)_2]^{n-}$ anion salts ($dmit^{2-}$ = 1,3-dithiole-2-thione-4,5-dithiolate anion, Scheme 1) have attracted much attention, because the electrical conductivities of some complexes are very high [1,2]. In particular, $TTF[Ni(dmit)_2]_2$ (TTF = tetrathiafulvalene) was reported to become a superconductor at low temperature [1]. An important goal of this research has been the understanding of the role of the intermolecular and intramolecular interactions in determining the electrical properties of this most unusual class of molecular solids.

To date, the research on the metal complexes of the $dmit^{2-}$ ligand mostly concentrated on the transition metals. One part of the research is the metal complexes with both a $dmit^{2-}$ ligand and an N_2 chelate ligand containing a pyridyl or related ring. Such complexes were reported to exhibit an intramolecular ligand-to-ligand charge transfer [3–5].

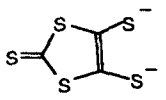

Scheme 1.

While the coordination properties and conductivities of $dmit^{2-}$ ligand with lanthanide elements have never been reported. Recently, we examined the reaction of lanthanide $dmit^{2-}$ with 1,10-phenanthroline, and the partial oxidation of the mixed-ligand complexes with iodine. In addition, we investigated the electrical conductivities of all these compounds.

EXPERIMENTAL

Reagents

The potassium salt K_2dmit is prepared following the method of Steimecke and co-workers [6]. 1,10-phenanthroline was purchased from BJCRF (China). Hydrated lanthanide chlorides were prepared by dis-

* Author to whom correspondence should be addressed.

solving the Anala R Ln_2O_3 (Ln = La, Nd, Sm, Gd, Er, Y) in 1 : 1 hydrochloric acid. All other chemicals were of A. R. grade. All reactions were carried out under inert atmosphere conditions.

Synthesis of the $K_2[Ln(dmit)(phen)_2Cl_3]\cdot 6H_2O$ *complexes (Ln = La, Nd, Sm, Gd, Er, Y)*

To the mixed methanol solution (2 cm^3) of $LnCl_3\cdot 6H_2O$ (Ln = La, Nd, Sm, Gd, Er, Y) (0.1 mmol) and 1,10-phenanthroline (0.2 mmol) was added dropwise a methanol solution of 0.1 mmol K_2dmit (1 cm^3) to give an orange precipitate of $K_2[Ln(dmit)(phen)_2Cl_3]\cdot 6H_2O$ immediately. The solid complex was collected by centrifuging, washed with methanol and dried under vacuum over P_2O_5. Yields were ca 60%. All the complexes are powdered solids and stable in air.

Iodine oxidation

Finely powdered $K_2[Ln(dmit)(phen)_2Cl_3]\cdot 6H_2O$ (Ln = La, Er) (0.05 mmol) were suspended in a hexane solution (30 cm^3) containing 0.1 mmol iodine. The solution was stirred at room temperature for 24 h to give an iodine-doped complex, which was washed with hexane (2 cm^3) several times, collected by centrifuging, and dried *in vacuo*.

Elemental analyses for $K_2[Ln(dmit)(phen)_2Cl_3]\cdot 6H_2O$ and the iodine-doped complexes are summarized in Table 1.

Chemical and physical measurements

The metal ion was determined by EDTA titration using Xylenol-orange as an indicator. Carbon, nitrogen and hydrogen were determined using an Elementar Vario EL (see Table 1). The IR spectra were recorded in the 4000–200 cm^{-1} region using KBr pellets and a 170 SX FTIR spectrometer (see Table 2). Electronic spectra were recorded on a Shimadzu UV-260 spectrophotometer in the 300–700 nm region in the DMF solution (see Table 3), and the powder electronic reflectance spectra were measured on a Shimadzu UV-240 spectrometer in the 300–700 nm region. Conductivity measurements were carried out with a DDS-11A type conductivity bridge using 10^{-3} $mol\cdot cm^{-3}$ solution in DMF at 25°C. Thermal analyses (TG and DTA) were performed on a Beijing PCD-2 thermobalance using about 10 mg powder sample and working at a heating rate of $10°C\cdot min^{-1}$ in static air. Low frequency (80–300 cm^{-1}) resonance Raman spectra were obtained using a SPEX 1403 Laser Raman spectrometer. Electrical conductivities were estimated on compressed pellets by the conventional two-probe technique [7].

RESULTS AND DISCUSSION

Composition of the complexes

Air-stable solid complexes were readily prepared by directly using hydrated lanthanide chlorides. The analytical data for the newly synthesized complexes, listed in Table 1, indicate that they had the general formula $K_2[Ln(dmit)(phen)_2Cl_3]\cdot 6H_2O$.

Table 1. Elemental analysis and molar conductance data

Compound	%C Found (Calc.)	%N Found (Calc.)	%H Found (Calc.)	%M Found (Calc.)	Molar conductance (Ω^{-1} cm^2 mol^{-1})
(1) $K_2[La(dmit)(phen)_2Cl_3]\cdot 6H_2O$	32.28 (32.81)	5.62 (5.67)	2.74 (2.86)	14.37 (14.05)	140.7
(2) $K_2[Nd(dmit)(phen)_2Cl_3]\cdot 6H_2O$	32.49 (32.64)	5.54 (5.64)	3.05 (2.84)	14.70 (14.51)	131.4
(3) $K_2[Sm(dmit)(phen)_2Cl_3]\cdot 6H_2O$	32.20 (32.43)	5.54 (5.61)	3.25 (2.82)	14.85 (15.04)	143.4
(4) $K_2[Gd(dmit)(phen)_2Cl_3]\cdot 6H_2O$	32.12 (32.21)	5.32 (5.57)	3.02 (2.80)	15.89 (15.63)	137.9
(5) $K_2[Er(dmit)(phen)_2Cl_3]\cdot 6H_2O$	31.52 (31.89)	5.46 (5.51)	2.56 (2.78)	16.70 (16.46)	140.7
(6) $K_2[Y(dmit)(phen)_2Cl_3]\cdot 6H_2O$	34.89 (34.56)	6.13 (5.97)	3.38 (3.01)	9.26 (9.47)	137.9
(7) $K_2[La(dmit)(phen)_2Cl_3]\cdot I_{3.5}$	24.15 (24.49)	4.01 (4.23)	1.03 (1.22)		
(8) $K_2[Er(dmit)(phen)_2Cl_3]\cdot I_{3.0}$	24.96 (25.15)	4.58 (4.35)	1.10 (1.25)		

Table 2. The IR spectra data (cm^{-1})

Compound	dmit C⋯S	dmit C⋯C	*phen*	RE—S	RE—N	ν(O—H)	δ(HOH)
(1)	1055s	1380w	1516s, 1423s, 843s, 728s	369w	264w	3333s	1647m
	1030s	1344w					
(2)	1055s	1378w	1516s, 1423s, 844s, 728s	368w	269w	3331s	1648m
	1030s	1344w					
(3)	1055s	1379w	1516s, 1422s, 844s, 728s	369w	274w	3337s	1649m
	1029s	1344w					
(4)	1055s	1380w	1517s, 1423s, 844s, 728s	367w	271w	3335s	1650m
	1030s	1344w					
(5)	1055s	1380w	1517s, 1423s, 844s, 728s	367w	269w	3335s	1651m
	1030s	1344w					
(6)	1055s	1381w	1517s, 1423s, 844s, 728s	368w	272w	3340s	1653m
	1031s	1345w					

Table 3. UV spectral data (nm)*

Compound	dmit π–π* band	*phen* π–π* band	RE ← S CT band
(1)	480	325	376
(2)	480	326	377
(3)	481	326	375
(4)	481	326	374
(5)	482	326	374
(6)	483	328	373

* In DMF.

Solubility and molar conductance

All the complexes are very soluble in DMF and DMSO, soluble in acetonitrile, acetone and nitromethane, and sparingly soluble in methanol, ethanol, ethylacetate, chloroform, benzene, hexane and ether. The molar conductance values of the complexes measured in DMF at 25°C lie in the range of 131–143 Ω^{-1} cm^2 mol^{-1} (Table 1), indicating that all the complexes are 2 : 1 type electrolytes [8]. This indicates that all the anions in the complexes are held in the coordination sphere of Ln^{3+}.

IR Spectra

The most important IR peaks of the ligand and the complexes are reported in Table 2.

Most of the observed IR bands are due to the coordinated ligands. The most characteristic absorptions, observed between 1500 and 1400 cm^{-1}, 840 cm^{-1} and 700 cm^{-1} in the spectra of the complexes are mainly ring vibrations of the bidentate coordinated 1,10-phenanthroline [9].

On the other hand, strong bands at ca 1050 and 1030 cm^{-1} appear in the spectra of the complexes and are easily assigned to the typical ν(C⋯S) stretching frequencies of the dmit ligand [6,10,11], indicating the bidentate behavior of the dithio in all the complexes.

In all the IR spectra of the complexes, strong bands which appear near 3330 and 1650 cm^{-1} are clearly due to ν(OH) and δ(HOH), respectively. The absorptions of ν(OH) of these complexes show that the water molecules are crystallized water molecules [12]. This inference is verified by the results of the TG-DTA analysis. But, in the IR spectra of (7) and (8), no such bands could be observed.

Electronic absorption and reflectance spectra

Table 3 shows electronic absorption spectra data for the complexes. The intense absorption bands centered at 480 nm in DMF are assignable to the π–π* transition of the dmit ligand. Similar absorptions are observed in other dmit-metal complexes such as Na_2dmit (514 in methanol), $[NBu^n_4]_2[Zn(dmit)_2]$ [6] (515 in DMSO) and [Pt(dmit)(bipym)] [13] (478 in DMSO). The intense bands appearing at ca 325 nm are attributed to π–π* transition of phen. The broad bands due to charge-transfer (CT) transition from the highest-filled molecular orbital of $dmit^{2-}$ to the 4f orbitals of the metal ions center at ca 375 nm in all the complexes. The band which can be assigned to the intramolecular ligand-to-ligand charge transfer (LLCT) transition could not be observed in the visible region absorption spectra [14].

The powder electronic reflectance spectra of (1) and (5) show the bands corresponding to those observed in solution, suggesting no significant intermolecular interaction in the solid state. This may be the reason why the complexes are almost insulators ($\sigma_{25\,°C} < 10^{-12}$ S cm^{-1}).

Thermal analyses

The TG and DTA curves for the complexes (1), (5) show that the water molecules contained in the complexes are all crystallized water molecules, because the only one endothermic peak appear at ca 95°C. And the percent of water [(1) : 10.3(f), 10.9(c); (5) : 10.1(f), 10.6(c)] are consistent with the results of elemental analysis. It is also proved by experiment that the residue contain K^+ ion.

Oxidation of the complexes by iodine-doping

The complexes (1) and (5) have been doped with iodine by reacting the finely powdered complexes suspended in hexane with an excess amount of iodine. A first indication on the nature of the iodine species present in these solids and the degree of the charge transfer can be found in the powder electronic reflectance spectra: it is known that the intense absorption maximum for a chain of I_3^- ions is in the 550 nm region [15]. In our case, the oxidized K_2[La(dmit)(phen)$_2$Cl$_3$]·$I_{3.5}$ compound exhibits a very broad intense absorption at 516 nm, and the oxidized K_2[Er(dmit)(*phen*)$_2$Cl$_3$]·$I_{3.0}$ compound also exhibits a broad absorption centering at 515 nm. These observations are consistent with the presence of I_3^- species in the studied compounds.

A definitive answer to this question is given by resonance Raman spectroscopy.

Complexes (7) and (8) exhibit a Raman peak at 106 cm^{-1} which is assignable to the symmetric stretching of the I_3^- ion [16]. Thus, complexes (7) and (8) are formulated as K_2[La(dmit)(*phen*)$_2$Cl$_3$]·$[I_3]_{1.17}$ and K_2[Er(dmit)(*phen*)$_2$Cl$_3$]·$[I_3]_{1.00}$, respectively.

The complexes (7) and (8) behave as typical semiconductors. Electrical conductivities measured for the compacted pellets indicate that the conductivities of the complexes are raised by the 10^5 order on doping iodine ($\sigma_{25°C}$ are 1.7×10^{-7} and 2.1×10^{-7} S cm^{-1} for (7) and (8), respectively).

In conclusion, stable lanthanide $dmit^{2-}$ can be obtained by means of forming mixed-ligand complexes. Electronic spectra suggest the existence of small covalency between Ln—S bond. No existence of intermolecular interaction and intramolecular ligand-to-ligand charge transfer transition determine the poor conductivity of the complexes. In the case of the planar transition-metal complexes, such as $Ni(dmit)_2^{2-}$, the segregated stacking of the constituent planar units including the presence of peripheral sulfur atoms leads to highly directional intermolecular π orbital interactions and, consequently, a quasi-1D electronic system. But in these lanthanide complexes, the Ln^{3+} ion is nine-coordinated with one $dmit^{2-}$ group, two bidentate 1,10-phenanthroline and three chlorine ions. Probably, this kind of coordination geometry may preclude the close intermolecular interactions which are required for good solid state conductivity, and the partial oxidation of the complexes with iodine make the conductivities be raised by the 10^5 order.

Acknowledgements—The authors are grateful to the China National Natural Science Foundation, Research Foundation of the state Education Commission of China for people who return to China and the Doctoral Research Foundation of Lanzhou University.

REFERENCES

1. Bousseau, M., Valade, L., Legros, J.-P., Cassoux, P., Carbauskas, M. and Interrante, L. V., *J. Am. Chem. Soc.*, 1986, **108,** 1908.
2. Sakamoto, Y., Matsubayashi, G. and Tanaka, T., *Inorg. Chim. Acta*, 1986, **113,** 137.
3. Miller, T. R. and Dance, G. I., *J. Am. Chem. Soc.*, 1973, **95,** 6970.
4. Vogler, A. and Kunkely, H., *J. Am. Chem. Soc.*, 1981, **103,** 1559.
5. Kumar, L., Puthraya, K. H. and Srivastava, T. S., *Inorg. Chim. Acta*, 1984, **86,** 173.
6. Steimecke, G., Seiler, H. J., Kirmse, R. and Hoyer, E., *Phosphorus Sulphur*, 1979, **7,** 49.
7. Araki, S., Ishida, K. and Tanaka, T., *Bull. Chem. Soc. Jpn.*, 1978, **51,** 407.
8. Geary, W. J., *Coord. Chem. Rev.*, 1971, **7,** 81.
9. Vicente, R., Ribas, J. and Sourisseau, C., *Polyhedron*, 1986, **5**(12), 2033.
10. Vicente, R., Ribas, J. and Cassoux, P., *Nouv. J. Chim.*, 1984, **8,** 653.
11. Schumaker, R. R. and Engler, E. M., *J. Am. Chem. Soc.*, 1977, **99,** 5521; Poleschner, H., John, W., Kempe, G., Hoyer, E. and Fanghanel, E., *Z. Chem.*, 1978, **18,** 345.
12. Nakamoto, K., *Infrared and Raman Spectra of Inorganic and Coordination Compounds*, 4th edn, pp. 251–252. John Wiley, 1986.
13. Matsubayashi, Gen-etsu, Yamaguchi, Yasuhiro and Tanaka, Toshio, *J. Chem. Soc., Dalton Trans.*, 1988, 2215.
14. Matsubayashi, Gen-etsu, Hirao, Motokazu and Tanaka, Toshio, *Inorg. Chim. Acta*, 1988, **144,** 217.
15. Redy, J. M., Knox, K. and Robin, M. B., *J. Chem. Phys.*, 1964, **40,** 1082.
16. Diel, B. N., Inabe, T., Lyding, J. W., Schoch, K. F. Jr., Kannewurf, C. R. and Marks, T. J., *J. Am. Chem. Soc.*, 1983, **105,** 1551.

Pergamon

PII: S0277-5387(97)00369-0

Polyhedron Vol. 17, No. 4, pp. 433–442, 1998
© 1998 Elsevier Science Ltd
All rights reserved. Printed in Great Britain
0277–5387/98 $19.00+0.00

On the hydrolysis of dimethyl-H-phosphonate. An ^{18}O-labelling and ^{31}P-NMR study

Michael C. Mitchell,[a] Roger J. Taylor[b] and Terence P. Kee[a]*

[a] School of Chemistry, University of Leeds, Woodhouse Lane, Leeds LS2 9JT, U.K.

[b] Novartis Pharmaceuticals UK Ltd., Hulley Road, Macclesfield, Cheshire SK10 2NX, U.K.

(Received 21 July 1997; accepted 3 September 1997)

Abstract—Quantitiative ^{31}P-NMR examination of the hydrolysis of dimethyl-H-phosphonate using ^{18}O-enriched water under base-catalysed conditions supports a mechanism involving exclusive [P—O] bond cleavage as opposed to the alternative [C—O] bond cleavage. © 1998 Elsevier Science Ltd. All rights reserved

Keywords: dimethyl-H-phosphonate; hydrolysis; bond cleavage.

As a class of compounds, H-phosphonate mono- and diesters have been known for many years yet only relatively recently have such compounds begun to be exploited in areas such as natural product, nucleotide [1], catalysis [2] and radical chemistry [3]. Indeed, the application of H-phosphonates in the synthesis of phosphorus-containing natural products including oligonucleotides [4] sugar-phosphates [5] and phospholipids [6], has become preferred to more well-established methodologies involving phosphite or phosphate precursors.

As a result of this wide applicability, there is a need to provide a solid foundation for the basic chemistry of H-phosphonates, especially concerning some of the more important transformations such as (i) hydrolysis, (ii) [P—H] exchange, (iii) transesterification and (iv) de-alkylation. Of these, the kinetics of [P—H]/[P—D] exchange processes have been examined previously [7] and we are currently extending this early work in the development of a semi-quantitative scale of relative kinetic acidity of the [P—H] function [8]. Transesterification is important in nucleotide chemistry and has consequently been the subject of several investigations [9]. Although it is well known that methyl esters of phosphorus(V) acids are readily de-methylated by simple organo–nitrogen bases [10], we have recently extended this methodology to H-phosphonates along with the immobilisation of H-phosphonic acid esters on ion-exchange resins [11].

Reactions involving the hydrolysis of phosphate and phosphonate esters are of fundamental importance. For example, compounds containing the phospho group [$-PO(OH)_2$] have myriad medicinal applications [12] yet phosphorus acids possess poor biological transport properties; at physiological pH the acid is strongly ionised [$pK_a(1)$ values [13] are typically of the order of 1–2], which in turn inhibits passage of the compound through cell membranes. One strategy to facilitate delivery of phosphonate-based drugs involves esterification of the parent phosphorus acid to afford a pro-drug diester [14], which then has increased access to the interior of a cell. The active drug is then released, via hydrolysis, at the precise point of need [14].

RESULTS AND DISCUSSION

Mechanisms of phosphorus ester hydrolysis

The process of H-phosphonate diester hydrolysis is illustrated in Scheme 1. As a consequence of there being two ester motifs within the compound, two hydrolytic transformations are possible; primary and secondary hydrolyses.

The hydrolytic behaviour of H-phosphonate esters in aqueous acidic and basic media has been examined previously. Hydrolysis of H-phosphonate diesters to H-phosphonate monoesters (primary hydrolysis) is found to occur much more readily under basic than acidic conditions; reaction being general base and

* Author to whom correspondence should be addressed.

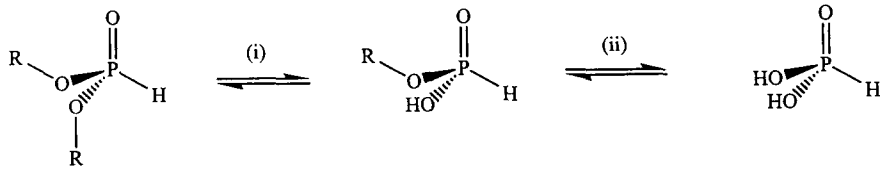

Scheme 1. The hydrolysis of dialkyl-H-phosphonate esters. (i) Primary hydrolysis. (ii) Secondary hydrolysis.

general acid catalysed, respectively [15]. In contrast, conversion of H-phosphonate monoesters to phosphorous acid (secondary hydrolysis) is more facile under acidic conditions [16]. The mechanisms of these hydrolyses have thus attracted much attention. What possibilities may be envisaged and how might we differentiate between them?

It has been suggested that H-phosphonate diesters hydrolyse both in alkali and acid with exclusive [P—O] bond fission [17]. This contrasts with the acid-catalysed hydrolysis of phosphate triesters which have been shown to proceed with both [P—O] and [C—O] bond cleavage. Evidence to support a mechanism involving [P—O] bond cleavage has been provided by Gerrard and co-workers through the hydrolysis of H-phosphonate diesters containing optically active ester functions [17]. Their work relied upon an examination of the optical purity of octan-2-ol produced during the hydrolysis of optically pure di-2-octyl-H-phosphonate, which revealed complete retention of octan-2-ol configuration, a result consistent only with exclusive [P—O] bond fission. However, since it is reasonable to suspect that steric requirements of the ester substituents should play a significant role in determining the relative rates of [P—O] and [C—O] bond cleavage in phosphorus ester hydrolysis, smaller esters such as dimethyl-H-phosphonate (DMHP) may afford different results.

Since it is obviously not possible to exploit optical activity in DMHP hydrolysis, we selected ^{18}O-isotopic labelling in conjunction with ^{31}P-NMR spectroscopy as a technique capable of differentiating between [P—O] and [C—O] bond cleavage in DMHP hydrolysis under either basic (Scheme 2) or acidic (Scheme 3) conditions and here report our studies under the former conditions.

^{18}O-labelling and ^{31}P-NMR spectroscopy as a mechanistic tool in phosphorus chemistry

The ^{31}P nucleus is one of the most attractive nuclei for NMR analysis, due to the relatively simple spectra often produced and wide chemical shift range. Furthermore, ^{31}P chemical shifts are very sensitive to small structural changes which can be measured easily [18]. Such structural changes include the replacement of a [^{16}O-P] motif for a [^{17}O-P] or [^{18}O-P] unit [19]. An ^{17}O atom directly bonded to ^{31}P results in a marked line-broadening of the ^{31}P resonance due to quadrupolar effects of the ^{17}O nucleus (nuclear spin $I = 5/2$). However, no such line-broadening is observed when ^{18}O is directly bonded to ^{31}P due to the ^{18}O nucleus possessing nuclear spin $I = 0$, and quadrupolar relaxation is an important phenomenon only for nuclei with $I > 1/2$. There is, however, a measurable isotopic shift of the ^{31}P-NMR resonance to lower frequency (by ca 3–7 Hz depending upon the operating frequency) upon replacing phosphorus-coordinated ^{16}O for ^{18}O which has been exploited in biochemistry for the

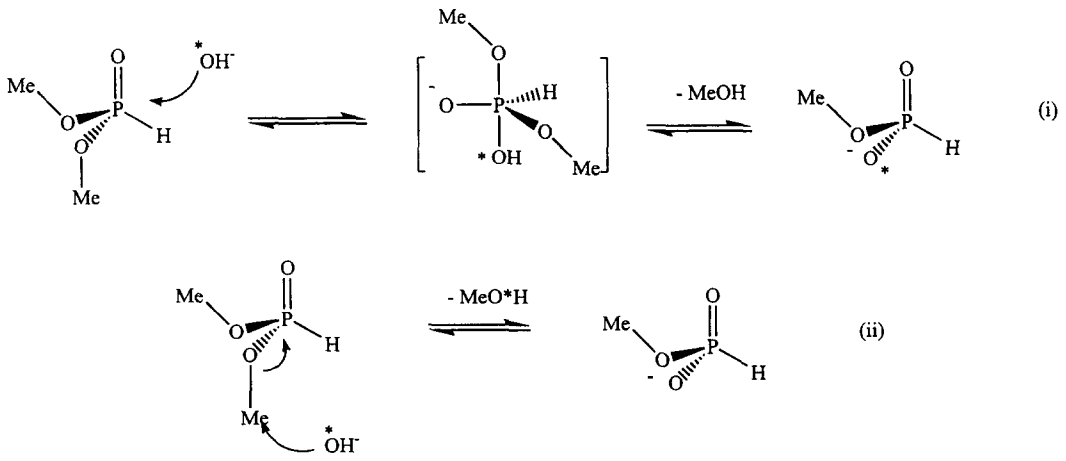

Scheme 2. Hydrolysis of DMHP under basic conditions with (i) [P—O] and (ii) [C—O] bond cleavage.

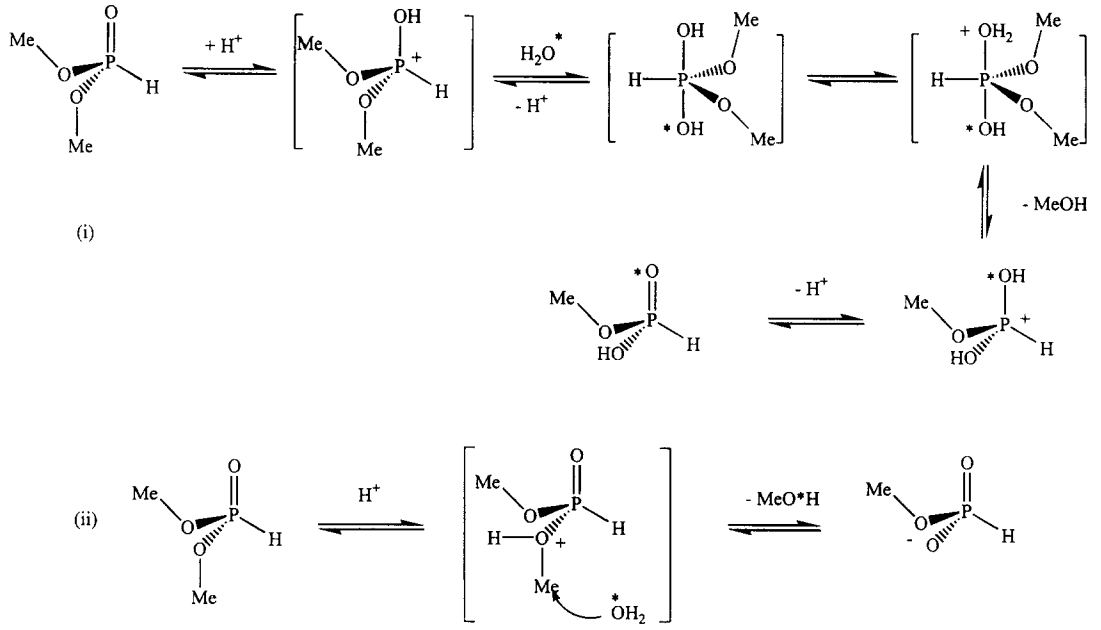

Scheme 3. Hydrolysis of DMHP under acidic conditions with (i) [P—O] and (ii) [C—O] bond cleavage.

identification of chiral [^{16}O, ^{17}O, ^{18}O]-phosphate esters [20] and in probing enzymatic mechanisms [21].

Thus, we designed a two-step experiment to probe [P—O] vs [C—O] bond cleavage in the base-catalysed hydrolysis of DMHP based on ^{18}O-labelling:

STEP 1. Preparation of a sample of ^{18}O-labelled water, of nominally 50:50 ^{18}O:^{16}O atom purity and determination of the atom purity (^{18}O:^{16}O) of the ^{18}O-labelled water, as accurately as possible, based upon the reaction with chlorodiphenylphosphine. Determination of atom purity (and evaluation of possible error limits during such a procedure) by $^{31}P\{^1H\}$ NMR spectroscopy.

STEP 2. Perform three reactions:

(a) dimethyl H-phosphonate (1 equiv.) + $H_2{}^{18}O$ (5 equivs.) in $CDCl_3$
(b) dimethyl H-phosphonate (1 equiv.) + $H_2{}^{18}O$ (5 equivs.) + NEt_3 (1 equiv.) in $CDCl_3$
(c) dimethyl H-phosphonate (1 equiv.) + NEt_3 (1 equiv.) in $CDCl_3$.

Examination of each reaction system by $^{31}P\{^1H\}$ NMR spectroscopy and determination of the extent of ^{18}O-incorporation into the products of hydrolysis and into dimethyl-H-phosphonate itself.

Preparation and assay of ^{18}O-labelled water

A sample of ^{18}O-labelled water of nominal 50:50 (^{18}O:^{16}O) isotopic composition was prepared by mixing equal quantities of ^{18}O-enriched water [^{18}O(97.9%):^{17}O(0.5%):^{16}O(1.6%)] and distilled water, under an atmosphere of dinitrogen. The atom purity (^{18}O:^{16}O) was assayed using $^{31}P\{^1H\}$ NMR spectroscopy by reaction with chlorodiphenylphosphine (Scheme 4) to afford, ^{18}O- and ^{16}O-isotopomers of diphenylphosphine oxide. The isotopomers returned ^{31}P NMR resonances separated by 3.4 Hz (operating frequency of 101.6 MHz; Fig. 1); the ^{18}O-isotopomer appearing to low frequency. Resolution of isotopomers was aided by the application of Lorentz–Gauss multiplication to the FID (LB = −1.00 Hz, GB = 10.0 %).

Di-2,6-*t*-butylpyridine was added to the reaction mixture to minimise acid-catalysed proton-exchange processes; processes which were found to cause broadening of the product signals [22]. The non-nucleophilic nature of di-2,6-*t*-butylpyridine is important since triethylamine or pyridine result in significant by-product formation.

The ratio of peak areas for the ^{18}O-P and ^{16}O-P

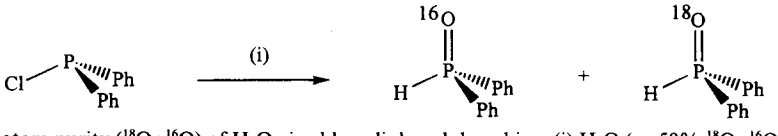

Scheme 4. Assay of atom purity (^{18}O:^{16}O) of H_2O via chlorodiphenylphosphine. (i) H_2O (ca 50% ^{18}O:^{16}O) (0.67 equivs), di-2,6-^{t}Bu-pyridine (0.67 equivs); $CDCl_3$. $\delta\delta_P$ (^{16}O-^{18}O) = 3.4 HZ (101 MHz).

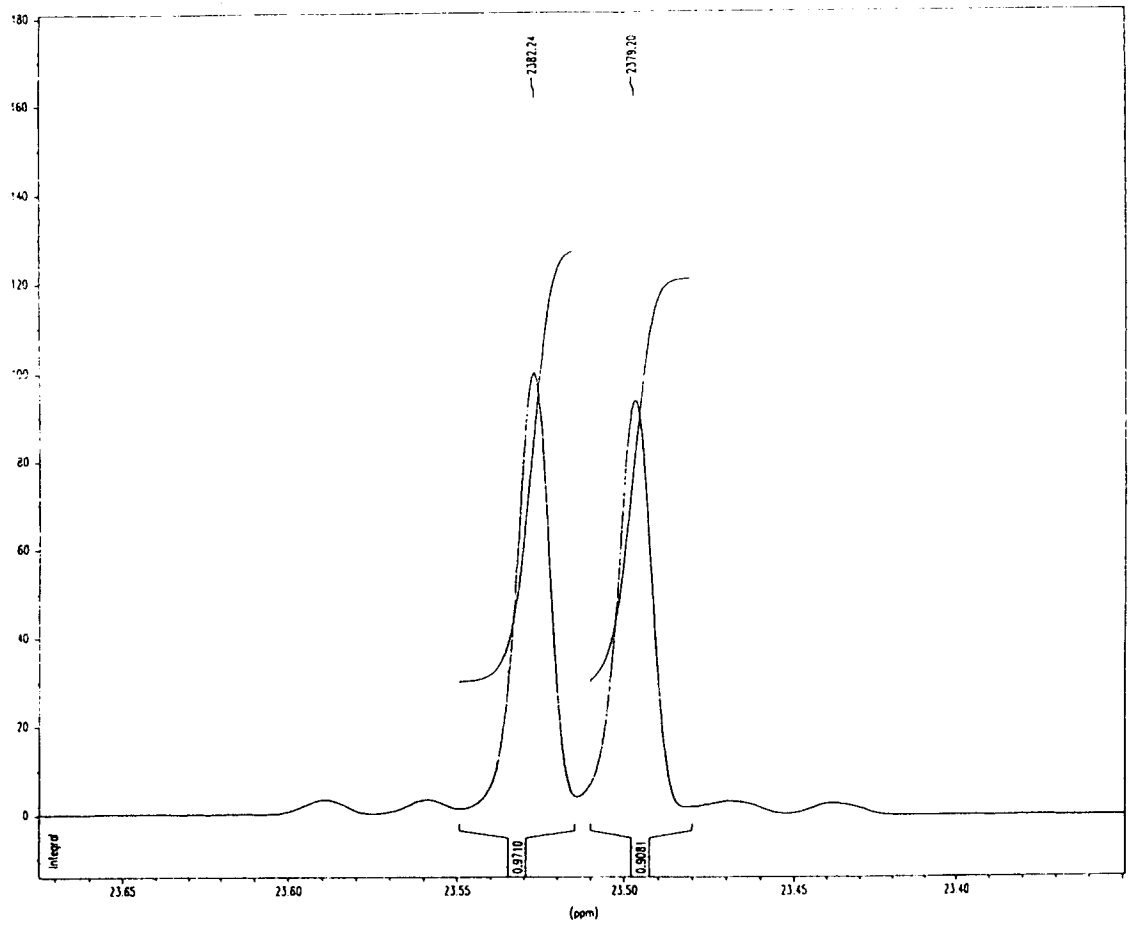

Fig. 1. ^{31}P-NMR spectroscopy of $Ph_2P(O)H$. (a) ^{16}O-P and (b) ^{18}O-P isotopomers.

isotopomers (Fig. 1) allowed the determination of the $^{18}O:{}^{16}O$ atom ratio to be 1 : 1.083; an ^{18}O-content of 48%.

The hydrolysis of DMHP with ^{18}O-enriched H_2O

Three reactions were performed concurrently, each composed of a solution of dimethyl-H-phosphonate (2.74×10^{-4} mol) in $CDCl_3$ with, respectively, the following additional components:

(a) $H_2{}^{18}O$ (48% atom purity ^{18}O, 5 equivs);
(b) $H_2{}^{18}O$ (5 equivs) and triethylamine (1 equiv.);
(c) triethylamine (1 equiv.) as a control system.

The fully proton-coupled ^{31}P NMR spectrum of each sample was collected at regular intervals. (see Experimental). Expansions of systems (a), (b) and (c) after 12 h reaction are shown in Fig. 2a–c, respectively; reaction systems (a) and (b) after 67 h reaction are illustrated in Fig. 3a, b. In each case, the doublet of septets resonance (δ_P 11.1, $^1J_{PH}$ 699 Hz, $^3J_{PH}$ 12.0 Hz) corresponds to dimethyl H-phosphonate, $(MeO)_2P(O)H$.

Comparison of the spectra in Fig. 2a–c illustrates several aspects of the hydrolysis of dimethyl H-phosphonate. Firstly, the reaction system in which only $H_2{}^{18}O$ is present (Fig. 2a) shows no evidence of hydrolysis after 12 h. The system containing both $H_2{}^{18}O$ and triethylamine (Fig. 2b) reveals hydrolysis to have occurred to an extent of ca 20%. This increased rate of hydrolysis in the presence of base is to be expected, given that hydrolysis of H-phosphonate diesters is known to be base-catalysed [15]. However, examination of Fig. 2c reveals evidence for hydrolysis even in the absence of $H_2{}^{18}O$. This suggests the presence of trace water in the system carried through presumably by the hygroscopic triethylamine; and background hydolysis involving such contamination must be considered when scrutinising data from this set of experiments. After 12 h, background hydrolysis in the system containing triethylamine only (Fig. 2c) has occurred to the extent of ca 4% and this defines the error range in the determination of ^{18}O-incorporation in our experiments. No further hydrolysis occurs in the absence of added water.

Examination of Fig. 2b reveals two hydrolysis prod-

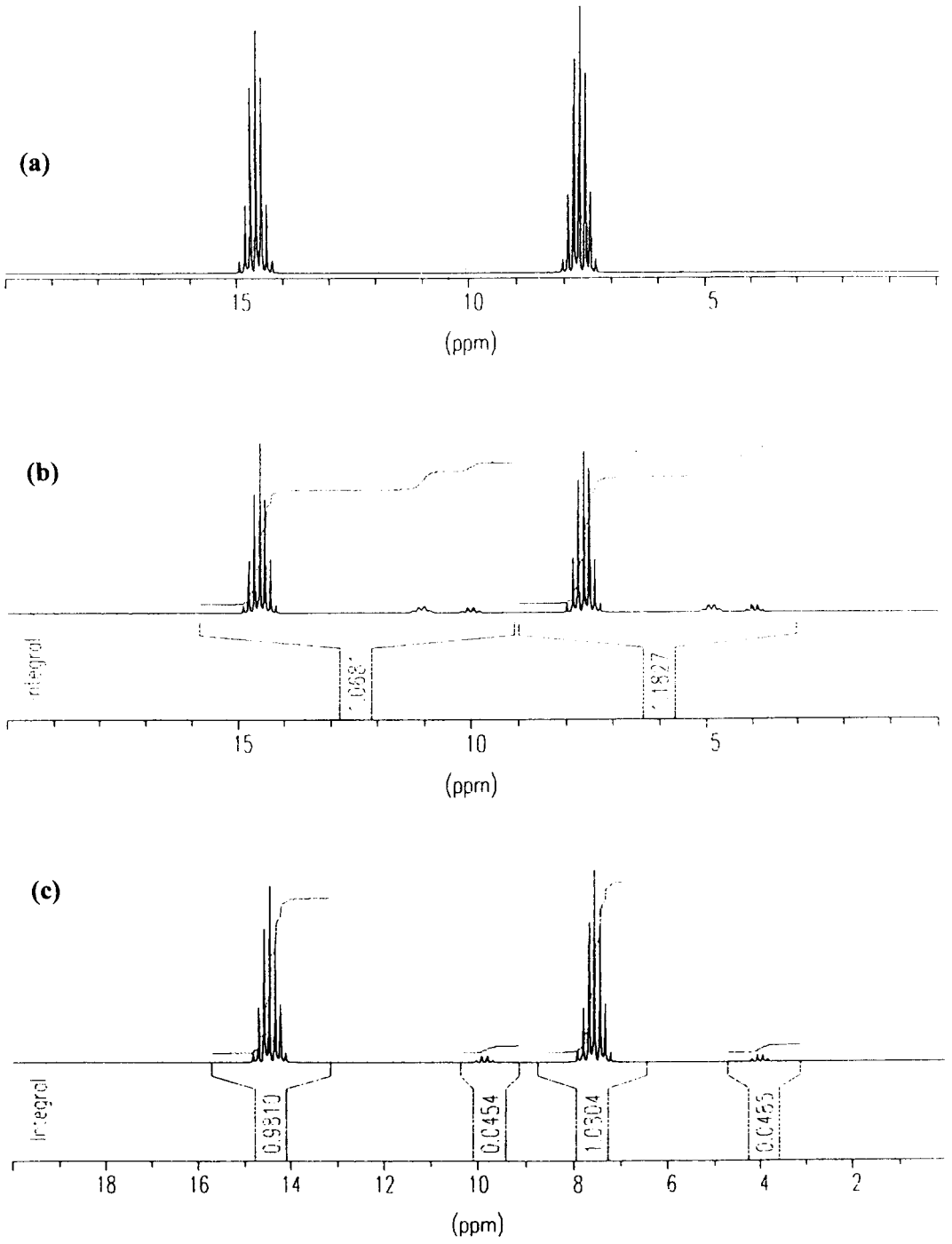

Fig. 2. ^{31}P-NMR spectra of DMHP after 12 h in the presence of (a) H_2O^*, (b) $H_2O^* + NEt_3$ and (c) NEt_3.

ucts in the ^{31}P NMR spectrum. One of the expected products, methyl-H-phosphonate, would be expected to afford a doublet of quartets in the ^{31}P NMR spectrum whilst the other logical product, phosphorus acid, should reveal itself as a doublet. However, ^{31}P-NMR reveals that both products display doublet of quartets splitting patterns. We suggest that one of these signals (expanded in Fig. 4a) may be assigned to the triethylammonium salt of methyl-H-phosphonic acid, whilst the other product may possibly be methyl-H-phosphonic acid, itself or perhaps the condensation product (MeO)HP(O)-O-P(O)H(OMe) formed by

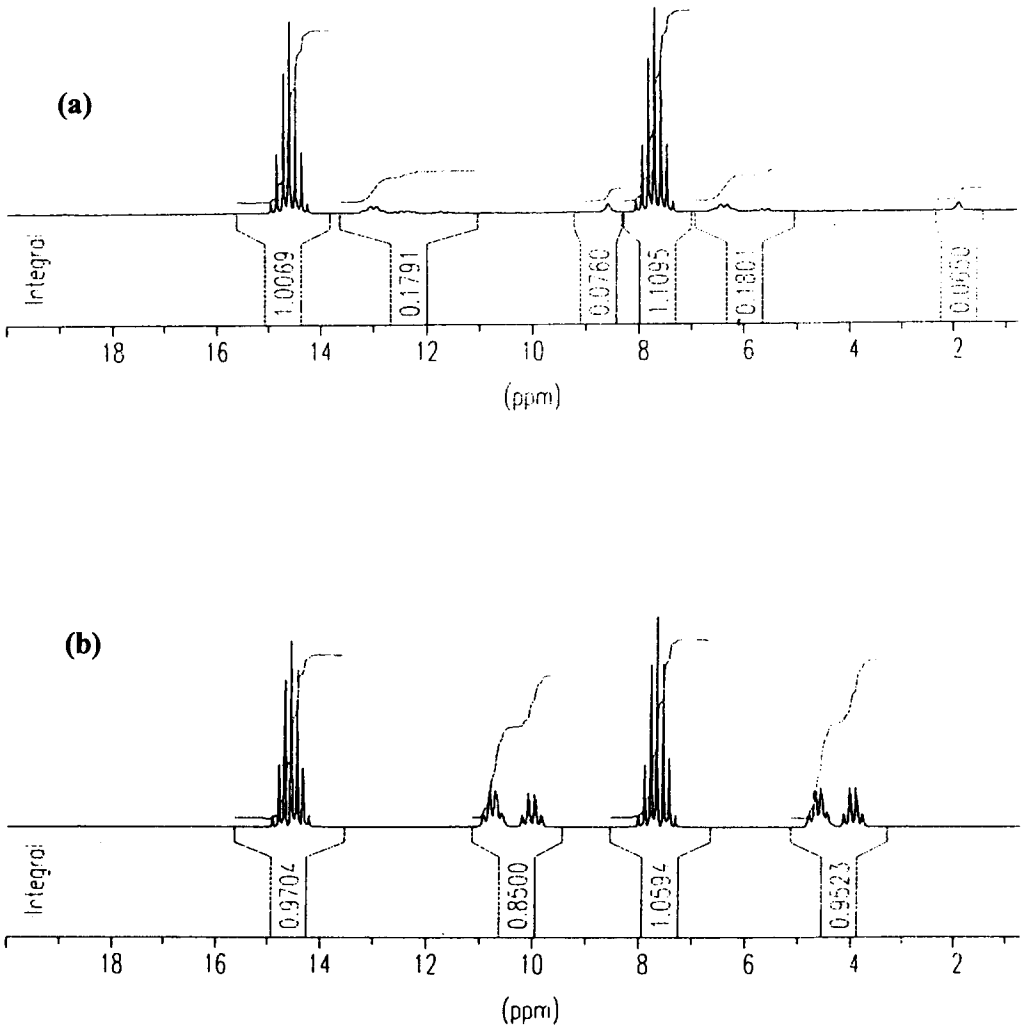

Fig. 3. ^{31}P-NMR spectra of DMHP after 67 h in the presence of (a) H_2O^* and (b) $H_2O^* + NEt_3$.

reaction of methyl-H-phosphonic acid with DMHP (Scheme 5).† The higher frequency multiplet is broader thus preventing observation of discrete ^{16}O- and ^{18}O-isotopomers; however, both isotopomers are observable in the low frequency multiplet (Fig. 4a).

After 67 h, systems (a) and (b) show further reaction (Fig. 3). The ^{31}P NMR spectrum of system (a) comprising dimethyl-H-phosphonate and $H_2{}^{18}O$ after 67 h (Fig. 3a) now reveals evidence of hydrolysis. However, inspection of the septet resonances of the DMHP shows that there is no evidence for concomitant ^{18}O-incorporation into dimethyl-H-phosphonate itself. This result seems to suggest that a mechanism of DMHP hydrolysis which proceeds as shown in Scheme 3(i) is unreasonable under the conditions here.

Further enlightening information emerges from system (b) (DMHP/$H_2{}^{18}O$/triethylamine; Fig. 3b). In this system, it is possible to observe all ^{18}O- and ^{16}O-isotopomeric resonances in the products of hydrolysis; expansions of which are shown in Fig. 4b and integrations of the peaks in the 10.2–9.8 ppm region shown in Fig. 5. In each case, zero filling to 64K points and Lorentz–Gauss multiplication was applied to the FID (LB = −0.30 Hz, GB = 40.0 %) to aid resolution of the isotopomeric peaks without distorting the shape. Integration returns an ^{18}O : ^{16}O isotopomer ratio of 44.7(5) : 55.3(5). Thus, incorporation of the ^{18}O-label during hydrolysis has occurred to the extent of 44.7(5)%. Since this experiment was performed with 48% ^{18}O-enriched water in the presence of triethylamine, which has already been shown (Fig. 2c) to result in background hydrolysis with *ca* 4% ^{16}O-incorporation, exclusive [P—O] bond cleavage during

† We are not certain of the assignements of these two species to ammonium salt and anhydride. Further experiments would be necessary to probe this in more detail. Nevertheless, it is clear that both species possess a single [MeOP] function resulting from partial hydrolysis.

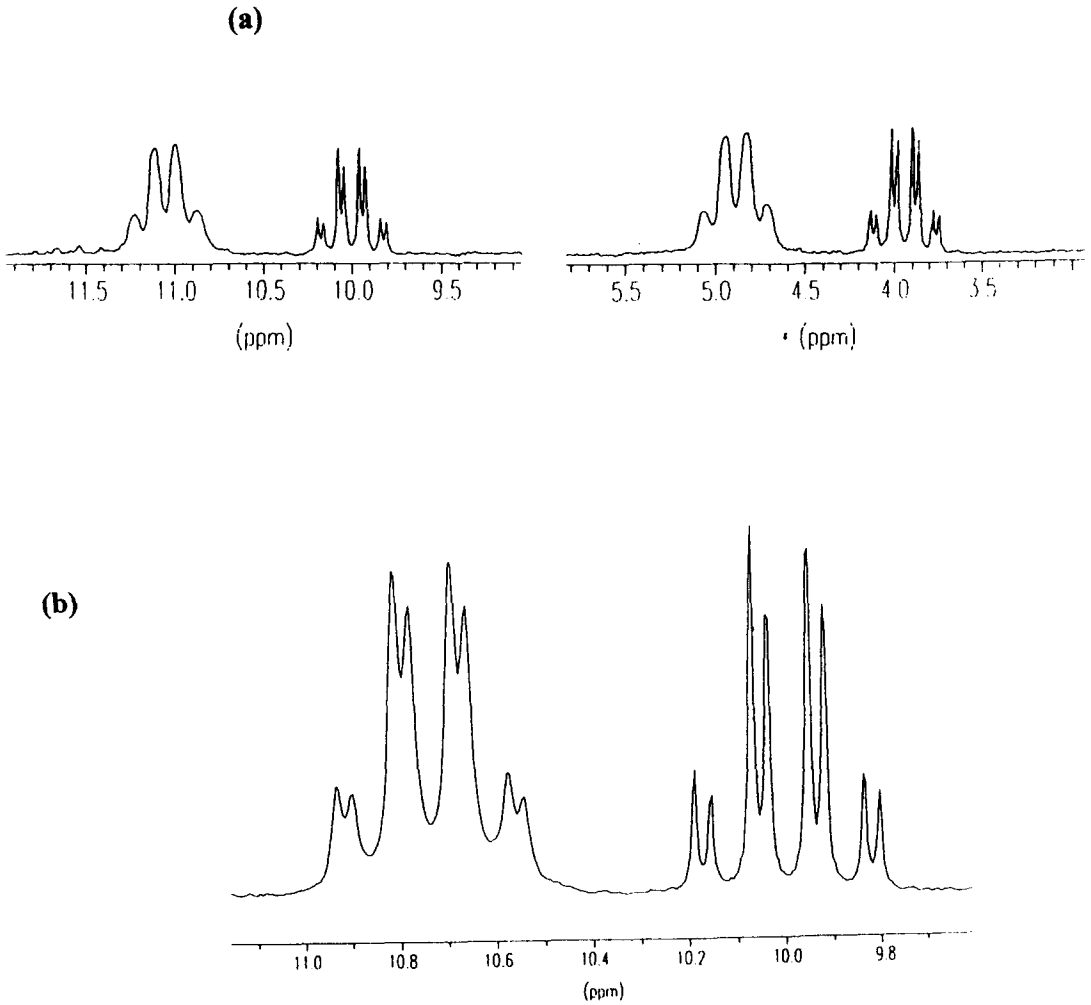

Fig. 4. (a) Expansion of selected regions Fig. 2(b). (b) Expansion of selected region of Fig. 3(b).

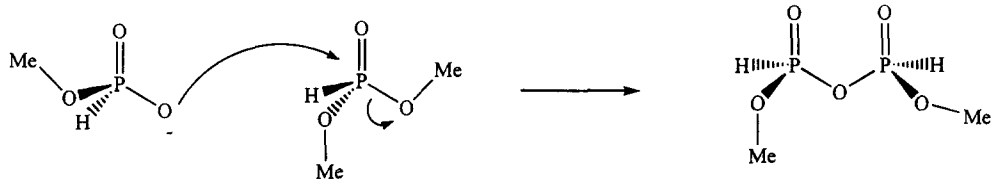

Scheme 5. Possible condensation reaction between DMHP and methyl-H-phosphonate.

hydrolysis would be expected to result in a ratio of methyl-H-phosphonic acid ^{18}O : ^{16}O isotopomers of ca 44 : 55 whereas exclusive [C—O] bond cleavage would return a ratio of 0 : 100. Consequently, within the bounds of experimental error, and allowing for trace-hydrolysis due to triethylamine, the experimental results strongly support a mechanism of base-catalysed DMHP hydrolysis which proceeds with exclusive [P—O] rather than [C—O] bond cleavage; supportive of the mechanism in Scheme 2(i).

EXPERIMENTAL

General procedures

All manipulations were performed under an atmosphere of dry dinitrogen gas using Schlenk and cannula techniques or in a dinitrogen-filled dry box, unless stated otherwise. NMR spectra were obtained on JEOL FX90Q, JEOL FX100, Bruker ARX 250 MHz and AM 400 instruments operating at 100.0

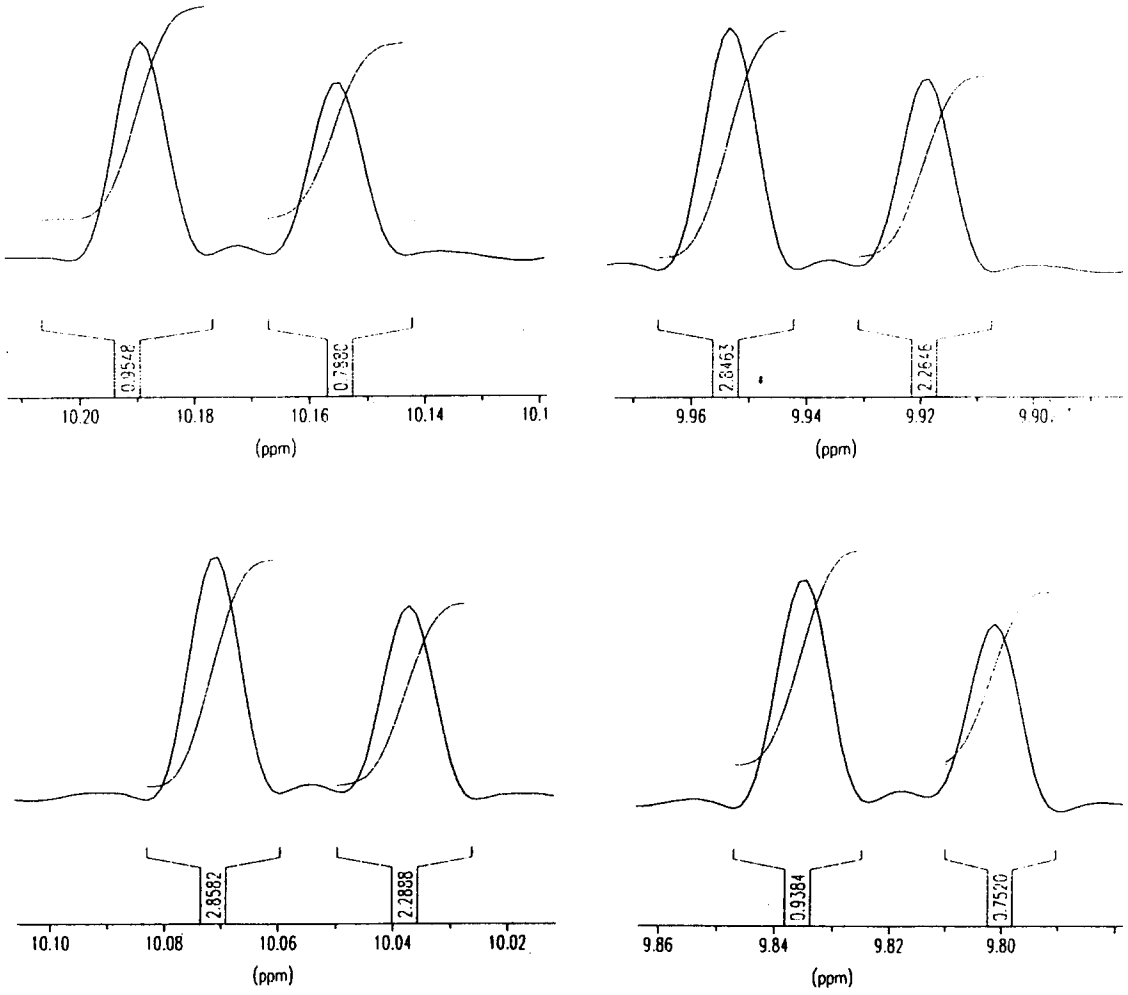

Fig. 5. Integration of expanded selected resonances of Fig. 4(b).

MHz, 250.133 MHz or 400.132 MHz for ^{1}H, 100.614 MHz or 62.895 MHz for ^{13}C and 36.2 MHz or 101.614 MHz for ^{31}P. Deuterated solvents were deoxygenated and where necessary ($CDCl_3$) dried by passage down a short column of basic (Brockman grade I) alumina before use. All spectra are reported at 298 K and referenced to 85% H_3PO_4 (^{31}P) as $\delta_P = 0$ ppm unless stated otherwise. ^{18}O-Enriched water (Euriso-Top) with a specification of $^{18}O(97.9\%):{}^{17}O(0.5\%):{}^{16}O(1.6\%)$ was purchased from MSD Isotopes and Ph_2PCl from Aldrich.

Assay of ^{18}O atom enrichment in ^{18}O-labelled water

A commercial sample of ^{18}O-enriched water $^{18}O(97.9\%):{}^{17}O(0.5\%):{}^{16}O(1.6\%)$ (50 μl, 0.056 g, 2.77 mmol) was added to distilled water (50 μl, 0.050 g, 2.78 mmol) under a dinitrogen atmosphere and sparged with dinitrogen. A sample of this mixture of $H_2{}^{18}O/H_2{}^{16}O$ isotopomers at a nominal atom ratio of ca $^{18}O:{}^{16}O$; 50:50 (1.5 μl, 9.1×10^{-5} mol) was added to a solution comprising Ph_2PCl (24 μl, 0.030 g, 0.14 mmol; 1.5 equivs), 2,6-di-*tert*-butylpyridine (20 μl, 0.017 g, 9.1×10^{-5} mol; 1.0 equiv.) and $CDCl_3$ (0.6 cm^3) in a 5 mm NMR tube. The NMR tube was closed with a push-on cap, sealed with cling-film and shaken briskly to ensure complete mixing of the components. The contents of the mixture were observed using $^{31}P\{^{1}H\}$ NMR spectroscopy. Spectra were recorded (141 scans) at 300 K on a Bruker 250 MHz spectrometer (101.268 MHz) over a spectroscopic width of 5102.04 Hz centred at 1518.83 Hz. Lorentz–Gauss multiplication was applied to the FID (LB = −1.00 Hz, GB = 10.0 %) and the resulting Fourier transformed spectrum was phased manually. Integration of the $^{18}O:{}^{16}O$ isotopomeric resonances afforded the relative quantities of each.

$\delta_P(CDCl_3)$ ppm	Assignment	% composition
23.53	$Ph_2P(O^{16})H$	52%
23.50	$Ph_2P(O^{18})H$	48%

Hydrolysis of $(MeO)_2P(O)H$ using ^{18}O-enriched water

Two reaction systems were prepared:

(1) To a solution of $(MeO)_2P(O)H$ (25 μl, 0.030 g, 2.73×10^{-4} mol) in $CDCl_3$ (0.6 cm^3) in a 5 mm NMR tube was added $H_2{}^{18}O$ (48 % atom purity ^{18}O) (23 μl, 0.026 g, 1.36 mmol) under an atmosphere of dinitrogen. The tube was sealed with a push-on cap, wrapped with cling-film and shaken briskly to afford a fully homogeneous solution. The fully proton-coupled ^{31}P NMR spectrum (101.268 MHz) was collected (2520 scans) on a Bruker 250 MHz spectrometer over a spectroscopic width of 8196.72 Hz; 16,384 data points; acquisition time 1.000 s; pulse delay 0.300 s; line-broadening 1.50 Hz. Resonances consistent with the formation of the hydrolysis products (MeO)(HO)P(O)H and $(HO)_2P(O)H$ were seen to develop over time, but the broad nature of these product resonances prevented resolution of ^{18}O : ^{16}O isotopomers. δ_P 11.14 [dsept, $^1J_{PH}$ 699.4 Hz, $^3J_{PH}$ 12.0 Hz; $(MeO)_2P(O)H$]; 9.68 [dq, br, $^1J_{PH}$ 669.4 Hz, $^3J_{PH}$ 12.0 Hz; (MeO)(HO)P(O)H]; 5.23 [d, br, $^1J_{PH}$ 674.4 Hz; $(HO)_2P(O)H$].

(2) The above procedure was repeated in the presence of NEt_3 (38 μl, 0.028 g, 2.73×10^{-4} mol) as an additional component in the reaction mixture and the mixture analysed analogously. δ_P 11.10 [dsept, $^1J_{PH}$ 698.4 Hz, $^3J_{PH}$ 12.0 Hz; $(MeO)_2P(O)H$]; 7.69 [dq, $^1J_{PH}$ 620.9 Hz, $^3J_{PH}$ 12.0 Hz; $(MeO)(H^{16}O)P(O)H$]; 6.98 {dq, $^1J_{PH}$ 613.9 Hz, $^3J_{PH}$ 12.0 Hz; $[HNEt_3]^+[(MeO)(^{16}O)P(O)H]^-$}; 7.66 [dq, $^1J_{PH}$ 620.9 Hz, $^3J_{PH}$ 12.0 Hz; $(MeO)(H^{18}O)P(O)H$]; 6.95 {dq, $^1J_{PH}$ 613.9 Hz, $^3J_{PH}$ 12.0 Hz; $[HNEt_3]^+[(MeO)(^{18}O)P(O)H]^-$}.

Acknowledgements—Grateful thanks are extended to the EPSRC and Novartis Pharmaceuticals U.K. Ltd (formally Ciba Central Research) for a CASE award (to M.C.M.) and to Albright and Wilson Ltd for generous supplies of chemicals.

REFERENCES

1. Stawinski, J., *Handbook of Organophosphorus Chemistry*, ed. R. Engel. Marcel Dekker, 1992, 377; Garegg, P. J., Regberg, T., Stawinski, J. and Stromberg, R., *Nucleosid. Nucleotid.*, 1987, **6,** 665; Garegg, P. J., Regberg, T., Stawinski, J. and Stromberg, R., *Chemica Scr.*, 1986, **26,** 59; Garegg, P. J., Lindh, I., Regberg, T., Stawinski, J. and Stromberg, R., *Tetrahedron Letts.*, 1986, **27,** 4051; Froehler, B. C. and Matteuchi, M. D., *Tetrahedron Letts.*, 1986, **27,** 469; Froehler, B. C., Ng, P. G. and Matteuchi, M. D., *Nucl. Acids Res.*, 1986, **14,** 5399; Garegg, P. J., Regberg, T., Stawinski, J. and Stromberg, R., *Chemica Scr.*, 1985, **25,** 280.
2. See for example; Yokomatsu, T., Yamagishi, T. and Shibuya, S., *J. Chem. Soc., Perkin Trans.* 1, 1997, 1527; Sardarian, A. R. and Kaboudin, B., *Tetrahedron Letts.*, 1997, **38,** 2543; Arai, T., Bougauchi, M., Sasai, H. and Shibasaki, M, *J. Org. Chem.*, 1996, **61,** 2926; Yokomatsu, T., Yamagishi, T, Matsumoto, K. and Shibuya, S., *Tetrahedron*, 1996, **52,** 11725; Sasai, H., Arai, S., Tahara, Y. and Shibasaki, M., *J. Org. Chem.*, 1995, **60,** 6656; Yokomatsu, T., Yoshida, Y. and Shibuya, S., *J. Org. Chem.*, 1994, **59,** 7930; Rath, N. P. and Spilling, C. D., *Tetrahedron Letts.*, 1994, **35,** 227; Yokomatsu, T., Yamagishi, T and Shibuya, S., *Tetrahedron: Asymmetry*, 1993, **4,** 1779; 1783.
3. Jang, D. O., *Tetrahedron Letts.*, 1996, **37,** 5367; Hubert, C., Oussaid, B., Etemad-Moghadam, G., Koenig, M. and Garrigues, B., *Synthesis*, 1994, 51.
4. Garegg, P. J., Lindh, I., Regberg, T., Stawinski, J., Henrichson, C. and Stromberg, R., *Tetrahedron Letts.*, 1986, **27,** 4055.
5. Nikolaev, A. V., Utkina, N. S., Shibaev, V. N., Ignatenko, A. V. and Kochetkov, N. K., *Bioorg. Khim.*, 1988, **14,** 555; Westerduin, P., Veeneman, G. H., van der Marel, G. A. and van Boom, J. H., *Tetrahedron Letts.*, 1986, **27,** 6271.
6. Lindh, I. and Stawinski, J., *J. Org. Chem.*, 1989, **54,** 1338.
7. Luz, Z. and Silver, B., *J. Am. Chem. Soc.*, 1961, **83,** 4518; Bailey, W. J. and Fox, R. B., *J. Org. Chem.*, 1963, 531.
8. Mitchell, M. C., Duxbury, J. and Kee, T. P., work in progress.
9. Lesnikowski, Z. J., *Bioorg. Chem.*, 1994, **22,** 128; Lesnikowski, Z. J., Zabawska, D., Jaworska-Maslanka, M. M., Schinazi, R. F. and Stec, W. J., *New. J. Chem.*, 1994, **18,** 1197; Lesnikowski, Z. J. and Schinazi, R. F., *J. Org. Chem.*, 1993, **58,** 6531; Lesnikowski, Z. J., *Bioorg. Chem.*, 1993, **21,** 127.
10. Gray, M. D. M. and Smith, D. J. H., *Tetrahedron Letts.*, 1980, **21,** 859.
11. Mitchell, M. C., Taylor, R. J. and Kee, T. P., unpublished results.
12. For leading references see, Allen, J. G., Atherton, F. R., Hall, M. J., Hassall, C. H., Holmes, S. W., Lambert, R. W., Nisbet, L. J. and Ringrose, P. S. *Nature*, 1978, **272,** 56; Hilderbrand, R. L., ed. *The Role of Phosphonates in Living Systems*, RCRC Press, Boca Raton, Fl., 1983; Cheng, L., Goodwin, C. A., Schully, M. F., Kakkar, V. V. and Claeson, G., *Tetrahedron Letts.*, 1991, **32,** 7333; *J. Med. Chem.*, 1992, **35,** 3364; Wang, C.-L. J., Taylor, T. L., Mical, A. J., Spitz, S. and Reilly, T. M., *Tetrahedron Letts.*, 1992, **33,** 7667; Green, D., Patel, G., Engendy, S., Baban, J. A., Claeson, G., Kakkar, V. V. and. Deadman, J., *Tetrahedron Letts.*, 1993, **34,** 6917; *Tetrahedron*, 1994, **50,** 5099; Shankar, R. and Scott, A. I., *Tetrahedron Letts.*, 1993, **34,** 231; Chen, S. and Yuan, C., *Synthesis*, 1993, 1074; Solodenko, V. A., Belik, M. Y., Galushko, S. V., Kukhar, V. P., Kozlova, E. V., Mironenko, D. A. and Svedas, V. K., *Tetrahedron: Asymmetry*, 1993, **4,** 1965; Chengzhi, C., Buechler, D., Lowe, D., Urwyler, S. and Shapiro, G. *Tetrahedron*, 1994, **50,** 5735; Nomizu, M., Otaka, A., Burke, Jr., T. R. and Roller, P. P., *Tetrahedron*, 1994, **50,** 2691; Green, O. M., *Tetrahedron Letts.*, 1994, **35,** 8081; Ojea, V., Ruiz, M., Shapiro, G. and Pombo-Villar, E., *Tetrahedron*

Letts., 1994, **35,** 3273; Mahajna, M. and Breuer, E., *J. Chem. Soc., Perkin Trans.* 1, 1994, 1847; Yi, B. and Burke, Jr., T. R., *Tetrahedron Letts.*, 1995, **36,** 4733; Berkowitz, D. B. and Smith, M. K., *J. Org. Chem.*, 1995, **60,** 1233; Campagne, J.-M., Coste, J. and Jouin, P., *Tetrahedron Letts.*, 1995, **36,** 2079; Deadman, J., Claeson, G. and Scully, M. F., *J. Enzyme Inhibition*, 1995, **9,** 29; Deadman, J., Engendy, S., Goodwin, C. A., Green, D., Baban, J. A., Patel, G., Skordalakes, E., Chino, N., Claeson, G., Kakkar, V. V. and Scully, M. F., *J. Med. Chem.*, 1995, **38,** 1511; Kitamura, M. Tokunaga, M. and Noyori, R., *J. Am. Chem. Soc.*, 1995, **117,** 2931; Jennings, L. J., Macchia, M. and Parkin, A., *J. Chem. Soc., Perkin Trans.* 1, 1992, 2197; Coe, D. M., Roberts, S. M. and Storer, R., *J. Chem. Soc., Perkin Trans.* 1, 1992, 2695; Lejczak, B., Kafarski, P. and Zygmunt, J., *Biochemistry*, 1989, **28,** 3459; Schultz, P. G., *Angew. Chem. Int. Ed. Engl.*, 1989, **28,** 1283; Meier, C., *Angew. Chem. Int. Ed. Engl.*, 1993, **32,** 1704; Hamilton, R., Walker, B. J. and Walker, B., *Tetrahedron Letts.*, 1993, **34,** 2847.

13. Guthrie, J. P., *Can J. Chem.*, 1979, **57,** 236.
14. Thompson, W., Nicholls, D., Mitchell, A. G., Corner, J. A., Irwin, W. J. and Freeman, S., *J. Chem. Soc. Perkin Trans.* 1. 1993, 2303.
15. Baddiley, J., Clark, V. M., Michalski, J. J. and Todd, A. R., *J. Chem. Soc.*, 1949, 815; Hammond, P. R., *J. Chem. Soc.*, 1962, 2521.
16. Dimroth, K. and Ploch, R., *Ber.*, 1957, 90, 801; Schofield, J. A. and Todd, A., *J. Chem. Soc.* 1961, 2316.
17. Gerrard, W., Green, W. J. and Nutkins, R. A. *J. Chem. Soc.*, 1952, 4076.
18. Harris, R. K. and Mann, B. E., eds. *NMR and the Periodic Table*, Academic Press, London, 1978, p 100.
19. Lowe, G., Potter, B. V. L. and Sproat, B. S., *J. Chem. Soc. Chem. Commun.*, 1979, 733.
20. Cullis, P. M. and Lowe, G., *J. Chem. Soc. Perkin Trans.* 1., 1981, 2317; Lowe, G., *Acc. Chem. Res.*, 1983, **16,** 244.
21. Jarvest, R. L., Lowe, G. and Potter, B. V. L., *J. Chem. Soc. Perkin Trans.* 1., 1981, 3186; Lowe, G., Cullis, P. M., Jarvest, R. L., Potter, B. V. L. and Sproat, B. S., *Phil. Trans. R. Soc. Lond. B*, 1981, **293,** 75; Holker, J. S. E.,. O'Brien, E., Moore, R. N. and Vederas, J. C., *J. Chem. Soc. Chem. Commun.*, 1983, 192; Gorst-Allman, C. P., Steyn, P. S. and Vleggaar, R., *J. Chem. Soc. Perkin Trans.* 1., 1983, 1357; Sankawa, U., Ebizuka, Y., Noguchi, H., Isikawa, Y., Kitaghawa, S., Yamamoto, Y., Kobayashi, T. and Iitak, Y., *Tetrahedron*, 1983, **39,** 3583; Lowe, G., Sproat, B. S. and Tansley, G., *Eur. J. Biochem.*, 1983, **130,** 341; Lee, S.-L., Hepburn, T. W., Swartz, W. H., Ammon, H. L., Mariano, P. S. and Dunaway-Mariano, D., *J. Am. Chem. Soc.*, 1992, **114,** 7346.
22. A reaction performed in the absense of di-2,6-*t*-butylpyridine resulted in a single, broad ^{31}P-NMR resonance at δ_P 23.8 ppm with a half-height linewidth of 12 Hz (operating frequency of 101.6 MHz).

Pergamon

PII: S0277-5387(97)00366-5

Polyhedron Vol. 17, No. 4, pp. 443–448, 1998
© 1998 Elsevier Science Ltd
All rights reserved. Printed in Great Britain
0277-5387/98 $19.00+0.00

Copper(II) diethylenetriamine perchlorato complexes bridged through varying length dicarboxylato spacers: synthesis, characterization and EPR studies

P. S. Subramanian, Paresh C. Dave, Vinod P. Boricha and D. Srinivas*

Sophisticated Analytical Instruments Laboratory, Central Salt & Marine Chemicals Research Institute, Gijubhai Badheka Marg, Bhavnagar 364 002, India

(Received 5 June 1997; accepted 3 September 1997)

Abstract—The synthesis and spectral characterization of dinuclear copper(II) complexes of the composition [(dien)CuLCu(dien)]$(ClO_4)_2$, where dien = diethylenetriamine and L^{2-} = oxalato, malonato, succinato, phthalato, isophthalato and terephthalato, are reported. IR spectra reveal that the mode of carboxylato coordination is *anti–anti* for oxalato complexes while it adopts chelate or polymeric *syn–anti* coordination for the rest of the complexes. The stereochemistry around copper is distorted square pyramidal. Oxalato forms two types of complexes I and II. EPR for I is characterized by a rhombic g tensor with $g_3 < g_1$ and g_2 and suggest that the unpaired electron has a predominant d_{z^2} character while II and the rest of the dicarboxylato complexes are characterized by an axial g tensor ($g_\parallel > g_\perp$) suggesting the occupancy of unpaired electron in a $d_{x^2-y^2}$ orbital. Frozen solution EPR spectra at 77 K indicate that the solvent molecule coordinates with the metal ion. Magnetic exchange in these complexes is intramolecular and both conjugated and unconjugated spacer dicarboxylato ligands propagate the exchange between the metal ions. © 1998 Elsevier Science Ltd. All rights reserved

Keywords: dinuclear Cu(II) complexes; EPR; exchange; spectroscopy.

Magnetic exchange interactions between transition metal ions bridged through multi-atomic ligands have been the subject of several investigations [1–4]. Among the bridging ligands the carboxylato group has been extensively investigated because of its occurrence in several metalloenzymes and its capability to form complexes with different metal ions in different modes of coordination, e.g. monodentate, bidentate (chelate), *syn–syn*, *syn–anti* and *anti–anti* [5–8]. Exchange in these type of complexes predominantly takes place through the superexchange mechanism via the carboxylato group and thus the mode of coordination plays a critical role on the magnitude of exchange interaction. IR spectroscopy has been proved to be a powerful tool in identifying the mode of coordination of the carboxylato ligands [5] while EPR has been used to study the intra/inter-molecular exchange interactions between the metal centers [9]. Recently, much attention has been paid by several groups of workers to understand the distance dependence of such exchange phenomenon in cases of favorable orbital overlap. Intramolecular long-range exchange coupling was observed in dinuclear Cu(II) complexes bridged through conjugated dicarboxylato ligands even for Cu···Cu separations greater than 10 Å [10–14].

We reported earlier [15] some dinuclear Cu(II) Schiff base complexes bridged through dicarboxylato ligands with varying chain lengths. Magnetic studies on those complexes have revealed the intermolecular exchange interaction as the efficient exchange pathway. In continuation to this we report here spectroscopic and EPR studies on dinuclear complexes of the composition [(dien]CuLCu(dien)]$(ClO_4)_2$, where dien = diethylenetriamine and L = dicarboxylato ligands viz. oxalato (**1**), malonato (**2**), succinato (**3**), phthalato (**4**), isophthalato (**5**) and terephthalato (**6**). Hendrickson *et al.* [16,17] and Kahn *et al.* [18] have

* Author to whom correspondence should be addressed. E-mail: general@cscsmcri.ren.nic.in

reported structural and magnetic properties of related oxalato bridged complexes, and Tsipis *et al.* [12] have reported phthalato bridged complexes. In the case of oxalato bridged complexes the exchange interaction between the dinuclear Cu(II) units is rather negligible, while in the phthalato complexes the two Cu(II) centers are coupled ferromagnetically with a singlet-triplet energy gap being 80 ± 10 cm^{-1} and $zJ' = -1.81$ cm^{-1}. In the present study the Cu $\cdots$ Cu separation is systematically varied with an interest to examine the effect of spacer units on the magnetic properties and to investigate whether the conjugated or unconjugated spacer units propagate the exchange interaction. Also the effect of mode of coordination on magnetism will be examined. Interestingly, EPR studies in polycrystalline and frozen solutions suggest that the exchange in the complexes under investigation takes place via intramolecular rather than intermolecular pathway.

EXPERIMENTAL

Synthesis

An aqueous solution of dicarboxylic acid (LH_2) (0.5 mmol, 25 ml) was added to a hot alcoholic solution (25 ml) of $Cu(CH_3COO)_2 \cdot H_2O$ (1 mmol) and the mixture was stirred for 30 min. To that was added dien (1 mmol) in 10 ml of alcohol in small fractions and stirring was continued for further 30 min while heating gently. The solution turned to bluish-violet. Then aqueous solution of $NaClO_4$ (1 mmol) was added and kept for slow evaporation. Good quality single crystals were obtained in 3–4 days. Oxalato complexes (**1**) have yielded two types of crystal (**I** and **II**). In the case of isophthalato (**5**) and terephthalato (**6**) complexes the sodium salts were used instead of their pure dicarboxylic acids. Microanalytical data: Found (calc.): Complex **1**, C, 19.3 (19.4); H, 4.2 (4.2); N, 13.7 (13.6). **2**, C, 21.0 (20.8); H, 4.6 (4.4); N, 13.1 (13.3). **3**, C, 22.3 (22.2); H, 4.9 (4.6); N, 13.0 (13.0). **4**, C, 25.3 (25.0); H, 4.5 (4.5); N, 12.3 (12.5). **5**, C, 25.3 (25.0); H, 4.6 (4.5); N, 12.8 (12.5). **6**, C, 22.5 (22.5); H, 4.6 (4.5); N, 12.9 (12.5).

CAUTION! Percholate salts can be potentially explosive during drying and grinding. So proper care should be exercised while handling such compounds. So far we have not experienced any problems during the preparation of samples.

Physical measurements

Elemental analyses of the complexes were carried out on a Perkin–Elmer PE 2400 Series II analyzer. FT–IR spectra were recorded for KBr pellets using a Biorad FTS-40 spectrophotometer. Electronic spectra in aqueous solutions were recorded on a Shimadzu UV-160 A UV-visible spectrophotometer. Cyclic voltammetric studies were carried out in aqueous solutions on a Princeton Applied Research Electrochemical system (model 273 A). Glassy carbon was used as a working electrode, Ag/AgCl was used as a reference electrode, Pt wire was used as an auxiliary electrode and 0.1 M tetraethylammonium tetrafluoroborate as a supporting electrolyte. Electron paramagnetic resonance (EPR) measurements were conducted on polycrystalline samples and frozen solutions using a Bruker ESP 300 X-band spectrometer and 100 kHz field modulation. DPPH was used as a field marker ($g = 2.0036$). Studies at liquid nitrogen temperature (77 K) were performed with a quartz inserting Dewar.

RESULTS AND DISCUSSION

All the complexes are deep bluish-violet and are soluble in several solvents. The elemental analyses data confirm the formation of dinuclear complexes. FT–IR spectra for oxalato and malonato complexes are shown in Fig. 1. Characteristic ligand bands for the complexes are observed in the finger print region. All the complexes except oxalato (**1**) showed similar spectral behavior. Selected IR data for the complexes are given in Table 1. The spectrum for oxalato differed in the positions of bands corresponding to carboxylato group. The bands for ν(NH) occurred in the range 3000–3250 cm^{-1} while ν(CH) of dien are observed in the range 2880–2970 cm^{-1}. Intense bands at 1144, 1106, 1049 and 629 cm^{-1} are attributed to perchlorato anion. While these bands were sharp and resolved, oxalato (**1**) and phthalato (**4**) complexes showed only partially resolved bands indicating two types of ClO_4^- ions, probably one being weakly coordinated and the other being free. Indeed the crystal structure of phthalato complex (**4**) reveals the weak coordination of perchlorate ion to one of the Cu(II) moieties [12]. Although two types of crystal phases (**I** and **II**) were obtained for oxalato both of them showed identical FT–IR spectra suggesting similar mode of coordination for COO^- moiety. The oxalato complexes also exhibited two partially resolved bands at 1652 and 1632, attributable to $\nu_{as}(COO^-)$ and a single band at 1462 cm^{-1} for $\nu_s(COO^-)$, while the rest of the complexes showed only a single intense band at 1603 for ν_{as} and 1405 cm^{-1} for ν_s. The two bands for oxalato indicate a difference in the strength of binding of carboxylato groups with the metal ions while the other acids (L) form a similar kind of binding. The $\Delta\nu$ ($\nu_{as} - \nu_s$) values can be used to determine the mode of coordination. These values for the present complexes (198–200 cm^{-1}) fall in the borderline for monodentate and bidentate chelation [5,19] and probably indicate that one of the oxygen atoms of the COO^- group makes a stronger coordination with the Cu(II) ion while the other participates in a relatively weaker coordination with the same or next nearest neighboring metal ion forming a one dimensional polymeric chain. In fact the crystal structures of succinato and

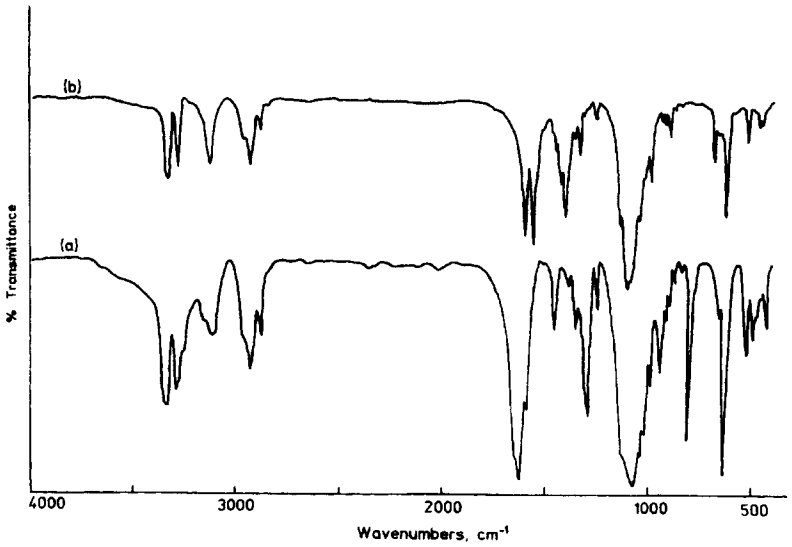

Fig. 1. FT–IR spectra for the KBr pellets of (a) [(dien)Cu(oxalato)Cu(dien)]$(ClO_4)_2$ **I** and (b) [(dien)Cu (malonato) Cu(dien)]$(ClO_4)_2$, **2**.

Table 1. IR, UV-visible and $E_{1/2}$ values for Cu(II)/Cu(I) redox couple for [(dien)CuLCu(dien)]$(ClO_4)_2$

L	$\nu_{as}(COO^-)$ cm^{-1}	$\nu_s(COO^-)$ cm^{-1}	$\Delta\nu$ cm^{-1}	ν(C—N) cm^{-1}	$\nu(ClO_4^-)$ cm^{-1}	$\lambda(\varepsilon)$ nm ($dm^3\ cm^{-1}\ mol^{-1}$)	$E_{1/2}$ V	ΔE mV
Oxalato **I**	1651, 1632	1459	192, 173	1205	1140, 1118, 1089, 625	623(162)	0.46	92
Oxalato **II**	1651, 1631	1461	190, 170	1254	1145, 1103, 1089, 624	623(162)	0.46	92
Malonato	1602	1405	197	1259	1143, 1106, 1083, 622	613(136)	0.46	59
Succinato	1603	1403	200	1259	1144, 1107, 1086, 623	615(152)	0.45	70
Phthalato	1603	1403	200	1258	1144, 1105, 1092, 623	607(140)	0.46	88
Isophthalato	1603	1404	199	1259	1144, 1107, 1085, 623	608(145)	0.45	96
Terephthalato	1603	1403	200	1259	1145, 1108, 1085, 623	614(174)	0.46	85

phthalato complexes do reveal this type of coordination [12,20]. Interestingly in the case of malonato, succinato, phthalato, isophthalato and terephthalato complexes, the carboxylato bands have shifted to a higher wave number suggesting the formation of chelate or *syn–anti* type of coordination for the carboxylato group while it adopts an *anti–anti* coordination in the oxalato complex. As the structural assignment of carboxylato complexes from IR data alone is not very reliable, a caution is made that the structures proposed are tentative.

Aqueous solutions of the complexes showed a broad band in the region 500–800 nm attributable to *d-d* transitions. In the case of oxalate this band is centered at 629 nm while the rest of the complexes showed a maximum at 614 nm (Table 1). This value falls in the range for square pyramidal geometry around copper(II) [21].

Cyclic voltammographs of the complexes in aqueous solutions showed a quasi reversible redox couple attributable to Cu(II)/Cu(I) with $E_{1/2}$ varying in a narrow range -0.45 to -0.46 V. However, the peak–peak separation (ΔE) is sensitive to the bridging ligand and varies from 59 to 96 mV in the order isophthalato > oxalato > phthalato > terephthalato > succinato > malonato and corresponds to involvement of one electron (Table 1). Probably the variation in ΔE might be associated with the changes in magnetic exchange interactions between the metal centers due to varying lengths of spacers and overlap of magnetic orbitals with the bridging ligand. These features suggest that both the copper centers have identical molecular geometries and exhibit a single redox couple.

All the complexes except oxalato (**I** and **II**) showed similar EPR spectral characteristics for their polycrystalline samples at 298 and 77 K. The spectra consist of a broad asymmetric resonance with a partially resolved parallel g feature. In spite of the fact that the two phases of the oxalato complex have shown identical IR and UV-visible spectra, their EPR are

quite different, while phase **I** showed three narrow and well resolved signals corresponding to a rhombic g tensor with $g_1 = 2.151$, $g_2 = 2.127$ and $g_3 = 2.050(3)$, phase **II** exhibited relatively broad features attributable to an axial g tensor ($g_\parallel = 2.182$ and $g_\perp = 2.086$). Representative spectra for oxalato (**I** and **II**) and malonato are depicted in Fig. 2. Hyperfine features due to copper could not be resolved due to exchange interactions. The sharp high field signals in the ESR spectra of Fig. 2 are g markers from DPPH. The spin Hamiltonian parameters listed in Table 2 indicate that oxalato I with $g_\parallel < g_\perp$ (g_1, g_2) has a d_{z^2} electronic ground state with a tetragonally compressed square pyramidal geometry while the rest of the complexes have tetragonally elongated square pyramidal geometry with the unpaired electron in $d_{x^2-y^2}$ orbital. The broad asymmetric resonance observed for the rest of the complexes is due to exchange interactions between metal ions while this is negligible for oxalato complexes as the magnetic orbitals of the metal ion and the oxalato group do not make a suitable overlap [16–18]. Terephthalato (**6**) [13] and phthalato (**5**) [12] complexes exhibit antiferro and ferromagnetic exchange interactions.

Table 2. EPR spin Hamiltonian parameters for polycrystals of $[(dien)CuLCu(dien)](ClO_4)_2$[a]

L	298 K			77 K		
	g_1	g_2	g_3	g_1	g_2	g_3
Oxalato **I**	2.151	2.127	2.050	2.151	2.130	2.051
Oxalato **II**	2.182	2.182	2.086	2.182	2.182	2.086
Malonato **2**	2.214	2.214	2.087	2.213	2.213	2.088
Succinato **3**	2.196	2.196	2.092	2.208	2.208	2.091
Phthalato **4**	2.186	2.186	2.078	2.218	2.218	2.092
Terephthalato **5**	2.213	2.213	2.090	2.215	2.215	2.091
Isophthalato **6**	2.221	2.221	2.091	2.221	2.221	2.091

[a] Error in g values is ± 0.003.

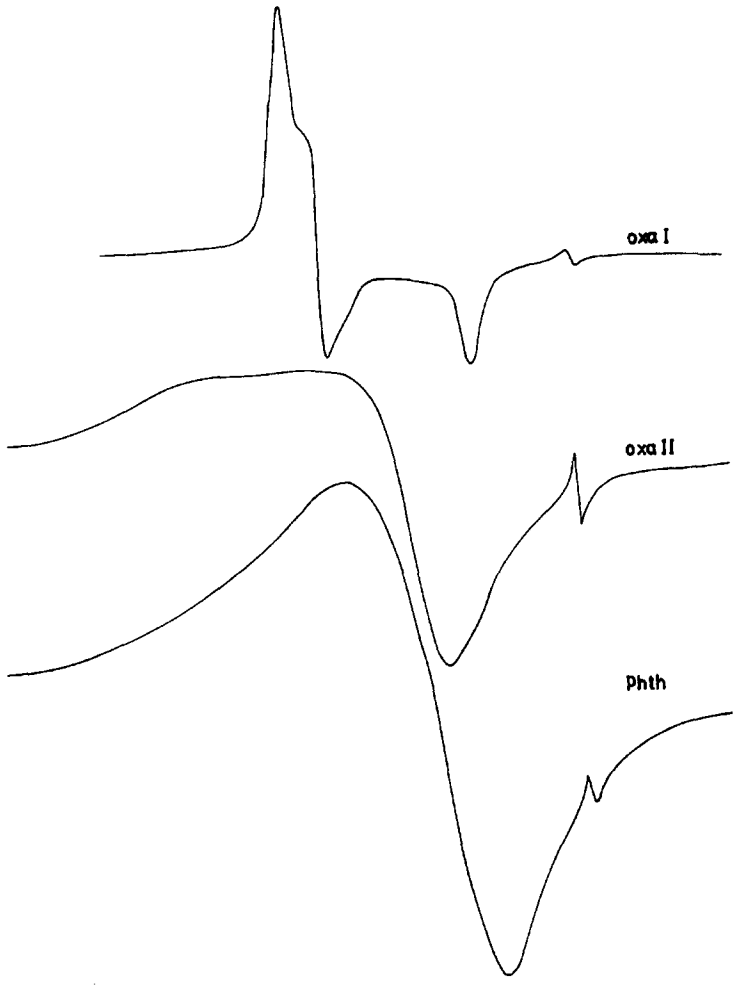

Fig. 2. X-band EPR spectra for polycrystalline samples of (a) oxalato **I**, (b) oxalato **II** and (c) phthalato at 77 K. Sharp high field signals are g markers from DPPH.

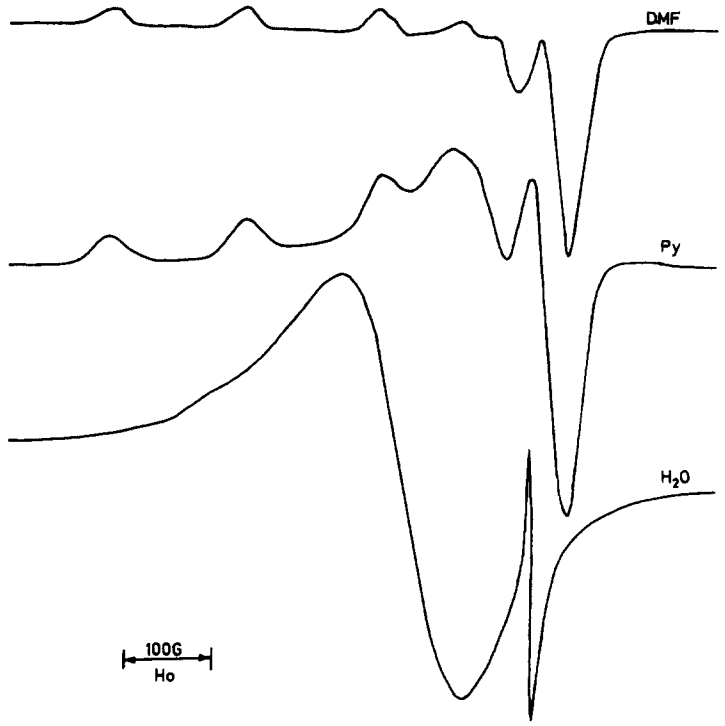

Fig. 3. X-band frozen solution EPR spectra for [(dien)Cu(malonato)Cu(dien)]$(ClO_4)_2$, **3** at 77 K.

Frozen solutions of the complexes in DMF and pyridine showed spectra characteristic of axial g and A tensors. Three of the four parallel hyperfine features due to copper are well resolved, while the fourth is overlapped by $g_\perp$ features which are partially resolved. Apart from these an extra line was observed in the highfield side which apparently coincides with the signals due to DPPH and is an "angular anomaly" due to power averaging [22]. Spectra for frozen aqueous solutions are similar that for their solid state. The spectra in different solvents for malonato are shown in Fig. 3. The spin Hamiltonian parameters (Table 3) vary with solvent and indicate the coordination of the solvent molecule with the metal ion. In the case of aqueous solutions the complexes adopt a suitable geometry so that the exchange interaction is significant. The spectroscopic and EPR investigations suggest the tentative molecular structures for the complexes as shown in Scheme 1. Identical spectra for polycrystalline samples as well as for the frozen aqueous solutions indicate that the exchange in these complexes is intramolecular rather than intermolecular. These results are consistent with the magnetic studies of Tsipis *et al.* for terephthalato and phthalato complexes [12,13]. Although the Cu···Cu separation varies due to variation length of the bridging dicarboxylato ligand, the identical spectral features for the malonato, succinato, phthalato, isophthalato and terephthalato complexes suggest that the exchange interaction in these complexes is not distant dependent and propagates through both conjugated and unconjugated bridges. The only important requirement is that the magnetic orbitals and the bridging ligand should make a proper overlap.

Table 3. EPR data for the frozen solutions of [(dien)Cu(malonato)Cu(dien)]$(ClO_4)_2$, **2** at 77 K[a]

Solvent	$g_\parallel$	$g_\perp$	g_{av}	$-A_\parallel$	$-A_\perp$
Water			2.096	[b]	[b]
DMF	2.238	2.072		188.1 (177.0)	18.0
Pyridine	2.219	2.067		188.0	20.2

[a] Error in g values ± 0.003 and A values are given in units of $\times 10^{-4}$ cm^{-1}. Error in $A_\perp$ is larger as these values were estimated from the linewidth of partially resolved g perpendicular features. Values in parentheses are for ^{65}Cu isotope.

[b] Not resolved.

CONCLUSIONS

Dinuclear Cu(II) dien complexes with dicarboxylato bridges were synthesized and characterized. The Cu···Cu separation is changed by varying the length of the spacer dicarboxylato ligand. The carboxylato group adopts *anti–anti* coordination in oxalato while *syn–anti* or chelate coordination for the rest

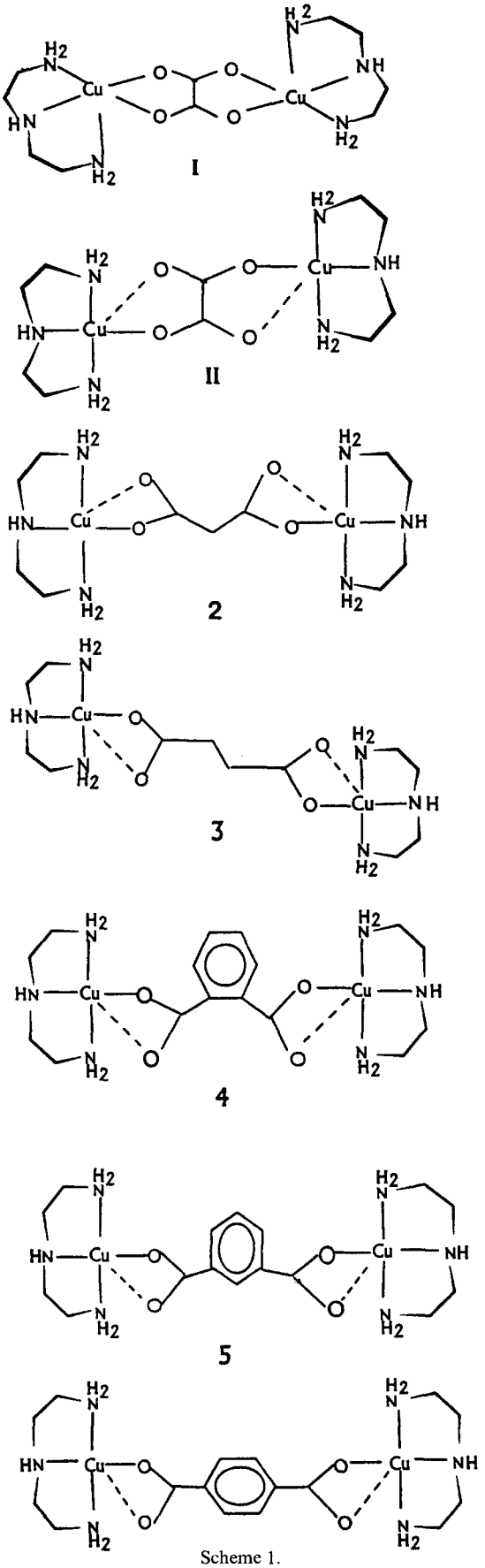

Scheme 1.

of the complexes. The geometry around copper is distorted square pyramidal. The intramolecular exchange interaction is rather negligible for oxalato complexes while the rest show similar magnetic behavior irrespective of chain length, suggesting a significant role of the overlap between the magnetic orbitals of the metal ion and the carboxylato group to propagate the exchange between the paramagnetic centers.

Acknowledgment—The authors acknowledge Dr S. D. Gomkale, Director, C.S.M.C.R.I., Bhavnagar for constant encouragement.

REFERENCES

1. *Magneto-Structural Correlations in Exchange Coupled Systems*, ed. D. Gatteschi, O. Kahn and R. D. Willet. NATO Advanced Study Institute Series. Reidel, Dordrecht, 1984.
2. Strothkamp, K. G. and Lippard, S. J., *Accts. Chem. Res.*, 1982, **15,** 318.
3. Doedens, R. J., *Prog. Inorg. Chem.*, 1976, **21,** 209.
4. Kahn, O., *Angew. Chem. Int. Ed. Engl.*, 1985, **24,** 834.
5. Mehrotra, R. C. and Bohra, R., *Metal Carboxylates.* Academic Press, New York, 1983.
6. Verdaguer, M., Gouteron, J., Jeannin, S., Jeannin, Y. and Kahn, O., *Inorg. Chem.*, 1984, **23,** 4291.
7. Bakalbassis, E. G., Mrozinski, J. and Tsipis, C. A., *Inorg. Chem.*, 1986, **25,** 3684.
8. Kramer, L. S., Clauss, A. W., Francesconi, L. C., Corlin, D. R., Hendrickson, D. N. and Stucky, G. D., *Inorg. Chem.*, 1981, **20,** 2070.
9. Bleaney, B. and Bowers, K. D., *Proc. R. Soc. London A*, 1952, **214,** 451.
10. Burger, K.-S., Chaudhuri, P., Wieghardt, K. and Nuber, B., *Chem. Eur. J.*, 1995, **1,** 583.
11. Bakalbassis, E. G., Tsipis, C. A. and Mrozinski, J., *Inorg. Chem.*, 1985, **24,** 4231.
12. Shakhatreh, S. K., Bakalbassis, E. G., Brudgam, I., Hartl, H., Mrozinski, J. and Tsipis, C. A., *Inorg. Chem.*, 1991, **30,** 2801.
13. Bakalbassis, E., Tsipis, C. A., Bozopoulos, A., Dreissig, W., Hartl, H. and Mrozinski, J., *Inorg. Chim. Acta*, 1991, **186,** 113.
14. Verdaguer, M., Gouteron, J., Jeannin, S., Jeannin, Y. and Kahn, O., *Inorg. Chem.*, 1984, **23,** 4291.
15. Subramanian, P. S. and Srinivas, D., *Polyhedron*, 1996, **15,** 985.
16. Hall, G. R., Duggan, D. M. and Hendrickson, D. N., *Inorg. Chem.*, 1975, **14,** 1956.
17. Felthouse, T. R., Laskowski, E. J. and Hendrickson, D. N., *Inorg. Chem.*, 1977, **16,** 1077.
18. Julve, M., Verdaguer, M., Gleizes, A., Philoche-Levisalles, M. and Kahn, O., *Inorg. Chem.*, 1984, **23,** 3808.
19. Deacon, G. B. and Phillips, R. J., *Coord. Chem. Rev.*, 1980, **33,** 227.
20. Pajunen, A., Pajunen, S., Kivikoski, J. and Valkonen, J., *Acta Crystallogr.*, 1996, **C52,** 2689.
21. Hathaway, B. J. and Tomlinson, A. G., *Coord. Chem. Rev.*, 1970, **5,** 1.
22. Gresmann, H. R. and Swalen, J. D., *J. Chem. Phys.*, 1962, **36,** 3221.

Pergamon

PII: S0277-5387(97)00367-7

Polyhedron Vol. 17, No. 4, pp. 449–455, 1998
© 1998 Elsevier Science Ltd
All rights reserved. Printed in Great Britain
0277-5387/98 $19.00+0.00

Reinvestigation of the crystal structure and cryomagnetic behaviour of copper(II) propionates

Y. H. Chung,[a] H. H. Wei,[a]* Y. H. Liu,[b] G. H Lee[b] and Yu Wang[b]

[a] Department of Chemistry, Tamkang University, Tamsui, Taiwan

[b] Instrumentation Center, College of Science, National Taiwan University, Taipei, Taiwan

(Received 10 April 1997; accepted 3 September 1997)

Abstract—Two different complexes of copper(II) propionates, $[Cu_2(C_2H_5CO_2)_4]$ (**1**) and $Na[Cu_4(C_2H_5CO_2)_9(H_2O)_3]$ (**2**) have been isolated from the reaction of $Cu(II)(NO_3)_2 3H_2O$ with propionic acid in an aqueous solution of NaOH. X-ray structural analysis revealed that complex **1** consists of a one-dimensional chain of an apical-to-basal Cu—O—Cu linkage of pairwise binuclear anhydrous cupric propionates, which agrees with results previously reported. Compound **2** consists of a cation Na^+ which interacts with six oxygen atoms of carboxylate groups, and anionic $[Cu_4(C_2H_5CO_2)_9(H_2O)_3]^-$ ion, which contains one isolated *syn–syn*-carboxylato dimeric copper(II) complex $[Cu_2(C_2H_5CO_2)_4(H_2O)_2]$, and a linear chain containing one *syn–syn*-carboxylato dimeric $[Cu_2(C_2H_5CO_2)_4]$ and its apical position linked by a carboxylate bridge with a unit of $[Cu(C_2H_5CO_2)(H_2O)]$. Cryomagnetic susceptibilities **1** and **2** have been measured over the temperature range 4–300 K. In **1**, the spins are coupled through an alternating one-dimensional antiferromagnetic interaction. In **2**, the cryomagnetic exchange interaction has been interpreted in terms of a strong antiferromagnetic interaction associated with the two paired dinuclear units of Cu(II)···Cu(II), and one mononuclear Cu(II) unit which complies with a Curie–Weiss law. © 1998 Elsevier Science Ltd. All rights reserved

Keywords: crystal structure; magnetic property; copper complexes; polynuclear complexes; propionate complexes.

The chemistry of the copper complexes with various carboxylates has been investigated for long time. A large number of binuclear copper(II) carboxylate adducts, $[Cu(RCO_2)L]_2$, have extensively been investigated in an effort to clarify the factors influencing the magnitude of the intramolecular magnetic exchange interaction which occurs between two Cu(II) ions in these compounds [1–7]. In most $[Cu(RCO_2)_2L]_2$ complexes, two copper(II) atoms are bridged in pairs by four *syn–syn*-carboxylato groups with two additional unidentate ligand (L) occupying the apical position.

Relatively few studies have been reported on the magneto-structural corrections in the non-adduct complex of copper(II) carboxylates such as $[Cu_2(RCO_2)_4]$ [4]. Although an X-ray crystallographic structure [8] and cryomagnetic data [9] of the dimeric copper(II) propionate $[Cu_2(C_2H_5CO_2)_4]$ have been reported in the past, the precise cryomagnetic behaviour, especially with regard to the X-ray structural data for this compound has, however, been rather controversial.

The contrasting structures of dimeric adduct $[Cu_2(RCO_2)_4L_2]$, and polymeric non-adduct $[Cu_2(RCO_2)_4]$ prompted us to reinvestigate in particular the cryomagnetic behaviour of the non-adduct copper(II) propionate $[Cu_2(C_2H_5CO_2)_4]$ compound. However, in the course of our synthetic investigations of the copper(II) propionic acid system, the products of a blue-green complex $[Cu_2(C_2H_5CO_2)_4]$ (**1**) and an emerald-green species $Na[Cu_4(C_2H_5CO_2)_9(H_2O)_3]$ (**2**) are isolated from the mixted aqueous solution of $Cu(NO_3)_2 \cdot 3H_2O$, propionic acid, and NaOH depending on their isolation conditions. The preparation, structure, EPR, and cryomagnetic behaviours of these two compounds are described in this paper.

* Author to whom correspondence should be addressed.

EXPERIMENTAL

Preparation of $[Cu_2(C_2H_5CO_2)_4]$ **(1)** *and* $Na[Cu_4(C_2H_5CO_2)_9(H_2O)_3]$ **(2)**

In the earliest report [9], unhydrated copper(II) propionate was prepared from excess of the diluted acid and copper carbonate and then dehydrated at 100°C over posphoric oxide. Here we modified the procedure as following: propionic acid (10 mmol) was dissolved in 50 cm^3 of water, and the resulting solution was adjusted to pH = 5.8 with ca 100 cm^3 of 0.25M NaOH. To this solution 25 cm^3 of aqueous $Cu(NO_3)_2 \cdot 3H_2O$ (60 mmol) was added under stirring. The resulting blue-green solution was allowed to stand in air at room temperature for one week and the earlier blue-green crystals of the compound **1** were filtered, after which the filtrate was concentrated (ca 3 weeks) to one third of its volume and the emerald-green crystals suitable for X-ray analysis of compound **2** were collected, washed with water, and air-dried at room temperature. Anal. Calc. (found) for $C_{12}H_{20}Cu_2O_8$ **(1)**: C, 33.40 (33.48) H, 4.60 (4.62)%. IR(cm^{-1}): 1628 (s), 1590, 1556 (s). Calc. (found) for $C_{27}H_{51}Cu_4NaO_{21}$ (2): C, 32.77 (32.56); H, 5.16 (5.21)%. IR (cm^{-1}): 1619 (s), 1592 (s), 1540.

X-ray crystallography

Intensities and lattice parameters of the blue-green crystal of **1** and the emerald-green crystal of **2** were measured at 25°C on an Enraf–Nonius CAD4 diffractometer by using monochromated Mo–K_α radiation. Crystal parameters and the selected data of collection and refinements of the complexes are summarized in Table 1. The structure was solved by heavy-atom method and subsequent difference Fourier maps, followed by full-matrix least-squares refinement based on F with the NRCVAX computer program [10]. The hydrogen atoms were placed at calculated positions with isotropic thermal parameters.

Physical measurements

Infrared spectra were recorded on a Bio-Rad FTS-40FTIR spectrophotometer as KBr pellets in the 4000–400 cm^{-1} region. X-band EPR spectra at 300 K for the complexes were recorded on a Bruker ECS-106 spectrometer. Temperature dependence of magnetic susceptibilities of the polycrystalline sample were measured between 4.2 and 300 K at a field of 1 T using a Quantum Design Model MPMS computer-controlled SQUID magnetometer. Diamagnetic corrections were made using Pascal's constants [11].

RESULTS AND DISCUSSION

Synthesis and structural characterizations of **1** *and* **2**

The reaction of $Cu(NO_3)_2 \cdot 3H_2O$ and NaOH with propionic acid in aqueous solution, on the time of

Table 1. Crystallographic data for compounds **1** and **2**

	1	**2**
Formula	$C_{12}H_{20}Cu_2O_8$	$C_{27}H_{51}Cu_4NaO_{21}$
Formula weight	419.37	988.85
Size, mm	0.05 × 0.13 × 0.40	0.40 × 0.50 × 0.50
T (K)	298	298
Crystal system	Triclinic	Monoclinic
Space group	$P\bar{1}$	$P2_1/n$
a, (Å)	5.1846(19)	13.470(6)
b, (Å)	8.4373(16)	26.370(14)
c, (Å)	9.523(3)	13.540(6)
α, (°)	91.732(20)	
β, (°)	91.79(3)	114.06440(0)
γ, (°)	105.06(3)	
V, Å^3	401.76(21)	4391(3)
Z	1	4
D_c, gcm^{-3}	1.73	1.496
$F(000)$	215	2038
λ[Mo–K_α], Å	0.7107	0.7107
μ, mm^{-1}	26.875	19.789
N	1415	6019
N_o ($I > 2\sigma(I)$)	1235	3942
R^a	0.024	0.046
$R_w{}^b$	0.023	0.050

$^a R = \Sigma|F_o\text{-}F_c|/\Sigma|F_o|$, $^b R_w = [\Sigma w^2(|F_o\text{-}F_c|^2/\Sigma w^2|F_o|^2]^{1/2}$

crystal growing, deposited the initial product blue-green crystal **1** from the mixed solution, and then deposited the emerald-green compound **2** after concentration of the solution.

The crystal structure of **1** is in good agreement with that previously reported [8] which shows the structure of the polymeric chain of $[Cu_2(C_2H_5CO_2)_4]$ (as shown in Fig. 1). The *syn–syn* propionate bridged Cu(II) dimer is self-assembly oxygen-bridged (apical) to the nearest dimers. This bridging arrangement gives rise to a Cu···Cu′ (apical) distance of 3.2442(3) Å, substantially longer than Cu···Cu of 2.5826(12) Å associated with the $Cu_2(C_2H_5CO_2)_4$ core. There was no doubt that the original Cu···Cu distances of 2.578(4) Å [8] are not significantly different from our refinement (2.5826(12) Å). The original Cu—O (basal) distance of 1.94 Å is shown to be somewhat shorter than the 2.0024(19) Å from our refinement, whereas the present Cu—O (apical) distance of 2.2259(19) Å is somewhat shorter at 2.28(1) Å in the original structure. The most important part of the previous determination was the geometry of their bridging propionate groups, the mean O—C—O angle (113°) was clearly quite different from our refinement value of 124.2°.

The crystal structure of **2** is shown in Fig. 2. Representative bond distances and angles are compiled in Table 2. The structure is composed of three units of formula $Na[Cu_4(C_2H_5CO_2)_9(H_2O)_3]$ (**2**); (i) the discrete hydrated binuclear $[Cu_2(C_2H_5CO_2)_4(H_2O)_2]$ (**a**), where two Cu(II) atoms are bridged by four propionate groups in *syn–syn* conformation; (ii) The bridged Cu(1)···Cu(2) distance, 2.5777(16) Å, which is close to that of **1** or to that of the well-known copper(II) acetate monhydrate dimer [12] and (iii) the polymeric chain of $[Cu_4(C_2H_5CO_2)_5(H_2O)]$ moiety, which consists of one unhydrated copper(II) propionate $[Cu_2(C_2H_5CO_2)_4]$ dimer (**b**), and its apical positions which are bridged by two additional *syn–anti*-propionate groups [O(15)—C(19)—O(16)] from the axial position of the central copper(II) [Cu $(C_2H_5CO_2)_2(H_2O)$] (**c**) moiety. In **c**, the Cu(4) atom is coordinated by one oxygen atom [O(16)] from the bridged *syn–anti*-propionate group, two oxygen atoms of O(17) and O(19) from monodentate propionate groups, one oxygen atom O(21) from an aqua ligand, and one oxygen atom O(19) from the neighbour **c** moiety, thus forming a distorted square pyramidal structure. In addition, the oxygen O(19) is self-assembling and bridged to the next Cu(4) of the neighbour **c** unit. These bridged Cu···Cu distances for Cu(1)···Cu(2), Cu(3)···Cu(3), and Cu(4)···Cu(4) in **a**, **b**, and **c** moieties are 2.5777(6), 2.6092(20), and 3.2146(20) Å, respectively.

Finally, it is noteworthy that Na^+ cation is six-coordinated with six oxygen atoms [O(2), O(9), O(13), O(15), O(18), and O(20)] of the subunits of **a**, **b**, and **c**, respectively, as shown in Fig. 2. The mean Na—O interatomic distance is 2.40 Å.

Magnetic properties

The room-temperature X-band (9.8 GHz) EPR spectra of the samples of **1** and **2** show a broad signal

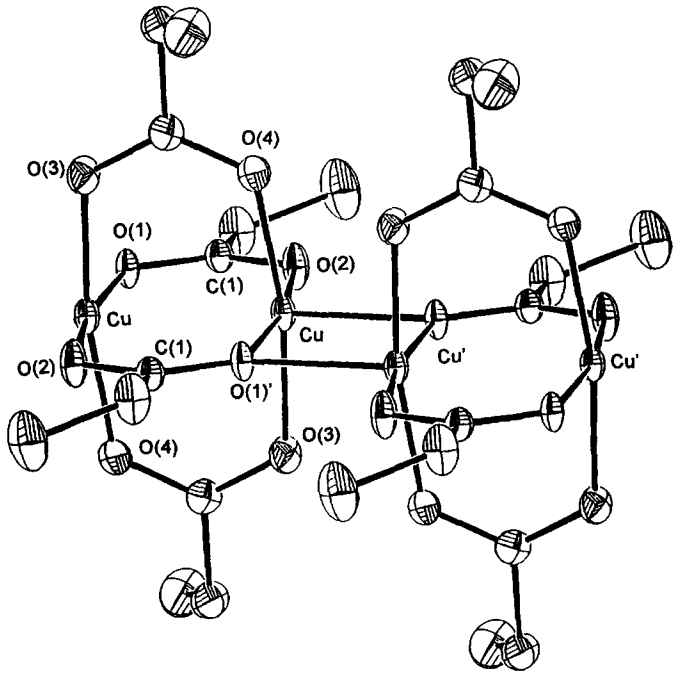

Fig. 1. ORTEP stereoview of **1** (30% probability thermal ellipsoids).

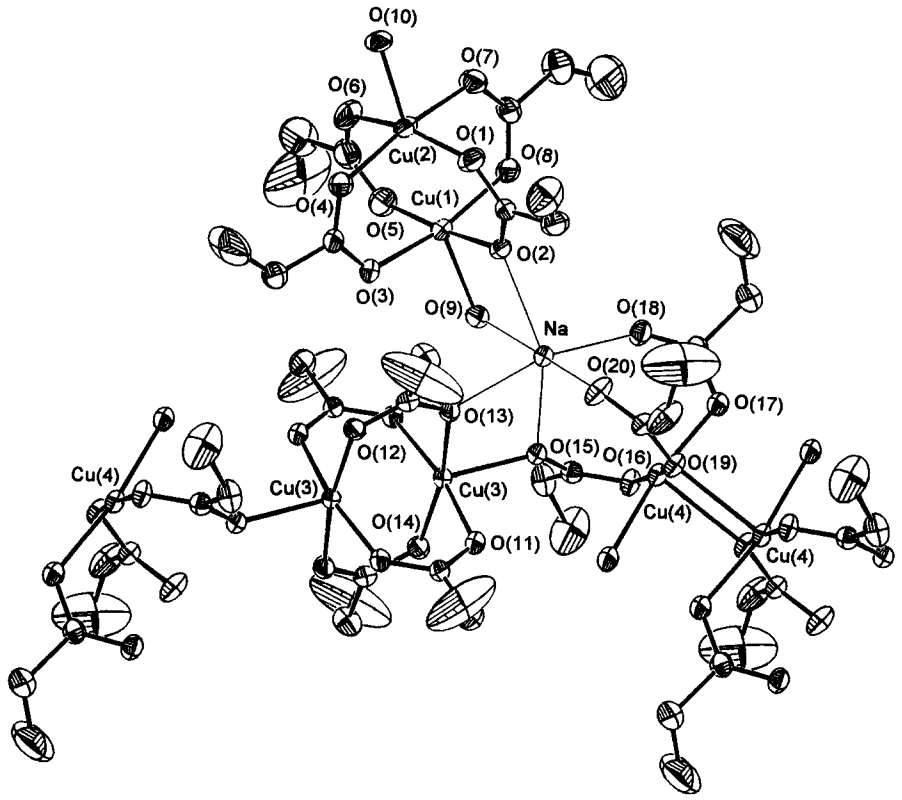

Fig. 2. ORTEP stereoview of **2** (30% probability thermal ellipsoids).

with a pronounced hump at $g = 2.07$ for **1** and 2.05 for **2** respectively. The results of the temperature dependence of magnetic measurements for $[Cu_2(C_2H_5CO_2)_4]$ **1** and $Na[Cu_4(C_2H_5CO_2)_9(H_2O)_3]$ **2** are illustrated in Figs 3 and 4, respectively.

The solid lines in Fig. 3 of compound **1** represent a best fit of data. As already mentioned in the molecular structure section, the bond distance of the two copper(II) ions Cu···Cu (basal) is shorter than that of the self-assembly oxygen-bridged Cu′···Cu′ (apical) in this polymeric chain. Thus there are two magnetic interactions present in the system. Consequently, the data were analyse by use of an analytical expression for the exchange interaction in an alternating chain of $S = 1/2$ ions developed by Hatifield [13,14] which has the following form:

$$\chi_m = Ng^2\mu_B^2[(A + B_x + C_x^2)/(1 + D_x + E_x^2 + F_x^3)] \quad (1)$$

with $x = J/kT$. The coefficients A–F are functions of the alternation parameter α defined by the Hamiltonian

$$H = -2J\sum_{i=1}^{n/2}[S_{2i}S_{2i-1} + \alpha S_{2i}S_{2i+1}] \quad (2)$$

where J and αJ are the coupling constants of Cu···Cu and Cu···Cu′ respectively. The data fit of this expression resulted (the solid lines in Fig. 3) in $J = -220$ cm^{-1}, $g = 2.07$ (from EPR) and the alternation parameter $\alpha = 0.10$. It is noteworthy that the original reported $2J$ value of 300 cm^{-1} for compound **1** [9], obtained from the simple Bleaney–Bowers equation of a two spin system with $H = 2JS_1S_2$, is smaller than that of $2J$ obtained by us.

The cryomagnetic susceptibility of compound **2** is illustrated in Fig. 4, in the form of χ_m(4Cu) and $\chi_m T$ vs T plots. Upon lowering the temperature from 300 K to about 90 K, the $\chi_m T$ value decreases from 0.86 cm^3 mol^{-1} K ($\mu_{eff} = 2.61\ \mu_B$) to a value of 0.39 cm^3 mol^{-1} K($\mu_{eff} = 1.75\ \mu_B$) indicating a strong antiferromagnetic interaction, whereas on reaching an extended plateau between 90 and 8 K, the values of $\chi_m T$ remain practically constant, and finally decreases below 8 K. In view of the crystal structure of **2**, magneto-structural correlation is complicated in the present system, nevertheless, the shorter distance between copper(II) atoms with bridging a *syn–syn* carboxylate dimer, the exchange coupling is always larger and antiferromagnetic in nature [4]. Clearly, as mentioned above in the structural analysis, this strong antiferromagnetic interaction should occur between Cu(1)···Cu(2) and Cu(3)···Cu(3). The magnetic interaction between the self-assembly oxygen-bridged Cu(4)···Cu(4) is also rather smaller in compound **1**. These become virtually diamagnetic at low temperature and Cu(4) dominates the magnetic response

Table 2. Selected bond distances (Å) and bond angles (°) of **1** and **2**

Compound **1**			
Cu—Cu	2.5826(12)	Cu—Cu′	3.2442(13)
Cu—O(1)	2.0024(19)	Cu—O(2)	1.9632(20)
Cu—O(3)	1.9378(21)	Cu—O(4)	1.9330(21)
Cu—O(1)′	2.2259(19)		
O(1)—Cu—O(2)	169.56(7)	O(3)—Cu—O(4)	169.69(8)
Cu—O(1)—Cu′	100.08(8)	O(1)—C(1)—O(2)	123.5(3)
O(3)—C(4)—O(4)	124.9(3)	Cu—O(2)—C(1)	122.40(18)
Cu(—O(1)—C(1)	124.41(17)	Cu′—O(1)—C(1)	135.31(17)
Compound **2**			
Cu(1)—Cu(2)	2.5777(16)	Cu(3)—Cu(3)	2.6092(20)
Cu(4)—Cu(4)	3.2146(20)	Cu(1)—O(2)	1.953(5)
Cu(1)—O(3)	1.958(5)	Cu(1)—O(5)	1.929(6)
Cu(1)—O(9)	2.175(5)	Cu(2)—O(4)	1.947(6)
Cu(2)—O(6)	1.982(7)	Cu(2)—O(7)	1.932(6)
Cu(2)—O(10)	2.102(6)	Cu(3)—O(11)	1.989(5)
Cu(3)—O(12)	1.987(5)	Cu(3)—O(13)	1.968(5)
Cu(3)—O(15)	2.120(5)	Cu(4)—O(16)	1.934(5)
Cu(4)—O(17)	1.969(5)	Cu(4)—O(19)	1.943(5)
Cu(4)—O(19)	2.299(5)	Cu(4)—O(21)	2.043(6)
Na—O(2)	2.420(6)	Na—O(9)	2.591(7)
Na—O(13)	2.387(6)	Na—O(15)	2.428(6)
Na—O(18)	2.301((6)	Na—O(20)	2.294(6)
O(3)—Cu(1)—O(8)	167.39(23)	O(2)—Cu(1)—O(5)	174.0(3)
O(2)—Cu(1)—O(9)	87.90(22)	O(5)—Cu(1)—O(9)	98.0(3)
O(3)—Cu(1)—O(9)	96.02(22)	O(1)—Cu(2)—O(6)	164.6(3)
O(1)—Cu(2)—O(4)	91.5(3)	O(4)—Cu(2)—O(7)	171.0(3)
O(1)—C(1)—O(2)	124.3(7)	O(3)—C(4)—O(4)	125.5(8)
O(5)—C(7)—O(6)	125.4(9)	O(7)—C(10)—O(8)	125.2(8)
O(11)—Cu(3)—O(12)	168.85(21)	O(13)—Cu(3)—O(14)	168.77(21
O(11)—C(13)—O(12)	124.4(7)	O(13)—C(16)—O(14)	125.1(7)
Cu(3)—O(15)—C(19)	134.4(5)	O(15)—C(19)—O(16)	122.4(7)
Cu(4)—O(16)—C(19)	112.3(5)	Cu(4)—O(19)—Cu(4)	98.29(19)
O(17)—Cu(4)—O(21)	169.85(21)	O(17)—C(22)—O(18)	125.1(7)

of the compound **2**. Accordingly, we attempted to fit the cryomagnetic data, however, an appropriate known theoretical model is not available, and after we tested a variety of models, the only one that gave a reasonable data fit involved two different dinuclear centres and one mononuclear centre in equal proportions, with different exchange constants. The magnetic susceptibility can be described by eqn (3),

$$\chi_m = \chi_1 + (1/2)\chi_2 + \chi_3 + N\alpha \qquad (3)$$

where χ_1, χ_2, and χ_3 are the temperature-dependent magnetic susceptibilities for the units of Cu(1)···Cu(2), Cu(3)···Cu(3), and Cu(4) respectively, and $N\alpha$ is the temperature-independent susceptibility. Assuming that the Cu(4) unit conforms to the Curie–Weiss law, with Weiss constant θ as an intermolecular exchange interaction, then $\chi_3 = C/(T-\theta)$. The sum of the exchange Hamiltonian of χ_1 and χ_2 is $H = -2J_1\Sigma S_1S_2 - 2J_2\Sigma S_1S_2$ where $S_1 = S_2 = 1/2$, has the Bleaney–Bowers expression (4) [15]

$$\chi_1 + (1/2)\chi_2 = (2Ng^2\mu_B^2/kT)\{[3+\exp(-2J_1/kT)]^{-1} + 1/2[3+\exp(-2J_2/kT)]^{-1}\} \qquad (4)$$

where J_1 and J_2 are the exchange interaction constants associated with Cu(1)···Cu(2) and Cu(3)···Cu(3) units respectively. With expression (3), and letting $J_1 > J_2$ [2–4], the best fit for **2** resulted in $J_1 = -225$ cm^{-1}, $J_2 = -160$ cm^{-1}, $g = 2.0$, $C = 0.39$ cm^3 mol^{-1} K, $\theta = -0.49$ K, and $N\alpha = 60 \times 10^{-6}$ cm^3 mol^{-1}. The solid line in Fig. 4 is calculated using the parameters derived above. The constant C value of 0.39 cm^3 mol^{-1} K is close to the value of 0.38 cm^3 mol^{-1} K for the noncoupled one spin $S = 1/2$ system; and the smaller θ value of -0.49 K indicates that a weak intermolecular antiferromagnetic interaction contributes to the bulk susceptibility at low temperature.

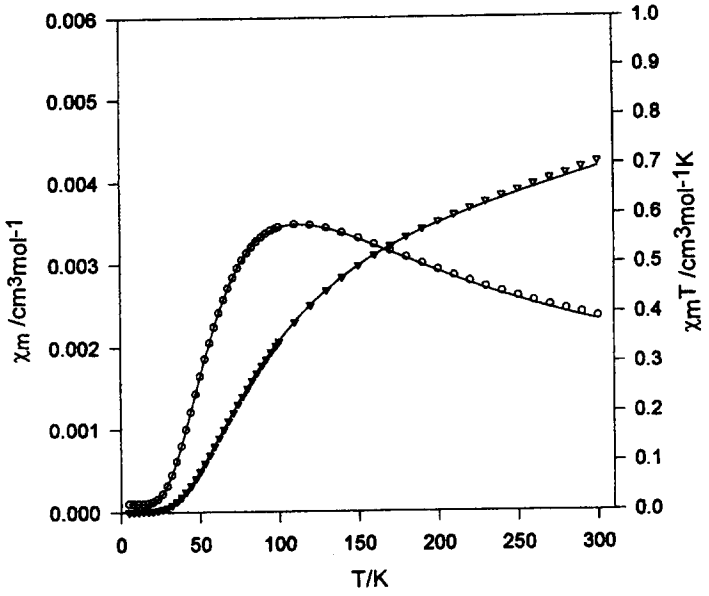

Fig. 3. Thermal variation of the molar magnetic susceptibility for **1** in the form χ_m and $\chi_m T$ vs T, the solid line is the best theoretical fit (see text).

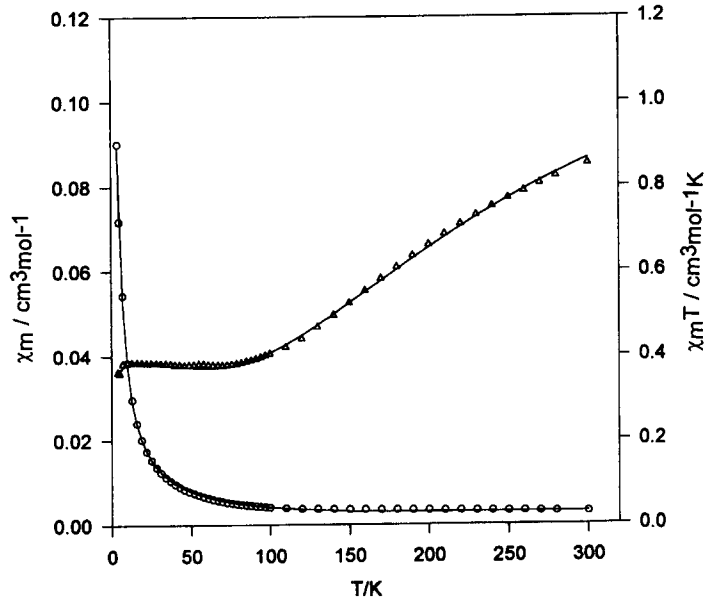

Fig. 4. Thermal variation of the molar magnetic susceptibility for **2** in the form χ_m and $\chi_m T$ vs T.

Finally, it is of interest to note that to our knowledge, compound **2** is the first example of a polymeric copper(II) compound built from a discrete copper(II) carboxylate dimer, carboxylato-bridged polymic chain, and the six-coordinated sodium cation.

SUPPLEMENTARY MATERIAL

Tables containing atom positions, anisotropic displacement parameters, hydrogen atom location, and bond lengths and angles have been deposited and are also available from the authors on request.

Acknowledgement—This work was supported by a grant of National Science of Council of Taiwan (NSC86–2113-M032-005).

REFERENCES

1. Doedens, R. J., *Prog. Inorg. Chem.*, 1976, **21**, 209.

2. Mehrotra, C. and Bohra, R. C., *Metal Carboxylates*, Academic Press, New York, 1983.
3. Melnik, M., *Coord. Chem. Rev.*, 1982, **42,** 259.
4. Kato, M., Y and Muto, Y., *Coord. Chem. Rev.*, 1988, **92,** 45.
5. Chiari, B., Piovesana, O., Tarantelli and Zanazzi, P. F., *Inorg. Chem.*, 1993, **32,** 4834.
6. Bürger, K. S., Chaudhuri, P. and Wieghardt, K., *Inorg. Chem.*, 1996, **35,** 2704.
7. Ueyama, N., Yamada, Y., Takeda, J., Okamura, T. and Mori, W., *Chem. Commun.*, 1996, 1377.
8. Simonov, Y. and Malinoskii, T. I., *Sov. Phys. Crystallogr.*, 1970, **15,** 310.
9. Martin, R. L. and Waterman, H., *J. Chem. Soc.*, 1957, 2545.
10. Gate, E. J., Le-Page, Y., Cherland, J. P., Lee, F. L. and White, P. S., *J. Appl. Cryst.*, 1989, **22,** 384.
11. Carlin, R. L., *Magnetochemistry*, Springer-Verlag, Berlin, 1986.
12. Mester de, P., Fletcher, S. R. and Skapsky, A. C., *J. Chem. Soc., Dalton Trans.*, 1973, 2575.
13. Hatifield, W. E., *J. Appl. Phys.*, 1981, **52,** 1985.
14. Hall, J. W., Marsh, W. E., Weller, R. R. and Hatifield, W. E., *Inorg. Chem.*, 1981, **20,** 1033.
15. Bleaney, B., and Bowers, K. D., *Proc. R. Soc. London*, 1952, **A214**, 451.
16. Kahn, O., *Molecular Magnetism*, VCH, New York, 1993, p. 26.

Pergamon

PII: S0277-5387(97)00365-3

Polyhedron Vol. 17, No. 4, pp. 457–461, 1998
© 1998 Elsevier Science Ltd
All rights reserved. Printed in Great Britain
0277-5387/98 $19.00+0.00

Tosylimido complexes of tungsten(VI)

Wa-Hung Leung*[a], Man-Ching Wu[a], Joyce L. C. Chim[a] and Wing-Tak Wong[b]

[a] Department of Chemistry, The Hong Kong University of Science and Technology, Clear Water Bay, Kowloon, Hong Kong

[b] Department of Chemistry, The University of Hong Kong, Pokfulam Road, Hong Kong

(Received 24 June 1997; accepted 27 August 1997)

Abstract—Treatment of $W(CO)_6$ with *N,N*-dichloro-*p*-toluenesulfonamide affords $[W(NTs)_2Cl_2]_x$ **1**, which reacts with bipy (2,2′-bipyridine) to give the adduct $W(NTs)_2Cl_2(bipy)$ **2**. The average W—N(imido), W—Cl and W—N (bipy) distances are 1.782, 2.352 and 2.284 Å, respectively. Reaction of $[W(NTs)_2Cl_2]_n$ with NaTp [Tp = hydrido(trispyrazolyl)borate] gives $TpW(NTs)_2Cl$ **4**. These tungsten(VI) tosylimido complexes undergo imido transfer reactions with tertiary phosphine to give W(IV) and the *N*-tosyl phosphinimine. © 1998 Elsevier Science Ltd. All rights reserved

Keywords: tosylimido; complexes; tungsten(VI).

While high-valent tosylimido-metal (M=NTs) species are often implicated as the active intermediates in metal-mediated olefin aziridination [1] and aminohydroxylation [2], well-defined isolated tosylimido-metal complexes are rather uncommon [3–5]. Sheldrick and coworkers first reported the synthesis of $W(NSO_2Ph)_2Cl_2(CH_3CN)_2$ by oxidative imination of $W(CO)_6$ with *N,N*-dichlorobenzenesulfonamide [3a]. Nevertheless, the reactivity of this tungsten(VI) benzensulfonylimido complex has not been explored. In an effort to develop metal-based reagents for amination of hydrocarbons, we here report the crystal structure and reactivity of a tosylimido complex of tungsten(VI).

RESULTS AND DISCUSSION

Synthesis of bis-tosylimido tungsten(VI) complexes

The tungsten(VI) bis-tosylimido complex $[W(NTs)_2Cl_2]_x$ **1** was prepared according to Sheldrick's procedure [3a] by oxidative imination of $W(CO)_6$ with *N,N*-dichloro-*p*-toluenesulfonamide, isolated as an air-sensitive yellow polymeric solid (eqn (1)).

$$W(CO)_6 + 2TsNCl_2 \rightarrow [W(NTs)_2Cl_2]_x + 6CO + Cl_2 \quad (1)$$

Complex **1** is insoluble in dichloromethane or toluene but readily dissolves in donor solvents such as THF and acetonitrile, in which $W(NTs)_2Cl_2(solv)_2$ are presumably formed. The IR spectrum of **1** is $\nu_{S=O}$ at 1158 cm^{-1} long with an intense band at 1098 cm^{-1}. The latter band is most likely due to $\nu_{W=N}$ which is extensively coupled with other stretching modes of the tosyl group. Polymeric **1** was found to be a good starting material for mononuclear tungsten tosylimido complexes, the syntheses of which are summarized in Scheme 1.

Adduct formation

Reactions of **1** with Lewis bases L gave adducts $W(NTs)_2Cl_2L_2$ [L = phosphines or pyridine]. Unlike

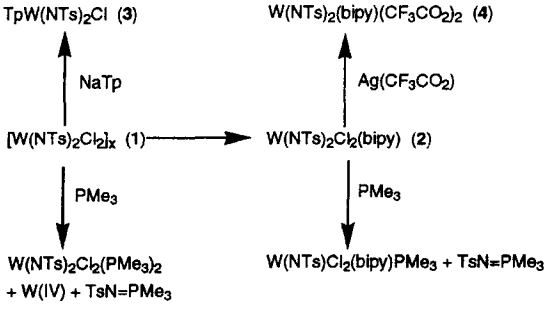

Scheme 1.

* Author to whom correspondence should be addressed.

1, these adducts are air-stable and can be recrystallized in air without decomposition. The structure of the bipy adduct $W(NTs)_2Cl_2(bipy)$ **2** has been established by X-ray crystallography. Figure 1 shows a perspective view of the molecule; selected bond lengths and angles are given in Table 2. The geometry around tungsten is octahedral with two *cis*-disposed tosylimides and two *trans*-disposed chlorides. The average W-N(imido) distance of ca 1.781 Å is comparable to that in $W(NSO_2Ph)_2Cl_2(CH_3CN)_2$ (1.78 Å) [3a] and the W(II) tosylimido analogue $[Tp'W(NTs)(CO)_2](I_3)$ [1.77(1) Å, Tp' = hydridotris(3,5-dimethylpyrazolyl) borate] [3b], indicative of the triple bond character of the W—NTs linkage. The W—N distances for these tosylimido complexes are, however, approaching the upper limit for alkylimido- and arylimido-tungsten(VI) complexes [6]. The W—N—S linkage in **2** is essentially linear (ca 171°), consistent with the *sp* hydridization for the imido nitrogen. The reactions of **1** with phosphines are complex and result in the formation of yellow adducts $W(NTs)_2Cl_2(PR_3)_2$ and reduction of W(VI) to W(IV) (see below).

Chloride substitution

Treatment of **1** with lithium alkoxides and alkyls gave intractable orange oils along with lithium chloride. There were no crystalline products isolated for the reaction of **1** with $Na(C_5H_5)$ or $Li(C_5Me_5)$. The interaction of **1** with NaTp [Tp = hydridotris (pyrazolyl)borate] yielded a yellow solid **4**, which is slightly soluble in THF and CH_2Cl_2 but readily dissolved in DMF. ^1H NMR and IR spectroscopies confirm that this yellow product contains the Tp ligand. Although X-ray quality could not be obtained, the analytical and spectroscopic data are adequate to characterize **4** as the half-sandwich compound $TpW(NTs)_2Cl$. The Tp' analogue $Tp'W(NSO_2Ph)_2Cl$ has been isolated recently by Sundermeyer and coworkers [3c]. Similarly, treatment of **1** with NaL_{OEt} (L_{OEt} = $CpCo[\{Et_2O\}_2P{=}O]_3$) gave the ether-soluble $L_{OEt}W(NTs)_2Cl$, isolated as a yellowish green powder. However the crude product was found to be contaminated with *p*-toluenesulfonamide and has not yet been obtained in a pure form.

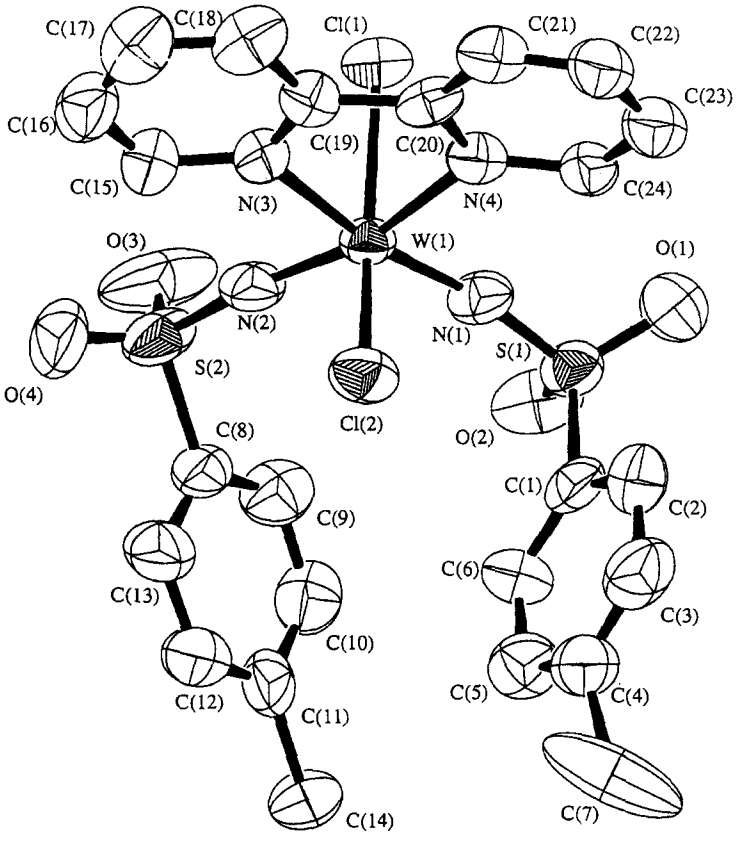

Fig. 1. Perspective view of $W(NTs)_2Cl_2(bipy)$ **2**.

Treatment of **1** with Ag(I) salts such as $AgCF_3CO_2$ and $AgCF_3SO_3$ did not lead to chloride abstraction. The chlorides in the adducts were, however, found to be more labile. For example, **2** undergoes metathesis with $AgCF_3CO_2$ slowly to give AgCl and $W(NTs)_2(bipy)(CF_3CO_2)_2$ **5**. The IR spectrum of **5** shows ν(C=O) bands at 1790, 1728 and 1674 cm^{-1}.

Reduction

No reactions between the above tungsten(VI) tosylimido complexes and olefins were observed under normal conditions. Reaction of **1** with tertiary phosphines such as PMe_3 and PMe_2Ph gave bluish green solutions, from which the *N*-tosyl phosphinimines and green oily materials were isolated along with the phosphine adducts $W(NTs)_2Cl_2(PR_3)_2$, identified by NMR spectroscopy. This suggests that imido transfer from **1** to phosphines occurred. The green oily material, presumably a reduced tungsten species, has not been characterized. Similarly treatment of **2** with PMe_3 gives $TsN{=}PMe_3$ and a green crystalline solid, which was characterized as the W(IV) imido species, $W(NTs)Cl_2(bipy)PMe_3$ (**6**), indicating that the bis-toyslimido-W(VI) complex undergoes imido transfer with phosphine to give monoimido-W(IV), as represented in eqn (2).

$$W(NTs)_2Cl_2(bipy) + 2PMe_3 \rightarrow W(NTs)Cl_2(bipy)PMe_3 + TsN{=}PMe_3 \quad (2)$$

Complex **6** is somewhat air-sensitive and decomposes in air to give a paramagnetic blue species even in the solid state.

While the W=N distance and the W—N—S(C) angle for **2** are not significantly different from those for normal W(VI) dialkylimido complexes [6], the former is apparently more reactive than the latter with respect to imido group transfer. Therefore it appears that the M=NR distance and M—N—R angle may not be a good indicator for the reactivity of imidometal complexes. On the other hand, the electronic factors, namely the electron deficiency of the imide ligand and the redox potential [7], of the imidometal complex have a profound influence on the metal-centered imido group transfer.

EXPERIMENTAL

All manipulations were carried out under nitrogen using standard Schlenck techniques. Solvents were purified, dried and distilled prior to use. Infrared spectra (Nujol) were recorded on a Perkin–Elmer 16 PC FT-IR spectrophotometer and mass spectra on a Finnigan TSQ 7000 spectrometer. ^1H NMR spectra were obtained on a Bruker ALX300 spectrometer. ^1H and ^{31}P chemical shifts (δ ppm) were reported with reference to $SiMe_4$ and H_3PO_4, respectively. Elemental analyses were performed by Medac Ltd, Brunel University, U.K.

The ligands bipy (2,2′-bipyridine) and NaTp (Tp = hydridotrispyrazolylborate) were obtained from Aldrich. The salt NaL_{OEt} (L_{OEt}=CpCo $[\{Et_2O\}_2P{=}O]_3$) was prepared according to the literature method [8].

Preparation of dichlorobis(tosylimido)tungsten(VI) (**1**)

This was prepared according to Sheldrick's procedure [3a]. To a solution $W(CO)_6$ (5.3 g, 15.06 mmol) ion CCl_4 (150 cm^3) was added dropwise a solution of *N,N*-dichloro-*p*-toluenesulfonamide (9.7 g, 40.42 mmol) in CCl_4 (70 mL) at 50–60°C. After addition, the reaction mixture was heated at reflux for 16 h. The resulting yellow solid was collected, washed with CCl_4 (3 × 20 ml) and dried *in vacuo* and is sufficiently pure for subsequent reactions (yield 8.4 g, 94%). ^1H NMR (CD_3CN): δ 2.50 (s, 6H, *p*-CH_3), 7.45 (d, J = 8 Hz, 4H, *m*-H), 7.81 (d, J = 8 Hz, 4H, *o*-H).

Preparation of 2,2′-bipyridinedichlorobis(tosylimido) tungsten(VI) (**2**)

To a suspension of **1** (0.55 g, 0.93 mmol) in CH_2Cl_2 (20 cm^3) was added 1 equiv. of bipy (0.15 g, 0.96 mmol) and the mixture was stirred at room temperature overnight. The solvent was pumped off and the residue was recrystallized from CH_2Cl_2/hexane to give orange crystals (yield 0.45 g, 65%). ^1H NMR ($CDCl_3$) δ 2.45 (s, 3H, *p*-CH_3), 7.27 (d, J = 7.8 Hz, 4H, *m*-H), 7.62 (d, J = 7.8 Hz, 4H, *o*-H), 7.67–9.72 (m, 8H, bipy). MS (FAB): m/z 750 $(M)^+$. Anal. Calc. for $[C_{24}H_{22}N_4Cl_2O_4S_2W]$: C, 38.5; H, 2.9; N, 7.5%. Found: C, 39.5; H, 3.2; N, 7.4%.

Preparation of chlorohydidotris(pyrazolyl)boratobis (tosylimido)tungsten(VI) (**3**)

To a suspension of **1** (0.5 g, 0.84 mmol) in THF (20 cm^3) was added 1 equivalent of NaTp (0.20 g, 0.85 mmol) and the mixture was stirred at room temperature overnight. The solvent was pumped off and the residue was recrystallized from THF/hexane to give a yellow crystalline solid (yield: 0.3 g, 47%). ^1H NMR ($CDCl_3$) δ 2.44 (s, 6H, *p*-CH_3), 4.62 (s, 1H, B*H*), 6.19 (t, J = 2.3 Hz, 2H, Tp), 6.39 (m, 1H, Tp), 7.24 (d, J = 7.8 Hz, 4H, *m*-H), 7.64 (d, J = 7.8 Hz, 4H, *o*-H), 7.46–7.99 (m, 6H, Tp). IR (cm^{-1}): 2538 $\nu_{B\text{-}H}$. MS (FAB): m/z 771 $(M+1)^+$, 735 $(M—Cl)^+$. Samples for analysis were recrystallised in air. Anal. Calc. for $[C_{23}H_{24}N_8BCl_8O_4S_2W \cdot H_2O]$: C, 34.9; H, 3.3; N, 14.1%. Found: C, 34.6; H, 3.1; N, 13.6%.

Reaction of **1** *with* NaL_{OEt}

To a solution of **1** (0.17 g, 0.29 mmol) in THF (20 cm^3) was added 1 equivalent of NaL_{OEt} (0.16 g, 0.29 mmol) and the mixture was stirred at room temperature overnight. The solvent was filtered and evaporated to dryness. The filtrate was recrystallized from ether/hexane to give pale yellowish green powder (yield 0.15 g). On the basis of NMR, the product was characterized as $L_{OEt}W(NTs)_2Cl$ contaminated with some *p*-toluenesulfonylamide (ca 10% by NMR). ^1H NMR ($CDCl_3$): δ 1.30 (overlapping t, 18 H, OCH_2CH_3), 2.43 (s, 6 H, *p*-CH_3), 4.21 (m, 12 H, OCH_2CH_3), 5.13 (s, 5H, C_5H_5), 7.33 (d, $J = 8.0$ Hz, 4 H, *m*-H) and 7.81 (d, $J = 8.0$ Hz, 4 H, *o*-H). $^{31}P\text{-}\{^1H\}$ NMR ($CDCl_3$): δ 116 (m). MS(FAB): 1094 $(M+1)^+$, 1059 $(M—Cl+1)^+$. Despite several attempts we have not been able to obtain analytical pure sample.

Preparation of 2,2′-bipyridinebis(tosylimido)bis (trifluoroacetato)tungsten(VI) (**5**)

To a solution of **2** (0.2 g, 0.27 mmol) in MeCN (20 cm^3) was added two equivalents of $AgCF_3CO_2$ (0.12 g, 0.53 mmol) and the mixture was stirred at room temperature overnight and filtered. The filtrate was evaporated to dryness and redissolved in THF. Addition of hexane and cooling at 0°C afforded a yellow crystalline product (Yield: 0.05 g, 25%). ^1H NMR ($CDCl_3$): δ 2.50 (s, 3H, *p*-CH_3), 2.53 (s, 3H, *p*-CH_3), 7.46 (d, $J = 7.8$ Hz, 4H, *m*-H), 7.82 (d, $J = 7.8$ Hz, 4H, *o*-H), 7.03–9.44 (m, 8H, bipy). MS (FAB): *m/z* 905 $(M+1)^+$. IR (cm^{-1}): 1790, 1728 and 1674 $\nu_{C=O}$. Samples for analysis were recrystallised in air. Anal. Calc. for $[C_{28}H_{22}N_4F_6O_8S_2W \cdot H_2O]$: C, 36.4; H, 2.6; N, 6.2%. Found: C, 36.3; H, 2.4; N, 5.8%.

Reaction of **1** *with* PMe_3

To a suspension of **1** (0.20 g, 0.34 mmol) in CH_2Cl_2 (10 cm^3) was added two equivalents of PMe_3 (0.68 mmol) and the mixture was stirred at room temperature overnight. The solvent was pumped off and the residue extracted with CH_2Cl_2. Recrystallization from CH_2Cl_2/hexane afforded a yellow solid and a green oil along with $TsN{=}PMe_3$ (δ^P 25.0). The yellow solid was identified as the phosphine adduct $W(NTs)_2Cl_2(PMe_3)_2$ by NMR spectroscopy. ^1H NMR ($CDCl_3$): δ 1.96 (d, $J = 19.8$ Hz, 18H, PMe_3), 2.33 (s, 6H, *p*-CH_3). 7.21 (d, $J = 7.8$ Hz, 4H, *m*-H), 7.73 (d, $J = 7.8$ Hz, 4H, *o*-H).

Reaction of **2** *with* PMe_3

To a solution of **2** (0.2 g, 0.27 mmol) in CH_2Cl_2 (20 cm^3) was added two equivalents of PMe_3 (0.53 mmol) and the mixture was stirred at room temperature overnight. The solvent was pumped off and the residue was recrystallized from CH_2Cl_2/hexane to give unreacted **2**, $Me_3P{=}NTs$ (δ^P 25.0), and a green solid (yield 25%). The green solid was identified as W(NTs) $Cl_2(PMe_3)$(bipy) by NMR spectroscopy and elemental analysis. ^1H NMR ($CDCl_3$): δ 1.16 (d, $J = 19.1$ Hz, 9H, PMe_3), 2.39 (s, 3H, *p*-CH_3), 7.27 (d, $J = 7.8$ Hz, 4H, *m*-H), 7.67 (d, $J = 7.8$ Hz, 4H, *o*-H), 6.72–9.46 (m, 8H, bipy). $^{31}P\text{-}\{^1H\}$ NMR ($CDCl_3$): δ 25.0 (s). Anal. Calc. for $[C_{20}H_{24}Cl_2N_3O_2PSW]$: C, 36.6; H, 3.7; N, 6.4%. Found: C, 36.0; H, 3.9; N, 6.0%.

X-ray structure determination of $W(NTs)_2Cl_2$(bipy) (**2**).

A summary of the crystal and data processing parameters for **2** is given in Table 1. Selected bond lengths and angles and final atomic coordinates are listed in Table 2. X-ray quality crystals of **2** were obtained from a saturated solution of CH_2Cl_2/hexane. Data were collected on a Rigaku AFC7R diffractometer at room temperature using graphite-monochromated Mo–K_α radiation. Intensity data were corrected for Lorentz and polarization effects. The structure was solved by Patterson method and refined by a full-matrix least-square analysis. All hydrogen atoms were refined isotropically and all other atoms were refined anisotropically. The hydrogen atoms were included as in idealized positions (C-H, 0.95 Å). List of final atomic coordinates, displacement factors and struc-

Table 1. Crystallographic data for $W(NTs)_2Cl_2$(bipy) (**2**)

Formula	$C_{24}H_{22}N_4Cl_2O_4S_2W$
M_r	749.34
Crystal system	monoclinic
Space group	$P2_1/c$ (No. 14)
a (Å)	10.741(4)
b (Å)	10.729(5)
c (Å)	24.471(3)
β (°)	97.93(2)
U (Å^3)	2793(1)
Z	4
ρ_{calcd} (g cm^{-3})	1.782
Color; habit	Yellow rods
λ (Å)	0.71073
T (K)	298
$2\theta_{max}$ (°)	50.0
μ (cm^{-1})	45.18
Unique reflections	5215 ($R_{int} = 0.023$)
Observed reflections	3290 ($I > 3.00\sigma(I)$)
Weighing scheme	$w^{-1} = \sigma^2(F) + 0.002F^2/4$
R^a	0.033
$R_w{}^b$	0.032
GoF^c	1.62

$^a R = \Sigma||F_o| - |F_c||/|F_o|$

$^b R_w = [\Sigma w(|F_o| - |F_c|)^2/\Sigma w|F_o|^2)]^{1/2}$

^{c} GoF $= [\Sigma w(|F_c| - |F_o|)^2/(N_{obs} - N_{param})]^{1/2}$

Table 2. Selected bond lengths (Å) and angles (°) for **2**

W—N(1)	1.778(6)	W—N(2)	1.785(6)
W—N(3)	2.279(6)	W—N(4)	2.288(6)
W—Cl(1)	2.351(2)	W—Cl(2)	2.353(2)
W—N(1)—S(1)	170.4(4)	W—N(2)—S(2)	172.1(4)
N(1)—W—N(3)	162.0(3)	N(1)—W—N(4)	91.8(3)
N(2)—W—N(3)	92.2(3)	N(2)—W—N(4)	162.7(3)
N(3)—W—N(4)	70.5(2)	Cl(1)—W—Cl(2)	157.87(8)
Cl(1)—W—N(2)	96.7(2)	Cl(1)—W—N(3)	82.5(2)
Cl(1)—W—N(4)	80.9(2)		

ture factors have been deposited as supplementary data with the Editor.

Acknowledgements—We thank The Hong Kong University of Science and Technology and The Hong Kong Research Grants Council for support.

REFERENCES

1. (a) Mahy, J. P., Battioni, P. and Mansuy, D. *J. Chem. Soc., Perkin Trans.* 2, 1988, 1517. (b) Evans, D. A., Faul, M. M. and Bilodeau, M. T., *J. Am. Chem. Soc.*, 1994, **116,** 2742. (c) Li, Z., Quan, W. and Jacobsen, E. N., *J. Am. Chem. Soc.*, 1995, **117,** 5889 and refs cited therein.
2. Li, G., Chang, H.-T. and Sharpless, K. B., *Angew. Chem. Int. Ed. Engl.*, 1996, **35,** 451 and refs cited therein.
3. W-tosylimido complexes: (a) Roesky H. W., Sundermeyer, J., Schimkowiak, J., Jones, P. G., Noltemeyer, M., Schroeder, T. and Sheldrick, G. M., *Z. Naturforsch.*, 1985, **40B,** 736. (b) Peréz, P. J., White, P. S., Brookhart, M. and Templeton, J. L., *Inorg. Chem.*, 1994, **33,** 6050. (c) Sundermeyer, J., Putterlik, J., Foth, M., Field, J. S. and Ramesar, N., *Chem. Ber.*, 1994, **127,** 1201.
4. Mo-tosylimido complex: Harlan, E. W. and Holm, R. H., *J. Am. Chem. Soc.*, 1990, **112,** 186.
5. The structure of the cycloaddition product of an Os(VIII) tosylimido complex with olefin have been characterized by X-ray crystallography: Hentges, S. G., Sharpless, K. B. and Tulip T. H., unpublished results (see ref. 6, p. 185).
6. (a) Nugent, W. A. and Mayer. J. M., *Metal-Ligand Multiple Bonds*, Wiley: New York, 1988. (b) Wigley, D. E., *Prog. Inorg. Chem.*, 1994, **42,** 239.
7. (a) Leung, W.-H, Wu, M.-C., Lau. T.-C. and Wong, W.-T., *Inorg. Chem.*, 1995, **34,** 4271. (b) Leung, W.-H., Hun, T. S. M., Hou H.-W. and Wong, K., Y. *J. Chem. Soc., Dalton Trans.*, 1997, 237.
8. Kläui, W. Z., *Naturforsch., B: Anorg. Chem. Org. Chem.*, 1979, **34B,** 1043.

Pergamon

PII: S0277-5387(97)00363-X

Polyhedron Vol. 17, No. 4, pp. 463–468, 1998
© 1998 Elsevier Science Ltd
All rights reserved. Printed in Great Britain
0277-5387/98 $19.00+0.00

The $[Cu([9]aneN_3)(OH)(OH_2)]^+$ catalysed hydrolysis of the phosphotriester 2,4-dinitrophenyl diethyl phosphate ([9]aneN$_3$ = 1,4,7-triazacyclononane)

Robert W. Hay* and Norman Govan

School of Chemistry, University of St Andrews, St Andrews KY16 9ST, U.K.

(Received 15 July 1997; accepted 26 August 1997)

Abstract—The hydrolysis of the phosphotriester 2,4-dinitrophenyl diethyl phosphate to diethyl phosphate is catalysed by the macrocyclic complex $[Cu([9]aneN_3)(OH_2)_2]^{2+}$ ([9]aneN$_3$ = 1,4,7-triazacyclononane). The pH dependence of the hydrolysis over the pH range 6.2 to 8.7 establishes that the active catalyst is the hydroxoaqua complex. The *pK* for the equilibrium $[Cu([9]aneN_3)(OH_2)_2]^{2+} \rightleftharpoons [Cu([9]aneN_3)(OH)(OH_2)]^+ + H^+$ determined by potentiometric titration is 7.5 at 35°C and $I = 0.1$ mol dm^{-3} so that catalysis at pH values close to neutrality is observed. Hydrolysis occurs by intramolecular attack of coordinated hydroxide on the phosphate triester which is bonded via the phosphoryl oxygen to the copper centre. © 1998 Elsevier Science Ltd. All rights reserved

Keywords: copper(II); triazacyclononane; hydrolysis; catalysis; phosphotriester.

A recent paper [1] has described the use of the complex $[Cu([9]aneN_3]^{2+}$ as a catalyst for the hydrolysis of the phosphodiester bis(4-nitrophenyl) phosphate (BNNP = 1). The complex is also active in the hydrolysis of peptides and proteins [2]. However, the mechanisms of these hydrolyses were not well defined. In the present paper we show that the complex is also a good catalyst for the hydrolysis of the water soluble phosphotriester 2,4-dinitrophenyl diethyl phosphate (**2**) and define the mechanism of the hydrolysis. X-ray crystallography has established that the complex $[Cu([9]aneN_3)Cl_2]$ [3] and the analogous bromo derivative [4] are five-coordinate with an approximate square pyramidal stereochemistry. In aqueous solution the halide ligands are displaced to give the diaqua complex. On the basis of previous studies on the activity of metal complexes on the hydrolysis of peptides [5] and phosphate esters [6] it is likely that the hydroxoaqua complex (**3**) is the active catalyst in the hydrolysis and this view is confirmed by the measurements described in this paper.

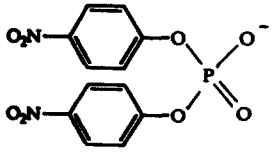

(1)

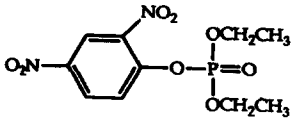

(2)

EXPERIMENTAL

Synthesis

1,4,7-Tris(*p*-toluenesulphonyl)-1,4,7-triazacyclononane. The disodium salt of the tritosylate of 1,5-diamino-3-azapentane [7] (53 g, 0.086 mol) was dissolved

* Author to whom correspondence should be addressed.

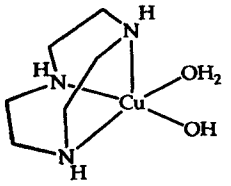

[Cu([9]aneN3)(OH)(OH2)]+

(3)

in dry DMF (350 cm^3) under an N_2 stream in a three necked flask fitted with a mechanical stirrer. The mixture was heated to 90°C in an oil bath and a solution of the ditosylate of 1,2-ethanediol [7] (32 g, 0.09 mol) in dry DMF added over a period of 45 min. Initially the solution became turbid, but on further heating at 105°C for 4 h in an oil bath, the contents of the flask turned a clear golden yellow. The solution was cooled to room temperature and the product precipitated as a white powder by slow addition of the DMF solution to water (2 dm^3) with rapid stirring. After filtration and washing with water (500 cm^3), the tosylate was recrystallised from $EtOH/H_2O$ and dried in a vacuum oven at 80°C. Yield: 38 g (74%), m.p. 220–223°C. ^1H NMR (TMS, $CDCl_3$) 2.60 (q, 12H phenyl), 3.45 (s, 12H, methyl), 2.40 (s, 9H, ethylene).

Hydrolysis of the tritosylate of 1,4,7-triazacyclononane was carried out as follows. The tritosylate (25 g) was dissolved in concentrated H_2SO_4 (120 cm^3) and the mixture heated with stirring on an oil bath at 130°C for 48 h. After cooling the solution was neutralised by the slow addition of NaOH (300 g) dissolved in water (600 cm^3). The resulting solution was cooled at 0°C overnight to allow Na_2SO_4 to crystallise. The supernatant was decanted into a continuous liquid–liquid extractor and extracted with $CHCl_3$, (200 cm^3). The $CHCl_3$ extracts were combined and the chloroform removed on a rotary evaporator. The residue obtained was dissolved in ethanol (25 cm^3) and the solution filtered from any insoluble material. The ligand trihydrochloride was precipitated by addition of concentrated HCl (10 cm^3). The solid product obtained was filtered off, washed with ethanol then diethyl ether and dried in air. Yield: 9 g. ^1H NMR (NaTMS, D_2O) 4.00 (s) with no evidence for aromatic protons.

[Cu([9]aneN$_3$)Cl$_2$]. The macrocyclic complex was prepared as follows. To a slurry of [9]aneN$_3$·3HCl (1.20 g, 5 mmol) in ethanol (15 cm^3) was added KOH (0.82 g, 15 mmol) and the mixture heated at 60°C for 20 min. After cooling the solution was filtered and added to a solution of $CuCl_2$ (0.85 g, 5 mmol) in ethanol (10 cm^3). Blue crystals formed on slow evaporation of the solvent. Found : C, 27.2; H, 6.0; N, 15.9. Calc. for $C_6H_{15}N_3CuCl_2$: C, 27.3; H, 5.7; N, 15.9%.

The ester 2,4-dinitrophenyl diethyl phosphate was prepared and purified as previously described [8].

CAUTION! The ester is a potent anticholinesterase agent and should be handled with care. Glassware was decontaminated with solutions of hypochlorite (bleach).

Physical measurements

The kinetics of hydrolysis of the phosphate triester to give diethyl phosphate were monitored spectrophotometrically at 400 nm (release of the 2,4-dinitrophenolate ion). Plots of ln $(A_\infty - A_t)$ vs time (A_∞ is the final absorbance and A_t the absorbance at time t) were linear for at least three half lives. The initial concentration of the triester employed in all the measurements was 8×10^{-5} mol dm^{-3}. Measurements were made at 35°C using an ionic strength of 0.1 mol dm^{-3} maintained using KNO_3. The kinetics were monitored using a Perkin–Elmer Lambda 5 spectrophotometer. Conductance measurements were made using 1×10^{-3} mol dm^{-3} aqueous solutions on an AGB 1000 conductivity meter and a dip-type cell with platinized electrodes. ^1H NMR spectra were determined at 300 MHz using TMS as reference in $CDCl_3$ solutions and NaTMS in D_2O solutions. Potentiometric titrations were carried out using a Radiometer Titralab system. Titrations were carried out at 35°C using KNO_3 to maintain the ionic strength at 0.1 mol dm^{-3}.

RESULTS AND DISCUSSION

Copper(II) forms a 1:1 complex with [9]aneN$_3$ ($\log K_{ML} = 16$) which is less thermodynamically stable than that of $[Cu(dien)]^{2+}$ ($\log K_{ML} = 18.0$) [9,10]. Formation constants of $[Ni([9]aneN_3)]^{2+}$ and $[Zn([9][aneN_3)]^{2+}$ ($\log K_{ML} = 16.2$ and 11.6 respectively) are substantially larger than those of $[Ni(dien)]^{2+}$ and $[Zn(dien)]^{2+}$ ($\log K_{ML} = 10.7$ and 8.9 respectively at 25°C) [10]. Normally macrocyclic copper(II) complexes form more thermodynamically stable complexes than those with analogous linear polyamines [9]. The anomalous behaviour with copper(II) has been attributed [9,10] to the steric constraints placed on copper(II) by the small triazamacrocycle. X-ray crystallography [3,4] has established that the complexes [Cu([9]aneN$_3$)X$_2$] (X = Cl, Br) have approximately square-pyramidal stereochemistry with an N_3X_2 donor set. The macrocyclic triamine is coordinated facially with N(2) and N(3) occupying equatorial sites and N(1) the apical site. The halide ligands occupy the two remaining equatorial positions.

In aqueous solution the complex [Cu([9]aneN$_3$)Cl$_2$] behaves as a 2:1 electrolyte with $\Lambda_M = 235$ S cm^2 mol^{-1} at 25°C due to displacement of the chloride ligands by water donors. In aqueous solution the complex has λ_{max} 656 nm ($\varepsilon = 47$ dm^3 mol^{-1} cm^{-1}) attri-

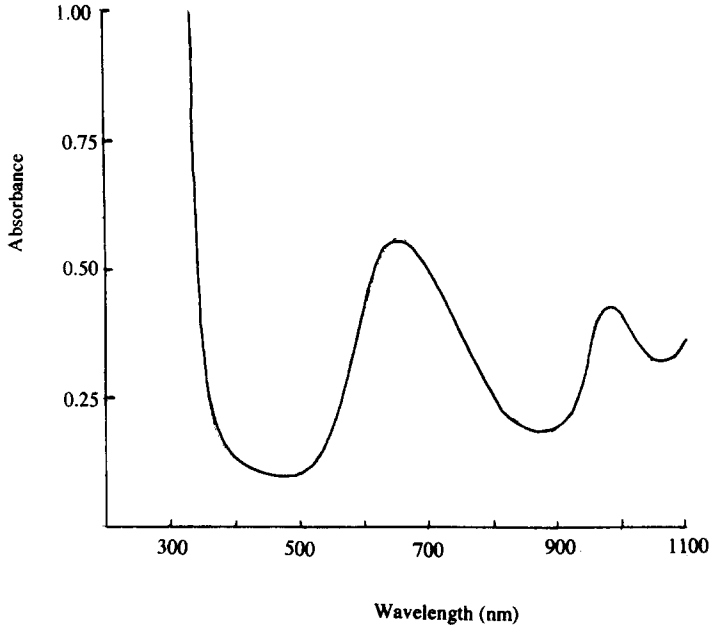

Fig. 1. The visible spectrum of $[Cu([9]aneN_3)Cl_2]$ in aqueous solution. The complex has $\varepsilon = 47$ dm^3 mol^{-1} cm^{-1} at 656 nm.

buted to the CuN_3O_2 chromophore (Fig. 1). The complex has a further band near 980 nm which is typically observed in square-pyramidal copper(II) complexes [14]. Potentiometric titration of an aqueous solution of the complex with sodium hydroxide gives a well defined end point after addition of one equivalent of base (Fig. 2), which can be attributed to the ionisation.

$$[Cu([9]aneN_3)(OH_2)_2]^{2+} \rightleftharpoons [Cu([9]aneN_3)(OH)(OH_2)]^{+} + H^{+}$$

The pK estimated from the potentiometric data is 7.5 at 35°C and $I = 0.10$ mol dm^{-3}. At pH values close to neutrality significant concentrations of the hydroxoaqua complex are present in solution. At higher pH formation of a dihydroxo-bridged dimer occurs and $[Cu[9]aneN_3)_2(OH)_2]$ has previously been characterised [15]. Formation of the dimer will be favoured by high metal complex concentrations.

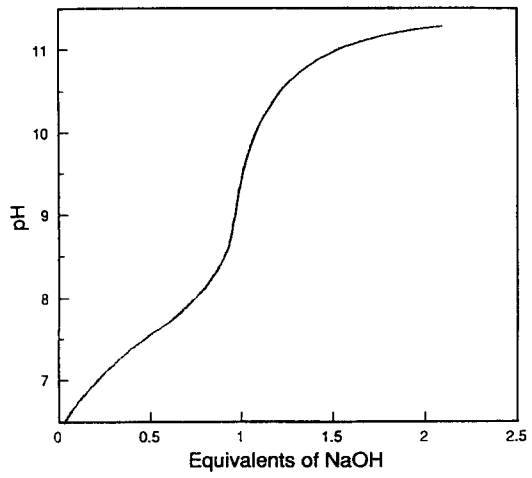

Fig. 2. Potentiometric titration of $[Cu([9]aneN_3)(OH_2)_2]^{2+}$ in aqueous solution at 35°C and $I = 0.1$ mol dm^{-3}.

Kinetic studies

In aqueous solution within the pH range 7–9 the hydrolysis of 2,4-dinitrophenyl diethyl phosphate to give diethyl phosphate and 2,4-dinitrophenoxide follows the rate expression [11]

$$k_{obs} = k_o + k_{OH}[OH^-] \quad (1)$$

where k_{obs} is the observed first order rate constant at constant pH, k_o represents the "spontaneous" water hydrolysis and k_{OH} is the second order rate constant for base hydrolysis. At 35°C and $I = 0.1$ mol dm^{-3}, $k_o = 2.26 \times 10^{-6}$ s^{-1} and $k_{OH} = 0.565$ dm^3 mol^{-1} s^{-1}. Using an activity coefficient of 0.768 calculated from the Davies' equation [12] and $pK_w = 13.712$ [13] in conjunction with eqn (1) the values of k_{obs} for the uncatalysed reaction are 2.40×10^{-6} s^{-1} at pH 7.0 and 3.69×10^{-6} s^{-1} at pH 8.

Catalysis of the reaction by $[Cu([9]aneN_3)(OH_2)_2]^{2+}$ was studied using an ester concentration of 8×10^{-5} mol dm^{-3} with the metal complex in large excess (2.5×10^{-3} mol dm^{-3}). Hydrolysis of 2,4-dinitrophenyl diethyl phosphate is subject to buffer catalysis [11] and therefore the metal complex was used as

Table 1. pH-Rate profile for the $[Cu([9]aneN_3)(OH_2)]^{2+}$ catalysed hydrolysis of 2,4-dinitrophenyl diethyl phosphate at 35°C and $I = 0.1$ mol dm^{-3}

pH	$10^4 k_{obs}$ (s^{-1})	pH	$10^4 k_{obs}$ (s^{-1})
6.20	1.98	7.53	11.90
6.51	3.02	7.85	14.90
6.67	3.86	8.13	16.68
6.93	4.34	8.38	15.82
7.21	7.62	8.71	16.10

The concentration of the metal complex was 2.5×10^{-3} mol dm^{-3} and the concentration of the phosphate ester 8×10^{-5} mol dm^{-3}. The quoted rate constants are the average values of at least three kinetic runs. The reactions were monitored by following the release of 2,4-dinitrophenoxide at 400 nm.

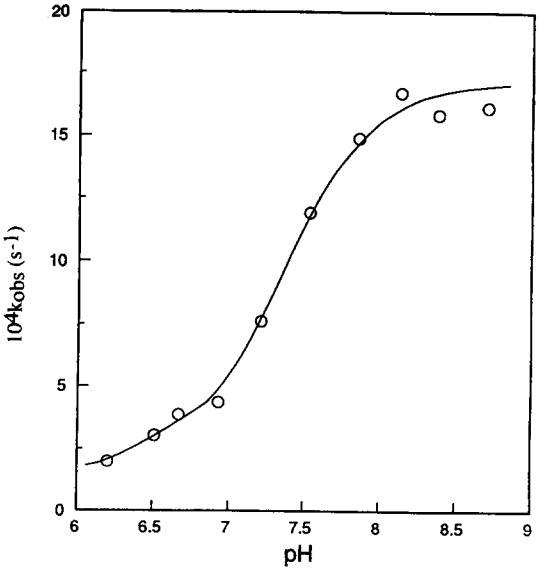

Fig. 3. pH-Rate profile for the $[Cu([9]aneN_3)(OH_2)_2]^{2+}$ catalysed hydrolysis of 2,4-dinitrophenyl diethyl phosphate at 35°C and $I = 0.1$ mol dm^{-3} (KNO_3). The total complex concentration was 2.5×10^{-3} mol dm^{-3} and the ester concentration 8×10^{-5} mol dm^{-3}.

the buffer. The pH was adjusted to the appropriate value by the dropwise addition of sodium hydroxide.

The pH-rate profile for the hydrolysis was studied over the pH range 6.20 to 8.71 (Table 1). Values of k_{obs} increase in a sigmoidal manner up to pH 8.5, Fig. 3, then begin to decline beyond pH 9.0. This behaviour is consistent with the hydroxoaqua complex being the active species in the hydrolysis. If α is the fraction of the total complex which is present as the hydroxoaqua species then values of k_{obs}/α should be constant if the hydroxoaqua complex is the active catalytic species. The results shown in Table 2 confirm that this is indeed the case. No evidence was obtained for saturation kinetics even with the metal complex in 50-fold excess over the substrate. The equilibrium constant K for the formation of the mixed ligand complex is therefore quite small.

$$[Cu([9]aneN_3)(OH_2)(OH)]^+ + O = P(OEt)_2OAr$$

$$\overset{K}{\rightleftharpoons} [Cu([9]aneN_3)(OH)(O = P(OEt)_2OAr)]^+$$

As the substitution reaction on copper(II) is rapid, formation of the mixed-ligand complex will be fast and the rate-determining step of the reaction is expected to be attack of coordinated hydroxide on the coordinated ester. However, the present results do not exclude the possibility of an intermolecular reaction involving attack of coordinated hydroxide on the free ester in solution. Recent studies [11] of the catalytic effects of a variety of bases and hydroxy complexes on the hydrolysis of 2,4-dinitrophenyl diethyl phosphate have shown that complexes such as $[Co(NH_3)_5OH]^{2+}$ lie on the Bronsted plot of $\log k_{cat}$ vs the pK_a of the conjugate acid, but that hydroxoaqua complexes such as $[Cu(tmen)(OH)(OH_2)]^+$ (tmen = *N,N,N′,N′*-tetramethylethylenediamine) are much more active than would be predicted from their pK_a. This result provides strong support for the occurrence of a cooperative type mechanism in such complexes in which attack of coordinated hydroxide occurs on the coordinated substrate which is also subject to Lewis acid catalysis by the metal ion.

Table 2. pH-Dependence as a function of α, the fraction of the metal complex ionised to the hydroxoaqua complex at 35°C and $I = 0.1$ mol dm^{-3}

pH	α	$10^4 k_{obs}$ (s^{-1})	$10^4 k_{obs}/\alpha$ (s^{-1})
6.93	0.21	4.34	20.5
7.21	0.34	7.62	22.4
7.53	0.52	11.90	22.8
7.85	0.69	14.90	21.6
8.13	0.81	16.68	20.6

α = the fraction of the total complex ionised to the hydroxoaqua complex calculated using a pK = 7.50.

One interesting feature of these reactions is that the diaqua complex also appears to exert a catalytic effect. Thus in the catalytic studies (Table 1) at pH 6.20, the value of $k_{obs} = 2 \times 10^{-4}$ s^{-1}. This pH is some 1.3 pH units lower than the pK_a of the complex. Other experiments established that free copper(II) and the ligand alone do not catalyse the reaction. At pH 6.20, k_{obs} for the uncatalysed reaction can be estimated from eqn (1) to be about 2.3×10^{-6} s^{-1} so that the rate enhancement is about 100-fold in the presence of the diaqua complex.

Experiments were also carried out to see if the reac-

Table 3. Relative catalytic effects of copper(II) complexes on the hydrolysis of 2,4-dinitrophenyl diethyl phosphate at 34°C and $I = 0.1$ mol dm^{-3} (KNO_3)

Copper complex	pH	k_{obs} (s^{-1})	$t_{1/2}$ (min)
$[Cu(tmen)(OH_2)_2]^{2+}$	7.0	4.48×10^{-3}	2.6
$[Cu(trimen)(OH_2)]^{2+}$	7.0	1.88×10^{-3}	6.1
$[Cu(dpa)(OH_2)_2]^{2+}$	7.0	9.21×10^{-3}	1.2
$[Cu(imid)_2(OH_2)_2]^{2+}$	7.0	4.89×10^{-4}	23.6
$[Cu(bipy)_2(OH_2)_2]^{2+}$	7.0	1.51×10^{-4}	76.5
$[Cu([9]aneN_3(OH_2)_2]^{2+}$	7.0	3.36×10^{-4}	34.4
$[Cu(glygly\text{-}2H)(OH_2)_2]^{2+}$	8.5	5.51×10^{-5}	209.6
Control	7.0	1.55×10^{-7}	52 days

The ester concentration employed in the measurements was 8×10^{-5} mol dm^{-3} and the catalyst concentration 2.5×10^{-3} mol dm^{-3}.

tion was truly catalytic and exhibited turnover. Turnover experiments were carried out at 25°C by pH-stat methods using a complex concentration of 5×10^{-5} mol dm^{-3} and an ester concentration of 7.5×10^{-4} mol dm^{-3} (15-fold excess of the ester). The release of H^+ at pH 7.0 was monitored by the addition of 0.01 mol dm^{-3} sodium hydroxide solution. The reaction was truly catalytic in the presence of $[Cu[9]aneN_3(OH_2)_2]^{2+}$ with 2.2 turnovers h^{-1}. This contrasts with a turnover rate of 20.6 turnovers h^{-1} by the complex $[Cu(tmen)(OH_2)_2]^{2+}$ and 31.2 turnovers h^{-1} by $[Cu(dpa)(OH_2)_2]^{2+}$ (dpa = 2,2′-dipyridylamine). The latter complex is a remarkably effective catalyst for the hydrolysis of the phosphotriester.

The high catalytic activity of a variety of copper(II) hydroxoaqua complexes (Table 3) (see Scheme 1 for structures) suggests that a bifunctional type of mechanism operates. For example, in the case of $[Cu([9]aneN_3)(OH_2)]^{2+}$ the value of $k_{cat}/\alpha = 21.6$ dm^3 mol^{-1} s^{-1} is nearly 40 times greater than k_{OH} (0.58 dm^3 mol^{-1} s^{-1}) at 35°C. Since the hydroxide ion is more than 10^6 stronger as a base than $[Cu([9]aneN_3)(OH_2)_2]^{2+}$ ($pK = 7.50$) this effectively excludes the copper complex acting as a general base catalyst. Lewis acid catalysis alone involving attack by "external" hydroxide on the coordinated ester does not account for the high catalytic activity observed. The effectiveness of the purely Lewis acid mechanism can be gauged by the fact that the base hydrolysis of trimethyl phosphate in the iridium(III) complex (**4**) is only accelerated by some 400-fold [16]. The hydrolysis of 4-nitrophenyl phosphate in the cobalt(III) complex

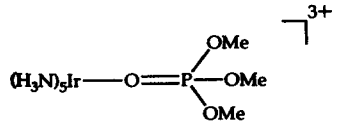

(4)

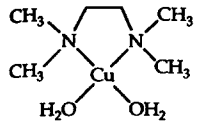

$[Cu(tmen)(OH_2)_2]^{2+}$

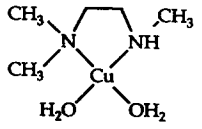

$[Cu(trimen)(OH_2)_2]^{2+}$

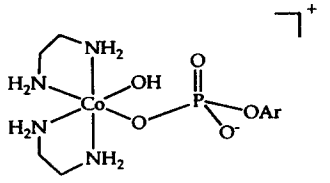

(5)

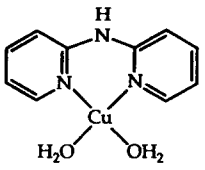

$[Cu(dpa)(OH_2)_2]^{2+}$

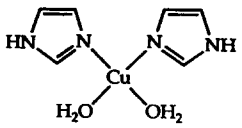

$[Cu(imid)_2(OH_2)_2]^{2+}$

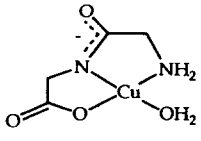

$[Cu(glygly\text{-}2H)(OH_2)]^{2+}$

Scheme 1.

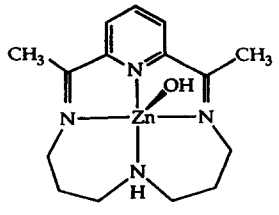

(6)

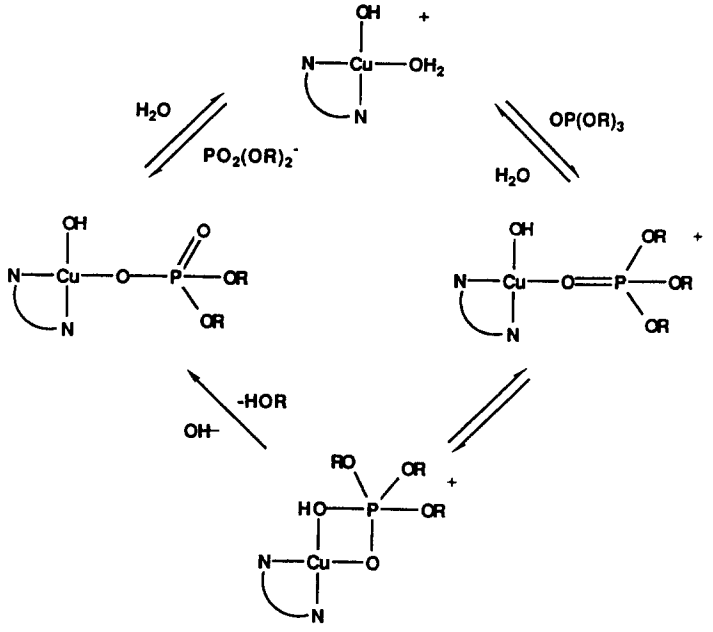

Scheme 2.

(**5**) has been shown to occur by intramolecular attack of coordinated hydroxide at phosphorus to give initially a five-coordinate phosphorane, which then decays to give $[Co(en)_2PO_4]$ containing bidentate phosphate and 4-nitrophenol [17]. The present results are similar to those of Breslow *et al.* [18] on the $[Zn(CR)OH]^+$ (**6**) catalysed hydrolysis of 2,4-dinitrophenyl diphenyl phosphate and of Morrow and Trogler [19] on the $[Cu(bipy)(OH)(OH_2)]^+$ catalysed hydrolysis of 4-nitrophenyl diethyl phosphate. All these reactions appear to involve intramolecular attack of coordinated hydroxide on the metal bound ester to give a phosphorane intermediate which then decays to products (Scheme 2). Such a "push–pull" type of mechanism, in which the metal ion polarises the P=O bond by its Lewis acid effect, and also delivers a coordinated hydroxide ion in an intramolecular reaction, accounts for the efficiency of the process.

REFERENCES

1. Burstyn, J. N. and Deal, K. A., *Inorg. Chem.*, 1993, **32,** 3585.
2. Hegg, E. L. and Burstyn, J. N., *J. Am. Chem. Soc.*, 1995, **117,** 7015.
3. Schwindinger, W. F., Fawcett, T. G., Lalancette, R. A., Potenza, J. A. and Schugar, H. J., *Inorg. Chem.*, 1980, **19,** 1379.
4. Bereman, R. D., Churchill, M. R., Schaber, P. M. and Winkler, M. E., *Inorg Chem.*, 1979, **18,** 3122.
5. See for example, Collman, J. P. and Buckingham, D. A., *J. Am. Chem. Soc.*, 1963, **85,** 3039; Buckingham, D. A., Collman, J. P., Happer, D. A. R. and Marzilli, L. G., *J. Am. Chem. Soc.*, 1967, **89,** 1082. For a review see Hay, R. W. in "*Reactions of Coordinated Ligands*", Vol 2 ed. Braterman, P. S., Plenum Press, 1989.
6. For a review see Chin, J., *Acc. Chem. Res.*, 1991, **24,** 145. See for example, Chin, J. and Zou, X., *J. Am. Chem. Soc.*, 1988, **110,** 223; Morrow, J. R. and Trogler, W. C., *Inorg. Chem.*, 1988, **27,** 3387.
7. Hay, R. W. and Norman, P. R., *J. Chem. Soc., Dalton Trans.*, 1979, 1441.
8. Hay, R. W. and Govan, N., *Polyhedron*, submitted for publication.
9. Kodama, M. and Kimura, E., *J. Chem. Soc., Dalton Trans.*, 1977, 1473 and references cited.
10. Yang, R. and Zompa, L. J., *Inorg. Chem.*, 1976, **15,** 1499.
11. Hay, R. W. and Govan, N., *Polyhedron*, 1996, **15,** 2381.
12. Davies, C. W., *J. Chem. Soc.*, 1938, 2093.
13. Harned, H. S. and Robinson, R. A., *Trans. Faraday Soc.*, 1940, **36,** 973.
14. Hathaway, B. J. and Billing, D. E., *Coord. Chem. Rev.*, 1970, **5,** 143.
15. Chaudhuri, P., Ventur, D., Weighhardt, K., Peters, E. M., Peters, K. and Simon, A., *Angew. Chem. Int. Ed. Engl.*, 1985, **24,** 57.
16. Hendry, P. and Sargeson, A. M., *J. Chem. Soc., Chem. Commun.*, 1982, 164.
17. Jones, D. R., Lindoy, L. F. and Sargeson, A. M., *J. Am. Chem. Soc.*, 1983, **105,** 7327.
18. Gellman, S. H., Petter, R. and Breslow, R., *J. Am. Chem. Soc.*, 1986, **108,** 2388.
19. Morrow, J. and Trogler, W. C., *Inorg. Chem.*, 1989, **28,** 2330.

Pergamon

PII: 80277-5387(97)00370-7

Polyhedron Vol. 17, No. 4, pp. 469–473, 1998
© 1998 Elsevier Science Ltd
All rights reserved. Printed in Great Britain
0277-5387/98 $19.00+0.00

The chemical reactivity of fullerene C_{60} towards *fac*-$Mo(CO)_3$(MeCN)(dppe) and $Mo(CO)_4$(dppe). Synthesis, characterization and reactions of the novel fullerene molybdenum derivative *fac*-$Mo(CO)_3$(dppe)(η^2-C_{60})

Li-Cheng Song,* Ying-Huai Zhu and Qing-Mei Hu

Department of Chemistry, Nankai University, Tianjin 300071, P.R. China

(Received 15 July 1997; accepted 20 August 1997)

Abstract—The acetonitrile ligand of *fac*-$Mo(CO)_3$(MeCN)(dppe)[dppe = bis-(1,2-diphenylphosphino)ethane] can be easily replaced by fullerene C_{60} in chlorobenzene at about 80°C to give exclusively *fac*-$Mo(CO)_3$(dppe)(η^2-C_{60}), whereas fullerene C_{60} reacted with $Mo(CO)_4$(dppe) in refluxing chlorobenzene to afford an isomeric mixture of *fac*- and *mer*-$Mo(CO)_3$(dppe)(η^2-C_{60}). These organomolybdenum C_{60} derivatives were characterized by elemental analysis and spectroscopic techniques. In addition, the η^2-C_{60} ligand in *fac*-$Mo(CO)_3$(dppe)(η^2-C_{60}) was also found to be easily displaced by MeCN, PPh_3 or pyridine to give corresponding *fac*-organomolybdenum complexes. © 1998 Elsevier Science Ltd. All rights reserved

Keywords: fullerene C_{60}; $Mo(CO)_3$(MeCN)(dppe); $Mo(CO)_4$(dppe); ligand substitution; synthesis; characterization.

Although C_{60} derivatives of group 8 to group 10 transition metals have been extensively studied [1–8], little is known about those of group 6 metals [9–11]. So far, structurally characterized organotransition metal C_{60} derivatives may fall into two categories: (1) fullerene core directly bonded to transition metals, such as (η^2-C_{60})M(PPh_3)$_2$(M = Pd, Pt) [1], (C_{60}){Pt(PEt_3)$_2$}$_6$ [2], (η^2-C_{60})Ni(PEt_3)$_2$ [3], (η^2-C_{60})IrCl(CO)(PPh_3)$_2$ [4], (η^2-C_{60})RhH(CO)(PPh_3)$_2$ [5], (η^2-C_{60})Os_3(CO)$_{10}$(PPh_3) [6], (C_{60})Ru_2(μ-Cl)$_2$$Cp^*_2$ [7], (η^2-C_{60})Fe(CO)$_4$ [8], (C_{60})[W(CO)$_3$(dppe)]$_n$(n = 1,2) [9a], [Mo(CO)$_3$(DDH)]$_2$$C_{60}$ · 2.5C_6H_6 (DDH = diacetyldihydrazone, H_2NN = C(Me) C(Me) = NNH_2) [10]; and *fac*/*mer*-W(CO)$_3$(dppb)(η^2-C_{60}) [11]; (2) fullerene core indirectly bonded to transition metals, such as (η^2-C_{60})[S_2Fe_2(CO)$_6$] [12] and (η^2-C_{60})[*o*-$(CH_2)_2C_5H_3$-η^5]Co(η^4-C_4Ph_4) [13]. In order to further develop the organometallic chemistry of group 6 metals' fullerene derivatives, we undertook this study. Herein we report the synthesis and structural characterization of fullerene molybdenum derivatives *fac*-$Mo(CO)_3$(dppe)(η^2-C_{60}) and *fac*/*mer*-$Mo(CO)_3$(dppe)(η^2-C_{60}), as well as η^2-C_{60} substitution reactions of *fac*-$Mo(CO)_3$(dppe)(η^2-C_{60}) with MeCN, Ph_3P and pyridine.

RESULTS AND DISCUSSION

We found that an equimolar amount of C_{60} reacted with *fac*-$Mo(CO)_3$(MeCN)(dppe) in chlorobenzene at about 80°C to give 84% of the product *fac*-$Mo(CO)_3$(dppe)(η^2-C_{60}) (Scheme 1).

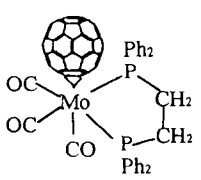

fac-isomer

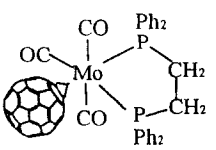

mer-isomer

Scheme 1.

* Author to whom correspondence should be addressed.

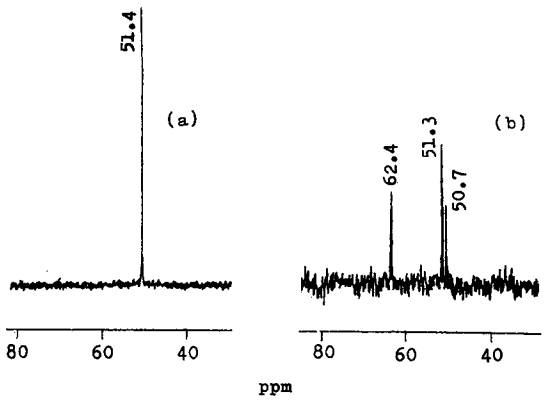

Fig. 1. (a) ^{31}P NMR spectrum of *fac*-Mo(CO)$_3$(dppe)(η^3-C$_{60}$), (b) ^{31}P NMR spectrum of *fac*- and *mer*-Mo(CO)$_3$(dppe)(η^2-C$_{60}$).

In principle, the product might exist as another isomer, i.e. *mer*-isomer or as a mixture of *fac*- and *mer*-isomers (Scheme 1). However, since its ^{31}P NMR spectrum (Fig. 1(a)) shows only one singlet at 51.4 ppm, the product should exist only as *fac*-isomer. This is because the *fac*-isomer has two P atoms in the same chemical environment and *mer*-isomer does not. The formation of only one isomer implies that the displacement of MeCN by C$_{60}$ took place completely with *fac*-configuration retention of the starting material.

The ^{1}H NMR spectrum of its ethylene group is also consistent with the *fac*-configuration of the product. It shows two kinds of resonances in an equal intensity, which were caused by two groups of hydrogen atoms: one at 2.60 ppm is on the same side of the equatorial plane (consisting of two equatorial CO, two P and two C of the ethylene group) as the C$_{60}$ cage, whereas the other at 2.40 ppm is on the opposite side of the plane as the C$_{60}$ cage. This assignment was made basically according to the electron-withdrawing effect of C$_{60}$ ligand.

In the ^{13}C NMR spectrum of the product, we observed 28 resonances in the fullerene sp^2-C area (133–152 ppm). This is actually in agreement with its Cs symmetry, although 32 peaks are theoretically expected for Cs symmetry. This is because the four carbon resonance peaks at 145.88, 142.85, 133.82 and 133.62 ppm each and have the intensity equivalent to two sp^2-C resonances [14].

In the IR spectrum of the product there are three absorption bands in the region 1880–1930 cm^{-1}, characteristic of the terminal carbonyls. The IR spectra of the product and its precursor determined in CH_2Cl_2 are shown in Fig. 2. In comparison with its precursor, the lowest ν_{CO} of the product shifts towards higher energy by about 72 cm^{-1}. Such an IR difference between them is obviously related to the stronger electron-withdrawing effect of C$_{60}$ ligand than MeCN ligand.

The UV spectrum of the product with that of free C$_{60}$ is shown in Fig. 3. As seen from Fig. 3 the first band at 280.7 nm for the product is much stronger than its second band at 350.5 nm, whereas the first band at 286.5 nm for free C$_{60}$ is smaller than its second band at 335.3 nm. This is probably due to the overlap of those two bands at around 280 nm, generated from C$_{60}$ ligand and the phenyl groups attached to P atoms in the product [15].

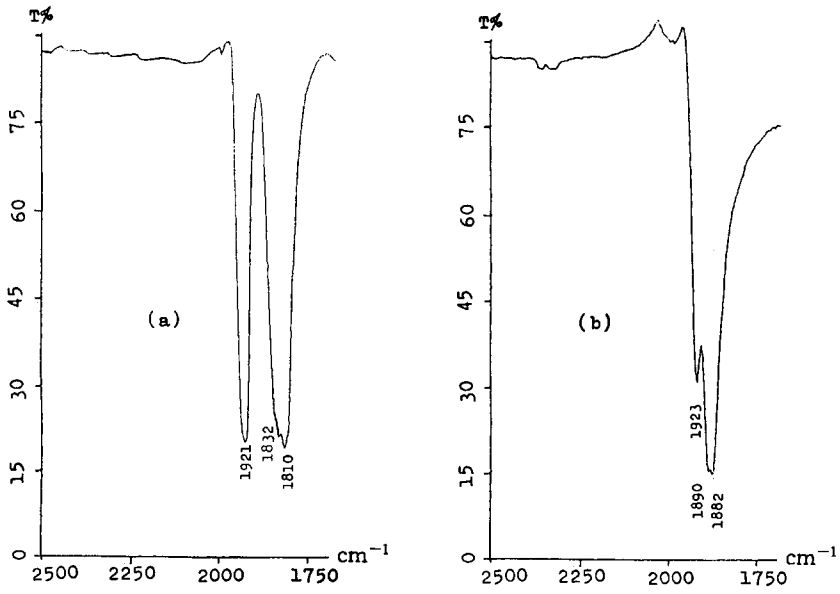

Fig. 2. (a) IR spectrum of *fac*-Mo(CO)$_3$(CH$_3$CN)(dppe), (b) IR spectrum of *fac*-Mo(CO)$_3$(dppe)(η^2-C$_{60}$).

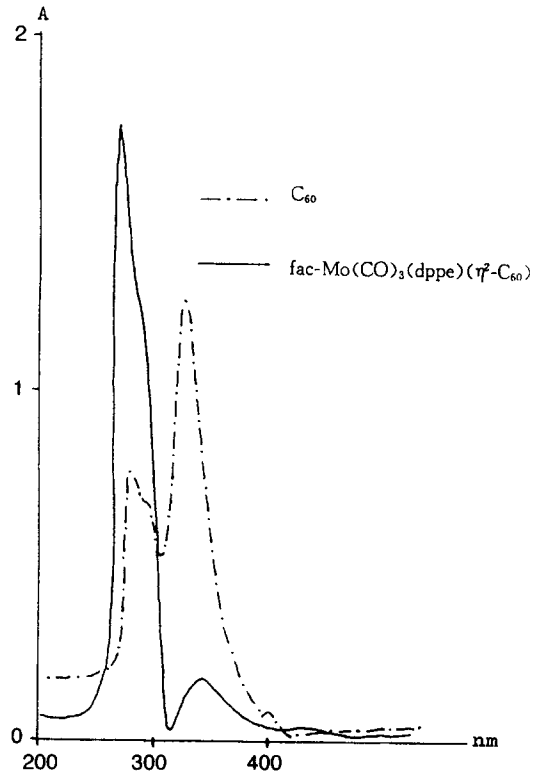

Fig. 3. UV-*vis* spectra of *fac*-Mo(CO)$_3$(dppe)(η^2-C_{60}) and C_{60} in toluene (1.85×10^{-5} M)

In addition, the C/H analysis for the product is satisfactory and its FD–MS spectrum displays a molecular ion peak at *m/z* 1296.

The product is somewhat air-sensitive, whose half-life of decomposition in CH_2Cl_2 is approximately 2.5 days. It is readily soluble in common organic solvents, for example, chlorobenzene, toluene, benzene, chloroform, dichloromethane and carbon disulphide, but it is hardly soluble in petroleum ether. Interestingly, the product *fac*-Mo(CO)$_3$(dppe)(η^2-C_{60}) can also take part in ligand displacement reactions. For example, addition of acetonitrile to a chlorobenzene solution of the product, followed by stirring the refluxing mixture for 6 h afforded 84% of *fac*-Mo(CO)$_3$(MeCN)(dppe) [16]; Similarly, the product reacted with pyridine or with PPh_3 in chlorobenzene to yield 91% of *fac*-Mo(CO)$_3$(dppe)(C_5H_5N) [17], and 85% of *fac*-Mo(CO)$_3$(PPh_3)(dppe) [17], respectively.

It is noteworthy that the thermal reaction of a slightly excessive Mo(CO)$_4$(dppe) with C_{60}, in contrast to that of Mo(CO)$_3$(MeCN)(dppe) with C_{60} mentioned above, gave a mixture of *fac*-Mo(CO)$_3$(dppe)(η^2-C_{60}) and *mer*-Mo(CO)$_3$(dppe)(η^2-C_{60}) in 43% yield. The two isomers are very close in polarity and thus could not be separated by conventional chromatography and recrystallization methods. Although the isomer mixture was claimed to be prepared by a photolytic procedure [9b], the thermal reaction procedure used here is much more convenient and produces the isomer mixture in higher yield. In addition, no detailed characterization data for the isomer mixture were given in the published paper [9b]. The ^{31}P NMR spectrum for this mixture (Fig. 1(b)) shows three signals, one at 51.3 ppm assigned to two identical P atoms of *fac*-isomer and two signals at 62.4 and 50.7 ppm in an equal intensity assigned to one P atom *cis* to C_{60} and the other P atom *trans* to C_{60} in *mer*-isomer respectively. The ^{1}H NMR spectrum for this mixture is similar to that of pure *fac*-isomer. However, the upfield broad singlet at 2.47 ppm is caused by *trans*-two hydrogens of CHCH in *fac*-isomer and two hydrogens of CH_2 attached to the *trans* P atom in *mer*-isomer, whereas the downfield singlet at 2.60 ppm is caused by *cis*- two hydrogens of CHCH in the *fac*-isomer and two hydrogens of CH_2 attached to the *cis* P atom in the *mer*-isomer due to the electron-withdrawing effect of the C_{60} ligand. While the IR spectrum of *fac*-isomer displays three terminal CO bands, that of this isomer mixture exhibits four bands within the terminal CO region. This is consistent with the observations that the number of IR active bands cannot exceed but may be less than the number of CO ligands in the complexes [18].

It follows that we have found a simple and convenient synthetic method for obtaining the single isomer *fac*-Mo(CO)$_3$(dppe)(η^2-C_{60}) in high yield. This method involves a ligand displacement reaction between C_{60} and *fac*-Mo(CO)$_3$(MeCN)(dppe) with *fac*-configuration retention of the starting material. We have also found that the thermal reaction between C_{60} and Mo(CO)$_4$(dppe) affords an isomer mixture of *fac*- and *mer*-Mo(CO)$_3$(dppe)(η^2-C_{60}) with more convenient manipulations and higher yield than the reported photolysis method [9b]. Finally, we have demonstrated that the η^2-C_{60} ligand in *fac*-Mo(CO)$_3$(dppe)(η^2-C_{60}) can also be displaced by MeCN, PPh_3 and C_5H_5N to give corresponding *fac*-organomolybdenum complexes in high yields.

EXPERIMENTAL

All reactions were carried out under a nitrogen atmosphere using standard Schlenk or vacuum-line techniques. Silica gel (10–40 μm) on TLC plates ($24 \times 16 \times 0.3$ cm) was activated for 3 h at 110°C, whereas silica gel (300–400 mesh) for column chromatography (15×2 cm) was activated for 1 h at 120°C. Toluene, THF, petroleum ether were dried and deoxygenated by distillation from sodium-/benzophenone ketyl. Chlorobenzene, MeCN and $CHCl_3$ were dried by distillation from P_2O_5. Pyridine and PPh_3 were chemical reagents used without further purification. Fullerene C_{60} was purchased from Yin-Han Fullerene High-Tech. Co. Ltd. *fac*-Mo(CO)$_3$(MeCN)(dppe) [16], dppe [19] and Mo(CO)$_4$(dppe) [20] were prepared according to the literature. The IR and UV-*vis* spectra were recorded on a Nicolet 170

SX FTIR spectrophotometer and a Shimadzu UV-240 spectrometer respectively, whereas the NMR spectra were determined on a Jeol FX qoQ or a Bruker AC-P 200 spectrometer. Elemental analysis and MS determinations were performed using a Yanaco CHN Corder MT-3 analyzer and a Zabspec spectrometer, respectively. Melting points were determined on a Yanaco MP-500 apparatus.

Reaction of fac-$Mo(CO)_3$(MeCN)(dppe) *with* C_{60} *and preparation of fac*-$Mo(CO)_3$(dppe)(η^2-C_{60})

A 100 cm^3 two-necked flask equipped with a magnetic stir-bar, a serum cap and a reflux condenser, was charged with 35 mg (0.056 mmol) of *fac*-$Mo(CO)_3$(MeCN)(dppe) and 40 cm^3 of chlorobenzene. To this solution was added 40 mg (0.056 mmol) of C_{60} in 40 cm^3 of chlorobenzene during about 2 h at room temperature. The reaction mixture was heated to about 80°C and then kept at this temperature for 6 h. After removal of the solvent under reduced pressure, the residue was purified by TLC (1:1 toluene: petroleum ether as eluent) to give 61 mg (84%) of *fac*-$Mo(CO)_3$(dppe)(η^2-C_{60}) as a dark green solid. m.p. 125–127°C. Found: C, 82.43; H, 2.21. Calc. for $C_{89}H_{24}MoO_3P_2$: C, 82.29; H, 1.85%, IR(CH_2Cl_2): $\nu_{C\equiv O}$, 1923 (s), 1890 (vs), 1882 (vs) cm^{-1}; ν_{C60} 1432 (m), 1182 (w), 588 (m), 518 (m) cm^{-1}. ^1H NMR ($CDCl_3$, TMS, 90 MHz): 2.40 (br. s, *trans*-CHCH), 2.60 (br.s, *cis*-CHCH), 7.20–7.60 (m, $4C_6H_5$) ppm. ^{31}P NMR ($CDCl_3$, H_3PO_4, 80.9 MHz): 51.4 ppm. ^{13}C NMR ($CDCl_3$, TMS, 50.3 MHz): 217.99, 210.63 (s, s, CO); 151.82, 151.59, 150.84, 150.76, 148.06, 147.94, 147.65, 147.29, 146.76, 146.59, 146.24, 146.04, 145.88 (2C), 145.18, 144.71, 144.67, 144.35, 143.47, 143.24, 142.85 (2C), 141.60, 135.70, 134.90, 134.63, 134.09, 133.82 (2C), 133.62 (2C), 133.38 (s, 28 resonances for C_{60}); 138.00, 137.39, 132.45, 132.20 (4 resonances for C_6H_5); 132.20, 130.51, 129.49, 129.30 (4 resonances for C_6H_5) ppm; 29.22, 28.14 (s, s, $2CH_2$) ppm. UV-*vis*(toluene, 1.85×10^{-5} M): λ_{max}(log ε) 280.7 (5.13), 350.5 (4.17), 433.3 (3.43), 537.7 (3.21) nm. FD–MS *m/z* (^{94}Mo, ^{31}P): 1296 (M^+).

Reaction of fac-$Mo(CO)_3$(dppe)(η^2-C_{60}) *with* MeCN *and preparation of fac*-$Mo(CO)_3$(MeCN)(dppe)

The same flask was charged with 3 mg (2.31×10^{-3} mmol) of *fac*-$Mo(CO)_3$(dppe)(η^2-C_{60}), 10 cm^3 of chlorobenzene and 10 cm^3 of MeCN. The dark green solution was refluxed for 6 h to give a light green solution. The same workup as above gave 1.20 mg (84%) of *fac*-$Mo(CO)_3$(MeCN)(dppe) as a pale yellow solid, which was identified by comparison of its m.p. and ^1H NMR spectrum with an authentic sample [16].

Reaction of fac-$Mo(CO)_3$(dppe)(η^2-C_{60}) *with pyridine and preparation fac*-$Mo(CO)_3$(dppe)(C_5H_5N)

Similarly, from 6 mg (4.62×10^{-3} mmol) of *fac*-$Mo(CO)_3$(dppe)(η^2-C_{60}), 10 cm^3 of chlorobenzene and 0.38 cm^3 of pyridine, 2.8 mg (92%) of *fac*-$Mo(CO)_3$(dppe) (C_5H_5N) as a light yellow solid was obtained and identified by comparison of its m.p. and IR spectrum with an authentic sample [17].

Reaction of fac-$Mo(CO)_3$(dppe)(η^2-C_{60}) *with* PPh_3 *and preparation of fac-Mo*$(CO)_3$(PPh_3)(dppe)

Similarly, from 6 mg (4.62×10^{-3} mmol) of *fac*-$Mo(CO)_3$(dppe)(η^2-C_{60}), 10 cm^3 of chlorobenzene and 1.3 mg (4.96×10^{-3} mmol) of PPh_3, 3.3 mg (85%) of *fac*-$Mo(CO)_3$ (dppe)PPh_3 as a light yellow solid was obtained and identified by comparison of its m.p. and IR spectrum with those of an authentic sample [17].

Reaction of $Mo(CO)_4$(dppe) *with* C_{60} *and preparation of a mixture of fac- and mer*-$Mo(CO)_3$(dppe)(η^2-C_{60})

The same flask charged with 40 mg (0.066 mmol) of $Mo(CO)_4$(dppe), 36 mg (0.05 mmol) of C_{60} and 50 cm^3 of chlorobenzene. The reaction mixture was refluxed for 12 h. Removal of the solvent gave a residue which was subjected to column chromatography using toluene as eluent. The green band was collected to give 28 mg (43%) of an isomer mixture of *fac*- and *mer*-$Mo(CO)_3$(dppe)(η^2-C_{60}) as a dark green solid. m.p. 120–128°C. Found: C, 82.30; H, 2.20. Calc. for $C_{89}H_{24}MoO_3P_2$: C, 82.29; H, 1.85% IR(CH_2Cl_2): $\nu_{C\equiv O}$, 1923 (s), 1891 (vs), 1880 (vs), 1856 (m) cm^{-1}; ν_{C60} 1429 (m), 1188 (w), 589 (m), 518 (m) cm^{-1}. ^1H NMR ($CDCl_3$, TMS, 90 MHz): 2.47 (br.s, *trans*-CHCH of *fac*-isomer and *trans*-CH_2 of *mer*-isomer, 2.60 (br.s, *cis*-CHCH of *fac*-isomer and *cis*-CH_2 of *mer*-isomer), 7.24–7.56 (m, $4C_6H_5$) ppm. ^{31}P NMR ($CDCl_3$, H_3PO_4 80.9 MHz): 62.4, 51.3, 50.7 ppm.

Acknowledgements—We are grateful to the National Natural Science Foundation of China and the Special Foundation of State Education Committee of China for financial support of this project.

REFERENCES

1. Fagan, P. J., Calabrese, J. C. and Malone, B., *Science*, 1991, **252,** 1160.
2. Fagan, P. J., Calabrese, J. C. and Malone, B., *J. Am. Chem. Soc.*, 1991, **113,** 9408.
3. Fagan, P. J., Calabrese, J. C. and Malone, B., *Acc. Chem. Res.*, 1992, **25,** 134.
4. Balch, A. L., Catalano, V. J. and Lee, J. W., *Inorg. Chem.*, 1991, **30,** 3980.
5. Balch, A. L., Lee, J. W., Noll, B. C. and Olmstead, M. M., *Inorg. Chem.*, 1993, **32,** 3577.
6. Park, J. T., Cho, J.-J. and Song, H.-J., *J. Chem. Soc., Chem. Commun.*, 1995, 15.
7. Mavunkal, I. J., Chi, Y., Peng, S.-M. and Lee, G.-H., *Organometallics*, 1995, **14,** 4454.
8. Douthwaite, R. E., Green, M. L. H., Stephens, A. H. H. and Turner, J. F. C., *J. Chem. Soc., Chem. commun.*, 1993, 1522.

9. (a) Shapley, J. R., Du, Y., Hsu, H.-F. and Way, J. J., *Proc-Electrochem. Soc.*, 1994, **94–24,** 1255. (b) Hsu, H.-F. and Shapley, J. R., *Proc-Electrochem. Soc.*, 1995, **95–10,** 1087.
10. Iglesias, M. and Santos, A., *Inorg. Chim. Acta*, 1996, **248,** 67.
11. Song, L.-C., Zhu, Y.-H. and Hu, Q.-M., *Polyhedron*, 1997, **16,** 2141.
12. Westmeyer, M. D., Galloway, C. P. and Rauchfuss, T. B., *Inorg. Chem.*, 1994, **33,** 4615.
13. Iyoda, M., Sultana, F., Sasaki, S. and Butenschön, *Tetrahedron Lett.*, 1995, **36,** 579.
14. Miles, W. H. and Smiley, P. M., *J. Org. Chem.*, 1996, **61,** 2559.
15. Dyer, J. R., *Applications of Absorption Spectroscopy of Organic Compounds*, p. 18, Prentice-Hall, Inc., London, 1965.
16. Kubas, G. J., Jarvinen, G. D. and Ryan, R. R., *J. Am. Chem. Soc.*, 1983, **105,** 1883.
17. Asali, K. J., Van Zyl, G. J. and Dobson, G. R., *Inorg. Chem.*, 1988, **27,** 3314.
18. Collman, J. P., Hegedus, L. S., *Principles and Applications of Organotransition Metal Chemistry*, p. 86, University Science Books, Mill Valley, California, 1980.
19. Chatt, J. and Hart, F. A., *J. Chem. Soc.*, 1960, 1378.
20. Grim, S. O., Briggs, W. L., Barth, R. C., Tolman, C. A. and Jesson, J. P., *Inorg. Chem.*, 1974, **13,** 1095.

Pergamon

PII: S0277-5387(97)00357-4

Polyhedron Vol. 17, No. 4, pp. 475–482, 1998
© 1998 Elsevier Science Ltd
All rights reserved. Printed in Great Britain
0277-5387/98 $19.00+0.00

The reactivity of neutral nitrogen donors in planar d_8 metal complexes. Part 3. The system chloro(2,2′:6′,2″-terpyridine)platinum(II) cation with pyridines and ammonia in methanol. Effect of basicity, π-acceptor capacity and steric hindrance

Bruno Pitteri,* Giampaolo Marangoni, Fabiano Visentin Viseutim, Lucio Cattalini and Tatiana Bobbo

Dipartimento di Chimica, Univeristà Cà Foscari di Venezia, Calle Larga S. Marta 2137, 30123–Venezia, Italy

(Received 30 July 1997; accepted 15 August 1997)

Abstract—The kinetics of the forward and reverse steps of the process $[Pt(NNN)Cl]^+ + am \rightleftharpoons [Pt(NNN)(am)]^{2+} + Cl^-$ (NNN = 2,2′:6′,2″-terpyridine; am = one of a number of pyridines and NH_3 covering a wide range of basicity) have been studied in methanol at 25°C. Both forward and reverse reactions obey the usual two-term rate law observed in square-planar substitution. The reactivity and the ability of the chloro-complex to discriminate among the nucleophiles, as well as the sensitivity of the rate of the chloro entry upon the nature of the displaced base and the steric factors in both the forward and reverse processes are discussed in terms of intimate mechanism and compared with data for a number of different Pt^{II} systems. The equilibrium constants for the reactions have been determined from the ratio of the rate constants. © 1998 Elsevier Science Ltd. All rights reserved

Keywords: nitrogen donors; pyridine; ammonia.

In a recent study of nucleophilicity and lability of neutral nitrogen donor bases towards planar tetracoordinate complexes and the relationships between reactivity and proton basicity, we reported kinetic and equilibrium data concerning the reversible displacement of am (am = a number of pyridines and some heterocyclic and aromatic amines) by chloride from the mono-cationic [1] $[Pt(SS)(am)Cl]^+$ and bis-cationic [2] $[Pt(SNS)(am)]^{2+}$ and [3] $[Pt(NSN)(am)]^{2+}$ complexes [SS = 1,2-bis(phenylsulfanyl) ethane; SNS = 2,6-bis(methylsulfanylmethyl)pyridine; NSN = bis(2-pyridylmethyl) sulphide] in MeOH at 25°C. The results were discussed in terms of intimate mechanism and bonding interactions in the ground and transition states.

In order to extend the experimental observations and the range of applicability of the proposed interpretation, we have now examined the system involving the tridentate aromatic nitrogen donor 2,2′:6′,2″-terpyridine (NNN) on measuring the rate of the processes

$$[Pt(NNN)Cl]^+ + am \rightarrow [Pt(NNN)am]^{2+} + Cl^- \quad (1)$$

(am = pyridines and ammonia) as well as those of the reverse reactions

$$[Pt(NNN)(am)]^{2+} + Cl^- \rightarrow [Pt(NNN)Cl]^+ + am \quad (2)$$

in methanol at 25°C. The results are herewith presented and discussed.

* Author to whom correspondence should be addressed.

EXPERIMENTAL

Materials

Platinum(II) chloride, $PtCl_2$, was obtained from Acros Chimica and 2,2′:6′,2″-terpyridine from Aldrich Chimica. Pure reagent-grade CH_3SO_3Na, $AgClO_4$, $LiClO_4$ (Fluka and Aldrich) were dried over P_2O_5 in a vacuum desiccator and used without further purification. Pyridines were recrystallized or distilled before use when necessary. CH_3OH (less than 0.1% water) and dimethylformamide (dmf) were pure reagent-grade products (Baker and BDH).

Instruments

Infrared spectra (4000–500 cm^{-1}, KBr discs; 600–50 cm^{-1}, polyethylene pellets) were recorded on a Nicolet Magna FT IR 750 spectrometer. Electronic spectra and kinetic measurements were obtained on a Perkin-Elmer Lambda 16 spectrophotometer. Proton NMR spectra were taken on a Bruker AC 200 F spectrometer. Conductivity measurements were carried out with a CDM 83 Radiometer Copenhagen conductivity meter and a CDC 334 immersion cell. Elemental analysis were performed by the Microanalytical Laboratory of the University of Padua.

Preparation of complexes

$[Pt(NNN)Cl](ClO_4)$ was prepared as reported in the literature [4].

All the complexes $[Pt(NNN)(am)](ClO_4)_2$ (am = pyridine, 3-methylpyridine, 4-methylpyridine, 4-cyanopyridine, 4-aminopyridine, 4-acetylpyridine, methylisonicotinate, 2-methylpyridine, 2,4-dimethylpyridine, ammonia) were prepared as follows. $AgClO_4$ (0.207 g, 1 mmol) was added to a warm solution (20 ml, 60°C) of $[Pt(NNN)Cl](ClO_4)$ (0.563 g, 1 mmol) in dmf and the mixture was stirred in the dark for 15 min. The AgCl formed was filtered off and, after addition of methanol (10 ml) and an excess of $LiClO_4$ (0.5 g), the solution was treated with 1 mmol of am and stirred at 60–70°C for 10 min. After cooling at room temperature, the microcrystalline product precipitated was filtered off, washed with methanol, diethyl ether and dried *in vacuo*. Yield: 70–90%.

Attempts to prepare analogous complexes with

Table 1. Analytical and physical data for the complexes

Complex	Analysis[a] (%) C	H	N	Cl	Colour	UV-VIS λmax[b]/nm (ε/dm^3 mol^{-1} cm^{-1})	Λ_m[c] (Ω^{-1} cm^2 mol^{-1})
$[Pt(NNN)Cl]Cl_4$[d]	32.1	2.1	7.3	12.3	Red-orange	332 (16,600)	73
	(32.0)	(2.0)	(7.5)	(12.6)		319 (12,100)	
$[Pt(NNN)(4\text{-}CNpy)](ClO_4)_2$	34.7	2.1	9.5	9.7	Yellow	339 (18,400)	154
	(34.5)	(2.1)	(9.6)	(9.7)		325 (11,200)	
$[Pt(NNN)(4\text{-}COOCH_3py)](ClO_4)_2$	34.4	2.4	7.1	9.4	Pale yellow	339 (18,400)	151
	(34.6)	(2.4)	(7.3)	(9.3)		325 (11,200)	
$[Pt(NNN)(4\text{-}COCH_3py)](ClO_4)_2$	35.0	2.4	7.2	9.4	Pale yellow	339 (18,400)	141
	(35.3)	(2.4)	(7.5)	(9.5)		325 (11,200)	
$[Pt(NNN)(py)](ClO_4)_2$	34.2	2.2	7.8	10.1	Cream	339 (19,500)	145
	(34.0)	(2.3)	(7.0)	(10.0)		325 (12,400)	
$[Pt(NNN)(4\text{-}Mepy)](ClO_4)_2$	34.7	2.6	7.7	10.0	Cream	340 (19,500)	147
	(35.0)	(2.5)	(7.8)	(9.8)		326 (12,400)	
$[Pt(NNN)(3\text{-}Mepy)](ClO_4)_2$	35.1	2.5	7.8	9.9	Pale yellow	342 (19,500)	141
	(35.0)	(2.5)	(7.8)	(9.8)		326 (12,400)	
$[Pt(NNN)(4\text{-}NH_2py)](ClO_4)_2$	33.2	2.6	9.6	9.8	Orange	339 (14,200)	146
	(33.3)	(2.4)	(9.7)	(9.8)		325 (11400)	
$[Pt(NNN)(2\text{-}Mepy)](ClO_4)_2$	35.1	2.6	7.6	9.8	Pale yellow	340 (19,500)	138
	(35.0)	(2.5)	(7.8)	(9.8)		326 (12,400)	
$[Pt(NNN)(2,4\text{-}Me_2py)](ClO_4)_2$	35.8	2.8	7.5	9.8	Pale yellow	340 (19,500)	145
	(36.0)	(2.7)	(7.6)	(9.7)		326 (12,400)	
$[Pt(NNN)(NH_3)](ClO_4)_2$	27.7	2.1	8.6	10.8	Cream	342 (20,000)	145
	(28.0)	(2.2)	(8.7)	(11.0)		326 (12,400)	

[a] Calculated values in parentheses

[b] In methanol

[c] In dimethylformamide

[d] ^1H NMR (δ 200 MHz, solvent dimethylformamide d [7], reference: solvent peak) 9.10 [2H, d, J = 4.7 Hz; H_a], 8.86–8.98 [5H, m, $H_{d,e,f}$], 8.78 [2H, t, d, J = 7.6 Hz, 1.5 Hz, H_c], 8.22 [≈2H, m, H_b] partially masked by solvent peak

am = aniline, morpholine, methylamine, and piperidine, under the same experimental conditions, always resulted in the formation of the hydroxo species $[Pt(NNN)OH](ClO_4)$.

Analytical and some physico-chemical data for the complexes are collected in Table 1. ^1H NMR data for $[Pt(NNN)Cl](ClO_4)$ are given according to the following scheme:

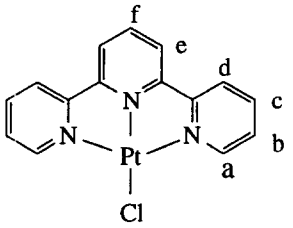

Scheme 1

Kinetics

The reactions were initiated by adding a 0.015 mol dm^{-3} dmf solution (2–10 μl) of the substrate complex. $[Pt(NNN)Cl](ClO_4)$ or $[Pt(NNN)(am)](ClO_4)_2$, to a methanolic solution (3 cm^3) of the appropriate reagent, the nitrogen base or chloride ion, respectively, previously brought to the reaction temperature (25°C) in a thermostated cell in the spectrophotometer. The concentration of the entering group was always large enough to provide pseudo-first-order conditions. After preliminary repetitive scan experiments in the range 260–360 nm to search for isosbestic points and spectral changes, the kinetics were studied by measuring the changing absorbance at suitable wavelengths as a function of time. Pseudo-first-order rate constants (k_{obs}, s^{-1}) were obtained either from the gradients of plots of $\log(D_t - D_\infty)$ vs time or from a non linear least-squares fit of experimental data to $D_t = D_\infty + (D_0 - D_\infty)\exp(-k_{obs}t)$ with D_0, D_∞, and k_{obs} as the parameters to be optimized (D_0 = absorbance after mixing of reactants, D_∞ = absorbance at completion of reaction). Rate constants were accurate within 5%.

RESULTS AND DISCUSSION

Kinetics of the displacement of chloride by am from $[Pt(NNN)Cl](ClO_4)$

The spectrum of the reaction mixtures evolves in all cases with time in a first order fashion and with well maintained isosbestic points, from that of the chloro substrate $[Pt(NNN)Cl]^+$ to that of an authentic sample of the substituted products $[Pt(NNN)(am)]^{2+}$ measured under the same experimental conditions, clearly indicating that the process studied is the displacement of the coordinated chloride by the nitrogen donor base. The observed rate constants, k_{obs}, collected in Table 2, obey the two-terms rate law $k_{obs} = k_1^f + k_2^f$ [am], typical of nucleophilic substitution at planar tetra-coordinate d^8 metal complexes [5] in which the k_1^f term refers to the solvolytic pathway involving the attack of the solvent as nucleophile, and k_2^f is the second-order rate constant for the direct attack of the nucleophile (am) at the substrate. The isosbestic points characteristic of the stage, the conditions of measurements, and the values of k_2^f, are all summarized in Table 3.

The k_1^f term, obtained as intercepts of the plots of k_{obs} vs am concentrations, is small and contribute little to the observed rates except at the lowest nucleophile concentrations. It may however be observed that on using a strong base, such as piperidine, no second order contribution can be detected and the only reaction product is the inert hydroxo species $[Pt(NNN)OH]^+$. For the same reason, i.e. the dominance of the solvent pathway in the chloride substitution, the nucleophilic attack of nitrogen donors at this substrate cannot be studied in water [6].

The specific second-order rate constants k_2^f (Table 4) obey the linear free energy relationship $\log k_2^f = \alpha pK_a + \text{constant}$, with $\alpha = 0.24$ (Fig. 1), as far as the entry of the isosteric pyridine, 4-cyanopyridine, 4-methylpyridine, 4-aminopyridine, 4-acetylpyridine, methylisonicotinate, and 3-methylpyridine is concerned. Ammonia is slightly less reactive as compared to the above mentioned pyridines, and this fact may be due to small differences in the solvation of the ligands and/or to a small contribution of π interactions for the latter reagents. Values of α for a number of platinum(II) complexes,

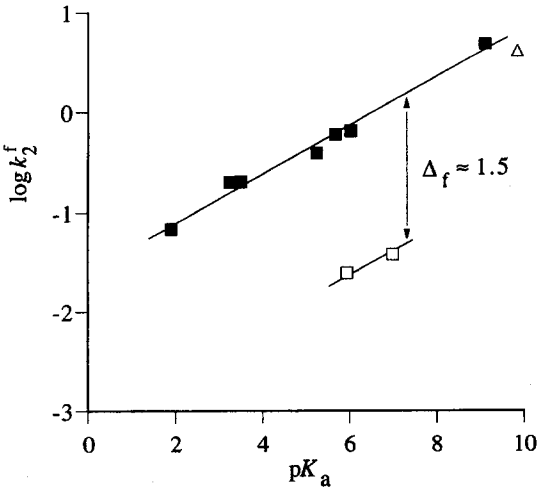

Fig. 1. $\log k_2^f$ for the reaction $[Pt(NNN)Cl]^+ + am \rightarrow [Pt(NNN)(am)]^{2+} + Cl^-$ plotted against pK_a of amH^+: ■, 4-cyanopyridine, 4-acetylpyridine, methylisonicotinate, pyridine, 4-methylpyridine, 3-methylpyridine, 4-aminopyridine; □, 2-methylpyridine and 2,4-dimethylpyridine; △, ammonia.

Table 2. First-order rate constants, k_{obs},[a] for the reaction $[Pt(NNN)Cl]^+ + am \rightarrow [Pt(NNN)(am)]^{2+} + Cl^-$ in methanol at 25°C ($I = 0.1$ mol dm^{-3}, CH_3SO_3Na)

am	[am]/ mol dm^{-3}	$10^3 k_{obs}$/ s^{-1}	am	[am]/ mol dm^{-3}	$10^3 k_{obs}$/ s^{-1}
4-Aminopyridine	0.001	4.5	Methylisonicotinate	0.01	3.42
	0.002	9.1		0.03	8.34
	0.003	13.4		0.05	10.94
	0.005	23.6		0.07	17.01
	0.007	36.5		0.10	20.84
	0.010	47.5			
			3-Methylpyridine	0.005	3.53
4-Cyanopyridine	0.2	19.3		0.010	6.77
	0.4	35.9		0.020	11.99
	0.6	48.7		0.025	15.20
	0.8	60.7		0.030	18.53
	1.0	75.4		0.040	23.23
				0.050	30.57
Pyridine	0.01	5.6		0.100	60.29
	0.02	10.7			
	0.03	14.7	2-Methylpyridine	0.0103	0.51
	0.05	23.9		0.0206	0.77
	0.07	31.4		0.0412	1.23
	0.10	40.7		0.0618	1.73
				0.0824	2.36
4-Methylpyridine	0.01	7.83		0.1030	2.76
	0.03	20.7			
	0.05	34.2	2,4-Dimethylpyridine	0.01	0.87
	0.07	47.1		0.03	1.57
	0.10	66.6		0.05	2.51
				0.06	2.87
4-Acetylpyridine	0.02	6.16		0.07	3.20
	0.03	8.53		0.10	4.20
	0.05	12.8			
	0.07	15.9	Ammonia	0.0015	5.68
	0.10	22.7		0.0029	11.46
				0.0058	22.8
				0.0087	36.9
				0.0116	46.5

[a] Errors on individual k_{obs} determinations are in ±5% range

allowing a comparison among the various substrates, are collected in Table 5, in which also the values of Δ_f [7], the usual parameter for the steric retardation observed by using 2-methyl-pyridines as nucleophiles, are reported.

Kinetics of the displacement of am by chloride from $[Pt(NNN)(am)Cl](ClO_4)_2$

When the substrates $[Pt(NNN)(am)]^{2+}$ are allowed to react with excess chloride ion, the spectral changes, again showing a first order dependence upon time, are exactly the reverse of those observed in the forward processes and with the same isosbestic points, as obviously expected for the displacement of the coordinated neutral base (am) by excess chloride ion. The reactions were studied at constant ionic strength ($I = 0.1$ mol dm^{-3}, CH_3SO_3Na). The observed rate constants, k_{obs}, collected in Table 3, obey the general relationship $k_{obs} = k_1^r + k_2^r[Cl^-]$, where k_1^r and k_2^r have the usual meaning. The k_1^r values are small as compared to $k_2^r[Cl^-]$ and almost negligible in most cases. The k_2^r values at $I = 0.1$ mol dm^{-3} are reported in Table 4 together with the corresponding values of k_2^{0r} extrapolated to zero ionic strength.

As previously found [2,3] also in this case the rate of processes between the mono-cationic platinum(II) substrate and neutral nitrogen donors is not influenced upon primary salt effect, whereas the rate of the reverse reactions between the bis-cationic species and chloride ion depends upon ionic strength. The extrapolation to zero ionic strength uses the Debye–Huckel relationship, $\log k_2^{0r} = \log k_2^r - 2\alpha Z_a Z_b I^{1/2}/(1+\beta I^{1/2})$, with $Z_a = +2$, $Z_b = -1$, $\alpha = 1.90$, and $\beta = 1.55$ (estimated from the dielectric constant of methanol at

Table 3. First-order rate constants, k_{obs},[a] for the reaction $[Pt(NNN)(am)]^{2+} + Cl^- \rightarrow [Pt(NNN)Cl]^+ + am$ in methanol at 25°C (I = 0.1 mol dm^{-3}, CH_3SO_3Na)

am	$[Cl^-]$/ mol dm^{-3}	$10^3 k_{obs}$/ s^{-1}	am	$[Cl^-]$/ mol dm^{-3}	$10^3 k_{obs}$/ s^{-1}
4-Cyanopyridine	0.00005	9.99	3-Methylpyridine	0.0004	3.24
	0.00010	17.76		0.0008	6.03
	0.00015	24.29		0.0012	9.46
	0.00020	31.91		0.0016	13.12
	0.00025	37.48		0.0020	16.48
	0.00030	45.03			
			4-Aminopyridine	0.002	0.26
Methylisonicotinate	0.0002	8.48		0.005	0.71
	0.0004	18.31		0.010	1.34
	0.0006	23.52		0.020	2.49
	0.0008	38.02		0.030	3.53
	0.0012	48.62			
			2-Methylpyridine	0.002	1.28
4-Acethylpyridine	0.0002	5.8		0.004	2.49
	0.0004	11.01		0.006	3.61
	0.0006	16.38		0.008	4.94
	0.0008	20.99		0.010	6.06
	0.0012	32.26		0.012	7.03
	0.0016	45.04	2,4-Dimethylpyridine	0.0002	0.09
Pyridine	0.0002	2.49		0.0004	0.15
	0.0004	4.78		0.0006	0.22
	0.0006	6.20		0.0008	0.29
	0.0008	8.95		0.0012	0.42
	0.0012	12.27		0.0016	0.56
	0.0016	19.12			
			Ammonia	0.0002	0.22
4-Methylpyridine	0.0002	1.17		0.0004	0.37
	0.0004	2.44		0.0006	0.56
	0.0006	3.13		0.0008	0.69
	0.0008	4.39		0.0012	1.09
	0.0012	6.00		0.0016	1.32
	0.0016	8.89			

[a] Errors on individual k_{obs} determinations are in ±5% range

25°C) [8]. As a consequence, also the equilibrium constants K depend upon ionic strength and in Table 4 are reported the values $K = k_2^f/k_2^r$ and $K^0 = k_2^f/k_2^{0r}$ determined from the ratios of the second-order rate constants for the forward and reverse reactions.

As far as the dependence of the reactivity upon the basicity of the leaving nitrogen base is concerned, the plot of $\log k_2^r$ vs pK_a (Fig. 2) leads to the linear free energy relationship $\log k_2^r = -0.53pK_a + \text{constant}$ for the complexes with the unhindered pyridine, 3-methylpyridine, 4-methylpyridine and 4-amino-pyridine. The substrates containing as leaving groups the bases with a more extended aromatic π system (4-cyano-, 4-acetylpyridine and methylisonicotinate) show the same dependence upon proton basicity, but the reactivity is slightly decreased in accordance with previous results [2,3].

The reactivity of the hindered substrates containing 2-methyl- and 2,4-dimethyl-pyridine allows to estimate a steric retardation factor $\Delta_r \approx 0.82$ (Fig. 2 and Table 5).

Ammonia is considerably more labile than expected from its basicity, reasonably for the same reasons reported above for its slightly low nucleophilicity.

On considering the second order rate constants (corrected to zero ionic strength) for the displacement, under the same experimental conditions, of chloride from $[Pt(NNN)Cl]^+$ by bromide (k_2^0 = 51.9 dm^3 mol^{-1} s^{-1}, n_{Pt}^0 = 4.18) and iodide (k_2^0 = 1941 dm^3 mol^{-1} s^{-1}, n_{Pt}^0 = 5.46) available from the literature [4], it is possible to estimate the k_2^f value for the entry of pyridine (n_{Pt}^0 = 3.19) from the n_{Pt}^0 relationship $\log k_2 = s(n_{Pt}^0) + \text{constant}$ [9]. The calculated (0.44) and experimental (0.432) values are practically the same. This nice agreement could be, to some extent, surprising on considering that (i) the nucleophilic discrimination factor has been obtained from the reactivity of two nucleophiles only and is therefore

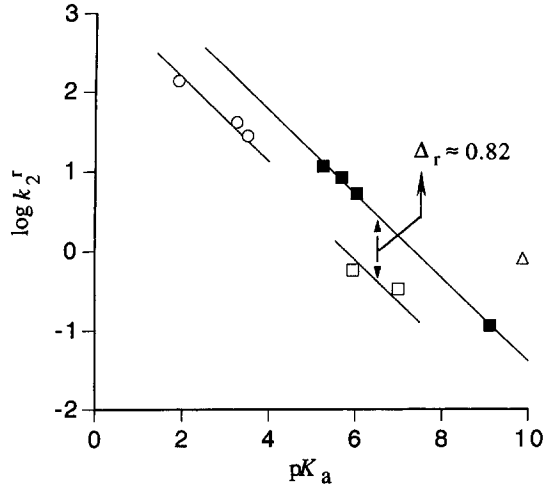

Fig. 2. $\log k_2^r$ for the reaction $[Pt(NNN)(am)]^{2+} + Cl^- \rightarrow [Pt(NNN)Cl]^+ + am$ plotted against pK_a of amH^+: ■, pyridine, 4-methylpyridine, 3-methylpyridine, 4-aminopyridine; ○, 4-acetylpyridine, methylisonicotinate, 4-cyanopyridine; □, 2-methylpyridine and 2,4-dimethylpyridine; △, ammonia.

affected by some error, (ii) the Debye–Huckel correction to zero ionic strength is approximate and (iii) the n_{Pt}^0 relationship is strictly obeyed only by neutral substrates reacting with purely σ donors. The difference in reactivity of pyridine towards the substrates $[Pt(NNN)Cl]^+$ ($k_2^f = 0.432$ dm^3 mol^{-1} s^{-1}), $[Pt(SNS)Cl]^+$ ($k_2^f = 0.0097$ dm^3 mol^{-1} s^{-1}) and $[Pt(SS)Cl_2]$ ($k_2^f = 0.283$ dm^3 mol^{-1} s^{-1}) can therefore be explained in terms of *trans*-labilizing effect and π interactions, as already reported in the study of the reactions of the same substrates with halide ions [4,10].

The parameter α_f (Table 5) is a measure of the ability of a substrate to discriminate among isosteric nitrogen donors and can be assumed to be a relative measure of its electrophilicity. This obviously implies that the intimate substitution mechanism must be the same for all the compared processes. The asynchronous substitution, characteristic of planar tetracoordinate platinum(II) complexes, offers the opportunity to describe as separated the energetic contributions of bond formation and bond rupture to the free energy of activation [11]. The relatively low discriminations among nitrogen donors (α_f, Table 5), together with the relatively high dependence of reactivity upon the basicity of the leaving nitrogen bases in the reverse processes (α_r, Table 5), strongly suggest a transition state for all these substitution in which the Pt—N bond is only partially formed in the rate determining transition state, whereas the Pt—Cl bond is practically formed to the same extent in the ground and transition states. This description is the same for all the substrates reported in Table 5.

At the same time, however, differences in electrophilicity emerge clearly on comparing the various substrates. It appears, as may be expected, that the electrophilicity increases among neutral substrates on moving from $[Pt(SS)Cl_2]$ [1] containing the aliphatic SS ligand, ($\alpha_f = 0.036$) to $[Pt(\alpha,\alpha'\text{-bipyridine})Cl_2]$ [12] ($\alpha_f = 0.06$) and [Pt(biacetylbis(N-methyl,N-phenyl)osazone)Cl_2] [13] ($\alpha_f = 0.05$), where the chelating ligands are capable of some π delocalization of negative charge during the nucleophilic attack. A further obvious increase of electrophilicity can be observed on moving from neutral to cationic species, and the presence of a very large π system in $[Pt(NNN)Cl]^+$ ($\alpha_f = 0.24$) leads to a discrimination larger than that observed with the substrate $[Pt(SNS)Cl]^+$ [2] ($\alpha_f = 0.15$).

On the contrary, the dependence of the reactivity upon the basicity of the nitrogen base in the reverse reactions (α_r, Table 5), is rather constant through all the compared substrates and may represent a limit value for platinum(II) complexes. This hypothesis requires further data to be confirmed.

The reactivity of the pyridine complex $[Pt(NNN)(py)]^{2+}$ at $I = 0$ mol dm^{-3} ($k_2^{0r} = 467$ dm^3 mol^{-1} s^{-1}) as compared with that of the mono-cationic $[Pt(SS)(py)Cl]^+$ ($k_2^{0r} = 0.078$ dm^3 mol^{-1} s^{-1}) [1] indicates that the nucleophilic attack of chloride occurs more easily at the bis-cationic than at the mono-cationic species and a comparison of the reactivity of chloride at the bis-cationic species $[Pt(NNN)(py)]^{2+}$ ($k_2^{0r} = 467$ dm^3 mol^{-1} s^{-1}) and $[Pt(SNS)(py)]^{2+}$ ($k_2^{0r} = 1.48$ dm^3 mol^{-1} s^{-1}) [2] provide a further evidence for the larger electrophilicity of the reaction centre for the former than the latter substrate.

The substrates can also be compared as far as steric retardation effects are concerned. Steric hindrance, as usually measured on using 2-methylpyridines as nucleophiles [1], is expressed by the value of $\Delta_f \approx 1.5$ [7] for the $[Pt(NNN)Cl]^+$ substrate (Fig. 1), which is comparable with the values of $\Delta_f \approx 1.6$ and 1.4 measured for the substrates $[Pt(SS)Cl_2]$ and $[Pt(SNS)Cl]^+$, respectively. It appears, therefore, that the limitation to free rotation around the Pt—N(am) bond in the trigonal bipyramidal transition state, due to the presence of two pyridine groups in the apical position, is not very different from that due to the presence of a single sulphur atom and a chloro ligand or two thioeteric sulphur atoms.

On comparing steric retardation parameters in the reverse processes, the steric factor $\Delta_r \approx 0.82$ in the present case is nearly the same as that measured for $[Pt(NSN)Cl]^+$ ($\Delta_r \approx 0.75$) [3]. In both cases two pyridine groups belonging to the chelating tridentate ligand occupy the apical positions in the trigonal bipyramidal transition states and the systems are, therefore, sterically comparable. It may be noted that the same observation was achieved on comparing the thermodynamic data concerning the relative stabilities of the corresponding halo platinum complexes. The steric retardation is slightly larger than that observed with the substrates $[Pt(SS)(am)Cl]^+$ ($\Delta_r \approx 0.6$) [1] and

Table 4. First- and second-order rate constants[a] and equilibrium constants for the reaction

$$[Pt(NNN)Cl]^+ + am \underset{k_1^r + k_2^r[Cl^-]}{\overset{k_1^f + k_2^f[am]}{\rightleftharpoons}} [Pt(NNN)(am)]^{2+} + Cl^-$$ in methanol at 25°C

am	λ/nm		[b]$10^3 k_2^f$/ dm^3 mol^{-1} s^{-1}	[b]$10^3 k_2^r$/ dm^3 mol^{-1} s^{-1}	$10^3 k_2^{0r}$/ dm^3 mol^{-1} s^{-1}	$10^2 K$ (k_2^f/k_2^r)	$10^2 K^0$ (k_2^f/k_2^{0r})	pK_a of amH$^+$
	Isosbestic point	*Used for calculations*						
4-Cyanopyridine	302, 336, 347	340	69±2	138000±3000	5658000	0.050±0.002	0.00122	1.90
Methylisonicotinate	302, 336, 347	342	200±20	41000±4000	1681000	0.49±0.07	0.0119	3.26
4-Acetylpyridine	302, 336, 347	340	202±7	27800±700	1140000	0.73±0.03	0.0177	3.51
Pyridine	302, 336, 347	340	432±8	11400±700	467000	3.8±0.2	0.0925	5.17
3-Methylpyridine	302, 336, 347	340	597±6	8400±200	344000	7.1±0.2	0.1735	5.68
4-Methylpyridine	302, 336, 347	340	654±3	5300±300	217000	12.3±0.7	0.3014	6.03
4-Aminopyridine	302, 336, 347	342	4900±200	115±3	4715	4300±200	103.92	9.12
2-Methylpyridine	302, 336, 347	342	24.7±0.6	580±10	23780	4.3±0.1	0.1039	5.94
2,4-Dimethylpyridine	302, 336, 347	342	38±1	337±3	13818	11.3±0.3	0.2750	6.99
Ammonia	312, 337, 347	342	4100±100	810±30	33211	510±20	12.35	9.85[c]

[a] Determined by weighted linear regression of k_{obs} values vs nucleophile concentration.

[b] $I = 0.1$ mol dm^{-3} (CH_3SO_3Na).

[c] pK_a value corrected according to Ref. 14.

Table 5. Discrimination (α) and steric hindrance (Δ) parameters for the reactions of pyridines with some platinum(II) chloro-complexes

Substrate	α_f	Δ_f	α_r	Δ_r	Ref.
[Pt(α,α'-bipyridine)Cl_2]	0.06				12
{Pt[biacetylbis(N-methyl,N-phenyl)osazone]Cl_2}	0.05				13
[Pt(SS)Cl_2]	0.036	1.6	−0.56	0.6	1
[Pt(SNS)$^+$	0.15	1.4	−0.45	0.57	2
[Pt(NSN)Cl]$^+$			−0.53	0.75	3
[Pt(NNN)Cl]$^+$	0.24	1.5	−0.53	0.82	p.w.

[Pt(SNS)(py)]$^{2+}$ ($\Delta_r \approx 0.57$) [2]. The values of Δ_r are always smaller than those of forward reactions Δ_f, as expected as a consequence of a partial compensation of steric hindrance in the ground and transition states for the nitrogen base displacement processes.

The ratio between the second-order rate constants for the forward and reverse reactions gives the corresponding equilibrium constants for the systems:

$$[Pt(NNN)Cl]^+ + am \rightleftharpoons [Pt(NNN)(am)]^{2+} + Cl^-$$

and the actual values of K and $I = 0.1$ mol dm^{-3} and K^0 at $I = 0$ mol dm^{-3} are reported in Table 4.

The plot of log K^0 versus pK_a (Fig. 3) is linear for the isosteric pyridines pyridine, 3-methylpyridine, 4-methylpyridine, and 4-aminopyridine and the free

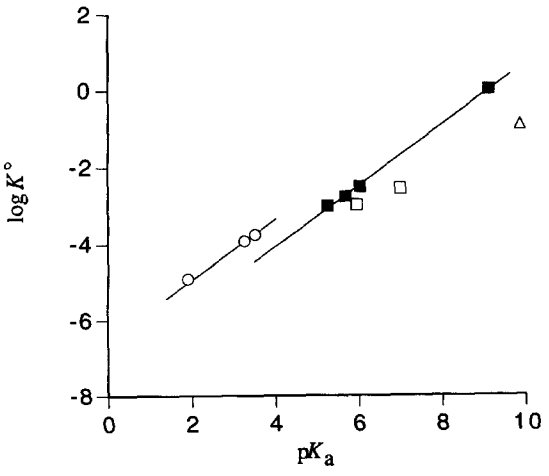

Fig. 3. log K^0 for the reaction [Pt(NNN)Cl]$^+$ + am $\rightleftharpoons$ [Pt(NNN)(am)]$^{2+}$ + Cl$^-$ plotted against pK_a of amH$^+$: ■, pyridine, 4-methylpyridine, 3-methylpyridine, 4-aminopyridine; ○, 4-acetylpyridine, methylisonicotinate, 4-cyanopyridine; □, 2-methylpyridine and 2,4-dimethylpyridine; △, ammonia.

energy relationship log $K^0 = 0.80$pK_a + constant can be derived. As expected the corresponding values for the 4-acetylpyridine, 4-cyanopyridine and methylisonicotinate is out of the line indicating an increased stability (4.3 kJ mol^{-1}), whereas the presence of hindered pyridines slightly decreases the stability.

The dependence of the stability of the complexes upon the basicity of pyridines is higher (0.80) for the presence bis-cationic substrates than that (0.58) measured with the mono-cationic substrates in the systems [Pt(SS)Cl_2] + am $\rightleftharpoons$ [Pt(SS)amCl]$^+$ + Cl$^-$. However, the values of the equilibrium constants are quite lower than those found in the previous case and this fact may reflect a larger tendency of Cl$^-$ to neutralize the positive charge in the bis-cationic than in mono-cationic substrate.

Acknowledgements—We thank the Italian Ministry of University and Consiglio Nazionale delle Ricerche (Rome) for financial support.

REFERENCES

1. Bellicini, M., Cattalini, L., Marangoni, G. and Pitteri, B., *J. Chem. Soc., Dalton Trans.*, 1994, 1805.
2. Pitteri, B., Marangoni, G. and Cattalini, L., *J. Chem. Soc., Dalton Trans.*, 1994, 3539.
3. Pitteri, B., Marangoni, G. and Cattalini, L., *Polyhedron*, 1995, **14**, 2331.
4. Pitteri, B., Marangoni, G., Cattalini, L. and Bobbo, T., *J. Chem. Soc., Dalton Trans.*, 1995, 3853.
5. Basolo, F. and Pearson, R. G., *Mechanism of Inorganic Reactions*, 2nd edn. Wiley, New York, 1967.
6. Annibale, G., private communication.
7. Δ can be regarded as the steric effect due to the introduction of a methyl group *ortho* to the nitrogen in the entering pyridine without any interference from the basicity change that might arise from the presence of the substituent.
8. Robinson, R. A. and Stokes, R. H., *Electrolyte Solutions*, 2nd edn. Butterworths, London, 1959, p. 231.
9. Cattalini, L., *Inorganic Reaction Mechanisms*, ed. J. O. Edwards. Wiley, New York, 1970.
10. Pitteri, B., Marangoni, G., Cattalini, L. and Canovese, *J. Chem. Soc., Dalton Trans.*, 1994, 169.
11. Tobe, M. L., *Comprehensive Coordination Chemistry*, ed. G. Wilkinson, R. D. Gillard and J. A. McCleverty, Vol. 1. Pergamon Press, Oxford, 1987.
12. Cattalini, L., Orio, A. and Doni, A., *Inorg. Chem.*, 1966, **5**, 1517.
13. Annibale, G., Cattalini, L., Maresca, L., Michelon, G. and Natile, G., *Inorg. Chim. Acta*, 1974, **10**, 211.
14. Benson, S. V., *J. Am. Chem. Soc.*, 1958, **80**, 5151.

Pergamon

PII: S0277-5387(97)00350-1

Polyhedron Vol. 17, No. 4, pp. 483–489, 1998
© 1998 Elsevier Science Ltd
All rights reserved. Printed in Great Britain
0277-5387/98 $19.00+0.00

Synthesis, structure and magnetic properties of transition metal complexes of the nitroxide 2′,5′-dihydro-4′,5′,5′-trimethyl-spiro-[4,5-diazafluorene-9,2′-imidazol]-1-oxyl

Frank Hintermaier and Wolfgang Beck*

Institut für Anorganische Chemie der Universität, Meiserstr. 1, D-80333 München, Germany

(Received 4 July 1997; accepted 14 August 1997)

Abstract—With the radical 2′,5′-dihydro-4′,5′,5′-trimethyl-spiro-[4,5-diazafluorene-9,2′-imidazol]-1-oxyl L a series of transition metal complexes has been prepared: $[ML_3](SbF_6)_2 \cdot 4H_2O$ with $M^{2+} = Mn^{2+}$ (**1**), Fe^{2+} (**2**), Co^{2+} (**3**), Ni^{2+} (**4**), Zn^{2+} (**5**). Reaction of L with Cu^{2+} in methanol yielded different products depending on the counterion. In the presence of weakly coordinating anions the Cu(I) complexes $[Cu_2L_3](SbF_6)_2 \cdot H_2O$ (**6**), $[Cu_2L_3](OTf)_2 \cdot 2MeOH$ (**7**) and $[Cu_2L_3](ClO_4)_2$ (**8**) were formed. Stronger coordinating counter ions gave the complexes $CuL_2Cl_2 \cdot H_2O$ (**9**), $CuL_2Br_2 \cdot H_2O$ (**10**) and $CuL_2(NO_3)_2$ (**11**). Also the synthesis of $[Ag_2L_3](SbF_6)_2 \cdot 2H_2O$ (**12**), $Pd(L)Cl_2 \cdot H_2O$ (**13**), $Pt(L)Cl_2 \cdot H_2O$ (**14**), $Ni(L)Cl_2$ (**15a**), $Ni(L)Cl_2 \cdot 4H_2O$ (**15b**) and $[Ru(bipy)_2(L)]Cl_2 \cdot 4H_2O$ (**16**) is reported. The magnetic moments of **1–6** and **10** correspond in the range 200–300 K to those expected for noninteracting spins of the metal ion and the radicals. At low temperatures spin pairing of metal and radical spins is observed for **1–3**. © 1998 Elsevier Science Ltd. All rights reserved

Keywords: nitroxide radicals; 3-imidazoline; transition metal complexes.

In continuation of our studies on the coordination chemistry of 3-imidazoline-1-oxyl-radicals [1,2] we report in this paper on transistion metal complexes of the radical 2′,5′-dihydro-4′,5′,5′-trimethyl-spiro-[4,5-diazafluorene-9,2′-imidazol]-1-oxyl L, which was previously reported [3].

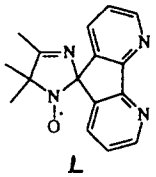

L

Due to its diazafluorene part L is a bidentate ligand and should reveal a coordination chemistry similar to that of 1,2-diimines [5], e.g. 2,2′-bipyridyl or *o*-phenanthroline. However the bite angle of L between the two donor *N*-atoms of the 4,5-diazafluorene part is only 38° [6,7] and therefore L should be a weaker ligand than 2,2′-bipyridyl or phenanthroline (bite angle 60°). Metal complexes of 4,5-diazafluorene [7,8], 4,5-diazafluorenone [9] and *N*,*N*′-methylen-2,2′-bisimidazole [10] have been reported.

RESULTS AND DISCUSSION

Complexes $[ML_3]^{2+}$ (*M = Mn, Fe, Co, Ni, Zn*)

The metal(II) chlorides MCl_2 (Mn^{2+}, Fe^{2+}, Co^{2+}, Ni^{2+} and Zn^{2+}) form with L in an H_2O/CH_3OH solution complexes of the type $[ML_3]^{2+}$ (**1–5**), which can

* Author to whom all correspondence should addressed.

be isolated as tetrahydrates of hexafluoroantimonate salts, using $AgSbF_6$.

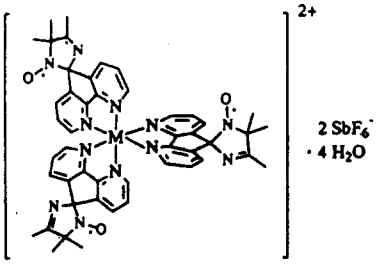

	1	2	3	4	5
M	Mn	Fe	Co	Ni	Zn

The same products were isolated when only two equivalents of L were used. In the FAB MS spectra of these compounds the ions $[ML_3(SbF_6)_2]^+$, $[ML_3(SbF_6)]^+$ and $[ML_3]^+$ were detected.

In the EPR spectra of **1–5** in methanolic solution only a triplet with slightly broadened lines of the nitroxide radical is observed at room temperature. These signals probably correspond to the dissociated nitroxide ligand while the intact complexes with small intramolecular superexchange should exhibit broad signals which may be unobservable at room temperature [4]. The EPR spectrum of the Mn complex **1** exhibits an additional sextet of the Mn^{2+} ion.

In the range 200–300 K, complexes **1, 2, 4** and **5** show magnetic moments which are close to the spin-only value for independent (noninteracting) spins of the metal ion and the nitroxide radicals (Table 1). For the cobalt complex **3** an orbital contribution has to be assumed [12]. The plots $1/\chi$ vs T obey the Curie Weiß law according to paramagnetic behaviour (Figs 1–5). At low temperature (4.2 K) a considerable decrease of the magnetic moment is found for **1–3** (Table 1) which we attribute to spin pairing of metal and radical spins.

Cu(I) and Ag(I) complexes

The reactions of L with *in situ* prepared solutions of $Cu(SbF_6)_2$ and $Cu(SO_3CF_3)_2$ (from $CuCl_2$ and $AgSbF_6$ or $AgSO_3CF_3$) or with $Cu(ClO_4)_2$ gave the complexes **6–8** in which the copper ion has the oxidation state +I. Thus a reduction of Cu(II) by methanol has occurred.

$[Cu_2L_3](SbF_6)_2 \cdot H_2O$	**6**
$[Cu_2L_3](SO_3CF_3)_2 \cdot 2$ MeOH	**7**
$[Cu_2L_3](ClO_4)_2 \cdot 3\ H_2O$	**8**

For **6** in the range 60–300 K a magnetic moment of $\mu_{eff} = 3.08\ \mu_B$ was observed which is close to that of 3.00 μ_B for Cu(I) (d^{10}) and three noninteracting radical spins ($S = 3 \cdot 1/2$).

The nitroxide reacts with $AgSbF_6$ to give the complex **9**.

$[Ag_2L_3](SbF_6)_2$ **9**

The formation of dinuclear complexes **7** and **9** is supported by FAB MS spectra in which the ions $[Cu_2L_3]^+$, $[Cu_2L_3 \cdot H_2O]^+$, $[Ag_2L_3]^+$ and $[Ag_2L_3SbF_6]^+$ could be detected. A force field calculation [13] shows that for **9** a structure with three bridging ligands, L is energetically favourable (Fig. 6).

With stronger coordinating anions during reactions of L copper(II) is not reduced and the green complexes **10–12** were obtained.

$CuL_2Cl_2 \cdot H_2O$	**10**
$CuL_2Br_2 \cdot H_2O$	**11**
$CuL_2(NO_3)_2$	**12**

The observed magnetic moment $\mu = 3.17\ \mu_B$ (Table 1) of **10** corresponds to three noninteracting spins (d^9 and two radical spins: $S = 3^1/_2$)

Complexes **10** and **11** may show a similar structure as has been reported for Cu(4,5-diazafluorene-9-one)$_2Cl_2$ [9] with hexacoordinated metal ion.

Table 1. Magnetic moments of **1–6, 10**

	S[11,12] (for independent metal and radical spins)		μ_B expected	$t\mu_B$ found	Θ (K)	Temperature (K)	μ_B found at low temperatures
1	(Mn^{2+}, high spin)	$5/2+3 \cdot 1/2$	6.64	6.37	~0	32–300	3.52(4.2 K)
2	(Fe^{2+}, high spin)	$4/2+3 \cdot 1/2$	5.75	5.77	−27	200–300	2.63(4.2 K)
3	(Co^{2+}, high spin)	$3/2+3 \cdot 1/2$	4.90	5.89	−19	190–300	2.06(4.2 K)
4	(Ni^{2+})	$1+3 \cdot 1/2$	4.12	4.25	−13	190–300	3.48(32.6 K)
5	(Zn^{2+})	$3 \cdot 1/2$	3.00	3.09	−6	190–300	2.90(32.5 K)
6	(Cu^{+})	$3 \cdot 1/2$	3.00	3.08	+4	60–300	
10	(Cu^{2+})	$1/2+2 \cdot 1/2$	3.00	3.17		60–300	1.43(4.2 K)

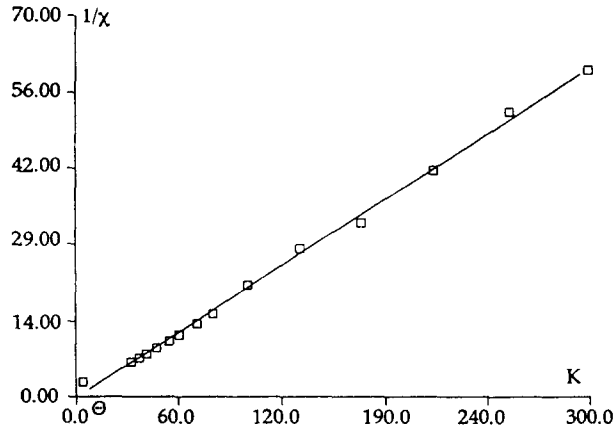

Fig. 1. $1/\chi$ (mol·cm^{-3}) vs T (K) for **1**.

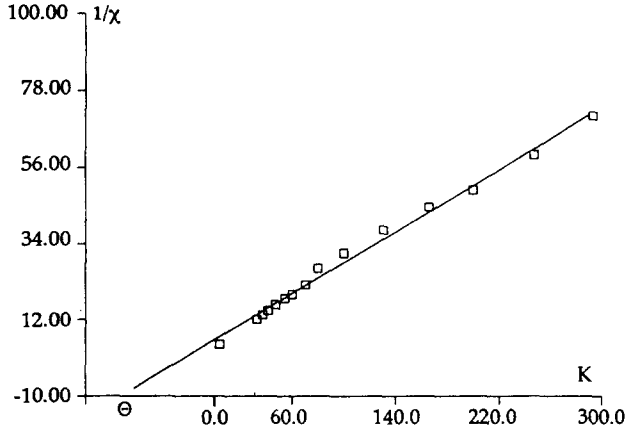

Fig. 2. $1/\chi$ (mol·cm^{-3}) vs T (K) for **2**.

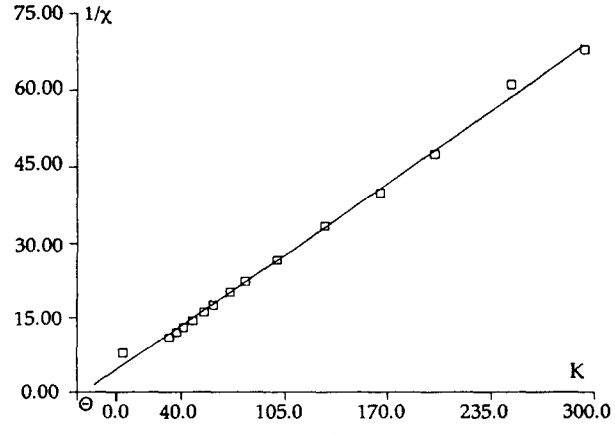

Fig. 3. $1/\chi$ (mol·cm^{-3}) vs T (K) for **3**.

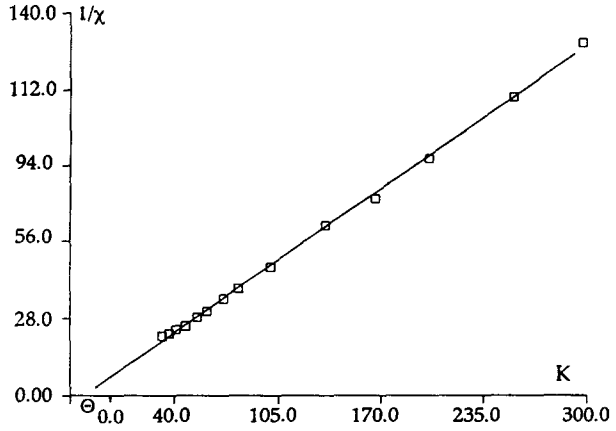

Fig. 4. $1/\chi$ (mol·cm^{-3}) vs T (K) for **4**.

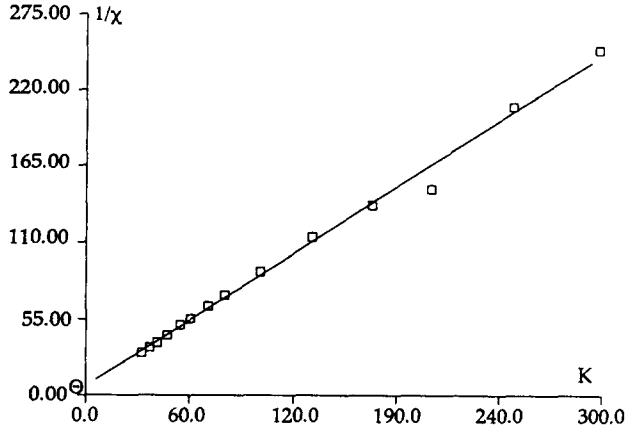

Fig. 5. $1/\chi$ (mol·cm^{-3}) vs T (K) for **5**.

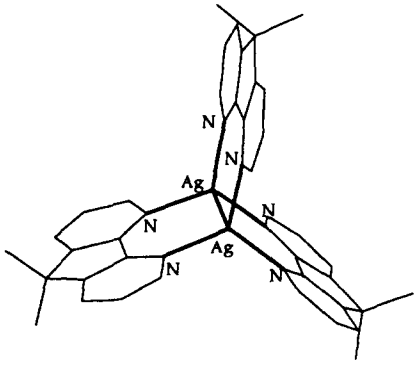

Fig. 6. Possible Structure of **9**.

Ni(II), Pd(II), Pt(II) and Ru(II) complexes

The reactions of the nitroxide L with Na_2PdCl_4, K_2PtCl_4, $NiCl_2 \cdot 6\,H_2O$ and $Ru(bipy)_2Cl_2$, respectively, gave the complexes **13–16**.

$Pd(L)Cl_2$	**13**
$Pt(L)Cl_2$	**14**
$Ni(L)Cl_2$	$Ni(L)Cl_2 \cdot 4\,H_2O$
15a	**15b**
$Ru(bipy)_2(L)]Cl_2 \cdot 4\,H_2O$	**16**

Complex **15** adds four equivalents of water on exposure to air in a reservible manner.

Ruthenium(II) complexes of diazabiarene ligands are of high interest due to their photo and redox chemistry [14]. Ruthenium(II) complexes of diazafluorene and diazafluorenenone have been previously described [7,8a].

The IR spectra of the complexes **1–16** are almost identical and differ only slightly from those of the free ligand L.

EXPERIMENTAL

The radical 2′,5′-dihydro-4′,5′,5′-trimethyl-spiro-[4,5-diazafluorene-9,2′-imidazol]-1-oxyl was prepared as described [4]. All other reagents and solvents were

purchased and used as received. The products were dried *in vacuo* (0.1 Torr) for 4–8 h. Elemental analyses: Heraeus VT. Metal analyses: AAS Perkin-Elmer 1100 B at the wave lengths Sb: 217.8 nm, Mn: 279.5 nm, Fe: 248.3 nm, Ni: 341.5 nm, Cu: 324.8 nm, Zn: 213.8 nm, and an ICP Jobin Y of JY 38 with an ICP 1500 plasmatherm generator for **6**. Dissolution with 65% HNO_3 (Merck Suprapur). EPR (X-band): Varian E-Line Spectrometer with a Varian E-101 microwave bridge. Magnetic measurements with 8–15 mg samples in the temperature range 30–300 K: Faraday-balance from the Institut für Physikalische Chemie der Universität München (Prof. Voitländer). IR: Nicolet 520 FT-IR-spectrometer in Hostaflon (2500–4000 cm^{-1}), in KBr (600–2500 cm^{-1} and sometimes in polyethylene (400–600 cm^{-1}). FAB–MS: Finnigan MAT 95 Q with Cs^+-gun in mNBA. Melting and decomposition points: Schmelzpunktsapparat Dr Tottoli from Büchi.

1. Solutions of 10.5 mg (0.0836 mmol) of $MnCl_2$ and of 57.5 mg (0.167 mmol) of $AgSbF_6$ in methanol were combined and boiled for 1 min. The solvent was removed *in vacuo* and the residue was treated with 10 ml of methanol. After separation of AgCl a methanol solution of 70.0 mg (0.252 mmol) of 2′,5′-dihydro-4′,5′,5′-trimethyl-spiro-[4,5-diazafluorene-9,2′-imidazol]-1-oxyl (L) was added. The mixture was stirred for 12 h, boiled for 1 min and evaporated to 3 ml. To this 20 ml of diethylether were added and the mixture was stirred for 2 h. The product was separated, washed with diethylether and dried *in vacuo*. Yield: 85 mg (71%) of an orange-yellow powder.

IR: ν = 2985 m, 2935 m, 1630 vs (C4 = N), 1604 vs (py), 1589 vs (py), 1465 s, 1418 s, 1384 s, 1365 m, 1165 s, 1145 s, 818 s, 794 s, 744 vs, 660 vs, br, 293 vs. FAB—MS: m/z = 1365 (5%, $[MnL_3(SbF_6)_2]^+$), 1129 (13%, $[MnL_3(SbF_6)]^+$), 893 (3%, $[MnL_3]^+$). $C_{48}H_{45}N_{12}O_3MnSb_2F_{12}\cdot 4H_2O$ (1436.44): Calc. C, 40.14; H, 3.72; N, 11.70; Mn, 3.83; Sb, 16.95. Found: C, 41.21; H, 3.60; N, 11.88; Mn, 3.29; Sb, 17.30%. EPR (MeOH): g = 2.0065, a_N = 13.5.

2. Same procedure as for **1**. 14.5 (0.144 mmol) mg of $FeCl_2$, 78.6 mg (0.229 mmol) of $AgSbF_6$ and 63.8 mg (0.229 mmol) of L. Yield: 45 mg (28%) of a bright yellow powder. Idential IR spectra as for **1**.

FAB–MS: m/z = 1441 (1%, $[FeL_3(SbF_6)_2\cdot 4H_2O]^+$), 1366 (3%, $[FeL_3(SbF_6)_2]^+$), 1130 (17%, $[FeL_3(SbF_6)]^+$), 894 (11%, $[FeL_3]^+$). $C_{48}H_{45}N_{12}O_3FeSb_2F_{12}\cdot 4H_2O$ (1437.35): Calc. C, 40.11; H, 3.72; N, 11.69; Fe, 3.89; Sb, 16.94. Found: C, 40.67; H, 3.78; N, 11.41; Fe, 4.90; Sb, 16.44%. EPR (MeOH): g = 2.0065, a_N = 13.6.

3. Same procedure as for **1**. 10.8 (0.084 mmol) mg of $CoCl_2$, 57.5 mg (0.167 mmol) of $AgSbF_6$ and 70.0 mg (0.252 mmol) of L. Yield: 92 mg (76%) of a bright brown powder.

FAB–MS: m/z = 1369 (3%, $[CoL_3(SbF_6)_2]^+$), 1133 (7%, $[CoL_3(SbF_6)]^+$), 896 (4%, $[CoL_3]^+$). $C_{48}H_{45}N_{12}O_3CoSb_2F_{12}\cdot 4H_2O$ (1440.43): Calc. C, 40.03; H, 3.71; N, 11.67. Found: C, 39.88; H, 3.54; N, 11.50%. EPR (MeOH): g = 2.0065, a_N = 13.5.

4. Same procedure as for **1**. 13.7 (0.106 mmol) mg of $NiCl_2$, 72.7 mg (0.215 mmol) of $AgSbF_6$ and 58.6 mg (0.210 mmol) of L. Yield: 43 mg (28%) of a bright brown powder.

FAB–MS: m/z = 1369 (5%, $[NiL_3(SbF_6)_2]^+$), 1132 (32%, $[NiL_3(SbF_6)]^+$), 896 (5%, $[NiL_3]^+$). $C_{48}H_{45}N_{12}O_3NiSb_2F_{12}\cdot 4H_2O$ (1440.21): Calc. C, 40.03; H, 3.71; N, 11.67; Ni, 4.01; Sb, 16.91. Found: C, 39.82; H, 3.76; N, 11.36; Zn, 4.42; Sb, 17.30%. EPR (MeOH): g = 2.0064, a_N = 13.5.

5. Same procedure as for **1**. 12.2 (0.090 mmol) mg of $ZnCl_2$, 61.6 mg (0.179 mmol) of $AgSbF_6$ and 50.0 mg (0.179 mmol) of L. Yield: 10 mg (8%) of a bright yellow powder. $C_{48}H_{45}N_{12}O_3ZnSb_2F_{12}\cdot 4H_2O$ (1446.88): Calc. C, 39.85; H, 3.69; N, 11.62; Zn, 4.52; Sb, 16.83. Found: C, 39.82; H, 3.75; N, 11.23; Zn, 3.86; Sb, 16.91%. EPR (MeOH): g = 2.0064, a_N = 13.5.

6. To a solution of 16.9 mg (0.125 mmol) of $CuCl_2$ in methanol 86.0 mg (0.250 mg) of $AgSbF_6$ were added. The mixture was boiled for 1 min, the methanol removed *in vacuo* and the residue treated with 14 ml of methanol. After separation of AgCl a solution of 70.0 mg (0.251 mmol) of L in 5 ml of methanol was added. The mixture was stirred for 15 h, the precipitate separated, washed with 2 ml of methanol and dried *in vacuo*. Yield: 46 mg (26%) of a bright yellow microcrystalline powder.

IR: ν = 2988 m, 1618 s (C4 = N), 1597 s (py), 1587 s (py), 1575 s, 1465 s, 1429 s, 1412 vs, 1385 s, 1365 m, 1146 s, 821 s, 792 s, 766 s, 747 vs, 660 vs, br, 291 vs. $C_{48}H_{45}N_{12}O_3Cu_2Sb_2F_{12}\cdot H_2O$ (1454.55): Calc. C, 39.63; H, 3.26; N, 11.56; Cu, 8.74; Sb, 16.74. Found: C, 39.90; H, 3.31; N, 11.45; Cu, 8.25; Sb, 16.66%. EPR: MeOH/H_2O (3/1): g = 2.0063, a_N = 13.6; MeOH: g = 2.0064, a_N = 13.7; MeCN: g = 2.0062, a_N = 13.5; acetone: g = 2.0064, a_N = 13.4.

7. Same procedure as for **6**. 13.0 mg (0.097 mmol) of $CuCl_2$, 49.7 mg (0.194 mmol) of AgO_3SCF_3 and 54.0 mg (0.194 mmol) L. Yield: 33 mg (26%) bright yellow powder.

IR: ν = 2982 m, 1630 m (C4 = N), 1597 m (py), 1586 m (py), 1573 m, 1465 m, 1430 m, 1410 s, 1384 m, 1277 vs, 1264 vs, 1225 s, 1165 s, 1032 vs, 747 s, 639 vs. FAB–MS: 980 (20%, $[Cu_2L_3\cdot H_2O]^+$), 962 (10%, $[Cu_2L_3]^+$), 932 (20%, $[Cu_2L_3\text{-}NO]^+$). $C_{50}H_{45}N_{12}O_9S_2Cu_2F_6\cdot 2CH_3OH$ (1327.27): Calc. C, 47.05; H, 4.03; N, 12.66; Cu, 9.58. Found: C, 46.77; H, 3.86; N, 12.76; Cu, 9.47%. EPR: MeCN: g = 2.0063, a_N = 13.5; MeOH: g = 2.0064, a_N = 13.5.

8. To a solution of 168 mg (0.600 mmol) L in 10 ml of methanol 0.2 mmol of $Cu(ClO_4)_2$ (as aquous solution) were added. The mixture was boiled for 15 min, the precipitate was separated, washed with methanol and dried *in vacuo*. Yield: 15 mg (6%) bright yellow powder.

IR: ν = 2990 m, 1618 m (C4 = N), 1597 m (py), 1586 m (py), 1574 m, 1465 m, 1428 m, 1410 vs, 1384

m, 1365 m, 1268 m, 1250 m, 1167 m, 1145 s, 1098 vs, 747 s, 624 s. $C_{48}H_{45}N_{12}O_{11}Cu_2Cl_2 \cdot 3H_2O$ (1218.02): Calc. C, 47.33; H, 4.22; N, 13.80. Found: C, 47.43; H, 4.17; N, 13.69%.

9. To a solution of 32.7 mg (0.095 mmol) of $AgSbF_6$ in 3 ml of methanol was added a solution of 53.0 mg (0.190 mmol) of L in 5 ml of methanol. The mixture was stirred for 12 h, the precipitate was separated, washed with methanol and dried *in vacuo*. Yield: 57 mg (78 %) of a bright orange powder.

IR: ν = 2982 m, 2939 m, 1630 s (C4 = N), 1597 s (py), 1587 s (py), 1577 s, 1466 m, 1432 m, 1413 vs, 1385 m, 1367 m, 1166 s, 1147 s, 817 s, 792 s, 766 m, 745 s, 657 vs, 639 s, 290 vs. FAB–MS: 1291 (1%, $[Ag_2L_3(SbF_6)]^+$), 1055 (1%, $[Ag_2L_3]^+$). $C_{48}H_{45}N_{12}O_3Ag_2Sb_2F_{12} \cdot 2H_2O$ (1454.55): Calc. C, 36.93; H, 3.16; N, 10.77; Sb, 15.60. Found: C, 36.63; H, 2.87; N, 10.42; Sb, 16.25%. EPR (MeCN): g = 2.0064, a_N = 13.4.

10. A solution of 16.9 mg (0.125 mmol) of $CuCl_2$ in 10 ml of methanol was treated with a solution of 70.0 mg (0.251 mmol) of L in 20 ml of methanol. The mixture was stirred for 12 h, the complex separated by centrifugation, washed twice with 2 ml of methanol and dried *in vacuo*. Yield: 42 mg (47%) of a bright green powder.

IR: ν = 2973 m, 2932 m, 1633 s (C4 = N), 1612 m, 1596 m (py), 1585 s (py), 1577 s, 1462 s, 1430 s, 1411 vs, 1381 s, 1361 m, 1267 m, 1251 s, 1166 s, 1142 s, 820 s, 791 s, 745 vs, 280 s, 273 s. $C_{32}H_{30}N_8O_2CuCl_2 \cdot H_2O$ (711.11): Calc. C, 54.05; H, 4.54; N, 15.76; Cu, 8.94. Found: C, 54.56; H, 4.48; N, 15.51; Cu, 8.83%.

11. Same procedure as for **10**. 34.8 mg (0.156 mmol) of $CuBr_2$ and 87.0 mg (0.312 mmol) of L. Yield: Grass green powder.

IR: ν = 2975 m, 1632 s (C4 = N), 1597 m (py), 1585 s (py), 1578 s, 1462 m, 1429 s, 1411 vs, 1381 m, 1361 m, 1267 m, 1251 m, 1166 s, 1142 s, 818 s, 791 s, 744 vs. $C_{32}H_{30}N_8O_2CuBr_2 \cdot H_2O$ (800.01): Calc. C, 48.04; H, 4.03; N, 14.01. Found: C, 48.35; H, 3.62; N, 14.03%.

12. Same procedure as for **10**. 84.0 mg (0.300 mmol) of L and 36.0 mg (0.149 mmol) of $Cu(NO_3)_2 \cdot 3H_2O$. Yield: 75 mg (67%) of a bright green powder.

IR: ν = 2990 m, 1632 s (C4 = N), 1598 m (py), 1585 s (py), 1473 s, 1412 vs, 1384 vs, 1293 vs, 817 s, 744 s. $C_{32}H_{30}N_{10}O_8Cu$ (746.20): Calc. C, 51.51; H, 4.05; N, 18.77. Found: C, 51.56; H, 4.01; N, 18.69%.

13. A solution of 56.5 mg (0.192 mmol) of Na_2PdCl_4 in 3 ml of water and 5 ml of methanol was combined with a solution of 53.6 mg (0.192 mmol) of L in 8 ml of methanol and 4 ml of water. After 12 h the precipitate was separated, washed with 8 ml methanol: water (1 : 1) and dried *in vacuo*. Yield 87.6 mg (96.4%) of an orange powder.

IR: ν = 2978 m, 1630 s (C4 = N), 1609 s (py), 1588 m (py), 1573 s, 1464 s, 1419 vs, 1411 vs, 1382 s, 1363 m, 1252 s, 1149 s, 773 s, 751 s, 348 s, 341 s. $C_{16}H_{15}N_4OPdCl_2 \cdot H_2O$ (474.66): Calc. C, 40.49; H, 3.61; N, 11.80. Found: C, 40.09; H, 3.71; N, 11.29%.

14. A solution of 41.5 mg (0.100 mmol) of K_2PtCl_4 in 4 ml of water and 2 ml of methanol was combined with a solution of 27.9 mg (0.100 mmol) of L in 4 ml of methanol and 12 ml of water. After 3 days the precipitate was separated, washed with methanol: water (1 : 3) and dried *in vacuo*. Yield: 37 mg (66 %) of an orange powder.

IR: ν = 2982 m, 1627 vs (C4 = N), 1615 vs (py), 1571 s (py), 1463 s, 1423 vs, 1410 vs, 1382 s, 1364 m, 1148 s, 754 s. $C_{16}H_{15}N_4OPtCl_2 \cdot H_2O$ (563.33): Calc. C, 34.11; H, 3.04; N, 9.95. Found: C, 34.23; H, 3.15; N, 9.72%.

15. 39.6 mg (0.167 mmol) $NiCl_2 \cdot 6H_2O$ were dissolved in 2 ml of methanol and 8 ml of water and combined with a solution of 45.0 mg (0.161 mmol) of L in 3 ml of methanol and 12 ml of water. After 1 day the solvent was removed *in vacuo*, the residue dissolved in 5 ml of methanol and the solution overlayered with 20 ml of diethylether. After 3 days the precipitate was separated, washed with diethylether and dried for 5 h at 65°C/0.1 torr. Yield: 37 mg (55%) orange-"rosa" coloured powder (**15a**). When **15a** was allowed to stand on air, the colour changed to yellow and the tetrahydrate **15b** was formed.

IR (**15b**): ν = 2991 m, 2978 m, 2970 m, 2932 m, 1627 s (C4 = N), 1594 m (py), 1584 m (py), 1568 s, 1464 m, 1428 s, 1402 vs, 1385 s, 1163 s, 810 s, 787 s, 748 s. $C_{16}H_{15}N_4ONiCl_2$ (**15a**) (408.94): Calc. C, 46.99; H, 3.70; N, 13.70. Found: C, 46.77; H, 3.97; N, 13.44%. $C_{16}H_{15}N_4ONiCl_2 \cdot 4H_2O$ (**15b**) (481.00): Calc. C, 39.95; H, 4.82; N, 11.65. Found: C, 40.41; H, 4.77; N, 11.69%.

16. 105 mg (0.196 mmol) of $Ru(bipy)_2Cl_2$ and 60.0 mg (0.215 mmol) of L in 7 ml of ethanol were refluxed for 3 h. The solvent was removed, the residue dissolved in CH_2Cl_2 and the product was precipitated by addition of pentane, washed twice by stirring in CH_2Cl_2 for 30 min and dried. Yield: 87 mg (51%) of a bright orange powder.

IR: ν = 2960 m, 2931 s, 2860 m, 1627 s (C4 = N), 1603 s (py), 1465 s, 1445 s, 1419 vs, 770 vs. $C_{36}H_{31}N_8ORuCl_2 \cdot 4H_2O$ (835.73): Calc. C, 51.74; H, 4.70; N, 13.41. Found: C, 51.94; H, 4.51; N, 13.11%. EPR (CH_2Cl_2): g = 2.0067, a_N = 13.3.

Acknowledgements—The authors wish to thank Deutsche Forschungsgemeinschaft and Fonds der Chemischen Industrie for generous support and DEGUSSA AG, Hanau, for the gift of chemicals. We thank Prof. J. Voitländer, München, for the use of the magnetic balance and the EPR spectrometer and Prof. W. Steglich, München, for MS spectra. The referees are thanked for valuable comments.

REFERENCES

1. Part from PhD thesis Frank Hintermaier, Universität München, 1995.
2. Hintermaier, F., Sünkel, K., Volodarsky, L. B. and Beck, W., *Inorg. Chem.*, 1996, **35**, 5500; Hintermaier, F., Mihan, S., Gerdan, M. Schönemann,

V., Trautwein, A. and Beck, W., *Chem. Ber.*, 1996, **129,** 571.
3. Hintermaier, F., Volodarsky, L. B., Polborn, K. and Beck, W., *Liebigs Ann. Chem.*, 1995, 2189.
4. Eaton, S. S. and Eaton, G. R., *Coord. Chem. Rev.*, 1988, **83,** 29.
5. (a) Jaeger, F. M. and van Dijk, J. A., *Z. anorg. allg. Chem.*, 1936, **227,** 273; (b) McKenzie, E. D. *Coord. Chem. Rev.* 1971, **6,** 187; (c) Lindoy, L. F. and Livingstone, S. E., *Coord. Chem. Rev.*, 1967, **2,** 173; (d) McWhinnie, W. R., *Coord. Chem. Rev.*, 1970, **5,** 293; (e) König, E., *Coord. Chem. Rev.*, 1968, **3,** 471; J. Reedijk in Comprehensive Coordination Chemistry ed. G. Wilkinson, R. D. Gillard and J. A. McCleverty. Pergamon Press, Oxford 1987.
6. Thummel, R. P., Lefoulon, F. and Mahadevan, R., *J. Org. Chem.*, 1985, **50,** 3824.
7. Henderson, L. J., Fronczek, F. R. and Cherry, W. R., *J. Am. Chem. Soc.* 1984, **106,** 5876.
8. (a) Thummel, R. P., Lefoulon, F. and Korp, J. D., *Inorg. Chem.*, 1987, **26,** 2370; (b) Wacholtz, W. M., Auerbach, R. A., Schmehl, R. H., Ollino, M. and Cherry, W. R., *Inorg. Chem.*, 1985, **24,** 1758; (c) Henderson, L. J. and Cherry, W. R., *J. Photochem.*, 1985, **28,** 143; (d) Zhu, L., Wang, Y., You, X., Yang, Y. and Huang. J., C. A., 1993, **119,** 107844 f.
9. (a) Balagopalakrishna, C., Rajasekharan, M. V., Bott, S., Atwood, J. L. and Ramakrishna, B. L., *Inorg. Chem.*, 1992, **31,** 2843; (b) Menon, S., Balagopalakrishna, C., Rajasekharan, M. V. and Ramakrishna, B. L., *Inorg. Chem.*, 1994, **33,** 950.
10. Goulle, V. and Thummel, R. P., *Inorg. Chem.* 1990, **29,** 1767.
11. Miller, J. S. and Epstein, A. J., *Angew. Chem.*, 1994, **106,** 399.
12. Weiss, A. and Witte, H., Magnetochemie, Verlag Chemie, Weinheim 1973.
13. Hyper ChemTM 3.0 for Windows, Autodesk Inc., 1993.
14. Juris, A., Balzani, V., Barigelletti, F., Campagna, S., Belser, P. and von Zelewsky, A., *Coord. Chem. Rev.*, 1988, **84,** 85; Belser, P. and von Zelewsky, A., *Helv. Chim. Acta*, 1980, **63,** 1675; Creutz, C. and Sutin, N., *Inorg. Chem.*, 1976, **15,** 496.

Pergamon

PII: S0277-5387(98)00351-3

Polyhedron Vol. 17, No. 4, pp. 491–495, 1998
© 1998 Elsevier Science Ltd
All rights reserved. Printed in Great Britain
0277-5387/98 $19.00+0.00

Switching and tuning processes in the interaction of protons with ferrocenyl amines

Angel Benito, Jose Manuel Lloris, Ramón Martínez-Máñez,* and Juan Soto

Departamento de Química, Universidad Politécnica de Valencia, Camino de Vera s/n, 46071 Valencia, Spain

(Received 24 June 1997; accepted 14 August 1997)

Abstract—Some new ferrocene-functionalized amines have been synthesized and characterized. Electrochemical and potentiometric studies have been carried out in THF: H_2O (60:40 v/v) to determine protonation constants of the oxidized and "reduced" species and the oxidation potential shift between pH acid and basic. Some electrochemical studies have also been performed in CH_2Cl_2: MeOH mixtures. The change in the acidity properties after oxidation and the related redox potential shift after protonation are discussed.
© 1998 Elsevier Science Ltd

Keywords: ferrocene; electroactive group; potentiometry; electrochemistry.

Ferrocene-functionalized polyamines are new receptors which have been reported to electrochemically recognize different substrates as consequence of the shift of the redox potential of the electroactive group [1–5]. Additionally we have recently shown that some of those receptors can quantitatively determine metal ions and anions in aqueous solutions [6]. It is known that amines can coordinate metal ions and, due to electrostatic forces, the oxidation potential of the redox groups is usually shifted to anodic potentials [1–7]. If the metal–ferrocenyl groups interaction is mainly electrostatic the presence of metal ions with the same charge would in principle produce the same shift of the oxidation potential. However, if the experiment is carried out in aqueous solutions different metal ions form different species in solution and therefore control of the pH can lead to selectivity in the recognition process. Working with amines the easiest coordination study is probably with protons. As a part of our interest in redox-active amines as receptors we have synthesized and studied the interaction of H^+, using potentiometric and electrochemical techniques, with some new receptors with the aim of determining (i) the effect that oxidation of the ferrocenyl groups has on the acidity of the ammonium groups and (ii) the effect that the protonation process has on the redox potential of the ferrocenyl groups.

* Author to whom correspondence should be addressed.

EXPERIMENTAL

Solvents and reagents

1,2-phenylenediamine, 1,3-phenylenediamine, 1,4-phenylenediamine and ferrocenecarbaldehyde were reagent quality and were used without further purification. Tetrahydrofuran (THF) used was freshly distilled from sodium benzophenone. Carbonate-free potassium hydroxide and hydrochloric acid solutions were used in the potentiometric and electrochemical experiments. Potassium nitrate (0.1 mol dm^{-3}) was used as supporting electrolyte in water. L^3 and L^4 were synthesized following literature procedures [8].

Synthesis of L^1, L^2 and L^5

Ferrocenecarboxaldehyde (856 mg, 4 mmol) was heated with 2 mmol of the corresponding diamine in benzene. After 2 h the solvent was removed under vacuum. The red solid was dissolved in tetrahydrofuran and heated under reflux in the presence of $LiAlH_4$ (10 mmol) for 1 h. The reaction mixture was cooled and small amounts of water were added cautiously in order to eliminate the excess of reductor. The resulting mixture was filtered and the solution evaporated under vacuum. Further addition of water and dichloromethane (30×3 cm^3) produced yellow organic phases which were dried with anhydrous mag-

nesium sulphate. The compounds were recrystallized from dichloromethane-hexane solutions.

N,N′-p-*phenylenbis*((*ferrocenylmethyl*)*amine*), L^1. (848 mg, 83%). Anal. Found: C, 67.40; H, 5.50; N, 5.60. Calc. for $C_{28}H_{28}N_2Fe_2$: C, 66.70; H, 5.60; N, 5.60%. IR (KBr disk): 3030w, 1610w, 1500s, 1470w, 1390m, 1280m, 1240w, 1220w, 1095m, 830m, 810s cm^{-1}. NMR ($CDCl_3$): ^1H δ 3.92 (s, 4H, CH_2), 4.18 (s, 10H, C_5H_5), 4.13 (t, 4H, C_5H_4), 4.24 (t, 4H, C_5H_4), 6.64 (s, 4H, C_6H_4). ^{13}C $\{^1H\}$ δ 44.7 (CH_2), 67.7 (C_5H_4), 68.0 (C_5H_4), 68.4 (C_5H_5), 86.9 (C_5H_4), 114.8 (C_6H_4), 141.0 (C_6H_4).

N,N′-m-*phenylenbis*((*ferrocenylmethyl*)*amine*), L^2. (859 mg, 86%). Anal. Found: C, 66.20; H, 5.50; N, 5.40. Calc. for $C_{28}H_{28}N_2Fe_2$: C, 66.70; H, 5.60; N, 5.60%. IR (KBr disk): 3060w, 1600s, 1500s, 1400m, 1210m, 1150w, 1100m, 810m, 740m cm^{-1}. ^1H δ 3.95 (s, 2H, CH_2), 4.18 (s, 10H, C_5H_5), 4.14 (t, 4H, C_5H_4), 4.25 (t, 4H, C_5H_4), 5.97 (t, 1H, C_6H_4), 6.10 (dd, 2H, C_6H_4), 7.04 (s, 1H, C_6H_4). ^{13}C $\{^1H\}$ δ 43.3 (CH_2), 67.7 (C_5H_4), 68.0 (C_5H_4), 68.4 (C_5H_5), 86.6 (C_5H_4), 97.2 (C_6H_4), 103.0 (C_6H_4), 130.1 (C_6H_4), 149.6 (C_6H_4).

N,N′-*propilenbis*((*ferrocenylmethyl*)*amine*), L^5. (763 mg, 82%). Anal. Found: C, 63.70; H, 6.20; N, 5.80. Calc. for $C_{25}H_{30}N_2Fe_2$: C, 63.90; H, 6.40; N, 6.00%. IR (KBr disk): 3095m, 2820m, 1640w, 1425s, 1312m, 1227m, 1110m, 1100s, 1035m, 960w, 822s, 808s cm^{-1}. ^1H δ 1.65 (q, 2H, CH_2), 2.69 (t, 4H, CH_2), 3.50 (s, 4H, CH_2), 4.09 (s, 10H, C_5H_5), 4.11 (s, 4H, C_5H_4), 4.17 (s, 4H, C_5H_4). ^{13}C $\{^1H\}$ δ 30.0 (CH_2), 47.9 (CH_2), 48.9 (CH_2), 67.7 (C_5H_4), 68.3 (C_5H_5), 86.8 (C_5H_4).

Physical measurements

NMR spectra were measured on a Bruker AC-200 FT spectrometer operating at 300 K. Chemical shifts for ^1H and ^{13}C $\{^1H\}$ spectra are referenced to TMS and $CDCl_3$, respectively. IR spectra were taken on a Perkin-Elmer 1750 spectrophotometer as KBr pellets. Electrochemical data were obtained with a programmable function generator Tacusel IMT-1, connected to a Tacusel PJT 120-1 potentiostat. The working electrode was platinum with a saturated calomel reference electrode separated from the text solution by a salt bridge containing the solvent/supporting electrolyte. The auxiliary electrode was platinum wire. Potentiometric titrations were carried out in THF: H_2O (60:40 v/v) using a reaction vessel water-thermostated at 25.0±0.1°C under nitrogen. The titrant was added by a Crison microburete 2031. The potentiometric measurements were made using a Crison 2002 pH-meter and a combined glass electrode. The titration system was automatically controlled by a PC computer using a program that monitored the e.m.f. values and the volume of titrant added. The electrode was calibrated as a hydrogen concentration proved by titration of known amounts of HCl with CO_2-free KOH solution and determining the equivalent point by Gran's method [9] which gives the standard potential E'^{O} and the ionic product of water ($K'_W = [H^+][OH^-]$). The logarithm of K'_W for the solvent used was found to be -15.1 ± 0.1 (25°C, 0.1 mol dm^{-3} tetrabutylammonium perchlorate). The computer program SUPERQUAD [10] was used to calculate the protonation and stability constants. The titration curves for each system (*ca.* 200 experimental points corresponding to at least three titration curves, pH = −log[H] range investigated 2.5–10, concentration of the ligand was *ca.* 1.2×10^{-3} mol dm^{-3}) were treated either as a single set or as separated entities without significant variations in the values of the stability constants. Finally the sets of data were merged together and treated simultaneously to give the stability constants.

RESULTS AND DISCUSSION

Synthesis and characterization

The reaction of ferrocenecarboxaldehyde with the diamines 1,3-, 1,4-phenylendiamine and 1,3-propylendiamine led to the corresponding Schiff base derivatives as red oils. IR spectra revealed that the condensation took place as can be observed by the strong ν(C=N) stretching vibration at about 1640 cm^{-1}. The IR also displayed for all the imine derivatives several characteristic ferrocene absorptions.

Reduction of the Schiff base derivatives with $LiAlH_4$ in tetrahydrofuran allowed isolation of the corresponding diamines L^1, L^2 and L^5. The IR showed that the imino group had been reduced by the absence of the ν(C=N) imine stretching peak. The lack after hydrogenation in the ^1H NMR of any imine protons at δ about 8.2 and the presence of characteristic CH_2 groups attached to ferrocenyl groups (δ about 3.5–3.9) also supports the proposed formulation. Similar synthetic procedures between ferrocenecarboxaldehyde and 1,2-phenylenediamine did not produce the expected Schiff-base derivatives but compounds L^3 and L^4 as we have reported [8].

Protonation behaviour

The protonation behaviour of L^1, L^2, L^3, L^4 and L^5 was studied by potentiometric titrations of acidified solutions of the amines in THF: H_2O (60:40 v/v) (0.1 mol dm^{-3} tetrabutylammonium perchlorate, 25°C). Basicity constants are gathered in Table 1. L^1, L^2 and L^3 behave as diprotic bases whereas only one protonation process was observed for the benzimidazol derivatives. As expected the diazaalkane derivative L^5 is more basic than the corresponding aryl amines L^1, L^2, L^3 and L^4, with the acidity of the first protonation constant following the order $L^2 > L^3 > L^4 > L^1 > L^5$. For the sake of comparison the basicity constants of the non-substituted 1,3- and 1,4-phenylenediamine

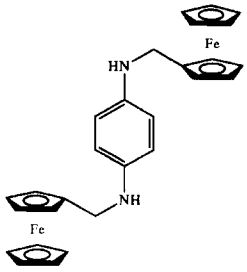

L^1

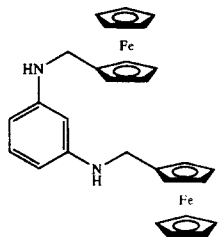

L^2

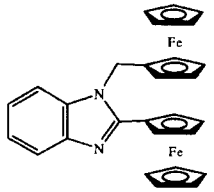

L^3

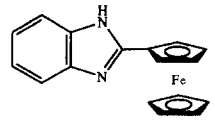

L^4

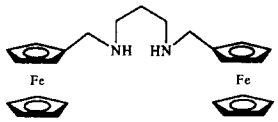

L^5

were also determined in THF : H_2O (60 : 40 v/v) mixtures, [log K ; 1,4-phenylenediamine : 5.80(1), 1.98(1) ; 1,3-phenylenediamine : 4.37(1), 1.19(2) ; for the processes, $L + H^+ \rightleftarrows LH^+$ and $LH^+ + H^+ \rightleftarrows LH_2^{+2}$, respectively]. It can be observed that the N-functionalization with ferrocenylmethyl groups reduces the basicity of the amine groups for the first protonation process but increases the basicity of the second protonation process of L^1 and L^2. Also for the sake of comparison we have determined the protonation constant for benzimidazole in THF : H_2O (60 : 40 v/v) and have obtained a value of log K = 3.09(1) for the process $L + H^+ \rightleftarrows LH^+$, indicating that the functionalization with a ferrocenyl group in the 2 position increases the basicity of the benzimidazol framework. A similar effect has been found in water when we compare the protonation constant for benzimidazole (log K = 5.47) and 2-methyl-benzimidazole (log K = 6.17) [11].

Electrochemical behaviour

Two related effects were studied electrochemically ; the possible modification of the acidity of the receptors by oxidation of the redox-active groups and the redox potential shift of the electro-active groups by addition of protons to the medium.

The receptors L^1–L^5 show an important difference with respect to the starting non-functionalized polyamines, due to the fact that L^1–L^5 are molecules whose basicity strength can be switched from "outside" by oxidation or reduction of the pendant redox-active ferrocenyl groups. That switching process between two different states containing oxidized or "reduced" ferrocenyl groups can be quantified from the study of the $E_{1/2}$–pH (half-wave potential vs pH) curves. Figure 1 shows an example of the shift of the oxidation potential of the receptor L^5. From the analysis of the $E_{1/2}$–pH curves it is possible to evaluate the protonation constants of the amines when the redox groups are oxidized. Table 2 shows the stepwise protonation constants for the oxidized L^1, L^2, L^3, L^4 and L^5 receptors obtained by fitting the $E_{1/2}$–pH curves with an equation which relates the half-wave potential with the proton concentration and the acidity constants for the "reduced" and the oxidized species [2]. As can be observed, oxidation of the ferrocenyl groups switches the acidity strength of the ammonium groups and oxidized species behave as stronger acids than the corresponding "reduced" species. Thus first protonation constants are reduced by 6 times for L^1 and by 38 times for L^4 due to the oxidation of the ferrocenyl groups. We and others have recently published that the change in the protonation constants is due mainly to electrostatic forces as a consequence of the existence of positively charged ferrocenyl groups after oxidation [12,13].

Another study on the ferrocene-functionalized

Table 1. Stepwise protonation constants (log K) of L^1, L^2, L^3, L^4 and L^5 determined in THF : H_2O (60 : 40 v/v) at 298.1 K in 0.1 mol dm^{-3} tetrabutylammonium perchlorate

Reaction	L^1	L^2	L^3	L^4	L^5
$L + H^+ \rightleftarrows HL^+$	5.59(1)[a]	3.93(1)	4.28(2)	4.80(1)	9.17(5)
$HL^+ + H^+ \rightleftarrows H_2L^{+2}$	3.69(4)	2.84(2)			7.19(3)

[a] Values in parentheses are standard deviations on the last significant figure.

Table 2. Stepwise protonation constants (log K) for the oxidized form of L^1, L^2, L^3, L^4 and L^5 determined in THF : H_2O (60 : 40 v/v) at 298.1 K in 0.1 mol dm^{-3} tetrabutylammonium perchlorate

Reaction	L^1	L^2	L^3	L^4	L^5
$^{ox}L + H^+ \rightleftharpoons {}^{ox}LH^+$	4.8(1)[a]	3.0(1)	2.78(6)	3.22(3)	7.9(1)
$^{ox}LH^+ + H^+ \rightleftharpoons {}^{ox}LH_2^{+2}$	1.8(1)	0.8(2)			5.5(1)

[a] Values in parentheses are standard deviations on the last significant figure.

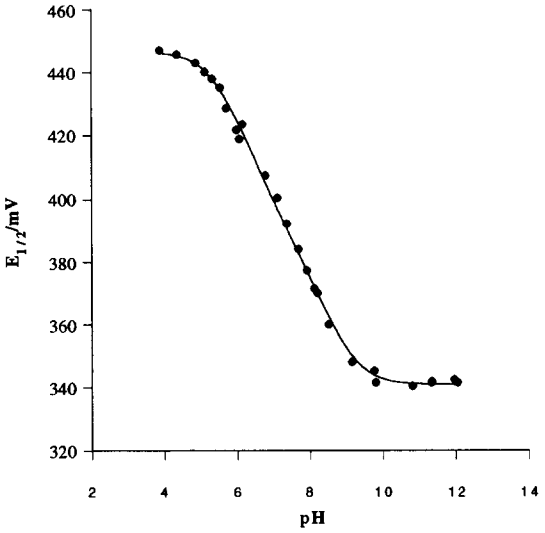

Fig. 1. Plot of the half-wave potential ($E_{1/2}$) vs pH for compound L^5.

amines is how the protonation of the amine groups affects the oxidation potential of the ferrocenyl moieties. For a fixed pH $E_{1/2}$ is a function of the acidity constants of the oxidized and "reduced" species and a steady shift is usually observed when the pH is changed. We can therefore say that the proton concentration can tune the value of the half-wave potential as can be observed for example in the $E_{1/2}$–pH curve shown in Fig. 1. On the other hand another interesting parameter is the maximum shift that can be achieved by changing the pH and can be measured as the difference between $E_{1/2}$ at basic pH and at pH = 0. That difference, ΔE, determined in THF : H_2O (60 : 40 v/v) was 79, 85, 42, 92 and 105 for molecules L^1, L^2, L^3, L^4 and L^5, respectively. We have recently shown that eqn (1) allows a prediction of the potential shift due to the coordination of H^+ in redox-functionalized polyamines as a function of the number of electrons involved in the electrochemical experiment (n); the number of redox groups (j); the distance between the protonation sites (i) and the ferrocenyl groups (r_{ji}) and the permittivity of the medium (ε) [12].

$$\Delta E = \frac{1}{jn}\left[\frac{14398}{\varepsilon}\sum_j\sum_i\frac{1}{r_{ji}} + \left(\frac{2\times10^6}{\varepsilon^2} + 1051\right)\sum_j\sum_i\frac{1}{r_{ji}^2}\right] \quad (1)$$

Distances can be calculated using molecular modeling programs such as PCMODEL [14]. The predicted ΔE values are 89, 92, 68, 165 and 93 mV, for L^1, L^2, L^3, L^4 and L^5, respectively. Although there is a good agreement between the predicted and the observed oxidation potential shift in L^1, L^2 and L^5 there is an important deviation for the benzimidazole derivatives probably due to the different nature of the protonated nitrogens.

The study of the change of $E_{1/2}$ as a function of the H^+ concentration shows for all the compounds studied in THF : H_2O (60 : 40 v/v) a steady one-wave shift, suggesting that the equilibrium is fast on the electrochemical time-scale. However the use of a different solvent may change the observed behaviour and produce a switching effect in the oxidation potential rather than a tuning process. Thus we have also studied the effect that the addition of H^+ has on the redox potential of L^1, L^2 and L^5 in dichloromethane : methanol (10 : 1) mixtures. Whereas no well defined voltammograms were observed for L^1, addition of acid (HCl, 0.1 M in dichloromethane : methanol 10 : 1) to L^2 and L^5 results in the appearance of a second wave at higher anodic potentials. After addition of two equivalents of acid the first wave disappears and only the second oxidation process is observed. The switching process is reversible and addition of KOH (KOH 0.1 M in dichloromethane : methanol 10 : 1) regenerates the first oxidation potential [8]. The ΔE between the first and the second wave is about 65 and 106 mV for L^2 and L^5, respectively. A similar behaviour has recently been observed for the benzimidazol derivatives L^3 and L^4.

Acknowledgements—We thank the Dirección General de Investigación Científica y Técnica (proyecto PB95-1121-C02-02) for support.

REFERENCES

1. Beer, P. D., Chen, Z., Drew, M. G. B., Kingston,

J., Ogden, M. and Spencer, P., *J. Chem. Soc., Chem. Commun.*, 1993, 1046; Beer, P. D., *Chem. Soc. Rev.*, 1989, **18,** 409.
2. Tendero, M. J. L., Benito, A., Martínez-Máñez, R., Soto, J., Payá, J., Edwards, A. J. and Raithby, P. R., *J. Chem. Soc., Dalton Trans.*, 1996, 343.
3. Tendero, M. J. L., Benito, A., Martínez-Máñez, R., Soto, J., García-España, E., Ramirez, J. A., Burguete, M. I. and Luis, S. V., *J. Chem. Soc., Dalton Trans.*, 1996, 2923.
4. Tendero, M. J. L., Benito, A., Martínez-Máñez, R. and Soto, J., *J. Chem. Soc., Dalton Trans.*, 1996, 4121.
5. Beer, P. D., Chen, Z., Drew, M. G. D., Johnson, A. O. M., Smith, D. K. and Spencer, P., *Inorg. Chim. Acta*, 1996, **246,** 143.
6. Padilla-Tosta, M. E., Martínez-Máñez, R., Pardo, T., Soto, J. and Tendero, M. J. L., *Chem. Commun.*, 1997, 887.
7. Tendero, M. J. L., Benito, A., Cano, J., Lloris, J. M., Martínez-Máñez, R., Soto, J., Edwards, A. J., Raithby, P. and Rennie, M. A., *J. Chem. Soc., Chem. Commun.*, 1995, 1643.
8. Benito, A., Martínez-Máñez, R., Payá, J., Soto, J., Tendero, M. J. L. and Sinn, E., *J. Organomet. Chem.*, 1995, **503,** 257.
9. Gran, G., *Analyst (London)*, 1952, **77,** 661; Rossotti, F. J. and Rossotti, H. J., *J. Chem. Educ.*, 1965, **42,** 375.
10. Gans, P., Sabatini, A. and Vacca, A., *J. Chem. Soc., Dalton Trans.*, 1985, 1195.
11. Lane, T. J. and Qinlan, K. P., *J. Am. Chem. Soc.*, 1960, **82,** 2994.
12. Benito, A., Martínez-Máñez, R., Soto, J. and Tendero, M. J. L., *J. Chem. Soc. Faraday Trans.*, 1997, **93,** 2175.
13. Plenio, H., Yang, J., Diodone, R. and Heinze, J., *Inorg. Chem.*, 1994, **33,** 4098.
14. PCMODEL, Molecular Modelling for Personal Computers and Workstations. Serene Software, 1988.

Pergamon

PII: S0277-5387(97)00353-7

Polyhedron Vol. 17, No. 4, pp. 497–505, 1998
© 1998 Elsevier Science Ltd
All rights reserved. Printed in Great Britain
0277-5387/98 $19.00+0.00

Generation of coordination networks with dicarboxylate-like ligands: synthesis and crystal structures of polymeric complexes of gadolinium(III) perchlorate with flexible double betaines

Ping-Rong Wei,* De-Dong Wu, Zhong-Yuan Zhou and Thomas C. W. Mak†

Department of Chemistry, The Chinese University of Hong Kong, Shatin, New Territories, Hong Kong

(Received 24 June 1997; accepted 13 August 1997)

Abstract—Three novel gadolinium(III) co-ordination polymers containing three flexible double betaines with different numbers of methylene bridges and a rigid *tris*(ethylene) bridge between two quaternary nitrogen atoms, namely $[\{Gd(L^1)_2(H_2O)_2\}_n](ClO_4)_{3n}\cdot nH_2O$ (**1**), $[\{Gd(L^2)_2(H_2O)_2\}_n](ClO_4)_{3n}\cdot nH_2O$ (**2**) and $[\{Gd(L^3)_2(H_2O)_2\}_n](ClO_4)_{3n}\cdot 8nH_2O$ (**3**) (L^1 = *N*,*N*′-dicarboxymethyl-*N*,*N*,*N*′,*N*′-tetramethyl-1,3-propanediammonium, $^-O_2CCH_2N^+Me_2$-$(CH_2)_3$-$N^+Me_2CH_2CO_2^-$; L^2 = *N*,*N*′-dicarboxymethyl-*N*,*N*,*N*′,*N*′-tetramethyl-1,4-butanediammonium, $^-O_2CCH_2N^+Me_2$-$(CH_2)_4$-$N^+Me_2CH_2CO_2^-$; L^3 = 1,4-diazoniabicyclo[2.2.2]octane-1,4-diacetate, $^-O_2CCH_2N^+(CH_2CH_2)_3N^+CH_2CO_2^-$), have been prepared and characterized by X-ray crystallography. Each complex contains paddlewheel-like dimeric subunits in which each pair of adjacent metal atoms is bridged by four μ-carboxylato-*O*,*O*′ groups that are orientated nearly perpendicular to each other about the metal–metal axis. The dimeric subunits are extended into a polymeric chain through the linkage of each metal center to the carboxylato groups of an adjacent dimer. Such infinite chains are extended into a plane wave-like layer structure in (**1**) and (**2**), and a three-dimensional framework in (**3**) by the cross-linkage of the molecular skeletons of double betaine ligands. The formation of hydrogen bonds further leads to a three-dimensional network in (**1**). The gadolinium(III) atom in each complex is surrounded in a distorted square-antiprismatic geometry by six carboxylato oxygen atoms and two aqua ligands. The carboxylato groups in the dimeric subunits adopt the common *syn–syn* bidentate bridging and unidentate co-ordination modes in (**1**), (**2**) and (**3**). In addition, the carboxylato groups in (**1**) and (**2**) also coordinate the metal atoms in an unusual *syn–skew* μ-*O*,*O*′ bridging mode. © 1998 Elsevier Science Ltd. All rights reserved

Keywords: gadolinium(III) perchlorate; coordination network; double betaine; dicarboxylate.

Metal co-ordination polymers of one-, two- and three-dimensional infinite frameworks have been the subject of intensive research for several decades, and major advances have been made in both their theoretical description and applications as new materials [1]. The chemistry of metal co-ordination polymers is among the most promising interfaces between synthetic chemistry and material science, as it provides a solid foundation for understanding how molecules can be organized and how functions can be achieved. Thus the structural design or modification of the framework has become a very active field in crystal engineering [2]. Our interest lies in the generation of polymeric structures in metal complexes by various double betaine ligands, each comprising two betaine moieties (betaine: $Me_3N^+CH_2CO_2^-$, IUPAC name: trimethylammonioacetate) in the same molecule and accordingly possessing pairs of anionic carboxylate groups and quaternary ammonio groups [3–6]. Recent studies have shown that variation of the double betaine ligands regarding the type of bridging unit, the flexibility of the molecular backbone and conformation preferences, as well as the metal ions employed and their counter anions, have a profound influence on the polymeric structures obtained [7–11].

* On sabbatical leave from the Department of Chemistry, Zhengzhou University, Zhengzhou 450052, P.R. China.

† Author to whom correspondence should be addressed.

In our latest attempts to prepare lanthanide complexes of betaines [12], we have obtained co-ordination polymers of neodymium and erbium perchlorates based on two-dimensional networks by using two flexible double betaines [13]. In the present work, we report the preparation and characterization of three new gadolinium(III) dicarboxylate-like complexes containing two- and three-dimensional frameworks constructed from three flexible double betaines with different numbers of methylene units and a rigid *tris*-(ethylene) bridge between two quaternary nitrogen atoms, namely $[\{Gd(L^1)_2(H_2O)_2\}_n](ClO_4)_{3n}\cdot nH_2O$ (**1**), $[\{Gd(L^2)_2(H_2O)_2\}_n](ClO_4)_{3n}\cdot nH_2O$ (**2**) and $[\{Gd(L^3)_2(H_2O)_2\}_n](ClO_4)_{3n}\cdot 8nH_2O$ (**3**) (L^1 = *N*,*N*′-dicarboxymethyl-*N*,*N*,*N*′,*N*′-tetramethyl-1,3-propanediammonium, $^-O_2CCH_2N^+Me_2$-$(CH_2)_3$-$N^+Me_2CH_2CO_2^-$; L^2 = *N*,*N*′-dicarboxymethyl-*N*,*N*,*N*′,*N*′-tetramethyl-1,4-butanediammonium, $^-O_2CCH_2N^+Me_2$-$(CH_2)_4$-$N^+Me_2CH_2CO_2^-$; L^3 = 1,4-diazoniabicyclo[2.2.2]octane-1,4-diacetate, $^-O_2CCH_2N^+(CH_2CH_2)_3N^+CH_2CO_2^-$).

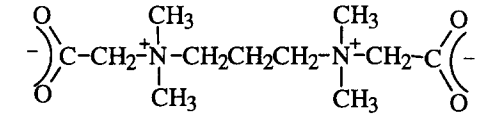

L^1

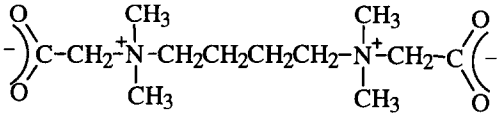

L^2

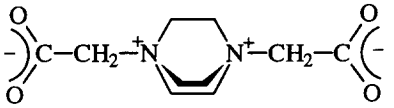

L^3

Structural formulas of L^1, L^2 and L^3

EXPERIMENTAL

Materials and measurements

The flexible double betaines L^1, L^2 and L^3 were synthesized as described previously [5(a),6]. The C, H and N microanalyses were carried out on a Perkin–Elmer 240 elemental analyser. Infrared spectra were recorded from KBr pellets in the range of 4000–400 cm^{-1} on a Perkin–Elmer 1600 FT-IR spectrometer.

Synthesis of complexes

$[\{Gd(L^1)_2(H_2O)_2\}_n](ClO_4)_{3n}\cdot nH_2O$ (**1**). Perchloric acid (2 N) was added slowly to an aqueous suspension (10 cm^3) of gadolinium oxide (Gd_2O_3 91 mg, 0.25 mmol) with stirring at about 60°C. The resulting clear solution of gadolinium(III) perchlorate (0.5 mmol) was mixed with an aqueous solution (5 cm^3) of L^1 (260 mg, 1.0 mmol). After stirring at about 60°C for a few minutes, the solution was filtered, and ethanol was diffused into the resulting solution over one week to yield colorless prismatic crystals. Found: C, 26.36; H, 5.07; N, 5.63. Calc. for $C_{22}H_{46}N_4O_{23}Cl_3Gd$: C, 26.47; H, 4.61; N, 5.61%. IR: 3449.2 (s), 2976.9 (w), 1617.9 (s), 1481.5 (m), 1435.2 (m), 1406.8 (m), 1336.5 (w), 1094.1 (s), 892.0 (w), 703.7 (w), 624.7 (m), 573.9 (w) and 481.8 (w) cm^{-1}.

$[\{Gd(L^2)_2(H_2O)_2\}_n](ClO_4)_{3n}\cdot nH_2O$ (**2**). To an aqueous solution (10 cm^3) of gadolinium(III) perchlorate (0.5 mmol) was added a solution of L^2 (274 mg, 1.0 mmol) in distilled water (5 cm^3) with stirring at about 60°C for a few minutes. After filtration, colorless block-like crystals were obtained by diffusing ethanol into the aqueous solution. Found: C, 27.63; H, 5.10; N, 5.32. Calc. for $C_{24}H_{54}N_4O_{23}Cl_3Gd$: C, 27.97; H, 5.24; N, 5.44%. IR: 3423.4 (s), 2980.5 (w), 1622.9 (s), 1483.2 (m), 1436.6 (m), 1407.5 (m), 1337.6 (w), 1138.7 (s), 1122.2 (s), 1081.5 (s), 895.1 (w), 720.5 (w), 627.3 (m), 570.4 (m) and 486.3 (w) cm^{-1}.

$[\{Gd(L^3)_2(H_2O)_2\}_n](ClO_4)_{3n}\cdot 8nH_2O$ (**3**) An aqueous solution (10 cm^3) of gadolinium(III) perchlorate (0.5 mmol) was mixed with a solution of L^3 (282 mg, 1.0 mmol) in water (5 cm^3). After stirring at about 60°C for a few minutes, a clear solution was obtained by filtration. The resulting solution was allowed to stand in air at room temperature for about a week to yield colorless prismatic crystals. Found: C, 22.31; H, 4.62; N, 5.44. Calc. for $C_{20}H_{54}N_4O_{30}Cl_3Gd$: C, 21.95; H, 4.93; N, 5.12%. IR: 3422.2 (s), 2988.9 (w), 1705.6 (m), 1644.4 (s), 1477.8 (w), 1444.4 (m), 1411.1 (m), 1322.2 (m), 1288.9 (m), 1138.9 (s), 1116.7 (s), 1088.9 (s), 905.6 (w), 877.8 (m), 850.0 (m), 682.3 (w), 627.8 (m) and 479.2 (w) cm^{-1}.

CAUTION. Metal perchlorate salts containing organic ligands are potentially explosive and should be handled with great care.

X-ray data collection and structure determination

Information concerning crystallographic data and structure refinement of the three complexes is summarized in Table 1. Raw intensities of complexes (**1**), (**2**) and (**3**) were collected at 293 K on a MSC/Rigaku RAXIS-IIC imaging plate system with a rotating anode X-ray source (Mo-K_α, λ = 0.71073 Å, 50 kV, 150 mA) [14], and corrected for absorption using the DIFABS program [15]. All calculations were performed on a PC 486 computer with the SHELXTL-PLUS program package [16]. Each crystal structure

Table 1. Data collection and processing parameters for complexes **1**–**3**

Complex	**1**	**2**	**3**
Formula	$C_{22}H_{46}N_4O_{23}Cl_3Gd$	$C_{24}H_{54}N_4O_{23}Cl_3Gd$	$C_{20}H_{54}N_4O_{30}Cl_3Gd$
Formula weight	998.2	1030.3	1094.3
Colour, habit	colorless prism	colorless block	colorless prism
Crystal size (mm^3)	$0.08\times0.12\times0.20$	$0.10\times0.18\times0.22$	$0.06\times0.20\times0.35$
Crystal system	Monoclinic	Triclinic	Monoclinic
Space group	$P2_1/c$ (No. 14)	$P\bar{1}$ (No. 2)	$P2_1/c$ (No. 14)
a (Å)	13.850(1)	12.035(2)	17.897(1)
b (Å)	25.711(1)	13.660(3)	14.731(1)
c (Å)	12.182(1)	14.881(3)	17.381(1)
α (°)	90	115.05(3)	90
β (°)	112.47(2)	106.10(3)	116.61(1)
γ (°)	90	97.44(3)	90
V (Å^3)	4008(2)	2041.9(10)	4097(2)
Z	4	2	4
$F(000)$	2020	1050	2228
D (calcd) (g cm^{-3})	1.654	1.676	1.774
μ (mm^{-1})	1.94	1.91	1.92
Collection range; $2\theta_{max}$	$\pm h, \pm k, l$; 45°	$\pm h, k, \pm l$; 45°	$\pm h, \pm k, l$; 45°
Unique data measured	8101	7458	7945
Observed data, n	6977 [$F \geqslant 6\sigma(F)$]	6399 [$F \geqslant 4\sigma(F)$]	6622 [$F \geqslant 6\sigma(F)$]
No. of variables, p	515	489	509
R	0.065	0.053	0.047
R'	0.083	0.071	0.058
S (goodness of fit)	1.24	1.36	1.26

$R = \Sigma\Delta/\Sigma|F_o|$, $R' = [\Sigma w\Delta^2/\Sigma\omega|F_o|^2]^{1/2}$ and $S = [\Sigma w\Delta^2/(n-p)]^{1/2}$ where $w = [\sigma^2(F_o)+K|F_o|^2]^{-1}\Delta = \|F_o|-F_c\|$; 10^4 K = 2, 8 and 2 for complexes **1**, **2** and **3**, respectively.

was solved with the Patterson superposition method. The non-hydrogen atoms were refined anisotropically, except for the oxygen atoms of the slightly disordered perchlorate groups in complexes (**1**) and (**2**), which were subjected to interatomic distance restraints of Cl—O = 1.42±0.01 Å and O···O = 2.31±0.02 Å and refined isotropically. All the hydrogen atoms were generated geometrically (C—H = 0.96 Å), assigned fixed isotropic thermal parameters, and included in the structure-factor calculations. Analytical expressions of neutral-atom scattering factors were employed, and anomalous dispersion corrections were incorporated [17]. Selected bond lengths and angles in Table 2. Additional information comprising atomic coordinates and thermal parameters has been deposited as Supplementary Material with the Editor.

RESULTS AND DISCUSSION

Description of structures

$[\{Gd(L^1)_2(H_2O)_2\}_n](ClO_4)_{3n}\cdot nH_2O$ (**1**). Complex (**1**) comprises a cationic polymer containing tetrakis(μ-carboxylato-*O*,*O*′)-bridged centrosymmetric dimeric subunits and discrete perchlorate anions, as well as lattice water molecules [Fig. 1(a)]. In each dimeric subunit, four carboxylato groups from respective L^1 ligands link a pair of gadolinium(III) atoms to generate a paddlewheel-like centrosymmetric [Gd_2(carboxylato-*O*,*O*′)$_4$] dimer, in both the usual *syn–syn* manner and an unusual *syn–skew* fashion. The latter mode, which is rarely encountered [18(a)], is intermediate between the *syn–syn* and *syn–anti* co-ordination modes commonly found in metal carboxylates [18(b)]. In the present complex one bridging carboxylato group coordinates the gadolinium(III) atom in an out-of-plane *skew* fashion [Gd(1)—O(5)—C(12)—C(13) 61.9°], while the other bridging carboxylato groups act in the most common *syn* mode [Gd(1)—O(4d)—C(11d)—C(10d) −178.8°, Gd(1)—O(3b)—C(11b)—C(10b) 146.7° and Gd(1)—O(6a)—C(12a)—C(13a) −159.9°]. The co-ordination sphere of each gadolinium(III) atom is completed by two unidentate carboxylato groups in the *syn* fashion [Gd(1)—O(7c)—C(22c)—C(21c) −167° and Gd(1)—O(1)—C(1)—C(2) −165.8°] and two aqua ligands in a distorted square antiprism. As shown in Fig. 1(b), one square face comprises four carboxylato oxygen atoms [O(4d), O(5), O(3b) and O(6a)] with a mean deviation of 0.043 Å from their least-square plane, whereas the other face as defined by two carboxylato oxygen atoms [O(1) and O(7c)] and two aqua oxygen atoms [O(1w) and O(2w)] has a mean deviation of 0.072 Å from their least-squares plane. The dihedral angle between the square faces is *ca.* 3.4°. The Gd—O distances lie between 2.320(4)

Table 2. Selected interatomic distances (Å) and angles (°) for complexes **1**–**3**

$[\{Gd(L^1)_2(H_2O)_2\}_n](ClO_4)_{3n} \cdot nH_2O$ (**1**)

Gd(1)—O(1)	2.347(4)	Gd(1)—O(5)	2.320(4)
Gd(1)—O(1W)	2.450(3)	Gd(1)—O(2W)	2.526(3)
Gd(1)—O(3b)	2.413(3)	Gd(1)—O(4d)	2.398(3)
Gd(1)—O(6a)	2.418(3)	Gd(1)—O(7c)	2.347(4)
Gd(1)···Gd(1a)	4.418(5)		
O(1)—Gd(1)—O(1W)	73.8(1)	O(1)—Gd(1)—O(2W)	71.3(1)
O(5)—Gd(1)—O(3b)	74.6(1)	O(5)—Gd(1)—O(4d)	74.8(1)
O(3b)—Gd(1)—O(6a)	76.6(1)	O(4d)—Gd(1)—O(6a)	77.7(1)
O(1W)—Gd(1)—O(7c)	69.6(1)	O(2W)—Gd(1)—O(7c)	72.5(1)
Hydrogen bonding:			
O(1W)···O(3W)	2.736(5)	O(3W)···O(3Wf)	2.761(5)

$[\{Gd(L^2)_2(H_2O)_2\}_n](ClO_4)_{3n} \cdot nH_2O$ (**2**)

Gd(1)—O(1)	2.382(4)	Gd(1)—O(5)	2.374(3)
Gd(1)—O(7)	2.387(4)	Gd(1)—O(1W)	2.497(4)
Gd(1)—O(2W)	2.438(4)	Gd(1)—O(3c)	2.416(4)
Gd(1)—O(4b)	2.318(5)	Gd(1)—O(6a)	2.381(3)
Gd(1)···Gd(1a)	4.479(5)		
O(1)—Gd(1)—O(1W)	71.1(1)	O(7)—Gd(1)—O(1W)	70.3(1)
O(1)—Gd(1)—O(2W)	71.8(1)	O(7)—Gd(1)—O(2W)	71.6(1)
O(5)—Gd(1)—O(3c)	75.4(1)	O(5)—Gd(1)—O(4b)	74.3(1)
O(3c)—Gd(1)—O(6a)	77.8(1)	O(4b)—Gd(1)—O(6a)	75.2(1)
Hydrogen bonding:			
O(1W)···O(3W)	2.787(5)	O(2W)···O(12)	2.860(5)

$[\{Gd(L^3)_2(H_2O)_2\}_n](ClO_4)_{3n} \cdot 8nH_2O$ (**3**)

Gd(1)—O(1)	2.377(4)	Gd(1)—O(5)	2.385(3)
Gd(1)—O(1W)	2.422(3)	Gd(1)—O(2W)	2.469(3)
Gd(1)—O(3b)	2.368(3)	Gd(1)—O(6a)	2.364(3)
Gd(1)—O(7c)	2.323(3)	Gd(1)—O(8d)	2.415(4)
Gd(1)···Gd(1a)	4.580(4)		
O(1)—Gd(1)—O(2W)	74.0(1)	O(1W)—Gd(1)—O(2W)	72.6(1)
O(1)—Gd(1)—O(3b)	77.1(1)	O(1W)—Gd(1)—O(3b)	71.0(1)
O(5)—Gd(1)—O(7c)	75.4(1)	0(6a)—Gd(1)—O(7c)	76.5(1)
O(5)—Gd(1)—O(8d)	73.8(1)	O(6a)—Gd(1)—O(8d)	72.6(1)
Hydrogen bonding:			
O(1w)···O(14)	2.851(4)	O(2w)···O(9w)	2.736(4)
O(3w)···O(1)	2.904(4)	O(4w)···O(2)	2.708(4)
O(4w)···O(5w)	2.806(4)	O(6w)···O(8w)	2.756(4)
O(9w)···O(10wd)	2.808(4)		

Symmetry code:

For (**1**): (a) −x, −y, −z; (b) −x, −0.5+y, 0.5−z; (c) x, y, 1+z; (d) x, 0.5−y, −0.5+z; (e) −x, −y, −1−z; (f) 1−x, −y, 1−z.

For (**2**): (a) 2−x, 1−y, 1−z; (b) 1+x, y, z; (c) 1−x, 1−y, 1−z; (d) 1−x, y, z; (e) 2−x, 2−y, 2−z.

For (**3**): (a) −x, −y, −z; (b) 1−x, −0.5+y, 0.5−z; (c) −x, −0.5+y, −0.5−z; (d) x, 0.5−y, 0.5+z; (e) −1+x, 0.5−y, −0.5+z.

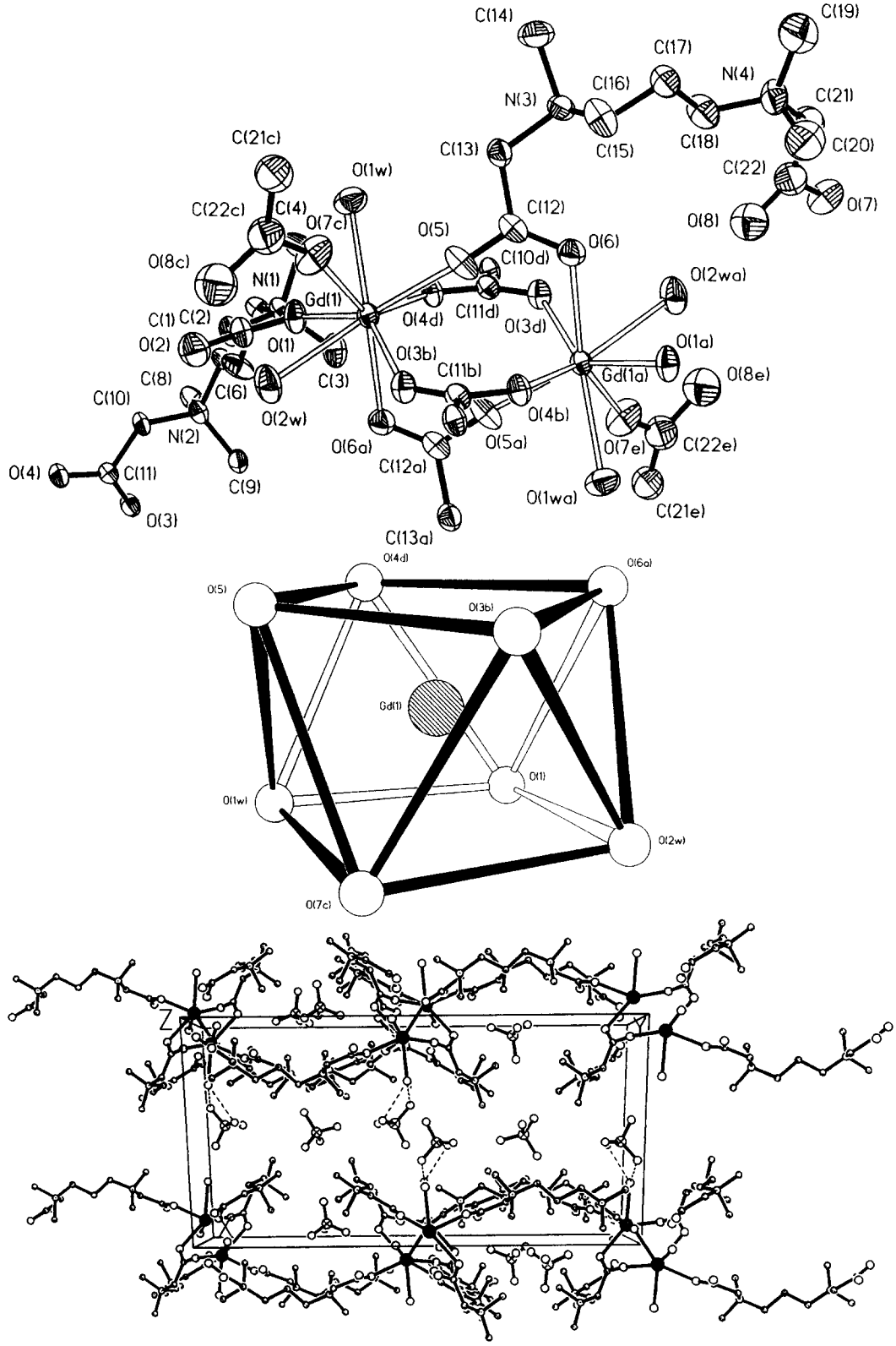

Fig. 1. (a) Structural skeleton of the asymmetric unit (35% thermal ellipsoids) of $[\{Gd(L^1)_2(H_2O)_2\}_n](ClO_4)_3n \cdot nH_2O$ (**1**) with atom labeling. (b) Perspective view showing the coordination polyhedron about the gadolinium(III) atom in (**1**). (c) Packing drawing of (**1**) showing the accommodation of perchlorate groups and lattice water molecules in the interlayer region between adjacent wavy coordination layers (see in cross section) matching the (100) planes. For clarity the Gd atoms are represented by large black circles.

and 2.526(3) Å, which are comparable to those found for other related gadolinium(III) carboxylates [19].

The molecular backbone of each of the two independent flexible double betaine ligands is extended to achieve a longer separation between its two quaternary nitrogen atoms. The conformation of the double betaine is similar to that in its hydrated form [5], but different from that in its mercury(II) adduct, in which the symmetry of the molecular backbone of L^1 has a C_2-axis at the middle methylene carbon atom [9(a)]. The Gd(1)···Gd(1a) separation is 4.418(5) Å, which is significantly larger than the average value [4.230 Å] in $[Gd_3(ClCH_2CO_2)_9(H_2O)_4]_n \cdot nH_2O$ [19]. A perspective view of complex (**1**) is shown in Fig. 1(c), where the dimeric subunits are extended into a polymeric chain running along the *b* direction. Such chains are further cross-linked by the molecular skeletons of double betaine ligands, thereby extending the structure into a wave-like layer corresponding to the plane (100). The perchlorate groups, one of which exhibits orientational disorder, are packed between the layers. The lattice water molecule O(3w) forms hydrogen bonds with aqua oxygen atom O(1w) and a symmetry-related lattice water molecule [O(3wf)] belonging to an adjacent layer [O(1w)···O(3w)···O(3wf)···O(1wf); O(1w)···O(3w) 2.736(5) Å, O(3w)···O(3wf) 2.761(5) Å], thereby leading to a three-dimensional network. A similar three-dimensional network formed by hydrogen bonding was also found in lanthanide(III) nicotinate [20].

$[\{Gd(L^2)_2(H_2O)_2\}_n](ClO_4)_{3n} \cdot nH_2O$ (**2**). The dimer in complex (**2**) is analogous to that of (**1**), being also a paddlewheel-like structure based on tetrakis(μ-carboxylato-*O*,*O*′) bridging [Fig. 2(a)]. The intra-dimeric Gd(1)···Gd(1a) separation [4.479(5) Å] and chemical environment of the gadolinium(III) atom in complex (**2**) are similar to those in (**1**), despite the fact that the two complexes crystallize in different space groups. Each gadolinium(III) atom is coordinated by six carboxylato oxygen atoms from L^2 ligands and two aqua ligands in an eight-coordination environment. The carboxylato groups of L^2 ligands in the dimeric subunits exhibit three different co-ordination modes: common bidentate bridging in the *syn–syn* configuration [Gd(1)—O(5)—C(13)—C(14) −162.6°, Gd(1a)—O(6)—C(13)—C(14) −166.2°], an unidentate mode [Gd(1)—O(1)—C(1)—C(2) 157.7°, Gd(1)—O(7)—C(19)—C(20) 157.5°], as well as an unusual *syn–skew* mode [Gd(1)—O(3c)—C(12c)—C(11c) −165.6°, Gd(1a)—O(4c)—C(12c)—C(11c) 117.9°]. The co-ordination geometry about each gadolinium(III) atom may be described as a square-antiprism with Gd—O distances in the range 2.318(5)–2.497(4) Å. One square face around the Gd(1) atom consists of oxygen atoms O(3c), O(4b), O(5) and O(6a) from different carboxylato groups with mean deviation 0.030 Å from their least-squares plane, and the other face is defined by two carboxylato oxygen atoms [O(1) and O(7)] and two aqua oxygen atoms [O(1w) and O(2w)] with a mean deviation of 0.010 Å from their least-squares plane. The dihedral angle between the square faces is *ca.* 1.6°. There are one complete and two independent "half molecules" of L^2 in the asymmetric unit of complex (**2**). Each half molecule has an inversion center located between the two middle methylene carbon atoms, being similar to that in its hydrated form [5], but different from that in its mercury(II) adduct, in which the molecular backbone of L^2 conforms to crystallographically imposed C_2 symmetry [9(a)]. A perspective view of complex (**2**) [Fig. 2(b)] shows that columns of paddlewheel-like [Gd_2(carboxylato-*O*,*O*′]$_4$ dimeric subunits stacked parallel to the *a* direction are cross-linked by the double betaine skeletons to generate a two-dimensional polymeric network corresponding to the (01$\bar{1}$) plane. The lattice water molecule O(3w) forms a hydrogen bond [O(3w)···O(1w) 2.787(5) Å] with an aqua ligand. The perchlorate groups, one of which forms an acceptor hydrogen bond [O(2w)···O(12) 2.860(5) Å] with an aqua ligand oxygen atom O(2w), occupy the inter-layer regions.

$[\{Gd(L^3)_2(H_2O)_2\}_n](ClO_4)_{3n} \cdot 8nH_2O$ (**3**). Complex (**3**) has a polymeric structure based on tetrakis(μ-carboxylato-*O*,*O*′)-bridged dimers [Fig. 3(a)] with an intra-dimeric Gd(1)···Gd(1a) distance of 4.580(4) Å, being a little longer than those in complexes (**1**) and (**2**). Each gadolinium(III) atom is coordinated by six carboxylato oxygen atoms from L^3 ligands and two aqua oxygen atoms in a square-antiprismatic geometry with Gd—O bond distances lying in the range 2.323(3)–2.469(3) Å, which are comparable to those in complexes (**1**) and (**2**). The mean deviations of the sets of oxygen atoms [O(1), O(3b), O(1w) and O(2w)] and oxygen atoms [O(5), O(7c), O(6a) and O(8d)] from their least-squares planes are 0.075 and 0.003 Å, respectively. The dihedral angle between the least-squares planes is *ca.* 2.1°. Unlike complexes (**1**) and (**2**), the carboxylato groups of L^3 ligands in complex (**3**) show two coordination modes: common *syn–syn* bridging bidentate [Gd(1)—O(5)—C(11)—C(12) −155.4°, Gd(1a)—O(6)—C(11)—C(12) −162.4°, Gd(1a)—O(7d)—C(20d)—C(19d) 146.9°, Gd(1)—O(8d)—C(20d)—C(19d) −169.3°] and unidentate [Gd(1)—O(1)—C(1)—C(2) −151.0°, Gd(1)—O(3b)—C(10b)—C(9b) −137.1°]. The two independent double betaine ligands in the asymmetric unit adopt an "S-shaped" conformation, similar to that in its hydrated form and hydrochloric acid adduct [6], but different from that in its cadmium bromide complex [21], in which the skeleton of L^3 exhibits a "C-shaped" conformation with the plane of one carboxylato group being approximately parallel to that of the other. The crystal structure of complex (**3**) is shown in Fig. 3(b), where the dimeric subunits are extended into plane wave-like layers corresponding to the (100) family of planes and further cross-linked by the double betaine skeletons to generate a three-dimensional polymeric framework. Hydrogen bonding plays an important role in consolidating this solid-state structure. The lattice water molecules form hydrogen bonds with one another [O(4w)···O(5w) 2.806(4) Å, O(6w)···O(8w)

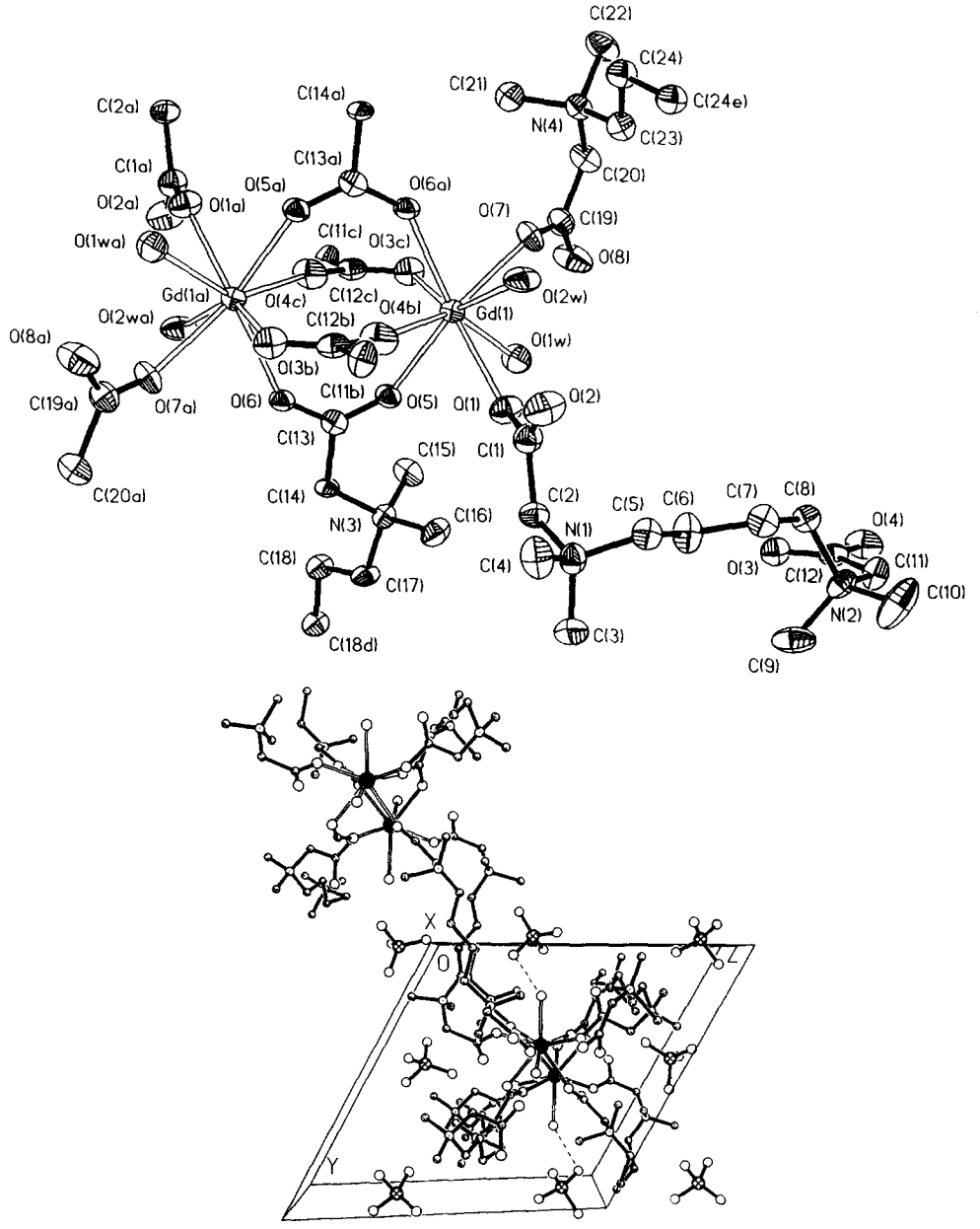

Fig. 2. (a) Structural skeleton of the asymmetric unit (35% thermal ellipsoids) of $[\{Gd(L^2)_2(H_2O)_2\}_n](ClO_4)_{3n} \cdot nH_2O$ (**2**) with atom labeling. (b) Packing drawing showing a plane wave-like layer (seen in cross section) corresponding to the $(01\bar{1})$ plane in the crystal structure of (**2**). The Gd atoms are represented by large black circles.

2.756(4) Å, O(9w)···O(10wd) 2.808(4) Å], and also donor hydrogen bonds [O(2w)···O(9w) 2.736(4) Å, O(1)···O(3w) 2.904(4) Å, O(2)···O(4w) 2.708(4) Å] with aqua ligand O(2w), co-ordinated caboxylato oxygen atom O(1), as well as unco-ordinated carboxylato oxygen atom O(2). The perchlorate groups, one of which forms an acceptor hydrogen bond [O(1w)···O(14) 2.851(4) Å] with aqua ligand O(1w), occupy the pockets and have no contact with the metal ions.

Summary

Lanthanide carboxylates have been widely studied, and most of them exhibit one- and two-dimensional polymeric structures [22]. Lanthanide co-ordination polymers with three-dimensional frameworks are very rare, although a three-dimensional lanthanide(III) nicotinate complex constructed from hydrogen bonding has been reported [20]. The present study has shown that novel lanthanide co-ordination polymers

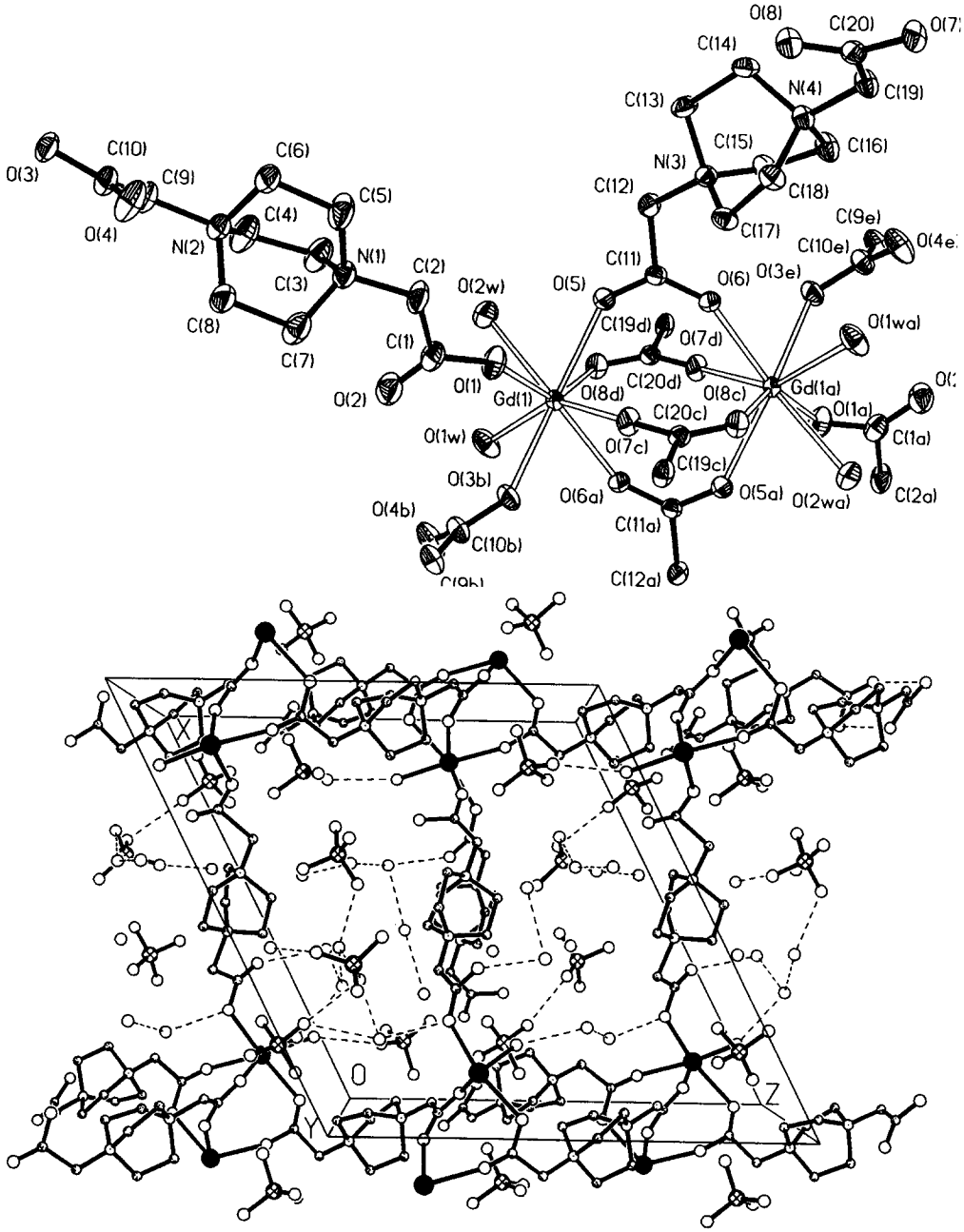

Fig. 3. (a) Structural skeleton of the asymmetric unit (35% thermal ellipsoids) of $[\{Gd(L^3)_2(H_2O)_2\}_n](ClO_4)_{3n} \cdot 8nH_2O$ (**3**) with atom labeling. (b) Packing drawing showing the three-dimensional coordination framework in the crystal structure of (**3**). The Gd atoms are represented by large black circles.

can be generated from gadolinium(III) perchlorate with flexible double betaines. The resulting three complexes in the present study are all based on the cross-linkage of paddlewheel-like tetrakis(carboxylato)-bridged dimers by the double betaine molecular backbones. Although they have the same metal-betaine ratio and nearly identical gadolinium co-ordination environments, complexes (**1**) and (**2**) have wave-like layer structures whereas (**3**) exhibits a three-dimensional framework. Variation of the bridging groups between two quaternary nitrogen atoms in three double betaines results in different crystal symmetries, co-ordination fashion of the carboxylato groups, as well as packing modes in the solid state.

Acknowledgement—This work is supported by Hong Kong Research Grants Council Earmarked Grant CUHK 303/96P.

REFERENCES

1. Pelhaes, P. and Drillon, M., *Organic and Inorganic Low-dimensional Crystalline Materials*, Plenum Press, New York, 1987.
2. (a) Sheats, J. E., Carraher, C. E. Jr., Pittman, C. U. Jr., Zeldin M. and Currell, B., *Inorganic and Metal-Containing Polymeric Materials*, Plenum Press, New York, 1990; (b) Laine, R. M., *Inorganic and Organometallic Polymers with Special Properties*, Kluwer, Dordrecht, 1992.
3. (a) Weiss, R., Roth, R., Lowack, R. H. and Bremer, M., *Angew. Chem. Int. Ed. Engl.*, 1990, **29**, 1132; (b) Wu, D.-D. and Mak, T. C. W., *J. Chem. Crystallogr.*, 1994, **24**, 689.
4. Wei, P.-R., Wu, D.-D. and Mak, T. C. W., *J. Mol. Struct.*, 1996, **372**, 181.
5. (a) Wu, D.-D., and Mak, T. C. W., *J. Mol. Struct.*, 1994, **326**, 193; (b) Wu, D.-D. and Mak, T. C. W., *J. Mol. Struct.*, 1996, **372**, 187.
6. Wu, D.-D. and Mak, T. C. W., *J. Chem. Crystallogr.*, 1997, **27**, 11.
7. (a) Wu, D.-D. and Mak, T. C. W., *J. Chem. Soc., Dalton Trans.*, 1995, 2671; (b) Wei, P.-R., Wu, B.-M., Leung, W.-P. and Mak, T. C. W., *Polyhedron*, 1996, **15**, 4041.
8. (a) Wu, D.-D. and Mak, T. C. W., *Polyhedron*, 1994, **13**, 3333; (b) Wu, D.-D. and Mak, T. C. W., *Struct. Chem.*, 1996, **7**, 205.
9. (a) Wu, D.-D. and Mak, T. C. W., *J. Chem. Soc., Dalton Trans.*, 1995, 139; (b) Wu, D.-D. and Mak, T. C. W., *Inorg. Chim. Acta*, 1995, **237**, 163.
10. Wu, D.-D. and Mak, T. C. W., *J. Chem. Crystallogr.*, 1996, **26**, 471.
11. Wei, P.-R., Wu, D.-D. and Mak, T. C. W., *Inorg. Chim. Acta*, 1996, **249**, 169.
12. (a) Chen, X.-M. and Mak, T. C. W., *Inorg. Chem.*, 1994, **33**, 2444; (b) Chen, X.-M. and Mak, T. C. W., *Polyhedron*, 1994, **13**, 1087; (c) Chen, X.-M., Aubin, S. M. J., Wu, Y.-L., Yang, Y.-S., Mak, T. C. W. and Hendrickson, D. N., *J. Am. Chem. Soc.*, 1995, **117**, 9600; (d) Chen, X.-M., Wu, Y.-L., Wang, R.-J. and Mak, T. C. W., *Polyhedron*, 1996, **15**, 739.
13. Wei, P.-R., Wu, D.-D., Zhou, Z.-Y., Li, S.-L. and Mak, T. C. W., *Polyhedron*, 1997, **16**, 749.
14. (a) Krause, K. L. and Phillips, G. N. Jr., *J. Appl. Crystallogr.*, 1992, **25**, 146; (b) Sato, M., Yamamoto, M., Imada, K., Katsube, Y., Tanaka, N. and Higashi, T., *J. Appl. Crystallogr.*, 1992, **25**, 348; (c) Tanner, J. and Krause, K. L., *The Rigaku Journal*, 1994, **11**, 4.
15. Walker, N. and Stuart, D., *Acta Crystallogr. Sect. A*, 1983, **39**, 158.
16. Sheldrick, G. M., In *Computational Crystallography*, ed. D. Sayre, Oxford University Press, New York, 1982, p. 506. Sheldrick, G. M., In *Crystallographic Computing 3: Data Collection, Structure Determination, Proteins, and Databases*, ed. G. M. Sheldrick, C. Kruger and R. Goddard, Oxford University Press, New York, 1985, p. 175.
17. *International Tables for X-ray Crystallography*, Vol. 4, ed. J. A. Ibers and W. C. Hamilton, Kynoch Press, Birmingham (now distributed by Kluwer Academic Press, Dordrecht), 1974, pp. 55, 99, 149.
18. (a) Mak, T. C. W. and Chen, X.-M., *J. Aust. Chem.*, 1991, **44**, 639; (b) Mehrotra, C. and Bohra, R., *Metal Carboxylates*, Academic Press, New York, 1983.
19. (a) Liu, S., Yang, L.-W., Rettig, S. J. and Orvig, C., *Inorg. Chem.*, 1993, **32**, 2773; (b) Sugita, Y. and Ouchi, A., *Bull. Chem. Soc. Jpn.*, 1987, **60**, 171.
20. Moore, J. W., Glick, M. D. and Baker, W. A. Jr., *J. Am. Chem. Soc.*, 1972, **94**, 1858.
21. Wu, D.-D. and Mak, T. C. W., *Inorg. Chim. Acta*, 1996, **253**, 15.
22. (a) Ouchi, A., Suzuki, Y., Ohki, Y. and Koizumi, Y., *Coord. Chem. Rev.*, 1988, **92**, 29; (b) Wei, P.-R., Jin, T.-Z., Yang, Q.-C. and Xu, G.-X., *J. Rare Earths*, 1992, **10**, 166.

Pergamon

PII: S0277-5387(97)00354-9

Polyhedron Vol. 17, No. 4, pp. 507–511, 1998
© 1998 Elsevier Science Ltd
All rights reserved. Printed in Great Britain
0277-5387/98 $19.00+0.00

Mass spectrometric and structural studies of some platinum-group metal complexes: the crystal and molecular structure of *trans*-$[Ru(NO)Cl_3(SbPh_3)_2]$

Sunil Chand,[a] Richard K. Coll[b]* and J. Scott McIndoe[b]

[a] Department of Chemistry, School of Pure & Applied Sciences, The University of the South Pacific, Suva, Fiji

[b] Department of Chemistry, The University of Waikato, Hamilton, New Zealand

(Received 21 April 1997; accepted 13 August 1997)

Abstract—The ruthenium triphenylstibine complexes $[RuCl_2(SbPh_3)_3]$ and $[RuCl_2(SbPh_3)_4]$, and the nitrosyl complexes $[Ru(NO)Cl_3(EPh_3)_2]$ for E = Sb, As, P; $[Rh(NO)Cl_2(EPh_3)_2]$ for E = As, P, have been investigated using electrospray mass spectrometry. The mass spectrometric evidence suggests that $[RuCl_2(SbPh_3)_4]$ is formed and not $[RuCl_2(SbPh_3)_3]$ as previously reported. *In situ* derivatisation in the presence of alkali metal ions gave simple spectra for the ruthenium nitrosyl complexes but not the rhodium complexes. The crystal and molecular structure for the ruthenium complex $[Ru(NO)Cl_3(SbPh_3)_2]$ has been determined by single crystal X-ray diffraction. There is a crystallographically imposed centre of inversion and the NO and chlorides are disordered. The triphenylstibine ligands are coordinated in the *trans* configuration (Ru–Sb = 2.649(1) Å). © 1998 Elsevier Science Ltd. All rights reserved

Keywords: ruthenium; nitrosyl; rhodium; triphenylstibine; electrospray mass spectrometry X-ray structure.

The preparation, reaction, and structural chemistries of nitrosyl-organopnictide and nitrosyl organochalcogenide complexes of platinum-group metals of the form $[M(NO)X_3L_2]$ for M = Ru, Os, X = halide, L = organopnictide or organochalcogenide, and $[M(NO)X_2L_2]$ for M = Rh, Ir, X = halide, L = organopnictide have been reported by us and other workers [1–18]. The chemistry of complexes with tertiary stibine and arsine ligands is in general much less well developed compared with their phosphine analogues despite the fact that they are good donor ligands. One reason for this may be the lack of suitable analytical probes for these ligands. Tertiary phosphines are conveniently studied using ^{31}P NMR spectroscopy, but there are no readily accessible NMR active nuclei available for the arsine and stibine ligands. There have been a number of X-ray structural investigations of these complexes, but again most of the studies have been carried out on organophosphine complexes with little data available for organoarsine or organostibine complexes [15,19–28].

The versatile new soft ionisation technique available in electrospray mass spectrometry [ESMS] is well suited to studying such complexes [29–30]. The soft ionisation process used in ESMS typically results in simple patterns in which the molecular ion peak or a simple adduct is clearly evident. At low cone voltage fragmentation is usually very limited, and fragmentation can easily be investigated by raising the cone voltage.

For neutral transition metal complexes good spectra can often be obtained by *in situ* derivatisation. For example this may involve the formation of adducts in which a halide or other negative ligand has been replaced by a neutral donor ligand that is present in the solvent. Common donor ligands include acetonitrile, water, and ammonia, and replacement of a halide ion by these ligands results in the formation of adducts with a single positive charge.

Here we have investigated the reported preparation of the complex $[RuCl_2(SbPh_3)_3]$ using ESMS. In

* Author to whom correspondence should be addressed.

addition we report ESMS for the complexes $[Ru(NO)Cl_3(EPh_3)_2]$ for E = P, As, Sb, and the five coordinate rhodium analogues, $[Rh(NO)Cl_2(EPh_3)_2]$ for E = P, As. During our studies of ruthenium organostibine complexes we isolated crystals of $[Ru(NO)Cl_3(SbPh_3)_2]$. Because of the paucity of data for organostibine complexes we have determined the structure by single crystal X-ray diffraction.

EXPERIMENTAL

The complexes $[RuCl_2(SbPh_3)_3]$, $[RuCl_2(SbPh_3)_4]$, $[Ru(NO)Cl_3(PPh_3)_2]$, $[Ru(NO)Cl_3(AsPh_3)_2]$, $[Ru(NO)Cl_3(SbPh_3)_2]$, $[Rh(NO)Cl_2(PPh_3)_2]$, and $[Rh(NO)Cl_2(AsPh_3)_2]$, were prepared by literature methods [1–3,7]. Recrystallisation by the slow evaporation of a chloroform solution produced red-orange, bipyramidal crystals of $[Ru(NO)Cl_3(SbPh_3)_2]$ suitable for X-ray analysis. Spectroscopic and analytical data for the recrystallised material were as observed previously for the bulk sample [1]: IR KBr disk ν(NO) 1840 cm^{-1}; ^1H NMR (δ ppm) 7.45 3-H, m; 7.75 2-H, m. Anal: found; C, 45.77; H, 3.19%; calc. for $C_{36}H_{30}Cl_3NORuSb_2$: C, 45.83; H, 3.20%.

Electrospray mass spectra were recorded in positive-ion mode on a VG Platform II instrument, using methanol as the mobile phase. No precautions were taken to exclude oxygen from the system. The samples were introduced via a microlitre syringe and a 10 μl sample loop fitted to a Rheodyne injector, with the mobile phase being delivered to the mass spectrometer by a Spectra System P1000 LC pump, at a flow rate of 0.01 ml min^{-1}. Nitrogen was employed both as the nebulising and drying gas. Fragmentation was investigated by varying the skimmer cone voltage, typically from 10 to 80 V. Spectra were typically acquired as 10 to 12 scans, and subsequently averaged. Isotope patterns for major species were recorded, and compared with calculated patterns obtained using the Isotope simulation program [31].

The crystal data, data collection parameters, and structure refinement details are summarised in Table 1. The unit cell parameters were determined by the least square refinement of 25 accurately centred high angle reflections. The data were collected at 168 K on a Siemens R3m Four-circle X-ray diffractometer with graphite-monochromated Mo–K_α radiation (λ = 0.71073 Å) using θ-scans to a maximum angle of $2\theta = 54°$. Reflection intensities were corrected for Lorentz and polarisation effects, and crystal stability was monitored by observation of three standard reflections after every 100 reflections: no movement or decay was observed. The absorption correction was based on ψ-scans and an ellipsoidal model, and the structure was solved in the centrosymmetric space group $P\bar{1}$ using the direct methods. The structure has been modelled with the chlorides and NO disordered over all four sites using a fractional occupancy [1/4 NO + 3/4 Cl] as recommended by the crystallographic referee. The nitrogen and oxygen atoms were inserted in calculated positions using Ru—N and N—O bond lengths taken from the literature [20]. The Ru—Cl, Ru—N, and N—O bond lengths were constrained to provide an acceptable refinement. All non-hydrogen atoms except the disordered nitrogen and oxygen atoms were modelled assuming anisotropic thermal vibration. Attempts to refine the nitrogen and oxygen atoms using isotropic thermal vibration were unsuccessful, and so these atoms were modelled using fixed temperature factors. Atomic scattering factors were taken from Crommer and Mann [32] and corrected for the effects of anomalous scattering using values from Crommer and Liberman [33]. The structure was solved using the direct methods and the refinement was carried out using a full-matrix least squares refinement procedure based on F^2. The final cycle of refinement based on 3283 unique observed data [$I > 2\sigma(I)$] and 208 variables converged with an

Table 1. Crystal data and structure refinement for $[Ru(NO)Cl_3(SbPh_3)_2)]$

Empirical formula	$C_{36}H_{30}Cl_3NORuSb_2$
Formula weight	943.53
Temperature	168(2) K
Wavelength	0.71073 Å
Crystal system	Triclinic
Space group	$P\bar{1}$
Unit cell dimensions	
a	9.842(4) Å
b	9.850(2) Å
c	10.419(4) Å
α	111.450(10)°
β	109.52(3)°
γ	92.44(3)°
Volume	870.3(5)Å
Z	1
Density (calculated)	1.800 mg/m^3
Absorption coefficient	2.229 mm^{-1}
Absorption correction	ψ-scans, ellipsoid model
Min/max transmission	0.477/0.531
F(000)	458
Crystal size	0.44 × 0.42 × 0.36 mm
Crystal colour/morphology	red-orange/bipyramid
θ range for data collection	2.24–27.00°
Index ranges	$-12 \leqslant h \leqslant 2$; $-11 \leqslant k \leqslant 11$, $-12 \leqslant l \leqslant 12$
Reflections collected	4540
Independent reflections	3682 [R_{int} = 0.0141]
Independent reflections [$I > 2\sigma(I)$]	3283
Refinement method	Full-matrix least-squares on F^2
Data/constraints/parameters	3682/12/208
Goodness-of-fit on F^2	1.028
Final R indices [$I > 2\sigma(I)$]	$R1$ 0.0548, $wR2$ 0.1458
R indices (all data)	$R1$ 0.0613, $wR2$ 0.1517
Largest diff. peak and hole	1.98 and −1.13 e Å^{-3}

Table 2. Selected bond lengths [Å] and angles [°] for [Ru(NO)$Cl_3(SbPh_3)_2$]

Ru(1)—Cl(1)	2.277(3)
Ru(1)—Cl(2)	2.345(2)
Ru(1)—Sb(1)	2.649(1)
Sb(1)—C(36)	2.095(8)
Sb(1)—C(16)	2.126(8)
Cl(1)—Ru(1)—Cl(2)	89.2(1)
Cl(2)—Ru(1)—Sb(1)	90.8(7)
C(31)—C(36)—Sb(1)	115.5(7)

$R = 0.0548$ and $Rw = 0.0613$, where the functions minimised are: $R = \Sigma(\|F_o\| - |F_c\|)/\Sigma(|F_o|$ and $Rw = \sqrt{[\Sigma w|F_o| - |F_c|^2)/\Sigma w|F_o|^2]}$. The data were processed and the structure solution and refinement carried out using the SHELXTL system of programs [34].

Selected atomic distances and angles are given in Table 2.

RESULTS AND DISCUSSION

Stephenson and Wilkinson (1966) [35] have reported that the reaction of hydrated ruthenium chloride with triphenylstibine at room temperature or under reflux results in the formation of the complex $[RuCl_2(SbPh_3)_3]$. Champness *et al.* (1993) have disputed the formation of $[RuCl_2(SbPh_3)_3]$ and their attempts to prepare this complex resulting in the formation of the complex $[RuCl_2(SbPh_3)_4]$ characterised by single-crystal X-ray diffraction [19]. As pointed out it is sometimes difficult to discriminate convincingly between these complexes on the basis of elemental analytical data or other spectroscopic evidence [19]. Although much structural information is provided by single-crystal X-ray studies, this does not provide information about the bulk material.

In this work the reaction of ruthenium chloride with excess triphenylstibine [6 : 1] under reflux gave a pink powder. The ESMS for this powder in the presence of a trace amount of CH_3CN contained evidence for the parent ion $[RuCl_2(SbPh_3)_4]^+$ [$M^+ = 1584$] and the adduct: $[RuCl_2(SbPh_3)_3(CH_3CN)]^+$ [$M^+ = 1273$]. A small peak assigned to the $[RuCl_2(SbPh_3)_3]^+$ ion [$M^+ = 1232$] was observed, but only a high cone voltage [> 80 V]. It is likely that this species has appeared as a result of fragmentation of the parent ion $[RuCl_2(SbPh_3)_4]^+$.

The product of the reaction of ruthenium chloride with triphenylstibine at room temperature gave a different, more complex, spectrum. The complexity of the spectrum indicated that a mixture of compounds had been produced in this reaction. There was no evidence for parent ions $[RuCl_2(SbPh_3)_3]^+$, $[RuCl_2(SbPh_3)_4]^+$, or any simple adducts of these ions. Hence our studies support those of Champness *et al.* (1993), and it seems there is some doubt over the existence of $[RuCl_2(SbPh_3)_3]$.

The nitrosyl complexes $[Ru(NO)Cl_3(EPh_3)_2]$ for E = Sb, As, P were also investigated using ESMS. None of the complexes gave simple spectra when measured in the presence of neutral donor species. Other workers have reported good ESMS for neutral metal carbonyl complexes by *in situ* derivatisation in the presence of anionic or cationic species [29–30]. For complexes containing basic carbonyl ligands, good spectra were obtained using Ag^+ ions. Non-polar, poorly basic carbonyl complexes required the presence of a nucleophile such as the methoxylate ion. This derivatisation reaction resulted in the formation of negative ion adducts of the form $[M + OMe]^-$.

In this work good spectra were obtained for ruthenium nitrosyl complexes in the presence of traces of alkali metal ions. The spectra for the complex $[Ru(NO)Cl_3(SbPh_3)_2]$ together with the isotope pattern and simulated spectra are shown in Fig. 1. Similar spectra were obtained for the triphenylphosphine and triphenylarsine complexes. The spectra suggest that simple 1 : 1 adducts are formed between the nitrosyl

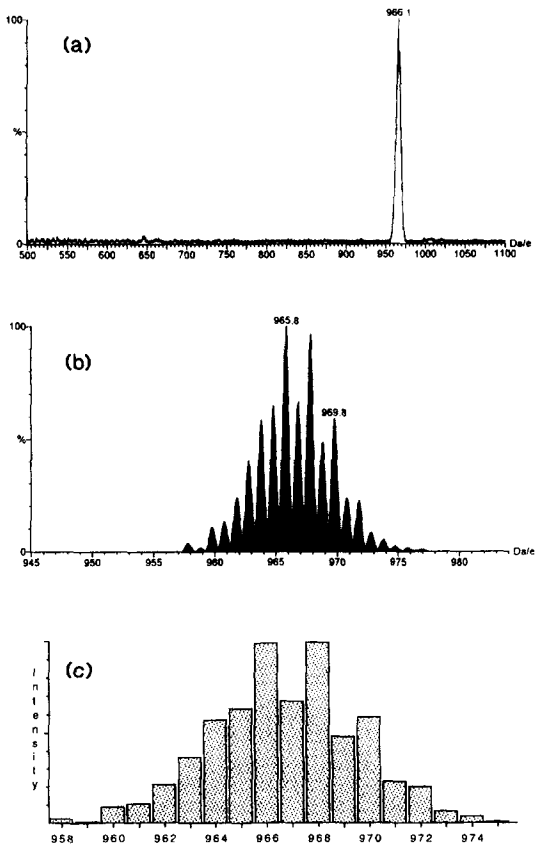

Fig. 1. Electrospray mass spectrum for [Ru(NO)$Cl_3(SbPh_3)_2] + Na^+$. (a) Mass spectrum; (b) isotope pattern for [Ru(NO)$Cl_3(SbPh_3)_2$)] + Na^+; (c) simulated mass spectrum for [Ru(NO)$Cl_3(SbPh_3)_2$)] + Na^+.

complex and the alkali metal ions. Good spectra were obtained using Li^+ Na^+ or K^+ ions, but not with Cs^+ or Rb^+. We also repeated our ESMS investigation of the complexes $[RuCl_2(SbPh_3)_3]$, and $[RuCl_2(SbPh_3)_4]$ in the presence of alkali metal ions, but were unable to obtain good spectra. Thus it seems likely that the nitrosyl oxygen is the basic centre despite the fact that the NO is bound in the linear fashion. Previous X-ray photoelectron studies have suggested that there is greater electron density on the nitrosyl ligand when it is coordinated in the bent fashion [36–42]. In view of this we also investigated some five-coordinate rhodium analogues: i.e. complexes of the form $[Rh(NO)Cl_2(EPh_3)_2]$. However, we were unable to obtain good spectra of parent ions or using any of the *in situ* derivatisation techniques described above. Previous studies have shown that the coordinated NO in these complexes is particularly labile and hence it seems likely that it is lost under the experimental conditions employed [1].

A view of the structure of $[Ru(NO)Cl_3(SbPh_3)_2]$ is shown in Fig. 2. Based on statistical analysis of the data and the recommendation of Brock and Dunitz (1994) [43] we have solved the structure in the centrosymmetric space group $P\bar{1}$, despite the fact that this imposes disorder.

The ruthenium atom lies on the origin and hence the structure has a crystallographically imposed centre of inversion and because of this, the NO and chlorides are disordered. The structure has been modelled with the chlorides and NO disordered over all four sites using a fractional occupancy of [1/4 NO + 3/4 Cl] and constrained bond lengths [see Experimental]. Crystallographically imposed disorder in NO complexes has also been reported for the related five-coordinated iridium and rhodium triphenylphosphine complexes $[Ir(NO)Cl_2(PPh_3)_2]$, and $[Rh(NO)Cl_2(PPh_3)_2]$ [4–5]. The triphenylstibine ligands in $[Ru(NO)Cl_3(SbPh_3)_2]$ are in the more common *trans* configuration as reported for other similar structures [4–5,9,12–13]. Few complexes are known in which the organopnictide or organochalcogenide ligand are coordinated in the *cis* configuration [1,15–18]. In fact the *cis* arrangement of the organopnictide ligands is only seen for complexes containing less bulky ligands such as Me_2PPh and Me_2AsPh [1,17].

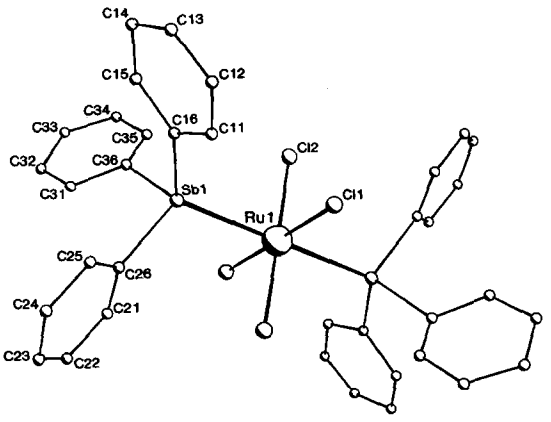

Fig. 2. Perspective view of the structure of [Ru $(NO)Cl_3(SbPh_3)_2$)]. The disorder NO has been omitted for clarity.

The structures for two analogous complexes have been reported previously: $[Ru(NO)Cl_3(PPh_3)_2]$ [12] and more recently $[Ru(NO)Cl_3(AsPh_3)_2]$ [20]. The triphenylphosphine and triphenylarsine analogues are isostructural with each other and with the related complex $[Os(NH_3)Cl_3(PPh_3)_2]$ [21]. All of these structures were solved in the space group $C2/c$. Close examination of the crystalline sample of $[Ru(NO)Cl_3(SbPh_3)_2]$ revealed that the sample contained crystals of two different morphologies: red thin plates, and red-orange bipyramids. We investigated both crystal types extensively and found no difference in unit cell parameters or any evidence for a unit cell similar to that seen for the phosphine or arsine analogues. Furthermore, there is no evidence in the spectra or analytical figures for the presence of any other compounds.

There are few reports of X-ray structural determinations of platinum group metal complexes containing organostibine ligands. Almost all of the reported complexes were carbonyl complexes [19,20–28] and the only closely comparable complexes are *mer*-$[OsBr_3(SbPh_3)_3]$ [23] and $[RuCl_2(SbPh_3)_4]$ [19]. The Ru—Sb bond length of 2.649(1) Å found in this work is at the long end of the range compared with the reported values [range 2.579(1)–2.654(2) Å]. Two of the values reported for $[OsBr_3(SbPh_3)_3$ [2.640(2), 2.644(2) Å] are a little shorter than found in this work. The third bond length reported for $[OsBr_3(SbPh_3)_3]$ [2.654(2) Å] is unusually long when compared with this work and the other reported values. This is somewhat surprising considering the osmium atom is formally in the +3 oxidation state whereas most of the other complexes are in the +2 or lower oxidation states. Interestingly the M—Sb bond lengths seen in the ruthenium (II) complex $[RuCl_2(SbPh_3)_4]$ [range 2.625(1)–2.632(1) Å] are significantly shorter than seen in either of $[OsBr_3(SbPh_3)_3]$ or in the present work, although they are similar to the other reported values. This difference may indicate a higher degree of metal-to-ligand π-back-bonding in the complex $[RuCl_2(SbPh_3)_4]$ due to the presence of the soft Ru(II) metal ion. In view of the disorder and constraints imposed upon the Ru—Cl bond lengths during refinement, comparisons with other data are unlikely to be meaningful. The C—Sb and C—C bond lengths in the ligands are similar to other reported values [9,11–13,19,21–28].

Supplementary material

Isotropic thermal parameters, atomic coordinates, a complete list of bond distances and angles, together

with observed and calculated structure factors have been deposited with the Cambridge Crystallographic Data Centre.

Acknowledgements—The authors acknowledge the University Grants Committees of The University of Waikato and The University of the South Pacific for the provision of funds for the purchase of equipment and chemicals. One of us, J.S.M., acknowledges The University of Waikato for the award of a post-graduate scholarship. We thank Prof. Brian Nicholson for helpful discussions.

REFERENCES

1. Coll, R. K. and Fergusson, J. E., *Inorg. Chim. Acta*, 1993, **207**(2), 191.
2. Robinson, S. D. and Uttley, M. F., *J. Chem. Soc., Dalton Trans.*, 1972, 1.
3. Robinson, S. D. and Uttley, M. F., *J. Chem. Soc. (A)*, 1971, 1254.
4. Golberg, S. Z., Kubiak, C., Meyer, C. D. and Eisenberg, R., *Inorg. Chem.*, 1975, **14**(7), 1650.
5. Mingos, D. M. P. and Ibers, J. A., *Inorg. Chem.*, 1971, **10**(5), 1035.
6. Araneo, A., Valenti, V. and Cariati, F., *J. Inorg. Nucl. Chem.*, 1970, **32**(6), 1877.
7. Baird, M. C., *Inorg. Chim. Acta*, 1971, **5**(1), 46.
8. Fergusson, J. E., Robinson, W. T. and Coll, R. K., *Inorg. Chim. Acta*, 1991, **181,** 37.
9. Coll, R. K., Fergusson, J. E., McKee, V., Page, C. T., Robinson, W. T. and Teow Sian Keong, *Inorg. Chem.*, 1987, **26**(1), 106.
10. Coll, R. K., Fergusson, J. E. and Teow Sian Keong, *Aust. J. Chem.*, 1986, **39**(7), 1161.
11. Fergusson, J. E., Page, C. T. and Robinson, W. T., *Inorg. Chem.*, 1976, **15**(9), 2270.
12. Haymore, B. L. and Ibers, J. A., *Inorg. Chem.*, 1975, **14**(12), 3060.
13. Schultz, A. J., Henry, R. L., Reed, J. and Eisenberg, R., *Inorg. Chem.*, 1974, **13**(3), 732.
14. Gupta, M., Seth, J. and Agarwala, U. C., *Indian J. Chem. Sect. A*, 1990, **29A**(2), 143.
15. Seddon, E. A. and Seddon, K. R., *Topics in Inorganic and General Chemistry*, Monograph 19, The Chemistry of Ruthenium, ed. R. J. H. Clark, Elsevier, 1984.
16. Fergusson, J. E. and Rodley, G. A., *Inorganic Chemistry Series* 2 : *Transition Metals Part* 2, Butterworths, London, 1975.
17. Townsend, R. E. and Coskran, K. J., *Inorg. Chem.*, 1971, **10**(8), 1661.
18. Innorta, G. and Modelli, A., *Inorg. Chim. Acta*, 1978, **31**(1), L367.
19. Champness, N. R., Levason, W. and Webster, M., *Inorg. Chim. Acta*, 1993, **208**(2), 189.
20. Souza, D. H. F., Oliva, G., Teixeira, A. and Batista, A. A., *Polyhedron*, 1995, **14**(8), 1031.
21. Bright, D. and Ibers, J. A., *Inorg. Chem.*, 1969, **8**(5), 1078.
22. Forbes, E. J., Jones, D. L., Paxton, K. and Hamor, T. A., *J. Chem. Soc., Dalton Trans.*, 1979, 879.
23. Hinckley, C. C., Matusz, M. and Robinson, P. D., *Acta Crystallogr. Sect. C*, 1988, **C44,** 1829.
24. Martin, L. R., Einstein, F. W. B. and Pomeroy, R. K., *Inorg. Chem.*, 1983, **22,** 1959.
25. Martin, L. R., Einstein, F. W. B. and Pomeroy, R. K., *Inorg. Chem.*, 1985, **24,** 2777.
26. Johnson, B. F. G., Lewis, J., Whitton, A. J. and Bott, S. G., *J. Organomet. Chem.*, 1990, **389,** 129.
27. Ang, H. G., Koh, C. H., Kon, L. L. and Kwik, W. L., *J. Organomet. Chem.*, 1993, **452,** 181.
28. Layer, T. M., Lewis, J., Martin, A., Raithby, P. R., Wing-Tak Wong, *J. Chem. Soc., Dalton Trans.*, 1992, 3411.
29. Henderson, W. and Nicholson, B. K., *J. Chem. Soc., Chem. Commun.*, 1995, 2531.
30. Henderson, W., McIndoe, J. S., Nicholson, B. K. and Dyson, P. J., *J. Chem. Soc., Chem. Commun.*, 1996, 1183.
31. Arnold, L. J., *J. Chem. Ed.*, 1992, **69,** 811.
32. Cromer, D. T. and Mann, J. B., *Acta Crystallogr. Sect. A*, 1968, **24,** 321.
33. Cromer, D. T. and Liberman, D., *J. Chem. Phys.*, 1970, **53,** 1891.
34. Sheldrick, G. M., SHELXTL user's manual, University of Cambridge.
35. Stephenson, T. A. and Wilkinson, G., *J. Inorg. Nucl. Chem.*, 1966, **28,** 945.
36. Su Chan-Cheng and Faller, J. W., *J. Organomet. Chem.*, 1975, **84**(1), 53.
37. Clark, D. T., Woolsey, I. S., Robinson, S. D., Laing, K. R. and Wingfield, J. N., *Inorg. Chem.*, 1977, **16**(5), 1201.
38. Brant, P. and Feltham, R. D., *J. Electron Spectrosc. Relat. Phenom.*, 1979, **16**(5), 379.
39. Feltham, R. D. and Brant, P., *J. Amer. Chem. Soc.*, 1982, **104**(3), 641.
40. Finn, P. and Jolly, W. L., *Inorg. Chem.*, 1972, **11**(4), 893.
41. Nefedov, V. I., Sinitsyn, N. M., Salyn, Ya V. and Bayer, L., *Soviet J. Coordination Chemistry*, 1975, **1**(12), 1332 [1618 : original Russian].
42. Pierpont, C. G., Pucci, A. and Eisenberg, R., *J. Amer. Chem. Soc.*, 1971, **93**(12), 3050.
43. Brock, C. P. and Dunitz, J. D., *Chem. Mater.*, 1994, **6,** 1118.

Pergamon

PII: S0277-5387(97)00343-4

Polyhedron Vol. 17, No. 4, pp. 513–517, 1998
© 1998 Elsevier Science Ltd
All rights reserved. Printed in Great Britain
0277-5387/98 $19.00+0.00

Effect of ligand and solvent on chloride ion coordination in anti-tumour copper(I) diphosphine complexes: synthesis of $[Cu(dppe)_2]Cl$ and analogous complexes (dppe = 1,2-bis(diphenylphosphino)ethane)

Jason S. Lewis,[a] Jamal Zweit[b] and Philip J. Blower[a]*

[a] Biosciences Department, The University, Canterbury CT2 7NJ, U.K.

[b] Joint Department of Physics, Institute of Cancer Research, Royal Marsden Hospital, Sutton SM2 5PT, U.K.

(Received 10 July 1997; accepted 8 August 1997)

Abstract—Complexes formed between copper(I) and 1,2-bis(diphenylphosphino)ethane (L^1) have previously been isolated as salts of the $[CuL^1_2]^+$ cation if only non-coordinating anions are present, or as $[Cu_2Cl_2L^1_3]$ if chloride is present. We describe the synthesis of $[CuL^1_2]Cl$, the stoichiometry of which is confirmed by elemental analysis, FAB mass spectroscopy and conductivity. Polar solvents (water–ethanol mixtures) lead to isolation of the latter, whereas solvents of lower polarity ($CHCl_3$, CH_2Cl_2) lead to isolation of the complexes containing coordinated chloride. Related ligands such as *cis*-1,2-bis(diphenylphosphino)ethene, 1,2-bis(diethylphosphino) ethane, 1,2-bis(dimethylphosphino)ethane and 1,2-bis(hydroxymethylphosphino)ethane, give salts $[CuL_2]Cl$. This behaviour, and that of other 1,2-bisphosphine ligands, is rationalised in terms of competition between chloride and phosphine ligands for binding sites on the metal, with the equilibrium position determined by solvent polarity, ligand structure and rigidity, and steric and electronic properties of the ligands. © 1998 Elsevier Science Ltd

Keywords: copper; phosphine.

INTRODUCTION

Copper(I) bis(diphosphine) complexes have been of interest because of their tumouricidal properties [1] and more recently, for their possible application as radiopharmaceuticals containing copper radioisotopes for medical imaging and radioisotope therapy [2,3]. Of the diphosphines tested, when complexed to copper, 1,2-bis(diphenylphosphino)ethane (L^1, see Fig. 1) produced the greatest increase in life span of rats with experimental cancers [4]. This ligand was tested in the form of the complex $[Cu_2Cl_2L^1_3]$, prepared by the reaction of CuCl with L^1 in chloroform. In contrast, reactions of CuCl with *cis*-bis(diphenylphosphino)ethene (L^2) and 1-(diethylphosphino)-2-(diphenylphospino)ethane give the salts $[CuL_2]Cl$, which were tested against tumours in this form [4,5]. Attempts to prepare the analogous complex of L^1, $[CuL^1_2]Cl$ for testing against tumours were not successful [1,5] and hence it could not be determined whether the relative tumouricidal effects of the complexes are related to their stoichiometry and charge. Progress in the application of the complexes requires understanding of the factors governing their structural and stoichiometric preferences. Here we describe the synthesis of the hitherto unreported complex $[CuL^1_2]Cl$ (**1**) and analogous complexes **2**–**5** with other 1,2-diphosphines L^2–L^5 (Fig. 1), and rationalise the equilibria between the complex types in terms of ligand electron donating power, chelate rigidity, and solvent polarity.

* Author to whom correspondence should be addressed. Tel: +44-(0)1227-766877 ext 4774 or +44-(0)1227-823475; Fax: +44-(0)1227-783059; e-mail: P.J.Blower@ukc.ac.uk

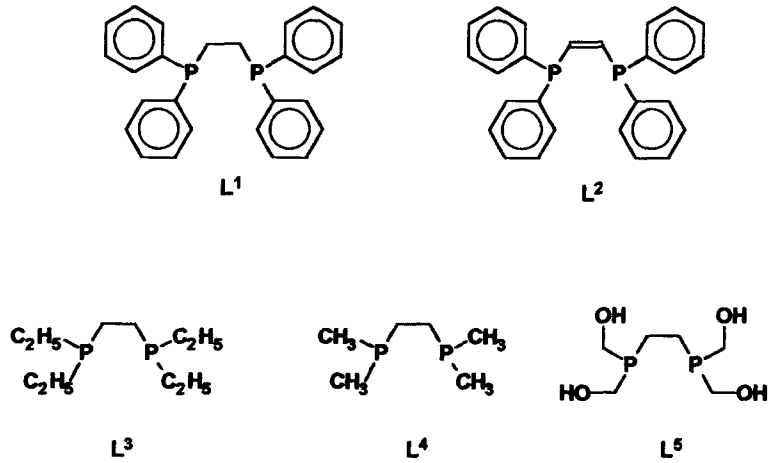

Fig. 1. Structures of ligands used in this work.

EXPERIMENTAL

All reactions were undertaken in air with anhydrous solvents unless otherwise indicated. C, H, N elemental analysis was performed by the Chemical Laboratory, University of Kent. ^{1}H NMR measurements were performed using a Jeol 270 MHz NMR spectrometer. Fast Atom Bombardment mass spectra were obtained using 3-nitrobenzyl alcohol as the matrix material at the EPSRC Mass Spectrometry Centre, Swansea, U.K. Infra-red spectra were recorded in the range 400–4000 cm^{-1} as Nujol mulls on KBr plates using a Perkin-Elmer infra-red spectrophotometer. Conductivities were measured using a Bibby MC1 conductivity meter on 1 mM solutions in anhydrous solvents, with $[Bu_4N]Cl$ solution as a calibrating standard. L^5 was prepared using published methods [6], as were the silver complexes $[AgL^1_2](NO_3)$ and $[AgL^2_2](NO_3)$ [7,8]. All chemicals were purchased from Aldrich, U.K. For thin layer chromatography (TLC), silica gel plates (Merck $60F_{254}$) and a mobile phase consisting of 0.9% saline (60%) and acetonitrile (40%) were used. The chromatograms were visualised with a UV lamp. Under these conditions the silver complexes $[AgL^1_2]^+$ and $[AgL^2_2]^+$ migrated with R_f 0.5, slightly lower than the values for their copper analogues.

Synthesis of $[Cu(L^1)_2]Cl$ (**1**) *and* $[Cu(L^2)_2]Cl$ (**2**) *from* $CuCl_2 \cdot 2H_2O$ *and diphosphines*

Typically L^1 or L^2 (52 mg, 0.13 mmol) was warmed in 2 ml of ethanol until fully dissolved. $CuCl_2 \cdot 2H_2O$ (8.5 mg, 0.05 mmol in 0.5 ml water) was added. An immediate loss of colour was observed and the resulting solution was allowed to stir at room temperature for a few minutes. The resulting white precipitate was isolated by filtration, yield 75% (L^1), 78% (L^2).

Synthesis of **1** *and* **2** *from* $[AgL^n_2](NO_3)$ (n = 1, 2) *and* $CuCl_2 \cdot 2H_2O$

The silver phosphine complex (96 mg, 0.1 mmol) was taken up in 2 ml ethanol. $CuCl_2 \cdot 2H_2O$ (1.7 mg, 0.01 mmol in 0.5 ml water) was added and the mixture stirred for 30 min. The silver chloride precipitate was removed by filtration and the filtrate analysed by thin layer chromatography.

Synthesis of $[Cu(L^3)_2]Cl$ (**3**) *and* $[Cu(L^4)_2]Cl$ (**4**)

The complexes were produced by modification of methods previously reported [5] for L^2. In brief, L^3 or L^4 (33 mg or 24 mg respectively, 0.16 mmol) was dissolved in 25 ml $CHCl_3$, and solid CuCl (8 mg, 0.08 mmol) was added. The mixture was stirred for 1 h at room temperature under a stream of nitrogen. The solvent was removed *in vacuo* to leave an oily residue. Diethyl ether was added and the compound was induced to crystallise by scratching. White crystals formed and were collected in air, yield 82% (L^3), 84%(L^4). The same complex, as identified by TLC, was obtained by using $CuCl_2 \cdot 2H_2O$ in place of CuCl.

Synthesis of $[CuL^5_2]Cl$ (**5**)

L^5 (0.075 g, 0.35 mmol) was taken up in 2 ml CH_2Cl_2. CuCl (0.017 g, 0.15 mmol) was added. The colourless solution was stirred for 1 hour at room temperature. The CH_2Cl_2 layer was extracted with 3×2 ml H_2O. The water fractions were collected and the water removed *in vacuo* to produce a colourless oil, yield 89%. ^{1}H NMR (D_2O): 4.4 (m, 16H, CH_2OH), 2.3 (m, 8H, CH_2CH_2). IR (Nujol mull): 3200–3400 (s, ν(O—H)).

RESULTS

Three approaches were employed in the synthesis of the bis(diphosphine) complexes of copper(I) chloride:

(a) reaction of CuCl with two mole-equivalents of diphosphine;
(b) reaction of $CuCl_2$ with 2.5–3 mole-equivalents of diphosphine;
(c) reaction of $CuCl_2$ with an excess of the labile silver complex of the diphosphine, $[AgL_2](NO_3)$.

All methods were successful in affording the complex salts in high yield (75–84% isolated). In method (b) the phosphine was used as a reducing agent as well as chelator, and for this reason additional phosphine was added. Method (c) was used with the more hydrophobic phosphines (L^1, L^2) in order to present the phosphine to the copper in a form that is more soluble in water or ethanol than the phosphine itself. This method also entails the phosphine acting as a reducing agent, and the reaction was accompanied by the precipitation of silver chloride which was removed by filtration. The reactions were conducted in either ethanol or water, except where literature methods were used. In all cases the complexes isolated were colourless crystalline solids (except $[CuL_2^5]Cl$ which was a colourless viscous oil) and had the stoichiometry $[CuL_2]Cl$. This formulation was consistent with elemental analysis and fast atom bombardment mass spectroscopy (Table 1). The latter all showed molecular ions corresponding to $[CuL_2]^+$ at 100% abundance. The conductivity measurements confirm that the complexes are fully ionised as 1 : 1 electrolytes in methanol solution, suggesting that chloride ion does not displace phosphine from the metal coordination sphere to a significant extent in that solvent. None of the spectroscopic techniques, however, can confirm unequivocally that the complexes exist as salts in the solid state rather than, for example, in the form $[CuCl(\eta^2\text{-}L)(\eta^1\text{-}L)]$ as found in the case where L = 2,3-bis(diphenylphosphino)maleic anhydride [3].

DISCUSSION

Previous attempts at synthesis of **1** have been unsuccessful: the $[CuL_2^1]^+$ cation has only been isolated previously in the form of salts of non-coordinating anions (trifluoroacetate, nitrate, dimesitylcuprate) [9–12]. Even weakly coordinating anions such as acetate [13] and nitrate [11] can displace one of the phosphine ligands in non-polar solvents (benzene) [13] containing an excess of L^1. The present work shows that this is primarily a solvent effect: with use of polar solvents (water/ethanol mixtures), it is not necessary to add an excess of diphosphine in order to suppress coordination of chloride ion, and chloride salt **1** can be isolated. It would now be of value to compare the anti-tumour efficacy of this complex with the other copper diphosphine complexes already examined [4], and with $[Cu_2Cl_2L_3^1]$ in particular. The conformationally rigid diphosphine L^2 does not appear to require highly polar solvents to form the corresponding chloride salt of the cationic complex: in previous reports complex **2** was isolated readily from chloroform solution [5].

The three complexes of 1,2-bis(dialkyl) phosphinoethane L^3, L^4, and L^5, (**3–5**) have not been

Table 1. Analytical and physical data

Complex	Formula	Microanalysis[a]	Conductivity[b]	FAB-MS	Rf[c]
1	$[CuL_2^1]Cl \cdot H_2O$	$CuC_{52}H_{50}P_4ClO$ C 68.7 (68.3) H 5.4 (5.5)	140.1	859 (100%, M^+); 461 (64%, M^+-L^1)	0.60
2	$[CuL_2^2]Cl \cdot 2H_2O$	$CuC_{52}H_{48}P_4ClO_2$ C 67.5 (67.3) H 5.0 (5.2)	139.5	855 (100%, M^+); 459 (96%, M^+-L^2)	0.61
3	$[CuL_2^3]Cl$	$CuC_{20}H_{48}P_4Cl$ C 46.8 (47.0) H 9.3 (9.5)	138.8	475 (100%, M^+); 269 (45%, M^+-L^3)	0.58
4	$[CuL_2^4]Cl$	$CuC_{12}H_{32}P_4Cl$ C 36.1 (36.1) H 8.0 (8.1)	146.4	363 (100%, M^+); 213 (52%, M^+-L^4)	0.58
5	$[CuL_2^5]Cl$	$CuC_{12}H_{32}P_4ClO_8$ C 27.6 (27.3) H 5.9 (6.1)	142.6	491 (100%, M^+)	n.d.[d]

[a] Calculated values in parenthesis.
[b] $\Omega^{-1}\,cm^{-1}\,mol^{-1}$. See experimental section for conditions. The standard compound $[Bu_4N]Cl$ gave a value of 142.1 under the same conditions.
[c] See experimental section for conditions.
[d] n.d. = not determined.

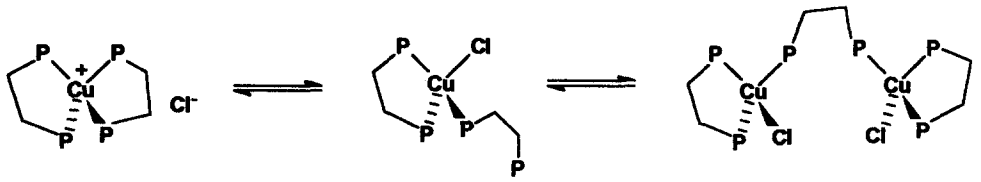

Fig. 2. Ligand exchange equilibria in copper(I) chloride complexes with 1,2-diphosphine ligands.

prepared previously, although the complex cation $[CuL^4_2]^+$ has been isolated in the solid state with a non-coordinating anion [14]. It is not necessary to use highly polar solvents to obtain the cationic complexes as chloride salts if the phosphines are alkylated rather than arylated: both L^3 and L^4 complex salts were isolated in good yield from chloroform solution. This is consistent with the earlier synthesis of $[Cu(eppe)_2]Cl$ (eppe = 1(diethylphosphino)-2-(diphenylphosphino) ethane) [8] under the same conditions.

While the results described here do not unequivocally eliminate the possibility that one or more of the complexes contain coordinated chloride ion in the solid state, they indicate that in polar solvents (e.g. methanol and, presumably, water which is of greatest relevance for the biomedical applications of these complexes) even the weakest chelator, L^1, forms a copper(I) complex that exists as 1 : 1 electrolyte with chloride as the counter ion, even in the absence of excess phosphine ligand. It appears that stronger electron donating phosphines, more rigid chelating geometries, and more polar solvents all favour displacement of chloride from the copper by phosphine groups. Thus, L^1 is a relatively weak donor and forms only non-electrolyte complexes in non-polar solvents. It displaces chloride only in polar solvents or when present in large excess, whereas the stronger (by virtue of alkyl substitution rather than aryl) and less sterically hindered donors L^3 and L^4 form 1 : 1 electrolytes in both polar and non-polar solvents and without any excess diphosphine. L^2 likewise displaces chloride more effectively than L^1, by virtue of its rigidity which entropically favours chelation. On the other hand, 2,3-bis(diphenylphosphino)maleic anhydride does not displace chloride readily: although it has a rigid chelating structure its electron donating ability is weaker than that of L^2 because of the anhydride group [3]. Upon hydrolysis of the anhydride group, however, the donor ability improves and it gives a complex analogous to that of L^2 [3].

In conclusion, by combining the experience described here with previous published work it is possible to rationalise qualitatively the coordination behaviour of the different diphosphine ligands with respect to their ability to displace chloride ion from the copper coordination sphere, as a function of the electron donating ability of the ligand, the conformational rigidity of the ligand, and the dielectric of the solvent. Chloride ion and 1,2-bis(diphosphine) ligands are thus well-matched in their affinity for the Cu^+ ion. The complex equilibria that occur, previously identified by ^{31}P NMR spectroscopy [5] in dichloromethane and dimethylacetamide solution and represented in part by Fig. 2, can be decisively controlled by relatively subtle modifications of the ligand or conditions.

Acknowledgments—We thank the Biotechnology and Biological Sciences Research Council (U.K.) and the Institute of Cancer Research for a CASE studentship (to J.S.L.).

REFERENCES

1. Berners-Price, S. J., Sadler, P. J., Phosphines and metal phosphine complexes: relationship of chemistry to anti-cancer and other biological activity. *Struct. Bonding* (Berlin), 1988, **70,** 27–102.
2. Lewis, J. S., Zweit, J., Dearling, J. L. J., Rooney, B. C., Blower, P. J., Copper(I) bis(diphosphine) complexes as a basis for radiopharmaceuticals for positron emission tomography and targeted radiotherapy. *Chem. Commun.*, 1996, 1093–1094.
3. Lewis, J., Heath, S. L., Powell, A. K., Zweit, J., Blower, P. J., Diphosphine bifunctional chelators for low-valent metal ions. Crystal structures of the copper(I) complexes $[CuClL^1_2]$ and $[CuL^1_2][PF_6]$ (L^1 = 2,3-bis(diphenylphosphino) maleic anhydride). *J. Chem. Soc., Dalton Trans.*, 1997, 855–861.
4. Mirabelli, C. K., Hill, D. T., Faucette, L. F., McCabe, F. L., Girard, G. R., Bryan, D. B., Sutton, B. M., Bartus, J. O., Crooke, S. T., Johnson, R. K., Antitumour activity of bis(diphenylphosphino)alkanes, their gold(I) coordination complexes and related compounds. *J. Med. Chem.*, 1987, **30,** 2181–2190.
5. Berners-Price, S. J., Johnson, R. K., Mirabelli, C. K., Faucette, L. F., McCabe, F. L., Sadler, P. J., Copper(I) complexes with bidentate tertiary phosphine ligands: solution chemistry and antitumor activity. *Inorg. Chem.*, 1987, **26,** 3383–3387.
6. Reddy, V. S., Katti, K. V., Barnes, C. L., Chemistry in environmentally benign media. 1. Synthesis and characterisation of 1,2-bis[bis (hydroxymethyl)phosphino]ethane (HMPE)—X-ray structure of $[Pt\{(HOH_2C)_2PCH_2CH_2P(CH_2OH)_2\}_2]Cl_2$. *Inorg. Chim. Acta*, 1995, **240,** 367–370.
7. Berners-Price, S. J., Brevard, C., Pagelot, A.,

Sadler, P. J., Stable, chelated, tetrahedral silver(I) complexes with bidentate phosphine ligands. A novel application of INEPT to $^{109}Ag\{^{31}P\}$NMR. *Inorg. Chem.*, 1985, **24,** 4278–4281.

8. Berners-Price, S. J., Brevard, C., Pagelot, A., Sadler, P. J., $[Cu(Ph_2PCH_2CH_2PEt_2)_2]Cl$: a chelated copper(I) complex with tetrahedral stereochemistry. Rate of inversion compared with those of isostructural silver(I) and gold(I) complexes. *Inorg. Chem.*, 1986, **25,** 596–599.
9. Dines, M. B., Phosphine and olefin complexes of copper(I) trifuoroacetate. *Inorg. Chem.*, 1972, **11,** 2949–2952.
10. Camus, A., Marsich, N., Nardin, G., Randaccio, L., The crystal and molecular structure of bis[1,2-bis(diphenylphosphino)ethane]copper(I) trifluoroacetate toluene solvate. *Transition Met. Chem.*, 1976, **1,** 205–206.
11. Anderson, W. A., Carty, A. J., Palenik, G. J., Schreiber, G., Nitrato and acetylacetonato complexes of copper(I). *Canadian J. Chem.*, 1971, **49,** 761–766.
12. Leoni, P., Pasquali, M., Ghilardi, C. A., Isolation and crystal and molecular structure of a rare example of a mononuclear organo-cuprate. *J. Chem. Soc., Chem. Commun.*, 1983, 240–241.
13. Edwards, D. A., Richards, R., Complexes of copper(I) acetate. Part I. Complexes with σ-donor ligands. *J. Chem. Soc., Dalton Trans.*, 1975, 637–643.
14. Darensbourg, D. J., Chao, C.-S., Reibenspies, J. H., Bischoff, C. J., Crystal structure and reactivity of $[Cu(dmpe)_2][Cu(Co(CO)_4)_2]$ (dmpe = 1,2-bis(dimethylphosphino)ethane): staggered and eclipsed conformations of $[(CO)_4Co\text{-}CuCo(CO)_4]^-$ anions. *Inorg. Chem.*, 1990, **29,** 2153–2157.

Pergamon

PII: S0277-5387(97)00341-0

Polyhedron Vol. 17, No. 4, pp. 519–522, 1998
© 1998 Elsevier Science Ltd
All rights reserved. Printed in Great Britain
0277-5387/98 $19.00+0.00

Synthesis and crystal structure of a monomeric aryloxo ytterbium dichloride $(ArO)YbCl_2(THF)_3$ (ArO=2,6-ditertbutyl-4-methylphenoxo)

Yingming Yao,[a] Qi Shen*[a] and Jie Sun[b]

[a] Chemistry Department of Suzhou University, Suzhou 215006 P.R. China

[b] Shanghai Institute of Organic Chemistry, Chinese Academy of Sciences, Shanghai 200032 P.R. China

(Received 25 November 1996; accepted 8 August 1997)

Abstract—The aryloxo ytterbium complex $(ArO)YbCl_2(THF)_3$ (ArO=2,6-ditertbutyl-4-methylphenoxo) has been prepared by the reaction of anhydrous $YbCl_3$ with ArONa in THF in the ratio of 1 : 1 at room temperature. The crystal structure was determined by X-ray diffraction. The molecular complex is a six-coordinate monomer. Two chlorine atoms, one oxygen atom of aryloxo and three oxygen atoms of THF coordinate to ytterbium atom to form a pseudo-octahedron. It belongs to orthorhombic crystal system, space group *Fddd*. The Yb—O(Ar) distance and the Yb—Cl distance are 2.083(5) Å and 2.555(2) Å, respectively. © 1998 Elsevier Science Ltd. All rights reserved

Keywords: synthesis; crystal structure; aryloxide; ytterbium; dichloride.

The large growth in organolanthanide chemistry has primarily centred on the complexes stabilized by cyclopentadienyl ligands. As their precursors, cyclopentadienyl lanthanide chlorides have been extensively studied including their syntheses and reactivities. In recent years, alkoxo and aryloxo ligands have become attractive monoanionic ligands, since they will form strong bonds with lanthanides and can be easily modified in steric bulk by substitution. The syntheses and reactivities of trialkoxo- and triaryloxo-lanthanide have been developed [1–11]. Recently, some alkyl and hydride lanthanide complexes have been synthesized and structurally characterized with bulky aryloxo as auxiliary ligand and they show good catalytic activity for cyclopolymerization of diene and for the polymerization of α-olefins [12–24]. However, the syntheses and structures of mononuclear alkoxo- and aryloxo-lanthanide dichlorides have not yet been studied. The dichlorides are considered to be the precursors for further transformation. We are investigating the synthesis and molecular structure and report here the synthesis and X-ray characterization of monomeric aryloxo ytterbium dichloride.

* Author to whom correspondence should be addressed.

EXPERIMENTAL

All manipulations were performed under argon using the Schlenk technique. THF was distilled from sodium benzophenone ketyl before use. Anhydrous $YbCl_3$ was prepared according to the literature [15]. ArONa was prepared from the reaction of ArOH and Na in THF. Metal and chlorine analyses were carried out using complexometric titration and the Volhard method, respectively. IR spectrum was recorded on a Nicolet-550 FTIR spectrometer as KBr pellets.

Synthesis of $(ArO)YbCl_2(THF)_3$

To a suspension of $YbCl_3$ (1.306 g, 4.67 mmol) in 20 cm^3 THF was slowly added a solution of ArONa (5.83 cm^3, 4.67 mmol) in THF at room temperature. After being stirred for 72 h, the NaCl was separated from the reaction mixture by centrifugation. The solvent was removed *in vacuo* to yield an orange-red powder (2.69 g, 85%). Found Yb, 25.8; Cl, 10.3. Calc. for $(ArO)YbCl_2(THF)_3$ Yb, 25.6; Cl, 10.5%. IR absorptions (cm^{-1}), 2957(s), 2918(w), 2873(w), 1634(s), 1434(s), 1396(m), 1362(m), 1231(m), 1151(s), 1065(m), 1027(w), 864(s), 771(s), 460(m). The powder was dissolved in THF and cooled to −5°C for crys-

tallization, the yellow crystals suitable for X-ray determination were obtained.

X-ray crystallography $(ArO)YbCl_2(THF)_3$

A yellow single crystal ($0.20 \times 0.20 \times 0.40$ mm) was sealed in a glass capillary under argon and mounted on a Rigaku AFC7R diffractometer. Intensity data were measured with ω-2θ scan type with MoK_α radiation, with $6.0 < 2\theta < 45.0°$, 8721 reflections were collected. Crystallographic data are listed in Table 1. The structure was solved by direct methods and expanded using Fourier techniques. The non-hydrogen atoms were refined anisotropically. The final cycle of full-matrix least-squares refinement was based on 1635 observed reflections [$F > 4.0\sigma(F)$] and 158 variable parameters and led to final $R = 0.0285$, $Rw = 0.0351$. All the calculations was performed by the program of Siemens SHELXTL PLUS (PC Version).

RESULTS AND DISCUSSION

Synthesis of the complex $(ArO)YbCl_2(THF)_3$

The synthesis and molecular structure of monoaryloxo-(alkoxo-)lanthanide dichloride has not been reported yet, although there are a few crystal structures of alkoxo lanthanide chlorides in the literature, which were obtained as byproducts in the syntheses of trialkoxo lanthanide complexes [16,17]. We found that the monoaryloxo ytterbium dichloriden can be synthesized by use of bulky 2,6-ditertbutyl-4-methylphenoxo-(ArO-) as ligand, anhydrous $YbCl_3$ reacts with one equivalent of ArONa in THF at room temperature and gives yellow $(ArO)YbCl_2(THF)_3$ in good yields.

$$YbCl_3 + ArONa \xrightarrow{THF} (ArO)YbCl_2(THF)_3 + NaCl\downarrow$$

The title complex has good solubility in THF, and slightly soluble in aromatic solvents. This complex can be recrystallized from THF solution to give yellow crystals suitable for X-ray determination.

The complex has no melting point, decomposed at above 109°C. The IR spectrum exhibits the characteristic absorption bands for aryloxo at ca 771, 864, 1151, 1434 and 2957 cm^{-1}, for coordinated THF at 1065 cm^{-1} [18], and for Ln—O mode at near 460 cm^{-1} [19].

Table 1. Crystal data and experimental parameters

Formual	$C_{27}H_{47}O_4Cl_2Yb$
Molecular weight	679.61
Crystal size (mm)	$0.20 \times 0.20 \times 0.40$
Crystal system	Orthorhombic
Crystal color and habit	Yellow, prismatic
Space group	*F*ddd (No. 70)
Lattice parameters	
a (Å)	16.192(3)
b (Å)	20.745(4)
c (Å)	36.879(7)
α (°)	90
β (°)	90
γ (°)	90
V (Å^3)	12388(6)
Dc (g·cm^{-1})	1.458
Z	16
μ (cm^{-1})	32.19
F(000)	5520
Temperature (°C)	20.0
Scan type	ω-2θ
Scan width (°)	$1.26 + 0.30 \tan\theta$
Scan speed (° min^{-1})	16.0
2θmax (°)	45.0
No. of unique reflections	8721
No. of reflections with $F \geqslant 4.0\sigma(F)$	1635
No. of parameters refined	158
R	0.0285
Rw	0.0351
G.O.F.	1.50

X-ray crystal structure

The molecular structure of the title compound is shown in Fig. 1. The important bond distances and bond angles are listed in Table 2.

The ytterbium atom is coordinated by two chlorine atoms, one oxygen atom of aryloxo and three oxygen atoms of THF, giving a six-coordinate, pseudo-octahedral complex. The geometry is related to that of the complex $CpYbCl_2(THF)_3$ [20]. The molecule lies on a two-fold axis which passes through the atoms O(3), Yb, O(1), C(1), C(4) and C(9).

It is interesting to compare the bond length values with those of other aryloxo complexes. The bond length of Yb—O(Ar) is 2.083(5) Å, subtraction of an ionic radius for six-coordinate Yb^{3+} (0.868 Å) [21] from this value gives 1.215 Å. Similar treatment of Ln—O(Ar) bond lengths for $[Yb(OC_6\text{-}H_3Ph_2\text{-}2,6)_3(THF)_2]$ [3], $Yb(OC_6H_2Bu^t_3\text{-}2,4,6)_3(THF)$ [5], $Sc(OC_6H_2Me\text{-}4\text{-}Bu^t_2\text{-}2,6)_3$ [1] gives 1.267, 1.27 and 1.30 Å, respectively. The present value is shorter than those of triaryloxo lanthanide complexes, almost certainly because of steric congestion caused by three bulky aryloxo ligands.

The bond length of Yb—Cl is 2.555(2) Å. This value is comparable with 2.52(5) Å in $YbCl_3(THF)_3$ [22] and 2.594 Å in $CpYbCl_2(THF)_3$ [20]. The Yb—O(THF) distances range from 2.292(4) Å to 2.434(5) Å and average 2.339(5) Å, and are well within the range of coordination bonds.

Acknowledgements—This work was supported by State Project for Basic Research, Chinese National Natural Science Foundation and the Laboratory of Organometallic Chemistry, Shanghai Institute of Organic Chemistry, Chinese Academy of Sciences.

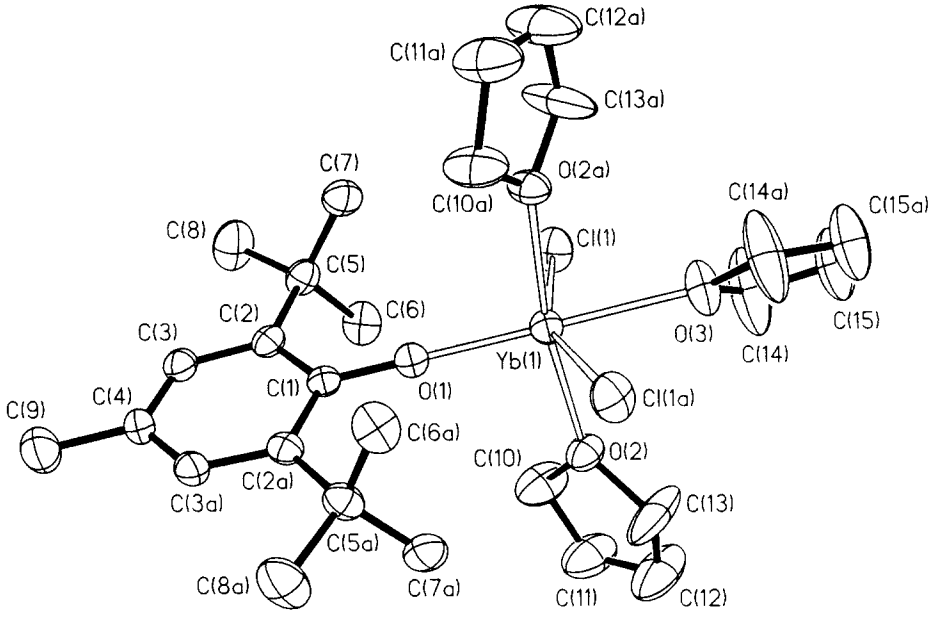

Fig. 1. Molecular structure of $(ArO)YbCl_2(THF)_3$.

Table 2. Some important bond lengths (Å) and angles (°) in $(ArO)YbCl_2(THF)_3$

Bond lengths			
Yb—Cl(1)	2.555(2)	O(1)—C(1)	1.352(9)
Yb—O(1)	2.083(5)	O(2)—C(10)	1.436(9)
Yb—O(2)	2.292(4)	O(2)—C(13)	1.446(11)
Yb—O(3)	2.434(5)	O(3)—C(14)	1.420(11)
		O(3)—C(14A)	1.419(11)
Bond angles			
Cl(1)—Yb—Cl(1A)	155.7(1)	O(1)—Yb—O(2)	94.6(1)
Cl(1)—Yb—O(1)	102.1(1)	O(1)—Yb—O(3)	180.0(1)
Cl(1)—Yb—O(2)	89.6(1)	O(1)—Yb—O(4)	94.3(2)
Cl(1)—Yb—O(2A)	88.4(1)	O(2)—Yb—O(3)	85.4(1)
Cl(1)—Yb—O(3)	77.9(1)	O(2)—Yb—O(2A)	170.9(2)
Yb—O(1)—C(1)	179.7(3)		

REFERENCES

1. Hitchcock, P. B., Lapper, M. F. and Singh, A., *J. Chem. Soc., Chem. Commun.*, 1983, 1499.
2. Hitchcock, P. B., Lappert, M. F. and Smith, R. G., *Inorg. Chim. Acta*, 1987, **139**, 183.
3. Deacon, G. B., Nickel, S., Mackinnon, P. and Tiekink, E. R. T., *Aust. J. Chem.*, 1990, **43**, 1245.
4. Stecher, H. A., Sen, A. and Rheingold, A. L., *Inorg. Chem.*, 1989, **28**, 3280.
5. Deacon, G. B., Feng, T., Nickel, S., Ogden, M. I. and White, A. H., *Aust. J. Chem.*, 1992, **45**, 671.
6. Qi, G. Z., Lin, Y. H., Hu, J. Y. and Shen, Q., *Polyhedron*, 1995, **14**, 413.
7. Bradley, D. C., Chudzynska, H., Hursthouse, M. B. and Moteralli, M., *Polyhedron*, 1991, **10**, 1049.
8. Evans, W. J., Olofson, J. M. and Ziller, J. W., *Inorg. Chem.*, 1989, **28**, 4308.
9. Evans, W. J., Golden, R. E. and Ziller, J. W., *Inorg. Chem.*, 1991, **30**, 4963.
10. Poncelet, O., Hurbert-Pflazgraf, L. G. and Daran, J. C., *J. Chem. Soc., Chem. Commun.*, 1989, 1846.
11. Stecher, H. A., Sen, A. and Rheingold, A. L., *Inorg. Chem.*, 1988, **27**, 1130.
12. Evans, W. J., Broomhall-Dillard, R. N. R. and Ziller, J. W., *Organomet.*, 1996, **15**, 1351.
13. Schaverien, C. J., Frijns, J. H. G., Heeres, H. J., Van den Hende, J. R., Teuben, J. H. and Spek, A. L., *J. Chem. Soc., Chem. Commun.*, 1991, 642.
14. Schaverien, C. J., *Organomet.*, 1994, **13**, 69.
15. Li, Y., Xu, X., Zhu, L. and Lu, G., *Chinese J. Appl. Chem.*, 1987, **5**, 82.

16. Evans, W. J. and Sollberger, M. S., *Inorg. Chem.*, 1988, **27**, 4417.
17. Evans, W. J., Sollberger, M. S. and Hanusa, T. P., *J. Am. Chem. Soc.*, 1988, **110**, 1841.
18. Xia, J. S., Jin, S. C. and Chen, W. Q., *Polyhedron*, 1996, **15**, 809.
19. Mehrotra, R. C. and Batwara, J. M., *Inorg. Chem.*, 1970, **9**, 2505.
20. Adam, M., Li, X. F., Oroschin, W. and Fischer, R. D., *J. Organomet. Chem.*, 1985, **296**, C19.
21. Shannon, R. D., *Acta Cryst., Sect. A*, 1976, **32**, 751.
22. Qian, C. T., Wang, B., Deng, D. L., Xu, C., Sun, X. Y. and Ling, R. G., *Jiegou Huaxie* (*Chinese J. Struct. Chem.*), 1993, **12**, 18.

Pergamon

PII: S0277-5387(97)00338-0

Polyhedron Vol. 17, No. 4, pp. 523–529, 1998
© 1998 Elsevier Science Ltd
All rights reserved. Printed in Great Britain
0277-5387/98 $19.00+0.00

Synthesis and characterization of rings with the atom combination Ga/As and In/As

Anahita Dashti-Mommertz, Bert Werner and Bernhard Neumüller*†

Fachbereich Chemie der Universität, Hans-Meerwein-Straße, D-35032 Marburg, Germany

(Received 19 June 1997; accepted 6 August 1997)

Abstract—The organogallium arsenide $[Pr^i(Cl)GaAsBu^t_2]_2$ (**1**) and the organoindium arsenide $[(PhCH_2)_2InAsBu^t_2]_2$ (**2**) have been prepared by the reaction of the corresponding halides Pr^iGaCl_2 and $(PhCH_2)_2InCl$ with Bu^t_2AsLi in THF and Et_2O, respectively. **1** and **2** have been fully characterized by elemental analysis and IR, NMR, and MS techniques as well as by X-ray diffraction. According to cryoscopic molecular weight determinations in benzene, **1** and **2** are present as dimers in solution. The structures of **1** and **2** display rhombic distorted four-membered rings M_2As_2 (M = Ga, In). © 1998 Elsevier Science Ltd. All rights reserved

Keywords: gallium arsenide; indium arsenide; crystal structures.

During the last ten years the synthesis and characterization of compounds possessing the element combination group 13/group 15 has developed into one of the most exciting areas in main group chemistry. The predominant important driving force for the research in this field is the potential employment of such compounds in MOCVD processes generating layers and thin films of group 13/15 semiconductor materials [1–3]. Nitrogen and phosphorus derivatives have been studied intensively, whereas arsenic and especially antimony compounds have not been investigated in great detail [1–4].

One approach to the better understanding of this class of compounds involves basic investigations such as optimizing the synthesis and studying the structural features of the compounds which often display rings and cages.

In this paper we report the reaction of an organogallium dichloride and a diorganoindium chloride with Bu^t_2AsLi to yield species with $R(Cl)GaAsBu^t_2$ and $R_2InAsBu^t_2$. The structural features of the products have been studied in solution and the solid state. Compounds of the type $R(Cl)GaAsR'_2$ have been investigated already by Wells *et al.* who reported a dimer–trimer equilibrium in solution. A crystal structure analysis was not carried out [5].

However, not only the degree of association is of interest in this case, but also, whether Cl or As in μ_2-bridging. One should expect As as a bridging atom, nevertheless, under certain conditions the chlorine atom can occupy this position [6,7].

EXPERIMENTAL

Instruments and materials

All experiments were carried out under an atmosphere of argon. Purification and drying of the solvents were done, using standard methods [8]. Pr^iGaCl_2 [34], $(PhCH_2)_2InCl$ [10,11], and Bu^t_2AsLi [35] were prepared by literature procedures.

The ^1H and ^{13}C NMR spectra were recorded on a Bruker AC-300 spectrometer (^1H, 300.134 MHz; ^{13}C, 75.469 MHz). The standard was TMS (external) with $\delta = 0.0$ ppm. The IR spectra were obtained using a Bruker IFS-88 instrument (Nujol mulls, CsI disks for the range 4000–500 cm^{-1}; polyethylene disks for the range 500–100 cm^{-1}). For the EI mass spectra a Varian CH7a mass spectrometer (70 eV) was used. The melting points were measured with a Dr Tottoli (Büchi) melting point apparatus in sealed capillaries under argon (values not corrected). The cryoscopic measurements were performed using a Normag molecular weight determination apparatus combined with a Beckmann thermometer.

* Author to whom correspondence should be addressed.

† Dedicated to Prof. Dr Manfred Weidenbruch on the occasion of his 60th birthday.

Synthesis of the compounds

Preparation of $[Pr^i(Cl)GaAsBu^t_2]_2$ (**1**). A solution of 1.81 g (9.25 mmol) of Bu^t_2AsLi in 10 ml of THF was added at −78°C to a solution of 1.70 g (9.25 mmol) of Pr^iGaCl_2 in 10 ml of THF. The green solution was stirred for 12 h until 20°C was reached. The color turned to yellow during this process. The solvent was removed under vacuum and the residue was treated with 10 ml of toluene. The suspension was filtered and the filtrate was reduced to dryness under vacuum. Recrystallization from toluene gives colorless crystals (2.69 g; 78.3%); m.p. 180°C. ^{1}H NMR (C_6D_6; ppm): 1.38 [d, 6H, CH (CH_3)$_2$], 1.39 (m, 1H, $CH(CH_3)_2$, AB_6 spin system), 1.41 [s, 18H, $C(CH_3)_3$]. ^{13}C NMR (C_6D_6; ppm): 20.2 [$CH(CH_3)_2$], 21.0 [$CH(CH_3)_2$], 32.6 [$C(CH_3)_3$], 43.8 [$C(CH_3)_3$]. Molecular weight determination (cryoscopic, benzene, $c = 0.0288$ mol/l): 703; $n = 2.1$. EI-MS: m/z (%) 190 (4) $[As(C_4H_9)_2]^+$, 179 (1) $(ClGaAs)^+$, 132 (2) $(AsC_4H_9)^+$, 105 (2) $(HGaC_3H_7)^+$, 75 (1) $(As)^+$, 69 (2) $(Ga)^+$, 57 (100) $(C_4H_9)^+$, 43 (14) $(C_3H_7)^+$. IR (cm^{-1}): 2719 w, 1198 w, 1160 vs, 1071 w, 1024 m, 977 m, 939 m, 918 m, 870 s, 845 m, 806 w, 654 vw, 522 m (νGaC), 395 m (νGaCl), 349 m (sh, νGa_2As_2), 327 m (νGa_2As_2), 266 m (br). Anal. calc. for $C_{22}H_{50}As_2Cl_2Ga_2$ (M_r 674.82) C, 39.16; H, 7.47; As, 22.20; Ga, 20.66. Found: C, 38.92; H, 7.34; As, 22.45; Ga, 20.36.

Preparation of $[(PhCH_2)_2InAsBu^t_2]_2$ (**2**). A solution of 0.64 g (3.26 mmol) of Bu^t_2AsLi in 15 ml of Et_2O was added to a solution of 1.04 g (3.13 mmol) of $(PhCH_2)_2InCl$ in 35 ml of Et_2O at 20°C. The mixture was stirred for 18 h while a voluminous colorless solid was formed. The solvent was removed under vacuum and the residue was extracted with four portions of 25 ml of boiling toluene. The filtrate was dried under vacuum and the colorless solid was recrystallized from *n*-pentane (1.10 g, 73% calculated from $(PhCH_2)_2$ InCl; mp 210°C dec). ^{1}H NMR (C_6D_6; ppm): 1.14 [s, 18 H, $C(CH_3)_3$], 2.56 (s, 4 H, CH_2Ph), 6.82–7.06 (m, 10 H, Ph—*H*). ^{13}C NMR (C_6D_6; ppm): 26.8 (CH_2Ph), 33.4 [$C(CH_3)_3$], 40.2 [$C(CH_3)_3$], 122.9 (C^4), 127.5 ($C^{3,5}$), 128.8 ($C^{2,6}$), 146.4 (C^1). Molecular weight determination (cryoscopic, benzene, $c = 0.0255$ mol/l): 895; $n = 1.8$. EI-MS: m/z (%) 190 (5) $(InAs)^+$, 132 (2) $(AsC_4H_9)^+$, 115 (1) $(In)^+$, 91 (66) $(CH_2Ph)^+$, 57 (100) $(C_4H_9)^+$. IR (cm^{-1}): 2720 w, 1594 m, 1302 w, 1262 m, 1206 m, 1154 m, 1069 m, 1036 m, 996 w, 936 w, 895 w, 880 m, 866 m, 795 s, 747 s, 695 s, 681 m, 660 m, 621 s, 534 s, 484 w ($\nu_{as}InC_2$), 447 w ($\nu_s InC_2$), 411 w, 329 w, 284 w (νIn_2As_2), 267 vw (νIn_2As_2), 209 vw, 167 vw, 119 vw. Anal. calc. for $C_{44}H_{64}As_2In_2$ (M_r 972.47): C, 54.34; H, 6.63; As, 15.41. Found: C, 54.07; H, 6.59; As, 15.19.

X-ray measurements and structure determination

The crystals were covered with a high-boiling paraffin oil and mounted on the top of a glass capillary under the flow of cold gaseous nitrogen. The orientation matrix and preliminary unit cell dimensions were determined from 25 reflections on a four-circle diffractometer with graphite-monochromated Mo-K_α radiation ($\lambda = 71.073$ pm; Siemens P4). The final cell parameters were determined from 25 high-angle reflections.

The intensities were corrected for Lorentz and polarization effects (for cell parameters and collection of the intensities, see Table 1). Both structures were solved with the program SHELXTL-Plus [36] (**1**: direct methods; **2**: Patterson method) and refined against F^2 by full-matrix least-squares using SHELXTL [37] (**1**) and SHELXL-93 [38] (**2**). The positions of the hydrogen atoms for **1** were calculated for ideal positions and refined with a common displacement parameter. The hydrogen atoms for **2** have been free refined. The calculation of the bond lengths, bond angles, and U_{eq} values was performed using the program PLATON [39]. Selected bond lengths and angles are listed in Table 2.

A comparison of M—As bond lengths is compiled in Table 3.

Table 1. Crystallographic data for $[Pr^i(Cl)GaAsBu^t_2]_2$ (**1**) and $[(PhCH_2)_2InAsBu^t_2]_2$ (**2**)

	1	**2**
Formula	$C_{22}H_{50}As_2Cl_2Ga_2$	$C_{44}H_{64}As_2In_2$
Formula weight	674.82	972.47
a (pm)	963.9(4)	1028.4(1)
b (pm)	1691.9(4)	1032.1(1)
c (pm)	1832.7(4)	1220.3(1)
α (°)		100.63(1)
β (°)		113.70(1)
γ (°)		107.77(1)
V ($pm^3 \cdot 10^6$)	2989(2)	1057.0(2)
Z	4	1
D_{calc} (g/cm^3)	1.500	1.528
Temp. (K)	223	223
Space group	Pbca (no. 61) [41]	$P\bar{1}$ (no. 2)
2θ range (°)	2–50	2–50
h	−1 to 11	−1 to 11
k	−1 to 20	−11 to 11
l	−21 to 21	−14 to 13
Absorpt. corr.	numerical	no
μ (cm^{-1})	41.9	26.7
Collected data	7013	4344
Unique data	2634	3644
Data with $F_o > 4\sigma(F_o)$	1458	3006
Refined parameter	128	345
R_1 [$F_o > 4\sigma(F_o)$][a]	0.0475	0.0212
wR_2[b]	0.0942	0.0470
Weight factor a[c]	0.0324	0.0287
$\Delta\rho_{max}/\Delta\rho_{min}$ ($e/pm^3 \cdot 10^6$)	1.02/−0.67	0.59/−0.72

[a] $R_1 = \Sigma\|F_o| - |F_c\|/\Sigma|F_o|$.
[b] $wR_2 = \{[\Sigma(F_o^2 - F_c^2)^2]/[w(F_o^2)^2]\}^{1/2}$.
[c] $w = 1/[\sigma^2(F_o^2) + (aP)^2]$ and $P = [\mathrm{Max}(F_o^2, 0) + 2F_c^2]/3$.

Table 2. Selected atomic distances (pm) and bond angles (°) in **1** and **2**

		1	
Ga1—As1	252.9(1)	As1—Ga1—As1a	88.16(3)
Ga1—As1a	252.0(1)	Ga1—As1—Ga1a	91.84(3)
Ga1—Cl1	223.0(2)	As1—Ga1—Cl1	106.68(6)
Ga1—Cl	198.7(7)	As1a—Ga1—Cl1	108.34(6)
As1—C2	200.8(7)	As1—Ga1—C1	124.8(2)
As1—C3	201.6(7)	Cl1—Ga1—C1	106.2(3)
		As1a—Ga1—C1	120.9(3)
		Ga1—As1—C2	112.7(2)
		Ga1—As1—C3	114.0(2)
		C2—As1—C3	111.4(3)
		C2—As1—Ga1a	111.8(2)
		C3—As1—Ga1a	113.8(2)
		2	
In1—As1	271.64(4)	As1—In1—As1a	83.18(1)
In1—As1a	271.21(5)	In1—As1—In1a	96.82(2)
In1—C1	221.1(3)	As1—In1—C1	114.2(1)
In1—C2	223.0(3)	As1—In1—C2	113.76(8)
As1—C3	200.9(3)	C1—In1—C2	106.6(1)
As1—C4	201.3(3)	C1—In1—As1a	123.4(1)
		C2—In1—As1a	114.4(1)
		In1—As1—C3	112.60(9)
		In1—As1—C4	108.74(8)
		C3—As1—C4	111.7(1)
		C3—As1—In1a	117.80(9)
		C4—As1—In1a	108.1(1)

Table 3. M—As bond lengths (M=Ga, In) for selected metal–arsenic compounds (pm)

Compound	M—As	Ref.
1	250.0(1), 252.9(1)	[a]
$[Ph_2GaAs(SiMe_3)_2]_2$	251.8(1), 253.0(1)	16
$[Me_2GaAsBu^t_2]_2$	254.1(1), 255.8(1)	17
$[Bu^n_2GaAsBu^t_2]_2$	254.8(3)–255.7(3)	17
$[Bu^t_2GaAs(SiMe_3)_2]_2$	263.0(1)	42
$Bu^t_2GaAsBu^t_2$	246.6(3)	18
$[(\{(Me_3Si)_2CH\}_2Ga)_2(Cl)\{As(SiMe_3)_2\}]$	250.3(1), 250.5(1)	43
$[\{Bu^t_2Ga\}_2(Cl)\{As(SiMe_3)_2\}]$	257.7(1)	42
$(Mes^*_2Ga)_2AsPh$[b]	240.1(1), 241.8(1)	44
$Bu^t_2GaAs(SiPh_3)[CH(SiMe_3)_2]$	245.8(1)	19
$[Me_2GaAsPr^i_2]_3$	249.8(2)–253.1(2)	45
$[(\{(Me_3Si)_2CH\}_2Ga)_3Ga_2(AsPh_2)(AsPh)\{(H)AsPh\}]$	245.0(1)–255.3(1)	46
2	271.21(5), 271.64(4)	[a]
$[Me_2InAsMe_2]_3$	265.7(3)–267.9(2)	29
$[Ph_2InAs(SiMe_3)_2]_2$	268.2(1)–268.9(1)	30
$[(Me_3CCH_2)_2InAs(SiMe_3)_2]_2$	275.2(1)	31
$[\{(Me_3CCH_2)_2In\}_2(Cl)\{As(SiMe_3)_2\}]$	269.4(3)	31
$[(Ph)\{(Me_3Si)_3C\}InAs(SiMe_3)_2]_2$	267.8(1), 268.0(1)	47

[a] This work.
[b] Mes* = $Pr^i_3C_6H_2$.

RESULTS AND DISCUSSION

Addition of Bu^t_2AsLi to Pr^iGaCl_2 in THF at $-78°C$ gives the organogallium arsenide $[Pr^i(Cl)GaAsBu^t_2]_2$ (**1**).

$$Pr^iGaCl_2 + LiAsBu^t_2 \rightarrow \underset{\mathbf{1}}{1/2[Pr^i(Cl)GaAsBu^t_2]_2} + LiCl \quad (1)$$

In a similar metathesis reaction $(PhCH_2)_2InCl$ reacts with Bu^t_2AsLi in Et_2O at room temperature to $[(PhCH_2)_2InAsBu^t_2]_2$ (**2**).

$$(PhCH_2)_2InCl + LiAsBu^t_2 \rightarrow \underset{\mathbf{2}}{1/2[(PhCH_2)_2InAsBu^t_2]_2} + LiCl \quad (2)$$

1 and **2** are air-sensitive colorless solids and soluble in non-polar solvents like *n*-pentane or toluene. According to cryoscopic measurements, **1** and **2** both possess a dimeric character in benzene.

A solution of **1** in C_6D_6 shows the typical AB_6 spin system for the Pr^i group [6–9]. Here the multiplet for the methine proton is partly covered by the singlet of the Bu^t groups at 1.41 ppm. The signal for the methylene protons in **2** at 2.56 exhibits a distinct low field shift in comparison to $In(CH_2Ph)_3$ [10,11] (1.81 ppm), $[(PhCH_2)_2InN(H)Bu^t]_2$ [7] (transoid derivative, AB spin system: 2.08, 2.28 ppm, $^2J(HH) = 11.1$ Hz) and $[(PhCH_2)_2InPPh_2]_3$ [12] (2.26 ppm). Higher values of 2.60 and 2.72 ppm have been observed for the bromides $(PhCH_2)_2InBr$ and $[PhCH_2InBr_2(THF)_2]$ [13].

1 and **2** possess C_i-symmetry leading to only two observal M_2As_2 ring vibrations caused by the rule of mutual exclusion [14]. We assign the two bands at 349, 327 cm^{-1} (**1**) and 284, 267 cm^{-1} (**2**), respectively, to those asymmetric ring vibrations. The absorption at 395 is caused by the terminal Ga—Cl bond [15]. For the M—C vibrations in **1** and in **2** the signals at 522 (**1**), 484 ($\nu_{as}InC_2$) and 447 cm^{-1} (ν_sInC_2) have been found. Both compounds are not very stable under EI mass spectra conditions. Prominent peaks of **1** are observed for $m/z = 57$ $(C_4H_9)^+$ and $m/z = 43$ $(C_3H_7)^+$. The spectrum of **2** exhibits peaks for $(InAs)^+$ ($m/z = 190$), for $(CH_2Ph)^+$ ($m/z = 91$) and for $(C_4H_9)^+$.

Description of the structures

Figure 1 shows the centrosymmetric dimer **1** with a planar rhombic distorted Ga_2As_2 four-membered ring. The Ga—As distances of 252.0(1) and 252.9(1) pm can be compared to 251.8(1) and 253.0(1) pm in $[Ph_2GaAs(SiMe_3)_2]_2$ [16]. The dimers $[Me_2GaAsBu^t_2]_2$ and $[Bu^n_2GaAsBu^t_2]_2$ [17] possess longer bond lengths of 255 pm (average) whereas the 263.0(1) pm in $[Bu^t_2GaAs(SiMe_3)_2]_2$ can be attributed mainly to the bulk of eight large substituents. The values for the first mentioned examples are due to the exchange of the electronegative Cl atom in **1** against an organic group. For gallium centers with the coordination number (CN) three, a shortening of the Ga—As bond should be observed such as the 246.6(3) pm for Bu^t $GaAsBu^t_2$ [18] and the 245.8(1) pm in $Bu^t_2GaAs(SiPh_3)$ $[CH(SiMe_3)_2]$ [19]. The rhombic distortion of M_2E_2 rings with group 13 metals is a generally observed feature. An angle larger than 90° can be found in almost all cases at the electronegative hetero-element E. Angles of 90° for M and E have been observed for the amid $[Me_2InN(SiMe_3)_2]_2$ [20]. There exist only few examples in which the group 15 element

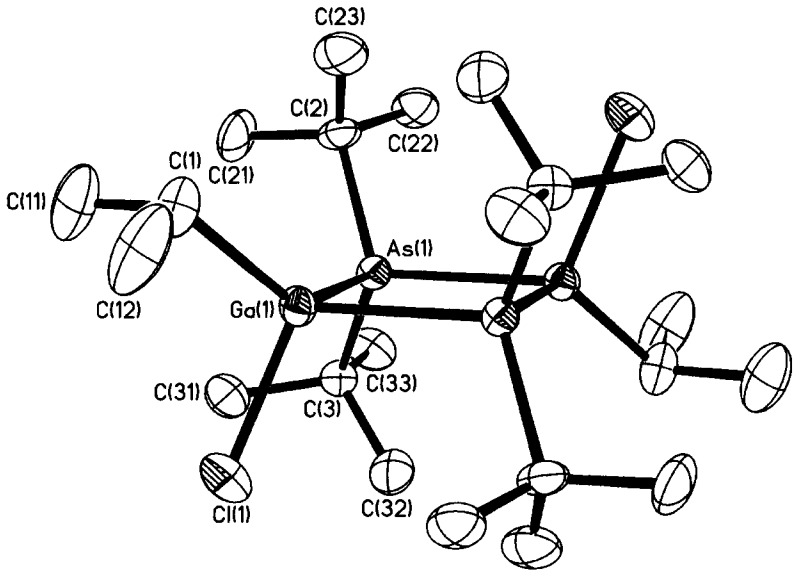

Fig. 1. Molecular structure of **1** (without H atoms). The thermal ellipsoids have a probability level of 50%.

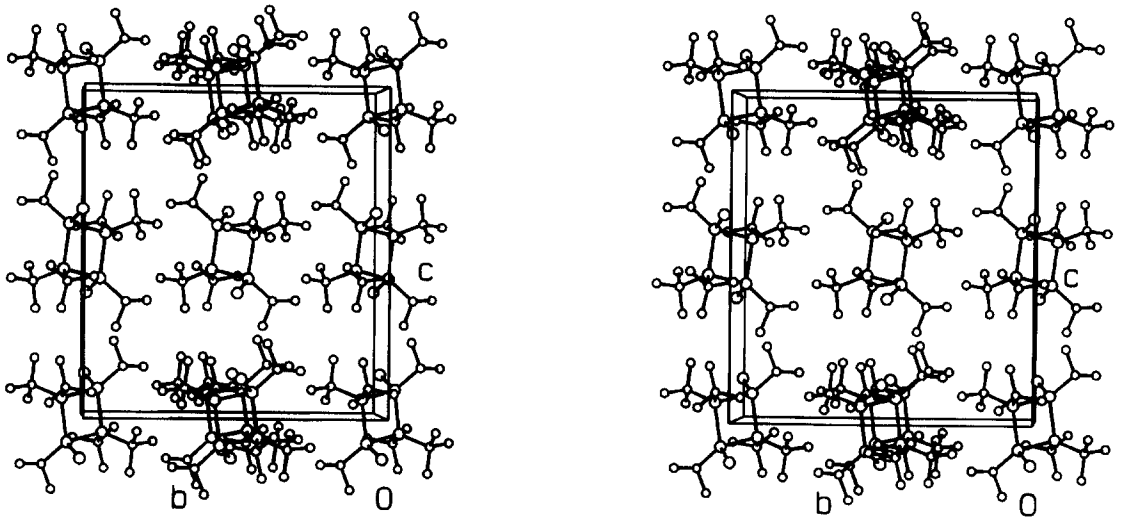

Fig. 2. Stereoscopic view of the unit cell of **1** (ORTEP) [40].

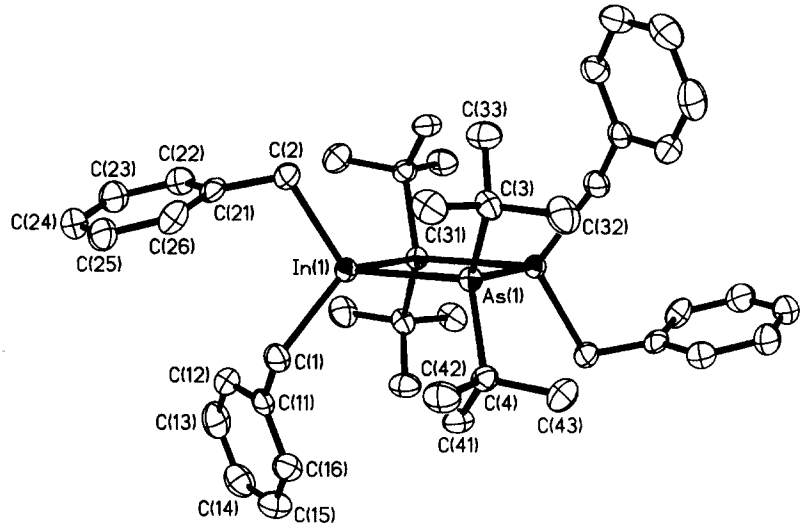

Fig. 3. Molecular structure of **2** (without H atoms).

does not occupy the μ_2-bridging position. In the case of $[Mes(Cl)InN(SiMe_3)_2]_2$ [7] this can be explained by the well-known low basicity of the $N(SiMe_3)_2$ group and in $[Bu^t(Cl)GaP(H)Mes']_2$ [Mes′ = 2,4,6-Bu^t_3 C_6H_2] [21] the bulky aryl substituent is responsible for this behavior. In both cases the Cl atoms occupy the bridging position. The Ga—Cl bond length of 223.0(2) pm is typical for a terminal Cl atom attached to a Ga center with CN four. 221.1(3) pm has been found for $[Mes^*GaCl_2(THF)]$ [22]. The shortening to 212.4(4) pm for $[Cp^*GaCl_2]_2$ [23], 215.1(2) pm for $[Bu^tGaCl_2]_2$ [24], 216 pm (average) for $[MesGaCl_2]_n$ [25] and to 218 pm (average) in $[GaCl_2(NPPh_3)]_2$ [26] are due to the two or more electronegative ligands coordinating the metal center. A low CN in combination with bulky substituents leads to Ga—Cl distances in the same range (Mes^*_2GaCl: 222.0(5) pm [22]; $Mes'GaCl_2$: 215.7(1) pm) [22,27]. The gallium atom in **1** shows no tendency to extend the coordination sphere to CN5 by intermolecular Ga···Cl contacts (Fig. 2), a characteristic behavior of Ga. Exceptions were observed if effects like intramolecular stabilization forces a higher CN, e.g. in $[2,6\text{-}(Me_2N\text{-}CH_2)_2C_6H_3Ga(N_3)_2]$ [28].

The centrosymmetric four-membered ring In_2As_2 in **2** exhibits in principle the same rhombic distortion as the Ga analogue in **1** (Fig. 3). The In—As distances of 271.21(5) and 271.64(4) pm are at the upper limit for this bond. $[Me_2InAsMe_2]_3$ [29] [265.7(3)–267.9(2) pm] and $[Ph_2InAs(SiMe_3)_3]_2$ [30] [268.2(1)–268.9(1) pm] have more typical bond lengths. A longer In—As bond of 275.2(1) pm [31] was found only in the steri-

cally crowded indium arsenide $[(Me_3CCH_2)_2InAs(SiMe_3)_2]_2$. An indicator of the sterical situation is the In—C bonds, which are relatively long [221.1(3); 223.0(3) pm] in comparison to $In(CH_2Ph)_3$ [218.6(7)–220.5(6) pm] [11] and $[(PhCH_2)_2InPPh_2]_3$ [218.5(4)–220.3(4) pm] [12].

1 possesses Ga···Ga contacts [362.7(1) pm] which are somewhat shorter than the sum of the van der Waals radii (380 pm). Recently, theoretical studies dealing with diamond shaped four-membered rings, like the ones present in **1** and **2**, verified that there is no evidence for a metal–metal bond. The contacts are rather forced by the ring geometry [32].

Acknowledgements—This work was supported by the Deutsche Forschungsgemeinschaft and the Fonds der Chemischen Industrie.

REFERENCES

1. Cowley, A. H. and Jones, R. A., *Angew. Chem., Int. Ed. Engl.*, 1989, **28,** 1208.
2. Cowley, A. H., *J. Organomet. Chem.*, 1990, **400,** 71.
3. Chemistry of Aluminium, Gallium, Indium and Thallium, ed. A. J. Downs, Blackie Academic and Professionals, London, 1993.
4. (a) For gallium and indium compounds, see: Gmelin Handbook of Inorganic Chemistry, Gallium, Organogallium Compounds, Part 1, Springer, Berlin (1987). In Weidlein, J., *Gmelin Handbook of Inorganic Chemistry, Organoindium Compounds*, Part 1, Springer, Berlin, 1991; (b) For new results in Ga(In)/Sb-chemistry see: Baldwin, R. A., Foos, E. E., Wells, R. L., White, P. S., Rheingold, A. L. and Yap, G. P. A., *Organometallics*, 1996, **15,** 5035.
5. Purdy, A. P., Wells, R. L., McPhail, A. T. and Pitt, C. G., *Organometallics*, 1987, **6,** 2099.
6. Neumüller, B., *Z. Naturforsch.*, 1990, **45B,** 1559.
7. Neumüller, B., *Z. Naturforsch.*, 1991, **46B,** 753.
8. Neumüller, B., *Chem. Ber.*, 1989, **122,** 2283.
9. Werner, B., Kräuter, T. and Neumüller, B., *Inorg. Chem.*, 1996, **35,** 2977.
10. Barron, A. R., *J. Chem. Soc., Chem. Commun.*, 1989, 1625.
11. Neumüller, B., *Z. Anorg. Allg. Chem.*, 1991, **592,** 42.
12. Werner, B. and Neumüller, B., *Organometallics*, 1996, **15,** 4258.
13. Werner, B., Kräuter, T. and Neumüller, B., *Z. Anorg. Allg. Chem.*, 1995, **621,** 346.
14. Weidlein, J., Müller, U. and Dehnicke, K., *Schwingungsspektroskopie*, 2nd ed., Thieme Verlag, Stuttgart, 1988.
15. Weidlein, J., Müller, U. and Dehnicke, K., *Schwingungsfrequenzen I*, Thieme Verlag, Stuttgart 1981.
16. Wells, R. L., Purdy, A. P., McPhail, A. T. and Pitt, C. G., *J. Organomet. Chem.*, 1986, **308,** 281.
17. Arif, A. M., Benac, B. L., Cowley, A. H., Geerts, R., Jones, R. A., Kidd, K. B., Power, J. M. and Schwab, S. T., *J. Chem. Soc., Chem. Commun.*, 1986, 1543.
18. Higa, K. T. and George, C., *Organometallics*, 1990, **9,** 275.
19. Petrie, M. A. and Power, P. P., *J. Chem. Soc., Dalton Trans.*, 1993, 1737.
20. Aitchison, K. A., Backer-Dirks, J. D. J., Bradley, D. C., Faktor, M. M., Frigo, D. M., Hursthouse, M. B., Hussain, B. and Short, R. L., *J. Organomet. Chem.*, 1989, **366,** 11.
21. Cowley, A. H., Jones, R. A., Mardones, M. A., Atwood, J. L. and Bott, S. G., *Heteroatom Chem.*, 1991, **2,** 11.
22. Petrie, M. A., Power, P. P., Dias, H. V. R., Ruhlandt-Senge, K., Waggoner, K. M. and Wehmschulte, R. J., *Organometallics*, 1993, **12,** 1086.
23. Beachley, O. T. Jr., Hallock, R. B., Zhang, H. M. and Atwood, J. L., *Organometallics*, 1985, **4,** 1675.
24. Power, M. B., Cleaver, W. M., Apblett, A. W., Barron, A. R. and Ziller, J. W., *Polyhedron*, 1992, **11,** 477.
25. Beachley, O. T. Jr., Churchill, M. R., Pazik, J. C. and Ziller, J. W., *Organometallics*, 1987, **6,** 2088.
26. Heshmatpour, F., Nußhär, D., Garbe, R., Wocadlo, S., Massa, W., Dehnicke, K., Goesmann, H. and Fenske, D., *Z. Anorg. Allg. Chem.*, 1995, **621,** 443.
27. Schulz, S., Pusch, S., Pohl, E., Dielkus, S., Herbst-Irmer, R., Meller, A. and Roesky, H. W., *Inorg. Chem.*, 1993, **23,** 3343.
28. Cowley, A. H., Gabbai, F. P., Olbrich, F., Gorbelin, S. and Lagow, R. J., *J. Organomet. Chem.*, 1995, **487,** C5.
29. Cowley, A. H., Jones, R. A., Kidd, K. B., Nunn, C. M. and Westmoreland, D. L., *J. Organomet. Chem.*, 1988, **341,** C1.
30. Wells, R. L., McPhail, A. T., Jones, L. J. and Self, M. F., *Polyhedron*, 1993, **12,** 141.
31. Jones, L. J. III, McPhail, A. T. and Wells, R. L., *Organometallics*, 1994, **13,** 3634.
32. Alemany, P. and Alvarez, S., *Inorg. Chem.*, 1992, **31,** 4266.
33. Perrin, D. D., Armarego, W. L. F. and Perrin, D. R., *Purification of Laboratory Chemicals*, 2nd ed., Pergamon Press, Oxford, 1980.
34. Niediek, K. and Neumüller, B., *Chem. Ber.*, 1994, **127,** 67.
35. Tzschach, A. and Deyling, W., *Z. Anorg. Allg. Chem.*, 1965, **336,** 36.
36. Sheldrick, G. M., *SHELXTL-Plus*, Release 4.2 for Siemens R3 Crystallographic Research Systems; Siemens Analytical X-ray Instruments, Inc., Madison, WI, U.S.A. (1990).
37. Sheldrick, G. M., *SHELXTL*, Release 5.03 for Siemens R3 Crystallographic Research Systems, Siemens Analytical X-ray Instruments, Inc., Madison, WI, U.S.A. (1995).
38. Sheldrick, G. M., *SHELXTL*-93, University of Göttingen (1993).
39. Spek, A. L., *PLATON*-94, Utrecht (1994).
40. Johnson, C. K., ORTEP. Report ORNL-3794,

Oak Ridge National Laboratory, Oak Ridge, TN, U.S.A., 1965.
41. *International Tables for Crystallography*, 2nd ed., Vol. A. Kluwer Academic Publishers, Dordrecht, 1989.
42. Wells, R. L., McPhail, A. T. and Alvanipour, A., *Polyhedron*, 1992, **11,** 839.
43. Wells, R. L., Pasterczyk, J. W., McPhail, A. T., Johansen, J. D. and Alvanipour, A., *J. Organomet. Chem.*, 1991, **407,** 17.
44. Petrie, M. A. and Power, P. P., *Inorg. Chem.*, 1993, **32,** 1309.
45. Cowley, A. H., Jones, R. A., Mardones, M. A. and Nunn, C. M., *Organometallics*, 1991, **10,** 1635.
46. Wells, R. L., Purdy, A. P., McPhail, A. T. and Pitt, C. G., *J. Chem. Soc., Chem. Commun.*, 1986, 487.
47. Wells, R. L., McPhail, A. T., Jones, L. J. III and Self, M. F., *J. Organomet. Chem.*, 1993, **449,** 85.

Pergamon

PII: S0277-5387(97)00340-9

Polyhedron Vol. 17, No. 4, pp. 531–538, 1998
© 1998 Elsevier Science Ltd
All rights reserved. Printed in Great Britain
0277-5387/98 $19.00+0.00

Spectroscopic and thermal study of dialkyl (α-anilino-*N*-benzyl)phosphonates and their palladium(II) dichloride adducts

Manda Ćurić,[a] Ljerka Tušek-Božić[a]* and Pietro Traldi[b]

[a] Department of Chemistry, Ruđer Bošković Institute, Bijenička c. 54, 10000 Zagreb, Croatia

[b] Servizio di Spettrometria di Massa, Area di Ricerca del CNR, Corso Stati Uniti 4, 35100 Padova, Italy

(Received 21 May 1997; accepted 6 August 1997)

Abstract—Spectroscopic (^{13}C NMR, UV/VIS, IR, FAB-mass) and thermal (TG, DTA) studies of dialkyl (α-anilino-*N*-benzyl)phosphonates and their palladium(II) dichloride adducts, *trans*-$Pd(L)_2Cl_2$, have been carried out to determine structural and decomposition properties of these biologically active compounds. Thermal decomposition of the complexes proceeds in two steps: dehalogenation coupled with deesterification is followed by complex pyrolysis which finally results in a mixture of Pd and P_2O_5. The main gas-phase fragmentation pathway consists of sequential losses of HCl giving rise to the mono- and bis-orthometallated species. These processes are in competition with the loss of the phosphonate ester groups. NMR and UV/VIS spectra have shown that complexes retain their integrity in chloroform, but dissociate readily in DMSO and DMF solutions, leaving free an organophosphorus ligand. The spectral and thermal properties of the complexes have been discussed with respect to their antitumor activity. © 1998 Elsevier Science Ltd. All rights reserved

Keywords: Palladium chloride; anilinobenzylphosphonate; complex; thermal analysis; spectroscopy.

There has been continuous interest in palladium(II) halide complexes with nitrogen donor ligands since they have been found to be effective in treating various types of animal and human carcinomas [1–4]. There is general agreement that DNA is an important pharmacological target for the Pd(II), like Pt(II), compounds [5]. The ability to break Pt,Pd—X bonds seems to be the rate determining step in their reaction with DNA strands [6]. Thus, in order to prepare compounds with higher efficiency, it is important to understand dissociation properties of palladium(II) complexes and their relationship with antitumor activity. In an effort of obtaining a new class of potentially useful antitumor and antiviral agents, we have recently reported the synthesis and characterization of palladium(II) halide complexes with several dialkyl phosphonates derived from quinoline and aniline [7–9]. Most of these compounds have been found effective *in vitro* against human and tumor cell lines. In this paper we describe the decomposition behavior of diethyl and dibutyl ester of (α-anilino-*N*-benzyl) phosphonic acid and their palladium(II) dichloride adducts investigated by means of ^{13}C NMR and electronic spectra, mass spectrometric measurements carried out under FAB conditions as well as by thermal (TG and DTA) analysis accompanied by the IR spectroscopic studies.

* Author to whom correspondence should be addressed. Fax: (385)-(1)-272-648; E-mail: tusek@olimp.irb.ir

EXPERIMENTAL

Materials

Diethyl and dibutyl (α-anilino-*N*-benzyl)phosphonates (L1 and L2) [10], prepared as previously described, were purified by repeated recrystallization from absolute ethanol. Their palladium(II) dichloride adducts, $Pd(L)_2Cl_2$ (L=L1, L2), were obtained by reaction of ligands with Na_2PdCl_4 in methanol according to published method [9]. All other reagents and solvents were of analytical grade and used without purification.

Physical measurements

^{13}C NMR spectra were recorded on a Varian 300 Gemini spectrometer in $CDCl_3$ containing TMS as an internal reference. Spectra were measured with proton broad band decoupling, attached proton test (APT) and gated decoupling techniques. Standard spectral parameters were as follows: operating frequency 75.46 MHz, sweep width 18 700 Hz, pulse width 5.0 μs, pulse delay 1.0 s, flip angle 34°, acquisition time 0.998 s, 11 K data points, digital resolution of 0.65 Hz per data point. The UV/VIS spectra were recorded on a Cary Model 17 spectrophotometer in $CHCl_3$ solution in the range of 260–600 nm. IR spectra were recorded on FT-2000 and 580 B Perkin-Elmer spectrophotometers using KBr (4000–250 cm^{-1}) and polyethylene (400–200 cm^{-1}) pellets. Mass spectrometric measurements were performed on a double-focusing reverse-geometry VG ZAB 2F instrument operating under FAB conditions by bombarding 3-nitrobenzyl alcohol sample solutions with 8 keV Xe atoms. Expected natural abundance isotope cluster patterns for various ion clusters were calculated with the Isotopic Distribution Program (IDS) contained in the FTMS 7.01 application program of the NICOS operating system using polynomial expansion, based on natural abundance of the isotopes. Thermogravimetric analyses (TG) were performed with a Cahn RG electromicrobalance in an air atmosphere at a heating rate of 4°C min^{-1} up to 800°C. Differential thermal analyses (DTA) were carried out on a Netzsch differential thermal analyser applying a heating rate of 2°C min^{-1} in a static air atmosphere. The reference substance was pure alumina. The X-ray powder diffraction patterns were taken with a Philips counter diffractometer (monochromatised Cu K_α radiation).

RESULTS AND DISCUSSION

Dialkyl (α-anilino-*N*-benzyl)phosphonates by reaction with $PdCl_4^{2-}$ form biologically active palladium dichloride adducts which have been found to possess *in vitro* cytostatic activity against human epidermoid carcinoma and murine leukemia cell lines [9]. It was found that butyl derivative is more effective than its ethyl analogue. In these square-planar complexes the two monodentate N-bonded ligands are coordinated mutually *trans* to the palladium(II) ion through the aniline nitrogen. The phosphoryl group is not involved in coordination to palladium and it is available for hydrogen bonding, which is known to have some importance in the approaching and binding of metal ions to nucleic acid constituents [11]. It has been suggested that the requirements for potential antitumor coordination compound are a pair of strongly bonded nitrogen donor ligands and a pair of moderately labile ligands such as halides [12]. Generally, it was noticed that the smaller antitumor activity show complexes containing labile ligands with the lower leaving ability. The spectroscopic and thermal studies presented for the free α-anilinobenzylphosphonates and their palladium complexes provided valuable

Table 1. ^{13}C NMR data[a]

Compound C Atom	L1	$Pd(L1)_2Cl_2$[b]	L2	$Pd(L2)_2Cl_2$[b]
C-1	135.92	133.00	135.94	133.44
C-2,6	127.79	127.87	127.74	128.11
C-3,5	128.49	128.43	128.47	128.67
C-4	127.86	128.10	127.71	128.24
C-7	146.33	142.56	146.29	142.90
	^3J(PC) = 14.8	*c*	^3J(PC) = 14.6	*c*
C-8,12	113.77	122.56	113.70	122.79
C-9,11	129.07	128.60	129.05	128.88
C-10	118.24	125.98	118.21	126.17
PCH	55.98	62.50	55.82	63.31
	^1J(PC) = 150.5	^1J(PC) = 150.3	^1J(PC) = 150.7	^1J(PC) = 141.4
OCH_2	63.11; 63.21	62.56; 63.42	66.63; 66.80	65.42; 67.15
	^2J(POC) = 6.7	^2J(POC) = 7.3	^2J(POC) = 6.9	^2J(POC) = 7.2
CH_3	16.14; 16.39	15.71; 15.80	13.27; 13.21	13.35; 13.41
	^3J(POCC) = 5.8	^3J(POCC) = 6.0		
$OCH_2CH_2CH_2CH_3$	—	—	32.06; 32.26	31.99; 32.04
			^3J(POCC) = 5.8	^3J(POCC) = 6.0
$OCH_2CH_2CH_2CH_3$	—	—	18.36; 18.23	18.34; 18.48

[a] Spectra recorded in $CDCl_3$ (δ in ppm, coupling constants in Hz).
[b] Data for the major isomer.
[c] The ^3J(PC) coupling is not visible, instead this resonance is doubled in intensity.

structural information as well as important information about stability of these compounds and the mode of their decomposition. The NMR and UV/VIS spectral analyses have shown that complexes retain their integrity in chloroform and dichloromethane solutions, but dissociate in dimethylformamide and dimethylsulphoxide. These solvents with strong complexing ability towards palladium(II) ion cleave the metal–nitrogen bond leaving free ligand molecules. ^{1}H NMR studies have shown that complexes are dissociated after 30 min [9]. This process may be stimulated by UV irradation. Therefore in this study we present only spectroscopic results obtained in a chloroform solution.

^{13}C NMR Spectra

The ^{13}C NMR chemical shifts and the carbon–phosphorus coupling constants for the organophosphorus ligands and their complexes are summarized in Table 1, according to the numbering scheme shown in Fig. 1. Spectral data of the free ligand [13] provided a basis for interpreting spectra of their palladium complexes. Broad-band decoupling, gated decoupling and APT spectra were also utilized in the spectral analysis.

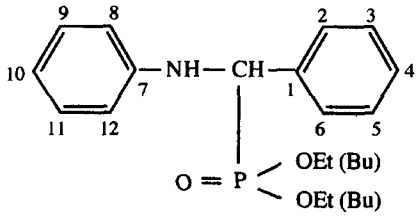

Fig. 1. Structure and numbering scheme for dialkyl (α-anilino-*N*-benzyl)phosphonates.

Signal assignment was ascertained on the basis of chemical shifts, signal intensities, spin–spin coupling constants and splitting patterns. The spectra of free ligands show that resonances of all alkyl carbons are doubled due to the non-equivalence of the two dialkyl ester groups. Two sets of separate resonances have been observed, also in their proton NMR spectra, as OR groups of the $P(O)(OR)_2$ moiety which is adjacent to a chiral center are diastereotopic [9,14]. The resonances of the alkyl carbons show also the signal splitting due to carbon–phosphorus couplings. The ^2J(POC) and ^3J(POCC) values are about 6.8 and 5.8 Hz, respectively. The benzylic PCH carbon shows one-bond PC coupling of about 150 Hz. For atomatic resonances it was observed that all *ortho* and *meta* carbons are magnetically equivalent as a consequence of the fast rotation on the timescale of NMR spectroscopy. The spectra of complexes show a great complexity due to the existence of more isomeric species with a different magnetic environment caused on one side by the presence of a new chiral center on the nitrogen atom, because of its coordination to palladium and, on the other side, by the restricted rotation around the C—N bond. Assuming that the arrangement of bonds around nitrogen approaches a tetrahedral configuration, similar to that at the adjacent asymmetric benzyl carbon atom, the simplified projection of three possible conformations of two diastereoisomers (a and b), one from each enantiomeric pair, is presented in Fig. 2. Furthermore, it could be assumed that the anilinobenzylphosphonate molecule, as a whole, is hindered in its rotation around the Pd—N coordination bond due to the proximity of the bulky phosphonate ester group. The major isomeric form, with a population of ca 70%, is most probably the less sterically hindered one. The splitting signals could be detected for almost all carbon atoms. In Table 1 only data for the major isomer obtained

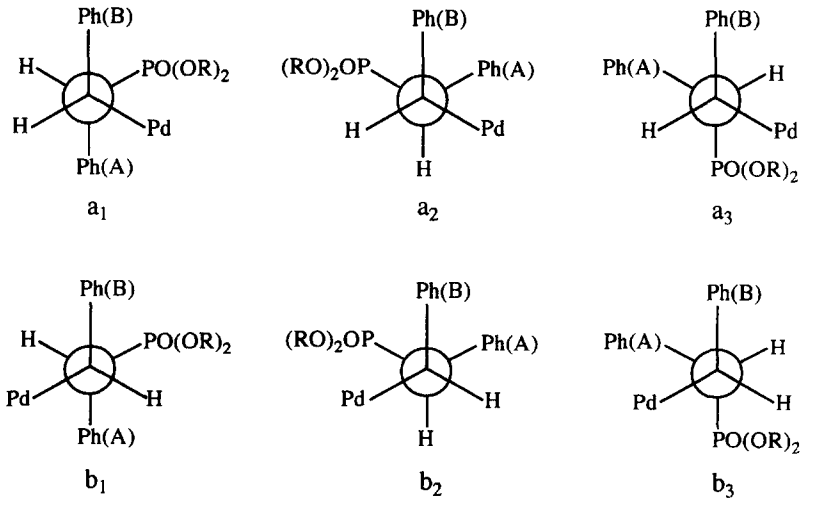

Fig. 2. Possible conformations of two diastereoisomers (a and b) of palladium(II) complexes of dialkyl (α-anilino-*N*-benzyl)phosphonates (R=Et, Bu).

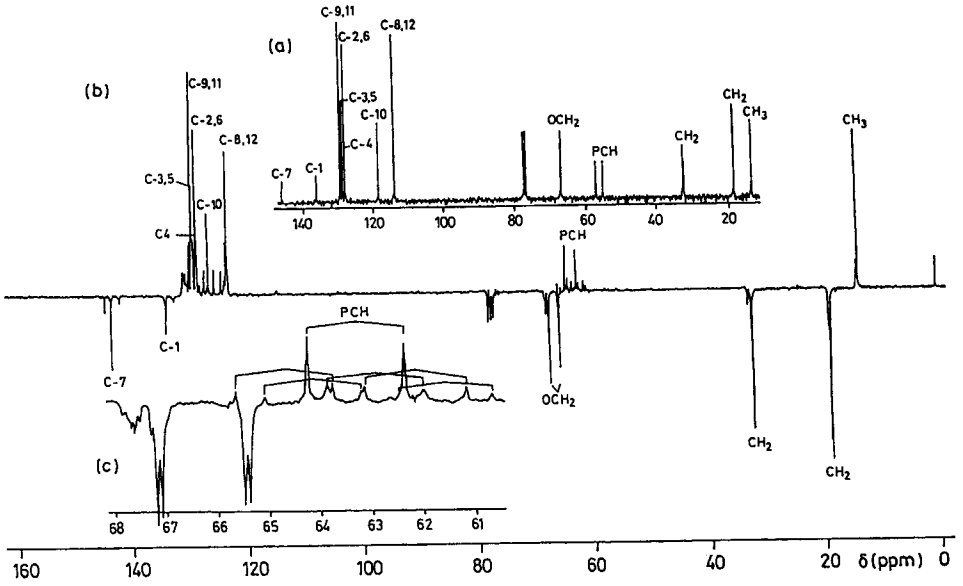

Fig. 3. ^{13}C NMR spectra of (a) L2, proton-decoupled spectrum; (b) $Pd(L2)_2Cl_2$, APT spectrum and (c) $Pd(L2)_2Cl_2$, APT spectrum showing an expansion of the doublet pattern for the PCH carbon.

from the proton decoupled spectra are given. The most pronounced shifts appear for the carbons of the PCH and $POCH_2$ groups as well as the carbons of the aniline ring which are close to the nitrogen bonded to the palladium(II) ion. In Fig. 3(c) it could be seen that the PCH carbon gives a pattern of multiplet doublets, and that one of the most intense doublets shows a downfield shift of 6.5 ppm with respect to this resonance in the free ligand. The nitrogen lone pair donation into the aniline ring is greatly reduced due to the palladium bonding, which should induce the significant chemical shift changes at the *ortho* and *para* positions [15, 16]. Thus, the moderate downfield shifts of about 9 and 8 ppm for the *ortho* carbons C-8, 12 and the *para* carbon C-10, respectively, along with an upfield shift of only 0.2–0.5 ppm for the *meta* carbons C-9 and C-11, could be observed in the spectra of complexes. The quaternary carbons C-1 and C-7 show an upfield shift of about 2.7 and 4 ppm, respectively. The coupling between phosphorus and the carbon atom C-7 ($\sim$14.6 Hz in free ligand) adjacent to nitrogen is not visible. Instead its signal is doubled in intensity. As expected, the resonances for the aromatic benzyl carbons C-2–C-6 remain almost unchanged upon complex formation.

Ultraviolet-visible spectra

The electronic absorption spectra of the free anilinobenzylphosphonate ligands in the 260–600 nm region show only one band at 292 nm (ε 10^3–10^4 M^{-1} cm^{-1}), which is in accordance with the spectra of the substituted anilino derivatives [17]. Their palladium complexes are characterized by one rather intense band at around 290 nm (ε 10^3–10^4 M^{-1} cm^{-1}) accompanied by a shoulder on the low energy side, as well as by a weaker absorption at 425 nm (ε 10^2–10^3 M^{-1} cm^{-1}). The former absorptions are predominantly originated form d–d transitions superimposed by the intraligand π–π^* transitions, while the band in the visible range is assignated to the metal-to-ligand charge-transfer transition. For the square-planar diamagnetic complexes three spin allowed d–d transitions are expected, corresponding to transitions from the three lower d-levels to the empty $d_{x^2-y^2}$ orbitals [18]. The ground state is $^1A_{1g}$ and the excited states related to these transitions are $^1A_{2g}$, $^1B_{1g}$ and ^1E_g in order of increasing energy. Strong charge-transfer or intraligand transitions may prevent the observation of these bands.

Mass spectra

The FAB mass spectra have been obtained for ligand L2 and its palladium complex. Their fragmentation pathway is very extensive and only the most abundant fragment ions are given in Table 2. The main decomposition pathway for the free ligand is the dissociation or complete loss of the phosphonate ester groups. The base peak at *m/z* 182 is formed by cleavage of the C—P bond. The further fragmentations include cleavage of the C—N and N—C bonds similarly as was observed in various benzylaniline derivatives [19, 20]. The presence of the phenyl groups could be detected by high abundance ions due to Ph^+ and Ph_2^+ at *m/z* 77 and *m/z* 154, respectively.

Table 2. Major fragments in mass spectra of L2 and $Pd(L2)_2Cl_2$[a]

Ionic species	Compound *m/z* (rel. int. %) L2	$Pd(L2)_2Cl_2$
$[MH]^-$		933–925 (0.1)
$[MH\text{-}HCl]^+$		897–889 (2)
$[MH\text{-}2HCl]^+$		859–853 (0.2)
$[MH\text{-}PO(OBu)_2]^+$		739–731 (0.3)
$[MH\text{-}2HCl\text{-}PO(OBu)_2]^+$		667–661 (0.2)
$[MH\text{-}PO(OBu)_2\text{-}(C_4H_8)_2]^+$		629–621 (0.3)
$[Pd(L\text{-}H)(C_6H_5NH_2)]^+$		577–571 (0.3)
$[MH\text{-}2PO(OBu)_2]^+$		546–538 (0.6)
$[Pd(L\text{-}H)]^+$		484–478 (4)
$[Pd(L\text{-}H\text{-}PO(OBu)_2)]^+$		290–284 (0.5)
$[LH]^+$	376 (9)	376 (4)
$[L]^+$	375 (3)	375 (6)
$[LH\text{-}PO(OBu)_2]^+$	183 (35)	183 (15)
$[L\text{-}PO(OBu)_2]^+$	182 (100)	182 (100)
$[C_6H_5C_6H_5]^+$	154 (3)	154 (6)
$[C_6H_5CHNH]^+$	105 (2)	105 (5)
$[C_6H_5CHN]$	104 (9)	104 (12)
$[C_6H_5N]^+$	91 (7)	91 (16)
$[C_6H_5]^+$	77 (10)	77 (31)

[a] L = parent ligand; M = parent complex.

In the spectrum of palladium complex the molecular ion as well as the fragment ions containing palladium are identified by the presence of the characteristic clusters of isotopic peaks due to the presence of the numerous palladium isotopes. The relative abundance of these fragment ions is relatively small and the theoretical isotopic mass distributions of Pd, PdCl and $PdCl_2$ clusters were also calculated to justify their assignments. The most intense fragment ions correspond to the fragments of the free non-coordinated ligand molecule. The fragmentation pathways, including possible structures of ions containing palladium, proposed on the basis of accurate mass measurements and isotopic cluster analysis, are reported in Scheme 1. Decomposition of the complex follows two fragmentation routes: one in which the protonated molecular ion sequentially loses hydrogen chloride and the other in which this loss is in competition with the loss of the dibutyl phosphonate ester group or its fragments. Further fragmentation is considered to involve the loss of the anilinobenzylphosphonate ligand molecule or its fragments. The molecular ion is protonated, since the anilino nitrogen as well as the phosphoryl oxygen, are known to be basic and hence, prone to protonation. The most important fragmentation pathways are the loss of one or both HCl molecules, which it may be assumed give rise to both mono- and bis-ortho-metallated species. The loss of the first HCl molecule gives $[Pd(L)(L\text{–}H)Cl+H)]^+$ ion, while the loss of the second should give an ion corresponding to the dimetallated complex $Pd(L\text{–}H)_2$. The most abundant palladium containing fragment ions are monopalladated ions containing both or only one organophosphonate ligand molecule. The high stability of such metallated systems is in agreement with the reported high stability of palladium(II) 5-membered cyclometallated systems having nitrogen donor ligands [21]. It is worth noting that dialkyl anilinobenzylphosphonates as secondary benzylamino derivatives do not form cyclopalladated complexes by reaction with $PdCl_4^{2-}$. Generally, it was shown that direct activation of C—H bonds by palladium(II) chlorides to afford corresponding palladacycles, is the most feasible in the case of tertiary amines and that secondary amines are usually inert toward such activation [22, 23]. Palladium(II) acetate was found to be a much better metallating reagent than tetrachloropalladate [24, 25]. It may be assumed that metallations of the chloropalladated compounds might occur in a matrix solution by the FAB-induced condensed phase reactions.

Thermal studies

Decomposition behavior of the ligands and their palladium complexes also was investigated by thermogravimetric measurements accompanied by the infrared spectroscopic study. The results obtained

Table 3. TG and DTA data

Compound	M.p.[a] (°C)	Temp. range, TG (°C)	Dehalogenation and pyrolysis[b], T, DTA (°C)
L1	97–99	169–838	103 (endo), 275 (exo), 335 (endo), 405 (endo)
$Pd(L1)_2Cl_2$	154–157	141–838	155 (endo), 210 (endo), 665 (exo), 704 (exo)
L2	55–56	166–820	55 (endo), 280 (exo), 325 (endo), 405 (endo)
$Pd(L2)_2Cl_2$	137–140	134–857	140 (endo), 220 (endo), 255 (endo), 565 (exo), 735 (exo)

[a] Data taken from Ref. 10. for the free ligands and from Ref. 9. for the complexes.
[b] Most of the DTA peaks above 300 are diffuse.

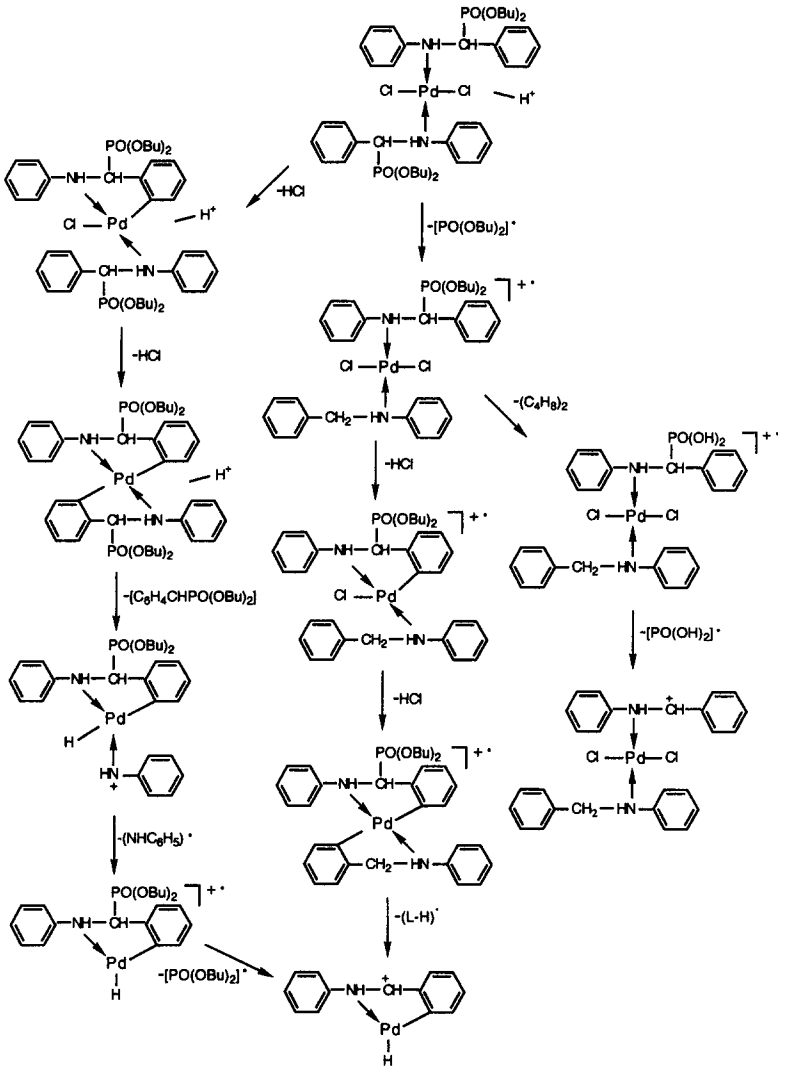

Scheme 1. FAB-induced decomposition pattern of complex $Pd(L2)_2Cl_2$.

from the TG and DTA curves are summarized in Table 3 and presented in Fig. 4 for L2 and its complex. The TG curves of the free ligands show a very sharp step between 170–240°C with a rapid weight loss of about 75%. This decomposition process could be ascribed to almost complete loss of the organic matter leaving P_2O_5 and appearing on the DTA curves as a strong exothermic effect centered at 275 and 280°C, respectively. The furthest weight loss over a broad step could be attributed to partial sublimation of P_2O_5 which takes place above 300°C [26]. Both ligands also show in a DTA curve, one endothermic effect at 55 and 105°C, respectively, which is not accompanied by the weight loss on the TG curve and corresponds approximately with the melting point values of these compounds [10].

The thermal decomposition of complexes occurs in two steps without formation of a stable intermediate. The first step between 135–280°C is attributed to the dehalogenation process overlapped with deesterification of the ligand which was confirmed by the subsequent infrared spectral study. It was shown that decomposition of the complexes started with their dehalogenation, as indicated by an intensity decrease of the Pd—Cl stretching vibration which appeared in both complexes at 332 cm^{-1}, while the loss of the alkyl ester group is accompanied by a decrease of the absorption bands arising from various modes of the P—O—Et(Bu) vibrations in the region of 1130–1035 cm^{-1} and C—C alkyl vibrations between 980–930 cm^{-1}, as well as by increasing of the ν(P=O) band at 1235 cm^{-1} [9, 27]. Furthermore, it was shown that a dehalogenation process was completed up to 300°C and that complexes were decomposed into a mixture of inorganic materials at 350–450°C. The final decomposition product as a mixture of metallic Pd and P_2O_5 was confirmed also by the X-ray diffraction analysis, as was obtained for palladium(II) halide

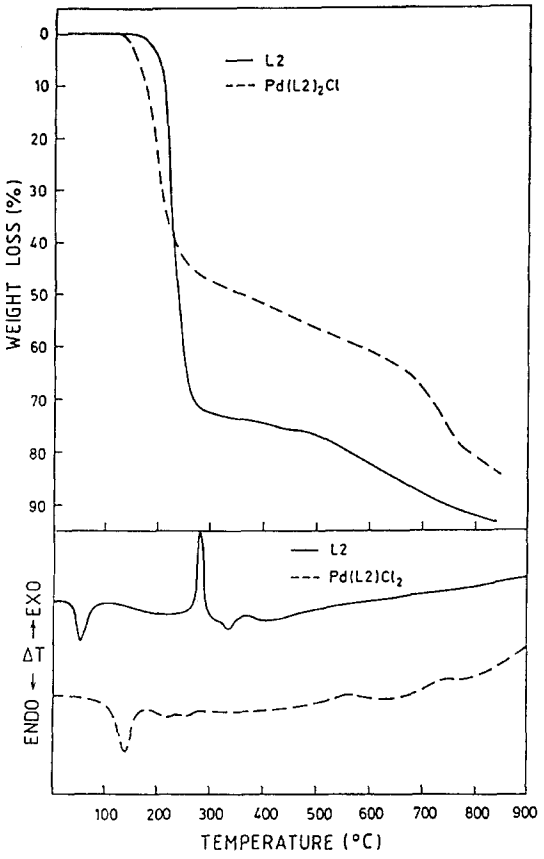

Fig. 4. TG–DTA curves for L2 and its complex $Pd(L2)_2Cl_2$.

complexes of various aminophosphonate derivatives [28]. Dehalogenation and deesterification of the complexes are accompanied by two endothermic effects in DTA curves and the first, more intense one, corresponds well with the melting point value of these compounds. This rather sharp thermal decomposition step is followed by a continuous weight loss with several unclear peaks in the DTA curves.

From the initial decomposition temperatures it could be concluded that the complex of diethyl ester is more stable than that of dibutyl ester. As the observed Pd—Cl stretching frequency is the same in both complexes indicating the similar palladium-chlorine bond strength, it may be presumed that the complex stability decreases with the length of the alkyl ester groups due to the increase of steric hindrance [29]. The observation is interesting in view of the importance of the Pd—Cl bond strength for the binding of the complexes to DNA strands, which in turn is related to their antitumor activity. The fact that ν(Pd—Cl) is not influenced by the length of the alkyl chain, indicates that other factors have a stronger influence to the complex activity. Lipophilicity of the complexes increases with increasing length of the alkyl chain and may facilitate the transport across the cellular membrane [30]. Furthermore, steric requirements of the complexes are growing in the same sequence, with the consequence of more severe damage of DNA after formation of the palladium-DNA complex. These effects are consistent with the rise in antitumor activity observed when increasing the length of the alkyl chain in palladium complexes of diethyl and dibutyl anilinobenzylphosphonates.

Acknowledgements—The financial support granted by the Ministry of Science, Technology and Informatics of the Republic of Croatia (grant No. 009806–07) is gratefully acknowledged. The authors thank Mr. Ž. Marinić and Mrs B. Metelko for recording the NMR spectra.

REFERENCES

1. Furlani, A., Scarcia, V., Faraglia, G., Sindellary, L., Trincia, L. and Nicolini, M., *Eur. J. Med. Chem.-Chim. Ther.*, 1986, **21**, 261.
2. Khokhar, A. R. and Lumetta, G. J., *Inorg. Chim. Acta.*, 1988, **153**, 255.
3. (a) Wimmer, F. L., Wimmer, S., Castan, P., Cros, S., Johnson, J. and Colacio-Rodrigues, E., *Anticancer Res.*, 1989, **9**, 791; (b) Castan, P., Colacio-Rodriguez, E., Beauchamp, A. L., Cros, S. and Wimmer, S., *J. Inorg. Biochem.*, 1990, **38**, 225.
4. Higgins III, D., Neely, L. and Fricker, S., *J. Inorg. Biochem.*, 1993, **49**, 149.
5. Bruhn, S. L., Toney, J. H. and Lippard, S. L., *Progress in Inorganic Chemistry: Bioinorganic Chemistry*, Vol. 38, ed. Lippard, S. L., Wiley, 1990, p. 477.
6. Bancroft, D. P., Lepre, C. A. and Lippard, S. J., *J. Am. Chem. Soc.*, 1990, **112**, 6860.
7. Tušek-Božić, Lj., Matijašić, I., Bocelli, G., Calestani, G., Furlani, A., Scarcia, V. and Papaioannou, A., *J. Chem. Soc., Dalton Trans.*, 1991, 195.
8. Tušek-Božić, Lj., Matijašić, I., Bocelli, G., Sgarabotto, P., Furlani, A., Scarcia, V. and Papaioannou, A., *Inorg. Chim. Acta.*, 1991, **185**, 229.
9. Ćurić, M., Tušek-Božić, Lj., Vikić-Topić, D., Scarcia, V., Furlani, A., Balzarini, J. and De Clercq, E., *J. Inorg. Biochem.*, 1996, **63**, 125.
10. Fields, E. K., *J. Am. Chem. Soc.*, 1952, **74**, 1520.
11. Reedijk, J., Fichtinger-Schepman, A. M. J., von Oasteron, A. T. and von de Putte, P., *Structure and Bonding* 67, Springer-Verlag, Berlin-Heidelberg, 1987.
12. Gill, D. S., *Platinum Coordination Complexes in Cancer Chemotherapy*, ed. Hacker, M. P., Douple, E. B. and Krakoff, I. H. Martinus Nijhoff, Boston, 1984, p. 267.
13. Ćurić, M., Tušek-Božić, Lj. and Vikić-Topić, D., *Magn. Reson. Chem.*, 1995, **33**, 27.
14. (a)Jagodić, V., *Croat, Chem. Acta*, 1976, **48**, 325; (b) Tušek, L.j. and Jagodić, V., *Croat. Chem. Acta*, 1977, **49**, 829.
15. Caubet, A., Moreno, V., Molins, E. and Miravitlles, C., *J. Inorg. Biochem.*, 1992, **48**, 35.
16. Vassilev, N. G. and Dimitrov, V. S., *Magn. Reson. Chem.*, 1994, **32**, 639.
17. Jaffe, H. H. and Orchin, M., *Theory and Appli-*

cations of Ultraviolet Spectroscopy. J Wiley, New York, 1962.
18. Kritzenberger, J., Yersin, H., Zabel, M. and Range, K. J., *Inorg. Chim. Acta*, 1993, **208,** 77.
19. Straub, R., Voyksner, R. D. and Keever, J. T., *J. Chromatography*, 1992, **627,** 173.
20. Dale, M. J., Jones, A. C., Langridge-Smith, P. R. R., Costello, K. F. and Cummins, P. G., *Analytical Chemistry*, 1993, **65,** 793.
21. Omae, I., *J. Organomet. Chem. Lib.*, 1986, **18,** 9.
22. Cope, A. C. and Friedrich, E. C., *J. Am. Chem. Soc.*, 1968, **90,** 909.
23. Dunina, V. V., Zalevskaya, O. A. and Potapov, V. M., *Zh. Obsch. Khim.*, 1984, **54,** 389.
24. Clark, P. W. and Dyke, S. F., *J. Organomet. Chem.*, 1985, **281,** 389.
25. (a) Fuchita, Y. and Tsuchiya, H., *Polyhedron*, 1993, **12,** 2079; (b) Fuchita, Y. and Tsuchiya, H., *Inorg. Chim. Acta*, 1993, **209,** 229.
26. Weast, R. C., *Handbook of Chemistry and Physics*, The Chemical Rubber Co., Cleveland, 1971–1972. p. B-117.
27. Thomas, L. C., *Interpretation of the Infrared Spectra of Organophosphorus Compounds*, Plenum, New York, 1974.
28. (a) Tušek-Božić, Lj. and Trojko, R., *Thermochim. Acta*, 1991, **189,** 175; (b) (a)Tušek-Božić, Lj., Ćurić, M. and Traldi, P., *Inorg. Chim. Acta*, 1997, **254,** 49.
29. Romero, M. A., Salas, J. M., Lopez, R. and Gutierrez, M. D., *Polyhedron*, 1988, **7,** 659.
30. (a) Kritzenberger, J., Bernhardt, G., Gust, R., Pistor, P., Schonenberger, H. and Yersin, H., *Monatsh. Chem.*, 1993, **124,** 587; (b) Souchard, J. P., Ha, T. T. B., Cros, S. and Johnson, N. P., *J. Med. Chem.*, 1991, **34,** 863.

Pergamon

PII: S0277-5387(97)00337-9

Polyhedron Vol. 17, No. 4, pp. 539–545, 1998
© 1998 Elsevier Science Ltd
All rights reserved. Printed in Great Britain
0277-5387/98 $19.00+0.00

Coordination geometries and cooperative ordering effects in copper(II) complexes with tridentate Schiff base dianions—VI† Structure and EPR spectra of (imidazole) (N-salicylidene-beta-alaninato)copper(II)

G. Plesch,[a]* V. Kettmann,[b] J. Sivý,[b] O. Švajlenová[b] and C. Friebel[c]

[a] Department of Inorganic Chemistry, Faculty of Natural Sciences, Comenius University, 842 15 Bratislava, Slovakia

[b] Department of Analytical Chemistry and Department of Chemical Theory of Drugs, Pharmaceutical Faculty, Comenius University, 832 32 Bratislava, Slovakia

[c] Department of Chemistry, Philipps University, D-350032 Marburg, Germany

(Received 22 April 1997; accepted 6 August 1997)

Abstract—The crystal and molecular structure of (imidazole)(*N*-salicylidene-*β*-alaninato)copper(II), monoclinic, space group C/2c, was solved by a single crystal X-ray structure analysis and refined to $R = 0.0577$ for 1286 observed reflections. The coordination polyhedron around Cu(II) is an axially elongated square-pyramid, the basal plane being formed by the (O, N, O) atoms of the tridentate Schiff base and the N atom of imidazole. The apex of the pyramid is occupied by the terminal carboxylic atom of adjacent molecule, thereby giving rise to centrosymmetric dimers. Non-parallel aligned stacks of dimeric units are propagated in the unit cell. The powder and single-crystal EPR spectra show cooperative g factors resulting from the weak coupling between two misaligned **g** tensors from dimeric units ordered in a disturbed-ferrodistortive way. Since the N–N axes, corresponding to g_y, are oriented nearly parallel, the g–g coupling shifts only the values of g_z and g_x. A complete consistency between the angular spectroscopic EPR behaviour and the X-ray structural data was found.
© 1998 Elsevier Science Ltd. All rights reserved

Keywords: copper(II) complex; *N*-salicylidene-*β*-alaninato; tridentate Schiff base; imidazole; X-ray crystal structure; single-crystal EPR spectra.

Since the first solution studies showed that the complexes of tridentate Schiff base dianions (TSB) are key intermediates in the metabolic reaction of amino acids [2], much work has been undertaken also on studies of these complexes in solid state. A great number of structures of copper(II) complexes containing various *N*-salicylidene-aminoacidato Schiff bases and different neutral ligands (L) have been determined by X-ray crystal structure analysis [3]. An examination of the structural data of these complexes showed the possibility of a mechanism for metabolic reactions of aminoacids catalyzed by the vitamin B_6 (or salicylaldehyde)- metal system [4,5].

The great flexibility of tridentate ligands connected with the variability of π–π interactions and hydrogen bonds leads to an extraordinary richness of cooperative ordering effects in the crystal structure, which is frequently connected with different coupling patterns ranging from ferrodistortive (parallel orientation of the main axes of coordination polyhedra) to antiferrodistortive (perpendicular orientation of the main axes of coordination polyhedra) [1,6–10]. The local symmetry in plane, where the chelate and neutral ligands are bound, undergoes only slight changes. On the other hand, a rich variety of axial distortions rang-

† For Part V. see ref. 1.

* Author to whom correspondence should be addressed. E-mail: plesch@fns.uniba.sk

ing from square-planar to square-pyramidal has been found. Such structural adaptability may be one of the reasons for the diversity of interactions of these complexes with biological systems.

A valuable tool for investigations on such complexes in the non-diluted state, where *g–g* coupling between non-aligned molecules frequently modifies the **g** tensor from molecular to cooperative, is the EPR spectroscopy. The single-crystal EPR spectra in particular allow, in connection with X-ray structural data, to find the best Cartesian coordinates within the structure of these low-symmetric Cu(II) complexes, giving the qualitative measure for the character of the chemical bonding [6,9].

In (2-methylimidazole)(*N*-salicylidene-glycinato)copper(II) the square-pyramids around Cu(II) are ordered on a slightly disturbed-antiferrodistortive way, forming a zig-zag chain, where members are connected in an axial direction via the bridging carboxylate oxygen belonging to the adjacent complex unit. From the cooperative $\mathbf{g}^c$ tensor of a single crystal and the X-ray structural data, the orthorhombic molecular *g* components have been evaluated [6]. An analogical X-ray structure has been reported for (imidazole)(*N*-salicylidene-glycinato)copper(II) [10]. On the other hand (1-methylimidazole)(*N*-salicylidene-*R,S*-valinato)copper(II) forms square-planar molecules associated to dimers [1]. Two misaligned stacks related by a glide plane are propagated in the structure. The interdimeric Cu · · · Cu distance between misaligned coordination polyhedra in this case amounts to 10.52 Å, which is too large for magnetic interactions between canted **g** tensors.

Since the imidazole group is found quite frequently in biological Cu(II) systems [11], we decided to continue our studies [1,6,7] of the influence of the Schiff base ligand on the structure of adducts of the type (TSB)Cu-(imidazole and its derivatives).

The *N*-salicylidene-*β*-alaninato ligand forms two fused six-membered chelate rings around Cu(II) instead of one six- and one five-membered as in *N*-salicylidene-glycinato dianion. In this paper the X-ray structure and single-crystal EPR spectra of (imidazole)(*N*-salicylidene-*β*-alaninato)copper(II) are reported.

EXPERIMENTAL

The title complex was prepared by treatment of $[Cu_2(N\text{-salicylidene-}\beta\text{-alaninato})_2(H_2O)]\text{-}(H_2O)$ [12] with an excess of imidazole in hot diluted ethanol (3 : 1). 5.45 g of the parent complex (10 mmol) was dissolved in the solvent at 70°C. By slow cooling of the filtered reaction mixture, a light green product containing well developed single crystals was obtained. The deposited product was ether washed and air dried. Analysis for $C_{13}H_{13}CuN_3O_3$ (formula weight 322.81) : Found% (Calc. %) : C 48.52 (48.37) ; H 4.09 (4.06) ; N 13.12 (13.02).

The crystal chosen for the X-ray structure analysis was of dimensions $0.4 \times 0.2 \times 0.2$ mm. Unit cell parameters were refined by a least-squares fit of the positional angles for 15 centred reflections.

Crystal data: monoclinic, space group C2/c, $a = 19.037(7)$ Å, $b = 9.789(6)$ Å, $c = 13.701(9)$ Å, $\beta = 95.82(6)°$, $V = 2540.1(3)$ Å^3, $Z = 8$, $\mu = 1.73$ mm^{-1}, $D_m = 1.69(1)$ g cm^{-1}, $D_x = 1.688$ g cm^{-1}, Mo-K_α radiation (0.71069 Å), $T = 293$ K.

Intensity data were collected up to $2\theta = 50°$ on a Syntex $P2_1$ diffractometer using the standard θ–2θ scan technique. The data were averaged to give 2053 unique reflections, 1286 of which were observed [$I \geqslant 2\sigma(I)$]. The structure was solved by the heavy-atom method and refined on F^2 by using the SHELXL93 program package [13] and anisotropic thermal parameters for the non-H atoms. All H atoms were located from a difference Fourier map but were not refined. The final residuals were $R(F) = 0.0577$, $wR(F^2) = 0.1108$, $S = 1.056$. In the final cycle the maximal ratio shift/e.s.d. was 0.008 and maximal and minimal heights in the difference map were 0.29 and -0.35 eÅ^{-3}, respectively.

The 35 GHz powder EPR spectrum of the ground sample was measured at room temperature on a Varian E-15 spectrometer using DPPH as an internal standard.

A well shaped monocrystal of the dimensions $0.2 \times 0.07 \times 0.02$ mm was fixed on a LiF cube, placed in a resonator and the EPR spectra at room temperature and 35 GHz were measured in three orthogonal planes. The angular dependence of the spectrum was measured in 15° steps at the modulation amplitude of 10 G and a microwave power of 5 mW.

RESULTS AND DISCUSSION

The complex molecule is characterized by an axially elongated square-pyramidal Cu(II) coordination (4 + 1), with the tridentate dianionic Schiff base (TSB) and the monodentate ligand (L) occupying the basal plane of the pyramid. The selected bond distances and angles are given in Table 1. The weakly coordinating carboxylic O3 atom of an adjacent complex molecule related by a centre of symmetry at 1/2, 1/2, 0 is located on the apical site. In this way, the Cu(II) complexes are bridged to dimers in which, due to extended bridge system, the intra-dimer Cu · · · Cu spacing of 5.292(3) Å is relatively large in comparison with other dimeric Cu(TSB) complexes [1,9,10,12,14] (Fig. 1). On the other hand, the closest inter-dimer Cu · · · Cu distance between the Cu(II) centres of the ferrodistortively ordered units comes to 6.167(3) Å. The bond lengths within the basal plane are : Cu—O1 1.892(5), Cu—O2 1.948(4), Cu—N1 1.929(5), and Cu—N2 1.970(5) Å, while the apical Cu—O3′ distance is 2.590(4) Å. The four basal donor atoms are not exactly planar and show a tetrahedral type of distortion with the following displacements from the mean plane of the

Table 1. Selected bond lengths [Å] and angles [deg] of (imidazole)(*N*-salicylidene-β-alaninato)copper(II)

Cu—O(1)	1.892(5)	O(1)—Cu—N(1)	93.4(2)
Cu—N(1)	1.929(5)	O(1)—Cu—O(2)	174.1(2)
Cu—O(2)	1.948(4)	N(1)—Cu—O(2)	92.1(2)
Cu—N(2)	1.970(5)	O(1)—Cu—N(2)	88.0(2)
O(1)—C(1)	1.304(8)	N(1)—Cu—N(2)	170.4(2)
O(2)—C(10)	1.259(7)	O(2)—Cu—N(2)	86.9(2)
O(3)—C(10)	1.218(7)	C(1)—O(1)—Cu	127.8(5)
N(1)—C(7)	1.275(9)	C(10)—O(2)—Cu	127.1(4)
N(1)—C(8)	1.440(8)	C(7)—N(1)—C(8)	118.7(6)
N(2)—C(11)	1.314(7)	C(7)—N(1)—Cu	124.0(5)
N(2)—C(13)	1.364(8)	C(8)—N(1)—Cu	117.3(5)
N(3)—C(11)	1.346(7)	C(11)—N(2)—C(13)	108.4(5)
N(3)—C(12)	1.368(9)	C(11)—N(2)—Cu	122.7(4)
C(8)—C(9)	1.495(9)	C(13)—N(2)—Cu	128.5(4)
C(9)—C(10)	1.512(8)	C(11)—N(3)—C(12)	107.9(5)
C(12)—C(13)	1.337(8)	O(1)—C(1)—C(6)	119.1(6)
		O(1)—C(1)—C(2)	121.9(8)
		N(1)—C(7)—C(2)	126.9(6)
		N(1)—C(8)—C(9)	112.8(5)
		C(8)—C(9)—C(10)	114.5(5)
		O(3)—C(10)—O(2)	124.1(5)
		O(3)—C(10)—C(9)	118.6(6)
		O(2)—C(10)—C(9)	117.3(6)
		N(2)—C(11)—N(3)	108.6(6)
		C(13)—C(12)—N(3)	107.0(6)
		C(12)—C(13)—N(2)	108.1(7)

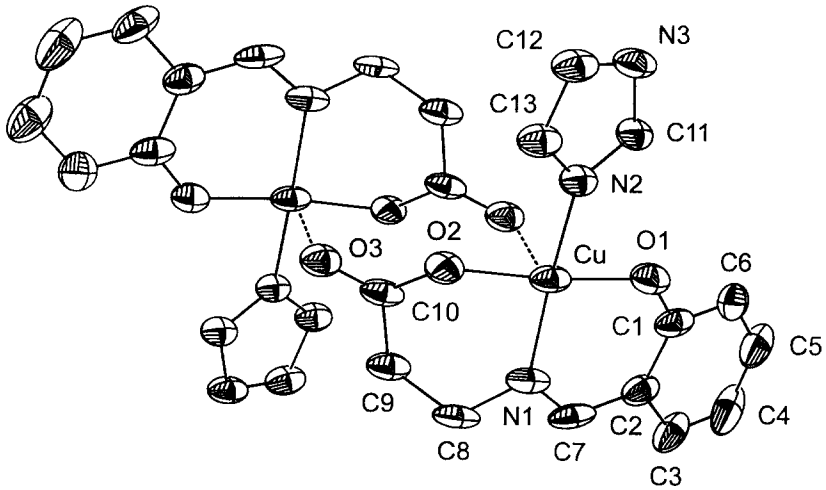

Fig. 1. A view of the binuclear complex $[Cu_2(sal\text{-}\beta\text{-}ala)_2(Im)_2]$, showing atom numbering of the reference molecule. Dashed lines represent the weak apical Cu—O′ interaction of 2.59 Å.

donor atoms: O1 0.103(5), N1 0.099(5), O2 0.102(5), N2 0.106(5) Å. The Cu atom is displaced by only 0.059(2) Å from this plane. The salicyladimine moiety is approximately planar (r.m.s. deviation 0.069 Å) but significantly folded relative to the basal coordination plane; the dihedral angle between the O_2N_2 basal plane and the mean plane of the salicyladimine moiety is 11.3(1)°. As a result, the six-membered chelate ring involving the salicyladimine part of the ligand shows considerable warping, with the endocylic torsion angles ranging from 18.6(8) to 16.4(5)°. The imidazole molecule is exactly planar (r.m.s. deviation 0.008 Å) and makes an angle of 21.5(2)° with the basal coordination plane.

The bond lengths and angles in the ligand part of the molecule are normal and well comparable with those found for related molecules [1,6,10]. The Cu—O bond length to phenolic oxygen O1 of the tridentate Schiff base is significantly shorter than the bonding to carboxylic oxygen O2, which indicates different bond

strengths. The apical Cu—O′ distance in the low-symmetry Cu(TSB)L complexes in inversely proportional to the average of bond distances in plane r_m, as well as to the experimental g values obtained from EPR. This fact shows analogy with the concept of tetragonality introduced by Hathaway [15] for complexes of tetragonal symmetry. Generally, the g_z value is most susceptible to shifts in tetragonality [15]. However, in complexes with g–g coupling between canted **g** tensors, where the experimental g_z value is hidden, the value of g_{av} can be taken as a measure of axial bond strength [1,7,8]. For example, in (1-methyl-imidazole)(*N*-salicylidene-*R*,*S*-valinato)copper(II) [1] Cu—O′ = no axial interaction, $r_m = 1.931(2)$ Å, $g_{av} = 2.097$; in the title complex Cu—O′ = 2.590(4) Å) $r_m = 1.936(4)$ Å, $g_{av} = 2.115$ and in (2-methylimidazole)(*N*-salicylidene-glycinato)copper(II) [6] Cu—O′ = 2.481(4) Å, $r_m = 1.961(5)$ Å $g_{av} = 2.126$. Similar results have been obtained by Warda [10].

The observed components $g_1 = 2.217$, $g_2 = 2.069$, $g_3 = 2.060$ of the EPR spectrum of the powdered sample (Fig. 2) give evidence that the experimental g factors result from a coupling of two magnetically non-equivalent Cu(II) complexes related by the glide plane of the monoclinic unit cell. For this case the following equations for experimental cooperative g values hold [6]:

$$g_1^c = \cos^2\gamma g_z + \sin^2\gamma(\cos^2\xi g_y + \sin^2\xi g_x),$$
$$g_2^c = \sin^2\gamma g_z + \cos^2\gamma(\cos^2\xi g_y + \sin^2\xi g_x)$$
$$g_3^c = \sin^2\xi g_y + \cos^2\xi g_x, \qquad (1)$$

where 2γ stands for the canting angle between the normal to equatorial planes of the coordination pyramids and ξ is the rotation angle around the g_z axis in this plane. From these equations the values of canting angle 2γ and molecular g parameters g_z and g_{xy} can be expressed [1,8] as a function of the well known parameter $G = (g_z - g_0)/(g_{xy} - g_0)$;

$$2\gamma = \arccos\{(g_1^c - g_2^c)(G+2)/[(g_1^c + g_2^c - 2g_0)(G-2) + 2(g_3^c - g_0)G]\},$$
$$g_z = [3g_{av}G - 2g_0(G-1)]/(G+2)$$
$$g_{xy} = [3g_{av} + g_0(G-1)]/(G+2) \approx (g_y + g_x)/2 \quad (2)$$

where $g_0 = 2.0023$.

A simple procedure, which is based on the consistency of G parameters for the complexes under investigation, has been proposed [1,8] for estimation of the anisotropy of g_{xy} components of **g** tensor with orthorhombic symmetry. For the range of $G = 4.65 \pm 0.25$, which is reasonable in our case [1,6,7,10], we obtain the following values: $g_z = 2.239 \pm 0.004$, $g_y = 2.060 \pm 0.010$, $g_x = 2.047 \pm 0.008$, $2\gamma = 40.4° \pm 3.4°$.

Looking at the mutual orientation of the magnetically non-equivalent Cu(II) coordination pyramids, we see nearly aligned N—N axes with an angle of 9.86(3)° (Fig. 3). Following to such small canting angle, the molecular $g_y \equiv g_3^c$ value corresponding to the N—N direction is observed rather exactly in the experimental EPR spectrum. On the other hand, the canting angle 2γ between the normals to the basic planes of the misaligned coordination polyhedra amounts to 40.26(3)°, which is in excellent agreement with the 2γ value calculated from EPR spectra. The ordering of the dimeric units of canted pyramids may be described as disturbed-ferrodistortive, where the closest inter-dimer Cu···Cu spacing responsible for

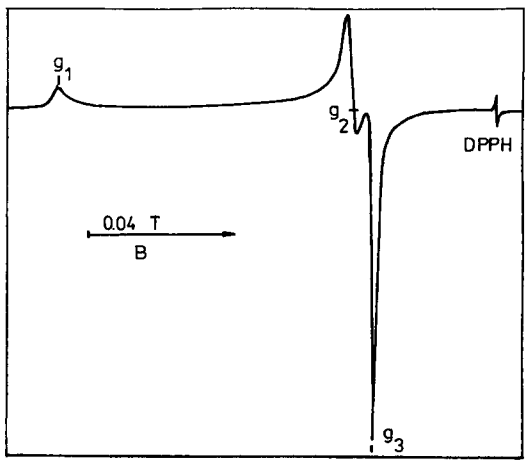

Fig. 2. The 35 GHz EPR powder spectrum of $[Cu_2(sal\text{-}\beta\text{-}ala)_2(Im)_2]$.

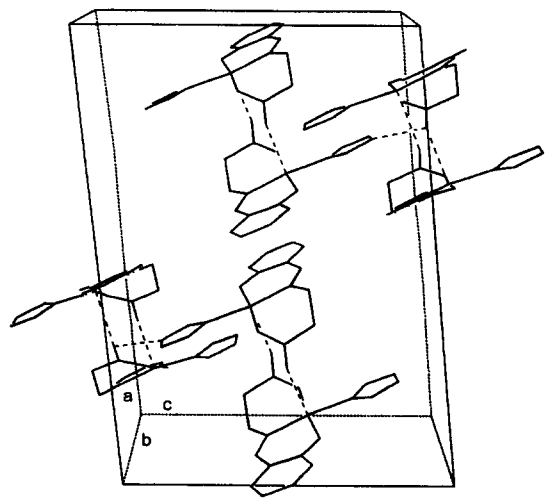

Fig. 3. View of the crystal packing of $[Cu_2(sal\text{-}\beta\text{-}ala)_2(Im)_2]$ centrosymmetric dimers propagated in the unit cell. In the disturbed-ferrodistortive ordering two stacks are related by a glide plane. The parallel orientation of aromatic parts of the ligands indicating π–π interactions is visible. The dashed lines represent the weak Cu—O′ apical interactions and the inter-dimeric hydrogen bonds.

the coupling of misaligned molecular **g** tensors is 7.359(4) Å.

Besides forming the weak apical Cu···O interaction, the carboxylate O3 atom of each complex molecule is also involved in an H bond interaction with the imidazole N3 atom (O···N = 2.748(3) Å) of a molecule related by a screw axis parallel with *b* (Fig. 3). The latter contact connects the dimers into helices going parallel to [0,1,0]. The chains are held together mainly by π–π stacking interactions between the aromatic rings of the Schiff-base ligands. All imidazole planes in the structure are lying parallel, which also contributes to the stabilisation of the crystal structure by π–π interactions.

A remarkable sharpness of all three components of the EPR powder signal suggested a single-crystal investigation. We succeeded in a quite favourable adjustment of the crystal, admitting to see all three main axes of the coupled crystal $\mathbf{g}^c$ tensor (Fig. 4). The diagonalisation of the $\mathbf{g}^2$ matrix obtained from angular measurements yields: $g_1^c = 2.219$, $g_2^c = 2.070$, $g_3^c = 2.059$, which is in excellent agreement with the results obtained from the EPR spectra of the ground sample. The extreme values g_1^c and g_3^c were observed in the plane perpendicular to the needle axis, whereas $g_2^c \equiv g_b$ was measured in both planes parallel to it. Analysing the cooperative **g** tensor in more detail, we have found a complete consistency between the angular spectroscopic EPR behaviour and the results of X-ray structural analysis. As already mentioned above, the N—N axes of two crystallographically non-equivalent complexes are tilted against the *ac** plane, perpendicular to the crystallographic *b* axis, by an angle of $\pm 4.93(3)^\circ$. Corresponding to such a small canting angle, the molecular g_y value is observed almost exactly in the *ac** plane, perpendicularly to the needle axis. On the other hand, the O—O axes of the misaligned complex molecules are strongly canted by an angle of $20.75(3)^\circ$ with respect to the crystallographic *b* axis. This canting, with regard of slight twisting, results in a canting angle $2\gamma = 40.26(3)^\circ$ between the normals to basic planes of coordination polyhedra, which correspond to g_z axes. If we neglect the slight twisting between g_y components, the g–g coupling influences only the g_z and g_x components of the misaligned molecular **g** tensors and the following equations for the experimental cooperative g values hold:

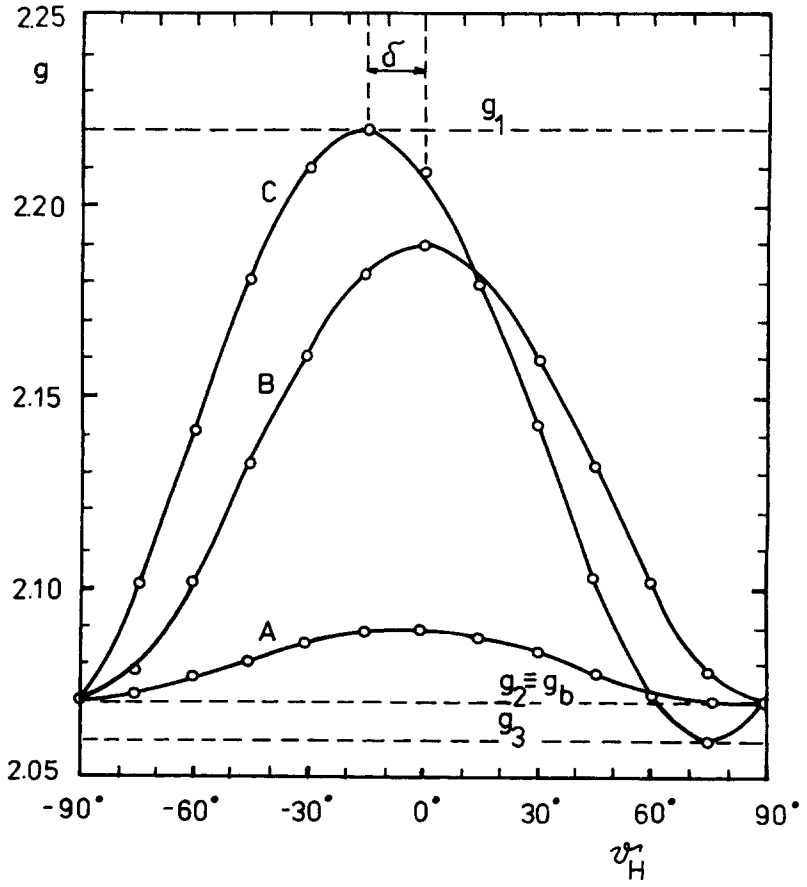

Fig. 4. Angular dependence of the single-crystal EPR spectra of $[Cu_2(sal\text{-}\beta\text{-}ala)_2(Im)_2]$ in three orthogonal planes (curves correspond to least-squares fit of the experimental results). The *C* plane, which is perpendicular to the needless axis, corresponds to (*ac**).

$$g_1^c = \cos^2 \gamma g_z + \sin^2 \gamma g_x$$

$$g_2^c = \sin^2 \gamma g_z + \cos^2 \gamma g_x \quad (3)$$

Using the angle γ obtained from X-ray structural analysis we obtain the values $g_x \equiv g_{OO} = 2.043$, $g_y \equiv g_{NN} = 2.060$, $g_z = 2.240$, which are in complete agreement with the molecular g parameters obtained from the powder EPR spectrum with a help of a simple approximation procedure [1,8], which can be used without any knowledge about the X-ray structure.

Considering the orientation of the g_1^c and g_3^c axes of the $\mathbf{g}^c$ tensor with respect to the roughly rectangular sectional area perpendicular to the crystallographic b axis, we have observed a phase shift by an angle $\delta \approx 17°$ (Fig. 4), which corresponds to the angle of 18.07(3)° between N—N and c^* axis found from X-ray structure analysis. From this finding we see that faces spread by the crystallographic b axis and a vector perpendicular to [010] running through the centres of symmetry of two adjacent misaligned dimers are preferred for the growth of crystals. Perpendicular to these faces we recognise the association of the complex units via π–π interactions between the aromatic systems of the ligands.

CONCLUSIONS

The reaction of [Cu_2(*N*-salicylidene-β-alaninato)$_2$(H_2O)]H_2O with imidazole leads to [Cu_2(*N*-salicylidene-β-alaninato)$_2$(imidazole)$_2$]. In the parent aqua-complex the dimer is realized [12] via double bridging through phenolic oxygens in basal planes (Cu—O = 1.92–2.01 Å) and the intradimeric Cu···Cu distance amounts to 3.03 Å. Due to superexchange interaction of a Cu—O—Cu type, the EPR spectra of this complex indicate [16] antiferromagnetic Cu··Cu coupling with a singlet–triplet separation being 565 cm^{-1}. In the imidazole adduct the neutral ligand is bound in-plane and the formation of dimers is achieved through weak axial Cu—O′ interaction with a length of 2.59 Å via the terminal carboxylic oxygens of the partner molecule. Due to the extended O—C—O bridge system, the intradimeric Cu···Cu spacing reaches 5.29 Å and no antiferromagnetic interaction is indicated by EPR. An analogical triatomic bridge system, however, constituting from NCS^- ambidentate ligands, is realised in [bis{(μ-isothiocyanato-N,S)(N-salicylidene-β-alaninato)}dicuprate(II)] [17] with intradimeric Cu···Cu distance of 5.77 Å.

Axial Cu—O′ interaction of different strength with the neighbouring complex molecule, which extends the square-planar coordination to (4+1), has been frequently observed in Cu(TSB)L adducts [6,10,18]. In Cu(II) complexes with tridentate Schiff bases having fused six- and five-membered chelate rings, the interaction with adjacent phenolic oxygen leads to dimers. On the other hand, zig-zag chains are formed by bonding to neighbouring terminal carboxylic oxygen. Although in the first case the intradimeric Cu···Cu spacing amounts only to 3.2–3.3 Å, no conditions for superexchange of antiferromagnetic type are given. The mutual perpendicular orientation of the bridging [Cu_2O_2'] and basal [CuN_2O_2] planes and the weak apical Cu—O′ bond, which is involved in the Cu—O′—Cu bridge do not allow an effective transfer of electron density between Cu(II) ions in dimers. In the carboxylato-bridged chains, the lowest Cu···Cu distances in the structure are in the range of 5.2–6.9 Å and they can be found between ferrodistortively ordered complex units, which are associated only by π–π interaction. The results presented here show that with tridentate *N*-salicylidene-β-alaninato Schiff base, which contains two conjugated six-membered chelate rings, the steric factors cause the formation of another type of dimers, where the Cu(II) ions are connected through triatomic O—C—O bridges from the carboxyl group of the partner molecule. The above described dimerisation and polymerisation are induced by cooperative ordering effects in solid state. Therefore, after dissolving the crystals, only monomeric complex units are present in diluted solution.

In [Cu_2(*N*-salicylidene-β-alaninato)$_2$(imidazole)$_2$] stacks of dimers, which are related by a screw axis going parallel to b, are propagated in the crystal structure. In such a way two stacks are ordered in a disturbed-ferrodistortive way. Since the interdimeric distance between misaligned coordination polyhedra amounts to 7.36 Å, weak coupling operates between canted **g** tensors and the experimental EPR spectra show cooperative character. From single-crystal EPR spectra, but also from powder EPR pattern, the orthorhombic molecular g components and the canting angle 2γ between the misaligned coordination polyhedra, which are in excellent agreement with the X-ray structure, were calculated.

Acknowledgements—Support of the Ministry of Education and Science of Slovak Republic (Grant Nos 1/1462/94 and 1223/94) is gratefully acknowledged.

Supplementary material available—Listing of atomic positions and anisotropic thermal parameters for non-H-atoms have been deposited at the Cambridge Crystallographic Data Centre.

REFERENCES

1. Plesch, G., Friebel, C., Warda, S. A., Sivý, J. and Švajlenová, O., *Transition Metal Chem.*, 1997, **22,** 433.
2. Metzler, D. E., Ikawa, M. and Snell, E. E., *J. Am. Chem. Soc.*, 1954, **76,** 648.
3. García Raso, A., Fiol, J. J. and Bádenas, F., *Polyhedron*, 1996, **15,** 4407, and references therein.
4. Bkouche-Waksman, I., Barbe, M. and Kvick, Å., *Acta Cryst.*, 1988, **B44,** 595.
5. Sivý, J., Kettmann, V., Krätsmár-Šmogrovič, J. and Breza, M., *Z. Naturforsch.*, 1994, **49c,** 571.

6. Sivý, J., Kettmann, V., Krätsmár-Šmogrovič, J., Švajlenová, O., Friebel, C. and Plesch, G., *Z. Anorg. Allg. Chem.*, 1990, **583,** 55.
7. Plesch, G., Friebel, C., Švajlenová, O. and Krätsmár-Šmogrovič, J., *Polyhedron*, 1991, **10,** 893.
8. Plesch, G., Friebel, C., Švajlenová, O. and Krätsmár-Šmogrovič, J., *Polyhedron*, 1995, **14,** 1185.
9. Friebel, C., Plesch, G., Kettmann, V., Krätsmár-Šmogrovič, J. and Švajlenová, O., *Inorg. Chim. Acta*, 1997, **234,** 273.
10. Warda, S. A., Bioanorganische Kupfer(II) Komplexe mit dreizähnigen O,N,O-Chelat Liganden und additiven einzähnigen Donorliganden, Verlag Shaker, Aachen, 1994.
11. Kaim, W. and Schwederski, B., *Bioanorganische Chemie*, Teubner, Stuttgart 1991.
12. Werner, P. E., Valent, A., Adelsköld, V. and Švajlenová, O., *Acta Chem. Scand.*, 1983, **A37,** 51.
13. Sheldrick, G. M., SHELXL93. A program for refinement of the crystal structures, Univ. Göttingen, 1995.
14. Korhonen, K. and Hämäläinen, R., *Acta Chem. Scand.*, 1979, **A33,** 569.
15. Hathaway, B. J. and Billing, D. E., *Coord. Chem. Rev.*, 1973, **5,** 143.
16. Jablokov, Ju. V., Krätsmár-Šmogrovič, J., Voronkova, V. K., Mosina, L. V., Švajlenová, O. and Žemlička, M., *Zh. neorg. khim.*, 1986, **31,** 707.
17. Kettmann, V., Krätsmár-Šmogrovič, J., Švajlenová, O. and Zemlička, M., *Z. Naturforsch.*, 1992, **47b,** 1565.
18. Pavelčík, F., Krätsmár-Šmogrovič, J., Švajlenová, O. and Majer, J., *Collect Czech. Chem. Commun.*, 1981, **46,** 3186.

Pergamon

PII: S0277-5387(97)00339-2

Polyhedron Vol. 17, No. 4, pp. 547–554, 1998
© 1998 Elsevier Science Ltd
All rights reserved. Printed in Great Britain
0277–5387/98 $19.00+0.00

Syntheses, crystal structures and solid state thermochromism of copper(II) complexes of *trans*-1,2-diaminocyclohexane

Chandi Pariya,* Fen-Ling Liao, Sue-Lein Wang and Chung-Sun Chung*

Department of Chemistry, National Tsing Hua University, Hsinchu, Taiwan 30043, Republic of China

(Received 20 June 1997; accepted 5 August 1997)

Abstract—The complexes $CuL_2X_2 \cdot nH_2O$ (L = *trans*-1,2-diaminocyclohexane; $n = 2$ when X is Cl and $n = 0$ when X is NO_3) have been synthesized. The complexes $[CuL_2(H_2O)_2]Cl_2$ (**1**) and $[CuL_2(NO_3)_2]$ (**2**) have been characterized by single crystal structural analyses and their thermochromism was studied in the solid state. Single crystal X-ray structure analysis of **1** and **2** shows that in both complexes copper ion possesses distorted (4+2) octahedral geometry with N_4O_2 chromophore. Complex **1** shows time-dependent reversible discontinuous thermochromism whereas, **2** shows reversible continuous thermochromism in the solid state. The discontinuous thermochromism in **1**, is due to the different ligand field strength between H_2O and Cl, and is associated with deaquation–anation reaction. The IR and electronic spectra of **2** vary with temperature, indicating reversible continuous thermochromism arising from axial interaction between semi-coordinated nitrate ions and CuN_4 plane. © 1998 Elsevier Science Ltd. All rights reserved

Keywords: copper(II) complexes; *trans*-1,2-diaminocyclohexane; syntheses; single crystal structure; thermochromism; TG-DTA.

Thermochromism which involves the change in color of a transition metal complex under thermal excitation is a subject of interest among coordination chemists. This occurs in solids [1] as well as in liquids [2]. The solid state thermochromism can be distinguished under two headings: discontinuous thermochromism, where the color change takes place suddenly and is associated with a first order structural phase transformation, and continuous thermochromism, where the color change is due to a gradual shift and/or broadening of the visible absorption bands upon stress with an increased population of the ground state vibrational levels. Thermochromic behaviour in copper(II) complexes with *N,N*-substituted ethylenediamines has been reported [3-9]. A discontinuous thermochromism in copper(II) halide (chloride and bromide) salts and copper(II) nitrate complexes of 2,2-dimethylpropane-1,3-diamine (dmpd) are extensively studied by Willett *et al.* [10–14]. The discontinuous thermochromism of copper(II) nitrate complexes of *N,N'*-dimethylethane-1,2-diamine is known [15]. A continuous thermochromism was reported for a series of $[Cu(dmpd)_2X_2]$ (X = Cl, Br and ClO_4) complexes by Pellacani *et al.* [16]. In transition metal complexes, thermochromic phase transitions are associated with a change in coordination geometry or in the effective ligand field strength of a coordinating ligand. The solid state thermochromic complexes are very important owing to their applicability as temperature sensors [17].

1,2-Diaminocyclohexane exists in two isomeric forms: *cis*- and *trans*- forms. *Trans*-isomer is more stable than *cis*- and probably because of this it has been well studied [18–24]. In this paper we report the preparation, characterization and thermochromic properties of *trans*-1,2-diaminocyclohexane complexes of CuX_2 (X = Cl and NO_3).

EXPERIMENTAL

Materials

High-purity (99%) *trans*-1,2-diaminocyclohexane (L) was purchased from Aldrich Chemical Company Inc. and used as received. All other chemicals used were of G.R. grade (Merck or Aldrich).

* Authors to whom correspondence should be addressed.

Physical measurements

The thermal analysis (TG–DTA) was carried out on a Seiko TG/DTA 300 simultaneous Thermo-Gravimetric/Differential Thermal Analyzer in a dynamic atmosphere of argon (100 ml min^{-1}). The sample was heated in an Al crucible at a rate of 10°C min^{-1} with an empty Al crucible as a reference. The enthalpy change of dehydration was calculated using a Seiko DSC 200 Differential Scanning Calorimeter with indium metal as the calibrant (rate of heating 10°C min^{-1}) in a dynamic atmosphere of argon (40 ml min^{-1}). The instruments used for recording the infrared (KBr discs and Nujol mulls) and electronic spectra (Nujol mulls) were BOMEM (Hartmann and Braun, MB-Series) and HITACHI (U-3300) spectrophotometer, respectively. The magnetic susceptibility and elemental analyses were performed on an EG and G PAR 155 Vibrating Sample magnetometer and a Heraeus CHN-O-Rapid instrument, respectively. For X-ray structure determination a Siemens R3m/V diffractometer was used.

Preparation of $[CuL_2(H_2O)_2]Cl_2$ (**1**)

$CuCl_2 \cdot 2H_2O$ (1 mmol) was dissolved in ethanol (10 cm^3). *Trans*-1,2-diaminocyclohexane (2 mmol) was then added to a $CuCl_2$ solution with stirring. The resulting pink solution on slow evaporation in a desiccator yielded the desired pink crystalline complex. The crystals were separated, washed with ethanol and dried in a desiccator. Recrystallization from hot water yielded pink crystals suitable for X-ray analysis. Found: C, 35.91; H, 8.10; N, 13.97. Calc. for $C_{12}H_{32}Cl_2N_4O_2Cu$ (**1**): C, 36.09; H, 8.08; N, 14.03%. μ_{eff} = 1.81 B.M.,[a] λ_{max} (Nujol) = 562 nm.

Preparation of $[CuL_2(NO_3)_2]$ (**2**)

$Cu(NO_3)_2 \cdot 3H_2O$ (1 mmol) was dissolved in methanol (10 cm^3). *Trans*-1,2-diaminocyclohexane (2 mmol) was then added to the above solution with stirring. The resulting pink solution was kept in a desiccator. After a few days fine pink crystals were separated out, filtered, washed with ethanol and dried in a desiccator. The recrystallization was from water yielding pink crystals suitable for X-ray analysis. Found: C, 34.53; H, 6.87; N, 20.12. Calc. for $C_{12}H_{28}N_6O_6Cu$ (**2**): C, 34.62; H, 6.78; N, 20.19%. μ_{eff} = 1.83 B.M.;[a] λ_{max} (Nujol) = 526 nm.

X-ray diffraction structural study

A crystal of dimensions 0.05 × 0.15 × 0.32 mm for **1** (0.05 × 0.12 × 0.22 for **2**) was selected for indexing and intensity data collection on a Siemens SMART-CCD diffractometer equipped with a normal focus, 3 kw sealed tube X-ray source. Intensity data were collected in 2082 (1271 for **2**) frames with increasing ω (width 0.3°/frame). Unit cell dimensions were determined by a least-squares fit of 3925 (3205 for **2**) reflections with $5 < 2\theta < 50°$. Absorption correction was based on 1671 (4301 for **2**) symmetry-equivalent reflections using the SHELXTL-PC program package ($T_{min,max}$ = 0.474, 0.928 and 0.487, 0.928 for **2**). On the basis of systematic absences, statistics of intensity distribution, and successful solution and refinement of the structure, the space group was determined to $P\bar{1}$ (No. 2) (and Pb_{ca} for **2** (No. 61)). Crystallographic data are summarized in Table 1.

[a] Non-S.I. Unit employed: B.M. 9.27 × 10^{-24} Am^2.

RESULTS AND DISCUSSION

Thermal analyses and thermochromism

The simultaneous thermogravimetric/differential thermal analysis (TG-DTA) of complexes **1** and **2** are shown in Figs 1 and 2, respectively. for complex **1**, $[CuL_2(H_2O)_2]Cl_2$ the weight loss observes in the TG curve in the temperature region (65–110°C) corresponds to the liberation of two molecules of H_2O. The DTA curve shows that the dehydration proceeds endothermically. The enthalpy change for this transformation was calculated from DSC curve (ΔH = 128.69 kJ mol^{-1}). The dehydrated species **1a**, CuL_2Cl_2 is stable in desiccator and can be stored for a long time. However, the species **1a**, rehydrates on standing in a humid atmosphere. On dehydration the color of the complex changes from pink to blue-violet. This color change is due to deaquation–anation reaction and is followed by the change of strength of the coordinating ligands. Thereafter an endothermic peak appears in the range 240–275°C where the TG curve changes quite sharply due to decomposition of *bis*-complex to *mono*-species and finally to metal salt. On the other hand complex **2**, changes its color from pink to blue-violet continuously and finally starts to decompose at 300°C. The thermal stability of the *bis*-nitro complex is more than the corresponding chloro species i.e. $CuL_2(NO_3)_2 > CuL_2Cl_2$.

Structure of $[CuL_2(H_2O)_2]Cl_2$ (**1**)

Figure 3 shows an ORTEP view and atom-numbering scheme of the dication $[CuL_2(H_2O)_2]^{2+}$ together with two chlorite ions and its packing arrangement is shown in Fig. 4. Selected atomic distances and bond angles are listed in Table 2. The copper ion in the complex possesses distorted (4+2) octahedral geometry having N_4O_2 chromophore. The two oxygen atoms of weakly coordinated water molecules in the *trans* position, Cu—O = 2.590(2) Å. Two 5-membered chelate rings are arranged in such a way

Table 1. Crystallographic and data collection parameters for complexes **1** and **2**

	1	**2**
Empirical formula	$C_{12}H_{32}Cl_2N_4O_2Cu$	$C_{12}H_{28}N_6O_6Cu$
Color	Pink	Pink
Formula weight (f_w)	398.9	415.9
Crystal size (mm)	$0.05 \times 0.15 \times 0.32$	$0.05 \times 0.12 \times 0.22$
Crystal system	Triclinic	Orthorhombic
Space group	$P\bar{1}$	Pb_{ca}
Unit cell dimensions		
a (Å)	6.1039(1)	9.9509(7)
b (Å)	7.0810(2)	8.0401(6)
c (Å)	12.0874(3)	23.1954(18)
α (°)	106.296(0)	–
β (°)	91.737(1)	–
γ (°)	108.359(1)	–
V (Å^3)	471.9(2)	1855.8(6)
Z	1	4
D_c (g cm^{-1})	1.404	1.489
Absorption coefficient (mm^{-1})	1.449	1.217
F(000)	211	876
Diffractometer used	Siemens SMART CCD	Siemens SMART CCD
Radiation, Mo–K_α (Å)	0.71073	0.71073
Temperature (K)	296	296
Monochromator	Highly oriented graphite crystal	Highly oriented graphite crystal
2θ Range (°)	2.5 to 57.2	2.5 to 57.7
Scan speed (sec frame^{-1})	10.00	10.00
Scan range (ω, °frame^{-1})	0.30	0.30
Index ranges	$-8 \leqslant h \leqslant 8$ $-9 \leqslant k \leqslant 9$ $-15 \leqslant l \leqslant 16$	$-13 \leqslant h \leqslant 11$ $-10 \leqslant k \leqslant 10$ $-30 \leqslant l \leqslant 23$
Reflections collected	4691 (4447 $\geqslant 3.0\sigma$ (I))	11024 (5979 $\geqslant 3.0\sigma$ (I))
Independent reflections	2180 (1820 $\geqslant 3.0\sigma$ (I)) ($R_{int} = 4.34\%$)	2266 (914 $\geqslant 3.0\sigma$ (I)) ($R_{int} = 5.85\%$)
System used	Siemens SHELXTL PLUS (VMS)	Siemens SHELXTL PLUS (VMS)
Solution	Direct Methods	Direct Methods
Refinement method	Full-Matrix Least-Squares	Full-Matrix Least-Squares
Extinction correction	$\chi = 0.0093$ (16), where $F^* = F[1 + 0.002 \chi F^2/\sin(2\theta)]^{-1.4}$	$\chi = 0.00040$ (12), where $F^* = F[1 + 0.002 \chi F^2/\sin(2\theta)]^{-1.4}$
Hydrogen atoms	Located on difference map	Located on difference map
Weighting scheme	$w^{-1} = \sigma^2(F) + 0.0010 F^2$	$w^{-1} = \sigma^2(F) + 0.0012 F^2$
Number of parameters refined	98	116
Final R indices (obs. data)	$R = 0.040$, $R_w = 0.0464$	$R = 0.0443$, $R_w = 0.0458$
Goodness-of-fit	1.21	1.08
Largest and mean Δ/σ	0.001, 0.000	0.001, 0.000
Data-to-parameter ratio	18.6 : 1	7.9 : 1
Largest difference peak/hole	0.46/−0.58 eÅ^{-3}	0.44/−0.84 eÅ^{-3}

that 6-membered cyclohexane rings are in *trans* chair–chair conformations. The average Cu—N bond distance 2.035(3) Å (Table 2) is an agreement with the values reported for other copper(II) diamine complexes [8]. The copper atom at the inversion center is co-planar with four ligand nitrogen atoms [N(1), N(2) and their centrosymmetrically related ones]. The geometry around copper is distorted square-planar, with an in-plane distortion introduced by the ligand bite angle N(1)—Cu—N(2) = 84.2(1)°.

Structure of $[CuL_2(NO_3)_2]$ (**2**)

An ORTEP view of the complex with the atom labelling scheme is shown in Fig. 5 and the packing arrangement is shown in Fig. 6. The structure consists of $[CuL_2]^{2+}$ cations and two NO_3 anions. The copper atom at the inversion center is co-planar with four ligand nitrogen atoms. The geometry around copper is distorted square-planar, with an in-plane distortion introduced by the ligand bite angle N(1)—

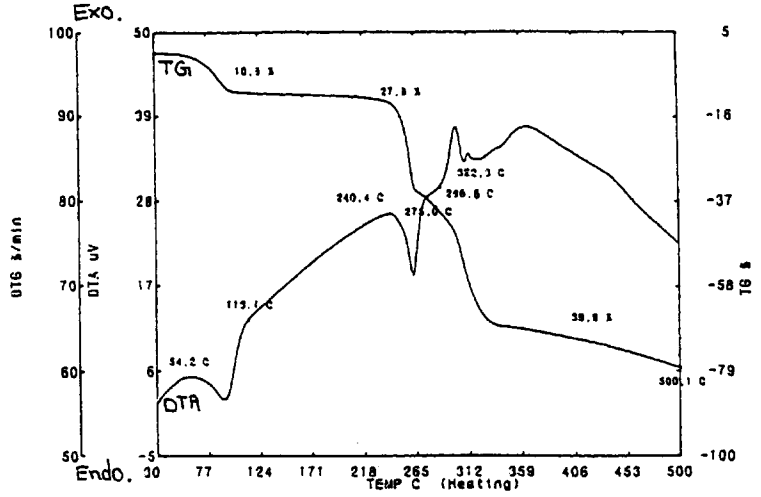

Fig. 1. Simultaneous TG–DTA (weight taken = 4.60 mg) curves for $CuL_2Cl_2 2H_2O$ (**1**).

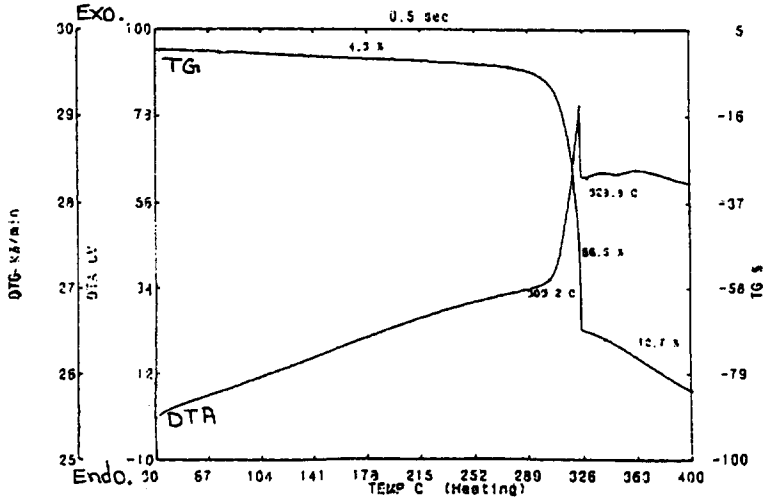

Fig. 2. Simultaneous TG–DTA (weight taken = 3.70 mg) curves for $CuL_2(NO_3)_2$ (**2**).

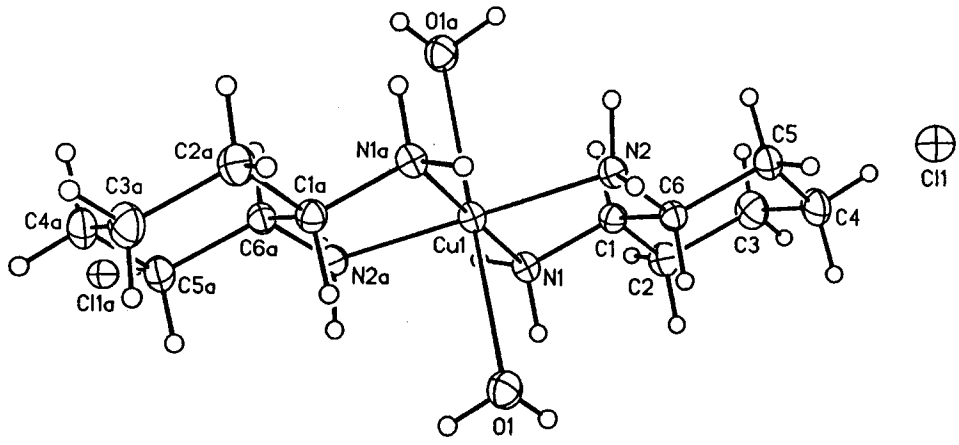

Fig. 3. ORTEP plot of $[CuL_2(H_2O)_2]Cl_2$ (**1**) with atom numbering scheme.

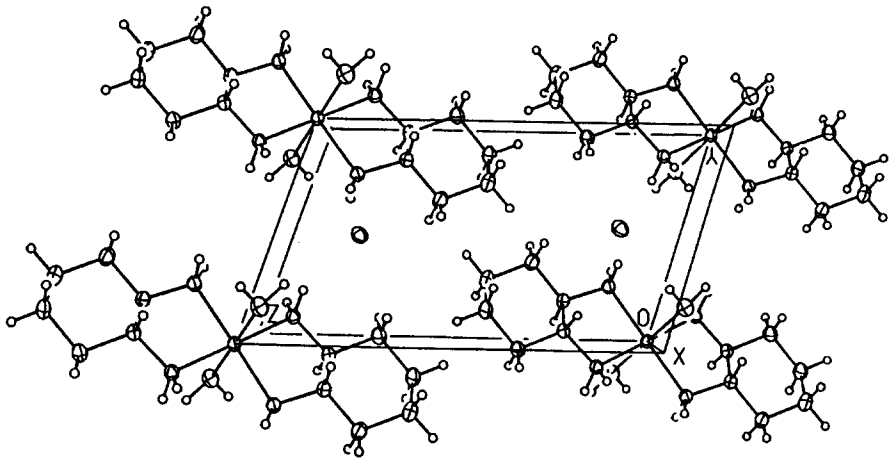

Fig. 4. Packing arrangement for $[CuL_2(H_2O)_2]Cl_2$ (**1**).

Table 2. Selected bond distances (Å) and angles (°) for complexes **1** and **2**

	1	**2**
Cu(1)—N(1)	2.044(2)	1.990(4)
Cu(1)—N(2)	2.027(3)	2.006(4)
Cu(1)—O(1/2)	2.590(2)	2.620(3)
O(1)—N(3)	—	1.216(7)
O(2)—N(3)	—	1.260(7)
O(3)—N(3)	—	1.231(6)
N(1)—C(1)	1.482(4)	1.473(7)
N(2)—C(6)	1.489(3)	1.487(7)
C(1)—C(2)	1.528(3)	1.531(8)
C(1)—C(6)	1.527(5)	1.494(8)
C(2)—C(3)	1.520(5)	1.534(8)
C(3)—C(4)	1.535(6)	1.490(9)
C(4)—C(5)	1.524(4)	1.530(9)
C(5)—C(6)	1.530(5)	1.525(8)
N(1)—Cu(1)—N(2)	84.2(1)	84.8(2)
N(1)—Cu(1)—N(1A)	180.0(1)	180.0(1)
N(2)—Cu(1)—N(1A)	95.8(1)	95.2(2)
N(1)—Cu(1)—N(2A)	95.8(1)	95.2(2)
N(2)—Cu(1)—N(2A)	180.0(1)	180.0(1)
N(1A)—Cu(1)—N(2A)	84.2(1)	84.8(2)
Cu(1)—N(1)—C(1)	107.2(2)	107.8(3)
Cu(1)—N(2)—C(6)	109.7(2)	109.4(3)
O(1)—N(3)—O(2)	—	119.5(5)
O(1)—N(3)—O(3)	—	120.1(5)
O(2)—N(3)—O(3)	—	120.3(5)
N(1)—C(1)—C(2)	113.5(3)	114.2(4)
N(1)—C(1)—C(6)	107.2(2)	107.7(4)
C(2)—C(1)—C(6)	110.9(2)	111.6(4)
C(1)—C(2)—C(3)	110.2(3)	108.8(5)
C(2)—C(3)—C(4)	111.6(3)	112.4(5)
C(3)—C(4)—C(5)	111.3(3)	114.0(5)
C(4)—C(5)—C(6)	110.0(3)	110.9(5)
N(2)—C(6)—C(1)	107.3(2)	108.4(4)
N(2)—C(6)—C(5)	113.4(2)	112.7(4)
C(1)—C(6)—C(5)	111.8(2)	111.3(5)

Cu—N(2) = 84.8(2)°. Two 5-membered chelate rings are arranged in such a way that 6-membered cyclohexane rings are in *trans*-chair–chair conformations. The weak coordinations, Cu—O(2) = 2.620(3) Å, of the two symmetry related oxygen atoms [O(2) and O(2a)] of the NO_3^- ion complete a distorted octahedron. O(3) of the nitrate is hydrogen bonded to one of the amino nitrogen atoms N(1) of the cation: O(3)···N(1) 3.028, O(3)···H(N1) 2.155 Å; N(1)—H(N1)—(O3) 163.34°. Similar type of hydrogen bonding between NO_3^- and nitrogen atoms were reported for copper(II) nitrate complexes of ligands 1,5-diazacyclooctane [25] and *N,N'*-dimethylethane-1,2-diamine [15]. The nitrate ion is a planar one. The N—O bond distances are almost equal (average being 1.236(7) Å).

Infrared and electronic spectra

The IR spectra of the complexes $[CuL_2(H_2O)_2]Cl_2$ (**1**) and $[CuL_2(NO_3)_2]$ (**2**) were taken at three stages, i.e. at room temperature, after heating at 110 and 140°C. We have some limitation for recording the spectra at higher temperature. After heating, the sample was treated with nujol and the spectra were recorded immediately at room temperature. Therefore, we have to consider that there is no change of the sample after addition of nujol. The IR spectra of complexes **1** and **1a,** reveal that amine are chelated and almost no significant change is observed in other variation bands, except for omission of the band for H_2O, after dehydration. To determine the coordination mode of the NO_3^- ions, we measured the combination band of the ν_1 symmetric stretching which appears in the region 1700–1800 cm^{-1} in the metallic complexes [26–28]. Here the IR spectra of the complexes do not differ much. Only the combination band of the NO_3^- appearing at 1748 cm^{-1}, broadens at a higher temperature and a small change in the relative intensities of the bands is observed.

The color change from pink **1** to blue-violet **1a**

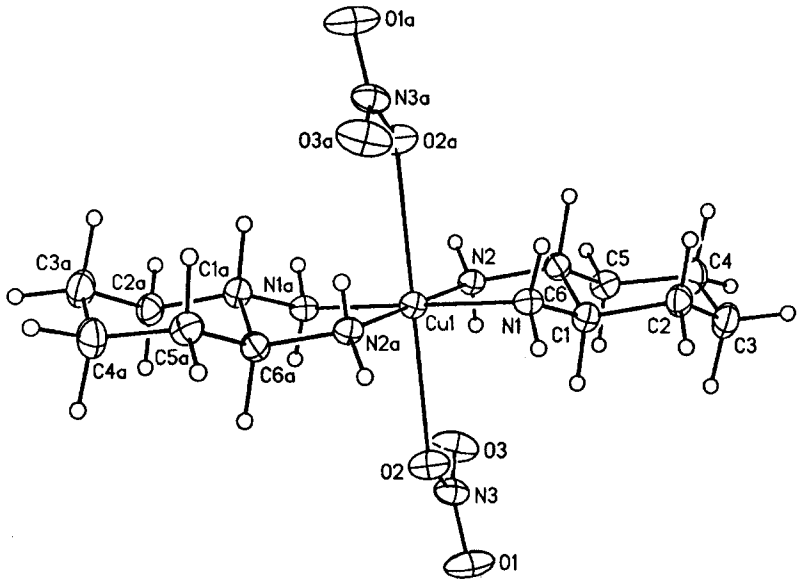

Fig. 5. ORTEP-plot of $[CuL_2(NO_3)_2]$ (**2**) with atom numbering scheme.

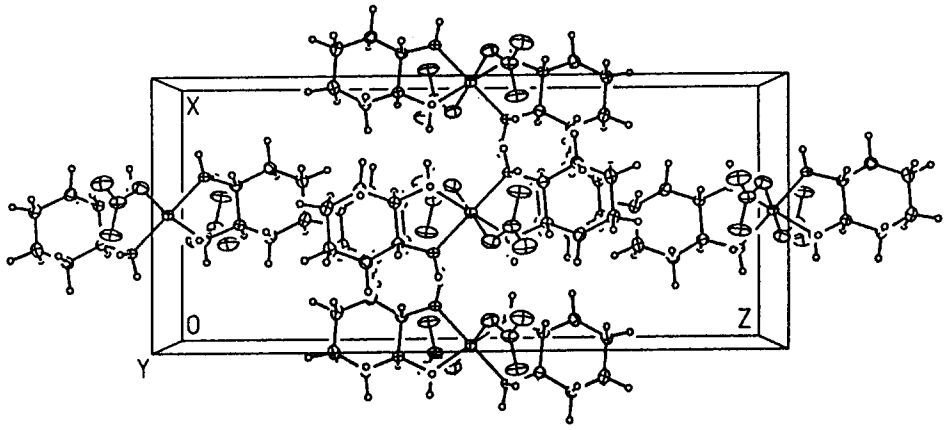

Fig. 6. Packing arrangement for $[CuL_2(NO_3)_2]$ (**2**).

associated with time dependent reversible thermochromism can be visually observed. The visible absorption spectra of the copper(II) complexes recorded at room temperature show a broad band at 562, 555 and 526 nm (Fig. 7) for **1**, **1a** and **2**, respectively. However, the absorption band becomes broader and λ_{max} is shifted to 542 nm for the species **2**, at higher temperature. Here also we have the same limitation as for the IR spectra at higher temperatures.

CONCLUSIONS

Complex **1** shows discontinuous thermochromism whereas **2** shows continuous thermochromism. In the former case the thermochromism is due to the change in ligand field strength of the coordinating H_2O and Cl. Whereas, in the latter case probably thermochromism is due to a temperature-dependent axial interaction between the anion and the CuN_4 plane, with a more square form being favored at a higher temperature [4].

Acknowledgements—We thank Dr K. Panneerselvam, Department of Physics for helpful discussions and to the National Science Council for support of this work under grants NSC86-2811-M-007-0038, NSC86-2113-M-007-023 and NSC87-2113-M-007-041. One of us (C.P.) thanks the NSC for a post-doctoral fellowship, to Professor N. Ray Chaudhuri, IACS, Calcutta, India for encouragement as well as to Mr Chi Wang and Dr Ta-Yung Chi for their assistance in the laboratory.

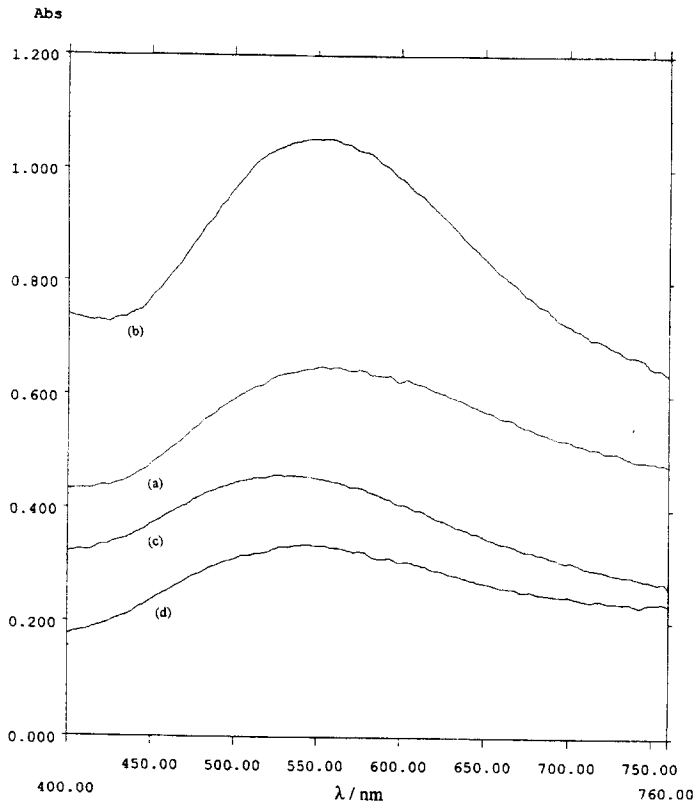

Fig. 7. Electronic spectra of $[CuL_2(H_2O)_2]Cl_2$ (**1**) at (a) room temperature (25°C); (b) after dehydration i.e. for CuL_2Cl_2 (**1a**) and $[CuL_2(NO_3)_2]$ (**2**) at (c) room temperature (25°C) and (d) after heating at 140°C.

REFERENCES

1. Bloomquist, D. R. and Willett, R. D., *Coord. Chem. Rev.*, 1982, **47,** 125.
2. Ouchi, A., Takeuchi, T. and Taminaga, I., *Bull. Chem. Soc. Jpn.*, 1970, **43,** 2609.
3. Grenthe, I., Paoletti, P., Sandstrom, M. and Glikberg, S., *Inorg. Chem.*, 1979, **18,** 2687.
4. Hatfield, W. E., Piper, T. S. and Klabunde, U., *Inorg. Chem.*, 1963, **2,** 629.
5. Yokoi, H., Sai, M. and Isobe, T, *Bull. Chem. Soc. Jpn.*, 1969, **42,** 2232.
6. Ferraro, J. R., Basile, L. J., Garcia-Ineguez, L. R., Paoletti, P. and Fabbrizzi, L., *Inorg. Chem.*, 1976, **15,** 2342.
7. Ferraro, J. R., Fabbrizzi, L. and Paoletti, P., *Inorg. Chem.*, 1977, **16,** 2127.
8. Fabbrizzi, L., Micheloni, M. and Paoletti, P., *Inorg. Chem.*, 1974, **13,** 3019.
9. Lever, A. B. P., Mantovani, E. and Donini, J. C., *Inorg. Chem.*, 1971, **10,** 2424.
10. Roberts, S. A., Bloomquist, D. R., Willett, R. D. and Dodgen, H. W., *J. Am. Chem. Soc.*, 1981, **103,** 2603.
11. Bloomquist, D. R., Willett, R. D. and Dodgen, H. W., *J. Am. Chem. Soc.*, 1981, **103,** 2610.
12. Bloomquist, D. R. and Willett, R. D., *J. Am. Chem. Soc.*, 1981, **103,** 2615.
13. Bloomquist, D. R., Pressprich, M. R. and Willett, R. D., *J. Am. Chem. Soc.*, 1988, **110,** 7391.
14. Menabue, L., Pellacani, G. C., Battaglia, L. P., Corradi, A. B., Sandrolini, F., Motori, A., Pylkki, R. J. and Willett, R. D., *J. Chem. Soc., Dalton Trans.*, 1984, 2187.
15. Koner, S., Ghosh, A., Ray Chaudhuri, N., Mukherjee, A. K., Mukherjee, M. and Ikeda, R., *Polyhedron*, 1993, **12,** 1311.
16. Battaglia, L. P., Corradi, A. B., Marcotrigiano, G., Menabue, L. and Pellacani, G. C., *J. Chem. Soc., Dalton Trans.*, 1981, 8.
17. Pariya, C., Ghosh, A. and Ray Chaudhuri, N., *J. Chem. Res.* (S), 1994, 428.
18. Khokhar, A. R., Xu, Q. and Al-Baker, S., *J. Inorg. Biochem.*, 1993, **52,** 51.
19. Xu, Q. and Khokhar, A. R., *J. Inorg. Biochem.*, 1992, **48,** 217.
20. Morooka, M., Ohba, S. and Miyamae, H., *Acta Cryst. Sect. B*, 1992, **48,** 667.
21. Morooka, M., Ohba, S., Saito, Y. and Miyamae, H., *Acta Cryst. Sect. B*, 1991, **47,** 910.
22. Farrell, N., Roberts, J. D. and Hacker, M. P., *J. Inorg. Biochem.*, 1991, **42,** 237.
23. Khokhar, A. R., Lumetta, G. J. and Bear, J. L., *J. Inorg. Biochem.*, 1988, **33,** 247.
24. Clark, R. J. H., Croud, V. B. and Khokhar, A. R., *Inorg. Chem.*, 1987, **26,** 3284.

25. Hoshino, N., Fukuda, Y., Sone, K., Tanaka, K. and Marumo, F., *Bull. Chem. Soc. Jpn.*, 1989, **62,** 1822.
26. Koner, S., Ghosh, A. and Ray Chaudhuri, N., *J. Chem. Soc., Dalton Trans.*, 1990, 1563.
27. Curtis, N. F. and Curtis, Y. M., *Inorg. Chem.*, 1965, **4,** 804.
28. Lever, A. B. P., Mantovani, E. and Ramaswamy, B. S., *Can. J. Chem.*, 1971, **49,** 1975.

Pergamon

PII: S0277-5387(97)00335-5

Polyhedron Vol. 17, No. 4, pp. 555–559, 1998
© 1998 Elsevier Science Ltd
All rights reserved. Printed in Great Britain
0277-5387/98 $19.00+0.00

Synthesis and X-ray crystal structure of $[(\eta^5\text{-}C_5H_5)Sm(\mu\text{-}OC_{20}H_{20}N_2O)]_2(\mu\text{-}THF)(THF)_2$: Mono(cyclopentadienyl)lanthanide complex bearing a C_2-symmetric tetradentate Schiff-base ligand

Qiancai Liu,† Mengxian Ding,* Yonghua Lin and Yan Xing

Polymer Chemistry Laboratory, Changchun Institute of Applied Chemistry, Chinese Academy of Sciences, 159 Renmin Street, Changchun 130022, P.R. China

(Received 17 April 1997; accepted 4 August 1997)

Abstract—$Cp_2SmCl(THF)$ reacts with 0.5 equivalent disodium salts of *trans*-(±)-*N*,*N*′-bis(salicylidene)-1,2-cyclohexanediamine give the title complex $[(\eta^5\text{-}C_5H_5)Sm(\mu\text{-}OC_{20}H_{20}N_2O)]_2(\mu\text{-}THF)(THF)_2$ (**1**). X-ray crystal determination shows that the molecule is a dimer, in which two $(\eta^5\text{-}C_5H_5)Sm(\mu\text{-}OC_{20}H_{20}N_2O)$ units are connected via a THF oxygen and two bridging oxygen atoms of Schiff base ligands. The average Sm—C distance is 2.78(7) Å, while those of Sm—O (bridging THF oxygen) and Schiff base oxygens are 2.79(3) and 2.43(4) Å, respectively. © 1998 Elsevier Science Ltd. All rights reserved

Keywords: Schiff base ligand; dimer; crystal structure.

There is a rapidly growing interest in chiral lanthanide complexes with optically active alcohols, phenols and chiral substituted cyclopentadiene as ligands, due to their excellent catalytic properties in polymerization and asymmetric synthesis [1–11]. Jacobsen *et al.* initially utilised chiral Schiff base manganese complexes based on optically active 1,2-diamines as catalysts for epoxidation of olefins [12], and Meunier *et al.* reported the synthesis, structure and catalytic activity of chiral Schiff base complexes and transition metal complexes by using ligands derived from 1,2-cyclohexanediamine or 2,2′-diamino-1,1′-binaphthyl [13]. However, the Schiff base complex of lanthanides, synthesising in non-aqueous conditions, are rare [14]. We are interested in the synthesis and catalytic properties of chiral lanthanide Schiff base complexes and isolated the first chiral bis(cyclopentadienyl) neodymium Schiff base complex with an optically active bidentate ligand [15] and the first mono(cyclopentadienyl)lanthanide complex bearing a C_2-symmetric Schiff base ligand [16] by the reaction of $Cp_3Ln(THF)$ with racemic *trans*-(±)-*N*,*N*′-bis(salicylidene)-1,2-cyclohexanediamine (**2**) [17]. In this paper, we wish to report a novel route to synthesise the types of complex. The crystal structure of $[(\eta^5\text{-}C_5H_5)Sm(\mu\text{-}OC_{20}H_{20}N_2O)]_2(\mu\text{-}THF)(THF)_2$ (**1**) will also be discussed.

EXPERIMENTAL

All reactions were carried out under an inert atmosphere of high-purity argon on a vacuum line. Transfer and handling of the complexes were facilitated by the use of Schlenk techniques. Tetrahydrofuran was refluxed and distilled over the sodium ketyl of benzophenone immediately before use. Anhydrous $SmCl_3$ and $Cp_2SmCl(THF)$ were prepared according to the literature [18–19]. *Trans*-(±)-*N*,*N*′-bis(salicylidene)-1,2-cyclohexanediamine was prepared by the reaction of racemic *trans*-1,2-cyclohexanediamine with salicylaldehyde in the boiling toluene by azeotropic dis-

† Present address: Institute of Applied Chemistry, East China University of Science and Technology, P.O. Box 421, 130 Meilong Road, Shanghai 200237, P.R. China. E-mail: jqsun@fudan.ac.cn.

* Author to whom correspondence should be addressed. E-mail: jqsun@fudan.ac.cn.

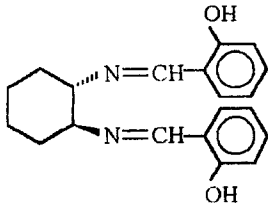

Trans-(±)-N,N'-Bis(salicylidene)-1,2-cyclohexanediamine(2)

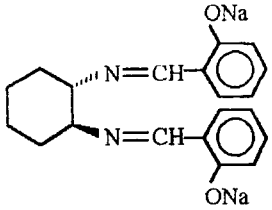

Disodium salt of **2**

tillation of water, the structure of which has been reported elsewhere [17]. Disodium salts of **2** were prepared by the reaction of **2** with NaH in THF. The analysis for Sm was accomplished using a literature method [20] with disodium EDTA.

Synthesis of $[(\eta^5\text{-}C_5H_5)Sm(\mu\text{-}OC_{20}H_{20}N_2O)]_2$ (μ-THF) $(THF)_2$ (**1**)

To a stirring 20 cm^3 THF solution of $Cp_2SmCl(THF)$ (2.57 mmol) was added disodium salts of *trans*-(±)-*N,N'*-bis(salicylidene)-1,2-cyclohexanediamine (**2**) (1.26 mmol) in THF (15 cm^3). After stirring for 16 h at room temperature, the reaction mixture was centrifuged to remove the solid materials and then concentrated under reduced pressure to ca. 15 cm^3 and then 20 cm^3 toluene was added. The resulting mixture was cooled to ca. −18°C and pale-yellow shuttle-shaped crystals were formed several weeks later (yield 12%). Found: Sm, 22.98. Calc. for $C_{62}H_{74}N_4O_7Sm_2$: Sm, 23.35%.

X-ray crystal structure determination of **1**

Suitable crystals of the title complex were sealed under argon in thin-walled glass capillaries for X-ray structure analysis. Unit cell and intensity data were obtained using standard procedures on a Siemens P4 four-circle diffractometer. The intensities were corrected for *Lp* effect and empirical absorptions. Experimental details are given in Table 1. The Sm atom position was located by the Patterson method and other non-hydrogen atoms by Fourier-difference tech-

Table 1. Summary of crystallographic data and data collection parameters for **1**

Formula	$C_{62}H_{74}N_4O_7Sm_2$
Mw	1287.95
Crystal dimension (mm)	0.40 × 0.24 × 0.16
Crystal system	Monoclinic
Cell constants	
a (Å)	18.284(4)
b (Å)	12.166(2)
c (Å)	26.230(5)
V (Å^3)	5808(2)
β (°)	95.44(3)
D_c (g·cm^{-3})	1.473
Space group	*Cc*
μ (mm^{-1})	2.057
F(000)	2616
Radiation (Å) Mo-K_α	0.71073
Monochromator	graphite
Scan mode	ω-2θ
2θ range (°)	3–46
h, k, l range	−1 to 20, −1 to 13, −28 to 28
Max. and min. transmission	0.67083 and 0.57092
Reflection collected	5160
No. of independent reflections	4487
Refinement parameters	626
R	0.0654
wR	0.1637

niques. All the positional and anisotropic thermal parameters for non-hydrogen atoms were refined by the full-matrix least-squares techniques. All hydrogen atoms were introduced in the calculated positions with a C—H bond distance of 0.96 Å. The calculations were performed on a Siemens Nixdorf PCD 4H computer with Siemens SHELXTL-Plus programs. Lists of final coordinates and thermal parameters, bond lengths and angles have been sent to the Editor as supplementary materials.

RESULTS AND DISCUSSION

It is now a general way [21] to synthesise organolanthanocene alkoxides or phenoxides by the reaction of Cp_3Ln moiety and organic acids stronger than C_5H_6 with the elimination of the latter. It is interesting to find that $Cp_3Yb(THF)$ reacts with **2** leading to the formation of $[(\eta^5\text{-}C_5H_5)Yb(\mu\text{-}OC_{20}H_{20}N_2O)]_2(\mu\text{-THF})(THF)$ (**3**) by the elimination of two C_5H_6 molecules, and which up to now, has been assigned as the only X-ray structurally determined example of mono (cyclopentadienyl)lanthanide phenoxide, by using the exchange reaction between Cp_3Ln and protic reagents. The X-ray determination of **3** indicates that two nitrogen atoms of the Schiff base can bond to the lanthanide center through their lone electron pairs. During the process of preparation of dinuclear bis(cyclopentadienyl)-samarium complex with one Schiff base as ligand, the title complex was isolated instead. We therefore postulated that the title complex may be formed as the following reaction:

$$2Cp_2SmCl(THF) + 2NaOC_{20}H_{20}N_2ONa \rightarrow [CpSm(\mu\text{-}OC_{20}H_{20}N_2O)]_2(\mu\text{-THF})(THF)_2 + 2CpNa + 2NaCl \quad (1)$$

Complex **1** is sensitive to air and moisture, but thermally stable and is only decomposed at $>226°C$. It is difficult to dissolve in aromatic solvents and only slightly soluble in THF, which may be the main reason for relative low yield. The molecular structure and atom numbering scheme of **1** is shown in Fig. 1. The selected bond lengths and bond angles are listed in Table 2. Complex **1** is a dimer composed of two $(\eta^5\text{-}C_5H_5)Sm(\mu\text{-}OC_{20}H_{20}N_2O)$ units connected via a bridging THF. Two oxygen atoms of the Schiff base ligands, and two free THF molecules are also found in the crystal. The 9-coordinated samarium atoms are each bonded to two nitrogen atoms and two oxygens of Schiff base, one Cp ring, one bridging oxygen from another Schiff base and oxygen from bridging THF to form a distorted pentagonal bipyramidal geometry with two nitrogen, two oxygens of Schiff base, one oxygen from bridging THF in pentagonal plane, while the centroid of Cp ring and bridging oxygen from

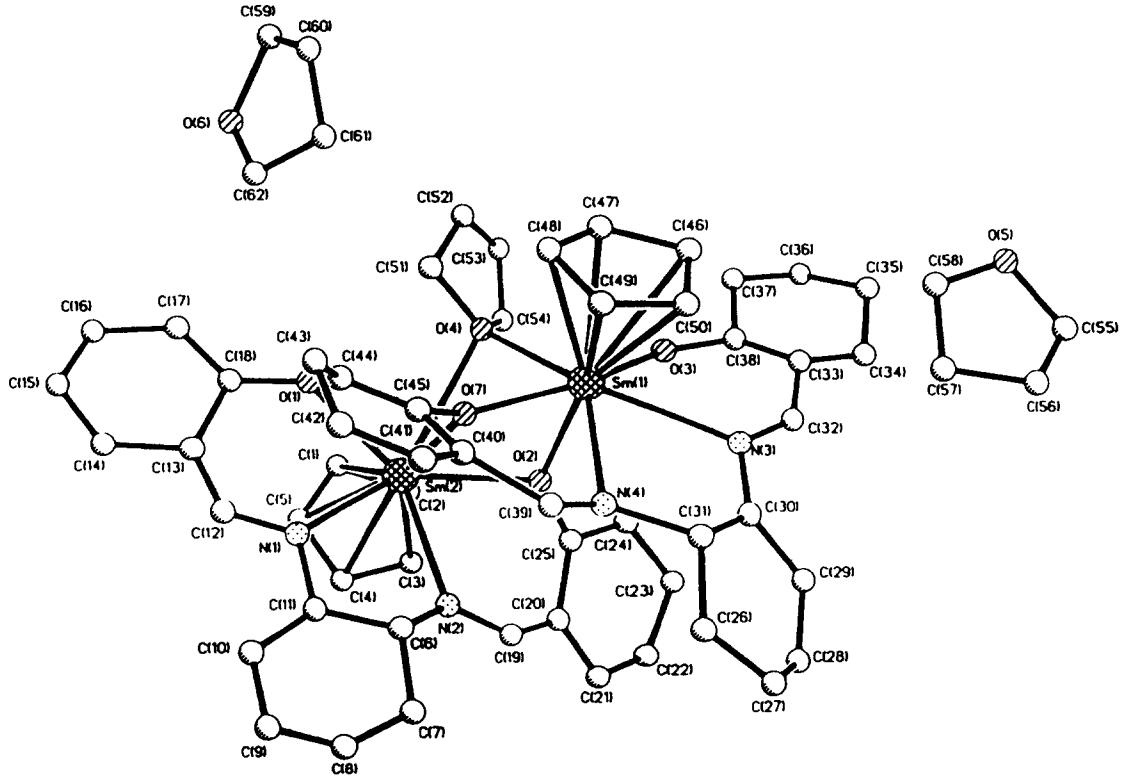

Fig. 1. The molecular structure and atomic numbering scheme for the complex $[(\eta^5\text{-}(c_5H_5)Sm(\mu\text{-}OC_{20}H_{20}N_2O)]_2(\mu\text{-THF})(THF)_2$ (**1**)

Table 2. Selected bond lengths (Å) and angles (°) for **1**

Sm(1)—C(46)	2.82(6)	Sm(1)—C(47)	2.72(7)
Sm(1)—C(48)	2.86(7)	Sm(1)—C(49)	2.75(7)
Sm(1)—C(50)	2.69(7)	Sm(1)—O(2)	2.37(5)
Sm(1)—N(3)	2.67(7)	Sm(1)—N(4)	2.65(5)
Sm(1)—O(3)	2.30(6)	Sm(1)—O(7)	2.28(5)
Sm(1)—O(4)	2.63(3)	Sm(2)—O(4)	2.95(3)
Sm(2)—O(1)	2.29(4)	Sm(2)—O(2)	2.46(3)
Sm(2)—O(7)	2.49(4)	Sm(2)—N(1)	2.55(5)
Sm(2)—N(2)	2.56(5)	Sm(2)—C(1)	2.77(8)
Sm(2)—C(2)	2.77(9)	Sm(2)—C(3)	2.85(6)
Sm(2)—C(4)	2.82(5)	Sm(2)—C(5)	2.73(7)

O(3)—Sm(1)—O(4)	80(2)	O(3)—Sm(1)—N(3)	64(2)
O(3)—Sm(1)—N(4)	131(2)	O(3)—Sm(1)—O(7)	146(2)
O(3)—Sm(1)—O(2)	84(2)	N(3)—Sm(1)—N(4)	69.2(14)
N(3)—Sm(1)—O(7)	140(2)	O(4)—Sm(1)—N(3)	141(2)
N(3)—Sm(1)—O(2)	89.9(14)	O(2)—Sm(1)—N(4)	82(2)
O(7)—Sm(1)—N(4)	73(2)	N(4)—Sm(1)—O(4)	137.0(12)
O(7)—Sm(1)—O(2)	74.1(11)	O(7)—Sm(1)—O(4)	68(2)
O(4)—Sm(1)—O(2)	70.6(11)	O(1)—Sm(2)—N(1)	76(2)
O(1)—Sm(2)—N(2)	142(2)	O(1)—Sm(2)—O(2)	136.0(14)
O(1)—Sm(2)—O(4)	72.6(14)	O(1)—Sm(2)—O(7)	84(2)
N(1)—Sm(2)—N(2)	67(2)	N(1)—Sm(2)—O(2)	132.6(13)
N(1)—Sm(2)—O(7)	85(2)	N(1)—Sm(2)—O(4)	135(2)
N(2)—Sm(2)—O(2)	71(2)	N(2)—Sm(2)—O(7)	85(2)
N(2)—Sm(2)—O(4)	130.9(13)	O(2)—Sm(2)—O(7)	68.9(13)
O(2)—Sm(2)—O(4)	64.0(13)	O(7)—Sm(2)—O(4)	60.5(14)

another Schiff base in the apical sites. It is interesting to find that the shadow of this complex looks like a butterfly. The Sm-bond distances range from 2.69(7)–2.86(7) Å with an average 2.78(7) Å, which is ca. 0.08 Å longer than that of **3** (2.70 Å). The Sm—O bond lengths change from 2.29(4) to 2.63(3) Å, with a specific example, Sm(2)—O(4) (2.95(3) Å), which is longer than that of Sm(1)—O(4) (2.63(3) Å), this indicates that the interaction of Sm(2) and O(4) is very weak. Why is the distance of Sm(2)—O(4) so long? This may be explained by the requirement of coordination saturation of the central atom.

However, the final *R* values and the esds for this complex are relatively higher, which is due to difficulty in obtaining fine crystals. Meanwhile many temperature factors for the complex are larger, which suggests that there might be some disorder caused by the use of a racemic ligand. Synthesis and catalytic properties of bis(cyclopentadienyl) or mono(cyclopentadienyl)lanthanide alkoxides or phenoxides with chiral C_2-symmetric chelating ligands are now under progress in this laboratory.

REFERENCES

1. Giardello, M. A., Sabat, M., Rheingold, A. L., Stern, C. L. and Marks, T. J., *J. Am. Chem. Soc.*, 1994, **116,** 10212.
2. Giardello, M. A., Conticello, V. P., Brard, L., Gagne, M. R. and Marks, T. J., *J. Am. Chem. Soc.*, 1994, **116,** 10241.
3. Fu, P. F., Brard, L., Li, Y. and Marks, T. J., *J. Am. Chem. Soc.*, 1995, **117,** 7157.
4. Gagne, M. R., Brard, L., Conticello, V. P., Giardello, M. A., Stern, C. L. and Marks, T. J., *Organometallics*, 1992, **11,** 2003.
5. Conticello, V. P., Brard, L., Giardello, M. A., Tuji, Y., Sabat, M., Stern, C. L. and Marks, T. J., *J. Am. Chem. Soc.*, 1992, **114,** 2761.
6. Giardello, M. A., Yamamoto, Y., Brard, L. and Marks, T. J., *J. Am. Chem. Soc.*, 1995, **117,** 3276.
7. Haar, C. M., Stern, C. L. and Marks, T. J., *Organometallics*, 1996, **15,** 1765.
8. Mitchell, J. P., Hajela, S., Brookhart, S. K., Hardcastle, K. I., Henling, L. M. and Bercaw, J. E., *J. Am. Chem. Soc.*, 1996, **118,** 1045.
9. Stendel, A., Stehr, J., Siebel, E. and Fisher, R. D., *J. Organomet. Chem.*, 1996, **510,** 197.
10. Shibasaki, M. and Sasai, H., *Pure & Appl. Chem.*, 1996, **58,** 113.
11. Molander, G. A., Schumann, H., Rosenthal, E. C. E. and Demtschuk, J., *Organometallics*, 1996, **18,** 3817; Geodheijt, M. S., Nijbacker, T., Akkerman, O. S., Bickelhaupt, F., Veldman, N. and Spek, A. L., *J. Organomet. Chem.*, 1997, **527,** 1.
12. Jacobsen, E. N., Zhang, W., Muci, A. R., Rcker, J. R. and Deng, L., *J. Am. Chem. Soc.*, 1991, **113,** 7063.
13. Bernardo, K., Leppard, S., Robert, A., Commenges, G., Dahan, F. and Meunier, B.,

Inorg. Chem., 1996, **35,** 387 and references cited therein.
14. Blech, P., and Floriani, C., *J. Chem. Soc., Dalton. Trans.*, 1990, 3557.
15. Liu, Q., Ding, M., Lin, Y. and Xing, Y., *J. Organomet. Chem.*, to be accepted.
16. Liu, Q., Ding, M., Lin, Y. and Xing, Y., submitted to *J. Organomet. Chem.*
17. Liu, Q., Ding, M., Lin, Y. and Xing, Y., *Acta Cryst. C*, 1997, in press.
18. Taylor, M. D. and Carter, C. P., *J. Inorg. Nucl. Chem.*, 1962, **42,** 387.
19. Magin, R. E., Manastyrskyj, S. and Dubeck, M., *J. Am. Chem. Soc.*, 1963, **85,** 672.
20 Ye, C. and Li, Y., *Youji Huaxue* (*Chin. J. Org. Chem.*), 1981, 210.
21. Wu, Z., Xu, Z., You, X., Zhou, X., Huang, X. and Chen, J., *Polyhedron*, 1994, **13,** 379 and references therein.

Pergamon

PII: S0277-5387(97)00330-6

Polyhedron Vol. 17, No. 4, pp. 561–576, 1998
© 1998 Elsevier Science Ltd
All rights reserved. Printed in Great Britain
0277-5387/98 $19.00+0.00

Tin(IV) and organotin(IV) complexes containing mono or bidentate N-donor ligands—IV.† 2-Methyl-, 2-isopropyl- and 4-methyl-imidazole derivatives: synthesis, characterization and behaviour in solution

Claudio Pettinari*, Maura Pellei, Fabio Marchetti, Carlo Santini and Michele Miliani

Dipartimento di Scienze Chimiche, Università degli Studi, via S. Agostino 1, 62032 Camerino, Macerata, Italy

(Received 5 June 1997; accepted 29 July 1997)

Abstract—The interaction between 4-methyl-, 2-methyl- and 2-isopropyl-imidazole, L^1, L^2 and L^3 respectively (L in general), and several tin(IV) and organotin(IV) acceptors in diethyl ether, acetonitrile, dichloromethane or chloroform, gives 1:1 $[(L^1)(C_6H_5)_3SnCl]\cdot 1/3H_2O$, $[(L^3)(C_6H_5)_3SnCl]$, $[(L^3)(CH_3)_3SnCl]$ and $[(L^3)(C_6H_5)_2SnCl_2]\cdot(H_2O)$, 2:1 $[(L)_2R_nSnX_{4-n}]\cdot zH_2O$ (L = L^1, R = Me, n = 1, 2 or 3, X = Cl, z = 0 or 6; L = L^1, R = Me, n = 2, X = Br or I, z = 0; L = L^1, R = Et, n = 2, X = Cl or Br, z = 0; L = L^1, R = Bu^n, n = 2 or 3, X = Cl or Br, z = 0; L = L^1, R = Ph, n = 2, X = Cl, z = 1; L = L^2, R = Me, n = 2 or 3, X = Cl, z = 0 or 1; L = L^2, R = Bu^n or Ph, n = 1, X = Cl, z = 2 or 3; L = L^3, R = Me, n = 2, z = 1) and 3:1 $(L^1)_3RSnCl_3$ (R = Bu^n or Ph) adducts. The derivative $[(L^1)_2(CH_3)_2SnCl_2]$ reacts with $AgNO_3$ and $NaBPh_4$ in ethanol and diethyl ether giving the complexes $[(L^1)_2(CH_3)_2Sn(NO_3)_2]\cdot H_2O$ and $[(L^1)_4(CH_3)_2Sn](BPh_4)_2$ respectively. The compounds were characterized by analytical and spectral data. The behavior in solution was investigated by conductivity, molecular weight determinations, ^1H, ^{119}Sn and ROESY NMR experiments. The triorganotin(IV) derivatives dissociate in chloroform and in acetone solution, the diorganotin(IV) derivatives dissociate only partly and the monoorganotin(IV) complexes probably retain the hexacoordinate configuration. The derivatives $[(L^1)_2(CH_3)_2SnX_2]$ (X = Cl or Br) react with 1,10-phenanthroline (Phen), yielding immediately the chelate adducts $[(Phen)(CH_3)_2SnX_2]$, upon complete displacement of the azole ligand, whereas the less basic 2-benzoylpyridine and the P-donors monodentate PR_3 (R = phenyl, benzyl or cyclohexyl) or bidentate $[PPh_2CH_2]_2$, are not able to displace the imidazole from the tin center. © 1998 Elsevier Science Ltd. All rights reserved

Keywords: tin(IV) complexes; organotin(IV) complexes; imidazole.

Heavy metals such as platinum, gold, ruthenium, rhodium, iridium, palladium, rhenium, titanium and tin can be the source of biologically active derivatives and occasionally became tools in chemotherapy against different kind of tumors in humans [1]. Since 1969, following the discovery of the antitumor activity of platinum complexes [2] it was tempting to study organotin(IV) compounds as possible candidates for antitumor agents and to identify compounds containing active antitumor organotin(IV) moieties $R_nSn^{(4-n)+}$ by antileukemia screening.

In discussing structure/activity relationships for tin(IV) and organotin(IV) derivatives $[(L)_xR_nSnX_{4-n}]$ three primary factors are involved: the nature of the organic group R, of the halide or pseudohalide X, and of the donor ligand. Examination of the structural data of tin(IV) compounds containing nitrogen-donor tested for antitumor activity revealed that active tin complexes had average tin–nitrogen bond lengths >2.39 Å, whereas inactive complexes had tin–nitro-

* To whom correspondence should be addressed.
† Part III is Ref. [7].

gen bonds <2.39 Å, which implies that a predissociation of the ligand may be an important step in the mode of action of these tin complexes [3], while the coordinated ligand may favor the transport of the active species to the site of action into cells, where they are released by hydrolysis.

A consideration of the published screening data for all the tin(IV) derivatives has revealed that many diorganotin(IV) compounds exhibit higher antitumor activity than the corresponding mono-, tri- and tetraorganotin(IV) or the inorganic tin(IV) chemicals, while, within the diorganotin(IV) class, the highest activity was given by the diethyl- and diphenyl-tin derivatives [4].

Now we are trying to extend our previous reports about the interaction of 1-benzylimidazole [5] (L^4), 4-phenylimidazole [6] (L^5) and 1-methylimidazole [7] (L^6) (Fig. 1) with several R_nSnX_{4-n} acceptors to a systematic study of tin(IV) and organotin(IV) complexes of imidazole.

We report here on the synthesis, spectroscopic characterization (IR and NMR data) and behavior in solution (conductivity and molecular weight measurements) of new adducts between R_nSnX_{4-n} (R = Me, Et, Bu^n and Ph; n = 1, 2 or 3; X = Cl, Br, I, NO_3 and BPh_4) acceptors and 4-methyl- (L^1), 2-methyl- (L^2) and 2-isopropyl-imidazole (L^3) donors (Fig. 1).

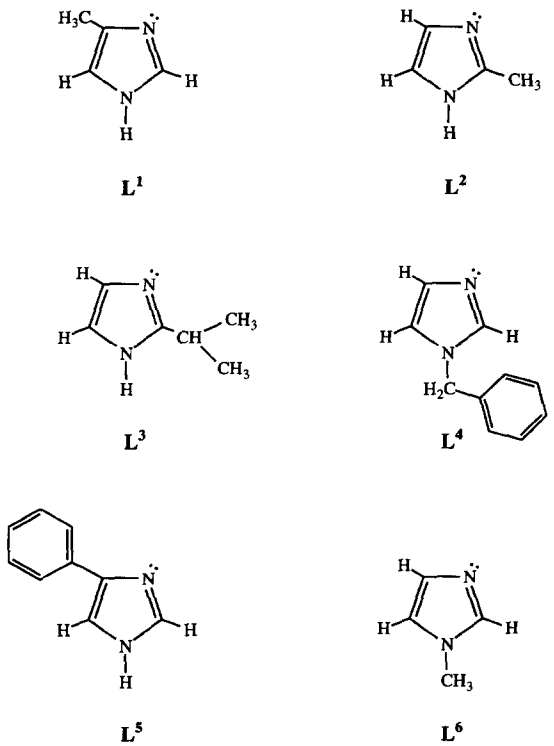

Fig. 1. Structure of the imidazole-type donors employed in the interaction with R_nSnX_{4-n} acceptors.

EXPERIMENTAL

The organotin(IV) halides were purchased from Alfa (Karlsruhe) and Aldrich (Milwaukee) and used as received. The ligands 4-methyl- (L^1), 2-methyl- (L^2) and 2-isopropyl-imidazole (L^3) were obtained from Aldrich and were crystallized from diethyl ether/petroleum ether (1 : 2).

The samples for microanalysis were dried *in vacuo* to constant weight (20°C, ca 0.1 Torr). Elemental analyses (C, H, N) were performed in house with a Carlo-Erba model 1106 instrument. IR spectra were recorded from 4000 to 100 cm^{-1} with a Perkin-Elmer System 2000 FT-IR instrument. ^1H and ^{119}Sn NMR spectra were recorded on a VXR-300 Varian spectrometer operating at room temperature (300 MHz for ^1H and 111.9 MHz for ^{119}Sn). The ROESY experiment was performed in accordance with procedure reported in literature [8] on a 7 mg/ml solution of compound **8** $[(L^1)_4(CH_3)_2Sn](BPh_4)_2$ in $CDCl_3$ at 25°C: mixing time = 300 msec, acquisition time = 0.5 s, 1 K (1024) data point. Melting points were taken on an IA 8100 Electrothermal instrument. The electrical conductance of the solutions was measured with a Crison CDTM 522 conductimeter at room temperature. The osmometric measurements were carried out at 40° over a range of concentrations with a Knauer KNA0280 vapor pressure osmometer calibrated with benzil. The solvent was Baker Analyzed Spectrophotometric grade chloroform. The results were reproducible to ±2%.

Reagents

Preparation of [bis(4-methylmidazole)trimethyltin (IV)] chloro, **1**. To a stirred refrigerated (0°C) diethyl ether solution (50 cm^3) of L^1 (1.0 g, 12.2 mmol), $(CH_3)_3SnCl$ (606 mg, 3.0 mmol) was added under N_2 stream. The mixture was stored at 0°C and stirred for 1 h. The colorless residue obtained was crystallized twice from diethyl ether to yield the analytical sample **1**. Compound **3** was obtained similarly.

Preparation of [bis(4-methylmidazole)tributyltin (IV)]chloro, **2**. To a stirred refrigerated (0°C) diethyl ether solution (50 cm^3) of L^1 (1.0 g, 12.2 mmol), $(C_4H_9)_3SnCl$ (1.0 g, 3.0 mmol) was added under N_2 stream. The mixture was stored at 0°C and stirred for 12 h. The solution was stored in a freezer overnight. After addition of petroleum ether (ca 20 cm^3) an oil was formed, which was separated from the solution. The oily residue was washed with diethyl ether/petroleum ether 1 : 1 (3 × 20 cm^3) and shown to be compound **2**.

Preparation of [bis(4-methylimidazole)dimethyldichlorotin(IV)], **4**. To a stirred diethyl ether solution (100 cm^3) of L^1 (1.0 g, 12.2 mmol), $(CH_3)_2SnCl_2$ (670 mg, 3.0 mmol) was added at room temperature. A colorless precipitate was formed immediately, which was filtered off after 10 h, washed with diethyl ether

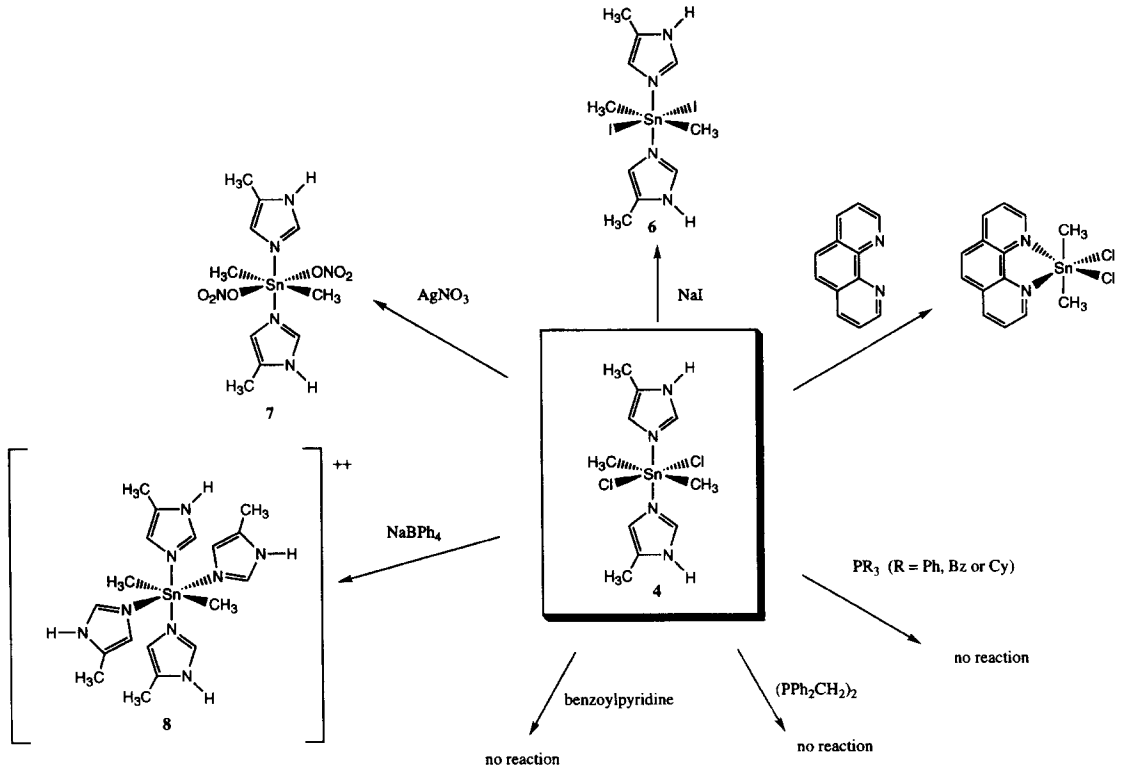

Scheme

and crystallized twice from dichloromethane and shown to be compound **4**. Compounds **5**, **9–13**, **15** and **16** were obtained similarly.

Preparation of [*bis*(4-*methylimidazole*)*dimethyldiiodotin*(*IV*)], **6**. A dry ethanol solution (100 cm^3) of compound **4** (576 mg, 1.5 mmol) was introduced into a 250 cm^3 round-bottomed flask fitted with a condenser. Sodium iodide (3.6 g, 24.0 mmol) was then added. The mixture was heated at reflux, under N_2 stream, with stirring for 10 days. It was then allowed to cool and the solvent was removed with a rotary evaporator. CH_2Cl_2 (50 cm^3) was then added, the suspension was filtered and the organic layer was dried on Na_2SO_4. It was then filtered and concentrated under reduced pressure. Petroleum ether (30 cm^3) was then added; the solution was left in the freezer for 1 day. A red-yellow precipitate was formed which was filtered off, washed with petroleum ether/Et_2O and crystallized twice from CH_2Cl_2/petroleum ether (1 : 2) to yield the analytical sample **6**.

Preparation of [*bis*(4-*methylimidazole*)*dimethyltin*(*IV*)*dinitrate*], **7**. A dry ethanol solution (100 cm^3) of compound **4** (500 mg, 1.3 mmol) was introduced into a 250 cm^3 round-bottomed flask fitted with a condenser. Silver nitrate (674 mg, 3.9 mmol) was then added. The mixture was heated at reflux, under N_2 stream, with stirring for 2 days. The pale-rose solution was then allowed to cool and the solvent was removed with a rotary evaporator. CH_2Cl_2 (50 cm^3) was added, the suspension was filtered and the organic layer was dried on Na_2SO_4. It was then filtered and concentrated under reduced pressure. Et_2O (30 cm^3) was then added. A colorless precipitate was formed which was filtered off, washed with diethyl ether and shown to be compound $(CH_3)_2Sn(NO_3)_2$. A diethyl ether solution of L^1 (250 mg, 3.0 mmol) was again added. The colorless precipitate obtained was filtered off, washed with diethyl ether and shown to be compound **7**.

Preparation of [*tetrakis*(4-*methylimidazole*)*dimethyltin*(*IV*)]*di*(*tetraphenylborate*), **8**. A dry ethanol solution (100 cm^3) of $(CH_3)_2SnCl_2$ (659 mg, 3.0 mmol) was introduced into a 250 cm^3 round-bottomed flask fitted with a condenser. $NaBPh_4$ (4.1 g, 12.0 mmol) was then added. The mixture was heated at reflux, under N_2 stream, with stirring for 1 day. It was then allowed to cool and the solvent was removed with a rotary evaporator. CH_2Cl_2 (50 cm^3) was then added, the suspension was filtered and the organic layer was dried on Na_2SO_4. It was then filtered and concentrated under reduced pressure. Et_2O (100 cm^3) and L^1 (905 mg, 12.0 mmol) were added. The mixture was stirred at room temperature for 2 h. The pale-rose solution was then concentrated under reduced pressure and *n*-hexane (30 cm^3) was added. A colorless precipitate was formed which was filtered off, washed with *n*-hexane and shown to be compound **8**.

Preparation of [*bis*(4-*methylimidazole*)*methyltrichlorotin*(*IV*)], **14**. To a stirred diethyl ether solution (100 cm^3) of L^1 (250 mg, 3.0 mmol), $(CH_3)SnCl_3$ (365 mg, 1.5 mmol) was added at room temperature. A colorless precipitate was formed immediately. It was filtered off after 2 min, washed with diethyl ether (3×15 cm^3), dried *in vacuo* to constant weight (20°C, ca 0.1 Torr) and shown to be compound **14**. If the reaction was carried out for a time longer than 2–3 min an oily product was obtained.

Preparation of [*bis*(2-*methylimidazole*)*trimethylchlorotin*(*IV*)], **17**. To a stirred refrigerated (0°C) CH_2Cl_2/CH_3CN solution (1 : 1, 50 cm^3) of L^2 (375 mg, 4.6 mmol), $(CH_3)_3SnCl$ (606 mg, 3.0 mmol) was added under N_2 stream. The colorless residue obtained was washed with diethyl ether, petroleum ether and dichloromethane, dried *in vacuo* to constant weight, and shown to be compound **17**. Compound **19** was obtained similarly.

Preparation of [*bis*(2-*methylimidazole*)*dimethyldichlorotin*(*IV*)], **18**. To a stirred CH_3CN solution (50 cm^3) of L^2 (375 mg, 4.6 mmol) was added a diethyl ether solution (50 cm^3) of $(CH_3)_2SnCl_2$ (670 mg, 3.0 mmol). The mixture was heated at reflux, under N_2 stream, with stirring for 1 day. The solution was then concentrated (20 cm^3) under reduced pressure and stored in a freezer overnight. The oily residue obtained was crystallized twice from CH_2Cl_2/CH_3CN (1 : 2) to yield the analytical sample **18**.

Preparation of [*bis*(2-*methylimidazole*)*phenyltrichlorotin*(*IV*)], **20**. To a stirred saturated diethyl ether/chloroform solution (1 : 1; 110 cm^3) of the ligand L^2 (250 mg, 3.0 mmol), $(C_6H_5)SnCl_3$ (544 mg, 1.8 mmol) was added at room temperature. A colorless precipitate was formed immediately. After 5 min the suspension was centrifuged and the residue was washed with diethyl ether to yield the analytical sample **20**.

Preparation of [(2-*isopropylimidazole*)*trimethylchlorotin*(*IV*)], **21**. To a stirred refrigerated (0°C) diethyl ether solution (50 cm^3) of L^3 (601 mg, 6.0 mmol), $(CH_3)_3SnCl$ (606 mg, 3.0 mmol) was added under N_2 stream. The mixture was stored at 0°C and stirred for 1 h. The colorless residue obtained was crystallized twice from diethyl ether to yield the analytical sample **21**. Compound **22** was obtained similarly.

Preparation of [(2-*isopropylimidazole*)*dimethyldichlorotin*(*IV*)], **23**. To a stirred diethyl ether/ dichloromethane (1 : 1) solution (100 cm^3) of L^3 (601 mg, 6.0 mmol), $(CH_3)_2SnCl_2$ (670 mg, 3.0 mmol) was added at room temperature. A colorless precipitate was formed immediately, which was filtered off after 10 h, washed with diethyl ether and crystallized twice from dichloromethane and shown to be compound **23**. Compound **24** was obtained similarly.

Preparation of [*dibromodimethyl*(1,10-*phenantroline*) *tin*(*IV*)]. To a stirred diethyl ether solution (100 cm^3) of 1,10-phenantroline (214 mg, 1.2 mmol), $[(L^1)_2(CH_3)_2SnBr_2]$ (280 mg, 0.6 mmol) was added at room temperature. The colorless precipitate became immediately pale pink; it was filtered off after 1 day, washed with diethyl ether and shown to be compound $[(Phen)(CH_3)_2SnBr_2]$. Compound $[(Phen)(CH_3)_2SnCl_2]$ was obtained similarly.

RESULTS AND DISCUSSION

Synthesis, reactivity and properties of the organotin(*IV*) *complexes*

Preparations of the organotin(IV) complexes were usually attempted with different stoichiometries in order to determine if more than one kind of derivative was afforded between the donors (L^1, L^2 and L^3) and a particular organotin(IV) acceptor. The complexes here discussed were the only ones that were isolated.

Interaction between various organotin(IV) compounds and excess L^1, L^2 or L^3 in organic solvent (diethyl ether, diethyl ether and dichloromethane, acetonitrile and dichloromethane or diethyl ether) produces the compounds **1–5, 9–24** listed in Table 1, according to eqn (1):

$$x(L) + (R_nSnX_{4-n}) \cdot zH_2O \xrightarrow{Solvent} [(L)_x(R_nSnX_{4-n})] \cdot zH_2O \quad \textbf{1–5, 9–24} \quad (1)$$

$$(L = L^1, L^2 \text{ or } L^3; R = Me, Et, Bu^n \text{ or } Ph; X = Cl \text{ or } Br; n = 1, 2 \text{ or } 3;$$

$$x = 1, 2 \text{ or } 3; z = 0, 1/3, 1, 2, 3 \text{ or } 6).$$

With the exception of compounds **3**, **21**, **22** and **24** (for which ligand-to-metal ratio of 1 : 1 was observed), and of **15** and **16** (ligand to metal ratio of 3 : 1) 2 : 1 adducts were always isolated. The first significant difference with respect to tin(IV) and organotin(IV) adducts of 1-benzyl-, 1-methyl- and 4-phenyl-imidazole is just in the obtaining of the 3 : 1 adducts **15** and **16**, likely due to the greater basicity of L^1 with respect to L^4 and L^5 or to the ability of L^1 to stabilize the tin(IV) adducts by formation of hydrogen bonds.

With the donors L^1 and L^2 2 : 1 adducts were obtained also with weak acceptors such as $(CH_3)_3SnCl$ and $(n\text{-}C_4H_9)_3SnCl$. The ligands L^1 and L^2 show the same behavior of L^5 which has been found in $[(L^5)(CH_3)_3Sn]Cl$ [6] able to saturate the coordination number equal to five upon displacement of the Cl from the coordination sphere of the tin centre and to stabilize the whole molecule involving the halide in a hydrogen bond network (Fig. 2).

With the exception of $[(L^3)_2(CH_3)_2SnCl_2] \cdot (H_2O)$ (**23**), 1 : 1 adducts were always obtained with the donor L^3, which is a more sterically hindered donor than those employed to date.

We also found that the reactions involving triorganotin(IV) chloride acceptors require a longer reac-

Table 1. Physical and analytical data of derivatives **1**–**24**

Compound and formula[a]	No.	Yield %	M.p. (°C)	Elemental analysis (%); Found (Calc.) C	H	N
$[(L^1)_2(CH_3)_3Sn]Cl$	(**1**)	95	85–88	36.8	6.0	15.8
$C_{11}H_{21}ClN_4Sn$				(36.4)	(5.8)	(15.4)
$[(L^1)_2(C_4H_9)_3Sn]Cl$	(**2**)	70	oil	49.5	8.1	11.6
$C_{20}H_{39}ClN_4Sn$				(49.0)	(8.0)	(11.4)
$[(L^1)(C_6H_5)_3SnCl]\cdot 1/3H_2O$	(**3**)	74	125 dec	55.7	4.7	6.1
$C_{22}H_{21.6}N_2O_{0.3}SnCl$				(56.5)	(4.5)	(6.0)
$[(L^1)_2(CH_3)_2SnCl_2]$	(**4**)	94	174–177	31.5	4.9	14.5
$C_{10}H_{18}Cl_2N_4Sn$				(31.3)	(4.7)	(14.6)
$[(L^1)_2(CH_3)_2SnBr_2]$	(**5**)	90	190–192	25.4	3.9	11.6
$C_{10}H_{18}Br_2N_4Sn$				(25.4)	(3.8)	(11.8)
$[(L^1)_2(CH_3)_2SnI_2]$	(**6**)	35	171–173	20.6	3.1	9.4
$C_{10}H_{18}I_2N_4Sn$				(21.2)	(3.2)	(9.9)
$[(L^1)_2(CH_3)_2Sn(NO_3)_2]\cdot H_2O$	(**7**)	24	176–179	25.9	4.4	18.2
$C_{10}H_{20}N_6O_7Sn$				(26.4)	(4.4)	(18.5)
$[(L^1)_4(CH_3)_2Sn](BPh_4)_2$	(**8**)	25	174–179	70.8	6.4	10.6
$C_{66}H_{70}B_2N_8Sn$				(71.1)	(6.3)	(10.0)
$[(L^1)_2(C_2H_5)_2SnCl_2]$	(**9**)	91	132–133	34.6	5.6	13.2
$C_{12}H_{22}Cl_2N_4Sn$				(35.0)	(5.4)	(13.6)
$[(L^1)_2(C_2H_5)_2SnBr_2]$	(**10**)	49	144–147	28.7	4.6	11.1
$C_{12}H_{22}Br_2N_4Sn$				(28.8)	(4.4)	(11.2)
$[(L^1)_2(C_4H_9)_2SnCl_2]$	(**11**)	88	143–145	41.1	6.8	11.9
$C_{16}H_{30}Cl_2N_4Sn$				(41.0)	(6.5)	(11.9)
$[(L^1)_2(C_4H_9)_2SnBr_2]$	(**12**)	69	143–145	34.8	5.7	10.4
$C_{16}H_{30}Br_2N_4Sn$				(34.5)	(5.4)	(10.0)
$[(L^1)_2(C_6H_5)_2SnCl_2]\cdot H_2O$	(**13**)	92	208–210	45.2	4.5	10.7
$C_{20}H_{24}Cl_2N_4OSn$				(45.7)	(4.6)	(10.7)
$[(L^1)_2(CH_3)SnCl_3]\cdot 6H_2O$	(**14**)	35	200 dec	20.7	5.0	10.6
$C_9H_{27}Cl_3N_4O_6Sn$				(21.1)	(5.3)	(10.9)
$(L^1)_3(C_4H_9)SnCl_3$	(**15**)	96	176–179	36.8	5.5	15.9
$C_{16}H_{27}Cl_3N_6Sn$				(36.4)	(5.2)	(15.9)
$(L^1)_3(C_6H_5)SnCl_3$	(**16**)	30	195–198	39.1	4.4	15.1
$C_{18}H_{23}Cl_3N_6Sn$				(39.4)	(4.2)	(15.3)
$[(L^2)_2(CH_3)_3Sn]Cl\cdot H_2O$	(**17**)	54	oil	34.6	5.8	14.4
$C_{11}H_{23}ClN_4OSn$				(34.6)	(6.1)	(14.7)
$[(L^2)_2(CH_3)_2SnCl_2]$	(**18**)	45	187–189	31.4	4.7	14.4
$C_{10}H_{18}Cl_2N_4Sn$				(31.3)	(4.7)	(14.6)
$[(L^2)_2(C_4H_9)SnCl_3]\cdot 2H_2O$	(**19**)	34	116–118	29.8	5.1	11.5
$C_{12}H_{25}Cl_3N_4O_2Sn$				(29.9)	(5.2)	(11.6)
$[(L^2)_2(C_6H_5)SnCl_3]\cdot 3H_2O$	(**20**)	56	>240	32.6	4.6	10.3
$C_{14}H_{23}Cl_3N_4O_3Sn$				(32.3)	(4.4)	(10.8)
$[(L^3)(CH_3)_3SnCl]$	(**21**)	45	oil	35.3	6.3	9.3
$C_9H_{19}ClN_2Sn$				(34.9)	(6.2)	(9.0)
$[(L^3)(C_6H_5)_3SnCl]$	(**22**)	57	151–152	57.5	5.3	5.7
$C_{24}H_{25}ClN_2Sn$				(58.2)	(5.1)	(5.6)
$[(L^3)_2(CH_3)_2SnCl_2]\cdot H_2O$	(**23**)	73	oil	36.9	6.1	12.6
$C_{14}H_{28}Cl_2N_4OSn$				(36.7)	(6.2)	(12.2)
$[(L^3)(C_6H_5)_2SnCl_2]\cdot H_2O$	(**24**)	83	135–137	45.6	4.7	6.2
$C_{18}H_{22}Cl_2N_2OSn$				(45.8)	(4.7)	(5.9)

[a] L^1 is 4-methylimidazole; L^2 is 2-methylimidazole; L^3 is 2-isopropylimidazole.

tion time than those involving diorganotin(IV) halides, which are slower with respect to those between the donors L^1, L^2 and L^3 and monoorganotin(IV) acceptors.

The compound $[(L^1)_2(CH_3)_2SnCl_2]$ **4** is converted into the analogous diiodide complex **6** on treatment with excess sodium iodide in ethanol solution. This conversion did not occur when diethyl- (**9**), di-*n*-butyl- (**11**) and diphenyl-tin(IV) (**13**) complexes were employed as starting material: in these cases both disproportionation of the tin(IV) halide in accordance with Kocheshkov reactions [9], and breaking of the donor-acceptor σ-bond occurred.

The substitution of the Cl^- with $[NO_3]^-$ or $[BPh_4]^-$ groups when ethanol solution of $AgNO_3$ or $NaBPh_4$ were added to ethanol solution of derivative **4**, pro-

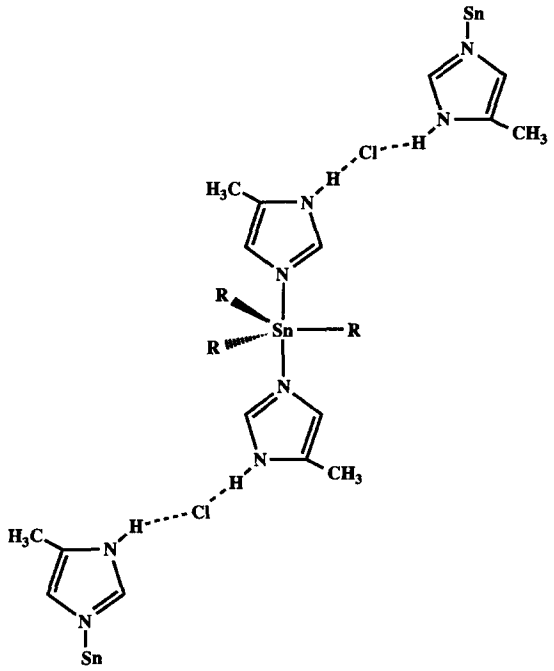

Fig. 2. Structure proposed for the 2:1 triorganotin(IV) adducts of L^1 and L^2.

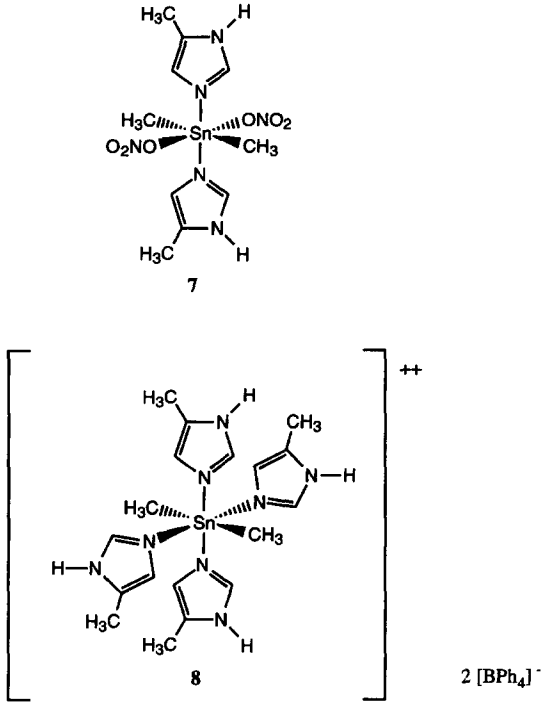

Fig. 3. Structure proposed for the adducts 7 and 8.

duced respectively the new complexes **7** and **8**, characterized by two different stoichiometries: 2:1 in the first and 4:1 in the second case. The formation of **8** gives further support [6,10] to the possibility of existence of the $[(CH_3)_2Sn]^{++}$ cation in the solid state, whereas the formation of **7** indicates the possibility of synthesis of imidazole-tin(IV) and organotin(IV) complexes containing coordinated mono- or bi-dentate nitrato groups (Fig. 3). This is a significative difference with respect to the early described organotin(IV) nitrato complexes of imidazoles, where the $[NO_3]^-$ group was always found to be ionic [10,11].

No adduct was obtained from reaction of L^2 with $(n\text{-}C_4H_9)_3SnCl$, $(C_6H_5)_3SnCl$, $(C_2H_5)_2SnCl_2$, $(n\text{-}C_4H_9)_2SnCl_2$ and $(C_6H_5)_2SnCl_2$, and of L^3 with $(n\text{-}C_4H_9)_3SnCl$, $(CH_3)_2SnCl_2$, $(C_2H_5)_2SnCl_2$, $(n\text{-}C_4H_9)_2SnCl_2$ and $(C_6H_5)SnCl_3$. These donors, which are more basic than L^4, L^5 and L^1, are also the most sterically hindered, due to the presence of a methyl (L^2) or an isopropyl (L^3) group near the coordination site. Moreover, we have found that the bond between L^2 and $(CH_3)_3SnCl$ or $(CH_3)_2SnCl_2$ and between L^3 and $(CH_3)_3SnCl$ is very weak. Compounds **17**, **18** and **21** are unstable not only in solution, but also in the solid state. When they are exposed to moisture for a long time, organotin(IV) oxides and hydroxides and/or the starting donor are often recovered. On the other hand complexes **1**–**16** are generally air-stable. Organotin(IV) oxides and/or hydroxides are also obtained upon prolonged standing of compounds **1**–**24** at 120°C. Diorgano- and triorgano-tin(IV) complexes are moderately soluble in chlorinated solvents (ca 3 mg/cm^3), acetone (*ca* 5 mg/cm^3) and DMSO (5–10 mg/cm^3) and insoluble in diethyl ether, ethanol, methanol and water. The monoorganotin(IV) adducts are generally less soluble in all the organic solvents commonly used.

The N_2-donor 1,10-phenanthroline is able to displace the 4-methylimidazole from its Me_2SnX_2 (X = Cl or Br) adducts, yielding the chelate *trans*-Me_2SnX_2(Phen) derivatives. On the other hand the 2-benzoylpyridine, which is less basic than imidazoles and Phen, in our conditions does not react with the diorganotin(IV)-4-methylimidazole derivatives. P-donors such as PPh_3, PBz_3 and $(PPh_2CH_2\text{-})_2$, more basic than benzoylpyridine, and PCy_3 more basic even than L^1 and Phen, are not able to replace the imidazole in the coordination sphere of tin(IV). This behavior is in accordance with the principle of the maximum hardness [12]. The reactivity of compound **4** is summarized in the scheme.

Several attempts to obtain crystals of adducts **1**–**24**, in suitable form for X-ray analyses, failed: in some cases amorphous powder was obtained, whereas in others one well-known hydrolysis products afforded.

IR Data

In Table 2 we report the most relevant infrared data (4000–100 cm^{-1}) for the ligands L^1, L^2 and L^3 and their tin(IV) and organotin(IV) complexes **1**–**24**. The spectra were recorded in nujol mull. By comparison with the data reported for other tin(IV) and organ-

otin(IV) adducts containing N-donor ligands [13], we suggest for adducts **1–24** the following assignments.

Ligand absorptions

In the 3200–3000 cm^{-1} region, the ligands exhibit weak bands typical of C—H stretching due to a pseudoaromatic ring, and in the region 1650–1500 cm^{-1} some more intense absorptions due to the ring breathing mode [14]. In the 2800–2600 cm^{-1} region the ligands exhibit a broad band typical of N—H stretching. In the tin(IV) and organotin(IV) adducts this band shifts in the 3400–3000 cm^{-1} region suggesting an important influence of the coordination to tin. The position and the broadening of the N—H stretching band are consistent with the presence of a hydrogen bond between the N—H moiety and the halide groups [6,15].

Sn—C stretching frequencies

In the triorganotin(IV) derivatives **1, 2** and **21** two strong or medium absorptions are observed at 555 and 546 cm^{-1}, 600 and 551 cm^{-1} and 550 and 542 cm^{-1} respectively. They are due to $\nu_{(asym)}$ and $\nu_{(sym)}$ Sn—C stretching vibrations and are consistent with an essentially trigonal pyramidal arrangement of organic groups with a marked deviation from planarity.

The appearance of only a single Sn—C bond (at 547 cm^{-1}) in the spectra of trimethyl tin(IV) complex of L^2 (**17**) and of triphenyltin(IV) complexes of L^1 (**3**) and L^3 (**22**) is taken to imply a C_{3v} symmetry of the C_3—Sn skeleton and in the first case a *trans*-pyramidal configuration of the two ligands [16].

Only a single Sn—C stretching vibration appeared in the spectra of dimethyltin(IV) complexes (**4–6** and **8**) of L^1, in accordance with a *trans*-octahedral configuration of the two alkyl groups [17]. Instead, two absorptions were observed in the spectra of the other diorganotin(IV) derivatives of L^1 (**9–13**), in the dimethyltin(IV) complex of L^2 (**18**) and in the diorganotin(IV) complexes of L^3 (**23** and **24**), in accordance with a markedly distorted *trans*-octahedral configuration of the two alkyl groups [18].

In the spectrum of derivative $[(L^1)_2(CH_3)_2Sn(NO_3)_2]\cdot H_2O$ (**7**) one broad absorption at ca 548 cm^{-1} and other less intense bands at 575, 526 and 514 cm^{-1} were found. In this case the presence of at least two markedly distorted *all-trans*-octahedral isomers is likely.

Sn—Cl stretching frequencies

In the triorganotin(IV) derivatives of L^1 (**1** and **2**) and L^2 (**17**) the tin-chloride stretching frequency is absent. On the basis of previous reports [19] on triorganotin(IV) complexes and in accordance with the X-ray crystal structure determination of [bis(4-phenylimidazole)trimethyltin(IV)]chloride [6] we have hypothesized an ionic formulation of the type $[(L)_2R_3Sn]^+[Cl]^-$. Whereas the Sn—Cl is present in the 1 : 1 triorganotin(IV) adducts of L^3, **21** and **22**.

In the di- and mono-organotin(IV) complexes the ν(Sn—Cl) are observed in the region 240–220 cm^{-1} and 330–260 cm^{-1} respectively.

Sn—N stretching frequencies

We are not able to assign the ν(Sn—N) vibrations, because they are likely hidden under some absorptions characteristic of the azole ring system [14].

Skeletal bending modes

In our alkyl complexes, the skeletal bending mode assignments are not straightforward. δ(C—Sn—C), δ(X—Sn—X), ρ(Sn—C_3), ρ(Sn—X_3) and ν(Sn—Br) fall in the region 190–120 cm^{-1} [20] and are far too close to resolve. However we are able to assign the bending of the phenyl groups in the aryltin(IV) derivatives **3, 13, 16, 20, 22** and **24** in the range 465–440 cm^{-1} respectively [21].

Other data

The nitrato complex **7** shows strong broad absorptions at 1410 and 1370 cm^{-1} due to ν_1 and ν_4 of NO_3 group. The separation of these two bands is of the same order of magnitude as that indicated for derivatives containing unidentate NO_3 [22]. In the far IR spectra this adduct exhibits also a broad absorption at ca 480 cm^{-1} due to Sn—O stretching vibration. This observation suggests that the nitrato group, upon complexation of tin(IV) by imidazole donors, remains in the coordination sphere of the metal.

Behavior in solution

The conductivity measurements (Table 3) were carried out in acetone solution for all the soluble compounds and in CH_2Cl_2 and DMSO only for selected derivatives, whereas the molecular weight determinations were performed in chloroform solution only on sufficiently soluble and stable adducts. The data show that triorganotin(IV) halide adducts **1–3, 17, 21** and **22** are not electrolytes in acetone and **1** also in CH_2Cl_2, even if they dissociate to a great extent in $CHCl_3$ solution (r = ratio between the vaporimetric molecular weight and formula weight lies in the range 0.38–0.48), in accordance with the non-ionic eqn (2) which indicates ligand loss in solution.

$$(L)_xR_3SnX \rightleftharpoons [(L)_{x-1}R_3SnX] + L \rightleftharpoons R_3SnX + xL \quad (2)$$

The diorganotin(IV) chloride and bromide adducts

Table 2. Selected IR data (4000–100 cm^{-1})[a] for the donors and their derivatives **1**–**24**

Compound	ν(C—H)azole	ν(N—H)	1650–1500	<600	ν(Sn—C)	ν(Sn—X)[b]	δ(X—Sn—Y)[c]	Other data
L^1	3085w	2700br	1649w, 1636sh, 1578m, 1534w, 1514w	356s, 346s, 286s, 279sh, 180m, 160s				
1	3119w, 3089w	3200br	1654w, 1647w, 1636w, 1599m, 1576w, 1560w	514w, 351w, 303w, 279w, 257w, 247w, 228w, 206w	555s, 546s		200m, 170s	
2		3200br	1596s, 1571s	458w, 411w, 396w, 350s, 279s, 255m, 250m, 228m	600sh, 511m		210s, 194s, 181s, 165s	
3	3132w, 3041w	3193w	1652w, 1644w, 1608sh, 1597m, 1579w, 1556w 1503m	571w, 396w, 352w, 322w	277s, 237m	216m	189s, 157s, 144s, 133s	δ(Ph): 452s ν(H_2O): 3360br
4		3240 br	1654w, 1646w, 1628w, 1577w, 1560w, 1506s	468w, 349m, 279w, 252sh	569s	234s		
5	3190w, 3141w	3300br	1651w, 1646w, 1629w, 1613sh, 1601m, 1503s	398w, 349m, 326w, 302w, 290w, 280w, 247w	568s	190s	225m, 202m, 170s, 162s	
6	3161w	3200br	1623w, 1598m, 1558w	398w, 376w, 351m, 327w, 303w, 291w, 280w, 267w, 255w, 247w	568s		225w, 170s	
7	3134w	3300br	1627m, 1597m, 1584sh, 1559w	481s, 381m, 279m, 227m	575w, 548m, 526w, 514m	204m	ν(NO_3): 1410br, 1370sh ν(H_2O): 3300br	
8	3148w	3300br	1650w, 1590br, 1570br	398w, 382w, 304w, 280w	569m		249m, 225w, 196sh	
9	3169w, 3112w	3200br	1645w, 1558m	485w, 346m, 296m, 278w	543m, 536m	220sh	205s, 196s, 176s, 168s	
10	3172w, 3130w	3200br	1652w, 1634w, 1594m, 1557w	416w, 347m, 292m, 280m	540m, 528s	202m	225w, 207w, 174s, 163s	
11	3130br	3050w	1651w, 1633w, 1597s, 1574w, 1538w, 1503s	456w, 400m, 348m, 285w, 274m, 257m, 245m	600sh, 569w	227s	212s, 198s	
12	3130br	3070w	1651w, 1626m, 1595m, 1574w, 1556w, 1537w, 1531w	520w, 408w, 397m, 348m, 288w, 279m, 274w, 252w, 244w	600sh, 559m	195m	226w, 217w, 206w, 179m, 163m	

Table 2—*Continued*

Compound	ν(C—H)azole	ν(N—H)	1650–1500	<600	ν(Sn—C)	ν(Sn—X)[b]	δ(X—Sn—Y)[c]	Other data
13	3140w	3383br	1593w, 1574w, 1530w	419w, 398w, 377w, 349w, 326w, 280sh	290m, 247m	227s	208s, 197s, 176s	δ(Ph) : 463m ν(H_2O) : 3360br
14	3138w	3250br	1622w, 1604w, 1558w, 1503sh	456w, 410w, 368w, 354w, 281m	563m, 525m	300br	262m, 256m, 247m	ν(H_2O) : 3300–2800br
15	3145w, 3133w, 3073w, 3047w	3390br, 3200br	1627w, 1606s, 1560w	419w, 396w, 365w, 353w, 326w, 255sh	610w	277s	225w, 205s, 181m, 170s	
16	3134w, 3043w	3350br	1652w, 1626w, 1605s, 1577sh, 1558w	366m, 325w	283s, 273s	283s	228m, 206m, 187m, 171m	δ(Ph) : 463m
L^2	3134w, 3106w	2700v br	1593s br, 1501m	470m, 410w, 377m, 355m, 324w, 302w, 285sh, 278s, 268s, 250sh, 227w, 220w, 209w, 193w, 181m				
17	3111w	3150br	1622w, 1589w, 1565m	385s, 274s	547s		210m, 174s, 170s	ν(H_2O) : 3300br
18		3200br	1627m, 1612m, 1566m	465m, 383m, 353w, 280s, 252sh	587s, 563s	229s	215s, 198s, 191s, 178s	
19	3138w, 3116w	3260br	1627m, 1558w, 1514w, 1503w	483s, 358w, 313sh, 238s	595m, 573m	260s br	226s, 203s	ν(H_2O) : 3450br
20	3108w	3200br	1630m, 1574w, 1557w, 1515w, 1504w	550br, 352w, 280m, 254w, 244w	290w, 265w	327w, 317w, 308w	225w, 208w	ν(H_2O) : 3360br δ(Ph) : 454w, 443w
L^3	3133w, 3113w	2900br	1560s, 1551s, 1512m	478m, 473m, 413s, 333m, 258w, 229m				
21	3161w, 3100w	3250br	1567m, 1558m	510w, 495m, 405m, 339m	550s, 542s	210br		
22	3104w, 3063w	3180br	1610w, 1577w, 1561m	569w, 495w, 403m, 341m	278s	225s	202s	δ(Ph) : 458m, 447m
23	3136w	3420br	1624s, 1559w	519w, 466m, 452m, 281m	570m, 552m	234m		ν(H_2O) : 3400br
24	3166w, 3138w	3000br	1615m, 1571w, 1560w	567m, 401w	307m, 290m	258m, 246w	221m, 200sh	δ(Ph) : 465m, 455m, 446sh

[a] In nujol ; [b] X = Cl or Br ; [c] X = Cl or Br, Y = X or N.

Table 3. Selected conductivity and molecular weight measurements of derivatives **1–24**

Compound	No.	Solvent	Conductivity[a] Conc.	Λ	FW	Molecular weight[b] MW	*r*	Conc.
$[(L^1)_2(CH_3)_3Sn]Cl$	(**1**)	Acetone	1.07	4.3	362.5	137	0.38	1.06
		CH_2Cl_2	0.99	0.2		151	0.41	1.84
		DMSO	1.00	14.7				
$[(L^1)(C_4H_9)_3Sn]Cl$	(**2**)	Acetone	1.09	1.6				
$[(L^1)_2(C_6H_5)_3SnCl]\cdot 1/3H_2O$	(**3**)	Acetone	0.96	9.8	473.6	194	0.41	0.96
						225	0.48	1.40
$[(L^1)_2(CH_3)_2SnCl_2]$	(**4**)	Acetone	0.98	20.8	383.9	310	0.81	1.32
		CH_2Cl_2	1.05	0.8		359	0.94	1.93
		DMSO	1.07	34.0				
$[(L^1)_2(CH_3)_2SnBr_2]$	(**5**)	Acetone	1.12	26.6	472.8	316	0.67	1.24
						359	0.76	1.47
$[(L^1)_2(CH_3)_2SnI_2]$	(**6**)	Acetone	1.07	124.1	566.8	199	0.35	0.35
						228	0.40	0.91
						277	0.49	1.80
$[(L^1)_2(CH_3)_2Sn(NO_3)_2]\cdot H_2O$	(**7**)	Acetone	0.53	39.2				
$[(L^1)_4(CH_3)_2Sn](BPh_4)_2$	(**8**)	Acetone	0.92	70.4	1115.7	179	0.16	1.42
		CH_2Cl_2	0.94	12.7		260	0.23	2.38
		DMSO	0.95	12.9				
$[(L^1)_2(C_2H_5)_2SnCl_2]$	(**9**)	Acetone	0.90	15.6	411.9	329	0.80	0.99
						384	0.93	2.25
						377	0.92	2.27
						369	0.90	3.45
$[(L^1)_2(C_2H_5)_2SnBr_2]$	(**10**)	Acetone	1.06	24.2				
$[(L^1)_2(C_4H_9)_2SnCl_2]$	(**11**)	Acetone	1.01	17.7	468.0	319	0.68	2.23
						368	0.79	4.07
$[(L^1)_2(C_4H_9)_2SnBr_2]$	(**12**)	Acetone	1.02	24.8				
$[(L^1)_2(C_6H_5)_2SnCl_2]\cdot H_2O$	(**13**)	Acetone	0.98	28.8				
$[(L^1)_2(CH_3)SnCl_3]\cdot 6H_2O$	(**14**)	Acetone	Insoluble					
		DMSO	0.90	59.0				
$(L^1)_3(C_4H_9)SnCl_3$	(**15**)	Acetone	0.97	13.7				
$(L^1)_3(C_6H_5)SnCl_3$	(**16**)	Acetone	1.04	16.4				
$[(L^2)_2(CH_3)_3Sn]Cl\cdot H_2O$	(**17**)	Acetone	1.03	11.6				
$[(L^2)_2(CH_3)_2SnCl_2]$	(**18**)	Acetone	1.23	49.5				
$[(L^2)_2(C_4H_9)SnCl_3]\cdot 2H_2O$	(**19**)	Acetone	0.99	66.7				
$[(L^2)_2(C_6H_5)SnCl_3]\cdot 3H_2O$	(**20**)	Acetone	Insoluble					
$[(L^3)(CH_3)_3SnCl]$	(**21**)	Acetone	0.99	3.2				
		CH_2Cl_2	1.00	0.0				
$[(L^3)(C_6H_5)_3SnCl]$	(**22**)	Acetone	1.00	3.5				
		CH_2Cl_2	1.09	0.0				
$[(L^3)_2(CH_3)_2SnCl_2]\cdot H_2O$	(**23**)	Acetone	0.98	3.9				
$[(L^3)(C_6H_5)_2SnCl_2]\cdot H_2O$	(**24**)	Acetone	0.97	54.4				
		CH_2Cl_2	1.11	1.1				

[a] In Ω^{-1} cm^2 mol^{-1} at room temperature; conc. is molar concentration ($\times 10^3$).
[b] 40°C, in $CHCl_3$; r = M.W./F.W.; conc. is: mg of compound/g of $CHCl_3$.

4, **5**, **9** and **11** are non-electrolytes and presumably dissociate partly in these solvents (r is in the range 0.67–0.94). We also found that the dissociation is not very dependent on the concentration of the solutions: for example r for compound **9** is 0.80 at conc. 0.99 mg/g and 0.90 at conc. 3.45 mg/g of $CHCl_3$.

The diorganotin(IV)diiodide adduct **6** exhibits a value of conductivity in acetone typical of a 1 : 1 electrolyte: it is also strongly dissociated in $CHCl_3$ solution. On the basis of this evidence we hypothesized an ionic nature in solution of complex **6** in accordance with eqn (3):

$$[(L^1)_2(CH_3)_2SnI_2] + n(\text{solvent}) \rightleftharpoons [(L^1)_2(CH_3)_2SnI(\text{solvent})_n]^+ + [I]^- \quad (3)$$

Compounds **7**, **8**, **14**, **18**, **19** and **24** are partly ionized: a similar behavior has been previously observed for analogous organotin(IV) complexes containing imidazole-type donors [5–7].

Table 4. ^{1}H NMR data for the donors and their derivatives **1–24**[a]

Compound	Solvent	N—H	CH_3 or i-C_3H_7	H azole	R—Sn	Other data
L[1]	$CDCl_3$	8.80br	2.27s	6.80s, 7.60s		
	Acetone	11.85br	2.22s	6.80s, 7.68s		
	EtOD		2.20s	6.70s, 7.46s		
1	$CDCl_3$	9.30br	2.32s	6.65s, 7.65s	0.70s	$^2J(^{119}Sn—^1H)$: 67.2 $^2J(^{117}Sn—^1H)$: 64.2
2	$CDCl_3$	10.50br	2.27s	6.69s, 7.56s	0.84t, 1.10–1.80m	$^2J(^{119}Sn—^1H)$: 63.1
3	Acetone		2.07s	6.57s, 7.37s	7.42m, 7.82d, 7.85d	$^2J(^{119}Sn—^1H)$: 63.8 H_2O: 3.45 br
4	$CDCl_3$	6.70br	2.36s	6.96s, 8.30br	1.16s, 1.22s, 1.25s 1.28s	$^2J(^{119}Sn—^1H)$: 92.3, 83.2, 79.8 $^2J(^{117}Sn—^1H)$: 86.4, 80.2, 76.5
5	$CDCl_3$	7.10br	2.40s	6.99s, 8.39s	1.25s, 1.35br, 1.44s	
6	$CDCl_3$	7.80br	2.39s	6.95s, 8.18s	1.04s, 1.20s, 1.60s	$^2J(^{119}Sn—^1H)$: 71.4, 76.2
7	Acetone	6.00br	2.37s	7.23s, 8.42s	0.75s, 0.80s, 0.85s	$^2J(^{119}Sn—^1H)$: 104.5 H_2O: 4.0br
8	$CDCl_3$	6.10br	2.01s 2.14s	6.46s, 6.56s 6.86s, 7.02s	0.71s	$^2J(^{119}Sn—^1H)$: 70.0 Ph: 6.79t, 6.97t, 7.00–7.40m, 7.48d
9	$CDCl_3$	8.0br	2.34s	7.00br, 8.00br	1.23t, 1.42t, 1.46t 1.74q	$^2J(Sn—^1H)$: 73 $^3J(^{119}Sn—^1H)$: 148.7, 149.6 $^3J(^{117}Sn—^1H)$: 142.0, 143.1
10	$CDCl_3$	12.40br 9.80br	2.35s	6.95s, 8.16s	1.16t, 1.35–1.60m 1.60–2.30m	
11	$CDCl_3$	13.20br	2.33s	6.96s, 8.04s	0.84t, 0.94t, 0.95t 1.20–1.50m 1.55–2.00m	
12	$CDCl_3$	13.06br	2.35s	6.95s, 8.09s	0.84t, 0.95t, 0.96t 1.15–1.50m 1.50–1.70m 1.70–2.10m	
13	Acetone		2.32s	7.20s, 8.40s	7.20–7.40m, 8.20d 8.21d	$^2J(^{119}Sn—^1H)$: 81.5
	EtOD		2.33s	7.85br, 8.65br	6.90–7.80m	

Table 4—*continued*

Compound	Solvent	N—H	CH_3 or i-C_3H_7	H azole	R—Sn	Other data
14	Acetone	12.00br	2.29s	7.34br, 8.45br	1.20s	$^2J(^{119}Sn—^1H)$: 130.0 H_2O: 4.10br
15	$CDCl_3$	10.80br 12.50br	2.12s 2.32s 2.39s	6.94s, 6.96s 7.13s, 7.26s 8.15m, 8.60s 8.72s, 8.80s	0.60–2.00m br	
16	Acetone	12.40br	2.26s	7.04s, 8.02s 8.33s, 8.47s	7.20–7.40m, 7.86d	$^2J(^{119}Sn—^1H)$: 143.2
L^2	$CDCl_3$	13.59s	2.60s	7.02s		
	Acetone	10.00br	2.32s	6.89s		
17	$CDCl_3$	8.85br	2.48s	6.92s	0.75s	$^2J(^{119}Sn—^1H)$: 65.2 $^2J(^{117}Sn—^1H)$: 62.3 H_2O: 1.60br
18	$CDCl_3$	10.56br	2.74s	7.11s	1.10s, 1.14s 1.19s, 1.23s	$^2J(^{119}Sn—^1H)$: 87.5, 94.7, 102.0
19	Acetone	6.7br	2.74s	7.43s	0.91t, 1.42ps 1.8–2.1m	H_2O: 2.20br
20	$CDCl_3$	7.0br	2.76s	7.15s	7.00–7.50br	
L^3	$CDCl_3$	11.04br	1.33s, 1.37s 3.13h	6.97s		H_2O: 1.60br
21	$CDCl_3$	9.95br	1.33s, 1.37s 3.13h	6.92s	0.72s	$^2J(^{119}Sn—^1H)$: 63.2 $^2J(^{117}Sn—^1H)$: 60.5
22	$CDCl_3$	6.5br	1.14s, 1.18s 2.95h	6.84s	7.72m,7.44m	
23	$CDCl_3$	13.3br	1.41s, 1.44s 3.41h	7.06s	1.05s	$^2J(^{119}Sn—^1H)$: 82.3 H_2O: 1.43br
24	$CDCl_3$	n.o.	1.44s, 1.48s 3.50h	7.10s	7.10–7.90m	

[a] δ in ppm, J in Hz; s = singlet, d = doublet, t = triplet, q = quartet, m = multiplet, ps = pseudosixtet, br = broad, h = heptet; n.o. = not observed.

The monoorganotin(IV) adducts **15** and **16** are not-electrolyte in acetone solution.

NMR spectroscopy

The ^{1}H NMR spectra of the donors L^1, L^2 and L^3 and of their organotin(IV) complexes **1–24** (Table 4) were recorded in $CDCl_3$ and for some derivatives in acetone or in EtOD, due to poor solubility in the former solvent. The ^{119}Sn spectra (Table 5) were carried out in $CDCl_3$ only on selected sufficiently soluble complexes.

The spectra of the triorganotin(IV) complexes **1, 2, 17** and **21** indicate a complete dissociation into the starting reagents. In fact, the Δ value (difference in chemical shift for the same type of proton in the free base and in its organotin(IV) complexes) is in the range 0.01–0.15 ppm.

Instead in the spectrum of the triphenyltin(IV) complexes **3** and **22** the signals of the ligand are displaced upfield and the Δ value is in the range (−0.15)–(−0.31) ppm. This peculiarity can be explained by considering the shielding effect exerted on CH_3, H2 and H5 protons by aromatic protons of the phenyl rings linked to tin(IV). In all these complexes the tin-proton coupling constants are of the same order of magnitude of those reported for the starting triorganotin(IV) acceptors [23].

In the spectra of the diorganotin(IV) complexes (**4–7, 9–13, 18, 23** and **24**) the signals of the ligands L^1, L^2 and L^3 are generally displaced to lower fields. The deshielding observed is attenuated at a position remote from the metal (methyl protons). The Δ observed is likely due to a σ-charge donation from the N-donor to tin(IV) acceptor and it is an evidence of the existence of the complexes in solution. However, the magnitude of the tin(IV)-proton coupling constants for all these diorganotin(IV) complexes, even if it is different from that reported in literature for the starting tetracoordinate diorganotin(IV) halides [24], is smaller with respect to that indicated for hexacoordinate undissociated organotin(IV) complexes containing N-donor ligands [25]: this suggests a partial dissociation of our complexes in chlorinate solution in accordance with the data derived from molecular weight measurements.

In the ^{1}H spectra of most of the complexes of L^1 more than one set of signals is observed for the imidazole ring protons and also for the two R groups linked to tin. None of the signals corresponds to those reported for the starting ligand and tin(IV) derivative employed [23]. It has been previously noted [26] that for $(L)_2R_2SnX_2$-type compounds *cis* and *trans* isomers are possible and also that organotin(IV) derivatives may undergo different equilibria in acetone solution. In our complexes there is also another possibility: the donor, in accordance with that previously observed in the derivatives of 4-phenylimidazole [6], may coordinate the tin atom not only by means of its N(3), but also by means of the N(1) atom. This is likely due to steric hindrance of the methyl group in the 4-position, which requires a metal/proton exchange between the two nitrogen sites [27]. At room temperature the metal/proton exchange is slow enough to allow the observation of signals due to both the organotin(IV) species in Fig. 4.

In order to confirm our hypothesis a variable temperature ^{1}H NMR experiment on a saturated solution ($CDCl_3$) of compound **4** was carried out. Some selected data are reported in Table 6. It should be noted that the magnitude of the tin-proton coupling constants becomes smaller when temperature increases; moreover the signals of the ligand upon complexation are more displaced downfield in the spectra recorded at lower temperatures. On the basis of this evidence we can hypothesize that the complex is more dissociated at high temperatures. In the spectra recorded at −45°C and at −30°C, the presence of seven different signals for the two methyl groups linked to tin is in accordance not only with the presence of isomers but also with the hypothesis of tin/proton "shuttling" between the two nitrogen sites. A similar pattern

Table 5. ^{119}Sn NMR data for some selected derivatives of L^1 and L^3

Compound	No.	Solvent	δ(^{119}Sn)
$[(L^1)_2(CH_3)_2SnCl_2]$	(**4**)	$CDCl_3$	−64.2, −117.3
$[(L^1)_2(CH_3)_2SnBr_2]$	(**5**)	$CDCl_3$	−119.2
$[(L^1)_2(C_2H_5)_2SnCl_2]$	(**9**)	$CDCl_3$	−92.2, −140.0, −184.0
$(L^1)_3(C_4H_9)SnCl_3$	(**15**)	$CDCl_3$	−285.3, −467.3, −474.0
$[(L^3)(CH_3)_3SnCl]$	(**21**)	$CDCl_3$	43.6
$[(L^3)(C_6H_5)_3SnCl]$	(**22**)	$CDCl_3$	−107.4
$[(L^3)(C_6H_5)_2SnCl_2]$	(**24**)	$CDCl_3$	[a]

[a] This compound is not very soluble in $CDCl_3$. After 30,000 cycles acquired, a broad signal likely due to oxide- or hydroxide-tin species is observed at ca 50 ppm.

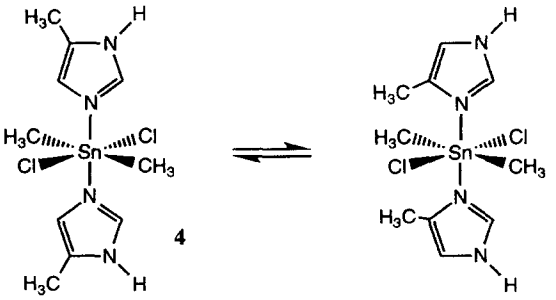

Fig. 4. Structure proposed for the 2 : 1 $(L^1)_2R_2SnX_2$ adducts: the 4-methylimidazole donor is able to coordinate by means of its N(1) or N(3) atom.

Table 6. Variable temperature ^1H NMR data of a $CDCl_3$ saturated solution of $[(L^1)_2(CH_3)_2SnCl_2]$ and $[(L^1)_2(C_2H_5)_2SnCl_2]$[a]

	$[(L^1)_2(CH_3)_2SnCl_2]$ (4)				$[(L^1)_2(C_2H_5)_2SnCl_2]$ (9)			
Temp.	H_2, H_4, H_5	4- or 5-CH_3	R—Sn	$^2J(^{119}Sn—^1H)$[b] $^2J(^{117}Sn—^1H)$	H_2, H_4, H_5	4 or 5-CH_3	R—Sn	$^2J(^{119}Sn—^1H)$[b] $^2J(^{117}Sn—^1H)$
−45°C	8.90(8)[c], 8.14(1)	2.38(30), 2.28(4)	1.23, 1.18, 1.13	ND[d]	8.20(1), 8.00(1.5)	2.35, 2.29, 2.22	1.76m, 1.66m, 1.43m	ND
	7.22(1), 6.79(8)	2.23(1), 2.20(1)	1.07, 1.03, 0.93	ND	6.95(1), 6.80(1.5)		1.19br, 0.91br	
			0.89					
−30°C	8.76(6), 8.14(1)	2.37(40), 2.28(6)	1.23, 1.18, 1.07	ND	8.18(1), 7.99(2)	2.33, 2.29, 2.26	1.77q, 1.75q, 1.68br	68
	7.22(1), 6.97(6)	2.23(1), 2.20(1)	1.04, 1.00, 0.92		6.98(1), 6.78(2)	2.20	1.44t, 1.41t, 1.20br	
			0.86				1.06t, 0.91br	
−15°C	8.67(6), 8.12(1)	2.37(40), 2.28(6)	1.25, 1.23, 1.18	ND	8.10(3), 8.00(1)	2.32, 2.29, 2.26	1.77q, 1.74q, 1.64br	71
	7.20(1), 6.97(6)	2.24(1), 2.20(1)	1.10, 1.07, 1.00	ND	7.95(3), 6.98(3)	2.19	1.44t, 1.41t, 1.11t	
					6.90(1), 6.80(3)		0.92t	
0°C	8.59(8), 8.10(1)	2.37(50), 2.29(4)	1.27, 1.23, 1.17	96, 110	8.10(2), 8.00(1)	2.32, 2.29, 2.26	1.77q, 1.75q, 1.64br	68
	7.21(1), 6.97(8)	2.24(1) 2.19(1)			7.95(1.5), 6.98(2)	2.18	1.45t, 1.42t, 1.16t	
					6.90(1), 6.80(1.5)		1.02t, 0.94t	
10°C	8.53(14), 8.10(1)	2.37(70), 2.29(6)	1.28, 1.22, 1.17	84, 90, 96	8.07(4), 7.95(1)	2.32, 2.29, 2.27	1.78q, 1.74q, 1.64br	73
	7.20(1), 6.97(1)	2.24(2), 2.18(1)			6.98(2), 6.92(2)	2.18	1.45t, 1.42t, 1.19t	
					6.85(1)		1.04t, 0.95t	
20°C	8.40(20), 8.06(1)	2.36(90), 2.29(6)	1.29, 1.23, 1.17	79, 83, 90	8.05(4), 7.98(1)	2.31, 2.29, 2.27	1.82q, 1.79q, 1.74q	73
	7.20(1), 6.97(20)	2.24(2), 2.18(1)			6.98(4), 6.87(1)	2.16	1.65m, 1.46t, 1.42t	
							1.24t, 0.98t	
30°C	8.33(20), 8.06(1)	2.36(90), 2.29(6)	1.29, 1.23, 1.17	79, 84, 89	8.0br, 7.0br	2.34br	1.74q, 1.46t, 1.42t	73
	7.20(1), 6.97(20)	2.24(2), 2.18(1)					1.23t	
40°C	8.23(20), 8.06(1)	2.35(55), 2.29(4)	1.29, 1.23, 1.17	80, 83, 86	8.05(6), 7.98(1)	2.31(12), 2.29(1)	1.82q, 1.79q, 1.74q	79
	7.20(1), 6.97(20)	2.23(1)			7.00(6), 6.85(1)	2.16(2)	1.47t, 1.42t, 1.26t	
							1.00t	
50°C	8.16(40), 8.06(1)	2.34(60), 2.28(4)	1.28, 1.24, 1.17	76, 81, 84	8.05(6), 7.98(1)	2.31(12), 2.29(1)	1.83q, 1.75m, 1.47t	78
	7.20(1), 6.97(40)	2.23(1)			7.00(6), 6.85(1)	2.16(2)	1.42t, 1.28t, 1.10t	

[a] In $CDCl_3$.
[b] J in Hz.
[c] Ratio of intensity in parentheses ( ).
[d] ND = Not distinguishable.

(Table 6) was also observed in the variable temperature ^{1}H NMR spectrum of **9**.

In the ^{1}H NMR spectrum of **8** two different resonances due to each CH_3, H2 and H4 or H5 of the imidazole moiety are observed upfield shifted with respect to the same resonance in the free donor ($\Delta = +0.26$ and $+0.13$, $+0.34$ and $+0.24$, and $+0.74$ and $+0.58$ respectively). This trend could be explained by considering the shielding effect exerted on CH_3, H2 and H4 or H5 by the aromatic protons of the BPh_4^- counter-ion. It has been previously reported that the existence of intermolecular and interionic contacts can be detected by Nuclear Overhauser Effects (NOEs) [28], which is the unique tool for investigating the aggregation and localization of the interacting fragments in solution. We have performed a ROESY experiment [8] on a saturated $CDCl_3$ solution of **8** at room temperature; however no cross peaks between the organometallic $(CH_3)_2(L^1)_4Sn^{++}$ moiety and BPh_4^- have been observed. In absence of crystal and molecular structure determination it is not possible to indicate if the BPh_4^- counter-ions interact, in the solid state, with the organometallic fragment.

^{119}Sn NMR signals of $[(L^1)_2R_2SnX_2]$ type compounds **4, 5** and **9** were observed in $CDCl_3$ solution (Table 5) between -64.2 and -184 ppm. The measured $\delta(^{119}Sn)$ values do not fit clearly into the reported ranges of $\delta(^{119}Sn)$ values of six-coordinate organotin(IV) compounds [23,24]. However these values are in accordance with the partial dissociation proposed on the basis of ^{1}H NMR data and molecular weight determinations. The presence of two and three signals in the spectra of derivatives **4** and **9** respectively, further supports the presence of isomers and/or of hydrolysis products. On the other hand, the ^{119}Sn chemical shift of compound **15** is typical of octahedral, pseudooctahedral or skewed trapezoidal environment [23,24]. Also on the basis of conductance values, we suggest for the 3:1 adducts **15** and **16** a non-ionic dissociation in solution such as in eqn (4):

$$(L^1)_3RSnCl_3 \rightleftharpoons (L^1)_{3-n}RSnCl_3 + nL^1 \qquad (4)$$

15, 16

(R = Bu^n, Ph)

In the absence of crystals suitable for X-ray analysis, we are not able to indicate with certainty the coordination number of tin in these compounds. In the solid state they could exist in a heptacoordinate form, but we cannot exclude the possibility of a hexacoordinate environment, with one imidazole donor out of the inner coordination sphere and hydrogen bonded to the other ligands or to the chlorides.

It has been reported [23,24] that the magnitude of the ^{119}Sn chemical shift of compounds having the same coordination number depends primarily on the electronegativity of the substituents at tin and on the geometric distortion which modify the interbond angles at tin: In our case the substitution of an R with a Cl group produces a significant upfield shift ($\delta(^{119}Sn)$ for **15**: -285.3, -467.3 and -474.0 ppm); a similar trend was previously observed in (β-diketonato)$_2$(CH_3)XSn (X = CH_3 or Cl) complexes [29].

The triorganotin(IV) derivatives **21** and **22** exhibit a single absorption at ca 43.6 and -107.4 ppm respectively, typical of four or five-coordinate central tin atom. These signals are upfield shifted with respect to those reported for the starting acceptors (Me_3SnCl: $+164.2$ ppm [30], Ph_3SnCl: -44.7 ppm) [31]. The shift is smaller than that observed in analogous 1-benzylimidazole derivatives [5].

CONCLUSIONS

The reactivity of alkyl-substituted imidazole donors towards organotin(IV) acceptors depends not only on the electronic and steric features of the groups bonded to tin, but also on the position of the alkyl substituent in the imidazole moiety and on the nature of the counter-ion: the ligand/metal ratio can range from 1:1 in $[(L^1)(C_6H_5)_3SnCl]\cdot 1/3H_2O$ to 4:1 in $[(L^1)_4(CH_3)_2Sn](BPh_4)_2$. The NMR data and molecular weight measurements indicate that the bonding interaction between L^1, L^2 and L^3 and R_nSnX_{4-n} generally increases with decreasing of n and that the donor is coordinated to tin through the nitrogen atom.

To date L^6 (1-methylimidazole) is the best imidazole-type donor investigated towards organotin(IV) acceptors: it can be deduced from the easy formation of adducts also with triorganotin(IV) acceptors and from the fairly good stability of them. The presence of a methyl substituent in the 4-position of the heterocyclic ring (L^1) seems to reduce the donating ability, with respect to the substitution in the 1-azole position (L^6), even if the pK_a of the two ligands is of the same order of magnitude [32].

On the other hand L^2 (2-methylimidazole) and L^3 (2-isopropylimidazole), which have a methyl and an isopropyl group respectively near to the coordination site, are the worst donor to date employed. Their reactions toward organotin(IV) acceptors were often unsuccessful and the few compounds obtained are not stable both in solution and in the solid state.

Combined analytical and spectral data (IR, far-IR, ^{1}H and ^{119}Sn NMR) suggest for the triorganotin(IV) adducts a bipyramid trigonal configuration, whereas a distorted octahedral or pseudooctahedral structure is likely for all the other derivatives.

Acknowledgements—We thank the MURST, CNR-Rome and the University of Camerino for financial help.

REFERENCES

1. Keppler, B. H., *Metal Complexes in Cancer Chemotherapy*, WCH Publishers, Weinheim (Federal Republic of Germany) (1993).

2. Rosemberg, B., van Camp, L., Troska, J. E. and Mansour, V. H., *Nature*, 1969, **222,** 385.
3. Crowe, A. J., Smith, P. J., Cardin, C. J., Parge, H. E. and Smith, F. E., *Cancer Lett.*, 1984, **24,** 45.
4. Crowe, A. J., *Drugs of the Future*, 1985, **3,** 229.
5. Pettinari, C., Marchetti, F., Cingolani, A. and Bartolini, S., *Polyhedron*, 1996, **15,** 1263.
6. Pettinari, C., Marchetti, F., Pellei, M., Cingolani, A., Barba, L. and Cassetta, A., *J. Organomet. Chem.*, 1996, **515,** 119.
7. Pettinari, C., Pellei, M., Miliani, M., Cingolani, A., Cassetta, A., Barba, L., Pifferi, A. and Rivarola, E., *J. Organomet. Chem.*, submitted.
8. Kessler, H., Griesinger, C., Kerssebaum, R., Wagner, K. and Ernst, R. R., *J. Amer. Chem. Soc.*, 1987, **109,** 607.
9. Kocheshkov, K. A., *Chem. Ber.*, 1926, **62,** 996.
10. Garcia Martinez, E., Sanchez Gonzalez, A., Casas, J. S., Sordo, J., Casellato, U. and Graziani, R., *Inorg. Chim. Acta*, 1992, **191,** 75.
11. Casas, J. S., Garcia Martinez, E., Sanchez Gonzalez, A., Sordo, J., Casellato, U., Graziani, R. and Russo, U., *J. Organomet. Chem.*, 1995, **493,** 107.
12. Pearson, R. G., *Acc. Chem. Res.*, 1993, **26,** 250.
13. (a) Ohkaku, N. and Nakamoto, K., *Inorg. Chem.*, 1993, **12,** 2440; (b) Beattie, I. R. and McQuillan, G. P., *J. Chem. Soc.*, 1963, 1519.
14. Nieuwpoort, G., Vos, J. G. and Groeneveld, W. L., *Inorg. Chim. Acta*, 1978, **29,** 117.
15. (a) Graziani, R., Casellato, U., Ettorre, R. and Plazzogna, G., *J. Chem. Soc., Dalton Trans.*, 1982, **805**; (b) Valle, G., Ettorre, R., Peruzzo, V. and Plazzogna, G., *J. Organomet. Chem.*, 1987, **326,** 169.
16. (a) Poller, R. C., *The Chemistry of Organotin Compounds*, Logos, London, 1970; (b) Newman, W. P., *The Organic Chemistry of Tin*, Wiley Interscience, New York, 1970; (c) Ho, B. W. K. and ZucKerman, J. J., *Inorg. Chem.*, 1973, **12,** 1552; (d) Huber, F., Vornefeld, M., Ruisi, G. and Barbieri, R., *App. Organomet. Chem.*, 1993, **7,** 243.
17. (a) Edgell, W. F. and Ward, C. H., *J. Mol. Spectrosc.*, 1962, **8,** 343; (b) Sandhu, J. K., Kaur, G., Holecek, J. and Licka, A., *J. Organomet. Chem.*, 1988, **345,** 51.
18. (a) May, J. R., McWhinnie, W. R. and Poller, R. C., *Spectrochim. Acta*, 1971, **27A,** 969; (b) Smith, A. L., *Spectrochim. Acta*, 1967, **24A,** 695; (c) Dance, M. S., McWhinnie, W. R. and Poller, R. C., *J. Chem. Soc., Dalton Trans.*, 1976, 2349.
19. Basu Baul, T. S., Dey, D., Mishra, D. D., Basaiawmoit, W. L. and Rivarola, E., *J. Organomet. Chem.*, 1993, **447,** 9.
20. Clark, R. J. H., Davies, A. G. and Puddephatt, R. J., *J. Chem. Soc. A*, 1968, 1828.
21. (a) Shobatake, K., Postmus, C., Ferraro, J. R. and Nakamoto, K., *Appl. Spectroscopy*, 1969, **23,** 12; (b) Bradbury, J., Forest, K. P., Nuttall, R. H. and Sharp, S. W., *Spectrochim. Acta*, 1967, **23,** 2701.
22. (a) Cotton, F. A. and Goodgame, D. M. L., *J. Chem. Soc.*, 1960, 5267; (b) Restivo, R. J., Costin, A., Ferguson, G. and Carty, A. J., *Can. J. Chem.*, 1975, **53,** 1949; (c) Anderson, W. A., Carty, A. J., Palenik, G. J. and Schreiber, G., *Can. J. Chem.*, 1971, **49,** 761.
23. Wrackmeyer, B., *Ann. Rep. NMR Spectrosc.*, 1985, **16,** 73.
24. Harrison, P. G., Investigating tin using spectroscopy. In *Chemistry of Tin*, Chapter 3, ed. P. G. Harrison. Chapman and Hall, London, 1989, pp. 61–115.
25. (a) Honnick, W. D., Hughes, M. C., Schaeffer, C. D. and Zuckerman, J. J., *Inorg. Chem.*, 1976, **15,** 1391 and references cited therein; (b) Lockart, T. P. and Manders, W. F., *Inorg. Chem.*, 1986, **25,** 892.
26. Donaldson, J. D. and Grimes, S. M., The inorganic chemistry of tin. In *Chemistry of Tin*, Chapter 4, ed. P. G. Harrison. Chapman and Hall, London, 1989, pp. 118–144 (and references cited therein).
27. (a) Borkett, N. F. and Bruce, M. I., *J. Organomet. Chem.*, 1974, **65,** C51; (b) Gassend, R., Marie, J. C. and Pommier, J. C., *J. Organomet. Chem.*, 1977, **132,** 69; (c) Angaroni, M. A., Ardizzoia, G. A., Beringhelli, T., D'Alfonso, G., La Monica, G., Masciocchi, N. and Moret, M., *J. Organomet. Chem.*, 1989, **363,** 409.
28. Neuhaus, D. and Williamson, N., *The Nuclear Overhauser Effect in Structural and Conformational Analysis*, VCH Publishers Inc., New York (1989).
29. (a) Pettinari, C., Rafaiani, G., Gioia Lobbia, G., Lorenzotti, A., Bonati, F. and Bovio, B., *J. Organomet. Chem.*, 1991, **405,** 75; (b) Bovio, B., Cingolani, A., Marchetti, F. and Pettinari, C., *J. Organomet. Chem.*, 1993, **458,** 39; (c) Pettinari, C., Marchetti, F., Leonesi, D., Rossi, M. and Caruso, F., *J. Organomet. Chem.*, 1994, **483,** 123.
30. van den Berghe, E. V. and van der Kelen, G. P., *J. Organomet. Chem.*, 1971, **26,** 207.
31. Holecek, J., Nadvornik, M., Handlir, K. and Licka, A., *J. Organomet. Chem.*, 1983, **241,** 177.
32. Grimmett, M. R., Imidazoles and their benzo derivatives: (i) structure. In *Comprehensive Heterocyclic Chemistry*, Vol. 5, Part 4a, ed. A. R. Katritzky, C. W. Rees and K. T. Potts. Pergamon Press, Oxford, 1984, p. 345.

Pergamon

PII: S0277-5387(97)00307-0

Polyhedron Vol. 17, No. 4, pp. 577–588, 1998
© 1998 Elsevier Science Ltd
All rights reserved. Printed in Great Britain
0277-5387/98 $19.00+0.00

Application of electrospray mass spectrometry to the characterisation of sulfonated and ferrocenyl phosphines

William Henderson* and Gregory M. Olsen

Department of Chemistry, University of Waikato, Private Bag 3105, Hamilton, New Zealand

(Received 13 May 1997; accepted 14 July 1997)

Abstract—A range of ferrocenyl-containing and sulfonated triphenylphosphines have been investigated by electrospray mass spectrometry. *In situ* formation of hydroxymethyl phosphonium salt derivatives of the ferrocenyl phosphines and *in situ* formation of silver(I) adducts of both the ferrocenyl and sulfonated phosphines provided a means of characterising such compounds. Results are discussed in terms of fragmentation and aggregation of the parent molecular ion species. Sulfonated phosphines, including their sodium adducts, were easily characterised by their negative-ion spectra. Aminoalkyl-ferrocenyl phosphines form strong $[M+H]^+$ ions in their positive-ion spectra. Ferrocenyl phosphines without amino functions give weaker $[M+H]^+$ ions and may also be complicated by the existence of $[M]^+$ ions. Less complex positive-ion mass spectra of these ferrocenyl phosphines can be observed following treatment with either a solution of $AgNO_3$ or a mixture of formaldehyde and HCl. © 1998 Elsevier Science Ltd. All rights reserved

Keywords: electrospray mass spectrometry; phosphines; ferrocene derivatives; sulfonated phosphines; water-soluble phosphines.

There is a vast literature on the chemistry of phosphines and their metal complexes [1]. Indeed, the action of some complexes, e.g. catalysts for organic synthesis, are intimately linked with the structure and characteristics of the phosphine ligand(s) coordinated [2–4]. Phosphines are important precursors for the development of such complexes and a considerable amount of data have been published on their characterisation. Recent evidence suggests that results derived from the relatively new technique of electrospray mass spectrometry (ESMS) are complementary to those obtained from other techniques such as electrochemistry or multinuclear magnetic resonance spectroscopy (NMR) [5].

In the past, mass spectrometry of either inorganic or organometallic compounds was dominated by the ionisation techniques of electron impact (EI) or fast atom bombardment (FAB). EI is largely limited to the analysis of neutral volatile species which for many reasons were also required to be thermally stable. FAB is more successful but was still disadvantaged by the relatively high degree of fragmentation, making identification of molecular ions difficult. The soft ionisation technique of electrospray (ES), which has proven particularly beneficial to biochemists for the characterisation of large organic molecules, e.g. proteins [6], has recently found favour among inorganic and organometallic chemists [5,7–12]. In general ESMS gives considerable control over the degree of fragmentation, by varying the skimmer cone voltage. In principle, the technique is applicable to any pre-existing cation, anion or neutral compound that can be modified by the addition of a suitable reagent to form an ion, providing that the ion is stable to the solution environment used in the mass spectrometer.

We recently described the ESMS analysis of a variety of hydroxymethylphosphines and their derivatives, including phosphine sulfides and phosphonium salts [12]. Results from this study identified the preferred fragmentation pathways for hydroxymethylphosphine derivatives and outlined a number of general routes for the detection of neutral phosphines, phosphine oxides and phosphine sulfides. Only weak ions are observed in the positive-ion ES mass spectra of many phosphines because they are weak

* Author to whom correspondence should be addressed.

bases, however it was demonstrated that the addition of a suitable reagent (either aqueous $AgNO_3$ or a mixture of 40% formaldehyde and concentrated HCl) could aid in the formation of cations for positive-ion ESMS. In this paper we report our studies on the further development of the ESMS technique for the analysis of other important types of phosphine ligands, particularly those which contain additional functional groups, such as sulfonated aryl phosphines, and ferrocene-derived phosphines.

The water-soluble sulfonated phosphines, $Ph_2P(C_6H_4SO_3Na)$ (TPPMS) and $P(C_6H_4SO_3Na)_3$ (TPPTS) were of particular interest since the introduction of the Rhone–Poulenc water-soluble rhodium hydroformylation catalyst $HRh(CO)(TPPTS)_3$ [3,4]. We have also examined a number of ferrocenyl phosphines (structures depicted in Scheme 1), which are of interest in the development of asymmetric catalysts [13] and compounds showing anti-cancer activity [14]. Few studies describe the use of ESMS for the analysis of ferrocenes [8,9] and no extensive studies, to the best of our knowledge, have been published on the ESMS of ferrocenyl- or sulfonated aryl phosphines.

The studies by Cole and co-workers [9] and ourselves [8] illustrate the difficulties which can arise in characterising molecular ions in the ESMS of ferrocene-derived compounds. The isotope pattern for the molecular ion is often complicated by the existence of both the ferricinium ion $[M]^+$ and the protonated ion $[M+H]^+$ with variable relative intensities. Intensities depend upon both the operating conditions of ESMS and the structure of the ferrocene. This complication may be avoided if a suitable ion can be formed which is less susceptible to electrochemical oxidation. The phosphine function on the compounds under investigation may be modified quite simply to form positively-charged species [12]. Positively-charged silver complex ions can be formed by the addition of a solution of $AgNO_3$, e.g. $[M+Ag]^+$, and hydroxymethyl phosphonium salts, e.g. $[M(CH_2OH)]^+$, may be formed by the addition of a solution of formaldehyde and HCl. Colton *et al.* have previously described the use of iodomethane as an alternative ionisation agent for the analysis of tertiary phosphines by ESMS [10,11].

EXPERIMENTAL

Materials

The ferrocenyl phosphines $FcCH_2P(CH_2OH)_2$ [19] and $FcCH_2PH_2$ [20] were prepared according to literature methods. The ferrocenyl phosphine $FcCH_2PPh_2$ [21] was prepared by reaction of Ph_2PCH_2OH with $[FcCH_2NMe_3]I$, full details of which will be published in due course. Sulfonated phosphines were also prepared using literature methods [15].

Instrumentation

Electrospray mass spectra were recorded in both positive-ion and negative-ion modes on a VG Platform II single quadrupole benchtop mass spectrometer (Fisons Instruments). Samples of either the ferrocenyl phosphines or the sulfonated phosphines were dissolved in 1 : 1 v/v acetonitrile–water. The solution, typically of approximate concentration 0.1 mM, may be further treated by the addition of 1–3 drops of either a 1 : 1 mixture of 40% formaldehyde and HCl or an aqueous solution of $AgNO_3$ (0.5 g/l). The Ag^+ concentration was semi-quantitative, deemed low if one drop of $AgNO_3$ was added and high if 3 drops of $AgNO_3$ were added to a solution of the phosphine. Samples were injected directly *via* a Rheodyne injector with a 10 μl sample loop. A Spectra-System P1000 LC pump delivered the solution to the vaporisation nozzle of the electrospray ion source (60°C) at a flow rate of 0.01 $cm^3\ min^{-1}$ and nitrogen was employed as both a drying and nebulising gas. Skimmer cone voltages were varied between 20 and 90 V, in order to investigate the effects of higher cone voltages on fragmentation of the parent ions. Spectra were typically an average between 10 and 20 scans, depending upon intensity. Theoretical isotope patterns were calculated using the *Isotope* program [22] and used to aid in assignment.

$^{31}P\text{-}\{^1H\}$ NMR spectra were recorded in 1 : 1 methanol : D_2O solution on a Bruker AC300P spectrometer at 121.5 MHz with external 85% H_3PO_4 (δ 0.0) as reference.

RESULTS AND DISCUSSION

Sulfonated phosphines

TPPTS and a crude sample of TPPMS, dissolved in 50% aqueous acetonitrile, were investigated by ESMS in negative-ion mode at a low cone voltage (20 V) either in combination with formic acid or $AgNO_3$, or as a neat solution. These phosphines, in contrast to neutral triphenylphosphine, exhibited strong ions in their negative-ion ES mass spectra. ESMS data are summarised in Table 1.

The ions $[P(m\text{-}C_6H_4SO_3)_3]^{3-}$ (m/z 166.3, the base peak) and $[P(m\text{-}C_6H_4SO_3)_3Na]^{2-}$ (m/z 261, 64%) dominate the negative-ion ES mass spectrum of TPPTS, as shown in Fig. 1. A number of minor ions including $[P(m\text{-}C_6H_4SO_3)_3H]^{2-}$ (m/z 250), $[P(O)(m\text{-}C_6H_4SO_3)_3]^{3-}$ (m/z 171.7), $[P(O)(m\text{-}C_6H_4SO_3)_3Na]^{2-}$ (m/z 269) and $[P(m\text{-}C_6H_4SO_3)_3Na_2]^-$ (m/z 545) can also be identified in the spectrum. The existence of the phosphine oxide derivatives in the ES mass spectra is consistent with the known chemistry of sulfonation of arylphosphines which can commonly produce phosphine oxides [4,15]. Two signals were observed at δ +32.5 and −4.2 in the $^{31}P\{^1H\}$ NMR spectrum of TPPTS in a 1 : 1 methanol : D_2O solution, and were

Table 1. Negative-ion electrospray mass spectral data for sulfonated phosphines TPPTS and TPPMS

Compound/mixture[a]	Major ESMS ions (m/z %)[b]
TPPTS	$[P(m\text{-}C_6H_4SO_3)_3Na_2]^-$ (545, 3%); $[P(O)(m\text{-}C_6H_4SO_3)_3Na]^{2-}$ (269, 6%); $[P(m\text{-}C_6H_4SO_3)_3Na]^{2-}$ (261, 64%); $[P(m\text{-}C_6H_4SO_3)_3H]^{2-}$ (250, 12%); $[P(O)(m\text{-}C_6H_4SO_3)_3]^{3-}$ (171.7, 10%); $[P(m\text{-}C_6H_4SO_3)_3]^{3-}$ (166.3, 100%).
TPPTS + HCOOH	$[P(m\text{-}C_6H_4SO_3)_3Na_2]^-$ (545, 9%); $[P(m\text{-}C_6H_4SO_3)_3NaH]^-$ (523, 11%); $[P(m\text{-}C_6H_4SO_3)_3H_2]^-$ (501, 9%); $[P(O)(m\text{-}C_6H_4SO_3)_3Na]^{2-}$ (269, 12%); $[P(m\text{-}C_6H_4SO_3)_3Na]^{2-}$ (261, 43%); $[P(m\text{-}C_6H_4SO_3)_3(NH_4)]^{2-}$ (258.5, 30%); $[P(m\text{-}C_6H_4SO_3)_3H]^{2-}$ (250, 100%); $[P(m\text{-}C_6H_4SO_3)_3]^{3-}$ (166.3, 50%).
TPPTS + $AgNO_3$	$[P(m\text{-}C_6H_4SO_3)_3Ag]^{2-}$ (303, 29%); unknown (275, 5%); $[Ag(NO_3)_2]^-$ (231, 100%); $[P(O)(m\text{-}C_6H_4SO_3)_3]^{3-}$ (171.7, 6%); $[P(m\text{-}C_6H_4SO_3)_3]^{3-}$ (166.3, 2%).
TPPMS	$[PhP(O)(m\text{-}C_6H_4SO_3)_2Na]^-$ (459, 2%); $[PhP(m\text{-}C_6H_4SO_3)_2Na]^-$ (443, 2%); $[Ph_2P(O)(m\text{-}C_6H_4SO_3)]^-$ (357, 12%); $[P(O)(m\text{-}C_6H_4SO_3)_3Na]^{2-}$ (269, 7%); $[P(O)(m\text{-}C_6H_4SO_3)_3H]^{2-}$ (258.5, 3%); $[PhP(O)(m\text{-}C_6H_4SO_3)_2]^{2-}$ (218, 100%); $[PhP(m\text{-}C_6H_4SO_3)_2]^{2-}$ (210, 77%); $[P(O)(m\text{-}C_6H_4SO_3)_3]^{3-}$ (171.7, 29%); $[P(m\text{-}C_6H_4SO_3)_3]^{2-}$ (166.3, 3%).
TPPMS + HCOOH	$[PhP(O)(m\text{-}C_6H_4\text{-}SO_3)_2Na]^-$ (459, 3%); $[PhP(O)(m\text{-}C_6H_4SO_3)_2(NH_4)]^-$ (454, 6%); $[PhP(O)(m\text{-}C_6H_4SO_3)_2H]^-$ (437, 7%); unknown (241, 8%); $[PhP(O)(m\text{-}C_6H_4SO_3)_2]^{2-}$ (218, 100%); $[PhP(m\text{-}C_6H_4SO_3)_2]^{2-}$ (210, 3%).
TPPMS + $AgNO_3$	$[PhP(O)(m\text{-}C_6H_4SO_3)_2Ag]^{2-}$ (545, 7%); $[PhP(m\text{-}C_6H_4SO_3)_2Ag]^{2-}$ (529, 5%); $[Ag_2(NO_3)_3]^-$ (402, 2%); $[Ph_2P(O)(m\text{-}C_6H_4SO_3)]^-$ (357, 6%); $[Ag(NO_3)_2]^-$ (231, 100%); $[PhP(O)(m\text{-}C_6H_4SO_3)_2]^{2-}$ (218, 84%); $[PhP(m\text{-}C_6H_4SO_3)_2]^{2-}$ (210, 6%); $[P(O)(m\text{-}C_6H_4SO_3)_3]^{3-}$ (171.7, 20%).

[a] TPPTS = $P(m\text{-}C_6H_4SO)_3^{-3}$ and TPPMS = $PPh_2(m\text{-}C_6H_4SO_3)^-$ both as their sodium salts.
[b] m/z values quoted are for the major peak in the isotope distribution pattern.

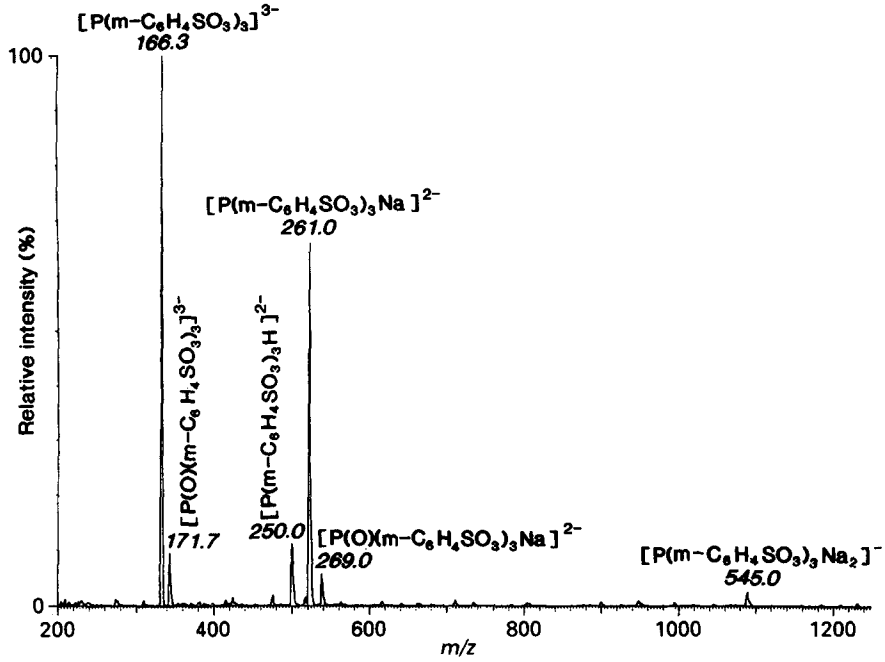

Fig. 1. Negative-ion ES mass spectrum (cone voltage 20 V) of TPPTS dissolved in 1 : 1 v/v acetonitrile–water.

assigned to the oxide of TPPTS and the free phosphine relatively. The minor protonated ions $[P(m\text{-}C_6H_4SO_3)_3NaH]^-$ (m/z 523), $[P(m\text{-}C_6H_4SO_3)_3H_2]^-$ (m/z 501) and the ammonium adduct $[P(m\text{-}C_6H_4SO_3)_3(NH_4)]^{2-}$ (m/z 258.5) were observed upon addition of formic acid to the neat solution. The ES mass spectrum was dominated by the signal at m/z 250 due to $[P(m\text{-}C_6H_4SO_3)_3H]^{2-}$. As expected, all the

sodium adducts decrease in intensity upon the addition of formic acid. The protonation pathway dominates if sufficient formic acid is added, the sodium adducts disappearing or representing only the minor ions in the ES mass spectra.

For TPPMS, $[P(O)(m\text{-}C_6H_4SO_3)_3H]^{2-}$ (*m/z* 171.7), $[Ph_2P(O)(m\text{-}C_6H_4SO_3)]^-$ (*m/z* 357), $[PhP(m\text{-}C_6H_4SO_3)_2]^{2-}$ (*m/z* 210) and the respective oxide $[PhP(O)(m\text{-}C_6H_4SO_3)_2]^{2-}$ (*m/z* 218, 100%) dominate the negative-ion ES mass spectrum. ESMS data suggests the mixture comprises the oxides of the mono-, di- and tri-sulfonated triphenyl phosphine in addition to the disubstituted phosphine $PhP(C_6H_4SO_3Na)_2$ (TPPDS). In contrast to TPPTS, the oxide peaks are highly significant ions in the negative-ion ES mass spectrum of the crude mixture of TPPMS. It seems probable that these oxides were formed as a direct result of the synthesis, as alluded to earlier, pre-existing in solution and not formed as a result of electrochemical oxidation in the ESMS. This hypothesis was later supported by data from $^{31}P\{^1H\}$ NMR using a 1 : 1 mixture of methanol and D_2O as solvent. Three signals were recorded in the chemical shift range of phosphine oxides at δ +34.4, +33.6 and +32.5 and were assigned to the mono-, di- and tri-sulfonated triphenylphosphine oxides. In addition, a single peak was recorded at δ −4.5 in the chemical shift range of free phosphines, assigned to the disulfonated analogue TPPDS. Thus, ESMS provides useful complementary information (to NMR spectroscopy) in the analysis of water-soluble sulfonated phosphines.

The major effect of adding formic acid to a solution of the crude TPPMS is the significant decrease in intensity of the ions $[P(O)(m\text{-}C_6H_4SO_3)_3]^{3-}$ (*m/z* 171.7) and $[PhP(m\text{-}C_6H_4SO_3)_2]^{2-}$ (*m/z* 210) whilst the oxide ion $[PhP(O)(m\text{-}C_6H_4SO_3)_2]^{2-}$ (*m/z* 218) maintains dominance. As indicated previously for TPPTS, the ions containing sodium decrease in intensity while the protonated ions and the ammonium adduct $[PhP(O)(m\text{-}C_6H_4SO_3)_2(NH_4)]^-$ (*m/z* 454) either appear or increase in intensity.

Addition of an aqueous solution of $AgNO_3$ to either a solution of TPPTS or TPPMS was investigated as an aid in identification. The ion $[Ag(NO_3)_2]^-$ (*m/z* 231, 100%) together with $[P(m\text{-}C_6H_4SO_3)_3Ag]^{2-}$ (*m/z* 303, 29%) represent the only ions of high intensity in the negative-ion ES mass spectrum of TPPTS. Interestingly the ion $[P(m\text{-}C_6H_4SO_3)_3Ag]^{2-}$ (*m/z* 303, 93%) increased in intensity upon the addition of formic acid to the mixture of TPPTS and $AgNO_3$.

Formic acid has been observed to aid in stripping residual Ag(I) from the surfaces inside the injector and/or capillary of the ESMS system, thus resulting in an increase in Ag(I) concentration. The ion $[Ag(NO_3)_2]^-$ (*m/z* 231, 100%) and the oxide $[PhP(O)(m\text{-}C_6H_4SO_3)_2]^{2-}$ (*m/z* 218, 84%) represent the major ions in the negative-ion ES mass spectrum of TPPMS. However, the Ag(I) complex ions $[PhP(m\text{-}C_6H_4SO_3)_2Ag]^-$ (*m/z* 529), $[PhP(O)(m\text{-}C_6H_4SO_3)_2Ag]^-$ (*m/z* 545) and $[Ag_2(NO_3)_3]^-$ (*m/z* 402) were also identified. The silver-nitrate ions observed at *m/z* 231 and *m/z* 402 were not unexpected given that comparably high concentrations of $AgNO_3$ were employed. Silver(I)-acetonitrile complexes $[Ag(CH_3CN)]^+$ (*m/z* 148) and $[Ag(CH_3CN)_2]^+$ (*m/z* 189) were the only species observed in the positive-ion ES mass spectrum following the addition of $AgNO_3$ to a solution of either TPPTS or TPPMS. Intense ions $[M+Ag]^+$ and $[2M+Ag]^+$ in the positive-ion ES mass spectra have been reported for solutions containing a neutral phosphine, e.g. PPh_3 and $AgNO_3$ [10,12]. Species such as $[\{P(m\text{-}C_6H_4SO_3)_3\}_2Ag]^{5-}$ (*m/z* 221.4) and $[\{PhP(m\text{-}C_6H_4SO_3)_2\}_2Ag]^{3-}$ (*m/z* 316.3) were not observed. For the former species, the high charge density of such an ion would likely result in association with H^+ or Ag^+, or dissociation of a phosphine ligand. For $[\{PhP(m\text{-}C_6H_4SO_3)_2\}_2Ag]^{3-}$ it is possible that the $AgNO_3$ concentration was too high.

Ferrocenyl phosphines

A number of ferrocenyl phosphines and aminoalkyl ferrocenyl phosphines **1, 2, 3** and **4** have also been studied by ESMS. Most compounds containing amino functions can be analysed easily by positive-ion ESMS; a strong $[M+H]^+$ ion is observed due to protonation of the basic nitrogen atom. Protonation can be achieved *in situ* either by interaction with water, a component of the mobile phase, or facilitated by the addition of acid. Results from the positive-ion ES mass spectral analysis of both the ferrocenyl phosphines and the amino ferrocenyl phosphines are presented in Table 2.

Nearly all the amino ferrocenyl phosphines (**3a, 3b** and **4b**) typically gave rise to a single peak due to the $[M+H]^+$ ion with the exception of PPFA (**4a**) which exhibits a strong $[M(O)+H]^+$ ion. In contrast, the corresponding phosphorus analogs are not as basic, typically giving rise to weaker $[M+H]^+$ ions. An unknown aggregate ion at *m/z* 998 and an unknown ion at *m/z* 387 both of variable percent intensity were repeatedly observed in the ES mass spectrum of BPPA. The intensity of these ions decreased over time as the spectra were being collected. Phosphine sulfide peaks of low percentage intensity were also observed in the ES mass spectra of BPPA and BPPFA. In most cases the M(S) peak cannot be discounted nor distinguished from $M(O)_2$ since the isotope patterns are very similar. However the ions of mass *m/z* 48 or *m/z* 64 higher than the $[M+Ag]^+$ ion, which were sometimes observed, are likely to be due to the phosphine derivatives $[M(O)(S)+Ag]^+$ and $[M(S)_2+Ag]^+$ respectively. The source of these species appears to be due to adventitious sulfur or sulfides in the system originating from previous solutions of metal–sulfide–thiolate clusters.

Increasing the cone voltage above 40 V can facilitate characterisation as the fragments formed provide further structural information concerning the original

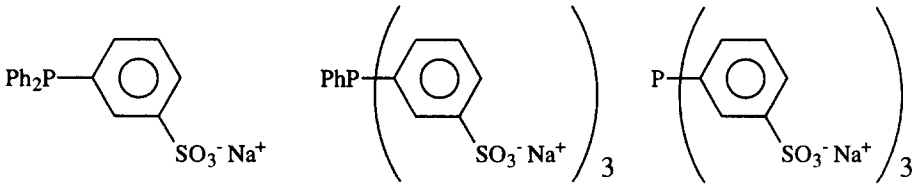

TPPMS TPPDS TPPTS

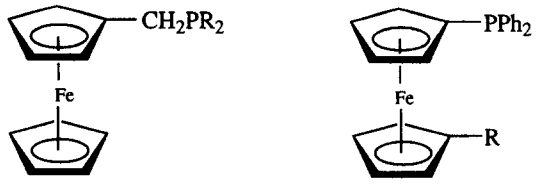

1 **2**

1a R = H
1b R = Ph
1c R = CH_2OH

2a R = H DPF
2b R = PPh_2 DPPF

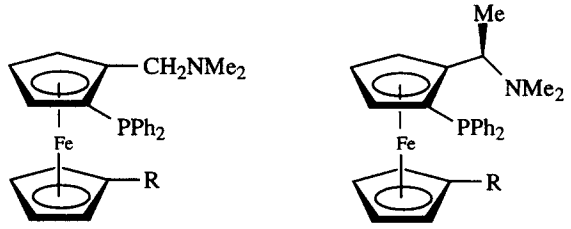

3 **4**

3a R = H PFMA
3b R = PPh_2 BPPA

4a R = H PPFA
4b R = PPh_2 BPPFA

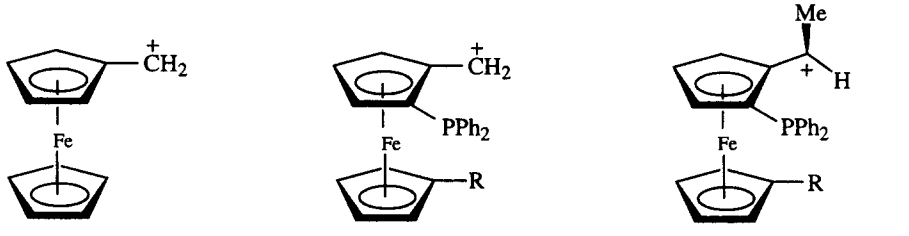

5 **6** **7**

6a R = H PFMA -NMe_2
6b R = PPh_2 BPPA -NMe_2

7a R = H PPFA -NMe_2
7b R = PPh_2 BPPFA -NMe_2

Scheme 1

Structures of sulfonyl and ferrocenyl phosphines employed in ESMS studies and structures of fragment carbocations observed in the positive-ion ES mass spectra of the ferrocenyl phosphines.

DPF = diphenylphosphinoferrocene.
DPPF = 1,1′-bis(diphenylphosphino)ferrocene.
PFMA = *N*,*N*-dimethyl-(2-(diphenylphosphino)ferrocenyl)-1-methylamine.
BPPA = *N*,*N*-dimethyl-(1′2-bis(diphenylphosphino)ferrocenyl)-1-methylamine.
PPFA = *N*,*N*-dimethyl-(2-(diphenylphosphino)ferrocenyl)-1-(methyl-1-methylamine).
BPPFA = *N*,*N*-dimethyl-(1′2-bis(diphenylphosphino)ferrocenyl)-1-(methyl-1-methylamine).

Table 2. Selected positive-ion electrospray mass spectral data for ferrocenyl phosphines with no added ionisation agents

Compound	Cone voltage (V)	Major ESMS ions (m/z, %)[a]
$FcCH_2PH_2$ (**1a**)	20	$[2M+H]^+$ (465, 12%); $[M]^+$ (232, 100%)
	50	$[M]^+$ (232, 27%); $[M-PH_2]^+$ (198, 38%); unknown (101, 100%)
	90	$[M-PH_2]^+$ (198, 38%)
$FcCH_2PPh_2$ (**1b**)	20	$[3M+Ag]^+$ (1261, 17%); $[M+Ag+CH_3CN+NO_3+H]^+$ (593, 78%); $[M+Ag+CH_3CN]^+$ (532, 24%); $[M+Ag]^+$ (491, 28%); $[M(O)+H+H_2O]^+$ (419, 33%); $[M(O)+H]^+$ (401, 57%); $[M+H]^+$ (385, 100%); unknown (288, 22); unknown (203, 26%)
	50	unknown (965, 20%); $[2M+Ag]^+$ (875, 100%); $[M(O)+H]^+$ (401, 12%); $[M+H]^+$ (385, 18%); unknown (233, 11); $[M-PPh_2]^+$ (198, 33%)
	90	unknown (965, 21%); $[2M+Ag]^+$ (875, 12%); unknown (351, 11%); $[M(O)-Cp^a]^+$ (335, 17%); $[M-PPh_2]^+$ (198, 100%)
$FcCH_2P(CH_2OH)_2$ (**1c**)	20	$[M(O)+H]^+$ (309, 5%); $[M+H]^+$ (293, 100%)
	50	$[M]^+$ (292, 7%)
	90	$[M-P(CH_2OH)_2]^+$ (198, 100%)
		$[M-P(CH_2OH)_2]^+$ (198, 100%)
DPF (**2a**)	20	$[3M+Ag]^+$ (1219, 13%); $[2M+Ag]^+$ (847, 6%); $[M(O)+H]^+$ (387, 19%); $[M+H]^+$ (371, 100%); $[M]^+$ (370, 20%); $[M-PPh_2+H]^+$ (186, 10%)
	50	$[2M+Ag]^+$ (847, 6%); $[M(O)+H]^+$ (387, 12%); $[M+H]^+$ (371, 100%); $[M]^+$ (370, 55%); $[M-PPh_2+H]^+$ (186, 26%)
	90	$[2M+Ag]^+$ (847, 65%); $[M+Ag]^+$ (477, 10%); $[M(O)+H]^+$ (387, 46%); $[M]^+$ (370, 28%); $[FeC_5H_4P(O)Ph_2]^+$ (321, 36%); $[FeC_5H_4PPh_2]^+$ (305, 5%); $[M-Ph]^+$ (293, 58%); $[M-PPh_2+H]^+$ (186, 100%)
DPPF (**2b**)	20	$[2M+Ag]^+$ (1217, 100%)
	50	$[2M+Ag]^+$ (1217, 100%); $[2M-PPh_2+Ag]^+$ (1033, 7%); $[M+Ag]^+$ (661, 5%); $[M-PPh_2+H]^+$ (370, 100%)
DPPF (**2b**)	90	$[2M+Ag]^+$ (1217, 5%); $[M+Ag]^+$ (661, 100%)
PFMA (**3a**)	20	$[M(S)+H]^+$ (460, 4%); $[M(O)+H]^+$ (444, 6%); $[M+H]^+$ (428, 100%); $[M-NMe_2]^+$ (383, 4%); $[C_5H_3(CH)PPh_2]^+$ (261, 11%)
	50	$[M+H]^+$ (428, 4%); $[M]^+$ (427, 13%); $[M(O)-NMe_2]^+$ (399, 5%); $[M-NMe_2]^+$ (383, 100%)
	90	$[2M+Ag]^+$ (961, 4%); $[M+Ag]^+$ (533, 3%); $[M(O)-NMe_2]^+$ (399, 9%); $[M-NMe_2]^+$ (383, 98%); $[M-NMe_2-Cp]^+$ (318, 100%); $[FeC_5H_4PPh_2]^+$ (305, 26%); $[C_5H_3(CH_2)PPh_2]^+$ (262, 6%)
BPPA (**3b**)	20	unknown (998, % variable); $[M(O)_2+H]^+$ (644, 29%); $[M(O)+H]^+$ (628, 43%); $[M+H]^+$ (612, 100%); $[FcP(O)Ph_2+H]^+$ (387, % variable)
	50	$[M(O)_2+H]^+$ (644, 16%); $[M(O)+H]^+$ (628, 54%); $[M+H]^+$ (612, 11%); $[M(O)_2-NMe_2]^+$ (599, 21%); $[M(O)-NMe_2]^+$ (583, 23%); $[M-NMe_2]^+$ (567, 100%)
	90	$[M+Ag]^+$ (718, 10%); $[M(O)_2-NMe_2]^+$ or $[M(S)-NMe_2]^+$ (599, 21%); $[M(O)-NMe_2]^+$ (583, 37%); $[M-NMe_2]^+$ (567, 100%); $[M-NMe_2-PPh_2]^+$ (382, 96%); $[FeC_5H_4P(S)Ph_2]^+$ (337, 32%); $[FeC_5H_4P(O)Ph_2]^+$ (321, 83%); $[FeC_5H_4PPh_2]^+$ (305, 48%)
PPFA (**4a**)	20	$[M(O)_2+H]^+$ (474, 29%); $[M(O)+H]^+$ (458, 100%)
	50	$[M(O)+H]^+$ (458, 29%); $[M(O)_2-NMe_2]^+$ (429, 42%); $[M(O)-NMe_2]^+$ (413, 100%)
	90	$[M(O)-NMe_2]^+$ (413, 66%); $[M(O)-NMe_2-Cp]^+$ (348, 54%); $[M-NMe_2-PPh_2]^+$ (212, 100%); $[P(O)Ph_2]^+$ (201, 15%)
BPPFA (**4b**)	20	$[M(O)_2+H]^+$ (658, 7%); $[M(O)+H]^+$ (642, 8%); $[M+H]^+$ (626, 100%); $[M-NMe_2]^+$ (581, 9%)
		$[2M+Ag]^+$ (1359, 11%); $[M+Ag]^+$ (732, 20%); $[M(O)_2-NMe_2]^+$ or $[M(S)-NMe_2]^+$ (613, 26%)
	50	$[M(O)-NMe_2]^+$ (597, 17%); $[M-NMe_2]^+$ (581, 100%); $[M(O)-NMe_2-PPh_2]^+$ (412, 12%); $[M-NMe_2-PPh_2]^+$ (396, 29%)
		$[M+Ag]^+$ (732, 18%); $[M-NMe_2H+Ag]^+$ (687, 16%); $[M(S)_2-NMe_2]^+$ (645, 7%); $[M(O)(S)-$
	90	$NMe_2]^+$ (629, 11%); $[M(O)_2-NMe_2]^+$ or $[M(S)-NMe_2]^+$ (613, 22%); $[M(O)-NMe_2]^+$ (597, 20%); $[M-NMe_2]^+$ (581, 62%); $[M(S)-NMe_2-PPh_2]^+$ (428, 17%); $[M(O)-NMe_2-PPh_2]^+$ (412, 31%); $[M-NMe_2-PPh_2]^+$ (396, 100%); $[M-NMe_2-2PPh_2+H]^+$ (212, 17%)

[a] m/z values quoted are for the major peak in the isotope distribution pattern.

ferrocene compound. More intense $[M]^+$ ions were observed at higher cone voltages and are presumed to be due to electrochemical oxidation of Fe^{II} to Fe^{III}. Higher cone voltages also appear to facilitate oxidation of the phosphine function to form $[M(O)+H]^+$ ions. Dominant fragment ions $[M-NMe_2]^+$ and $[M(O)-NMe_2]^+$, which are stable carbonium ions (structures **6a, 6b, 7a** and **7b**), were observed at higher cone voltages, resulting from the cleavage of the CH_2—N bond in the amino ferrocenyl phosphines. This fragmentation pathway has also been reported for $FcCH_2NMe_2$ [8]. Predictably, the same stable carbonium fragment ion $[FcCH_2]^+$ **5** (*m/z* 198) was observed at higher cone voltages for those ferrocenylmethyl phosphines in which the phosphine function is separated from the cyclopentadienyl ring by a methylene unit.

Of interest was the appearance of a number of ions which were shown (by their isotope patterns) to contain silver. In particular, those ferrocenyl phosphines which contain a diphenylphosphine moiety appeared to show a strong tendency to coordinate to Ag^I. $[M+Ag]^+$ and $[2M+Ag]^+$ ions were observed for DPF, DPPF, $FcCH_2PPh_2$, PFMA and BPPFA, even though no Ag^I salts had been added to the samples prior to analysis. The existence of these ions were proposed to result from adventitious silver, a contaminant in the ESMS system. Indeed, such phenomena are not uncommon; Ag^I ions have been observed lingering in the capillary system of our ESMS instrument on previous occasions. The $[3M+Ag]^+$ ion was also observed in the positive-ion ES mass spectra of DPF and $FcCH_2PPh_2$ (20 V), consistent with a coordination number of 3 for Ag^+. In the positive-ion ES mass spectrum of DPPF only the $[M+Ag]^+$ and $[2M+Ag]^+$ ions were observed, suggesting this particular ferrocenyl phosphine has a very high affinity for Ag^I. The $[2M+Ag]^+$ complex ion is consistent with known tetrahedral four-coordinate Ag^I systems, and such an observation is supported by the knowledge that DPPF is an excellent chelating ligand and has a vast coordination chemistry which has been studied in great detail [13,16].

We have previously reported the ease with which hydroxymethyl phosphonium salts may be generated from the respective neutral phosphines, for positive-ion ES mass spectral analyses [12]. As a direct consequence of this work we wished to investigate whether similar derivatives of ferrocenyl phosphines could also be formed *in situ*. The aminoalkyl ferrocenyl phosphine derivatives were subjected to a similar regime in order to obtain comparative data. Results are presented in Table 3. The positive-ion ES mass spectra of the ferrocenyl phosphonium salt derivatives proved to be less complex when compared with the ES mass spectra obtained without the addition of formaldehyde and HCl. The hydroxymethyl phosphonium cations $[M(CH_2OH)]^+$ were the major ions in the mass spectra of $FcCH_2PPh_2$, $FcCH_2P(CH_2OH)_2$ and DPF. $FcCH_2PH_2$, a primary phosphine, underwent a significant but expected transformation to the *tris*-hydroxymethyl phosphonium salt $[FcCH_2P(CH_2OH)_3]^+$ (*m/z* 323). The reagent system, formaldehyde and HCl, is employed for the synthesis of hydroxymethyl phosphonium salts from either primary, secondary or tertiary phosphines and was originally reported by Hoffman [17]. Hemiformal adducts $[M(CH_2O)_n(CH_2OH)]^+$ ($n = 1, 2$) were also observed in these mass spectra; these are not unusual for hydroxymethylphosphine derivatives [18]. Both the hydroxymethyl phosphonium salt $[M+CH_2OH]^+$ (*m/z* 585) and the *bis*-hydroxymethyl phosphonium salt $[M+2CH_2OH]^{2+}$ (*m/z* 308) of DPPF were observed but they were only minor ions in the mass spectrum. DPPF appeared to be more susceptible to fragmentation, under these conditions the $[C_5H_5PPh_2CH_2OH]^+$ ion at (*m/z* 281) being the base peak in the mass spectrum, even at relatively low cone voltages (e.g. 20 V). The same ion was observed as the base peak in the mass spectra of BPPA and BPPFA. These three ferrocenes have one feature in common, namely a PPh_2 function on each cyclopentadienyl ring. We postulate that both these phosphine functions may become modified to form the *bis*-hydroxymethyl phosphonium salt, as observed in the mass spectrum of DPPF. However, because both these positively charged phosphorus atoms are directly attached to the cyclopentadienyl ring there is a strong possibility that the delocalised π-electron density in the ring may be disturbed due to an inductive effect. This would ultimately result in weakening the π-interaction between the Fe atom and the ring, resulting in fragmentation. It is also notable that a similar effect is not observed for either DPF or PFMA whose structures in contrast to the previous ferrocenes contain only one PPh_2 function on only one of the cyclopentadienyl rings. It seems feasible to suggest that the inductive effect is not strong enough in this system to facilitate fragmentation.

As expected, the protonated ion $[M+H]^+$ (*m/z* 428) represented the base peak in the mass spectrum of the amino ferrocenyl phosphine PFMA with added CH_2O/HCl, however the phosphonium salt $[M+CH_2OH]^+$ (*m/z* 458) was also observed. Unexpectedly, the $[M+H]^+$ ion was comparatively weak in the mass spectra of the remaining amino ferrocenyl phosphines (i.e. BPPA, PPFA and BPPFA) treated with CH_2O/HCl. A significant contribution was made by the doubly-charged ions $[M+CH_2OH+H+CH_3CN+H_2O]^{2+}$ (*m/z* 259) and $[M+CH_2OH+H]^{2+}$ (*m/z* 229.5) in the mass spectrum of PFMA, which form when both the P atom and the N atom are positively charged. A similar ion $[M+CH_2OH+H]^{2+}$ (*m/z* 328.5) was observed in the mass spectrum of BPPFA. Major fragment ions $[FcCH_2]^+$ **5** (*m/z* 198) and $[M-PPh_2]^+$ (*m/z* 370), formed in the mass spectra of the ferrocenylmethyl phosphines at higher cone voltages, were similar to those reported earlier for the same compound without the addition of CH_2O/HCl. The fragment ion $[C_5H_3(CHMe)PPh_2CH_2OH]^+$ (*m/z*

Table 3. Selected positive-ion electrospray mass spectral data for ferrocenyl phosphines[a] treated with a 1 : 1 mixture of formaldehyde and HCl

Compound	Cone voltage (V)	Major ESMS ions (m/z %)[b]
$FcCH_2PH_2$ (**1a**)	20	$[M+3CH_2O+CH_2OH]^+$ (353, 15%); $[M+2CH_2O+CH_2OH]^+$ (323, 100%)
	50	$[M+2CH_2O+CH_2OH]^+$ (323, 15%); $[M-PH_2]^+$ (198, 100%)
	90	$[M-PH_2]^+$ (198, 100%)
$FcCH_2PPh_2$ (**1b**)	20	$[M+CH_2O+CH_2OH]^+$ (445, 8%); $[M+CH_2OH]^+$ (415, 100%)
	50	$[M+CH_2OH]^+$ (415, 27%); $[P(O)Ph_2]^+$ (201, 5%); $[M-PPh_2]^+$ (198, 26%); unknown (142, 100%)
	90	$[M-PPh_2]^+$ (198, 100%)
$FcCH_2P(CH_2OH)_2$ (**1c**)	20	$[M+CH_2O+CH_2OH]^+$ (353, 62%); $[M+CH_2OH]^+$ (323, 100%)
	50	$[M+CH_2O+CH_2OH]^+$ (353, 7%); $[M+CH_2OH]^+$ (323, 11%); $[M-P(CH_2OH)_2]^+$ (198, 100%)
	90	$[M-P(CH_2OH)_2]^+$ (198, 100%)
DPF (**2a**)	20	$[M+CH_2O+CH_2OH]^+$ (431, 9%); $[M+CH_2OH]^+$ (401, 100%); $[C_5H_5PPh_2CH_2OH]^+$ (281, 68%)
	50	$[M+CH_2O+CH_2OH]^+$ (431, 6%); $[M+CH_2OH]^+$ (401, 100%); $[C_5H_5PPh_2CH_2OCH_2OH]^+$ (311, 6%); $[C_5H_5PPh_2CH_2OH]^+$ (281, 63%)
	90	$[M]^+$ (370, 18%); $[FeC_5H_4PPh_2]^+$ (305, 100%); $[M-Ph]^+$ (293, 11%)
DPPF (**2b**)	20	$[M(O)+CH_2OH]^+$ (601, 7%); $[M+CH_2OH]^+$ (585, 7%); $[M+2CH_2OH]^{2+}$ (308, 22%); $[C_5H_5PPh_2CH_2OH]^+$ (281, 100%)
	50	$[M+H]^+$ (555, 10%); $[FeC_5H_4PPh_2]^+$ (305, 7%); $[C_5H_5PPh_2CH_2OH]^+$ (281, 100%); $[C_5H_5PPh_2H]^+$ (251, 9%)
	90	$[M+H]^+$ (555, 12%); $[M(O)-PPh_2+H]^+$ (386, 83%); $[M-PPh_2+H]^+$ (370, 100%); $[M(O)-PPh_2-Cp]^+$ (321, 10%); $[FeC_5H_4PPh_2]^+$ (305, 10%); $[C_5H_5PPh_2H]^+$ (251, 9%)
PFMA (**3a**)	20	$[M+CH_2OH+CH_3CN+H_2O]^+$ (517, 11%); $[M+CH_2OH]^+$ (458, 20%); $[M(O)+H]^+$ (444, 8%); $[M+H]^+$ (428, 100%); $[C_5H_3(CH_2)PPh_2CH_2OH]^+$ (293, 29%); unknown (273, 72%); $[M+CH_2OH$
PFMA (**3a**)		$+H+CH_3CN+H_2O]^{2+}$ (259, 67%); $[M+CH_2OH+H]^{2+}$ (229.5, 40%)
	50	$[M+H]^+$ (428, 12%); $[M-NMe_2]^+$ (383, 100%); $[C_5H_3(CH_2)PPh_2CH_2OH]^+$ (293, 27%); unknown (273, 47%); $[M+CH_2OH+H+CH_3CN+H_2O]^{2+}$ (259, 65%)
	90	$[M+H]^+$ (428, 16%); $[M-NMe_2]^+$ (383, 62%); $[M(O)-NMe_2-Cp]^+$ (334, 22%); $[FeC_5H_3(CH_2)PPh_2+H]^+$ (317, 100%); $[FeC_5H_4PPh_2]^+$ (305, 33%); $[M+CH_2OH+H+CH_3CN+H_2O]^{2+}$ (259, 17%); $[M+CH_2OH+H+H_2O]^{2+}$ (238.5, 30%)
BPPA (**3b**)	20	$[M+CH_2OH+H]^{2+}$ (321.5, 9%); $[C_5H_5PPh_2CH_2OH]^+$ (281, 100%)
	50	$[M-NMe_2]^+$ (567, 9%); $[C_5H_5PPh_2CH_2OH]^+$ (281, 100%); $[C_5H_5PPh_2H]^+$ (251, 7%)
	90	$[M+H]^+$ (612, 12%); $[M(O)-NMe_2]^+$ (583, 12%); $[M-NMe_2]^+$ (567, 100%); $[M-NMe_2-PPh_2]^+$ (382, 29%); $[FeC_5H_4PPh_2]^+$ (305, 10%); $[FeC_5H_3PPh_2]^+$ (304, 34%); $[C_5H_5PPh_2H]^+$ (251, 16%); $[P(O)Ph_2]^+$ (201, 43%)
PPFA (**4a**)	20	$[M(O)+H]^+$ (458, 4%); $[M+H]^+$ (442, 6%); $[C_5H_3(CHMe)PPh_2CH_2OH]^+$ (307, 100%); $[PPh_2(CH_2OH)_2]^+$ (247, 42%); $[P(O)Ph_2(CH_2OH)]^+$ (233, 36%); $[PPh_2(CH_2OH)+H]^+$ (217, 35%); unknown (203, 86%)
	50	$[M(O)+H]^+$ (458, 4%); $[M(O)-NMe_2]^+$ (413, 6%); $[M-NMe_2]^+$ (397, 10%); $[C_5H_3(CHMe)PPh_2CH_2OH]^+$ (307, 100%); $[PPh_2(CH_2OH)_2]^+$ (247, 17%); $[P(O)Ph_2(CH_2OH)]^+$ (233, 40%); $[PPh_2(CH_2OH)+H]^+$ (217, 19%); unknown (203, 96%)
	90	$[M(O)+H]^+$ (458, 13%); $[M-NMe_2]^+$ (397, 11%); $[M-NMe_2-Cp]^+$ (332, 22%); $[C_5H_3(CHMe)PPh_2H]^+$ (277, 24%); $[C_5H_3(CH)PPh_2]^+$ (261, 26%); $[M-NMe_2-PPh_2]^+$ (212, 100%); unknown (203, 77%)
BPPFA (**4b**)	20	$[M+H]^+$ (626, 5%); $[M+CH_2OH+H]^{2+}$ (328.5, 27%); $[C_5H_3(CHMe)PPh_2CH_2OH]^+$ (307, 86%); $[C_5H_5PPh_2CH_2OH]^+$ (281, 100%)
	50	$[M(O)-NMe_2]^+$ (597, 36%); $[M-NMe_2]^+$ (581, 41%); $[C_5H_3(CHMe)PPh_2CH_2OH]^+$ (307, 60%); $[C_5H_5PPh_2CH_2OH]^+$ (281, 100%); $[C_5H_3(CHMe)PPh_2H]^+$ (277, 21%)
	90	$[M(O)-NMe_2]^+$ (597, 7%); $[M-NMe_2]^+$ (581, 53%); $[M(O)-PPh_2-NMe_2]^+$ (412, 15%); $[M-PPh_2-NMe_2]^+$ (396, 100%); $[FeC_5H_4PPh_2]^+$ (305, 26%); $[C_5H_3(CH(CH_3))PPh_2H]^+$ (277, 22%); $[C_5H_3(CH)PPh_2]^+$ (261, 16%); $[P(O)Ph_2]^+$ (201, 14%)

[a] For structures see Scheme 1.

[b] m/z values quoted are for the major peak in the isotope distribution pattern.

Table 4. Selected positive-ion electrospray mass spectral data for ferrocenyl phosphines[a] with added $AgNO_3$

Compound	Ag^+ Conc.[b]	Major ESMS ions (m/z, %)[c]
$FcCH_2PH_2$ (**1a**)	Low	$[2M+Ag]^+$ (571, 4%); $[M(O)+NH_4]^+$ (266, 14%); $[M]^+$ (232, 100%)
	High	$[3M+Ag]^+$ (803, 12%); $[2M+Ag]^+$ (571, 100%); $[M+Ag+CH_3CN]^+$ (380, 6%); $[M+Ag]^+$ (339, 7%); $[M]^+$ (232, 13%)
$FcCH_2PPh_2$ (**1b**)	Low	$[3M+Ag]^+$ (1261, 100%); $[2M+Ag]^+$ (875, 5%); $[M(O)+NH_4]^+$ (418, 4%); $[M(O)+H]^+$ (401, 11%); $[M]^+$ (384, 23%)
	High	$[2M+Ag]^+$ (875, 35%); $[M+Ag+CH_3CN]^+$ (532, 59%); $[M+Ag]^+$ (491, 100%); $[M]^+$ (384, 16%)
$FcCH_2P(CH_2OH)_2$ (**1c**)	Low	$[3M+Ag]^+$ (983, 100%); $[2M+Ag]^+$ (691, 51%); $[M(O)+H]^+$ (309, 11%); $[M]^+$ (292, 5%)
	High	$[2M+Ag]^+$ (691, 13%); $[M+Ag+CH_3CN]^+$ (440, 76%); $[M+Ag]^+$ (399, 100%)
DPF (**2a**)	Low	$[3M+Ag]^+$ (1219, 100%); $[2M+Ag]^+$ (847, 56%); $[M]^+$ (379, 19%)
	High	$[2M+Ag]^+$ (847, 50%); $[M+Ag+CH_3CN]^+$ (518, 100%)
DPPF (**2b**)	Low	$[2M(O)+Ag]^+$ (1249, 10%); $[M+M(O)+Ag]^+$ (1233, 49%); $[2M+Ag]^+$ (1217, 100%)
	High	$[M+NO_3+2Ag]^+$ (832, 37%); $[M(S)+Ag]^+$ or $[M(O)_2+Ag]^+$ (693, 11%); $[M(O)+Ag]^+$ (677, 40%); $[M+Ag]^+$ (661, 100%); $[M+2Ag]^{2+}$ (385, 22%)
BPPA (**3b**)	Low	$[M(S)+H]^+$ or $[M(O)_2+H]^+$ (644, 16%); $[M(O)+H]^+$ (628, 31%); $[M+H]^+$ (612, 100%)
	High	$[M(S)+Ag]^+$ or $[M(O)_2+Ag]^+$ (754, 9%); $[M+Ag]^+$ (718, 100%); $[M(O)_2+H]^+$ or $[M(S)+H]^+$ (644, 8%); $[M(O)+H]^+$ (628, 13%); $[M+H]^+$ (612, 42%)

[a] For structures see Scheme 1.
[b] For details of low and high Ag^+ concentrations refer to experimental section.
[c] m/z values quoted are for the major peak in the isotope distribution pattern.

307) was observed as the base peak in the mass spectrum of PPFA and as a major ion in the mass spectrum of BPPFA at low cone voltages. A similar ion $[C_5H_3(CH_2)PPh_2CH_2OH]^+$ (m/z 293) of low intensity was also observed in the mass spectrum of PFMA. Cleavage of the C—N bond is anticipated under these conditions to form the carbonium ion $[M-NMe_2]^+$ observed in the mass spectrum of BPPFA and PPFA at higher cone voltages and is likely to be more stable than the equivalent ion formed from BPPA or PFMA. Further fragmentation is likely to result for BPPFA to form the m/z 307 ion for reasons discussed earlier, however no explanation can be given for the existence of the same ion in the mass spectrum of PPFA. At high cone voltages cleavage of the C—P bond of the diphenylphosphino group and the cyclopentadienyl ring of the ferrocenes (**2–4**) was observed, rather than loss of a cyclopentadienyl moiety. This alternative fragmentation route becomes available at higher cone voltages and is consistent with the knowledge that such a process requires more energy than the cleavage of either a C—N bond or loss of a cyclopentadienyl moiety.

$[M+Ag]^+$ and $[2M+Ag]^+$ ions were observed in the positive-ion ES mass spectra of a number of ferrocenyl phosphines due to adventitious Ag^+ in the ESMS system. This information, in addition to supporting evidence from previous studies [10,12], suggested that the deliberate addition of Ag^I may aid in characterisation of ferrocenyl phosphines. A number of the ferrocenyl phosphines were treated with an aqueous solution of $AgNO_3$ and the positive-ion ES mass spectra recorded at a cone voltage of 20 V. Data is given in Table 4. All of the ferrocenylmethyl phosphines (**1**) showed $[3M+Ag]^+$, $[2M+Ag]^+$ and $[M+Ag]^+$ ions. Typically the $[3M+Ag]^+$ and $[2M+Ag]^+$ ions were dominant at low Ag^+ concentrations, however upon increasing the Ag^+ concentration, the $[2M+Ag]^+$ and $[M+Ag]^+$ ions become more prominent. This observation is demonstrated by comparison of the positive-ion ES mass spectra of $FcCH_2PPh_2$ with added $AgNO_3$, as depicted in Fig. 2 [(a): high Ag^+ concentration, (b): low Ag^+ concentration]. Both $[M(O)+H]^+$ and $[M]^+$ ions were observed in nearly all the mass spectra, however they were predominantly of low intensity with the exception of $FcCH_2PH_2$ and BPPA. The primary phosphine, $FcCH_2PH_2$, seemed particularly sensitive to the mild oxidising properties of Ag^+, the $[M]^+$ ion constituting the major peak in the mass spectrum at low Ag^+ concentration. For **1b** a highly characteristic aggregate ion $[M+Ag+CH_3CN]^+$ (m/z 532) was also recorded, a familiar feature of all positive-ion ES mass spectra when employing $AgNO_3$ as a reagent [13]. The major ion observed in the ES mass spectrum of BPPA at low Ag^+ concentration was the $[M+H]^+$ (m/z 612) ion, however the $[M+Ag]^+$ (m/z 718) ion dominates at higher Ag^+ concentrations. For aminoferrocenyl phosphines there appears to be competition between the protonation pathway which results in the formation of the $[M+H]^+$ ion and the complexation pathway to form either the $[M+Ag]^+$ or $[2M+Ag]^+$

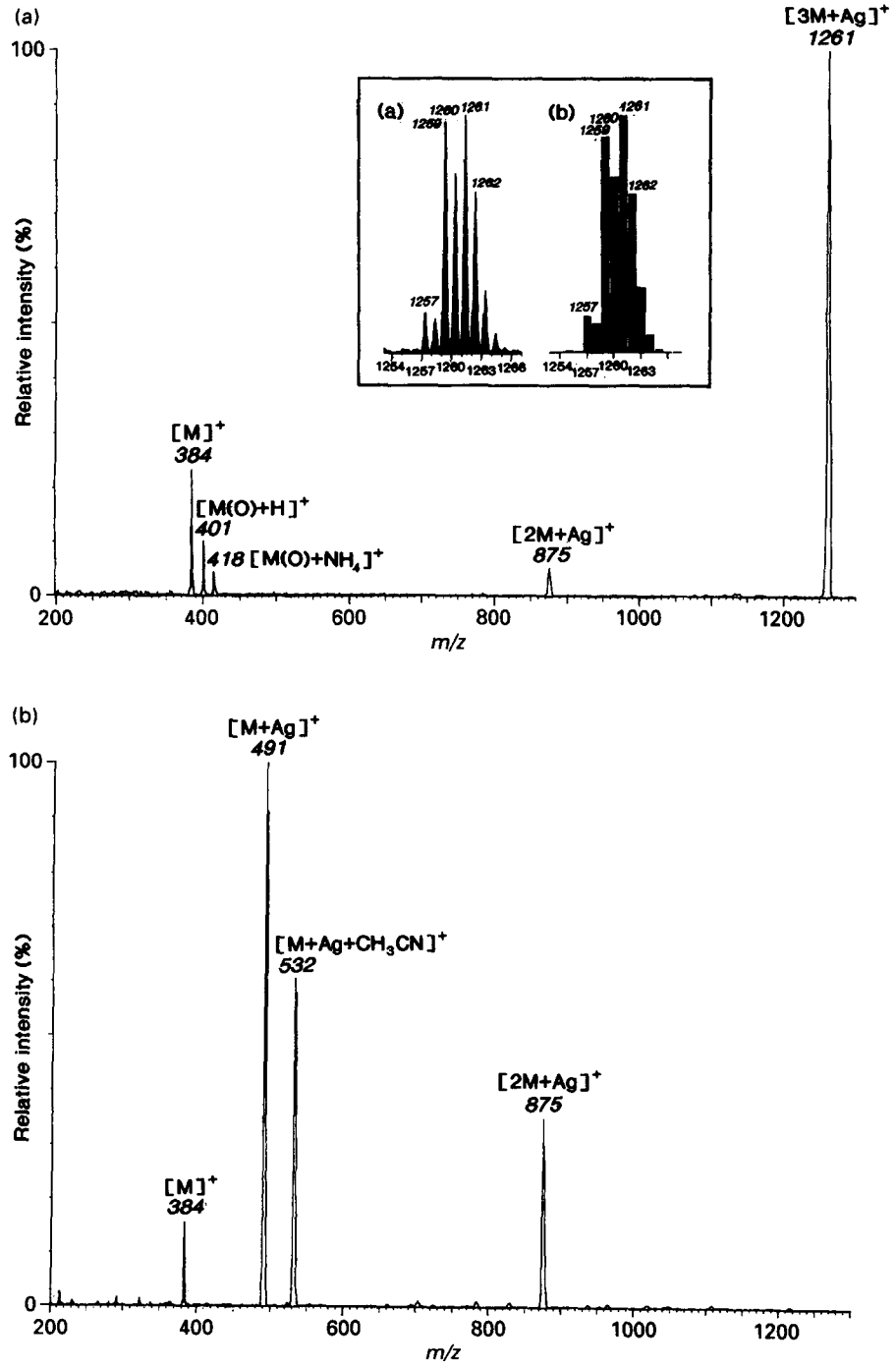

Fig. 2. Positive-ion ES mass spectra (cone voltage 20 V) of $FcCH_2PPh_2$ dissolved in 1 : 1 acetonitrile–water solution, with addition of $AgNO_3$. (a) Low concentration of Ag^+; (b) high concentration of Ag^+. M refers to $FcCH_2PPh_2$. The inset shows: (a) observed and (b) calculated isotope patterns for the $[3M+Ag]^+$ ion (*m/z* 1261).

ions. When the Ag^+ concentration is relatively low the protonation pathway appears to dominate.

CONCLUSIONS

Sulfonated phosphines may be easily characterised by negative-ion ESMS, as expected. Intense signals are observed for the singly-, doubly- and triply-charged phosphines and their oxides of TPPMS, TPPDS and TPPTS respectively. Singly- and doubly-charged sodium, protonated or ammonium adducts of the phosphines and their oxides are easily identified by analysis of the isotope patterns. Characterisation may be facilitated by the addition of formic acid or to a lesser extent, following the addition of an aqueous solution of $AgNO_3$.

A strong phosphonium ion, $[M(CH_2OH)]^+$ appears in the positive-ion mass spectra of those ferrocene phosphines that contain only one phosphine group, following the addition of formaldehyde and HCl. Amino ferrocenyl phosphines do not require such a reagent, forming strong $[M+H]^+$ ions in the positive-ion mass spectra. Fragment ions become pronounced for both the amino ferrocenyl phosphines and those ferrocenyl phosphines which contain more than one phosphine function, following the addition of formaldehyde and HCl. Silver complexes, $[3M+Ag]^+$, $[2M+Ag]^+$ and $[M+Ag]^+$, which have distinctive isotope patterns, were commonly recorded in the positive-ion ES mass spectra for the ferrocenylmethyl phosphines treated with $AgNO_3$. Both reagents therefore aid in identification and help to alleviate the difficulties associated with distinguishing between $[M]^+$ and $[M+H]^+$ ions which are common to the positive-ion ES mass spectra of ferrocenyl phosphines.

Acknowledgements—This work was supported by the University of Waikato and the Cancer Society of New Zealand. Samples of TPPTS, TPPMS and a number of ferrocenyl phosphine derivatives were kindly supplied by Professors B. H. Robinson and J. Simpson, University of Otago. We would also like to thank Mr Nick Goodwin who provided samples of $FcCH_2PPh_2$, $FcCH_2PH_2$ and $FcCH_2P(CH_2OH)_2$. We also acknowledge the New Zealand Lottery Grants Board for a grant-in-aid towards the purchase of an electrospray mass spectrometer, and Wendy Jackson for technical assistance.

REFERENCES

1. See for example: Dias, P. B., de Piedade, M. E. M. and Simões, J. A. M., *Coord. Chem. Rev.*, 1994, **135/136**, 737; Mayer, H. A. and Kaska, W. C., *Chem. Rev.*, 1994, **94,** 1239; Newkome, G. R., *Chem. Rev.*, 1993, **93,** 2067; Cotton, F. A. and Hong, B., *Prog. Inorg. Chem.*, 1992, **40,** 179; Bader, A. and Lindner, E., *Coord. Chem. Rev.*, 1991, **108,** 27; Hartley, F. R., ed., *The Chemistry of Organophosphorus Compounds*, Vol. 1. Wiley, New York, 1990.
2. See for example: Horváth, I. T. and Rábai, J., *Science*, 1994, **266,** 72; Brown, J. M., *Chem. Soc. Rev.*, 1993, **93,** 25; Sawamura, M. and Ito, Y., *Chem. Rev.*, 1992, **92,** 857; Noyori, R., *Chemtech.*, 1992, **22,** 360.
3. Herrmann, W. A. and Kohlpaintner, C. W., *Angew. Chem. Int. Ed. Engl.*, 1993, **32,** 1524 and references therein; Barton, M. and Atwood, J. D., *J. Coord. Chem.*, 1991, **24,** 43; Sinou, D., *Bull. Soc. Chim. Fr.*, 1987, 480.
4. Kuntz, E. G., 1987, *Chemtech.*, **17,** 570; Cornils, B. and Wiebus, E., *Rec. Trav. Chim. Pays-Bas*, 1996, **115,** 211.
5. See: Hop, C. E. C. A. and Bakhtiar, R., *J. Chem. Educ.*, 1996, **73,** A162, and references therein; Colton, R., D'Agostino, A. and Traeger, J. C., *Mass Spectrom. Rev.*, 1995, **14,** 79, and references therein.
6. See: Przybylski, M. and Glocker, M. O., *Angew. Chem. Int. Ed. Engl.*, 1996, **35,** 807; Smith, R. D., Loo, J. A., Ogorzalek Loo, R. R., Busman, M. and Udseth, H. R., *Mass Spectrom. Rev.*, 1991, **10,** 359; Smith, R. D., Loo, J. A., Edmonds, C. J., Bavinga, C. J. and Udseth, H. R., *Analyt. Chem.*, 1990, **62,** 882; Fenn, J. B., Mann, M., Meng, C. K., Wong, S. F. and Whitehouse, C. M., *Mass Spectrom. Rev.*, 1990, **9,** 37; Fenn, J. B., Mann, M., Meng, C. K., Wong, S. F. and Whitehouse, C. M., *Science*, 1989, **246,** 64; Wong, S. F., Meng, C. K. and Fenn, J. B., *J. Phys. Chem.*, 1988, **92,** 546; Whitehouse, C. M., Dreyer, R. M., Yamashita, M. and Fenn, J. B., *Analyt. Chem.*, 1985, **57,** 675.
7. For selected examples see: Henderson, W., McIndoe, J. S., Nicholson, B. K. and Dyson, P. J., *Chem. Commun.*, 1996, 1183; Henderson, W. and Nicholson, B. K., *Polyhedron*, 1996, **15,** 4015; Ferrer, M., Reina, R., Rossell, O., Seco, M. and Segalés, G., *J. Organomet. Chem.*, 1995, **515,** 205; Russell, K. C., Leize, E., Van Dorsselaer, A. and Lehn, J.-M., *Angew. Chem. Int. Ed. Engl.*, 1995, **34,** 209. Arakawa, R., Matsuo, K., Ohno, T. and Haga, M., *Inorg. Chem.*, 1995, **34,** 2464; Marken, F., Bond, A. M. and Colton, R., *Inorg. Chem.*, 1995, **34,** 1075; Bond, A. M., Colton, R., Mah, Y. A. and Traeger, J. C., *Inorg. Chem.*, 1994, **33,** 2548; Caudle, M. T., Stevens, R. D. and Crumbliss, A. L., *Inorg. Chem.*, 1994, **33,** 6111; Dakternieks, D., Zhu, H., Tiekink, E. R. T. and Colton, R., *J. Organomet. Chem.*, 1994, **476,** 33; Stewart, I. I. and Horlick, G., *Analyt. Chem.*, 1994, **66,** 3983.
8. Henderson, W., Oliver, A. G. and Downard, A. J., *Polyhedron*, 1996, **15,** 1165.
9. Xu, X., Nolan, S. P. and Cole, R. B., *Analyt. Chem.*, 1994, **66,** 119.
10. Canty, A. J. and Colton, R., *Inorg. Chim. Acta*, 1994, **220,** 99.
11. Colton, R., Traeger, J. C. and Harvey, J., *Org. Mass. Spectrom.*, 1992, **27,** 1030.
12. Henderson, W. and Olsen, G. M., *Polyhedron*, 1996, **15,** 2105.
13. Gan, K.-S. and Hor, T. S. A., *Ferrocenes: Homogeneous, Catalysis, Organic Synthesis, Materials Science* (ed. A. Togni and T. Hayashi), VCH Publishers, Weinheim, 1995, pp. 3–96; Butler, I. R., Cullen, W. R., Rettig, S. J. and White, A. S. C., *J. Organomet. Chem.*, 1995, **492,** 157; Togni, A.,

Breutel, C., Schnyder, A., Spindler, F., Landert, H. and Tijani, A., *J. Am. Chem. Soc.*, 1994, **116,** 4062; Kagan, H. B., Diter, P., Gref, A., Guillaneux, D., Masson-Szymczak, A., Rebiere, F., Riant, O., Samuel, O. and Taudien, S., *Pure Appl. Chem.*, 1996, **68,** 29.

14. Duffy, N. W., McAdam, C. J., Robinson, B. H. and Simpson, J., *Inorg. Chem.*, 1994, **33,** 5343; Hill, D. T., Girard, G. R., McCabe, F. L., Johnson, R. K., Stupik, P. D., Zhang, J. H., Reiff, W. M. and Eggleston, D. S., *Inorg. Chem.*, 1989, **28,** 3529. Viotte, M., Gautheron, B., Nifant'ev, I. and Kuz'mina, L. G., *Inorg. Chim. Acta*, 1996, **253,** 71.
15. Bartik, T., Bartik, B., Hanson, B. E., Guo, I. and Tóth, I., *Organometallics*, 1993, **12,** 164; Larpent, C., Dabard, R. and Patin, H., *Inorg. Chem.*, 1987, **26,** 2922; Kuntz, E. G., French Patent 2314910, 20.06, 1975 and U.S. Patent Re 31812, 29.05, 1982; Ahrland, S., Chatt, J., Davies, N. and Williams, N., *J. Chem. Soc.*, 1958, 276.
16. For selected recent references see: Casagrande, O. L. Jr, Gerbase, A. E., Stedile, F. C., da Cunha, F. O. V., Amaral, L. and Baumvol, I. J. R., *Polyhedron*, 1997, **16,** 171; Avent, A. G., Bedford, R. B., Chaloner, P. A., Dewa, S. Z. and Hitchcock, P. B., *J. Chem. Soc., Dalton Trans.*, 1996, 4633; Yam, V. W.-W., Choi, S. W.-K. and Cheung, K.-K., *J. Chem. Soc., Dalton Trans.*, 1996, 3411; Li, G., Li, S., Tan, A. L., Yip, W.-H., Mak, T. C. W. and Hor, T. S. A., *J. Chem. Soc., Dalton Trans.*, 1996, 4315; Zanello, P., Opromolla, G., Giorgi, G., Sasso, G. and Togni, A., *J. Organomet. Chem.*, 1996, **506,** 61; Munyejabo, V., Damiano, J.-P., Postel, M., Bensimon, C. and Roustan, J. L., *J. Organomet. Chem.*, 1995, **491,** 61; Zhou, M., Xu, Y., Tan, A.-M., Leung, P.-H., Mok, K. F., Koh, L.-L. and Hor, T. S. A., *Inorg. Chem.*, 1995, **34,** 6425.
17. Hoffman, A., *J. Am. Chem. Soc.*, 1921, **43,** 1684.
18. Vullo, W. J., *J. Org. Chem.*, 1968, **33,** 3665.
19. Goodwin, N. J., Henderson, W. and Sarfo, J. K., *Chem. Commun.*, 1996, 1551.
20. Goodwin, N. J., Henderson, W. and Nicholson, B. K., *Chem. Commun.*, 1997, 31.
21. Marr, G. and White, T., *J. Chem. Soc., Perkin I*, 1973, 1955; Pauson, P. L. and Watts, W. E., *J. Chem. Soc.*, 1963, 2990; Charrier, C. and Mathey, F., *Tetrahedron Lett.*, 1978, 2407; Marr, G., Wakefield, R. J. and White, T. M., *J. Organomet. Chem.*, 1975, **88,** 357.
22. Arnold, L. J., *J. Chem. Educ.*, 1992, **69,** 811.

Pergamon

PII: S0277-5387(97)00355-0

Polyhedron Vol. 17, No. 4, pp. 589–597, 1998
© 1998 Elsevier Science Ltd
All rights reserved. Printed in Great Britain
0277-5387/98 $19.00+0.00

The exceptional structural versatility of 2,2′-dipyridylamine (Hdpa) and its ions $[dpa]^-$ and $[H_2dpa]^+$

F. Albert Cotton,*[a] Lee M. Daniels,[a] Glenn T. Jordan IV[a] and Carlos A. Murillo*[a,b]

[a] Laboratory for Molecular Structure and Bonding, Department of Chemistry, Texas A&M University, College Station, TX 77843-3255, U.S.A.

[b] Department of Chemistry, University of Costa Rica, Ciudad Universitaria, Costa Rica

(Received 16 June 1997; accepted 8 July 1997)

Abstract—This report describes several cobalt compounds that contain 2,2′-dipyridylamine (Hdpa) and its ionic forms, dpa^- and H_2dpa^+. It was carried out with the aim of structurally characterizing various coordination modes of such species. The reaction of two equivalents of Hdpa with one equivalent of $[Co(H_2O)_6](ClO_4)_2$ produces the octahedral complex $[Co(Hdpa)_2((CH_3)_2CO)_2](ClO_4)_2$. Under mild aerobic conditions, Co(II) is oxidized to Co(III) to yield the six-coordinate peroxo bridged compound $[Co_2(Hdpa)_4(\mu\text{-}O_2)(\mu\text{-}OH)](ClO_4)_3 \cdot 3$acetone (**I**), the neutral Hdpa ligand chelates to the metal and shows significant puckering of the pyridyl rings. The tetrahedral complex, $Co(Hdpa)Cl_2$ (**II**), is prepared from the reaction of anhydrous $CoCl_2$ and Hdpa; puckering of the pyridyl groups is significantly smaller than that found for **I**. The deprotonated ligand reacts with $CoCl_2$ to produce the neutral molecule, $Co(dpa)_2$ (**III**) in which the dipyridyl groups are almost planar. The reaction of Hdpa and $[Co(H_2O)_6](ClO_4)_2$ in the presence of excess HCl yields the salt, $[H_2dpa]_2[CoCl_4]$ (**IV**). The crystal structures of **I, II, III,** and **IV** are presented. In structures **I–III,** the ligands chelate to the metal atom through the nitrogen atoms of the pyridyl rings in an anti–anti configuration. The structure of **IV** is also in an anti–anti configuration with the proton residing between the two nitrogen atoms of the pyridyl rings. © 1998 Elsevier Science Ltd

Keywords: cobalt and dipyridylamine compounds; crystal structure.

2,2′-Dipyridylamine and its anion have been observed to coordinate to metal atoms in a variety of ways [1], as shown in Fig. 1. Our own interest in this type of ligand was first stimulated by the discovery of the binding mode of type **d** in the compounds $Cu_3(dpa)_4Cl_2$ [2,3], $Cu_3(dpa)_4Br_2$ [2] and $Ni_3(dpa)_4Cl_2$ [4] by Hathaway and others. It was later reported [5] that a similar trinuclear cobalt(II) compound had an unsymmetrical chain of cobalt atoms. This peculiar observation caused us to make a first report on our work [1c]. While further investigating the cobalt system, we found a type of crystal in which the trinuclear $Co_3(dpa)_4Cl_2$ unit is present along with a mononuclear species of the type $Co(H_ndpa)_2$ [6]. From the structural data on this compound, it was not clear whether this mononuclear species was the divalent cation $Co(Hdpa)_2^{2+}$ or the neutral complex $Co(dpa)_2$. We therefore undertook a structural investigation of various binding modes of 2,2′-dipyridylamine and its ions in cobalt complexes to get an overview of the structural trends.

The complexation of Hdpa to cobalt ions has been known for a long time. For example, the synthesis of $Co(Hdpa)Cl_2$ was first published in 1957 [7]. A series of such complexes which contain four- or six-coordinate Co atoms were prepared later [8]. Early studies of complexes of Hdpa and its anion also include other elements of the first transition series, namely Fe [9], Cu [10] and Ni [11]. This report describes a complex in which the cobalt atom is six-coordinate, two four-coordinate complexes, and a compound containing the H_2dpa cation. A report on various compounds that contain linear trinuclear

* Authors to whom correspondence should be addressed.

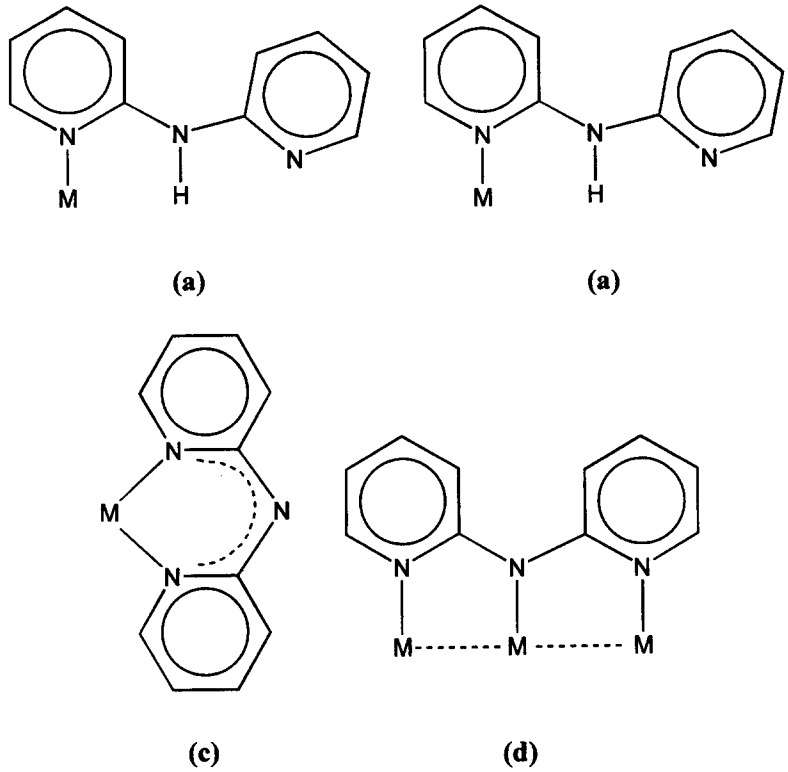

Fig. 1. A representation of the binding modes of Hdpa or its anion to metal centers.

species of the type $Co_3(dpa)_4X_2$ has already appeared [6].

EXPERIMENTAL

Materials and methods

Except where noted, all manipulations were carried out by employing standard Schlenk techniques under an atmosphere of nitrogen. Tetrahydrofuran, toluene, diethyl ether, and hexanes were freshly distilled from Na/K benzophenone and dichloromethane was distilled from P_2O_5 prior to use. Acetone was distilled from K_2CO_3, CH_3CN was distilled from CaH_2, and methanol was distilled from magnesium turnings. Dimethyl sulfoxide was used as received. Anhydrous $CoCl_2$ was purchased from Alfa and stored in the dry box. Cobalt perchlorate hexahydrate was obtained from Aldrich Chemical Company. Hdpa was also purchased from Aldrich and sublimed prior to use. Infrared spectral data were recorded as KBr pellets on a Perkin–Elmer 16PC FT-IR spectrophotometer at 2 cm^{-1} resolution. Electronic absorption spectra were measured on a Cary 17 spectrophotometer.

Preparations

Reaction of $[Co(H_2O)_6](ClO_4)_2$ *with Hdpa.* In a small Schlenk tube, 0.187 g (1.09 mmol) of Hdpa was dissolved in 5 ml of CH_3CN. In a separate Schlenk tube, 0.181 g (0.495 mmol) of $[Co(H_2O)_6](ClO_4)_2$ was dissolved in 5 ml of CH_3CN. The two solutions were mixed to give an orange solution. Diethyl ether was added to precipitate a pale orange powder. This solid was repeatedly washed with more Et_2O and then dried under vacuum. IR (KBr, cm^{-1}): 3314 (m), 3243 (w), 3207 (w), 3141 (w), 3095 (w), 2999 (w), 2937 (w), 2320 (m), 2289 (m), 1631 (vs), 1583 (s), 1525 (m), 1472 (vs), 1434 (m), 1416 (m), 1354 (m), 1268 (w), 1237 (m), 1166 (s), 1095 (vs), 1009 (s), 930 (w), 903 (m), 881 (w), 842 (w), 792 (s), 771 (s), 751 (m), 623 (s), 534 (m), 430 (m), 422 (m). While the product is only slightly soluble in CH_3CN and acetone, it was found to be soluble in acetone containing a small amount of water. A non-deoxygenated acetone solution layered with hexanes produced orange crystals of $[Co(Hdpa)_2((CH_3)_2CO)_2](ClO_4)_2$. Also produced by this diffusion method were small black crystals of $[Co_2(Hdpa)_4(\mu\text{-}O_2)(\mu\text{-}OH)]\text{-}(ClO_4)_3 \cdot 3$acetone **(I)** arising from the oxidation of Co(II) to Co(III). We made no attempts to optimize the yields, which were roughly 80% $[Co(Hdpa)_2((CH_3)_2CO)_2](ClO_4)_2$ and 5% **I**. [CAUTION: Perchlorate complexes can potentially explode and should be handled with care!]

$Co(Hdpa)Cl_2$ **(II)**. The procedure was modified from that described by Bailar and Kirschner [7]. In a 50 ml Schlenk flask, 0.318 g (2.45 mmol) of anhydrous $CoCl_2$ was dissolved in 15 ml of CH_3CN to give a royal blue solution. In a separate Schlenk flask, 0.428

g (2.50 mmol) of Hdpa was dissolved in 10 ml of CH_3CN. The Hdpa solution was added to the stirred cobalt solution via cannula; a bright blue powder immediately precipitated. Stirring was continued for several minutes, and the supernatant liquid was seen to be colorless. The mixture was filtered and the blue powder was washed with copious amounts of CH_3CN. Yield: 0.694 g (94.3%). The solid is insoluble in most organic solvents, but readily soluble in DMSO. Blue crystals were grown from a concentrated DMSO solution layered with CH_2Cl_2 and then layered with diethyl ether. IR (KBr, cm^{-1}): 3326 (w), 3299 (w), 3249 (w), 3210 (w), 3146 (w), 3118 (vw), 3092 (vw), 3063 (vw), 1640 (vs), 1617 (w), 1592 (w), 1582 (vs), 1529 (s), 1476 (vs), 1434 (s), 1422 (m), 1236 (s), 1173 (m), 1161 (s), 1023 (m), 1018 (m), 909 (m), 764 (vs), 655 (m), 520 (m), 418 (m).

$Co(dpa)_2$ (**III**). In a 100 ml round-bottom flask, 0.963 g (5.62 mmol) of Hdpa was dissolved in 30 ml of toluene. The solution was cooled to −78°C and 4.1 ml of 1.4 M CH_3Li was added. The solution immediately turned milky white. The reaction mixture was warmed to near room temperature upon which 0.344 g (2.64 mmol) of anhydrous $CoCl_2$ was added from a solid addition tube. After several minutes of stirring, 20 ml of THF was added forming a dark red-brown solution. The reaction was stirred overnight at room temperature. Most of the product precipitated from the solution as an orange powder. It was collected by filtration, washed twice with small amounts of THF, and dried under vacuum to yield 0.700 g (66.4%) of $Co(dpa)_2$. Crystals were obtained from work-up of the filtrate. The filtrate was evaporated to dryness and the residue dissolved in 25 ml of toluene to give a deep wine-red solution. This solution was filtered through Celite and layered with 40 ml of hexanes. Red crystals (0.0395 g, 3.75%) grew after two weeks of diffusion. IR (KBr, cm^{-1}): 3051 (w), 1609 (s), 1533 (s), 1440 (vs), 1250 (m), 1241 (m), 1146 (s), 1111 (w), 1095 (w), 1045 (w), 1006 (s), 894 (m), 849 (m), 786 (m), 767 (s), 733 (m), 726 (m), 656 (w), 553 (w). UV/vis (CH_2Cl_2): λ = 390 nm; 355 nm; 342 nm.

[H_2dpa]$_2$[$CoCl_4$] (**IV**). In a 50 ml Schlenk flask, 0.343 g (2.00 mmol) of Hdpa was dissolved in 6 ml of CH_3OH. In a separate flask, 0.364 g of [$Co(H_2O)_6$](ClO_4)$_2$ was dissolved in 6 ml of CH_3OH. The pink cobalt solution was added to the stirred Hdpa. The color changed from pink to orange. The solution was concentrated to 5 ml upon which a white powder began to precipitate, presumably Hdpa. Five ml of CH_3CN were added to redissolve the powder, restoring the original orange color. Aqueous 6 M HCl, 0.7 ml, was then added which immediately formed a blue solution and a blue powder. The mixture was filtered and the clear blue filtrate was layered with 20 ml of hexanes. Small sky blue crystals grew at the solvent interface after several days. IR (KBr, cm^{-1}): 3273 (w), 3243 (w), 3211 (w), 3182 (w), 3135 (w), 3082 (w), 3054 (w), 3019 (w), 2990 (w), 1653 (s), 1601 (s), 1557 (s), 1497 (m), 1481 (m), 1452 (s), 1304 (w), 1265 (w), 1243 (m), 1157 (m), 1005 (w), 982 (w), 944 (w), 897 (m), 767 (s), 688 (w), 673 (w), 530 (m). [CAUTION: Perchlorate complexes can potentially explode and should be handled with care!]

[$Co(CH_3CN)_6$][$CoCl_3(CH_3CN)$]$_2$·CH_3CN. This compound was prepared by dissolving anhydrous $CoCl_2$ in a minimal amount of CH_3CN. The resulting royal blue solution was layered with diethyl ether to produce large rectangular, royal blue crystals. These crystals are extremely solvent sensitive and rapidly turn pink in the presence of moisture.

Structure determinations

Single crystal X-ray diffraction studies of **I, II,** and **III** were carried out at −60°C with a Nonius FAST area detector, utilizing the program MADNES [12]. X-ray diffraction data for **IV** were collected on a Nonius CAD4 diffractometer at −105°C. In structures **I** and **II,** the positions of the heavy atoms were found via direct methods from the SHELXTL package [13]. In structures **III** and **IV,** the metal atoms were located by the Patterson method. For all structures, subsequent cycles of least-squares refinement followed by difference–Fourier syntheses, revealed the positions of the remaining non-hydrogen atoms. In most cases, hydrogen atoms were located in difference–Fourier maps and then refined isotropically. Other details of data collection and refinement are given in Table 1. Selected bond distances and angles for compounds **I**–**IV** are provided in Tables 2–5, respectively. Supplementary data for **I, II, III, IV** and [$Co(CH_3CN)_6$][$CoCl_3(CH_3CN)$]$_2$·CH_3CN have been deposited with the Cambridge Crystallographic Data Centre.†

RESULTS AND DISCUSSION

[Co_2(Hdpa)$_4$(μ-O_2)(μ-OH)](ClO_4)$_3$·3acetone (**I**)

The reaction of [$Co(H_2O)_6$](ClO_4)$_2$ with two equivalents of Hdpa in CH_3CN gives an orange solution from which a pale orange solid can be obtained by the addition of Et_2O. The infrared spectrum reveals N—H absorptions at 3324, 3243, and 3207 cm^{-1}, as well as strong bands at 2320 and 2289 cm^{-1} corresponding to C≡N. This product is readily soluble in acetone containing ca 5% water and gives poorly formed crystals of [Co(Hdpa)$_2$((CH_3)$_2$CO)$_2$](ClO_4)$_2$ in which a six-coordinate divalent cobalt atom is bonded to two chelating and puckered Hdpa molecules and two acetone molecules. Its identity was established by X-ray crystallography [14], but crystallographic disorder

† Supplementary material available: Tables of positional parameters for **I, II, III, IV** and [$Co(CH_3CN)_6$][$CoCl_3$(CH_3CN)]$_2$·CH_3CN, full tables of displacement parameters and molecular dimensions (39 pages).

Table 1. Crystal data and structure refinement for $[Co_2(Hdpa)_4(\mu\text{-}O_2)(\mu\text{-}OH)](ClO_4)_3 \cdot 3$acetone (**I**), $Co(Hdpa)Cl_2$ (**II**), $Co(dpa)_2$ (**III**), and $[H_2dpa]_2[CoCl_4]$ (**IV**)

Empirical formula	$C_{49}H_{55}C_{13}Co_2N_{12}O_{18}$	$C_{10}H_9Cl_2CoN_3$	$C_{20}H_{16}CoN_6$	$C_{20}H_{20}Cl_4CoN_6$
Formula weight	1324.26	301.03	399.32	545.15
Space group	$P2_1/c$	$P\bar{1}$	$I2/a$	$C2/c$
a (Å)	11.232(1)	7.363(1)	12.325(1)	14.421(5)
b (Å)	22.95(1)	8.647(2)	10/689(5)	11.097(1)
c (Å)	22.084(3)	9.387(3)	14.229(1)	14.460(5)
α (°)	90	75.14(2)	90	90
β (°)	93.22(1)	89.73(2)	107.94(1)	100.74(2)
γ (°)	90	85.84(2)	90	90
V (Å^3)	5684(3)	576.1(2)	1783.4(9)	2273(1)
Z	4	2	4	4
d_{calc} (g cm^{-1})	1.548	1.735	1.487	1.593
Crystal size (mm)	$0.18 \times 0.12 \times 0.10$	$0.30 \times 0.15 \times 0.08$	$0.18 \times 0.15 \times 0.13$	$0.22 \times 0.20 \times 0.18$
Absorption coefficient (mm^{-1})	0.807	1.925	0.980	1.246
Data collection instrument	FAST	FAST	FAST	CAD4
Radiation (monochromated in incident beam) Mo-K_α	0.71073 Å	0.71073 Å	0.71073 Å	0.71073 Å
Orientation reflections, number, range (θ)	250, 9.0–20.0	119, 6.8–20.8	214, 9.0–20.8	25, 13–19
Temperature (K)	213(2)	213(2)	213(2)	168(2)
Scan method	Frame data from ω scans	Frame data from ω scans	Frame data from ω scans	ω scans
Data collected range, θ(°)	2.18–22.55	2.24–22.47	2.43–22.53	2.33–22.45
No. unique data, total	7230	2961	1164	1466
Number of parameters refined	808	169	155	181
Final R indices [$I > 2\sigma(I)$][a,b]	$R1 = 0.070$, $wR2 = 0.154$	$R1 = 0.032$, $wR2 = 0.080$	$R1 = 0.033$, $wR2 = 0.076$	$R1 = 0.032$, $wR2 = 0.079$
R indices (all data)[a,b]	$R1 = 0.104$, $wR2 = 0.177$	$R1 = 0.035$, $wR2 = 0.085$	$R1 = 0.038$, $wR2 = 0.079$	$R1 = 0.064$, $wR2 = 0.089$
Quality-of-fit indicator[c]	1.057	1.138	1.095	1.050
Largest shift/e.s.d. final cycle	0.078	<0.001	<0.001	<0.001
Largest peak, final cycle (e Å^{-3})	0.62(9)	0.36(8)	0.31(5)	0.28(7)
Weighting coefficients **a**, **b**[b]	0.591, 29.47	0.0317, 0.6999	0.0185, 4.990	0.0506, 0.4463

[a] $R1 = \Sigma||F_0| - |F_c||/\Sigma|F_0|$.
[b] $wR2 = [\Sigma w(F_0^2 - F_c^2)^2/\Sigma w(F_0^2)^2]^{1/2}$, $w = 1/[\sigma^2(F_0^2) + (\mathbf{a} \cdot p)^2 + \mathbf{b} \cdot p]$, $p = [(F_0^2) + 2(F_c^2)]/3$.
[c] Quality-of-fit $= |\Sigma w(|F_0^2| - |F_c^2|)^2/(N_{obs} - N_{parameters})]^{1/2}$.

prevented a full refinement of the structure. However, when crystals are grown from non-deoxygenated wet acetone, a second type of crystal can also be obtained. The dark, almost black crystals are the peroxo dinuclear complex **I**; the structure of the cation is shown in Fig. 2. The molecule consists of two pseudo octahedral Co(III) metal centers. Each metal atom is attached to two chelating Hdpa ligands and the centers are united by a peroxo group and a hydroxo group. The bridging hydroxo moiety is hydrogen bonded to an interstitial acetone molecule; the O···O separation is 2.81 Å. This type of complex is well established [15] and the O—O distance of 1.390(6) Å is in the expected range [16]. Other peroxo complexes of cobalt with Hdpa have been reported [17], but they have not been structurally characterized. One attempt to do such a characterization failed since the crystals turned out to be $[Co(Hdpa)_2(CO_3)]ClO_4$ [18].

The N—Co—N bond angles for $[Co(Hdpa)_2(CO_3)]ClO_4$ and for **I** are close to 90°, as expected for a six-coordinate cobalt atom. The presence of two chelating Hdpa groups and two additional ligands in the coordination sphere forces the Hdpa ligand to adopt a configuration in which the dihedral angles between the two pyridyl groups range from 36.9 to 43.3°. The non-planarity of the Hdpa ligand is typically found in six- [19], some five- [1b,20], and four-coordinate square planar Pd complexes [21].

$Co(Hdpa)Cl_2$ (II)

In acetonitrile, $CoCl_2$ dissolves to give a deep royal blue solution which upon layering with Et_2O yields royal blue crystals of $[Co(CH_3CN)_6][CoCl_3(CH_3CN)]_2 \cdot CH_3CN$ [22]. This material is composed of octahedral $[Co(CH_3CN)_6]^{2+}$ cations and tetrahedral $[CoCl_3(CH_3CN)]^-$ anions, the dimensions of which are very similar to those previously reported for compounds containing such ions [23]. The ionic

Table 2. Selected bond lengths (Å) and angles (°) for [Co_2(Hdpa)$_4$(μ-O_2)(μ-OH)] (ClO_4)$_3$ · 3acetone (**I**)

Co(1)—O(2)	1.872(4)	Co(2)—N(9)	1.936(5)
Co(1)—O(3)	1.928(5)	Co(2)—N(12)	1.940(6)
Co(1)—N(1)	1.943(5)	Co(2)—N(10)	1.953(6)
Co(1)—N(6)	1.946(5)	Co(2)—N(7)	2.016(5)
Co(1)—N(3)	1.952(6)	O(1)—O(2)	1.390(6)
Co(1)—N(4)	2.014(6)	O(3)—H(3)	0.72(7)
Co(2)—O(1)	1.861(4)	H(3)—O(18)	2.09(7)
Co(2)—O(3)	1.929(5)		
O(2)—Co(1)—O(3)	83.8(2)	O(3)—Co(2)—N(9)	91.1(2)
O(2)—Co(1)—N(1)	90.2(2)	O(1)—Co(2)—N(12)	87.8(2)
O(3)—Co(1)—N(1)	91.7(2)	O(3)—Co(2)—N(12)	90.2(2)
O(2)—Co(1)—N(6)	92.4(2)	N(9)—Co(2)—N(12)	178.6(2)
O(3)—Co(1)—N(6)	88.7(2)	O(1)—Co(2)—N(10)	88.9(2)
N(1)—Co(1)—N(6)	177.4(2)	O(3)—Co(2)—N(10)	172.4(2)
O(2)—Co(1)—N(3)	86.6(2)	N(9)—Co(2)—N(10)	90.7(2)
O(3)—Co(1)—N(3)	170.4(2)	N(12)—Co(2)—N(10)	87.9(2)
N(1)—Co(1)—N(3)	88.2(2)	O(1)—Co(2)—N(7)	179.5(2)
N(6)—Co(1)—N(3)	91.7(2)	O(3)—Co(2)—N(7)	95.9(2)
O(2)—Co(1)—N(4)	178.6(2)	N(9)—Co(2)—N(7)	88.6(2)
O(3)—Co(1)—N(4)	97.7(2)	N(12)—Co(2)—N(7)	91.9(2)
N(1)—Co(1)—N(4)	89.8(2)	N(10)—Co(2)—N(7)	91.5(2)
N(6)—Co(1)—N(4)	87.6(2)	O(2)—O(1)—Co(2)	110.9(3)
N(3)—Co(1)—N(4)	92.0(2)	O(1)—O(2)—Co(1)	111.9(3)
O(1)—Co(2)—O(3)	83.6(2)	Co(1)—O(3)—Co(2)	119.4(3)
O(1)—Co(2)—N(9)	91.7(2)	O(3)—H(3)—O(18)	173(8)

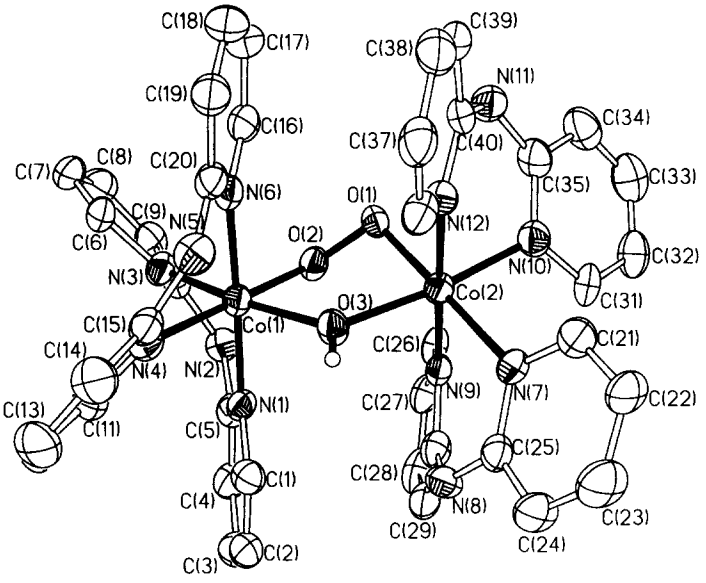

Fig. 2. Molecular structure of the cation in [Co_2(Hdpa)$_4$(μ-O_2)(μ-OH)](ClO_4)$_3$ · 3acetone (**I**).

complex [$Co(CH_3CN)_6$][$CoCl_3(CH_3CN)$]$_2$ reacts with an acetonitrile solution of Hdpa to give an insoluble blue precipitate which dissolves in DMSO to produce, upon layering with CH_2Cl_2/Et_2O, dark blue crystals of **II**.

The mononuclear complex has a distorted tetrahedral geometry as shown in Fig. 3. The angles around the cobalt atom range from 94.0 to 116.5°, which is a large deviation from the idealized angle of 109.5°. The complex is stabilized by intermolecular hydrogen

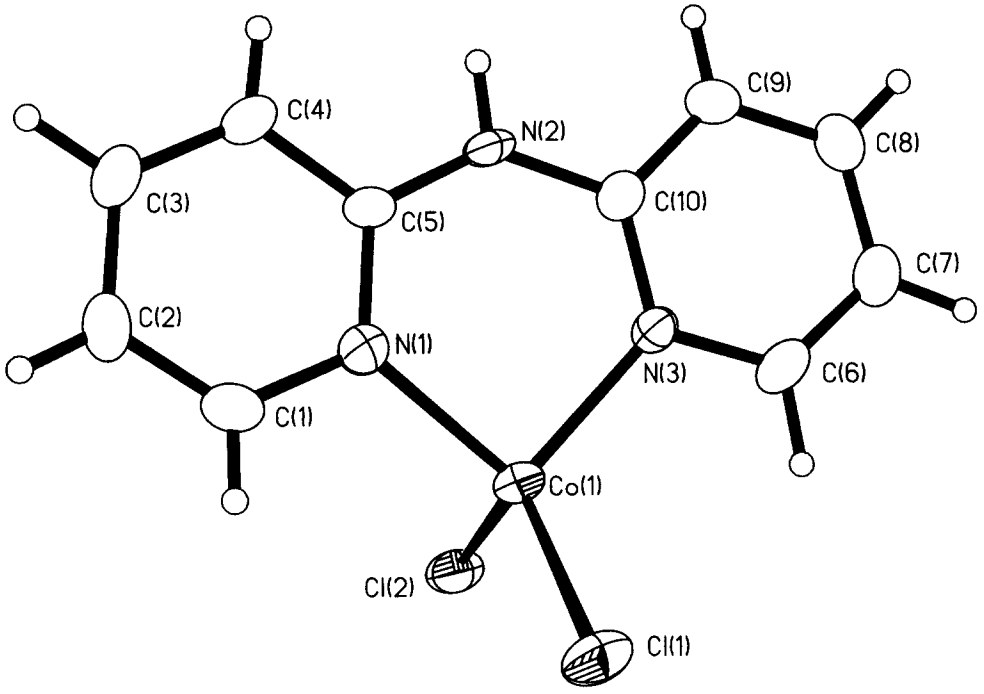

Fig. 3. Molecular structure of $Co(Hdpa)Cl_2$ (**II**).

Table 3. Selected bond lengths (Å) and angles (°) for $Co(Hdpa)Cl_2$ (**II**)

Co(1)—Cl(1)	2.220(1)	N(1)—C(5)	1.351(4)
Co(1)—Cl(2)	2.242(1)	N(2)—C(5)	1.373(4)
Co(1)—N(1)	2.008(3)	N(2)—C(10)	1.382(4)
Co(1)—N(3)	1.998(3)	N(3)—C(6)	1.356(5)
N(1)—C(1)	1.361(5)	N(3)—C(10)	1.348(4)
N(3)—Co(1)—N(1)	94.0(1)	Cl(1)—Co(1)—Cl(2)	111.17(4)
N(1)—Co(1)—Cl(1)	116.49(9)	C(5)—N(2)—C(10)	133.7(3)
N(3)—Co(1)—Cl(1)	112.79(9)	C(5)—N(1)—Co(1)	123.6(2)
N(3)—Co(1)—Cl(2)	113.29(9)	C(10)—N(3)—Co(1)	123.6(2)
N(1)—Co(1)—Cl(2)	108.1(1)		

bonding between N—H···Cl units as shown in Fig. 4. The N(2A)···Cl(2C) separation of 3.28 Å is similar to that found in complexes of the type $CoCl_2$(formamidine)$_2$ [24]. The N(1)—Co(1)—N(3) angle is only 94.0(1)°, but the small steric hindrance of the chloride ions allows the Hdpa fragment to the almost planar. The dihedral angle between the pyridyl groups is 5.6°, which is slightly smaller than that found in a copper analog (7.3°) [25]. A relatively small torsion angle is also found in copper(I) complexes such as [(Hdpa)CuI_2Cu(Hdpa)] and [Cu(Hdpa)$_2$][Cu(dpa)X_2], X = Cl, Br and I [26], but it can be slightly larger in others such as [Cu(Hdpa)$_2$]Cl in which one of the dihedral angles is 5.6° and the other is 16.7° [25,27]. However, in all pseudo-tetrahedral complexes with chelating Hdpa, there is a distinctive characteristic; the angle about the amine nitrogen attached to the pyridyl groups is in the range of 133.6 and 135.1°. This is also true for [Cu(Hdpa)$_2$]$(ClO_4)_2$ (134(1)°) [10]. This angle decreases slightly (131.1(4), 129.9(2) and 132.1(2)°) for the two polymorphs of the non-coordinated Hdpa molecule [28].

$Co(dpa)_2$ (**III**)

The reaction of Lidpa with $CoCl_2$ in a non-coordinating solvent such as toluene allows the isolation of bright red crystals of $Co(dpa)_2$, the structure of which is shown in Fig. 5. The four-coordinate cobalt atom is surrounded by two dpa anions which are related by a crystallographic 2-fold axis. The mol-

Table 4. Selected bond lengths (Å) and angles (°) for $Co(dpa)_2$ (**III**)[a]

Co(1)—N(3)	1.963(2)	H(6)—N(2B)	2.44(3)
Co(1)—N(1)	1.972(2)	C(1)—C(2)	1.354(5)
N(1)—C(1)	1.364(4)	C(2)—C(3)	1.387(5)
N(1)—C(5)	1.367(4)	C(3)—C(4)	1.353(5)
N(2)—C(5)	1.346(4)	C(4)—C(5)	1.424(4)
N(2)—C(10A)	1.344(4)	C(6)—C(7)	1.358(4)
N(3)—C(6)	1.378(4)	C(7)—C(8)	1.395(4)
N(3)—C(10)	1.371(4)	C(8)—C(9)	1.355(4)
C(1)—C(2)	1.354(5)	C(9)—C(10)	1.425(4)
C(6)—H(6)	0.97(3)		
N(3)—Co(1)—N(1)	120.66(9)	C(10)—N(3)—C(6)	118.9(2)
C(1)—N(1)—C(5)	118.6(3)	C(10)—N(3)—Co(1)	122.7(2)
C(1)—N(1)—Co(1)	118.4(2)	C(6)—N(3)—Co(1)	118.3(2)
C(5)—N(1)—Co(1)	122.8(2)	C(6)—H(6)—N(2B)	177(2)
C(5)—N(2)—C(10A)	128.2(2)		

[a] Atoms labeled with "A" are generated by a 2-fold axis and the atoms labeled as "B" correspond to an amido nitrogen from a neighboring molecule.

Table 5. Selected bond lengths (Å) and angles (°) for $[H_2dpa]_2[CoCl_4]$ (**IV**)

Co(1)—Cl(2)	2.266(1)	N(2)—C(10)	1.391(5)
Co(1)—Cl(1)	2.280(1)	N(2)—H(10)	1.06(7)
N(1)—C(1)	1.361(5)	N(1)—H(11)	1.33(3)
N(2)—C(5)	1.372(5)	N(3)—H(11)	1.36(3)
Cl(2)—Cl(1)—Cl(1)	109.68(4)	C(5)—N(2)—C(10)	129.2(4)
C(5)—N(1)—H(11)	103(1)	C(10)—N(2)—H(10)	114(4)
C(10)—N(3)—H(11)	105(1)	C(5)—N(2)—H(10)	117(4)

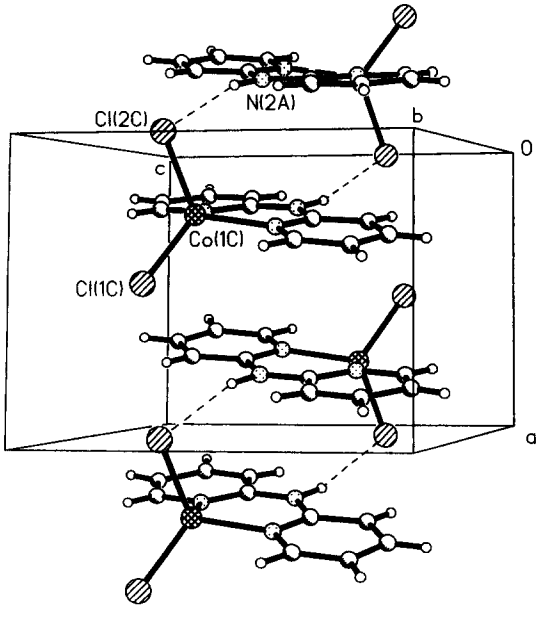

Fig. 4. Packing diagram of $Co(Hdpa)Cl_2$ (**II**) showing the hydrogen bonding.

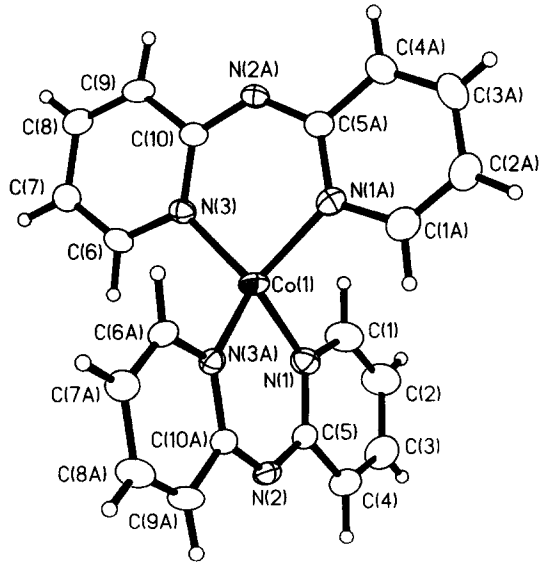

Fig. 5. Molecular structure of $Co(dpa)_2$ (**III**).

ecules pack in such a way as to show significant C—H···N interactions [29]. The C(6)···N(2B) separation is 3.41(3) Å and the N(2B)···H(6) distance is 2.44(3) Å. The nearly planar dpa^- anions display a torsion angle of the pyridyl groups of 3.6° and a C—N—C angle of 128.2(2)° at the bridging nitrogen. This angle is significantly smaller than those found in pseudo tetrahedral complexes where the neutral Hdpa molecule serves as a ligand (*vide supra*). The equivalent angles are even smaller (127.9°) in the copper analog [30] and in a Cu(3,3′-dimethyldpa)$_2$ [31] complex (128.1°). The N(1)—Co—N(3A) angle in **III** is 94.5(1)°, which is similar to that found in **II**.

It is reasonable to expect a decrease of the pyridyl—N—pyridyl angle for the anionic ligand relative to the neutral ligand since the lone pair of electrons would be expected to push the rings more strongly than a hydrogen atom. Another important observation is that there exists a marked difference in the C—C distances of the pyridyl rings with alternating long and short distances (see Table 3) which is very possibly due to the contribution of canonical forms such as **b**, which tends to localize single and double bonds.

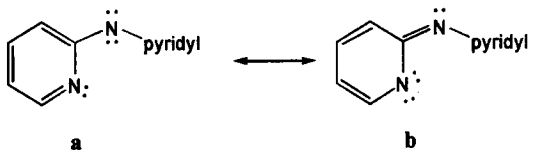

a **b**

$[H_2dpa]_2[CoCl_4]$ (**IV**)

From the reaction mixture which contained $[Co(H_2O)_6][ClO_4]_2$, neutral Hdpa and an acidic solution of HCl in a methanol/acetonitrile mixture, sky blue crystals of a cation containing H_2dpa^+ species can be isolated. A drawing of an H_2dpa^+ cation and the corresponding $CoCl_4^{2-}$ anion is shown in Fig. 6. The anion dimensions are typical [32] of those found for other tetrahedral tetrachlorocobaltate species. The additional proton is located between the atoms N(1) and N(3) which provides certain similarities to the metal chelated dpa and Hdpa species. The torsion angle between the pyridyl groups is 7.0° and the angle of 129.2(4)° for the C(5)—N(2)—C(10) unit is smaller than the corresponding angle formed by the chelating Hdpa groups but larger than those found in complexes containing chelating anionic dpa groups. The ions pack in the crystal forming hydrogen bonds between the N(2)—H groups and a chloride ion of the $CoCl_4^{2-}$ anion.

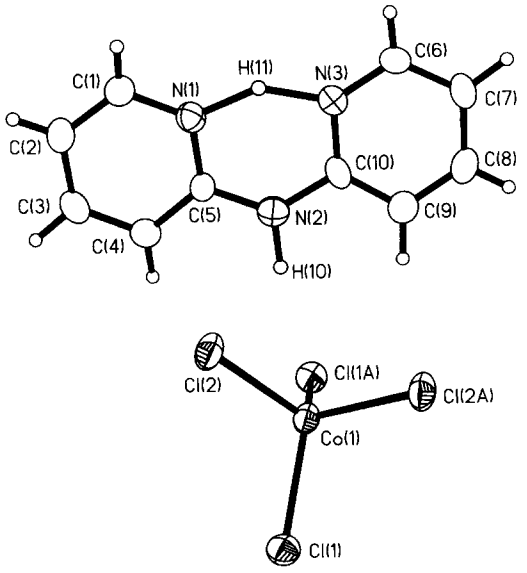

Fig. 6. Molecular structure of an H_2dpa^+ cation and the $CoCl_4^{2-}$ anion in $[H_2dpa]_2[CoCl_4]$ (**IV**).

Summary

2,2′-Dipyridylamine is known to act as a monodentate or a chelating bidentate ligand. The molecule can be deprotonated and the corresponding anion can be a chelating bidentate ligand or can be bridging a chain of three metal atoms. Under acidic conditions, the ligand can form the corresponding H_2dpa^+ cation. Structurally, such species have characteristics that make their identification relatively simple. In six-coordinate and square planar complexes, the neutral ligand chelates to the metal atom in such a way that a significant puckering of the pyridyl rings is observed (ca 35°); that puckering is significantly smaller (ca 5–7°) in four-coordinate pseudo tetrahedral complexes even though the N—M—N angles are only slightly greater than 90°. The anionic-chelating dpa^- groups in pseudo tetrahedral complexes are essentially planar (torsion angles of 3.6° or less) and have pyridyl—N—pyridyl angles which are ca 5° smaller than the corresponding ones in pseudo tetrahedral complexes which contain the chelating neutral ligand (127 vs 132° or more). The characteristic difference provides a general and reliable way to distinguish between structures **b** and **c** (Fig. 1), even when the presence or absence of a hydrogen atom on the bridging nitrogen atom cannot be established by other methods.

Acknowledgements—We are grateful to the Vicerrectoría de Investigación U.C.R. and the Department of Chemistry for support of work at the University of Costa Rica and to the National Science Foundation for support of work at Texas A&M University.

REFERENCES

1. See for example: (a) Howie, R. A. and McQuillan, G. P., *J. Chem. Soc., Dalton Trans.*, 1986, 759 and references therein. (b) Johnson, J. E. and

Jacobson, R. A., *J. Chem. Soc., Dalton Trans.*, 1973, 580; (c) Cotton, F. A., Daniels, L. M. and Jordan IV, G. T., *J. Chem. Soc., Chem. Commun.*, 1997, 421.
2. Wu, L.-P., Field, P., Morrissey, T., Murphy, C., Nagle, P., Hathaway, B., Simmons, C. and Thorton, P., *J. Chem. Soc., Dalton Trans.*, 1990, 3835.
3. Pyrka, G. J., El-Mekki, M. and Pinkerton, A. A., *J. Chem. Soc., Chem. Commun.*, 1991, 84.
4. Aduldecha, S. and Hathaway, B., *J. Chem. Soc., Dalton Trans.*, 1991, 993.
5. Yang, E.-C., Cheng, M.-C., Tsai, M.-S. and Peng, S.-M., *J. Chem. Soc., Chem. Commun.*, 1994, 2377.
6. Cotton, F. A., Daniels, L. M., Jordan IV, G. T. and Murillo, C. A., *J. Am. Chem. Soc.*, 1997, **119,** 10377.
7. Bailar Jr, J. C. and Kirschner, S., *Inorg. Synth.*, 1957, **5,** 184.
8. Goodgame, M., *J. Chem. Soc. (A)*, 1966, 63.
9. Burbridge, C. D. and Goodgame, D. M. L., *J. Chem. Soc. (A)*, 1967, 694.
10. Johnson, J. E., Beineke, T. A. and Jacobson, R. A., *J. Chem. Soc. (A)*, 1971, 1371.
11. (a) Burbridge, C. D. and Goodgame, D. M. L., *J. Chem. Soc. (A)*, 1968, 237; (b) Hurley, T. J. and Robinson, M. A., *Inorg. Chem.*, 1968, **7,** 33.
12. Pflugrath, J. and Messerschmitt, A., MADNES, Munich Area Detector (New EEC) System, Version EEC 11/1/89, with enhancements by Nonius Corporation, Delft, The Netherlands. A description of MADNES appears in: A. Messerschmitt and J. Pflugrath *J. Appl. Cryst.*, 1987, **20,** 30.
13. SHELXTL Version 5; Siemens Industrial Automation, Inc., Madison, WI, U.S.A.
14. [Co(Hdpa)$_2$(acetone)$_2$][ClO_4]$_2$ crystallizes in space group $C2/c$ with cell parameters $a = 24.186(5)$ Å, $b = 10.274(2)$ Å, $c = 16.363(3)$ Å, $\beta = 127.94(3)$°, $V = 3207(1)$ Å^3, and $Z = 4$. Data were gathered on a Nonius FAST diffractometer at −60°C. Refinement of 210 parameters with all 2026 independent reflections produced a residual of $wR2 = 0.208$ ($R1 = 0.076$ based on the 1771 reflections having $I > 2\sigma I$). The cation has crystallographic two-fold symmetry. The unique Co—N bond distances are 2.080(5) Å and 2.089(5) Å, and the Co—O(acetone) distance is 2.177(4) Å. The two acetone ligands are cis to each other, and the least-squares planes based on each dpa ligand make an angle of 64(deg). The N—Co—N angle of the chelate is 86.1(2)°.
15. Gajda, T., Henry, B. and Delpuech, J.-J., *Inorg. Chem.*, 1997, **36,** 1850.
16. Cotton, F. A. and Wilkinson, G., *Advanced Inorganic Chemistry*, 5th ed. Wiley, New York, 1988.
17. Johnson III, W. L. and Geldard, J. F., *Inorg. Chem.*, 1978, **17,** 1675.
18. Williams, A. F., Bocquet, B. and Bernardinelli, G., *Acta Cryst.*, 1987, **C43,** 883.
19. For other examples see: Fuller, C. C. and Jacobson, R. A., *Inorg. Chim. Acta*, 1981, **48,** 191 and references therein.
20. Ugozzoli, F., Lanfredi, A. M. M., Marsich, N. and Camus, A., *Inorg. Chim. Acta*, 1977, **256,** 1.
21. Freeman, H. C. and Snow, M. R., *Acta Cryst.*, 1965, **18,** 845.
22. The royal blue crystals of [$Co(CH_3CN)_6$][$CoCl_3(CH_3CN)$]$_2$·CH_3CN crystallize in space group $P2_1/n$ with the following unit cell parameters: $a = 8.925(1)$ Å, $b = 8.4197(5)$ Å, $c = 24.163(1)$ Å, $\beta = 93.471(7)$°, $V = 1812.4(2)$ Å^3, and $Z = 4$. Data were collected at −90°C on a Nonius FAST diffractometer with Mo-Kα radiation. A complete listing of bond lengths and angles, as well as displacement parameters are provided as supplementary material.
23. (a) For complexes containing the [$Co(CH_3CN)_6$]$^{2+}$ cation see: Veith, M., Gödicke, B. and Huch, V., *Z. Anorg. Allg. Chem.*, 1989, **579,** 99. (b) For complexes containing the [$CoCl_3(CH_3CN)$]$^-$ anion see: (i) Kireeva, O. K., Bulychev, B. M., Streltsova, N. R., Belsky, V. K. and Dunin, A. G., *Polyhedron*, 1992, **11,** 1801; (ii) Hartung, J., Beyer, L., Gutiérrez-Puebla, E., Fernández, V. and Olk, B., *Z. Naturforsch.*, 1992, **47b,** 183.
24. Arnold, D. I., Cotton, F. A., Maloney, D. J., Matonic, J. H. and Murillo, C. A., *Polyhedron*, 1997, **16,** 133 and references therein.
25. Spodine, E., Atria, A. M., Baggio, R. and Garland, M. T., *Acta, Cryst.*, 1996, **C52,** 1407.
26. Bowmaker, G. A., Healy, P. C., Kepert, D. L., Kildea, J. D., Skelton, B. W. and White, A. H., *J. Chem. Soc., Dalton Trans.*, 1989, 1639.
27. Pyrka, G., Seeney, R. J. and Pinkerton, A. A., *Acta Cryst.*, 1991, **C47,** 510.
28. (a) Johnson, J. E. and Jacobson, R. A., *Acta Cryst.*, 1973, **B29,** 1669; (b) Pyrka, G. L. and Pinkerton, A. A., *Acta Cryst.*, 1992, **C48,** 91.
29. For complete details on the hydrogen bonding interactions see: Cotton, F. A., Daniels, L. M., Jordan, IV, G. T. and Murillo, C. A., *J. Chem. Soc., Chem. Commun.*, 1997, 1673.
30. Rodig, O. R., Brueckner, T., Hurlburt, B. K., Schlatzer, R. K., Venable, T. L. and Sinn, E., *J. Chem. Soc., Dalton Trans.*, 1981, 196.
31. Baxter, C. E., Rodig, O. R., Schlatzer, R. K. and Sinn, E., *Inorg. Chem.*, 1979, **18,** 1918.
32. For example see: (a) Van Berkel, P. M., Driessen, W. L., Hämäläinen, R., Reedijk, J. and Turpeinen, U., *Inorg. Chem.*, 1994, **33,** 5920; (b) Antolini, L., Marcotrigiano, G., Menabue, L. and Pellacani, G. C., *Inorg. Chem.*, 1979, **18,** 2652; (c) Smith, H. W. and Stratton, W. J., *Inorg. Chem.*, 1977, **16,** 1640.

Pergamon

PII: S0277-5387(97)00287-8

Polyhedron Vol. 17, No. 4, pp. 599–602, 1998
© 1998 Elsevier Science Ltd
All rights reserved. Printed in Great Britain
0277-5387/98 $19.00+0.00

Oxidation state determination of plutonium aquo ions using x-ray absorption spectroscopy

Steven D. Conradson,[a]* Ilham Al Mahamid,[b] David L. Clark,[c,d] Nancy J. Hess,[e] Eric A. Hudson,[b] Mary P. Neu,[c,d] Phillip D. Palmer,[c] Wolfgang H. Runde[d,f] and C. Drew Tait[c,d]

[a]Chemical Science and Technology Division and the Materials Science and Technology Division, Los Alamos National Laboratory, Los Alamos, NM 87545, Mail Stop D-429, U.S.A.

[b]The Lawrence Berkeley National Laboratory, Berkeley, Mail Stop 70A-3317, CA 94550, U.S.A.

[c]Chemical Science and Technology Division and the Materials Science and Technology Division, Los Alamos National Laboratory, Los Alamos, NM 87545, Mail Stop G-739, U.S.A.

[d]The G. T. Seaborg Institute for Transactinium Science, Livermore, CA, U.S.A.

[e]The Materials Science Division, Pacific Northwest Laboratory, Richland, WA 99352, Mail Stop K2-44, U.S.A.

[f]Chemical Science and Technology Division and the Materials Science and Technology Division, Los Alamos National Laboratory, Los Alamos, NM 87545, Mail Stop J514, U.S.A.

(Received 2 June 1997; accepted 23 June 1997)

Abstract—Four oxidation states (III, IV, V, and VI) of Pu may coexist under environmentally relevant conditions. An efficient method to determine the states actually present in various matrices would enhance the ability to model the fate and transport of plutonium in process streams and in the environment. This communication establishes that the L_3 X-ray absorption near-edge structure (XANES) spectra of Pu are primarily determined by the valence state and the presence or absence of the trans dioxo moiety, consistent with previous U and Np XANES studies. The edge energies were observed to shift progressively to higher energy with increasing valence, with an average 1.68 eV increase per formal oxidation state increase. In addition, the general spectral shape of the (III) and (IV) species is clearly different from the dioxo-containing (V) and (VI) species, with the first maximum much larger and sharper for the (III) and (IV) spectra than for the (V) and (VI) spectra. © 1998 Elsevier Science Ltd. All rights reserved

Keywords: XANES; plutonium; oxidation state.

Chemical speciation, as the determinant of reactivity of the key radionuclides in nuclear waste (Sr, Cs, U, Np, Pu, Am, and Tc), is critical towards understanding and predicting their fate and transport in the environment [2–6]. The number of accessible oxidation states for transuranic ions in aqueous solution adds to the complexity of their chemistry. For plutonium, four oxidation states (III, IV, V, and VI) may coexist in aqueous solution [7]. X-ray absorption near-edge structure (XANES) spectroscopy is an established technique for the determination of oxidation state and local chemical environment, even at relatively low concentrations and without requiring extensive sample preparation that could induce artifacts [8]. The determination of edge energies and near-edge features of known Pu aquo species for different oxidation states will allow the determination of predominant oxidation states in complex matrices such as solution/solid-surface interfaces, amorphous solids, or radioactive tank wastes [9]. While XANES spectra of U and the complete suite of accessible Np oxidation states have been reported [10,11], there have been no systematic studies performed for Pu. We report here

* Author to whom correspondence should be addressed.

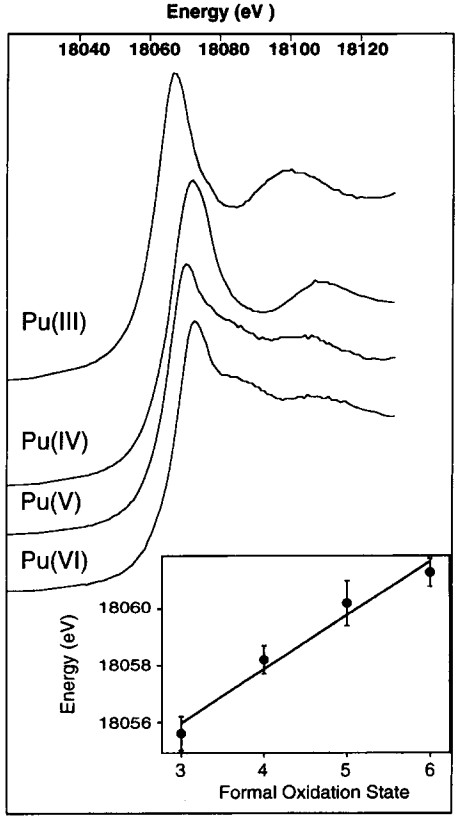

Fig. 1. Plutonium XANES spectra for the aquo (III), (IV), (V), and (VI) species. The edge energies, as measured by the inflection point of the arctangent part of the fits, are inset.

the edge energies and near-edge features for plutonium aquo ions in oxidation states (III–VI).

Aqueous plutonium solutions containing a single oxidation state were prepared electrochemically [12], and the stability of the stock solutions was verified both before and after XANES analysis with UV–vis–NIR absorption spectroscopy. Each stock solution contained greater than 98% of a single plutonium species, although any effect of the X-ray beam on the actual sample was not directly addressed. Similar chemical environments around each of the plutonium cations were produced by preparing and studying the aquo complexes. Aquo ions of Pu^{3+}, Pu^{4+}, and PuO_2^{2+} were prepared in 1 M $HClO_4$, while PuO_2^{+} was prepared in perchlorate solution at pH 3 and subsequently stabilized with respect to disproportionation by adjusting the pH of the solution to 6 [12]. X-ray absorption measurements were performed in transmission ($Pu^{III,IV,VI}$) or fluorescence (Pu^{V}) mode at the Pu L_3-edge [13] and calibrated against a Zr foil [14]. The energies of the Pu absorption edges were determined in two ways: (1) as the inflection point of the edge and (2) as the energy of the arctangent in least squares fits of the XANES region using an arctangent plus Gaussian functions [15]. In the latter case, the arctangent represents the $2p_{3/2} \rightarrow$ continuum transition, and thus coincides with the onset of the absorbance, while the Gaussians fit the higher order features, including the main peak and the first EXAFS oscillations. The initial peak, or 'white line', has historically been assigned to the allowed bound final state $2p_{3/2} \rightarrow 6d$ transition [10,11,16,17], but recent work suggests that it may be better explained as EXAFS. A theoretical analysis of the transition will be reported elsewhere [18]. The type of fits described here are comparable to XANES fits reported for U and Np [10,11,16,17].

Pu L_3 edge spectra of the aquo ions are shown in Fig. 1, where significant shifts to higher energy with increasing valence are observed. In addition, the general shape of the near edge spectra for the (III) and (IV) species is clearly different from those of the dioxo-containing (V) and (VI) species (Fig. 1). Specifically, the main peak is much more distinct for the (III) and (IV) spectra, whereas the (V) and (VI) spectra exhibit a prominent shoulder on the high energy side of this peak. These characteristics are similar to the L_3 XANES of $U^{IV,VI}$ and $Np^{III-VII}$ [10,17]. The energies of the edge and 'white line' positions are listed in Table 1. The edge energy shifts determined by the second derivatives generally increase with the formal oxidation state of the absorbing metal atom, such that

Table 1. XANES data for plutonium aquo complexes in different oxidation states[a]

Sample	2nd der. crossing	Arctan			Gaussians		
		edge	height	width	1st	2nd	3rd
Pu^{3+}	18060.1	18055.6±0.6	0.339±0.006	0.19±0.02	18064.0	18070.3	—
Pu^{4+}	18063.2	18058.2±0.5	0.337±0.005	0.19±0.03	18068.3	18075.6	—
PuO_2^{+}	18062.6	18059.7±0.2	0.322±0.005	0.23±0.03	18067.3	18071.6	—
PuO_2^{+}	18062.6	18060.2±0.8	0.327±0.004	0.15±0.02	18065.7	18072.1	18099.8
PuO_2^{2+}	18064.8	18061.3±0.5	0.323±0.007	0.22±0.02	18068.9	18078.4	—
PuO_2^{2+}	18064.8	18061.2±0.6	0.321±0.005	0.18±0.03	18068.9	18080.0	18103.2

[a] All energy positions are in eV, where the energy axis had been calibrated using the XANES edge from Zr foil at 17,999.35 eV. The arctan height, width, and edge are taken from variables k[1], k[2], and k[3], respectively, as defined in ref. [13].

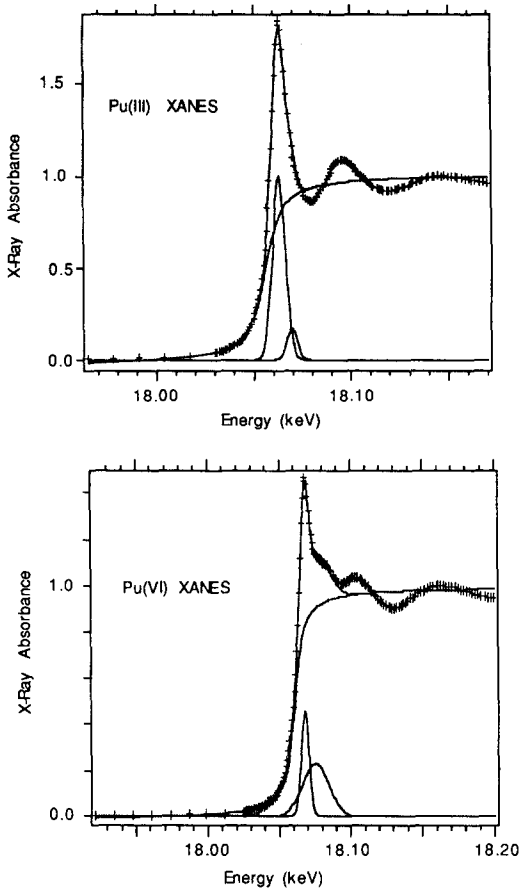

Fig. 2. Representative fits of the XANES for Pu^{III} and Pu^{VI}, representing the aquo- and dioxo-containing species, respectively.

(III), (IV/V), and (VI) are readily distinguished (Table 1). We note that while the overall shapes of the near edge spectra for (IV) and (V) states allow unambiguous assignment, their energies as determined by using only 2nd derivatives are quite similar. If the trend in edge shift reflects the charge, this might be explained by the increase in covalency (and diminution of difference in Pu charge) associated with the presence of the dioxo moiety in (V) and (VI) states. However, when fit to an arctangent and 2 Gaussians (Fig. 2), [15] which might be more sensitive to valence and less so to the positions and shapes of the other features of the edge, the arctangent (ionization) energies do increase progressively with formal oxidation state. The inset of Fig. 1 shows the excellent linear correlation between the arctan-based edge position and Pu oxidation state ($r^2 = 0.997$). Addition of a third Gaussian to the XANES deconvolution for the (V) and (VI) species affected the edge position only marginally (Table 1), and the general conclusion of higher edge position with oxidation state remains. Therefore, the arctangent fitting strategy avoids interference from the 'white line' when determining the energy of the edge.

This work shows that the primary determinants of Pu XANES are the valence state and the presence or absence of the trans-dioxo moiety, consistent with previous U and Np XANES studies [16,17,19,20]. Furthermore, this work establishes that XANES spectroscopy provides a rapid and straightforward means for determination of the average valence of Pu in species with primarily oxygen ligation, using a combination of the spectral features (III and IV vs V and VI) and the calculated arctangent edge energy. We anticipate that these findings will aid in our ability to determine the oxidation state of Pu in a variety of important complex chemical matrices such as aging radioactive wastes, process stream residues, glasses, ceramics, and soils.

Acknowledgements—This research was supported by the Nuclear Material Stabilization Task Group, the Office of Basic Energy Sciences, and the Office of Health and Environmental Research. These latter two programs are from the U.S. Department of Energy under contracts W-7405-ENG-36 and DE-AC03-76SF00098 with the University of California. W.R. acknowledges postdoctoral support from the Glenn T. Seaborg Institute for Transactinium Studies. XAS experiments were performed at the Stanford Synchrotron Radiation Laboratory, which is supported by the U.S. DOE Office of Basic Energy Sciences. Raymond C. Gatti and Scott A. Carpenter are acknowledged for their participation in sample preparation and XANES measurements.

Supplementary data—Figures of the fits for all 4 Pu oxidation states is available. Ordering information is given on any current masthead page.

REFERENCES

1. (a) LANL Mailstop D429; (b) LBNL Mailstop 70A-3317; (c) LANL Mail Stop G739; (d) G. T. Seaborg Institute; (e) PNNL Mailstop K2-44; (f) LANL Mailstop J514.
2. Dozol, M. and Hagemann, R., *Pure and Appl. Chem.*, 1993, **65,** 1081.
3. Clark, D. L., Hobart, D. E. and Neu, M. P., *Chem. Rev.*, 1995, **95,** 25.
4. Kim, J. I., *Mater. Res. Soc. Symp. Proc.*, 1993, **294,** 3.
5. (a) Fuger, J., *J. Nucl. Mater.*, 1993, **201,** 3; (b) Choppin, G. R., *Radiochim. Acta*, 1983, **32,** 43.
6. Hobart, D. E., *Proc. Robert A. Welch Conf. Chem. Res.*, 1990, **34,** 379.
7. Weigel, F., Katz, J. J. and Seaborg, G. T., *The Chemistry of the Actinide Elements*; (Katz, J. J., Seaborg, G. T. and Morss, L. R., eds) Vol. 1, 781, Chapman and Hall, London (1986).
8. Bianconi, A., *X-Ray Absorption: Principles, Applications, Techniques of EXAFS, SEXAFS and XANES*; Koningsberger, D. C. and Prins, R., Eds., Vol. 92, 573, John Wiley & Sons: New York (1988).
9. Brown, G. E., *Mineral–Water Interface Geochemistry*; Hochella, M. F. and White, A. F.,

Eds; Vol. 23; 309, Mineralogical Society of America, Washington, D.C. (1990).
10. Morris, D. E., Allen, P. G., Berg, J. A., Chisholm-Brause, C. J., Conradson, S. D., Donohoe, R. J., Hess, N. J., Musgrave, J. A. and Tait, C. D., *Environ. Sci. Techn.*, 1996, **30,** 2322.
11. Bertram, S., Kaindl, G., Jove, J. and Pages, M., *Physica B*, 1989, **158,** 508.
12. ^{242}Pu was purified using ion chromatography (Lewatit MP-500) of Pu^{VI} in 9 M HCl ($PuCl_6^{2-}$), and eluted using 0.5 M HCl. Purified Pu^{IV} was oxidized to Pu^{IV} in fuming $HClO_4$, and the resulting solution diluted with 1 M $HClO_4$, and analyzed spectrophotometrically at 830 nm ($\varepsilon = 525$ M^{-1} cm^{-1}). Pu^{V} was prepared by placing Pu^{VI} in 0.2 M ClO_4, adjusting the pH to 3 using NH_4OH, followed by electrochemical reduction at a potential of 0.54 V (*vs* SCE). The pH was adjusted to 6, and the solution analyzed spectrophotometrically at 569 nm ($\varepsilon = 19$ M^{-1} cm^{-1}). Pu^{III} solutions were obtained by electrolytic reduction of Pu^{VI} at 0.51 V (*vs* SCE) in 1 M $HClO_4$, and analyzed spectrophotometrically at 600 nm ($\varepsilon = 37.5$ M^{-1} cm^{-1}). The Pu^{III} solution was oxidized electrochemically to Pu^{IV} at 1.2 V (*vs* SCE) in 1 M $HClO_4$. At this potential, Pu^{V} and Pu^{VI} could form, but the rate of formation for such irreversible reactions is small. Pu^{IV} is analyzed spectrophotometrically at 470 nm ($\varepsilon = 56.5$ M^{-1} cm^{-1}). Final Pu solution concentrations were 0.10 M for all samples except for Pu^{V}, which was 0.008 M.
13. XANES data were recorded at 295 K at the Stanford Synchrotron Radiation Laboratory (SSRL): unfocused beamline 4-2, Si(220), double-crystal monochromator, 3.0 GeV, 60–100 mA. The XANES region was taken as extending above the Pu edge to 18,120 eV.
14. The Pu L_3 edge spectrum normalized by setting the value of a polynomial fit through the pre-edge region to zero and that of a polynomial fit through the EXAFS region to unity at 18,120 eV. The spectra were calibrated by comparison of spectra for Zr foil, where the first inflection point was defined to be 17,999 eV.
15. Fit = k[0] + (k[1]* arctan (k[2]*(x−k[3]))) + (k[4]* exp $(-((x-k[5])/k[6])^2)$) + (k[7]* exp $(-((x-k[8])/k[9]^2))$, where x is the X-ray energy in eV and the k's are the fit parameters.
16. Kalkowski, G., Kaindl, G., Bertram, S., Schmiester, G., Rebizant, J., Spirlet, J. C. and Vogt, O., *Solid State Commun.*, 1987, **64,** 193.
17. Kalkowski, G., Kaindl, G., Brewer, W. D. and Krone, W., *Phys. Rev. B*, 1987, **35,** 2667.
18. Conradson, S. D., Rehr, J. and Mustre De Leon, J., work in progress.
19. Agarwal, B. K., *X-ray Spectroscopy*, 2nd ed.; Springer-Verlag, Berlin (1991).
20. Ghatikar, M. N. and Padilia, B. D., *J. Phys. C*, 1978, **11,** 1941.

Pergamon

PII: S0277-5387(97)00170-8

Polyhedron Vol. 17, No. 4, pp. 603–606, 1998
© 1998 Elsevier Science Ltd
All rights reserved. Printed in Great Britain
0277-5387/98 $19.00+0.00

Synthesis and X-ray crystal structure of N,N′,N″-tris(2-thienylmethyl)-cis-1,3,5-triaminocyclohexane copper(II) dichloride

Neng Ye[a], Robin D. Rogers[b], Martin W. Brechbiel[c] and Roy P. Planalp[a]*

[a] Department of Chemistry, University of New Hampshire, Durham, NH 03824, U.S.A.

[b] Department of Chemistry, The University of Alabama, Tuscaloosa, AL 35487, U.S.A.

[c] Chemistry Section, Radiation Oncology Branch, National Institutes of Health, Bethesda, MD 20892, U.S.A.

(Received 16 December 1996; accepted 22 April 1997)

Abstract—The title complex was synthesized by reaction of *N,N′,N″*-tris(2-thienylmethyl)-*cis*-1,3,5-triaminocyclohexane (tachthioph) with copper(II) chloride in acetonitrile or methanol. Crystallographic characterization of Cu(tachthioph)$Cl_2 \cdot$MeCN reveals a typical Jahn–Teller-distorted square-pyramidal CuN_3Cl_2 coordination sphere. There is no interaction with the 2-methylenethiophene pendant arms. © 1998 Elsevier Science Ltd. All rights reserved

Keywords: copper complexes; square-pyramidal; nitrogen donor ligands.

Tridentate ligand complexes of copper(II) chloride are of interest in bond cleavage of biological molecules, in that they catalyze hydrolysis of both unactivated peptide linkages and phosphodiester bonds [1]. Although Co^{III} complexes enhance rates of amide hydrolysis, only a few Cu^{II} complexes have been found to possess the appropriate properties for the catalytic hydrolysis of amide linkages [2,3]. We discuss herein the synthesis and X-ray structural characterization of *N,N′,N″*-tris(2-thienylmethyl)-*cis*-1,3,5-triaminocyclohexane copper(II) dichloride.

EXPERIMENTAL

Materials and methods

Anhydrous grade MeOH was obtained from Fisher. Et_2O was distilled from Na/K. $CuCl_2$ was from Aldrich. Tachthioph was prepared as previously reported [4].

Fast atom bombardment (FAB-MS) mass spectra were obtained on an Extrel 4000. Elemental analyses were performed by the University Instrumentation Center at UNH.

Preparation of Cu(tachthioph)Cl_2 To a colorless solution of tachthioph (0.0198 g, 4.74×10^{-5} mol) in MeOH (2 mL) was added a greenish–brown solution of $CuCl_2$ (0.0082 g, 6.1×10^{-5} mol) in MeOH (2 mL), affording a dark green solution. After standing for 2 h, ether (10 mL) was diffused, through the vapor phase, into the solution overnight. The green prisms were isolated, washed with ether, and dried under reduced pressure. Yield 0.015 g (2.7×10^{-5} mol, 57%). Anal. Calcd for $C_{21}H_{27}CuN_3S_3Cl_2 \cdot H_2O$: C, 44.24; H, 5.12; N, 7.37. Found: C, 44.79; H, 5.05; N, 7.56. MS (FAB, glycerol/H_2O matrix) *m/z*: 515 $[M\text{-}Cl]^+$, 480 $[M\text{-}2Cl]^+$. UV–vis (Methanol): λ_{max} 233.5 nm ($\varepsilon = 3.12 \times 10^4$).

Crystal structure determination

$[C_{21}H_{27}Cl_2CuN_3S_3][CH_3CN]$, green fragment, $0.20 \times 0.12 \times 0.04$ mm, $fw = 593.13$, triclinic, $a = 8.8282(5)$, $b = 10.9528(6)$, $c = 15.4888(9)$ Å, $\alpha = 72.061(1)°$, $\beta = 74.761(1)°$, $\gamma = 67.109(1)°$, $V = 1295.05(13)$ Å^3, space group $P\bar{1}$, $Z = 2$, $D_c = 1.521$ g/cm^3, μ (Mo-Kα) = 1.312 mm^{-1}, $\lambda = 0.71073$ Å.

* Author to whom correspondence should be addressed.

Crystals were obtained by diffusion of ether, through the vapor phase, into an acetonitrile solution of Cu(tachthioph)Cl_2. A fragment was taken directly from the crystals in supernatant, sealed in epoxy and mounted on a glass fiber. Data were collected on a Siemens SMART/CCD area detector diffractometer ($-9 \leqslant h \leqslant 9$, $-12 \leqslant k \leqslant 12$, $-12 \leqslant l \leqslant 17$; $1.40 \leqslant \theta \leqslant 23.26°$) at -100°C with graphite-monochromated Mo-Kα radiation. 5262 reflections were measured, 3576 reflections were unique, and 3079 reflections with $I > 2\sigma(I)$ were considered to be observed for purposes of R value computation. The data were corrected for Lorentz and polarization factors.

The structure was solved by direct methods. Six positions were found to be disordered between *S* and *C*. It was not possible to resolve separate positions for each disordered pair, therefore each position was refined with partial *S* and partial *C* occupancy. The disorder was deduced to be 85%/15%. Thus, S(1C9), S(2C14), S(3C19) were refined at 85% occupancy sulfur and 15% occupancy *C*. Similarly, positions *C*(9S1), *C*(14S2), and *C*(19S3) were refined as 85% *C* and 15% *S*. The geometrically constrained hydrogen atoms were placed in calculated positions and allowed to ride on the bonded atom with $B = 1.2 \times$ Ueqv (C). The methyl hydrogen atoms were included as a rigid group with rotational freedom at the bonded carbon atom ($B = 1.2 \times$ Ueqv(*C*)). The remaining three hydrogen atoms were located from a difference Fourier map and allowed to ride on the bonded N atoms with $B = 1.2 \times$ Ueqv (*N*). Refinement of the non-hydrogen atoms was carried out with anisotropic temperature factors. Final values of R(all data) = 4.78%, R_w (all data) = 10.75%, R(obs data) = 3.74%, and

Table 1. Selected bond distances (Å) and angles (°), and the torsion angles (C—C—C—C, °) of Cu(tachthioph)$Cl_2 \cdot$ MeCN

Cu—N(2)	2.065(3)	N(2)—C(3)	1.497(4)	C(12)—C(13)	1.507(5)
Cu—N(1)	2.069(3)	N(3)—C(17)	1.479(4)	C(13)—C(14S2)	1.441(5)
Cu—N(3)	2.288(3)	N(3)—C(5)	1.500(4)	C(14S2)—C(15)	1.455(5)
Cu—Cl(2)	2.2914(10)	N(4)—C(22)	1.122(6)	C(15)—C(16)	1.339(6)
Cu—Cl(1)	2.3216(9)	C(1)—C(6)	1.516(5)	C(17)—C(18)	1.516(5)
S(1C9)—C(11)	1.699(5)	C(1)—C(2)	1.530(5)	C(18)—C(19S3)	1.488(5)
S(1C9)—C(8)	1.702(4)	C(2)—C(3)	1.523(5)	C(19S3)—C(20)	1.437(5)
S(2C14)—C(16)	1.691(4)	C(3)—C(4)	1.532(5)	C(20)—C(21)	1.330(6)
S(2C14)—C(13)	1.711(4)	C(4)—C(5)	1.536(5)	C(22)—C(23)	1.454(7)
S(3C19)—C(21)	1.670(5)	C(5)—C(6)	1.526(5)		
S(3C19)—C(18)	1.704(4)	C(7)—C(8)	1.501(5)	N(2)—Cu—N(1)	91.30(11)
N(1)—C(7)	1.492(4)	C(8)—C(9S1)	1.418(5)	N(2)—Cu—N(3)	92.06(11)
N(1)—C(1)	1.499(4)	C(9S1)—C(10)	1.369(5)	N(1)—Cu—N(3)	86.43(11)
N(2)—C(12)	1.495(4)	C(10)—C(11)	1.341(7)	N(2)—Cu—Cl(2)	87.66(9)

N(1)—Cu—Cl(2)	175.10(8)	C(3)—C(2)—C(1)	113.0(3)
N(3)—Cu—Cl(2)	98.39(7)	N(2)—C(3)—C(2)	112.2(3)
N(2)—Cu—Cl(1)	154.91(9)	N(2)—C(3)—C(4)	110.3(4)
N(1)—Cu—Cl(1)	87.47(8)	C(2)—C(3)—C(4)	110.6(3)
N(3)—Cu—Cl(1)	112.85(7)	C(3)—C(4)—C(5)	115.6(3)
Cl(2)—Cu—Cl(1)	91.44(4)	N(3)—C(5)—C(6)	110.8(3)
C(7)—N(1)—C(1)	111.4(3)	N(3)—C(5)—C(4)	111.8(3)
C(7)—N(1)—Cu	112.9(2)	C(6)—C(5)—C(4)	110.9(3)
C(1)—N(1)—Cu	117.8(2)	C(1)—C(6)—C(5)	113.9(3)
C(12)—N(2)—C(3)	115.0(3)	N(1)—C(7)—C(8)	113.6(3)
C(12)—N(2)—Cu	109.0(2)	N(2)—C(12)—C(13)	116.5(3)
C(3)—N(2)—Cu	116.2(2)	N(3)···C(17)—C(18)	114.6(3)
C(17)—N(3)—C(5)	111.0(3)	N(4)—C(22) C(23)	179.1(5)
C(17)—N(3)—Cu	120.3(2)		
C(5)—N(3)—Cu	110.8(2)		
N(1)—C(1)—C(6)	111.1(3)		
N(1)—C(1)—C(2)	111.5(3)		
C(6)—C(1)—C(2)	111.0(3)		

C(1)—C(2)—C(3)—C(4) 52.30(39)	C(4)—C(5)—C(6)—C(1) 50.22(39)
C(2)—C(3)—C(4)—C(5) 49.48(41)	C(5)—C(6)—C(1)—C(2) 54.28(39)
C(3)—C(4)—C(5)—C(6) 48.23(41)	C(6)—C(1)—C(2)—C(3) 55.29(39)

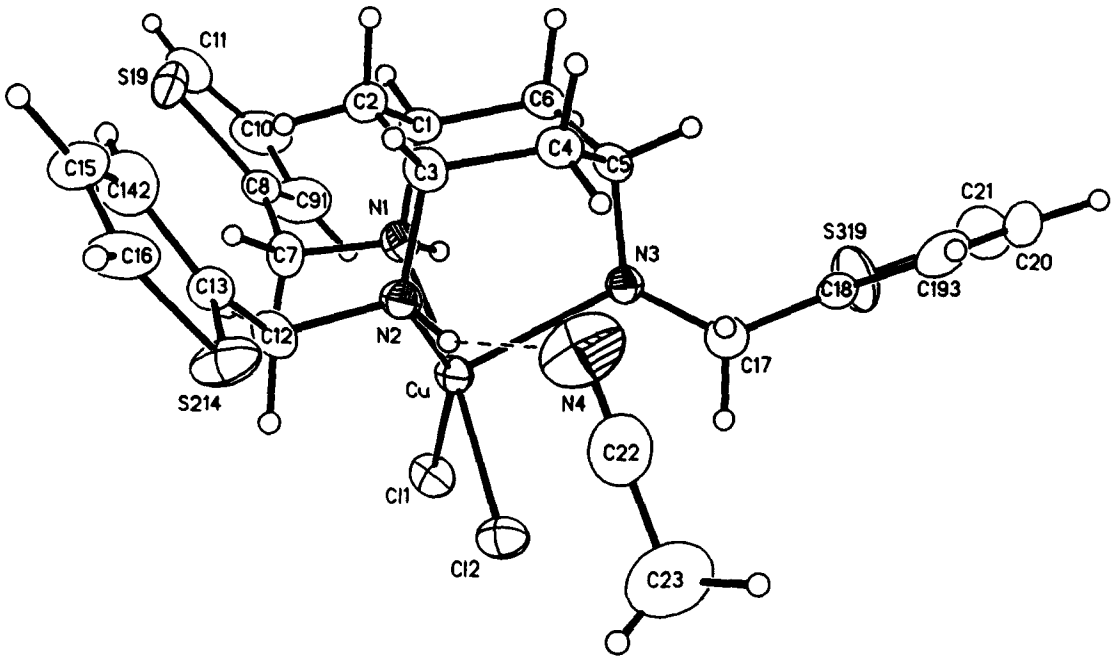

Fig. 1. ORTEP view of $Cu(tachthioph)Cl_2 \cdot MeCN$ with S/C atoms in major occupancy positions and 50% probability ellipsoids.

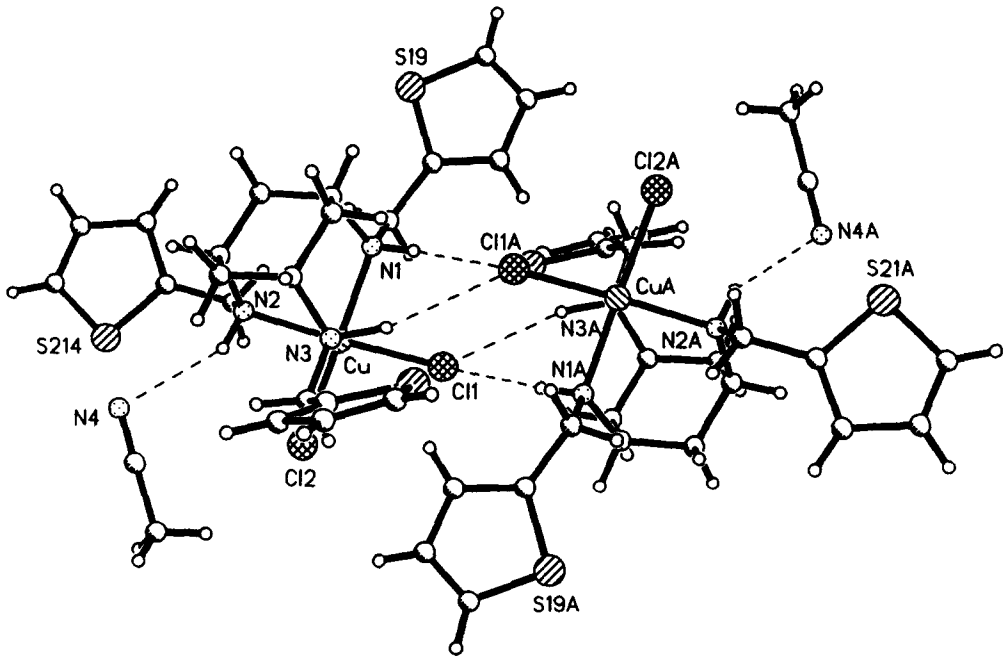

Fig. 2. A view of the hydrogen-bonded dimer of the $Cu(tachthioph)Cl_2 \cdot MeCN$.

R_w(obs data) = 8.90% were obtained with a GOF (on F^2) of 1.045 and SHELX-93 weight parameters of 0.0434 and 1.5816.

RESULTS AND DISCUSSION

The preparation of Cu(tachthioph)Cl_2 is straightforward. The acetonitrile solvate Cu(tachthioph)$Cl_2 \cdot$MeCN provided acceptable single crystals for diffraction study. A view of the molecule Cu(tachthioph)Cl_2 is provided in Fig. 1. Selected bond distances and angles are in Table 1. The metal coordination sphere is distorted square pyramidal, with N(3) in the apical position and N(1), N(2), Cl(1) and Cl(2) forming the square base. The distortion leads N(1) and Cl(2) towards the apical sites of a trigonal bipyramidal and N(2), N(3) and Cl(1) toward the equatorial sites. The apical bond distance Cu—N(3) of 2.288(3) Å is substantially longer than the basal ones as is typical of Jahn–Teller-distorted copper(II). This may be compared with the apical Cu—N distances of 2.246(4) and 2.231(4) Å in square-pyramidal Cu(1,4,7-triazacyclononane)Cl_2 [5] and Cu(1,4,7-triazacyclononane)Br_2 [6], respectively. Comparison may also be made to Cu(1,3,5-triamino-1,3,5-trideoxy-*cis*-inositol)$_2^{2+}$ [7] (Cu(taci)$_2^{2+}$), which is similar to the title compound in that it contains copper(II) coordinated by a *cis*-1,3,5-triaminocyclohexane-derivative group. In this octahedrally-coordinated complex, the longer Cu^{II}—N distance is 2.322(6) Å. The shorter Cu—N distances of the title compound are 2.065(3) (N(2)) and 2.069(3) Å (N(1)), which compare favourably with those of 2.086(4) Å for Cu(taci)$_2^{2+}$ and 2.063(4), 2.038(4) Å in Cu(1,4,7-triazacyclononane)Cl_2.

Copper(II)—chloride distances of Cu(tachthioph)Cl_2 (Cu—Cl(2) = 2.2914(10), Cu—Cl(1) = 2.3216(9) Å) are comparable to those of Cu(1,4,7-triazacyclononane)Cl_2 (2.268(1), 2.312(1) Å). The Cu—Cl(1) bond distance is significantly longer than Cu—Cl(2) due to the two hydrogen bonds accepted by Cl(1) (*vide infra*). The bite angles of N—Cu—N of Cu(tachthioph)Cl_2 (N = N(1), N(2), or N(3)) are 91.30(11), 92.06(11) and 86.43(11)° as compared to 85.7(2), 90.1(2), 89.9(2) and 94.3(2) in Cu(taci)$_2^{2+}$. The torsion angles C—C—C—C of the cyclohexyl ring, a measure of ligand distortion induced by the metal pushing the nitrogens outward (Table 1) [8,9] are not significantly different from those of Cu(cis-1,3,5-triaminocyclohexane)$_2^{2+}$, which range from 50.6(13) to 52.9(13)° [10].

The atoms N(1) and N(3) form single hydrogen bonds to Cl($\bar{1}$) in a molecule related by a crystallographic center of inversion resulting in a hydrogen-bonded dimer (H(1)$\cdots$Cl(1a) = 2.529(3) Å, N(1)—H(1)$\cdots$Cl(1a) = 167.34(6)°; H(3)$\cdots$Cl(1a) = 2.777(3) Å, N(3)—H(3)$\cdots$Cl(1a) = 158.79(6)°). The hydrogen bonding is completed by interactions to two terminal solvent molecules. N(2) donates a single hydrogen bond to the N atoms of the solvent (H(2)$\cdots$N(4) = 2.582(5) Å; N(2)—H(2)$\cdots$N(4) = 148.7(1)°) and the solvent methyl group participates in a very weak interaction with Cl(2) (H(23C)$\cdots$Cl(2) = 2.844(5) Å; C(23)—H(23C)$\cdots$Cl(2) = 132.2(1)°).

Acknowledgement—R.P. thanks the NIH for support.

REFERENCES

1. Hegg, E. L. and Burstyn, J., *J. Am. Chem. Soc.*, 1995, **117,** 7015.
2. Reddy, K., Jacobson, A., Kung, J. and Sayre, L., *Inorg. Chem.*, 1991, **30,** 3520.
3. Sayre, L., Reddy, K., Jacobson, A. and Tang, W., *Inorg. Chem.*, 1992, **31,** 935.
4. Bowen, T., Planalp, R. and Brechbiel, M. W., *Bioorg. Med. Chem. Lett.*, 1996, **6,** 807.
5. Schwindinger, W. F., Fawcett, T. G., Lalancette, R. A., Potenza, J. and Schugar, H., *Inorg. Chem.*, 1980, **19,** 1379.
6. Bereman, R. D., Churchill, M., Schaber, P. and Winkler, M., *Inorg. Chem.*, 1979, **18,** 3122.
7. Hegetschweiler, K., Gramlich, V., Ghisletta, M. and Samaras, H., *Inorg. Chem.*, 1992, **31,** 2341.
8. Hilfiker, K. A., Rogers, R., Brechbiel, M. W. and Planalp, R., *Inorg. Chem.*, 1997, **36,** 4600.
9. Choquette, D. M., Buschmann, W. E., Olmstead, M. M. and Planalp, R., *Inorg. Chem.*, 1993, **32,** 1062.
10. Ammeter, H., Bürgi, H., Gamp, E., Meyer-Sandrin, V. and Jensen, W., *Inorg. Chem.*, 1979, **18,** 733.
11. SHELXTL Version 5, Siemens Industrial Automation, Inc., Analytical Instrumentation Business Unit, Madison, WI, USA, 1995.

Pergamon

PII: S0277-5387(97)00356-2

Polyhedron Vol. 17, No. 4, pp. 607–611, 1998
© 1998 Elsevier Science Ltd
All rights reserved. Printed in Great Britain
0277-5387/98 $19.00+0.00

The preparation and crystal structure of $(dppe)(CO)_3Re\text{-}OC(O)O\text{-}Re(CO)_3(dppe)$

Santosh K. Mandal,[a] Douglas M. Ho,[b] Guang Qing Li[c] and Milton Orchin[c]*

[a] Department of Chemistry, Morgan State University, Baltimore, MD 21251, U.S.A.

[b] Department of Chemistry, Princeton University, Princeton, NJ 08544, U.S.A.

[c] Department of Chemistry, University of Cincinnati, Cincinnati, OH 45221, U.S.A.

(Received 6 February 1997; revised 8 April 1997)

Abstract—The title compound is readily prepared from the rhenium carboxylate, $(dppe)(CO)_3ReC(O)OCH_3$, by prolonged stirring of a solution of the carboxylate in benzene/H_2O or THF/H_2O. The reaction involves the unusual *in situ* conversion of Re—C bonds to Re—O bonds. The X-ray structure of the title compound shows that the μ_2,η^2-carbonato ligand is present in the symmetrical *syn, syn* conformation in the solid state in contrast to the alternate *syn, anti* geometry reported for the related complex, $(diars)(CO)_3ReOC(O)ORe(CO)_3(diars)$.
© 1998 Elsevier Science Ltd. All rights reserved

Keywords: rhenium; 1,2-bis(diphenylphosphino)ethane; rhenium carboxylate complex; bridging carbonato complex; crystal structure.

There are now many examples of functional groups directly bonded to transition metals through a metal–carbon bond and many, although fewer, examples of organometallic compounds involving metal–oxygen single bonds (such as transition metal alkoxides). The facile insertion of CO_2 into an M—O bond of alkoxides leading to organometallic carbonates is a reaction that has become of increasing interest because of its relevance to reversible sequestering of this "green house" gas. Such insertion reactions and the wide variety of complexes that are thereby generated have been summarized in a recent excellent review [1]. Although there are now numerous examples of μ_2,η^2 organometallic carbonates and some bicarbonates [2–8], there are fewer examples of transition metals bridged by a single carbonato linkage, i.e. M—OC(O)O—M. These include complexes where M=Rh [4], Cu [9–11], Cr [12], Re [13], and Mn [14]. In only the last case has the formation of the bridging carbonato complex involved the conversion of M—C to M—O bonds. We wish to report here on the transformation of *fac*-$(dppe)(CO)_3Re\text{–}C(O)OC_2H_5$ to *fac*-$(dppe)(CO)_3Re\text{–}OC(O)O\text{–}Re(CO)_3(dppe)$. The X-ray crystal study of the bridging carbonato complex is also reported.

* Author to whom correspondence should be addressed.

EXPERIMENTAL

All reactions were carried out under an atmosphere of argon. Solvents were used directly from bottles of certified purity. *fac*-$(dppe)(CO)_3ReC(O)OC_2H_5$ was prepared according to the literature method [15]. The IR spectra were recorded on a Perkin–Elmer 1600 Series FT-IR instrument. NMR spectra were recorded on a Bruker AC 250 (250.133 MHz, ^1H; 62.896 MHz, ^{13}C; 101.256 MHz, ^{31}P) spectrometer. Melting points were recorded on a Mel-Temp apparatus and are uncorrected. Elemental analyses were performed by Galbraith Laboratories, Inc.

Preparation of $(dppe)(CO)_3Re\text{–}OC(O)O\text{–}Re(CO)_3(dppe)$

A 0.50 g sample of *fac*-$(dppe)(CO)_3ReC(O)OC_2H_5$ was stirred with benzene or THF (50 cm^3) in the presence of water (0.5 cm^3) under argon for 7 d. The solution was evaporated to dryness and the solid residue was recrystallized from a dichloromethane/hexane mixture. The white precipitate that separated was collected by filtration, washed with hexane (3×15 cm^3), and dried *in vacuo*. Data: m.p. 160–162°C. IR (cm^{-1}, CH_2Cl_2): $\nu_{(C\equiv O)}$ 2028s, 1945s, 1887s and $\nu_{(C\equiv O)}$

1534m. Anal. Found: C, 48.89; H, 3.50. Calc. for $C_{59}H_{48}O_9P_4Re_2 \cdot CH_2Cl_2$: C, 48.62; H, 3.40. ^1H NMR (δ, $CDCl_3$): 7.45 (m, 40H, C_6H_5), 5.29 (s, 2H, CH_2Cl_2), 2.61 (m, 8H, CH_2). ^{13}C NMR (δ, CD_2Cl_2): 166.7 (μ-CO_3). ^{31}P NMR (δ, CD_2Cl_2, reference: 85% H_3PO_4): 33.6 (s).

Reaction of (dppe)$(CO)_3$Re–OC(O)O–Re$(CO)_3$(dppe) *with* HCl

A solution of 0.22 g of (dppe)$(CO)_3$Re–OC(O)O–Re$(CO)_3$(dppe) in benzene (40 cm^3) was treated with excess of concentrated HCl (5 cm^3). After stirring for 2 h, the excess acid was removed by extraction with water. The benzene solution was then concentrated and mixed with hexane, and the resultant mixture was cooled. The white microcrystals that separated were collected by filtration, washed with hexane (3×15 cm^3) and dried under vacuum to give *fac*-(dppe)$(CO)_3$ReCl in essentially quantitative yield. This complex has been reported previously [16].

Reaction of (dppe)$(CO)_3$Re–OC(O)O–Re$(CO)_3$(dppe) *with* p-*toluenesulfonic acid monohydrate*

A solution of 0.50 g of (dppe)$(CO)_3$Re–OC(O)O–Re$(CO)_3$(dppe) in 50 cm^3 of dichloromethane was stirred with a 10-fold excess of *p*-toluenesulfonic acid monohydrate (98.5%) at room temperature for 1 h. The excess acid was removed by extraction with water. The dichloromethane solution was concentrated and mixed with hexane, and the resultant mixture was cooled. The white microcrystals that separated were collected by filtration, washed with hexane (3×15 cm^3), and dried under vacuum to give *fac*-(dppe)$(CO)_3$ReOTs in about 68% yield. This compound has been characterized previously [17].

Single crystal X-ray diffraction study of (dppe)$(CO)_3$Re–OC(O)O–Re$(CO)_3$(dppe)$\cdot 2C_6H_6$

A colorless prism 0.12 mm × 0.20 mm × 0.28 mm in size was sealed in a glass capillary and then transferred to a Siemens R3 m/v diffractometer. Crystal data: $C_{59}H_{48}O_9P_4Re_2 \cdot 2C_6H_6$; monoclinic, space group $C2/c$ (No. 15); $a = 31.537(3)$ Å, $b = 9.437(1)$ Å, $c = 22.139(3)$ Å, $\beta = 98.52(1)°$, $V = 6516(1)$ Å^3, $Z = 4$, $D_{calcd} = 1.58$ gcm^{-3}. The cell dimensions were refined with monoclinic constraints employing 25 centered reflections having $11° < \theta < 17.5$. One quadrant of data ($-40 < h < 40$, $0 < k < 12$, $0 < l < 28$) was collected at 298 K out to a θ maximum of 27.5° using Mo—K_α ($\lambda = 0.071073$ Å) and 1.2 degree ω scans. A total of 8143 reflections were measured, 7488 were unique [$R_{(int)} = 0.0226$] and 5980 were observed [$F > 3\sigma(F)$]. Corrections were made for Lorentz-polarization and absorption effects. The minimum and maximum transmission factors were 0.5138 and 0.9730, respectively. The structure was solved by heavy-atom methods and refined on F by full-matrix least-squares with SHELXTL-PLUS [18]. The non-hydrogen atoms were refined with anisotropic displacement coefficients and the hydrogen atoms were included with a riding model. The refinements converged to $R(F) = 0.0391$ and $wR(F) = 0.0304$ with 419 variables; where $R(F) = \Sigma(||F_o| - |F_c||)/\Sigma|F_o|$ and $wR(F) = [\Sigma(W||F_o| - |F_c||^2)/\Sigma W|F_o|^2]^{1/2}$. The goodness-of-fit was 1.27. The final atomic coordinates and equivalent isotropic displacement parameters are given in Table 1, selected bond distances and angles are presented in Table 2, and a labeled diagram of the structure is provided as Fig. 1. Further details are given in the Supplementary Material.

RESULTS AND DISCUSSION

A bridging Re carbonato complex analogous to the one we report here has been prepared previously [13] from the methyl carbonato complex, Re$(CO)_3$(diars)OC(O)OCH_3. In this instance and in the preparation of a Cu bridging carbonato complex [9], the M—O bond is present in the precursor complex. In a preparation of the Re bridging carbonato compound we report here, the precursor complex is Re(dppe)$(CO)_3$C(O)OC_2H_5 in which the Re is bonded to a carbon atom. On prolonged stirring in benzene/water (or THF/H_2O) at room temperature, the Re-carbon bond in the starting compound is replaced by the Re-oxygen bonds of the bridging carbonato linkage. We have observed a similar transformation in the manganese analog [14] but were unable to secure a definite X-ray crystal structure of the bridging carbonato complex. The crystal structure reported here confirms the μ_2,η^2 linkage of our Re complex. The molecule possesses crystallographic 2-fold symmetry and an ReOC(O)ORe core with a *syn,syn* conformation. The Re—O, O—C(O)O and OC(=O)O distances are 2.127(3), 1.315(5) and 1.228(9) Å, respectively, and are normal. The ReOC(O)ORe core within the related (diars)$(CO)_3$ReOC(O)ORe$(CO)_3$(diars) [13] exhibits an alternate *syn,anti* geometry with comparable distances of 2.138(6), 1.308(10) and (*syn*) and 2.143(6), 1.296(10) and 1.245(10) Å (*anti*), respectively. The ReO—C(O)—ORe angle in our (dppe) complex is 111.4(6)° while that in the diars complex is 116.7(8)°. To the best of our knowledge, these two values represent the present lower and upper bounds for dinuclear centers bridged solely by the carbonato ligand. The 111.4(6)° value in our dppe complex is also comparable to the average value of 111° observed in transition metal carbonates, M–OC(O)–OCH_3.

There is a prior interesting report of the conversion of an M—C bond to an M—O bond consisting of the decarbonylation of an Mo–C(O)OMe complex to the corresponding Mo–OMe complex [19]. We suspect that this reaction proceeds by prior dissociation at the

Table 1. Crystallographic data for (dppe)(CO)$_3$Re–OC(O)O–Re(CO)$_3$(dppe) · 2C$_6$H$_6$

Empirical formula	$C_{71}H_{60}O_6P_4Re_2$
Color and habit	Colorless prisms
Formula weight	1553.59
Temperature (K)	294
Radiation	Mo—K_α (λ = 0.071073 Å)
Monochromator	Highly oriented graphite crystal
Crystal system	Monoclinic
Space group	$C2/c$ (#15)
Unit cell dimensions	a = 31.537(3) Å
	b = 9.437(1) Å
	c = 22.139(3) Å
	β = 98.52(1)°
Volume (Å^3), Z	6516(1), 4
Density (calculated) (g/cm^3)	1.58
Absorption coefficient (cm^{-1})	39.13
F (000)	3072
2θ range	4.0–55.0°
Scan type	ω
h, k, l Limits	−40–40, 0–12, 0–28
Reflections collected	8143 total, 7488 independent, $R_{(int)}$ = 0.0226
Reflections observed	5980, $F > 3\sigma(F)$
Absorption correction	Semi-empirical (XEMP)
Min./Max. transmission	0.5138/0.9730
Refinement method	Full-matrix least-squares (XLS)
Goodness-of-fit	S = 1.27
Final residuals	$R(F)$ = 0.0391, w$R(F)$ = 0.0304
Max./min. excursions (e Å^{-3})	1.23 and −0.78

Table 2. Selected bond distances (Å) and angles (°) for (dppe)(CO)$_3$Re–OC(O)O–Re(CO)$_3$(dppe) · 2C$_6$H$_6$

Re—P(1)	2.476(1)	Re—P(2)	2.458(1)
Re—O(4)	2.127(3)	Re—C(1)	1.897(5)
Re—C(2)	1.946(5)	Re—C(3)	1.919(5)
P(1)—C(5)	1.837(5)	P(1)—C(7)	1.828(5)
P(1)—C(13)	1.830(5)	P(2)—C(6)	1.829(5)
P(2)—C(19)	1.820(4)	P(2)—C(25)	1.832(5)
O(1)—C(1)	1.159(6)	O(2)—C(2)	1.133(7)
O(3)—C(3)	1.162(6)	O(4)—C(4)	1.315(5)
O(4′)—C(4)	1.315(5)	O(5)—C(4)	1.228(9)
C(5)—C(6)	1.532(6)		

P(1)—Re—P(2)	81.5(1)	P(1)—Re—O(4)	79.4(1)
P(2)—Re—O(4)	80.6(1)	P(1)—Re—C(1)	94.6(2)
P(2)—Re—C(1)	96.1(2)	O(4)—Re—C(1)	173.6(2)
P(1)—Re—C(2)	96.4(2)	P(2)—Re—C(2)	175.4(1)
O(4)—Re—C(2)	95.0(2)	C(1)—Re—C(2)	88.1(2)
P(1)—Re—C(3)	173.0(2)	P(2)—Re—C(3)	91.7(2)
O(4)—Re—C(3)	97.8(2)	C(1)—Re—C(3)	87.8(2)
C(2)—Re—C(3)	90.3(2)	Re—P(1)—C(5)	107.0(2)
Re—P(1)—C(7)	117.2(2)	C(5)—P(1)—C(7)	106.4(2)
Re—P(1)—C(13)	120.2(2)	C(5)—P(1)—C(13)	102.0(2)
C(7)—P(1)—C(13)	102.5(2)	Re—P(2)—C(6)	104.9(2)
Re—P(2)—C(19)	120.1(2)	C(6)—P(2)—C(19)	104.9(2)
Re—P(2)—C(25)	117.4(1)	C(6)—P(2)—C(25)	105.7(2)
C(19)—P(2)—C(25)	102.3(2)	Re—O(4)—C(4)	125.8(3)
Re—C(1)—O(1)	178.0(5)	Re—C(2)—O(2)	176.7(4)
Re—C(3)—O(3)	174.7(4)	O(4)—C(4)—O(4′)	111.4(6)
O(4)—C(4)—O(5)	124.3(3)	P(1)—C(5)—C(6)	110.0(3)
P(2)—C(6)—C(5)	108.8(3)	P(1)—C(7)—C(8)	123.6(4)
P(1)—C(7)—C(12)	118.5(4)	P(1)—C(13)—C(14)	120.7(4)
P(1)—C(13)—C(18)	120.8(4)	P(2)—C(19)—C(20)	121.8(4)
P(2)—C(19)—C(24)	119.5(4)	P(2)—C(25)—C(26)	118.7(4)
P(2)—C(25)—C(30)	122.7(4)		

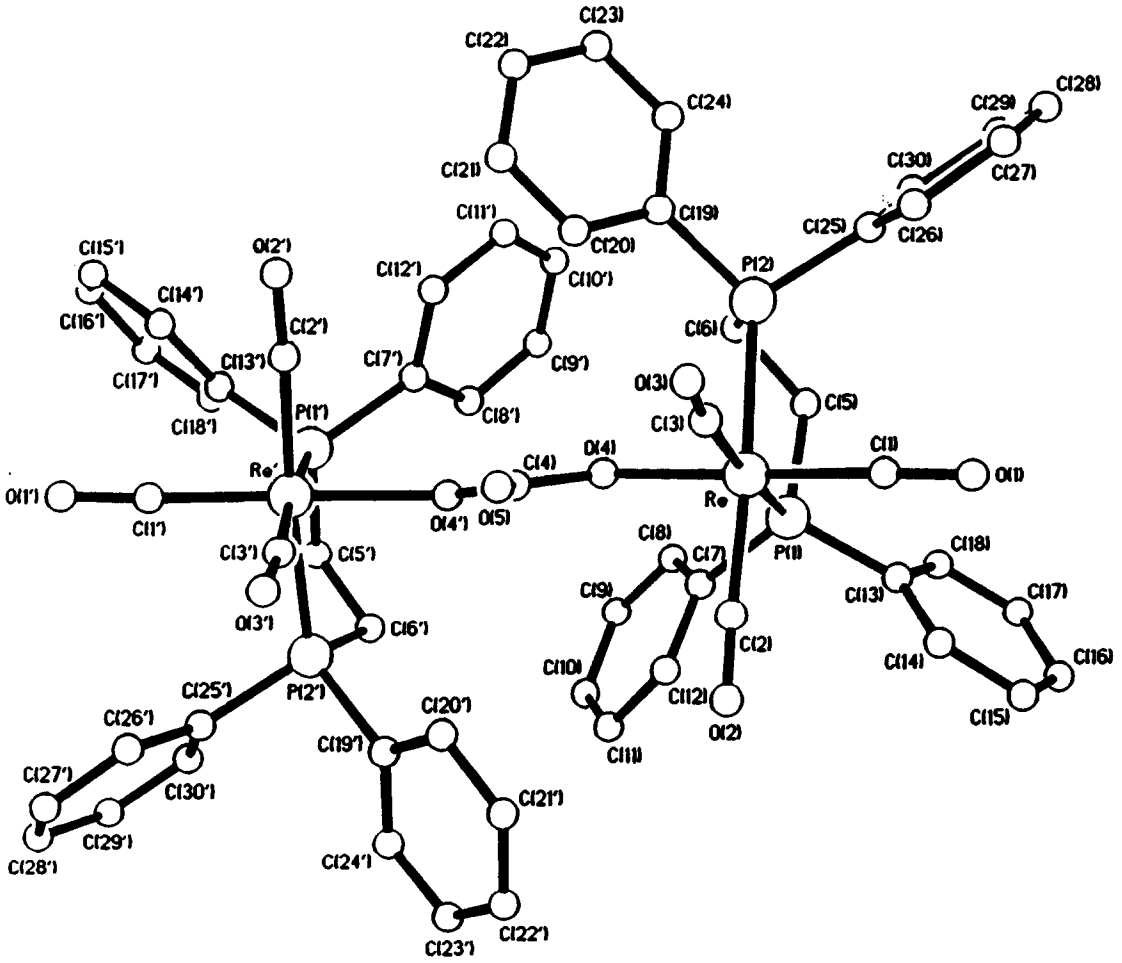

Fig. 1. Perspective drawing of molecule $(dppe)(CO)_3Re–OC(O)O–Re(CO)_3(dppe)$.

acyl oxygen bond, followed by decarbonylation of the cation.

If only a small sample of the bridging carbonato complex is desired, the most convenient preparation consists of dissolving the methoxide, *fac*-$Re(CO)_3(dppe)OCH_3$ [17] in a minimum of benzene whereupon the desired transformation occurs in about 1 h. The properties of the bridging carbonato complex obtained by this procedure were indistinguishable from those of the carbonato complex obtained from the ethyl carboxylate. The crystal used for the X-ray diffraction study was obtained from the alkoxide in this fashion. Apparently the alkoxide, which is known to be a scavenger for carbon dioxide, reacts with adventitious carbon dioxide to form the corresponding methyl carbonate. The conversion of the methyl carbonate to the bridging carbonato complex is analogous to that reported for the related Re(diars) complex [13] and requires a very small quantity of water. Our benzene solvent was not dried but when benzene that had been carefully dried and degassed was used, no bridging bicarbonato complex was formed. On treatment of the bridging carbonato complex with HCl or *p*-toluenesulfonic acid monohydrate, CO_2 is immediately evolved and the corresponding covalent compounds $Re(CO)_3(dppe)Cl$ and $Re(CO)_3(dppe)OTs$ are formed, respectively, in high yield.

REFERENCES

1. Gibson, D. H., *Chem. Rev.*, 1996, **96,** 2063.
2. Palmer, D. A. and Van Eldik, R., *Chem. Rev.*, 1983, **83,** 651.
3. Mandal, S. K., Ho, D. M. and Orchin, M., *Organometallics*, 1993, **12,** 1714.
4. Yoshida, T., Thorn, D. L., Okano, T., Ibers, J. A. and Otsuka, S., *J. Am. Chem. Soc.*, 1979, **101,** 4212.
5. Ganguly, S., Mayue, J. T. and Roundhill, D. M., *Inorganic Chem.*, 1992, **31,** 3831.
6. Flynn, B. R. and Vaska, L., *J. Am. Chem. Soc.*, 1973, **95,** 5081.
7. Tsuda, T., Chujo, Y. and Saegusa, T., *J. Am. Chem. Soc.*, 1980, **102,** 431.

8. Sullivan, B. P. and Meyer, T. J., *J. Chem. Soc., Chem. Commun.*, 1984, 1244.
9. Yamamoto, T., Kubota, M. and Yamamoto, A., *Bull. Chem. Soc. Japan*, 1980, **53,** 680.
10. Menif, R., Reibenspies, J. and Martell, A. E., *Inorganic Chem.*, 1991, **30,** 3446.
11. Kitajima, N., Fujisawa, K., Koda, T., Hikichi, S. and Moro-oka, Y., *J. Chem. Soc., Chem. Comm.*, 1990, 1357.
12. Bang, E., Eriksen, J., Glerup, J., Monsted, L., Monsted, O. and Weihe, H., *Acta Chem. Scand.*, 1991, **45,** 367.
13. Simpson, R. D. and Bergman, R. G., *Organometallics*, 1992, **11,** 4306.
14. Li, G. Q., Burns, R. M., Mandal, S. K., Krause, J. A. and Orchin, M., *J. Organomet. Chem.*, in press.
15. Mandal, S. K., Ho, D. M. and Orchin, M., *Polyhedron*, 1992, **11,** 2055.
16. Zingales, F., Graziani, M., Faraone, F. and Belluco, U., *Inorg. Chim. Acta*, 1967, 172.
17. Mandal, S. K., Ho, D. M. and Orchin, M., *Inorganic Chem.*, 1991, **30,** 2244.
18. SHELXTL-PLUS 3.43 for R3/V and R3m/V Crystallographic Systems. Sheldrick, G. M., University of Goettingen, Germany, and Siemans/Nicolet Analytical X-Ray Instruments, Inc., Madison, WI, 1988.
19. Leoni, P., Pasquali, M., Salsini, L., Bugno, C., Braga, D. and Sabatino, P., *J. Chem. Soc., Dalton Trans.*, 1989, 155.

Pergamon

PII: S0277-5387(97)00407-5

Polyhedron Vol. 17, No. 4, pp. 613–616, 1998
© 1998 Elsevier Science Ltd
All rights reserved. Printed in Great Britain
0277-5387/98 $19.00+0.00

Synthesis and structural characterisation of the zinc carboxylate bis(Ferrocenedicarboxylato) bis(1-methylimidazole)dizinc(II). A structure displaying a bimetallic macrocyclic framework

Thomas A. Zevaco,[a]* Helmar Görls[b] and Eckhard Dinjus[c]

[a] Projektgruppe "CO_2-Chemie" an der Friedrich-Schiller-Universität Jena, Lessingstraße 12, 07743 Jena, Germany

[b] Institut für Anorganische und Analytische Chemie der Universität, August Bebel Straße 2, 07743 Jena, Germany

[c] Forschungszentrum Karlsruhe GmbH, Institut für Technische Chemie-Chemisch-Physikalische Verfahren, Postfach 3640, 76021 Karlsruhe, Germany

(Received 21 July 1997; accepted 1 October 1997)

Abstract—The synthesis, spectral characterisation and X-ray structure determination of the first zinc(II) ferrocenedicarboxylate $[Zn(1,1'\text{-Ferdc})(1\text{-methylimidazole})_2]_2$, **1**, ($1,1'\text{-}H_2$ferdc = 1,1′-ferrocenedicarboxylic acid) is described. The molecular structure of **1** consists of a centrosymmetric cyclic dimer exhibiting a slightly distorted tetrahedral geometry around the zinc atoms. The ferrocenedicarboxylic acid acts as a *syn*-bound O,O′-bridging ligand. © 1998 Elsevier Science Ltd. All rights reserved

Keywords: crystal structure; zinc complex; carboxylate; imidazole; ferrocene; dimer.

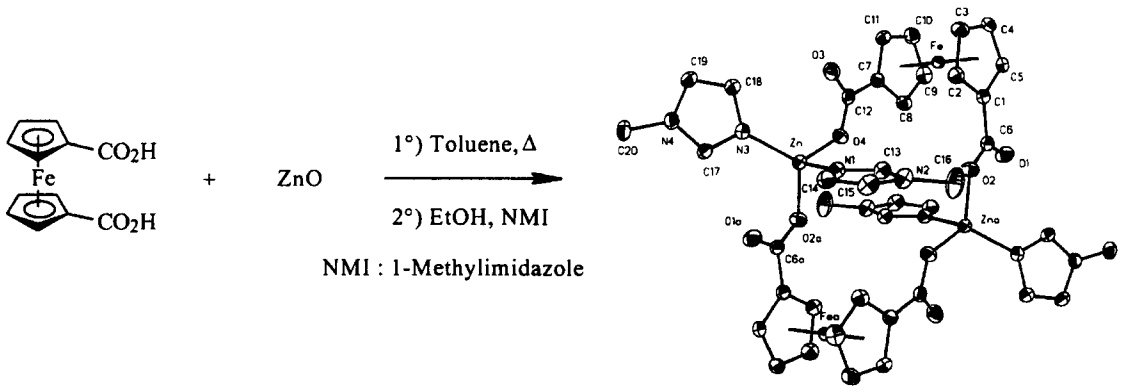

The zinc(II) carboxylates are known to be effective catalysts for the copolymerisation of CO_2 and epoxides [1]. The most efficient carboxylates are obtained from dicarboxylic acids and display most of the time polymeric structures [2]. The solid state structure of such carboxylates as well as the exact nature of the active site remain controversial. We became interested in systems involving soluble zinc(II) carboxylates which should allow an easier investigation of the reac-

* Author to whom correspondence should be addressed.

tion of carbon dioxide with epoxides. Carboxylic acids based on a ferrocene moiety afford monomeric as well as polymeric transition metal carboxylates [3–6]. Structural characterisations of mono- and dicarboxylato derivatives of ferrocene have been undertaken in the case of copper [5,6] and iron [4]. Surprisingly, no crystallographic data were available, to our knowledge, for ferrocenecarboxylates of zinc(II). The steric restrictions induced by the ferrocene fragment as well as the dependence of structure on additional coligands might produce new versatile zinc carboxylates. We decided therefore to undertake the synthesis and structural characterisation of such zinc carboxylates. We report here the first X-ray structure determination of a zinc(II) ferrocenecarboxylate.

The reaction of the 1,1′-ferrocenedicarboxylic acid [7] (1 equiv.), noted 1,1′-H_2Ferdc, with zinc oxide (1 equiv.) under reflux in toluene afforded an amorphous orange solid. After filtration, the orange precipitate was dissolved in a hot ethanolic solution of 1-methylimidazole (10 mol%), and was allowed to stand ca two weeks at 4°C and afforded orange needles (yield 40%). The spectroscopic results [8,9] suggest a non-polymeric compound presenting a "*O,O′*-bis(monodentate)" co-ordination of the dicarboxylate ligand with the formula [Zn(1,1′-ferdc)(1-methylimidazole)$_2$]$_n$. Successive recrystallisations yield finally to prismatic single crystals suitable for an X-ray structural characterisation.

Crystal data for **1**. $C_{40}H_{40}N_8O_8Zn_2Fe_2 \cdot 2C_2H_5OH$, Mr = 1187.52 gmol^{-1}, orange prisms, size 0.40 × 0.38 × 0.36 mm^3, triclinic, space group P-1 (No. 2), a = 10.114(2), b = 10.515(2), c = 13.735(4) Å, α = 112.07(1), β = 105.48(1), γ = 103.83(1)°, V = 1296.1(5) Å^3, Z = 1, $\rho_{calcd.}$ = 1.531 gcm^{-3}, μ (Mo–K_α) = 15.31 cm^{-1}, ψ-scan (*trans*$_{min}$: 0.531; *trans*$_{max}$ 0.991), F(000) = 616, 5558 reflections in h, $\pm k$, $\pm l$, measured in the range 2.43° ≤ Θ ≤ 26.29°, 5249 independent reflections, R_{int} = 0.022, 4713 reflections with $F_o > 4\sigma(F_o)$, 335 parameters, R = 0.041, wR^2 = 0.114, GOF = 1.024, largest difference peak: 1.19 e Å^{-3}.

X-ray diffraction data. CAD4 diffractometer using graphite-monochromated Mo–K_α radiation. The crystals were mounted in a cold nitrogen stream. Data were corrected for Lorentz, polarisation effects, and for absorption [17]. The structure was solved by direct methods (SHELXS) [18] and refined by full-matrix least squares techniques against F^2 (SHELXL-93) [19]. The hydrogen atoms were included at calculated positions with fixed thermal parameters; all nonhydrogen atoms were refined anisotropically. XP (Siemens Analytical X-ray Instruments, Inc.) was used for structure representations.

The molecular structure with atomic labelling is given in Fig. 1. The molecule is a centrosymmetric, cyclic dimer constituted by the linkage of two (1-methylimidazole)$_2$Zn ($O_2CC_5H_4$-Fe-$C_5H_4CO_2$) units. Only one example of such a cyclic bimetallic framework was previously reported in the case of the ferrocenophane [Fe(C_5H_4Se)$_2$Zr(C_5H_4-^{t}Bu)$_2$]$_2$ [10].

The so-formed macrocycle presents two bridging *O,O′*-ferrocenedicarboxylato moieties with a monodentate *syn*-co-ordination of the carboxy groups. The neutral imidazole ligands can be classified in two groups: the "exocyclic" imidazoles pointing out of the macrocycle and the "endocyclic" imidazoles pointing towards the cavity of the macrocycle. The overall conformation of this macrocycle can be regarded as an *anti* conformation in respect to the usual definition used with [1,1′] ferrocenophanes [11]. The shortest non-bonding contacts found within the dimer occur between acidic sp^2 carbons of the exocyclic imidazole moieties and pendant oxygen atoms of the carboxy groups [O(3)···C(18): 3.116(3) Å; O(3)···H(18): 2.450(3) Å and O(1a)···C(17): 2.973(3) Å; O(1a)···H(17): 2.254(3) Å]. These distant contacts cannot be considered as hydrogen bonds owing to the inappropriate angular geometry [12].

Each zinc atom occupies the centre of a tetrahedron characterised by a dihedral angle of 89.3(1)° between the planes defined by N(3)—Zn—N(1) and O(4)—Zn—O(2a). The angles within the polyhedron are shifted from the theoretical value and range from 97.0(1)° to 118.8(1)°, the N(3)—Zn—O(4) angle being the greatest observed in the molecule.

The Zn—O bond lengths, 1.982(3) and 1.975(3) Å, are within the range reported for tetrahedral environments [13]. The carboxylato groups are bound in a monodentate configuration as shown by the distances measured between pendant carboxylic oxygens and zinc atom [2.975(3) and 2.815(3) Å]. The Zn—N bond lengths, 1.997(3) and 2.010(3) Å, are similar to those found in other tetrahedral zinc complexes of imidazole derivatives as already documented with, e.g. [Zn(imidazole)$_2$(O_2CCH_3)$_2$] [14] [Zn—N: 1.996(2)–2.003(3) Å] and are shorter than those found in octahedral imidazole complexes like [Zn(quinaldinato)$_2$(1-methylimidazole)$_2$] [15] (2.144(2) Å). The η^5-C_5H_4 planes in the ferrocenedicarboxylate ligands are essentially coplanar, displaying a dihedral angle of 1.5(1)°; the cyclopentadienyles ligands deviate from the eclipsed conformation by 4.5(1)°. Individual Fe—C_{ring} distances range from 2.036(4) to 2.054(4) Å [mean Fe-ring distance: 1.652(3) Å] and are comparable to those found in other ferrocenecarboxylato compounds [4–6] [2.030(6)–2.071(3) Å]. As was found to be the case for ferrocenecarboxylato compounds of copper(II) [4,5], the O_2C—C_4H_5 fragments are not strictly planar. The torsionnal angles for theses moieties are 6.5(1)° and 12.5(1)° about the C(6)—C(1) and C(12)—C(7) linkages respectively.

The other bond lengths and bond angles found within the ferrocenecarboxylic acid and 1-methylimidazole molecules are in good agreement with those previously reported [15,16].

The crystal structure of the complex consists of separated discrete molecular units and ethanol molecules of solvatation which are separated by normal

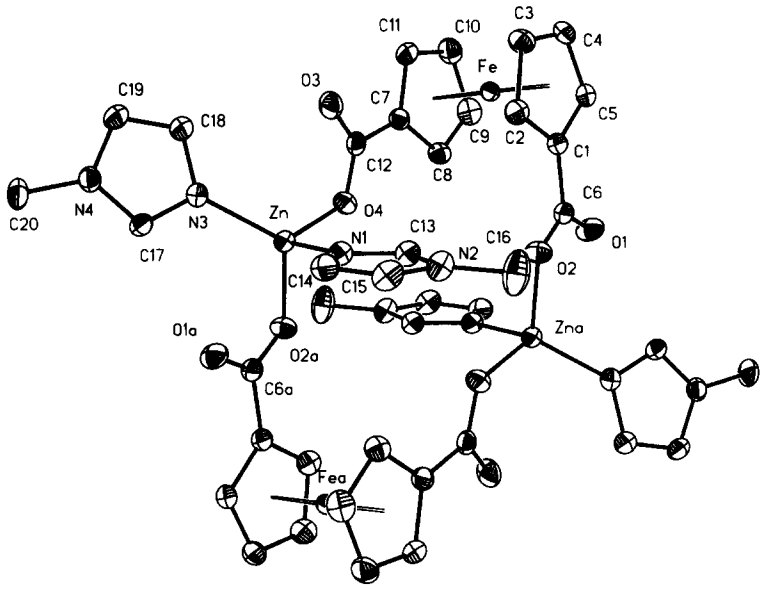

Fig. 1. Molecular structure of $[Zn_2(1,1'\text{-Ferdc})_2(1\text{-methylimidazole})_4]\cdot 2EtOH$ with 50% probability thermal ellipsoids. Solvent molecules and hydrogen atoms are omitted for clarity. Symmetry transformation used to generate equivalent atoms: (a): $1-x, -y, -z$. Key bond lengths (Å) and angles (°): Zn—O(4), 1.982(3), Zn—O(3) 2.975(3), Zn—O(2a) 1.975(3), Zn—O(1a) 2.815(3), Zn—N(3) 1.997(3), Zn—N(1) 2.010(3), C(6)—O(1) 1.230(5), C(6)—O(2) 1.289(4), C(3)—O(12) 1.243(5), C(4)—O(12) 1.281(4), Fe—Fe(a) 9.474(3), Zn—Zn(a) 5.682(3), Fe—Zn 5.696(3). N(1)—Zn—N(3) 112.25(9), O(2a)—Zn—O(4) 113.71(8), O(2a)-Zn-N(3) 112.07(8), N(3)—Zn—O(4) 101.95(9), O(1a)—C(6a)—O(2a) 122.4(2), O(3)—C(12)—O(4) 124.8(3).

Van der Waals distances. The crystal structure exhibits no abnormally short intermolecular contacts.

More work is currently in progress to control the degree of oligomerisation of such bimetallic compounds. Likewise, the dependence of the dimeric structure on the nature of the present neutral coligands has to be rationalised.

Acknowledgments—The authors wish to thank the Max Planck Gesellschaft for financial support and for a postdoctoral fellowship (T.A.Z.).

REFERENCES

1. (a) Inoue, S., *Makromol. Chem., Rapid Commun.*, 1980, **1,** 775; (b) Soga, K., Uenishi, K., Ikeda, S., *J. Polym. Sci. Polym. Chem. Ed.*, 1979, **17,** 415.
2. (a) Motika, S. A., Pickering, T. L., Rokicki, A. and Stein, B. K., U.S. Pat. 5,026,676; (b) Sun, H.-N., U.S. Pat. 4,783,445; (c) Rokicki, A., U.S. Pat. 4,943,677; (d) Karipides, A., *Acta Cryst.*, 1980, **B36,** 1659.
3. Togni, A. and Hayashi; T., *Ferrocenes*, VCH, Weinheim, 1995. p. 317 and references cited therein.
4. Christie, S. D., Subramanian, S., Thompson, L. K. and Zaworotko, M. J., *J. Chem. Soc., Chem. Commun.*, 1994, 2563.
5. Churchill, M. R., Li, Y.-J., Nalewajek, D., Schaber, P. and Dorfman, J., *Inorg. Chem.*, 1985, **24,** 2684.
6. (a) Latif Abuhijleh, A. and Woods, C., *J. Chem. Soc., Dalton Trans.*, 1992, 1249; (b) Latif Abuhijleh, A., Pollitte, J. and Woods, C., *Inorg. Chim. Acta.*, 1994, **215,** 131.
7. The 1,1′-ferrocenedicarboxylic acid was prepared according to the following reference: Rausch, M. D. and Ciappenelli, D. J., *J. Organomet. Chem.*, 1967, **10,** 127.
8. Spectroscopic data for $[Zn_2(1,1'\text{-Ferdc})_2(1\text{-methylimidazole})_4]\cdot 2EtOH$ IR (cm^{-1}, KBr pellet): 3118 m for [$\nu(C_{sp^2}$-H)]; 2924 and 2854 m for [$\nu(C_{sp^3}$-H)]; 1608 vs, 1580 s for [ν_{as}(COO)]; 1540 m for [ν_s(C = N)]; 1332 vs for [ν_s(COO)]; 658 m for [δ(COO)]; 1244, 1230m [ν(ring Im.)]; 864, 660 m [δ (ring Im.)]. The $\delta[\nu_{as\text{-}s}$(COO)] value of 275 cm^{-1} suggests a terminal co-ordination of the carboxylate [9]. ^{1}H-NMR in dmso d_6, δ ppm (multiplicity, attribution): 7.72 (s, imidazole H2); 7.45 (s, imidazole H4); 6.90 (s, imidazole H5); 4.36 (s, broad, H2-5_{Cp}); 3.77 (s, CH_3). ^{13}C-NMR, δ ppm: 183.03(-COO); 71.72, 70.27, 66.57 (C1, C2-C5 and C3-C4 of the Cp ring); 141.11, 134.74, 119.88 (imidazole C2, C4 and C5 sp^2), 30.91(imidazole C sp^3).
9. Deacon, G. B. and Phillips, R. J., *Coord. Chem. Rev.*, 1980, **33,** 227.
10. Broussier, R., Gobet, Y., Amardeil, R., Da Rold, A., Kubicki, M. M. and Gautheron, B., *J. Organomet. Chem.*, 1993, **445,** C4.
11. (a) Löwendahl, J.-M. and Hakansson, M., *Organometallics*, 1995, **14,** 4736; (b) Mueller-Westerhof, U. T., Swiegers, G. F. and Haas, T. J., *Organometallics*, 1992, **11,** 3411.

12. (a) Desiraju, G. R., *Acc. Chem. Res.*, 1996, **29,** 441; (b) Subramanian, S. and Zaworotko, M. J., *Coord. Chem. Rev.*, 1994, **137,** 357.
13. Kennard, C. H. L., Smith, G., O'Reilly, E. J., Stadnicka, K. M. and Oleksyn, B. J., *Inorg. Chim. Acta*, 1982, **59,** 241.
14. Horrocks W. D., Jr, Ishley, J. N. and Whittle, R. R., *Inorg. Chem.*, 1982, **21,** 3265.
15. Zevaco, T. A., Görls, H. and Dinjus, E., *Inorg. Chim. Acta*, in press.
16. (a) Palenik, G. J., *Acta Cryst.*, 1969, **24,** 2744; (b) Takusagawa, F. and Koetzle, T., *Acta Cryst.*, 1979, **B35,** 2888.
17. *MOLEN, An Interactive Structure Solution Procedure*, Enraf-Nonius, Delft, The Netherlands, 1990.
18. Sheldrick, G. M., *Acta Cryst.*, 1990, **A46,** 467.
19. Sheldrick, G. M., University of Göttingen, Germany, 1993.

Pergamon

PII: S0277-5387(97)00361-6

Polyhedron Vol. 17, No. 4, pp. 617–621, 1998
© 1998 Elsevier Science Ltd
All rights reserved. Printed in Great Britain
0277-5387/98 $19.00+0.00

COMMUNICATION

Synthesis, structure, and characterization of $(MePh_2P)_{10}Au_{12}Ag_{13}Br_9$: The first example of a neutral bi-icosahedral Au–Ag cluster with a novel seven-membered satellite ring of bridging ligands

Boon K. Teo,[a]* Hy Dang,[a] Charles F. Campana[b] and Hong Zhang[a]*

[a] Department of Chemistry, University of Illinois at Chicago, Chicago, IL 60607

[b] Siemens Analytical X-Ray Instruments, Madison, WI 53719

(Received 11 July 1997)

Abstract—The synthesis, structure, and characterization of the first example of a neutral vertex-sharing bi-icosahedral bimetallic (Au–Ag) cluster, $(MePh_2P)_{10}Au_{12}Ag_{13}Br_9$, with a novel 7-membered satellite ring of bridging halide ligands are reported. © 1998 Elsevier Science Ltd. All rights reserved

Keywords: cluster of clusters; bi-icosahedral cluster; mixed-metal cluster; rotamer; roulettamer

Many high nuclearity clusters consist of smaller clusters as building blocks [1–3]. These clusters may be termed "clusters of clusters". Our recent synthetic and structural efforts in this area led to a series of vertex-sharing polyicosahedral mixed-metal clusters with the icosahedron as the basic building block [4–11]. Particularly interesting is the bi-icosahedral series wherein the relative rotation (Θ, in degrees) of the two icosahedra gives rise to different metal configurations (rotameric forms, R(Θ)), as exemplified by R(9) of $[(p\text{-}Tol_3P)_{10}Au_{13}Ag_{12}Cl_7]^{2+}$ (**1**) [4] and R(36) of $[(Ph_3P)_{10}Au_{13}Ag_{12}Br_8]^+$ (**2**) [5]. Here R(0) represents the staggered-eclipsed-staggered (ses) and R(36) the staggered-staggered-staggered (sss) configurations of the four metal pentagons of the bi-icosahedral metal framework. In fact, **1** and **2** are examples of two series of bi-icosahedral bimetallic clusters of the general formulas $[(R_3P)_{10}Au_{13}Ag_{12}X_7]^{2+}$ and $[(R_3P)_{10}Au_{13}Ag_{12}X_8]^+$, respectively, with a satellite ring of five or six halide ligands (hereafter referred to as 5- and 6-ring series, respectively) bridging the two inner silver pentagons, as portrayed in Chart I(a) and (b) for **1** and **2**, respectively. Within each series, different bridging ligand arrangements (roulettameric forms) have been observed. For example, for the 6-ring series, the roulettameric-rotameric forms, ranging from qd_5-R(0) [6]. to $o\text{-}q_2d_4$-R(0) [7], to $o\text{-}t_2d_4$-R(18) [8], to $p\text{-}t_2d_4$-R(36) [5], to $p\text{-}d_2t_4$-R(36) [9], have been observed. Here, d, t, and q denote double, triple, and quadruple bridging, respectively. We report herein the synthesis and structure of a new bi-icosahedral Au–Ag cluster $(MePh_2P)_{10}Au_{12}Ag_{13}Br_9$ (**3**) with an unprecedented roulettameric form which represents the first example of a novel 7-membered satellite ring (hereafter referred to as the 7-ring series) of bridging halide ligands (see Chart I(c)).

The title cluster compound **3** was synthesized by reducing a mixture of $MePh_2PAuBr$ and $[MePh_2PAgBr]_4$ in absolute ethanol with $NaBH_4$. The dark brown product, after removal of unreacted starting materials and impurities, was purified by recrystallization twice from CH_2Cl_2. Rectangular plate crystals of **3** were grown from CH_2Cl_2/EtOH (5 : 1

* Authors to whom correspondence should be addressed.

ratio) and characterized by X-ray crystallography,† elemental analysis,‡ ^{31}P NMR, and UV-Vis spectroscopy (*vide infra*). The results are consistent with the formulation $(MePh_2P)_{10}Au_{12}Ag_{13}Br_9 \cdot 9EtOH$. Figures 1(a) and (b) portray the molecular architecture of **3** while Fig. 1(c) depicts the 7-membered satellite ring of bridging bromide ligands. The metal framework can be described as two Au-centered icosahedra sharing a vertex (Ag13). There are 10 $MePh_2P$ ligands, each coordinated to one of the 10 peripheral Au atoms with an average Au-P distance of 2.29 Å. Seven bridging bromide ligands (Br1 to Br7) connect the two Ag_5 pentagons while two terminal bromide ligands (Br8 and Br9) coordinate to the two apical Ag atoms (Ag11 and Ag12) with an average Ag—Br distance of 2.53 Å. The two metal icosahedra are rotated by ca 36°, giving rise to the R(36) rotameric form of the metal configuration. The crystal structure showed that the title cluster is a neutral molecule with no anions, which is consistent with its solubility in nonpolar solvents such as toluene and insolubility in polar solvents such as CH_3CN. Hence, the title compound represents the first example of a neutral bimetallic bi-icosahedral Au—Ag cluster since all previously known bi-icosahedral Au—Ag clusters bear either +2 (5-ring series) or +1 (6-ring series) charges. As such, the title cluster completes the sequence of the progression from 5- to 6- to 7-membered satellite rings of bridging halide ligands for this particular series of bimetallic bi-icosahedral clusters, as exemplified by **1, 2,** and **3,** along with the change in the overall charge from +2 to +1 to 0, respectively (cf Chart I). This charge difference is due to the fact that these bi-icosahedral clusters conform to the Polyoctet rule of $8n = 8 \times 2 = 16$ electron system (namely, 25(M)–7(X) – 2 = 16, 25(M)–8(X) – 1 = 16, and 25(M)–9(X) = 16, for **1, 2,** and **3,** respectively) [11].

The most important structural feature of **3** is the 7-membered satellite ring of the bridging ligands around the "equator" of the bi-icosahedral metal core (see Fig. 1(c)). The seven bridging bromide ligands form a slightly distorted heptagon with an average Br ··· Br distance of 3.96 Å, very close to the van der Waals contact of 3.90 Å [12]. The seven bridging bromide ligands are coplanar with the shared vertex lying in the plane. The common plane bisects the cluster into two icosahedra. All seven bridging Br ligands can be considered as double bridging with an average Ag—Br distance of 2.70 Å. However, there are additional contacts at Ag9 ··· Br1, 3.41 Å; Ag5 ··· Br3, 3.37 Å; Ag10 ··· Br5, 3.23 Å and Ag1 ··· Br7, 3.34 Å so that Br1, Br3, Br5 and Br7 may also be considered as semi-triple bridging. All bromide ligands form extensive hydrogen bonds with the phosphine ligands. It is apparent that, with the less bulky $MePh_2P$ (in comparison with Tol_3P in **1** or Ph_3P in **2**), the "equatorial ring" of the bi-icosahedral cluster allows the accommodation of seven halide ligands.

The $^{31}P\{^1H\}$NMR spectrum (81.015 MHz, CH_2Cl_2 at RT) of **3** consists of a doublet at 47.9 ppm (standard 85% H_3PO_4) with ^3J(P–Ag) of 78 Hz. We interpret the doublet as due to the *para* Ag atom of the inner Ag_5 pentagon of the same icosahedron.§ The electronic spectrum (in CH_2Cl_2) of **3** (λ_{max}(nm), $\varepsilon \times 10^{-4}$ (M^{-1} cm^{-1}): 328, 5.16; 420, 2.19; 505, 2.54) is very similar to those observed for other vertex-sharing bi-icosahedral clusters [4–9]. However, the lowest-energy absorption, observed at 505 nm, is red shifted by 20 nm from **2**. This band, interpreted by us as the plasmon frequency [13], is sensitive to, and hence highly characteristic of, the metal combination, the ligand environment, as well as the overall charge. We believe the observed 20 nm shift of this absorption band to a longer wavelength is primarily due to a combination of the increased number of bridging halide ligands (from 6 to 7) and the reduced charge (from +1 to 0) in going from **2** to **3**.

As observed in other vertex-sharing polyicosahedral Au–Ag clusters [4–11], the metal–metal bond lengths of **3** follow the trend of Au–Au < Au–Ag ⩽ Ag–Ag (see Fig. 1 caption), indicating the bonding strength of Au–Au > Au–Ag ⩾ Ag–Ag. More importantly, the intraicosahedral metal–metal distances are shorter than the intericosahedral distances, indicating that intraicosahedral bonding is significantly stronger than the intericosahedral bonding. These observations provide strong structural support for the "cluster of clusters" description [11] of this class of vertex-sharing polyicosahedral clusters

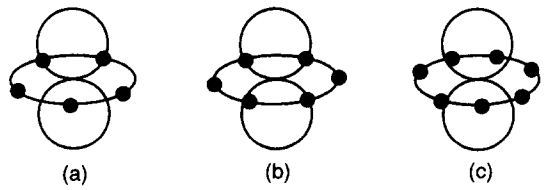

Chart I. Schematic representations of the 5-, 6-, and 7-membered satellite rings of bridging ligands (solid dots on ellipses) in vertex-sharing bi-icosahedral (open circles) clusters.

† Crystal data: Single-crystal X-ray diffraction data were collected at 173°K, using Siemens SMART X-ray diffractometer equipped with a CCD area detector and a Mo-target X-ray tube ($\lambda = 0.71073$ Å). $(MePh_2P)_{10}Au_{12}Ag_{13}Br_9 \cdot 9EtOH$: monoclinic $P2_1/c$, $a = 19.3984(5)$, $b = 29.9067(8)$, $c = 28.8959(7)$ Å, $\beta = 107.651(1)°$; $V = 15974.5(7)$ Å^3, and $Z = 4$. Anisotropic (heavy atoms)-isotropic (carbon atoms) refinement gave $R_1 = 7.1\%$ for 5166 independent reflections ($2\Theta \leqslant 45°$) with $I > 3\sigma$. Atomic coordinates, bond lengths and angles, and thermal parameters have been deposited at the Cambridge Crystallographic Data Center. See Notice to Authors, Issue No. 1.

‡ Anal. by Midwest Microlab (Indianapolis, IN) for dried crystalline samples of $(MePh_2P)_{10}Au_{12}Ag_{13}Br_9$ (MW = 6487.22), Calc. (found): C, 24.07 (24.65); H, 2.02 (2.09)%.

§ Further splittings due to the three *meta* Ag atoms and the two *ortho* Ag atoms were too small to be observed [14].

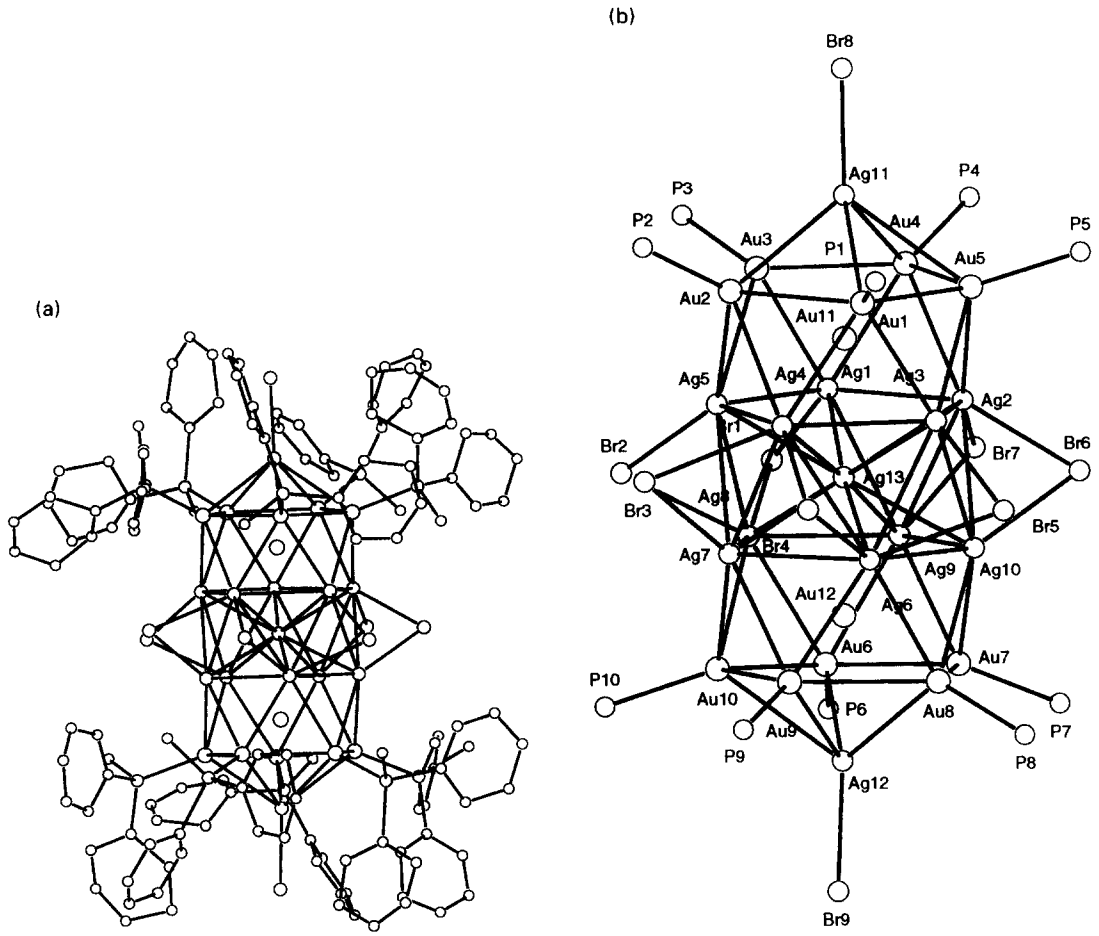

Fig. 1. The molecular architecture of the title cluster $(MePh_2P)_{10}Au_{12}Ag_{13}Br_9$(**3**): (a) general view; (b) the $P_{10}Au_{12}Ag_{13}Br_9$ core (same orientation as in (a)); and (c) the projection of the two silver pentagons onto the plane of the seven bridging Br ligands which form a 7-membered satellite ring around the equator of the bi-icosahedral cluster. The 7-membered Br ring can be described as a distorted heptagon with the following van der Waals contacts: Br1 ··· Br2, 4.00 Å; Br2 ··· Br3, 3.98 Å; Br3 ··· Br4, 3.83 Å; Br4 ··· Br5, 3.95 Å; Br5 ··· Br6, 3.99 Å; Br6 ··· Br7, 3.98 Å; Br7 ··· Br1, 3.96 Å. Some important metal–metal distances (in Å) are (averaged over the idealized D_{5d} symmetry and indicated by a representative bond): Au11—Au1, 2.695; Au11—Ag1, 2.874; Au11—Ag11, 2.804; Au11—Ag13, 2.699; Ag13—Ag1, 2.863; Au1—Au2, 2.894; Au1—Ag3, 2.904; Au1—Ag11, 2.995; Ag1—Ag2, 2.975; Ag1—Ag8, 3.101. Other important distances (averaged) are: Au—P, 2.29 Å; Ag—Br (terminal), 2.53 Å; Ag—Br (bridging), 2.70 Å. See text.

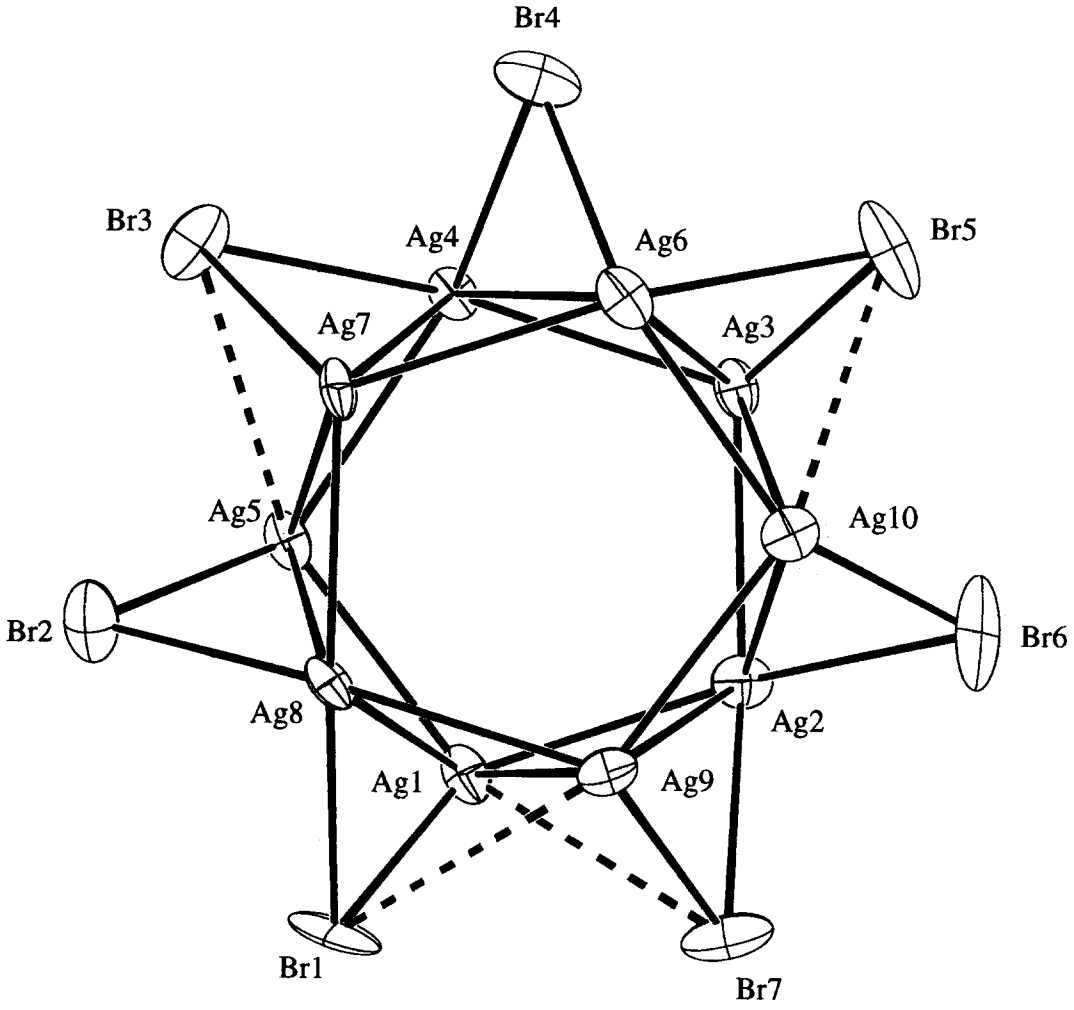

Fig. 1(c).

wherein the 13-atom centered icosahedron serves as the basic building block. In comparison with **2**, however, there is a slight but significant expansion of the two inner Ag pentagons, resulting in an increase in the average intraring Ag—Ag distance from 2.914 Å in **2** to 2.975 Å in **3** and an increase in the average intericosahedral Ag—Ag distance from 2.978 Å in **2** to 3.101 Å in **3**. These expansions are consistent with the increase in the number of bridging Br ligands from 6 (in **2**) to 7 (in **3**). Concomitantly, the average (icosahedral center)-to-(shared vertex) distance decreases from 2.845 Å in **2** to 2.699 Å in **3**.

Finally, the title compound **3** also represents the largest polyicosahedral Au–Ag clusters reported to date using $MePh_2P$ as ligands [14] which has a smaller cone angle [15] than Ph_3P. Apparently the sterically less bulky $MePh_2P$ allows the formation of the 7-membered ring of bridging Br ligands. Furthermore, this ligand also greatly enhances the solubility of these clusters in common organic solvents. As such it opens the door to other vertex-sharing mixed-metal polyicosahedral clusters based on this phosphine ligand as well as to further examples of vertex-sharing bi-icosahedral clusters with a 7-membered satellite ring of bridging halide ligands (work in progress).

Acknowledgment—The authors thank the National Science Foundation and ACS-PRF for the financial support of this research.

REFERENCES

1. Whoolery, A. J. and Dahl, L. F., *J. Am. Chem. Soc.*, 1991, **113**, 6683.
2. Zheng, Z., Knobler, C. B., Mortimer, M. D., Kong, G. and Hawthorne, M. F., *Inorg. Chem.*, 1996, **35**, 1235.
3. Kester, J. G., Keller, D., Huffman, J. C., Benefiel, M. A., Geiger, Jr. W. E., Atwood, C., Siedle, A. R., Korba, G. A. and Todd, L. J., *Inorg. Chem.*, 1994, **33**, 5438.

4. Teo, B. K. and Zhang, H., *Inorg. Chem.*, 1991, **30,** 3115.
5. Teo, B. K., Shi, X. and Zhang, H., *J. Chem. Soc. Chem. Comm.*, 1992, 1195.
6. Teo, B. K., Shi, X. and Zhang, H., *J. Cluster Sci.*, 1993, **4**(4), 471.
7. Teo, B. K., Shi, X. and Zhang, H., *J. Am. Chem. Soc.*, 1991, **113,** 4329.
8. Teo, B. K. and Zhang, H., *Angew. Chem., Int. Ed. Engl.*, 1992, **31,** 445.
9. Teo, B. K., Zhang, H. and Shi, X., *Inorg. Chem.*, 1990, **29,** 2083.
10. Teo, B. K., Zhang, H. and Shi, X., *J. Am. Chem. Soc.*, 1990, **112,** 8552; Teo, B. K., Hong, M., Zhang, H. and Huang, D., *Angew. Chem., Int. Ed. Engl.*, 1987, **26,** 897; Teo, B. K., Shi, X. and Zhang, H., *Inorg. Chem.*, 1993, **32,** 3987.
11. For reviews, see Teo, B. K. and Zhang, H., *Coord. Chem. Rev.*, 1995, **143,** 611; Teo, B. K., Zhang, H. and Shi, X., in *The Chemistry of the Copper and Zinc Triads*, ed. Welch, A. J. and Chapman, S. K., The Royal Society of Chemistry, 211 (1993).
12. Pauling, L., *The Nature of the Chemical Bond*, 3rd Ed. Cornell University Press, Ithaca, New York, 1960, p. 260.
13. Teo, B. K., Keating, K. and Kao, Y.-H., *J. Am. Chem. Soc.*, 1987, **109,** 3494.
14. Copley, R. C. B. and Mingos, D. M. P., *J. Chem. Soc., Dalton Trans.*, 1992, 1755.
15. Tolman, C. A., *Chem. Rev.*, 1977, **77,** 313.

Pergamon

PII: S0277-5387(97)00362-8

Polyhedron Vol. 17, Nos. 5–6, pp. 623–624, 1998
© 1998 Elsevier Science Ltd
All rights reserved. Printed in Great Britain
0277–5387/98 $19.00+0.00

Foreword

Recent advances in metal alkoxide and amide chemistry*

It is difficult to know to whom credit should be given for the synthesis of the first metal alkoxide, perhaps, in part, because one has to agree on the distinction between a metal and a metalloid. Ebelman [1] can reasonably be championed as the father of the field of SOL–GEL chemistry: $Si(OEt)_4 + H_2O \rightarrow SiO_2 + EtOH$. Probably Frankland [2] can be considered the patriarch of metal-amides following his discovery of zinc diethylamide. However, as we approach the turn of the third millennium, it is clear that one man, Donald Bradley, has, more than any other, contributed to the field of metal-alkoxides and amides during the latter half of the 20th century. He and his group pioneered the syntheses and characterizations of numerous metal-alkoxides and amides and mixed metal-alkoxides. In 1956, he formulated a structural theory for metal alkoxides [3] and later one for metal oxo-alkoxides [4]. He and his group were the first to recognize the importance of π-donation and the stabilization of otherwise coordinatively unsaturated species by either π-effects, as in $Mo(NMe_2)_4$ [5], or by steric effects as in $Cr(O^tBu)_4$ [6] and a host of three coordinate metal complexes such as $Cr(NPr^i_2)_3$ [7]. Some 30 years later this has led to the extensive use of π-donor ligands (alkoxides, siloxides, aryloxides, amides and imides) in organometallic chemistry as π-buffers and cyclopentadienyl alternatives [8]. However, Don Bradley was always attracted to the utility of metal-alkoxides and amides in the synthesis of high purity metal-oxides and nitrides [9] and I recall, as a graduate student in the 1960s, watching coworkers studying the hydrolysis of highly purified metal alkoxides and the ammonolysis of metal-amides together with the subsequent pyrolysis of the polymeric products. The target compounds of these endeavors were materials such as lithium niobate, silicon- and aluminum-nitride. What heresy this seemed to this author when one could have been recording the electronic and paramagnetic resonance spectra of say three coordinate transition metal ions and determining the ligand field parameters for metal ions in trigonal planar fields. Well the 1960s were the halcion days for Ligand Field theory, so the reader should forgive this author for some of his lack of foresight for the materials chemistry revolution based on the molecular approach, Le Chemie Douce, which was to explode in the 1980s. Of course, ^{17}O NMR spectroscopy, solid-state magic angle spinning NMR spectroscopy and even single crystal X-ray diffraction were either not available or were far from routine in the 1960s and 1970s and so it is now in the 1990s that we witness the world discovering at a rapid pace that which Don Bradley envisaged during his pioneering studies in the 1950s and 1960s. Every current journal in the field of inorganic chemistry seems to carry new work on metal or mixed metal-alkoxides/alcoholates and oxo-alkoxides and, with each structure, we see further verification of Bradleys structural theories. How many people, and how many times have metal-amide aminolyses been reinvestigated in the pursuit of the chemical vapor deposition of metal-nitride films? Others have surely perfected Bradley's dreams in the syntheses of high purity metal-oxide and -nitride films. Many a patent has been filed and several industrial processes now use this methodology. Even extension of the chemistry of trivalent amides of the 2nd and 3rd row transition metal ions molybdenum and tungsten has allowed a new lease of life to d^3-metal chemistry with the recent isolation of terminal phosphide and arsenide ligands, the cleavage of dinitrogen and the formation and characterization of the first terminal metal-carbide, $[L_3M{\equiv}C]^-$ [10].

Don Bradley has made numerous other significant contributions, particularly in the area of main group 13 : 15 semiconductor precursors but, in keeping with the policy laid down by the founding Editor of this journal, Sir Geoffrey Wilkinson, this is a thematic issue—one on recent developments of metal-alkoxide and amide chemistry. It is thus not an honor issue in the normal sense, but more a tribute to one of inorganic chemistry's true pioneers. What more can a chemist want from his colleagues than to be admired as a human being, highly respected as a scientist and to know that his or her thoughts and work have influenced others, both in his time and, indeed, will continue to do so in life's long afterglow.

MALCOLM H. CHISHOLM
Indiana University
Bloomington, IN 47405
July 1997

* The publisher would like to state that the paper 'Synthesis and characterization of titanium and zirconium complexes bearing diphenyltriazenido ligands' by C. H. Winter *et al.* was published in *Poly.*, 1997, **16**, 4017–4022.

Pergamon

PII: S0277-5387(97)00469-5

Polyhedron Vol. 17, No. 5–6, pp. 625–639, 1998
© 1998 Published by Elsevier Science Ltd
All rights reserved. Printed in Great Britain
0277–5387/98 $19.00+0.00

Group 2/titanium heterometallic alkoxides; their reproducible syntheses and characterization. Crystal structures of the compounds $[SrTi_4(OEt)_{18}]$ and $[Sr_2Ti(OPr^i)_8(Pr^iOH)_3] \cdot 2Pr^iOH$

Ian Baxter,[a] Simon R. Drake,[b] Michael B. Hursthouse,[a]* K. M. Abdul Malik,[a] D. Michael P. Mingos,[b]* John C. Plakatouras,[b] and David J. Otway[b]*

[a]Department of Chemistry, University of Wales Cardiff, P.O. Box 912, Park Place, Cardiff, CF1 3TB, Wales, U.K.

[b]Department of Chemistry, Imperial College of Science, Technology and Medicine, South Kensington, London SW7 2AY, U.K.

(Received 5 November 1997; accepted 10 November 1997)

Abstract—The reactions of either (i) bulk metal in alcohol (EtOH or Pr^iOH); or (ii) the preformed metal alkoxides, $[M(OR)_2(ROH)_x]_n$ with a stoichiometric amount of $Ti(OPr^i)_4$ at reflux yielded the novel hydrocarbon soluble molecular aggregates $[MTi_2(OEt)_{10}(EtOH)_5]_n$ [M = Sr (**1**) and Ba (**2**)]; $[MTi_4(OEt)_{18}]$ [M = Sr (**3**) and Ba (**4**)]; $[M_2Ti(OEt)_8(EtOH)_5]_n$ [M = Sr (**5**) and Ba (**6**)]; and $[Sr_2Ti(OPr^i)_8(Pr^iOH)_3] \cdot 2Pr^iOH$ (**7**). All complexes have been characterized by elemental analyses and spectroscopic methods; (**3**) and (**7**) have also been characterized by X-ray crystallography. The structure of (**3**) is based on a "bow-tie" Ti_2SrTi_2 unit where the strontium is coordinated to two face sharing bioctahedral $Ti_2(OEt)_9^-$ units, via two "terminal" and two "bridging" ethoxo ligands from each $Ti_2(OEt)_9^-$ unit. In (**7**) the Sr_2Ti unit forms a triangle, bridged by three μ_2-Pr^iO ligands and capped by two μ_3-Pr^iO ligands, and further supported by six terminal Pr^iO/Pr^iOH ligands.
© 1998 Published by Elsevier Science Ltd. All rights reserved

Keywords: titanium; strontium; isopropoxide; ethoxide; crystal structure.

In recent years, heterometallic alkoxides have been used as polymerization catalysts and as molecular precursors for high purity ceramic metal oxide superconductors and other speciality materials [1–3]. It is well established that, for obtaining semiconductors or superconductors by MOCVD techniques, the use of a "single source" precursor (in which the different elements are incorporated in a single precursor molecule) increases the quality of the final material [4]. The initial problem, however, is the synthesis of heterometallic compounds with the required ratios of the metals.

* Authors to whom correspondence should be addressed. Tel.: 01222 874068. Fax: 01222 874029.
E-mail: hursthouse@cardiff.ac.uk.

The use of heterometallic alkoxides as precursors for metal oxides gives rise to several important advantages over the use of traditional ceramic routes to these materials [3]. Firstly, the heterometallic oxides may be prepared directly from solutions via a sol-gel process [5], thus avoiding the use of calcination; if the products obtained are amorphous they can be converted into crystalline solids by the use of hydrothermal techniques [6]. Secondly, the purity and stoichiometry of the heterometallic oxides formed is wholly dependent on the stoichiometry of the parent molecular alkoxide complex [1].

Group 2 metal titanates are useful sol-gel precursors in the preparation of dense ferroelectric materials, thin film electronic components, and piezoelectric materials [1,5,7–20]. $BaTiO_3$ (which is just one of plethora of possible phases that metal titanates can

adopt, e.g. $BaTi_4O_9$, $Ba_4Ti_{13}O_{30}$, $Ba_6Ti_{17}O_{40}$) was first processed from metal alkoxide compound in 1969 by Mazdiyasni *et al.* [3]. They hydrolysed a 1 : 1 solution of barium isopropoxide and titanium amyloxide with three equivalents of water and observed an exothermic reaction. The $BaTiO_3$ was formed as a precipitate and dried at 50°C for 12 h (*in vacuo*). This powder was then calcined at 700°C, compacted under pressure, and sintered at 1300°C. This process (and its strontium equivalent) was patented by these workers in 1972 [8] and has remained the benchmark ever since. However, no attempt was made to isolate and structurally characterize the intermediate materials.

In the late 1970s and early 1980s Turova and coworkers [21–23] performed a series of syntheses to obtain various heterometallic alkoxides including some barium titanium alkoxides; however no conclusive data (e.g. NMR, X-ray, TGA studies) were published. Indeed, it is only recently that some data on the structures of this type of complex has started to appear in the literature [24,25]. For example, $[Ba_4Ti_{13}(\mu_3\text{-}O)_{12}(\mu_5\text{-}O)_6(\mu_1,\text{-}\eta^1\text{-}OCH_2CH_2OCH_3)_{12}(\mu_1,\mu_3,\text{-}\eta^2\text{-}OCH_2CH_2OCH_3)_{12}]$ was prepared from the methoxyethoxides of barium and titanium with the addition of six equivalents of water over a period of two months, and considered to be a possible precursor for the phase $Ba_4Ti_{13}O_{30}$ (a high frequency resonator) [26]. Similarly, $[Ba_4Ti_4(\mu_4\text{-}O)_4(\mu_3\text{-}OR)_2(\mu\text{-}OR)_8(OR)_6(ROH)_4][Ba_4Ti_4(\mu_4\text{-}O)_4(\mu_3\text{-}OR)_2(\mu\text{-}OR)_9(OR)_5(ROH)_3]$, a possible precursor for $BaTiO_3$ was prepared from a 1 : 1 mixture of barium metal and $Ti(OPr^i)_4$ in refluxing isopropanol [25]. The colour of the solution was stated to be "transparent dark yellow", suggesting that the solution had started to decompose. [These reactions normally produce colourless crystals from *clear* solutions of isopropanol or ethanol]. Hubert-Pfalzgraf *et al.* [7] recently isolated the mixed metal and mixed ligand compound $[Ba_2Ti_2(tmhd)_4(OEt)_{10}]$ by the reaction of $[Ti(OEt)_4]$ with "$Ba(tmhd)_2$". The structures of the compounds $[MTi_4(OEt)_{18}]$ (M = Ca and Ba) have been reported [27].

Apart from these compounds, we are not aware of any other structurally characterized Group 2/titanium alkoxide species. Some Group 1 metal titanates, e.g. $[LiTi(OPr^i)_5]_2$ have recently been structurally characterized and their NMR and infrared spectra discussed [28]. The dimeric complex was made from "BuLi and $Ti(OPr^i)_4$ in isopropanol. Also recently the syntheses of two $[MTi(OCH_2Pr^i)_5]$ complexes (M = Na or K) have been reported [29]. Many research groups [7,30–40] have produced heterometallic alkoxides and recent examples include: $[BaCu(C_2H_4O_2)_n(C_2H_4O_2)_2]$ (n = 3 or 6) [41], $[H_4BaCu_4(tmhd)_4(OCH_2CH_2OCH_3)_6]$ [42], $[Y_2Ba_2(O)(OEt)_8(tmhd)_6]$ (tmhd = 2,2-6,6-tetramethylheptanedionate) [41], $[BaY_2\{OCH(CF_3)_2\}_4(tmhd)_4]$ [44] and $[Mg_2Sb_4(OEt)_{16}]$ [45].

This paper aims to rectify the general lack of information on Group 2/titanium heterometallic alkoxides and describes the syntheses and characterization of several products obtained from reactions utilizing different stoichiometries of the metals (Ba/Sr : Ti), and also with different alkoxides (e.g. OEt, OPr^i). Single crystal X-ray studies of two of these materials are also reported.

RESULTS AND DISCUSSION

Syntheses of compounds (1)–(7)

Four different ratios of Group 2 metal ethoxide to titanium ethoxide [1 : 1, 1 : 2, 1 : 4, and 2 : 1 (M^{II} : Ti)] were studied, because these ratios mirror those found in the solid state end products. It was hoped that compounds with the correct in-built stoichiometry would be isolated. All reactions were carried out at reflux in EtOH or Pr^iOH with stirring for 1 h after addition of the titanium complex. (i) The use of one equivalent of $Ti(OEt)_4$ does not produce a 1 : 1 compound, but as seen for the isopropoxide based materials, 2 : 1 M : Ti compound [of the same formula as (**5**) and (**6**) below] are regularly obtained; (ii) two equivalents of $Ti(OEt)_4$ produce M = Sr (**1**) and M = Ba (**2**), (iii) four equivalents $Ti(OEt)_4$ M = Sr (**3**) and M = Ba (**4**), (iv) half an equivalent $Ti(OEt)_4$ M = Sr(**5**) and M = Ba (**6**), and (v) Pr^iOH, half an equivalent $Ti(OPr^i)_4$ (**7**). Formation of the 1 : 1 M^{2+} : Ti^{4+} stoichiometric compounds was not possible, due to the preference of these materials to form triangular based compounds [see structures of (**3**) and (**7**) later]. Similar behaviour was also noted for the isopropoxide compound (**7**) (i.e. when either a 1 : 1 or 2 : 1 ratio of the metals is utilized, *only* the 2 : 1 complex is formed). The reactions proceeded rapidly and generally without any colour change.

The heterometallic ethoxides could also be synthesized directly from the metal, without the need to use the preformed Group 2 ethoxide, in which case the metal was placed in a Schlenk tube, ethanol added with $Ti(OEt)_4$ (stoichiometrically as required) and the reaction mixture warmed to reflux. This resulted in a more rapid and vigorous reaction than that with the preformed ethoxide. Dissolution of the metal (pieces or chunks) was completed after 1.5 h. During this reaction a number of unusual colours were observed:

$$\text{Colourless} \xrightarrow{1\text{ min}} \text{Grey} \xrightarrow{10\text{ min}} \text{Purple/Pink} \xrightarrow{10\text{ min}} \text{Royal Blue} \xrightarrow{1\text{ h}} \text{Colourless}$$

The blue colour appeared to be generated by a Ti^{3+} species formed *in situ* which was then reoxidized to Ti^{4+} in the final complex (the products were all colourless crystals). Similar observations were also made earlier [28] during the synthesis of Group 1 titanates,

e.g., $[LiTi(OPr^i)_5]_2$. The formulations were based on C, H microanalyses, IR and multinuclear NMR studies. Complexes **3** and **7** were also characterized by X-ray analysis.

General physical data

The physical data for (**1**)–(**7**) are summarized in Table 1. The melting points of the compounds are considerably different from those of the starting materials (strontium and barium ethoxide), suggesting that they are definitely mixed metal compounds. All the compounds were extremely air and moisture sensitive. They were isolated as colourless crystalline solids, but with differences in their crystallinities; (i) the 1 : 2 compounds (**1**) and (**2**) were obtained as very large crystalline masses; (ii) the 1 : 4 complexes (**3**) and (**4**) were microcrystalline; and finally the 2 : 1 complexes (**5**)–(**7**) were obtained as large parallelpiped crystals that tended to grow upwards from the bottom of the Schlenk. They are all highly soluble in aromatic and hydrocarbon solvents and also in hot alcoholic solutions, but are *virtually insoluble* at 25 C in their respective parent alcohols. The 1 : 4 (M : Ti) complexes (**3**) and (**4**) are also soluble in long chain hydrocarbons such as hexadecane. None of the compounds sublime into the vapour phase, because they decompose to mixed metal oxides.

TGA/DSC studies

The results of TGA/DSC studies are summarized in Table 1. As expected, the compounds do indeed decompose to the stoichiometrically correct oxides except $[SrTi_4(OEt)_{18}]$ which partially sublimes before decomposing. The DSC results show that only the 1 : 4 stoichiometry complexes have definite melting points (ca 130 °C), whereas the other materials appear to dissolve in the released solvent (EtOH or Pr^iOH) at lower temperatures (50–100 °C), rather than actually melting.

Infrared spectroscopy

The infrared spectra of complexes (**1**)–(**7**) (Table 2) are very similar, and dominated by ligand vibrations [28]. The ν(M—O) bands are assigned on the basis of previous work on titanium alkoxides including extensive deuterium labeling studies of $Ti(OPr^i\text{-}d_7)_4$ by Hampden-Smith *et al.* [28].

NMR spectroscopy

Multinuclear NMR (^1H and $^{13}C\{^1H\}$ NMR (Table 3)) studies of (**1**)–(**7**) were carried out in C_6D_6 and C_7D_8 over a range of temperatures. The Sr based compounds gave sharper, well defined spectra, as observed

Table 1. Physical data for heterometallic alkoxide complexes (**1**)–(**7**)

Complex		Melting Point °C	TGA °C	DSC °C, Mcal/mg	Solubility† H	A	C
$[SrTi_2(OEt)_{10}(EtOH)_5]_n$	(**1**)	85–90	2 step loss to give $SrTi_2O_5$ by 400	55, −7.7 des; 281, −20.7 dec	s	s	s
$[BaTi_2(OEt)_{10}(EtOH)_5]_n$	(**2**)	45–50 dissolves	3 step loss to give $BaTi_2O_5$ by 350	69, −57.6 des; 308, −28.2 dec	s	s	s
$[SrTi_4(OEt)_{18}]$	(**3**)	125–129	2 step loss to give $SrTi_4O_9$ by 350 (some sub.)	130, −3.9 mpt; 270, −61.8 dec 193, −2.8 dec; 326, −7.5 dec	s	s	s
$[BaTi_4(OEt)_{18}]$	(**4**)	129–132	2 step loss to give $BaTi_4O_9$ by 830	134, −2.0 mpt; 285; −17.5 dec	s	s	s
$[Sr_2Ti(OEt)_8(EtOH)_5]_n$	(**5**)	des. 65	6 step loss to give Sr_2TiO_4 by 950	68, −40.4 des; 161, −8.7 dec 397, 7.9 dec; 916, −6.5 dec	s	s	s
$[Ba_2Ti(OEt)_8(EtOH)_5]_n$	(**6**)	des. 125	3 step loss to give Ba_2TiO_4 by 830	75, −39.8 des; 303, −10.7 dec	s	s	s
$[Sr_2Ti(OPr^i)_8(Pr^iOH)_5]_n$	(**7**)	52–55	3 step loss to give Sr_2TiO_4 by 950	69, −36.8 des; 364; −10.4 dec 914, −7.8 dec	s	s	s

des = desolvates. Solubility: H = hydrocarbon; A = aromatic; C = coordinating; s = soluble.
†All compounds are soluble in EtOH at 70 °C, but insoluble below ~25 °C.

Table 2. Selected infrared data for the heterometallic alkoxides of Sr and Ba (**1**)–(**7**) (cm^{-1})

Compound		ν(O—H)[b]	ν(C—H)[a]		δ(C—H)[a]		ν(CCO)[b]		ν(C—C)[b]	γ(CH_2)[b]	δ(CCO)[b]	ν(M—O)[b]
EtOH		3401	2975	2885	1423	1381	1093	1051	880	804	432	—
				1331								
$[SrTi_2(OEt)_{10}(EtOH)_5]_n$	(**1**)	3373	2969	2924	1470	1442	1117	1099	885	799	443	596
			2856		1375	1355	1070	1054				530
$[BaTi_2(OEt)_{10}(EtOH)_5]_n$	(**2**)	3321	2969	2924	1471	1442	1152	1098	883	799	435	584
			2862		1374	1355	1070	1054				534
$[SrTi_4(OEt)_{18}]$	(**3**)		2969	2924	1471	1441	1151	1099	885	802	450	597
			2855		1380	1355	1070	1050				526
$[BaTi_4(OEt)_{18}]$	(**4**)		2968	2924	1471	1441	1146	1098	886	803	445	596
			2854		1374	1355	1070	1053				528
$[Sr_2Ti(OEt)_8(EtOH)_5]_n$	(**5**)	3173	2962	2923	1444	1380	1138	1096	884	800	434	596
			2866				1054					550
$[Ba_2Ti(OEt)_8(EtOH)_5]_n$	(**6**)	3156	2968	2923	1470	1442	1138	1098	884	799	429	584
			2864		1374	1355	1053					536
$[Sr_2Ti(OPr^i)_8(Pr^iOH)_5]_n$	(**7**)	3185	2963	2861	1462	1372	1157	1131	844	818	461	592
					1326		1017		828			564

[a]hexachlorobutadiene mull.
[b]Nujol Mull.

Table 3. Room temperature ^1H and $^{13}C\{^1H\}$ NMR data (δ/ppm) for the heterometallic alkoxides of Sr and Ba (**1**)–(**7**)

Compound		^1H[a]			$^{13}C\{^1H\}$[b]		
		CH_3	CH_2	OH	CH_3	CH_2	Solvent
$[SrTi_2(OEt)_{10}(EtOH)_5]_n$	(**1**)	1.09, 1.22	3.61, 4.33	4.65	18.33, 19.25	58.20, 68.93	C_6D_6
		1.35, 1.56	4.47				
$[BaTi_2(OEt)_{10}(EtOH)_5]_n$	(**2**)	1.14, 1.37	3.63, 4.42	5.23	18.42, 19.23	57.61, 64.17	C_6D_6
					19.44	67.50	
$[SrTi_4(OEt)_{18}]$	(**3**)	1.03, 1.22	3.49, 4.31	2.96 (weak)	19.79, 19.69	57.59, 65.91	C_6D_6
		1.38, 1.58	4.36		24.84, 26.12	68.12, 70.31	
$[BaTi_4(OEt)_{18}]$	(**4**)	1.05, 1.28	3.49, 4.33	3.79 (weak)	17.81, 19.41	57.27, 65.45	C_6D_6
		1.41	4.43			67.26, 70.12	
$[Sr_2Ti(OEt)_8(EtOH)_5]_n$	(**5**)	1.11, 1.29	3.81, 4.14	9.53	18.65, 19.44	57.23, 65.03	C_6D_6
		1.50	4.36		19.82	68.66	
$[Ba_2Ti(OEt)_8(EtOH)_5]_n$	(**6**)	1.18, 1.36	3.69, 4.32	6.06	18.76, 19.21	57.75, 64.19	C_6D_6
		1.53	4.43		19.46	67.81, 70.03	
$[Sr_2Ti(OPr^i)_8(Pr^iOH)_5]$	(**7**)	1.26	4.30[c]	5.19	26.47	66.02[c]	C_7D_8

[a]270 MHz.
[b]67.94 MHz.
[c]Actually *CH* and *CH*.

for other alkoxide complexes, e.g. the Group 2 ethoxides [46]. ^1H variable temperature NMR has proved very useful in studying these compounds.

1 : 2 *Stoichiometry compounds* (**1**) *and* (**2**)

The ^1H NMR spectrum for (**1**) shows some very broad peaks for the ethyl resonances. There appears to be at least three ethyl environments for the complex in solution. A variable temperature study of (**1**) revealed some interesting results; the OH resonance shifts upfield and at 70°C only two 2 ethyl environments are observed (one very broad and one sharp). The $^{13}C\{^1H\}$ spectrum shows two methyl resonances and at least four methylene resonances.

The ^1H NMR spectrum in C_6D_6 at room temperature of (**2**) shows one sharp and one broad ethyl environments. However on raising the temperature to 75°C the whole spectrum sharpens up; four ethyl resonances can be clearly seen, some of which were probably obscured by overlapping peaks at room temperature. The OH resonance shifts from δ 5.23 to

4.42 on raising the temperature to 75°C. This data is corroborated by the $^{13}C\{^1H\}$ NMR spectrum which shows three ethyl environments both at room temperature and at 75°C.

1 : 4 *stoichiometry compounds* (**3**) *and* (**4**)

The ^1H NMR of (**3**) in C_6D_6 at room temperature shows four ethyl environments and only one OH environment with a pair of sharp, well defined ethyl proton multiplets and three poorly defined pairs of resonances. At higher temperatures (70°C) the spectrum is better resolved with two ethyl environments observed, one sharp and the other broad; further, as the temperature is increased, the OH proton resonance shifts from δ 2.96 to δ 1.34. This suggests that there are only two ethyl environments at high temperature. In contrast, the $^{13}C\{^1H\}$ NMR spectrum shows there are four environments at both high and room temperatures.

The ^1H NMR of (**4**) in C_6D_6 at room temperature shows three ethyl environments (one sharp and two very broad), which on warming to 70°C merge to form just two (sharp) environments. At high temperatures the ethanol/ethoxide ligands are probably undergoing rapid exchange and so all that is observed in the spectrum is two sharp peaks. Also on warming the OH resonance shifts from δ 3.79 to δ 2.13. Integration shows the complex to have the formula $[BaTi_4(OEt)_{18}]$, but the crystals are probably wet. The $^{13}C\{^1H\}$ NMR corroborates this, showing three environments at room temperature.

2 : 1 *stoichiometry compounds* (**5**), (**6**) *and* (**7**)

Both compounds (**5**) and (**6**) show three environments for the alkoxide/alcohol ligands attached to the two metals. Compound (**5**), after careful drying in the glovebox, produced a spectrum (at room temperature) which is consistent with the formula $[Sr_2Ti(OEt)_8(EtOH)_5]_n$. The variable temperature study of (**5**) in C_6D_6 shows that the OH resonance associated with these peaks shifts by about 3 ppm down field over a 50°C range. Also two of the ethyl resonances broaden and lose all resolution as the temperature is raised; these peaks appear to be associated with the OH peak because they all broaden and decrease in intensity together (i.e. they are EtOH solvate/solvent). The $^{13}C\{^1H\}$ shows a similar set of environments to the proton NMR with three ethyl environments observed at both room temperature and 75°C.

The ^1H NMR of (**6**) in C_6D_6 at room temperature shows two ethyl environments and one OH environment with integrations consistent with the formulation $[Ba_2Ti(OEt)_8(EtOH)_5]_n$. On warming to 70°C, a third ethyl environment is seen, suggesting that this peak, at room temperature, overlapped with the other two. The $^{13}C\{^1H\}$ NMR spectra at both room temperature and 70°C show three ethyl environments.

The room temperature ^1H NMR spectrum of (**7**) in d_8-toluene reveals the presence of only one isopropoxide environment, with the methyl resonance observed at δ 1.42 and the methylene resonance at δ 4.47, in a ratio of 6 : 1. The resonance for the alcohol proton was found to be dependent on solvent, concentration and also temperature, and was observed between 3 and 6 ppm, with a OH : CH integration ratio of 0.4. A rapid proton exchange between the alcohol and alkoxide ligands is proposed at room temperature. On warming to 47°C the characteristic multiplet pattern of the CH peak is observed, with a similar shift of the alcohol proton peak from δ 6 to 2.95. On cooling a solution of the mixed metal isopropoxide in d_8-toluene down to −80°C, no significant changes in the spectrum were observed and we were unable to obtain a low temperature limiting spectrum due to sample precipitation and solution viscosity effects.

The ^1H and $^{13}C\{^1H\}$ NMR spectra of the alkoxides (**1**)–(**7**) show that it is possible to obtain some information on the ratio of alcohol to alkoxide ligands in the complexes, but further information (e.g. whether a species has a certain number of μ_3- or μ_3-bonded ligands) is not feasible due to the fast exchange regimes observed herein. A possibility would be to use ^{17}O NMR as shown by Day *et al.* [47] in a number of studies on titanium polyoxoalkoxides complexes such as $[\{Ti_7O_4\}(OEt)_{20}]$ and $[\{Ti_{11}O_{13}\}(OPr^i)_{18}]$. They have utilized 40 atom% ^{17}O-enriched H_2O to hydrolyze titanium alkoxides (such as $[Ti(OPr^i)_4]$ and $[Ti(OEt)_4]$), and then by studying the products via ^{17}O and $^{13}C\{^1H\}$ NMR spectroscopies it has been possible to assign the oxo-ligands thus obtained as either μ_3 or μ_2-bonded groups. However, such studies were not carried out in the present work, although we believe that there are grounds for a future study into this area using such materials.

Mass spectrometry

Mass spectrometric results were obtained for all the alkoxides (**1**)–(**7**), but no conclusive evidence of heterometallic molecules was observed in the gas phase. The ions observed all corresponded to $Ti(OR)_4$ break-up fragments and clusters of $[Ti(OR)_4]_n$ (R = Et or Pr^i) with the highest mass ions observed corresponding to the ion $[Ti_4(OEt)_{15}]^+$ {for (**3**) and (**4**)}. Similar results have been observed for a number of other heterometallic compounds, and this is probably due to breakdown of the heterometallic ensemble under the high vacuum utilized in the mass spectrometer.

X-RAY CRYSTAL STRUCTURES

Although all the heterometallic compounds were crystalline products, X-ray quality single crystals were

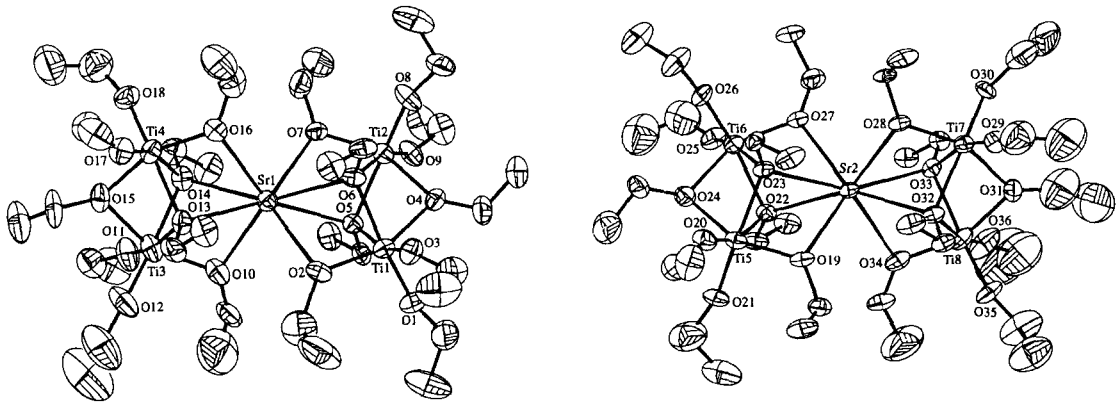

Fig. 1. Structures of the two independent molecules of $[SrTi_4(OEt)_{18}]$ (**3**) with the hydrogen atoms omitted for clarity. Thermal ellipsoids are drawn at 35% probability.

obtained only for (**3**) and (**7**) and for these two compounds full structural determinations were undertaken.

Structure of $[SrTi_4(OEt)_{18}]$ (**3**)

The crystal structure of (**3**) consists of discrete molecules of $[SrTi_4(OEt)_{18}]$ held together by van der Waals' forces. There are two molecules per asymmetric unit with very similar bond lengths and angles, differing mainly in the relative orientations of some of the ethoxy ligands. The structures of the two molecules are shown in Fig. 1, and selected geometry parameters are listed in Table 4. There are no solvate molecules in the lattice. The structure is based on a "bow-tie" or spiro Ti_2SrTi_2 unit where the strontium is coordinated to two face sharing bioctahedral $Ti_2(OEt)_9^-$ units. Each $Ti_2(OEt)_9^-$ unit utilizes two "terminal" and two "bridging" ethoxo ligands for coordination with the central strontium atom which achieves a coordination number of eight. The geometry around each Sr is best described as distorted square antiprismatic as indicated by the dihedral angles between the two $SrTi_2$ planes are 63.4 and 62.3° in the two molecules, respectively. For an ideal square antiprismatic geometry, the value of this angle is 45° and the four oxygen atoms on each $Ti_2(OEt)_9^-$ unit are staggered with respect to those of the second $Ti_2(OEt)_9^-$ unit. In contrast, an eclipsed arrangement would give a dihedral angle of 0 or 90°. The geometry around the titanium atoms is distorted octahedral with three different kinds of ethoxo ligands bonded to each metal. The Ti···Ti and Ti···Sr nonbonded distances in the two molecules fall into the very narrow ranges 3.027(2)–3.039(2) Å and 3.458(4)–3.479(3) Å, respectively. The Ti—O—Ti angles involving the μ_2-bridging ligands [91.8(2)–95.5(2)°] are close to the corresponding angles involving the μ_3-bridging ligands [91.5(2)–92.4(2)°]. However, the Ti—O—Sr angles involving the μ_2-bridging ligands [99.0(2)–100.0(2)°] are wider than the corresponding angles involving the μ_3-bridging ligands [93.38(14)–95.5(2)°].

The Ti—O distances span the range 1.774(6)–2.149(4) Å and can be grouped into four distinct categories: (i) the Ti—O (terminal) distances, range 1.764(6)–1.814(5), average 1.783 Å; (ii) the Ti—O (μ_2-Ti_2 bridging) distances, range 2.041(5)–2.077(6), average 2.059 Å, (iii) the Ti—O (μ_2-TiSr bridging) distances, range 1.875(5)–1.920(5), average 1.902 Å, and (iv) the Ti—O (μ_3-Ti_2Sr bridging) distances, range 2.081(4)–2.149(4), average 2.111 Å. The observed trend, Ti—O (μ_3-Ti_2Sr bridging) > Ti—O (μ_2-Ti_2 bridging) > Ti—O (μ_2-TiSr bridging) > Ti—O (terminal), underlines the dependence of the bond strength on the charge distribution of the ligand atom.

The Sr—O bond distances involve two types of bridging (i.e. μ_2- and μ_3-) ethoxide ligands, and lie in the narrow range 2.563(4)–2.620(5), average 2.594 Å; but unlike the Ti—O distances, these values appear not to be significantly dependent on the nature of bridging oxygen atoms. In fact, the average values for the Sr—O (μ_2-) and Sr—O (μ_3-) bonds, 2.605 and 2.590 Å, respectively, are nearly the same. This is somewhat surprising, since the bonds involving the μ_3-ligands are generally expected to be longer than those involving the μ_2-ligands. The fact that this does not happen with strontium in the present structure may be explained by assuming that the distortion in the $Ti_2(OEt)_9^-$ core would be bigger if the situation were different and that this is not thermodynamically favourable.

Complex (**3**) is a novel strontium titanium alkoxide which has coordinatively saturated the strontium metal centre via the use of μ_2- and μ_3-bridging ethoxide ligands from two Ti_2O_9 units. A similar structural framework was observed for $[BaZr_4(OPr^i)_{18}]$ [48], but no reliable results were reported therein due to incomplete model and unsatisfactory refinement.

Table 4. Selected bond lengths (Å) and angles (°) for $[SrTi_4(OEt)_{18}]$ (**3**)

Sr(1)—O(14)	2.578(4)	Sr(1)—O(10)	2.585(5)
Sr(1)—O(13)	2.589(4)	Sr(1)—O(5)	2.591(5)
Sr(1)—O(7)	2.596(4)	Sr(1)—O(6)	2.604(5)
Sr(1)—O(2)	2.619(5)	Sr(1)—O(16)	2.620(5)
Ti(1)—O(1)	1.785(5)	Ti(1)—O(3)	1.814(5)
Ti(1)—O(2)	1.896(5)	Ti(1)—O(4)	2.074(5)
Ti(1)—O(6)	2.082(4)	Ti(1)—O(5)	2.149(4)
Ti(2)—O(9)	1.792(4)	Ti(2)—O(7)	1.915(5)
Ti(2)—O(4)	2.065(5)	Ti(2)—O(5)	2.085(5)
Ti(2)—O(6)	2.127(4)	Ti(3)—O(12)	1.764(6)
Ti(3)—O(11)	1.790(5)	Ti(3)—O(10)	1.897(6)
Ti(3)—O(15)	2.077(6)	Ti(3)—O(13)	2.090(5)
Ti(3)—O(14)	2.139(5)	Ti(3)—Ti(4)	3.039(2)
Ti(4)—O(18)	1.769(5)	Ti(4)—O(17)	1.794(4)
Ti(4)—O(16)	1.878(5)	Ti(4)—O(15)	2.050(6)
Ti(4)—O(14)	2.087(5)	Ti(4)—O(13)	2.129(4)
Sr(2)—O(19)	2.563(4)	Sr(2)—O(33)	2.582(5)
Sr(2)—O(28)	2.589(4)	Sr(2)—O(32)	2.592(5)
Sr(2)—O(23)	2.596(5)	Sr(2)—O(22)	2.598(5)
Sr(2)—O(27)	2.599(4)	Sr(2)—O(34)	2.600(5)
Ti(5)—O(21)	1.783(5)	Ti(5)—O(20)	1.805(5)
Ti(5)—O(19)	1.920(5)	Ti(5)—O(24)	2.059(5)
Ti(5)—O(23)	2.081(4)	Ti(5)—O(22)	2.134(4)
Ti(6)—O(25)	1.776(4)	Ti(6)—O(27)	1.905(5)
Ti(6)—O(24)	2.054(5)	Ti(6)—O(22)	2.089(4)
Ti(6)—O(23)	2.119(4)	O(19)—C(37)	1.403(7)
Ti(7)—O(30)	1.785(4)	Ti(7)—O(28)	1.900(5)
Ti(7)—O(31)	2.049(6)	Ti(7)—O(32)	2.119(4)
Ti(7)—O(33)	2.125(4)	Ti(7)—Ti(8)	3.027(2)
Ti(8)—O(36)	1.768(5)	Ti(8)—O(35)	1.780(5)
Ti(8)—O(34)	1.906(6)	Ti(8)—O(31)	2.041(5)
Ti(8)—O(33)	2.102(4)	Ti(8)—O(32)	2.115(4)
O(14)—Sr(1)—O(10)	62.9(2)	O(14)—Sr(1)—O(13)	55.78(12)
O(10)—Sr(1)—O(13)	62.8(2)	O(14)—Sr(1)—O(5)	153.23(14)
O(10)—Sr(1)—O(5)	95.7(2)	O(13)—Sr(1)—O(5)	130.95(13)
O(14)—Sr(1)—O(7)	143.36(14)	O(10)—Sr(1)—O(7)	126.81(14)
O(13)—Sr(1)—O(7)	94.86(13)	O(5)—Sr(1)—O(7)	61.95(13)
O(14)—Sr(1)—O(6)	133.45(12)	O(10)—Sr(1)—O(6)	143.6(2)
O(13)—Sr(1)—O(6)	152.48(14)	O(5)—Sr(1)—O(6)	55.87(13)
O(7)—Sr(1)—O(6)	63.63(13)	O(14)—Sr(1)—O(2)	97.3(2)
O(10)—Sr(1)—O(2)	85.1(2)	O(13)—Sr(1)—O(2)	144.4(2)
O(5)—Sr(1)—O(2)	63.03(14)	O(7)—Sr(1)—O(2)	117.7(2)
O(6)—Sr(1)—O(2)	62.6(2)	O(14)—Sr(1)—O(16)	61.2(2)
O(10)—Sr(1)—O(16)	117.0(2)	O(13)—Sr(1)—O(16)	63.0(2)
O(5)—Sr(1)—O(16)	145.0(2)	O(7)—Sr(1)—O(16)	87.1(2)
O(6)—Sr(1)—O(16)	97.1(2)	O(2)—Sr(1)—O(16)	128.25(14)
O(1)—Ti(1)—O(3)	98.0(2)	O(1)—Ti(1)—O(2)	101.8(2)
O(3)—Ti(1)—O(2)	100.8(2)	O(1)—Ti(1)—O(4)	94.4(2)
O(3)—Ti(1)—O(4)	95.5(2)	O(2)—Ti(1)—O(4)	155.0(2)
O(1)—Ti(1)—O(6)	162.6(2)	O(3)—Ti(1)—O(6)	95.7(2)
O(2)—Ti(1)—O(6)	85.9(2)	O(4)—Ti(1)—O(6)	73.7(2)
O(1)—Ti(1)—O(5)	94.9(2)	O(3)—Ti(1)—O(5)	164.8(2)
O(2)—Ti(1)—O(5)	84.4(2)	O(4)—Ti(1)—O(5)	75.4(2)
O(6)—Ti(1)—O(5)	70.2(2)	O(8)—Ti(2)—O(9)	99.5(2)
O(8)—Ti(2)—O(7)	99.1(2)	O(9)—Ti(2)—O(7)	102.6(2)
O(8)—Ti(2)—O(4)	95.8(2)	O(9)—Ti(2)—O(4)	95.0(2)
O(7)—Ti(2)—O(4)	154.5(2)	O(8)—Ti(2)—O(5)	165.4(2)
O(9)—Ti(2)—O(5)	93.8(2)	O(7)—Ti(2)—O(5)	83.6(2)
O(4)—Ti(2)—O(5)	77.0(2)	O(8)—Ti(2)—O(6)	95.2(2)
O(9)—Ti(2)—O(6)	161.9(2)	O(7)—Ti(2)—O(6)	85.2(2)

Table 4—*Continued.*

O(4)—Ti(2)—O(6)	72.9(2)	O(5)—Ti(2)—O(6)	70.6(2)
O(12)—Ti(3)—O(11)	99.1(3)	O(12)—Ti(3)—O(10)	101.5(3)
O(11)—Ti(3)—O(10)	99.7(2)	O(12)—Ti(3)—O(15)	95.6(2)
O(11)—Ti(3)—O(15)	97.2(2)	O(10)—Ti(3)—O(15)	153.7(2)
O(12)—Ti(3)—O(13)	162.4(2)	O(11)—Ti(3)—O(13)	96.0(2)
O(10)—Ti(3)—O(13)	84.9(2)	O(15)—Ti(3)—O(13)	73.3(2)
O(12)—Ti(3)—O(14)	94.5(2)	O(11)—Ti(3)—O(14)	165.1(2)
O(10)—Ti(3)—O(14)	83.5(2)	O(15)—Ti(3)—O(14)	75.3(2)
O(13)—Ti(3)—O(14)	69.7(2)	O(18)—Ti(4)—O(17)	99.8(2)
O(18)—Ti(4)—O(16)	99.6(2)	O(17)—Ti(4)—O(16)	102.7(2)
O(18)—Ti(4)—O(15)	95.3(2)	O(17)—Ti(4)—O(15)	94.5(2)
O(16)—Ti(4)—O(15)	154.8(2)	O(18)—Ti(4)—O(14)	164.8(2)
O(17)—Ti(4)—O(14)	93.9(2)	O(16)—Ti(4)—O(14)	83.6(2)
O(15)—Ti(4)—O(14)	77.0(2)	O(18)—Ti(4)—O(13)	95.4(2)
O(17)—Ti(4)—O(13)	161.3(2)	O(16)—Ti(4)—O(13)	85.3(2)
O(15)—Ti(4)—O(13)	73.1(2)	O(14)—Ti(4)—O(13)	70.0(2)
O(19)—Sr(2)—O(33)	143.53(14)	O(19)—Sr(2)—O(28)	126.05(12)
O(33)—Sr(2)—O(28)	63.8(2)	O(19)—Sr(2)—O(32)	95.1(2)
O(33)—Sr(2)—O(32)	56.14(12)	O(28)—Sr(2)—O(32)	62.1(2)
O(19)—Sr(2)—O(23)	61.77(14)	O(33)—Sr(2)—O(23)	154.28(13)
O(28)—Sr(2)—O(23)	98.9(2)	O(32)—Sr(2)—O(23)	134.70(13)
O(19)—Sr(2)—O(22)	64.60(13)	O(33)—Sr(2)—O(22)	129.85(13)
O(28)—Sr(2)—O(22)	146.57(14)	O(32)—Sr(2)—O(22)	150.88(14)
O(23)—Sr(2)—O(22)	55.5(2)	O(19)—Sr(2)—O(27)	117.4(2)
O(33)—Sr(2)—O(27)	97.15(13)	O(28)—Sr(2)—O(27)	86.45(14)
O(32)—Sr(2)—O(27)	144.78(13)	O(23)—Sr(2)—O(27)	61.27(12)
O(22)—Sr(2)—O(27)	63.12(13)	O(19)—Sr(2)—O(34)	85.0(2)
O(33)—Sr(2)—O(34)	62.65(14)	O(28)—Sr(2)—O(34)	117.2(2)
O(32)—Sr(2)—O(34)	62.08(13)	O(23)—Sr(2)—O(34)	141.4(2)
O(22)—Sr(2)—O(34)	94.1(2)	O(27)—Sr(2)—O(34)	129.96(13)
O(21)—Ti(5)—O(20)	99.7(2)	O(21)—Ti(5)—O(19)	97.5(2)
O(20)—Ti(5)—O(19)	104.5(2)	O(21)—Ti(5)—O(24)	98.1(2)
O(20)—Ti(5)—O(24)	93.8(2)	O(19)—Ti(5)—O(24)	153.5(2)
O(21)—Ti(5)—O(23)	166.7(2)	O(20)—Ti(5)—O(23)	93.0(2)
O(19)—Ti(5)—O(23)	82.8(2)	O(24)—Ti(5)—O(23)	77.2(2)
O(21)—Ti(5)—O(22)	96.7(2)	O(20)—Ti(5)—O(22)	159.3(2)
O(19)—Ti(5)—O(22)	85.6(2)	O(24)—Ti(5)—O(22)	71.4(2)
O(23)—Ti(5)—O(22)	70.0(2)	O(26)—Ti(6)—O(25)	99.4(2)
O(26)—Ti(6)—O(27)	102.8(2)	O(25)—Ti(6)—O(27)	98.9(2)
O(26)—Ti(6)—O(24)	94.6(2)	O(25)—Ti(6)—O(24)	97.8(2)
O(27)—Ti(6)—O(24)	153.4(2)	O(26)—Ti(6)—O(22)	162.0(2)
O(25)—Ti(6)—O(22)	94.8(2)	O(27)—Ti(6)—O(22)	85.7(2)
O(24)—Ti(6)—O(22)	72.5(2)	O(26)—Ti(6)—O(23)	95.1(2)
O(25)—Ti(6)—O(23)	164.9(2)	O(27)—Ti(6)—O(23)	82.1(2)
O(24)—Ti(6)—O(23)	76.5(2)	O(22)—Ti(6)—O(23)	70.2(2)
O(29)—Ti(7)—O(30)	99.3(2)	O(29)—Ti(7)—O(28)	102.9(2)
O(30)—Ti(7)—O(28)	99.0(2)	O(29)—Ti(7)—O(31)	94.7(2)
O(30)—Ti(7)—O(31)	97.0(2)	O(28)—Ti(7)—O(31)	153.9(2)
O(29)—Ti(7)—O(32)	96.7(2)	O(30)—Ti(7)—O(32)	162.8(2)
O(28)—Ti(7)—O(32)	83.2(2)	O(31)—Ti(7)—O(32)	75.6(2)
O(29)—Ti(7)—O(33)	163.8(2)	O(30)—Ti(7)—O(33)	93.1(2)
O(28)—Ti(7)—O(33)	85.3(2)	O(31)—Ti(7)—O(33)	73.3(2)
O(32)—Ti(7)—O(33)	70.02(14)	O(36)—Ti(8)—O(35)	99.0(3)
O(36)—Ti(8)—O(34)	99.4(3)	O(35)—Ti(8)—O(34)	100.8(2)
O(36)—Ti(8)—O(31)	97.3(3)	O(35)—Ti(8)—O(31)	96.2(2)
O(34)—Ti(8)—O(31)	153.9(2)	O(36)—Ti(8)—O(33)	96.2(2)
O(35)—Ti(8)—O(33)	162.9(2)	O(34)—Ti(8)—O(33)	84.3(2)
O(31)—Ti(8)—O(33)	74.0(2)	O(36)—Ti(8)—O(32)	166.2(2)
O(35)—Ti(8)—O(32)	93.7(2)	O(34)—Ti(8)—O(32)	83.3(2)
O(31)—Ti(8)—O(32)	75.9(2)	O(33)—Ti(8)—O(32)	70.5(2)

Table 4—*Continued.*

Ti(1)—O(2)—Sr(1)	99.0(2)	Ti(2)—O(4)—Ti(1)	94.3(2)
Ti(2)—O(5)—Ti(1)	91.6(2)	Ti(2)—O(5)—Sr(1)	95.0(2)
Ti(1)—O(5)—Sr(1)	93.45(14)	Ti(1)—O(6)—Ti(2)	92.3(2)
Ti(1)—O(6)—Sr(1)	94.7(2)	Ti(2)—O(6)—Sr(1)	93.6(2)
Ti(2)—O(7)—Sr(1)	99.3(2)	Ti(3)—O(10)—Sr(1)	99.9(2)
Ti(3)—O(13)—Ti(4)	92.2(2)	Ti(4)—O(13)—Sr(1)	94.1(2)
Ti(3)—O(13)—Sr(1)	94.8(2)	Ti(4)—O(14)—Ti(3)	91.9(2)
Ti(4)—O(14)—Sr(1)	95.5(2)	Ti(3)—O(14)—Sr(1)	93.92(14)
Ti(4)—O(15)—Ti(3)	94.8(2)	Ti(4)—O(16)—Sr(1)	99.6(2)
Ti(5)—O(19)—Sr(2)	100.0(2)	Ti(6)—O(22)—Ti(5)	91.8(2)
Ti(6)—O(22)—Sr(2)	95.2(2)	Ti(5)—O(22)—Sr(2)	93.38(14)
Ti(5)—O(23)—Ti(6)	92.4(2)	Ti(5)—O(23)—Sr(2)	94.7(2)
Ti(6)—O(23)—Sr(2)	94.5(2)	Ti(5)—O(24)—Ti(6)	95.0(2)
Ti(6)—O(27)—Sr(2)	100.0(2)	Ti(7)—O(28)—Sr(2)	99.8(2)
Ti(8)—O(31)—Ti(7)	95.5(2)	Ti(8)—O(32)—Ti(7)	91.3(2)
Ti(8)—O(32)—Sr(2)	94.53(14)	Ti(7)—O(32)—Sr(2)	94.1(2)
Ti(8)—O(33)—Ti(7)	91.5(2)	Ti(8)—O(33)—Sr(2)	95.13(14)
Ti(7)—O(33)—Sr(2)	94.2(2)	Ti(8)—O(34)—Sr(2)	99.6(2)

Structure of $[Sr_2Ti(OPr^i)_8(Pr^iOH)_3]\cdot 2Pr^iOH$ (7)

The crystal structure of (7) consists of trinuclear molecules of $[Sr_2Ti(OPr^i)_8(Pr^iOH)_3]$ held together by strong hydrogen bonds involving the two solvated Pr^iOH molecules and forming a polymeric chain along the *a*-axis. The structure of a single complex molecule together with the associated solvate species is shown in Fig. 2, and selected bond lengths and angles are given in Table 5.

Complex (7) consists of a triangle of two strontium and one titanium atoms with metal–metal non-bonded distances of Sr(1)···Sr(2) 3.6350(13), Ti(1)···Sr(1) 2.399(2) and Ti(1)···Sr(2) 2.390(2) Å. The molecule is stabilized by a belt of three μ_2-isopropoxide ligands around the metal triangle and two μ_3-isopropoxide ligands above and below the plane of the metal atoms. Each metal centre is further coordinated by two terminally placed Pr^iO/Pr^iOH ligands. The basic Sr_2TiO_5 framework is similar to those observed in several other complexes, e.g., $[Ca_3(OPh)_5(hmpa)_6]^+[OPh]^-\cdot 2PhOH$ [49], $[Sr_3(OPh)_6(hmpa)_5]$ [49] and $[Sr_3(tmhd)_3(OSiPh_3)_3]\cdot 0.5C_6H_5Me$ [50]. The molecule possesses a crystallographic mirror plane of symmetry passing through the Sr, Ti and the μ_2-O atoms; the two uncoordinated Pr^iOH molecules also lie on the mirror plane. The overall structure is based on three octahedra, each sharing two of its "faces" with the other octahedra in a bifacial manner. The octahedral geometries around the metal centres are distorted, those around the Sr atoms very severely, due to the strain caused by the formation of bridges involving both μ_2- and μ_3-isopropoxide groups. The Sr···Sr and Sr···Ti distances are close to the respective values observed in other complexes, e.g., Sr···Sr 3.544(2)–3.654(2) Å in $[Sr_3(tmhd)_3(OSiPh_3)_3]\cdot 0.5C_6H_5Me$ [50], and Sr···Ti 3.458(4)–3.479(3) Å in (3). The μ_2-bridging oxygen atoms O(1), O(2) and O(3) are exactly planar, and the Sr—O—Sr/Ti angles involving these bridges are quite similar [96.0(2)–98.0(2)°]. The Sr—O—Sr/Ti angles involving the μ_3-oxygen atoms [O(4), O(4′)] are somewhat narrower [92.12(14)–93.7(2)°].

The Ti—O distances show considerable variations [1.816(4)–2.116(4) Å] depending on the nature of the alkoxide linkage. The unique distance involving the terminal ligands, 1.816(4) Å, is significantly shorter than those involving the μ_2-[O(1), O(3)] and μ_3-[O(4)] bridging groups, 1.991(6), 2.017(5), and 2.116(4) Å, respectively. These bond lengths correspond, respectively, to the Ti—O—C bond angles of 157.8 (average), 127.6 (average) and 131.0(4)°. The general increase in bond angle with decreasing bond length may be interpreted as due to an increase in the *s*-character of the oxygen bonding orbital. The Ti—O distance in the present compound involving the μ_3-ligand is very close to the average value in (3), but the average values involving the μ_2-SrTi bridging and terminal ligands [2.004 and 1.816(4) Å] are somewhat longer than the corresponding values [1.902 and 1.783 Å] in (3).

The Sr—O distances [2.399(6)–2.589(4)] also show considerable variations and fall into four different categories, i.e., (i) 2.399(6) and 2.426(6), average 2.413 Å for the μ_2-O (Sr_2 bridging), (ii) 2.493(6), 2.524(6), average 2.507 Å for the μ_2-O (SrTi bridging), (iii) 2.520(4), 2.528(4), average 2.524 Å for the μ_3-O (Sr_2Ti bridging), and (iv) 2.535(4), 2.589(4), average 2.562 Å for the terminal ligands. The order of these bond lengths is as expected, but the average value (2.502 Å) is considerably shorter than that (2.594 Å) in (3) and ~2.60 Å in the ionic oxides SrO and Sr_2TiO_4. The shorter Sr—O distances in (7) compared

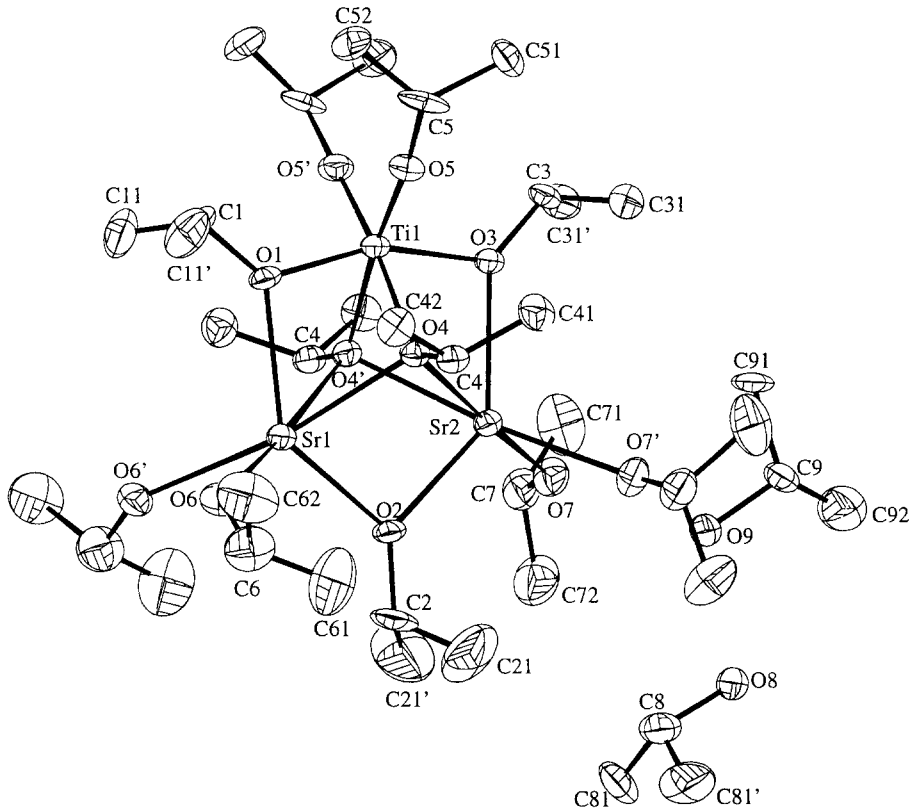

Fig. 2. Structure of the $[Sr_2Ti(OPr^i)_8(Pr^iOH)_3]\cdot 2Pr^iOH$ (**7**) with the hydrogen atoms omitted for clarity. Thermal ellipsoids are drawn at 50% probability. The primed atoms are related to the unprimed ones by a mirror plane of symmetry.

Table 5. Bond lengths (Å) and angles (°) for $[Sr_2Ti^i(OPr^i)_8(Pr^iOH)_3]\cdot 2Pr^iOH$

Sr(1)—O(2)	2.399(6)	Sr(1)—O(1)	2.493(6)
Sr(1)—O(4)	2.528(4)	Sr(1)—O(6)	2.589(4)
Sr(2)—O(2)	2.426(6)	Sr(2)—O(4)	2.520(4)
Sr(2)—O(3)	2.524(6)	Sr(2)—O(7)	2.535(4)
Ti(1)—O(5)	1.816(4)	Ti(1)—O(1)	1.991(6)
Ti(1)—O(3)	2.017(5)	Ti(1)—O(4)	2.116(4)
O(2)—Sr(1)—O(1)	134.4(2)	O(2)—Sr(1)—O(4)	76.7(2)
O(1)—Sr(1)—O(4)	64.40(14)	O(4)—Sr(1)—O(4)#1	61.2(2)
O(2)—Sr(1)—O(6)	108.4(2)	O(1)—Sr(1)—O(6)	107.29(14)
O(4)—Sr(1)—O(6)	111.12(14)	O(4)#1—Sr(1)—O(6)	170.18(14)
O(6)—Sr(1)—O(6)#1	75.7(2)	O(2)—Sr(2)—O(4)	76.4(2)
O(4)—Sr(2)—O(4)#1	61.4(2)	O(2)—Sr(2)—O(3)	134.9(2)
O(4)—Sr(2)—O(3)	65.19(14)	O(2)—Sr(2)—O(7)	106.7(2)
O(4)—Sr(2)—O(7)	171.93(14)	O(4)#1—Sr(2)—O(7)	111.65(14)
O(3)—Sr(2)—O(7)	108.73(14)	O(7)#1—Sr(2)—O(7)	74.9(2)
O(5)—Ti(1)—O(5)#1	94.9(3)	O(5)—Ti(1)—O(1)	97.6(2)
O(5)—Ti(1)—O(3)	96.5(2)	O(1)—Ti(1)—O(3)	159.1(3)
O(5)—Ti(1)—O(4)#1	170.0(2)	O(5)—Ti(1)—O(4)	95.1(2)
O(1)—Ti(1)—O(4)	81.2(2)	O(3)—Ti(1)—O(4)	82.2(2)
O(4)#1—Ti(1)—O(4)	74.9(2)		
Ti(1)—O(1)—Sr(1)	98.0(2)	Sr(1)—O(2)—Sr(2)	97.7(2)
Ti(1)—O(3)—Sr(2)	96.0(2)	Ti(1)—O(4)—Sr(2)	93.6(2)
Ti(1)—O(4)—Sr(1)	93.7(2)	Sr(2)—O(4)—Sr(1)	92.12(14)

Symmetry transformations used to generate equivalent atoms: #1 $(x, y, 0.5-z)$.

with (**3**) may be correlated to the coordination number of strontium in the two compounds (six vs eight). The Sr—O bond lengths observed in the present complexes may also be compared with those observed in the two other strontium alkoxides, $[Sr_4(OPh)_8(PhOH)_2(thf)_2]$ [51] [average distances: Sr—O (terminal) 2.499 Å, Sr—O (μ_2-Sr_2 bridging) 2.449 Å, and Sr—O (μ_3-Sr_3 bridging) 2.535 Å] and $[Sr(OC_6H_2Bu^t_3)_2(thf)_3 \cdot 0.5thf]$ [52] (average distance: Sr—O (terminal) 2.314 Å].

This trinuclear isopropoxide supported aggregate has three alcohol groups present. On the basis of stereochemical considerations and bond length data, these three alcohols are most likely to be attached terminally solely to the two Sr atoms. Certainly the long Sr—O bonds [2.589(4) Å for Sr(1)—O(6) and 2.535(4) Å for Sr(2)—O(7)] involving the terminal ligands are compatible with this suggestion. The fact that the Sr(1)—O(6)/O(6′) bonds are longer than the Sr(2)—O(7)/O(7′) bonds also suggest that, most probably, two of the three alcoholic protons are attached to the O(6) and O(6′) atoms whilst the third is disordered between the O(7) and O(7′) atoms. Attachment of any alcohol molecule to Ti(1) is ruled out because of its high charge and relatively short Ti—O (terminal) bond.

The overall polyhedron observed for (**7**) is not very different to that observed for one half of $[SrTi_4(OEt)_{18}]$ (**3**) except that instead of a dimeric Ti_2O_9 unit as in (**3**), a dimeric Sr_2O_9 unit is observed in (**7**). An interesting aspect of the crystal structure of (**7**) is the role played by the two uncoordinated Pr^{i}OH molecules. As mentioned earlier, these species are involved in strong hydrogen bonding, between themselves and also with the Pr^{i}OH molecules coordinated to the two strontium atoms, and form a chain structure along the *a*-axis. The O···O distances involved in the unique hydrogen bonds are O(6)···O(8) (at $-0.5+x$, $-0.5-y$, z) 2.656, O(7)···O(9) (at x, y, $0.5-z$) 2.646, O(8)···O(9) (at x, y, z) 2.448 Å. The OH hydrogen atoms were not located, and so the donor and acceptor atoms could not be identified. However, the O···O distances are quite short and this indicates the presence of very strong hydrogen bonds between these atoms. In fact, the distance between the pair of solvated Pr^{i}OH molecules (2.448 Å) is one of the shortest to be found for such hydrogen bonded species. Such a network of hydrogen bonds could have important implications on the properties of this material.

With the structural data collected so far it is possible to infer the structures of the remaining complexes, i.e. the barium analogues of (**3**) and (**7**) are of similar structure; also the 2:1 (M^{II}:Ti^{4+}) ethoxide based complexes (**5**) and (**6**) probably have the same structural make-up as compound (**7**). A similar comparison may be drawn for the 1:2 stoichiometry complexes (**1**) and (**2**), with their structures comprising half of that observed for (**3**). It may be possible for this unit to dimerize and form a complex similar to that observed for $[BaZr_2(OPr^i)_{10}]_2$, an isopropoxide-linked (through barium) dimer [48].

CONCLUSIONS

The present study suggests that it is possible to produce heterometallic alkoxide complexes with a predefined stoichiometry. This could have important possibilities for ceramic production with only the phase required being grown from a specific precursor via sol-gel processing.

The interesting structural motifs observed for (**3**) and (**7**) may be extended to the other predefined stoichiometry complexes. The triangular based metal core is not unusual in itself, having been observed for a number of mixed metal alkoxides [1,48], but the lack of any coordinated solvent in the crystal structure of (**3**) is quite unusual. Both the IR and NMR studies of this complex suggest the presence of free or coordinated alcohol, but the X-ray structure does not show the presence of any alcohol. This may be due to desolvation when handling the crystals, or alternatively the sample was slightly "damp" with alcohol when subjected to IR and NMR analyses.

The TGA/DSC results show that the crystalline solids are converted to their metal oxides at relatively low temperatures. But large scale trials (and analysis of the residues by X-ray powder diffraction) are required. This may prove to be an area of future study in Group 2/titanium heterometallic alkoxides.

EXPERIMENTAL

General procedures and instrumentation

All manipulations were carried out under an atmosphere of dry (molecular sieves) argon (using standard dry-box and Schlenk techniques). All solvents were rigorously dried and then distilled from their respective drying agents by standard methods. Elemental analyses were performed by the microanalytical department of Imperial College. The melting points were measured under argon in sealed capillaries and are uncorrected values. Infrared spectra were recorded on a Perkin-Elmer FTIR 1720 spectrometer as Nujol or hexachlorobutadiene (HCB) mulls between 25×4 mm KBr plates. The solvents were pre-dried with 4 Å molecular sieves prior to use, and the samples were protected from the atmosphere by an O-ring-sealed Presslok holder. NMR data were recorded on a Jeol GS 270 NMR spectrometer, using the protio impurities of the deuterated solvent as reference for ^{1}H spectra and the ^{13}C resonance of the solvent as a reference for $^{13}C\{^1H\}$ spectra. The NMR samples were prepared in the glovebox using Wilmad 5 mm NMR tubes equipped with J. Youngs valves to ensure reproducibility of NMR spectra and ensure sample stability. All chemical shifts are positive to high frequency of the standard. Mass spectrometric studies were performed on

a Kratos MS 30 (University of London Mass Spectrometry Service at the Royal School of Pharmacy) or a VG Autospec-Q (Imperial College Mass Spectrometry Service) operating in Electron Impact (positive) mode (70 eV) using a direct insertion probe and operating over the temperature range 50–200°C. Some samples were involatile under these conditions and thus the "softer" Fast Atom Bombardment (positive) mode (30–35 eV) was utilized where necessary. The samples were prepared in micro sure-seal bottles. Controlled thermal analyses were studied using a Polymer Laboratories 1500H simultaneous thermal analyzer (STA), controlled by a Omni Pro 486DX-33 PC. The measurements were carried out in alumina crucibles (sample mass ~10–25 mg) under an atmosphere of flowing (25 cm^3/min) nitrogen gas, using heating rates of 5 or 10°C/min.

Starting materials

Strontium and barium metal granules were purchased from Alfa Chemicals and stored in an inert atmosphere glove-box. Larger samples of the metal were purchased from Inorgtech and stored under oil prior to use. When utilized they were washed three times with *n*-pentane/hexane to remove this oil. Nujol and hexachlorobutadiene were obtained from Aldrich Chemicals and dried over 4 Å molecular sieves prior to use. Ethanol (EtOH) and isopropanol (Pr^iOH) were also purchased from Aldrich, and dried and distilled before use. All gases were purchased from BOC Ltd.

NOTE: Strontium and barium metals and their solutions are toxic and must be handled with care and kept under an inert atmosphere. The materials described herein should be prepared under dry argon using thoroughly degassed and dry solvents.

Synthesis of $[SrTi_2(OEt)_{10}(EtOH)_5]_n$ **(1)**

Strontium metal pieces (0.86 g, 9.77 mmol) was placed in a flame dried Schlenk with EtOH (30 cm^3) and $Ti(OEt)_4$ (2 equiv., 19.54 mmol, 3.83 cm^3) and solution refluxed at 80°C. The metal dissolved in an hour leaving a clear solution. On standing at −25°C the solution yielded a large crop of colourless crystals which were filtered off. Yield: 6.32 g, 70%, two crops. Found: C, 42.12; H, 9.23. $C_{30}H_{80}O_{15}SrTi_2$ requires: C, 41.69; H, 9.33%. ^1H NMR: (C_6D_6, 67.94 MHz, 70°C), δ 1.06 (t, CH_3), 1.36 (s, CH_3), 2.76 (s, O*H*), 3.57 (q, CH_2), 4.39 (s, br, CH_2). $^{13}C\{^1H\}$ NMR: (C_6D_6, 67.94 MHz, 70°C), δ 18.33 (s, CH_3), 19.25 (s, CH_3), 58.20 (s, CH_2), 68.93 (s, vbr, CH_2). Mass spectrometry: only $Ti(OEt)_4$ breakup observed.

Synthesis of $[BaTi_2(OEt)_{10}(EtOH)_5]_n$ **(2)**

Barium metal pieces (1.36 g, 9.9 mmol) were placed in a flame dried Schlenk with EtOH (30 cm^3) and $Ti(OEt)_4$ (2 equiv., 19.8 mmol, 3.88 cm^3) and the solution refluxed at 80°C. All the metal dissolved over 1 h. On standing at −25°C the solution yielded a large crop of colourless crystals which were carefully filtered off. Yield: 6.91 g, 83%, two crops. Found: C, 38.89; H, 8.96. $C_{30}H_{80}O_{15}BaTi_2$ requires: C, 39.42; H, 8.82%. ^1H NMR: (C_6D_6, 270 MHz, 75°C), δ 1.05 (t, CH_3), 1.17 (t, CH_3), 1.35 (s, CH_3), 1.51 (t, CH_3), 3.38 (s, br, O*H*), 3.50 (d, CH_2), 4.28 (q, CH_2), 4.33 (q, CH_2), 4.42 (d, CH_2). $^{13}C\{^1H\}$ NMR: (C_6D_6, 67.94 MHz, 75°C), δ 18.17 (s, CH_3), 19.07 (s, CH_3), 19.16 (s, CH_3), 57.28 (s, CH_2), 64.13 (s, CH_2), 67.83 (s, br, CH_2). Mass spectrometry: only $Ti(OEt)_4$ breakup observed.

Synthesis of $[SrTi_4(OEt)_{18}]$ **(3)**

Strontium metal pieces (0.46 g, 5.23 mmol) were placed in a flame dried Schlenk and EtOH (30 cm^3) added. There was a vigorous exothermic reaction with hydrogen released and the solution turning grey. Then $Ti(OEt)_4$ (4 equivs, 20.9 mmol, 5.2 cm^3) was added and the solution heated to reflux with stirring. After 40 min, all the metal had dissolved with the product starting to deposit out of solution. Therefore more ethanol (20 cm^3) was added and the solution heated to 85°C for 1 h. This solution was then allowed to cool very slowly, producing large plate/flake like crystals. Yield: 4.79 g, 67%. Found: C, 40.02; H, 8.68. $C_{36}H_{90}O_{18}SrTi_4$ requires: C, 39.66; H, 8.82%. ^1H NMR: (C_6D_6, 270 MHz, 70°C), δ 1.00 (t, CH_3), 1.34 (s, O*H*), 1.37 (s, CH_3), 3.50 (q, CH_2), 4.40 (s, CH_2). $^{13}C\{^1H\}$ NMR: (C_6D_6, 67.94 MHz, 70°C), δ 17.95 (s, CH_3), 19.24 (s, CH_3), 24.87 (s, CH_3), 26.02 (s, CH_3), 58.99 (s, CH_2), 68.6 (m, CH_2). Mass spectrometry: only $Ti(OEt)_4$ breakup observed.

Synthesis of $[BaTi_4(OEt)_{18}]$ **(4)**

Barium metal ribbon (0.705 g, 5.13 mmol) was placed in a flame dried Schlenk and EtOH (30 cm^3) added. The metal dissolved very rapidly (i.e. 10 min) and the solution turned purple. Then $Ti(OEt)_4$ (4 equivs, 5.1 cm^3, 20.51 mmol) was added and the solution stirred at reflux for 1 h. The purple colour was discharged yielding a colourless solution. The solution was then allowed to return to room temperature very slowly when a large crop of small white feather like crystals were obtained. Yield: 6.09 g, 84%. Found: C, 38.26; H, 7.89. $C_{36}H_{90}O_{18}BaTi_4$ requires: C, 37.93; H, 7.96%. ^1H NMR: (C_6D_6, 270 MHz, 70°C), δ 0.99 (t, CH_3), 1.32 (s, CH_3), 2.13 (s, O*H*), 3.43 (q, CH_2), 4.38 (d, CH_2). Mass spectrometry: only $Ti(OEt)_4$ breakup observed.

Synthesis of $[Sr_2Ti(OEt)_8(EtOH)_5]_n$ **(5)**

Strontium metal ribbon (0.883 g, 10.03 mmol) and EtOH (30 cm^3) were placed in flame dried Schlenk

and stirred at reflux. Then $Ti(OEt)_4$ (1.24 cm^3, 0.5 equivs, 5.01 mmol) was added slowly to the reaction. The colour of the solution changed to purple to grey to blue and finally back to colourless. After all the metal had dissolved in 45 min, the solution was allowed to return to room temperature slowly. A large crop of crystals deposited, which were filtered off. Yield: 5.91 g, 85%. Found: C, 37.98; H, 8.76. $C_{26}H_{70}O_{13}Sr_2Ti$ requires: C, 38.39; H, 8.67%. ^1H NMR: (C_6D_6, 270 MHz, 75°C), δ 1.13 (t, CH_3), 1.23 (t, CH_3), 1.48 (t, CH_3), 3.77 (d, CH_2), 4.21 (q, CH_2), 4.36 (q, CH_2), 7.84 (s, O*H*). $^{13}C\{^1H\}$ NMR: (C_6D_6, 67.94 MHz, 75°C), δ 18.49 (s, CH_3), 19.19 (s, CH_3), 19.53 (s, CH_3), 57.66 (s, CH_2), 64.94 (s, CH_2), 68.73 (s, CH_2). Mass spectrometry: only $Ti(OEt)_4$ breakup observed.

Synthesis of $[Ba_2Ti(OEt)_8(EtOH)_5]_n$ (**6**)

Barium metal ribbon (1.36 g, 9.90 mmol) was placed in a flame dried Schlenk and EtOH (25 cm^3) added. An instant reaction occurred with hydrogen evolution and the solution became purple in colour. Then $Ti(OEt)_4$ (0.5 equiv., 1.23 cm^3, 4.45 mmol) was added and the solution set to stir at reflux for 1 h. On allowing to slowly cool to room temperature, a large crop of large needle-like crystals deposited out of solution. Yield: 2.23 g, first crop; 3.81 g, second crop; overall yield 71%. Found: C, 34.89; H, 7.67 $C_{26}H_{70}O_{13}Ba_2Ti$ requires: C 34.19; H, 7.73%. Mass spectrometry: only $Ti(OEt)_4$ breakup observed.

Synthesis of $[Sr_2Ti(OPr^i)_8(Pr^iOH)_3]\cdot 2Pr^iOH$ (**7**)

Strontium metal chunks (4.12 g, 46.8 mmol) and isopropanol (60 cm^3) were refluxed for 5 h in a flame dried Schlenk. The metal reacted with vigorous hydrogen gas evolution and dissolved to yield a near colourless solution of the alkoxide. Titanium isopropoxide $[Ti(OPr^i)_4]$ (6.4 cm^3, 23.4 mmol) was added carefully to the hot solution (an immediate, highly exothermic reaction involving the release of more gas was observed) and left to stir for 2 h at reflux. Filtration and subsequent cooling of the solution gave a large crop of white crystals. Yield: three crops of 10.22, 9.89 and 5.4 g, total yield 62%. Found: C, 46.93; H, 9.66 $C_{39}H_{96}O_{13}Sr_2Ti$ requires: C, 47.02; H, 9.71%. ^1H NMR: (C_6D_6, 270 MHz, 65°C), δ 1.24 (d, $^2J = 5.94$ Hz, CH_3), 3.27 (s, O*H*), 4.26 (s, br, $^2J = 5.94$ Hz, C*H*). $^{13}C\{^1H\}$ NMR: (C_6D_6, 67.94 MHz, 20°C), δ 26.47 (s,

Table 6. Crystallographic data for complexes (**3**) and (**7**)

	(**3**)	(**7**)
Formula	$C_{36}H_{90}O_{18}SrTi_4$	$C_{39}H_{96}O_{13}Sr_2Ti$
Molecular weight	1090.30	996.26
Colour; habit	clear blocks	clear blocks
Crystal size (mm)	$0.30\times0.20\times0.18$	$0.28\times0.22\times0.17$
Crystal system	monoclinic	orthorhombic
Space group	$P2_1/n$	*Pnam*
a (Å)	28.618(5)	23.449(1)
b (Å)	20.251(8)	13.187(2)
c (Å)	20.192(4)	17.315(7)
β (°)	109.00(10)	—
V (Å^3)	11,065(5)	5354(2)
Z	8	4
D_{calc} (g cm^{-3})	1.309	1.236
μ (mm^{-1})	1.569	2.181
$F(000)$	4608	2128
Total no. of reflections	36,460	15,288
Absorption correc. factors	0.879–1.008	0.923–1.021
No. of unique data	16,176	4222
R_{int}	0.0869	0.0545
θ range (°)	1.80–25.16	2.10–25.03
Data/parameter	16,176/1117	4222/293
Goodness-of-fit on F^2	0.799	0.848
ρ_{min}/ρ_{max}	−0.355/0.678	−0.625/0.972
R^a	0.1250(0.0566)^b	0.0872(0.0592)^b
$wR_2{}^b$	0.1317(0.1193)^b	0.1613(0.1421)^b

Details in common: cell refinement by 250 reflections; fast area detector; Mo–K_α radiation, $\lambda = 0.71069$ Å, $T = 150$ *K*, refinement on F^2 using all unique data.

$^aR = \Sigma(\Delta F)/\Sigma(F_o)$; $wR_2 = [\Sigma\{w(\Delta F^2)^2\}/\Sigma\{w(F_o^2)^2\}]^{1/2}$.

^{b}The *R*-values calculated for data with $I > 2\sigma(I)$ only are given in parentheses.

CH_3), 66.02 (s, CH). Mass spectrometry: only ligand breakup observed.

X-ray crystallography for (**3**) *and* (**7**)

X-ray measurements for both compounds were made at 150 K using Mo–K_α radiation ($\lambda = 0.71069$ Å, graphite monochromator) on a Delft instrument FAST TV area detector diffractometer equipped with a rotating anode generator (50 Kv, 50 mA), a buffer board, a DEP image intensifier and an Oxford Cryostream low-temperature cooling system by following previously described procedures [53]. The data were corrected for Lorentz and polarization effects and also for absorption using the program DIFFABS [54]. The crystal data and details of data collection and structure refinements are presented in Table 6.

The structures were solved via direct methods (SHELX-S) [55] and difference electron density syntheses, and refined by full-matrix least squares on F^2 (SHELXL-93) [56] using all the unique data with intensities greater than 0. The secondary carbon atoms [C(3) and C(19)] in (**3**) and the tertiary carbon atoms [C(5) and C(9)] in (**7**) were disordered and two positions for each were refined with partial occupancies (0.50). All non-hydrogen atoms were anisotropic, with ISOR restraints being used for several atoms in both structures. The hydrogen atoms belonging to the partially occupied carbon atoms and neutral alcohol molecules in (**7**) were ignored; others were included in calculated positions (riding model). The final R-values are given in Table 6.

Atom coordinates, H-atom parameters, thermal parameters, full bond length and angles listings, and lists of observed and calculated structure factors have been deposited as supplementary material. All calculations were performed on Pentium 200 MHz personal computer. Sources of scattering factors are as in Ref. 70. The diagrams were drawn with the program SNOOPI [57].

Acknowledgements—We would like to thank the EPSRC (M.B.H., K.M.A.M., D.J.O., J.C.P.), the CASE sponsor Inorgtech, the Royal Society, and the Nuffield Foundation for financial support.

REFERENCES

1. Caulton, K. G. and Hubert-Pfalzgraf, L. G., *Chem. Rev.*, 1990, **90,** 969, and references therein.
2. Bradley, D. C., Mehrotra, R. C. and Gaur, D. P., *Metal Alkoxides*. Academic Press, London, 1978, and references therein.
3. Cowley, A. H. and Jones, R. A., *Angew. Chem. Int. Edn. Engl.*, 1989, **28,** 1208.
4. Mazdiyasni, K. S., Dollof, K. S. and Smith, J. S., *J. Amer. Ceram. Soc.*, 1969, **52,** 523.
5. Klee, M. and Brand, W., *K. Keramiek*, 1987, **4,** 60, and references therein.
6. Phule, P. P. and Risbud, S. H., *J. Mater. Sci.*, 1990, **25,** 1169, and references therein.
7. Hubert-Pfalzgraf, L. G., *Polyhedron*, 1994, **13,** 1181.
8. U.S. Patent 3,647,364, 1972.
9. Kasai, T. and Ozaki, Y., *Yogyo-Kyokai-Shi*, 1987, **95,** 912.
10. Nonaka, T., Kaneko, K., Hasegawa, T., Kishio, K., Takahashi, Y., Kobayashi, K., Kitazawa, K. and Fueki, K., *Jpn. J. Appl. Phys.*, 1988, **27,** L867.
11. Katayama, S. and Sekine, M., *J. Mater. Chem.*, 1991, **1,** 1031.
12. Plourde, J. K., Linn, D. F., O'Bryan, H. M. and Thomson, J. Jr, *J. Amer. Ceram. Soc.*, 1975, **58,** 418.
13. Cross, L. E., *Amer. Ceram. Soc. Bull.*, 1984, **63,**586.
14. Mazdiyasni, K. S., *Amer. Ceram. Soc. Bull.*, 1984, **63,** 591.
15. O'Bryan, H. and Thomson, J., *J. Amer. Ceram. Soc.*, 1985, **68,** C70.
16. Pfaff, G., *J. Mater. Chem.*, 1992, **2,** 591.
17. Sharma, H. B., Tandon, R. P., Mansingh, A. and Rup, R., *J. Mater. Sci. Lett.*, 1993, **12,** 1795.
18. Azuma, T., Takahashi, S. and Kuwabara, M., *Jpn. J. Appl. Phys.*, 1993, **32,** 4089.
19. Hayashi, T., Ohji, N., Hirohara, K., Fukunaga, T. and Maiwa, H., *Jpn. J. Appl. Phys.*, 1993, **32,** 4092.
20. Dutta, P. K., Gallagher, P. K. and Twu, J., *Chem. Mater.*, 1993, **5,** 1739.
21. Turevskaya, E. P., Turova, Ya. N. and Novoselova, A. V., *Dokl. Akad. SSSR.*, 1978, **247,** 883.
22. Yanovskaya, M. I., Yorova, N. Ya, Turevskaya, E. P., Novoselova, A. V., Venevtsev, Y. N., Sagitov, S. I. and Soboleva, E. M., *Izv. Akad. Nauk. SSSR, Neorg. Mater.*, 1981, **17,** 307.
23. Torova, N. Ya and Yanovskaya, M. I., *Izv. Akad. Nauk. SSSR, Neorg. Mater.*, 1983, **19,** 693.
24. Campion, J. F., Payne, D. A., Chae, H. K., Mauri, J. K. and Wilson, S. R., *Inorg. Chem.*, 1991, **30,** 3244.
25. Yanovsky, A. I., Yanovskaya, M. I., Limar, V. K., Kessler, V. G., Turova, N. Ya and Struchkov, Y., *J. Chem. Soc., Chem. Commun.*, 1991, 1605.
26. Moulson, A. J. and Herbert, J. M., *Electroceramics: Materials. Properties and Applications*. Chapman and Hall, London, 1990.
27. Turevskaya, E. P., Kessler, V. G., Turova, N. Y., Pisaresky, A., Yanovsky, A. I. and Struchkov, Y., *J. Chem. Soc., Chem. Commun.*, 1994, 2003.
28. Hampden-Smith, M. J., Williams, D. S. and Rheingold, A. L., *Inorg. Chem.*, 1990, **29,** 4076.
29. Boyle, T. and Bradley, D. C., *Inorg. Chem.*, 1995, **34,**
30. Coan, P. S., Streib, W. E. and Caulton, K. G., *Inorg. Chem.*, 1991, **30,** 5019.
31. Coan, P. S., Streib, W. E. and Caulton, K. G., *Inorg. Chem.*, 1992, **31,** 4207.
32. Vaartstra, B. A., Streib, W. E. and Caulton, K. G., *J. Amer. Chem. Soc.*, 1990, **112,** 8593.
33. Samuels, J. A., Chiang, W.-C., Huffman, J. C., Trojan, K. L., Hatfield, W. E., Baxter, D. V. and Caulton, K. G., *Inorg. Chem.*, 1994, **33,** 2167.
34. Yanovskaya, M. I., Turevskaya, E. P., Kessler,

V. G., Obvintseya, I. E. and Turova, N. Ya, *Integ. Ferro.*, 1992, **1,** 343.
35. Kirby, K. E., *Mat. Res. Bull.*, 1988, **23,** 881.
36. Foulon, J. D., Miele, P. and Hovnanian, N., *Zeit. Krist.*, 1994, **209,** 282.
37. Boulmaâz, S., Hubert-Pfalzgraf, L. G., Halut, S. and Daran, J. C., *J. Chem. Soc., Chem. Commun.*, 1994, p. 601 and p. 705.
38. Daniele, S., Hubert-Pfalzgraf, L. G., Daran, J. C. and Halut, S., *Polyhedron*, 1994, **13,** 927.
39. Bidell, W., Döring, J., Bosch, H. W., Hund, H.-U., Plappert, E. and Berke, H., *Inorg. Chem.*, 1993, **32,** 502.
40. Love, C. P., Torardi, C. C. and Page, C. J., *Inorg. Chem.*, 1992, **31,** 1784.
41. Sauer, N. N., Garcia, E., Salazar, K. V., Ryan, R. R. and Martin, J. A., *J. Amer. Chem. Soc.*, 1990, **112,** 1525.
42. Bidell, W., Shklover, V. and Berke, H., *Inorg. Chem.*, 1992, **31,** 5561.
43. Miele, P., Foulon, J. D., Hovnanian, N. and Cot, L., *J. Chem. Soc., Chem. Commun.*, 1993, 29.
44. Labrize, L., Hubert-Pfalzgraf, L. G., Daran, J. C. and Halut, S., *J. Chem. Soc., Chem. Commun.*, 1993, 1556.
45. Bemm, U., Lashgari, K., Norrestam, R., Nygren, M. and Westin, G., *J. Solid State Chem.*, 1993, **103,** 366.
46. (a) Arunasalam, V.-C., Baxter, I., Drake, S. R., Hursthouse, M. B., Malik, K. M. A. and Otway, D. J., *Inorg. Chem.*, 1995, **34,** 5295; (b) Arunasalam, V.-C., Drake, S. R., Hursthouse, M. B., Malik, K. M. A., Miller, S. A. S. and Mingos, D. M. P., *J. Chem. Soc., Dalton Trans.*, 1996, 2435.
47. Day, V. W., Eberspacher, T. A., Klemeperer, W. G. and Park, C. W., *J. Amer. Chem. Soc.*, 1993, **115,** 8469, and references therein.
48. Vaartstra, B. A., Huffman, J. C., Streib, W. E. and Caulton, K. G., *Inorg. Chem.*, 1991, **30,** 3068.
49. Caulton, K. G., Chisholm, M. H., Drake, S. R., Folting, K., Huffman, J. C. and Streib, W. E., *Inorg. Chem.*, 1993, **32,** 1370.
50. Baxter, I., Darr, J. A., Drake, S. R., Hursthouse, M. B., Malik, K. M. A. and Mingos, D. M. P., *J. Chem. Soc., Dalton Trans.*, 1997, 2875.
51. Caulton, K. G., Chisholm, M. H., Drake, S. R. and Streib, W. E., *Inorg. Chem.*, 1990, **29,** 2707.
52. Drake, S. R., Hursthouse, M. B., Malik, K. M. A. and Otway, D. J., *Polyhedron*, 1992, **11,** 1995.
53. Darr, J. A., Drake, S. R., Hursthouse, M. B. and Malik, K. M. A., *Inorg. Chem.*, 1993, **32,** 5704.
54. Walker, N. P. C. and Stuart, D., *Acta Cryst., Sect. A*, 1983, **39,** 158, adapted for FAST geometry by A. Karaulov, University of Wales Cardiff, 1991.
55. Sheldrick, G. M., *Acta Crystallogr. Sect. A*, 1990, **46,** 467.
56. Sheldrick, G. M., SHELXL-93 program for crystal structure refinement. University of Göttingen, Germany, 1993.
57. Davies, K., SNOOPI Program for crystal structure drawing. University of Oxford, 1983.

Pergamon

PII: S0277-5387(97)00468-3

Polyhedron Vol. 17, No. 5–6, pp. 641–657, 1998
© 1998 Published by Elsevier Science Ltd
All rights reserved. Printed in Great Britain
0277-5387/98 $19.00+0.00

Insertion reactions of small molecules into group 2 metal alkoxides; structural characterization of $[Mg_9(\mu_5\text{-}CO_3)(O_2COMe)_8(\mu_3\text{-}OMe)_8(MeOH)_{13}]\cdot MeOH\cdot C_7H_8$

V. Cumaran Arunasalam,[a] Ian Baxter,[b] Jawwad A. Darr,[a]‡ Simon R. Drake,[a] Michael B. Hursthouse,*[b] K. M. Abdul Malik[b] and D. Michael P. Mingos*[a]

[a]Department of Chemistry, Imperial College of Science, Technology and Medicine, South Kensington, London SW7 2AY, U.K.

[b]Department of Chemistry, University of Wales Cardiff, P.O. Box 912, Park Place, Cardiff CF1 3TB, U.K. (e-mail: malikka@cardiff.ac.uk)

(Received 5 November 1997; accepted 10 November 1997)

Abstract—The SO_2 inserted compounds $[M(O_2SOMe)_2(MeOH)_2]_\infty$ (M = Mg **1**; M = Ca **2**) were synthesized from the reaction of the corresponding $[M(OMe)_2]_\infty$ complexes in methanol, followed by recrystallization from either *n*-hexane or toluene. The reaction of COS or CS_2 gas with $[M(OMe)_2]_\infty$ in methanol, yielded the inserted products $[M(\{OCS\}OMe)_2(MeOH)_x]_n$ ($x = 2$, M = Mg **3**; $x = 3$, $n = 2$, M = Ca **4**) and $[M(S_2COMe)_2(MeOH)_x]_n$ ($x = 6$, M = Mg **5**; $x = 4$, M = Ca **6**), respectively. The analogous reaction of $[M(OMe)_2]_\infty$ (M = Mg, Ca) with CO_2 gas gave the mixed methoxide/methylcarbonato compounds $[Mg(O_2COMe)(OMe)(MeOH)_{1.5}]_n$ **7a** and $[Ca(O_2COMe)(OMe)(MeOH)]_n$ **8**. Recrystallization of **7a** from a "wet" hydrocarbon solvent mixture led to the crystalline product $[Mg_9(CO_3)(O_2COMe)_8(OMe)_8(MeOH)_{13}]\cdot MeOH\cdot C_7H_8$ **7b**. The corresponding insertion reaction of CO_2 gas with $[M(OEt)_2]_\infty$ (M = Mg, Ca) gave the mixed ethoxide/ethylcarbonato compounds $[M(O_2COEt)(OEt)(EtOH)_2]_n$ (M = Mg **9**; M = Ca **10**). Similarly, the reaction of CO_2 gas with $[Mg(OR)_2]_\infty$ (R = Pr^i, Bu^t) in the parent alcohol, resulted in the $[Mg(O_2COR)(OR)(ROH)]_n$ compounds (R = Pr^i **11**; R = Bu^t **12**). All compounds have been characterized by spectroscopic techniques including NMR (^{1}H and ^{13}C) and IR spectroscopy, and in selected cases by TGA/DSC. Complex **7b** was unambiguously characterized by single crystal X-ray diffraction. It was established that **7b** is a nonameric complex comprising of two Mg_4O_4 cubes, with a remote ninth magnesium atom held in position via two bridging methylcarbonato groups and an unusual μ_5-carbonate ligand. © 1998 Published by Elsevier Science Ltd. All rights reserved

Keywords: insertion reactions; magnesium; calcium; ethoxide; methoxide.

INTRODUCTION

The insertion reactions of one-carbon-atom molecules (C_1 chemistry) are an important area of research. Although the major raw material for C_1 based chemistry is CO, CO_2 may also serve as a convenient reagent in reactions which mimic Fischer–Tropsch (F-T) process [1,2]. CO_2 is used as an industrial feedstock in the production of urea, carboxylic acids and organic carbonates [1,3]. Another promising area of current research is the laboratory synthesis of organic substances derived from CO_2, ranging from hydrocarbons to cyclic lactones [4]. In insertion reactions, an atom or a group of atoms is formally inserted between two atoms which were initially bound together, resulting in no change in the formal oxidation state of the metal [5].

$$M{-}X + YZ \rightarrow M{-}(YZ){-}X$$

* Author to whom correspondence should be addressed. Tel.:01222 874068. Fax: 01222 874029. E-mail: hursthouse@cardiff.ac.uk.

‡ Current Postal Address: Department of Chemistry, University Park, Nottingham, NG7 2RD, UK.

One of the most common insertion reactions is that involving CO_2 and metal–carbon bonds of Grignard reagents [6–8]. The resulting carboxylate is subsequently hydrolysed to yield the corresponding organic acid. Insertion reactions of CO_2 have been extensively reported for metal–hydrogen, metal–carbon and metal–nitrogen bound compounds [9]. In contrast, the analogous carbon dioxide insertion reactions into M—OR bonds is an underdeveloped area with only few examples of authenticated insertion products [5].

The related insertion reactions of SO_2, COS and CS_2 have recently attracted attention. Such reactions are also of interest in their own right because of their roles in catalyst poisoning and air pollution treatment [10]. The detrimental environmental effects of SO_2 has resulted in a renewed interest in the chemistry of this ligand. Reactions of SO_2 with metal complexes have been exhaustively reported [11], in particular with the class "b" or soft metals [12]. Structural studies of these complexes reveal, as expected, S-co-ordinated SO_2 moieties. In contrast, class "a" and borderline metals have been relatively neglected. SO_2 is also extensively used as a feedstock in organic syntheses [13], for example, organomagnesium compounds are known to react with SO_2 to give sulfinic acids upon hydrolysis [12]. Insertion reactions of SO_2 into transition metal–carbon bonds to yield sulfinato-complexes have been widely studied [13]. In contrast, only a few SO_2 insertions reactions into metal–oxygen bonds have been reported [14,15]. Although magnesium and calcium complexes have found applications within SO_2 chemistry, there is a lack of reports on well characterized SO_2 complexes of the Group 2 metals. Furthermore, SO_2 complexes which are S-bonded have been observed frequently, while O-bonded complexes are rather rare. The reactions of COS with transition metals have also been widely studied and the area has been reviewed by Ibers [10,16]. Insertion reactions of COS into metal–hydrogen bonds have been widely reported [17], but the corresponding reactions into metal–oxygen bonds have been relatively neglected. Similarly, the co-ordination chemistry of CS_2 has been extensively studied since the preparation of the first transition-metal CS_2 complexes in 1967 [18]. In fact, CS_2 has proved to be a versatile ligand which forms complexes with almost every transition metal [10].

We have previously reported the reactions of the related molecules COS and SO_2 with $[Ca(OMe)_2]_\infty$, which led to the insertion products $[Ca(\{OCS\}OMe)_2(MeOH)_3]_2$ and $[Ca(O_2SOMe)_2(MeOH)_2]_\infty$, respectively [19, 20]. More recently, we reported the insertion reactions of COS gas with magnesium and strontium alkoxide compounds to give the inserted complexes $[Mg(\{OCS\}OEt)_2(EtOH)_4]$ and $[Sr_3(\{OCS\}OEt)_6(EtOH)_8]$ [21]. Such compounds are also of interest in their own right because of their potential as models for catalyst poisoning [10].

As early as 1897, Szarvasy [22] prepared a magnesium methylcarbonato-complex "$[Mg(O_2COMe)_2]_n$" from the reaction of magnesium methoxide with carbon dioxide. However, it was not until 60 years later that its use was first reported in synthetic organic reactions for introducing a carboxyl group into active hydrogen compounds such as primary nitro-alkanes [23]. Complexes of the general formula "$[M(O_2COR)_2]_n$" (M = Ca, Ma) are the suggested intermediates to oil-lube additives, the colloidal magnesium and calcium carbonates [24].

$$M(OR)_2 \xrightarrow{CO_2} [M(O_2COR)_2]_n \xrightarrow[H_2O,oil]{surfactant,\ promoters} MCO_3 + 2ROH$$

Scheme 1.

The only commercially available Group 2 metal alkylcarbonato complex is "$[Mg(O_2COMe)_2]_n$" [25] (Aldrich) which is available as either dimethylformide (5M) or methanol (0.5M) solutions [26]. However, this complex has not been fully characterized by spectral and structural methods. In the present paper, we report the preparation and properties of a range of inserted products of CO_2, SO_2, COS and CS_2 with magnesium and calcium alkoxides, and an X-ray structural characterization of the partially hydrolysed product $[Mg_9(\mu_5\text{-}CO_3)(\mu_2\text{-}O_2COMe)_4(O_2COMe)_4(\mu_3\text{-}OMe)_8(MeOH)_{13}]\cdot MeOH\cdot C_7H_8$, which may be viewed as an intermediate in the formation of colloidal magnesium carbonate.

EXPERIMENTAL

General procedures and instrumentation

All manipulations of reactants and products were carried out under nitrogen atmosphere (Schlenk techniques), argon atmosphere (Miller Howe 160 FF glove-box) or *in vacuo*, with exclusion of moisture and oxygen. Elemental analyses were performed by the microanalytical department of Imperial College. Melting points were measured under argon in sealed capillaries using an "Electrothermal" apparatus and are uncorrected. Infrared spectra were recorded on a Perkin–Elmer FTIR 1720 spectrometer as Nujol or hexachlorobutadiene (HCB) mulls between 25 × 4 mm KBr plates. The Nujol and HCB were both pre-dried with 4 Å molecular sieves prior to use and the samples were protected from the atmosphere by an O-ring sealed Presslock™ holder (Aldrich). Solution NMR spectra were recorded on a Jeol GS 270 MHz NMR spectrometer. ^1H NMR spectra were recorded for 16 scans at 270.16 MHz, whilst $^{13}C\{^1H\}$ NMR solution spectra were obtained at 67.94 MHz. Chemical shifts were referenced to tetramethylsilane (ca 1%) added by volume or using the *protio* impurities of the deuterated solvent. ^1H and $^{13}C\{^1H\}$ solid state NMR spectra were collected at 300.00 and 75.67 MHz, respectively, on a Bruker instrument at University College, London University Solid State NMR service. Mass spectra

were run on a VG Autospec. instrument at Imperial College. Controlled thermogravimetric analysis (TGA) and differential scanning calorimetric (DSC) measurements were done using a Polymer Laboratories 1500H simultaneous thermal analyzer, controlled by a Omni Pro 486DX-33 PC. The measurements were carried out in alumina crucibles (sample mass 11–25 mg) under an atmosphere of flowing (30 cm^3 min^{-1}) nitrogen gas, using a heating rate of 16 C min^{-1}.

CAUTION: Care should be taken by conducting all reactions in a ventilated fume cupboard.

Starting materials

All Group 2 alkoxide starting materials were prepared as described previously [21]. $[Mg(OR)_2]_n$ (R = Et, Pr^i, Bu^t) were prepared from the reaction of dibutylmagnesium (Aldrich) in *n*-hexane or heptane with the desired alcohol. $[Mg(OMe)_2]_n$ and $[Ca(OR)_2]_n$ (R = Me, Et) were prepared from the reaction of metal chips (Johnson Matthey) in alcohol. $[Ca(OMe)_2(MeOH)_2]_n$ was prepared from the corresponding homoleptic complexes or as described previously [21,27]. CO_2 was purchased from BOC and used as obtained. SO_2, COS and CS_2 were purchased from Aldrich Chemical Company.

Preparation of the SO_2 inserted complexes

$[Mg(O_2SOMe)_2(MeOH)_2]_n$ **1**. To a suspension of magnesium methoxide $\{[Mg(OMe)_2]_n\}$ (1.00 g, 11.63 mmol) in methanol (30.0 cm^3) was bubbled SO_2 gas at room temperature. This resulted in a vigorous exothermic reaction and dissolution of the methoxide to give a clear solution. The resulting solution was stirred for a further 30 min and a crystalline solid isolated at −20 C (2.19 g, 67%), m.p. desolvates >56 C (Found: C, 16.7; H, 4.8%. $C_4H_{14}MgO_8S_2$ requires C, 17.3; H, 5.0%); ν_{max}/cm^{-1} (Nujol) 3387 m, 1261 m, 1160 m, 1090 s, 1021 s, 987 s, 799 m, 725 m, 680 m, 599 m, 443 w, 353 w; (HCB) 3363 m, 2952 s, 2846 s, 1471 s, 1455 s, 1403 s; *m/z* (FAB^+) 214 [$Mg(O_2SOMe)_2$, 7], 115 [$Mg(O_2SOMe)$, 35], 95 [O_2SOMe, 20], 44 [SO_2, 40%].

$[Ca(O_2SOMe)_2(MeOH)_2]_n$ **2**. A similar experimental work up as that described for **1**, starting from calcium methoxide (1.35 g, 13.23 mmol) in methanol (30.0 cm^3) to obtain crystals of **2** at 0 C (1.83 g, 47%), m.p. desolvates >55 C (Found: 16.4; H, 4.6%. $C_4H_{14}CaO_8S_2$ requires C, 16.3; H, 4.8%); ν_{max}/cm^{-1} (Nujol) 3345 m, 1433 m, 1261 m, 1141 s, 1106 s, 1064 s, 1061 s, 1029 s, 855 w, 800 m, 722 m, 671 s, 646 s, 560 m, 458 w, 428 m, 309 m; (HCB) 3333 m, 2929 m, 2827 m, 1453 w, 1432 m; *m/z* (FAB^+) 595 [$Ca_3(O_2SOMe)_5$, 5], 461 [$HCa_2(O_2SOMe)_4$, 15], 365 [$Ca_2(O_2SOMe)_3$, 5], 135 [$Ca(O_2SOMe)$, 65], 95 [O_2SOMe, 16], 44 [SO_2, 36%].

Preparation of the COS inserted complexes

$[Mg(\{OCS\}OMe)_2(MeOH)_2]_n$ **3**. To a suspension of magnesium methoxide (1.25 g, 14.53 mmol) in methanol (30.0 cm^3) was bubbled COS gas at room temperature. This resulted in a vigorous exothermic reaction and precipitation of a white solid. The resulting solid was insoluble in alcohol and isolated by filtration. Yield: 2.50 g (63%) m.p. desolvates >67 C (Found: C, 26.2; H, 4.9%. $C_6H_{14}MgO_6S_2$ requires C, 26.7; H, 5.2%); ν_{max}/cm^{-1} (Nujol) 3428 s, 3287 s, 1505 s, 1431 s, 1261 m, 1246 m, 1186 s, 1125 s, 1105 s, 1043 s, 1020 s, 798 m, 733 s, 685 s, 671 s, 551 s, 513 s, 433 s, 342 m, 302 m; (HCB) 3436 s, 3311 s, 3093 s, 2991 s, 2941 s, 2836 s, 1505 s, 1449 s, 1432 s, 1375 s; *m/z* (FAB^-) 321 [$Mg_2(\{OCS\}OMe)_3$, 4], 115 [$Mg(\{OCS\}OMe)$, 23], 91 [$\{OCS\}OMe$, 48], 60 [COS, 15%].

$[Ca(\{OCS\}OMe)_2(MeOH)_3]_2$ **4**. To a suspension of calcium methoxide (1.75 g, 17.12 mmol) in methanol (30.0 cm^3) was bubbled COS gas at room temperature. This resulted in an exothermic reaction and dissolution of the methoxide to yield a yellow solution. The volume of the solution was reduced to ca 5 cm^3 and left to stand at room temperature for 12 h when a crystalline solid was isolated (2.64 g, 54%), m.p. desolvates >75 C (Found: C, 25.9; H, 5.9%. $C_7H_{18}CaO_7S_2$ requires C, 26.4; H, 5.7%); ν_{max}/cm^{-1} (Nujol) 3170 s, 1688 s, 1607 s, 1324 s, 1306 s, 1244 m, 1193 s, 1088 s, 1053 s, 1019 s, 923 m, 872 w, 820 m, 722 m, 680 m, 613 m, 558 s, 512 s, 327 s; (HCB) 3174 s, 2942 s, 2872 m, 2838 m, 2811 m, 1689 m, 1462 s, 1401 s, 1380 m, 1324 m, 1303 m; *m/z* (FAB^+) 131 [$Ca(\{OCS\}OMe)$, 15], 91 [$\{OCS\}OMe$, 58], 60 [COS, 12%].

Preparation of the CS_2 inserted complexes

$[Mg(S_2COMe)_2(MeOH)_6]_n$ **5**. To a suspension of magnesium methoxide (1.25 g, 14.53 mmol) in methanol (30.0 cm^3) was added CS_2 (2.18 cm^3, 36.33 mmol) at room temperature. This was an exothermic reaction, and on stirring the methoxide dissolved slowly to yield a yellow solution. The solution was stirred for a further 30 min and the volume reduced *in vacuo* by half; a crystalline solid was isolated at −20 C (3.49 g, 56%), m.p. disolvates >65 C (Found: C, 28.2; H, 6.8%. $C_{10}H_{30}MgO_8S_4$ requires C, 27.9; H, 7.0%); ν_{max}/cm^{-1} (Nujol) 3115 s, 1512 m, 1419 s, 1299 w, 1261 m, 1237 m, 1188 s, 1130 s, 1110 s, 1093 s, 1054 s, 1043 s, 1016 s, 951 s, 925 m, 801 m, 722 m, 657 s, 621 m, 574 m, 470 s, 424 s, 403 s, 341 m; (HCB) 3103 s, 2966 s, 2962 s, 2842 s, 2825 s, 2796 s, 1520 s, 1505 s, 1444 s, 1429 s, 1418 w; *m/z* (FAB^+) 286 [$HMg_6(O)_5(OMe)_2$, 15], 247 [$HMg_5(O)_4(OMe)_2$, 16], 227 [$Mg_3(OMe)_5$, 26], 141 [$Mg_2(OMe)_3$, 10], 116 [$Mg(S_2CO)$, 22], 76 [CS_2, 100%].

$[Ca(S_2COMe)_2(MeOH)_4]_n$ **6**. A similar experimental work up as described for **5** was used, starting from calcium methoxide (1.50 g, 14.70 mmol) in methanol

($30.0\ cm^3$). The volume of the solution was reduced to ca $5\ cm^3$, and then left to stand at $-20°C$. A crystalline solid was isolated after 4 h (3.80 g, 65%), m.p. desolvates $>60°C$ (Found: C, 25.0; H, 5.3. $C_8H_{22}CaO_6S_4$ requires C, 25.1; H, 5.8%); ν_{max}/cm^{-1} (Nujol) 3561 w, 3185 w, 1524 w, 1347 m, 1261 m, 1193 s, 1146 s, 1093 s, 1047 s, 1018 s, 945 m, 800 m, 723 m, 588 m, 564 m, 468 m, 352 m; (HCB) 3662 w, 3182 m, 2966 s, 2962 s, 2842 s, 2825 s, 2796 s, 1520 s, 1444 s, 1432 s, 1418 w, 1350 m; *m/z* (FAB^+) 229 [$Ca_3(O)(OMe)_3$, 23], 183 [$Ca_3(O)_2(OMe)$, 18], 127 [$Ca_2(O)(OMe)_2$, 16], 132 [$Ca(S_2CO)$, 9], 76 [CS_2, 100%].

Preparation of CO_2 *inserted complexes*

$[Mg(O_2COMe)(OMe)(MeOH)_{1.5}]_n$ **7a**. To a suspension of magnesium methoxide (1.30 g, 15.11 mmol) in methanol ($30.0\ cm^3$) was bubbled CO_2 gas at room temperature. This resulted in an exothermic reaction and dissolution of the methoxide after ca 30 min. The solution was reduced to dryness *in vacuo* to yield a white solid (2.08 g, 85%), m.p. decomposes $>300°C$ (Found: C, 29.4; H, 6.3%. $C_{4.5}H_{12}MgO_{5.5}$ requires C, 30.3; H, 6.7%); ν_{max}/cm^{-1} (Nujol) 3269 s, 1690 s, 1655 s, 1335 s, 1261 w, 1192 m, 1101 s, 1056 s, 1040 s, 934 m, 849 m, 825 s, 713 m, 629 m, 455 m; (HCB) 3273 s, 2950 s, 2924 s, 2826 s, 1690 s, 1655 s, 1457 s, 1404 s, 1339 s; *m/z* (EI^+) 227 [$Mg_3(OMe)_5$, 3], 181 [$Mg_3(O)(OMe)_3$, 10], 99 [$Mg(O_2COMe)$, 10], 77 [H_2O_2COMe, 64], 44 [CO_2, 25%].

$[Mg_9(CO_3)(O_2COMe)_8(OMe)_8(MeOH)_{13}]\cdot MeOH\cdot C_7H_8$ **7b**. In an attempt to grow single crystals of **7a**, the compound was first dissolved in methanol and then the solvent removed, which resulted in a white paste. This was redissolved in a mixture of toluene and hexane (2:1 *v/v*). Slow crystallizations over a period of 48 h at room temperature yielded a very small crop of needle-like crystals, which was crystallographically characterized as **7b**.

$[Ca(O_2COMe)(OMe)(MeOH)]_n$ **8**. To a suspension of the calcium methoxide (0.75 g, 7.35 mmol) in methanol ($30.0\ cm^3$) was bubbled CO_2 gas at room temperature for 30 min. This resulted in an exothermic reaction and precipitation of a white solid. The compound is insoluble in methanol and was isolated by filtration (1.02 g, 78%), m.p. decomposes $>300°C$ (Found: C, 26.3; H, 5.2%. $C_4H_{10}CaO_5$ requires C, 26.9; H, 5.6%); ν_{max}/cm^{-1} (Nujol) 3209 w, 1723 m, 1682 s, 1645 s, 1403 w, 1350 m, 1332 s, 1316 s, 1262 w, 1191 w, 1102 m, 1089 m, 1049 w, 1027 w, 918 w, 826 m, 820 m, 722 w, 698 w, 618 m, 373 w; (HCB) 3216 w, 2995 m, 2954 m, 2857 w, 2833 w, 1721 m, 1681 s, 1644 s, 1446 m, 1403 w, 1352 m, 1332 s, 1312 s; *m/z* ($EI.^+$) 405 [$Ca_5(CO_3)_2(O_2COMe)_3$, 20], 305 [$Ca_2(O_2COMe)_3$, 17], 263 [$Ca_3(CO_3)(OMe)_3$, 24], 229 [$Ca_3(O)(OMe)_3$, 40], 181 [$Ca_3(O)(OMe)_3$, 76], 127 [$Ca_2(O)(OMe)_2$, 37], 77 [H_2O_2COMe, 75], 44 [CO_2, 100%].

$[Mg(O_2COEt)(OEt)(EtOH)_2]_n$ **9**. A similar experimental work up as that described for **7a** was used, starting from magnesium ethoxide (1.50 g, 13.16 mmol) in ethanol ($20.0\ cm^3$), to yield a white solid (2.60 g, 79%), m.p. decomposes $>300°C$ (Found: C, 42.1; H, 8.7%. $C_9H_{22}MgO_6$ requires C, 43.2; H, 8.8%); ν_{max}/cm^{-1} (Nujol) 3445 m, 3231 m, 1652 s, 1326 s, 1175 s, 1104 s, 1056 s, 1014 m, 887 s, 824 s, 810 m, 722 s, 626 s, 433 s, 352 s; (HCB) 3446 m, 3219 m, 2979 s, 2931 s, 2854 s, 2823 m, 1651 s, 1471 s, 1411 s, 1377 s, 1329 s; *m/z* ($E.I.^+$) 134 [$Mg_3(O)_2(OCH_2)$, 12], 94 [$Mg_2(O)(OCH_2)$, 15], 76 [$H_2O_2COCH_2$, 20], 44 [CO_2, 25%].

$[Ca(O_2COEt)(OEt)(EtOH)_2]_n$ **10**. Experimental work up as described for **8** was used, starting from tetra-ethanol solvated calcium ethoxide (2.50 g, 7.96 mmol) in ethanol ($20.0\ cm^3$), to yield a white solid (1.61 g, 76%), m.p. decomposes $>300°C$ (Found: C, 39.8; H, 7.5%. $C_9H_{22}CaO_6$ requires C, 40.6; H, 8.3%); ν_{max}/cm^{-1} (Nujol) 3317 w, 1655 s, 1401 s, 1320 s, 1265 w, 1176 w, 1106 s, 1057 w, 1017, 985 w, 888 w, 825 m, 722 w, 615 w, 407 w, 353 w; (HCB) 3253 w, 2980 m, 2934 m, 2907 w, 1654 s, 1486 m, 1402 s, 1378 s, 1320 s; *m/z* ($E.I.^+$) 170 [$Ca_2(CO_3)(OCH_2)$, 7], 89 [H_2O_2COEt, 47], 44 [CO_2, 100%].

$[Mg(O_2COPr^i)(OPr^i)(Pr^iOH)]_n$ **11**. Experimental work up as described for **7a** was used, starting from magnesium *iso*-propoxide (2.00 g, 14.08 mmol) in *iso*-propoxide (2.00 g, 14.08 mmol) in *iso-propanol* (20.0 *cm*^{3}), to yield a white solid (3.53 g, 82%), m.p. decomposes $>300°C$ (Found: C, 48.3; H, 9.2%. $C_{10}H_{22}MgO_5$ requires C, 48.8; H, 8.9%); ν_{max}/cm^{-1} (Nujol) 3455 m, 3310 m, 1654 s, 1406 m, 1338 s, 1311 s, 1261 m, 1180 s, 1148 m, 1115 s, 1076 s, 954 m, 921 m, 856 m, 819 s, 727 m, 616 m, 479 m, 391 s, 316 m; (HCB) 3481 w, 3280 w, 2980 s, 2934 m, 2877 m, 1651 s, 1471 m, 1403 s, 1383 s, 1339 m, 1314 s; *m/z* ($E.I.^+$) 134 [$Mg_3(O)_2(OCH)$, 45], 105 [$H_2O_2COPr^i$, 20], 93 [$Mg_2(O)(OCH)$, 10], 90 [$H_2O_2COCH(Me)$, 70], 44 [CO_2, 100%].

$[Mg(O_2COBu^t)(OBu^t)(Bu^tOH)]_n$ **12**. To a suspension of magnesium *tert*-butoxide (1.25 g, 14.53 mmol) in *tert*-butanol ($20.0\ cm^3$) was bubbled CO_2 gas at room temperature. This resulted in an exothermic reaction and precipitation of a white solid, which was insoluble in and separated by filtration (3.59 g, 86%), m.p. decomposes $>300°C$ (Found: C, 53.4; H, 9.1%. $C_{13}H_{28}MgO_5$ requires C, 54.2; H, 9.7%); ν_{max}/cm^{-1} (Nujol) 3459 w, 3256 w, 3189 w, 1634 s, 1395 s, 1260 m, 1239 m, 1200 s, 1088 m, 1026 m, 954 s, 884 m, 823 m, 796 m, 766 m, 737 m, 574 m, 494 s, 422 m, 369 m, 330 m; (HCB) 3444 w, 3248 w, 3193 w, 2969 s, 2931 m, 2870 m, 1634 s, 1479 m, 1465 m, 1398 s, 1361 s.

Preparation of Carbon-13 labelled $^{13}CO_2$ *inserted compounds*

Compounds **13**, **14** and **15** were prepared by following procedures adopted for the corresponding

unlabelled CO_2 inserted compounds as described above.

$[Mg(O_2{}^{13}COMe(OMe)(MeOH)_{1.5}]_n$ **13**. ν_{max}/cm^{-1} (Nujol) 3404 m, 3256 m, 1604 s, 1300 s, 1193 m, 1099 s, 1059 s, 931 m, 799 s, 721 w, 628 m, 444 s, 303 m; (HCB) 3401 s, 3250 s, 2952 s, 2826 s, 1603 s, 1448 s, 1409 s, 1311 s.

$[Ca(O_2{}^{13}COMe)(OMe)(MeOH)_n$ **14**. ν_{max}/cm^{-1} (Nujol) 3213 s, 2003 w, 1674 m, 1633 s, 1597 s, 1132 s, 1307 s, 1290 s, 1191 m, 1155 m, 1099 s, 1086 s, 1048 s, 1027 s, 909 s, 796 s, 722 m, 696 m, 617 s, 372 m, 285 s; (HCB) 3217 w, 2995 w, 2953 w, 2852 w, 2833 w, 1676 m, 1634 s, 1598 s, 1442 m, 1308 s.

$[Ca(O_2{}^{13}COEt)(OEt)(EtOH)_2]_n$ **15**. ν_{max}/cm^{-1} (Nujol) 3207 m, 1621 s, 1298 s, 1172 m, 1156 m, 1102 s, 1081 s, 1056 s, 970 m, 881 s, 795 s, 722 m, 607 m, 476 s, 327 s, 289 s, 279 s (Nujol); (HCB) 3200 m, 2971 s, 2922 s, 2727 m, 2606 m, 1625 s, 1466 m, 1455 m, 1371 s.

Crystal structure determination of compound **7b**

X-ray measurements were made at 150(2) K using Mo–K_α radiation ($\lambda = 0.71069$ Å, graphite monochromator) on a Delft Instruments FAST TV area detector diffractometer equipped with a rotating anode generator (50 kV, 50 mA), a buffer board, a DEP image intensifier, and an Oxford Cryostream low temperature cooling system by following previously described procedure [28]. The cell parameters were obtained from the least-squares refinement of the diffractometer angles for 250 reflections. A total of 12,049 intensity data were collected from a volume corresponding to slightly more than a hemisphere of reciprocal space [$2.15 \leqslant \theta \leqslant 25.38^\circ$); $-12 \leqslant h \leqslant 10$, $-18 \leqslant k \leqslant 18$, $-25 \leqslant l \leqslant 18$], which gave 10,590 ($R_{int} = 0.0373$) unique data with intensities greater than zero. The data were corrected for Lorentz and polarization factors but not for absorption.

The structure was solved by direct methods (SHELXS86) [29] and difference electron density syntheses, and refined on F^2 by full matrix least-squares (SHELXL93) [30] using all unique data. All non-hydrogen atoms were refined anisotropically. The crystal was a poor diffractor and the data set contained an unusually large number of "unobserveds". Free refinement at the initial stage resulted in very elongated ellipsoids or "non-positive-definite" displacement coefficients for several atoms. Bond lengths associated with several terminal groups were also unrealistic. So the final cycles of refinement were carried out with (a) ISOR = 0.015 restraints for several atoms and (b) bond length constraints for several methoxy/methanol groups. The hydrogen atoms of the MeOH molecules were all ignored; other hydrogen atoms in the complex were included in calculated positions (riding model) with $U_{iso} = n \times U_{eq}$ of the parent carbon ($n = 1.2$ for CH and 1.5 for CH_3 groups). Residual electron densities ranged from -0.36 to 0.75 $eÅ^{-3}$ and indicated no features of stereochemical significance. The crystal data are summarized in Table 1, and selected bond lengths and angles are presented in Table 2. The final R-values are given in Table 1. Sources of scattering factors as in Ref. 30. The diagrams were drawn with the program SNOOPI [31]. The calculations were done on Pentium P5-90 personal computer. Further crystallographic details, fractional atom co-ordinates, thermal parameters, hydrogen

Table 1. Crystal data for $[Mg_9(\mu_5\text{-}CO_3)(O_2COMe)_8(\mu_3\text{-}OMe)_8(MeOH)_{13}]\cdot MeOHC_7H_8\cdot$ (**7b**)

Formula	$[C_{38}H_{100}Mg_9O_{48}]\cdot CH_3OH\cdot C_7H_8$
FW	1668.15
Crystal system	triclinic
Space group	$P\bar{1}$
a (Å)	11.300(5)
b (Å)	17.187(8)
c (Å)	21.829(8)
α (°)	91.438(12)
β (°)	97.42(2)
γ (°)	90.14(2)
V (Å^3)	4203(3)
Z	2
Temperature (K)	150(2)
λ(Mo–K_α) (Å)	0.71069
Data/parameter	10,590/950
R^a	0.1577(0.0789)^c
wR^b	0.2715(0.1949)^c

$^aR = \Sigma(F_o - F_c)/\Sigma(F_o)$.
$^bwR = [\Sigma\{\omega(F_o^2 - F_c^2)^2\}/\Sigma\{w(F_o^2)^2\}]^{1/2}$, $w = 1/[\sigma^2(F_o^2)]$.
^{c}The R-values for data with $I > 2\sigma(I)$ are given in parentheses.

Table 2. selected IR data (cm^{-1}) for complexes **1**–**7a** and **8**–**15**

Complex	ν(X=Y)	ν(X—Y)	ν_{as} (X—Z)	ν_s(X—Z)	$\pi(XZ_3)$
(**1**)	1160	987	—	—	
(**2**)	1141	1064	—	—	
(**3**)	1186	—	1505	—	
(**4**)	1193	923	1688, 1607	—	
(**5**)	1188	951	—	—	
(**6**)	1193	925	—	—	
(**7a**)	—	—	1690, 1655	1335	849, 825
(**8**)	—	—	1723–1645	1350–1316	826, 820
(**9**)	—	—	1652	1326	824, 810
(**10**)	—	—	1655	1320	825
(**11**)	—	—	1654	1338, 1311	856, 811
(**12**)	—	—	1634	1260	823
(**13**)	—	—	1650, 1604	1300	799
(**14**)	—	—	1674–1597	1332–1290	796
(**15**)	—	—	1621	1290	795

Spectra obtained from Nujol mull. ν_{as} = asymmetric stretch; ν_s = symmetric stretch; π = out of plane bend. X = S, Y = O for **1** and **2**; X = C, Y = S and Z = O for **3** and **4**; X = C, Y = S for **5** and **6**, X = C and Z = O for **7a**–**15**.

atom parameters, and full list of interatomic distances and angles are deposited as supplementary material.

RESULTS AND DISCUSSION

Synthesis

The insertion reactions of the small molecules SO_2, COS, CO_2 and CS_2 into Group 2 metal–alkoxide bonds described herein involved addition of the gases SO_2, COS, CO_2 and liquid CS_2, respectively, to the alkoxide compounds in solution. Such reactions have been studied previously using either condensation [6,7] or autoclave [32] techniques.

The reactions of CO_2, SO_2 and COS as gases with metal alkoxide suspensions/solutions at ambient temperatures resulted in exothermic reactions. The reactions were complete within ca 30 min. Similarly, reactions involving CS_2 proceeded exothermically and were accompanied by dissolution of the alkoxides. In contrast, the insertion of CO_2 into molybdenum–alkoxide [32] bonds requires harsher conditions (high pressures of CO_2 and reflux temperatures).

The molecules SO_2, COS and CS_2 produced the double insertion products **1**–**6** when M = Mg or Ca. Structural studies have shown that the inserted products adopt the range of bonding modes illustrated in Fig. 1. In contrast, the CO_2 reactions appear to proceed via a single insertion process. Scheme 2 illustrates a generalized reaction scheme for CO_2 insertions into a range of magnesium and calcium alkoxides to yield the alkoxy–alkylcarbonato complexes **7a**–**12**.

$$[M(OR)_2]_n + 2ROH \xrightarrow{CO_2} [M(O_2COR)(OR)(ROH)_x]_z$$

Scheme 2

Unfortunately, it did not prove possible to obtain single crystals of these products and recrystallization resulted in the formation of oligomeric species presumably due to hydrolysis reactions involving traces of moisture. For example, the X-ray structure of **7b** revealed, very surprisingly, the incorporation of a CO_3^{2-} group in a monomeric metal framework. It has not proved possible to confirm unambiguously the origin of this CO_3^{2-} ligand in complex **7b**, but it could result from the hydrolysis of small quantities of $[Mg(O_2COMe)(OMe)(MeOH)_{1.5}]_n$ **7a** with the elimination of methanol and the formation of magnesium carbonate; "$[Mg(CO)_3]_n$" (Scheme 3).

$$\text{"}[Mg(\mu_2\text{-}O_2COMe)(OMe)(MeOH)_{1.5}]\text{"} \xrightarrow{H_2O} \text{"}[Mg(CO_3)]_n\text{"} + 3.5MeOH$$

Scheme 3.

Complex **7b** probably represents an intermediate in this hydrolysis process. The overall reaction is given in Scheme 4.

$$9[Mg(O_2COMe)(OMe)(MeOH)_{1.5}]_n\ \mathbf{7a} + H_2O \xrightarrow{C_7H_8\text{/n-hexane}} 1.5MeOH + [Mg_9(CO_3)(O_2COMe)_8 \times (OMe)_8(MeOH)_{13} \cdot MeOH \cdot C_7H_8\ \mathbf{7b}$$

Scheme 4

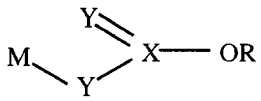

(a) unidentate

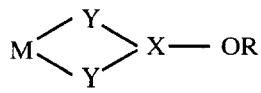

(b) chelating $\kappa^2 Y,Y'$

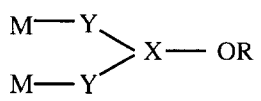

(c) bridging $1\kappa Y,2\kappa Y'$

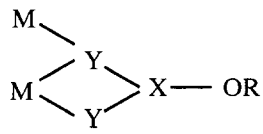

(d) chelating bridging μ_2, $1{:}2\kappa^2 Y;2\kappa Y'$

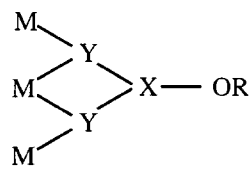

(e) chelating bridging μ_3, $1{:}2\kappa^2 Y;2{:}3\kappa^2 Y'$

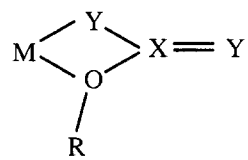

(f) chelating $\kappa^2 Y,O$

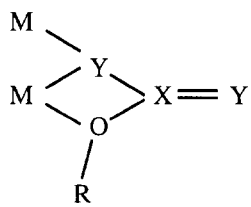

(g) chelating bridging μ_2, $1{:}2\kappa^2 Y;2\kappa O$

Key; CO_2, X = C, Y = O; SO_2, X = S, Y = O; COS, X = C, Y = S, O; CS_2, X = C, Y = S.

Fig. 1. Potential co-ordination modes for inserted moieties.

The reaction of CO_2 with the tetra-ethanol solvated calcium ethoxide $[\{Ca(OEt)_2(EtOH)_4\}_n]$ in toluene resulted in an increase in viscosity and "gelling" of the solution. However, on refluxing, evolution of CO_2 was observed and this was accompanied by a decrease in viscosity, implying a decarboxylation or extrusion reaction [21]. Significantly, the same reaction in ethanol resulted in precipitation of the complex $[Ca(O_2COEt)(OEt)(EtOH)_2]_n$ **10**. Further investigations support the view that CO_2 insertion into the Ca—OEt bond is occurring, but in toluene the ethylcarbonato ligand is unstable due to the absence of donor ligands such as ethanol co-ordinated to the metal. Similar observations were reported by Saegusa *et al.* [33], with *tert*-butyl isocyanide ligand stabilising the *tert*-butylcarbonato group by its σ-donating property.

$^{13}CO_2$ enrichment studies were performed for a range of magnesium and calcium alkoxides, which yielded the complexes **13**–**15**. Reaction conditions and work-up were similar to those of the unlabelled CO_2 experiments.

The insertion reactions of CO_2, SO_2 and COS into the Group 2 metal–alkoxide bonds are irreversible, and the resultant products **1**–**4** and **7a**–**15** are stable under reduced pressures (ca 1×10^{-2} Torr) and temperatures (up to 80°C). In contrast, the CS_2 inserted complexes **5** and **6** were unstable in the solid state.

Physical properties

Complexes **1**, **2** and **4**–**6** were isolated from methanol solutions as crystalline solids, whilst the complex

$[Mg(\{OCS\}OMe)_2(MeOH)_2]_n$ **3** was isolated as a white precipitate from methanol. Complexes **1**, **2** and **4**–**6** are soluble in methanol, in contrast, complex **3** is insoluble, indicating that it is a polymeric compound. Interestingly, the SO_2, COS and CS_2 calcium complexes **2**–**4** and **6** are soluble in methanol, whilst the CO_2 derivative **8** is insoluble. This may be due to the formation of the *bis*-inserted products with SO_2, COS and CS_2 in contrast to the mono-inserted products with CO_2. The solubilities of the inserted methoxide derivatives are significantly greater than those for $[Mg(OMe)_2]_n$ and $[Ca(OMe)_2]_n$, especially in DMSO [21]. The magnesium carbonato-derivatives **7a**, **9** and **11** are soluble in their parent alcohol and were isolated by removing the solvent. Complexes **8**, **10** and **12** were isolated as white insoluble precipitates.

The magnesium alkoxy alkycarbonato complexes **7**, **9** and **11** show good solubilities in their respective parent alcohols and DMSO, and are moderately soluble in toluene, whilst their calcium counterparts **8**, **10** are insoluble in their parent alcohols. This disparity in solubilities suggests different degrees of oligomerization; the calcium complexes are polymeric whilst the magnesium derivatives are more discrete oligomers. A noteworthy exception is the magnesium *tert*-butoxide derivative **12**, which is insoluble in *tert*-butanol.

Complexes **1**–**12** are air sensitive and readily hydrolyze to yield the corresponding metal carbonates, sulfites, thiocarbonates or dithiocarbonates. They are, however, stable at room temperature under an inert atmosphere and can be stored indefinitely in a glovebox. Furthermore, these complexes did not show sharp melting points, but decomposed at high temperatures.

Infra-red spectra

Sulphur dioxide inserted compounds. Complexes **1** and **2** exhibited asymmetric and symmetric stretching modes associated with alkylsulfito ligands corresponding to O-co-ordination: 1160 and 987 cm^{-1} (for **1**) and 1141 and 1064 cm^{-1} (for **2**), respectively, [34,35]. Similar stretching frequencies were observed for the recently structurally characterized iridium complex with an O-co-ordinated methylsulfito ligand [36]. Methylsulfito deformation vibrations δ(O—S—O) were observed at 680 cm^{-1} for **1**, and at 671 and 646 cm^{-1} for **2**. IR spectroscopic studies suggest different methylsulfito co-ordination modes in complexes **1** and **2**.

Carbonyl sulfide inserted compounds. IR spectra of complexes **3** and **4** are clearly different and imply dissimilar methylthiocarbonato co-ordination modes. Complex **4** exhibits ν(CO) stretching vibrations at 1688 and 1607 cm^{-1}, suggesting two distinct co-ordination modes (Table 2). In contrast, complex **3** displays a single ν(CO) stretching vibration at significantly lower frequency 1505 cm^{-1}. Similar stretching vibrations have been observed at 1620 and 1568 cm^{-1} for $[Sr_3(\{OCS\}OEt)_6(EtOH)_8]$ and 1568 cm^{-1} for $[Mg(\{OCS\}OEt)_2(EtOH)_4]$ [21]. The ν(C=S) stretching mode was observed at 1186 and 1193 cm^{-1} for **3** and **4**, respectively. Furthermore, complex **4** exhibited a ν(C—S) stretching mode at 923 cm^{-1}, suggesting two distinct methylthiocarbonato co-ordination modes. These peaks can be compared with the ν(C=S) stretching frequencies for $[Sr_3(\{OCS\}OEt)_6(EtOH)_8]$ and $[Mg(\{OCS\}OEt)_2(EtOH)_4]$ at 1176 and 1174 cm^{-1}, respectively, and ν(C—S) stretching mode at 930 cm^{-1} for $[Sr_3(\{OCS\}OEt)_6(EtOH)_8]$ [21]. Additional bands associated with methylthiocarbonato complexes are observed at 1125, 685, 671, 551 and 513 cm^{-1} for complex **3**, and 680, 613, 558, 512 cm^{-1} for complex **4**. Similar vibrational frequencies have been previously reported for manganese alkythiocarbonato complexes [37]. IR data for compound **3** suggest that the ligands display a mode of co-ordination similar to that illustrated in Fig. 1 (f) or (g), whilst complex **4** exhibits two distinct co-ordination modes [see Fig. 1, (b) and (g)].

Carbon disulfide inserted compounds. Characteristic IR group stretching modes associated with the dithiocarbonato ligand were observed for complexes **5** and **6** [38–40]. Complexes **5** and **6** exhibited bands corresponding to the ν(C=S) stretching modes at 1188 and 1193 cm^{-1} respectively, while the ν(C—S) stretching vibrations were observed at 951 cm^{-1} and 925 and 945 cm^{-1}, respectively (Table 2). The presence of both ν(C=S) and ν(C—S) stretching vibrations suggests that either unidentate co-ordination is present or, more likely, the chelating $\kappa^2 Y,O$ (Y = S) co-ordination mode is involved [Fig. 1, (f)].

Carbon dioxide inserted compounds. IR spectra of complexes **7a**–**12** exhibited characteristic stretching modes of the alkylcarbonato ligands (Table 2). The spectrum for **8** reveals three distinct asymmetric (1723, 1682, 1645 cm^{-1}) and symmetric (1350, 1331, 1316 cm^{-1}) stretching vibrations associated with methylcarbonato ligands, implying three different co-ordination modes for this ligand. The precise modes are hard to define due to the range of the potential bonding types (see Fig. 1). Similar stretching vibrations were also observed for complex **7a**. In contrast, the IR spectra for compounds **9**, **10**, **11** and **12** revealed two strong bands associated with the alkylcarbonato ligands in the region 1720–1520 cm^{-1} and 1350–1280 cm^{-1}, respectively, which could be assigned to the asymmetric ν_{as}(C—O) and symmetric ν_s(C—O) stretching modes, while a medium or weak out of plane bending (π) peak is observed between 856–810 cm^{-1} (Table 2). The ν(C—O)R stretching vibration expected around 1200–1100 cm^{-1} could not be assigned owing to overlap with ν(C—O) stretching modes of the alkoxide and alcohol ligands. Similar frequency ranges were reported by other workers [32,34,41–44]. The stretching and deformational vibrational frequencies associated with the alkyl vibrations were observed at their characteristic ranges.

Carbon-13 labelled $^{13}CO_2$ studies confirmed these assignments with an observed shift to lower frequencies for those bands associated with C—O vibrations in complexes **13–15**. The observed frequency shift was in close agreement with the calculated values, assuming the simple harmonic oscillator model (see Table 2). Comparison of the IR spectra of complexes **8** and **14** shows the expected shift to lower frequencies in **14**. In general, the IR bands corresponding to the ν_{as}(C—O) and ν_s(C—O) stretching modes were broad and yielded little structural information. It can be suggested, however, that a range of alkylcarbonato co-ordination modes are present.

Nuclear magnetic resonance spectra

Sulphur dioxide inserted compounds. ^{1}H NMR spectroscopic studies (Table 3) in $(CD_3)_2SO$ for complexes **1** and **2** at room temperature revealed a single broad resonance in each spectrum associated with methanol and methylsulfito ligands, indicative of an exchange process occurring between methanol and methylsulfito groups which is fairly fast compared to the NMR timescale. Similar fluxional behaviour was observed in the ^{13}C-$\{^1H\}$ NMR study for complex **2**, while the methylsulfito ligand were resolved in the corresponding spectrum for complex **1** (Table 4).

Carbonyl sulfide inserted compounds. ^{1}H NMR spectroscopic studies in $(CD_3)_2SO$ for complexes **3** and **4** clearly differentiated the methanol and methylthiocarbonato resonances (Table 3). The spectrum for complex **3** displayed two signals associated with two distinct methylthiocarbonato environments, whilst a single resonance was observed for **4**. Similar solution behaviour was observed in the ^{13}C-$\{^1H\}$ NMR spectra of **3** and **4** (Table 4). A characteristic thiocarbonato carbon signal, {O*C*S}OMe was observed in the ^{13}C-$\{^1H\}$ NMR spectra, and as expected, this was observed down-field from the carbonato carbon resonances. Darensbourg *et al.* [45,46] observed similar chemical shift positions for COS insertion products with tungsten alkoxides.

Carbon disulfide inserted compounds. ^{1}H NMR spectroscopic studies in $(CD_3)_2SO$ for complexes **5** and **6** (Table 3) revealed resonances due to both methanol and methylditiocarbonato ligands. Complex **5** displayed two signals, albeit at similar chemical shift positions, corresponding to two distinct methyldithiocarbonato environments, whilst a single resonance was observed for complex **6**, indicative of either one methyldithiocarbonato ligand environment or fluxional behaviour. ^{13}C-$\{^1H\}$ NMR solution studies (Table 4) exhibited a single distinctive resonance down-field for both **5** and **6** corresponding to the methyl group of the methyldithiocarbonato ligand. The dithiocarbonato carbon resonance S_2COMe was observed at low field (ca δ 230) with respect to the

Table 3. ^{1}H NMR data (δ, ppm) for complexes **1–7a** and **8–15**

Complex	ROH CH_3	XYZOR/OR CH_3	ROH CH or CH_2	XYZOR/OR CH or CH_2	ROH OH
(**1**)	3.09	3.09 (12 H, br)	—	—	4.33 (2 H)
(**2**)	3.12	3.12 (12 H, br)	—	—	4.18 (2 H)
(**3**)	3.15 (6 H)	3.01 (3 H), 3.36 (3 H)	—	—	4.33 (2 H)
(**4**)	3.09 (9 H)	3.28 (6 H)	—	—	4.19 (3 H)
(**5**)	3.11, 3.12 (18 H)	3.68 (3 H), 3.69 (3 H)	—	—	4.12 (6 H)
(**6**)	3.13 (12 H)	3.69 (6 H)	—	—	4.07 (4 H)
(**7a**)	3.18 (4.5 H)	3.22–3.47 (3 H, m, OCH_3), 3.74, 3.84 (3 H, O_2COCH_3)	—	—	4.58 (1.5 H, br)
(**8**)	3.14, 3.15 (3 H)	3.76 (6 H)	—	—	4.23, 4.24 (1 H)
(**9**)	1.00–1.10	1.00–1.10 (12 H, m)	3.41 (4 H, m, CH_2)	3.80 (4 H, q, CH_2)	4.41 (2 H, t)
(**10**)	1.01–1.09	1.01–1.09 (12 H, m)	3.42 (4 H, m, CH_2)	3.80 (4 H, q, CH_2)	4.43 (2 H, t)
(**11**)	1.01 (6 H, d)	1.08 (12 H, d)	3.74 (1 H, m, CH)	4.53 (2 H, m, CH)	4.45 (1 H)
(**12**)	1.09 (9 H)	1.31 (18 H)	—	—	4.19 (1 H)
(**13**)	2.87 (4.5 H)	3.16 (3 H, s, OCH_3), 3.41 (3 H, s, $O_2{}^{13}COCH_3$)	—	—	4.18 (1.5 H)
(**14**)	3.15 (3 H),	3.35 (3 H), 3.37 (3 H)	—	—	4.21 (1 H)
(**14**)[a]	3.37	3.37	—	—	4.99
(**15**)	1.04	1.04 (12 H, m)	3.44 (4 H, q, CH_2)	3.79 (4 H, q, CH_2)	4.46 (2 H)
(**15**)[a]	1.16 (br)	1.16 (br)	3.58 (br, CH_2)	3.58 (br, CH_2)	5.30, 6.11 (br)

ROH = parent alcohol.

[a] δ_H(MAS ECHO solid state); XYZOR = O_2SOMe (**1** and **2**), {OCS}OMe (**3** and **4**), S_2COMe (**5** and **6**), O_2COR (**7a–12**), $O_2{}^{13}COR$ (**13–15**).

All peaks are singlets unless stated otherwise; d = doublet; t = triplet; q = quartet; m = multiplet; br = broad.

Table 4. ^{13}C NMR data (δ, ppm) for complexes **1**–**7a** and **8**–**15**

	ROH CH_3	XYZOR/OR CH_3	ROH C_α	XYZOR/OR C_α	XYZOR Y = C
$[Mg(O_2SOR^1)_2(R^1OH)_2]_n$ (**1**)	49.05	44.88	—	—	—
$[Ca(O_2SOR^1)_2(R^1OH)_2]$ (**2**)	48.82 (br)	48.82 (br)	—	—	—
$[Mg(\{OCS\}OR^1)_2(R^1OH)_2]_n$ (**3**)	49.03	50.36, 52.16	—	—	184.92
$[Ca(\{OCS\}OR^1)_2(R^1OH)_3]_2$ (**4**)	49.24	52.01	—	—	184.94
$[Mg(S_2COR^1)_2(R^1OH)_6]_n$ (**5**)	49.10	58.14	—	—	231.00
$[Ca(S_2COR^1)_2(R^1OH)_4]_n$ (**6**)	48.86	57.79	—	—	230.84
$[Mg(O_2COR^1)(OR^1)(R^1OH)_{1.5}]_n$ (**7a**)	49.31, 49.53	52.94	—	—	158.49, 158.73
δ_C(CPMAS solid state)	49.76	53.13	—	—	160.20, 164.38
$[Ca(O_2COR^1)(OR^1)(R^1OH)]_n$ (**8**)	48.85	52.39	—	—	158.25
δ_C(CPMAS solid state)	49.53	52.25, 53.21, 54.10	—	—	158.14, 159.72
$[Mg(O_2COR^2)(OR^2)(R^2OH)_2]_n$ (**9**)	15.07	18.70	56.24	60.62	158.02
δ_C(CPMAS solid state)	14.88	18.01	57.72	61.72	159.36
$[Ca(O_2COR^2)(OR^2)(R^2OH)_2]_n$ (**10**)	15.67	19.09	56.67	60.45	158.38
δ_C(CPMAS solid state)	14.51	16.37, 17.74	61.64 (br)	61.64 (br)	158.89
$[Mg(O_2COR^3)(OR^3)(R^3OH)]_n$ (**11**)	22.45	25.66	62.19	67.18	157.77
δ_C(CPMAS solid state)	22.53	25.22	65.44	68.75	158.72
$[Mg(O_2COR^4)(OR^4)(R^4OH)]_n$ (**12**)	28.33	28.50, 31.42	67.00	75.66 (br)	157.79 (br)
δ_C(CPMAS solid state)	28.82	31.21, 35.77	68.49	76.23 (br)	157.76 (br)
$[Mg(O_2{}^{13}COR^1)(OR^1)(R^1OH)_{1.5}]_n$ (**13**)	48.77	52.36	—	—	157.89, 163.55
δ_C(CPMAS solid state)	49.72	53.22	—	—	159.96, 164.47
$[Ca(O_2{}^{13}COR^1)(OR^1)(R^1OH)]_n$ (**14**)[a]	48.87	52.30	—	—	158.23, 164.13
δ_C(CPMAS solid state)	49.12	49.12	—	—	157.66, 157.98, 158.43, 159.76, 164.80
$[Ca(O_2{}^{13}COR^2)(OR^2)(R^2OH)_2]_n$ (**15**)	15.34	18.76	56.17	59.82	157.66
δ_C(CPMAS solid state)	15.01	18.35	57.40	58.96	156.49, 159.00, 167.46

R^1 = Me; R^2 = Et; R^3 = Pr^i; R^4 = Bu^t; C_α = $C\{CH_3\}_3$/CH/CH_2 carbon (as appropriate) for that particular alcohol/inserted alkoxide/alkoxide.

ROH = parent alcohol; XYZOR = O_2SOR^1 (**1** and **2**), $\{OCS\}OR^1$ (**3** and **4**), S_2COR^1 (**5** and **6**), O_2COR (**7a**–**12**), $O_2{}^{13}COR$ (**13**–**15**).

All peaks are singlets unless stated otherwise.

br = broad.

[a]contains free $^{13}CO_2$ peak at δ 124.55.

carbonato (see later) and thiocarbonato and free CS_2 carbon signals (free CS_2 at ca δ 192). Other workers have also noted the dithiocarbonato carbon signal in a similar position [38,46,47].

Carbon dioxide inserted compounds. ^1H NMR studies in $(CD_3)_2SO$ for complexes **7a**–**12** revealed (Table 3) resonances associated with alkyl groups at chemical shift positions comparable with their respective alkoxide compounds [21]. Complex **7a** exhibited well resolved signals corresponding to methanol, methoxide and methylcarbonato ligands. In contrast, there was a lack of peak resolution for complexes **8**–**12**, indicative of superimposed signals or exchange processes occurring between alkoxide and alkycarbonato ligands which are rapid compared to the NMR timescale at room temperature. A noteworthy feature of the ^1H NMR spectra of complexes **9** and **10** is the multiplicity exhibited by OH and CH_2 protons of the ethanol ligands; OH and CH_2 resonances are resolved into triplets and pseudo quintets respectively (^3J = 4.95 Hz) indicative of a slow intra-molecular exchange process.

^{13}C-$\{^1H\}$ NMR solution studies for complexes **7a**–**12** (Table 4) also demonstrated fluxional behaviour between the alkoxide and alkycarbonato ligands. However, complexes **9** and **10** displayed an apparent shift to lower field (ca 3 ppm) of the ethylcarbonato α-carbon compared with their alkoxide signals (δ 60.6 for compound **9** compared to δ 58.4 for the corresponding alkoxide). The appearance of a very diagnostic signal at low field associated with the carbonato carbon, O_2COR (ca 157–166; cf free CO_2 at ca δ 124), is significant in the characterization for alkycarbonato complexes. This resonance has been found to be relatively unaffected by the alkyl substituents, it is possibly dependent on the mode of co-ordination [43,44].

Complexes **13**–**15**, the carbon-13 labelled $^{13}CO_2$ inserted compounds, allowed definitive assignments of the carbonato carbon signal $O_2{}^{13}COR$ to be made. Also evident from the ^{13}C-$\{^1H\}$ NMR spectra are the

weaker signals which were previously absent in the non-enriched complexes. In general, the carbonato signals derived from the carbon-13 labelled compounds yielded one or more intense resonances in solution than the analogous non-enriched complexes.

^{13}C-$\{^1H\}$ CPMAS NMR solid state studies were performed in order to provide additional structural information. The solution ^{13}C-$\{^1H\}$ NMR spectrum of complex **7a** revealed two almost identically shifted resonances associated with the carbonato carbon, while the solid state spectrum exhibited two signals separated by ca δ 4 ppm, indicative of two distinct methylcarbonato environments for the latter. Thus, exchange processes or time averaging effects are present in solution which give almost identical methylcarbonato environments. This is further supported by the presence of two signals (separated by ca δ 4 ppm) from the analogous carbon-13 labelled compound **13**. Similarly, the solution $^{13}C\{^1H\}$NMR of complex **14** exhibited two resonances for the carbonato carbon, but in the solid state, five well resolved signals were observed indicative of five distinct methylcarbonato environments. These findings were also observed for other complexes, although in some cases only one resonance was detected in both solution and solid state at comparable chemical shift positions.

The resonances corresponding to alkyl carbons of the alkoxide and alcohol ligands are similarly well resolved in the solid state spectra. For example, ^{13}C-$\{^1H\}$NMR spectrum for complex **8** in solution exhibits a single broad resonance due to the methoxide and methylcarbonato carbons, whilst the corresponding solid state spectrum is sufficiently discriminating to reveal a signal corresponding to the methoxide carbon and two signals due to the methlycarbonato carbons. This lends further support for the occurrence of exchange processes in solution at room temperature.

Multinuclear NMR (^1H and ^{13}C-$\{^1H\}$) variable temperature studies were investigated to determine the thermal stabilities of the alkycarbonato ligand. ^1H NMR variable temperature studies (20–80°C) for complex **10** resulted in a loss of resolution of the signals on increasing the temperature, accompanied by an up-field shift of the OH signal, while the other signals remained constant. Similar observations were noted for the complex $[\{Ca(OEt)_2(EtOH)_4\}_n]$ [21]. In contrast, no apparent changes were observed in the ^{13}C-$\{^1H\}$ NMR on increasing the temperature. Thus, the ethylcarbonato complex is thermally stable up to a temperature of 80°C. In contrast, solution NMR studies described by Chisholm *et al.* [32] on molybdenum alkoxy alkycarbonato complexes demonstrated decarboxylation at 80°C.

TGA/DSC and mass spectrometry studies

Thermogravimetric analysis (TGA) and differential scanning calorimetry (DSC) studies were performed on complexes **2**, **4**, **6** and **7a**. The TGA analyses for compounds **2** and **4** revealed the loss of the co-ordinated methanol molecules below 100°C, followed by the decomposition of the homoleptic insertion products with the liberation of either SO_2 or COS gas [19–21].

The DSC curve of complex $[Ca(S_2COMe)_2(MeOH)_4]_n$ **6** provided several interesting features. An endotherm was observed over the range 32–100°C and three distinct peaks were apparent. The first is centred at 38°C, the second at 65°C and the third at 81°C. This was mirrored in the TGA plot with a single rapid weight loss of 72.8% corresponding to four methanol molecules and breakdown of the CS_2 inserted ligands. This intermediate was stable at 400°C whereupon a further weight loss of 7.8% was observed to give a residue of 18.5% at this temperature (CaS would give a residue of 18.8%). This weight loss is consistent with an endotherm centred at 447°C (-26.92 mcal mg^{-1}) in the DSC plot. A further slight weight loss between 480°C and 1200°C (to yield a residue of 13.7%) was proposed as loss of sulphur to give calcium metal (expected 10.5%).

The DSC curve of $[Mg(O_2COMe)(OMe)(MeOH)_{1.5}]_n$ **7a** shows two endotherms with shoulders. The first peak is broad and centred at 92°C (-81.27 mcal mg^{-1}), which is mirrored in the TGA plot with a 53.1% weight loss corresponding to loss of methanol and CO_2 (calculated 51.7%). The second endothermic reaction is observed at ca 440°C (-36 mcal mg^{-1}); this process is coupled with a simultaneous weight loss of 27.4% for methoxide and methyl groups to yield magnesium oxide residue by 460°C (final residue 22.5%; expected for MgO 22.5%). The first derivative curve of the TGA plot for complex **7a** suggests two overlapping reactions in the ranges 42–175°C and 375–470°C. The presence of these reactions is further supported by observations of shoulders in the corresponding DSC spectrum.

TGA/DSC studies have confirmed the stability of the inserted complexes to 80°C. Complexes **7a**, **2** and **4** decompose to the metal oxide powders, whilst complex **6** decomposes to yield the metal sulfide by 450°C with subsequent gradual sublimation of sulfur to yield the metal.

X-ray structural studies

The crystal structures of the inserted products **2** and **4** have been communicated previously [19,20]. In the present paper we describe for the first time the crystal structure of the interesting product **7b**.

The structure of the SO_2 inserted product **2** has been shown to be polymeric consisting of infinite zig-zag chains of $[Ca(O_2SOMe)(MeOH)_2]$ [19]. The methylsulfito ligand in this compound acts as both chelating and bridging ligand, whilst the methanol molecules are unidentate and terminally co-ordinated. The eight co-ordinate calcium centres are co-ordinated to two oxygen atoms of two bridging methylsulfito ligands

which are chelated to adjacent calcium atoms, two oxygen atoms from a co-ordinated methanol molecules and four oxygen atoms belonging to two chelating methylsulfito ligands. Compound **4** was shown to be centrosymmetric dimer with both *O*, *S*- and *O*,*O*-chelating methylthiocarbonato ligands and two bridging *O*,*O*-methylthiocarbonato ligands [20]. Each calcium is eight co-ordinate due to a chelating *O*,*S*-methylthiocarbonato ligand, a chelating and bridging *O*,*O*-methylthiocarbonato ligand, three oxygen atoms belonging to three terminally co-ordinated methanol molecules and one carbonyl oxygen chelating the second calcium and involved in the bridge formation.

Complex **7b** was obtained from complex **7a** as outlined in the Experimental Section. Slow crystallization from a mixture of slightly wet toluene and hexane (2 : 1 *v*/*v*) over 48 h at room temperature yielded needle-like colourless crystals, suitable for X-ray crystallography. The present study has revealed the true identity of this crystalline material **7b** as the nonameric metal aggregate $[Mg_9(CO_3)(O_2COMe)_8(OMe)_8(MeOH)_{13}]$; the crystals also contain one methanol and one toluene solvate (per complex mole) in the lattice.

The structure of **7b** is shown in Fig. 2, and the inner core is illustrated in Fig. 3. Selected interatomic distances and angles are presented in Table 5. The compound consists of nine magnesium atoms, each of them having six-co-ordinate, distorted octahedral geometries. The gross molecular structure consists of two distorted Mg_4O_4 cubes linked through a μ_5-carbonato and two bridging methylcarbonato groups; the ninth magnesium is linked to the Mg_4O_4 cubes through the unique carbonato and two other bridging methylcarbonato groups.

In both the cubane frameworks, the magnesium atoms are held in place by four μ_3-methoxide ligands, each magnesium being bonded facially to the oxygen atoms of three such ligands. However, there is no systematic pattern in the distribution of the ligands in the remaining co-ordination sites around the magnesium atoms. In the cubane containing Mg(1)–Mg(4), Mg(1) is also co-ordinated to two terminal methanol groups and a terminal methylcarbonato ligand, whilst Mg(3) and Mg(4) are each co-ordinated to two bridging methylcarbonato ligands and the μ_5-carbonate. The co-ordination geometry around Mg(2) is augmented by three terminal methanol ligands only. In the second cube containing Mg(5)–Mg(8), the octahedral co-ordination geometries are completed by two terminal methanols and a terminal methylcarbonato group for both Mg(6) and Mg(8), one terminal methanol, one terminal methylcarbonato group and one oxygen of the μ_5-carbonato ligand for Mg(7), and two bridging methylcarbonato ligands and one oxygen atom from the μ_5-carbonato group for Mg(5). The three terminal sites around the remaining magnesium

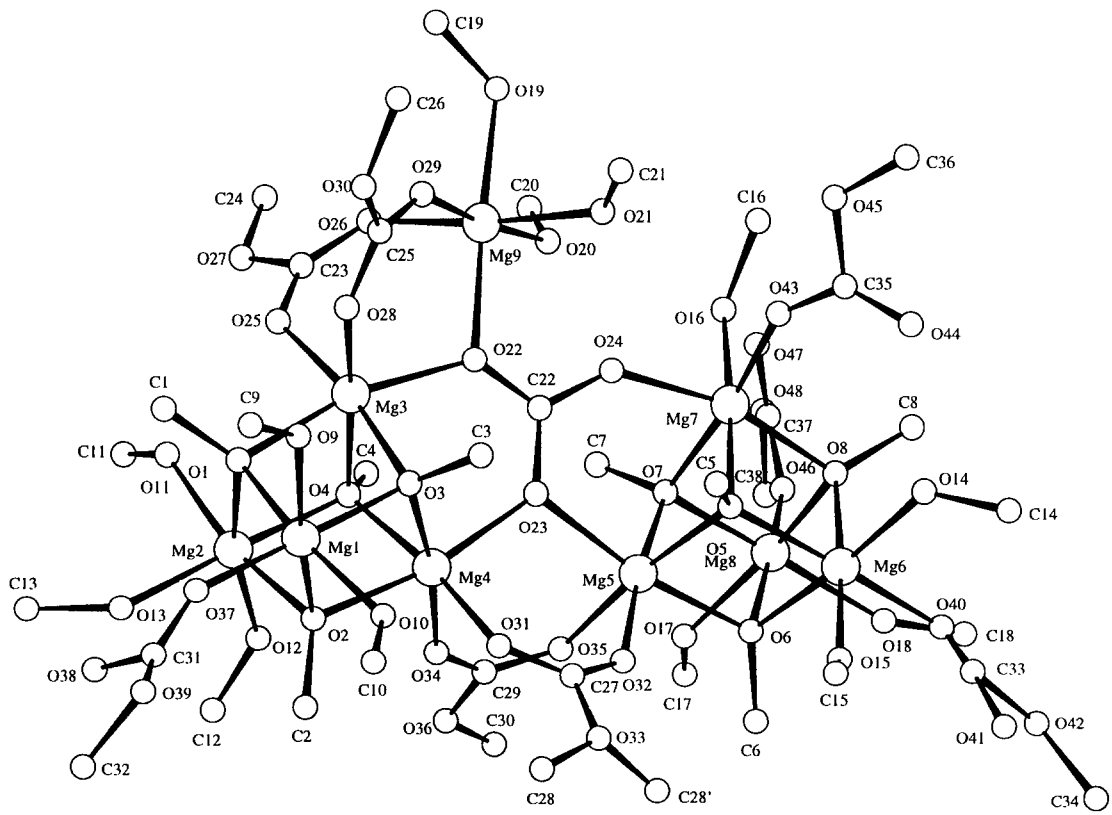

Fig. 2. The molecular structure of $[Mg_9(CO_3)(O_2COMe)_7(OMe)_9(MeOH)_{13}]$ **7b**, showing the atom numbering scheme.

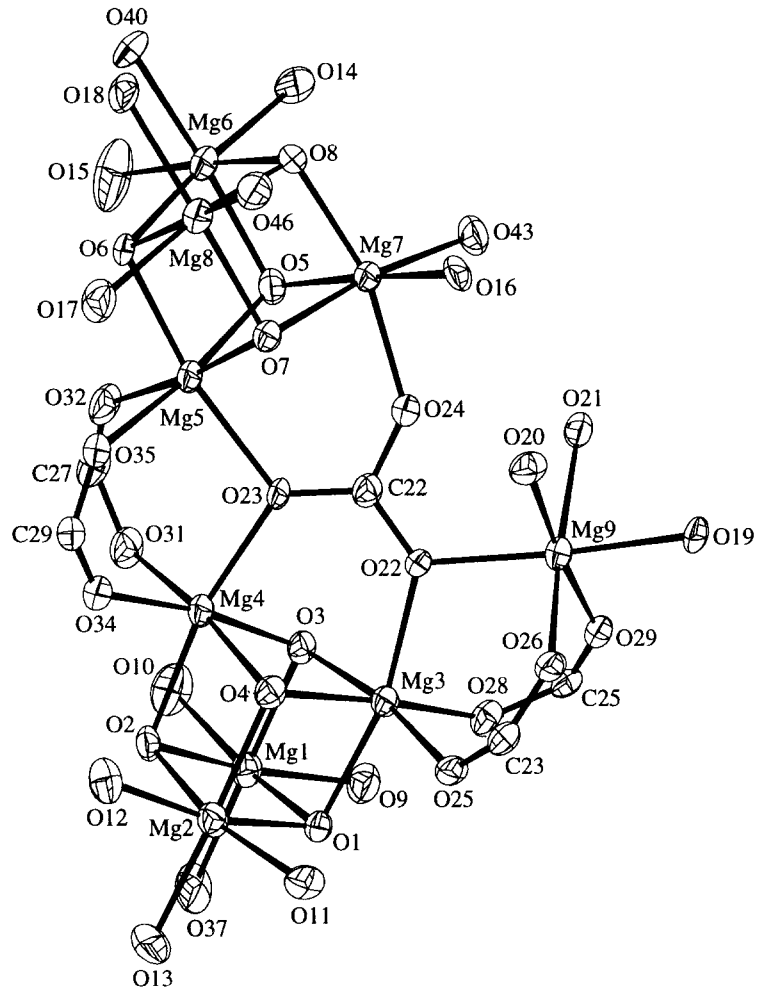

Fig. 3. A view of the $[Mg_9(CO_3)(O_2C)_7(O)_{22}]$ central core of complex **7b**.

atom, Mg(9) are occupied by three methanol molecules.

The Mg···Mg non-bonded distances involving the pair of magnesium atoms linking the two cubes [Mg(4)···Mg(5)], or one cube and the Mg(9) octahedron [Mg(3)···Mg(9)] are nearly identical and have values of 3.486(4) and 3.489(5) Å, respectively. The corresponding distances within the cubes are much smaller (by ca 0.34 Å) and lie in the narrow range 2.978(4)–3.186(5) Å (average value 3.119 Å).

The Mg—O bond distances in the complex **7b** may be divided into several groups. Those involving the μ-methoxide ligands in the cubane moieties span the range 2.050(7)–2.134(6) Å, average 2.089 Å. These bond lengths may be compared with the range 2.05–2.14 Å for μ_3-methoxide ligands in the recently reported complex "$[Mg(OMe)_2 \cdot 3.5MeOH]$" [48]. The internal O—Mg—O angles in both the cubes for complex **7b** are all acute [80.2(3)–87.3(3)°, average 82.8°] and the Mg—O—Mg angles are all obtuse [91.5(3)–100.1(3)°, average 96.6°]. O—Mg—O and Mg—O—Mg angles for "$[Mg(OMe)_2 \cdot 3.5MeOH]$" have been observed in similar ranges of 78.4–85.5° and 92.9–101.4°, respectively [48]. The second set of Mg—O bond distances involve the thirteen neutral methanol molecules which are all bonded terminally to the magnesium atoms. These distances range from 2.046(8)–2.155(8) Å, and have an average value of 2.102 Å. These distances are ca 0.03 Å longer than the Mg—O(μ_3-OMe) distances. Similar differences in the metal–oxygen bond lengths involving the μ_3-capping alkoxide groups and terminally bound neutral alcohol ligands have been observed in other cases, e.g. "$[Mg(OMe)_2 \cdot 3.5MeOH]$" [48] and $[Ca_4(O\text{-}Et)_4(tmhd)_4(EtOH)_4]$ [27]. The third set of Mg—O bond distances involve the terminally bound methylcarbonato ligands. The Mg—O bond distances in this group lie in the range 1.988(8) to 2.177(14) Å, with an average of 2.059 Å. The fourth set of Mg—O distances also involves the methylcarbonato groups, but this time they are co-ordinated in a slightly asymmetric bridging manner ($1\kappa O, 2\kappa O'$). The Mg—O bond distances are in the range 2.043(7)–2.166(7) Å, with an average of 2.076 Å. As expected the Mg—O(bridging)

Table 5. Selected bond lengths (Å) and angles (°) for $[C_{38}H_{100}Mg_9O_{48}]$, CH_3OH, C_7H_8 (**7b**)

Mg(1)—O(37)	1.988(8)	Mg(1)—O(3)	2.050(7)
Mg(1)—O(1)	2.071(6)	Mg(1)—O(10)	2.082(8)
Mg(1)—O(2)	2.102(7)	Mg(1)—O(9)	2.107(7)
Mg(2)—O(13)	2.046(8)	Mg(2)—O(4)	2.058(7)
Mg(2)—O(1)	2.090(7)	Mg(2)—O(2)	2.094(6)
Mg(2)—O(11)	2.126(7)	Mg(2)—O(12)	2.155(8)
Mg(3)—O(3)	2.052(6)	Mg(3)—O(25)	2.051(6)
Mg(3)—O(28)	2.067(7)	Mg(3)—O(4)	2.114(7)
Mg(3)—O(22)	2.118(6)	Mg(3)—O(1)	2.119(6)
Mg(4)—O(4)	2.068(6)	Mg(4)—O(31)	2.069(7)
Mg(4)—O(34)	2.075(7)	Mg(4)—O(3)	2.083(7)
Mg(4)—O(23)	2.107(6)	Mg(4)—O(2)	2.134(6)
Mg(5)—O(32)	2.043(7)	Mg(5)—O(7)	2.074(6)
Mg(5)—O(6)	2.095(7)	Mg(5)—O(5)	2.110(7)
Mg(5)—O(23)	2.148(6)	Mg(5)—O(35)	2.166(7)
Mg(6)—O(5)	2.056(8)	Mg(6)—O(15)	2.071(8)
Mg(6)—O(8)	2.104(7)	Mg(6)—O(14)	2.102(8)
Mg(6)—O(6)	2.121(7)	Mg(6)—O(40)	2.177(14)
Mg(7)—O(24)	2.031(7)	Mg(7)—O(43)	2.038(6)
Mg(7)—O(5)	2.064(6)	Mg(7)—O(8)	2.078(7)
Mg(7)—O(16)	2.102(6)	Mg(7)—O(7)	2.131(7)
Mg(8)—O(46)	2.032(8)	Mg(8)—O(7)	2.054(7)
Mg(8)—O(18)	2.088(8)	Mg(8)—O(8)	2.106(7)
Mg(8)—O(6)	2.112(7)	Mg(8)—O(17)	2.139(8)
Mg(9)—O(29)	2.042(7)	Mg(9)—O(19)	2.089(6)
Mg(9)—O(26)	2.094(7)	Mg(9)—O(20)	2.104(7)
Mg(9)—O(21)	2.121(7)	Mg(9)—O(22)	2.118(6)

O(37)—Mg(1)—O(3)	179.2(3)	O(37)—Mg(1)—O(1)	97.1(3)
O(3)—Mg(1)—O(1)	83.5(2)	O(37)—Mg(1)—O(10)	92.7(3)
O(3)—Mg(1)—O(10)	86.8(3)	O(1)—Mg(1)—O(10)	168.5(3)
O(37)—Mg(1)—O(2)	97.4(3)	O(3)—Mg(1)—O(2)	83.2(3)
O(1)—Mg(1)—O(2)	82.5(3)	O(10)—Mg(1)—O(2)	90.2(3)
O(37)—Mg(1)—O(9)	92.1(3)	O(3)—Mg(1)—O(9)	87.3(3)
O(1)—Mg(1)—O(9)	90.2(3)	O(10)—Mg(1)—O(9)	95.6(3)
O(2)—Mg(1)—O(9)	168.6(3)	O(13)—Mg(2)—O(4)	177.8(3)
O(13)—Mg(2)—O(1)	97.9(3)	O(4)—Mg(2)—O(1)	83.0(3)
O(13)—Mg(2)—O(2)	95.8(3)	O(4)—Mg(2)—O(2)	82.4(2)
O(1)—Mg(2)—O(2)	82.2(2)	O(13)—Mg(2)—O(11)	92.9(3)
O(4)—Mg(2)—O(11)	89.1(3)	O(1)—Mg(2)—O(11)	88.1(3)
O(2)—Mg(2)—O(11)	167.7(3)	O(13)—Mg(2)—O(12)	92.7(3)
O(4)—Mg(2)—O(12)	86.1(3)	O(1)—Mg(2)—O(12)	167.5(3)
O(2)—Mg(2)—O(12)	90.3(3)	O(11)—Mg(2)—O(12)	97.9(3)
O(3)—Mg(3)—O(25)	171.0(3)	O(3)—Mg(3)—O(28)	89.0(3)
O(25)—Mg(3)—O(28)	95.9(3)	O(3)—Mg(3)—O(4)	87.0(2)
O(25)—Mg(3)—O(4)	87.4(3)	O(28)—Mg(3)—O(4)	173.3(3)
O(3)—Mg(3)—O(22)	88.3(2)	O(25)—Mg(3)—O(22)	98.6(2)
O(28)—Mg(3)—O(22)	97.0(3)	O(4)—Mg(3)—O(22)	88.3(3)
O(3)—Mg(3)—O(1)	82.3(2)	O(25)—Mg(3)—O(1)	89.9(2)
O(28)—Mg(3)—O(1)	93.1(3)	O(4)—Mg(3)—O(1)	81.0(2)
O(22)—Mg(3)—O(1)	166.0(3)	O(4)—Mg(4)—O(31)	171.5(3)
O(4)—Mg(4)—O(34)	88.3(3)	O(31)—Mg(4)—O(34)	93.5(3)
O(4)—Mg(4)—O(3)	87.3(3)	O(31)—Mg(4)—O(3)	89.9(3)
O(34)—Mg(4)—O(3)	172.4(3)	O(4)—Mg(4)—O(23)	90.6(2)
O(31)—Mg(4)—O(23)	97.5(3)	O(34)—Mg(4)—O(23)	96.1(3)
O(3)—Mg(4)—O(23)	90.2(2)	O(4)—Mg(4)—O(2)	81.1(2)
O(31)—Mg(4)—O(2)	90.5(3)	O(34)—Mg(4)—O(2)	91.5(3)
O(3)—Mg(4)—O(2)	81.7(3)	O(23)—Mg(4)—O(2)	168.6(3)
O(32)—Mg(5)—O(7)	173.6(3)	O(32)—Mg(5)—O(6)	92.7(3)
O(7)—Mg(5)—O(6)	80.9(3)	O(32)—Mg(5)—O(5)	92.4(3)
O(7)—Mg(5)—O(5)	87.2(3)	O(6)—Mg(5)—O(5)	80.4(3)
O(32)—Mg(5)—O(23)	94.6(3)	O(7)—Mg(5)—O(23)	91.8(2)
O(6)—Mg(5)—O(23)	169.7(2)	O(5)—Mg(5)—O(23)	92.1(3)

Table 5—*continued.*

O(32)—Mg(5)—O(35)	90.2(3)	O(7)—Mg(5)—O(35)	89.3(3)
O(6)—Mg(5)—O(35)	91.2(3)	O(5)—Mg(5)—O(35)	171.3(3)
O(23)—Mg(5)—O(35)	96.0(3)	O(5)—Mg(6)—O(15)	96.7(4)
O(5)—Mg(6)—O(8)	81.7(3)	O(15)—Mg(6)—O(8)	176.7(4)
O(5)—Mg(6)—O(14)	94.8(3)	O(15)—Mg(6)—O(14)	90.7(4)
O(8)—Mg(6)—O(14)	92.2(3)	O(5)—Mg(6)—O(6)	81.0(3)
O(15)—Mg(6)—O(6)	93.2(4)	O(8)—Mg(6)—O(6)	83.8(3)
O(14)—Mg(6)—O(6)	174.6(3)	O(5)—Mg(6)—O(40)	164.2(5)
O(15)—Mg(6)—O(40)	94.3(5)	O(8)—Mg(6)—O(40)	86.7(4)
O(14)—Mg(6)—O(40)	96.4(4)	O(6)—Mg(6)—O(40)	87.0(4)
O(5)—Mg(6)—C(33)	170.7(5)	O(15)—Mg(6)—C(33)	75.4(5)
O(8)—Mg(6)—C(33)	106.0(5)	O(14)—Mg(6)—C(33)	90.3(5)
O(6)—Mg(6)—C(33)	94.3(5)	O(40)—Mg(6)—C(33)	19.9(5)
O(24)—Mg(7)—O(43)	87.4(2)	O(24)—Mg(7)—O(5)	88.9(3)
O(43)—Mg(7)—O(5)	96.1(2)	O(24)—Mg(7)—O(8)	164.0(3)
O(43)—Mg(7)—O(8)	106.7(2)	O(5)—Mg(7)—O(8)	82.1(3)
O(24)—Mg(7)—O(16)	90.2(3)	O(43)—Mg(7)—O(16)	88.5(2)
O(5)—Mg(7)—O(16)	175.3(3)	O(8)—Mg(7)—O(16)	97.7(3)
O(24)—Mg(7)—O(7)	86.2(3)	O(43)—Mg(7)—O(7)	172.8(3)
O(5)—Mg(7)—O(7)	86.9(3)	O(8)—Mg(7)—O(7)	80.2(3)
O(16)—Mg(7)—O(7)	88.5(3)	O(46)—Mg(8)—O(7)	100.7(3)
O(46)—Mg(8)—O(18)	91.6(3)	O(7)—Mg(8)—O(18)	166.7(3)
O(46)—Mg(8)—O(8)	103.7(3)	O(7)—Mg(8)—O(8)	81.3(3)
O(18)—Mg(8)—O(8)	90.8(3)	O(46)—Mg(8)—O(6)	172.4(3)
O(7)—Mg(8)—O(6)	81.0(3)	O(18)—Mg(8)—O(6)	87.5(3)
O(8)—Mg(8)—O(6)	83.9(3)	O(46)—Mg(8)—O(17)	87.1(3)
O(7)—Mg(8)—O(17)	88.6(3)	O(18)—Mg(8)—O(17)	97.2(3)
O(8)—Mg(8)—O(17)	166.4(3)	O(6)—Mg(8)—O(17)	85.4(3)
O(29)—Mg(9)—O(19)	90.1(3)	O(29)—Mg(9)—O(26)	94.9(3)
O(19)—Mg(9)—O(26)	89.4(3)	O(29)—Mg(9)—O(20)	175.1(3)
O(19)—Mg(9)—O(20)	85.3(3)	O(26)—Mg(9)—O(20)	86.8(3)
O(29)—Mg(9)—O(21)	89.7(3)	O(19)—Mg(9)—O(21)	84.2(3)
O(26)—Mg(9)—O(21)	172.1(3)	O(20)—Mg(9)—O(21)	88.1(3)
O(29)—Mg(9)—O(22)	92.2(2)	O(19)—Mg(9)—O(22)	176.4(3)
O(26)—Mg(9)—O(22)	93.1(3)	O(20)—Mg(9)—O(22)	92.3(3)
O(21)—Mg(9)—O(22)	93.2(3)		
Mg(1)—O(1)—Mg(2)	97.6(3)	Mg(1)—O(1)—Mg(3)	95.5(3)
Mg(2)—O(1)—Mg(3)	97.2(3)	Mg(2)—O(2)—Mg(1)	96.5(3)
Mg(2)—O(2)—Mg(4)	96.5(2)	Mg(1)—O(2)—Mg(4)	95.8(3)
Mg(1)—O(3)—Mg(3)	98.2(3)	Mg(1)—O(3)—Mg(4)	99.0(3)
Mg(3)—O(3)—Mg(4)	92.1(3)	Mg(2)—O(4)—Mg(4)	99.7(2)
Mg(2)—O(4)—Mg(3)	98.4(3)	Mg(4)—O(4)—Mg(3)	90.8(3)
Mg(6)—O(5)—Mg(7)	98.9(3)	Mg(6)—O(5)—Mg(5)	100.0(3)
Mg(7)—O(5)—Mg(5)	91.5(3)	Mg(5)—O(6)—Mg(8)	97.6(3)
Mg(5)—O(6)—Mg(6)	98.4(3)	Mg(8)—O(6)—Mg(6)	94.4(3)
Mg(8)—O(7)—Mg(5)	100.1(3)	Mg(8)—O(7)—Mg(7)	99.1(3)
Mg(5)—O(7)—Mg(7)	90.6(3)	Mg(7)—O(8)—Mg(6)	96.9(3)
Mg(7)—O(8)—Mg(8)	99.2(3)	Mg(6)—O(8)—Mg(8)	95.0(3)
C(22)—O(22)—Mg(3)	129.7(5)	C(22)—O(22)—Mg(9)	119.5(5)
Mg(3)—O(22)—Mg(9)	110.8(3)	C(22)—O(23)—Mg(4)	126.3(6)
C(22)—O(23)—Mg(5)	123.5(6)	Mg(4)—O(23)—Mg(5)	110.2(2)
C(22)—O(24)—Mg(7)	137.9(6)	O(24)—C(22)—O(22)	118.0(8)
O(24)—C(22)—O(23)	119.4(9)	O(22)—C(22)—O(23)	122.6(8)

methylcarbonato bond lengths are longer than those of the terminally bound ligands.

Finally, at the very centre of this molecule is a highly unusual bridging chelating μ_5-carbonate group ($1:2\kappa^2O;3:4\kappa^2O';5\kappa O''$) [49]. This ligand acts as a focal point holding together not only the two cubes, but also the single remote Mg(9) atom. The Mg—O(μ_5-CO_3) bond distances lie in the range 2.031(7)–2.148(6) Å, with an average bond length of 2.123 Å. This value is similar to that observed in

[$4MgCO_3 \cdot 4H_2O$], which has an average Mg—O(CO_3) distance of 2.10 Å [50]. The μ_3-carbonate ligand takes up a planar geometry with near equivalent C—O bond lengths and angles indicative of a fully delocalized system.

CONCLUSION

This study has shown that the Group 2 metal alkoxides are capable of undergoing a wide range of insertion reactions with unsaturated inorganic molecules. COS, CS_2 and SO_2 insert into both the alkoxide bonds to give well defined monomeric and oligomeric products which are more amenable to characterization than the parent alkoxides. CO_2 inserts into only one of the alkoxide bonds and the resultant compounds are difficult to characterize by structural techniques. Recrystallization of $[Mg(OMe)(O_2COMe)(MeOH)_{1.5}]_n$ has resulted in the isolation and definitive characterization of a hydrocarbon soluble intermediate in the formation of magnesium carbonate. The nonameric complex $[Mg_9(CO_3)(O_2COMe)_8(OMe)_8(MeOH)_{13}]$ **7b** contains methylcarbonato, methoxide and neutral methanol ligands. The presence of the μ_5-carbonate ligand in the structural core of this nonameric complex is unique. It is probable that partial hydrolysis may have occurred during recrystallization. The analogous CO_2 insertion reactions for calcium alkoxides have also been studied; however, unlike their magnesium analogues they are insoluble in non-co-ordinating solvents, suggesting the presence of polymeric species.

The isolation of what effectively is a partially hydrolyzed alkoxide carbonato-complex (**7b**) has implications for use of this compound as a sol-gel precursor to magnesium carbonate and ultimately the corresponding metal oxide. The solubility of this carbonate containing species in hydrocarbon solvent systems suggests that in principle relatively large aggregates can be formed and solubilized as long as the aggregate has a hydrophobic exterior.

Acknowledgements—The authors would like to thank the EPSRC (M.B.H., K.M.A.M. and J.A.D.) and Exxon Chemical Ltd (V.C.A.), and BP for endowing D.M.P.M.'s chair. Thanks are also due to Hilary O'Callaghan and Patrick Barrie who performed some of the spectroscopic/analytical measurements.

REFERENCES

1. Darensbourg, D. J. and Kudaroski, R. A., *Adv. Organomet. Chem.*, 1983, **22,** 129, and references therein.
2. For example see: Chisholm, M. H., *Chem. Soc. Rev.*, 1995, 79 and references therein.
3. (a) Mastrorilli, P., Moro, G., Nobile, C. F. and Latronio, M., *Inorg. Chim. Acta*, 1992, **192,** 189; (b) Amatore, C., Jutand, A., Khalil, F. and Nielsen, M. F., *J. Am. Chem. Soc.*, 1992, **114,** 7076; (c) Aida, T. and Inoue, S., *J. Amer. Chem. Soc.*, 1983, **105,** 1304; (d) Whitlock, B. J. and Whitlock, Jr. H. W., *J. Org. Chem.*, 1974, **39,** 3144.
4. Denise, B. and Sneeden, R. P. A., *Chemtech.*, 1982, **12,** 108.
5. Cotton, F. A. and Wilkinson, G. In *Advanced Inorganic Chemistry*, 4th edn. John Wiley & Sons, New York, 1980.
6. Palmer, D. A. and Eldik, R. V., *Chem. Rev.*, 1983, **83,** 651, and references therein.
7. Krishnamurthy, K. V., Harris, G. M. and Sastri, V. S., *Chem. Rev.*, 1970, **70,** 171 and references therein.
8. Weidlein, J., *Z. Anorg. Allg. Chem.*, 1970, **378,** 245.
9. (a) US Patent, 4,957,642; Karsch, H. H., *Chem. Ber.*, 1977, **110,** 2213; (b) Crutchley, R. J., Powell, J., Faggiani, R. and Lock, C. J., *Inorg. Chim. Acta*, 1977, **24,** L15; (c) Ashworth, T. V. and Singleton, E., *J. Chem. Soc., Chem. Commun.*, 1976, 204; (d) Walther, D., Ritter, U., Kempe, R., Sieler, J. and Undeutsch, B., *Chem. Ber.*, 1992, **125,** 1523; (e) Chisholm, M., Budzichowski, T. A., Feher, F. J. and Ziller, J. W., *Polyhedron*, 1992, **11,** 1575; (f) Hursthouse, M. B., Malik, M. A., Motevalli, M. and O'Brien, P., *J. Chem. Soc., Chem. Commun.*, 1991, 1690.
10. Ibers, J. A., *Chem. Soc. Rev.*, 1982, **11,** 57 and references therein.
11. (a) Wojcicki, A., *Adv. Organomet. Chem.*, 1974, **12,** 31; (b) Kitching, W. and Fong, C. W., *Organomet. Chem. Rev. A*, 1970, **5,** 281 and references therein.
12. (a) Alcock, N. W., Platt, A. W. G., Powell, H. H. and Pringle, P. G., *J. Organomet. Chem.*, 1989, **361,** 409; (b) Kubat-Martin, K. A., Kubas, G. J. and Ryan, R. R., *Organometallics*, 1988, **7,** 1657; (c) Braga, D. and Roulet, R., *J. Organomet. Chem.*, 1985, **286,** C8; (d) Joseph, M. F. and Baird, M. C., *Inorg. Chim. Acta*, 1985, **96,** 229; (e) Pandit, S. K., Gopinathan, S. and Gopinathan, C., *Ind. J. Chem.*, 1982, **21A,** 78; (f) Sonsale, A. Y., Chatterjee, A. K., Gopinathan, S. and Gopinathan, C., *Ind. J. Chem.*, 1981, **20A,** 1121; (g) Bhaduri, S., Johnson, B. F. G., Khair, A., Ghatak, I. and Mingos, D. M. P., *J. Chem. Soc., Dalton Trans.*, 1980, 1572; (h) Mingos, D. M. P., *Transition Met. Chem.*, 1978, **3,** 1; (i) Huber, V. F. and Padberg, F. J., *Z. Anorg. Allg. Chem.*, 1967, **351,** 1.
13. (a) Pinnick, H. W. and Reynolds, M. A., *J. Org. Chem.*, 1979, **44,** 160; (b) Masilamani, D. and Rogic, M. M., *J. Amer. Chem. Soc.*, 1978, **100,** 4634.
14. (a) Esmadi, F. T. and Dohaidel, M. K., *Polyhedron*, 1990, **9,** 1633; (b) Schenk, W. A. and Karl, U., *Z. Naturforsch.*, 1989, **44b,** 993; (c) Critchlow, P. B. and Robinson, S. D., *Inorg. Chem.*, 1978, **17,** 1902; (d) Dobson, A. and Robinson, S. D., *Inorg. Chem.*, 1977, **16,** 1321; (e) von Werner, K., Beck, W. and Bohner, U., *Chem. Ber.*, 1974, **107,** 2434; (f) Barlex, D. M. and Kemmitt, R. D. W., *J. Chem. Soc., Dalton Trans.*, 1972, 1436.

15. Ghilardi, C. A., Midollini, S. and Sacconi, L., *Inorg. Chem.*, 1977, **16,** 2377.
16. Ibers, J. A., Gaffney, T. R. and Schramm, K. D., *IUPAC Coord. Chem.*, 1981, **21,** 141.
17. (a) Darensbourg, D. J. and Rokicki, A., *Organometallics*, 1982, **1,** 1685; (b) Darensbourg, D. J. and Rokicki, A., *J. Amer. Chem. Soc.*, 1982, **104,** 349; (c) Ashworth, T. V., Nolte, M. and Singleton, E., *J. Organomet. Chem.*, 1976, **121,** C57.
18. Baird, M. C. and Wilkinson, G., *J. Chem. Soc. A*, 1967, 865.
19. Arunasalam, V.-C., Baxter, J., Hursthouse, M. B., Malik, K. M. A., Mingos, D. M. P. and Plakatouras, J. C., *J. Chem. Soc., Chem. Commun.*, 1994, 2695.
20. Arunasalam, V.-C., Baxter, I., Hursthouse, M. B., Malik, K. M. A., Mingos, D. M. P. and Plakatouras, J. C., *Polyhedron*, 1995, **14,** 1105.
21. (a) Arunasalam, V.-C., Ph.D. thesis, Univ. of London, 1995; (b) Bezougli, I. K., Bashall, A., McPartlin, M. and Mingos, D. M. P., *J. Chem. Soc., Dalton Trans.*, 1997, 287.
22. Markies, P. R., Akkerman, O. S., Bickenhaupt, F., Smeets, W. J. J. and Spek, A. L., *Adv. Organomet. Chem.*, 1991, **32,** 147.
23. (a) Williams, R. A., Hanusa, T. P. and Huffman, C., *Organometallics*, 1990, **9,** 1128; (b) Williams, R. A., Hanusa, T. P. and Huffman, J. C., *J. Chem. Soc., Chem. Commun.*, 1988, 1045.
24. Marsh, J. F., *Chemistry and Industry*, 1987, 470.
25. Szarvasy, E., *Ber.*, 1897, **20,** 1836.
26. *Catalogue of Handbook of Fine Chemicals*. Aldrich Chemical Company, Dorset, 1993.
27. Arunasalam, V.-C., Baxter, I., Drake, S. R., Hursthouse, M. B., Malik, K. M. A. and Otway, D. J., *Inorg. Chem.*, 1995, **34,** 5295.
28. Darr, J. A., Drake, S. R., Hursthouse, M. B. and Malik, K. M. A., *Inorg. Chem.*, 1993, **32,** 5704.
29. Sheldrick, G. M., *Acta Crystallogr.*, 1990, **A46,** 467.
30. Sheldrick, G. M., SHELXL93 program for crystal structure refinement. University of Gottingen, Germany, 1993.
31. Davies, K., SNOOPI program for crystal structure drawing. University of Oxford, U.K., 1983.
32. Chisholm, M. H., Cotton, F. A., Extine, M. W. and Reichert, W. W., *J. Amer. Chem. Soc.*, 1978, **100,** 1727.
33. Tsuda, T., Sanada, S., Ueda, K. and Saegusa, T., *Inorg. Chem.*, 1976, **15,** 2329.
34. Nakamoto, K., In *Infrared and Raman Spectra of Inorganic and Co-ordination Compounds*, 4th edn. John Wiley & Sons, New York, 1986.
35. Robinson, E. A., *Can. J. Chem.*, 1961, **39,** 247.
36. Randall, S. L., Miller, C. A., Janik, T. S., Churchill, M. R. and Atwood, J. D., *Organometallics*, 1994, **13,** 141.
37. Goodsel, A. J. and Byholder, G., *J. Amer. Chem. Soc.*, 1972, **94,** 6725.
38. Kim, Y.-J., Osakada, K., Sugita, K., Yamamoto, T. and Yamamoto, A., *Organometallics*, 1988, **7,** 2182.
39. (a) Contreras, L., Monge, A., Pizzano, A., Ruiz, C., Sanchez, L. and Carmona, E., *Organometallics*, 1992, **11,** 3971; (b) Carmona, E., Galindo, A., Gutierrez-Puebla, E., Monge, A. and Puerta, C., *Inorg. Chem.*, 1986, **25,** 3804.
40. (a) Colthup, N. B. and Powell, L. P., *Spectrochim. Acta*, 1987, **43A,** 317; (b) Little, L. H., Poling, G. W. and Leja, J., *Can. J. Chem.*, 1961, **39,** 745.
41. Tsuda, T. and Saegusa, *Inorg. Chem.*, 1972, **11,** 2561.
42. Yamamoto, T., Kuboto, M. and Yamamoto, A., *Bull. Chem. Soc. Jpn.*, 1980, **53,** 680.
43. Kato, M. and Ito, T., *Inorg. Chem.*, 1985, **24,** 504.
44. Kato, M. and Ito, T., *Inorg. Chem.*, 1985, **24,** 509.
45. Darensbourg, D. J., Mueller, B. L., Bischoff, C. J., Chojnacki, S. S. and Reibenspies, J. H., *Inorg. Chem.*, 1991, **30,** 2418.
46. Darensbourg, D. J., Sanchez, K. M., Reibenspies, J. H. and Rheingold, A. L., *J. Amer. Chem. Soc.*, 1989, **111,** 7094.
47. Simpson, R. D. and Bergman, R. G., *Angew. Chem. Int. Ed. Engl.*, 1992, **31,** 220.
48. Starikova, Z. A., Yanovsky, A. I. and Turova, N. Ya., *Polyhedron*, 1997, **6,** 967.
49. Examples of μ-CO_3^{2-} groups: (a) Harada, H., Kodera, M., Vuckovic, G., Matsumoto, N. and Kida, S., *Inorg. Chem.*, 1991, **30,** 1190; (b) Jameson, D. L., Xie, C.-L., Hendrickson, D. N., Potenza, J. A. and Schugar, H. J., *J. Amer. Chem. Soc.*, 1987, **109,** 740; (c) Churchill, M. R., Lashewycz, R. A., Koshy, K. and Dasgupta, T. P., *Inorg. Chem.*, 1981, **20,** 376.
50. Akao, M., Marumo, F. and Iwai, S., *Acta Crystallogr.*, 1974, **B30,** 2670.

Pergamon

PII: S0277-5387(97)00418-X

Polyhedron Vol. 17, No. 5–6, pp. 659–674, 1998
© 1998 Elsevier Science Ltd
All rights reserved. Printed in Great Britain
0277–5387/98 $19.00+0.00

β-Diketonate derivatives of titanium alkoxides: X-ray crystal structures and solution dynamics of the binuclear complexes $[\{Ti(OR)_3(dik)\}_2]$†

R. John Errington,* John Ridland, William Clegg, Robert A. Coxall and Jan M. Sherwood

Department of Chemistry, Bedson Building, University of Newcastle upon Tyne, NE1 7RU, U.K.

(Received 8 August 1997; accepted 26 September 1997)

Abstract—The crystal structures of the 2,4-pentanedionato (acetylacetonato, acac) and 2,2,6,6-tetramethylheptane-3,5-dionato (tmhd) compounds $[\{Ti(OR)_3(dik)\}_2]$ (dik = acac, R = Me, Et, Pr^i; dik = tmhd, R = Me, Pr^n, Pr^i), obtained from reactions between $Ti(OR)_4$ and one equivalent of dikH, have been determined for the first time. In the solid state, these compounds adopt centrosymmetric, alkoxide-bridged binuclear structures which in solution undergo ligand redistribution to give mixtures of $[\{Ti(OR)_3(dik)\}_2]$, $[Ti(OR)_2(dik)_2]$ and $Ti(OR)_4$. When R = Pr^i, the equilibrium favours the mononuclear compounds, whereas when R = Me, Et or Pr^n the binuclear compounds can be observed in the ^{1}H NMR spectra. Variable-temperature ^{1}H NMR spectra provide an insight into the dynamic behaviour of the methoxides $[\{Ti(OMe)_3(dik)\}_2]$, and possible ligand exchange mechanisms are discussed. No conclusive evidence was obtained for the existence of dimeric or monomeric $[Ti(OBu^t)_3(dik)]$ in the solid state or in solution. © 1998 Elsevier Science Ltd. All rights reserved

Keywords: titanium alkoxides; β-diketonates; crystal structures; NMR; solution dynamics.

While the number of X-ray crystal structures of metal alkoxides continues to grow, detailed knowledge of their solution behaviour is remarkably sparse. In order to develop a better understanding of the solution dynamics in these systems, we have been studying early transition-metal alkoxides and their derivatives [1], particularly with regard to hydrolytic aggregation and sol–gel processing. β-Diketones are used as "modifiers" in sol–gel processing, but the literature is somewhat ambiguous about the structures and behaviour of the species present in solution before, and during, hydrolysis (details are discussed later in the paper). Titanium tetraalkoxides have been previously described to react with one or two equivalents of β-diketones (dikH) to give products formulated as $[Ti(OR)_3(dik)]$ and $[Ti(OR)_2(dik)_2]$ respectively [2]. Bradley and Holloway first showed that the mononuclear, octahedral disubstituted complexes $[Ti(OR)_2(dik)_2]$ have *cis* alkoxide groups, and their ^{1}H NMR investigations demonstrated the non-rigid nature of these structures in solution [3]. More detailed studies subsequently provided evidence for an intramolecular structural rearrangement via a twist mechanism [4]. By comparison, the nature of the monosubstituted compounds $[Ti(OR)_3(dik)]$ is less well established and, although their involvement in the β-diketone modified sol–gel hydrolysis of titanium alkoxides has been discussed [5], no crystal structures of representative examples have been determined. In this paper we describe the solid-state structures of a range of such compounds obtained from reactions involving pentane-2,4-dione (acacH) and 2,2,6,6-tetramethylheptane-3,5-dione (tmhdH). In addition, the solution behaviour of these compounds is discussed in the light of variable-temperature ^{1}H NMR results.

EXPERIMENTAL

All manipulations were carried out under dry, oxygen-free nitrogen using standard Schlenk techniques, or in a dry box fitted with a recirculation system. Hydrocarbon solvents were dried over and distilled

* Author to whom correspondence should be addressed.

† Dedicated to Professor Don Bradley on the occasion of his 73rd birthday.

from sodium-benzophenone prior to use. Propan-2-ol and ethanol were dried over sodium, and methanol was dried over magnesium. Pentane-2,4-dione (acetylacetone, acacH) was fractionally distilled and stored under oxygen-free nitrogen. 2,2,6,6-Tetramethylheptane-3,5-dione (tmhdH), $Ti(OEt)_4$, $Ti(OPr^n)_4$ and $Ti(OPr^i)_4$ were used as received without further purification. $Ti(OBu^t)_4$ was prepared by adding *tert*-butanol to an "ammonia-neutralised" $TiCl_4$ solution in heptanes according to a method developed by Haslam [6], followed by distillation of the crude alkoxide. $Ti(OMe)_4$ was prepared by addition of $Ti(OPr^i)_4$ to a 40-molar excess of refluxing methanol, with subsequent collection of the resultant solid. IR spectra were recorded as mineral oil mulls between CsI plates on a Perkin–Elmer 598 spectrometer or on a Mattson Genesis FTIR spectrometer. Ambient-temperature ^1H and ^{13}C NMR spectra were recorded on a Bruker WP 200 spectrometer. ^{13}C and variable-temperature ^1H NMR spectra were recorded on JEOL Lambda 500 or Bruker AMX500 spectrometers. Elemental analyses were performed by the University of Newcastle upon Tyne microanalytical service.

Preparation of $[\{Ti(OMe)_3(acac)\}_2]$ **1**

(a) Methanol (10 cm^3, 247.2 mmol) was added to $Ti(OPr^i)_4$ (6.44 g, 22.65 mmol) and the mixture was stirred for 1 h to precipitate $[\{Ti(OMe)_4\}_4]$. The solvents were removed and the solids washed with hexanes (15 cm^3) then dried *in vacuo*. Yield of $[\{Ti(OMe)_4\}_4]$ 3.90 g, 100%. Toluene (20 cm^3) was added, the suspension was heated to 65–70 °C and pentane-2,4-dione (2.33 cm^3, 22.65 mmol) was then added by syringe to give a clear, dark red solution. A colourless microcrystalline solid was obtained by reduction of solvent volume and storage at −30 °C. The solid was collected by filtration, washed with cold toluene (acetone/solid CO_2 slush bath) and dried *in vacuo*. Yield 1.15 g, 21%. Found: C, 40.05; H, 6.66. $C_{16}H_{32}O_{10}Ti_2$ requires C, 40.02; H, 6.72%.

(b) $[\{Ti(OMe)_4\}_4]$ (1.00 g, 1.45 mmol) and $[Ti(OPr^i)_2(acac)_2]$ (2.12 g, 5.81 mmol) were placed in a Schlenk flask and dissolved in toluene (20 cm^3) to give a clear, pale yellow solution. Subsequent removal of solvents yielded a yellow oil (2.39 g). Crystals suitable for X-ray analysis were obtained by treatment of the oil with methanol (10 cm^3, 247.2 mmol), reduction of the solvent volume and storage at −5 °C. Yield: 0.39 g, 14%. Found: C, 39.27; H, 6.50. $C_{16}H_{32}O_{10}Ti_2$ requires C, 40.02; H, 6.72%.

Preparation of $[\{Ti(OEt)_3(acac)\}_2]$ **2**

Pentane-2,4-dione (3.37 cm^3, 32.82 mmol) was added slowly by syringe to a commercial solution of $Ti(OEt)_4$ in heptanes (Tilcom ETOL) (15.25 g, 32.82 mmol) to give a pale yellow solution. Removal of the solvents *in vacuo* yielded a yellow oil which subsequently crystallised. Yield 9.84 g. The crude product was washed with cold hexanes (15 cm^3, acetone/liquid N_2 slush bath) and dried *in vacuo*. Yield: 7.32 g, 79%. Crystals suitable for X-ray analysis were obtained by recrystallisation from hexanes (12 cm^3). Found: C, 47.28; H, 7.43. $C_{22}H_{44}O_{10}Ti_2$ requires C, 46.82; H, 7.86%. δ_H ($C_6D_5CD_3$, 200 MHz) 5.52, 5.48 (singlets, 2H), 4.82 (br, 12H), 2.03, 1.99, 1.98, 1.89 (singlets, 12H), 1.49 (br, 18H). δ_C ($C_6D_5CD_3$, 50.32 MHz) 191.9, 188.5, 103.5, 102.7, 73.1, 72.6, 69.0, 27.2, 26.7, 20.0 and 19.6.

Preparation of $[\{Ti(OPr^i)_3(acac)\}_2]$ **3**

(a) Pentane-2,4-dione (3.83 cm^3, 37.34 mmol) was added dropwise to $Ti(OPr^i)_4$ (10.62 g, 37.34 mmol) in hexanes (10 cm^3) at 0 °C to give a yellow solution. Crystals suitable for X-ray diffraction were obtained by recrystallisation of a portion of the crude product from propan-2-ol. Yield: 5.41 g, 45%. Found: C, 52.53; H, 9.20. $C_{28}H_{56}O_{10}Ti_2$ requires C, 51.86; H, 8.70%. δ_C ($C_6D_5CD_3$, 50.32 MHz) 190.0, 186.3, 101.5, 77.7, 75.4, 25.8, 25.7, 24.8, 24.7 and 24.5.

(b) $Ti(OPr^i)_4$ (2.75 cm^3, 9.32 mmol) was added to a solution of $[Ti(OPr^i)_2(acac)_2]$ (3.40 g, 9.32 mmol) in propan-2-ol (10 cm^3). Colourless crystals formed on storage at −30 °C. The solids were collected by filtration, washed with hexanes and dried *in vacuo*. Yield: 2.80 g, 46%. The unit cell was confirmed as that of compound **2** by X-ray diffraction.

Preparation of $[\{Ti(OMe)_3(tmhd)\}_2]$ **4**

2,2,6,6-Tetramethylheptane-3,5-dione (2.30 cm^3, 11.00 mmol) was added slowly by syringe to a clear solution of $Ti(OMe)_4$ (1.89 g, 11.0 mmol) in toluene (30 cm^3) at 30 °C. The resulting clear solution was stirred for 2 h before removal of the solvents *in vacuo*. The crude resinous product (3.58 g, 100%) was taken up in hexanes (10 cm^3) to give a cloudy solution, from which a finely divided white precipitate (0.76 g in total) was removed by filtration. Treatment of the solution with hexanes led to no further precipitation. The solvents were removed to yield a cloudy oil 2.90 g, 81%. Crystals suitable for X-ray diffraction were obtained by recrystallisation from hexanes (*ca.* 12 cm^3) at −30 °C. A sample was removed from the mother liquor and dried *in vacuo*. Found: C, 52.92; H, 9.14. $C_{28}H_{56}O_{10}Ti_2$ requires C, 51.86; H, 8.70%. δ_C ($C_6D_5CD_3$, 50.32 MHz) 201.5, 198.7, 93.7, 93.5, 64.3, 41.6 and 29.2.

Preparation of $[\{Ti(OEt)_3(tmhd)\}_2]$ **5**

2,2,6,6-Tetramethylheptane-3,5-dione (3.45 cm^3, 16.50 mmol) was added slowly by syringe to a commercial solution of $Ti(OEt)_4$ in heptanes (Tilcom

ETOL) (7.67 g, 16.5 mmol of Ti). The exothermic reaction produced a pale yellow solution. Reduction of the solvent volume *in vacuo* after 15 min resulted in rapid crystallisation of a colourless solid. The mixture was warmed to 60°C to dissolve the solids and the solution was left to cool to ambient temperature. The resulting crystalline solid was collected by filtration, washed with hexanes (2 × 5 cm^3) and dried *in vacuo*. Yield 3.75 g, 62%. δ_H ($C_6D_5CD_3$, 200 MHz) 6.13, 6.08, 6.06 (singlets, 2H), 4.99 (s), 4.79 (q), 4.57 (br) (total 12H), 1.64 (br), 1.47 (br), 1.27 (s) (total 54H). δ_C ($C_6D_5CD_3$, 50.32 MHz) 201.4, 198.3, 92.9, 72.2, 68.79, 41.2, 29.2, 19.9 and 19.8.

Preparation of $[\{Ti(OPr^n)_3(tmhd)\}_2]$ **6**

2,2,6,6-Tetramethylheptane-3,5-dione (4.54 cm^3, 21.75 mmol) was added dropwise to $Ti(OPr^n)_4$ (6.18 g, 21.75 mmol) in hexanes (20 cm^3). The solvent volume was reduced under reduced pressure until crystallisation commenced. The product was collected by filtration, washed with cold hexanes (20 cm^3, acetone/liquid N_2 slush bath) and dried *in vacuo*. Crystals suitable for X-ray diffraction were obtained by recrystallisation from hexanes (ca 10 cm^3). Yield: 4.30 g, 48%. Found: C, 59.23; H, 10.39. $C_{40}H_{80}O_{10}Ti_2$ requires C, 58.82; H, 9.87%. δ_H ($C_6D_5CD_3$, 200 MHz) 6.13, 6.08, 6.05 (singlets, 2H), 5.04 (br), 4.88 (br), 4.72 (t), 4.48 (br) (total 12H), 2.06 (br), 1.85 (sext), 1.65 (br) (total 12H), 1.51, 1.47, 1.42, 1.27 (singlets, 36H), 1.20 (m, 18H). δ_C ($C_6D_5CD_3$, 50.32 MHz) 202.4, 201.2, 200.1, 93.4, 93.3, 93.1, 79.0, 78.5, 78.0, 74.8, 42.3, 41.5, 41.2, 29.3, 28.7, 28.1, 27.6, 27.5, 27.1, 11.9, 11.7 and 11.2.

Preparation of $[\{Ti(OPr^i)_3(tmhd)\}_2]$ **7**

2,2,6,6-Tetramethylheptane-3,5-dione (3.40 cm^3, 16.70 mmol) was added dropwise to $Ti(OPr^i)_4$ (4.66 g, 16.37 mmol) in hexanes (10 cm^3) at 0°C. A pale yellow colour developed. A colourless crystalline solid was obtained at −30°C after reduction of the solvent volume. The product was collected by filtration, washed with ice-cold hexanes (20 cm^3) and dried *in vacuo*. Yield: 2.36 g, 35%. Crystals suitable for X-ray diffraction were obtained by recrystallisation of a portion of the crude product from hexanes at −5°C. Found: C, 59.41; H, 10.45. $C_{40}H_{80}O_{10}Ti_2$ requires C, 58.82; H, 9.87%. δ_H ($C_6D_5CD_3$, 200 MHz) 6.04 (s, 2H), 5.12 (sept, 2H), 4.73 (sept, 4H), 1.54 (d, 6H), 1.48 (s, 18H), 1.46 (d, 30H), 1.28 (s, 18H). δ_C ($C_6D_5CD_3$, 50.32 MHz) 201.2, 198.0, 93.08, 78.3, 77.2, 41.6, 41.5, 29.3, 29.1, 27.6 and 26.5.

Attempted preparation of $[Ti(OBu^t)_3(tmhd)]$ **8**

2,2,6,6-Tetramethylheptane-3,5-dione (1.46 cm^3, 7.00 mmol) was added to $Ti(OBu^t)_4$ (2.06 g, 6.06 mmol) in hexanes (10 cm^3). Colourless prisms were obtained from the colourless solution at −30°C. These were collected by filtration, washed with 2 × 5 cm^3 hexanes and dried *in vacuo*. Yield: 1.03 g. IR 1600 m, 1570 m, 1530 m, 1500 m, 1355 s, 1290 w, 1250 w, 1230 m, 1200 m, 1180 m, 1145 m, 1040 m, 1010 s, 970 w, 875 m, 790 m, 760 w, 740 w, 630 w, 585 m, 505 w, 495 w, 435 w and 375 w cm^{-1}. δ_C ($C_6D_5CD_3$, 50.32 MHz) 200.7, 197.1, 92.51, 83.8, 41.7, 41.4, 32.6, 29.3 and 29.1.

Preparation of $[Ti(OMe)_2(acac)_2]$ **9**

Pentane-2,4-dione (3.98 cm^3, 38.73 mmol) was added slowly by syringe to a suspension of $[\{Ti(OMe)_4\}_4]$ (3.33 g, 4.84 mmol) in toluene (30 cm^3) to give a pale yellow solution. Filtration and removal of the solvents *in vacuo* yielded a yellow oil which subsequently crystallised. Yield: 5.68 g, 95%. δ_H ($C_6D_5CD_3$, 200 MHz) 5.45 (s, 2H), 4.49 (s, 6H), 1.95 (s, 6H), 1.84 (s, 6H).

Preparation of $[Ti(OEt)_2(acac)_2]$ **10**

Pentane-2,4-dione (5.03 cm^3, 48.99 mmol) was added slowly by syringe to a commercial solution of $Ti(OEt)_4$ in heptanes (Tilcom ETOL) (11.38 g, 24.50 mmol of Ti). A pale yellow colour developed. Removal of the solvents *in vacuo* gave a quantitative yield of an orange oil which subsequently crystallised. δ_H ($C_6D_5CD_3$, 200 MHz) 5.50 (s, 2H), 4.80 (q, 4H), 1.98 (s, 6H), 1.89 (s, 6H), 1.46 (t, 6H). δ_C ($C_6D_5CD_3$, 50.32 MHz) 192.0, 188.5, 103.6, 73.1, 27.5, 26.8 and 19.7.

Preparation of $[Ti(OPr^i)_2(acac)_2]$ **11**

Pentane-2,4-dione (8.06 cm^3, 78.5 mmol) was added slowly by syringe to a solution of $Ti(OPr^i)_4$ (10.93 g, 38.4 mmol) in hexanes (10 cm^3) to give an orange solution. The solution was cooled to −30°C for 2 weeks to give **11** as colourless to pale yellow needles. These were removed by filtration and dried *in vacuo*. Yield: 1.82 g, 13%. δ_H ($C_6D_5CD_3$, 200 MHz) 5.47 (s, 2H), 5.19 (sept, 2H), 1.97 (s, 6H), 1.88 (s, 6H), 1.54 (d, 6H), 1.48 (d, 6H).

Preparation of $[Ti(OMe)_2(tmhd)_2]$ **12**

2,2,6,6-Tetramethylheptane-3,5-dione (6.20 cm^3, 30.13 mmol) was added slowly by syringe to a solution of $Ti(OMe)_4$ (2.55 g, 14.8 mmol) in toluene (30 cm^3) at 40°C. A pale yellow colour developed. A colourless microcrystalline solid was obtained by cooling the solution to −30°C after reducing its volume *in vacuo*. The product was collected by filtration, washed with cold hexanes (acetone/liquid N_2 slush bath) and dried *in vacuo*. Yield: 3.59 g, 75%. δ_H ($C_6D_5CD_3$, 200 MHz)

6.07 (s, 2H), 4.50 (s, 6H), 1.42 (s, 18H), 1.26 (s, 18H). δ_C ($C_6D_5CD_3$, 50.32 MHz) 201.5, 198.7, 93.7, 64.3, 41.3 and 29.2.

Preparation of $[Ti(OEt)_2(tmhd)_2]$ **13**

2,2,6,6-Tetramethylheptane-3,5-dione (4.51 cm^3, 23.85 mmol) was added slowly by syringe to a commercial solution of $Ti(OEt)_4$ in heptanes (Tilcom ETOL) (5.54 g, 11.90 mmol of Ti) to give a pale yellow solution. Removal of the solvents *in vacuo* after 15 min yielded a viscous, pale yellow oil. A pale brown waxy solid was obtained by extraction with hexanes and cooling the solution to −30°C. Yield: 3.99 g, 99%. δ_H ($C_6D_5CD_3$, 200 MHz) 6.04 (s, 2H), 4.75 (q, 4H), 1.44 (t, 6H), 1.43 (s, 18H), 1.25 (s, 18H). δ_C ($C_6D_5CD_3$, 50.32 MHz) 201.4, 198.3, 93.4, 72.1, 41.6, 41.3, 29.2, 29.1 and 19.9.

Preparation of $[Ti(OPr^n)_2(tmhd)_2]$ **14**

2,2,6,6-Tetramethylheptane-3,5-dione (2.83 cm^3, 13.57 mmol) was added slowly by syringe to a solution of $Ti(OPr^i)_4$ (1.81 g, 6.36 mmol) in hexanes (10 cm^3). The resulting colourless solution was heated to 54°C and stirred for 30 min before removal of the solvent under reduced pressure until crystallisation commenced. Hexanes (5 cm^3) were added and the solution was cooled to −30°C. The colourless crystalline solid was collected by filtration, washed with ice-cold hexanes (5 cm^3) and dried *in vacuo*. δ_H ($C_6D_5CD_3$, 200 MHz) 6.05 (s, 2H), 4.73 (t, 4H), 1.84 (sext, 4H), 1.46 (s, 18H), 1.28 (s, 18H), 1.20 (t, 6H).

Preparation of $[Ti(OPr^i)_2(tmhd)_2]$ **15**

2,2,6,6-Tetramethylheptane-3,5-dione (5.77 cm^3, 27.65 mmol) was added slowly by syringe to a water-cooled solution of $Ti(OPr^i)_4$ (3.93 g, 13.83 mmol) in hexanes (10 cm^3). The resulting pink solution was stirred for 20 min then solvent was removed *in vacuo* until crystallisation commenced. The solution was cooled to −30°C overnight to give a colourless solid which was collected by filtration, washed with cold hexanes (acetone/CO_2 slush bath) and dried *in vacuo*. Yield: 1.91 g, 26%. δ_H ($C_6D_5CD_3$, 200 MHz) 6.04 (s, 2H), 5.12 (sept, 2H), 1.47 (s, 18H), 1.28 (s, 18H), 1.54 (d, 6H), 1.46 (d, 6H). δ_C ($C_6D_5CD_3$, 50.32 MHz) 201.2, 198.0, 93.1, 78.3, 41.7, 41.7, 29.3, 29.1, 26.7 and 26.5.

Table 1. Crystallographic data

Compound	**1**	**2**	**3**	**4**	**6**	**7**
Formula	$C_{16}H_{32}O_{10}Ti_2$	$C_{22}H_{44}O_{10}Ti_2$	$C_{28}H_{56}O_{10}Ti_2$	$C_{28}H_{56}O_{10}Ti_2$	$C_{40}H_{80}O_{10}Ti_2$	$C_{40}H_{80}O_{10}Ti_2$
M	480.2	564.4	648.5	648.5	816.8	816.8
Crystal system	monoclinic	monoclinic	triclinic	monoclinic	triclinic	triclinic
Space group	$P2_1/c$	$P2_1/n$	$P\bar{1}$	$P2_1/c$	$P\bar{1}$	$P\bar{1}$
a (Å)	8.2967(9)	8.8660(12)	9.5051(18)	7.2822(7)	10.0871(10)	10.3288(9)
b (Å)	19.498(2)	16.069(2)	9.8682(19)	19.410(2)	13.5226(13)	11.0355(9)
c (Å)	7.8539(9)	10.4965(14)	11.667(2)	12.4726(12)	18.640(2)	11.7479(10)
α (°)			66.507(5)		86.722(3)	67.892(2)
β (°)	115.695(2)	103.640(4)	70.059(5)	100.697(2)	80.568(2)	73.336(2)
γ (°)			66.087(4)		72.723(2)	70.773(2)
V (Å)^3	1144.9(2)	1453.2(3)	896.2(3)	1732.3(3)	2394.9(4)	1150.9(2)
Z	2	2	1	2	2	1
D_c (g cm^{-3})	1.393	1.290	1.202	1.243	1.133	1.180
μ (mm^{-1})	0.742	0.595	0.491	0.508	0.380	0.396
$F(000)$	504	600	348	696	888	444
Crystal size, mm	0.44 × 0.40 × 0.20	0.38 × 0.26 × 0.24	0.28 × 0.26 × 0.22	0.52 × 0.38 × 0.36	0.50 × 0.46 × 0.42	0.66 × 0.64 × 0.30
θ_{max} (°)	28.5	28.3	28.4	28.5	25.0	28.3
Maximum indices h, k, l	11, 25, 10	11, 20, 13	12, 13, 15	9, 24, 16	13, 17, 25	13, 14, 15
Reflections measured	7073	8913	5581	10,735	12,471	7179
Unique reflections	2642	3323	3857	3974	8258	4989
R_{int}	0.0352	0.0169	0.0504	0.0304	0.0304	0.0209
Transmission factors	0.819–0.880	0.768–0.928	0.872–0.910	0.715–0.809	0.776–0.822	0.837–0.913
Number of refined parameters	133	160	227	191	543	248
Weighting parameters a, b	0.0483, 0.9626	0.0342, 0.8979	0.1113, 0	0.0348, 0.9377	0.2732, 3.6570	0.0333, 0.5401
Extinction coefficient x	0.0042(10)	0.0013(7)	0	0.0009(4)	0	0.0003(9)
Rw (all data, on F^2)	0.1019	0.0795	0.2232	0.0889	0.4587	0.0836
R (data with $F^2 > 2\sigma(F^2)$)	0.0351(2466)	0.0297(3069)	0.0857(1933)	0.0315(3390)	0.1404(5584)	0.0298(4634)
Goodness of fit on F^2	1.130	1.072	0.908	1.063	1.066	1.081
Max., min. el. density, eÅ^{-3}	0.64, −0.53	0.34, −0.32	0.58, −1.01	0.35, −0.30	2.17, −1.50	+0.33, −0.30

Preparation of $[Ti(OBu^t)_2(tmhd)_2]$ **16**

2,2,6,6-Tetramethylheptane-3,5-dione (2.93 cm^3, 14.05 mmol) was added to $Ti(OBu^t)_4$ (2.18 g, 6.41 mmol) in hexanes (5 cm^3). The white precipitate produced was dissolved by adding hexanes (5 cm^3) and warming to 55°C. Colourless prisms were obtained by cooling to −30°C. These were collected by filtration, washed with ice-cold hexanes (10 cm^3) and dried *in vacuo*. Yield: 0.39 g, 11%. IR 1600 s, 1570 s, 1525 s, 1500 s, 1355 s, 1290 w, 1250 w, 1230 m, 1200 m, 1180 s, 1145 m, 1040 s, 1010 s, 970 w, 875 m, 790 s, 760 w, 740 w, 628 m, 585 m, 500 w, 435 w and 375 w cm^{-1}. δ_H ($C_6D_5CD_3$, 200 MHz) 6.00 (s, 2H), 1.64 (s, 18H), 1.47 (s, 18H), 1.29 (s, 18H). δ_C ($C_6D_5CD_3$, 50.32 MHz) 200.7, 197.1, 92.5, 83.8, 41.7, 41.4, 32.6, 29.3 and 29.1.

X-ray crystallography

Crystal data for all six structures are given in Table 1 together with other information on the structure determination procedures. Crystals were examined at 160 K on a Siemens SMART CCD diffractometer with Mo–K_α radiation ($\lambda = 0.71073$ Å); cell parameters were refined from all strong reflections, and intensities were integrated from narrow frames (0.3° in ω) covering more than a hemisphere of data in each case. Absorption corrections were based on multiple and symmetry-equivalent reflections.

The structures were determined variously by heavy-atom and direct methods, and refined by full-matrix least squares on F^2 values for all data, with weighting $w^{-1} = \sigma^2(F_o^2) + (aP) + (bP)$, where $P = (F_o^2 + 2F_c^2)/3$. Anisotropic displacement parameters were refined for non-hydrogen atoms, and isotropic hydrogen atoms were included with riding model constraints. An isotropic extinction parameter x was refined, whereby F_c is multiplied by $(1 + 0.001xF_c^2\lambda^3/\sin 2\theta)^{-1/4}$. Residuals are defined as $Rw = \{\Sigma[w(F_o^2 - F_c^2)^2]/\Sigma[w(F_o^2)^2]\}^{1/2}$ for all data, conventional $R = \Sigma||F_o| - |F_c||/\Sigma|F_o|$ for reflections having $F_o^2 > 2\sigma(F_o^2)$. The structure of **3** shows minor disorder in two of the three Pr^i groups, which was resolved and refined with restraints. The structure of **6** has two independent molecules, both of which are extremely disordered, and only a relatively poor refinement could be achieved with many restraints and constraints.

Programs were standard Siemens data collection (SMART) and integration (SAINT) software [7], SHELXTL [8] and local programs. Atomic coordinates, displacement parameters and full geometry have been deposited at the Cambridge Crystallographic Data Centre.

RESULTS AND DISCUSSION

Solid-state structures

Colourless crystalline compounds $[\{Ti(OR)_3(dik)\}_2]$ were prepared from $Ti(OR)_4$ and one equivalent of dikH in appropriate solvents (Scheme 1). No solid products were obtained from the 1:1 reaction between $Ti(OBu^t)_4$ and acacH, and only crystalline **16** was isolated in the attempted preparation of **8** from $Ti(OBu^t)_4$ and tmhdH. Where crystalline products were obtained from oils, complete separation from oily material was often difficult, resulting in micro-

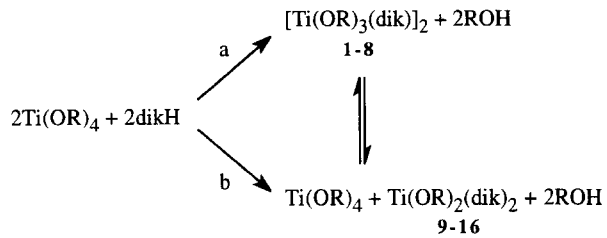

Compd.	R	dik
1, 9	Me	acac
2, 10	Et	acac
3, 11	Pr^i	acac
4, 12	Me	tmhd
5, 13	Et	tmhd
6, 14	Pr^n	tmhd
7, 15	Pr^i	tmhd
8, 16	Bu^t	tmhd

Scheme 1

analysis results which deviated slightly from expected values.

Crystals of **1–4, 6** and **7** were suitable for X-ray diffraction studies and the structures are shown in Figs 1–6. Selected bond lengths and angles are collected in Table 2. All of these compounds have binuclear, centrosymmetric structures and the asymmetic alkoxide bridges reflect the stronger *trans* influence of the terminal alkoxides compared with the β-diketonates. The greatest difference between the two bridging bond distances occurs in the isopropoxides, which may be related to the much smaller amount (if any) of the

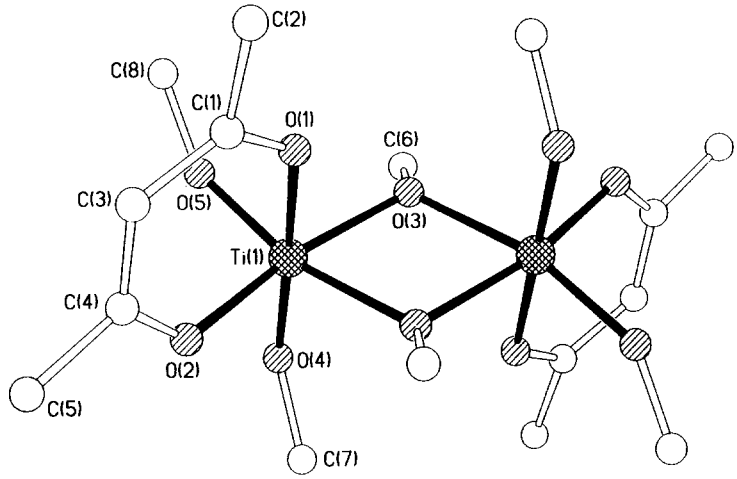

Fig. 1. The structure of $[\{Ti(OMe)_3(acac)\}_2]$ (**1**).

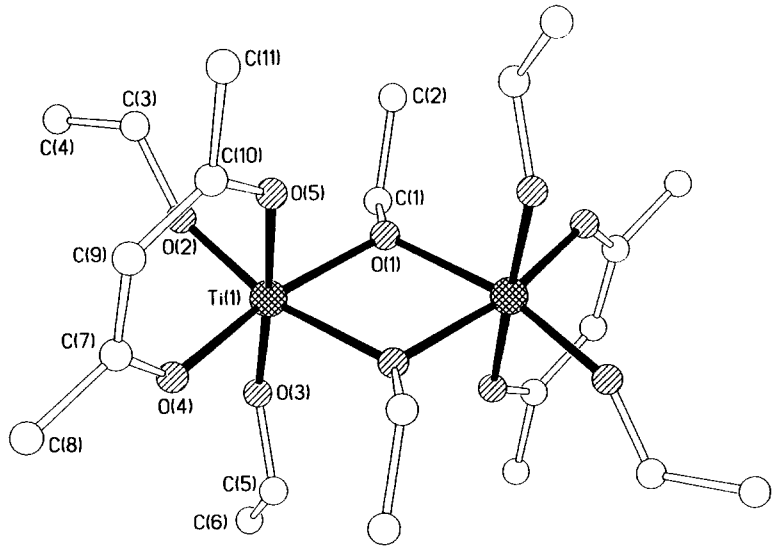

Fig. 2. The structure of $[\{Ti(OEt)_3(acac)\}_2]$ (**2**).

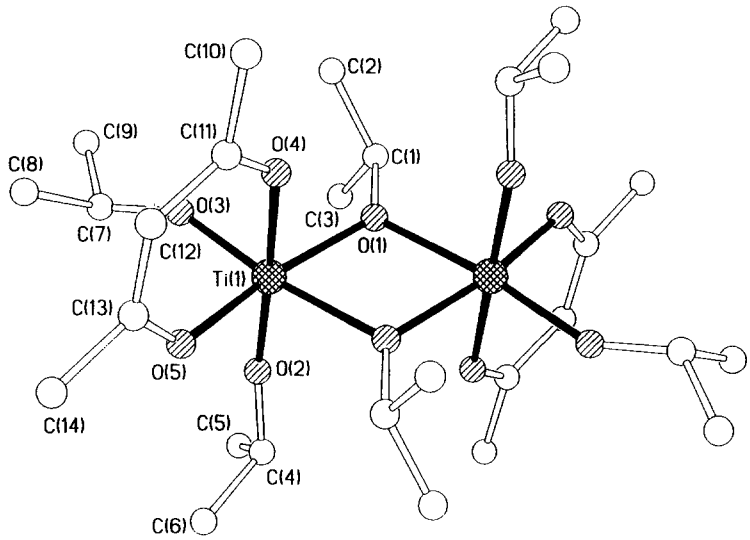

Fig. 3. The structure of $[\{Ti(OPr^i)_3(acac)\}_2]$ (**3**).

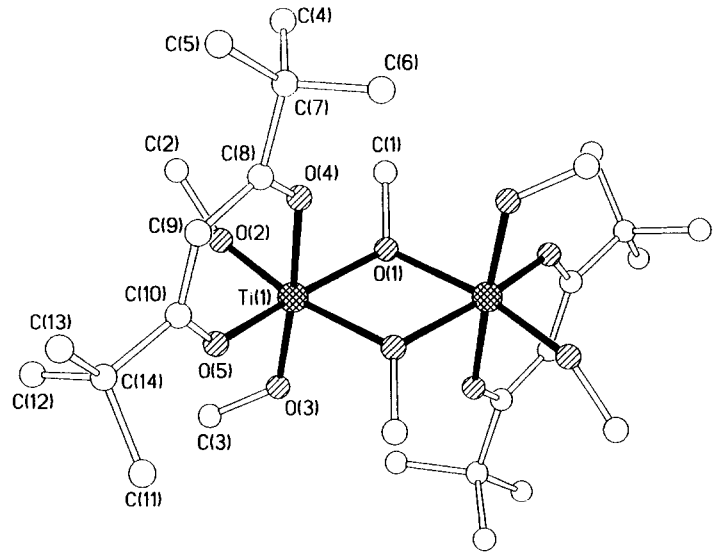

Fig. 4. The structure of $[\{Ti(OMe)_3(tmhd)\}_2]$ (**4**).

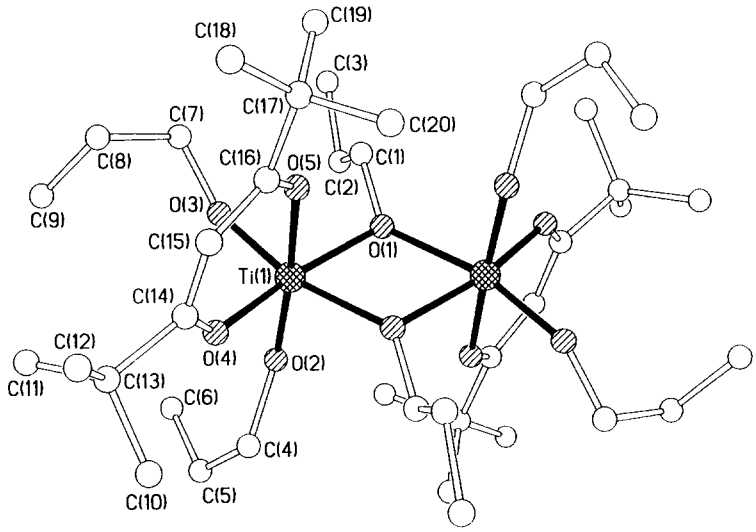

Fig. 5. The structure of $[\{Ti(OPr^n)_3(tmhd)\}_2]$ (**6**).

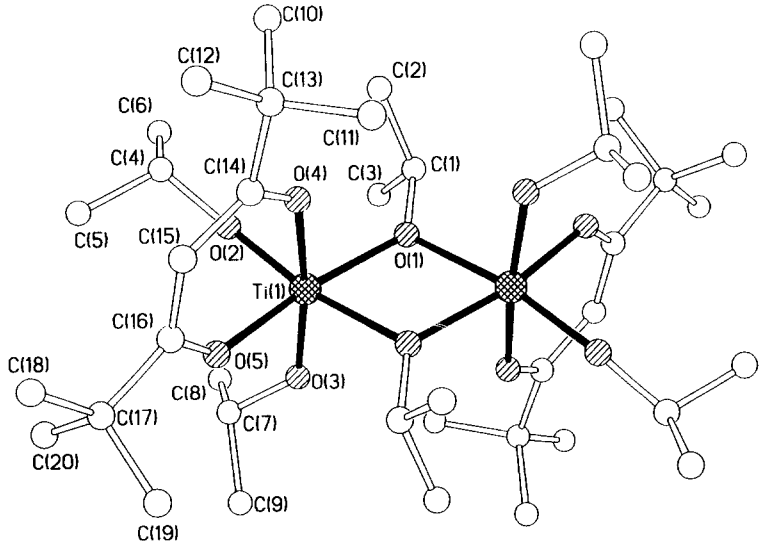

Fig. 6. The structure of $[\{Ti(OPr^i)_3(tmhd)\}_2]$ (**7**).

Table 2. Selected bond lengths (Å) and angles (°) for **1–4, 6** and **7**

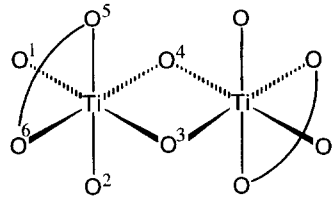

Compound	1	2	3	4	6	7
Ti—O^1	1.8038(13)	1.8047(11)	1.784(4)	1.7953(12)	1.783(7)	1.8017(9)
Ti—O^2	1.8004(14)	1.7961(10)	1.782(4)	1.8182(11)	1.792(6)	1.8160(9)
Ti—O^3	2.0562(13)	2.0642(10)	2.101(3)	2.0649(11)	2.069(6)	2.0941(9)
Ti—O^4	1.9996(13)	1.9909(10)	1.969(3)	1.9710(11)	1.940(6)	1.9677(9)
Ti—O^5	2.0789(13)	2.0844(11)	2.073(4)	2.0788(11)	2.055(2)	2.0753(9)
Ti—O^6	2.0168(13)	2.0200(10)	2.030(3)	2.0089(11)	1.998(2)	2.0434(9)
O^3—Ti—O^4	74.41(6)	73.98(4)	75.00(13)	74.20(5)	72.3(2)	73.35(4)
O^5—Ti—O^6	82.52(5)	81.92(4)	81.95(14)	80.93(4)	80.41(7)	80.53(4)
O^1—Ti—O^2	98.37(6)	97.21(5)	96.4(2)	95.71(5)	96.9(4)	96.28(4)

dimeric structure observed in the ^{1}H NMR spectra of these compounds by comparison with the primary alkoxide analogues, as discussed in the next section. The bond lengths are generally similar to those in the monomeric **11**, although the angles between terminal alkoxides and the angles subtended by the acac ligands are smaller than the analogous angles in **11** [99.8° and 83.59° (average) respectively] [9]. These results demonstrate that the steric bulk of the isopropoxide ligand is not sufficient to prevent association of the five-coordinate fragments Ti(OPr^i)$_3$(dik) by the formation of alkoxide bridges but, as discussed below, it does influence the lability of the dimeric species. Solid-state IR data for the binuclear alkoxides **1–7** (from mineral oil mulls) are collected in Table 3 for comparison with those for the mononuclear bis-diketonates **9–15**, which are given in Table 4.

A related binuclear structure has been reported for the chloro complex [{TiCl$_3$(acac)}$_2$], which undergoes ligand redistribution in solution to give $TiCl_4$ and [TiCl$_2$(acac)$_2$] [10], and similar behaviour has been proposed for the alkoxide analogues [11]. In view of the ambiguity associated with previous descriptions of the monosubstituted compounds [Ti(OR)$_3$(dik)] in the literature, we undertook a detailed NMR investigation of the solution properties of the structurally characterised dimers [{Ti(OR)$_3$(dik)}$_2$], and the results are described below.

Solution studies

In the ^{1}H NMR spectra of the isopropoxide complexes **3** and **7**, the major peaks present are due to a mixture of Ti(OPr^i)$_4$ and the bis-diketonate complexes **11** and **15** respectively, indicating that ligand redistribution occurs readily in solutions of the substituted secondary alkoxide complexes [{Ti(OPr^i)$_3$(dik)}$_2$], and that the equilibrium shown in Scheme 1 lies well towards the monomeric species at concentrations used to obtain the NMR spectra. Figure 7 shows the ^{1}H NMR spectrum of a solution of **3** at 273 K. The broadened methine septet and methyl doublet are due to the isopropoxide ligands of Ti(OPr^i)$_4$, while the sharp methine signal and the two sets of sharp doublets are due to the diastereotopic isopropoxide groups of the bis-acetylacetonate **11**. The remaining major singlets are due to the methine proton and the non-equivalent methyl groups of the acac ligands in **11**. The dimeric structure of **3** (Fig. 3) would be expected to give an ^{1}H NMR spectrum containing three methine septets and six methyl doublets due to the three diastereotopic isopropoxide groups, in addition to a singlet due to the methine peak of acac and two singlets due to the non-equivalent methyl groups of the acac ligands. Given the dynamic nature of the dimeric methoxide structures discussed below, the isopropoxide methine peaks would be expected to be significantly broadened, while rapidly exchanging acac methyl groups would give rise to a singlet in the ^{1}H NMR spectrum. There are small peaks in the ^{1}H NMR spectrum of **3** which may be due to the dimeric structure, (any associated isopropoxide methine peaks must be broadened into the baseline), although such peaks are even less evident in the ^{1}H NMR spectrum of **7**.

In the ^{1}H NMR spectra of products from attempted preparations of the tertiary alkoxide derivatives [Ti(OBu^t)$_3$(acac)] and the tmhd analogue **8**, only peaks due to Ti(OBu^t)$_4$ and [Ti(OBu^t)$_2$(dik)$_2$] are present (Fig. 8). This suggests that with bulky alkoxide groups either the equilibrium shown in Scheme 1 lies

Table 3. IR data for the binuclear complexes $[\{Ti(OR)_3(dik)\}_2]$[a]

dik = acac			dik = tmhd			
R = Me (**1**)	R = Et (**2**)	R = Pr^i (**3**)	R = Me (**4**)	R = Et (**5**)	R = Pr^n (**6**)	R = Pr^i (**7**)[b]
2955 s	2930 s	2970 s	2922 s	2956 s	2965 s	2935 sh
2910 s	2840 s	2950 s	2852 s	2923 s	2930 s	2910 s
2798 m		2850 s	2792 m	2851	2870 s	2840 s
	1602 s	1608 s	1592 m	1597 m	1595 s	1585 m
1586 s			1565 s	1577s	1577 s	1565 s
			1550 s	1556 m	1552 s	1547 s
1520 s	1520 s	1520 s	1530 s	1531 m	1531 s	1525 s
			1499 s	1504 s	1496 s	1495 s
1447 s	1462 s	1466 s	1452 s	1401 m	1463 s	1447 s
1371 s			1375 s		1377 s	1370 s
1358 sh	1375 s	1360 s	1355 s	1358 s	1358 s	1350 s
1323 m		1327 m				1320 m
			1292 w	1294 w	1292 m	1285 w
1275 m	1278 m	1275 m			1271 w	
			1245 w	1248 w	1248 m	1241 w
			1228 m		1228 m	1225 w
	1182 m		1172 w	1177 w	1173 m	
1154 m		1157 s	1151 s	1149 m	1147 m	1155 m
1111 s		1126 s	1117 w	1124 s	1119 s	1120 s
	1107 s			1109 s		
1090 m	1065 s		1078 s	1062 m	1076 s	
1037 s	1042 m		1034 m	1043 m	1045 m	
	1022 m				1018 m	
		1001 s	967 w	968 w	995 s	1005 s
					968 m	970 m
929 m	921 m	943 m	937 w	920 m	935 w	935 m
				910 m	908 w	
	888 m			889 m	887 m	
			872 m	873 m	872 m	870 w
		852 m				840 w
807 m		823 m				820 w
			795 m	794 w	795 m	795 w
	773 m	767 m	765 w	763 w	762 w	760 w
			738 w	737 w	739 w	735 w
722 w	722 w	721 w	724 w			
677 m	668 m	658 m				
	657 m	623 s	623 m	623 m	623 s	630 s
600 s	603 s		598 s	596 s	598 s	
583 s		560 s	573 m	578 s		590 s
547 w	546 m		526 m	528 s	542 s	558 m
510 s	527 m		504 m	507 s	523 s	
442 s	481 m		484 w		496 s	
420 m	432 m	450sbr	432 w	426 m	428 m	
400 w	385 w	390 m	410 w			
		340 m	355 w		355 w	
325 w	310 w		330 w	315 w	320 w	
295 w		288 w	295 w			
275 w						

[a] Nujol mulls on CsI plate except where indicated.
[b] Nujol mull on KBr plates.

even further towards the monomeric species and the concentration of dimer is too low to be observed by ^{1}H NMR, or the monosubstituted compounds are not formed. In this regard, it should be noted that the product from the attempted synthesis of $Ti(OBu^t)_3$(acac) was a liquid, and attempts to crystallise **8** from the 1 : 1 reaction between $Ti(OBu^t)_4$ and tmhdH yielded only the bis-diketonate **16**.

Table 4. IR data for the mononuclear complexes $[\{Ti(OR)_2(dik)\}_2]$[a]

dik = acac			dik = tmhd			
R = Me (**9**)	R = Et (**10**)	R = Pr^i (**11**)	R = Me (**12**)	R = Et (**13**)	R = Pr^n (**14**)	R = Pr^i (**15**)
2950 s	2963 s	2955 s	2966 s	2960 s	2960 s	2948 s
2925 s	2923 s	2910 s	2922 s	2918 s	2928 s	2915 s
2870 s		2860 s			2860 s	
2856 s	2855 s	2845 s	2859 s	2849 s	2845 s	2848 s
2810 m			2804 m			
		1600 sh		1599 s	1595 s	
1590 s	1589 s	1585 s	1590 br	1581 s	1580 s	1590 sh
					1565 s	1560 s
				1552 s	1550 s	
1520 s	1525 s	1520 s		1537 s	1530 s	1525 s
				1508 s	1500 s	1490 s
			1425 m			
			1350 s	1356 s	1355 s	1350 s
						1320 m
1285 s	1278 m	1275 s	1295 m	1294 m	1295 w	1290 m
			1244 s	1248 m	1245 w	1245 m
			1228 s	1227 m	1225 m	1225 m
1190 w	1187 m		1197 m			
		1160 m	1171 s	1176 m	1175 w	1160 m
1155 m			1150 s	1147 s	1145 m	1130 s
1120 m	1106 m	1120 s		1107 s	1110 m	
	1064 m		1075 s		1075 m	
1030 sh	1026 m	1020 sh	1022 m	1026 w	1025 w	
		1010 sh				
		990 s			995 s	995 s
950 w			969 m	968 m	970 s	
940 w	917 m	930 m	931 w	916 s		
			872 s	874 s	875 m	870 m
830 w		855 s				850 m
	795 m		796 s	795 s	795 m	795 m
780 m	770 w	775 m	777 m			765 w
	722 w		764 m	762 m	765 w	740 w
			738 m		740 w	
675 m	661 w	665 m				
610 m	623 m	620 s	621 s	623 br	630 s	630 s
600 s			600 s			
590 s	593 m	585 m				585 m
560 m	548 m					
			504 s	503 m	510 w	505 m
			480 m	478 w	485 w	480 m
450 m	445 m	445 m				455 m
		440 m				
420 m			429 m	430 w	435 w	430 w
	410 m		409 w			
360 m	344 m	355 m	355 w	340 w	355 m	355 w
			330 m			
	250 w					

[a] Nujol mulls on CsI plates.

The ^{1}H NMR spectra of **1** and **4** show that ligand redistribution also occurs upon dissolution of these methoxide derivatives, but now the dimeric solid-state structures shown in Figs 1 and 4 can be identified as major components. Variable-temperature studies (Figs 9 and 10) reveal similar solution behaviour for the two compounds and also provide some insight into the dynamic nature of the dimeric structures in solution. At 303 K, the methoxide regions (between 4.0 and 4.7 ppm) of the ^{1}H NMR spectra contain one sharp peak due to the bis-diketonate complexes **9** or **12** in addition to two broad resonances and other

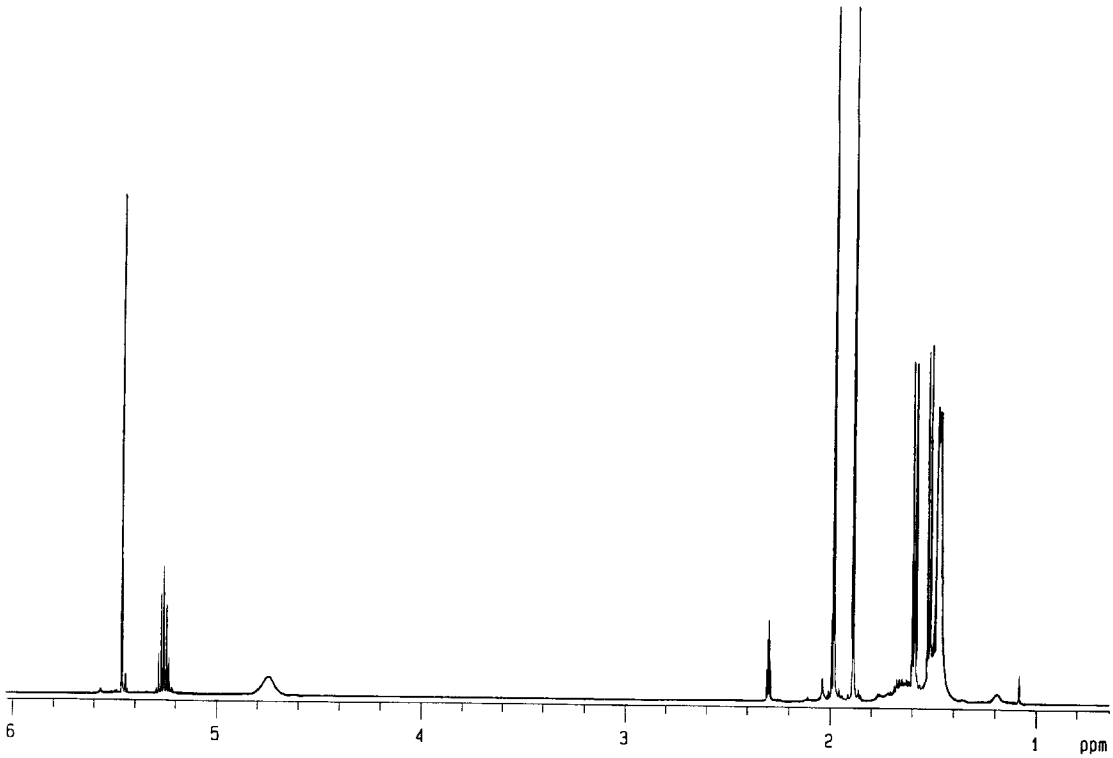

Fig. 7. ^{1}H NMR spectrum ($C_6D_5CD_3$, 273 K) of $[\{Ti(OPr^i)_3(acac)\}_2]$ (**3**).

minor peaks. At this temperature, the two broader, upfield peaks due to the methyl (1.8–2.1 ppm) or *tert*-butyl (1.2–1.6 ppm) groups of the diketonate ligands are those of **9** or **12** respectively, while the slightly lower-field singlet in each spectrum is due to rapidly exchanging alkyl substituents of the diketonate ligands in dimeric **1** or **4**. As the sample is cooled, the signals due to diketonate alkyl substituents in **9** and **12** sharpen, while the singlet due to methyl or *tert*-butyl groups in dimeric **1** or **4** broadens then splits into two singlets which sharpen down to 223 K. At 223 K the three methoxide resonances of dimeric **1** (Fig. 1) or **4** (Fig. 4) are clearly visible, in addition to the singlet due to **9** or **12** and other minor peaks, some of which are presumably due to $Ti(OMe)_4$. The ^{1}H NMR spectrum of $[\{Ti(OMe)_4\}_4]$ at 304 K contains four peaks at 4.16, 4.49, 4.50 and 4.65 ppm in the ratio 6:4:4:2, and is consistent with the structure shown in Fig. 11 if the terminal methoxide peaks are accidently equivalent or rapidly exchanging. These chemical shifts are somewhat temperature dependent, but peaks in the low-temperature ^{1}H NMR spectrum of **4** at 4.22, 4.46, 4.59 and 4.74 ppm can be assigned to $[\{Ti(OMe)_4\}_4]$ and similar peaks are observed in the low-temperature spectrum of **1**. The spectra in Figs 9 and 10 also show that the lower-field terminal methoxide peaks broaden and coalesce while the peak due to the bridging methoxide is still visible. This indicates that exchange between the two types of terminal methoxide in the dimers **1** and **4** is more rapid than terminal-bridging methoxide exchange, and possible mechanisms are discussed in more detail below.

Although the ethoxide and *n*-propoxide resonances in the variable-temperature ^{1}H NMR spectra of **2** and **6** respectively are complex and difficult to assign, the *β*-diketonate resonances behave in a similar fashion to those of **1** and **4**, suggesting that all of these primary alkoxide derivatives have similar solution dynamics. These NMR studies therefore demonstrate that the edge-shared bioctahedral structures of dimeric primary and secondary alkoxide complexes $[\{Ti(OR)_3(dik)\}_2]$ are dynamic in solution, and that ligand redistribution occurs when these compounds dissolve to give equilibrium mixtures of $Ti(OR)_4$, $[Ti(OR)_2(acac)_2]$ and $[\{Ti(OR)_3(dik)\}_2]$. To confirm this we synthesised **3** from a mixture of $Ti(OPr^i)_4$ and $[Ti(OPr^i)_2(acac)_2]$, and similarly prepared **1** by treating a mixture of $[\{Ti(OMe)_4\}_4]$ and $[Ti(OPr^i)_2(acac)_2]$ with methanol. These transformations must involve the transfer of a *β*-diketonate ligand from one titanium to another, presumably via a binuclear intermediate, and this process must be associated with the dynamic solution behaviour of the symmetric dimers $[\{Ti(OR-)_3(dik)\}_2]$. Scheme 2 shows a proposed mechanism for the ligand exchange processes observed in the ^{1}H NMR studies and for *β*-diketonate and alkoxide ligand transfer. The rapid exchange processes observed in mononuclear $[Ti(OR)_2(dik)_2]$ **V** have previously been ascribed to a fluxional twist mechanism

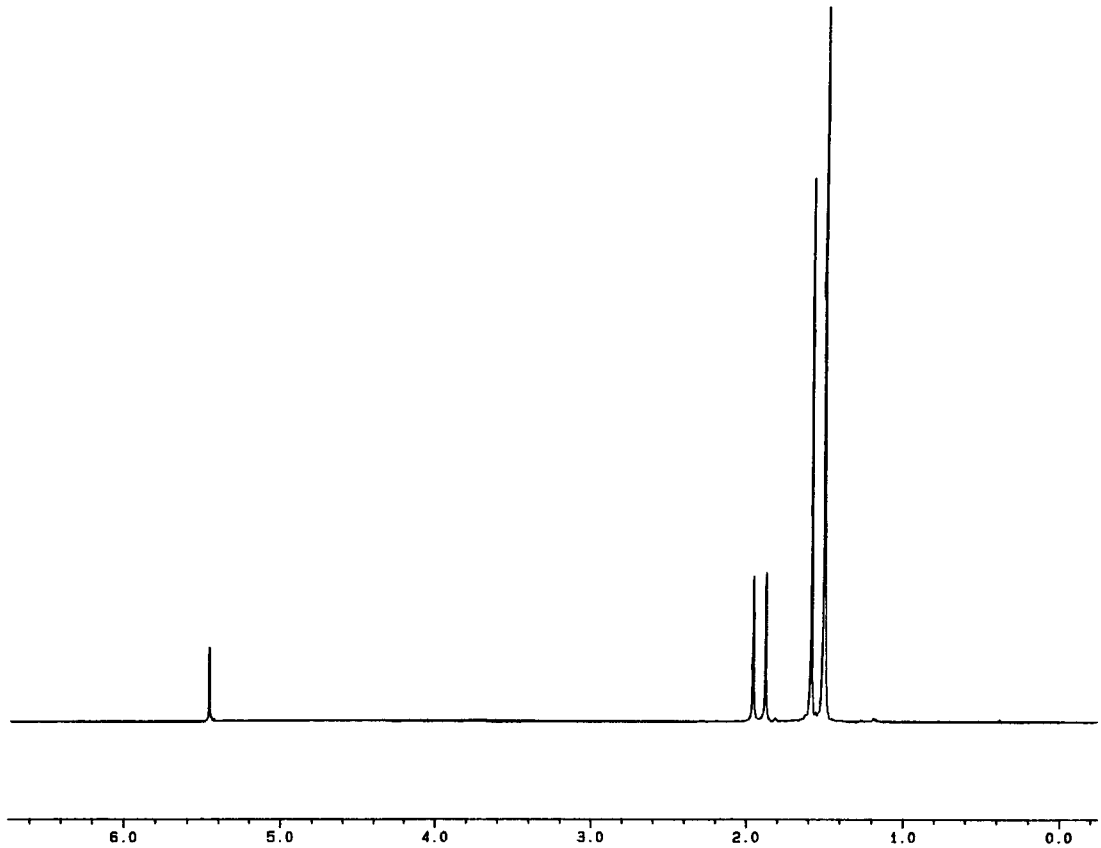

Fig. 8. ^{1}H NMR spectrum ($C_6D_5CD_3$, 297 K) of the product from the 1 : 1 reaction between $Ti(OBu^t)_4$ and acacH after removal of the volatiles.

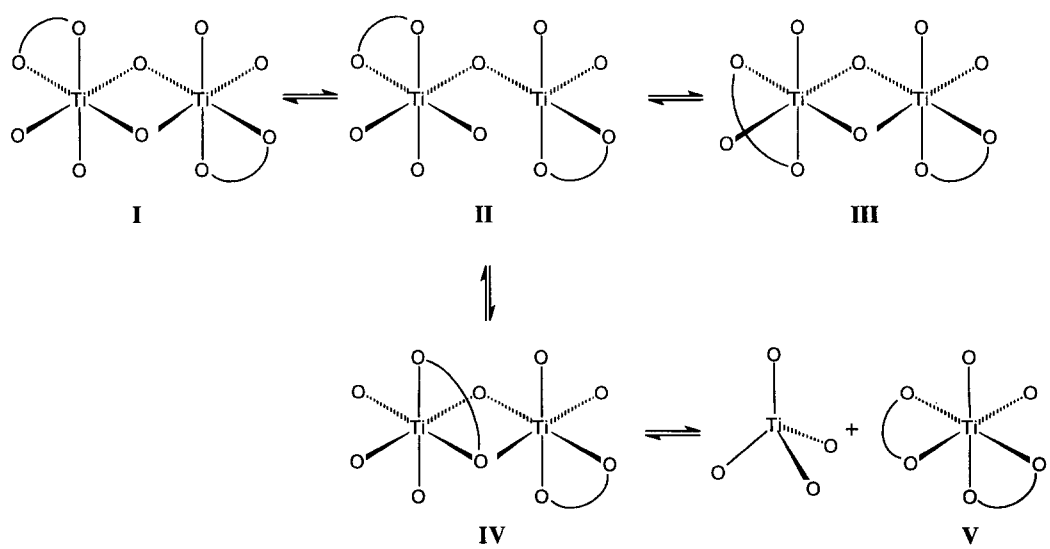

Scheme 2

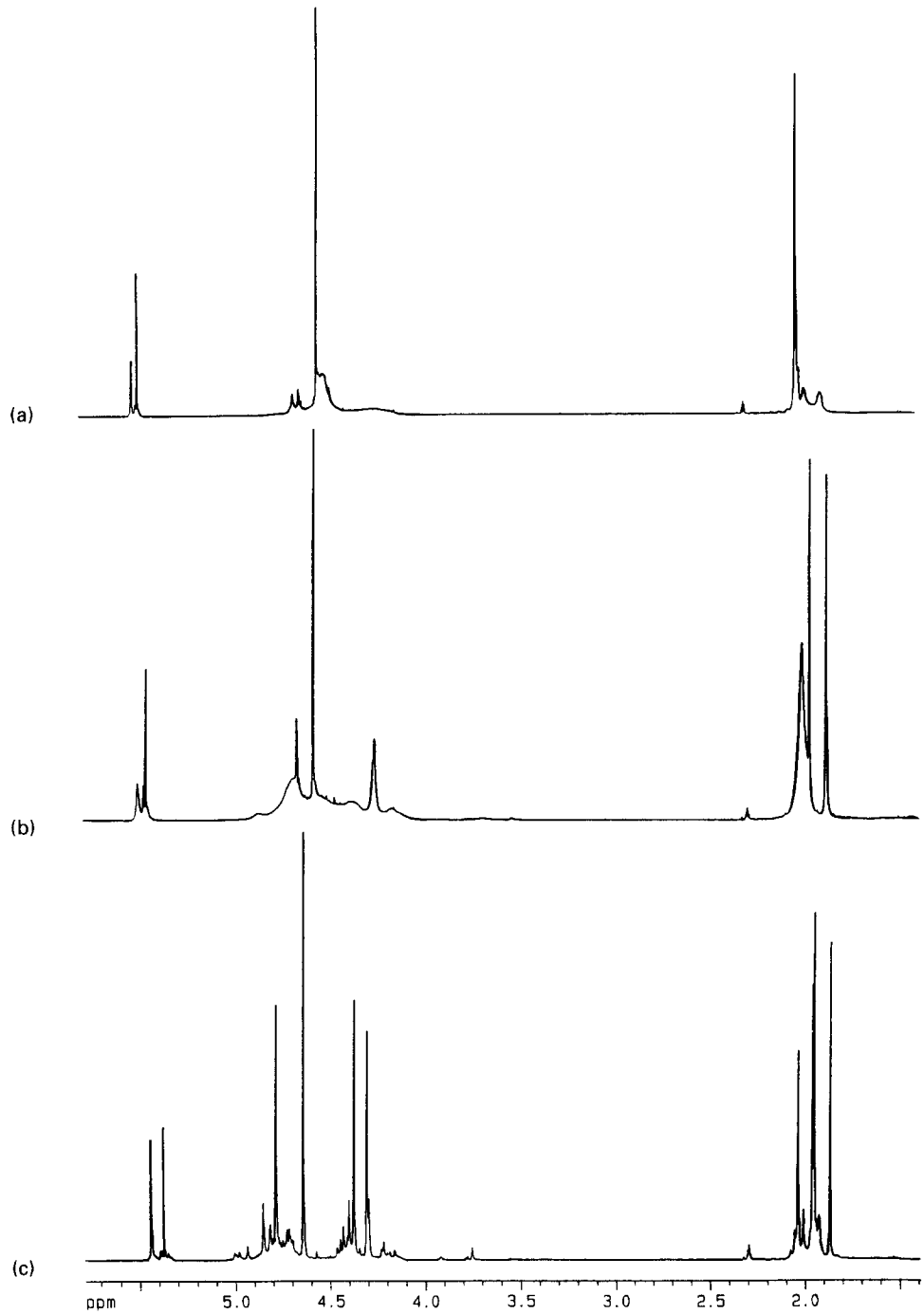

Fig. 9. Variable temperature ^{1}NMR spectra ($C_6D_5CD_3$) of $[\{Ti(OMe)_3(acac)\}_2]$ (**1**) : (a) 303 K ; (b) 273 K ; (c) 223 K

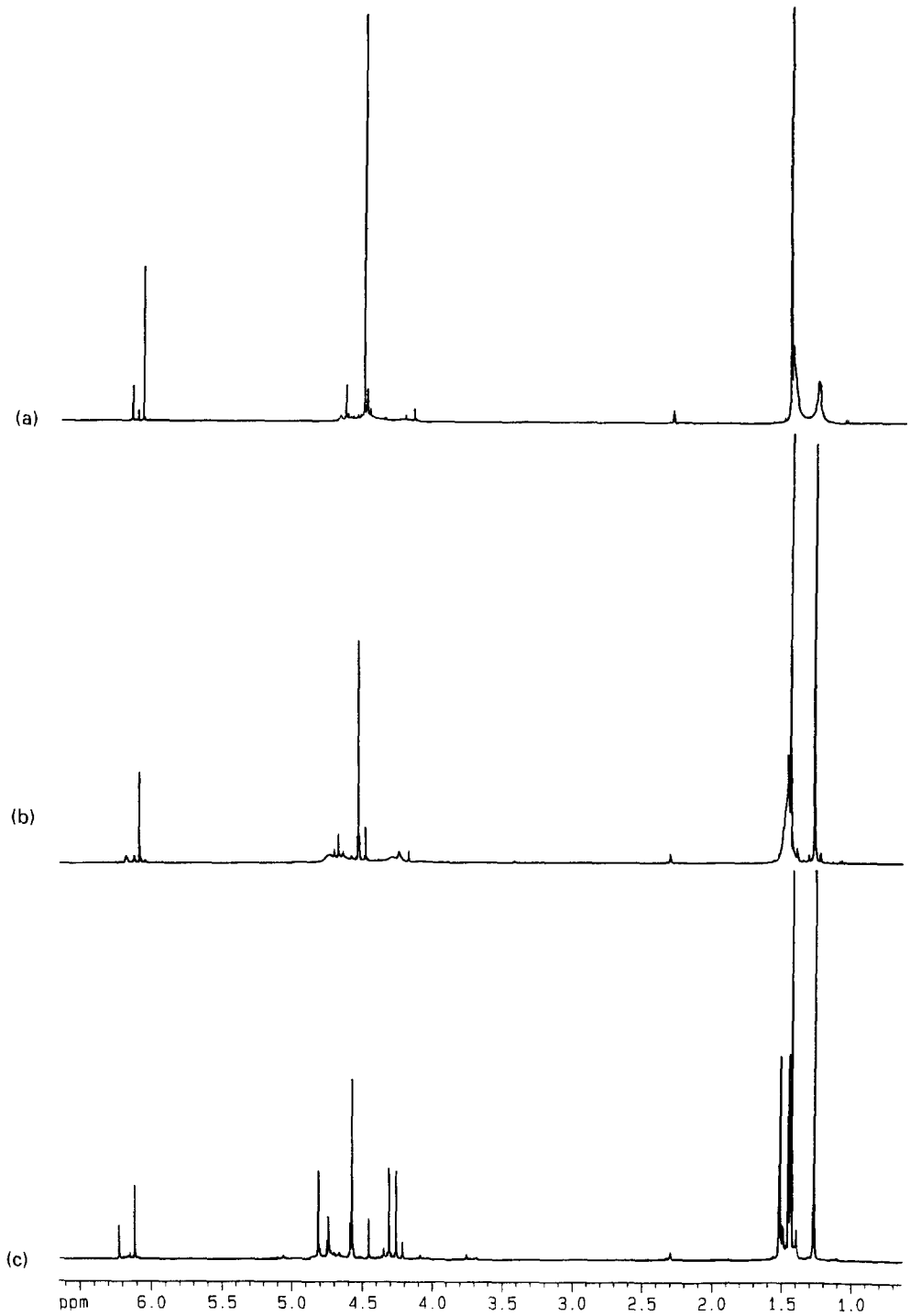

Fig. 10. Variable temperature ^{1}NMR spectra ($C_6D_5CD_3$) of [{Ti(OMe)$_3$(tmhd)}$_2$] (**4**): (a) 303 K; (b) 273 K; (c) 223 K.

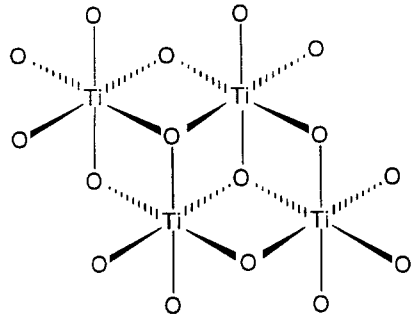

Fig. 11. The core structure of $[\{Ti(OMe)_4\}_4]$.

[4] and, since the alkyl substituents of the diketonate ligands in $[\{Ti(OR)_3(dik)\}_2]$ **I** exchange more rapidly than those in **V**, it seems plausible to propose a similar mechanism for dimeric **I**. Such a process would exchange the alkyl groups of the diketonate and interchange the terminal alkoxide ligands. Cleavage of the longer bridging bond *trans* to a terminal alkoxide would generate 5- and 6-coordinate metal centres as in **II**. Berry pseudo-rotation at the 5-coordinate centre provides another mechanism for exchange of the terminal alkoxides and of the alkyl substituents on the β-diketonate, while rotation of the 6-coordinate fragment would either exchange terminal and bridging alkoxides, as in **III**, or bring the β-diketonate into a bridging position as in **IV**. Dissociation of **IV** would then produce $Ti(OR)_4$ and $[Ti(OR)_2(dik)_2]$. Studies in coordinating solvents are now in progress to provide further information about the mechanistic aspects of these ligand exchange processes.

CONCLUSIONS

Previous solution studies of $Ti(OR)_3(dik)$ complexes have been somewhat ambiguous. Molecular weight determinations on isolated solids gave values which were concentration dependent and smaller than those expected for binuclear species [2(b)], and results from EXAFS studies of $Ti(OR)_4$/acac systems (R = Pr^i and Et) were interpreted in terms of monomeric, five-coordinate $[Ti(OR)_3(acac)]$ for R = Pr^i, or a mixture of monomeric $[Ti(OR)_3(acac)]$ and dimeric $[\{Ti(OR)_3(acac)\}_2]$ for R = Et [5]. Our results demonstrate conclusively that centrosymmetric, binuclear $[\{Ti(OR)_3(dik)\}_2]$ can be isolated in the solid state for primary and secondary alkoxide derivatives, and that disproportionation occurs in solution to give $Ti(OR)_4$ and $[Ti(OR)_2(dik)_2]$. For R = Pr^i, disproportionation is essentially complete, but for primary alkoxides the dimeric species are present in solutions of appropriate concentrations for NMR studies (*ca.* 0.2 M). Based on the ^1H NMR results, mechanisms can be proposed to account for the fluxional and dynamic processes associated with ligand exchange and ligand transfer. No conclusive evidence has yet been obtained as to the nature of the compounds obtained from 1 : 1 reactions between $Ti(OBu^t)_4$ and acacH or tmhdH, so it is still unclear whether $Ti(OBu^t)_3(dik)$ can be prepared and, if so, whether these compounds are mononuclear or binuclear.

These results illustrate the complex nature of sol–gel precursor solutions generated from 1 : 1 reactions between $Ti(OR)_4$ and dikH and should help in understanding the subsequent hydrolysis and aggregation processes. We will describe the results of our hydrolysis studies on such systems in a forthcoming paper.

Acknowledgements—We are grateful to Prof. W. McFarlane and Dr N. H. Rees for recording the NMR spectra. This work was supported by Tioxide Specialties (part-time studentship to J.R.) and by the EPSRC.

REFERENCES

1. Errington, R. J., Kerlogue, M. D. and Richards, D. G., *J. Chem. Soc., Chem. Commun.*, 1993, 64; Clegg, W., Elsegood, M. R. J., Errington, R. J. and Havelock, J., *J. Chem. Soc., Dalton Trans.*, 1996, 681–690.
2. (a) Schmidt, F., *Angew. Chem.*, 1952, **64,** 536; (b) Yamamoto, A. and Kambara, S., *J. Am. Chem. Soc.*, 1957, **79,** 4344.
3. Bradley, D. C. and Holloway, C. E., *J. Chem. Soc., Chem. Commun.*, 1965, 284; Bradley, D. C. and Holloway, C. E., *J. Chem. Soc. (A)*, 1969, 282.
4. Fay, R. C. and Lindmark, A. F., *J. Am. Chem. Soc.*, 1983, **105,** 2118.
5. Léaustic, A., Babonneau, F. and Livage, J., *Chem. Mater.*, 1989, **1,** 240; Léaustic, A., Babonneau, F. and Livage, J., *Chem. Mater.*, 1989, **1,** 248.
6. GB patent 787,180 to E. I. Dupont et Nemours, 1957.
7. SMART (CCD data collection software) and SAINT (frame integration), Siemens Analytical X-ray Instruments Inc., Madison, WI, U.S.A., 1994.
8. Sheldrick, G. M., SHELXTL User Manual, Version 5. Siemens Analytical X-ray Instruments Inc., Madison, WI, U.S.A., 1995.
9. Errington, R. J., Ridland, J., Clegg, W. and Coxall, R. A., unpublished results.
10. Serpone, N., Bird, P. H., Bickley, D. G. and Thompson, D. W., *J. Chem. Soc., Chem. Commun.*, 1972, 217.
11. Holloway, C. E. and Sentek, A. E., *Can. J. Chem.*, 1971, **49,** 519.

Pergamon

PII: S0277-5387(97)00402-6

Polyhedron Vol. 17, No. 5–6, pp. 675–688, 1998
© 1998 Elsevier Science Ltd
All rights reserved. Printed in Great Britain
0277-5387/98 $19.00+0.00

Chromium(VI) nitrido complexes: reactions with Brønsted acids and synthesis of organometallic derivatives

Aaron L. Odom and Christopher C. Cummins*

Department of Chemistry, Massachusetts Institute of Technology, Cambridge, MA 02139, U.S.A.

(Received 28 May 1997; accepted 26 September, 1997)

Abstract—The chromium(VI) nitrido complex $NCr(N\text{-}i\text{-}Pr_2)_3$ was prepared in 67% yield by vanadium(III)-mediated deoxygenation of coordinated nitric oxide. The iodide complex $NCr(I)(N\text{-}i\text{-}Pr_2)_2$, prepared by treatment of $NCr(N\text{-}i\text{-}Pr_2)_3$ with lutidinium iodide, was converted to $NCr(CH_2SiPhMe_2)(N\text{-}i\text{-}Pr_2)_2$ upon treatment with $Mg(CH_2SiPhMe_2)_2$. $NCr(N\text{-}i\text{-}Pr_2)_3$ reacts with 1 equiv. of phenol or $HOC(CF_3)_2Me$ to produce the mono-alkoxide complexes $NCr(OPh)(N\text{-}i\text{-}Pr_2)_2$ or $NCr(OC(CF_3)_2Me)(N\text{-}i\text{-}Pr_2)_2$ in respective yields of 89 and 77%. Spin saturation transfer measurements performed on $NCr(OC(CF_3)_2Me)(N\text{-}i\text{-}Pr_2)_2$ are indicative of $Cr—N_{amido}$ bond rotation with a first-order rate constant of ca 13 s^{-1}. Addition of an excess of $HOC(CF_3)_2Me$ to $NCr(N\text{-}i\text{-}Pr_2)_3$ produced the mono-amido complex $NCr(OC(CF_3)_2Me)_2(N\text{-}i\text{-}Pr_2)$ in 86% yield. Subjecting $NCr(N\text{-}i\text{-}Pr_2)_3$ to refluxing HS-*t*-Bu provided $NCr(S\text{-}t\text{-}Bu)_2(N\text{-}i\text{-}Pr_2)$ in 73% yield. Black $NCr(S\text{-}t\text{-}Bu)_2(N\text{-}i\text{-}Pr_2)$ evinces a monomeric structure in the solid state, according to single-crystal X-ray diffraction data, with a $Cr—N_{nitrido}$ distance of 1.543(6) Å. Bis-thiolate $NCr(S\text{-}t\text{-}Bu)_2(N\text{-}i\text{-}Pr_2)$ forms an adduct with $Cu(Et_2dtc)$, $NCr(N\text{-}i\text{-}Pr_2)[(\mu\text{-}S\text{-}t\text{-}Bu)_2Cu(Et_2dtc)]$, which was also characterized by X-ray diffraction. Reaction of $NCr(N\text{-}i\text{-}Pr_2)_3$ with two equiv. of phenol gave $NCr(OPh)_2(N\text{-}i\text{-}Pr_2)$ in 81% yield. Dialkyl $NCr(CH_2SiMe_3)_2(N\text{-}i\text{-}Pr_2)$ was obtained from $NCr(OPh)_2(N\text{-}i\text{-}Pr_2)$ upon treatment with $LiCH_2SiMe_3$ in 57% yield. Insertion of *tert*-butylisonitrile was observed upon treatment of $NCr(CH_2SiMe_3)_2(N\text{-}i\text{-}Pr_2)$ with excess *t*-BuNC to give $NCr(C(=N\text{-}t\text{-}Bu)CH_2SiMe_3)(CH_2SiMe_3)(N\text{-}i\text{-}Pr_2)$, which was isolated in 70% yield. The latter η^2-iminoacyl compound was characterized by X-ray diffraction, revealing a pseudo-square pyramidal ligand arrangement.
© 1998 Elsevier Science Ltd. All rights reserved

Keywords: chromium; nitrido; iminoacyl; protonolysis; amido; nitrosyl.

Recent developments in the activation of small molecules have led to the discovery of new routes to terminal nitrido complexes. For example, three-coordinate $Mo(N[R]Ar)_3$, where R is $C(CD_3)_2(CH_3)$ and Ar is 3,5-$C_6H_3Me_2$, was found to react with dinitrogen to form $NMo(N[R]Ar)_3$ via a linear μ-dinitrogen dinuclear complex intermediate [1]. In addition, the cleavage of nitric oxide to nitride and oxo functionalities by two metal centers was achieved. Bradley's nitrosyl $ONCr(N\text{-}i\text{-}Pr_2)_3$ [2], in particular, was found to serve as an oxo donor to $V(Mes)_3(THF)$ [3,4].

Much of the interest in reactions that produce terminal nitrido complexes stems from the possibility of producing useful chemical feedstocks like ammonia from strategic starting materials. Reactions that convert dinitrogen or NO_x gases to nitrido complexes could represent a useful first step toward achieving this goal. Also important in this context is to elucidate the chemistry of the resulting nitrido complexes. In a study conducted by Chisholm and co-workers [5] reactions of $NM(O\text{-}t\text{-}Bu)_3$, where M = Mo and W, with excess *i*-PrOH were investigated. Treatment of $NMo(O\text{-}t\text{-}Bu)_3$ with isopropanol led to exclusive alkoxide substitution given $NMo(O\text{-}i\text{-}Pr)_3$. The tungsten derivative $NW(O\text{-}t\text{-}Bu)_3$, in contrast, was exhaustively attacked by isopropanol giving $W(O\text{-}i\text{-}Pr)_6$.

In addition to chemistry where the nitrido nitrogen is an active participant, there is also an extensive chemistry in which a nitrido nitrogen acts as a spectator ligand [6–8]. For example, molybdenum(VI) nitrides can be synthesized with soft ligands such as thiolates [9] or hard ligands such as amides [1,8,10].

* Author to whom correspondence should be addressed.

Molybdenum organometallic complexes also have been synthesized [11] including the σ organometallic complex NMo(neopentyl)$_3$ [7]. Chromium(VI) derivatives with this large variety of ligands offer an exciting new field of study [12].

RESULTS AND DISCUSSION

Synthesis of NCr(N-*i*-Pr$_2$)$_3$ (3) *and nitric oxide cleavage*

Bradley and co-workers synthesized Cr(N-*i*-Pr$_2$)$_3$ (**1**) by addition of 3 equiv. of LiN-*i*-Pr$_2$ to ethereal CrCl$_3$ [13]. Treatment of **1** with nitric oxide results in a rapid reaction to produce orange ONCr(N-*i*-Pr$_2$)$_3$ (**2**) [2]. The π acidic nitrosyl ligand induces a diamagnetic $\{ONCr\}^4$ low-spin electronic configuration, which results in a low N—O stretching frequency of 1643 cm^{-1}. Deoxygenation of **2** by two equiv. of V(mesityl)$_3$(THF)[3] gave rise to NCr(N-*i*-Pr$_2$)$_3$ (**3**) and OV(mesityl)$_3$, but the latter is trapped by an additional equiv. of V(mesityl)$_3$(THF) to form O[V(mesityl)$_3$]$_2$ [14]. The nitrido complex was easily separated from the vanadium(IV) μ-oxo species by pentane extraction [4].

The physical properties of beet-colored **3** are significantly different from those of **2** and **1**, consistent with the large difference in formal oxidation state. The solid state structure of **3** as determined by X-ray diffraction revealed an average Cr—N$_{amido}$ bond length that is ~0.3 Å shorter than found in **1**. The Cr—N$_{nitrido}$ distance of 1.544(3) Å in **3** is ~0.15 Å shorter than Cr—N$_{nitrosyl}$ bonds in ONCr[N(SiMe$_3$)$_2$]$_3$ and ONCr(I)(N[R]Ar$_F$)$_2$, where R = C(CH$_3$)(CD$_3$)$_2$ and Ar$_F$ = 2,5-C$_6$H$_3$FMe [15]. In addition, the ^{1}H NMR spectrum of **3** exhibits broad resonances for the amido ligands at room temperature. The broad nature of the peaks is attributed to hindered rotation around the Cr—N$_{amido}$ bonds and contrasts with the narrow line widths found in the ^{1}H NMR spectrum of ONCr(N-*i*-Pr$_2$)$_3$ (**2**).

Bis-amido chromium(VI) complexes (scheme 1)

(*i*) *Synthesis of* NCr(I)(N-*i*-Pr$_2$)$_2$(**4a**). Lutidinium iodide is conveniently synthesized in anhydrous form by the reaction of 2,6-lutidine, *tert*-butyl alcohol and ISiMe$_3$ in dry ether. Addition of 2.5 equiv. of lutidinium iodide to 1 equiv. of **3** initiated a color change of the reaction mixture to orange-red. Protolytic amido replacement was found to have occurred giving NCr(I)(N-*i*-Pr$_2$)$_2$ (**4a**) [16]. The lutidine by-product was easily separated by recrystallization. An attempt to produce NCr(I)$_2$(N-*i*-Pr$_2$) under forcing conditions only resulted in an intractable product and starting materials.

The ^{1}H NMR spectrum of **4a** is indicative of hindered rotation [17,26] around the Cr—N$_{amido}$ bonds. Four doublets are observed in the spectrum. These correspond to the diastereotopic methyl hydrogens, which are differentiated further by being syn or anti with respect to the nitrido nitrogen. Two septets are also observed in the spectrum, septets which correspond to methine hydrogens located syn and anti with respect to the nitrido group. A dramatic slowing of the Cr—N$_{amido}$ rotation rate in **4a** versus **3** is explicable in terms of a qualitative molecular orbital picture for the two molecules [18]. In NCr(N-*i*-Pr$_2$)$_3$ (**3**), the chromium has a degenerate set of two orbitals available for π bonding to the three amido substituents. The three amido π donor orbitals must compete for

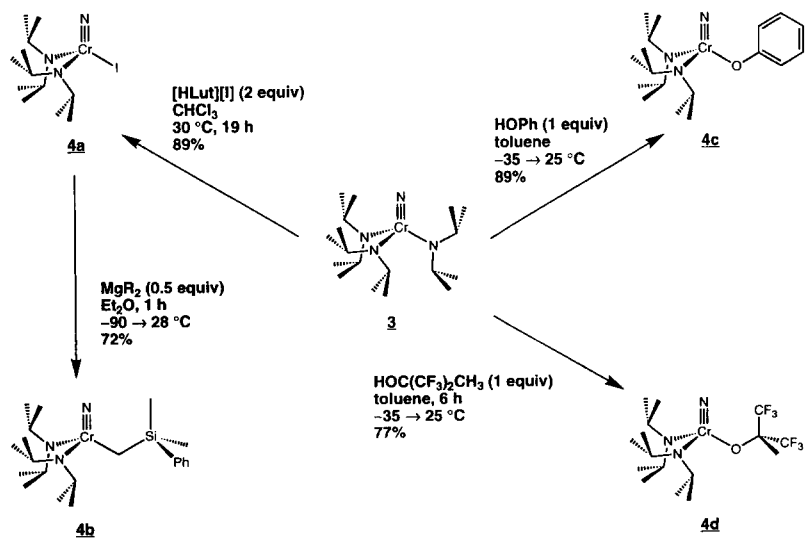

Scheme 1.

the two metal π acceptor orbitals, resulting in a bond order for the amido substituents of one and two-thirds. The iodide complex **4a** has only two amides to donate into the two metal orbitals with proper symmetry for π bonding. Therefore, the amido substituents in NCr(I)(N-*i*-Pr_2)$_2$ may form two double bonds (formally) to the chromium center. The hindered rotation observed for **4a** is even more dramatic in light of the steric difference between NCr(I)(N-*i*-Pr_2)$_2$ (**4a**) and NCr(N-*i*-Pr_2)$_3$ (**3**). The iodide complex **4a,** which presumably is less sterically congested, exhibits characteristics indicative of slower amido rotation.

(*ii*) *Synthesis and thermal decomposition of* NCr($CH_2SiPhMe_2$)(N-*i*-Pr_2)$_2$ (**4b**). A nitrido alkyl complex NCr($CH_2SiPhMe_2$)(N-*i*-Pr_2)$_2$ (**4b**) was produced by addition of Mg($CH_2SiPhMe_2$)$_2$ to a cold solution of **4a** in ether [16]. NCr($CH_2SiPhMe_2$)(N-*i*-Pr_2)$_2$ **4b** is a rare example of a chromium(VI) organometallic complex [19]. The σ alkyl complex **4b** also is a rare example of an alkyl nitrido complex [7,11]. Orange NCr($CH_2SiPhMe_2$)(N-*i*-Pr_2)$_2$ (**4b**) was isolated in 72% recrystallized yield and has a ^{1}H NMR spectrum with four doublets and two septets assignable to the amido hydrogens.

The alkyl-nitrido complex **4b** is stable in solution at room temperature for hours without appreciable decomposition, but the compound decomposes at 60°C with a first order rate constant of $(2.4 \pm 0.1) \times 10^{-4}$ s^{-1} [16]. The data for the decomposition are consistent with β-hydrogen abstraction [20] from one of the amido substituents by the departing alkyl. The products included $PhSiMe_3$ (GC/MS and ^{1}H NMR), the imine Me_2C=N-*i*-Pr (tentative ^{1}H NMR identification), and diisopropylamine (^{1}H NMR). We have not characterized a black solid (possibly CrN [21]) produced during the thermolysis.

(*iii*) *Synthesis of* NCr(OPh)(N-*i*-Pr_2)$_2$ (**4c**). Addition of one equiv. of phenol to **3** in toluene caused the solution to change color to orange over a few minutes. The phenoxide NCr(OPh)(N-*i*-Pr_2)$_2$ (**4c**) product, which was purified by recrystallization from ether, was isolated in 88% yield.

Phenoxide **4c** is stable for long durations in solution at room temperature, and exhibits slightly different NMR properties from **4a** and **4b**. The compound displays four peaks for the methyl hydrogens and two peaks for the methine hydrogens as in the previously discussed bis-amido compounds. However, the peaks in NCr(OPh)(N-*i*-Pr_2)$_2$ are significantly broadened which suggests faster rotation around the Cr—N_{amido} bonds than in NCr(I)(N-*i*-Pr_2)$_2$ and NCr($CH_2SiPhMe_2$)(N-*i*-Pr_2)$_2$. The less hindered rotation is indicative of the greater π donating ability of the phenoxide ligand relative to the alkyl or iodide ligands.

(*iv*) *Synthesis of* NCr($OC(CF_3)_2Me$)(N-*i*-Pr_2)$_2$ (**4d**) *and spin saturation transfer* Phenol and HOC(CF_3)$_2$Me are often compared due to their similar pK_a' [22] but dramatically different π basicity [23]. Addition of one equiv. of HOC(CF_3)$_2$Me to a stirring solution of **3** cleanly produced NCr($OC(CF_3)_2Me$)(N-*i*-Pr_2)$_2$ (**4d**), which was isolated in 77% yield.

The ^{1}H NMR spectrum has the four-doublets-two-septets pattern indicative of hindered rotation about the Cr—N_{amido} bonds. The compound **4d,** unlike phenoxide **4c,** has sharp peaks in its spectrum corresponding to the amido ligands. The more hindered rotation found for **4d** relative to **4c** can be attributed to decreased π donation by the fluorinated alkoxide ligand relative to phenoxide and to the larger steric demands of the alkoxide ligand.

Magnetization transfer between the two methine hydrogens in **4d** was measured using the method of Dahlquist, Longmuir and Du Vernet [24]. The experiment was performed in C_6D_6 at room temperature, and the data are plotted in Fig. 1. The data were fit to $A_0 e^{-Xt}$, where t is the delay time and A_0 is the intensity of the selectively-irradiated peak in the difference spectrum at t = 0. The difference curve fit converged at A_0 = 178 (0.77) and X = 13.99 (0.096) with R = 0.9997. The sum curve fit converged at A_0 = 187 (0.59) and X = 0.428 (0.016) with R = 0.983. From the values of X a rate constant for amido rotation equal to 13.5 (0.1) s^{-1} is obtained, which correlates to $\Delta G^{\ddagger}$ = 16 kcal/mol [25].

Mono-amido chromium(VI) nitrido complexes (scheme 2)

(*i*) *Synthesis of* NCr($OC(CF_3)_2Me$)$_2$(N-*i*-Pr_2) (**5a**) *and spin saturation transfer.* Addition of excess

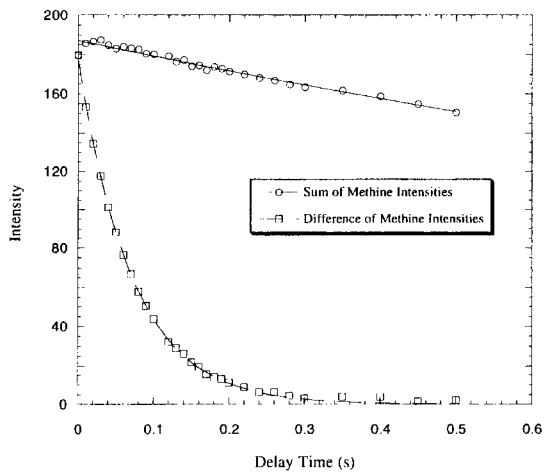

Fig. 1. Sum and difference in intensity plot for the two septets in NCr($OC(CF_3)_2Me$)(N-*i*-Pr_2)$_2$ (**4d**) in C_6D_6. The lines were fit to the equation $A_0 e^{-Xt}$, where A_0 is the initial intensity of the selectively pulsed peak and t is the delay time in seconds. X in the sum plot is equal to 1/T1. In the difference plot X is equal to 1/T1 + k(1) + k(−1). The sum curve fit converged at A_0 = 187(0.59) and X = 0.428(0.016) with R = 0.983. The difference curve fit converged at A_0 = 178 (0.77) and X = 13.99 (0.096) with R = 0.9997. The fits indicate a rate constant for the amido rotation of 13.5 (0.1) s^{-1} for k(1) + k(−1) which correlates to $\Delta G^{\ddagger}$ = 16 kcal/mol.

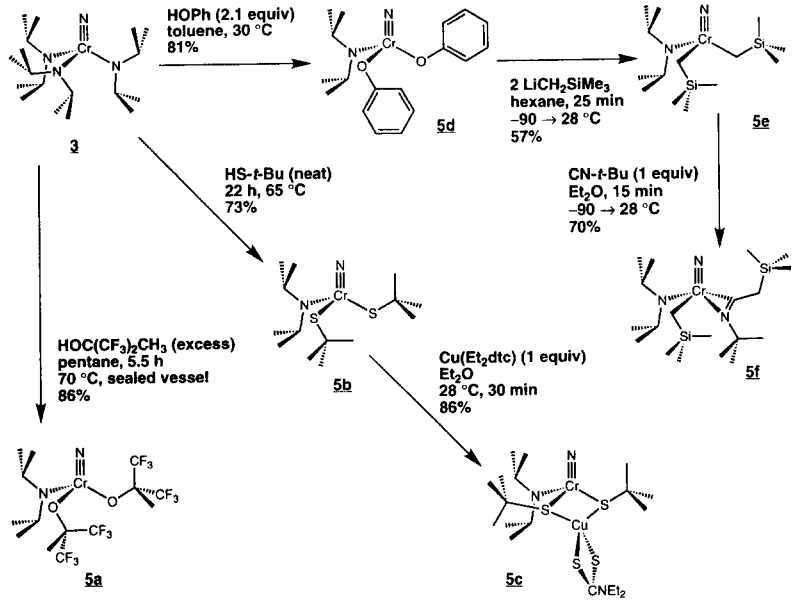

Scheme 2.

$HOC(CF_3)_2Me$ to **3** produced the bis-alkoxide complex $NCr(OC(CF_3)_2Me)_2(N\text{-}i\text{-}Pr_2)$ (**5a**). The reaction was quite slow and required heating at 70°C in a concentrated solution of the alcohol for 5 h. The production of **5a** was very clean and yielded 86% of the purified complex. This is in contrast to the reaction of **4a** with lutidinium iodide, which did not result in the clean production of $NCr(I)_2(N\text{-}i\text{-}Pr_2)$.

An alternative synthesis of **5a** involves heating $NCr(I)(N\text{-}i\text{-}Pr_2)_2$ in the neat alcohol for 12 h. Under these conditions $[H_2N\text{-}i\text{-}Pr_2]$ [I] precipitates from the solution, and **5a** is produced in 64% yield.

The ^1H NMR spectra of all of the mono-amido complexes exhibit two doublets for the methyl hydrogens and two septets for the methine hydrogens of the diisopropylamide. The inequivalence of the *iso*-propyl groups is attributed to syn and anti differentiation with respect to the nitrido functionality and is indicative of significant amido—chromium multiple bond character.

Table 1. Selected bond distances (Å) and angles (°) for $NCr(S\text{-}t\text{-}Bu)_2(N\text{-}i\text{-}Pr_2)$ (**5b**)

Cr(1)—N(2)	1.543(6)
Cr(1)—N(1)	1.780(6)
Cr(1)—S(1)	2.217(3)
Cr(1)—S(2)	2.235(3)
N(2)—Cr(1)—N(1)	106.3(3)
N(2)—Cr(1)—S(1)	107.7(2)
N(2)—Cr(1)—S(2)	107.5(2)
N(1)—Cr(1)—S(1)	109.6(2)
N(1)—Cr(1)—S(2)	108.8(2)
C(11)—S(1)—Cr(1)	113.8(3)
C(21)—S(2)—Cr(1)	111.8(3)

Spin saturation transfer experiments carried out for $NCr(OC(CF_3)_2Me)_2(N\text{-}i\text{-}Pr_2)$ (**4a**) did not indicate magnetization transfer between the methyl hydrogens of the amido substituent even at 90°C. The lack of transfer suggests a rotation rate constant of less than $\sim 0.3\ s^{-1}$ at that elevated temperature, and the activation energy required for rotation can be estimated to be $\geqslant 22$ kcal/mol. The activation energies associated with Cr—N_{amido} rotation in **4d** and **5a** are comparable with some of the larger $M{=}ER_2$ (where E is carbon or nitrogen) bond rotation activation energies found in the literature. The $M_2(NR_2)_6$ complexes of molybdenum and tungsten, where R is methyl or ethyl, have activation energies for amido rotation of 11 to 14 ± 0.5 kcal/mol [26]. Schrock and co-workers have measured the activation energies required for alkylidene rotation in several tantalum complexes [27]. $Cp_2Ta(Cl)(CHC(CH_3)_3)$, $Cp_2Ta(CH_2Ph)(CHPh)$ and $Cp_2Ta(CH_3)(CH_2)$ are reported to have values of $\Delta G^{\ddagger}$ for Ta=C rotation of 16.8 ± 0.1, 19.3 ± 0.1 and $\geqslant 21.4$ kcal/mol, respectively.

(ii) Synthesis and X-ray crystal structure of $NCr(S\text{-}t\text{-}Bu)_2(N\text{-}i\text{-}Pr_2)$ (**5b**). Group 6 nitrides with soft ligands such as thiolates are rare [9]. The scarcity of reports involving high oxidation state nitrido thiolate complexes could be construed as indicative of instability in this class of compounds. The most common decomposition route for thiolate complexes is S—S bond formation giving reduction at the metal center [28]. This decomposition can occur by thiolate radical loss from the metal with subsequent S—S bond formation, by reductive elimination of two thiolates on the same metal center or by dimerization with

Table 2. Selected bond distances (Å) and angles (°) for NCr(N-*i*-Pr$_2$)[(μ-S-*t*-Bu)$_2$Cu(Et$_2$dtc)] (**5c**)

Cr—N(1)	1.805(13)
Cr—N(2)	1.547(13)
Cr—S(1)	2.240(6)
Cr—S(2)	2.247(6)
Cu—S(1)	2.277(5)
Cu—S(2)	2.250(5)
Cu—S(3)	2.395(5)
Cu—S(4)	2.370(5)
Cr—Cu	2.607(4)
N(2)—Cr—N(1)	107.0(6)
N(1)—Cr—S(1)	111.2(5)
N(2)—Cr—S(1)	108.9(5)
N(1)—Cr—S(2)	111.0(5)
N(2)—Cr—S(2)	109.5(5)
S(1)—Cr—S(2)	109.2(2)
N(1)—Cr—Cu	136.5(4)
N(2)—Cr—Cu	116.4(5)
S(1)—Cr—Cu	55.4(2)
S(2)—Cr—Cu	54.62(14)
S(2)—Cu—S(1)	107.8(2)
S(1)—Cu—S(4)	122.4(2)
S(2)—Cu—S(4)	120.0(2)
S(1)—Cu—S(3)	110.9(2)
S(2)—Cu—S(3)	116.2(2)
S(4)—Cu—S(3)	75.9(2)
S(1)—Cu—Cr	54.1(2)
S(2)—Cu—Cr	54.53(14)
S(3)—Cu—Cr	140.4(2)
S(4)—Cu—Cr	143.6(2)
Cr—S(1)—Cu	70.5(2)
Cr—S(2)—Cu	70.8(2)
C(11)—S(1)—Cr	115.8(6)
C(11)—S(1)—Cu	113.3(6)
C(21)—S(2)—Cr	115.1(6)
C(21)—S(2)—Cu	113.8(6)
C(1)—S(3)—Cu	83.3(6)
C(1)—S(4)—Cu	84.3(6)

Table 3. Selected bond distances (Å) and angles (°) for NCr(C(=N-*t*-Bu)CH$_2$SiMe$_3$)(CH$_2$SiMe$_3$)(N-*i*-Pr$_2$) (**5f**)

Cr(1)—N(11)	1.77(2)
Cr(1)—N(12)	1.90(2)
Cr(1)—N(13)	1.59(2)
Cr(1)—C(11)	2.50(2)
Cr(1)—C(121)	1.67(2)
N(12)—C(121)	1.56(3)
N(12)—C(126)	1.55(3)
N(13)—Cr(1)—C(121)	103.9(10)
N(13)—Cr(1)—N(11)	110.6(9)
C(121)—Cr(1)—N(11)	120.9(10)
C(121)—Cr(1)—N(12)	51.4(8)
N(11)—Cr(1)—N(12)	133.7(9)
N(13)—Cr(1)—N(12)	115.5(10)
N(11)—Cr(1)—C(11)	95.3(8)
N(12)—Cr(1)—C(11)	66.6(8)
N(13)—Cr(1)—C(11)	108.4(9)
C(121)—Cr(1)—C(11)	117.6(9)
Si(11)—C(11)—Cr(1)	121.0(10)
C(121)—N(12)—Cr(1)	56.4(10)
C(126)—N(12)—C(121)	114(2)
C(126)—N(12)—Cr(1)	170(2)

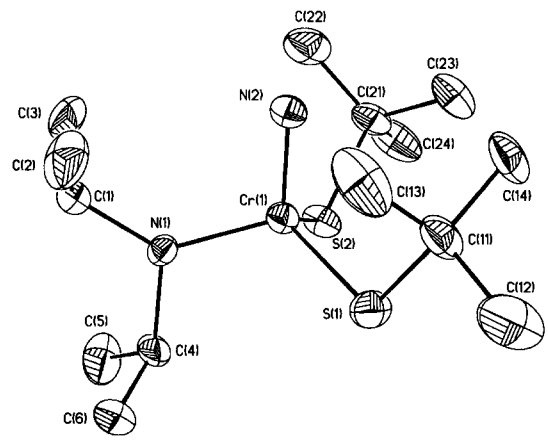

Fig. 2. ORTEP diagram of NCr(S-*t*-Bu)$_2$(N-*i*-Pr$_2$) (**5b**). The ellipsoids are at the 35% probability level.

reductive elimination from two metal centers. The decomposition mechanisms listed above allow the metal center to access its lower oxidation states and would seem to be favorable for a chromium(VI) thiolate complex. It was found, however, that refluxing *tert*-butylthiol will convert **3** to the quite stable thiolate complex NCr(S-*t*-Bu)$_2$(N-*i*-Pr$_2$) (**5b**) in 73% yield. The dark, highly crystalline product forms green or blue solutions depending on the solvent.

An X-ray diffraction study carried out on **5b** yielded a model exhibiting a monomeric structure in the solid state (Fig. 2). All of the structurally characterized chromium(VI) nitrido complexes are monomeric in the solid state, which contrasts with the polymeric structures of many molybdenum and tungsten nitrido compounds [29]. The nitrido nitrogen is surrounded closely by an isopropyl group from the amido substituent and the two *tert*-butyl groups of the thiolates. The structure exhibits a Cr—N(2) distance of 1.543(6) Å which is a typical Cr—$N_{nitrido}$ distance for this class of complexes [4,12,16]. The Cr(1)—N(1) distance in **5b** is ~0.09 Å shorter than the average Cr—N_{amido} distance in Cr(N-*i*-Pr$_2$)$_3$ and ~0.06 Å shorter than in NCr(N-*i*-Pr$_2$)$_3$. The shortening of the metal—N_{amido} bond is consistent with increased π bonding in the mono-amido Cr(VI) complex.

(iii) Synthesis and X-ray crystal structure of NCr(N-*i*-Pr$_2$)[(μ-S-*t*-Bu)$_2$Cu(Et$_2$dtc)] (**5c**). A blue ethereal solution of NCr(S-*t*-Bu)$_2$(N-*i*-Pr$_2$) (**5b**) gives an orange-brown reaction mixture when added to a slurry of Cu(Et$_2$dtc) [30]. The resultant complex NCr(N-*i*-Pr$_2$)[(μ-S-*t*-Bu)$_2$Cu(Et$_2$dtc)] (**5c**) has *tert*-butyl thiolate ligands bridging the chromium and cop-

Table 4. Summary of crystal data for $NCr(S\text{-}t\text{-}Bu)_2(N\text{-}i\text{-}Pr_2)$ (**5b**), $NCr(N\text{-}i\text{-}Pr_2)[(\mu\text{-}S\text{-}t\text{-}Bu)_2Cu(Et_2dtc)]$ (**5c**) and $NCr(C(=N\text{-}t\text{-}Bu)CH_2SiMe_3)(CH_2SiMe_3)(N\text{-}i\text{-}Pr_2)$ (**5f**)

Compound	**5b**	**5c**	**5f**
Empirical formula	$C_{14}H_{32}CrN_2S_2$	$C_{19}H_{42}CrCuN_3S_4$	$C_{19}H_{45}CrN_3Si_2$
Space group	$P2_1/n$	$P2_1/n$	P1
a, Å	9.891(8)	13.501(8)	7.6178(10)
b, Å	12.334(8)	9.974(9)	10.1373(13)
c, Å	16.537(10)	20.97(2)	18.181(2)
α, degrees	90	90	89.358(2)
β, degrees	94.56(4)	98.16(7)	80.999(4)
γ, degrees	90	90	71.845(2)
Z	4	4	2
V, Å^3	2011(2)	2795(4)	1316.6(3)
ρ_{calcd}, g/cm^3	1.138	1.322	1.069
Cryst. dimens, mm	$0.40 \times 0.30 \times 0.10$	$0.45 \times 0.26 \times 0.09$	$0.71 \times 0.14 \times 0.12$
Cryst. color	black	black	yellow-green
R1(F)	0.0642	0.1148	0.0924
Rw(F^2)	0.1231	0.2905	0.1809
GOF ($I > 2\sigma I$)	1.289	1.152	1.125
ψ-scans max. trans.	0.1372	0.1685	0.7189
ψ-scans min. trans.	0.1125	0.1095	0.6096
temp., K	188(2)	130(2)	193(2)

per metal centers and is synthesized in 73% purified yield. The solid state structure of **5c** (Fig. 3) as determined by X-ray diffraction shows a $NCr(N\text{-}i\text{-}Pr_2)(S\text{-}t\text{-}Bu)_2$ fragment which is essentially unperturbed from the structure of **5b** (Fig. 2). The complex exhibits a pseudo-tetrahedral arrangement of sulfurs around the copper(I) metal center. The *tert*-butyl substituents enclose the nitrido nitrogen while the $Cu(Et_2dtc)$ fragment occupies a position on the opposite side of the S(1)—S(2)—N(1) plane [31].

(*iv*) *Synthesis of* $NCr(OPh)_2(N\text{-}i\text{-}Pr_2)$ (**5d**). Treatment of a toluene solution of **3** with two equiv. of phenol results in a rapid color change to dark orange and production of $NCr(OPh)_2(N\text{-}i\text{-}Pr_2)$ (**5d**). The reaction is complete in less than thirty min in dramatic contrast to the conditions for the synthesis of **5a**.

The bis-phenoxide complex **5d** is easily synthesized and isolated but is, however, somewhat thermally sensitive. The complex decomposes in solution at room temperature to yield an intractable solid. The nature of this decomposition, although currently unknown, is probably the result of Cr—O homolytic bond cleavage to reduce the oxidation state of the metal and produce phenoxide radical [32].

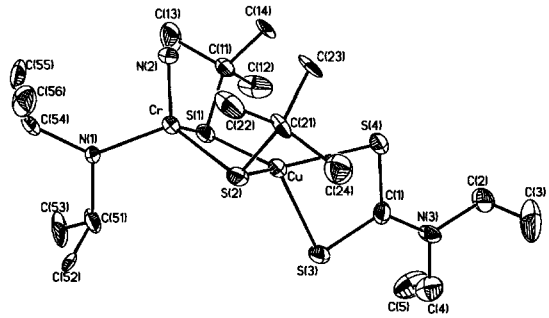

Fig. 3. ORTEP diagram of $NCr(N\text{-}i\text{-}Pr_2)[(\mu\text{-}S\text{-}t\text{-}Bu)_2Cu(Et_2dtc)]$ (**5c**). The ellipsoids are at the 35% probability level.

(*v*) *Synthesis and thermolysis of* $NCr(CH_2SiMe_3)_2(N\text{-}i\text{-}Pr_2)$ (**5e**). Addition of two equiv. of $LiCH_2SiMe_3$ to a cold solution of **5d** in pentane results in the formation of the chromium(VI) organometallic complex $NCr(CH_2SiMe_3)_2(N\text{-}i\text{-}Pr_2)$ (**5e**). The highly lipophilic compound was purified by recrystallization from hexamethyldisiloxane at -35°C in 57% yield.

The complex **5e** exhibits thermal stability similar to that found for **4b**. The compound can be stirred at room temperature overnight without substantial decomposition, but it decomposes rapidly at 60°C. The decomposition, though not as clean as found for **4b**, may proceed by a similar β-hydrogen abstraction mechanism. The ^1H NMR spectrum of the decomposition products revealed tetramethylsilane, $HN\text{-}i\text{-}Pr_2$ and the imine $Me_2C{=}N\text{-}i\text{-}Pr$ to be among the products. There is also a black solid produced during the thermolysis.

(*vi*) *Reactivity of* **5e** *with tert*-butyisonitrile. *The synthesis and X-ray crystal structure of* $NCr(C(=N\text{-}t\text{-}Bu)CH_2SiMe_3)(CH_2SiMe_3)(N\text{-}i\text{-}Pr_2)$ (**5f**). Addition of *t*-butyl isonitrile to an ethereal solution of **5e** produced a color change to yellow-green, forming the iminoacyl $NCr(C(=N\text{-}t\text{-}Bu)CH_2SiMe_3)(CH_2SiMe_3)(N\text{-}i\text{-}Pr_2)$ (**5f**). Only a single insertion reaction occurs even with 24 h exposure of the dialkyl to 10 equiv. of *t*-butyl isonitrile. The greater reactivity of $NCr(CH_2$

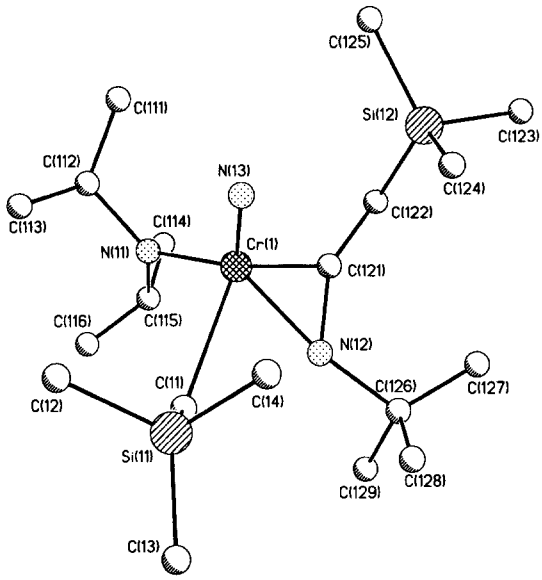

Fig. 4. PLUTO diagram of NCr(C(=N-*t*-Bu)CH_2 $SiMe_3$)(CH_2SiMe_3)(N-*i*-Pr_2) (**5f**). One of the two chemically equivalent molecules in the asymmetric unit is shown.

$SiMe_3)_2$(N-*i*-Pr_2) (**5e**) relative to NCr(C(=N-*t*-Bu)CH_2SiMe_3)(CH_2SiMe_3)(N-*i*-Pr_2) (**5f**) towards insertion can be attributed to electronic differences between the two complexes. The dialkyl can be described as a 14e complex with an available low energy orbital in the plane normal to the nitrido vector and passing through chromium. The iminoacyl complex **5f** has a 16e metal center and no low energy orbitals available, such that a second insertion reaction is unfavorable. Accordingly, treatment of the 16e monoalkyl complex **4b** with 10 equiv. of *t*-butyl isonitrile also gave no reaction even after 24 h reaction time.

An X-ray diffraction study (Fig. 4) carried out on **5f** clearly revealed the presence of an η^2-iminoacyl group. The four different ligands reside in a pseudo square pyramidal arrangement with the η^2-iminoacyl, amido and alkyl substituents residing in the basal plane and the nitrido nitrogen occupying the axial site.

Reactivity of the nitrido nitrogen in chromium(VI) nitrido complexes

(*i*) *Reaction of* 3 *with nucleophiles.* Nitrido complexes often react with nucleophiles to produce complexes with lower oxidation states for the central metal [8]. Nitrides react with phosphines to produce phosphiniminato complexes [33] or with sulfur to produce thionitrosyls [34]. Reactions of this type that effect a reduction of the metal center would seem favorable for chromium(VI). However, a clean addition reaction involving the nitrido nitrogen has not been observed. The microscopic reverse of the nitrosyl deoxygenation reaction does not occur on treatment of NCr(N-*i*-$Pr_2)_3$ (**3**) with 10 equiv. of pyridine-*N*-oxide or trimethylamine-*N*-oxide in CH_2Cl_2 over several d. Nitrido **3** does not react with a concentrated solution of S_8 in CS_2 even after two d. In addition, **3** does not react with neat triethylphosphine even with 24 h of reaction time. This lack of reactivity towards phosphines is especially intriguing due to the reactivity of NCr^{V}(TPP) with PMe_3 to produce $Me_3P{=}NCr^{III}$(TPP) [35].

(*ii*) *Reaction of* NCr(N-*i*-$Pr_2)_3$ *with water.* The nitrido functionality, although stable to a number of protic reagents, does react with water. Addition of 2 equiv. of water to a THF solution of **3** resulted in the precipitation of an insoluble black material, which has not been characterized. However, addition of a THF solution of **3** to an excess of water resulted in smooth hydrolysis of the nitrido nitrogen to form [H_2N-*i*-$Pr_2]_2[Cr_2O_7]$, which was isolated in 73% recrystallized yield.

EXPERIMENTAL

General considerations

All manipulations were carried out in a Vacuum Atmospheres dry box under a purified nitrogen atmosphere unless stated otherwise. Anhydrous ether was purchased from Mallinckrodt and freshly distilled from purple sodium benzophenone ketyl. Toluene was purchased from Mallinckrodt and purified by refluxing over molten sodium under nitrogen for at least two d. Pentane (EM Science) was distilled from purple sodium benzophenone ketyl. Distilled solvents were transferred under vacuum to glass vessels and stored in a Vacuum Atmospheres dry box prior to use. Nitric oxide (grade 5.0) was purchased from BOC corporation and used as supplied. *Tert*-butyl mercaptan was purchased from Aldrich, dried over activated 3 Å sieves for two d and then was distilled under nitrogen prior to use. *Tert*-butylisonitrile was purchased from Aldrich, degassed and stored over 3 Å sieves prior to use. Hexafluoro-2-methylisopropanol (hexafluoro-*tert*-butanol) purchased from PCR Chemical Company was degassed and dried over 3 Å sieves prior to use. (*N*,*N*-diethyldithiocarbaminato)copper(I) [30] and V(mesityl)$_3$(THF) [3] were made according to published procedures. All other solvents, including deuterated solvents, were degassed and stored over activated 3 Å sieves for at least 24 h before use. The sieves were activated by heating at approximately 200°C *in vacuo* overnight. Other chemicals were purchased from commercial sources and used as received. Cr(N-*i*-$Pr_2)_3$ [13], and (ON)Cr(N-*i*-$Pr_2)_3$ [2], were made according to literature methods. NCr(I)(N-*i*-$Pr_2)_2$ and NCr(CH_2SiMe_2Ph)(N-*i*-$Pr_2)_2$ were prepared as previously communicated [16].

Infrared spectra were recorded on a Perkin Elmer

1600 Series FTIR or a Biorad FTS 135. ^{1}H, ^{13}C, ^{15}N and ^{19}F NMR spectra were recorded on Varian VXR-500, Varian XL-300, or Varian Unity-300 spectrometers. ^{1}H and ^{13}C chemical shifts are reported with reference to solvent resonances (residual C_6D_5H in C_6H_6 as 7.15 ppm; C_6D_6 as 128.0 ppm; $CHCl_3$ in $CDCl_3$ as 7.24 ppm; $CDCl_3$ as 77.0 ppm) and were recorded at room temperature unless otherwise stated. ^{19}F NMR chemical shifts are reported with reference to external $CFCl_3$ as 0.00 ppm. ^{15}N NMR chemical shifts are reported with respect to external nitromethane at 380.2 ppm (relative to liquid NH_3 at 0.00 ppm). Combustion analysis were performed by Oneida Research Services, Whitesboro, NY or by Microlytics, South Deerfield, MA. Melting points were obtained in sealed glass capillaries and are uncorrected.

Synthesis and reactivity studies

(*i*) *Synthesis of* $NCr(N\text{-}i\text{-}Pr_2)_3$ (**3**). $(ON)Cr(N\text{-}i\text{-}Pr_2)_3$ (1.094 g, 2.859 mmol, 1 equiv.), V(mesityl)$_3$(THF) (2.983 g, 6.207 mmol, 2.17 equiv.), 35 ml of toluene and a stir bar were loaded into a 300 ml glass vessel equipped with a side arm. The mixture was stirred in a 65°C oil bath for 60 min, during which the solution turned from brown to red. The volatiles were removed *in vacuo*, and the contents of the bomb were extracted with pentane. The resultant beet solution was filtered through a bed of Celite on a sintered glass frit. Extraction left a less soluble, highly pyrophoric black solid on the frit. The product was recrystallized from ether in 67% yield (0.701 g, 1.91 mmol). ^{1}H NMR ($CDCl_3$): δ 3.93 (v br s, 1H), 1.28 (v br s, 6H). ^{13}C NMR ($CDCl_3$): δ 54 (v br s), 27 (v br s), 23 (v br s). FTIR ($NCr(N\text{-}i\text{-}Pr_2)_3$, $CHCl_3$) 1054.0 cm^{-1}. FTIR ($^{15}NCr(N\text{-}i\text{-}Pr_2)_3$, $CHCl_3$) 1029.0 cm^{-1}. ^{15}N NMR ($^{15}NCr(N\text{-}i\text{-}Pr_2)_3$, C_6D_6) δ 979. M.p. ca 110°C (subl). EIMS (high res.) calc. 366.281435 (M^+); found 366.28109, error range 0.00071. Anal. calcd for $C_{18}H_{42}N_4Cr$: C, 58.98; H, 11.55; N, 15.28; Found: C, 59.11; H, 11.13; N, 15.26.

(*ii*) *Reaction of* **4a** *with lutidinium iodide*. Into a 120 ml glass bomb equipped with a stopcock was loaded lutidinium iodide (108 mg, 2.5 equiv., 0.459 mmol), **4a** (72.2 mg, 1 equiv., 0.184 mmol), 7 ml of $CHCl_3$ and 7 ml of THF. The solution was placed in a 75°C oil bath and stirred for 18 h. A small amount of green insoluble material formed, and the ^{1}H NMR spectrum in $CDCl_3$ exhibited peaks corresponding only to the starting materials.

(*iii*) *NMR tube thermolysis of* $NCr(CH_2SiPhMe_2)(N\text{-}i\text{-}Pr_2)_2$ (**4b**) In a sealable NMR tube was loaded 40 mg of **4b** and 995 mg of C_6D_6. The sealed tube was heated to 60°C in an oil bath and was checked periodically over 7 h. All starting material had been consumed by the 7 h mark according to ^{1}H NMR analysis. The spectrum showed $PhSiMe_3$ (s, 0.18 ppm; m, 7.19 ppm; m, 7.44) which was also seen in the GC/MS of the reaction products ($M^+ = 150$). Also observed in the ^{1}H NMR was $HN\text{-}i\text{-}Pr_2$ (d, 0.93 ppm; sept, 2.76 ppm) and peaks attributable to $Me_2C{=}N\text{-}i\text{-}Pr$ (d, 1.14 ppm; s, 1.35 ppm; s, 1.80 ppm; sept, 3.43 ppm). No other peaks were observed in the NMR spectrum. A black insoluble material was formed during the thermolysis.

(*iv*) *Preparation of* $NCr(N\text{-}i\text{-}Pr_2)_2(OPh)$ (**4c**). In a 125 ml Erlenmeyer flask was loaded $NCr(N\text{-}i\text{-}Pr_2)_3$ (750 mg, 2.05 mmol, 1 equiv.), 40 ml of toluene and a stir bar. The solution was frozen in a cold well at liquid nitrogen temperature and then removed to a stir plate. Once the solution could be stirred as a cold slurry, a −35°C solution of HOPh (193 mg, 2.04 mmol, 1 equiv.) in 20 ml of toluene was added dropwise. The solution was allowed to warm and stir for 30 min. and the reaction mixture changed from a beet color to dark orange. The product was recrystallized from ether in 89% yield (653 mg, 1.82 mmol). ^{1}H NMR (300 MHz, $CDCl_3$): δ = 1.20 (br app s, 6H, Pr-*i*-CH_3), 1.25 (br app s, 6H, *i*-PrCH_3), 1.43 (br app s, 6H, *i*-PrCH_3), 1.84 (br app s, *i*-PrCH_3), 3.75 (br app s, 2H, *i*-PrCH), 5.04 (br app s, 2H, *i*-PrCH), 6.76 (t, J_{HH} = 6.6 Hz, 1H, p-Ph), 6.95 (d, J_{HH} = 8.1 Hz, 2H, m-Ph), 7.15 (t, J_{HH} = 7.8 Hz, 4H, o-Ph). $^{13}C\{^{1}H\}$ NMR (300 MHz, $CDCl_3$ −20°C): δ = 21.207 (*i*-PrCH_3), 21.502 (*i*-PrCH_3), 30.240 (*i*-PrCH_3), 30.546 (*i*-PrCH_3), 55.440 (*i*-PrCH), 58.417 (*i*-PrCH), 166.838 (ipso-OPh), 128.997 (o-OPh), 119.090 (m-OPh), 117.720 (p-OPh). M.p. 64–65°C. EIMS (low res.): *m/z* (%): 359 (23.76) [$M^{+\bullet}$]. Anal. calcd for $C_{18}H_{33}N_3OCr$: C, 60.14; H, 9.25; N, 11.69. Found: C, 60.40; H, 9.55; N, 11.50.

(*v*) *Preparation of* $NCr(N\text{-}i\text{-}Pr_2)_2(OC(CH_3)(CF_3)_2)$ (**4d**). In a 20 ml scintillation vial $NCr(N\text{-}i\text{-}Pr_2)_3$ (286 mg, 0.764 mmol, 1 equiv.), 10 ml of toluene and a stirbar were cooled to −35°C. To the cool, stirring solution was added a −35°C solution of $HOC(CH_3)(CF_3)_2$ (139 mg, 0.764 mmol, 1 equiv.) in 6 ml of toluene dropwise over a few min. The mixture was warmed to room temp. and stirred for 6 h. The volatiles were removed under vacuum and the orange product was recrystallized from pentane in 77% yield (262 mg, 0.586 mmol). ^{1}H NMR (300 MHz, $CDCl_3$): δ = 1.25 (m, 12H, *i*-PrCH_3), 1.45 (d, J_{HH} = 6.0 Hz, 6H, *i*-PrCH_3), 1.64 (s, 3H, *i*-PrCH_3), 1.78 (d, J_{HH} = 6.0 Hz, 6H, *i*-OPrCH_3), 3.71 (sept, J_{HH} = 6.0 Hz, 2H, *i*-PrCH), 4.94 (sept, J_{HH} = 6.0 Hz, 2H, *i*, PrCH). ^{19}F NMR (300 MHz, $CDCl_3$): δ = −78.51 ppm. $^{13}C\{^{1}H\}$ NMR (500 MHz, C_6D_6): δ = 20.2 (*i*-PrCH_3), 21.2 ($OC(CH_3)(CF_3)_2$), 29.79 (*i*-PrCH_3), 30.2 ($OC(CH_3)(CF_3)_2$), 55.7 (*i*-PrCH), 58.4 (*i*-PrCH), 79.9 ($OC(CH_3)(CF_3)_2$). M.p. 149–151°C. EIMS (low res.): *m/z* (%): 447(12.48) [$M^{+\bullet}$]. Anal. calcd for $C_{16}H_{31}N_3OF_6Cr$: C, 42.95; H, 6.98; N, 9.39. Found: C, 43.23; H, 7.15; N, 9.18.

(*vi*) *Spin saturation transfer experiments*. The magnetization transfer experiments were done by ^{1}H NMR using the method of Dahlquist, Longmuir and Du Vernet [24] in C_6D_6 at 294(1) K. In **4d**, mag-

netization transfer between the methine hydrogens of the amido substituents was examined. The technique involves a selective 180° pulse on one of the two methine peaks followed by a full spectrum 90° pulse. At zero delay time, the selectively-irradiated peak (P_1) appears inverted relative to the remainder of the spectrum. The delay time (t) between the selective and full spectrum pulses was varied. The peak heights of P_1 and the peak related to P_1 by rotation (P_2) vary with t if magnetization transfer occurs. The spectra are subtracted from the simple 90° pulse spectrum of the complex. At a delay time of zero P_1 displays twice the intensity in the difference spectrum, and all the other peaks (including P_2) are effectively eliminated in the subtraction. The sum of the intensities for P_1 and P_2 in the difference spectrum vary with the delay time as $A_0 e^{-(1/T1)t}$, where A_0 is the intensity of P_1 in the difference spectrum at $t = 0$ and T1 is the magnetization relaxation rate. A separate T1 determination gave the relaxation rates for P_1 and P_2 to be the same within the error of the experiment ($T1_{P1} = 1.667 \pm 0.01329$ s, $T1_{P2} = 1.664 \pm 0.01575$ s). The difference in the intensities of P_1 and P_2 in the difference spectra vary with t as $A_0 e^{-((1/T1)+k(1)+k(-1))t}$, where k(1) is the rate constant for the conversion of P_1 and P_2 and k(−1) is the rate constant for the conversion of P_2 to P_1. The sum and difference in the intensities for P_1 and P_2 are plotted and fit in Fig. 1. The fit was done to the equation $A_0 e^{-Xt}$. The difference in X for the sum and difference lines is the value k(1)+k(−1) and constitutes the rate constant for one full rotation. A_0 was refined and varies slightly in the sum and difference plots. The variation of A_0 is attributed to a small intensity value for P_2 in the $t = 0$ spectrum from incomplete quenching. The difference curve fit converged at $A_0 = 178$ (0.77) and $X = 13.99$ (0.096) with $R = 0.9997$. The sum curve fit converged at $A_0 = 187$ (0.59) and $X = 0.428$ (0.016) with $R = 0.983$. The fits indicate a value of 13.5 (0.1) s^{-1} for k(1)+k(−1) which correlates to $\Delta G^{\ddagger} = 16$ kcal/mol [25].

In **5a**, magnetization transfer between the methyl doublets was examined, but no transfer was observed. The lack of magnetization transfer is indicative of $k(1)+k(-1) \ll 1/T1$. The T1 values in s for the two doublets were found to be (2.365 ± 0.032883, 2.348 ± 0.02388) and (2.737 ± 0.2093, 2.783 ± 0.2198) by an inversion recovery experiment [37]. Therefore, placing the rate constant for the rotation at 0.3 s^{-1} is a conservative estimate, and the "real" activation energy could be much higher than 22 kcal/mol.

(*vii*) *Preparation of* NCr(N-*i*-Pr_2)(OC(CH_3)(CF_3)$_2$)$_2$ (**5a**). *Method A.* In a 20 ml scintillation vial was loaded NCr(N-*i*-Pr_2)$_3$ (0.571 g, 1.56 mmol, 1 equiv.), a stir bar and 5 ml of pentane. To the stirring solution was added HOC(CH_3)(CF_3)$_2$ (8 g, 440 mmol, 28 equiv.) dropwise. After a few min. of stirring the dark orange solution was transferred to a 120 ml glass bomb equipped with a stopcock. The solution was removed from the drybox and heated in an oil bath at 70°C with stirring. After heating $5\frac{1}{2}$ h the volatiles were removed *in vacuo* and the resulting orange solid was recrystallized from pentane to yield dark crystals of **5a** in 86% yield (0.704 g, 1.33 mmol).

Method B. In a 100 ml glass vessel equipped with a Teflon stopcock was loaded Cr(N)(I)(N-*i*-Pr_2)$_2$ (81 mg, 0.206 mmol, 1 equiv.), HOC(CH_3)(CF_3)$_2$ (3 g, 165 mmol, 800 equiv.) and a stir bar. The reaction mixture was heated at 74°C for 12 h to yield a colorless precipitate (likely [H_2N-*i*-Pr_2] [I]) and an orange solution. The volatiles were removed *in vacuo* and the resulting orange solid was extracted into a minimum of pentane and filtered. Cooling the solution gave the product as thin orange plates in 64% yield (57 mg, 0.132 mmol). ^{1}H NMR (300 MHz, $CDCl_3$): $\delta = 1.15$ (d, $J_{HH} = 6.5$ Hz, 6H, *i*-PrCH_3), 1.82 (s, $J_{HH} = 6.5$ Hz, 6H, *t*-BuCH_3), 4.16 (sept, $J_{HH} = 6.5$ Hz, 1H, *i*-PrCH), 5.51 (sept, $J_{HH} = 6.5$ Hz, 1H, *i*-PrCH). ^{13}C{^{1}H} NMR (500 MHz, C_6D_6): $\delta = 18.88$ (*i*-Pr*C*H_3), 19.35 (*i*-Pr*C*H_3), 28.89 (OC(*C*H_3)(CF_3)$_2$), 64.96 (*i*-Pr*C*H), 65.19 (*i*-Pr*C*H), 81.70 (O*C*(CH_3)(CF_3)$_2$), 124.28 (OC(CH_3)(*C*F_3)$_2$). M.p. 112–113°C. Anal. calcd for $C_{12}H_{20}N_2O_2F_{12}Cr$: C, 31.83; H, 3.82; N, 5.30. Found: C, 32.05; H, 3.89; N, 5.17.

(*viii*) *Preparation of* NCr(N-*i*-Pr_2)(S-*t*-Bu)$_2$ (**5b**). A 300 ml two neck flask equipped with a gas adapter was loaded with NCr(N-*i*-Pr_2)$_3$ (352 mg, 0.960 mmol) and a stir bar. The remaining neck was stoppered with a septum and then the flask was removed from the dry box. Dry *t*-butylmercaptan (160 ml, 1.42 mol) was transferred to the reaction flask via canula. The septum was replaced under counterflow of nitrogen with a water cooled condenser and the solution was refluxed for 22 h. The volatiles were removed *in vacuo*. The black solid was extracted with pentane and filtered through a sintered glass frit using celite as a filtering agent. The pentane solution yielded black needle crystals in 73% yield (232 mg, 0.696 mmol) on concentrating and cooling. ^{1}H NMR (300 MHz, $CDCl_3$): $\delta = 1.30$ (d, $J_{HH} = 6$ Hz, 6H, *i*-PrCH_3), 1.49 (d, $J_{HH} = 6$ Hz, 6H, *i*-PrCH_3), 1.70 (s, 18H, *t*-BuCH_3), 3.71 (sept, $J_{HH} = 6$ Hz, 1H, *i*-PrCH), 5.60 (sept, $J_{HH} = 6$ Hz, 1H, *i*-PrCH). ^{13}C{^{1}H} NMR (300 MHz, $CDCl_3$): $\delta = 18.76$ (*i*-PrCH_3), 28.72 (*i*-PrCH_3), 35.37 (*t*-BuCH_3), 50.62 (*t*-BuC), 58.74 (*i*-PrCH), 59.48 (*i*-PrCH). ^{13}C NMR (300 MHz, $CDCl_3$): $\delta = 18.76$ (q, *i*-PrCH_3), 28.72 (q, *i*-PrCH_3), 35.37 (q, *t*-BuCH_3), 50.62 (s, *t*-BuC), 58.74 (d, *i*-PrCH), 59.48 (d, *i*-PrCH). EIMS (low res.): *m/z* (%): 344(24)[$M^{+\bullet}$]. Anal. calcd for $CrN_2S_2C_{14}H_{32}$: C, 48.80; H, 9.36; N, 8.13. Found: C, 49.05; H, 9.82; N, 8.22.

(*ix*) *Preparation of* NCr[(μ-S-*t*-Bu)$_2$Cu(Et$_2$dtc)](N-*i*-Pr_2) (**5c**). To a slurry of Cu(Et$_2$dtc) (0.129 g, 0.652 mmol, 1 equiv.) in 10 ml of ether was added a solution of **5b** (0.225 g, 0.652 mmol, 1 equiv.) in 5 ml of ether. During the addition, a rapid color change from the blue of **5b** to dark brown occurred. The solution was homogeneous a few min. after the addition was complete. The solution was allowed to stir for 30 min. before the volatiles were removed

under vacuum. The dark brown product was recrystallized from ether in 86% yield (0.304 g). ^{1}H NMR (300 MHz, C_6D_6): δ = 0.691 (d, J_{HH} = 6 Hz, 6H, *i*-PrC*H*$_3$), 1.04 (t, J_{HH} = 7 Hz, 6H, EtC*H*$_3$), 1.59 (d, J_{HH} = 6 Hz, 6H, *i*-PrC*H*$_3$), 1.83 (s, 18H, *t*-BuC*H*$_3$), 3.17 (sept, J_{HH} = 6 Hz, 1H, *i*-PrC*H*), 3.70 (quar., J_{HH} = 7 Hz, 4H, EtC*H*$_2$) 3.77 (sept, J_{HH} = 6 Hz, 1H, *i*-PrC*H*). ^{13}C{^{1}H} NMR (300 MHz, C_6D_6): δ = 12.88 (*i*-PrC*H*$_3$), 19.56 (EtC*H*$_3$), 29.90 (*i*-PrC*H*$_3$), 34.63 (*t*-BuC*H*$_3$), 47.85 (EtC*H*$_2$), 54.08 (*t*-BuC), 57.24 (*i*-PrC*H*), 57.99 (*i*-PrC*H*). M.p. 99–102°C. Anal. calcd for $CrCuN_3S_4C_{19}H_{42}$: C, 41.02; H, 7.61; N, 7.55. Found: C, 40.81; H, 7.28; N, 7.53.

(*x*) *Preparation of* NCr(N-*i*-Pr$_2$)(OPh)$_2$ (**5d**). Into a one neck 150 ml round bottom flask was loaded a stir bar, 20 ml of toluene and NCr(N-*i*-Pr$_2$)$_3$ (604 mg, 1.65 mmol, 1 equiv.). Into this stirring solution was added phenol (326 mg, 2.1 equiv., 3.47 mmol) in 13 ml of toluene dropwise via pipette. During addition the solution changed from beet to dark orange in color. After thirty min. of reaction time, the volatiles were removed under vacuum. The resultant black solid was recrystallized to give a black powder in 81% yield (458 mg, 1.33 mmol). ^{1}H NMR (300 MHz, $CDCl_3$): δ = 1.15 (d, J_{HH} = 6.6 Hz, 6H, *i*-PrCH$_3$), 1.78 (d, J_{HH} = 6.6 Hz, 6H, *i*-PrCH$_3$), 4.07 (sept, J_{HH} = 6.6 Hz, 1H, *i*-PrCH), 5.19 (sept, J_{HH} = 6.6 Hz, 1H, *i*-PrCH), 6.84 (t, J_{HH} = 7.2 Hz, 2H, p-Ph), 7.04 (d, J_{HH} = 7.8 Hz, 4H, m-Ph), 7.13 (app. q, J_{HH} = 7.2 Hz, 4H, o-Ph). ^{13}C{^{1}H} NMR (300 MHz, $CDCl_3$): δ = 20.53 (*i*-PrCH$_3$), 29.28 (*i*-PrCH$_3$), 63.77 (*i*-PrCH), 64.29 (*i*-PrCH), 116.97 (p-Ph), 122.33 (m-Ph), 129.29 (o-Ph), 167.33 (ipso-Ph). ^{13}C NMR (300 MHz, $CDCl_3$): δ = 20.53 (q, J_{CH} = 128 Hz, *i*-PrCH$_3$), 29.28 (q, J_{CH} = 128 Hz, *i*-PrCH$_3$), 63.77 (d, J_{CH} = 128 Hz, *i*-PrCH), 64.29 (d, J_{CH} = 128 Hz, *i*-PrCH), 116.97 (d, J_{CH} = 167.3 Hz, p-Ph), 122.33 (d, J_{CH} = 158.9 Hz, m-Ph), 129.29 (d, J_{CH} = 159.7 Hz, o-Ph), 167.33 (s, ipso-Ph). EIMS (low res.): *m/z* (%): 352(27.67) [M$^+$]. Anal. calcd for $C_{18}H_{24}N_2O_2Cr$: C, 61.35; H, 6.86; N, 7.95. Found: C, 61.11; H, 6.91; N, 7.64.

(*xi*) *Preparation of* NCr(N-*i*-Pr$_2$)(CH$_2$SiMe$_3$)$_2$ (**5e**). NCr(N-*i*-Pr$_2$)(OPh)$_2$ (0.786 g, 2.23 mmol, 1 equiv.), a stir bar and 55 ml of hexane were loaded into a 250 ml round bottom flask. The flask was moved to a liquid nitrogen temperature cold well, and the solution was frozen. Once the solution was frozen the flask was removed to a stir plate to thaw. When the slurry could be stirred a near frozen solution of LiCH$_2$SiMe$_3$ (0.420 g, 4.46 mmol, 2 equiv.) in 55 ml of hexane was added dropwise over a few min. As the reaction mixture warmed the NCr(N-*i*-Pr$_2$)(OPh)$_2$ slowly went into solution and a colorless solid precipitated from the brown solution. The solution was allowed to stir for 5–10 min. after all the NCr(N-*i*-Pr$_2$)(OPh)$_2$ had dissolved (about 25 min. reaction time). The mixture was refrozen in the cold well and allowed to warm again until fluid. The cold solution was filtered into a chilled filter flask through a sintered glass frit using celite as a filtering agent. The filtered product was recrystallized from hexamethyldisiloxane giving light orange needles in 57% yield (432 mg, 1.27 mmol). The lipophilic purified material is thermally sensitive, but can be kept in solution at −35°C for long periods of time without noticeable decomposition. The material may also be kept in solution at room temperature overnight without substantial decomposition (<10%). M.p. 56–57°C. ^{1}H NMR (300 MHz, C_6D_6, 25°C): δ = −0.318 (d, J_{HH} = 10 Hz, 2H, CH$_2$), 0.347 (s, 18H, SiMe$_3$ CH$_3$), 0.870 (d, 6H, J_{HH} = 6.5 Hz, *i*-PrCH$_3$), 1.26 (d, 6H, J_{HH} = 6.5 Hz, *i*-PrCH$_3$), 2.12 (d, J_{HH} = 10 Hz, 2H, CH$_2$), 2.98 (sept, J_{HH} = 6.5 Hz, 1H, *i*-PrCH), 5.96 (sept, J_{HH} = 6.5 Hz, 1H, *i*-PrCH). ^{13}C{^{1}H} NMR (300 MHz, C_6D_6): d = 2.07 (s, SiCH$_3$), 21.1 (s, *i*-PrCH), 29.48 (s, *i*-PrCH), 56.47 (s, *i*-PrCH$_3$), 58.60 (s, *i*-PrCH$_3$), 69.16 (s, CH$_2$SiCH$_3$). ^{13}C NMR (300 MHz, C_6D_6, 25°C): δ = 2.07 (d, J_{CH} = 118 Hz, SiCH$_3$), 21.1 (s, J_{CH} = 133 Hz, *i*-PrCH), 29.48 (s, J_{CH} = 133 Hz, *i*-PrCH), 56.47 (s, J_{CH} = 117 Hz, *i*-PrCH$_3$), 58.60 (s, J_{CH} = 117 Hz, *i*-PrCH$_3$), 69.16 (s, J_{CH} = 116 Hz, CH$_2$SiCH$_3$). MS low res. EI: *m/z* (%): 340(0.42) [M$^+$]. Anal. calcd for $CrN_2Si_2C_{14}H_{36}$: c, 49.37; H, 10.65; N, 8.22. Found: C, 49.22; H, 11.11; N, 8.57.

(*xii*) *NMR tube thermolysis of* NCr(N-*i*-Pr$_2$)(CH$_2$SiMe$_3$)$_2$ (**5e**). In a sealable NMR tube was loaded ~12 mg of **5e** and 700 mg of C_6D_6. The tube was partially evacuated then sealed. The solution was warmed to 60°C in an oil bath. The thermolysis was complete after 5 h as indicated by the ^{1}H NMR spectrum of the solution. The spectrum exhibited decomposition products which included SiMe$_4$ (s, 0.018 ppm), HN-*i*-Pr$_2$ (d, 0.935 ppm; sept, 2.76 ppm) and Me$_2$C=N-*i*-Pr (d, 1.14 ppm; s, 1.35 ppm; s, 1.80 ppm; sept, 3.34 ppm) in a molar ratio of 3.29:1.85:2.18.

(*xiii*) *Preparation of* NCr(C(=N-*t*-Bu)CH$_2$SiMe$_3$)(CH$_2$SiMe$_3$)(N-*i*-Pr$_2$) (**5f**). A solution of **5e** (32.3 mg, 1 equiv., 0.0948 mmol) and 3 ml of ether in a 20 ml scintillation vial was frozen in the box cold well. The solution was allowed to warm until stirring before a cold solution of *tert*-butylisonitrile (10 μl, 1.0 equiv., 0.0948 mmol) in 2 ml of ether was added. The solution rapidly changed color from orange to yellow-green. After 15 min. of reaction time the volatiles were removed *in vacuo* and the resulting solid was recrystallized from hexamethyldisiloxane. **5f** was isolated in 70% yield (28.2 mg). ^{1}H NMR (300 MHz, C_6D_6): δ = 0.214 (s, 9H, SiCH$_3$), 0.711 (s, 9H, SiCH$_3$), 0.683 (d, 6H, J_{HH} = 6 Hz, *i*-PrCH$_3$), 0.713 (d, 6H, J_{HH} = 6 Hz, *i*-PrCH$_3$), 1.26 (d, J_{HH} = 11.7 Hz, H, CH$_2$), 1.38 (d, J_{HH} = 11.7 Hz, H, CH$_2$), 1.77 (d, J_{HH} = 6 Hz, H, CH$_2$), 1.81 (d, J_{HH} = 6 Hz, H, CH$_2$), 2.72 (d, J_{HH} = 11.7 Hz, H. CH$_2$), 2.86 (sept, J_{HH} = 6 Hz, 1H, *i*-PrCH), 3.31 (sept, J_{HH} = 6 Hz, 1H, *i*-PrCH). ^{13}C{^{1}H} NMR (300 MHz, C_6D_6): d = 2.07 (s, SiCH$_3$), 21.1 (s, *i*-PrCH), 29.48 (s, *i*-PrCH), 56.47 (s, *i*-PrCH$_3$), 58.60 (s, *i*-PrCH$_3$), 69.16 (s, CH$_2$SiCH$_3$). ^{13}C NMR (300 MHz, C_6D_6, 25°C): δ = (q, J_{CH} = 118 Hz, SiCH$_3$), (s, J_{CH} = 133 Hz, *i*-PrCH), (s, J_{CH} = 133 Hz, *i*-PrCH), (s, J_{CH} = 117 Hz, *i*-PrCH$_3$), (s, J_{CH} = 117 Hz, *i*-PrCH$_3$), (s, J_{CH} = 116 Hz, CH$_2$S-

iCH_3). MS low res. EI: *m/z* (%): 423(1.25) [M^+]. MS high res. EI: found: 423.25573 (0.00083) [M^+], calc.: 423.255715. M.p. 83–84°C. Anal. calcd for $CrN_3C_{19}H_{45}Si_2$: C, 53.85; H, 10.70; N, 9.92. Found: C, 54.64; H, 10.93; N, 9.96.

(*xiv*) *Reaction of* **3** *with excess water.* To a mixture of deoxygenated water (10 ml, ~1000 equiv.) and 12 ml of THF was added **3** (0.187 g, 0.510 mmol, 1 equiv.) as a solution in 20 ml of THF dropwise. The solution gradually took on an orange color as the addition was carried out. Once the addition was complete, the volatiles were removed *in vacuo*. The product [H_2N-*i*-Pr_2]$_2$[Cr_2O_7] was recrystallized from acetonitrile in 73% (0.153 g) yield. ^{1}H NMR (300 MHz, D_2O): δ = 1.28 (d, J_{HH} = 6 Hz, 24H, CH_3), 3.50 (sept, J_{HH} = 6 Hz, 4H, *i*-PrCH). Anal. calcd for $Cr_2N_2C_{12}H_{32}O_7$: C, 34.29; H, 7.67; N, 6.66. Found: C, 33.95; H, 7.51; N, 6.53.

(*xv*) *Extended Hückel calculations.* The calculations were done using the X-ray structural coordinates for NCr(N-*i*-Pr_2)$_3$ (**3**), monosubstituted NCr(N-*i*-Pr_2)$_2$(CH_2Si(Ph)Me_2) (**4b**), and disubstituted NCr(S-*t*-Bu)$_2$(N-*i*-Pr_2) (**5b**) as input for YAeHMOP ver 2 [38]. In each case the entire molecule was used in the calculation. The LUMO in each molecule was an orbital with metal-ligand π^* character with respect to all of the π donors. The calculated energies for the LUMOs of **3**, **4b** and **5b** were −9.567, −9.816, and −9.384 eV, respectively.

Crystallographic studies

X-ray diffraction data were collected using a Siemens Diffractometer. The detector includes a Mo Kα sensitive phosphor behind a Beryllium window which is 6 cm from the sample. The phosphor, which is activated by the crystal's X-ray diffraction, sends a signal via a fiber optic taper to a Charge Coupled Device (CCD). The CCD is cooled to ca. −55°C to reduce thermal noise. The CCD is read and the data collection controlled by a computer with a Pentium processor. The software for data collection, Siemens Molecular Analysis Research Tool (SMART v4.050), was developed by Siemens Industrial Automation, Inc. The data collection was done using a Siemens Platform three circle goniometer (χ set to 54.78°) and a water cooled Mo X-ray tube (λ = 0.71073 Å) operating at 50 kV/40 mA. A single crystal graphite monochromator was used. Prior to sample exposure the X-rays were columnated to 0.8 or 0.5 mm. The instrument is equipped with a Molecular Structure Corp. low temperature controller with a liquid nitrogen cooled inner stream and a heated dry N_2 outer stream. The temperatures were determined by a thermistor located within the low temperature device near the exit port and are uncorrected.

An initial unit cell determination was done using ω scans. Three sets of fifteen frames were collected with a −0.3° scan width. The starting positions for the first, second and third runs were (2θ = 337.02°, ω = 337.02°, φ = 0°), (2θ = 337.02°, ω = 337.02°, φ = 90°), and (2θ = 22.98°, ω = 22.98°, φ = 0°), respectively. From this frame data, a set of intense reflections were chosen and an initial cell was found through repeated least squares and Bravais lattice analysis.

The data were collected using ω scans in four separate runs using a −0.3° scan width. The first through fourth starting positions and number of frames collected were (2θ = −25°, ω = −26°, φ = 0°, no. frames = 606), (2θ = −25°, ω = −21°, φ = 88°, no. frames = 435), (2θ = −25°, ω = −23°, φ = 180°, no. frames = 230), and (2θ = −25°, ω = −23°, φ = 180°, no. frames = 50), respectively. The data collected constitute approximately a hemisphere plus an additional 40% of the Ewald sphere. The fourth run duplicates the first 50 frames of the initial run, and the data are corrected for crystal degradation by analyzing the intensity differences in reflections measured in these redundant frames. The data collections were done using 10 s correlated frames (2 × 5 s frames analyzed for anomalous intensity) with a 7 s total read out time. The total data collection time is approximately 6.5 h. Data storage, reduction and structure solution were done on a Silicon Graphics Indy equipped with a MIPS R5000 processor running at 180 MHz and 3 Gigabytes of a total disk space. Using the initial cell, the frame data were integrated to hkl/intensity data using the Siemens program package SAINT v4.050. The final unit cell was determined by SAINT using all the observed data.

The structures were solved and refined using SHELXTL Version 5.03, a program developed by G. M. Sheldrick and Siemens Industrial Automation, Inc. For absorption of a semi-empirical ψ-scan absorption correction was used, which includes all of the data as the basis set.

NCr(S-*t*-Bu)$_2$(N-*i*-Pr_2) (**5b**). Crystals grown from a concentrated ether solution at −35°C were quickly moved from a scintillation vial to a microscope slide containing Paratone N (an Exxon product). Under the microscope a black plate was selected and mounted on a glass fiber using wax. A total of 5293 reflections were collected ($-10 \leqslant h \leqslant 8$, $-13 \leqslant k \leqslant 13$, $-18 \leqslant l \leqslant 18$) in the θ range of 2.06 to 20.00° of which 1861 were unique (R_{int} = 0.0605). The structure was solved by direct methods in conjunction with standard difference Fourier techniques. All non-hydrogen atoms were refined anisotropically. Hydrogen atoms were placed in calculated (d_{C-H} = 0.96 Å) positions. The largest peak and hole in the difference map were 0.254 and −0.315 e/Å^3, respectively. The least squares refinement converged normally.

NCr[(μ-S-*t*-Bu)$_2$Cu(Et_2dtc)](N-*i*-Pr_2) (**5c**). Crystals grown from a concentrated ether solution at −35°C were quickly moved from a scintillation vial to a microscope slide containing Paratone N. Under the microscope a black plate was selected and mounted on a glass fiber. A total of 7473 reflections were collected

($-12 \leqslant h \leqslant 14$, $-11 \leqslant k \leqslant 9$, $-23 \leqslant l \leqslant 19$) in the θ range of 1.69 to 20.00° of which 2590 were unique ($R_{int} = 0.0899$). The structure was solved by direct methods in conjunction with standard difference Fourier techniques. All non-hydrogen atoms were refined anisotropically. Hydrogen atoms were placed in calculated ($d_{C-H} = 0.96$ Å) positions. The largest peak and hole in the difference map were 2.813 and -0.810 e/Å^3, respectively. The residual electron density resides near the S, Cu and Cr atoms. The least squares refinement converged normally.

NCr(C(=N-*t*-Bu)CH_2SiMe_3)(CH_2SiMe_3)(N-*i*-Pr_2) (**5f**). Crystals grown from a concentrated hexamethyldisiloxane solution at −35°C were quickly moved from a scintillation vial to a microscope slide containing Paratone N. Under the microscope a yellow plate was selected and mounted on a glass fiber. A total of 3916 reflections were collected ($-7 \leqslant h \leqslant 8$, $-11 \leqslant k \leqslant 11$, $-20 \leqslant l \leqslant 20$) in the θ range of 2.12 to 20.00 giving 2999 independent reflections ($R_{int} = 0.0449$). The structure was solved by direct methods in conjunction with standard difference Fourier techniques. The structure suffers from pseudo-symmetry problems. The two molecules in the asymmetric unit sit on either side of a pseudo-inversion center which tries to relate the alkyl and iminoacyl ligands on the two molecules. The pseudo-inversion center creates a pseudo-mirror plane in the molecule in P(−1) which runs through the $N_{iminoacyl}$—$N_{nitrido}$—N_{amido} atoms. Attempts to refine the structure in P(−1) as a disorder problem were less successful than refinement of models in P(1) with no inversion center between molecules. The Cr(1)—C(11) distance was restrained to be within a 3 σ range of 2.3 Å with σ of 0.05 Å. Only the Cr and Si atoms were refined anisotropically. Hydrogen atoms were placed in calculated ($d_{C-H} = 0.96$ Å) positions. The largest peak and hole in the difference map were 0.573 and -1.034 e/Å^3, respectively.

CONCLUDING REMARKS

Chromium(VI) nitrido compounds are available through nitric oxide cleavage using Cr(N-*i*-Pr_2)$_3$ and V(mesityl)$_3$(THF). The nitrido functionality displays remarkable kinetic stability towards a variety of acidic reagents. Among the products available by protolytic removal of one amido substituent were found to be NCr(I)(N-*i*-Pr_2)$_2$ (**4a**), NCr(OPh)(N-*i*-Pr_2)$_2$ (**4c**) and NCr($OC(CF_3)_2Me$)(N-*i*-Pr_2)$_2$ (**4d**). The monoalkyl complex NCr(N-*i*-Pr_2)$_2$($CH_2Si(Ph)Me_2$) (**4b**) was synthesized from the reaction of **4a** with Mg($CH_2SiPhMe_2$)$_2$. The products available by protolytic removal of two amido substituents were NCr($OC(CF_3)_2Me$)$_2$(N-*i*-Pr_2) (**5a**), NCr(S-*t*-Bu)$_2$(N-*i*-Pr_2) (**5b**) and NCr(OPh)$_2$(N-*i*-Pr_2) (**5d**). Thiolate **5b** coordinates Cu(Et_2dtc) to produce the bridging thiolate complex NCr(N-*i*-Pr_2)[(μ-S-*t*-Bu)$_2$Cu(Et_2dtc)] (**5c**). The reaction of **5d** with 2 equiv. of $LiCH_2SiMe_3$ produces NCr(N-*i*-Pr_2)(CH_2SiMe_3)$_2$ (**5e**). The chromium(VI) alkyl complexes **5e** and **4b** were found to decompose thermally with products indicative of β-hydrogen abstraction from the amido ligands. The 14e alkyl **5e** reacts with *tert*-butyl isonitrile to give an iminoacyl alkyl complex. The nitrido nitrogen is stable to some harsh acidic conditions, i.e. refluxing HS-*t*-Bu, but does undergo hydrolysis upon treatment with excess water.

Our results for the protolytic replacement of the amido substituents in nonpolar media on the complex NCr(N-*i*-Pr_2)$_3$ (**3**) are suggestive of two important kinetic factors which affect the viability of an amido protonation. The first is sterics. In a nonpolar environment, a mechanism involving the prior coordination of the incoming protic reagent with concomitant or subsequent proton transfer should be favored. Prior coordination of the protic reagent (e.g. an oxygen or sulfur lone pair) reduces the amount of charge separation in the intermediate or transition state vis-á-vis simple proton transfer followed by attack of the conjugate base. For such a mechanism, steric constraints at the metal center and at the incoming protic reagent could be exceedingly important but difficult to assess. The Lewis acidity of the metal center may play a role in the ease of coordination of an incoming Brønsted acid. Extended Hückel calculations incorporating the X-ray crystal structure coordinates of NCr(N-*i*-Pr_2)$_3$ (**3**), NCr(N-*i*-Pr_2)$_2$($CH_2Si(Ph)Me_2$) (**4b**), and NCr(S-*t*-Bu)$_2$(N-*i*-Pr_2) (**5b**) suggest that the LUMO energies decrease in the order **5b** > **3** > **4b**. This trend is consistent with the observation that **5b** is inert to excess HS-*t*-Bu, whereas **3** is attacked readily by the same reagent. Thus, we may propose that the greater the Lewis acidity of the chromium nitrido amido in question, the more readily will alcoholysis or thiolysis proceed.

In more polar media, the reactions may proceed by mechanisms involving greater charge separation in the transition states or intermediates. Accordingly, reaction of an almost 1:1 solution of THF/water with **3** provided [H_2N-*i*-Pr_2]$_2$[Cr_2O_7] in high yield.

Chromium(VI) nitrido complexes are now available for comparison with their molybdenum and tungsten analogs. Further investigation into the chemistry of these new complexes will serve to substantiate trends in nitrido chemistry of group 6. In addition, pseudo-tetrahedral high oxidation state chromium compounds comprise a new area of study in the already active area of chromium(VI) chemistry [36].

Acknowledgements—For funding C.C.C. thanks the National Science Foundation (CAREER Award CHE-9501992), DuPont (Young Professor Award), the Packard Foundation (Packard Foundation Fellowship), Union Carbide (Innovation Recognition Award), and 3M (Innovation Fund Award). C.C.C. is a Sloan Foundation Fellow (1997-2000). A.L.O. is grateful to Texaco for a fellowship and Marc Johnson for invaluable discussion.

REFERENCES

1. (a) Laplaza, C. E. and Cummins, C. C., *Science*, 1995, **268,** 861; (b) Laplaza, C. E., Johnson, M. J. A., Peters, J. C., Odom, A. L., Kim, E., Cummins, C. C., George, G. N. and Pickering, I. J., *J. Am. Chem. Soc.*, 1996, **118,** 8623–8638.
2. (a) Bradley, D. C. and Newing, C. W., *J. Chem. Soc., Chem. Commun.*, 1970, 219; (b) Bradley, D. C., Hursthouse, M. B. and Newing, C. W., *J. Chem. Soc. D*, 1971, 411; (c) Bradley, D. C., Hursthouse, M. B., Newing, C. W. and Welch, A. H., *J. Chem. Soc., Chem. Commun.*, 1972, 567.
3. (a) Seidel, W. and Kreisel, G., *Z. Anorg. Allg. Chem.*, 1977, **435,** 146; (b) Seidel, W. and Kreisel, G., *Z. Chem.*, 1974, **14,** 25.
4. Odom, A. L., Cummins, C. C. and Protasiewicz, J. D., *J. Am. Chem. Soc.*, 1995, **117,** 6613–6614.
5. (a) Chisholm, M. H., Hoffmann, K. M. and Huffman, J. C., *Inorg. Chem.*, 1983, **22,** 2903–2906; (b) Chan, D. M.-T., Chisholm, M. H., Folting, K., Huffman, J. C. and Marchant, N. S., *Inorg. Chem.*, 1986, **25,** 4170.
6. (a) Dehnicke, K. and Strahle, J., *Angew. Chem. Int. Ed. Engl.*, 1992, **31**; (b) Dehnicke, K. and Strahle, J., *Angew. Chem. Int. Ed. Engl.*, 1992, **31,** 955–978.
7. Herrmann, W. A., Bogdanovic, S., Poli, R. and Prierweier, T., *J. Am. Chem. Soc.*, 1994, **116,** 4989–4990.
8. Nugent, W. A. and Mayer, J. M., *Metal–Ligand Multiple Bonds*. John Wiley and Sons, 1988.
9. A high yielding synthesis of the stable complex $NMo(S\text{-}t\text{-}Bu)_3$ was recently discovered. Unpublished results, A. L. Odom and C. C. Cummins.
10. (a) Gebeyehu, Z., Weller, F., Neumuller, B. and Dehnicke, K., *Z. Anorg. Allg. Chem.*, 1991, **593,** 99; (b) Johnson, M. J. A., Lee, P. M., Odom, A. L., Davis, W. M. and Cummins, C. C., *Angew. Chem. Int. Ed. Engl.*, 1997, **36,** 87.
11. (a) Belmonte, P. A. and Own, Z.-Y., *J. Am. Chem. Soc.*, 1984, **106,** 7493–7496; (b) Caulton, K. G., Chisholm, M. H., Doherty, S. and Foltrig, K., *Organometallics*, 1995, **14,** 2585–2588; (c) Holl, M. M. B., Wolczanski, P. T. and Duyne, G. D. V., *J. Am. Chem. Soc.*, 1990, **112,** 7989–7994; (d) Shapley, P. A. and Wepsiec, J. P., *Organometallics*, 1986, **5,** 1515–1517; (e) Shapley, P. A., Kim, H. S. and Wilson, S. R., *Organometallics*, 1988, **7,** 928–933.
12. The synthesis and solid state structure of $NCr(O\text{-}t\text{-}Bu)_3$ was recently reported. Chiu, H.-T., *et al. Chem. Commun.*, 1996, 139.
13. (a) Bradley, D. C., Hursthouse, M. B. and Newing, C. W., *J. Chem. Soc., Chem. Commun.*, 1971, 411; (b) Alyea, E. C., Basi, J. S., Bradley, D. C. and Chisholm, M. H., *J. Chem. Soc. D*, 1968, 495.
14. Vivanco, M., Ruiz, J., Floriani, C., Chiesi-Villa, A. and Rizzoli, C., *Organomet.*, 1993, **12,** 1802.
15. The $Cr—N_{nitrosyl}$ distance in $ONCr(I)(N[R]Ar_F)$, where $R = C(CH_3)(CD_3)_2$ and $Ar_F = 2,5\text{-}C_6H_3FMe$, was found to be 1.70(3) Å. Unpublished results, A. L. Odom and C. C. Cummins. The $Cr—N_{nitrosyl}$ distance in $ONCr[N(SiMe_3)_2]_3$ is 1.738(20) Å. D. C. Bradley, M. B. Hursthouse, C. W. Newing and A. H. Welch. *J. Chem. Soc., Chem. Commun.*, 1972, 567.
16. Odom, A. L. and Cummins, C. C., *Organometallics*, 1996, **15,** 898.
17. (a) Chetcuti, M. J., Chisholm, M. H., Folting, K., Haitko, D. A., Huffman, J. C. and Janos, J., *J. Am. Chem. Soc.*, 1983, **105,** 1163; (b) Cowley, A. H., Pagel, D. J. and Walker, M. L., *J. Am. Chem. Soc.*, 1978, **100,** 7065.
18. Cotton, F. A., *Chemical Applications of Group Theory*. John Wiley and Sons, 1990.
19. (a) Danopoulos, A. A., Leung, W.-H., Wilkinson, G., Hussain-Bates, B. and Hursthouse, M. B., *Polyhedron*, 1990, **9,** 2625; (b) Meijboom, N., Schraverien, C. J. and Orpen, A. G., *Organomet.*, 1990, **9,** 774; (c) Noh, S.-K., Heintz, R. A., Haggerty, B. S., Rheingold, A. L. and Theopold, K. H., *J. Am. Chem. Soc.*, 1992, **114,** 1892; (d) Sullivan, A. C., Wilkinson, G., Hussain-Bates, B. and Hursthouse, M. B., *J. Chem. Soc., Dalton Trans.*, 1988, 53.
20. Song, J. I., Berno, P. and Gambarotta, S., *J. Am. Chem. Soc.*, 1994, **116,** 6927.
21. (a) Maury, F., *J. de Physique IV*, 1995, **5,** 449; (b) Lee, S. C., Ho, W. Y., Lai, F. D., *Mater. Chem. and Phys.*, 1996, **43,** 266–273; (c) Mills, T., *J. Less-Common Met.*, 1970, **22,** 373 and references therein.
22. Phenol and $HOC(CF_3)_2Me$ have $pK_a's$ of ~ 10 and ~ 9.6, respectively; (a) Patai, S., *The Chemistry of the Hydroxyl Group*, ed. S. Patai. Wiley, 1971; (b) Willis, C. J., *Coord. Chem. Rev.*, 1988, **88,** 133.
23. Schrock, R. R., *Polyhedron*, 1995, **14,** 3177–3195.
24. Dahlquist, F. W., Longmuir, K. J. and Vernet, R. B. D., *J. of Mag. Res.*, 1975, **17,** 406–410.
25. Kegley, S. E. and Pinhas, A. R., *Problems and Solutions in Organometallic Chemistry*. University Science Books, 1986.
26. Chisholm, M. H., Folting, K., Huffman, J. C. and Rothwell, I. P., *Organometallics*, 1982, **1,** 251–259.
27. Guggenberger, L. J. and Schrock, R. R., *J. Am. Chem. Soc.*, 1975, **97,** 6578–6579.
28. (a) Deutsch, E., Root, M. J. and Nosco, D. L., *Advances in Inorganic and Bioinorganic Mechanisms*, ed. A. G. Sykes, Academic Press, 1982; (b) Dilworth, J. R., *Sulfur, its Significance for Chemistry, for the Geo-, Bio-, and Cosmosphere and Technology*, ed. A. Muller and B. Krebs. Elsevier Science Publishers, 1984; (c) Stiefel, E. I., Miller, K. F., Bruce, A. E., Corbin, J. L., Berg, J. M. and Hodgson, K. O., *J. Am. Chem. Soc.*, 1980, **102,** 3624; (d) Millar, M., Lee, J. F., Koch, S. A. and Fikar, R., *Inorg. Chem.*, 1982, **21,** 4105–4106; (e) Boyd, I. W., Dance, I. G., Landers, A. E. and Wedd, A. G., *Inorg. Chem.*, 1979, **18,** 1875; (f) Boorman, P. M., Chivers, T., Mahadev, K. N. and O'Dell, B. D., *Inorg. Chim. Acta*, 1976, **19,** L35.
29. Molybdenum(VI) and tungsten(VI) nitrides display a "shish kebob" polymer structure in the solid state when sterically allowed. For example see the structures of $NM(O\text{-}t\text{-}Bu)_3$, where M—Mo and W. (a) Chan, D. M.-T., Chisholm, M. H., Folting, K., Huffman, J. C. and Marchant,

N. S., *Inorg. Chem.*, 1986, **25,** 4170–4174; (b) Chisholm, M. H., Hoffman, D. M. and Huffman, J. C. *Inorg. Chem.*, 1983, **22,** 2903–2906. For examples of molybdenum(VI) and tungsten(VI) complexes where the polymeric structure is sterically prohibited see the solid state structures of $NMo(NPh_2)_3$ and $NMo(NRAr)_3$. (a) Gebeyehu, Z., Weller, F., Neumuller, B. and Dehnicke, K., *Z. Anorg. Allg. Chem.*, 1991, **593,** 99; (b) Laplaza, C. E., Odom, A. L., Davis, W. M., Cummins, C. C. and Protasiewicz, J. D., *J. Am. Chem. Soc.*, 1995, **117,** 4999. Chromium(VI) complexes do not exhibit a tendency to form such polymers regardless of steric constraints. See ref. 4, ref. 12 and ref. 16.

30. (a) Hesse, R., *Ark. Kemi.*, 1963, **20,** 481. Bonamico, M., Dessy, G., Mugnoli, A., Vaciago, A. and Zambonelli, L., *Acta Cryst.*, 1965, **19,** 886; (b) Fredga, A., *Recl. Trav. Chim. Pays-Bas.*, 1950, **69,** 416. 949.
31. Heterobinuclear complexes with bridging thiolates similar to this one have appeared in the literature. (a) Boorman, P. M., Kraatz, H.-B., Parvez, M. and Ziegler, T., *J. Chem. Soc., Dalton Trans.*, 1993, 433; (b) Huang, Y., Drake, R. H. and Stephan, D. W., *Inorg. Chem.*, 1993, **32,** 3022; (c) Otsuka, S., Okura, N. and Payne, N. C., *J. Chem. Soc., J. Chem. Commun.*, 1982, 531. (d) Wark, T. A. and Stephan, D. W., *Inorg. Chem.*, 1987, **26,** 363.
32. (a) Musso, H., *Angew. Chem. Int. Ed. Eng.*, 1963, **2,** 723–735; (b) Scott, A. I., *Quarterly Rev.*, 1966, 1; (c) Taylor, W. I. and Battersby, A. R. In *Oxidative Coupling of Phenols*, ed. W. I. Taylor and A. R. Battersby. New York, 1967.
33. (a) Pawson, D. and Griffith, W. P., *J. Chem. Soc., Dalton Trans.*, 1975, 417–423; (b) Schmidt, I., Kynast, U., Hanich, J. and Dehnicke, K., *Z. Naturforsch.*, 1984, **39B,** 1248–1251; (c) Dehnicke, K., Prinz, H., Kafitz, W. and Kujanek, R., *Liebigs Ann. Chem.*, 1981, 20–27; (d) Chatt, J. and Dilworth, J. R., *J. Indian Chem. Soc.*, 1977, **54,** 13–18.
34. (a) Hursthouse, M. B. and Motevalli, M., *J. Chem. Soc., Dalton Trans.*, 1979, 1362–1366; (b) Bishop, M. W., Chatt, J. and Dilworth, J. R., *J. Chem. Soc., Dalton Trans.*, 1979, 1–5.
35. Buchler, J. W., Dreher, C. and Lay, K.-L., *Chem. Ber.*, 1984, **117,** 2261–2274.
36. The extensive reaction chemistry of chromium complexes within biological systems is an active area of research. For examples see (a) Anderson, R. A., *Sci. Total Environ.*, 1981, **17,** 13–29; (b) Jennette, K. W., *Environmental Health Perspectives*, 1981, **40,** 233–252; (c) Moghaddas, S., Gelerinter, E. and Bose, R. N., *J. of Inorg. Biochem.*, 1995, **57,** 135–146; (d) Molyneux, M. J., Davis, M. J., *Carcinogenesis*, 1995, **16,** 875–882; (e) T. Norseth, *Environmental Health Perspectives*, 1981, **40,** 121–130. For examples of some recent advances in the inorganic chemistry of chromium(VI) see (a) Danopoulos, A. A., Wilkenson, G., Sweet, T. K. N. and Hursthouse, M. B., *J. Chem. Soc., Dalton Trans.*, 1995, 2111–2123; (b) Cook, G. K. and Mayer, J. M., *J. Am. Chem. Soc.*, 1995, **116,** 1855. Chromium(VI) complexes also are commonly employed in organic synthesis. See for examples (a) Cainelli, G. and Cardillo, G., *Chromium Oxidation in Organic Chemistry*. Springer-Verlag, Berlin, 1984; (b) Leung, W. H., Chow, E. K. F., Wu, M. C., Kum, P. W. Y. and Yeung, L. L., *Tet. Letters*, 1995, **36,** 107–108.
37. Vold, R. L., Wangh, J. S., Klein, M. P. and Phelps, D. E., *J. Chem. Phys.*, 1968, **48,** 3831.
38. Landrum, G. A., YAeHMOP: Yet another extended Hückell molecular orbital package. YAeHMOP is freely available on the WWW at URL: http://overlap.chem.cornell.edu:8080/yaehmop.html.

Pergamon

PII: S0277-5387(97)00379-3

Polyhedron Vol. 17, No. 5–6, pp. 689–704, 1998
© 1998 Elsevier Science Ltd
All rights reserved. Printed in Great Britain
0277-5387/98 $19.00+0.00

Heterometallic alkoxides containing alkoxometallate(IV) ligands: synthesis and structural comparison

Ram C. Mehrotra and Anirudh Singh

Department of Chemistry, University of Rajasthan, Jaipur 302004, India

(Received 12 May 1997; accepted 2 September 1997)

Abstract—A brief account of heterometallic alkoxides containing alkoxometallate(IV) (e.g., $\{M_2(OR)_9\}^-$, $\{M(OR)_5\}^-$, and $\{M(OR)_6\}^-$) ligands have been presented, with an emphasis on the correlation of their structural features on the basis of steric and allied factors. © 1998 Elsevier Science Ltd. All rights reserved

Keywords: heterometallic alkoxides; nonaalkoxodimetallars; pentaalkoxometallates; hexaalkoxometallates.

The synthesis and characterization of a large number of stable heterometallic alkoxides [1–10] having two or more different metals in a molecular species has added a new dimension to our existing knowledge of heterometallic coordination chemistry. In view of the difficulties [11] in obtaining crystallographically suitable crystals for structural elucidation, doubts were expressed on the entity of such derivatives which appear to derive their stability mainly from a suitable juxtaposition of alkoxide (μ_2- or μ_3-) bridges between dissimilar metals. In 1989 Bradley described our work as "extremely important advances in the synthesis of heterometallic alkoxides, i.e. compounds containing two, three or four different metals in a cluster molecule" [12]. This work has now been followed with a crystallographic characterization of a number of these derivatives.

The synthesis of volatile and soluble (in organic solvents) sodium nona-alkoxodizirconates $NaZr_2(OR)_9$, by Bartley and Wardlaw [13] in 1958, added an entirely new dimension to the chemistry of heterometallic alkoxides, which were initially conceived as alkoxo salts by Meerwein and Bersin [14]. In fact, the first nona-alkoxodistannate derivative, $NaSn_2(OEt)_9$, was also described by Bradley *et al.* [15] in 1957 as an intermediate in their efforts to synthesize tin tetraalkoxides by the reactions of $SnCl_4$ with alkali metal alkoxides.

Mehrotra and Agrawal (1967) drew pointed attention to the uniqueness of $\{Zr_2(OPr^i)_9\}^-$ derivatives based on the non-conducting behaviour of $KZr_2(OPr^i)_9$ [16]; a simple structure was suggested [1] in 1978 involving two $\{Zr(OPr^i)_6\}$ octahedra sharing a face which appears to be confirmed by the X-ray structures [6–9,17,18] determined since 1984. The versatility of $\{M_2(OR)_9\}^-$ groups in responding to the desire of different metal atoms to achieve their preferred coordination state and geometry by the formation of alkoxo bridges (μ_2 or μ_3) with the heterometal atoms, has been demonstrated in a number of publications [19–27] from our laboratories. Veith *et al.* [28] recently (1996) re-emphasized "the versatility of $M_2(OR)_9$ groups in responding to the need of different metal atoms in order to build heterometallic alkoxide clusters".

Bradley [29] has also collaborated recently in a metrical comparison of an interesting series of derivatives $[MTi(OPr^i)_5]n$ (M=Li($n = 2$), Na($n = \infty$), K($n = \infty$)). Although all three congeners are dimeric [30] in benzene, only the lithium derivative exhibits in the solid state a dimeric structure with the standard M_4O_{16} arrangement involving titanium and lithium atoms in distorted trigonal–bipyramidal and tetrahedral geometries, respectively. However, sodium and potassium analogues depict polymeric structures with linear and non-linear alternating chains [29]. This has been ascribed to larger Na and K atoms leading to tight ion pairs being formed between the more electropositive alkali metal cations and the $\{Ti(OPr^i)_5\}^-$ anions.

In this article an attempt has been made for correlation amongst different types of heterometallic alkoxides of tetravalent metals on lines similar to that suggested for homometallic alkoxides by Bradley [31].

Consistent with the predominating influence of steric factors [32,33] in homometallic alkoxides, the bulk of the attached alkoxo groups in the chelating alkoxometallate ligands plays an important role in determining the geometry of the overall heterometallic system. The oligomerization in homometallic alkoxides arises from the tendency of the metal atom to attain the desired coordination state in the most economical manner [31] by alkoxo (μ_2-/μ_3-) bridge formation. Interestingly, the desired sterically permissible coordination state of the central heterometal atom can be attained by the requisite number of alkoxo group ligation from the potentially multidentate chelating alkoxometallate (e.g. $\{M_2(OR)_9\}^-$, $\{M(OR)_4\}^-$, $\{M(OR)_5\}^-$, or $\{M(OR)_6\}^{2-}$) ligands. For example, in $Ln\{(\mu_2\text{-}OPr^i)_2Al(OPr^i)_2\}_3$ [1,34] (Ln = a lanthanide) and $Ni\{(\mu_2\text{-}OMe)_3Al(OMe)\}_2$ [35] the bi- and tridentate, ligating modes of $\{Al(OPr^i)_4\}^-$ and $\{Al(OMe)_4\}^-$ respectively provide an octahedral environment of alkoxo ligands around both the lanthanide and nickel atoms. The role of the steric factor is reflected in the tertiary butoxo analogue, $Ni\{(\mu_2\text{-}OBu^t)_2Al(OBu^t)_2\}_2$ [36], in which $\{Al(OBu^t)_4\}^-$ units behave as bidentate ligands and provide a tetrahedral environment around nickel.

With the help of the above generalizations, we have been predicting mainly on the basis of NMR and other physicochemical data, the plausible structures of heterometallic alkoxides. Most of these (e.g. $KZr_2(OPr^i)_9(DME)$ [37], $(Pr^iOH)_2K\{Al(OPr^i)_4\}$ [38], $Er\{Al(OPr^i)_4\}_3$ [39], $Pr\{Zr_2(OPr^i)_9\}Cl_2$ [40], $[Cd\{Zr_2(OPr^i)_9\}(\mu\text{-}Cl)]_2$ [26] have been confirmed later by X-ray crystallographic determinations.

Compared to the tetrahedral $\{Al(OPr^i)_4\}^-$ and octahedral $\{M(OPr^i)_6\}^-$ (M=Nb or Ta) entities with bi- (and in some cases tri-) dentate ligands [3,6–10,18], a tetravalent metal like zirconium is capable of achieving hexacoordinate configuration in $\{Zr_2(OR)_9\}^-$ ligands with two face sharing octahedra and even simple models of these clearly depicted their capability of chelating another metal in a bidentate as well as tri- and tetradentate manner [6–10,18]; this has been confirmed later by X-ray crystallographic studies. In addition, $\{M(OR)_5\}^-$ and $\{M(OR)_6\}^{2-}$ units are also beginning to demonstrate their potentiality as chelating ligands.

In view of the X-ray crystallographic structures of a large number of title compounds being available during the last 12–13 years from ours as well as other laboratories, the main purpose of this article is to attempt for the first time a correlation of as many of these as possible in a logical fashion.

METHODS OF PREPARATION

The versatility of alkoxometallate(IV) groups such as $\{M_2(OR)_9\}^-$, $\{M(OR)_5\}^-$, and $\{M(OR)_6\}^{2-}$ (where M = a tetravalent metal, R = an alkyl or fluorinated alkyl) as chelating ligands, has resulted in a variety of novel heterometallic alkoxides. The synthetic route for these include the following:

(a) Reactions involving union of two different metal alkoxides [13,16,41–48];
(b) Interactions of alkali and alkaline earth metals with an appropriate metal isopropoxide isopropylate, $M_2(OPr^i)_8(Pr^iOH)_2$ (M=Zr, Hf, or Sn) [16,19,41,49];
(c) Reactions of metal (U [17], Sn [15]) chlorides or their complexes (e.g., $Nb_2Cl_4(OMe)_4(HOMe)_2$ [50]) with alkali metal alkoxides;
(d) Reactions of metal halides (chloride [19–27,40,51–53], iodide [28,54]/fluoride [53]) or their complexes [55,56] with alkali metal alkoxometallate(IV) ligands;
(e) Reactions of metal amides (e.g. $LiNMe_2$ [49b], $NaN(SiMe_3)_2$ [57], $Ba\{N(SiMe_3)_2\}_2(THF)_2$ [49a], $Sn\{N(SiMe_3)_2\}_2$ [58], $Pb\{N(SiMe_3)_2\}_2$ [58]) with tetravalent metal alkoxide alcoholates (e.g. $Zr_2(OPr^i)_8(Pr^iOH)_2$ [49,49b,58] and $M_2(OBu^t)_8(HOBu^t)$ (M = Th [57], U [48]));
(f) Reactions of $(NH_4)_2Ce(NO_3)_6$ with alkali metal t-butoxides [59];
(g) Reactions of potassium hydride with $Zr_2(OPr^i)_8(Pr^iOH)_2$ [37];
(h) Reaction of a metal chloride (e.g. $NbCl_5$ [50]) with magnesium in methanol.

The letter designations correspond to the letters used in Table 1 to identify synthetic routes to title derivatives.

STRUCTURAL INTERRELATIONSHIPS AND RESULTING DIVERSITIES

Solid state structural studies have been performed on a variety of system containing one or more $\{M_2(OR)_9\}^-$, $\{M(OR)_5\}^-$, and $\{M(OR)_6\}^{2-}$ units. Although a complete analysis of each structure is not the aim of this article, a brief summary of basic trends and general types of structures will be presented.

Out of the many operative factors [1,60] such as: (i) the empirical formula of the compound; (ii) the bulk of the alkoxo group; (iii) the size and formal oxidation state of the metal atom(s) in the basic skeleton; (iv) the presence of lone pair(s) of electrons on the metal atom(s); and (v) the d^n electron configuration for the transition metals (leading to pronounced ligand field effects), the steric factor and/or the presence of lone pair(s) appear to play a predominant role.

Bradley's proposal [31] for the lowest oligomerization state of homometallic alkoxides has been extended by Caulton *et al.* [44] in a modified form for heterometallic alkoxides, $M_aM'_b(OR)_m$. These types of derivatives with a low m/(a+b) ratio generally prefer closed polyhedral structures, in order

Table 1. Some heterometallic alkoxides containing $\{M_2(OR)_9\}^-$, $\{M(OR)_5\}^-$ and $\{M(OR)_6\}^{2-}$ units (M = a tetravalent metal, R=Me, Et, Pr^n, Pr^i, Bu^t)

Compound	Method of preparation	Characterization
Nonaalkoxodimetallate derivatives		
$Li\{Zr_2(OR)_9\}$ [13] (R=Et, Pr^n, Pr^i Bu^n)	a	Anal; MW
$Li\{Zr_2(OPr^i)_9\}(Pr^iOH)$ [49b]	e	^1H, ^{13}C NMR; X-ray
$M'\{M_2(OPr^i)_9\}$ [1,16] (M′=Li, Na, K, Rb, Cs; M=Zr, Hf, Sn)	a	Anal; ^1H, ^{13}C NMR; IR; MW
$[Na\{Ce_2(OBu^t)_9\}]$ [59]	f	Anal; IR; ^1H, ^{13}C NMR; X-ray
$[(DME)K\{Zr_2(OPr^i)_9\}]$ [37]	g (followed by interaction with DME)	^1H, ^{13}C NMR; X-ray
$[K\{Zr_2(OBu^t)_9\}]$ [43]	a	Anal; ^1H, ^{13}C NMR
$[Na\{Th_2(OBu^t)_9\}]$ [57]	e	Anal; IR; ^1H NMR; X-ray
$[K\{U_2(OBu^t)_9\}]$ [17]	c	^1H NMR; X-ray
$Be\{Zr_2(OPr^i)_9\}Cl$ [51]	d	Anal; IR; 1H, ^{13}C NMR; MW
$[Mg\{Ti_2(OEt)_8Cl\}(\mu\text{-}Cl)]_2$ [79]	$MgCl_2+4Ti(OEt)_4$	Anal; IR; X-ray
$[Mg\{Zr_2(OPr^i)_9\}(\mu\text{-}Cl)]_2$ [19]	d	Anal; IR; ^1H, ^{13}C NMR; MW
$[Ba\{Zr_1(OPr^i)_9\}_2]$ [49a]	b,e	Anal; IR; ^1H, ^{13}C NMR; X-ray
$[Ba\{Zr_2(OPr^i)_9\}(\mu\text{-}OPr^i)]_2$ [49a]	b,e	Anal; IR; ^1H, ^{13}C NMR; X-ray
$[M'\{Zr_2(OPr^i)_9\}Cl]_2$ (M′=Zn [25], Cd [25,26])	d	Anal; IR; ^1H, ^{13}C NMR; MW; X-ray [26]
$M'\{M_2(OPr^i)_9\}_2$ (M′=Mg, Ca, Sr, Ba [19], M=Zr, Hf; M′=Zn, Cd [25], M=Zr)	b	Anal; IR; ^1H NMR; MW
	d	Anal; IR; ^1H, ^{13}C NMR; MW
$[M'\{Sn_2(OPr^i)_9\}Cl]_2$ [27] (M′=Mg, Zn, Cd)	d	Anal; IR; ^1H, ^{13}C, ^{119}Sn NMR; MW
$[M'\{Sn_2(OPr^i)_9\}(OPr^i)]$ [27] (M′=Ba, Cd)	c(M′=Cd), b(M′=Ba)	Anal; IR, ^1H, ^{13}C, ^{119}Sn NMR; MW
$[M'\{Sn_2(OPr^i)_9\}_2]$ [27] (M′=Mg, Ba, Zn, Cd)	b(M′=Ba), d	Anal; IR; ^1H, ^{13}C, ^{119}Sn NMR; MW
$Ln\{Zr_2(OPr^i)_9\}Cl_2$ [40] (Ln=Y, La, Pr, Nd, Sm, Ho, Lu)	d	Anal; IR; ^1H, ^{13}C NMR; MW; UV-vis (Ln=Pr, Nd, Ho); Magnetic studies (Ln=Pr, Nd, Ho)
$Ln\{Zr_2(OPr^i)_9\}_2Cl$ [40] (Ln=Y, La, Pr, Nd, Sm, Ho, Lu)	d	Anal; IR; ^1H, ^{13}C NMR; MW; UV-vis (Ln=Pr, Nd, Ho); Magnetic studies (Ln=Pr, Nd, Ho)
$Ln\{Zr_2(OPr^i)_9\}_3$ [40,63] (Ln=La, Pr, Nd, Sm, Ho, Lu)	d	Anal; IR; ^1H, ^{13}C NMR; MW; UV-vis and Magnetic studies (Ln=Pr, Nd, No)
$Ln\{Sn_2(OPr^i)_9\}_xCl_{3-x}$ [40,70] (Ln=Y, La, Pr, Nd, Lu; x = 2,3)	d	Anal; IR; ^1H, ^{13}C, ^{119}Sn NMR; Mw; UV-vis (Ln=Pr, Nd)
$[Na(MeOH)_6][Nb_2(OMe)_9]$ [50]	c	X-ray
$[Mg(MeOH)_6]_2[Nb_2(OMe)_9]Cl_3$ [50]	h	X-ray
$[Mg(MeOH)_6][Nb_2(OMe)_9]I\cdot 2MeOH$ [50]	h	X-ray
$M'\{Zr_2(OPr^i)_9\}Cl$ (M′=Mn [20], Fe [21], Co [22], Ni [23], Cu [24,53], Sn [52])	d	Anal; IR; MW; UV-vis; Magnetic studies; X-ray
$M'\{Zr_2(OPr^i)_9\}_2$ (M′=Mn [20], Fe [21], Co [22], Ni [23], Cu [24])	d	Anal; IR; MW; UV vis; Magnetic studies
$Fe\{Zr_2(OPr^i)_9\}_3$	d	Anal; IR; MW; Magnetic studies
$[Cd\{M_2(OPr^i)_9\}I]$ (M=Ti [54], Zr [61], Hf [54], Sn [28])	d	Anal; IR; ^1H, ^{13}C, ^{113}Cd, ^{119}Sn NMR; MW; X-ray
$[Sn\{Zr_2(OPr^i)_9\}(\mu\text{-}I)]_2$ [28]	d	Anal; IR; ^1H, ^{13}C, ^{119}Sn NMR; MW; X-ray
$[Pb\{Zr_2(OPr^i)_9\}(\mu\text{-}OPr^i)]_2$ [44,58]	a	Anal; IR; ^1H, ^{13}C, ^{207}Pb NMR; X-ray

Table 1.—*Continued.*

Compound	Method of preparation	Characterization
Pentaalkoxometallate derivatives		
$[M'\{Ti(OPr^i)_5\}]_n$ (M′=Li(n = 2) [16,30], Na [29], K [29] (n = ∞)	a	Anal; IR; ^1H, ^{13}C, ^7Li, ^{23}Na, ^{39}K NMR; MS; X-ray (Li [30], Na [29], K [29])
$[M'\{M(OBu^t)_5\}]_n$ M′=Li [16], Na [16], K [16,43] M=Ti [16], Zr [16,43], Sn [42]	a	Anal; ^1H, ^{13}C NMR; MW; IR; X-ray [42,43]
Hexaalkoxometallate derivatives		
$[Na_2\{Zr\{OCH(CF_3)_2\}_6(C_6H_6\}_2]$ [47]	a,c	Anal; IR; ^1H, ^{19}F NMR; X-ray
$[Na_2\{Zr[OCH(CF_3)_2]_6(C_6H_6)]$ [47]	a,c	Anal; IR; ^1H, ^{19}F NMR; X-ray
$[Tl_2\{\{Zr[OCH(CF_3)_2]_6]$ [46,47]	a	Anal; ^1H, ^{19}F, ^{205}Tl NMR; X-ray
$[\{(COD)Rh\}_2\{Ti(OPr^n)_6\}]$ [56]	d	Anal; ^1H NMR; X-ray
$[\{(COD)Rh\}_2\{Sn(OEt)_6\}]$ [55]	d	Anal; ^1H, ^{13}C, ^{119}Sn NMR; X-ray
$Zn\{Sn(OEt)_6\}$	d	Anal; ^1H, ^{13}C, ^{119}Sn NMR
$[Tl_2\{Sn(OEt)_6\}]_x$ [45]	a	Anal; ^1H, ^{119}Sn NMR; X-ray
$Sn\{Zr(OPr^i)_6\}$ [58]	e	Anal; ^1H, ^{13}C, ^{119}Sn NMR
$M'\{Zr(OBu^t)_6\}$ [58] (M′=Sn, Pb)	a,e	Anal; ^1H, ^{13}C, $^{119}Sn/^{207}Pb$ NMR
Heterotrimetallic alkoxides		
$[\{Cd(OPr^i)_3\}Ba\{M_2(OPr^i)_9\}]_2$ (M=Ti [54], Zr [61], Hf [54])	d	Anal; ^1H, ^{13}C, ^{113}Cd NMR; MW; X-ray
$[\{Zr_2(OPr^i)_9\}Ln\{Al(OPr^i)_4\}_2]$ [40] (Ln=Y, La, Pr, Nd, Lu)	d	Anal; IR; ^1H, ^{13}C, ^{27}Al NMR; MW
$[\{Zr_2(OPr^i)_9\}M'\{Al(OPr^i)_4\}]$ [71,72] (M′=Mn, Fe, Co, Ni, Cu)	d	Anal; IR; UV-vis; MW; Magnetic studies

to endow suitably high coordination states to all metals.

Nonaalkoxodimetallate derivatives

Out of a number of alkoxometallate(IV) units mentioned above, the ligands of the type $\{M_2(OR)_9\}^-$ have so far been most extensively employed for the synthesis of derivatives which are generally volatile and soluble in organic solvents from which X-ray suitable crystals can be sometimes obtained.

The structure of an apparently free nonaalkoxodimetallate anion [50], $\{M_2(OR)_9\}$, shown in Fig. 1, can be envisaged as a face shared bi-octahedron:

The above structure in a simple anionic form is depicted in a few niobium(IV) solvent separated ion pair derivatives [50]: $[Na(MeOH)_6][Nb_2(OMe)_9]$, $[Mg(MeOH)_6]_2[Nb_2(OMe)_9]Cl_3$, and $[Mg(MeOH)_6][Nb_2(OMe)_9]I.2\,MeOH$.

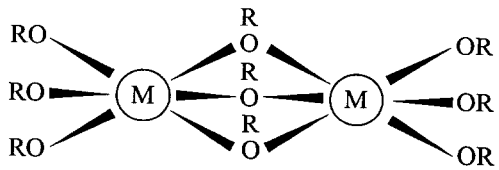

Fig. 1. Schematic structural representation of nonaalkoxodimetallate anion (M = a tetravalent metal).

This behaviour of the above methoxo complexes might arise from the unique property of solubility of methoxides of niobium in contrast to the insolubility of methoxides of other metals like Ti, Zr, Hf, Th, and Sn. Being a stronger donor, methyl alcohol saturates coordinatively the other metals (Na and Mg), and thus reduces their tendency to form methoxo bridges with $Nb_2(OMe)_9$ moiety. In almost all the other cases investigated so far, the confacial bi-octahedral unit $\{M_2(OR)_9\}^-$ forms alkoxo bridges with central metal atom(s), binding them in tetra-, tri-, or bi-dentate fashion.

(a) Tetra-dentate mode of coordination

A critical survey of a large number of such derivatives indicates the following idealized core structure (Fig. 2) in which all metals attain a six-coordination state.

The effect of factors such as size of M, size and valency of M′, bulk of alkoxo group, nature and presence of X···X (as a bidentate neutral ligand or zero/one/two monovalent unidentate ligand(s)).

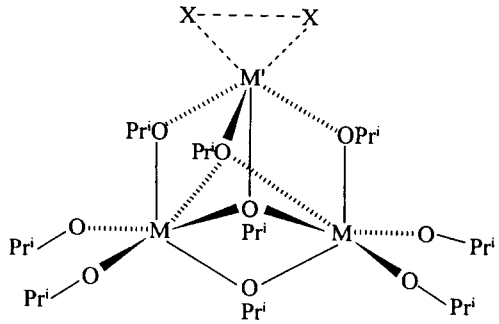

Fig. 2. Schematic structural representation of X-ray determined heterotrinuclear metal alkoxides in which all metal atoms attain coordination number six (e.g. (i) M=Zr(IV), M′=K, R=Pr^i, X···X=MeOC$_2$H$_4$OMe(**1**); (ii) M=Zr(IV), M′=Pr(III), R=Pr^i, X=Cl(**2**)).

The X-ray structural investigations on a number of other heterotrinuclear metal alkoxides such as [NaCe$_2$(OBu^t)$_9$] (**3**) [59], [NaTh$_2$(OBu^t)$_9$] (**4**) [59], [KU$_2$(OBu^t)$_9$] (**5**) [17], [CuCl{Zr$_2$(OPr^i)$_9$}] (**6**) [59], and [ICd{M$_2$(OPr^i)$_9$}] (M = Ti (**7**) [54], Zr (**8**) [61], Hf (**9**) [54], and Sn (**10**) [28]) revealed the presence of the generic structure shown in Fig. 3, wherein heterometal atoms or species are again bonded in tetradentate (η^4) fashion.

M=Ce (**3**) [59], M′=Na, R=Bu^t; M=Th (**4**) [57], M′=Na, R=Bu^t;

M=U (**5**) [17], M′=K, R=Bu^t; M=Zr, M′=CuCl (**6**) [53], R=Pr^i;

M=Ti (**7**) [54], M′=CdI, R=Pr^i; M=Zr (**8**) [61], M′=CdI, R=Pr^i

M=Hf (**9**) [54], M′=CdI, R=Pr^i; M=Sn (**10**) [28], M′=CdI, R=Pr^i

The structures of (**3**), (**4**), and (**5**) (Fig. 3) show that with bulkier OBu^t groups, the central metal (M′) Na or K is not ligated further and remains tetra-coordinate.

Another remarkable class of crystallographically characterized alkoxides include the dimeric [Ba{Zr$_2$(OPr^i)$_9$}(μ-OPr^i)]$_2$ (**11**) [49] and [Cd{Zr$_2$(OPr^i)$_9$}(μ-Cl)]$_2$ (**12**) (Fig. 4) [26]. In both these cases the heteroatom barium or cadmium is tetradentally bonded with a {Zr$_2$(OPr^i)$_9$}$^-$ unit, and the centrosymmetric dimers consist of two triangular BaZr$_2$(μ_3-OPr^i)$_2$(μ_2-OPr^i)$_3$(OPr^i)$_4^+$ or CdZr$_2$(μ_3-OPr^i)$_2$(μ_2-OPr^i)$_3$(OPr^i)$_4^+$ units linked by the barium or cadmium atoms via two isopropoxo and chloro bridges, respectively. all metal atoms are six coordinate and adopt distorted octahedral geometry.

By contrast, derivatives (**6**), (**7**), (**8**), (**9**) and (**10**) are monomeric with five-coordinate geometry around the copper atom in (**6**) and the cadmium atom in (**7**), (**8**), (**9**) and (**10**). The dimeric structure shown in Fig. 4 for the analogous chloro derivative is inhibited due to steric congestion in the cases of (**6**)–(**10**), arising from the smaller size (72 pm) of copper(II) (**6**) and the larger size (220 pm) of the iodo ligand [(**7**)–(**10**)].

An interesting derivative Ba{Zr$_2$(OPr^i)$_9$}$_2$ [49a] with eight coordinated barium has also been crystallographically characterized. The structure consists of a "bow tie" or spiro Zr$_2$BaZr$_2$ unit, wherein barium is coordinated tetradentally by two face-shared bioctahedral {Zr$_2$(OPr^i)$_9$}$^-$ units to yield almost a staggered conformation of eight-coordinate polyhedron around barium.

There are several interesting features in the solid state structures of nonaalkoxodimetallate derivatives which might be emphasized.

A general trend has been observed in heterometallic alkoxides containing alkoxometallate(IV) units such as {M$_2$(OPr^i)$_9$}$^-$ (M=Ce, Ti, Zr, Hf, Th, or U),

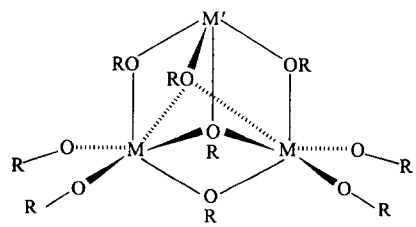

M = Ce (**3**),[59] M′ = Na, R = Bu^t; M = Th (**4**),[57] M′ = Na, R = Bu^t;

M = U (**5**),[17] M′ = K, R = Bu^t; M = Zr, M′ = CuCl (**6**),[53] R = Pr^i;

M = Ti (**7**),[54] M′ = CdI, R = Pr^i; M = Zr (**8**),[61] M′ = CdI, R = Pr^i

M = Hf (**9**),[54] M′ = CdI, R = Pr^i; M = Sn (**10**),[28] M′ = CdI, R = Pr^i

Fig. 3. Schematic representation of X-ray crystallographically determined structures of some monomeric heterobimetallic alkoxides.

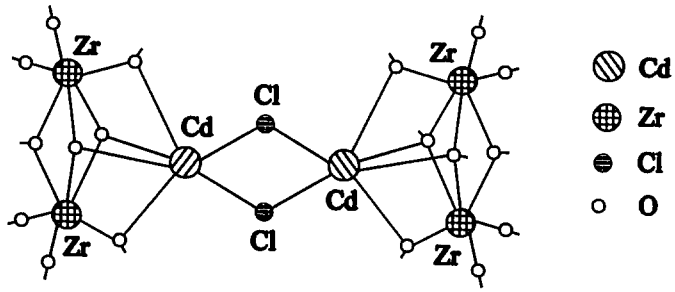

Fig. 4. X-ray crystal structure of $[Cd\{Zr_2(OPr^i)_9\}(\mu\text{-}Cl)]_2$ [26], depicted without the isopropyl group.

$\{M(OR)_5\}^-$ (M=Ti (R=Pr^i), Zr(R=Bu^t), and $\{M(OR)_6\}^{2-}$ (M=Ti (R=Pr^n), Zr(R=$CH(CF_3)_2$) that the $p\pi$–$d\pi$ interactions tend to make M—O_t distances shorter and M—O_t—C angles larger (approaching linearity) than those at the bridging sites (see Table 2). By contrast, a recent publication dealing with $Cd\{Sn_2(OPr^i)_9\}I$ revealed that Sn—O_t distances and Sn—O_t—C bond angles do not follow the above trend; this might arise from differences in main group and transition metal derivatives. A plausible suggestion could be that a short M—O_t bond results from a high degree of ionic character in early transition metal derivatives and an enhanced covalent nature of the Sn—O_t bond, but this difference in behaviour requires further intensive investigations.

Further, as expected from electronic considerations, M—μ_3—O are longer than M—μ_2—O which in turn are longer than M—O_t (terminal) distances. In the case of $\{M_2(OR)_9\}^-$ derivatives, both the above features are illustrated by a few examples in Table 2.

However, the more generally observed feature of increasing bond length with a higher bridging order appears to be reversed in a few cases (e.g. (**3**) [59], (**4**) [57], (**5**) [17], Table 2). These exceptions appear to be corroborative of the overshadowing tendency of such derivatives for attaining compactness of the structures in the process of which alkali metal atoms are apparently tucked in tighter to the "basket" formed by the four alkoxo oxygen atoms of $\{M_2(OR)_9\}^-$ unit.

(*b*) *Tri- and bi-dentate mode of coordination*

The possibility for $\{Zr_2(OPr^i)_9\}^-$ ligand to behave in a tridentate(η^3) manner suggested earlier for derivatives $[Co\{Zr_2(OPr^i)_9\}_2]$ [22] and $[Cu\{Zr_2(OPr^i)_9\}^2]$ [24] on the basis of electronic and other physicochemical data has now been X-ray crystallographically confirmed in cases of $LiZr_2(OPr^i)_9$ (Pr^iOH) (**11**) [49b] (Fig. 5) and $[Sn\{Zr_2(OPr^i)_9\}(\mu\text{-}I)]_2$ (**12**) [28] (Fig. 6). The small lithium ion (78 pm) interacts with a $\{Zr_2(OPr^i)_9\}^-$ unit via only three isopropoxo groups, rather than four, utilized by its heavier congeners such as Na^+ (98 pm) and K^+ (133 pm). Lithium appears to be too small to span the distance between isopropoxo groups on two different zirconium(IV) centres; the fourth coordination site on lithium is consequently occupied by an isopropanol molecule, which is hydrogen bonded to oxygen of a terminal isopropoxo group.

The derivative $[Sn\{Zr_2(OPr^i)_9\}(\mu\text{-}I)]_2$ (**12**) [28] (Fig. 6) consists of $\{Zr_2(OPr^i)_9\}^-$ unit interacting with Sn(II) in a tridentate (η^3) fashion as depicted for (**11**).

The structures of (**11**) and (**12**) clearly depict the influence of the nature (i.e. size and/or the presence of a lone pair of electrons) of the heterometal in determining the structural forms adopted by a heterometallic system. Tin(II) with its stereochemically active lone pair of electrons appears to inhibit the $\{Zr_2(OPr^i)_9\}^-$ ligand to bind it in a tetradentate fashion.

A remarkable result in this area is the structural characterization of $[Pb\{Zr_2(OPr^i)_9\}(\mu\text{-}OPr^i)]_2$ (**13**) [44,58] (Fig. 7), which shows a serpentine (not *closo*) structure with six-coordinate zirconium and four-coordinate lead.

Although the size of Pb(II) (132 pm) is larger than tin(II) (93 pm) the $\{Zr_2(OPr^i)_9\}^-$ unit binds the former in a bidentate (η^2) manner. This unusual ligating behaviour which was first suggested in derivatives of the types $Ln\{Zr_2(OPr^i)_9\}_3$ [40,62,63] (Ln = a lanthanide metal) and $Fe\{Zr_2(OPr^i)_9\}_3$ [64] has now been actually confirmed by X-ray crystallographic studies of (**13**). The bidentate coordination of $\{Zr_2(OPr^i)_9\}^-$ ligand is possibly due to the presence of a lone pair of electrons coupled with weaker Lewis acid character of lead(II) in this system.

The above description shows a delicate balance amongst the nature and size of the metal atom, the steric bulk of alkoxo ligand, and stoichiometry of the resulting stable heterobimetallic alkoxides. The current investigations in our laboratories reveal even more fascinating possibilities in these directions.

Pentaalkoxometallate derivatives

The role of steric effect in determining stoichiometry and structure of a heterometallic alkoxide is further well illustrated by the comparative stability of $M'M_2(OR)_9$ and $M'M(OR)_5$. For example, with isopropoxo(R) ligands all the tetravalent metals (M)

Table 2. Comparison of average metal–oxygen bond length (pm) and metal–oxygen–carbon bond angles (°) in some structurally characterized heterobimetallic alkoxides

Compound	M—O terminal	M—Oμ_2	M—Oμ_3	M—O—C terminal	Geometry	Ref.
$[Na\{Th_2(OBu^t)_9\}]$	Th—O 216	Th—O 237 Na—O 261	Th—O 249 Na—O 240	167.6	Th: distorted octahedron Na: distorted-bipyramid with one missing equatorial ligand	57
$[K\{U_2(OBu^t)_9\}]$	U—O 213	U—O 226 Na—O 294	U—O 244 Na—O 275	170.5	U: distorted octahedron K: distorted trigonal bipyramid with one missing equatorial ligand	17
$[ClCu\{Zr_2(OPr^i)_9\}]$	Zr—O 193	Zr—O 215 Cu—O 200	Zr—O 224 Cr—O 220	173.6	Zr: distorted octahedron Cu: distorted trigonal bipyramid	53
$[ICd\{Ti_2(OPr^i)_9\}]$	Ti—O 178	Ti—O 199 Cd—O 234	Ti—O 216 Cd—O 228	165.2	Ti: distorted octahedron Cd: distorted trigonal bipyramid	54
$[ICd\{Sn_2(OPr^i)_9\}]$	Sn—O 197	Sn—O 210 Cd—O 230	Sn—O 220 Cd—O 237	126.9	Sn: distorted octahedron Cd: distorted trigonal bipyramid	28
$[Cd\{Zr_2(OPr^i)_9\}(\mu\text{-}Cl)]_2$ (Fig. 4)	Zr—O 193	Zr—O 212 Cd—O 236	Zr—O 227 Cd—O 240	165.8	Zr: distorted octahedron Cd: distorted octahedron, tending to approach a bicapped tetrahedral arrangement	26
$[Sn\{Zr_2(OPr^i)_9\}(\mu\text{-}I)]_2$ (Fig. 6)	Zr—O 195	Zr—O 216 Sn—O 220	Zr—O 233 Sn—O 239		Zr: distorted octahedron Sn: distorted trigonal-bipyramid or distorted octahedron in which one of the axial sites is occupied by a pair of non-bonding electrons	28
$[Pb\{Zr_2(OPr^i)_9\}(\mu\text{-}OPr^i)]_2$ (Fig. 7)	Zr—O 193	Zr—O 221 Pb—O 232	Zr—O 225 Pb—O 272	164.8	Zr: distorted octahedron Pb: pseudo trigonal-bipyramid with one vacant equatorial position	44, 58
$[Li\{Ti(OPr^i)_5\}]_2$ (Fig. 8)	Ti—O 181	Ti—O 189 Li—O 193	Ti—O 199 Li—O 198	170.2 (axial), 140.3 (equatorial)	Ti: distorted trigonal-bipyramid Li: distorted tetrahedra	30
$[Na\{Ti(OPr^i)_5\}]_\infty$	Ti—O 181	Ti—O 190 Na—O 230			Ti: distorted trigonal-bipyramid Na: highly distorted tetrahedra	30
$[K\{Ti(OPr^i)_5\}]_\infty$ (Fig. 9)	Ti—O 181	Ti—O 188 K—O 282	Ti—O 198 K—O 278		Ti: distorted trigonal-bipyramid K: extremely distorted trigonal bipyramid	29
$[K\{Zr(OBu^t)_5\}]_2$ (Fig. 10)	Zr—O 195	Zr—O 204 K—O 277	Zr—O 204 K—O 292	169.6	Zr: trigonal bipyramid K: distorted trigonal-bipyramid	43
$[Na_2Zr\{OCH(CF_3)_2\}_6(C_6H_6)_2]$ (Fig. 12)	Zr—O 200	Zr—O 209 Na—O 241		179.7	Zr: octahedron Na: bent two coordinate environment of sodium is supplemented by bonding to four fluorines (one from each CF_3 group) and each sodium is η^6-bonded with benzene molecule	47
$[Tl_2Zr\{OCH(CF_3)_2\}_6]$ (Fig. 11)		Zr—O 206 Tl—O 280			Zr: slightly distorted octahedron Tl: three coordinate thallium atoms are in contact with six fluorines (one from each CF_3 group)	46, 47
$[\{(COD)Rh\}_2\{Ti(OPr^n)_6\}]$ (Fig. 13)	Ti—O 180	Ti—O 203		160.2	Ti: octahedron Rh: square planar	56
$[\{(COD)Rh\}_2\{Sn(OEt)_6\}]$	Sn—O 198	Sn—O 209		125.5	Sn: distorted octahedron Rh: square planar	55
$[Tl_2\{Sn(OEt)_6\}]_\infty$ (Fig. 15)		Sn—O 208	Sn—O 220		Sn: distorted octahedron Tl: distorted trigonal bipyramid with the lone pair occupying the vacant equational coordination site	45

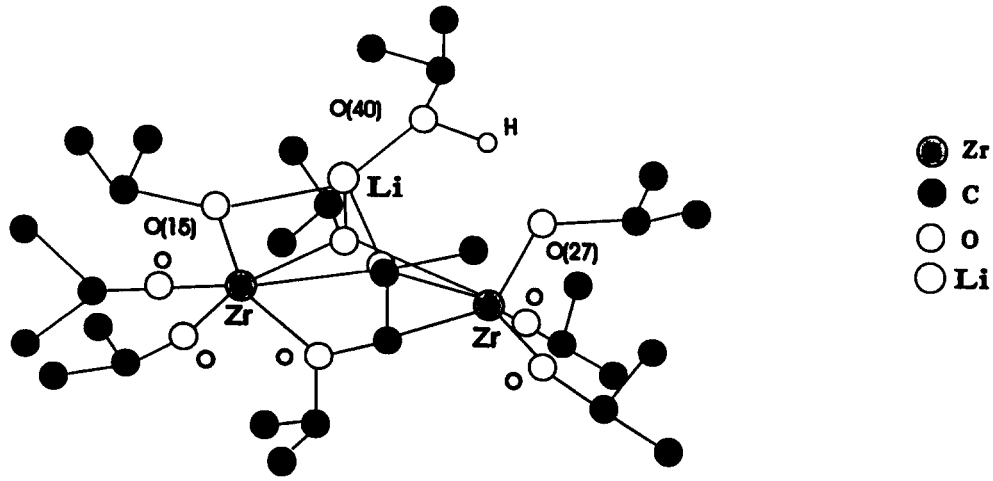

Fig. 5. X-ray crystal structure of $[LiZr_2(OPr^i)_9(Pr^iOH)]$ [49b].

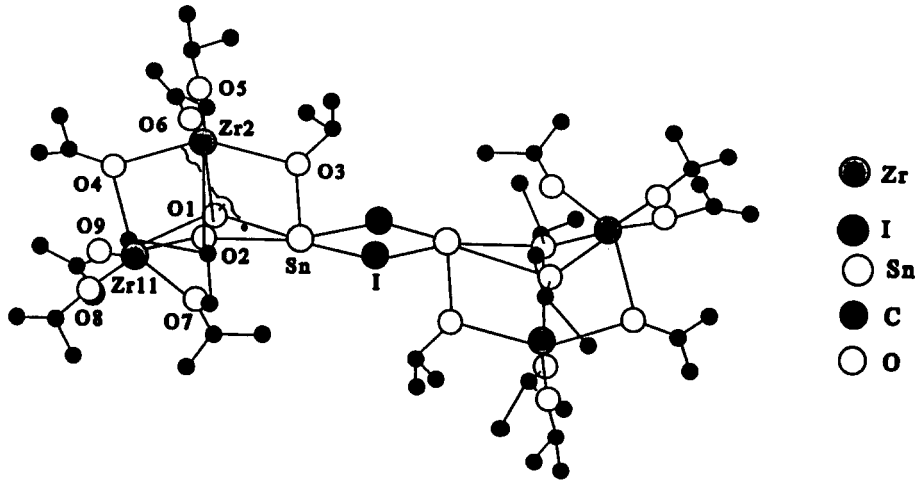

Fig. 6. X-ray crystal structure of $[Sn\{Zr_2(OPr^i)_9\}(\mu\text{-}I)]_2$ [28].

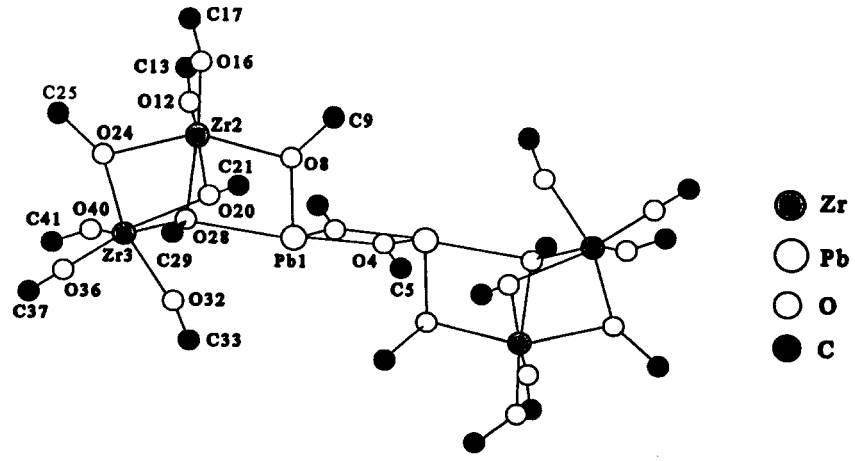

Fig. 7. X-ray crystal structure of $[Pb\{Zr_2(OPr^i)_9\}(\mu\text{-}OPr^i)]_2$ [44,58].

[17,28,37,54,57] such as Ce^{4+} (94 pm), Ti^{4+} (64 pm), Zr^{4+} (87 pm), Hf^{4+} (84 pm), Th^{4+} (99 pm), U^{4+} (97 pm), and Sn^{4+} (74 pm) form derivatives of the type $M'M_2(OR)_9$, while stable analogous tertiarybutoxo derivatives are known only for Ce (**3**) [59], Zr, Hf [43], Th (**4**) [57] and U (**5**) [17], when M′=Na or K. Although thermal stability of all these has not been investigated, the molecule $MZr_2(OBu^t)_9$ appears to be sterically strained leading to disproportionation to more stable $MZr(OBu^t)_5$. The tetravalent titanium and tin are relatively too small to accommodate six bulky OBu^t, groups around themselves and afford stable derivatives of formula $M'M(OBu^t)_5$ [42,64] only; it is also worth mentioning that analogous isopropoxo derivatives [16,29,30,64] for both of these metals are known. It is interesting that the derivative $[KZr(OBu^t)_5]_2$ isolated in 1967 by Mehrotra and Agrawal [16] has now been X-ray crystallographically [43] characterized showing six OBu^t groups around each larger zirconium atoms.

The above description shows that with a fine tuning in the size of the ligand, derivatives of different stoichiometries of the same tetravalent metal can be obtained as being revealed by current investigations in our laboratories.

Amongst the alkali metal derivatives of the type $M'M(OR)_5$, the lithium pentaisopropoxotitanate [30] (**14**) is dimeric (Fig. 8) to provide four- and five-coordination states to lithium and titanium centres, respectively.

By contrast, analogous derivatives of sodium and potassium are polymeric [30]. The importance of metal ion size is reflected in the fact that the infinite linear chains formed in $[NaTi(OPr^i)_5]_\infty$ (**15**) [29] consist of alternative five coordinate titanium centres and tetrahedral sodium atoms, whereas although potassium analogue $[KTi(OPr^i)_5]_\infty$ (**16**) [29] (Fig. 9) is structurally similar to (**15**), it consists of nonlinear continuous chains with potassium atoms in an extremely distorted form from idealized trigonal–bipyramidal geometry, revealing an arrangement between the ideal square bipyramid and trigonal–bipyramid. In both cases, the alkali metal acts as a bridge between discrete, mononuclear, trigonal bipyramidal pentaisopropoxotitanate units. This type of decreased linearity with increased alkali metal radii has also been observed for the other inorganic systems [65].

From the above descriptions two interesting questions arise: (i) why are the derivatives (**15**) and (**16**) of heavier alkali metals polymeric, when the lithium analogue (**14**) is a discrete dimeric molecule; and (ii) why are the polymeric chains non-linear in (**16**)?

To identify definite factors for such abnormalities would be a difficult task with the limited physicochemical data available to date. However, some logical explanations can be put forward. For example, the increase in alkali metal–titanium distances (290 pm, (**14**); 329 pm, (**15**); 336–355 pm, (**16**)) on descending the group could be responsible for nonlinearity of the polymeric chains in (**16**); and adoption of polymeric structures by (**15**) and (**16**), in contrast to the lithium analogue (**14**). This may be a consequence of the magnitudes of alkali metal (M′)/metal(M) radii ratios: in the $M'Ti(OPr^i)_5$ series; discrete molecules have been obtained for M′/M ratios of less than 1.4, whereas for M′/M ratios greater than 1.4, polymeric structures have been identified. This conclusion appears to be corroborated in $M'\{Sn(OBu^t)_3\}$ systems, in which due to the large size (93 pm) of Sn(II) both lithium and sodium derivatives are discrete dimeric solids with M′/Sn(II) ratios attaining values in the range 0.82 to 1. However, in the analogues of potassium and its heavier congeners, the ionic form is attained even with potassium when the M′/Sn(II) ratio becomes 1.40.

Apart from the size of the alkali metal present, the increase in the bulk of the alkoxo group from OPr^i to OBU^t has a predominant role in determining the stability and structures of derivatives of the type

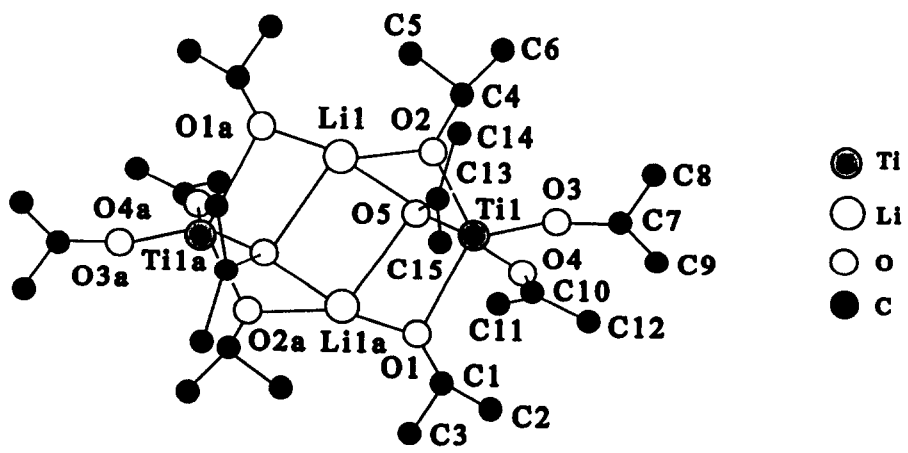

Fig. 8. X-ray crystal structure of $[LiTi(OPr^i)_5]_2$ [30].

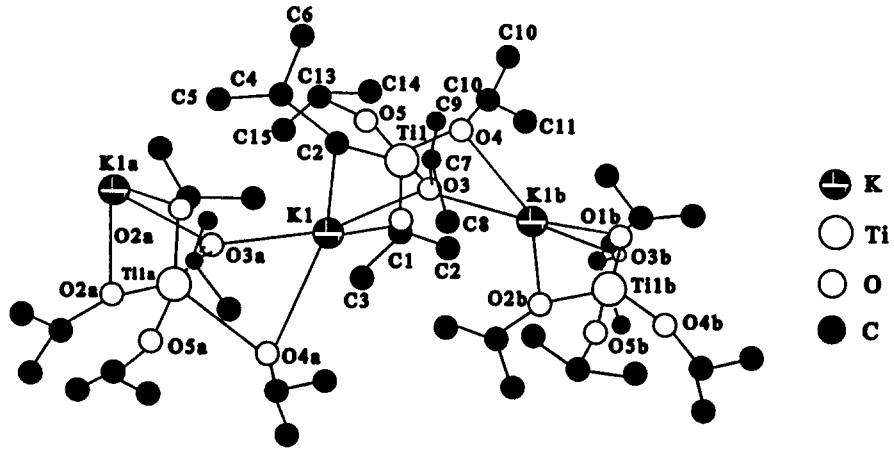

Fig. 9. X-ray crystal structure of $[KTi(OPr^i)_5]_\infty$ [29].

$M'M(OR)_5$. An interesting example arising from such influences is the crystallographically characterized discrete dimeric molecule $[KZr(OBu^t)_5]_2$ (**17**) [43] (Fig. 10), which is composed of two five-coordinate inequivalent zirconium centres, each depicting trigonal–bipyramidal geometry, and the two five-coordinate potassium atoms.

From the above crystallographic investigations structural correlationships between the two discrete dimeric molecules $[LiTi(OPr^i)_5]_2$ and $[KZr(OBu^t)_5]_2$ can be envisaged. For example, these structures appear to be related to the more symmetric $M'_2M_2(\mu_3\text{-}OR)_2(\mu_2\text{-}OR)_4$ unit shown in (I). In this M and M′ can have a varying number of terminal alkoxo ligands either on M, M′, or both in a process to attain sterically allowed coordinative saturation. For example, $Li_2Ti_2(OPr^i)_{10}$ adopts structure(II), with two terminal isopropoxo groups on each titanium (at site M) and no terminal ligand on lithium (at site M′), as in (II). In view of the larger size of K^+ ion compared to that of Li^+, a third μ_3-OR group is required to satisfy coordinative saturation of K^+ centres, as in (III).

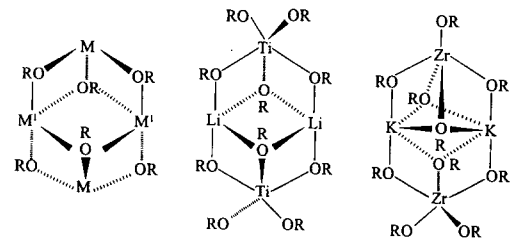

(I) (II) (III)

Hexaalkoxometallate derivatives

Veith and co-workers [67,68], who have contributed richly in the area of heavy *p*-block metal anion complexes, emphasized that the "sandwich" type structure(IV) (based on the desire of metal ions to achieve their preferred coordination number and geometry involving the formation of alkoxo (μ_2- or μ_3-) bridg-

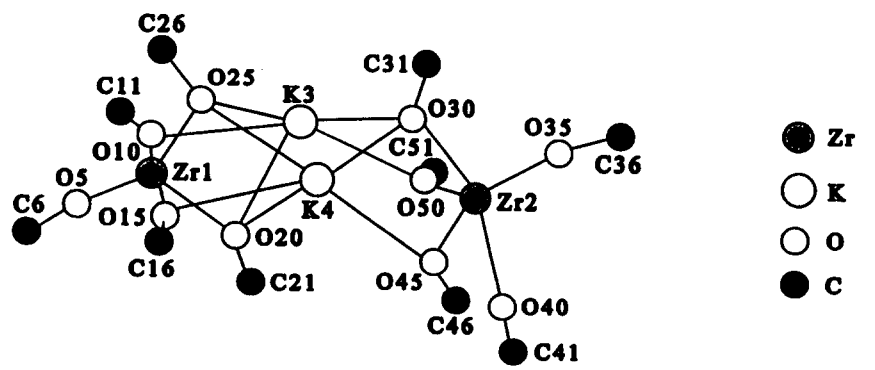

Fig. 10. X-ray crystal structure of $[KZr(OBu^t)_5]_2$. [43].

ing), when R is the sterically bulky OBu^t group, is of wide occurrence, and acceptability in heterobimetallic alkoxides involving the heavy main group ion (M′) contain a lone pair of electrons.

The presence of this type of basic skeleton has been crystallographically [46,47] established in the case of $Tl_2Zr\{OCH(CF_3)_2\}_6$ (**19**) (Fig. 11); the presence of M′ ··· F interactions with the CF_3 group plays a role in satisfying the coordination sphere of the thallium ion (M′) and in preventing further association of the trinuclear unit.

The structure of (**19**) (Fig. 11) is centrosymmetric, containing a crystallographic inversion centre at the zirconium atom, which is surrounded by six fluoroalkoxo groups in a distorted octahedron, capped on *trans* faces by Tl^+ ions giving the overall molecular unit $Tl(\mu_2\text{-}OR_f)_3Zr(\mu_2\text{-}OR_f)_3\,Tl(R_f{=}CH(CF_3)_2)$:

Interestingly, in other derivatives such as $Na_2Zr\{O\text{-}CH(CH_3)_2\}_6(C_6H_6)_2$ (**20**) [47], $Na_2Zr\{OCH(CF_3)\}_6(C_6H_6)$ (**21**) [47], $\{(COD)Rh\}_2\{Ti(OPr^n)_6\}$ (**22**) [56], and $\{(COD)RH\}_2\{Sn(OEt)_6\}$ (**23**) [55], the generic basic structural skeleton (V) $M'(\mu_2\text{-}OR)_2(OR)_2M(\mu_2\text{-}OR)_2M'$ is present.

The derivative (**20**) [47] depicts a special feature in that the Na^+ cations (M′) are loosely coordinated by

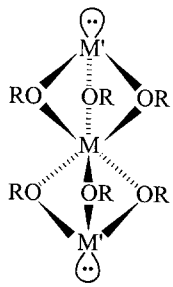

(IV)

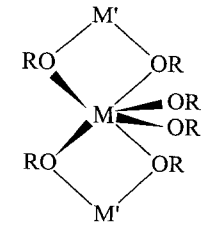

(V)

η^6-benzene ligands (one to each Na^+); this prevents further association of the complexed unit by satisfying the coordination state of sodium cations. The structure of (**20**) shown in Fig. 12 is again a sandwich type compound similar to the thallium analogue (**19**) (Fig. 11) with the difference that lone pair sites are occupied by benzene ligands in (**20**) along with the presence of four doubly-bridged instead of six doubly-bridged fluoroalkoxo groups in (**19**). Crystallographic studies have also shown evidence of secondary heterometal (Na or Tl) ··· F interactions.

It is interesting that in the absence of one of the two η^6-ligated benzene molecules, the species $Na_2Zr\{O\text{-}CH(CF_3)_2\}_6(C_6H_6)$ adopts a structure with an infinite chain of alternating benzene and $Na_2Zr\{O\text{-}CH(CF_3)_2\}_6$ links.

It may not be out of place to mention that in view of the versatility of a $\{Zr_2(OPr^i)_9\}^-$ ligand which offers a variety of synthetic and structural possibilities and choices, it should be of considerable interest to investigate the chemistry of the $[Zr_2\{OCH(CF_3)_2\}_9^-$ ligand.

The derivatives (**22**) [56] and (**23**) [55] are structurally quite similar in adopting the basic skeleton shown in (**V**), wherein the heterometal (M′) sites are occupied by (COD) Rh^+ species and M=Ti (R=Pr^n) [56] or Sn (R=Et) [55] respectively. While the structure of the titanium derivative (**22**) (Fig. 13) possesses

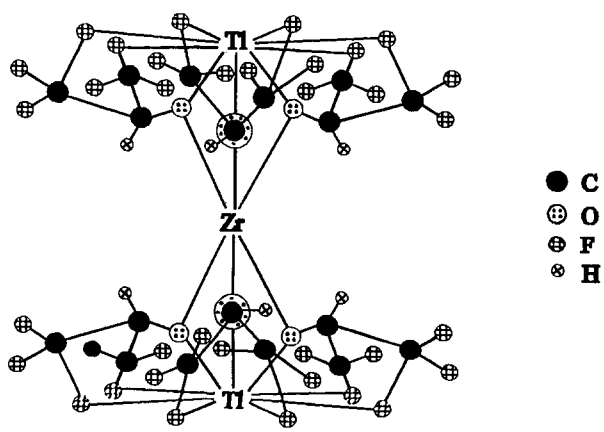

Fig. 11. X-ray crystal structure of $Tl_2Zr\{OCH(CF_3)_2\}_6$ [46,47].

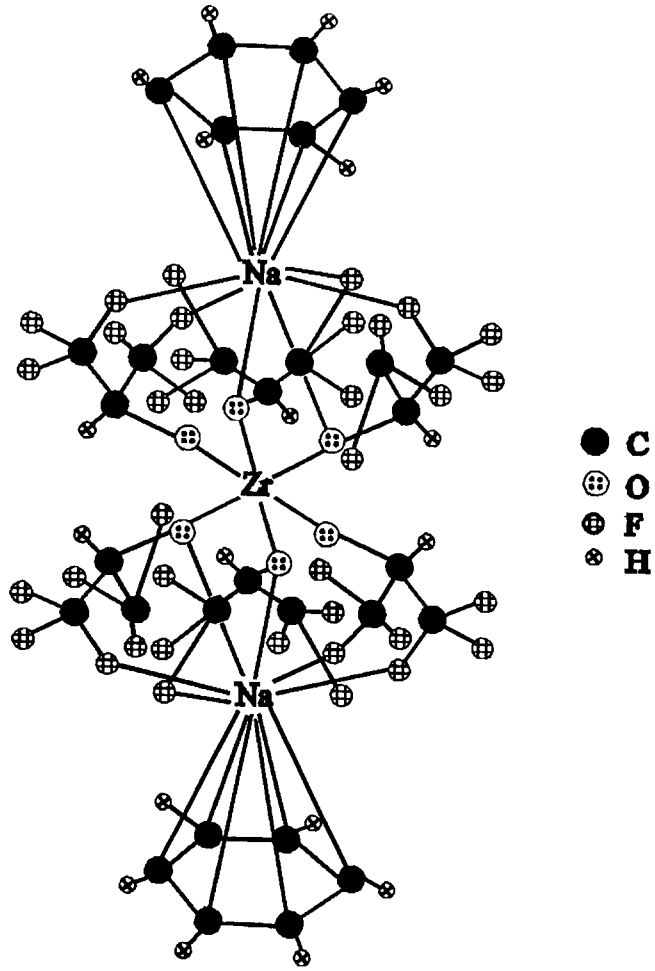

Fig. 12. X-ray crystal structure of $Na_2Zr\{OCH(CF_3)_2\}_6(C_6H_6)_2$.

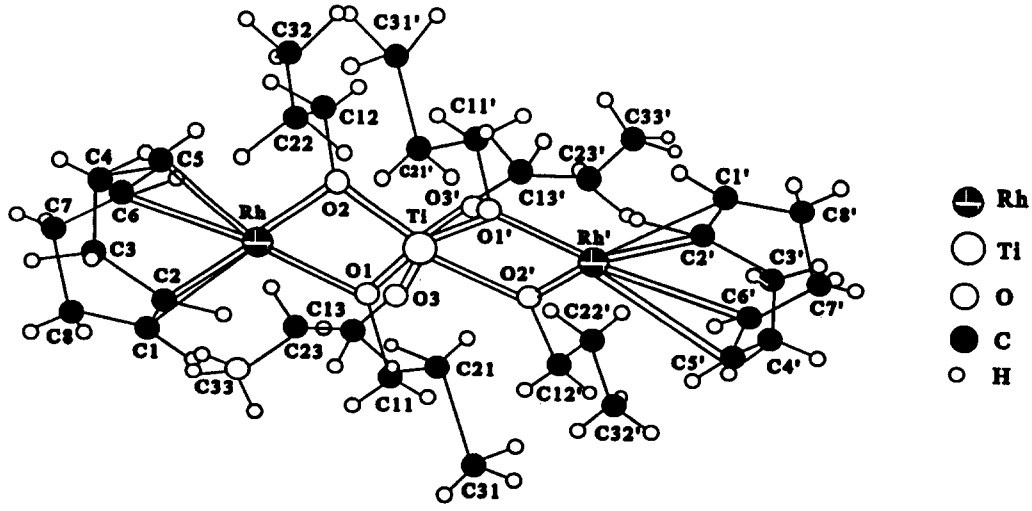

Fig. 13. X-ray crystal structure of $\{(COD)Rh\}_2\{Ti(OPr^n)_6\}$ [56].

a rigorous crystallographic C_2 symmetry, that of the tin derivative (**23**) depicts only approximate idealized C_2 symmetry. The most noticeable difference between the two is the different bonding mode for the two terminally bonded alkoxo groups which have a nearly linear (160(1)°) in (**22**) and a more bent angle (125.5°) in the case of (**23**). The acute M—O_t—C (terminal) bond angles appear to be a general feature in main group metal alkoxide [28,42,55,69] chemistry.

The structure (Fig. 14) for $(DME)_2$ $Na_2Ce(\mu_3\text{-}OBu^t)_2$ $(\mu_2\text{-}OBu^t)_2$ $(OBu^t)_2$ [59], is interesting in that (DME) Na^+ electrophiles occupy adjacent faces of the octahedron rather than *trans* faces, which would give a more linear Na/Ce/Na geometry.

Each sodium atom in the above structure (Fig. 14) is five-coordinate. The cerium atom adopts a distorted octahedral geometry wherein two OBu^t groups are terminal, two are double (μ_2-) bridging and two are triple (μ_3-) bridging.

Detailed investigations on similar derivatives of other tetravalent metals would be expected to throw light on the above mentioned structural diversities.

By contrast, $Tl_2Sn(OEt)_6$ (**24**) [45] exists, due to the lone pair on thallium, as a one dimensional polymer in the solid state (Fig. 15) with two types of ethoxo ligands, i.e. two double (μ_2-) bridging ethoxo ligands that bridge Tl and Sn and one triple (μ_3-) bridging ethoxo ligand that bridges two Tl centres and one Sn atom. Each Sn(IV) centre is in an octahedral environment while each Tl(I) centre adapts a distorted trigonal–bipyramidal geometry, with a lone pair occupying the vacant equatorial coordination site.

In view of the recent novel developments in the chemistry of the $\{Sn_2(OPr^i)_9\}^-$ ligand in our [27,40,51,70] as well as other [28] laboratories, it might also be of interest to investigate the Tl/Sn/OPr^i systems.

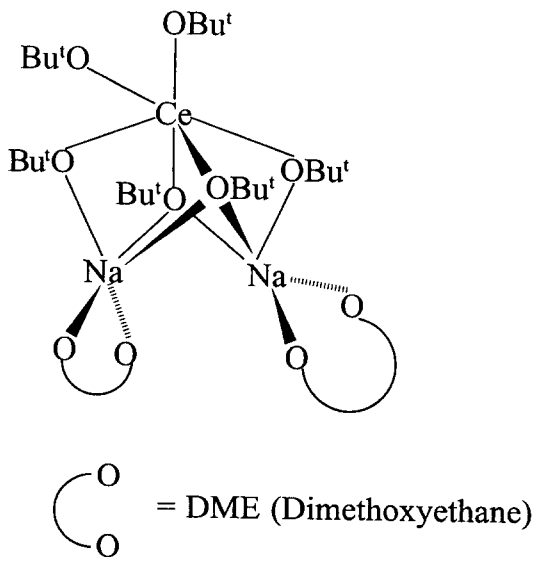

Fig. 14. Schematic structural representation of X-ray determined heterobimetallic alkoxide of cerium(IV) $(DME)_2$ $Na_2Ce(OBu^t)_6$ [59].

Heterotrimetallic alkoxides

Synthesis (by metathesis reaction) and characterization by physicochemical methods of a large number of interesting heterotrimetallic derivatives have been reported from our laboratories. However, X-ray crystal structures of only three derivatives $[\{Cd(OPr^i)_3\}Ba\{M_2(OPr^i)_9\}]_2$ (M=Ti (**25**) [54], Zr (**26**) [61], and Hf (**27**) [54]) have been elucidated so far.

The formation of the derivative (**26**) by the reaction shown below

$$2\{Zr_2(OPr^i)_9\}CdI + 2KBa(OPr^i)_3 \rightarrow [\{Cd(OPr^i)_3\}Ba\{Zr_2(OPr^i)_9\}]_2 + 2KI$$

has a distinctive feature, i.e. the exchange of central metal atoms between the two precursors used for its synthesis. This change is possibly favoured by the greater oxophilicity of barium(II) and its tendency for higher coordination numbers.

The structure shown in Fig. 16 depicts a crystallographic centre of symmetry and all Ba and Zr atoms as six-coordinate, while cadmium atoms are four-coordinate.

Hopefully, this interesting development will soon be followed by structural elucidation of other ter- as well as higher heterometallic alkoxides [40,52,71–73].

CONCLUSIONS

After the three seminal papers in 1957 [15], 1958 [13], and 1967 [16] on the title compounds, a new upsurge occurred in the field due to their X-ray structural elucidation and fastly emerging applications as precursors for novel materials by the Sol–Gel [74,75] and MOCVD [12] processes. It is gratifying to the authors that except for the series of soluble and volatile $M'_2Zr_3(OPr^i)_{14}$ (where M'=Li, Na, K) species reported [16] in 1967, all the other observations and inferences noted in the above publication [16] have been broadly corroborated during the last three decades by more sophisticated techniques. In addition to various suggestions for future lines of investigation mentioned in this paper already, it would also be interesting to establish the identity of these $M'_2Zr_3(OPr^i)_{14}$ complexes, particularly in view of the recent developments in the tetraisopropoxoaluminates of magnesium [76] and barium [77] with compositions different from the conventional $M'\{Al(OPr^i)_4\}_2$ (M'=Mg, Ca, Sr, Ba, etc.) described earlier from our laboratories [70] in our pursuit of "single source" precursors for a desired ceramic material. Furthermore, the synthesis and X-ray crystal structure [79] of a novel type of derivative $[Mg\{Ti_2(OEt)_8Cl\}(\mu\text{-}Cl)]_2$ with a $\{Ti_2(OEt)_8Cl\}^-$ in place of the usual

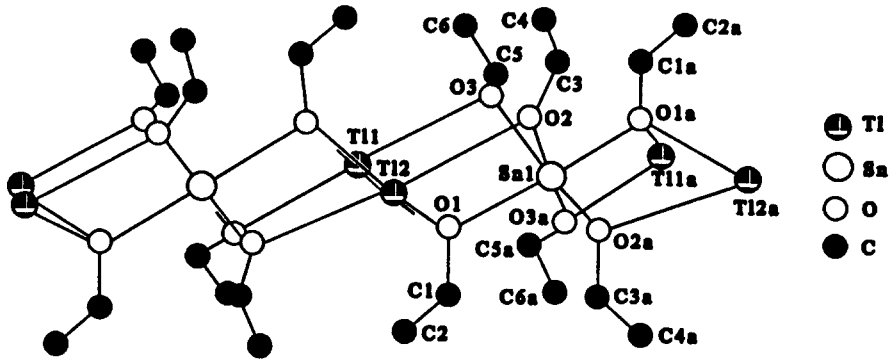

Fig. 15. X-ray crystal structure of $[Tl_2Sn(OEt)_6]_\infty$.

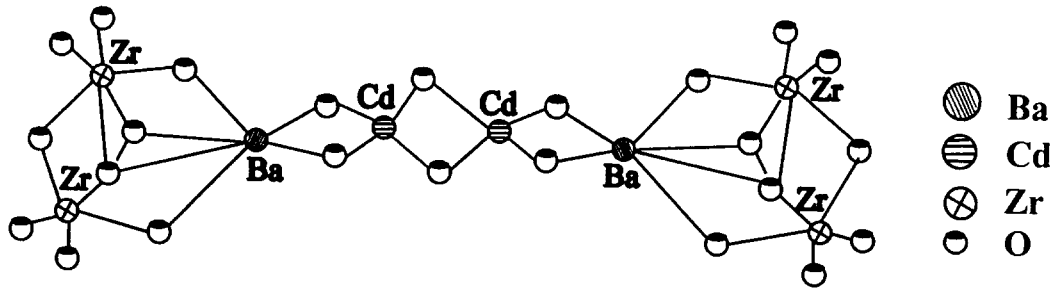

Fig. 16. X-ray crystal structure of $[\{Cd(OPr^i)_3\}Ba\{Zr_2(OPr^i)_9\}]_2$ [61].

$\{M_2(OR)_9\}^-$ unit has opened up a new dimension in heterometallic alkoxide chemistry; our recent [40,80] findings in this particular area are rather exciting, but the same are not being included in this article for sake of brevity.

Acknowledgements—Thanks are due to the Department of Science and Technology, New Delhi, for financial support of our work and to Professor D. C. Bradley, FRS, for his continued encouragement.

In view of the close association of one of the authors of this article with Professor Bradley in the formative years (1950–52) of homometallic alkoxide chemistry, and his highly innovative contributions to this field, we deem it a privilege to dedicate this article to Don C. Bradley on the occasion of his 73rd birthday.

REFERENCES

1. Bradley, D. C., Mehrotra, R. C. and Gaur, D. P., *Metal Alkoxides*. Academic Press, London, 1978.
2. Mehrotra, R. C. and Mehrotra, A., *Inorg. Chem. Acta Rev.*, 1972, **5,** 127.
3. Mehrotra, R. C., *Adv. Inorg. Chem. Radiochem.*, 1983, **26,** 269.
4. Mehrotra, R. C., *Chemtracts*, 1990, **2,** 389.
5. Veith, M., Weidner, S., Kunze, K., Käfer, D., Hans, J. and Huch, V., *Coord. Chem. Rev.*, 1994, **137,** 297.
6. Caulton, K. G. and Hubert-Pfalzgraf, L. G., *Chem. Rev.*, 1990, **90,** 969.
7. Mehrotra, R. C., Singh, A. and Tripathi, U. M., *Chem. Rev.*, 1991, **91,** 1287.
8. Mehrotra, R. C., Singh, A. and Sogani, S., *Chem. Rev.*, 1994, **94,** 1643.
9. Mehrotra, R. C., Singh, A. and Sogani, S., *Chem. Soc. Rev.*, 1994, **23,** 215.
10. Mehrotra, R. C. and Singh, A., *J. Ind. Chem. Soc.*, 1993, **70,** 885.
11. Bradley, D. C., *Phil. Trans. R. Soc. Lond.*, 1990, **A330**, 167.
12. Bradley, D. C., *Chem. Rev.*, 1989, **89,** 1317.
13. Bartley, W. G. and Wardlaw, W., *J. Chem. Soc.*, 1958, 421.
14. Meerwein, H. and Bersin, T., *Ann.*, 1929, **476,** 113.
15. Bradley, D. C., Caldwell, E. V. and Wardlaw, W., *J. Chem. Soc.*, 1957, 4775.
16. Mehrotra, R. C. and Agrawal, M. M., *J. Chem. Soc. (A)*, 1967, 1026.
17. Coton, F. A., Marler, D. O. and Schwotzer, W., *Inorg. Chem.*, 1984, **23,** 4211.
18. Mehrotra, R. C. and Singh, A., *Prog. Inorg. Chem.*, 1997, **46,** 239.
19. (a) Sogani, S., Singh, A. and Mehrotra, R. C., *Indian J. Chem.*, 1995, **34A,** 449; (b) Govil, S. and Mehrotra, R. C., *Aust. J. Chem.*, 1975, **28,** 2125.

20. Dubey, R. K., Singh, A. and Mehrotra, R. C., *Indian J. Chem.*, 1992, **31A,** 156.
21. Shah, A., Singh, A. and Mehrotra, R. C., *Inorg. Chim. Acta*, 1988, **141,** 289.
22. Dubey, R. K., Singh, A. and Mehrotra, R. C., *Inorg. Chim. Acta*, 1986, **118,** 151.
23. Jain, R., Rai, A. K. and Mehrotra, R. C., *J. Inorg. Chem. (China)*, 1987, **3,** 96.
24. Dubey, R. K., Singh, A. and Mehrotra, R. C., *Polyhedron*, 1987, **6,** 427.
25. Sogani, S., Singh, A. and Mehrotra, R. C., *Main Group Met. Chem.*, 1990, **13,** 375.
26. Sogani, S., Singh, A., Bohra, R., Mehrotra, R. C. and Noltemeyer, M., *J. Chem. Soc., Chem. Commun.*, 1991, 738.
27. Sogani, S., Singh, A. and Mehrotra, R. C., *Polyhedron*, 1995, **14,** 621.
28. Veith, M., Mathur, S. and Huch, V., *J. Chem. Soc., Dalton Trans.*, 1996, 2485.
29. Boyle, T. J., Bradley, D. C., Hampden-Smith, M. J., Patel, A. and Ziller, J. W., *Inorg. Chem.*, 1995, **34,** 5893.
30. Hampden-Smith, M. J., Williams, D. S. and Rheingold, A. L., *Inorg. Chem.*, 1990, **29,** 4076.
31. Bradley, D. C., *Nature*, 1958, **182,** 1211.
32. Bradley, D. C., Mehrotra, R. C. and Wardlaw, W., *J. Chem. Soc.*, 1952, 2027.
33. Mehrotra, R. C., *J. Indian Chem. Soc.*, 1953, **30,** 585.
34. Mehrotra, R. C. and Agrawal, M. M., *J. Chem. Soc., Chem. Commun.*, 1968, 469.
35. Mehrotra, R. C. and Singh, J., *Can. J. Chem.*, 1984, **62,** 1003.
36. Garg, G., Dubey, R. K., Singh, A. and Mehrotra, R. C., *Polyhedron*, 1991, **10,** 1733.
37. Vaartstra, B. A., Streib, W. E. and Caulton, K. G., *J. Am. Chem. Soc.*, 1990, **112,** 8593.
38. Meese-Marktscheffel, J. A., Weimann, R., Schumann, H. and Gilje, J. W., *Inorg. Chem.*, 1993, **32,** 5894.
39. Wijk, M., Norrestam, R., Nygren, M. and Westin, G., *Inorg. Chem.*, 1996, **35,** 1077.
40. Tripathi, U. M., Singh, A. and Mehrotra, R. C., unpublished result. U. M. Tripathi, Ph.D. thesis, University of Rajasthan, Jaipur, India, 1992.
41. Agrawal, M. M., Ph.D. thesis, University of Rajasthan, Jaipur, India, 1968.
42. Veith, M. and Reimers, M., *Chem. Ber.*, 1990, **123,** 1941.
43. Teff, D. J., Huffman, J. C. and Caulton, K. G., *Inorg. Chem.*, 1994, **33,** 6289.
44. Teff, D. J., Huffman, J. C. and Caulton, K. G., *Inorg. Chem.*, 1995, **34,** 2491.
45. Hampden-Smith, M. J., Smith, D. E. and Duesler, E. N., *Inorg. Chem.*, 1989, **28,** 3999.
46. Samuels, J. A., Zwanziger, J. W., Lobkovsky, E. B. and Caulton, K. G., *Inorg. Chem.*, 1992, **31,** 4046.
47. Samuels, J. A., Lobkovsky, E. B., Streib, W. E., Folting, K., Huffman, J. C., Zwanziger, J. W. and Caulton, K. G., *J. Am. Chem. Soc.*, 1993, **115,** 5093.
48. Van der Sluys, W. G. and Sattelberger, A. P., *Chem. Rev.*, 1990, **90,** 1027.
49. (a) Vaarstra, B. A., Huffman, J. C., Streib, W. E. and Caulton, K. G., *Inorg. Chem.*, 1991, **30,** 3068; (b) Vaarstra, B. A., Huffman, J. C., Streib, W. E. and Caulton, K. G., *J. Chem. Soc., Chem. Commun.*, 1990, 1750.
50. Cotton, F. A., Diebold, M. P. and Roth, W. J., *Inorg. Chem.*, 1988, **27,** 3596.
51. Sogani, S., Singh, A. and Mehrotra, R. C., unpublished results. S. Sogani, Ph.D. thesis, University of Rajasthan, Jaipur, India, 1992.
52. Mathur, S., Singh, A. and Mehrotra, R. C., unpublished result. S. Mathur, Ph.D. thesis, University of Rajasthan, Jaipur, India, 1992.
53. Vaartstra, B. A., Samuels, J. A., Barash, E. H., Martin, J. D., Streib, W. E., Gasser, C. and Caulton, K. G., *J. Organomet. Chem.*, 1993, **449,** 191.
54. Veith, M., Mathur, S. and Huch, V., *Inorg. Chem.*, 1996, **35,** 7295.
55. Wark, T. A., Gulliver, E. A. and Hampden-Smith, M. J., *Inorg. Chem.*, 1990, **29,** 4360.
56. Day, V. W., Eberspacher, T. A., Haq, J., Klemperer, W. G. and Zhong, B., *Inorg. Chem.*, 1995, **34,** 3549.
57. Clark, D. L. and Watkin, J. G., *Inorg. Chem.*, 1993, **32,** 1766.
58. Teff, D. J., Huffman, J. C. and Caulton, K. G., *Inorg. Chem.*, 1996, **35,** 2981.
59. Evans, W. J., Deming, T. J., Olofson, J. M. and Ziller, Z. W., *Inorg. Chem.*, 1989, **28,** 4027.
60. Chisholm, M. H., in *Inorganic Chemistry: Toward the 21st Century*, ed. M. H. Chisholm. ACS Symposium Series 211, Washington, 1983.
61. Veith, M., Mathur, S. and Huch, V., *J. Am. Chem. Soc.*, 1996, **118,** 903.
62. Tripathi, U. M., Singh, A. and Mehrotra, R. C., *Polyhedron*, 1991, **10,** 949.
63. Garg, G., Singh, A. and Mehrotra, R. C., *Indian J. Chem.*, 1995, **34A,** 484.
64. Singh, A. and Mehrotra, R. C., unpublished results.
65. Evans, W. J., Boyle, T. J. and Ziller, Z. W., *Organometallics*, 1992, **11,** 3903.
66. Veith, M. and Rosler, R., *Z. Naturforsch.*, 1986, **41B,** 1071.
67. Veith, M., *Angew. Chem., Int. Ed. Engl.*, 1987, **26,** 1.
68. Veith, M., Käfer, D. and Huch, V., *Angew. Chem., Int. Ed. Engl.*, 1986, **25,** 376.
69. Cayton, R. H., Chisholm, M. H., Davidson, E. R., Distasi, V. F., Du, P. and Huffman, J. C., *Inorg. Chem.*, 1991, **30,** 1020.
70. Tripathi, U. M., Singh, A. and Mehrotra, R. C., *Polyhedron*, 1995, **14,** 2461.
71. Dubey, R. K., Shah, A., Singh, A. and Mehrotra, R. C., *Recl. Trav. Chim. Pays-Bas.*, 1988, **107,** 237.
72. Dubey, R. K., Singh, A. and Mehrotra, R. C., *J. Organomet. Chem.*, 1988, **341,** 569.
73. Gupta, R., Shah, A., Singh, A. and Mehrotra, R. C., *New J. Chem.*, 1991, **15,** 665.
74. Dislich, H., *Angew. Chem., Int. Ed. Engl.*, 1971, **10,** 363.
75. Mehrotra, R. C., *J. Non-Cryst. Solids*, 1988, **100,** 1.
76. Meese-Marktscheffel, J. A., Fukuchi, R., Kida, M., Tachibana, G., Jensen, C. M. and Gilje, J. W., *Chem. Mater.*, 1993, **5,** 755.

77. Bhagat, M., Singh, A. and Mehrotra, R. C., *Main Group Met. Chem.*, 1997, **20,** 89.
78. Mehrotra, R. C., Goel, S., Goel, A. B., King, R. B. and Nainan, K. C., *Inorg. Chim. Acta*, 1978, **29,** 141.
79. Malpezzi, L., Zucchini, U. and Dall'Occo, T. *Inorg. Chem. Acta*, 1991, **180,** 245.
80. Bhagat, M., Singh, A. and Mehrotra, R. C. *Indian J. Chem.*, 1997, **36A,** in press.

Pergamon

PII: S0277-5387(97)00360-4

Polyhedron Vol. 17, No. 5-6, pp. 705-711, 1998
© 1998 Elsevier Science Ltd
All rights reserved. Printed in Great Britain
0277-5387/98 $19.00+0.00

Preparation, characterization and electronic structure of $W_2(NMe_2)_2(OR_f)_4$, where $R_f = CMe_2CF_3$, $CMe(CF_3)_2$ and $C(CF_3)_3$, as deduced by photoelectron spectroscopic studies and the single crystal X-ray structure for $R_f = OCMe(CF_3)_2$*

Theodore A. Budzichowski,[a] Malcolm H. Chisholm,[a] Darin B. Tiedtke,[a] Nadine E. Gruhn[b] and Dennis L. Lichtenberger[b]

[a] Department of Chemistry and Molecular Structure Center, Indiana University, Bloomington, IN 47405, U.S.A.

[b] Department of Chemistry and Center for Gas-Phase Electron Spectroscopy, University of Arizona, P.O. Box 210041, Tucson, AZ 85721, U.S.A.

(Received 26 May 1997; revised 13 August 1997)

Abstract—The compounds $W_2(NMe_2)_2(OCMe_2CF_3)_4$, **1**, $W_2(NMe_2)_2(OCMe(CF_3)_2)_4$, **2**, and $W_2(NMe_2)_2(OC(CF_3)_3)_4$, **3**, have been obtained from reactions between $W_2(NMe_2)_6$ and the respective fluoroalcohol in hydrocarbon solvents. The compounds **2** and **3** appear inert to further reaction with their fluoroalcohol at room temperature while **1** reacts further to give $W_2(OCMe_2CF_3)_6$. In solution NMR data indicate that all three compounds exist in a mixture of *anti*- and *gauche*-rotamers with restricted rotations about both W—N and W≡W bonds on the NMR time-scale. The solid-state molecular structure of **2** reveals a centrosymmetric $NO_2W{\equiv}WO_2N$ core with W—W = 2.3107(6) Å, W—N = 1.914(4) Å, W—O = 1.959(3) and 1.907(3) Å and angles W—W—O/N within the range 100 to 110°. The gas phase photoelectron spectra for **1**, **2** and **3** were obtained and are compared with that for $W_2(NMe_2)_6$. The introduction of the fluoroalkoxide ligands has a pronounced effect in stabilizing the metal and nitrogen lone-pair based ionizations, and this effect is amplified by the successive replacement of each methyl group by a trifluoromethyl group. Also for the compounds **1**, **2**, and **3** the lowest ionization bands clearly reveal the removal of the degeneracy of the W—W π MOs as expected for *anti* and *gauche* complexes. © 1998 Elsevier Science Ltd. All rights reserved

Keywords: $W_2(NMe_2)_2(OR_f)_4$; photoelectron spectroscopic studies; single crystal X-ray structure.

The reactivity of a metal center is greatly influenced by the nature of the metal, its electronic configuration and the set of attendant ligands. These effects are clearly evident for $M_2(OR)_6$ compounds, where M = Mo and W, that share a common ethane-like structure $O_3M{\equiv}MO_3$, where the triple bond is cylindrical being composed of one σ and two π components $\sigma^2\pi^4$ [1,2]. The marked differences in reactivity as a function of metal is seen in the reductive cleavage of nitriles by $W_2(O^tBu)_6$, eqn (1), [3], whereas the complex $Mo_2(O^tBU)_6$ is inert with respect to reaction with MeC≡N under similar conditions.

(1) $W_2(O^tBu)_6 + MeC{\equiv}N \xrightarrow[\text{hexane}]{0\,^\circ C}$

$$(^tBuO)_3W{\equiv}N + (^tBuO)_3W{\equiv}CMe$$

However, upon changing the alkoxide from O^{t}Bu to $OCMe_2CF_3$ Schrock and co-workers noted [4] not a reductive cleavage analogous to (**1**) but rather a reversible Lewis base association, eqn (2).

* Dedicated to Professor D. C. Bradley, in appreciation and respect for his pioneering work on metal amides and metal alkoxides.

(2) $W_2(OCMe_2CF_3)_6 + 2MeC{\equiv}N \underset{\text{toluene-}d_8}{\rightleftharpoons} W_2(OCMe_2CF_3)_6(NCMe)_2$

In our studies of the activation of CO we have seen similar differences and noted that the behavior of $W_2(NMe_2)_2(OR_f)_4$ compounds (R_f = a fluoroalkyl group) is markedly different from that of $W_2(NMe_2)_6$ [5]. In this paper we report the preparation and characterization of a series of $W_2(NMe_2)_2(OR_f)_4$ compounds for which photoelectron spectroscopy reveals an interesting trend with the increase of substitution of Me by CF_3.

RESULTS AND DISCUSSION

Syntheses

The compounds $W_2(NMe_2)_2(OR_f)_4$, where $R = CMe_2CF_3$, **1**, $R = CMe(CF_3)_2$, **2**, and $R = C(CF_3)_3$, **3**, were prepared according to the alcoholysis reaction shown in eqn 3.

(3) $W_2(NMe_2)_6 + 4R_fOH \xrightarrow[\text{hydrocarbon}]{22\,^\circ C} W_2(NMe_2)_2(OR_f)_4 + 4HNMe_2$

The reaction involving $R_f = CMe_2CF_3$ represents a partial alcoholysis as in the presence of excess $Me_2(CF_3)COH$ the homoleptic alkoxide $W_2(OCMe_2CF_3)_6$ is formed. However, under similar conditions the compounds **2** and **3** are inert to further alcoholysis. In the case of the preparation of **3** the amine salt $Me_2NH_2^+OC(CF_3)_3^-$ is formed and is removed by vacuum sublimation at 45 °C, 10^{-2} Torr. A similar finding has been reported for the preparation of $Mo_2(NMe_2)_2(OC(CF_3)_3)_4$ in the reaction between $Mo_2(NMe_2)_6$ and $(CF_3)_3COH$ [6].

The new compounds **1**, **2** and **3** are orange, hydrocarbon-soluble, air-sensitive, crystalline solids at room temperature. They show moderate thermal stability and may be sublimed in the temperature range 85–110 °C at 10^{-3} Torr, with only minor decomposition. In solution the NMR data indicate the presence of *gauche*- and *anti*-rotamers with the *gauche* being the major rotamer. There is restricted rotation about both the W≡W and W—N bonds. The coalescence of proximal and distal NMe groups does not occur below 110 °C in toluene which places $\Delta G^{\neq}_{\text{rotation}} > 17$ kcal/mol in contrast to 11 kcal/mol in $W_2(NMe_2)_6$ [7].

Solid-state and molecular structure of $W_2(NMe_2)_2(OCMe(CF_3)_2)_4$, **2**, *and a discussion of bonding*

Compound **2** crystallizes from hexanes in the space group C_2/c with four molecules in the unit cell. A drawing of the molecular structure with the atom label scheme is shown in Fig. 1. Pertinent bond distances and bond angles are given in Table 1. The molecule is situated at a crystallographic inversion center which relates both halves of the molecule as shown. The staggered *anti* $NO_2W{\equiv}WO_2N$ unit is unexceptional and the W—W distance of 2.3207(6) Å is as expected [1,2]. The two W—O distances, 1.959(3) and 1.907(3) Å are longer than those seen in $W_2(OR)_6$ compounds which fall in a very narrow range 1.88(1) Å [8] and the W—N distances 1.914(4) Å are notably shorter than that in $W_2(NMe_2)_6$, 1.98(1) Å (ave) [7]. This is understandable in terms of the $OCMe(CF_3)_2$ ligand being a weaker σ- and π-donor relative to OR (R = alkyl) and NMe_2. Thus the successive replacement of the W—NMe_2 bonds by $OCMe(CF_3)_2$ bonds leads to

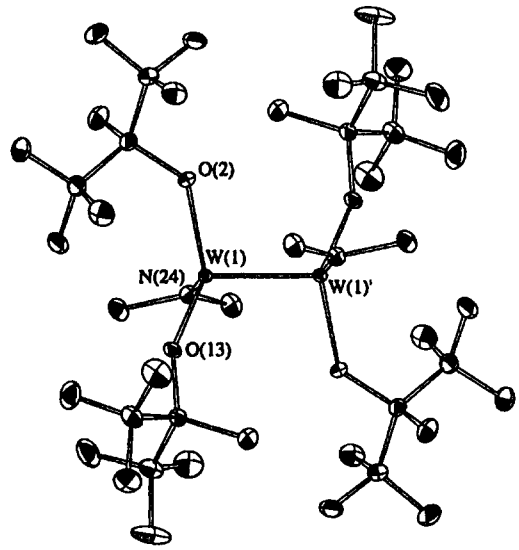

Fig. 1. An ORTEP drawing of the $W_2(NMe_2)_2(OCMe(CF_3)_2)_4$ molecule.

Table 1. Selected bond distances (Å) and bond angles (°) for $W_2(NMe_2)_2(OCMe(CF_3)_2)_4$

A	B	Distance
W(1)	W(1)′	2.3107(6)
W(1)	O(2)	1.959(3)
W(1)	O(13)	1.907(3)
W(1)	N(24)	1.914(4)
F	C	1.33(1) (ave)

A	B	C	Angle
W(1)′	W(1)	O(2)	100.78(10)
W(1)′	W(1)	O(13)	110.57(11)
W(1)′	W(1)	N(24)	99.85(14)
O(2)	W(1)	O(13)	115.45(15)
O(2)	W(1)	N(24)	117.90(17)
O(13)	W(1)	N(24)	110.42(17)

enhanced π-donation by the Me_2N ligands that remain at the W_2^{6+} center.

To a first order approximation one might expect the electron releasing properties of an alkoxide to correlate with the pKa of the free alcohol which are 18.6 for ^tBuOH, 11.4 for Me_2CF_3COH, 9.6 for $Me(CF_3)_2COH$, and 5.4 for $(CF_3)_3COH$ [9]. It should be noted too that with the change in pKa of the alcohol there is a similar change in the ionization energy of the oxygen lone-pair: compare 10.22 eV for ^tBuOH, 11.11 eV for CF_3Me_2COH and 11.93 eV for $(CF_3)_2MeCOH$, for example [10]. Thus for a compound of formula $W_2(NMe_2)_2(OR)_4$ the successive substitution of CF_3 for Me on the ^tBu group would lead to an increase in W—N π-bonding. This should manifest itself in (i) shorter W—N bonds, (ii) an increase in the barrier to W—N bond rotation and (iii) an increase in the kinetic barrier for subsequent alcoholysis to give $W_2(OR)_6$ since protonation of the amide nitrogen represents an important component to this ligand exchange reaction. Within the series of compounds reported here this is seen. As described elsewhere the metal centers become more Lewis acidic as the RO^- ligands donate less electron density to the metal centers [11]. This can be understood as the LUMOs of the M_2 complexes are the M—M δ and δ^* orbitals which, in the presence of π-donor ligands are raised in energy, since they are the metal receptor d orbitals for ligand to metal π-bonding [12].

Photoelectron spectroscopy

The He I photoelectron spectra of the low-valence regions of $W_2(NMe_2)_6$, $W_2(NMe_2)_2(OCMe_2(CF_3))_4$, $W_2(NMe_2)_2(OCMe(CF_3)_2)_4$, and $W_2(NMe_2)_2(OC(CF_3)_3)_4$ are shown in Fig. 2. The ionizations are represented by asymmetric Gaussian peaks [13], parameters for which are listed in Table 2. In this energy region, the spectrum of $W_2(NMe_2)_6$ contains ionizations that originate from the M—M σ orbital, the M—M π orbitals, and the six amide-based nitrogen lone-pair orbitals, while the spectra of the mixed amide/alkoxide compounds contain ionizations that originate from the M—M σ orbital, the M—M π orbitals, and the two amide-based nitrogen lone-pair orbitals. The primary orbital character associated with an ionization has been assigned by comparison to the PES of other triply-bonded Mo_2- and W_2-containing alkoxide and amide ligands [14,15], by comparison within this series of compounds, and by comparison to the results of Fenske–Hall calculations [16] on the model systems $M_2(NH_2)_2(OH)_4$ (M = Mo, W). The assignments listed in Table 2 reflect the primary character of the corresponding valence metal or ligand orbitals. However, it must be remembered that a completely accurate description of an orbital from which an ionization originates includes additional mixing with other valence metal or ligand orbitals.

The spectrum of $W_2(NMe_2)_6$ is shown in Fig. 2(A).

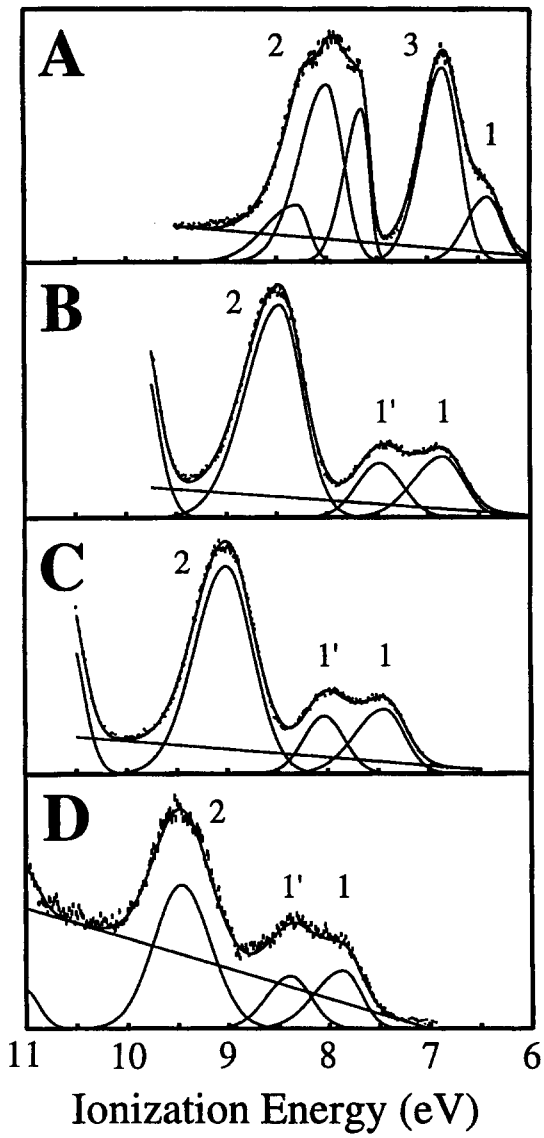

Fig. 2. He I photoelectron spectra of compounds of (**A**) $W_2(NMe_2)_6$, (**B**) $W_2(NMe_2)_2(OCMe_2(CF_3))_4$, (**C**) $W_2(NMe_2)_2(OCMe(CF_3)_2)_4$, and (**D**) $W_2(NMe_2)_2(OC(CF_3)_3)_4$.

Several differences are evident between the spectrum of this compound and the previously reported PES of $Mo_2(NMe_2)_6$ [13]. For $Mo_2(NMe_2)_6$, there is a complex series of overlapping ionizations in this region. The leading edge of the overlapping ionizations has been assigned to the nitrogen lone-pair orbitals of a_{2g} and a_{1u} symmetry that do not have the correct symmetry to interact with any of the metal-based orbitals and are nearly degenerate in energy. The spectrum of $W_2(NMe_2)_6$, in contrast, has two separate bands in this region. The band at lowest ionization energy has a shoulder on the low ionization energy side (labeled 1 in Fig. 2A) that is assigned to ionization from the W—W π orbital, which has been destabilized from the position of the Mo—Mo π ionization as is

Table 2. Fit parameters for photoelectron spectra

Compound	Position (eV)	Halfwidth High	Halfwidth Low	Rel. Area	Label	Assignment
$W_2(NMe_2)_6$	6.41	0.41	0.33	1.00	1	W—W π
	6.85	0.51	0.40	3.96	3	N l.p.
	7.64	0.23	0.16	0.95	2	W—W σ, N l.p.
	7.91	0.56	0.39	4.26		
	8.29	0.55	0.32	1.95		
$W_2(NMe_2)_2(OCMe_2(CF_3))_4$	6.85	0.67	0.47	1.23	1	W—W π
	7.48	0.52	0.52	1.00	1′	W—W π
	8.47	0.81	0.54	5.01	2	W—W σ, N l.p.
$W_2(NMe_2)_2(OCMe(CF_3)_2)_4$	7.44	0.69	0.47	1.37	1	W—W π
	8.04	0.48	0.47	1.00	1′	W—W π
	9.01	0.75	0.62	5.18	2	W—W σ, N l.p.
$W_2(NMe_2)_2(OC(CF_3)_3)_4$	7.85	0.68	0.46	1.16	1	W—W π
	8.38	0.48	0.47	1.00	1′	W—W π
	9.44	0.75	0.62	3.51	2	W—W σ, N l.p.

typically seen for W-based versus Mo-based ionizations in compounds with multiple metal–metal bonds [17]. The main portion of this band (band 3) is assigned to ionization from the same non-interacting nitrogen lone-pair orbitals (a_{2g} and a_{1u}) that are the highest occupied molecular orbitals for $Mo_2(NMe_2)_6$. The ionization energies of these nitrogen lone-pairs are approximately the same for the Mo and W compounds, being shifted only 0.09 eV to higher ionization energy for the W analogue. The ionization band labeled 2 in Fig. 2(A) contains ionizations from the nitrogen lone-pair orbitals of e_g and e_u symmetry, as well as ionization from the W—W σ bond, based on the separations observed between the σ and π ionizations of other M—M triple-bonded complexes [10].

The spectra of the three mixed amide/alkoxide compounds are shown in Fig. 2(B)–(D). These compounds each have two ionizations from nitrogen lone-pairs in this region, which are assigned to band 2. The non-interacting lone-pair ionizations in band 3 for $W_2(NMe_2)_6$ are gone. Two small ionizations of about equal intensity are seen at the low ionization energy side of the spectra. While at first consideration it might be thought that the first two ionization bands, labeled 1 and 1′ in Fig. 2, could be assigned to the W—W π and σ ionizations, the data are not consistent with this assignment. Bands 1 and 1′ have relative areas (1 : 1′) ranging from 1.37 : 1.00 to 1.16 : 1.00. In general, the observed relative areas of the σ and π ionizations of tungsten and molybdenum hexaalkoxides are about 1 : 2 [14]. Also, bands 1 and 1′ are separated from each other by 0.53 eV to 0.63 eV for these compounds, while other W—W triple bonded systems have σ and π ionizations that are separated by 1.52 eV [$W_2(OCMe_3)_6$] to 1.74 eV [$W_2(OCMe(CF_3)_2)_6$] [10]. The bands 1 and 1′ are assigned to the two W—W π ionizations, which in the lowered symmetry of these molecules are no longer expected to be degenerate. These molecules are known to exist in an *anti* conformation in the crystalline phase and as a mixture of *anti* and *gauche* (primarily *gauche*) conformations in solutions. The gas-phase conformation is not explicitly known. However, Fenske–Hall calculations on the model complex $W_2(NH_2)_2(OH)_4$ predict that in the ground state these two metal based orbitals will be most separated in energy for the *anti* conformation and will be very little separated in the *gauche* conformation. This is because in the C_{2h} symmetry of the *anti* conformation the W—W π orbitals transform as b_u and a_u symmetry orbitals, which will have greatly different amounts of overlap with the alkoxide oxygen lone-pair orbitals. The Fenske–Hall calculations would therefore suggest the observed splitting of the π ionizations indicates that these molecules exist primarily in the *anti* conformation in the gas phase. The ionization band labeled 2, which is assigned to the two nitrogen lone-pair ionizations must also contain the W—W σ band ionization.

As fluorines are added to the alkoxide ligands, all of the ionizations in this region shift to lower ionization energy. These shifts are influenced by two factors. The first of these is the change in net charge potential felt at the metal or nitrogen centers, which is the result of the σ-donating ability and orbital charge distribution of the alkoxide ligands. The second factor is the orbital overlap interactions of the metal with the oxygen lone-pair orbitals of the alkoxides, forming bonding and anti-bonding pairs. As fluorines are added to the alkoxides, the oxygen lone-pairs are lowered in energy, thereby reducing their interactions with the W—W π orbital. The ionization labeled 1 shifts 0.59 eV as the number of fluorines per alkoxide is increased from three to six, and 0.41 eV as the number of fluorines is increased from six to nine. The non-additivity

of these shifts is likely due to geometry changes in the alkoxide ligands upon fluorination. The shifts of the W—W π ionizations with successive fluorinations of the alkoxide ligands are comparable to the shift of the W—W π ionizations when four amide ligands of $W_2(NMe_2)_6$ are replaced with four trifluoroalkoxide ligands.

While to this point we have considered the trends observed for the metal-based ionizations, the nitrogen-based ionizations give the most information about the reactivity of these molecules. Ionization band 2 is stabilized to approximately the same extent as the M—M π ionizations, and there is only a small amount of broadening of band 2 as fluorines are added to the alkoxides, which indicates that the W—W σ-bond ionization and amide nitrogen lone-pair ionizations are being stabilized by approximately the same amount. The nitrogen lone-pairs of the amides are stabilized by the same charge effect that causes some of the stabilization of the M—M π-bond ionizations. In addition, these two ligands orbitals interact with the W—W δ and δ^* orbitals in a π symmetry fashion [13]. The W—W δ and δ^* orbitals, in turn, have σ symmetry with respect to the four alkoxy ligands, which allows the alkoxides to directly remove electron density from the nitrogen lone-pairs. As previously noted, the pKas of the free alcohols are significantly lowered by successive substitution of CF_3 for Me on the ^{t}Bu group. The ionization energy of the oxygen lone-pairs for the free alcohols is stabilized by about 0.8 eV per successive substitution of CF_3 for Me, while the amide nitrogen lone-pair ionization energies are stabilized by approximately 0.5 eV per successive substitution. This would suggest that the pKas of the amide lone-pairs are being lowered approximately 5/8 as much as the pKas of the free alcohols. Due to the decrease of electron density at the nitrogens and the resulting lowering of pKa, the nitrogen lone-pairs are stabilized to such an extent that the amide ligands are no longer basic enough to be protonated and allow further ligand exchange.

EXPERIMENTAL SECTION

General methods

Standard air-sensitive Schlenk line and dry-box techniques were used. Aromatic and aliphatic hydrocarbon solvents were dried over sodium or potassium benzophenone ketyl under a N_2 flow, subjected to three freeze-thaw-degas cycles before use, and stored over 4 Å molecular sieves. The fluoroalcohols (from PCR) were distilled and subjected to three freeze-thaw-degas cycles prior to use.

Spectroscopic methods

Infrared spectra were obtained on a Perkin–Elmer 283 Spectrophotometer as Nujol mulls between NaCl plates or as pressed KBr pellets. ^{1}H NMR spectra were recorded on either a Varian GEM-300, a Nicolet 360, Varian I-400, or a Bruker AM-500 NMR spectrophotometer in dry, degassed toluene-d_8 or benzene-d_6. ^{1}H NMR chemical shifts are in ppm relative to the protio impurity in benzene-d_6 set at δ 7.15 or the CHD_2 quintet of toluene-d_8 set at δ 2.09. ^{13}C NMR spectra were recorded on Varian GEM-300, Varian I-400, or Bruker AM-500 spectrophotometers at 75, 100 and 125 MHz, respectively. ^{13}C NMR chemical shifts are in ppm relative to the triplet of benzene-d_6 set at δ 128.0 ppm or the downfield singlet of toluene-d_8 set at δ 137.5. ^{19}F NMR spectra were recorded on a Varian GEM-300 or a Nicolet 360 spectrophotometer at 282 and 340 MHz, respectively. ^{19}F NMR chemical shifts are in ppm relative to the external reference of CF_3COOH set at δ −76.5.

Photoelectron spectra were recorded using an instrument that features a 36 cm hemispherical analyzer (McPherson) and custom designed sample cells and detection and control electronics. The instrument and data collection and manipulation procedures have been described in detail elsewhere [19]. During collection the instrument resolution (measured using the full-width-at-half-maximum of the argon $^2P_{3/2}$ ionization) was 0.020–0.030 eV.

All samples sublimed cleanly with no detectable evidence of decomposition products in the gas phase or as a solid residue. The sublimation temperatures (in C, at 10^{-4} torr) were: $W_2(NMe_2)_6$, 99–102°; $W_2(NMe_2)_2(OCMe_2(CF_3))_4$, 94–98°; $W_2(NMe_2)_2(OCMe(CF_3)_2)_4$, 92–100°; $W_2(NMe_2)_2(OC(CF_3)_3)_4$, 67–73°. Temperatures were monitored using a "*K*" type thermocouple passed through a vacuum feedthrough and attached directly to the sample cell.

The spectra are represented analytically with the best fit of asymmetric Gaussians [13]. Each Gaussian is defined by its position, amplitude, half-width on the high binding energy side, and half-width on the low binding energy side.

Preparation of $W_2(OCMe_2CF_3)_4(NMe_2)_2$ (**1**). $W_2(NMe_2)_6$ (167 mg, 0.264 mmol) was dissolved in hexanes (10 ml). $HOCMe_2CF_3$ (203 mg, 1.58 mmol) was added to the solution via gas-tight ml syringe. The reaction was allowed to stir for 6 h and became dark red in color. The solvent was removed under vacuum. **1** was obtained in crystalline form (248 mg, 83%) from benzene 80°C to 23°C. ^{1}H NMR (300 MHz, toluene-d_8, 23°C): δ 4.10, 2.51, 1.90, 1.66, 1.16, 0.95 (6:6:6:6:6:6 for *gauche* rotamer) and 4.15, 2.37, 1.41, 1.35 (6:6:12:12 for *anti* rotamer). ^{19}F NMR (282 MHz, C_6D_6 ext. ref. to CF_3COOH at −23°C): δ −83.4, −83.8 (1:1 for *gauche* rotamer) and −83.6 (for *anti* rotamer).

Preparation of $W_2(OC(CF_3)_2Me)_4(NMe_2)_2$ (**2**). $W_2(NMe_2)_6$ (2.20 g, 3.48 mmol) was dissolved in 25 ml of hexanes. The fluoroalcohol (4.3 g, 24 mmol) was then added to the solution via syringe and the reaction stirred for several hours. An instantaneous reaction was evident based on the observation of a

color change to deep red, and microcrystals of the sparingly soluble product were formed. After 2 h, the solvent was evaporated *in vacuo* (23°C, 0.01 Torr) and 2.49 g of **2** (61% yield) was crystallized from hexanes (65 to −35°C). The crystalline material was dried *in vacuo* (23°C, 2 h, 0.01 Torr) prior to use. ^{1}H NMR (300 MHz, toluene-d_8, 23°C): δ 4.22, 2.47, 1.54 (6:6:12 for *anti* rotamer), 4.30, 2.34, 2.07, 1.21 (septet, $J_{H-F} = 1.5$ Hz) (6:6:6:6 for *gauche* rotamer). $^{13}C\{^1H\}$ NMR (75 MHz, toluene-d_8, 23°C): δ 82.36, 60.42, 39.37, 19.42 (s for *anti* rotamer), 82.60, 82.13, 60.11, 40.04, 20.24, 19.57 (s for *gauche* rotamer). ^{19}F NMR (340 MHz, toluene-d_8, 23°C): δ −78.75 (q, J_{F-F} = 10 Hz), −79.59 (q, $J_{F-F} = 10$ Hz) (*anti* rotamer), −78.87 (q, 6F, $J_{F-F} = 9$ Hz), −79.04 (s, 12F), −79.96 (q, 6F, $J_{F-F} = 9$ Hz) (*gauche* rotamer).

Preparation of $W_2(OC(CF_3)_3)_4(NMe_2)_2$ (**3**). $W_2(NMe_2)_6$ (167 mg, 0.264 mmol) was dissolved in hexanes (10 ml). $(CF_3)_3COH$ (500 mg, 2.12 mmol) was added to the solution via gas-tight ml syringe. The reaction was allowed to stir for 6 h and became pale orange–red in color. The solvent was removed under vacuum and $[Me_2NH_2][OC(CF_3)_3]$ was sublimed *in vacuo* at 60°C. **3** was obtained in microcrystalline form (195 mg, 53%) rom toluene 110°C to 23°C. ^{1}H NMR (300 MHz, toluene-d_8, 23°C): δ 2.42 (s, 12 H), 4.21 (6 H), 4.53 (6 H).

Crystallographic study.

General operating procedures and listings of programs have been previously given [19].

$W_2(NMe_2)_2(OCMe(CF_3)_2)_4$. A summary of crystal data collection is given in Table 3.

The structure was solved by initially locating the tungsten position from a Patterson map (SHELXS-86). The remaining non-hydrogen atoms were obtained from subsequent iterations of least-squares refinement and difference Fourier calculation. The center of the molecule is at a crystallographic center of symmetry. The difference Fouriers of the asymmetric unit had two persistent peaks of 4.1 and 2.6 e/Å^3 in the vicinity of the tungsten atom but at chemically unreasonable positions. It was then noted that each was separated from its symmetry equivalent position by 2.30 Å as compared with the observed W—W distance of 2.311 Å. It was therefore assumed that a small amount of disorder was present and two additional tungsten atoms, W(27) and W(28) in the tables of atomic coordinates were included in the refinement. The occupancies initially refined to approximately 2.0 and 1.5% and were fixed at these values for the final cycles of refinement. At these low levels of occupancy, any light atoms associated with the disorder would not be expected to be observed. Hydrogens were included in fixed calculated positions.

In the final cycles of refinement, the ordered non-hydrogen atoms were varied with anisotropic thermal parameters and the two disordered atoms were varied with isotropic thermal parameters to a final $R(F) = 0.029$ for the 244 total variables using all of the unique data. Data having $F < 3\sigma(F)$ were given zero weight and are indicated with asterisks in the appendix of F_o and F_c. The largest peak in the final difference map was 1.5 e/A^3 in the vicinity of the disorder. All other peaks were less than 0.9 e/A^3 and the deepest hole was −1.2 e/A^3.

Table 3.

Empirical formula	$C_{20}H_{24}F_{24}NO_4W_2$
Color of crystal	orange
Crystal dimensions	0.15 × 0.15 × 0.20
Space group	C2/c
Cell dimensions	
T (°C)	−167
a (Å)	18.226(4)
b (Å)	14.121(3)
c (Å)	13.552(3)
β (deg)	108.73(1)
Z (molecules/cell)	4
V (Å^3)	3303.04
d_{calcd} (g/cm^3)	2.373
λ (Å)	0.71069
MW	1180.08
μ (cm^{-1})	72.728
Detector-to-sample distance (cm)	22.5
Sample-to-source distance (cm)	23.5
Av ω scan width at half height	0.25
Scan speed (deg/min)	8.0
Scan width (deg + dispersion)	2.0
Individual background (s)	4
Aperture size (mm)	3.0 × 4.0
2θ range (deg)	6–55
Total no. of reflections collected	5624
no. of unique intensities	3809
no. with $F > 0.0$	3639
no. with $F > 3\sigma(F)$	3409
$R(F)$	0.0292
$R_w(F)$	0.0293
Goodness of fit for last cycle	1.058
Maximum δ/σ for last cycle	0.002

Acknowledgements—T.A.B., M.H.C. and D.B.T. thank the National Science Foundation for support. D.L.L. and N.E.G. acknowledge support by the National Science Foundation, the U.S. Department of Energy (Division of Chemical Sciences, Office of Basic Energy Sciences, Office of Energy Research) for contributions to the equipment, and the Materials Characterization Program, Department of Chemistry, University of Arizona.

REFERENCES

1. Cotton, F. A. and Walton, R. A., In *Multiple Bonds Between Metal Atoms*, 2nd edn., Oxford University Press, 1993.
2. Chisholm M. H., *Acc. Chem. Res.*, 1990, **23**, 419.

3. Schrock, R. R., Listeman, M. L. and Sturgeoff, L. G., *J. Am. Chem. Soc.*, 1982, **104,** 4291.
4. Freudenberger, J. H., Pedersen, S. F. and Schrock, R. R., *Bull. Soc. Chim. France*, 1985, 349.
5. (a) Budzichowski, T. A., Chisholm, M. H., Tiedtke, D. B., Huffman, J. C. and Streib, W. E., *Organometallics*, 1995, **14,** 2318; (b) Blower, P. J., Chisholm, M. H., Clark, D. L. and Eichhorn, B. W., *Organometallics*, 1986, **5,** 2125.
6. Abbot, R. G., Cotton, F. A. and Falvello, L. R., *Polyhedron*, 1991, **9,** 1821.
7. Chisholm, M. H., Cotton, F. A., Extine, M. W. and Stults, B. R., *J. Am. Chem. Soc.*, 1976, **98,** 4477.
8. (a) R = ^{i}Pr: Chisholm, M. H., Clark, D. L., Folting, K., Huffman, J. C. and Hampden-Smith, M. J., *J. Am. Chem. Soc.*, 1987, **109,** 7750; (b) R = cyclohexyl and W_2(pinacolate)$_3$: Chisholm, M. H., Folting, K., Hampden-Smith, M. J. and Smith, C. A., *Polyhedron*, 1987, **6,** 1747.
9. Serjeant, E. P. and Dempsey, P., In *Ionization Constants of Organic Acids in Aqueous Solution*, Pergamon Press, Oxford, 1979.
0. Pollard, J. R., Ph.D. Dissertation, University of Arizona, 1996.
11. Chisholm, M. H., Tiedtke, D. B., Huffman, J. C. and Streib, W. E., *Polyhedron*, this issue.
12. See figures portraying the influence of RO π donation on the M—M HOMO and LUMO: Chisholm, M. H., *J. C. S. Dalton Trans.*, 1996, 1781.
13. Lichtenberger, D. L. and Copenhaver, A. S., *J. Elect. Spec. Rel. Phen.*, 1990, **50,** 353.
14. Bursten, B. E., Cotton, F. A., Green, J. C., Seddon, E. A. and Stanley, G. G., *J. Am. Chem. Soc.*, 1980, **102,** 4579.
15. Kober, E. M. and Lichtenberger, D. L., *J. Am. Chem. Soc.*, 1985, **107,** 7199.
16. Hall, M. B. and Fenske, R. F., *Inorg. Chem.*, 1972, **11,** 768.
17. Lichtenberger, D. L. and Johnston, R. L., In *Metal–Metal Bonds and Clusters in Chemistry and Catalysis*, ed. J. P. Fackler, Jr., Plenum, New York, 1990, p. 275.
18. Lichtenberger, D. L., Renshaw, S. K. and Bullock, R. M., *J. Am. Chem. Soc.*, 1993, **115,** 3276–3285, and references therein.
19. Chisholm, M. H., Folting, K., Huffman, J. C. and Kirkpatrick, C. C., *Inorg. Chem.*, 1984, **23,** 1021.

Pergamon

PII: S0277-5387(97)00374-4

Polyhedron Vol. 17, No. 5-6, pp. 713-723, 1998
© 1998 Elsevier Science Ltd
All rights reserved. Printed in Great Britain
0277-5387/98 $19.00+0.00

Synthesis, characterization and reactivity of crown ether adducts of barium carboxylates: $Ba(O_2CCH_3)_2(18\text{-crown-6})\cdot 4H_2O$ and $Ba(O_2C(CH_2)_4CO_2)(18\text{-crown-6})\cdot 8H_2O$

Leo Archer, Mark J. Hampden-Smith* and Eileen Duesler

Department of Chemistry and Center for Micro-Engineered Materials, University of New Mexico, Albuquerque, New Mexico, 87131, U.S.A.

(Received 3 July 1997; accepted 8 August 1997)

Abstract—The compounds $Ba(O_2CCH_3)_2(18\text{-crown-6})\cdot nH_2O$ and $Ba(O_2C(CH_2)_4CO_2)(18\text{-crown-6})\cdot nH_2O$ were prepared by the reaction between barium carbonate and the appropriate organic acid in the presence of 18-crown-6. These compounds were characterized by a variety of spectroscopic and analytical methods which showed that various hydrates could be formed. The species $Ba(O_2CCH_3)_2(18\text{-crown-6})\cdot 4H_2O$ (**1**) and $Ba(O_2C(CH_2)_4CO_2)(18\text{-crown-6})\cdot 8H_2O$ (**2**) were structurally characterized by single-crystal X-ray diffraction. In the solid state compound **1** was comprised of a Ba atom in the center of the 18-crown-6 ring with chelating acetate ligands being in the axial positions of the equitorial coordination plane. Water molecules were hydrogen bonded to the oxygen atoms of the acetate ligands. Compound **2** is an infinite polymer in the solid state with the Ba atom also in the center of the 18-crown-6 ring with each carboxylate group chelating to one Ba and each adipate bridging through the second carboxylate group of the dicarboxylate to another Ba atom. Compound **1** crystallizes in the monoclinic space group $P2_1/c$ with cell dimensions of $a = 9.512(1)$ Å, $b = 7.811(1)$ Å, $c = 16.906(1)$ Å, $\beta = 99.049(8)^\circ$, $V = 1240.5(3)$ Å^3 and $Z = 2$. Compound **2** crystallizes in the triclinic space group $P\bar{1}$ with cell dimensions of $a = 8.525(1)$ Å, $b = 9.769(1)$ Å, $c = 10.200(1)$ Å, $\alpha = 106.59(1)^\circ$, $\beta = 90.37(1)^\circ$, $\gamma = 110.34(1)^\circ$, $V = 757.4(1)$ Å^3 and $Z = 1$. Compounds **1** and **2** thermally decompose to evolve the 18-crown-6 ligand intact at approximately 200°C, prior to the thermal decomposition of the carboxylate ligand to form $BaCO_3$. Compounds **1** or **2** were mixed with $Ti(O\text{-}i\text{-}Pr)_4$ in ethanol, spin coated onto Pt substrates and heated to 400°C followed by annealing at 700°C for 1 h in air. Coumpound **1** resulted in formation of a mixture of $BaTiO_3$, $BaCO_3$ and TiO_2, while **2** produced only $BaCO_3$ films. The difference in reactivity of **1** and **2** may be connected to the availability of a thermal window for ester elimination as indicated by the TGA results. © 1998 Elsevier Science Ltd. All rights reserved

Keywords: crown ether adducts; barium carbonate; organic acid.

In the past few years, the technological and commercial value of metal alkoxide compounds is beginning to be realized by their use as precursors for the formation of metal oxide materials [1–4]. The flexibility that metal alkoxide precursors provide, enables the formation of materials with a wide variety of compositions and microstructures. The pioneering work in the development of general synthetic strategies to these precursors and the recognition that they have value as precursors to materials was conducted in the research group of Professor Don Bradley, to whom this volume is dedicated [5,6].

* Author to whom correspondence should be addressed.

The conversion of metal alkoxide precursors to metal oxide materials has been performed using a variety of different reaction strategies including hydrolysis and thermolysis, the initial understanding of which was also pioneered by the same research team [2,7–13]. Bradley *et al.* were also amongst the first to recognize that metal alkoxide compounds could undergo ester elimination reactions which give rise to metal-oxo-metal bonds which are a fundamental building block of metal oxide materials [14]. The original studies involved the reactions between titanium alkoxides and silicon alkoxyacetates which resulted in the formation of metal siloxides. Since this time, a large variety of reactions between metal

alkoxides and metal carboxylates have been shown to result in the formation of metal oxide compounds, particularly in the formation of perovskite phase mixed metal oxides such as $BaTiO_3$ [8,9]. However, although the formation of esters has been established during some of these reactions, the reaction mechanism is not always clear as a result of the presence of other species such as free alcohol, free carboxylic acid and water, which together can also react to form esters as products [8]. To better understand the nature of the reaction between metal alkoxides and metal carboxylates, a number of research groups have been studying reactions between these reagents under conditions where there is less ambiguity in the interpretation of the reaction pathway by virtue of the absence of interfering species [8,9]. Our studies have focused on the investigation of some model tin-containing systems where the reactions can be followed conveniently by multinuclear NMR spectroscopy [15,16]. The general principles deduced from these reactions can then be applied to more technologically relevant systems in an attempt to control the outcome of these reactions [17,18].

In this paper, we describe the synthesis and characterization of two new barium carboxylate compounds which were prepared to investigate their reactivity towards titanium alkoxides to form barium titanate. In this context it is relevant to briefly review the formation of Group 2 element-containing materials.

There is considerable interest in the synthesis of derivatives of the Group 2 elements which have properties which make them suitable as precursors for the formation of Group 2 element-containing thin films [9]. These materials include perovskite phase ferroelectric ceramics such as $PbTiO_3$, $Ba_{1-x}Sr_xTiO_3$, $Pb_{1-x}Zr_xTiO_3$, and $SrBi_2Ta_2O_9$ [8,19,20], dielectric materials such as Sr_2AlTaO_6 [21,22], ceramic superconductors such as $YBa_2Cu_3O_{7-x}$ [23–25], magnetic materials such as $BaFe_{12}O_{19}$ [26,27], and display materials such as Ce-doped MS, where M = Ca, Sr, Ba and Ce-doped $CaGa_2S_4$. The precursor design criteria depend on which method of film deposition is employed. Chemical vapor deposition requires that the precursors have suitable volatility to be transported intact to at heated surface while liquid phase deposition techniques require that the precursors be soluble [28,29]. In each case, once the precursor is delivered to the substrate, it is desirable that it reacts in a way which involves complete elimination of the supporting organic ligands and formation of the desired product. The films are usually required to have the properties of high purity, a high level of crystallinity, theoretical density and be deposited at the lowest possible temperature.

The synthesis of suitable precursors of the Group 2 elements has presented a particular problem for the formation of Group 2 element-containing materials. The origin of this problem lies in the tendency of the Group 2 elements to form oligomeric species as a result of their high coordination numbers (typically Ca, Sr and Ba prefer coordination numbers of 8–12) and the resulting small charge-to-size ratio which is not conducive to the formation of high vapor pressure species for chemical vapor deposition applications. Recently, major advances have been made in the design of low nuclearity Group 2 element compounds through the use of neutral multidentate ligands to consume coordination sites at the Group 2 metal center. The most success in terms of preparing volatile Group 2 element compounds for CVD has been with the use of cyclic or acyclic polyethers or polyamines in conjunction with fluorinated β-diketonates and β-ketoiminates [22,30–38]. However, while β-diketonates appear to be the ligands which impart the highest volatility to metal–organic compounds, their thermal decomposition is often the source of problems associated with impurity incorporation in the film. This is especially true for the case of fluorinated β-diketonates which typically deposit metal fluorides, or at best, fluoride or carbon contaminated films [39,40].

As a result of this problem, we have been searching for alternative supporting ligands and reaction strategies which avoid the problems associated with fluorinated β-diketonates. These strategies include ester elimination reactions between metal carboxylate and metal alkoxide compounds to form metal oxides or sulfides according to the stoichiometry of eqn (1) [15,16,41]; ether elimination between metal alkoxides or siloxides [9,18] according to equation (2) and the elimination of anhydrides according to the stoichiometry of eqn (3) [42–44].

$$M(OR)_n + M'(OECR')_n \rightarrow MM'E_{n/2} + nRO_2CR' \quad (E = O \text{ or } S) \quad (1)$$

$$M(OR)_n + M'(OR')_n \rightarrow MM'O_{n/2} + nROR' \quad (2)$$

$$M(OECR)_n \rightarrow ME + n/2(RCO)_2E \quad (E = O \text{ or } S) \quad (3)$$

We have demonstrated that these are viable reaction strategies to make thin films of a variety of different materials under unusually mild conditions.

In this paper, we describe the synthesis, characterization and reactivity of two new barium carboxylate species which were prepared with the intention that (a) they have a low nuclearity and (b) to study their thermal reactivity. Crown ether ligands were used to induce low nuclearity in these compounds and carboxylate ligands were chosen for their potential reactivity towards other metal alkoxide compounds via ester elimination. The aim of this study was to determine whether the polyether ligands could be removed from the coordination sphere of Ba prior to thermal decomposition of the carboxylate ligands. If this is the case, then this provides a "thermal window" for the reaction of the unassociated barium carboxylate compound with a metal alkoxide to undergo ester elimination and remove the carboxylate

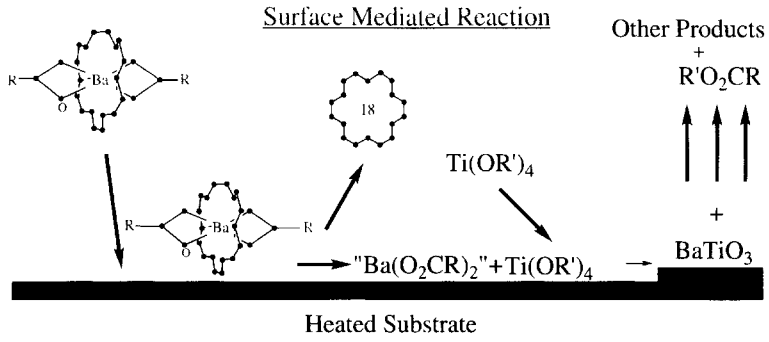

Fig. 1. Schematic representation of proposed substrate activated thermal "window" within which ester elimination may take place.

ligand intact and thus avoid formation of carbonates which would normally be expected in these systems. This strategy is illustrated schematically in Fig. 1, where a volatile metal carboxylate is delivered to a surface, the polyether ligand dissociates releasing a reactive "$M(O_2CR)_2$" species which can react with a metal alkoxide via ester elimination and the remaining alkoxide ligands are removed by thermally-induced elimination.

EXPERIMENTAL

All manipulations were carried out under an atmosphere of dry dinitrogen using standard Schlenk techniques. Hydrocarbon and ethereal solvents were distilled from sodium benzophenone ketyl and stored over 4 Å molecular sieves. The metal starting materials $BaCO_3$, $Ba(O_2CCH_3)_2$ and the carboxylic acids were purchased from Aldrich Chemical Co. The 18-crown-6 polyether was obtained from Strem Chemicals. All starting materials were used without further purification.

Elemental analyses (EA) were performed by Mrs R. Ju at the Department of Chemistry, University of New Mexico. Nuclear magnetic resonance spectra were recorded on a Bruker AC-250P NMR spectrometer by using the protio impurities of the deuterated solvents as reference for the ^1H NMR. Infrared data were recorded on a Perkin–Elmer model 1620 FTIR spectrophotometer. Thermogravimetric analyses were conducted on a Perkin–Elmer model TGA 7 analyzer in the temperature range of 30–900 C at 10 °C/min ramp rate. Powder X-ray diffraction data were recorded on a Siemens D5000 instrument. Thin films were placed upon a piece of plasticine on a thin film mount. The data were taken from 10–90°, the preset time was 8.0 s with a 0.040° step size. Single-crystal X-ray diffraction data were collected on a Nicolet R3m/v diffractometer. The structures were solved by either the Patterson method or direct methods using SHELXTL Plus and refined by the full-matrix least-squares method.

Synthesis and characterization

Synthesis of $Ba(O_2CCH_3)_2$(18-crown-6)·$4H_2O$ (**1**). $Ba(O_2CCH_3)_2$ (1.69g, 6.6 mmol) was dissolved in 25 cm^3 of distilled water and this solution was added to a solution of 18-crown-6 (1.75g, 6.6 mmol) dissolved in 25 cm^3 of distilled water. The mixture was stirred for 2 h. The solvent was removed under vacuum until a white crystalline (by XRD) solid remained. Yield: 3.37 g (98.5%). Colorless crystalline plates suitable for single-crystal X-ray diffraction analysis were obtained after recrystallization from water (Fig. 2). Similar results were obtained when $BaCO_3$ and acetic acid were used as reagents in plave of barium acetate. Elem. anal.: found % (calc. for $BaC_{16}H_{42}O_{16}$, $Ba(O_2CCH_3)_2$(18-crown-6)·$6H_2O$): C, 30.63 (30.61); H, 6.69 (6.74). Thermogravimetric analysis: Observed weight loss 66.24%, expected weight loss 66.65% (based on $BaCO_3$ formation, and $Ba(O_2CCH_3)_2$(18-crown-6)·$4H_2O$ starting material); ^1H NMR (250 MHz, 25 °C, D_2O): 3.57 ppm, s, crown; 1.72 ppm, s,

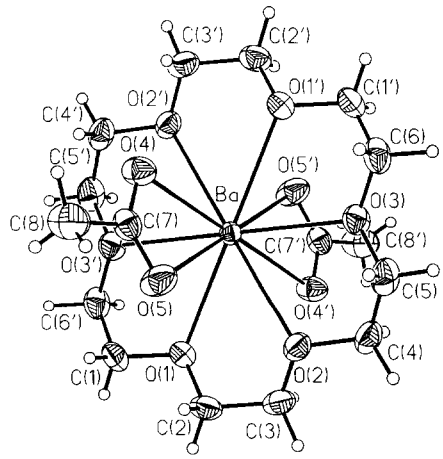

Fig. 2. The solid-state molecular structure of $Ba(O_2CCH_3)_2$(18-crown-6)·$4H_2O$.

$C(O)CH_3$. IR (KBr, cm^{-1}): 3440 w, 3249 w, 2911 w, 1560 w, 1419 w, 1350 w, 1324 m, 1270 m, 1224 m, 1090 w, 996 m, 964 w, 931 m, 919 w, 829 w, 668 w.

Synthesis of $Ba(O_2C(CH_2)_4CO_2)$(18-crown-6)·$8H_2O$ (**2**). A colloidal solution of $BaCO_3$ (1.00g, 5.1 mmol) and 18-crown-6 (1.34g, 5.1 mmol) in 100 cm^3 of H_2O was heated to 70°C and stirred for 5 min. The $BaCO_3$ was only slightly soluble but the solution went completely clear upon addition of $HO_2C(CH_2)_4CO_2H$ (0.741g, 5.1 mmol). The solution was filtered and the solvent was removed under vacuum. Crystals suitable for single-crystal X-ray diffraction analysis were obtained from $EtOH/H_2O$ (Fig. 3). Elem. anal.: found % (calc. for $BaC_{18}H_{42}O_{15}$, $Ba(O_2C(CH_2)_4CO_2)$(18-crown-6)·$5H_2O$): C 33.66 (33.95), H 6.01 (6.65). Thermogravimetric analysis: observed weight loss 68.08%, expected weight loss 68.97% (based on $BaCO_3$ formation, and $Ba(O_2C(CH_2)_4CO_2)$(18-crown-6)·$5H_2O$ starting material); ^1H NMR (250 MHz, 25°C, D_2O): 3.56 ppm, s, crown; 2.01 ppm, t, O_2CCH_2-; 1.36 ppm, t, -$(CH_2)_2$-. IR (KBr): 3447 m, 2924 m, 1653 s, 1515 m, 1465 m, 1400 m, 1345 m, 1280 m, 1248 m, 1106 m, 1050 m, 965 m, 825 m, 668 m.

X-ray crystallographic data

Crystal data for $Ba(O_2CCH_3)_2$(18-crown-6)·$4H_2O$. $C_{16}H_{38}O_{14}Ba$, monoclinic, $P2_1/c$, $a = 9.5117(12)$, $b = 7.8112(9)$, $c = 16.906(2)$ Å, $\beta = 99.049(8)°$, $V = 1240.5(3)$ $Å^3$; $Z = 2$; $D_c = 1.584$g cm^{-3}; μ(Mo–K_α) = 23.73 cm^{-1}; $T = 25°C$, Siemens R3m/v, Mo–K_α. Of 3832 data ($4 < 2\theta < 55$), 2838 were independent, and 2036 were observed [$2\sigma(F_o)$]. The structure was solved by the Patterson method. Refinement: all non-hydrogen atoms anisotropic, all hydrogen atoms included in positions found in difference maps, $R(F) = 2.09\%$, $R(wF) = 2.23\%$, $GOF = 1.01$, $N_o/N_v = 13.5$, $\Delta(\rho) = 0.28$ $eÅ^3$, $\Delta/\sigma_{(max)} = 0.078$. SHELXTL software used for all computations (G. Sheldrick, Siemens XRD, Madison, WI, U.S.A.). An empirical (ψ-scan) correction was performed. The ratio of the transmission coefficients was 1.60. Crystallographic data are summarized in Table 1 and bond lengths and angles are reported in Table 2. Atomic positional parameters have been deposited with the Director, Cambridge Crystallographic Data Base.

Crystal data for $Ba(O_2C(CH_2)_4CO_2)$(18-crown-6)·$8H_2O$. $C_{18}H_{44}O_{18}Ba$, triclinic, $P\bar{1}$, $a = 8.5250(10)$, $b = 9.7690(10)$, $c = 10.2000(20)$ Å, $\alpha = 106.59(1)°$, $\beta = 90.37(8)°$, $\gamma = 110.34(1)°$, $V = 757.48(3)$ $Å^3$; $Z = 1$; $D_c = 1.504$g cm^{-3}; μ(Mo–K_α) = 23.73 cm^{-1}; $T = 25°C$, Siemens R3m/v, Mo–K_α. Of 6820 data ($2° \leqslant 2\theta° \leqslant 55°$), 3410 were independent, and 3321 were observed [$2\sigma(F_o)$]. The structure was solved by the Patterson method. Refinement: Fixed isotropic U set to 1.25 U (equiv.) of parent atom, all non-hydrogen atoms are isotropic, all hydrogen atoms included in positions found in difference maps, $R(F) = 4.44\%$, $R(wF) = 4.99\%$, $GOF = 0.89$, $N_o/N_v = 9.2$, $\Delta(\rho) = 2.87$ $eÅ^{-3}$, $\Delta/\sigma_{(max)} = 0.078$. SHELXTL software used for all computations (G. Sheldrick, Sie-

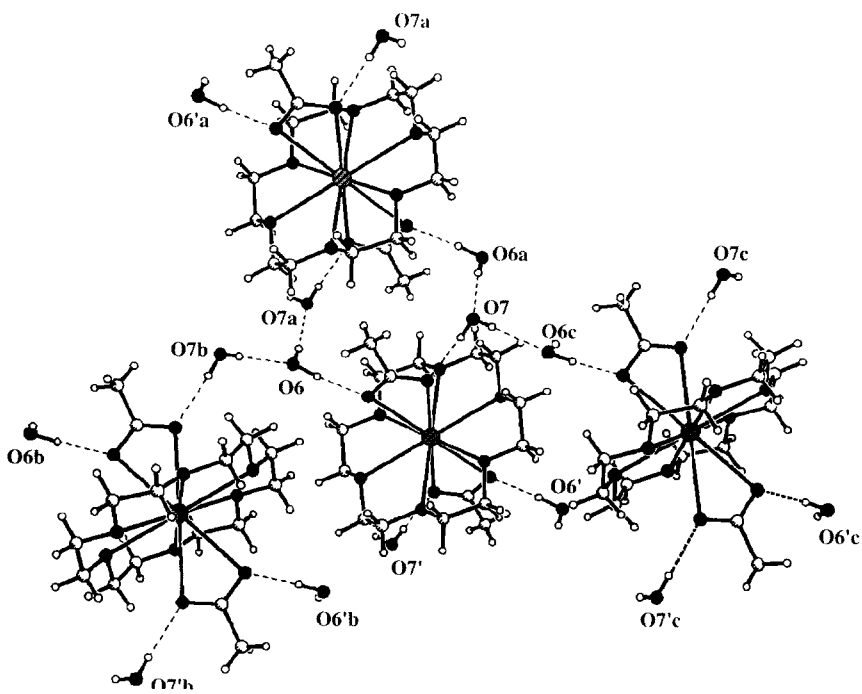

Fig. 3. The crystal structure of $Ba(O_2CCH_3)_2$(18-crown-6)·$4H_2O$.

Table 1. Crystallographic data for **1** and **2**

	1	**2**
Empirical formula	$C_{16}H_{38}BaO_{14}$	$C_{18}H_{48}BaO_{18}$
Formula weight	591.8	685.9
Color, habit	Colorless transparent plate	Clear transparent prism
Unit cell dimension		
a (Å)	9.512(1)	8.525(1)
b (Å)	7.811(1)	9.769(1)
c (Å)	16.906(1)	10.200(1)
α (°)	—	106.59(1)
β (°)	99.05(1)	90.37(1)
γ (°)	—	110.34(1)
Crystal system	Monoclinic	Triclinic
Space group	$P2_1/c$	$P\bar{1}$
T° K	293	293
λ Å	0.71073	0.71073
Z	2	1
Crystal size mm	$0.092 \times 0.161 \times 0.483$	$0.207 \times 0.276 \times 0.276$
Volume (Å^3)	1240.5(3)	757.4(1)
Reflection collected	3832	6820
Reflection used	2036	3321
Abspt. coeff. mm^{-1}	1.663	1.382
$R(F)$%	2.09	4.44
$R_w(F)$%	1.97	4.36

Table 2. Relevant bond lengths (Å) and angles (°) for **1**

Ba—O(1)	2.828(2)	Ba—O(2)	2.835(2)
Ba—O(3)	2.753(2)	Ba—O(4)	2.885(2)
Ba—O(5)	2.877(2)	O(2)—C(4)	1.431(4)
C(1)—O(1)	1.423(4)	C(5)—O(3)	1.445(4)
O(1)—C(2)	1.435(3)	O(5)—C(7)	1.251(3)
C(3)—O(2)	1.425(4)	O(4)—C(7)	1.246(4)
O(3)—C(6)	1.422(4)		
O(1)—Ba—O(2)	60.9(1)	O(1)—Ba—O(3)	120.3(1)
O(2)—Ba—O(3)	60.7(1)	O(1)—Ba—O(4)	108.0(1)
O(2)—Ba—O(4)	112.8(1)	O(3)—Ba—O(4)	104.8(1)
O(1)—Ba—O(5)	74.1(1)	O(2)—Ba—O(5)	70.9(1)
O(3)—Ba—O(5)	98.1(1)	O(4)—Ba—O(5)	45.0(1)
O(3)—Ba—O(1A)	59.7(1)	O(2)—Ba—O(1A)	119.1(1)
O(5)—Ba—O(1A)	105.9(1)	O(4)—Ba—O(1A)	72.0(1)
O(1)—Ba—O(2A)	119.1(1)	O(4)—Ba—O(2A)	67.2(1)
O(3)—Ba—O(2A)	119.3(1)	O(2)—Ba—O(3A)	119.3(1)
O(5)—Ba—O(2A)	109.1(1)	O(4)—Ba—O(3A)	75.2(1)
O(1)—Ba—O(3A)	59.7(1)	O(1)—Ba—O(4A)	72.0(1)
O(5)—Ba—O(3A)	81.9(1)	O(3)—Ba—O(4A)	75.2(1)
O(2)—Ba—O(4A)	67.2(1)	O(5)—Ba—O(4A)	135.0(1)
O(2)—Ba—O(5A)	109.1(1)	O(1)—Ba—O(5A)	105.9(1)
O(4)—Ba—O(5A)	135.0(1)	O(3)—Ba—O(5A)	81.9(1)
Ba—O(5)—C(7)	95.6(2)	Ba—O(4)—C(7)	95.3(2)
O(1)—Ba—O(2A)	119.1(1)	O(1)—Ba—O(4A)	72.0(1)
O(1)—Ba—O(3A)	59.7(1)	O(3)—Ba—O(4A)	75.2(1)
O(2)—BaO(4A)	67.2(1)	O(2)—Ba—O(4A)	67.2(1)
O(2)—Ba—O(5A)	109.1(1)	O(1)—Ba—O(5A)	105.9(1)
O(4)—Ba—O(5A)	135.0(1)	O(3)—Ba—O(5A)	81.9(1)

Table 3. Relevant Bond lengths(Å) and Angles(°) for **2**

Ba—O(1)	2.805(3)	Ba—O(2)	2.794(3)
Ba—O(3)	2.792(3)	Ba—O(4)	2.979(4)
Ba-O(5)	2.761(4)	Ba—C(7)	3.234(5)
O(1)—C(1)	1.424(5)	O(1)—C(6A)	1.428(7)
O(2)—C(2)	1.436(6)	O(2)—C(3)	1.426(8)
O(3)—C(4)	1.428(5)	O(3)—C(5)	1.431(6)
O(4)—C(7)	1.253(6)	O(5)—C(7)	1.247(6)
O(1)—Ba—O(2)	60.3(1)	O(1)—Ba—O(3)	119.4(1)
O(2)—Ba—O(3)	60.3(1)	O(1)—Ba—O(4)	69.7(1)
O(2)—Ba—O(4)	76.1(1)	O(3)—Ba—O(4)	106.3(1)
O(1)—Ba—O(5)	113.8(1)	O(2)—Ba—O(5)	92.7(1)
O(3)—Ba—O(5)	79.8(1)	O(4)—Ba—O(5)	44.6(1)
O(2)—Ba—O(1A)	119.7(1)	O(3)—Ba—O(1A)	60.6(1)
O(4)—Ba—O(1A)	110.3(1)	O(5)—Ba—O(1A)	66.2(1)
O(4)—Ba—O(2A)	103.9(1)	O(3)—Ba—O(2A)	119.7(1)
O(5)—Ba—O(3A)	100.2(1)	O(5)—Ba—O(2A)	87.3(1)
O(1)—Ba—O(4A)	110.3(1)	O(4)—Ba—O(3A)	73.7(1)
O(5)—Ba—O(4A)	135.4(1)	O(2)—Ba—O(4A)	103.9(1)
Ba—O(5)—C(7)	100.8(3)	Ba—O(4)—C(7)	90.1(3)
O(4)—C(7)—O(5)	121.9(4)		

mens XRD, Madison, WI, U.S.A.). An empirical (ψ-scan) correction was performed. The ratio of the transmission coefficients was 1.12. Crystallographic data are summarized in Table 1 and bond lengths and angles are reported in Table 3. Atomic positional parameters have been deposited with the Director, Cambridge Crystallographic Data Base.

Spin-coating experiments

The following is the general procedure used for thin film deposition: A mixture of 0.100 g (0.16 mmol) of $Ba(O_2CCH_3)_2$(18-crown-6) and 0.0452 g (0.16 mmol) $Ti(O\text{-}i\text{-}Pr)_4$ was dissolved in 1.5 cm^3 of EtOH. A Pt/Si/SiO_2 wafer was placed upon a rotating mount and spun at 3000 rpm. A syringe containing the mixture of barium and titanium precursors was used to drop the solution on the wafer, three drops at a time followed by heating in an oven (in air) to 200°C for 5 min. When 21 drops, approximately 0.3 cm^3, were added the film was placed in an oven at 200°C for 5 min for the last time. The films were then annealed at 700°C for 1 h.

RESULTS AND DISCUSSION

The preparation of **1** involved adding the polyether ligand to barium acetate dissolved in water and stirring the solution. The solvent was removed under vacuum and crystalline powder remained (XRD). Compound **1** was recrystallized from H_2O. Compound **2** was synthesized by adding 18-crown-6 to a heated aqueous suspension of $BaCO_3$ and then reacting the mixture with adipic acid. The solvent was removed under vacuum and the crystalline powder (XRD) was recrystallized in a EtOH/H_2O mixture to give single-crystals of sufficient quality to be analyzed by single-crystal X-ray diffraction. The coordinated H_2O was removed under vacuum from complexes **1** and **2** but the resulting species, while dehydrated, exhibited relatively low solubility in other solvents other than water. Furthermore, care has to be taken not to remove the crown ether ligands during dehydration.

The thermogravimetric analysis and single-crystal structural data for **1** agree with the presence of four water molecules of crystallization. However, the sample submitted for elemental analysis was recrystallized from water and is consistent with the presence of six water molecules of crystallization. The difference in water content probably results from the recrystallization process. In the case of **2** elemental and thermogravimetric analyses show that the sample contains five water molecules whereas the recrystallized sample contains eight water molecules of crystallization. Again the difference in degree of hydration probably originates from the different methods by which the fractions were obtained.

There are two peaks in the ^1H NMR spectrum of **1** at 1.72 and 3.57 ppm consistent with the methyl protons of the acetate ligand and the methylene protons of the 18-crown-6, respectively. The ^1H NMR spectroscopic data for **2** shows a singlet associated with the methylene protons of the crown ether at 3.56 ppm and two multiplets derived from the methylene protons of the adipate ligand. The solution ^1H NMR spectra are consistent with the empirical formulae.

The presence of two ν(O—H) vibrational bands in the IR spectrum of **1** is consistent with the compound having two types of H_2O of crystallization with

ν(O—H) at 3421 cm^{-1} and 3249 cm^{-1}. The infra red spectroscopic data for **2** show a peak at 3447 cm^{-1} also consistent with the presence of H_2O. In **1**, the $\nu_{asym}(CO_2)$ can be assigned to the peak at 1560 cm^{-1} and $\nu_{sym}(CO_2)$ is likely the peak observed at 1419 cm^{-1}. These values are consistent with a general trend of values observed by Deacon *et al.* for a series of metal carboxylate and metal trifluorocarboxylate complexes [45]. Deacon *et al.* further suggest that it is possible to infer the mode of coordination of the carboxylate group to the metal center by measuring the difference between the asymmetric and symmetric $\nu(CO_2)$ stretches, $\Delta(CO_2)$. The literature values for a chelating or bridging mode of coordination in acetato complexes is $\Delta(CO_2) < 150$ cm^{-1}. The observed $\nu_{asym}(CO_2)$ and $\nu_{sym}(CO_2)$ peak positions lead to a $\Delta(CO_2)$ of 141 which is consistent with either a chelating or bridging mode of acetate coordination.

The assignment of the $\nu(CO_2)$ peaks associated with the metal adipate precursor is not as simple because there are four peaks which could be assigned to $\nu(CO_2)$. Deacon *et al.* warn that their conclusions are less likely to extend to other more complex carboxylate precursors such as those containing dicarboxylates [45]. Thus assigning structural inference in the adipate complex would be at best speculative and have not been attempted here.

The title compounds were structurally characterized in the solid state by single-crystal X-ray diffraction. The molecular structure and atom numbering scheme for **1** is shown in Fig. 2 and a view of the crystal structure of **1** is presented in Fig. 3 emphasizing the nature of water binding. In **1** the Ba atom lies in the center of the 18-crown-6 ring with chelating acetate ligands being in the axial positions of the equitorial coordination plane. Analogous structures have been observed for $Ba(hfac)_2$(18-crown-6) [32,33] and $Ba(O_2CC\text{-}t\text{-}Bu)_2$(18-crown-6) [46]. The Ba—O ether and carboxylate bond distances are similar in both **1** and $Ba(O_2CC\text{-}t\text{-}Bu)_2$(18-crown-6) and have average values of 2.805(45) Å and 2.823(10) Å ($Ba—O_{ether}$) and 2.881(6) Å and 2.834(18) Å ($Ba—O_{carboxylate}$), respectively. The O—C—O angles of the carboxylate ligands in the above compounds are almost identical at 123.8(3)° and 123.8(9)°, respectively.

There are two distinct types of water molecules involved in the hydrogen bonding in **1**. The water molecules of both types hydrogen bond to a carboxylate oxygen atom and two adjacent water molecules [O(6)···O(5) 2.808, O(6)···O(7a) 2.900 Å; O(7)···O(4) 2.864, O(7)···O(6c) 2.893 Å], however, the O···O distance between one type of water molecule and a carboxylate oxygen atom is larger by ca 0.06 Å. The fact that the water molecules are not coordinated to the barium atom suggests that the ten coordinate barium center is coordinatively saturated.

Both **1** and **2** are quite similar in their local geometry as shown by the molecular structure of **2** in Fig. 4. As in **1**, the barium atom in **2** resides at the center of the 18-crown-6 ring. Although compound **2** has a dicarboxylate ligand capable of chelating to the barium atom through both carboxylate groups, it instead bridges between two barium atoms to form an infinite polymer. This geometry allows the barium atom to sit at the center of the 18-crown-6 ring. It is expected based on size comparisons that this configuration provides the best interaction for the barium atom with the six oxygen atoms of the 18-crown-6 ether [47]. As in **1**, the oxygen atoms of the carboxylate ligands in **2** have hydrogen bonds from surrounding water molecules. However, the carboxylate groups in **2** are not symmetrically bound to the barium atom as in **1**. Two types of $Ba—O_{carboxylate}$ bond distances exist; a long bond at 2.979(4) Å and a short bond at 2.761(4) Å. The $Ba—O_{ether}$ bond distances are all similar and have an average value of 2.797(7) Å. The reason for the asymmetric bonding of the adipate ligand is not clear but may be a result of both hydrogen bonding and/or crystal packing. The $[Ba(O_2C(CH_2)_4CO_2)$(18-crown-6)$\cdot 8H_2O]_n$ chains pack in a staggered fashion such that the crowns of adjacent chains are aligned with the adipate bridges to give an [-adipate-crown-adipate-crown-]$_n$ sequence approximately perpendicular to the chain direction. This packing arrangement creates large serpentine channels in the crystal in which the waters of hydration reside, see Fig. 5.

The TGA data for **1** and **2** are shown in Fig. 6a and

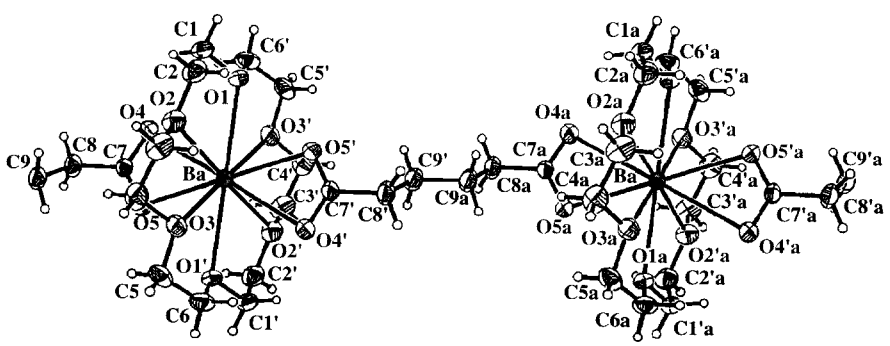

Fig. 4. The molecular structure of $Ba(O_2C(CH_2)_4CO_2)$(18-crown-6)$\cdot 8H_2O$.

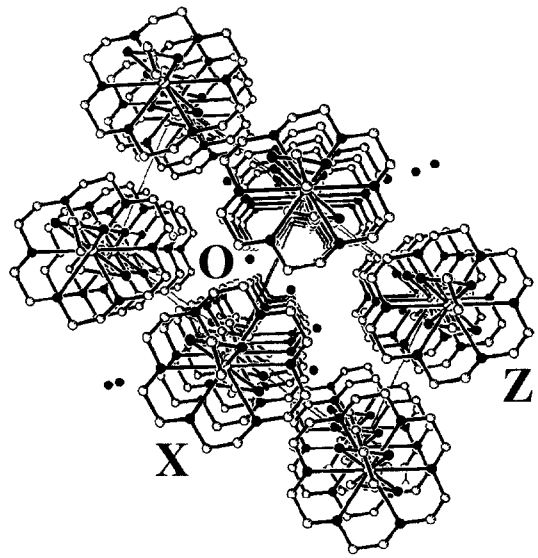

Fig. 5. The crystal structure of $Ba(O_2C(CH_2)CO_2)(18\text{-crown-}6)\cdot 8H_2O$.

6b. For **1** (see Fig. 6a), the total weight loss of ~66% is consistent with the decomposition to form $BaCO_3$ which was confirmed by powder XRD. The weight loss takes place in four distinct steps. The first two

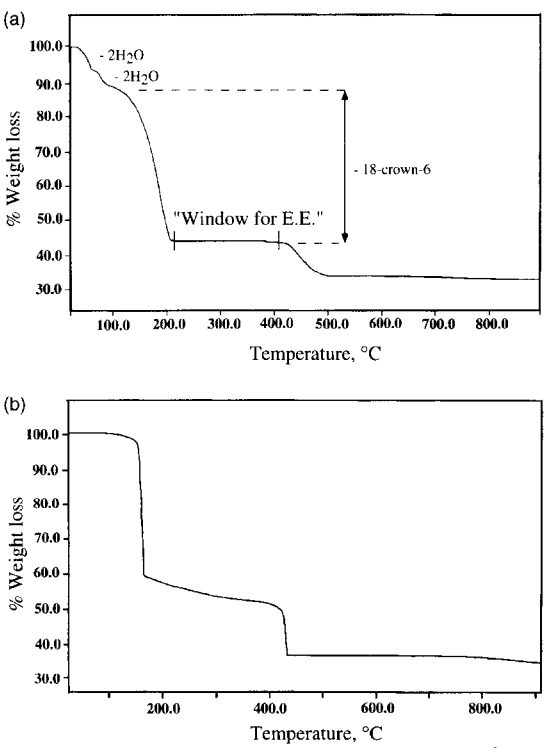

Fig. 6. Thermal gravimetric analysis data for (a) $Ba(O_2CCH_3)_2(18\text{-crown-}6)\cdot 4H_2O$ and (b) $Ba(O_2C(CH_2)_4CO_2)(18\text{-crown-}6)\cdot 5H_2O$.

occur between 50°C and 120°C and are consistent with loss of four water molecules, two in each step. This corresponds to the two different types of waters of crystallization observed by the IR spectroscopy data and shown in the crystal structure. The next step is consistent with loss of the 18-crown-6 ligand. Separate sublimation experiments reveal that the 18-crown-6 ligand is removed intact from the complex (as determined by ^1H NMR) on heating to 200°C. There is no further weight loss until around 410°C where reaction of the remaining organic substituents takes place with the formation of $BaCO_3$. This weight loss is complete by 500°C. The TGA data show that after the loss of water and crown ether, the barium acetate formed does not undergo a weight change over a temperature range of ~200°C. This provides a "window" for ester elimination where the barium acetate remains intact and is available to react with another species such as a metal alkoxide.

The TGA data for **2** (Fig. 6b) exhibits a two stage weight loss to give a product with mass, within the error limits, expected for formation of $BaCO_3$. The first stage of the decomposition begins at about 100°C and ends around 170°C. The total weight loss suggests the removal of the 18-crown-6 ligand and five equivalents of H_2O (55% calc., observed ~ 53.5%). The small step up to the inflection point corresponds closely to the loss of three equivalents of H_2O (~ 8.5%). The remaining weight loss corresponding to the reaction of the adipate ligand (calc. ~15%, observed ~14.5%) to form $BaCO_3$ at ~450°C. For **2**, there does not appear to be a thermal "window" for ester elimination analogous to the TGA of **1** above, because there is significant weight loss between the onset of thermal decomposition and the formation of $BaCO_3$ (i.e. there is no flat region in the TGA plot as there is for **1**). This may make this species unsuitable for clean reaction with a metal alkoxide.

Compound **1** was dehydrated and used as a precursor to form $BaTiO_3$ films via spin-coating by reaction with $Ti(O\text{-}i\text{-}Pr)_4$. An ethanol solution of **1** and $Ti(O\text{-}i\text{-}Pr)_4$ in a 1 : 1 mol ratio were spun onto a Pt/Si/SiO_2 wafer and between each coating the substrate and film were heated to 200°C for 5 min in air. The films were amorphous at this temperature (by XRD). On heating to 700°C for 1 h in air, X-ray diffraction showed the presence of crystalline perovskite phase $BaTiO_3$ and crystalline $BaCO_3$ (°) as the only crystalline phases (Fig. 7). The presence of some $BaCO_3$ is not unexpected since the deposition and annealing steps were performed in air and when dehydrated **1** was used to deposit a film without titanium precursor only $BaCO_3$ was deposited (XRD). Scanning electron microscopy revealed the film was approximately 10 μm thick and fairly extensively cracked as would be expected for such a thick film. The cross-sectional and surface views are shown in Fig. 8. Auger electron spectroscopy analysis of the film reveals the presence of Ba : Ti : O and C in the ratios of approximately 2 : 3 : 8 : 1, respectively. These data are consistent with

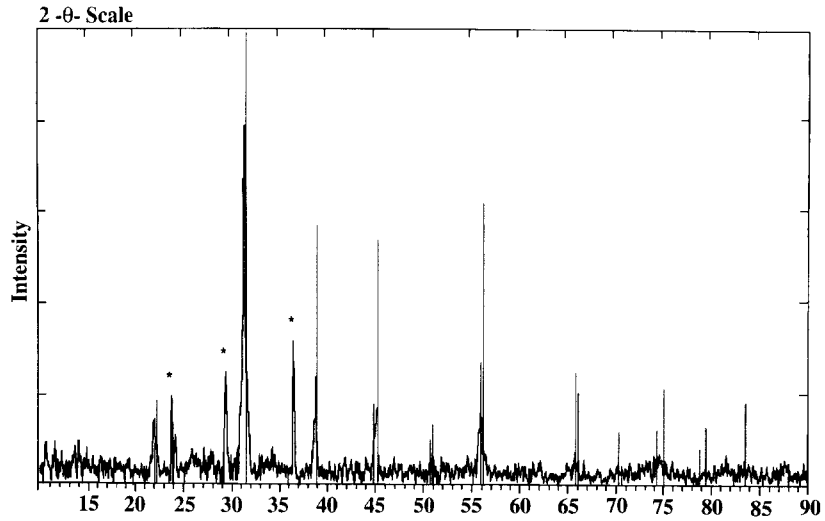

Fig. 7. X-ray diffraction data for thin film deposited by spin-coating an ethanol solution of $Ba(O_2CCH_3)_2$(18-crown-6) and $Ti(O\text{-}i\text{-}Pr)_4$.

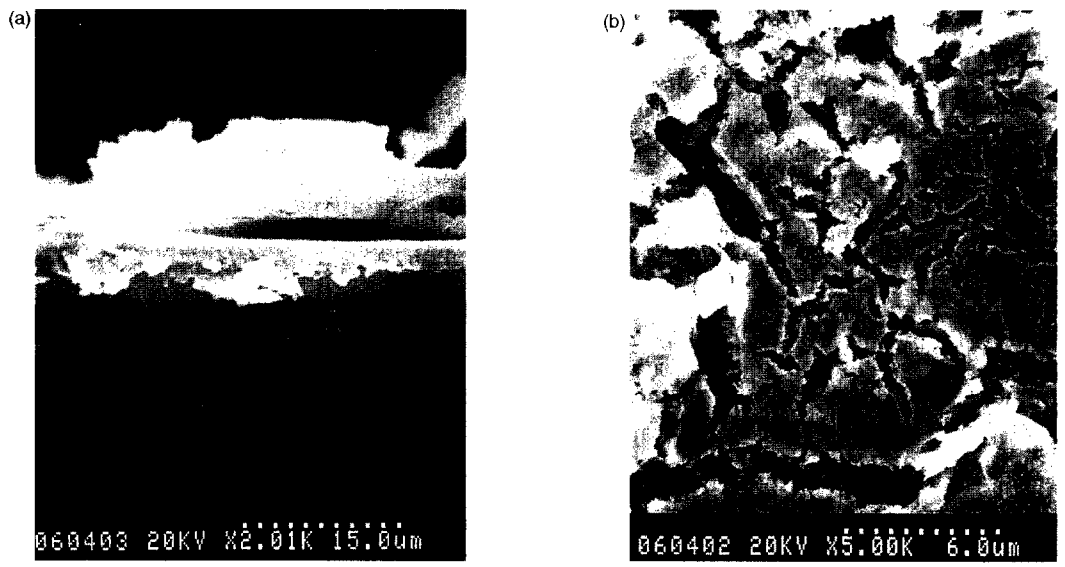

Fig. 8. (a) Scanning electron micrograph of a cross-section of the $BaTiO_3$ film formed from the deposition of $Ba(O_2CCH_3)_2$(18-crown-6) and $Ti(O\text{-}i\text{-}Pr)_4$ annealed at 700°C for 1 h. (b) Scanning electron microscopic image of the surface of the $BaTiO_3$ film formed from the deposition of $Ba(O_2CCH_3)_2$(18-crown-6) and $Ti(O\text{-}i\text{-}Pr)_4$ annealed at 700°C for 1 h.

the presence of $BaTiO_3$ and $BaCO_3$, as observed by X-ray diffraction and also the presence of amorphous TiO_2. Numerous attempts were made to determine the nature of the organic byproducts formed during this reaction both *in situ* using quadrupole mass spectroscopy and *ex situ* by conduction solid state experiments, but no unambiguous evidence for the formation of an ester could be obtained.

Attempts to form films under similar conditions from **2** proved unsuccessful with TiO_2 and $BaCO_3$ being the only identifiable crystalline phases present by XRD. When control experiments using **1** and **2** were performed without a titanium source, the only species obtained was barium carbonate as determined by XRD.

SUMMARY AND CONCLUSIONS

The synthesis and characterization of two new barium carboxylates has been described. The acetate complex is monomeric and may prove useful as a source of barium for CVD The oligomeric nature of the adipate complex rules out it usefulness as a CVD

precursor. The thermal behavior of **1** demonstrates the loss of the crown and carboxylate ligand takes place in two distinct steps while for **2**, there is significant weight loss from the onset of loss of the crown ether ligand to the onset of reaction of the adipate ligands. The reaction of compound **1** with $Ti(O\text{-}i\text{-}Pr)_4$ resulted in formation of $BaTiO_3$, although no evidence for a mechanism which involved ester elimination was obtained. Coumpound **2** did not form barium titanate under analogous conditions which may indicate the significance of the TGA data which showed the absence of a thermal "window" for ester elimination for **2**.

Acknowledgments—We would like to thank Texas Instruments for their financial support of this project, the NSF Chemical Instrumentation program for the purchase of a low field NMR spectrometer and AFOSR and the Camille and Henry Dreyfus Foundation for the purchase of the X-ray diffractometer. M.H.-S. would like to thank Prof. Don Bradley for many helpful discussions and much encouragement over the last 15 years.

REFERENCES

1. Klein, L. C., *Sol–Gel Technology for Thin Films, Fibers, Preforms, Electronics and Specialty Shapes*, Noyes Publications, Park Ridge, 1988.
2. Brinker, C. J. and Scherer, G. W., *Sol–Gel Science: The Physics and Chemistry of Sol–Gel Processing*, Academic Press, Boston, 1990.
3. Caulton, K. G. and Hubert-Pfalzgraf, L. G., *Chem. Rev.*, 1990, **90,** 969.
4. Hubert-Pfalzgraf, L. G., *New J. Chem.*, 1987, **11,** 663.
5. Bradley, D. C., Mehrotra, R. C. and Gaur, D. P., *Metal Alkoxides*, Academic Press, London, 1978.
6. Bradley, D. C., *Coord. Chem. Rev.*, 1967, **2,** 299.
7. Bradley, D. C. and Holloway, H., *Can. J. Chem.*, 1962, **40,** 1176.
8. Chandler, C. D., Roger, C. and Hampden-Smith, M. J., *Chem. Rev.*, 1993, **93,** 1205.
9. Wojtczak, W. A., Fleig, P. and Hampden-Smith, M. J., *Adv. Organomet. Chem.*, 1996, **40,** 215–340.
10. Day, V. W., Eberspacher, T. A., Klemperer, W. G. and Park, C. W., *J. Am. Chem. Soc.*, 1993, **115,** 8469.
11. Hubert-Pfalzgraf, L. G., *Polyhedron*, 1994, **13,** 1181.
12. Turova, N. Y., Tureskaya, E. P., Kessler, V. G., Yanovsky, A. I. and Struchkov, Y. T., *J. Chem. Soc. Chem. Commun.*, 1993, 21.
13. Caulton, K. G., Chisholm, M. H., Drake, S. R. and Streib, W. E., *Angew. Chem. Int. Ed. Engl.*, 1990, **29,** 1483.
14. Bradley, D. C. and Thomas, I. M., *J. Chem. Soc., A.*, 1959, 3404.
15. Caruso, J., Hampden-Smith, M., Rheingold, A. L. and Yap, G., *J. Chem. Soc. Commun.*, 1995, **2,** 157.
16. Caruso, J., Roger, C., Schwertfeger, F., Hampden-Smith, M., Rheingold, A. and Yap, G., *Inorg. Chem.*, 1995, **34,** 449.
17. Wojtczak, W., Atanasova, P., Duesler, E. and Hampden-Smith, M. J., *Inorg. Chem.*, 1996, **35,** 6995.
18. Wojtczak, W. A., Hampden-Smith, M. J. and Duesler, E. N., *Inorg. Chem.*, 1996, **35,** 6638.
19. Warren, W. L., Dimos, D. B., Tuttle, B. A., Nasby, R. D. and Pike, G. E., *Appl. Phys. Lett.*, 1994, **65,** 1018.
20. Boyle, T. J., Bucheit, C. D., Rodriguez, M. A., Al-Shareef, H. N., Hernandez, B. A., Scott, B. and Ziller, J. W., *J. Mater. Res.*, 1996, **9,** 2246.
21. Han, B., Neumayer, D. A., Goddreau, B. H., Marks, T. J. Zhang, H. and Dravid, V. P., *Chem. Mater.*, 1994, **6,** 18.
22. Marks, T. J., *Pure Appl. Chem.*, 1995, **67,** 313–318.
23. Larbalestier, D. C., *MRS Bulletin*, 1992, **XVII,** 16.
24. Sheng, Z. Z. and Hermann, A. M., 1988, **332,** 138.
25. Bednorz, J. G. and Muller, A. K., *Z. Physik. B.*, 1986, **64,** 189.
26. Hibst H., *Angew. Chem., Int. Ed. Engl.*, 1982, **21,** 270.
27. Hibst, H. and Schwab, E. in *Materials Science and Technology*, ed. R. W. Cahn, P. Haasen and E. J. Kramer, VCH, Weinhiem 1994.
28. Kodas, T. T. and Hampden-Smith, M. J., *The Chemistry of Metal CVD*. VCH, Weinheim, 1994.
29. Rees, W. S., in *CVD of Semiconductors*, ed. W. S. Rees, VCH, Weinheim, 1996.
30. Kobayashi, I., Wakao, Y., Tomigana, K. and Okada, M., *Jpn. J. Appl. Phys.*, 1994, **33,** 4680–4683.
31. Neumayer, D. A., Studebaker, D. B., Hinds, B. J., Stern, C. L. and Marks, T. J., *Chem. Mater.*, 1994, **6,** 878–880.
32. Norman, J. A. T. and Pez, G. P., *J. Chem. Soc., Chem. Commun.*, 1991, **14,** 971–2.
33. Timmer, K., and Meinema, H. A., *Inorganica Chimica Acta*, 1991, **187,** 99–106.
34. Feil, W. A., Wessels, B. W., Tonge, L. M. and Marks, T. J., *J. Appl. Phys.*, 1990, **67,** 3858–61.
35. Gilbert, S. R., Wessels, B. W., Studebaker, D. B. and Marks, T. J., *Appl. Phys. Lett.*, 1995, **66,** 3298–300.
36. Wessels, B. W. Zhang, J. M., DiMeo, F. Jr., Richeson, D. S., Marks, T. J., DeGroot, D. C. and Kannewurf, C. R., *Proc. SPIE-Int. Soc. Opt. Eng.*, 1991, **1394,** 232–7.
37. Wills, L. A., Wessels, B. W., Richeson, D. S. and Marks, T. J., *Appl. Phys. Lett.*, 1992, **60,** 41–3.
38. Zhang, J. M., Wessels, B. W., Richeson, D. S. and Marks, T. J., *J. Cryst. Growth*, 1991, **107,** 705–9.
39. Purdy, A. P., Berry, A. D., Holm, R. T., Fatemi, M. and Gaskill, D. K. *Inorg. Chem.*, 1989, **28,** 2799–803.
40. Gardiner, R. A., Gordon, D. C., Stauf, G. T. and Vaartstra, B. A., *Chem. Mater.*, 1994, **6,** 1967–1970.
41. Caruso, J., Alam, T. M. and Hampden-Smith, M. J., *J. Chem. Soc., Dalton Transactions*, 1996, 2659.
42. Nyman, M., Duesler, E. N. and Hamden-Smith, M. J., *Adv. Mater., CVD*, 1995, **2,** 171.

43. Shang, G., Duesler, E. N. and Hampden-Smith, M. J. *Adv. Mater. CVD*, 1996, **2,** 242–246.
44. Shang, G., Duesler, E. N. and Hampden-Smith, M. J., *J. Chem. Soc., Chem. Commun.*, 1996, 1733.
45. Deacon, G. B. and Phillips, R. J., *Coord. Chem. Rev.*, 1980, **33,** 227.
46. Rheingold, A. L., White, C. B., Haggerty, B. S., Kirlin, P. and Gardiner, R. A., *Acta Cryst.*, 1993, **C49,** 808.
47. Hay, B. P., and Rustad, J. R., *J. Am. Chem. Soc*, 1994, **116,** 6316–26.

Pergamon

PII: S0277-5387(97)00373-2

Polyhedron Vol. 17, No. 5–6, pp. 725–736, 1998
© 1998 Elsevier Science Ltd
All rights reserved. Printed in Great Britain
0277–5387/98 $19.00+0.00

Synthesis and reactivity of η^6-arene ruthenium anilide complexes

James M. Boncella,* Tegan M. Eve, Barry Rickman and Khalil A. Abboud

Department of Chemistry and Center for Catalysis, University of Florida, Gainesville, Florida 32611-7200, U.S.A.

(Received 23 June 1997; accepted 8 August 1997)

Abstract—The compounds, $(\eta^6\text{-}C_6Me_6)Ru(PMe_3)(R)(NR'R'')$; (R=Ph, R′=H, R″=Ph, **3**; R=Me, R′=H, R″=Ph, **4**; R=Ph, R′=H, R″=*p*-tol, **5**; R=Me, R′=Me, R″=Ph, **6**) are synthesized through the interaction of $(\eta^6\text{-}C_6Me_6)Ru(PMe_3)(R)(I)$ and the corresponding anilide salt, KNR′R″ in THF at low temperature. The reactions between these complexes and the unsaturated electrophilic reagents, CO_2 and dimethylacetylene dicarboxylate (DMAD) have been described. The typical reaction involves net insertion of the electrophile into the Ru anilide bond. Complex **6** reacts with H_2O giving the hydroxide complex, **11**, which reacts with CO_2 giving the bicarbonato complex, **12**. The X-ray crystal structure of **3** is reported. Compound **3** crystallizes in the monoclinic space group, $P2_1/n$, $a = 12.013(2)$ Å, $b = 16.700(3)$ Å, $c = 12.414(1)$ Å, $\beta = 97.35(2)$, $V = 2470.0(7)$ Å^3 and $Z = 4$. © 1998 Elsevier Science Ltd. All rights reserved

Keywords: η^6-arene ruthenium anilide complexes; unsaturated electrophilic reagents; CO_2; DMAD.

We have been interested in the chemistry of late (group 8–10) transition metal amide complexes to investigate their reactivity and to examine the possibility of using them in stoichiometric or catalytic C—N bond forming reactions. The relative scarcity [1] of ruthenium compounds of this type sparked our interest in their chemistry. Our attention has been focused on the $(\eta^6\text{-}C_6Me_6)Ru(PMe_3)(R)(NHR)$ class of compounds because of their ease of preparation and the fact that they are isoelectronic with the $Cp^*Ir(PMe_3)(R)X$ (X = NHR, OR, etc.) compounds which have been demonstrated to participate in an interesting array of reactions [2]. Furthermore, the chemistry of $(\eta^6\text{-}C_6Me_6)Ru(PMe_3)(Ph)NHPh$ can be compared with other 18 e$^-$ group 8 anilide and imido complexes such as $(PMe_3)_4Ru(H)(NHPh)$[1h] and (*p*-Cym)OsNR [3]. In this paper we describe the synthesis, and characterization of a series of arene Ru anilide complexes. The reactivity of these molecules with the unsaturated electrophiles, CO_2 and dimethylacetylene dicarboxylate (DMAD) are also reported. The reaction of a hydroxide derivative with CO_2 to give a bicarbonato complex is also described.

* Author to whom correspondence should be addressed.

EXPERIMENTAL

All procedures were performed using either Schlenk or dry box techniques, under an inert atmosphere of either argon or nitrogen. Pentane and diethyl ether (Et_2O) were distilled from sodium/benzophenone and subsequently degassed. Methylene chloride was distilled from P_2O_5 and degassed. Tetrahydrofuran (THF) was dried by refluxing over potassium metal prior to distillation and then degassed after distillation. Deuterated solvents were dried over molecular sieves and degassed prior to use. ^1H, ^{13}C, and ^{31}P NMR spectra were recorded on a Varian VXR-300 (300 MHz), or a General Electric QE-300 (300 MHz) spectrometer. Chemical shifts for ^1H and ^{13}C spectra were referenced to residual proton signals in the solvent and are reported relative to TMS; shifts for ^{31}P spectra are reported relative to external 85% H_3PO_4. Elemental analyses were performed by the University of Florida Analytical Services or Atlantic Microlab, Inc., Norcross, Georgia. Infrared spectra were recorded on a Perkins Elmer 1200 series spectrometer from KBr pellets which were prepared in an inert atmosphere glove box. Mass spectroscopy data were obtained with a Finnigan 4500 Gas Chromatograph/Mass Spectrometer using FAB techniques.

The following compounds were purchased from Aldrich Chemical Co., and were used without further purification: dimethylacetylene dicarboxylate, phenyl lithium, methyl lithium, sodium iodide, and para-toluidine. Aniline and *N*-methyl aniline were distilled from sodium metal.

The potassium amides were synthesized by reacting the appropriate aniline and KH in THF, with KN(Me)Ph being prepared by modified literature procedures [4]. $(\eta^6\text{-}C_6Me_6)Ru(PMe_3)Cl_2$ was prepared according to literature methods [5], and $(\eta^6\text{-}C_6Me_6)Ru(PMe_3)I_2$ was prepared by ion exchange with NaI and $(\eta^6\text{-}C_6Me_6)Ru(PMe_3)Cl_2$ under reflux in acetone following the procedure used for the synthesis of $Cp^*Rh(PMe_3)I_2$ [6].

Preparation of $(\eta^6\text{-}C_6Me_6)Ru(PMe_3)(Ph)I$ (**1**)

To a stirring solution of $(\eta^6\text{-}C_6Me_6)Ru(PMe_3)I_2$ (1.037 g, 1.748 mmol) in 75 ml of THF was added dropwise 1.07 ml of a 1.8 M solution of LiPh in toluene/Et_2O (1.9 mmol). The solution immediately turned from purple to orange-red. After 45 min the solvent was removed under reduced pressure to leave an orange-red oil. The product was extracted with Et_2O until the extracts were colorless. The combined extracts were reduced in volume and cooled to -20°C giving deep red crystals of **1** (0.599 g, 1.102 mmol) in 63% yield. Anal. Calc. for $C_{21}H_{32}IPRu$: C, 46.41; H, 5.94. Found: C, 46.11; H, 5.95.

Preparation of $(\eta^6\text{-}C_6Me_6)Ru(PMe_3)(Me)I$ (**2**)

To a stirring solution of $(\eta^6\text{-}C_6Me_6)Ru(PMe_3)I_2$ (3.50 g, 5.90 mmol) in 125 ml of THF was added dropwise 5.15 ml of a 1.26 M solution of LiMe in Et_2O (6.49 mmol). The solution immediately turned from purple to orange-red. After 45 min the solvent was removed under reduced pressure to leave a red oil. The product was extracted with Et_2O until the extracts were colorless. The combined extracts were reduced in volume and cooled to -20°C giving deep red crystals of **2** (2.12 g, 4.40 mmol) in 75% yield. Anal. Calc. for $C_{16}H_{30}IPRu$: C, 39.93; H, 6.28. Found: C, 39.04; H, 6.21. HRMS (FAB) (Calc.): 466.993 $(M\text{-}CH_3)^+$. (Found): 467.010 $(M\text{-}CH_3)^+$.

Preparation of $(\eta^6\text{-}C_6Me_6)Ru(PMe_3)(NHPh)(Ph)$ (**3**)

To a cold (-78°C) stirring solution of **1** (0.730 g, 1.436 mmol) in 100 ml of THF was added a solution of KNHPh (0.264 g, 2.015 mmol) in 25 ml of THF. After 45 min the reaction mixture was allowed to come to room temperature, whereupon it slowly turned from clear red to brown with white precipitates. After stirring 2 h longer, the solvent was removed under reduced pressure to leave a sticky solid. The product was extracted with Et_2O until the extracts were colorless. The combined extracts were reduced in volume and cooled to -50°C giving deep red crystals of 3 (0.404 g, 0.795 mmol) in 55% yield. IR (KBr): 3330.6 cm^{-1} ($\nu_{N\text{-}H}$). Anal. Calc. for $C_{27}H_{38}NPRu$: C, 63.74; H, 7.53; N, 2.75. Found: C, 62.85; H, 7.58; N, 2.67. HRMS (FAB) (Calc.): 509.1779 $(M+1)^+$. (Found): 509.1659 $(M+1)^+$.

Preparation of $(\eta^6\text{-}C_6Me_6)Ru(PMe_3)(NHPh)(Me)$ (**4**)

To a cold (-78°C) stirring solution of **2** (0.320 g, 0.665 mmol) in 50 ml of THF was added a solution of KNHPh (0.31 g, 0.997 mmol) in 25 ml of THF. After 45 min the reaction mixture was allowed to come to room temperature, whereupon it slowly turned from clear red to red-brown with white precipitates. After stirring 2 h longer, the solvent was removed under reduced pressure to leave a sticky solid. The product was extracted with Et_2O until the extracts were colorless. The combined extracts were reduced in volume and cooled to -50°C giving large, opaque red crystals of **5** (0.320 g, 0.718 mmol) in 72% yield. IR (KBr): 3329.7 cm^{-1} ($\nu_{N\text{-}H}$). Anal. Calc. for $C_{22}H_{36}NPRu$: C, 59.17; H, 8.13; N, 3.14. Found: C, 59.25; H, 8.18; N, 3.10.

Preparation of $(\eta^6\text{-}C_6Me_6)Ru(PMe_3)(NHC_6H_4CH_3)(Ph)$ (**5**)

To a cold (-78°C) stirring solution of **1** (0.980 g, 1.875 mmol) in 75 ml of THF was added a solution $KNHC_6H_4CH_3$ (0.393 g, 2.705 mmol) in 30 ml of THF. After 30 min the reaction mixture was allowed to come to room temperature, whereupon it slowly turned from clear red to orange-brown with white precipitates. After stirring 1 h longer, the solvent was removed under reduced pressure to leave a solid. The product was extracted with diethyl ether until the extracts were colorless. The combined extracts were reduced in volume and cooled to -50°C giving powdery orange crystals of **8** (0.608 g, 1.163 mmol) in 62% yield. IR (KBr): 3361.4 cm^{-1} ($\nu_{N\text{-}H}$). Anal. Calc. for: $C_{28}H_{40}NPRu$ C, 64.34; H, 7.71; N, 2.68. Found: C, 64.26; H, 7.72; N, 2.63.

Preparation of $(\eta^6\text{-}C_6Me_6)Ru(PMe_3)(NMePh)(Me)$ (**6**)

To a cold (-78°C) stirring solution of **2** (0.250 g, 0.519 mmol) in 40 ml of THF was added a solution of KNMePh (0.113 g, 0.778 mmol) in 25 ml of THF. After 45 min the reaction mixture was allowed to come to room temperature, whereupon it slowly turned from clear red to red-brown with white precipitates. After stirring 2 h longer, the solvent was removed under reduced pressure to leave a solid. The product was easily extracted with a small volume (25 ml) of diethyl ether. The extract was reduced in volume and

cooled to -50°C giving large, red crystals of **6** (0.130 g, 0.282 mmol) in 54% yield. Anal. Calc. for $C_{23}H_{38}NPRu$: C, 59.98; H, 8.32; N, 3.04. Found: C, 59.77; H, 8.28; N, 2.94.

Reaction of **3** *with carbon dioxide. Synthesis of* (η^6-C_6Me_6)Ru(PMe_3)(OC(O)NHPh)(Ph) (**7**)

Charging a sealable NMR tube with ~30 mg of **3** in C_6D_6 with an atmosphere of carbon dioxide afforded a maximum 57% yield of insertion product, **7**, leaving the remaining **3** unchanged. Vigorous bubbling of carbon dioxide through solutions of **3** (0.100 g, 0.197 mmol) in 25 ml of either toluene or diethyl ether for 0.5 h, followed by removal of the solvent under reduced pressure resulted in 70% and 43% respective yields of **7**.

Reaction of **4** *with carbon dioxide. Synthesis of* (η^6-C_6Me_6)Ru(PMe_3)(OC(O)NHPh)(Me) (**8**)

Vigorous bubbling of carbon dioxide through a stirring solution of **5** (0.551 g, 1.234 mmol) in 40 ml of diethyl ether for 0.5 h caused a color change from bright red to pale red-yellow. The solution was left stirring under an atmosphere of carbon dioxide for an additional 0.5 h, during which time a yellow precipitate formed. Removal of the solvent under reduced pressure resulted in a quantitative yield of product **8**. The reaction may also be carried out in a sealable NMR tube as described in the reaction of 3 with carbon dioxide to give 100% conversion to **8**. IR (KBr): 3301.7 cm^{-1} (ν_{N-H}); 1638.1 cm^{-1} ($\nu_{C=O}$). Anal. Calc. for $C_{23}H_{36}NO_2PRu$: C, 56.31; H, 7.40; N, 2.86. Found: C, 56.39; H, 7.44; N, 2.85.

Synthesis of (η^6-C_6Me_6)Ru(PMe_3)(OC(O)$NHC_6H_4CH_3$)(Ph) (**9**)

Vigorous bubbling of carbon dioxide through a stirring solution of **5** (0.702 g, 1.343 mmol) in 50 ml of toluene for 20 min caused a color change from bright red to pale brown-yellow. The solution was left stirring under an atmosphere of carbon dioxide for an additional 0.5 h, during which time a drab green oil formed. Removal of the solvent under reduced pressure left the green oil which was extracted into diethyl ether until the extracts were colorless. The combined extracts were reduced in volume and cooled to -20°C giving a dark green powder of **9**. The reaction may also be carried out in a sealable NMR tube as described in the reaction of 3 with carbon dioxide to give 100% conversion to **9**. IR (KBr): 3281.8 cm^{-1} (ν_{N-H}); 1631.8 cm^{-1} ($\nu_{C=O}$). Anal. Calc. for $C_{29}H_{40}NO_2PRu$: C, 61.47; H, 7.12; N, 2.47. Found: C, 61.25; H, 7.18; N, 2.41.

Synthesis of (η^6-C_6Me_6)Ru(PMe_3)[(MeOOC) C=C (COOMe)(NHPh)](Me) (**10**)

To a stirring solution of **4** (0.109 g, 0.244 mmol) in 30 ml of THF two equivalents of DMAD (0.06 ml) were added. The color of the solution immediately changed from red to dark green. The solution was allowed to stir for 0.5 h, after which the solvent was removed under reduced pressure leaving a thick, dark green oil. The oil was washed with 15 ml of pentane to remove excess DMAD, and the product was then extracted into diethyl ether until extracts were colorless. The combined extracts were reduced in volume and cooled to -50°C giving dark green powder as the product **9** (0.046 g, 0.078 mmol) in 32% yield. When this reaction is carried out in a sealed NMR tube with 0.020 g of 5 and a 10% excess of DMAD the reaction is observed to go to completion with the excess of DMAD left unreacted. IR (KBr): 3311.4 cm^{-1} (ν_{N-H}); 1702.0 cm^{-1} ($\nu_{C=O}$). Anal. Calc. for $C_{28}H_{42}NO_4PRu$: C, 57.13; H, 7.19; N, 2.38. Found: C, 57.03; H, 7.17; N, 2.41.

Synthesis of (η^6-C_6Me_6)Ru(PMe_3)(OC(O)OH) (Me)·H_2O (**11**)

Vigorous bubbling of carbon dioxide through a stirring solution of **6** (0.085 g, 0.185 mmol) in 40 ml of diethyl ether for 0.5 h caused a color change from bright red to pale yellow. The solution was left stirring under an atmosphere of carbon dioxide for an additional 0.5 h, during which time a pale yellow precipitate formed. The solvent was filtered off and the powder dried under reduced pressure to give 11 (0.058 g, 0.145 mmol) in 78% yield. IR (KBr): 1607.8 cm^{-1} ($\nu_{C=O}$). Anal. Calc. for $C_1H_{31}O_3PRu$: C, 47.10; H, 7.67. Found: C, 47.08; H, 7.35. Compound **11** can also be synthesized by bubbling CO_2 through a toluene solution of the hydroxide complex, **12** (*vide infra*).

Reaction of **6** *with water. Synthesis of* (η^6-C_6Me_6)Ru(PMe_3)(OH)(Me)·xH_2O (**12**)

A stirring solution of 10 (0.065 g, 0.141 mmol) in 20 ml of diethyl ether was prepared. Fifteen ml (six-fold excess) of deionized, degassed water was syringed into the solution three times at twenty minute intervals to give 18 equivalents of water. After the last addition the solution was stirred for 1 h, during which time a color change from bright red to yellow-brown was observed. Removal of solvent under reduced pressure afforded a brown oil. 15 ml of pentane was added to this oil and stirred for 1 h, after which the yellow-brown pentane solution was filtered off leaving a yellow powder. Drying the powder under reduced pressure afforded 12 in undetermined yield. IR (KBr): 3220 cm^{-1} (ν_{O-H}, broad).

X-ray crystal structure of **3**

Data were collected at room temperature on a Siemens R3m/V diffractometer equipped with a graphite monochromator utilizing MoK_α radiation ($\lambda = 0.71069$ Å). 50 reflections with $20.0° \leqslant 2\theta \leqslant 22.0°$ were used to refine the cell parameters. 9211 reflections (two equivalent sets) were collected using the ω-scan method (1.2° scan range and 3–6° scan speed depending on intensity). Four reflections were measured ever 96 reflections to monitor instrument and crystal stability (maximum correction on **I** was <1%). Absorption corrections were not applied based because of the crystal shape and small size.

The structure was solved by the heavy-atom method in SHELXTL plus [7] from which the locations of the Ru atom was obtained. All of the non-H atoms were located from a subsequent Difference Fourier map. The structure was refined in SHELXTL plus using full-matrix least squares. The non-H atoms were treated anisotropically. The H-atoms on C21 were calculated in idealized positions and the thermal parameter of H21c was fixed at 0.08. The rest of the H-atoms were obtained from a subsequent Difference Fourier map and were refined without any constraints, except H6′b and the H-atoms on Cl′ which have their thermal parameters fixed at 0.08. 409 parameters were refined and $\Sigma w\ (|F_o|-|F_c|)^2$ was minimized; $w = 1/(\sigma|F_o|)^2$, $\sigma(F_o) = 0.5\ k\mathbf{I}^{-1/2}\ \{[\sigma(\mathbf{I})]^2+(0.02\mathbf{I})^2\}^{1/2}$, **I**(intensity) = $(\mathbf{I}_{peak}-\mathbf{I}_{background})$(scan rate), and $\sigma(\mathbf{I}) = (\mathbf{I}_{peak}+\mathbf{I}_{background})^{1/2}$(scan rate), k is the correction due to decay and Lp effects, 0.02 is a factor used to down weight intense reflections and to account for instrument instability. The linear absorption coefficient was calculated from values from the *International Tables for X-ray Crystallography* [8]. Scattering factors for non-hydrogen atoms were taken from Cromer and Mann [9] with anomalous-dispersion corrections from Cromer and Liberman [10], while those of hydrogen atoms were from Stewart *et al.* [11].

RESULTS AND DISCUSSION

We have found that reaction of KNR′R″ with (η^6-C_6Me_6)Ru(PMe_3)(R)I in THF proceeds rapidly to give good to moderate yields of the corresponding anilide complexes as shown in eqn (1).

In our experience, the success of the synthesis of anilide complexes via nucleophilic displacement of leaving groups from η^6-arene complexes of ruthenium is dependent upon the nature of the leaving group and the nature of the metal associated with the anilide anion. The chemistry in eqn (1) works most efficiently when I^- is the leaving group and K^+ is the anilide counterion. This chemistry stands in contrast to earlier results from this laboratory [1g] which showed that the reaction between (η^6-C_6Me_6)Ru(PMe_3)Cl_2 and LiNHPh proceeds via a complicated mechanism involving the loss of PMe_3 to give the bimetallic complex [(η^6-C_6Me_6)$_2$Ru$_2$(μ_2-NHPh)$_3$]$^+$ as the anilide containing product. The presence of both the I^- and the R group in the starting material leads to cleaner and more predictable chemistry.

Compounds **3**–**6** are red, crystalline solids that are thermally stable, but air and moisture sensitive in solution and the solid state. They are soluble in ethereal solvents and aromatic hydrocarbons, and have been characterized via ^1H, ^{13}C and ^{31}P NMR spectroscopy. The NMR data for all the compounds reported are found in Tables 1–3. The ^1H NMR spectra typically display a single peak arising from the C_6Me_6 group as well as a doublet from the coordinated PMe_3 group. The methyl group in compounds **4** and **6** is responsible for a doublet at −0.13 and 0.40 ppm, respectively. There are a series of doublets and triplets in the aromatic region of the spectra that are due to the phenyl groups of the anilide or the Ru phenyl groups.

The NMR spectra of compound **6** are more complicated than those of **3**–**5** since more aromatic peaks are observed than can be accounted for if there is free rotation of the phenyl group in both the ^1H and ^{13}C spectra. In ^{13}C NMR spectrum of **6**, six peaks assignable to the aromatic carbons of **6** are observed. This observation is consistent with slow rotation of the

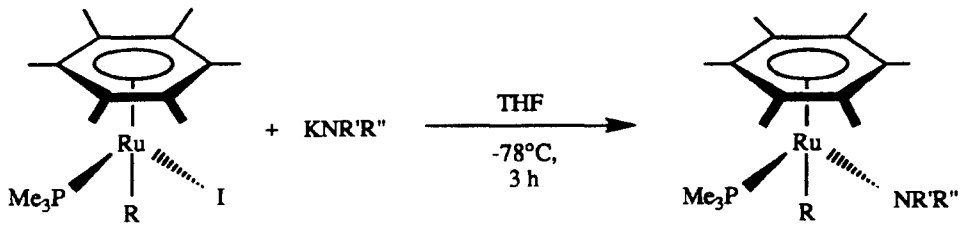

3; **R=Ph, R'=H, R"=Ph**
4; **R=Me, R'=H, R"=Ph**
5; **R=Ph, R'=H, R"=*p*-tol**
6; **R=Me, R'=Me, R"=Ph**

(1)

Table 1. ^{1}H NMR data[a]

Compound	δ ppm	Mult.	J. Hz	Integ.	Assignt.
(η^6-C_6Me_6)Ru(PMe_3)(Ph)I (**1**)[b]	1.19	d	$J^2_{P\,H} = 9$	9	–P<u>Me</u>$_3$
	1.67	s		18	–C_6(C<u>H</u>$_3$)$_6$
	7.03	m		4	aromatic
	8.59	m, br		1	aromatic
(η^6-C_6Me_6)Ru(PMe_3)(Me)I (**2**)[b]	0.75	d	$J^3_{P-H} = 11$	3	–<u>Me</u>
	1.17	d	$J^2_{P-H} = 9$	9	–P<u>Me</u>$_3$
	1.72	s		18	–C_6(C<u>H</u>$_3$)$_6$
(η^6-C_6Me_6)Ru(PMe_3)(NHPh)Ph (**3**)[b]	0.86	d	$J^2_{P-H} = 8.5$	9	–P<u>Me</u>$_3$
	1.34	s, br		1	–N<u>H</u>Ph
	1.64	s		18	–C_6(C<u>H</u>$_3$)$_6$
	6.41	m, br		3	aromatic
	7.13	m, br		+slvt	aromatic
(η^6-C_6Me_6)Ru(PMe_3)(NHPh)Me (**4**)[d]	−0.13	d	$J^3_{P-H} = 9$	3	–<u>Me</u>
	0.81	s, br		1	–N<u>H</u>Ph
	1.13	d	$J^2_{P\,H} = 9$	9	–P<u>Me</u>$_3$
	1.95	s		18	–C_6(C<u>H</u>$_3$)$_6$
	5.76	t of t		1	aromatic
	6.01	d, br		2	aromatic
	6.66	t, br		2	aromatic
(η^6-C_6Me_6)Ru(PMe_3)($NHC_6H_4CH_3$)Ph (**5**)[d]	0.91	s, br		1	N<u>H</u>C$_6$H$_4$Me
	1.08	d	$J^2_{P-H} = 6$	9	–P<u>Me</u>$_3$
	1.94	s		18	–C_6(C<u>H</u>$_3$)$_6$
	2.06	s		3	NHC$_6$H$_4$<u>Me</u>
	6.05	d		2	aromatic
	6.55	d		2	aromatic
	6.85	t		1	aromatic
	7.00	t, br		2	aromatic
(η^6-C_6Me_6)Ru(PMe_3)(NMePh)Me (**6**)[b]	0.40	d	$J^3_{P-H} = 9$	3	–<u>Me</u>
	0.85	d	$J^2_{P-H} = 9$	9	–P<u>Me</u>$_3$
	1.61	s		18	–C_6(C<u>H</u>$_3$)$_6$
	2.84	s		3	–N<u>Me</u>Ph
	6.51	t		1	aromatic
	6.67	m, br		2	aromatic
	7.25	t		1	aromatic
	7.38	t		1	aromatic
(η^6-C_6Me_6)Ru(PMe_3)(OC(O)NHPh)Ph (**7**)[b]	1.08	d	$J^2_{P\,H} = 8.5$	9	–P<u>Me</u>$_3$
	1.70	s		18	–C_6(C<u>H</u>$_3$)$_6$
	6.38	d		1	aromatic
	6.60	s, br		1	–OCON<u>H</u>Ph
	7.09	m, br		+slvt	aromatic
	7.56	d		2	aromatic
	8.16	d		1	aromatic
(η^6-C_6Me_6)Ru(PMe_3)(OC(O)NHPh)Me (**8**)[d]	0.32	d	$J^3_{P-H} = 6$	3	–<u>Me</u>
	1.26	d	$J^2_{P-H} = 9$	9	–P<u>Me</u>$_3$
	1.95	s		18	–C_6(C<u>H</u>$_3$)$_6$
	6.38	s, br		1	–OCON<u>H</u>Ph
	6.76	t		1	aromatic
	7.13	t		2	aromatic
	7.29	d		2	aromatic
(η^6-C_6Me_6)Ru(PMe_3)[(MeOOC)C=C(COOMe)(NHPh)](Me) (**9**)[c]	−0.26	d	$J^3_{P-H} = 9$	3	–<u>Me</u>
	1.18	d	$J^2_{P-H} = 9$	9	–P<u>Me</u>$_3$
	1.96	s		18	–C_6(C<u>H</u>$_3$)$_6$
	3.57	s		3	–OC<u>H</u>$_3$
	3.59	s		3	–OC<u>H</u>$_3$
	5.93	s, br		1	–dmadN<u>H</u>Ph
	6.60	d		2	aromatic
	6.71	t		1	aromatic
	7.12	t		2	aromatic

Table 1—*Continued.*

Compound	δ ppm	Mult.	J. Hz	Integ.	Assignt.
(η^6-C_6Me_6)Ru(PMe_3)(OC(O)$NHC_6H_4CH_3$)Ph (**10**)[b]	1.06	d	$J^2_{P-H} = 9$	9	$-PMe_3$
	1.69	s		18	$-C_6(CH_3)_6$
	2.11	s		3	NHC_6H_4Me
	6.63	s, br		1	NHC_6H_4Me
	7.00	d		2	aromatic
	7.11	m, br		+slvt	aromatic
	7.44	m, br		3	aromatic
	8.13	m, br		1	aromatic
(η^6-C_6Me_6)Ru(PMe_3)(OC(O)OH)Me·H_2O (**11**)[c]	0.33	d	$J^3_{P-H} = 9$	3	$-Me$
	1.22	d	$J^2_{P-H} = 9$	9	$-PMe_3$
	1.91	s		18	$-C_6(CH_3)_6$
	11.08	s, br		1	$-OCO_2H$
(η^6-C_6Me_6)Ru(PMe_3)(OH)Me·xH_2O (**12**)[b]	−4.40	s, br		1	$-OH$
	0.38	d	$J^3_{P-H} = 9$	3	$-Me$
	1.04	d	$J^2_{P-H} = 9$	9	$-PMe_3$
	1.75	s		18	$-C_6(CH_3)_6$
	3.99	s, br			$-xH_2O$

[a] All spectroscopic data were collected at 23°C. The multiplicity doublet is apparent splitting patterns when refering to the PMe_3 ligands and do not necessarily reflect the true coupling constants.
[b] C_6D_6.
[c] $CDCl_3$.
[d] CD_2Cl_2.

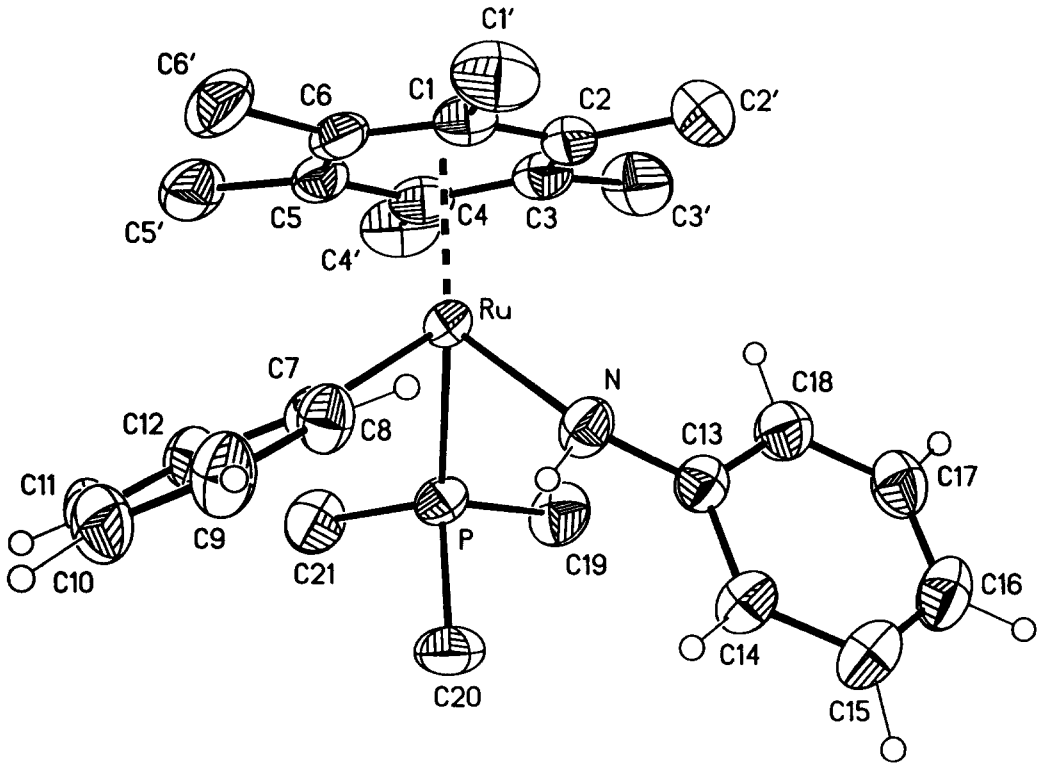

Fig. 1. Thermal ellipsoid plot of compound **3**.

Table 2. $^{13}C\{^1H\}$ NMR data[a]

Compound	δ ppm	Mult.	J. Hz	Assignt.
(η^6-C_6Me_6)Ru(PMe_3)(Ph)I (**1**)[c]	16.6	s		$-C_6(\underline{C}H_3)_6$
	19.2	d	$J^1_{P-C} = 32$	$-P\underline{Me}_3$
	98.0	d	$J^2_{P-C} = 3$	$-\underline{C}_6(CH_3)_6$
	121.0	s		aromatic
	125.7	s		aromatic
	127.0	s		aromatic
	140.2	d	$J^2_{P-C} = 15$	*ipso*-C
	147.1	s		aromatic
(η^6-C_6Me_6)Ru(PMe_3)(Me)I (**2**)[b]	−6.3	d	$J^2_{P-C} = 20$	$-\underline{Me}$
	16.3	s		$-C_6(\underline{C}H_3)_6$
	18.6	d	$J^1_{P-C} = 31$	$-P\underline{Me}_3$
	95.7	d	$J^2_{P-C} = 3$	$-\underline{C}_6(CH_3)_6$
(η^6-C_6Me_6)Ru(PMe_3)(NHPh)Ph (**3**)[b]	15.6	s		$-C_6(\underline{C}H_3)_6$
	16.7	d	$J^1_{P-C} = 28$	$-P\underline{Me}_3$
	98.9	d	$J^2_{P-C} = 3.6$	$-\underline{C}_6(CH_3)_6$
	108.9	s		aromatic
	117.1	s, br		aromatic
	121.4	s		aromatic
	128.3	s		aromatic
	161.5	s		aromatic
	170.2	d	$J^2_{P-C} = 22$	Ru-*ipso*-C
(η^6-C_6Me_6)Ru(PMe_3)(NHPh)Me (**4**)[b]	1.89	d	$J^2_{P-C} = 20$	$-\underline{Me}$
	15.3	s		$-C_6(\underline{C}H_3)_6$
	15.7	d	$J^1_{P-C} = 28$	$-P\underline{Me}_3$
	96.6	d	$J^2_{P-C} = 3.8$	$-\underline{C}_6(CH_3)_6$
	107.6	s		aromatic
	108.9	s		aromatic
	128.6	s		aromatic
	162.1	d	$J^3_{P-C} = 2.5$	*ipso*-C
(η^6-C_6Me_6)Ru(PMe_3)($NHC_6H_4CH_3$)Ph (**5**)[d]	16.2	s		$-C_6(\underline{C}H_3)_6$
	17.2	d	$J^1_{P-C} = 28$	$-P\underline{Me}_3$
	20.1	s		NHPh–$\underline{CH}_3$
	99.6	d	$J^2_{P-C} = 3.8$	$-\underline{C}_6(CH_3)_6$
	116.1	s		aromatic
	116.9	s, br		aromatic
	121.1	s		aromatic
	128.9	s		aromatic
	140.5	s		aromatic
	159.6	d		aromatic
	170.8	d	$J^2_{P-C} = 22$	Ru-*ipso*-C
(η^6-C_6Me_6)Ru(PMe_3)(NMePh)Me (**6**)[b]	2.61	d	$J^2_{P-C} = 22$	Ru-$\underline{Me}$
	15.6	s		$-C_6(\underline{C}H_3)_6$
	16.0	d	$J^1_{P-C} = 28$	$-P\underline{Me}_3$
	42.0	s		$-N\underline{Me}Ph$
	97.0	d	$J^2_{P-C} = 3$	$-\underline{C}_6(CH_3)_6$
	107.6	s		aromatic
	111.7	s		aromatic
	121.3	s		aromatic
	127.0	s		aromatic
	129.5	s		aromatic
	161.7	d	mom0]1.71	*ipso*-C
			$J^3_{P-C} = 1.5$	
(η^6-C_6Me_6)Ru(PMe_3)(OC(O)NHPh)Me (**8**)[d]	1.87	d	$J^2_{P-C} = 20$	Ru–$\underline{Me}$
	15.4	d	$J^1_{P-C} = 28$	$-P\underline{Me}_3$
	15.7	s		$-C_6(\underline{C}H_3)_6$
	95.7	d	$J^2_{P-C} = 3.3$	$-\underline{C}_6(CH_3)_6$
	117.1	s		aromatic
	120.0	s		aromatic
	128.7	s		aroamtic
	142.9	s		carbonyl
	159.8	d	$J^5_{P-C} = 4.3$	*ipso*-C

Table 2—*Continued.*

Compound	δ ppm	Mult.	J. Hz	Assignt.
(η^6-C_6Me_6)Ru(PMe_3)[(MeOOC)C=C(COOMe)(NHPh)](Me) (**9**)[c]	−1.71	d	$J^2_{P-C} = 19$	Ru–Me
	15.9	s		$-C_6(CH_3)_6$
	17.4	d	$J^1_{P-C} = 30$	$-PMe_3$
	49.2	s		methoxy C
	51.3	s		methoxy C
	99.2	d	$J^2_{P-C} = 3.2$	$-C_6(CH_3)_6$
	115.7	s		aromatic
	118.6	s		aromatic
	128.8	s		aromatic
	132.4	d	$J^3_{P\ C} = 4.6$	Ru—C=C
	145.7	s		*ipso*-C
	162.7	d	$J^2_{P-C} = 17$	Ru—C=C
	163.5	d	$J^3_{P\ C} = 1.6$	Ru—C—C=O
	176.2	s		—C=C—C=O
(η^6-C_6Me_6)Ru(PMe_3)($OC(O)NHC_6H_4CH_3$)Ph (**10**)[b]	15.7	s		$-C_6(CH_3)_6$
	15.9	d	$J^1_{P\ C} = 29$	$-PMe_3$
	20.7	s		NHPh–CH_3
	97.7	d	$J^2_{P-C} = 2.3$	$-C_6(CH_3)_6$
	117.8	s		aromatic
	121.9	s, br		aromatic
	126.0	s		aromatic
	127.0	s		aromatic
	129.3	s		aromatic
	136.4	s		aromatic
	139.9	s		aromatic
	140.6	d		carbonyl
	160.2	s		aromatic
	167.8	d	$J^2_{P-C} = 24$	Ru-*ipso*-C
(η^6-C_6Me_6)Ru(PMe_3)(OC(O)OH)Me · H_2O (**11**)[c]	2.07	d	$J^2_{P-C} = 20$	Ru–Me
	15.1	d	$J^1_{P-C} = 28.5$	$-PMe_3$
	15.4	s		$-C_6(CH_3)_6$
	95.2	d	$J^2_{P\ C} = 3$	$-C_6(CH_3)_6$
	161.8	s		carbonyl
(η^6-C_6Me_6)Ru(PMe_3)(OH)Me · xH_2O (**12**)[b]	1.24	d	$J^2_{P-C} = 20$	Ru–Me
	14.6	d	$J^1_{P-C} = 27$	$-PMe_3$
	15.3	s		$-C_6(CH_3)_6$
	95.0	d	$J^2_{P-C} = 3$	$-C_6(CH_3)_6$

[a] All spectroscopic data were collected at 23°C. The multiplicity doublet is apparent splitting patterns when referring to the PMe_3 ligands and do not necessarily reflect the true coupling constants.
[b] C_6D_6.
[c] $CDCl_3$.
[d] CD_2Cl_2.

phenyl group on the NMR timescale and probably arises from steric interactions between the MeNPh group and the rest of the molecule. Hindered rotation about P—Ph and Rh—Ph groups has been observed in the isoelectronic, and closely related compounds, Cp*Rh(Ph)(X)(PR_3) [6]. Though we have not investigated the low temperature NMR behavior of compounds **3–5,** observable barriers to rotation about the Ru—Ph and N—Ph bonds might be expected by analogy with the Rh compounds.

Crystals of **3** suitable for a single crystal X-ray diffraction study were grown by slowly cooling a saturated Et_2O solution of **3** to −40°C. A thermal ellipsoid plot of **3** is shown in Fig. 1, while data collection parameters and selected bond lengths and angles are found in Tables 4 and 5. The compound has the expected three legged piano stool geometry with the PMe_3, NHPh, and Ph groups defining the "legs" of the piano stool. The angles between these groups are slightly less than 90° and suggest a significant steric influence from the C_6Me_6 group as is consistent with the observed hindered rotation of the phenyl groups in NMR spectra of **6**. The geometry about the nitrogen atom of the anilide is planar as is typically observed

Table 3. $^{31}P\{^1H\}$ NMR data[a]

Compound	δ ppm	mult.
(η^6-C_6Me_6)Ru(PMe_3)(Ph)I (**1**)[c]	38.32	s
(η^6-C_6Me_6)Ru(PMe_3)(Me)I (**2**)[c]	2.68	s
(η^6-C_6Me_6)Ru(PMe_3)(NHPh)Ph (**3**)[b]	5.27	s
(η^6-C_6Me_6)Ru(PMe_3)(OC(O)NHPh)Ph (**4**)[b]	5.92	s
(η^6-C_6Me_6)Ru(PMe_3)(NHPh)Me (**5**)[b]	9.58	s
(η^6-C_6Me_6)Ru(PMe_3)(OC(O)NHPh)Me (**6**)[b]	48.16	s
(η^6-C_6Me_6)Ru(PMe_3)[(MeOOC)C=C(COOME)(NHPh)](Me) (**7**)[b]	44.04	s
(η^6-C_6Me_6)Ru(PMe_3)($NHC_6H_4CH_3$)Ph (**8**)[d]	46.05	s
(η^6-C_6Me_6)Ru(PMe_3)(OC(O)$NHC_6H_4CH_3$)Ph (**9**)[b]	5.84	s
(η^6-C_6Me_6)Ru(PMe_3)(NMePh)Me (**10**)[b]	9.10	s
(η^6-C_6Me_6)Ru(PMe_3)(OC(O)OH)Me·H_2O (**11**)[c]	10.21	s
(η^6-C_6Me_6)Ru(PMe_3)(OH)Me·xH_2O (**12**)[b]	8.16	s

[a] All spectroscopic data were collected at 23° C.
[b] C_6D_6.
[c] $CDCl_3$.
[d] CD_2Cl_2.

in transition metal amide complexes even when the metal center is electronically saturated as in groups 8–10. The Ru—N—C(13) angle of 135° is also indicative of the steric congestion in the coordination sphere.

The bond lengths are generally unremarkable with the exception of the rather short distance of 1.360(5) between C13 and N in the anilide group. Shortened C—N bonds in other anilides of late transition metal complexes have been observed previously, and are consistent with some amount of stabilization of the nitrogen lone pair through π interaction with the phenyl ring [12]. Given the electronic saturation of the metal center in these complexes, π donation from the N to the metal is not possible, and interaction between the phenyl ring and the amide N may help to stabilize the complex.

We have explored the reactivity of compounds **3–6** with the unsaturated electrophiles CO_2 and DMAD. The reaction between CO_2 and compounds **3–5** results in the net insertion of the CO_2 into the Ru—N bond to give a metal carbamate complex as is shown in eqn (2). Given the electronic saturation at the metal centre, it is likely that these reactions occur via direct attack of the N lone pair on CO_2 followed by Ru—O bond formation. This type of reactivity is well precedented in other group 8–10 metal amido complexes [13]. Interestingly, the complexes display a range of reactivity with CO_2. When the reaction between **3** and excess CO_2 was monitored by ^1H NMR spectroscopy, the reaction proceeded to only 70% conversion, while the same reaction with **4** or **5** resulted in quantitative conversion to products. It would appear that the increased electron richness of the *p*-toluamide ligand in **5** and the better electron donating Me group in **4** (vs the Ph group in **3**) make the N atom more nucleophilic in **4** and **5** which allows the reaction to go to completion.

The differences in the reactivity of **3–5** are more obvious when these compounds are allowed to react with DMAD. Thus, while the anilide and *p*-toluamide complexes, **3** and **5** do not react with DMAD, complex **4** reacts to give a quantitative yield of the insertion product, **9**, eqn (3). It would appear that this difference in reactivity is due to the increased electron donating ability of the Me group of **4** relative to the Ph groups of **3** and **5** and is consistent with the reac-

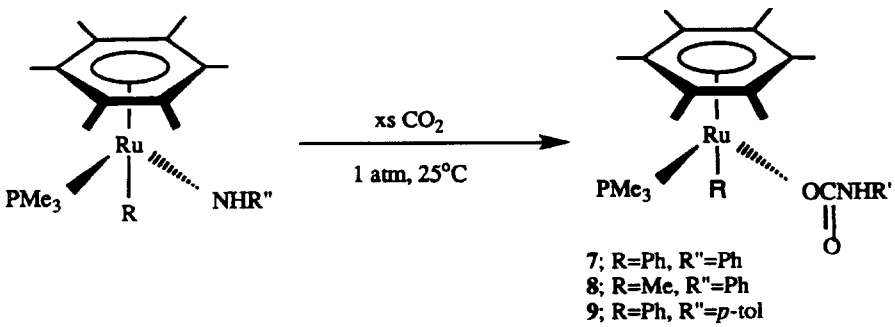

7; R=Ph, R"=Ph
8; R=Me, R"=Ph
9; R=Ph, R"=*p*-tol

(2)

Table 4. Crystallographic data

A. Crystal data (298 K)	**3**
a (Å)	12.013(2)
b (Å)	16.700(3)
c (Å)	12.414(1)
β (°)	97.35(2)
V (Å^3)	2470.0(7)
^{d}calc (g cm^{-3}) (298 K)	1.37
Empirical formula	$C_{27}H_{38}NPRu$
Formula wt, g	508.6
Crystal system	Monoclinic
Space group	$P2_1/n$
Z	4
F(000) electrons	1064
B. Data collection (298 K)	
Radiation λ (Å)	Mo–K_α, 0.71073
Mode	ω-scan
Scan range	Symmetrically over 1.2 about $K_{\alpha 1,2}$ maximum
Background	offset 1.0 and −1.0 in ω from $K_{\alpha 1,2}$ maximum
Scan rate (°) min^{-1}	3–6
2θ range (°)	3–50
Range of $h\ k\ l$	$0 \leqslant h \leqslant 14$
(2 equivalent sets)	$-19 \leqslant k \leqslant 19$
	$-14 \leqslant l \leqslant 14$
Total reflections measured	9211 (two equivalent sets)
Unique reflections	4356
Absorption coeff. μ (Mo–K_α), cm^{-1}	7.13
C. Structure refinement	
S, Goodness-of-fit	1.08
Reflections used, $I > 2\sigma(I)$	3174
No. of variables	409
R, wR* (%)	2.74, 3.18
R, wR*, all data (%)	4.95, 3.96
$R_{int.}$ (%)	1.54
Max. shift/esd	0.001
Min. peak in diff. four. map (e Å^{-3})	−0.32
Max. peak in diff. four. map (e Å^{-3})	0.43

* Relevant expressions are as follows, where in the footnote F_o and F_c represent, respectively, the observed and calculated structure-factor amplitudes.

Function minimized was $w(|F_o| - |F_c|)^2$, where $w = (\sigma(F))^{-2}$

$R = \Sigma(||F_o| - |F_c||)/\Sigma|F_o|$

$wR = [\Sigma w(|F_o| - |F_c|)^2/\Sigma/F_o|^2]^{1/2}$

$S = [\Sigma w(|F_o| - |F_c|)^2/(m-n)]^{1/2}$.

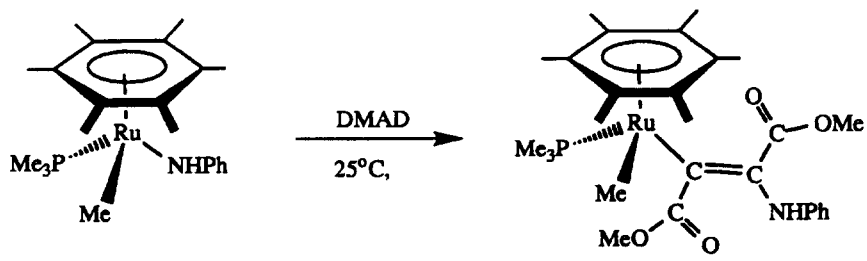

4 **10**

(3)

Table 5. Bond lengths (Å) and angles (°) for compound 3

1	2	3	1–2 (Å)	1–2–3(°)
P	Ru	N	2.2919(9)	84.76(9)
N	Ru	C7	2.121(3)	84.18(12)
C7	Ru	P	2.096(3)	86.55(9)
C13	N	Ru	1.360(5)	135.4(2)
C1	Ru		2.263(4)	
C2	Ru		2.301(4)	
C3	Ru		2.329(4)	
C4	Ru		2.228(4)	
C5	Ru		2.241(3)	
C6	Ru		2.268(3)	

tivity of these compounds with CO_2. Unfortunately, we cannot rule out the possibility that the observed differences in reactivity with DMAD are due to the difference in the steric effects of the Ru—Me and Ru—Ph groups.

The *N*-methyl anilide complex, **6,** is considerably more reactive than **3–5**. Instead of reacting with CO_2 to give the expected carbamate complex, the product of the reaction between **6** and CO_2 is the bicarbonate complex, $(\eta^6\text{-}C_6Me_6)Ru(PMe_3)(HCO_3)$, **11**. We believe that the conversion of **6** to **11** involves traces of H_2O in the CO_2 which either converts **11** to a hydroxide, **12,** which reacts further with CO_2, or that the product carbamate complex reacts with H_2O giving **11** as the reaction product.

In order to test this hypothesis, complex **6** was converted to the hydroxide complex, **12** through its reaction with water. Compound **12** is isolated as a yellow powder that is soluble in ethereal solvents, and insoluble in aliphatic hydrocarbons. The ^1H NMR spectrum of **12** shows two broad peaks at −4.40 and 3.99 ppm respectively that might be assigned to the hydroxide proton. Given the variability of the integration of the peak at 3.99 ppm from sample to sample, we are inclined to assign the peak at −4.40 ppm to the hydroxide proton by analogy with $Cp^*Ir(PMe_3)Ph(OH)$[2a], and the peak at 3.99 ppm to the water of hydration [14]. When **12** is allowed to react with CO_2, it is rapidly and quantitatively converted into the bicarbonate complex, **11** as shown in eqn (4). The nucleophilicity of the hydroxide group in **12** is expected and the reaction between other late transition metal hydroxides and unsaturated electrophiles is well precedented [2a,15].

Preliminary studies indicate that compound **12** does not react with ethylene at low to elevated temperatures and 1 atm pressure. This lack of reactivity differs from the related complex $Cp^*Ir(OH)(Me)(PMe_3)$, which has been shown to react with ethylene via a complicated mechanism with the net result being insertion of the ethylene into the Ir—O bond [2]. We are continuing to investigate the reactivity of **12** with a variety of substrates.

In summary, the synthesis of a series of anilide complexes of the type, $(\eta^6\text{-}C_6Me_6)Ru(PMe_3)(R)NR'Ph$, can be achieved via nucleophilic displacement of iodide from the corresponding precursor complexes using potassium anilides. Unsaturated electrophiles react with the anilide complexes by attacking the lone pair of the anilide nitrogen and resulting in net insertion of the electrophile into the Ru N bond. The nucleophilicity of the N (or in the case of **12,** O) atom of these complexes is likely due to the fact that the Ru atom in these 18 e^- complexes cannot function as a π acceptor toward the anilide or hydroxide donors.

SUPPLEMENTARY MATERIAL AVAILABLE

Positional parameters, and a complete listing of bond lengths and angles.

Acknowledgements—We wish to thank the donors of the Petroleum Research Fund for partial support of this work. We also wish to thank the National Science Foundation for partial support of this work in the form of an REU grant that supported TME and BR.

REFERENCES

1. (a) Bryndza, H. E., Tam, W., *Chem. Rev.*, 1988, **88,** 1163. (b) Fryzuk, M. D., Montgomery, D. C. and *Coord. Chem.*, 1989, **95,** 1–40. (c) Lappert, M. F., Power, P. P., Sanger, A. R. and Srivastrava, R. C., *Metal and Metalloid Amides*, Halstead Press: Chatham, Kent, England, 1980, pp. 488–533. (d) Roundhill, D. M., *Chem. Rev.*, 1992, **92,** 1. (e) Koelliker, R. and Milstein, D., *J. Am. Chem. Soc.*, 1991, **113,** 8524. (f) Hartwig, J. F., Anderson, R.

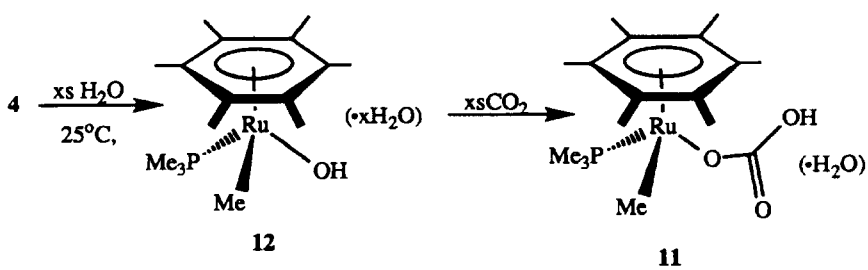

12 **11**

(4)

A. and Bergman, R. G., *J. Am. Chem. Soc.*, 1989, **111,** 2717. (g) Martin, G. C., Palenik, G. J. and Boncella, J. M., *Inorg. Chem.*, 1990, **29,** 2027. (h) Martin, G. C., Boncella, J. M. and Wurcherer, E. J., *Organometallics*, 1991, **10,** 2804. (h) Hartwig, J. F., Anderson, R. A. and Bergman, R. G., *Organometallics*, 1991, **10,** 1875.

2. (a) Glueck, D. S. and Bergman, R. G., *Organometallics*, 1990, **9,** 2862. (b) Glueck, D. S. and Bergman, R. G., *Organometallics*, 1991, **10,** 1462. (c) Glueck, D. S. and Bergman, R. G., *Organometallics*, 1991, **10,** 1479. (d) Worpel, K. A. and Bergman, R. G., *J. Am. Chem. Soc.*, 1993, **115,** 7888. (e) Ritter, J. C. M. and Bergman, R. G., *Am. Chem. Soc.*, 1997, **119,** 2580.
3. (a) Michelman, R. I., Andersen, R. A. and Bergman, R. G., *J. Am. Chem. Soc.*, 1993, **115,** 5100. (b) Michelman, R. I., Andersen, R. A. and Bergman, R. G., *Organometallics*, 1993, **12,** 2741.
4. Reetz, M. J., Urz, R. and Schuster, T., *Synthesis*, 1983, 540.
5. (a) Bennett, M. A,. Huang, T. W., Matheson, T. W. and Smith, A. K., *Inorg. Synth.*, 1982, **21,** 74. (b) Werner, H. and Kletzin, H., *J. Organomet. Chem.*, 1982, **228,** 289.
6. Feher, F. J. and Jones, W. D., *Inorg. Chem.*, 1984, **23,** 2376.
7. Sheldrick, G. M. SHELXTL plus. Nicolet XRD Corporation, Madison, Wisconsin, U.S.A. (1990).
8. *International Tables for X-ray Crystallography* Vol. IV, p. 55. Birmingham : Kynoch Press. (Present distributor, D. Reidel, Dordrecht.), (1974).
9. Cromer, D. T. and Mann, J. B., *Acta Cryst.*, 1968, **A24,** 321–324.
10. Cromer, D. T. and Liberman, D., *J. Chem. Phys.*, 1970, **53,** 1891–1898.
11. Stewart, R. F., Davidson, E. R. and Simpson, W. T., *J. Chem. Phys.*, 1965, **42,** 3175–3187.
12. (a) Villaneuva, L. A., Abboud, K. A. and Boncella, J. M., *Organometallics*, 1994, **13,** 3921. (b) Rahim, R. and Ahmed, K. J., *Organometallics*, 1994, **13,** 1751. (c) Vanderlende, D. D., Abboud, K. A. and Boncella, J. M., *Inorg. Chem.*, 1995, **24,** 5319.
13. (a) Klein, D. P., Hayes, J. C. and Bergman, R. G., *J. Am. Chem. Soc.*, 1988, **110,** 3704. (b) Boncella, J. M. and Villanueva, L. A., *J. Organomet. Chem.*, 1994, **465,** 297. (c) Rahim, M., White, C., Rheingold, A. L. and Ahmed, K. J., *Organometallics*, 1993, **12,** 2401. (d) Villanueva, L. A., Abboud, K. A. and Boncella, J. M., *Organometallics*, 1992, **11,** 2963.
14. Burn, M. J., Fickes, M. G., Hartwig, J. F., Hollander, F. J. and Bergman, R. G., *J. Am. Chem. Soc.*, 1993, **115,** 5875.
15. (a) Green, L. M. and Meek, D. W., *Organometallics*, 1989, **8,** 659. (b) Alsfasser, R., Trofimenko, S., Looney, A., Parkin, G. and Vahrenkamp, H., *Inorg. Chem.*, 1991, **30,** 4098.

Pergamon

PII: S0277-5387(97)00371-9

Polyhedron Vol. 17, No. 5–6, pp. 737–744, 1998
© 1998 Elsevier Science Ltd
All rights reserved. Printed in Great Britain
0277-5387/98 $19.00+0.00

Triamidostannates(II) as nucleophiles: synthesis of allyltriamidostannanes

Konrad W. Hellmann,[a] Claudia Bott,[a] Lutz H. Gade,[a]* Ian J. Scowen,[b] and Mary McPartlin[b]

[a] Institut für Anorganische Chemie, Universität Würzburg, Am Hubland, D-97074 Würzburg, Germany

[b] School of Applied Chemistry, University of North London, Holloway Road, London N7 8DB, U.K.

(Received 30 April 1997; revision 8 August 1997

Abstract—A series of triamido stannanes of the general types $HC\{SiMe_2NR\}_3SnCH_3$ [R = p-Tolyl (**3**), t-Butyl (**4**)] and $MeSi\{SiMe_2N(R)\}_3SnR'$ [R = p-Tolyl and R' = $CH_2CH{=}CH_2$ (**5**), $CH_2CH{=}CHCH_3$ (**6**), $CH_2CH{=}CHC_6H_5$ (**7**), $CH_2(CH_3)C{=}CH_2$ (**8**); R = t-Butyl and R' = $CH_2CH{=}CH_2$ (**9**), $CH_2CH{=}CHCH_3$ (**10**)] have been synthesized by reacting the lithium triamidostannates $[HC\{SiMe_2NR\}_3SnLi(THF)_n]$ and $[MeSi\{SiMe_2NR\}_3SnLi(THF)_n]$ with the respective alkyl halides. For $HC\{SiMe_2NtBu\}_3SnCH_3$ a single crystal X-ray structure analysis established the detailed structural arrangements in this new class of compounds.
© 1998 Elsevier Science Ltd. All rights reserved

Keywords: tin; metal amides; tripodal amido ligands; metal nucleophiles.

We recently reported the synthesis and crystal structures of a series of group 14 triamido metallates which are stabilized by the tripodal amido ligands previously developed by us [1]. The alkali metal stannates were not only found to display a rich structural chemistry but have been employed in the synthesis of a variety of transition metal–tin heterobimetallics, essentially functioning as soft "donor ligands" [2]. A remarkable feature of their reactivity is the relative inertness to oxidative degradation in the coupling reactions leading to these species, a situation which is attributed to the electronegative substituents coordinated to the divalent tin centres. The most remarkable manifestation of this property is the synthesis and first structural characterization of a metal–metal bonded Ag—Sn complex as well as the stable metal–metal bonds established for several Au—Sn heterobimetallics containing gold in the oxidation states I, II and III [3].

In this paper we report first results of our investigations into the use of the triamido stannates as nucleophiles in the synthesis of new organo-tin reagents. Of these new systems allyltin derivatives were of special interest in view of their manifold application in organic synthesis [4–6].

EXPERIMENTAL

All manipulations were performed under an inert gas atmosphere of dried argon in standard (Schlenk) glassware which was flame dried with a Bunsen burner prior to use. Solvents were dried according to standard procedures and saturated with Ar. The deuterated solvents used for the NMR spectroscopic measurements were degassed by three successive "freeze–pump–thaw" cycles and dried over 4 Å molecular sieves. The centrifuge employed in some of the syntheses was a Rotina 48 by Hettich Zentrifugen, Tuttlingen, Germany, which was equipped with a specially designed Schlenk-tube rotor [7].

The ^{1}H-, ^{13}C-, ^{29}Si-, and ^{119}Sn-NMR spectra were recorded on a Bruker AC 200 spectrometer equipped with a B-VT-2000 variable temperature unit (at 200.13, 50.32, 39.76 and 74.63 MHz, respectively) with tetramethylsilane and $SnMe_4$ as references. Elemental analyses were carried out in the microanalytical laboratory of the Chemistry Department at Würzburg. The stannates $[HC\{SiMe_2N(4\text{-}CH_3C_6H_4)\}_3SnLi$-

* Author to whom correspondence should be addressed.

Dedicated to Prof. Don Bradley, the pioneer of metal amide chemistry.

$(THF)_3$] (**1a**), [$HC\{SiMe_2N[C(CH_3)_3]\}_2SnLi(THF)$] (**1b**) and [$MeSi\{SiMe_2N(4\text{-}CH_3C_6H_4)\}_3Sn\text{-}Li(THF)_3$] (**2a**), [$MeSi\{SiMe_2N[C(CH_3)_3]\}_3Sn\text{-}Li(THF)$] (**2b**) were prepared as reported previously by us [1,3]. All other chemicals used as starting materials were obtained commercially and used without further purification.

PREPARATION OF THE COMPOUNDS

$HC[SiMe_2N(4\text{-}CH_3C_6H_5)]_3SnMe$ (3)

$HC[SiMe_2N(4\text{-}CH_3C_6H_5)]_3SnLi(THF)_3$ (0.88 g, 1.04 mmol) (**1a**) and MeI (64 μl, 1.05 mmol) were stirred in thf (30 ml) at room temperature for 1 h. The solvent was removed *in vacuo* and the residue extract with toluene (20 ml). After filtration over Celite to remove the LiI formed in the reaction the colourless solution was concentrated to 8 ml and then stored at -35°C. Compound **3** was obtained as a colourless, crystalline solid after 24 h. Yield: 0.60 g (90%). ^{1}H-NMR (200.13 MHz, [D$_6$]benzene, 295 K): $\delta = -0.44$ (s, 1 H, HC), 0.33 [s, 3H, $SnCH_3$, $^2J(^{117/119}Sn\text{-}^1H) = 69$ Hz (broad)], 0.48 (s, 18 H, $Si(CH_3)_2$), 2.14 (s, 9 H, $CH_3C_6H_4$), 6.87 (m, 12 H, $CH_3C_6H_4$); $\{^1H\}^{13}$C-NMR (50.32 MHz, [D$_6$]benzene, 295 K): $\delta = -8.5$ ($SnCH_3$), 5.2 ($Si(CH_3)_2$), 10.5 (CH), 20.7 ($CH_3C_6H_4$), 125.6 (C^3), 129.9 (C^4), 130.3 (C^2), 147.7 (C^1). IR (KBr): 3010 w cm^{-1}, 2950 w, 2910 w, 2860 w, 1610 m, 1510 s, 1440 w, 1360 m, 1300 m, 1285 s, 1250 s, 1180 w, 1115 w, 1015 w, 980 w, 940 w, 925 w, 900 m, 845 s, 810 s, 775 m, 685 w; $C_{29}H_{43}N_3Si_3Sn$ (636.28); calcd C 54.74, H 6.76, N 6.61; found C 54.70, H 6.73, N 6.57.

$HC\{SiMe_2N[C(CH_3)_3]\}_3SnMe$ (4)

To a stirred solution of $HC[SiMe_2NC(CH_3)_3]_3SnLi(THF)$ (**1b**) (1.05 g, 2.60 mmol) in diethylether (30 ml) MeI (0.16 ml, 2.60 mmol) was added through a syringe at room temperature. After stirring for 5 h the solvent was removed *in vacuo*. The residue was extracted with pentane (20 ml) and the solution was filtered through Celite. After concentration to 8 ml the solution was stored at -35°C. Compound **4** was obtained as a yellow crystalline solid within 48 h.

Yield: 1.07 g (77%); ^{1}H-NMR (200.13 MHz, [D$_6$]benzene, 295 K): $\delta = -0.93$ [s, 1 H, HC, $^4J(^{117/119}Sn\text{-}^1H) = 13.4$ Hz], 0.45 (s, 18 H, $Si(CH_3)_2$), 1.07 [s, 3 H, $SnCH_3$, $^2J(^{117/119}Sn\text{-}^1H) = 56.8/59.5$ Hz], 1.24 (s, 27 H, $C(CH_3)$). $\{^1H\}^{13}$C-NMR (50.32 MHz, [D$_6$]benzene, 295 K): $\delta = -6.8$ ($SnCH_3$), 9.6 ($Si(CH_3)_2$), 14.5 (CH), 35.4 ($C(CH_3)$), 54.7 ($C(CH_3)$); $\{^1H\}^{29}$Si-NMR (39.76 MHz, [D$_6$]benzene, 295 K): $\delta = 0.8$ ($Si(CH_3)_2$); $\{^1H\}^{119}$Sn-NMR (74.63 MHz, [D$_6$]benzene, 295 K): $\delta = -57.3$; IR (Nujol): $\nu = 3130$ vw cm^{-1}, 1997 vw, 1591 w, br, 1256 w, 1117 w, 1017 w, 868 w, 787 w, 719 w, 691 w; $C_{20}H_{49}N_3Si_3Sn$ (534.58) calcd C 44.94, H 9.24, N 7.86; found C 45.12, H 918, N 7.69.

General procedure for preparation of $MeSi[SiMe_2N(4\text{-}CH_3C_6H_4)]_3Sn(allyl)$ (5–8)

To solutions of $MeSi[SiMe_2N(4\text{-}CH_3C_6H_4)]_3SnLi(THF)_3$ (0.88 g, 1.06 mmol) in toluene (30 ml) an equimolar amount of RX (X=Br, Cl; 1.06 mmol) was added in each case at room temperature and the reaction mixture was subsequently stirred for 1 h. After removal of LiX by centrifugation, the solvent was removed *in vacuo*. The residues were washed with cold pentane (5 ml). After drying for several hours compounds **6–9** were obtained as colourless analytical pure solids.

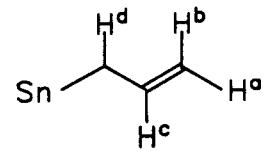

$MeSi[SiMe_2N(4\text{-}CH_3C_6H_4)]_3SnCH_2CH{=}CH_2$ (5)

Yield: 0.63 g, (86%); ^{1}H-NMR (200.13 MHz, [D$_6$]benzene, 295 K): $\delta = 0.18$ (s, 3H, CH_3Si), 0.56 (s, 18H, $Si(CH_3)_2$), 1.92 (d, $^3J_{HH} = 8.4$ Hz, $^2J_{SnH} = 99.4$ Hz, 2H, H^d), 2.11 (s, 9H, 4-$CH_3C_6H_4$), 4.20 (d, $^3J_{HH} = 16.8$ Hz, 1H, H^a), 4.35 (d, $^3J_{HH} = 9.13$ Hz, 1H, H^b), 4.87 (m, 1H, H^c), 6.91 (d, $^3J_{HH} = 8.2$ Hz, 6H, H^2), 7.05 (d, 6H, H^3); $\{^1H\}^{13}$C-NMR (50.32 MHz, [D$_6$]benzene, 295 K): $\delta = -15.0$ (CH_3Si), 3.4 ($Si(CH_3)_2$), 20.0 ($SnCH_2$), 20.7 (4-$CH_3C_6H_4$), 115.1 ($CH{=}CH_2$), 117.0 ($CH{=}CH_2$), 126.4 (C^2), 130.1 (C^3), 131.3 (C^4), 147.7 (C^1); $\{^1H\}^{29}$Si-NMR (39.76 MHz, [D$_6$]benzene, 295 K): $\delta = 4.4$ ($Si(CH_3)_2$), -91.4 ($SiCH_3$); $\{^1H\}^{119}$Sn-NMR (74.63 MHz, [D$_6$]benzene, 295 K): $\delta = -160.4$; $C_{31}H_{47}N_3Si_4Sn$ (692.77); calcd C 53.75, H 6.84, N 6.07; found C 53.58, H 6.97, N 5.99.

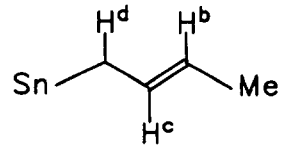

$MeSi[SiMe_2N(4\text{-}CH_3C_6H_4)]_3SnCH_2CH{=}CHCH_3$ (6)

Yield: 0.60 g (80%); ^{1}H-NMR (200.13 MHz, [D$_6$]benzene, 295 K): $\delta = 0.19$ (s, 3H, CH_3Si), 0.56 (s, 18H, $Si(CH_3)_2$), 1.15 (d, $^3J_{HH} = 5.1$ Hz,

$^5J_{SnH}$ = 43.7 Hz, 3H, CH=CHCH$_3$), 1.90 (dd, ^3J_HcHd = 6.9 Hz, ^4J_HbHd = 1.1 Hz, $^2J_{SnH}$ = 96.1 Hz, 2H, H^3), 2.10 (s, 9H, 4-CH$_3$C$_6$H$_4$), 4.4–4.6 (m, 2H, H^c u. H^b), 6.92 (d, $^3J_{HH}$ = 8.2 Hz, 6H, H^2), 7.07 (d, 6H, H^3); {^{1}H}^{13}C-NMR (50.32 MHz, [D$_6$]benzene, 295 K): δ = −15.0 (CH$_3$Si), 3.4 (Si(CH$_3$)$_2$), 17.9 (CH=CHCH$_3$), 18.9 (SnCH$_2$), 20.7 (4-CH$_3$C$_6$H$_4$), 117.0 (CH=CHCH$_3$), 126.4 (C^2), 130.0 (C^3), 130.1 (CH=CHCH$_3$), 131.1 C^4), 147.9 (C^1); {^{1}H}^{29}Si-NMR (39.76 MHz, [D$_6$]benzene, 295 K): δ = 4.1 (Si(CH$_3$)$_2$), −91.4 (SiCH$_3$); {^{1}H}^{119}Sn-NMR (74.63 MHz, [D$_6$]benzene, 295 K): δ = −71.9. C$_{32}$H$_{49}$N$_3$Si$_4$Sn (706.79): calcd C 54.38, H 6.99, N 5.95; found C 54.46, H 6.87, N 5.74.

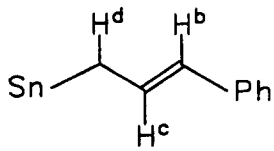

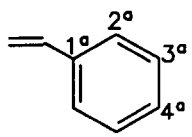

MeSi[SiMe$_2$N(4-CH$_3$C$_5$H$_4$)]$_3$SnCH$_2$CH=CHC$_6$H$_5$ (**7**)

Yield: 0.62 g (76%); ^{1}H-NMR (200.13 MHz, [D$_6$]benzene, 295 K): δ = 0.17 (s, 3H, CH$_3$Si), 0.53 (s, 18H, Si(CH$_3$)$_2$), 2.02 (d, $^3J_{HH}$ = 8.4 Hz, $^2J_{SnH}$ = 101.1 Hz, 2H, H^d), 2.14 (s, 9H, 4-CH$_3$C$_6$H$_4$), 5.14 (dt, ^3J_HbHc = 16.1 Hz, ^3J_HdHc = 8.4 Hz, 1H, H^c), 5.43 (d, $^3J_{HH}$ = 15.4 Hz, 1H, H^b), 6.92 (d, $^3J_{HH}$ = 8.2 Hz, 6H, H^2), 7.07 (d, 6H, H^3), 7.0–7.2 (m, 5H, CH=CHC$_6$H$_5$); {^{1}H}^{13}C-NMR (50.32 MHz, [D$_6$]benzene, 295 K): δ = −15.1 (CH$_3$Si), 3.4 (Si(CH$_3$)$_2$), 19.8 (SnCH$_2$), 20.7 (4-CH$_3$C$_6$H$_4$), 117.0 (CH=CHC$_6$H$_5$), 123.7 (CH=CHC$_6$H$_5$), 126.1 (C^{2a}), 126.5 (C^2), 126.7 (C^{4a}), 128.4 (C^{3a}), 130.2 (C^3), 131.3 (C^4), 137.9 (C^{1a}), 147.8 (C^1); {^{1}H}^{29}Si-NMR (39.76 MHz, [D$_6$]benzene, 295 K): δ = 4.4 (Si(CH$_3$)$_2$), −91.5 (SiCH$_3$); {^{1}H}^{119}Sn-NMR (74.63 MHz, [D$_6$]benzene, 295 K): δ = −50.4; C$_{37}$H$_{51}$N$_3$Si$_4$Sn (768.87); calcd C 57.80, H 6.69, N 5.47; found C 57.98, H 6.61, N 5.69.

MeSi[SiMe$_2$N(4-CH$_3$C$_6$H$_4$)]$_3$SnCH$_2$CCH$_3$=CH$_2$ (**8**)

Yield: 0.58 g (78%); ^{1}H-NMR (200.13 MHz, [D$_6$]benzene, 295 K): δ = 0.19 (s, 3H, CH$_3$Si), 0.56 (s, 18H, Si(CH$_3$)$_2$), 0.98 (s, br, $^4J_{SnH}$ = 18.3 Hz, 3H, CCH$_3$CH=CH$_2$), 1.99 (s, $^2J119_{SnH}$ = 96.5 Hz,

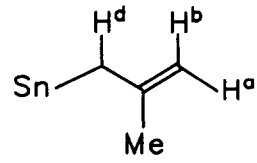

$^2J119_{SnH}$ = 99.4 Hz, 2H, H^d), 2.12 (s, 9H, 4-CH$_3$C$_6$H$_4$), 3.95 (q, $^4J_{HH}$ = 0.8 Hz, $^4J_{SnH}$ = 36.9 Hz, 1H, H^b), 4.07 (t, $^4J_{HH}$ = 1.8 Hz, $^4J_{SnH}$ = 26.7 Hz, 1H, H^a), 6.92 (d, $^3J_{HH}$ = 8.2 Hz, 6H, H^2), 7.11 (d, 6H, H^3); {^{1}H}^{13}C-NMR (50.32 MHz, [D$_6$]benzene, 295 K): δ = −15.0 (CH$_3$Si), 3.4 (Si(CH$_3$)$_2$), 20.7 (4-CH$_3$C$_6$H$_4$), 23.4 (SnCH$_2$), 24.0 (CCH$_3$=CH$_2$), 112.1 (CCH$_3$=CH$_2$), 127.1 (C^2), 130.0 (C^3), 131.5 (C^4), 139.3 (CCH$_3$=CH$_2$), 147.7 (C^1); {^{1}H}^{29}Si-NMR (39.76 MHz, [D$_6$]benzene, 295 K): δ = 4.1 (Si(CH$_3$)$_2$), −91.8 (SiCH$_3$); {^{1}H}^{119}Sn-NMR (74.63 MHz, [D$_6$]benzene, 295 K): δ = −105.5; C$_{32}$H$_{49}$N$_3$Si$_4$Sn (706.79); calcd C 54.38, H 6.99, N 5.95; found C 54.51, H 7.11, N 6.04.

General procedure for the preparation of MeSi{SiMe$_2$N[C(CH$_3$)$_3$]}$_3$Sn(allyl) (**9**, **10**)

To a solution of MeSi{SiMe$_2$N[C(CH$_3$)$_3$]}$_3$SnLi(THF) (0.43 g, 0.68 mmol) in toluene (30 ml) an equimolar amount RX (X=Cl, Br, 0.68 mmol) was added and the reaction mixture subsequently stirred for 7 days at room temperature. After centrifugation of the LiX the solvent was removed *in vacuo*. The residue was washed with pentane (5 ml) and compounds **9** and **10** were obtained as colourless solids after vacuum-drying for several hours.

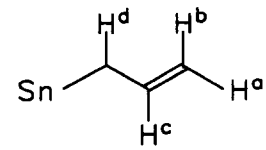

MeSi{SiMe$_2$N[C(CH$_3$)$_3$}$_3$SnCH$_2$CH=CH$_2$(**9**)

Yield: 0.33 g (81%); ^{1}H-NMR (200.13 MHz, [D$_6$]benzene, 295 K): δ = 0.08 (s, 3H, CH$_3$Si), 0.57 (s, 18H, Si(CH$_3$)$_2$), 1.33 (s, 27H, C(CH$_3$)), 2.79 (d, $^3J_{HH}$ = 8.0 Hz, $^2J_{SnH}$ = 81.1 Hz, 2H, H^d), 4.9–5.1 (m, 2H, H^b u. H^a), 6.0–6.3 (m, 1H, H^c); {^{1}H}^{13}C-NMR (50.32 MHz, [D$_6$]benzene, 295 K): δ = −13.9 (CH$_3$Si), 7.9 (Si(CH$_3$)$_2$), 36.2 (C(CH$_3$)$_3$), 40.1 (SnCH$_2$), 58.5 (C(CH$_3$)$_3$), 117.6 (CH=CH$_2$), 135.9 (CH=CH$_2$); {^{1}H}^{29}Si-NMR (39.76 MHz, [D$_6$]benzene, 295 K): δ = −3.2 (Si(CH$_3$)$_2$), −98.6 (SiCH$_3$); {^{1}H}^{119}Sn-NMR (74.63 MHz, [D$_6$]benzene, 295 K):

$\delta = -108.1$; $C_{22}H_{53}N_3Si_4Sn$ (590.72); calcd C 44.73, H 9.04, N 7.11; found C 44.95, H 9.19, N 7.28.

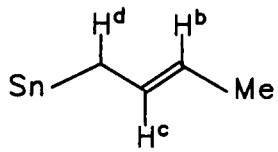

$MeSi\{SiMe_2N[C(CH_3)_3]\}_3SnCH_2CH{=}CHCH_3$ (**10**)

Yield: 0.33 g (79%); ^{1}H-NMR (200.13 MHz, [D$_6$]benzene, 295 K): $\delta = 0.09$ (s, 3H, CH_3Si), 0.58 (s, 18H, $Si(CH_3)_2$), 1.35 (s, 27H, $C(CH_3)$), 1.64 (d, $^3J_{HH} = 5.1$ Hz, 3H, $CH{=}CHCH_3$), 2.76 (d, $^3J_{HH} = 7.7$ Hz, $^2J_{SnH} = 78.6$ Hz, 2H, H^d), 5.2–5.5 (m, 1H, H^b), 5.7–5.9 (m, 1H, H^c); {^{1}H}^{13}C-NMR (50.32 MHz, [D$_6$]benzene, 295 K): $\delta = -13.9$ (CH_3Si), 7.9 ($Si(CH_3)_2$), 18.1 ($CH{=}CHCH_3$), 36.4 ($C(CH_3)_3$), 39.0 ($SnCH_2$), 58.5 ($C(CH_3)_3$), 125.6 ($CH{=}CHCH_3$), 132.2 ($CH{=}CH_2$); {^{1}H}^{29}Si-NMR (39.76 MHz, [D$_6$]benzene, 295 K): $\delta = -3.4$ ($Si(CH_3)_2$), -98.3 ($SiCH_3$); {^{1}H}^{119}Sn-NMR (74.63 MHz, $= -107.1$; $C_{23}H_{55}N_3Si_4Sn$ (604.75); calcd C 45.68, H 9.17, N 6.95; found C 45.93, H 9.04, N 6.88.

X-ray crystallographic study of **4**

Crysta data. $C_{20}H_{49}N_3Si_3Sn$, $M = 534.58$, hexagonal space group $P6_3$ (no. 173), $a = b = 10.2554(11)$, $c = 15.441(2)$ Å, $U = 1406.4(3)$ Å^3, $Z = 2$, $F(000) = 564$, $D_{calc} = 1.262$ Mg m^{-3}, μ(Mo-K_α) = 1.047 mm^{-1}.

Data collection. X-ray intensity data were collected from a colourless block shaped crystal of **4** (0.44 × 0.48 × 0.80 mm) in the θ-range 2.29–24.99° ($-1 \leqslant h \leqslant 11$, $-12 \leqslant k \leqslant 1$, $-1 \leqslant l \leqslant 18$) using a Siemens P4 four-circle diffractometer with graphite monochromated Mo-K_α radiation ($\lambda = 0.71073$ Å). A total of 2342 independent reflections were collected of which 929 were unique ($R_{int} = 0.0218$).

Structure solution and refinement [8].

The metal position was deduced from a Patterson synthesis and the remaining non-hydrogen atoms of the structure were identified in a series of Fourier and difference-Fourier maps. Hydrogen atoms were included in idealized positions and assigned $U_{iso} = 1.2\ U_{eq}$ of the parent carbon atom (methine) or $1.5\ U_{eq}$ of the parent carbon atom (methyl). After refinement with isotropic displacement parameters for all non-hydrogen atoms, an empirical absorption correction was applied (T_{max} 0.853, T_{min} 0.448). In the final cycles of full-matrix least squares refinement on F^2, non-hydrogen atoms were assigned anisotropic displacement parameters and refinement converged at $R_1 = 0.0518$, $wR_2 = 0.1336$ [$I > 2\sigma(I)$] and $R_1 = 0.0557$, $wR_2 = 0.1623$ (all data). The largest peak and trough in the final difference-Fourier map were 1.80 and -1.19 eÅ^{-3}, respectively, and the Flack absolute structure parameter refined to 0.26(12). We attribute the relatively high values of these parameters to the presence of a small quantity of complex of opposite chirality in the crystal but found no improvement in refinement by modelling racemic twinning. Supplementary data containing fractional atomic coordinates, thermal parameters and tables of bond lengths and angles have been deposited at the Cambridge Crystallographic Centre (CCDC).

RESULTS AND DISCUSSION

The reaction of the two previously reported lithium triamidostannates $[HC\{SiMe_2N(4\text{-}CH_3C_6H_4)\}_3SnLi(THF)_3]$ (**1a**), $[HC\{SiMe_2N[C(CH_3)_3]\}_3SnLi(THF)]$ (**1b**) with methyl iodide in ether solvents demonstrates to which degree the reactivity of the tin nucleophiles depends on the ligand periphery of the tripodal amido ligand. Whereas complete conversion of compound **1a** to the respective methyl stannane $[HC\{SiMe_2N(4\text{-}CH_3C_6H_4)\}_3SnMe]$ (**3**) has occurred after ca 30 min reaction time the analogous transformation using **1b** as starting material to give $[HC\{SiMe_2N[C(CH_3)_3]\}_3SnMe]$ (**4**) requires several hours reaction time (eqn 1). This probably is a consequence of the steric shielding of the nucleophilic centre by the bulky *tert*-butyl-groups in the latter.

The formulation of the methyl stannanes **3** and **4** is established by elemental analysis and the ^{1}H-, ^{13}C- and ^{29}Si-NMR spectroscopic data are consistent with the proposed structures of the compounds. The formation of the methyl–tin bonds could be directly inferred from the observed $^2J(^{117/119}Sn\text{-}^1H)$ coupling in **4**

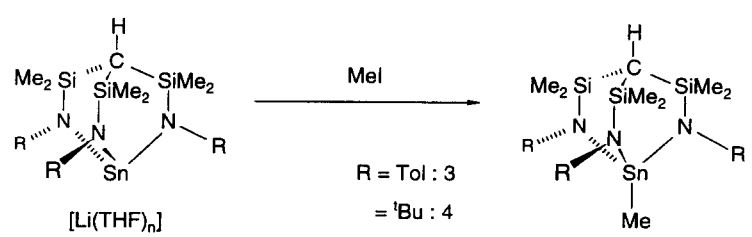

(1)

[56.8/59.5 Hz]. In the ^{1}H-NMR spectrum of **3** the tin satellites of the methyl group were broad and the coupling constants of ^{117}Sn and ^{119}Sn isotopomers not resolved [^2J(SnH) = 69 Hz].

In order to establish the detailed structural parameters of these new triamidotin compounds a single crystal X-ray structure analysis of **4** was carried out. The molecular structure of **4** is shown in Fig. 1 and the principal metric parameters are listed in Table 1. Compound **4** crystallizes in the hexagonal space group $P6_3$ and the threefold symmetrical molecules are aligned along the crystallographic 3-fold axis, with the metal atom, the Sn-bound methyl group and the bridge head CH-unit on the 3-fold axis. As in the previously studied tripodal triamidotin compounds, the structural centre piece is the [2,2,2]bicyclooctane-related cage comprising the trisilylmethane unit and the triamidotin unit. These two units are slightly twisted with respect to each other [torsion angle C(1)—Si(1)—N(1)—Sn(1) 23.3(6)°] which is to be seen as a consequence of the steric repulsion of the methyl groups within the trisilylmethane unit rather than being due to the geometrical requirements of Sn—N binding in the molecule.

Although **4** is the first triamidotin(IV) compound containing a tripodal amido ligand to be structurally characterized, there are a number of crystal structures previously reported for the triamido stannates(II) and their Sn–metal bonded derivatives. It was therefore of particular interest to compare the metric parameters of the cage structure in these different systems. The ∠(N—Sn—N) angles in the triamidostannates(II) are close to 90° indicating little or no s–p hybridization at the tin atoms. These angles are increased in the Sn—M-heterobimetallics to values between 100 and 102°, while the ∠[N(1)—Sn(1)—N(1′)] value in the structure of **4** is 103.5(4)°. This may be indicative of a certain degree of s–p-hybridization in the tetravalent tin compound, given the low steric demand of the methyl group occupying the fourth coordination site. Another interesting feature is the contraction of the Sn—N bond in the Sn(IV) complex [d{Sn(1)—N(1)} = 2.093(10) Å] compared to those determined in the triamidostannates(II) containing tripodal amidoligands with a trisilylmethane framework which lie in the range of 2.15 Å [1]. Remarkably, the Sn—N bond lengths in the heterobimetallic systems are scattered around the value determined for **4** (although significant variations are observed). These structural parameters clearly set the tetravalent organotin compound **4** apart from the divalent tin derivatives of the tripodal amido ligands we previously characterized, although they lie well within the range of previously characterized alkyltriamidotin com-

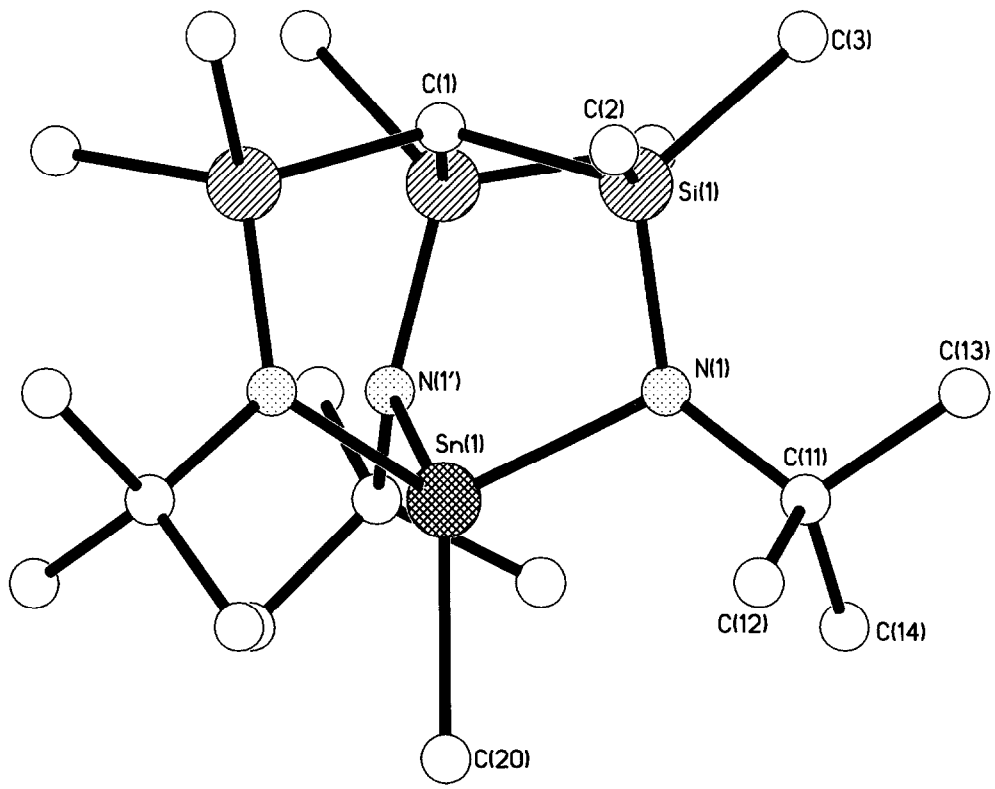

Fig. 1. (a) The X-ray structure of **4** viewed perpendicular to the 3-fold axis showing the atomic numbering scheme; (b) a view down the 3-fold axis showing the helical twist in the tripod ligand.

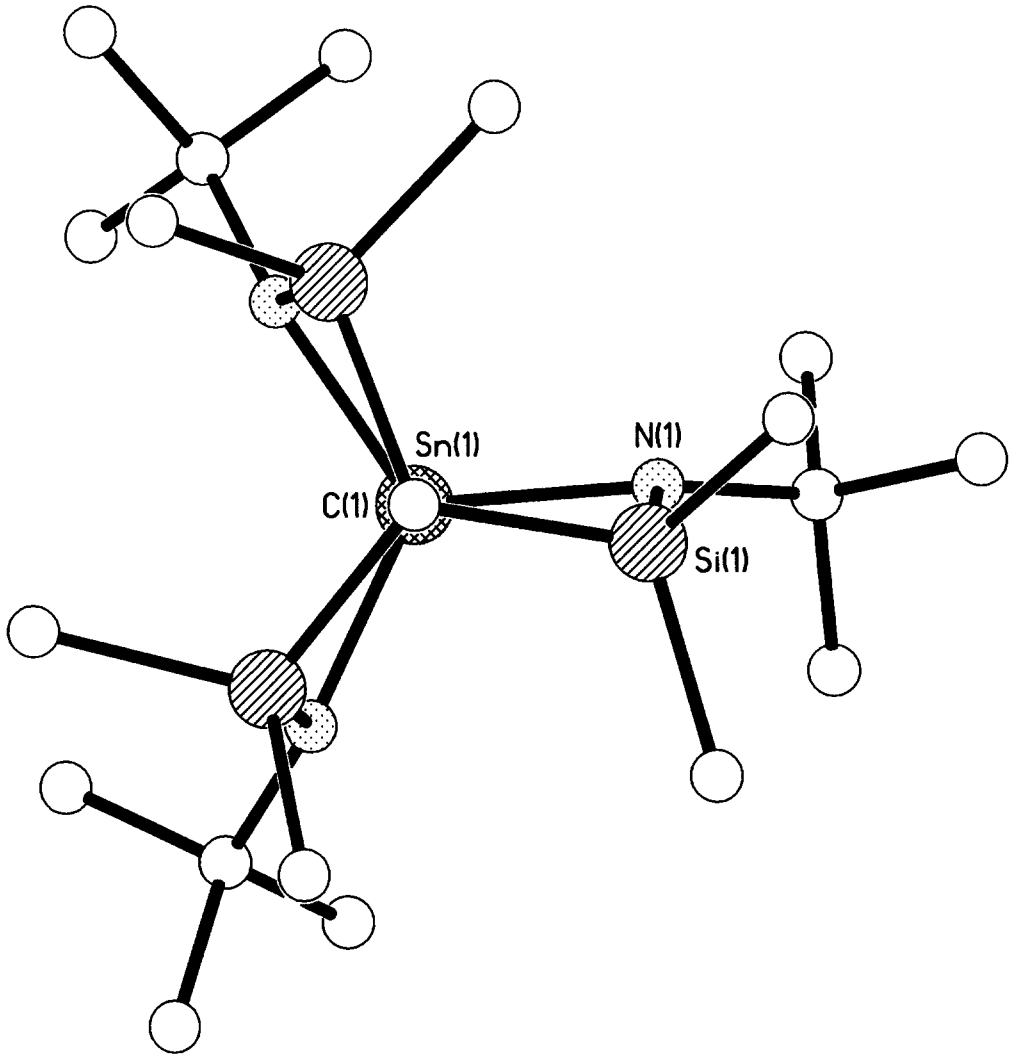

Fig. 1—*Continued.*

Table 1. Selected bond lengths [Å] and angles [°] for **4**

Sn(1)—N(1)	2.093(10)	N(1)—Sn(1)—N(1′)[a]	103.5(4)
Sn(1)—C(20)	2.09(3)	N(1)—Sn(1)—C(20)	114.9(3)
C(1)—Si(1)	1.893(8)	C(11)—N(1)—Si(1)	125.7(11)
Si(1)—N(1)	1.724(12)	C(11)—N(1)—Sn(1)	119.4(10)
		Si(1)—N(1)—Sn(1)	110.4(5)

[a] Symmetry related atom at $-y+1, x-y+1, z$.

pounds [9]. The relatively high esd on the Sn—Me bond length is attributed to the slight disorder in the crystal (see Experimental section) and therefore does not permit its further discussion.

As stated above, one of the aims of this study was the preparation of a series of allyl triamidostannanes. For this purpose the two triamidostannates [MeSi $\{SiMe_2N(4\text{-}CH_3C_6H_4)\}_3$Sn-Li(THF)$_3$] (**2a**), [MeSi $\{SiMe_2N[C(CH_3)_3]\}_3$SnLi(THF)] (**2b**) containing a trisilylsilane ligand backbone were employed as metal nucleophiles. These systems were chosen since they are easier to isolate and to handle than the trisilylmethane analogues. In the reactions with a series of allyl halides a similarly marked difference in reactivity between the *p*-tolyl-*N* and the *tert*-butyl-*N* substituted species was observed. While the conversions of the former were

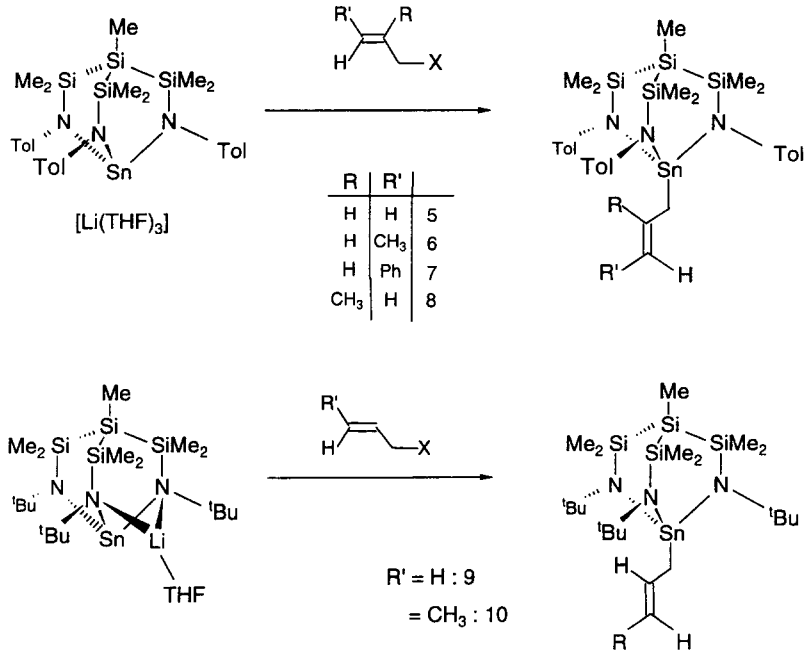

Scheme 1.

complete within less than 1 h of reaction time, the reaction of the stannate **2b** with the allyl halides took approximately 7 days to go to completion (Scheme 1). The formulation of the allyltriamidostannanes **5**–**10** was substantiated by the analytical and ^{1}H-, ^{13}C-, ^{119}Sn- and ^{29}Si-NMR spectroscopic data. The proton signals of the allyl CH_2/CHR groups which are bonded directly to the tin atoms are associated with sets of $^{117/119}$Sn satellites which were not resolved into the two isotopomers in most cases. The ^{2}J(Sn—H) coupling constants lie in the range of 96–100 Hz in **5**–**8** and are 81.1 and 78.6 Hz for **9** and **10**, respectively. In compound **8**, bearing the 2-methylallyl group ^{4}J(Sn—H) satellites were also observed with the proton signals of the methyl group [^{4}J(Sn—H) = 18.3 Hz)] and the olefinic protons [H^{b}: ^{4}J(Sn—H) = 36.9, H^{a}: ^{4}J(Sn—H) = 26.7 Hz (for labelling see Experimental section)].

CONCLUSIONS

The triamidostannates containing tripodal amido ligands which we reported previously are metal nucleophiles which may be employed in the synthesis of new organotin compounds. We are currently studying the synthetic potential of particularly the allyl tin compounds reported in this paper and plan to extend the study to include chiral amido ligands in the future.

Acknowledgements—We thank the Deutsche Forschungsgemeinschaft, the Fonds der Chemischen Industrie, the Engineering and Physical Science Research Council (U.K.), the DAAD and the British Council (ARC grant to L.H.G. and M.McP.) for financial support and Wacker Chemie AG for generous gifts of basic chemicals. Thanks is also due to Prof. H. Werner (Würzburg) for his continued interest and support of this work.

REFERENCES

1. (a) Hellmann, K. W., Steinert, P. and Gade, L. H., *Inorg. Chem.*, 1994, **33**, 3859; (b) Hellmann, K. W., Gade, L. H., Gevert, O., Steinert, P. and Lauher, J. W., *Inorg. Chem.*, 1995, **34**, 4069.
2. (a) Hellmann, K. W., Friedrich, S., Gade, L. H., Li, W. S. and McPartlin, M., *Chem. Ber.*, 1995, **128**, 29. (b) Memmler, H., Kauper, U., Gade, L. H., Stalke, D. and Lauher, J. W., *Organometallics*, 1996, **15**, 3637.
3. (a) Contel, M., Hellmann, K. W., Gade, L. H., Scowen, I. J., McPartlin, M. and Laguna, M., *Inorg. Chem.*, 1996, **35**, 3713. (b) Findeis, B., Gade, L. H., Scowen, I. J. and McPartlin, M., *Inorg. Chem.*, 1997, **36**, 960. (c) Findeis, B., Contel, M., Gade, L. H., Laguna, M., Gimeno, M. C., Scowen, I. J. and McPartlin, M., *Inorg. Chem.*, 1997, **36**, 2386.
4. (a) Marshall, J. A., *Chem. Rev.*, 1996, **96**, 31. Yamamoto, Y., ed., *Organotin Compounds in Organic Synthesis*: *Tetrahedron*, 1987, **45**, 909. (b) Omae, I., *Organotin Chemistry*, Elsevier, Amsterdam, 1989.
5. Nozaki, H., In *Organometallics in Synthesis—A Manual*, ed. M. Schlosser, Wiley, 1994, p. 535.
6. Pereyre, M., Quintard, J.-P. and Rahm, A., *Tin in Organic Synthesis*, Butterworth, London, 1987.
7. Hellmann, K. W. and Gade, L. H., *Verfahrenstechnik*, 1987, **31**(5), 70.

8. SHELXTL PC-version 5.03, Siemens Analytical X-Ray, Madison, WI, USA, 1994.
9. (a) Rannenberg, M. and Weidlein, J., *Z. Naturforsch. B*, 1991, **46,** 459. (b) Plass, W. and Verkade, J. G., *Inorg. Chem.*, 1993, **32,** 5145. (c) Laplaza, C. E., Davis, W. M. and Cummins, C. C., *Organometallics*, 1995, **14,** 577.

Pergamon

PII: S0277-5387(97)00372-0

Polyhedron Vol. 17, No. 5–6, pp. 745–748, 1998
© 1998 Elsevier Science Ltd
All rights reserved. Printed in Great Britain
0277-5387/98 $19.00+0.00

Sterically induced *cis* isomerism in an Sb(III) imido dimer; synthesis, structure and solution dynamics of $[(Me_2N)Sb(\mu\text{-}NDipp)]_2$ (Dipp = 2,6-$Pr^i_2C_6H_3$)

Michael A. Beswick, Christopher N. Harmer, Alexander D. Hopkins, Michael A. Paver, Paul R. Raithby and Dominic S. Wright*

Chemistry Department, Lensfield Road, Cambridge CB2 1EW, U.K.

(Received 14 April 1997; accepted 4 August 1997)

Abstract—The reaction of $[Sb(NMe_2)_3]$ with the sterically bulky amine $[DippNH_2]$ gives the unusual *cis* dimer $[(Me_2N)Sb(\mu\text{-}NDipp)]_2$ **1**, containing a puckered Sb_2N_2 core. ^1H NMR studies show that the *cis* conformation is retained in solution. © 1998 Elsevier Science Ltd. All rights reserved

Keywords: *cis* isomerism; Sb(III) imido dimer; puckered Sb_2N_2 core.

We here report that the reaction of $[Sb(NMe_2)_3]$ with 2,6-diisopropylaniline ($DippNH_2$) (1 : 1 equivalents) (Scheme 1) gives the puckered *cis* dimer $[(Me_2N)Sb\{\mu\text{-}N(Dipp)\}]_2$ **1** [1]. Variable-temperature ^1H NMR studies illustrate that the *cis* conformation is retained in solution at and below room temperature. In earlier studies of dimethylamido Group 15 reagents [2] we showed that the reactions of a range of primary amines (RNH_2) with $[E(NMe_2)_3]$ (E = Sb or Bi; $x = 0-2$) give the *trans* dimers $[(Me_2N)E(\mu\text{-}R)]_2$ in the solid state and that the *cis–trans* equilibria occurring in solution for these species are markedly dependent on the degree of intramolecular bonding between functional groups (present on R) and the metal centres

$$2[Sb(NMe_2)_3] + 2[DippNH_2] \xrightarrow{\text{toluene}} [(Me_2N)Sb(\mu\text{-}NDipp)]_2 + 4Me_2NH$$

Scheme 1.

[2b,3]. The study presented here was undertaken in order to examine the potential disruption of the planar Sb_2N_2 units of these dimers by sterically demanding organic substituents, and the possible formation of monomeric species $[(Me_2N)Sb{=}NR]$.

A low-temperature (150 K) X-ray study was undertaken on **1** [4]. This shows that the complex exists as dimers, $[(Me_2N)Sb\{\mu\text{-}N(Dipp)\}]_2$, in the solid state. There are two crystallographically independent chemically equivalent molecules in the asymmetric unit which differ only slightly in their bond lengths and angles (one of which is shown in Fig. 1a). There are major distortions introduced by the incorporation of the sterically bulky Dipp groups into the Sb_2N_2 core framework. The bond lengths and angles within the planar cores of the *trans* dimers $[(Me_2N)Sb(\mu\text{-}NR)]_2$ [R = 3,4,5-$(MeO)_3C_6H_2$, 4-methylpyrid-2-yl] [2b] are similar to those found in **1** (Sb—N av. 2.06 Å, N—Sb—N av. 76.8°, Sb—N—Sb av. 100.6°). However, the Sb_2N_2 rings of **1** are butterfly shaped (with an average angle of 153.4° between the N wing-tips) (Fig. 1b).

The folding of these ring units and the surprising *cis* conformation of the NMe_2 groups with respect to the core stems from the extreme steric confrontation between the Pr^i substituents of the Dipp groups and the NMe_2 groups. In a planar *trans* arrangement these units would be brought into direct contact on each side of the Sb_2N_2 ring (Fig. 2a). However, the adoption of

* Author to whom correspondence should be addressed.

Dedicated to Prof. Don Bradley on the occasion of his 73rd birthday and in recognition of his immense and fundamental contributions to the development of metal alkoxide and amide chemistry.

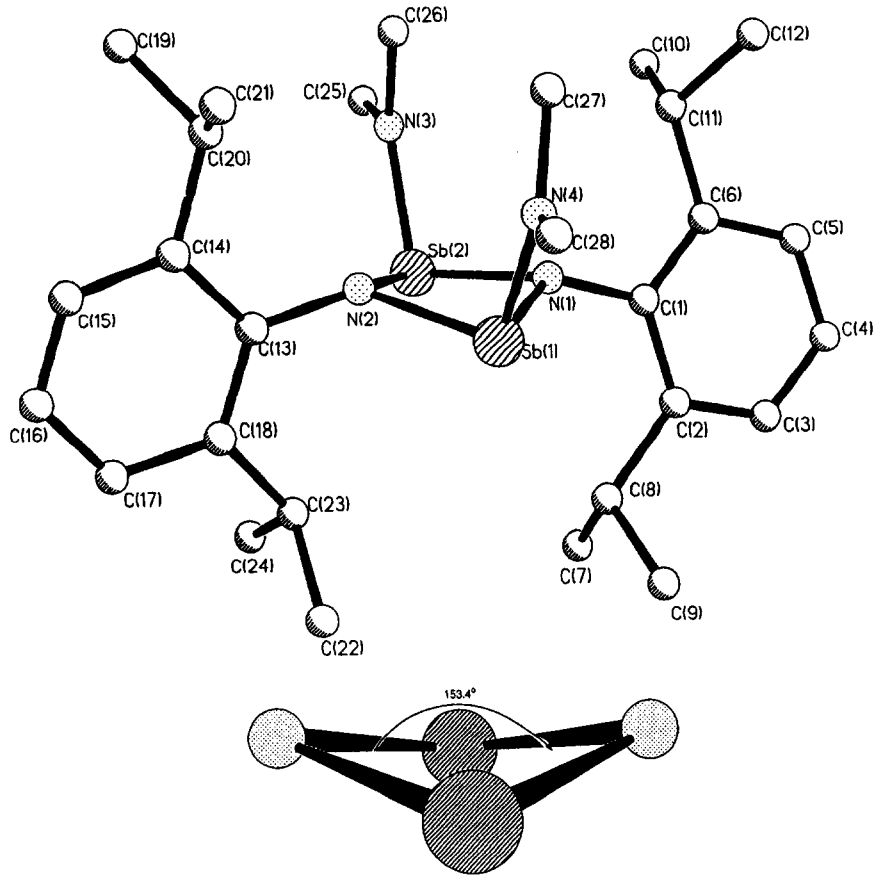

Fig. 1. Molecular structure of complex **1**. Hydrogen atoms have been omitted for clarity. Key bond lengths (Å) and angles (°): molecule A—Sb(1)—N(1) 2.062(8), Sb(1)—N(2) 2.056(8), Sb(1)—N(4) 1.983(8), Sb(2)—N(2) 2.048(7), Sb(2)—N(1) 2.052(8), Sb(2)—N(3) 1.976(9), Sb(1)···Sb(2) 3.179(1), N(4)—Sb(1)—N(2) 104.5(3), N(4)—Sb(1)—N(1) 101.9(3), N(2)—Sb(1)—N(1) 76.1(3), N(3)—Sb(2)—N(2) 101.5(3), N(3)—Sb(2)—N(1) 104.3(4), N(2)—Sb(2)—N(1) 76.5(3), Sb(2)—N(1)—Sb(1) 101.2(4), Sb(2)—N(2)—Sb(1) 101.6(3): molecule B—Sb(3)—N(5) 2.086(8), Sb(3)—N(6) 2.063(8), Sb(3)—N(7) 1.998(9), Sb(4)—N(5) 2.053(8), Sb(4)—N(6) 2.086(8), Sb(4)—N(8) 2.003(8), Sb(1)···Sb(2) 3.171(1), N(7)—Sb(3)—N(5) 105.2(3), N(7)—Sb(3)—N(6) 100.2(3), N(5)—Sb(3)—N(6) 77.3(3), N(8)—Sb(4)—N(5) 100.2(3), N(8)—Sb(4)—N(6) 104.7(3), N(5)—Sb(4)—N(6), 77.5(3), Sb(3)—N(5)—Sb(4) 100.0(3), Sb(3)—N(6)—Sb(4) 99.7(3).

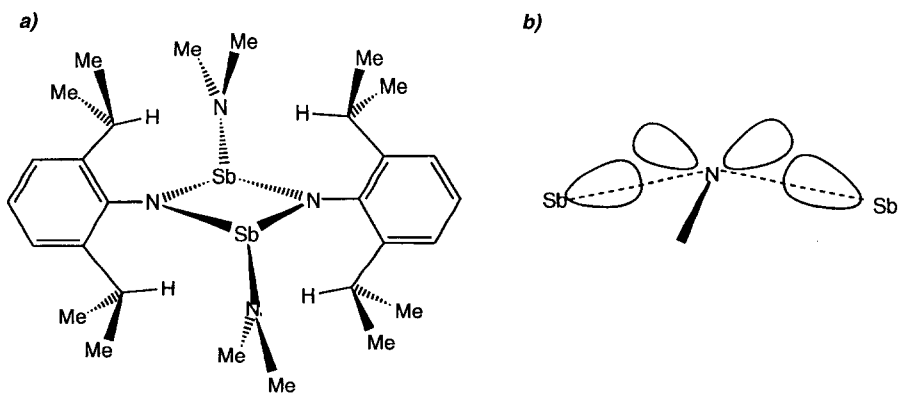

Fig. 2. (a) alternative planar *trans* arrangement showing steric congestion on both sides of the Sb_2N_2 ring, (b) disruption of the Sb—N bonding in the puckered rings of **1**.

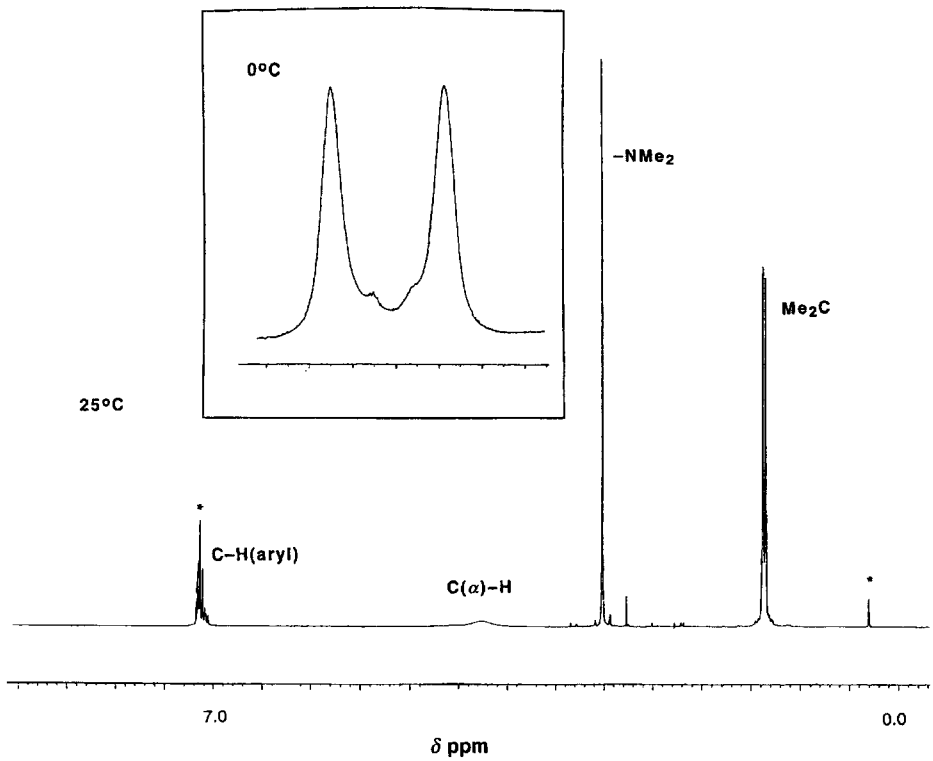

Fig. 3. ^{1}H NMR spectrum of **1** in toluene (250 MHz) (boxed inset shows the C(α)—H protons at 0°C).

a *cis* arrangement provides an overall release from the inherent steric congestion at the periphery of the core. By pivoting the DippN moieties away from the crowded side of the ring, maximum space is made available for the accommodation of the NMe_2 and Pr^i groups. This pivoting clearly disrupts the alignment of the Sb and N orbitals involved in ring bonding, which can no longer retain optimum overlap, and puckering of the ring results (Fig. 2b). The butterfly-shaped Sb_2P_2 core of the dimeric Sb(III) phosphinidine complex $[SbP(2,4,6\text{-}Bu^t_3C_6H_2)]_2$ (fold angle 103.2°) occurs as a result of an Sb—Sb bond [2.723(1) Å] [5]. The much longer Sb···Sb contacts in **1** (av. 3.18 Å) indicate that such bonding is not induced by the weakening of the Sb_2N_2 ring. Instead there is a compensatory shortening of the Sb—$N(Me_2)$ bonds compared to those present in the planar *trans* dimers [av. 1.99 Å in **1**; cf av. 2.02 Å] [2b].

Variable-temperature ^{1}H NMR studies show that the *cis* structure of **1** is maintained in toluene over a wide temperature range. Even at room temperature, two ill-defined overlapping septets [centred at δ 4.25] are observed for the α-C—H atoms of the two Pr^i substituents of each Dipp group. These are rendered inequivalent in the sterically congested *cis* structure by restricted rotation of the Me_2CH groups (Fig. 3). Although still poorly resolved, these resonances are fully separated at ca 0°C. Separate Me resonances for the Pr^i groups could not be resolved over the same temperature range, implying that there is little difference between their chemical environments. It cannot be deduced whether the interchange of the α-C—H protons of the Pr^i groups at higher temperature occurs by butterfly wing flapping (accompanied by N and Sb configurational inversion) or by simple rotation of the imido C—N bonds. However, no dissociation of **1** into monomers could be detected (down to ca −80°C), making a dissociation/re-association process less likely. In addition, rapid rotation of the Sb—NMe_2 bonds gives rise to only one Me resonance for **1**.

Although previous NMR studies of the dimers $[(Me_2N)Sb(\mu\text{-}NR)]_2$ [2b] and $[Bu^tSb(\mu\text{-}NBu^t)]_2$ [6] have shown that the distribution of the *cis* and *trans* isomers in solution is affected by the steric bulk and donor ability of the bridging imido groups, the observation of a *cis* dimer structure for **1** in the solid state and the persistence of this conformation in solution are unprecedented for such compounds. For the chloro-bridged amido Sn(II) complexes $[Sn(\mu\text{-}Cl)NR_2]_2$, *cis* and *trans* structures have been characterized in the solid state [7]. However, no correlation between the character of the organic substituents (R) and the preference for the *cis* or *trans* conformation appears to exist for these species.

Acknowledgements—We thank the EPSRC, U.K. (MAB, CNH, ADH), the Royal Society (PRR, DSW) and Jesus College Cambridge (fellowship for MAP) for financial support.

REFERENCES

1. *Synthesis of* **1**. To a solution of $DippNH_2$ (1.3 ml, 6.89 mmol), in toluene was added $[Sb(NMe_2)_3]$ (6.89 mmol). Heating to reflux led to the formation of a yellow solution. The solution was filtered (Celite) and the solvent was removed under vacuum to yield a light yellow solid. This was redissolved in hexane (10 ml) and the solution was reduced to ca 7 ml. The yellow precipitate produced was gently heated back into solution and storage (20°C, 12 h) gave yellow crystals of **1**, yield 1.18 g (50%); m.p. 155°C; Elemental analysis, found C, 47.9; H, 6.6; N, 7.6. Calc. C, 49.3; H, 6.8; N, 8.2; IR (solid, Nujol): ν_{max}/cm^{-1} major bands at 3046(w) (aryl C—H str.), 2777(m) (C(α)—H str.), other bands at 1182(s), 1099(m), 939(m), 849(m), 772(s), 656(m); ^1H NMR [250 MHz, +25°C, d_8-toluene], 7.1 (mult., 3H, aryl C—H), 4.25 (m, 2H, C(α)—H), 3.05 (s, 6H, Me2N—), 1.35 (d, 12H, Me_2C of Dipp).
2. (a) Edwards, A. J., Leadbeater, N. E., Paver, M. A., Raithby, P. R., Russell, C. A. and Wright, D. S., *J. Chem. Soc., Dalton Trans.*, 1994, 1479; (b) Edwards, A. J., Paver, M. A., Raithby, P. R., Rennie, M.-A., Russell, C. A. and Wright, D. S., *J. chem. Soc., Dalton Trans.*, 1994, 2963.
3. Studies of related Bi systems, Beswick, M. A., Davies, M. K., Paver, M. A., Raithby, P. R., Steiner, A. and Wright, D. S., unpublished results.
4. *Crystal data for* **1**: $C_{28}H_{117}N_4Sb_2$ $F_w = 682.19$, monoclinic, space group $P2_1/n$, $a = 17.084(3)$, $b = 18.929(6)$, $c = 19.768(4)$ Å, $\beta = 99.79(2)°$, $V = 6300(3)$ Å^3, $Z = 8$, $\rho_{calc.} = 1.439$ Mg m^{-3}, $\lambda = 0.71073$ Å, $T = 150(2)$ K, $\mu(MoK_\alpha) = 1.736$ mm^{-1}. Data were collected on a Siemens-Stoe AED diffractometer using an oil-coated rapidly-cooled crystal of dimensions $0.30 \times 0.25 \times 0.20$ mm in an oil drop by the θ/ω method ($2.60° \leqslant 2\theta \leqslant 22.51°$). Of a total of 8561 collected reflections, 8239 were independent. The data were corrected for absorption by a semi-empirical method based on ψ-scans. The structure was solved by direct methods and refined by full-matrix least-squares on F^2 to final values of $R1(F > 4\sigma(F)) = 0.0479$ and $\omega R2 = 0.0926$ and $R1 = 0.1276$ and $\omega R2 = 0.2019$ (all data) [$R1 = \Sigma|F_o - F_c|/\Sigma F_o$ and $\omega R2 = (\Sigma\omega(F_o^2 - F_c^2)^2/\ \Sigma\omega(F_o^2)^2)^{0.5}$] [8]; largest peak and hole in the final difference map 0.568 and -0.628 eÅ^{-3}.
5. Jutzi, P., Meyer, U., Opiela, S., Olmstead, M. and Power, P. P., *Organometallics*, 1990, **9**, 1459.
6. Kuhn, N. and Scherer, O. J., *Z. Naturforsch., Teil B*, 1979, **34**, 888.
7. Chorley, R. W., Hitchcock, P. B., Jolly, B. S., Lappert, M. F. and Lawless, G. A., *J. Chem. Soc., Chem. Commun.*, 1991, **5**, 2511.
8. Sheldrick, G. M., SHELXL, Göttingen, 1993.

Pergamon

PII: S0277-5387(97)00394-X

Polyhedron Vol. 17, No. 5-6, pp. 749-758, 1998
© 1998 Elsevier Science Ltd
All rights reserved. Printed in Great Britain
0277-5387/98 $19.00+0.00

Molybdenum and tungsten Cp* complexes that contain 2,2′-diamidodiphenylamido or 2-amido-2′-oxydiphenylamido ligands

Shi'ang Cai, Richard R. Schrock,* Rhett R. Kempe and W. M. Davis

Department of Chemistry 6-331, Massachusetts Institute of Technology Cambridge, MA 02139, U.S.A.

(Received 25 April 1997; accepted 1 August 1997)

Abstract—Cp^*MCl_4 compounds (M = Mo or W) react with 2-amino-2′-hydroxydiphenylamine ($[H_2NNHOH]$) to yield complexes of the type Cp*M[HNNO]Cl. An X-ray study of the one electron reduction product, $\{Na(C_2H_5)_2O\}\{Cp^*Mo[HNNO]Cl\}$, showed it to contain square pyramidal $\{Cp^*Mo[HNNO]Cl\}^-$ ions weakly connected by bridging Na(ether) units. Cp* W[HNNO]Cl could be oxidized readily by AgOTf in acetonitrile to produce $\{Cp^*W[HNNO]Cl\}^+OTf^-$. Both Cp*M[HNNO]Cl compounds are reduced by hydrazine to give the diamagnetic compound, $Cp^*M[HNNO](NH_3)$. An X-ray structure of $Cp^*Mo[HNNO](NH_3)$ showed that the almost planar $[HNNO]^{3-}$ ligand and the ammonia ligand occupy the four basal positions in an approximately square pyramidal "piano stool" complex. Red crystalline Cp*W[HNNNH]Cl ($[HNNNH]^{3-} = [(2\text{-}NHC_6H_4)_2N]^{3-}$) could be prepared from Cp^*WCl_4 and 2,2′-diaminodiphenylamine. It can be oxidized with AgOTf or $NOPF_6$ to yield $\{Cp^*W[HNNNH]Cl\}X$ (X = OTf or PF_6). $\{Cp^*W[HNNNH]Cl\}PF_6$ reacts with three equivalents of NH_2NMe_2 to afford $Cp^*W[HNNNH](NNMe_2)$, with four equivalents of isopropylamine to produce Cp*W[HNNNH](N-*i*-Pr), and with water in the presence of K_2CO_3 to yield Cp*W[HNNNH](O). Cp*W[(HNNNH]Cl reacts with dimethyl zinc at 80° to give Cp*W[HNNNH]Me, which can be subsequently oxidized by silver triflate to give $\{Cp^*W[HNNNH]Me\}OTf$. Deprotonation of $\{Cp^*W[HNNNH]Me\}OTf$ with DBU yielded an imido complex, $Cp^*W[(2\text{-}N\text{-}C_6H_4)(2'\text{-}NH\text{-}C_6H_4)N]Me$ via loss of one of the two ligand NH protons. © 1998 Elsevier Science Ltd. All rights reserved

Keywords: molybdenum; tungsten; 2,2′-diamidodiphenylamido; 2-amido-2′-oxydiphenylamido.

In the past few years we have synthesized and explored the chemistry of relatively high oxidation state tungsten or molybdenum complexes that will activate and reduce dinitrogen. In a series of studies we focused on complexes that contain the Cp^*MMe_3 core (M = W [1–5], Mo [3,6,7], or Re[8]). Some of the results that have emerged from these studies are as follows: (i) metals in a relatively high oxidation state (e.g. W(III) or W(IV)) can bind N_2 or partially reduce (N_2H_x) ligands; (ii) a 2π, 1σ arrangement of orbitals in such circumstances is favorable for stabilizing N_2H_x ligands; and (iii) a complex that contains bound hydrazine is a likely intermediate in which the N—N bond is cleaved to give ammonia. Recent investigations of the chemistry of tungsten and molybdenum phosphine complexes that is relevant to dinitrogen fixation has also begun to focus on the "mid" oxidation states for binding partially reduced (N_2H_x) ligands [9].

Unfortunately, there is at least one significant disadvantage to complexes that contain the Cp^*MMe_3 core. If we are to have any hope of reaching our long-term goal of developing a catalytic system for the reduction of dinitrogen using protons and electrons, methyl ligands eventually are protonated and lost as methane. Complexes that contain monodentate alkoxide ligands [10] did not prove to be suitable, in part because alkoxides also are readily protonated and can undergo ligand redistribution reactions that significantly complicate the chemistry in which we are interested. Therefore we looked for multidentate trianionic ligands that could take the place of the three methyl groups in the Cp^*MMe_3 core and that would be less susceptible than methyl ligands toward protonation and subsequent dissociation from the metal.

2,2′-Diaminodiphenylamine [11] and 2-amino-2′-hydroxydiphenylamine can be prepared by reducing

* Author to whom correspondence should be addressed.

the corresponding nitro compounds [12]. We felt that trianions derived from such compounds, $[HNNNH]^{3-}$ or $[HNNO]^{3-}$ (see below), would bind to Mo or W to yield complexes that contain Cp*M(HNNNH) or Cp*M(HNNO) cores. The *o*-phenylene rings should enforce planarity of the ligand system and therefore should encourage formation of pseudo five-coordinate complexes having a "piano stool" geometry. They also should discourage protonation of the amido nitrogen atoms. In this paper we report the synthesis of MCp*[HNNO] (M = Mo or W) and WCp*[HNNNH] complexes, X-ray structures of two MoCp*[HNNO] derivatives, and some chemistry that suggests that such ligands may prove useful for high oxidation state Mo or W chemistry.

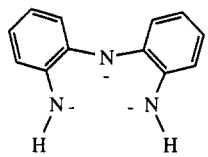

$[HNNNH]^{3-}$

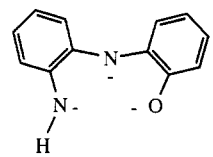

$[HNNO]^{3-}$

RESULTS AND DISCUSSION

Complexes containing the Cp*M[HNNO] *Core* (M = Mo, W)

Cp^*MoCl_4 reacts with 2-amino-2′-hydroxydiphenylamine in the presence of three equivalents of triethylamine to yield the 2-amido-2′-oxydiphenylamido ($[HNNO]^{3-}$) derivative **1a** [eqn (1)] as brown-black microcrystals in 65% isolated yield. An analogous reaction starting with Cp^*WCl_4 yielded Cp*W[HNNO]Cl (**1b**). Both **1a** and **1b** show ESR signals at $g \approx 2$, consistent with the presence of one unpaired electron. Although resonance forms can be drawn in which the metal is in a more reduced state, we prefer to view these as d^1 M(V) complexes.

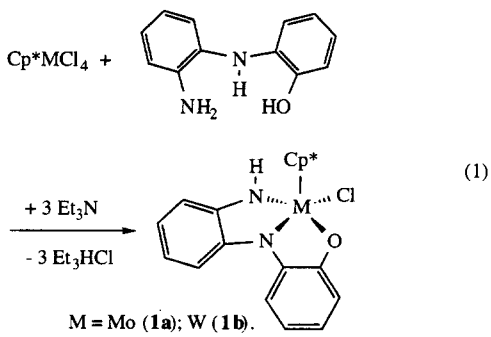

(1)

Reaction of **1a** with Cp_2Co yields a diamagnetic species that we formulate as the d^2 complex, $\{Cp_2Co\}\{Cp^*Mo[HNNO]Cl\}$ (**2**) formed by one electron reduction of **1a** (Scheme 1). Reduction of **1a** with sodium amalgam in THF yields an analogous species (**3**) that is isolated as a sodium salt containing one equivalent of diethyl ether. The proton on nitrogen in the HNNO ligand could be observed at 7.80 ppm in the proton NMR spectrum of **3** as a broad singlet, but not in **2** (at 22°C), perhaps because in **2** the NH proton cannot be differentiated from aryl protons between 7.20 and 6.00 ppm. An X-ray study of **3** showed it to contain approximately square pyramidal $\{Cp^*Mo[HNNO]Cl\}^-$ ions weakly connected by bridging Na(ether) units (Fig. 1, Table 1) in a manner such that the O(2)—Na(1)—Na(2)—O(3) axis serves as a C_2 axis. The $[HNNO]^{3-}$ ligand is approximately planar. Unfortunately, the structure had to be refined with the Cp* and phenyl rings as rigid groups, and therefore the quality is not high. The Na—Cl bond lengths are ~2.70 Å, but the Na(1)—N(2) distance (2.55 Å) and Na(2)—O(1) distance (2.51 Å) suggest that these interactions are significant and that the sodium ions therefore are pseudo five-coordinate. The core bond lengths and angles in the $\{Cp^*Mo[HNNO]Cl\}^-$ ion are shown in Fig. 2 in order to illustrate that the approximately square pyramidal MoN_2OCl core geometry is roughly the same as that found for a more accurately determined structure discussed below. Reduction of **1b** proceeds similarly to yield what appears, by proton NMR, to be the tungsten analog of **2**, but this compound was not characterized further.

Cp*W[HNNO]Cl could be oxidized readily by AgOTf in acetonitrile to produce $\{Cp^*W[HNNO]Cl\}^+$ OTf^- (**4**) essentially quantitatively. The NH proton in **4** was located at 11.37 ppm in the proton NMR spectrum. We assume that there is no room for the triflate ion to bind strongly to the metal and therefore have formulated **4** as an ionic species. In contrast, **1a** was not oxidized under similar conditions to an analogous Mo(VI) species.

Compounds **1a** and **1b** are both reduced by hydrazine (2 equiv.) to give diamagnetic compounds with the formula Cp*M[HNNO](NH_3) (**5a** and **5b**, respectively). The only other observable product of these high yield reactions was $N_2H_5^+$ (according to NMR spectra), presumably as the chloride salt. The proton on nitrogen in the HNNO ligand and the ammonia protons could not be observed readily in either **5a** or **5b** as a consequence of facile proton exchange between these sites at room temperature. At low temperature the rate of the exchange process is slow enough that the HNNO proton can be observed near 8 ppm (8.34 ppm in **5a**; 8.27 ppm in **5b**) and the NH_3 proton around 3 ppm (2.96 ppm in **5a**; 3.68 ppm in **5b**). **5a** is also formed upon addition of excess hydrazine to **3**.

We speculate that the mode of formation of compounds **5a** and **5b** from **1a** and **1b** involves formation and decomposition of intermediate hydrazido(1-) species, Cp*M[HNNO](N_2H_3), as shown in eqns (2) and (3). This proposal is based on the fact that the W(V) complex, $Cp^*WMe_3(N_2H_3)$, which is pro-

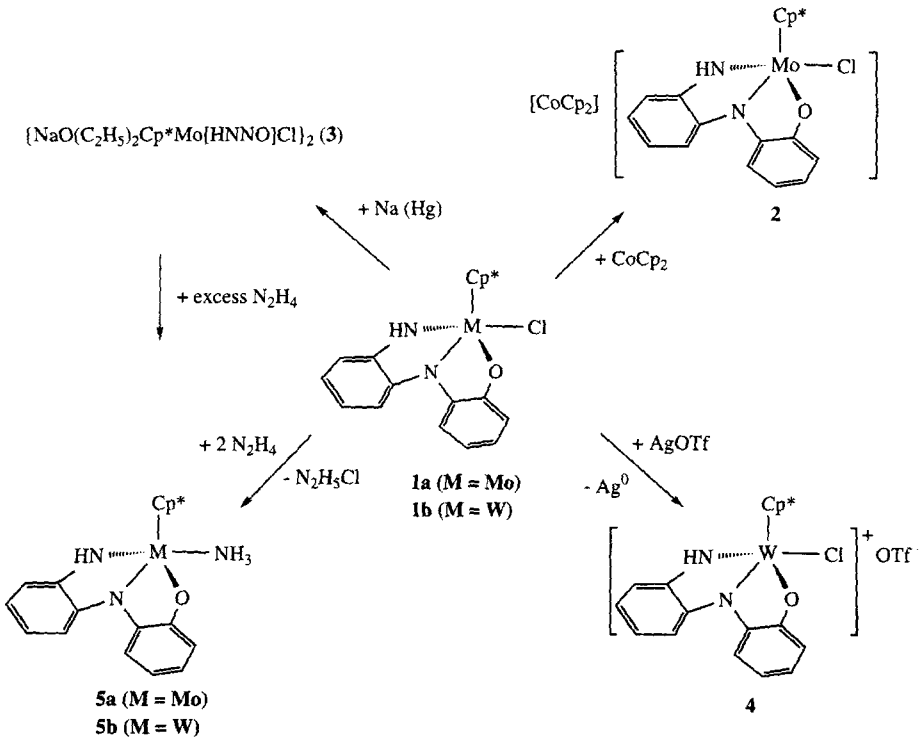

Scheme. 1.

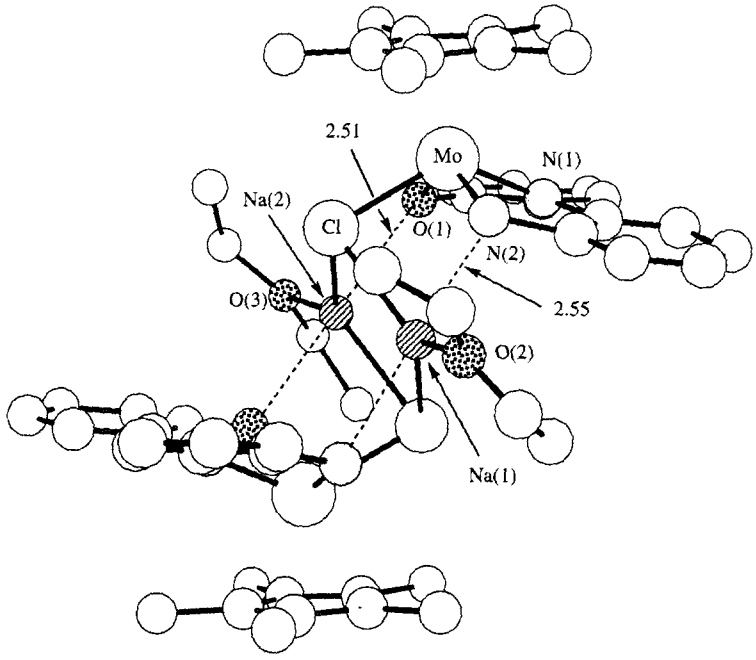

Fig. 1. Molecular structure of $\{Na[O(C_2H_5)_2]Cp^*Mo[(2\text{-}NH\text{-}C_6H_3)(2'\text{-}O\text{-}C_6H_4)N]Cl\}_2$ (3). Hydrogen atoms are omitted for clarity.

posed to be formed upon deprotonation of $[Cp^*WMe_3(N_2H_4)]^+$, decomposes to yield 0.5 equiv. of $Cp^*Me_3W{=}NNH_2$, 0.5 equiv. of $Cp^*Me_3W{=}NH$, and 0.5 equiv. of NH_3 [1]. Since the proposed $Cp^*M[HNNO](N_2H_3)$ compounds would also contain the metal in the M(V) oxidation state, we propose

Table 1. Selected bond lengths (Å) and bond angles (°) in $\{Na[O(C_2H_5)_2]Cp^*Mo[HNNO]Cl\}_2$ (**3**)

Mo—O(1)	2.13(2)	Mo—N(1)	2.01(1)
Mo—N(2)	1.94(2)	Mo—Cl	2.510(4)
Na(1)—Cl	2.70(2)	Na(2)—Cl	2.72(2)
Na(1)—N(2)	2.55(2)	Na(2)—O(1)	2.51(2)
Na(1)—O(2)	2.20(4)	Na(2)—O(3)	2.36(3)
O(1)—Mo—N(1)	73(1)	O(1)—Mo—Cl	84.9(5)
N(1)—Mo—N(2)	81(1)	N(1)—Mo—Cl	131.1(4)
N(2)—Mo—Cl	80.6(6)	N(2)—Mo—O(1)	128.7(9)
Na(1)—Cl—Na(2)	85.1(4)	Cl—Na(1)—Cl′	95.4(7)

Table 2. Selected bond lengths (Å) and bond angles (°) in $Cp^*Mo[HNNO](NH_3)$ (**5a**)

Mo—O(1)	2.049(5)	Mo—N(1)	2.226(6)
Mo—N(2)	2.024(6)	Mo—N(3)	2.017(6)
Mo—C(13)	2.238(7)	Mo—C(15)	2.356(7)
Mo—C(17)	2.435(7)	Mo—C(19)	2.296(7)
Mo—2(21)	2.208(7)		
O(1)—Mo—N(1)	77.0(2)	O(1)—Mo—N(2)	77.1(2)
N(1)—Mo—N(3)	87.9(2)	N(2)—Mo—N(3)	75.3(2)
N(3)—Mo—O(1)	126.0(2)	N(2)—Mo—N(1)	131.3(2)

that they also are likely to be unstable with respect to an intermolecular decomposition reaction shown in eqn (3). However, details of the decomposition reaction are unclear at this stage. It is also not clear why M(IV) ammonia complexes are formed rather than M = NNH_2 or M = NH species.

$$Cp^*M[HNNO]Cl + 2N_2H_4 \rightarrow N_2H_5Cl + \text{“}Cp^*M[HNNO](N_2H_3)\text{”} \quad (2)$$

$$\text{“}Cp^*M[HNNO](N_2H_3)\text{”} \rightarrow Cp^*M[HNNO](NH_3) + 0.5N_2 \quad (3)$$

Crystals of **5a** suitable for X-ray studies were obtained by recrystallization from an ether solution layered with pentane. The core structure of **5a** (Fig. 3) is similar to that found in **3** (Fig. 2). Relevant bond lengths and angles are listed in Table 2 and the core of **5a** is compared to that of **3** in Fig. 2. The 2-amidophenyl-2′-oxydiphenylamido ligand and the ammonia ligand occupy the four basal positions in a square pyramidal or “piano stool” arrangement typically found for pseudo-five-coordinate monocylopentadienyl complexes [13]. The $[HNNO]^{3-}$ ligand is close to being planar and the two Mo—N and one Mo—O bonds are all essentially the same length and relatively short (2.02 to 2.05 Å). The N(3)—Mo—N(2) and N(2)—Mo—O(1) bond angles are essentially equal, but the N(3)—Mo—N(1) bond angle is larger than the O(1)—Mo—N(1) bond angle by ~10°, perhaps because of steric repulsion between the proton on N(3) and the protons on ammonia. The Mo—N(1) distance (2.225(6) Å) is what one might expect for a dative Mo—N bond. The Cp* ligand is coordinated in an acentric fashion, with the Mo—C(17) distance being statistically longer that the other Mo—C distances. This circumstance is not unusual [14] and probably can be ascribed to greater repulsive forces between the ammonia ligand and the Cp* ligand compared to those between the flat HNNO ligand and the Cp* ligand. The protons on the ammonia ligand were not located in the X-ray study.

Synthesis and reactivity of complexes containing the $Cp^*W[(2\text{-}NH\text{-}C_6H_4)_2N]$ *core*

$Cp^*W[HNNNH]Cl$ (**6**; Scheme 2; $[HNNNH]^{3-}$ = $[(2\text{-}NHC_6H_4)_2N]^{3-}$) could be prepared from Cp^*WCl_4 and 2,2′-diaminodiphenylamine in the presence of at least three equivalents of triethylamine. Compound **6** is a red crystalline solid that is relatively soluble in CH_2Cl_2 and THF, but sparingly soluble in CH_3CN and hydrocarbons. It can be stored in air over a period of several weeks without significant decomposition. It does not react with water or methanol in the presence of triethylamine, nor does it react readily with NH_3 or N_2H_4. Compound **6** was not reduced by cobaltocene or zinc amalgam. It did react with excess sodium

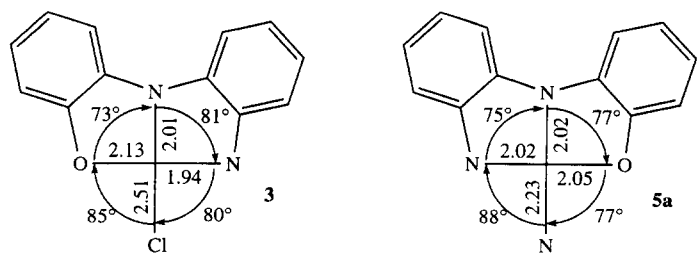

O-Mo-N =129°; N-Mo-Cl = 131° O-Mo-N =126°; N-Mo-N = 131°

Fig. 2. A comparison of bond lengths and angles in **3** and **5a**.

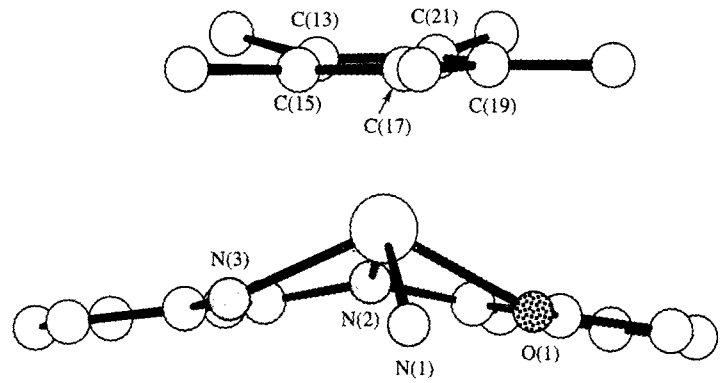

Fig. 3. Molecular structure of Cp*Mo[(2-NH-C_6H_4)(2'-O-C_6H_4)N](NH_3) (**5a**). Hydrogen atoms are omitted for clarity.

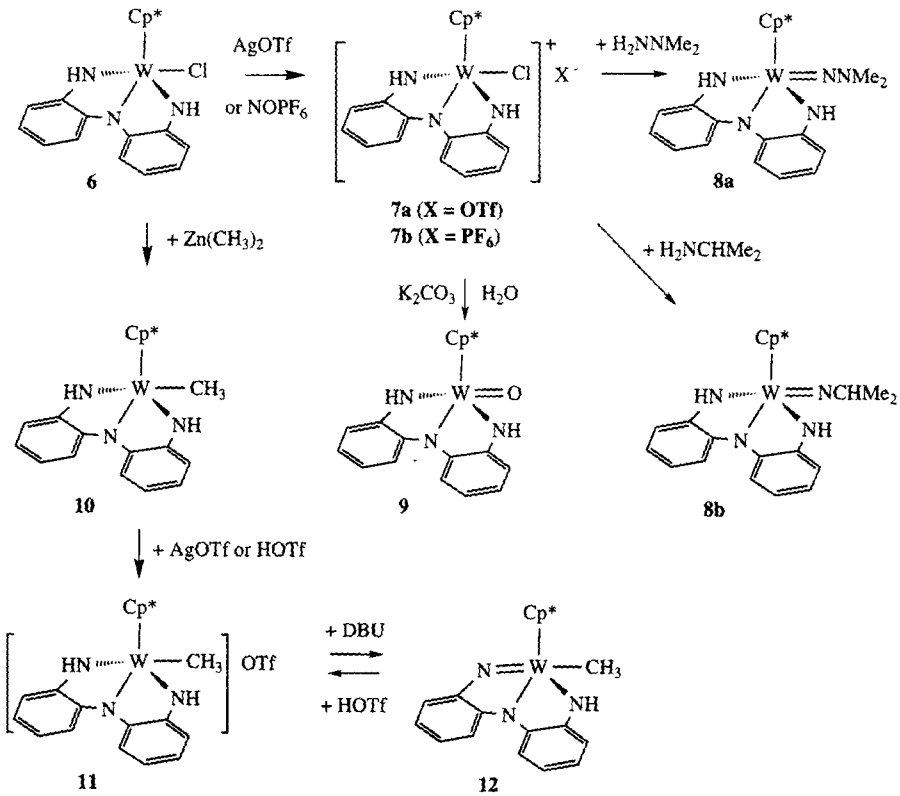

Scheme. 2.

amalgam in THF to produce an extremely air-sensitive diamagnetic species in low yield (30% from acetonitrile), but this product was not characterized.

Compound **6** can be oxidized readily. For example, it reacts cleanly with AgOTf or $NOPF_6$ to afford {Cp*W[HNNNH]Cl}X (X = OTf, **7a**; PF_6, **7b**) quantitatively. Both compounds are soluble in acetonitrile, but insoluble in other common organic solvents. ^1H NMR spectra of the two in CD_3CN are almost identical, consistent with their proposed ionic nature. The $[HNNNH]^{3-}$ ligand NH resonance is found as a broad singlet at 10.22 ppm in the proton NMR spectrum in CD_3CN.

Compound **7b** reacts with three equivalents of NH_2NMe_2 to afford Cp*W[HNNNH]($NNMe_2$) (**8a**) in moderate (37% isolated) yield. Compound **7b** also reacts with four equivalents of isopropylamine to produce Cp*W[HNNNH](N-*i*-Pr) (**8b**), and with water in the presence of K_2CO_3 to yield Cp*W[HNNNH](O) (**9**). Proton NMR spectra of **8** and **9** in C_6D_6 reveal the $[HNNNH]^{3-}$ ligand NH resonance at ~6.5 ppm.

Compound **6** reacts with dimethyl zinc slowly at

room temperature, and at 80° Cp*W[HNNNH]Me (**10**) is formed in good yield (67% isolated) in 1 h. Compound **10** is oxidized quantitatively by silver triflate to give {Cp*W[HNNNH]Me}OTf (**11**). Interestingly, an attempt to protonate **10** with one equivalent of triflic acid in CH_2Cl_2 led (slowly over a period of 3 days) to its oxidation to give **11** in moderate yield (65% isolated). The proton NMR spectrum of **11** in CD_3CN showed a resonance at 0.71 ppm, for the methyl group. Only four different aromatic protons were observed, consistent with the molecule having mirror symmetry. Compound **11** is a rare example of a cationic W(VI) alkyl complex (cf. $[Cp^*WMe_5]^+$). [15].

Deprotonation of **11** with DBU did not give $Cp^*W[HNNNH](CH_2)$, but an imido complex, $Cp^*W[(2\text{-}N\text{-}C_6H_4)(2'\text{-}NH\text{-}C_6H_4)N]Me$ (**12**), formed via loss of one of the two ligand NH protons. The NMR spectrum of **12** is relatively complex, as expected for a molecule having no symmetry. Normally eight proton resonances are observed in the aromatic region, but if **12** is contaminated with a trace of a proton source, even DBUHOTf, only four different aromatic proton resonances are observed, consistent with protonation and deprotonation of **12** being a fast and reversible process. Addition of one equivalent of HOTf to **12** yields **11** quantitatively. Formation of **12** should be compared to deprotonation of $[Cp^*WMe_5]^+$ to yield unstable $Cp^*WMe_3(CH_2)$ [15].

CONCLUSIONS

Multidentate amido ligands that contain *o*-phenylene links between amido nitrogens show some promise as supporting ligands for high oxidation state Cp*Mo or Cp*W chemistry. Among the interesting features of complexes that contain such ligands are the planar tridentate ligand backbone, the stability of the backbone to proton abstraction and cleavage reactions, and the ability of several complexes to be smoothly oxidized or reduced. For steric reasons, the parent (proton-substituted) versions of the two ligands described here are likely to be the only ones that can be put on Cp*M complexes to give approximately square pyramidal complexes. Conversely, more steric protection against bimolecular reactions is likely to be required if multidentate amido ligands are employed in the absence of other bulky ligands. In this context it should be noted that several tantalum complexes have been prepared that contain a pentafluorophenyl-substituted or trimethylsilyl-substituted version of the $[HNNNH]^{3-}$ ligand [16]. Other types of conformationally rigid multidentate amido ligands have appeared in the literature relatively recently [17–25]. It is interesting to note that cationic zirconium(IV) complexes containing the $[(t\text{-}BuN\text{-}o\text{-}C_6H_4)_2O]^{2-}$ ligand [22] are catalysts for the living polymerization of 1-hexene at room temperature or below. We expect that other examples of the utility of appropriately substituted multidentate amido ligands in high oxidation state chemistry, especially those that contain the *o*-phenylene backbone, will be forthcoming.

EXPERIMENTAL

General details

Standard experimental procedures can be found elsewhere [1]. All NMR chemical shifts are reported in ppm downfield from TSM (^1H and ^{13}C) external reference. Microanalyses (C, H, N) were performed in our laboratory using a Perkin–Elmer PE2400 microanalyzer. Cp^*MoCl_4 [26], Cp^*WCl_4 [15], 2,2′dinitrodiphenylamine [11], and 2-nitro-2′-hydroxydiphenylamine [12] were prepared as described in the literature.

Preparation of compounds

Cp*Mo[HNNO]Cl (**1a**). A yellow solution of 2-amino-2′-hydroxy diphenylamine (0.537 g, 2.68 mmol) and Et_3N (0.841 g, 8.31 mmol) in THF (10 ml) was added dropwise to a slurry of purple Cp^*MoCl_4 (1.00 g, 2.68 mmol) in 50 ml of THF at −40° C. The solution color changed to red-brown and some solid precipitated. The mixture was warmed to room temperature, stirred for 22 h, and filtered. The solid was washed with THF until the washings were colorless. The solvents were removed from the red-brown filtrate and the brown residue was recrystallized from a small amount of dichloromethane to give almost black microcrystals; yield 0.810 g (65%): ESR (CH_2Cl_2) $g = 1.98$; $\Delta_{1/2} = 9.9$ g. Anal. Calc. for $C_{22}H_{24}ClMoN_2O$: C, 56.97; H, 5.22; N, 6.04; Cl, 7.64. Found: C, 56.30; H, 5.19; N, 6.00; Cl, 7.69.

Cp*W[HNNO]Cl (**1b**). A yellow solution of 2-amino-2′-hydroxy diphenylamine (1.91 g, 9.55 mmol) and NEt_3 (3.00 g, 29.65 mmol) in THF (20 ml) was added to a red suspension of Cp^*WCl_4 (4.40 g, 9.55 mmol) in THF (100 ml) at −40° C. The solution color changed gradually to green-brown as a white solid deposited. The mixture was warmed to room temperature and stirred for 42 h. The reaction mixture was filtered and the solid was washed with THF until the washings were colorless. The volatile solvents were removed from the green-brown filtrate *in vacuo* and the residue was washed with cold dichloromethane (4 × 5 ml) to give a green solid; yield 4.48 g (85%): ESR (CH_2Cl_2) $g = 1.93$; $\Delta\nu_{1/2} = 18.5$ g. Anal. Calc. for $C_{22}H_{24}ClN_2OW$: C, 47.89; H, 4.38; N, 5.08. Found: C, 48.23; H, 4.44; N, 5.04.

$\{Cp_2Co\}\{Cp^*Mo[HNNO]Cl\}$ (**2**). A solution of 40 mg (0.21 mmol) of cobaltocene in 5 ml ether was added dropwise to a red-brown solution of 0.100 g (0.21 mmol) Cp*Mo[HNNO]Cl in 10 ml of THF. The color of the solution changed immediately to red.

After 24 h pentane was layered on top of the solution and the sample was kept at −30°C for 24 h to give brown microcrystals; yield 0.120 g (0.18 mmol, 86%): ^{1}H NMR (THF-d_8) δ 7.20–6.00 (m, 8, Ar*H*), 3.95 (s, 10, Cp), 1.25 (s, 15, Cp*). The $[HNNO]^{3-}$ ligand's NH proton was not located. It is believed either to be in the region of 7.20–6.00 ppm or to be too broad at 22°C to be observed readily. Anal. Calc. For $C_{32}H_{34}ClCoMoN_2O$: C, 58.86; H, 5.25; N, 4.29. Found: C, 58.87; H, 5.44; N, 4.08.

$\{Na[O(C_2H_5)_2]Cp^*Mo[HNNO]Cl\}_2$ (**3**). Sodium amalgam (1 equiv. of 0.05% Na/Hg) was added to a red brown solution of 200 mg (0.43 mmol) Cp*Mo[HNNO]Cl in 10 ml of THF. The mixture was stirred until the color changed to orange (20–30 min). The mixture was filtered and the residue was washed with THF until the washings were colorless. The solvents were removed from the orange filtrate *in vacuo* to give an orange glass. The orange glass was dissolved in a mixture of ether and pentane (1 : 1; 10 ml) and 10 ml of pentane was layered on top. Large brown crystals formed with time; yield 160 mg (0.33 mmol, 77%): ^{1}H NMR (THF-d_8) δ 7.80 (br s, 1 N*H*), 6.89–6.55 (m, 8, Ar*H*), 3.43–3.30 (q, 4, ether CH_2), 1.14–1.03 (t, 6, ether CH_3), 1.11 (s, 15 Cp*). Anal. Calc. for $C_{26}H_{34}ClMoN_2NaO_2$: C, 55.67; H, 6.11; N, 4.99. Found: C, 55.42; H, 5.76; N, 5.32.

$\{Cp^*W[HNNO]Cl\}OTf$ (**4**). A solution of AgOTf (0.265 g, 1.03 mmol) in CH_3CN (5 ml) was added dropwise to a green suspension of Cp*W[HNNO]Cl (0.570 g, 1.03 mmol) in CH_3CN (10 ml). A gray solid formed immediately and the color of the solution changed to red. The mixture was stirred at room temperature for 4 h and filtered. The solvent was removed from the filtrate *in vacuo* and the residue was extracted with dichloromethane. The red extract was reduced in volume and diethyl ether (15 ml) was layered on top. The mixture was cooled to −30 C to produce red-purple crystals which were isolated by filtration and dried *in vacuo*; yield 0.662 g (91%): ^{1}H NMR ($CDCl_3$ δ 11.37 (s, 1, N*H*), 7.65–6.80 (4 doublets and 4 triplets, 8, Ar*H*), 2.59 (s, 15, Cp*). Anal. Calc. for $C_{23}H_{24}ClF_3N_2O_4SW$: C, 39.42; H, 3.45; N, 4.00. Found: C, 39.52; H, 3.75; N, 3.85.

Cp*Mo[HNNO](NH_3) (**5a**). Hydrazine (28.9 μl, 0.91 mmol) was added to a red-brown solution of Cp*Mo[HNNO]Cl (0.210 g, 0.45 mmol) in THF (10 ml) at −40°C. The mixture was allowed to warm to room temperature. Over a period of 22 h the color changed gradually to green and a white solid formed. The mixture was filtered and the solvent was removed from the filtrate *in vacuo*. The residue was dissolved in ether (5 ml) and pentane was added just short of precipitating the product. Upon cooling this solution to −40°C, green crystals were formed and isolated by filtration; yield 0.188 g (93%): ^{1}H NMR (THF-d_8, −88°C) δ 8.34 (br s, 1 N*H*), 7.90–6.66 (m, 8, Ar*H*), 2.96 (br s, 3, NH_3), 1.1 (s, 15, Cp*). Anal. Calc. for $C_{22}H_{27}MoN_3O$: C, 59.32; H, 6.11; N, 9.43. Found: C, 59.44; H, 5.84; N, 9.19.

Cp*W[HNNO](NH_3) (**5b**). Hydrazine (73 μl, 2.29 mmol) was added to a green suspension of Cp*W[HNNO]Cl (0.418 g, 0.76 mmol) in THF (20 ml). The mixture was stirred at room temperature for 72 h. The color gradually changed to green-brown and a white solid formed. The mixture was filtered and the filtrate was reduced in volume *in vacuo*. Pentane (20 ml) was added to precipitate the product; yield 0.376 g (93%): ^{1}H NMR (THF-d_8, 23°C) δ 7.84–6.60 (m, 8, Ar*H*), 1.17 (s, 15, Cp*): ^{1}H NMR (THF-d_8, −84°C) δ 8.27 (br s, 1, N*H*), 7.85–6.58 (m, 8, Ar*H*), 3.68 (br s, 3, NH_3), 1.39 (s, 15, Cp*).

Cp*W[HNNNH]Cl (**6**). A solution of 2,2′-diaminodiphenylamine (2.86 g, 14.4 mmol) and triethylamine (4.50 g, 44.5 mmol) in THF (20 ml) was added dropwise to a red suspension of Cp^*WCl_4 (6.62 g, 14.4 mmol) in THF (100 ml) at −40°C. The color changed to dark red immediately and a white solid gradually deposited. After the addition was completed, the mixture was warmed to room temperature and stirred for 22 h. The reaction mixture was filtered and the solid was washed with THF until the washings were almost colorless. All volatile components were removed from the filtrate *in vacuo* and the red residue was dissolved in a minimum amount of hot dichloromethane. The solution was cooled to −40°C to yield small red crystals, which were isolated by filtration and dried *in vacuo*; yield 5.98 g (76%): ESR (CH_2Cl_2) $g = 1.94$; $\Delta\nu_{1/2} = 20.0$ g; IR (KBr, Nujol) cm^{-1} 3322 (ν_{NH}). Anal. Calc. for $C_{22}H_{25}ClN_3W$: C, 47.98; H, 4.58; N, 7.63. Found: C, 47.87; H, 4.70; N, 7.89.

$\{Cp^*W[HNNNH]Cl\}OTf$ (**7a**). A solution of AgOTf (1.706 g, 6.64 mmol) in CH_3CN (10 ml) was added dropwise to a red slurry of Cp*W[HNNNH]Cl (3.66 g, 6.64 mmol) in CH_3CN (50 ml) at room temperature. Silver metal formed and the solution changed to red-brown. The mixture was stirred for 1 h and filtered and the solid was washed with CH_3CN until the washings were colorless. The filtrate was reduced in volume (10 ml) and CH_2Cl_2 added to precipitate the product; yield 4.46 g (96%): ^{1}H NMR (CD_3CN) δ 10.23 (br s, 2, N*H*), 7.83 (d, 2, Ar*H*), 7.28 (d, 2, Ar*H*), 7.11 (t, 2, Ar*H*), 6.90 (t, 2, Ar*H*), 2.49 (s, 15, Cp*); IR (KBr, Nujol) cm^{-1} 3307 (ν_{NH}).

$\{Cp^*W[HNNNH]Cl\}PF_6$ (**7b**). A solution of $NOPF_6$ (0.284 g, 1.62 mmol) in CH_3CN (5 ml) was added dropwise to a cold (−40°C) suspension of Cp*W[HNNNH]Cl (0.894 g, 1.62 mmol) in CH_3CN (10 ml). Gas evolved and the color changed to yellow-brown. The mixture was warmed to room temperature and stirred for another hour. Solvents were removed *in vacuo* leaving a brown solid; yield 1.10 g (98%): ^{1}H NMR (CD_3CN) δ 10.22 (br s, 2, N*H*), 7.84 (d, 2, Ar*H*), 7.27 (d, 2, Ar*H*), 7.12 (t, 2, Ar*H*), 6.90 (t, 2, Ar*H*), 2.49 (s, 15, Cp*); IR (KBr, Nujol) cm^{-1} 3352 (ν_{NH}). Anal. Calc. for $C_{22}H_{25}ClF_6N_3PW$: C, 37.98; H, 3.62; N, 6.04. Found: C, 37.76; H, 3.65; N, 6.10.

Cp*W[HNNNH](η^1-NNMe$_2$) (**8a**). 1,1-Dimethylhydrazine (38 μl, 0.51 mmol) was added to a yellow-brown solution of $\{Cp^*W[HNNNH]Cl\}PF_6$ (0.116 g,

0.17 mmol) in CH_3CN (15 ml) at −40°C. The solution changed to green, then a yellow precipitate formed. The mixture was allowed to warm to room temperature and was stirred for 30 min. The reaction mixture was filtered and the yellow solid was washed with cold CH_3CN (5 ml) and dried *in vacuo*; yield 0.035 g (37%): ^{1}H NMR (C_6D_6) δ 8.11–6.90 (m, 8, Ar*H*), 6.35 (s, 2, N*H*), 3.04 (s, 6, NN*Me*$_2$), 1.50 (s, 15, Cp*); ^{1}H NMR (CD_2Cl_2) δ 7.86–6.75 (m, 8, Ar*H*), 6.69 (s, 2, N*H*), 3.63 (s, 6, NN*Me*$_2$), 1.60 (s, 15, Cp*); ^{13}C{^{1}H} NMR (CD_2Cl_2) δ 153.5–115.0 (6 singlets, Ar*C*), 111.8 (s, *C*$_5$Me$_5$), 48.9 (s, NN*Me*$_2$), 10.4 (s, C$_5$*Me*$_5$). Anal. Calc. for $C_{24}H_{31}N_5W$: C, 50.27; H, 5.45; N, 12.21. Found: C, 50.64; H, 5.22; N, 12.26.

Cp*W[HNNNH](N-*i*-Pr) (**8b**). A solution of *i*-PrNH_2 (0.49 ml, 5.75 mmol) in CH_3CN (5 ml) was added dropwise to a brown solution of {Cp*W[HNNNH]Cl}PF_6 (1.00 g, 1.44 mmol) in CH_3CN (10 ml) at −40°C. The solution changed to red immediately and a red precipitate formed. The mixture was warmed to room temperature and stirred for 16 h. The mixture was then cooled to −40°C and allowed to stand at this temperature for 12 h. The red solid was collected by filtration and washed with cold CH_3CN (5 ml). It was then extracted with toluene until the extracts were colorless. Solvents were removed from the combined extracts to give the red product; yield 0.575 g (70%): ^{1}H NMR (CD_2Cl_2) δ 7.75–6.68 (m, 8, Ar*H*), 6.49 (s, 2, N*H*), 5.63 (septet, 1, NC*H*Me$_2$), 1.74 (s, 15, Cp*), 1.29 (d, 6, NCH*Me*$_2$). Anal. Calc. for $C_{25}H_{32}N_4W$: C, 52.46; H, 5.63; N, 9.79. Found: C, 52.17; H, 5.83; N, 9.71.

Cp*W[HNNNH](O) (**9**). This complex could be prepared either from {Cp*W[HNNNH]Cl}PF_6 or {Cp*W[HNNNH]Cl}OTf. Degassed H_2O (29 μl, 1.61 mmol) was added to a mixture of {Cp*W[HNNNH]Cl}OTf (0.750 g, 1.07 mmol) and K_2CO_3 (0.760 g, 5.50 mmol) in CH_3CN (20 ml) at 0°C. The mixture was stirred at 0°C for 2 h, then warmed to room temperature and stirred for another 18 h. The volatile components were removed *in vacuo*. The residue was extracted with dichloromethane until the extracts were colorless. Dichloromethane was removed from the combined extracts *in vacuo* and the brown crystalline solid was washed with CH_3CN (2 × 5 ml) and dried *in vacuo*; yield 0.555 g, 98%): ^{1}H NMR ($CDCl_3$) δ 7.80–6.76 (m, 8, Ar*H*), 6.59 (s, 2, N*H*), 1.83 (s, 15, Cp*); IR (KBr, Nujol) cm^{-1} 3376 and 3247 (ν_{NH}), 885 (ν_{WO}). Anal. Calc. for $C_{22}H_{25}N_3OW$: C, 49.73; H, 4.74; N, 7.91. Found: C, 49.84; H, 5.07; N, 7.87.

Cp*W[HNNNH]Me (**10**). $ZnMe_2$ (0.16 ml, 2.32 mmol) was added to a suspension of Cp*W[HNNNH]Cl (0.920 g, 1.67 mmol) in toluene (15 ml). The reaction flask was sealed with a septum and was heated at 80°C for 1 h. The solution changed to red-purple and a green solid deposited. The mixture was cooled to room temperature and filtered. The green solid was washed with toluene until the washings were almost colorless. The residue was extracted with diethyl ether until the extracts were colorless. The combined ether extracts were chromatographed on a short alumina column using diethyl ether as eluent solvent. A red-purple band was collected. The volume of the solution was then reduced to ~3 ml *in vacuo*. The solution was cooled to −40°C. The red-purple solid was collected by decanting the supernatant liquid and was dried *in vacuo*; yield 0.570 g (64%): ESR (CH_2Cl_2) $g = 1.98$; $\Delta\nu_{1/2} = 17.3$ g. Anal. Calc. for $C_{23}H_{28}N_3W$: C, 52.09; H, 5.32; N, 7.92. Found: C, 52.39; H, 5.42; N, 7.89.

{Cp*W[HNNNH]Me}OTf (**11**). *Method A*. A cold (−40°C) solution of Cp*W[HNNNH]Me (0.114 g, 0.21 mmol) in CH_2Cl_2 (5 ml) was added quickly to a suspension of triflic acid (19 μl, 0.21 mmol) in CH_2Cl_2 (10 ml) at −40°C. The mixture was slowly warmed to room temperature and stirred for 3 days. The solution gradually changed from red-purple to green and a small amount of white solid formed. The mixture was filtered through a frit and the green filtrate reduced in volume (3 ml). Diethyl ether (15 ml) was layered on top. Green crystals grew slowly at 22°C. The crystals were isolated by decanting the mother liquor; yield 95 mg (65%): ^{1}H NMR (CD_3CN) δ 9.80 (br s, 2, N*H*), 7.68 (d, 2, Ar*H*), 7.07 (t, 2, Ar*H*), 7.05 (d, 2, Ar*H*), 6.85 (t, 2, Ar*H*), 2.31 (s, 15, Cp*), 0.71 (s, 3, *Me*). Anal. Calc. for $C_{24}H_{28}F_3N_3O_3SW$: C, 42.43; H, 4.15; N, 6.18. Found: C, 43.01; H, 4.26; N, 6.50.

Method B. To a purple solution of Cp*W[HNNNH]Me (0.300 g, 0.57 mmol) in THF (5 ml) was added dropwise a solution of AgOTf (0.145 g, 0.57 mmol) in THF (5 ml) at room temperature. A silver mirror formed immediately and a green solid deposited. Acetonitrile (10 ml) was added to the reaction mixture and the mixture was stirred for 30 min. The resulting mixture was filtered through a medium frit bedded with Celite. The green filtrate was reduced to ~3 ml *in vacuo*. Diethyl ether (15 ml) was layered on top. Green crystals formed with time at room temperature. The crystals were collected by decanting the supernatant liquid and dried *in vacuo*; yield 0.353 g (92%).

Cp*W[(2-N-C_6H_4)(2′-NH-C_6H_4)N]Me (**12**). DBU (27.3 μl, 0.18 mmol) was added to a green slurry of {Cp*W[HNNNH]Me}OTf (0.124 g, 0.18 mmol) in CH_2Cl_2 (10 ml) at −40°C. The color of the solution changed to red immediately. The mixture was warmed to room temperature and stirred for 1 h. All volatile components were removed *in vacuo* and the residue was extracted with diethyl ether until the extracts were colorless. The solvents were removed from the red extracts to give a red solid; yield 0.080 g (83%): ^{1}H NMR (CD_2Cl_2) δ 8.25 (br s, 1, N*H*), 7.54–6.26 (m, 8, Ar*H*), 2.01 (s, 15, Cp*), 0.46 (s, 3, *Me*); ^{1}H NMR ($CDCl_3$) δ 8.17 (br s, 1, N*H*), 7.61–6.30 (m, 8, Ar*H*), 2.01 (s, 15, Cp*), 0.54 (s, 3, *Me*); ^{13}C{^{1}H} NMR ($CDCl_3$) δ 158.8–114.6 (11 singlets, Ar*C*), 113.6 (s, *C*$_5$Me$_5$), 18.4 (s, W*Me*), 11.2 (s, C$_5$*Me*$_5$). Anal Calc. for $C_{23}H_{27}N_3W$: C, 52.19; H, 5.14; N, 7.94. Found: C, 52.61; H, 5.30; N, 8.15.

Crystal structure of $\{Na[O(C_2H_5)_2]Cp^*Mo[HNNO]Cl\}_2$ (**3**). An orange-brown prismatic crystal of dimension $0.25 \times 0.28 \times 0.47$ mm was mounted in a glass capillary in a nitrogen atmosphere. The data were collected at room temperature on a Rigaku diffractometer with a graphite-monochromated Mo–K_α radiation ($\lambda = 0.71069$ Å). Of the 3276 reflections that were collected, 3131 were unique, and equivalent reflections were merged. The intensities of three representative reflections measured after every 150 reflections remained constant throughout data collection, obtained from a least-squares refinement using the setting angles of 23 carefully centered reflections in the range $13.94° < 2\theta < 20.44°$ corresponded to a monoclinic cell with the dimensions $a = 15.367(4)$ Å, $b = 20.850(3)$ Å, $c = 12.271(2)$ Å and $\beta = 113.71(3)$ for $Z = 4$. Based on systematic absences the space group was determined to be C_2 (#5). The calculated density is 1.456 g/cm^3. A numerical absorption correction, using the program DIFABS, was applied, resulting in transmission factors ranging from 0.76 to 1.32. The structure was solved by Patterson's method. The final cycle of full matrix least-squares refinement was based on 1288 observed reflections ($I > 4\sigma(I)$) and 91 variable parameters and converged (largest parameter shift was 3.8 times its esd) with unweighted and weighted agreement factors of $R = 0.082$ and $R_w = 0.091$. The maximum and minimum peaks on the final difference Fourier correspond to 1.13 and -0.93 e$^-$/Å^3, respectively. All calculations were performed using the TEXAN crystallographic software package. Due to a disorder problem the pentamethylcyclopentadienyl ligand and all phenyl rings were refined as rigid groups.

Crystal structure of $Cp^*Mo[HNNO](NH_3)$ (**5a**). A green prismatic crystal with dimensions $0.3 \times 0.2 \times 0.2$ mm was mounted on a glass fiber under a stream of cold nitrogen gas from a liquid nitrogen bath. Data were collected at $-72°$C on an Enraf–Nonius CAD 4 diffractometer with a graphite-monochromated Mo–K_α radiation ($\lambda = 0.71069$ Å). Of the 8525 reflections that were collected, 4146 were unique, and equivalent reflections were merged. The intensities of three representative reflections measured after every 60 min remained constant throughout data collection, obtained from a least-squares refinement using the setting angles of 25 carefully centered reflections in the range $18.00° < 2\theta < 26.00°$ corresponded to a tetragonal cell with the dimensions $a = 19.105(2)$ Å and $c = 12.271(2)$ Å for $Z = 8$. Based on systematic absences the space group was determined to be $P4_2/n$ (#86). The calculated density is 1.322 g/cm^3. An empirical absorption correction, based on azimuthal scans of five reflections, was applied, resulting in transmission factors ranging from 0.95 to 1.00. The structure was solved by Patterson's method. The final cycle of full matrix least-squares refinement was based on 2044 observed reflections ($I > 4\sigma(I)$) and 252 variable parameters and converged (largest parameter shift was 0.00 times its esd) with unweighted and weighted agreement factors of $R = 0.045$ and $R_w = 0.037$. The maximum and minimum peaks on the final difference Fourier correspond to 0.47 and -0.69 e$^-$/Å^3, respectively. All calculations were performed using the TEXAN crystallographic software package.

Supplementary information covering experimental details, labelled ORTEP drawing, final positional parameters, final thermal parameters, and final observed and calculated structure factors for $\{NaO(C_2H_5)_2Cp^*Mo[(2\text{-}NH\text{-}C_6H_4)(2'\text{-}O\text{-}C_6H_4)N]Cl\}_2$ (16 pp) and $Cp^*Mo[(2\text{-}NH\text{-}C_6H_4)(2'\text{-}O\text{-}C_6H_4)N](NH_3)$ (20 pp) is available upon request.

Acknowledgements—R.R.S. thanks the National Institutes of Health for support (GM 341978) and R.R.K. thanks the German Academic Exchange Service for a HEP postdoctoral fellowship.

REFERENCES

1. Glassman, T. E., Vale, M. G., Schrock, R. R. and Kol, M., *J. Am. Chem. Soc.*, 1993, **115,** 1760.
2. Glassman, T. E., Vale, M. G. and Schrock, R. R., *J. Am. Chem. Soc.*, 1992, **114,** 8098.
3. Glassman, T. E., Vale, M. G. and Schrock, R. R., *Organometallics*, 1991, **10,** 4046.
4. Glassman, T. E., Liu, A. H. and Schrock, R. R., *Inorg. Chem.*, 1991, **30,** 4723.
5. O'Regan, M. B., Liu, A. H., Finch, W. C., Schrock, R. R. and Davis, W. M., *J. Am. Chem. Soc.*, 1990, **112,** 4331.
6. Schrock, R. R., Glassman, T. E. and Vale, M. G., *J. Am. Chem. Soc.*, 1991, **113,** 725.
7. Schrock, R. R., Kolodziej, R. M., Liu, A. H., Davis, W. M. and Vale, M. G., *J. Am. Chem. Soc.*, 1990, **112,** 4338.
8. Vale, M. G. and Schrock, R. R., *Organometallics*, 1993, **12,** 1140.
9. Hidai, M. and Mizobe, Y., *Chem. Rev.*, 1995, **95,** 1115.
10. O'Regan, M. B., Vale, M. G., Payack, J. F. and Schrock, R. R. *Inorg. Chem.*, 1992, **31,** 1112.
11. Tomlinson, M. L., *J. Chem. Soc.*, 1939, 158.
12. Wilshire, J. F. K. *Aust. J. Chem.*, 1988, **41,** 995.
13. Kubacek, P., Hoffmann, R. and Havlas, Z. *Organometallics*, 1982, **1,** 180.
14. Sundermeyer, J., Radius, U. and Burschka, C. *Chem. Ber.*, 1992, **125,** 2379.
15. Liu, A. H., Murray, R. C., Dewan, J. C., Santarsiero, B. D. and Schrock, R. R., *J. Am. Chem. Soc.*, 1987, **109,** 4282.
16. Schrock, R. R., Lee, J., Liang, L.-C. and Davis, W. M., *Inorg. Chim. Acta*, in press.
17. Guérin, F., McConville, D. H. and Vittal, J. J., *Organometallics*, 1995, **14,** 3154.
18. Guérin, F., McConville, D. H. and Vittal, J. J., *Organometallics*, 1996, **15,** 5586.
19. Guérin, F., McConville, D. H. and Payne, N. C. *Organometallics*, 1996, **15,** 5085.
20. Guérin, F., McConville, D. H. and Vittal, J. J., *Organometallics*, 1997, **16,** 1491.

21. Fryzuk, M. D., Love, J. B., Rettig, S. J. and Young, V. G., *Science*, 1977, **275,** 1445.
22. Baumann, R., Davis, W. M. and Schrock, R. R., *J. Am. Chem. Soc.*, 1997, **119,** 3830.
23. Cloke, F. G. N., Hitchcock, P. B. and Love, J. B., *J. Chem. Soc., Dalton Trans.*, 1995, 25.
24. Horton, A. D., de With, J., van der Linden, A. J. and van de Weg, H., *Organometallics*, 1996, **15,** 2672.
25. Clark, H. C. S., Cloke, F. G. N., Hitchcock, P. B., Love, J. B. and Wainwright, A. P., *J. Organomet. Chem.*, 1995, **501,** 333.
26. Murray, R. C., Blum, L., Liu, A. H. and Schrock, R. R., *Organometallics*, 1985, **4,** 954.

Pergamon

PII: S0277-5387(97)00313-6

Polyhedron Vol. 17, No. 5–6, pp. 759–768, 1998
© 1998 Elsevier Science Ltd
All rights reserved. Printed in Great Britain
0277-5387/98 $19.00+0.00

Supramolecular assemblies of tungsten complexes with unusual chelating groups†

Timothy E. Baroni,[a] Vladimir Kolesnichenko,[a] Lawrence Seib,[a] Joseph A. Heppert,[a]* Louise M. Liable-Sands,[b] Glenn P. A. Yap[b] and Arnold E. Rheingold[b]

[a] Department of Chemistry, University of Kansas, Lawrence, KS 66045, U.S.A.;

[b] Department of Chemistry and Biochemistry, University of Delaware, Newark, DE, U.S.A.

(Received 28 May 1997; accepted 17 July 1997)

Abstract—Metal complexes of ligands with η^1-*O* coordinated carbonyl moieties are well-known throughout the inorganic literature. However, metal complexes containing authentic acid chloride ligands have not previously been isolated. The synthesis and characterization of compounds with the formula $W(X)Cl_3(OPh\text{-}2\text{-}COCl)$ (**2**) [X = O (**2a**), NC_6H_3-2,6-$(CH_3)_2$ (**2b**), and Ph_2C_2 (**2c**)] are reported. The crystal structures of **2a** and **2c** were solved, showing the interaction of the acid chloride carbonyl moiety with the tungsten center. Complex **2c** adopts a channelled structure having six-fold symmetric voids in the solid state. As was anticipated, the coordinated acid chloride of **2a** reacts readily with nucleophiles to produce the ester $WOCl_3(OPh\text{-}2\text{-}COPr^n)$ (**3**) and the amide $WOCl_3(OPh\text{-}2\text{-}CONHBu^t)$ (**4a**). A related amide complex $WOCl_3(OPh\text{-}2\text{-}CONH_2)$ (**4b**), synthesized by the reaction of $WOCl_4$ with salicylamide, displays an infinite-chain structure supported by hydrogen bonding between the amide group and the oxo ligand of an adjacent tungsten complex. The η^1-*O* coordinated nitro compounds $W(X)Cl_3(OPh\text{-}2\text{-}NO_2)$ (**5**) [X = O (**5a**), NC_6H_3-2,6-$(CH_3)_2$ (**5b**), and Ph_2C_2 (**5c**)] have also been isolated and the crystal structure of **5c** is reported. © 1998 Elsevier Science Ltd. All rights reserved

Keywords: tungsten; salicylate; acid chloride; hydrogen bonding; materials.

During the 100 years of research that have gone into the development of the field of coordination chemistry, it has become apparent that virtually every generalization about the nature of metal ligand bonding is confounded by a range of exceptions. For example, arguments can be made regarding the tendency of carbon monoxide and other π-acceptor ligands to bind to transition metals with low formal oxidation states, but there are noteworthy examples of carbonyl ligand binding to formally highly oxidized metals. Although suitable ligands for supporting early transition metals in ultimate or penultimate formal oxidation states are typically ionic and strongly electron donating species such as halide, oxide, alkyl amide (R_2N^-), alkyl imido ($R\text{-}N^{-2}$) [1], alkoxide [2,3,4,5], thiolate [6], β-diketonate, cyclopentadienide and carboxylate [7] ligands, there are numerous examples of neutral σ-donor and π-acceptor ligands that support such complexes. While very weakly binding, the η^1-*O* coordinated carbonyl moieties is a class of ligands that pervades the literature in transition metal complexes for both high and low formal oxidation states.

Carboxylates [7], esters, aldehydes [8], ketones, and amides [9] are particularly common as η^1-*O* bound ligands, and are frequently encountered in association with highly Lewis acidic materials. The importance of such functional groups perhaps stems either from their ubiquitous presence in biological systems [10], or from their involvement in industrially important catalytic processes [11]. The stabilization of complexes containing such extraordinarily weak σ-donor ligands is usually accomplished by incorporating that σ-donor into ligand with another coordinating moiety, predisposing the system to a chelating interaction.

One ligand moiety in the group of carbonyl compounds for which there were previously no examples is the acid chloride. Access to a group of stable metal acid chlorides could provide a ready pathway for ligand-based electrophilic attachment of metals to tar-

† Dedicated to Prof. D. C. Bradley on the occasion of his 73rd birthday.

* Author to whom correspondence should be addressed.

get molecules. Two other functional groups whose coordination chemistry has not been greatly elaborated for high oxidation state metals are nitro groups and primary or secondary amides (Fig. 1). Both η^1-*O* nitro and amide substituents provide the opportunity for constructing hydrogen bonded motifs of transition metal complexes for use in a range of materials applications.

In this paper, we report the synthesis of η^1-*O* coordinated complexes of these ligands with tungsten(VI) complexes, specifically those containing an oxo, aryl imido or η^2-diphenylacetylene units. We have begun to examine both the reactivity of these complexes and their potential to organize stable early transition metal compounds into inorganic/organic hybrid supramolecular materials.

RESULTS AND DISCUSSION

Synthesis and characterization of W(=X)Cl_3(OPh-2-Y) *complexes*

The complexes were synthesized in the same manner as analogous biphenolate and salicylate complexes [12]. The parent metal complex W(=X)Cl_4 was combined with the appropriate phenol in dichloromethane at ambient temperature [Eq. (1)] yielding the chelated phenoxide complex. The compounds were isolated as deep red to red-orange crystalline materials from dichloromethane/hexane solutions.

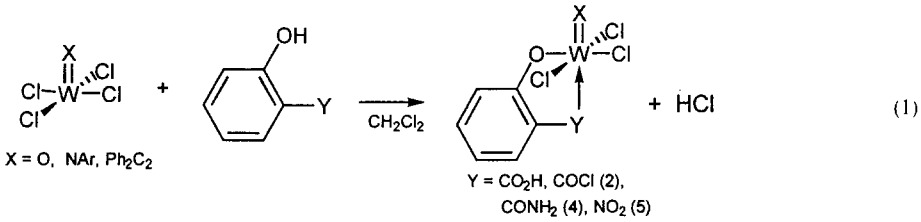

(1)

There is a considerable interest in compound **2**, as no acid chloride complexes have been reported previously. X-ray crystallographic studies of **2a** and **2c** will be discussed below. Given the inherent electrophilicity of both the tungsten and carbonyl moieties in complex **2**, either site may be attacked by nucleophiles. This behavior was examined through reactions of **2a** with alcohols or amines. Complex **2a** reacts with η-propanol to yield **3** with and fumes of HCl [Eq. (2)]. The reaction produces an ester which is isolated in modest yield (54%). The regiochemistry of propyl attachment is confirmed by a heteronuclear multiple bond connectivity (HMBC) NMR experiment [14]. HMBC shows coupling between the ^{1}H nuclei on the

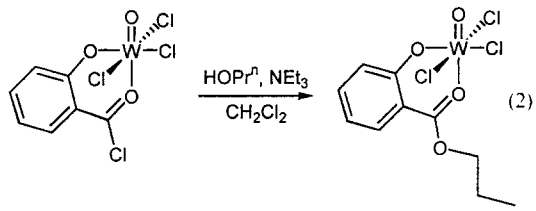

(2)

a carbon of the *n*-propyl group to the carbonyl carbon of the ester. Low yields of amide products, such as the *N*-*t*-butyl salicylamide complexes (**4a**), can be obtained through similar reactions between **2a** and amines. It is unclear whether the low yields observed in these reactions are due to the formation of side products or to difficulty in separating the amide product from *t*-butylammonium chloride (*vide infra*).

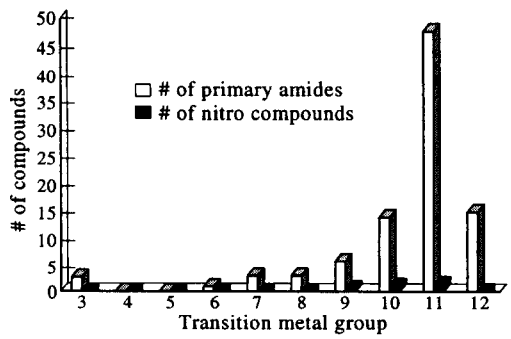

Fig. 1. Frequency of primary amides and nitro groups as η^1-*O* ligands in the Cambridge Structural Database (CSD) [13].

The unsubstituted salicylamide complex **4b** is readily prepared through the combination of $WOCl_4$ with salicylamide in a method analogous to the preparation of the salicylic acid compounds [12]. Because amides are well known synthons for supramolecular assembly in biological [15] and inorganic systems [16], complex **4b** also has potential for building similar structures. The poor solubility of **4b** in non-donor solvents like dichloromethane, chloroform, and toluene is probably caused by intermolecular associations in the solid state. Complex **4b** is more soluble in ether, THF, and very soluble in DMF. The amide groups are not likely to engage in hydrogen bonding with the carbonyl in an adjacent tungsten complex, due to steric hindrance

generated by η^1-*O* coordination of the amide. However, the terminal oxo group is accessible and does form a hydrogen bond with an adjacent amide molecule (*vide infra*).

Efforts were made to employ the nitro complexes **5** as hydrogen bond acceptors with hydrogen bond donors complexes. Given the fact that the amide N-H groups in **4b** will hydrogen bond to an oxo moiety, a carboxylic acid should also form a hydrogen bond with the oxo group of **5a**. Crystallization of an equimolar mixture of $WOCl_3$(OPh-2-NO_2) (**5a**) and $WOCl_3$(Hsal) in dichloromethane yielded only powdered $WOCl_3$(Hsal). Apparently, neither the nitro nor the terminal oxo groups of **5a** are sufficiently basic to bind the $WOCl_3$(Hsal) acid. It may be that the hydrogen bond donor (the Hsal complex) simply does not have the proper complementarity to form a hydrogen bond with the nitro group or the oxo group [17]. Alternatively, the formation of strong intermolecular hydrogen bonding in the $WOCl_3$(Hsal) lattice may favor the fractionation of the pure acid from **5a**. We are currently examining other hydrogen bond donors that will complement the use of **5** as a Brønsted base in supramolecular assemblies.

X-ray structure data

Compounds **2a, 2c, 4b,** and **5c,** have been characterized by X-ray crystallography. Selected bond distances and angles comparing these complexes are listed in Table 1. It is interesting to note the similarities of the nitro compound **5c** (Fig. 2) to the salicylic acid [12] and acid chloride **2c** (Fig. 3) complexes, the latter two having an obvious structural similarity. The W—$C_{C\equiv C}$ distances of all three diphenylacetylene compounds are identical within the 3σ crystallographic convention. The W—O_{trans} distances of **2c** and **5c** are slightly longer than that of the salicylate

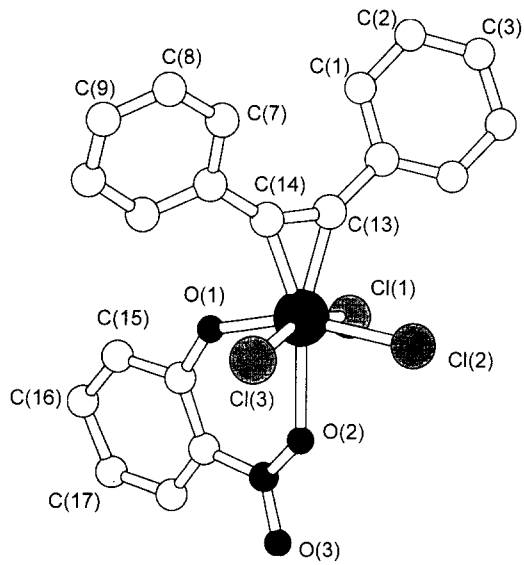

Fig. 2. Ball and stick diagram of the molecular structure of W(η^2-Ph_2C_2)Cl_3(OPh-2-NO_2) (**5c**).

Table 1. Selected bond distances (Å) and angles (°) for comparison in selected W(X)Cl_3(OPh-2-Y) compounds

	Oxo		Diphenylacetylene		
Y =	-CO_2H···dme	-COCl (**2a**)	-COCl (**2c**)	-CO_2H	-NO_2 (**5c**)
W—Cl_{avg}	2.32(2)	2.31(2)	2.36(4)	2.36(3)	2.34(3)
W=O	1.68(1)	1.657(7)	—	—	—
W—C_{avg}	—	—	2.026(7)	2.014(10)	2.016(9)
W—O_{trans}	2.21(2)	2.318(6)	2.271(4)	2.211(6)	2.274(7)
W—O_{Ph}	1.88(1)	1.873(6)	1.905(5)	1.928(6)	1.933(6)
W—O_{Ph}—C	139(2)	141.75	137.3(4)	136.7(5)	135.0(6)
O—A—B	121.5(7)	116.9(7)	115.4(6)	119.6(8)	118.6(9)
W—O—A—B	174.0(7)	176.4(4)	172.6	174.9	175.3

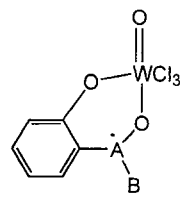

A = C, B = OH
A = C, B = Cl (2a)

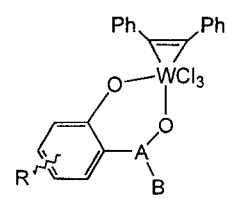

A = C, B = OH, R = 5-Cl
A = C, B = Cl, R = H (2c)
A = N, B = O, R = H (5c)

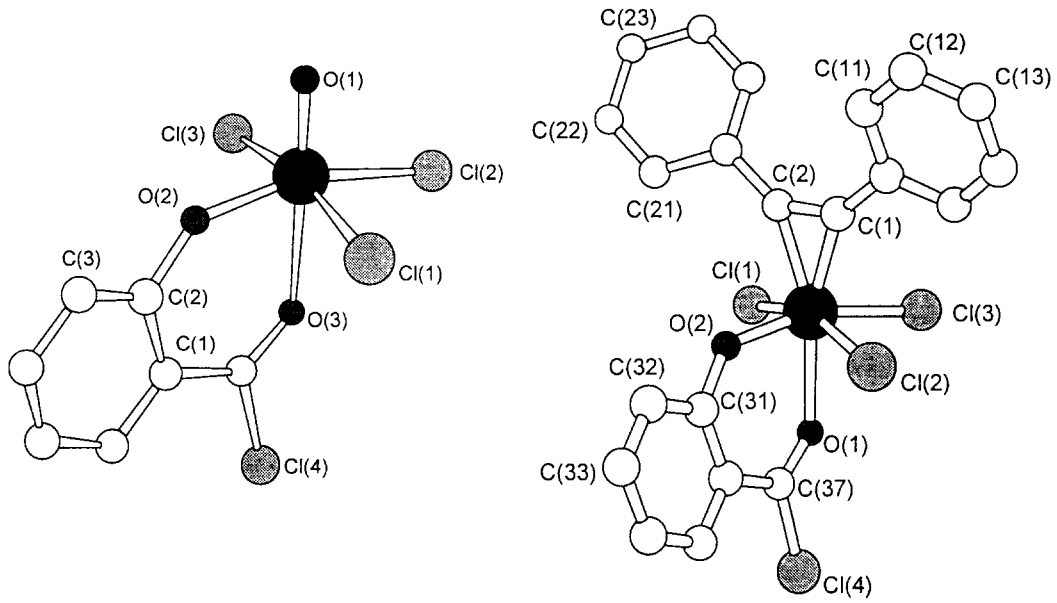

Fig. 3. Ball and stick diagrams of the molecular structures of $WOCl_3(OPh\text{-}2\text{-}COCl)$ (**2a**) and $W(\eta^2\text{-}Ph_2C_2)Cl_3(OPh\text{-}2\text{-}COCl)$ (**2c**).

(Y = -CO_2H) by about 0.061(2) Å. This is probably due to the reduced σ-donor ability of the acid chloride and nitro groups compared to the acid. In all of the complexes, the W—O_{trans} bonds are severely weakened by the *trans* influence of the multiply bonded oxo or acetylene units. The η^1-*O* coordination of the respective groups does not seem to generate significant strain within the chelant moiety. The bond angles and distances in the carboxylate, acid chloride, and nitro groups are consistent with sp^2 hybridized central atom. Also noted in the table are the dihedral angles created by the chelant moiety and the tungsten center. As expected, these angles show the nearly planar arrangement of the coordinating group. The nitro group in **5c** has equal N—O bond lengths of 1.238(10) and 1.233(9) Å indicating that there is significant delocalization in this subunit. This is counter to the expectation that the bonded N—O unit will donate more electron density to tungsten and thereby exhibit greater N—O single bond character than the uncoordinated N—O group. The W—O interaction is evidently too weak to significantly perturb bonding in the NO_2 unit.

Relatively few coordination compounds containing acid chloride or nitroarene ligands exist for comparison with **2c** and **5c**. Even fewer examples of these complexes are observed among the early transition metals. A cobalt(III) complex of 3-(dimethylamino)-2-aminoacrylyl chloride (**I**) is the only example of an η^1-*O* bonded acid chloride [18]. Like the *o*-hydroxybenzoylchloride ligand in **2c**, the 3-(dimethylamino)-2-aminoacrylyl chloride binding to cobalt is stabilized *via* a chelate interaction. the acid chloride functionality in **2**, the chemistry of **I** is atypical of acid

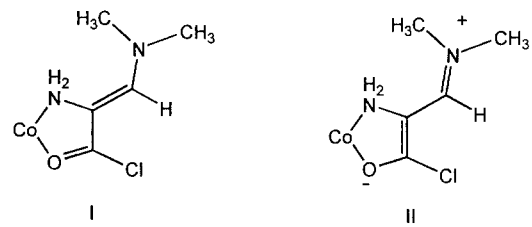

chlorides [19]. The complex is unreactive to water and actually crystallizes as a hydrated salt. The reduced electrophilicity of the acid chloride carbon has its origins in strong π-donation by the dimethylamino group, which results in a ligand having primarily enolate character (**II**).

Monodentate nitroarene complexes are also very rare for the early transition metals (see Fig. 1), although a range of examples have been structurally characterized for Group 9 and 10 metals [20]. Nitro group coordination in these complexes is stabilized by the formation of either *o*-nitrophenolate or *o*-nitrophenyl chelates. Typical M—O distances in four and six coordinate palladium and rhodium complexes are 2.135(4) and 2.138(3) Å, respectively. These M—O distances are slightly shorter than the distance found in **5c**. The Pd—O bond of the *o*-nitrophenyl chelate is easily disrupted through the addition of phosphine and pyridine ligands, indicating that coordination of the nitro group to the palladium is extremely weak [20]. The nitro group of **5c** can also be compared with the coordination of nitrate ion [21]. The coordination of the *o*-nitrophenolate anion is naturally restricted to

an η^1-*O* mode by the six-membered ring formed by the phenolate unit. Crystallographically characterized metal nitrates are analyzed by a comparison of the metal oxygen distances, where M—O_{short} is the distance to the closer oxygen and M—O_{long} is the distance to the further oxygen [21]. The W—O_{short} distance in **5c** of 2.274(7) Å is longer than the characteristic M—O_{short} distance for third row transition metal nitrates. This long bond results from the strong *trans* influence of the acetylene ligand and the poor localization of negative charge density on the oxygens of the nitro group. The W—O_{long} distance is 4.342(7) Å, significantly longer than any reported for simple nitrate salts (M—O_{long} = 3.5 Å). The geometrical constraints imposed by the chelate ring will only permit η^1-*O* coordination mode of the NO_2 group.

The complexes all crystallize in different space groups, the most unusual being $R\bar{3}$ for **2c**. This complex crystallizes in a three-fold symmetric group due to π-interactions [22] between the salicoyl and acetylene units of neighboring molecules. The diphenylacetylene ligand is involved in two types of interactions: (1) π-stacking of C(21)—C(26) ring of the diphenyl acetylene to the C(31)—C(36) ring in an adjacent salicoyl chloride ligand at a distance of 3.749 Å and an interplanar angle of 0° and (2) a C—H $\cdots$ π interaction of the other acetylene phenyl group [C(11)—C(16)] to C(32) of a different salicoyl chloride unit at a distance of 3.654 Å and an angle of 132.9°. With an additional contact of a C—H $\cdots$ π interaction with another adjacent aryl ring C(13)—H(13) $\cdots$ [C(11)—C(26)] at a distance of 3.654 Å and a C—H $\cdots$ centroid angle of 117.3°, the molecule forms an unusual lattice structure that is highly ordered. The hexagonal crystallographic axis corresponds to the *c*-axis of the cell, generating a hexagonal-shaped channel (Fig. 4). The channel has a diameter of approximately 5–6 Å (accounting for large atom radii and hydrogen atoms) and is devoid of solvent molecules. The closest distance between carbon nuclei across the channel is 8.5 Å, while the closest carbon–chlorine distance is 7.8 Å. The absence of solvent is confirmed by NMR characterization of the bulk material. This is an unusual channel structure for a non-covalently bonded system [23]. Future studies will address the idea that molecules assembled by multiple π-interactions can be used to construct other materials containing large unoccupied void volumes.

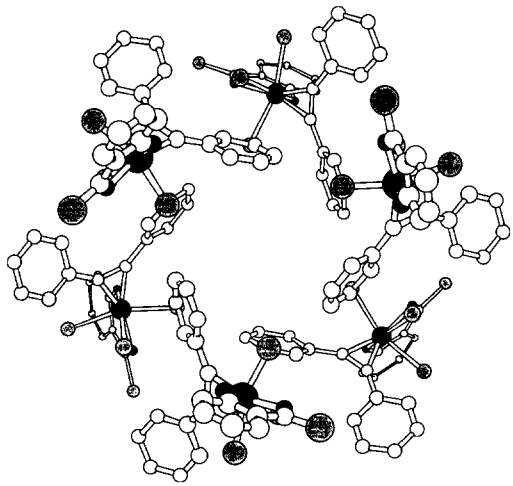

Fig. 4. View of W(η^2-Ph_2C_2)Cl_3(OPh-2-COCl) (**2c**) down the *c* crystallographic axis.

The acid chloride complex **2a** does not exhibit the same channel structure as **2c**. Its structure is typical of tungsten oxo compounds [24], with relevant bond distances and angles listed in Table 1. The only significant structural differences between the two oxo complexes in Table 1 is in the oxo ligand and the chelant moiety. The terminal oxo group bonds at a slightly shorter distance in **2a** than in related salicylate complexes [12]. This may be due to the decreased electron donating ability of the acid chloride compared to the acid, which allows the oxo ligand to interact more strongly with tungsten. This hypothesis is verified by the fact that the W—$O_{carbonyl}$ bond length is much longer in the acid chloride than the corresponding acid (by 0.108 Å). In all other respects, such as W—Cl and W—O_{Ph} bond lengths and corresponding bond angles, the molecular units of **2a** and **2c** are quite similar. Also, complex **2a** bears resemblance to **2c** in the intermolecular associations that are formed. The oxo group forms a 3.39(1) Å C—H $\cdots$ O hydrogen bond with the hydrogen atom on C(3) [25]. The C—H $\cdots$ O interaction lies along the *a* direction of the unit cell. Yet another close contact is observed between Cl(3) and the carbonyl carbon C(7) of an adjacent molecule. The atoms are separated by 3.488(9) Å, at an angle of 90° between the metal chloride bond and the plane of the acid chloride group. The two molecules involved in this interaction are related by the screw-axis in the crystal. The atomic organization of this contact is reminiscent of a nucleophilic substitution at a carbonyl carbon [26]. Lastly, the aromatic rings of the salicoyl chloride ligands stack at a distance of 4.033(6) Å and an interplanar angle of 0° [22].

The structure of the amide **4b** is a classic octrahedral tungsten oxychloride complex (Fig. 5, Table 2). It displays the *trans* effect typical of an oxo ligand with a long bond to the neutral η^1-*O* amide group [W—O_{amide} = 2.271(4) Å]. While the molecular unit appears to be rather mundane, the intermolecular interactions are quite fascinating. There is a hydrogen bond from the amide group of one tungsten atom to the oxo group of the adjacent molecule. This N—H $\cdots$ O_{oxo} interaction is 3.067(9) Å, with an apparent N—H $\cdots$ O angle of 117.7(10)° (Fig. 6). Actually, N—H $\cdots$ O interactions of this type are very common in organometallic coordination chemistry [9]. An average N—H $\cdots$ O distance of the interaction described here is 3.02(1) Å, with an angle of 155.9(5)°. The hydrogen bond between the amide and oxo group in **4b** continues through the lattice, making an infinite

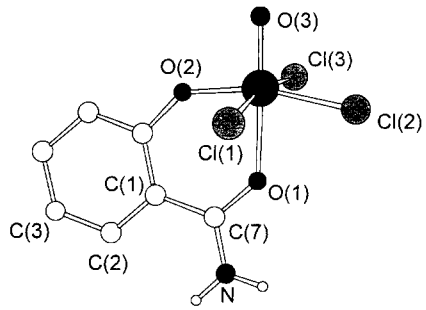

Fig. 5. Ball and stick diagram of the molecular structure of $WOCl_3(OPh\text{-}2\text{-}CONH_2)$ (**4b**).

Table 2. Pertinent bond distances (Å) and angles (°) in $WOCl_3(OPh\text{-}2\text{-}CONH_2)$ (**4b**)

W—Cl (avg)	2.329(15)	O(1)—WCl (avg)	83.3(4)
W—O(1)	2.147(9)	O(3)—W—Cl (avg)	97.6(15)
W—O(2)	1.875(8)	W—O(2)—C(6)	139.3(7)
W—O(3)	1.676(9)	N—C(7)—O(1)	117.9(11)
N—C(7)	1.290(15)		
O(1)—C(7)	1.285(15)		

one dimensional chain of hydrogen bonds. These one dimensional chains of complexes are arranged in a herringbone pattern. These strands are in turn held together by two other non-covalent interactions: (1) A close contact, possibly a van der Walls interaction, between a chloride ligand [Cl(3)] and an adjacent arene ring at a distance of 3.434 Å with an 89.9° contact angle, and (2) A C—H···Cl interaction between C(3) of the arene ring and Cl(1) of a nearby complex at a distance of 3.696 Å and an angle of 118.1°. Hydrocarbon C—H···Cl interactions are well known and have been observed in the assembly of other hydrogen bonded complexes [27]. All of these interactions help to stabilize the crystal lattice, which contributes to the poor solubility of **4b** in non hydrogen bonding solvents (*N*- or *O*-atom donor solvents). According to the Cambridge Structural Database (CSD), only one other group 6 complex with a coordinating primary amide moiety has been documented: $MoO_2Cl_2(CH_3CONH_2)$ [28]. This complex shows an analogous intermolecular oxo-amide hydrogen bond motif in the solid state at a distance of 3.042 Å and an angle of 158°.

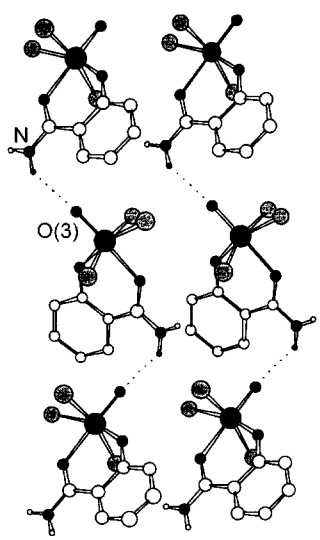

Fig. 6. Infinite chain of hydrogen bonding by N—H···O=W groups in $WOCl_3(OPh\text{-}2\text{-}CONH_2)$ (**4b**).

EXPERIMENTAL

General procedures

All experiments were performed under a nitrogen atmosphere in a HE-553-2 Vacuum Atmospheres dry box or using standard Sclenk techniques. Benzene, toluene, hexane, and diethyl ether were purified by distillation over Na/benzophenone. Dichloromethane and *t*-butylamine were purified by distillation over CaH_2, followed by purging with dry nitrogen. NMR solvents (Cambridge Isotope Laboratories) were dried with 5 Å molecular sieves and degassed with dry nitrogen prior to use. Salicylic acid (H_2sal), and 2-nitrophenol ($HOPh\text{-}2\text{-}NO_2$) were used as received from Aldrich. Thionyl chloride was used as received from Eastman-Kodak. $W(=NC_6H_3\text{-}2,6\text{-}Me_2)Cl_4$ and $W(\eta^2\text{-}Ph_2C_2)Cl_4$ were prepared using published procedures. $WOCl_4$ was received as a gift from Hercules Research Company.

NMR spectra were recorded on Bruker AM-500 or DRX-400, Varian XL-300, or General Electric QE-300 spectrometers. ^1H and ^{13}C data are listed in parts per million (ppm) downfield from tetramethylsilane with ^1H data referenced by the solvent's residual proton peak. All NMR spectra are recorded at ambient temperature (~20°C) in $CDCl_3$ unless otherwise noted. All coupling constants are linked in hertz (Hz). Elemental analyses were performed by Desert Analytics (P.O. Box 41838, Tucson, AZ 85717).

Preparation of salicoyl chloride (HOPh-2-COCl) (**1**)

This procedure is based on several literature methods [29]. Salicylic acid (10.0 g, 72.4 mmol) was placed in a 250 cm^3 flask with a magnetic stirbar. A small amount of aluminum chloride (0.3 g, 2.25 mmol) was added, followed by dry benzene (60 cm^3). The mixture was fitted with a reflux condenser and thionyl chloride (7.92 cm^3, 108.6 mmol, 1.5 equiv.) was added

by syringe. As the yellow mixture was refluxed for 5 h, it became orange colored. The volume was then reduced to 30 cm^3 *in vacuo* and was stirred overnight. The volume of the viscous solution was further reduced *in vacuo* until the exterior of the flask was no longer cool to the touch. This gelatinous product was vacuum distilled twice into a liquid nitrogen cooled flask (to insure the complete removal of the solvent). The product is a colorless, non-viscous liquid at room temperature, whose density (1.3112 g/cm^3) and freezing point (18°C) match the literature values [30]. This material was stored at −20°C to prolong shelf life as autocondensation occurs more quickly at room temperature. The solid was melted immediately prior to each use and handled under nitrogen to prevent hydrolysis. Yield: 34% (2.90 cm^3, 3.80 g, 24.3 mmol).

Preparation of $WOCl_3$(OPh-2-COCl) (**2a**)

$WOCl_4$ (2.5017 g, 7.32 mmol) was slurried in dichloromethane (20 cm^3) in a 50 cm^3 Schlenk flask with a magnetic stirbar. Salicoyl chloride (0.87 cm^3, 7.28 mmol) was added slowly by syringe. The slurry became blood red upon addition of the first drop of salicoyl chloride. The addition of salicoyl chloride produced copious amounts of HCl over the 5 min required to add the liquid. The reaction was stirred an additional 25 min then the solvent was removed *in vacuo*. The product was recrystallized from toluene layered with hexane to yield a deep crimson microcrystalline material. X-ray quality crystals were recrystallized from dichloromethane layered with hexane. Yield: 96% (3.1811 g, 7.07 mmol). NMR data: ^1H (300 MHz): δ 8.48 (H, dd, 6-position of OPh-2-COCl), 8.01 (H, dt, 5-position), 7.46 (H, dt, 4-position), 7.22 (H, dd, 3-position). ^{13}C (500 MHz, $CDCl_3$): δ 178.86 (-COCl), 159.67, 140.25, 136.16, 129.40, 123.59 123.10. Mass spectrum (EI): 460 [M^+], 427 [$WOCl_3$(OPh-2-COCl)$^+$], 307 [$WOCl_3^+$], 272, 240 [$C_{14}H_8O_4^+$], 120 [$C_6H_4CO_2^+$], 92 [$C_6H_4O^+$], 64 [$COCl^+$]. Anal. calcd for $C_7H_7O_3WCl_4$. Calc.: 18.21% C; 0.87% H. Found: 18.89% C; 0.62% H.

Preparation of W(=NC_6H_3-2,6-Me_2)Cl_3(OPh-2-COCl) (**2b**)

This compound was prepared in a manner similar to **2a**. W(=NC_6H_3-2,6-Me_2)Cl_4 (1.6070 g, 3.61 mmol) was slurried in dichloromethane (30 cm^3) and salicoyl chloride (0.43 cm^3, 3.60 mmol) was added by syringe. The product was recrystallized from dichloromethane and isolated as a black microcrystalline material. Yield: 76% (1.5550 g, 2.75 mmol). NMR data: ^1H (400 MHz): δ 8.41 (H, dd, 6-H of -OPh-2-COCl), 7.93 (H, dt, 5-H), 7.35 (H, t, 4-H), 7.31 (2H, d, *m*-H's of imido), 7.08 (H, d, 3-H of -OPh-2-COCl), 6.74 (H, t, *p*-H of imido), 3.22 (6H, s, NC_6H_3-2,6-($\underline{C}H_3$)$_2$). ^{13}C: δ 180.73 (-$\underline{C}$OCl), 162.52, 150.13, 144.69, 141.33, 136.24, 133.15, 126.89, 126.42, 122.83, 121.56, 18.44 (NC_6H_3-2,6-($\underline{C}H_3$)$_2$). Anal. $C_{15}H_{13}NO_2WCl_4$. Calc.: 31.89% C; 2.32% H; 2.48% N; 25.10% Cl. Found: 31.53% C; 2.02% H; 2.37% N; 25.28% Cl.

Preparation of W(η^2-Ph_2C_2)Cl_3(OPh-2-COCl) (**2c**)

This compound was also prepared in a manner similar to **2a**. W(Ph_2C_2)Cl_4 (1.2087 g, 2.40 mmol) was slurried in 30 cm^3 dichloromethane and salicoyl chloride (0.28 cm^3, 2.35 mmol) was added by syringe. The solution was filtered through Celite and the volume reduced *in vacuo* to yield purplish–black blocks suitable for X-ray diffraction. Yield: 70% (1.0520 g, 1.69 mmol). NMR data: ^1H (400 MHz): δ 8.45 (H, dd, 6-H of -OPh-2-C = OCl), 8.16 (4H, *o*-H's of Ph_2C_2), 7.84 (H, dt, 5-H, of -OPh-2COCl), 7.77 (4H, t, *m*-H's of Ph_2C_2), 7.63 (2H, t, *p*-H's of Ph_2C_2), 7.36 (4-H of -OPh-2-COCl), 6.94 (3-H of -OPh-2-COCl). ^{13}C (partial): δ 179.79, (-$\underline{C}$OCl), 163.20, 141.41, 138.17, 136.41, 134.72, 134.11, 129.43, 125.44, 122.35, 119.47. Anal. calcd for $C_{21}H_{14}O_2WCl_4$. Calc.: 40.42% C; 2.26% H; 22.73% Cl. Found: 40.34% C; 1.98% H; 22.38% Cl.

Preparation of $WOCl_3$(OPh-2-COOPr^n) (**3**)

A 50 cm^3 Schlenk flask was charged with **2a** (0.8061 g, 1.79 mmol), a magnetic stirbar, and dichloromethane (25 cm^3). In a separate Schlenk flask, 1-propanol (0.13 cm^3, 1.74 mmol) and triethylamine (0.25 cm^3, 1.79 mmol) were mixed with dichloromethane (10 cm^3). The solution of **2a** was cooled to −78°C and the 1-propanol/triethylamine solution was added dropwise over 15 min. Fumes evolved during the addition (presumably HCl). After stirring an additional 45 min at −78°C, the reaction was allowed to warm to room temp (over thirty minutes) and stripped to dryness *in vacuo*. The dark red residue was taken up in hot hexane (5 × 10 cm^3) and filtered through Celite. The hexane was concentrated and allowed to cool, producing crystals of **3**. Yield: 54% (0.4673 g, 0.09 mmol). NMR data: ^1H (400 HMz): δ 8.24 (H, dd, 6-H), 7.86 (H, dt, 5-H) 7.35 (H, t, 4-H), 7.18 (H, d, 3-H), 4.65 (2H, t, $OC\underline{H}_2CH_2Ch_3$), 1.96 (2H, q, $OCH_2C\underline{H}_2CH_3$), 1.11 (3H, t, $OCH_2CH_2C\underline{H}_3$). ^{13}C: δ 169.77 (ester), 160.65, 137.37, 131.75, 129.30, 123.17, 118.94, 71.98 ($O\underline{C}H_2CH_2CH_3$), 22.26 ($OCH_2\underline{C}H_2CH_3$), 10.64 ($OCH_2CH_2\underline{C}H_3$).

Preparation of $WOCl_3$(OPh-2-CONHBu^t) (**4a**)

This compound was synthesized in a similar fashion to the ester complex **3**. A toluene solution of *t*-butylamine (0.27 cm^3, 2.57 mmol) was added to a toluene solution of **2a** (0.4673 g, 1.04 mmol) at −78°C. The reaction was filtered to remove the by-product, *t*-butylammonium chloride. The solid salt was washed with hot toluene (2 × 10 cm^3) and the filtrate solution

concentrated *in vacuo*. The solution was warmed to 60°C and allowed it to stand, yielding deep red block crystals. The poor yield may be due to association of the product with the *t*-butylammonium chloride. This hypothesis was corroborated by the fact that the precipitate yielded bright red solution upon cleaning the filter frit with acetone. Yield: 11% (0.0580 g, 0.012 mmol). NMR data (300 MHz): ^{1}H: δ 7.73 (H, t), 7.64 (H, d), 7.26 (H, t) 6.98 (H, bs, -CONH(CH$_3$)$_3$), 1.60 [9H, s, -CONH(CH$_3$)$_3$].

Preparation of $WOCl_3(OPh\text{-}2\text{-}CONH_2)$ **(4b)**

$WOCl_4$ (2.1900 g, 6.41 mmol) was weighed into a 50 cm^3 Schlenk flask with a magnetic stirbar. Dichloromethane (30 cm^3) was added via cannula, followed by solid salicylamide (0.8795 g, 6.41 mmol) from an addition tube. Upon addition of the salicylamide, a deep reddish-purple color developed and as the reaction proceeded, microcrystals of the same color began to precipitate. The mixture was stirred for eight hours, then the solid microcrystalline product was harvested by filtration (2.465 g 5.57 mmol). The supernatant solution volume was reduced and cooled to −20°C, yielding X-ray quality crystals (0.213 g, 0.48 mmol). Yield: 94% (2.678 g [total], 6.05 mol). NMR data: ^{1}H (300 MHz): δ 7.85 (H, t), 7.75 (H, d), 7.35 (H, t), 7.24 (H, d), 7.03 (H, broad s, CONH), 6.61 (H, broad s, CONH). The complex was not soluble enough in $CDCl_3$ to obtain a ^{13}C NMR spectrum. Anal. $C_7H_6O_3NWCl_3$. Calc.: 19.01% H, 3.17% N. Found: 19.24% C; 1.29% H, 3.22% N.

Preparation of $WOCl_3(OPh\text{-}2\text{-}NO_2)$ **(5a)**

A 50 cm^3 Schlenk flask was charged with $WOCl_4$ (1.3650 g, 4.00 mmol), a magnetic stirbar, and dichloromethane (30 cm^3). Solid 2-nitrophenol (0.5593 g, 4.02 mmol) was added by addition tube and the solution immediately changed to a deep red color. The mixture was stirred for 6 h, then filtered through Celite. The volume was reduced to 5 cm^3 and allowed to stand, producing blood red blocks. The liquid was decanted and the material dried for 6 h at room temperature (10^{-6} torr). The material appeared glassy rather than microcrystalline. Yield: 75% (1.3270 g, 2.99 mmol). NMR data: ^{1}H (300 MHz): δ 8.40 (H, dd, 6-H), 7.97 (H, dt, 5-H), 7.45 (H, dt, 4-H), 7.29 (H, d, 3-H). ^{13}C: δ 211.08 (C-NO$_2$), 195.24, 194.56 (O—C$_{ipso}$), 185.37, 183.52, 180.78. Anal. calcd for $C_6H_4O_4NWCl_3$. Calc.: 16.22% C; 0.91% H; 3.15% N. Found: 16.16% C; 0.68% H; 3.07% N.

Preparation of $W(=NC_6H_3\text{-}2,6\text{-}Me_2)Cl_3(OPh\text{-}2\text{-}NO_2)$ **(5b)**

This synthesis was carried out in a manner similar to that of **5a**. The filtrate was concentrated to 20 cm^3 and warmed to 40°C. Thin brown parallel-piped shaped crystals formed after standing overnight at room temperature. Two crops of these crystals yielded only small amounts of material (0.129 g, 0.23 mmol). The supernate was cooled to −20°C to produce more crystals which had a different morphology from the first crops. This material was block shaped and the blocks were clumped together. Both sets of crystals have identical ^{1}H and ^{13}C NMR spectra. Yield: 70% (0.727 g [total], 1.33 mmol). NMR data: ^{1}H (300 MHz): δ 8.32 (H, dd, 6-H), 7.86 (H, dt, 5-H), 7.30 (3H, mult, 4-H of OPh-2-NO$_2$ and *m*-H's of imido), 7.14 (H, d, 3-H), 6.72 (H, t, *p*-H of imido), 3.20 (6H, s, NC$_6$H$_3$-2,6-(CH$_3$)$_2$). ^{13}C: δ 157.05, 149.76, 144.43, 139.46, 136.27, 133.11, 126.96, 126.48, 125.84, 124.13, 18.01 (NC$_6$H$_3$-2,6-(CH$_3$)$_2$). Analytical Data for $C_{14}H_{13}O_3N_2WCl_3$. Calc.: 30.71% C; 2.39% H; 5.12% N. Found: 30.40% C; 2.21% H; 4.98% N.

Preparation of $W(\eta^2\text{-}Ph_2C_2)Cl_3(OPh\text{-}2\text{-}NO_2)$ **(5c)**

This synthesis was carried out in a manner similar to that of **5a**. The filtrate was concentrated to 5 cm^3 and layered with 7 cm^3 hexane. After standing at room temperature for 3 days, shiny, red–orange, X-ray quality needles were harvested by decanting the supernate solution. Yield: 87% (0.872 g, 1.44 mmol). NMR data: ^{1}H (300 MHz): δ 8.36 (H, dd, 6-H of OPh-2-NO$_2$), 8.17 (4H, dd, *o*-H's of Ph's), 7.79 (5H, t, *m*-H's of Ph's overlapped with 5-H of OPh-2-NO$_2$), 7.65 (2H, t, *p*-H's of Ph's), 7.33 (H, t, 4-H), 7.01 (H, d, 3-H). ^{13}C: δ 252.22 (Ph$_2$C$_2$), 158.52, 139.81, 138.14, 135.05, 134.79, 134.41, 129.51, 127.36, 125.35, 124.30. Anal. calcd for $C_{20}H_{13}O_3NWCl_3$. Calc.: 39.60% C; 2.33% H; 2.31% N. Found: 39.71% C; 2.07% H, 2.26% N.

Crystallographic structure determinations

Crystal, data collection, and refinement parameters are given in Table 3. Suitable crystals for single-crystal X-ray diffraction were sectioned and mounted in a thin-walled capillary flushed with nitrogen. The unit-cell parameters were obtained by the least-squares refinement of the angular settings of 24 reflections ($20 \leqslant 2\theta \leqslant 25$) for all structures except **2a** ($48 < 2\theta < 50$).

The systematic absences in the diffraction data are uniquely consistent with $P2_1/n$ for **2a** and **4b** while **5c** was assigned to *Pccn*. The unit-cell parameters, photographic data, systematic absences and occurrences of equivalent reflections in **2c** are consistent with rhombohedral space groups without *c*-glide absences. The *E*-statistics and the chemical composition suggested the space group, $R\bar{3}$, and this solution gave chemically reasonable and computationally stable results during refinement.

The structures were solved by direct methods, completed by subsequent difference Fourier syntheses and refined by full-matrix least-squares procedures. Semi-

Table 3. Summary of X-ray diffraction data for crystallographically characterized compounds

Compound	**2a**	**2c**	**4b**	**5c**
Empirical formula	$C_7H_4Cl_4O_3W$	$C_{21}H_{14}Cl_4O_2W$	$C_7H_6Cl_3NO_3W$	$C_{20.50}H_{15}Cl_4NO_3W$
Formula weight	461.77	623.97	458.30	648.98
Crystal color, habit	Deep red prism	Deep red block	Dark red block	Red thin plate
Space group	$P2_1/n$	$R\bar{3}$	$P2_1/n$	$Pccn$
V, Å^3	1161.2(3)	9997(7)	1111.7(7)	4439(2)
Z (molecule/cell)	4	18	4	8
$R(F)$, %	0.045[b]	0.0351[b]	0.0438[a]	0.0330[b]
Rw (F), %	0.071	0.0755[b,c]	0.0537[a]	0.0710[b,c]
Temperature (C)	−120	25(2)	23(2)	−35(2)
Radiation	Cu-$K\alpha$ (λ = 1.54178 Å)		Mo-$K\alpha$ (λ = 0.71073 Å)	
a (Å)	11.579(2)	32.453(8)	5.5687(5)	26.590(5)
b [Å)	7.909(2)	—	14.618(2)	10.370(2)
c (Å)	12.705(1)	10.961(4)	13.683(3)	16.097(2)
α ( )	—	—	—	—
β ( )	93.57(1)	—	93.78(1)	—
γ ( )	—	120	—	—

[a] Quantity minimized = $\Sigma\Delta^2$; $R = \Sigma\Delta/\Sigma(F_o)$; $R(w) = \Sigma\Delta w^{1/2}/\Sigma(F_o \cdot w^{1/2})$, $\Delta = |(F_o - F_c)|$.
[b] Quantity minimized = $R(wF^2) = \Sigma[w(F_o^2 - F_c^2)^2]/\Sigma[(wF_o^2)^2]^{1/2}$; $R = \Sigma\Delta/\Sigma(F_o))$, $\Delta = |(F_o - F_c)|$.
[c] $R(wF^2)$, %.

empirical ellipsoid absorption corrections were applied to **2c** and **4b**, and a semi-empirical lamina absorption correction was applied to **5c**; all data with a glancing angle of $\leqslant 3^\circ$ to the prominent face [0 0 1] were rejected, affecting 163 reflections. One-half of a molecule of dichloromethane was located on a two-fold axis in **5c**. All non-hydrogen atoms were refined with anisotropic displacement parameters and all hydrogen atoms were treated as idealized contributions. Several of the remaining peaks from the difference map (1.06 to 1.46 e/Å^3 for **2c**, and 1.01 to 2.56 e/Å^3 for **4b**) were in chemically unreasonable positions (i.e. positions near the heavy atoms: 1.15 Å from W and 1.64 Å from Cl for **2c** and 0.86 to 1.58 Å from W for **4b**) and were considered noise. The structure of **2a** was solved using TeXsan software and Cromer and Waber's neutral atom scattering factors [31]. All software and sources of the scattering factors for **2c**, **4b**, and **5c** are contained in either SHELXTL version 4.2 or the SHELXTL version 5.03 program libraries (G. Sheldrick, Siemens XRD, Madison, WI).

CONCLUSIONS

A wide variety of weakly-coordinated functional groups can be used to satisfy the coordination sphere of the $W(X)Cl_3(OR)$ fragment. The electrophilic acid chloride complexes, $W(X)Cl_3(OPh\text{-}2\text{-}COCl)$, may have synthetic utility for the metallation of alcohols, amines, and nucleophilic metal complexes. Both $W(\eta^2\text{-}C_2Ph_2)Cl_3(OPh\text{-}2\text{-}COCl)$ and $WOCl_3(OPh\text{-}2\text{-}CONH_2)$ produce interesting lattice structures. $W(\eta^2\text{-}C_2Ph_2)Cl_3(OPh\text{-}2\text{-}COCl)$ arranges in a three-fold symmetric space group through weak intermolecular contacts involving the aryl subunits of the diphenyl acetylene and salicoyl chloride ligands. These contacts generate a star-shaped void whose internal diameter is 5–6 Å. This is a very unusual feature in non-covalently bonded solids. $WOCl_3(OPh\text{-}2\text{-}CONH_2)$ forms an infinite one-dimensional hydrogen bonded herringbone in the solid phase.

Acknowledgement—The authors acknowledge the donors of the Petroleum Research Fund administered by the American Chemical Society for support of this research.

REFERENCES

1. Templeton, J. L., *Adv. Organomet. Chem.*, 1987, **29**, 1.
2. Wilkinson, G., ed., *Comprehensive Coordination Chemistry*. pp. 335–364, Pergamon Press, New York (1987).
3. Person, C., Oskarsson, A. and Andersson, C., *Polyhedron*, 1992, **16**, 2039.
4. Bell, A., *J. Mol. Cat.*, 1991, **76**, 165.
5. Morton, M. D., Heppert, J. A., Dietz, S. D., Huang, W. H., Ellis, D. A., Grant, T. A., Eilerts, N. W., Barnes, D. L., Takusagawa, F. and VanderVelde, D., *J. Am. Chem. Soc.*, 1993, **115**, 7916.
6. Wilkinson, G., ed., *Comprehensive Coordination Chemistry*. pp. 633–660, Pergamon Press, New York (1987).
7. Wilkinson, G., ed., *Comprehensive Coordination Chemistry*. pp. 461–486, Pergamon Press, New York (1987).
8. Kovalenko, Y. V., Abramenko, V. L. and Sergienko, V. S., *Z. Neorg. Khimii*, 1994, **39**, 1653.
9. Biradha, K., Desiraju, G. R., Braga, D. and Grepioni, F., *Organometallics*, 1996, **15**, 1284.
10. (a) Rydon, H. N., ed., *Amino Acids, Peptides, and*

Related Compounds, Butterworths, Boston (1976); (b) See also [15a].
11. (a) Patai, S., *The Chemistry of Carboxylic Acids and Esters*, Interscience-Publishers, New York (1969); (b) Gutte, B., ed., *Peptides: Synthesis, Structures, and Applications*, Academic Press, San Diego (1995).
12. (a) Baroni, T. E., Heppert, J. A., Hodel, R. R., Kingsborough, R. P., Morton, M. D., Rheingold, A. L. and Yap, G. P. A., *Organometallics*, 1996, **15,** 4872 and its correction; (b) Baroni, T. E., Bembenek, S., Heppert, J. A., Hodel, R. R., Laird, B. B., Morton, M. D., Barnes, D. L. and Takusagawa, F., manuscript submitted to *Inorg. Chem.*
13. A connectivity search for η^1-*O*-bound nitro or primary amide moieties to each of the transition metal groups in the CSD resulted in the hits tabulated here.
14. Bax, A. and Summers, M. F., *J. Am. Chem. Soc.*, 1986, **108,** 2093.
15. (a) Creighton, T. E., *Proteins: Structures and Molecular Properties*, pp. 226–238, W. H. Freeman & Co., New York (1993); (b) LaBrenz, S. R. and Kelly, J. W., *J. Am. Chem. Soc.*, 1995, **117,** 1655.
16. (a) Kabanos, T. A., Keramidas, A. D., Papaioannou, A. and Terzis, A., *Inorg. Chem.*, 1994, **33,** 845; (b) Kawamoto, T., Prakash, O., Ostrander, R., Rheingold, A. L. and Borovik, A. S., *Inorg. Chem.*, 1995, **34,** 4294; (c) See also refs [17] and [28].
17. (a) Subramanian, S. and Zaworotko, M. J., *Coord. Chem. Rev.*, 1994, **137,** 357; (b) Desiraju, G. R., *Angew. Chem. Int. Ed. Engl.*, 1995, **34,** 2311.
18. Jackson, W. G., Sargeson, A. M., Tucker, P. A. and Watson, A. D., *J. Am. Chem. Soc.*, 1981, **103,** 533.
19. Patai, S., ed., *The Chemistry of Acyl Halides*, Interscience, New York (1972).
20. (a) Vincente, J., Martín, J., Chicote, M. T., Solans, X. and Miravitlles, C., *J. Chem. Soc., Chem. Commun.*, 1985, 1004; (b) Vincente, J., Chicote, M. T., Martín, J. and Artiago, M., *J. Chem. Soc., Chem. Commun.*, 1988, 141.
21. Wilkinson G., ed., *Comprehensive Coordination Chemistry*, pp. 413–434, Pergamon Press, New York, (1987). *Nitroalkanes* or *nitroarenes* are not expressly discussed in this section but their structural similarity to *nitrates* (where one oxygen is replaced by an R group) warrants this reference.
22. (a) Bürgi, H.-B. and Dunnitz, J. D., eds., *Structure Correlation*, pp. 523–529. VCH, New York (1994); (b) Desiraju, G. R. and Gavezzotti, A., *Acta Cryst., Sect. B.*, 1989, **B45,** 473. (c) Kawamoto, T., Hammes, B. S., Haggerty, B., Yap, G. P. A., Rheingold, A. L. and Borovik, A. S., *J. Am. Chem. Soc.*, 1996, **118,** 285. (d) Karpishin, T. B., Stack, T. D. B. and Raymond, K. N., *J. Am. Chem. Soc.*, 1993, **115,** 6115.
23. (a) Russel, V. A., Evans, C. C., Li, W. and Ward, M. D., *Science*, 1997, **276,** 575; (b) Pinnavaia, T. J. and Thorpe, M. F., eds., *Access in Nanoporous Materials*, Plenum Press, New York (1995).
24. (a) Lehtonen, A. and Sillanpää, R., *J. Chem. Soc., Dalton Trans.*, 1994, 2119. See also ref. [3] and [4].
25. Sharma, C. V. K., Panneerselvam, K., Pilati, T. and Desiraju, G. R., *J. Chem. Soc., Perkin Trans.*, 1993, **2,** 2209.
26. (a) Rauk, A., *Orbital Interaction Theory of Organic Chemistry*, John Wiley & Sons, Inc., New York (1994); (b) Traven, V. F., *Frontier Orbitals and Properties of Organic Molecules*, Ellis Horwood Limited, New York (1992).
27. James, S. L., Verspui, G., Spek, A. L. and van Koten, G., *J. Chem. Soc., Chem. Commun.*, 1996, 1309.
28. Sergienko, V. S., Ovchinnikova, N. A., Porai-Koshits, M. A. and Glushkova, M. A., *Russ. J. Coord. Chem.*, 1987, **12,** 961.
29. (a) McMaster, L. and Ahmann, F. F., *J. Am. Chem. Soc.*, 1928, **50,** 145; (b) Anschütz, L., *J. Lieb. Ann. der Chemie.*, 1927, **B454**, 71.
30. Lide, D. R., ed., *CRC Handbook of Chemistry and Physics*, 71st Edition (1990).
31. Cromer, D. T. and Waber, J. T., *International Tables for X-ray Crystallography*, Vol. 4, Table 2.2A, The Kynoch Press, Birmingham (1974).

Pergamon

PII: S0277-5387(97)00317-3

Polyhedron Vol. 17, No. 5–6, pp. 769–771, 1998
© 1998 Elsevier Science Ltd
All rights reserved. Printed in Great Britain
0277-5387/98 $19.00+0.00

Crystal and molecular structure of $[Li_3(\mu_2\text{-}OAr)_3]$ (OAr = 2,6-diphenyl-3,5-di-tert-butylphenoxide); a cluster containing short Li—O distances†

Jonathan S. Vilardo, Phillip E. Fanwick and Ian P. Rothwell*

Department of Chemistry, 1393 Brown Building, Purdue University, West Lafayette, IN 47907-1393, U.S.A.

(Received 23 April 1997; accepted 17 July 1997)

Abstract—Reaction of 2,6-diphenyl-3,5-di-*tert*-butylphenol (HOAr) with one equivalent of *n*-BuLi in toluene generates the hydrocarbon soluble cluster $[Li_3(\mu_2\text{-}OAr)_3]$ **1**. The molecular structure of **1** consists of a six-membered ring (crystallographically imposed C_3 axis) of Li and O(aryloxide) atoms with alternating Li—O distances of 1.78(1) and 1.840(7) Å. © 1998 Elsevier Science Ltd. All rights reserved

Keywords: crystal structure; molecular structure; $Li_3(\mu_2\text{-}OAr)_3$.

The structural chemistry of Group 1 metal compounds continues to attract considerable research attention [1]. This interest stems not only from the diverse structures adopted by these compounds but also by the recognition that the degree of aggregation of lithium reagents can strongly influence their reactivity [2]. In the case of lithium aryloxides the degree of oligomerization is sensitive to the steric nature of the phenoxide nucleus as well as the presence of Lewis bases. In the presence of THF the parent lithium phenoxide has been shown to adopt a hexameric structure $[(\mu_3\text{-}PhO)Li(THF)]_6$ in both the solid state (hexagonal prismatic) and solution (^{7}Li NMR) [3]. In contrast the lithium 2,6-di-*tert*-butylphenoxide forms the dinuclear $[Li(\mu_2\text{-}OC_6H_3Bu^t_2\text{-}2,6)(THF)]_2$ [4]. We have recently begun to investigate the transition metal chemistry of 3,5-disubstituted-2,6-diphenylphenoxides [5]. The presence of the *meta*-substituents severely reduces the tendency to undergo cyclometallation of the *ortho*-phenyl rings. In the case of 2,6-diphenyl-3,5-di-*tert*-butylphenoxide (the phenol first being synthesized by Barton *et al.* [6]) the bulky meta substituents render the ligand metallation

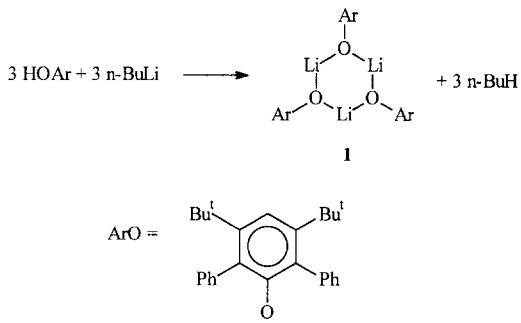

1

'immune' [5]. Furthermore they force the phenyl rings to adopt a conformation essentially perpendicular to the central phenoxide ring leading to a bulkier phenoxide ligand. In this note we report on the structure of the lithium derivative of this bulky phenol.

RESULTS AND DISCUSSION

The addition of a hexane solution of *n*-butyl lithium to a benzene solution of 2,6-diphenyl-3,5-di-*tert*-butylphenol (HOAr) [6] leads to a solution from which the lithium aryloxide **1** can be obtained as white crystals upon cooling a saturated toluene solution.

† Dedicated to Professor Don Bradley in recognition of his seminal contributions to metal alkoxide chemistry.

* Author to whom correspondence should be addressed.

The ^{1}H NMR spectrum of **1** in C_6D_6 shows a single set of aryloxide proton resonances. The molecular structure of **1** determined by X-ray diffraction is shown in Fig. 1. The molecule adopts a trinuclear structure with a crystallographically imposed three-fold rotation axis making the three lithium atoms and aryloxide ligands equivalent. The lithium atoms in **1** are formally two coordinate with C(22) and C(21) of the *ortho*-phenyl rings at distances of 2.478(8) and 2.689(8) Å. The presence of lithium bonds to unsaturated and saturated carbon fragments is an important characteristic of many lithium aggregates that typically do not contain Lewis bases [2c]. There is a distinct asymmetry to the aryloxide bridges in **1** as shown by the Li—O distances of 1.775(7), 1840(8) Å and Li—O—C angles of 113.8(3), 134.9(3)°. The short Li—O distance represents the shortest value for this parameter for a phenoxide bound to lithium.

In Table 1 are listed the molecular structures and Li-O(aryloxide) distances for lithium phenoxides contained in the Cambridge Crystallographic Database [3,4,7–18]. It can be seen that the two previously characterized trinuclear structures both contain 4-coordinate lithium atoms with the metal being chelated by the nitrogen atoms of amine or imine functionalities contained in the ortho positions of the phenoxide. The closest structural analogues to **1** are in fact the trimeric lithium amido compounds $[Li\{N(SiMe_3)_2\}]_3$ [19] and $[Li\{N(CH_2Ph)_2\}]_3$ [20] which contain a six membered ring of alternating Li and N(amido) atoms.

EXPERIMENTAL

All operations were carried out under a dry nitrogen atmosphere in a vacuum atmospheres Dri-Lab or by standard Schlenk Techniques. The hydrocarbon solvents were distilled from sodium benzophenone and stored under nitrogen until needed. 2,6-diphenyl-3,5-di-*tert*-butylphenol was made by a previous reported method [6] ^{1}H NMR spectra were recorded on a Varian Associates Gemini-200 spectrometer and referenced to protio impurities of commercial C_6D_6. The

Table 1. Selected structural parameters for lithium aryloxides

Compound	Aryloxide	Li—O	Ref.
$[Li(OAr)(THF)]_6$ two crystalline forms; two chair Li_3O_3 rings stacked upon one another, 4-coord Li	μ_3-OC_6H_5	1.911(21)–1.990(22); 1.895(21)–1.992(22)	[3]
$[Li(OAr)(THF)]_4(HOAr)$ distorted cube with one edge opened up by bridging phenol ligand, 4-coord Li	μ_3-OC_6H_5	1.91(2)–2.05(2)	[7]
$[Li(OAr)(NMC)]_4$ regular cube, 4-coord Li	μ_3-OC_6H_5	1.88(2)–2.00(2)	[8]
$[Li_4(OAr)_3(NCS)(HMPA)_4]$ cube, 4-coord Li, bridging HMPA, terminal NCS	μ_3-OC_6H_5	1.89(2)–2.02(2)	[9]
$[Li_4(OAr)_2(I)_2]$ cube 4-coord Li	μ_3-$OC_6H_2(CH_2NMe_2)_2$-2,6-Me-4	1.903(7)–1.934(9)	[10]
$[Li(OAr)]_4Li_4O_4$ cube, 4-coord Li, with sodiated methyl groups; Na atoms interact with phenoxide groups	μ_4-$OC_6H_2\{CH_2Na(TMEDA)\}$-2-Me_2-4,6	1.97(2) (av.)	[11]
$[Li(OAr)]_3$ planar Li_3O_3 ring, 4-coord Li	μ_2-$OC_6H_2(CH{=}NPr^i)_2$-2,6-Me-4	1.85(2)–1.90(3)	[12]
$[Li(OAr)]_3$ planar Li_3O_3 ring, 4-coord Li	μ_2-$OC_6H_2(CH_2NMe_2)_2$-2,6-Me-4	1.846(9)–1.887(9)	[13]
$[Li(OAr)(OEt_2)]_2$ planar Li_2O_2 ring, 3-coord Li	μ_2-$OC_6H_2Bu^t_2$-2,6-Me-4	1.849(11), 1.867(10)	[14]
$[Li(OAr)(OEt_2)]_2$ planar Li_2O_2 ring, 3-coord Li	μ_2-$OC_6H_2Bu^t_2$-2,6	1.828(7), 1.867(7)	[4]
$[Li(OAr)(OEt_2)]_2$ planar Li_2O_2 ring, 3-coord Li	μ_2-$OC_6H_3Bu^t_2$-2,6	1.830(7), 1.880(7)	[15]
$[(18\text{-crown-6})Li_2(OAr)_2]$ planar Li_2O_2 ring, 5-coord Li	μ_2-OC_6H_5	1.855(12)–1.895(12)	[16]
$[(15\text{-crown-5})Li_4(OAr)_4]$ two crystalline forms, 4- and 6-coord Li	μ_2-OC_6H_5	1.836(9)–1.939(8)	[17]
$[(\text{cyclohexano-15-crown-5})_2Li_4(OAr)_4]$ 4- and 6-coord Li	μ_2-OC_6H_5	1.859(8)–1.910(8)	[18]

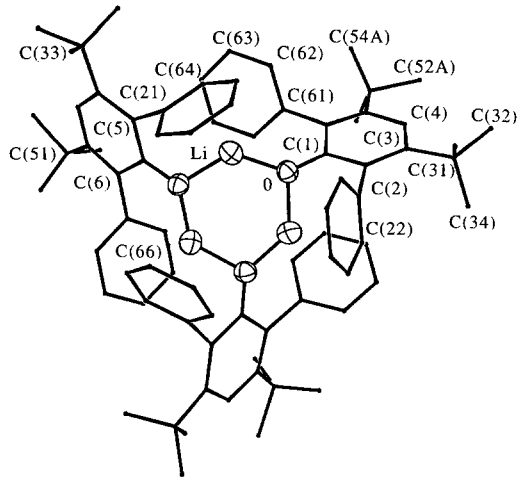

Fig. 1. Molecular structure of **1** showing the atomic numbering scheme. Selected bond lengths (Å) and angles ( ): Li—O 1.775(7), Li—O 1.840(8), O—Li—O 129.7(4), Li—O—Li 110.0(4), Li—O—C(1) 113.8(3), Li—O—C(1) 134.9(3).

X-ray diffraction study was carried out 'in house' at Purdue University.

Lithium-2,6-*diphenyl*-3,5-*di*-tert-*butylphenoxide* $[Li_3(OAr)_3]$ **1**

To a 100 cm^3 round bottom flask containing a suspension of 2,6-diphenyl-3,5-di-*tert*-butylphenol (5.0 g, 14 mmol) in toluene (50 cm^3) was added 2.5 molar *n*-butyllithium in hexane (5.6 cm^3, 14 mmol). The reaction mixture was stirred at room temperature for 1 h and the solvent removed *in vacuo* to give an off-white powder. Recrystallization of the resulting crude solid from toluene afforded colorless crystals which were washed with hexane and dried *in vacuo* to yield 3.0 g (60%). Anal. calcd for $C_{26}H_{29}OLi$: C, 85.69; H, 8.02. Found: C, 85.39; H, 8.17. ^1H NMR (C_6D_6, 30 °C): δ 6.85–7.3 (m, aromatics, 11H), 1.34 (s, Bu^t, 18H).

Acknowledgment—We thank the National Science Foundation (Grant CHE-9700269) for financial support of this research.

REFERENCES

1. (a) Sapse, A.-M. and Schleyer, P. v. R., ed. *Lithium Chemistry*. Wiley, New York, 1995; (b) Mulvey, R. E., *Chem. Soc. Rev.*, 1991, **20,** 167.
2. (a) Collum, D. B., *Acc. Chem. Res.*, 1992, **25,** 448; (b) Gregory, K., Schleyer, P. v. R. and Snaith, R., *Adv. Inorg. Chem.*, 1991, **37,** 47; (c) Goldfuss, B., Schleyer, P. v. R. and Hampel, F., *J. Am. Chem. Soc.*, 1996, **118,** 12,183 and refs therein.
3. Jackman, L. M., Cizmeciyan, D., Williard, P. G. and Nichols, M. A., *J. Am. Chem. Soc.*, 1993, **115,** 6262.
4. Huffman, J. C., Geerts, R. L. and Caulton, K. G., *J. Cryst. Spectrosc.*, 1984, **14,** 541.
5. (a) Lockwood, M. A., Clark, J. R., Parkin, B. C., Fanwick, P. E. and Rothwell, I. P., *J. Chem. Soc., Chem. Commun.*, 1996, 1973; (b) Vilardo, J. S., Lockwood, M. A., Hanson, L. G., Clark, J. R., Parkin, B. C., Fanwick, P. E. and Rothwell, I. P., *J. Chem. Soc., Dalton Trans.*, 1997, 3353.
6. Barton, D. H. R., Donnelly, D. M. X., Guiry, P. J. and Reibenspies, J. H., *J. Chem. Soc., Chem. Commun.*, 1990, 1110.
7. Pink, M., Zahn, G. and Sieler, J., *Z. Anorg. Allg. Chem.*, 1994, **620,** 749.
8. Walther, D., Ritter, U., Gessler, S., Sieler, J. and Kunert, M., *Z. Anorg. Allg. Chem.*, 1994, **620,** 101.
9. Raithby, P. R., Reed, D., Snaith, R. and Wright, D. S., *Angew. Chem., Int. Ed. Engl.*, 1991, **30,** 1011.
10. van der Schaaf, P. A., Hogerheide, M. P., Grove, D. M., Spek, A. L. and van Koten, G., *J. Chem. Soc., Chem. Comm.*, 1992, 1703.
11. Harder, S. and Streitwieser, A., *Angew. Chem., Int. Ed. Engl.*, 1993, **32,** 1066.
12. Korobov, M. S., Minkin, V. I., Nivorozhkin, L. E., Kompan, O. E. and Struchkov, Yu. T., *Zh. Obshch. Khim.*, 1989, **50,** 429.
13. van der Schaaf, P. A., Jastrzebski, J. T. B. H., Hogerheide, M. P., Smeets, W. J. J., Spek, A. L., Boersma, J. and van Koten, G., *Inorg. Chem.*, 1993, **32,** 4111.
14. Cetinkaya, B., Gumrukcu, I., Lappeter, M. F., Atwood, J. L. and Shakir, R., *J. Am. Chem. Soc.*, 1980, **102,** 2086.
15. Kociok-Kohn, G., Pickardt, J. and Schumann, H., *Acta Cryst., Sect. C (Cr. Str. Comm.)*, 1991, **47,** 2649.
16. Watson, K. A., Fortier, S., Murchie, M. P., Bovenkamp, J. W., Rodrigue, A., Buchanan, G. W. and Ratcliffe, C. I., *Can. J. Chem.*, 1990, **68,** 1201.
17. Murchie, M. P., Bovenkamp, J. W., Rodrigue, A., Watson, K. A. and Fortier, S., *Can. J. Chem.*, 1988, **66,** 2515.
18. Watson, K. A., Fortier, S., Murchie, M. P. and Bovenkamp, J. W., *Can. J. Chem.*, 1991, **69,** 687.
19. Barr, D., Clegg, W., Mulvey, R. E. and Snaith, R., *J. Chem. Soc., Chem. Commun.*, 1984, 285.
20. Mootz, Von D., Zinnius, A. and Bottcher, B., *Angew Chem.*, 1969, **81,** 398.

Pergamon

PII: S0277-5387(97)00316-1

Polyhedron Vol. 17, No. 5–6, pp. 773–779, 1998
© 1998 Elsevier Science Ltd
All rights reserved. Printed in Great Britain
0277-5387/98 $19.00+0.00

'1,3-Dimetallabenzene' derivatives of niobium and tantalum

Patrick N. Riley, Robert D. Profilet, Michelle M. Salberg, Phillip E. Fanwick and Ian P. Rothwell*

Department of Chemistry, 1393 Brown Building, Purdue University, West Lafayette, IN 47907-1393, U.S.A.

(Received 23 April 1997; accepted 17 July 1997)

Abstract—The alkylidyne bridged compounds $[(cb)_2M(\mu\text{-}CSiMe_3)_2M(cb)_2]$ (**1a**, M = Nb; **1b**, M = Ta; cb = carbazole) react thermally with one equivalent of alkynes EtC≡CEt and $Me_3SiC{\equiv}CH$ to produce new organometallic derivatives **2** and **3**, respectively. The molecular structures of **2** and **3** are shown to consist of non-planar six-membered di-metallacycles originating from insertion of an alkyne unit into one of the alkylidyne bridges of **1**. Treatment of **1b** with 3,5-di-*tert*-butyl-2,6-diphenylphenol (ArOH) leads to the monophenoxide $[(ArO)(cb)Ta(\mu\text{-}CSiMe_3)_2Ta(cb)_2]$ **4**. Treatment of **4** with $Me_3SiC{\equiv}CH$ leads to the corresponding metallacycle $[(ArO)(cb)Ta(\mu\text{-}CSiMe_3)\{\mu\text{-}C(SiMe_3)CHC(SiMe_3)\}Ta(cb)_2]$ **5**. Structural parameters for **2b**, **3a**, **3b** and **5** obtained by X-ray diffraction show delocalization is present with four equivalent M—C and two equivalent C—C distances. The non-planar structure is best described as a twist of the planar [M(μ-C)—M] and [C—C—C] units within the ring. The non-planar structure of **2a** and **2b** is maintained in solution as evidenced by diastereotopic methylene protons for the CH_2CH_3 substituents. At elevated temperatures coalescence to a simple A_2B_3 pattern is observed. From the coalescence temperatures of 328 K for **2b** an activation barrier of 16.1(5) kcal mol^{-1} can be estimated for the adoption of a planar structure. The insertion of $Me_3SiC{\equiv}CH$ produces a 2,4,6-substitution pattern for **3a**, **3b** and **5** with the 5-H (*beta* to two metal centers) being downfield shifted to δ 8.43 (**3a**), 8.64 (**3b**) and 9.03 ppm (**5**). © 1998 Elsevier Science Ltd. All rights reserved

Keywords: niobium; tantalum; alkylidyne bridged compounds.

Metallacyclic compounds of the transition metals are an important class of organometallic species [1]. This is particularly the case where such compounds represent intermediates in catalytic cycles [2]. In a number of cases metallacyclic compounds exhibit properties that are derived directly from their cyclic nature. One important subset of such molecules are those deemed to possess aromatic character [3]. The work of Bleeke *et al.* has led to the generation of iridacycles whose structure and reactivity make a compelling case for being considered iridabenzenes [3]. During our investigation of the Group 5 metal chemistry of carbazole ligands we have isolated a series of dimetallacyclic compounds and in this paper we discuss the structure and reactivity of these molecules that can potentially be considered '1,3-dimetallabenzenes' [4].

RESULTS AND DISCUSSION

Synthesis of compounds

The alkylidyne bridged compounds $[(cb)_2M(\mu\text{-}CSiMe_3)_2M(cb)_2]$ (**1a**, M = Nb; M = Ta, **1b**; cb = carbazole) [5] are only sparingly soluble in cold hydrocarbon solvents yielding blue and red solutions, respectively. When C_6D_6 solutions of **1** and excess 3-hexyne or $Me_3SiC{\equiv}CH$ are heated at 100°C a slow (monitored by ^1H NMR) conversion to much more soluble organometallic derivatives takes place. The resulting products have been characterized as arising from insertion of 1 equiv. of alkyne into a single alkylidyne bridge (Scheme 1). The new compounds **2** and

* Author to whom correspondence should be addressed.

† Dedicated to Professor Don Bradley in recognition of his seminal contributions to metal amide chemistry.

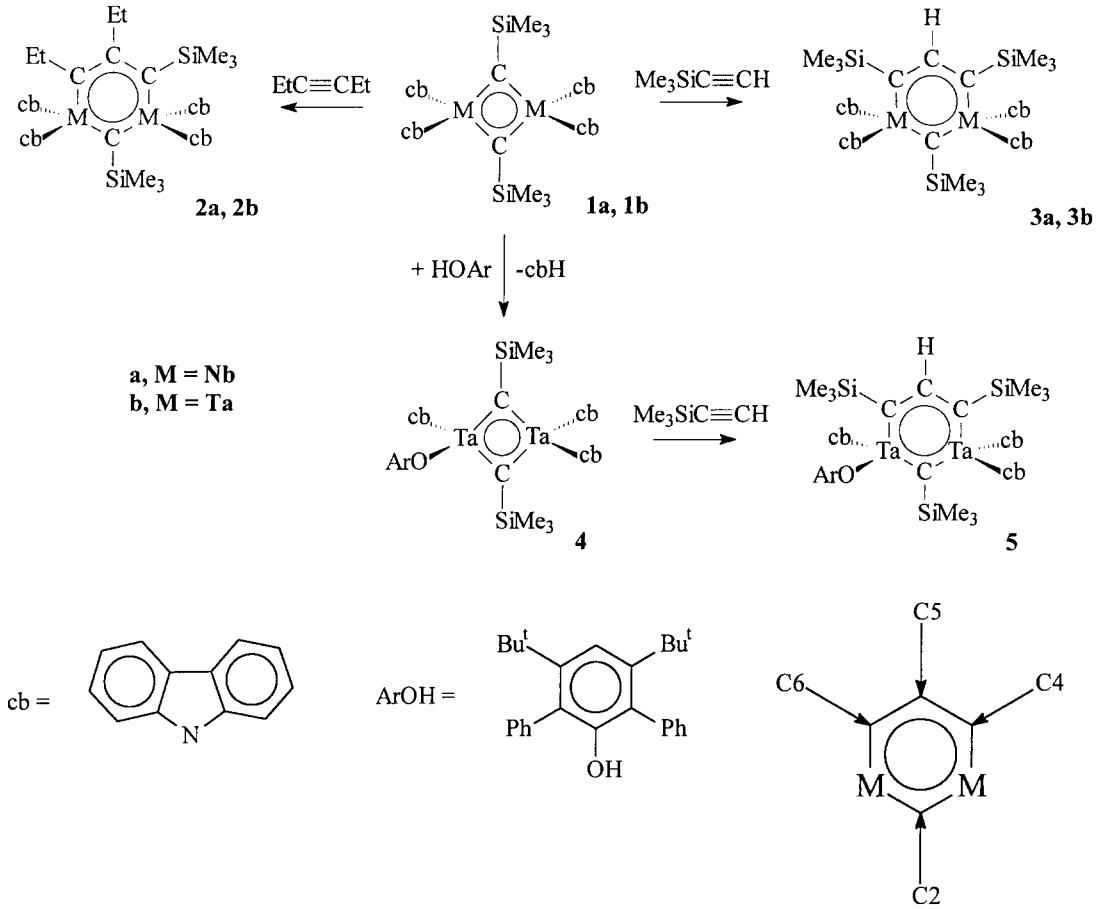

Scheme 1.

3 can be obtained crystalline from toluene or benzene solutions layered with hexane.

Attempts to obtain analogous compounds starting with the previously reported compound $[(Ph_2\text{-}2,6\text{-}C_6H_3O)_2Ta(\mu\text{-}CSiMe_3)_2Ta(OC_6H_3Ph_2\text{-}2,6)_2]$ [6] failed. The dark green tetra-phenoxide did not react with $Me_3SiC{\equiv}CH$ in C_6D_6 solution when heated at 100°C for days. The addition of the bulky, metallation immune phenol 3,5-di-*tert*-butyl-2,6-diphenylphenol (HOAr) [7,8] to benzene solutions of **1b** was found to lead to the clean formation of a soluble, monophenoxide $[(ArO)(cb)Ta(\mu\text{-}CSiMe_3)_2Ta(cb)_2]$ **4** and 1 equiv. of carbazole. This compound does react with one equivalent of $Me_3SiC{\equiv}CH$ to produce the corresponding dimetallacycle $[(ArO)(cb)Ta(\mu\text{-}CSiMe_3)\{\mu\text{-}C(SiMe_3)CHC(SiMe_3)\}Ta(cb)_2]$ **5**.

Solid state structures

The derivatives **2b, 3a, 3b** and **5** have been subjected to single crystal X-ray diffraction analysis. The molecular structures of **2b** and **3a** are shown in Figs 1 and 2. The tantalum complex **3b** (benzene solvate) is isomorphous and isostructural with **3a** (toluene solvate) and selected structural parameters are given in Tables 1 and 2. The molecular structure of **5** is shown in Fig. 3 with structural parameters contained in Table 3. The most noticeable feature of the molecular structures is the non-planarity of the six-membered ring. This distortion is most succinctly defined by the angle θ between the two planes defined by the [MCM] and [CCC] atoms within the six-membered ring. The carbon fragment and the atoms directly bound to it form a planar unit. The substituent to the carbon atom C(2) (Scheme 1) is also in the same plane as the [MC(2)M] unit. For the four molecules structurally characterized the value of θ lies in the narrow range 52–57 . The structures of **2b, 3** and **5** contrasts with that observed for the di-tungsten compound $[(Pr^iO)_2W(\mu\text{-}CSiMe_3)\{\mu\text{-}C(SiMe_3)CHC(SiMe_3)\}W(OPr^i)_2]$ **6** reported and analyzed a number of years ago by Chisholm and Heppert [9]. In d^1–d^1 **6** a much more severe distortion was observed leading to a structure best described as containing a dimetallated allyl ligand. Inspection of the interatomic distances for **2b, 3** and **5** (Fig. 4, Tables 1–3) show that the twisting does

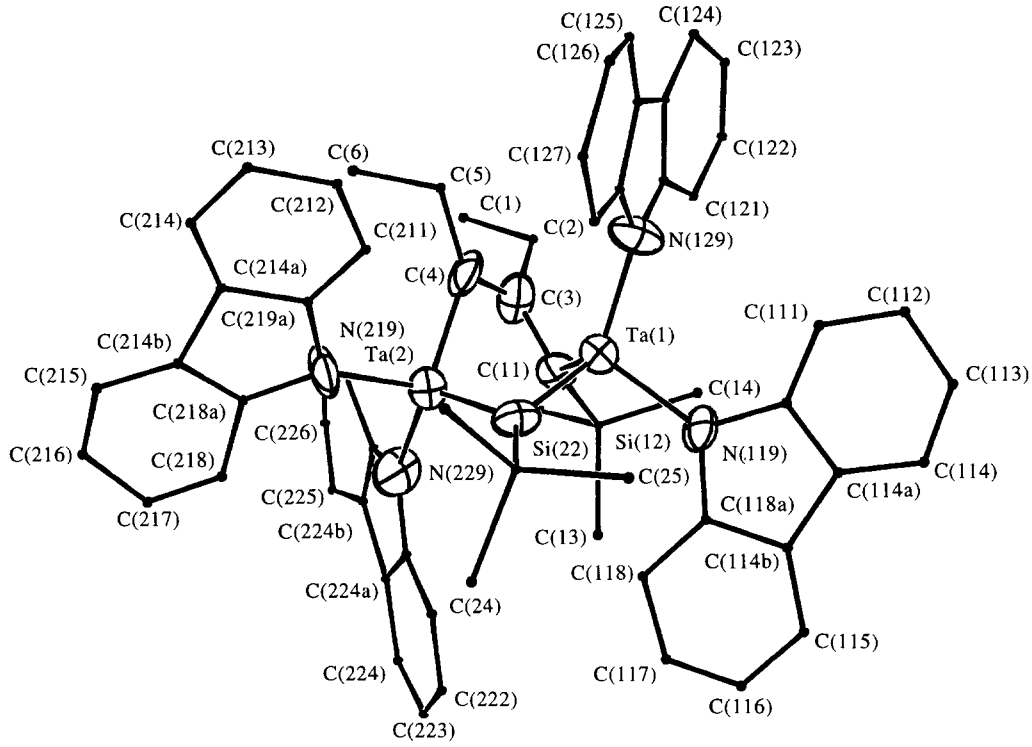

Fig. 1. Molecular structure of $[(cb)_2Ta(\mu\text{-}CSiMe_3)\{\mu\text{-}C(Et)C(Et)C(SiMe_3)\}Ta(cb)_2]$ **2b** showing the atomic numbering scheme.

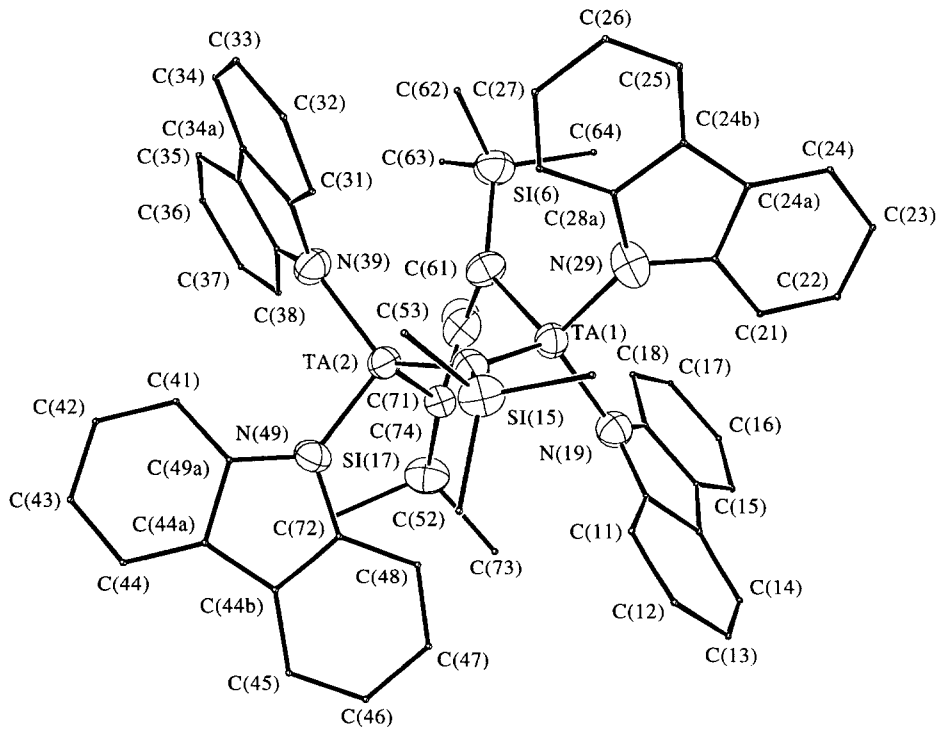

Fig. 2. Molecular structure of $[(cb)_2Ta(\mu\text{-}CSiMe_3)\{\mu\text{-}C(SiMe_3)CHC(SiMe_3)\}Ta(cb)_2]$ **3b** (benzene solvate) showing the atomic numbering scheme. An identical numbering scheme used for isostructural **3a** (toluene solvate).

Table 1. Selected bond distances (Å) and angles (°) for $[(cb)_2Ta(\mu\text{-}CSiMe_3)\{\mu\text{-}C(Et)C(Et)C(SiMe_3)\}Ta(cb)_2]$ **2b**

Ta(1)—Ta(2)	2.864(1)	Ta(1)—N(119)	2.03(1)
Ta(1)—N(129)	2.08(2)	Ta(2)—N(219)	2.02(1)
Ta(2)—N(229)	2.07(2)	Ta(1)—C(21)	1.99(2)
Ta(2)—C(21)	2.04(2)	Ta(1)—C(11)	2.11(2)
Ta(2)—C(4)	2.04(2)	C(3)—C(4)	1.48(3)
C(3)—C(11)	1.40(3)		

N(119)—Ta(1)—N(129)	105.8(7)	N(219)—Ta(2)—N(229)	104.9(7)
Ta(1)—C(21)—Ta(2)	90.5(7)	Ta(1)—C(11)—C(3)	93(1)
Ta(2)—C(4)—C(3)	98(1)	C(4)—C(3)—C(11)	119(2)

Table 2. Selected bond distances (Å) and angles (°) for $[(cb)_2M(\mu\text{-}CSiMe_3)\{\mu\text{-}C(SiMe_3)C(H)C(SiMe_3)\}M(cb)_2]$ (M = Nb, **3a**; Ta, **3b**)

	3a. C_7H_8	**3b.** C_6H_6
M(1)—M(2)	2.876(1)	2.8801(5)
M(1)—N(19)	2.048(8)	2.053(6)
M(1)—N(29)	2.052(9)	2.036(7)
M(2)—N(39)	2.046(7)	2.054(6)
M(2)—N(49)	2.047(8)	2.035(6)
M(1)—C(51)	1.975(9)	1.988(8)
M(1)—C(61)	2.03(1)	2.058(8)
M(2)—C(51)	2.026(9)	1.998(7)
M(2)—C(71)	2.04(1)	2.033(7)
C(61)—C(67)	1.41(1)	1.41(1)
C(67)—C(71)	1.40(1)	1.42(1)
N(19)—M(1)—N(29)	107.2(4)	106.8(3)
N(39)—M(2)—N(49)	106.7(3)	106.1(3)
M(1)—C(51)—M(2)	91.5(4)	92.5(3)
M(1)—C(61)—C(67)	95.8(6)	95.3(5)
M(2)—C(71)—C(67)	93.0(6)	93.1(5)
C(61)—C(67)—C(71)	121.3(9)	124.9(7)

bring C(4) to within 2.5–2.7 Å of the second metal center. This distance is, however, much longer than typically found for alkyl groups bound to Nb, Ta and also exceeds the distance to π-bound carbon groups such as η^6-arene ligands attached to these metal centers [10]. We, therefore, conclude that this is a non-bonding contact. Within the six-membered ring there is little structural evidence for localization of the bonding. The M—C(2) distances scan the narrow range of 1.975(9)–2.04(2) Å, negligibly longer than those found for the alkylidyne bridges in the 1,3-dimetallacyclobutadiene substrates **1a** and **1b**, 1.948(4)–1.971(3) Å. The M—C(4) and M—C(6) distances are comparable to each other in all four structures, 2.03(1)–2.11(2) Å, and only slightly longer than these distances. The C(4)—C(5) and C(5)—C(6) distances of 1.40(3)–1.48(3) Å are slightly longer than the value of 1.39 Å typically quoted for benzene [11].

The M—N distances to the carbazole ligands are 2.02(1)–2.08(2) Å, indistinguishable from values of 2.021(4)–2.065(2) Å found in **1a, 1b** [5]. Similarly, the orientation of the wedge shaped carbazole ligands is very similar to that observed in **1a, 1b** and a series of isocyanide derivatives [5]. The presence of the aryloxide ligand in **5** does not appear to dramatically affect the bonding of the adjoining carbazole ligand.

Solution structure and fluxionality

The ^{1}H NMR spectra of the 3-hexyne derivatives **2a** and **2b** are highly informative. The non-equivalent ethyl groups lead to two resolvable sets of multiplets. The non-planar structure yields a well-resolved ABX_3 pattern for one of the CH_2CH_3 groups while the other group [presumably attached to C(5)] is close to an A_2X_3 pattern. The presence of diastereotopic methylene protons for the C(6)-ethyl substituent confirms a non-planar structure is maintained in solution. As the temperature of a sample of **2b** in toluene-d_8 is raised, the diastereotopic methylene protons broaden and eventually coalescence at 55°C. From the coalescence temperature an activation barrier of 16.1(5) Kcal mol^{-1} is estimated. This barrier represents the energy loss on forming a planar structure for **2b**; i.e. the barrier to interconversion of the two enantiomers of **2b**.

The most interesting feature of the ^{1}H NMR of the 2,4,6-tris(trimethysilyl) derivative **3** and **5** is the chemical shift of the resonance for the proton C(5)—*H*. This appears as a singlet at δ 8.43, 8.64 and 9.03 ppm for **3a, 3b** and **5**, respectively. This particular proton is β-to two metal centers which may account for its low field position. These chemical shifts do compare with a value of δ 8.48 ppm for the β-proton in the vinyl ligand in $[Ta(OC_6H_3Bu^t\text{-}CMe_2CH_2)(OC_6H_3Bu^t_2\text{-}2,6)(Cl)(CH{=}CHPh)]$, [12] implying that there may be little ring current present in these compounds.

EXPERIMENTAL

All operations were carried out under a dry nitrogen atmosphere or *in vacuo* either in a Vacuum Atmo-

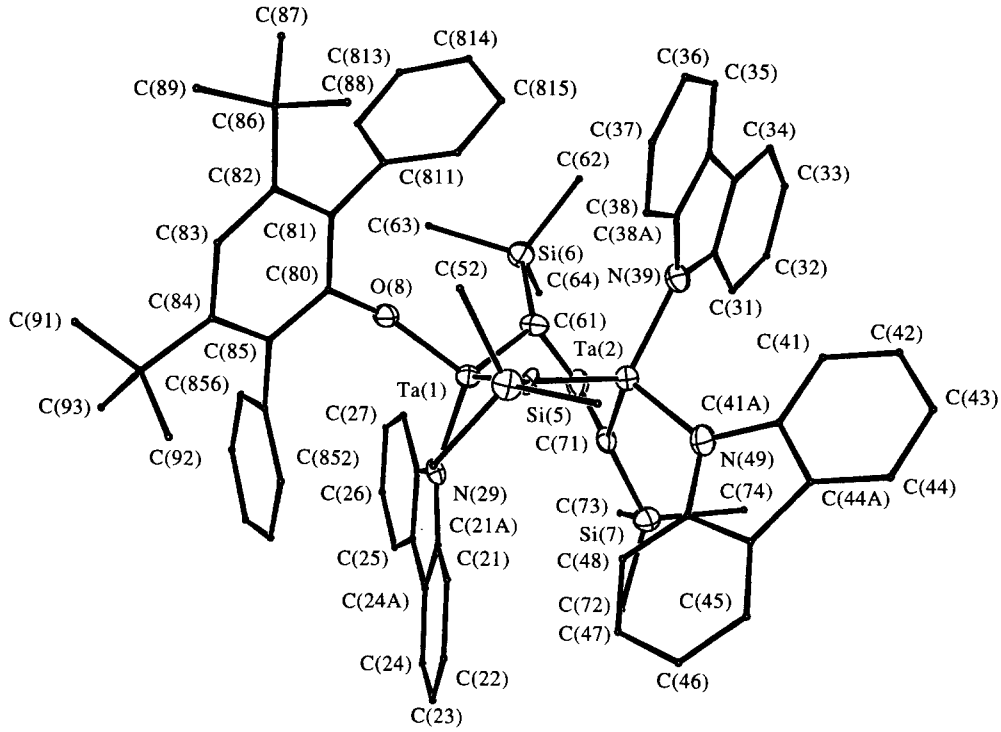

Fig. 3. Molecular structure of $[(ArO)(cb)Ta(\mu\text{-}CSiMe_3)\{\mu\text{-}C(SiMe_3)CHC(SiMe_3)\}Ta(cb)_2]$ **5** showing the atomic numbering scheme.

Table 3. Selected bond distances (Å) and angles (°) for $[(ArO)(cb)Ta(\mu\text{-}CSiMe_3)\{\mu\text{-}C(SiMe_3)C(H)C(SiMe_3)\}Ta(cb)_2]$ **5**

Ta(1)—Ta(2)	2.9592(7)	Ta(1)—O(8)	1.887(4)
Ta(1)—N(29)	2.064(5)	Ta(2)—N(39)	2.040(6)
Ta(2)—N(49)	2.041(6)	Ta(1)—C(50)	1.989(6)
Ta(2)—C(50)	2.005(6)	Ta(1)—C(61)	2.032(7)
Ta(2)—C(71)	2.031(6)	C(61)—C(67)	1.43(1)
C(71)—C(67)	1.42(1)		

O(8)—Ta(1)—N(29)	110.1(2)	N(39)—Ta(2)—N(49)	103.2(2)
Ta(1)—C(50)—Ta(2)	95.6(3)	C(50)—Ta(1)—C(61)	102.9(3)
C(50)—Ta(2)—C(71)	103.1(3)	Ta(1)—C(61)—C(67)	115.2(5)
Ta(2)—C(71)—C(67)	96.3(4)	C(61)—C(67)—C(71)	126.9(6)
Ta(1)—O(8)—C(80)	150.7(4)		

sphere Dri-Lab or by standard Schlenk techniques. Hydrocarbon solvents were dried by distillation from sodium/benzophenone and stored under dry nitrogen. Trimethylsilylacetylene and 3-hexyne were purchased from Aldrich Chemical Company and dried over molecular sieves prior to use. The ligand 2,6-diphenol-3,5-di-*tert*-butylphenol was prepared according to a literature procedure [7]. The compounds $[(cb)_2M(\mu\text{-}CSiMe_3)_2M(cb)_2]$ (**1a**, M = Nb; **1b**, M = Ta) were obtained by previously published procedures [5]. The ^1H and ^{13}C NMR spectra were recorded on Varian Associates Gemini 200 and General Electric QE-300 spectrometers. Microanalyses were performed in-house at Purdue University.

Preparation of $[(cb)_2Nb(\mu\text{-}CSiMe_3)\{\mu\text{-}C(Et)C(Et)C(SiMe_3)\}Nb(cb)_2$ **2a**

To a toluene (20 cm^3) solution of $[(cb)_2Nb(\mu\text{-}CSiMe_3)_2Nb(cb)_2]$ **1a** (0.40 g, 0.40 mmol) was added 1 equiv. of 3-hexyne (0.03 g, 0.40 mmol). The solution was heated at 110°C for 72 h. The resulting solution was filtered and the filtrate dried *in vacuo* to leave a

dark red solid. This solid was washed with hexane and dried *in vacuo*. The residue was recrystallized from a concentrated solution of toluene layered with hexane. Yield = 0.16 g (0.15 mmol, 38%). ^{1}H NMR (C_6D_6, 30°C): δ −0.77 (s, SiMe_3); 0.33 (s, Nb_2CSiMe_3); 0.13, 0.81 (t, CH_2CH_3); 1.56, 2.32 (br, CH_2CH_3). ^{13}C NMR (C_6D_6, 30°C): δ 1.3 (SiMe_3); 5.6 (Nb_2CSiMe_3).

Preparation of [(cb)$_2$Ta(μ-CSiMe$_3$){μ-C(Et)C(Et)C(SiMe$_3$)}Ta(cb)$_2$] **2b**

To a toluene (20 cm^3) solution of [(cb)$_2$Ta(μ-CSiMe$_3$)$_2$Ta(cb)$_2$] **1b** (0.50 g, 0.42 mmol) was added 1 equiv. of 3-hexyne (0.04 g, 0.42 mmol). The solution was heated at 110°C for 72 h. The resulting solution was filtered and the filtrate dried *in vacuo* to leave a dark red solid. This solid was washed with hexane and dried *in vacuo*. The residue was recrystallized from a concentrated solution of toluene layered with hexane. Yield = 0.30 g (0.23 mmol, 55%). Anal. calcd for $Ta_2C_{62}H_{60}N_4Si_2$: C, 58.21; H, 4.73; N, 4.38. Found: C, 57.91; H, 4.77; N, 4.22. ^{1}H NMR (C_6D_6, 30°C): δ −0.75 (s, SiMe_3); 0.34 (s, Ta_2CSiMe_3); 0.21, 0.84 (t, CH_2CH_3); 1.85, 2.40, 2.68 (br, CH_2CH_3); 6.59 (t, cb *meta-H*); 8.71 (d, cb *ortho-H*). ^{13}C NMR (C_6D_6, 30°C): δ 1.4 (SiMe_3); 6.7 (Ta_2CSiMe_3); 16.0 (CH_2CH_3); 27.2, 27.7 (CH_2CH_3); 253.9 (C*C*SiMe$_3$); 257.3 (C*C*Et); 393.0 (Ta$_2$-μ—*C*SiMe$_3$).

Preparation of [(cb)$_2$Nb(μ-CSiMe$_3$){μ-C(SiMe$_3$)CHC(SiMe$_3$)}Nb(cb)$_2$] **3a**

To a toluene (15 cm^3) solution of [(cb)$_2$Nb(μ-CSiMe$_3$)$_2$Nb(cb)$_2$] **1a** (0.25 g, 0.24 mmol) was added an excess of Me$_3$SiC≡CH (0.12 g, 1.22 mmol). The solution was heated at 110°C for 20 h. The resulting solution was filtered and the filtrate dried *in vacuo* to leave a dark red solid. This solid was washed with hexane and dried *in vacuo*. The residue was recrystallized from a concentrated solution of toluene layered with hexane. Yield = 0.04 g (0.04 mmol, 15%). ^{1}H NMR (C_6D_6, 30°C): δ −0.70 (s, SiMe_3); 0.07 (s, Nb_2CSiMe_3); 8.43 (s, C(5)-*H*); 8.60 (d, cb *ortho-H*). ^{13}C NMR (C_6D_6, 30°C): δ 0.10 (SiMe_3); 5.8 (Nb_2-μ-CSiMe_3); 267.9 (Nb*C*SiMe_3).

Preparation of [(cb)$_2$Ta(μ-CSiMe$_3$){μ-C(SiMe$_3$)CHC(SiMe$_3$)}Ta(cb)$_2$] **3b**

To a toluene (15 cm^3) solution of [(cb)$_2$Ta(μ-CSiMe$_3$)$_2$Ta(cb)$_2$] (0.10 g, 0.08 mmol) was added as excess of Me$_3$SiC≡CH (0.15 g, 1.83 mmol). The solution was heated at 110°C for 18 h. The resulting solution was filtered and the filtrate dried *in vacuo* to leave a dark red solid. This solid was washed with hexane and dried *in vacuo*. The residue was recrystallized from a concentrated solution of toluene layered with hexane. Yield = 0.02 g (0.02 mmol, 20%). Anal. calcd for $Ta_2C_{61}H_{60}N_4Si_3 \cdot C_7H_8$: C, 58.87; H, 4.94; N, 4.04. Found: C, 58.13; H, 5.03; N, 4.00. Crystals suitable for X-ray diffraction were obtained from a benzene solution layered with hexane. ^{1}H NMR (C_6D_6, 30°C): δ −0.63 (s, SiMe_3); 0.14 (s, Ta_2CSiMe_3); 8.64 (s, C(5)-*H*); 8.73 (d, cb *ortho-H*). ^{13}C NMR (C_6D_6, 30°C): δ −0.30 (SiMe_3); 5.6 (Ta_2-μ-CSiMe_3); 255.0 (Ta*C*SiMe$_3$); 386.5 (Ta_2-μ-*C*SiMe$_3$).

Preparation of [(ArO)(cb)Ta(μ-CSiMe$_3$)$_2$Ta(cb)$_2$], **4**

To a toluene (15 cm^3) solution of [(cb)$_2$Ta(μ-CSiMe$_3$)$_2$Ta(cb)$_2$] **1b** (0.50 g, 0.42 mmol) was added 2.2 equiv. of 2,6-diphenol-3,5-di-*tert*-butylphenol (0.33 g, 0.92 mmol). The solution was heated at 100°C for 6 d, then allowed to cool slowly during which time a yellowish-brown solid precipitated from solution. The solid was washed with hexane and dried *in vacuo*. Yield = 0.11 g (19%). Anal. calcd for $Ta_2C_{70}H_{71}N_3Si_2O$: C, 60.56; H, 5.15; N, 303. Found: 63.78; H, 5.06; N, 3.99. ^{1}H NMR (C_6D_6, 30°C): δ −0.18 (s, Ta_2CSiMe_3); 1.19 (s, C*C*Me$_3$). ^{13}C NMR (C_6D_6, 30°C): δ 5.32 (s, Ta$_2$-μ—CSiMe_3); 33.1 (CMe_3); 37.6 (*C*Me$_3$); 398.5 (Ta$_2$-μ-*C*SiMe$_3$).

Preparation of [(ArO)(cb)Ta(μ-CSiMe$_3$){μ-C(SiMe$_3$)CHC(SiMe$_3$)}Ta(cb)$_2$], **5**

To a C_6D_6 solution of [(OAr)(cb)Ta(μ-CSiMe$_3$)$_2$Ta(cb)$_2$] **4** (0.05 g, 0.04 mmol) was added one equiv. of Me$_3$SiC≡CH (0.004 g, 0.04 mmol). The solution was heated at 100°C for 96 h. The orange solution was filtered then layered with hexane producing yellow crystals of product which were washed with hexane and dried *in vacuo*. ^{1}H NMR (C_6D_6, 30°C): δ −0.79, −0.35 (s, SiMe_3); 0.53 (s, Ta_2CSiMe_3); 1.02, 1.12 (s, CCMe_3); 9.03 (s, C(5)-*H*). ^{13}C NMR (C_6D_6, 30°C): δ 0.45, 0.85 (SiMe_3); 7.77 (Ta$_2$-μ—CSiMe_3); 33.0, 33.6 (CCMe_3); 239.2 (Ta*C*SiMe$_3$); 361.1 (Ta$_2$-μ—*C*SiMe$_3$).

Crystallographic studies— Crystal data, data collection and experimental details of the crystallographic study are contained in the supplementary material.

Acknowledgment—We thank the National Science Foundation (Grant CHE-9700269) for financial support of this research.

REFERENCES

1. Collman, J. P., Hegedus, L. S., Norton, J. R. and Finke, R. G., In *Principles and Applications of Organotransition-Metal Chemistry*, Ch. 9. University Science Books, Mill Valley, CA, 1987.
2. Constable, E. C., *Polyhedron*, 1984, **3,** 1037.
3. Bleeke, J. R., *Acc. Chem. Res.*, 1991, **24,** 271.

4. Profilet, R. D., Fanwick, P. E. and Rothwell, I. P., *Angew, Chem., Int. Ed. Eng.*, 1992, **31,** 1261.
5. Riley, P. N., Profilet, R. D., Fanwick, P. E. and Rothwell, I. P., *Organometallics*, 1996, **15,** 5502.
6. Fanwick, P. E., Ogilvy, A. E. and Rothwell, I.P., *Organometallics*, 1987, **6,** 73.
7. Barton, D. H. R., Donnelly, D. M. X., Guiry, P. J. and Reibenspies, J. H., *J. Chem. Soc., Chem. Commun.*, 1990, 1110.
8. Vilardo, J. S., Lockwood, M. A., Hanson, L. G., Clark, J. R., Parkin, B. C., Fanwick, P. E. and Rothwell, R. P., *J. Chem. Soc., Dalton Trans.*, 1997, 3353.
9. Chisholm, M. H., Huffman, J. C. and Heppert, J. A., *J. Am. Chem. Soc.*, 1985, **107,** 5116.
10. Wexler, P. A., Wigley, D. E., Koerner, J. B. and Albright, T. A., *Organometallics*, 1991, **10,** 2319.
11. Morrison, R. T. and Boyde, R. N., *Organic Chemistry*, 5th edn. Allyn and Bacon, Boston, 1987.
12. Clark, J. R. and Rothwell, I. P., to be published.

Pergamon

PII: S0277-5387(97)00311-2

Polyhedron Vol. 17, No. 5–6, pp. 781–790, 1998
© 1998 Elsevier Science Ltd
All rights reserved. Printed in Great Britain
0277-5387/98 $19.00+0.00

Preparation of volatile molecular lithium–niobium alkoxides. Crystal structures of $[Nb(\mu\text{-}OCH_2SiMe_3)(OCH_2SiMe_3)_4]_2$ and $[LiNb(\mu_3\text{-}OCH_2SiMe_3)\text{-}(\mu_2\text{-}OCH_2SiMe_3)_2(OCH_2SiMe_3)_3]_2$†

Subhash C. Goel, Jennifer A. Hollingsworth, Alicia M. Beatty, Kerry D. Robinson, and William E. Buhro*

Department of Chemistry, Washington University, St. Louis, Missouri 63130-4899, U.S.A.

(Received 29 May 1997; accepted 9 July 1997)

Abstract—New heterometallic alkoxides $[LiNb(OCH_2CMe_3)_6]_2$ (**4**), $LiNb(OCH_2CMe_3)_6(Me_3CCH_2OH)_2$ (**5**), and $[LiNb(OCH_2SiMe_3)_6]_2$ (**6**) have been prepared from the corresponding homometallic alkoxides. All are moderately soluble in hydrocarbons and sublime in moderate to good recoveries. The structure of **6** determined crystallographically contains an $Nb_2Li_2(\mu\text{-}O)_4(\mu_3\text{-}O)_2$ central-core geometry. Compound **4** appears to be isostructural on the basis of ^1H NMR data. Bulk pyrolysis of **4** gives crystalline $LiNbO_3$ under N_2 at 600°C. However, $LiNbO_3$ films are not obtained from **4** by spray MOCVD under conditions that give $LiNbO_3$ films from $[LiNb(OEt)_6]_x$. Crystallographic structure determination for the precursor compound $[Nb(\mu\text{-}OCH_2SiMe_3)(OCH_2SiMe_3)_4]_2$ (**3**) reveals an edge-shared bioctahedral geometry in which the μ-O atoms are distinctly pyramidal. This structure is maintained in solution; the pyramidal bridge configurations allow coexistence of syn and anti dimeric isomers. Precursor **3** also exhibits a dimer-monomer equilibrium for which $\Delta H = 63(3)$ kJ/mol and $\Delta S = 180(10)$ J/(K mol). © 1998 Elsevier Science Ltd. All rights reserved

Keywords: preparation; volatile; double alkoxide; crystal structure; dynamic behavior; precursor.

Herein we report the first *molecular* lithium–niobium (double) alkoxides of empirical formula $LiNb(OR)_6$. Unlike known *nonmolecular* lithium–niobium alkoxides [1,2], the new compounds are soluble in hydrocarbon solvents and sublime intact (*in vacuo*). On the basis of these characteristics, the new $LiNb(OR)_6$ derivatives may be useful lithium niobate ($LiNbO_3$) precursors [3].

Bradley and others have established the utility of alkoxide precursors to oxide materials by sol–gel processing (SGP) and metallo–organic chemical vapor deposition (MOCVD) [3–6]. Problems are often encountered with heterometallic alkoxides such as those from the $LiNb(OR)_6$ family. Although the known $LiNb(OR)_6$ compounds (R = Me, Et, *i*-Pr, *t*-Bu) [1] are sufficiently soluble in their respective parent alcohols for SGP of $LiNbO_3$ films, they dissociate to LiOR and $Nb(OR)_5$ upon volatilization, precluding $LiNbO_3$ growth by standard MOCVD [1,3].

The poor volatiles and hydrocarbon solubilities of $LiNb(OR)_6$ compounds are likely due to nonmolecular solid-state structures. $[LiNb(OEt)_6]_x$ is a helical polymer in the solid state, in which polymerization is achieved through μ-alkoxide bridges [2]. To our knowledge no other $[LiNb(OR)_6]_x$ compound has been structurally characterized (until now); however, the others likely exhibit related nonmolecular structures with extensive alkoxide bridging. Nonmolecularity limits the performance of alkoxide compounds as oxide precursors [5,7].

Despite these shortcomings, Wernberg, Gysling, and Braunstein *were* able to grow epitaxial $LiNbO_3$ by *spray* MOCVD using $[LiNb(OEt)_6]_x$ [8,9]. In spray

† This paper is dedicated to Professor Donald C. Bradley in honor of his pioneering contributions to inorganic and materials chemistry, and on the occasion of his 73rd birthday.

* Author to whom correspondence should be addressed; buhro@wuchem.wustl.edu.

MOCVD a precursor *solution* is misted, evaporated, and the resulting dispersed precursor is rapidly vaporized just before entry into the film-deposition zone. This precursor-introduction method allows modestly volatile precursors to be effectively employed (volatilized), here without prior dissociation of the Li and Nb components. Wernberg and Gysling obtained precursor solutions of $[LiNb(OEt)_6]_\infty$ in toluene after long stirring periods (48 h), during which depolymerization of the nonmolecular structure apparently occurred [8]. We sought to improve the solubility and volatility of $[LiNb(OR)_6]_x$ precursors to increase the convenience of the spray MOCVD process and to determine if such enhancements increase the quality of the deposited $LiNbO_3$ films. We also sought to examine the MOCVD performance of alkoxides lacking H atoms β to oxygen.

We report that the new molecular derivatives $[LiNb(OR)_6]_2$ where R = CH_2CMe_3 and CH_2SiMe_3 dissolve rapidly and sublime *in vacuo* in moderate recoveries. The dimeric molecular structure of $[LiNb(OCH_2SiMe_3)_6]_2$ has been determined crystallographically, and the two compounds (R = CH_2CMe_3 and CH_2SiMe_3) appear to be isostructural on the basis of solution-phase spectral data. We have also prepared an alcohol adduct of empirical formula $LiNb(OCH_2CMe_3)_6(Me_3CCH_2OH)_2$; this compound exhibits the highest sublimation recovery of the new $LiNb(OR)_6$ derivatives. Our unsuccessful efforts to use one of the compounds as an $LiNbO_3$ precursor by spray MOCVD are discussed.

In the course of the work $LiOCH_2CMe_3$, $LiOCH_2SiMe_3$, and $[Nb(OCH_2SiMe_3)_5]_2$ were isolated and fully characterized, the latter by single-crystal X-ray diffraction. We also report the dynamic NMR behavior of $Nb(OCH_2SiMe_3)_5$, which includes monomer–dimer equilibria and alkoxide–ligand site exchange.

EXPERIMENTAL

General methods

All ambient-pressure procedures were carried out under dry nitrogen using standard inert-atmosphere techniques. $LiN(SiMe_3)_2$ was prepared from $HN(SiMe_3)_2$ and *n*-BuLi in hexane by modification of a literature procedure [10], and was sublimed (90–100°C, 10^{-4} torr) before use. $Nb(O\text{-}i\text{-}Pr)_5$ was prepared by a literature procedure [11]. Niobium pentachloride ($NbCl_5$) was obtained from Strem and used as received. 2,2-Dimethylpropan-1-ol (Me_3CCH_2OH), trimethylsilylmethanol (Me_3SiCH_2OH), and NH_3(g) were obtained from Aldrich and used as received. Trimethylsilylmethanol was stored over type 4A molecular sieves before use. Hexane, benzene, and toluene were distilled from sodium benzophenone ketyl.

C, H, and N analyses were performed by Oneida Research Services, Whitesboro, NY. For total metal analyses (Li+Nb), samples were hydrolyzed with a few drops of conc. NH_3(aq) in a quartz crucible, carefully dried, ignited over a gas-burner flame, and weighed as $LiNbO_3$. NMR spectra were recorded at a field corresponding to 300 MHz for ^1H and 75 MHz for ^{13}C. All reported sublimation temperatures correspond to the oil-bath temperatures employed.

Preparation of $LiOCH_2CMe_3$ (1)

Me_3CCH_2OH (3.0 g, 34 mmol) and $LiN(SiMe_3)_2$ (5.0 g, 30 mmol) were combined in benzene (25 cm^3) at room temperature, giving an exothermic reaction. The reaction mixture was stirred for 30 min, and then benzene and other volatiles were removed under reduced pressure. The residual solid was sublimed (135–140°C, 10^{-4} torr) to yield the product as a white solid (2.30 g, 22.8 mmol, 82%). M.p.: 220–223°C. Found: C, 63.49; H, 11.75. Calc. for $C_5H_{11}OLi$: C, 63.83; H, 11.78%.

1 is soluble in hydrocarbon solvents. ^1H NMR (δ, benzene-d_6, *unsublimed* **1**): 3.82 (s, 0.1 × 2 H, OCH_2), 3.67 (s, 0.9 × 2 H, OCH_2), 1.04 (s, 0.1 × 9 H, Me) 1.00 (s, 0.9 × 9 H, *Me*). ^1H NMR (δ, benzene-d_6, *sublimed* **1**): 3.82 (s, 0.1 × 2 H, OCH_2), 3.71 (s, 0.9 × 2 H, OCH_2), 1.04 (s, 0.1 × 9 H, *Me*) 1.01 (s, 0.9 × 9 H, *Me*). $^{13}C\{^1H\}$ NMR (ppm, benzene-d_6): 77.20 (OCH_2, minor), 76.92 (OCH_2, major), 34.31 (CMe_3), 27.64 (*Me*, minor), 26.96 (*Me*, major). IR (KBr, cm^{-1}): 2951 vs, 2864 m, 2791 w, 2690 w, 2643 vw, 1478 w, 1457 w, 1957 w, 1357 m, 1250 vw, 1106 vs, 1086 s, 1020 w, 891 vw, 748 vw, 570 m, 511 w, 573 w.

Preparation of $LiOCH_2SiMe_3$ (2)

Me_3SiCH_2OH (1.30 cm^3, 1.07 g, 10.3 mmol) and $LiN(SiMe_3)_2$ (1.67 g, 10.0 mmol) were combined in benzene (10 cm^3) at room temperature, giving an exothermic reaction. The reaction mixture was stirred for 30 min, and then benzene and other volatiles were removed under reduced pressure. The residual solid was sublimed (140–145°C, 10^{-4} torr) to yield the product as a white solid (0.83 g, 7.5 mmol, 75%). M.p.: 222°C. Found: C, 43.67; H, 10.02. Calc. for $C_4H_{11}OSiLi$: C, 43.61; H, 10.06%.

2 is soluble in hydrocarbon solvents. ^1H NMR (δ, benzene-d_6): 3.74 (s, 2H OCH_2), 0.20 (s, 9 H, $SiMe_3$). $^{13}C\{^1H\}$ NMR (ppm, benzene-d_6): 57.02 (OCH_2), −2.84 ($SiMe_3$). IR (KBr, cm^{-1}): 2957 m, 2896 w, 2740 m, 1615 w, 1418 vw, 1245 s, 1045 w, 857 vs, 837 sh s, 757 vw, 695 w, 671 vw, 528 b m, 442 b m.

Preparation of $Nb(OCH_2CMe_3)_5$ [12]

$NbCl_5$ (4.0 g, 14.8 mmol) and Me_3CCH_2OH (10.0 g, 113.5 mmol) were combined in benzene (60 cm^3). Excess anhydrous NH_3 gas was then added according

to the literature procedure [12] for the preparation of $Nb(OCH_2CH_2CHMe_2)_5$. The product was purified by sublimation (120°C, 10^{-2} torr), yielding a white solid (5.12 g, 9.7 mmol, 65%). ^1H NMR (δ, benzene-d_6): 4.25 (s, 10 H, OCH_2), 1.04 (s, 45 H, *Me*). $^{13}C\{^1H\}$ NMR (ppm, benzene-d_6): 85.26 (OCH_2), 33.96 (CMe_3), 26.61 (*Me*).

Synthesis of $[Nb(OCH_2SiMe_3)_5]_2$ (**3**)

Me_3SiCH_2OH (4.06 cm^3, 3.35 g, 32.1 mmol) and $Nb(O\text{-}i\text{-}Pr)_5$ (2.50 g, 6.43 mmol) were combined in benzene (50 cm^3). The solution was refluxed on a variable-return fractionating column [13]. Distillate was collected at 1–2 drops/min over 4–5 h to separate the liberated *i*-PrOH as its azeotrope with benzene. The azeotrope distilled initially at 72°C. As the reaction progressed the distillation temperature slowly increased to the boiling point of pure benzene (80.1 C), at which point the solution was allowed to cool. The benzene was removed under reduced pressure and the residual solid was sublimed (120–125°C, 10^{-4} torr) to yield **3** (2.95 g, 2.42 mmol, 75%) as a white crystalline solid. M.p.: 111–112°C. Found: C, 39.55; H, 9.43. Calc. for $C_{20}H_{55}O_5Si_5Nb$: C, 39.44; H, 9.10%.

3 is moderately soluble in hydrocarbon solvents. ^1H NMR (δ, benzene-d_6, 25°C): 4.75 (s, terminal OCH_2, anti dimer, 0.21×16 H), 4.72–4.67 ("m", vertical and μ OCH_2, syn dimer, low intensity), 4.52 (br s, μ OCH_2, anti dimer, 0.21×4 H), 4.43 (s, horizontal OCH_2, syn dimer, small shoulder), 4.40 (s, OCH_2, monomer, 0.79×10 H), 0.42 (s, μ *Me*, anti dimer, 0.21×18 H), 0.27 (s, terminal *Me*, anti dimer, 0.21×48 H), 0.17 (s, *Me*, monomer 0.79×45 H). ^1H NMR (δ, toluene-d_8, 25°C): 4.72 (br s, terminal OCH_2, anti dimer, 0.06×10 H), 4.68 (br s, μ or vertical OCH_2, syn dimer, 0.19×4 H), 4.66 (br s, μ or vertical OCH_2, syn dimer, 0.19×4 H), 4.55 (br s, μ or vertical OCH_2, syn dimer, 0.19×4 H), 4.51 (br s, horizontal OCH_2, syn dimer, 0.19×8 H), 4.44 (s, OCH_2, monomer, 0.750×10 H), 4.34 (br s, μ OCH_2, anti dimer, 0.06×4 H); 0.380 (br "m", μ *Me*, dimer, 0.25×18 H), 0.248 (br "m", terminal *Me*, dimer, 0.25×72 H), 0.173 (s, *Me*, monomer, 0.75×45 H). (See Results and Discussion for definition of "vertical" and "horizontal".) $^{13}C\{^1H\}$ NMR (ppm, benzene-d_6): 70.24 (OCH_2, monomer), 3.03 (*Me*, monomer). IR (KBr, cm^{-1}): 2957 m, 2898 w, 2858 w, 2796 w, 1416 w, 1246 s, 1209 vw, 106 sh w, 1070 s, 1049 s, 1037 m, 990 w, 855 vs, 761 m, 697 m, 673 m, 600 m, 569 s, 517 m, 449 m.

Preparation of $[LiNb(OCH_2CMe_3)_6]_2$ (**4**)

$LiOCH_2CMe_3$ (**1**, 0.71 g, 7.6 mmol) and $Nb(OCH_2CMe_3)_5$ (4.00 g, 7.57 mmol) were combined in benzene (20 cm^3) and the mixture was warmed (50–60°C) to produce a homogeneous solution. The solution was then evaporated *in vacuo* to *ca.* half its original volume. Product **4** crystallized upon cooling (−6°C), and was separated from the supernatant liquid and dried *in vacuo* (2.50 g). The supernatant liquid was evaporated and the residue sublimed (120–125°C, 10^{-4} torr) to yield additional **4** (1.42 g). Total yield: 3.92 g, 3.15 mmol, 83%. M.p.: 181–210°C. Found (sublimed **4**): C, 58.44; H, 10.98. Calc. for $C_{30}H_{66}O_6LiNb$: C, 57.86; H, 10.68%.

4 is moderately soluble in hydrocarbon solvents. ^1H NMR (δ, benzene-d_6): 4.28 (pseudo t, $^2J_{Ha\text{-}Hb} = 6.1$ Hz, 4 H, μ_3 $OCH_aH_bCMe_3$), 4.17 (br s, 20 H, terminal and μ_2 OCH_2), 1.10 (br s, 18 H, μ_3 $OCH_aH_bCMe_3$), 1.05 (s, 54 H, terminal *Me*), 1.04 (s, 36 H, μ_2 *Me*). ^1H NMR spectra of aged samples were considerably more complex. $^{13}C\{^1H\}$ NMR (ppm, benzene-d_6): 83.50 (μ_3 OCH_2), 82.48 (μ_2 OCH_2), 81.87 (terminal OCH_2), 34.42 (μ_3 CMe_3), 33.88 (terminal CMe_3), 33.82 (μ_2CMe_3), 27.35 (μ_3 CMe_3), 27.15 (terminal CMe_3), 26.56 (μ_2 CMe_3). IR (cm^{-1}, KBr): 2953 vs, 2901 m, 2866 s, 2692 vw, 1479 m, 1463 m, 1393 m, 1362 m, 1290 vw, 1259 vw, 1218 vw, 1072 vs, 1023 vs, 935 vw, 903 vw, 751 w, 650 s, 604 m, 462 m.

Pure **4** (0.220 g, 0.177 mmol) sublimed at 120–125°C, 10^{-4} torr (0.103 g, 0.083 mmol, 47% recovery). The ^1H NMR spectrum of the sublimate resembled that for *aged* **4**.

Preparation of $LiNb(OCH_2CMe_3)_6(Me_3CCH_2OH)_2$ (**5**)

Me_3CCH_2OH (2.0 g, 23 mmol), $LiOCH_2CMe_3$ (**1**, 0.53 g, 5.8 mmol), and $Nb(OCH_2CMe_3)_5$ (3.00 g, 5.67 mmol) were dissolved in benzene (10 cm^3). A white solid precipitated. The reaction mixture was warmed to redissolve the solid product, transferred to a water bath (50–55°C) in a Dewar flask, and allowed to cool slowly to room temperature. Colorless crystals of **5** formed, which were separated from the supernatant liquid and dried *in vacuo* (4.12 g, 5.15 mmol, 91%). M.p.: 182–191°C. Found: C, 60.02; H, 11.35. Calc. for $C_{40}H_{90}O_8LiNb$: C, 60.13; H, 11.35%.

Compound **5** is moderately soluble in hydrocarbon solvents. ^1H NMR (δ, benzene-d_6): 4.30 (s, 12 H, OCH_2), 3.35 (s, 4 H, CH_2 of alcohol), 3.32 (s, 2 H, *HO*), 1.16 (s, 54 H, *Me*), 0.82 (s, 18 H, *Me* of alcohol). $^{13}C\{^1H\}$ NMR (ppm, benzene-d_6): 82.11 (OCH_2 of alkoxy ligand), 74.11 (OCH_2 of alcohol), 34.04 (CMe_3 of alkoxy ligand), 32.60 (CMe_3 of alcohol), 27.43 (*Me* of alkoxy ligand), 26.09 (*Me* of alcohol). IR (cm^{-1}, KBr): 3430 b vw, 2951 vs, 2904 m, 2865 m, 2833 sh, w, 2701 vw, 1479 w, 1462 w, 1391 w, 1361 w, 1260 vw, 1217 vw, 1066 vs, 1022 s, 935 vw, 902 vw, 751 vw, 634 m, 597 sh w, 451 w.

Pure **5** (1.32 g, 1.65 mmol) sublimed at 120–125°C, 10^{-4} torr with loss of Me_3CCH_2OH to yield $[LiNb(OCH_2CMe_3)_6]_2$ (**4**) (0.85 g, 0.70 mmol, 82%). Calc. for $C_{30}H_{66}O_6LiNb$: Li + Nb, 16.03. Found: Li + Nb, 15.83. The ^1H NMR matched that of crystallized **4** (see above).

Preparation of $[LiNb(OCH_2SiMe_3)_6]_2$ (**6**)

$LiOCH_2SiMe_3$ (**2**, 0.45 g, 4.10 mmol) and $[Nb(OCH_2SiMe_3)_5]_2$ (**3**, 2.50 g, 2.05 mmol) were combined in benzene (10 cm^{-3}) and the mixture was warmed (50–60°C) to produce a homogeneous solution. Colorless crystals of **6** were deposited upon cooling to room temperature (20 h), which were separated from the supernatant liquid and dried *in vacuo* (1.29 g, 0.90 mmol, 44%). M.p.: 130–134°C. Found: C, 40.00; H, 9.40. Calc. for $C_{24}H_{66}O_6Si_6NbLi$: C, 40.08, H, 9.25%.

Compound **6** is moderately soluble in hydrocarbon solvents. ^1H NMR (δ, benzene-d_6): 4.53 (br s, 20 H, terminal and μ_2-OCH_2), 4.44–4.40 (m, 4 H, μ_3-OCH_aH_bSiMe$_3$), 0.26 (s, 90 H, terminal and μ_2 *Me*), 0.17 (s, 18 H, μ_3 *Me*). ^1H NMR spectra of aged samples were considerably more complex. $^{13}C\{^1H\}$ NMR (ppm, benzene-d_6): 67.28 (terminal-OCH_2), 66.61 (μ_3-OCH_2), 65.79 (μ_2-OCH_2), −1.54 (terminal Si*Me*$_3$), −2.36 (μ_2 Si*Me*$_3$), and −3.15 (μ_3 Si*Me*$_3$). IR (KBr, cm^{-1}): 2955 m, 2899 w, 2855 w, 2794 vw, 1416 vw, 1246 s, 1105 sh w, 1056 sh m, 1037 m, 853 vs, 760 w, 696 w, 673 w, 595 vw, 539 s, 501 m.

Pure **6** (0.26 g, 0.18 mmol) sublimed at 155–160°C, 10^{-4} torr (0.11 g, 0.077 mmol, 42% recovery). The ^1H NMR spectrum of the sublimate matched that of crystallized **6** (see above).

NMR study of the monomer–dimer equilibrium of **3**

A 0.0058 M sample was prepared by dissolving pure **3** in toluene-d_8. NMR probe temperatures were calibrated with methanol and ethylene-glycol standards. Spin-lattice relaxation times (T_1 values) for the ^1H resonances in **3** were determined with 180–90° inversion–recovery experiments at 298 K and 338 K. Cycle times for collection of FID pulses were set to 5× the longest T_1 to ensure quantitative integrations. Data were obtained by integrating methyl resonances; the total dimer contribution was determined by summing the dimer Me resonances. Data from OCH_2 resonances did not extend the temperature range over which meaningful results could be obtained; furthermore, integrations were less reliable due to monomer–dimer overlap at high temperatures and substantial peak broadening at low temperatures. The sample was not entirely dissolved at low temperatures; here the actual concentration was determined by: {[total (monomer + dimer) Me integration ÷ solvent Me integration]$_{lo\,T}$ ÷ [total (monomer + dimer) Me integration ÷ solvent Me integration]$_{hi\,T}$} × 0.0058 M. Data (T (K), [monomer]^2/[dimer]): 309, 3.98×10^{-2}; 298, 2.50×10^{-2}; 288, 9.92×10^{-3}; 278, 3.02×10^{-3}; 267, 6.24×10^{-4}; 257, 1.78×10^{-4}; 247, 6.16×10^{-5}; 236, 2.06×10^{-5}; 226, 9.38×10^{-6}. Thermodynamic quantities were determined by linear least-squares fitting of the data to $\{-\ln[\text{monomer}]^2/[\text{dimer}]\} = \Delta H/RT - \Delta S/R$: $\Delta H = 63(3)$ kJ/mol and $\Delta S = 180(10)$ J/K mol. Errors were estimated by standard procedures.

NMR study of the fluxional behavior of **3**

Exchange of vertical and horizontal terminal ligands (refer to Results and Discussion) in the anti dimer of **3** was observed at both the slow- and fast-exchange limits. A rate constant, ΔG, and error estimates were extracted from the coalescence data by standard methods. Data from OCH_2 resonances: ^1H NMR (δ, toluene-d_8, low-temperature limit) 4.76 (s), 4.70 (s); $T_c = 253(5)$ K; $\Delta\nu = 19.2(2)$ Hz. The rate constant $k_{253} = 42.7(4)$ s^{-1}, and $\Delta G_{253} = 54.0(4)$ kJ/mol.

Crystal structure determination for $[Nb(OCH_2SiMe_3)_5]_2$ (**3**)

A colorless prism ($0.25 \times 0.54 \times 0.42$ mm) obtained by slowly cooling a benzene solution of **3** was sealed in a glass capillary under N_2. Cell constants were determined from the setting angles of 25 centered reflections at 296 K using monochromated Mo-K_α radiation ($\lambda = 0.71073$ Å) on a Siemens R3m/V diffractometer. Three standard reflections were measured every 97 reflections; no significant decay was observed. A total of 6269 reflections ($+h$, $\pm k$, $\pm l$) were collected. Lorentz, polarization, and empirical corrections were applied to the data set, from which 4802 unique reflections with $F > 6\sigma(F)$ were used in the subsequent structure analysis with the Siemens SHELXTL PLUS program package.

The space-group ($P\bar{1}$) was assigned from statistical data and subsequently confirmed by successful refinement and convergence. The position of the niobium atom was determined by direct methods. The remaining non-hydrogen atoms were found by successive full-matrix least-squares refinements and difference Fourier map calculations, and were then refined anisotropically. All hydrogen atoms were placed at idealized positions ($d_{C-H} = 0.96$ Å) and refined with a common, isotropic thermal parameter using the riding model. A final $R(F_o)$ value of 0.0330 was obtained. Crystallographic data are listed in Table 1. Atomic positional parameters and other details of data collection and analysis are summarized in the supplementary material.

Crystal structure determination for $[LiNb(OCH_2SiMe_3)_6]_2$ (**6**)

The same techniques employed for **3** were used for **6**, except for the differences noted below. A colorless plate ($0.20 \times 0.72 \times 0.40$ mm) grown directly from the reaction mixture at room temperature was used in the analysis. Cell constants were determined from the setting angles of 20 centered reflections, and data were

Table 1. Crystallographic data for **3** and **6**

	3	**6**
Chemical formula	$C_{40}H_{110}Nb_2O_{10}Si_{10}$	$C_{24}H_{66}LiNbO_6$
a (Å)	11.360 (3)	12.921 (5)
b (Å)	12.100 (3)	20.742 (9)
c (Å)	14.863 (5)	16.637 (6)
α (°)	109.10 (2)	—
β (°)	111.46 (2)	96.22 (3)
γ (°)	91.21 (2)	—
V (Å^3)	1773.3 (9)	4433 (3)
Z	1	4
Formula weight	1218.0	719.2
Space group	$P\bar{1}$	$P2_1/n$
T (°C)	22	23
λ (Å)	0.71073	0.71073
ρ_{calcd} (g/cm^3)	1.141	1.078
μ (cm^{-1})	5.31	4.61
$R(F_o)^a$	0.0330	0.0693
$R_w(F_o)^b$	0.0427	0.1765
GOF	1.07	1.007 (on F^2)

$^a R(F_o) = \Sigma\|\|F_o| - |F_c\|\|/\Sigma|F_o|$.
$^b R_w(F_o) = \Sigma_w\|\|F_o| - |F_c\|^2/\Sigma w|F_o|^2)^{1/2}$; $w = [\sigma^2(F_o) + g(F_o)^2]^{-1}$.

collected in the ω mode. A total of 8346 reflections ($+h$, $+k$, $\pm l$) were collected and the $P2_1/n$ space group was assigned.

The position of the niobium atom was determined by heavy-atom methods. All non-hydrogen atoms were refined anisotropically using F^2 refinements of 7735 independent reflections. Because of disorder (see below), some of the Si—C bond distances were restrained to 1.87(1) Å during refinement. Hydrogen atoms were placed at idealized positions and refined with common isotropic thermal parameters using a riding model. Hydrogen atoms attached to disordered carbon atoms were assigned the appropriate site-occupancy factors. Some unresolved disorder remained, as evidenced by large thermal parameters for several carbon atoms. A final $R(F_o)$ value of 0.0693 was obtained. Crystallographic data are listed in Table 1. Atomic positional parameters and other details of data collection and analysis are summarized in the supplementary material.

The crystallographically unique portion of the molecule exhibited some disorder caused by conformational variations and apparent thermal motion of the pendant trimethylsilyl groups. Si(1) and its attached methylene and methyl groups were dissolved cooperatively over two related sets at 52% and 48% occupancies. Other methyl groups were also disordered: C(31)/C(31B), 51%/49%; C(42)/C(42B), 65%/35%; C(52)/C(52B), 57%/43%; and C(63)/C(63B), 52%/48%.

RESULTS AND DISCUSSION

$LiOCH_2CMe_3$ (**1**) *and* $LiOCH_2SiMe_3$ (**2**)

The new lithium alkoxides add to the presently known volatile examples [14]. They were prepared by alcoholysis as shown in eq. (1), and sublimed *in vacuo* at 135–145°C/10^{-4} Torr:

$$LiN(SiMe_3)_2 + ROH \xrightarrow[R = CH_2CMe_3\ (1)\ \ CH_2SiMe_3\ (2)]{} LiOR + HN(SiMe_3)_2 \quad (1)$$

^{1}H and ^{13}C NMR of **2** showed only one set of resonances corresponding to —CH_2 and $SiMe_3$ protons; however, compound **1** showed two sets of resonances for —CH_2 and CMe_3 protons suggesting that **1** existed as two different oligomers. Prior to sublimation **1** was a mixture of these postulated oligomers in a 9:1 ratio. The major oligomer sublimed with small downfield ^{1}H resonance shifts ($\Delta\delta$ OCH_2: 0.035 ppm; $\Delta\delta$ CH_3: 0.010 ppm). The minor oligomer sublimed inconsistently. It appeared to be the heavier oligomer as it sometimes remained in the sublimation vessel after sublimation of the major oligomer. On other occasions, the minor oligomer sublimed with the major oligomer with approximate retention of the oligomeric ratio.

$[Nb(OCH_2SiMe_3)_5]_2$ (**3**)

Compound **3** was prepared from Nb(O-*i*-Pr)$_5$ by alcohol exchange, and structurally characterized as shown in Fig. 1. The molecular structure is an edge-shared bioctahedral dimer with 8 terminal alkoxide ligands (4 "vertical" and 4 "horizontal" according to their dispositions in the dimer as oriented in Fig. 1) and 2 bridging alkoxide ligands, as is typical of $Nb(OR)_5$ compounds. Both $[Nb(\mu\text{-}OMe)(OMe)_4]_2$ [15] and $[Nb(\mu\text{-}OEt)(OCH_2CMe_3)_4]_2$ [16] exhibit solid-state structures similar to that of **3**.

However, the configuration of the bridging oxygen atoms in **3** differs from those in the previously known structural homologs. In **3**, the μ-O atoms (O2 and O2A, Fig. 1) are pyramidalized; the sum of the bond angles about these centers is 350.0 degrees. The corresponding bridging-oxygen centers in $[Nb(\mu\text{-}OMe)(OMe)_4]_2$ [15] and $[Nb(\mu\text{-}OEt)(OCH_2CMe_3)_4]_2$ [16] approach planarity more closely, having sums of the bond angles about them of 354.5, 355.0 and 357.0 degrees, respectively. The pyramidality of the bridging centers in **3** and the steric bulk of the bridging ligand allows syn and anti isomers of the dimeric structure to exist in solution (see below). In the solid state **3** adopts the anti geometry, in which the α-carbon atoms of the bridging alkoxide ligands are on the opposite sides of the horizontal plane defined by O4, O5, Nb, NbA, O4A, and O5A atoms (Fig. 1).

Variable-temperature ^{1}H NMR experiments

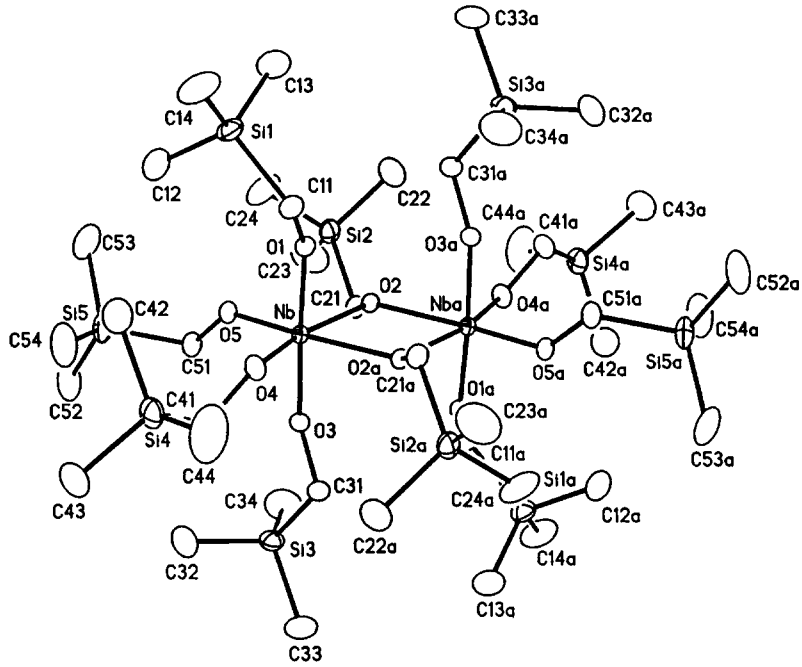

Fig. 1. Thermal ellipsoid plot (20% probability contours) of $[Nb(\mu\text{-}OCH_2SiMe_3)(OCH_2SiMe_3)_4]_2$ (**3**). Hydrogen atoms were omitted for clarity. Selected bond distances (Å): Nb—O(1), 1.902 (3); Nb—O(2), 2.134 (2); Nb—O(3), 1.902 (3); Nb—O(4), 1.919 (2); Nb—O(5), 1.896 (2); Nb—O(2A), 2.174 (2); O(1)—C(11), 1.415 (5); O(2)—C(21), 1.451 (4); O(3)—C(31), 1.408 (5); O(4)—C(41), 1.418 (4); O(5)—C(51), 1.423 (4). Selected angles (°): O(1)—Nb—O(2), 90.2 (1); O(1)—Nb—O(3), 174.6 (1); O(2)—Nb—O(3), 91.2 (1); O(1)—Nb—O(4), 86.4 (1); O(2)—Nb—O(4), 163.7 (1); O(3)—Nb—O(4), 90.8 (1); O(1)—Nb—O(5), 95.7 (1); O(2)—Nb—O(5), 94.6 (1); O(3)—Nb—O(5), 89.4 (1); O(4)—Nb—O(5), 101.6 (1); O(1)—Nb—O(2A), 88.8 (1); O(2)—Nb—O(2A), 71.7 (1); O(3)—Nb—O(2A), 86.6 (1); O(4)—Nb—O(2A), 92.3 (1); O(5)—Nb—O(2A), 165.6 (1); Nb—O(1)—C(11), 144.0 (2); Nb—O(2)—C(21), 121.1 (1); Nb—O(3)—C(31), 151.3 (2); Nb—O(4)—C(41), 133.0 (2); Nb—O(5)—C(51), 136.8 (3); C(21)—O(2)—Nb(A), 120.6 (2); Nb—O(2)—Nb(A), 108.3 (1).

revealed dynamic equilibria between three species in solution, which we identify as monomeric, syn-dimeric, and anti-dimeric isomers of **3** (see Scheme 1). The monomer, producing a singlet resonance (Fig. 2), dominated at higher temperatures and represented at least 75% of the isomer population at room tem-

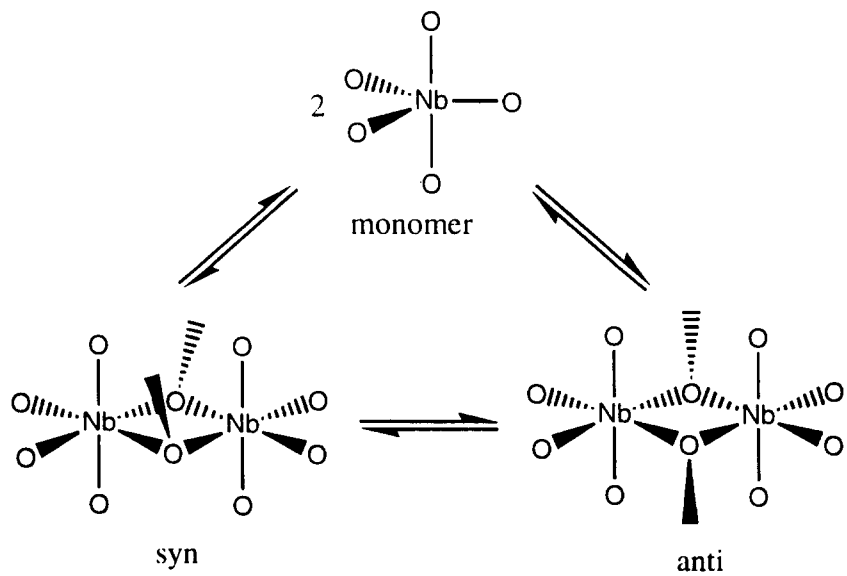

Scheme 1. Monomer-dimer equilibria for **3**.

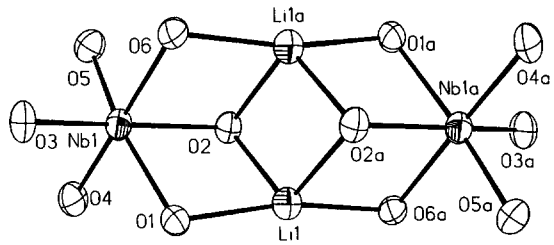

Fig. 2. Variable-temperature ^{1}H NMR spectra of $Nb(OCH_2SiMe_3)_5$ (**3**). (a) In the 205 K spectrum the 2 singlets assigned to terminal OCH_2 protons and the singlet assigned to bridging OCH_2 protons of the anti dimer are indicated by arrows. The horizontal OCH_2 protons of the syn dimer are also present at 205 K as a broad shoulder downfield of the bridging ligand of the anti dimer. This resonance sharpens as the dimer equilibrium shifts toward the syn isomer as indicated in the 226 K spectrum. Vertical and bridging ligands of the syn dimer are poorly resolved. The emerging monomer OCH_2 singlet is evident in the 257 K spectrum, and becomes the highest-intensity resonance in the higher T spectra (see the 360 K spectrum). (b) The monomer methyl resonance is indicated by arrows in the dimer-dominated equilibrium at 226 K and in the monomer-dominated equilibrium at 360 K.

perature and above. The anti isomer, producing 3 alkoxide resonances in the expected intensity ratios of 4:4:2 (Fig. 2), dominated at the lowest temperatures. The syn isomer, producing 4 alkoxide resonances in the ratios of 4:2:2:2 (some of which were obscured), was in its greatest relative abundance at intermediate temperatures (Fig. 2). The two dimers contributed greater than 90% to the total isomer population at temperatures below −35°C. Integrated intensities as a function of temperature allowed determination of the thermodynamic parameters for the equilibrium [total dimer] = [2 monomer]: ΔH = 63(3) kJ/mol and ΔS = 180(10) J/(K mol). This ΔH value was similar to that for the corresponding equilibrium in the Nb(O-*i*-Pr)$_5$ system (ΔH = 75(13) kJ/mol) [17].

Variable-temperature ^{1}H NMR spectra of the *anti*-**3** isomer (Fig. 2) also revealed site exchange of terminal alkoxide ligands that we label horizontal and vertical (according to the Fig. 1, Scheme 1 orientation). This type of exchange has been noted previously in 3 homologous $Nb(OR)_5$ compounds. The ΔG_{253} = 54.0(4) kJ/mol we measured from coalescence data for **3** is within the range of values determined for $[Nb(OMe)_5]_2$, $[Nb(OEt)_5]_2$, and $[Nb(O\text{-}i\text{-}Bu)_5]_2$ (50.6(4), 48.1(1.2), and 64.8(1.2) kJ/mol, respectively) [18,19]. The dynamic behavior of **3** is quite comparable to that in all earlier studies on homologous $Nb(OR)_5$ compounds and their tantalum analogs, except to our knowledge discrete syn and anti dimeric (edge-shared bioctahedral) isomers have not been previously observed in these systems.

$[LiNb(OCH_2CMe_3)_6]_2$ (**4**), $LiNb(OCH_2CMe_3)_6(Me_3CCH_2OH)_2$ (**5**), *and* $[LiNb(OCH_2SiMe_3)_6]_2$ (**6**)

The new Li–Nb heterometallic alkoxides were prepared by combining the corresponding homometallic alkoxides. The structure of **6** is shown in Fig. 3 and 4. Crystals of **4** grown from benzene proved to be unsuitable for single-crystal X-ray diffraction; however, we surmised that **4** is isostructural to **6** on the basis of spectroscopic data discussed below.

The central core of **6** (Fig. 3) contains an $Nb_2Li_2(\mu\text{-}O)_4(\mu_3\text{-}O)_2$ unit that is geometrically similar to the central units in $[MSn(O\text{-}t\text{-}Bu)_3]_2$ (M = Li, Na) [20] and $[LiTi(O\text{-}i\text{-}Pr)_5]_2$ [21]. The compound initially identified as $[LiNb(OEt)_5(OH)]_2$ also has an $Nb_2Li_2(\mu\text{-}O)_4(\mu_3\text{-}O)_2$ central core and an overall structure related to that of **6** [22], a reformulation of this compound as $[LiNbO(OEt)_4(EtOH)]_2$ has recently been suggested [7].

The structure of **6** differs from those of the related examples outlined above in a significant aspect: **6** possesses *asymmetrically* bridging μ_3-OR ligands. The triply bridging atom O2 lies closer to Li1 than to Li1 A by 0.187 (26) Å. That asymmetry is apparently manifested in the ^{1}H NMR of **6**, in which the methylene protons on the μ_3 ligand, μ_3-$OCH_aH_bSiMe_3$, produce an AB multiplet. If the μ_3 ligand bridged symmetrically, then its methylene protons would be chemically equivalent and appear as a singlet. All other features in the ^{1}H NMR spectrum of **6** are consistent with the solid-state structure, with the terminal, μ_2, and μ_3 ligands appearing as separate Me resonances in 6:4:2 ratios. Thus, the structure and bridge asymmetry of **6** observed in the solid state are apparently maintained upon dissolution.

The similarity of the ^{1}H NMR spectra of **6** and **4** suggest that they are isostructural. Like the spectrum of **6**, the spectrum of **4** contains a multiplet (in this case a pseudotriplet) that we assign to the μ_3-$OCH_aH_bCMe_3$ ligands in an asymmetrically bridged structure homologous to that for **6**. The spectrum of **4** also contains Me resonances in 6:4:2 ratios that we assign to the terminal, μ_2, and μ_3 ligands, respectively.

Both **6** and **4** underwent structural changes in solution upon standing, as evidenced by the increasingly complex ^{1}H NMR spectra obtained from aged samples. This may indicate that their dimeric molecular structures are unstable in solution with respect to oligomerization. Consequently, characteristic spectra for **4** and **6** were recorded immediately after dissolution of crystalline materials.

The structure of the alcohol adduct **5** is unknown,

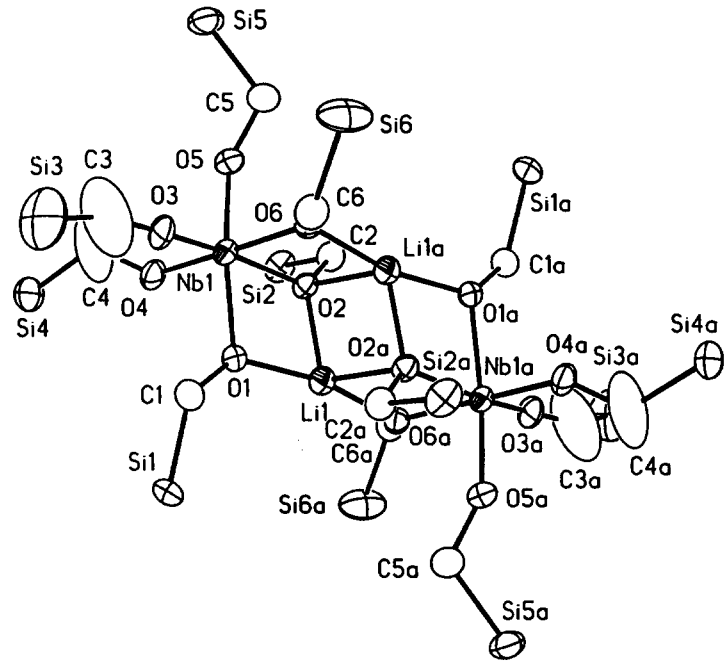

Fig. 3. Thermal ellipsoid plot (20% probability contours) comprising the central core of $[LiNb(\mu_3\text{-}OCH_2SiMe_3)(\mu_2\text{-}OCH_2SiMe_3)_2(OCH_2SiMe_3)_3]_2$ (**6**). Selected bond distances (Å): Nb(1)—O(1), 2.052 (4); Nb(1)—O(2), 2.054 (4); Nb(1)—O(3), 1.881 (5); Nb(1)—O(4), 1.902 (5); Nb(1)—O(5), 1.896 (5); Nb(1)—O(6), 2.037 (4); Li(1)—O(1), 1.980 (12); Li(1)—O(2), 1.976 (13); Li(1)—O(2A), 2.163 (13); Li(1)—O(6A), 1.974 (12); O(2)—Li(1A), 2.163 (13). Selected angles (°): O(1)—Nb(1)—O(2), 76.7 (4); O(1)—Nb(1)—O(3), 92.6 (2); O(2)—Nb(1)—O(3), 164.1 (2); O(1)—Nb(1)—O(4), 89.5 (2); O(2)—Nb(1)—O(4), 98.4 (2); O(3)—Nb(1)—O(4), 93.1 (2); O(1)—Nb(1)—O(5), 167.6 (2); O(2)—Nb(1)—O(5), 91.3 (2); O(3)—Nb(1)—O(5), 99.8 (2); O(4)—Nb(1)—O(5), 88.9 (2); O(1)—Nb(1)—O(6), 91.5 (2); O(2)—Nb(1)—O(6), 81.1 (2); O(3)—Nb(1)—O(6), 87.6 (2); O(4)—Nb(1)—O(6), 178.8 (2); O(5)—Nb(1)—O(6), 90.0 (2); O(1)—Li(1)—O(2), 80.2 (5); O(1)—Li(1)—O(2A), 104.6 (6); O(1)—Li(1)—O(6A), 168.5 (7); O(2)—Li(1)—O(2A), 103.9 (5); O(2)—Li(1)—O(6A), 109.3 (6); O(2A)—Li(1)—O(6A), 79.8 (4); Nb(1)—O(2)—Li(1), 100.8 (4); Nb(1)—O(6)—Li(1A), 102.4 (4); Nb(1)—O(1)—Li(1), 100.8 (4); Li(1)—O(2)—Li(1A), 76.1 (5).

although we infer that **5** is molecular rather than nonmolecular on the basis of its solubility, volatility, and the structures of the analogs **4** and **6**. The ^1H NMR spectrum of **5** is very simple, with all OCH_2CMe_3 ligands apparently equivalent. Presumably, the simplicity results from alkoxide–ligand site exchange among chemically inequivalent positions, although we did not investigate the variable-temperature NMR behavior of **5** to support this presumption. We note that **5** sublimed to give **4** in almost twice the recovery that was achieved in the sublimation of pure **4**, and that **4** sublimed in better recovery from the mother liquor remaining after crystallization of **4** than as a pure substance. Perhaps the alcohol ligands in **5** and residual alcohol present in the mother liquor inhibited oligomerization of **4** to nonvolatile structures during sublimation.

Attempted spray MOCVD using $[LiNb(OCH_2CMe_3)_6]_2$ (**4**)

To obtain a preliminary indication of the suitability of **4** as an $LiNbO_3$ precursor, samples of **4** were decomposed in quartz tubes under flowing N_2 at 600°C. Dark mirror coatings formed on the interior tube walls, which were found to be crystalline $LiNbO_3$ by X-ray powder diffraction (XRD), a promising indicator for the applicability of **4** as a spray MOCVD precursor.

We then assembled a hot-wall spray MOCVD reactor following closely the design reported by Wernberg, Gysling, and Braunstein [9]. We successfully reproduced the deposition of $LiNbO_3$ from $[LiNb(OEt)_6]_x$ using the solvent-evaporation-zone temperature, the precursor-decomposition-zone temperature, and the carrier gas (5% O_2 in Ar) and flow rate they reported [9].

However, we failed to deposit $LiNbO_3$ from **4** using the same experimental parameters. Precursor-decomposition-zone temperatures and carrier-gas flow rates above and below those employed with $[LiNb(OEt)_6]_x$ were also examined without success. The minimal deposits obtained did not produce detectable XRD intensities. In most runs, a much larger quantity of white solid collected as a non-adherent coating at the outlet constriction in the reactor and beyond. This material was insoluble in organic solvents, amorphous by XRD, and annealed (500°C) to give crystalline $LiNbO_3$ and traces of $LiNb_3O_8$. Gravimetric analyses established that most of the

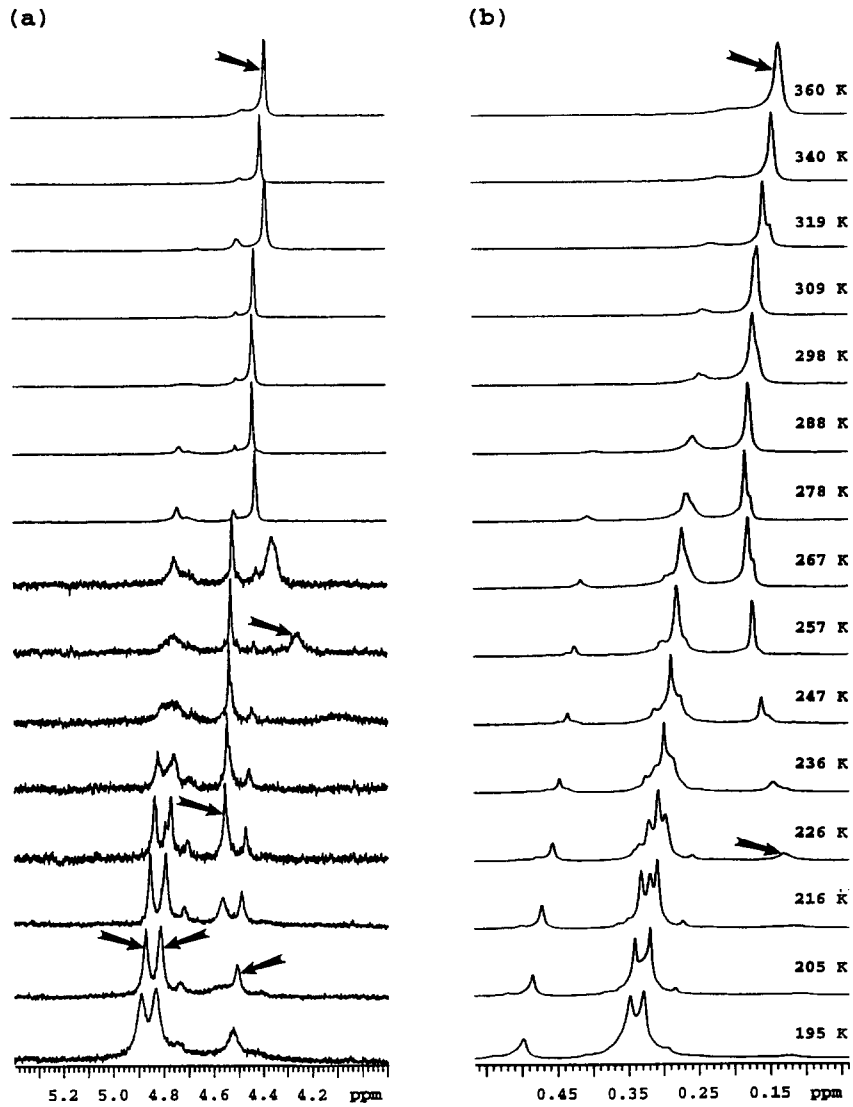

Fig. 4. Thermal ellipsoid plot (20% probability contours) of $[LiNb(\mu_3\text{-}OCH_2SiMe_3)(\mu_2\text{-}OCH_2SiMe_3)_2(OCH_2SiMe_3)_3]_2$ (**6**). Methyl-carbon and hydrogen atoms were omitted for clarity.

organic content had been removed from the material during passage through the reactor. These observations suggest that dissociation of the Li and Nb components of **4** was not occurring, but that **4** decomposed homogeneously in the gas phase to produce particles [23] rather than heterogeneously at the substrate to produce a film.

We expected that $[LiNb(OEt)_6]_n$ and **4** would exhibit differing decomposition behavior. In a classic study Bradley and Faktor established that alkoxide compounds having hydrogen atoms β to oxygen may decompose autohydrolytically in the gas phase at elevated temperatures and atmospheric pressure (Scheme 2) [24]. By this mechanism alkoxide decomposition is initiated by a trace of H_2O, which generates metal oxide and byproduct alcohol hydrolytically. The liberated alcohol is dehydrated to alkene on hot reactor surfaces, generating twice the original trace amount of H_2O. Each successive cycle doubles the amount of metal oxide and H_2O produced; hence, the mechanism is autohydrolytic. Because $[LiNb(OEt)_6]_n$ possesses hydrogens β to oxygen whereas **4** does not, only the former may decompose autohydrolytically.

We suggest that autohydrolysis is the likely decomposition mechanism for $[LiNb(OEt)_6]_n$ during spray MOCVD of $LiNbO_3$, although the mechanism has not been investigated [25]. If autohydrolytic $[LiNb(OEt)_6]_n$ decomposition initiates at the leading edge of the deposition substrate, then the H_2O concentration may increase steadily towards the trailing edge of the substrate, possibly causing nonuniform film growth. We considered that use of precursors like **4**, for which autohydrolysis is inoperative, might increase the area over which uniform $LiNbO_3$ films may be grown. Unfortunately, to date neither **4** nor its analogs have given $LiNbO_3$ films. Assigning the differing behaviors

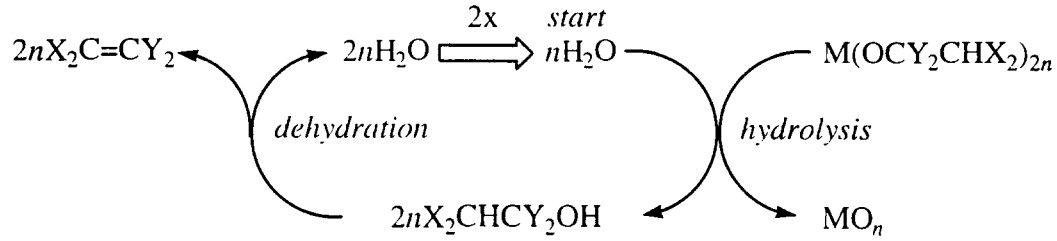

Scheme 2. Autohydrolytic decomposition of alkoxide precursors.

of $[LiNb(OEt)_6]_n$ and **4** to the presence and absence of autohydrolysis, respectively, is tempting but currently speculative.

SUMMARY

To our knowledge **6** is the only completely characterized *molecular* $LiNb(OR)_6$ compound. The homolog **4** is spectroscopically similar to **6** and is presumably isostructural. All of **4**–**6** are moderately soluble and volatile, although the alcohol adduct **5** and impure **4** sublime in the greatest recoveries. Under static conditions, **4** decomposes to $LiNbO_3$ at temperatures comparable to those for $[LiNb(OEt)_6]_x$. However, in preliminary studies **4** has not been a similarly successful spray MOCVD precursor, perhaps for lack of the autohydrolytic decomposition pathway.

Acknowledgements—This work was funded by an NSF-PYI award to WEB (CHE-9158369) generously supported by the Eastman Kodak Co. We are grateful to A. A. Wernberg and H. J. Gysling for numerous helpful discussions, and to T. J. Boyle for sharing information prior to publication. We thank A. d'Avignon for expert advice and assistance with NMR spectroscopy. Washington University's X-ray Crystallography Facility was funded by the NSF Chemical Instrumentation Program (CHE-8811456). The Washington University High-Resolution NMR Service Facility was funded in part by NIH Biomedical Research-Support Shared-Instrument Grants RR-02004, RR-05018, and RR-07155, and a gift from the Monsanto Co. JAH is currently a NASA Graduate Research Fellow.

REFERENCES

1. Mehrotra, R. C., Agrawal, M. M. and Kapoor, P. N., *J. Chem. Soc. A*, 1968, 2673.
2. Eichorst, D. J., Payne, D. A., Wilson, S. R. and Howard, K. E., *Inorg. Chem.*, 1990, **29,** 1458.
3. Chandler, C. D., Roger, C. and Hampden-Smith, M. J., *Chem. Rev.*, 1993, **93,** 1205.
4. Caulton, K. G. and Hubert-Pfaltzgraf, L. G., *Chem. Rev.*, 1990, **90,** 969.
5. Bradley, D. C., *Chem. Rev.*, 1989, **89,** 1317.
6. Brierley, C. J., Trundle, C., Considine, L., Whatmore, R. W. and Ainger, F. W., *Ferroelectrics*, 1989, **91,** 181.
7. Herrmann, W. A., Huber, N. W. and Runte, O., *Angew. Chem. Int. Ed. Engl.*, 1995, **34,** 2187.
8. Wernberg, A. A. and Gysling, H. J., *Chem. Mater.*, 1993, **5,** 1056.
9. Wernberg, A. A., Gysling, H. J. and Braunstein, G., *J. Crystal Growth*, 1994, **140,** 57.
10. Wannagat, U. and Niederprüm, H., *Chem. Ber.*, 1961, **94,** 1540.
11. Bradley, D. C., Chakravarti, B. N., Chatterjee, A. K., Wardlaw, W. and Whitley, A., *J. Chem. Soc.*, 1958, 99.
12. Bradley, D. C., Chakravarti, B. N., Chatterjee, A. K. and Wardlaw, W., *J. Chem. Soc.*, 1956, 4439.
13. Goel, S. C. and Buhro, W. E., *Inorg. Synth.*, 1997, **31,** 294.
14. Chisholm, M. H., Drake, S. R., Naiini, A. A. and Streib, W. E., *Polyhedron*, 1991, **10,** 805.
15. Pinkerton, A. A., Schwarzenbach, D., Hubert-Pfalzgraf, L. G. and Reiss, J. G., *Inorg. Chem.*, 1976, **15,** 1196.
16. Boyle, T. J., Alam, T. M., Dimos, D., Moore, G. J., Buchheit, C. D., Al-Shareef, H. N., Mechenbier, E. R., Bear, B. R. and Ziller, J. W., *Chem. Mater.*, 1997, **12,** 3187–3198.
17. Bradley, D. C. and Holloway, C. E., *J. Chem. Soc. (A)*, 1968, 219.
18. Riess, J. G. and Pfalzgraf, L. G., *Bull. Soc. Chim. Fr.*, 1968, 2401.
19. Holloway, C. E., *J. Coord. Chem.*, 1971, **1,** 253.
20. Veith, M. and Rösler, R., *Z. Naturforsch.*, 1986, **41b,** 1071.
21. Hampden-Smith, M. J., Williams, D. S. and Rheingold, A. L., *Inorg. Chem.*, 1990, **29,** 4076.
22. Yanovskii, A. I., Turevskaya, E. P., Turova, N. Ya. and Struchkov, Yu T., *Sov. J. Coord. Chem.*, 1985, **11,** 63.
23. Kodas, T. T. and Hampden-Smith, M. J. in *The Chemistry of Metal CVD*, ed. T. T. Kodas and M. J. Hampden-Smith, VCH, Weinheim, 1994, pp. 484–487.
24. Bradley, D. C. and Faktor, M. M., *Trans. Faraday Soc.*, 1959, 55.
25. Other alkoxide decomposition mechanisms have been found in other instances. For example, for decomposition of $[Cu(O\text{-}t\text{-}Bu)]_4$ see: Jeffries, P. M., Dubois, L. H. and Girolami, G. S., *Chem. Mater.*, 1992, **4,** 1169.

Pergamon

PII: S0277-5387(97)00310-0

Polyhedron Vol. 17, No. 5-6, pp. 791-802, 1998
© 1998 Elsevier Science Ltd
All rights reserved. Printed in Great Britain
0277-5387/98 $19.00+0.00

Organoamidometallics—VI.† A new synthetic route to [*N*,*N*′-bis(polyfluorophenyl)ethane-1,2-diaminato(2-)]dipyridineplatinum(II) complexes and the preparation of [*N*-phenyl-*N*′-(polyfluorophenyl)ethane-1,2-diaminato(2-)] dipyridineplatinum(II) complexes‡

Glen B. Deacon,* Bryan M. Gatehouse, Scott T. Haubrich, Joanne Ireland and Eric T. Lawrenz

Chemistry Department, Monash University, Clayton, Victoria 3168, Australia

(Received 22 April 1997; accepted 7 July 1997)

Abstract—Reaction of $[Pt(en)Cl_2]$ (en = ethane-1,2-diamine) with thallium(I) carbonate (or in some cases K_2CO_3) and a polyfluorobenzene in hot pyridine (py) or 3-methylpyridine (tmpy) yields the [*N*,*N*′-bis (polyfluorophenyl)ethane-1,2-diaminato(2-)]platinum(II) complexes, $[Pt\{N(R)CH_2\}_2L_2]$ (L = py, R = *p*-HC_6F_4, C_6F_5, *p*-BrC_6F_4, *p*-IC_6F_4, *p*-MeC_6F_4, *p*-$C_6F_5C_6F_4$, 2,3,5-$F_3C_6H_2$, *p*-$O(H)CC_6F_4$, *p*-$MeOC_6F_4$; L = tmpy, R = *p*-HC_6F_4). Yields were markedly greater with the use of Tl_2CO_3 than reported for reactions of $[Pt(en)Cl_2]$ with thallium(I) polyfluorobenzoates. A new class of platinum(II) amides, namely [*N*-(phenyl)-*N*′-(polyfluorophenyl)ethane-1,2-diaminato(2-)]platinum(II) complexes, $[Pt\{N(Ph)CH_2CH_2N(R)\}L_2]$ (L = py, R = *p*-HC_6F_4, C_6F_5, *p*-MeC_6F_4, *p*-ClC_6F_4, *p*-BrC_6F_4; L = 4-methylpyridine, R = *p*-HC_6F_4), has been prepared by reaction of $[Pt(PhNHCH_2CH_2NH_2)I_2]$ with Tl_2CO_3 or a thallium(I) polyfluorobenzoate and a polyfluoroaromatic compound in pyridine or 4-methylpyridine. The complexes where R = *p*-MeC_6F_4, *p*-ClC_6F_4, *p*-BrC_6F_4 could be prepared only with Tl_2CO_3, which also provided cleaner products where both routes were used. The crystal structure of $[Pt\{N(Ph)CH_2CH_2N(p\text{-}MeC_6F_4)\}(py)_2]$ has been determined and shows a slightly distorted square planar coordination for platinum, with two amide and two *cis* pyridine nitrogen donors.
© 1998 Elsevier Science Ltd. All rights reserved

Keywords: platinum; organoamide; polyfluorophenyl; thallium(I) carbonate; CO_2 formation; X-ray structure.

The platinum(II) organoamides $[Pt\{N(R)CH_2\}_2(py)_2]$ (R = polyfluoroaryl) [1] have high biological activity against murine L1210 leukeamia cells and the *cis*-$[Pt(NH_3)_2Cl_2]$ (cisplatin) resistant variant [2]. Activity is also shown by representative compounds against HT-29 and BE human colon carcinoma cells in culture and against P388 leukeamia in mice, where the complexes R = *p*-HC_6F_4, C_6F_5, or *p*-IC_6F_4, have very good activity [2]. Recently, $[Pt\{N(p\text{-}HC_6F_4)CH_2\}_2(py)_2]$ has been shown to be active against the mouse plasmacytoma ADJ/PC6 [3(a)], a cell line in wide use for screening antitumour behavior of platinum complexes [3(b)]. The compounds are of particular interest, since the nitrogen donor atoms have no hydrogen substituents, a normal requirement for active platinum(II) complexes [4], and since *cis*-$PtCl_2(py)_2$ is inactive *in vivo* [2,5].

Unusually for platinum(II) organoamides [6–9], the complexes are stable to water [1], and this contrasts the extreme moisture sensitivity of simple analogues

* Author to whom correspondence should be addressed.

† Part V is [16(d)].

‡ Dedicated to Professor Don Bradley, F.R.S., on the occasion of his 73rd birthday, in recognition of his outstanding and pioneering contribution to the chemistry of metal alkoxides and amides, and with thanks for professional advice, encouragement, and friendship over many years.

(e.g. $[Pt\{N(R)CH_2\}_2(bpy)]$ R = Me or H, bpy = 2,2′-bipyridine) [10]. Hitherto, the complexes have been prepared in yields of 6–44% by novel decarboxylation reactions from $[Pt(en)Cl_2]$ (en = ethane-1,2-diamine) and thallium(I) pentafluoro- or 2,3,5,6-tetrafluorobenzoate, usually with an added polyfluorobenzene (eq. (1) and (2)) [1].

$$[Pt(en)Cl_2] + 2TlO_2CC_6F_5 + 4py \rightarrow [Pt\{N(p\text{-}HC_6F_4)CH_2\}_2(py)_2] + 2TlCl + 2CO_2 + 2pyHF \quad (1)$$

$$[Pt(en)Cl_2] + 2TlO_2CC_6F_4H\text{-}p + 2RF + 4py \rightarrow [Pt\{N(R)CH_2\}_2(py)_2] + 2TlCl + 2CO_2 + 2p\text{-}H_2C_6F_4 + 2pyHF \quad (2)$$

Higher yield syntheses would be of major benefit, not only because of the cost of reagents, but also because of the need to generate sufficient amounts for continuing biological testing. A key step in the synthesis is considered to be deprotonation of $[Pt(en)Cl_2]$ by a highly carbanionic C_6F_5 or p-HC_6F_4 group generated by decarboxylation [1]. We have recently shown that deprotonation of $[Pd\{NH(R)CH_2CH_2NR'_2\}Cl_2]$ (R = polyfluorophenyl, R′ = Me or Et) compounds to give palladium(II) organoamides, $[Pd\{N(R)CH_2CH_2NR'_2\}(py)Cl]$, can be achieved with Tl_2CO_3 in pyridine [11]. This has now led to a successful attempt to prepare the target $[Pt\{N(R)CH_2\}_2(py)_2]$ complexes, including three new examples, by reaction of $[Pt(en)Cl_2]$ with Tl_2CO_3 (and some cases K_2CO_3) and a polyfluorobenzene labile to nucleophilic substitution, in pyridine. These syntheses are now described together with preparations of a new class of platinum(II) organoamides, namely $[Pt\{N(Ph)CH_2CH_2N(R)\}L_2]$ complexes (e.g. L = py, R = C_6F_5 or p-HC_6F_4), where use of Tl_2CO_3 proved more successful than thallium(I) polyfluorobenzoates. The structure of a typical new complex, $[Pt\{N(Ph)CH_2CH_2N(p\text{-}MeC_6F_4)\}(py)_2]$, has been determined by X-ray crystallography.

RESULTS AND DISCUSSION

Synthesis of $[Pt\{N(R)CH_2\}_2(py)_2]$ *complexes*

The previously synthesized and characterized [*N*,*N*′-bis(polyfluorophenyl)ethane-1,2-diaminato (2-)]dipyridineplatinum(II) complexes **1a–1g** [1] have now been prepared by reactions between dichloro(ethane-1,2-diamine)platinum(II), a polyfluoroaromatic compound, and thallium(I) or potassium carbonate in pyridine (eq. (3)). Three new organoamidoplatinum(II) complexes **1h, 1i** and **1j** were synthesized in pyridine or 3-methylpyridine (tmpy).

$$[Pt(en)Cl_2] + 2M_2CO_3 + 2RF + 2L \rightarrow [Pt\{N(R)CH_2\}_2L_2] + 2MCl + 2CO_2 + 2H_2O + 2MF \quad (3)$$

M = Tl; L = py; R = p-HC_6F_4 **1a**, C_6F_5 **1b**, p-BrC_6F_4 **1c**, p-IC_6F_4 **1d**, p-MeC_6F_4 **1e**, p-$C_6F_5C_6F_4$ **1f**, 2,3,5-$F_3C_6H_2$ **1g**, p-$O(H)CC_6F_4$ **1h**, p-$MeOC_6F_4$ **1i**; L = tmpy; R = p-HC_6F_4 **1j**; M = K, **1a–1c**.

Details of the preparations are given in Table 1. Syntheses of **1a** with differing mole ratios of M_2CO_3 : $[Pt(en)Cl_2]$ have shown that for M = K or Tl, a 2 : 1 stoichiometry gives higher yields (based on platinum) than a 1 : 1 stoichiometry. Raising the ratio to 4 : 1 for M = K gives only a minor increase in yield. These results are consistent with the stoichiometry of reaction (3). The reactions are sensitive to variation of the cation M. Thus, in the synthesis of **1a**, Tl_2CO_3 is more effective than K_2CO_3, whilst no **1a** could be isolated after use of Na_2CO_3. Similarly, in the syntheses of **1c** and **1d**, Tl_2CO_3 gave a considerably higher yield than K_2CO_3. The effects of the different cations, Tl > K > Na, are not understood at this stage. They cannot be related to the lattice energies of the metal chloride products, since NaCl has the highest lattice energy [12(a)–(c)], but reaction (3) fails with M = Na. The reaction mixtures are heterogenous with a number of reactants and products evidently near insoluble in pyridine or tmpy. In these circumstances, subtle solubility differences may have a considerable effect on the outcome. Possibly the solubility of TlCl compared with that of Tl_2CO_3 is more favourable than for NaCl in relation to Na_2CO_3. All three metal chlorides are reported to be insoluble in dry pyridine [12(d)–(f)], but subtle differences may be revealed by quantitative measurements, as observed for these salts in the polar organic solvent methanol, where the solubilities are TlCl < KCl < NaCl [13]. A similar sequence for pyridine would favour reaction (3), M = Tl. The variability in reactivity of K_2CO_3 with different fluorocarbons (reasonably reactive with C_6F_5H, C_6F_6, C_6F_5Br but unreactive with C_6F_5I) could reflect the effect of the added fluorocarbon on relative solubilities. Certainly, the reactivity of C_6F_5I to nucleophilic substitution (see reaction path) is not expected to be dramatically different from that of C_6F_5Br [14].

The yields from the preparations (3) are compared with those from reactions (1) and (2) in Table 2. From reaction (3) with M = K, the yields are generally comparable with those from (1) or (2), except in the synthesis of **1d** where reaction (2) is more effective. However, for M = Tl, reaction (3) normally gives *much* higher yields than (1) or (2), and this is particularly evident in the syntheses of **1d** in pyridine and of the new complex **1j** in tmpy. Moreover, the successful synthesis of **1h** and the detection of **1i** contrasts earlier failures to obtain these products by reaction (2) [1]. The successful synthesis of **1h** also led to an attempt to induce reaction (3) with the substrates $C_6F_5CF_3$ and o-$H_2C_6F_4$, which had failed in reaction

Table 1. Synthesis of $[Pt\{N(R)CH_2\}_2L_2]$ complexes from $[Pt(en)Cl_2]$, a polyfluorobenzene and a metal carbonate in a pyridine[a]

M_2CO_3 (M)	Amount (mmol)	Polyfluoroarene	Amount (mmol)	Temperature (°C)	Time (h)	Product	Yield[b] (%)	CO_2 (%)
Tl	1.0	C_6F_5H	9.0	115–120	1	**1a**	24	100
Tl	2.0	C_6F_5H	9.0	115–120	1	**1a**	60 (42)	100
K	1.0	C_6F_5H	9.0	115–120	1	**1a**	21	100
K	2.0	C_6F_5H	9.0	115	1	**1a**	44	100
K	4.0	C_6F_5H	9.0	115	1	**1a**	49	
K[c]	2.0	C_6F_5H	18.0	110–115	1	**1a**	30	60
Na	2.0	C_6F_5H	9.0	115–120	1	—	—	trace
K	2.0	C_6F_6	8.7	120	1	**1b**	43	100
Tl	2.0	C_6F_6	9.0	115	1	**1b**	62 (44)	100
K	2.0	BrC_6F_5	8.0	115	1	**1c**	26	30
Tl	2.0	BrC_6F_5	8.0	115	1	**1c**	60 (28)	100
K	2.0	IC_6F_5	8.0	115	1	—	—	15
Tl	2.0	IC_6F_5	8.0	115	1	**1d**	73 (28)	100
Tl	2.0	MeC_6F_5	8.0	115	1.5	**1e**	27 (23)	40
Tl	2.0	$C_6F_5C_6F_5$	6.0	115	1	**1f**	44 (6)	100
Tl	2.0	1,2,3,5-$C_6F_4H_2$	9.0	115	2	**1g**	36 (22)	45
Tl	2.0	$C_6F_5C(H)O$	3.0	60–70	1	**1h**	20 (—)	80
Tl	2.0	$MeOC_6F_5$	9.0	115	2	**1i**	8[d] (—)	85
Tl[e]	2.0	C_6F_5H	9.0	110–115	1	**1j**	29	100
Tl	2.0	C_6F_5H	18.0	100–110	1	**1j**	55 (29)	100

[a] All reactions with $[Pt(en)Cl_2]$ (1.0 mmol) in 10 cm^3 of pyridine or substituted pyridine.
[b] Yield of recrystallized, spectroscopically pure, product. Figures in parentheses are reported yields from reaction (1) or (2) [1].
[c] $KHCO_3$ used: At 80°C (1.5 h) **1a** (7%) and CO_2 (7%) were obtained.
[d] Because of the low yield, this compound was identified only by ^1H and ^{19}F NMR spectroscopy.
[e] $TlO_2CC_6F_5$ was used instead of Tl_2CO_3.

(2) [1], but no organoamidoplatinum(II) complexes were isolated despite evolution of the expected CO_2. Thus, reaction (3), M = Tl has a *major* advantage over (1) or (2) in terms of yield. In addition, it eliminates the need (and cost) to synthesize $TlO_2CC_6F_5$ or $TlO_2CC_6F_4H$-*p* from Tl_2CO_3 and the poly-

Table 2. Syntheses of [*N*-Phenyl-*N'*-(polyfluorophenyl)ethane-1,2-diaminato(2-)]dipyridineplatinum(II) complexes[a]

TlO_2CR (R)	Amount (mmol)	M_2CO_3 (M)	Amount (mmol)	Polyfluoroarene	Amount (mmol)	Temperature (°)	Time (min)	Product	Yield[b] (%)
C_6F_5	2.0			C_6F_5H	18.0	80–85	45	**2a**	25
		Tl	2.0	C_6F_5H	18.0	80–85	45	**2a**	25
		K	2.0	C_6F_5H	18.0	115	360	—	—
C_6F_5	2.0			C_6F_5H	18.0	85–90	45	**2b**[c]	36
p-HC_6F_4	2.0			C_6F_6	26.0	85–90	60	—	—
p-HC_6F_4	4.0			C_6F_6	43.3	95–100	45	**2c**	41[d]
		Tl	2.0	C_6F_6	17.4	80–85	60	**2c**	32
p-HC_6F_4	2.0			C_6F_5Me	39.5	85	45	—	—
		Tl	2.0	C_6F_5Me	15.8	80–85	60	**2d**	6[b], 26[e]
		Tl	2.0	C_6F_5Cl	15.5	80–85	60	**2e**	17
p-HC_6F_4	2.0			C_6F_5Br	40.1	85–88	60	—	—
p-HC_6F_4	4.0			C_6F_5Br	40.1	90–95	50	—	—
		Tl	2.0	C_6F_5Br	16.0	80–85	60	**2f**	24

[a] All reactions with $[Pt\{NH(Ph)CH_2CH_2NH_2\}I_2]$ (1.0 mmol) in 10 cm^3 of pyridine or, in one case, 4-methylpyridine.
[b] Yield of recrystallized material which was analytically pure.
[c] 4-Methylpyridine was used as the solvent.
[d] Not reproducible.
[e] Yield of recrystallized material which was spectroscopically pure.

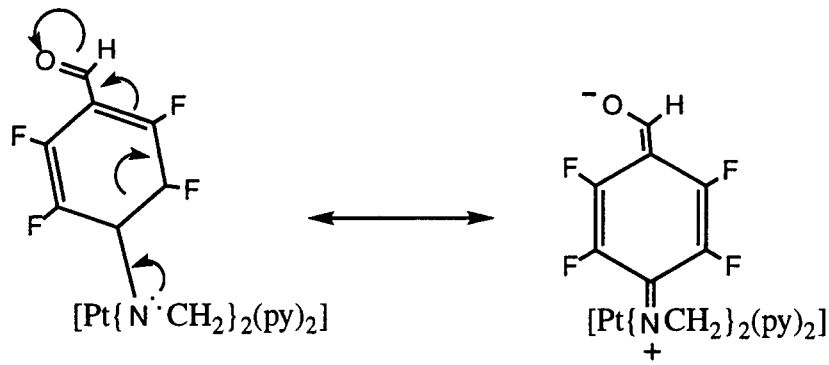

fluorobenzoic acids, and obviates the carbonation preparation of p-$HC_6F_4CO_2H$, which is not commercially available.

The crude products **1c**–**1e** showed the presence of small amounts of impurities, attributable to other isomers, $[Pt\{N(m\text{-}XC_6F_4)CH_2\}_2(py)_2]$ and $[Pt\{N(o\text{-}XC_6F_4)CH_2\}_2(py)_2]$ (X = Br, I or Me), which were removed by a single recrystallization. The complexes **1a**–**1g** had spectroscopic properties in agreement with those previously reported [1], whilst the new complexes **1h** and **1j** were microanalytically pure and had ^1H and ^{19}F NMR spectra (Experimental Section) consistent with the proposed structures, including $^3J_{Pt,H(py)}$ coupling constants. Complex **1j** gave a parent ion in the mass spectrum whereas **1h** gave no platinum containing peaks. Fragment ions indicative of the various ligands were evident. The infrared spectrum of **1h** gave an aldehyde ν(C=O) absorption at 1687 cm^{-1}. This is at lower energy than that of $C_6F_5C(H)O$ (1715 cm^{-1}) [15] suggesting that delocalization of the amido nitrogen lone pair into the polyfluorophenyl ring, established by X-ray diffraction of several polyfluorophenyl-substituted organoamidoplatinum(II) complexes [16], is extended to the carbonyl oxygen.

The aldehyde proton was observed at 9.79 ppm in the ^1H NMR spectrum, which is near the high frequency limit owing to the electron-withdrawing effect of the fluorocarbon substituent. Because the new complex **1i** was obtained only in low yield, it was identified solely by ^1H and ^{19}F NMR spectroscopy (Experimental Section).

The reaction path for the Tl_2CO_3 *based synthesis*

Reaction (3) is considered to involve initially the formation of $[Pt(en)(py)_2]CO_3$ (reaction 4)), since this complex was identified in the insoluble material from heating $[Pt(en)Cl_2]$ and Tl_2CO_3 in pyridine at 110°C. Formation of carbonato complexes from metal chlorides and ionic carbonates is a standard preparative method [17], but is unlikely here in a polar solvent which coordinates well to platinum.

$$[Pt(en)Cl_2] + Tl_2CO_3 + 2py \rightarrow [Pt(en)(py)_2]CO_3 + 2TlCl \quad (4)$$

That $[Pt(en)(py)_2]CO_3$ can be a precursor of the complexes **1** was shown by the reaction of the authentic compound (from $[Pt(en)(py)_2]Cl_2$ and Ag_2CO_3) with C_6F_5H in toluene/pyridine at 110°C, when CO_2 and **1a** were obtained. (The reaction could not be induced in toluene alone.)

$$2[Pt(en)(py)_2]CO_3 + 2C_6F_5H \xrightarrow{py} \mathbf{1a} + 2H_2O + 2CO_2 + [Pt(en)(py)_2]F_2 \quad (5)$$

Little CO_2 was evolved during reaction (4), hence deprotonation of $[Pt(en)(py)_2]^{2+}$ by CO_3^{2-}, giving the amide nucleophile $[Pt(NHCH_2)_2(py)_2]$ (which substitutes into polyfluoroarenes in the proposed path for reactions (1) and (2) [1]), can be ruled out, because the coproduced bicarbonate ions (reaction (6)) would decompose into CO_2 at the reaction temperature.

$$[Pt(en)(py)_2]CO_3 + Tl_2CO_3 \not\rightarrow [Pt(NHCH_2)_2(py)_2] + 2TlHCO_3 \quad (6)$$

This is demonstrated by the thermal decomposition of potassium bicarbonate in pyridine at 90–100°C.

$$2KHCO_3 \rightarrow H_2O + CO_2 + K_2CO_3 \quad (7)$$

In addition, $[Pt(en)Cl_2]$ does not react with C_6F_5H in pyridine in the absence of added base, e.g. CO_β^{2-} in the present systems. Thus a path involving displacement of a coordinated —NH_2 group of ethane-1,2-diamine by pyridine, and nucleophilic attack of the free —NH_2 on the polyfluoroarene can be excluded. Accordingly, we propose that hydrogen bonding between —NH_2 and CO_3^{2-}, e.g. in $[Pt(en)(py)_2]CO_3$, although insufficient to cause deprotonation (see reaction (6)), is strong enough to generate partial lone pair character on nitrogen and hence promote nucleophilic substitution in the polyfluoroarene, e.g. for C_6F_5H in Scheme 1.

Thus CO_2 evolution derives from thermal decomposition of HCO_3^- and reaction of pyridinium fluoride (Scheme 1) with CO_3^{2-} or HCO_3^-, e.g. $2pyHF + Tl_2CO_3 \rightarrow 2TlF + CO_2 + H_2O$. The plausibility of this reaction, which is consistent with pK_a values ($pyH^+ = 5.25$, $H_2CO_3 = 6.37$ and $HCO_3^- = 10.25$), was shown by CO_2 formation on

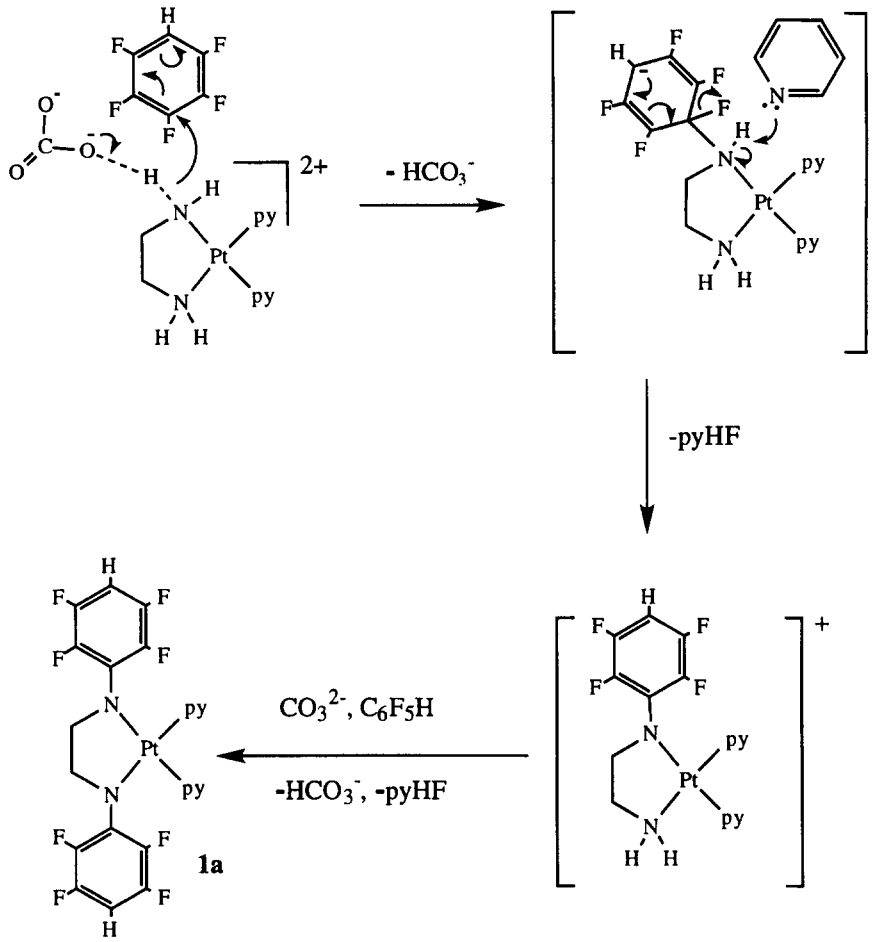

Scheme 1.

reaction of pyridinium mesitylenesulfonate with Tl_2CO_3 [18]. The proposed path explains the key observation that CO_2 evolution only occurs on addition of the polyfluoroarene. It is also consistent with a lower reaction temperature for reaction (3), RF = C_6F_5CHO, than for other polyfluoroarenes (Table 1), since the Meisenheimer intermediate (e.g. Scheme 1) can be stabilized by delocalization of charge onto the carbonyl oxygen. It is of interest that **1a** can also be prepared by reaction of $[Pt(en)Cl_2]$ with $KHCO_3$ and C_6F_5H in pyridine, but only at a temperature where decomposition of bicarbonate ions into carbonate, e.g. reaction (7), is observed.

Preparation of [N-(phenyl)-N′-(polyfluorophenyl) ethane-1,2-diaminato(2-)]dipyridineplatinum(II) complexes

Reactions utilizing thallium(I) polyfluorobenzoates or thallium(I) carbonate were also used to produce a new class of platinum(II) amides, namely [*N*-(phenyl) *N*′-(polyfluorophenyl)ethane-1,2-diaminato(2-)] dipyridineplatinum(II) complexes (eq. (8)–(10)). The complexes **2a–f** are light sensitive, especially when in solution, and great care was taken to minimize the exposure to light during their synthesis. Only three compounds, **2a–c**, were able to be synthesized by reac-

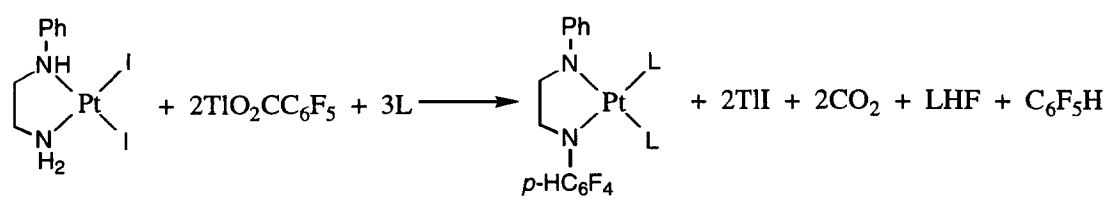

L= py **2a** or 4-methylpyridine (fmpy) **2b** (8)

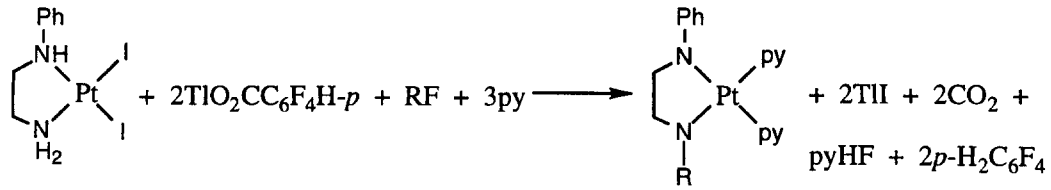

$$+ 2TlO_2CC_6F_4H\text{-}p + RF + 3py \longrightarrow + 2TlI + 2CO_2 + pyHF + 2p\text{-}H_2C_6F_4$$

R=C_6F_5 **2c** (9)

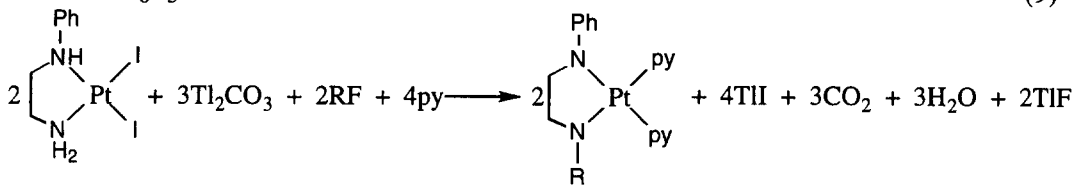

$$2 + 3Tl_2CO_3 + 2RF + 4py \longrightarrow 2 + 4TlI + 3CO_2 + 3H_2O + 2TlF$$

R=*p*-HC_6F_4 **2a**, C_6F_5 **2c**, *p*-MeC_6F_4 **2d**, *p*-ClC_6F_4 **2e**, *p*-BrC_6F_4 **2f** (10)

tions (8) and (9). All attempts to obtain **2d** and **2f** by reaction (9) failed, whilst the preparation of **2c** by (9) was not reproducible. However, reaction (10) has been established as a general route by the successful syntheses of **2a** and **2c–2f**. When the preparation of **1a** was attempted with potassium carbonate, little CO_2 was evolved and no ether soluble products were formed. In general, it was observed that the reactions involving thallium(I) carbonate were cleaner and contained less dark coloured impurities than those involving thallium(I) polyfluorobenzoates (see Table 2). The syntheses (8)–(10) involve polyfluorophenylation of a single —NH_2 group by paths analogous to those for the two —NH_2 groups in reactions (1)—(3) respectively, together with the deprotonation of a coordinated —NHPh group.

All compounds (**2a–2f**) were obtained analytically pure. The infrared spectra of the complexes indicated the presence of the polyfluoroaromatic group by strong ν(CF) absorptions in the region 1000–900 cm^{-1}, as expected [1]. The presence of the monosubstituted phenyl group was indicated by strong characteristic absorptions at 749–746 cm^{-1} and 702–691 cm^{-1} for all complexes [19]. The electron impact mass spectra of the complexes **2a–2f** confirmed the presence of the organoamide and pyridine ligands, with $[PhNHCH_2CH_2NH(R)]^+$ as the highest observed peak in all spectra. The Fast Atom Bombardment mass spectrum of **2a** showed a protonated molecular ion. The UV-Vis spectra gave electronic absorption maxima and extinction coefficients in the range for platinum(II) polyfluorophenylamides [1]. Upon exposure to light, the absorption band weakened and insoluble decomposition products were formed.

Table 3. $^3J_{H,Pt}$ coupling constants (Hz) for **2a–2f**

Complex	CH_2NPh	H2,6(py) ppm	$^3J_{H,Pt}$	H2,6(py) ppm	$^3J_{H,Pt}$
2a	25	8.80	29	8.88	38
2b	—	8.59	32	8.69	23
2c	26	8.77	28	8.84	37
2d	—	8.83	29	8.86	35
2e	25	8.82	38	8.90	38
2f	—	8.82	29	8.89	38

The ^{19}F NMR chemical shifts of **2a–2f** were in good agreement with those calculated by use of substituent chemical shifts [1,20]. The ^1H NMR spectra revealed two different pyridine ligands and CH_2 groups, as expected from the unsymmetrical nature of the organoamide ligands. One CH_2 resonance is fairly constant (3.06–3.10 ppm) for all complexes **2a–2f** (Experimental Section), whilst the other resonance shows greater variation, 3.27–3.46 ppm. Thus, it can be concluded that the former is adjacent to the NPh group, whilst the latter is next to the varying NR group. The low frequency resonance is always a triplet as expected for CH_2 adjacent to the NPh group, whilst the other peak is always an unresolved complex multiplet since coupling is expected with *ortho*-fluorines in addition to the adjacent CH_2 group. The inequivalent pyridine ligands give overlapping, but distinctly recognizable *ortho* resonances. Only one resonance each is seen for the *meta* and *para* protons, but the peaks are unresolved multiplets in contrast to their usually well defined splitting patterns.

For **2a, 2c** and **2e**, ^{195}Pt satellites are observed on the resonance of the CH_2NPh group and the $^3J_{H,Pt}$ coupling constants (Table 3) approach the values for the CH_2 group in complexes of the type $[Pt\{N(R)CH_2\}_2(py)_2]$ (27–30 Hz) [1]. Approximate $^3J_{H,Pt}$ coupling constants can be determined from the overlapping H2,6 resonances of both pyridine ligands (Table 4). The larger, usually higher frequency values (32–38 Hz), which are similar to those of **1a–1e** (33–34 Hz) [1], may plausibly be assigned to the pyridine *trans* to —N(R) (R = polyfluorophenyl). However,

Table 4. Selected bond distances (Å) and angles (°) for **2d**

Pt—N(1)	1.991(5)	N(1)—Pt—N(2)	82.1(2)
Pt—N(2)	2.023(7)	N(1)—Pt—N(3)	173.7(3)
Pt—N(3)	2.042(5)	N(1)—Pt—N(4)	93.0(2)
Pt—N(4)	2.052(7)	N(2)—Pt—N(3)	94.0(2)
C(1)—N(1)	1.40(1)	N(2)—Pt—N(4)	175.1(2)
C(10)—N(2)	1.37(1)	N(3)—Pt—N(4)	90.9(2)
N(1)—C(8)	1.46(1)	C(1)—N(1)—C(8)	117.6(5)
N(2)—C(9)	1.47(1)	C(8)—N(1)—Pt	114.1(4)
		C(1)—N(1)—Pt	128.3(5)
		C(10)—N(2)—C(9)	118.6(6)
		C(9)—N(2)—Pt	107.8(3)
		C(10)—N(2)—Pt	127.1(4)

this must be qualified by the difficulty in resolving the overlapping satellites, the two high J values for **2e**, and inversion of the J value/frequency relationship with **2b**.

X-ray crystal structure of [Pt{N(Ph)CH_2CH_2N(*p*-MeC_6F_4)}$(py)_2$] **2d**

The molecular structure of [Pt{N(Ph)CH_2CH_2N(*p*-MeC_6F_4)}$(py)_2$] **2d** is displayed in Fig. 1. Crystallographic details are given in the Experimental Section, and selected bond distances and angles in Table 4. Two amide and two pyridine nitrogen donor atoms have an approximately square planar arrangement around platinum, with N—Pt—N bond angles (Table 4) distorted from 90°, the smallest being the bite angle of the chelating amide. The platinum centre is only 0.0411 Å out of the plane of donor atoms. The bond angles about the polyfluorophenylamide nitrogen N(1) (Σ360°) and phenylamide nitrogen N(2) (Σ354°) are distorted from tetrahedral (Σ328.5°) towards trigonal (Σ360°), indicative of substantial delocalization of the amide ion lone pair into the phenyl and polyfluorophenyl rings. This is confirmed by the bond distances between the amide nitrogens and carbon atoms of the polyfluorophenyl and phenyl groups, N(1)—C(1) = 1.40(1) and N(2)—C(10) = 1.37(1) Å, respectively, which are closer to N—C aromatic distances than to an N—C single bond length. Near triangular amide nitrogen stereochemistry and short N—C bond lengths, have also been observed in other fluorocarbon-stabilized platinum(II) amides [16], and in anilido-, *N*-phenylanilido and *N*-methylanilido-platinum(II) complexes, *trans*-[PtH(NHPh)$(PEt_3)_2$] [9], [PtCl$(NPh_2)(PEt_3)_2$] [21] and [PtMe(NMePh)$(Me_2PCH_2)_2$] [22], respectively. The Pt—N(py) bond distances (2.042(5), and 2.052(7) Å) are longer than in [Pt{N(*p*-HC_6F_4)CH_2}$_2$$(py)_2$] (1.98 Å) [16(a)] but comparable with those observed for other polyfluorophenylamidoplatinum(II) complexes (2.037–2.065 Å) [16(b)–16(d)]. No significant difference between the bond length *trans* to NPh or N(*p*-MeC_6F_4) is observed. The Pt—N(amide) bond distances (1.991(5) and 2.023(7) Å) are shorter than those observed for [Pt{N(*p*-HC_6F_4)CH_2}$_2$$(py)_2$] (2.08 Å) [16(a)], though in the range (1.995–2.017 Å) for other polyfluorophenylamidoplatinum(II) complexes [16(b)–16(d)]. The *p*-MeC_6F_4 and C_6H_5 rings are inclined at 56.2 and 47.9° respectively to the coordination plane, whilst the pyridines *trans* to NPh and N(*p*-MeC_6F_4) are inclined at 63.6° and 33.1° respectively, to the coordination plane, with a dihedral angle between the two pyridines of 67.2°. The larger inclination of the pyridine *trans* to NPh is due to the bulky *p*-MeC_6F_4 group *cis* to the pyridine.

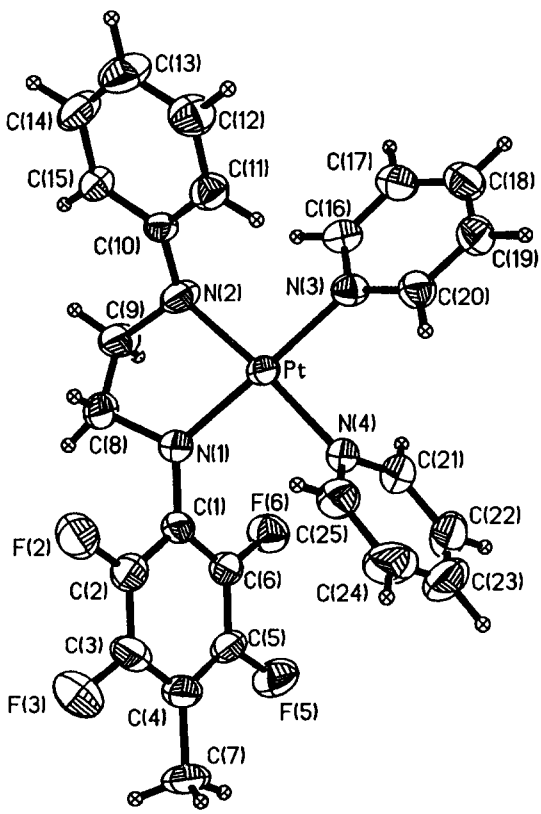

Fig. 1. The molecular structure of [Pt{N(Ph)CH_2CH_2N-(*p*-MeC_6F_4)}$(py)_2$] **2d**.

The new complexes **2** retain the stability to water observed for the complexes **1**, hence introduction of an NPh group does not create hydrolytic instability, although the complexes *trans*-[PtH(NHPh)$(PEt_3)_2$] [9], [PtCl$(NPh_2)(PEt_3)_2$] [21] and [PtMe(NMePh)$(Me_2PCH_2)_2$] [22] are moisture-sensitive. As judged by N—C(Ar) distances and sums of bond angles at amide nitrogen atoms, the extent of delocalization of the amide lone pair appears similar in water-stable and water-sensitive organoamidoplatinum(II) complexes (Table 4 and [9,16,21,22]). Possibly then, the origin of the water-stability of the polyfluorophenylamidoplatinum(II) complexes arises because the fluorocarbon substituents prevent release of electron density to the amide nitrogen on approach of an electrophile ($H^{\delta+}$ of water). However, electron release is

possible with unidentate phenylamide ligands. The stability of the Pt—NPh(CH_2—) bond of the complexes **2** by contrast with Pt—NMePh of [PtMe(NMePh)(Me_2PCH_2)$_2$] may derive from steric inhibition of the approach of water with the pyridine ligands and aryl groups substantially inclined to the coordination plane.

EXPERIMENTAL

General methods

Microanalyses were performed by Campbell Microanalytical Laboratories, University of Otago, New Zealand. Infrared spectra in the range 4000–650 cm^{-1} were recorded with a Perkin-Elmer 1600 F.T.I.R. spectrophotometer as Nujol and hexachlorobutadiene (HCB) mulls. ^1H and ^{19}F NMR spectra were recorded with a Bruker AM300 spectrometer; the solvent used was $(CD_3)_2CO$. Proton chemical shifts are referenced to internal tetramethylsilane and fluorine chemical shifts to internal trichlorofluoromethane. Mass spectra were recorded with a VG Micromass 7070F or VG-TRIO GC-Mass spectrometer. FAB mass spectra were recorded with a Kratos (AEI) MS30 mass spectrometer by Professor J. M. Miller, Brock University, Canada, using 3-nitrobenzyl alcohol as the matrix liquid. For platinum containing ions, clusters with the correct isotope pattern were observed. UV/Visible spectra were recorded with a Hitachi 150-20 spectrophotometer, the solvent being 95% ethanol. Molar (decadic) absorption coefficients are given in units of $dm^3\ mol^{-1}\ cm^{-1}$.

Solvents and reagents

Nitrogen gas was purified by passage through copper "catalyst" (BASF R3-11) and molecular sieves (4 Å). Diethyl ether was of anhydrous analytical grade. Light petroleum refers to the fraction boiling between 60–80°C. All pyridines were distilled and stored under nitrogen. Pyridine and 3-methylpyridine were refluxed over and distilled from potassium hydroxide pellets and stored over molecular sieves (4 Å). 4-Methylpyridine (fmpy) was dissolved in 20% (by volume) sulfuric acid when the non-basic impurities were removed by steam distillation. After addition of solid sodium hydroxide, fmpy was separated by decantation and then dried over and distilled from sodium hydroxide pellets. Literature methods were used to prepare thallium(I) pentafluorobenzoate [23], thallium(I) 2,3,5,6-tetrafluorobenzoate [23], potassium tetrachloroplatinate [24], dichloroethane-1,2-diamineplatinum(II) (by application [25(a)] of the Dhara method [25(b)]) and ethane-1,2-diaminedipyridineplatinum(II) chloride [26]. Polyfluoroaromatics were purchased from Bristol Organics, Imperial Smelting and Aldrich and were used without purification. Thallium(I) carbonate (Johnson Matthey) and *N*-phenylethane-1,2-diamine (Aldrich) were used without purification. Potassium and sodium carbonate were anhydrous and from Ajax chemicals.

Ethane-1,2-diaminedipyridine(II) carbonate

Ethane-1,2-diaminedipyridineplatinum(II) chloride (0.10 g, 0.20 mmol) was dissolved in water (10 cm^3) and freshly prepared silver(I) carbonate (0.60 g, 0.20 mmol) was added. The solution was stirred in the dark for 1 h. Silver chloride was filtered off and the filtrate was concentrated *in vacuo* until a precipitate formed. IR: 3417s(br), 3060s, 1647m, 1602m, *1458m*, 1448s, *1443s*, 1410w, 1370w, 1320w, 1157s, 1132m, 1073w, 1052s, 883w, 762m, 696m cm^{-1}. (Stretching frequencies italicized are assigned to ν(CO) of CO_3^{2-}.)

Diiodo(N-phenylethane-1,2-diamine)platinum(II)

Potassium iodide (8.8 g, 53 mmol) in water (10 cm^3) was stirred with a solution of K_2PtCl_4 (2.2 g, 5.3 mmol) in water (50 cm^3) for 1.5 h to give a dark brown solution. *N*-Phenylethane-1,2-diamine (0.8 g, 5.9 mmol) was added and the mixture stirred overnight. The resulting yellow precipitate was collected, washed with water, then resuspended in water (50 cm^3) and KI (5.0 g, 30 mmol) added. After 1 h the yellow solid was collected, washed with water, ethanol and ether and dried overnight under vacuum. Yield 2.8 g, 90%. m.p. 210–212°C (dec). Found: C, 16.9; H, 1.7; N, 5.1. $C_8H_{11}I_2N_2Pt$ requires: C, 16.4; H, 2.1; N, 4.8%. IR: 3219m, 3170w, 3127w, 1804w, 1634w, 1611s, 1492m, 1479m, 1415w, 1378w, 1197m, 1154m, 1075m, 1046s, 1022s, 780w, 759m, 721m, 693s cm^{-1}.

Syntheses of [N,N'-Bis(polyfluorophenyl)ethane-1,2-diaminato(2-)]dipyridineplatinum(II) complexes **1**

The compounds were prepared by three methods.

Method 1. Syntheses of complexes 1 using thallium (I), potassium or sodium carbonate. Dichloroethane-1,2-diamineplatinum(II) and thallium(I), potassium or sodium carbonate were placed in a Schlenk flask which was fitted with a condenser and connected to a barium hydroxide trap. The system was purged with nitrogen, and pyridine or a substituted pyridine and the appropriate polyfluoroaromatic compound were added by syringe. The mixture was then heated with stirring. The evolved CO_2 was swept into the barium hydroxide trap by nitrogen and was determined gravimetrically as $BaCO_3$ and the yields are given in Table 1. After the reaction was complete, the reaction mixture was cooled and the solvent removed *in vacuo*. The residue was stirred in light petroleum for at least 1 h, and the liquid was then decanted off. The residue was extracted with acetone which was filtered and concentrated *in vacuo* to 50 cm^3. Decolourizing char-

coal was added for complexes **1c, 1d** and **1i,** where the solutions were very dark. Light petroleum (20 cm^3) was added and evaporation continued until crystallization occurred, except for **1d,** which was crystallized from acetone alone, and **1h** and **1e,** where the acetone extract was evaporated to dryness. Products were recrystallized from acetone/light petroleum, except for **1c** (from Tl_2CO_3), **1d,** and **1e,** which were recrystallized from acetone, and **1h** and **1i,** which were purified by chromatography (below). Similar procedures were used for reactions with potassium and sodium carbonate. Reaction conditions and yields of products are indicated in Table 1. Complexes **1a–1g** were identified by the ^1H and ^{19}F NMR spectra, which were identical with those reported [1].

Method 2. Synthesis of **1a** *using potassium bicarbonate.* Dichloroethane-1,2-diamineplatinum(II), potassium bicarbonate, pyridine and pentafluorobenzene were stirred and heated under nitrogen. Work up was as for method 1. Conditions, amounts of reagents and the yield are given in Table 1.

Method 3. Synthesis of **1j** *using thallium(I) pentafluorobenzoate.* Dichloroethane-1,2-diamineplatinum (II), thallium(I) pentafluorobenzoate, 3-methylpyridine and pentafluorobenzene were stirred and heated under nitrogen. Work up was as for method 1. Conditions, amounts of reagents and the yield are given in Table 1.

[*N,N'-Bis*(2,3,5,6-*tetrafluoro*-4-*formylphenyl*)*ethane*-1,2-*diaminato*(2-)]*dipyridineplatinum(II)* **1h**

The crude black product was dissolved in a minimum of 1:1 acetone/light petroleum and passed through a neutral alumina column with elution by 1:1 acetone/light petroleum. The first yellow-orange band was collected, the solvent partly evaporated and more light petroleum added. Cooling at −10°C overnight gave orange-red crystals. m.p. 226–227°C (dec). Found: C, 41.0; H, 1.9; N, 7.4. $C_{26}H_{16}F_8N_4O_2Pt$ requires: C, 40.9; H, 2.1; N, 7.3%. ^{19}F NMR: −151.0, m, 4F, F3,5; −153.7, m, 4F, F2,6. ^1H NMR: 3.54, s with ^{195}Pt satellites $^3J_{H,Pt}$ 26 Hz, 4H, CH_2; 7.42, t, 4H, H3,5 (py); 7.96, t, 2H, H4 (py); 8.76, d with ^{195}Pt satellites $^3J_{H,Pt}$ 36 Hz, 4H, H2,6 (py); 9.79, s, 2H, CHO. UV/Visible spectrum: 430 nm (ε 71.4×10^3). IR: 2926m, 2862w, 2782m, 1687vs, 1624vs, 1607s, 1547m, 1508w, 1484vs, 1459m, 1449s, 1394vs, 1341m, 1315m, 1304m, 1228m, 1183s, 1090w, 1071m, 1017m, 957m, 819w, 776m, 701m cm^{-1}. Mass spectrum: *m/z* 408 [0.5%, $C_{16}H_4F_8N_2O_2^+$]; 380 [1.2%, $C_{15}H_4F_8N_2O^+$]; 219 [0.5%, *p*-$CHOC_6F_4NCH_2CH_2^+$]; 207 [18%, *p*-$CHOC_6F_4NHCH_3^+$]; 178 [52%, *p*-$CHOC_6F_4H^+$]; 79 [100%, py^+].

[*N,N'-Bis*(2,3,5,6-*tetrafluoro*-4-*methoxyphenyl*)*ethane*-1,2-*diaminato*(2-)]-*dipyridineplatinum(II)* **1i**

The crude product was dissolved in acetone and passed through a neutral alumina column. The first yellow-orange band was collected, and the solution was concentrated *in vacuo* until a precipitate formed. The product which contained impurities was isolated. ^{19}F NMR: −153.3 d, 4F, F(2,6); −163.0 d, 4F, F(3,5). ^1H NMR: 3.08, s with ^{195}Pt satellites $^3J_{Pt,H}$ 27 Hz, 4H, CH_2; 3.76, s, 6H, CH_3; 7.25, t, 4H, H3,5 (py); 7.83, t, 2H, H4 (py); 8.61, s with ^{195}Pt satellites $^3J_{Pt,H}$ 30 Hz, 4H, H2,6 (py).

[*N,N'-Bis*(2,3,5,6-*tetrafluorophenyl*)*ethane*-1,2-*diaminato*(2-)]*di*(3-*methylpyridine*)*platinum(II)* **1j**

This complex was prepared both from Tl_2CO_3 and from $TlO_2CC_6F_5$ (Table 1). m.p. 160–161°C (dec). Found: C, 42.3; H, 2.6; N, 7.8. $C_{26}H_{20}F_8N_4Pt$ requires: C, 42.5; H, 2.7; N, 7.6%. ^{19}F NMR: −144.8, m, 4F, F3,5; −150.6, m, 4F, F2,6. ^1H NMR: 2.15, s, 6H, CH_3; 3.16, s with ^{195}Pt satellites $^3J_{H,Pt}$ 27 Hz, 4H, CH_2; 6.28, tt, 2H, *p*-HC_6F_4; 7.12, t, 2H, H5 (py); 7.64, d, 2H, H4 (py); 8.35, d, 2H, H6 (py); 8.50, d with ^{195}Pt satellites $^3J_{H,Pt}$ 38 Hz, 2H, H2 (py). UV/Visible spectrum: 358 nm (ε 9.0×10^3). IR: 2925w, 2902w, 2849w, 1634s, 1579m, 1496vs, 1474vs, 1445s, 1335m, 1283w, 1166w, 1149m, 1126vs, 1088m, 1044w, 982w, 926vs, 882m, 805m, 770m, 705w cm^{-1}. Mass spectrum: *m/z* 735 [1.9%, M^+]; 380 [1.9%, $C_{12}H_{13}N_2Pt^+$]; 354 [4%, $C_{14}H_6F_8N_2^+$]; 288 [1%, $C_6H_7NPt^+$]; 93 [100%, 3-$Mepy^+$].

Reaction path studies

Thermal stability of thallium(I) carbonate in pyridine. Thallium(I) carbonate (0.94 g, 2.0 mmol) was heated with stirring in pyridine at 115°C for 6.25 h. No CO_2 evolution was evident.

Attempted reaction of thallium(I) carbonate and pentafluorobenzene. Thallium(I) carbonate (2.0 mmol) and pentafluorobenzene (18.0 mmol) were heated in pyridine at 110°C for 1 h under nitrogen. No CO_2 evolution was evident and thallium(I) carbonate was recovered.

Attempted reaction of [*Pt*(*en*)*Cl*$_2$], *pentafluorobenzene and pyridine.* [Pt(en)Cl_2] (1.0 mmol), pentafluorobenzene (18.0 mmol) and pyridine (10 cm^3) were heated at 110°C for 1 h. No reaction was evident. No ether soluble products were obtained and only starting material was identified by infrared spectroscopy.

Reaction of [*Pt*(*en*)*Cl*$_2$], *Tl*$_2$CO$_3$, and pyridine. [Pt(en)Cl_2] (1.0 mmol), Tl_2CO_3 (2.0 mmol) and pyridine (10 cm^3) were heated at 110°C for 1 h. Only a slight liberation of CO_2 was evident. A sample of the insoluble material was isolated and its infrared spectrum was shown to be identical with that of [Pt(en)$(py)_2$]CO_3. Pentafluorobenzene was then added at 110°C producing CO_2 almost immediately. The reaction mixture was heated and stirred for an additional 30 min. Work up as for method 1 produced **1a** (30%), and CO_2 (70%).

Synthesis of **1a** *from ethane-1,2-diaminedipyridineplatinum(II) carbonate.* Ethane-1,2-diaminedipyridineplatinum(II) carbonate (0.10 g, 0.20 mmol) and pentafluorobenzene (1.0 cm^3, 9.0 mmol) were stirred in toluene (10 cm^3) at 110 °C for 1 h under nitrogen. Only a trace amount of CO_2 was detected. Pyridine (5 cm^3) was added at 110 °C and CO_2 was evolved. The resulting yellow reaction mixture was heated and stirred for a further 3 h. Work up was as for method 1 and yielded **1a,** as well as unreacted $[Pt(en)(py)_2]CO_3$.

Syntheses of [N-Phenyl-N′-(polyfluorophenyl)ethane-1,2-diaminato(2-)]dipyridineplatinum(II) complexes **2**

From thallium(I) penta- or 2,3,5,6-tetra-fluorobenzoate or thallium(I) carbonate. Diiodo(*N*-phenylethane-1,2-diamine)platinum(II), thallium(I) penta- or 2,3,5,6-tetra-fluorobenzoate or carbonate, and a polyfluorobenzene were reacted together in pyridine or 4-methylpyridine as in method 1 for $[Pt\{N(R)CH_2\}L_2]$ complexes. Yields of CO_2 were approximately quantitative for successful reactions. After reaction, the solvent was removed under vacuum. The residue was stirred in light petroleum for at least 1 h, and then extracted with ether, the solution being protected from the light at all times. The filtered ether extract was concentrated under reduced pressure to 50 cm^3. Light petroleum (20 cm^3) was added and evaporation continued until crystallization occurred. Reaction conditions and yields are indicated in Table 2. $^3J_{H,Pt}$ coupling constants are given in Table 3. Where the same complex was obtained from more than one reaction, the products had identical spectroscopic properties.

A similar procedure was used in the attempted synthesis of **2a** with potassium carbonate as the reagent. Little CO_2 evolution was observed, and no ether soluble products were obtained.

[N-(Phenyl)-N′-(2,3,5,6-tetrafluorophenyl)ethane-1,2-diaminato(2-)]dipyridineplatinum(II) **2a**

Orange powder. m.p. 145–147 °C (dec). Found: C, 45.1; H, 3.1; F, 11.8; N, 8.5. $C_{24}H_{20}F_4N_4Pt$ requires: C, 45.4; H, 3.2; F, 12.0; N, 8.8%. ^{19}F NMR: −144.7, m, 2F, F3,5; −152.0, m, 2F, F2,6. ^1H NMR: 3.08, t, $^3J_{H,H}$ 6 Hz, 2H, CH_2NPh; 3.41, m, 2H, $CH_2N(p\text{-}HC_6F_4)$; 6.16, m, 2H, *p*-HC_6F_4+H4 (Ph); 6.56, d, $^3J_{H,H}$ 8 Hz, 2H, H2,6 (Ph); 6.65, t, $^3J_{H,H}$ 9 Hz, 2H, H3,5 (Ph); 7.31, m, 4H, H3,5 (py); 7.82, m, 2H, H4 (py); 8.80, d, $^3J_{H,H}$ 5 Hz, 2H, H2,6 (py *trans* to NPh); 8.88, d, $^3J_{H,H}$ 5 Hz, 2H, H2,6 (py *trans* to $N(p\text{-}HC_6F_4)$). UV/Visible spectrum: 342 nm (ε 5.3×10^3). IR: 3063w, 3017w, 2998w, 2915w, 2805w, 1632s, 1604m, 1590s, 1560w, 1490s, 1449s, 1330m, 1312s, 1281m, 1236m, 1155w, 1138s, 1102w, 1061s, 989m, 971m, 934s, 908s, 875m, 837m, 768m, 758s, 746m, 717w, 699s cm^{-1}. Mass spectrum: *m/z* 284 [6%, LH_2^+]; 191 [3%, $p\text{-}HC_6F_4NCH_2CH_2^+$]; 178 [5%, $p\text{-}HC_6F_4NCH_3^+$]; 163 [1%, $p\text{-}HC_6F_4N^+$]; 149 [2%, $p\text{-}HC_6F_4^+$]; 106 [95%, $C_6H_5NCH_3^+$]; 79 [100%, py^+]; 77 [20%, $C_6H_5^+$]; 52 [70%, $C_4H_4^+$]. FAB Mass spectrum: *m/z* 636 [80%, MH^+]; 557 [30%, $(MH-py)^+$]; 488 [10%, $(MH-C_6F_4H)^+$]; 451 [10%, $Pt\{(p\text{-}HC_6F_4)NCH_2\}(py)^+$]; 352 [20%, $(Ptpy_2-H)^+$]; 274 [20%, $Ptpy^+$]; 136 [15%, $C_6H_5NCH_2CH_2NH_2^+$]; 105 [30%, $C_6H_5NCH_3^+$]; 80 [100%, pyH^+].

[N-(Phenyl)-N′-(2,3,5,6-tetrafluorophenyl)ethane-1,2-diaminato(2-)]bis(4-methylpyridine)platinum(II) **2b**

Yellow powder. m.p. 149–151 °C. Found: C, 47.1; H, 4.0; F, 11.6; N, 8.7. $C_{26}H_{24}F_4N_4Pt$ requires: C, 47.1; H, 3.7; F, 11.5; N, 8.4%). ^{19}F NMR: −144.7, m, 2F, F3,5; −152.3, m, 2F, F2,6. ^1H NMR: 2.28, s, 6H, CH_3 (fmpy); 3.06, t, $^3J_{H,H}$ 6 Hz, 2H, $CH_2N(Ph)$; 3.42, m, 2H, CH_2N (*p*-HC_6F_4); 6.15, m, 2H, *p*-HC_6F_4+H4 (Ph); 6.58, d, $^3J_{H,H}$ 8 Hz, 2H, H2,6 (Ph); 6.67, t, $^3J_{H,H}$ 8 Hz, 2H, H3,5 (Ph); 7.11, m, 4H, H3,5 (py); 8.59, d, $^3J_{H,H}$ 6 Hz, 2H, H2,6 (py *trans* to $N(p\text{-}HC_6F_4)$ 8.69, m, 2H, H2,6 (py *trans* to NPh). UV/Visible spectrum: 333 nm (ε 4.3×10^3). IR: 3041w, 2916w, 2866w, 2798w, 1920w, 1804w, 1619s, 1492s, 1363w, 1326m, 1282w, 1243w, 1209m, 1136s, 1098w, 1065m, 984m, 933s, 913m, 813s, 748m, 721m, 700m cm^{-1}. Mass spectrum: *m/z* 284 [9%, LH_2^+]; 178 [5%, $p\text{-}HC_6F_4NCH_3^+$]; 165 [3%, $p\text{-}HC_6F_4NH_2^+$]; 149 [2%, $C_6F_4H^+$]; 118 [2%, $C_6H_5NCH_2CH^+$]; 106 [100%, $C_6H_5NCH_3^+$]; 93 [75%, $Mepy^+$]; 77 [15%, $C_6H_5^+$].

[N-(Pentafluorophenyl)-N′-(phenyl)ethane-1,2-diaminato(2-)]dipyridineplatinum(II) **2c**

Yellow/orange crystals. m.p. 164–166 °C. Found: C, 44.3; H, 3.1; F, 14.6; N, 8.8. $C_{24}H_{19}F_5N_4Pt$ requires: C, 44.1; H, 2.9; F, 14.5; N, 8.6%. ^{19}F NMR: −151.8, dd, $^3J_{F,F}$ 20 Hz, $^4J_{F,F}$ 8 Hz, 2F, F2,6; −168.8, t, $^3J_{F,F}$ 21 Hz, 2F, F3,5; −178.0, m, 1F, F4. ^1H NMR: 3.09, t, $^3J_{H,H}$ 6 Hz, 2H, CH_2NPh; 3.27, m, 2H, $CH_2N(C_6F_5)$; 6.13, t, $^3J_{H,H}$ 7 Hz, 1H, H4 (Ph); 6.46, d, $^3J_{H,H}$ 8 Hz, 2H, H2,6 (Ph); 6.60, m, 2H, H3,5 (Ph); 7.31, m, 4H, H3,5 (py); 7.84, m, 2H, H4 (py); 8.77, m, 2H, H2,6 (py *trans* to NPh); 8.84, m, 2H, H2,6 (py *trans* to $N(C_6F_5)$). UV/Visible spectrum: 339 nm (ε 4.3×10^3). IR: 3056w, 3011w, 2922w, 2900w, 2811w, 1619s, 1606w, 1588s, 1506m, 1488s, 1450m, 1336m, 1240w, 1210w, 1174m, 1090s, 1070m, 1028s, 984s, 953m, 920m, 830w, 766m, 746s, 722w, 691s cm^{-1}. Mass spectrum: *m/z* 302 [8%, LH_2^+]; 298 [5%, $L-2H^+$]; 196 [3%, $C_6F_5NCH_3^+$]; 183 [2%, $C_6F_5NH_2^+$]; 167 [1%, $C_6F_5^+$]; 118 [2%, $C_6H_5NCH_2CH^+$]; 106 [100%, $C_6H_5NCH_3^+$]; 79 [75%, py^+]; 77 [20%, $C_6H_5^+$].

[*N*-(*Phenyl*)-*N'*-(2,3,5,6-*tetrafluoro*-4-*methylphenyl*) *ethane*-1,2-*diaminato*(2-)]*dipyridine-platinum*(*II*) **2d**

Orange crystals. m.p. 149–151°C. Found: C, 46.0; H, 3.5; N, 8.5. $C_{25}H_{22}F_4N_4Pt$ requires: C, 46.2; H, 3.4; N, 8.6%. ^{19}F NMR: −149.9, m, 2F, F3,5; −152.1, m, 2F, F2,6. ^1H NMR: 1.90, t, $^4J_{H,F}$ 2 Hz, 3H, *p*-$CH_3C_6F_4$; 3.09, t, $^3J_{H,H}$ 6 Hz, 2H, CH_2NPh; 3.29, m, 2H, $CH_2N(p\text{-}MeC_6F_4)$; 6.07, t, $^3J_{H,H}$ 7 Hz, 1H, H4 (Ph); 6.44, d, $^3J_{H,H}$ 8 Hz, 2H, H2,6 (Ph); 6.59, t, $^3J_{H,H}$ 7 Hz, 2H, H3,5 (Ph); 7.28, m, 4H, H3,5 (py); 7.81, m, 2H, H4 (py); 8.83, m, 2H, H2,6 (py *trans* to NPh); 8.86 m, 2H, H2,6 (py *trans* to N(*p*-MeC_6F_4)). UV/Visible spectrum: 337 nm (ε 3.8×10^3). IR: 3068w, 2928w, 2857w, 2816w, 1646w, 1610m, 1587s, 1482s, 1450m, 1334m, 1241w, 1210w, 1163m, 1088w, 1069m, 988m, 961w, 926s, 905m, 856w, 828w, 762m, 746m, 722m, 693s cm^{-1}. Mass spectrum: *m/z* 298 [10%, LH_2^+]; 276 [5%, $PtpyH_2^+$]; 193 [8%, *p*-$MeC_6F_4NHCH_3^+$]; 178 [2%, *p*-$MeC_6F_4NH^+$]; 106 [100%, $C_6H_5NCH_3^+$]; 79 [80%, py^+].

[*N*-(4-*Chloro*-2,3,5,6-*tetrafluorophenyl*)-*N'*-(*phenyl*) *ethane*-1,2-*diaminato*(2-)]*dipyridineplatinum*(*II*) **2e**

Orange powder. m.p. 162–164°C. Found: C, 43.0; H, 2.8; N, 8.4. $C_{24}H_{19}ClF_4N_4Pt$ requires: C, 43.0; H, 2.9; N, 8.4%. ^{19}F NMR: −148.6, m, 2F, F3,5; −151.1, m, 2F, F2,6. ^1H NMR: 3.10, t, $^3J_{H,H}$ 6 Hz, 2H, $CH_2N(Ph)$; 3.43, m, 2H, $CH_2N(p\text{-}ClC_6F_4)$; 6.09, t, $^3J_{H,H}$ 7 Hz, 1H, H4 (Ph); 6.43, d, $^3J_{H,H}$ 8 Hz, 2H, H2,6 (Ph); 6.59, m, 2H, H3,5 (Ph); 7.32, m, 4H, H3,5 (py); 7.84, m, 2H, H4 (py); 8.82, d, $^3J_{H,H}$ 5 Hz, 2H, H2,6 (py); 8.90, m, 2H, H2,6 (py). UV/Visible spectrum: 343 nm (ε 6.1×10^3). IR: 3076w, 2922w, 2806w, 1918w, 1830w, 1803w, 1624m, 1611s, 1588m, 1478s, 1451m, 1438m, 1335m, 1296w, 1280w, 1242w, 1210w, 1152s, 1072m, 985s, 940m, 877w, 828w, 758m, 749m, 722m, 694m cm^{-1}. Mass spectrum: *m/z* 318 [15%, LH_2^+]; 212 [10%, *p*-$ClC_6F_4NCH_3^+$]; 118 [10%, $C_6H_5NCH_2CH^+$]; 106 [100%, $C_6H_5NCH_3^+$]; 79 [30%, py^+].

[*N*-(4-*Bromo*-2,3,5,6-*tetrafluorophenyl*)-*N'*(*phenyl*) *ethane*-1,2-*diaminato*(2-)]*dipyridine-platinum*(*II*)-0.25 *diethyl ether* **2f**

Orange/brown powder. m.p. 152–154°C (dec). Found: C, 41.1; H, 2.9; N, 7.8. $C_{25}H_{21.5}BrF_4N_4O_{0.25}Pt$ requires: C, 41.0; H, 2.9; N, 7.7%. ^{19}F NMR: −140.9, m, 2F, F3,5; −150.3, m, 2F, F2,6. ^1H NMR: 1.13, t, 1.5H, CH_3 (ether); 3.10, t, $^3J_{H,H}$ 6 Hz, 2H, $CH_2N(Ph)$; 3.40, 1H, CH_2 (ether); 3.46, m, 2H, $CH_2N(p\text{-}BrC_6F_4)$; 6.13, t, $^3J_{H,H}$ 7 Hz, 1H, H4 (Ph); 6.48, d, $^3J_{H,H}$ 8 Hz, 2H, H2,6 (Ph); 6.62, t, $^3J_{H,H}$ 8 Hz, 2H, H3,5 (Ph); 7.31, m, 4H, H3,5 (py); 7.83, m, 2H, H4 (py); 8.82, d, $^3J_{H,H}$ 5 Hz, 2H, H2,6 (py *trans* to NPh); 8.89, d, $^3J_{H,H}$ 5 Hz, 2H, H2,6 (py *trans* to N(*p*-BrC_6F_4)). UV/Visible spectrum: 345 nm (ε 5.9×10^3). IR: 3074w, 2878w, 2831w, 2803w, 1803w, 1611m, 1606m, 1587s, 1477s, 1451m, 1438m, 1334m, 1278m, 1242w, 1210w, 1177w, 1148s, 1083w, 1071m, 1027w, 985s, 940m, 815m, 758s, 748m, 727w, 702m cm^{-1}. Mass spectrum: *m/z* 362 [5%, LH_2^+]; 284 [5%, *p*-$BrC_6F_4NCH_2CH_2N^+$]; 245 [2%, *p*-$BrC_6F_4NH_3^+$]; 106 [100%, $C_6H_5NCH_3^+$]; 79 [80%, py^+].

CRYSTALLOGRAPHY

Crystal Data for [Pt{N(Ph)CH_2CH_2N(*p*-MeC_6F_4)}$(py)_2$] **2d**

$PtC_{25}H_{22}F_4N_4$; *fw* = 649.6 g/mol; Monoclinic, space group $P2_1/c$. a = 13.845(3), b = 9.790(3), c = 18.405(6) Å; β = 110.73(1)°; V = 2333(1) Å^3, D_c = 1.85 g/cm^3; Z = 4; $F(000)$ = 1256; μ = 61.26 cm^{-1} for Mo-K_α radiation (λ = 0.71073 Å); 293(1) K. Cell parameters were determined from 24 accurately centred reflections measured between $24° < 2\theta < 30°$ and were calculated by the standard Philips program.

Structure determination

A representative yellow-orange acicular crystal of approximate dimensions ($0.10\times0.15\times0.30$ mm) was used for data collection. Intensity measurements were made on a Philips PW1100 diffractometer using graphite monochromated Mo-K_α radiation $6° < 2\theta \leqslant 60°$, operating in an ω scan mode with a symmetric scan range of $\pm(0.80+0.2\tan\theta)°$ in ω from the calculated Bragg scattering angle at a scan rate of 0.03° sec^{-1}. A total of 6800 unique data were collected ($\pm h$, $+k$, $+l$), 3408 of which were considered to be observed [$F \geqslant 6\sigma(F)$], and used in the final refinement. Three standard reflections monitored every 4 h showed no significant variation in intensity over the data collection period. Intensity data were processed as described previously [27]. A face-indexed numerical absorption correction was applied [28], on six crystal faces, the maximum and minimum transmission factors being 0.583 and 0.390, respectively. The atomic scattering factors for neutral atoms were taken from [29] and were corrected for anomalous dispersion by using values from [29]. All calculations were performed on a VAX 6250 computer. The program used for least-squares refinement was that due to Sheldrick [28].

The structure was solved by conventional Patterson and Fourier methods. Final refinement was full-matrix least-squares employing anisotropic thermal parameters for all non hydrogen atoms (single isotropic thermal parameter for hydrogen fixed at 0.08 Å^2—positioned in geometrically idealized positions: C—H 0.96 Å). At convergence (308 variables, 3408 observed data) R was 0.036 and wR 0.035 where

$$wR = \Sigma(|F_o| - |F_c|)\omega^{1/2}/\Sigma|F_o|\omega^{1/2}$$

and $\omega = [\sigma^2(F_o)]^{-1}$. The goodness of fit value $([\Sigma\omega(|F_o| - |F_c|)^2/(N_{observ.} - N_{params.})]^{1/2})$ was 1.29.

Acknowledgements—We would like to thank the Australian Research Council and the Monash Research Fund for support, and Professor J. M. Miller, Brock University, for the FAB mass spectrum.

REFERENCES

1. Buxton, D. P., Deacon, G. B., Gatehouse, B. M., Grayson, I. L., Thomson, R. J. and Black, D. St. C., *Aust. J. Chem.*, 1986, **39,** 2013.
2. Webster, L. K., Deacon, G. B., Buxton, D. P., Hillcoat, B. M., James, A. M., Roos, I. A. G., Thomson, R. J., Wakelin, L. P. G. and Williams, T. L., *J. Med. Chem.*, 1992, **35,** 3349.
3. (a) Webster, L. K., Deacon, G. B. and Rainone, S., Unpublished results; (b) Goddard, P., Valenti, L. and Kelland, L. R., *Anticancer Research*, 1994, **14,** 1065.
4. (a) Van der Veer, J. L. and Reedijk, J., *Chem. Br.*, 1988, **20,** 775; (b) Reedijk, J., *Pure Appl. Chem.*, 1987, **59,** 181; (c) Farrell, N., *Transition Metal Complexes as Drugs and Chemotherapeutic Agents*, Kluwer Academic Publishers, Dordrecht, 1989; (d) Reedijk, J., *Inorg. Chim. Acta*, 1992, **198,** 838; (e) Reedijk, J., *J. Chem. Soc., Chem. Commun.*, 1996, 801; (f) Hambley, T. W., *Chem. in Aust.*, 1991, **58,** 263.
5. Farrell, N., Ha, T., Souchard, J. P., Wimmer, F. L., Cros, S. and Johnson, N. P., *J. Med. Chem.*, 1989, **32,** 2240.
6. Lappert, M. F., Power, P. P., Sanger, A. R. and Srivastava, R. C., *Metal and Metalloid Amides*, Ellis Horwood, Chichester, 1980.
7. Fryzuk, M. D. and Montgomery, C. D., *Coord. Chem. Rev.*, 1989, **95,** 1.
8. Bryndza, H. E. and Tam, W., *Chem. Rev.*, 1988, **88,** 1163.
9. Cowan, R. L. and Trogler, W. C., *J. Am. Chem. Soc.*, 1989, **111,** 4750.
10. (a) Watt, G. W. and Upchurch, D. G., *J. Am. Chem. Soc.*, 1968, **90,** 914; (b) Watt, G. W. and Upchurch, D. G., *J. Am. Chem. Soc.*, 1967, **89,** 177.
11. Deacon, G. B. and Ingram, W. L., Unpublished results.
12. *Gmelins Handbuch der Anorganische Chemie*, (a) Syst. Nr. 21, p. 312; (b) Syst. Nr. 22, p. 359; (c) Syst. Nr. 38, p. 259; (d) Syst. Nr. 21, p. 367; (e) Syst. Nr. 22, p. 464; (f) Syst. Nr. 38, p. 281, Verlag. Chemie, Weinheim/Berlin, 1928/1937, 1953/1940.
13. Stephen, H. and Stephen, T., eds, *Solubilities of Inorganic and Organic Compounds*, Vol. 1, Part 1, Pergamon, Oxford, 1963.
14. (a) Banks, R. E., *Fluorocarbons and Their Derivatives*, Oldbourne Press, London, 1964; (b) Burdon, J., *Tetrahedron*, 1965, **21,** 3373; (c) Burdon, J., Coe, P. L., Marsh, C. R. and Tatlow, J. C., *Tetrahedron*, 1966, **22,** 1183.
15. Pouchert, C. J., ed., *The Aldrich Library of FT-IR Spectra*, Vol. 2, Ed. 1, Spectrum 129C, Aldrich Chemical Co. Inc., 1985.
16. (a) Deacon, G. B., Gatehouse, B. M., Grayson, I. L. and Nesbit, M. C., *Polyhedron*, 1984, **3,** 753; (b) Buxton, D. P., Deacon, G. B., Gatehouse, B. M., Grayson, I. L. and Wright, P. J., *Acta Cryst.*, 1985, **C41,** 1049; (c) Buxton, D. P., Deacon, G. B., Gatehouse, B. M., Grayson, I. L. and Black, D. St. C., *Aust. J. Chem.*, 1988, **41,** 943; (d) Deacon, G. B., Gatehouse, B. M., Ireland, J., *Aust. J. Chem.*, 1991, **44,** 1669.
17. Oldham, C., in *Comprehensive Coordination Chemistry*, ed. G. Wilkinson, R. D. Gillard and J. A. McCleverty, Vol. 2, Ch 15.6, Pergamon, Oxford, 1987.
18. Chow, A., MSc. Thesis, Monash University, 1996.
19. Williams, D. H. and Fleming, I., *Spectroscopic Methods in Organic Chemistry*, 5th ed., McGraw-Hill, London, 1995.
20. Bruce, M. I., *J. Chem. Soc. (A)*, 1968, 1459.
21. Eadie, D. T., Pidcock, A., Stobart, S. R., Brennan, E. T. and Cameron, T. S., *Inorg. Chim. Acta*, 1982, **65,** L111.
22. Bryndza, H. E., Fultz, W. C. and Tam, W., *Organometallics*, 1985, **4,** 939.
23. Deacon, G. B., Faulks, S. J. and Miller, J. M., *Transition Met. Chem.*, 1980, **5,** 305.
24. Brauer, G., ed., *Handbook of Preparative Inorganic Chemistry*, Vol. 2, 2nd edn, Academic, New York, 1965.
25. (a) Buxton, D. P., Ph.D. Thesis Monash University, 1986; (b) Dhara, S. C., *Indian J. Chem.*, 1970, **8,** 193.
26. *Gmelins Handbook of Inorganic Chemistry Main Series*, Vol. 68D, Verlag Chemie, Weinheim, 1957.
27. Fallon, G. D. and Gatehouse, B. M., *J. Solid State Chem.*, 1980, **34,** 193.
28. Sheldrick, G. M., *SHELX-76 Program for Crystal Structure Determination*, Cambridge, England, 1975.
29. Ibers, J. A. and Hamilton, W. C., eds, *International Tables for X-ray Crystallography, Vol. IV*, Kynoch Press, Birmingham, 1974.

Pergamon

PII: S0277-5387(97)00397-5

Polyhedron Vol. 17, No. 5–6, pp. 803–810, 1998
© 1998 Elsevier Science Ltd
All rights reserved. Printed in Great Britain
0277-5387/98 $19.00+0.00

The synthesis of olefin, carbonyl and thiolate complexes of platinum(IV) in the [(η^5-C_5Me_5)Pt(IV)] system. Crystal and molecular structure of (η^5-C_5Me_5)$PtMe_2$[S(p-$CH_3(C_6H_4)$)]†

William A. Howard and Robert G. Bergman

Department of Chemistry, University of California, Berkeley, CA 94720, USA

(Received 9 June 1997; accepted 1 July 1997)

Abstract—A number of Cp*$PtMe_2X$ and Cp*$PtMe_2(L)^+(OTf)^-$ complexes have been prepared [Cp* = η^5-C_5Me_5; OTf = OSO_2CF_3; X = OTf, I, N_3, S(*p*-tol); L = CO, C_2H_4, CH_2=CHMe, NH_3, NH_2Bu^t]. The complexes Cp*$PtMe_2(CO)^+(OTf)^-$, Cp*$PtMe_2(C_2H_4)^+(OTf)^-$, and Cp*$PtMe_2(CH_2$=$CHMe)^+(OTf)^-$ represent a rare type of compound in which a π acid ligand is coordinated to a high valent metal center predominantly through σ-donation and π-backbonding plays only a limited role in the metal–ligand interaction. The arylthiolate complex, Cp*$PtMe_2$[S(*p*-tol)], has been structurally characterized by X-ray diffraction. © 1998 Elsevier Science Ltd. All rights reserved

Keywords: platinum; Pt(IV); pentamethylcyclopentadienyl; alkene; azide; carbonyl; thiolate; azide; triflate complexes.

Although alkoxide complexes of platinum(II) have been well-studied [1], such derivatives of platinum(IV) are much rarer [2], and so the chemistry and the physical properties of these compounds have not been thoroughly examined. Bradley has done extensive work on the use of metal alkoxides as precursors for the deposition of metal oxides [3], and we have recently described the use of volatile *cis*-bis(η^2,η^1-pent-4-en-1-yl)platinum in the deposition of pure thin platinum films [4]. We sought to synthesize various alkoxide derivatives of platinum(IV) in order to study their fundamental chemistry and to examine their potential as precursors in chemical vapor deposition.

The pentamethylcyclopentadienyl ligand (*abbr.* Cp*) has been used to stabilize a variety of alkoxo and amido derivatives of the late transition metals such as Cp*$Ir(PPh_3)(OEt)(H)$ [5] and Cp*$Ni(PMe_3)(NH(p\text{-tol}))$ [6], but this ligand has not been used extensively in platinum chemistry. In fact, only seven [Cp*Pt] compounds had been reported in the literature before 1990 [7]. Since platinum(IV) complexes are invariably six-coordinate, the three-coordinate monovalent Cp* ligand seems ideally suited as an ancillary ligand for stabilizing alkoxide derivatives of Pt(IV). Useful synthetic routes into [Cp*Pt(IV)] compounds were provided independently by the research groups of Sharp [8] and Roesky [9] in 1990. These researchers described a number of [Cp*Pt(IV)] derivatives with halide and methyl ligands, but [Cp*Pt(IV)] complexes with oxygen-, nitrogen-, or sulfur-based ligands were not reported.

The goals of this work are to synthesize new derivatives of [Cp*Pt(IV)] having bonds between Pt and electronegative atoms such as O, S and N and to study the physical and chemical properties of these compounds. Although we have not been able to isolate and fully characterize simple Cp*-substituted platinum alkoxides or aryloxides, we have found the Cp* ligand to be useful for stabilizing several unusual [Pt(IV)-ligand] moieties, including some with Pt—O and Pt—S bonds. Platinum(IV) complexes with triflate, olefin, carbonyl, and arylthiolate functional groups have been isolated and are described herein.

RESULTS AND DISCUSSION

As shown in Scheme 1, Cp*$PtMe_2(OTf)$ (OTf = OSO_2CF_3) may be isolated as an air-stable,

† Dedicated to Professor Donald C. Bradley, whose research has greatly influenced much of the work that has gone on in our group during the past several years.

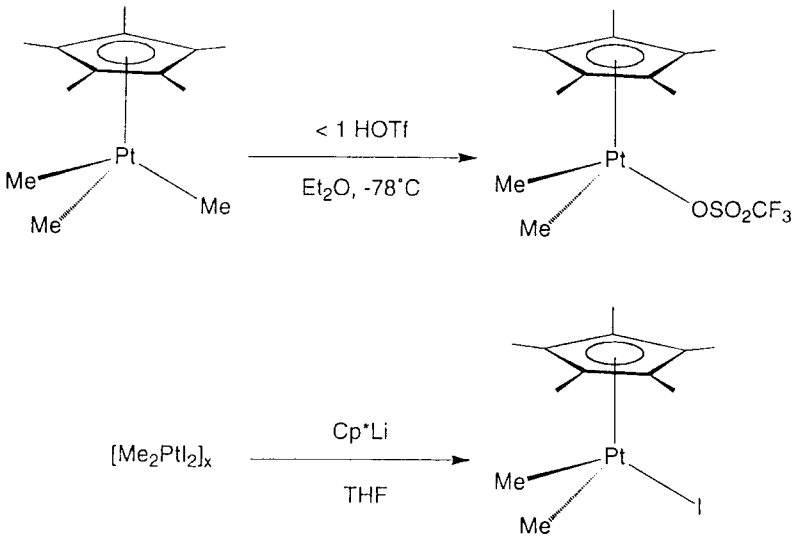

Scheme 1.

bright orange crystalline solid in greater than 90% yield by reaction of Cp^*PtMe_3 [9] with slightly less than one equivalent of trifluoromethanesulfonic acid (i.e., triflic acid) at −78°C. Using more triflic acid only results in a lower yield of $Cp^*PtMe_2(OTf)$. The presence of the triflate ligand in $Cp^*PtMe_2(OTf)$ is confirmed by a singlet in the ^{19}F NMR spectrum (CD_2Cl_2) at −15.8 ppm and by very strong absorptions at 1294 cm^{-1}, 1250 cm^{-1}, 1176 cm^{-1}, and 1032 cm^{-1} in the infrared spectrum [10]. Also shown in Scheme 1 is the synthesis of Cp^*PtMe_2I, which may be isolated in 59% yield as an air-stable, reddish orange solid from the reaction of $[Me_2PtI_2]_x$ with Cp*Li at room temperature, similar to Sharp's synthesis of Cp^*PtMe_2Br [8].

The results of investigating the reactivity of $Cp^*PtMe_2(OTf)$ are illustrated in Scheme 2. The triflate ligand is easily displaced from the platinum center in $Cp^*PtMe_2(OTf)$ by various dative ligands (L) such as C_2H_4, CH_2=CHMe, Co, NH_3, and

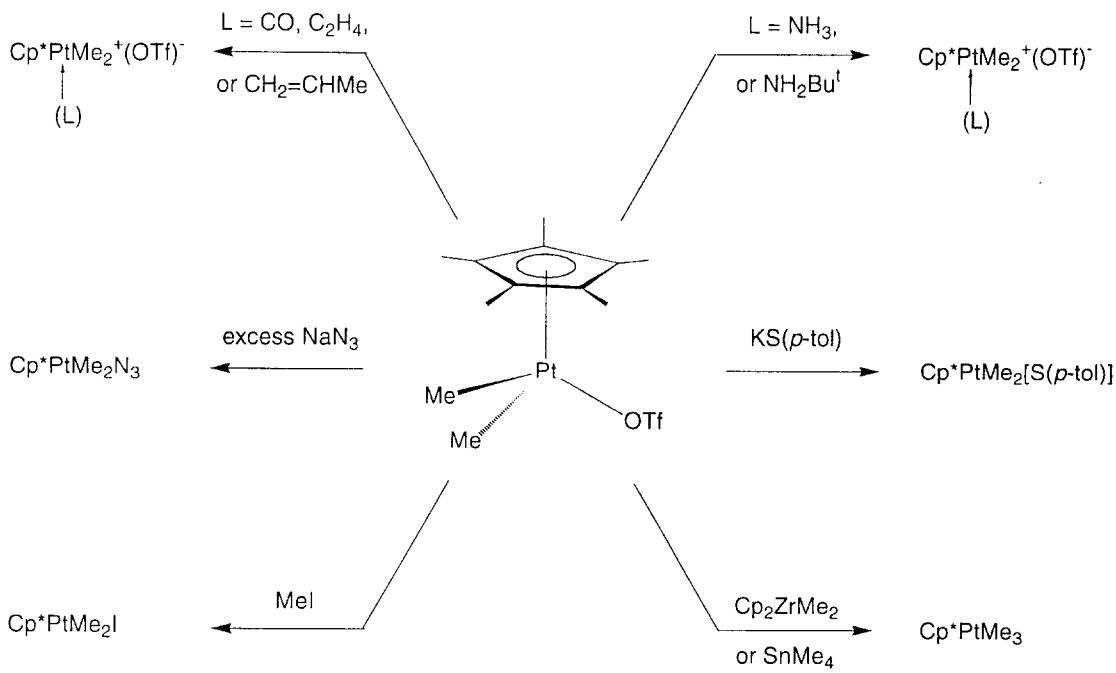

Scheme 2.

NH_2Bu^t to afford the salts $Cp^*PtMe_2(L)^+(OTf)^-$, all of which may be isolated in ca. 85–95% yields. The bound ethylene ligand in $Cp^*PtMe_2(C_2H_4)^+(OTf)^-$ has resonances in the ^1H NMR spectrum at 3.71 ppm (s, $^2J_{Pt-H} = 52$ Hz) and in the $^{13}C\{^1H\}$ NMR spectrum at 72.3 ppm (s, $^1J_{Pt\,C} = 101$ Hz). The carbonyl ligand of $Cp^*PtMe_2(CO)^+(OTf)^-$ is characterized by a ν_{CO} stretching frequency of 2114 cm^{-1} in the infrared spectrum and by a singlet at 155.9 ppm in the $^{13}C\{^1H\}$ NMR spectrum (CD_2Cl_2). Ethylene coordination and carbon monoxide coordination to $Cp^*PtMe_2(OTf)$ are reversible, so that $Cp^*PtMe_2(OTf)$ may be regenerated simply by evaporating a solution of $Cp^*PtMe_2(L)^+(OTf)^-$ (L = C_2H_4, CO) to dryness. Both $Cp^*PtMe_2(NH_3)^+(OTf)^-$ and $Cp^*PtMe_2(NH_2Bu^t)^+(OTf)^-$ are stable under reduced pressure, however.

The π acidic carbonyl and olefin ligands in $Cp^*PtMe_2(L)^+(OTf)^-$ (L = CO, C_2H_4, CH_2=CHMe) are coordinated to cationic platinum (IV) centers. To our knowledge, only a handful of platinum(IV) carbonyl complexes [11–13] and only one other platinum(IV) olefin derivative [14] have been reported previously. In $Cp^*PtMe_2(L)^+(OTf)^-$ (L = CO, C_2H_4, CH_2=CHMe), the carbonyl and olefin ligands are bound to the platinum centers primarily through σ donation, and very little, if any, π backbonding is expected [15]. Indeed, the ν_{CO} stretching frequency in $Cp^*PtMe_2(CO)^+(OTf)^-$ is much higher than those for some Pt(II)carbonyl derivatives (1968–2044 cm^{-1}) and intermediate between those of other platinum(IV) carbonyl compounds (2060–2191 cm^{-1}) (see Table 1). Nevertheless, the ν_{CO} value for $Cp^*PtMe_2(CO)^+(OTf)^-$ is lower than 2143 cm^{-1}, the stretching frequency for free CO [16], which indicates that some degree of π backbonding does stabilize the [Pt—CO] bond.

In the absence of a dative trapping ligand, $Cp^*PtMe_2(OTf)$ slowly decomposes at room temperature to a mixture of compounds, one component of which is Cp^*PtMe_3. Presumably Cp^*PtMe_3 is formed when $Cp^*PtMe_2(OTf)$ abstracts a methyl group from another molecule of $Cp^*PtMe_2(OTf)$. Qualitatively, the rate of thermal decomposition is solvent dependent; $Cp^*PtMe_2(OTf)$ decomposes faster in THF than in benzene.

Table 1. ν_{CO} Stretching frequencies for carbonyl complexes of platinum(IV) and [Cp*Pt(II)]

Compound	ν_{CO} (cm^{-1})	Reference
$[PtCl_5(CO)]^-$	2191	12
$Cp^*PtMe_2(CO)^+(OTf)$	2114	this work
fac-$[Pt(I)(Me)_3(SMe_2)(CO)]$	2090	13
[Pt(Me)(I)(Cl)(py)(CO) $\{CH(py)CH_2CH_3\}]^+(Cl)^-$	2060	11
Cp*Pt(CO)(Cl)	2044	7c
Cp*Pt(CO)Pt(CO)Cp	2005, 1984	7c
$[Cp^*Pt(CO)]_2$	1989, 1968	7c

The formation of Cp^*PtMe_3 in the thermal degradation of $Cp^*PtMe_2(OTf)$ suggests that the electrophilic $Cp^*PtMe_2(OTf)$ has an affinity for methyl groups. Indeed, $Cp^*PtMe_2(OTf)$ can also abstract a methyl group from either Cp_2ZrMe_2 (Cp = η^5-C_5H_5) or $SnMe_4$ immediately to yield Cp^*PtMe_3 [17], but there is no reaction with $SiMe_4$.

$Cp^*PtMe_2(OTf)$ also demonstrates an affinity for halides and pseudohalides. Thus, treatment of a benzene solution of $Cp^*PtMe_2(OTf)$ with MeI slowly yields Cp^*PtMe_2I and MeOTf [18] within three hours at room temperature; no reaction was observed, however, between $Cp^*PtMe_2(OTf)$ and PhBr [19]. $Cp^*PtMe_2(OTf)$ readily reacts with excess NaN_3 in THF to yield $Cp^*PtMe_2N_3$, which exhibits a very strong $\nu(N_3)$ absorption in the infrared spectrum at 2008 cm^{-1} [20].

Sharp has indicated that the reaction of Cp^*PtMe_2Br with $LiNHBu^t$ only gives back the starting materials in low yields with no tractable products [8]. We reasoned that $Cp^*PtMe_2(OTf)$ may serve as a more useful precursor for amide and alkoxide derivatives of [Cp*Pt(IV)] since the triflate ligand is a better leaving group than the bromide ligand. A red solid, tentatively characterized as $Cp^*PtMe_2(OPh)$ [21], may be isolated by treating Cp*PtMe(OTf) with LiOPh in Et_2O at −78°C, but the yield is low and some other [Cp*Pt] by-products, one of which is Cp^*PtMe_3, are also formed.

Both $Cp^*PtMe_2(OTf)$ and Cp^*PtMe_2I react cleanly, however, with the sulfur-based nucleophile KS(*p*-tol) to afford $Cp^*PtMe_2[S(p\text{-tol})]$, which has been characterized by X-ray diffraction. An ORTEP diagram is shown in Fig. 1 while relevant crystallographic and metrical data are given in Tables 2 and 3. The X-ray study revealed the [Pt—S] bond length of 2.344(1) Å to be similar to the sum of the covalent radii (2.35 Å) of six-coordinate platinum(IV) (1.31 Å) and sulfur (1.04 Å) [22], and the [Pt—S—C] bond angle to be 108.4(2)°. With a maximum difference of 0.043(6) Å, there is little variation among the five aromatic [C—C] bond lengths in the Cp* ligand, contrasting with the structure of Cp^*PtMe_2Cl in which the Cp* ligand shows a small deviation toward "diene-like" geometry [9].

Although we are unaware of any other structurally characterized arylthiolate complexes of platinum(IV) with two-coordinate sulfur atoms, the cubic complex $[PtMe_3(\mu\text{-}SPh)]_4$, which contains four-coordinate sulfur atoms, has been structurally characterized [23]. The average [Pt—S] bond length [2.506(5) Å] and the average [Pt—S—C] bond angle [118.1(7)°] in $[PtMe_3(\mu\text{-}SPh)]_4$ are longer and greater, respectively, than those in $Cp^*PtMe_2[S(p\text{-tol})]$, which may be attributed to differences in the coordination numbers of the sulfur atoms. Some arylthiolate complexes of platinum(II) with two-coordinate sulfur atoms have been structurally characterized [24,25], and the

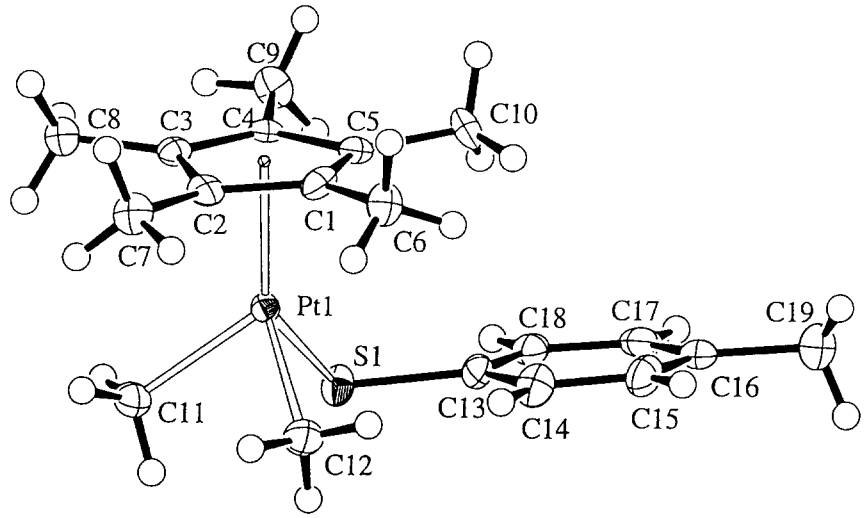

Fig. 1.

Table 2. Crystal and intensity collection data for Cp*PtMe$_2$[S(*p*-tol)]

Formula	$C_{19}H_{28}SPt$
Formula weight	483.6
Lattice	Primitive
Cell constants	a = 8.41400(10) Å
	b = 12.72130(10) Å
	c = 16.9927(3) Å
	α = 90.0°
	β = 97.578(1)°
	γ = 90.0°
	V = 1802.96(4) Å^3
Z	4
radiation (λ, Å)	Mo Kα (0.71069)
Space group	$P2_1/c$ (No. 14)
ρ (calcd), g cm^{-3}	1.781
μ (Mo Kα), cm^{-1}	78.60
Goodness of fit	1.06
R	0.021
R_w	0.027

Table 3. Selected bond lengths Å and angles (deg.) for Cp*PtMe$_2$[S(*p*-tol)]

Pt—S	2.344(1)	S—C(13)	1.790(4)
Pt—C(11)	2.075(5)	C(1)—C(2)	1.446(7)
Pt—C(12)	2.067(5)	C(2)—C(3)	1.453(6)
Pt—C(1)	2.265(5)	C(3)—C(4)	1.410(6)
Pt—C(2)	2.196(4)	C(4)—C(5)	1.437(6)
Pt—C(3)	2.300(4)	C(5)—C(1)	1.421(6)
Pt—C(4)	2.324(4)		
Pt—C(5)	2.306(4)		
Pt—S—C(13)	108.4(2)°	S—Pt—C(11)	86.1(1)°
S—Pt—C(12)	92.2(1)°	C(11)—Pt—C(12)	82.5(2)°

geometry of the [Pt—S—C] moieties in these compounds is similar to that of Cp*PtMe$_2$[S(*p*-tol)]. For example, the [Pt—S] bond length in [Cp(CO)Mn{μ-C(PMe$_3$) C$_6$H$_4$Me}Pt(*p*-tol)(PMe$_3$)] is 2.365(3) Å and the [Pt—S—C] bond angle is 109.3(3)° [26].

EXPERIMENTAL DETAILS

General considerations

Unless otherwise noted, all reactions and manipulations were carried out under nitrogen using standard Schlenk and vacuum techniques or in a Braun inert atmosphere box (N_2). Infrared spectra were taken on a Mattson Galaxy 3000—Fourier Transform Infrared spectrometer (FTIR). All ^{1}H, ^{13}C{^{1}H}, and ^{19}F NMR spectra were obtained at room temperature on a Bruker AMX-400 spectrometer at the frequencies 400 MHz, 100.6 MHz, and 376.5 MHz, respectively. ^{19}F NMR spectra were referenced externally to trichlorofluoromethane. Elemental analyses were performed by the University of California-Berkeley Microanalytical facility on a Perkin Elmer 2400 series II CHNO/S Analyzer. The single crystal X-ray analysis of Cp*PtMe$_2$[S(*p*-tol)] was carried out by Dr Frederick J. Hollander at the University of California, Berkeley X-ray facility.

Unless otherwise noted, reagents were purchased from commercial suppliers and used without further purification. Hexanes, pentane, diethyl ether, tetrahydrofuran, benzene, and toluene were distilled from sodium/benzophenone ketyl under N_2 prior to use. Methylene chloride was distilled from CaH_2 under N_2. $(Me_2PtI_2)_x$ [27], Cp*PtMe$_3$ [9], Cp*Li [28], and Cp_2ZrMe_2 [29] were synthesized according to published procedures. KS(*p*-tol) was synthesized by

treating a hexane solution of KH with a hexane solution of $HSC_6H_4CH_3$ and was recrystallized from hexane at $-35°C$.

Cp*PtMe$_2$(OTf)

Under N_2, a $-78°C$ solution of HOTf (260 μl, 2.94 mmol) in Et_2O (10 ml) was added slowly by cannula to a stirred solution of Cp*PtMe$_3$ (1.22 g, 3.25 mmol) in Et_2O (20 ml) which was immersed in a $-78°C$ bath. The mixture, which turned orange immediately, was allowed to warm to room temperature and stirred for 15 min. The volatile components were removed *in vacuo*, leaving a dark orange residue. The remainder of this procedure was carried out in the air. The product was extracted into C_6H_6 (10 ml), and the black extract was passed through a fritted column containing silanized silica (60 Å). The column was washed with C_6H_6 until the washes were colorless, and all washes were combined with the original filtrate. The volatile components of the bright orange filtrate were removed *in vacuo* leaving an orange crystalline solid which was washed with pentane (2×10 ml portions) and vacuum-dried. Yield: 1.41 g (94% based on HOTf). Anal. Calc. for $C_{13}H_{21}F_3O_3SPt$: C, 30.65%; H, 4.15%. Found: C, 30.45%; H, 4.42%. IR (KBr pellet, cm^{-1}): 2960 (m), 2897 (m), 2854 (w), 2802 (w), 1628 (w), 1527 (m), 1483 (w), 1452 (s), 1383 (s), 1350 (m), 1294 (vs), 1250 (vs), 1176 (vs), 1076 (w), 1032 (vs), 957 (w), 835 (m), 798 (w), 768 (m), 644 (vs), 615 (w) 582 (m), 548 (w), 521 (m). ^1H NMR (CD_2Cl_2): δ 1.79 ppm [s, 15 H, $\{\eta^5\text{-}C_5(CH_3)_5\}$, $^3J_{Pt\text{-}H} = 21$ Hz]; δ 1.40 ppm [s, 6 H, $2\{CH_3\}$, $^2J_{Pt\ H} = 70$ Hz]. ^{19}F NMR (CD_2Cl_2): -15.8 ppm [s]. $^{13}C\{^1H\}$ NMR (CD_2Cl_2): 7.3 ppm [s, 2 C, 2 $\{CH_3\}$, $^1J_{Pt\text{-}C} = 724$ Hz]; 8.8 ppm [s, 5 C, $\{\eta^5\text{-}C_5(CH_3)_5\}$]; 109.3 ppm [s, 5 C, $\{\eta^5\text{-}C_5(CH_3)_5\}$, $^1J_{Pt\ C} = 40$ Hz]; 119.0 ppm [q, 1 C, $\{OSO_2CF_3\}$, $^1J_{C\text{-}F} = 312$ Hz].

Cp*PtMe$_2$I

A mixture of Cp*Li (0.17 g, 1.22 mmol) and $(Me_2PtI_2)_x$ (0.50 g, 1.05 mmol) in THF (5 ml) was stirred at room temperature overnight (ca 12 h). The volatile components were removed *in vacuo* leaving a dark brown–black residue. The remainder of this procedure was carried out in the air. The product was extracted from the dark residue with C_6H_6 (10 ml) and the extract was passed through a fritted column containing silica gel (60 Å particles). The silica column was washed with C_6H_6 until the washes were colorless, and these washes were combined with the initial C_6H_6 extract. The volatile components of the filtrate were removed *in vacuo* leaving a reddish orange crystalline solid which was washed with pentane (10 ml) at $-78°C$ and vacuum-dried. Yield: 0.30 g (59%). Anal. Calc. for $C_{12}H_{21}IPt$: C, 29.58%; H, 4.34%. Found: C, 29.47%; H, 4.42%. IR (KBr pellet, cm^{-1}): 2976 (s), 2958 (s), 2893 (vs), 2852 (m), 2721 (w), 1522 (s), 1493 (m), 1443 (vs), 1427 (s), 1377 (vs), 1350 (s), 1225 (vs), 1200 (m), 1153 (s), 1074 (w), 1022 (vs), 953 (w), 833 (w), 793 (w), 609 (w), 544 (m). ^1H NMR (CD_2Cl_2): δ 1.87 ppm [s, 15 H, $\{\eta^5\text{-}C_5(CH_3)_5\}$, $^3J_{Pt\text{-}H} = 14$ Hz]; δ 1.19 ppm [s, 6 H, 2 $\{CH_3\}$, $^2J_{Pt\text{-}H} = 81$ Hz]. $^{13}C\{^1H\}$ NMR (CD_2Cl_2): -6.1 ppm [s, 2 C, 2 $\{CH_3\}$, $^1J_{Pt\text{-}C} = 678$ Hz]; 8.6 ppm [s, 5 C, $\{\eta^5\text{-}C_5(CH_3)_5\}$]; 107.0 ppm [s, 5 C, $\{\eta^5\text{-}C_5(CH_3)_5\}$, $^1J_{Pt\text{-}C} = 20$ Hz].

Cp*PtMe$_2$(C$_2$H$_4$)(OTf)

C_2H_4 (1 atm) was admitted to a Schlenk tube containing an orange, homogeneous solution of Cp*PtMe$_2$(OTf) (0.30 g, 0.59 mmol) in C_6H_6 (5 ml). The mixture, which immediately became cloudy and off-white, was stirred 5 min. at room temperature. The reaction mixture was then allowed to settle and the supernatant was decanted off the off-white product. The product was washed with benzene (2×5 ml) and pentane (1×10 ml) and dried by exposure to a gentle stream of air. Yield: 0.29 g (91%). Anal. Calc. for $C_{15}H_{25}F_3O_3SPt$: C, 33.52%; H, 4.69%. Found: C, 33.39%; H, 4.72%. IR (KBr pellet, cm^{-1}): 2983 (s), 2916 (s), 2899 (s), 2860 (w), 2825 (w), 1616 (w), 1525 (w), 1506 (m), 1460 (s), 1429 (s), 1383 (s), 1350 (w), 1261 (vs), 1221 (vs), 1198 (m), 1157 (vs), 1076 (w), 1036 (vs), 957 (w), 837 (w), 802 (w), 764 (w), 752 (w), 729 (w), 654 (s), 638 (s), 617 (w), 573 (m), 552 (w), 517 (m), 461 (w). ^1H NMR (CD_2Cl_2): δ 1.96 ppm [s, 15 H, $\{\eta^5\text{-}C_5(CH_3)_5\}$, $^3J_{Pt\text{-}H} = 11$ Hz]; δ 1.02 ppm [s, 6 H, 2 $\{CH_3\}$, $^2J_{Pt\ H} = 70$ Hz]; δ 3.71 ppm [s, 4 H, $\{C_2H_4\}$, $^2J_{Pt\ H} = 52$ Hz]. ^{19}F NMR (CD_2Cl_2): -16.2 ppm [s]. $^{13}C\{^1H\}$ NMR (CD_2Cl_2): 2.6 ppm [s, 2 C, $2\{CH_3\}$, $^1J_{Pt\text{-}C} = 563$ Hz]; 8.2 ppm [s, 5 C, $\{\eta^5\text{-}C_5(CH_3)_5\}$]; 112.0 ppm [s, 5 C, $\{\eta^5\text{-}C_5(CH_3)_5\}$, $^1J_{Pt\text{-}C} = 20$ Hz]; 72.3 ppm [s, 2 C, $\{C_2H_4\}$, $^1J_{Pt\text{-}C} = 101$ Hz]; 121.6 ppm [q, 1 C, $\{OSO_2CF_3\}$, $^1J_{C\text{-}F} = 330$ Hz).

Cp*PtMe$_2$(CH$_2$=CHMe)(OTf)

CH_2=CHMe (1 atm) was admitted to a Schlenk tube containing an orange, homogeneous solution of Cp*PtMe$_2$(OTf) (0.30 g, 0.59 mmol) in C_6H_6 (5 ml). The mixture, which immediately became cloudy and pale yellow, was stirred 5 min. at room temperature. The very thick reaction mixture was centrifuged, washed with benzene (2×5 ml) and pentane (2×10 ml), and dried by exposure to a gentle stream of air. Yield: 0.30 g (92%). Anal. Calc. for $C_{16}H_{27}F_3O_3SPt$: C, 34.84%; H, 4.93%. Found: C, 34.24%; H, 4.88%. IR (KBr pellet, cm^{-1}): 2981 (s), 2958 (s), 2897 (vs), 2850 (m), 2804 (w), 1632 (w), 1527 (m), 1498 (w), 1452 (s), 1383 (s), 1350 (m), 1294 (s), 1250 (s), 1165 (s), 1074 (w), 1030 (s), 835 (w), 800 (w), 766 (w), 752 (w), 638 (s), 615 (w), 579 (m), 550 (w), 521 (m), 494 (w), 436 (w), 415 (w). ^1H NMR (CD_2Cl_2): δ 1.92 ppm [s, 15 H, $\{\eta^5\text{-}C_5(CH_3)_5\}$]; δ 0.65 ppm [s, 3 H, $\{CH_3\}$, $^2J_{Pt\ H} = 71$ Hz]; δ 1.21 ppm [s, 3 H, $\{CH_3\}$, $^2J_{Pt\text{-}H} = 70$

Hz]; δ 1.71 ppm [d, 3H, $\{CH_2{=}CH(CH_3)\}$, $^4J_{H-H} = 6$ Hz, $^3J_{Pt-H} = 37$ Hz]; δ 3.64 ppm [m, 2 H, $\{CH_2{=}CH(CH_3)$, CH_2 proton *cis* to $CH_3\}$; δ 4.38 ppm [m, 1 H, $\{CH_2{=}CH(CH_3)$, CH_2 proton *trans* to $CH_3\}$]. ^{19}F NMR (CD_2CL_2): -16.1 ppm [s]. $^{13}C\{^1H\}$ NMR (CD_2Cl_2): 3.2 ppm [s, 1 C, $\{CH_3\}$, $^1J_{Pt-C} = 578$ Hz]; 5.7 ppm [s, 1 C, $\{CH_3\}$, $^1J_{Pt-C} = 606$ Hz]; 8.4 ppm [s, 5 C, $\{\eta_5C_5(CH_3)_5\}$; 111.9 ppm [s, 5 C $\{\eta^5$-$C_5(CH_3)_5\}$; 18.4 ppm [s, 1 C, $\{CH_2{=}CH(CH_3)\}$]; 71.1 ppm [s, 1 C, $\{CH_2{=}CH(CH_3)]$, $^1J_{Pt-C} = 108$ Hz]; 93.4 ppm [s, 1 C, $\{CH_2{=}CH(CH_3)\}$, $^1J_{Pt\ C} = 83$ Hz]; 121.5 ppm [q, 1 C, $\{OSO_2CF_3\}$, $^1J_{C-F} = 312$ Hz].

$Cp^*PtMe_2(CO)(OTf)$

CO (1 atm) was admitted to a Schlenk tube containing an orange, homogeneous solution of $Cp^*PtMe_2(OTf)$ (0.21 g, 0.42 mmol) in C_6H_6 (5 ml). The mixture, which immediately became cloudy and off-white, was stirred 30 min. at room temperature. The off-white solid was then allowed to settle, isolated by filtration, and dried by exposure to a gentle stream of air. Yield: 0.19 g (86%). Anal. Calc. for $C_{14}H_{21}F_3O_4SPt$: C, 31.29%; H, 3.94%. Found: C, 31.27%; H, 3.99%. IR (KBr pellet): 2983 (m), 2926 (s), 2897 (m), 2852 (w), 2114 (vs), 1612 (s), 1502 (m), 1462 (s), 1425 (s), 1385 (m), 1269 (vs), 1240 (vs), 1221 (s), 1153 (vs), 1078 (w), 1030 (vs), 874 (w), 837 (w), 752 (w), 696 (w), 638 (vs), 571 (m), 517 (m), 472 (m), 442 (w), 417 (m). ^{1}H NMR (CD_2Cl_2): δ 2.12 ppm [s, 15 H, $\{\eta^5$-$C_5(CH_3)_5\}$, $^3J_{Pt-H} = 10$ Hz]; δ 1.20 ppm [s, 6 H, 2 $\{CH_3\}$, $^2J_{Pt-H} = 69$ Hz]. ^{19}F NMR (CD_2Cl_2): -16.1 ppm [s]. $^{13}C\{^1H\}$ NMR (CD_2Cl_2): -1.6 ppm [s, 2 C, 2 $\{CH_3\}$, $^1J_{Pt-C} = 505$ Hz]; 8.8 ppm [s, 5 C, $\{\eta^5$-$C_5(CH_3)_5\}$]; 113.1 ppm [s, 5 C, $\{\eta^5$-$C_5(CH_3)_5\}$, $^1J_{Pt-C} = 20$ Hz]; 121.6 ppm [q, 1 C, $\{OSO_2CF_3\}$, $^1J_{C\ F} = 311$ Hz]; 155.9 ppm [s, 1 C, $\{CO\}$].

$Cp^*PtMe_2(NH_3)(OTf)$

NH_3 (1 atm) was admitted to a Schlenk tube containing an orange, homogeneous solution of $Cp^*PtMe_2(OTf)$ (0.30 g, 0.59 mmol) in C_6H_6 (10 ml). The mixture, the color of which immediately became tan, was stirred 5 min. at room temperature. The volatile components were removed under reduced pressure, leaving a tan crystalline solid behind. Yield: 0.28 g (89%). Anal. Calc. for $C_{13}H_{24}F_3NO_3SPt$: C, 29.66%; H, 4.59%; N, 2.66%. Found: C, 29.60%; H, 4.65%; N, 2.63%. IR (KBr pellet, cm^{-1}): 3280 (s), 3244 (s), 3215 (s), 3169 (s), 2949 (s), 2904 (s), 2816 (w), 1585 (w), 1510 (m), 1452 (s), 1385 (s), 1362 (m), 1325 (vs), 1277 (vs), 1257 (vs), 1236 (vs), 1157 (vs), 1103 (w), 1074 (w), 1034 (vs), 949 (w), 852 (w), 833 (w), 800 (w), 756 (m), 640 (vs), 575 (m), 542 (w), 517 (s), 480 (w), 438 (w), 422 (w). ^{1}H NMR (CD_2Cl_2): δ 1.83 ppm [s, 15 H, $\{\eta^5$-$C_5(CH_3)_5\}$]; δ 0.92 ppm [s, 6 H, $\{CH_3\}$, $^2J_{Pt-H} = 74$ Hz]; δ 3.41 ppm [br, 3 H, $\{NH_3\}$]. ^{19}F NMR (CD_2Cl_2): -16.2 ppm [s]. $^{13}C\{^1H\}$ NMR (CD_2Cl_2): -0.5 ppm [s, 2 C, 2 $\{CH_3\}$, $^1J_{Pt-C} = 664$ Hz]; 8.2 ppm [s, 5 C, $\{\eta^5$-$C_5(CH_3)_5\}$]; 106.5 ppm [s, 5 C, $\{\eta^5$-$C_5(CH_3)_5\}$, $^1J_{Pt-C} = 30$ Hz]; 124.1 ppm [q, 1 C, $\{OSO_2CF_3\}$, $^1J_{C-F} = 322$ Hz].

$Cp^*PtMe_2(NH_2Bu^t)(OTf)$

NH_2Bu^t vapor (1 atm) was admitted to a Schlenk tube containing an orange, homogeneous solution of $Cp^*PtMe_2(OTf)$ (0.20 g, 0.40 mmol) in C_6H_6 (10 ml). The mixture, which immediately became cloudy and yellow, was stirred 30 min. at room temperature. The reaction mixture was then allowed to settle, yielding a pale yellow crystalline solid under a pale orange supernatant. The solid was isolated by filtration, washed with pentane (1 × 10 ml), and vacuum-dried. Yield: 0.19 g (84%). Anal. Calc. for $C_{17}H_{32}F_3NO_3SPt$: C, 35.05%; H, 5.54%, N, 2.40%. Found: C, 35.25%; H, 5.56%; N, 2.12%. IR (KBr pellet, cm^{-1}): 3255 (s), 3224 (s), 3151 (s), 2972 (s), 2910 (s), 2823 (w), 1601 (m), 1510 (m), 1446 (s), 1377 (s), 1263 (vs), 1223 (vs), 1205 (s), 1188 (s), 1157 (vs), 1074 (w), 1032 (s), 931 (w), 893 (m), 831 (w), 752 (m), 638 (s), 573 (m), 542 (w), 517 (s), 447 (m), 440 (m). ^{1}H NMR (CD_2Cl_2): δ 1.84 ppm [s, 15 H $\{\eta^5$-$C_5(CH_3)_5\}$, $^3J_{Pt-C} = 12$ Hz]; δ 0.99 ppm [s, 6 H, 2 $\{CH_3\}$, $^2J_{Pt\ H} = 73$ Hz]; δ 1.15 ppm [s, 9 H, $\{NH_2C(CH_3)_3\}$]; δ 3.94 ppm [br, 2 H, $\{NH_2C(CH_3)_3\}$]. ^{19}F NMR (CD_2Cl_2): -16.0 ppm [s]. $^{13}C\{^1H\}$ NMR (CD_2Cl_2): 3.3 ppm [s, 2 C, 2 $\{CH_3\}$, $^1J_{Pt-C} = 671$ Hz]; 9.0 ppm [s, 5 C, $\{\eta^5$-$C_5(CH_3)_5\}$]; 107.3 ppm [s, 5 C, $\{\eta^5$-$C_5(CH_3)_5\}$, $^1J_{Pt-C} = 25$ Hz]; 29.7 ppm [s, 3 C, $\{NH_2C(CH_3)_3\}$]; 56.3 ppm [s, 1 C, $\{NH_2C(CH_3)_3\}$]; 121.3 ppm [q, 1 C, $\{OSO_2CF_3\}$, $^1J_{C-F} = 321$ Hz].

$Cp^*PtMe_2N_3$

At -35°C, THF (3 ml) was added to a mixture of $Cp^*PtMe_2(OTf)$ (0.18 g, 0.35 mmol) and NaN_3 (0.12 g, 1.80 mmol). The mixture was stored at -35°C for 30 min. and then allowed to warm to room temperature and stirred for 20 min. The volatile components were removed *in vacuo* and the product was extracted from the solid residue into pentane (2 × 10 ml, 4 × 5 ml). The first extract was orange and the final extract was colorless. The extracts were filtered and combined. The filtrate was concentrated under reduced pressure so that the volume was approx. $\frac{1}{2}$ the original volume. The product, an orange crystalline solid, was crystallized from this concentrated pentane solution at -78°C, isolated by filtration, and dried *in vacuo*. Yield: 0.06 g (41%). Anal. Calc. for $C_{12}H_{21}N_3Pt$: C, 35.82%; H, 5.26%; N, 10.44%. Found: C, 35.42%; H, 5.23%; N, 9.99%. IR (KBr pellet, cm^{-1}): 2974 (s), 2960 (s), 2897 (s), 2812 (m), 2008 (vs), 1518 (s), 1446 (vs), 1431 (vs), 1381 (vs), 1354 (s), 1282 (vs), 1230 (s), 1205 (s), 1153 (s), 1095 (w), 1072 (m), 1028 (m), 951 (w), 837 (m), 798 (w),

619 (m), 582 (m), 548 (s). ^{1}H NMR (CD_2Cl_2): δ 1.78 ppm [s, 15 H, $\{\eta^5$-$C_5(CH_3)_5\}$, $^3J_{Pt-H} = 13$ Hz]; δ 0.96 ppm [s, 6 H, 2 $\{CH_3\}$, $^2J_{Pt-H} = 77$ Hz]. $^{13}C\{^1H\}$ NMR (CD_2Cl_2): -0.3 ppm [s, 2 C, 2 $\{CH_3\}$, $^1J_{Pt-C} = 710$ Hz]; 8.1 ppm [s, 5 C, η^5-$C_5(CH_3)_5\}$]; 106.0 ppm [s, 5 C, $\{\eta^5$-$C_5(CH_3)_5\}$, $^1J_{Pt-C} = 26$ Hz].

Cp*PtMe$_2$[S(p-tol)]

At -35°C, THF (3 ml) was added to a mixture of Cp*PtMe$_2$OTf (0.18 g, 0.35 mmol) and KS(*p*-tol) (0.06 g, 0.37 mmol). The mixture was stored at -35°C for 30 min. and then allowed to warm to room temperature and stirred for 15 min. The volatile components were removed *in vacuo* and the product was extracted from the solid residue into pentane (3×10 ml, 2×5 ml). The first extract was red and the final extract was colorless. The extracts were filtered and combined. The filtrate was concentrated under reduced pressure so that the volume was approx. $\frac{2}{3}$ the original volume. The product, an orange crystalline solid, was crystallized from this concentrated pentane solution at -78°C, isolated by filtration, and dried *in vacuo*. Yield: 0.11 g (61%). Anal. Calc. for $C_{19}H_{28}SPt$: C, 47.19%; H, 5.84%. Found: C, 47.29%; H, 5.70%. IR (KBr pellet, cm^{-1}): 3059 (w), 2956 (m), 2895 (m), 2856 (m), 2812 (m), 1884 (w), 1630 (w), 1593 (w), 1514 (m), 1483 (s), 1444 (s), 1423 (s), 1383 (s), 1356 (m), 1259 (w), 1225 (m), 1211 (w), 1198 (m), 1176 (w), 1155 (m), 1101 (w), 1080 (s), 1016 (m), 951 (w), 933 (w), 847 (w), 829 (w), 806 (vs), 702 (w), 685 (w), 627 (m), 609 (m), 586 (w), 546 (m), 494 (vs), 465 (w), 449 (w), 440 (w), 417 (w). ^{1}H NMR (CD_2Cl_2): δ 1.73 ppm [s, 15 H, (η^5-$C_5(CH_3)_5$, $^3J_{Pt-H} = 9$ Hz]; δ 0.78 ppm [s, 6 H, 2 (CH_3), $^2J_{Pt-H} = 80$ Hz]; δ 2.21 ppm [s, 3 H, $\{SC_6H_4(CH_3)\}$]; δ 6.84 ppm [d, 2 H, $\{SC_6H_4(CH_3)\}$, $^3J_{H-H} = 8$ Hz]; δ 7.08 ppm [d, 2 H, $\{SC_6H_4(C_3)\}$, $^3J_{H-H} = 8$ Hz]. $^{13}C\{^1H\}$ NMR (CD_2Cl_2): -3.9 ppm [s, 2 C, 2 (CH_3), $^1J_{Pt-C} = 690$ Hz]; 8.1 ppm [s, 5 C, (η^5-$C_5(CH_3)_5$]; 132.9 ppm [s, 5 C, (η^5-$C_5(CH_3)_5$, $^1J_{Pt-C} = 30$ Hz]; 21.1 ppm [s, 1 C, $SC_6H_4(CH_3)$]; 105.7 ppm [s, 2 C, $SC_6H_4(CH_3)$]; 128.9 ppm [s, 2 C, $SC_6H_4(CH_3)$]; 133.5 ppm [s, 1 C, $SC_6H_4(CH_3)$]; 137.1 ppm [s, 1 C, $SC_6H_4(CH_3)$].

Formation of Cp*PtMe$_2$[S(*p*-tol)] *from* Cp*PtMe$_2$I

THF-d_8 (1 ml) was added to a mixture of Cp*PtMe$_2$I (0.006 g, 0.01 mmol) and KS(*p*-tol) (0.006 g, 0.04 mmol). ^{1}H NMR spectroscopy revealed the formation of Cp*PtMe$_2$[S(*p*-tol)] to be complete within 30 min. at room temperature.

Reversibility of C_2H_4 *coordination to* Cp*PtMe$_2$(OTf)

A solution of Cp*PtMe$_2$(C_2H_4)$^+$(OTf)$^-$ (0.02 g, 0.04 mmol) in CH_2Cl_2 (5 ml) was magnetically stirred as the volatile components were slowly removed under reduced pressure, leaving a yellowish orange solid. ^{1}H NMR analysis (CD_2Cl_2) revealed the solid to be a mixture of Cp*PtMe$_2$(C_2H_4)$^+$(OTf)$^-$ (76%) and Cp*PtMe$_2$(OTf) (24%).

Reactivity of Cp*PtMe$_2$OTf *toward* SnMe$_4$

$SnMe_4$ (2 μl, 0.01 mmol) was added to a solution of Cp*PtMe$_2$OTf (0.007 g, 0.01 mmol) in $CDCl_3$ (1 ml). ^{1}H NMR spectroscopy revealed the formation of Cp*PtMe$_3$ to be complete within 5 min. at room temperature [17].

Reactivity of Cp*PtMe$_2$(OTf) *toward* Cp$_2$ZrMe$_2$

$CDCl_3$ (1 ml) was added to a mixture of Cp*PtMe$_2$-(OTf) (0.01 g, 0.02 mmol) and Cp$_2$ZrMe$_2$ (0.005 g, 0.02 mmol). ^{1}H NMR spectroscopy revealed the formation of Cp*PtMe$_3$ to be complete within 20 min. at room temperature [17].

Reactivity of Cp*PtMe$_2$(OTf) *toward* MeI

MeI (1 μl, 0.02 mmol) was added to a solution of Cp*PtMe$_2$(OTf) (0.006 g, 0.01 mmol) in C_6D_6 (1 ml). ^{1}H NMR spectroscopy revealed the formation of Cp*PtMe$_2$I and MeOTf to be complete within 3 h at room temperature [18].

X-Ray Structure Determination of Cp*PtMe$_2$[S(*p*-tol)]

Crystal data and refinement parameters for Cp*PtMe$_2$[S(*p*-tol)] are summarized in Table 2. An orange polyhedral crystal of Cp*PtMe$_2$[S(*p*-tol)] (approximate dimensions $0.12 \times 0.15 \times 0.27$ mm), obtained from a concentrated pentane solution at -35°C, was mounted on a glass fiber using Paratone N hydrocarbon oil. All measurements were made on a Siemens SMART diffractometer using graphite monochromated Mo Kα radiation ($\lambda = 0.71073$ Å). Cell constants and an orientation matrix, obtained from a least-squares refinement using the measured positions of 5800 reflections with $I > 10\sigma(I)$ in the range $3.00 < 2\Theta < 45.00$°, correspond to a primitive monoclinic cell. Systematic absences were uniquely consistent with the space group $P2_1/c$ (No. 14). The data were collected at a temperature of -142 ± 1°C. Data were integrated using the program SAINT with box parameters of $1.6 \times 1.6 \times 0.6$° to a maximum 2Θ value of 52.1°. The data were corrected for Lorentz and polarization effects. No decay correction was applied. Analysis of the data with XPREP indicated the space group and allowed for calculation of the absorption coefficient. The structure was solved by direct methods and expanded using Fourier techniques. All non-hydrogen atoms were refined anisotropically. Hydrogen atoms were included in idealized positions after location on a difference Fourier map,

but not refined. All calculations were performed using the teXsan crystallographic software package of Molecular Structure Corporation.

Acknowledgements—Funding through NIH Grant No. GM-25459 is gratefully acknowledged. We thank Dr F. J. Hollander, Director of the UC Berkeley X-ray diffraction facility (CHEXRAY), for the structural characterization of $Cp^*PtMe_2[S(p\text{-tol})]$.

REFERENCES AND NOTES

1. Bryndza, H. E. and Tam, W., *Chem. Rev.*, 1988, **88,** 1163–1188.
2. For some examples of Pt(IV) alkoxide compounds see (a) Monaghan, P. K. and Puddephatt, R. J., *Inorg. Chim. Acta*, 1982, **65,** L59; (b) Monaghan, P. K. and Puddephatt, R. J., *Organometallics*, 1984, **3,** 444–449; (c) Appleton, T. G., Hall, J. R., Neale, D. W. and Williams, M. A., *J. Organomet. Chem.*, 1984, **276,** C73; (d) Akl, N. and Tayim, H. A., *J. Organomet. Chem.*, 1985, **297,** 371.
3. Bradley, D. C., *Chem. Rev.*, 1989, **89,** 1317–1322.
4. Tagge, C. D., Simpson, R. D., Bergman, R. G., Hostetler, M. J., Girolami, G. S. and Nuzzo, R. G., *J. Am. Chem. Soc.*, 1996, **118,** 2634–2643.
5. Glueck, D. S., Winslow, L. J. N. and Bergman, R. G., *Organometallics*, 1991, **10,** 1462–1479.
6. Holland, P. L., Andersen, R. A. and Bergman, R. G., *J. Am. Chem. Soc.*, 1996, **118,** 1092–1104.
7. For some examples of [Cp*Pt] complexes reported before 1990, see (a) Taylor, S. H. and Maitlis, P. M., *J. Organomet. Chem.*, 1977, **139,** 121–123; (b) O'Hare, D., *Organometallics*, 1987, **6,** 1766–1772. (c) Boag, N. M., *Organometallics*, 1988, **7,** 1446–1449; (d) Dixon, A. J., Firth, S., Haynes, A., Poliakoff, M., Turner, J. J. and Boag, N. M., *J. Chem. Soc., Dalton Trans.*, 1988, 1505–1507; (e) Boag, N. M., *J. Chem. Soc. Chem. Commun.*, 1988, 617–619; (f) Yang, D. S., Bancroft, G. M., Puddephatt, R. J., Bursten, B. E. and McKee, S. D., *Inorg. Chem.*, 1989, **28,** 872–877.
8. Roth, S., Ramamoorthy, V. and Sharp, P. R., *Inorg. Chem.*, 1990, **29,** 3345–3349.
9. Rockensüss, W., Roesky, H. W., Gilje, J. W. and Noltemeyer, M., *Eur. J. Solid State Inorg. Chem.*, 1990, **27,** 599–615.
10. The 1294 cm^{-1} and 1032 cm^{-1} frequencies are believed to correspond to the asymmetric and symmetric stretches, respectively, of the SO_3 portion of the triflate anion; the 1250 cm^{-1} and 1176 cm^{-1} frequencies most probably correspond to the asymmetric and symmetric stretches of the CF_3 portion of the triflate ligand. See Johnston, D. H. and Shriver, D. F., *Inorg. Chem.*, 1993, **32,** 1045–1047.
11. Gillard, R. D., Pilbrow, M. F., Leonard, S., Rendle, M. C. and Tipper, C. F. H., *Polyhedron*, 1982, **1,** 689–692.
12. Belli Dell'Amico, D., Calderazzo, F., Marchetti, F. and Merlino, S., *J.C.S. Dalton Trans.*, 1982, 2257–2260.
13. Scott, J. D. and Puddephatt, R. J., *Organometallics*, 1986, **5,** 1253–1257.
14. Parsons, E. J., Larsen, R. D. Jennings, P. W., *J. Am. Chem. Soc.*, 1985, **107,** 1793–1794.
15. For reviews concerning late metal compounds in which the carbonyl ligand bonds to the metal center primarily through σ donation, see (a) Ellis, J. E. and Beck, W., *Angew. Chem. Int. Ed. Engl.*, 1995, **34,** 2489–2491; (b) Aubke, F. and Wang, C., *Coord. Chem. Rev.*, 1994, **137,** 483–524.
16. Aubke, F. and Wang, C., *Coord. Chem. Rev.*, 1994, **137,** 483–524.
17. The expected by-products in these reactions are Cp_2 for (Me)(OTf) and Me_3Sn (OTf), respectively, and ^1H NMR data for both of these compounds have been published. In the reaction with $SnMe_4$, the observed ^1H NMR data for the by-product are as follows: [$CDCl_3$, δ 0.81 ppm, s, $J_{Sn\ H} = 65$ Hz. The reported ^1H NMR data for $SnMe_3(OTf)$ are: [$CDCl_3$, δ 0.74 ppm, $J_{Sn-H} = 62.8$ Hz] [17a]. In the reaction with Cp_2ZrMe_2, the observed ^1H NMR data for the by-product are as follows: [$CDCl_3$, δ 0.58 ppm, s, {Me}; δ 6.36 ppm, s, 2 {Cp}]. The reported ^1H NMR data for $Cp_2Zr(Me)(OTf)$ are: [$CDCl_3$, δ 0.57 ppm, s, {Me}; δ 6.34 ppm, s, 2 {Cp}] [17b]. (a) Kapoor, R., Sood, V. and Kapoor, P., *Polyhedron*, 1995, **14,** 489–494; (b) Luinstra, G. A., *J. Organomet. Chem.*, 1996, **517,** 209–215.
18. MeOTf was identified as the by-product by comparison with the ^1H NMR spectrum of an authentic sample of MeOTf. ^1H NMR data for MeOTf (C_6D_6): δ 2.97 ppm [s].
19. ^1H NMR spectroscopy revealed no reaction between $Cp^*PtMe_2(OTf)$ and PhBr in C_6D_6 after two days at room temperature.
20. Some IR stretching frequencies for platinum(II) azides have been reported to be in the range 2032–2080 cm^{-1}. See Bowman, K. and Dori, Z., *Inorg. Chem.*, 1970, **9,** 395–397.
21. ^1H NMR data for $Cp^*PtMe_2(OPh)$ (CD_2Cl_2): δ 0.41 ppm [s, 6 H, 2 {CH_3}, $^2J_{Pt-H} = 79$ Hz]; δ 1.77 ppm [s, 15 H, η^5-$C_5(CH_3)_5$}, $^3J_{Pt-H} = 7$ Hz]; δ 6.86 ppm [d, 2 H, {OC_6H_5}, $^3J_{H-H} = 8$ Hz]; δ 6.95 ppm [t, 1 H, {OC_6H_5}, $^3J_{H\ H} = 7$ Hz[; δ 7.27 ppm [t, 2 H, {OC_6H_5}, $^3J_{H\ H} = 8$ Hz].
22. Pauling, L., *The Nature of the Chemical Bond*, 3rd edn. Cornell University Press, Ithaca, 1960.
23. Craig, D. C. and Dance, I. G., *Polyhedron*, 1987, **6,** 1157–1159.
24. Cooper, M. K., Hair, N. J. and Yaniuk, D. W., *J. Organomet. Chem.*, 1978, **150,** 157–170.
25. Jeffery, J. C., Navarro, R., Razay, H. and Stone, F. G. A., *J.C.S. Dalton Trans.*, 1981, 2471–2478.
26. This similarity in [Pt—S] bond lengths is due to the fact that platinum(II) and platinum(IV) have nearly identical radii. See (a) Shannon, R. D., *Acta Crystallogr.*, 1976, **A32,** 751. (b) Hartley, F. R., *The Chemistry of Platinum and Palladium*. Applied Science Publishers, London, 1973, Chapter 2, p. 8.
27. Clark, H. C. and Manzer, L. E., *J. Organomet. Chem.*, 1973, **59,** 411–428.
28. Schock, L. E. and Marks, T. J., *J. Am. Chem. Soc.*, 1988, **110,** 7701–7715.
29. Samuel, E. and Rausch, M. D., *J. Am. Chem. Soc.*, 1973, **95,** 6263–6267.

Pergamon

PII: S0277-5387(97)00293-3

Polyhedron Vol. 17, No. 5–6, pp. 811–819, 1998
© 1998 Elsevier Science Ltd
All rights reserved. Printed in Great Britain
0277–5387/98 $19.00+0.00

Bimetallic mixed-metal complexes of the salen(ᵗBu) ligands

Michael S. Hill, Pingrong Wei and David A. Atwood*†

Center for Main Group Chemistry, Department of Chemistry, North Dakota State University, Fargo, North Dakota 58105, U.S.A.

(Received 30 April 1997; accepted 25 June 1997)

Abstract—The Salen(ᵗBu) ligands, Salen(ᵗBu), (N,N′-ethylenebis(3,5-di-*tert*-butylsalicylideneimine) and Salpen(ᵗBu), (N,N′-propylenebis(3,5-di-*tert*-butylsalicylideneimine) can be combined with $GaEt_3$ to prepare the 'open' monometallic compounds, Salen(ᵗBu)H($GaEt_2$) (**1**) and Salpen(ᵗBu)($GaEt_2$) (**2**). These, in turn, can be converted to the bimetallic derivatives, Salen(ᵗBu)($GaEt_2$)$_2$ (**3**) and Salpen(ᵗBu)($GaEt_2$)$_2$ (**4**) by addition of $GaEt_3$. Alternatively, **3** and **4** can be made by the addition of two moles of $GaEt_3$ to the appropriate ligand. This was the method used to prepare Salben(ᵗBu)($GaEt_2$)$_2$ (**5**) (Salben(ᵗBu) = N,N′-butylenebis(3,5-di-*tert*-butylsalicylideneimine) and Salhen(ᵗBu)($GaEt_2$)$_0$ (**6**) [Salhen(ᵗBu) = N,N′-hexylenebis(3,5-di-*tert*-butylsalicylideneimine]. Compounds **1** and **2** can be utilized to form the unique mixed-metal derivatives L($GaEt_2$)(MR_2) (where L = Salen(ᵗBu), M : R = Al, Me (**7**); Al, Et (**9**); and L = Salpen(ᵗBu), M : R = Al, Me (**8**); Al, Et (**10**). At ambient temperatures in non-polar solvents, **7**–**12** do not undergo exchange of either the alkyl or MR_2 groups. All of the compounds were characterized by Mp, analyses, ^{1}H NMR, IR and, in the case of **1** and **3**–**6**, by X-ray crystallography. © 1998 Elsevier Science Ltd. All rights reserved

Keywords: Group 13; salen(ᵗBu); bimetallic.

The Salen [1] class of ligands has been used extensively to support transition metal bonding schemes [2] and to a much lesser extent those of the main group elements. Some Group 13 examples include those incorporating aluminum [3] and gallium [4] alkyls, aluminum alkoxides [5] and aluminum cations [6]. The dominant structural motif for these complexes is one in which one metal is coordinated by all of the heteroatoms of the ligand in a planar arrangement [Fig. 1(a)]. In fact, many of the applications associated with these ligands rely upon this arrangement and the predominance of the chelate effect. For the main group elements there has historically been only one exception to this coordination mode. This is the bimetallic complex, Salpen($GaMe_2$)$_2$, which was formed using an excess of $GaMe_3$ in a heated, sealed tube reaction [4]. Unfortunately, these relatively harsh reaction conditions have given the false impression that extreme measures must be taken in order to prevent the Salen ligand from forming the monometallic chelate.

The Salen ligands have been shown to support bimetallic formulations for an alkyl borane [7] and a number of borates having the arrangement shown in Fig. 1(b) [8]. However, this is not surprising considering that boron generally does not go beyond a coordination number of four (a monomeric, fully chelated derivative would be five-coordinate). What we have recently discovered, however, is that the heavier congeners of the Group 13 elements, and in particular gallium, readily form open structures with the Salen ligands. Not only does this imply that monometallic [Fig. 1(c)] and bimetallic [Fig. 1(b)] open structures are accessible but that mixed metal derivatives may also readily be formed [Fig. 1(d)].

The potential isolation of dialkyl Group 13 derivatives having an open structure was implied in the proposed mechanism of formation of some of the first Salen-Al derivatives [3] as well as some tmtaa derivatives [9]. In this mechanism 1 equiv. of alkane is eliminated as the slow first step, followed by ring closure and elimination of a second equivalent of alkane. Under the conditions that were employed,

* Author to whom correspondence should be addressed.

† Dedicated to Prof. D. C. Bradley on the occasion of his 73rd birthday.

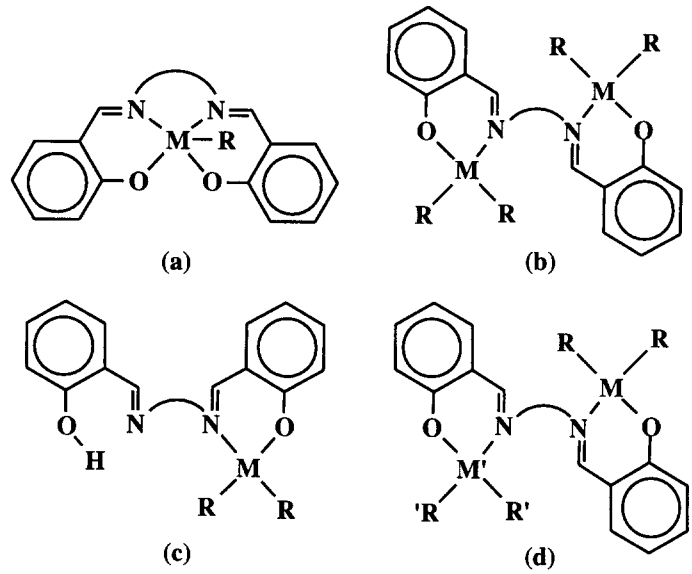

Fig. 1. General depiction of the structures that the Salen ligands adopt with the Group 13 elements.

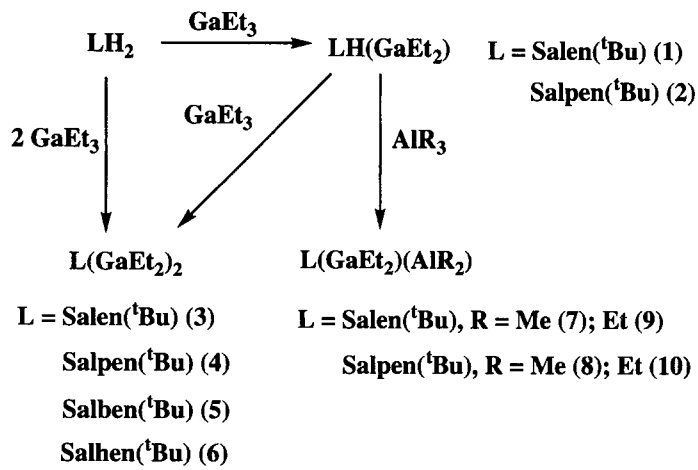

Scheme 1. Reactions leading to the formation of **1**–**10**.

however, the Salen intermediates were not able to be isolated.

One considerable limitation in using the Salen ligands lies in the fact that they are generally insoluble when bound in a neutral complex. Occasionally, this problem can be tempered somewhat by use of the Acen ligand [Figure 2(b)]. In order to avoid solubility problems altogether we have begun investigating derivatives that feature pendant alkyl groups. One such Salen derivative is Salen('Bu)H_2 [10] which possesses tertiary butyl groups at two positions on each of the phenol rings. The present work will explore the isolation and subsequent reactions of open Salen('Bu)–gallium combinations.

RESULTS AND DISCUSSION

Synthesis and Characterization

The monometallic compounds, **1** and **2**, are prepared in high yield by the addition of $GaEt_3$ to the ligand at 25°C. They can be refluxed in toluene for up to 4 h with effecting ring closure. Under these conditions the same reaction with either aluminum [11] or indium [12] reagents leads to ring closure and formation of the five-coordinate monometallic derivatives. Thus, the R_2Ga^- unit appears to be remarkably stable in relation to the aluminum and indium derivatives. The aqueous stability of Me_2Ga^+ serves as an

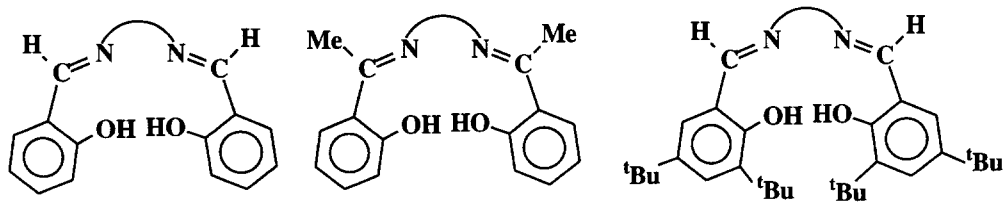

Fig. 2. General depiction of the Salen (a), Acen (b) and Salen('Bu) (c) ligands.

example of this fact [13]. The ^{1}H NMR data for **1** and **2** are consistent with an asymmetric structure in solution (Table 1). Specifically, there are two resonances for the imine (N=C*H*) groups. Addition of another mole of Et_3Ga to **1** and **2** leads to formation of the symmetric bimetallic derivatives, **3** and **4**. Alternatively, **3** and **4** (as well as **5** and **6**) can be formed by the addition of 2 moles of $GaEt_3$ to one of the ligands. Based upon the ^{1}H NMR data, these compounds are symmetric in solution. The Ga-Et resonances for **1–6** are fairly consistent and are similar to the shifts reported for other compounds containing the GaEt group such as the monometallic derivatives, LGaEt [L = Salen('Bu), Salophen('Bu) and Salomphen('Bu)] [14].

Formation of **1** or **2**, *in situ*, followed by addition of AlR_3, affords the mixed-metal derivatives, **7–10**. They are readily characterized by their distinctive ^{1}H NMR data in which there are two sets of resonances that can be ascribed to each of the MR_2 groups. The ethyls on each metal are equivalent as was seen in the homobimetallic complexes, **3–6**. There are two imine peaks (2H, total) that integrate with each set of the Ga-ethyl groups (CH_2CH_3, 6 H) in a 1 : 3 ratio. In contrast, the imine is observed as a sharp singlet for **3–6**. The CH : Me integration of 1 : 3 would also be observed if the solution consisted of a mixture of the respective bimetallic derivatives, $L(GaEt_2)_2$ and $L(AlR_2)_2$. However, in an equilibrium mixture these two species would be present with the mixed-metal as well and the ^{1}H NMR spectra would be correspondingly more complex. Thus, at ambient temperatures there is no evidence for either metal or alkyl exchange in solution **7–10**. A similar observation (that of a 'rigid' solution state geometry) has been made for Group 13 derivatives of the reduced Salen ligand, Salan [15].

Structural Characterization

A summary of data collection parameters and selected bond lengths and angles for compounds **1** and **3–6** are listed in Tables 2 and 3. In all of the structures (Figs 3–7) the gallium atoms are coordinated by the ligand and the two alkyl groups in a distorted Td geometry. Deviation from ideal angles are seen in a narrowed N—Ga—O angle and consequently widened C—Ga—C angles. According to Bent's Rule bonds to more electronegative atoms contain more *p* character [16]. Thus, the angles that the Salen ligands make are close to what would be observed in a tetraligated complex containing two heteroatoms and two alkyl functionalities. In $Me_2AlOAr(NH_2^tBu)$ [Ar = 2,6-('Bu)$_2$Ph], for instance, the O—Al—N angle is 99.2 (2)° while the C—Al—C angle is 115.9 (4)° [17]. This partially accounts for the stability of the MR_2 unit in these ligands. The Ga—O [av. = 1.92 (2) Å] and Ga—N [2.07 (3) Å] bond distances in the five-coordinate 'closed' structure of Salen('Bu)GaEt [14] the distances in **1**, and **3–6** are longer than [av. Ga—O = 1.87 (2); Ga—N = 2.02 (1) Å]. This is in keeping with the trend for larger bond lengths with increasing coordination numbers.

In bimetallic Salen borate derivatives [$L(BOR_2)_2$ (R = Me, Et)] highly ordered secondary structures are found in the packing diagrams of the compounds where L = Salben('Bu), Salpten('Bu) and Salhen('Bu). However, in **4–6** the length of the ligand backbone does not affect the packing diagrams of the compounds in any systematic way. Moreover, there are no significant deviations in the bond lengths and angles that can be correlated to the length of the ligand backbone.

EXPERIMENTAL

General considerations

All manipulations were conducted using Schlenk techniques in conjunction to an inert atmosphere glove box. All solvents were rigorously dried prior to use. NMR data were obtained on JEOL-GSX-400 and -270 instruments at 270.17 (^{1}H) MHz in $CDCl_3$ unless otherwise indicated. Chemical shifts are reported relative to $SiMe_4$ and are in ppm. Elemental analyses were obtained on a Perkin–Elmer 2400 Analyzer. Infrared data were recorded as KBr pellets on a Matheson Instruments 2020 Galaxy Series spectrometer and are reported in cm^{-1}. Both the infrared and elemental analyses for the compounds are listed in the supporting information. The reagent, 3,5-di-

Table 1. Selected ^{1}H NMR data for compounds **1**–**10**[a]

Compound	**1**	**2**	**3**	**4**	**5**	**6**	**7**	**8**	**9**	**10**
GaR_2	0.38 (m)	0.36 (m)	0.43 (m)	0.41 (m)	0.41 (m)	0.39 (m)	0.42 (m)	0.38 (m)	0.45 (m)	0.42 (m)
	1.06 (t)	1.05 (t)	1.09 (t)	1.08 (t)	1.04 (t)	1.05 (t)	1.10 (t)	1.07 (t)	1.04 (m)	1.07 (m)
AlR_2							−0.70 (s)	−0.74 (s)	−0.08 (s)	−0.08 (s)
									1.04 (m)	1.07 (m)
Ph-^{t}*Bu*	1.21 (s), 1.26 (s)	1.26 (s), 1.31 (s)	1.23 (s)	1.28 (s)	1.26 (s)	1.24 (s)	1.22 (s), 1.24 (s)	1.27 (s), 1.29 (s)	1.23 (s), 1.24 (s)	1.30 (s), 1.32 (s)
	1.38 (s), 1.45 (s)	1.40 (s), 1.46 (s)	1.40 (s)	1.43 (s)	1.40 (s)	1.41 (s)	1.39 (s), 1.40 (s)	1.41 (s), 1.42 (s)	1.40 (s), 1.41 (s)	1.44 (s), 1.45 (s)
N=C*H*	8.05 (s), 8.37 (s)	8.05 (s), 8.39 (s)	8.00 (s)	8.04 (s)	8.00 (s)	8.01 (s)	7.97 (s), 8.05 (s)	8.02 (s), 8.11 (s)	7.99 (s), 8.08 (s)	8.06 (s), 8.16 (s)

[a] Samples were run in $CDCl_3$ at 270 MHz.

tert-butyl-2-hydroxybenzaldehyde was prepared according to the literature [18].

Details of the crystal data and a summary of data collection parameters for the complexes are given in Table 3. Data were collected on a Siemens CCD diffractometer using graphite monochromated Mo-K_α (0.71073 Å) radiation. All calculations were performed on a PC using the Siemens software package, SHELXTL-Plus.

Synthesis of salen(^{t}Bu)HGaEt$_2$ (**1**)

A solution of $GaEt_3$ (0.32 g, 2.03 mmol) in toluene (5 cm^3) was added to a stirred solution of Salen(^{t}Bu)H$_2$ (1.00 g, 2.03 mmol) in toluene (5 cm^3) at room temperature. The initial pale yellow solution became pale green upon stirring for 5 h. Removal of the solvent *in vacuo* yielded a green solid which was recrystallized at 25°C from methanol to yield the title compound as pale green needles (0.98 g, 77%). M.p. 99–100°C. A similar procedure performed with an additional 4 h reflux yielded an identical product in similar yield. ^{1}H NMR: 3.81–3.84 (br.s, 4H, CH_2H_2), 6.80 (d, 1H, Ph-*H*), 7.05 (d, 1H, Ph-*H*), 7.36–7.40 (m, 2H, Ph-*H*).

Synthesis of salpen(^{t}Bu)HGaEt$_2$ (**2**)

This compound was synthesized by an identical procedure to that outlined above from Salpen(^{t}Bu)H$_2$ (1.00 g, 1.98 mmol) and $GaEt_3$ (0.31 g, 1.98 mmol), *in vacuo* removal of the solvent yielded the title compound as pale green solid in stoichiometric yield. M.p. 52–56°C. ^{1}H NMR: 2.06–2.12 (m, 2H, $CH_2CH_2CH_2$), 3.51–3.70 (m, 4H, $CH_2CH_2CH_2$), 6.85 (d, 1H, Ph-*H*), 7.08 (d, 1H, Ph-*H*), 7.39–7.45 (m, 2H, Ph-*H*).

Synthesis of salen(^{t}Bu)(GaEt$_2$)$_2$ (**3**)

A solution of triethyl gallium (0.64 g, 4.06 mmol) in toluene (5 cm^3) was added at room temperature to a stirred solution of Salen(^{t}Bu)H$_2$ (1.00 g, 2.03 mmol) in toluene (20 cm^3). The resulting yellow solution was stirred for 24 h at which point removal of solvent resulted in a yellow solid which was recrystallized from toluene at −30°C to yield the title compound as a pale green crystalline solid (1.44 g, 95%). M.p. 109–111°C. Subsequent recrystallisation of a small portion realized crystals suitable for X-ray analysis. ^{1}H NMR: 3.70 (s, 4H, CH_2CH_2), 6.79 (d, 2H, Ph-*H*), 7.44 (d, 2H, Ph-*H*).

Synthesis of salpen(^{t}Bu)(GaEt$_2$)$_2$ (**4**)

This compound was synthesized via similar method to that above from triethylgallium (0.31 g, 1.98 mmol) and Salpen(^{t}Bu)H$_2$, (0.50 g, 0.99 mmol), recrystallisation from hexane at −30°C yielding the title

Table 2. Selected bond distances (Å) and angles (°) for compounds **1, 3, 4, 5** and **6**

Salen('Bu)HGaEt$_2$ (**1**)

Ga(1)—N(1)	2.03 (1)	Ga(1)—O(1)	1.871 (8)
Ga(1)—C(1)	1.97 (2)	Ga(1)—C(3)	1.89 (2)

N(1)—Ga(1)—O(1)	92.3 (4)	O(1)—Ga(1)—C(3)	109.3 (7)
O(1)—Ga(1)—C(1)	110.5 (5)	C(3)—Ga(1)—C(1)	123.4 (8)
C(3)—Ga(1)—N(1)	107.7 (6)	C(1)—Ga(1)—N(1)	109.1 (6)

Salen('Bu)(GaEt$_2$)$_2$ (**3**) (one molecule only)

Ga(1)—O(1)	1.874 (5)	Ga(1)—C(35)	1.98 (1)
Ga(1)—C(33)	1.99 (1)	Ga(1)—N(1)	2.010 (6)
Ga(2)—O(2)	1.868 (5)	Ga(2)—C(37)	1.93 (1)
Ga(2)—C(39)	1.956 (9)	Ga(2)—N(2)	2.030 (6)

O(1)—Ga(1)—C(35)	107.8 (3)	O(1)—Ga(1)—C(33)	109.2 (3)
C(35)—Ga(1)—C(33)	124.1 (5)	O(1)—Ga(1)—N(1)	92.4 (2)
C(35)—Ga(1)—N(1)	111.8 (4)	C(33)—Ga(1)—N(1)	106.9 (4)
O(2)—Ga(2)—C(37)	107.0 (3)	O(2)—Ga(2)—C(39)	110.1 (3)
C(37)—Ga(2)—C(39)	127.3 (5)	O(2)—Ga(2)—N(2)	91.1 (2)
C(37)—Ga(2)—N(2)	105.2 (4)	C(39)—Ga(2)—N(2)	110.4 (4)

Salpen('Bu)(GaEt$_2$)$_2$ (**4**)

Ga(1)—O(1)	1.863 (6)	Ga(1)—C(40)	1.95 (1)
Ga(1)—C(38)	1.95 (1)	Ga(1)—N(1)	2.024 (6)
Ga(2)—O(2)	1.858 (6)	Ga(2)—C(34)	1.95 (1)
Ga(2)—C(36)	1.99 (1)	Ga(2)—N(2)	2.028 (6)

O(1)—Ga(1)—C(40)	104.7 (4)	O(1)—Ga(1)—C(38)	110.3 (4)
C(40)—Ga(1)—C(38)	126.4 (5)	O(1)—Ga(1)—N(1)	92.5 (2)
C(40)—Ga(1)—N(1)	110.0 (4)	C(38)—Ga(1)—N(1)	107.6 (4)
O(2)—Ga(2)—C(34)	107.0 (3)	O(2)—Ga(2)—C(36)	109.8 (4)
C(34)—Ga(2)—C(36)	125.7 (6)	O(2)—Ga(2)—N(2)	91.9 (3)
C(34)—Ga(2)—N(2)	109.6 (5)	C(36)—Ga(2)—N(2)	107.4 (4)

Salben('Bu)(GaEt$_2$)$_2$ (**5**) (one molecule only)

Ga(1)—O(1)	1.88 (1)	Ga(1)—C(37)	1.95 (2)
Ga(1)—C(35)	1.96 (2)	Ga(1)—N(1)	2.02 (1)
Ga(2)—O(2)	1.88 (1)	Ga(2)—C(39)	1.99 (4)
Ga(2)—C(41)	2.05(4)	Ga(2)—N(2)	2.03 (1)

O(1)—Ga(1)—C(37)	107.3 (7)	O(1)—Ga(1)—C(35)	110.2 (6)
C(37)—Ga(1)—C(35)	125.8 (8)	O(1)—Ga(1)—N(1)	90.9 (6)
C(37)—Ga(1)—N(1)	110.3 (8)	C(35)—Ga(1)—N(1)	106.7 (6)
O(2)—Ga(2)—C(39)	105 (1)	O(2)—Ga(2)—C(41)	108 (1)
C(39)—Ga(2)—C(41)	134 (2)	O(2)—Ga(2)—N(2)	91.0 (6)
C(39)—Ga(2)—N(2)	108 (1)	C(41)—Ga(2)—N(2)	102 (1)

Salhen('Bu)(GaEt$_2$)$_2$ (**6**)

Ga(1)—O(1)	1.886 (4)	Ga(1)—C(19)	1.949 (7)
Ga(1)—C(21)	1.956 (7)	Ga(1)—N(1)	2.013 (5)

O(1)—Ga(1)—C(19)	108.0 (3)	O(1)—Ga(1)—C(21)	109.9 (3)
C(19)—Ga(1)—C(21)	124.6 (3)	O(1)—Ga(1)—N(1)	91.5 (2)
C(19)—Ga(1)—N(1)	109.0 (3)	C(21)—Ga(1)—N(1)	108.8 (3)

compound as a pale green crystals suitable for X-ray analysis (0.61 g, 81%). M.p. 104–106°C. ^{1}H NMR: 2.08–2.16 (m, 2H, $CH_2CH_2CH_2$), 3.53–3.56 (m, 4H, CH_2-N), 6.86 (d, 2H, Ph–*H*), 7.48 (d, 2H, Ph–*H*), 8.04 (s, 2H, Ph-C*H*).

*Synthesis of salben('*Bu)(GaEt$_2$)$_2$ (**5**)

This compound was synthesized *via* similar method to that above from triethylgallium (0.42 g, 2.65 mmol) and Salben('Bu)H$_2$, (0.69 g, 1.33 mmol), recrys-

Table 3. Data collection and processing parameters for compounds **1**, **3**–**6**

Complex	**1**	**3**	**4**	**5**	**6**
Formula	$C_{36}H_{57}GaN_2O_3$	$C_{60}H_{99}Ga_3N_3O_3$	$C_{41}H_{68}Ga_2N_2O_2$	$C_{863}H_{105}Ga_3N_3O_3$	$C_{29}H_{45}GaNO$
Formula weight	619.56	1119.58	760.41	1161.66	493.38
Crystal size (mm)	$0.60 \times 0.50 \times 0.50$	$(0.40)^3$	$0.50 \times 0.40 \times 0.40$	$(0.40)^3$	$(0.40)^3$
Crystal system	Orthorhombic	Triclinic	Triclinic	Triclinic	Monoclinic
Space group	$Pna2_1$	$P\bar{1}$	$P\bar{1}$	$P\bar{1}$	$C2/c$
a (Å)	10.7206 (6)	10.9678 (6)	12.1087 (9)	9.7232 (6)	15.080 (1)
b (Å)	16.3322 (9)	15.5929 (9)	12.8082 (9)	14.5796 (9)	16.917 (1)
c (Å)	21.109 (1)	19.893 (1)	16.042 (1)	24.978 (2)	23.208 (1)
α (°)	90	78.107 (1)	111.073 (1)	106.664 (1)	90
β (°)	90	76.264 (1)	90.862 (2)	94.251 (1)	100.586 (2)
γ (°)	90	89.602 (1)	106.834 (1)	94.286 (1)	90
V (Å^3)	3695.9 (4)	3230.6 (3)	2202.2 (3)	3365.7 (4)	5819.9 (7)
Z	4	2	2	2	8
F(000)	1336	1194	812	1242	2120
D(calcd) (g cm^{-3})	1.113	1.151	1.147	1.146	1.126
μ (mm^{-1})	0.774	1.282	1.255	1.233	0.964
θ_{range} (°)	1.58–20.00	1.08–19.00	1.37–20.00	0.86–17.00	1.79–19.99
Refl. (collected)	10732	8944	6596	7053	8413
Refl. (independent)	3008 [$F \geqslant 4\sigma(F)$]	5128 [$F \geqslant 4\sigma(F)$]	3963 [$F \geqslant 4\sigma(F)$]	3829 [$F \geqslant 4\sigma(F)$]	2702 [$F \geqslant 4\sigma(F)$]
No. of variables,	369	622	424	650	289
$R1$ (%)*[a]	8.28	6.37	7.23	9.70	5.71
R (all data) (%)	8.90	7.07	8.21	12.22	8.09

[a]* $R = (\Sigma||F_o| - |F_c||)/\Sigma|F_o|$.

tallisation from toluene at −30°C yielded the title compound as pale yellow crystals suitable for X-ray analysis (0.76 g, 75%). M.p. 129–131°C. ^{1}H NMR: 1.73 (m, 4H, CH_2CH_2), 3.51 (m, 4H, CH_2-N), 6.84 (d, 2H, Ph-*H*), 7.42 (d, 2H, Ph-*H*), 8.00 (s, 2H, Ph-C*H*).

Synthesis of salhen(^{t}Bu)$(GaEt_2)_2$ (**6**)

This compound was synthesized via similar method to that above from triethylgallium (0.51 g, 3.20 mmol) and Salhen(^{t}Bu)H_2, (0.88 g, 1.60 mmol), recrystallisation from toluene at −30°C yielding the title compound as pale yellow crystals suitable for X-ray analysis (0.95 g, 74%). M.p. 109–110°C. ^{1}H NMR: 1.70 (m, 4H, CH_2CH_2), 3.47 (m, 4H, CH_2-N), 6.85 (d, 2H, Ph-*H*), 7.43 (d, 2H, Ph-*H*).

Synthesis of salen(^{t}Bu)$(GaEt_2)(AlMe_2)$ (**7**)

A solution of triethylgallium (0.32 g, 2.03 mmol) in toluene (5 cm^3) was added at room temperature to a

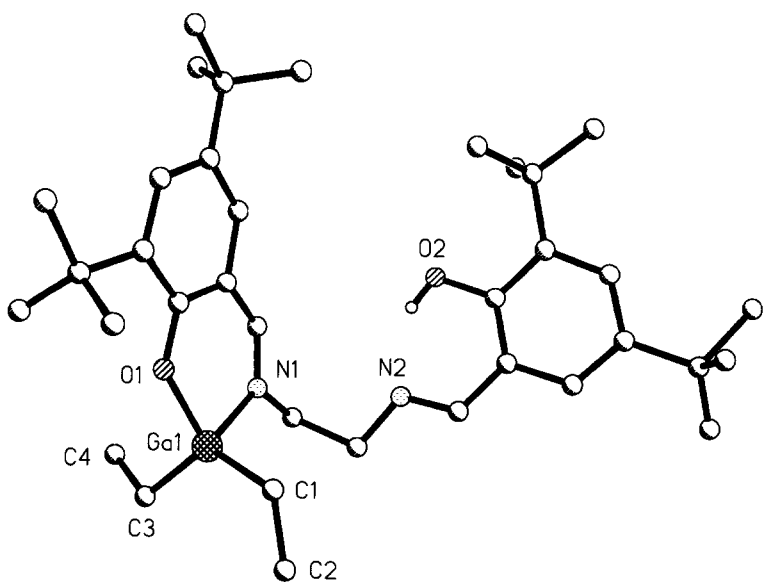

Fig. 3. Molecular structure and atom numbering scheme for Salen(^{t}Bu)H$(GaEt_2)$ (**1**).

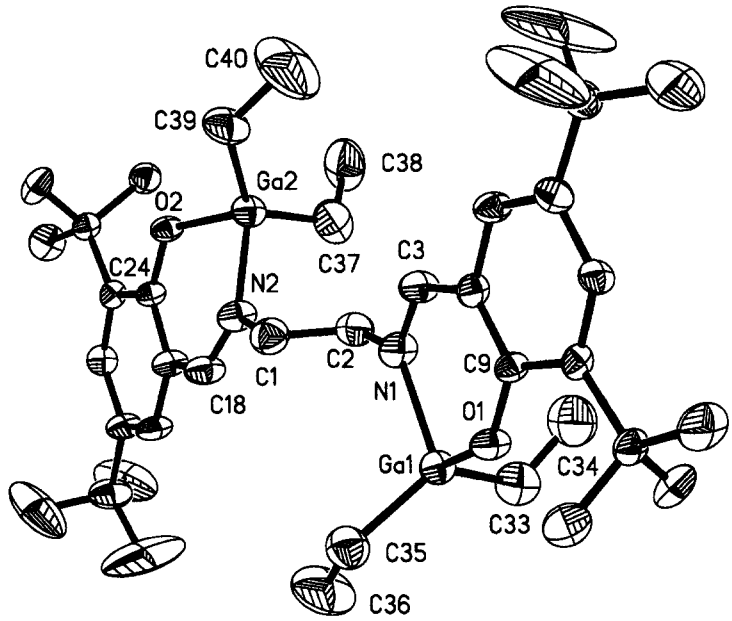

Fig. 4. Molecular structure and atom numbering scheme for Salen('Bu)$(GaEt_2)_2$ (**3**).

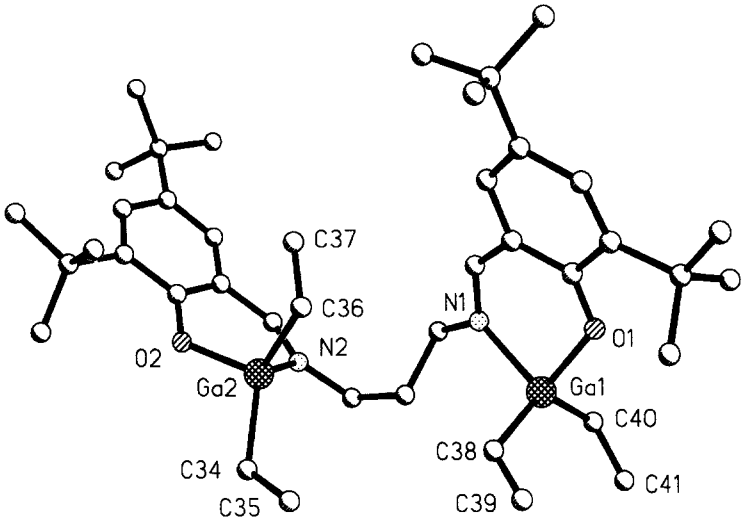

Fig. 5. Molecular structure and atom numbering scheme for Salpen('Bu)$(GaEt_2)_2$ (**4**).

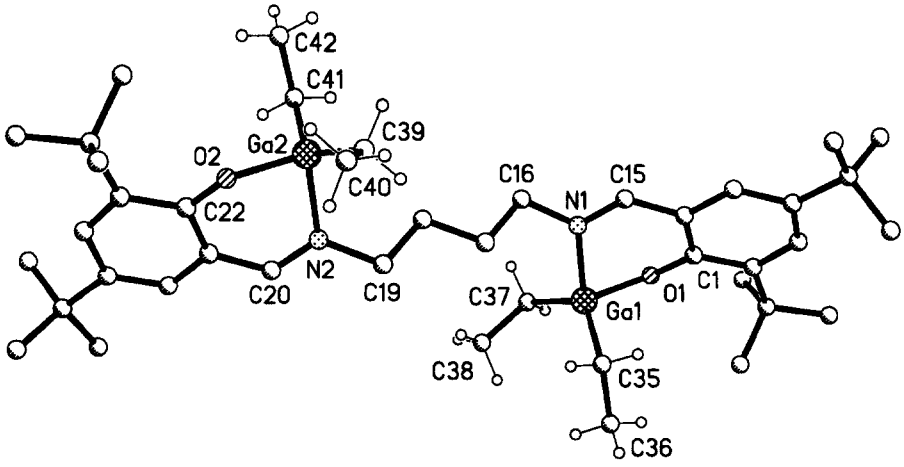

Fig. 6. Molecular structure and atom numbering scheme for Salben('Bu)$(GaEt_2)_2$ (**5**).

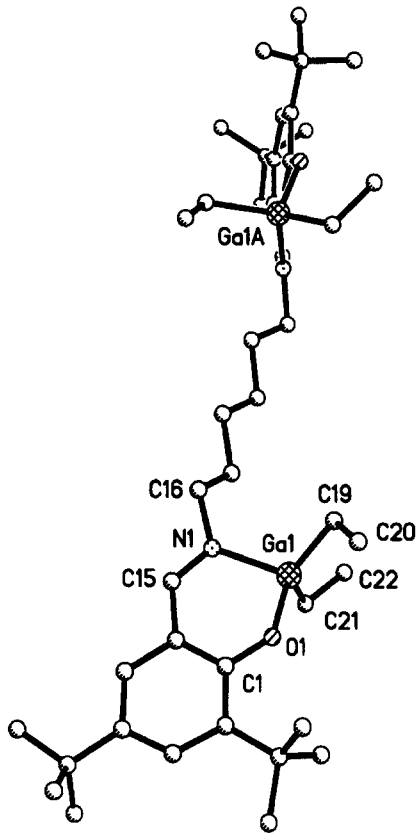

Fig. 7. Molecular structure and atom numbering scheme for Salhen('Bu)($GaEt_2$)$_2$ (**6**).

stirred solution of Salen('Bu)H_2 (1.00 g, 2.03 mmol) in toluene (15 cm^3). The resulting pale yellow solution was stirred for 15 min at which point a solution of trimethyl aluminum (0.147 g, 2.03 mmol) in toluene (5 cm^3) was added. After stirring for 2 h the solvent was removed under reduced pressure to yield a yellow solid which was crystallised as rectangular pale green blocks from toluene at −30°C (0.98 g, 72%). M.p. 108–110°C. ^{1}H NMR: 3.71–3.97 (m, 4H, CH_2-N), 6.76 (m, 1H, Ph-H), 6.90 76 (m, 1H, Ph-H), 7.43 (d, 1H, Ph-H), 7.52 (d, 1H, PhH), 7.97 (s, 1H, PhCH).

Synthesis of salpen('Bu)($GaEt_2$)($AlMe_2$) (**8**)

This compound was synthesized via a similar procedure to that outlined above employing triethyl gallium (0.31 g, 1.98 mmol), Salpen('Bu)H_2 (1.00 g, 1.98 mmol) and trimethylaluminum (0.142 g, 1.98 mmol), and recovered in stoichiometric yield by removal of solvent under reduced pressure. M.p. 84–86°C. ^{1}H NMR: 2.08–2.24 (m, 2H, $CH_2CH_2CH_2$) 3.56–3.65 (m, 4H, CH_2-N), 6.85 (m, 1H, Ph-H), 6.99 (m, 1H, Ph-H), 7.47 (d, 1H, Ph-H), 7.54 (d, 1H, PhH).

Synthesis of salen('Bu)($GaEt_2$)($AlEt_2$) (**9**)

This compound was synthesized with a similar procedure to that outlined above employing triethyl gallium (0.24 g, 1.52 mmol), Salen('Bu)H_2 (0.75 g, 1.52 mmol) and triethylaluminum (0.17 g, 1.52 mmol), and recovered in stoichiometric yield by removal of solvent under reduced pressure. M.p. 138–141°C (dec). ^{1}H NMR: 3.71–3.82 (m, 4H, CH_2-N), 6.76 (m, 1H, Ph-H), 6.88 (m, 1H, Ph-H), 7.44 (d, 1H, Ph-H), 7.50 (d, 1H, PhH).

Synthesis of salpen('Bu)($GaEt_2$)($AlEt_2$) (**10**)

This compound was synthesized with a similar procedure to that outlined above employing triethyl gallium (0.24 g, 1.52 mmol), Salpen('Bu)H_2 (0.77 g, 1.52 mmol) and triethylaluminum (0.17 g, 1.52 mmol), and recovered in stoichiometric yield by removal of solvent under reduced pressure. M.p. 93–94°C. ^{1}H NMR: 2.10–2.22 (m, 2H, $CH_2CH_2CH_2$), 3.57–3.62 (m, 4H, CH_2-N), 6.88 (m, 1H, Ph-H), 7.00 (m, 1H, Ph-H), 7.49 (d, 1H, Ph-H), 7.57 (d, 1H, Ph-H).

CONCLUSION

A wide range of bimetallic and mixed-metal group 13 compounds are accessible when using the Salen('Bu) ligands. Their formation relies on the fact that the chelated $GaEt_2$ fragment is remarkably stable. For example, it does not undergo intramolecular alkane elimination with the phenol portion of the ligand, nor does it react with MeOH under ambient conditions. Furthermore, the mixed-metal derivatives do not undergo scrambling of either the -R or -MR_2 groups.

Acknowledgements—Gratitude is expressed to the National Science Foundation (Grant 9452892) and the donors of the Petroleum Research Fund (Grant 31901-AC3), administered by the American Chemical Society, for support. The receipt of an NSF-CAREER (1996–2000) award is also gratefully acknowledged.

REFERENCES

1. "Salen" is the name that has historically been used to describe the entire class of such ligands possessing various diamino backbones. However, it is also the specific name of the ethyl derivative, $SalenH_2$.
2. (a) Holm, R. H., Everett, G. W. Jr. and Chakravorty, A., *Prog. Inorg. Chem.*, 1966, **7**, 83; (b) Hobday, M. D. and Smith, T. D., *Coord. Chem. Rev.*, 1972, **9**, 311.
3. Dzugan, S. J. and Goedken, V. L., *Inorg. Chem.*, 1986, **25**, 2858.
4. Chong, K. S., Rettig, S. J., Storr, A. and Trotter, J., *Can. J. Chem.*, 1977, **55**, 2540.
5. Gurian, P. L., Cheatham, L. K., Ziller, J. W. and Barron, A. R., *J. Chem. Soc., Dalton Trans.*, 1991, 1449.
6. (a) Atwood, D. A., Jegier, J. A. and Rutherford, D., *J. Am. Chem. Soc.*, 1995, **117**, 6779; (b) Davidson, M. G., Lambert, C., Lopez-Solera, I.,

Raithby, P. R. and Snaith, R., *Inorg. Chem.*, 1995, **34,** 3765; (c) Atwood, D. A., Jegier, J. A. and Rutherford, D., *Inorg. Chem.*, 1996, **35,** 63.
7. Atwood, D. A., Jegier, J. A., Remington, M. P. and Rutherford, D., *Aust. J. Chem.*, 1996, **49,** 1333.
8. Wei, P. and Atwood, D. A., *Inorg. Chem.*, 1997, **36,** 4060.
9. (a) Goedken, V. L., Ito, H. and Ito, T., *J. Chem. Soc., Chem. Commun.*, 1984, 1453; (b) Alcock, N. W., Blacker, N. C., Wallbridge, M. G. H. and Barker, J., *J. Organomet. Chem.*, 1991, **419,** C23; (c) Atwood, D. A., Atwood, V. O., Cowley, A. H., Atwood, J. L. and Roman, E., *Inorg. Chem.*, 1992, **31,** 3871.
0. Transition metal-Salen('Bu) derivatives are well known; (a) Lee, N. H., Muci, A. R. and Jacobsen, E. N., *Tetrahedron Let.*, 1991, **32,** 3055; (b) Jacobsen, E. N., Zhang, W., Muci, A. R., Ecker, J. R. and Deng, L., *J. Am. Chem. Soc.*, 1991, **113,** 7063; (c) Baran, P., Bottchner, A., Elias, H., Haase, W., Huber, M., Fuess, H. and Paulus, H., *Z. Naturforsch.*, 1992, **47B,** 1681; (d) Bottcher, A., Elias, H., Muller, L. and Paulus, H., *Angew. Chem. Int. Ed. Engl.*, 1992, **31,** 623; (e) Herrmann, W. A., Rauch, M. U. and Artus, G. R., *Inorg. Chem.*, 1996, **35,** 1988.
11. Atwood, D. A., Hill, M. S., Jegier, J. A. and Rutherford, D., *Organometallics*, 1997, **16,** 2659.
12. Hill, M. S. and Atwood, D. A., *Main Group Chem.*, in press.
13. Beachley, O. T., Jr., Kirss, R. U., Bianchini, R. J. and Royster, T. L., *Organometallics*, 1987, **6,** 724.
14. Atwood, D. A., and Hill, M. S., *Chem. Ber.*, submitted.
15. Atwood, D. A. and Rutherford, D., *Comm. Inorg. Chem.*, 1996, **19,** 25.
16. Bent, H. A., *J. Chem. Educ.*, 1960, **37,** 616; Bent, H. A., *Chem. Rev.*, 1961, **61,** 275.
17. Jegier, J. A. and Atwood, D. A., *Bull. Soc. Chim. Fr.*, 1996, **133,** 965.
18. Casiraghi, G., Casnati, G., Puglia, G., Sartori, G., and Terenghi, G., *J. Chem. Soc., Perkin Trans.*, 1980, 1862.

Pergamon

PII: S0277-5387(97)00292-1

Polyhedron Vol. 17, No. 5–6, pp. 821–830, 1998
© 1998 Elsevier Science Ltd
All rights reserved. Printed in Great Britain
0277-5387/98 $19.00+0.00

Chemical routes to barium–cerium oxides: the quest for mixed-metal precursors. Molecular structure of $Ba_4Ce_2(\mu_6\text{-}O)(thd)_4(\mu_3\text{-}OPr^i)_8(OPr^i)_2$*

Liliane G. Hubert-Pfalzgraf,[a]† Christine Sirio[a] and Claudine Bois[b]

[a] Laboratoire de Chimie Moléculaire, URA-CNRS, Université de Nice Sophia Antipolis, Parc Valrose, 06 108 Nice Cédex 2, France

[b] Laboratoire de Chimie des Métaux de Transition, URA-CNRS, 4 Place Jussieu 75 230 Paris Cédex 05, France

(Received 29 April 1997; accepted 25 June 1997)

Abstract—Various synthetic routes to Ba–Ce mixed-metal species have been investigated No reaction was observed between $Ce_2(OPr^i)_8(Pr^iOH)_2$ (**1**) and barium isopropoxide. The enhanced acidity of the alcohol molecules of **1** has been used as a means to access to Ba–Ce species and to fix the stoichiometry between the metals. $Ba_2Ce_4(OPr^i)_{20}$ (**2**) has been obtained. This species is unstable in the presence of isopropanol giving $BaCe_4(OPr^i)_{18}$ (**3**). The reaction between **1** 2,2,6,6-tetramethylheptane-3,5-dione (thdH) and barium isopropoxide gives $Ba_4Ce_2(\mu_6\text{-}O)(thd)_4(\mu_3\text{-}OPr^i)_8(OPr^i)_2$ (**4**) independently of the stoichiometry used for the reaction. The reactions between **1**, barium isopropoxide and acetylacetone are more complex and different compounds, namely $Ba_2Ce_2O(acac)_2(OPr^i)_8$ (**5**) or $BaCe_2(acac)(OPr^i)_9$ (**6**) are formed depending on the experimental conditions. All compounds have been characterized by elemental analysis, FT-IR, ^1H and ^{13}C NMR. **4** was also characterized by X-ray diffraction. Hydrolysis–polycondensation reactions have been estimated for **4** and for **6**. © 1998 Elsevier Science Ltd. All rights reserved

Keywords: cerium, barium, mixed-metal alkoxides, β-diketonates, sol-gel.

Cerium is involved in a variety of advanced oxide materials such as sensors, γ-scintillators, high Te superconductors [1]. Among them, barium cerates are of particular interest since solid electrolytes based on such formulations have been reported to have ionic conductivities similar to those of yttria stabilized zirconia (YSZ) but at lower temperatures [2]. The Ce(IV) isopropoxide solvate $Ce_2(OPr^i)_8(Pr^iOH)_2$ (**1**) has been known for many years namely as early as 1956, due to the contribution of Don Bradley to metal alkoxide chemistry [3]. It represents the most commonly used starting material for cerium(IV) chemistry with anionic oxygen donor ligands and organometallics [4].

We wish to report here our investigations between **1** and various barium species for the formation of Ba–Ce mixed-metal species. Whereas no reaction was observed by mixing the isopropoxides of the different metals at room temperature, the building up of Ba–Ce species could be achieved by the assistance of ancillary ligands, namely β-diketones or by using the enhanced acidity of the isopropanol ligand for the incorporation of barium. $Ba_2Ce_4(OPr^i)_{20}$, (**2**) $BaCe_4(OPr^i)_{18}$ (**3**), $Ba_4Ce_2O(thd)_4(OPr^i)_{10}$ (**4**), $Ba_2Ce_2O(acac)_2(OPr^i)_8$ (**5**) and $BaCe_2(acac)OPr^i)_9$ (**6**) were obtained and characterized by elemental analysis, FT-IR, ^1H and ^{13}C NMR. They represent, to the best of our knowledge, the first mixed-metal Ba-Ce species reported so far. The molecular structure of **4** was established by X-ray

* Dedicated to Prof. D. C. Bradley on the occasion of his 73rd birthday.

† Author to whom correspondence should be addressed.

diffraction. Hydrolysis-polycondensation reactions were investigated for **4** and **6**.

EXPERIMENTAL

All reactions were achieved under inert atmosphere using Schlenk tube techniques. Solvents were dried and purified by distillation. $Ce_2(OPr^i)_8(Pr^iOH)_2$ (**1**) [5] and $Ba[N(SiMe_3)_2]_2(THF)_2$ [6] were obtained according to the literature. ^1H, ^{13}C NMR and IR spectra were run on Bruker AC-200 and IR-FTS 45 spectrometers respectively. IR spectra were obtained as Nujol mulls. Analyses were obtained from the Centre de Microanalyses du CNRS. TGA analyses of the powders obtained after hydrolysis were done with a Setaram system using a temperature ramp of 5°C/min.

Hydrolyses experiments were achieved in THF; water was added in THF (2 moles/l)

Synthesis of $[BaCe_2(OPr^i)_{10}]m$ (**2**)

1 (3.2 g, 3.7 mmol) in 20 cm^3 of toluene were added to barium chips (0.5 g, 3.7 mmol). Ammonia was bubbled through the medium for activation of the metal. The solution became brown. After consumption of barium, the medium was evaporated to dryness and the solid was redissolved in 10 cm^3 of hexane. $[BaCe_2(OPr^i)10]_m$ (2.6 g, 70%) was obtained at −25°C.

(3.2 g, 3.7 mmol) of **1** were added to $Ba[N(SiMe_3)_2]_2(THF)_2$ (2.3 g, 3.9 mmol) in 10 cm^3 of hexane. The solution turned yellow. $[BaCe_2(OPr^i)_{10}]_m$ (3.15 g, 80%) was isolated at 25°C. Calc. for $C_{30}H_{70}O_{10}BaCe_2$, 35.7; H, 7.5; Ba, 13.6; Ce, 27.8. Found: C, 35.3; H, 7.2; Ba, 13.8; Ce, 27.40%. IR (cm^{-1}): 1360sh, 1329m, 1160m, 1138m, 1124s, 991m, 976s, 966m, 944sh, 837m, 825m, 814m, 525m, 520sh, 466m, 442m, 412sh, 397m (νM—OR). ^1H NMR (C_7D_8, 25°C, ppm): 5.3m (1H, CH), 5.2 sept (J = 6.1 Hz, 4H, CH) 4.9m (5H, CH); 1.73, 1.4d (J = 6.1 Hz, 6:54, 60H, CH_3). ^1H NMR (C_7D_8, −70°C, ppm): 5.4, 5.2, 5.1, 4.9m (2:2:1:5, 10H, CH); 1.8, 1.7d (J = 6 Hz, 12:18, 30H, CH_3), 1.5d [30H, CH_3]. $^{13}C\{^1H\}$ NMR (C_6D_6, ppm): 78.3, 77.5, 71.0 (CH); 31.9, 28.3, 23.0 (CH_3).

Synthesis of $BaCe_4(OPr^i)_{18}$ (**3**)

Addition of isopropanol (0.5 cm^3) to a solution of **2** obtained from (2.75 mmol) of **1** and (2.78 mmol) of barium in toluene (10 cm^3) gave $BaCe_4(OPr^i)_{18}$ (65%). Anal. calcd for $C_{54}H_{126}O_{18}BaCe_4$: C, 36.8; H, 7.2; Ce, 31.8; Ba, 7.8. Found: C, 37.1; H, 7.4; Ce, 32.5; Ba, 8.4%. IR (cm^{-1}); 1358m, 1338s, 1327s, 1160s, 1128s, 1124s, 993s, 977s, 957s, 942sh, 918sh, 837m, 824m, 576m, 526s, 463sh, 445m, 416m, 401sh [ν(M—OR]. ^1H NMR (C_6D_6, 25°C, ppm): 5.3, 5.2, 4.95 sept (J = 6 Hz, 4:8:6, 18H, CH); 1.9, 1.6, 1.5, 1.4d (J = 6Hz, 12:36:30:30, 108H, Me) $^{13}C\{^1H\}$ NMR (C_6D_6, ppm): 79.3, 78.2, 77.8, 69.6 (CH); 28.7, 28.6, 28.4, 26.0 CH_3.

Synthesis of $Ba_4Ce_2O(thd)_4(OPr^i)_{10}$ (**4**)

thdH (0.17 cm^3, 0.82 mmol) was added to **1** (0.36 g, 0.42 mmol) in 20 cm^3 of toluene. This solution, which turned immediately from yellow to orange, was added to $[Ba(OPr^i)_2]_\infty$ (0.44g, 1.7 mmol) in 20 cm^3 of toluene. Crystals of **4** (0.35 g, 76%) were obtained at 4°C.

A suspension of $[Ba(OPr^i)_2]_\infty$ (0.6 g, 2.4 mmol) in 10 cm^3 of hexane was added to 0.5 g (0.6 mmoles) of $Ce(thd)_4$ in 15 cm^3 hexane. Solubilisation of $[Ba(OPr^i)_2]_\infty$ was observed. After 18 h., (0.5 g, 73%) of **4** were obtained. **4** was also formed by reacting **1** with $Ba(thd)_2$ (1:2 stoichiometry) but in poor yield (~20%). It is non-volatile (Dec: 150°C) Anal. Calcd for $C_{74}H_{146}O_{19}Ba_4Ce_2$: Ce, 12.9; Ba, 25.3; Found: Ce, 13.2; Ba, 25.6%. IR (cm^{-1}): 1589s, 1575s [ν(C=O)]; 1533m, 1502s [ν(C=C)] 1461s, 1417s, 1378s, 1366s, 1357s; 1270w, 1241m, 1224m, 1180m, 1159s, 1128s, 1117s, 979s, 949s, 864s, 842m, 819m; 790m, 753m, 730m; 594s, 567m, 525m, 470m, 458s, 416s, 397s (νM—O). ^1H NMR (C_6D_6, ppm): 6.0s (4H, CH, thd); 5.3, 4.5 sept (J = 6Hz, 8:2, 10H, CH, Pr^i); 1.7d (J = 6 Hz, 48H, Me, Pr^i); 1.4s (72H, Me, thd); 1.10d (J = 6Hz, 12H, Me, Pr^i). $^{13}C\{^1H\}$ NMR (C_6D_6, ppm): 190 (C=O), 89.5 (CH, thd); 82.3, 70.0 (CH, Pr^i); 41.3 (C, thd); 29.2, 28.7, 27.4 (Me, Pr^i, thd).

Synthesis of $Ba_2Ce_2O(acac)_2(OPr^i)_8$ (**5**)

Acetylacetone (0.25 cm^3, 2.4 mmol) were added to **1** (1.0 g, 1.15 mmol) dissolved in 40 cm^3 of toluene. The resulting orange solution was added to $[Ba(OPr^i)_2]_\infty$ (1.8 g, 17.1 mmol) in 10 cm^3 of toluene. The reaction medium became yellow. After stirring for 18 h and filtration, $Ba_2Ce_2O(acac)_2(OPr^i)_8$ (0.5 g, 35%) crystallized at 30°C. Anal. Calcd for $C_{34}H_{70}O_{13}Ba_2Ce_2$: C, 32.9; H, 5.7; Ce, 22.6; Ba, 22.1, Found: C, 32.6; H, 5.4; Ce, 22.4; Ba, 23.1% IR (cm^{-1}): 1604s [ν(C=O)]; 1507s [ν(C=C)]; 1406m, 1357m, 1329sh; 1260w, 1239m, 1156s, 1125s, 1010m, 992s, 953s, 906m, 838m, 817m; 770m, 753m; 589m, 563m, 520m, 487m, 460m, 457w, 409w, 397w [ν(M—)O]. ^1H NMR (C_6D_6, ppm): 5.5s (2H, CH, acac); 5.3, 4.8 sept (J = 6 Hz, 6:2, 8H, CH, Pr^i); 2.0s (12H, Me, acac); 1.8, 1.66, 1.31d (J = 6Hz, 12:24:12, 48H, Me, Pr^i). $^{13}C\{^1H\}$ NMR (C_6D_6, ppm): 186.6 (C=O); 99.8 (CH, acac); 92.5, 79.1, 69.2 (CH, Pr^i); 29.0; 28.4, 28.2 (CH_3, Pr^i, acac).

Synthesis of $BaCe_2(acac)(OPr^i)_9$ (**6**)

acacH (0.4 cm^3, 3.6 mmol) was added to **1** (1.7 g, 1.95 mmol) in 15 cm^3 of toluene. The orange solution

obtained was added to $[Ba(OPr^i)_2]_x$ (0.95 g, 3.7 mmol) in 20 cm^3 of toluene. After stirring and filtration, $BaCe_2(acac)(OPr^i)_9$ was crystallised out (1.6 g, 81%) at 4°C.

Same product from acacH (3.85 mmol) $[Ce(OPr^i)_4(Pr^iOH)]_2$ (3.85 mmol) in 30 cm^3 of toluene and $[Ba(OPr^i)_2]_x$ (2.2 mmol). (97%). MP: 165°C, Anal. Calcd for $C_{32}H_{70}O_{11}BaCe_2$: C, 36.7; H, 6.7; Ce, 26.8; Ba, 13.1. Found: C, 36.3; H, 6.5; Ce, 27.2; Ba, 13.8%. IR (cm^{-1}): 1588m, 1545m [ν(C=O)]; 1504m [ν(C=C)]; 1359sh, 1327m; 1249m, 1188sh, 1159s, 1124s, 992s, 977s, 957s, 946sh, 907sh, 838m, 826m, 818m; 776m, 653m, 522m, 512sh, 465m, 443m, 413m, 400m, 397m [ν(M—O)]. ^1H NMR ($CDCl_3$, 25°C, ppm): 5.45s (1H, CH, acac); 5.05, 4.7m (4:5, 9H, CH, Pr^i); 1.96s (6H, Me, acac); 1.6, 1.4d (J = 6 Hz, 24:30, 54H, Me, Pr^i). ^1H NMR ($CDCl_3$, −45°C, ppm): 5.4s (1H, CH, acac); 4.95, 4.85, 4.6m (1:2:6, 9H, CH, Pr^i); 1.8s (6H, Me acac); 1.3, 1.15d (J = 6 Hz, 30:24, 54H, Me, Pr^i). $^{13}C\{^1H\}$ NMR (C_6D_6, ppm): 186.6 (C=O); 103 (CH, acac); 92.9, 78.8, 70.4 (CH, Pr^i); 28.8, 28.5, 28.1 (CH_3, Pr^i, acac).

Unit cell parameters (−100°C): a = 18.07, b = 12.91, c = 19.24 Å; β = 96.23°.

The various compounds are soluble in polar solvents (THF, Et_2O, DME), slightly soluble in toluene or isopropanol and insoluble in hexane. **3** is insoluble in isopropanol.

Crystallography of $Ce_2Ba_4O(thd)_4(OPr^i)_{10}.C_7H_8$

Data were collected with two different crystals, the first of them being deteriorated after a few hours. Unit cell dimensions with estimated standard deviations were obtained from least squares refinements of the setting angles of 25 well-centered reflections. Two standard reflections were monitored periodically; for the first crystal, their intensities showed a regular decay; a correction was applied. Crystallographic data and other pertinent informations are summarized in Table 1. Corrections were made for Lorentz and polarization effects. Empirical absorption corrections (Difabs) [7] and a secondary extinction corrections were applied.

Computations were performed by using CRYSTALS [8]. Atomic form factors for neutral Ba, Ce, O and C were taken from Ref. [9], anomalous dispersion was taken in account. All atoms were anisotropically refined, except those of the toluene molecule. Least-squares refinements were carried out, in three blocks, by minimizing the function $\Sigma w(|F_o|-|F_c|)^2$, where F_o and F_c are the observed and calculated structure factors. Models reached convergence with $R = \Sigma(\|F_o|-|F_c\|)/\Sigma|F_o|$ and $Rw = [\Sigma(|F_o|-|F_c|)^2/\Sigma w(F_o)^2]^{1/2}$ having values listed in Table 1. The weighting scheme was unity. Criteria for a satisfactory complete analysis were the ratios of rms shift to standard deviation being less than 0.1 and no significant features in the final map. The structure consists of a centrosymmetric $Ce_2Ba_4O(thd)_4(OPr^i)_{10}$ molecule, O(1) lies on an inversion center. The structure also contains a disordered toluene molecule near an inversion center (0,1/2,1/2), its atoms were introduced with an occupancy factor of 0.5, except C(100), since C(100)′ (′: $-x$, $1-y$, $1-z$) is another atom of the ring, and C(102) which cannot be distinguished from the methyl group of the centrosymmetric molecule. The view of the molecule is done using Cameron [10].

Supplementary Material deposited at the Cambridge Crystallographic Data Centre: Tables of atomic coordinates, of anisotropic thermal parameters, of non-essential bond lengths and angles, list of observed and calculated structure factors.

RESULTS AND DISCUSSION

Synthesis and characterization

No reaction was observed between $Ce_2(OPr^i)_8(Pr^iOH)_2$, **1** and $[Ba(OPr^i)_2]_x$ in toluene at room temperature. Heating leads to the conversion of **1** into various oxo species [11] and was thus precluded. The formation of mixed-metal species was thus achieved at room temperature by using either the enhanced acidity of the coordinated alcohol molecules or by adding ancillary ligands, namely β-diketones to the mixture of metal alkoxides. By contrast to the former, the latter strategy does not allow to fix the stoichiometry between the metals [13]. Scheme 1 summarizes the various synthetic routes developed for access to Ba-Ce species. Characterization was achieved by elemental analysis, FT-IR and ^1H and ^{13}C NMR.

The reactivity of the coordinated alcohol molecules of $Ce_2(OPr^i)_8(Pr^iOH)_2$ was investigated toward barium bis(trimethylsilylamide) and metallic barium. Whereas $Ba[N(SiMe_3)_2]_2(THF)_2$ corresponds to a labile species, the barium chips need activation by ammonia, as observed previously for the synthesis of BaZr species [12] or other barium derivatives [14]. The mixed-metal species isolated in high yield ($\geq$70%) from hexane displays the expected stoichiometry between the metals and corresponds to $[BaCe_2(OPr^i)_{10}]m$, **2**. This species is unstable in the presence of isopropanol. Addition of small amounts of isopropanol (5% in volume) affords a new species, namely $Ce_4Ba(OPr^i)_{18}$, **3**, in which the stoichiometry between the metals has been modified. **3** is obtained in high yield (~65%), together with insoluble barium isopropoxide. The dissociation of **2** into the homometallic alkoxides $[Ba(OPr^i)_2]_x$ and $Ce_2(OPr^i)_8(Pr^iOH)_2$ is complete in pure isopropanol.

In the absence of crystals suitable for X-ray analysis, the structural information of **2** and **3** was gained by ^1H and ^{13}C NMR. Variable temperature ^1H NMR spectra point out the fluxional nature of compounds **2** and **3**. The CH groups of **2** resonate as three septuplets in a 1:4:5 integration ratio at room tempera-

Table 1. Crystal data for $[Ba_4Ce_2O(thd)_4(O^iPr)_{10}]$, C_7H_8

Fw	2261.70
a (Å)	12.876(4)
b (Å)	14.683(4)
c (Å)	15.138(7)
α (°)	74.43(3)
β (°)	65.28(2)
γ (°)	84.45(3)
V (Å^3)	2504(2)
Z	1
Space group	$P-1$
Systematic absences	none
Crystal shape	parellelepiped
Linear absorption coefficient μ (cm^{-1})	25.04
Density ρ(g cm^3)	1.44
Diffractometer	CAD4-Enraf–Nonius
Radiation	Mo K_α (λ = 0.71069 Å)
Scan type	$\omega/2\theta$
Scan range (°)	0.8 + 0.345 tgθ
θ limits (°)	1–20
Temperature of measurement (°C)	−100
Octants collected	−11,12; −13,14; 0,14
Nb of unique data collected	4792
Nb of unique data used for refinement	4141 $(F_o)^2 > 3\sigma(F_o)^2$
$R = \Sigma\|\|F_o\| - \|F_c\|\|/\Sigma\|F_o\|$	0.049
$Rw = [\Sigma w(\|F_o\| - F_c\|)^2/\Sigma wF_o^2]^{1/2}$	0.057
Absorption correction	DIFABS (min = 0.87, max = 1.16)
Exctinction parameter ($\times 10^{/-6}$)	116
Nb of variables	471
$\Delta\rho$min (e/Å^3)	−1.0
$\Delta\rho$max (e/Å^3)	1.1

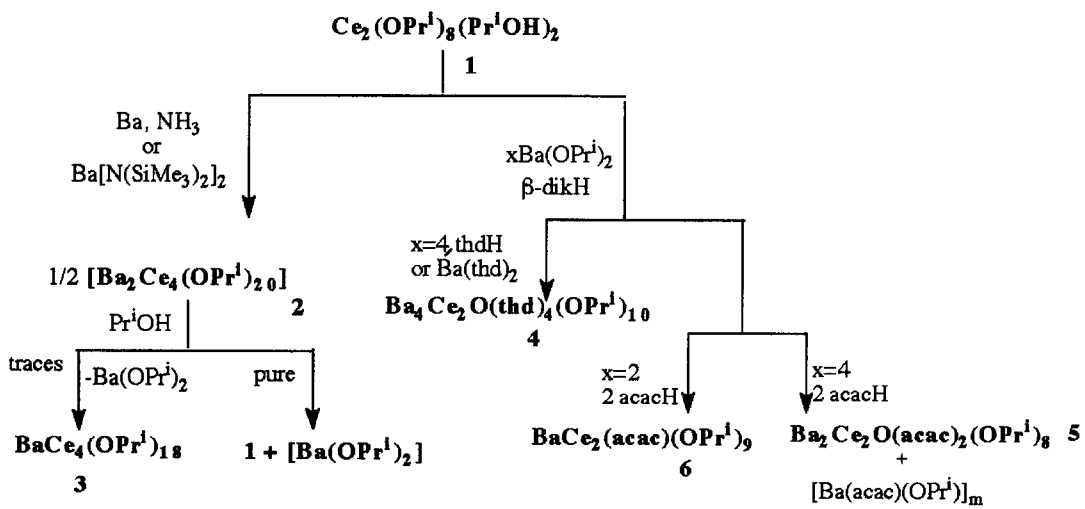

Scheme 1. Various synthetic routes to Ba–Ce species (all reactions in toluene at room temperature if not otherwise stated).

ture. At low temperature (−70°C), four multiplets are observed, their integration ratio being 2 : 2 : 1 : 5. The ^{1}H NMR as well as the ^{13}C NMR data indicate the presence of at least four types of magnetically non-equivalent alkoxide ligands. They are consistent with a dinuclear structural unit $Ba_2Ce_4(\mu_3\text{-}OPr^i)_4(\mu\text{-}OPr^i$-

$)_8(OPr^i)_8$ in which all metals are 6-coordinate, analogous to that of $Ba_2Zr_4(OPr^i)_{20}$ [12]. It is built up on the $[Ce_2(\mu_3\text{-}OR)_2(\mu\text{-}OR)_3(OR)_4]^-$ fragment which has found precedent in $NaCe_2(OBut)_9$ [15]. The ligating ability of $M_2(OR)_9^-$ fragments has been well documented for tetravalent transition metals namely titanium [16], zirconium [17] and hafnium [18]. The integration ratio observed for **2** suggests that the most shielded multiplet at 4.9 ppm can be attributed to the OR ligands in terminal positions on cerium atoms, as well as to these bridging the cerium atoms. Structure A represents a structural type based on the assembly of two triangular units which has been observed for mixed-metal species having a $M_2M'_4$ stoichiometry, the bridging ligands being alkoxides [12,13] or chlorides as observed for $Cd_2Zr_4(\mu_3\text{-}OR)_4(\mu\text{-}OR)_6(OR)_8(\mu\text{-}Cl)_2$ [19], $Pr_2Al_4(\mu\text{-}OR)_8(OR)_8(\mu\text{-}Cl)_2(ROH)_2$ [20], R = Pr^i or $[MgTi_2(\mu_3\text{-}OR)_2(\mu\text{-}OR)_2(OR)_4(\mu\text{-}Cl)_2]_2(\mu\text{-}Cl)_2$ (R = Et) [13].

The 1 : 4 stoichiometry analogous to that of compound **3** has been observed for $BaM_4(OR)_{18}$ (M = Ti [16], Zr [12,17], an hydrolysis product, $BaZr_4(\mu_3\text{-}OH)(OPr^i)_{17}$ [21], $Sm_4Ti(\mu_5\text{-}O)(OPr^i)_{14}$ [22] and $YPr_4(\mu_5\text{-}O)(OPr^i)_{13}$ [23]. Compound **3** derives from **2** in the presence of isopropanol. Its spectroscopic data (FT-IR spectra as well as the chemical shifts in the ^1H NMR spectra) are quite similar to those of compound **2** and thus suggest small structural modifications. ^1H NMR spectra show three multiplets (integration ratio 4 : 8 : 6) for the CH groups at room temperature. Four types of magnetically different CH are observed in the ^{13}C NMR spectrum. These data are consistent with a structure of type B in which two $Ce_2(OR)_{9-}$ moieties are assembled around a central, eight coordinate barium atom. That structural type corresponds to the structures observed in the solid state for the $BaM_4(OR)_{18}$ species [12,16].

The use of β-diketones can be another way to promote the formation of mixed-metal species [13]. The reaction between $Ce(OPr^i)_2(thd)_2$, obtained *in situ* by reacting $Ce_2(OPr^i)_8(Pr^iOH)_2$, **1** and 4 equiv. of thdH, and barium isopropoxide (stoichiometry Ce : Ba 2 : 4) leads to a yellow solution. A mixed-metal species, $Ba_4Ce_2O(OPr^i)_{10}(thd)_4$, **4** crystallized out in high yield (76%). It is also easily obtained by reaction between cerium tetramethylheptanedionate and barium isopropoxide. By contrast, the reaction between barium tetramethylheptanedionate and cerium isopropoxide affords **4** in a poor yield. The FT-IR spectrum of **4** shows ν(C=O) absorption bands characteristic of tetramethylheptanedionate ligands. Their frequencies (1589, 1575 cm^{-1}) suggest that the β-diketonate ligands are linked to the barium atoms, rather than to the cerium ones.

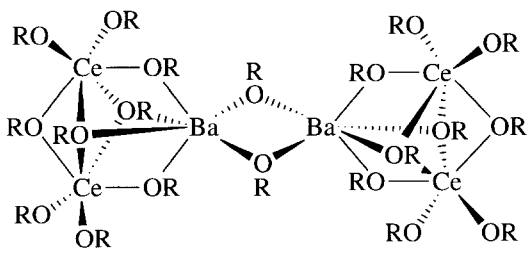

A

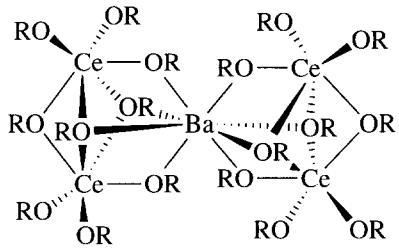

B

This was confirmed by single crystal X-ray diffraction studies of **4**. Its molecular structure depicted in Fig. 1, corresponds to a centrosymmetrical hexanuclear cluster $Ba_4Ce_2(\mu_6\text{-}O)(\eta^2\text{-}thd)_4(\mu_3\text{-}OPr^i)_8(OPr^i)_2$. Selected bond lengths and angles are collected in Table 2. The hexanuclear cluster is a distorted octahedron with the metals assembled around a central oxo ligand O(1) and the two cerium atoms in the apical positions. All Ba_2Ce faces of the octahedron are capped by triply-bridging alkoxide ligands. The barium atoms bear also chelating tetramethylheptanedionates and are thus hexacoordinated. The cerium atoms are linked to one terminal OR group and are hexacoordinated. The cerium-oxygen bond distances spread over the range 2.06(1)–2.300(8) Å, with the cerium oxo bond distances having values intermediate between terminal and triply bridging Ce—OR bonds. The barium-oxygen ones are, as expected on the basis on the metal radii, longer and very from 2.561(9) to 3.006(1) Å. These distances vary in the order Ba—O(thd) (av. 2.572) < Ba-μ_3-OPr^i (2.803 Å av.) < Ba-μ_6O (av. 3.005 Å). The octahedron is flattened (non-bonding distances Ba(2)···Ba′(2) and Ce(1)···Ce′(1) are 6.068(1) and 4.47(2) Å, respectively) and the surrounding of the μ_6-oxo ligand O(1) is thus highly distorted since the Ce-O(1) bond lengths have a value of 2.24(1) Å only. These data are consistent with the distances reported in the literature for cerium and barium derivatives in which the metals have similar coordination numbers [11,24,25]. The Ce—O bond distances of **4** are for instance shorter than for $Ce_4(\mu_4\text{-}O)(OPr^i)_{14}$ [11]. The terminal Ce—OR bonds are associated to large Ce—O—C angles [171.2(10)°]. The structural type of **4** has precedent in the literature, it is related to that of $Zr_2Co_4(\mu_6\text{-}O)(acac)_4(\mu\text{-}OPr^n)_8(OPr^n)_2$ [26] and of $Ba_2Y_4(\mu_6\text{-}O)(thd)_4(\mu_3\text{-}OEt)_8$ [27]. The obtaining of oxo species is quite common for large, oxophilic metals such as

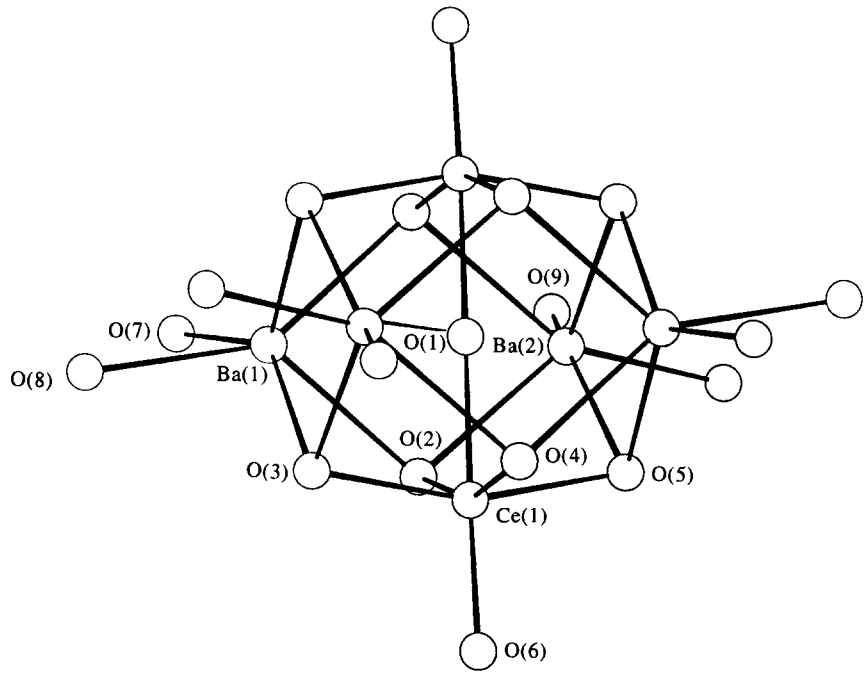

Fig. 1. Metal oxygen core of $Ce_2Ba_4(\mu\text{-}O)(thd)_4(\mu_3\text{-}OPr^i)_8(OPr^i)_2$ showing the atom numbering scheme.

lanthanides [1]. Various sources of the oxo ligand have been discussed. **4** is obtained in high and reproducible yields. These observations are in the favor of C—O bond cleavage reactions of the OR group as the origin of the O^{2-} ligand rather than adventitious hydrolysis.

The ^1H NMR spectra of **4** show two types of methine groups for the alkoxide ligands in a 4 : 1 integration ratio, all β-diketonate ligands appear magnetically equivalent. These data account for the retention of the solid state structure upon dissolution.

Acetylacetone is a more convenient β-diketone for sol–gel applications [28]. However, the reactions between **1**, barium isopropoxide and acetylacetone are less selective than for tetramethylheptanedione and three different compounds are formed by using a synthetic procedure similar to that of **4**. The mixed-metal species $Ba_2Ce_2O(acac)_2(OPr^i)_8$ (**5**) is isolated in about 35% yield. Attempts to increase the yield of **3** by adjusting the reaction conditions acacH-**1**-$Ba(OPr^i)_2$ (2 : 1 : 2 stoichiometry) did not give access to **5**, but afforded a new Ba—Ce species, $BaCe_2(acac)(OPr^i)_9$, **6**, isolated in ~80% yield together with a barium acetylacetonatoisopropoxide derivative characterized by ν(CO) stretching frequencies at 1588, 1548 cm^{-1}. **6** was also obtained by reaction between **2** and acetylacetone. No crystals suitable for a complete X-ray analysis could be obtained for **5** and **6**. By contrast with our observations with titanium ethoxide [28b], barium acetylacetonate is inert toward **1**. FT-IR spectra suggest that the acetylacetonate ligands are linked to the barium centers [ν(C=O) 1604; 1588, 1545 cm^{-1}) for **5** and for **6**, respectively. ^1H NMR spectra indicate that the β-diketonate ligands are magnetically equivalent. Variable temperature ^1H NMR spectra account for the fluxionality of species **5** and **6**. The CH groups of the alkoxide ligands of **5** resonate as two septuplets at 5.3 and 4.8 ppm displaying an integration ratio of 6 : 2 in the ^1H NMR spectrum and as three peaks in the ^{13}C NMR. The low temperature spectra (−45°C) of compound **6** show three types of CH groups in a 1 : 2 : 6 integration ratio. The overall NMR data are consistent with structure C for **5** and structure D for **6**.

The structures are based on tetranuclear or triangular units, respectively, with bridging alkoxide ligands and the alkaline earth metals bearing the acetylacetonate moieties. All metals are 6-coordinate. For structure C, the metals are assembled by a central μ4-oxo ligand and two faces of the tetrahedron are capped by triply bridging alkoxide ligands. The structure is thus related to that of $Pb_2Ti_2(\mu_4\text{-}O)(\mu_3\text{-}OPr^i)_2(\mu\text{-}OPr^i)_4(OPr^i)_4$ and of its acetylacetonate derivative [29]. The triangular unit of structure D is capped by two triply bridging alkoxide ligands. Structure D derives from structure A by cleavage of the bridging Ba—OR—Ba bond by the chelating acetylacetone ligand.

The reactions between cerium isopropoxide, barium isopropoxide and β-diketones, namely 2,2,6,6-tetramethylheptane-3,5-dione or acetylacetone, are less selective for the latter. Similar observations have been reported in the literature. For instance, the reaction between $Zr(OR)_4$ and $Co(acac)_2$ (1 : 2.5 stoichiometry) afforded $Zr_2Co_2(acac)_2(\mu_3\text{-}OR)_2(\mu\text{-}OR)_4(OR)_4$ and $Zr_2Co_4(\mu_6\text{-}O)(\mu\text{-}OR)_8(OR)_2(acac)_4$ (R = Pr^n) [26,30]. No influence of the stoichiometry

Table 2. Selected bond lengths (Å) and angles (°) for $Ce_2Ba_4O(thd)_4(OPri)_{10}.C_7H_8$

Ba(1)—Ba(2)	4.296(1)	Ba(1)—Ba(2)′	4.246(1)
Ba(1)—Ce(1)	3.738(1)	Ba(1)—Ce(1)′	3.739(1)
Ba(2)—Ce(1)	3.772(1)	Ba(2)—Ce(1)′	3.751(1)
Ce(1)—O(1)	2.2234(9)	Ce(1)—O(2)	2.320(8)
Ce(1)—O(3)	2.298(8)	Ce(1)—O(4)	2.273(8)
Ce(1)—O(5)	2.291(8)	Ce(1)—O(6)	2.06(1)
Ba(1)—O(1)	3.006(1)	Ba(1)—O(2)	2.786(8)
Ba(1)—O(3)	2.801(8)	Ba(1)—O(4)′	2.83(1)
Ba(1)—O(5)′	2.793(9)	Ba(1)—O(7)	2.562(9)
Ba(1)—O(8)	2.570(9)	Ba(2)—O(1)	3.034(1)
Ba(2)—O(2)	2.79(1)	Ba(2)—O(3)′	2.814(9)
Ba(2)—O(4)′	2.810(8)	Ba(2)—O(5)	2.824(8)
Ba(2)—O(9)	2.571(8)	Ba(2)—O(10)	2.585(8)
O(1)—Ce(1)—O(2)	78.6(2)	O(1)—Ce(1)—O(3)	80.5(2)
O(2)—Ce(1)—O(3)	88.3(3)	O(1)—Ce(1)—O(4)	80.1(2)
O(2)—Ce(1)—O(4)	158.6(3)	O(3)—Ce(1)—O(4)	88.2(3)
O(1)—Ce(1)—O(5)	80.0(2)	O(2)—Ce(1)—O(5)	87.8(3)
O(3)—Ce(1)—O(5)	160.5(3)	O(4)—Ce(1)—O(5)	88.5(3)
O(1)—Ce(1)—O(6)	176.6(3)	O(2)—Ce(1)—O(6)	99.0(4)
O(3)—Ce(1)—O(6)	102.0(4)	O(4)—Ce(1)—O(6)	102.3(3)
O(5)—Ce(1)—O(6)	97.5(4)		
O(2)—Ba(1)—O(3)	70.3(2)	O(2)—Ba(1)—O(4)′	79.6(3)
O(3)—Ba(1)—O(4)′	119.6(2)	O(2)—Ba(1)—O(5)′	119.4(3)
O(3)—Ba(1)—O(5)′	82.0(3)	O(4)′—Ba(1)—O(5)′	69.0(2)
O(2)—Ba(1)—O(7)	99.9(3)	O(3)—Ba(1)—O(7)	143.1(3)
O(4)′—Ba(1)—O(7)	91.8(3)	O(5)′—Ba(1)—O(7)	130.5(3)
O(2)—Ba(1)—O(8)	129.9(3)	O(3)—Ba(1)—O(8)	91.7(3)
O(4)′—Ba(1)—O(8)	144.6(3)	O(5)′—Ba(1)—O(8)	102.7(3)
O(7)—Ba(1)—O(8)	66.9(3)	O(2)—Ba(2)—O(3)′	118.8(2)
O(2)—Ba(2)—O(4)′	79.8(3)	O(3)′—Ba(2)—O(4)′	68.9(3)
O(2)—Ba(2)—O(5)	69.4(2)	O(3)′—Ba(2)—O(5)	81.2(3)
O(4)′—Ba(2)—O(5)	118.5(2)	O(2)—Ba(2)—O(9)	106.7(3)
O(3)′—Ba(2)—O(9)	123.5(3)	O(4)′—Ba(2)—O(9)	89.5(3)
O(5)—Ba(2)—O(9)	149.3(3)	O(2)—Ba(2)—O(10)	127.7(3)
O(3)′—Ba(2)—O(10)	105.1(3)	O(4)′—Ba(2)—O(10)	146.1(3)
O(5)—Ba(2)—O(10)	92.3(3)	O(9)—Ba(2)—O(10)	65.4(3)
Ce(1)—O(1)—Ce(1)′	180.0	Ba(1)—O(2)—Ba(2)	100.7(3)
Ba(1)—O(2)—Ce(1)	93.7(3)	Ba(2)—O(2)—Ce(1)	94.7(3)
Ba(1)—O(2)—C(1)	120.3(7)	Ba(2)—O(2)—C(1)	115.4(8)
Ce(1)—O(2)—C(1)	126.2(8)	Ce(1)—O(3)—C(4)	128.5(10)
Ba(1)—O(3)—Ba(2)′	98.3(3)	Ba(1)—O(3)—Ce(1)	93.8(3)
Ba(2)′—O(3)—Ce(1)	93.9(3)	Ba(1)—O(3)—C(4)	121.8(11)
Ba(2)′—O(3)—C(4)	113.8(9)	Ce(1)—O(4)—C(7)	137.7(8)
Ba(1)′—O(4)—Ba(2)′	99.3(3)	Ba(1)′—O(4)—Ce(1)	93.6(3)
Ba(2)′—O(4)—Ce(1)	94.5(3)	Ba(1)—O(4)—C(7)	111.2(8)
Ba(2)′—O(4)—C(7)	113.5(6)	Ce(1)—O(5)—C(10)	120.7(8)
Ba(1)′—O(5)—Ba(2)	98.2(3)	Ba(1)′—O(5)—Ce(1)	94.2(3)
Ba(2)—O(5)—Ce(1)	94.5(2)	Ba(1)′—O(5)—C(10)	120.5(8)
Ba(2)—O(5)—C(10)	122.3(7)	Ce(1)—O(6)—C(13)	171.1(10)
Ba(1)—O(7)—C(16)	138.1(9)	Ba(1)—O(8)—C(22)	138.1(8)
Ba(2)—O(9)—C(27)	140.5(8)	Ba(2)—O(10)—C(33)	139.3(8)

Symmetry code: ′ $-x, -y, -z$

between the reactants seems to have been reported so far for the M : M′(OR)/thdH systems. Another surprising feature is that, independently of the synthetic route used-addition of the β-diketone, use of cerium β-diketonate derivatives-, all β-diketonate ligands are borne by the barium centers in the final product. The β-diketonate ligands are generally linked to the two different metals for most structurally characterized

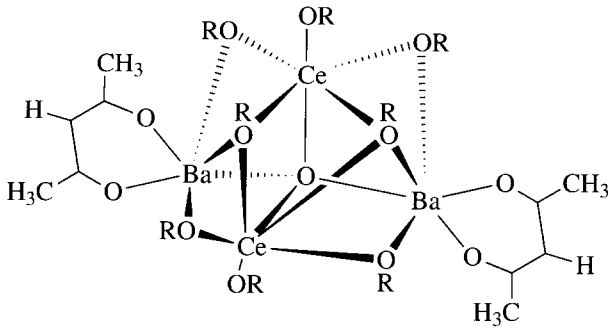

C

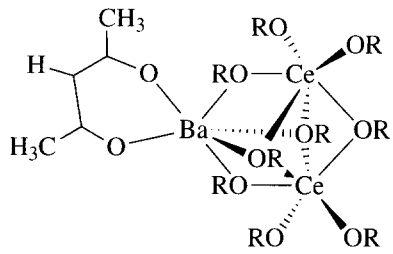

D

mixed-metal β-diketonatoalkoxides known so far and their formation proceeds via ligand redistribution reactions [13,31]. Our observations indicate thus a higher affinity of barium vs cerium for the chelating β-diketonate.

Hydrolysis–polycondensation reactions

None of the Ba–Ce species reported is volatile but their solubility allows their transformation by solution routes. The hydrolysis polycondensation reactions of **4** and of **6** were investigated in THF solutions (0.01 M). Hydrolysis was achieved at room temperature by addition of water diluted in THF and for an hydrolysis ratio $h = 100$ ($h = [H_2O]/[CeBa\ precursor]$). Formation of precipitates, white and yellow, respectively, occurs immediately. FT-IR spectra of these powders show the presence of $\nu(C{=}O)$ absorption bands at 1589, 1576 and 1588 and 1545 cm^{-1} respectively. These observations indicate the presence of residual β-diketonate ligands and thus of differential hydrolysis as generally observed for diketonatoalkoxides [24,21,28].

TGA measurements performed under nitrogen indicate that the loss of the organic residues occurs essentially between ~100°C and 600°C. An endothermic peak is observed around 800°C on the TDA profile of the powder (**4a**) resulting from the hydrolysis of **4**. X-ray powder diffraction (XRD) at various temperatures was achieved. Whereas the powder resulting hydrolysis of **6** was amorphous at room temperature, that derived from **4** indicated the presence of some metastable (decomposition occurred around 200°C) crystalline material. Crystallisation started at ≈600°C for **4a** (Fig. 2). At 800°C, barium carbonate (orthorhombic) and cubic cerium oxide are clearly identified. Crystalline barium cerate $BaCeO_3$ is obtained at 1000°C together with an amorphous barium oxide matrix. The powder derived from the hydrolysis of **6** leads to barium cerate and cubic cerium oxide which are crystallized at 900°C. In both cases, $BaCeO_3$ is obtained together with a binary oxide as a result of the stoichiometry of the mixed-metal species used as precursor.

Solid state routes to $BaCeO_3$ are essentially based on the reactions between barium carbonate and cerium oxide and occur around 1350°C [32]. Thus, despite the quite high conditions of crystallisation of $BaCeO_3$ via the above chemical routes, a reduction of about 450°C is observed. The mildest conditions of crystallization of the $BaCeO_3$ perovskite phase (750°C) have been reported so far with a modified Pechini process, EDTA being used instead the usual citric acid [2b]. Facile formation of barium carbonate has been reported previously for chemical routes [2a], as a result, treatment at 1000°C was necessary in order to get rid of that undesired phase. Conversion of the $BaCe_2(acac)(OPr^i)_9$ species **6** appears more interesting than that of **4** which generates barium carbonate as intermediate. The formation of barium carbonate can result from the decomposition of the β-diketonate ligand. However, no barium carbonate was detected in the powders resulting from the hydrolysis-polycondensation for other mixed-metal barium species supported by β-diketonate ligands such as $Ba_2Ti_2(thd)_4(OEt)_8(EtOH)_2$ or $Ba_2Ti_2(acac)_4(OEt)_8$ [28b]. The facile formation of $BaCO_3$ suggests easy segregation of the Ba–Ce species in the course of the polycondensation process as well as C—C bond cleavage reactions of the organic moieties during the thermal treatment (no absorption bands characteristics of $BaCO_3$ were observed by FT-IR on the amorphous powders obtained at room temperature) [34]. This was confirmed by the fact that hydrolysis of a mixture of barium and cerium isopropoxides (Ba : Ce, 1 : 1 stoichiometry) gave results similar to these based on the use of Ba–Ce species. Facile segregation could be favored by the fact that all β-diketonate ligands are linked to barium. Strong assembling and chelating ligands seem thus required for a better homogeneity. On the other hand, the easy conversion of $Ba_2Ce_4(OPr^i)_{20}$ into $BaCe_4(OPr^i)_{18}$ (and/or its complete dissociation) in the presence of isopropanol shows that the parent alcohol is not necessarily the best solvent for the processing of mixed-metal species.

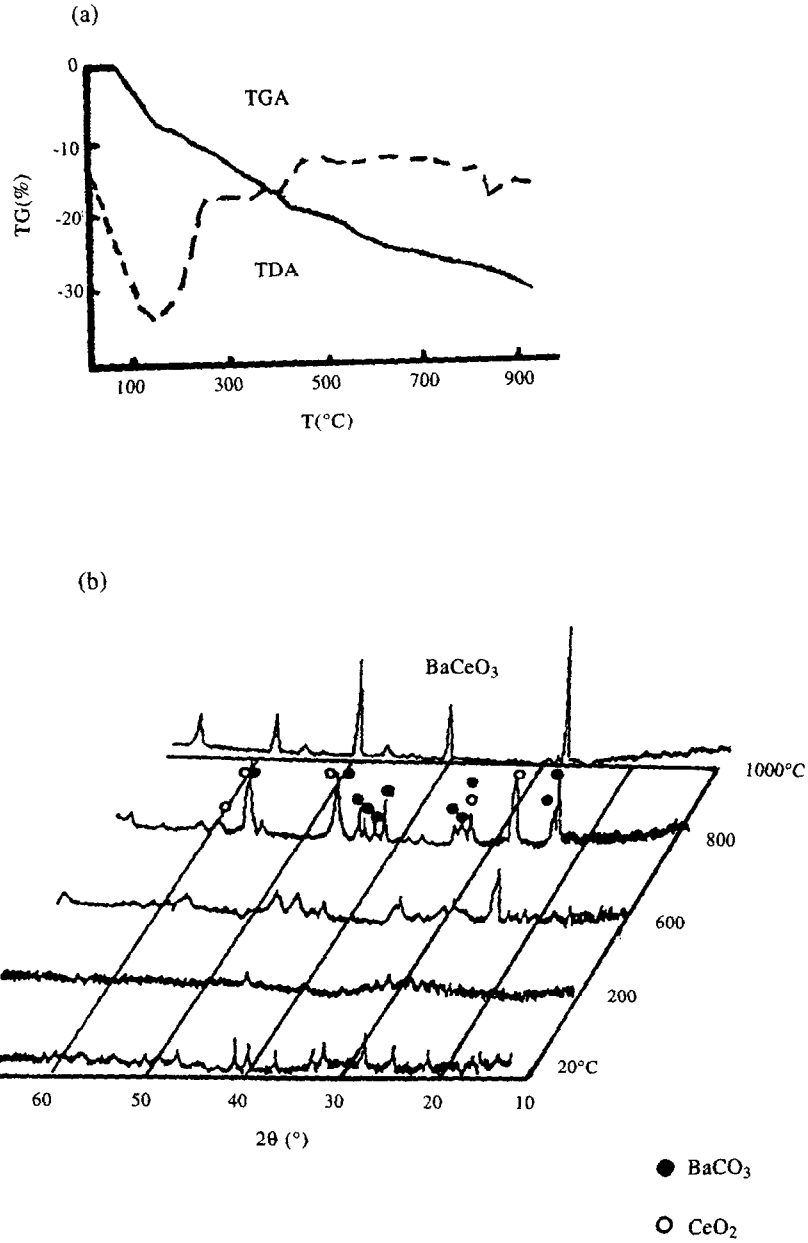

Fig. 2. X-ray diffraction patterns of the powders resulting from the hydrolysis of **4** and of **6** in THF.

REFERENCES

1. Hubert-Pfalzgraf L. G., *New J. Chem.*, 1995, **19**, 727.
2. (a)Tamiguchi N., Hatoh, K., Nikura, J., Gamo, T. and Iwahara, H., *Sol. State Ionics*, 1992, **53–56**, 998; (b) Agarwal, V. and Liu, M., *J. Electrochem. Soc.*, 1996, **143**, 3239.
3. Bradley, D. C., Chatterjee, A. K. and Wardlaw, W., *J. Chem. Soc.*, 1956, 2260.
4. Gulino, A., Casarin, M., Conticello, V. P., Gaudiello, J. G., Mauermann, H., Fragalar, I. and Marks, T. J., *Organometallics*, 1988, **7**, 2360.
5. Vaartstra, B. A., Huffman, J. C., Gradeff, P. S., Hubert-Pfalzgraf, L. G., Daran, J. C., Parraud, S. and Caulton, K. G., *Inorg. Chem.*, 1990, **29**, 3126.
6. Vaartstra, B. A., Huffman, J. C., Streib, W. E. and Caulton, K. G., *Inorg. Chem.*, 1991, **30**, 121.
7. Walker, N. J. and Stuart, D., *Acta Cryst.*, 1983, **39A**, 158.
8. Watkin, J., Carruthers, J. R. and Betteridge, P. W., *CRYSTALS*, An Advanced Crystallographic Program System; Chemical Crystallography Laboratory, University of Oxford, Oxford, England, 1988.
9. *International Tables for X-ray Crystallography*, Vol. IV, Kynoch Press, Birmingham, (1974).
10. Pearce, L. J. and Watkin, D. J., *Chemical Crystallography Laboratory*, Oxford, 1992.

11. Sirio, C., Hubert-Pfalzgraf, L. G. and Bois, C., *Polyhedron*, 1997, **16,** 1129.
12. Vaartstra, B. A., Streib, W. E. and Caulton, K. G., *Inorg. Chem.*, 1991, **30,** 3068.
13. Caulton, K. G. and Hubert-Pfalzgraf, L. G., *Chem. Rev.*, 1990, **90,** 969; Hubert-Pfalzgraf, L. G., *Polyhedron*, 1994, **13,** 1181.
14. Darr, J. A., Drake, S. R., Williams, D. J. and Slawin, A. M., *J. Chem. Soc., Chem. Commun.*, 1993, 866.
15. Evans, W. J., Deming, T. J., Olofson, J. M. and Ziller, J. W., *Inorg. Chem.*, 1989, **28,** 4027.
16. Yanovskii, A. I., Turevskaya, E. P., Yanovskaya, I. M., Kessler, V. G., Turova, N. Ya., Pisareivskii, and Yu, T., Struchkov, *Rus. J. Inorg. Chem.*, 1995, **40,** 339.
17. Turevskaya, E. P., Berdyev, D. V. and Turova, N. Ya., *J. Sol–Gel Science*, 1997, **8,** 111; Turevskaya, E. P., Berdyev, D. V., Turova, N. Ya. and Yanovskaya, I. M., *Rus. J. Inorg. Chem.*, 1995, **40,** 1527.
18. Veith, M., Mathur, S. and Huch, V., *Inorg. Chem.*, 1996, **35,** 726.
19. Sogani, S., Singh, A., Bohra, R., Mehrotra, R. C. and Noltemeyer, M., *J. Chem. Soc., Chem. Commun.*, 1991, 738.
20. Tripathi, U. M., Singh, A., Mehrotra, R. C., Goel, S. C., Chiang, M. Y. and Buhro, W. E., *J. Chem. Soc., Chem. Commun.*, 1992, 152.
21. Kuhlman, R., Vaartstra, B. A., Streib, W. E., Huffman, J. C. and Caulton, K. G., *Inorg. Chem.*, 1993, **32,** 1272.
22. Daniele, S., Hubert-Pfalzgraf, L. G., Daran, J. C. and Halut, S., *Polyhedron*, 1994, **13,** 927.
23. Hubert-Pfalzgraf, L. G., Daniele, S., Bennaccur, A., Duran, J. C. and Vaissermann, J., *Polyhedron*, 1997, **16,** 1223.
24. Ribot, F., Toledano, P. and Sanchez, C., *Chem. Mater.*, 1991, **3,** 759.
25. Hubert-Pfalzgraf, L. G., Labrize, F., Bois, C. and Vaissermann, J., *Polyhedron*, 1994, **15,** 2163.
26. Schmid, R., Mosset, A. and Galy, J., *Inorg. Chim. Acta*, 1991, **179,** 167.
27. Miele, P., Foulon, J. C., Hovnanian, N. and Cot, L., *J. Chem. Soc., Chem. Commun.*, 1993, 29.
28. (a)Livage, J. and Henry, M., *Prog. Solid State Chem.*, 1987, **11,** 664; (b) Kessler, V. G., Hubert-Pfalzgraf, L. G., Daniele, S. and Gleizes, A., *Chem. Mater.*, 1994, **6,** 2336.
29. Daniele, S., Papiernik, R., Hubert-Pfalzgraf, L. G., Jagner, S. and Hakansson, M., *Inorg. Chem.*, 1995, **34,** 628.
30. Schmid, R., Mosset, A. and Galy, J., *Acta Cryst.*, 1991, **C47,** 750.
31. Labrize, F., Hubert-Pfalzgraf, L. G., Vaissermann, J. and Knobler, C. B., *Polyhedron*, 1996, **15,** 577 and refs therein.
32. Rauch, W. and Liu, M., *Role of Ceramics in Advanced Electrochemical Systems*, Eds, American Chemical Society, Kumta P. N., Rohrer, G. S. and Balachandrau, U, 1996.
34. Borup, B., Folting, K. and Caulton, K. G., *Chem. Mater.*, 1997, **9,** 1021.

Pergamon

PII: S0277-5387(97)00291-X

Polyhedron Vol. 17, No. 5–6, pp. 831–843, 1998
© 1998 Elsevier Science Ltd
All rights reserved. Printed in Great Britain
0277–5387/98 $19.00+0.00

Copper(II)/alkaline-earth metal(II) and copper(II)/lanthanides(III) mixed metal complexes containing bifunctional pyridyl alcohol or amino alcohol ligands†

Suning Wang

Department of Chemistry, Queen's University, Kingston, Ontario, Canada K7L 3N6

(Received 17 March 1997; accepted 25 June 1997)

Abstract—The utility of bifunctional ligands such as hydroxypyridine and 1,3-bis(dimethylamino)-2-propanol in the synthesis of mixed metal complexes containing lanthanides, alkaline-earth metals, and copper is examined. The focus of this article is on the syntheses, crystal structures, thermal and magnetic properties of the mixed metal complexes obtained by our group. The role of these mixed metal complexes in the precursor solution for the $YBa_2Cu_3O_{7-x}$ film is also discussed. © 1998 Elsevier Science Ltd. All rights reserved

Keywords: copper; lanthanides; alkaline-earth metal; structures; properties.

The recent intense research interest in mixed metal complexes containing copper, lanthanides, and alkaline-earth metal ions was motivated, to a large extent, by the discovery of high T_c copper oxide based superconductors nearly a decade ago [1]. The most important member of the copper oxide based superconductors is the $YBa_2Cu_3O_{7-x}$ superconductor (1-2-3 superconductor). It has been well established that the replacement of the yttrium ion by members of the lanthanide family does not significantly perturb the superconductivity of the 1-2-3 superconductor. Other important copper oxide based superconductors include $Bi_2Sr_2CaCu_2O_{8+x}$ and $Bi_2Sr_2Ca_2Cu_3O_{10+x}$. The T_c of these superconductors is well above the boiling point of liquid nitrogen, making some of the practical applications possible. Bulk powder samples of these superconductors can be obtained readily by conventional ceramic production techniques. The production of high quality superconductive films, a highly desired form for practical applications, still remains, however, as a non-trivial task. The commonly used chemical method for film production of superconductors is *via* chemical vapor deposition (CVD). The CVD method has been demonstrated to be able to produce good quality of films, but limited by the availability of volatile precursor compounds [2]. Alternatively, one can mix the corresponding compounds of all components together in solution and coat them onto the substrate via spin coating or dip coating process. This method requires that all components are soluble in solution. One way to improve the solubility of the metal compounds in organic solvents is to bind suitable organic ligands to the metal centers. Due to the inherent different nature of the metal ions present in superconductors, their requirements for ligands are quite different. For example, a copper(II) ion binds well with oxygen or nitrogen donor atoms in an essentially covalent fashion while lanthanide(III) ions have a poor affinity to neutral nitrogen donor atoms and a relatively good affinity to negatively charged donor atoms such as oxygen, due to the ionic nature of the lanthanide–ligand bond [3]. Our strategy was therefore to employ bifunctional ligands which contain both a neutral coordinating site and a negatively charged coordinating site so that they can bind to two different metal ions (Fig. 1).

The bifunctional ligands (Fig. 2) used in our study include 2-hydroxyl pyridine (2-PyOH), 1,3-bis(dimethylamino)-2-propanol (bdmapH), and 2,6-bis[(dimethylamino)methyl]-4-methylphenol(bdmmpH). A variety of mixed metal complexes have been synthesized by using these ligands. This review

† Dedicated to Prof. D. C. Bradley on the occasion of his 73rd birthday.

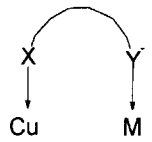

$M = Y^{3+}$, Ln^{3+}, alkaline-earth met

Fig. 1. The selective binding of a bifunctional ligand to two different metal ions.

will focus on the syntheses and structures of the mixed metal complexes. Magnetic properties and the relevance of these compounds to superconductors will be addressed.

The serendipitous discovery of $Y_2Cu_8(\mu_4\text{-}O)_2(\mu\text{-}2\text{-}PyO)_{12}(\mu\text{-}Cl)_2(NO_3)_4(H_2O)$ *and* $Nd_2Cu_8(\mu_4\text{-}O)_2(\mu\text{-}2\text{-}PyO)_{12}(\mu\text{-}Cl)_2(OCH_3)_4(H_2O)_4$

The 2-hydroxyl pyridine ligand has been demonstrated earlier by Goodgame and coworkers to be very useful in the synthesis of mixed metal compounds such as [4] $Cu_4Ln_2(2\text{-}PyO)_8(2\text{-}PyOH)_4(OH)_2(NO_3)_4(H_2O)_2$. Most of the earlier syntheses carried out by Goodgame's team were done in either aqueous solutions or in methanol by using copper(II) nitrate or copper(II) hydroxide as the copper source. With the hope to obtain new mixed metal complexes which are soluble in organic solvents, we tried a few modifications to Goodgame's syntheses by using $Cu(OCH_3)_2$, instead of $Cu(NO_3)_2$ or $Cu(OH)_2$, as the starting material and CH_2Cl_2 or THF as the solvents. The dark green crystals isolated initially from the reaction of $Y(NO_3)_3 \cdot 4H_2O$, $Cu(OCH_3)_2$, and 2-hydroxyl pyridine in a 1 : 4 : 6 ratio in CH_2Cl_2 was found to have the formula of $Y_2Cu_8(\mu_4\text{-}O)_2(\mu\text{-}2\text{-}PyO)_{12}(\mu\text{-}Cl)_2(NO_3)_4(H_2O)_2$ (**1**), an entirely different compound from that of Goodgame! Compound **1** can also be obtained by using methanol as the solvent. The key difference between the composition of compound **1** and those of Goodgame's compounds is the presence of the chloride ligands in **1**, which is responsible for the formation of a new molecule with beautiful and unique structural features. Where did the chlorine come from? After analyzing the starting materials, we found out that the chlorine came with $Cu(OCH_3)_2$ (about 3%, sufficient to produce compound **1** in a quantitative yield!). The company who supplied this compound told us that due to technical problems it is difficult to keep the chlorine content in $Cu(OCH_3)_2$ below 1%. Without the chlorine impurity, it is very likely that we would have reproduced Goodgame's compound. In order to introduce the chloride ligands into the reaction mixture in a controlled fashion, we replaced $Y(NO_3)_3 \cdot 4H_2O$ with $YCl_3 \cdot xH_2O$ in the reaction which did not yield crystalline products. The replacement of $Y(NO_3)_3 \cdot 4H_2O$ by $NdCl_3 \cdot 6H_2O$, however, produced dark green crystals with the formula of $Nd_2Cu_8(\mu_4\text{-}O)_2(\mu\text{-}2\text{-}PyO)_{12}(\mu\text{-}Cl)_2(OCH_3)_4(H_2O)_4$ (**2**).

The structures [5,6] of compounds **1** and **2** resemble each other, as shown in Figs 3 and 4. The Y^{III} and Nd^{III} ions are surrounded by negatively charged oxygen atoms from the deprotonated 2-PyOH, the oxo, the nitrate, or the methoxyl ligands while the pyridyl groups are bound exclusively to the copper(II) centers, demonstrating the preferential coordinating pattern of the 2-PyOH ligand. The oxo ligands were believed to come from the reaction of H_2O with base such as the methoxy ligand. The most important feature in these two structures is the central core unit $M_2Cu_4O_{10}$ where the M^{III} ions are linked to the four copper(II) ions *via* eight oxygen atoms of $2\text{-}PyO^-$ and two oxide ligands. The structural feature displayed by the central core units of **1** and **2** closely resembles that [1] found in 1-2-3 superconductor (Fig. 5).

Magnetic susceptibility measurements revealed that antiferromagnetic exchanges between Cu^{II}–Cu^{II} centers, Nd^{III}–Nd^{III} centers, and Cu^{II}–Nd^{III} centers dominate in these two compounds.

Several other interesting copper(II)/lanthanides (III) mixed metal complexes containing either 2-hydroxyl pyridine or 6-methyl 2-hydroxyl pyridine ligands and displaying complex structural features have been reported by Winpenny and co-workers [7] which further demonstrated the usefulness of 2-hydroxyl pyridine based ligands for the syntheses of copper/lanthanides compounds. However, there is one weakness associated with the 2-hydroxyl pyridine compounds, that is, most of them have very poor solubility in common organic solvents, limiting their practical applications.

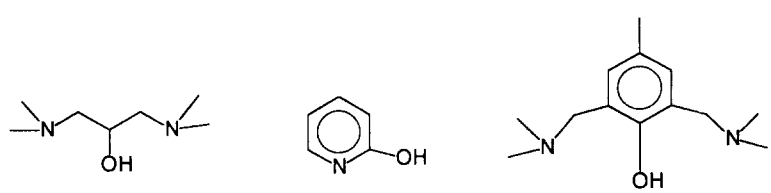

bdmapH 2-PyOH bdmmpH

Fig. 2. The bifunctional ligands.

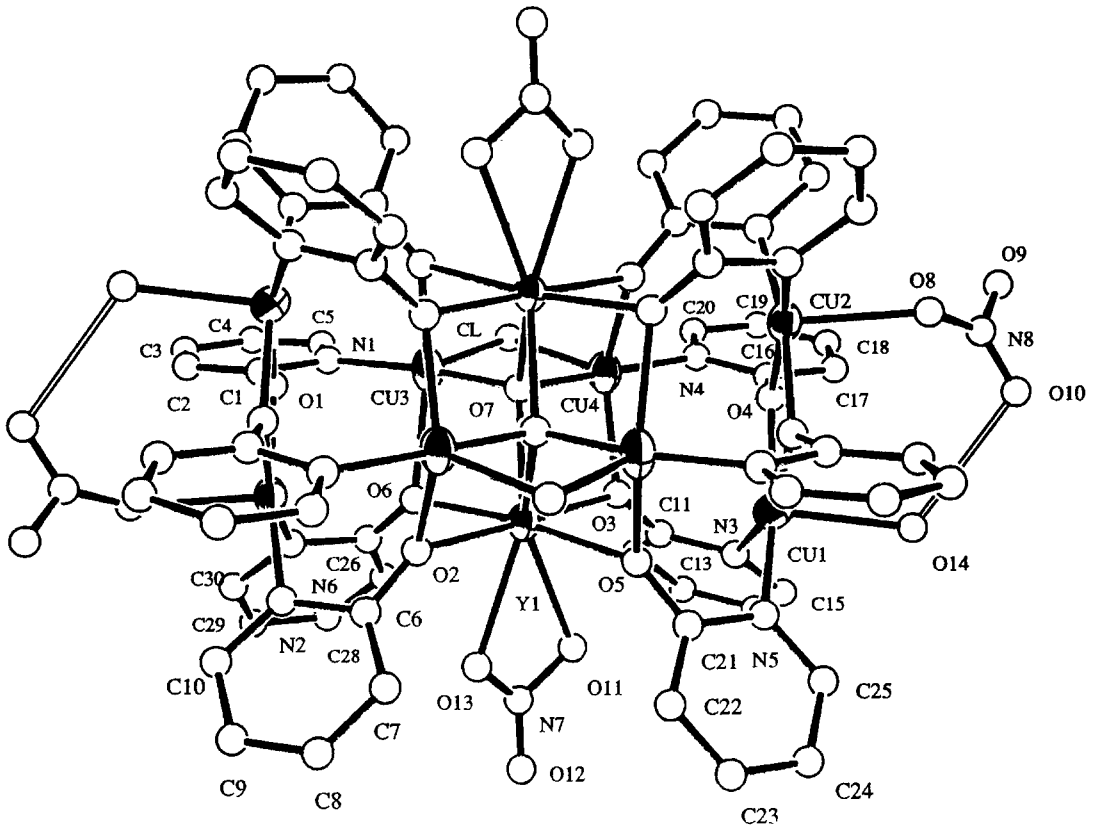

Fig. 3. The crystal structure of $Y_2Cu_8(\mu_4\text{-}O)_2(\mu\text{-}2\text{-}PyO)_{12}(\mu\text{-}Cl)_2(NO_3)_4(H_2O)_2$ (**1**).

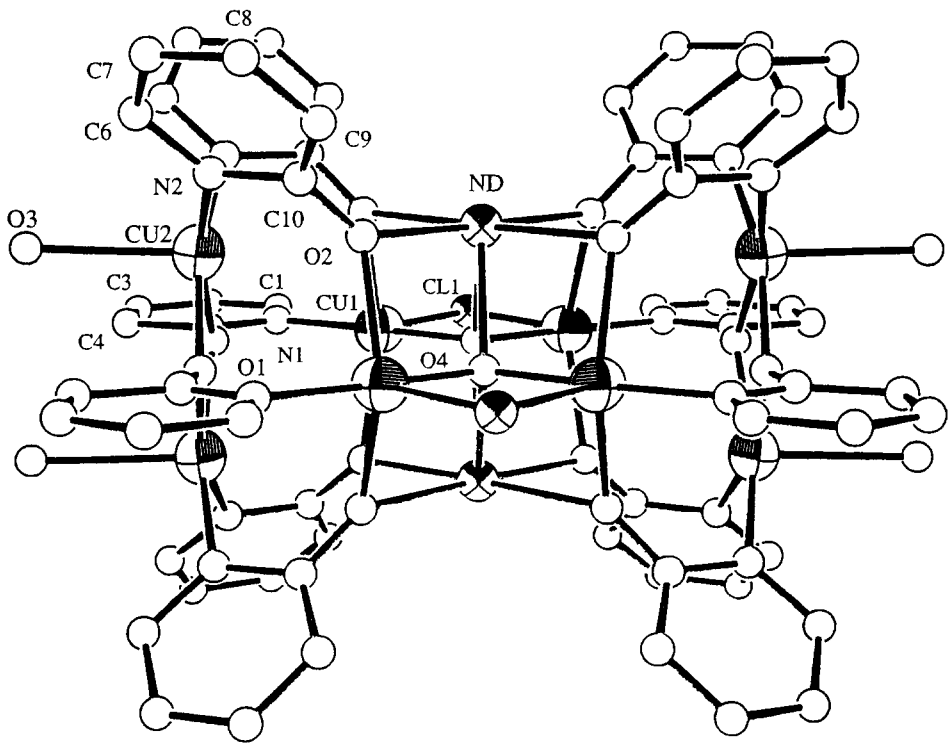

Fig. 4. The crystal structure of $Nd_2Cu_8(\mu_4\text{-}O)_2(\mu\text{-}2\text{-}Pyo)_{12}(\mu\text{-}Cl)_2(OCH_3)_4(H_2O)_4$ (**2**).

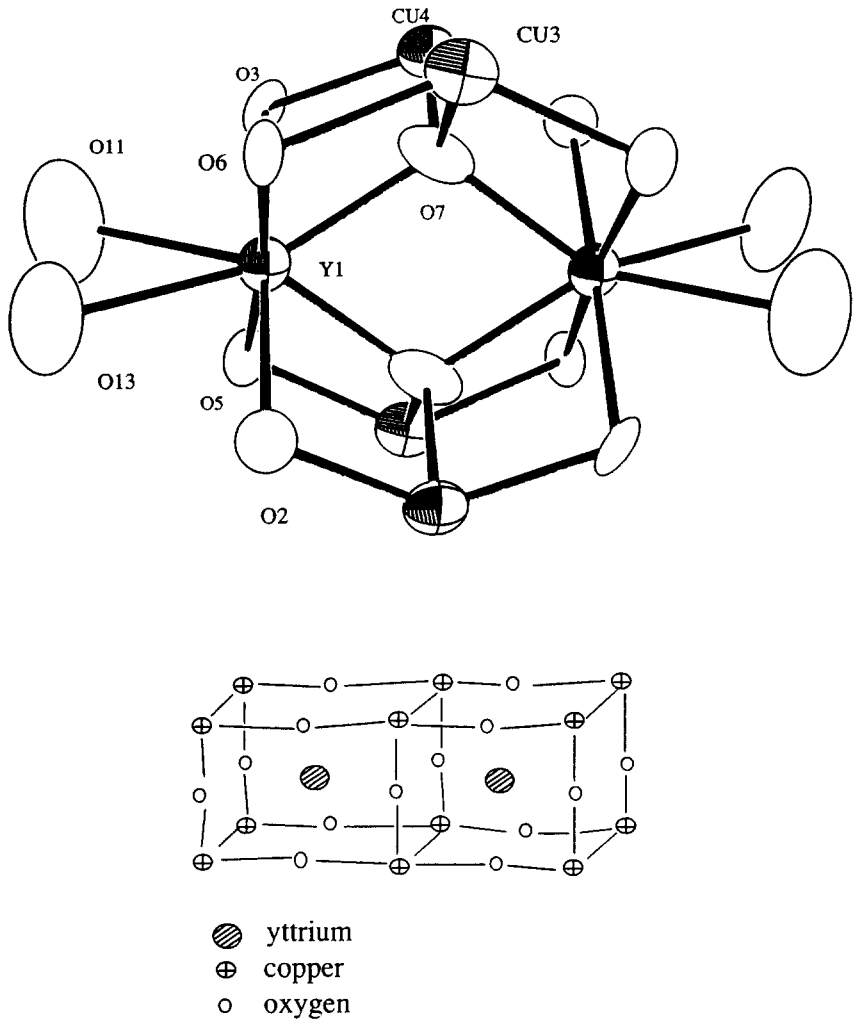

Fig. 5. The core structure of compound **1** and the bonding environment of yttrium in 1-2-3 superconductor.

Copper(II)/lanthanides(III) complexes of 1,3-*bis(dimethylamino)-2-propanol*

To improve the solubility of the mixed metal compounds, we decided to investigate the coordination chemistry of 1,3-bis(dimethylamino)-2-propanol (bdmapH). The bdmapH ligand has several advantages over the 2-hydroxyl pyridine ligand. First of all, it has three binding sites, two neutral amino groups and one hydroxyl group which can be deprotonated readily to bind to a highly electropositive metal ion such as a lanthanide ion. Secondly, it contains four methyl groups which would enhance the solubility of the metal complexes in organic solvents.

The syntheses of our mixed metal complexes of bdmapH are based on two routes. In the first route, $Ln(O_2CR)_3$ and $Cu(O_2CR)_2$, where R is either a methyl group or a trifluoromethyl group, were used as the starting material to react with the bdmapH ligand. The products from the reactions where acetate compounds were used usually have poor solubility and are difficult to grow single crystals. The reactions where trifluoroacetate compounds were employed often produced soluble crystalline products. The compound that we have been able to isolate successfully is a trinuclear complex [8] with the formula of $LaCu_2(bdmap)_3(O_2CCF_3)_4$ (**3**). The reaction scheme for compound **3** is shown in eq. (1).

$$\begin{aligned} &La(O_2CCF_3)_3 + 0.5\,Cu(O_2CCF_3)_2 \\ &\qquad + 1.5\,Cu(OCH_3)_2 + 3bdmapH \\ &= LaCu_2(bdmap)_3(O_2CCF_3)_4 + 3CH_3OH. \end{aligned} \quad (1)$$

The metal atoms in compound **3** has a triangular arrangement (Fig. 6). The lanthanum(III) ion is linked to two copper(II) ions *via* three oxygen atoms of the deprotonated bdmapH ligands (bdmap). Two of the oxygen atoms act as doubly bridging atoms while the third one acts as a triply bridging atom. The two copper(II) ions are bridged together by one bdmap ligand. The lanthanum ion is surrounded predominately by oxygen atoms. The two La—N bonds are very long [2.85(2) Å], reflecting the poor affinity

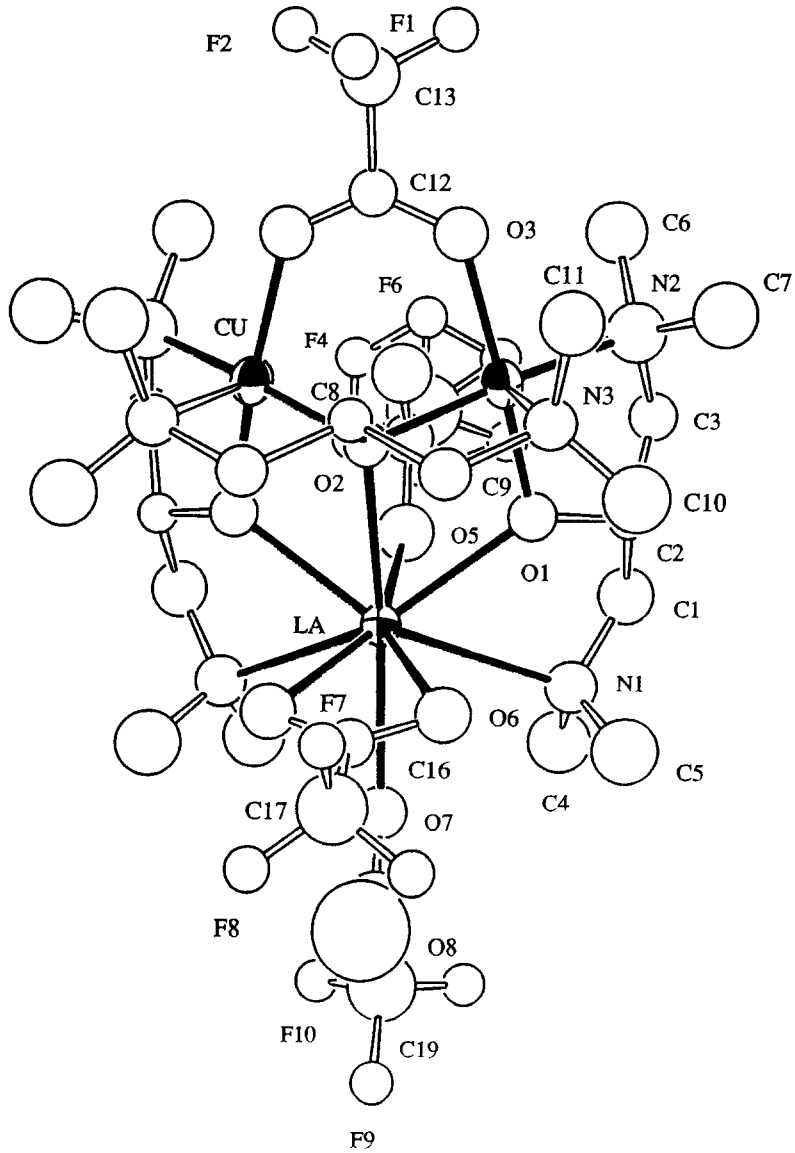

Fig. 6. The crystal structure of $LaCu_2(O_2CCF_3)_4(bdmap)_3$ (**3**).

of lanthanide ions to the neutral amino binding site. The Cu—Cu separation distance is 3.265(6) Å. The magnetic exchange between these two CU^{II} ions was found to be weakly antiferromagnetic ($J = -6.0$ cm^{-1}), established by magnetic susceptibility measurements. Compound **3** is soluble in common organic solvents such as CH_2Cl_2 and THF. Upon heated under oxygen, it decomposes cleanly to the corresponding oxide composition $LaCu_2O_{3.5}$ at 420°C. A triangular structure similar to that of **3** has been observed in compound $[YCu_2(OCH_2CH_2OCH_3)_3(hfacac)_2(tmhd)_2]$ where tmhd = 2,2,6,6-tetramethylheptane-3,5-dionate and the bifunctional ligand, 2-methoxy ethanol, was used as the bridging ligand [9].

In the second route $Ln(O_2CR)_3$ was replaced with $Ln(hfacac)_3$ (hexafluoroacetylacetonato). $Cu(O_2CR)_2$ or $Cu(OCH_3)_2$ was used as the copper(II) starting material to react with the bdmapH ligand. Various products have been isolated from the reactions, depending on the starting materials of lanthanum and copper and their relative ratio. One major factor contributed to the complexity of these reactions is the poor stability of the hfacac ligand towards nucleophiles [10] which has also been observed by other research groups [11]. A typical decomposition reaction of the neutral hfacacH molecule in the presence of a base is shown in Scheme 1.

The reaction of $Cu(O_2CCH_3)_2(H_2O)$, $Ln(hfacac)_3$, Ln = Pr, Nd, and bdmapH in a 1 : 2 : 3 ratio in THF yielded a trinuclear compound with the formula of $LnCu_2(hfacac)(bdmap)_3(O_2OCH_3)_2(O_2CCF_3)(hfacacH)$ (**4**). The trifluoroacetate ligand came from the decomposition of one of the hfacac ligand. In the

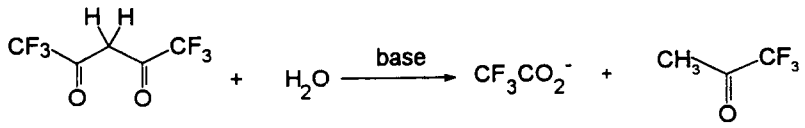

Scheme 1.

crystal lattice, the neutral hfacacH molecule exists in an enol form stabilized by the formation of hydrogen bonds between the oxygen atoms of the hfacacH and the non-coordinating amino group [N(4)] in the complex. As shown in Fig. 7, the basic structural features of **4** resemble that of **3**. The lanthanide ion in **4** is linked to two copper(II) ions through three oxygen atoms of the bdmap ligands in a similar fashion as that observed in **3**. Unlike compound **3** where two amino groups are weakly bound to the lanthanide ion, in compound **4** only one amino group is bound to the lanthanide center, perhaps due to the increased steric bulkiness imposed by the hfacac ligand and the hydrogen bond formation. The magnetism in compound **4** has been found to be dominated by the paramagnetic lanthanide(III) ion. Upon heated under oxygen, compound **4** decomposed to the corresponding oxide composition of $LnCu_2O_{3.5}$ at approximate 310°C, about 100°C lower than that of **3**. The presence of the hfacac ligand in **4** apparently helped to lower the thermal decomposition temperature [12].

The reaction of $Cu(OCH_3)_2$, $Ln(hfacac)_3$, Ln = Pr, Y, and bdmapH in a 1 : 1 : 2 ratio in THF, attempted for the synthesis of $LnCu(bdmap)_2(hfacac)_3$ yielded an unusual blue compound with the formula of $LnCu(bdmapH)_2(hfacac)_2(O_2CCF_3)L$ (**5**) where L = 2-methyl-2,4,6-tris(trifluoromethyl)-1,3-dioxane-4,6-diolato. The trifluoroacetate ligand in the com-

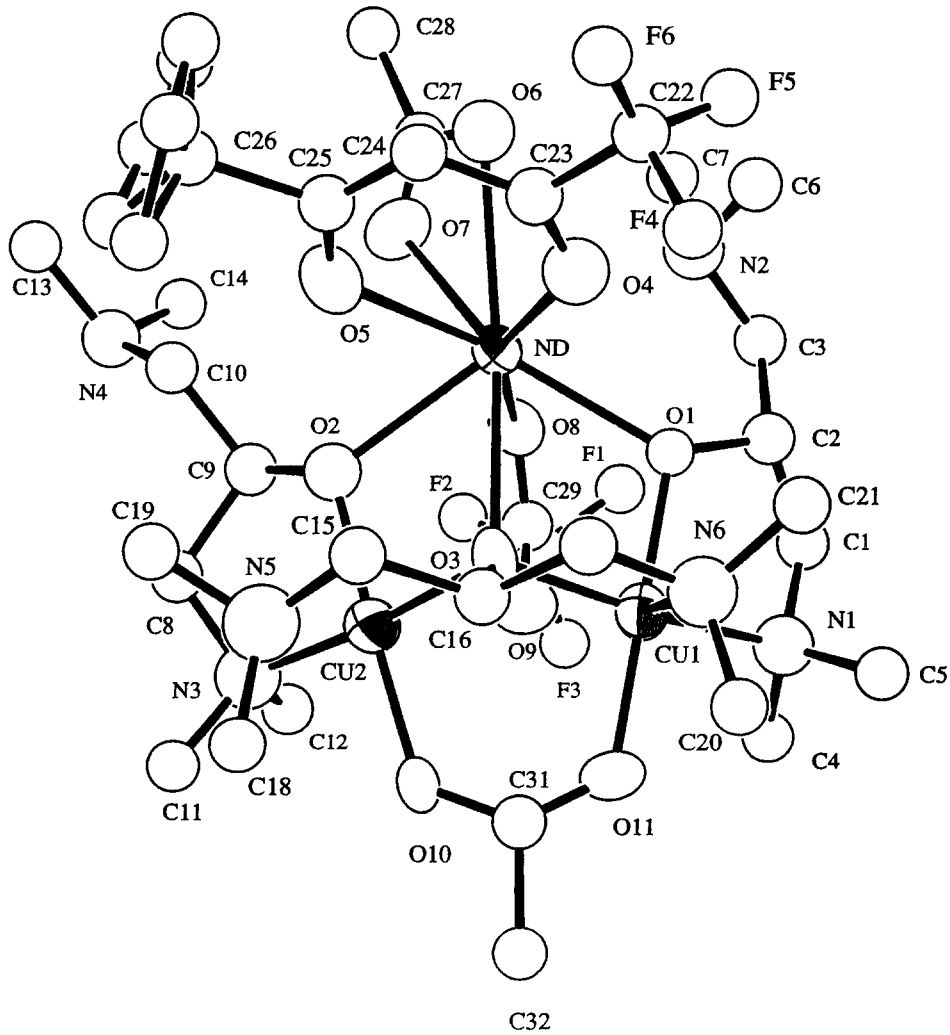

Fig. 7. The crystal structure of $NdCu_2(hfacac)(bdmap)_3(O_2CCH_3)_2(O_2CCF_3)(hfacacH)$ (**4**).

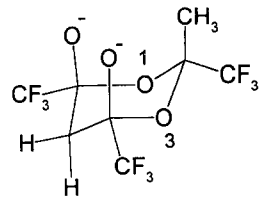

Fig. 8. The 2-methyl-2,4,6-tris(trifluoromethyl)-1,3-dioxane-4,6-diolato ligand.

pound was again formed from the decomposition of the hfacac ligand. The unusual ligand L can be viewed as a derivative of 1,3-dioxane-4,6-diol, as shown in Fig. 8. The L ligand has a chair conformation with two trifluoromethyl groups occupying the 4 and 6 equatorial positions and two oxygen atoms occupying the 4 and 6 axial position. The CF_3 and CH_3 groups on position 2 display a 50%/50% disorder over the axial and the equatorial positions. The ligand L can be considered as the cycloaddition product of a 1,1,1-trifluoro-2,2-propanediol molecule to the hfacac ligand, promoted by the metal complex (Scheme 2). The 1,1,1-trifluoro-2,2-propanediol is the hydration product of tirfluoroacetone. The adventitious water molecules in the solvent and bdmapH are believed to be responsible for the diol formation. The details of the formation mechanism of ligand L have not yet been understood.

The complicated structure of compound **5** is better shown by using a line drawing diagram (Fig. 9). The lanthanide ion is linked to the copper(II) ion *via* two

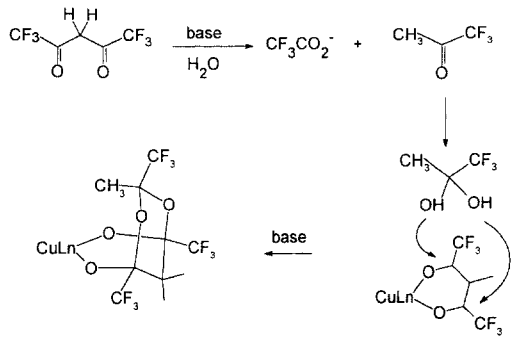

Scheme 2.

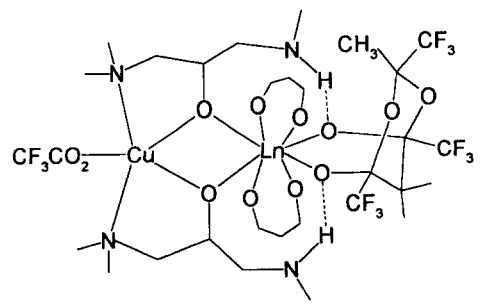

Fig. 9. The structure of compound **5**, LnCu(bdmapH)$_2$(hfacac)$_2$(O_2CCF_3)L.

oxygen atoms of the bdmapH ligand. The proton originally bound to the oxygen atom of the bdmapH is shifted to the non-coordinating amino site and forms a hydrogen bond with the oxygen atom of the L ligand. The lanthanide ion is surrounded again by negatively charged oxygen atoms only.

Alkaline-earth metal(II)/copper(II) complexes of 1,3-*bis(dimethylamino)*-2-*propanol*

The bdmapH ligand is useful not only in the syntheses of lanthanides/copper complexes, but also in the syntheses of alkaline-earth metal/copper complexes, due to the similar ionic nature of lanthanide-ligand bonds and alkaline-earth metal–ligand bonds. We have found that various mixed metal complexes containing alkaline-earth metal ions and copper(II) ions can be obtained readily by using reactions similar to those for the syntheses of lanthanides/copper complexes. The structures and compositions of these new complexes are highly dependent on the reaction conditions, stoichiometry, and the reagents. For example, from the reaction of $Ca(O_2CCF_3)_2$, $Cu(OCH_3)_2$, and bdmapH in a 1 : 1 : 2 ratio in THF, a dinuclear complex with the formula of $CaCu((O_2CCF_3)_2(bdmap)_2(H_2O)$ (**6**) was isolated [13]. As shown in Fig. 10, the linkage between Ca^{II} and Cu^{II} in compound **6** resembles that found in compound **5**, that is, these two metal ions are linked together through the oxygen atoms of the bdmap ligands. The copper(II) center has a square pyramidal geometry with the O(6) atom occupying the axial position [Cu—O(6) = 2.397(8) Å]. As found in the Ln/Cu complexes, the Ca—N bonds are much longer than those of Ca—O bonds, again reflecting the relatively poor affinity of the highly electropositive Ca^{II} ion towards the neutral amino group. Compound **6** forms a dimer in the solid state through the formation of intermolecular hydrogen bonds between the non-coordinating oxygen atom of the trifluoroacetate ligand and the H_2O ligand. There is also an intramolecular hydrogen bond between O(7) and O(4) [2.72(1) Å].

Interestingly, from the analogous reaction of $Sr(O_2CCF_3)_2$, $Cu(OCH_3)_2$, and bdmapH in a 1 : 1 : 2 ratio in THF, a tetranuclear complex with the formula of $[SrCu(O_2CCF_3)_2(bdmap)_2]_2$ (**7**) was obtained [13]. Compound **7** consists of two dinuclear units $SrCu(O_2CCF_3)_2(bdmap)_2$, joined together through two trifluoroacetate bridges. As shown in Fig. 11, the structure of the dinuclear portion is similar to that of compound **6**. The coordination environment of the Sr^{II} ion on **7** resembles that of the Ca^{II} ion in **6**. The difference between **6** and **7** is due to the coordinated H_2O ligand which is absent in **7**. In **7**, the coordination site occupied by a H_2O in **6** is filled by the oxygen atom of the bridging trifluoroacetate ligand. It is very likely that the water molecule in **6** came from the bdmapH reagent which is difficult to be completely

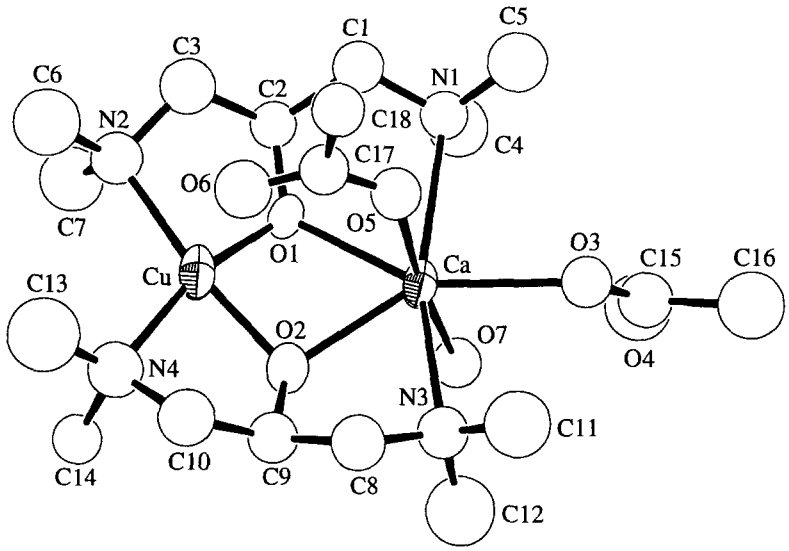

Fig. 10. The crystal structure of $CaCu(O_2CCF_3)_2(bdmap)_2(H_2O)$ (**6**). For clarity, the fluorine atoms are omitted.

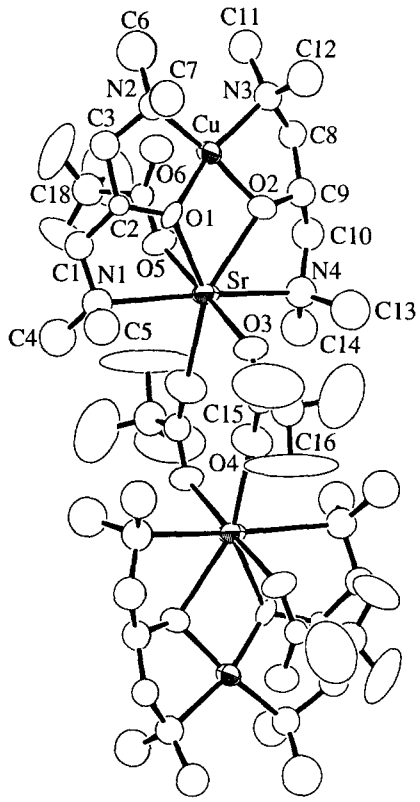

Fig. 11. The crystal structure of $[SrCu(O_2CCF_3)_2(bdmap)_2(H_2O)]_2$ (**7**).

free of water. However, it is not obvious why the Ca^{II} ion in **6** picked up the water while the Sr^{II} ion in **6** did not. One possible explanation is that the Ca^{II} ion has a higher tendency to undergo hydration due to its relatively small size, in comparison to that of the Sr^{II} ion.

When $Sr(O_2CCF_3)_2$, $Cu(OCH_3)_2$, and bdmapH were reacted in a 1:2:3 ratio in THF, a trinuclear complex with the formula of $SrCu_2(O_2CCF_3)_3(bdmap)_3$ (**8**) was produced [14]. The structure of **8** is very similar to that of $LaCu_2(O_2CCF_3)_4(bdmap)_3$ (**3**) (Fig. 12). The Sr^{II} ion is linked to the two copper(II) ions by three oxygen atoms of the bdmap ligands in a similar fashion as that observed in **3**. The Cu–Cu separation distance is 3.271(4) Å, similar to that found in **3**. Magnetic exchanges between the two copper(II) ions in **8** was found to be weakly antiferromagnetic with the exchange constant $J = -17\ cm^{-1}$.

When $Sr(O_2CCF_3)_2$, $Cu(OCH_3)_2$ and bdmapH were reacted in a 1:2:4 ratio in THF, an interesting hex-

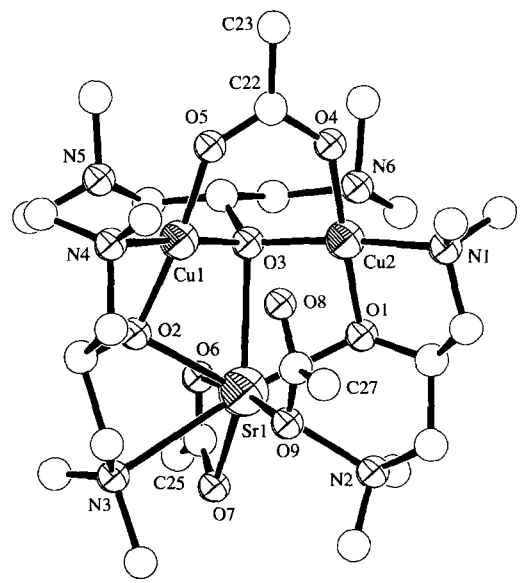

Fig. 12. The crystal structure of $SrCu_2(O_2CCF_3)_3(bdmap)_3$ (**8**). For clarity, the fluorine atoms are omitted.

anuclear complex with the formula of $Sr_2Cu_4(O_2CCF_3)_4(bdmap)_6(\mu_3\text{-}OH)_2$ (**9**) was isolated [13]. The presence of excess bdmapH ligand in this reaction was necessary to ensure the formation of the hydroxide ligands. The structure of compound **9** is given in Fig. 13. There are two $SrCu(O_2CCF_3)_2(bdmap)_2$ units in **9** with a structure somewhat resembling that of **7**, except that one of the amino group is not coordinated to the Sr^{II} center, but formed a hydrogen bond with the hydroxide ligand. These two SrCu units are linked to the dinuclear $Cu_2(OH)_2$ unit *via* two bdmap ligands and the two hydroxide ligands. The $Cu_2(OH)_2$ portion is planar with a short Cu^{II}–Cu^{II} distance [2.865(5) Å] and unusually small Cu—O—Cu angle [93.5(7)°] which would result in a ferromagnetic exchange between the two Cu^{II} centers, based on some of the well established empirical relationship between the exchange constant *J*, Cu—Cu distance, and Cu—O—Cu angle. Unfortunately we have not been able to carry out the study of magnetic properties of this compound.

When the trifluoroacetate salts were replaced with the corresponding acetate salts in the syntheses described above, there were either no reactions or the products were too insoluble to grow single crystals. The only acetate analogous compound [14] which we were able to synthesize is $SrCu_2(O_2CCH_3)_3(bdmap)_3$ (**10**) with a structure identical to that of **8**.

Unlike the lanthanides/copper complexes which undergo facile thermal decomposition to form the corresponding oxides even in the presence of fluorinated ligands such as trifluoroacetate or hfacac, the thermal decomposition patterns of alkaline-earth metal/copper complexes are dramatically affected by the presence of fluorinated ligands [13,14]. For example, upon heated under oxygen, compound **6** decomposed to CaF_2/CuO at about 280°C while compound **7** decomposed to SrF_2/CuO at 390°C. Compound **8** decomposed thermally to SrF_2/2CuO at about 400°C while the acetate analogous compound **10** decomposed initially to form $Sr(CO_3)$/2CuO and did not form SrO/2CuO until about 800°C. We concluded that the presence of fluorinated ligand does lower the thermal decomposition temperature, but the fluorine contamination becomes a serious problem with the alkaline-earth metal compounds due to the high stability of the MF_2 phase. The fluorine contamination problems could be overcome by introducing oxide or hydroxide ligands into the complexes. For example, we have observed that compound **9**, $Sr_2Cu_4(O_2CCF_3)_4(bdmap)_6(\mu_3\text{-}OH)_2$, decomposed cleanly to the SrO/2CuO composition at about 330°C. No fluorine contamination was observed in spite of the presence of trifluoroacetate ligands. The difference between compound **9** and compound **6**, **7**, or **8** is the presence of two hydroxide ligands which bind to both Sr^{II} and Cu^{II} ions. We believe that these hydroxide ligands prevented the formation of the SrF_2 phase.

The reaction of $Ba(O_2CCF_3)_2$ with $Cu(OCH_3)_2$ and bdmapH always yielded blue oily products. The com-

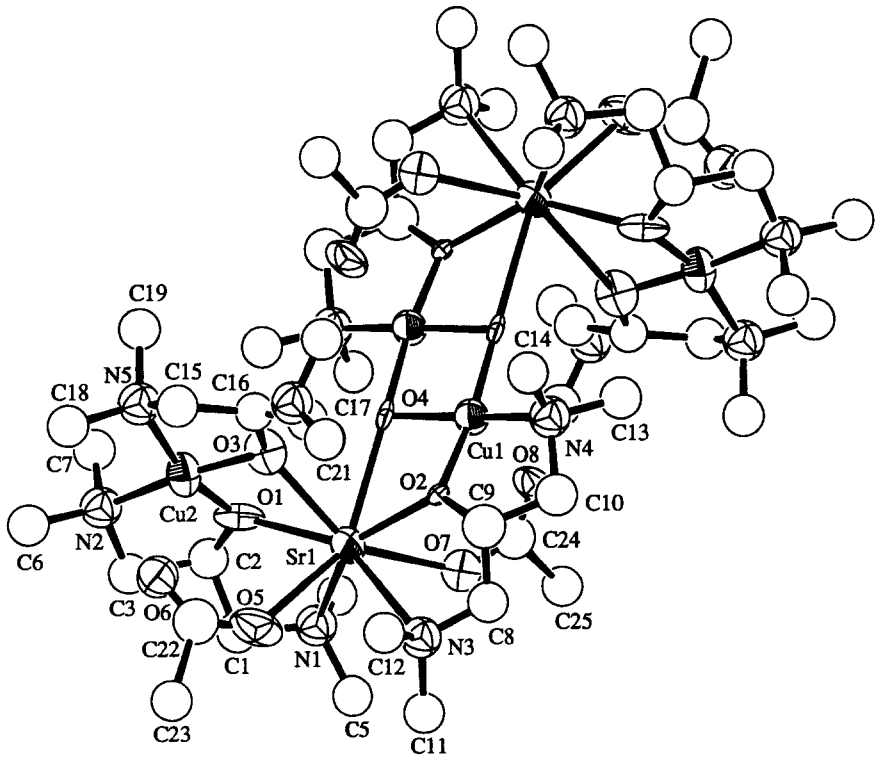

Fig. 13. The crystal structure of $Sr_2Cu_4(O_2CCF_3)_4(bdmap)_6(\mu_3\text{-}OH)_2$ (**9**). For clarity, the fluorine atoms are omitted.

position of these products still remains as a mystery to us. To encourage the formation of crystalline products, we added 2-hydroxyl pyridine to the reaction. The only crystalline compound isolated from these reactions was $BaCu_4(bdmap)_4(2\text{-}PyO)_4(O_2CCF_3)_2$ (**11**) which can be obtained in good yield from the reaction of $Ba(O_2CCF_3)_2$, $Cu(OCH_3)_2$, bdmapH, and 2-PyOH in a 1 : 4 : 4 : 4 ratio in THF [15]. Compound **11** has an interesting sandwich structure with the Ba^{II} ion seating in the center of the sandwich as shown in Fig. 14. The Ba^{II} ion is surrounded by eight oxygen atoms, 4 from the 2-PyO and 4 from the bdmap ligands. The nitrogen atoms are coordinated exclusively to the copper(II) ions. The two dinuclear copper(II) units are twisted about 60° from each other. The Cu—Cu distances in the dinuclear units are 2.919(7) Å and 2.921(7) Å while the Cu—O—Cu angles range from 89(1) to 97(1)°. The magnetic exchange in this complex has been found to be weakly antiferromagnetic.

Lanthanides/copper complexes of 2,6-bis[(dimethylamino)methyl]-4-methylphenol

We have demonstrated that 1,3-bis(dimethylamino)-2-propanol is a very useful ligand for the syntheses of mixed metal complexes involving lanthanides, alkaline-earth metal, and copper. However, it is difficult to control the products formed from the reactions due to their high dependency on the stoichiometry of all starting materials and reaction conditions. We were therefore interested in developing a more systematic and controlled approach for the synthesis of mixed metal complexes. One possibility is to use copper(II) complexes which contain appro-

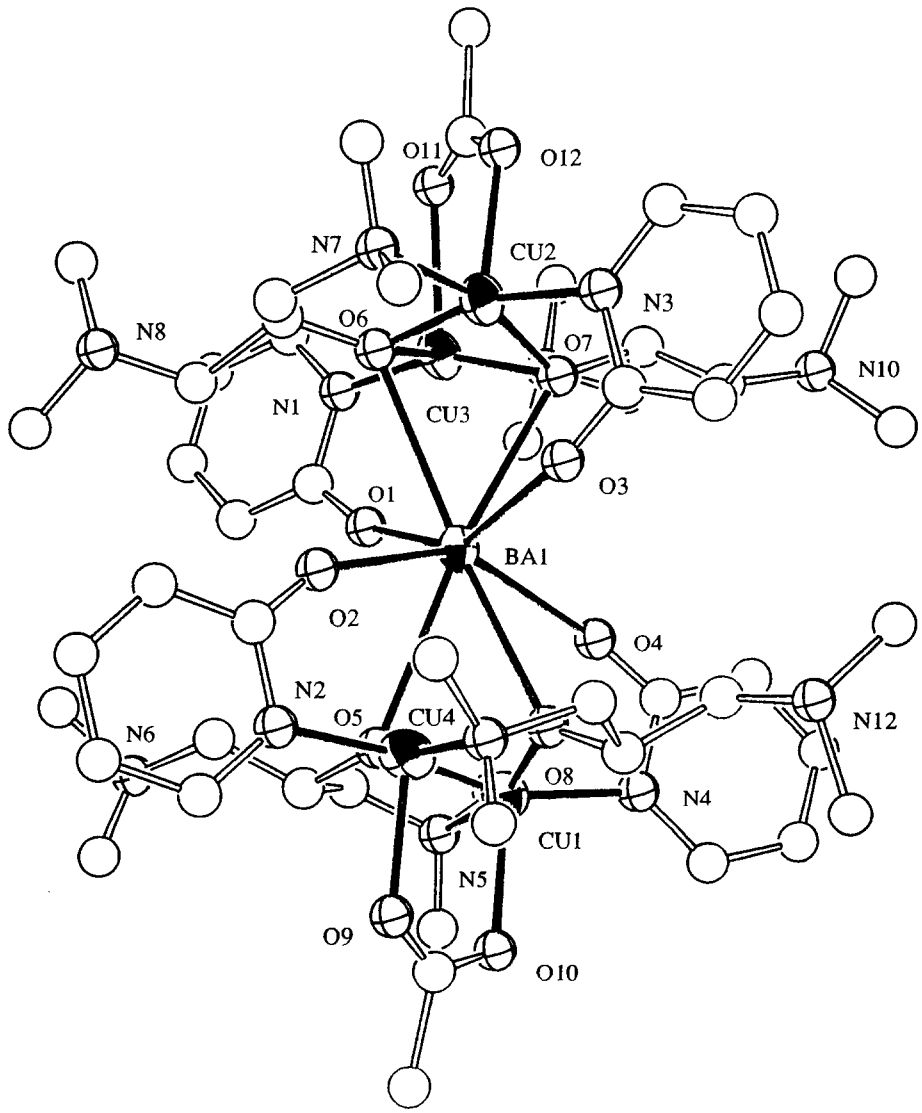

Fig. 14. The crystal structure of $BaCu_4(bdmap)_4(2\text{-}PyO)_4(O_2CCF_3)_2$ (**11**). For clarity, the fluorine atoms are omitted.

priate aminoalcohol ligands and vacant binding sites as the starting material. We have not been able to synthesize such a copper complex by using the bdmapH ligand. We have succeeded, however, in synthesizing a useful mononuclear copper(II) complex by using the bdmmpH ligand, $Cu(bdmmp)_2(H_2O)$ (**12**). The structure [16] of **12** is shown in Fig. 15. The oxygen atom of the phenolato group is bound to one copper(II) ion only, making it possible to bind to a second metal center such as a lanthanide ion. The other important feature of this compound is that it contains a coordinated H_2O ligand which forms two hydrogen bonds with two non-coordinating amino groups. This H_2O could potentially serve as a source of oxide or hydroxide ligands which are capable of bridging several metal ions. Indeed, when compound **12** was reacted with $Ln(hfacac)_3$ (Ln = Pr) in a 1 : 1 ratio, a dinuclear complex with the formula of $LnCu(bdmmp)(bdmmpH)(OH)(hfacac)_3$ (**13**) was obtained. The H_2O ligand in **12** became a bridging hydroxide ligand for the Cu^{II} and the Ln^{III} ions in **13** by losing one of its protons to the amino group [16]. We believe that the conversion of H_2O to OH^- in **13** is promoted by both the basic amino group and the lanthanide(III) ion which is known to have a high affinity toward water molecules. The singly coordinated oxygen atom from one of the bdmmp ligand in **12** became a bridging ligand to link the Cu^{II} and Ln^{III} ions together in **13**. For clarity, the structure of **13** is represented as a line drawing diagram in Scheme 3. When $Ln(hfacac)_3$ is replaced with $Ln(O_2CCF_3)_3$ (Ln = La) in the reaction, a tetranuclear complex with the formula of $[LnCu(bdmmp)(bdmmpH)(OH)(O_2CCF_3)_3]_2$ (**14**) was obtained. Compound **14** contains two dinuclear LnCu units linked together through four bridging trifluoroacetate ligands. The structure of the dinuclear LnCu unit in **14** is similar to that of **13** as shown in Scheme 3. The difference between compound **13** and compound **14** lies on the difference between the hfacac ligand and the trifluoroacetate ligand—the former almost always functions as a bidentate chelate ligand while the latter has the tendency to function as a bridging ligand.

Compound **13** is one of the few rare examples of discrete dinuclear CuLn complexes. The Pr–Cu separation distance in **13** is 3.538(2) Å. Magnetic susceptibility data indicated that the magnetic exchange between the Pr^{III} ion and the Cu^{II} ion is weakly antiferromagnetic [16].

Production of superconducting films by using a solution precursor system

One advantage provided by the bdmapH ligand is that it significantly improves the solubility of the metal compounds in organic solvents. For example, the mixture of $Y(O_2CCH_3)_3$, $Ba(O_2CCH_3)_2$, and $Cu(O_2CCH_3)_2$ in a 1 : 2 : 3 ratio produces precipitates in the solvents such as THF. The addition of acetic acid to the THF solution (1 : 5) improves the solubility at high temperature, but results in co-precipitation when the solution is cooled to ambient temperature. We have found that the co-precipitation can be prevented by adding a small amount of bdmapH to the solution (2 bdmapH per copper) [8a]. The solution obtained is dark blue and homogeneous. The viscosity of this solution can be adjusted readily by adjusting the amount of solvents. We believe that the bdmapH ligand forms complexes with the metal ions in the solution to increase their solubility. Although we have not been able to isolate any crystalline mixed metal compounds directly from the solution of the mixture, we believe that it is likely that some of the complexes formed in solution may be the same or related to those we obtained by independent syntheses, as described in earlier sections. The precursor solution made of $Y(O_2CCH_3)_3$, $Ba(O_2CCH_3)_2$, $Cu(O_2CCH_3)_2$, and bdmapH can be coated readily to a MgO (100) substrate via a spin-coating process. Subsequent heating and annealing treatments produced 1-2-3 films on the substrate. Superconducting films oriented along C

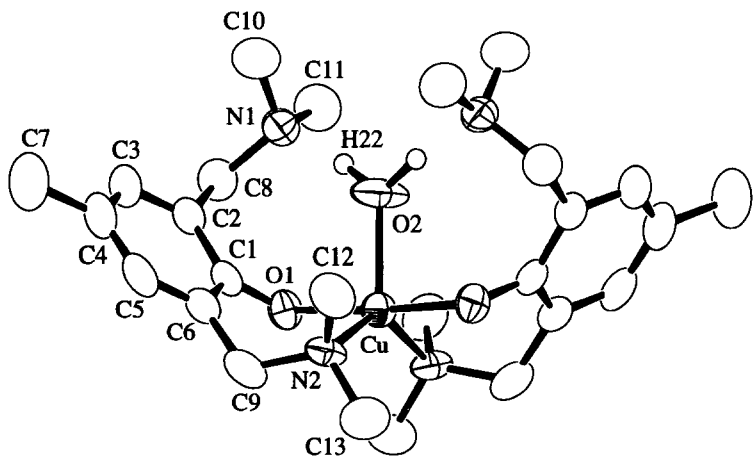

Fig. 15. The crystal structure of $Cu(bdmmp)_2(H_2O)$ (**12**).

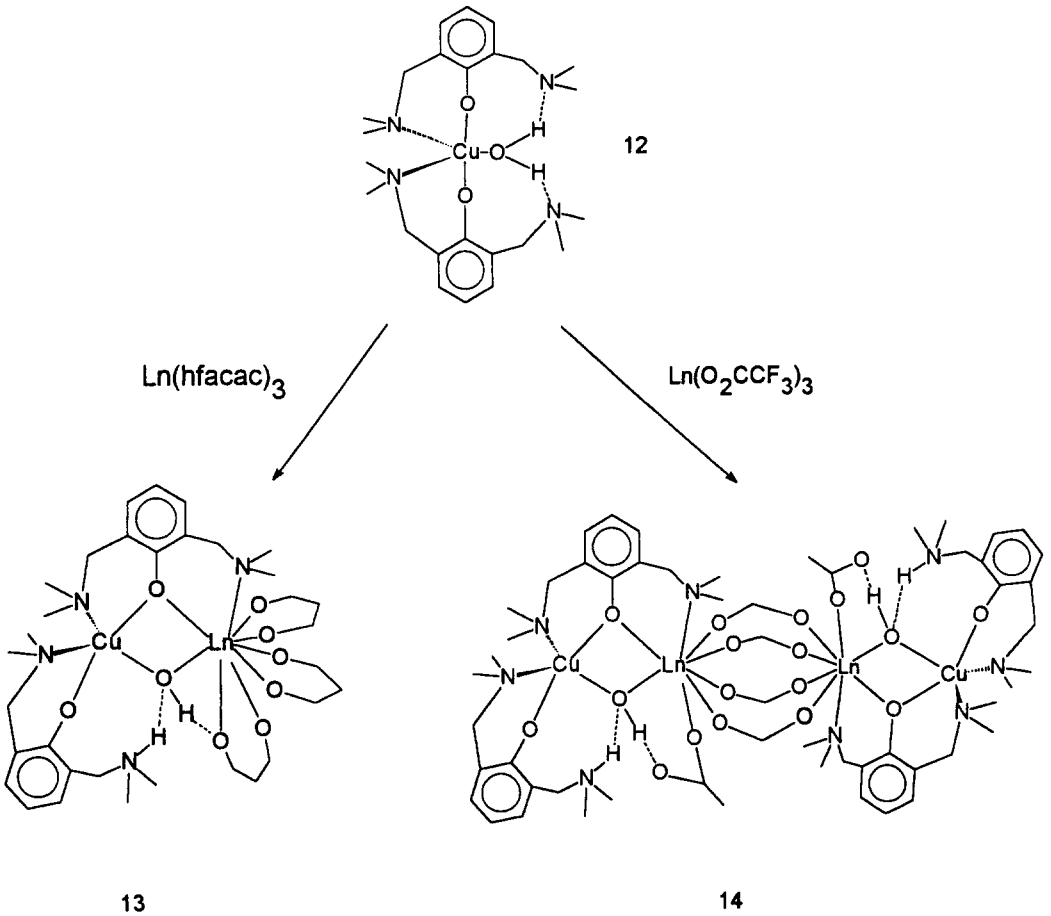

Scheme 3.

axis were obtained by repeated coating, heating, and annealing processes [17].

Summary

2-Hydroxyl pyridine and amino alcohol are efficient ligands for binding to both copper(II) ions and electropositive ions such as alkaline-earth metal and lanthanide ions. The structures and compositions of the mixed metal complexes obtained by using these ligands are highly dependent on the stoichiometry of the starting materials, the solvents, and the adventitious water molecules in the system. The $Cu(bdmmp)_2(H_2O)$ compound is a useful precursor complex for the systematic syntheses of mixed metal complexes. The presence of fluorinated ligands in the complexes generally lowers the thermal decomposition temperature substantially. However, fluorine contamination due to the formation of the MF_2 phase become a serious problem for complexes containing alkaline-earth metal ions. Introducing oxide or hydroxide bridging ligands in these complexes could minimize this problem. The bdmapH ligand is a useful cross-linking reagent for 1-2-3 superconducting films produced by a solution precursor system *via* spin coating. Magnetic exchange between paramagnetic lanthanide ions and copper(II) ions are weak. The magnetic exchange between copper(II) centers in these complexes are usually dominated by antiferromagnetism.

Acknowledgement—The author thanks the students and postdoctorals who contributed to the work described here and NSERC of Canada for financial support.

REFERENCES

1. (a) Rao, C. N., *Chemistry of Advanced Materials*, Blackwell Scientific Publications, London, (1993); (b) Segal, D., *Chemical Synthesis of Advanced Ceramic Material*, Cambridge University Press, Cambridge, 1989; (c) Brinker, C. J., Clark, D. E. and Ulrich, D. R. (ed.), *Mater. Res. Sym. Proc.*, 1988, **121**; Zelinski, B. J. J., Brinker, C. J., Clark, D. E. and Ulrich, D. R., *Mater. Res. Sym. Proc.*, 1990, **180**; (d) Rupich, M. W., Lagos, B. and Hachey, J. P., *Appl. Phys. Lett.*, 1989, **55**, 2449; (e) Rice, C. E., Van Dover, R. B. and Fisanick, G. J., *Appl. Phys. Lett.*, 1987, **51**, 1842; (f) Love, C. P., Torardi, C. C. and Page, C. J., *Inorg. Chem.*, 1992, **31**, 1784.

2. *High T_c Superconductor Thin Films*, L. Correra, Ed., Elsevier Science Publishers, Amsterdam, (1992).
3. Cotton, F. A. and Wilkinson, G., *Adv. Inorg. Chem.*, 5th Edn., John Wiley & Sons, New York (1988).
4. Goodgame, D. M. L., Williams, D. J. and Winpenny, R. E. P., *Polyhedron*, 1989, **12,** 1531.
5. Wang, S., *Inorg. Chem.*, 1991, **30,** 2252.
6. Wang, S., Pang, Z. and Wagner, M. J., *Inorg. Chem.*, 1992, **31,** 5381.
7. (a) Blake, A. J., Gould, R. O., Milne, P. E. Y. and Winpenny, R. E. P., *J. Chem. Soc. Chem. Commun.*, 1991, 1453; (b) Blake, A. J., Milne, P. E. Y., Thornton, P. and Winpenny, R. E. P., *Angew. Chem. Int. Ed. Engl.*, 1991, **30,** 1139.
8. (a) Wang, S., Pang, Z., Smith, K. D. L. and Wagner, M. J., *J. Chem. Soc., Dalton Trans.*, 1994, 955; (b) Wang, S., Pang, Z., Smith, K. D. L. and Wagner, M. J., *J. Chem. Soc. Chem. Commun.*, 1992, 1594.
9. Bidell, W., Döring, J., Bosch, H. W., Hund, H.-U, Plappert, E. and Berke, H., *Inorg. Chem.*, 1993, **32,** 502.
10. March, J., *Adv. Organic Chem.* 3rd Edn., John Wiley & Sons, New York (1985).
11. Poncelet, O., Hubert-Pfalzgraf, L. G. and Daran, J. C., *Polyhedron*, 1990, **9,** 1305.
12. (a) Wang, S., Pang, Z., Smith, K. D. L., Hua, Y., Deslippe, C. and Wagner, M. J., *Inorg. Chem.*, 1995, **34,** 908; (b) Wang, S., Pang, Z. and Smith, K. D. L., *Inorg. Chem.*, 1993, **32,** 4992.
13. Breeze, S. R. and Wang, S., *Inorg. Chem.*, 1994, **33,** 5113.
14. Breeze, S. R., Wang, S. and Thompson, L. K., *Inorg. Chim. Acta*, 1996, **250,** 163.
15. Wang, S., Trepanier, S. J. and Wagner, M. J., *Inorg. Chem.*, 1993, **32,** 833.
16. Chen, L., Breeze, S. R., Rousseau, R. J., Wang, S. and Thompson, L. K., *Inorg. Chem.*, 1995, **34,** 454.
17. Breeze, S. and Wang, S., *J. Mat. Res.*, 1997, submitted.

Pergamon

PII: S0277-5387(97)00281-7

Polyhedron Vol. 17, No. 5–6, pp. 845–850, 1998
© 1998 Elsevier Science Ltd
All rights reserved. Printed in Great Britain
0277–5387/98 $19.00+0.00

Homoleptic trisaminopyridinato M^{III} complexes (M = Ti, V and Cr), synthesis, structure and EPR investigations†

Anke Spannenberg,[a] Annegret Tillack,[a] Perdita Arndt,[a] Reinhardt Kirmse[b] and Rhett Kempe[a]*

[a] Abteilung Komplexkatalyse, IfOK an der Universität Rostock, Buchbinderstraße 5–6, 18055 Rostock, Germany

[b] Institut für Anorganische Chemie, Universität Leipzig, Talstr. 35, 04103 Leipzig, Germany

(Received 27 May 1997; accepted 23 June 1997)

Abstract—The synthesis of a series of trisaminopyridinato metal(III) complexes (metal = Ti, V and Cr) is reported. The titanium complex is synthesized by reduction of the monochloro Ti^{IV} complex (4-Me-TMS-APy)$_2$Ti(NMe$_2$)Cl (4-methyl-2-trimethylsilylaminopyridine = 4-Me-TMS-APyH) using sodium amalgam as a reducing agent. The vanadium complex is prepared *via* a salt elimination route using $VCl_3(THF)_3$ and 3 equiv of *in situ* lithiated 4-Me-TMS-APyH. The chromium complex is made *via* benzene elimination from $Ph_3Cr(THF)_3$ and 3 equiv of 4-Me-TMS-APyH. All three compounds are paramagnetic and the IR spectra of the compounds fit very well in the finger print range. The X-ray crystal structure analyses of the titanium and the chromium complexes establish their mononuclear structures with a strongly disturbed octahedral coordination geometry. The EPR spectra of the Ti^{III} and Cr^{III} complexes are reported. © 1998 Elsevier Science Ltd. All rights reserved

Keywords: aminopyridinato ligands; titanium; vanadium; chromium; EPR spectra.

M^{III} amido complexes of the early transition metals were first described by Bürger and Wannagat [1] and simultaneously exploited by Bradley *et al.* [2]. They were investigated with regard to structural aspects and the nature of the amido metal bond [3]. Approaches nowadays using chelating amido ligands are focused on the design of well defined reactive pockets at such reduced metal centers, for instance, to activate substrates *via* oxidative addition pathways [4]. We are interested in following this tendency by exploring the capability of aminopyridinato ligands [5–7]. Due to the flexibility in the binding mode of such ligands it might be possible to stabilize reduced and thus reactive early transition metal centers *via* steric shielding, on the one hand, and to offer furthermore the opportunity of creating a reactive pocket *via* ligand rearrangement and/or metal pyridine bond cleavage if substrates are present in order to activate them. In this paper we report on the synthesis and structure of trisaminopyridinato complexes, (4-Me-TMS-APy)$_3$M (M = Ti, V, Cr and 4-Me-TMS-APyH = 4-methyl-2-trimethylsilylaminopyridine) as well as on EPR investigations of the three complexes. Amidinato ligands might be considered as the most related ligand system to aminopyridinato ligands and selected examples of six-coordinated complexes have been published for vanadium [8], titanium [9], and chromium [10].

EXPERIMENTAL

Materials and procedures

Solvents were dried and freshly distilled from sodium tetraethylaluminate under argon prior to use. 4-Methyl-2-trimethylsilylaminopyridine was prepared according to a method published previously [7] as well as (4-Me-TMS-APy)$_2$Ti(NMe$_2$)Cl. Trichlorotris-(tetrahydrofuran)vanadium(III) [16] and triphenyl-

* Author to whom correspondence should be addressed.

† Dedicated to Don Bradley in recognition of his outstanding contributions to amido metal chemistry.

tris(tetrahydrofuran)chromium(III) [17] were synthesized according to literature methods. All manipulations were performed with rigorous exclusion of oxygen and moisture using standard Schlenk-technique.

Physical measurements

Elemental analyses were performed with a Leco CHNS-932 elemental analyzer. The IR-spectra were recorded on a Nicolet Magna 550 spectrometer. X-ray data were collected on a STOE-IPDS diffractometer using monochromated Mo-K_α radiation. The structures were solved by direct methods (SHELXS-86) [18] and refined by full matrix least square techniques against F^2 (SHELXL-93) [19], XP (Siemens Analytical X-ray Instruments, Inc.) was used for structure representations. Further details of the crystal structure investigations are available upon request from the Director of the Cambridge Crystallographic Data Center, 12 Union Road, GB-Cambridge CB2 1EZ (U.K.), on quoting the full journal citation. EPR spectra of $\approx 1 \times 10^{-2}$ M solutions of the compounds in hexane were recorded with a Bruker ESP 300E spectrometer at X-band frequency ($n \approx 9.5$ GHz) at $T = 295$ K and 110 K.

Preparation of tris(4-methyl-2-trimethylsilylamino-pyridinato)titanium(III), (1)

486 mg (1 mmol) of (4-Me-TMS-APy)$_2$Ti(NMe$_2$)Cl was added to a slurry of 23 mg (1 mmol) of sodium as sodium amalgam in 30 cm^3 of hexane and stirred for 24 h at room temperature. The reaction mixture was filtered, the solvent was reduced to half *in vacuo* and stored at -78 °C to yield 269 mg (46%) of **1**. IR (Nujol, cm^{-1}): 1600 and 1535 ν(ar C=C), 1316, 1292, 1245 δ_S(CH$_3$—Si), 1172, 1022, 962, 873 ν(N—Si), 843 γ(CH$_3$—Si), 788 δ(ar C—H), 766 γ(CH$_3$—Si), 727 δ(ar C—H), 589. $C_{27}H_{45}N_6Si_3Ti$ (585.83): Calc. C 55.36, H 7.74, N 14.35; found C 53.64, H 7.71, N 13.93%. We attribute the low carbon values of **1** and **3** to metal (Ti, V as well as Si) carbide formation.

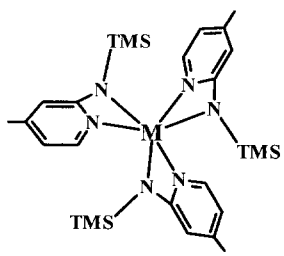

M = Ti, V and Cr

Preparation of tris(4-methyl-2-trimethylsilylamino-pyridinato)chromium(III), (2)

To a solution of 999 mg (2 mmol) of triphenyltris(tetrahydrofuran)chromium(III) in 30 cm^3 of THF was added 1.3 cm^3 (6 mmol) of 4-methyl-2-trimethylsilylaminopyridine at -40 C. The mixture was stirred for 24 h at room temperature. The solvent was removed *in vacuo*, the residue was taken up with hexane and filtered. At -78 °C 696 mg (59%) of **2** was slowly crystallized. IR (Nujol, cm^{-1}): 1606 and 1532 ν(ar C=C), 1326, 1293, 1243 δ_S(CH$_3$—Si), 1172, 1024, 970, 873 ν(N—Si), 840 γ(CH$_3$—Si), 783 δ(ar C—H), 766 γ(CH$_3$—Si), 730 δ(ar C—H), 591. $C_{27}H_{45}N_6Si_3Cr$ (589.95): Calc. C 54.97, H 7.69, N 14.25; found C 55.12, H 7.98, N 14.16%.

Preparation of tris(4-methyl-2-trimethylsilylamino-pyridinato)vanadium(III), (3)

To a solution of 1.9 cm^3 (9 mmol) of 4-methyl-2-trimethylsilylaminopyridine in 30 cm^3 of THF was added slowly *via* stirring 5.6 cm^3 (9 mmol) of a 1.6 M hexane solution of *n*-butyllithium at -40 °C. This mixture was stirred for 2 h at room temperature. 1.121 g (3 mmol) of trichlorotris(tetrahydrofuran)-vanadium(III) was partly solved in 25 cm^3 of THF. The lithiated ligand was added to this mixture and stirred for an additional 48 h at room temperature. The solvent was removed *in vacuo*, the residue was taken up with hexane and filtered off from LiCl. Crystallisation from hexane at -78 °C yielded 1.272 g (72%). IR (Nujol, cm^{-1}): 1603 and 1538 ν(ar C=C), 1315, 1291, 1247 δ_S(CH$_3$—Si), 1172, 1021, 969, 870 ν(N—Si), 840 γ(CH$_3$—Si), 787 δ(ar C—H), 767 γ(CH$_3$—Si), 729 δ(ar C—H), 592. $C_{27}H_{45}N_6Si_3V$ (588.89): Calc. C 55.07, H 7.70, N 14.27; found C 53.69, H 7.53, N 13.92%.

RESULTS AND DISCUSSION

The reduction of (4-Me-TMS-APy)$_2$Ti(NMe$_2$)Cl (smoothly prepared *via* amine elimination starting from (Me$_2$N)$_3$TiCl [11] and 2 equiv of 4-Me-TMS-APyH) with sodium amalgam in hexane leads to (4-Me-TMS-APy)$_3$Ti (**1**) according to Scheme 1. It is proposed that after the reduction the dimethylamido ligand is exchanged by an aminopyridinato ligand. Thus titanium dimethylamido species should be obtained as byproducts. Unfortunately, no such amido complexes were detected by NMR, which might be explained by possible paramagnetism. A salt elimination reaction of 3 equiv of *in situ* lithiated 4-Me-TMS-APyH and TiCl$_3$(THF)$_3$ failed. Compound **1** is a dark purple complex. Solution magnetic susceptibility measurements on **1** obtained in benzene solution by the method of Evans [12] gave $\mu_{eff} = 1.99$ μ_b, which is in accordance with one unpaired electron. Due to its paramagnetic nature an X-ray analysis was

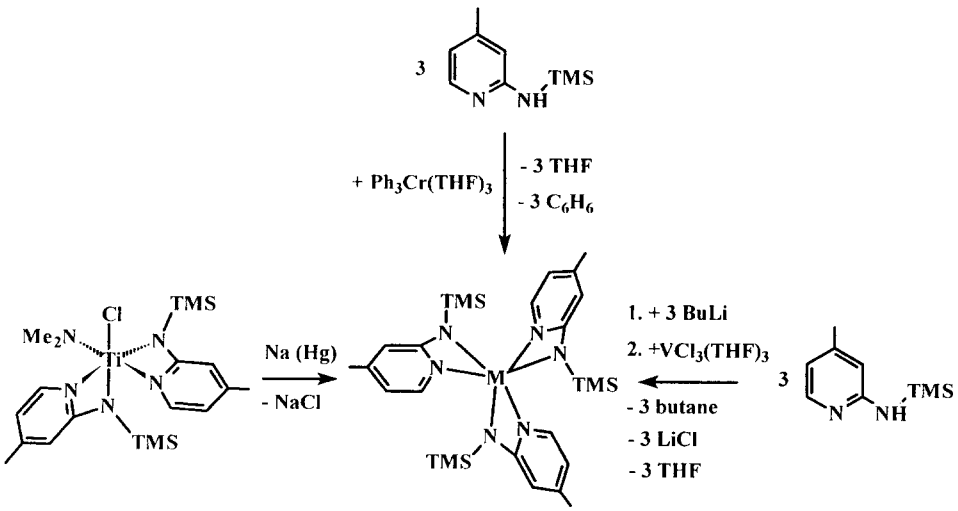

Scheme 1. Synthesis of **1**, **2** and **3**.

carried out. Suitable crystals could be obtained after keeping a highly saturated hexane solution over two weeks at −78°C. A perspective ORTEP drawing of the molecular structure of **1** is shown in Fig. 1 as well as key bond distances and angles. Some important crystallographic features are shown in Table 1. The coordination geometry is best described as strongly disturbed octahedral. The virtual D_3 symmetry common to all of the homoleptic tris-chelated compounds [10] is not accomplished due to ligand asymmetry. The averaged Ti—N_{amido} bond length in **1** (2.09 Å {0.2 Å longer than the titanium amido bond normally [7]}), is different compared to the averaged Ti—$N_{pyridine}$ distance in **1**. The latter is 2.15 Å and only slightly shorter as the common titanium pyridine bond length [7]. Thus a weak metal amido and a typical pyridine bond are observed. Due to the analogy of the bonding situation of (4-Me-TMS-APy)$_2$Ti(NMe$_2$)Cl [7] and **1** in the solid state a similar behaviour in solution like ligand rotation *via* pyridine titanium bond cleavages is proposed.

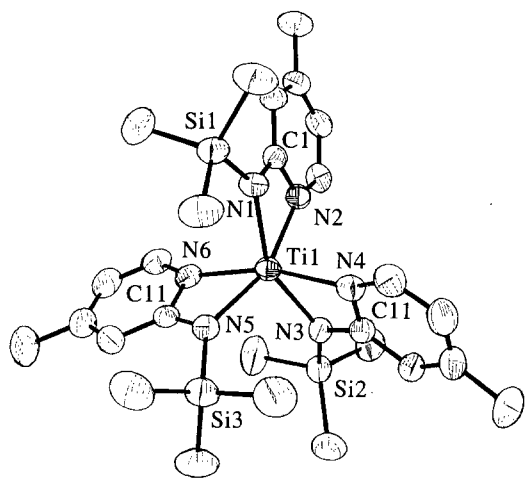

Fig. 1. Structural representation of **1**. Hydrogen atoms are omitted for clarity. The thermal ellipsoids correspond to 30% probability. Selected bond lengths (Å) and angles (°): C(1)—N(2) 1.359(4), C(1)—N(1) 1.370(4), C(6)—N(3) 1.369(4), C(6)—N(4) 1.372(4), C(11)—N(5) 1.351(4), C(11)—N(6) 1.383(4), N(1)—Ti(1) 2.069(3), N(2)—Ti(1) 2.186(3), N(3)—Ti(1) 2.094(3), N(4)—Ti(1) 2.137(3), N(5)—Ti(1) 2.103(2), N(6)—Ti(1) 2.126(3), N(2)—C(1)—N(1) 111.4(3), N(3)—C(6)—N(4) 109.9(3), N(5)—C(11)—N(6) 110.7(3), N(5)—Ti(1)—N(6) 64.28(10), N(3)—Ti(1)—N(4) 64.05(10), N(1)—Ti(1)—N(2) 63.90(10).

The reaction of 3 equiv of 4-Me-TMS-APyH with $Ph_3Cr(THF)_3$ leads *via* benzene elimination [13] to (4-Me-TMS-APy)$_3$Cr (**2**), a dark red chromium compound analogous to **1** (Scheme 1). The use of aryl elimination routes to synthesize Cr^{III} amido complexes is unusual and offers an attractive alternative approach to salt elimination routes. The high magnetic susceptibility of $\mu_{eff} = 4.47\ \mu_b$ indicates **2** to have three unpaired electrons. The single-crystal X-ray structure analysis of **2** establishes its monomeric structure as shown in Fig. 2 including principal bond distances and angles. Crystallographic data are listed in Table 1. The chromium complex is isomorphous to **1** and the general structural arrangements are equivalent. The averaged Cr—N_{amido} bond length (2.06 Å) is equal to the averaged Cr—$N_{pyridine}$ (2.04 Å) distance. Thus a delocalised binding mode with equivalent nitrogen metal bonds as those known for benzamidinate [14] complexes is proposed for **2**, which is in contrast to the binding situation in complex **1**.

Table 1. Crystallographic data for **1** and **2**

Compound	**1**	**2**
Formula	$C_{27}H_{45}N_6Si_3Ti$	$C_{27}H_{45}N_6Si_3Cr$
Mol. mass	585.9	590.0
Cryst. color	black-purple	red-brown
Cryst. descript	prism	needle-like
Cryst. size (mm)	$0.4 \times 0.4 \times 0.2$	$0.7 \times 0.1 \times 0.05$
Cryst. system	triclinic	triclinic
Space group	$P-1$(#2)	$P-1$(#2)
a (Å)	9.707(1)	9.665(2)
b (Å)	10.862(1)	10.809(2)
c (Å)	16.720(2)	16.778(3)
α (°)	90.67(1)	91.41(1)
β (°)	93.54(1)	93.12(1)
γ (°)	99.61(1)	98.69(1)
Z	2	2
T (K)	293(2)	293(2)
μ (mm^{-1})	0.374	0.459
Absorp. corr.	no	no
θ range (°)	1.90–24.41	1.91–24.35
Largest diff. (e $Å^{-3}$) peak/hole	0.24/−0.39	0.32/−0.31
No. of rflns. (measd.)	11196	11002
No. of rflns. (indep.)	5258	5191
R (int)	0.081	0.083
No. of rflns. (obsd.) $I > 2\sigma(I)$	3145	1670
No. of parameters	335	335
$R1$ [$I > 2\sigma(I)$]	0.047	0.060
$wR2$ (all data)	0.137	0.142

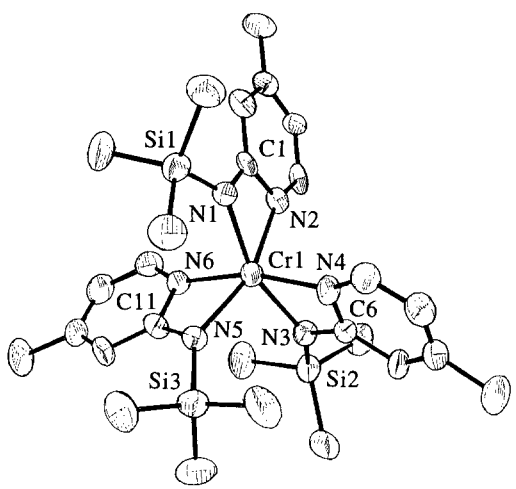

Fig. 2. Perspective ORTEP drawing of the molecular structure of **2**. All nonhydrogen atoms are represented by thermal ellipsoids drawn to encompass 30% probability. Selected bond lengths (Å) and angles (°): C(1)—N(1) 1.341(8), C(1)—N(2) 1.377(9), C(6)—N(3) 1.361(7), C(6)—N(4) 1.359(9), C(11)—N(6) 1.355(7), C(11)—N(5) 1.354(7), N(1)—Cr(1) 2.056(6), N(2)—Cr(1) 2.054(5), N(3)—Cr(1) 2.079(6), N(4)—Cr(1) 2.024(6), N(5)—Cr(1) 2.066(5), N(6)—Cr(1) 2.027(5), N(1)—C(1)—N(2) 112.6(7), N(3)—C(6)—N(4) 109.6(7), N(6)—C(11)—N(5) 110.0(6), N(6)—C(11)—C(12) 118.9(6), N(1)—Cr(1)—N(2) 66.7(2), N(6)—Cr(1)—N(5) 65.6(2), N(4)—Cr(1)—N(3) 65.6(2).

The reaction of 3 equiv of *in situ* generated "4-Me-TMS-APyLi" with $VCl_3(THF)_3$ affords $(4\text{-Me-TMS-APy})_3V$ (**3**), a dark orange crystalline material according to Scheme 1. Compound **3** is a paramagnetic high-spin complex. Solution magnetic susceptibility measurements [12] on **3** obtained in benzene solution gave $\mu_{eff} = 3.67\ \mu_b$, significantly higher than 2.83 μ_b, the spin-only value for two unpaired electrons. The IR spectra of **1**, **2** and **3** are in accordance to each other as seen in the finger print plot (Fig. 3). Thus an analogous structural arrangement is assumed. **1**, **2** and **3** are very sensitive to air and moisture and very well soluble in hydrocarbon solvents. Due to the extremely high solubility the isolated yields of crystalline materials are always moderate.

The trisaminopyridinato M^{III} complexes have been studied by EPR in solutions at $T = 295$ K and 110 K. EPR spectra were obtained for the Ti^{3+} ($3d^1$) and the Cr^{3+} ($3d^3$) complexes, but not for the V^{3+} ($3d^2$) species. The room-temperature EPR spectra observed consist of a symmetrical single line with linewidths of 3 mT for Ti^{3+} and more than 200 mT for Cr^{3+}. The isotropic g values are found to be $g_0 = 1.936 \pm 0.003$ and $g_0 = 2.000 \pm 0.005$ for the titanium and the chromium complex, respectively. In Fig. 4(a) the frozen solution EPR spectrum of **1** is shown. The spectrum of the titanium complex consists of the liquid solution of a single line also. However, the linewidth is larger ($\Delta B_{pp} = 6.5$ mT) and slightly anisotropic indicating a small **g** anisotropy. It is also centered at $g = 1.936$.

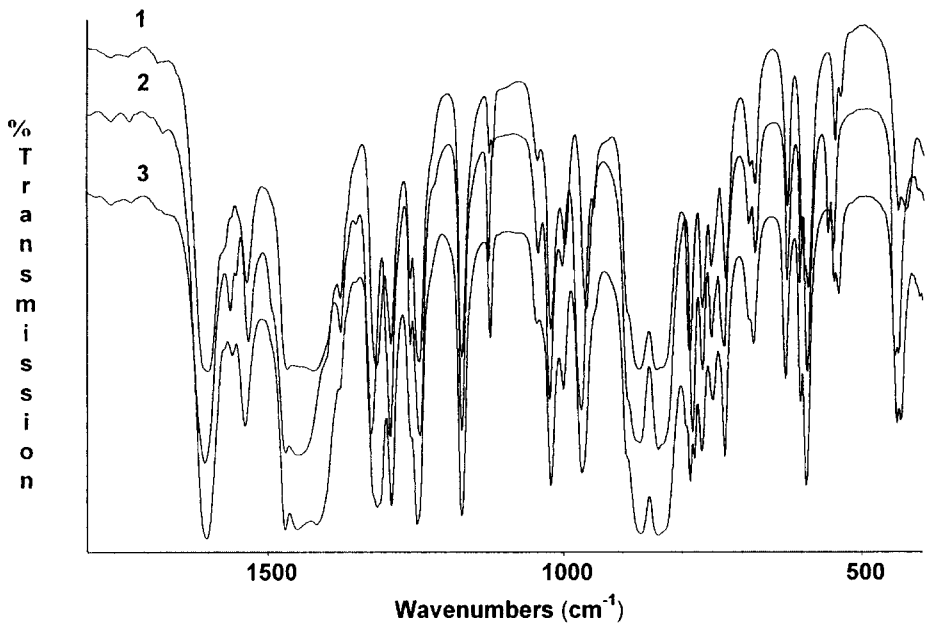

Fig. 3. IR spectra (Nujol) of **1**, **2** and **3** in the finger print range.

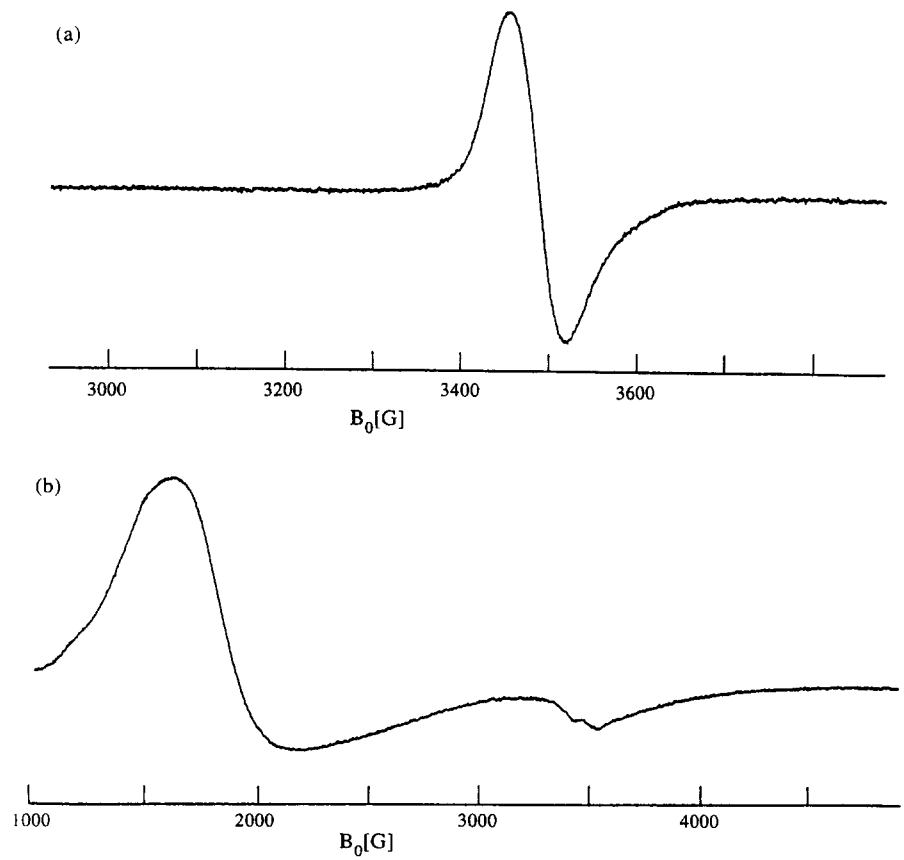

Fig. 4. X-band EPR spectra of (4-Me-TMS-APy)$_3$Ti (a) and (4-Me-TMS-APy)$_3$Cr (b) in frozen hexane, $T = 110$ K.

Due to the small anisotropy of the line observed the individual components of the **g** tensor cannot be derived (nor by the simulation programs available). The observation of ^{47,49}Ti hyperfine interactions is prevented because of the large linewidth and the low natural abundance of the isotopes ^{47}Ti and ^{49}Ti. Figure 4(b) represents the frozen solution EPR spectrum of the chromium complex. In the field range up to 1 T no additional EPR signals were observed. The spectrum consists of signals in the $g = 6$–4 and $g = 2$ region which is in agreement with a $S = 3/2$ spin-system having a fine structure interaction $\mathbf{S} \times \mathbf{D} \times \mathbf{S}$ which exceeds the electron Zeeman interaction $m_B \mathbf{g} \times \mathbf{B} \times \mathbf{S}$ in magnitude. According to the numerous $\mathbf{S} = 3/2$ spectra simulations published by Mabbs and Collision [15] the fine structure parameter D is found to be $\geqslant 1$ cm^{-1}; also a rhombic distortion is indicated (see $g = 2$ region). The EPR spectra are in good agreement with what can be drawn from the crystal structure analyses which provide disturbed octahedral symmetries for the complexes under study. For the vanadium(III) complex no EPR spectrum has been observed in the temperature range applied. This is not surprising, since for V^{3+} in an octahedral environment the orbital ground state is a triplet one which will be split by lower-symmetric ligand field components. Obviously, this splitting is not large and thus results in short spin-lattice relaxation times which prevent the detection of EPR spectra in the temperature range studied.

Acknowledgements—We thank Professor U. Rosenthal for generous support and helpful discussions. Financial support by the Max-Planck-Gesellschaft and the Fonds der Chemischen Industrie is gratefully acknowledged.

REFERENCES

1. Bürger, H. and Wannagat, U., *Monatsh. Chem.*, 1963, **94,** 1007; Bürger, H. and Wannagat, U., *Monatsh. Chem.*, 1964, **95,** 1099.
2. Basi, J. S. and Bradley, D. C., *Proc. Chem. Soc. (London)*, 1963, 305; Eller, P. G., Bradley, D. C., Hursthouse, M. B. and Meek, D. W., *Coord. Chem. Rev.*, 1977, **241,** 1.
3. Lappert, M. F., Power, P. P., Sanger, A. R. and Srivastava, R. C., *Metal and Metalloid Amides.* Ellis Horwood Ltd., Chichester, England, 1980.
4. Cummins, C. C., Lee, J., Schrock, R. R. and Davis, W. M., *Angew. Chem.*, 1992, **104,** 1510; *Angew. Chem. Int. Ed. Engl.*, 1992, **31,** 1501.
5. Aminopyridinato ligands are deprotonated α-aminopyridines if they coordinate in a strained η^2 fashion: Chakravarty, A. R., Cotton, F. A. and Shamshoum, E. S., *Inorg. Chim. Acta*, 1984, **86,** 5; (b) Calhorda, M. J., De C. T. Carrondo, M. A. A. F., Gomes da Costa, R., Dias, A. R., Duarte, M. T. L. S. and Hursthouse, M. B., *J. Organomet. Chem.*, 1987, **320,** 53; (c) Edema, J. J. H., Gambarotta, S., Meetsma, A., Spek, A. L. and Veldman, N., *Inorg. Chem.*, 1991, **30,** 2062; Oberthür, M., Arndt, P. and Kempe, R., *Chem. Ber.*, 1996, **129,** 1087; Spannenberg, A., Arndt, P., Oberthür, M. and Kempe, R., *Z. Anorg. Allg. Chem.*, 1997, **623,** 389.
6. Kempe, R., Brenner, S. and Arndt, P., *Organometallics*, 1996, **15,** 1071.
7. Kempe, R. and Arndt, P., *Inorg. Chem.*, 1996, **35,** 2644.
8. Cotton, F. A., Daniels, L. M. and Murillo, C. A., *Inorg. Chem.*, 1993, **32,** 2881.
9. Cotton, F. A. and Wojtczak, W. A., *Polyhedron*, 1994, **13,** 1337.
10. Cotton, F. A., Daniels, L. M., Maloney, D. J. and Murillo, C. A., *Inorg. Chim. Acta*, 1996, **242,** 31.
11. Benzing, E. and Kornicker, W., *Chem. Ber.*, 1961, **94,** 2263.
12. Sur, S. K., *J. Magn. Reson.*, **82,** 169; Evans, D. F., *J. Chem. Soc.*, 1959, 2003.
13. Kurras, E., Rosenthal, U., Mennenga, H. and Oehme, G., *Angew. Chem.*, 1973, **85,** 913; *Angew. Chem. Int. Ed. Engl.*, 1973, **12,** 854.
14. Edelmann, F. T., *Coord. Chem. Rev.*, 1994, **137,** 403.
15. Mabbs, F. E. and Collison, D., *Electron Paramagnetic Resonance of d Transition Metal Compounds.* Elsevier, Amsterdam, 1992, Chapter 12.
16. Fackler, J. P., Jr., *Inorg. Synth.*, 1982, **XXI,** 138.
17. Herwig, W. and Zeiss, H., *J. Am. Chem. Soc.*, 1959, **81,** 4798.
18. Sheldrick, G. M., *SHELXS*-86, *Acta Crystallogr. Sect. A*, 1990, **46,** 467.
19. Sheldrick, G. M., *SHELXL*-93, unpublished.

Pergamon

PII: S0277-5387(97)00288-X

Polyhedron Vol. 17, No. 5–6, pp. 851–856, 1998
© 1998 Elsevier Science Ltd
All rights reserved. Printed in Great Britain
0277-5387/98 $19.00+0.00

Mono-phenoxy oxo complexes of tungsten(VI)†

Mark W. Glenny,[a] Alastair J. Nielson[b]* and Clifton E. F. Rickard[a]

[a]Department of Chemistry, The University of Auckland, Private Bag 92019, Auckland, New Zealand

[b]Department of Chemistry, Massey University at Albany, Private Bag 102904, North Shore Mail Centre, Auckland, New Zealand

(Received 7 May 1997; accepted 23 June, 1997)

Abstract—The complexes $[WOCl_3(OAr)]_x$ (Ar = 4-*tert*-butylphenyl **1**, 2,6-dimethylphenyl **2**, 2,6-di-*iso*-propylphenyl **3**) are prepared by reacting HOAr with an excess of $[WOCl_4]$ but are thermodynamically unstable forming bis-phenoxide complexes on standing. Debutylation occurs with 2,6-di-*tert*-butylphenol but a monophenoxide **4** was prepared with the lithium phenoxide. The complex debutylates and forms bis-phenoxides on standing. An X-ray crystal structure of **2** shows a dimeric chloro-bridged structure with terminal oxo and 2,6-dimethylphenoxide ligands. The oxo ligand acts essentially as a $1\sigma, 2\pi$ donor to tungsten [W—O(1) bond length 1.679(4) Å] and the phenoxide as a $1\sigma, 1\pi$ donor [W—O(2) bond length 1.820(4) Å]. The phenyl ring positions to reduce interactions of the methyl substituents with the oxo and chloro ligands but NMR spectra show rapid phenoxide rotation in solution. Variable temperature NMR spectral studies of **4** show the *tert*-butyl groups lock the rotation which may be important in the debutylation process. The complexes have limited catalytic potential due to instability. © 1998 Elsevier Science Ltd. All rights reserved

Keywords: phenoxide; oxo; tungsten.

Phenoxide complexes of tungsten are of interest in the field of C—H activation [1], alkene metathesis [2] and polymerisations [3]. Most often the complexes used contain two or more phenoxides which are effective π-donor ligands. However the number of phenoxides in a complex is not always easy to control. This is demonstrated in the preparation of a series of complexes with the general formula $[WCl_{6-x}(OAr)_x]$ ($x = 2$, 3 and 4) where the reaction was sensitive to the phenol used and did not seem to follow any definite pattern with regard to the steric or electronic properties of the phenol [4]. Our interest in phenoxide complexes of tungsten is in the production of cost effective complexes for use in catalytic processes. We report here the preparation and properties of monophenoxy-oxo complexes of tungsten(VI) which are derived from the inexpensive compound $[WOCl_4]$ and commercially available phenols using simple reaction procedures.

RESULTS AND DISCUSSION

Initial attempts to replace one of the chloro ligands in $[WOCl_4]$ with a phenoxide ligand using a 1:1 ratio of reactants, invariably led to mixtures containing mono and bis-phenoxide complexes which proved difficult to separate analytically pure. However, an appreciable excess of $[WOCl_4]$ was found to suppress formation of the bis-phenoxide which was always present with $[WOCl_4]$:phenol ratios less than about 1.5:1. Thus when a dichloromethane solution of *p*-*tert*-butylphenol was added to $[WOCl_4]$ dissolved in diethyl ether, the purple monophenoxide complex $[WOCl_3(OC_6H_4Bu^t\text{-}4)]_x$ **1**, was formed in 90% yield.

$$\text{excess } [WOCl_4] + HOC_6H_4Bu^t\text{-}4 \rightarrow [WOCl_3(OC_6H_4Bu^t\text{-}4)]_x \ \mathbf{1}$$

If toluene was used in place of diethyl ether, the reaction produced significant amounts of the bis-phenoxide complex, probably as a result of the lower solubility of $[WOCl_4]$ in this solvent. Complex **1** formed as a somewhat impure powder which failed to

* Author to whom correspondence should be addressed.

† Dedicated to Professor D. C. Bradley on the occasion of his 73rd birthday.

produce crystals for a structure determination. Both the ^1H and ^{13}C-$\{^1H\}$ NMR spectra showed single resonances for the appropriate hydrogen and carbon atoms with the *ipso* carbon resonance occurring at δ 160.29 in the ^{13}C-$\{^1H\}$ NMR spectrum.

Reaction of 2,6-dimethylphenol, or its trimethylsilyl ether derivative, with $[WOCl_4]$ gave a crystalline purple complex analysing as the mono phenoxide $[WOCl_3(OC_6H_3Me_2\text{-}2,6)]_x$, which was shown to be a chloro-bridged dimer **2** by X-ray crystallography.

$$\text{excess } [WOCl_4] + HOC_6H_3Me_2\text{-}2,6 \rightarrow [WOCl_3(OC_6H_3Me_2\text{-}2,6)]_2$$

$$\text{excess } [WOCl_4] + Me_3SiOC_6H_3Me_2\text{-}2,6 \rightarrow [WOCl_3(OC_6H_3Me_2\text{-}2,6)]_2$$

The structure (Fig. 1) showed the molecule to be dimeric with the two halves centrosymmetrically related. Each tungsten atom adopts a distorted octahedral coordination geometry with chloro ligands making up the asymmetric bridge. The oxo ligand lies *trans* to the longer bridge with a terminal chloride ligand lying *trans* to the other. The remaining coordination sites are filled by terminal phenoxide and chloride ligands which are mutually *trans*. Selected bond lengths and angles are contained in Table 1. The W—Cl(1) distance [2.394(2) Å] is marginally shorter than the equivalent W—Cl bond in the structurally related complex $[WCl_4(NCHMe_2)]_2$ [2.418(4) Å] [5], but the W—Cl(1′) distance [2.876(2) Å], *trans* to the oxo ligand, is considerably longer than in the imido complex [2.736(5) Å] reflecting the stronger *trans* influence of the oxo ligand [6]. The W—Cl(3) bond length in **2** [2.303(2) Å], is of similar magnitude to the analogous bond in the imido complex [2.285(4) Å], and both these distances are similar to the remaining *trans* related terminal W—Cl bonds in the imido complex [W—Cl, 2.310(4) and 2.285(4) Å]. The equivalent positions to these two chlorides are occupied by *trans* oriented phenoxide and chloro ligands in **2**, where the W—Cl(2) distance is lengthened to 2.325(2) Å, indicating the phenoxide exerts a *trans* influence. A similar situation exists in $[WCl(NPh)(OEt)_2(\mu\text{-}OEt)]_2$

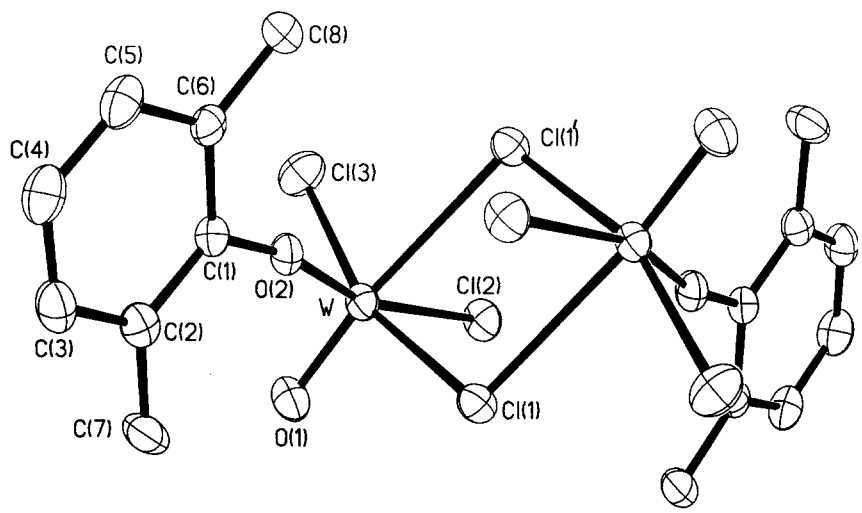

Fig. 1. ORTEP diagram of **2**. Thermal elipsoids shown at 50% probability level.

Table 1. Selected bond lengths (Å) and angles (°) for **2**

W—O(1)	1.679(4)	W—Cl(1)	2.394(2)
W—O(2)	1.820(4)	W—Cl(1′)	2.876(2)
W—Cl(3)	2.303(2)	O(2)—C(1)	1.375(6)
W—Cl(2)	2.325(2)		

O(1)—W—O(2)	101.2(2)	O(2)—W—Cl(1′)	82.73(14)
O(1)—W—Cl(1)	97.1(2)	Cl(1)—W—Cl(2)	86.44(9)
O(1)—W—Cl(2)	96.7(2)	Cl(3)—W—Cl(1)	160.50(6)
O(1)—W—Cl(3)	102.0(2)	Cl(1)—W—Cl(1′)	77.10(7)
O(1)—W—Cl(1′)	173.0(2)	Cl(2)—W—Cl(3)	87.47(9)
O(2)—W—Cl(1)	89.50(14)	Cl(2)—W—Cl(1′)	79.31(7)
O(2)—W—Cl(2)	162.03(13)	W—Cl(1)—W(1′)	102.90(7)
O(2)—W—Cl(3)	90.62(14)	C(1)—O(2)—W	167.6(4)

where an alkoxide ligand lies *trans* to a chloro ligand [7].

It is of interest to assess the π-donor contributions from the oxo and phenoxide ligands in **2**, especially in view of the phenoxide ligand preferring a terminal position rather than the expected bridging mode. The W—O(1) bond length [1.679(4) Å] is significantly shorter than those found for $[WCl_2(O)_2(bipy)]$ (bipy = 2,2′-bipyridyl), [1.745(3) and 1.792(2) Å] [8] and $[WCl_2(O)(NCMe_3)(bipy)]$ [1.716(5) Å] [9] where neither the oxo or imido ligands appear to dominate the π-donation. While the oxo ligands in these complexes may be lengthened somewhat by a hydrogen bond type interaction to the bipy ligand, the short W—O(1) bond in **2** is probably best represented by a 1σ, 2π donor interaction which leaves the phenoxide ligand as a 1σ, 1π donor if the electron count is to be maximised. However, significant orbital sharing can still be expected so that the oxo and phenoxide ligands cannot be regarded as pure 1σ, 2π or 1σ, 1π donors, respectively. The W—O(2) bond distance [1.820(4) Å] is similar to those found in $[WCl_4(OC_6H_3Ph_2\text{-}2,6)_2]$ where a high degree of ligand to metal π-donation is expected [4]. The W—O(2)—C(1) bond angle [167.6(4)°] is larger than that found for the two phenoxides in $[WCl_4(OC_6H_3Ph_2\text{-}2,6)_2]$ [141.8(6) and 149.3(6)°] [4] being closer to linearity than expected but may be influenced by crystal packing forces in much the same way as W—N—C bond angles are in imido complexes [10]. The phenyl ring rotates only slightly to remove unfavourable steric interactions of the *ortho* methyl groups with O(1) and Cl(1′) which appears to allow the C(1) *p*-orbital to maximise overlap with the O(2)—W(1) π-donor system. In the absence of strong crystal packing forces, there would seem to be conflict in the solid state between steric and electronic influences which could be more significant if there were larger substituents in the *ortho* positions. In solution however, the phenoxide ligand is rotating rapidly on the NMR time scale as only one methyl resonance is observed. π-Donation is maximised in the complex apparently by having a terminal phenoxide ligand rather than a weaker π-donor chloro ligand. Overall the bonding situation in solution for the terminal phenoxide is reflected by the *ipso* carbon resonance in the $^{13}C\text{-}\{^1H\}$ NMR spectrum which appears at δ 164.16.

Several exploratory reactions were carried out to determine the reactivity of **2**. The chloro bridge remains intact after dissolving the solid in thf (tetrahydrofuran) or diethyl ether but addition of pyridine (py) gave $[WOCl_3(OC_6H_3Me_2\text{-}2,6)(py)]$ as shown by a 1:1 ratio of phenoxide and py ligands in the ^1H NMR spectrum. Insertion of carbon monoxide into the M—O phenoxide bond did not occur, even under pressure with heating in benzene while reaction with *tert*-butylisocyanate yielded a mixture of products. Reduction with 2 equiv. of Na/Hg amalgam in the presence of trimethylphosphine gave an unstable complex identified as $[WOCl(OC_6H_3Me_2\text{-}2,6)(PMe_3)_3]$ on the basis of its ^1H NMR spectrum. This showed a 1:3 phenoxide to PMe_3 ligand ratio with a triplet and doublet in a 2:1 ratio for the phosphines thus indicating a *mer* geometry [11].

In an attempt to resolve the issue of conflict between electronic and steric influences suggested by the X-ray crystal structure of **2**, an excess of $[WOCl_4]$ was reacted with phenols bearing larger substituents in the 2,6 positions of the phenyl ring. Reaction with 2,6-di-*iso*-propylphenylphenol gave the complex $[WOCl_3(OC_6H_3Pr^i_2\text{-}2,6)]_x$ **3**, for which NMR spectra showed a single species with an *ipso* carbon resonance at δ 161.34. When the complex was allowed to stand for several days in the solid state or heated in a solvent, NMR spectra and elemental analysis showed the presence of the bis-phenoxide complex $[WOCl_2(OC_6H_3Pr^i_2\text{-}2,6)]_x$.* Indeed NMR spectra of **2**, left to stand for several days at room temperature, also showed the presence of the analogous bis-phenoxide complex.

Reaction of 2,6-di-*tert*-butyl-4-methylphenol, or the trimethylsilyl ether derivative, with excess $[WOCl_4]$ again led to a purple solid but NMR spectra indicated one of the *tert*-butyl groups had been removed. We believe the complex is $[WOCl_3(OC_6H_3Bu^t\text{-}2\text{-}Me\text{-}4)]_x$ but it also appears to form a bis-phenoxide on standing. Lithium 2,6-di-*tert*-butyl-4-methylphenoxide reacted with an excess of $[WOCl_4]$ to form a single product with an *ipso* carbon resonance at δ 165.07 which is apparently $[WOCl_3(OC_6H_2Bu^t_2\text{-}2,6\text{-}Me\text{-}4)]_x$ **4**. However NMR spectra show that on recrystallisation or allowing the complex to stand, de-*tert*-butylation and the formation of the bis-phenoxide complexes takes place.

The ^1H and $^{13}C\text{-}\{^1H\}$ NMR spectra of a freshly prepared sample of **4** show two resonances for the *tert*-butyl groups. This suggests a structure similar to that of the dimeric complex **2** where the phenoxide ligand does not rotate about the asymmetric centre. The chemical shift difference, Δ, of the two non-equivalent *tert*-butyl groups in the ^1H NMR spectrum show a significant solvent dependence, on changing $CDCl_3$ to the more anisotropic toluene-d^8 (Δ_{CDCl_3} = 0.006 ppm; $\Delta_{toluene\text{-}d^8}$ = 0.15 ppm). The non-equivalent aromatic protons display characteristic first order splitting patterns with a coupling constant typical of a *meta* arrangement (1.9 Hz). Variable temperature ^1H NMR spectral studies in toluene-d^8 showed the *tert*-butyl group proton resonances broadened but did not coalesce up to the boiling point of the solvent (110°C) indicating the *tert*-butyl groups effectively lock the phenoxide into a specific conformation. In contrast, the spectra of the *iso*-propyl and methyl analogues, **3** and **2**, show the phenoxides are free to rotate.

* A range of bis phenoxide complexes have been prepared and will be reported at a later date.

EXPERIMENTAL

Elemental analysis were obtained by Dr A. G. Cunninghame and associates, University of Otago, New Zealand. All reactions and subsequent manipulations were carried out under dry, oxygen-free nitrogen using standard bench-top techniques. $[WOCl_4]$ was prepared by reaction of H_2WO_4 in thionyl chloride [13] and phenols were used as received. The trimethylsilylethers were prepared by reacting sodium amide with the appropriate phenol in diethyl ether, adding chlorotrimethylsilane and fractionally distilling the product. Hexane and diethyl ether were dried over and distilled from sodium wire/benzophenone under nitrogen and dichloromethane from finely ground calcium hydride. ^{1}H NMR (400.14 MHz) and ^{13}C-$\{^1$H$\}$ NMR (100.6 MHz) spectra were recorded on a Bruker AM400 spectrometer.

Preparation of $[WOCl_3(C_6H_4Bu^t\text{-}4)]_x$ (**1**)

A solution of *p-tert*-butylphenol (0.30 g, 2.0 mmol) in dichloromethane (25 cm^3) was added to a solution of $[WOCl_4]$ (1.71 g, 5.0 mmol) in diethyl ether (25 cm^3) and dichloromethane (40 cm^3) and the resulting purple solution stirred overnight. Removal of the solvent followed by drying *in vacuo* afforded a purple amorphous solid which was extracted into hexane (40 cm^3) and filtered through celite. Removal of the solvent afforded the analytically pure complex. Yield 0.82 g (90%) of **1** as a moisture-sensitive purple powder. ^{1}H NMR ($CDCl_3$) δ, 1.34 (s, 9H, ^{t}Bu), 7.18 (d, 2H$_m$, $^3J_{HH}$ = 8.7 Hz), 7.54 (d, 2H$_o$, $^3J_{HH}$ = 8.7 Hz). ^{13}C-$\{^1$H$\}$ NMR ($CDCl_3$) δ 31.48 (CMe_3), 34.75 (CMe_3), 120.14 and 126.43 (C_o and C_m), 155.03 (C_p), 160.29 (C_{ipso}). Found: C, 26.67; H, 2.89. Calc. for $C_{10}H_{13}Cl_3O_2W$: C, 26.37; H, 2.89%.

Preparation of $[WOCl_2(\mu\text{-}Cl)(O\text{-}C_6H_3Me_2\text{-}2,6)]_2$ (**2**)

Method A. A solution of 2,6-dimethylphenol (0.45 g, 3.68 mmol) in diethyl ether (20 cm^3) was added dropwise to a solution of $[WOCl_4]$ (1.75 g, 5.12 mmol) in diethyl ether (50 cm^3) and the resulting purple solution stirred overnight. The workup was identical to that of **1** using hexane as the extraction solvent. Removal of the solvent afforded analytically pure **2** as a moisture-sensitive purple glassy solid (1.5 g, 95%) which was recrystallised from hexane at -20°C. ^{1}H NMR ($CDCl_3$) δ, 2.66 (s, 6H, 2Me), 6.95 (d, 1H$_p$, $^3J_{HH}$ = 7.6 Hz), 7.23 (d, 2H$_m$, $^3J_{HH}$ = 7.6 Hz). ^{13}C-$\{^1$H$\}$ NMR ($CDCl_3$) δ, 17.19 (Me), 128.34 (C_m), 132.61 (C_p), 134.25 (C_o), 164.16 (C_{ipso}). Found: C, 22.44; H, 2.12. Calc. for $C_{16}H_{18}Cl_6O_4W_2$: C, 22.48; H, 2.12%.

Method B. A solution of 2,6-dimethylphenyltrimethylsilylether (0.71 g, 3.65 mmol) in diethyl ether (15 cm^3) was added dropwise to a solution of $[WOCl_4]$ (3.13 g, 9.16 mmol) in diethyl ether (70 cm^3) and the mixture stirred overnight. Workup as for method A afforded an identical product to method A. Yield 1.44 g (92%).

Preparation of $[WOCl_3(OC_6H_3Pr^i_2\text{-}2,6)]_x$ (**3**)

In an analogous procedure to that of **1**, $[WOCl_4]$ (1.5 g, 4.39 mmol) and 2,6-di-*iso*-propylphenol (0.50 g, 2.80 mmol) afforded 1.2 g (92%) of **3** as a moisture-sensitive purple wax. ^{1}H NMR ($CDCl_3$) δ, 1.35 (d, 12H, $CHMe_2$, $^3J_{HH}$ = 6.7 Hz), 3.08 (sept, 2H, $2CHMe_2$, $^3J_{HH}$ = 6.7 Hz), 7.10 (t, 1H$_p$, $^3J_{HH}$ = 7.7 Hz), 7.31 (d, 2H$_m$, $^3J_{HH}$ = 7.7 Hz). ^{13}C-$\{^1$H$\}$ NMR ($CDCl_3$) δ, 23.92 ($CHMe_2$), 30.20 ($CHMe_2$), 123.83 (C_m), 133.25 (C_p), 145.15 (C_o), 161.34 (C_{ipso}). Found: C, 26.32; H, 3.47. Calc. for $C_{12}H_{17}Cl_3O_2W$: C, 29.81; H, 3.54%.

Preparation of $[WOCl_3(OC_6H_2Bu^t_2\text{-}2,6\text{-}Me\text{-}4)]_x$ (**4**)

A solution of lithium 2,6-di-*tert*-butyl-4-methylphenoxide was prepared by the addition of *n*-BuLi (1.8 M, 1.6 cm^3, 2.88 mmol) in hexane to a solution 2,6-di-*tert*-butyl-4-methylphenol (0.62 g, 2.81 mmol) in diethyl ether (30 cm^3) at 0°C followed by stirring for 4 hours at room temperature. This solution was then added dropwise to a solution of $[WOCl_4]$ (1.75 g, 5.12 mmol) in diethyl ether (50 cm^3) at -78°C over a period of 20 minutes then stirred at room temperature overnight. After removal of the solvent and drying *in vacuo*, the purple wax was washed with cold (-78°C) hexane (10 cm^3) and further dried. Workup as for **1** afforded 1.0 g (68%) of **4** as a moisture-sensitive waxy solid. ^{1}H NMR ($CDCl_3$) δ, 1.55 (s, 9H, Bu^t), 1.55 (s, 9H, Bu^t), 2.84 (s, 3H, Me), 7.23 (d, 1H$_m$, $^4J_{HH}$ = 1.9 Hz), 7.27 (d, 1H$_m$, $^4J_{HH}$ = 1.9 Hz). ^{13}C-$\{^1$H$\}$ NMR ($CDCl_3$) δ, 30.31 (Me), 30.59 (CMe_3), 34.10 (CMe_3), 35.54 (CMe_3), 36.03 (CMe_3), 125.56 and 127.36 (C_m), 144.21 (C_p), 147.49 and 147.73 (C_o), 165.07 (C_{ipso}).

Crystallography

Data were collected on a Siemens SMART diffractometer. The data collection covered a nominal sphere of reciprocal space, by a combination of four sets of exposures. Each set had a different phi angle for the crystal and each exposure covered 0.3° in α. Coverage of the unique data set is at least 98% complete to 56° in 2θ. Crystal decay was monitored by repeating the initial frames at the end of data collection and analysing the duplicate reflections. Unit cell parameters were obtained by least squares fit of all data with $I > 10\sigma(I)$. Lorentz and polarisation reflections were applied and absorption corrections by the method of Blessing [14].

The structure was solved by Patterson and Fourier techniques and refined by full matrix least squares.

All non-hydrogen atoms were allowed to assume anisotropic thermal motion. Hydrogen atoms were placed geometrically and refined with a riding model with U_{iso} constrained to 1.2 times U_{eq} of the carrier atom. Data collection and refinement parameters are given in Table 2 and Table 1 lists important bond lengths and angles. The structure is illustrated in Fig. 1 which gives the numbering scheme. Programs used were SHELXS [15] for structure solution and SHELXL [16] for refinement.

CONCLUSIONS

This work shows that monophenoxy derivatives of $[WOCl_4]$ can be prepared but the complexes are not particularly stable. This feature seems to increase as the size of the substituents in the 2,6-positions of the phenyl ring become larger. Methyl and *iso*-propyl substituents allow rapid rotation of the phenoxide ligand to occur but *tert*-butyl groups lock this process. This could well be a factor in the debutylation which takes place on standing, and may be related to similar debutylations of 2,6-di-*tert*-butyl substituted phenols initiated by strong Lewis acids such as $AlCl_3$ which is utilised extensively in phenol chemistry [12]. Overall, these monophenoxy-oxo complexes do not appear to rate as potential catalysts due to their inherent instability.

REFERENCES

1. Kerschner, J. L., Torres, E. M., Fanwick, P. E. and Rothwell, I. P., *Organometallics*, 1989, **8,** 1424 and refs therein.
2. Quignard, F., Leconte, M. and Basset, J. M., *J. Mol. Catal.*, 1986, **36,** 13.
3. Nakayama, Y., Mashima, K. and Nakamura, A., *J. Chem. Soc., Chem. Commun.*, 1992, 1496; Bell, A., *J. Mol. Catal.*, 1992, **76,** 165.
4. Quignard, F., Leconte, M., Basset, J. M., Hsu, L. H., Alexander, J. J. and Shore, S. G., *Inorg. Chem.*, 1987, **26,** 4272.
5. Ashcroft, B. R., Clark, G. R., Nielson, A. J. and Rickard, C. E. F., *Polyhedron*, 1986, **5,** 2081.
6. Nugent, W. A. and Mayer, J. M., *Metal–Ligand Multiple Bonds*, Wiley, New York (1988).
7. Bates, P. R., Nielson, A. J. and Waters, J. M., *Polyhedron*, 1987, **6,** 163.

Table 2. Data collection and processing parameters for **2**

Formula	$C_{16}H_{18}Cl_8O_4W_2$
Molecular weight	427.35
Crystal system	Triclinic
Space group	P-1
a (Å)	8.199(5)
b (Å)	8.286(5)
c (Å)	9.057(3)
I (°)	109.88(6)
θ (°)	90.89(6)
K (°)	102.37(5)
V (Å^3)	562.6(5)
Z	2
d(calc) (g cm^{-3})	2.523
F(000)	396
T (mm^{-1})	10.95
Radiation Mo-K_α (Monochromatic) Σ (Å)	0.71069
Temperature (K)	203
Diffractometer	Siemens SMART
Scan Technique	Area detector
2Π (min–max) (°)	2.4–28.3
h, k, l range	$-10 \leqslant h \leqslant 10$, $-10 \leqslant k \leqslant 10$, $-11 \leqslant l \leqslant 11$
No. of reflections	4351
No. of independent reflections	2486 R_{int} 0.0256
No. of observed reflections $I > 2[(I)]$	2449
Crystal size (mm)	0.43 × 0.32 × 0.24
A (min–max)	0.080–0.184
Least squares weights (a, b)	0.0473, 2.01
No. of variables in LS	127
Goodness of fit on F^2	1.084
Function minimised	$\Sigma w(F_o^2 - F_c^2)^2$
R and $wR2$ (obs. data)	0.0316 0.0837
Peak height in final density map (min–max)	eÅ^{-3} +1.98–2.06

$R = \Sigma \|F_o| - |F_c\| / \Sigma |F_o| \Sigma\ wR2 = \{\Sigma[w(F_o^2 - F_c^2)^2] / \Sigma\{w(F_o^2)^2]\}^{1/2}$
$w = 1.0/[^2(F_o^2) + a*P^2 + b*P]$, $P = (F_o^2 + 2F_c^2)/3$.

8. Herrmann, W. A., Thiel, W. R. and Herdtweek, E., *Chem. Ber.*, 1990, **123,** 271.
9. Clegg, W., Errington, R. J., Hockless, D. C. R. and Redshaw, C., *J. Chem. Soc., Dalton Trans.*, 1993, 1965.
10. Wigley, D. E., *Prog. Inorg. Chem.*, 1994, **42,** 239.
11. Clark, G. R., Nielson, A. J. and Rickard, C. E. F., *J. Chem. Soc., Dalton Trans.*, 1995, 1907.
12. Masashi, M. T., Watanabe, H. and Tsuge, O., *Org. Prep. Proced. Int.*, 1974, **6,** 117; Masashi, M. T. and Takehiko, Y., *Org. Prep. Proced. Int.*, 1978, **10,** 143; Masashi, M. T. and Takehiko, Y., *J. Org. Chem.*, 1979, **44,** 3037.
13. Nielson, A. J. and Anderson, R. A., *Inorg. Synth.*, 1985, **23,** 195.
14. Blessing, R. H., *Acta Cryst.*, 1995, **A51,** 33.
15. Sheldrick, G. M., SHELXS, Institut Fur Anorganisch Chemie, Universitat Gottingen, Germany (1990).
16. Sheldrick, G. M., SHELXL-93, Institut Fur Anorganisch Chemie, Universitat Gottingen, Germany (1990).

Pergamon

PII: S0277-5387(97)00290-8

Polyhedron Vol. 17, No. 5–6, pp. 857–867, 1998
© 1998 Elsevier Science Ltd
All rights reserved. Printed in Great Britain
0277-5387/98 $19.00+0.00

Pyridine, isocyanide, carbodiimide and allene adducts of hexakis(trifluoromethyl *t*-botoxy)ditungsten. A comparison of ligand binding to $W_2(O^tBu)_6$ and $W_2(OCMe_2CF_3)_6$†

Theodore A. Budzichowski, M. H. Chisholm,* Kristen Folting, John C. Huffman, William E. Streib and Darin B. Tiedtke

Department of Chemistry and Molecular Structure Center, Indiana University, Bloomington, IN 47405, U.S.A.

(Received 2 May 1997; accepted 23 June 1997)

Abstract—$W_2(OR)_6$ compounds, where R = ^{t}Bu and CMe_2CF_3, both reversibly bind pyridine in hydrocarbon solvents to form adducts $W_2(OR)_6L_2$. Pyridine binds more strongly to the fluoroalkoxide but the structural parameters of the compounds $W_2(OCMe_2CF_3)_6(C_6H_5N)_2$ and $W_2(O^tBu)_6(4\text{-}CH_3C_6H_4N)_2$ reveal an essentially identical $W_2O_6N_2$ core with W—W = 2.39(1) Å, W—O = 1.92–1.95 Å and W—N = 2.26(1) Å. Both compounds were crystallographically characterized in the space group $C2/c$ and each molecule has rigorous C_2 symmetry. Allene and 1,3-di-*p*-tolylcarbodiimide form 1 : 1 adducts with $W_2(OCMe_2CF_3)_6$ in which the substrate is bound parallel to the M-M axis, i.e. μ-η^2,η^2-C_3H_4 and μ-η^2,η^2-ArNCNAr-$W_2(OCMe_2CF_3)_6$. Also $W_2(OCMe_2CF_3)_6$ and $W_2(OSi^tBuMe_2)_6$ bind two equivalents of xylylisocyanide to afford $W_2(OR)_6(\eta^1\text{-CNAr})_2$. For $W_2(OCMe_2CF_3)_6(\eta^1\text{-CNAr})_2$, the molecular structure has been determined by X-ray crystallography and shows a nearly eclipsed central $W_2O_6C_2$ skeleton with W—W = 2.44(1) Å, W—O = 1.94(1) Å (av.) and W—C = 2.14(1) Å, whereas the W—W—O angles span the range 105–114°, the W—W—C angles are 83(1)°. Similarly, $W_2(OCMe(CF_3)_2)_4(NMe_2)_2$ forms a *bis* adduct upon reaction with the isocyanide. However, the molecular structure of $W_2(OCMe(CF_3)_2)_4(NMe_2)_2(\eta^1\text{-CNAr})_2$ shows a staggered arrangement of the two ligands about the ditungsten center where W—W = 2.382(1) Å, W—O = 2.00(1) Å (av.), W—N = 1.93(1) Å (av.) and W—C = 2.14(1) Å (av.) with a C—W—W—C dihedral angle of 41.9°. These reactions and their products are compared for $W_2(OR)_6$ compounds where R = ^{t}Bu, ^{t}BuMe$_2$Si and CMe_2CF_3. © 1998 Elsevier Science Ltd. All rights reserved

Keywords: tungsten; M-M triple bonds; alkoxides; isocyanide; carbodiimide; allene.

The reactivity of a metal center is greatly influenced by its attendant ligands and perhaps nowhere is this more apparent than in catalysis. In our studies of the reactivity of compounds containing $(M{\equiv}M)^{6+}$ bonds we find that the nature of the metal, Mo versus W, and the attendant ligand set greatly influence reactivity but in a way in which we do not yet fully understand. For example, $W_2(O^tBu)_6$ and NO react in the presence of pyridine (py) to give $W(O^tBu)_3(NO)(py)$ [1] by cleavage of the W—W triple bond whereas NO and $W_2(OSi^tBuMe_2)_6$ yield N_2 and oxotungsten siloxides [2]. $Mo_2(O^tBu)_6$ dissolves in acetonitrile whereas $W_2(O^tBu)_6$ and MeC≡N react virtually instantaneously at room temperature to give $(^tBuO)_3W{\equiv}N$ and $(^tBuO)_3W{\equiv}CMe$ [3]. $W_2(OCMe_2CF_3)_6$ and MeC≡N on the other hand react in solution to give an equilibrium wherein acetonitrile forms a σ- or η^1-N bound adduct, eq. (1) [4].

$$W_2(OCMe_2CF_3)_6 + 2MeC{\equiv}N \rightleftharpoons W_2(OCMe_2CF_3)_6(NCMe)_2 \quad (1)$$

While some of these remarkable differences in reactivity may be traced to thermodynamics, we are inclined to the view that kinetic factors are also important if not the dominant factors influencing reactivity

* Author to whom correspondence should be addressed.

† Dedicated to Professor D. C. Bradley, a life long friend and mentor.

[5]. Thus the frontier orbital energies of the substrates and metal centers involved are most significant. In this paper we compare further some reactivity studies of $W_2(OCMe_2CF_3)_6$, and other W_2^{6+} complexes supported by poorer π-donors, with the closely related compound $W_2(O^tBu)_6$.

RESULTS AND DISCUSSION

Syntheses and reactivity studies

Pyridine binds to both $W_2(O^tBu)_6$ and $W_2(OCMe_2CF_3)_6$ in hydrocarbon solutions. By ^1H NMR spectroscopy the binding is seen to be reversible according to eq. (2). The position of the equilibrium lies in favor of the binding to the trifluorobutoxide compound but an accurate measurement of K_{eq} has not been determined by these NMR studies. The equilibrium is dynamic on the NMR time-scale as is rotation about the M—M bond axis and for R = ^{t}Bu these are not frozen out until *ca* -30°C in toluene-d_8.

$$W_2(OR)_6 + 2py \rightleftharpoons W_2(OR)_6(py)_2 \qquad (2)$$

Crystals suitable for an X-ray study were obtained for $W_2(O^tBu)_6$(4-Me-py)$_2$ from hexane and for $W_2(OCMe_2CF_3)_6(py)_2$ from benzene. Both compounds are dark brown, hydrocarbon-soluble, air-sensitive crystalline compounds.

Allene, $CH_2{=}C{=}CH_2$, and 1,3-di-*p*-tolylcarbodiimide form 1 : 1 adducts with $W_2(OCMe_2CF_3)_6$ while $W_2(OSi^tBuMe_2)_6$ is unreactive with these substrates. The new 1 : 1 adducts are green, hydrocarbon-soluble, air-sensitive crystalline compounds. Formation of these 1 : 1 adducts parallels the behavior of $W_2(O^tBu)_6$ [6]. However, the compound $W_2(O^tBu)_6(C_3H_4)$ is thermally unstable and, in solution, reacts to give the products derived from propyne, namely $W(O^tBu)_3$(CMe) and $W(O^tBu)_3$(CH) though that latter compound can only be detected in solution because it rapidly decomposes in the absence of a Lewis base such as py or quinuclidine [7]. Further reaction with allene gives the more thermally stable compound $W_2(O^tBu)_6(\mu\text{-}\eta^1,\eta^3\text{-}C_3H_4)(\eta^2\text{-}C_3H_4)$ [6a]. No such reactivity is observed for $W_2(OCMe_2CF_3)_6(C_3H_4)$, and the 1:1 adduct is unreactive in the presence of excess allene.

$W_2(OCMe_2CF_3)_6$, $W_2(OSi^tBuMe_2)_6$ and $W_2(OCMe(CF_3)_2)_4(NMe_2)_2$ react with aryl isocyanides to form bis adducts. For the fluoroalkoxide complexes, the xylylisocyanide adducts formed crystals suitable for X-ray studies. The coordination of the isocyanide ligand is evidently sufficiently strong that significant dissociation is not observed in solution at room temperature. The formation of the 2 : 1 adducts in the reactivity of these alkoxide supported W_2-complexes differs from the formation of the 1 : 1 adducts in the chemistry of $W_2(O^tBu)_6$. In the latter case, the isocyanide [8] and the carbonyl [9] form a bridge across the two metal atoms. The mixed amido-fluoroalkoxide compound $W_2(NMe_2)_2(OCMe(CF_3)_2)_6$ also forms a 2 : 1 adduct with xylylisocyanide and pyridine.

NMR and other spectral characterization data are given in the Experimental Section.

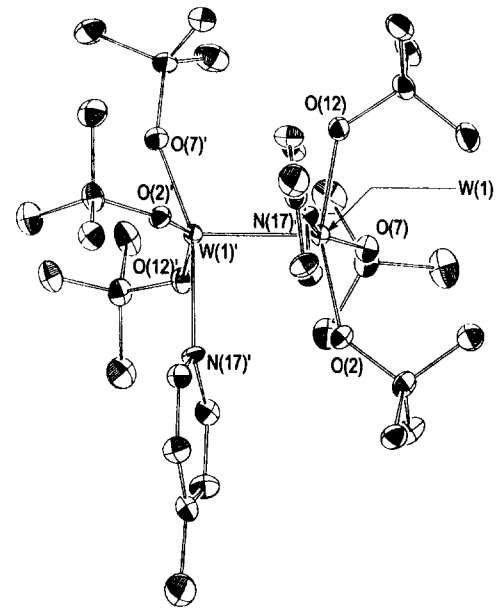

Fig. 1. An ORTEP drawing of the $W_2(O^tBu)_6$(4-Me-py)$_2$ molecule.

Crystal and molecular structures

$W_2(O^tBu)_6$(4-Me-py)$_2$ and $W_2(OCMe_2CF_3)_6(py)_2$ both crystallize in the space group $C2/c$ with crys-

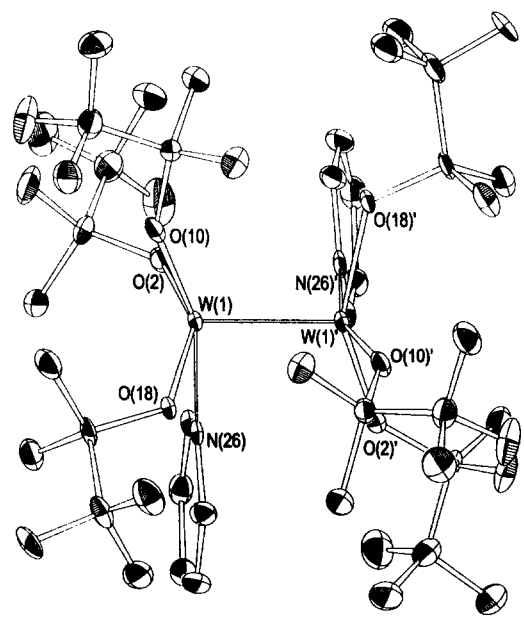

Fig. 2. An ORTEP drawing of the $W_2(OCMe_2CF_3)_6(py)_2$ molecule.

Table 1. Selected bond distances (Å) and angles (°) for $W_2(O^tBu)_6(4\text{-Me-py})_2$

W(1)′—W(1)	2.397(1)
W(1)—O(2)	1.941(4)
W(1)—O(7)	1.930(4)
W(1)—O(12)	1.941(4)
W(1)—N(17)	2.254(5)
O(2)—C(3)	1.445(7)
O(7)—C(8)	1.420(7)
O(12)—C(13)	1.446(7)

W(1)′—W(1)—O(2)	103.5(1)
W(1)′—W(1)—O(7)	112.3(1)
W(1)′—W(1)—O(12)	100.6(1)
W(1)′—W(1)—N(17)	88.4(1)
O(2)—W(1)—O(7)	92.5(2)
O(2)—W(1)—O(12)	151.0(2)
O(2)—W(1)—N(17)	82.4(2)
O(7)—W(1)—O(12)	93.1(2)
O(7)—W(1)—N(17)	159.3(2)
O(12)—W(1)—N(17)	82.3(2)
W(1)—O(2)—C(3)	136.8(4)
W(1)—O(7)—C(8)	152.5(4)
W(1)—O(12)—C(13)	132.2(3)
W(1)—N(17)—C(18)	121.8(4)
W(1)—N(17)—C(22)	123.3(4)

tallographically imposed C_2 symmetry. ORTEP drawings of $W_2(O^tBu)_6(4\text{-Me-py})_2$ and $W_2(OCMe_2(CF_3))_6(py)_2$ are given in Figs 1 and 2, respectively, and selected bond distances and bond angles are given in Tables 1 and 2. A view looking down the M—M axis for each molecule is given in Fig. 3.

Table 2. Selected bond distances (Å) and angles (°) for $W_2(OCMe_2CF_3)_6(py)_2$

W(1)—W(1)′	2.3903(8)
W(1)—O(2)	1.954(5)
W(1)—O(10)	1.923(5)
W(1)—O(18)	1.958(5)
W(1)—N(26)	2.273(7)
C—F	1.34 (av.)

W(1)′—W(1)—O(2)	106.6(2)
W(1)′—W(1)—O(10)	109.4(2)
W(1)′—W(1)—O(18)	102.7(1)
W(1)′—W(1)—N(26)	89.3(2)
O(2)—W(1)—O(10)	93.2(2)
O(2)—W(1)—O(18)	146.5(2)
O(2)—W(1)—N(26)	81.9(2)
O(10)—W(1)—O(18)	92.1(2)
O(10)—W(1)—N(26)	161.2(2)
O(18)—W(1)—N(26)	82.6(2)
W(1)—O(2)—C(3)	136.2(5)
W(1)—O(10)—C(11)	148.3(5)
W(1)—O(18)—C(19)	127.2(5)
W(1)—N(26)—C(27)	122.0(5)
W(1)—N(26)—C(31)	121.6(5)

The two molecules are seen to be remarkably similar in their solid-state structures. The W—W distances, 2.40(1) Å and the W—O distances, which range from 1.92 to 1.96 Å, are essentially identical within the 3σ criterion. Despite the more favorable binding of pyridine to $W_2(OCMe_2CF_3)_6$ this is not reflected in the W—N distances: 2.27(1) Å versus 2.25(1) Å for the 4-Me-pyridine ligand in $W_2(O^tBu)_6(4\text{-Me-py})_2$. However, once again within the criterion of 3σ these W—N distances have to be viewed equivalent. Thus, the structures of the pyridine adducts offer no insight to the rather different reactivities of the two $W_2(OR)_6$ compounds.

$W_2(OCMe_2CF_3)_6(4\text{-Me-}C_6H_4CNCC_6H_4\text{-4-Me})$ crystallized in the space group $P\bar{1}$ with a molecule of *n*-hexane at the crystallographic center of symmetry. The *n*-hexane was refined at 78% partial occupancy and the three carbon atoms in the asymmetric unit of this solvent molecule showed some disorder. Despite these problems the structure of the ditungsten complex was refined satisfactorily, at least with respect to

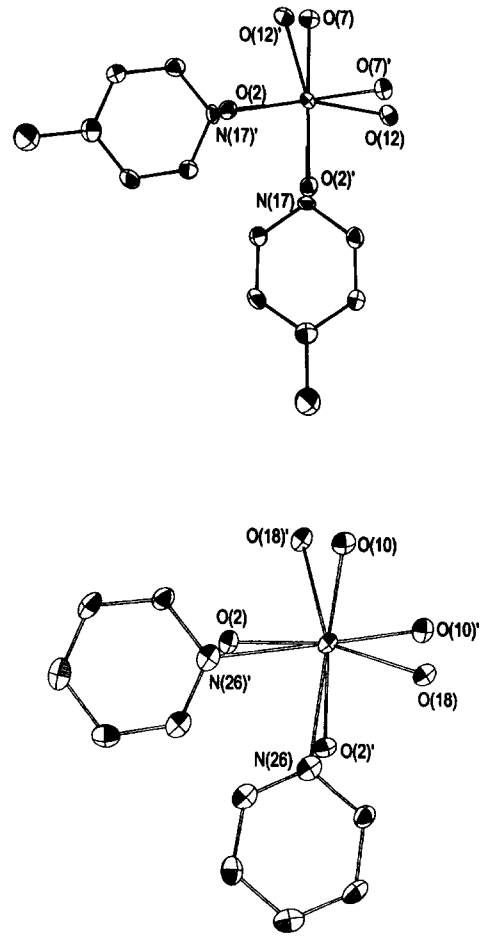

Fig. 3. Views of the central skeleton of the $W_2(O^tBu)_6(4\text{-Me-py})_2$ and $W_2(OCMe_2CF_3)_6(py)_2$ molecules looking down the M—M—axis.

gross features of the molecular geometry. An ORTEP drawing of the molecule is given in Fig. 4. The bridging carbodiimide lies parallel to the M—M axis in a $\mu\eta^2,\eta^2$ manner. This imposes an eclipsed geometry for the O_3WWO_3 skeleton. Selected bond distances and bond angles are given in Table 3.

The W—W distance of 2.52 Å is the range expected for a $(W{\equiv}W)^{8+}$ moiety consistent with the view that the carbodiimide is partially reduced. This is also reflected in the η^2-C—N distances of 1.28 Å and the N—C—N angle of 155°. The W—N distances, 2.08(1) Å (av.) and the W—C distances 2.19(1) Å (av.) also imply a strongly bound carbodiimide ligand. There is very little difference in the metrical parameters reported for $W_2(O^tBu)_6(\mu\eta^2,\eta^2\text{-ArNCNAr})$ by Cotton *et al.* [6b] with those found for the present structure.

$W_2(OCMe_2CF_3)_6(\mu\text{-}CH_2CCH_2)$. An ORTEP view of the molecule is given in Fig. 5 with selected bond distances and bond angles listed in Table 4. Superficially, the molecule is similar to the carbodiimide structure described previously but the W—W distance of 2.59 Å is significantly longer implying a greater degree of oxidation of the ditungsten center. Also the C—C—C angle of 141° deviates more from linearity than does the N—C—N angle. The C—C distances of 1.46 Å (av.) are comparable to Csp^2–Csp^2 single bond distances, certainly greatly reduced from those in free allene. The structure resembles in every way that of $W_2(O^tBu)_6(\mu\eta^2,\eta^2\text{-}C_3H_4)$ reported earlier [6a]. The W—O distances of the OR ligands trans to the W—C bonds are longer than those that are mutually trans implying that the allene ligand exerts a higher trans-influence [10] than the fluoroalkoxide.

$W_2(OCMe_2CF_3)_6(CNxylyl)_2$. An ORTEP drawing of the molecule is given in Fig. 6 and selected bond distances and bond angles are given in Table 5. The molecule has virtual but not crystallographically imposed C_2 symmetry. The W—W distance of 2.44(1) Å is longer than that expected for a triple bond but only slightly, c.f. the pyridine adducts described earlier. This can be understood in terms of the xylylisocyanide ligands acting as π-acceptor ligands. The central $W_2O_6C_2$ core is very similar to that seen for the $W_2(OCMe_2CF_3)_6(CO)_2$ molecule [11]. Note the

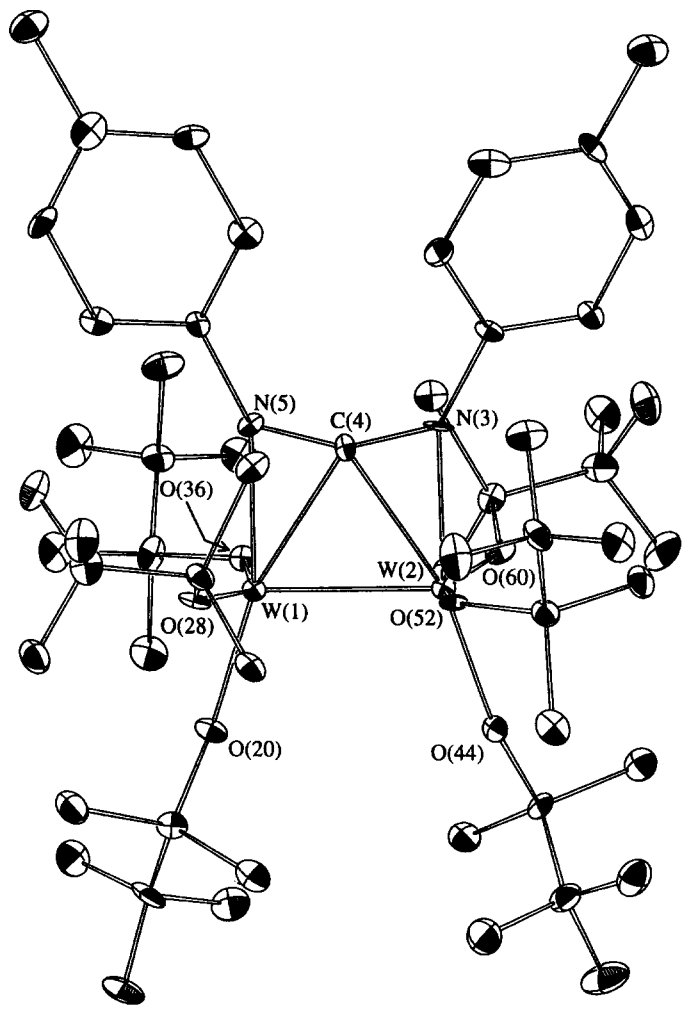

Fig. 4. An ORTEP drawing of the $W_2(OCMe_2CF_3)_6(\mu\text{-}4\text{-}Me\text{-}C_6H_4CNCC_6H_44\text{-}Me)$ molecule.

Table 3. Selected bond distances (Å) and angles (°) for $W_2(OCMe_2CF_3)_6(\mu\text{-}CH_2CCH_2)$

W(1)—W(2)	2.5930(6)
W(1)—O(6)	1.904(6)
W(1)—O(14)	1.936(6)
W(1)—O(22)	1.889(6)
W(1)—C(3)	2.118(9)
W(1)—C(4)	2.092(9)
W(2)—O(30)	1.889(6)
W(2)—O(38)	1.947(6)
W(2)—O(46)	1.898(6)
W(2)—C(4)	2.084(9)
W(2)—C(5)	2.144(9)
C—F	1.34(1) av.
C(3)—C(4)	1.464(12)
C(4)—C(5)	1.455(12)

W(2)—W(1)—O(6)	98.5(2)
W(2)—W(1)—O(14)	116.2(2)
W(2)—W(1)—O(22)	105.9(3)
W(2)—W(1)—C(3)	91.8(2)
W(2)—W(1)—C(4)	51.5(3)
O(6)—W(1)—O(14)	86.2(3)
O(6)—W(1)—O(22)	155.2(2)
O(6)—W(1)—C(3)	85.7(3)
O(6)—W(1)—C(4)	97.0(3)
O(14)—W(1)—O(22)	87.2(3)
O(14)—W(1)—C(3)	151.8(3)
O(14)—W(1)—C(4)	167.5(3)
O(22)—W(1)—C(3)	88.9(3)
O(22)—W(1)—C(4)	94.5(3)
C(3)—W(1)—C(4)	40.7(3)
W(1)—W(2)—O(30)	106.4(2)
W(1)—W(2)—O(38)	113.9(2)
W(1)—W(2)—O(46)	100.7(2)
W(1)—W(2)—C(4)	51.8(2)
W(1)—W(2)—C(5)	91.7(2)
O(30)—W(2)—O(38)	86.9(3)
O(30)—W(2)—O(46)	152.6(2)
O(30)—W(2)—C(4)	96.0(3)
O(30)—W(2)—C(5)	89.1(3)
O(38)—W(2)—O(46)	86.2(3)
O(38)—W(2)—C(4)	165.6(3)
O(38)—W(2)—C(5)	154.1(3)
O(46)—W(2)—C(4)	97.3(3)
O(46)—W(2)—C(5)	85.8(3)
C(4)—W(2)—C(5)	40.2(3)
W(1)—O(6)—C(7)	136.9(5)
W(1)—O(14)—C(15)	144.5(6)
W(1)—O(22)—C(23)	151.9(5)
W(2)—O(30)—C(31)	152.8(6)
W(2)—O(38)—C(39)	142.3(5)
W(2)—O(46)—C(47)	134.5(5)
W(1)—C(3)—C(4)	68.7(5)
W(1)—C(4)—W(2)	76.8(3)
W(1)—C(4)—C(3)	70.6(5)
W(1—C(4)—C(5)	148.0(7)
W(2)—C(4)—C(3)	145.9(7)
W(2)—C(4)—C(5)	72.1(5)
C(3)—C(4)—C(5)	141.3(8)
W(2)—C(5)—C(4)	67.7(5)

Table 4. Selected bond distances (Å) and angles (°) for $W_2(OCMe_2CF_3)_6(\mu\text{-}N(C\text{-}p\text{-tolyl})_2)$

W(1)—W(2)	2.5064(8)
W(1)—O(20)	1.888(8)
W(1)—O(28)	1.949(8)
W(1)—O(36)	1.913(7)
W(1)—N(5)	2.088(9)
W(1)—C(4)	2.19(1)
W(2)—O(44)	1.891(8)
W(2)—O(52)	1.922(8)
W(2)—O(60)	1.950(7)
W(2)—N(3)	2.066(9)
W(2)—C(4)	2.19(1)
C—F	1.34(1) (av.)
N(3)—C(4)	1.28(2)
N(5)—C(4)	1.28(2)

W(2)—W(1)—O(20)	109.2(3)
W(2)—W(1)—O(28)	99.1(2)
W(2)—W(1)—O(36)	109.2(2)
W(2)—W(1)—N(5)	89.9(3)
W(2)—W(1)—C(4)	55.2(3)
O(20)—W(1)—O(28)	88.7(3)
O(20)—W(1)—O(36)	89.0(3)
O(20)—W(1)—N(5)	160.7(4)
O(20)—W(1)—C(4)	164.3(4)
O(28)—W(1)—O(36)	150.7(3)
O(28)—W(1)—N(5)	85.2(3)
O(28)—W(1)—C(4)	92.7(4)
O(36)—W(1)—N(5)	87.4(3)
O(36)—W(1)—C(4)	97.2(4)
N(5)—W(1)—C(4)	34.8(4)
W(1)—W(2)—O(44)	109.7(2)
W(1)—W(2)—O(52)	108.4(3)
W(1)—W(2)—O(60)	98.8(2)
W(1)—W(2)—N(3)	89.8(3)
W(1)—W(2)—C(4)	55.1(3)
O(44)—W(2)—O(52)	90.0(3)
O(44)—W(2)—O(60)	88.9(3)
O(44)—W(2)—N(3)	160.4(4)
O(44)—W(2)—C(4)	164.7(4)
O(52)—W(2)—O(60)	151.5(3)
O(52)—W(2)—N(3)	86.2(4)
O(52)—W(2)—C(4)	96.2(4)
O(60)—W(2)—N(3)	85.5(4)
O(60)—W(2)—C(4)	92.3(4)
N(3)—W(2)—C(4)	34.7(4)
W(1)—O(20)—C(21)	146.8(7)
W(1)—O(28)—C(29)	127.5(7)
W(1)—O(36)—C(37)	148.5(7)
W(2)—O(44)—C(45)	147.2(7)
W(2)—O(52)—C(53)	149.2(7)
W(2)—O(60)—C(61)	126.7(7)
W(2)—N(3)—C(4)	78.0(7)
W(2)—N(3)—C(6)	148.8(8)
C(4)—N(3)—C(6)	132.5(1)
W(1)—N(5)—C(4)	76.9(7)
W(1)—N(5)—C(13)	150.4(8)
C(4)—N(5)—C(13)	131.9(1)
W(1)—C(4)—W(2)	69.8(3)
W(1)—C(4)—N(3)	137.0(9)
W(1)—C(4)—N(5)	68.3(6)
W(2)—C(4)—N(3)	67.2(6)
W(2)—C(4)—N(5)	138.0(9)
N(3)—C(4)—N(5)	154.7(12)

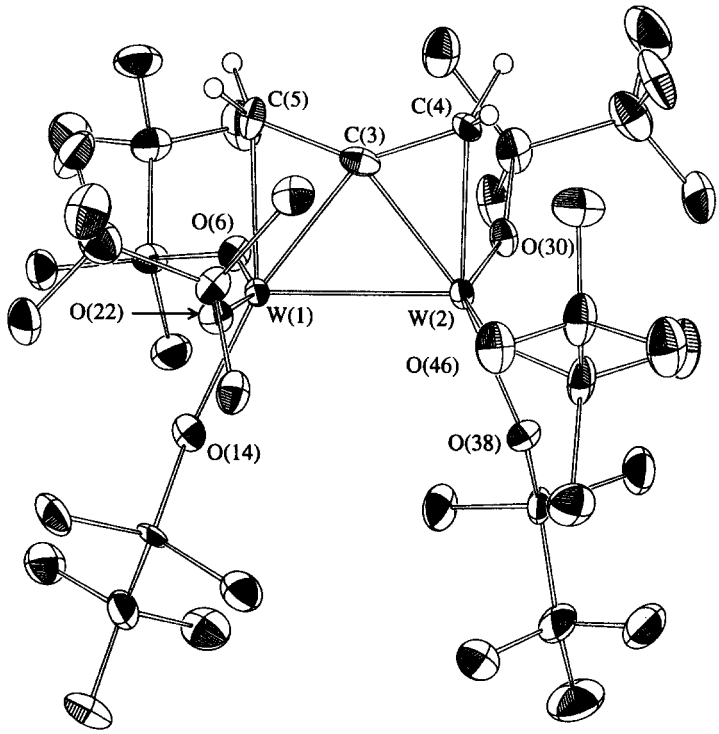

Fig. 5. An ORTEP drawing of the $W_2(OCMe_2CF_3)_6(\mu\text{-}CH_2CCH_2)$ molecule.

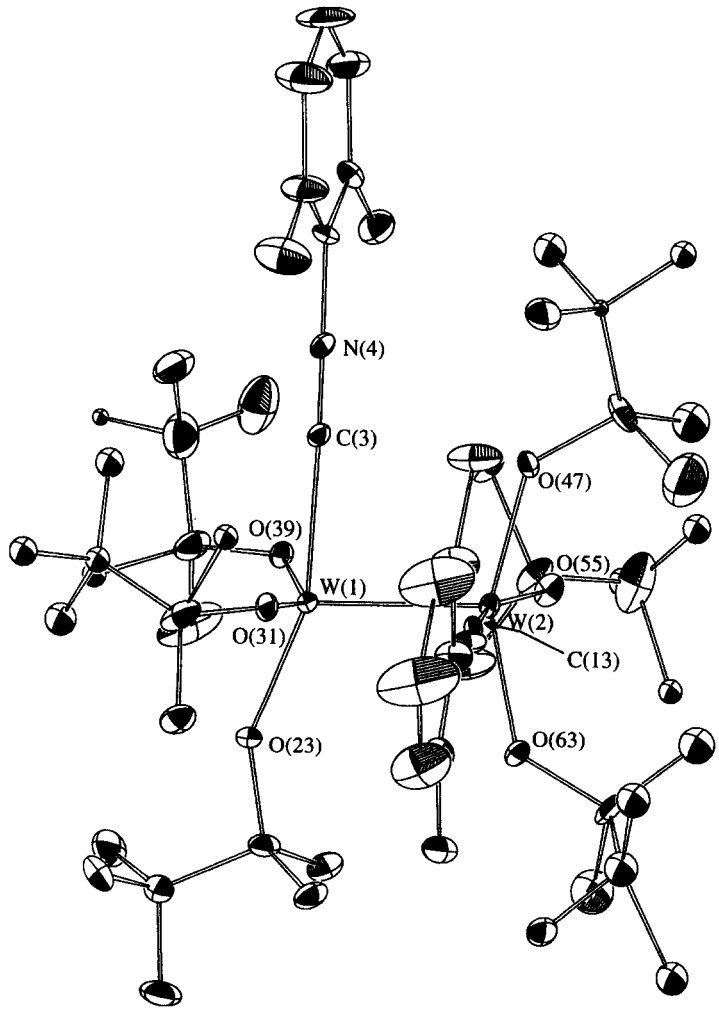

Fig. 6. An ORTEP drawing of the $W_2(OCMe_2CF_3)_6(CNxylyl)_2$ molecule.

Table 5. Selected bond distances (Å) and angles (°) for $W_2(OCMe_2CF_3)_6(NCxylyl)_2$

W(1)—W(2)	2.4427(6)
W(1)—O(23)	1.936(6)
W(1)—O(31)	1.933(6)
W(1)—O(39)	1.935(6)
W(1)—C(3)	2.152(9)
W(2)—O(47)	1.939(6)
W(2)—O(55)	1.937(6)
W(2)—O(63)	1.930(6)
W(2)—C(13)	2.143(10)
N(4)—C(3)	1.15(1)
N(14)—C(13)	1.160(1)
W(2)—W(1)—O(23)	113.1(2)
W(2)—W(1)—O(31)	100.3(2)
W(2)—W(1)—O(39)	106.2(2)
W(2)—W(1)—C(3)	86.3(2)
O(23)—W(1)—O(31)	92.3(3)
O(23)—W(1)—O(39)	91.9(3)
O(23)—W(1)—C(3)	160.5(3)
O(31)—W(1)—O(39)	149.0(3)
O(31)—W(1)—C(3)	82.6(3)
O(39)—W(1)—C(3)	83.3(3)
W(1)—W(2)—O(47)	101.6(2)
W(1)—W(2)—O(55)	114.1(2)
W(1)—W(2)—O(63)	105.0(2)
W(1)—W(2)—C(13)	84.3(2)
O(47)—W(2)—O(55)	92.2(3)
O(47)—W(2)—O(63)	148.3(3)
O(47)—W(2)—C(13)	82.1(3)
O(55)—W(2)—O(63)	92.3(3)
O(55)—W(2)—C(13)	161.6(3)
O(63)—W(2)—C(13)	83.8(3)
W(1)—O(23)—C(24)	147.9(6)
W(1)—O(31)—C(32)	133.1(7)
W(1)—O(39)—C(40)	141.5(8)
W(2)—O(47)—C(48)	131.2(6)
W(2)—O(55)—C(56)	148.1(6)
W(2)—O(63)—C(64)	134.1(6)
W(1)—C(3)—N(4)	178.0(8)
W(2)—C(13)—N(14)	176.5(8)

W—W—C angles are 83° (av.) and the dihedral angle between the two W—W—C planes is close to 90° which facilitates a mixing of W—W d_π and Wd_π—CNπ^* bonding as described for the dicarbonyl adduct previously [11]. A view looking down the M—M axis of the central $W_2O_6(CN)_2$ core is shown in Fig. 7.

$W_2(OCMe(CF_3)_2)_4(NMe_2)_2(CNxylyl)_2$. An ORTEP diagram of the molecule showing the atom numbering scheme is given in Fig. 8. Selected bond distances and angles are given in Table 6. The molecular structure contrasts with that seen for the *bis*-isocyanide and *bis*-carbonyl adducts of $W_2(OCMe_2CF_3)_6$ in that the core is made up of two staggered four coordinate W atoms, where the C(47)—W(1)—W(2)—C(57) angle is 41.9°. The W—W distance of 2.380(1) Å is only slightly

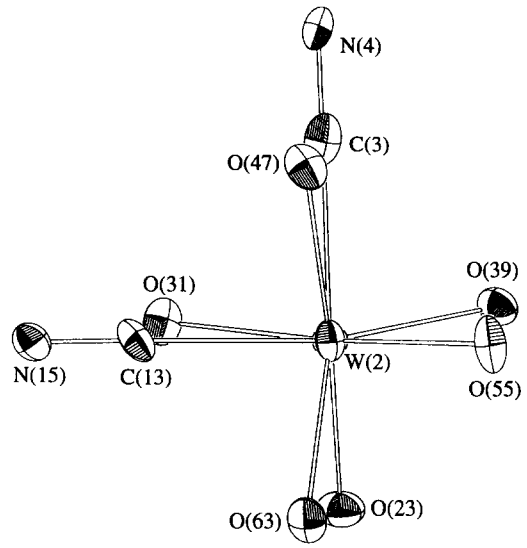

Fig. 7. A view of the central skeleton of the $W_2(OCMe_2CF_3)_6(CNxylyl)_2$ molecule looking down the M—M bond axis.

longer than that observed in $W_2(OCMe(CF_3)_2)_4(NMe_2)_2$ and significantly shorter than the W—W distances in the *bis*-carbonyl and *bis*-isocyanide adducts of $W_2(OCMe_2CF_3)_6$. The two W—W—C angles are 90.2(2)° and 88.6(2)°. The W—N distances of 1.93(1) Å (av.) and W—O distances of 2.00(2) Å (av.) are notably longer than in the parent compound $W_2(OCMe(CF_3)_2)_4(NMe_2)_2$ [12] which reflects the increase in coordination number at the metal center.

EXPERIMENTAL

General operating procedures for the manipulation of air-sensitive samples were observed.

Preparation of $[W_2(O^tBu)_6(py)_2]$. Pyridine (1 cm^3) was added to a solution of $W_2(O^tBu)_6$ [13] (153 mg, 0.190 mmol) in 10 cm^3 of dry, degassed benzene at 23°C. The solution was stirred at 23°C for 1 h and the solvent was reduced under vacuum. Crystallization in dry, degassed toluene at −20°C gave dark red microcrystals in 81% yield. The crystals obtained when using pyridine were not suitable for a single crystal X-ray study. The use of 4-Me-pyridine during the preparation did afford crystals (from hexanes) of $[W_2(O^tBu)_6(4\text{-Me-py})_2]$ (**1-Me**) suitable for study by X-ray analysis. ^{1}H NMR for **1** (300 MHz, C_7D_8, −30°C) δ = 8.43 (br. multiplets, 2H), 6.85 (br. multiplets, 1H), 6.55 (br. multiplets, 2H), 2.40 (18H), 1.53 (18H), 1.20 (18H). ^{1}H NMR for **1** (300 MHz, C_7D_8, 16°C) δ = 1.59 (54H). $^{13}C\{^1H\}$ NMR for **1** (75 MHz, C_7D_8, −30°C) δ = 151.3, 135.0, 122.5 (NC_5H_5); 82.0, 76.4, 74.4 ($C(CH_3)$); 34.8, 33.4, 33.1 ($C(CH_3)$).

Preparation of $[W_2(OCMe_2CF_3)_6(py)_2]$. Pyridine (1 cm^3) was added to a solution of $W_2(OCMe_2CF_3)_6$ [4] (170 mg, 0.15 mmol) in 10 cm^3 of dry, degassed benzene at 23°C. The solution was stirred at 23°C for 1 h

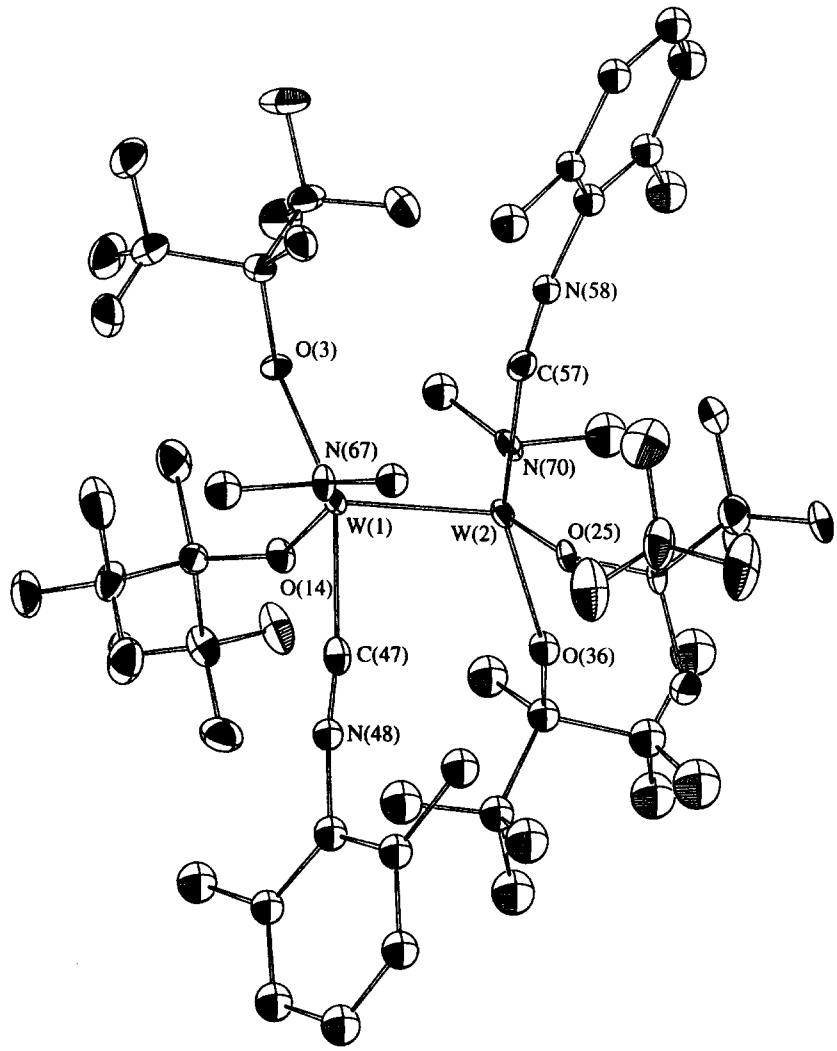

Fig. 8. An ORTEP drawing of the $W_2(OCMe(CF_3)_2)_4(NMe_2)_2(CNxylyl)_2$ molecule.

and the solvent was reduced under vacuum. Crystallization from dry, degassed benzene (65–23°C) gave X-ray quality black crystals in 68% yield. ^1H NMR (300 MHz, C_7D_8, −80°C) $\delta = 8.43$ (br. multiplets, 2H), 6.85 (br. multiplets, 1H), 6.55 (br. multiplets, 2H), 1.95 (6H), 1.50 (6H), 1.33 (6H), 1.31 (6H), 0.92 (6H), 0.86 (6H). $^{19}F\{^1H\}$ NMR (283 MHz, C_7D_8, 16°C, ext. ref. CF_3CO_2H $\delta = -78.45$) $\delta = -80.8$ (br. 12F), −82.2 (6F). $^{19}F\{^1H\}$ NMR (283 MHz, C_7D_8, −50°C, ext. ref. CF_3CO_2H $\delta = -78.45$) $\delta = -78.8$ (6F), −79.0 (6F), −80.1 (6H).

Preparation of $W_2(OCMe_2CF_3)_6(CN\text{-}2,6\text{-}Me_2C_6H_3)_2$. $W_2(OCMe_2CF_3)_6$ [4] (200 mg, 0.18 mmol) and xylylisocyanide (91 mg, 0.71 mmol) solids were added to a 30 cm^3 Schlenk flask in a nitrogen glove box. Hexanes (3 cm^3) were added and the solution was concentrated. Brown, tetragonal thin plates (199 mg, 81%) were obtained at −35°C. Recrystallization from Et_2O at −35°C yielded crystals for the X-ray study. ^1H NMR (300 MHz, C_7D_8, 23°C): δ 2.52 (s, 12H), 2.29 (s, 6H), 2.21 (s, 6H), 1.49 (s, 6H), 1.20 (s, 12H), 1.18 (s, 6H), 6.5–6.9 (br. multiplets 6H). $^{19}F\{^1H\}$ NMR (340 MHz, C_7D_8, 23°C): δ −75.9 (s, 6F), −76.2 (s, 6F), −84.4 (s, 6F).

Preparation of $W_2(OSi^tBuMe_2)_6(CN\text{-}2,6\text{-}Me_2C_6H_3)_2$. $W_2(OSi^tBuMe_2)_6$ [2] (25 mg, 0.022 mmol) and $CN\text{-}2,6\text{-}Me_2C_6H_3$ (34 mg, 0.22 mmol) were dissolved in 0.6 cm^3 of toluene-d_8 in an NMR tube. The kinetically labile **4** did not yield a crystalline compound. ^1H NMR (300 MHz, C_7D_8, −20°C): δ 6.6–7.1 (br, 6H), 2.0 (s, 12H), 1.16 (s, 18H), 1.06 (s, 18H), 0.943 (s, 18H), 0.34 (s, 6H), 0.33 (s, 6H), 0.26 (s, 18H), 0.24 (s, 6H).

Preparation of $W_2(OCMe(CF_3)_2)_4(NMe_2)_2(CN\text{-}2,6\text{-}Me_2C_6H_3)_2$. $W_2(OC(CF_3)_2Me)_4(NMe_2)_2$ [13] (150 mg, 0.13 mmol) and $CN\text{-}2,6\text{-}Me_2C_6H_3$ were combined in a 30 cm^3 Schlenk flask in a nitrogen glove box. THF (10 cm^3) was added to the flask followed by reduction in volume to concentrate the solution. Crystallization at −35°C gave bundles of deep red fibers which were separated by sublimation of excess isocyanide at 23°C to give 160 mg (85%). Recrystallization from CH_2Cl_2

Table 6. Selected bond distances (Å) and angles (°) for $W_2(NMe_2)_2(OCMe(CF_3)_2)_4(CNxylyl)_2$

W(1)—W(2)	2.3820(6)
W(1)—O(3)	2.003(5)
W(1)—O(14)	1.993(5)
W(1)—N(67)	1.933(6)
W(1)—C(47)	2.133(9)
W(2)—O(25)	2.018(5)
W(2)—O(36)	1.986(6)
W(2)—N(70)	1.926(7)
W(2)—C(57)	2.147(8)
C—F	1.34(1) (av.)
N(48)—C(47)	1.16(1)
N(58)—C(57)	1.42(1)

W(2)—W(1)—O(3)	114.8(2)
W(2)—W(1)—O(14)	102.4(2)
W(2)—W(1)—N(67)	104.5(2)
W(2)—W(1)—C(47)	88.6(2)
O(3)—W(1)—O(14)	87.2(2)
O(3)—W(1)—N(67)	95.4(3)
O(3)—W(1)—C(47)	156.4(3)
O(14)—W(1)—N(67)	149.0(3)
O(14)—W(1)—C(47)	84.4(3)
N(67)—W(1)—C(47)	80.9(3)
W(1)—W(2)—O(25)	108.4(2)
W(1)—W(2)—O(36)	113.3(2)
W(1)—W(2)—N(70)	99.3(2)
W(1)—W(2)—C(57)	90.2(2)
O(25)—W(2)—O(36)	84.0(2)
O(25)—W(2)—N(70)	149.5(3)
O(25)—W(2)—C(57)	80.7(3)
O(36)—W(2)—N(70)	96.80(26)
O(36)—W(2)—C(57)	155.1(3)
N(70)—W(2)—C(57)	86.7(3)
W(1)—O(3)—C(4)	143.8(5)
W(1)—O(14)—C(15)	140.2(5)
W(2)—O(25)—C(26)	139.3(5)
W(2)—O(36)—C(37)	145.2(5)
C(47)—N(48)—C(49)	173.0(8)
C(57)—N(58)—C(59)	172.3(8)
W(1)—N(67)—C(68)	134.6(5)
W(1)—N(67)—C(69)	114.1(5)

gave X-ray quality deep red cubes. ^{1}H NMR (300 MHz, C_7D_8, 80°C): δ 6.6–7.0 (br, 6H), 4.64 (s, 6H), 2.58 (s, 6H), 2.39 (s, 12H), 1.69 (s, 12H). ^{1}H NMR (300 MHz, C_7D_8, −40°C): δ 6.6–7.0 (br, 6H), 4.55 (s, 3H), 4.52 (s, 3H), 2.53 (s, 3H), 2.14 (s, 3H), 2.02 (s, 3H), 1.76 (s, 3H), 1.71 (s, 3H), 1.19 (s, 3H).

Preparation of $W_2(OCMe_2CF_3)_6(\mu,\eta^2,\eta^2\text{-}CH_2CCH_2)$. $W_2(OCMe_2CF_3)_6$ [4] (25 mg, 0.022 mmol) was dissolved in 0.6 cm^3 of C_7D_8 in an NMR tube equipped with a J. Young valve. Allene (10 equiv.) was transferred at −196°C to the NMR tube by means of a calibrated gas manifold. The reaction mixture was thawed and placed at −35°C for 24 h. Analysis by ^{1}H NMR spectroscopy at −20°C allows an estimated yield of 85% with the remaining tungsten containing compound being $W_2(OCMe_2CF_3)_6$. Addition of a large excess of allene (>20 equiv.) results in the formation of a transparent solid proposed to be polyallene. ^{1}H NMR (300 MHz, C_7D_8, −20°C): δ 1.66, 1.37, 1.04 (s, 12H), 7.57 (s, 4H). $^{13}C\{^1H\}$ NMR (75 MHz, C_7D_8, −20°C): δ 265.1, 95.0, 85.1 (q), 81.4 (q), 25.1 (s), 24.8 (s), 24.1 (s). $^{19}F\{^1H\}$ NMR (340 MHz, C_7D_8, −20°C): δ −80.4 (s, 6F), −81.0 (s, 12F).

Preparation of $W_2(OCMe_2CF_3)_6(\mu,\eta^2,\eta^2\text{-4-Me-C}_6H_4N{=}C{=}N{=}C_6H_4\text{-4-Me})$. $W_2(OCMe_2CF_3)_6$ [4] (275 mg, 0.244 mmol) 4-Me-C_6H_4-N=C=N-C_6H_4-4-Me (119 mg, 0.535 mmol) were combined in a 30 cm^3 Schlenk flask in a nitrogen atmosphere glove box. Hexanes (5 cm^3) were added to the Schlenk flask. Reduction of the volume followed by crystallization at −35°C afforded dark green cubes (280 mg, 85%) that were suitable for X-ray analysis. ^{1}H NMR (300 MHz, C_7D_8, 23°C): δ 6.99 (d, $^3J_{HH}$ = 32 Hz), 6.80 (d, $^3J_{HH}$ = 32 Hz), 1.85, 1.71, 1.46 (s, 12H). $^{19}F\{^1H\}$ NMR (340 MHz, C_7D_8, 23°C): δ −80.0 (s, 6F), −80.8 (s, 12F).

Single crystal X-ray crystallographic studies— General operating procedures and listings of programs have been previously given [14]. A summary of crystallographic data is given in Table 7. Complete listings of atomic coordinates have been deposited with the Cambridge Crystallographic Data Center.

CONCLUSIONS

The molecular structures of the pyridine, carbodiimide and allene adducts of $W_2(O^tBu)_6$ and $W_2(OCMe_2CF_3)_6$ are remarkably similar and belie the otherwise very different reactivities of the two complexes. This, of course, supports the view that structural data rarely provide much insight into reactivity. The relative thermal stability of the allene adduct reported here leads us to propose that the greater reactivity of the *t*-butoxide arises because the more basic ^{t}BuO ligand promotes an allene to propyne isomerization. That $W_2(OCMe_2CF_3)_6(\mu,\eta^2,\eta^2\text{-}CH_2CCH_2)$ does not react with additional allene to give a compound of the type $W_2(OR)_6(\mu,\eta^1,\eta^3\text{-}C_3H_4)(\eta^2\text{-}C_3H_4)$ as seen for R = ^{t}Bu may reflect the less easily oxidized and less π-basic W_2 core when supported by $(CF_3)Me_2CO$ ligands. This too may be the reason for the formation of the 2:1 isocyanide and carbonyl adducts with $W_2(OCMe_2CF_3)_6$ as compared to the $W_2(O^tBu)_6(\mu\text{-L})$ compounds (L = CO, CNAr). The latter contain highly reduced C—O and C—N bonds as a result of extensive back-bonding from the W_2 $d\pi$ electrons [8,9].

In the compound $W_2(OCMe(CF_3)_2)_4(NMe_2)_2$ which contains both strongly π-donating amide ligands and weakly π-donating $(CF_3)_2MeCO$ ligands the metal centers are sufficiently Lewis acidic to bind xylylisocyanide (2 equiv.). This contrasts with the behavior of $W_2(NMe_2)_6$ and testifies to the electronic

Table 7. Summary of crystal data

	I[a]	II[b]	III[c]	IV[d]	V[e]	VI[f]
Empirical formula	$C_{36}H_{68}N_2O_6W_2$	$C_{34}H_{46}F_{18}N_2O_6W_2$	$C_{27}H_{40}F_{18}O_6W_2$	$C_{39}H_{50}F_{18}N_2O_6W_2$; $1/2C_6H_{14}$	$C_{42}H_{54}F_{18}N_2O_6W_2$	$C_{38}H_{42}F_{24}N_4O_4W_2$
Color of crystal	Black	Black	Black	Black	Dark Brown	Red
Crystal dimensions (mm)	$0.13 \times 0.13 \times 0.24$	$0.20 \times 0.24 \times 0.40$	$0.08 \times 0.20 \times 0.25$	$0.24 \times 16 \times 0.22$	$0.10 \times 0.15 \times 0.15$	$0.16 \times 0.20 \times 0.20$
Space group	$C2/c$	$C2/c$	$P2_1/c$	$P\bar{1}$	$P\bar{1}$	$P\bar{1}$
Cell dimensions						
Temperature (°)	−160	−170	−165	−169	−171	−170
a (Å)	30.636(14)	23.733(6)	16.816(3)	14.634(3)	11.659(2)	11.101(2)
b (Å)	10.818(3)	10.458(2)	10.633(1)	15.408(3)	21.373(3)	21.323(3)
c (Å)	20.357(9)	20.396(4)	21.616(3)	12.428(2)	10.944(2)	10.666(1)
α (°)				113.27(1)	97.14(1)	94.87(1)
β (°)	143.58(1)	125.17(1)	102.71(1)	93.22(1)	114.78(1)	109.14(1)
γ (°)				81.34(1)	84.00(1)	95.43(1)
Z	4	4	4	2	2	2
V (Å^3)	4005.69	4138.24	3770.32	2545.02	2452.47	2356.07
Calculated Density (p, g cm^{-3})	1.646	2.049	2.062	1.821	1.886	2.033
Wavelength (Å)	0.71069	0.71069	0.71069	0.71069	0.71069	0.71069
Molecular Weight	992.64	1276.32	1170.28	1395.59	1392.57	1442.44
Linear Absorption Coefficient (cm^{-1})	59.032	57.970	63.512	47.208	48.988	51.184
Detector to sample distance (cm)	22.5	22.5	22.5	22.5	22.5	22.5
Sample to source distance (cm)	23.5	23.5	23.5	23.5	23.5	23.5
average ω scan width at half height (deg)	0.25	0.25	0.25	0.25	0.25	0.25
scan speed (deg/min)	5.0	8.0	8.0	6.0	6.0	8.0
scan width (deg + dispersion)	1.8	2.0	2.0	2.0	2.0	2.0
individual background (s)	10	4	4	6	6	4
aperature size (mm)	3.0×4.0	3.0×4.0	3.0×4.0	3.0×4.0	3.0×4.0	3.0×4.0
2θ range (deg)	6–50	6–55	6–45	6–45	6–45	6–45
Total no. of reflections collected	7601	10195	7566	9685	8550	10037
no. of unique intensities	3543	4778	4946	6686	6442	6164
no. with $F > 0.00$	3405	4527	4580	6237	6122	5847
no. with $F > \sigma(F)$	3308					
no. with $F > 2.33\sigma(F)$	3158					
no. with $F > 3*\sigma(F)$		4150	4169	5770	5745	5440
$R(F)$	0.0309	0.0470	0.0366	0.0564	0.0422	0.0363
$Rw(F)$	0.0332	0.0492	0.0362	0.0548	0.0452	0.0375
goodness of fit for last cycle	0.985	1.288	1.156	1.661	1.533	1.145
maximum δ/σ for last cycle	0.05	0.002	0.23	0.02	0.27	0.035

[a] **I** = $W_2(O^tBu)_6(4\text{-Mepy})_2$.
[b] **II** = $W_2(OCMe_2CF_3)_2(py)_2$.
[c] **III** = $W_2(OCMe_2CF_3)_6(\mu\text{-}CH_2CCH_2)$.
[d] **IV** = $W_2(OCMe_2CF_3)_6(\mu\text{-CN-}p\text{-tolyl})_2$.
[e] **V** = $W_2(OCMe_2CF_3)_6(CNxylyl)_2$.
[f] **IV** = $W_2(NMe_2)(OCMe(CF_3)_2)_6(CNxylyl)_2$.

influence of the $OCMe(CF_3)_2$ ligands at the ditungsten center.

Obviously the results reported here merely add to our knowledge of the chemistry of $W_2(OR)_6$ compounds but do not provide quantitative information concerning the factors influencing the vastly different reactivity seen toward certain substrates such as MeC≡N. However, more quantitative studies are underway.

Acknowledgements—We thank the National Science Foundation for support and D.B.T. thanks General Electric for a fellowship.

REFERENCES

1. Chisholm, M. H., Cotton, F. A., Extine, M. W. and Kelly, R. L., *Inorg. Chem.*, 1979, **18,** 116.
2. Chisholm, M. H., Cook, C. M. and Streib, W. E., *Inorganica Chim. Acta*, 1992, **198–200,** 63.
3. Schrock, R. R., Listemann, M. L. and Sturgeoff, L. G., *J. Am. Chem. Soc.*, 1982, **104,** 4291.
4. Freudenberger, J. H., Pedersen, S. F. and Schrock, R. R., *Bull. Soc. Chim. France*, 1985, 349.
5. Budzichowski, T. A., Chisholm, M. H. and Folting, K., *Chem.—A Eur. J.*, 1996, **2,** 110.
6. (a) μ-allene: Cayton, R. H., Chacon, S. J., Chisholm, M. H., Hampden-Smith, M. J., Huffman, J. C., Folting, K., Ellis, P. D. and Huggins, B. A., *Angew. Chem. Int. Ed. Engl.*, 1989, **28,** 1523; Chacon, S. T., Chisholm, M. H., Hampden-Smith, M. J., Huffman, J. C. and Folting, K., *Organometallics*, 1991, **10,** 3722; (b) 1,3-di-*p*-tolyl-carbodiimide: Cotton, F. A., Schwotzer, W. and Shamshoum, E. S., *Organometallics*, 1985, **4,** 461.
7. Chisholm, M. H., Folting, K., Hoffman, D. M. and Huffman, J. C., *J. Am. Chem. Soc.*, 1984, **106,** 6794.
8. Chisholm, M. H., Clark, D. L., Ho, D. and Huffman, J. C., *Organometallics*, 1987, **6,** 1532.
9. Chisholm, M. H., Hoffman, D. M. and Huffman, J. C., *Organometallics*, 1985, **4,** 987 and refs therein.
10. Appleton, T. G., Clark, H. C. and Manzer, L. E., *Coord. Chem. Rev.*, 1973, **10,** 352.
11. Budzichowski, T. A., Chisholm, M. H., Tiedtke, D. B., Huffman, J. C. and Streib, W. E., *Organometallics*, 1995, **14,** 2318.
12. For the preparation and structure see this issue of *Polyhedron*.
13. Akiyama, M., Chisholm, M. H., Cotton, F. A., Extine, M. W., Haitko, D. A., Little, D. and Fanwick, P. E., *Inorg. Chem.*, 1979, **18,** 2321.
14. Chisholm, M. H., Folting, K., Huffman, J. C. and Kirkpatrick, C. C., *Inorg. Chem.*, 1984, **23,** 1021.

Pergamon

PII: S0277-5387(97)00289-1

Polyhedron Vol. 17, No. 5-6, pp. 869-877, 1998
© 1998 Elsevier Science Ltd
All rights reserved. Printed in Great Britain
0277-5387/98 $19.00+0.00

Isolation and structural characterization of the polymetallic zirconium alkoxide complexes, $Zr_3O(OCH_2CMe_3)_9Cl$, $Zr_3O(OCMe_3)_9(OH)$, and $Na_4Zr_6O_2(OEt)_{24}$†

William J. Evans,* Mohammad A. Ansari and Joseph W. Ziller

Department of Chemistry, University of California Irvine, Irvine, CA 92697-2025, U.S.A.

(Received 30 April 1997; accepted 23 June, 1997)

Abstract—Three polymetallic zirconium alkoxide complexes have been isolated and structurally characterized which show that by proper combination of zirconium precursor and alkoxide, this small class of compounds can be expanded. The trimetallic neopentoxide complex $[(NpO)_2Zr]_3(\mu\text{-}ONp)_3(\mu_3\text{-}Cl)(\mu_3\text{-}O)$, **1**, ($Np = CH_2CMe_3$) can be isolated from the reaction of $ZrCl_4$ with four equivalents of $KOCH_2CMe_3$ in THF. The trimetallic *tert*-butoxide complex, $[(^tBuO)_2Zr]_3(\mu\text{-}O^tBu)_2(\mu\text{-}OH)(\mu_3\text{-}O^tBu)(\mu_3\text{-}O)$, **2**, can be isolated from the reaction of $ZrCl_4$ with 3.3 equivalents of $LiOCMe_3$ in THF. The reaction of $Zr(OEt)_4$ with one equivalent of $NaOSiMe_3$ in THF formed the mixed-metal polymetallic complex, $\{Na_2[(EtO)Zr]_3(\mu\text{-}OEt)_7(\mu_3\text{-}OEt)_2(\mu_3\text{-}O)\}_2$, **3**. These results show that the common $M_3(\mu\text{-}E)_3(\mu_3\text{-}E)_2$ structural motif with E being a ligand donor atom can be obtained with zirconium alkoxides. © 1998 Elsevier Science Ltd. All rights reserved

Keywords: zirconium; alkoxide; polymetallic; heterometallic; oxide.

Zirconium is a desirable metallic component in a variety of materials which have useful practical properties [1]. Attempts to manufacture defect-free zirconium-containing materials using molecular zirconium chemistry [2] as an alternative route to the usual thermal/mechanical techniques are hampered by the fact that there are few polymetallic zirconium precursors in the literature. Indeed, this problem was recognized as early as 1985 [3], but still has not been rectified. Crystallographically characterized homometallic molecular compounds containing three or more zirconium atoms are limited to: $Zr_3S_3(S^tBu)_2(BH_4)_4(THF)_2$ [3], $[Zr_3O(OH)_3(C_6H_5CO_2)_3(C_5H_5)_3][C_6H_5CO_2]$ [4], $Zr_3O(CCO)(O_2CN^iPr_2)_6(C_5H_5)_2$ [5], $Zr_3O(OH)_4Cl_3(C_5Me_5)_3$ [6], $Zr_4[CH_3C(CH_2O)_3]_2(O^iPr)_{10}$ [7], $Zr_4O(O^iPr)_{10}(acac)_4$ [8], $Zr_5H_4Cl_{14}(PR_3)_5$ ($PR_3 = PMe_3, PEt_3, PhMe_2$) [9], $Zr_5(tritox)_5(N)(NH)_4(NH_2)_4$ [10], $Zr_6(tritox)_6(N)(NH)_6(NH_2)_3$ [10], $Zr_6S_6(S^tBu)_4(BH_4)_8(THF)_2$ [11], $Zr_6Cl_{14}H_4(PR_3)_4$ (R = Me, Et, Pr) [12], $(Zr_6Cl_{18}H_5)(HPPh^tBu_2)$ [12], and $Zr_{13}O_8(OMe)_{36}$ [13]. The number of crystallographically characterized polyzirconium alkoxide complexes, a class of compounds which would be desirable as precursors for sol gel processing, is particularly small despite the fact that zirconium alkoxide compounds have been known for many years [14].

In comparison to this limited collection of polymetallic zirconium complexes, an extensive variety of polymetallic alkoxides is available for other metals [15]. For example, neighboring element yttrium forms numerous classes of polymetallic species with simple alkoxide ligands and polymetallic alkoxides of

* Author to whom correspondence should be addressed.

† Dedicated to Professor Donald C. Bradley, who has given us such a rich legacy of alkoxide chemistry.

titanium, lanthanides, actinides, and the Groups 5 and 6 transition metals are also known. The polymetallic alkoxides of these neighboring elements frequently contain a central trimetallic core connected by triply bridging ligands above and below the triangular plane and three doubly bridging ligands in the plane. In alkoxide complexes, the ligand donor atoms, E, in this $M_3(\mu_3\text{-}E)_2(\mu\text{-}E)_3$ unit, are typically oxygen atoms provided by alkoxide, hydroxide, or oxide ligands or, in some cases, they are halide ions. This trimetallic core appears to be a good building block for making larger arrays of yttrium, lanthanide, and actinide polymetallic species. For example, the yttrium *tert*-butoxide complex $Y_3(\mu_3\text{-}O^tBu)(\mu_3\text{-}Cl)(\mu\text{-}O^tBu)_3(O^tBu)_3Cl(THF)_2$ can be converted to $Y_{14}(O^tBu)_{28}Cl_{10}O_2(THF)_4$, which contains four $Y_3(\mu_3\text{-}E)_2(\mu\text{-}E)_3$ units [16].

Formation of trimetallic zirconium analogs of the common yttrium alkoxides, $Y_3(\mu\text{-}O^tBu)_3(\mu_3\text{-}Z)_2(O^tBu)_4L_2$ (Z = O'Bu, Cl, O; L = ether or alcohol), would require some modification of the ligand content to achieve charge balance, since Zr^{IV} requires one more anionic ligand per metal than Y^{III}. This could be accomplished by replacement of both neutral L ligands by OR^- and by replacing one of the monoanionic ligands by dianionic oxide, e.g. $Zr_3(\mu\text{-}OR)_3(\mu_3\text{-}O)(\mu_3\text{-}OR)(OR)_6$. If no dianionic ligands are present in a trimetallic zirconium analog of $Y_3(OR)_9L_2$, charge balance would require an extra ligand, e.g. $Zr_3(\mu\text{-}OR)_3(\mu_3\text{-}OR)_2(OR)_7$. This would require at least one zirconium center to be 7-coordinate instead of the favored 6-coordination. If these $Zr_3O(OR)_{10}$ or $Zr_3(\mu\text{-}OR)_{12}$ complexes are too sterically crowded to be stable, polymetallic species could only form if smaller ligands can be substituted for alkoxides. Halide and hydroxide monoanions and oxide and sulfide dianions would be the most useful in this regard.

The $M_3(\mu_3\text{-}E)_2(\mu\text{-}E)_3$ core has actually been observed for zirconium when E = S in the case of $Zr_3S_3(S^tBu)_2(BH_4)_4(THF)_2$ [3]. Since this complex has three dianionic sulfide ligands, only six monoanions are required and there is room for two THF ligands to bind. A complex containing two of these trimetallic units is also known, $Zr_6S_6(S^tBu)_4(BH_4)_8(THF)_2$ [3]. The isolation of the actinide alkoxide complex $U_3(O^tBu)_{10}O$ [17] indicates that the tetravalent nature of a metal does not prohibit formation of trimetallic alkoxide complexes of formula $M_3(\mu_3\text{-}E)_2(\mu\text{-}E)_3$ with tetravalent metals, but the larger size of the actinide metals reduces the problems with steric crowding. Polymetallic $Ti_4(OMe)_{16}$ [18], $Ti_4(OEt)_{16}$ [19], $W_4(OEt)_{16}$ [20], and $Th_4(OEt)_{16}(py)_2$ [21] complexes are known, but have structures which lack one of the μ_3-ligands in the $M_3(\mu_3\text{-}E)_2(\mu\text{-}E)_3$ structure.

To determine if polymetallic zirconium alkoxide complexes related to species such as $Y_3(\mu\text{-}O^tBu)_3(\mu_3\text{-}Z)_2(O^tBu)_4(THF)_2$ [16], $Zr_3S_3(S^tBu)_2(BH_4)_4(THF)_2$ [3], and $U_3(O^tBu)_{10}O$ [17] could be formed with simple alkoxide ligands, we have examined several combinations of zirconium precursors with alkoxide ligands known to give polymetallic species with other metals. We report here the isolation of three examples of trimetallic zirconium alkoxides which demonstrate that polymetallic zirconium complexes of this type are accessible with the proper combination of ligands. An attempt to make a mixed sulfide alkoxide is also reported.

EXPERIMENTAL

The chemistry described below was performed under nitrogen using Schlenk, vacuum line, and glove box techniques. Solvents were purified as previously described [22]. NMR spectra were recorded at 25°C using a General Electric QE 300 spectrometer. Elemental analyses were performed by Analytische Laboratorien, Gummersbach, Germany and on a Carlo Erba EA 108 instrument. LiO'Bu was obtained by reacting HO'Bu and *n*-butyllithium in hexanes and was dried under high vacuum. $ZrCl_4$ and $Zr(OEt)_4$ (Aldrich) were used as obtained.

$[(Me_3CCH_2O)_2Zr]_3(\mu\text{-}OCH_2CMe_3)_3(\mu_3\text{-}Cl)(\mu_3\text{-}O)$, **1**

In the glovebox, a freshly prepared sample of $KOCH_2CMe_3$, obtained by reacting KH (160 mg, 4.0 mmol) with $HOCH_2CMe_3$ (350 mg, 4.0 mmol) in 10 cm^3 of THF, was added to a solution of $ZrCl_4$ (233 mg, 1.0 mmol) in 10 cm^3 of THF. The resulting cloudy solution was stirred for 48 h and centrifuged to remove a small amount of pale yellow solid. The supernatant was evaporated to dryness using a rotary evaporator. Recrystallization from hexane did not produce high quality crystals, but recrystallization from toluene at −40°C was successful (170 mg, 45%). Anal. Calcd for $C_{45}H_{45}O_{10}ClZr_3$: C, 48.72; H, 9.00; Zr, 24.67. Found: C, 49.09; H, 9.10; Zr, 24.50. IR (Nujol): 1458 s, 1375 s, 1142 w, 1110 m, 1010 w, 725 m, 665 w, 650 m cm^{-1}. ^1H NMR (C_6D_6) δ 4.25 (s, 6H, $CH_2C(CH_3)_3$), 4.01 (s, 6H, $CH_2C(CH_3)_3$), 3.94 (s, 6H, $CH_2C(CH_3)_3$), 1.16 (s, 27H, $CH_2C(CH_3)_3$), 1.06 (s, 27H, $CH_2C(CH_3)_3$), 1.16 (s, 27H, $CH_2C(CH_3)_3$). ^{13}C NMR (C_6D_6): δ 82.3 ($CH_2C(CH_3)_3$), 80.3 ($CH_2C(CH_3)_3$), 33.6 ($CH_2C(CH_3)_3$), 33.0 ($CH_2C(CH_3)_3$), 26.4 ($CH_2C(CH_3)_3$), 26.2 ($CH_2C(CH_3)_3$).

$[(Me_3CO)_2Zr]_3(\mu\text{-}OCMe_3)_2(\mu\text{-}OH)(\mu_3\text{-}OCMe_3)(\mu_3\text{-}O)$, **2**

A mixture of $LiOCMe_3$ (266 mg, 3.33 mmol) and Li_2S (16 mg, 0.33 mmol) in 10 cm^3 of THF was added to a vial containing $ZrCl_4$ (233 mg, 1.0 mmol) in 10 cm^3 of THF. The resulting mixture was stirred for 24 h and centrifuged to remove a small amount of solid. The solution was evaporated to dryness and then extracted with hexanes. Slow evaporation of the hexanes solution at ambient temperature for several days

produced crystalline **2** (270 mg, 84%). X-ray quality crystals were grown from toluene at −40°C. Anal. Calcd for $C_{36}H_{82}O_{11}ClZr_3$: C, 44.78; H, 8.57; Zr, 28.36. Found: C, 43.38; H, 8.34; Zr, 28.10. IR (Nujol): 1458 s, 1375 s, 1142 w, 1110 m, 1010 w, 725 m, 665 w, 650 m cm^{-1}. ^1H NMR (C_6D_6) δ 1.85 (s, $C(CH_3)_3$), 1.74 (s, $C(CH_3)_3$), 1.68 (s, $C(CH_3)_3$), 1.57 (s, $C(CH_3)_3$), 1.52 (s, $C(CH_3)_3$), 1.49 (s, H, $C(CH_3)_3$), 1.47 (s, H, $C(CH_3)_3$), 1.46 (s, H, $C(CH_3)_3$). ^{13}C NMR (C_6D_6): 76.3 (s, $C(CH_3)_3$, 75.7 (S, $C(CH_3)_3$), 74.3 (s, $C(CH_3)_3$), 73.6 (s, $C(CH_3)_3$), 34.1 (s, $C(CH_3)_3$), 33.8 (s, $C(CH_3)_3$), 33.2 (s, $C(CH_3)_3$), 32.9 (s, $C(CH_3)_3$), 33.6 (s, $C(CH_3)_3$), 32.3 (s, $C(CH_3)_3$). **2** can also be made analogously in similar yield in the absence of Li_2S.

$\{Na_2[(EtO)Zr]_3(\mu\text{-}OEt)_7(\mu_3\text{-}OEt)_2(\mu_3\text{-}O)\}_2$, **3**

A suspension of $Zr(OEt)_4$ (271 mg, 1 mmol) in 10 cm^3 of THF was reacted with $NaOSiMe_3$ (112 mg, 1 mmol) in 5 cm^3 of THF. Most of the $Zr(OEt)_4$ went into solution as the mixture was stirred over a 48 h period. The resultant solution was centrifuged to remove a small amount of solid (~20 mg). The volume of the supernatant was reduced to half using a rotary evaporator and then transferred to the freezer at −38°C to give colorless crystals (30 mg, 10%). Anal. Calcd for $C_{48}H_{120}O_{26}Na_4Zr_6$: C, 32.89; H, 6.90; Zr, 31.23. Found: C, 32.74; H, 6.80; Zr, 31.45. ^1H NMR (THF-d_8) δ 4.33 (m, 4H, CH_2CH_3), 4.25 (m, 6H, CH_2CH_3), 4.12 (m, 14H, CH_2CH_3), 1.43 (m, 9H, CH_2CH_3), 1.34 (m, 21H, CH_2CH_3), 1.26 (m, 6H, CH_2CH_3). ^{13}C NMR (THF-d_8) 73.0, 65.1, 63.8 (CH_2CH_3), 21.5, 20.9, 14.7 (CH_2CH_3). IR (Nujol): 1460 s, 1376 s, 1244 w, 1152 w, 1089 w, 1055 m, 930 m, 833 m, 722 w cm^{-1}.

General aspects of X-ray data collection, structure determination, and refinement

Crystals were coated with Paratone oil, mounted on a glass fiber, and transferred to the nitrogen cold stream of a Siemens P4 diffractometer. Determination of Laue symmetry, crystal class, unit cell parameters and the crystal's orientation matrix was carried out according to standard procedures [23]. Intensity data were collected at 163 K using a 2θ–ω scan technique with Mo-K_α radiation (details are given in Table 1). No significant decay was observed during data collection. Data were corrected for Lorentz and polarization effects and were placed on an absolute scale. The raw data were processed with a modified version of CARESS [44]. All calculations were carried out using the SHELXL program [25]. The analytical scattering factors for neutral atoms were used throughout the analysis [26]. All of the structures were solved by direct methods and refined on F^2 by full-matrix least squares techniques.

$[(Me_3CCH_2O)_2Zr]_3(\mu\text{-}OCH_2CMe_3)_3(\mu_3\text{-}Cl)(\mu_3\text{-}O)$, **1**

The diffraction symmetry of a colorless crystal of dimensions $0.40 \times 0.33 \times 0.27$ mm was $2/m$ with systematic absence $h01$ for $h+1 = 2n+1$. The two possible space groups are Pn and $P2/n$. The noncentrosymmetric space group Pn was found to be the correct choice. At convergence $wR2 = 0.1011$ and GOF = 1.047 to 257 variables against all 7360 unique data. As a comparison for refinement on F, $R1 = 0.0359$ for those 6886 data with $F > 4\sigma$ (F). It was necessary to constrain the geometry of the neopentoxide ligands defined by atoms C(41)–C(45) by using the atoms C(8)–C(10) as a reference model.

$[(Me_3CO)_2Zr]_3(\mu\text{-}OCMe_3)_2(\mu\text{-}OH)(\mu_3\text{-}OCMe_3)(\mu_3\text{-}O)$, **2**

The diffraction symmetry of a colorless crystal of dimensions $0.16 \times 0.17 \times 0.60$ mm was $2/m$ with systematic absence $0k0$ for $k = 2n+1$. The two possible space groups are $P2_1$ and $P2_1/m$. The centrosymmetric space group $P2_1/m$ was found to be the correct choice. At convergence $wR2 = 0.0999$ and GOF = 1.055 for 241 variables against all 4455 unique data. As a comparison for refinement on F, $R1 = 0.0407$ for those 3516 data with $F > 4\sigma$ (F).

$\{Na_2[(EtO)Zr]_3(\mu\text{-}OEt)_7(\mu_3\text{-}OEt)_2(\mu_3\text{-}O)\}_2$, **3**

A colorless crystal of dimensions $0.05 \times 0.13 \times 0.36$ mm was mounted on a glass fiber and transferred to a Siemens P4 rotating anode diffractometer. There were no systematic absences nor diffraction symmetry other than the Friedel condition. The centrosymmetric space group $P\bar{1}$ was assigned and later determined to be the correct choice. The molecule is located on an inversion center. Carbon atoms C(18), C(19) and C(24) are disordered. Two components (site occupancy = 0.5) were included for each of the three atoms to account for this disorder. Hydrogen atoms associated with C(19B) were not included. At convergence, $wR2 = 0.1550$ and GOF = 1.017 for 371 variables against all 4955 unique data. As a comparison for refinement on F, $R1 = 0.0563$ for those 3163 data with $F > 4\sigma$ (F).

RESULTS AND DISCUSSION

$[(Me_3CCH_2O)_2Zr]_3(\mu\text{-}OCH_2CMe_3)_3(\mu_3\text{-}Cl)(\mu_3\text{-}O)$, **1**

The reaction of $ZrCl_4$ with 4 equiv. of $KOCH_2CMe_3$ in THF gives a white microcrystalline product which upon recrystallization from toluene gives **1** in 45% yield. The ^1H NMR spectrum of **1** in C_6D_6 contains three resonances of equal intensity in the methylene region and three larger resonances of equal intensity in the methyl region which indicated that **1** was not a

simple monometallic $Zr(OR)_4$ or bimetallic $(RO)_3Zr(\mu\text{-}OR)_2Zr(OR)_3$ complex. The ^{13}C NMR spectrum contained six resonances, two each in the methyl region, the methylene region, and the quaternary carbon region. X-ray crystallography revealed that **1** is a trimetallic zirconium alkoxide which has retained one chloride ligand per three metals and has incorporated an oxide ligand, i.e. $Zr_3O(OCH_2CMe_3)_9Cl$, **1**. The source of the oxide ligand is unknown, but the isolation of oxide/alkoxide complexes in reactions of this type is not uncommon [4,5,27–29].

The structure of complex **1**, Figs 1 and 2, is analogous to those of compounds such as $Y_3(\mu\text{-}O^tBu)_3(\mu_3\text{-}O^tBu)(\mu_3\text{-}Cl)(O^tBu)_4L_2$ [16], $La_3(\mu\text{-}O^tBu)_3(\mu_3\text{-}O^tBu)_2(O^tBu)_4(^tBuOH)_2$ [16], and $Zr_3S_3(S^tBu)_2(BH_4)_4(THF)_2$ [3]. Replacement of two neutral ligands with monoanions and incorporation of a dianionic oxide achieves charge balance in this $M_3(\mu\text{-}E)_3(\mu_3\text{-}E)_2$ structure which contains all six-coordinate zirconium centers. Hence, the three zirconium atoms comprise a triangle which has $\mu\text{-}OCH_2CMe_3$ ligands bridging each edge. Each zirconium is ligated by two terminal neopentoxide ligands. Above the zirconium triangle is a μ-Cl ligand and below is a μ_3-O ligand. Each zirconium center has a distorted octahedral environment and overall the complex has three fold rotational symmetry.

Selected bond lengths and angles are given in Table 2. All of the bridging Zr—OR distances are within the narrow range 2.161(4)–2.171(4) Å and as expected they are longer than the 1.914(4)–1.947(4) Å terminal Zr—OR distances. These distances are comparable to the average bridging (2.170 Å) and terminal (1.943 Å) Zr—O^{i}Pr distances in $[(^iPrO)_3Zr(\mu\text{-}O^iPr)(^iPrOH)]_2$ [30]. The 2.082(3)–2.090(3) Å $Zr\text{–}\mu_3\text{-}O$ distances are intermediate between these ranges. In comparison, the corresponding Zr—μ_3-O distances in $[Zr_3(\mu_3\text{-}O)(\mu\text{-}OH)_3(C_6H_5COO)_3(\eta^5\text{-}C_5H_5)_3][C_6H_5COO]$ range from 2.059(4) to 2.079(4) Å [5]. Since no compound containing a Zr_3—(μ_3-Cl) arrangement has previously been reported in the literature, no direct comparisons can be made with the 2.847(1)–2.886(1) Å Zr—μ_3-Cl distances, but an analogous arrangement occurs in several yttrium complexes. For example, in $Y_3Cl_2(O^tBu)_7(THF)_2$ and $Y_3Cl(O^tBu)_8(THF)_2$ [17], Y—μ_3-Cl distances are 2.831(10)–2.885(10) and 2.820(5)–2.897(2) Å, respectively. Considering the differences in the ionic radii of six-coordinate Zr^{IV} (0.72 Å) and Y^{III} (0.90 Å), the distances found in **1** are longer than expected [31]. On the other hand, the 3.2956(8)–3.3021(7) Å Zr···Zr distances are shorter than the 3.50–3.63 Å Y···Y distances in $Y_3Cl(O^tBu)_8(THF)_2$. The Zr···Zr distances in **1** are also on the short end of the 3.278(2)–3.574(2) Å range of distances in $Zr_3S_3(S^tBu)_2(BH_4)_4(THF)_2$ [3] and are shorter than the 3.468(1)–3.507(1) Å range in $Zr_6S_6(S^tBu)_4(BH_4)_8(THF)_2$ [3]. The sulfur compounds may have

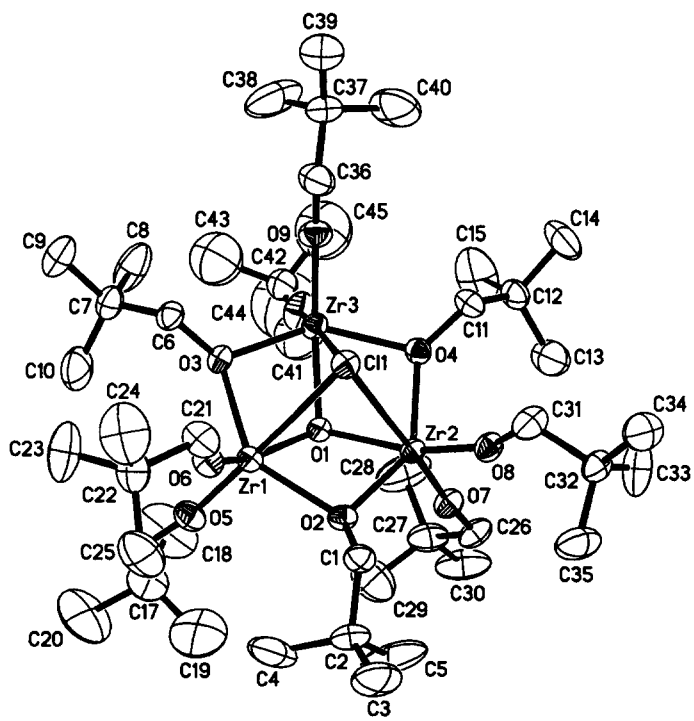

Fig. 1. Molecular structure of $Zr_3O(OCH_2CMe_3)_9Cl$, **1**, with thermal ellipsoids drawn at the 50% probability level.

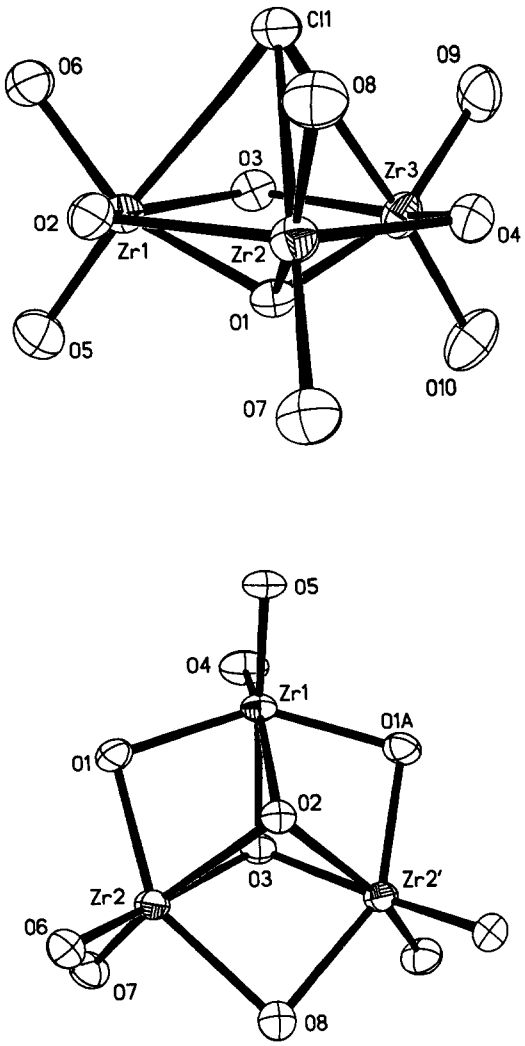

Fig. 2. Side view of metal oxygen halide framework of $Zr_3O(OCH_2CMe_3)_9Cl$, **1**, and top view of metal oxygen framework of $Zr_3O(OCMe_3)_9(OH)$, **2**.

longer Zr···Zr distances due to the larger size of the bridging atoms.

$[(Me_3CO)_2Zr]_3(\mu\text{-}OCMe_3)_2(\mu\text{-}OH)(\mu_3\text{-}OCMe_3)(\mu_3\text{-}O)$, 2

In an attempt to make a mixed ligand zirconium *tert*-butoxide sulfide of formula $Zr_3(\mu\text{-}OR)_3(\mu_3\text{-}S)(\mu_3\text{-}OR)(OR)_6$, $ZrCl_4$ was treated with 3.33 equiv. of $LiOCMe_3$ and 0.33 equiv. of Li_2S. Again the ^1H and ^{13}C NMR spectra of the product were not structurally definitive and the complex was characterized by X-ray crystallography, Figs 2 and 3.

The product isolated from this reaction, **2**, was indeed a trimetallic zirconium alkoxide, but no sulfur was incorporated. Instead, incorporation of oxide and hydroxide ligands occurred. Since **2** can be obtained in similar yields in reactions in the absence of lithium sulfide, it is unlikely that it is formed by hydrolysis of a sulfide intermediate. Again the source of the oxide and hydroxide ligands is not known, but the synthesis of **2** is reproducible and the compound is readily isolated as the favored product of this ligand metal combination.

The structures of **1** and **2** are closely related. Both contain a $Zr_3(\mu_3\text{-}O)(\mu_3\text{-}Z)(\mu_2\text{-}O)_3$ core as a structural feature. In the case of **2**, the triply bridging atoms are supplied by one *tert*-butoxide ligand and one oxide and the doubly bridging oxides arise from two *tert*-butoxide ligands and the hydroxide. The hydrogen on the hydroxide was not located crystallographically, but the bond distances are consistent with its location on O(8). The 2.101(7) Å average Zr—μ_3-O distance is similar to that observed in **1**. The terminal Zr—O(O^{t}Bu) distances range from 1.918(4) to 1.961(3) Å and are shorter than the bridging 2.162(3) and 2.182(3) Å Zr—O(μ_2-O^{t}Bu) distances which are shorter than the 2.391(4) and 2.373(3) Å Zr—O(μ_3-O^{t}Bu) lengths. The 2.326(3) Å Zr—O(8) distance is significantly longer than the other Zr—O(μ_3-O) distances and is consistent with a Zr—OH bond [4]. The 3.2207(7) and 3.2533(8) Å Zr···Zr distances are slightly shorter than those in **1**.

$\{Na_2[(EtO)Zr]_3(\mu\text{-}OEt)_7(\mu_3\text{-}OEt)_2(\mu_3\text{-}O)\}_2$, 3

In contrast to zirconium alkoxides in which the R group is propyl or larger, zirconium ethoxide, '$Zr(OEt)_4$' is essentially insoluble in THF. However, a suspension of this material in THF reacts with sodium salts such as $NaOSiMe_3$ and $NaOCH_2CH_3$ to form solutions from which crystals of the mixed-metal $Na_4Zr_6(OEt)_{24}O_2$, **3**, were isolated. In our hands, $NaOSiMe_3$ was the best reagent to reproducibly introduce sodium and solubilize $Zr(OEt)_4$. Since NMR spectra were not informative, **3** was characterized by X-ray diffraction.

Complex **3** (Fig. 4), consists of six octahedrally coordinated zirconium centers and four five coordinate sodium atoms bridged with ethoxide ligands and two μ_5-O ligands. The condensed ZrO_6 units are reminiscent of the condensed MO_6 units in polymolybdates and polytungstates [32]. Complex **3** contains $Zr_3(\mu_3\text{-}O)(\mu\text{-}OR)_3$ subunits and can be considered as two $[(EtO)_3Zr_3(\mu_3\text{-}O)(\mu\text{-}OEt)_9]^{2-}$ units bridged with four sodium atoms. Four alkali metals have previously been observed to connect pairs of zirconium atoms in $K_4Zr_2O(O^iPr)_{10}$, a complex which also can be formed by a variety of alkali metal reagents [28]. As usual, the terminal Zr—O distances, 1.937(6)–1.951(7) Å, are longer than the bridging ones. The bridging ethoxide ligands are of two types: in each half of the structure, three connect zirconium atoms and six bridge zirconium to sodium. The Zr—O distances for the zirconium bridging ligands, 2.139(7)–2.197(6) Å have larger values than the Zr—O dis-

Table 1. Crystallographic data for $[(Me_3CCH_2O)_2Zr]_3(\mu\text{-}OCH_2CMe_3)_3(\mu_3\text{-}Cl)(\mu_3\text{-}O)$, **1**, $[(Me_3CO)_2Zr]_3(\mu\text{-}OCMe_3)_2(\mu\text{-}OH)(\mu_3\text{-}OCMe_3)(\mu_3\text{-}O)$, **2**, and $\{Na_2[(EtO)Zr]_3(\mu\text{-}OEt)_7(\mu_3\text{-}OEt)_2(\mu_5\text{-}O)\}_2$, **3**

Compound	**1**	**2**	**3**
Formula	$C_{52}H_{107}ClO_{10}Zr_3$	$C_{36}H_{82}O_{11}Zr_3$	$C_{48}H_{120}Na_4O_{26}Zr_6$
Formula weight	1201.49	964.68	1752.72
Space group	*P*n	$P2_1/m$	$P\bar{1}$
a (Å)	15.431(3)	10.787(2)	12.116(2)
b (Å)	13.6242(10)	20.517(2)	12.741(2)
c (Å)	15.536(4)	11.276(2)	14.284(2)
α (°)			99.61(2)
β (°)	96.63(2)	100.56(2)	104.33(1)
γ (°)			110.42(1)
Z	2	2	1
V (Å^3)	3244.4(10)	2453.2(7)	1922.5(5)
D, calculated (g cm^{-3})	1.230	1.31	1.52
Radiation (λ)	0.7107	0.71073	0.7107
Abs. coefficient μ (mm^{-1})	0.560	0.671	0.872
*R*1, $[I > 2\sigma(I)]$	0.0359	0.041	0.056
w*R*2, all data	0.1011	0.100	0.155
GOF on F^2	1.05	1.06	1.017

tances of the ligands connecting zirconium to sodium, 2.020(6)–2.074(6) Å.

The formation of direct zirconium analogs of the common $Y_3(\mu\text{-}O^tBu)_3(\mu_3\text{-}Z)_2(O^tBu)_4L_2$ compounds of yttrium is not possible using just the eleven ligands in these systems. For charge balance, either an extra alkoxide (requiring 7-coordinate zirconium) or an oxide ligand must be incorporated. In each of the new complexes described here, an oxide ligand has been incorporated. In addition, in the case of **1** and **2**, halide and hydroxide ligands are found in the products. Inclusion of such small monoanionic ligands aids in forming polymetallic species since it reduces the steric crowding around the Zr_3 unit.

The isolation of **1–3** shows that analogs of $Y_3(\mu\text{-}O^tBu)_3(\mu_3\text{-}Z)_2(O^tBu)_4L_n$ complexes can indeed be made with zirconium if oxide, halide and hydroxide ligands are incorporated. This means that a variety of polymetallic zirconium species should be accessible if the necessary coligands required for charge balance and steric minimization can be included. Deliberate incorporation of the most desirable of these ligands, oxide and hydroxide, is not easy since the salts of these ligands are typically insoluble in the ether solvents commonly used. Furthermore, simple addition of these salts provides no guarantee that they will be incorporated as was observed in the reaction leading to complex **2**. On the other hand, hydrolysis of Zr—OR groups and C—O cleavage reactions can occur in these systems and can provide these ligands [27–29]. The incorporation of oxide into each of the complexes reported here is reminiscent of the consistent formation of the oxide $Y_5O(O^iPR)_{13}$ in preparations of '$Y(O^iPr)_3$' [29].

The progression of ligand sizes in the three structures reported here shows how ligand bulk can affect aggregation. The ethoxide group is the least sterically demanding and allows the most aggregation. Neopentoxide is next largest in this series and the structure of **1** shows that these ligands are not too bulky to form a $[(RO)_2Zr(\mu\text{-}OR)]_3$ unit provided there are small ligands in the μ_3-capping positions. The structure of complex **2** suggests that a trimeric $[(^tBuO)_2Zr]_3$ unit cannot accommodate three doubly-bridging μ-O^{t}Bu ligands around the triangle and will require either μ-OH or μ-O ligands to form a $M_3(\mu_3\text{-}E)_2(\mu\text{-}E)_3$ structure.

CONCLUSIONS

This study shows that trimetallic zirconium alkoxide complexes can be obtained from combinations of monozirconium precursors with simple alkoxide reagents. As is the case for other early metal and f element alkoxide systems, the syntheses are highly dependent on the precise combination of reagents. Structurally, there are similarities with other early metal and f element alkoxide complexes which may be useful in designing more extended systems with zirconium.

Acknowledgments—For support of this research, we thank the Division of Chemical Sciences of the Office of Basic Energy Sciences of the Department of Energy and the Phillips Laboratory Propulsion Directorate of Edwards Air Force Base. Helpful discussions with Dr J. Lichtenhan are gratefully acknowledged.

Table 2. Important angles (°) and distances (Å) for $[(Me_3CCH_2O)_2Zr]_3(\mu\text{-}OCH_2CMe_3)_3(\mu_3\text{-}Cl)(\mu_3\text{-}O)$, **1**, $[(Me_3CO)_2Zr]_3(\mu\text{-}OCMe_3)_2(\mu\text{-}OH)(\mu_3\text{-}OCMe_3)(\mu_3\text{-}O)$, **2**, and $\{Na_2[(EtO)Zr]_3(\mu\text{-}OEt)_7(\mu_3\text{-}OEt)_2(\mu_5\text{-}O)\}_2$, **3**

1		**2**		**3**	
μ_3-O— or μ_5-O—Zr					
Zr(1)—O(1)	2.082(3)	Zr(1)—O(3)	2.108(4)	Zr(1)—O(1)	2.186(5)
Zr(2)—O(1)	2.090(3)	Zr(2)—O(3)	2.094(2)	Zr(2)—O(1)	2.169(5)
Zr(3)—O(1)	2.089(3)			Zr(3)—O(1)	2.169(5)
Bridging μ-O—Zr					
Zr(1)—O(2)	2.171(4)	Zr(1)—O(1)	2.182(3)	Zr(1)—O(2)	2.184(6)
Zr(2)—O(2)	2.168(3)	Zr(2)—O(1)	2.162(2)	Zr(1)—O(3)	2.191(6)
Zr(1)—O(3)	2.161(4)	Zr(1)—O(2)	2.391(4)	Zr(2)—O(2)	2.150(6)
Zr(3)—O(3)	2.164(4)	Zr(2)—O(2)	2.373(3)	Zr(2)—O(8)	2.139(7)
Zr(2)—O(4)	2.161(3)	Zr(2)—O(8)	2.326(3)	Zr(3)—O(3)	2.169(6)
Zr(3)—O(4)	2.167(4)			Zr(3)—O(8)	2.197(6)
				Zr(2)—O(9)	2.074(6)
				Zr(3)—O(11)	2.020(6)
				Zr(3)—O(12)	2.040(6)
				Zr(1)—O(4)	2.038(6)
				Zr(1)—O(5)	2.023(6)
				Zr(2)—O(7)	2.072(6)
Terminal Zr—O					
tZr(1)—O(5)	1.91(4)	Zr(1)—O(5)	1.960(4)	Zr(1)—O(6)	1.937(6)
Zr(1)—O(6)	1.938(4)	Zr(2)—O(6)	1.961(3)	Zr(2)—O(10)	1.942(6)
Zr(2)—O(7)	1.914(4)	Zr(2)—O(7)	1.913(3)	Zr(3)—O(13)	1.951(7)
Zr(2)—O(8)	1.946(4)				
Zr(3)—O(9)	1.947(4)				
Zr(3)—O(10)	1.926(4)				
Miscellaneous					
Zr(1)—Cl(1)	2.886(1)			Na(1)—O(1′)	2.666(6)
Zr(2)—Cl(1)	2.847(1)			Na(1)—O(5′)	2.361(7)
Zr(3)—Cl(1)	2.866(1)			Na(1)—O(7)	2.393(6)
				Na(1)—O(9)	2.384(7)
				Na(1)—O(11′)	2.363(7)
				Na(2)—O(1′)	3.018(6)
				Na(2)—O(4)	2.301(6)
				Na(2)—O(7)	2.368(7)
				Na(2)—O(9′)	2.357(6)
				Na(2)—O(12′)	2.306(7)
Angles					
O(1)—Zr(1)—O(2)	74.02(13)	O(1)—Zr(1)—O(2)	75.14(7)	O(2)—Zr(1)—O(3)	89.3(2)
O(1)—Zr(1)—O(3)	73.86(13)	O(1)—Zr(1)—O(1′)	144.32(14)	O(2)—Zr(1)—O(4)	87.8(2)
O(1)—Zr(2)—O(2)	73.93(13)	O(1)—Zr(1)—O(2)	75.14(7)	O(2)—Zr(1)—O(5)	166.4(2)
O(1)—Zr(2)—O(4)	74.10(13)	O(1)—Zr(1)—O(3)	74.96(7)	O(3)—Zr(1)—O(4)	169.1(2)
O(1)—Zr(3)—O(3)	73.66(13)	O(1)—Zr(2)—O(3)	75.66(12)	O(2)—Zr(2)—O(7)	90.5(2)
O(1)—Zr(3)—O(4)	74.00(13)	O(1)—Zr(2)—O(8)	147.14(10)	O(2)—Zr(2)—O(8)	92.7(2)
Zr(1)—O(1)—Zr(2)	104.40(13)	O(4)—Zr(1)—O(5)	101.6(2)	O(2)—Zr(2)—O(9)	169.6(2)
Zr(1)—O(1)—Zr(3)	104.68(13)	O(6)—Zr(2)—O(7)	98.90(13)	O(2)—Zr(2)—O(10)	91.8(2)
Zr(2)—O(1)—Zr(3)	104.11(14)	Zr(1)—O(1)—Zr(2)	95.70(11)	O(1)—Zr(3)—O(13)	161.6(2)
Zr(1)—O(2)—Zr(2)	98.90(13)	Zr(1)—O(3)—Zr(2)	100.07(12)	O(3)—Zr(3)—O(8)	87.9(2)
Zr(1)—O(3)—Zr(3)	99.55(14)	Zr(2)—O(3)—Zr(2′)	101.9(2)	O(3)—Zr(3)—O(11)	92.7(2)
Zr(2)—O(4)—Zr(3)	99.17(14)	Zr(2)—O(8)—Zr(2′)	88.73(14)	O(3)—Zr(3)—O(12)	169.9(2)
Zr(1)—Cl(1)—Zr(2)	70.19(3)			Zr(1)—O(1)—Zr(2)	104.1(2)
Zr(1)—Cl(1)—Zr(3)	70.07(3)			Zr(1)—O(1)—Zr(3)	104.3(2)
Zr(2)—Cl(1)—Zr(3)	70.45(3)			Zr(2)—O(1)—Zr(3)	104.6(2)
				Zr(1)—O(1)—Na(1′)	89.4(2)
				Zr(1)—O(1)—Na(1′)	163.1(3)
				Zr(1)—O(2)—Zr(2)	104.8(2)
				Zr(1)—O(3)—Zr(3)	104.2(3)
				Zr(1)—O(4)—Na(2)	111.4(2)
				Zr(1)—O(5)—Na(1′)	102.7(2)
				Zr(2)—O(8)—Zr(3)	104.7(2)
				Zr(2)—O(12)—Zr(3)	104.7(2)

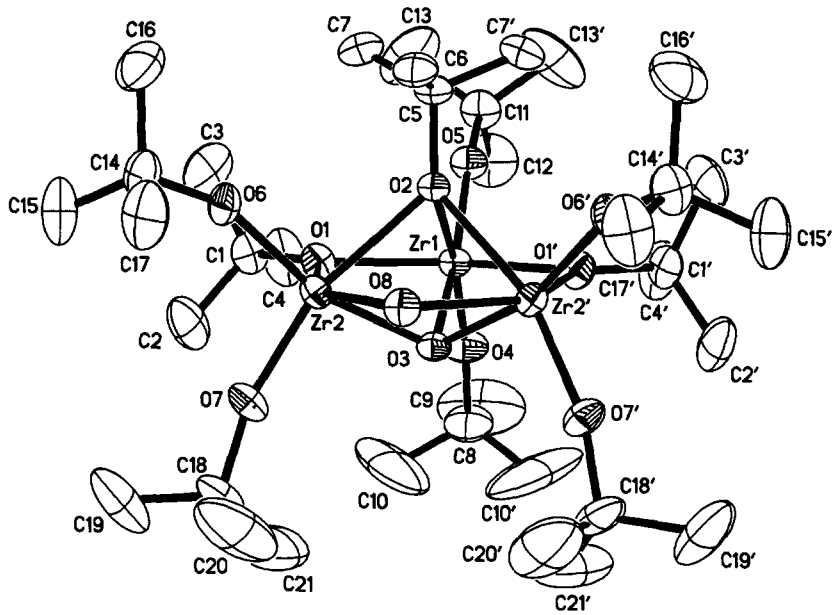

Fig. 3. Molecular structure of $Zr_3O(OCMe_3)_9(OH)$, **2**, with thermal ellipsoids drawn at the 50% probability level.

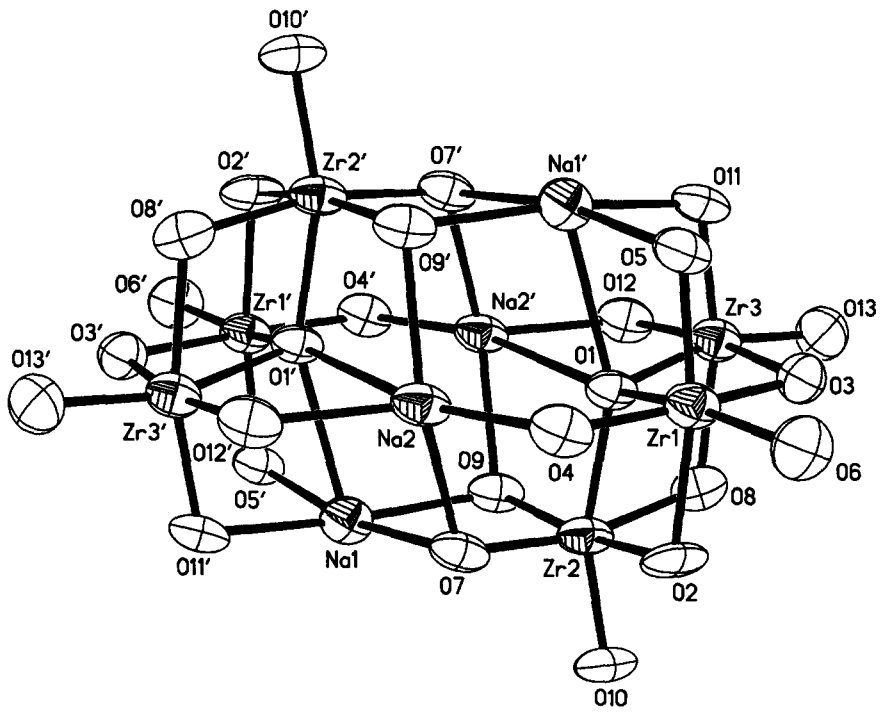

Fig. 4. Molecular structure of $Na_4Zr_6O_2(OEt)_{24}$, **3**, with thermal ellipsoids drawn at the 50% probability level and CH_2CH_3 groups deleted for clarity.

REFERENCES

1. (a) Mazdiyasni, K. S., Lynch, C. J. and Smith II, J. S., *J. Am. Ceram. Soc.*, 1967, **50,** 532; (b) Haertling, G. H. in *Industrial Applications of Rare Earth Elements*, ed. K. A. Gschneidner, Jr., *ACS Symp. Ser.*, 1980, **164**; (c) Buchanan, R. C. in *Ceramic Materials for Electronics*, Marcel Dekker, New York (1991). *Ullmann's Encyclopedia of Industrial Chemistry*, 5th Ed. 1996, **A28,** 557.
2. (a) Bradley, D. C., *Polyhedron*, 1994, **13,** 1111; (b) Bradley, D. C., *Chem. Rev.*, 1989, **89,** 1317; (c) Hubert-Pfalzgraf, L. G., *New J. Chem.*, 1995, **19,** 727; (d) Caulton, K. G. and Hubert-Pfalzgraf, L. G., *Chem. Rev.*, 1990, **90,** 969.
3. Coucouvanis, D., Lester, R. K., Kanatzidis, M. G. and Kessissoglou, D. P., *J. Am. Chem. Soc.*, 1985, **107,** 8279.
4. Thewalt, U., Doppert, K. and Lasser, W., *J. Organomet. Chem.*, 1986, **308,** 303.
5. Calderazzo, F., Englert, U., Guarini, A., Marchetti, F., Pampaloni, G., Segre, A. and Tripepi, G., *Chem. Eur. J.*, 1996, **2,** 412.
6. Babcock, L. M., Day, V. W. and Klemperer, W. G., *Inorg. Chem.*, 1989, **28,** 806.
7. Boyle, T. J., Schwartz, R. W., Doedens, R. J. and Ziller, J. W., *Inorg. Chem.*, 1995, **34,** 1110.
8. Tolédano, P., In, M. and Sanchez, C., *C. R. Acad. Sci. Paris, Sér. II*, 1991, **311,** 1161.
9. Cotton, F. A., Lu, J., Shang, M. and Wojtczak, W. A., *J. Am. Chem. Soc.*, 1994, **116,** 4364.
10. Holl, M. M. B. and Wolczanski, P. T., *J. Am. Chem. Soc.*, 1992, **114,** 3854.
11. Coucouvanis, D., Hadjikyriacou, A., Lester, R. and Kanatzidis, M. G., *Inorg. Chem.*, 1994, **33,** 3645.
12. (a) Cotton, F. A., Feng, X., Shang, M. and Wojtczak, W. A., *Angew. Chem. Int. Ed. Engl.*, 1992, **31,** 1050; (b) Chen, L., Cotton, F. A. and Wojtczak, W. A., *Inorg. Chem.*, 1996, **35,** 2988.
13. Morrison, B., *Acta Cryst.*, 1977, **33B,** 303.
14. (a) Bradley, D. C., Abd-el Halim, F. M., Sadek, E. A. and Wardlaw, W., *J. Chem. Soc.*, 1952, 2032; (b) Bradley, D. C., Sinha, R. N. P. and Wardlaw, W., *J. Chem. Soc.*, 1958, 4651.
15. Only some reviews [2] are given here. (a) Bradley, D. C., Mehrotra, R. C. and Gauer, D. P., *Metal Alkoxides*, Academic Press, New York (1978); (b) Mehrotra, R. C., Kapoor, P. N. and Batwara, J. W., *Coord. Chem. Rev.*, 1989, **31,** 67; Mehrotra, R. C., Singh, A. and Tripathi, U. M., *Chem. Rev.*, 1991, **91,** 1287.
16. (a) Evans, W. J., Sollberger, M. S. and Hanusa, T. P., *J. Am. Chem. Soc.*, 1988, **110,** 1841; (b) Evans, W. J. and Sollberger, M. S., *Inorg. Chem.*, 1988, **27,** 4417; Andersen, R. A., Templeton, D. H. and Zalkin, A., *Inorg. Chem.*, 1978, **17,** 1962; (c) Bradley, D. C., Chudzynska, H., Hursthouse, M. B. and Motevalli, M., *Polyhedron*, 1991, **10,** 1049.
17. (a) Cotton, F. A., Marler, D. O. and Schwotzer, W., *Inorg. Chem.*, 1984, **23,** 4211; (b) Cotton, F. A., Marler, D. O. and Schwotzer, W., *Inorg. Chim. Acta*, 1984, **95,** 207.
18. Ibers, J. A., *Nature (London)*, 1963, **197,** 686.
19. Wright, D. A. and Williams, D. A., *Acta Cryst., Sect. B*, 1968, **24,** 1107; (b) Watenpaugh, K. and Caughlan, C. N., *Chem. Commun.*, 1967, 76; (c) Witters, R. W. and Caughlan, C. N., *Nature (London)*, 1965, **205,** 1312.
20. Chisholm, M. H., Huffman, J. C., Kirkpatrick, C. C., Leonelli, J. and Folting, K., *J. Am. Chem. Soc.*, 1981, **103,** 6093.
21. (a) Barnhart, D. M., Clark, D. L., Gordon, J. C., Huffman, J. C. and Watkin, J. G., *Inorg. Chem.*, 1994, **33,** 3939; (b) Clark, D. L., Crumbine, S. K., Scott, B. L. and Watkin, J. G., *J. Am. Chem. Soc.*, 1995, **117,** 9089.
22. Evans, W. J., Chamberlain, L. R., Ulibarri, T. A. and Ziller, J. W., *J. Am. Chem. Soc.*, 1988, **110,** 6423.
23. XSCANS Software Users Guide, Version 2.1, Siemens Industrial Automation, Inc.; Madison, WI, 1994.
24. Broach, R. W., Argonne National Laboratory, Illinois, 1978.
25. Sheldrick, G. M., Siemens Analytical X-Ray Instruments, Inc.; Madison, WI, 1994.
26. *International Tables of X-Ray Crystallography*, Vol. C., Kluwer Academic Publishers, Dordrecht (1992).
27. (a) Mehrotra, R. C. and Singh, A., *Chem. Soc. Rev.*, 1996, 1; (b) Hubert-Pfalzgraf, L. G., Daniele, S., Bennaceur, A., Daran, J.-C. and Vaissermann, J., *Polyhedron*, 1997, **16,** 1223; (c) Schmid, R., Ahamdane, H. and Mosset, A., *Inorg. Chim. Acta*, 1991, **190,** 237; (d) Daniele, S., Hubert-Pfalzgraf, L. G., Daran, J.-C. and Toscano, R. A., *Polyhedron*, 1993, **12,** 2091.
28. Vaartstra, B. A., Streib, W. E. and Caulton, K. G., *J. Am. Chem. Soc.*, 1990, **112,** 8593.
29. Poncelet, O., Sartain, W. J., Hubert-Pfalzgraf, L. G., Folting, K. and Caulton, K. G., *Inorg. Chem.*, 1989, **28,** 263.
30. Vaartstra, B. A., Huffman, J. C., Gradeff, P. S., Hubert-Pfalzgraf, L. G., Daran, J.-C., Parraud, S., Yunlu, K. and Caulton, K. G., *Inorg. Chem.*, 1990, **29,** 3126.
31. Shannon, R. D., *Acta Cryst.*, 1976, **A32,** 751.
32. (a) Pope, M. T., *Heteropoly and Isopoly Oxometalates*, Springer-Verlag, Berlin (1983); (b) Day, V. W. and Klemperer, W. G., *Science*, 1985, **228,** 533.

Pergamon

PII: S0277-5387(97)00270-2

Polyhedron Vol. 17, No. 5–6, pp. 879–889, 1998
© 1998 Elsevier Science Ltd
All rights reserved. Printed in Great Britain
0277–5387/98 $19.00+0.00

Syntheses of trirhenium alkoxide clusters in the presence of trimethylphosphine†

Wei-Wei Zhuang,[a] Simon G. Bott,[b] Arne Schmitz,[a] and David M. Hoffman[a]*

[a]Department of Chemistry, University of Houston, Houston, TX 77204, U.S.A.

[b]Department of Chemistry, University of North Texas, Denton, TX 76203, U.S.A.

(Received 30 April 1997; accepted 12 June 1997)

Abstract—The THF adduct of rhenium trichloride, $Re_3(\mu\text{-}Cl)_3Cl_6(THF)_3$, reacts with trimethylphosphine and $NaOPr^i$ to give the chloro-hydride $Re_3(\mu\text{-}OPr^i)_3Cl(H)(OPr^i)_4(PMe_3)$ and the dimer $\{Re_3(\mu\text{-}OPr^i)_3Cl(OPr^i)_4\}_2(\mu\text{-}Cl)_2$ in moderate yields. On the basis of spectroscopic studies and an X-ray crystal structure, the hydride ligand in the chloro–hydride cluster is proposed to occupy a site *trans* to Cl and *cis* to PMe_3. The hydride ligand is proposed to originate from isopropoxide β-hydrogen elimination. Ethylene and 2-butyne react with the phosphine-hydride cluster to yield ethyl and 2-butenyl clusters, respectively, and sodium isopropoxide reacts to give $Re_3(\mu\text{-}OPr^i)_3(H)(OPr^i)_5(PMe_3)$. The latter compound is more conveniently prepared by reacting PMe_3 with the homoleptic isopropoxide cluster $Re_3(\mu\text{-}OPr^i)_3(OPr^i)_6$. In contrast, the analogous reaction of PMe_3 with the homoleptic neopentoxide cluster $Re_3(\mu\text{-}OCH_2Bu^t)_3(OCH_2Bu^t)_6$ gives a simple phosphine adduct, $Re_3(\mu\text{-}OCH_2Bu^t)_3(OCH_2Bu^t)_6(PMe_3)$. The reaction of $Re_3(\mu\text{-}Cl)_3Cl_6(THF)_3$ with trimethylphosphine and sodium neopentoxide produces the reduced cluster $Re_3(\mu\text{-}Cl)(\mu\text{-}OCH_2Bu^t)_2Cl(OCH_2Bu^t)_4(PMe_3)_2$ in low yield. There are 13 electrons available for Re–Re bonding in the reduced cluster but its structure is not significantly different from similar 12-electron clusters. © 1998 Elsevier Science Ltd. All rights reserved

Keywords: rhenium; alkoxide; clusters; phosphine; hydride; β-hydrogen elimination.

We recently reported the synthesis of homoleptic trirhenium(III) alkoxide clusters [1–3] and used them as sources of hydride clusters (*via* alkoxide β-hydrogen elimination) in reactions with alkenes and alkynes [4,5]. As part of our studies, we became interested in preparing derivatives with halide ligands that could be used to synthesize alkyl, cationic and reduced alkoxide clusters. Reactions of $Re_3Cl_9(THF)_3$ with less than 9 equiv. of sodium alkoxides does not give clean alkoxide-halide products, producing instead mixtures that include the homoleptic alkoxide clusters. We therefore turned to reactions of $Re_3Cl_9(THF)_{3-n}(PMe_3)_n$ clusters [6] with sodium alkoxides in the expectation the phosphine ligands could block complete substitution of the halides and stabilize the resulting halides to oligomerization *via* chloride or alkoxide bridges.

Herein we report on reactions of $Re_3Cl_9(THF)_3$ with sodium isopropoxide and neopentoxide in the presence of trimethylphosphine that yield $\{Re_3(\mu\text{-}OPr^i)_3Cl(OPr^i)_4\}_2(\mu\text{-}Cl)_2$, $Re_3(\mu\text{-}OPr^i)_3Cl(H)(OPr^i)_4(PMe_3)$ and $Re_3(\mu\text{-}Cl)(\mu\text{-}OCH_2Bu^t)_2Cl(OCH_2Bu^t)_4(PMe_3)_2$ clusters, and chemistry derived from or motivated by the isolation of these products, including the synthesis of $Re_3(\mu\text{-}OCH_2Bu^t)_3(OCH_2Bu^t)_6(PMe_3)$, $Re_3(\mu\text{-}OPr^i)_3H(OPr^i)_5(PMe_3)$, $Re_3(\mu\text{-}OPr^i)_3Cl(Et)(OPr^i)_4(NCMe)$ and $Re_3(\mu\text{-}OPr^i)_3Cl(\eta\text{-}C(Me)=C(H)Me)(OPr^i)_4$.

RESULTS AND DISCUSSION

A summary of our synthetic results is presented in Scheme 1. The X-ray crystal structures of $\{Re_3(\mu\text{-}OPr^i)_3Cl(OPr^i)_4\}_2(\mu\text{-}Cl)_2$, $Re_3(\mu\text{-}OPr^i)_3Cl(H)(OPr^i)_4(PMe_3)$, $Re_3(\mu\text{-}Cl)(\mu\text{-}OCH_2Bu^t)_2Cl(OCH_2Bu^t)_4(PMe_3)_2$ and $Re_3(\mu\text{-}OCH_2Bu^t)_3(OCH_2Bu^t)_6(PMe_3)$ were determined.

* Author to whom correspondence should be addressed.

† Dedicated to Professor D. C. Bradley on the occasion of his 73rd birthday.

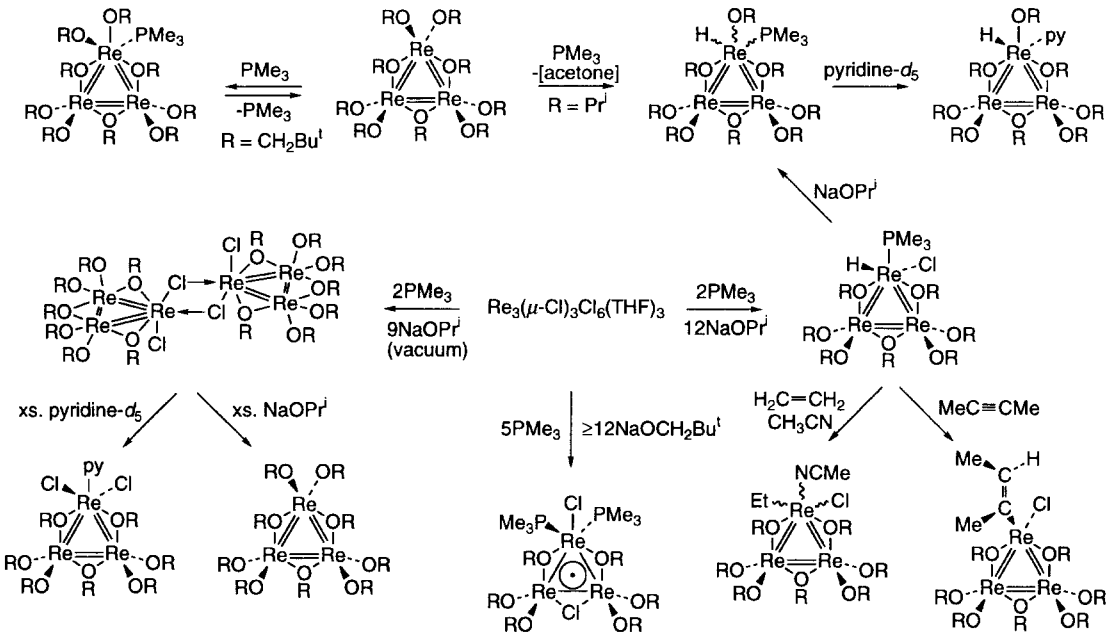

Scheme 1.

$\{Re_3(\mu\text{-}OPr^i)_3Cl(OPr^i)_4\}_2(\mu\text{-}Cl)_2$

The addition of 2–3 equiv. of PMe_3 to $Re_3(\mu\text{-}Cl)_3Cl_6(THF)_3$ in THF, which presumably forms $Re_3(\mu\text{-}Cl)_3Cl_6(PMe_3)_2(THF)$ or a mixture of $Re_3(\mu\text{-}Cl)_3Cl_6(PMe_3)_3$ and starting material [6,7], followed by the slow addition of 9 equiv. of $NaOPr^i$ to the reaction mixture produces, after workup, dark red crystals of the cluster dimer $\{Re_3(\mu\text{-}OPr^i)_3Cl(OPr^i)_4\}_2(\mu\text{-}Cl)_2$ in moderate yield. In the synthesis it is critical for phosphine to be removed *in vacuo* from the reaction mixture after the $NaOPr^i$ addition or otherwise the product cannot be isolated. When $NaOPr^i$ is added to the cluster dimer, the known homoleptic isopropoxide cluster [1,2] $Re_3(\mu\text{-}OPr^i)_3(OPr^i)_6$ is produced. Several attempts to prepare the cluster dimer without using phosphine in the reaction mixture failed, but it is reasonable to expect that the proper reaction conditions to produce the dimer in the absence of phosphine will be found eventually.

The room temperature ^1H NMR spectrum of $\{Re_3(\mu\text{-}OPr^i)_3Cl(OPr^i)_4\}_2(\mu\text{-}Cl)_2$ in C_6D_6 consists of four broad doublets of equal intensity arising from the methyl groups of the terminal isopropoxide ligands, two broad doublets and one sharp doublet arising from the methyl groups of the bridging isopropoxide ligands, and two broad septets (2:2) and one misshapen septet (relative intensity 3) arising from the methine groups. The misshapen septet is a broad septet of relative intensity 2 overlapping a septet of intensity 1. All of the broad resonances become sharp as the sample is cooled from room temperature to 10°C. The data are consistent with the structure shown in Scheme 1 (i.e. a structure with virtual C_s symmetry) and the solid state structure (*vide infra*). It should be noted that the room temperature ^1H NMR spectrum recorded for a $CDCl_3$ solution is identical to that reported by Wilkinson and co-workers for a compound with the proposed formulation $Re_3(\mu\text{-}Cl)(\mu\text{-}OPr^i)_2Cl(OPr^i)_5$ [8]. It is clear '$Re_3(\mu\text{-}Cl)(\mu\text{-}OPr^i)_2Cl(OPr^i)_5$' is in fact the dimer $\{Re_3(\mu\text{-}OPr^i)_3Cl(OPr^i)_4\}_2(\mu\text{-}Cl)_2$ on the basis of our NMR data and X-ray crystal structure. However, all attempts to prepare the cluster dimer using the reported procedure [8], which did not involve trimethylphosphine, have thus far failed.

To probe the cause of the broadening in the ^1H NMR resonances at room temperature, high temperature spectra were collected for a toluene-d_8 solution. At 85°C, the temperature at which some decomposition occurs, the spectrum consists of three septets in a 1:2:4 ratio and three doublets in a 2:4:8 ratio where the doublets of intensity 4 and 2 are in the bridging isopropoxide region. The doublet that was sharp in the room temperature spectrum remained sharp over the entire temperature range examined. The doublet of intensity 8 could be interpreted as a sharp doublet superimposed on a very broad doublet. If this interpretation is correct, the data are consistent with a dynamic process that gives the molecule two perpendicular mirror planes (i.e. gives it virtual C_{2v} symmetry). A plausible mechanism to account for this data is a dimer $\rightleftharpoons$ monomer equilibrium; the monomer $Re_3(\mu\text{-}OPr^i)_3Cl_2(OPr^i)_4$ would have virtual C_{2v} symmetry because of rapid C—O bond rotation coupled with rapid inversion at oxygen for the bridg-

ing isopropoxide ligands. Another possibility is a process involving Cl debridging and the bond rotation shown in **I**. Indirect support for the equilibrium pro-

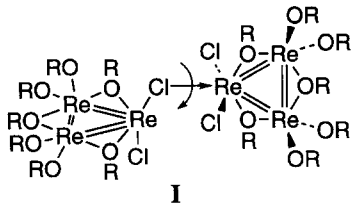

I

posal comes from the reaction of $\{Re_3(\mu\text{-}OPr^i)_3Cl(O\text{-}Pr^i)_4\}_2(\mu\text{-}Cl)_2$ with pyridine-d_5 in benzene-d_6, which gives an ^1H NMR spectrum consisting of three septets in a 4 : 2 : 1 ratio and four doublets in a 4 : 4 : 4 : 2 ratio. The spectroscopic data are consistent with formation of the pyridine adduct $Re_3(\mu\text{-}OPr^i)_3Cl_2(OPr^i)_4(py)$ having the C_{2v} structure shown in Scheme 1.

$Re_3(\mu\text{-}OPr^i)_3Cl(H)(OPr^i)_4(PMe_3)$

The addition of 2–4 equiv. of PMe_3 to $Re_3(\mu\text{-}Cl)_3Cl_6(THF)_3$ in THF followed by the slow addition of 12 equiv. of $NaOPr^i$ to the reaction mixture produces, after workup, green blocks of $Re_3(\mu\text{-}OPr^i)_3Cl(H)(OPr^i)_4(PMe_3)$ in moderate yield. The dimer $\{Re_3(\mu\text{-}OPr^i)_3Cl(OPr^i)_4\}_2(\mu\text{-}Cl)_2$ can be found in the mother liquor.

The spectroscopic data for $Re_3(\mu\text{-}OPr^i)_3Cl(H)(O\text{-}Pr^i)_4(PMe_3)$ are consistent with the structure shown in Scheme 1 and the solid state structure (*vide infra*). The ^1H NMR spectrum (C_6D_6) consists of seven equal intensity doublets, four in the bridging and three in the terminal isopropoxide ligand regions, arising from the methyl protons, a doublet arising from the phosphine methyl protons, four methine septets in a 1 : 2 : 2 : 2 ratio, and a doublet at $\delta -6.3$ due to the hydride ligand with phosphorous coupling (42 Hz). In the IR spectrum there is a sharp, medium intensity band at 1979 cm^{-1} that can be assigned to a terminal hydride stretch; as a comparison, the Re—H stretching bands for $Re_3(\mu\text{-}OPr^i)_3(H)(OPr^i)_5$ and $Re_3(\mu\text{-}OPr^i)_3(H)(OPr^i)_5(py)$ occur at 1991 and 2002 cm^{-1}, respectively [2].

We have reported recently several examples of trirhenium(III) alkoxide clusters acting as sources of terminal hydride clusters *via* observed or proposed alkoxide β-hydrogen elimination reactions [1–5]. On this basis, we propose that the source of the hydride ligand in $Re_3(\mu\text{-}OPr^i)_3Cl(H)(OPr^i)_4(PMe_3)$ is isopropoxide β-hydrogen elimination. In an attempt to observe acetone, the reaction to form the hydride cluster was carried out in an NMR tube but the ^1H NMR spectra of the mixture were too complex to conclude whether acetone was present.

$Re_3(\mu\text{-}OPr^i)_3(H)(OPr^i)_5(PMe_3)$

The NMR-tube scale reaction of $Re_3(\mu\text{-}OPr^i)_3Cl(H)(OPr^i)_4(PMe_3)$ with excess $NaOPr^i$ in benzene-d_6 gives a new hydride cluster, $Re_3(\mu\text{-}OPr^i)_3(H)(OPr^i)_5(PMe_3)$. On a large scale, $Re_3(\mu\text{-}OPr^i)_3(H)(OPr^i)_5(PMe_3)$ is more conveniently synthesized by the reaction of $Re_3(\mu\text{-}OPr^i)_3(OPr^i)_6$ with excess PMe_3 in hexanes, from which the hydride can be isolated as green crystalline blocks in moderate yield. When the reaction of $Re_3(\mu\text{-}OPr^i)_3(OPr^i)_6$ with excess PMe_3 is carried out in an NMR tube, $Re_3(\mu\text{-}OPr^i)_3(H)(OPr^i)_5(PMe_3)$ is formed in $\geqslant 95\%$ yield (*vs* C_6Me_6 internal standard) within minutes, and 1 equiv. of acetone is produced for every molecule of product cluster. The cluster $Re_3(\mu\text{-}OPr^i)_3(OPr^i)_6$ is known to exist in solution as an equilibrium mixture of $Re_3(\mu\text{-}OPr^i)_3(H)(OPr^i)_5$ and acetone [1,2]. In these reactions the phosphine acts as a trapping reagent to form the phosphine-hydride cluster in the same way that pyridine, olefins and alkynes can act as hydride traps to form a pyridine adduct, and alkyl and alkenyl clusters [1,2,4].

The ^1H NMR spectrum of $Re_3(\mu\text{-}OPr^i)_3(H)(OPr^i)_5(PMe_3)$ in CD_2Cl_2 consists of eight equal intensity methyl doublets, with five in the terminal and three in the bridging isopropoxide regions, a doublet arising from the phosphine methyl protons, and four methine septets in a 1 : 1 : 2 : 4 ratio. Three of the septets are not well resolved. The pattern of methyl resonances indicates clearly that the cluster has mirror symmetry but the stereochemistry at the unique Re is ambiguous (i.e. it is unclear whether there is a *trans* or *cis*-P—Re—H arrangement, and if it is *cis*, whether the hydride is in the plane of the Re_3 triangle). In the closely related, structurally characterized hydride cluster $Re_3(\mu\text{-}OPr^i)_3(H)(OPr^i)_5(py)$ the hydride is perpendicular to the Re_3 plane and there is a *trans*-py-Re-H arrangement. The cluster $Re_3(\mu\text{-}OPr^i)_3(H)(OPr^i)_5(PMe_3)$ can be converted to the pyridine adduct by adding a drop of pyridine-d_5 to a benzene-d_6 solution of $Re_3(\mu\text{-}OPr^i)_3(H)(OPr^i)_5(PMe_3)$. On the basis of the structural precedent of $Re_3(\mu\text{-}OPr^i)_3(H)(OPr^i)_5(py)$ and the conversion of the phosphine cluster to the pyridine adduct, it is reasonable to suggest that $Re_3(\mu\text{-}OPr^i)_3(H)(OPr^i)_5(PMe_3)$ has a structure analogous to the pyridine adduct. On the other hand, the P-H coupling constant in $Re_3(\mu\text{-}OPr^i)_3(H)(OPr^i)_5(PMe_3)$ is about 15 Hz less (27 *vs* 42 Hz) than the coupling constant in $Re_3(\mu\text{-}OPr^i)_3Cl(H)(O\text{-}Pr^i)_4(PMe_3)$, which an X-ray crystallographic study (*vide infra*) shows has a *cis*-P—Re—H arrangement. This suggests $Re_3(\mu\text{-}OPr^i)_3(H)(OPr^i)_5(PMe_3)$ has *cis*-P—Re—H stereochemistry. A crystal structure of $Re_3(\mu\text{-}OPr^i)_3(H)(OPr^i)_5(PMe_3)$ is needed to resolve the structural ambiguity.

The IR spectrum of $Re_3(\mu\text{-}OPr^i)_3(H)(OPr^i)_5(PMe_3)$ has a medium intensity band at 1923 cm^{-1} that can be assigned to a terminal Re—H stretch.

$Re_3(\mu\text{-}OCH_2Bu^t)_3(OCH_2Bu^t)_6(PMe_3)$

The synthesis of $Re_3(\mu\text{-}OPr^i)_3(H)(OPr^i)_5(PMe_3)$ from PMe_3 and $Re_3(\mu\text{-}OPr^i)_3(OPr^i)_6$ suggested that the

analogous neopentoxide cluster, $Re_3(\mu\text{-}OCH_2Bu^t)_3(H)(OCH_2Bu^t)_5(PMe_3)$, might also be synthesized by reacting $Re_3(\mu\text{-}OCH_2Bu^t)_3(OCH_2Bu^t)_6$ with PMe_3. The reaction produces, however, only the simple phosphine adduct $Re_3(\mu\text{-}OCH_2Bu^t)_3(OCH_2Bu^t)_6(PMe_3)$ as crystalline green blocks in moderate yield. Some PMe_3 is lost from the cluster when it is held under dynamic vacuum for an extended period of time, which may account for why the chemical analysis is close to a $Re_3(\mu\text{-}OCH_2Bu^t)_3(OCH_2Bu^t)_6$ stoichiometry. When the reaction is carried out in an NMR tube (benzene-d_6; 5–6 equiv. of PMe_3), the phosphine adduct forms within several hours in >95% yield (*vs* C_6Me_6 internal standard). In contrast, we reported recently that the NMR tube-scale reactions of $Re_3(\mu\text{-}OCH_2Bu^t)_3(OCH_2Bu^t)_6$ with PMe_2Ph under forcing conditions produces what appears to be $Re_3(\mu\text{-}OCH_2Bu^t)_3(H)(OCH_2Bu^t)_5(PMe_2Ph)$ [$\delta(ReH)$ −3.1, J_{PH} = 30 Hz, C_6D_6] but the hydride was not formed cleanly [3]. The difference in reactivity of $Re_3(\mu\text{-}OCH_2Bu^t)_3(OCH_2Bu^t)_6$ and $Re_3(\mu\text{-}OPr^i)_3(OPr^i)_6$ with PMe_3 under mild conditions—formation of $Re_3(\mu\text{-}OCH_2Bu^t)_3(OCH_2Bu^t)_6(PMe_3)$ *vs* $Re_3(\mu\text{-}OPr^i)_3(H)(OPr^i)_5(PMe_3)$ and acetone—is consistent with our previous findings [2] that $K_{eq} \approx 6 \times 10^{-4}$ M at room temperature for the equilibrium $Re_3(\mu\text{-}OPr^i)_3(OPr^i)_6 \rightleftharpoons Re_3(\mu\text{-}OPr^i)_3(H)(OPr^i)_5 + O{=}CMe_2$ and the analogous neopentoxide β-hydrogen elimination equilibrium, if it exists at all, favors strongly the homoleptic cluster [3].

The room temperature ^1H NMR spectrum of $Re_3(\mu\text{-}OCH_2Bu^t)_3(OCH_2Bu^t)_6(PMe_3)$ is fully consistent with the structure shown in Scheme 1 and the solid state structure (*vide infra*), having three AB quartets, a singlet and two doublets (due to weak P–H coupling) in the methylene region, and six singlets in the Bu^t region in a 1:1:1:2:2:2 ratio. The phosphine peak is obscured in the spectrum by one of the methyl resonances at ≈1 ppm, which was proven by preparing the PMe_3-d_9 complex and obtaining its $^2H\{^1H\}$ spectrum. To test the stability of the adduct in solution, a toluene-d_8 solution containing excess PMe_3 was heated in the NMR probe. At 60°C, the adduct was stable, but at 80°C complete dissociation occurred giving $Re_3(\mu\text{-}OCH_2Bu^t)_3(OCH_2Bu^t)_6$ and free PMe_3. Upon cooling the sample, the adduct reformed slowly.

$Re_3(\mu\text{-}Cl)(\mu\text{-}OCH_2Bu^t)_2Cl(OCH_2Bu^t)_4(PMe_3)_2$

The successful isolation of the isopropoxide derivatives $Re_3(\mu\text{-}OPr^i)_3Cl(H)(OPr^i)_4(PMe_3)$ and $\{Re_3(\mu\text{-}OPr^i)_3Cl(OPr^i)_4\}_2(\mu\text{-}Cl)_2$ from reactions of sodium isopropoxide and rhenium chloride in the presence of trimethylphosphine prompted us to attempt similar reactions using sodium neopentoxide. Various stoichiometries were used but in only one case was a clean product isolated. The reaction of $Re_3(\mu\text{-}Cl)_3Cl_6(THF)_3$ in THF with five equiv. of PMe_3 followed by the slow addition of ⩾12 equiv. of $NaOCH_2Bu^t$ gave low (≈12%), reproducible yields of the reduced cluster $Re_3(\mu\text{-}Cl)(\mu\text{-}OCH_2Bu^t)_2Cl(OCH_2Bu^t)_4(PMe_3)_2$, which was identified by X-ray crystallography. Electron counting indicates there are 13 electrons available for Re—Re bonding in the cluster. Consistent with the compound being paramagnetic, the ^1H NMR spectrum has only broad, ill-defined resonances that do not sharpen when the sample is warmed or cooled.

The identity of the reducing agent in the synthesis of $Re_3(\mu\text{-}Cl)(\mu\text{-}OCH_2Bu^t)_2Cl(OCH_2Bu^t)_4(PMe_3)_2$ has not been determined. Walton and co-workers [9,10], however, have observed reduction of rhenium(III) chloride by monodentate tertiary phosphines under forcing conditions to yield the Re^{II} dimers $[ReCl_2(PR_3)_2]_2$ and Wilkinson *et al.* have reported reduction of $Re_3Cl_3(CH_2SiMe_3)_6$ by PMe_3 to give the Re^{II} dimer $[ReCl(CH_2SiMe_3)(PMe_3)_2]_2$ [11]. These reports suggest the preparation of $Re_3(\mu\text{-}Cl)(\mu\text{-}OCH_2Bu^t)_2Cl(OCH_2Bu^t)_4(PMe_3)_2$ involves phosphine reduction of rhenium(III). More logical preparations of the reduced cluster using reducing agents such as magnesium and Na/Hg have thus far failed.

Only two other examples of well characterized 13-electron Re_3 clusters are known. Wilkinson, Hursthouse and co-workers reported the crystal structure of the hexanuclear cluster **II** [12,13] in which the extra

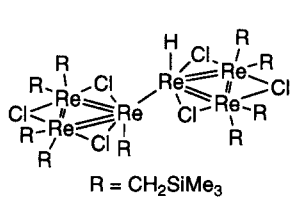

II

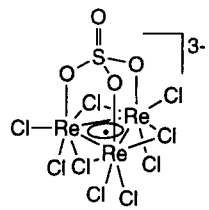

III

electron has been used to couple two 13-electron Re_3 fragments *via* a Re—Re bond, and Mertis *et al.* reported the electrochemical reduction of Re_3Cl_9 in aqueous hydrochloric acid from which the triply-bridged sulphato derivative **III** could be isolated [14].

Reactions of $Re_3(\mu\text{-}OPr^i)_3Cl(H)(OPr^i)_4(PMe_3)$ *with ethylene and 2-butyne*

To test the reactivity of the Re—H bond in $Re_3(\mu\text{-}OPr^i)_3Cl(H)(OPr^i)_4(PMe_3)$, reactions with ethylene and 2-butyne were carried out. The reaction of ethylene with $Re_3(\mu\text{-}OPr^i)_3Cl(H)(OPr^i)_4(PMe_3)$ gave the ethyl cluster $Re_3(\mu\text{-}OPr^i)_3Cl(Et)(OPr^i)_4(MeCN)$ in low yield after a workup that included exposure to excess acetonitrile. The reaction carried out in an NMR tube was not clean, which accounts for the low yield of the large scale reaction. The reaction of $Re_3(\mu\text{-}OPr^i)_3Cl(H)(OPr^i)_4(PMe_3)$ with 2-butyne gave the 2-butenyl cluster $Re_3(\mu\text{-}OPr^i)_3Cl(\eta\text{-}C(Me){=}CMe(H))(OPr^i)_4(PMe_3)$ in 44% yield as green needles after workup and crystallization from CH_2Cl_2/CH_3CN.

Proton NMR spectra for the ethyl and 2-butenyl clusters indicate they have virtual mirror symmetry in solution as illustrated in Scheme 1. The ethyl ligand in $Re_3(\mu\text{-}OPr^i)_3Cl(Et)(OPr^i)_4(MeCN)$ gives rise to a quartet and triplet. The stereochemistry at the Re(Cl)Et(MeCN) center cannot be assigned on the basis of NMR spectra but it is likely that the strong σ-donor ethyl ligand is perpendicular to the Re_3 plane as in the case of the hydride ligand in structurally characterized $Re_3(\mu\text{-}OPr^i)_3H(OPr^i)_5(py)$ [2]. The butenyl proton of $Re_3(\mu\text{-}OPr^i)_3Cl(\eta\text{-}C(Me)=CMe(H))(OPr^i)_4$ appears as a quartet and one of the methyl groups gives rise to a doublet. NOE experiments suggest the methyl groups are mutually *cis*, as expected for an insertion product.

X-ray crystal structures of $Re_3(\mu\text{-}OCH_2Bu^t)_3(OCH_2Bu^t)_6(PMe_3)$, $Re_3(\mu\text{-}OPr^i)_3Cl(H)(OPr^i)_4(PMe_3)$, $\{Re_3(\mu\text{-}OPr^i)_3Cl(OPr^i)_4\}_2(\mu\text{-}Cl)_2$ *and* $Re_3(\mu\text{-}Cl)(\mu\text{-}OCH_2Bu^t)_2Cl(OCH_2Bu^t)_4(PMe_3)_2$

Thermal ellipsoid plots are shown in Figs 1–4 and selected bond distances and angles are presented in Tables 1 and 2. The clusters $Re_3(\mu\text{-}OCH_2Bu^t)_3(OCH_2Bu^t)_6(PMe_3)$, $Re_3(\mu\text{-}OPr^i)_3Cl(H)(OPr^i)_4(PMe_3)$, $\{Re_3(\mu\text{-}OPr^i)_3Cl(OPr^i)_4\}_2(\mu\text{-}Cl)_2$ crystallize with CH_2Cl_2 in the lattice.

The cluster $\{Re_3(\mu\text{-}OPr^i)_3Cl(OPr^i)_4\}_2(\mu\text{-}Cl)_2$ is situated about an inversion center and $Re_3(\mu\text{-}Cl)(\mu\text{-}OCH_2Bu^t)_2Cl(OCH_2Bu^t)_4(PMe_3)_2$ is bisected by a crystallographic two-fold axis. The hydride ligand in $Re_3(\mu\text{-}OPr^i)_3Cl(H)(OPr^i)_4(PMe_3)$ was not located crystallographically, but there is a 'missing' ligand at Re(1) *trans* to Cl(1) that is the likely hydride site. This assignment is consistent with the spectroscopic data as well. There are no unusual bond angles associated with the clusters, but there are some interesting differences in analogous bond distances.

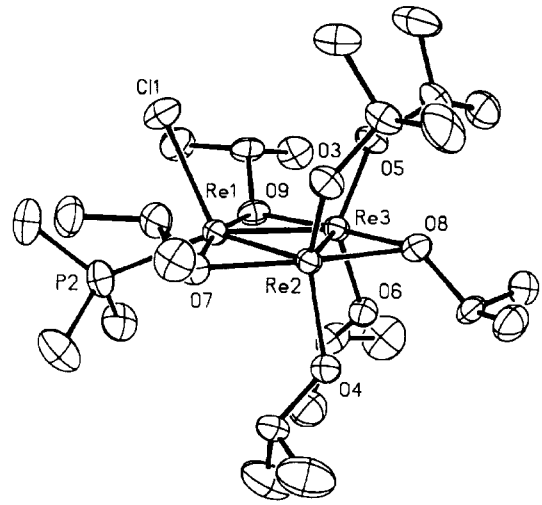

Fig. 2. Molecular structure of $Re_3(\mu\text{-}OPr^i)_3Cl(H)(OPr^i)_4(PMe_3)$ (40% probability ellipsoids).

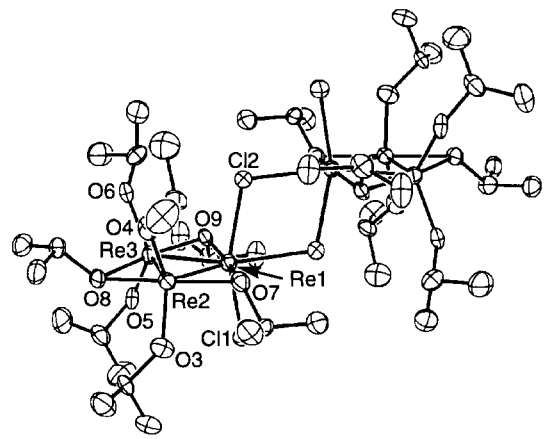

Fig. 3. Molecular structure of $\{Re_3(\mu\text{-}OPr^i)_3Cl(OPr^i)_4\}_2(\mu\text{-}Cl)_2$ (30% probability ellipsoids).

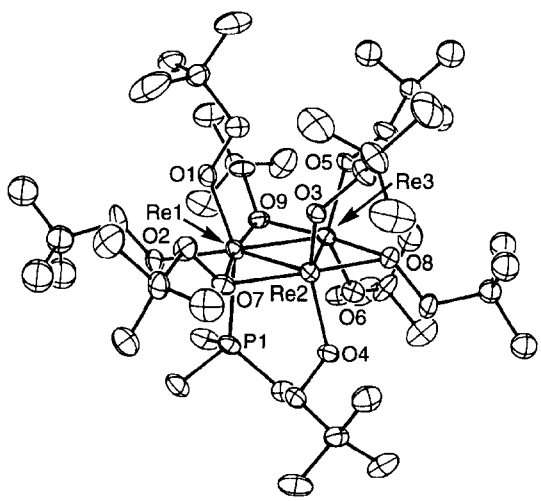

Fig. 1. Molecular structure of $Re_3(\mu\text{-}OCH_2Bu^t)_3(OCH_2Bu^t)_6(PMe_3)$ (40% probability ellipsoids).

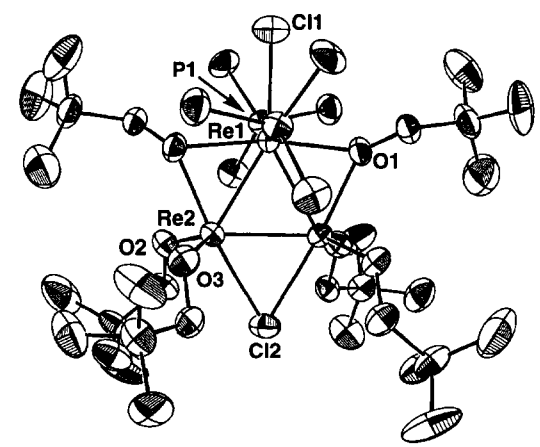

Fig. 4. Molecular structure of $Re_3(\mu\text{-}Cl)(\mu\text{-}OCH_2Bu^t)_2Cl(OCH_2Bu^t)_4(PMe_3)_2$ (50% probability ellipsoids).

Table 1. Selected bond distances (Å) and angles (°) for $Re_3(\mu\text{-}OCH_2Bu^t)_3(OCH_2Bu^t)_6(PMe_3)$, $Re_3(\mu\text{-}OPr^i)_3Cl(H)(O\text{-}Pr^i)_4(PMe_3)$, and $\{Re_3(\mu\text{-}OPr^i)_3Cl(OPr^i)_4\}_2(\mu\text{-}Cl)_2$

	$Re_3(\mu\text{-}OCH_2Bu^t)_3$ $(OCH_2Bu^t)_6(PMe_3)$	$Re_3(\mu\text{-}OPr^i)_3Cl$- $(H)(OPr^i)_4(PMe_3)$	$\{Re_3(\mu\text{-}OPr^i)_3Cl$- $(OPr^i)_4\}_2(\mu\text{-}Cl)_2$
Re(1)—Re(2)	2.385(1)	2.379(1)	2.385(1)
Re(1)—Re(3)	2.388(1)	2.374(1)	2.392(1)
Re(2)—Re(3)	2.388(1)	2.375(1)	2.376(1)
Re(2)—O(3)	1.903(7)	1.890(6)	1.875(11)
Re(2)—O(4)	1.922(7)	1.913(6)	1.911(11)
Re(2)—O(7)	2.088(8)	2.073(6)	2.083(11)
Re(2)—O(8)	2.098(7)	2.091(6)	2.116(11)
Re(3)—O(8)	2.125(7)	2.098(5)	2.123(10)
Re(1)—O(7)	2.121(7)	2.137(5)	2.103(11)
Re(3)—O(5)	1.904(7)	1.887(7)	1.860(11)
Re(3)—O(6)	1.906(7)	1.912(5)	1.893(10)
Re(3)—O(9)	2.120(7)	2.079(5)	2.096(10)
Re(1)—O(9)	2.127(7)	2.125(5)	2.110(10)
Re(1)—X	2.488(3)[b]	2.421(2)[c]	2.344(4)[d]
Re(1)—Y	1.963(7)[b]	—	2.432(4)[d]
Re(1)—Z	2.047(8)[b]	2.534(3)[c]	2.634(4)[d]
O(3)—Re(2)—O(4)	123.8(3)	124.7(2)	125.5(5)
O(5)—Re(3)—O(6)	123.6(3)	125.5(2)	125.9(5)
Re(2)—O(8)—Re(3)	68.9(2)	69.1(2)	68.2(3)
Re(1)—O(7)—Re(2)	69.0(2)	68.8(2)	69.5(3)
Re(1)—O(9)—Re(3)	68.4(2)	68.8(1)	69.3(3)
X—Re(1)—Y	156.8(2)[b]	—	160.1(1)[d]
X—Re(1)—Z	74.9(2)[b]	91.0(1)[c]	84.0(1)[d]
Y—Re(1)—Z	81.9(3)[b]	—	76.2(1)[d]
Re(1,2)—Re(3)—O(5)[a]	117.8	120.8	120.4
Re(1,2)—Re(3)—O(6)[a]	118.6	113.7	113.5
Re(1,3)—Re(2)—O(3)[a]	115.9	118.5	118.5
Re(1,3)—Re(2)—O(4)[a]	120.3	116.7	115.8
Re(2,3)—Re(1)—X[a]	94.8[b]	116.4[c]	100.2[d]
Re(2,3)—Re(1)—Y[a]	108.3[b]	—	99.7[d]
Re(2,3)—Re(1)—Z[a]	169.5[b]	152.6[c]	175.8[d]

[a] Re(n,m) is the midpoint between atoms Re(n) and Re(m).
[b] X = P(1), Y = O(1) and Z = O(2).
[c] X = Cl(1) and Z = P(2).
[d] X = Cl(1), Y = Cl(2) and Z = Cl(2′).

Table 2. Selected bond distances (Å) and angles (°) for $Re_3(\mu\text{-}Cl)(\mu\text{-}OCH_2Bu^t)_2Cl(OCH_2Bu^t)_4(PMe_3)_2$

Re(1)—Re(2)	2.4182(7)	Re(2)—O(1′)	2.073(7)
Re(2)—Re(2′)	2.4801(4)	Re(2)—O(2)	1.900(7)
Re(1)—P(1)	2.474(3)	Re(2)—O(3)	1.915(8)
Re(1)—Cl(1)	2.453(5)	Re(2)—Cl(2)	2.440(4)
Re(1)—O(1)	2.118(7)		
Re(2)—Re(1)—P(1)	100.26(7)	O(2)—Re(2)—O(3)	120.8(3)
Re(2)—Re(1)—P(1′)	94.12(2)	Re(1)—O(1)—Re(2′)	70.5(2)
P(1)—Re(1)—P(1′)	163.25(8)	Re(2)—Cl(2)—Re(2′)	61.1(1)
Cl(1)—Re(1)—P(1)	81.63(8)	Re(2,2′)—Re(1)—P(1)[a]	98.4(1)
Cl(1)—Re(1)—O(1)	95.3(2)	Re(1,2′)—Re(2)—O(2)[a]	120.6(2)
O(1)—Re(1)—O(1′)	169.5(2)	Re(1,2)—Re(2)—O(3)[a]	118.4(2)

[a] Re(n,m) is the midpoint between atoms Re(n) and Re(m).

The Re—Re bond distances [2.374(1)–2.392(1) Å] in $Re_3(\mu\text{-}OCH_2Bu^t)_3(OCH_2Bu^t)_6(PMe_3)$, $Re_3(\mu\text{-}OPr^i)_3Cl(H)(OPr^i)_4(PMe_3)$ and $\{Re_3(\mu\text{-}OPr^i)_3Cl(OPr^i)_4\}_2(\mu\text{-}Cl)_2$ are comparable to those found in $Re_3(\mu\text{-}OCH_2Bu^t)_3(OCH_2Bu^t)_6$, $[Na(THF)_2][Re_3(\mu\text{-}OCH_2Bu^t)_3H(OCH_2Bu^t)_6]$, $Re_3(\mu\text{-}OPr^i)_3(H)(OPr^i)_5$, $Re_3(\mu\text{-}OPr^i)_3(H)(OPr^i)_5(py)$, and $Re_3(\mu\text{-}OPr^i)_3(\eta\text{-}CPh{=}CH_2)(OPr^i)_5$ [2.357(1)–2.383(2) Å] [2–4] but the distances in the reduced cluster $Re_3(\mu\text{-}Cl)(\mu\text{-}OCH_2Bu^t)_2Cl(OCH_2Bu^t)_4(PMe_3)_2$ are slightly longer [2.4182(7) and 2.4801(4) Å]. In the latter case, the longer of the two distances is associated with the chlorine-bridged Re(2)—Re(2′) bond. For comparison, the Re–Re distances in $Re_3(\mu\text{-}Cl)_3(OBu^t)_6$ are 2.436(3)–2.439(3) Å and the chlorine-bridged Re–Re distance in $Re_3(\mu\text{-}Cl)(\mu\text{-menthoxo})_2Cl(menthoxo)_5$ is 2.422(3) Å while the alkoxide-bridged distances are 2.368(3) and 2.376(3) Å [8]. It is tempting to suggest that the slightly longer Re–Re distances in the reduced cluster indicate the added electron occupies a Re–Re antibonding MO but the effect, if it exists at all, is small and we hesitate to draw any firm conclusions.

The Re–P distances in $Re_3(\mu\text{-}OCH_2Bu^t)_3(OCH_2Bu^t)_6(PMe_3)$ [2.488(3) Å] and $Re_3(\mu\text{-}Cl)(\mu\text{-}OCH_2Bu^t)_2Cl(OCH_2Bu^t)_4(PMe_3)_2$ [2.474(3) Å] are not significantly different from one another but they are both shorter than the distances in $Re_3(\mu\text{-}OPr^i)_3Cl(H)(OPr^i)_4(PMe_3)$ [2.534(3) Å] and $Re_3(\mu\text{-}Cl)_3Cl_6(PMe_3)_3$ [2.634(4) Å] [7]. In all the clusters, the $Re\text{–}O_{terminal}$ distances are not significantly different from each other with the exception of Re(1)—O(1) and Re(1)—O(2) in $Re_3(\mu\text{-}OCH_2Bu^t)_3(OCH_2Bu^t)_6(PMe_3)$, which are, respectively, greater than 0.09 Å and 0.13 Å longer than the other terminal distances. It appears that the sterically congested Re(1) site in $Re_3(\mu\text{-}OCH_2Bu^t)_3(OCH_2Bu^t)_6(PMe_3)$ is associated with longer distances with respect to the other alkoxide clusters.

The $Re\text{–}Cl_{terminal}$ distance in $Re_3(\mu\text{-}OPr^i)_3Cl(H)(OPr^i)_4(PMe_3)$ [2.421(2) Å] is almost 0.1 Å longer than the $Re\text{–}Cl_{terminal}$ distance in $\{Re_3(\mu\text{-}OPr^i)_3Cl(OPr^i)_4\}_2(\mu\text{-}Cl)_2$ [2.344(4) Å], where the distance is comparable to those in $Re_3(\mu\text{-}Cl)_3Cl_6(PMe_3)_3$ [2.310(3) Å]. In the phosphine-hydride cluster the terminal chlorine is *trans* to H, which has a high *trans* influence, and in the latter, chlorine is *trans* to a bridging chloride, a low *trans* influence ligand [15]. The $Re\text{–}Cl_{bridge}$ distances in the cluster dimer are longer than the $Re\text{–}Cl_{terminal}$ distance, and the Re–Cl(2′) distance is especially long, suggesting that the dimer is held together weakly.

EXPERIMENTAL

General techniques and reagents

All manipulations were carried out in a nitrogen-filled glovebox or by using standard Schlenk techniques. Solvents were purified by using standard techniques and stored in the drybox over molecular sieves until they were needed. Rhenium metal was purchased from Cleveland Refractory Metals. The compounds $Re_3(\mu\text{-}Cl)_3Cl_6(THF)_3$ [13, 16, 17], $Re_3(\mu\text{-}OPr^i)_3(OPr^i)_6$ and $Re_3(\mu\text{-}OCH_2Bu^t)_3(OCH_2Bu^t)_6$ were prepared according to the literature methods [1–3]. Proton and ^{13}C NMR spectra were referenced internally to solvent proton and carbon-13 resonances, respectively. Spectra were collected on a 300-MHz instrument. Elemental analyses were performed by Oneida Research Services, Whitesboro, NY.

Syntheses

$\{Re_3(\mu\text{-}OPr^i)_3Cl(OPr^i)_4\}_2(\mu\text{-}Cl)_2$. Trimethylphosphine (1.8 mmol) was added *via* a calibrated vacuum manifold to a frozen red solution of $Re_3Cl_9(THF)_3$ (0.98 g, 0.90 mmol) in THF (50 cm^3). The color of the solution gradually changed to purple as it was stirred at room temperature for 12 h. Sodium isopropoxide (0.66 g, 8.1 mmol) was then added slowly and the color of solution gradually changed to brown over a period of 0.5 h. At this point the flask was attached to a vacuum line and the stopcock was opened to vacuum for about 1 min. The stopcock was closed and the mixture was stirred at room temperature for another 6 h. The volatile components were then removed under reduced pressure. The brown residue was extracted with hexanes (5×15 cm^3), and the combined extracts were filtered through Celite. The volatile components were removed *in vacuo* from the filtrate, the residue was dissolved in CH_2Cl_2, and the resulting solution was concentrated *in vacuo* to ≈ 10 cm^3. The flask was transferred to a freezer where it was kept at $-35°C$ for 12 h, producing dark red crystals. Yield 0.35 g (37%) (Found: C, 23.45; H, 4.45. $C_{42}H_{98}Cl_4O_{14}Re_6$ requires C, 24.18; H, 4.73%). ^1H NMR (C_6D_6, 10°C): δ 1.15 (d, 12, $J_{HH} = 6$ Hz, $OCHMe_2$), 1.20 (d, 12, $J_{HH} = 6$ Hz, $OCHMe_2$), 1.29 (d, 12, $J_{HH} = 6$ Hz, $OCHMe_2$), 1.32 (d, 12, $J_{HH} = 6$ Hz, $OCHMe_2$), 1.73 (d, 12, $J_{HH} = 6$ Hz, $OCHMe_2$), 2.03 (d, 12, $J_{HH} = 6$ Hz, $OCHMe_2$), 2.26 (d, 12, $J_{HH} = 6$ Hz, $OCHMe_2$), 4.43 (sept, 4, $J_{HH} = 6$ Hz, $OCHMe_2$), 5.20 (sept, 6, $J_{HH} = 6$ Hz, $OCHMe_2$), 5.62 (sept, 4, $J_{HH} = 6$ Hz, $OCHMe_2$). $^{13}C\{^1H\}$ NMR (C_6D_6): δ 26.7 (4, $OCHMe_2$), 27.4 (4, $OCHMe_2$), 27.5 (4, $OCHMe_2$), 28.0 (4, $OCHMe_2$), 28.3 (4, $OCHMe_2$), 29.7 (4, $OCHMe_2$), 30.1 (4, $OCHMe_2$), 70.1 (4, $OCHMe_2$), 71.6 (2, $OCHMe_2$), 76.5 (4, $OCHMe_2$), 76.8 (4, $OCHMe_2$). IR (Nujol, CsI, cm^{-1}): 1319m, 1167m, 1146w, 1099s, 980s, 955s, 914s, 849s, 833s, 721w, 638m, 615m, 601m, 538w, 444w, 432w.

$Re_3(\mu\text{-}OPr^i)_3Cl(H)(OPr^i)_4(PMe_3)$. Trimethylphosphine (1.8 mmol) was added *via* a calibrated vacuum manifold to a frozen red solution of $Re_3Cl_9(THF)_3$ (0.98 g, 0.90 mmol) in THF. The mixture was warmed to room temperature and the color gradually changed to purple as it was stirred for 12 h. Sodium isopropoxide (0.90 g, 11 mmol) was added slowly and the color of the solution gradually changed to green

over a period of 15 min. After 2 h, the volatile components were removed under reduced pressure, and the residue was extracted with hexanes (4×15 cm^3). The extracts were combined and filtered through Celite. The volatile components were removed *in vacuo* from the green filtrate, and the residue was dissolved in CH_2Cl_2/CH_3CN (5:1). The solution was concentrated to 5 cm^3 and the flask was transferred to the freezer where it was kept at −35 °C for 12 h. The product crystallized as green blocks. Yield 0.31 g (38%) (Found: C, 26.41; H, 4.96. $C_{24}H_{59}ClO_7PRe_3$ requires C, 26.57; H, 5.48%). ^{1}H NMR (C_6D_6): δ −6.32 (d, 1, $^2J_{PH}$ = 42 Hz, Re-*H*), 1.05 (d, 6, J_{HH} = 6 Hz, OCH*Me*$_2$), 1.16 (d, 9, $^2J_{PH}$ = 9 Hz, P*Me*$_3$), 1.24 (d, 6, J_{HH} = 6 Hz, OCH*Me*$_2$), 1.33 (d, 6, J_{HH} = 6 Hz, OCH*Me*$_2$), 1.39 (d, 6, J_{HH} = 6 Hz, OCH*Me*$_2$), 1.72 (d, 6, J_{HH} = 6 Hz, OCH*Me*$_2$), 1.79 (d, 6, J_{HH} = 6 Hz, OCH*Me*$_2$), 1.81 (d, 6, J_{HH} = 6 Hz, OCH*Me*$_2$), 4.55 (sept, 2, J_{HH} = 6 Hz, OC*H*Me$_2$), 4.72 (sept, 2, J_{HH} = 6 Hz, OC*H*Me$_2$), 4.96 (sept, 1, J_{HH} = 6 Hz, OC*H*Me$_2$), 5.08 (sept, 2, J_{HH} = 6 Hz, OC*H*Me$_2$). ^{13}C{^{1}H} NMR (C_6D_6): δ 15.0 (d, 3, J_{PC} = 23 Hz, P*Me*$_3$), 26.6 (4, OCH*Me*$_2$), 27.2 (2, OCH*Me*$_2$), 27.4 (2, OCH*Me*$_2$), 27.5 (2, OCH*Me*$_2$), 28.5 (4, OCH*Me*$_2$), 72.4 (1, OCHMe$_2$), 73.0 (2, OCHMe$_2$), 76.0 (2, OCHMe$_2$), 77.8 (2, OCHMe$_2$). ^{31}P{^{1}H} NMR (C_6D_6): −11.0. IR (Nujol, KBr, cm^{-1}): ν (Re—H) 1979m, 1452s, 1418m, 1400w, 1371s, 1319s, 1285m, 1208m, 1165s, 1101s, 1044m, 963s, 874m, 845s, 833s, 733m, 700m, 671w, 625m, 615m, 596m, 569w, 536w, 469s, 451s, 419s, 405s.

$Re_3(\mu\text{-}OPr^i)_3Cl(CH_2CH_3)(OPr^i)_4(CH_3CN)$. Ethylene (0.90 mmol) was added *via* a calibrated vacuum manifold to a frozen green solution of $Re_3(\mu\text{-}OPr^i)_3Cl(H)(OPr^i)_4(PMe_3)$ (0.20 g, 0.18 mmol) in hexane. The solution was warmed to 50 °C and stirred at this temperature for 2 days. The solution volume was then reduced *in vacuo* to 2 cm^3. Acetonitrile (20 cm^3) was added, which caused a green solid to precipitate. Yield: 0.042 g (21%). ^{1}H NMR (C_6D_6): δ 0.05 (t, 3, J_{HH} = 8 Hz, CH_2CH_3), 0.58 (s, 3, CH_3CN), 0.97 (d, 6, J_{HH} = 6 Hz, OCH*Me*$_2$), 1.14 (d, 6, J_{HH} = 6 Hz, OCH*Me*$_2$), 1.18 (d, 6, J_{HH} = 6 Hz, OCH*Me*$_2$), 1.28 (d, 6, J_{HH} = 6 Hz, OCH*Me*$_2$), 1.70 (d, 6, J_{HH} = 6 Hz, OCH*Me*$_2$), 1.80 (d, 6, J_{HH} = 6 Hz, OCH*Me*$_2$), 1.81 (d, 6, J_{HH} = 6 Hz, OCH*Me*$_2$), 3.43 (q, 2, J_{HH} = 8 Hz, CH_2CH_3), 4.43 (sept, 2, J_{HH} = 6 Hz, OC*H*Me$_2$), 4.90 (2 overlapping sept, 3, OC*H*Me$_2$), 5.15 (sept, 2, J_{HH} = 6 Hz, OC*H*Me$_2$). ^{13}C{^{1}H} NMR (C_6D_6): δ −1.37 (1, CH_3CN), 23.7 (1, CH_2CH_3), 26.5 (1, CH_2CH_3), 26.6 (2, OCH*Me*$_2$), 27.3 (4, OCH*Me*$_2$), 27.4 (4, OCH*Me*$_2$), 27.7 (2, OCH*Me*$_2$), 29.4 (2, OCH*Me*$_2$), 67.5 (1, OCHMe$_2$), 72.9 (2, OCHMe$_2$), 74.8 (2, OCHMe$_2$), 77.8 (2, OCHMe$_2$), 93.4 (1, CH_3CN). IR (Nujol, KBr, cm^{-1}): 1373m, 1364m, 1319w, 1200w, 1167w, 1103s, 961s, 928s, 845s, 833s, 723w, 698w, 635w, 623w, 615w, 596w, 534w, 465m, 457m, 442m, 430m.

$Re_3(\mu\text{-}OPr^i)_3Cl(\eta\text{-}C(Me)=C(H)Me)(OPr^i)_4$. 2-Butyne (0.90 mmol) was added *via* a calibrated vacuum manifold to a frozen green solution of $Re_3(\mu\text{-}OPr^i)_3Cl(H)(OPr^i)_4(PMe_3)$ (0.20 g, 0.18 mmol) in hexanes (15 cm^3). The solution was warmed to 50 °C and left to stir at this temperature for 12 h. The mixture was filtered, and the volatile components were removed *in vacuo* from the filtrate. The green residue was dissolved in CH_2Cl_2/CH_3CN (5:1) and the solution was concentrated *in vacuo* to 5 cm^3. The flask was transferred to a freezer where it was kept at −35 °C for 12 h. The product crystallized as green needles. Yield: 0.86 g (44%) (Found: C, 28.31; H, 5.34. $C_{25}H_{56}ClO_7Re_3$ requires C, 28.25; H, 5.31). ^{1}H NMR (C_6D_6): δ 1.10 (d, 6, J_{HH} = 6 Hz, OCH*Me*$_2$), 1.15 (d, 6, J_{HH} = 6 Hz, OCH*Me*$_2$), 1.25 (d, 6, J_{HH} = 6 Hz, OCH*Me*$_2$), 1.28 (d, 6, J_{HH} = 6 Hz, OCH*Me*$_2$), 1.53 (s, 3, *Me*C=CHMe), 1.71 (d, 6, J_{HH} = 6 Hz, OCH*Me*$_2$), 1.76 (d, 6, J_{HH} = 6 Hz, OCH*Me*$_2$), 1.81 (d, 6, J_{HH} = 6 Hz, OCH*Me*$_2$), 2.15 (d, 3, J_{HH} = 6.6 Hz, MeC=CH*Me*), 4.45 (q, 1, J_{HH} = 6.3 Hz, MeC=C*H*Me), 4.53 (sept, 2, J_{HH} = 6 Hz, OC*H*Me$_2$), 4.90 (2 overlapping sept, 3, OC*H*Me$_2$), 5.18 (sept, 2, J_{HH} = 6 Hz, OC*H*Me$_2$). ^{13}C{^{1}H} NMR (C_6D_6): δ 9.5 (1, MeC-CH*Me*), 22.9 (1, *Me*CCHMe), 26.0 (2, OCH*Me*$_2$), 26.8 (2, OCH*Me*$_2$), 26.9 (2, OCH*Me*$_2$), 27.0 (2, OCH*Me*$_2$), 27.5 (2, OCH*Me*$_2$), 28.0 (2, OCH*Me*$_2$), 28.7 (2, OCH*Me*$_2$), 72.1 (2, OCHMe$_2$), 72.7 (2, OCHMe$_2$), 72.9 (1, OCHMe$_2$), 79.5 (2, OCHMe$_2$), 119 (1, MeC=*C*HMe), 128 (1, Me*C*=CHMe). IR (Nujol, KBr, cm^{-1}): ν(C=C) 1582w, 1319m, 1167w, 1130w, 1099s, 949s, 845m, 837m, 721m, 694m, 637w, 619w, 480s, 465s, 413w, 403w.

$Re_3(\mu\text{-}OPr^i)_3H(OPr^i)_5(PMe_3)$. Trimethylphosphine (0.78 mmol) was added *via* a calibrated vacuum manifold to a frozen green solution of $Re_3(OPr^i)_9$ (0.14 g, 0.13 mmol) in hexanes (15 cm^3). The solution was warmed to room temperature and stirred for 12 h. The volatile components were then removed under reduced pressure. The green residue was dissolved in CH_2Cl_2/CH_3CN (5:1), and the solution was concentrated *in vacuo* to 3 cm^3. The flask was transferred to a freezer where it was kept at −35 C for 12 h. The product crystallized as green blocks, which were isolated by removing the mother liquor with a pipet and washing with cold CH_2Cl_2 (2×5 cm^3). Yield: 0.77 g (56%) (Found: C, 29.04; H, 5.99. $C_{27}H_{66}O_8PRe_3$ requires C, 29.26; H, 6.00%). ^{1}H NMR (CD_2Cl_2): δ −4.40 (d, 1, $^2J_{PH}$ = 27 Hz, Re-*H*), 0.74 (d, 6, J_{HH} = 6 Hz, OCH*Me*$_2$), 0.79 (d, 6, J_{HH} = 6 Hz, OCH*Me*$_2$), 0.90 (d, 6, J_{HH} = 6 Hz, OCH*Me*$_2$), 1.06 (d, 6, J_{HH} = 6 Hz, OCH*Me*$_2$), 1.13 (d, 6, J_{HH} = 6 Hz, OCH*Me*$_2$), 1.21 (d, 9, $^2J_{PH}$ = 7.5 Hz, P*Me*$_3$), 1.47 (d, 6, J_{HH} = 6 Hz, OCH*Me*$_2$), 1.53 (d, 6, J_{HH} = 6 Hz, OCH*Me*$_2$), 1.55 (d, 6, J_{HH} = 6 Hz, OCH*Me*$_2$), 4.01 (sept, 1, J_{HH} = 6 Hz, OC*H*Me$_2$), 4.41 (sept, 1, J_{HH} = 6 Hz, OC*H*Me$_2$), 4.51 (sept, 4, J_{HH} = 6 Hz, OC*H*Me$_2$), 4.61 (sept, 2, J_{HH} = 6 Hz, OC*H*Me$_2$). ^{13}C{^{1}H} NMR (CD_2Cl_2): δ 13.7 (d, 3, J_{PC} = 17 Hz, P*Me*$_3$), 26.3 (2, OCH*Me*$_2$), 26.4 (2, OCH*Me*$_2$), 26.5 (2, OCH*Me*$_2$), 26.7 (2, OCH*Me*$_2$), 27.27 (2, OCH*Me*$_2$), 27.32 (2, OCH*Me*$_2$), 27.7 (2, OCH*Me*$_2$), 30.2 (2, OCH*Me*$_2$),

72.1 (2, $OCHMe_2$), 72.3 (2, $OCHMe_2$), 72.6 (2, $OCHMe_2$), 72.9 (2, $OCHMe_2$). $^{31}P\{^1H\}$ (CD_2Cl_2): −27.5 (s). IR (Nujol, CsI, cm^{-1}) ν(Re—H) 1923m, 1622m, 1371s, 1319s, 1283m, 1206w, 1165s, 1105s, 1028w, 963s, 833s, 731m, 679m, 623s, 594s, 573s, 536m, 430m.

$Re_3(\mu\text{-}OCH_2Bu^t)_3(OCH_2Bu^t)_6(PMe_3)$. Trimethylphosphine (1.1 mmol) was added *via* a calibrated vacuum manifold to a frozen green solution of $Re_3(OCH_2Bu^t)_9$ (0.30 g, 0.22 mmol) in hexanes (20 cm^3). The solution was warmed to room temperature and stirred for 12 h. The volatile components were then removed under reduced pressure. The green residue was dissolved in CH_2Cl_2, the solution was concentrated *in vacuo* to 4 cm^3, and the flask was transferred to a freezer where it was kept at −35°C for 12 h. The product crystallized as green blocks, which were isolated by removing the mother liquor *via* a pipet and washing with cold CH_2Cl_2 (2 × 5 cm^3). Yield: 0.23 g (73%) (Found: C, 39.76; H, 7.54. $C_{48}H_{108}O_9PRe_3$ requires C, 40.63; H, 7.67%). ^1H NMR (C_6D_6): δ 0.98 (s, 18, OCH_2CMe_3), ≈1 (PMe_3, see text), 1.025 (s, 9, OCH_2CMe_3), 1.03 (s, 18, OCH_2CMe_3), 1.25 (s, 9, OCH_2CMe_3), 1.37 (s, 9, OCH_2CMe_3), 1.41 (s, 18, OCH_2CMe_3), 3.16 and 4.36 (AB q, 2, J_{HH} = 10 Hz, OCH_2CMe_3), 3.55 and 4.89 (AB q, 2, J_{HH} = 10 Hz, OCH_2CMe_3), 3.94 (d, 2, $^4J_{PH}$ = 2.7 Hz, OCH_2CMe_3), 4.37 (d, 2, $^4J_{PH}$ = 2.7 Hz, OCH_2CMe_3), 4.43 (s, 2, OCH_2CMe_3), 4.58 and 4.83 (AB q, 2, J_{HH} = 12 Hz, OCH_2CMe_3). $^{31}P\{^1H\}$ (C_6D_6): δ −22.3. IR (Nujol, KBr, cm^{-1}): 2951s, 2911s, 2864s, 1478s, 1464m, 1443w, 1416w, 1391s, 1373w, 1360s, 1300w, 1271w, 1258w, 1213m, 1142w, 1080m, 1065m, 1038s, 1013s, 972s, 932w, 907w, 783w, 754w, 737m, 671m, 638w, 619w, 604w, 584w, 482m, 469s, 453m, 436m.

$Re_3(\mu\text{-}Cl)(\mu\text{-}OCH_2Bu^t)_2Cl(OCH_2Bu^t)_4(PMe_3)_2$. Trimethylphosphine (4.5 mmol) was added *via* a calibrated vacuum manifold to a frozen red solution of $Re_3Cl_9(THF)_3$ (0.98 g, 0.90 mmol) in THF. The color of the solution gradually changed to purple as it was stirred at room temperature for 12 h. Sodium neopentoxide (1.2 g, 11 mmol) was then added slowly until the solution turned green. The mixture was stirred at room temperature for 12 h during which time the green color persisted. (If the green color did not persist, more $NaOCH_2CMe_3$ (≈0.5 g) was added until the green color returned.) The volatile components were then removed under reduced pressure, and the residue was extracted with hexanes (5 × 20 cm^3). The extracts were combined and filtered through Celite. The green filtrate was concentrated *in vacuo* to *ca* 5 cm^3 and the flask was transferred to a freezer where it was stored at −35°C for 12 h. The product formed as small green crystals. The crystals were isolated and washed with acetonitrile (2 × 10 cm^3), and then dried *in vacuo* for 4 h. Yield: 0.15 g (12%) ^1H NMR (C_6D_6): δ 0.8 (br), 5.3 (br). IR (Nujol, KBr, cm^{-1}): 1416w, 1391m, 1377s, 1362m, 1298w, 1279m, 1258w, 1217w, 1042s, 1007s, 955s, 855w, 756w, 739w, 729w, 675s.

Crystal structure determination of $\{Re_3(\mu\text{-}OPr^i)_3(Cl(OPr^i)_4\}_2(\mu\text{-}Cl)_2 \cdot 2CH_2Cl_2$

Crystal data. $C_{42}H_{98}O_{14}Cl_4Re_6 \cdot 2CH_2Cl_2$, M = 2256.26, orthorhombic, space group $Pbca$, a = 17.300(3), b = 17.800(3), c = 23.533(3) Å, U = 7247 Å^3, T = −50°C, Mo-K_α (λ = 0.71073 Å), Z = 4, D_c = 2.07 g cm^{-3}, $F(000)$ = 4256, μ = 104.7 cm^{-1}. Crystal size: 0.18 × 0.22 × 0.44 mm.

Data collection. The air sensitive brown prismatic blocks were manipulated under mineral oil. Nicolet R3 four-circle diffractometer equipped with an LT-2 low-temperature device, ω mode with scan width $\Delta\theta = 1.30 + (K_{\alpha 2} - K_{\alpha 1})$°, scan speed range 1.5–15.0° min^{-1}, graphite-monochromated Mo-K_α radiation; 5236 reflections measured ($4 \leqslant 2\theta \leqslant 45$°, h, k, l), 3278 independent with $I > 3\sigma(I)$. Lorentz and polarization corrections were applied, as well as a semi-empirical absorption correction based on ten reflections having chi values between 70 and 90°. Two standard reflections were measured every 2 h or after every 100 data collected, and these showed no significant variation.

Structure solution and refinement. The Laue symmetry was determined to be mmm, and from the systematic absences the space group was shown to be $Pbca$. The structure was solved by interpretation of a Patterson map, which revealed the positions of three independent Re atoms in the asymmetric unit, consisting of one-half molecule situated about an inversion center. Remaining atoms were found in subsequent difference Fourier syntheses. The hydrogen atoms were placed in calculated positions and constrained to riding motion, with a single variable isotropic temperature factor for all of them. A molecule of methylene chloride solvent was also located and refined with 70% occupancy factors. After all shift/esd ratios were less than 0.1 convergence was reached with R, R_w = 0.037, 0.037 (GOF = 1.33). The weighting scheme was $w = [\sigma(F)]^{-2}$. No unusually high correlations were noted between any of the variables in the last cycle of full-matrix least squares refinement, and the final difference density map showed a maximum peak of about 1.1 e/Å^3. All calculations were made using Nicolet's SHELXTL PLUS (1987) package of programs [18].

Crystal structure determination of $Re_3(\mu\text{-}OPr^i)_3Cl(H)(OPr^i)_4(PMe_3) \cdot CH_2Cl_2$

Crystal data. $C_{24}H_{59}O_7PClRe_3 \cdot CH_2Cl_2$, M = 1169.78, triclinic, space group $P\bar{1}$, a = 11.365(3), b = 11.857(3), c = 16.101(2) Å, α = 80.44(1), β = 84.60(1), γ = 69.50(1)°, U = 2003 Å^3, T = −50°C, Mo-K_α (λ = 0.71073 Å), Z = 2, D_c = 1.94 g cm^{-3}, $F(000)$ = 1116, μ = 94.4 cm^{-1}. Crystal size: 0.12 × 0.17 × 0.60 mm.

Data collection. The air sensitive dark green columns were manipulated under mineral oil. Nicolet R3 four-circle diffractometer equipped with an LT-2 low-

temperature device, ω mode with scan width $\Delta\theta = 1.25 + (K_{\alpha 2} - K_{\alpha 1})^\circ$, scan speed range 1.5–15.0° min^{-1}, graphite-monochromated Mo-K_α radiation; 7066 reflections measured ($4 \leqslant 2\theta \leqslant 50^\circ$, h, $\pm k$, $\pm l$), 5948 independent with $I > 3\sigma(I)$. Lorentz and polarization corrections were applied, as well as a semi-empirical absorption correction based on psi scans of ten reflections having chi values between 70 and 90°. Two standard reflections were measured every 2 h or after every 100 data collected, and these showed no significant variation.

Structure solution and refinement. The Laue symmetry was determined to be $\bar{1}$, and the space group was shown to be $P\bar{1}$ or $P1$. $P\bar{1}$ was assumed from the beginning because the unitary structure factors displayed centric statistics. The structure was solved by interpretation of a Patterson map, which revealed the positions of the Re atoms. Remaining atoms were found in subsequent difference Fourier syntheses. The hydrogen atoms were placed in calculated positions and constrained to riding motion, with a single variable isotropic temperature factor for all of them. The hydrogen atom that is postulated to be attached to Re(1) was not located. After all shift/esd ratios were less than 0.1 convergence was reached with R, $R_w = 0.029$, 0.031 (GOF = 1.81). The weighting scheme was $w = [\sigma(F)]^{-2}$. No unusually high correlations were noted between any of the variables in the last cycle of full-matrix least squares refinement, and the final difference density map showed a maximum peak of about 1.5 e/Å^3 between Re(1) and Re(3). This density was assumed to be spurious since the IR spectrum indicated the presence of a terminal rather than a bridging hydride ligand. All calculations were made using Nicolet's SHELXTL PLUS (1987) package of programs [18].

Crystal structure determination of $Re_3(\mu\text{-}OCH_2Bu^t)_3(OCH_2Bu^t)_6(PMe_3)\cdot CH_2Cl_2$

Crystal data. $C_{48}H_{108}O_9PRe_3\cdot CH_2Cl_2$, $M = 1504.06$, monoclinic, space group $P2_1/c$, $a = 17.506(6)$, $b = 18.990(8)$, $c = 19.332(7)$ Å, $\beta = 93.12(3)^\circ$, $U = 6417$ Å^3, $T = -50$°C, Mo-K_α ($\lambda = 0.71073$ Å), $Z = 4$, $D_c = 1.56$ g cm^{-3}, $F(000) = 3000$, $\mu = 58.7$ cm^{-1}. Crystal size: $0.40 \times 0.50 \times 0.60$ mm.

Data collection. The air sensitive bright green prismatic blocks were manipulated under mineral oil. Nicolet R3 four-circle diffractometer equipped with an LT-2 low-temperature device, ω mode with scan width $\Delta\theta = 1.30 + (K_{\alpha 2} - K_{\alpha 1})^\circ$, scan speed range 2.0–15.0° min^{-1}, graphite-monochromated Mo-K_α radiation; 8350 reflections measured ($4 \leqslant 2\theta \leqslant 45^\circ$, h, k, $\pm l$), 6103 independent with $I > 3\sigma(I)$. Lorentz and polarization corrections were applied, as well as a semi-empirical absorption correction based on ten reflections having chi values between 70 and 90°. Two standard reflections were measured every 2 h or after every 100 data collected, and these showed no significant variation.

Structure solution and refinement. The Laue symmetry was determined to be $2/m$, and from the systematic absences the space group was shown to be $P2_1/c$. The structure was solved by interpretation of a Patterson map, which revealed the positions of the Re atoms. Remaining atoms were found in subsequent difference Fourier syntheses. The hydrogen atoms were placed in calculated positions and constrained to riding motion, with a single variable isotropic temperature factor for all of them. Three of the Bu^t groups were found to be disordered, and these were treated by introducing ideal rigid bodies at each location and allowing them to rotate independently while constraining the isotropic temperature factors to be equal. The occupancy factors refined to 70 : 30 for C7 : C7′ and C22 : C22′, and 60 : 40 for C37 : C37′. A very heavily disordered molecule of methylene chloride was also located, and the two major orientations were refined as ideal rigid bodies having 50% occupancies. After all shift/esd ratios were less than 0.2 convergence was reached with R, $R_w = 0.036$, 0.037 (GOF = 1.39). The weighting scheme was $w = [\sigma(F)]^{-2}$. No unusually high correlations were noted between any of the variables in the last cycle of full-matrix least squares refinement, and the final difference density map showed a maximum peak of about 1.8 e/Å^3 located near Re. All calculations were made using Nicolet's SHELXTL PLUS (1987) package of programs [18].

Crystal structure determination of $Re_3(\mu\text{-}Cl)(\mu\text{-}OCH_2Bu^t)_2Cl(OCH_2Bu^t)_4(PMe_3)_2$

Crystal data. $C_{36}H_{84}Cl_2O_6P_2Re_3$, $M = 1304.52$, monoclinic, space group $C2/c$, $a = 12.239(1)$, $b = 19.644(2)$, $c = 20.825(2)$ Å, $\beta = 102.238(6)^\circ$, $U = 4893.0(8)$ Å^3, $T = 23$°C, Mo-K_α ($\lambda = 0.71073$ Å), $Z = 4$, $D_c = 1.77$ g cm^{-3}, $F(000) = 2548$, $\mu = 77.16$ cm^{-1}. Crystal size: $0.06 \times 0.09 \times 0.11$ mm.

Data collection. A dark block was mounted in a 0.7-mm O.D. Lindeman capillary under nitrogen. Enraf-Nonius CAD-4 diffractometer, ω mode with scan width $\Delta\theta = 0.8 + 0.35 \tan\theta$, scan speed range (0.67–8° min^{-1}, graphite-monochromated Mo-K_α radiation; 4660 reflections measured ($2 \leqslant 2\theta \leqslant 50^\circ$, h, k, $\pm l$), 4456 unique ($R_{int} = 0.020$), 2435 observed with $F > 6\sigma(F)$. Lorentz and polarization corrections were applied, as well as a semi-empirical absorption correction based on five reflections having chi values between 70 and 90°. Three standard reflections were measured every 3600 sec and these showed no significant variation.

Structure solution and refinement. The structure was solved by interpretation of a Patterson map, which revealed the positions of the two independent Re atoms. Remaining atoms were found in subsequent difference Fourier syntheses. Hydrogen atoms were entered in idealized geometries and allowed to ride on

the appropriate carbon atom [$U(H) = 1.3U_{eq}(C)$]. All non-hydrogen atoms were refined with anisotropic thermal parameters. Convergence was reached with R, $R_w = 0.032$, 0.036 (GOF = 1.48). The weighting scheme was $w = [0.04F^2 + (\sigma F)^2]^{-1}$. The final difference map showed a maximum peak of about 0.83 e/Å^3 near the Re atoms. All calculations were made using the MolEN package of programs [19].

CONCLUSION

The isopropoxide clusters $Re_3(\mu\text{-}OPr^i)_3Cl(H)(OPr^i)_4(PMe_3)$ and $\{Re_3(\mu\text{-}OPr^i)_3Cl(OPr^i)_4\}_2(\mu\text{-}Cl)_2$ were prepared from rhenium chloride and sodium isopropoxide in the presence of trimethylphosphine. In the chloro–hydride cluster the hydride ligand is proposed to occupy a site *trans* to Cl and *cis* to PMe_3. The source of the hydride ligand is thought to be isopropoxide β-hydrogen elimination. Reactions of the hydride cluster under mild conditions with ethylene and 2-butyne yield ethyl and 2-butenyl clusters, respectively, and the reaction with sodium isopropoxide gives $Re_3(\mu\text{-}OPr^i)_3(H)(OPr^i)_5(PMe_3)$. The cluster $Re_3(\mu\text{-}OPr^i)_3(H)(OPr^i)_5(PMe_3)$ is more conveniently prepared by reacting PMe_3 with $Re_3(\mu\text{-}OPr^i)_3(OPr^i)_6$, a reaction in which PMe_3 traps $Re_3(\mu\text{-}OPr^i)_3(H)(OPr^i)_5$ from its equilibrium with $Re_3(\mu\text{-}OPr^i)_3(OPr^i)_6$ and acetone. The analogous reaction of PMe_3 with the less sterically crowded homoleptic neopentoxide cluster $Re_3(\mu\text{-}OCH_2Bu^t)_3(OCH_2Bu^t)_6$ gives the phosphine adduct $Re_3(\mu\text{-}OCH_2Bu^t)_3(OCH_2Bu^t)_6(PMe_3)$. In contrast to the reactions of rhenium chloride with trimethylphosphine and sodium isopropoxide, a similar reaction involving sodium neopentoxide gave the reduced cluster $Re_3(\mu\text{-}Cl)(\mu\text{-}OCH_2Bu^t)_2Cl(OCH_2Bu^t)_4(PMe_3)_2$. This cluster has 13 electrons available for Re–Re bonding, but its structure is not significantly different from similar 12-electron clusters. Trimethylphosphine is apparently the reducing agent in the preparation of the reduced cluster.

Acknowledgments—Acknowledgement for support is made to the Robert A. Welch Foundation. We are grateful to J. Korp for his technical assistance with the X-ray crystallographic analyses.

Supplementary Data—Atomic coordinates, thermal parameters, bond lengths and angles, have been deposited at the Cambridge Crystallographic Data Centre (CCDC).

REFERENCES

1. Hoffman, D. M., Lappas, D. and Wierda, D. A., *J. Am. Chem. Soc.*, 1989, **111,** 1531.
2. Hoffman, D. M., Lappas, D. and Wierda, D. A., *J. Am. Chem. Soc.*, 1993, **115,** 10538.
3. Zhuang, W. W., Truitt, B. E. and Hoffman, D. M., *Inorg. Chem.*, 1997, **36,** 3330.
4. Hoffman, D. M., Lappas, D. and Wierda, D. A., *Organometallics*, 1997, **16,** 972.
5. Zhuang, W. W. and Hoffman, D. M., *Organometallics*, 1997, **16,** 3102.
6. Cotton, F. A. and Walton, R. A., *Multiple Bonds Between Metal Atoms*, p. 539. Clarendon Press, Oxford (1993).
7. Esjornson, S. M. V., Fanwick, P. E. and Walton, R. A., *Polyhedron*, 1990, **9,** 1165.
8. Wong, A. C. C., Wilkinson, G., Hussain, B., Motevalli, M. and Hursthouse, M. B., *Polyhedron*, 1988, **7,** 1363.
9. Cotton, F. A., Frenz, B. A., Ebner, J. R. and Walton, R. A., *J. Chem. Soc., Chem. Commun.*, 1974, 4.
10. Ebner, J. R. and Walton, R. A., *Inorg. Chem.*, 1975, **14,** 1987.
11. Edwards, P., Mertis, K., Wilkinson, G., Hursthouse, M. B. and Malik, K. M. A., *J. Chem. Soc., Dalton Trans.*, 1980, 334.
12. Mertis, K., Edwards, P. G., Wilkinson, G., Malik, K. M. A. and Hursthouse, M. B., *J. Chem. Soc., Chem. Commun.*, 1980, 654.
13. Mertis, K., Edwards, P. G., Wilkinson, G., Malik, K. M. A. and Hursthouse, M. B., *J. Chem. Soc., Dalton Trans.*, 1981, 705.
14. Mertis, C., Psaroudakis, N., Terzis, A. and Houndas, A., *Polyhedron*, 1991, **10,** 741.
15. Cotton, F. A. and Wilkinson, G., *Advanced Inorganic Chemistry, 5th edn.*, p. 1300. John Wiley & Sons, Chichester (1988).
16. Lincoln, R., Wilkinson, G., Walton, R. A. and Wood, T. E., *Inorg. Synth.*, 1980, **20,** 41.
17. Lincoln, R., Wilkinson, G., Walton, R. A. and Wood, T. E., *Inorg. Synth.*, 1980, **20,** 44.
18. Sheldrick, G. M., SHELXTL PLUS, Release 3.4 for the Nicolet R3m/v Crystallographic System, Nicolet Instrument Corp., Madison, 1987.
19. MolEN, An Interactive Structure Solution Program, Enraf-Nonius, Delft, 1990.

Pergamon

PII: S0027-5387(97)00260-X

Polyhedron Vol. 17, No. 5–6, pp. 891–897, 1998
Published by Elsevier Science Ltd
Printed in Great Britain
0277-5387/98 $19.00+0.00

Alkoxy(siloxy) complexes of tin, lead and bismuth†

Karl W. Terry,[a] Kai Su,[a] T. Don Tilley[a]* and Arnold L. Rheingold[b]

[a]Department of Chemistry, University of California, Berkeley, CA 94720-1460, and the Chemical Sciences Division, Lawrence Berkeley Laboratory, 1 Cyclotron Road, Berkeley, CA 94720, U.S.A.

[b]Department of Chemistry, University of Delaware, Newark, Delaware 19716, U.S.A.

(Received 29 April 1997; accepted 11 June 1997)

Abstract—By reaction of $PbCl_2$ with 3 equivalents of $NaOSi(O^tBu)_3$, the ate complex $NaPb[OSi(O^tBu)_3]_3$ was obtained. This compound possesses a structure containing a 3-coordinate, trigonal prismatic lead center, and a 6-coordinate Na atom encapsulated in an oxygen matrix formed by the bridging siloxy and *tert*-butoxy groups of the $-OSi(O^tBu)_3$ ligands. The neutral lead complex $Pb[OSi(O^tBu)_3]_2 \cdot {}^tBuOH \cdot CH_3CN$ was obtained from reaction of $Pb_3(\mu\text{-}O^tBu)_6$ with $HOSi(O^tBu)_3$. The tin complex $KSn[OSi(O^tBu)_3]_3$, prepared from $SnCl_2$ and $KOSi(O^tBu)_3$, is isomorphous with $NaPb[OSi(O^tBu)_3]_3$. The bismuth compounds $Bi[OSi(O^tBu)_3]_3$ and $Bi[OSi(O^tBu)_2Ph]_3$ were obtained by similar methods. © 1998 Elsevier Science Ltd. All rights reserved

Keywords: tin; lead; bismuth; alkoxide; siloxide; precursor.

The pioneering work of Donald Bradley and coworkers has sparked considerable interest in the synthesis and characterization of binary metal alkoxides and 'double alkoxides' [1]. Such compounds display interesting structures and often provide convenient chemical pathways to metal oxide materials. Much of the recent interest in alkoxide complexes stems from their use as ceramic precursors, *via* the sol–gel process involving hydrolysis of M—OR bonds, or *via* chemical vapor deposition routes to thin films [2]. We have been exploring an alternative route to mixed-metal alkoxides *via* low-temperature thermolyses of single-source molecular precursors containing $-OSi(O^tBu)_3$ and $-O_2P(O^tBu)_2$ ligands [3,4]. For example, we have found that the alkoxy(siloxy) complex $Zr[OSi(O^tBu)_3]_4$ readily converts at low temperatures (100–150°C) to homogeneous zirconia–silica materials [4]. These conversions typically occur at low temperature, give materials with high surface areas, and are compatible with nonpolar media. Here we describe the synthesis of main group-metal alkoxy(siloxy) complexes, and structural information for lead and tin derivatives.

† Dedicated to Professor Donald Bradley, in recognition of his many pioneering contributions to the field of metal alkoxide and metal amide chemistry.

* Author to whom correspondence to be addressed.

EXPERIMENTAL

All manipulations were performed under an atmosphere of argon or nitrogen using Schlenk techniques and/or a Vacuum Atmospheres glovebox. Dry, oxygen-free solvents were employed throughout. Elemental analyses were performed at Mikroanalytiches Labor Pascher or Desert Analytics Laboratories. Infrared spectra were recorded on a Perkin–Elmer 1330 or a Mattson Galaxy Series Fourier Transform infrared spectrometer. NMR spectra were obtained with a GE QE-300 instrument at 300 (^1H), 75.5 (^{13}C) and 59.6 (^{29}Si) MHz, or on a Bruker AMX 400 spectrometer at 400 (^1H) and 100.6 (^{13}C) MHz. Thermal analyses were performed on a Dupont 951 Thermogravimetric Analyzer. The compounds $HOSi(O^tBu)_3$ [5], $NaOSi(O^tBu)_3$ [6], $KOSi(O^tBu)_3$ [7], $HOSi(O^tBu)_2Ph$ [3b], $[Pb(O^tBu)_2]_3$ [8], and $Bi(O^tBu)_3$ [9] were prepared according to literature procedures.

$NaPb[OSi(O^tBu)_3]_3$. 1,2-Dimethoxyethane (120 cm^3) was added to a solid mixture of $PbCl_2$ (3.00 g, 0.0108 mol) and $NaOSi(O^tBu)_3$ (9.27 g, 0.0324 mol). The reaction mixture was stirred for 1 h and then refluxed for 8 h. The volatile material was removed

under dynamic vacuum and the remaining white solid was dried for 12 h under dynamic vacuum. The product was extracted into pentane (75 cm^3), and concentration and cooling (to -30 °C) of this solution yielded 7.31 g (66%) in three crops. Anal. Calcd for $C_{36}H_{81}NaO_{12}PbSi_3$: C, 42.4; H, 8.00. Found: C, 41.9; H, 7.68. ^1H NMR (300 MHz, benzene-d_6, 22 °C) δ 1.50 (s, CMe_3). $^{13}C\{^1H\}$ NMR (75.5 MHz, benzene-d_6, 22 °C) δ 32.33 (CMe_3) 71.91 (CMe_3). ^{29}Si NMR (59.6 MHz, benzene-d_6, 22 °C) δ −88.67. IR (Nujol, CsI, cm^{-1}): 1382 s, 1360 vs, 1236 s, 1360 vs, 1210 s sh, 1190 vs, 1040 vs br, 1020 vs, 1000 vs, 980 vs, 960 s sh, 910 w sh, 822 s, 790 w sh, 700 s, 695 s sh, 512 m, 484 m, 424 m, 380 w, 350 w, 300 w.

$Pb[OSi(O^tBu)_3]_2 \cdot {}^tBuOH \cdot CH_3CN$. Benzene (100 cm^3) was added to a solid mixture of $[Pb(O^tBu)_2]_3$ (6.73 g, 0.0063 mol) and $HOSi(O^tBu)_3$ (10.08 g, 0.038 mol). The mixture was stirred for 0.5 h and then the volatile material was removed under dynamic vacuum. The remaining white solid was dried for 12 h under dynamic vacuum. This solid was dissolved in benzene (70 cm^3), and concentration of this solution followed by layering with acetonitrile afforded 8.38 g of the product as colorless crystals in 52% yield. Anal. Calcd for $C_{30}H_{67}NO_9PbSi_2$: C, 42.4; H, 7.95. Found: C, 42.5; H, 7.82. ^1H NMR (300 MHz, dichloromethane-d_2, 22°C): δ 1.34 (s, 63 H, $SiOCMe_3$, $HOCMe_3$) 1.97 (s, 3 H, NCMe). IR (Nujol, CsI, cm^{-1}): 2307 vw, 2275 w, 1383 m, 1360 s, 1238 m, 1210 m sh, 1190 s, 1040 s br, 1020 s sh, 955 s, 910 w sh, 822 m, 797 w sh, 628 w, 510 m, 480 m, 436 m, 375 w br, 340 w br.

$KSn[OSi(O^tBu)_3]_3$. A 5.00 g sample of $KOSi(O^tBu)_3$ (16.7 mmol) and 1.05 g of $SnCl_2$ (5.52 mmol) were combined in a 100 cm^3 Schlenk flask in the glovebox. After the solution was stirred at room temperature for 30 min, it was heated at reflux for 17 h. Vacuum evaporation of the solvent and subsequent recrystallization from cold pentane (−78 °C) gave 4.0 g (4.22 mmol, 81%) of $KSn[OSi(O^tBu)_3]_3$ (m.p. 89 °C dec). Anal. Calcd for $C_{36}H_{81}KO_{12}Si_3Sn$: C, 45.6; H, 8.61. Found: C, 46.0; H, 8.66. ^1H NMR (benzene-d_6, 400 MHz) δ 1.48. $^{13}C\{^1H\}$ NMR (benzene-d_6, 100.6 MHz) δ 32.3 ($OCMe_3$), 73.5 ($OCMe_3$). IR (Nujol, NaCl, cm^{-1}): 1460 s, 1448 s, 1382 m, 1362 s, 1243 s, 1190 s, 1065 vs, 1025 s, 913 m, 821 w, 702 m, 649 w, 517 w, 491 w, 425 w.

$Bi[OSi(O^tBu)_3]_3$. Method 1: THF (30 cm^3) was added to a solid mixture of $BiCl_3$ (0.300 g, 0.952 mmol) and $NaOSi(O^tBu)_3$ (0.818 g, 2.85 mmol) at room temperature. The cloudy solution was stirred for 11 h. The volatile material was removed under dynamic vacuum and the remaining white residue was dried under dynamic vacuum for 12 h. Extraction of the white residue with pentane (20 cm^3), concentration, and cooling gave the product as white crystals (0.276 g, 29%). Method 2: THF (30 cm^3) was added to a solid mixture of $BiCl_3$ (0.300 g, 0.952 mmol) and $KOSi(O^tBu)_3$ (0.864 g, 2.85 mmol) at room temperature. Workup is similar to that in Method 1 above. The yield was 0.281 g (30%). Method 3: Benzene (30 cm^3) was added to a solid mixture of $Bi(O^tBu)_3$ (0.334 g, 0.780 mmol) and $HOSi(O^tBu)_3$ (0.619 g, 2.34 mmol). The clear solution was stirred for 1 h. The volatile material was removed under dynamic vacuum and the remaining white residue was dried for 12 h under dynamic vacuum. Dissolution in pentane, filtration, and concentration gave 0.246 g (32%). Anal. Calcd for $C_{36}H_{81}BiO_{12}Si_3$: C, 43.3; H, 8.71. Found C, 43.2; H, 8.22. ^1H NMR (300 MHz, benzene-d_6, 22 °C) δ 1.49 (s, 81 H, CMe_3). $^{13}C\{^1H\}$ NMR (75.5 MHz, benzene-d_6, 22 °C) δ 32.00 (CMe_3), 72.93 (CMe_3). IR (Nujol, CsI, cm^{-1}): 1385 m, 1361 s, 1240 m, 1209 m sh, 1190 s, 1055 vs, 1020 m sh, 907 vs, 827 w, 798 vw, 698 m, 634 w, 544 w, 488 m, 455 w sh, 420 vw, 375 vw sh, 350 vw sh.

$Bi[OSi(O^tBu)_2Ph]_3$. Toluene (25 cm^3) was added to a solid mixture of $Bi(O^tBu)_3$ (0.300 g, 0.700 mmol) and $(^tBuO)_2PhSiOH$ (0.564 g, 2.10 mmol). The colorless solution was stirred for 1.5 h and then the volatiles were removed under dynamic vacuum. The remaining white residue was dissolved in pentane (10 cm^3). The pentane was removed under dynamic vacuum to remove traces of *tert*-butyl alcohol. The white solid was redissolved in pentane (10 cm^3). Filtration, concentration and cooling to −78 °C gave the product (0.330 g, 47%) as a white crystalline solid. Anal. Calcd for $C_{42}H_{69}BiO_9Si_3$: C, 49.9; H, 6.88. Found C, 49.6; H, 7.11. ^1H NMR (300 MHz, benzene-d_6, 22 °C) δ 1.40 (s, 54 H, CMe_3), 7.21, 7.23, 7.26, 7.28 (m, 9 H, Ph) 8.12, 8.12, 8.14, 8.15 (m, 6 H, Ph). IR (Nujol, CsI, cm^{-1}): 3060 vw sh, 3020 vw sh, 1616 vw, 1590 vw, 1428 m, 1388 m, 1362 s, 1240 m, 1200 m sh, 1188 m, 1120 s, 1050 s, 1020 s sh, 900 s, 822 w, 808 m, 790 m, 712 s, 645 m, 545 m, 480 m br, 350 w br.

X-ray structure determinations for $Na[Pb[OSi(O^tBu)_3]_3$ *and* $KSn[OSi(O^tBu)_3]_3$. Crystal, data collection, and refinement parameters are collected in Table 1. Colorless crystals of both compounds were photographically characterized and determined to belong to the monoclinic crystal system. Systematic absences in the diffraction data uniquely determined the space group. Azimuthal scans indicated that no correction for absorption was required for $KSn[OSi(O^tBu)_3]_3$; standard ψ-scan data were used to provide a correction for $NaPb[OSi(O^tBu)_3]_3$. The structures were solved by direct methods, completed from difference Fourier maps, and refined with anisotropic thermal parameters for all nonhydrogen atoms, except for the carbon atoms in $NaPb[OSi(O^tBu)_3]_3$ which were held isotropic to conserve data. Hydrogen atomat contributions were idealized. In $KSn[OSi(O^tBu)_3]_3$, several of the *tert*-butyl groups were rotationally disordered over two sites in varying degrees; in two cases, the groups at C(9) and C(33) were disordered over two sites about equally and both sites were refined. At C(25) and C(29), the second form was only about 10% occupied and was ignored. All computations used SHELXTL 4.2 or 5.1 software (G. Sheldrick, Siemens XRD, Madison, WI.).

Table 1. Crystallographic data for $NaPb[OSi(O^tBu)_3]_3$ and $KSn[OSi(O^tBu)_3]_3$

	$NaPb[OSi(O^tBu)_3]_3$	$KSn[OSi(O^tBu)_3]_3$
Formula	$C_{36}H_{81}NaO_{12}PbSi_3$	$C_{36}H_{81}KO_{12}Si_3Sn$
Formula weight	1020.48	948.1
Crystal system	monoclinic	monoclinic
Space group	$P2_1/n$	$P2_1/n$
a(Å)	14.963(2)	14.981(3)
b(Å)	21.919(3)	21.632(4)
c(Å)	17.628(2)	17.693(4)
β(°)	112.72(1)	112.17(1)
V(Å^3)	5333.2(12)	5310(2)
Z	4	4
ρ_{calc} (g cm^{-3})	1.271	1.186
μ (Mo-K_α) (cm^{-1})	32.34	6.74
T (K)	295	245
diffractometer	Siemens P4	Siemens P4
λ(Å)	0.71073	0.71073
2θ range (°)	4–45 ($\pm h$, $+k$, $+l$)	4–50 ($\pm h$, $+k$, $-l$)
rfns (collctd, indpdnt, obsrvd)	6224, 5779, 2628 ($2\sigma I$)	9664, 9345, 5286 ($2\sigma I$)
$R(F)$, $R(wF)$ [a](%)	6.10, 5.99	6.16, 8.18
GOF	1.38	1.63
N_o/N_v	8.8	12.5

[a] $R(F) = \Sigma\Delta/\Sigma(F_o)$; $R(wF) = \Sigma[\Delta\omega^{1/2}]/[F_o w^{1/2}]$; $\Delta = |F_o - F_c|$; $w^{-1} = \sigma^2(F_o) + gF_o^2$

RESULTS AND DISCUSSION

Lead complexes

Addition of 2 or 3 equiv. of $NaOSi(O^tBu)_3$ to $PbCl_2$ in THF or 1,2-dimethoxyethane (DME) gave the monomeric 'ate' complex $NaPb[OSi(O^tBu)_3]_3$ [eq. (1)]. Crystals suitable for X-ray crystallography were obtained by crystallization of the compound from pentane at −35°C. An ORTEP drawing is shown in Fig. 1, and bond distances and angles are listed in Table 2. The 6-coordinate sodium atom is encapsulated in an oxygen matrix formed by bridging siloxy and *tert*-butoxy groups from the $-OSi(O^tBu)_3$ ligands. The lead atom is 3-coordinate and possesses a trigonal prismatic coordination geometry that presumably reflects the presence of a stereochemically active lone pair. For comparison, the complex $Pb_3(\mu\text{-}O^tBu)_6$ possesses a geometry similar to $NaPb[OSi(O^tBu)_3]_3$ in that the terminal lead atoms are 3-coordinate and trigonal prismatic [8]. The Pb-O distances in $NaPb[OSi(O^tBu)_3]_3$ range from 2.12 to 2.15 Å and are slightly shorter than the terminal Pb—O distances in $Pb_3(O^tBu)_6$ (2.17 Å). The O—Pb—O angles in the latter complex (av. 80.3°) are more acute than those observed in $NaPb[OSi(O^tBu)_3]_8$ (av. 87.3°).

Unlike many other alkoxy(siloxy) complexes which are quite thermally labile, $NaPb[OSi(O^tBu)_3]_3$ displays a sharp melting point at 174–175°C. Thermogravimetric analysis (TGA) of the compound under oxygen (Fig. 2) revealed a precipitous weight loss with an onset temperature of *ca* 300°C. The weight loss at 1100°C was *ca* 70%. The TGA trace of this compound under argon displayed an onset temperature of *ca* 200°C and a gradual weight loss of 60% to 400°C. Powder X-ray diffraction (PXRD) of the black material obtained from thermolysis of $NaPb[OSi(O^tBu)_3]_3$ heated to 400°C and held at that temperature under oxygen showed the presence of Pb metal as the only crystalline product present.

$$PbCl_2 + 3\,NaOSi(O^tBu)_3 \xrightarrow{THF} \quad (1)$$

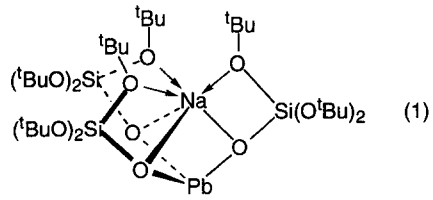

In an attempt to form a neutral lead(II) siloxide, the trimeric complex $Pb_3(O^tBu)_6$ [8] was stirred with 6 equiv. of $HOSi(O^tBu)_3$ in benzene. Removal of the volatile material and drying under extended dynamic vacuum gave an extremely soluble, waxy solid. Dis-

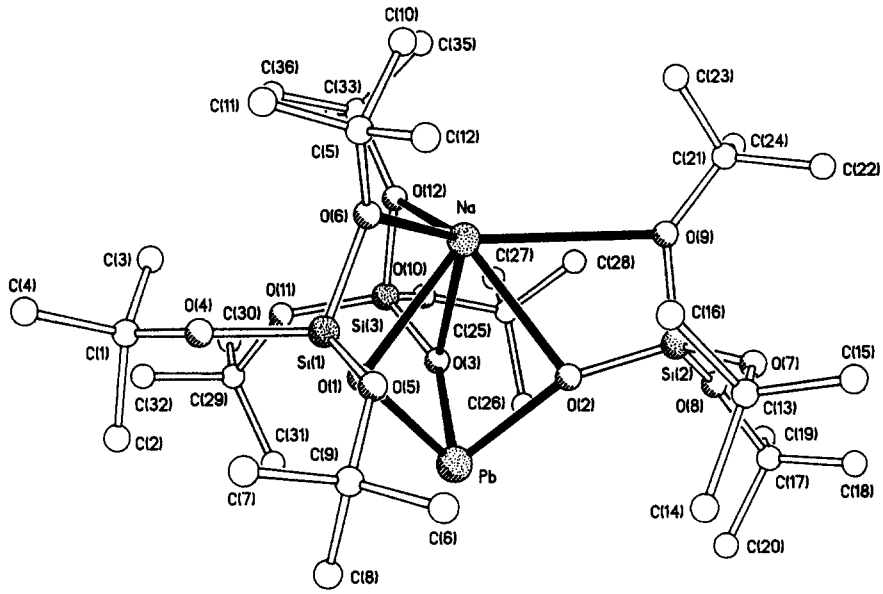

Fig. 1. View of the molecular structure of $NaPb[OSi(O^tBu)_3]_3$, drawn with arbitrary-radius atomic spheres for clarity, rather than thermal ellipsoids, due to high thermal activity in the ^{t}Bu groups.

Table 2. Selected interatomic distances (Å) and angles ( ) for $NaPb[OSi(O^tBu)_3]_3$

Na—Pb	3.150(6)	Pb—O(1)	2.143(15)
Pb—O(2)	2.119(15)	Pb—O(3)	2.152(14)
Na—O(2)	2.420(20)	Na—O(1)	2.504(14)
Na—O(6)	2.518(17)	Na—O(3)	2.619(15)
Na—O(12)	2.455(16)	Na—O(9)	2.858(23)
Si(1)—O(4)	1.634(16)	Si(1)—O(1)	1.559(14)
Si(1)—O(6)	1.628(12)	Si(1)—O(5)	1.604(16)
Si(2)—O(7)	1.610(20)	Si(2)—O(2)	1.580(18)
Si(2)—O(9)	1.559(18)	Si(2)—O(8)	1.524(19)
Si(3)—O(10)	1.604(15)	Si(3)—O(3)	1.550(17)
Si(3)—O(12)	1.635(11)	Si(3)—O(11)	1.620(16)
Na—O(6)—C(5)	133(1)	O(2)—Pb—O(3)	86.9(6)
Na—O(12)—C(33)	128(1)	O(12)—Na—O(6)	120.0(6)
Na—O(9)—C(21)	129(2)	O(12)—Na—O(9)	111.8(7)
Na—O(1)—Pb	85.0(5)	O(6)—Na—O(9)	122.7(7)
Na—O(2)—Pb	87.6(7)	O(12)—Na—O(2)	126.2(6)
Na—O(3)—Pb	82.0(5)	O(12)—Na—O(3)	58.7(4)
Na—O(1)—Si(1)	98.5(6)	O(12)—Na—O(1)	105.6(5)
Na—O(2)—Si(2)	109.8(8)	O(6)—Na—O(1)	60.3(4)
Na—O(3)—Si(3)	96.6(6)	O(6)—Na—O(2)	105.6(6)
Na—O(6)—Si(1)	96.1(6)	O(6)—Na—O(3)	129.0(5)
Na—O(9)—Si(2)	92.2(8)	O(9)—Na—O(1)	126.6(6)
Na—O(12)—Si(3)	100.7(6)	O(9)—Na—O(2)	54.8(5)
Pb—O(1)—Si(1)	152(1)	O(9)—Na—O(3)	97.5(6)
Pb—O(2)—Si(2)	147(1)	O(1)—Na—O(2)	72.6(6)
Pb—O(3)—Si(3)	155(1)	O(1)—Na—O(3)	71.0(4)
O(1)—Pb—O(2)	86.4(6)	O(2)—Na—O(3)	71.1(5)
O(1)—Pb—O(3)	87.7(5)		

solution in benzene and layering with acetonitrile afforded colorless crystals of $Pb[OSi(O^tBu)_3]_2 \cdot {}^t$BuOH · NCMe. Addition of *tert*-butyl alcohol to a dichloromethane-d_2 solution of $Pb[OSi(O^tBu)_3]_2 \cdot {}^t$BuOH · NCMe results in an upfield shift of the ^{t}Bu resonance without separation of the resonances due to $OSi(O^tBu)_3$ and HO^tBu. Attempts to form $Pb[OSi(O^tBu)_3]_2 \cdot {}^t$BuOH · NCMe by the reac-

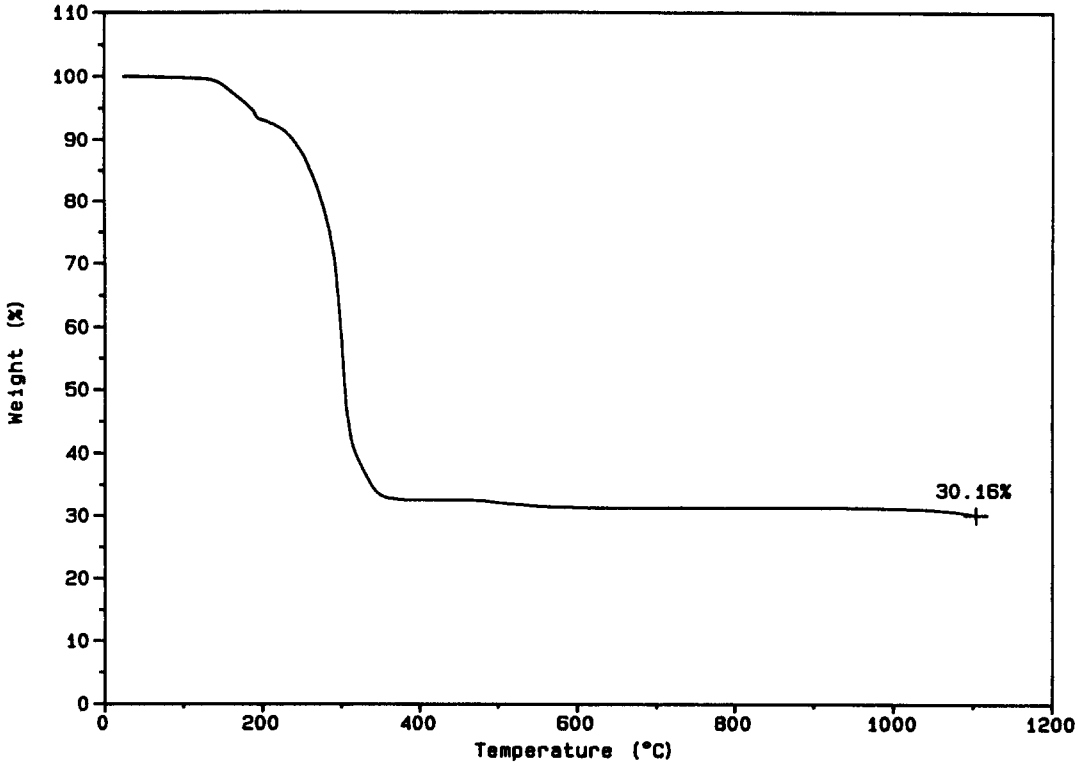

Fig. 2. Thermal gravimetric analysis curve for $NaPb[OSi(O^tBu)_3]_3$ under oxygen.

tion of $PbCl_2$ with $HOSi(O^tBu)_3$ in refluxing toluene/acetonitrile in the presence of pyridine were unsuccessful. In addition, there was no reaction between $Pb[OSi(O^tBu)_3]_2 \cdot {}^tBuOH \cdot NCMe$ and $NaOSi(O^tBu)_3$ in benzene-d_6 at room temperature.

The tin complex $KSn[OSi(O^tBu)_3]_3$

Reaction of $SnCl_2$ with 3 equiv. of $KOSi(O^tBu)_3$ in THF resulted in formation of the ate complex $KSn[OSi(O^tBu)_3]_3$ in near quantitative yield [eq. (2)]. The product was crystallized from cold pentane and isolated in 80% yield as colorless needles. A TGA analysis of $KSn[OSi(O^tBu)_3]_3$ revealed a rapid weight loss starting at 200°C, with the decomposition being completed at about 350°C (88% weight loss).

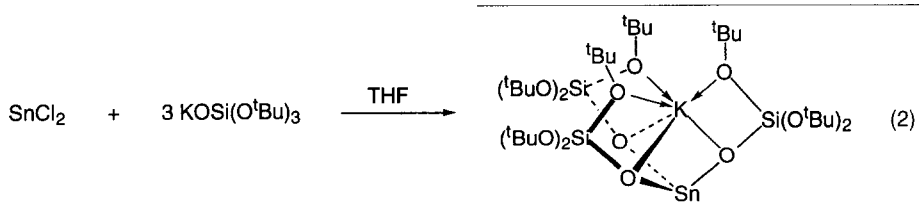

(2)

Related Sn^{II} heterobimetallic complexes of the type $[MSn(^tOBu)_3]_n$ have been reported [10], and Caulton and coworkers have described potassium siloxide 'ate' complexes of tin(II), such as $(DME)_2K(\mu\text{-}OSiPh_3)_3Sn$ and $K(\mu\text{-}OSiMe_2{}^tBu)_3Sn$ [11].

The molecular structure of the compound is shown in the ORTEP drawing of Fig. 3, and selected bond distances and angles are given in Table 3. The structure is isomorphous with $NaPb[OSi(O^tBu)_3]_3$, and in many respects the molecules are similar. The K···Sn separation of 3.483(2) Å is somewhat greater than the corresponding Na···Pb distance of 3.150(6) Å, resulting in a slightly expanded $M(\mu\text{-}O)_3M'$ cage for the former compound. For comparison, the K···Sn distances in $(\eta^2\text{-}DME)_2K(\mu\text{-}OSiPh_3)_3Sn$ and $(\eta^2\text{-}DME)(\eta^1\text{-}DME)K(\mu\text{-}OSiPh_3)_3Sn$ are 3.515, 3.460 and 3.480 Å, respectively. Note that the K—O—Sn angles (54°) are considerably more acute than the Na—O—Pb angles (85°) in $NaPb[OSi(O^tBu)_3]_3$, which reflects different ionic radii for the component metal centers. The O—Sn—O angles in $KSn[OSi(O^tBu)_3]_3$ (av. 89°) are very similar to the corresponding angles observed for $(\eta^2\text{-}DME)_2K(\mu\text{-}$

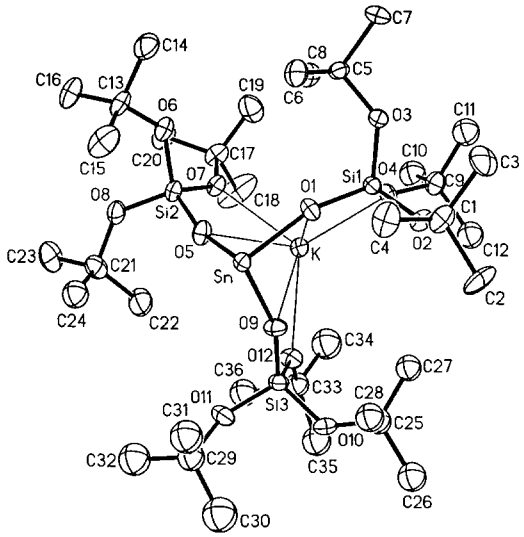

Fig. 3. ORTEP view of the molecular structure of KSn[O-Si(O^{t}Bu)$_3$]$_3$

OSiPh$_3$)$_3$Sn and (η^2-DME)(η^1-DME)K(μ-OSiPh$_3$)$_3$Sn (87–90°). Such acute angles have been rationalized on the basis of Fenske-Hall calculations as arising from a compromise between maximizing Sn—O σ-interactions while minimizing unfavorable Sn—O π-interactions and O—O nonbonded contacts [11].

Bismuth complexes

Addition of THF to a solid mixture of 3 equiv. of NaOSi(O^{t}Bu)$_3$ or KOSi(O^{t}Bu)$_3$ and BiCl$_3$ resulted in formation of Bi[OSi(O^{t}Bu)$_3$]$_3$. This complex was also obtained by addition of benzene to a solid mixture of 3 equiv. of HOSi(O^{t}Bu)$_3$ and Bi(O^{t}Bu)$_3$ [9]. Isolation was achieved by crystallization from pentane at −78 °C. Hydrolysis of Bi[OSi(O^{t}Bu)$_3$]$_3$ with excess water in benzene-d_6 resulted in formation of HOSi-(O^{t}Bu)$_3$ (3 equiv. by ^{1}H NMR spectroscopy) and a white precipitate. This complex is quite thermally labile, as shown by a TGA analysis under oxygen, which revealed a low onset temperature for decomposition at *ca* 90 °C followed by an abrupt weight loss of approximately 40% to just under 200 °C. This is followed by a smoother weight loss of approximately 25% to 375 °C.

A bismuth alkoxy(siloxy) complex was also formed in the reaction of Bi(O^{t}Bu)$_3$ with 3 equiv. of HOSi-Ph(O^{t}Bu)$_2$. This highly soluble complex, Bi[OSi-Ph(O^{t}Bu)$_2$]$_3$, was isolated as a white solid from pentane at −78 °C. Crystals suitable for X-ray crystallography were not obtained via repeated crystallizations.

Acknowledgements—This work was supported by the Director, Office of Energy Research, Office of Basic Energy

Table 3. Selected interatomic distances (Å) and angles (°) for KSn[OSi(O^{t}Bu)$_3$]$_3$

K—Sn	3.483(2)	Sn—O(1)	2.058(6)
Sn—O(5)	2.038(5)	Sn—O(9)	2.054(6)
K—O(7)	2.704(7)	K—O(1)	2.822(6)
K—O(4)	2.730(6)	K—O(5)	2.865(6)
K—O(12)	2.730(8)	K—O(9)	2.797(6)
Si(1)—O(1)	1.563(6)	Si(2)—O(7)	1.635(5)
Si(1)—O(2)	1.612(8)	Si(2)—O(8)	1.611(7)
Si(1)—O(3)	1.624(8)	Si(3)—O(9)	1.565(7)
Si(1)—O(4)	1.649(5)	Si(3)—O(10)	1.616(9)
Si(2)—O(5)	1.580(8)	Si(3)—O(11)	1.592(7)
Si(2)—O(6)	1.621(8)	Si(3)—O(12)	1.634(6)
K—O(4)—C(9)	125.8(5)	O(5)—Sn—O(9)	88.6(3)
K—O(7)—C(17)	123.7(5)	O(1)—K—O(4)	54.4(2)
K—O(12)—C(33)	126.8(7)	O(1)—K—O(5)	61.0(2)
K—O(1)—Sn	54.1(2)	O(4)—K—O(5)	112.9(2)
K—O(5)—Sn	55.3(2)	O(1)—K—O(7)	96.9(2)
K—O(9)—Sn	53.4(2)	O(5)—K—O(7)	54.1(2)
K—O(1)—Sn(1)	99.8(3)	O(1)—K—O(9)	62.2(2)
K—O(4)—Si(1)	101.1(3)	O(4)—K—O(9)	100.8(2)
K—O(5)—Si(2)	98.3(3)	O(5)—K—O(9)	60.6(2)
K—O(7)—Si(2)	103.2(3)	O(7)—K—O(9)	112.8(2)
K—O(9)—Si(3)	100.1(2)	O(1)—K—O(12)	115.0(2)
K—O(12)—Si(3)	100.9(3)	O(4)—K—O(12)	124.2(2)
Sn—O(1)—Si(1)	159.2(5)	O(5)—K—O(12)	97.1(2)
Sn—O(5)—Si(2)	158.4(5)	O(7)—K—O(12)	118.7(2)
Sn—O(9)—Si(3)	159.7(4)	O(9)—K—O(12)	54.4(2)
O(1)—Sn—O(9)	89.8(3)	O(4)—K—O(7)	117.0(2)
O(1)—Sn—O(5)	89.6(2)		

Sciences, Chemical Sciences Division, of the U.S. Department of Energy under Contract No. DE-AC03-76SF00098.

REFERENCES

1. (a) Bradley, D. C., *Chem. Rev.*, 1989, **89,** 1317; (b) Bradley, D. C., *Polyhedron*, 1994, **13,** 1111; (c) Bradley, D. C. and Faktor, M. M., *J. Chem. Soc., Faraday Trans.*, 1959, **55,** 2117.
2. (a) Klein, L. C., *Sol–Gel Technology for Thin Films, Fibers, Preforms, Electronics and Specialty Shapes*, Noyes Publications, Park Ridge (1988); (b) Brinker, C. J. and Scherer, G. W., *Sol–Gel Science, The Physics and Chemistry of Sol–Gel Processing*, Academic Press, San Diego (1990); (c) Livage, J., Henry, M. and Sanchez, C., *Prog. Solid State Chem.*, 1989, **18,** 259; (d) Hubert-Pfalzgraf, L. G., *New J. Chem.*, 1987, **11,** 663; (e) Caulton, K. G. and Hubert-Pfalzgraf, L. G., *Chem. Rev.*, 1990, **90,** 969; (f) Hubert-Pfalzgraf, L. G., *Polyhedron*, 1994, **8,** 1181.
3. (a) Terry, K. W., Gantzel, P. K. and Tilley, T. D., *Chem. Mater.*, 1992, **4,** 1290; (b) Terry, K. W., Lugmair, C. G., Gantzel, P. K. and Tilley, T. D., *Chem. Mater.*, 1996, **8,** 274; (c) Su, K., Tilley, T. D. and Sailor, M. J., *J. Am. Chem. Soc.*, 1996, **118,** 3459; (d) Lugmair, C. G., Tilley, T. D. and Rheingold, A. L., *Chem. Mater.*, 1997, **9,** 339; (g) Su, K. and Tilley, T. D., *Chem. Mater.*, 1997, **9,** 588.
4. (a) Terry, K. W. and Tilley, T. D., *Chem. Mater.*, 1991, **3,** 1001; (b) Terry, K. W., Lugmair, C. G. and Tilley, T. D., *J. Am. Chem. Soc.*, in press.
5. Abe, Y. and Kijima, I., *Bull. Chem. Soc. Jpn.*, 1969, **42,** 1118.
6. McMullen, A. K., Tilley, T. D., Rheingold, A. L. and Geib, S. J., *Inorg. Chem.*, 1989, **28,** 3772.
7. Terry, K. W., Ph. D. Thesis, University of California at San Diego, 1993.
8. Goel, S. C., Chiang, M. Y. and Buhro, W. E., *Inorg. Chem.*, 1990, **29,** 4640.
9. (a) Evans, W. J., Hain, J. H. Jr. and Ziller, J. W., *J. Chem. Soc., Chem. Commun.*, 1989, 1628; (b) Massiani, M. C., Papiernik, R., Hubert-Pfalzgraf, L. G. and Daran, J. C., *J. Chem. Soc., Chem. Commun.*, 1990, 301.
10. (a) Veith, M., *Chem. Rev.*, 1990, **90,** 3; (b) Veith, M. and Roesler, R., *Z. Naturforsch., B: Anorg. Chem., Org. Chem.*, 1986, **41B,** 1071; (c) Mehrotra, R. C., Singh, A. and Sogani, S., *Chem. Rev.*, 1994, **94,** 1643.
11. McGeary, M. J., Cayton, R. H., Folting, K., Huffman, J. C. and Caulton, K. G., *Polyhedron*, 1992, **11,** 1369.

Pergamon

PII: S0277-5387(97)00256-8

Polyhedron Vol. 17, No. 5–6, pp. 899–915, 1998
© 1998 Elsevier Science Ltd
All rights reserved. Printed in Great Britain
0277-5387/98 $19.00+0.00

Physicochemical approach to the studies of metal alkoxides†

N. Ya. Turova,[a]* E. P. Turevskaya,[a] M. I. Yanovskaya,[b] A. I. Yanovsky,[c] V. G. Kessler[a] and D. E. Tcheboukov[a]

[a]M. V. Lomonosov Moscow State University, Faculty of Chemistry, 119899, Moscow, Russia

[b]L. Ya. Karpov Institute of Physical Chemistry, 103064, Moscow, Russia

[c]A. N. Nesmeyanov Institute of Organoelement Compounds of Russian Academy of Sciences 117813, Moscow, Russia

(Received 24 April 1997; accepted 11 June, 1997)

Abstract—The review provides a description of main events in the development of chemistry of metal alkoxides in Russian and summarizes the results obtained by the authors. The studies of solubility and vapor pressure in the $M(OR)_n$-ROH (R = Li, Mg, Ca, Sr, Ba, Tl) systems permitted the determination of the composition of the solvates formed and the optimization of the isolation conditions for distinct derivatives. The electrochemical synthetic approach to the alkoxide and 2-methoxyethoxide derivatives of III–VIII Group elements has been elaborated. Improvement of the MCl_n with NaOR metathesis conditions led to practically quantitative yields of alkoxides.

The examples of the structures of polynuclear oxoalkoxides, earlier erroneously considered to be ortho-derivatives, i.e. '$M(OR)_n$', are given. It has been stated that among the alkoxoderivatives of Zr and Hf these are only $M(OC_2H_4OMe)_4$ and $M(OR)_4 \cdot ROH$ (R = Pr^i, Bu^t) that exist as individual compounds, while the samples of those with different R contain oxocomplexes of $M_3O(OR)_{10}$ and $M_4O(OR)_{14}$ composition. The questions connected with the origin of oxogroups in the molecules of alkoxides and their influence on the properties of the samples are discussed. The irreproducibility of the physicochemical constants for the samples (physical state, melting points, solubility in alcohols, intensity of coloration) is caused by different 'chemical' (synthetic procedures, isolation conditions) and thermal prehistory and storage times; it originates from the difference in their molecular composition (different fractions of different types of oligomeric and polymeric $[M(OR)_n]_m$ and $M_xO_y(OR)_z$ aggregates).

Formation of bimetallic alkoxides is studied using the plotting of 20°C solubility isotherms in $M(OR)_n$–$M'(OR)_m$–Solvent systems. Different kinds of systems are considered and the composition and structure of bimetallic complexes and oxocomplexes, originating from their decomposition, are described. Decomposition of alkoxomolybdates and -tungstates in solutions may result in crystallization of complex oxides as the final products. The example of $MTiO_3$ (M = Mg, Ba) oxide preparation is discussed as most illustratively demonstrating the need in studies of metal alkoxides interaction in solution for the optimization of synthesis of oxides by the sol-gel technique. © 1998 Elsevier Science Ltd. All rights reserved

Keywords: Metal alkoxides; electrochemical synthesis; oxoalkoxides; physicochemical analysis.

The studies of metal alkoxides started in Russia about 100 years ago. In 1899 at the Sankt-Peterburg University, V. E. Tishchenko (an apprentice of Butlerov and Mendeleev) presented a thesis entitled 'On the action of aluminium amalgam on alcohols: aluminium alkoxides, their properties and reactions' [1]. In spite of the national celebrity status, which the Tishchenko reaction (the transformation of aldehydes into esters on action of $Al(OR)_3$) received, this latter work remained unknown by foreign chemists, as it was published only in Russian in the Journal of Russian Physicochemical Society. However, in this work (i) some general methods of synthesis of metal alkoxides have been elaborated, the regularities of variations in the values of physicochemical constants along hom-

* Author to whom correspondence should be addressed.

† Dedicated to Professor D. C. Bradley on the occasion of his 73rd birthday.

ologous series (ii), and on the ramification of organic radicals (iii) were formulated, the main thermolysis pathways (iv) and main directions of metal alkoxides application in organic synthesis (v) were determined. This work undoubtedly represented the first systematic investigation of the properties of one of the most important classes of alkoxides, performed at very high standard and might serve as an example of fundamental and comprehensive approach to the problem even for the modern researchers.

In the 1950s the group under Professor A. N. Nesmeyanov at the Institute of Organic Chemistry of the USSR Academy of Sciences initiated one of the first systematic studies of titanium alkoxides. The synthetic approaches to these compounds (in particular, $TiCl_4$ alcoholysis reactions in presence of NH_3 or Py) were worked out and the products of their partial haloidation and hydrolysis were investigated for the first time [2].

Fundamental synthetic and physicochemical studies of lithium alkoxides were carried out in Moscow at the L. Ya. Karpov Institute of Physical Chemistry in the early 1960s by T. V. Talalaeva *et al.* [3]. The synthesis of nearly all representatives of the LiOR homologous series was reported and the molecular complexities of these compounds were determined. The structures of aggregates present in solid, liquid and gaseous phases ($n = 3$–9), were deduced on the basis of IR and NMR spectral data compared with those calculated theoretically in relation to different structural models.

The first X-ray single crystal investigation of the structure of a metal alkoxide, namely $W(OPh)_6$, was carried out in 1957 by Yu. T. Struchkov at the Moscow State University. It has been found that in the octahedral molecule of this compound, the Ph-rings are placed around the W atom in rendered conformation (like propeller blades) thus totally protecting it sterically [4]. The authors referred to this circumstance to explain the unusually high stability of tungsten phenoxide to hydrolysis even in acidic media. Later, during many years it was Yu. T. Struchkov, who headed the X-ray structure studies of homo- and heterometallic alkoxides at A. N. Nesmeyanov Institute of Organoelement Compounds of Russian Academy Sciences. More than 50 structures of metal alkoxides (of the total of several hundreds known today) [5] were determined in his laboratory.

In 1957 at the Department of Inorganic Chemistry of the Moscow State University, a study of beryllium alkoxides was initiated by Professor A. V. Novoselova in connection with the problem of the preparation of high purity materials for the nuclear industries [6]. Her laboratory was one of the centers of physicochemical analysis of inorganic compounds and, naturally, this approach (plotting of property versus composition diagrams) was applied to the studies of metal alkoxides. The objects of our studies became methoxides and ethoxides of magnesium and alkaline earth metals and, later, the derivatives of a broad spectrum of elements—from Ia to VIIIb Groups of the Periodic Table. The following standard research scheme was usually applied:

—Optimization of synthesis, isolation and purification conditions for distinct derivatives.

—Investigation of their physicochemical properties such as solubility in organic solvents, thermal properties, spectral characteristics, crystal structure etc. (in connection with the chemical and thermal prehistory and 'age' of the samples).

—Study the complex formation with the derivatives of other elements, investigation of properties and crystal structures of bimetallic complexes.

—One of the most important directions was connected with the studies of oxoalkoxides—the conditions of their formation, their properties and molecular structures and the determination of the possible origin of oxogroups in the coordination spheres of metal atoms.

—Optimization of preparation conditions for some simple and complex oxides produced from metal alkoxides.

The results obtained in all of the mentioned research directions were produced to contribute to the elaboration of the scientific principles of sol–gel technology [7].

Studying the literature on the chemistry of metal alkoxides during the past 40 years, we paid special attention to the works of Professor D. C. Bradley, whose classic investigations promoted the creation of the modern science of metal alkoxide chemistry. Being unfortunately not acquainted with him personally, we nevertheless consider him as our teacher in the field of chemistry that we have chosen for our research. In addition to the MSU employees, these are the former graduates of the abovementioned laboratory working at Karpov Institute and Institute of Organoelement Compounds who counterpart in our research activity.

1. SYNTHESIS OF METAL ALKOXIDES

The provision of the industries of oxide materials with a broad assortment of accessible alkoxide derivatives that can be prepared using simple and inexpensive techniques is one of the principal conditions of its development. In spite of the considerable attention that is paid in the modern literature to the derivatives of alcohols with more and more sterically demanding and ramified radicals, our research remained concentrated mainly on the derivatives of the first representatives of the homologous series and those of 2-methoxyethanol.

Having experimentally analyzed the numerous (but not always reliable) literature data and having optimized the known approaches and developed some new techniques, we have concentrated our attention on three main approaches applicable in both laboratory and industrial practice.

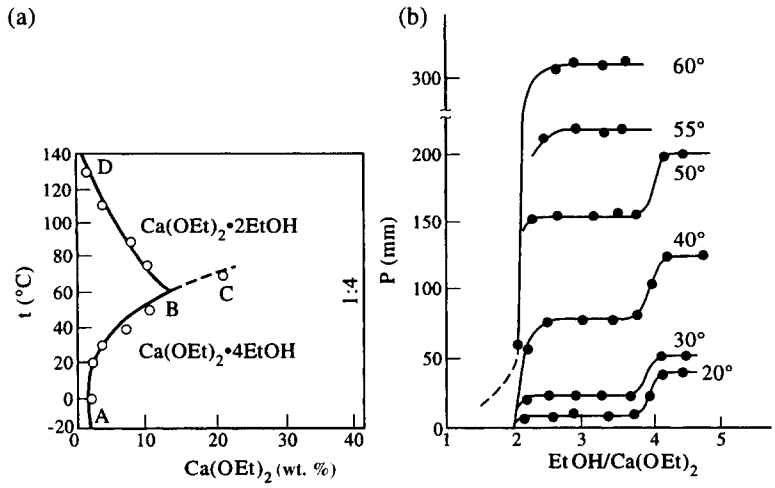

Fig. 1. Solubility (a) and vapor pressure (b) in the $Ca(OEt)_2$–EtOH system.

For the preparation of the derivatives of akaline, alkaline earth metals, magnesium and aluminium, the reaction of metals with alcohols did not meet any obstacles in the synthesis of methoxides, ethoxides etc. however the conditions of their isolation and the compositions of the solvates formed could be improved. For this purpose, the solubility polytherms in $M(OR)_n$ (s)–ROH (l) were investigated, and the tensimetric study of $M(OR)_n$ (s)–ROH (g), where M = Li, Mg, Ca, Sr, Ba, R = Me, Et was carried out [8]. As examples, the state diagram in the $Ca(OEt)_2$–EtOH binary system and the vapor pressure isotherms in it are given in Fig. 1. There was established the existence of a 1:4 solvate, that loses two moles of EtOH under mother liquor at 60°C forming a 1:2 solvate. The solubility of the latter decreases with temperature due to the exothermal effect of its dissolution (−29.5 kJ/mol). The thermodynamic functions of the reaction.

$$Ca(OEt)_2 \cdot 4EtOH(s) \Leftrightarrow Ca(OEt)_2 \cdot 2EtOH(s) + 2EtOH(g)$$

are $\Delta H_T = 162.5$, $\Delta G_{298} = 39.1$ kJ/mol, $\Delta S_T = 414.1$ J/mol K. Considerable increase in the solubility of 1:4 solvate with temperature (ΔH of dissolution = +37.8 kJ/mol) permits its recrystallization from alcohol. The loss of the last ROH molecule by disolvate (as it also takes place in the case of other metal alkoxide solvates) is accompanied by partial solvolysis and appearance of oxogroups in its structure. The latter, even in microammounts, changes considerably the properties of the samples (see below). In spite of the idea of ionic nature of alkaline earth solvates being well-established in the literature, the publications of the last years testify their molecular nature. Cubane-like molecules were found in the structures of $Mg(OMe)_2 \cdot 3.5$ MeOH [9] and $Ba(O\text{-}Bu^t)_2 \cdot {}^tBuOH$ [10].

Interaction of thallium metal with EtOH is worth special mention. Contradiction in the literature data left it unclear that TlOEt might be prepared if the presence of water, which is the other product of this reaction. The investigation of the TlOEt solubility polytherm in EtOH has shown that this system undergoes layering and thus water is quantitatively transferred into the upper alcohol layer, while the alkoxide—free from hydrolysis products—forms a lower layer as a heavy viscous oil (Fig. 2) [11].

For the preparation of Group III–VIII metal alkoxides, the application of the electrochemical method, based on anodic dissolution of metals in anhydrous alcoholic media in presence of conductive additives, proved to be the most promising. This technique was patented by the Monsanto Corporation in 1972 for the preparation of ethoxides of Si, Ge, Ti, Zr, Ta [12],

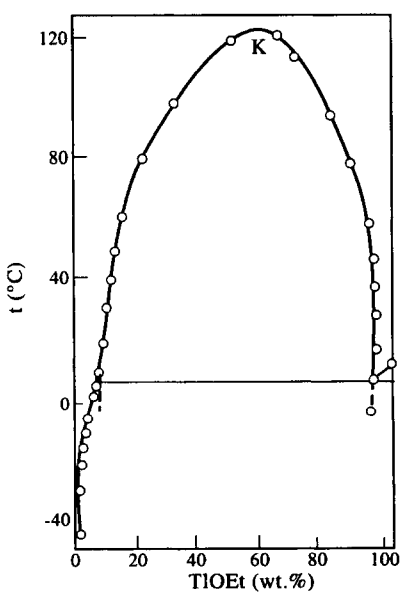

Fig. 2. Solubility polytherm in the TlOEt–EtOH system.

and was applied by Lehmkuhl *et al.* for the synthesis of Fe^{II}, Co and Ni alkoxides [13]. We have substantially widened the spectrum of products prepared by this method [14a]. The preparation techniques exploiting this approach were developed for soluble $M(OR)_n$, M = Sc, Y, La, Ln [14b], Ti, Zr, Hf, Nb [14a], Ta [14c], R = Me, Et, Pr^i, Bu^n; $MO(OR)_4$, M = Mo, W, R = Me, Et, Pr^i [14d]; 2-methoxyethoxides of Y, Ln, Sn^{II}, Zr, Hf, Nb, Ta, Fe^{III}, Co, Ni [14e], which are concentrated in electrolyte and several insoluble products such as $Bi(OMe)_3$ [14f], $Cr(OR)_3$ (R = Me, Et, $MeOC_2H_4$) [14g], $V(OR)_3$ [14d], $Ni(OR)_2$ (R = Me, Pr^n, Pr^i) [14h], $Cu(OR)_2$, R = ^{n}Bu, C_2H_4OMe [14i], $Re_4O_2(OMe)_{16}$ [14j], which precipitates from it in the cell. $[Bu_4N]Br$ or cheaper reagents such as lithium salts were used as conductive additives. It is worth noting that the oxidation state of a metal in the derivative to be prepared is dependent upon the nature of alcohol. Thus in contrast to the anodic oxidation of iron in aliphatic alcohols, which provides a route to air-sensitive solid $Fe(OR)_2$ [13], the same process, when carried out in 2-methoxyethanol, gives a liquid $Fe_n(OC_2H_4OMe)_{3-2n}$, which is perfectly stable and soluble in donor organic solvents [14e]. The latter can serve as a versatile precursor of Fe_2O_3-based materials. The anodic oxidation of several metals in the same $MeOC_2H_4OH$-based electrolyte turned to be a very convenient route to prepare film-forming solutions (with prescribed stoichiometries such as ZrO_2-Y_2O_3, $PbZr_{1-x}Ti_xO_3$, $Ba_xSr_{1-x}TiO_3$) [15]*.

One of the most attractive advantages of the electrochemical technique is provided by its simplicity: as the initial reagents are used pure metals (which, in contrast to anhydrous halides, are easier to handle and are always commercially available), the volumes of organic solvents applied are also considerably reduced. One disadvantage of this technique one can mention is the difficulty to remove the admixtures of alkoxide chlorides or bimetallic alkoxides in the case when LiCl is used as a conductive additive [14c]. When the industrial application is considered, these are such features as its high productivity, continuous and non-pollutive character (as hydrogen is the major side-product) that are of prime importance. At present the technological schemes are developed for electrochemical production of a number of derivatives, first and foremost for the large-scale production of $Ti(OBu)_4$ [16].

Besides the electrochemical synthesis, especially in the cases when its application is impossible due to cathodic reduction of an alkoxide formed (leading to lower oxidation state derivatives or to electrochemical refinement of the metal), we applied the well-known metathesis reaction:

$$MCl_n + n\text{NaOR} \rightarrow M(OR)_n + n\text{NaCl}\downarrow$$

M = In, Y, La, Ln, Ti, Ge, Bi, V^{IV}, $[VO]^{2+}$, $[VO]^{3+}$, Nb, $[NbO]^{3+}$, W, $[M'O]^{4+}$, $[M'O_2]^{2+}$ (M′ = Mo, W), Fe^{III}

Low yields of final products, described in literature, were increased to practically quantitative ones due to elimination of the alcoholysis processes for MCl_n (strong Lewis acids), which is accompanied by formation of alkoxide chlorides and subsequently the polymeric oxoalkoxides. For this purpose the initial chloride was always introduced into reaction with NaOR on cooling and vigorous stirring in the form of solution or suspension in ether or hydrocarbon solvent. Destruction of bimetallic alkoxide chloride intermediates was achieved by prolonged heating of the reaction mixtures under reflux or by complete removal of the solvent [17, 14b, f, d].

2. OXOALKOXIDES

Polymeric metal oxoalkoxides obtained by hydrolysis or thermolysis of $M(OR)_n$ were for a long time considered as being of practical interest as materials for thermally stable, hydrophobic and protective coatings [18, 19]. A new period in the history of oxoalkoxides was connected with the oligomeric oxoalkoxide complexes, which were structurally characterized at the end of the 1960s [20]. The role played by these derivatives in the chemistry of metal alkoxides turned out to be extremely important. A whole series of compounds, described as '$M(OR)_n$' were found in particular to contain oxogroups in their structures. The latter usually have the structural function of polydentate bridges and therefore were present in the composition in very low quantities. This circumstance, in combination with the presence of solvating alcohol molecules or alcohol molecules included into the holes of the crystal lattice (originating from the complex shape of oxoalkoxide molecules), leads in many cases to microanalysis data that do not differ from those of $M(OR)_n$. The IR spectra in such cases give very often insufficient information as the M—O—M vibration frequencies rarely are characteristic enough. Therefore, the main role in the characterization of oxoalkoxides should be played by X-ray single crystal studies.

A well-known example is provided by crystalline isopropoxides of rare earth elements which turned in fact to be pentanuclear oxocomplexes $Ln_5(\mu_5\text{-}O)(\mu_3\text{-}OR)_4(\mu\text{-}OR)_4(OR)_5$ [21,22]. 'Crystalline aluminium ethoxide' (formed on prolonged heating of polymeric $Al(OEt)_3$ under benzene with subsequent evacuation and recrystallization from CS_2) was found to be in fact

* The application of 2-methoxyethoxides in general has granted a considerable progress in sol–gel technology. On the first hand, due to the possibility of chelation they turned out to be better soluble than $M(OA1K)_n$—the derivatives of the same metals in alcohols, THF and even hydrocarbons. On the other hand, they seem to be rather more stable to hydrolysis, and in some cases to redox processes, and form more stable sols when the excess of water is applied.

an oxoethoxide—$Al_{10}(\mu_4\text{-}O)_2(\mu_3\text{-}O)_2(\mu\text{-}OEt)_{14}(OEt)_{18}$ (Fig. 3a). The molecule consists of two pentamers bound by planar μ_3-O-groups in a $[Al_2O_2]$ cycle. Aluminium atoms possess tetrahedral, octahedral and trigonal bipyramidal coordination. Such decanuclear molecules are, according to mass-spectral data, also present in the gas phase [23]. It is worth noting that the known '$Fe(OEt)_3$' (dark orange–brown crystals that precipitate quantitatively from solutions in alcohol) is isomorphous to the described Al compound and is also an oxoderivative, but easier isolable and more stable [17e].

The crystalline product that precipitates from the yellow solutions of $Ca(OEt)_2$, obtained on reflux (on drying of the alcohol, for example) possesses '$Ca(OEt)_2 \cdot 2EtOH$' composition, but its crystal structure is built up of $Ca_6(\mu_4\text{-}O)_2(\mu_3\text{-}OEt)_4(OEt)_4 \cdot 14EtOH$ hexanuclear molecules, consisting of two $[Ca_4O_4]$ cubes sharing a common $[Ca_2O(oxo)_2]$ face [24] (Fig. 3b), its metal–oxygen core is analogous to that of $Li_5Sm(OBu^t)_8$ [25].

The structure of the well-known catalyst and reductive agent '$AlCl(OPr^i)_2$', which is widely used in organic synthesis, is actually built up of $Al_4(\mu_4\text{-}O)(\mu\text{-}OPr^i)_5[H(OPr^i)_2]Cl_4$ tetrahedral molecules, which are also present in the gas phase (Fig. 3c). All Al atoms in this structure are pentacoordinated (trigonal bipyramids); two of the four terminal OR-groups are connected by a hydrogen bond (i.e. one of them should be a solvating alcohol molecule) [26]. The molecules of crystalline 'lead isopropoxide obtained by anodic oxidation of lead in alcohol are octahedral $Pb_6(\mu_3\text{-}O)_4(\mu_3\text{-}OPr^i)_4$ aggregates with oxo- and alkoxide groups placed in turn over the faces of octahedron (Fig. 3d). This compound is a structural analog of tin and lead hydroxides—$M_6O_4(OH)_4$ [27].

The most impressive result was obtained on investigation of the physicochemical characteristics and, in particular, mass-spectra of zirconium and hafnium alkoxides ['$M(OR)_4$']. The amorphous samples having this composition, in fact contain admixtures of oxocomplexes such as $M_3O(OR)_{10}$ and $M_4O(OR)_{14}$, which are present in the solid state, in solution and in the gas phase [28]. The structure of the trinuclear species, deduced on the basis of NMR data, is analogous to that of the known triangular Th, Mo and U^{IV} oxoalkoxide clusters, i.e. $M_3(\mu_3\text{-}O)(\mu_3\text{-}OR)(\mu\text{-}OR)_3(OR)_6$, R = ^{i}Pr, ^{t}Bu [29–31], while that of tetranuclear ones contains an $[M_4]$ tetrahedron. As the ultimate proof, confirming the presence of oxoligands in the species of '$Hf(OEt)_4$' one can consider the isolation from its solution in toluene of the hexanuclear $[Hf_3O(OEt)_{10}(EtOH)]_2$ complex, whose structure is built up of two abovementioned triangular fragments connected by two extra solvating alcohol molecules (Fig. 3e). These are only liquid $M(OC_2H_4OMe)_4$ and $M(OR)_4 \cdot ROH$ solvates (R = ^{i}Pr, ^{t}Bu, M = Zr, Hf,) that can be considered to be individual products [28].

The minimal nuclearity among the oxoalkoxide species is demonstrated by tantalum oxoisopropoxide, $Ta_2(\mu\text{-}O)(\mu\text{-}OPr^i)(OPr^i)_7 \cdot {}^i$PrOH. This compound is a structural analog of $[M(OPr^i)_4 \cdot {}^i PrOH]_2$ (M = Zr, Hf) [32], containing however a bridging oxogroup instead of μ-OR-group in its structure (Fig. 3f). This compound is formed on short-time reflux of $Ta(OPr^i)_5$ in alcohol (for example, in the course of electrosynthesis). On long-term storage of such a solution, a product of rather more profound condensation, characterized as $Ta_7(\mu_3\text{-}O)(\mu\text{-}O)_8(\mu\text{-}OPr^i)_4(OPr^i)_{13}$ (Fig. 3g) [14c] is precipitated.

In spite of quite the considerable number of oxoalkoxides known at present, the satisfactory and ultimate answer to the question about their possible origin still cannot be given. It is very important to mention that the majority of the abovementioned species were isolated on prolonged storage (after heat treatment of solutions etc.) and are therefore the products of some kind of decomposition processes. The presence of oxogroups in the structures of the first isolated compounds of this kind, i.e. $Ti_7O_4(OEt)_{20}$, $Nb_8O_{10}(OEt)_{20}$* [20] and $Zr_{13}O_8(OMe)_{36}$ [33] was explained by occurrence of uncontrolled reactions of microhydrolysis.

Later, however, it has been proved that the same compounds are also formed under the conditions of complete isolation from moisture; the first one was prepared on heating of $Ti(OEt)_4$ solutions in alcohol in an autoclave [34], the second—on storage of liquid $NbO(OEt)_3$ samples in the sealed samples [17c]. The oxogroups apparently originate under these conditions due to quite different processes, such as ether elimination for example:

$$—M—OR + RO—M— \xrightarrow[-R_2O]{} —M—O—M—$$

This kind of decomposition, which was observed for the first time by Bradley (who described the formation of two oxo-tertbutoxides $NbO(OBu^t)_3$ and $Nb_2O(OBu^t)_8$ on action of ^{t}BuOH on $Nb(OEt)_5$ [35]), is very characteristic of the alkoxides of rhenium [36], tungsten and especially molybdenum [14d, 37]. It proved to be practically impossible to isolate the derivatives of $Mo(OR)_6$ series (its tungsten analogs are not much more stable either). The following sequence of transformations takes place on storage:

$$M(OR)_6 \xrightarrow[R_2O]{} MO(OR)_4 \xrightarrow[-R_2O]{} MO_2(OR)_2$$

and is accelerated by the traces of moisture, on heating and especially in presence of alkali alkoxides (see below).

This reaction may play a very important role in the processes of hydrolysis of metal alkoxide, when the precipitation of crystalline oxide phases takes place already from the solutions in organic solvents. For

* It was recently proved that $Ta_8O_{10}(OEt)_{20}$, isomorphous to its niobium analog, crystallizes on hydrolysis from $Ta(OEt)_5$ solution in EtOH.

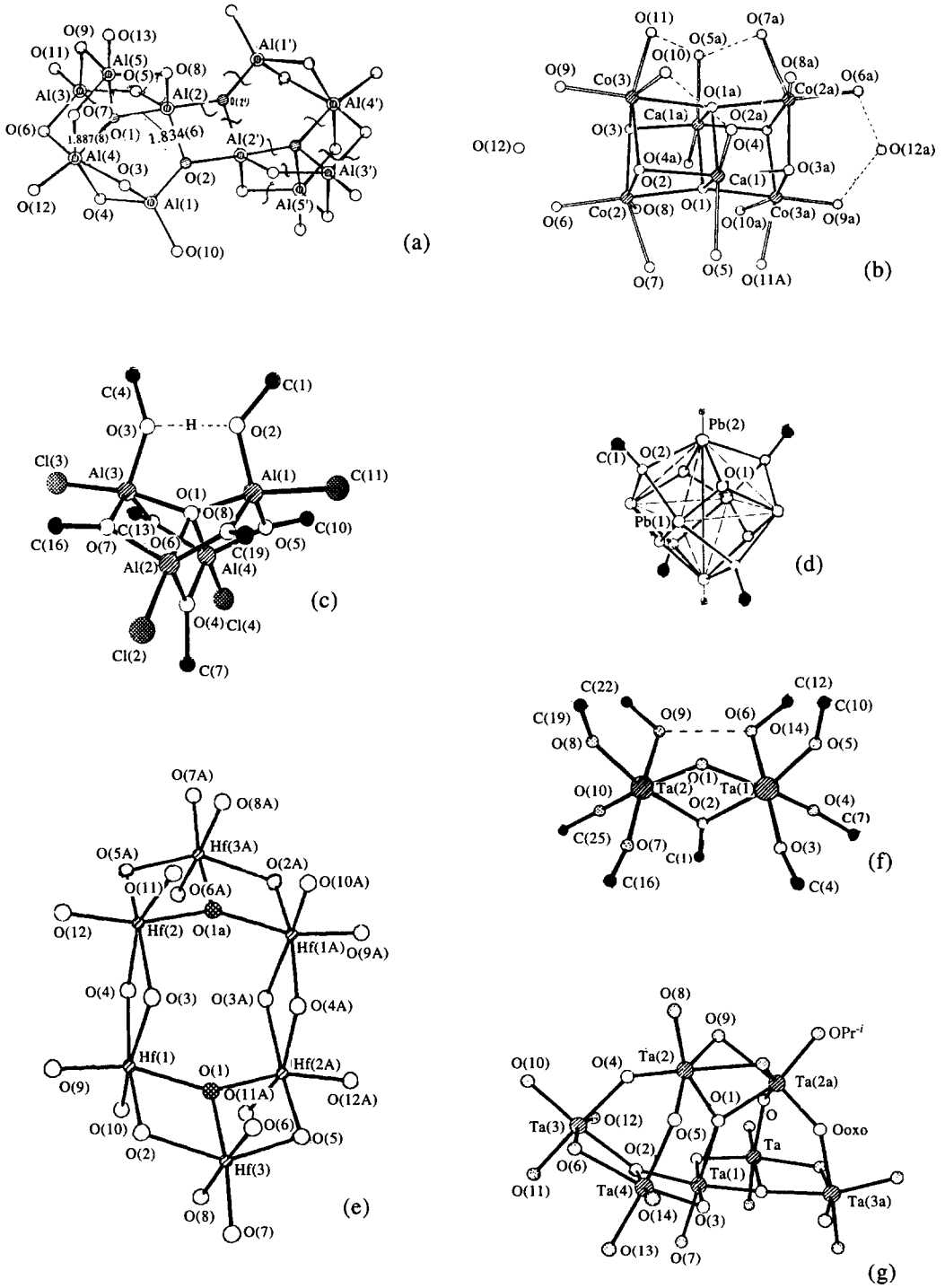

Fig. 3. Structures of oxoalkoxide complexes: $M_{10}(\mu_4\text{-}O)_2(\mu_3\text{-}O)_2(\mu\text{-}OEt)_{14}(OEt)_8$, M = Al, Fe (a), marks show the points of fraction leading to oligomeric molecules detected in the gas phase; $Ca_6(\mu_4\text{-}O)_2(\mu_3\text{-}OEt)_4(OEt)_4 \cdot 14EtOH$ (b); $Al_4(\mu_4\text{-}O)(\mu\text{-}OPr^i)_5[H(OPr^i)_2]Cl_4$ (c); $Pb_6(\mu_3\text{-}O)_4(\mu_3\text{-}OPr^i)_4$ (d); $[Hf_3O(OEt)_{10}(EtOH)]_2$ (e); $Ta_2(\mu\text{-}O)(\mu\text{-}OPr^i)(OPr^i)_7 \cdot {}^iPrOH$ (f); $Ta_7(\mu_3\text{-}O)(\mu\text{-}O)_8(\mu\text{-}OPr^i)_4(OPr^i)_{13}$ (g).

example, in action of the excess of water on $Bi(OEt)_3$ in benzene, the formation of α-Bi_2O_3 phase was observed (the presence of ether was detected by GLC). At the same time, the precipitates obtained in ethanol were always amorphous, while in 2-methoxyethanol the formation of very stable sols took place; in both latter cases no trace of ether could be detected [38].

The appearance of oxogroups in the molecules of alkaline and alkaline earth metals and lanthanum (and, possibly, lanthanides) alkoxides can be caused by uncontrolled oxidation (by the traces of oxygen dissolved in the solvents used or present in atmosphere). The primary products of oxidation contain —OOR and —OOH groups [39], which undergo radical decomposition that produces water, and gives rise to oxo- and HCOO-groups in the structures of the species.* The yellow coloration observed in the samples is due to the presence of free radicals R$^{\cdot}$ producing a sharp singlet in the ESR spectra of these samples [40]. Such reactions can occur only in the case of the most ionic alkoxides, for which dissociation in solutions is accompanied by liberation of OR^- anions, able to react with O_2. These are 2-methoxyethoxides that demonstrate the most pronounced trend toward oxidation. Thus among the derivatives of lanthanides, only the derivative of yttrium (which is the most electronegative element among them) might be isolated free from oxogroups as $[Y(OC_2H_4OMe)_3]_{10}$ [41]. Gadolinium 2-methoxyethoxide can be isolated already as $Gd_6(\mu_4\text{-}O)(OR)_{16}$ [42]. On reaction of Ba with the same alcohol under the most complete isolation from oxygen and moisture, Caulton *et al.* were only able to isolate an oxoalkoxide $Ba(\mu_6\text{-}O)(OR)_{10}\cdot 4ROH$ composition [43]. At the same time the derivatives of MeOH and *t*-ROH turn to be much more stable to oxidation, for example, such lanthanum derivatives as $La_3(OBu^t)_9(^tBuOH)_2$ [44] and $[La(OCPh_3)_3]_2\cdot 3C_7H_8$ [45] have recently been isolated and structurally characterized.

The most pronounced difference between oxo- and orthoforms can be observed in case of polymeric $M(OR)_n$. The oligomeric nature of oxoalkoxides containing minimal amounts of oxogroups originating from uncontrolled microhydrolysis or -oxidation leads to a substantial increase in their solubility and reactivity. Thus, $[Ba(OBu^n)_2]_x$, synthesized by reaction of Ba with alcohol in hydrocarbon is totally insoluble in butanol and does not react with $Ta(OBu)_5$. However, when [mol9]0.05 of the oxogroup per Ba atom appears in its composition, it can be dissolved in BuOH to up to the concentration of ~40 wt%, which permits the preparation of its mixed solutions with tantalum butoxide, containing metals in any desired ratios [40,46]. Therefore, the solubility in alcohols or reactivity in the reactions of complex formation can serve as the 'indicators' of purity of the samples of $M(OR)_n$. At the same time, the $M(OR)_2\cdot 4ROH$, M = Mg, Ca, Ba, R = Me, Et, being soluble in alcohols are comparably stable to oxidation [8], due presumably to the solvation effect.

Also at the same time, the multinuclear $M_xO_y(OR)_z$, which have good solubility in hydrocarbons, can only usually be dissolved in alcohols on heating (or mechanical destruction under solvent) due to solvolytic destruction of their huge molecules. Therefore, their solubility never reaches the equilibrium values [17c]. The only exception to this rule seems to be $Ta_2O(OPr^i)_8\cdot {}^iPrOH$, whose molecules, presumably, remain intact in solution in alcohol [14c].

Formation of oxoalkoxides occurs, naturally, also in the course of controlled oxidation of low-valent $M(OR)_x$ derivatives by oxygen. As an example of such a process we can mention the formation of $MoO_2(OR)_2$ in the colored electrolytes (containing admixtures of Mo^V) put in contact with dry air [14d].

3. PARTICULAR FEATURES OF THE PHYSICOCHEMICAL BEHAVIOR OF METAL ALKOXIDES. 'COORDINATION POLYMERISM'

During the last two decades, the data on irreproducibility of characteristics of distinct alkoxides, such as $Al(OEt)_3$ [47], $Al(OPr^i)_3$ [20], $Ga(OPr^i)_3$ [20], $Ti(OMe)_4$ [48], have been quoted many times in literature.

It was found out that the variations in the values of 'physicochemical constants' of the samples, i.e. physical state, melting and sublimation points, solubility in alcohols, intensity of coloration etc., are dependant upon their 'prehistory', that is the thermal regime of their synthesis, nature of solvent, they were separated from, their storage time ('age') and so on, and are characteristic of the majority of the alkoxide derivatives of Group III–VIII metal alkoxides. The data obtained using such techniques as mass spectrometry, cryoscopy, IR spectroscopy and X-ray powder diffraction proved metal alkoxides to be able to form in each case, species of different sizes and structures capable of undergoing mutual transformations. The presence of different oligomeric and polymeric species in one and the same sample hinders its crystallization and causes irreproducibility of its characteristics. The assembly of these phenomena we have designated by a term 'coordination polymerism'. The simplest examples of such phenomena are provided by the existence of two different forms of titanium methoxide and of tungsten oxomethoxide. The well-known tetranuclear $[Ti(OMe)_4]_4$ molecules exist in the structure of crystals obtained from solutions in toluene. The action of alcohol provides the samples that are insoluble in organic solvents and possess polymeric structure according to

* Formation of formate groups independent of the alkoxide group R is due to oxidative destruction of C—C bonds and can be observed due to rather characteristic HCOO valence bands in IR spectra.

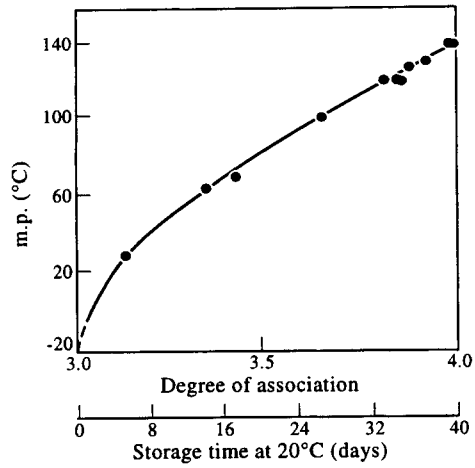

Fig. 4. Melting point versus molecular complexity ('age' of the samples) diagram for $[Al(OPr^i)_3]_n$.

the IR data obtained [48]. The oligomeric form of tungsten methoxide crystallized out from solutions in toluene or THF and was built up of $[WO(OMe)_3(\mu\text{-}OMe)]_2$ dimeric molecules [49]. From the solutions in alcohol (obtained by metathesis of $WOCl_4$ with NaOMe) the polymeric form, containing in its structure the asymmetric W=O···W bridges (analogous to those existing in the structure of $WOCl_4$) was obtained [50].

A classic example of an alkoxide, which samples demonstrate variable molecular composition, is provided by $Al(OPr^i)_3$, whose transformations in solutions were very thoroughly studied in the 1960s and 70s by vibration and NMR spectroscopy and tensimetry [20,51–53]. The freshly distilled liquid samples contain the trimeric $[(RO)_2Al(\mu\text{-}OR)_2]_2AlOR$ molecules, which have a chain structure with a pentacoordinate central Al atom and tetrahedrally coordinated peripheric ones [51] (its structural analog is the crystalline aluminium alkoxide chloride $Al_3Cl_5(\mu\text{-}OPr^i)_4$ [54]). On prolonged storage (about 40 days), the samples solidify forming crystals built up of tetrameric $Al[(\mu\text{-}OR)_2Al(OR)_2]_3$ molecules [55] (their structure was earlier predicted by Bradley [52]). The process of 'aging', i.e. the increase in the melting point up to 140°C and in the molecular complexity from 3 to 4 can be illustrated by Fig. 4, which plots the melting points vs. storage time in the phase diagram for trimer–tetramer system. Thus, in contrast to the data of Figgen and Gerding [53a], there are no different distinct solid forms of $Al(OPr^i)_3$, however two kinds of species coexist in the samples in different ratios. They are conserved in solution in hydrocarbons but on action of alcohol commence the crystallization of the form consisting of tetrameric molecules; the concentration of solutions decreases to a value corresponding to the equilibrium solubility of the latter. The samples that contain both kinds of species, when treated with alcohol, first undergo the extraction of unlimited soluble trimer, and thus provide very concentrated solutions. From the latter the tetrameric form subsequently crystallizes and thus the concentration decreases until it reaches the same value of equilibrium solubility. It is possible to suppose that in solution in alcohol, the molecules of trimer that contain pentacoordinate metal atoms are solvated and form larger aggregates *via* hydrogen bonding, which decompose producing tetrameric molecules, containing hexacoordinated Al atoms. Thus the steric unsaturation of the coordination polyhedron of the central aluminium atom makes the phase containing it unstable thermodynamically [55]. In the mass-spectra of some samples of aluminium isopropoxide, reported in [53b,c] in addition to the fragments of trimer and tetramer were found several ions with high m/z, which we could attribute to the fragments of oxodecamers [presumably analogous to $Al_{10}O_4(OEt)_{22}$]: $Al_9O_4(OPr)^+_{18}$ (1369), $Al_8O_4(OPr)^+_{15}$ (1165), $Al_7O_3(OPr)^+_{14}$ (1063), $Al_7O_4(OPr)^+_{12}$ (969), $Al_6O_3(OPr)^+_{11}$ (859).

Even greater pronounced coordination polymerism is characteristic of 2-methoxyethoxides. Presence of the ether function in the molecule provides an alternative for the saturation of the coordination sphere of the metal atom—in addition to OR-bridging groups these are oxygen atoms of ether groups that can enter it due to chelation. THe analysis of the structures of $M(OC_2H_4OMe)_n$ shows that the alkoxy oxygen atoms can be mono-, bi- and tridentate, while the ether oxygen atoms can be monodentate or not be coordinated at all. These factors provide an additional basis for coordination polymerism. This is probably the reason for the fact that most of the known 2-methoxyethoxides are liquids; the crystals can usually be obtained with low yields from the solutions in hydrocarbons.

Properties of the samples of $Al(OEt)_3$, described in the literature, appeared so different that it was usually supposed that several forms of this product existed, and in particular, polymeric β-form ('solvated') and oligomeric α-form ('non-solvated'). The first one can be obtained on prolonged heating of metal with an excess of alcohol in the presence of $HgCl_2$. The second is obtained from xylene or on heating of the first one, especially when carried out in the presence of aromatic hydrocarbons. The latter form is soluble and highly reactive. Its properties vary over a wide range, from viscous liquid to an amorphous solid with a m.p. of about 105–146°C, depending on the conditions of the synthesis of samples (heating rate etc.). The action of alcohol on the soluble liquid samples again transforms them into polymeric solids. In addition, there are two crystalline forms known (obtained from solutions in alcohol or in CS_2), to which the compositions '$Al(OEt)_3$' (shown to be $Al_{10}O_4(OEt)_{22}$, as it was mentioned above [23]) and '$Al(OEt)_2(OH)$' were ascribed. In the mass-spectra of all the forms, in addition to the fragments of $[Al(OEt)_3]_n$, where $n = 2$–4, fragments of oxoethoxides were found, containing from 4 to 10 metal atoms per fragment (Fig. 5). Relative intensities

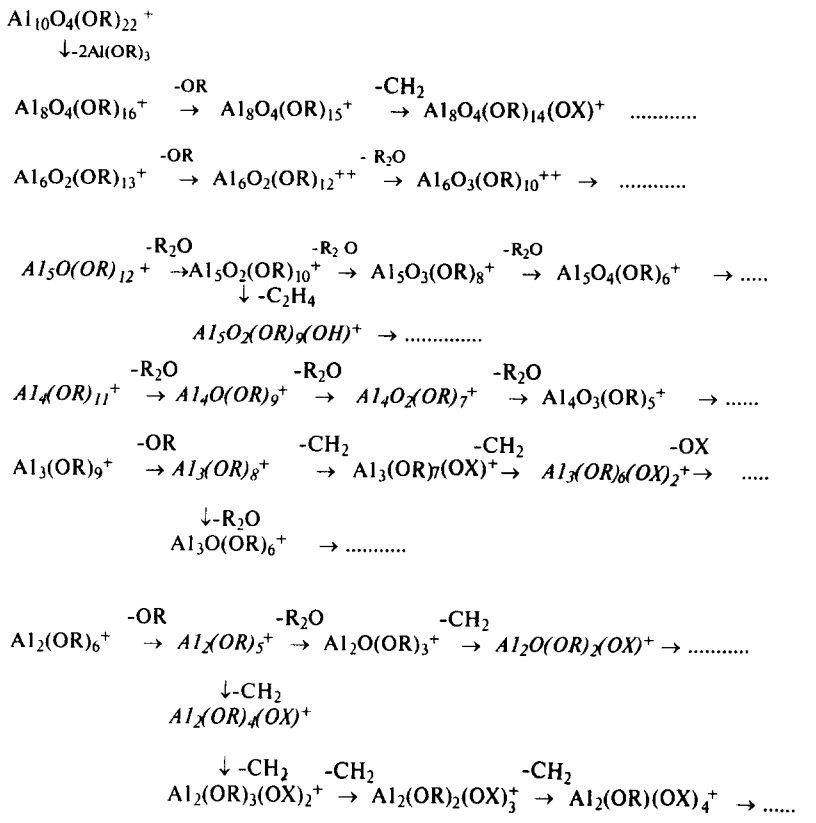

Fig. 5. Fragmentation scheme in the mass-spectra of $[Al(OMe)_3]_n$ and $[Al(OEt)_3]_n$ (the ions, observed by Oliver and Worrall [56], are printed in italic, X = H for methoxide and Me for ethoxide).

of peaks corresponding to ortho- and oxoforms testify that the composition of the samples can vary in a comparably wide range depending on the conditions of their synthesis and their thermal prehistory* [47].

Some information about the structure of oligomeric oxoalkoxides present in the amorphous samples, solutions or gas phase, can be obtained by reconstructing them from the X-ray molecular structures of polynuclear oxoalkoxide species, considering the oxo-groups as the points of condensation. Thus, in the molecule of $Al_{10}O_4(OEt)_{22}$ (Fig. 3a), one can trace the fragments corresponding to the tetra-, penta-, hexa- and octanuclear oxocomplexes, detected in the mass-spectra. It should be noted that the average molecular complexity for the '$Al(OEt)_3$' samples (corresponding to the decamer) in solution [58] and in the gas phase is the same (4.4). The same types of ortho- and oxo-oligomeric fragments were found in the mass-spectra of $Al(OMe)_3$ [47] (Fig. 5). On storage, the samples of polymeric methoxide and ethoxide undergo partial crystallization (with conservation of a major part as an amorphous matrix) with the formation of a layered structure of bayerite $Al(OH)_3$-type, which after 5 years of storage is converted to the more stable gibbsite $Al(OH)_3$-type [59].

'True' $Fe(OEt)_3$ is a polymer with the same kind of structure. It precipitates as yellow powder on action with liquid ethoxides of titanium or niobium on solutions of $Fe_{10}O_4(OEt)_{22}$ in alcohol [60a]. Apparently, the exchange reaction of the oxocomplexes of two metals in solution leads to formation of the least soluble product, which is iron ethoxide. Mass-spectra of iron ethoxide contain the fragments of oxoalkoxide species (from penta- to binuclear) and those of $Fe(OEt)_3$ monomers and dimers.

The properties of the samples of $Fe(OPr^i)_3$, which do not contain oxocomplexes, also vary over a wide range: m.p. 88–150°C (the latter value was obtained

*To be able to judge if the mass-spectral data provide adequate information about the molecular composition of the condensed phase, we compared them with those of X-ray single crystal, cryoscopic, ebulloscopic etc. studies of more than 50 oligomeric alkoxides and oxoalkoxides [57]. It was found that the size of species present in the samples is usually not dependent on their physical state. Mass-spectra of polymers, which are difficult to reproduce, contain only small fragments. As the first step of fragmentation is connected with the loss of an OR-group, it is possible to distinguish the oxofragments, formed under fragmentation due to electron impact or via loss of an ether molecule by an ortho-fragment and those originating from really existing oxoalkoxide molecules.

after a year of storage), color changes on action of ROH on the melt or on 'aging' from reddish brown to light yellow, solubility decreases from ~7% to 0. Fragments of orthotrimers, dimers and monomers were detected in the mass-spectra.

In addition to the examples discussed above, the coordination polymerism has been observed for samples of '$Zr(OR)_4$' and '$Hf(OR)_4$' [28], $NbO(OR)_3$ [17c], $MoO(OR)_4$ [37] and $MO_2(OR)_2$ (M = Mo, W) [37,70]. It is worth noting that for molybdenum oxoalkoxides, the polymerization occurs in presence of NaOR admixtures and proceeds *via* formation of OR-bridges, while dioxoderivatives of both molybdenum and tungsten undergo spontaneous polymerization with formation of oxobridges of M=O···M type. Polymerism of nickel ethoxide and isopropoxide is due to the presence of both octahedrally and tetrahedrally coordinated nickel atoms in their polymeric structures [14h].

The existence of different molecular forms was observed even for some heterometallic alkoxides. Thus, melting of $[NaWO_2(OC_2H_4OMe)_3]_2$ is associated with transformation of *cis*-$[WO_2]$ groups (where W=O bonds are terminal) into W=O···W chains, and of tetranuclear oligomers into a polymeric structure [70].

The data presented above, permits the tracing of some regularities in the transformations of properties of distinct alkoxide samples that occur due to poly- and oligomerization:

1. Molecular complexity increases on aging and on action of alcohols due, presumably to solvation of the 'young' forms, containing sterically unsaturated metal atoms. The next step is connected with formation of hydrogen bonds between solvated molecules and subsequent condensation with formation of OR-bridges and release of solvating alcohol molecules. This process is followed by the increase in the melting and sublimation temperatures, and decrease in solubility and weakening of coloration. In the mass-spectra, the increased evaporation temperature increases the fraction of low-nuclearity fragments.

2. Thermal treatment of the samples or their dissolution in aromatic hydrocarbon solvents leads to their oligomerization (in the latter case, probably, due to partial breakage of alkoxide bridges and formation of π-complexes). Products of this process display lower thermal constants, higher solubility in alcohols and more intense color. Their mass-spectra contain fragments corresponding to polynuclear oligomers present in the condensed phase. The scheme of these transformations is shown in Fig. 6.

Mastering these regularities, it is possible in many cases to modify the molecular composition of the samples and their properties. Describing the behavior of samples of distinct alkoxides it is very often difficult to distinguish the influence of the two main factors—non-uniform molecular composition of orthoforms and presence of oxoderivatives.

4. BIMETALLIC ALKOXIDES AND SYNTHESIS OF COMPLEX OXIDES

Heterometallic alkoxides have recently become a topic of special attention as the precursors of complex oxide materials for modern industries [71]. Their studies mainly deal with their preparation, the compounds described recently being characterized usually by X-ray single crystal studies, IR and NMR spectral data.

For determination of the composition and relative stability of bimetallic alkoxides, formed in solution and in the solid state, we applied the approach of physicochemical analysis based on investigation of the solubility isotherms in $M(OR)_n$–$M'(OR)_m$–L systems, where L is the solvent (alcohol, ether, hydrocarbon etc.) at 20°C. This approach, usually applied to the studies of inorganic salts interaction in aqueous media, turned out to be very fruitful for the studies of metal alkoxides. It permits us to test the interaction of components in the possible range of M : M′ ratios and determine the composition of the complexes formed in this system.

Let us consider examples of different types of interaction in ternary systems, displayed graphically in the Gibbs–Roseboom triangular diagrams (Fig. 7).

1. In the NaOMe–$Fe(OMe)_3$–MeOH system, no interaction takes place; polymeric iron methoxide remains insoluble at any concentration of NaOMe and the $Fe(OMe)_3$ crystallization curve lies on the side of the triangle [72].

2. Polymeric $Ba(OBu^n)_2$ dissolves in solutions of $Ti(OBu)_4$ in alcohol due to formation of the complex of composition $BaTi_4(OR)_{18}$ (which does not exist however in the solid state) as the curve corresponding to the crystallization of barium butoxide lies along the 1:4 section of the diagram [73]*.

3. Both components, i.e. $Bi(OEt)_3$ and $WO(OEt)_4$, are poorly soluble in pure alcohol, but in the presence of each other are transferred into solution due to formation of complexes with 3:2 and 1:1 compositions [75].

4. Both components $Ba(OMe)_2$ and $Ta(OMe)_5$ are soluble in alcohol, but the extrapolation of the $Ba(OMe)_2$·MeOH crystallization curve to the opposite side of the triangle testifies the formation of a 1:2 complex in solution (in an analogous system, containing isopropoxides as components, there exists a crystalline complex with *cis*-$[(^iPrOH)_2BaTa_2(OPr^i)_{12}]$ structure) [46].

---

*The consideration of more than 200 systems of AX_n–BX_m–L type, covering a wide spectrum of compounds and solvents, led us to a conclusion that there exists a connection between the position of the poorly soluble component crystallization curve in the diagram and the composition of the complex, which it forms in solution. The M : M′ ratio in the complex can be found by extrapolation of the crystallization curve for the poorly soluble component to the opposite side of the triangle [74].

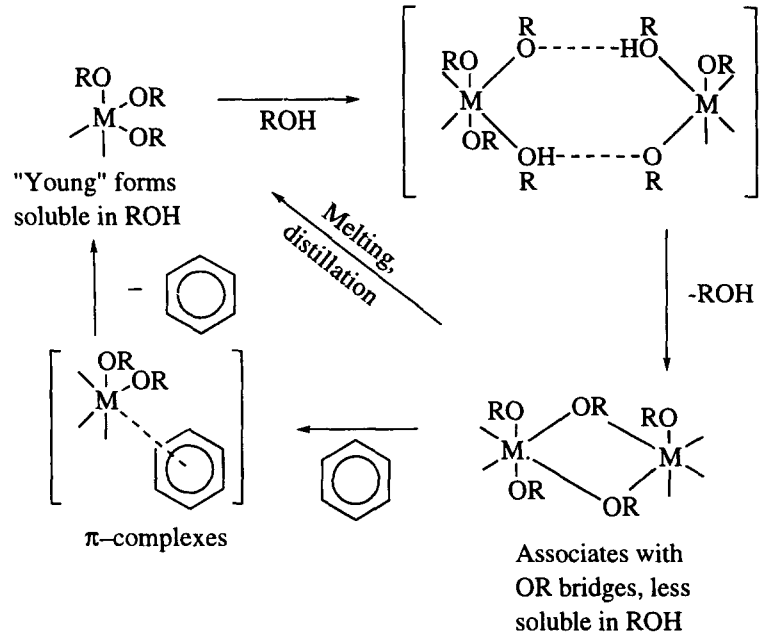

Fig. 6. General scheme of changes in molecular compositions of metal alkoxides under the action of different factors.

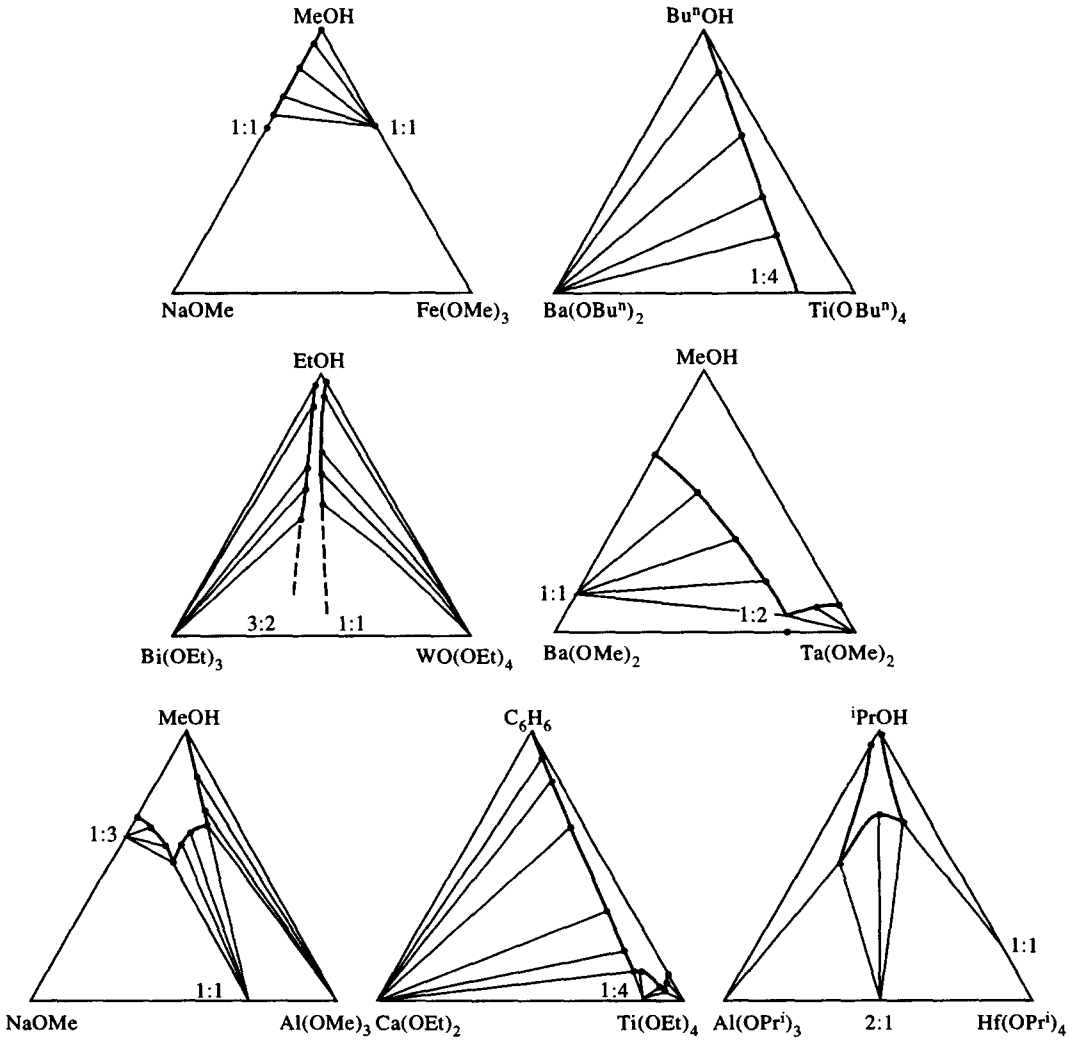

Fig. 7. Solubility isotherms in $M(OR)_n$–$M'(OR)_m$–L systems at 20 °C (wt %).

5. In the following three systems we observed the formation of crystalline bimetallic complexes $NaAl(OMe)_4$, $Ca[Ti_2(OEt)_9]_2$ and *cis*-$(Pr^iO)_2Hf[Al(OPr^i)_4]_2$. It is interesting to note that the first exists in the alkaline alkoxide excess and undergoes solvolysis in pure alcohol (analogous to hydrolysis of sodium aluminate). Therefore the eutonic point (corresponding the equilibrium of three phases) is situated on the 1:1 section of the diagram [76]. Calcium ethoxotitanate is formed in the excess of $Ti(OEt)_4$ [77], as the acidity of the latter exceeds substantially that of $Al(OR)_3$ and the difference in acidity for the two components in this system is more pronounced than in the previous one. Finally, in the system, formed by two 'acidic' alkoxides like those of Hf and Al the complex can stay in equilibrium with the solutions of both components and does not undergo solvolysis on action of alcohol.

The results were obtained by investigation of more than 50 systems, where the formation of alkoxoaluminates, -titanates, -zirconates, -hafnates, -niobates, -tanatlates, -molybdates, -tungstates and -ferrates (see Table 1) permitted the optimization for the conditions of their synthesis and those of the preparation of solutions for sol–gel application.

Let us consider the molecular structures of some of the complexes discovered in the abovementioned systems. Among the alkoxotitanates of alkaline earth elements, there are complexes of 1:4 composition, which possess the highest stability. Crystal structures of calcium and barium ethoxotitanates were found to be built up of $M^{II}[Ti_2(OEt)_9]_2$ symmetric molecules, where the central atom coordinates two $[Ti_2(OR)_9]$ groups (two octahedra sharing a common face). They are attached to the M^{II} ions *via* two μ_3- and two μ_2-OR-groups. The coordination number of barium and, quite unexpectedly, calcium atoms is equal to 8 (Fig. 8a) [73b]. These molecules as well as those of $BaZr_4(O-Pr^i)_{18}$ and $BaZr_4(OH)(OPr^i)_{17}$ described by Caulton [86] are highly stable. They are present in solutions of all barium alkoxotitanates (even in the cases when their existence in the solid state has not been proved) and in gas phase for alkoxozirconates [85].

Quite an unexpected result was obtained when investigating interactions of magnesium and titanium ethoxides. It turned out that the complex formed has a variable $MgTi_{4-x}(OEt)_{16-4x}\cdot(EtOH)_{2x}$ composition and conserves a structure analogous to that of $[Ti(OEt)_4]_4$ [20], where part of the $[Ti(OR)_4]$ group is substituted by $[Mg(OR)_2(ROH)_2]$. It is possibly due to the striking likeness of the Ti and Mg covalent radii (Fig. 8b) [83]. Formation of complexes with a variable composition is quite unusual for alkoxides having molecular structures.

The $NaMO_2(OC_2H_4OMe)_3]_2$ (M = Mo, W) and $[NaWO(OEt)_5(EtOH)]_2$ (Fig 8c, d) [75a] complexes are examples of the same tetranuclear type structure. While in the structure of the first of these two complexes, the bonding parameters (such as M—O bond lengths and M—O—C valent angles) change regularly depending on the nature of the OR-groups (terminal, μ_2-, μ_3-). Those having a sodium ethoxotungstate structure are independent of the structural function of the ligand, which permits one to consider all OR-groups as terminal and the molecule as an aggregate of ion pairs, i.e. $[Na(EtOH)_2]_2^+$ $[WO(OEt)_5]_2^-$. An example of a heteronuclear compound, containing a metal–metal bond in its structure is provided by the $(MeO)_2MoO(\mu\text{-}OMe)_3ReO(OMe)_2$ molecule (two octahedra sharing a common face) obtained by anodic dissolution of rhenium in methanol in the presence of $MoO(OMe)_4$ [89].

In addition to complex formation, there are the decomposition processes leading to the formation of bimetallic oxoalkoxides that are characteristic of the majority of the abovementioned systems. Besides the factors affecting the decomposition of homometallic alkoxides that have been considered above, one should at this point emphasize the role of alkaline or alkaline earth alkoxides (or, possibly, in some cases, the products of their uncontrolled oxidation) in the decomposition of the bimetallic complexes. Thus on the $MoO(OR)_4$ interaction with NaOR (R = Et, ^{i}Pr) in alcohols, these are $[NaMo_2O_4(OR)_5(ROH)]_2$ complexes that can be isolated and they already contain one extra μ-O-group per molybdenum atom than the initial species (Fig. 8e) [75]. Interaction of $MoO(OR)_4$ with the excess of NaOR or action of the latter on $[NaMo_2O_4(OR)_5(ROH)]_2$ complexes leads to crystallization Na_2MoO_4 already at room temperature.* (It is worth noting that microadmixtures of NaOR promote polymerization of $MoO(OR)_4$ and thus stabilize their samples against ether elimination.) The same reaction provided an access to the crystalline phases of Na_2WO_4, Bi_2MoO_6 (ferroelectric), cubic solid solutions in the Bi_2O_3-WO_3 system (δ'-phase, ionic conductor due to mobility of oxygen ions).

The extreme trend to oxidation, demonstrated by butoxides of lithium, barium etc. leads to a rapid increase of their solubility in the solutions of $Ti(OBu)_4$ in comparison with that displayed in the diagrams (Fig. 7) and provides a route to solutions with the desired component ratios.

The composition (stoichiometry) and structures of oxoalkoxo complexes are in general quite different from those found for bimetallic complexes free from oxoligands in the same systems (Table 1). This permits them to be used as precursors of the oxide phases in the sol–gel route. A good example can be seen in the preparation of $BaTiO_3$. In freshly prepared solutions containing Ba : Ti = 1:1, these are the above-

* 2-methoxyethoxomolybdates are more stable due, apparently, to the chelation of alkaline or alkaline earth metal (Li, Na, Ba) atoms in their structures, the ratio of the size and effective charge being optimal for $NaMoO_2(OC_2H_5OMe)_3]_2$.

Table 1. Complex formation in systems $M(OR)_n$–$M'(OR)_m$–L at 20°C (composition of the complexes is designated by M : M′ : ROH ratio; by * are marked the complexes, for which the X-ray structures have been determined)

System	M	R	Composition of the complex in solid state	in solution	Ref.	Isolated oxoalkoxo complexes	Alkoxy-derived oxide materials
$M(OR)_n$–$Al(OR)_3$–THF	Li	^{t}Bu	1:1	1:1	[79]	—	
$M(OR)_n$–$Al(OR)_3$–ROH	Na	Me, Et	1:1	1:1	[76]	—	$Na_2O \cdot nAl_2O_3$
$M(OR)_n$–$Al(OR)_3$–ROH	Mg	Et	1:2	1:2; 3:2	[80]	—	n = 5,7,9,11,13,
$M(OR)_n$–$Al(OR)_3$–ROH	Ba	Et	1:2; 3:2	1:2; 3:2	[81]	—	ceramics
$M(OR)_n$–$Al(OR)_3$–C_nH_n	Ti	Et	—	2:1	[82]	—	(solid electrolyte)
$M(OR)_n$–$Al(OR)_3$–ROH	Zr(Hf)	^{i}Pr	1:2*	?	[78]	—	—
$M(OR)_n$–$Ti(OR)_4$–ROH	Mg	Me	no interaction	—	[83]	—	—
$M(OR)_n$–$Ti(OR)_4$–ROH	Mg	Et	1:x:2*	1:4(?)	,,	—	
$M(OR)_n$–$Ti(OR)_4$–ROH	Mg	Bu	—	—	,,	1:1, viscous liquid	$MgTiO_3$
$M(OR)_n$–$Ti(OR)_4$–C_nH_n	Ca	Et	1:4*	1:4	[73, 77]	—	ceramics [83]
$M(OR)_n$–$Ti(OR)_4$–ROH	Sr	^{i}Pr	—	—		$Sr_6Ti_4O_4(OR)_{20}$, $Sr_4Ti_4O_4(OR)_{14} \cdot 2ROH$	—
$M(OR)_n$–$Ti(OR)_4$–ROH	Ba	Me	1:4	—	[84]	$Ba_2[Ti_4O(OR)_{18}(ROH)_2] \cdot ROH$* [84]	
$M(OR)_n$–$Ti(OR)_4$–ROH	Ba	Et	1:4*; 1:2:5	1:4	[73a,b]	$Ba_4Ti_2O(OR)_{14} \cdot 8ROH$*	$BaTiO_3$
$M(OR)_n$–$Ti(OR)_4$–C_nH_n	Ba	Et	1:4	1:4			Powders, films
$M(OR)_n$–$Ti(OR)_4$–ROH	Ba	^{i}Pr	—	1:4	[73c]	$[BaTiO(OR)_4(ROH)_{7,8}]_4$	[73d]
$M(OR)_n$–$Ti(OR)_4$–ROH	Ba	^{n}Bu	—	1:4	[73a]	1:1 (?), viscous liquid	—
$M(OR)_n$–$Zr(OR)_4$–ROH	Ba	Et	1:4*	—	[85, 86]	$Ba_4Zr_2O(OR)_{14} \cdot 8ROH$	—
$M(OR)_nZr(OR)_4$–ROH	Ba	^{i}Pr	1:4*; 1:2*; 2:1:5		,,	$BaZrO(OR)_4 \cdot ROH$	—
$M(OR)_n$–$M(OR)_5$–ROH (M^V = Nb, Ta)	Li	Me, Et	[1:1], *	1:1	[87a, 46, 85a]	$LiTa_9O_{13}(OEt)_{20} \cdot 2EtOH$*	$LiNbO_3$, powders,
	Li	^{n}Bu				$[LiM^VO(OEt)_4(EtOH)]_2$*	films [87b]
$M(OR)_n$–$M(OR)_5$–ROH	Li	^{i}Pr	—	1:1	[46]	—	—
$M(OR)_n$–$M(OR)_5$–ROH	Mg	Me, Bu^n	—	1:2	[46]	$[MgTaO(OBu)_3(BuOH)]_4$*	$BaMg_{1/3}Ta_{2/3}O_3$
$M(OR)_n$–$M(OR)_5$–ROH	Mg	Et	1:2:2*	1:2	[46]	—	—
$M(OR)_n$–$M(OR)_5$–ROH	Ba	Me, Et	—	1:2	[46, 87]	$[BaM^VO(OEt)_5(EtOH)_{1.5}]_4$*	—
$M(OR)_n$–$M(OR)_5$–ROH	Ba	^{i}Pr	1:2:2*	—	[46]	—	—
$M(OR)_n$–$M(OR)_5$–ROH	Ba	^{n}Bu	no interaction	—	[46]	—	—
$M(OR)_n$–$M(OR)_5$–ROH	Sc	^{i}Pr	—	1:2	[87a]	—	—
$M(OR)_n$–$M(OR)_5$–ROH	La	^{i}Pr	1:2*	1:2(?)	[87a]	—	—
NaOR–$MoO(OR)_4$–ROH	—	Et, ^{i}Pr	–	1:1	[75a]	$[NaMo_2O_4(OR)_5 \cdot (ROH)]_2$*	Na_2MoO_4, Na_xMoO_4, films
$M(OR)_n$–$WO(OR)_4$–ROH	Na	Et	[1:1:2]$_2$*	1:1	[75a]	—	—
	Bi	Et	—	3:2; 1:1	1:1	[75a]	Bi_2WO_6, δ*-phase [75b]
$M(OR)_n$–$MoO_2(OR)_2$–ROH	Na	$MeOC_2H_4$	[1:1]$_2$*	1:1	[75]	—	
	Bi	,,	—	2:3	[75a]	—	Bi_2MoO_6 [75b]
$M(OR)_n$–$Fe(OR)_3$–ROH	Li, Na	Me	no interaction		[72, 88]	$Na_2Fe_6O(OMe)_{18} \cdot 6MeOH$	
$M(OR)_n$–$Fe(OR)_3$–ROH	Li, Na, K	Et	no interaction	—	[72]	3:1; 1:1 (in solution)	—
$M(OR)_n$–$Fe(OR)_3$–ROH	Ba	Et	no interaction	—	[72]	3:2; 1:2 (in solution)	—
$M(OR)_n$–$Fe(OR)_3$–ROH	Y	^{i}Pr	—	1:2; 1:3	[60a]		$YFeO_3$, $Y_3Fe_5O_{12}$ [60b]

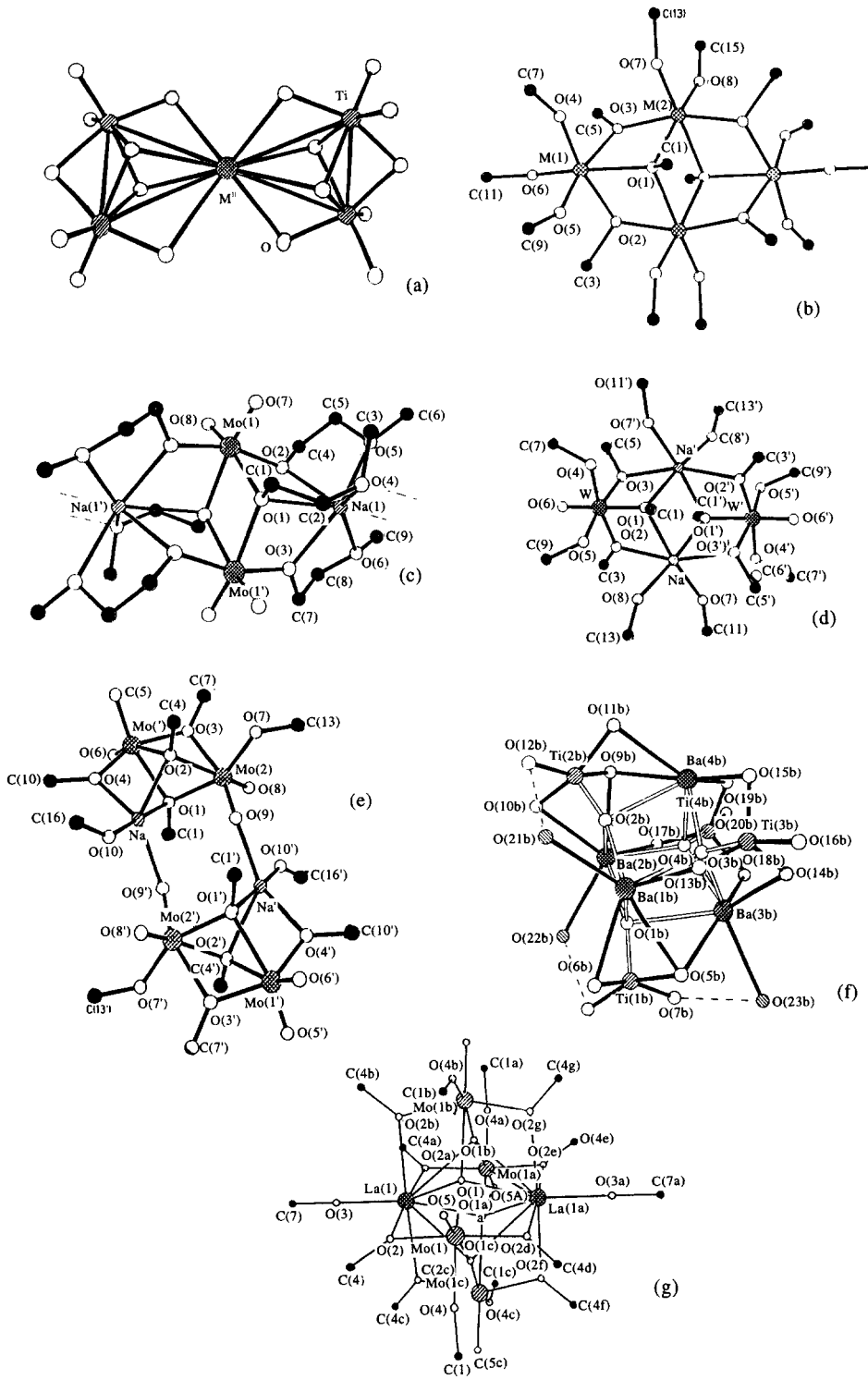

Fig. 8. Structures of selected bimetallic alkoxides: $M^{II}[Ti_2(OEt)_9]_2(M^{II} = Ca, Ba)$ (a); $[Mg_xTi_{4-x}(OEt)_{16-4x}(EtOH)_{2x}]$ (b); $[NaMO_2(OC_2H_4OMe)_3]_2$, M = Mo, W (c); $[NaWO(OEt)_5(EtOH)]_2$ (d); $[NaMo_2O_4(OR)_5(ROH)]_2$ (R = Et, ^{i}Pr) (e); $[BaTiO(OPr^i)_4(^iPrOH)_{7.8}]_4$ (f); $La_2Mo_4O_4(\mu\text{-}OPr^i)_8(OPr^i)_6$ (g).

mentioned complexes with 1:4 compositions and free $Ba(OR)_2$ that are present. This explains the fact that their application for the preparation of single-phase $BaTiO_3$ always leads to a failure. However, if before hydrolysis they were subjected to prolonged reflux, giving rise to formation of 1:1 complexes, $BaTiO_n(OR)_{6-2n}$, true precursors of barium titanate, they can produce its single-phase samples when

applied in sol–gel synthesis. One of the latter compounds, $[BaTiO(OPr^i)_4(^iPrOH)_{7/8}]_4$ (Fig. 8f) was isolated and subjected to X-ray single crystal investigation. In the center of its molecule lies a distorted $[Ba_4O_4]$ cube with metal atoms and oxoligands put in place of the vertexes. The oxoligands belong to $[TiO(OR)_4]$ groups; the solvate molecules, attached to Ba atoms, form intramolecular hydrogen bonds with the nearest OR-groups [73c]. It is worth noting that the Ba—O—Ti bridging fragments are already present in the structure of this molecule. The cubane-like structures related to this one have recently been found for $[BaNbO(OEt)_5(HOEt)_{1.5}]_4$ [87a] and $[MgTaO(OBu^n)_5(Bu^nOH)]_4$ [46]. One can suppose that this structural type may be observed for oxocomplexes of such stoichiometry containing atoms of bi- and polyvalent metals independently on the nature of the latter and the organic radicals.

For the preparation of $MgTiO_3$ it was found to be highly advantageous to use the solutions of butoxides, prepared by reaction of magnesium metal with $Ti(OBu)_4$ in butanol in 1:1 ratio. The reaction is accompanied by partial reduction of Ti^{IV} compounds into green $Ti^{III,IV}$ derivatives. Their subsequent oxidation by dry air leads to formation of soluble $MgTiO_n(OBu)_{6-2n}$ [83].

Here are some other examples of heterometallic alkoxide structures. A complex possessing an unusual $LiTa_9O(OEt)_{20}\cdot 2EtOH$ composition has an uncompleted Keggin structure of nine $[TaO_6]$ octahedra surrounding a $[LiO_4]$ tetrahedron, having one free vertex turned into the outer space [46]. On interaction of '$La(OPr^i)_3$' with $MoO(OPr^i)_4$ in hexane on heating, a hexanuclear $La_2Mo_4O_8(\mu\text{-}OR)_8(OR)_6$ molecule having a tetragonal bipyramidal *trans*-$[La_2Mo_4]$ metal atom arrangement was formed (Fig. 8g). It differs from the other known hexanuclear molecules with 2:4 metal atom ratios by the absence of μ_6-O atom in its center [90].

In conclusion, let us consider the role played by oxogroups in the process of complex formation. The example dealing with the interaction of butoxides of lithium and tantalum has already been discussed above. The isopropoxides of Zr (Hf, Ta) react with $Al(OPr^i)_3$ only after prolonged heating of solutions in alcohol [78]. One can suppose, therefore, that the complex formation for alkaline or alkaline earth alkoxides does not need any 'activation' because of the practically inevitable presence of microamounts of oxogroups in their samples.

It is very interesting to note that from solutions, which certainly contain oxocomplexes, may crystallize bimetallic alkoxides free from these ligands. For example, we can mention $HfAl_2(OPr^i)_{10}$ or $LaNb_2(OPr^i)_{13}$, precipitating from solution containing $La_5O(OR)_{13}$ [87], $Ba[Zr_2(OEt)_9]_2$, formed in the presence of zirconium oxoethoxide [85] and so on. The crystallization of this or that product depends upon their solubility; that is the least soluble compound that precipitates, the mother liquor being depleted or enriched in oxoligands [the analogous situation being described for the crystallization of $Fe(OEt)_3$].

We have proved that the isopropoxides of the late transition metals (Fe, Co, Ni etc.) in contradiction with the data of [91–93], do not interact with the isopropoxides of Al, Nb, Ta on complete isolation from moisture and the data on formation of volatile bimetallic species does not take place. On prolonged heating in the presence of traces of moisture, the dissolution of polymeric $M(OR)_2$ does occur giving rise to bimetallic oxoalkoxo-complexes as viscous non-volatile liquids described, for example, by Teyssie *et al.* [94]. In spite of the absence of complex formation between the methoxides of sodium and iron (Fig. 7), the interaction of NaOMe with the solution of $FeCl_3$ in methanol (apparently containing oxogroups, formed on alcoholysis of the chloride) gives a crystalline $Na_2[Fe_6(\mu_6\text{-}O)(OMe)_{18}]\cdot 6MeOH$ complex [88].

CONCLUSIONS

We would like to underline, that the physicochemical approach that we applied to the studies of metal alkoxides is the natural development of ideas and methodology, demonstrated in the pioneering works of D. C. Bradley. To the latter belong the detailed investigation of the properties of alkoxides and the regularities of their variation along the homologous series and in the groups of the Periodic Table, determination of the molecular composition of the samples and the structures of the species present. The Structural Theory developed by D. C. Bradley has acted as a powerful driving force for the initiation of wide-range structure studies that are carried out at present.

Investigation of the decomposition pathways of metal alkoxides and reactions of their hydrolysis laid the scientific background of the modern sol–gel route to oxide materials.

Acknowledgements—The authors are indebted to the Russian Foundation for Basic Research (Project No 96-33553) and INTAS (Grant 94-771).

REFERENCES

1. Tischtschenko, W. E., *Zhurn. Russ. Fiz.-Khim. Obsch.*, 1899, **31**, 694, 784 (Russ.).
2. Nogina, O. V., Freydlina, R. Kh. and Nesmeyanov, A. N., *Izv. AN SSSR, Ser. khim.*, 1950, 327; 1951, 518; 1952, 74, 1037; 1954, 41; 1961, 437; *Dokl. AN SSSR*, 1952, **85**, 571.
3. (a) Talalaeva, T. V., Zareva, G. V., Simonov, A. P. and Kocheshkov, K. A., *Izv. AN SSSR, Ser. khim.*, 1964, 638 (Russ.).; (b) Simonov, A. P., Shigorin, D. N., Talalaeva, T. V. and Kocheshkov, K. A., *Optika i Spektroskopiya*, 1964, **17**, 848 (Russ.).
4. Struchkov, Yu. T. and Lobanova, G. M., *Vestnik Mosk. Univ.*, 1959, 178 (Russ.).

5. Struchkov, Yu. T., Turova, N. Ya. and Yanovsky, A. I., in *Correlations, Transformations and Interactions in Organic Crystal Chemistry*, p. 289 Oxford University Press (1994).
6. Turova, N. Ya., Novoselova, A. V. and Semenenko, K. N., *Zh. Neorg. Khim.*, 1959, **4,** 997; 549 (Russ.).
7. Turova, N. Ya., Turevskaya, E. P., Kessler, V. G. and Yanovskaya, M. I., *J. Sol–Gel Sci. Technol.*, 1994, **2,** 17.
8. (a) Turowa, N. Ya., Popowkin, B. A. and Nowoselowa, A. W., *Z. Anorg. Allg. Chem.*, 1969, **365,** 100; (b) Turova, N. Ya. and Novoselova, A. V., *Bull. Acad. Sci. USSR, Div. Chem. Sci.*, 1970, 709.
9. Starikova, Z. A., Yanovsky, A. I., Turevskaya, E. P. and Turova, N. Ya., *Polyhedron*, 1997, **16,** 967.
10. Borup, B., Samuels, J. A., Streib, W. E. and Caulton, K. G., *Inorg. Chem.*, 1994, **33,** 997.
11. Turevskaya, E. P., Turova, N. Ya. and Novoselova, A. V., *Russ. J. Inorg. Chem.*, 1975, **20,** 839.
12. Gerr. Offen. Pat. 2005.835 (1970); Fr. Pat. 2.091.229 (1972).
13. Lehmkuhl, H. and Eisenbach, W., *Ann. Chem.*, 1975, 672.
14. (a) Shreider, V. A., Turevskaya, E. P., Kozlova, N. I. and Turova, N. Ya., *Inorg. Chim. Acta*, 1981, **13,** L73; (b) Kozlova, N. I., Turova, N. Ya. and Turevskaya, E. P., *Sov. J. Coord. Chem.*, 1982, **8,** 339; (c) Turova, N. Ya., Korolev, A. V., Tchebukov, D. E. and Belokon', A. I., *Polyhedron*, 1996, **15,** 3869; (d) Kessler, V. G., Turevskaya, E. P. and Kucheiko, S. I., *MRS Symp. Proc.*, 1994, **346,** 3; *J. Gen. Chem. USSR*, 1990, **60,** 99; (e) Turova, N. Ya., Turevskaya, E. P., Kessler, V. G., Kozlova, N. I. and Belokon', A. I., *Russ. J. Inorg. Chem.*, 1992, **37,** 26; (f) Kucheiko, S. I., Kessler, V. G. and Turova, N. Ya., *Sov. J. Coord. Chem.*, 1987, **13,** 586; (g) Rogova, T. V., private communication; (h) Rogova, T. V. and Turova, N. Ya., *Sov. J. Coord. Chem.*, 1985, **11,** 448; (i) Turevskaya, E. P., Kozlova, N. I., Turova, N. Ya., Popovkin, B. A. and Yanovskaya, M. I., *Superconductivity: Phys. Chem. Technol.*, 1989, **2,** 925; (j) Kessler, V. G., Shevel'kov, A. V. and Khvorykh, G. V., *Russ. J. Inorg. Chem.*, 1995, **40,** 1424.
15. (a) Maleto, M. I., Solov'yeva, L. I., Turevskaya, E. P., Vorotilov, K. A. and Yanovskaya, M. I., *Thin Solid Films*, 1994, **249,** 1; (b) Solov'yeva, L. I., Obvintseva, I. E., Yanovskaya, M. I., Vorotilov, K. A. and Vasil'yev, V. A., *Inorg. Mater.*, 1996, **32,** 767; (c) Vorotilov, K. A., Yanovskaya, M. I., Solov'yeva, L. I., Valeev, A. S. and Petrovsky, V. I., *Microelectronic Eng.*, 1995, **29,** 41.
16. Kovsman, E. P., Andruseva, S. I., Solov'yeva, L. I., Adamova, M. N. and Rogova, T. V., *J. Sol–Gel Sci. Technol.*, 1994, **2,** 61.
17. (a) Turova, N. Ya., Rogova, T. V., Kucheiko, S. I. and Turevskaya, E. P., Pat. USSR No. 1310381 (1987); C.A. 1987, **107,** P 153.915; (b) Turevskaya, E. P. and Turova, N. Ya., *Koord. Khim.*, 1989, **15,** 373; *ibid*, 1988, **14,** 926 (Russ.); (c) Kessler, V. G., Turova, N. Ya., Yanovsky, A. I. Belokon', A. I. and Struchkov, Yu. T., *Russ. J. Inorg. Chem.*, 1991, **36,** 938; (d) Kucheiko, S. I., Turova, N. Ya. and Kozlova, N. I., *Sov. J. Coord. Chem.*, 1985, **11,** 961; (e) Turova, N. Ya., Rogova, T. V. and Kozlova, N. I., *Sov. J. Coord. Chem.*, 1983, **9,** 685; (f) Rogova, T. V. and Turova, N. Ya., *ibid*, 1985, **11,** 366.
18. Bradley, D. C., *Coord. Chem. Rev.*, 1967, **2,** 299.
19. Andrianov, K. A. Polymers with Inorganic Main Chains, Moscow, Publishing-House of the Acad. Sci. USSR, 1962 (Russ.).
20. Bradley, D. C., Mehrotra, R. C. and Gaur, D. P., Metal Alkoxides. Academic Press (1978).
21. Poncelet, O., Sartain, W. J., Hubert-Pfalzgraf, L. G., Folting, K. and Caulton, K. G., *Inorg. Chem.*, 1989, **28,** 263.
22. Bradley, D. C., Chudzynska, H., Frigo, D. M., Hammond, M. E., Hursthouse, M. B. and Mazid, M. A., *Polyhedron*, 1990, **9,** 719.
23. Yanovsky, A. I., Turova, N. Ya. and Kozlova, N. I., *Sov. J. Coord. Chem.*, 1987, **13,** 149.
24. Turova, N. Ya., Turevskaya, E. P., Yanovsky, A. I. and Struchkov, Yu. T., *J. Chem. Soc., Chem. Commun.*, 1993, 21.
25. Schumann, H., Kociok-Koehn, G., Dietrich, A. and Goezlitz, F. H., *Z. Naturforsch.*, 1991, **46B,** 896.
26. Turova, N. Ya., Yanovsky, A. I., Kessler, V. G., Kozlova, N. I. and Struchkov, Yu. T., *Russ. J. Inorg. Chem.*, 1991, **36,** 1404.
27. Yanovsky, A. I., Turova, N. Ya., Turevskaya, E. P. and Struchkov, Yu. T., *Sov. J. Coord. Chem.*, 1982, **8,** 76.
28. Turevskaya, E. P., Kozlova, N. I., Turova, N. Ya., Berdyiev, D. V., Kessler, V. G. and Grishin, Yu. K., *Russ. Chem. Bull.*, 1995, 734.
29. Chisholm, M. H., Folting, K., Huffman, J. C. and Cober, E. M., *Inorg. Chem.*, 1985, **24,** 241.
30. Cotton, F. A., Marler, D. O. and Schwotzer, W., *Inorg. Chim. Acta*, 1984, **85,** 207.
31. Clark, D. L. and Watkin, J. G., *Inorg. Chem.*, 1993, **32,** 1766.
32. Vaartstra, B. A., Huffman, J. C., Gradeff, P. S., Hubert-Pfalzgraf, L. G., Daran, J., Parrand, S., Yunlu, K. and Caulton, K. G., *Inorg. Chem.*, 1990, **29,** 3126.
33. Morosin, B., *Acta Cryst.*, 1977, **B33,** 303.
34. Schmid, R., Mosset, A. and Galy, J., *J. Chem. Soc., Dalton Trans.*, 1991, 1999.
35. Bradley, D. C., Chakravarti, B. N., Chatterjee, A. K., Wardlaw, W. and Whitley, A., *J. Chem. Soc.*, 1958, 99.
36. Bol'shakov, A. M., Glushkova, M. A. and Buslaev, Yu. A., *Sov. J. Coord. Chem.*, 1978, **4,** 1075.
37. Kozlova, N. I., Kessler, V. G., Turova, N. Ya. and Belokon', A. I., *Sov. J. Coord. Chem.*, 1989, **15,** 867.
38. Turevskaya, E. P., Bergo, V. B., Yanovskaya, M. I. and Turova, N. Ya., *Russ. J. Inorg. Chem.*, 1996, **41,** 695.
39. Le Berre, A., *Bull. Soc. Chim. France*, 1961, 1198; 1543.
40. Turova N. Ya., Turevskaya, E. P., Yanovskaya, M. I., Kotova, N. M. and Shfirina, R. R., *Russ. J. Inorg. Chem.*, 1993, **38,** 1055.
41. Poncelet, O., Hubert-Pfalzgraf, L. G., Duran, J.-C. and Astier, R., *J. Chem., Soc., Chem. Commun.*, 1989, 1846.

42. Hubert-Pfalzgraf, L. G., private communication.
43. Caulton, K. G., Chisholm, M. H., Drake, S. R. and Huffman, J. C., *J. Chem. Soc., Chem. Commun.*, 1990, 1498.
44. Bradley, D. C., Chudzynska, H., Hursthouse, M. B. and Motevalli, M., *Polyhedron*, 1991, **10,** 1049.
45. Evans, W. J., Golden, R. E. and Zieler, J. W., *Inorg. Chem.*, 1991, **30,** 4963.
46. Tchebukov, D. E., Turova, N. Ya., Korolev, A. V. and Belokon', A. I., *Russ. J. Inorg. Chem.*, 1997, **42,** 10.
47. Turova, N. Ya., Kozlova, N. I. and Yanovskaya, M. I., *Sov. J. Coord. Chem.*, 1980, **6,** 260.
48. Kakos, G. A. and Winter, G., *Austral. J. Chem.*, 1968, **21,** 793.
49. Clegg, W., Errington, J. R. and Redshaw, C., *J. Chem. Soc., Dalton Trans.*, 1992, 3189.
50. Kucheiko, S. I., Turova, N. Ya., Kozlova, N. I. and Zhadanov, B. V., *Sov. J. Coord. Chem.*, 1985, **11,** 867.
51. Bradley, D. C., *Adv. Inorg. Chem. Radiochem.*, 1972, **15,** 259; *Uspekhi Khimii*, 1978, **47,** 638 (Russ.).
52. Bradley, D. C., *Adv. in Chem. Ser.*, 1959, **23,** 10.
53. (a) Figgen, W. and Gerding, H., *Rec. Trav. Chim.*, 1970, **89,** 175; *ibid*, 1971, **90,** 410; (b) Daasch, L. W. and Fales, H. M., *Org. Mass-Spectrom.*, 1969, **2,** 1043; (c) Brown, L. M. and Mazdiyasni, K. S., *Anal. Chem.*, 1969, **41,** 1243.
54. Yanovsky, A. I., Kozunov, V. A., Turova, N. Ya., Furmanova, N. G. and Struchkov, Yu. T., *Doklady Chem. Proc. Acad. Sci. USSR*, 1979, **244,** 26.
55. Turova, N. Ya., Kozunov, V. A., Yanovsky, A. I., Bokii, N. G., Struchkov, Yu. T. and Tarnopol'sky, B. L., *J. Inorg. Nucl. Chem.*, 1979, **41,** 5.
56. Oliver, J. G. and Worrall, I. J., *J. Chem. Soc.*, 1970A, 2347.
57. Kozlova, N. I., Turova, N. Ya. and Nekrasov, Yu. S., *Sov. J. Coord. Chem.*, 1980, **6,** 124.
58. Ulich, H. and Nespital, W., *Z. Phys. Chem.*, 1933, **165,** 294.
59. Rogova, T. V., Turova, N. Ya. and Novoselova, A. V., *Doklady Chem. Proc. Acad. Sci. USSR*, 1985, **285,** 355.
60. (a) Rogova, T. V., Turova, N. Ya. and Kozlova, N. I., *Sov. J. Coord. Chem.*, 1986, **12,** 440; (b) Yanovskaya, M. I., Rogova, T. V., Ivanov, S. A., Kolganova, N. V. and Turova, N. Ya., *J. Mater. Sci. Lett.*, 1987, **6,** 274.
70. Kessler, V. G., Tchebukov, D. E. and Turova, N. Ya., *Russ. J. Inorg. Chem.*, 1993, **38,** 23.
71. Caulton, K. G. and Hubert-Pfalzgraf, L. G., *Chem. Rev.*, 1990, **90,** 969.
72. Rogova, T. V., Turova, N. Ya., Chernova, N. A. and Novoselova, A. V., *Sov. J. Coord. Chem.*, 1985, **11,** 710.
73. (a) Turevskaya, E. P., Yanovskaya, M. I., Limar, V. K. and Turova, N. Ya., *Russ. J. Inorg. Chem.*, 1993, **38,** 563; (b) Turevskaya, E. P., Kessler, V. G., Turova, N. Ya., Yanovsky, A. I. and Struchkov, Yu. T., *J. Chem. Soc., Chem. Commun.*, 1994, 2303; (c) Yanovsky, A. I., Yanovskaya, M. I., Limar, V. K., Kessler, V. G., Turova, N. Ya. and Struchkov, Yu. T., *ibid*, 1991, 1605; (d) Vorotilov, K. A., Obvintseva, I. E., Petrovsky, V. I., Yanovskaya, M. I., Turevskaya, E. P. and Turova, N. Ya., *Ferroelectrics*, 1991, **123,** 261.
74. Turova, N. Ya., *Sov. J. Coord. Chem.*, 1984, **10,** 644.
75. (a) Turova, N. Ya., Kessler, V. G. and Kucheiko, S. I., *Polyhedron*, 1991, **10,** 2617; (b) Yanovskaya, M. I., Turevskaya, E. P., Kessler, V. G., Obvintseva, I. E. and Turova, N. Ya., *Integrated Ferroelectrics*, 1992, **1,** 343.
76. Karpovskaya (Yanovskaya), M. I., Turova, N. Ya. and Novoselova, A. V., *Russ. J. Inorg. Chem.*, 1978, **23,** 766.
77. Turevskaya, E. P., Turova, N. Ya. and Novoselova, A. V., *Russ. J. Inorg. Chem.*, 1978, **23,** 355.
78. Turevskaya, E. P., Berdyev, D. V., Turova, N. Ya., Starikova, Z. A., Yanovsky, A. I., Struchkov, Yu. T. and Belokon', A. I., *Polyhedron*, 1997, **16,** 663.
79. Kozlova, N. I., Karpovskaya (Yanovskaya), M. I. and Turova, N. Ya., *Russ. J. Inorg. Chem.*, 1979, **24,** 107.
80. Karpovskaya (Yanovskaya), M. I., Turova, N. Ya., Kozlova, N. I., Rogova, T. V. and Novoselova, A. V., *Doklady Chem. Proc. Acad. Sci. USSR*, 1978, **239,** 111.
81. Turevskaya, E. P., Turova, N. Ya., Yanovskaya, M. I. and Novoselova, A. V., *Russ. J. Inorg. Chem.*, 1979, **24,** 1005.
82. Turevskaya, E. P. Turova, N. Ya. and Novoselova, A. V., *Inorg. Mat.*, 1980, **16,** 1805.
83. Kotova, N. M., Yanovskaya, M. I. and Turova, N. Ya., *Russ. J. Inorg. Chem.*, 1995, **40,** 1773.
84. Kotova, N. M., Yanovskaya, M. I. and Turova, N. Ya., *ibid*, 1998, **43,** 3.
85. Turevskaya, E. P., Berdyev, D. V. and Turova, N. Ya., *ibid*, 1995, **40,** 1589.
86. (a) Vaartstra, B. A., Huffman, J. C., Streib, W. E. and Caulton, K. G., *Inorg. Chem.*, 1991, **30,** 3068; (b) Kuhlmann, R., Vaartstra, B. A., Streib, W. E., Huffman, J. C. and Caulton, K. G., *ibid*, 1993, **32,** 1272.
87. (a) Turevskaya, E. P., Turova, N. Ya., Korolev, A. V., Yanovsky, A. I. and Struchkov, Yu. T., *Polyhedron*, 1995, **14,** 1531; (b) Yanovskaya, M. I., Turevskaya, E. P., Leonov, A. P. and Ivanov, S. A., *J. Mater. Sci.*, 1988, **23,** 395.
88. Hegetschweller, K., Schmalle, H. W., Streit, H. M., Gramlich, V., Hund, H.-U. and Erni, I., *Inorg. Chem.*, 1992, **31,** 1299.
89. Kessler, V. G., Seisenbaeva, G. A., Shevel'kov, A. V. and Khvorykh, G. V., *J. Chem. Soc., Chem. Commun.*, 1995, 1779.
90. Kessler, V. G., Turova, N. Ya., Panov, A. N., Yanovsky, A. I. and Struchkov, Yu. T., *Polyhedron*, 1996, **15,** 335.
91. Singh, J. V., Jain, N. C. and Mehrotra, R. C., *Synth. React. Inorg. Met-Org. Chem.*, 1979, **9,** 79.
92. Jain, R., Rai, A. K. and Mehrotra, R. C., *Z. Naturforsch*, 1985, **B40,** 1371.
93. Dubey, R. K., Singh, J. V. and Mehrotra, R. C., *Bull. Soc. Chem. Jap.*, 1988, **61,** 983.
94. Ouhadi, T., Bione, J. P., Stevens, C., Warin, R., Hodes, L. and Teyssie, P., *Inorg. Chim. Acta*, 1976, **19,** 203.

Pergamon

PII: S0277-5387(97)00262-3

Polyhedron Vol. 17, No. 5–6, pp. 917–923, 1998
© 1998 Elsevier Science Ltd
All rights reserved. Printed in Great Britain
0277-5387/98 $19.00+0.00

Ortho-substituted aryl diamido complexes of zirconium: observation of rotameric isomers†

Frédéric Guérin, Orin Del Vecchio and David H. McConville*

Department of Chemistry, University of British Columbia, 2036 Main Mall, Vancouver, British Columbia, Canada V6T 1Z1

(Received 10 April 1997; accepted 11 June 1997)

Abstract—Zirconium complexes bearing a series of ortho-substituted aryl diamido ligands [2,6-$(RNCH_2)_2NC_5H_3]^{2-}$ (R = 2-PhC_6H_4 (BPhP); 2-$^iPrC_6H_4$ (BMPP); 2-$^tBuC_6H_4$ (BMBP), 2-^{i}Pr-6-MeC_6H_3 (MPPP)) have been synthesized. The mixed amide complexes [2,6-$(RNCH_2)_2NC_5H_3$]$Zr(NMe_2)_2$ are prepared in high yield from 2,6-$(RHNCH_2)_2NC_5H_3$ and $Zr(NMe_2)_4$. The mixed amides react with excess $ClSiMe_3$ to afford the dichlorides [2,6-$(RNCH_2)_2NC_5H_3$]$ZrCl_2$ in nearly quantitative yield. Dimethyl complexes are prepared from [2,6-$(RNCH_2)_2NC_5H_3$]$ZrCl_2$ and 2 equiv. of MeMgCl. NMR spectroscopy has been used to identify rotameric isomers derived from restricted rotation about the N—C_{ipso} bond of the ligand. The aryl groups in (BPhP)ZrX_2 complexes freely rotate at all temperatures (−80 to +80°C) while (BMPP)ZrX_2 (X = NMe_2, Cl, Me) derivatives adopt *meso* and *rac* rotamers at low temperatures. In contrast, (BMBP)ZrX_2 and (MPPP)ZrX_2 (X = NMe_2, Cl, Me) compounds are locked at all temperatures. (BMBP)$ZrCl_2$ is isolated as a single isomer, likely the *meso* rotamer, while (MPPP)$ZrCl_2$ is a near statistical mixture of *meso* and *rac* isomers. © 1998 Elsevier Science Ltd. All rights reserved

Keywords: zirconium complexes; isomer; rotamer.

Tremendous progress has been made over the past 15 years on the design and preparation of single-site group 4 catalysts for the polymerization of α-olefins [1–3]. Efforts in this area have been concerned with the way in which the catalytic activity and stereoregularity can be altered with changes to the ancillary ligands. For example, the ingeniously designed C_2-symmetric compound *rac*-ethylenebis(η^5-tetrahydroindenyl) $ZrCl_2$ [4] and the left/right C_s-symmetric derivative isopropyl(η^5-Cp-1-η^5-fluorenyl)$ZrCl_2$ [5] are catalyst precursors for the isospecific and syndiospecific polymerization of propylene, respectively. Building upon the structure/property relationship in metallocene complexes, Waymouth and Coates recently reported the details of a new zirconium catalyst that takes advantage of an 'oscillating' ligand environment [6]. The putative cationic complex $[(2\text{-Ph-indenyl})_2ZrP]^+$ (**I**) (P = polymer chain) can adopt one of two possible isomeric structures; a *rac* species which polymerizes propylene in an isospecific manner or a *meso* complex

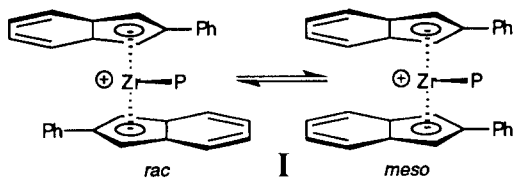

I

which gives rise to blocks of atactic polypropylene. The interconversion of these species on the polymerization time scale affords stereoblock polypropylene, a thermoplastic elastomer.

Although the metallocene class of compounds have been successful, there is a growing interest in alternative ligand systems; in particular, attention has focused on nitrogen-based ligands [7–13]. For example, chelating diamide complexes of titanium serve as precursors for the highly active [14] and living [15] polymerization of α-olefins. In addition, pyridine diamide complexes of zirconium are active catalysts for the polymerization of ethylene [16]. With the oscillating catalyst tenet in hand, we set out to prepare diamide ligands bearing potentially oscillating aryl substituents at nitrogen. Herein we describe the syn-

† Dedicated to Professor D. C. Bradley on the occasion of his 73rd birthday.

* Author to whom correspondence should be addressed.

thesis and fluxional behavior of ortho-substituted aryl diamido complexes of zirconium.

RESULTS AND DISCUSSION

2,6-Bis(bromomethyl)pyridine [17] reacts with 2 equiv. of LiNHR (R = 2-PhC_6H_4; 2-$^iPrC_6H_4$; 2-$^tBuC_6H_4$, 2-^{i}Pr-6-MeC_6H_3) in THF at −78°C to afford the pyridine diamine ligands (**1a–d**) in 63–93% yield (Scheme 1).

The ligands are white crystalline solids, except **1a** which was isolated as a yellow oil. We have previously reported [16,18] that amine elimination reactions [19] are an excellent method for appending bulky chelating diamide ligands to zirconium. The pyridine diamine ligands **1a–d** react cleanly with $Zr(NMe_2)_4$ [20] at 23°C to afford the mixed amide complexes (**2a–d**) in nearly quantitative yield as evidenced by ^{1}H NMR spectroscopy. The reaction between $Zr(NMe_2)_4$ and the 2-*tert*-butyl substituted ligand **1c** is fast at −80°C, as no intermediates are observed by ^{1}H NMR spectroscopy. These aminolysis reactions are unaffected by the presence of excess dimethylamine [21], hence we observe only the kinetic products. The amide complexes **2a–c** are isolated as yellow solids in >90% yield, however, the high solubility of compound **2d** in hexanes limits its isolation.

The temperature invariant proton NMR spectrum of complex **2a** exhibits a single sharp resonance for the methylene protons of the ligand (CH_2N) and a singlet for the dimethylamido groups. These resonances are consistent with some degree of free rotation about the N—C_{ipso} bond which yields a structure with local C_{2v}-symmetry. Using the X-ray coordinates [16] of $[(RNCH_2)_2NC_5H_3]ZrMe_2$ (R = 2,6-$Et_2C_6H_3$) as a starting point, modelling studies [22] on derivative **2a** predict a large barrier to rotation about the N—C_{ipso} bond when the *o*-phenyl groups pass by the dimethylamido groups (**A**). Therefore, the spectroscopically observed C_{2v}-symmetry likely arises from the *o*-phenyl groups passing by the methylene protons of the ligand backbone. Furthermore, these calculations suggest that the ease of rotation decreases in the following way: *o*-Ph > *o*-^{i}Pr > *o*-^{t}Bu (*vide infra*).

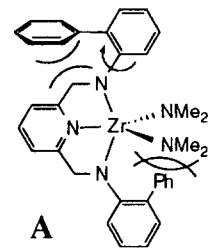

A

The room temperature ^{1}H NMR spectrum of complex **2b** exhibits a single sharp resonance for the methylene protons of the ligand (CH_2N) and a single doublet for the isopropyl methyl groups. Again these resonances are consistent with some degree of free rotation about the N—C_{ipso} bond (C_{2v}-symmetry). The low temperature (−80°C) limiting ^{1}H NMR spectrum of compound **2b** in d_8-toluene shows three $N(CH_3)_2$ resonances in a ratio of 1 : 1 : 1.2. In addition, overlapping resonances are observed for the methylene protons of the ligand (CH_2N—two AB quartets), the isopropyl methyls ($CHMe_2$—four doublets), and the isopropyl methines ($CHMe_2$—two septets). These resonances are in agreement with about a 1.67 : 1 mixture of the C_s-symmetric *meso* and C_2-symmetric *rac* rotameric isomers in solution at −80°C (Fig. 1). The above resonances coalesce at −40°C

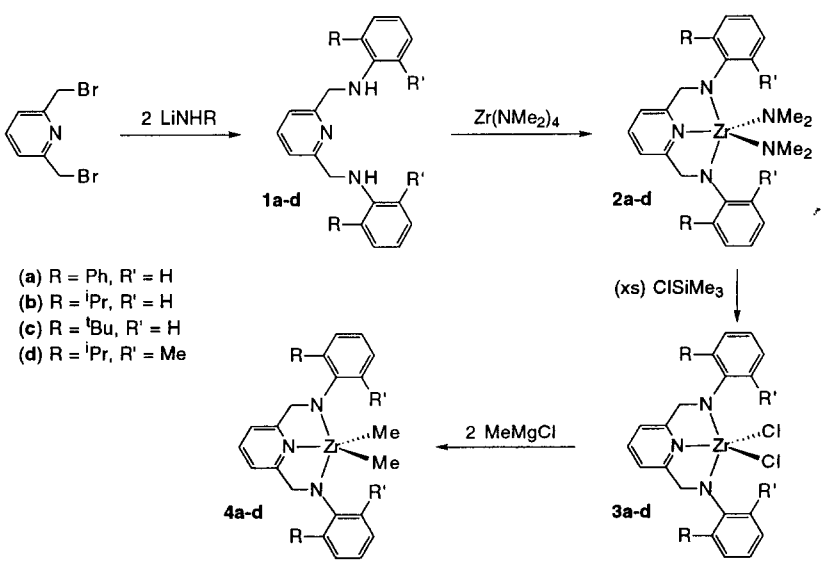

Scheme 1.

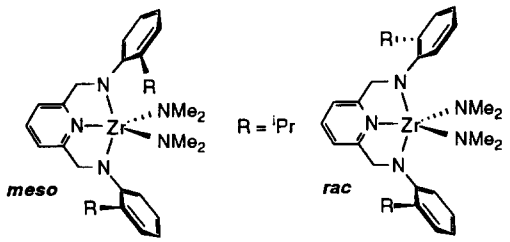

Fig. 1.

yielding a barrier to rotation of the aryl groups of $\Delta G\ddagger = 11.2$ (5) kcal mol^{-1}.

In contrast to both **2a** and **2b**, the room temperature ^{1}H NMR spectrum of compound **2c** shows resonances for two distinct species whose relative intensities do not change from -80°C to $+80$°C. Consistent with the presence of the *rac* isomer is an AB quartet for the ligand methylene protons (CH_2N), a single sharp resonance for the chemically equivalent dimethylamido groups, and a singlet for the equivalent ^{t}Bu groups. In addition to these resonances, the *meso* isomer displays a separate singlet for the ligand methylene protons, two inequivalent dimethylamido resonances, and a singlet for the *tert*-butyl group. Although an AB pattern is expected for the ligand methylene protons, if the chemical shift difference between H_A and H_B is small ($\Delta\nu \leqslant 0.4$ Hz), an apparent singlet is observed [23]. Integration of the $N(CH_3)_2$ groups indicates a *meso*/*rac* ratio of about 2.6 : 1. As noted above, this ratio is unaffected by added dimethylamine. The carbon NMR spectrum of **2c** also shows two species in about a 2.6 : 1 ratio.

Jordan has reported [21] that the reaction of $(EBI)H_2$ [EBI = 1,2-bis(1-indenyl)ethane] with Zr $(NMe_2)_4$ yields $(EBI)Zr(NMe_2)_2$ in a *meso*/*rac* ratio of 1 : 13. However, the reaction of $Me_2Si(C_5H_4$-3-^{t}Bu$)_2$ and $Zr(NMe_2)_4$ yields $[Me_2Si(C_5H_3$-3-^{t}Bu$)_2]Zr(NMe_2)_2$ in a *meso*/*rac* ratio of 2 : 1 [24]. In the latter example the higher *meso* preference is assigned to a lateral deformation of the *ansa* ligand system. We speculate that a similar 'deformation' may occur in these systems whereby the metal adopts a square-based pyramidal (sbp) geometry instead of a trigonal bipyramidal (tbp) confirmation, thus relieving the steric strain associated with the *meso* isomer relative to the *rac* (Fig. 2).

The energy difference between sbp and tbp geometries is expected to be quite small given the d^0 electronic configuration of zirconium. In fact, this change in hybridization has been observed for other

Fig. 2.

d^0 group 4 complexes bearing the pyridine diamide ligand. The mononeophyl complex $[2,6\text{-}(RNCH_2)_2NC_5H_3]TiBr(CH_2CMe_2Ph)$ (R = 2,6-$Me_2C_6H_3$) [25] displays a sbp geometry in the solid state with the largest group ($-CH_2CMe_2Ph$) occupying the apical position. This geometry minimizes the interaction between the orthomethyl groups of the aryl and the bulky neophyl ligand. We should add that it is not possible to distinguish between the proposed sbp and tbp complexes by NMR spectroscopy since both compounds possess C_s-symmetry.

The proton NMR spectrum of compound **2d**, which bears an isopropyl group in the 2-position and a methyl moiety in the 6-position of the aryl, shows resonances for two rotameric isomers. In this case, there is a slight bias for the *rac* isomer (*meso*/*rac*, 1 : 1.13). The near 1 : 1 correspondence between these species is also observed in the carbon NMR spectrum of **2d**. Given that these species do not interconvert (from -80°C to $+80$°C), even in the presence of excess dimethylamine, suggests that during the aminolysis reaction the aryl groups have little influence on one another; in other words, a near statistical distribution of isomers is produced.

The mixed amide complexes **2a–d** react with excess $ClSiMe_3$ to afford the dichloride derivatives (**3a–d**) in 80–96% isolated yield (Scheme 1). Upon addition of $ClSiMe_3$ the solutions turn black which we attribute to minor impurities given the high isolated yields. The orthophenyl substituted complex **3a** displays limited solubility in common organic solvents. The ^{1}H NMR spectrum of **3a** shows a sharp singlet for the ligand methylene protons (CH_2N), consistent with rapid rotation about the N—C_{ipso} bond. The proton NMR spectrum of **3b** at 23°C shows broad featureless resonances for the methylene (CH_2N), the isopropyl methine, and the isopropyl methyl protons of the ligand. At temperatures above $+60$°C the spectrum is consistent with rapid rotation of the aryl group. The low temperature (-60°C) limiting spectrum of **3b** displays resonances for the two rotamers in a ratio of about 2 : 3, however, it is not possible to discern which isomer predominates since the spectra of C_s- and C_2-symmetric compounds are indistinguishable (requires NMR active groups in the equatorial plane of a tbp). In this case the barrier to aryl group rotation is $\Delta G\ddagger = 13.8$ (5) kcal mol^{-1}.

The *meso*/*rac* ratio in the mixed amide complex **2c** is 2.6 : 1. Interestingly, upon reaction with excess $ClSiMe_3$ a single isomer of the dichloride complex **3c** is formed. We have followed this reaction by ^{1}H NMR spectroscopy and found that no other products are formed. It is not possible to determine which isomer is present, however, the following results suggest that the *meso* rotamer is formed preferentially. The reaction of **3c** with two equiv. of $PhCH_2MgCl$ yields the *meso* dibenzyl complex (**5c**) in quantitative yield by proton NMR spectroscopy [eq. (1)].

The ^{1}H NMR spectrum of **5c** shows a single AB quartet for the ligand methylene protons (CH_2N),

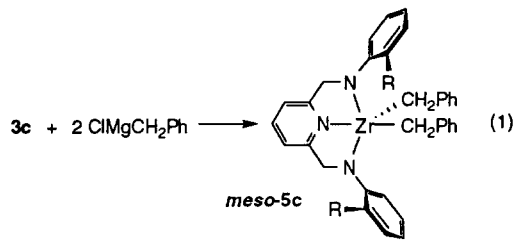

one *tert*-butyl resonance, and two benzyl resonances ($ZrCH_2Ph$); all in accordance with the presence of the *meso* isomer. Compound **5c** can also be prepared from $Zr(CH_2Ph)_4$ [26] and ligand **1c**. As noted above, a sbp geometry in compound **5c** would reduce the steric interactions between the benzyl groups and the *tert*-butyl groups. The monoalkyl derivatives [2,6-$(RNCH_2)_2NC_5H_3$]ZrClR′ and (R = 2-^{t}BuC$_6$H$_4$; R′ = CH_2CMe_2Ph, CH_2SiMe_3), prepared from compound **3c** and the corresponding alkylating reagent, also display resonances associated with only the *meso* isomer [27].

As expected, the proton NMR spectrum of compound **3d** displays resonances for two rotamers in a ratio of about 1 : 1.15. It would appear that no change in the isomeric ratio, within limits of detection, takes place during the metathesis reaction with $ClSiMe_3$. Furthermore, no change in this ratio is observed upon heating to 80°C.

The dichloride complexes **3a–c** react with 2 equiv. of methyl Grignard to afford the dimethyl derivatives (**4a–c**) in 67–85% yield as white crystalline solids (Scheme 1). The spectroscopic data for the Zr–Me groups is consistent with other related dimethyl species [17]. The proton NMR spectrum of the 2-phenylaryl substituted complex **4a** displays resonances for a single C_{2v}-symmetric species down to −80°C.

The 2-isopropylaryl substituted complex **4b** exhibits fluxional behavior. A stacked plot of a portion of the ^{1}H NMR spectrum of complex **4b** at several temperatures is shown in Fig. 3. The spectrum at 23°C displays a singlet at 4.84 ppm for the ligand methylene protons (CH_2N), a septet at 3.57 ppm for the isopropyl methine ($CHMe_2$), a doublet at 1.31 ppm for the chemically equivalent isopropyl methyl groups ($CHMe_2$), and a singlet for the Zr–Me_2 groups at 0.46 ppm. The low temperature limiting spectrum (−60°C) shows an AB quartet for the ligand methylene protons, a broad resonance for the isopropyl methine, a broad pattern for the isopropyl methyl groups, and three broad zirconium methyl resonances in a ratio of 1 : 1.3 : 1. We assign these resonances to a *meso/rac* mixture in a ratio of 1.5 : 1. The above resonances coalesce at −20°C yielding a barrier to rotation of the aryl groups of $\Delta G‡ = 12.0$ (5) kcal mol^{-1}.

The reaction of **3c** with bulky alkylating reagents affords exclusively *meso* type complexes (*vide supra*). Interestingly, the reaction of **3c** with two equiv. of methyl Grignard yields a mixture of rotameric isomers

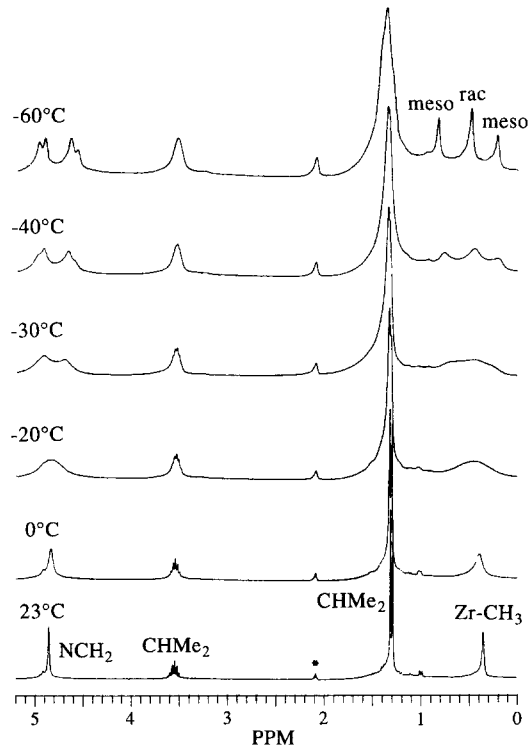

Fig. 3. Variable temperature ^{1}H NMR spectra of **4b** in d_8-toluene (* denotes solvent).

in a ratio of about 3 : 1 (*meso/rac*). The temperature invariant (−80°C to +80°C) ^{1}H NMR spectrum of **4c** shows two slightly off-centred AB quartets for the ligand methylene protons, two *tert*-butyl resonances, and three Zr–*Me* singlets (ratio, 1.5 : 1 : 1.5). Interestingly, the 2-*tert*-butyl substituted ligand appears to isomerize readily under metathetical type conditions, yet is stable to such processes under thermal conditions. We are currently examining the details of the transformation. Consistent with the lack of rotation in the 2,6-disubstituted aryl complexes [17,26], the dimethyl compound **4d** shows the same *meso/rac* ratio (1 : 1.14) as does the dichloride precursor **3d**.

EXPERIMENTAL

General details

All experiments were performed under a dry nitrogen atmosphere using standard Schlenk Techniques or in an Innovative Technology Inc. glovebox. Solvents were distilled from sodium/benzophenone ketyl (THF, hexanes, diethylether) or molten sodium (toluene). 2-Isopropylaniline, 2-*tert*-butylaniline, 2-phenylaniline, and 2-isopropyl-6-methylaniline were purchased from Aldrich and distilled under reduced pressure before use. MeMgCl and $ZrCl_4$ were purchased from Aldrich and used as received. 2,6-

Bis(bromomethyl)pyridine was prepared using previously reported synthesis [18]. Unless otherwise specified, proton (300 MHz) and carbon (75.46 MHz) NMR spectra were recorded in C_6D_6 at approximately 23°C on a Varian 300-XL spectrometer. The proton chemical shifts were references to internal C_6D_5H ($\delta = 7.15$ ppm) and the carbon resonances to C_6D_6 ($\delta = 128.0$ ppm). Some resonances are obscured by C_6D_6 and/or are overlapping. The elemental analysis were performed using sealed tin cups on a Fisons Instruments model 1108 elemental analyzer by Mr Peter Borda of this department. The following abbreviations for the ligands are used: 2,6-$(RHNCH_2)_2$ NC_5H_3 ($(BPhP)H_2$, R = 2-PhC_6H_4; $(BMPP)H_2$, R = 2-$^i PrC_6H_4$; $(BMBP)H_2$, R = 2-$^t BuC_6H_4$, $(MPPP)H_2$, R = 2-^{i}Pr-6-MeC_6H_3).

(BPhP)H$_2$ (**1a**). A THF (150 cm^3) solution of LiNHR (5.144 g, 29.4 mmol) was added slowly to a stirring THF (100 cm^3) solution of 2,6-bis(bromomethyl)pyridine (3.890 g, 14.7 mmol) at −78°C. The mixture was warmed to room temperature and stirred for 12 h. The solution was quenched with a saturated $NaHCO_3$ solution (100 cm^3) and extracted with dichloromethane. The solvent was removed *in vacuo* to give a yellow oil (**1a**) which was used as isolated (6.000 g, 13.6 mmol, 93%). ^{1}H NMR δ 7.50 (d, 4H, m Ar/Ph), 7.09–7.40 (m, 10H, Ar/Ph), 6.97 (t, 1H, py), 6.80 (t, 2H, Ar/Ph), 6.73 (d, 2H, Ar/Ph), 6.60 (d, 2H, Ar), 5.15 (t, 2H, N*H*), 4.08 (d, 4H, NCH_2). ^{13}C{^{1}H} δ 158.28, 145.17, 140.31, 136.79, 130.61, 129.84, 129.16, 128.17, 127.39, 119.27, 117.64, 111.26, 49.25. MS (EI) *m/z* 441.220 (M^+). Calcd for $C_{31}H_{27}N_3$: 441.220.

(BMPP)H$_2$ (**1b**). The preparation of compound **1b** is identical to **1a** except for the work up. LiNHR (5.335 g, 37.4 mmol) and 2,6-bis(bromomethyl)pyridine (5.000 g, 18.9 mmol) yield a white solid. The solid was dissolved in a minimal amount of an ether, hexanes added until the solution is cloudy, and cooled to −30°C. A white crystalline solid (**1b**) was isolated by filtration and dried under vacuum (4.500 g, 12.0 mmol, 63%). ^{1}H NMR δ 7.18 (dd, 2H, Ar), 7.11 (dd, 2H, Ar), 6.97 (m, 1H, py), 6.84 (td, 2H, Ar), 6.77 (d, 2H, py), 6.62 (dd, 2H, Ar), 4.77 (br s, 2H, N*H*), 4.29 (s, 4H, NCH_2), 2.87 (sept, 4H, C*H*Me$_2$), 1.23 (d, 12H, CH*Me*$_2$). ^{13}C{^{1}H} δ 158.68, 144.98, 136.94, 132.43, 127.21, 125.31, 119.77, 118.09, 111.33, 49.61, 27.70, 22.49. MS (EI) *m/z* 373.252 (M^+). Calcd for $C_{25}H_{31}N_3$: 373.252.

(BMBP)H$_2$ (**1c**). The preparation of compound **1c** is identical to **1b**. LiNHR (5.865 g, 37.8 mmol) and 2,6-bis(bromomethyl)pyridine (5.000 g, 18.9 mmol) gave **1c** as a white crystalline solid (5.820 g, 14.4 mmol, 76%). ^{1}H NMR δ 7.35 (d, 2H, Ar), 7.16 (dd, 2H, Ar), 7.02 (td, 1H, py), 6.84 (d, 2H, Ar), 6.82 (t, 2H, py), 6.628 (d, 2H, Ar), 4.24 (broad s, 2H, NH), 4.32 (s, 4H, NCH_2), 1.49 (s, 18H, *t*-Bu). ^{13}C{^{1}H} δ 158.39, 146.24, 137.04, 133.55, 54.52, 55.33, 54.48, 56.22, 49.82, 34.41, 30.08. MS (EI) *m/z* 401.283 (M^+). Calcd for $C_{27}H_{35}N_3$: 401.283.

(MPPP)H$_2$ (**1d**). The preparation of compound **1d** is identical to **1b**. LiNHR (7.750 g, 49.9 mmol) and 2,6-bis(bromomethyl)pyridine (5.000 g, 18.9 mmol) gave **1d** as a white crystalline solid (4.910 g, 12.2 mmol, 65%). ^{1}H NMR δ 7.13 (d, 2H, Ar), 7.00–7.03 (m, 5H, py/Ar), 6.75 (d, 2H, py), 4.34 (s, 2H, N*H*), 4.18 (s, 4H, NCH_2), 3.45 (sept, 2H, C*H*Me$_2$), 2.31 (s, 6H, Me), 1.21 (d, 12H, CH*Me*$_2$). ^{13}C{^{1}H} δ 159.01, 145.46, 141.45, 136.75, 131.21, 128.88, 124.13, 123.39, 120.29, 55.33, 27.99, 24.16, 19.03. MS (EI) *m/z* 401.283 (M^+). Calcd for $C_{27}H_{35}N_3$: 401.283.

(BPhP)Zr(NMe$_2$*)*$_2$ (**2a**). A toluene solution of $Zr(NMe_2)_4$ (3.635 g, 13.6 mmol) was added to a toluene solution (50 cm^3) of **1a** (6.000 g, 13.6 mmol) and stirred for 12 h. The solvent was removed *in vacuo* and the resulting solid extracted with hexanes (3 × 50 cm^3) and filtered through Celite. The volume of the filtrate was reduced and the solution cooled to −30°C, affording **2a** as a yellow crystalline solid (7.715 g, 12.5 mmol, 92%). ^{1}H NMR δ 7.74 (d, 2H, Ar/Ph), 7.71 (d, 2H, Ar/Ph), 7.32–7.36 (m, 4H, Ar/Ph), 6.98–7.11 (m, 8H, Ar/Ph), 6.56 (t, 1H, py), 6.00 (d, 2H, py), 4.66 (s, 4H, NCH_2), 2.94 (s, 12H, N*Me*$_2$). ^{13}C{^{1}H} δ 164.67, 153.33, 143.59, 137.46, 135.30, 131.95, 128.45, 128.32, 128.196, 127.76, 126.34, 122.55, 116.93, 63.29, 41.92.

(BMPP)Zr(NMe$_2$*)*$_2$ (**2b**). The preparation of compound **2b** is identical to **2a**. $Zr(NMe_2)_4$ (2.150 g, 8.03 mmol) and **1b** (3.000 g, 8.03 mmol) gave **2b** as a yellow crystalline solid (4.100 g, 7.44 mmol, 93%). ^{1}H NMR δ 7.41 (dd, 2H, Ar), 7.32 (dd, 2H, Ar), 7.21 (td, 2H, Ar), 1.11 (td, 2H, Ar), 8.87 (t, 1H, py), 6.42 (d, 2H, py), 4.93 (s, 4H, NCH_2), 3.53 (sept, 4H, C*H*Me$_2$), 2.76 (s, 12H, NMe$_2$), 1.29 (d, 12H, CH*Me*$_2$). ^{13}C{^{1}H} δ 164.64, 152.91, 145.71, 137.59, 129.27, 126.32, 126.14, 124.04, 117.34, 67.26, 42.03, 27.29, 25.23.

(BMBP)Zr(NMe$_2$*)*$_2$ (**2c**). The preparation of compound **2c** is identical to **2a**. $Zr(NMe_2)_4$ (2.150 g, 8.04 mmol) and **1c** (3.000 g, 8.03 mmol) gave **2c** a yellow crystalline solid (3.987 g, 7.24 mmol, 90%). The following data is for both rotamers (*meso*/*rac*, 2.6 : 1). ^{1}H NMR δ 7.48 (t, Ar), 7.24 (t, Ar), 7.07 (t, Ar), 6.90 (t, py), 6.49 (d, py), 4.91 (s, *meso* NCH_2), 4.90 (AB quartet, $^2J_{HH}$ = 20.0 Hz, *rac* NCH_2), 3.01 (s, *meso* N*Me*$_2$), 2.65 (s, *rac* N*Me*$_2$), 2.42 (s, *meso* N*Me*$_2$), 1.57 (s, *rac* C*Me*$_3$), 1.51 (s, *meso* C*Me*$_3$). ^{13}C{^{1}H} δ 163.88, 163.14, 156.07, 154.46, 146.67, 137.73, 132.32, 132.12, 128.90, 127.94, 126.95, 126.76, 124.30, 123.73, 117.25, 68.40, 43.25, 42.15, 41.05, 36.56, 32.64, 32.41.

(MPPP)Zr(NMe$_2$*)*$_2$ (**2d**). The preparation of compound **2d** is identical to **2a**. $Zr(NMe_2)_4$ (2.671 g, 10.0 mmol) and **1d** (4.010 g, 10.0 mmol) gave **2d** as a yellow crystalline solid (3.090 g, 5.34 mmol, 54%). The following data is for both rotamers (*meso*/*rac*, 1 : 1.13). ^{1}H NMR δ 7.23–7.27 (m, Ar/Ph), 7.05–7.16 (m, Ar/Ph), 6.93 (t, py), 6.48 (d, py), 4.68 (AB quartet, $^2J_{HH}$ = 20.3 Hz, *rac* NCH_2), 4.65 (AB quartet, $^2J_{HH}$ = 20.3 Hz, *meso* NCH_2), 4.00 (sept, *meso* C*H*Me$_2$), 3.82 (sept, *rac* C*H*Me$_2$), 2.88 (s, *meso* N*Me*$_2$), 2.57 (s, *rac* N*Me*$_2$), 2.32 (s, *rac* Me), 2.30 (s, *meso* N*Me*$_2$), 2.19 (s, *meso* Me), 1.39 and 1.38 (d, *meso*

CHMe_2), 1.32 and 1.29 (d, *rac* CHMe_2). $^{13}C\{^1H\}$ δ 164.12, 163.81, 152.39, 152.12, 146.41, 146.38, 137.60, 137.54, 135.37, 135.10, 123.86, 123.77, 117.25, 65.06, 64.92, 42.59, 41.33, 40.08, 27.64, 26.92, 26.76, 24.28, 24.04, 19.16, 19.07.

(*BPhP*)$ZrCl_2$ (**3a**). Excess $ClSiMe_3$ (2 cm^3) was added dropwise to a toluene solution (50 cm^3) of compound **2a** (2.315 g, 3.74 mmol) at 23°C. The solution was stirred for 12 h during which time **3a** precipitated as a beige solid. Hexanes (100 cm^3) was added and the solution was cooled to −30°C for 12 h. The solid was isolated by filtration and dried under vacuum (2.152 g, 3.57 mmol, 96%). ^1H NMR δ 8.44 (d, 2H, Ph), 7.80–7.90 (m, 4H, Ph), 6.90–7.40 (m, 12H, Ar/Ph), 6.39 (t, 1H, py), 5.84 (d, 2H, py), 4.54 (s, 4H, NCH_2). Compound **3a** is poorly soluble in organic solvents which precludes its convenient characterization by $^{13}C\{^1H\}$ NMR.

(*BMPP*)$ZrCl_2$ (**3b**). The preparation of compound **3b** is identical to **3a**. Excess $ClSiMe_3$ (2 cm^3) and **2b** (1.500 g, 2.72 mmol) affords **3b** as a beige solid (1.190 g, 2.23 mmol, 82%). ^1H NMR δ 7.98 (br d, 2H, Ar), 7.29 (m, 2H, Ar), 7.15 (m, 4H, Ar), 6.89 (t, 1H, py), 6.34 (d, 2H, py), 4.73 (br s, 4H, NCH_2), 3.48 (br sept, 4H, C*H*Me_2), 1.33 (br s, 12H, CHMe_2). $^{13}C\{^1H\}$ (d_8-toluene, 80°C) δ 164.31, 147.20, 146.33, 138.63, 130.34, 127.41, 127.33, 126.74, 117.71, 69.32, 27.60, 25.01.

(*BMBP*)$ZrCl_2$ (**3c**). The preparation of compound **3c** is identical to **3a**. Excess $ClSiMe_3$ (2 cm^3) and **2c** (1.000 g, 1.73 mmol) affords **3c** as a beige solid (0.860 g, 1.54 mmol, 89%). ^1H NMR δ 7.95 (d, 2H, Ar), 7.47 (d, 2H, Ar), 7.18 (m, 4H, Ar), 6.81 (t, 1H, py), 6.34 (d, 2H, py), 4.78 (AB quartet, $^2J_{HH}$ = 20.1 Hz, 4H, NCH_2), 1.47 (s, 18H, *t*-Bu). $^{13}C\{^1H\}$ δ 162.66, 147.23, 146.05, 138.79, 131.46, 131.01, 127.46, 127.16, 117.76, 70.21, 37.09, 33.31.

(*MPPP*)$ZrCl_2$ (**3d**). The preparation of compound **3d** is identical to **3a**. Excess $ClSiMe_3$ (2 cm^3) and **2d** (1.700 g, 2.94 mmol) affords **3d** as a beige solid (1.327 g, 2.36 mmol, 80%). The following data is for both rotamers (*meso*/*rac*, 1:1.15). ^1H NMR (CD_2Cl_2) δ 8.04 (t, py), 7.52 (d, py), 7.09–7.25 (m, Ar), 5.06 (AB quartet $^2J_{HH}$ = 21.3 Hz, NCH_2), 5.05 (AB quartet $^2J_{HH}$ = 21.3 Hz, NCH_2), 3.56 (sept, C*H*Me_2), 3.48 (sept, C*H*Me_2), 2.35 (s, Me), 2.31 (s, Me), 1.35 (d, CHMe_2), 1.32 (d, CHMe_2), 1.18 (d, CHMe_2), 1.16 (d, CHMe_2). $^{13}C\{^1H\}$ NMR ($CDCl_2$) δ 164.16, 164.12, 147.52, 147.38, 145.22, 145.19, 141.53, 139.92, 136.18, 136.05, 129.33, 128.74, 128.70, 128.51, 127.41, 126.87, 125.59, 125.21, 124.77, 118.74, 67.20, 67.16, 28.03, 27.91, 27.73, 27.54, 23.81, 23.42, 19.50, 19.46.

(*BPhP*)$ZrMe_2$ (**4a**). MeMgCl (3.70 cm^3, 0.99 M, 3.67 mmol) were added to a CH_2Cl_2 (25 cm^3) solution of compound **3a** (1.000 g, 1.66 mmol) at −78°C. The mixture was stirred for 12 h and then the solvent removed *in vacuo*. The resulting solid was extracted with toluene and filtered through Celite. The solvent was removed *in vacuo* and the remaining solid dissolved in a minimum amount of CH_2Cl_2 and cooled to −30°C for 12 h. **4a** was isolated as a white crystalline solid and dried under vacuum (0.625 g, 1.11 mmol, 67%). ^1H NMR δ 8.10 (d, 2H, Ph), 7.73 (d, 4H, Ph), 7.38 (d, 2H, Ar/Ph), 7.28–7.31 (m, 2H, Ar/Ph), 7.08–7.15 (m, 6H, Ar/Ph), 6.99 (m, 2H, Ar/Ph), 6.49 (t, 1H, py), 5.93 (d, 2H, py), 4.62 (s, 4H, NCH_2), 0.73 (s, 6H, Zr-*Me*). $^{13}C\{^1H\}$ NMR δ 164.02, 148.94, 142.66, 137.59, 136.82, 133.01, 129.06, 128.68, 128.49, 128.17, 126.84, 125.21, 116.97, 64.51, 42.38 (Zr-*C*H_3). Anal. Calcd for $C_{33}H_{31}N_3Zr$: C, 70.67; H, 5.57; N, 7.49. Found: C, 70.60; H, 5.55; N, 7.19.

(*BMPP*)$ZrMe_2$ (**4b**). MeMgCl (0.78 cm^3, 3.0 M, 2.35 mmol) was added to a diethylether (23 cm^3) solution of compound **3b** (0.500 g, 0.94 mmol) at 23°C. The mixture was stirred for 12 h and then the solvent removed *in vacuo*. The resulting solid was extracted with toluene and filtered through Celite. The solvent was removed *in vacuo* and the remaining solid dissolved in a minimum amount of diethylether and cooled to −30°C for 12 h. **4b** was isolated as a white crystalline solid and dried under vacuum (0.445 g, 0.90 mmol, 85%). ^1H NMR δ 7.69 (m, 2H, Ar), 7.36 (m, 2H, Ar), 7.20 (m, 4H, Ar), 6.87 (t, 1H, py), 6.38 (d, 2H, py), 4.84 (s, 4H, NCH_2), 3.57 (sept, 4H, C*H*Me_2), 1.31 (d, 12H, CHMe_2), 0.46 (br s, 6H, Zr-*Me*). $^{13}C\{^1H\}$ NMR δ 164.02, 148.50, 147.54, 131.08, 129.27, 127.21, 127.67, 126.29, 117.35, 58.31, 41.23 (Zr-*C*H_3), 27.25, 25.39. Anal. Calcd for $C_{27}H_{35}N_3Zr$: C, 65.81; H, 7.16; N, 8.53. Found: C, 66.03; H, 7.18; N, 8.68.

(*BMBP*)$ZrMe_2$ (**4c**). The preparation of compound **4c** is identical to **4b**. MeMgCl (0.52 cm^3, 3.0 M, 1.55 mmol) and **3c** (0.350 g, 0.62 mmol) gave **4c** as a white crystalline solid (0.234 g, 0.45 mmol, 73%). The following data is for both rotamers (*meso*/*rac*, 3:1). ^1H NMR δ 7.78 (d, Ar), 7.54 (d, Ar), 7.20 (m, Ar), 6.87 (t, py), 6.43 (d, py), 4.91 (AB quartet, $^2J_{HH}$ = 20.7 Hz, *meso* NCH_2), 4.83 (AB quartet, $^2H_{HH}$ = 20.7 Hz, *rac* NCH_2), 1.55 (s, *rac t*-Bu), 1.49 (s, *meso t*-Bu), 0.82 (s, *meso* Zr-Me), 0.62 (s, *rac* Zr-Me), 0.26 (s, *meso* Zr-Me). $^{13}C\{^1H\}$ NMR δ 163.66, 163.21, 149.43, 147.18, 137.90, 133.98, 132.75, 130.93, 127.06, 126.92, 126.02, 125.88, 117.47, 70.03, 69.71, 45.71 (Zr-CH_3), 44.73 (Zr-*C*H_3), 39.57, 37.18, 33.34. Anal. Calcd for $C_{29}H_{39}N_3Zr$: C, 66.87; H, 7.55; N, 8.07. Found: C, 66.64; H, 7.77; N, 7.91.

(*MPPP*)$ZrMe_2$ (**4d**). The preparation of compound **4d** is identical to **4b**. MeMgCl (0.75 cm^3, 3.0 M, 2.23 mmol) and **3d** (0.500 g, 0.89 mmol) gave **4d** as a white crystalline solid (0.316 g, 0.61 mmol, 69%). The following data is for both rotamers (*meso*/*rac*, 1:1.4). ^1H NMR δ 7.00–7.23 (m, Ar), 6.91 (t, py), 6.45 (d, py), 4.75 (AB quartets $^2J_{HH}$ = 20.8 Hz, NCH_2), 4.74 (AB quartets $^2J_{HH}$ = 20.8 Hz, NCH_2), 3.90 (sept, C*H*Me_2), 2.38 (s, Me), 2.11 (s, Me), 1.45 (d, CHMe_2), 1.43 (d, CHMe_2), 1.25 (d, CHMe_2), 1.23 (d, CHMe_2), 0.45 (s, *meso* Zr-*Me*), 0.39 (s, *rac* Zr-*Me*), 0.32 (s, *meso* Zr-*Me*). $^{13}C\{^1H\}$ NMR δ 164.23, 164.17, 147.78, 147.75, 147.28, 137.79, 136.43, 129.28, 128.67, 128.51, 125.97, 125.64, 124.54, 117.42, 65.96, 44.35, 43.71,

42.67, 28.63, 28.51, 27.71, 23.75, 23.63, 21.40, 19.09. Anal. Calcd for $C_{29}H_{29}N_3Zr$: C, 66.87; H, 7.55; N, 8.07. Found: C, 66.79; H, 7.51; N, 8.24.

(BMBP)Zr(CH$_2$Ph)$_2$ (**5c**). $PhCH_2MgCl$ (2.50 cm^3, 0.89 M, 2.22 mmol) was added to a diethylether (25 cm^3) solution of compound **3c** (0.500 g, 0.89 mmol) at −30°C. The mixture was stirred for 12 h and then the solvent removed *in vacuo*. The resulting solid was extracted with toluene and filtered through Celite. The solvent was removed *in vacuo* and the remaining solid dissolved in a minimum amount of diethylether and cooled to −30°C for 12 h. **5c** was isolated as a bright yellow crystalline solid and dried under vacuum (0.438 g, 0.65 mmol, 73%). ^{1}H NMR δ 7.50 (m, 1H, Ar), 7.42 (m, 1H, Ar), 7.18 (m, 4H, Ar and Ph), 7.04 (m, 2H, Ar and Ph), 6.81 (t, 2H, Ar and Ph), 6.73 (t, 1H, py), 6.35 (d, 2H, py), 5.71 (m, 2H, Ph), 4.66 (AB quartet, $^2J_{HH}$ = 20.5 Hz, 4H, NHH_2), 2.34 (s, 2H, CH_2Ph), 1.80 (s, 2H, CH_2Ph), 1.46 (s, 18H, CMe_3). $^{13}C\{^1H\}$ δ 161.91, 149.65, 148.98, 146.61, 137.36, 137.07, 132.96, 131.10, 130.31, 130.12, 127.36, 126.56, 126.32, 124.95, 124.14, 119.58, 117.07, 69.41, 65.16, 56.69, 37.17, 33.47. Anal. Calcd for $C_{41}H_{47}N_3Zr$: C, 73.17; H, 7.04; N, 6.24. Found: C, 73.10; H, 7.15; N, 6.39.

CONCLUSIONS

A series of ortho-substituted aryl diamide complexes of zirconium have been prepared in high yield. Depending on the size of the ortho substituent on the aryl group, rotameric isomers, derived from restricted rotation about the N—C_{ipso} bond, can be observed spectroscopically and the barriers to isomerization measured. In the case of the 2-phenylaryl moiety, rapid isomerization is observed at all temperatures regardless of the substituents bound to zirconium in the equatorial plane. The 2-isopropylaryl substituted complexes exhibit fluxional behavior with the low temperature limiting ^{1}H NMR spectra showing resonances for species consistent with *meso* and *rac* rotamers. In contrast, the 2-*tert*-butylaryl derivatives are 'locked' as five coordinate species but can isomerize during metathesis reactions at the metal center. The 2-isopropyl-6-methyl complexes are also locked, however, the rotameric ratios remain the same in all derivatives of this ligand system. We are currently studying the α-olefin polymerization chemistry of these and other complexes.

Acknowledgements—Funding from the NSERC (Canada) in the form of a Research Grant to D.H.M. and Union Carbide Canada is gratefully acknowledged.

REFERENCES

1. Bochmann, M. J., *Chem. Soc., Dalton Trans.*, 1996, 255.
2. Brintzinger, H. H., Fischer, D., Mülhaupt, R., Rieger, B. and Waymouth, R. M., *Angew. Chem., Int. Ed. Engl.*, 1995, **34,** 1143.
3. Mohring, P. C., Coville, N. J. *J. Organomet. Chem.*, 1994, **479,** 1.
4. Kaminsky, W., Kulper, K., Brintzinger, H. H. and Wild, F. R. W. P., *Angew. Chem., Int. Ed. Engl.*, 1985, **24,** 507.
5. Ewan, J. A., Jones, R. L., Razavi, J. A., *J. Am. Chem. Soc.*, 1988, **110,** 6255.
6. Coates, G. W., Waymouth, R. M., *Science*, 1995, **267,** 21.
7. Tinkler, S., Deeth, R. J., Duncalf, D. J. and McCamley, A., *J. Chem. Soc., Chem. Commun.*, 1996, 2623.
8. Aoyagi, K., Gantzel, P. K., Kalai, K. and Tilley, T. D., *Organometallics*, 1996, **15,** 923.
9. Warren, T. H., Schrock, R. R. and Davis, W. M., *Organometallics*, 1996, **15,** 562.
10. Horton, A. D., de With, J., van der Linden, A. J., van de Weg, H., *Organometallics*, 1996, **15,** 2672.
11. Cloke, F. G. N., Geldbach, T. J., Hitchcock, P. B., and Love, J. B., *J. Organomet. Chem.*, 1996, **506,** 343.
12. Clark, H. C. S., Cloke, F. G. N., Hitchcock, P. B., Love, J. B. and Wainwright, A. P., *J. Organomet. Chem.*, 1995, **501,** 333.
13. Herrmann, W. A., Denk, M., Albach, R. W., Behm, H. and Herdtweck, E., *Chem. Ber.*, 1991, **124,** 683.
14. Scollard, J. D., McConville, D. H., Payne, N. C and Vittal, J. J., *Macromolecules*, 1996, **29,** 5241.
15. Scollard, J. D. and McConville, D. H., *J. Am. Chem. Soc.*, 1996, **118,** 10008.
16. Guérin, F., McConville, D. H. and Vittal, J. J., *Organometallics*, 1996, **15,** 5586.
17. Haeg, M. E., Whitlock, B. J. and Whitlock Jr., H. W., *J. Am. Chem. Soc.*, 1989, **111,** 692.
18. Scollard, J. D., McConville, D. H. and Vittal, J. J., *Organometallics*, 1995, **14,** 5478.
19. Lappert, M. F., Power, P. P., Sanger, A. R. and Srivastava, R. C., *Metal Metalloid Amides*; Ellis Horwood: Chichester (1980).
20. Bradley, D. C. and Thomas, I. M., *Proc. Chem. Soc., London*, 1959, 225.
21. Diamond, G. M., Rodewald, S. and Jordan, R. F., *Organometallics*, 1995, **14,** 5.
22. Calculations were performed using CAChe Scientific software by Tektronix.
23. Lambert, J. B., Shurvell, H. F., Lightner, D. and Cooks, R. G., *Introduction to Organic Spectroscopy*; Macmillan Publishing Company: New York, 1987, 68.
24. Diamond, G. M., Jordan, R. F. and Petersen, J. L., *Organometallics*, 1996, **15,** 4045.
25. Guérin, F., McConville, D. H. and Payne, N. C., *Organometallics*, 1996, **15,** 5085.
26. Schrock, R. R. and Wengrovius, J. H., *J. Organomet. Chem.*, 1981, **205,** 319.
27. Guérin, F. and McConville, D. H., unpublished results.

Pergamon

PII: S0277-5367(97)00261-1

Polyhedron Vol. 17, No. 5–6, pp. 925–934, 1998
© 1998 Elsevier Science Ltd
All rights reserved. Printed in Great Britain
0277-5387/98 $19.00+0.00

A new trend in metal–alkoxide chemistry: the elaboration of monophasic organic–inorganic hybrid materials

R. Corriu

Laboratoire de Chimie Moléculaire et Organisation du solide, UMR 5637, Université Montpellier II, Département de Chimie Organique Fine, CC 007, Place E. Bataillon, 34095 Montpellier Cedex 5, France

(Received 11 June 1997)

Abstract—The elaboration of monophasic organic inorganic hybrid materials is an important extension of metal alkoxide chemistry. These solids are obtained by hydrolytic polycondensation from a molecular precursor containing -Si(OR)$_3$ groups (at least two) covalently bound to an organic moiety. Using solid state ^{13}C NMR it is possible to demonstrate that, in all cases studied until now, the organic units are bound to the oxide matrix after hydrolysis. ^{29}Si permits the evaluation of the degree of polycondensation. All the solids obtained are kinetically controlled: their texture is highly dependent on all the parameters governing the kinetics of polycondensation (catalyst, temperature, solvent, concentrations, etc.). It is also possible to demonstrate that the geometry of the organic molecule is an important factor for both the texture and the short range organization of the solid. Weak interactions (charge transfer complexes) have been evidenced as possible controlling parameters for the solid formation. Short range organization in the hybrid material can be demonstrated using the easy polymerisation of bisacetylenic units which has been observed by heating the solid formed by hydrolytic polycondensation of [(MeO)$_3$Si]$_2$C$_4$.

The relationship between the porosity formed in the solid after elimination of the organic unit and the size of this unit was considered. A mild selective cleavage for Si—C bonds has been found and used for eliminating the organic moiety. After cleaving and recovering the organic molecule a monodispersed porosity is observed. However, there is no relation between the size of the pores and the size of the molecule. This fact is certainly due to a reorganization of the solid occurring during the Si—C bond cleavage. © 1998 Elsevier Science Ltd. All rights reserved

Keywords: monophasic hybrid materials; kinetic control of solid formation; shortage organisation; rearrangement of the solid.

The elaboration of solids by sol–gel is one of the natural extensions of metal alkoxide chemistry [1–3]. This way permits access to materials through a very simple one pot procedure summarized in Scheme 1. The molecular precursor undergoes an inorganic polymerization which leads to a highly crosslinked solid through a hydrolytic polycondensation of which the two first steps are:

(i) The nucleophilic attack of water at the metal which can be catalyzed (or not), the possible catalysts being acids, bases, or nucleophiles.

(ii) The condensation reaction which corresponds to the M—O—M bond formation and which can occur either via a homo or a hetero condensation [1–3].

The process is highly complex when polysubstitutions and polycondensations are occurring. These reactions are in competition with redistribution reactions. Moreover they can lead either to cyclic or linear oxide units. In the case of silica, generally considered as the most simple [1–4], Scheme 2 presents some of the possibilities [5]. It is interesting to point out the complexity of these processes and also the lack of basic knowledge of the kinetics where polyfunctional metals are involved. For instance in the case of silicon, the kinetics of monofunctional alkox-

† This paper is dedicated to Professor Bradley in recognition of his pioneering work and great influence in metal alkoxide chemistry.

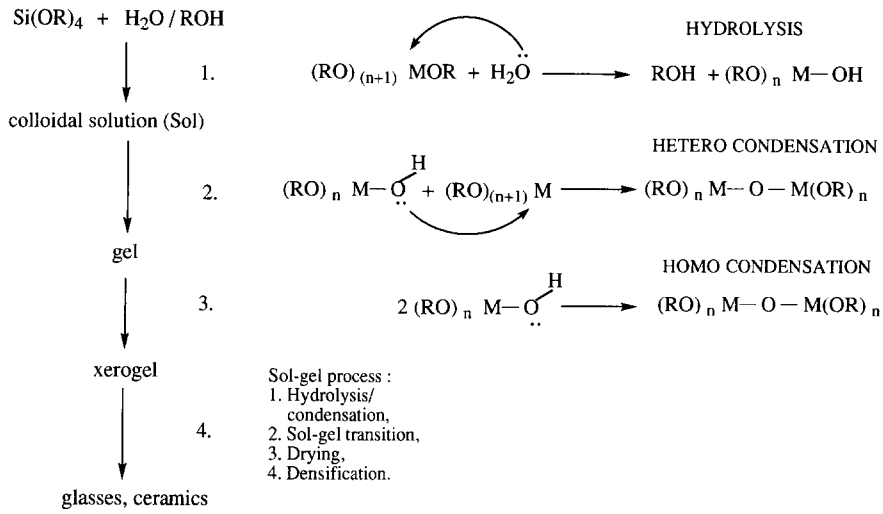

Scheme 1.

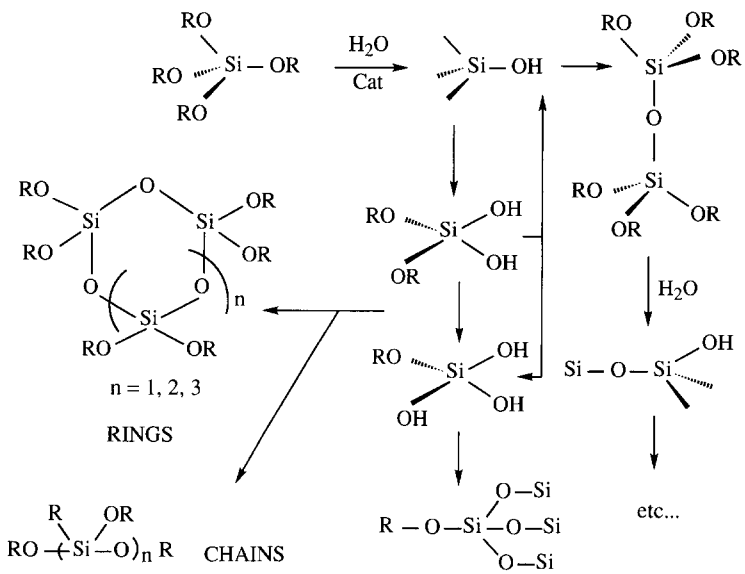

Scheme 2.

ysilane R_3SiOR are known [6]. However the only reliable results concerning the relative successive rates of Si—OR hydrolysis in $Si(OR)_4$ were reported only recently by Chojnowski *et al.* [7].

Although the fundamental knowledge is poor, the sol–gel route nevertheless remains very attractive because of the very convenient access to the solid, and because of the wide possibilities opened by this method.

The organic–inorganic hybrid materials is one of them [8]. This new class of solids corresponds to a new field of investigations growing up very quickly [9] and opening the elaboration of new materials. This review will be limited to our recent interest devoted to the study of the *monophasic* organic–inorganic hybrid solids [10].

These kind of hybrids are formed by organic units bound to an inorganic matrix by at least one metal carbon covalent bond. They are obtained with precursors from which the inorganic matrix can be built up around the organic moiety through the hydrolytic polycondensation as illustrated in Scheme 3 [8–10].

Obviously the number of metals which permit this polycondensation with conservation of the covalent metal–carbon bonds is limited. For example, Si, P, Ge, As, B, Sn are opening possibilities. However between them, silicon seems to be the most convenient from many aspects: well known chemistry [6], stability of Si—C bond, well documented sol–gel methodology [1–2], facility of identification and commercially available starting reagents.

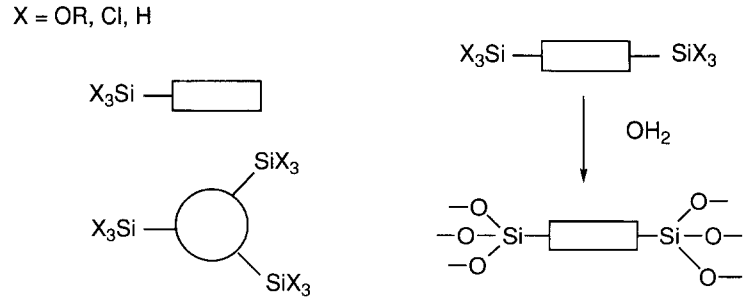

Scheme 3.

Identification of the solids

The preparation of solids is performed by hydrolytic polycondensation from a molecular precursor containing SiX_3 groups covalently bound to an organic unit [10–21]. The inorganic matrix is built up around the organic moieties by polycondensation of SiX_3.

In all cases studied until now, it is possible to demonstrate, by use of ^{13}C solid state NMR, that the organic structure is maintained during the solid's formation procedure, without Si—C bond cleavage. This cleavage should be detected by modification of both the ^{13}C and ^{29}Si signals. In this last case, the formation of Q units in the range of -100 to -110 ppm could be observed. It is also possible to estimate the degree of polycondensation around silicon by ^{29}Si NMR [8f–10b]. One illustrative example is given in the case of polycondensation of precursor A and B [17–19] (Fig. 1).

Table 1 lists most the organic spacer which have been studied until now.

Kinetic control of the solid

It is very important to point out that the texture* of all the solids obtained is kinetically controlled. This means that all parameters which can modify the kinetics of the polycondensation process are of importance for the nature of the material elaborated. It is possible to demonstrate that BET and porosity of the solids obtained from the same precursor, are highly sensitive to all the parameters able to modify the kinetics of polycondensation (nature of the leaving group, solvent, concentration of the reagents, catalyst temperature, etc.). A few examples are given in Table 2 [11–19].

The nature of the organic units can also be a drastic parameter. The comparison of the solids obtained from the polycondensation performed in the same experimental conditions from the two spacers represented in the Scheme 4 is well illustrated [17–19].

With the rigid spacer ($n = 0$), a hydrophilic solid is obtained instead of a hydrophobic one with the more flexible ($n = 2$). In this last case, the organic groups are located at the surface, in agreement with both the reactivity observed towards $Cr(CO)_6$, and with the mass peaks detected by SIMS (Secondary Ion Mass Spectrometry) [22] which are characteristic of phenyl (77) and tolyl (91) and which do not exhibit any SiOH (45). In contrast, the rigid spacer exhibits very poor reactivity in accordance with the hydrophilicity observed and the results of SIMS. The phenyl groups are not chemically accessible. They cannot be detected by SIMS, only SiOH (45) is observed at the surface of the solid.

The experiments described show that the nature of the organic spacer is an important factor in the control of the formation of the solid in the polycondensation reaction. They suggest that interactions between the organic units might play an important role in the formation of the solid. Two obvious conclusions can be revealed from this assumption. If this hypothesis is correct, weak interactions should be able to modify the nature of the solid. Moreover, the possible interactions between the organic spacers during the formation of the solid might induce a short range organisation between the organic units. These two points will be illustrated.

Weak interactions and solid organisation

The great influence of the weak interactions can be evidenced by studying the effect of charge transfer complexes on the solid formation. It is known that terthiophene and TCNQ can form such complexes [29]. We have used this weak interaction in order to consider its influence on the formation on monophasic hybrid solids. As illustrated in Scheme 5 bis(trimethoxylsilyl) terthiophene (**I**) is giving a charge complex (**II**) with TCNQ [14]. By cohydrolysis with $Si(OMe)_4$, a solid (**III**) is obtained which exhibits a poor specific surface (6 $m^2\ g^{-1}$), a visible absorption similar to (**II**) and a higher conductivity (10^{-6} s cm^{-1} instead of 10^{-10}). The absorption spectrum provides

*The texture of the solid is the sum of the macroscopic parameters which permits the identification = density, specific surface area (BET), volume and nature of porosity, granulometry, etc....

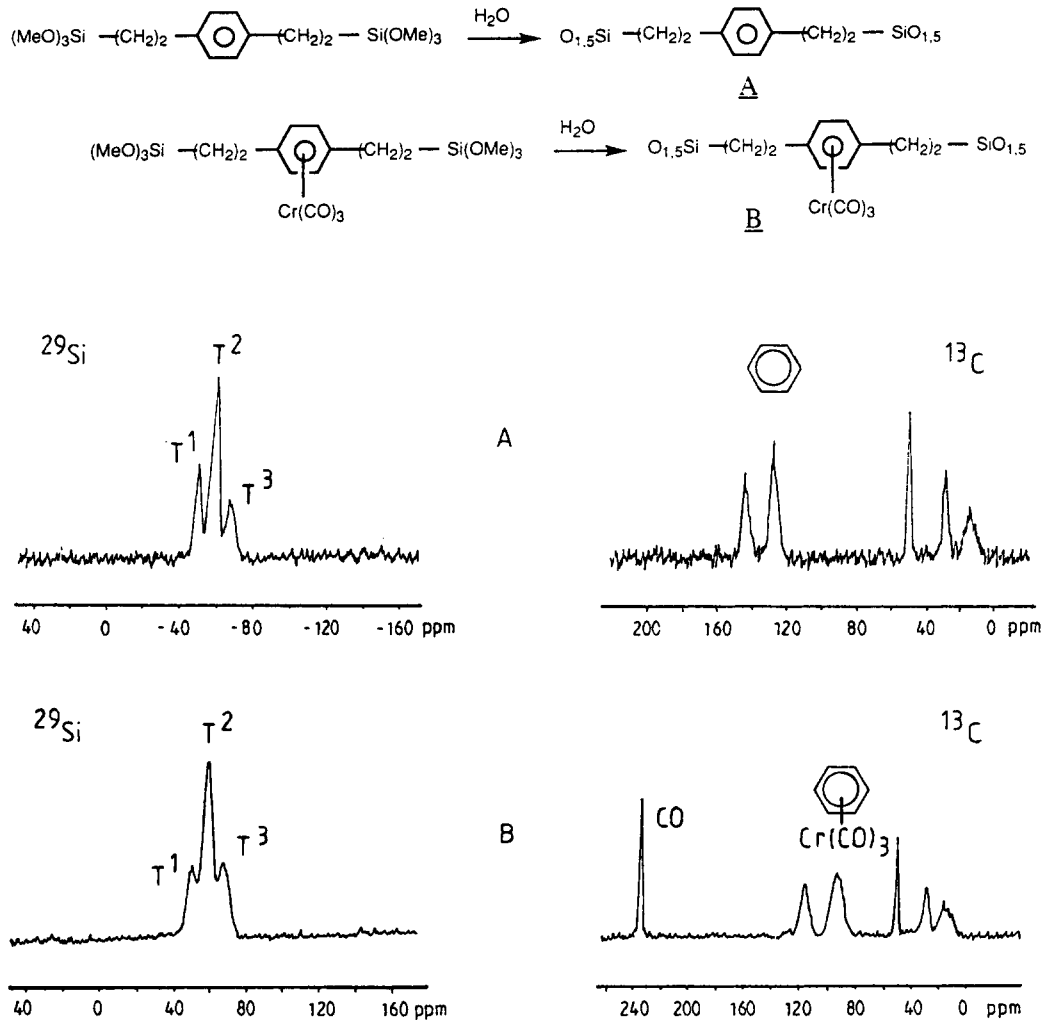

Fig. 1. ^{29}Si and ^{13}C NMR features observed before (A) and after complexation (B) with $Cr(CO)_3$.

evidence that the charge transfer complex is maintained in the solid. Washing with ether–acetone mixture, we observe the disappearance of both conductivity and visible spectrum corresponding to the destruction of the charge transfer complex [14]. This experiment illustrates how weak this interaction is since a washing permits its elimination. It is interesting to compare the BET measured on (**III**) and (**IV**) (6 and 9 $m^2\ g^{-1}$ respectively) with the value of the solid (**IV'**) (566 $m^2\ g^{-1}$) obtained from hydrolytic polycondensation performed on (**I**) in the same experimental conditions.

The two solids (**IV**) and (**IV'**) have the same IR and NMR features but are corresponding to two different arrangements in the solid.

A possible short range organisation in the solid

For the detection of possible short range organisation in the solid, diyne units have been chosen because of their very selective reactivity. The polymerization of the diacetylene groups occurs topochemically [24–26], that is, a particular arrangement of the triple bonds with respect to one another is required. As illustrated in Scheme 6, the 1–4 addition, leading to enyne formation, requires the diacetylene units to be parallel to each other [27].

Gels containing diacetylene units have been prepared from 1,4-bis(trimethoxy-silyl)buta-1,3 diyne. These solids exhibit the NMR and IR features of the starting precursor: ^{13}C NMR $\delta = 79.4$ and 87.8 *C*—*C*≡*C*—Si, IR: $\nu = 2202$ and 2091 cm^{-1}. After heating at 200°C under argon, the formation of enynes and the associated crosslinking in the solid was detected by spectroscopy (^{13}C NMR $\delta = 133$, ^{29}Si NMR; $\delta = -74$, IR $\nu = 2169\ cm^{-1}$) [28]. Moreover, the same spectroscopic features were found regardless of whether gelation was performed before the crosslinking (route A) or whether the crosslinking was induced by irradiation before the gelation (route B) (Scheme 7).

It is interesting to compare this polymerization with the crosslinking observed in the case of polymers $[—SiR_2—C{\equiv}C—C{\equiv}C—]_n$ for which the DTA curve

Table 1. Listing of most of the monophasic organic inorganic hybrid materials prepared

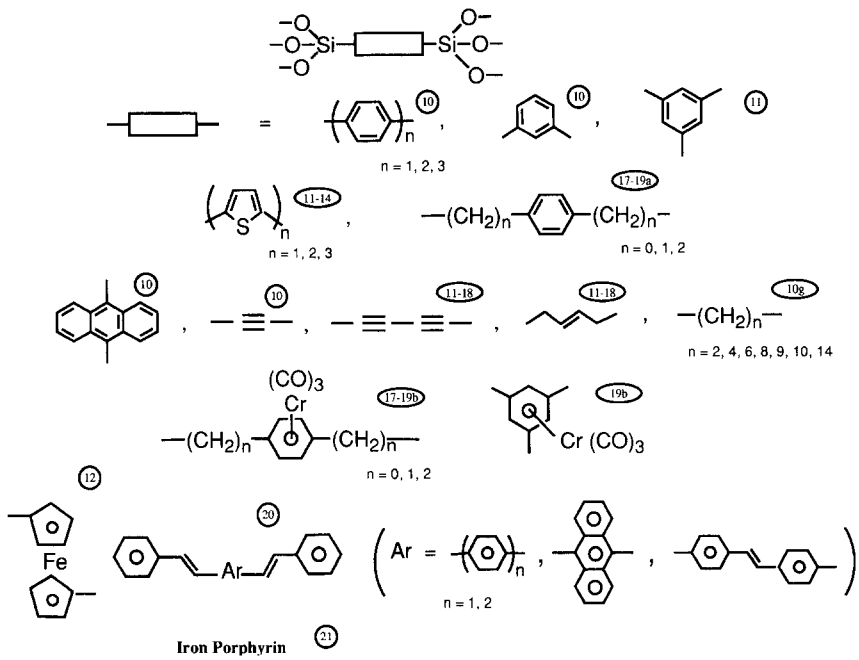

Table 2. Kinetic control of the texture of monophasic organic inorganic hybrid materials

No	Precursors	c[a]	Solv.[b]	Catalyst[c]	t (min)[d]	S[e]
1		3	MeOH	$NH_4F(10^{-3})$	10^{-1}	1030
2	$Si(OMe)_3$	1	MeOH	$NH_4F(10^{-3})$	10	516
3		1	THF	$NH_4F(10^{-3})$	1	493
4		0.5	THF	$NH_4OH(2.6)$	45	1260
5		0.5	THF	$NH_4OH(10^{-2})$	95	380
6	$Si(OMe)_3$	0.5	THF	$HCl(5\ 10^{-3})$	600	129
7		0.5	MeOH	$HCl(10^{-2})$	95	770
8	$(CH_2)_2Si(OMe)_3$	0.5	MeOH	$NH_4F(10^{-2})$	45	5
9		0.5	MeOH	$NH_4OH(10^{-2})$	8×10^4	4
10		0.5	THF	$NH_4F(10^{-2})$	3900	7
11		0.5	THF	$NH_4OH(10^{-2})$	360	0
12	$(CH_2)_2Si(OMe)_3$	0.5	THF	$HCl(10^{-2})$	30	8
13		3	MeOH	$NH_4F(10^{-3})$	60	325
14	$(MeO)_3Si$ ⌒ $Si(OMe)_3$	1	MeOH	$NH_4F(10^{-3})$	2×10^4	0
15		0.1	MeOH	$NH_4OH(2.6)$	30	977

[a] c = concentration [mol L^{-1}].
[b] Solv. = Solvent.
[c] Value in parentheses is the concentration of the catalyst [mol L^{-1}].
[d] t = Gel time.
[e] Specific surface area.

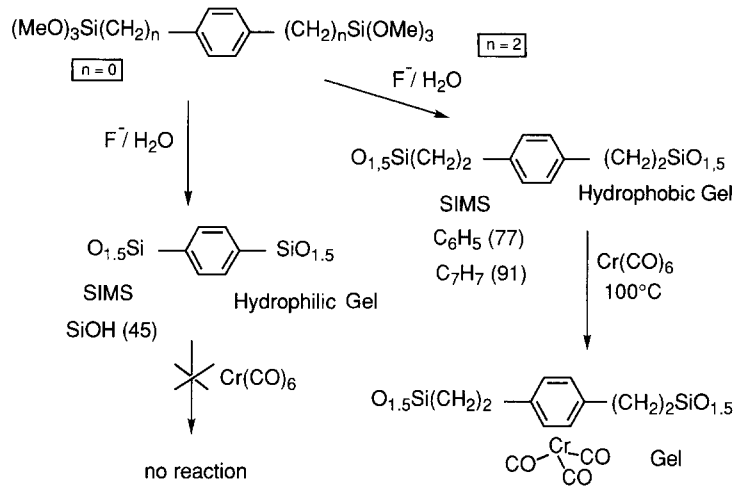

Scheme 4.

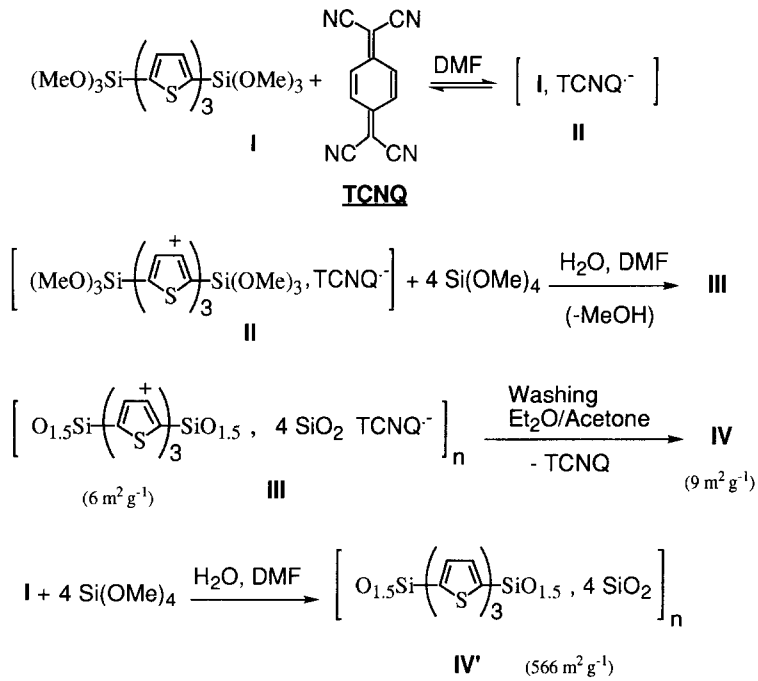

	Absorption			Conductivity
II	847	749	647 nm	10^{-10} S cm^{-1}
III	855	752	684 nm	10^{-6} S cm^{-1}

Scheme 5.

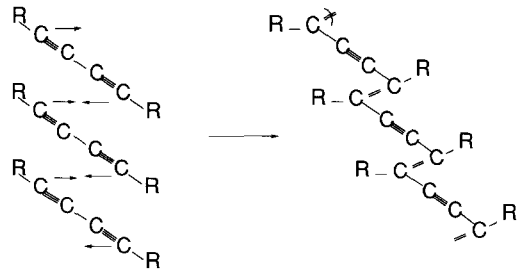

Scheme 6.

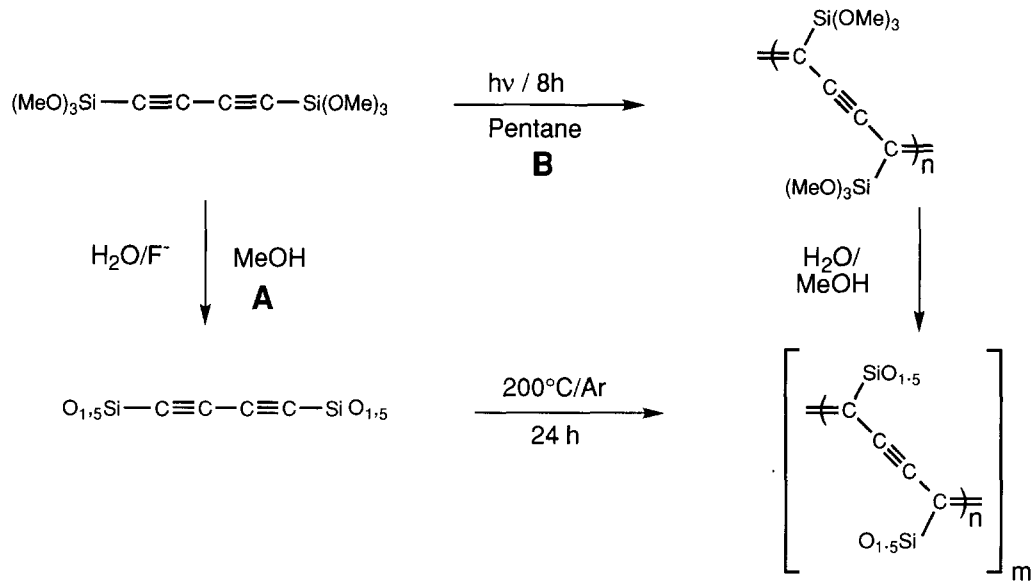

Scheme 7.

is highly dependent on the organization in the solid [27]. In the DTA curve of crystalline polymers of this type (R = Me, Et), a sharp peak occurs at 200°C that can be attributed to the crosslinking reaction. In contrast, the poor crystalline (R≡Ph) or non-crystalline polymers (R≡$SiMe_3$) are crosslinked only between 250 and 350°C. In the case of gels, the crosslinking reaction starts at lower temperatures as shown in Fig. 2. The DTA curve exhibits an exothermic transformation between 120 and 350°C with a maximum at 250°C.

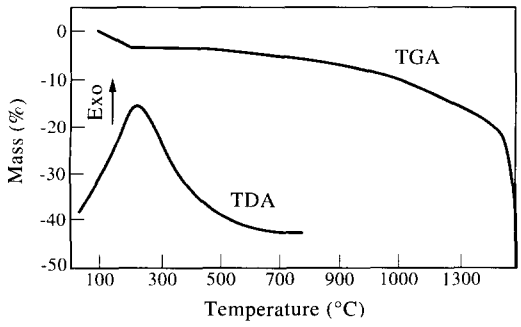

Fig. 2. TDA and TGA curves observed.

The facile reaction between the diyne fragments at a relatively low temperature within the amorphous gel may be indicative of a favourable arrangement of the diyne moieties. The enyne formation involves parallelism between several diacetylenic units inside the solid. These results suggest the formation of short range organization in the silica network that permit the 1–4 addition between the organic units, and which is too short for detection by XRD.

Finally the last example discussed in this review is in connection with the possibilities open by molecular imprinting.

Structure of the organic spacer and porosity

It is beneficial to include organic moieties in solids and to induce a porosity by their elimination. Generally the elimination of the organic part is performed by oxidative reactions (air, ozone, etc.) which completely destruct the molecular skeleton, with an increase of the specific surface area [29]. Since the oxidation methods are liable to provide some modifications of the silica network, because of the local increase of temperature, and in order to avoid the

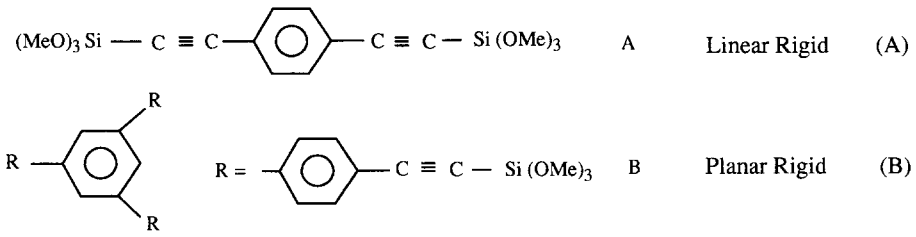

Scheme 8.

sacrificial route, we have prepared systems in which it is possible to perform a chemically induced selective cleavage.

During our previous work [30] we have observed that Si—C≡C—C≡C— may be cleaved by H_2O (or MeOH) in the presence of NH_4F at 60°C leading to the formation of SiOH or (SiOMe) one part, and HC≡C—C≡CH species as the other part. By extension of this method, it is possible to cleave the Si–ethynyl bonds selectively and to recover the organic molecules almost quantitatively (80–95%). This chemical cleavage is followed by a thermal treatment at 600°C, after which the remaining amount of carbon is very low (less than 0.5%) [31,32].

As a first step, we studied the silica gels containing organic molecules with a well determined geometry and precursors (A), (B) and (C) have been prepared. (See Scheme 8).

The gelation of (A), (B) and (C) is performed in the same conditions [room temperature, no catalyst, solvent = THF, precursor concentration 1M or 3M under inert atmosphere (nitrogen) and stirring, aging

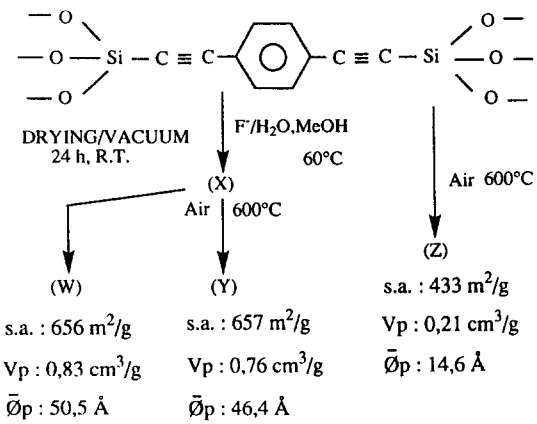

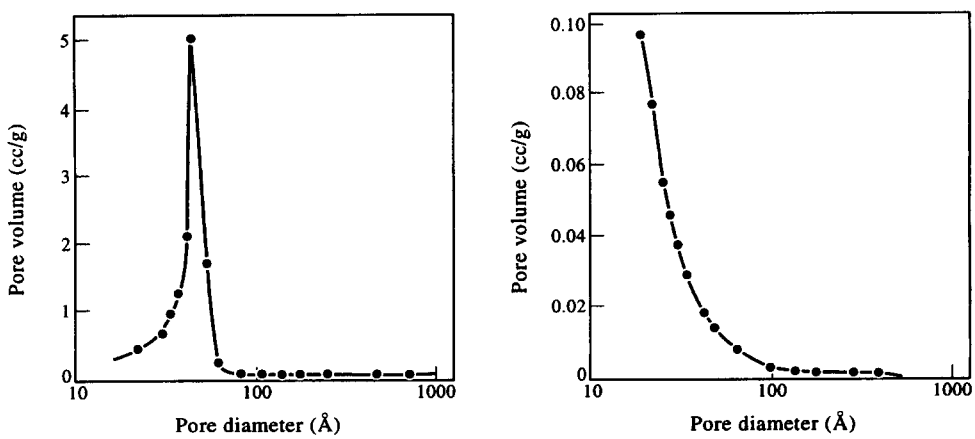

Scheme 9.

Table 3. Comparison of specific surface area of (A), (B), and (C) before and after elimination of the organic moiety. (Chemical treatment followed by heating at 600°C)

	A Linear rigid	B Planar rigid	C Linear flexible
Specific surface m^2/g BET before treatment	19	25	6
After treatment	657	706	407
Pore vol. (cm^3/g)	0.76	1.16	0.72
Pore size (Å)	46	65	70
Size of the molecule which was eliminated (Å)	8	7	8.4↔4.6

one week, filtration, washing with Et_2O, grinding and drying at room temperature under vacuum]. The cleavage of Si—C≡C bonds permits the almost quantitative separation of the organic moiety. Table 3 gives the specific areas and porosity measured: in all cases the specific surface area increases with elimination of the organic moiety. Moreover the porosities are highly depending on the geometric feature of the molecule.

It is also of interest to compare the selective cleavage reported here with the sacrificial route using air oxidation. The oxidation route (600°C/air) leads to a highly dispersed microporosity. In contrast, a very narrow porosity is obtained when the chemical cleavage is followed by a thermal treatment performed in the same conditions (600°C/air). This difference was observed with (A), (B) and (C).

Scheme 9 shows the difference between the two routes in the case of (A).

Another interesting observation (cf. Table 3) is the fact that in all cases, the size of the pores is wider than the size of the molecule eliminated. This result is in agreement with the presence of a short range organization induced by the organic moieties inside the amorphous solid network, and also with a possible reorganization of the silica network induced by the F^- catalyst during the chemical cleavage of the Si—C≡C— bond.

CONCLUSION

The results presented here show the wide possibilities which are presented by the monophasic organic–inorganic hybrid solids. These materials are prepared by the elaboration of an oxide network (generally SiO_2) around an organic moiety using an hydrolytic polycondensation. This method of elaboration permits the formation of kinetically controlled solids. Factors influencing the kinetics of polycondensation, and also weak interactions between the organic units are able to modify the nature and the texture of the resulting solid. The materials obtained exhibit a short range organization which can be evidenced by chemical reactivity and by porosities studies performed after elimination of organic units.

REFERENCES

1. Bradley, D. C., Mehrotra, R. C. and Gaur, D. P., *Metal Alkoxides*, Academic Press, N.Y. (1978).
2. Livage, J., Henry, M. and Sanchez, C., *Prog. Solid State Chem.*, 1988, **18,** 259.
3. (a) Yajima, S., Hayashi, J. and Omori, M., *Chem. Lett.*, 1975, 931; (b) Yajima, S., Okamura, K, and Hayashi, J., *ibid*, 1975, 1209.
4. (a) Aelion, R., Loebel, A. and Eirich, F., *Rec. Trav. Chim.*, 1950, **69,** 61; (b) *J. Am. Chem. Soc.*, 1950, **72,** 5705; (c) Grubb, W. T., *ibid.*, 1954, **76,** 3408.
5. Corriu, R. J. P., Leclercq, Vioux, A., Pauthe, M. and Phalippou, J., in *Ultrastructure Processing of Advanced Ceramics* (Eds J. D. Mackenzie and D. R. Ulrich), p. 113, J. Wiley & Sons (1988).
6. Eaborn, C., *Organosilicon Compounds*, Butterworths, London (1960).
7. Chojnowski, J., Cypryk, M., Kazmierski, K. and Rozga, K., *J. Non-Cryst. Solids*, 1990, **125,** 40.
8. (a) For a general survey see *Hybrid Organic–inorganic Composites*, Ed. *ACS Symp.*, ser. no. 585, American Chemical Society, San Diego, DC (1994); *New J. Chem.*, 1994, **18,** 989. (b) Schmidt, H. K., *Mater. Res. Soc. Symp. Proc.*, 1984, **32,** 327; (c) Schmidt, H. K., *Inorganic and Organometallic Polymers*, ACS Symp., ser. no. 360, p. 333. American Chemical Society, Washington, DC (1988); (d) Schmidt, H. K., *Mater. Res. Soc. Symp. Proc.*, 1990, **180,** 961 and refs therein; (e) Mackenzie, J. D., *J. Sol–Gel Sci. Tech.*, 1994, **2,** 81; and refs therein; (f) Schubert, U., Hüsing, N. and Lorenz, A. *Chem. Mater.*, 1995, **7,** 2010; (g) Loy, D. A. and Shea, K. J., *Chem. Rev.*, 1995, **95,** 1431.
9. (a) Judenstein, P. and Sanchez, C., *J. Mater. Chem.*, 1996, **6,** 511; (b) Corriu, R. J. P. and LeClercq, *Augewichem. Int. Ed. Engl.*, 1996, **35,** 1920, *Tailor-Made Silicon–Oxygen Compounds—From Molecules to Materials*, R. Corriu and P. Jutzi Eds, Vieweg, Braunschweig, Wiesbaden, 1996.
10. (a) Shea, K. J., Loy, D. A. and Webster, O. W., *Chem. Mater.*, 1989, **1,** 574; (b) Shea, K. J., Loy, D. A. and Webster, O. W., *J. Am. Chem. Soc.*, 1992, **114,** 6700 and refs therein; (c) Choi, K. M. and Shea, K. J., *J. Phys. Chem.*, 1994, **98,** 3207; (e) Choi, K. M., Hemminger, J. C. and Shea, K. J., *ibid.*, 1994, **116,** 9052; (d) Choi, K. M. and

Shea, K. J., *ibid.*, 1995, **99,** 4720; (f) Oviatt, H. W., Shea, K. J., Kalluri, S., Shi, Y., Steier, W. H. and Dalton, L. R., *Chem. Mater.*, 1995, **7,** 493; (g) Oviatt, H. W. Jr, Shea, K. J. and Small K. J., *Chem. Mater.*, 1993, **5,** 943; (h) Loy, D. A., Jamison, G. M., Baugher, B. M., Myers, S. A., Assink, R. A. and Shea, K. J., *Chem. Mater.*, 1996, **8,** 656.

11. (a) Corriu, R. J. P., Moreau, J. J. E., Thepot, P. and Wong Chi Man, M., *Chem. Mater.*, 1992, **4,** 1217; (b) Corriu, R. J. P., Moreau, J. J. E. and Wong Chi Nan, M., *J. Sol–Gel Sci. Tech.*, 1994, **2,** 87.
12. (a) Audebert, P., Calas, P., Cerveau, G., Corriu, R. J. P. and Costa, N., *J. Electroanalytical Chem.*, 1994, **372,** 275; (b) Cerveau, G., Corriu, R. J. P. and Costa, N., *J. Non Cryst. Solids*, 1993, **163,** 226.
13. Sauvajol, J. L., Chorro, C., Lère-Porte, J. P., Corriu, R. J. P., Moreau, J. J. E., Thépot, P. and Wong Chi Man, M., *Synth. Metals*, 1994, **62,** 233.
14. Corriu, R. J. P., Moreau, J. J. E., Thépot, P., Wong Chi Man, M., Chorro, C., Lère-Porte, J. P. and Sauvajol, J. L., *Chem. Mater.*, 1994, **6,** 640.
15. Moran M., Caudrado, I., Pascual, M. C., Casado, C. M. and Losada, J., *Organometallics*, 1992, **11,** 1210.
16. Choi, K. M. and Shea, K. J., *Chem. Mater.*, 1993, **5,** 1067.
17. (a) Cerveau, G., Corriu, R., and Lepeytre, C., *J. Mater. Chem.*, 1995, **5,** 793; (b) Cerveau, G., Chorro, C., Corriu, R., Lepeytre, C., Lère-Porte, J. P., Moreau, J., Thépot, P. and Wong Chi Man, M., *ACS Symp. Ser.*, 1995, **585,** 210.
18. Corriu, R. J. P., Moreau, J. J. E., Thépot, P. and Wong Chi Man, M., *J. Mater. Chem.*, 1994, **4,** 987.
19. (a) Cerveau, G., Corriu, R. and Lepeytre, *J. Organomet. Chem.*, in press.
20. Corriu, R., Hesemann, P. and Lanneau, G., *Chem. Commun.*, 1996, 1845.
21. Battioni, P., Cardin, E., Louloudi, M., Schöllhorn, B., Spyroulias, G. A., Mansuy, D. and Traylor, T. G., *Chem. Commun.*, 1996, 2037.
22. Cerveau, G., Corriu, R., Lepeytre, C., Aubagnac, J. L., Combarieu, R. and De Puydt, Y., *J. of Non-Crystalline Solids*, in press.
23. (a) Hotta, S. and Waragai, K., *Synth. Met.*, 1989, **32,** 395; (b) Hotta, S. and Waragai, K., in *The Physics and Chemistry of Organic Superconductors*, Springer Verlag, Berlin (1990) p. 391.
24. Brefort, J. L., Corriu, R. J. P., Gerbier, Ph., Guerin, C., Henner, B. J. L., Jean, A., Kulhman, T., Garnier, F. and Yassar, A., *Organometallics*, 1992, **11,** 2500.
25. (a) Bässler, H., Enkelmann, V. and Sixl, H., *Adv. Polym. Sci.*, 1984, 63; (b) Chance, R. R., Pattel, G. N., *J. Polym. Sci. Polym. Phys. Ed.*, 1978, **16,** 859; (c) Chance, R. R., Pattel, G. N., Turi, E. A. and Khanna, Y. P., *J. Am. Chem. Soc.*, 1978, **100,** 1307; (d) Patil, A. O., Desmpande, D. D., Talwar, S. S. and Biswas, A. B., *J. Polym. Sci. Polym. Chem. Ed.*, 1981, **19,** 1155; (e) Kato, J., Nakamura, K., Yamazakis, S. and Amano, T., *J. Polym. Sci. Part A Polym. Chem.*, 1989, **27,** 1853.
26. (a) Corriu, R. J. P., Guerin, C., Henner, B. J. L., Jean, A. and Mutin, P. H., *J. Organomet. Chem.*, 1990, **396,** C3; (b) Corriu, R. J. P., Gerbier, Ph., Guerin, C., Henner, B. J. L., Jean, A. and Mutin, P. H., *Organometallics*, 1992, **11,** 2507.
27. Corriu, R. J. P., Gerbier, Ph., Guerin, C., Henner, B. J. L. and Fourcade, R. J., *J. Organomet. Chem.*, 1993, **449,** 111.
28. Melreyer, A. J. and Baughmann, R. H., *J. Polymer Sci. Polymer Phys. Ed.*, 1989, **27,** 1853 and refs therein.
29. Loy, D. A., Buss, R. J., Assink, R. A., Shea, K. J. and Oviatt, H. W., *Polym. Prep. Am. Soc.*, 1993, **34,** 244.
30. Corriu, R., Moreau, J., Thépot, P. and Wong Chi Man, M., *Chem. Mater.*, 1996, **8,** 100.
31. Chevalier, P., Corriu, R., Moreau, J. and Wong Chi Man, M., *J. Sol–Gel Science and Technology*, 1997, **8,** 603.
32. Cerveau, G., Chevalier, P., Corriu, R., Lepeytre, C., Lère-Porte, J. P., Moreau, J., Thepot, P. and Wong Chi Man, M., in *Tailor-Made Silicon–Oxygen Compounds—From Molecules to Materials*, p. 273, R. Corriu and P. Jutzi Eds, Vieweg Pub., Braunschweig, Wiesbaden, 1996.

Pergamon

PII: S0277-5387(97)00243-X

Polyhedron Vol. 17, No. 5–6, pp. 935–942, 1998
© 1998 Elsevier Science Ltd
All rights reserved. Printed in Great Britain
0277-5387/98 $19.00+0.00

Bis-amido- complexes of heavier Group 15 metal chlorides with the sterically hindered, N-functionalised amido ligand, $[\{2\text{-}(6\text{-Me})C_5H_3N\}NSiMe_3]^-$†

Colin L. Raston,[a]* Brian W. Skelton,[b] Vicki-Anne Tolhurst[a] and Allan H. White[b]

[a] Department of Chemistry, Monash University, Clayton, Melbourne, Victoria, 3168, Australia

[b] Department of Chemistry, University of Western Australia, Nedlands, Western Australia, 6709, Australia

(Received 17 May 1997; accepted 7 June 1997)

Abstract—The reaction of the lithium amide, [2-(6-methyl)pyridyl]trimethylsilylamido-lithium, with antimony(III) or bismuth(III) trichloride in diethyl ether gives the bis-amido antimony(III) or bismuth(III) chloride $[\{2\text{-}(6\text{-Me})C_5H_3N\}NSiMe_3]MCl_2$ [M = Sb (**1**) or Bi (**2**)] as colourless or yellow prisms respectively. The antimony complex is monomeric in the solid state whereas the bismuth complex is dimeric with bridging chlorides. © 1998 Elsevier Science Ltd. All rights reserved

Keywords: antimony(III); bismuth(III); amido-complexes; N-functionalised; lithium; chloro.

Compounds containing heavier Group 15 elements (As, Sb, Bi) have attracted interest in recent times because of their importance as heterogeneous catalysts (in particular bismuth [1]) as well as precursors for superconducting materials in MOCVD processes [2,3]. Many trivalent phosphorus and arsenic amides have been well characterised. In comparison structurally characterised amide compounds of Sb^{III} and Bi^{III} are limited. This is a result of the inherent instability of such complexes [4].

The majority of arsenic, antimony and bismuth amides which have been structurally characterised have been in the 3+ oxidation state, and have largely been found with 'simple', or unfunctionalised amide ligands in trigonal pyramidal coordination geometries about the metal centre. In the related fields of Group 15 metal alkyl and thiol chemistry the use of bulky ligands with the donor functional groups capable of also interacting with the metal centres have been investigated. Examples include the bulky N-functionalised alkyl ligand-$C(SiMe_3)_2C_5H_4N$-2 [5] and the aryl ligand (dimethylamino)methyl benzene [6], as well as the thiol ligands pyridine-2-thiolate and 3-(trimethylsilyl)pyridine-2-thiolate [7]. These studies give hypercoordinated products where the coordination number has been expanded through intermolecular Lewis base-metal/metalloid interactions.

To date this approach of incorporating functional groups has not been explored for amide complexes of arsenic, antimony and bismuth. To this effect, we have undertaken studies involving the bulky amide ligand **A** derived from the amine group deprotonation of 6-methyl-2-trimethylsilylaminopyridine **HN′pyMe** (**HA**). We have previously used this ligand to stabilise low aggregate complexes of late transition metals by acting as a two electron-pair donor through the amido atom and the N-pyridyl functionalities [8,5]. Herein we report the synthesis and structural elucidation, by X-ray diffraction, of the bis-amido complexes of antimony and bismuth containing **A**. Our interest in preparing these compounds arose out of two important considerations; firstly to ascertain how such compounds would compare structurally with other structurally characterised pntictide amides given the

† Dedicated to Don Bradley on the occasion of his 73rd birthday.

* Author to whom correspondence should be addressed.

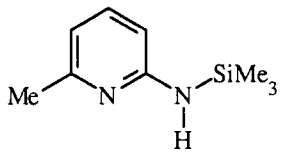

HN'pyMe (**HA**)

presence of a potentially ligating pyridyl nitrogen, and secondly to investigate the potential use of these compounds as starting reagents for mixed Group 13/15 single source precursors for MOCVD.

EXPERIMENTAL

Syntheses

All manipulations were carried out using standard Schlenk and glove box techniques under an atmosphere of high purity argon or nitrogen. Solvents were dried then freeze/thaw degassed prior to use. The aryl amide [HN'pyMe] **HA**, was prepared according to the literature procedure [9]. Bu^{n}Li was obtained from Metallgesellschaft (AG), Germany, as a 1.60 M solution in hexane and was standardised prior to use. All other reagents were obtained from Aldrich and the $SbCl_3$ and $BiCl_3$ were purified by sublimation before use. ^{1}H NMR spectra were recorded on a Bruker AC-200 spectrometer in deuterated benzene and referenced to the residual ^{1}H resonances of the solvent (δ 7.15). ^{13}C NMR spectra were recorded in deuterated benzene on a Bruker AC-200 spectrometer operating at 50 MHz using broad band proton decoupling and were referenced to the ^{13}C resonances of the deuterated solvent (δ 128.0). ^{15}N NMR spectra were recorded in deuterated benzene on a Bruker DRX500 spectrometer operating at 50.7 MHz using broad band proton decoupling and were referenced to the external ^{15}N resonance of nitromethane (δ 0). Elemental analyses were performed by the Chemical and Micro-Analytical Services Pty. Ltd, Melbourne. Melting points were determined in sealed glass capillaries under argon and are uncorrected.

Synthesis of chloro-bis[6-*methyl*-2-*pyridyltrimethylsilylamido*-N,N']-*antimony(III)*, **1**. A solution of $(LiN'pyMe)_2$ (0.76 g, 2.04 mmol) in diethyl ether was slowly added to a stirred solution of $SbCl_3$ (0.44 g, 1.93 mmol) in diethyl ether (20 cm^3) at -80°C. A white precipitate was gradually formed upon addition. The mixture was stirred and allowed to warm to room temperature overnight. The suspension was filtered and volatiles were removed from the filtrate *in vacuo*. Colourless crystals of the **1** were grown from hexane at room temperature (0.43 g, 43%).

M.p. 93–95°C; ^{1}H NMR (200 MHz, C_6D_6) δ 0.41, 0.45 (2 × 9H, s, SiCH_3), 1.75, 1.80 (2 × 3H, s, CH_3), 6.17–5.95 (2 × 2H, m, C_5H_3N) 6.96–6.78 (2 × 1H, m, C_5H_3N); ^{13}C NMR (50 MHz, C_6D_6) δ 2.22, 3.49 (SiCH$_3$), 20.3, 21.6 (CH$_3$), 109.8, 109.9, 112.1, 113.4, 139.2, 140.8, 152.8, 154.1, 161.4 (C_5H_3N); ^{15}N NMR (50.7 MHz, C_6D_6) $\delta -119$ (C_5H_3N); anal: found C 41.58, H 5.87, N 10.65, calc. for $C_{18}H_{30}N_4Si_2SbCl$ C 41.91, H 5.86, N 10.86.

Synthesis of chloro-bis[6-*methyl*-2-*pyridyltrimethylsilylamido*-N,N']-*bismuth(III)*, **2**. A solution of LiN'PyMe in diethyl ether was prepared from HN'PyMe (0.70 g, 3.9 mmol) and Bu^{n}Li (2.4 ml of a 1.6 M hexane solution) at 0°C. After stirring for 2 h, the yellow solution was gradually added to a solution of $BiCl_3$ (0.53 g, 1.6 mmol) in diethyl ether (20 cm^3). A white precipitate was gradually formed upon addition. The resulting yellow mixture was stirred and allowed to warm to room temperature overnight with stirring for 16 h. The solution was filtered and volatiles removed *in vacuo*. Yellow prisms of **2** were grown from toluene at -30°C (0.61 g, 60%).

M.p. 185–187°C; ^{1}H NMR (200 MHz, C_6D_6) δ 036, 0.49 (2 × 9H, s, SiCH_3), 1.75, 2.36 (2 × 3H, s, CH_3), 6.35–6.91 (2 × 2H, m, C_5H_3N), 7.03–7.22 (2 × 1H, m, C_5H_3N); ^{13}C NMR (50 MHz, C_6D_6) δ 0.19, 2.46 (SiCH$_3$) 22.51, 24.52 (CH$_3$), 106.69, 110.95, 112.19, 113.69, 130.76, 137.51, 138.95, 152.49, 156.94, 163.69 (C_5H_3N); ^{15}N NMR (50.7 MHz, C_6D_6) δ -126 (C_5H_3N); anal: found C 35.19, H 4.81, N 9.67%, calc. for $C_{18}H_{30}N_4Si_2BiCl$ C 34.65, H 5.01, N 9.29%.

Crystal structure determinations

Crystals of **1** suitable for X-ray structure determination were grown from hexane solutions at ambient temperature and were mounted in sealed capillaries under an argon atmosphere. Crystals of compounds **2** suitable for X-ray structure determination were grown from toluene solutions at -30°C and were mounted in sealed capillaries under an argon atmosphere. Unique room temperature four circle diffractometer data sets were measured using an Enraf–Nonius CAD4 diffractometer ($2\theta/\theta$ scan mode; monochromatic Mo-K_α radiation, $\lambda = 0.7107$ Å; $T \sim 295$ K) yielding 7576 independent reflections, 4552 with $I \geqslant 3.0\sigma(I)$ being considered 'observed' for **1** and 5510 independent reflections, 3830 being considered 'observed' for **2** and used in the full matrix least squares refinements after absorption correction. Anisotropic thermal parameters found were refined for the non-hydrogen atoms (x, y, z, U_{iso}) being included constrained at estimated values. Convention residuals R, R_w [statistical weights, derivative of $\sigma^2(I) = \sigma^2(I_{diff}) + 0.0004\sigma^4(I_{diff})$] are quoted at convergence. Neutral atom complex scattering factors were employed, computation using the XTAL 3.4 program system implemented by S. R. Hall [10]. A summary of crystal and solution and refinement data is given in Table 1. Non-hydrogen and important hydrogen atom coordinates are given in supplementary material. Molecular projections showing numbering schemes are given in Figs 1 and 2. Important molec-

Table 1. Crystallographic data

	$C_{18}H_{30}N_4Si_2SbCl$ (1)	$C_{18}H_{30}N_4Si_3BiCl$ (2)
Formula	$C_{18}H_{30}N_4Si_2SbCl$	$C_{18}H_{30}N_4Si_2BiCl$
M	515.85	603.07
System	triclinic	triclinic
Space group	$P\bar{1}$ (no. 2)	$P\bar{1}$ (no. 2)
T (K)	298	298
a (Å)	17.355(7)	11.155(5)
b (Å)	14.481(5)	11.02(1)
c (Å)	10.317(4)	10.457(5)
α (°)	110.05(3)	94.71(6)
β (°)	91.99(3)	96.00(3)
γ (°)	95.53(3)	109.20(6)
V (Å^3)	2418	1198
Z	4	2
ρ_{calcd} (g cm^{-3})	1.41	1.671
$F(000)$	1048	588
μ_{Mo} (cm^{-1})	13.5	76
Crystal size	$0.47 \times 0.25 \times 0.18$ mm	$0.25 \times 0.40 \times 0.12$ mm
$A^*_{min,max}$	1.24, 1.49 (gaussian)	3.1, 6.2 (analytical)
$2\theta_{max}$ (°)	48	55
N, N_0	7576, 4552	5510, 3830
R^a	0.061	0.059
R_w^b	0.067	0.060

[a] $R = \Sigma||F_o| - |F_c||/\Sigma|F_o|$.
[b] $R_w = (\Sigma||F_o| - |F_c||^2/\Sigma w|F_o|^2)^{1/2}$.

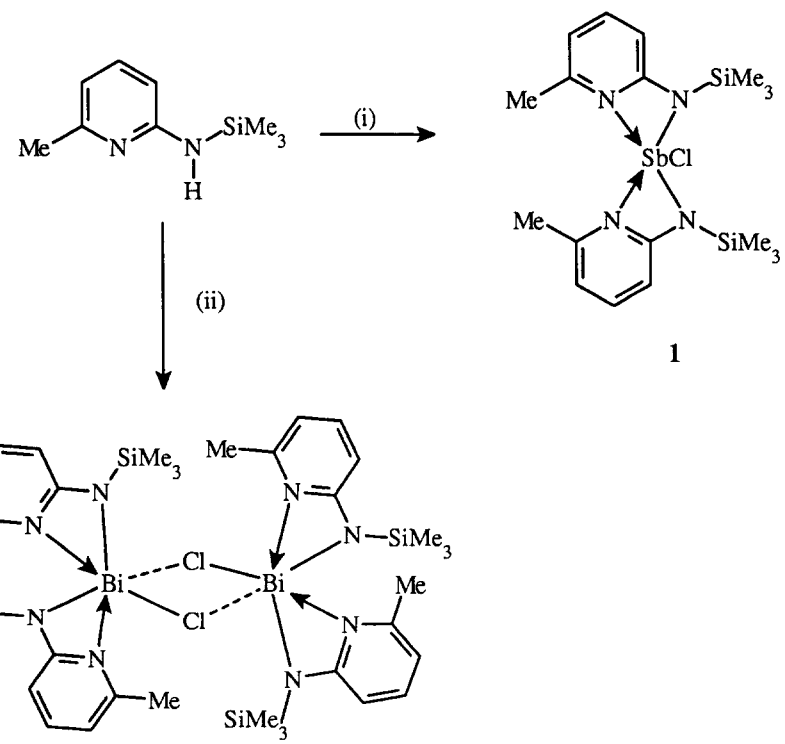

2

Scheme 1. (i) 1. Bu^{n}Li, 0°C, Et_2O; 2. 0.5 $SbCl_3$, −80°C (ii) 1. Bu^{n}Li, 0°C, Et_2O; 2. 0.5 $BiCl_3$, −80°C

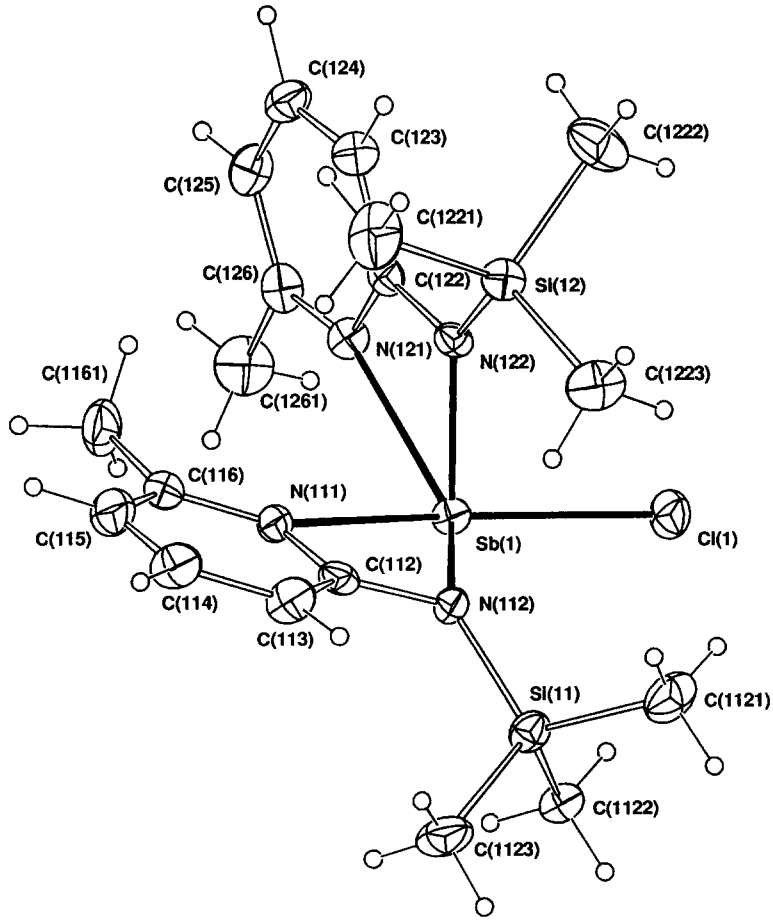

Fig. 1. Molecular projection of $[\{2\text{-}(6\text{-Me})C_5H_3N\}NSiMe_3]_2SbCl$ **1** showing atom labelling scheme. Thermal ellipsoids are drawn at the 20% probability level.

ular geometries are given in Table 2. Thermal ellipsoids are drawn at the 20% probability level. Anisotropic thermal parameters were refined for all non-hydrogen atoms in each structure.

RESULTS AND DISCUSSION

The monomeric diamido antimony chloride and the dimeric diamido bismuth chloride complexes **1** and **2** were prepared *via* the metathesis between the metal trichlorides and the lithiated complex of **A** in the appropriate stoichiometric amounts (Scheme 1). Compounds **1** and **2** were isolated as colourless and yellow crystals, respectively. Both are thermally stable, air and moisture sensitive, and have been characterised using ^1H, ^{13}C and ^{15}N NMR spectroscopy, microanalysis, and X-ray single crystal diffraction studies.

While complexes **1** and **2** are isolated from the stoichiometric reactions with the lithiated complex of **A**, surprisingly compound **1** is also formed for a 1:1 ratio of amide to $SbCl_3$. In addition complex **2** forms from the reaction with a ratio of amide to $BiCl_3$ of 3:1. This can be attributed to the redistribution of the ligands while in solution and the preferential crystallisation of the monochloride complexes as the least soluble species. Redistribution reactions have been noted for both antimony and bismuth aryl and alkyl complexes [11,12].

The thermal stability of these compounds is in contrast to complexes formed using the conjugate base of the analogous alkyl ligand, 2-[bis(trimethylsilyl) methyl]pyridine (R). In this case, the treatment of $AsCl_3$ and $SbCl_3$ with 2 equiv. of the lithium derivative of this ligand yielded intractable oils accompanied by the rapid loss of $ClSiMe_3$ while for the analogous reaction with $BiCl_3$, a red crystalline solid was obtained only below 0°C. Above 0°C this solid decomposes to give orange crystals which by X-ray structure determination has been shown to be the substituted allylic complex, (E)-$[BiR(CH_2CH{=}C)$-$(SiMe_3)(C_5H_4N\text{-}2)]\{R = [C(SiMe_3)_2C_5H_4N\text{-}2]^-\}$ [5]. This stability difference can possibly be explained by a combination of two characteristics; firstly, the addition of a methyl group on the six position of the pyridyl ring increases the steric bulk of the ligand enough to help stabilise the compound, secondly, considering the M—N bond is stronger than the M—C bond, the

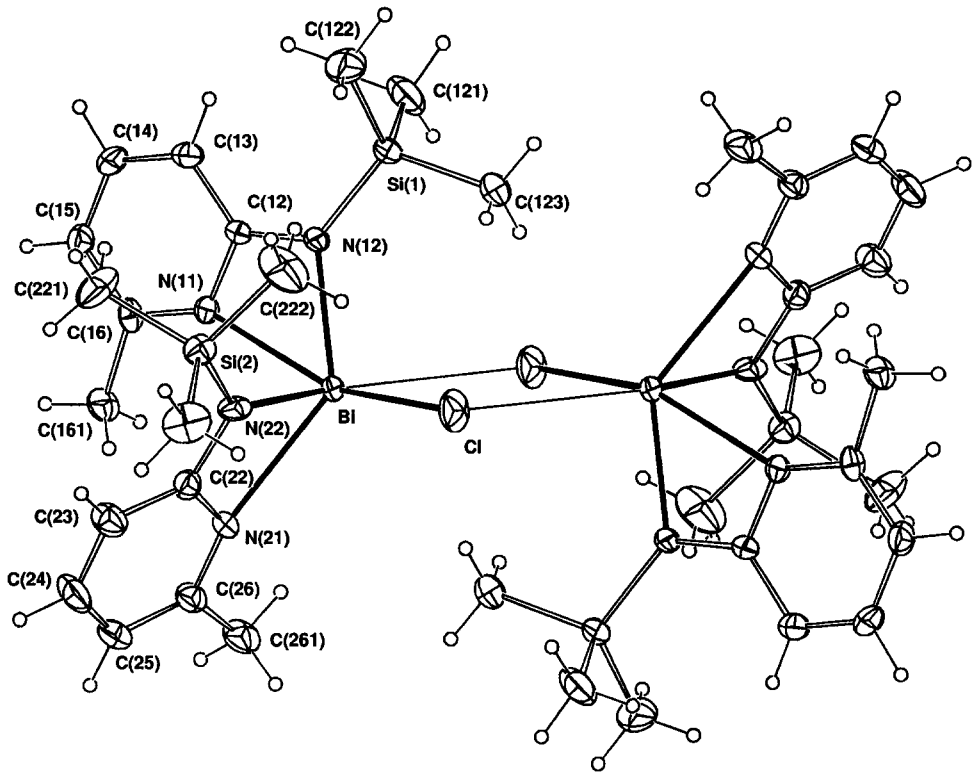

g. 2. Molecular projection of [{2-(6-Me)C_5H_3N}$NSiMe_3$]$_2$BiCl **2** showing atom labelling scheme. Thermal ellipsoids are drawn at the 20% probability level.

Table 2. Molecular core geometries, $ClM(C_9H_{15}N_2Si)_2$, **1** and **2**

Compound (mol)	Sb(1, 2), **1**	Bi, **2**
Distances (Å)		
M—Cl	2.492(4), 2.502(4)	2.629(4)
M—N(11)	2.401(8), 2.397(8)	2.49(1)
M—N(21)	2.607(9), 2.63(1)	2.60(1)
M—N(12)	2.127(8), 2.108(9)	2.271(8)
M—N(22)	2.095(7), 2.074(3)	2.15(1)
N(12)—Si(1)	1.735(9), 1.76(1)	1.75(1)
N(22)—Si(2)	1.757(8), 1.771(8)	1.75(1)
M···Cl′		3.554(6)
M···M′		4.838(3)
Angles (°)		
Cl—M—N(11)	146.1(2), 144.3(2)	153.5(3)
Cl—M—N(12)	90.2(2), 90.0(2)	99.8(3)
Cl—M—N(21)	116.7(2), 114.4(2)	109.6(3)
Cl—M—N(22)	88.9(2), 88.5(2)	88.0(3)
N(11)—M—N(12)	59.5(3), 59.1(3)	57.4(3)
N(11)—M—N(22)	81.7(7), 80.8(3)	80.2(4)
N(12)—M—N(21)	140.7(7), 143.6(3)	135.0(4)
N(12)—M—N(22)	98.6(3), 100.4(3)	92.2(4)
N(21)—M—N(22)	56.4(3), 56.3(3)	56.8(4)
Ligand plane parameters (C_5N) (Ligands 1, 2)		
X^2 (1,2)	1.0, 1.0; 1.9, 3.6	0.6, 0.9
δM	0.29(2), 0.16(2); 0.29(2), 0.06(2)	0.12(2), 0.35(2)
δCl	1.11(2), −1.91(2); 1.27(3), −2.10(3)	0.87(4), −1.94(3)

replacement of the alkyl group with an amido moiety may increase the stability of the R_2MCl compound. Increasing the stability of compounds by the addition of a methyl moiety to the 6 position pyridyl ring has been highlighted in a comparison of Group 11 compounds where the compounds, $[\{2\text{-Me-}C_5H_3N\text{-}6\text{-}C(SiMe_3)_2\}M]_2$ (M=Cu, Ag, Au), are substantially more stable than the unsubstituted analogues $[\{C(SiMe_3)_2C_5H_4N\text{-}2\}M]_2$ (M=Cu, Ag, Au) [13].

The ^1H and ^{13}C NMR spectra of the diamido antimony chloride and diamido bismuth chloride complexes exhibit two sets of resonances due to the amido ligands being inequivalent. This is supported by the solid state structures from X-ray determination. No significant differences are seen between the coordinated ligand in both compounds and the free ligand; the J_{H-H} values of the pyridyl *m*-protons for the antimony and bismuth compounds are 7.21 and 8.48 Hz, respectively (*cf.* 7.31 for the free ligand). The ^{15}N NMR spectra show a significant upfield shift from the N(pyridyl) from the free ligand (δ −105) through the bis-amido antimony compound (δ −119) to the bismuth diamide (δ −126). This corresponds to the interaction between the metal and the N(pyridyl) becoming stronger as the metal becomes more electropositive. No N(amido) resonance was observed due to relaxation time and concentration problems. A downfield shift in ^{13}C NMR spectra for carbons associated with amido moieties bound to Group 15 elements has been noted before and is attributed to the increasing size of the central atom [14,15].

X-ray structure commentary

Structure of **1**. The compound chloro-bis[6-methyl-2-pyridyltrimethylsilylamido-*N*,*N'*]-antimony (**1**) crystallises as colourless prismatic crystals in the triclinic space group $P\bar{1}$ (no. 2) with four molecules in the unit cell. Two pseudosymmetrically related molecules make up the asymmetric unit of the structure. Both of these are identical within experimental error and can be best described as bis-amido antimony monochloride (Fig. 1).

Primary coordination places the antimony in a three coordinate trigonal pyramidal environment where the stereochemically active lone pair of the antimony occupies the vertex of the pyramid which is common for antimony(III) compounds. Internal coordination from the pyridyl nitrogen centres gives the antimony an overall five coordinate, distorted trigonal bipyramidal environment. To our knowledge, this compound is the first monochloride antimony(III) which has internal coordination from a Lewis basic pyridyl nitrogen. The ligands chelate the antimony centre, forming four membered rings and are bound *cis* with one of the amido ligands bound in the equatorial positions and the other having the amide nitrogen occupying the third equatorial position and the pyridyl nitrogen coordinated at the axial position. The chloride moiety occupies the remaining axial position. It is the steric constraint caused by the bite angle of the ligand and the influence of the antimony lone pair of electrons which prevents the coordination environment from being ideal trigonal bipyramidal. The trimethylsilyl group of the equatorial bound amide ligand is such that it is situated above the pyridyl ring of the other ligand while its associated trimethylsilyl group is directly opposite the pyridyl ring on the N—N—N plane. This results in the two ligands being inequivalent.

Important bond distances and angles for **1** and **2** are given in Table 2. Discussions on the diamido antimony complex will use the molecular geometries of the Sb(1) structure. The Sb—N (amide) bond distances are 2.095(8) and 2.127(8) Å for the equatorial/equatorial bound ligand and equatorial/axial bound ligand, respectively. These are comparable to the Sb—N bond distances of the four membered cyclic diamido compound $Me_2Si(N^tBu)_2SbCl$ which are 1.995(6) Å [16]. The lengthening of the Sb—N bond in the pyridyl amide in compound **1** is in accordance with the higher coordination number of the antimony centre in this compound compared to the diamido compound.

The Sb—N(pyridyl) bond distances of 2.401(8) and 2.607(9) Å for the axial and equatorial nitrogen centres are substantially longer than those of the amido nitrogen centres. The significant difference in the two bond lengths can be attributed to the lone pair of the antimony pushing the equatorial bound pyridyl ring away from the antimony through lone pair/bonding pair repulsions. However, the distances are in the range for the Sb—N(pyridyl) bond distances for the four coordinate antimony compound $[C(SiMe_3)_2C_5H_4N\text{-}2]SbCl_2$ and the six coordinate antimony compound $[Sb(2\text{-}SC_5H_4N)_3]$. These bond distances have the range of 2.371–2.837 Å, respectively [5,7].

The Sb—Cl bond distance of 2.492(4) Å is comparable to the Sb–Cl bond distance of 2.472(3)° for the cyclic antimony diamido species, $Me_2Si(N^tBu)_2SbCl$ [15], and in contrast exhibits no weak Sb···Cl interactions between each molecule. The N—Si bond distances of 1.735(9) and 1.757(8) Å are not significantly different to that of a typical silylamide (*ca* 1.73 Å [4]). However they are significantly longer than those found in the lithium amide LiA [1.705(5) Å] [9]. This is consistent with the largely covalent nature of the Sb—N bond placing minimal additional electronic charge density on the nitrogen centre.

The N(amide)—Sb—Cl bond angles of 88.9(2) and 90.2(2)° are as expected for a trigonal bipyramidal coordination geometry where the chloride occupies an axial position and the amides occupy equatorial positions. In comparison, the N(pyridyl)—Sb—Cl bond angle of the equatorial/equatorial ligand is much larger, being 116.7(2)°, for two reasons. Firstly, the acute ligand bite angles of 56.4(3) and 59.5(3)°, themselves prohibit an approach to a near ideal bipyramidal geometry. The difference in the bite angles of

the two ligands is in accordance with the lengthening of the N—Sb bond distance of the equatorial/equatorial ligand compared to the equatorial/axial ligand caused by the interaction of the lone pair of electrons on the antimony of the former ligand. Secondly, the stereochemically active lone pair of electrons of the antimony centre contributes to the distortion. These two factors can also be seen in the Cl—Sb—N(pyridyl) bond angle of the equatorial/axial ligand. At 146.1(2)°, it is significantly more acute when compared with the 180° for an ideal trigonal bipyramidal coordination geometry. All other bond distances and angles for the diamido antimony (**1**) are unexceptional.

Structure of **2**. The compound chloro-bis[6-methyl-2-pyridyltrimethylsilylamido-*N*,*N*′]-bismuth (**2**) crystallises as yellow prismatic crystals in the triclinic space group $P\bar{1}$ (no. 2) with two molecules in the unit cell, the asymmetric unit comprising of a discrete, dimeric molecule with crystallographic C_i symmetry and a four membered planar Bi_2Cl_2 ring core (Fig. 2). This compound is best described as a chloro-bridged bis-amido bismuthine.

As with the diamido antimony chloride complex **1**, the amido ligands chelate the bismuth centre, forming four membered chelate rings. The diamido bismuth chloride, complex **2**, also exhibits both primary coordination from the amido nitrogens of the ligand and dative bonding with the pyridyl nitrogens. Overall, the bismuth centre is six coordinate and has a distorted octahedral environment. This deviation from an ideal octahedron is most probably due to both the stereochemically active lone pair on the bismuth atom and the small bite angle of the ligand. The arrangement of the ligands around the bismuth atom is similar to that of the antimony compound in that one amido ligand has both the N(amide) and N(pyridyl) occupying two equatorial positions while the other amido ligand has the N(amide) coordinated at an equatorial position and the N(pyridyl) coordinated at the axial position. The chloro-moiety again occupies the axial position of the first bismuth atom but bridges to the second bismuth through the equatorial position. This difference in structure from the bismuth diamide compared to the antimony diamide can be attributed to the difference in atomic size of the bismuth compared to antimony. As such, higher coordination numbers and higher association of bismuth compounds are well documented [17–20].

Important bond angles and distances are given in Table 2. The Bi—N(amide) bond distances are 2.15(1) and 2.271(8) Å for the equatorial/equatorial bound ligand and equatorial/axial bound ligand, respectively. These distances are comparable to the Bi—N bond distances of the four membered cyclic diamido compound $Me_2Bi(N^tBu)_2BiCl$ and the triamido bismuthine compound $Bi(NPh)_3$ which are 2.124(9) [16] and 2.17(2)–2.26(3) Å [21], respectively.

As expected, the Bi—N(pyridyl) bond distances of 2.49(1) and 2.60(1) Å for the axial and equatorial nitrogen centres are again substantially longer than the Bi—N(amide) bond distances. These bond distances are comparable with the four coordinate bismuth compound $[C(SiMe_3)_2C_5H_4N\text{-}2]BiCl_2$ whose Bi—N(pyridyl) bond length is 2.485(9)° [5] and are relatively short when compared with the six coordinate trithiol bismuth compound $[Bi(2\text{-}SC_5H_3N\text{-}3\text{-}SiMe_3)_3]$ whose Bi—N(pyridyl) bond lengths are 2.69(2)–2.83(2)° [7]. In a similar manner to a pattern identified by Cowley *et al.* [6], when comparing similar arsenic, antimony and bismuth triaryl compounds that exhibit internal coordination, the average difference in the Bi—N bond lengths of **2** is 0.33 Å which is considerably smaller than the average difference in the Sb—N bond lengths in **1** which is 0.408 Å. This reflects the stronger interaction of the more Lewis acidic bismuth centre with the nitrogen atom compared to the interaction within the antimony complex **1**.

The Bi—Cl bond distance 2.629(4) Å is comparable to the Bi—Cl bond distance of 2.748(4) Å for the chloro bismuth compound $Me_2Bi(N^tBu)_2BiCl$ [16]. The bismuth diamide also exhibits a weak Bi···Cl interaction of 3.554(6) Å to the next molecule to forming a weak dimeric compound. Again, this is comparable to $Me_2Bi(N^tBu)_2BiCl$ which has a weak Bi···Cl interaction distance of 3.047(4) Å where the molecules form an infinite chain [16]. The N—Si bond distance of 1.75(1) Å is not significantly different to that of a typical N—Si bond distance (1.73 Å) which shows that there is a large covalent nature associated with the Bi—N bond similar to the Sb—N in the previously described compound.

The N(amide)—Bi—Cl bond angles of 88.0(3) and 99.8(3)° are as expected for a distorted octahedral coordination geometry where the chloride and N(amide) are *cis* relative to each other. The equatorial bound N(pyridyl)—Bi—Cl bond angle is much larger at 109.6° while the axial bound pyridyl ring has an N(pyridyl)—Bi—Cl bond angle of 153.5(3)°, which is again much smaller than the expected 180°. Again, these distortions from ideal octahedral geometry can be explained by the effect of the stereochemically active lone pair of the bismuth and the acute bite angles of the ligands [57.4(3)° and 56.8(3)°]. All other bond distances and bond angles for the bismuth diamide compound **2** are unexceptional.

CONCLUSION

We have been able to prepare and structurally characterise products obtained from the reaction of amide HN′pyMe with Bu″Li and the metal trichloride (M = Sb, Bi) in the ratio of 2 : 1. The product obtained from the antimony trichloride reaction has been isolated as monomeric $(MepyN')_2SbCl$ while the product obtained from the bismuth trichloride reaction has been obtained as the weakly dimeric compound $[(MepyN')_2BiCl]_2$. The difference in association

between the two compounds can be attributed to the larger atomic size of bismuth compared to antimony, which allows the bismuth centre to coordinate to the chloride atom of the next molecule. The increase in atomic size from arsenic to bismuth may also explain the difficulty in isolating the analogous arsenic diamide. Both compounds exhibit covalent character unlike the largely ionic nature of the corresponding lithium amide. We are currently pursuing the chemistry of these compounds as well as the synthesis of the mono-amido- and tris-mido-compounds of the heavier Group 15 elements.

Acknowledgment—We gratefully acknowledge support of this work by the Australian Research Council and Monash University.

Supplementary data available—Lists of atomic coordinates, U_{ij} values, bond distances and angles, and summaries of the X-ray diffraction data (x pages) for compounds **1** and **2**. Ordering information is given on any current masterhead page.

REFERENCES

1. Grasselli, R. K. and Burrington, J. D., *Adv. Catal.*, 1981, **30,** 133.
2. Cowley, A. H. and Jones, R. A., *Angew. Chem. Int. Ed. Engl.*, 1989, **28,** 1208.
3. Higa, K. T. and George, C., *Organometallics*, 1990, **9,** 275.
4. Lappert, M. F., Power, P. P., Sanger, A. R. and Srivastava, R. C., *Metal and Metalloid Amides*, Ellis Horwood Limited, Chichester, (1980).
5. Jones, C., Engelhardt, L. M., Junk, P. C., Hutchings, D. S., Patalinghug, W. C., Raston, C. L. and White, A. H., *J. Chem. Soc., Chem. Commun.*, 1991, 1560.
6. Kamepalli, S., Carmalt, C. J., Culp, R. D., Cowley, A. H. and Jones, R. A., *Inorg. Chem.*, 1996, **35,** 6179.
7. Block, E., Ofori-Okai, G., Kang, H., Wu, J. and Zubieta, J., *Inorg. Chem.*, 1991, **30,** 4784.
8. Engelhardt, L. M., Jacobson, G. E., Patalinghug, W. C., Skelton, B. W., Raston, C. L. and White, A. H., *J. Chem. Soc., Dalton Trans.*, 1991, 2859.
9. Engelhardt, L. M., Jacobson, G. E., Junk, P. C., Raston, C. L., Skelton, B. W. and White, A. H., *J. Chem. Soc., Dalton Trans.*, 1988, 1011.
10. Hall, S. R., Flack, H. D. and Stewart, J. M., *The XTAL* 3.4 *Reference Manual*, Universities of Western Australia, Geneva and Maryland.
11. Li, X.-W., Lorberth, J., Massa, W. and Wocadlo, S., *J. Organomet. Chem.*, 1995, **485,** 141.
12. Hendershot, D. G., Pazik, J. C. and Berry, A. D., *Chem. Mater.*, 1992, **4,** 833.
13. van den Anker, T. R. and Raston, C. L., *J. Organomet. Chem.*, 1995, **500,** 289.
14. Ando, F., Hayashi, T., Ohashi, K. and Koketsu, J., *J. Inorg. Nucl. Chem.*, 1975, **37,** 2011.
15. Moedritzer, K., *Inorg. Chem.*, 1964, **3,** 604.
16. Veith, M. and Bertsch, B., *Z. Anorg. Allg. Chem.*, 1988, **557,** 7.
17. Lorberth, J., Massa, W., Wocadlo, S., Sarraje, I., Shin, S.-H. and Li, X.-W., *J. Organomet. Chem.*, 1995, **485,** 149.
18. Clegg, W., Errington, R. J., Fisher, G. A., Hockless, D. C. R., Norman, N. C., Orpen, A. G. and Statford, S. E., *J. Chem. Soc., Dalton Trans.*, 1992, 1967.
19. Clegg, W., Farrugia, L. J., McCamley, A., Norman, N. C., Orpen, A. G., Pickett, N. L. and Statford, S. E., *J. Chem. Soc., Dalton Trans.*, 1993, 2579.
20. Schier, A., Wallis, J. M., Müller, G. and Schmidbaur, H., *Angew. Chem. Int. Ed. Engl.*, 1986, **25,** 757.
21. Clegg, W., Compton, N. A., Errington, R. J., Norman, N. C. and Wishart, N., *Polyhedron*, 1989, **8,** 1579.

Pergamon

PII: S0277-5387(97)00241-6

Polyhedron Vol. 17, No. 5–6, pp. 943–946, 1998
© 1998 Elsevier Science Ltd
All rights reserved. Printed in Great Britain
0277–5387/98 $19.00 + 0.00

Synthesis and structural characterization of titanium complexes containing a sulfinyl-bridged *bis*(phenolato) ligand†

Jun Okuda,* Stefan Fokken, Hak-Chul Kang and Werner Massa

Institut für Anorganische Chemie und Analytische Chemie der Johannes Gutenberg-Universität Mainz, J.-J.-Becher-Weg 24, D-55099 Mainz, Germany

(Received 2 May 1997; accepted 7 June 1997)

Abstract—Titanium complexes containing the novel tridentate 2,2′-sulfinylbis(6-*tert*-butyl-4-methylphenoxo) ligand (sibmp) were synthesized and characterized. Treatment of titanium tetra-*iso*-propoxide with 2,2′-sulfinylbis(6-*tert*-butyl-4-methylphenol) (sibmpH_2) in 1 : 1 molar ratio afforded red–orange, sparingly soluble di-*iso*-propoxo derivative [Ti(sibmp)(O-*i*-Pr)$_2$]$_2$·0.5 Et_2O. The single-crystal structure analysis was performed and revealed a dimeric centrosymmetric structure with a planar Ti_2O_2 core. The titanium center is approximately octahedral with a S=O function intramolecularly coordinated at the titanium center. Treatment of sibmpH_2 with titanium tetra-*iso*-propoxide in 2 : 1 molar ratio gave yellow Ti(sibmp)$_2$ with a C_2-symmetric spirocyclic structure. The dark red dichloro complex [Ti(sibmp)Cl_2] was prepared by reacting titanium tetrachloride with sibmpH_2. © 1998 Elsevier Science Ltd. All rights reserved

Keywords: bis(phenolato) ligand; tridentate ligand; titanium alkoxide; L-alkene polymerization catalyst.

Homogeneous 1-alkene polymerization catalysts based on titanium complexes with bulky bidentate bis(phenolato) ligands [1] are currently of some interest as alternatives for the widely used metallocene catalysts. We are studying the coordination chemistry of various sterically demanding dianionic ligands related to the 2,2′-methylenebis(6-*tert*-butyl-4-methylphenolato) ligand (mbmp) [2], which have been modified to contain a bridge different from the methylene link [3a,b,9]. In particular, it was noted that the sulfide bridge imparts significant increase in the polymerization activity of the titanium complexes containing the 2,2′-thiobis (6-*tert*-butyl-4-methylphenolato) (tbmp) when activated with methyl aluminoxane [1]. We describe here the synthesis and characterization of complexes incorporating the tridentate 2,2′-sulfinylbis(6-*tert*-butyl-4-methylphenolato) ligand along with the structure determination of a dimeric titanium complex that reveal an intramolecularly coordinated O-sulfinyl function [4].

RESULTS AND DISCUSSION

When a solution of freshly distilled Ti(O-*i*-Pr)$_4$ in diethyl ether was layered at room temperature with a solution of 2,2′-sulfinylbis(6-*tert*-butyl-4-methylphenol) (sibmpH_2) [5] in diethyl ether, a nearly quantitative yield of Ti(sibmp) (O-*i*-Pr)$_2$ was obtained over a period of 24 h as well-formed orange-red crystals which retain approximately 0.25 equiv. of diethyl ether molecule per titanium in the lattice. The ether molecules could be completely removed in vacuum to give analytically pure Ti(sibmp) (O-*i*-Pr)$_2$ as red powder. In contrast to soluble Ti(mbmp) (O-*i*-Pr)$_2$ [2c], but very similar to Ti(tbmp) (O-*i*-Pr)$_2$ [3], Ti(sibmp) (O-*i*-Pr)$_2$ turned out to be only sparingly soluble in most of the common non-polar and polar organic solvents. Only in hot (170) dimethyl sulfoxide was it possible to attain sufficient solubility to record a ^{1}H NMR spectrum that is compatible with the formulation Ti(sibmp) (O-*i*-Pr)$_2$. Crystals of the diethyl ether solvate were, however, suitable for single-crystal X-ray diffraction (Fig. 1). The compound crystallized in the centrosymmetric space group *P*1 with two monomeric units per unit cell. The dimeric structure is bridged by two *iso*-propoxo ligands which together

* Author to whom correspondence should be addressed.

† Dedicated to D. C. Bradley on the occasion of his 73rd birthday.

with the two titanium centers form a planar Ti_2O_2 core, typical for many doubly oxygen-bridged dititanium complexes [6]. Each titanium center is octahedrally coordinated by two bridging *iso*-propoxo groups and one terminal *iso*-propoxo group facing the sibmp ligand. Most notably, the sulfinyl bridge *trans* to the terminal *iso*-propoxo group is intramolecularly coordinated at the titanium center *via* the oxygen atom. The titanium–oxygen bond length of 2.149(3) Å appears to be slightly longer than that for other neutral oxygen donors coordinated at a tetravalent titanium center. For example, the titanium–oxygen bond distance in the titanium adduct of an organic carbonyl derivative such as ethyl acetate is 2.029(3) Å ($[TiCl_4(H_3CCOOC_2H_5)]_2$) [7] and phosphoryl derivatives such as $POCl_3$ in $[TiCl_4(POCl_3)]_2$ show a corresponding value of 2.10(2) Å [8]. The somewhat unexpected dimeric structure may be ascribed to the higher Lewis-acidity of the titanium center, since the S=O bridge can be assumed to increase the Brönsted acidity of the OH function substantially, thus decreasing the basicity of the phenolate anion and leading to a more Lewis-acidic metal center. In agreement with this explanation, the π-donor property of the phenoxo ligands is not pronounced, as evidenced by the averaged Ti—O bond lengths of 1.897(3) and 1.933(3) Å, typical for a Ti—O single bond, and concomitantly, the angles at the oxygen of 139.2(3) and 140.6(2)° are significantly less obtuse. In comparison, $Ti(mbmp)Cl_2$ contains corresponding bond distances of 1.742(3) and 1.759(3) Å and bond angles of 143.5(3) and 155.8(3)° [2a,c], reflecting a strong $p\pi$–$d\pi$ interaction.

An example of mononuclear titanium complex containing the sibmp ligand was obtained by slowly adding neat $Ti(O\text{-}i\text{-}Pr)_4$ to a solution of two equivalents of $sibmpH_2$ in diethyl ether to give the spirocyclic complex $Ti(sibmp)_2$ which was isolated as yellow crystals soluble in diethyl ether. $Ti(sibmp)_2$ shows NMR spectroscopic features that are similar to those of the complex $Ti(mbmp)_2$ previously described by us [2c]. Thus the molecule of $Ti(sibmp)_2$ does not possess any mirror plane, resulting in sibmp ligands of which the two phenoxo groups are inequivalent. For the probable octahedral geometry with intramolecular S=O—coordination, $Ti(sibmp)_2$ is expected to adopt a C_2-symmetrical structure as depicted in Scheme 1. Treatment of $sibmpH_2$ with titanium tetrachloride in 1 : 1 molar ratio in dichloromethane at room temperature afforded $Ti(sibmp)Cl_2$ as dark red micro-crystals. Because of the Lewis acidity comparable to that of $Ti(mbmp)Cl_2$ [2c], labile Lewis base adducts are formed with both diethyl ether and THF.

In conclusion, a new tridentate ligand sibmp has been introduced that promises to become a useful ancillary ligand for Lewis-acidic metal centers, in particular for homogeneous polymerization catalysts [9].

EXPERIMENTAL

General considerations

All operations were performed under an inert atmosphere of argon using standard Schlenk-line or glovebox techniques. THF and diethyl ether were distilled from sodium benzophenone ketyl. Pentane and hexane were purified by distillation from sodium/triglyme benzophenone ketyl. 2,2′-Thiobis(6-*tert*-butyl-4-methylphenol) was prepared according to a procedure described in ref. [10]. All other chemicals were commercially available and used as received unless otherwise stated. ^1H NMR and ^{13}C NMR spectra were recorded on a Bruker AMX 200 or AM 400 spectrometer. Mass spectra were obtained on a Varian CH7 spectrometer. Elemental analyses were performed by the Microanalytical Laboratory of this department.

2,2′-*Sulfinylbis*(6-tert-*butyl*-4-*methylphenol*). 2,2′-Sulfinylbis(6-*tert*-butyl-4-methylphenol) was prepared by oxidation of 2,2′-thiobis(6-*tert*-butyl-4-methylphenol) with hydrogen peroxide and isolated as colorless crystals in 91% yield; ^1H NMR ($CDCl_3$, 25°C): δ 1.38 (s, 18 H, $C(CH_3)_3$), 2.20 (s, 6

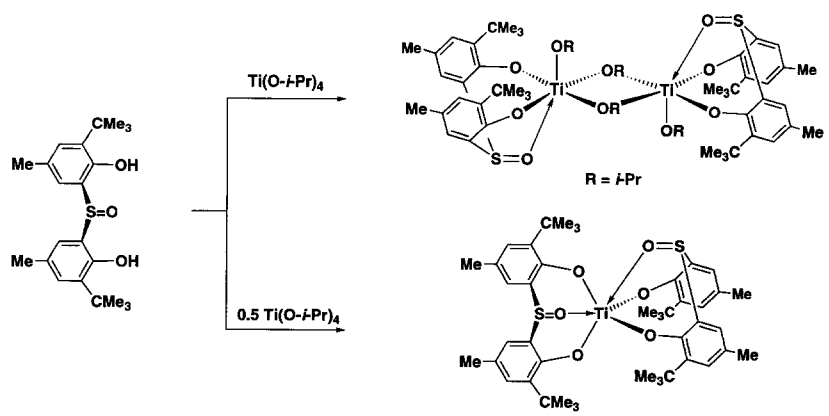

Scheme 1.

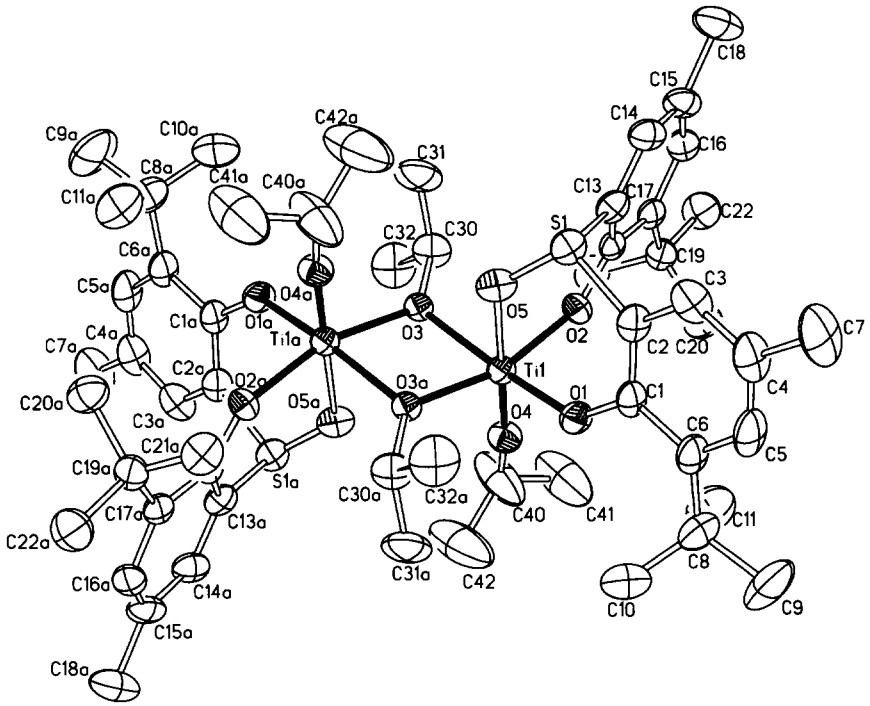

Fig. 1. ORTEP view of the molecular structure of [Ti(sibmp) (O-*i*-Pr)$_2$]$_2$·0.5 Et$_2$O. Thermal ellipsoids are drawn at the 50% probability level. Hydrogen atoms are omitted for the sake of clarity. Selected bond distances (Å) and angles (°): Ti—O(1) 1.897(3), Ti—O(2), 1.933(3); Ti—O(5) 2.450(1); S(1)—O(5), 1.490(3); Ti(1)—O(3), 2.037(2); Ti(1)—O(3a), 2.008(2); Ti(1)—O(4), 1.763(3); O(1)—Ti(1)—O(2), 89.42(12); O(3)—Ti(1)—O(3a), 74.65(11); O(4)—Ti(1)—O(5), 179.15(12); C(1)—O(1)—Ti(1), 139.2(3); S(1)—O(5)—Ti(1), 121.9(2); Ti(1)—O(3)—Ti(1), 105.35(11).

H, 4-CH$_3$), 6.63 (s, 2 H, 3-C$_6$H$_2$), 7.19 (s, 2 H, 5-C$_6$H$_2$), 9.33 (s, 2 H, OH); ^{13}C{^{1}H} NMR (CDCl$_3$, 25°C): δ 20.74 (4-CH$_3$), 29.42 (C(CH$_3$)$_3$), 35.16 (C(CH$_3$)$_3$), 121.98 (C-2), 124.24 (C-3), 128.75 (C-4), 131.96 (C-5), 139.87 (C-6), 155.44 (C-1); IR (Nujol): ν 3140 br (OH), 1439 s, 1390 m, 1245 s, 1204 s, 957 m, 860 m, 757 m cm^{-1}; EI MS: *m/z* 374 (46%, M$^+$). Anal. Calcd for C$_{22}$H$_{30}$O$_3$S: C, 70.55; H, 8.07. Found: C, 70.32; H, 8.14.

Bis{2,2′-*sulfinylbis*(6-tert-*butyl*-4-*methylphenolato*)}-*titanium*. A solution of sibmpH$_2$ (753 mg, 2.01 mmol) in diethyl ether was slowly treated with titanium tetra(*iso*-propoxide) (0.295 cm^3, 1.01 mmol) under vigorous stirring. After stirring for 2 h, the microcrystalline precipitate was filtered off, washed with hexane and dried *in vacuo*. Yellow crystals (470 mg) were isolated in 30% yield. ^{1}H NMR (CDCl$_3$, 25°C): δ 1.23, 1.51 (s, 18 H, 6,6′-C(CH$_3$)$_3$), 2.21, 2.22 (s, 6 H, 4,4′-CH$_3$), 6.81, 7.03 (d, $^4J_{HH}$ = 1.5 Hz, 2 H, 3,3′-C$_6$H$_2$), 7.13 (2 overlapping d, $^4J_{HH}$ = 1.5 Hz, 4 H, 5,5′-C$_6$H$_2$); ^{13}C{^{1}H} NMR (CDCl$_3$, 25°C): δ 20.74 (4,4′-CH$_3$), 29.35, 29.88 (C(*C*H$_3$)$_3$), 35.23, 35.71 (C(*C*H$_3$)$_3$), 123.93, 124.64 (C-3,3′), 125.56, 127.03 (C-2,2′), 126.91, 128.25 (C-4,4′), 131.49, 133.16 (C-5,5′), 139.04, 139.40 (C-6,6′), 158.11, 159.26 (C-1,1′); EI MS: *m/z* 792 (100%, M$^+$). Anal. Calcd for C$_{44}$H$_{56}$O$_6$S$_2$Ti: C, 66.65; H, 7.12. Found: C, 66.08; H, 6.86.

Dichloro{2,2′-*sulfinylbis*(6-tert-*butyl*-4-*methylphenolato*)}*titanium*. A solution of sibmpH$_2$ (1.72 g, 4.59 mmol in 8 cm^3) in dichloromethane was slowly added to a solution of titanium tetrachloride (0.87 g, 4.59 mmol) in dichloromethane. Immediate color change of the solution to dark brown was observed. After cooling to −78°C for 24 h, the mother liquor was filtered off and the dark brown crystals dried *in vacuo* to afford 2.10 g (93%) of the product. ^{1}H NMR (CD$_2$Cl$_2$, 25°C): δ 1.39 (s, 18 H, C(CH$_3$)$_3$), 2.29 (s, 6 H, 4-CH$_3$), 7.06 (d, $^4J_{HH}$ = 1.8 Hz, 2 H, 3-C$_6$H$_2$), 7.27 (d, $^4J_{HH}$ = 1.8 Hz, 2 H, 5-C$_6$H$_2$); ^{13}C{^{1}H} NMR (CD$_2$Cl$_2$, 25°C): δ 20.69 (4-CH$_3$), 29.25 (C(*C*H$_3$)$_3$), 35.38 (C(*C*H$_3$)$_3$), 124.12 (C-3), (C-2, -4 not detected), 133.40 (C-5), 144.96 (C-6), 156.96 (C-1); EI MS: *m/z* 490 (14%, M$^+$). Anal. Calcd for C$_{22}$H$_{30}$O$_3$Cl$_2$STi: C, 53.78; H, 5.74. Found: C, 53.80; H, 6.02.

Di(iso-*propoxo*){2,2′-*sulfinylbis*(6-tert-*butyl*-4-*methylphenolato*)}*titanium*. A hexane solution of sibmpH$_2$ (1.20 g, 3.20 mmol in 7 cm^3) was layered on top of an ethereal solution of titanium tetra(*iso*-propoxide) (0.91 g, 3.20 mmol in 10 cm^3). After standing for 4 h at room temperature precipitation of orange crystals was complete. The mother liquor was filtered off, and the crystals were washed with 10 cm^3 of hexane to give 1.57 g of product (91%). Single crystals suitable for X-ray diffraction could be obtained by this method. ^{1}H NMR ((CD$_3$)$_2$SO, 170°C): δ 1.09 (br s, 12 H, CH(CH$_3$)$_2$), 1.39 (s, 18 H, ((CH$_3$)$_3$), 2.15 (s, 6 H, 4-CH$_3$), 3.60 (br m, 1 H, C*H*(CH$_3$)$_2$), 3.84 (br m, 1 H, C*H*(CH$_3$)$_2$),

6.87 (br s, 2 H, 3-C_6H_2), 7.00 (br s, 2 H, 5-C_6H_2); IR (Kbr): ν 2959 m, 1439 s, 1296 m, 1273 m, 1128 ms, 1024 m, 985 m, 860 m, 825 s, 624 m, 552 m, 536 m, 460 m cm^{-1}; EI MS: m/z 538 (23%, $M^+/2$), 479 (16%, $M^+/2-C_3H_7O$): Anal. Calcd for $C_{28}H_{42}O_5STi$: C, 62.44; H, 7.86. Found C, 62.56; H, 8.04.

Crystal data for [Ti(sibmp)(O-i-Pr)$_2$]$_2$·0.5 Et_2O. Orange–red cubes, $C_{30}H_{47}O_{5.5}STi$, $M_r = 575.64$, triclinic, space group P1, $a = 9.567(1)$, $b = 13.784(1)$, $c = 13.965(2)$ Å, $\alpha = 112.30(1)$, $\beta = 95.06(1)$, $\gamma = 108.39(1)^\circ$, $V = 1570.9(3)$ Å^3, $Z = 2$, $D_{calc} = 1.217$ g cm^{-3}, $F(000) = 618$. Data in the range $3 < 2\theta < 58^\circ$ were collected at 293(2) K using Cu-$K\alpha$ radiation on a Enraf–Nonius CAD4 diffractometer. The structure was solved by direct methods and refined by full-matrix least squares techniques against all F^2 data. GOF = 1.035, w$R_2 = 0.1455$ for all 4269 reflections and $R = 0.0514$ for 3405 observed reflections $I > 2\sigma(I)$.

Acknowledgements—Generous financial support by the Volkswagen-Foundation, the Deutsche Forschungsgemeinschaft (SFB 260), the Fonds der Chemischen Industrie, and BASF AG (Kunststofflaboratorium) is gratefully acknowledged.

Supplementary material available—Listings of all crystal data and refinement parameters, atomic parameters including hydrogen atoms, thermal parameters, torsional angles, bond lengths and angles, and stereodrawing of unit cell for [Ti(sibmp)(O-*i*-Pr)$_2$]$_2$·0.5 Et_2O (9 pages). Ordering information is given on any current masthead page.

REFERENCES

1. (a) Kakugo, M., Miyatake, T. and Mizunuma, K., *Chem. Express*, 1987, **2,** 445; (b) Miyatake, T., Mizunuma, K., Seki, Y. and Kakugo, M., *Makromol. Chem., Rapid Commun.*, 1989, **10,** 349; (c) Miyatake, T., Mizunuma, K. and Kakugo, M., *Makromol. Chem., Macromol. Symp.*, 1993, **66,** 203; (d) Schaverien, C. J., van der Linden, A. J. and Orpen, A. G., *Am. Chem. Soc., Polym. Div., Polymer Prepr.*, 1994, **35,** 672; Schaverien, C. J., van der Linden, A. J. and Orpen, A. G., *J. Am. Chem. Soc.*, 1995, **117,** 3008.
2. (a) Floriani, C., Corazza, F., Lesueur, W., Chiesi-Villa, A. and Guastini, C., *Angew. Chem.*, 1989, **101,** 93; *Angew. Chem., Int. Ed. Engl.*, 1989, **28,** 66; (b) Corazza, R., Floriani, C., Chiesi-Villa, A. and Guastini, C., *Inorg. Chem.*, 1991, **30,** 146; (c) Okuda, J., Fokken, S., Kang, H.-C. and Massa, W., *Chem. Ber.*, 1995, **128,** 221; (d) Schermerhorn, E. J., Master's Thesis, State University of New York at Albany, 1993; (e) Chisholm, M. H., Huang, J.-H., Huffman, J. C., Streib, W.E. and Tiedke, D., *Polyhedron*, 1997, **16,** 2941.
3. (a) Fokken, S., Spaniol, T. P., Kang, H. C., Massa, W. and Okuda, J., *Organometallics*, 1996, **15,** 5069; (b) Fokken, S. Ph.D. Thesis, University of Marburg, 1997; (c) Porri, L., R. A., Colombo, P., Moano, E., Capelli, S. and Meille, S. V., *J. Organomet. Chem.*, 1996, **514,** 213.
4. For other examples of titanium complexes containing a tridentate ligand, see: (a) Menge, W. M. P. B. and Verkade, J. G., *Inorg. Chem.*, 1991, **30,** 4628; (b) Naiini, A. A., W. M. P. B. and Verkade, J. G., *Inorg. Chem.*, 1991, **30,** 5009; (c) Cummins, C. C., Schrock, R. R. and Davis, W. M., *Organometallics*, 1992, **11,** 1452; (d) Nugent, W. A. and Harlow, R. L., *J. Am. Chem. Soc.*, 1994, **116,** 6142; (e) Harlow, R. L., *Acta Cryst.*, 1983, **39,** 1344.
5. Chandrasekaran, A., Day, R. O. and Holmes, R. R., *Organometallics*, 1996, **15,** 3182.
6. For other examples with $Ti_2(\mu$-O-*i*-Pr$)_2$ units, see: (a) Siedle, A. R. and Huffman, J. C., *Inorg. Chem.*, 1990, **29,** 3131; (b) Sabat, M., Gross, M. F. and Finn, M. G., *Organometallics*, 1992, **11,** 745; (c) Fisher, J., van der Sluys, W. G., Huffman, J. C. and Sears, J., *Synth. React. Inorg. Met.-Org. Chem.*, 1993, **23,** 479.
7. Brun. L., *Acta Cryst.*, 1966, **20,** 739.
8. Bränden, C.-I. and Lindqvist, I., *Acta Chem. Scand.*, 1960, **14,** 726.
9. The polymerization activity for ethylene follows the order for titanium(IV) complexes: mbmp < sobmp (ref. [9c]) < sibmp < tbmp: (a) Sernetz, F. G., Mülhaupt, R., Fokken, S. and Okuda, J., *Macromolecules*, 1997, **30,** 1562; (b) Sernetz, F. G. Ph.D. Thesis, University of Freiburg, 1996; Related sulfonyl-bridged bisphenolato (sobmp) complexes are accessible in a manner analogous to sibmp complexes.
10. Prakasha, T. K., Day, R. O. and Holmes, R. R., *J. Am. Chem. Soc.*, 1993, **115,** 2690.

Pergamon

PII: S0277-5387(97)00242-8

Polyhedron Vol. 17, No. 5–6, pp. 947–952, 1998
© 1998 Elsevier Science Ltd
All rights reserved. Printed in Great Britain
0277-5387/98 $19.00+0.00

Chelating amides of lithium. Synthesis, structure and coordination chemistry†

Michael D. Fryzuk,* Garth R. Giesbrecht, Samuel A. Johnson, James E. Kickham and Jason B. Love

Department of Chemistry, 2036 Main Mall, Vancouver, B.C., Canada V6T 1Z1

(Received 10 April 1997; accepted 6 June 1997)

Abstract—A limited review of the use of mixed-donor ligands that contain amides is presented. By combining amides with phosphines and amines in a chelating array, a variety of tridentate and macrocyclic ligands have been prepared. The synthesis and structures of a variety of lithium derivatives are presented since these are the typical starting materials in the preparation of transition metal, main group and lanthanide complexes that incorporate these ligand systems. It is found that the structures of these lithium derivatives depend on the nature of the other donors present in the chelating array. © 1998 Elsevier Science Ltd. All rights reserved

Keywords: amide; phosphine; amine; tridentate; macrocycle; lithium.

One of the tenets of inorganic chemistry is that steric hindrance can force low coordination numbers [1]. For this reason, bulky ligands have prospered in all areas of coordination chemistry ranging from organometallic complexes to catalyst precursors. It is only fitting that due credit be given to D. C Bradley who was one of the pioneers of this idea some forty years ago [2]. In the research to be summarized here, the connection to Bradley and co-workers is particularly strong since they were one of the first groups to investigate the preparation of late metal–amide complexes [3]. The use of the bulky *bis*(trimethylsilylamide) donor, $[N(SiMe_3)_2]^-$ [4,5], to generate Co^I, Ni^I and Co^{II} amides also having monodentate phosphine donors provided the seeds of inspiration for the design [6] of tridentate amidodiphosphine ligands of the type **I** (Fig. 1). As it turned out, not only could this ligand bind to the late metals [7] but its coordination chemistry with the early metals and the lanthanides was also particularly rich [8].

From a practical point of view, the synthesis of metal amides relies on access to alkali metal amide precursors, for example, amides of lithium in particular have been shown to be extremely useful in this regard [9]. In addition, lithium amides have been widely used in organic chemistry since they are mild bases capable of deprotonating a wide variety of substrates [10]. For these reasons, the solid state and solution structures of such species have been the subject of considerable research [9–14]. In this paper, we outline some of our efforts in the synthesis and structures of lithium amides that are part of a tridentate or a macrocyclic array of donors. In addition, we review some of the coordination chemistry that these amide-based ligands display.

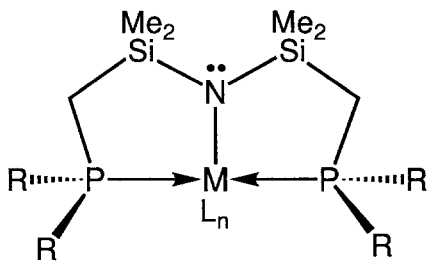

I

Fig. 1. Complexed tridentate amidodiphosphine ligand **I**.

Acyclic tridentate amide arrays

Our first ligand design utilized the readily available starting material, 1,3-bis(chloromethyl)tetra-

† Dedicated to D. C. Bradley on the occasion of his 73rd birthday

* Author to whom correspondence should be addressed.

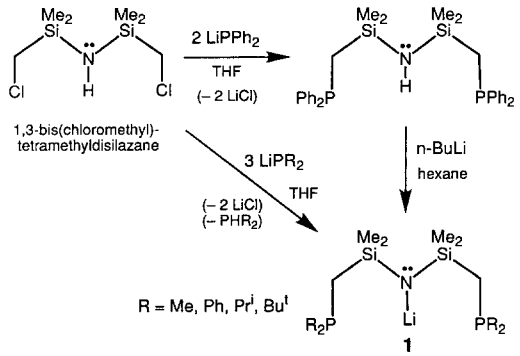

Scheme 1.

methyldisilazane, $HN(SiMe_2CH_2Cl)_2$, to prepare a series of tridentate ligands that incorporated an amide unit with two flanking phosphine donors [15,16]. The general synthetic sequence is shown in Scheme 1; diaryl or dialkylphosphide nucleophiles react smoothly with the commercially available, starting disilazane to produce either the amine or the amide derivatives, depending on the basicity of the phosphide.

The lithium amidodiphosphine derivative **1** serves as the key starting material in the preparation of both early and late transition metal complexes. However, its solid state and solution structure could not be unambiguously determined. The structure shown in Scheme 1 as an acyclic monomer was based more on convenience than spectroscopic data, and on the basis of recent studies of lithium disilylamides, is probably naive and unrealistic. A more reasonable structure is a dimer involving each amide bridging two lithiums as shown in **2** (Fig. 2). Although we have no direct evidence for this dimeric form or its structure, it is known that the phosphine donors do not coordinate to the lithium ions at any temperature since $^{31}P\{^1H\}$ NMR spectra show no coupling to ^7Li. Solution molecular weight studies in benzene were not reproducible. The propensity for lithium amide structures to incorporate robust amide bridges [9–11] is the sole rationale for the proposed structure of **2**.

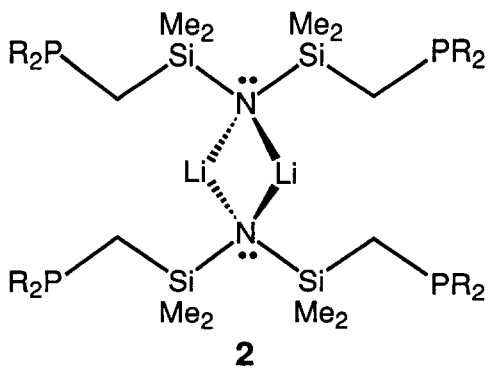

Fig. 2. Proposed solution structure of **1**.

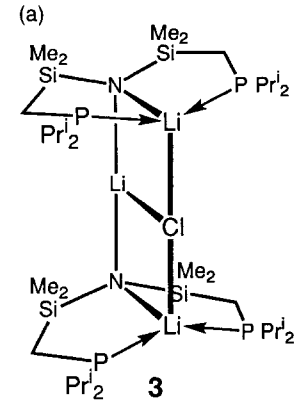

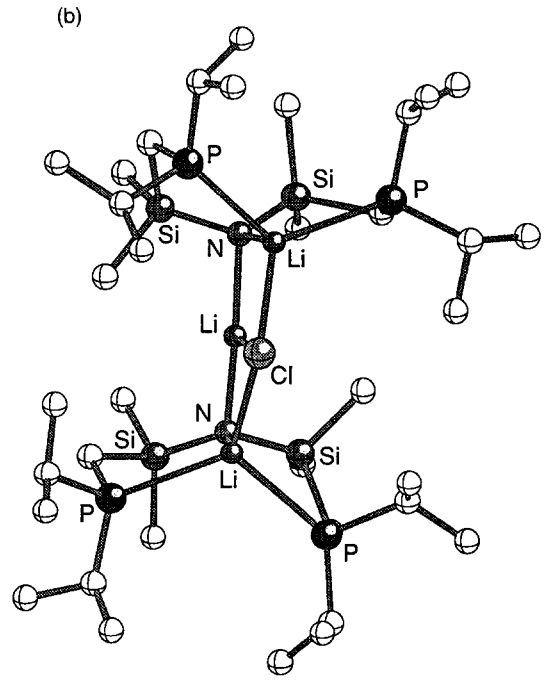

Fig. 3. Solid state structure of **3**.

Recently, we have obtained some structural data on derivatives of the lithium amidodiphosphine **1** (R = Pr^i) [17]. An X-ray crystal structure of the LiCl adduct, $\{LiN(SiMe_2CH_2PPr^i_2)_2\}_2LiCl$ (**3**) (Fig. 3), shows a ladder motif involving three lithium ions; in this case, the phosphine donors bind to the lithium centres both in solution (on the basis of ^7Li and $^{31}P\{^1H\}$ NMR spectroscopic studies) and in the solid state. A related adduct was also structurally characterized; addition of $LiAlMe_4$ to **1** produced the adduct $LiN(SiMe_2CH_2PPr^i_2)_2 \cdot LiAlMe_4$ (**4**) (Fig. 4). In the solid state, **4** is a dimer as shown below, but the solution NMR data suggest that this dimer can break up rather easily to form monomer **4**.

An even more complicated adduct was isolated from the reaction of **1** (R = Pr^i) with $NaBEt_4$; the solid state structure shows an infinite polymeric form of the formula $\{LiN(SiMe_2CH_2PPr^i_2)_2 \cdot NaBEt_4\}_x$ (**5**).

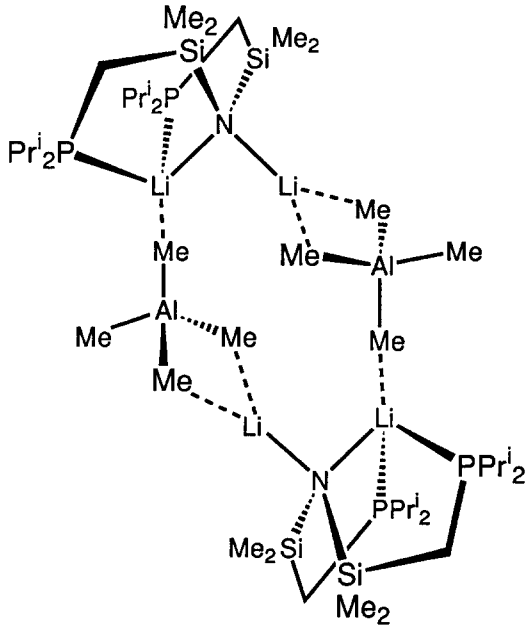

4

Fig. 4. Solid state structure of **4**.

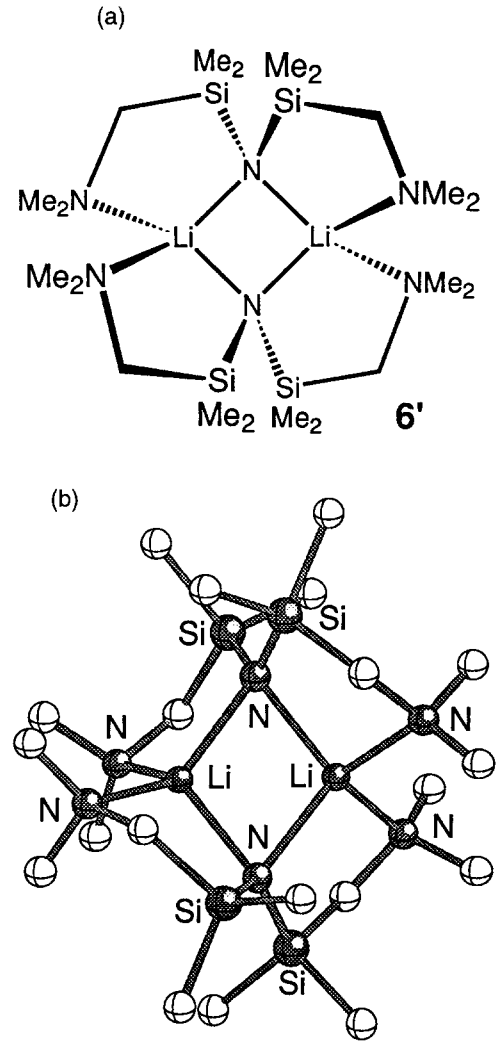

Fig. 5. Solid state structure of **6**.

We have examined the coordination chemistry of **1** with many metals in all the parts of the periodic table. Some of the early work has been reviewed [6–8]. More recently, we have continued our efforts by examining main group elements such as Al and Ga and the Group 3 element Sc [18,19], as well as the ability of this ligand to stabilize unusual oxidation states such as Zr^{III} [20].

Buoyed by our success of combining the amide donor with phosphines in an acyclic chelating array, we decided to try and synthesize a tridentate system with the amide donor flanked by amine donors, in this case, NMe_2 units [21]. Attempts to extend the synthesis of **1** shown in Scheme 1 to the all nitrogen analogue initially met with failure. For example, the reaction of $LiNMe_2$ with the disilazane did not produce any products that could be conclusively identified. However, an efficient synthesis was achieved by a protection-deprotection sequence as shown in Scheme 2. The NMe_2 donor is introduced first before amine exchange with ammonia to produce the disilyltriamine. Subsequent deprotonation produces the dimeric amidodiamine **6**.

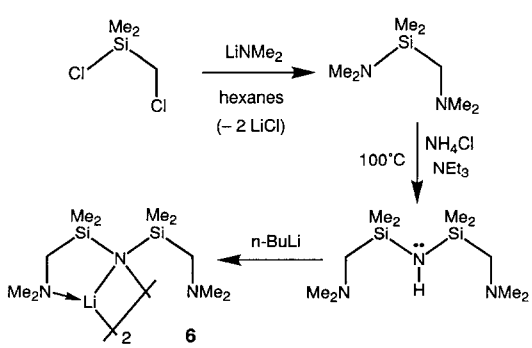

Scheme 2.

In contrast to the aforementioned amidodiphosphine **1** for which we proposed a dimeric formulation as **2**, the dimeric form of **6** is evident from symmetry considerations at low temperature in solution (by ^1H NMR spectroscopy) and from the X-ray crystal structure. The overall D_2 geometry is shown in Fig. 5 as **6'**.

As is often seen in lithium amide structures, a dimer is formed having the amide unit bridging two lithium ions; in this case, the dimethylamino donors bind to the lithium in contrast to that proposed for **2** where no evidence for phosphine coordination to lithium was evident.

The coordination chemistry with the amidodiamine **6** has been initiated [21]. With the Group 4 elements, distorted octrahedral complexes have been isolated as shown in eq. (1).

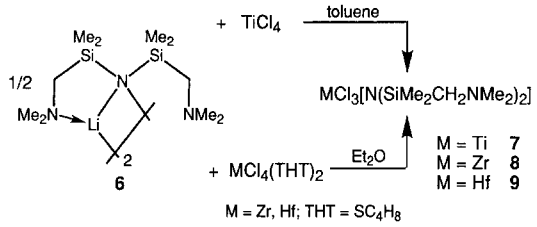

The titanium complex **7** displays a meridional arrangement of the tridentate ancillary ligand while both the heavier members **8** and **9** have the ligand in a facial orientation (Fig. 6). In these latter derivatives the distortion from octrahedral is so large that a bicapped tetrahedral [22] description could also be applicable.

Attempts to prepare a yttrium complex with this ligand system have met with mixed results. Shown below (Fig. 7) is the X-ray structure of the main product isolated from this reaction; the product has the molecular formula $[(Me_2NCH_2SiMe_2)_2N]YCl(\mu\text{-}Cl)_2Li[HN(SiMe_2CH_2NMe_2)_2]$ (**10**) wherein one equivalent of the ligand has been protonated and is bound to coordinated LiCl while the other is the expected, tridentate amidodiamine ligated to the yttrium. The source of the proton in the triamine bound in a bidentate fashion to the lithium ion is under investigation [23].

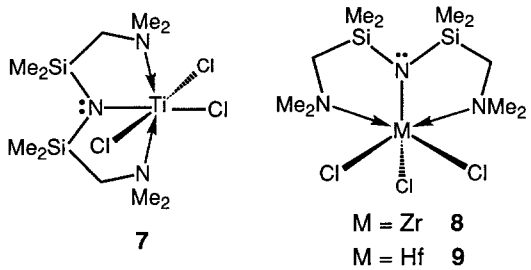

Fig. 6. Geometry of amidodiamine complexes of Ti, Zr and Hf.

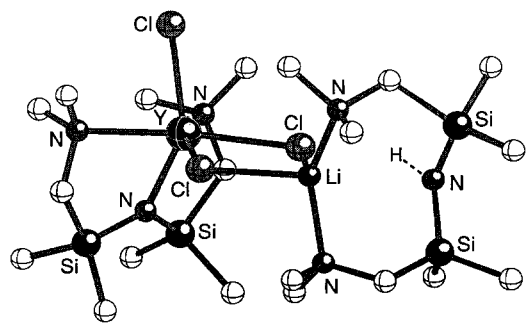

Fig. 7. Solid state structure of **10**.

Cyclic tetradentate diamide arrays

In the tridentate systems described above, the amide unit serves to anchor the ligand to the metal thereby forcing the ligand arms to bind by the virtue of their proximity, in other words, by the chelate effect. However, while the stability of the flanking arms binding to the metal is enhanced by this design, we have amassed considerable evidence that is consistent with facile phosphine and amine arm dissociations [21,22], at least for complexes of the early metals. While such kinetic processes could be beneficial (e.g., liberating sites on the metal for activation), we were also interested in designing new ligand systems that would be resistant to ligand dissociation. It seemed logical that a cyclic system could achieve this goal because the ligands would be constrained by the intrinsic inability of an appropriately designed cyclic system to expand [24]. One possible macrocyclic system is shown in Fig. 8 as **II**.

In this macrocyclic system, two amides and two phosphines are arranged trans to each other in a 12-membered ring. The synthesis of this ligand is shown in Scheme 3. The first step follows the general sequence shown in Scheme 1 wherein addition of two equiv. of primary phosphide to the disilazane generates a material that still has protons attached to the phosphorus atoms; subsequent addition of another equivalent of the disilazane and four equiv. of n-BuLi results in excellent yields of *syn*-$Li_2(THF)[P_2N_2]$ (**11**) and *anti*-$Li_2(THF)_2[P_2N_2]$ (**12**) [25]. We ascribe the high chemical yield in this last step as due to the template effect by the dilithio diamide-bridged motif. The two isomeric forms of this macrocyclic precursor can be separated by fractional crystallization and each form displays unique coordination behaviour with transition and main group elements.

The coordination chemistry of these new macrocyclic diamidodiphosphines is in progress and already we are seeing some differences in reactivity of metal complexes that incorporate this ligand system. For

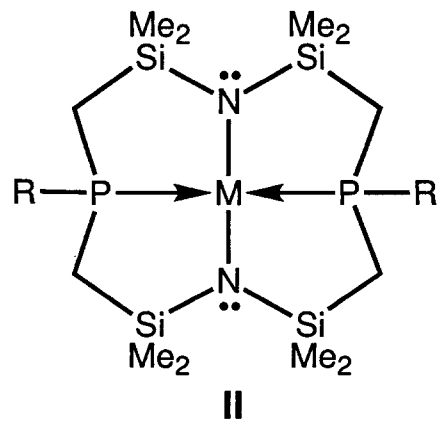

Fig. 8. Complexed macrocyclic diamidodiphosphine ligand **II**.

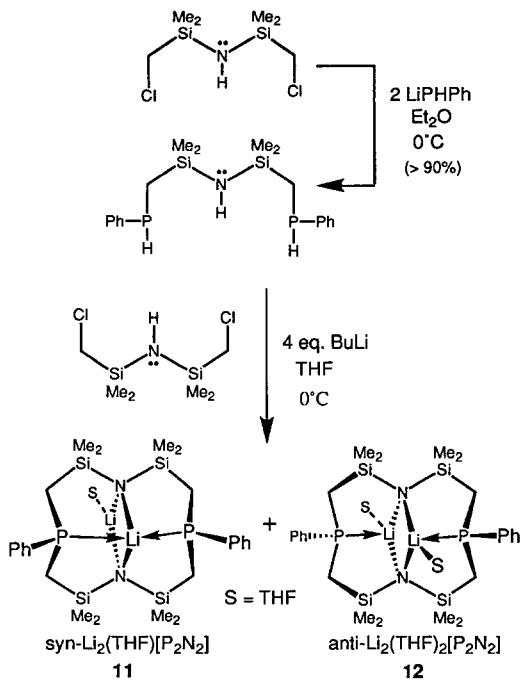

Scheme 3.

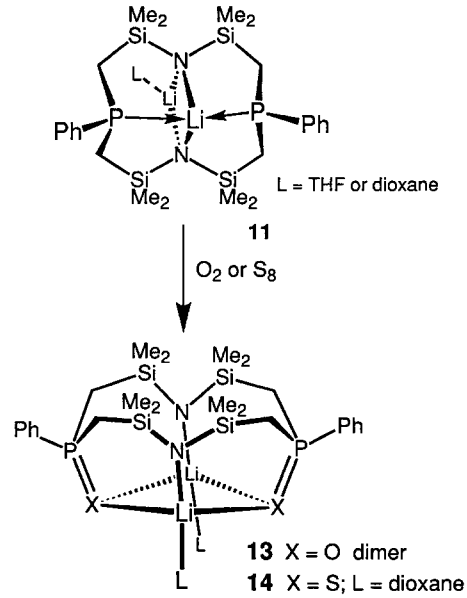

Scheme 4.

example, dinuclear zirconium dinitrogen complexes of the *syn*-$[P_2N_2]$ macrocycle show intriguing reactivity with dihydrogen and silanes without loss of the coordinated N_2 fragments [26].

Recent work from our laboratory has also shown that the phosphine donors of the macrocyclic arrays can be oxidized to generate the corresponding phosphine oxide and sulfide derivatives; we have been able to structurally characterize the corresponding *syn* derivatives that were prepared by the general route in Scheme 4; the reaction of the *syn* dilithio derivative **11** (either the THF or dioxane adduct) with dioxygen

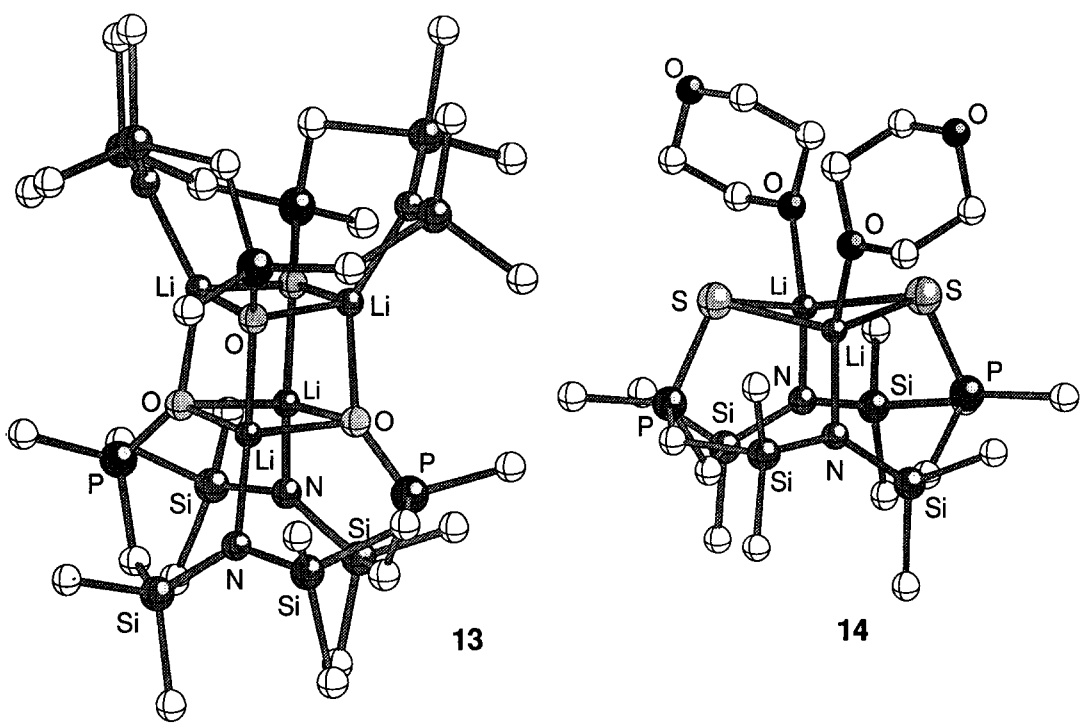

Fig. 9. Solid state structures of **13** and **14**.

or molecular sulfur produces the corresponding oxide **13** and the sulfide **14,** respectively [27]. The solid state structures (Fig. 9) are also given and show that the phosphine oxide derivative has a dimeric structure involving a cube of lithium ions and four oxygens from the phosphine oxide functionalities. The sulfide derivative was recrystallized from dioxane and this is apparently a strong enough donor for lithium to break up any dimeric forms that are similar to **13**. The coordination chemistry of these new macrocyclic ligands is in progress.

CONCLUSION

By building on the early work of Bradley and others who initiated studies on metal amide complexes, a huge literature now exists on the coordination chemistry and reactivity of amide derivatives [28]. Our approach has been to use the amide unit as an integral part of a chelating structure that when coordinated to a metal forces multidentate interactions. The starting point has typically involved the synthesis of lithium amides having chelating donors such as phosphines but recently we have included amine donors and most recently phosphine oxide and sulfides. What is evident at this stage is that the structures of the lithium amides vary from system to system; nevertheless, these derivatives do serve as efficient reactants for the incorporation of these mixed donor ancillary ligands onto transition metals and other elements.

Acknowledgements—Funding for the research was generously provided by NSERC of Canada. We also thank Dr Steven J. Rettig for his continued enthusiasm and dedication in solving many of the X-ray structures discussed here.

REFERENCES

1. Eller, P. G., Bradley, D. C., Hursthouse, M. B. and Meek, D. W., *Coord. Chem. Rev.*, 1977, **24,** 1.
2. Bradley, D. C., Mehrotra, and Wardlaw, W., *Prog. Inorg. Chem.*, 1960, **2,** 303.
3. Bradley, D. C., Hursthouse, M. B., Smallwood, R. J. and Welch, A. J., *Chem. Commun.*, 1972, 872.
4. Wannagat, U., *Pure Appl. Chem.*, 1969, **19,** 329.
5. Harris, D. H. and Lappert, M. F., *J. Organomet. Chem. Libr.*, 1976, **2,** 13.
6. Fryzuk, M. D., *Can. J. Chem.*, 1992, **70,** 2839.
7. Fryzuk, M. D., Montgomery, C. D., *Coord. Chem. Rev.*, 1989, **95,** 1.
8. Fryzuk, M. D., Berg, D. J. and Haddad, T. S., *Coord. Chem. Rev.*, 1990, **99,** 137.
9. Pauer, F. and Power, P. P. In *Lithium Chemistry*; p. 295, A.-M. Sapse and P. von Ragué Schleyer, Ed.; John Wiley & Sons: New York (1995).
10. Collum, D. B., *Acc. Chem. Res.*, 1993, **26,** 227.
11. Gregory, K., von Ragué Schleyer, P., Snaith, R., *Adv. Inorg. Chem.*, 1991, **37,** 47.
12. Romesberg, F. E. and Collum, D. B., *J. Am. Chem. Soc.*, 1994, **116,** 9198.
13. Lucht, B. L. and Collum, D. B., *J. Am. Chem. Soc.*, 1995, **117,** 9863.
14. Lucht, B. L. and Collum, D. B., *J. Am. Chem. Soc.*, 1996, **118,** 2217.
15. Fryzuk, M. D., MacNeil, P. A., Rettig, S. J., Secco, A. S. and Trotter, J., *Organometallics*, 1982, **1,** 918.
16. Fryzuk, M. D., Carter, A. and Westerhaus, A., *Inorg. Chem.*, 1985, **24,** 642.
17. Fryzuk, M. D., Giesbrecht, G. and Rettig, S. J., *Organometallics*, 1997, **16,** 725.
18. Fryzuk, M. D., Giesbrecht, G. R., Olovsson, G. and Rettig, S. J., *Organometallics*, 1996, **15,** 4832.
19. Fryzuk, M. D., Giesbrecht, G. R. and Rettig, S. J., *Organometallics*, 1996, **15,** 3329.
20. Fryzuk, M. D., Mylvaganam, M., Zaworotko, M. J. and MacGillivray, L. R., *Polyhedron*, 1996, **15,** 689.
21. Fryzuk, M. D., Hoffman, V., Kickham, J. E., Rettig, S. J. and Gambarotta, S., *Inorg. Chem.*, 1997, **36,** 3480.
22. Fryzuk, M. D., Carter, A. and Rettig, S. J., *Organometallics*, 1992, **11,** 469.
23. Fryzuk, M. D. and Kickham, J. E., 1997, unpublished results.
24. Lindoy, L. F., *The Chemistry of Macrocylic Ligand Complexes*, Cambridge University Press, Cambridge (1989).
25. Fryzuk, M. D., Love, J. B. and Rettig, S. J., *J. Chem. Commun.*, 1996, 2783.
26. Fryzuk, M. D., Love, J. B., Rettig, S. J. and Young, V. G., *Science*, 1997, **275,** 1445.
27. Fryzuk, M. D., Johnson, S. A. and Rettig, S. J., 1997, unpublished results.
28. Lappert, M. F., Power, P. P., Sanger, A. R. and Srivastava, R. C., *Metal and Metalloid Amides*, Ellis Horwood, Chichester (1980).

Pergamon

PII: S0277-5387(97)00244-1

Polyhedron Vol. 17, No. 5–6, pp. 953–958, 1998
© 1998 Elsevier Science Ltd
All rights reserved. Printed in Great Britain
0277-5387/98 $19.00+0.00

Trivalent uranium chemistry: molecular structure of $[(Me_3Si)_2N]_3U$

Joanne L. Stewart* and Richard A. Andersen

Department of Chemistry, University of California and Chemical Sciences Division, Ernest Orlando Lawrence Berkeley National Laboratory, Berkeley, CA 94720, U.S.A.

(Received 18 April 1997; accepted 5 June 1997)

Abstract—The X-ray crystal structure (−110°C); space group $P\bar{3}$ 1c, $a = b = 16.370(2)$ Å, $c = 8.302(1)$ Å, $\alpha = \beta = 90°$, $\gamma = 120°$, $V = 1926.7(1)$ Å^3, $Z = 2$; shows that the geometry of $U[N(SiMe_3)_2]_3 \cdot 1/3$ cyclohexane is pyramidal, consistent with deductions made on the basis of infrared spectroscopy. The U—N distance is 2.320(4) Å and the N—U—N angle is 116.24(7)°. The solid state magnetic susceptibility from 35–280 K gives μ_{eff} of 3.354(4) with $\theta = -13$ K and 3.385(4) B.M. with $\theta = -11$ K at 5 and 40 kGauss, respectively. The effective magnetic moments are similar to that found for UF_3 and other trivalent uranium metallocenes, consistent with a $5f^3$ electron configuration. © 1998 Elsevier Science Ltd. All rights reserved

Keywords: uranium (III); sylylamide; X-ray; magnetic moment.

The idealized geometry of binary, three-coordinate compounds, ML_3, is either trigonal planar (D_{3h} symmetry), pyramidal (C_{3v}) or T-shaped (C_{2v}). Molecular orbital models based upon Walsh diagrams [1a,b], VSEPR concepts based upon electron pair repulsion [1c], or a pure electrostatic model (the polarized-ion model) [1d,e] have been used to rationalize molecular geometry. The metal trihalides have been studied extensively at high temperature in the gas phase [2a,b] and in the solid state by matrix isolation spectroscopy [2c]. The principal difficulty in studies of molecules formed under 'extreme' conditions is establishing the identity and constitution of the species under study, as illustrated by a study of matrix-isolated TiF_n species [2d]. One way around some of these problems is to prepare and isolate ML_3 compounds that can be shown to be pure, monomeric compounds by normal physical studies. This is a rather difficult task since three-coordinate molecules are coordinatively unsaturated and the compounds often exist in equilibrium among various species depending upon the phase, temperature, solvent, etc. One way to prevent molecular association is to use sterically bulky ligands. Many examples of the use of steric effects to prevent association are in the literature of ML_3 compounds [3]. A particularly illustrative example is found in organoaluminum chemistry; Me_3Al is a dimer in the solid state [4a,b], though its vapor is composed of monomer and dimer species [4c]. The organoaluminum compound with bulky ligands, $(Me_3C)_3Al$, is a monomer under all conditions [4d].

The bis(trimethylsilyl)amido ligand, $(Me_3Si)_2N$, forms an extensive set of ML_2 [5] and ML_3 [6] compounds with the *np*, 3*d*, and 4*f* block metals. For $M[N(SiMe_3)_2]_3$ only monomeric compounds are known in the solid state and in gas phase though the geometry depends upon the phase. The *p*-block metals where M is Al, Ga, In, Tl are isostructural in the solid state with $P\bar{3}1c$ symmetry [7]. The molecules have trigonal planar geometry and their idealized symmetry is D_3 since the ligands are molecular propellars with the Me_3Si-blades giving the molecules a 'handedness'. In the first-row transition series, where M is Ti, V, Cr, Mn, and Fe, the molecules are isostructural with the *np*-block metals [8] and the geometry is trigonal planar [3,8]. Compounds where M is Sc or the 4*f*-block metal, Nd, Eu, or Yb crystallize in the space group $P\bar{3}$ 1c, though the geometry is nonplanar in each case [3,9]. The gas phase structures, where M is Ce, Pr, and La have been determined by electron diffraction and these

* Address all correspondence to this author at Chemistry Department, University of California, Berkeley, California 94720, U.S.A.

This paper is dedicated to Don Bradley who, along with U. Wannagat, was the pioneer in silylamide chemistry, on the occasion of his 73rd birthday.

are also pyramidal [10]. Perhaps the most interesting example in the $[(Me_3Si)_2N]_3M$ series is that of scandium, which is found to be pyramidal in solid state by X-ray diffraction [9b] though planar in gas phase by electron diffraction [11].

Several years ago we prepared the silylamide derivative of the heaviest, naturally occurring element, uranium and showed that the molecule is monomeric in gas phase [12]. Though the solid state structure was not available, we suggested that the molecule was pyramidal on the basis of its infrared spectrum. In this paper we show that this deduction is correct.

Molecular structure

An ORTEP diagram of $[(Me_3Si)_2N]_3U$ is shown in Fig. 1. Table 1 lists the crystal data. The molecule crystallizes in the space group $P\bar{3}1c$ as do all trissilylamide metal compounds that have been crystallographically characterized. The uranium compound is pyramidal, and the uranium atom is disordered above and below the plane defined by the three nitrogen atoms by 0.456(1) Å. The U—N distance of 2.320(4) Å is unique though two comparisons may be made. The Nd—N and Ce—N distances in $[(Me_3Si)_2N]_3Nd$ in the solid state and $[(Me_3Si)_2N]_3Ce$ in the gaseous state are 2.29(2) Å [4c] and 2.33(4) Å [5], respectively. The radii tabulated by Shannon [8] show that trivalent uranium in six coordination is 0.02 Å larger than trivalent cerium and 0.05 Å larger than neodymium. Extrapolation of these values gives a U—N distance of 2.34 or 2.35 Å, close to that observed.

The reason for the pyramidal geometry of $[(Me_3Si)_2N]_3U$ is not straightforward. The pyramidal geometry observed in the crystal structures of $[(Me_3Si)_2N]_3M$, where M is Sc or Eu, was suggested to be due to the lack of M—N π-bonding in these compounds, the explicit deduction being that the planarity of $[(Me_3Si)_2N]_3M$ was due to M—N π-bonding [9b]. A comprehensive study of the gas phase photoelectron spectroscopy of planar or pyramidal $[(Me_3Si)_2N]_3M$ compounds showed that the extent of M—N

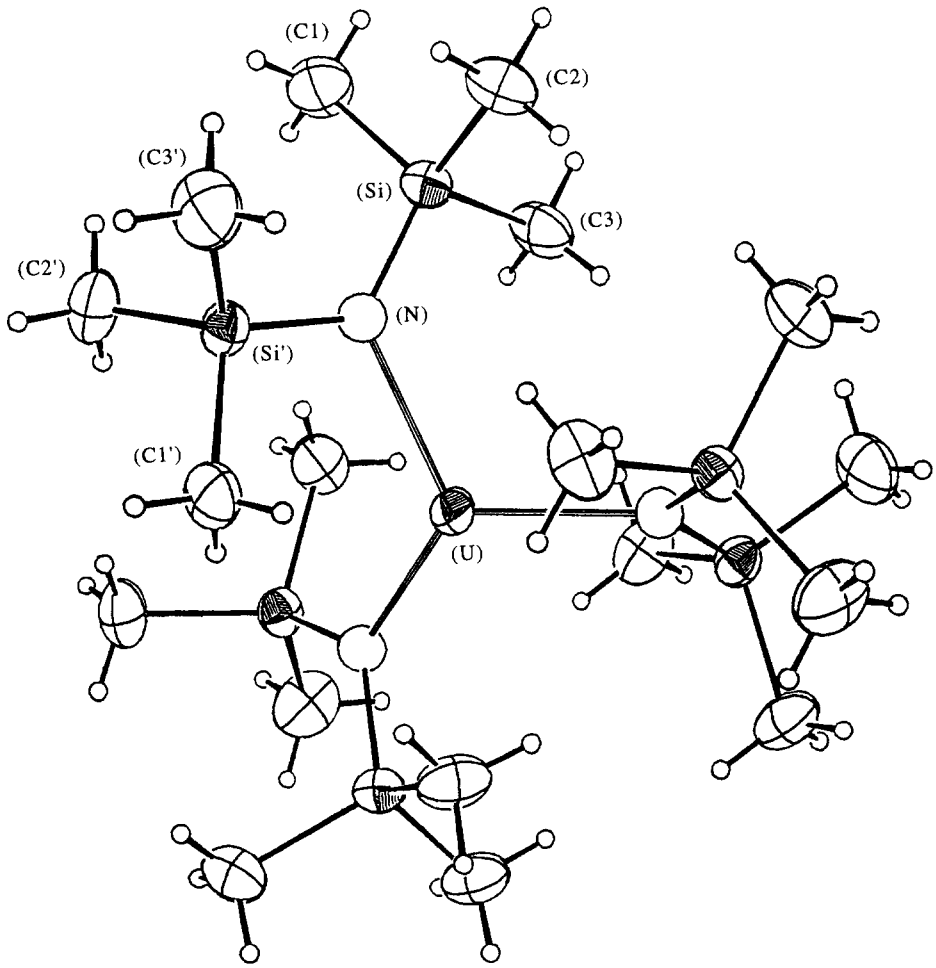

Fig. 1. ORTEP diagram, down the 3-axis of $[(Me_3Si)_2N]_3U \cdot \frac{1}{3}(C_6H_{12})$ at -110°C, 50% thermal ellipsoids, showing one of the two disordered uranium sites. U—N = 2.320(4) Å, N—Si = 1.713(1) Å, N—U—N = 116.24(7)°, Si—N—Si = 125.8(2)°, U—N—Si (ave.) = 117(4.5)°.

Table 1. Crystal data for $U[N(SiMe_3)_2]_3 \cdot 1/3(C_6H_{12})$ (-110 ± 4°C)

Space group	$P\bar{3}\,1c$
a, b (Å)	16.370(2)
c (Å)	8.302(1)
α (°)	90
β (°)	90
γ (°)	120
V (Å^3)	1926.7(1)
Z	2
Fw	747.24
d (calc.) g/cm^3	1.29
μ (calc.) 1/cm	41.88
Radiation	Mo-K_α ($\lambda = 0.71073$ Å)
Monochromator	highly oriented graphite
Scan range, type	$3 \leqslant 2\theta \leqslant 45°$, θ–2θ
Scan speed (°/min)	0.84–6.7, variable
Scan width (°)	$\Delta\theta = 0.60 + 0.35 \tan\theta$
Reflections collected	1886; $+h$, $+k$, $\pm l$
Unique reflections	845
Reflections, $F_o^2 > 3\sigma(F_o^2)$	654
R (%)	2.17
R_w (%)	2.90
R_{all} (%)	4.95
GOF	1.267
g (e^{-2})	$1.7(3) \times 10^{-7}$
Largest Δ/σ in final least-square cycle	0.02

Intensity standards: 4, 4, −4; 11, −5, −1; −5, 11, 1; measured every hour of X-ray exposure time. Over the period of data collection there was a 1.4% decay in intensity.

Orientation standards: 3 reflections were checked after every 100 measurements. Crystal orientation was redetermined if any of the reflections were offset from their predicted positions by more than 0.1°. Reorientation was required once throughout the data collection. The cell constants listed were determined at the end of data collection.

π-bonding in these compounds is insignificant [14]. Hence, differential π-bonding cannot account for the change in geometry. Solid state packing forces are likely to be unimportant (except for scandium) since La, Ce, and Pr are pyramidal in the gaseous state [10] as are Nd [9c] and Eu [9b] in the solid state.

Both electrostatic and covalent models have been used to rationalize the geometry of nonlinear ML_2 species and nonplanar ML_3 species. In the electrostatic, or polarized-ion model for ML_3 compounds, the geometry is largely determined by the size of the central ion and the size of the anionic ligands, L. Qualitatively, as the LML angle gets smaller than 120°, L···L repulsions will develop which will be destabilizing. For the smaller metals, i.e., those of the 3*d*-transition series, the planar geometry is determined largely by the L···L repulsions. As the metal ions get larger the intra-ligand repulsions become less destabilizing on bending and the pyramidal geometry is less unfavorable. In addition, bending LML away from 120° induces a dipole moment in the direction opposite of the bending. The interaction of the induced dipole moment with the negatively charged ligands is stabilizing (a charge-dipole interaction). Since the induced dipole moment is proportional to the polarizability, which is proportional to the size of the metal ion, the largest ions should be the most pyramidal. This is consistent with the experimental facts [10].

The polarized-ion model has been used in a quantitative manner to account for the non-linear geometry of gaseous BaF_2 [15], and in a qualitative way to rationalize the geometry and the thermodynamic properties of gaseous alkaline earth halides, oxides, and metallocenes [1d,16,17]. It has been pointed out in a theoretical study on ML_2 species, that bond angle calculations using this method are very sensitive to the polarizability value (α_m) chosen for the metal [18c]. This sensitivity to parameter choice decreases as the polarizability of the metal increases.

A covalent or orbital hybridization model has also been used to explain the non-linear geometry of ML_2 and the pyramidal geometry of ML_3 compounds [18]. The stability of the non-linear or non-planar configurations are rationalized by the involvement of metal *d*-orbitals in bonding. For example, *ab initio* calculations have been performed on $U(CH_3)_3$ which serves as a model compound for the pyramidal com-

pound $U[CH(SiMe_3)]_3$ [19]. The pyramidal geometry is said to be due to the involvement of 6*d* orbitals in the U—C bonding. It is crucial to remember that the polarized-ion model is purely electrostatic and it allows electron exchange (covalency) by polarization, whereas the molecular orbital model introduces polarization by including *d*-orbitals. Both models account for the experimental facts, and arguments over which model is to be preferred are largely semantic [20].

EXPERIMENTAL

The silylamide, $[(Me_3Si)_2N]_3U$, was prepared as previously described [12]. The infrared spectrum and melting point were identical to those previously reported but the ^1H NMR spectrum (20°C, C_6D_6) is a singlet at -11.4 ($\nu_{1/2} = 15$ Hz) rather than at -18.1 ppm as previously described. A plot of the inverse susceptibility as a function of temperature for $[(Me_3Si)_2N]_3U$ is shown in Fig. 2. The magnetic moment (μ_B) is 3.354(4) B.M. ($\Theta = -13$ K) at 5 kGauss and 3.385(4) B.M. ($\Theta = -11$ K) at 40 kGauss over the temperature range of 35–280 K. The shape of the curve and the magnetic moment are similar to those previously reported for other trivalent uranium compounds [21].

X-ray crystallography of $[(Me_3Si)_2N]_3U_{1/3}(C_6H_{12})$

Deep purple crystals of the compound were obtained by slow cooling of a saturated cyclohexane solution to -15°C. Crystals of appropriate size were mounted in 0.3 mm thin-walled quartz capillaries in an inert-atmosphere glove box. The capillaries were removed from the box and flame sealed. Preliminary precession photographs indicated trigonal Laue symmetry and yielded preliminary cell dimensions.

The crystal used for data collection was of approximate dimensions 0.39 mm × 0.20 mm × 0.20 mm. It was transferred to an Enraf–Nonius CAD-4 diffractometer and cooled to -110°C by a cold flow apparatus previously calibrated by a thermocouple placed at the sample position. The crystal was centered in the beam. Accurate cell dimensions and orientation matrix were determined by a least-squares fit to the setting angles of the unresolved MoKα components of 24 symmetry related reflections with 2θ between 24 and 30°. The search yielded the same Laue symmetry as the precession photographs and systematic absences indicated the space group to be either $P31c$ or $P\bar{3}\,1c$. The normalized structure factor statistics suggested the choice of the acentric space group, however, a successful solution in the acentric group could not be achieved. A successful solution was found using the space group $P\bar{3}\,1c$. The final cell parameters and specific data collection parameters are given in Table 1.

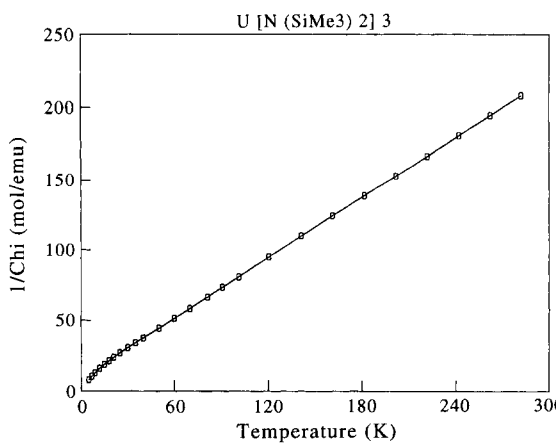

Fig. 2. Plot of inverse magnetic susceptibility *vs* temperature (K) for $[(Me_3Si)_2N]_3U$.

The 1886 raw intensity data were converted to structure factor amplitudes and their esds by correction for scan speed, background and Lorentz-polarization effects. Inspection of the intensity standards showed no appreciable decay in intensity (1.4%) during data collection. Inspection of the azimuthal scan data showed a variation $I_{min}/I_{max} = 0.90$ for the average curve. An empirical correction for absorption, based on the azimuthal scan data, was applied to the intensities. Removal of systematically absent data and averaging of redundant data left 905 unique data. The redundant data were averaged with an agreement factor, based on F_{obs}, of 1.5% for observed and accepted data and 3.9% for all data.

The structure was solved by Patterson methods and refined *via* standard least-squares and Fourier techniques. In a difference Fourier map calculated following refinement of all non-hydrogen atoms with anisotropic thermal parameters, peaks corresponding to the expected positions of all of the hydrogen atoms were found, as well as a large peak near the origin (*vide infra*). All hydrogens were included in the structure factor calculations in their expected positions based on idealized bonding geometry. All hydrogens were assigned isotropic thermal parameters 1.15 Å^2 larger than the equivalent B_{iso} of the atom to which they were bonded. None of the hydrogens were refined in least squares.

After the hydrogen atoms were included in the structure, a model for the electron density near the origin was developed. Hursthouse and Rodesiler found that $Fe[N(SiMe_3)_2]_3$ crystallized with a channel running down the *z*-axis that is large enough to accommodate a benzene molecule [8d]. Successful refinement of solvent molecules in the channel has not been achieved in any of the tris(bis(trimethylsilyl)amido) metal structures. In $[(Me_3Si)_2N]_3U$, the large peak near the origin in the difference Fourier map was able to be refined with anisotropic thermal parameters as a carbon atom with 1/3 occupancy. The symmetry generated positions gave reasonable bond lengths and angles that showed the atom to be part of a disordered

cyclohexane ring. The hydrogen atoms of the cyclohexane molecule were not included. The thermal parameters showed the carbon atom to be severely anisotropic: B(1,1) = 4.7(6), B(2,2) = 3.7(5), B(3,3) = 19(1), with the motion (or disorder) in the z-direction. This model accounted nicely for the electron density found in the channel and the largest peaks in the final difference Fourier map are now associated with the uranium and are not found in the channel. A packing diagram, that shows the C_6H_{12} molecule is in the Supplementary Material.

The quantity minimized by the least squares was $\Sigma w(|F_o| - |F_c|)^2$, where w is the weight of a given observation. The p-factor, used to reduce the weight of intense reflections, was set to 0.03 throughout the refinement. The analytical forms of the scattering factor tables for the neutral atoms were used and all non-hydrogen scattering factors were corrected for both the real and imaginary components of anomalous dispersion.

Inspection of the residuals ordered in ranges of $\sin(\theta/\lambda)$, $|F_o|$, and parity and value of the individual indices showed no unusual features or trends. A secondary extinction parameter was refined in the final cycles of least squares. Seven reflections were rejected as "bad" data in the final refinement, based on their high values of $w \times \Delta^2$. The highest and lowest peaks in the final difference Fourier map had electron densities of 0.364 and -0.215 $e^{-1}/Å^3$, respectively, and were associated with the uranium atom.

Acknowledgements—This work was supported by the Director, Office of Energy Research, Office of Basic Energy Sciences, Chemical Sciences Division of the U.S. Department of Energy under Contract No. DE-AC03-76SF00098. We thank Dr F. J. Hollander, staff crystallographer of the University of California, Berkeley CHEXRAY facility for his help with the X-ray crystallography.

Supplementary material—Positional parameters, a table of bond lengths and angles, anisotropic thermal parameters, and structure factor tables (11 pages).

REFERENCES

1. (a) Burdett, J. K., *Molecular Shapes*, Wiley, New York (1980); (b) Albright, T. A., Burdett, J. K. and Whangbo, M. H., *Orbital Interactions in Chemistry*, Wiley, New York (1985); (c) Gillespie, R. J., *Molecular Geometry*, Van Nostrand-Rheinhold, London (1972); (d) Drake, M. C. and Rosenblatt, G. M., *J. Electrochem. Soc.*, 1979, **126,** 1387; (e) Hildebrand, D. L., *ibid.* 1979, **126,** 1396.
2. (a) Hargittai, M., *Coord. Chem. Rev.*, 1988, **91,** 35; (b) Haregittai, M., in *Stereochemical Applications of Gas-Phase Electron Diffraction*, p. 383, Hargittai, I. (ed.) VCH Publishers, Part B, (1988); (c) Nakamoto, K., p. 108, *Infrared and Raman Spectra*, Wiley, New York, 4th ed. (1986); (d) Beattie, I. R., Jones, P. J. and Young, N. A., *Angew Chem. Int. Ed.*, 1989, **28,** 313.
3. Eller, P. G., Bradley, D. C., Hursthouse, M. B. and Meek, D. W., *Coord. Chem. Rev.*, 1977, **24,** 1.
4. (a) Rundle, R. E., *J. Am. Chem. Soc.*, 1947, **69,** 1327; (b) Hoffman, J. C. and Streib, W. E., *J. Chem. Soc., Chem. Comm.*, 1971, 911; (c) Almenningen, A., Halvorsen, S. and Haaland, A., *Acta Chem. Scand.*, 1971, **25,** 1937; (d) Lehmkuhl, H., Olbrysch, O. and Nehl, H., *Annalen.*, 1973, 708.
5. Power, P. P., *Comments Inorg. Chem.*, 1989, **8,** 177.
6. Lappert, M. F., Power, P. P., Sanger, A. R. and Srivastava, R. C., *Metals and Metalloid Amides*, Ellis Horwood, Chichester (1980).
7. (a) Pump, J., Rochow, E. G. and Wannagat, U., *Angew. Chem. Int. Ed. Eng.*, 1963, **2,** 264; (b) Bürger, H., Chicon, J., Goetze, U., Wannagat, U. and Wismar, H. J., *J. Organomet. Chem.*, 1971, **33,** 1; (c) Krommes, P. and Lorberth, J., *Ibid.*, 1977, **131,** 415; (d) Sheldrick, G. M. and Sheldrick, W. S., *J. Chem. Soc. (A)*, 1969, 2279; (e) Allman, R., Henke, W., Krommes, P. and Lorbeth, J., *J. Organomet. Chem.*, 1978, **162,** 283.
8. (a) Bürger, H. and Wannagat, U., *Monatsh. Chem.*, 1963, **94,** 1007; (b) Bürger, H. and Wannagat, U., *Ibid.*, 1964, **95,** 1099; (c) Alyea, E. C., Bradley, D. C. and Copperthwaite, R. G., *J. Chem. Soc., Dalton Trans.*, 1972, 1580; (d) Hursthouse, M. B. and Rodesiler, P. F., *Ibid.*, 1972, 2100.
9. (a) Bradley, D. C., Ghotra, J. S. and Hart, F. A., *J. Chem. Soc., Dalton Trans.*, 1973, 1021; (b) Ghotra, J. S., Hursthouse, M. B. and Welch, A. J., *J. Chem. Soc. Chem. Comm.*, 1973, 669; (c) Andersen, R. A., Templeton, D. H. and Zalkin, A., *Inorg. Chem.*, 1978, **17,** 2317.
10. Fjeldberg, T. and Andersen, R. A., *J. Mol. Struct.*, 1985, **129,** 93.
11. Fjeldberg, T. and Andersen, R. A., *J. Mol. Struct.*, 1985, **128,** 49.
12. Andersen, R. A., *Inorg. Chem.*, 1979, **18,** 1507.
13. Shannon, R. D., *Acta Cryst.*, 1976, **32A,** 751.
14. Green, J. C., Payne, M., Seddon, E. A. and Andersen, R. A., *J. Chem. Soc., Dalton Trans.*, 1982, 887.
15. Guido, M. and Gigli, G., *J. Chem. Phys.*, 1976, **65,** 1397.
16. (a) Guido, M. and Gigli, G., *J. Chem. Phys.*, 1974, **61,** 4138; (b) Hildenbrand, D. L., *J. Electrochem. Soc.*, 1979, **126,** 1396.
17. (a) Andersen, R. A., Boncella, J. M., Burns, C. J., Green, J. C., Hohl, D. and Rosch, N., *J. Chem. Soc., Chem. Comm.*, 1986, 405; (b) Andersen, R. A., Blom, R., Burns, C. J. and Volden, H. V., *Ibid.*, 1987, 768; (c) Andersen, R. A., Boncella, J. M., Burns, C. J., Blom, R., Haaland, A. and Volden, H. V., *J. Organomet. Chem.*, 1986, **312,** C49; (d) Andersen, R. A., Blom, R., Boncella, J. M., Burns, C. J. and Volden, H. V., *Acta Chem. Scand.*, 1987, **41A,** 24; (e) Green, J. C., Hohl, D. and Rosch, N., *Organometallics*, 1987, **6,** 712.
18. (a) Hayes, E. F., *J. Phys. Chem.*, 1966, **70,** 3740; (b) Coulson, C. A., *Isr. J. Chem.*, 1973, **11,** 683; (c) Meyers, C. E., Norman, L. J. and Loew, L. M., *Inorg. Chem.*, 1978, **17,** 1581; (d) De Kock,

R. L., Peterson, M. A., Timmer, L. K., Baerends, E. J. and Vernooijs, P., *Polyhedron*, 1990, **9,** 1919.
19. Ortiz, J. V., Hay, P. J. and Martin, R. L., *J. Am. Chem. Soc.*, 1992, **114,** 2736.
20. Burns, C. J. and Bursten, B. E., *Comments Inorg. Chem.*, 1989, **9,** 61.
21. (a) Kanellakopulos, B., in *Organometallics of the f-Elements*, p. 1, Marks, T. J. and Fischer, R. D. (eds). D. Reidel, Dordrecht (1979); (b) Kanellakopulos, B., in *Gmelin Handbuch der Anorganische Chemie*, Uranium Suppl. A.6, (1983) p. 1; (c) Kanellakopulos, B., Fischer, E. O., Dornberger, E. and Baumgärtner, F., *J. Organomet. Chem.*, 1970, **24,** 507.

Pergamon

PII: S0277-5387(97)00315-X

Polyhedron Vol. 17, No. 5–6, pp. 959–963, 1998
© 1998 Elsevier Science Ltd
All rights reserved. Printed in Great Britain
0277-5387/98 $19.00+0.00

Changes in molecular geometry caused by oxidation in Ru_2 paddlewheel complexes: from Ru_2^{4+} to Ru_2^{5+} †

F. A. Cotton* and A. Yokochi

Department of Chemistry, Texas A&M University, College Station, TX77843-3255, U.S.A.

(Received 29 March 1997; accepted 5 June 1997)

Abstract—$[Ru_2(chp)_4(thf)][BF_4]$(Hchp = 2-chloro-6-hydroxypyridine) has been prepared and structurally characterized. The Ru–Ru distance is 2.2660(6) Å. Comparison of the structure of this Ru_2^{5+} compound with that of the previously known Ru_2^{4+} complex, $Ru_2(chp)_4(thf)$, reveals that the changes caused by the increase in oxidation state are similar to those previously observed for the Ru_2^{5+} to Ru_2^{6+} oxidation, with the metal–metal bond becoming slightly longer, by 0.005(1) Å, and all the metal–ligand bond lengths decreasing slightly.
© 1998 Elsevier Science Ltd. All rights reserved

Keywords: paddlewheel complexes; ruthenium; diruthenium; bond lengths; metalometal bonds.

Recognition of the existence of compounds containing multiply-bonded dimetal units occurred more than 30 years ago [1]. Soon after the earliest work, which dealt with dirhenium and dimolybdenum compounds, the first diruthenium compound, $Ru_2(O_2CCH_3)_4Cl$ was reported by Geoffrey Wilkinson and coworkers [2a]. A few years later it was found to have a Ru–Ru bond [2b] and thus a vigorous and fruitful effort began whereby dozens of diruthenium compounds containing Ru_2^{4+}, Ru_2^{5+} and Ru_2^{6+} cores have been prepared and characterized.

In the investigation of these molecules, as well as multiply-bonded dimetal compounds of other transition elements, the length of the metal–metal bond and its relation to bond order, has been one of the main areas in which research has focused [1]. Because changes in the ligand set surrounding the dimetal unit may have large effects on the molecular geometry [1], it is desirable to structurally compare molecules in which the only change is in the electron configuration [3].

Recently, we published a study in which the structure of an Ru_2^{6+} compound, $[Ru_2(ap)_4Cl][FeCl_4]$ (Hap = 2-anilinopyridine), was compared with that of an Ru_2^{5+} complex which contains exactly the same set of ligands, $Ru_2(ap)_4Cl$ [4]. Despite the fact that Ru_2^{4+} compounds have been known for almost as long as those of Ru_2^{5+} [1], there has not been, to date, a similar study in which two complexes of diruthenium containing exactly the same ligand set, but with these two core oxidation states, are compared. Since we have recently reported the structure of 0,4-$Ru_2(chp)_4(thf)$ (Hchp = 2-chloro-6-hydroxypyridinate) [5], the preparation and structural characterization of $[Ru_2(chp)_4(thf)]^+$ became our goal in order to make such a comparison.

EXPERIMENTAL

The work described here was carried out under an atmosphere of dry N_2 except where otherwise indicated. Solvents were of commercial grade, and freshly distilled from Na/K under an atmosphere of dry N_2 prior to use. $Ru_2(chp)_4Cl$ [6] and $Ru_2(chp)_4(thf)$ [5] were prepared according to published procedures. $AgBF_4$ was purchased from the Aldrich Chemical Co. and used as received. The IR spectrum was recorded from a KBr pellet on a Perkin–Elmer 1600-PC spectrophotometer. The magnetic susceptibility measurements were performed using a modified Gouy method, using a Johnson Mathey MSB-1 balance. Before calculating magnetic moments, the magnetic sus-

* Author to whom correspondence should be addressed.

† Dedicated to Prof. D. C. Bradley on the occasion of his 73rd birthday.

ceptibilities were corrected for diamagnetic contributions from the ligands and counterions by using correction coefficients estimated from Pascal's constants [7]. Both of the samples used for the magnetic measurement were ground and subjected to a vacuum for 1 h prior to use.

Synthesis of $[Ru_2(chp)_4(thf)][BF_4]$

In a Schlenk tube equipped with a magnetic stirring bar were placed, under an atmosphere of dry N_2, 0.15 g of $Ru_2(chp)_4Cl$ and 0.04 g $AgBF_4$. After the tube was sealed with a rubber septum and connected to a vacuum line, 10 cm^3 of THF, freshly distilled from Na/K under an atmosphere of dry N_2, were introduced using a syringe. This immediately resulted in a purple solution from which a fine, white precipitate, presumably AgCl, started forming. Stirring was continued for 2 h, and the solution filtered through a short plug of Celite and layered with 30 cm^3 of hexanes. Diffusion of the hexanes into the THF solution yielded a large crop of small prismatic crystals. Yield 0.142 g (88%).

IR (KBr, cm^{-1}): 2924 w, 1950 m, 1533 m, 1442 s, 1434 s, 1388 w, 1348 m, 1261 w, 1174 w, 1084 s, 1016 m, 929 w, 791 m, 720 m, 667 w, 630 m.

X-ray crystallography

While all the crystals examined were well shaped, their diffraction patterns revealed them to be twinned to a certain extent. However, careful choosing and trimming of a crystal yielded a specimen which did not appear to be twinned by inspection of axial diffraction photographs.

The crystal was mounted on the end of a thin quartz fiber with the aid of a small amount of a hydrocarbon grease and rapidly placed in the cold stream equipping the Nonius FAST area detector diffractometer. General procedures for this instrument have been reported elsewhere [8], but changes which have since been implemented in data collection and reduction have not yet been fully described, and are given below. The new procedures were devised to ensure that more accurate intensities are obtained, and that substantial amounts of redundant data, in the form of reflections equivalent both through azimuthal vector rotation and symmetry equivalents, are measured in order that an accurate empirical absorption correction may be performed.

After optical centering of the crystal in the X-ray beam, centering of reflections for crystal orientation, determination and refinement of crystallographic parameters and verification of crystallographic symmetry through the use of axial images, the instrument was set for data collection. The detector was set at a distance of 40 mm from the crystal, and the swing angle driven to 19°. This detector position allows data to be collected up to $2\theta = 51°$, and works well for crystals where the longest axis of the (primitive) unit cell does not exceed 30 Å. These parameters may be suitably modified to minimize reflection overlap in crystals with longer axes. Raw data were collected as series of oscillation images, each representing a 0.2° increment of one of three scans. One 220° scan about the ϕ axis was done with $\kappa = 33°$, and $\omega = 180°$. Subsequently, two 72° rotations about the ω axis were performed, one with $\omega = 205°$, $\kappa = -160°$ and $\phi = -75°$, and a second with ϕ rotated 90° from this, i.e., $\phi = 165°$ [9].

The images thus obtained were processed with an off-line version of MADNES [10], using an ellipsoid fit procedure as described by Kabsch [11]. Prior to extraction of reflection intensities from the images, a small portion of the data was processed in order to determine the appropriate size of the 'shoebox' to be fitted around each reflection, that both includes the complete reflection, and minimizes the amount of background measured, thus further decreasing the likelihood that the refection intensities may be skewed by encroachment by neighboring reflections. In this case a width of 0.7 mm and a length of 0.16° were deemed appropriate. Using these parameters, the three sets of images were processed, yielding three separate sets of data. These files contain F^2 and $\sigma(F^2)$ is given for each reflection, as well as additional information specifying where each reflection was positioned, both physically on the detector, and rotational angle in the general scan.

The three data files were then processed and fused into one file, containing the intensity data along with crystal dependent polar coordinates for the direction of the incident and reflected beams as found for each reflection, by using a locally modified version of the program ABSURD [12]. The data were corrected for absorption anisotropy effects and merged using a local adaptation of the program SORTAV [13]. In this case a total of 19,622 reflections were processed, with maximum and minimum transmission coefficients of 0.891(10) and 0.659(5), yielding 6549 unique reflections after merging ($R_{merge} = 4.96\%$).

A solution was obtained by using direct methods as programmed in SHELXS-86 [14], from which the complete molecule of $[Ru_2(chp)_4(thf)]^+$ was found. Remaining atoms were found by successive iterations of least squares cycles followed by Fourier synthesis using the program SHELXL-93 [15]. All hydrogen atoms in the main molecule were found and were freely refined in the final least squares cycle. Selected crystallographic parameters and details of the refinement are given in Table 1, and a listing of selected bond lengths and angles is found in Table 2. A thermal ellipsoid plot of the $[Ru_2(chp)_4(thf)]^+$ molecule is given in Fig. 1.

In addition to a molecule of $[Ru_2(chp)_4(thf)]^+$, a $[BF_4]^-$ counterion and a THF molecule of crystallization, the unit cell also contains an area of diffuse solvent which was modeled as a highly disordered THF molecule, in which the atoms were refined with a common isotropic displacement parameter.

Table 1. Crystal data and structure refinement for $[Ru_2(chp)_4(thf)][BF_4]\cdot 2THF$

Empirical formula	$C_{32}H_{36}BCl_4F_4N_4O_7Ru_2$
Formula weight	1019.48
Space group	$P2_1/n$
Unit cell dimensions	$a = 14.691(2)$ Å $\alpha = 90°$
	$b = 11.670(2)$ Å $\beta = 104.71(2)°$
	$c = 22.635(5)$ Å $\gamma = 90°$
Volume	3753.3(11) Å^3
Z	4
Density (calculated)	1.804 g/cm^3
Crystal size	$0.2 \times 0.1 \times 0.1$ mm
Absorption coefficient	1.162 mm^{-1}
Data collection instrument	Nonius FAST
Wavelength	0.71073 Å
Orientation reflections, number, range (θ)	250, 8–20
Temperature	293(2) K
Scan method	Ellipsoid-mask fit
Theta range for data collection	2.26–25.09°
Reflections collected	19,622
Independent reflections	6549 [R(int) = 0.0496]
Data/restraints/parameters	6549/53/642
Max. and min. transmission	0.891(10) and 0.659(5)
Refinement method	Full-matrix least-squares on F^2
Final R indices [$I > 2\sigma(I)$]	$R1 = 0.043$, $wR2 = 0.104$
R indices (all data)	$R1 = 0.072$, $wR2 = 0.119$
Goodness-of-fit on F^2	1.064
Largest shift/esd, final cycle	0.001
Largest peak, final cycle	0.81(11) e/Å^3

Table 2. Selected bond lengths (Å) and angles (°) for $[Ru_2(chp)_4(thf)][BF_4]\cdot 2THF$

Ru(1)—O(3)	1.976(4)
Ru(1)—O(1)	1.977(4)
Ru(1)—O(2)	1.978(4)
Ru(1)—O(4)	1.981(4)
Ru(1)—O(5)	2.212(3)
Ru(1)—Ru(2)	2.2660(6)
Ru(2)—N(1)	2.098(4)
Ru(2)—N(3)	2.100(4)
Ru(4)—N(4)	2.103(5)
Ru(2)—N(2)	2.107(5)
O(3)—Ru(1)—Ru(2)	91.80(10)
O(1)—Ru(1)—Ru(2)	91.73(10)
O(2)—Ru(1)—Ru(2)	91.29(11)
O(4)—Ru(1)—Ru(2)	91.58(10)
O(5)—Ru(1)—Ru(2)	179.70(11)
N(1)—Ru(2)—Ru(1)	87.71(12)
N(3)—Ru(2)—Ru(1)	87.52(12)
N(4)—Ru(2)—Ru(1)	87.45(12)
N(2)—Ru(2)—Ru(1)	87.63(12)

Magnetic susceptibility measurements

Magnetic susceptibility of $[Ru_2(chp)_4(thf)][BF_4]$. Since this compound is not air sensitive or moisture sensitive, the sample was prepared, and the measurement made, in air. In a carefully calibrated tube were placed 0.1201 g of finely powdered $[Ru_2(chp)_4(thf)][BF_4]$, and the measurement made. Calculations revealed a magnetic moment of 3.82 B.M.

Magnetic susceptibility of $Ru_2(chp)_4(thf)$. This compound is exceedingly air sensitive, both in solution and as a solid. For this reason, the preparation of the sample was carried out under an atmosphere of dry Ar. In the sample tube were placed 0.1325 g of $Ru_2(chp)_4(thf)$, and the tube sealed with the aid of a rubber septum. The sample was then rapidly transferred to the balance, and from the measurement a magnetic moment of 2.87 B.M. was calculated.

DISCUSSION

Synthesis of $[Ru_2(chp)_4(thf)][BF_4]$

The synthesis of the compound was quite straightforward, consisting in the mere removal of the axial halide from $Ru_2(chp)_4Cl$ with $AgBF_4$ in THF. The reactants were placed together in the Schlenk tube under an atmosphere of dry N_2 because of the extremely hygroscopic character of $AgBF_4$. When the silver salt is allowed to absorb atmospheric moisture undesirable side products are formed in which the water is found coordinated to the diruthenium unit [16].

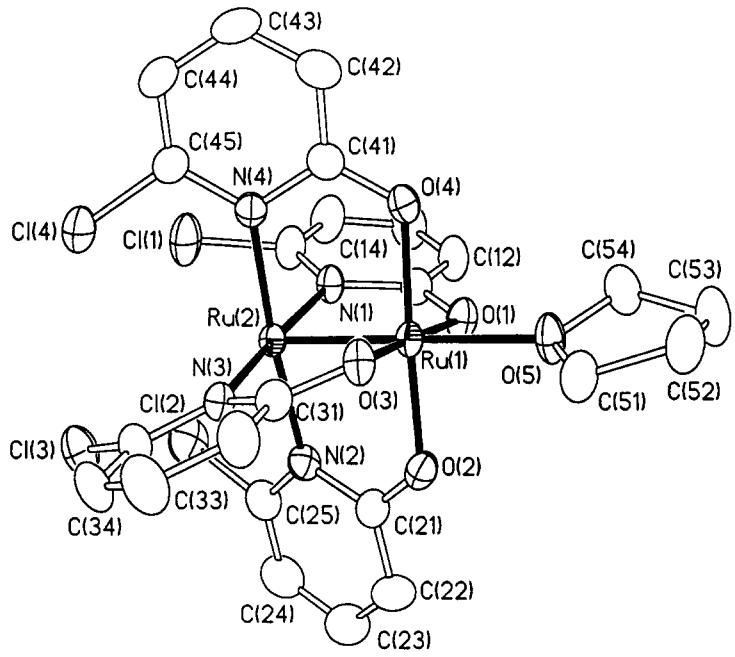

Fig. 1. Thermal ellipsoid plot of $[Ru_2(chp)_4(thf)]^+$.

Magnetic properties

As expected the Ru_2^{5+} compound has magnetic properties consistent with the presence of three unpaired electrons per formula unit, thus confirming the $\pi^{*2}\delta^{*1}$ electronic configuration for this molecule. The Ru_2^{4+} complex is paramagnetic, with magnetic properties consistent with the existence of two unpaired electrons per molecule. This rules out the possibility of a $\pi^{*4}\delta^{*0}$ ground state, but cannot distinguish between the other two reasonable options, $\delta^{*2}\pi^{*2}$ or $\pi^{*3}\delta^{*1}$. A choice between these two can be made on the basis of the molecular structure.

Structure of $[Ru_2(chp)_4(thf)]^+$ *and comparison with* $Ru_2(chp)_4(thf)$

The structure determined for $[Ru_2(chp)_4(thf)]^+$ is that which was expected: the four chp^- ligands remain arranged about the Ru_2 unit such that all four chlorine atoms are at the same end of the molecule, and the molecule of THF is found coordinated to the axial position unencumbered by the pendant halogens, i.e., the 0,4-regioisomer. The length of the Ru–Ru bond is found to be 2.2660(6) Å, well within the range expected for Ru_2^{5+} compounds, intermediate between $Ru_2(chp)_4Cl$ (Ru–Ru = 2.2835(15) Å) [17] and $[\{Ru_2(chp)_4\}_2]^{2+}$ (Ru—Ru = 2.254(1) Å) [5].

In going from the Ru_2^{4+} to the Ru_2^{5+} state the Ru–Ru bond lengthens slightly, while all the metal–ligand bonds shorten significantly, as had been found for the Ru_2^{5+} to Ru_2^{6+} oxidation,[4] and these changes are summarized in Table 3. These changes are consistent with the changes observed in electronic ground state for the Ru_2 unit, and clearly show that in the ground state of the Ru_2^{4+} complex the electronic configuration is $\delta^{*2}\pi^{*2}$ for the following reasons. While an oxidation resulting from the removal of an antibonding δ^* electron from the Ru–Ru bond, accompanied by a slight increase in electrostatic repulsion between the two metal atoms would result in the slight increase found in metal–metal distance, removal of a strongly antibonding π^* electron would result in a large decrease in metal–metal distance, unlikely to be completely offset by the electrostatic effect referred to. The fact that δ^* electrons are only weakly antibonding was first proven by the series of compounds $[Re_2Cl_4(PMePh_2)_4]^{n+}$ (n = 0, 1, 2), in which removal of the δ^* electrons results in only small changes in metal–metal bond length [3].

The increased electrostatic attraction between the metal atoms and the anionic chp^- ligands results in the shortening of the M–N and $M–O_{chp}$ bonds. The same is true for the $Ru–O_{thf}$ bond since even though this ligand is neutral, it has an electrostatic dipole moment such that a partial negative charge lies on the O. This, in combination with the fact that the thf is a monodentate ligand, and therefore somewhat more susceptible to deformation by packing forces [17], explains the large decrease in $Ru–O_{thf}$ bond length.

CONCLUSIONS

From the comparison of the structures and magnetic properties of these two complexes it is clear that

Table 3. Comparison of selected bond lengths (Å) in $Ru_2(chp)_4(thf)$ and $[Ru_2(chp)_4(thf)]^+$. Numbers in parentheses are either crystallographic s.u.'s or average crystallographic s.u.'s

	Ru–Ru	Average Ru—N	Average Ru—O_{chp}	Ru—O_{thf}
$Ru_2(chp)_4(thf)$	2.2609(8)	2.121(5)	2.047(4)	2.251(4)
$[Ru_2(chp)_4(thf)]^+$	2.2660(6)	2.102(4)	1.978(4)	2.212(3)
Δ	0.0051	−0.019	−0.069	−0.039

the oxidation arises from the removal of a weakly antibonding δ^* electron, changing the electronic configuration from $\pi^{*2}\delta^{*2}$ to $\pi^{*2}\delta^{*1}$. In removing this weakly antibonding electron from the Ru–Ru orbital manifold the gains achieved in bonding are easily offset by the increased electrostatic repulsion between the metal atoms caused by the oxidation, and results in a slight increase in metal–metal distance, a change similar to that observed for the Ru_2^{5+} to Ru_2^{6+} oxidation.

Acknowledgment—We thank the National Science Foundation for financial support.

REFERENCES

1. Cotton, F. A. and Walton, R. A., *Multiple Bonds Between Metal Atoms*, 2nd edn. Oxford University Press, Oxford, 1993.
2. (a) Stephenson, T. A. and Wilkinson, G. J., *J. Inorg. Nucl. Chem.*, 1966, **28,** 2285; (b) Bennett, M. J., Caulton, K. G. and Cotton, F. A., *Inorg. Chem.*, 1969, **9,** 1.
3. See, for example, Cotton, F. A., Falvello, L. R., Tomas, M. and Walton, R. A., *J. Am. Chem. Soc.*, 1983, **105,** 4950.
4. Cotton, F. A. and Yokochi, A., *Inorg. Chem.*, 1997, **36,** 567.
5. Cotton, F. A., Kim, Y. and Yokochi, A., *Inorg. Chim. Acta*, 1995, **236,** 55.
6. Chakravorty, A. R., Cotton, F. A. and Tocher, D. A., *Inorg. Chem.*, 1985, **24,** 1263.
7. *Theory and Application of Molecular Paramagnetism*, ed. E. A. Boudreaux and L. N. Mulay, John Wiley and Sons, New York (1976).
8. Cotton, F. A., Haefner, S. C. and Sattelberger, A. P., *Inorg. Chem.*, 1995, **34,** 1875.
9. For triclinic crystals, due to the low symmetry of these systems, a fourth scan of 60° about ω is usually added with $\omega = 180°$, $\kappa = 33°$, $\phi = -110°$.
10. Pflugrath, J. and Messerschmitt, A., MADNES, Munich Area Detector (New EEC) system, version EEC 11/09/89, with enhancements by Nonius Corp., Delft, The Netherlands. A description of MADNES can be found in Messerschmitt A. and Pflugrath, J. *J. Appl. Cryst.*, 1987, **20,** 306.
11. Kabsch, W., *J. Appl. Cryst.*, 1988, **21,** 67; Kabsch, W., *J. Appl. Cryst.*, 1988, **21,** 916.
12. Evans, P. R., ABSURD—Absorption Correction for the Area Detector, MRC Laboratory of Molecular Biology, Cambridge, UK (1990).
13. Blessing, R. H., *Acta Cryst.*, 1995, **A51,** 33.
14. Sheldrick, G. M., in *Crystallographic Computing* 3, ed. G. M. Sheldrick, C. Krüger and R. Goddard. Oxford University Press, Oxford (1985).
15. Sheldrick, G. M., in *Crystallographic Computing* 6, ed. H. D. Flack, L. Parkanyi and K. Simon. Oxford University Press, Oxford (1993).
16. Cotton, F. A. and Yokochi, A., in preparation.
17. Cotton, F. A. and Yokochi, A., *Inorg. Chem.*, 1997, **36,** 2461.

Pergamon

PII: S0277-5387(97)00245-3

Polyhedron Vol. 17, No. 5–6, pp. 965–968, 1998
© 1998 Elsevier Science Ltd
All rights reserved. Printed in Great Britain
0277-5387/98 $19.00+0.00

$MoO(O^iPr)_4$ decomposition pathways on ageing: spontaneous and nearly quantitative transformation into $Mo_6O_{10}(O^iPr)_{12}$

Vadim G. Kessler,[a]* Andrei V. Shevelkov[a] and Lars A. Bengtsson-Kloo[b]

[a] Department of Inorganic Chemistry, Lomonosov Moscow State University, Vorobjovy Gory, 119899 Moscow, Russia

[b] Inorganic Chemistry 1, Dept of Chemistry, Lund University, P.O. Box 124, S-221 00 Lund, Sweden

(Received 3 March 1997; accepted 5 June 1997)

Abstract—Liquid samples of $MoO(O^iPr)_4$ (**I**), kept at room temperature in complete isolation from oxygen and moisture, nearly completely solidify after approximately 2 months of storage. GLC-MS analysis of the liquid residue showed it containing approximately equal amounts of ^iPrOH and acetone and excess of $^iPr_2O$. Multinuclear NMR (^{13}C, ^{17}O and ^{95}Mo) investigation of this reaction in solution in toluene proved that acetone and ether elimination occur simultaneously. The solid product of the reaction was identified as $Mo_6O_{10}(O^iPr)_{12}$ (**II**). © 1998 Elsevier Science Ltd. All rights reserved

Keywords: $MoO(O^iPr)_4$; acetone; ether.

The preparation and properties of $MoO(O^iPr)_4$ (**I**) have been first described by Chisholm *et al.* in the fundamental work devoted to the investigation of the oxidation of $Mo_2(OR)_6$ and $[Mo(OR)_4]_x$ ($x = 1$ or 2) compounds by molecular oxygen [1]. While the dimeric isopropoxide of molybdenum(IV) (Mo=Mo) undergoes a facile one-step, oxidative addition process in hydrocarbon media, leading directly to **I**:

$$Mo_2(O^iPr)_8 + O_2 \rightarrow 2MoO(O^iPr)_4) \quad (1)$$

the derivative of molybdenum(III) Mo≡Mo) follows a complex oxidation pathway associated with the formation of two structurally identified intermediates—$Mo_3O(O^iPr)_{10}$ and $Mo_6O_{10}(O^iPr)_{12}$ (**II**). The average reaction equation can in this case be formulated as

$$Mo_2(O^iPr)_6 + O_2 \rightarrow MoO_2(O^iPr)_2 + 2^iPrO\cdot \quad (2)$$

The free radicals thus formed recombine to give an equimolar mixture of acetone and isopropanol. Only microamounts of **I** were obtained by Chisholm and co-workers using reaction (1). For the synthetic purposes, the same authors prepared it by metathesis of $MoOCl_4$ with ROH in the presence of Et_3N [2]. No ageing phenomenon was noticed for **I**, described as a yellow liquid, distillable at 60°C/10^{-4} torr without decomposition. In later publications the preparation of the samples of **I** (identical in appearance and spectral characteristics to those mentioned in [1,2]) by metathesis of $MoOCl_4$ with NaOR and by anodic oxidation of molybdenum metal in ROH was described [3,4]. The tendency to ether elimination, being a general feature of molybdenum(VI) alkoxides [4], was also observed for **I** and the phenomenon becomes especially pronounced in reactions with the alkoxides of electropositive metals, for example [5]

$$2La(O^iPr)_3 + 4MoO(O^iPr)_4 \rightarrow$$

$$La_2Mo_4O_8(O^iPr)_{14} + 4^iPr_2O \quad (3)$$

The later publications also emphasis the inapplicability of distillation for the purification of **I**, because of contamination with dioxoderivative caused by ether elimination [3]. The samples of **I** described in [3–5] were purified by extraction with hexane and thus the contamination by alkaline metals might not be totally excluded.

* Author to whom correspondence should be addressed.

The present communication is devoted to the description of phenomena observed for the spectrally pure samples of **I** on storage.

EXPERIMENTAL

All compounds described in this work are highly sensitive to moisture and oxygen and therefore all operations with them were carried out under inert atmosphere conditions employing a vacuum line or a glove box.

Dehydration of alcohols, ROH, was performed by refluxing over magnesium (R = Me), and aluminum (R = ^{i}Pr) alkoxides with subsequent distillation. Toluene and hexane were refluxed over sodium and then distilled over $LiAlH_4$. Pyridine was stored over anhydrous KOH and distilled over a fresh portion of KOH prior to use.

The carbon and hydrogen contents in the samples were determined using conventional combustion techniques. The molybdenum content was determined gravimetrically as MoO_3. Hydrated oxides were precipitated from solutions by hot 1:1 diluted HNO_3, washed with the deionized water on the filter and annealed to constant weight at 400°C. The lithium content was determined by flame photometry with an FLAPHO-4 device.

IR spectra were recorded with a Specord IR 75 in Nujol or hexachlorobutadiene mulls. Crystalline solid samples were identified using powder diffractometry (DRON 3M). GLC-MS tests were carried out using an MAT 311A Varian device (source temperature 200°C, SE-30 separation column). All NMR spectra were recorded on a Varian Unity 300 MHz spectrometer. TMS was used as reference for the ^{13}C spectra, ^{17}O-enriched (approx. 2%) water for the ^{17}O and MoO_4^{2-} (aq) for the ^{95}Mo spectra.

*Preparation of the spectrally pure samples of **I** and decomposition study.*

Approximately 1 g of $MoO(OMe)_4$ prepared by anodic oxidation of molybdenum in methanol [6], and containing less than 10 ppm of Li because of repeated recrystallisation prior to use, was dissolved in 20 cm^3 ^{i}PrOH. The solution was slowly evaporated to dryness in dynamic vacuum at room temperature. This operation was repeated trice. The product turned to be a bright yellow solid (mp 18°C) identified by IR and ^{13}C NMR spectra as pure $MoO(P^iPr)_4$. About 5 g $MoO(O^iPr)_4$ was dissolved in toluene to give a 1 M solution. An analogous sample, to which 0.2 g pyridine was added, was also prepared. Both solutions were sealed in evacuated ampoules and stored in darkness.

*X-ray single crystal investigation of **II**.*

A crystal was chosen from the crop that precipitated from the solution of **I** after two months of storage. It was sealed in a glass capillary tube under argon in a dry box, and mounted on the goniometer head of a CAD4 diffractometer. Unit cell parameters were obtained by indexing 25 randomly found reflections in an angular range $3.6 < \theta < 12.7°$ at ambient temperature. The triclinic unit cell parameters $a = 13.289(8)$, $b = 11.469(8)$, $c = 10.047(6)$ Å, $\alpha = 106.86(9)$, $\beta = 91.5(1)$, $\gamma = 98.95(9)°$ were refined based on 24 well-centered reflections in the angular range $8 < \theta < 12°$ and appeared to differ slightly from those obtained for $Mo_6O_{10}(O^iPr)_{12}$: $a = 13.082$, $b = 11.478$, $c = 9.760$ Å, $\alpha = 106.40$, $\beta = 91.85$, $\gamma = 99.81°$ [1]. Data collection in the angular range $1 < \theta < 4°$ was performed, and intensities of observed reflections were compared with those simulated using the cell dimensions and atomic parameters listed in [1]. A comparison of related intensities of 45 reflections showed no difference between the investigated and reported phases, and proved their chemical identity. However, minor structural changes due to the organic tail rotation on going from 160 to 291 K cannot be ruled out, and the increase in the unit cell volume could be indicative of this.

RESULTS AND DISCUSSION

The unusual ageing phenomenon described in this paper was first observed for the liquid samples of **I** sealed in the evacuated glass ampules and left for prolonged storage in a darkness at room temperature (24°C). It was observed that their colour slowly changed from bright yellow to dark reddish-brown. After approximately 2 weeks the precipitation of a solid started. The samples solidified nearly completely in 9–10 weeks being transformed into a reddish-orange solid and minor amounts of a pale non-viscous liquid. The molybdenum content in the liquid phase was very low (2%), while the IR spectrum in the Mo=O and Mo—OR vibration region revealed the pattern characteristic of **I** (see [1–3]). This made us believe that the liquid phase could be a mixture of the organic products of decomposition of **I**. It was subjected to a GLC-MS investigation that showed it to consist of three main components: acetone and isopropanol in approximately equal amounts, and excess of isopropylether. The presence of the latter compound was anticipated and the mechanism of its formation has been discussed in the literature [4]. In contrast, the presence of an equimolar mixture of the ketone and alcohol was unexpected and may be explained by three different scenarios. The simplest one can be regarded as a spontaneous radical decomposition, analogous, for example, to that of $U(OMe)_6$, subjected to laser irradiation [7]:

$$2MoO(P^iPr)_4 \rightarrow 2MoO(O^iPr)_3 + 2^iPrO\cdot \quad (4a)$$

$$2^iPrO\cdot \rightarrow {}^iPrOH + CH_3COCH_3 \quad (4b)$$

However, the activation energy for such a reaction

ought to be rather high, and would therefore presumably require a photochemical initiation, which is unlikely considering that the samples were stored in darkness. The second possibility involves a β-hydrogen transfer from the methyne group of the ligand directly to the metal atom, analogous to that observed for $[Re(O^iPr)_3]_3$ [8], followed by the interaction of a hydride intermediate with an unreacted molecule of **I**:

$$MoO(O^iPr)_4 \rightarrow MoO(O^iPr)_3H + CH_3COCH_3 \quad (5a)$$

$$MoO(O^iPr)_3H + MoO(O^iPr)_4 \rightarrow 2MoO(O^iPr)_3 + {}^iPrOH \quad (5b)$$

The third reaction pathway may be analogous to the mechanism established for the catalytical activity of molybdenum oxides in the methanol conversion into formaldehyde [9] and involves the β-hydrogen transfer from the ligand to the oxo oxygen atom, again followed by the interaction with a molecule of **I**:

$$MoO(O^iPr)_4 \rightarrow Mo(O^iPr)_3(OH) + CH_3COCH_3 \quad (6a)$$

$$Mo(O^iPr)_3(OH) + MoO(O^iPr)_4 \rightarrow 2MoO(O^iPr)_3 + {}^iPrOH \quad (6b)$$

All these possible explanations are associated with the reduction of **I** and the formation of Mo^V derivatives. The identification of the solid product of ageing proved this to be the case. The solid formed revealed an IR spectrum identical to that described for compound **II** [1] and was by microanalysis found to have almost the same composition, i.e. $Mo_6O_{10}(O^iPr)_{12}$ (see Fig. 1). In addition, its X-ray powder pattern turned out to be very similar to that calculated for **II** using the unit cell parameters given in [1].

In order to investigate the kinetics of the above mentioned decomposition processes, the ^{13}C and ^{17}O NMR spectra were recorded for the samples of the 1 M solution of **I** in toluene approximately every second week for 2 months. The spectra of the freshly prepared samples were in agreement with the presence of pure **I** in the solution (^{13}C δ, ppm: 78.2 (*C*H), 23.1 and 20.2 (CH_3); ^{17}O δ, ppm: 897 sharp (*O*=Mo, to compare with 894 in ref [1]) and 292 broad (R*O*—Mo). After the first 2 weeks of storage two sharp and intense new peaks appeared in the low-field region: at 99.7 ppm, corresponding to a R_2C=O group coordinated by a metal centre, and at 61.7 ppm, presumably originating from the *C*H fragments in isopropylether. The peak at 78 ppm becomes noticeably broadened, most likely because of exchange with released molecules of isopropyl alcohol. In the high-field region a new peak at 26.5 ppm appears, that with a certainty can be attributed to the CH_3 groups of acetone. The changes are even more pronounced after approximately 4 weeks of storage. It should be noted that at this point the peak at 78 ppm splits further into two broad resonances at 81 (weaker) and 76 (stronger), thus indicating the appearance of structurally distinguishable alkoxide ligands. The ^{17}O spectrum also demonstrates rather important changes: both resonances observed for **I** are shifted up-field to 868 and 188 ppm, respectively, and two new sharp peaks corresponding to oxoligands appear at 573 and 84 ppm. A considerable change is also observed in the ^{95}Mo: the peak at +47 ppm, corresponding to pure **I** [10] is considerably decreased in intensity and a new broad peak at −17 has become predominant.

All these observations are in agreement with the simultaneous elimination of acetone and ether and partial reduction of Mo^{VI} into Mo^V, that eventually transforms $MoO(O^iPr)_4$ (**I**) nearly quantitatively into $Mo_6O_{10}(O^iPr)_{12}$ (**II**). This suggestion is further supported by the X-ray pattern identification of a crystal formed on ageing of a solution of **I** in toluene with compound **II**.

It is to be noted that the addition of amines to the samples of **I** prevents coloration and thus is likely to hinder the described decomposition pathway.

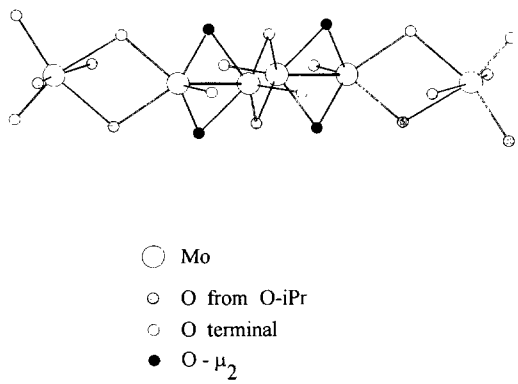

Fig. 1. Molecular structure of $Mo_6O_{10}(O^iPr)_{12}$ (**II**), generated using the atomic coordinates published by Chisholm *et al.* [1]; carbon atoms are omitted for clarity.

REFERENCES

1. Chisholm, M. H., Folting, K., Huffman, J. C. and Kirkpatric, C. C., *Inorg. Chem.*, 1984, **23,** 1021.
2. Chisholm, M. H., Folting, K., Huffman, J. C. and Kirkpatric, C. C., *J. Am. Chem. Soc.*, 1981, **103,** 5967.
3. Turova, N. Ya. and Kessler, V. G., *Russ. J. General Chem.* (*Russ*), 1990, **60,** 113.
4. Turova, N. Ya., Kessler, V. G. and Kucheiko, S. I., *Polyhedron*, 1991, **10,** 2617.
5. Kessler, V. G., Turova, N. Ya., Panov, A. N., Yanovsky, A. I., Pisarevsky, A. P. and Struchkov, Yu. T., *Polyhedron*, 1996, **15,** 335.
6. Kessler, V. G., Mironov, A. V., Turova, N. Ya., Yanovsky, A. I. and Struchkov, Yu. T., *Polyhedron*, 1993, **12,** 1573.

7. Van der Sluys, W. G. and Sattelberger, A. P., *Chem. Rev.*, 1990, **90,** 1027.
8. Hoffman, D. M., Lappas, D. and Wierda, D. A., *J. Am. Chem. Soc.*, 1989, **111,** 1531.
9. McCarron, E. M. and Harlow, R. L., *J. Am. Chem. Soc.*, 1983, **105,** 6179.
10. Fedotov, M. A., Kessler, V. G., Turova, T. Ya., unpublished.

Pergamon

PII: S0277-5387(97)00222-2

Polyhedron Vol. 17, No. 5–6, pp. 969–976, 1998
© 1998 Elsevier Science Ltd
All rights reserved. Printed in Great Britain
0277-5387/98 $19.00+0.00

Organoimido and organodi-imido vanadium complexes†

Dale E. Wheeler,[a] Ji-Fang Wu[b] and Eric A. Maatta[b]*

[a] Department of Chemistry, University of Wisconsin-Parkside, Kenosha, WI 53141-2000, U.S.A.

[b] Department of Chemistry, Kansas State University, Manhattan, KS 66506-3701, U.S.A.

(Received 24 April 1997; accepted 17 May 1997)

Abstract—Reactions of the *p*-tolylimido vanadium(V) complex $[V(NTol)Cl_3]$, **1**, with sodium dithiocarbamate salts $Na[S_2CNR_2]$ yield an homologous series of organoimido vanadium(V) dithiocarbamate systems $[TolN{\equiv}V(S_2CNR_2)_xCl_{(3-x)}]$ [$x = 1$: R = Et (**2a**), Me (**2b**); $x = 2$: R = Et (**3a**), Me (**3b**); $x = 3$: R = Et (**4a**), Me (**4b**)]; the electronic and ^{51}V NMR spectra of these complexes are described. Zn reduction of complexes **3** affords impure products whose ESR spectra are consistent with the presence of the V(IV) systems $[V(NTol)(S_2CNR_2)_2]$, **5**. Reaction of $VOCl_3$ with 0.5 equiv. of *p*-OCN—C_6H_4–NCO yields the *p*-phenylenediimido complex $[Cl_3V{\equiv}NC_6H_4N{\equiv}VCl_3]$, **6**. Dissolution of **6** in THF produces an adduct $[(THF)_3Cl_3V{\equiv}NC_6H_4N{\equiv}VCl_3(THF)_3]$, **7**, whose THF ligands are weakly bound. $VOCl_3$ reacts with an equimolar amount of *p*-OCN—C_6H_4—NCO to produce the mononuclear complex *p*-$[Cl_3V{\equiv}NC_6H_4$—NCO], **8**. The reaction of **8** with $OWCl_4$ in refluxing toluene affords an insoluble product analyzing as the expected heterobinuclear system $[Cl_3V{\equiv}NC_6H_4N{\equiv}WCl_4]$, **9**, but treatment of this product with THF yields a mixture shown by ^1H NMR to contain both **7** and its ditungsten analogue $[(THF)Cl_4W{\equiv}NC_6H_4N{\equiv}WCl_4(THF)]$, indicating that an unusual intermetallic exchange of imido ligands has occurred. The chloride ligands of **6** can be substituted by $[S_2CNEt_2]$ or [O'Bu] anions to afford $[(Et_2NCS_2)_3V{\equiv}NC_6H_4N{\equiv}V(S_2CNEt_2)_3]$, **11**, and $[('BuO)_3V{\equiv}NC_6H_4N{\equiv}V(O'Bu)_3]$, **12**, respectively. © 1998 Elsevier Science Ltd. All rights reserved

Keywords: organoimido vanadium(V) dithiocarbamate systems; intermetallic exchange; imido ligands.

The first examples of vanadium dithiocarbamate complexes, $V(S_2CNR_2)_4$, were prepared by Bradley and Gitlitz by the action of CS_2 on the corresponding tetrakis(dialkylamides) $V(NR_2)_4$ [1]. Subsequent investigations [2] revealed that $V(S_2CNEt_2)_4$ was thermally and oxidatively unstable and that upon exposure to O_2, the oxo vanadium dithiocarbamates $O{\equiv}V(S_2CNEt_2)_3$ [3] and $O{\equiv}V(S_2CNEt_2)_2$ [4] were produced. Since oxo and organoimido ligands are isoelectronic, and often form congruent sets of transition metal complexes [5], we became interested in the arylimido analogues of these oxo-vanadium systems. In this contribution, we report an homologous series of tolylimido vanadium dithiocarbamate complexes of the form $[TolN{\equiv}V(S_2CNR_2)_xCl_{(3-x)}]$ and describe the preparation and preliminary reactivity studies of a divanadium phenylenedi-imido complex *viz.*, $[Cl_3V{\equiv}NC_6H_4N{\equiv}VCl_3]$.

RESULTS AND DISCUSSION

Tolylimido vanadium(V) complexes

The starting material for these syntheses is *p*-tolylimido vanadium(V) trichloride [6], $V(NTol)Cl_3$, **1**, which is one of a large number of arylimido vanadium(V) complexes conveniently prepared from the reaction of $VOCl_3$ with the corresponding arylisocyanate ArNCO [7]. The substitution reactions of **1** with anhydrous sodium dithiocarbamates $Na[S_2CNR_2]$ (R = Me, Et) in CH_2Cl_2 at room temperature occur as shown in eq. (1). All of these solid products display good solubility in chlorinated hydrocarbon solvents and are moderately soluble in toluene, with the diethyl dithiocarbamate species as a class displaying higher solubility than the dimethyl derivatives.

* Author to whom correspondence should be addressed.

† Dedicated with respect to Professor Donald C. Bradley, an inspiring scientist and a true gentleman.

$$\mathbf{1} + x\,Na[S_2CNR_2] \xrightarrow{CH_2Cl_2} TolN{\equiv}V(S_2CNR_2)_xCl_{(3-x)} + x\,NaCl \quad (1)$$

$x = 1$: R = Et, **2a**; R = Me, **2b**

$x = 2$: R = Et, **3a**; R = Me, **3b**

$x = 3$: R = Et, **4a**; R = Me, **4b**

The ^1H NMR spectra of the monosubstituted species **2a** and **2b** each reveal a single environment for the alkyl groups within the dithiocarbamate ligands, suggesting that the dithiocarbamates bind in the equatorial plane *cis* to the tolylimido ligand, but this observation alone is insufficient to deduce their probable geometries. For the disubstituted systems **3a** and **3b**, ^1H NMR spectra again indicate that the dithiocarbamates are contained in the equatorial plane *cis* to the tolylimido ligand: for **3a**, the S_2CNEt_2 groups produce a single methyl triplet δ 1.27 and a pair of methylene ABX_3 multiplets (due to the diastereotopic CH_2 protons) centered at δ 3.78 while for **3b**, a single resonance for the S_2CNMe_2 groups is observed at δ 3.36. These observations are consistent with a pseudo-octahedral structure for complexes **3** in which the chlorine atom occupies the position *trans*-to the tolylimido ligand as shown in Fig. 1. For the trisubstituted complexes **4**, ^1H NMR spectra suggest the adoption of a pentagonal bipyramidal structure (Fig. 1). Thus, the methyl groups of the S_2CNEt_2 ligands of **4a** appear as two triplets of relative intensity 5:1, as observed for the isoelectronic species $[PhN{\equiv}Mo(S_2CNEt_2]^+$ [9]; the methyl groups of the S_2CNMe_2 ligands of **4b** appears as five singlets of relative intensity 2:1:1:1:1. Pentagonal bipyramidal structures have been established crystallographically both for $O{\equiv}V(S_2CNEt_2)_3$ [3b] and $[Ph_3CN{\equiv}Mo(S_2CNMe_2)_3]^+$ [10].

The ^{51}V NMR spectra of these complexes have been recorded as $CDCl_3$ solutions and the results are collected in Table 1. For the mono-substituted complexes **2**, the ^{51}V chemical shifts are perturbed only slightly upfield of that of the $V(NTol)Cl_3$ parent (**1**, 305; **2a**, 301; **2b**, 289 ppm). Incorporation of a second dithiocarbamate ligand induces a moderate upfield shift (**3a**, 166; **3b**, 161 ppm), while extreme upfield shifts are observed for the tris(dithiocarbamate) complexes (**4a**,

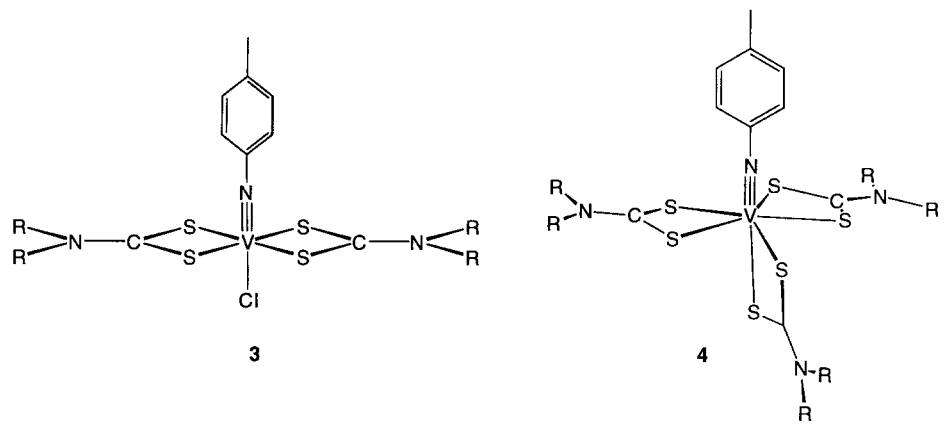

Fig. 1. Proposed structures for complexes **3** and **4**.

Table 1. ^{51}V NMR[a] and visible spectral[b] Data for $V(NTol)(S_2CNR_2)_xCl_{(3-x)}$ Complexes

Complex	$\delta(^{51}V)$ (ppm)	fwhm (Hz)	λ_{max} (nm)
$V(NTol)(S_2CNEt_2)Cl_2$ (**2a**)	301	415	530
$V(NTol)(S_2CNMe_2)Cl_2$ (**2b**)	289	439	520
$V(NTol)(S_2CNEt_2)_2Cl$ (**3a**)	166	2610	393
$V(NTol)(S_2CNMe_2)_2Cl$ (**3b**)	161	1870	540
$V(NTol)(S_2CNEt_2)_3$ (**4a**)	−565	1780	520
$V(NTol)(S_2CNMe_2)_3$ (**4b**)	−574	1530	393

[a] $CDCl_3$ solution, 298 K, 105.2 MHz, relative to external $VOCl_3/CDCl_3$ (75% v/v), positive values denote downfield chemical shifts.

[b] $C_6H_5CH_3$ solution, 298 K.

−565; **4b**, −574 ppm). The linewidths of these resonances in all cases are sufficiently broad (*ca* 400–2600 Hz) so as to preclude the resolution of ^{51}V–^{14}N spin coupling; such coupling constants have been observed to range from 92–112 Hz in related $V(NR)X_3$ systems (R = alkyl, aryl; X = alkoxide, aryloxide, alkyl) [7b,11]. Within each set, the ^{51}V chemical shift of a given S_2CNMe_2 complex is observed at slightly higher field than that of its S_2CNEt_2 counterpart, an observation which is consistent with the greater electron donation capability of the S_2CNMe_2 ligand. It is interesting to note that the progressive upfield shift in $\delta(^{51}V)$ observed upon successive replacement of chloride by S_2CNR_2 ligands in this series is opposite to the effect induced by replacement of chloride by monodentate thiolates. Thus, Preuss [12] finds that successive substitution of chloride by *tert*-butyl thiolate in the series $[V(N^tBu)(S^tBu)_xCl_{(3-x)}]$ drives the ^{51}V chemical shifts downfield ($x = 0$, 8; $x = 1$, 232; $x = 2$, 330; $x = 3$, 467 ppm).

The electronic spectra of complexes **2, 3,** and **4** in the range 350–700 nm have been recorded as toluene solutions (Table 1). In all cases, shoulders in the visible region are observed superimposed upon an intense and broad feature tailing out of the UV region. The energies of these visible region absorptions increase with progressive incorporation of dithiocarbamate ligands. As previously noted for the series $[V(NTol)(OR)_xCl_{(3-x)}]$ (R = ^{t}Bu,2,6-$Me_2C_6H_3$) [7b], there is a correlation between $\delta(^{51}V)$ and (ΔE^{-1}) for the $[V(NTol)(S_2CNR_2)_xCl_{(3-x)}]$ complexes as shown in Fig. 2. Such a correlation implies that the dominant factor governing the observed ^{51}V chemical shifts is the paramagnetic shielding term σ_{para} [7b,13].

Attempts to generate the d^1 systems $[V(NTol)(S_2CNR_2)_2]$ from the corresponding $[V(NTol)(S_2CNR_2)_2Cl]$ complexes **3,** as shown in eq. (2), have been only partially successful. Thus, treatment of either **3a** or **3b** with an excess of Zn powder in CH_2Cl_2 at room temperature afforded dark yellow–brown solutions after 18 h reaction time. Workup led to dark brown powders which displayed broad and indistinct ^1H NMR spectra. ESR spectra of these products (298 K, $CDCl_3$ solution) revealed the characteristic eight line spectra expected for V(IV) with a d^1_{xy} configuration (**5a**: $g = 1.976$, $A(^{51}V) = 89.1$ G; **5b**: $g = 1.991$, $A(^{51}V) = 89.9$ G). While these values are very close to those reported for the analogous vanadyl

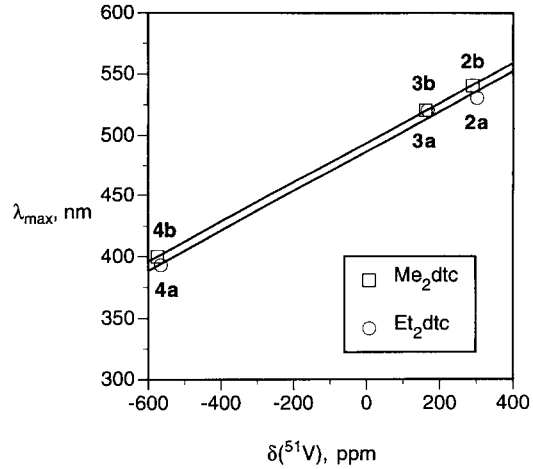

Fig. 2. Correlation of $\delta(^{51}V)$ with visible region λ_{max}. See text for numbering scheme.

complexes [2,4b], elemental analysis results on complexes **5** indicated that these products were not obtained in a pure state.

Phenylenedi-imido vanadium(V) complexes

A variety of organodi-imido bridged systems $[L_nM{\equiv}N{-}R{-}N{\equiv}ML_n]$ are known for M = Mo, W, Re and U, but to our knowledge no such complexes have been reported for vanadium [14–17]. An entry point to such systems is provided by the *p*-phenylenedi-imido complex $[Cl_3V{\equiv}NC_6H_4N{\equiv}VCl_3]$, **6,** which can be prepared in high yield as shown in eq. (3). **6** is obtained as a brown solid which is soluble (with adduct formation) in THF, but which is insoluble in other common organic solvents suggesting that unsolvated **6** exists as an intermolecularly associated species in the solid state. When **6** is dissolved in THF, an intense yellow–brown solution is formed from which a brown solid product **7** can be obtained. The ^1H NMR spectrum of **7** reveals the incorporation of three THF ligands per vanadium atom [eq. (4)].

The THF ligands are easily lost from **7**; storage *in vacuo* induces the formation of a complex shown by elemental analysis to be a mono-THF complex of **6,** *viz.* $[Cl_3V{\equiv}NC_6H_4N{\equiv}VCl_3]\cdot THF$, in which we believe the THF molecule to be simply a guest in the

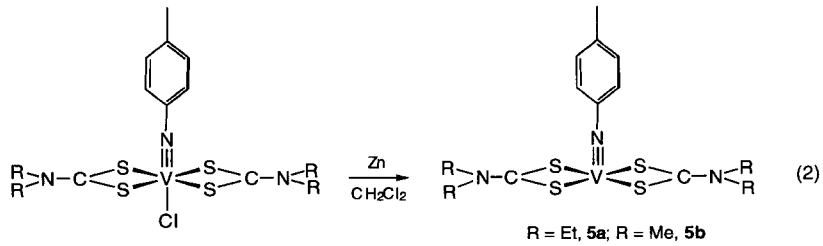

(2)

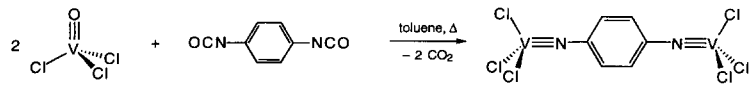

6 (3)

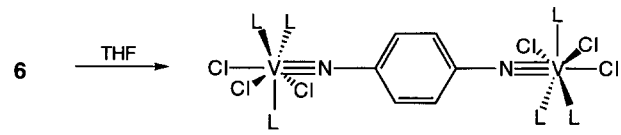

7 (L = THF) (4)

lattice. Similar facile loss of coordinated THF has been noted for analogous [ArN≡VCl_3] systems, for which both mono- and bis-THF adducts can be isolated [7b,18]. The ^{51}V NMR spectrum ($CDCl_3$, 298 K) of **7** displays a broad (fwhm = 2200 Hz) resonance at δ 380 ppm; the corresponding resonance for [TolN≡VCl_3(THF)] is observed at δ 374 ppm (fwhm = 1900 Hz) [7b].

The reaction between $VOCl_3$ and an equimolar amount of *p*-phenylene diisocyanate affords the mononuclear complex [OCN—C_6H_4N≡VCl_3], **8**, in high yield as shown in eq. (5). The ^{51} NMR resonance for **8** is observed at δ 283 ppm (fwhm = 750 Hz), within the range previously observed for various *p*-substituted phenylimido vanadium trichloride complexes, [X—C_6H_4N≡VCl_3] [7b].

The presence of the pendant isocyanate function within **8** suggested the possibility of using it to construct heterobimetallic phenylenedi-imido systems of the type [Cl_3V≡NC_6H_4N≡ML_n], but our preliminary investigations of such reactions have uncovered unexpected results. Thus, reaction between **8** and $WOCl_4$ in refluxing toluene [eq. (6)] produces a brown powder whose elemental analysis is a reasonable agreement with that expected for the presumptive product [Cl_3V≡NC_6H_4N≡WCl_4], **9**. As observed for **6**, **9** is insoluble in common non-donor solvents, but is readily soluble in THF. Surprisingly, however, the ^{1}H NMR spectrum of the material obtained after workup of a solution of **9** in THF revealed the presence of both **7** and its ditungsten analogue [(THF)Cl_4W≡N-C_6H_4N≡WCl_4(THF)] [14c]; the spectrum contained no resonances attributable to a THF complex of **9**. Thus, we conclude that an unusual example of an intermetal exchange of imido ligands [19] has occurred leading to a net disproportionation of **9**. As shown in Scheme 1 (which is a simplistic representation that does not attempt to account for additional intermolecular associations), a plausible intermediate in this redistribution reaction is a heterobimetallic *bis*-(μ-imido) species. At this stage, the actual nature of the brown product isolated from the reaction of eq. (6) remains uncertain—as does any potential involvement of THF in promoting the disproportionation—and distinguishing among the possibilities shown in Scheme 1 (i.e. authentic **9**, or the *bis*-(μ-imido) species, or a 1 : 1 mixture of homobimetallic species **6** and **10**) is not yet possible.

The chloride ligands of **6** undergo substitution by dithiocarbamates and *tert*-butoxide in reactions analogous to those of eq. (1) but, in reactions designed to replace either one or two chlorides at each vanadium center, ^{1}H NMR spectra of the products indicated that mixtures of variously substituted products were obtained. A pure product, **11**, has been obtained in the case of complete substitution of all six chlorides by [S_2CNEt_2] as shown in eq. (7). **11** is obtained as a mahogany solid in *ca* 60% yield. No discernable ^{51}V NMR resonance could be observed for **11**, presumably due to the extreme breadth of the signal. Similarly, the reaction of **6** with 6 equiv. of KO^{t}Bu proceeds with complete chloride substitution to pro-

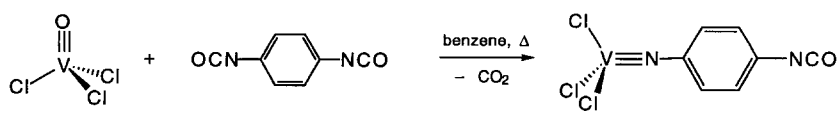

8 (5)

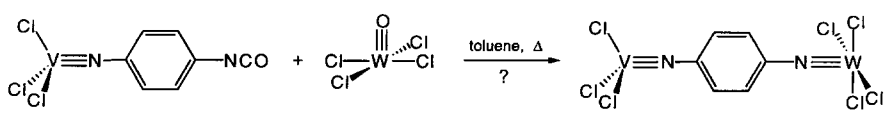

8 9 (6)

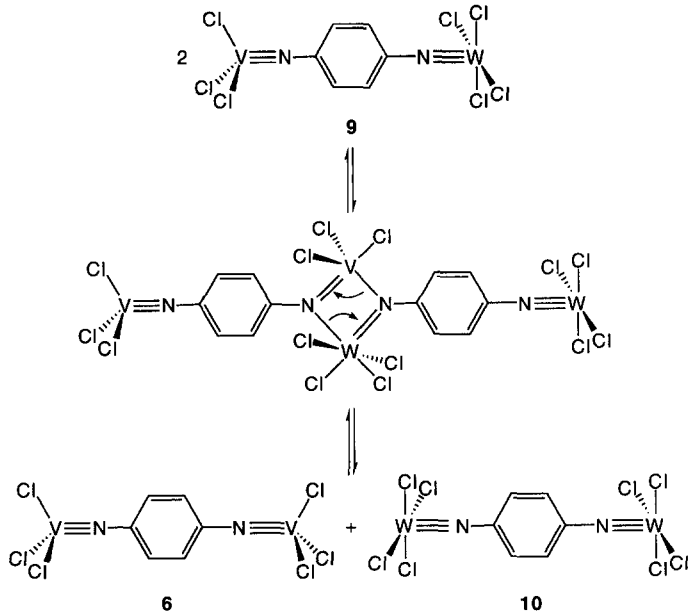

Scheme 1. A possible pathway for the disproportionation of **9**.

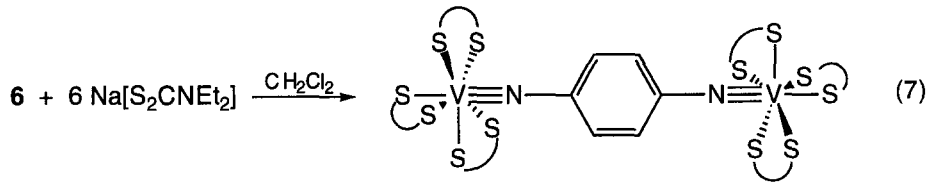

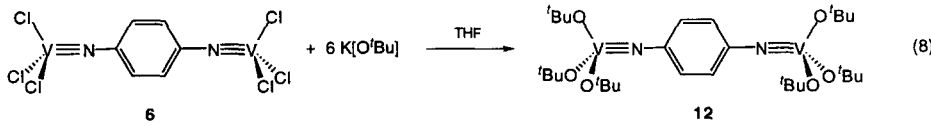

duce the hexakis(*tert*-butoxide) product **12** [eq. (8)]. **12** is obtained as a dark orange powder which is extremely soluble in common organic solvents, including hexane. The ^{51}V NMR resonance for **12** is observed at δ −638, a value only slightly downfield of that for the corresponding tolylimido system [TolN≡V(O^{t}Bu)$_3$] (δ −654) [7b]. Although the resonance for **12** is relatively narrow (fwhm = 345 Hz), ^{51}V–^{14}N spin coupling could not be resolved in this case; for [TolN≡V(O^{t}Bu)$_3$], this coupling constant was observed to be 111 Hz [7b].

EXPERIMENTAL

All reactions and manipulations were carried out either *in vacuo* or under an atmosphere of purified dry nitrogen. Solvents employed were dried and distilled prior to use. Sodium dialkyldithiocarbamate salts were prepared by treatment of the corresponding amine with NaOH in the presence of CS_2, and were dried *in vacuo* at 100°C prior to use. V(NTol)Cl$_3$ was prepared as previously described [7b]. Other reagents were obtained from commercial sources.

Elemental analyses were performed by Galbraith Laboratories, Knoxville, TN. ^1H (400.1 MHz) and ^{51}V (105.2 MHz) NMR spectra were obtained on an IBM/Bruker WM-400 instrument at 298 K and are referenced to internal Me_4Si and external $VOCl_3/CDCl_3$ (75% v/v), respectively. ESR spectra were recorded with a Bruker ER 200D spectrometer operating near 9.27 GHz and were calibrated using DPPH as an external field marker. Electronic spectra in the range 350–700 nm were recorded with a Cary 14 spectrophotometer.

V(NTol)(S$_2$CNEt$_2$)Cl$_2$ (**2a**)

A portion of V(NTol)Cl$_3$ (0.500 g, 1.91 mmol) was placed in a reaction flask and *ca* 5 g of Celite was

added as a filtration aid. An addition sidearm containing $Na(S_2CNEt_2]$ (0.326 g, 1.91 mmol) was attached, and 25 cm^3 of CH_2Cl_2 was introduced by vacuum distillation. After complete dissolution of the vanadium complex, the dithiocarbamate salt was added to the stirred solution at room temperature, causing a rapid color change from dark green to orange–red. After 30 min, the reaction was filtered on a medium porosity sintered glass frit and the filtrate was taken to dryness. The dark red–purple solid product was triturated with pentane (*ca* 30 cm^3), collected by filtration and dried *in vacuo*. If necessary, the product can be recrystallized to remove traces of V(NTol)$(S_2CNEt_2)_2Cl$ (**3a**) by the addition of hexane to a concentrated CH_2Cl_2 solution. Anal. Calcd (found) for $C_{12}H_{17}N_2S_2Cl_2V$: C, 38.41 (38.92); H, 4.57 (4.89); N, 7.47 (7.49). ^1H NMR ($CDCl_3$): δ 7.24 (AA′BB′ q, $J_{AB} = 7.92$ Hz, 4 H, $C_6H_4CH_3$), 3.86 (q, 4H, CH_2CH_3), 2.43 (*s*, 3H, $C_6H_4CH_3$), 1.34 (t, 6H, CH_2CH_3). ^{51}V NMR ($CDCl_3$): δ 301 (fwhm = 415 Hz). λ_{max} ($C_6H_5CH_3$): 530 nm.

V(NTol)$(S_2CNMe_2)Cl_2$ (**2b**)

Prepared and purified as for **2a,** using V(NTol)Cl_3 (0.500 g, 1.91 mmol) and $Na[S_2CNMe_2]$ (0.273 g, 1.91 mmol); the product is a dark red solid. ^1H NMR ($CDCl_3$): δ 7.24 (AA′BB′ q, $J_{AB} = 8.02$ Hz, 4H, $C_6H_4CH_3$), 3.36 (s, 6H, CH_3), 2.43 (s, 3H, $C_6H_4CH_3$). ^{51}V NMR ($CDCl_3$): δ 289 (fwhm = 439 Hz). λ_{max} ($C_6H_5CH_3$): 540 nm.

V(NTol)$(S_2CNEt_2)_2Cl$ (**3a**)

Prepared as for **2a,** using V(NTol)Cl_3 (0.500 g, 1.91 mmol) and $Na[S_2CNEt_2]$ (0.652 g, 3.80 mmol) and stirring at room temperature for 60 min. The dark red product is obtained as the CH_2Cl_2 hemisolvate. Anal. Calcd (found) for $C_{17.5}H_{28}N_3Cl_2S_4V$: C, 39.19 (39.07); H, 5.23 (5.53); N, 7.84 (7.72). ^1H NMR ($CDCl_3$): δ 7.30 (AA′BB′ q, $J_{AB} = 8.32$ Hz, 4 H, $C_6H_4CH_3$), 5.29 (s, 1H, CH_2Cl_2) 3.82 (ABX_3 m, 4H, CH_2CH_3), 3.74 (ABX_3 m, 4H, CH_2CH_3), 2.43 (s, 3H, $C_6H_4CH_3$), 1.27 (t, 12H, CH_2CH_3). ^{51}V NMR ($CDCl_3$): δ 166 (fwhm = 2610 Hz). λ_{max} ($C_6H_5CH_3$): 520 nm.

V(NTol)$(S_2CNMe_2)_2Cl$ (**3b**)

Prepared as for **2a,** using V(NTol)Cl_3 (0.500 g, 1.91 mmol) and $Na[S_2CNMe_2]$ (0.545 g, 3.81 mmol), and stirring at room temperature for 60 min; the product is a dark red solid which can be purified by recrystallization from CH_2Cl_2/hexane. ^1H NMR ($CDCl_3$): δ 7.31 (AA′BB′ q, $J_{AB} = 8.06$ Hz, 4 H, $C_6H_4CH_3$), 3.36 (s, 12H, CH_3), 2.42 (s, 3H, $C_6H_4CH_3$). ^{51}V NMR ($CDCl_3$): δ 161 (fwhm = 1870 Hz). λ_{max} ($C_6H_5CH_3$): 520 nm.

V(NTol)$(S_2CNEt_2)_3$ (**4a**)

Prepared as for **2a,** using V(NTol)Cl_3 (0.500 g, 1.91 mmol) and $Na[S_2CNEt_2]$ (0.978 g, 5.72 mmol), and stirring at room temperature for 90 min; the product is a dark yellow solid which can be purified by recrystallization from CH_2Cl_2/hexane. Anal. Calcd (found) for $C_{22}H_{37}N_3S_6V$: C, 43.98 (43.60); H, 6.21 (6.22); N, 9.24 (9.18). ^1H NMR ($CDCl_3$): δ 7.03 (AA′BB′ q, $J_{AB} = 8.08$ Hz, 4H, $C_6H_4CH_3$), 3.81 (m, br, 12H, CH_2CH_3), 2.27 (s, 3H, $C_6H_4CH_3$), 1.27 (t, br, 15H, CH_2CH_3), 1.17 (t, br, 3H, CH_2CH_3). ^{51}V NMR ($CDCl_3$): δ −565 (fwhm = 1780 Hz). λ_{max} ($C_6H_5CH_3$): 393 nm.

V(NTol)$(S_2CNMe_2)_3$ (**4b**)

Prepared as for **2a,** using V(NTol)Cl_3 (0.500 g, 1.91 mmol) and $Na[S_2CNMe_2]$ (0.818 g, 5.72 mmol), and stirring at room temperature for 90 min; the product is a dark yellow solid which can be purified by recrystallization from CH_2Cl_2/hexane. ^1H NMR ($CDCl_3$): δ 7.04 (AA′BB′ q, $J_{AB} = 8.14$ Hz, 4 H, $C_6H_4CH_3$), 3.42 (s, 6H, CH_3), 3.37, 3.35, 3.31, 3.28 (s, 3H each, CH_3), 2.27 (s, 3H, $C_6H_4CH_3$). ^{51}V NMR ($CDCl_3$): δ −574 (fwhm = 1530 Hz). λ_{max} ($C_6H_5CH_3$): 390 nm.

V(NTol)$(S_2CNEt_2)_2$ (**5a**)

A reaction vessel was charged with **3a** (0.300 g, 0.616 mmol) and Zn powder (1.45 g; 22.2 mmol), and CH_2Cl_2 (*ca* 50 cm^3) was admitted by vacuum distillation. The reaction mixture was stirred at room temperature for 24 h, and the color of the solution changed from orange–red to yellow–brown. The mixture was filtered, the filtrate was taken to dryness and the resultant dark brown powder was triturated with pentane, and dried *in vacuo*. Elemental analyses were not satisfactory. ESR ($CDCl_3$, 298 K): octet, $g = 1.976$, $A(^{51}V) = 89.1$ G.

V(NTol)$(S_2CNME_2)_2$ (**5b**)

Prepared as for **5a,** using **3b** (0.300 g, 0.695 mmol) and Zn powder (1.36 g, 20.8 mmol) and stirring at room temperature for 18 h; the product is a dark brown powder. Elemental analyses were not satisfactory. ESR ($CDCl_3$, 298 K): octet, $g = 1.991$, $A(^{51}V) = 89.9$ G.

p-$[Cl_3V{\equiv}NC_6H_4N{\equiv}VCl_3]$ (**6**)

A portion of $VOCl_3$ (2.5 cm^3, 26 mmol) in toluene (*ca* 120 cm^3) was added to a reaction flask bearing a reflux condenser, and an additional sidearm containing *p*—OCN—C_6H_4—NCO (2.00 g, 12 mmol) was attached. As the solution was being warmed to reflux temperature, the diiocyanate was added in por-

tions over a few minutes. After 45 h of refluxing, the dark green–brown solution was cooled and the dark brown solid product was collected by filtration, washed with CH_2Cl_2 until the washings were colorless, and dried *in vacuo* at 55°C for 12 h to yield 4.23 g (84%) of **6**. anal. Calcd (found) for $C_6H_4N_2Cl_6V_2$: C, 17.21 (17.35); H, 0.96 (1.11); N, 6.69 (6.79).

p-[(THF)$_3$Cl$_3$V≡NC$_6$H$_4$N≡VCl$_3$(THF)$_3$] (**7**)

At room temperature, 0.25 g of **6** were dissolved in 50 cm^3 of THF, and the intense yellow–brown solution was stirred at room temperature for 30 min. Evaporation of the solvent afforded a brown solid, which was dried *in vacuo* for 6 h. ^{1}H NMR ($CDCl_3$): δ 7.78 (s, 4 H, C_6H_4), 4.04 (t, 24H, OCH_2CH_2), 1.96 (quintet, 24H, OCH_2CH_2). ^{51}V NMR ($CDCl_3$): δ 380 (fwhm = 2200 Hz). The THF ligands of **7** are weakly bound and storage *in vacuo* induces the loss of five of them, forming a brown mono(THF) adduct, **6**·THF. Anal. Calcd (found) for $C_{10}H_{12}N_2OCl_6V_2$: C, 24.47 (24.69); H, 2.46 (2.92); N, 5.71 (5.76).

p-[Cl$_3$V≡NC$_6$H$_4$—NCO] (**8**)

A solution of $VOCl_3$ (2.8 cm^3, 29 mmol) in 25 cm^3 of benzene was added dropwise over the course of 1 h to a stirred solution of *p*-OCN—C_6H_4—NCO (4.88 g, 30 mmol) in *ca* 100 cm^3 of benzene at 60°C. The green solution was refluxed for 36 h and solvent was removed *in vacuo*. The brown solid residue was washed with hexane (*ca* 30 cm^3), collected by filtration and dried *in vacuo* at 60°C to yield 6.74 g (79%) of **8**. Anal. Calcd (found) for $C_7H_4N_2OCl_3V$: C, 29.05 (28.94); H, 1.39 (1.45); N, 9.65 (9.68). ^{1}H NMR ($CDCl_3$): δ 7.32 (AA′BB′ q, J_{AB} = 8.30 Hz, 4 H, C_6H_4). ^{51}V NMR ($CDCl_3$): δ 283 (fwhm = 750 Hz).

p-[Cl$_3$V≡NC$_6$H$_4$N≡WCl$_4$] (**9**)

A mixture of $WOCl_4$ (0.36 g, 1.03 mmol) and **8** (0.30 g, 1.03 mmol) was dissolved in toluene (*ca* 50 cm^3) forming a green solution. The solution was refluxed for 24 h, during which time the color became yellow–brown. After cooling to room temperature, the brown solid product was collected by filtration, washed with CH_2Cl_2 until the washings no longer showed a green color, and dried under vacuum to yield 0.36 g (60%) of a product analyzing as **9**. Anal. Calcd (found) for $C_6H_4N_2Cl_7VW$: C, 12.27 (12.36); H, 0.69 (1.20); N, 4.77 (4.07).

p-[(Et$_2$NCS$_2$)$_3$V≡NC$_6$H$_4$N≡V(S$_2$CNEt$_2$)$_3$] (**11**)

A portion of Na[S$_2$CNEt$_2$] (1.03 g, 6.0 mmol) was added to a suspension of **6** (0.42 g, 1.0 mmol) in 50 cm^3 CH_2Cl_2 containing *ca* 5 g of Celite as a filtration aid. The red reaction mixture was stirred at room temperature for 90 min and filtered. The residue remaining on the frit was washed with CH_2Cl_2 (2 × 50 cm^3); these washings were combined with the filtrate and taken to dryness. The dark red solid residue was washed with hexane (50 mL) and dried under vacuum to yield 0.65 g (59%) of mahogany **11**. anal Calcd (found) for $C_{36}H_{64}N_8S_{12}V_2$: C, 39.46 (39.86); H, 5.89 (6.06); N, 10.23 (10.33). ^{1}H NMR ($CDCl_3$): δ 6.78 (s, 4H, C_6H_4), 3.80 (m, br, 24H, CH_2), 1.25, 1.16 (overlapped m, br, 36H, CH_3).

p-[('BuO)$_3$V≡NC$_6$H$_4$N≡V(O'Bu)$_3$] (**12**)

A portion of K[O'Bu] (2.50 g, 22.3 mmol) was added to a solution of **6** (1.50 g, 3.58 mmol) in 100 mL of THF containing *ca* 3 g of Celite as a filtration aid. An orange color developed immediately and the reaction was stirred at room temperature for 18 h, filtered and the filtrate was taken to dryness. The solid residue was extracted into hexane (50 cm^3), filtered and taken to dryness yielding 1.77 g (77%) of dark orange **12**. ^{1}H NMR($CDCl_3$): δ 7.06 (s, 4H, C_6H_4), 1.41 (s, 54H, CH_3). ^{51}V NMR ($CDCl_3$): δ −638 (fwhm = 345 Hz).

Acknowledgements—We thank the National Science Foundation and the Division of Chemical Sciences, Office of Basic Energy Sciences, Department of Energy for support of this work.

REFERENCES

1. (a) Bradley, D. C. and Gitlitz, M. H., *J. Chem. Soc., Chem. Commun.*, 1965, 289, (b) Bradley, D. C. and Gitlitz, M. H., *J. Chem. Soc. (A)* 1969, 1152.
2. Bradley, D. C., Rendall, I. F. and Sales, K. D. *J. Chem. Soc., Dalton Trans.*, 1973, 2228.
3. (a) Casey, A. T., Mackey, D. J., Martin, R. L. and White, A. H., *Aust. J. Chem.*, 1972, **25,** 477; (b) Dewan, J. C., Kepert, D. L., Raston, C. L., Taylor, D., White, A. H. and Maslen, E. N., *J. Chem. Soc., Dalton Trans.*, 1973, 2082.
4. (a) McCormick, B. J., *Inorg. Chem.*, 1968, **7,** 1965; (b) McCormick, B. J. and Bellot, E. H., *ibid.*, 1970, **9,** 1779.
5. Wigley, D. E., *Prog. Inorg. Chem.*, 1994, **42,** 239.
6. Maatta, E. A., *Inorg. Chem.*, 1984, **23,** 2560.
7. (a) Bradley, D. C., Hursthouse, M. B., de M. Jelfs, A. N. and Short, R. L., *Polyhedron*, 1983, **2,** 849; (b) Devore, D. D., Lichtenhan, J. D., Takusagawa, F. and Maatta, E. A., *J. Am. Chem. Soc.*, 1987, **109,** 7408.
8. Young, C. G., Broomhead, J. A. and Boreham, C. J., *J. Chem. Soc., Dalton Trans.*, 1983, 2135.
9. Maatta, E. A. and Wentworth, R. A. D., *Inorg. Chem.*, 1979, **18,** 2409.
10. Bishop, M. W., Chatt, J., Dilworth, J. R., Neaves, B. D., Dahlstrom, P., Hyde, J. and Zubieta, J., *J. Organomet. Chem.*, 1981, **213,** 109.

11 (a) Preuss, F., Towae, W., Kruppa, V. and Fuchslocher, E., *Z. Naturforsch.*, 1984 **39b,** 1510; (b) Nugent, W. A. and Harlow, R. L., *J. Chem. Soc., Chem. Commun.*, 1979, 342.
12. Preuss, F., Noichl, H. and Kaub, J., *Z. Naturforsch.*, 1986, **41b,** 1085.
13. Figgis, B. N., Kidd, R. G. and Nyholm, R. S., *Proc. R. Soc. London, A*, 1962, **269,** 469.
14. (a) Maatta, E. A. and Devore, D. D., *Angew. Chem. Int. Ed. Engl.*, 1988, **27,** 569; (b) Maatta, E. A. and Kim, C., *Inorg. Chem.*, 1989, **28,** 623; (c) Liang, M. and Maatta, E. A., *ibid.*, 1992, **31,** 953; (d) Stark, J. L., Rheingold, A. L. and Maatta, E. A., *J. Chem. Soc., Chem. Commun.*, 1995, 1165.
15. Rosen, R. K., Andersen, R. A. and Edelstein, N. M., *J. Am. Chem. Soc.*, 1990, **112,** 4588.
16. Clegg, W., Errington, R. J., Hockless, D. C. R., Kirk, J. M. and Redshaw, C., *Polyhedron*, 1992, **11,** 381.
17. Hogarth, G., Mallors, R. L. and Norman, T., *J. Chem. Soc., Chem. Commun.*, 1993, 1721.
18. Carofiglio, T., Floriani, C., Chiesi-Villa, A. and Guastini, C., *Inorg. Chem.*, 1989, **28,** 4417.
19. Jolly, M., Mitchell, J. P. and Gibson, V. C., *J. Chem. Soc., Dalton Trans.*, 1992, 1331.

Pergamon

PII: S0277-5387(97)00207-6

Polyhedron Vol. 17, No. 5–6, pp. 977–982, 1998
© 1998 Elsevier Science Ltd
All rights reserved. Printed in Great Britain
0277–5387/98 $19.00+0.00

Azido and amido derivatives of aluminium(III)†

Joel S. Silverman, Claire J. Carmalt, Deborah A. Neumayer,‡
Alan H. Cowley,* Brian G. McBurnett and Andreas Decken¶

Department of Chemistry & Biochemistry, The University of Texas at Austin, Austin, TX 78712, U.S.A.

(Received 9 May 1997; accepted 12 May 1997)

Abstract—The piperidinyl-substituted aluminium azide, $[(pip)_2AlN_3]_2$ (**5**) (pip = piperidinyl, $\overline{N(CH_2)_4CH_2}$), has been synthesised via the reaction between $[(pip)_2AlCl]_2$ and one equivalent of NaN_3. A related pyrrolyl derivative, $[(Me_2N(H))Al(pyr)_3]$ (**7**) (pyr = pyrrolyl, $\overline{N(CH)_3CH}$), was prepared via the dimethylamine elimination reaction between $[Al_2(NMe_2)_6]$ and six equivalents of pyrrole. A third aluminium amido complex, $[Li(Al(NH^tBu)_4)]_2$ (**9**), has been isolated from the salt elimination reaction between $AlCl_3$ and an excess of $LiNH^tBu$. all three compounds have been characterised by X-ray crystallography; compounds **5** and **9** are dimeric in the solid state, whereas **7** is monomeric. © 1998 Elsevier Science Ltd. All rights reserved

Keywords: aluminium; azide; amide; X-ray.

The Group 13 nitrides (AlN, GaN, InN) continue to generate significant interest for applications in advanced microelectronic and optoelectronic devices [1]. In the context of metalorganic chemical vapour deposition (MOCVD) techniques, these materials are currently prepared by the reaction of ER_3 (E = Al, Ga, In; R = alkyl) with ammonia at temperatures in excess of 900°C [1]. Unfortunately, the use of such high temperatures results in a loss of stoichiometry due to nitrogen deficiency and also introduces thermal stresses in the resulting films. Accordingly, attention has turned recently to the development of single-source precursors in an attempt to lower the thermal budget [1]. Our own work focused initially on a new class of GaN precursors that embody labile amido substituents and an azide nitrogen source, a prime example being $[(Me_2N)Ga(N_3)(\mu\text{-}NMe_2)]_2$ (**1**) [2]. However, the solid state structure of **1** comprises a polymeric chain of dimeric units, thus limiting the volatility of this precursor. In a subsequent development, we discovered [3] that treatment of **1** with pyridine afforded $[Ga(N_3)_3(py)_3]$ (**2**) (py = pyridine), the first example of a structurally characterised tris-(azide) of gallium [4]. The use of azides as the nitrogen source has also been investigated for precursors to aluminium nitride (AlN). Thus, Gladfelter, Evans *et al.* deposited AlN on several substrates at temperatures as low as 400°C by using dialkylaluminium azides [5]. Moreover, a trisazido-aluminium complex possessing a structure similar to that of **2**, $[Al(N_3)_3(py)_3]$ (**3**), has been reported and some related azides, $[Me_2N(CH_2)_3]_2Al(N_3)$ (**4**) and $[AlMe_2(N_3)(N(H_2)^tBu)]$ have been used to grow epitaxial AlN films above 800°C [6]. A number of aluminium amido complexes of the type $[R_{3-n}Al(NR'_2)_n]$ (R = Me, Et, n = 1 or 3) have been used to grow AlN at lower temperatures; however, the resulting AlN films were found to be contaminated with high levels of carbon [7].

In order to explore further the utility of azides or amides as the nitrogen source in AlN precursors we have synthesised a number of azido or amido aluminium precursors which possess an all nitrogen coordination sphere.

RESULTS AND DISCUSSION

With a view to developing an AlN precursor featuring an azide nitrogen source, the colourless crystalline compound **5** was prepared in high yields by means of a two-step procedure as summarised in Scheme 1. Analytical and spectroscopic data were consistent with the empirical formulation, $[(pip)_2AlN_3]_2$ (**5**) (pip = piperidine, $\overline{N(CH_2)_4CH_2}$);

* Author to whom correspondence should be addressed.

† Dedicated to Professor Donald C. Bradley, a true pioneer, with admiration and affection.

‡ Current address: Thomas J. Watson Research Center, IBM, P.O. Box 218, Yorktown Heights, NY 10598.

¶ Current address: Department of Chemistry, University of New Brunswick, Fredericton, New Brunswick, Canada, E3B 5AB.

$$AlCl_3 + 2Li(pip) \xrightarrow[-2LiCl]{\text{pentane, -78 °C}} [(pip)_2AlCl]_2$$

$$[(pip)_2AlCl]_2 \xrightarrow[\text{dibenzo-18-crown-6}]{CH_2Cl_2} [(pip)_2AlN_3]_2 \quad \mathbf{5}$$

$$pip = \overline{N(CH_2)_4CH_2}$$

Scheme 1.

however, in order to establish both the degree of oligomerisation and the stereochemistry at aluminium it was necessary to appeal to X-ray crystallography. Compound **5** crystallises in the triclinic space group $P\bar{1}$ and the solid state comprises an array of dimeric units (Fig. 1): a selection of bond lengths and angles

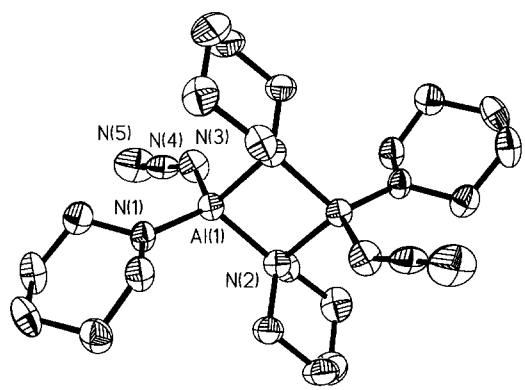

Fig. 1. Molecular structure of $[(pip)_2AlN_3]_2$ (**5**) showing the atom numbering scheme. Ellipsoids are drawn at the 30% level. Hydrogen atoms are omitted.

appears in Table 1. The dimer is formed by means of two bridging piperidinyl (pip) groups, and the resulting Al_2N_2 core is planar by virtue of its location on a crystallographic centre of symmetry. The nonbridging positions are occupied by pip and N_3 groups, resulting in the overall geometry about the aluminium centre being approximately tetrahedral [*av.* N—Al—N 108.9(2) Å]. The Al—N_3 bond distances of 1.805(5) Å in **5** are considerably shorter than those in $[Al(N_3)_3(py)_3]$ **3** [*av.* Al—N 1.971(2) Å] and $N_3Al[(CH_2)_3NMe_2]_2$ **4** (Al—N 1.897(2) Å) even though all three complexes involve terminal azide ligands [6]. The metrical parameters for the azide moieties are typical of those reported for a variety of covalent azides both in terms of the N—N—N bond angle [176.5(7)°] and also with respect to the observation of two significantly different N—N bond distances [1.169(6) and 1.122(6) Å] [8]. The average Al—N(pip) bond lengths are 1.765(4) (terminal pip) and 1.935(5) Å (bridging pip), both of which correspond well to those previously reported for $[Al_2(NMe_2)_6]$ [9] and $[Al_2(pyd)_6]$ (**6**) (pyd = pyrrolidine, $\overline{N(CH_2)_3CH_2}$) [10]. Only one other piperidinyl aluminium complex has been crystallographically characterised prior to **5**,

Table 1. Selected bond lengths (Å) and angles (°) for **5**, **7** and **9**

Compound **5**		Compound **7**		Compound **9**	
Al(1)—N(1)	1.765(4)	Al(1)—N(3)	1.824(2)	Al(1)—N(4)	1.795(4)
Al(1)—N(3)	1.805(4)	Al(1)—N(1)	1.826(2)	Al(1)—N(3)	1.887(4)
Al(1)—N(2)	1.927(4)	Al(1)—N(2)	1.827(2)	Al(1)—N(1)	1.891(4)
Al(1)—N(2a)	1.942(4)	Al(1)—N(4)	1.933(2)	Al(1)—N(2)	1.894(4)
N(3)—N(4)	1.169(6)			Li(1)—N(2a)	2.052(1)
N(4)—N(5)	1.122(6)			Li(1)—N(1)	2.08(1)
				Li(1)—N(3)	2.10(1)
N(1)—Al(1)—N(3)	114.7(2)	N(3)—Al(1)—N(1)	109.93(9)	N(4)—Al(1)—N(1)	121.5(2)
N(1)—Al(1)—N(2a)	114.7(2)	N(3)—Al(1)—N(2)	111.2(1)	N(4)—Al(1)—N(1)	122.0(2)
N(3)—Al(1)—N(3)	114.7(2)	N(1)—Al(1)—N(2)	112.55(9)	N(3)—Al(1)—N(1)	97.8(2)
N(1)—Al(1)—N(3)	114.7(2)	N(3)—Al(1)—N(4)	108.8(1)	N(4)—Al(1)—N(1)	110.0(2)
N(3)—Al(1)—N(3)	114.7(2)	N(1)—Al(1)—N(4)	106.48(9)	N(3)—Al(1)—N(1)	99.7(2)
N(2)—Al(1)—N(3)	114.7(2)	N(2)—Al(1)—N(4)	107.6(1)	N(1)—Al(1)—N(1)	102.1(2)
N(5)—N(4)—N(3)	176.5(7)			N(2a)—Li(1)—N(1)	124.3(5)
				N(2a)—Li(1)—N(3a)	88.0(4)
				N(1)—Li(1)—N(3a)	138.4(5)

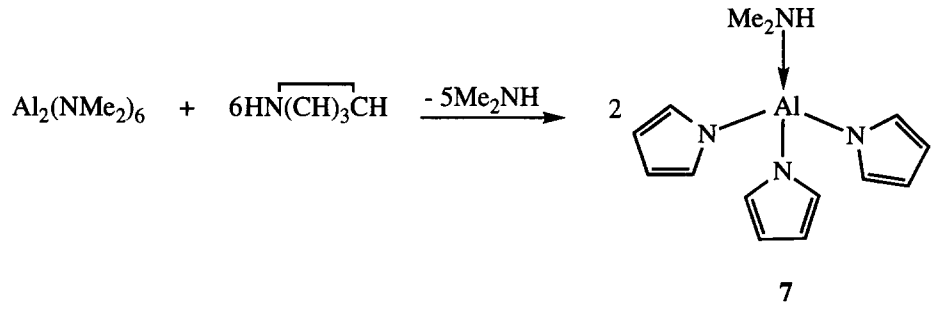

7

Scheme 2.

namely the lithium salt $[(thf)_2LiAl(pip)_4]$ [10]. It is also worth noting that the structure of **5** is similar to that of the related gallium complex $[(Me_2N)Ga(N_3)(\mu\text{-}NMe_2)]_2$ **1**, which is also dimeric by virtue of bridging dimethylamido groups [3].

With a view to investigating the use of the pyrrolyl group as the nitrogen source and in an attempt to isolate a mononuclear, monomeric AlN precursor, $[Al_2(NMe_2)_6]$ was treated with six equivalents of pyrrole at room temperature in hexane solution (Scheme 2). Elemental analytical data, together with ^1H and ^{13}C NMR spectral information, were consistent with the formation of a complex of formula $[(Me_2N(H))Al(pyr)_3]$ (**7**) (pyr = pyrrole, N(CH)$_3$CH). We note, however, that the N—H resonance for the Me_2NH group was not observed in the ^1H NMR spectrum of **7**. An X-ray crystallographic study revealed that the solid state structure of **7** comprises monomeric units, one of which is depicted in Fig. 2; selected bond lengths and angles are presented in Table 1. It is interesting to note the formation of the monomeric amine adduct, $[(Me_2N(H))Al(pyr)_3]$ **7**, rather than a dimeric species of the type $[Al_2(pyr)_6]$ (**8**). Compound **6** [10] is similar to the anticipated product **8**; however, the preparation of **6** involves the reaction of alane with three equivalents of pyrrolidine rather than amine elimination, hence a compound analogous to **7** is not possible. Compound **7** crystallises in the triclinic space group $P\bar{1}$ with no unusually short intermolecular contacts between the monomeric units. The geometry about the aluminium center is approximately tetrahedral [*av.* N—Al—N 109.44(9) Å] with the average Al—N_{pyr} bond length of 1.825(2) Å being much shorter than the N → Al donor bond from the Me_2NH ligand [Al—N(4) 1.933(2) Å] as expected. In a related complex, $[Me_3Al(NH_2{}^tBu)]$ [11], the N → Al bond length of 2.027(3) Å is slightly longer than that in **7** which probably results from increased steric interactions from the *tert*-butyl group. The average Al—N_{pyr} bond length is similar to the terminal Al—N bond lengths found in dimeric species such as **6** [10] and $[Al_2(NMe_2)_6]$ [9].

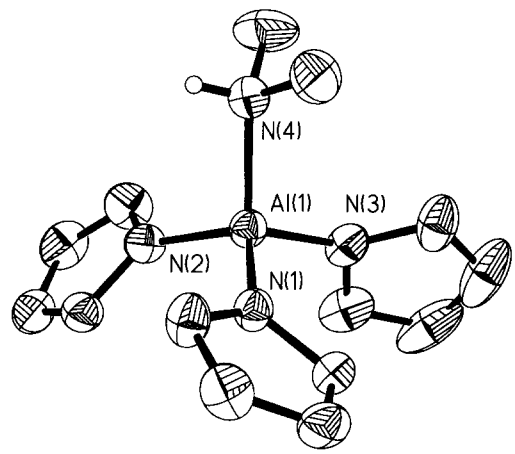

Fig. 2. Molecular structure of $[(Me_2N(H))Al(pyr)_3]$ (**7**) showing the atom numbering scheme. Ellipsoids are drawn at the 30% level. Hydrogen atoms are omitted.

The reaction between $AlCl_3$ and three equivalents of $LiNH^tBu$ was carried out in an attempt to form an example of an aluminium trisamide of the type $[Al(NH^tBu)_3]_n$. However, analytical and spectroscopic

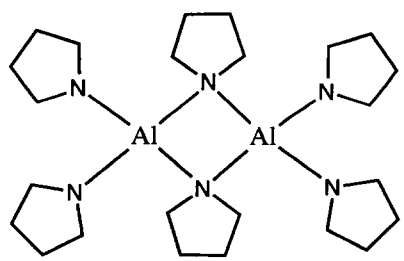

6

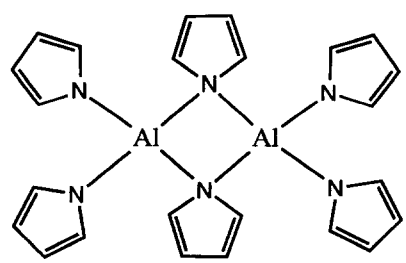

8

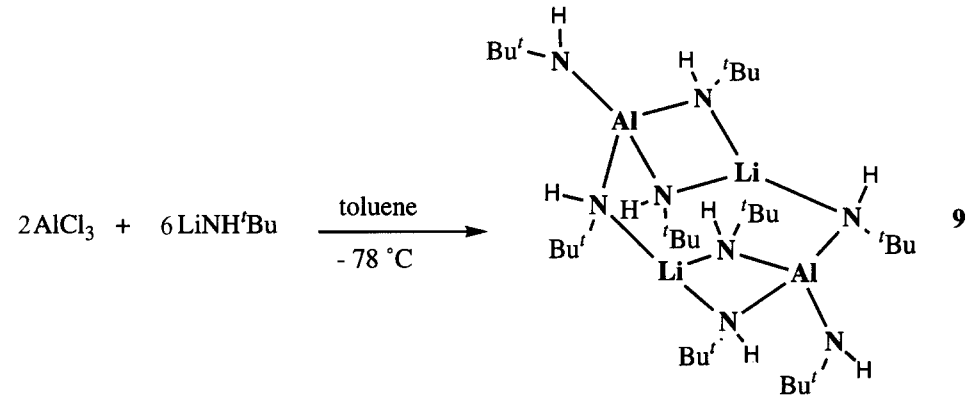

Scheme 3.

data were indicative of the formation of a lithium salt of formula $[Li(Al(NH^tBu)_4)]_2$ (**9**) (Scheme 3). The ^1H NMR of **9** exhibits a sharp singlet resonance in the ^tBu region, suggesting dynamic behaviour and, as in the case of **7**, the N—H resonances for the NH^tBu groups were not observed. An X-ray crystallographic study revealed that the solid state structure of **9** comprises dimeric units; selected bond lengths and angles are presented in Table 1. Compound **9** crystallises in the triclinic space group $P\bar{1}$ with no unusually short intermolecular contacts between dimeric units. The dimer is formed by means of two lithium cations bridging two $[Al(NH^tBu)_4]^-$ anions as shown in Fig. 3 (the Al—N—Li skeleton is shown in bold-face in Scheme 3). In turn each lithium cation in **9** is bonded to three nitrogen atoms of a NH^tBu group (*av.* Li—N 2.08(1) Å) with only a weak interaction to Al [Al(1)—Li(1a) 2.701(9) Å and Al(1)—Li(1) 3.236(9) Å]. The geometry about the aluminium center is approximately tetrahedral [*av.* N—Al—N 108.85(2) Å] with the terminal Al—N(4) bond length of 1.795(4) Å being shorter than the bridging Al—N bond lengths [*av.* 1.891(4) Å] as expected. These metrical parameters are similar to those reported for some related lithium salts of aluminium amides which have been reported previously, namely $[(pydH)_2LiAl(pyd)_4]$ [10], $[(thf)_2LiAl(pip)_4$ [10], and $[(thf)_2LiAl(NMe_2)_4]$ [12], all of which can be described as a solvated lithium cation bound to a tetrahedral $[Al(NR_2)_4]^-$ anion. Other pertinent lithium salts are $[(thf)_nLiAl(mes)_2(NH^tBu_2)_2]$ [13] (mes = 2,4,6-trimethylphenyl) (n = 1 or 2) and $[(thf)_4Li][Al(^tBu)_2(^tBu)(NDipp)]$ [13], (Dipp = 2,6-diisopropylphenyl), the latter being an anion–cation pair with no contacts between Li and the nitrogen of the amide for steric reasons.

In summary, three new aluminium complexes have been synthesised and structurally characterised. Complexes **5** and **7** are possible precursors for AlN and detailed chemical vapour deposition experiments are in progress.

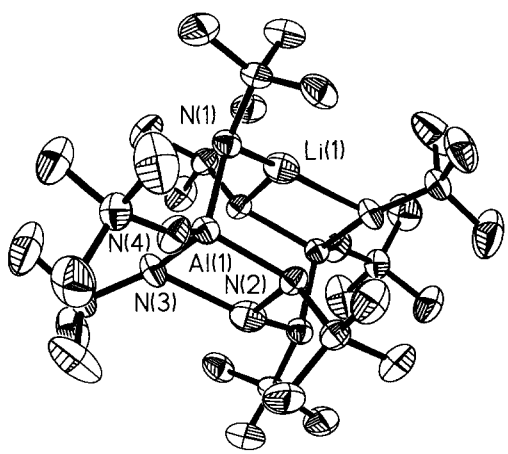

Fig. 3. Molecular structure of $[Li(Al(NH^tBu)_4)]_2$ (**9**) showing the atom numbering scheme. Ellipsoids are drawn at the 30% level. Hydrogen atoms are omitted.

EXPERIMENTAL

General procedures

All manipulations were performed under a dry, oxygen-free dinitrogen or argon atmosphere using standard Schlenk techniques or a HE-493 Vacuum Atmospheres drybox. Unless otherwise stated, all solvents were dried over sodium and distilled from sodium benzophenone ketyl under argon prior to use. The reagent $[Al_2(NMe_2)_6]$ was prepared according to the literature method [9]. All other reagents were obtained from commercial sources and used without further purification. Elemental analyses were performed by Atlantic Microlab, Inc., Norcross, GA.

Physical measurements

Mass Spectra (CIMS) were run on a Finnagan MAT 4023 instrument, and NMR spectra were recorded on a GE QE-300 spectrometer (^1H 300.19 MHz; ^{13}C, 75.48). NMR spectra are referenced to

C_6D_6 which was dried over sodium-potassium alloy and distilled prior to use; ^1H and ^{13}C chemical shifts are reported relative to $Si(CH_3)_4$ (0.00 ppm). Melting points were obtained in sealed glass capillaries under argon and are uncorrected.

Synthesis of $[(pip)_2AlN_3]_2$ **5**

n-Butyllithium (16.2 cm^3, 1.6 M solution in hexane) was added dropwise to a stirred solution of piperidine (2.76 g, 32.4 mmol) in diethyl ether (40 cm^3) at −78°C. After stirring for 12 h and being allowed to warm to room temperature, the resulting yellow solution was added dropwise to a solution of $AlCl_3$ (2.16 g, 16.2 mmol) in diethyl ether (30 cm^3) at −78°C. The solution was stirred for 12 h, pumped to dryness *in vacuo* to give a yellow oil which was dissolved in pentane (40 cm^3). After filtration over Celite, the solvent was removed *in vacuo* giving a yellow oil which was redissolved in CH_2Cl_2 (40 cm^3). Sodium azide (1 g, 16.2 mmol) and dibenzo-18-crown-6 (0.1 g) were added and the solution was stirred for 12 h, after which time the mixture was filtered over celite and the solvent removed *in vacuo*. Pentane (20 cm^3) was added and the resulting solution was stored at −20°C. After a few days at this temperature, X-ray quality crystals of **5** were obtained, m.p. 87–88°C. FTIR 2132.40 cm^{-1} (N_3). HRMS: calcd mass for $C_{20}H_{41}N_{10}Al_2$ 475.314649; found 475.312555. ^1H NMR (300.15 MHz, C_6D_6) δ 0.90 (t, 8H, *p*-$\overline{N(CH_2)_4CH_2}$), 1.27 (t, 16H, *m*-$\overline{N(CH_2)_4CH_2}$), 2.46 (d, 16H, *o*-$\overline{N(CH_2)_4CH_2}$), $^{13}C\{^1H\}$ NMR (75.14 MHz, C_6D_6) δ 22.9 (*o*-$\overline{N(CH_2)_4CH_2}$), 23.6 (*m*-$\overline{N(CH_2)_4CH_2}$), 44.7 (*p*-$\overline{N(CH_2)_4CH_2}$).

Synthesis of $[(Me_2N(H))Al(pyr)_3]$ **7**

Pyrrole (0.59 g, 8.8 mmol) was dissolved in hexane (10 cm^3) and added dropwise to a solution of $[Al(NMe_2)_3]_2$ (0.46 g, 2.9 mmol) in hexane (50 cm^3) at 25°C resulting in the immediate formation of white precipitate. The reaction mixture gradually turned pink as it was stirred for 15 h. The solvent was removed *in vacuo* giving a pink solid which was dissolved in toluene, filtered over celite, and stored at −20°C. X-ray quality crystals of **7** were obtained after 24 h (0.72 g, 92%), m.p. 80°C (dec), 140–142°C (melts). HRMS: calcd mass for $C_{14}H_{19}N_4Al$ 271.148942; found 271.150338. ^1H NMR (300.15 MHz, C_6D_6) δ 1.27 [s, 6H, $N(CH_3)_2$], 6.64 [d, 6H, β-$\overline{N(CH)_3CH}$], 2.46 [d, 6H, α-$\overline{N(CH)_3CH}$], $^{13}C\{^1H\}$ NMR (75.14 MHz, C_6D_6) δ 37.55 [$N(CH_3)_3$], 111.41 [β-$\overline{N(CH)_3CH}$], 112.33 [α-$\overline{N(CH)_3CH}$].

Synthesis of $[Li(Al(NH^tBu)_4)]_2$ **9**

t-Butyllithium (11.6 cm^3, 1.7 M solution in pentane) was added dropwise to a solution of $^tBuNH_2$ (2.0 cm^3, 1.39 g, 1.9 mmol) in hexane (30 cm^3) at −78°C resulting in a cloudy white slurry. The stirred slurry

Table 2. Crystal data, details of intensity, measurement and structure refinement for **5**, **7** and **9**

	5	**7**	**9**
Formula	$C_{10}H_{20}AlN_5$	$C_{14}H_{19}AlN_4$	$C_{16}H_{40}AlLiN_4$
Fw	237.29	270.31	322.44
T(K)	293(2)	293(2)	293(2)
λ	0.71073	0.71073	0.71073
Cryst syst	Triclinic	Triclinic	Triclinic
Space group	$P\bar{1}$	$P\bar{1}$	$P\bar{1}$
a (Å)	9.384(2)	7.7272(7)	10.268(2)
b (Å)	9.794(2)	9.6883(5)	10.767(2)
c (Å)	15.224(3)	10.808(2)	11.152(3)
α (°)	96.40(2)	71.27(1)	92.95(3)
β (°)	94.60(2)	87.84(1)	117.18(3)
γ (°)	109.94(2)	88.970(9)	99.02(3)
V (Å^3)	1296.6(5)	765.8(2)	1072.6(4)
Z	4	2	2
d (calc) (g/cm^3)	1.216	1.172	0.998
Abs. coeff (cm^{-1})	1.40	1.25	0.97
Crystal size, mm	0.22 × 0.32 × 0.32	1.13 × 0.63 × 0.22	0.43 × 0.28 × 0.19
θ (°)	2.24–24.98	2.46–27.40	2.63–25.13
Total no. of rflns	5535	3346	4470
No. of obsd rflns	4529	2678	3762
No. of ref params	290	181	227
GOF on F^2	1.032	1.275	1.038
$wR2/R1^a$[$I > 2\sigma(I)$]	0.1465/0.0784	0.1373/0.0462	0.1796/0.0688

^{a} $R1 = \Sigma||F_o| - |F_c||/\Sigma|F_o|$, $wR2 = [\Sigma[w(F_o^2 - F_c^2)^2]/\Sigma[w(F_o^2)^2]]^{1/2}$, $1/[\sigma^2(F_o^2) + (aP)^2 + bP]$ where $P = [Max(0, F_o^2)/3 + 2F_c^2/3]$

was allowed to warm to 25°C over a 2 h period. The resulting ^{t}BuN(H)Li reagent was added dropwise over a 1.5 h period to a solution of $AlCl_3$ (0.84 g, 6.3 mmol) in hexane (30 cm^3) at −78°C. The reaction mixture was stirred for 15 h then filtered over Celite. The volume of the resulting clear, colourless solution was reduced by half and stored at −20°C. X-ray quality crystals of **9** were obtained after 12 h (1.22 g, 60%), m.p. 155°C (dec). HRMS: calcd mass for $C_{32}H_{80}N_8Al_2Li$ 637.630388; found 637.629682. ^{1}H NMR (300.15 MHz, C_6D_6) δ 1.43 (s, 36H, ^{t}Bu).

X-ray crystallography

Crystals of **5** were grown from pentane solutions at −20°C whereas crystalline samples of **7** and **9** were grown from toluene solutions stored at −20°C. Crystals of **5, 7** and **9** were mounted in thin-walled glass capillaries and sealed under argon. Data were collected on an Enraf Nonius diffractometer at 25°C with graphite monochromated Mo-Kα radiation (λ = 0.71073 Å). Accurate unit cell parameters were determined by recentering 25 optimal high angle reflections. Three standard reflections were measured every 1800 s during data collection, and no decreases in intensities were noted. Corrections were applied for Lorentz-polarization and absorption effects. The structures were solved for the heavy atoms by direct methods. Subsequent difference syntheses gave all other non-hydrogen atomic positions and these were refined by full-matrix least squares on F^2 using the Siemens SHELXL PLUS 5.0 (PC) software package [14]. All non-hydrogen atoms were allowed anisotropic thermal motion. Hydrogen atoms were included at calculated positions (C—H 0.96 Å) and were refined using a riding model and a general isotropic thermal parameter. Crystallographic data and details of the data collection procedures and structure refinement for **5, 7** and **9** are presented in Table 2. Further details on the crystal structure analysis are available on request from the Director of the Cambridge Crystallographic Data Centre, 12 Union Road, Cambridge CB2 1EZ, U.K. by quoting the full journal citation.

Acknowledgements—We are grateful to the Science and Technology Center Program of the National Science Foundation (CHE-08920120), the National Science Foundation (CHE-9629088), and the Robert A. Welch Foundation for generous financial support.

REFERENCES

1. Neumayer, D. A. and Ekerdt, J. G., *Chem. Mater.*, 1996, **8,** 9.
2. Neumayer, D. A., Cowley, A. H., Decken, A., Jones, R. A., Lakhotia, V. and Ekerdt, J. G., *J. Am. Chem. Soc.*, 1995, **115,** 5893.
3. Carmalt, C. J., Cowley, A. H., Culp, R. D. and Jones, R. A., *Chem. Commun.*, 1996, 1453.
4. Uncoordinated $Ga(N_3)_3$ was first prepared over 40 years ago. See Wiberg, E. and Michand, H., *Z. Naturforsch., Teil B*, 1954, **9,** 502. Subsequent to our work [3], a synthetic route to **2** involving the intermediacy of uncoordinated $Ga(N_3)_3$ has been published along with an X-ray crystal structure. See, Fischer, R. A., Miehr, A., Herdtweck, E., Mattner, M. R., Sussek, H., Ambacher, O., Metzger, T., Born, E., Weinkauf, S., Pulham, C. R. and Parsons, S., *Chem. Eur.*, 1996, **2,** 1353.
5. Boyd, D. C., Haasch, R. T., Mantell, D. R., Schulze, R. K., Evans, J. F. and Gladfelter, W. L., *Chem. Mater.*, 1989, **1,** 119.
6. Fischer, R. A., Miehr, A., Sussek, H., Pritzkow, H., Herdtweck, E., Müller, J., Ambacher, O. and Metzger, T., *Chem. Commun.*, 1996, 2685.
7. Baixia, L., Yinkui, L. and Yi, L., *J. Mater. Chem.*, 1993, **3,** 117.
8. For a review of covalent azides, see Tornieporth-Oetting, I. C. and Klapötke, T. M., *Angew. Chem., Int. Ed. Engl.*, 1995, **34,** 511.
9. Waggoner, K. M., Olmstead, M. M. and Power, P. P., *Polyhedron*, 1990, **9,** 257.
10. Andrianarison, M. M., Ellerby, M. C., Gorrell, I. B., Hitchcock, P. B., Smith, J. D. and Stanley, D. R., *J. Chem. Soc., Dalton Trans.*, 1996, 211.
11. Atwood, D. A. and Rutherford, D., *Main Group Chemistry*, 1996, **1,** 431.
12. Böck, St., Nöth, H. and Rahm, P., *Z. Naturforsch., Teil B*, 1988, **43,** 53.
13. Rutherford, D. and Atwood, D. A., *J. Am. Chem. Soc.*, 1996, **118,** 11535.
14. Sheldrick, G. M., *SHELXTL PC Version* 5.0, Siemens Analytical X-ray Instruments, Inc., 1994.

Pergamon

PII: S0277-5387(97)00205-2

Polyhedron Vol. 17, No. 5–6, pp. 983–991, 1998
© 1998 Elsevier Science Ltd
All rights reserved. Printed in Great Britain
0277-5387/98 $19.00+0.00

1,3-Diphenylamidine and methylaminopyridine compounds of gallium†

Yoshihiro Koide,[a] Julie A. Francis,[a] Simon G. Bott[b]* and Andrew R. Barron[a]*

[a]Department of Chemistry, Rice University, Houston, TX 77005, U.S.A.

[b]Department of Chemistry, University of Houston, Houston, TX 77204, U.S.A.

(Received 7 April 1997; accepted 12 May 1997)

Abstract—Reaction of $Ga(^tBu)_3$ with the 1,3-diphenylamidine [PhN(H)C(H)=NPh, H-dpam] yields monomeric $(^tBu)_2Ga(dpam)$ (**1**). The partial hydrolysis of **1** results in the isolation of $(^tBu)_2Ga(\mu\text{-dpam})(\mu\text{-OH})Ga(^tBu)_2$ (**2**), whose structure consists of a gallium dimer in which the amidine and hydroxide ligands bridge two $Ga(^tBu)_2$ moieties. Reaction of $[Me_2Ga(\mu\text{-Cl})]_2$ with H-dpam results in the complex $[H_2\text{-dpam}][Me_2GaCl_2]$ (**3**). The solid state structure of **3** indicates the presence of a hydrogen bonded cation–anion complex, in which the core has a twisted eight-membered ring configuration. The versatility of amidines as both chelating and bridging ligands to gallium is discussed with respect to the predominance of bridging and chelating modes of coordination of carboxylates and triazenides, respectively. Reaction of 2-(methylamino)pyridine (H-map) with $Ga(^tBu)_3$ allows for the isolation of $(^tBu)_2Ga(map)$ (**4**). In contrast, reaction with $[(^tBu)_2Ga(\mu\text{-Cl})]_2$ and $[Me_2Ga(\mu\text{-Cl})]_2$ yields the Lewis acid base adducts, $(^tBu)_2GaCl(H\text{-map})$ (**5**) and $Me_2GaCl(H\text{-map})$ (**6**), respectively. Reaction of compound **6** with $^nPrNH_2$ does not result in the deprotonation of the H-map ligand, but ligand metathesis and the formation of $(^tBu)_2GaCl(NH_2{}^nPr)$ (**7**). The structures of **2, 3, 6,** and **7** have been determined by X-ray crystallography. © 1998 Elsevier Science Ltd. All rights reserved

Keywords: amidine; aminopyridine; hydrogen bonding; hydrolysis; gallium.

We have become interested in the structural relationships between potentially isolobal [1] (and isoelectronic) ligands as they pertain to their coordination to the Group 13 metals: aluminum, gallium and indium. Our initial studies in this area involved a comparison of carboxylates (**I**) [2] and their isolobal analogs, 1,3-diphenyl triazenide ligands (**II**) [3,4,5,6]. We have demonstrated that despite the clear isolobal relationship between the parent ligands [7], the propensity of triazenides to act as a chelating rather than bridging ligand (as is observed for carboxylates) to aluminum, gallium or indium, suggests that they are better considered equivalent to acetylacetenoates. While we originally ascribed the differences in coordination of carboxylates and triazenides to the greater steric strain that would be imposed on a chelating carboxylate than is observed for the triazenide [8], it is possible that the presence of aryl (or alkyl) substituents on the 1,3 positions of the triazenide may add a steric component to the difference in observed coordination. In order to determine if it is steric rather than ring strain factors controlling the preferred coordination mode for carboxylates and triazenides it would be desirable to study a hybrid class of ligand, such as a dialkylamidines (**III**) [9]. A particular advantage of the amidines is that the steric bulk at both carbon (*R'*) and nitrogen (*R*) may be tuned as desired. Dialkylamidine complexes of transition metals have been well studied; however, compared to the extensive chemistry of carboxylate compounds a limited number of compounds

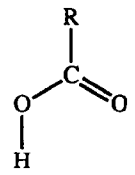

(**I**)

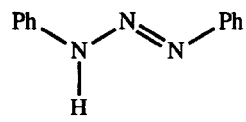

(**II**)

* Authors to whom correspondence should be addressed.

† Dedicated to Professor D. C. Bradley, FRS for his seminal contributions to the chemistry of alkoxide and amide compounds of the main group and transition metals.

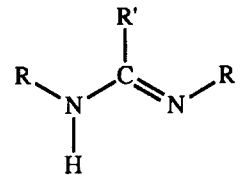

(III)

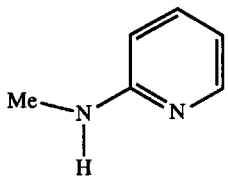

(IV)

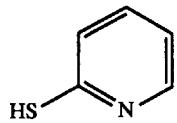

(V)

of the Group 13 metals have been reported for amidines [10,11]. The dialkylamidine compounds of gallium were shown by X-ray crystallography to be both chelating and bridging, suggesting that amidines are potentially more flexible ligands for the Group 13 metals than either carboxylates or triazenides. Our studies involve the reactions of 1,3-diphenylamidine (H-dpam, **III**, R = Ph, R' = H).

Alternative isolobal (and isoelectronic) analogs of an amidine are 2-(methylamino)pyridine (H-map, **IV**) and 2-mercaptopyridine ligand (H-Spy, **V**). The latter has previously been demonstrated to form both bridging and chelating complexes with aluminum, gallium and indium [12,13].

In order to determine the relative coordination modes for these isolobal ligands we have investigated the reactions of 1,3-diphenylamidine (H-dpam) and 2-(methylamino)pyridine (H-map) with gallium trialkyls and di-alkyl chlorides. The initial results of this study are presented herein.

RESULTS AND DISCUSSION

Amidine compounds

Reaction of $Ga(^tBu)_3$ with one equivalent of H-dpam yields $(^tBu)_2Ga(dpam)$ (**1**), with the con-

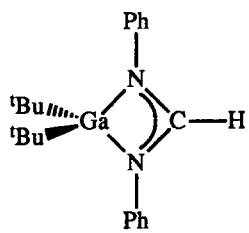

(1)

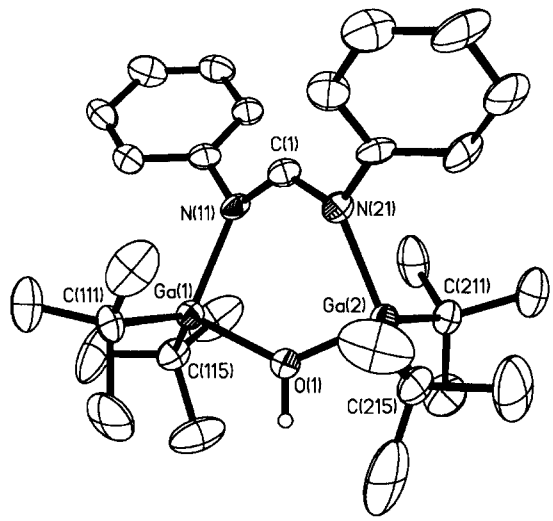

Fig. 1. The molecular structure of one of the crystallographically independent molecules of $(^tBu)_2Ga(\mu$-dpam$)(\mu$-OH$)Ga(^tBu)_2$ (**2**). Thermal ellipsoids are shown at the 30% level and organic hydrogen atoms are omitted for clarity.

comitant liberation of iso-butane. Based upon mass spectrometry (M^+ = 378) compound **1** appears to be isostructural to the 1,2,3-triphenylamidine compound Me_2Ga(PhNCPhNPh) [11].

Compound **1** undergoes partial hydrolysis to liberate dpam-H and the dimeric hydroxide compound, $(^tBu)_2Ga(\mu$-dpam$)(\mu$-OH$)Ga(^tBu)_2$ (**2**), whose molecular structure is shown in Fig. 1; selected bond lengths and angles are given in Table 1. Two independent molecules are present in the asymmetric unit; however, all bond lengths and angles are close to or within experimental error between the two molecules (see Table 1). The Ga_2ON_2C cycle occupies a twist boat conformation (see Fig. 2) as a consequence of the steric interaction between the *tert*-butyl and phenyl groups [2]. The coordination around each gallium is distorted tetrahedral, with the smallest angles being

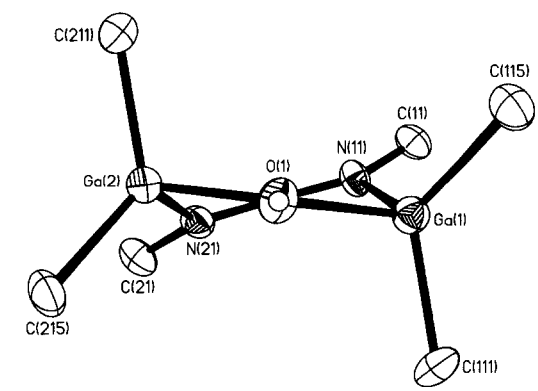

Fig. 2. Partial coordination of $(^tBu)_2Ga(\mu$-dpam$)(\mu$-OH$)Ga(^tBu)_2$ (**2**) viewed along the O(1)···C(1) vector demonstrating the twist boat conformation of the Ga_2ON_2C cycle.

Table 1. Selected bond lengths (Å) and angles (°) for (^{t}Bu)$_2$Ga(μ-dpam)(μ-OH)Ga(^{t}Bu)$_2$ (**2**)

Molecule 1		Molecule 2	
Ga(1)—O(1)	1.933(6)	Ga(3)—O(2)	1.938(5)
Ga(1)—N(11)	2.028(7)	Ga(3)—N(31)	2.020(7)
Ga(1)—C(111)	2.038(9)	Ga(3)—C(311)	1.99(1)
Ga(1)—C(115)	2.010(8)	Ga(3)—C(315)	2.00(1)
Ga(2)—O(1)	1.938(6)	Ga(4)—O(2)	1.945(6)
Ga(2)—N(21)	2.032(6)	Ga(4)—N(41)	2.020(6)
Ga(2)—C(211)	2.001(9)	Ga(4)—C(411)	1.999(9)
Ga(2)—C(215)	2.01(1)	Ga(4)—C(415)	1.999(8)
N(11)—C(1)	1.30(1)	N(31)—C(2)	1.33(1)
N(11)—C(11)	1.42(1)	N(31)—C(31)	1.414(9)
N(21)—C(1)	1.34(1)	N(41)—C(2)	1.331(9)
N(21)—C(21)	1.42(1)	N(41)—C(41)	1.43(1)
O(1)—Ga(1)—N(11)	93.8(3)	O(2)—Ga(3)—N(31)	93.4(2)
O(1)—Ga(1)—C(111)	104.4(3)	O(2)—Ga(3)—C(311)	105.3(3)
O(1)—Ga(1)—C(115)	106.7(3)	O(2)—Ga(3)—C(315)	105.4(3)
N(11)—Ga(1)—C(111)	108.3(3)	N(31)—Ga(3)—C(311)	110.5(4)
N(11)—Ga—(1)—C(115)	113.3(4)	N(31)—Ga(3)—C(315)	113.6(3)
C(111)—Ga(1)—C(115)	125.2(4)	C(311)—Ga(3)—C(315)	123.5(4)
O(1)—Ga(2)—N(21)	94.4(2)	O(2)—Ga(4)—N(41)	94.3(3)
O(1)—Ga(2)—C(211)	103.9(3)	O(2)—Ga(4)—C(411)	104.4(3)
O(1)—Ga(2)—C(215)	105.4(3)	O(2)—Ga(4)—C(415)	105.4(3)
N(21)—Ga(1)—C(211)	110.5(3)	N(41)—Ga(4)—C(411)	110.4(3)
N(21)—Ga(1)—C(215)	112.9(3)	N(41)—Ga(4)—C(415)	112.7(3)
C(211)—Ga(2)—C(215)	124.6(4)	C(411)—Ga(4)—C(415)	124.5(3)
Ga(1)—O(1)—Ga(2)	132.0(3)	Ga(3)—O(2)—Ga(4)	132.4(3)
Ga(1)—N(11)—C(1)	127.9(6)	Ga(3)—N(31)—C(2)	127.7(5)
Ga(1)—N(11)—C(11)	118.2(5)	Ga(3)—N(31)—C(31)	118.1(6)
C(1)—N(11)—C(11)	112.9(7)	C(2)—N(31)—C(31)	113.5(6)
Ga(2)—N(21)—C(1)	125.6(5)	Ga(4)—N(41)—C(2)	126.2(6)
Ga(2)—N(21)—C(21)	119.1(5)	Ga(4)—N(41)—C(41)	118.5(4)
C(1)—N(21)—C(21)	114.2(6)	C(2)—N(41)—C(41)	113.6(7)
N(11)—C(1)—N(21)	128.1(8)	N(31)—C(2)—N(41)	128.0(8)

intra-ring, i.e., N—Ga—O [93.4(2)–94.4(2)°]. The Ga—N bond lengths [2.020(7)–2.032(6) Å] are within the range reported for chelating amidine compounds of gallium [2.009(2)–2.141(2) Å] [10,11]. As is typical for amidine ligands the N—C bond distances within the amidine core [1.30(1)–1.34(1) Å] are intermediate between those of isolated N—C single (*ca* 1.45 Å) and N=C double bond (*ca* 1.28 Å) lengths, consistent with delocalization of the N···C···N π-bond. The Ga—O—Ga angle [132.0(3), 132.4(3) Å] is smaller than that reported for [(^{t}Bu)$_2$Ga(μ-OH)]$_3$ (**VI**) [143.0(2) Å] [14].

Whereas Barker *et al.* have previously reported that the reaction of 1,2,3-triphenylamidine with $GaMe_3$ yields Me_2Ga(PhNCPhNPh) [11], the reaction of H-dpam with [$Me_2Ga(\mu$-Cl)]$_2$ does not result in alkane elimination but the formation of the salt, [H_2-dpam][Me_2GaCl_2] (**3**) (see Experimental), whose formation presumably occurs *via* the series of reactions shown in Eqs 1–3. We note that while Me_2Ga(PhNCPhNPh) [11] and Me_2Ga(PhNCMeNPh) [10] have been previously reported, we were unable to isolate Me_2Ga(dpam) under the present reaction conditions.

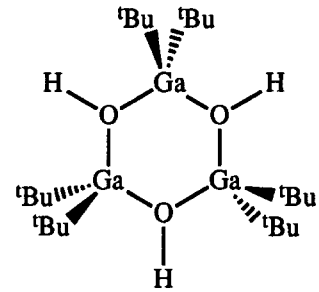

(VI)

$$Me_2GaCl + H\text{-dpam} \rightarrow Me_2Ga(dpam) + HCl \quad (1)$$

$$H\text{-dpam} + HCl \rightarrow [H_2\text{-dpam}]Cl \quad (2)$$

$$Me_2GaCl + [H_2\text{-dpam}]Cl \rightarrow [H_2\text{-dpam}][Me_2GaCl_2] \quad (3)$$

The structure of [H_2-dpam][Me_2GaCl_2] (**3**) is shown in Fig. 3; selected bond lengths and angles are given in Table 2. The coordination environment about

Table 2. Selected bond lengths (Å) and angles (°) for $[H_2$-dpam$][Me_2GaCl_2]$ (**3**)

Ga(1)—Cl(1)	2.307(4)	Ga(1)—C(11)	1.95(2)
N(2)—C(2)	1.31(1)	N(2)—C(3)	1.40(2)
Cl(1)—Ga(1)—Cl(1a)	97.4(1)	Cl(1)—Ga(1)—C(11)	106.3(6)
C(11)—Ga(1)—C(11a)	130.3(5)	C(1)—N(2)—C(3)	127(1)
N(2)—C(2)—N(2a)	125(1)		

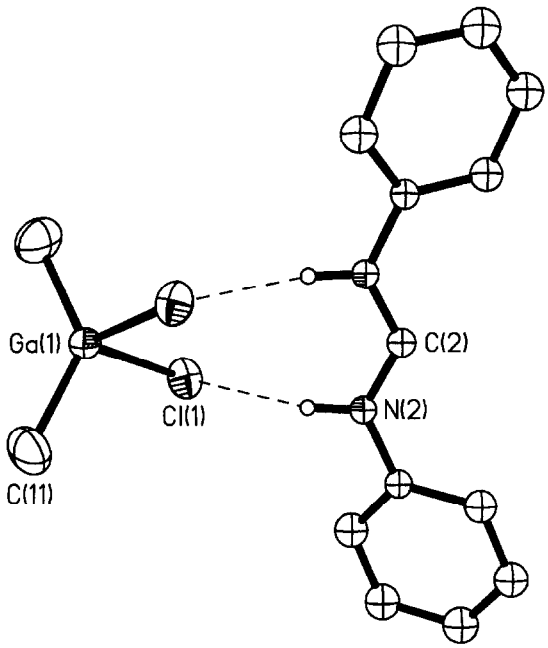

Fig. 3. The structure of $[H_2$-dpam$][Me_2GaCl_2]$ (**3**). Thermal ellipsoids are shown at the 30% level and organic hydrogen atoms are omitted for clarity.

Ga(1) is similar to previously characterized anion in $[Me_4As][Me_2GaCl_2]$ [15]. The Ga(1)—Cl(1) bond distance [2.307(4) Å] is slightly longer than non-hydrogen bonded terminal analogs [2.276(4), 2.277(4) Å] consistent with the hydrogen bonding interaction. Similarly, the Cl(1)—Ga(1)—Cl(1a) bond angle in **3** [97.4(1)°] is smaller than that in $[Me_4As][Me_2GaCl_2]$ [99.7(1)°], presumably due to the constraints of the two N—H···Cl hydrogen bonds. The hydrogen bonded anion–cation complex forms an unusual twisted 8-membered ring (see Fig. 4). The N—H···Cl hydrogen bonding distances [2.13(4) Å] is slightly shorter than recently observed for $[H_2N^iPr_2][MeGaCl_3]$, 2.43(7), 2.60(7) Å [16].

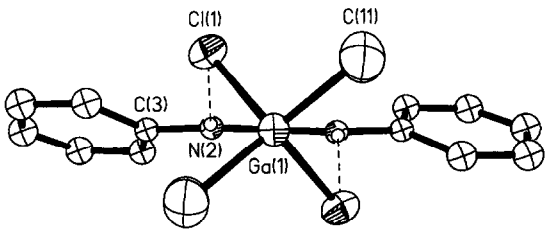

Fig. 4. $[H_2$-dpam$][Me_2GaCl_2]$ (**3**) viewed along the Ga(1)···C(1) vector demonstrating the conformation of the $GaCl_2H_2N_2C$ cycle.

Amidines: intermediaries between carboxylates and triazenides

We have previously suggested that the propensity of carboxylate ligands to act as bridging rather than chelating ligands to the Group 13 metals is due to the topotactic nature of the reaction [2], since no reorganization of the O—C—O framework is required in going from the 'free' carboxylic acid to the bridging carboxylate ligand. In particular the O—C—O angle in the free ligand (*ca* 123°) is similar to the range we have reported for bridging complexes (122–125°), and distinct to that observed and calculated for chelating carboxylates [2,17]. This is represented graphically in Fig. 5. In contrast, the N—N—N angle in bridging triazenide complexes is significantly larger than that for free and chelating triazenides (see Fig. 5) in accord with the observed preference of the latter mode of coordination.

The observations herein, and previously [10,11], that amidines exist as both bridging and chelating ligands suggests that they are more flexible ligands to Group 13 metals than either triazenides or carboxylates. This effect may be expected based on the rationale used for the triazenide and carboxylate preferential binding [2,8]. Thus, from Fig. 5 it is seen that the N—C—N angle in 'free' amidines occurs in between the values observed for chelating and bridging coordination. Furthermore, in both carboxylates and triazenides the intra-ligand angle is essentially invariant; however, the N—C—N angle in amidines may be

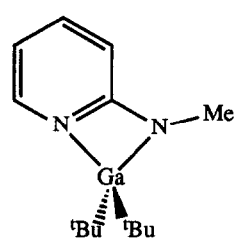

(**4**)

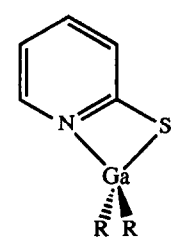

(**VII**)

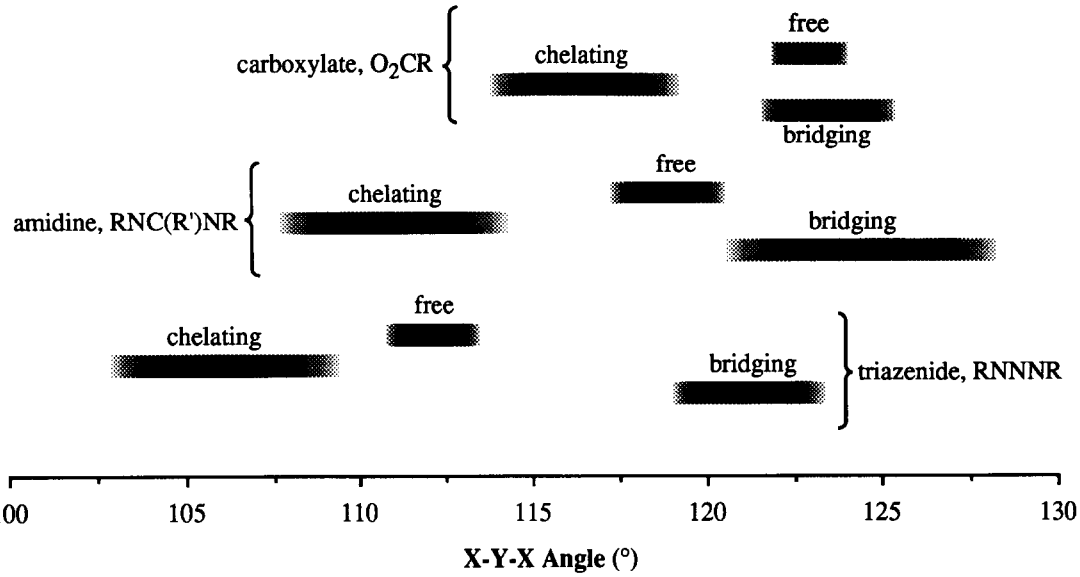

Fig. 5. Graphical representation of the X—Y—X bond angle (°) for triazenides, amidines, and carboxylates in chelating and bridging complexes as well as the 'free' ligand.

increased through the use of sterically demanding groups at either or both C and N. Thus, amidine ligands offer an entry into a diverse range of Group 13 metal complexes. Our studies in this regard are continuing.

2-(*Methylamino*)*pyridine compounds*

Reaction of $Ga(^tBu)_3$ with 2-(methylamino)pyridine (H-map) yields $(^tBu)_2Ga$(2-map) (**4**). Mass spectra of compound **4** indicate it to be monomeric in the gas phase (see Experimental), and thus analogous to $(R)_2Ga(Spy)$ (**VII**, R = Me,^{t}Bu).

As was observed for H-dpam (*vide supra*), the reaction of H-map with $[R_2Ga(\mu\text{-Cl})]_2$ (R = Me,^{t}Bu) does not result in alkane elimination, but yields the Lewis acid–base complexes, Me_2GaCl(2-map) (**5**) and $(^tBu)_2$ GaCl(2-map) (**6**). The molecular structure of Me_2GaCl(2-map) (**6**) has been determined by X-ray crystallography and is shown in Fig. 6; selected bond lengths and angles are given in Table 3.

The 2-(methylamino)pyridine ligand in compound **6** coordinates *via* the pyridine nitrogen, consistent with the greater Lewis basicity of pyridine over a secondary amine. It is interesting to note that the configuration of the Me_2GaCl moiety in the solid state (**VIII**) with respect to the 2-(methylamino)pyridine ligand precludes N—H···Cl hydrogen bonding (i.e. **IX**). In addition to the lack of intra-molecular N—H···Cl hydrogen bonding, there is no evidence for inter-molecular hydrogen bonding from the crystal packing. The ν(N—H) stretch in the IR spectra of compound **6** is unchanged between solution (3327 cm^{-1}, CH_2Cl_2) and the solid state (3329 cm^{-1}, KBr disk), suggesting that no N—H···Cl hydrogen bonding occurs to the methyl amine of the H-map ligand. Similarly the change observed for compound **5** (3346 cm^{-1}, CH_2Cl_2 versus 3354 cm^{-1}, KBr disk) is consistent with no hydrogen bonding.

Reaction of compound **6** with ^{n}PrNH$_2$ does not result in the deprotonation of the H-map ligand, but ligand metathesis and the formation of $(^tBu)_2$

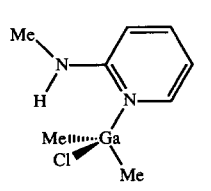

(VIII)

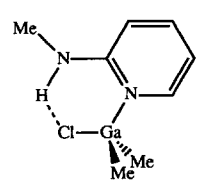

(IX)

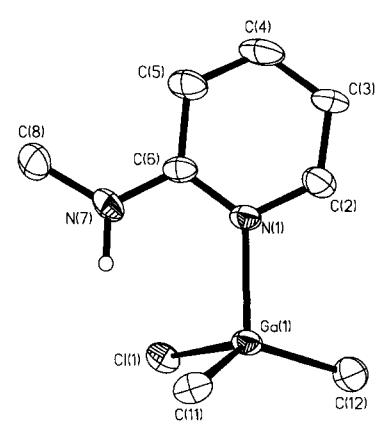

Fig. 6. The molecular structure of Me_2GaCl(H-map) (**6**). Thermal ellipsoids are shown at the 30% level and organic hydrogen atoms are omitted for clarity.

Table 3. Selected bond lengths (Å) and angles (°) for Me_2GaCl[H-map] (**6**)

Ga(1)—Cl(1)	2.276(1)	Ga(1)—N(1)	2.066(3)
Ga(1)—Cl(11)	1.945(5)	Ga(1)—C(12)	1.958(4)
Cl(1)—Ga(1)—N(1)	99.18(9)	Cl(1)—Ga(1)—C(11)	106.8(1)
Cl(1)—Ga(1)—C(21)	107.5(1)	N(1)—Ga(1)—C(11)	108.0(2)
N(1)—Ga(1)—C(21)	106.8(2)	C(11)—Ga(1)—C(21)	125.5(2)

Table 4. Selected bond lengths (Å) and angles (°) for (^{t}Bu)$_2$GaCl($NH_2{}^n$Pr) (**7**)

Ga(1)—Cl(1)	2.285(2)	Ga(1)—N(1)	2.067(4)
Ga(1)—C(11)	1.979(7)	Ga(1)—C(21)	1.987(6)
Cl(1)—Ga(1)—N(1)	94.1(1)	Cl(1)—Ga(1)—C(11)	107.9(2)
Cl(1)—Ga(1)—C(21)	109.3(2)	N(1)—Ga(1)—C(11)	105.7(2)
N(1)—Ga(1)—C(21)	111.0(2)	C(11)—Ga(1)—C(21)	124.5(2)

GaCl($NH_2{}^n$Pr) (**7**), whose structure has been confirmed by X-ray crystallography. The molecular structure of compound **7** is shown in Fig. 7; selected bond lengths and angles are given in Table 4. The Ga(1)—N(1) distance [2.067(4) Å] is similar to that observed for the pyridine donor in compound **6** (*vide supra*). In addition the Ga(1)—Cl(1) bond [2.285(2) Å] is essentially the same as that observed for compound **6**; however, while there is no evidence for intramolecular hydrogen bonding in **7**, the crystal packing (Fig. 8) shows strong inter-molecular N—H···Cl hydrogen bonding.

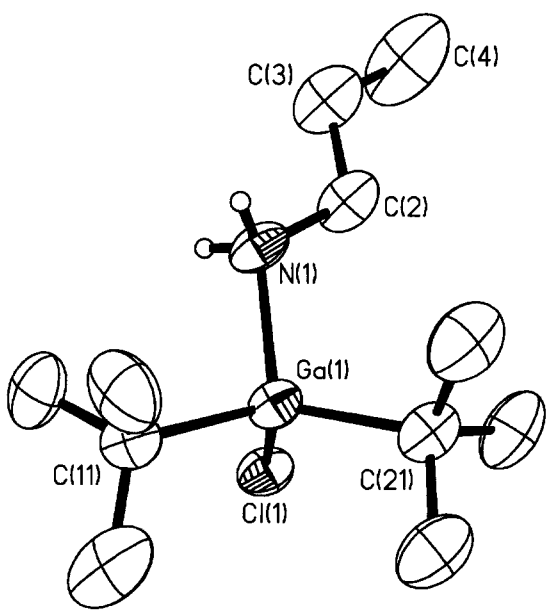

Fig. 7. The molecular structure of (^{t}Bu)$_2$GaCl($NH_2{}^n$Pr) (**7**). Thermal ellipsoids are shown at the 30% level and hydrogen atoms are omitted for clarity.

EXPERIMENTAL

All operations were carried out using Schlenk techniques or in an argon atmospheric VAC glovebox. The synthesis of Ga(^{t}Bu)$_3$ [18,19] [(^{t}Bu)$_2$Ga(μ-Cl)]$_2$ [20], and [Me_2Ga(μ-Cl)]$_2$ [21] are reported elsewhere. ^{1}H and ^{13}C NMR analysis was carried out on a Bruker WM-250 MHz spectrometer. Mass spectra analysis was obtained on a Finnegan MAT95 mass spectrometer with an electron beam energy of 70 eV for EI mass spectra. IR analysis was carried out on a Perkin–Elmer 1600 Series FT-IR spectrometer using Nujol mulls.

(^{t}Bu)$_2$Ga(dpam) (**1**)

H-dpam (1.82 g, 8.31 mmol) was dissolved in degassed toluene (50 cm^3) and the solution was cooled to −78°C. Ga(^{t}Bu)$_3$ (2.0 cm^3, 8.31 mmols) was then added slowly and the mixture was left to stir overnight while warming to room temperature. The solution was filtered, concentrated *in vacuo*, and cooled (−22°C). Several crops of pale yellow crystals were collected by filtration and subsequent recooling of the filtrate. MS (EI, %): *m/z* 378 (M^+, 7), 321 (M^+—^{t}Bu, 98), 265 (M^+—2^{t}Bu, 80), 196 (dpam, 7), 57 (^{t}Bu, 27). IR (cm^{-1}): 2961 (m), 2924 (m), 2338 (m), 1265 (s), 1084

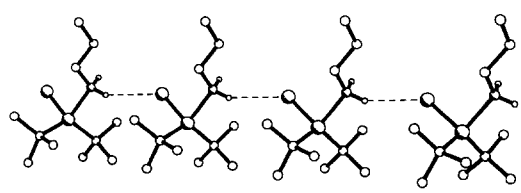

Fig. 8. A view of the inter-molecular hydrogen bonding observed in the solid state for $Me_2GaCl(NH_2{}^n Pr)$ (**7**).

(s), 1011 (s), 794 (s). ^{1}H NMR (C_6D_6): δ 8.32 [1H, s, C*H*N], 7.12 [2H, dd, J(H—H) = 7.8 Hz, *m*-C*H*], 6.87 [1H, t, J(H—H) = 7.8 Hz, *p*-C*H*], 6.82 [2H, d, J(H—H) = 7.8 Hz, *o*-C*H*], 1.29 [18H, s, C(CH_3)$_3$]. ^{13}C NMR (C_6D_6): δ 155.56 (N*C*N), 144.98 (N*C*), 130.11 (*o*-*C*H), 124.78 (*p*-*C*H), 119.06 (*m*-*C*H), 30.53 [C(*C*H$_3$)$_3$].

(^{t}Bu)$_2$Ga(μ-dpam)(μ-OH)Ga(^{t}Bu)$_2$ (**2**)

To a hexane (50 cm^3) suspension of H-dpam (1.0 g, 5.1 mmol) was added Ga(^{t}Bu)$_3$ (1.2 g, 5.0 mmol) dropwise to provide a clear solution. The solution was allowed to stir at ambient temperature for 1 h. The solvents and volatiles were removed *in vacuo* to yield the colorless solids. The product was re-dissolved in wet CH_2Cl_2 and recrystallized at -24°C. Yield: 69%. MS (EI, %): *m*/*z* 523 [M$^+$—^{t}Bu, 100], 321. IR (cm^{-1}): 2928 (m), 2839 (m), 1650 (vs), 1589 (s), 1532 (m), 1489 (m), 1308 (w), 1292 (w), 1201 (m), 1025 (w). ^{1}H NMR: δ 7.33 [2H, dd, J(H—H) = 7.8 Hz, *m*-C*H*], 7.09 [1H, t, J(H—H) = 7.8 Hz, *p*-C*H*], 7.08 [2H, d, J(H—H) = 7.8 Hz, *o*-C*H*], 2.36 (1H, s, O*H*), 1.28 [1H, s, NC(*H*)N], 1.04 [36H, s, C(CH_3)$_3$]. ^{13}C NMR: δ 129.8 (*m*-*C*H), 126.0 (*p*-*C*H), 124.8 (*o*-*C*H), 31.7 [C(*C*H$_3$)$_3$], 24.1 (N*C*N).

[H_2-dpam][Me_2GaCl_2] (**3**)

To a CH_2Cl_2 solution (2.0 cm^3) of H-dpam (0.42 g, 2.2 mmol) was added dropwise an Et_2O solution (2.0 cm^3) of [Me_2Ga(μ-Cl)]$_2$ (0.29 g, 2.2 mmol) at -78°C. The solution mixture was stirred overnight and allowed to rise to anambient temperature. The solvents and volatiles were removed under vacuum to yield a yellow oily residue. The residue was sublimed at *ca* 140°C to obtain pale yellow crystals. Yield: 49%. MS (EI, %): *m*/*z* 294 (M$^+$—2 Cl, 38), 279 [(M$^+$—2 Cl—Me, 100]. IR (cm^{-1}): 3398 (w), 1650 (vs), 1590 (s), 1495 (w). 1307 (w), 1201 (w). ^{1}H NMR: δ 7.2 (2H, br s, N—*H*), 7.2–6.8 (10H, m, C_6H_5), 2.11 [1H, s, NC(*H*)N], 0.30 [6H, s, Ga—CH_3]. ^{13}C NMR (δ): 129.8 (*o*-*C*H), 123.9 (*p*-*C*H), 120.0 (*m*-*C*H), 1.76 (Ga—*C*H$_3$).

(^{t}Bu)$_2$Ga(map) (**4**)

To H-map (0.9 g, 8.31 mmol) in hexane (50 cm^3) was added Ga(^{t}Bu)$_3$ (2.0 g, 8.31 mmol) at -78°C. After warming to room temperature and stirring overnight, the mixture was filtered, and after removal of all volatiles yielded a yellow oil. MS (EI, %): *m*/*z* 233 (M$^+$—^{t}Bu, 18), 177 (M$^+$—2^{t}Bu, 20), 107 (map, 82), 57 (^{t}Bu, 12). R(cm^{-1}): 2960 (s), 2837 (s), 1608 (s), 1501 (m), 1419 (m), 1296 (m), 1086 (s), 1009 (s), 799 (s), 656 (m). ^{1}H NMR (C_6D_6): δ 7.02 [1H, d, J(H—H) = 7.5, 6-C*H*], 6.92 [1H, dd, J(H—H) = 7.5, 4-C*H*], 5.81 [1H, dd, J(H—H) = 7.5, 5-C*H*], 5.77 [1H, d, J(H—H) = 6.8 Hz, 3-C*H*], 2.67 (3H, s, NCH_3), 1.22 [18H, s, C(CH_3)$_3$]. ^{13}C NMR (C_6D_6): δ 144.3 (6-*C*H), 140.2 (4-*C*H), 107.1 (5-*C*H), 103.8 (3-*C*H), 30.6 [C(*C*H$_3$)$_3$], 24.1 (N*C*H$_3$).

(^{t}Bu)$_2$GaCl(H-map) (**5**)

To neat H-map (0.40 g, 3.9 mmol) was added [(^{t}Bu)$_2$Ga(μ-Cl)]$_2$ (0.86 g, 3.9 mmol) at ambient temperature. The resulting colorless oily product was agitated for 1 h. Hexane (2 cm^3) was added and stirred additional 1 h. The solvent and volatiles were removed *in vacuo* to yield a colorless solid. The material was recrystallized from CH_2Cl_2 at -24°C. Yield: 79%. MS (EI, %): *m*/*z* 269 (M$^+$—^{t}Bu, 36), 233 (M$^+$—^{t}Bu—Cl, 18), 183 [(^{t}Bu)$_2$GaCl, 75]. IR (cm^{-1}): 3309 (s, br), 2952 (s), 2939 (s), 2839 (s), 1711 (w), 1661 (s), 1625 (vs), 1581 (vs), 1540 (s), 1474 (s), 1423 (m), 1362 (w), 1350 (w), 1172 (s), 1078 (w), 997 (w), 814 (m), 508 (w). ^{1}H NMR: δ 7.65 [1H, d, J(H—H) = 7.5, 6-C*H*], 6.73 [1H, dd, J(H—H) = 7.5, 4-C*H*], 5.92 [1H, dd, J(H—H) = 7.5, 5-C*H*], 5.61 [1H, d, J(H—H) = 6.8 Hz, 3-C*H*], 1.99 [3H, d, J(H—H) = 5.0 Hz, NCH_3], 1.36 [18H, s, C(CH_3)$_3$]. ^{13}C NMR: δ 144.8 (6-*C*H), 140.7 (4-*C*H), 111.4 (5-*C*H), 108.1 (3-*C*H), 30.9 [C(*C*H$_3$)$_3$], 28.5 [N*C*H$_3$].

Me_2GaCl(H-map) (**6**)

To neat H-map (0.20 g, 1.9 mmol) was added [Me_2Ga(μ-Cl)]$_2$ (0.25 g, 1.9 mmol) at ambient temperature. The resulting colorless oily product was agitated for 30 min and then set in a freezer (-24°C) overnight to obtain crystalline solids. Yield: 93%. MS (EI, %): *m*/*z* 227 [M$^+$—Me, 15], 207 (M$^+$—Cl, 10), 191 (M$^+$—Cl—CH_4, 15), 121 (MeGaCl, 21), 108 (map-H, 100), 99 (GaMe_2, 41). IR (cm^{-1}): 3682 (w), 3331 (m, br), 1663 (s), 1626 (s), 1579 (s), 1537 (m), 1472 (m), 1170 (m), 1007 (w). ^{1}H NMR: δ 7.49 [1H, d, J(H—H) = 7.5, 6-C*H*], 7.40 (1H, br, N—*H*), 6.70 [1H, dd, J(H—H) = 7.5, 4-C*H*], 5.86 [1H, dd, J(H—H) = 7.5, 5-C*H*], 5.58 [1H, d, J(H—H) = 6.8 Hz, 3-C*H*], 1.97 [3H, d, J(H—H) = 5.0 Hz, NCH_3], 0.26 (6H, s, Ga—CH_3). ^{13}C NMR: δ 158.8 (6-*C*H), 143.8 (6-*C*H), 141.4 (4-*C*H), 112.7 (5-*C*H), 108.3 (3-*C*H), 29.0 (N*C*H$_3$), -2.9 (Ga—*C*H$_3$).

(^{t}Bu)$_2$GaCl(NH$_2$^{n}Pr) (**7**)

To (^{t}Bu)$_2$GaCl(H-map) (1.1 g, 4.1 mmol) was added NH$_2$^{n}Pr (0.25 g, 4.2 mmol) and the mixture stirred for 1 h. As this slightly exothermic reaction cooled down to ambient temperature, needle like crystals were formed. Yield: 96%. MS (EI, %): *m*/*z* 220 (M$^+$—^{t}Bu, 37). ^{1}H NMR: δ 2.21 (1H, br, NH$_a$), 1.86 (1H, br, NH$_b$), 1.24 [18H, s, C(CH$_3$)$_3$], 1.07 [2H, t, J(H—H) = 7.2 Hz, NH$_2$CH_2], 0.68 [2H, qt,

Table 5. Summary of X-ray diffraction data

Compound	(^{t}Bu)$_2$Ga(μ-dpam)(μ-OH)Ga(^{t}Bu)$_2$ (**2**)	[H$_2$-dpam][Me$_2$GaCl$_2$] (**3**)	Me$_2$GaCl(H-map) (**6**)	(^{t}Bu)$_2$GaCl(NH$_2$^{n}Pr) (**7**)
Formula	$C_{29}H_{48}Ga_2N_2O$	$C_{15}H_{19}Cl_2GaN_2$	$C_8H_{14}ClGaN_2$	$C_{11}H_{27}ClGaN$
Cryst size (mm)	$0.21 \times 0.24 \times 0.26$	$0.09 \times 0.10 \times 0.28$	$0.18 \times 0.21 \times 0.24$	$0.10 \times 0.12 \times 0.45$
Cryst system	triclinic	orthorhombic	monoclinic	triclinic
Space group	$P\bar{1}$	*Pbcn*	$P2_1/n$	$P\bar{1}$
a (Å)	11.592(1)	18.648(2)	8.945(2)	6.3492(7)
b (Å)	16.712(2)	11.135(1)	11.305(2)	10.907(1)
c (Å)	17.009(2)	8.543(1)	11.273(2)	12.510(1)
α (°)	79.146(8)			109.412(8)
β (°)	89.238(8)		106.50(1)	97.407(8)
γ (°)	73.688(8)			97.010(9)
V (Å^3)	3103.1(6)	1773.9(4)	1093.0(3)	787.6(1)
Z	4	4	4	2
D (calcd) (g/cm^3)	1.242	1.378	1.479	1.160
μ (cm^{-1})	17.51	18.41	27.09	18.62
T (K)	298	298	298	298
2θ range (°)	3.0–44.0	3.0–44.0	3.0–55.0	3.0–50.0
No. collected	7576	1292	2787	2808
No. ind	7576	1292	2639	2808
No. obsd	4429 ($\|F_0\| > 6.0\sigma\|F_0\|$)	449 ($\|F_0\| > 6.0\sigma\|F_0\|$)	1739 ($\|F_0\| > 6.0\sigma\|F_0\|$)	2294 ($\|F_0\| > 6.0\sigma\|F_0\|$)
Weighting scheme	$w^{-1} = 0.04\ (\|F_0\|)^2 + \sigma(\|F_0\|)^2$	$w^{-1} = 0.04\ (\|F_0\|)^2 + \sigma(\|F_0\|)^2$	$w^{-1} = 0.04\ (\|F_0\|)^2 + \sigma(\|F_0\|)^2$	$w^{-1} = 0.04\ (\|F_0\|)^2 + \sigma(\|F_0\|)^2$
R	0.0413	0.0482	0.0324	0.0517
R_w	0.0502	0.0585	0.0335	0.0556
Largest diff peak (eÅ^{-3})	0.37	0.38	0.45	0.83

J(H—H) = 7.2 Hz, $NH_2CH_2CH_2$], 0.35 [3H, t, J(H—H) = 7.2 Hz, $NH_2CH_2CH_2CH_3$].

Crystallographic studies

Crystals of compounds **2, 3, 6,** and **7** were sealed in a glass capillary under argon and mounted on the goniometer of an Enraf–Nonius CAD-4 automated diffractometer. Data collection and cell determinations were performed in a manner previously described [22], using the $\theta/2\theta$ scan technique. Pertinent details are given in Table 3. The structures were solved by Patterson or direct Fourier methods, and the model refined using full-matrix least squares techniques. All non-hydrogen atoms were refined anisotropically, except for compound **3** in which Ga(1), Cl(1), and C(11) were the only atoms refined anisotropically. Except for the hydroxide and amine hydrogens, all hydrogen atoms were calculated and constrained to 'ride' upon the appropriate atoms [d(C—H) = 0.95 Å, U(H) = $1.3B_{eq}$(C)]. The hydroxide and amine hydrogens were located in the difference map, and their isotropic thermal parameter was allowed to 'ride' upon the heavy atom [U(H) = $1.3B_{eq}$(O) or $1.3B_{eq}$(N)]. All computations were performed using MolEN [23] or SHELX86 [24]. A summary of cell parameters, data collection, and structure solution is given in Table 5. Scattering factors were taken from ref. [25].

Acknowledgments—Financial support for this work was provided by the National Science Foundation, the Office of Naval Research and the Robert A. Welch Foundation. The authors acknowledged the assistance of Dr N. McMahon (Rice University) for mass spectrometry measurements.

REFERENCES

1. Hoffmann, R., *Angew. Chem., Int. Ed. Engl.*, 1982, **21,** 711.
2. Bethley, C. E., Aitken, C. L., Koide, Y., Harlan, C. J., Bott, S. G. and Barron, A. R., *Organometallics*, 1997, **16,** 329.
3. Leman, J. T., Barron, A. R., Ziller, J. W. and Kren, R. M., *Polyhedron*, 1989, **8,** 1909.
4. Leman, J. T. and Barron, A. R., *Organometallics*, 1989, **8,** 1828.
5. Leman, J. T., Roman, H. A. and Barron, A. R., *J. Chem. Soc., Dalton Trans.*, 1992, 2183.
6. Leman, J. T., Roman, H. A. and Barron, A. R., *Organometallics*, 1993, **12,** 2988.
7. Moor, D. S. and Robinson, S. D., *Adv. Inorg. Chem. Radiochem.*, 1986, **30,** 1.
8. Leman, J. T., Braddock-Wilking, J., Coolong, A. J. and Barron, A. R., *Inorg. Chem.*, 1993, **32,** 4324.
9. (a) Barker, J. and Kilner, M., *Coord. Chem. Rev.*, 1994, **133,** 219; (b) Patai, S., Ed., *The Chemistry of Amidines, and Imidates*, Vol. 2. Wiley, New York (1991).
10. (a) Ergezinger, C., Weller, F. and Dehnicke, K., *Z. Naturforsch., Tiel B*, 1988, **43,** 1621; (b) Hausen, H. D., Gerstner, F. and Schwarz, W., *J. Organomet. Chem.*, 1978, **145,** 277; (c) Kottmair-Maierson, D., Lechler, R. and Weidlein, J., *Z. Anorg. Allg. Chem.*, 1991, **593,** 111; (d) Dehnicke, K., *Chem. Ztg.*, 1990, **114,** 295.
11. Barker, J., Blacker, N. C., Phillips, P. R., Alcock, N. W., Errington, W. and Wallbridge, M. G. H., *J. Chem. Soc., Dalton Trans.*, 1996, 431.
12. Kumar, R., de Mel, V. S. J. and Oliver, J. P., *Organometallics*, 1989, **8,** 2488.
13. Landry, C. C., Hynes, A., Barron, A. R., Haiduc, I. and Silvestru, C., *Polyhedron*, 1996, **15,** 391.
14. Atwood, D. A., Cowley, A. H., Harris, P. J., Jones, R. A., Koshmieder, S. U., Nunn, C. M. and Bott, S. G., *Organometallics*, 1993, **12,** 24.
15. Hausen, H. D., Guder, H. J. and Schwarz, W., *J. Organomet. Chem.*, 1977, **132,** 37.
16. Niemeyer, M., Goodwin, T. J., Risbud, S. H. and Power, P. P., *Chem. Mater.*, 1996, **8,** 2745.
17. (a) Reger, D. L., Knox, S. J. and Lebioda, L., *Organometallics*, 1990, **9,** 2218; (b) Einstein, F. W. B., Gilbert, M. M. and Tuck, D. G., *J. Chem. Soc., Dalton Trans.*, 1973, 248; (c) Hausen, H.-D., *J. Organomet. Chem.*, 1972, **39,** C37.
18. Kovar, R. A., Derr, H., Brandau, D. and Callaway, J. O., *Inorg. Chem.*, 1975, **14,** 2809.
19. Schwering, H.-U., Jungk, E. and Weidlein, J., *J. Organomet. Chem.*, 1975, **91,** C4.
20. Cleaver, W. M. and Barron, A. R., *Chemtronics*, 1989, **4,** 146.
21. Tuck, D. G., In *Comprehensive Organometallic Chemistry*, Vol. 7, ch. 7, Eds G. Wilkinson, F. G. A. Stone and E. W. Abel, Pergamon Press, Oxford (1983).
22. Mason, M. R., Smith, J. M., Bott, S. G. and Barron, A. R., *J. Am. Chem. Soc.*, 1993, **115,** 4971.
23. MolEN, Enraf–Nonius, MolEN, An Interactive Structure Solution Procedure; Enraf–Nonius, Delft, Netherlands, 1990.
24. SHELX86, G. M. Sheldrick, in *Crystallographic Computing*, pp. 184–189, Eds G. M. Sheldrick, C. Kruger and R. Goddard, Oxford University Press (1985).
25. *International Tables for X-Ray Crystallography*, Vol. 4, Kynoch Press, Birmingham (1974).

Pergamon

PII: S0277-5387(97)00223-4

Polyhedron Vol. 17, No. 5–6, pp. 993–998, 1998
© 1998 Elsevier Science Ltd
All rights reserved. Printed in Great Britain
0277-5387/98 $19.00+0.00

Synthesis and structure of the novel octalithium–dipotassium mixed oxide–alkoxide cage complex $[Li_8K_2(O)(Bu^tO)_8 \cdot 2TMEDA]$†

Fiona M. Mackenzie,[a] Robert E. Mulvey,[a]* William Clegg[b] and Lynne Horsburgh[b]

[a] Department of Pure and Applied Chemistry, University of Strathclyde, Glasgow G1 1XL, U.K.

[b] Department of Chemistry, University of Newcastle, Newcastle upon Tyne NE1 7RU, U.K.

(Received 2 May, 1997; accepted 5 May 1997)

Abstract—The title compound crystallises as a hexane hemisolvate from 1 : 1 : 1 or 2 : 1 : 2 reaction mixtures of the lithium primary amide $Bu^tN(H)Li$, potassium *t*-butoxide Bu^tOK, and the diamine TMEDA in hexane solution. An X-ray crystallographic study reveals that it exists as a discrete cage species with a central oxo (O^{2-}) anion, coordinated to the eight cations of a surrounding 16-vertex (Li_8O_8) polyhedron, two opposing sides of which are each bridged by a TMEDA-chelated K^+ cation. Made up of μ_3O-Li_3 and μ_2O-Li_2 interactions, the Li_8O_8 polyhedron can be regarded in common terminology for alkali metal based structures, as an incomplete stack arrangement of two tetrameric $(Li—O)_4$ cyclic rings. The eight Li^+ cations form a distorted dodecahedron and the eight alkoxide O atoms form a distorted square antiprism. © 1998 Elsevier Science Ltd. All rights reserved

Keywords: alkali metals; alkoxide; cage complex; crystal structure; oxide.

The growing technological importance of metal oxides in, for example, electronic and ceramic materials, has rekindled enthusiasm for fundamental studies of metal alkoxides, which make excellent precursors for the deposition of metal oxides. This point is highlighted in a recent review by Bradley [1]. Intermediate in composition between molecular metal alkoxides and macromolecular metal oxides, metal oxide alkoxide combinations represent a structural link between the two extremities; as such, they have attracted special attention. Here, in this paper, we report an unprecedented mixed alkali metal oxide alkoxide in $[Li_8K_2(O)(Bu^tO)_8 \cdot 2TMEDA]$, (**1**). This was produced unexpectedly during a study of lithium amide/potassium alkoxide reactions, the intended aim of which was to grow crystals of a model superbase comparable to the previously reported trimetallic lithium–sodium–potassium formulation $[\{LiNaK[PhN(H)]_2(Bu^tO) \cdot 2TMEDA\}_2]$ [2].

RESULTS AND DISCUSSION

Synthesis and characterisation

Treating the lithium primary amide $Bu^tN(H)Li$,[3] freshly prepared from equimolar amounts of *n*-butyllithium and *t*-butylamine, with potassium *t*-butoxide (Bu^tOK) in the presence of N, N, N′, N′-tetramethylethylenediamine (TMEDA) resulted in mauve coloured solutions which deposited large colourless rhombic crystals of $\mathbf{1} \cdot \frac{1}{2}C_6H_{14}$. Two distinct stoichiometries of the respective reactants, 1 : 1 : 1 and 2 : 1 : 2, gave this same crystalline product, and both reactions were found to be reproducible. Disregarding the oxide component, the yield of **1** can be estimated to be typically 45–50%, based on consumption of potassium *t*-butoxide (weighed as the anhydrous

* Author to whom correspondence should be addressed.

† Dedicated to Professor Don Bradley on the occasion of his 73rd birthday in recognition of his outstanding contributions to metal alkoxide and amide chemistry.

material). No other solid products were forthcoming from the filtrates (following removal of **1**) despite prolonged cooling at freezer temperatures. These observations imply that the formation of **1** is probably kinetically driven. Considering only the 1 : 1 : 1 reaction, all of the amide anions, nearly all of the K^+ cations, and (since the yield of **1** falls well short of quantitative) some butoxide anions, Li^+ cations and TMEDA molecules, must remain in solution. Clearly, therefore, given the complexity of this mixture, a variety of aggregated species could be present in solution, of which **1** is presumably the least soluble. Once isolated, the rhombic crystals of $\mathbf{1} \cdot \frac{1}{2}C_6H_{14}$ are robust, showing no visible signs of decomposition when stored in an argon-filled dry box for several weeks. Their melting point (218–220 °C) distinguishes them from the reactants Bu'OK (m.p. 256–258 °C) and $[\{Bu'N(H)Li\}_8]$ (decomp. to dark brown solid from about 260 °C), both of which could have potentially crystallised in an unreacted state from solution. The absence of amide groups was confirmed by the lack of N—H bonds in the IR spectrum of **1**: the air-exposed spectrum revealed the presence of both lithium and potassium through the hydroxide (O—H) stretches at 3676 and 3506 cm^{-1} respectively. As its highly polar core is hidden by an outer shell of lipophilic *t*-butyl groups (see discussion of structure below), **1** possesses appreciable solubility in arene solvents, thus enabling a ^1H NMR spectrum to be recorded in deutero–toluene solution. Importantly, the integration ratio found for Bu^t : TMEDA (8 : 2) is in agreement with the stoichiometry determined by the X-ray diffraction study, confirming that the crystal structure is representative of the bulk solid product. Furthermore, the presence of chemically distinct types of $Bu'O^-$ anions in the crystal structure is echoed by the observation of a series of overlapping Bu^t(*Me*) resonances, centred at 1.52 ppm. This chemical shift value intimates a lower shielding of the Bu^t hydrogen atoms compared to those in pure Bu'OK (corresponding value, 1.01 ppm), which is consistent with the lower ionicity of the small alkali metal.

An essential question regarding the synthesis of **1** remains to be answered: what is the source of the oxido (O^{2-}) ligand? We believe it stems from a trace amount of moisture in Bu'OK, a solid noted for its strong hygroscopic nature. This reactant was used as supplied by Aldrich, and as no special precautions were taken when transferring it in the open atmosphere to the Schlenk tube, it could have easily picked up moisture during the process. On the other hand, if moisture had been present prior to the addition of the alkoxide, then the lithium amide (or at an earlier stage, *n*-butyllithium) would surely have removed it according to the decomposition reaction shown in eq. (1). Metal alkoxides are known to react stoichiometrically with water to form the corresponding alcohol and metal oxide [1]. Equation (2) illustrates this reaction for an alkali metal (M). Such a process could have occurred *in situ* here, as a pre-requisite to the formation of **1**. In this connection, the formula of **1** is best represented as $(Bu'OK)_2(Bu'OLi)_6(Li_2O)(TMEDA)_2$, i.e., containing one molecule of lithium oxide. Whether this molecule is generated directly through the reaction in equation 2 (with M = Li) or indirectly by a metal exchange process involving an *in situ* form of K_2O, remains an open question.

$$Bu'N(H)Li + H_2O \rightarrow Bu'NH_2 + LiOH \quad (1)$$

$$2ROM + H_2O \rightarrow 2ROH + M_2O \quad (2)$$

Moisture is often suspected to be the source, when oxygen centres turn up adventitiously in structures determined by X-ray diffraction. A good example, pertinent to **1**, is crystalline $[(Bu'OLi)_{10}(LiOH)_6]$ [4], which was obtained by exposing a concentrated Bu'O-Li/hexane solution to moist air over a prolonged period; but this product of partial hydrolysis differs from **1** by having hydroxide (OH^-), rather than oxide, anions. However, the latter anions do appear in the monolithium-tetramagnesium cresylate $[LiMg_4O(R)_7 \cdot 4THF]$ [R=*o*-Me(C_6H_4)O] [5] and the tetradecalithium amide $[Li_{14}(O)\{(H)N(c\text{-}C_5H_9)\}_{12}]$ [6], both of which were synthesised serendipitously from reactions that may have inadvertently involved trace quantities of moisture. Unexpected oxide–alkoxide complexes of barium have also been recently reported in $[H_4Ba_6(O)(OCH_2CH_2OCH_3)_{14}]$ [7] and $[H_3Ba_6(O)(OBu^t)_{11}(OCEt_2CH_2O)(THF)_3]$ [8]: the sources of their oxo components are not known.

Returning to **1**, its synthesis can be regarded in part as an incomplete metathetical process between lithium *t*-butylamide and potassium *t*-butoxide as two molecules of the latter compound remain incorporated within the cage framework of the lithium *t*-butoxide derived product. There is some similarity here with the aforementioned trimetallic dimer $[\{LiNaK[PhN(H)]_2(Bu'O) \cdot 2TMEDA\}_2]$ [2], since it also contains cocomplexed potassium *t*-butoxide molecules which resist metathesis (in contrast to sodium *t*-butoxide molecules in the same reaction mixture which react with lithium anilide to formally produce lithium *t*-butoxide and sodium anilide molecules). This preference of the potassium alkoxide for co-complexation over anion exchange has also been demonstrated in the synthesis of the twenty-membered polyhedral cage species $[\{(cyNLi)_3Sb\}_2(Bu'OK)_3 \cdot (toluene)_x]$ [9].

X-ray crystallographic study

The crystal structure of $\mathbf{1} \cdot \frac{1}{2}C_6H_{14}$ shows a discrete, molecular arrangement (Fig. 1), built around an oxo (O^{2-}) core. Directly surrounding the core is a 16-vertex (Li_8O_8) polyhedral cage, the oxygen atoms of which belong to butoxide anions. In keeping with the terminology commonly used in alkali metal architecture, this polyhedron is best described as a 'stack' of two tetrameric $(Li—O)_4$ cyclic rings [10]. Figure 2 emphasises this point in showing one ring stacked on

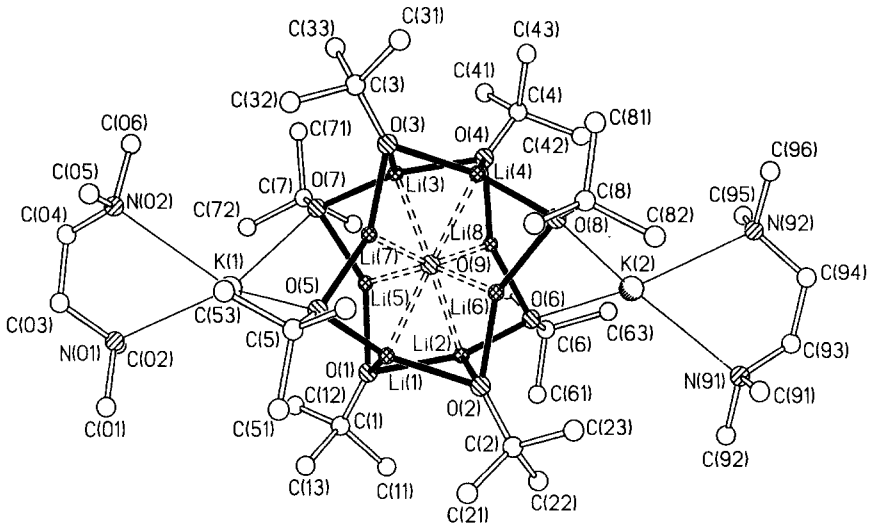

Fig. 1. Molecular structure of **1** without hydrogen atoms.

top of the other (the central oxo is also visible). These rings are highly puckered (r.m.s. deviations 0.269 and 0.261 Å from their respective mean planes, which are inclined at only 0.7° to each other). Stacked-ring structures, as typified by the sodium *t*-butoxide hexamer [made up of two trimeric $(Na—O)_3$ rings, as pictured in Fig. 3], [11] generally have each cation in the 'top' ring bonded to its vertical anion neighbour in the 'bottom' ring and *vice versa*: overall this creates a cage with an enclosed volume which is usually vacant. In **1**, this volume is, in contrast, occupied by the oxo anion, and as a consequence the intermolecular ring to ring bonding is incomplete: between the rings there are four bonded pairs [Li(1)—O(2), Li(2)—O(2), Li(3)—O(3), Li(4)—O(4)] and four non-bonded pairs [Li(5)/O(5), Li(6)/O(6), Li(7)/O(7), Li(8)/O(8)]. Positioned at the outermost points of the polyhedron, the oxygen atoms in this latter group make up for the lack of these bonds by interacting with a K^+ cation: O(5), O(7) and O(6), O(8) each 'chelate' to one of two K^+ cations (Fig. 4). Occupying positions at opposite ends of an axis running through the oxo centre [K···O(9)···K angle, 166.9°], the K^+ cations are also each chelated by a single TMEDA molecule. The eight *t*-butyl groups projecting outwards from the core complete the structure.

Table 1 lists selected bond lengths and angles within **1**. Two distinct sets of Li^+ cations make up the μ_8-coordination of the oxo centre. The four-coordinate type [Li(1) to Li(4)], which participate in intermolecular ring to ring bonding, form long bonds to this oxygen (mean length, 2.195 Å); the other set not involved in the intermolecular ring to ring bonding [Li(5) to Li(8)] are drawn closer to O(9) (mean length, 1.895 Å), reflecting their smaller overall coordination number (three). This $\mu_8O—Li_8$ coordination is unusual. It contrasts with the oxide amide cage species $[Li_{14}(O)\{(H)N(c\text{-}C_5H_9)\}_{12}]$ [6], the Li—O bonds of which are similar in length [1.888(10) Å] to the short

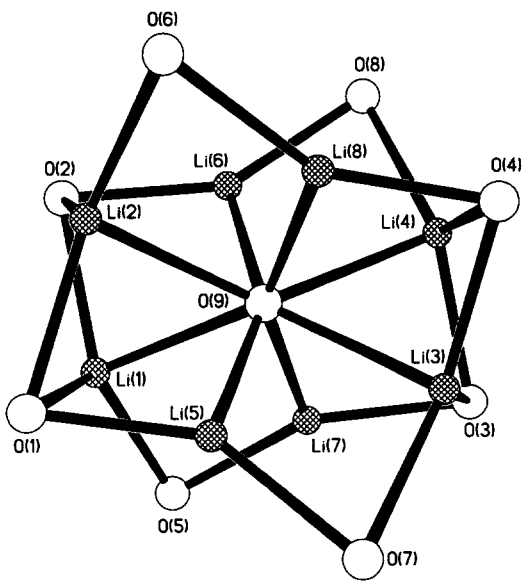

Fig. 2. Core of **1** emphasising its stacked-ring nature.

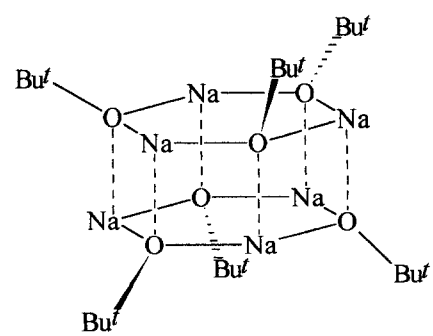

Fig. 3. Hexameric stack structure of sodium *t*-butoxide.

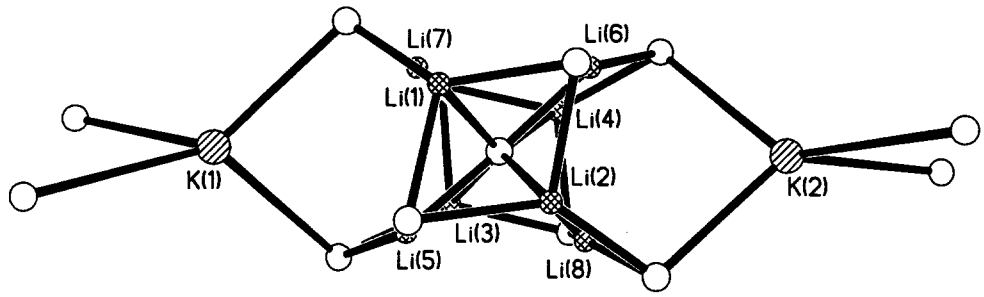

Fig. 4. Section of **1** showing the metal-ligand coordinations.

set in **1**. It also differs from the μ_5O—$LiMg_4$ coordination upon which the oxide cresylate structure of $[LiMg_4O(R)_7 \cdot 4THF]$ [R=*o*-Me(C_6H_4)O] is founded [its solitary Li—O (oxo) bond is 1.89(2) Å long] [5]. The bond angles around O(9) cover a wide range [61.2(2)—151.3(3)°]; this oxo anion lies essentially at the centroid of the Li_8 polyhedron, which is a distorted dodecahedron. Turning to the Li—O (butoxide) bonds, the twelve involving Li(1) to Li(4) are generally longer (mean value, 2.006 Å) than the eight involving Li(5) to Li(8) (mean value, 1.901 Å). The eight oxygen atoms form a distorted square antiprism (seen perpendicular to the two square faces in Fig. 2). Due in part to the incomplete intermolecular ring to ring bonding, the butoxide anions separate into those μ_3O—Li_3 bonded [O(1) to O(4)] and those μ_3O—Li_2K bonded [O(5) to O(8)]. No regular hexameric $[(Bu^tOLi)_6]$ unit or fragment thereof, which would be based predominately on μ_3O—Li_3 bridging, is therefore evident, in contrast to that recently reported for the partially-hydrolysed butoxide $[(Bu^tOLi]_{10} \cdot (LiOH)_6]$: the starting point for aggregation is presumably a short-lived monomeric Li_2O molecule, which would have a strong attraction for Bu^tOLi molecules as they form. The K—O bonds which open up the stacked-ring $(Li_4O_4)_2$ substructure have a mean length of 2.795 Å. Both types of butoxide O atoms [O(1) to O(4); O(5) to O(8)] occupy distorted tetrahedral environments [mean bond angles: 105.3 and 106.8°, respectively], characteristically with obtuse C—O—M and acute M—O—M angles (excepting Li—O—K angles which span the range 75.7–119.8°). The four-coordinate set of Li^+ cations deviate more from an ideal tetrahedral geometry than the three-coordinate set do from an ideal trigonal planar geometry as indicated by their respective mean bond angles (104.2 and 119.3°). Due to a reduction in angular constraints, the mean bond angle about the larger K^+ cations (109.3°) more closely approaches the tetrahedral value, though individually the bond angles are severely distorted, primarily as a consequence of the limited bite size of TMEDA (mean bond angle subtended at K^+ by the diamine is 64.1°).

In conclusion, a new mixed lithium–potassium, mixed oxide–alkoxide salt has been synthesised, though the origin of the oxide component remains uncertain. An X-ray diffraction study has revealed an incomplete stack arrangement of two tetrameric $(Li—O)_4$ cyclic rings with an encapsulated oxo core; two open faces, one on either side of the stack, are each bridged by a TMEDA-chelated K^+ cation.

EXPERIMENTAL

Synthesis of $[Li_8K_2(O)(Bu^tO)_8 \cdot 2TMEDA]$, **1**

Reactions were carried out in Schlenk tubes under a protective atmosphere of dry, oxygen-free argon gas. Freshly distilled *tert*-butylamine (10 mmol) was slowly added to a hexane solution of Bu^nLi (10 mmol) at room temperature, and the mixture was stirred for about 30 min by which time gas evolution (butane) had ceased. The resulting pale yellow solution was injected *via* a gas-tight syringe to a white suspension of Bu^tOK (10 mmol) in hexane. A reaction ensued immediately, following which a fine, beige precipitate was obtained. The mixture was subsequently surrounded by a hot water bath maintained at 60°C for one hour. TMEDA (10 mmol) was then introduced to produce a slightly cloudy, mauve solution, which was subsequently filtered through celite. Cooling of the filtrate (to 4°C), yielded large colourless rhombic crystals of **1**. IR spectra (Nujol mull; cm^{-1}) 2954s, 2858s, 2725w, 2367m, 1470m, 1384m, 1344w, 1304w, 1212m, 1153m, 1081w, 1027w, 988m, 948w, 783w, 724m and 611w; (after exposing mull to air for 2 s) 3676s, 3506m, 2929s, 2850s, 1463s, 1378s, 1212m, 1166w, 1093w, 1034m, 984w, 895w, 822w, 717m and 597w. Elemental analyses, Found C, 54.1; H, 11.0; N, 6.4; Li, 5.2; K, 8.1. Calc. for $C_{47}H_{111}N_4O_9Li_8K_2$; C, 55.9; H, 11.0; N, 5.5; Li, 5.5; K, 7.7%. ^{1}H NMR (400 MHz, toluene-d_8, 25°C) δ 1.52 (overlapping s, 36H, CH_3 of Bu^t), 2.09 (s, 12H, CH_3 of TMEDA), 2.20 (s, 4H, CH_2 of TMEDA).

X-ray crystallography

Crystal data for $\mathbf{1} \cdot \frac{1}{2}C_6H_{14}$: $C_{44}H_{104}K_2Li_8N_4O_9 \cdot \frac{1}{2}C_6H_{14}$, $M = 1011.1$, monoclinic, space group $P2_1/c$, $a = 25.5528(15)$, $b = 13.9207(8)$, $c = 19.5913(11)$ Å, $\beta = 100.518(2)°$, $v = 6851.8(7)$ Å^3, $Z = 4$, $D_c = 0.979$

Table 1. Selected bond lengths (Å) and angles (°) for **1**

Li(1)—O(1)	2.024(7)	Li(1)—O(2)	2.019(7)
Li(1)—O(5)	1.939(7)	Li(1)—O(9)	2.198(7)
Li(2)—O(1)	2.062(8)	Li(2)—O(2)	2.012(7)
Li(2)—O(6)	2.013(7)	Li(2)—O(9)	2.155(7)
Li(3)—O(3)	1.997(6)	Li(3)—O(4)	1.986(6)
Li(3)—O(7)	2.063(7)	Li(3)—O(9)	2.197(7)
Li(4)—O(3)	1.972(7)	Li(4)—O(4)	1.967(7)
Li(4)—O(8)	2.020(7)	Li(4)—O(9)	2.230(7)
Li(5)—O(1)	1.878(7)	Li(5)—O(7)	1.957(7)
Li(5)—O(9)	1.887(7)	Li(6)—O(2)	1.887(8)
Li(6)—O(8)	1.947(8)	Li(6)—O(9)	1.883(7)
Li(7)—O(3)	1.869(7)	Li(7)—O(5)	1.888(7)
Li(7)—O(9)	1.906(6)	Li(8)—O(4)	1.856(7)
Li(8)—O(6)	1.929(7)	Li(8)—O(9)	1.903(6)
K(1)—O(5)	2.711(3)	K(1)—O(7)	2.916(3)
K(2)—O(6)	2.770(3)	K(2)—O(8)	2.781(3)
K(1)—N(01)	2.881(4)	K(1)—N(02)	2.920(4)
K(2)—N(91)	2.870(5)	K(2)—N(92)	2.889(4)

O(5)—Li(1)—O(2)	137.8(3)	O(5)—Li(1)—O(1)	116.7(4)
O(2)—Li(1)—O(1)	105.3(3)	O(5)—Li(1)—O(9)	95.3(3)
O(1)—Li(1)—O(9)	84.5(2)	O(2)—Li(1)—O(9)	84.2(3)
O(6)—Li(2)—O(1)	139.2(3)	O(2)—Li(2)—O(6)	116.6(4)
O(2)—Li(2)—O(1)	104.2(3)	O(6)—Li(2)—O(9)	97.0(3)
O(2)—Li(2)—O(9)	85.4(3)	O(1)—Li(2)—O(9)	84.7(3)
O(4)—Li(3)—O(7)	141.8(3)	O(3)—Li(3)—O(7)	114.8(3)
O(4)—Li(3)—O(3)	103.3(3)	O(7)—Li(3)—O(9)	95.8(3)
O(3)—Li(3)—O(9)	85.4(2)	O(4)—Li(3)—O(9)	84.7(3)
O(3)—Li(4)—O(8)	139.8(3)	O(4)—Li(4)—O(8)	115.2(3)
O(4)—Li(4)—O(3)	105.0(3)	O(8)—Li(4)—O(9)	95.5(3)
O(3)—Li(4)—O(9)	85.1(3)	O(4)—Li(4)—O(9)	84.2(3)
O(1)—Li(5)—O(7)	147.6(4)	O(9)—Li(5)—O(7)	110.7(3)
O(1)—Li(5)—O(9)	98.0(3)	O(2)—Li(6)—O(8)	149.3(4)
O(9)—Li(6)—O(8)	110.6(4)	O(9)—Li(6)—O(2)	97.3(3)
O(3)—Li(7)—O(5)	153.9(4)	O(5)—Li(7)—O(9)	107.7(3)
O(3)—Li(7)—O(9)	97.9(3)	O(4)—Li(8)—O(6)	152.0(4)
O(9)—Li(8)—O(6)	109.1(3)	O(4)—Li(8)—O(9)	97.2(3)
Li(5)—O(1)—Li(1)	81.5(3)	Li(5)—O(1)—Li(2)	81.7(3)
Li(1)—O(1)—Li(2)	67.9(3)	Li(6)—O(2)—Li(2)	80.4(3)
Li(6)—O(2)—Li(1)	83.3(3)	Li(2)—O(2)—Li(1)	69.0(3)
Li(7)—O(3)—Li(4)	85.4(3)	Li(7)—O(3)—Li(3)	80.2(3)
Li(4)—O(3)—Li(3)	69.2(3)	Li(8)—O(4)—Li(4)	82.7(3)
Li(8)—O(4)—Li(3)	84.8(3)	Li(4)—O(4)—Li(3)	69.6(3)
Li(7)—O(5)—Li(1)	81.1(3)	Li(7)—O(5)—K(1)	94.8(2)
Li(1)—O(5)—K(1)	103.0(2)	Li(8)—O(6)—Li(2)	77.3(3)
Li(8)—O(6)—K(2)	88.3(2)	Li(2)—O(6)—K(2)	109.3(2)
Li(5)—O(7)—Li(3)	75.8(3)	Li(5)—O(7)—K(1)	75.7(2)
Li(3)—O(7)—K(1)	119.8(2)	Li(6)—O(8)—Li(4)	77.1(3)
Li(6)—O(8)—Li(2)	83.3(2)	Li(4)—O(8)—K(2)	117.3(2)
Li(6)—O(9)—Li(5)	151.3(3)	Li(8)—O(9)—Li(7)	148.0(3)
Li(7)—O(9)—Li(2)	137.5(3)	Li(6)—O(9)—Li(3)	134.7(3)
Li(2)—O(9)—Li(3)	138.6(2)	Li(8)—O(9)—Li(1)	137.7(3)
Li(3)—O(9)—Li(1)	136.2(3)	Li(5)—O(9)—Li(4)	135.2(3)
Li(2)—O(9)—Li(4)	136.2(3)	Li(1)—O(9)—Li(4)	137.6(2)
Li(6)—O(9)—Li(8)	91.6(3)	Li(5)—O(9)—Li(8)	96.7(3)
Li(6)—O(9)—Li(7)	96.2(3)	Li(5)—O(9)—Li(7)	91.2(3)
Li(6)—O(9)—Li(2)	76.8(3)	Li(5)—O(9)—Li(2)	79.1(3)
Li(8)—O(9)—Li(2)	74.4(3)	Li(5)—O(9)—Li(3)	74.0(3)
Li(8)—O(9)—Li(3)	78.1(3)	Li(7)—O(9)—Li(3)	74.4(2)
Li(6)—O(9)—Li(1)	78.6(3)	Li(5)—O(9)—Li(3)	76.8(3)
Li(7)—O(9)—Li(1)	74.3(2)	Li(6)—O(9)—Li(4)	73.4(3)
Li(8)—O(9)—Li(4)	75.0(3)	Li(7)—O(9)—Li(4)	77.7(3)
Li(2)—O(9)—Li(1)	63.2(2)	Li(3)—O(9)—Li(4)	61.2(2)
O(5)—K(1)—O(7)	90.93(9)	N(01)—K(1)—N(02)	64.23(12)
O(5)—K(1)—N(01)	139.74(11)	N(01)—K(1)—O(7)	127.82(11)
O(5)—K(1)—N(02)	122.22(11)	O(7)—K(1)—N(02)	104.15(12)
O(6)—K(2)—O(8)	93.48(9)	N(91)—K(2)—N(92)	63.91(13)
O(6)—K(2)—N(91)	118.46(14)	O(8)—K(2)—N(91)	137.26(15)
O(6)—K(2)—N(92)	136.59(10)	O(8)—K(2)—N(92)	112.48(12)

g cm^{-3}, $\mu = 0.18$ mm^{-1} (Mo-Kα radiation, $\lambda = 0.71073$ Å), $F(000) = 2224$, $T = 160$ K, crystal size $0.60 \times 0.42 \times 0.18$ mm. Measurements were made on a Siemens SMART CCD area-detector diffractometer. Cell parameters were refined from the observed ω angles of all strong reflections in the complete data set. Intensities were integrated from several series of frames, each 0.3° in ω, covering more than a hemisphere of reciprocal space. No absorption or extinction corrections were necessary. 33833 reflections were collected ($\theta_{max} = 25°$, maximum indices 34, 18, 26), giving 11981 unique data, $R_{int} = 0.0548$.

The structure was determined by direct methods and refined by full-matrix least-squares on F^2 values, with weighting $w^{-1} = \sigma^2(F_o^2) + (0.1315P)^2 + 4.2059P$, where $P = (F_o^2 + 2F_c^2)/3$. Anisotropic displacement parameters were refined for all non-hydrogen atoms, and isotropic hydrogen atoms were included with riding model constraints. Two-fold disorder of orientation was resolved for one Bu^t group; no hydrogen atoms were included for the *n*-hexane solvent molecule positioned on an inversion centre, for which the displacement parameters are rather large, indicating possible unresolved disorder. At convergence, $wR = \{\Sigma[w(F_o^2 - F_c)^2]/\Sigma[w(F_o^2)^2]\}^{1/2} = 0.2675$ for all data, conventional $R = 0.0911$ on F values of 6935 reflections with $F_o^2 > 2\sigma(F_o^2)$, goodness of fit = 1.047 for all F^2 values and 644 refined parameters. A final difference syntheses shows no features outside the range $+0.73$ to -0.34 e$Å^{-3}$.

Programs were standard Siemens control (SMART) and integration (SAINT) software [12], SHELXTL [13], and local programs. Atomic coordinates, displacement parameters and full geometry have been deposited at the Cambridge Crystallographic Data Centre.

Acknowledgements—We thank the Associated Octel Co. Ltd. (Ellesmere Port, U.K.) and the EPSRC for sponsoring this research.

REFERENCES

1. Bradley, D. C., *Chem. Rev.*, 1989, **89,** 1317.
2. Mackenzie, F., Mulvey, R. E., Clegg, W. and Horsburgh, L., *J. Am. Chem. Soc.*, 1996, **118,** 4721.
3. Barnett, N. D. R., Clegg, W., Horsburgh, L., Lindsay, D. M., Liu, Q.-Y., Mackenzie, F. M., Mulvey, R. E. and Williard, P. G., *J. Chem. Soc., Chem. Commun.*, 1996, 2321.
4. Lambert, C., Hampel, F., Schleyer, P. v. R., Davidson, M. G. and Snaith, R., *J. Organomet. Chem.*, 1995, **487,** 139.
5. Henderson, K. W., Mulvey, R. E., Reinhard, F. B. M., Clegg, W. and Horsburgh, L., *J. Am. Chem. Soc.*, 1994, **116,** 10777.
6. Clegg, W., Horsburgh, L., Dennison, P. R., Mackenzie F. M. and Mulvey, R. E., *J. Chem. Soc., Chem. Commun.*, 1996, 1065.
7. Caulton, K. G., Chisholm, M. H., Drake, S. R. and Huffman, J. C., *J. Chem. Soc., Chem. Commun.*, 1990, 1498.
8. Caulton, K. G., Chisholm, M. H., Drake, S. R. and Folting, K., *J. Chem. Soc., Chem. Commun.*, 1990, 1349.
9. Barr, D., Edwards, A. J., Paver, M. A., Raithby, P. R., Rennie, M.-A., Russell, C. A. and Wright, D. S., *Angew. Chem. Int. Ed. Engl.*, 1995, **34,** 1012.
10. Mulvey, R. E., *Chem. Soc. Rev.*, 1991, **20,** 167.
11. Weiss, E., *Angew, Chem. Int. Ed. Engl.*, 1993, **32,** 1501.
12. SMART (CCD data collection software) and SAINT (frame integration), Siemens Analytical X-ray Instruments Inc., Madison WI, USA (1994).
13. Sheldrick, G. M., SHELXTL User Manual, Version 5. Siemens Analytical X-ray Instruments Inc., Madison WI, USA (1995).

Pergamon

PII: S0277-5387(97)00206-4

Polyhedron Vol. 17, No. 5–6, pp. 999–1000, 1998
© 1998 Elsevier Science Ltd
All rights reserved. Printed in Great Britain
0277-5387/98 $19.00+0.00

Reactions of the stable bis(amino)silylene Si[{N(CH$_2$Bu^t)}$_2$C$_6$H$_4$-1,2] with multiply bonded compounds†

Barbara Gehrhus and Michael F. Lappert*

The Chemistry Laboratory, University of Sussex, Brighton BN1 9QJ, U.K.

(Received 14 April 1997; accepted 5 May 1997)

Abstract—Treatment of the title silylene [abbreviated as Si(NN)] under mild conditions with various unsaturated organic compounds has yielded the following series of tetravalent silicon compounds: Si(NN)Si(NN)(X)Y [XY = OCRR′ (R,R′ = Ph$_2$; Ph,Me or Ad′; Ad′ = Ad minus H, Ad = adamantyl), NCBu^t or C(SiMe$_3$)CPh], 2-C$_6$H$_4$Si(NN)N(R)CHR′ [R,R′ = SiMe$_3$,Ph or Bu^t,(H)Si(NN)], 2-C$_6$H$_4$Si(NN)OSi(H){N(R)C$_6$H$_4$NR-2}CPh (R = CH$_2$Bu^t), Si(NN)(Bu^t)X [X = CN or Si(NN)CN], [Si(NN)]$_2$NAd and Si(NN)N(Ad)N:NAd. © 1998 Elsevier Science Ltd. All rights reserved

Keywords: silicon; silylenes; oxidative addition reactions; organosilicon compounds.

Recently we reported the isolation of the thermally stable bis(amino)silylene Si[{N(CH$_2$Bu^t)}$_2$C$_6$H$_4$-1,2], **1** and showed that **1** is highly reactive towards MeI, EtOH or a chalcogen [1]. We now present extensions of this study of the reactivity of **1** by focusing on reactions with compounds containing multiple bonds, as summarised in Scheme 1.

The treatment of **1** with (i) RR′CO, (ii) Bu^{t}CN or (iii) PhCCSiMe$_3$ gave (i) the disilaoxetane (cf. [2]) **2** (R = R′ = Ph), **3** (R = Me, R′ = Bu^t), or **4** (RR′ = Ad′; Ad′ = Ad minus H, Ad = adamantyl), (ii) the disilazetine (cf. [3]) **5** or (iii) the disilabutene (cf. [4]) **6**. These reactions are believed to have proceeded *via* a three-membered ring intermediate **A** which with a second molecule of **1** gave the appropriate compound Si(NN)Si(NN)(X)Y [X-Y = OCRR′, NCBu^t or C(SiMe$_3$)CPh]. Attempts to isolate compound **A**, but using an excess of the unsaturated organic reagent, were unsuccessful, although a stable silaoxirane [5] and silacyclopropene [6] have recently been described.

Reaction of **1** with the imine Ph(R)C:NR′ (R,R′ = Ph,SiMe$_3$ or H,Bu^t) did not give a four-membered ring product. Instead we propose that an azasilacyclopentane intermediate underwent an intramolecular rearrangement to afford compound **7** or (after formal insertion of **1** into a C—H bond) **8**, respectively. The mechanism leading to **7** and **8** is similar to that described for the gas phase reaction of dimethylsilylene with benzophenone yielding a siloxaindane [7].

However (cf. compound **2**), when **1** was added slowly to a hot solution of Ph$_2$CO in benzene, the fused tetracyclic ring compound **9** was obtained. The reaction pathway is believed to have some similarities with that described above for **7**, whereby the oxo (O in place of NSiMe$_3$) analogue of **7** is a further intermediate which reacts with **1**.

Treatment of **1** with *t*-butyl isonitrile led to different products depending on the reaction conditions. When **1** was added slowly to an excess of Bu^{t}NC the 1:1 oxidative adduct **10** was formed; but by reversing the order of addition compound **11** was isolated. A silaketenimine (or a Lewis acid–base adduct) (cf. [8]) is proposed to have been the common intermediate which either rearranged to **10** or with **1** afforded **11**.

A similar dependence upon reaction conditions was shown when **1** was treated with adamantyl azide. In this system, a silaimine (cf. [9]) is a plausible inter-

* Author to whom correspondence should be addressed.

† Dedicated to Professor Donald Bradley, as a mark of friendship and esteem.

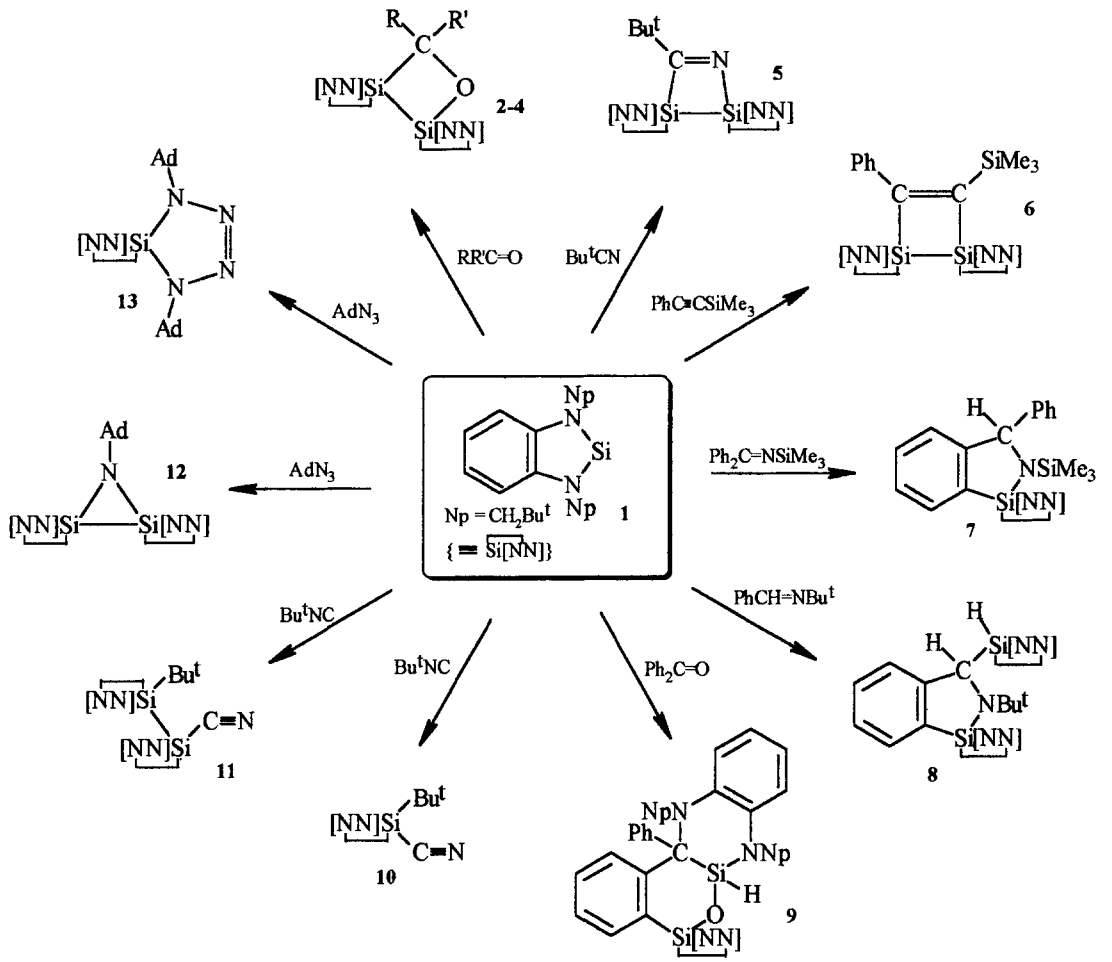

Scheme 1.

mediate which reacts with silylene **1** (adding the azide to a solution of **1**) to give **12**, or with azide (adding **1** to a solution of azide) to form **13**.

Each of the compounds **2**–**13** has been fully characterised by their NMR and MS spectra and gave satisfactory elemental analytical data [for example, ^{29}Si NMR spectral chemical shifts (δ): **2** 9.66, 21.96; **3** 6.44, 19.97; **4** 5.03, 21.04; **5** 19.02, 26.33; **6** −9.11, 13.03, 22.58; **7** 6.44, −5.49; **8** −4.16, −12.66; **9** −15.45, −28.18; **10** −17.84; **11** −15.96, −39.31; **12** −28.49 and **13** −38.13]. The structures of the crystalline compounds **2, 5, 8, 9** and **11** have been further established by single crystal X-ray diffraction studies. Detailed experimental data as well as mechanistic aspects will be described in the full papers.

In conclusion, the reactions of Scheme 1 demonstrate that **1**, although thermally stable, is a highly reactive species and shows distinct differences to the reaction behaviour of its transient relatives.

Acknowledgements—We are grateful to the European Union for the award of a category 30 TMR fellowship to B.G. and the E.P.S.R.C. for other support.

REFERENCES

1. Gehrhus, B., Hitchcock, P. B., Lappert, M. F., Heinicke, J., Boese, R. and Bläser, D., *J. Organomet. Chem.*, 1996, **521,** 211.
2. Schäfer, A., Weidenbruch, M. and Pohl, S., *J. Organomet. Chem.*, 1985, **282,** 305.
3. Weidenbruch, M., Flintjer, B., Pohl, S. and Saak, W., *Angew. Chem, Int. Ed. Engl.*, 1989, **28,** 95.
4. Belzner, J., Ihmels, H., Kneisel, B. O. and Herbst-Irmer, R., *J. Chem. Soc., Chem. Commun.*, 1994, 1989.
5. Belzner, J., Ihmels, H., Pauletto, L. and Noltemeyer, M., *J. Organomet. Chem.*, 1996, **61,** 3315.
6. Belzner, J. and Ihmels, H., *Tetrahedron Lett.*, 1993, **41,** 6541.
7. Ando, W., Masayuki, I. and Sekiguchi, A., *J. Am. Chem. Soc.*, 1977, **99,** 6448.
8. Weidenbruch, M., Bran-Roth, B., Pohl, S. and Saak, W., *Angew. Chem, Int. Ed. Engl.*, 1990, **29,** 90; Takeda, N., Suzuki, H., Tokitoh, N. and Okazaki, R., *J. Am. Chem. Soc.*, 1997, **119,** 1456.
9. Denk, M., Hayashi, R. K. and West, R., *J. Am. Chem. Soc.*, 1994, **116,** 10813.

Pergamon

PII: S0277-5387(97)00328-8

Polyhedron Vol. 17, No. 5–6, pp. 1001–1004, 1998
© 1998 Elsevier Science Ltd
All rights reserved. Printed in Great Britain
0277–5387/98 $19.00+0.00

First structural characterization of a zinc-*bis*(dialkylamide) compound: $Zn\{N[C(CH_3)_2(CH_2)_3C(CH_3)_2]\}_2$†

William S. Rees, Jr,*[a] Oliver Just,[a] Herbert Schumann*[b] and Roman Weimann[b]

[a] School of Chemistry and Biochemistry, and School of Materials Science and Engineering and Molecular Design Institute, Georgia Institute of Technology, Atlanta, GA 30332-0400, U.S.A.

[b] Institut für Anorganische und Analytische Chemie der Technischen Universität Berlin, Straße des 17. Juni 135, D-10623 Berlin, Germany

(Received 2 May 1997)

Abstract—The reaction of two molar equivalents of $Li\{N[C(CH_3)_2(CH_2)_3C(CH_3)_2]\}$ with $ZnCl_2$ in diethyl ether yields the title compound **1**, which was characterized by ^1H, ^{13}C and ^{14}N NMR, melting point, elemental analysis, mass spectrometry and single crystal X-ray diffraction. The structural characterization permits the first direct comparison of di(aryl)amide and di(triorganosilyl)amide examples with a di(alkyl)amide composition, thereby probing the nature of the Zn–N interaction. © 1998 Elsevier Science Ltd. All rights reserved

Keywords: di(alkyl)amide composition; Zn–N interaction.

The II–VI wide band gap semiconductor ZnSe, operating in the blue region of the visible spectrum, possesses potential as one component of versatile optoelectronic devices [1–10] however, achievement of reproducible, high level *p*-type doping presents a significant challenge in improving and controlling their luminescent properties [11–15]. Zinc *bis*(disilyl) amide compounds have been shown to meet some of these demands; however, it has been of interest to prepare silicon-free analogs [16,17]. In this report, the attention is focused on obtaining a novel zinc amide of related interest to the above study. To facilitate the preservation of the zinc–nitrogen bond during the thermal growth process, an appropriate ligand, possessing easily splittable and stable fragments, was selected. This approach involves the use of silicon-free ligands to prepare homoleptic zinc-*bis*(dialkylamide) compounds $Zn[NR_2]_2$, featuring the metal atom in a low-coordination sphere. Compounds possessing such a structure might have a different stability, compared with $Zn\{N[Si(CH_3)_3]_2\}_2$ [18]. To date, little has been done on the zinc-*bis*(amide) compounds to test the validity of this relationship. The commensurately scarce structural information on silicon-free zinc amide compounds is complemented by dimeric species having the metal atom stabilized by an alkyl group or an intermolecular coordinative bond derived from a localized lone-pair presence on nitrogen: $[MeZnN(C_6H_5)_2]_2$ [19], $\{Zn[N(C_6H_5)_2]_2\}_2$ [20] and $[HZnN(CH_3)CH_2CH_2N(CH_3)_2]_2$ [20].

RESULTS AND DISCUSSION

During the investigation of the gas phase decomposition mechanism of zinc-*bis*(amide) compounds, a need emerged for examples which contained substituents at the nitrogen atom other than silicon [16,17]. It was surmised that the consequence of removing the stabilization imparted to the Zn—N bond by the silyl units might lend additional insight into the mechanism of incorporation of nitrogen into epitaxially grown ZnSe. The structural variation chosen for this exploration was one which employed tertiary carbon atoms at the amide linkage. From earlier work, it was known that *t*-Bu groups can be inserted successfully in the place of one of the tri-

* Authors to whom correspondence should be addressed.

† Dedicated, with great fondness, to Professor Donald Bradley on the wondrous occasion of his birthday.

methylsilyl moieties [25a]. Thus, eq. (1) represents, to our knowledge, the initial report of the preparation, isolation and definitive structural characterization of a zinc-*bis*(amide) devoid of any stabilization attributed to silicon-containing species. The utilization of lithium tetramethylpiperidide in a reaction with zinc dichloride cleanly produces a homoleptic zinc-*bis*(dialkylamide) derivative, which was purified by repeated sublimation, to yield colorless and thermally stable needles [21]. The molecular composition of compound **1**, determined by X-ray diffraction techniques [22], is depicted in Fig. 1.

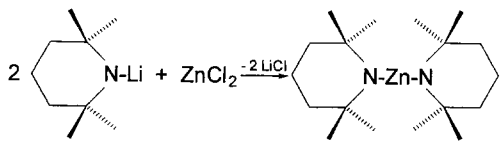

(1)

Our studies on compounds with differently bonded nitrogen atoms in zinc-*bis*(*bis*(trimethylsilyl)amide) [18] (I) and zinc-*bis*(tetramethylpiperidide) (II) aimed also at elucidating the distinction in the stability of the Zn—N bonds displayed by these compounds. Because of the different electronic nature of (II), π-overlap between the fully occupied, unhybridized p-orbital on the nitrogen and available empty 4p-orbitals on the zinc atom may perturb the Zn—N σ-bond. However, no obstacles exist for such a favorable electron density flow from the p-orbital on the trigonal–planar nitrogen, perpendicular to the Zn, N, Si plane, toward the zinc atom in (I). The ability of silicon to stabilize an adjacent negative charge by electrostatic forces is well known [18]. The Zn—N bond in (II) also is reflected in the fact that the strong partially positive charged zinc atom lacks any associated σ-electron-donating groups. By attaching the metal atom to a robust and space-requiring ligand, such as tetramethylpiperidide, the molecule resides in a kinetically stable state, limiting the exposure not only of the metal center to a possible nucleophilic approach, but also shielding the nitrogen atoms against electrophilic attack. Thus, it is possible to stabilize the Zn—N bond, without relying on the employment of silicon atom substituent imparted stabilization. It is noted that the absence of any phenyl rings in (II) removes from consideration the argument relating to interactions of π-systems with the central metal atom to impart stability in such low coordination number, homoleptic transition element *bis*(disilylamide) compounds [23].

The Zn—N interatomic distance for compound **1** (Table 1) is highly commensurate with the GPED value of $Zn\{N[Si(CH_3)_3]_2\}_2$ [24], as well as displaying consistency with the value portrayed by $Zn\{N[Si(CH_3)_3][C(CH_3)_3]\}_2$ [25a], however, the data reported for $Zn\{N[Si(C_6H_5)_2(CH_3)]_2\}_2$ [23] is longer (0.03 Å) than that for the other three examples available for comparison. In the case of the latter compound, the interatomic distance elongation most likely is attributable to the intramolecular stress induced by the sterically encumbered nature of the *bis*(triorganosilyl)amide ligand selected for the investigation. The good level of agreement between the other values (Table 1) would indicate that the range for a typical covalent Zn—N interatomic distance falls within 1.81–1.82 Å.

To probe the stress placed upon the Zn—N interaction in these compounds the ^{14}N NMR data may be compared for $Zn\{N[C(CH_3)_2(CH_2)_3C(CH_3)_2]\}_2$ and $Zn\{N[Si(CH_3)_3][C(CH_3)_3]\}_2$. They are almost identical (at -267 and -290 ppm respectively) and indicate a comparable degree of orbital hybridization and bond ionicity for the electronically stabilized *di*(silyl) example and the relatively unstabilized *tetra*(organo) example.

The stability imparted by the trimethylsilyl moiety to metal–nitrogen interactions in element amide complexes was recognized by Bradley in 1972 [26]. Over the ensuing quarter century, this observation has been applied to the successful isolation of hundreds of

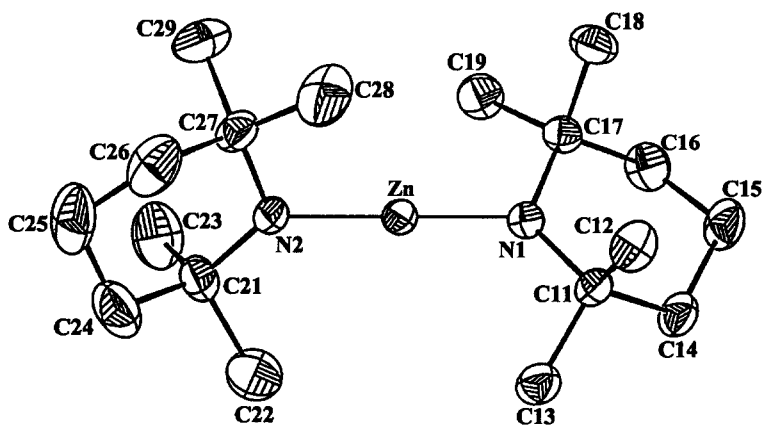

Fig. 1. ORTEP representation with atom-numbering scheme of the solid state molecular structure of compound **1**.

Table 1. Selected interatomic angles [°] and interatomic distances [Å] for structurally characterized representatives of four different zinc amides

Data	$Zn[N(TMS)_2]_2$[a]	$Zn[N(TMS)(t\text{-}Bu)]_2$	$Zn\{N[SiMePh_2]_2\}_2$	$Zn\{\overline{N[C(CH_3)_2(CH_2)_3C(CH_3)_2]}\}_2$
Zn—N	1.824(14)	1.823(8) 1.812(8)	1.850(3)	1.819(2) 1.822(2)
N—Zn—N		179.4(5)	177.5(2)	179.41(9)
N—E[b]	1.728(7)	1.639(12) [Si] 1.694(12) [Si] 1.449(14) [C] 1.387(15) [C]	1.717(5)	1.467(3) 1.469(3) 1.465(4) 1.470(3)
Zn—N—E	114.8(10)	117.3(7) [Si] 115.9(7) [Si] 119.2(8) [C] 119.9(9) [C]	116.9(3)	118.5(2) 117.8(2) 118.9(2) 118.5(2)
E—N—E	130.4(20)	123.5(8) 124.2(8)	130.2(3)	120.4(2) 120.1(2)
Reference	24	25	23	This work

[a] gas-phase electron diffraction.

[b] E = Si for $Zn[N(TMS)_2]_2$, $Zn[N(TMS)(t\text{-}Bu)]_2$ and $Zn\{N[SiMePh_2]_2\}_2$. E = C for $Zn\{\overline{N[C(CH_3)_2CH_2CH_2CH_2C(CH_3)_2]}\}_2$ (this work). TMS = $Si(CH_3)_3$.

examples of compounds of this popular ligand. Thus, the present initial structural characterization of a *bis*(dialkylamide) compound of zinc has potential ramification in other areas of metal–nitrogen chemistry. These presently are undergoing active exploration, and will be described as they become available. Therefore, $Zn\{\overline{N[C(CH_3)_2(CH_2)_3C(CH_3)_2]}\}_2$, while sterically stabilized, apparently exhibits only slightly less covalent character than $Zn\{N[Si(CH_3)_3]_2\}_2$. Such comparison previously has been conducted for Ga, Ge, Sn and Li homologues of $^-\{\overline{N[C(CH_3)_2(CH_2)_3C(CH_3)_2]}\}$ and $^-\{N[Si(CH_3)_3]_2\}$ [27].

Acknowledgements—We gratefully acknowledge the Office of Naval Research for financial support and the Deutsche Forschungsgemeinschaft (DFG) for granting a postdoctoral research fellowship to O.J.

REFERENCES

1. Nakanishi, K., Suemune, I., Fujii, Y., Kuroda, Y. and Yamanishi, M., *Appl. Phys. Lett.*, 1991, **59,** 1401.
2. Zmudzinski, C. A., Guan, Y. and Zory, P. S., *IEEE Photon. Technol. Lett.*, 1990, **2,** 94.
3. Haase, M. A., Qiv, J., DePuydt, J. M. and Cheng, H., *Appl. Phys. Lett.*, 1991, **59,** 1272.
4. Qiv, J., DePuydt, J. M., Cheng, H. and Haase, M. A., *Appl. Phys. Lett.*, 1991, **59,** 1992.
5. Haase, M. A., Cheng, H., Misemer, D. K., Strand, T. A. and DePuydt, J. M., *Appl. Phys. Lett.*, 1991, **59,** 3619.
6. Jeon, H., Ding, J., Patterson, W., Nurmikiko, A. V., Xie, W., Grilla, D. C., Kobayashi, M. and Gunshor, R. L., *Appl. Phys. Lett.*, 1991, **59,** 3619.
7. Menner, R., DimmLer, B., Mauch, R. H. and Schock, H. W., *J. Crystal Growth*, 1988, **86,** 906.
8. Katayama, H., Oda, S. and Kukimoto, H., *Appl. Phys. Lett.*, 1975, **27,** 697.
9. Rohde, H. J., *Thin Solid Films*, 1983, **110,** L125.
10. Okuyama, H., Miyajima, T., Morinaga, Y., Hiei, F., Ozawa, M. and Akimoto, K., *Electron. Lett.*, 1992, **28,** 3619.
11. Wright, P. J., Cockayne, B., Catell, A. F., Dean, P. J., Pitt, A. D. and Blackmore, G. W., *J. Crystal Growth*, 1982, **59,** 155.
12. Stutius, W., *J. Crystal Growth*, 1982, **59,** 1.
13. Stutius, W., *J. Appl. Phys.*, 1982, **53,** 284.
14. Stutius, W., *Appl. Phys. Lett.*, 1982, **40,** 246.
15. Catell, A. F., Cockayne, B., Dexter, K., Kirton, J. and Wright, P. J., *IEEE Trans. Electron Devices ED*, 1983, **30,** 471.
16. Rees, Jr, W. S., Green, D. M., Anderson, T. J., Bretschneider, E., Pathangey, B. and Kim, J., *J. Electronic Materials*, 1992, **21,** 361.

17a. Rees, Jr, W. S., Anderson, T. J., Green, D. M. and Bretschneider, E., In *Wide Band Gap Semiconductors*, ed. T. D. Moutakas, J. I. Pankove and Y. Hamakawa, *Mat. Res. Soc. Symp. Proc.*, 1992, **242,** 281.

17b. Rees, Jr, W. S., Green, D. M., Hesse, W., Anderson, T. J. and Pathangey, B., In *Chemical Perspectives of Microelectronic Materials III*, ed. C. R. Abernathy *et al.*, *Mat. Res. Soc. Symp. Proc.*, 1993, **282,** 63.

17c. Rees, Jr, W. S. and Just, O., In *Gas-Phase and Surface Chemistry in Electronic Materials Processing*, ed. T. J. Mountziaris, G. R. Paz-Pujalt,

F. T. J. Smith and P. R. Westmoreland, *Mat. Res. Soc. Symp. Proc.*, 1994, **334,** 219.

17d. Gaul, D. A., Rees, Jr, W. S. and Just, O., In *Metal–Organic Chemical Vapor Deposition of Electronic Ceramics II*, ed. S. B. Desu, D. B. Beach and P. C. Van Buskirk, *Mat. Res. Soc. Symp. Proc.*, 1996, **415,** 117.

18. Bürger, H., Sawodny, W. and Wannagat, U., *J. Organomet. Chem.*, 1965, **3,** 113.

19. Bell, N. A., Shearer, H. M. M. and Spencer, C. B., *Acta Cryst.*, 1983, **C39,** 1182.

20. Bradley, D. C., *Inorg. Macromol. Rev.*, 1970, **1,** 141.

21. General comments: due to the extreme oxygen- and moisture-sensitivity of the zinc amides, all manipulations were performed under dried and purified nitrogen or argon atmosphere on the vacuum line by employing standard Schlenk or inert gas-filled glove box techniques. The solvents were degassed and freshly distilled from sodium or potassium/benzophenone prior to use. All obtained compounds have been characterized by satisfactory elemental analysis, NMR, as well as mass spectroscopy.

Physical measurements: ^{1}H, ^{13}C and ^{14}N NMR spectra were recorded on Varian Gemini 300 MHz and Bruker 400 MHz instruments respectively; microanalysis was performed on a Perkin-Elmer 2400 Series II Elemental Analyzer; mass spectrum was obtained on a VG Instruments 70SE spectrometer; zinc content was determined on a Perkin-Elmer OPTIMA 3000 ICP-OES analyzer.

Experimental procedure: to a solution of 11.15 g (78.93 mmole) of tetramethylpiperidine in 100 mL of diethyl ether in a 250 mL Schlenk flask, 41.5 mL of a *n*-BuLi/hexane solution (1.90 mol/L) was added through a syringe at 0°C over a period of 30 min. The formed pale yellow solution then was refluxed for 1 h and, after attaining ambient temperature on its own, was stirred for an additional hour at this temperature. A solution of 5.37 g (39.40 mmole) of zinc dichloride in 100 mL of diethyl ether was added through a cannula to the formed lithium tetramethylpiperidide at 0°C over a period of 1 h. After stirring overnight, lithium chloride was separated by Schlenk filtration and the diethyl ether was removed at reduced pressure. The crude reaction product was isolated from the salt residue by vapor transfer. Ensuing sublimation of this material afforded zinc-*bis*(tetramethylpiperidine) as colorless and crystalline needles. Yield: 4.4 g (32%); m.p. = 59°C; sublimation conditions: 135°C/0.01 Torr; ^{1}H NMR [C_6D_6, δ, ppm], 1.72–1.64 (m, 4H, CH_2), 1.35 (t, 8H, CH_2), 1.25 (s, 24H, CH_3); ^{13}C NMR [C_6D_6, δ, ppm], 52.96 (s, $C(CH_3)_2$), 39.45 (s, CCH_2), 36.82 (s, $C(CH_3)_2$), 19.50 (s, CCH_2CH_2); ^{14}N NMR [C_6D_6, δ, ppm], −267.52 (s); MS (EI, 70 eV, m/z (%), 185°C): 345 [M^+], 330 [M^+-CH_3], 315 [M^+-$2CH_3$], 204 [M^+-$\overline{N[C(CH_3)_2(CH_2)_3C(CH_3)_2}$], 126 [$C(CH_3)_2(CH_2)_3C(CH_3)_2]^+$; Anal. Calcd. for $C_{18}H_{36}N_2Zn_1$: C, 62.50; H, 10.49; Zn, 18.90. Found: C, 62.25; H, 10.61; Zn, 19.10.

22. Crystal data: $C_{18}H_{36}N_2Zn_1$, crystal size: $(0.27 \times 0.25 \times 0.30)$ mm^3, $M_r = 345.86$, monoclinic, space group $P2_1/n$, $a = 11.465(3)$ Å, $b = 11.643(4)$ Å, $c = 15.676(3)$ Å, $\beta = 110.587(14)°$, $V = 1958.9(9)$ Å^3, $Z = 4$, $D_{calc} = 1.173$ g/cm^{-3}, $R = 0.0490$, $R_w = 0.0356$, $T = 185$K, absorption coefficient = 1.251 mm^{-1}, $F(000) = 752$, diffractometer: Enraf-Nonius CAD-4, radiation: $Mo_{K\alpha} = 0.71069$ Å, aperture: 2.1 mm, scan angle: $(0.80 + 0.35 \tan\theta)°$, variable scan time: max. 45 s, scan technique: ω-2θ, theta range for data collection: $2° < 2\theta < 50°$, index ranges: $0 \leqslant h \leqslant 13$, $0 \leqslant k \leqslant 13$, $-18 \leqslant l \leqslant 18$, reflections collected: 3896, independent reflections: 3159 [R(int) = 0.0262], goodness-of-fit: 1.025, largest diff. peak and hole: max. 0.382 eÅ^{-3} and min. −0.359 eÅ^{-3}.

23. Power, P. P., Ruhlandt-Senge, K. and Shoner, S. C., *Inorg. Chem.*, 1991, **30,** 5013.

24. Haaland, A., Hedberg, K. and Power, P. P., *Inorg. Chem.*, 1984, **23,** 1972.

25a. Rees, Jr, W. S., Green, D. M. and Hesse, W., *Polyhedron*, 1992, **11,** 1667.

25b. One can also replace, in selected examples, the trimethylsilyl group with a dimethylsilyl group, see: Rees, Jr, W. S., Just, O., Schumann, H. and Weimann, R., *Angew. Chem. Int. Ed. Engl.*, 1996, **35,** 419.

26. Bradley, D. C., Ghotra, J. S. and Hart, F. A., *J. Chem. Soc., Chem. Commun.*, 1972, 349.

27a. Chorley, R. W., Hitchcock, P. B., Lappert, M. F., Leung, W. P., Power, P. P. and Olmstead, M. M., *Inorg. Chim. Acta*, 1992, **198/200,** 203.

27b. Linti, G., Frey, F. and Polborn, K., *Chem. Ber.*, 1994, **127,** 1387.

Pergamon

PII: S0277-5387(97)00272-6

Polyhedron Vol. 17, No. 5-6, pp. 1005-1034, 1998
© 1998 Elsevier Science Ltd
All rights reserved. Printed in Great Britain
0277-5387/98 $19.00+0.00

New perspectives in the tailoring of hetero (bi- and tri-) metallic alkoxide derivatives†

Michael Veith,* Sanjay Mathur* and Charu Mathur

Institute of Inorganic Chemistry, University of Saarland, P.O. 151150, D-66041 Saarbrücken, Germany

(Received 22 April 1997)

Abstract—Metal alkoxides containing more than one sort of metallic element are predominantly known in the field of heterobimetallic derivatives. In order to pass to heterotrimetallic homoleptic alkoxides bimetallic alkoxides have to be prepared which are at the same time heterobimetallic and heteroleptic. They serve as starting materials in salt elimination reactions leading to heterotrimetallic homoleptic alkoxides. The structural entity serving as a building block in these reactions must be kinetically stable in order to survive in the synthetic procedures. Besides heterotermetallic alkoxides, heterobimetallic alkoxides with halides and cyclopentadienyl as ancillary ligands and transition metal complexes of new mixed-metal alkoxy derivatives are presented. Besides the syntheses and the structural characterization reactivity, spectral aspects in view of dynamic or static structures and applications of hetero(bi- and tri-)metallic alkoxides are discussed. © 1997 Elsevier Science Ltd. All rights reserved.

Keywords: heterobimetallic alkoxides; heterotrimetallic alkoxides; heteroleptic alkoxides; transition metal complexes of heterometal alkoxides.

1. INTRODUCTION

Within the realm of M–O–C derivatives, metal alkoxide chemistry has seen an impressive growth over the last decade. The importance of metallo–organic derivatives as versatile precursors to ultra-pure oxide-ceramics [1] in conjunction with the fact that most of the advanced ceramics are multimetallic in nature e.g., $YBa_2Cu_3O_{7-\delta}$ [2], $HgBa_2CuO_4$ [3], $Bi_2Sr_2CaCu_2O_8$ [4] has led to the present interest in the tailoring of heterometal alkoxides. The chemical synthesis routes provide better control over purity, composition, homogeneity and microstructure which are crucial parameters for high performance materials. In addition, the precursors used are generally readily purifiable (*via* crystallization/distillation) and the possibility of variable atomic ratios in the precursors allow for novel compositions not easily obtainable, by other conventional routes. The versatility of chemical routes largely depends on the availability of heterometal molecules as precursors and in view of the metal combinations being immense, a large number of new heterometal alkoxides and allied derivatives with novel structural and bonding features have been characterized in the recent years [5]. However, the formation of a thermodynamically favoured heterometal alkoxide assembly is subject to various factors such as the atomic size of the metallic elements and steric bulk of the alkoxo ligands and the synthesis of a heterometal precursor with targeted ratio of metallic elements cannot be achieved by simply mixing the two or more components in required molar ratios. The metal stoichiometry in the isolated product is thus often inappropriate for the material science requirements. The appropriate metal ratio is of prime consideration in assessing the feasibility of heterometal alkoxides as precursors to useful multi-component metal oxides. Moreover, the growing realization that a 'single-source' precursor with different metals assembled in one molecule in the desired metal ratios (for instance '$YBa_2Cu_3(OR)_{13}$' for $YBa_2Cu_3O_{7-\delta}$) can lead to morphologically pure samples of multi-component ceramics, constitutes one of the continuing synthetic challenges in heterometal alkoxide chemistry. Of central importance to this theme are the developments of new synthetic principles (e.g., the use of novel alkoxometallate units or metallic elements in

† Dedicated to Prof. D. C. Bradley for his pioneering work on metal alkoxides and on the occasion of his 73rd birthday.

* Authors to whom correspondence should be addressed.

unusual oxidation states) which will allow the rational synthesis of stable heterometallic systems with desired metal combinations. It is relevant to mention that the existence of heterotermetallic alkoxides as discrete molecular species in the solution and solid state has been recently established [6], employing coordinatively unsaturated species $\{M'(OPr^i)_3\}^-$ (M = Ba, Sr, Ca) towards well-characterised halide heterobimetallic alkoxides, $ICd\{M_2(OPr^i)_9\}$ (M = Sn, Ti, Zr, Hf).

A comprehensive discussion of the various aspects of metal alkoxide chemistry has been made in some recent reviews [5]. In view of the above and the limited scope of the present article, this review is not intended to be an all-inclusive treatment of heterometal alkoxide chemistry and we confine to the research carried out in our laboratories on heterometal alkoxide derivatives, however, a relevant reference is made to other recent examples not covered in earlier reviews. Owing to the pronounced tendency of heterometal alkoxides to undergo redistribution reactions, dynamic rearrangement of the ligands around the metallic centres and rapid site exchange among alkoxy groups, the spectroscopic pattern of heterometal systems are often deceptive and present an over-simplified picture of metal stoichiometry and molecular symmetry [5b]. In view of the above, special emphasis is given in this article, to the heterometal alkoxide derivatives whose identity has been established by X-ray crystallography. We outline in this review our recent research on three new classes of heterometal alkoxide derivatives namely (i) hetero*ter*metallic alkoxides (ii) hetero*bi*metallic alkoxides with *halide(s)* and *cyclopentadienyl* as ancillary ligand(s) and (iii) the *transition metal complexes* of new mixed-metal alkoxy derivatives. The subject matter entails the synthesis, structure, reactivity, spectral aspects and applications of the hetero (bi- and tri-) metallic alkoxides.

2. HETEROBIMETALLIC ALKOXIDES

2.1 *Homoleptic heterobimetallic alkoxides*

The reactions involving component alkoxides (Lewis acid–base interactions) or metathesis of all the metal–halogen bonds in metal halides by alkali metal alkoxometallates (salt elimination reactions) represent the most general synthetic routes to heterobimetallic alkoxy derivatives based on only one type of alkoxy ligands (homoleptic).

2.1.1 *Synthesis*

(*i*) *Lewis acid–base reactions.* The ability of metal alkoxides ($M(OR)_x$) to form mixed-metal species $MM'(OR)_{x+y}$ is well-known [7] and is exemplified among the alkali metal derivatives of a large number of metal alkoxides (eqs 1–9) [8–17]. The oligomeric nature of the constituent alkoxides is not considered in the equations illustrated below. Some of the reactions (eqs 2, 4, 6 and 7) do not represent pure Lewis acid–base interactions as the product formation involves addition or release of neutral molecules (alcohol, THF, dioxane), however, in view of their similar formation (donor–acceptor interaction of two component alkoxides), they are included in the following discussion.

$$M'OBu^t + M(OBu^t)_2 \rightarrow 1/n\{M'M(OBu^t)_3\}_n \quad (1)$$

M = Ge, Sn, Pb

M′ = Li, Na, K, Rb, Cs

$$KOPr^i + Al(OPr^i)_3 \xrightarrow{2Pr^iOH} 1/n\{KAl(OPr^i)_4(Pr^iOH)_2\}_n \quad (2)$$

$$M'OBu^t + M(OBu^t)_3 \rightarrow 1/n\{M'M(OBu^t)_4\}_n \quad (3)$$

M = Sb; M′ = K, Rb, Cs

M = Bi; M′ = K

$$2KOBu^t + Sb(OBu^t)_3 \xrightarrow{C_4H_8O_2} K_2Sb(OBu^t)_5 \cdot (C_4H_8O_2) \quad (4)$$

$$M'OPr^i + Ti(OPr^i)_4 \rightarrow 1/n\{MTi(OPr^i)_5\}_n \quad (5)$$

M′ = Li, Na, K

$$KOPr^i + 2Ti(OPr^i)_4 \xrightarrow{2THF} (THF)_2KTi_2(OPr^i)_9 \quad (6)$$

$$2LiOPr^i + [Hf(OPr^i)_4 \cdot Pr^iOH]_2 \rightarrow \{LiHf(OPr^i)_5\}_2 + 2Pr^iOH \quad (7)$$

$$KOBu^t + M(OBu^t)_4 \rightarrow 1/n\{KM(OBu^t)_5\}_n \quad (8)$$

M = Sn, Zr

$$LiOEt + Nb(OEt)_5 \rightarrow 1/n\{LiNb(OEt)_6\}_n \quad (9)$$

In analogy to alkali metal alkoxometallates, a large number of molecular heterobimetallic alkoxides of various di-, tri-, tetra- and penta-valent metallic elements have been obtained following the Lewis acid–base principle. Some typical examples are shown below (eqs 10–15) [18–22].

$$2/m[M(OBu^t)_2]_m + 1/n[M'(OBu^t)_2]_n \rightarrow M'\{M(OBu^t)_3\}_2 \quad (10)$$

M = Ge, Sn m = 2; M = Pb m = 2

M′ = Mg, Ca, Sr, Ba

$$6/n[Pb(OPr^i)_2]_n + 6/n[Zr(OPr^i)_4]_n \rightarrow Pb_4Zr_2(OPr^i)_{16} + Pb_2Zr_4(OPr^i)_{20} \quad (11)$$

$$4/n[Pb(OPr^i)_2]_n + 2/n[Zr(OPr^i)_4]_n \rightarrow Pb_4Zr_2(OPr^i)_{16} \quad (12)$$

$$1/n[Ba(OPr^i)_2]_n + 3Ti(OPr^i)_4 \rightarrow \{Ti(OPr^i)_5\}Ba\{Ti_2(OPr^i)_9\} \quad (13)$$

$$1/2[Al(OPr^i)_3]_4 + 1/2[Hf(OPr^i)_4 \cdot Pr^iOH]_2 \rightarrow Al_2Hf(OPr^i)_{10} + Pr^iOH \quad (14)$$

$$1/n[Ba(OPr^i)_2]_n + Nb_2(OPr^i)_{10} \xrightarrow{Pr^iOH} BaNb_2(OPr^i)_{12}(Pr^iOH)_2 \quad (15)$$

The heterometal alkoxides based on Lewis acid–base reactions generally involve the reaction of an alkoxide of molecular nature with unsaturated metal alkoxides $[M(OR)_x]_n$ [5a]. However, mixing two component metal alkoxides do not always result in a heterobimetallic compound and this synthetic strategy is found to be inoperative in many cases, for instance, K, Rb and Cs *tert*-butoxides react with $Sn(OBu^t)_4$ to form compounds $MSn(OBu^t)_5$ (M = K, Rb, Cs), however, no heterometal derivatives are formed with lithium and sodium *tert*-butoxides [15]. Similarly, attempts made to use $As(OBu^t)_3$ as a Lewis acid in the reaction with alkali metal *tert*-butoxides $MOBu^t$ (M = Li, Na, K, Rb, Cs) failed even at elevated temperatures and after long reaction times [10]. Furthermore, no heterometal derivative results in the reaction involving Sn^{II} and Ge^{II} *tert*-butoxides whereas, $Sn_2(OBu^t)_4$ and $Pb_3(OBu^t)_6$ react in appropriate molar ratio to yield $PbSn_2(OBu^t)_6$, which has been characterised in the solid state [18b]. Although depolymerization of $[Pb(OPr^i)_2]_n$ takes place in the presence of $[Zr(OPr^i)_4]_n$ to yield Pb–Zr mixed metal alkoxides, no mixed-metal species is formed when $Ti(OPr^i)_4$ is used [19]. $[Sr(OBu^t)_2]_n$ undergo a facile reaction with $Sn_2(OBu^t)_4$ to form $SrSn_2(OBu^t)_6$ while $[Ca(OBu^t)_2]_n$ do not react even under drastic conditions; this discriminating reactivity of calcium and strontium *tert*-butoxides toward $Sn_2(OBu^t)_4$ is shown to be selective for the quantitative separation of Sr and Ca [18].

(*ii*) *Salt elimination reactions.* Substitution of all halide ligands in a metal halide by anionic alkoxometallates is another synthetic pathway for the construction of heterometal alkoxide molecules (eqs 16–20) [5a,c,d,23–25]. The alkali metal derivatives (eqs 1–9) described in the preceding sub-section are interesting reagents to transfer metallo-ligands of the type $\{M^{II}(OR)_3\}^-$, $\{M^{III}(OR)_4\}^-$, $\{M^{IV}(OR)_5\}^-$, $\{M^{V}(OR)_6\}^-$ and $\{M_2^{IV}(OR)_9\}^-$ to an electropositive metal centre and have been used as building blocks in the construction of a variety of heterometal alkoxides.

$$2M'Br + Na_2M_2(OBu^t)_6 \rightarrow 2M'M(OBu^t)_3 + 2NaBr \quad (16)$$

M = Ge, Sn, Pb; M′ = In, Tl

$$[6M'X_2 + 4Na_2M_2(OBu^t)_6 \rightarrow 3M'_2M_2(OBu^t)_8 + 8NaX] \quad (17)$$

M′ = Co, Ni; M = Ge

M′ = Mg, Cr, Mn, Co, Ni; M = Sn

M′ = Co; M = Pb

$$M'Cl_2 + Na_2M_2(OBu^t)_6 \rightarrow M'M_2(OBu^t)_6 + 2NaCl \quad (18)$$

M′ = Mg, Cr, Mn, Zn; M = Ge

M′ = Mn, Zn; M = Pb

$$ErCl_3 + 3/n[KAl(OPr^i)_4]_n \rightarrow Er\{Al(OPr^i)_4\}_3 + 3KCl \quad (19)$$

$$MCl_2 + 2/n[KAl(OR)_4]_n \rightarrow M\{Al(OR)_4\}_2 + 2KCl \quad (20)$$

M = Be, Mg, Zn, Cd, Hg, Mn, Fe, Co, Ni, Cu;

OR = OPr^i, OBu^t

The transmetallation reactions using large, soft and polarizable metal cations (e.g., Tl^+, Ba^{2+}) represent another means of inducing salt-elimination reactions as shown in the following examples (eqs 21–23) [5a,26].

$$TlSn(OBu^t)_3 + InBr \rightarrow InSn(OBu^t)_3 + TlBr \quad (21)$$

$$ZnCl_2 + Tl_2Sn(OEt)_6 \rightarrow (EtO)ZnSn(OEt)_5 + 2TlCl \quad (22)$$

$$2Ba\{OCH(CF_3)_2\}_2 + CuCl_2 \rightarrow BaCu\{OCH(CF_3)_2\}_4 + BaCl_2 \quad (23)$$

Although anion-exchange reactions between a mixed metal alkoxide $MM'(OR)_x$ (M = an alkali metal) and a metal halide ($M''X_n$) appears a possible synthetic route to build heteronuclear species, the transfer of $\{M'(OR)_x\}^-$ moiety does not always take place as desired and in a number of cases, no reaction occurs when an alkali metal alkoxide is treated with a metal halide (eqs 24–26) [10,20].

$$CuCl_2 + 2/n[KTi(OPr^i)_5]_n \rightarrow Cu(OPr^i)_2 + 2Ti(OPr^i)_4 + 2KCl \quad (24)$$

$$CaCl_2 + 2/n[KSb(OBu^t)_4]_n \rightarrow Ca(OBu^t)_2 + 2Sb(OBu^t)_3 + 2KCl \quad (25)$$

$$CuI + 1/n[KSb(OBu^t)_4]_n \rightarrow 1/4[Cu(OBu^t)]_4 + Sb(OBu^t)_3 + KI \quad (26)$$

(*iii*) *Miscellaneous methods.* Other common preparative routes to heterobimetallic alkoxides involve

(i) the reaction of two different metals with an alcohol (eq. 27) [27] (ii) the reaction of a metal with a metal alkoxide in the presence of parent alcohol (eqs 28–29) [28,29] (iii) reaction of a metal amide [19], alkyl [30] or hydride [31] with a metal alkoxide alcoholate (eqs 30–32) and (iv) alcoholysis of a mixture of two different metal amides (eq. 33) [32].

$$Mg + 2Al + 10Pr^iOH \rightarrow (Pr^iOH)_2MgAl_2(OPr^i)_8 + 4H_2 \quad (27)$$

$$2Ba + 2[Zr(OPr^i)_4 \cdot Pr^iOH]_2 \xrightarrow{4Pr^iOH} Ba_2Zr_4(OPr^i)_{20} + 2H_2 \quad (28)$$

$$M + 4Ti(OEt)_4 \xrightarrow{2EtOH} M\{Ti_2(OEt)_9\}_2 + H_2 \quad (29)$$

$M = Ba, Ca$

$$6Pb[N(SiMe_3)_2]_2 + 3[Zr(OPr^i)_4 \cdot Pr^iOH]_2 \xrightarrow{6Pr^iOH} Pb_2Zr_4(OPr^i)_{20} + Pb_4Zr_2(OPr^i)_{16} + 12HN(SiMe_3)_2 \quad (30)$$

$$2CuX + [Zr(OPr^i)_4 \cdot Pr^iOH]_2 \rightarrow Cu_2Zr_2(OPr^i)_{10} + 2XH \quad (31)$$

$X = mesityl$

$$KH + [Zr(OPr^i)_4 \cdot Pr^iOH]_2 \rightarrow KZr_2(OPr^i)_9 + Pr^iOH + H_2 \quad (32)$$

$$Y[N(SiMe_3)_2]_3 + 2Ba[N(SiMe_3)_2]_2 + 8Bu^tOH \rightarrow YBa_2(OBu^t)_7(Bu^tOH) + 7HN(SiMe_3)_2 \quad (33)$$

In an interesting synthetic approach, heterometallic Ce^{IV} alkoxides $(DME)_2Na_2Ce(OBu^t)_6$ and $NaCe_2(OBu^t)_9$ have been obtained by the reaction of ceric ammonium nitrate with appropriate amounts of sodium *tert*-butoxide (eqs 34–35) [33].

$$(NH_4)_2Ce(NO_3)_6 + 8NaOBu^t \xrightarrow{THF/DME} (DME)_2Na_2Ce(OBu^t)_6 + 2NH_3 + 6NaNO_3 + 2Bu^tOH \quad (34)$$

$$2(NH_4)_2Ce(NO_3)_6 + 13NaOBu^t \rightarrow NaCe_2(OBu^t)_9 + 4NH_3 + 12NaNO_3 + 4Bu^tOH \quad (35)$$

2.1.2 *Structural and spectral features*

The binding mode (terminal, μ_2- or μ_3-) of alkoxy ligands and the nature of metal atoms play a governing role in the structural frameworks (e.g., molecular or polymeric linear arrays or closed polyhedral units) formed among the various thermodynamically accessible heterometal alkoxo clusters (Table 1). The bridging propensity of the alkoxide groups and the strength of alkoxy bridges between similar as well as different metal atoms generally preclude the coordination expansion of metallic constituents by any alternative mechanism, for instance, adding up solvent molecules (containing a donor atom) as donor ligands. In view of the above, the number of doubly (μ_2-) and triply (μ_3-) bridging alkoxide groups are important in determining the nuclearity of the resulting complex and their presence can result in different frameworks e.g., the potassium penta-*tert*-butoxy stannate, $[KSn(OBu^t)_5]$ [15] devoid of alkoxy groups in μ_3-configuration is a one-dimensional polymer (Fig. 9) whereas, zirconium compound with an identical formulation $[KZr(OBu^t)_5]$ [16] but containing a triply bridging alkoxy group is observed as a dimer in the solid state (Fig. 10). The effect of the size of metal atoms is evident in the solid state structures of $(DME)KZr_2(OPr^i)_9$ [31] and $(Pr^iOH)LiZr_2(OPr^i)_9$ [29]; whereas potassium derivative shows a closed triangular (KZr_2) structure, the smaller lithium atom ($Li^+ = 0.70$ Å; $K^+ = 1.33$ Å) fails to adopt a closed MM'_2 structural motif and displays an open structure.

A remarkable variety of structures [5,8,18,34] is observed among the tris-(*tert*-butoxo)stannate (-germanate or plumbate) derivatives of the alkali (eq. 1) and alkaline earth (eq. 10) metals. Whereas the stannates of lithium and sodium form cage-like molecular structures (**I**), the similar derivatives of heavier K, Rb and Cs are polymeric (**II**) (see Fig. 1). The Li and Na compounds are dimers of formula $M_2Sn_2(\mu_3\text{-}OBu^t)_2(\mu_2\text{-}OBu^t)_4$ (**I**) with no terminal ligands on either of the metallic elements and pyramidal tin(II) presumably possesses a stereochemically active electron lone pair. The polycyclic $Sn_2O_6M_2$ (M = Li, Na) core consists of two analogous seco-norcubane subunits, sharing a face. Alternatively, the structure can be viewed as two pyramidal $Sn(OBu^t)_3^-$ units linked by two alkali metal atoms. The heavier congeners (K, Rb, Cs) form a one-dimensional chain of interlinked SnO_3M units (**II**), the alkali metals are additionally coordinated by two oxygen atoms of a second cage to give a polymeric arrangement in the crystal. The higher coordination number observed for heavier alkali metal atoms is possibly favoured by their larger size. The room temperature ^1H NMR spectra of the alkali metal alkoxo-stannates show a single alkoxide environment. In case of $M_2Sn_2(OBu^t)_6$ (M = Li, Na) derivatives, the cryoscopic measurements indicate that a dimeric structure is maintained in the solution. However, the gas phase nuclearity as determined by mass spectroscopy, shows the sodium compound to be dimer while lithium analog is a monomer.

The general structural type (Fig. 2) observed in the interaction of Lewis basic *tert*-butoxides of divalent Ge, Sn and Pb with polymeric alkoxides of alkaline earth metals (eq. 10) can be designated as a bis (Janus-head) structural motif (**III**) [34]. The metal-oxygen framework, as found in the X-ray crystallographic

Table 1. The thermodynamically accessible metal stoichiometries as observed in the crystallographically characterised homoleptic hetero-(bi- and tri-) metallic alkoxides

Cluster	Coordination number			μ_2-OR[a]	μ_3-OR[b]	Examples
	M	M′	M″			
$[MM'X_n]$	3	3	—	3	—	$[MSn(OBu^t)_3]$ (M = Tl, In) [39]
$[MM'X_n]_2$	4	3	—	4	2	$[MSn(OBu^t)_3]_2$ (M = Li, Na) [8]
	4	5	—	4	2	$[LiTi(OPr^i)_5]_2$ [11]
	3	6	—	4	2	$[LiHf(OPr^i)_5]_2$ [14]
	5	5	—	4	3	$[KZr(OBu^t)_5]_2$ [16]
$[MM'X_n]_n$	5	3	—	3	—	$[KSn(OBu^t)_3]_n$ [8]
	6	4	—	4	—	$[KAl(OPr^i)_4(Pr^iOH)_2]_n$ [9]
	4	4	—	4	—	$[KM'(OBu^t)_4]_n$ (M = Bi, Sb) [10]
	4	5	—	4	—	$[NaTi(OPr^i)_5]_n$ [12]
	5	5	—	3	1	$[KTi(OPr^i)_5]_n$ [12,13]
	4	4	—	5	—	$[KSn(OBu^t)_5]_n$ [15]
	4	6	—	4	—	$[LiNb(OEt)_6]_n$ [17]
$[MM'_2X_n]$	6	3	—	6	—	$[MM'_2(OBu^t)_6]$ (M = Mg, Ca, Pb, Cd, Mn, Eu, M′ = Ge; M = Sr, Ba, Ca, Pb, Cd, M′ = Sn; M = Sr, M′ = Pb) [18b]
	5	6	—	2	2	$[(DME)_2Na_2Ce(OBu^t)_6]$ [33]
	5	5	—	3	2	$[YBa_2(OBu^t)_7(Bu^tOH)]$ [32]
	6	4	—	4	—	$[MgAl_2(OPr^i)_8(Pr^iOH)_2]$ [27]
	4	4	—	4	—	$[NiAl_2(OBu^t)_8]$ [13], $[MgAl_2(OBu^t)_8]$ [25]
	4	6	—	2	2	$[LiZr_2(OPr^i)_9(Pr^iOH)]$ [29]
	4	6	—	3	2	$[(DME)KZr_2(OPr^i)_9]$ [31], $[(THF)_2KTi_2(OPr^i)_9]$ [13]
	4	6	—	3	2	$[KU_2(OBu^t)_9]$ [45]
	4	6	—	3	2	$[NaM'_2(OBu^t)_9]$ (M′ = Ce [33], Th [34])
	4	6	—	4	—	$[Al_2Hf(OPr^i)_{10}]$ [21]
	6	6	—	4	—	$[BaNb_2(OPr^i)_{12}(Pr^iOH)_2]$ [22]
	6	6	—	5	—	$[(Pr^iO)La\{Nb_2(OPr^i)_{12}\}]$ [22]
$[MM'_2X_n]_2$	3,4	6	—	8	—	$[Pb_2Zr(OPr^i)_8]_2$ [19]
	4	6	—	8	2	$[PbZr_2(OPr^i)_{10}]_2$ [19]
	6	6	—	8	4	$[BaZr_2(OPr^i)_{10}]_2$ [46]
$[MM'_2X_n]_n$	5	4	—	3	2	$[K_2Sb(OBu^t)_5\cdot(C_4H_8O_2)]_n$ [10]
	4	6	—	4	2	$[Tl_2Sn(OEt)_6]_n$ [26c]
$[MM'_3X_n]$	6	4	—	6	—	$[Er\{Al(OPr^i)_4\}_3]$ [24]
	6	6,5	—	5	2	$[BaTi_3(OPr^i)_{14}]$ [20]
$[M_2M'_2X_n]$	4	3	—	6	—	$[M_2M'_2(OBu^t)_8]$ (M = Co, M′ = Ge; M = Mg, Cr, Mn, Co, Ni, M′ = Sn) [23]
	2	6	—	6	—	$[Cu_2Zr_2(OPr^i)_{10}]$ [30]
$[M_2M'_3X_n]$	4,5	4	—	8	—	$[Mg_2Al_3(OPr^i)_{13}]$ [37]
$[MM'_4X_n]$	8	6	—	6	4	$[M\{Ti_2(OEt)_9\}_2]$ (M = Ba, Ca) [42]
$[M_2M'_2M''_4X_n]$	4	6	6	12	4	$[\{Cd(OPr^i)_3\}M'\{M''_2(OPr^i)_9\}]_2$ (M′ = Ba, Sr, Ca; M″ = Sn, Ti, Zr, Hf) [6,13,14]
$[M_2M'_2M''_2X_n]$	6	6	6	6	4	$[Ba_2Ti_2Zr_2(OPr^i)_{20}]$ [13]

[a] μ_2-OR = doubly bridging alkoxo ligands.
[b] μ_3-OR = triply bridging alkoxo ligands.

studies [18], displays two trigonal bipyramids joined together at a common apex, defined by the heterometal partner. Consequently in all structures, the central element is six-fold coordinated by the alkoxide oxygens while the outer metals occupying the terminator positions are three-fold coordinated and possess presumably a lone pair of electrons. The detailed comparison of bond lengths and angles in the different derivatives show that the ability of the monoanionic $M(OBu^t)_3^-$ unit to accommodate a metal atom with respect to its size follows the order $Sn(OBu^t)_3^- < Ge(OBu^t)_3^- < Pb(OBu^t)_3^-$ [18b]. This trend is especially evident in the transition metal derivatives (see sub-section 2.1.2).

Although a large number of heterometallic alkoxides containing aluminium are based on the $\{Al(OPr^i)_4\}^-$ unit [5c], the ligating properties of this monoanionic alkoxometallate unit is not well-established. Most of the studies propose a bidentate ligating mode which indeed has been observed in the solid

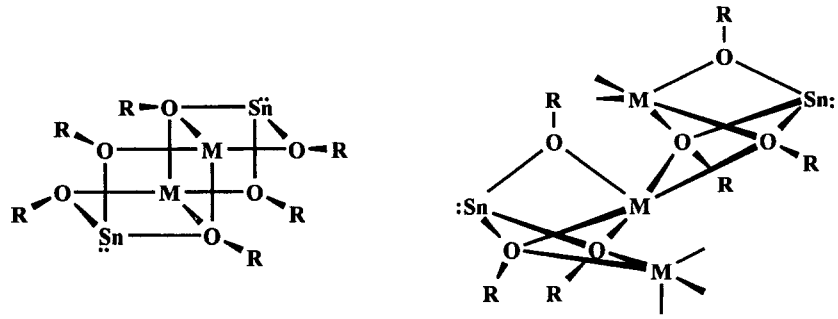

I II

(R = Bu^t)

Fig. 1. Schematic representation of the metal–oxygen core observed in the structures of $[M\{Sn(OBu^t)_3\}]_2$ (M = Li, Na) (**I**) and $[M\{Sn(OBu^t)_3\}]_n$ (M = K, Rb, Cs) (**II**) [8].

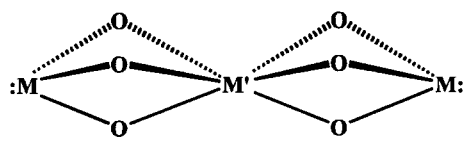

III

Fig. 2. Schematic representation of the metal–oxygen skeleton observed in $M'M_2(OBu^t)_6$ derivatives [18].

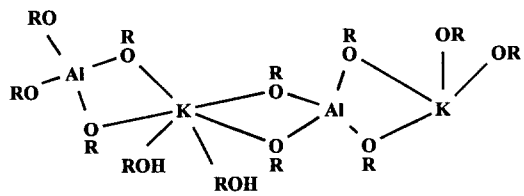

(R = Pr^i)

Fig. 3. Representation of a section of the solid state structure of $[(Pr^iOH)_2K\{Al(OPr^i)_4\}]_n$ polymer [9].

state structures of $[ClPr\{Al(OPr^i)_4\}_2(Pr^iOH)]_2$ [35], and $[Mg\{Al(OPr^i)_4\}_2(Pr^iOH)_2]$ [27]. However, other structurally characterised examples with an $\{Al(OPr^i)_4\}^-$ unit bridging (i) two metals through single alkoxide bridges (e.g., $[Mo_2(O_2CCH_3)_2\{Al(OPr^i)_4\}_2]$ [36] or (ii) two metals by a double OR bridge to one and a single bridge to the second (e.g., $[Mg_2Al_3(OPr^i)_{13}]$ [37]) are also known.

The attempts made to establish the identity and formulation of heterometal alkoxides by single crystal X-ray diffraction analysis are generally frustrated by their organic periphery (which makes them extremely soluble in common organic solvents) and physical state (viscous liquids or waxy solids). These problems can be overcome, in some cases, by using coordinating solvents (alcohol, THF, ether, pyridine, DME) which serve as neutral ligands and complete the coordination sphere of involved metal(s) to offer more tractable (coordinatively saturated) systems suitable for single crystal X-ray crystallography. A structural study performed on the single crystals obtained from an isopropanol solution of potassium tetraisopropoxyaluminate, $KAl(OPr^i)_4$ (eq. 2), revealed a polymer of composition $[(Pr^iOH)_2K\{Al(OPr^i)_4\}]_n$ [9] with chains of alternating K and Al atoms joined by doubly bridging isopropoxy groups (Fig. 3). Aluminium is present in a tetrahedral environment while potassium additionally coordinated by two neutral Pr^iOH molecule displays a severely distorted octahedral coordination sphere.

The alkali metal alkoxy antimonates and bismuthates obtained according to eq. 3 exhibit only one signal in their ^1H NMR spectra. The X-ray structural study performed on crystalline samples of $KSb(OBu^t)_4$ [10] and $KBi(OBu^t)_4$ [10] reveal the compounds to be made up of one-dimensional arrangements of $M(OBu^t)_4^-$ ($M = Sb^{III}$, Bi^{III}) units linked through potassium atoms situated at inversion centres and coordinated by four alkoxo groups in a single plane. The coordination figure of both Sb^{III} and Bi^{III} resembles a ψ-trigonal bipyramid where one of the equatorial site is occupied by the electron lone pair. Although identical in stoichiometry, the two compounds crystallise with slightly different structures (Fig. 4), whereas the *pseudo*-trigonal bipyramid $Sb(OBu^t)_4^-$ unit possesses a two fold axis of symmetry [Fig. 4(a)], the analogous $Bi(OBu^t)_4^-$ unit lacks it [Fig. 4(b)].

The crystal structure of $K_2Sb(OBu^t)_5 \cdot$ dioxane [10] obtained (eq. 4) on varying the K : Sb metal stoichiometry in eq. 3 reveals an infinite array of molecules linked through the oxygen atoms of dioxane molecules (Fig. 5). The repeating unit consists of an O_5 trigonal bipyramid, the equatorial edges of which

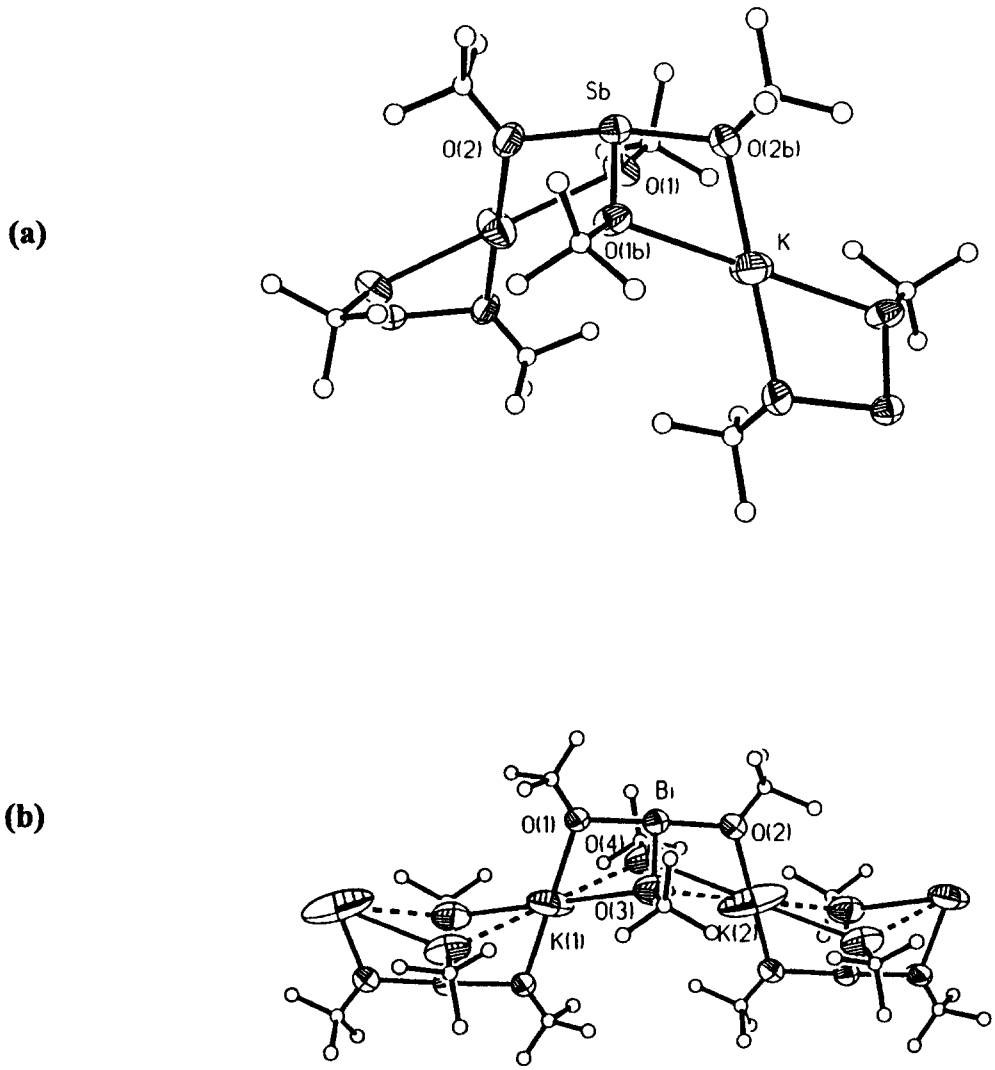

Fig. 4. A section of the one-dimensional structures of (a) $[KSb(OBu^t)_4]_n$ and (b) $[KBi(OBu^t)_4]_n$ [10].

are centred by two potassium and one antimony atom. Antimony(III) bonded to four oxygen atoms exhibits a *pseudo*-trigonal bipyramidal coordination while potassium atoms are trigonally bipyramidally coordinated.

Among the alkali metal titanium alkoxide derivatives $M\{Ti(OPr^i)_5\}$ (M = Li, Na, K), (eq. 5) described by Hampden-Smith *et al.* [11], the lithium derivative is found to be dimeric in the solid state. The X-ray structure of $[LiTi(OPr^i)_5]_2$ (Fig. 6) shows two approximately trigonal-bipyramidal titanium atoms joined by lithium bridges. If the terminal OPr^i ligands on titanium atoms are removed, the core structure parallels the metal–oxygen framework observed for $[LiSn(OBu^t)_3]_2$ (Fig. 1). All the derivatives undergo an alkoxide ligand exchange process that is rapid on the ^1H NMR time scale at ambient temperature. However, low-temperature (−20°C) NMR studies reveal two types of ligand environments for $[LiTi(OPr^i)_5]_2$ in intensity ratio 4 : 1 which is consistent with the empirical formula $[LiTi(OPr^i)_5]$ but not with the solid state structure which shows three different alkoxide environments. A limiting spectrum displaying the three unique isopropoxy environments could not be obtained even at −120°C.

The use of alkali metal NMR in examining the solution behaviour of $[MTi(OPr^i)_5]$ derivatives along with the X-ray structural characterization of Na and K substituted titanium isopropoxide derivatives is recently reported [12]. Both $[NaTi(OPr^i)_5]_n$ and $[KTi(OPr^i)_5]_n$ are polymeric species wherein the alkali metal acts as a bridge between discrete mononuclear trigonal-bipyramidal $Ti(OPr^i)_5^-$ units. The one-dimensional polymer $[NaTi(OPr^i)_5]_n$ is linear and exhibits alternating five coordinate titanium moieties and tetrahedrally surrounded sodium atoms. With respect to the coordination numbers of the metallic elements, the structure is comparable to that of

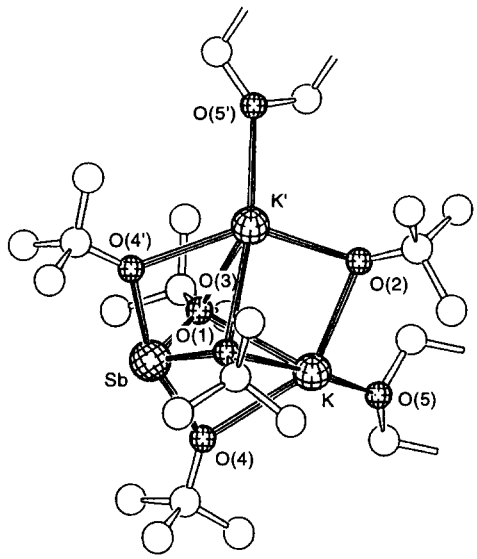

Fig. 5. A section of the dioxane-bridged structure of $[K_2Sb(OBu^t)_5 \cdot \text{dioxane}]$ [10].

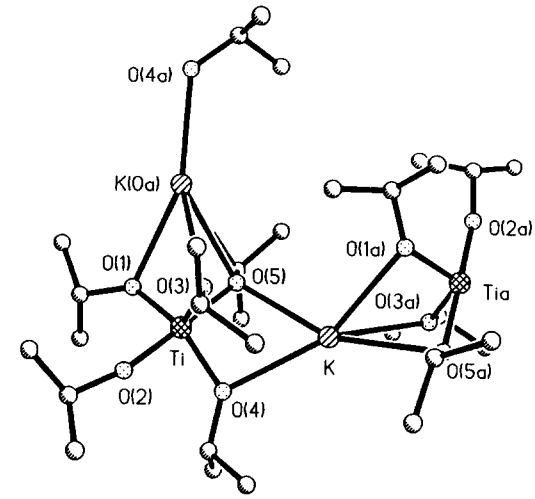

Fig. 7. A portion of the one-dimensional structure observed for $[KTi(OPr^i)_5]_n$ [13].

$[KSn(OBu^t)_5]_n$. In contrast to the sodium derivative, the potassium analog exhibits a penta-coordination for the K atoms. The non-linear continuous chain found in the solid state is a reminiscent of the structure observed for $[KSn(OBu^t)_3]_n$ with K atoms being present in a highly distorted trigonal-bipyramidal geometry. We have simultaneously solved the structure for potassium derivative (Fig. 7) [13].

The seco-norcubane core ($M_2M'_2O_6$) (**I**) is a recurrent structural feature among heterometallic alkoxides based on M:M' = 1:1 stoichiometry; a modification of this framework has been observed in the solid state structure of $[LiHf(OPr^i)_5]_2$ [14] (eq. 7) which displays a dimeric arrangement with two Hf^{IV} atoms present in a distorted octahedron of OPr^i ligands while the lithium atoms are three-fold coordinated and display a trigonal pyramidal geometry (Fig. 8). The central $Li_2Hf_2O_6$ unit in $[LiHf(OPr^i)_5]_2$ (Fig. 8) is an interesting variant of the metal–oxygen core observed in $[LiSn(OBu^t)_3]_2$ (Fig. 1) and $[LiTi(OPr^i)_5]_2$ (Fig. 6) with lithium occupying the position of tin (titanium) and hafnium that of lithium. Thus in

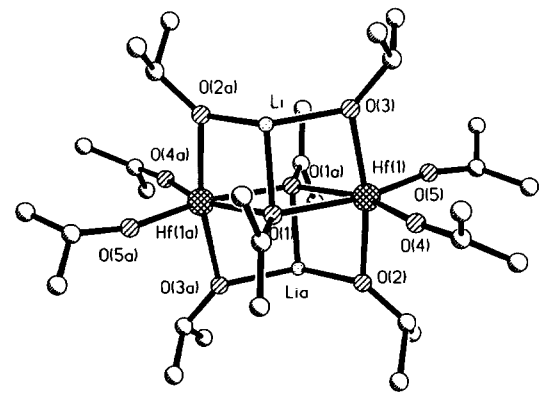

Fig. 8. Molecular structure of $[LiHf(OPr^i)_5]_2$. Unlabelled atoms are carbon [14].

contrast to the four coordinate lithium atoms in Sn^{II} and Ti^{IV} derivatives, the lithium centres in Hf^{IV} compound are three coordinate. Further, the hafnium derivative is stereochemically rigid and the spectral data indicate that the dimeric form persists in solution.

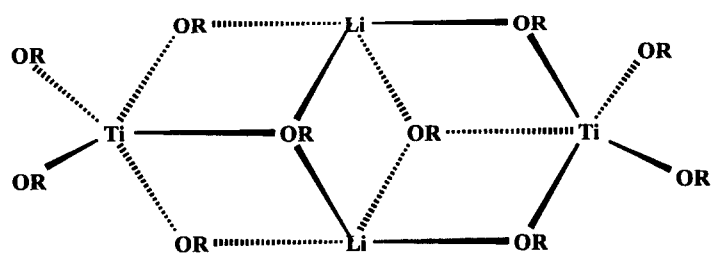

(R = Pr^i)

Fig. 6. Schematic representation of the molecular structure of $[LiTi(OPr^i)_5]_2$ [11].

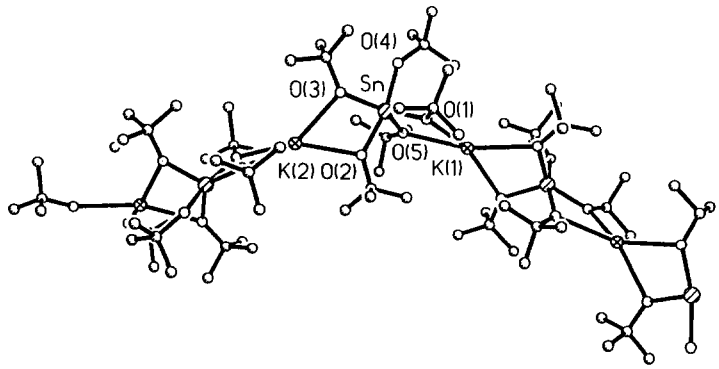

Fig. 9. A section of the crystal structure of $[KSn(OBu^t)_5 0.5C_7H_8]_n$ [15]. The toluene molecule is not shown.

The ligand geometries at heterometal centres in the above examples based on $M_2M'_2O_6$ core can be attributed to the tendency of the metallic element to achieve a preferred configuration or higher coordination numbers. Thus tin(II), devoid of any terminal ligands in $[M\{Sn(OBu^t)_3\}]_2$ (M = Li, Na) derivatives possesses a stereochemically active lone pair and the preferred pyramidal configuration whereas the tendency of larger tetravalent metals to be in a hexa-coordination is reflected in $[LiHf(OPr^i)_5]_2$ where a bond to lithium is sacrified to attain an octahedral ligand environment for Hf^{IV}.

The structural characterisation of $[KSn(OBu^t)_5]_n$ [15] (eq. 8) reveals that the compound crystallises with a half molecule of toluene per repeating unit. In the crystal, four- and five-fold coordinated potassium and tin(IV) atoms, respectively are interlinked via alkoxy bridges to give a one dimensional helical chain $(O_2SnO_2K)_n$ (Fig. 9). Alternatively, the polymer results from the trigonal bipyramids of *tert*-butoxy ligands built about Sn^{IV} which are interlinked by two structurally different potassium atoms.

In contrast to the polymeric structure observed for $[KSn(OBu^t)_5]_n$ (Fig. 9), the zirconium analogue [16] is dimeric in the solid state (Fig. 10). Both the metals (K and Zr) are five-coordinate, however, the disposition of two $Zr(OBu^t)_5^-$ unit is asymmetric with one Zr atom sharing four of its OBu'-groups in bridging the '$KZr(OBu^t)_5$' fragments while the other shares only three. This makes Zr^{IV} centres inequivalent (Fig. 10), however potassium centres are equalised by a mirror plane. The molecule is highly fluxional and even at −75°C, the ^1H NMR spectrum remains a singlet.

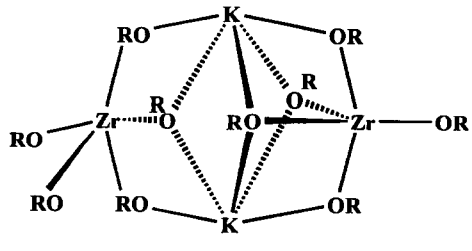

(R = Bu^t)

Fig. 10. Schematic representation of the molecular structure of $[KZr(OBu^t)_5]_2$ [16].

On the basis of solubility differences, two structurally and stoichiometrically different products $[Pb_2Zr_4(OPr^i)_{20}]$ and $[Pb_4Zr_2(OPr^i)_{16}]$ can be isolated from a 1:1 mixture of lead and zirconium isopropoxides (eq. 11) [19]. Both the products were also obtained by mixing lead amide and zirconium isopropoxide in 2:1 molar ratio, in the presence of isopropanol (eq. 30). The latter derivative could be obtained quantitatively on employing the correct stoichiometry of component alkoxides (eq. 12). A rigorous centrosymmetric structure is observed in $Pb_4Zr_2(OPr^i)_{16}$ where two $(Pr^iO)_3Zr(\mu_2\text{-}OPr^i)_3Pb$ are linked by a $Pb_2(OPr^i)_4$ unit (Fig. 11a). The solid state structure of $Pb_2Zr_4(OPr^i)_{20}$, with Pb : Zr ratio 1 : 2, can be derived from that of $Pb_4Zr_2(OPr^i)_{16}$ by replacing the $Pb(OPr^i)_2$ units with a $Zr(OPr^i)_4$ moiety on either side of the $Pb_2(OPr^i)_4$ core (Fig. 11b).

Formation of the alkali and alkaline earth metal alkoxometallates of compositions $M_2M'_3(OPr^i)_{14}$ and $M''M'_3(OPr^i)_{14}$ (M = Na, K; M' = Zr^{IV}, Hf^{IV}; M'' = Mg, Ca, Sr, Ba), respectively is reported and the proposed structures of these derivatives suggest a hexa-coordination for the tetravalent metals [7]. However, there is no report available on the existence of a $M_3(OPr^i)_{14}^{-2}$ substructure in the solid state, although a modification of $M_3(OR)_{14}^{-2}$ structural unit has been observed in the solid state structure of heterobimetallic acetato-*oxo*-alkoxide $PbZr_3O(OAc)_2(OPr^i)_{10}$ [1e]. In order to examine the formation of a dianionic sequestering unit $\{Ti_3(OPr^i)_{14}\}^{2-}$, a Ba–Ti mixed metal alkoxide was prepared by reacting $Ba(OPr^i)_2$ with $Ti(OPr^i)_4$ (eq. 13) [20] in 1:3 stoichiometry. The analytical and cryoscopic data of the crystalline product indicate the formation of a monomeric heterometal species with the anticipated Ba : Ti (1 : 3) stoichiometry and possibly the $Ti_3(OPr^i)_{14}^{2-}$ unit. The solid state structure, however, revealed a

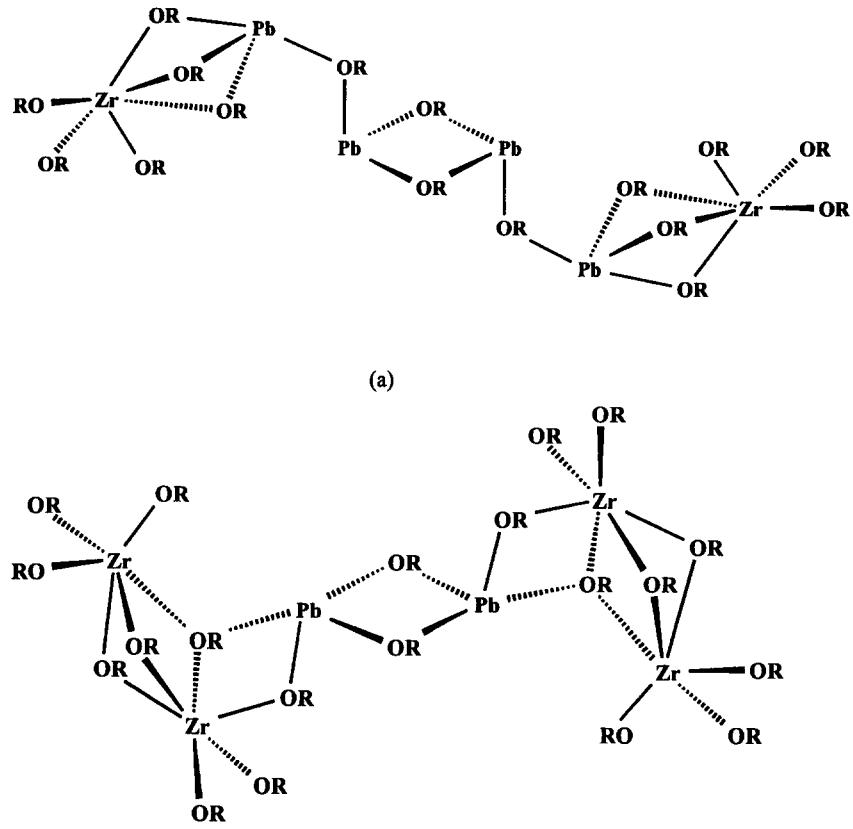

Fig. 11. Schematic representation of the molecular structures of (a) $[Pb_4Zr_2(OPr^i)_{16}]$ and (b) $[Pb_2Zr_4(OPr^i)_{20}]$ [19].

different geometry and arrangement of ligands but with the desired Ba : Ti metal ratio. The X-ray structure (Fig. 12) shows Ba^{2+} in a distorted trigonal prismatic geometry formed by the tetra- and bi-dentate interaction of monoanionic $\{Ti_2(OPr^i)_9\}^-$ and $\{Ti(OPr^i)_5\}^-$ units, respectively. The ^1H NMR spectrum at $-53^\circ C$ shows seven sets of methyl resonances

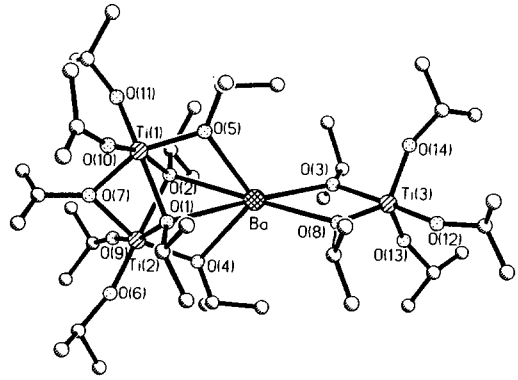

Fig. 12. The molecular structure of $[BaTi_3(OPr^i)_{14}]$ [20].

whose relative and total intensities are consistent with the retention of heterometal framework in solution. The above observations are corroborated by ^{13}C CP MAS NMR data.

Recently, the X-ray structure determination [21] of a previously reported hafnium-aluminium heterometal derivative, $Al_2Hf(OPr^i)_{10}$, (eq. 14) confirmed the proposed structure of Mehrotra *et al.* [38]. The molecule (Fig. 13) consists of an octahedrally coordinated Hf^{IV} atom bearing two bidentate $Al(OPr^i)_4^-$ sub-units and two terminal OPr^i ligands. The aluminium atoms are slightly distorted from a regular tetrahedral geometry.

The barium–niobium heterobimetallic isopropoxide obtained from the isopropanol solution of two alkoxides (Ba : Nb = 1 : 2, eq. 15) is shown by X-ray crystallographic study to have the composition $[Ba\{Nb(OPr^i)_6\}_2(Pr^iOH)_2]$ [22]. The molecule consists of a chain of three octahedra built around one barium(II) and two niobium(V) atoms. The central BaO_6 octahedron shares two neighbouring edges with the peripheral NbO_6 units to give a molecular framework shown in Fig. 14.

The lanthanum–niobium isopropoxide LaN-

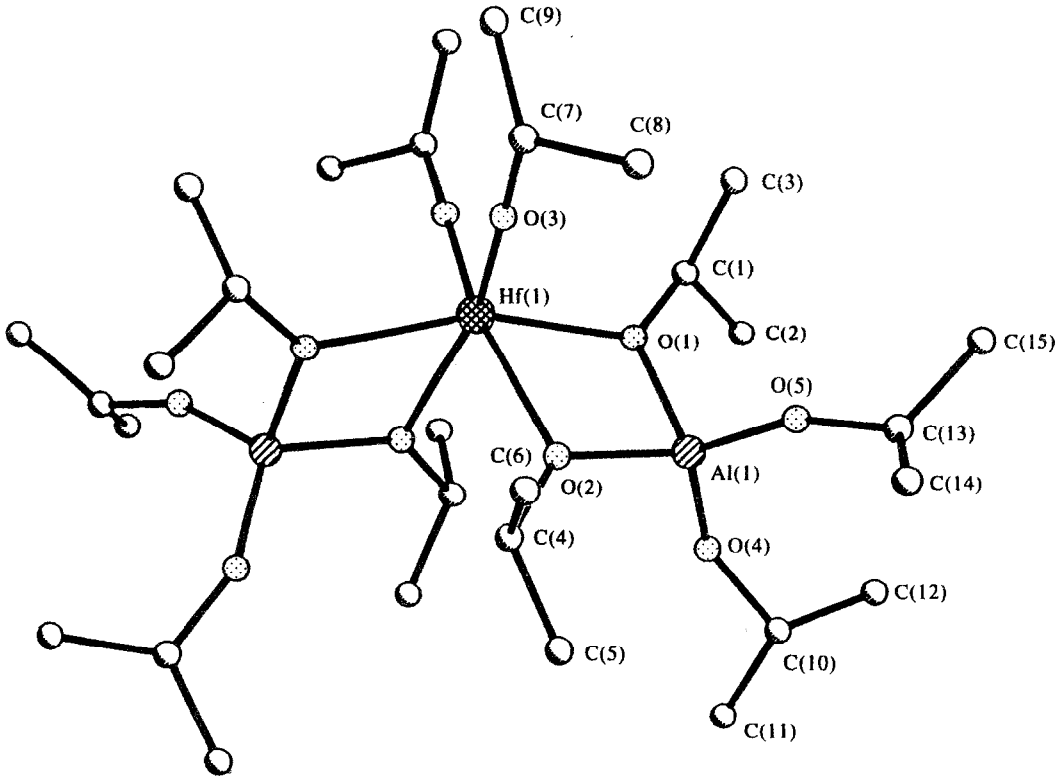

Fig. 13. A ball and stick representation of the molecular structure of $[Al_2Hf(OPr^i)_{10}]$ [21].

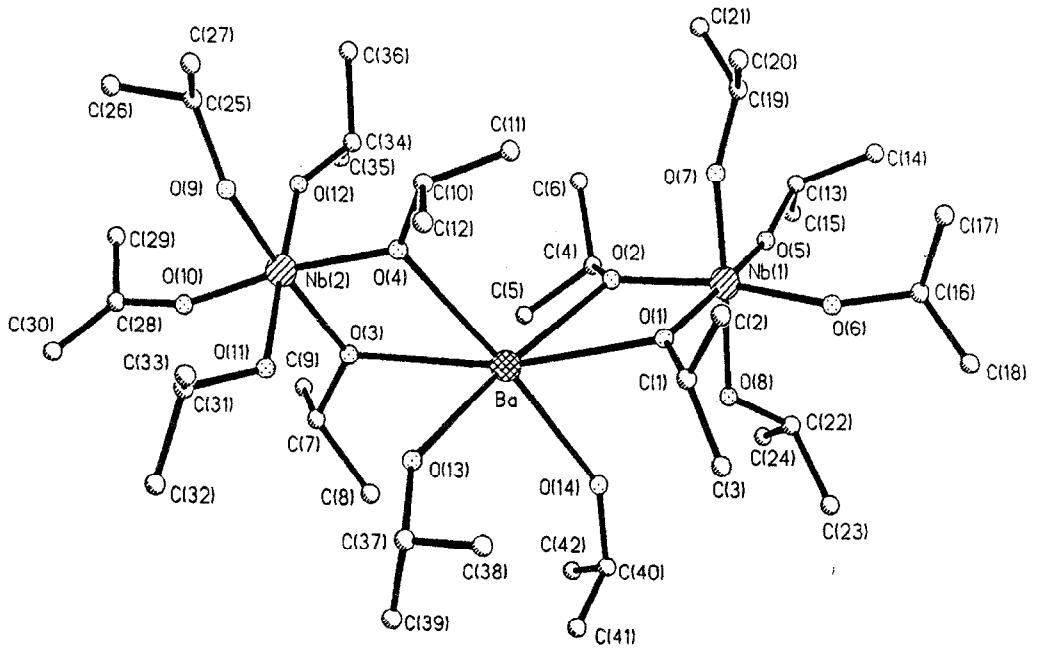

Fig. 14. Molecular structure of $[Ba\{Nb(OPr^i)_6\}_2(Pr^iOH)_2]$ [22].

$b_2(OPr^i)_{13}$ [22] crystallises from the solutions containing two alkoxides in La : Nb = 1 : (1–3) molar ratios. The molecule (Fig. 15) in the solid state reveals the central La atom in a strongly distorted octahedron of OPr^i ligands which shares a face with one NbO_6 octahedra and an edge with the other. The noteworthy

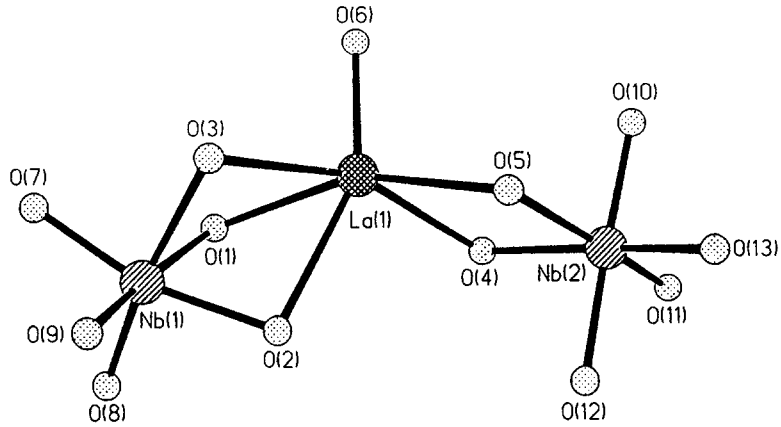

Fig. 15. Metal–oxygen core of $[(Pr^iO)La\{Nb(OPr^i)_6\}_2]$ [22].

structural feature is the ambidentate (bi- and tri-) ligating behaviour of $\{Nb(OPr)_6\}^-$ moiety.

Following the salt elimination principle, we have reported on the synthesis, structural characterization and reactivity of a variety of heterometal derivatives formed by the use of chelating $\{M(OBu^t)_3\}^-$ ($M = Ge^{II}$, Sn^{II}, Pb^{II}) anions toward main group and transition metals [5a,18]. Unlike the solid state structures observed for the alkali metal tris-(*tert*-butoxy) stannates (-germanates or -plumbates) (Fig. 1), the analogous derivatives of monovalent indium and thallium (eq. 16) are obtained as monomeric cage (**IV**) of the type $M(\mu\text{-}OBu^t)_3M'$ (M = Sn, Ge; M′ = In Tl; M = Pb, M′ = Tl) (Fig. 16). The $M'MO_3$ core represents a distorted trigonal bipyramid where the oxygen and metal atoms occupy the equatorial and apical positions, respectively. The cationic fragment $\{Sn(\mu\text{-}OBu^t)_3Pb\}^+$ with a structure similar to that of $MM'(OBu^t)_3$ (**I**) compounds has been observed as a component of the multimetallic compound $Pb_7Sn_6I_8(OBu^t)_{18}$ [25].

Depending upon the size of metal and the geometrical softness of the $\{M(OBu^t)_3\}^-$ ligands, two structural forms are observed for the transition metal derivatives; the smaller 3d cations form compounds of the general formula $(OR)M(\mu\text{-}OR)_2M'(\mu\text{-}OR)_2M'(\mu\text{-}OR)_2M(OR)$ (**V**) (M = Sn, Ge, Pb; M′ = Ni, Cr, Co, Mn) (eq. 17) with the main group and transition metal stoichiometry being 1 : 1. The metal–oxygen

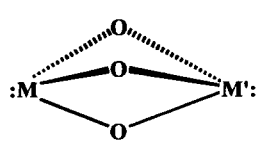

IV

Fig. 16. Schematic representation of the metal oxygen core of the $M'(OBu^t)_3M$ (M = Ge, Sn, Pb; M′ = In, Tl) compounds [39].

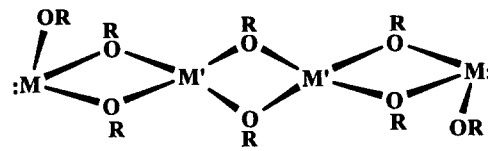

V

(R = Bu^t)

Fig. 17. Schematic representation of the solid-state structures observed for $[M'_2M_2(OBu^t)_8]$ (M = Ge, Sn, Pb; M′ = Mg, Ni, Cr, Co, Mn) derivatives [23].

skeleton (Fig. 17) of these derivatives exhibits a bidentate ligating mode of $\{M(OR)_3\}^-$ (M = Sn(II), Ge(II), Pb(II)) units in contrast to the tridentate behaviour observed in the structural types **I**–**IV**. The transition metal in the observed framework (**V**) occupies a four fold-coordination site which can be described as a spiro metallic centre in a distorted oxygen tetrahedron. The overall metal–oxygen skeleton (**V**) can be seen as three four-membered rings arranged in a perpendicular manner. The transition metals (M′) are quasi-tetrahedrally coordinated while the group 14 elements bearing a dangling alkoxo ligand are in a pyramidal 3-fold oxygen environment. On the other hand, if tris-(*tert*-butoxy)-germanate or -plumbate, is used against metal halides of Cr, Mn or Zn compounds with the general formula $M(\mu\text{-}OR)_3M'$ $(\mu\text{-}OR)_3M$ are obtained (eq. 18) which have a structure similar to alkaline earth derivatives (**III**) based on tridentate $\{M(OR)_3\}^-$ units. In all these derivatives (**I**–**V**), the terminal positions of main group elements present in the subvalent state (ns^2 configuration) function as potential Lewis basic sites which have been used to obtain transition metal derivatives (see sub-section 2.1.3) [34].

The X-ray diffraction analysis performed recently on an erbium–aluminium (Er : Al = 1 : 3) bimetallic isopropoxide (eq. 19) reveals a molecular formula

$ErAl_3(OPr^i)_{12}$ [24] analogous to that proposed for $LnAl_3(OPr^i)_{12}$ [7] compounds (Ln = lanthanide atom). In the light of structure determination (Fig. 18), the molecular formula can be precisely expressed as $Er\{(\mu_2\text{-}OPr^i)_2Al(OPr^i)_2\}_3$ where each of the three tetrakis-isopropoxy aluminate ligands coordinate the central atom Er^{III} *via* two OPr^i groups. The structural framework of $Er\{Al(OPr^i)_4\}_3$ differs from the related compound $Al\{Al(OPr^i)_4\}_3$ [39,40] in the coordination figures of hexa-coordinate central atoms. In case of aluminium isopropoxide, the central Al^{III} has almost an ideal octahedral geometry, whereas, the erbium complex displays a distorted trigonal prismatic coordination for Er^{III} which is in accordance with the tendency of lanthanide elements to prefer a prismatic geometry (over octahedral).

It has been reported that the complex formation of $Al(OPr^i)_3$ with $[Ni(OPr^i)_2]_n$ do not give the previously reported $[Ni\{Al(OPr^i)_4\}_2]$ and only the mixture of two corresponding alkoxides results [41]. However, we have been able to synthesise and structurally characterise the analogous *tert*-butoxide derivative. The sublimable nature of $[Ni\{Al(OBu^t)_4\}_2]$ speaks for the stability of such derivatives. The compound i shown by the X-ray crystallographic study [13] is monomeric in the solid state and the structure (Fig. 19) [27] is similar to that proposed by Mehrotra *et al.* for $M\{Al(OR)_4\}_2$ derivatives [5c,d] (eq. 20). The molecular architecture can be viewed as bidentate interactions of two tetrahedral $Al(OBu^t)_4^-$ moieties to the Ni^{2+} centre. The two '$NiAl(OBu^t)_2$' four-membered rings fused at a common end (Ni^{II}) are perpendicular to each other. Both Ni^{II} and Al^{III} are quasi-tetrahedrally coordinated by the *tert*-butoxy ligands, the distortion being more significant in the case of nickel.

The heterobimetallic compound $[Mg\{Al(OBu^t)_4\}_2]$ [25] with Mg:Al stoichiometry appropriate for $MgAl_2O_4$ spinel is obtained from the reaction of

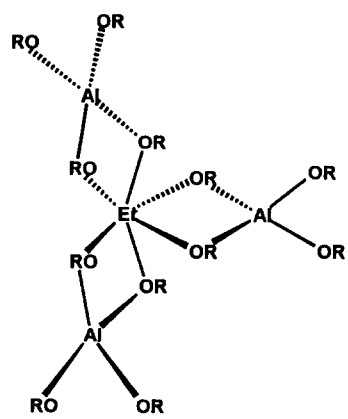

(R = Pr^i)

Fig. 18. Schematic representation of the molecular framework of $Er\{Al(OPr^i)_4\}_3$ [24].

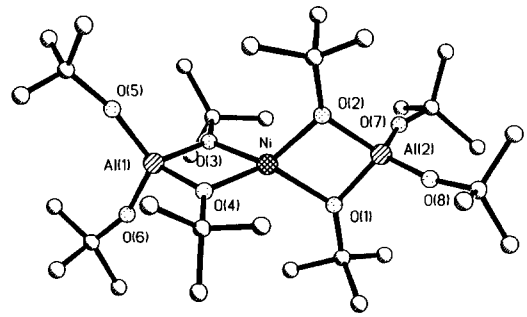

Fig. 19. Ball and stick drawing of the molecular structure of $[Ni\{Al(OBu^t)_4\}_2]$ [13].

$MgCl_2$ with $NaAl(OBu^t)_4$ in 1 : 2 molar ratio. The X-ray diffraction study shows a spirocyclic core made up of two planar AlO_2Mg four-membered rings joined at magnesium (Fig. 20). With two terminal ligands present on each of the aluminium atoms, all the metallic elements are present in a four-fold coordination of oxygen atoms. The angular distortions, due to the formation of four-membered $Al(\mu\text{-}OBu^t)_2Mg$ rings, are reflected in the distorted tetrahedral geometries of Mg^{II} and Al^{III} centres.

The isopropoxide analogue of $[Mg\{Al(OBu^t)_4\}_2]$ derivative is synthesised by the reaction of the two metals in isopropanol (eq. 27). The compound crystallises as $[(Pr^iOH)_2Mg\{Al(OPr^i)_4\}_2]$ [27] and the solid state structure (Fig. 21) exhibits two $\{Al(OPr^i)_4\}^-$

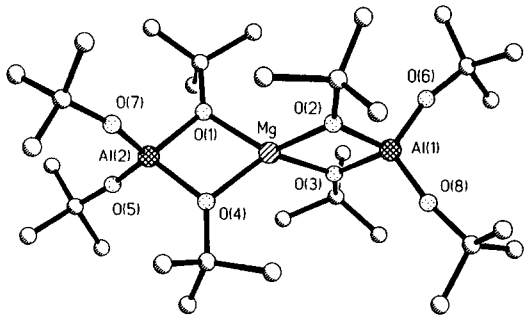

Fig. 20. Molecular structure of $[Mg\{Al(OBu^t)_4\}_2]$ [25].

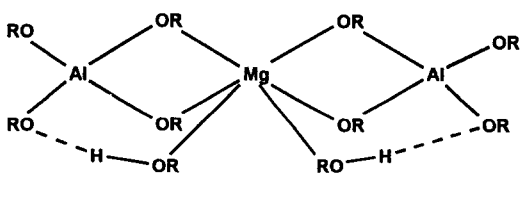

(R = Pr^i)

Fig. 21. Schematic representation of the molecular structure observed for $[(Pr^iOH)_2Mg\{Al(OPr^i)_4\}_2]$ [27].

units coordinating the central atom Mg^{II} in a bidentate fashion. The coordination sphere of magnesium is completed by two adduct alcohol molecules which show Al(R)—O···H(OR)M interactions with one of the terminal OPr^i-groups of each $\{Al(OPr^i)_4\}^-$ moiety.

The effect of the ramification of alkyl group on the coordination numbers of the metals present in the heterometallic alkoxides is nicely illustrated in the derivatives $[Mg\{Al(OBu^t)_4\}_2]$ and $[Mg\{Al(OPr^i)_4\}_2 \cdot (Pr^iOH)_2]$. Whereas the central atom Mg^{II} is tetra-coordinate in the *tert*-butoxide derivative, it achieves a hexa-coordination by two coordinating alcohol molecules in the latter case. Although both the heterometal precursors have a Mg : Al ratio suitable for $MgAl_2O_4$ ceramic, the 'base free' *tert*-butoxide compound appears to be a better choice as the presence of stabilising ligands in the latter case can lead to a higher percentage of carbonaceous impurities in the resulting mixed-metal oxide.

The $M'\{M_2(OR)_9\}_2$ (M′ = Ba, Ca; M = Ti, Zr) derivatives [20,42,43] (eqs 28 and 29) contain a central eight coordinated metal atom bound to two face-sharing biooctahedral $M_2(OR)_9^-$ units. Although the X-ray data in the case of Ba–Zr mixed-metal compound, could not be refined satisfactorily, the molecule is proposed to have a similar spiro $M_2M'M_2$ arrangement. A similar structure has been proposed for the derivative $[Ba\{Ti_2(OPr^i)_9\}_2]$ (Fig. 22) [20].

A Cu^I–Zr^{IV} mixed-metal species is obtained by the reaction of copper(I) mesityl and zirconium isopropoxide isopropanolate (eq. 31) [30]. The X-ray diffraction study shows the molecule, $Cu_2Zr_2(OPr^i)_{10}$, to result from a union of confacial bioctahedral $Zr_2(OPr^i)_9^-$ substructure and a bent $(Cu_2(OR))^+$ unit bound together by the two bridging OPr^i groups of $Zr_2(OPr^i)_9$ fragment. The eight membered metal-oxygen ring (Fig. 23) is essentially planar.

The yttrium–barium (1 : 2) heterobimetallic $YBa_2(OBu^t)_7(Bu^tOH)$ [32] obtained by the alcoholysis of a mixture of yttrium and barium amides (eq. 33) displays a triangular structure (Fig. 24) commonly adopted by $M'M_2$ heterometallic alkoxides. All metals are five-coordinate, with the terminal ligand on one of the barium atoms being an alcohol molecule. The crystal structure comprises chains of YBa_2 triangles held together by hydrogen bonds between adduct alcohol molecule of one YBa_2 unit to a terminal alkoxo group of another unit.

The sodium–thorium heterometallic alkoxide $NaTh_2(OBu^t)_9$, described by Clark *et al.*, involves the deprotonation of the coordinated alcohol in $Th_2(OBu^t)_8(Bu^tOH)$ with $NaN(SiMe_3)_2$ [44]. The crystal structure (Fig. 25) shows discrete $NaTh_2(OBu^t)_9$ molecules. There is no terminal ligand attached on the alkali atom, however, no intermolecular interactions between the sodium atom of one molecule and oxygen atoms of adjacent molecules are observed. A similar structure is observed for the related derivatives $KU_2(OBu^t)_9$ and $NaCe_2(OBu^t)_9$, reported by Cotton *et al.* [45] and Evans *et al.* [33], respectively.

Heterometal alkoxides of Ce^{IV} have been obtained, using ceric ammonium nitrate and sodium *tert*-butoxide as starting materials (eqs 34 and 35). The derivatives $(DME)_2Na_2Ce(OBu^t)_6$ [33] and $NaCe_2(OBu^t)_9$ [33] characterised by single crystal X-ray diffraction technique reveal molecular frameworks based on

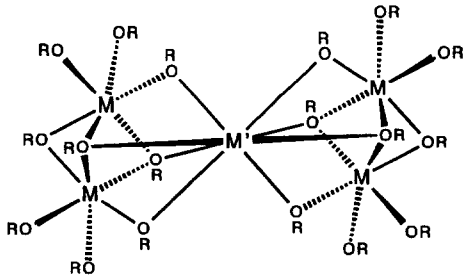

(R = Et, Pr^i)

Fig. 22. Schematic representation of the structure of $[M'\{M_2(OR)_9\}_2]$ (M′ = Ba, M = Ti, Zr; M′ = Ca, M = Ti) derivatives [20,42,43].

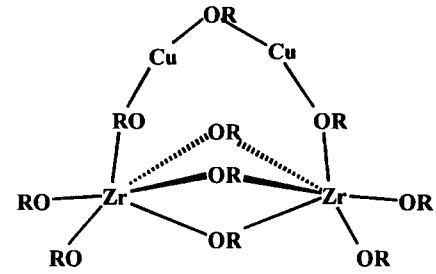

(R = Pr^i)

Fig. 23. Schematic representation of the molecular structure of $Cu_2Zr_2(OPr^i)_{10}$ [30].

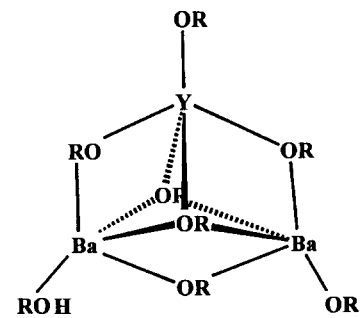

(R = Bu^t)

Fig. 24. Schematic representation of the molecular structure of $YBa_2(OBu^t)_7(Bu^tOH)$ [32].

(R = Et, Pr^i)

Fig. 22. Schematic representation of the structure of $[M'\{M_2(OR)_9\}_2]$ (M′ = Ba, M = Ti, Zr; M′ = Ca, M = Ti) derivatives [20,42,43].

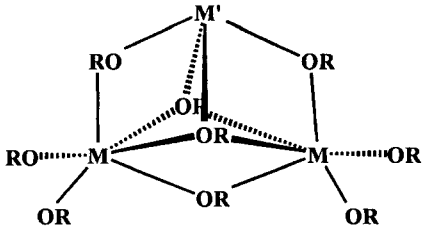

(R = Bu^t)

Fig. 25. Schematic representation of the molecular structure observed for M'$\{M_2(OBu^t)_9\}$ (M' = Na, M = Th^{IV}, Ce^{IV}; M' = K, M = U^{IV}) derivatives [33,44,45].

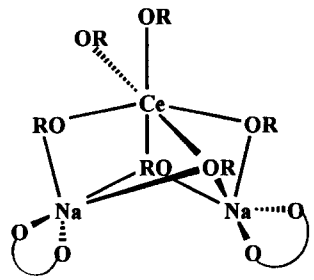

(R = Bu^t)

Fig. 26. Schematic representation of the molecular structure of $[(DME)_2Na_2Ce(OBu^t)_6]$ [3].

Na_2Ce and $NaCe_2$ triangles, respectively (Figs 25 and 26). Whereas cerium is hexa-coordinate in both the derivatives, the sodium atoms display penta- and tetra-coordination, respectively.

2.1.3 *Reactions*

Heterobimetallic alkoxides with subvalent main group metals (ns^2 configuration) situated at the apices of one or two (fused) trigonal bipyramids act as excellent electron donors to various transition metal carbonyls. This synthetic strategy has allowed the construction of a large number of derivatives with one-dimensional arrays of metallic elements held together by direct metal–metal and M—O(R)—M bonds [34]. The difference in the reactivity of the ns^2 elements follow the sequence $In^I \gg Ge^{II} > Sn^{II} > Tl^I, Pb^{II}$. The efforts made to attach transition metal carbonyl at Tl^I or Pb^{II} ends were not successful. For a particular ns^2 element, the reactivity follow the order: $Ni(CO)_4 > Fe_2(CO)_9 > Mo(CO)_6 > Cr(CO)_6 > W(CO)_6$. A number of metal carbonyl complexes of mixed-metal alkoxides have been characterised in the solid state. Some representative frameworks of the heterometal assemblies containing three or four different metals are shown in Fig. 27.

The pronounced tendency of metal atoms to increase their coordination numbers makes the heterobimetallic alkoxides labile species and neutral metal alkoxide molecules can be added as building blocks, to modify the coordination figure of the central metal atom or to change the nuclearity of the complex [5,7]. Three soluble barium–titanium containing heterobimetallic isopropoxides with manipulable Ba : Ti stoichiometries and nuclearity have been obtained by using $Ti(OPr^i)_4$ as a building block towards polymeric $[Ba(OPr^i)_2]_n$ [20]. The dimeric compound $[BaTi_2(OPr^i)_{10}]_2$ with Ba : Ti ratio 1 : 2, reacts with one equivalent of $Ti(OPr^i)_4$ to afford mononuclear species $BaTi_3(OPr^i)_{14}$ which can be converted into $BaTi_4(OPr^i)_{18}$ by an additional mole of $Ti(OPr^i)_4$ (eq. 36).

$$1/2[BaTi_2(OPr^i)_{10}]_2 \xrightarrow{Ti(OPr^i)_4} BaTi_3(OPr^i)_{14} \xrightarrow{Ti(OPr^i)_4} BaTi_4(OPr^i)_{18} \quad (36)$$

A similar interconversion has been reported for Pb–Zr mixed-metal alkoxides where the lead-rich derivative $[Pb_4Zr_2(OPr^i)_{16}]$ can be converted into the zirconium-rich analogue $[Pb_2Zr_4(OPr^i)_{20}]$ by reacting it with an appropriate amount of zirconium alkoxide and *vice-versa* (eqs 37 and 38) [19].

$$Pb_4Zr_2(OPr^i)_{16} + 6Zr(OPr^i)_4 \rightarrow 2Pb_2Zr_4(OPr^i)_{20} \quad (37)$$

$$Pb_2Zr_4(OPr^i)_{20} + 6/n[Pb(OPr^i)_2]_n \rightarrow 2Pb_4Zr_2(OPr^i)_{16} \quad (38)$$

Discrete heterometallic alkoxy derivatives have a defined stoichiometry at the molecular level and are thus attractive precursors in sol–gel processing of mixed-metal oxides. Although extensive studies have been made to understand the initial stages of hydrolysis and the mechanisms of conversion of homo-metallic alkoxides to metal oxides, the key studies using heterometallic precursors are missing, however, a few scattered reports available show interesting structural and nuclearity changes. The controlled hydrolysis reaction (eq. 39) of $[LiTi(OPr^i)_5]_2$ proceeds with the retention of metal stoichiometry, however the degree of aggregation grows and the resulting molecule $[LiTiO(OPr^i)_3]_4$ [46] is tetrameric, possibly due to the greater bridging ability of an oxo (O^{2-}) ligand in comparison to the alkoxide group.

$$2[LiTi(OPr^i)_5]_2 + 4H_2O \rightarrow [LiTiO(OPr^i)_3]_4 + 8Pr^iOH \quad (39)$$

However, the controlled hydrolysis of $Ba\{Zr_2(OPr^i)_9\}_2$ shows no change in the metal ratios or segregation of the molecule and $BaZr_4(OPr^i)_{17}(OH)$ [46] is obtained with a structure similar to that of parent compound (Fig. 22).

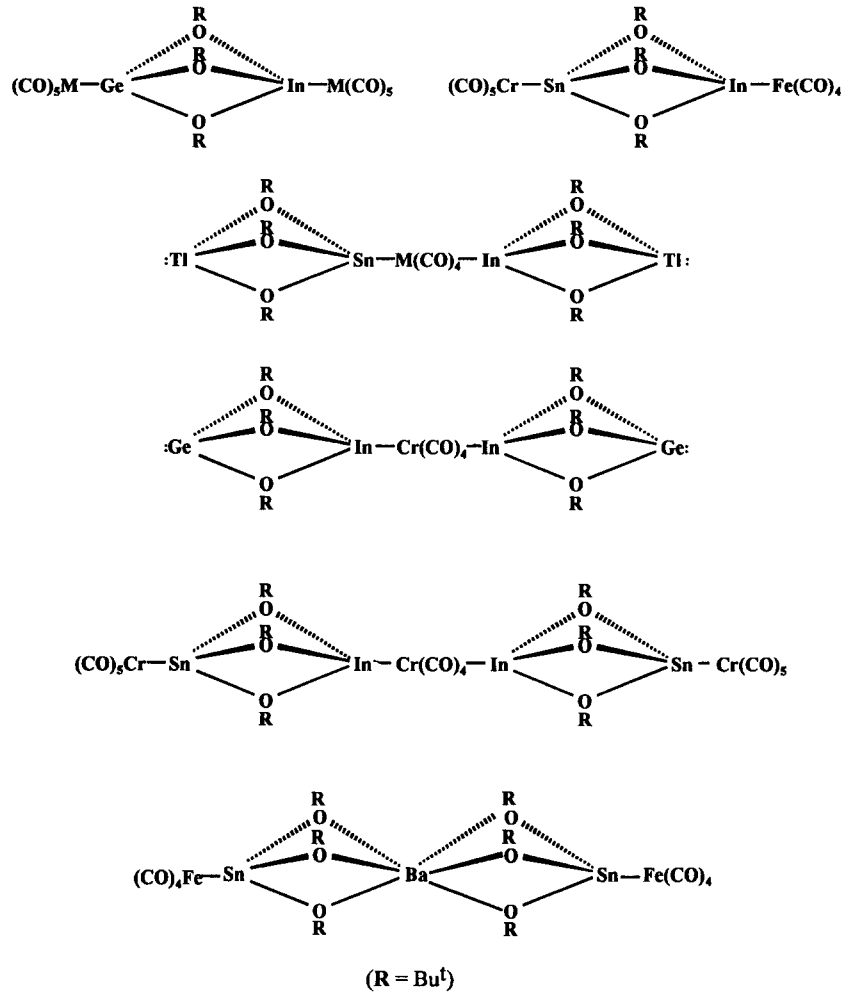

Fig. 27. Schematic representation of the frameworks observed in the transition metal derivatives of some mixed-metal alkoxides [34].

2.2 *Heteroleptic heterobimetallic alkoxides*

In contrast to the large number of reports available on the structural characterization of homoleptic heterometal alkoxides, the structurally characterized examples of halide heterometallic alkoxides are scarce. Prior to our investigations, the well-characterised chloride heterobimetallic alkoxides were limited to $[ClMg\{Ti_2(OEt)_8Cl\}]_2$ [47], $[ClM\{Zr_2(OPr^i)_9\}]_2$ (M = Cd [48], Cu [30]) and $[ClPr\{Al(OPr^i)_4\}_2(Pr^iOH)]_2$ [35]. Although a large number of chloro alkoxometallates are reported, the absence of single crystal X-ray diffraction studies together with *oxo* forming and salt retaining [49] tendency of heterometal alkoxide derivatives has made their formulation and identity ambiguous. In our continuing investigations on halo-functionalised heterometallic alkoxides, we have found that these 'intermediates' are generally soluble and stable compounds (most of them sublime/distill *in vacuo* without any extensive decomposition) and show enormous potential as attractive synthons for incorporating other ligands (OR^-, $OSiMe_3^-$, $OSiPh_3^-$, $C_5H_5^-$) in the heterometal assembly. It is worth noting that use of halide heterobimetallic alkoxides towards cyclopentadienyl reagents has furnished the first examples of an elusive class of cyclopentadienyl containing heterobimetallic alkoxides [50,51]. More interestingly, the metathesis of metal–halogen bonds using suitable alkalimetal alkoxometallates has offered novel molecular alkoxide assemblies containing three different metals (see Section 3) [6,14]. Although the class of heteroleptic alkoxides would, in principle, include the heterometal alkoxide derivatives based on other hetero-ligands such as hydride, oxide, β-diketonates, carboxylates, siloxides, aryloxides, etc., the present article is limited to heterobimetallic derivatives containing halide and cyclopentadienyl as ancillary ligands.

2.2.1 *Synthesis*

(*i*) *Salt elimination reactions.* In view of our interest in the halo-alkoxometallates as interesting synthons (see Section 3) and dearth of information about their structural features, we have investigated the solution and solid state characterization of a number of halide heterobimetallic derivatives illustrated in eqns 40–46 [6,13,14,51,52]

$$MX_2 + KM'_2(OPr^i)_9 \rightarrow XM\{M'_2(OPr^i)_9\} + KX \quad (40)$$

$M = Cd$; $X = I$; $M' = Sn^{IV}, Ti^{IV}, Zr^{IV}, Hf^{IV}$

$M = Fe, Cu$; $X = Cl$; $M' = Ti^{IV}, Hf^{IV}$

$$MX_2 + KM'_2(OPr^i)_9 \rightarrow \tfrac{1}{2}[XM\{M'_2(OPr^i)_9\}]_2 + KX \quad (41)$$

$M = Sn$; $X = Cl$; $M' = Zr, Hf$

$M = Pb$; $X = I$; $M' = Ti, Zr$

$$BaI_2 + KM_2(OPr^i)_9 \rightarrow \tfrac{1}{2}[IBa\{M_2(OPr^i)_9\}]_2 + KI \quad (42)$$

$M = Sn, Ti, Zr, Hf$

$$CdI_2 + KTa(OPr^i)_6 \xrightarrow{2Pr^iOH} [ICd\{Ta(OPr^i)_6\}(Pr^iOH)_2] + KI \quad (43)$$

$$2CdI_2 + 2KOPr^i + Nb(OPr^i)_5 \xrightarrow{C_7H_8} \tfrac{1}{2}[I_2Cd_2Nb(OPr^i)_7]_2 + 2KI \quad (44)$$

$$2MCl_3 + 2KM'_2(OPr^i)_9 \rightarrow 2/n[Cl_2M\{M'_2(OPr^i)_9\}]_n + 2KCl \quad (45)$$

$M = Bi$; $M' = Ti, Zr, Hf$; $n = 2$

$M = In, Y$; $M' = Ti, Zr, Hf$; $n = 1$

$$SnI_4 + nKTi(OPr^i)_5 \rightarrow [I_{4-n}Sn\{Ti(OPr^i)_5\}_n] + nKI \quad (46)$$

$n = 1$–3

The first examples of cyclopentadienyl containing heterobimetallic alkoxides have been synthesised by treating various alkali metal alkoxometallates with cyclopentadienyl tin(II) chloride (eqs 47 and 48). Alternatively, these heteroleptic derivatives become accessible on reacting well-characterised halide–heterobimetallic alkoxides with sodium cyclopentadienide [50,51]

$$(C_5H_5)SnCl + KM(OBu^t)_3 \rightarrow (C_5H_5)Sn(\mu\text{-}OBu^t)_2M(OBu^t) + KCl \quad (47)$$

$M = Sn, Ge$

$$(C_5H_5)SnCl + KM_2(OPr^i)_9 \rightarrow (C_5H_5)Sn\{M_2(OPr^i)_9\} + KCl \quad (48)$$

$M = Zr, Hf$

(*ii*) *Miscellaneous methods.* The Lewis acid–base interaction of a metal halide and alkoxide (eqs 49 and 50) provides an alternative to the salt elimination reaction for the synthesis of halo functionalised heteremetal alkoxides [47,53]

$$MgCl_2 + 2Ti(OEt)_4 \rightarrow \tfrac{1}{2}[ClMg\{Ti_2(OEt)_8Cl\}]_2 \quad (49)$$

$$BiCl_3 + OV(OPr^i)_3 \xrightarrow{3HOC_2H_4OCH_3} \tfrac{1}{2}[BiCl_3OV(OC_2H_4OCH_3)_3]_2 + 3Pr^iOH \quad (50)$$

2.2.2 *Structural and spectral features*

In the course of our ongoing investigations, we have synthesised and characterised a large number of heteroleptic heterometal alkoxides based on chelating alkoxometallate units of the type $\{M(OR)_3\}^-$ (M = Ge, Sn, Pb), $\{M(OR)_4\}^-$ (M = Al, Ga, Sb, Bi), $\{M(OR)_5\}^-$ (M = Sn, Ti, Zr, Hf), $\{M(OR)_6\}^-$ (M = Nb, Ta) and $\{Ma_2(OR)_9\}^-$ (M = Sn, Ti, Zr, Hf). The structurally characterised examples of various heteroleptic heterobimetallic alkoxides are assembled in Table 2.

Salient features of the structurally characterised compounds based on face-sharing bioctahedral $\{M_2(OR)_9\}^-$ sub-structure are (i) the gradation of the metal–oxygen bond lengths within the $M_2(OPr^i)_9^-$ unit [M—O (terminal) < M—(μ_2-OM) (doubly bridging, μ_2-) < M-(μ_3-OM) (triply bridging, μ_3-)] which corroborates the loss of electron density at the oxygen with each successive bridge and (ii) the greater opening of the terminal M—O—C bond angles which is presumably a consequence of metal–oxygen multiple bond order and steric factors. The most commonly observed mode of ligation for $M_2(OPr^i)_9^-$ type sequestering anions is the use of four alkoxy oxygen atoms (two terminal and two bridging) to form a pocket to accommodate the cationic fragment. The size of the pocket depends on the size of the M^{IV} cation and M ··· M vector and its compatibility to the size of heterometal partner decides the stability of the resulting complex. The chemistry of confacial bioctahedral $M_2(OR)_9^-$ units is dominated by the use of zirconium and the formation of analogous bioctahedral substructure by tetravalent tin, titanium and hafnium was not investigated before. The solid state structures of $ICdSn_2(OPr^i)_9$ [52], $ICdTi_2(OPr^i)_9$ [6] and $ICdHf_2(OPr^i)_9$ [6] derivatives reported by us, provide the first structural evidence for the existence of a $M_2(OPr^i)_9^-$ unit, based on Sn^{IV}, Ti^{IV} and Hf^{IV}. Owing to the facts, such as (i) the monomeric and non-adduct forming behaviour of $Ti(OPr^i)_4$ [7] (cf. isopropoxides

Table 2. The thermodynamically accessible metal stoichoimetries found in the crystallographically characterised heteroleptic heterobimetallic alkoxo clusters

Clusters	Coordination number				Examples
	M	M′	μ_2-OR[a]	μ_3-OR[b]	
$[MM'X_n]$	3	3	2	—	$[CpSnGe(OBu^t)_3]$ [51][c] $[CpPbSn(OBu^t)_3]$ [50][c]
	5	6	2	—	$[ICd\{Ta(OPr^i)_6\}(Pr^iOH)_2]$ [13]
$[MM'_2X_n]$	4	4	4	—	$[(C_5HMe_4)_4Ti_2(OMe)_4Mg]$ [65][c]
	5	6	3	2	$[ClCu\{M'_2(OPr^i)_9\}]$ (M′ = Ti [20], Zr [30], Hf [14]), $[ICd\{M'_2(OPr^i)_9\}]$ (M′ = Sn, Ti, Zr, Hf) [6,52], $[ClFe\{M'_2(OPr^i)_9\}]$ (M = Ti, Hf) [13]
	6	6	3	2	$[Cl_2Y\{M'_2(OPr^i)_9\}]$ (M = Ti [20], Zr [13], $[(Pr^iO)ClY\{Ti_2(OPr^i)_9\}]$ [13]
	6	5	4	—	$[I_2Sn\{Ti(OPr^i)_5\}_2]$ [13]
	3	6	3	2	$[CpSn\{Zr_2(OPr^i)_9\}]$ [50][c]
$[MM'_2X_n]_2$	7	4	8	—	$[ClPrAl_2(OPr^i)_8(Pr^iOH)]_2$ [35]
	6	6	6	4	$[ClMg\{Ti_2(OEt)_8Cl\}]_2$ [47]
	6	6	6	4	$[IBa\{M'_2(OPr^i)_9\}]_2$ (M′ = Sn, Ti, Zr, Hf) [13]
	6	6	6	4	$[ClCd\{Zr_2(OPr^i)_9\}]_2$ [48]
	4	6	6	2	$[ClSn\{M'_2(OPr^i)_9\}]_2$ (M′ = Zr, Hf) [50]
	5	6	4	4	$[ISn\{M'_2(OPr^i)_9\}]_2$ (M′ = Zr, Hf) [13,52]
	6	6	4	4	$[Cl_2Bi\{Zr_2(OPr^i)_9\}]_2$ [13]
$[M_4M'_2X_n]$	4	6	4	—	$[I_2Cd_2Nb(OPr^i)_7]_2$ [13]
$[MM'_8X_n]$	5	4	—	8	$[LnNa_8(OBu^t)_{10}Cl]$ [60]

[a] μ_2-OR = doubly bridging alkoxo ligands.
[b] μ_3-OR = triply bridging alkoxo ligands.
[c] The contribution of cyclopentadienyl ligand in the ligand count is being considered to be unity.

of tetravalent Sn, Zr and Hf are dimeric alcoholates $[M(OPr^i)_4 \cdot Pr^iOH]_2$) (ii) the known heterometal compounds where the use of homometallic Ti and Zr alkoxides as building blocks results in the formation of products with different metal ratios as well as different structural features and (iii) the 'belief' that smaller Ti^{4+} cation cannot achieve hexa-coordination due to the steric bulk of OPr^i ligands [19b] which results from the paucity of structurally characterised six-coordinate titanium isopropoxide derivatives, the use of alkali metal alkoxo-titanates in the formation of heterometal derivatives remain unexplored. In view of above and the importance of titanium containing ceramics [54] we have synthesised a number of mixed-metal derivatives based on mono-anionic $\{Ti_2(OPr^i)_9\}^-$ and $\{Ti(OPr^i)_5\}^-$ units (Tables 1 and 2).

The iodide cadmium nonaisopropoxo-distannate (-dititanate, -dizirconate and -dihafnate) derivatives [6,52] (eq. 40) are isostructural and the molecule can be viewed as a tetra-dentate interaction of the anionic con-facial bioctahedral $\{M_2(OPr^i)_9\}^-$ (M = Sn, Ti, Zr, Hf) unit to a cationic CdI^+ fragment. The coordination polyhedron of cadmium bearing iodide as a terminal ligand resembles a distorted trigonal bipyramid whereas each tetravalent metal centre (Sn, Ti, Zr, Hf) is hexa-coordinate and displays a distorted octahedral geometry.

In the case of $ICd\{Ti_2(OPr^i)_9\}$ derivative (Fig. 28), the Cd-(μ_2-OTi) distances are found to be longer than Cd-(μ_3-OTi) distances. The relatively small size of titanium atom results in shorter Ti—OPr^i terminal distances which consequently show longer Cd—μ_2-OTi contacts. The pocket formed by short μ_3- and long μ_2-contacts is not suitable for binding Cd^{2+} strongly and the poor fit of Cd^{2+} in the 'arms' of

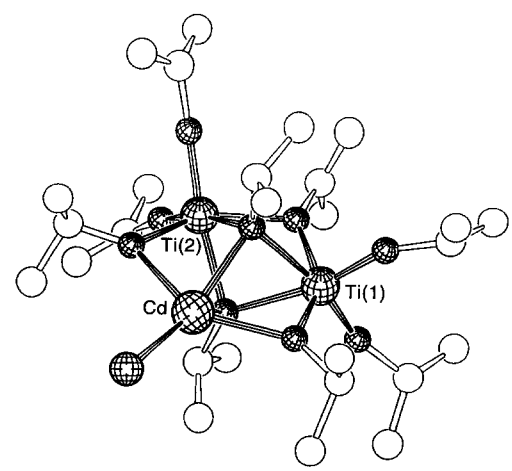

Fig. 28. Molecular structure of $ICd\{Ti_2(OPr^i)_9\}$ [6b].

$Ti_2(OPr^i)_9^-$ unit is evident in the thermal lability of $ICd\{Ti_2(OPr^i)_9\}$, whereas the $ICd\{M_2(OPr^i)_9\}$ derivatives based on larger Zr^{IV} and Hf^{IV} atom sublime almost quantitatively, when heated *in vacuo* [6b]. The cryoscopic and multinuclear spectroscopic data indicate the $ICd\{M_2(OPr^i)_9\}$ derivatives to be monomeric in solution which is corroborated by the solid state CP MAS ^{113}Cd NMR studies. The ^1H NMR spectra of these derivatives suggest a C_{2v} molecular symmetry in the solution as displayed in a characteristic set of four signals in the intensity ratio 4:2:2:1. Further, the similar ^{113}Cd chemical shifts in solution and solid state indicate that the binding mode of $M_2(OPr^i)_9^-$ unit to cadmium is retained in both the states. The mononuclear nature of the iodo-heterobimetallic derivatives in the vapour phase can be inferred in a representative case on recording a chemical ionization mass spectrum (M^+) for $ICd\{Hf_2(OPr^i)_9\}$ which exhibits a molecular ion corresponding to the monomer [6b].

The presence of an NMR active heterometal partner, as shown for cadmium compounds, facilitates the probing of structural behaviour of heterometal alkoxide derivatives in the solution and solid state. This assumes special significance among heterometal alkoxides where the ^1H and ^{13}C NMR spectra are often not structurally diagnostic, due to the high fluxionality of these derivatives in solution. In view of the above, our initial investigations were focused on metals (^{113}Cd, ^{119}Sn, ^{207}Pb) whose coordination state could be studied by NMR spectroscopy in both the solution and solid state.

New bimetallic halide isopropoxides of divalent Sn and Pb are accessible by the metathesis reactions of their halides and alkali metal salts of $M_2(OPr^i)_9^-$ anions containing Ti, Zr and Hf atoms (eq. 41) [50,52]. In contrast to the monomeric Cd^{II} derivatives, $ICd\{M_2(OPr^i)_9\}$, the analogous derivatives of Sn^{II} and Pb^{II} are found to be dimeric species. The molecular structure of $[ISn\{M_2(OPr^i)_9\}]_2$ (M = Zr, Hf) shows (Fig. 29) a tridentate interaction of $M_2(OPr^i)_9$ unit with Sn^{II} which deviates from the typical tetra-dentate ligating mode of $M_2(OR)_9^-$ moieties presumably due to the presence of the stereochemically active lone pair at tin. The central $Sn_2I_2O_6$ unit can be described as two SnI_2O_3 trigonal bipyramids joined along a common edge. Alternatively, when the lone pair of electrons at tin(II) is considered to be stereochemically active, the tin geometry resembles a distorted octahedron in which one of the axial sites is occupied by the non-bonding electron pair.

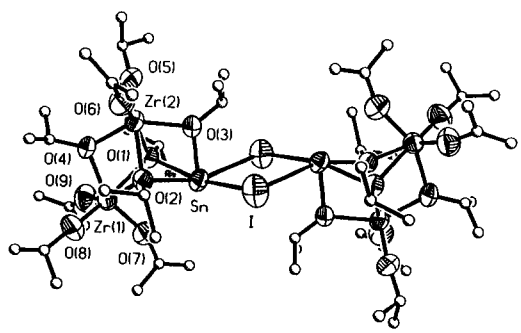

Fig. 29. Molecular structure of $[ISn\{Zr_2(OPr^i)_9\}]_2$ [52].

Whereas $[ISn\{Zr_2(OPr^i)_9\}]_2$ [52] is a centrosymmetric dimer, the chloride tin-dizirconate (dihafnate) molecule [50] adopts, in the solid state, a dimeric form *via* long Sn···Cl interactions (Fig. 30) between chlorine of one molecule and the tin atom of a second molecule, nevertheless their deviation from C_i symmetry is small. The bidentate coordination of the $M_2(OPr^i)_9^-$ unit has also been observed in $[Pb_2Zr_4(OPr^i)_{20}]$ [12]. If the long Sn···Cl interactions are taken into account, the coordination sphere of tin(II) can be termed as '3 + 1'. Most striking is the change in the ligating behaviour of $M_2(OPr^i)_9^-$ units to similar SnX^+ (X = Cl, I) fragments; the $M_2(OPr^i)_9$ sub-structures act as bi- and tri-dentate ligands for chloride and iodide derivatives, respectively. As inferred by the cryoscopic studies (molecular complexity, $\eta = 1.4$–1.6), the dimeric form of $[XSn\{M_2(OPr^i)_9\}]_2$ derivatives is not maintained in the solution. A 2 monomer ⇔ dimer equilibrium, is indicated in the solution by ^{119}Sn NMR spectra which has been confirmed by variable temperature ^{119}Sn NMR studies. The effect of the nature of metal atoms is seen among iodo derivatives of bivalent cadmium and tin. The $ICd\{M_2(OPr^i)_9\}$ derivatives (Fig. 28) exhibit a closed triangular (CdM_2) framework however, the replacement of $Cd^{(II)}$ by Sn^{II} of almost similar size (Cd^{2+} = 0.99 Å, Sn^{2+} = 1.02 Å) gives an open structure (Fig. 29). This possibly results from the tendency of tin(II) atom to achieve a pyramidal configuration and to retain a stereochemically active lone pair consequently, a dimeric framework is preferred (despite the bulk of iodide ligands) over a monomeric closed triangular structure. The role of halide ligands in the nuclearity and coordination numbers of metals has also been observed for Cd–Zr mixed-metal alkoxides where the substitution of chloride, in the dimeric $[ClCd\{Zr_2(OPr^i)_9\}]_2$ [45] containing a six-coordinate cadmium, by bulkier iodide ligand produces monomeric $ICd\{Zr_2(OPr^i)_9\}$ with a five coordinate cadmium.

The discovery of the super-conducting properties of a number of copper containing oxide-ceramic [55] materials has resulted in an unprecedented search for soluble copper containing derivatives which can be used as precursors to ceramic materials *via* sol–gel processes. The reactions of copper(II) chloride with $KM_2(OPr^i)_9$ (M = Ti, Hf) in 1:1 stoichiometry offered halide heterobimetallic alkoxide of the type $ClCu\{M_2(OPr^i)_9\}$ (eq. 40) [14,20]. The zirconium analogue $ClCu\{Zr_2(OPr^i)_9\}$ is also known [30]. Their solid state structures resemble closely to the structures observed for $ICd\{M_2(OPr^i)_9\}$ compounds, a perspective drawing is shown for the titanium analog

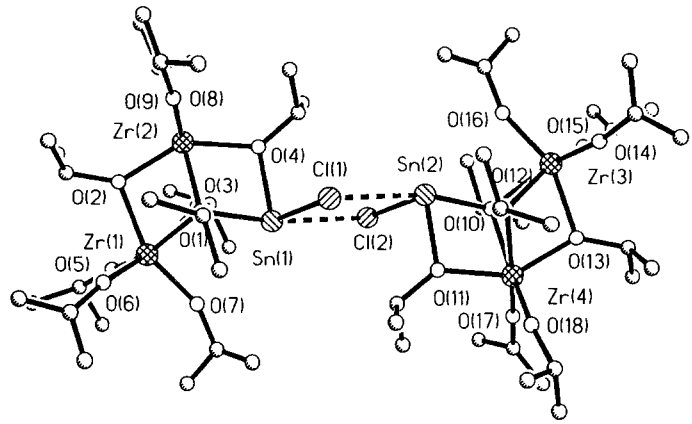

Fig. 30. Molecular structure of $[ClSn\{Zr_2(OPr^i)_9\}]_2$ [50].

(Fig. 31). The $\{(Pr^iO)_3M(\mu_2\text{-}OPr^i)_3M(OPr^i)_3\}^-$ unit coordinate Cu^{II} through four oxygen atoms of the OPr^i groups, two of which also bridge the two M^{IV} centres. The core of the molecules comprise a heterometallic isosceles CuM_2 triangle with similar non-bonded $Cu\cdots M$ distances; the triangular base is capped on both the sides by a μ_3-OPr^i ligand, two Cu—M and the third M—M side of the triangular core are each bridged by a μ_2-OPr^i group.

The five-coordinate copper in $ClCu\{M_2(OPr^i)_9\}$ derivatives (M = Ti, Zr, Hf) constitute a distorted trigonal bipyramid with four oxygen and one chlorine ligand where the axial (doubly bridging) OPr^i ligands are bound to copper in a symmetrical fashion. Among the equatorial ligands, the average Cu—(μ_3-O) distance is longer than the copper contact to much larger chloride ion and chloride is apparently the most tightly bound ligand to copper. This observation can be understood in terms of Jahn-Teller distortion (Cu^{II}, d^9) which makes copper coordination sphere flexible to display both normal coordinated (Cu—L) and longer semi-coordinated ($Cu\cdots L$) bonds [56,57]. In view of the above, the copper coordination in $ClCu\{M_2(OPr^i)_9\}$ derivatives can be viewed as '3+2' with three strong (Cl, O_{a1}, O_{a2}) and two weak (O_{e1}, O_{e2}) interactions.

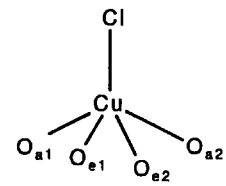

In view of the paramagnetic influence of Cu^{II}, these derivatives exhibit simple Curie–Law behaviour deduced from a linear relationship between the change in ^1H NMR isotropic shift with respect to the temperature. The monomeric nature of $ClCu\{M_2(OPr^i)_9\}$ derivatives is supported by the cryoscopic measurements which rules out the possibility of interacting paramagnetic centres to give dimeric diamagnetic species of the type '$Cu(\mu\text{-}Cl)_2Cu$'.

Iodide heterobimetallic derivatives of barium of the formula $[IBa\{M_2(OPr^i)_9\}]_2$ (M = Sn, Ti, Zr, Hf) [13] (eq. 42) are dimeric in the solution and solid state. The molecular structure (Fig. 32) can be analysed as a union of three face-sharing octahedra built about

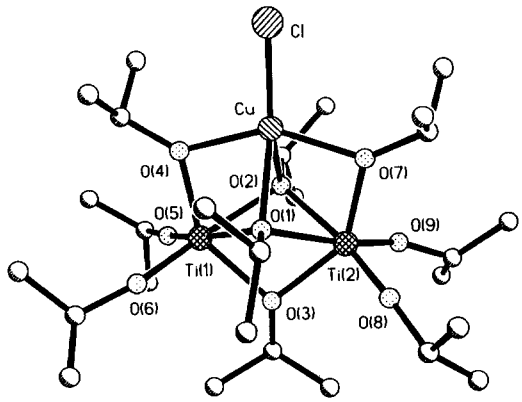

Fig. 31. Molecular structure of $ClCu\{Ti_2(OPr^i)_9\}$ [20].

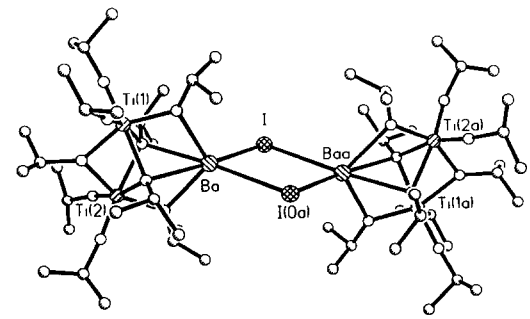

Fig. 32. Molecular structure of $[IBa\{Ti_2(OPr^i)_9\}]_2$ [13].

two Ti (Sn, Zr, Hf) and one Ba atom. The monomeric formulation 'IBa$\{Ti_2(OPr^i)_9\}$' of these derivatives is a ligand deficient modification of M_3L_{11} structural unit observed in the solid state structures of $[Cl_2Y\{Ti_2(OPr^i)_9\}]$ [20] and $[(OPr^i)ClY\{Ti_2(OPr^i)_9\}]$ [13]. Owing to the ligand deficit, the simplest structural change to attain a M_3L_{11} motif involves the dimerisation *via* 'terminal' iodide ligands. The other MM'_2L_{10} derivatives supporting the proposed dimerisation are $[ClCd\{Zr_2(OPr^i)_9\}]_2$ [48] and $[BaZr_2(OPr^i)_{10}]_2$ [46].

Although structurally characterised halide heterobimetallic alkoxides based on tri-, tetra-, penta- and nona-alkoxometallate are known, reports available on halo-functionalised heterometal alkoxy derivatives based on $M(OPr^i)_6^-$ fragments (M = Nb, Ta) are relatively scarce. Equation 43 illustrates the synthesis of a monomeric monoiodo cadmium hexaisopropoxo-tantalate [13]. The molecule (Fig. 33) is formed by the bidentate ligation of $Ta(OPr^i)_6^-$ unit to Cd^{II} bearing an iodide ligand. The cadmium atom is additionally coordinated by two alcohol molecules to display a quasi-trigonal bipyramidal geometry whereas the ligand disposition around tantalum represents a slightly distorted octahedron.

An attempted synthesis of a halide-free Cd—Nb mixed metal alkoxide with 1 : 1 metal stoichiometry gave a dimeric iodo-complex with Cd–Nb stoichiometry 2 : 1 (eq. 44) [13]. The molecular structure reveals two tetrahedral Cd^{II} fragments '$ICd(OPr^i)_3$' and '$I_2Cd(OPr^i)_2$' (Fig. 34) bound to the octahedral $Nb(OPr^i)_6^-$ moiety in bi- and mono-dentate fashion, respectively. The observation of two resonances, corresponding to two chemically inequivalent Cd^{II} centres in the solution and solid state ^{113}Cd CP MAS NMR spectra provides evidence that the heterometallic framework observed in the solid state is also maintained in the solution.

As indicated in eqs 40–43, the reactions of divalent metal halides with alkali metal alkoxometallates in 1 : 1 stoichiometry offer mono-halo heterometallic derivatives. In a similar manner di- and tri-halo functionalised heterometallic alkoxides are obtained on employing tri- and tetravalent metal halides, respectively. Dichloro-yttrium-nonaisopropoxo-dimetallate compounds of the type $Cl_2Y\{M_2(OPr^i)_9\}$ (M = Ti, Zr, Hf) [13,20] have been synthesised (eq. 45) quantitatively by the equimolar reaction of YCl_3 and $KM_2(OPr^i)_9$ derivatives. The derivatives are stereochemically rigid and the NMR spectra are indicative of the structural pattern existing in the solution.

The X-ray diffraction analysis performed on a representative titanate derivative reveals a monomeric species (Fig. 35) formed by a face-sharing fusion of three octahedra built about a yttrium and two titanium atoms. Each metal atom bears two terminal ligands which are chlorides in the case of yttrium. The central $M_3O_9Cl_2$ unit of the compound represent a modified M_3X_{11} structural type observed in other metal alkoxides e.g., $La_3(OBu^t)_9$ $(Bu^tOH)_2$ [58]. In contrast to the monomeric yttrium derivatives, the analogous bismuth derivatives [13] have a dimeric structure. The molecular structure of $[Cl_2Bi\{Zr_2$

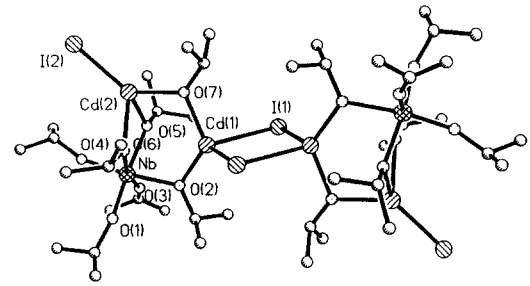

Fig. 34. Molecular structure of $[I_2Cd_2Nb(OPr^i)_7]_2$ [13].

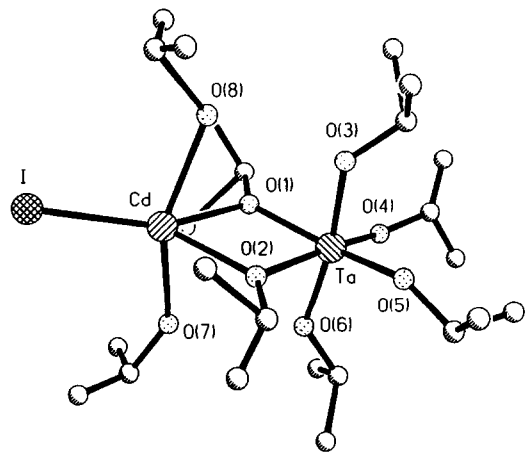

Fig. 33. Molecular structure of $[ICd\{Ta(OPr^i)_6\}(Pr^iOH)_2]$ [13].

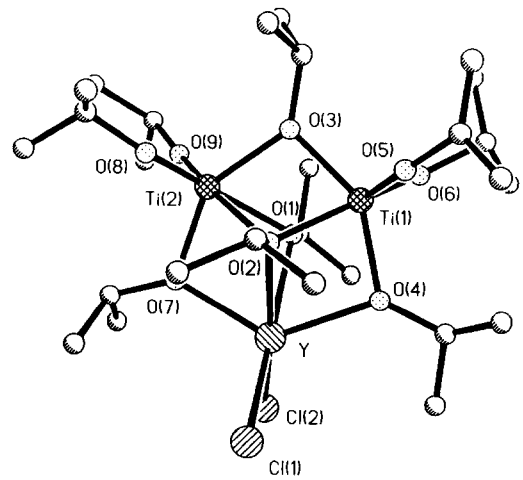

Fig. 35. Molecular structure of $[Cl_2Y\{Ti_2(OPr^i)_9\}]$ [20].

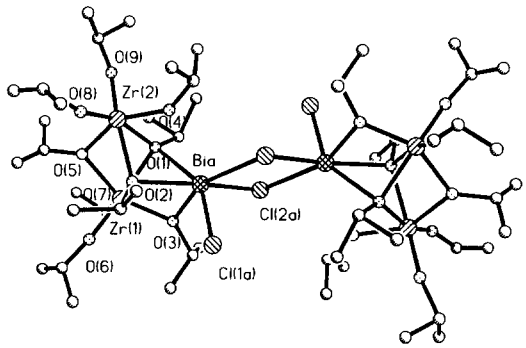

Fig. 36. Molecular structure of $[Cl_2Bi\{Zr_2(OPr^i)_9\}]_2$ [13].

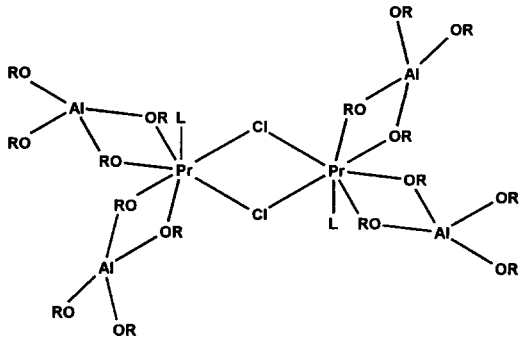

(R = Pr^i; L = Pr^iOH)

Fig. 38. Schematic representation of the molecular structure of $[ClPr\{Al(OPr^i)_4\}_2(Pr^iOH)]_2$ [35].

$(OPr^i)_9\}]_2$ is shown in Fig. 36. One of the chlorine atoms present at bismuth interact with the bismuth atom of another '$Cl_2Bi\{Zr_2(OPr^i)_9\}$' unit to give the observed dimeric form. Similar to the solid state structures of $[ISn\{M_2(OPr^i)_9\}]_2$ compounds, the $[Cl_2Bi\{Zr_2(OPr^i)_9\}]_2$ derivative displays a tridentate behaviour of $M_2(OPr^i)_9$ (M = Zr, Hf) units.

A series of iodo-heterobimetallic Sn^{IV}–Ti^{IV} derivatives [13] are obtained by the interaction of SnI_4 and $KTi(OPr^i)_5$ in appropriate molar ratios (eq. 46). The derivatives are highly fluxional at room temperature, however, structurally diagnostic spectra are obtained on lowering the temperature. The cryoscopic and VT ^{119}Sn NMR studies indicate the monomeric behaviour in solution. The X-ray diffraction study performed on a diiodo-derivative shows (Fig. 37) a six-coordinate tin(IV) surrounded by two iodide and two bidentate $\{Ti(OPr^i)_5\}^-$ ligands. The two titanium atoms are present in a distorted trigonal bipyramidal arrangement of alkoxo ligands.

The chloro(propan-2-ol)bis(tetraisopropoxoaluminato)-prasesodymium(III) dimer, $[ClPr\{Al(OPr^i)_4\}_2(Pr^iOH)]_2$ [35] represent the only halide heterometallic alkoxide based on a bidentate $\{Al(OPr^i)_4\}^-$ moiety (Fig. 38). The centrosymmetric dimer consists of two triangular $Al_2Pr(\mu\text{-}OPr^i)_4(OPr^i)_4(Pr^iOH)^+$ units linked by two chloride bridges. Praseodymium is hepta-coordinate and the coordination polyhedron formed by five oxygens and two bridging chlorine atoms can be envisaged as a distorted capped trigonal prism.

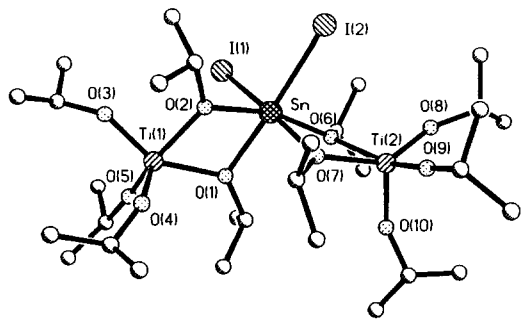

Fig. 37. Molecular structure of $[I_2Sn\{Ti(OPr^i)_5\}_2]$ [13].

Although the reactions involving metal halides and an alkali metal reagent proceed quantitatively in most of the cases and the desired target product is obtained in a 'clean' way (no undesirable side products), examples are known where alkali metal or halide ions remain attached to give 'ate' complexes. This problem of salt retention is more frequently encountered in the homo- as well as hetero-metallic alkoxide chemistry of yttrium and lanthanide metals. Evans *et al.* have reported [59] on the simple chloro-alkoxometallates of the type $Y_3(OBu^t)_8Cl(THF)_2$ and $Y_3(OBu^t)_7Cl_2(THF)_2$ obtained as the major products in the reactions of YCl_3 with 3 and 2 equiv. of $NaOBu^t$, respectively. Mixed-metal alkoxides representing a new class of $LnNa_8(OBu^t)_{10}Cl$ (Ln = Y, Eu) complexes [60] are obtained in high yields (70–90%) in the reactions involving $LnCl_3$ and 10 equiv. of $NaOBu^t$. Interestingly, a hydroxy derivative $YNa_8(OBu^t)OH$ belonging to this class is also formed in a similar reaction between YCl_3 and $NaOBu^t$ (which reportedly was contaminated by impurities such as NaOH). Other typical examples include chloride heterobimetallic aryloxide of the type $[ClM(OR)_3Na]$ (M = La, Y; R = $C_6H_2(CH_2NMe_2)$-2-6-Me-4) [61] and $[ClY_2(OR')_6Na]$ (R' = $C_6H_4(CH_2NMe_2)$) [61] obtained in the reaction of lutetium or yttrium trichloride with three equivalents of sodium aryloxides. The problem of salt retention is more frequently observed in the case of smaller alkali-metal ions (Li^+, Na^+) and can be overcome to a certain extent by using potassium derivatives presumably due to the higher insolubility of KCl, in common organic solvents, in comparison to that of LiCl and NaCl. However, this problem is not always eliminated by the use of heavier alkali metals, e.g. the reaction of anhydrous $LnCl_3$ (Ln = Nd, Er, Lu) with potassium arlyoxide results, irrespective of the amount (3 or 4 equiv.) of KOAr used, in the formation of $KLn(OAr)_4$ derivatives [62].

The halide heterobimetallic ethoxide $[ClMg\{Ti_2(OEt)_8Cl\}]_2$ (eq. 49) obtained by the dissolution of $MgCl_2$ in $Ti(OEt)_4$ is the only well-characterised derivative that represent an alternative synthetic route to halide heterometallic alkoxides. The molecule is observed as a centrosymmetric dimer in the solid state and the overall structure is similar to that of $[IBa\{Ti_2(OPr^i)_9\}]_2$ derivative (Fig. 32). The central atom, magnesium, coordinated by the three oxygen and one chlorine atom of the modified face-sharing biocta-hedral unit $\{Ti_2(OEt)_8Cl\}^-$ and bearing a 'terminal' chloride ligand dimerises ($Mg(\mu\text{-}Cl)_2Mg$) to achieve the M_3X_{11} form.

A new chloro bismuth–vanadium heterobimetallic oxoalkoxide $[BiCl_3OV(OC_2H_4OCH_3)_3]_2$ [53] is obtained (eq. 50) by the reaction of $BiCl_3$ with $OV(OPr^i)_3$ in 2-methoxyethanol. The X-ray structural study reveals the vanadium atom in a distorted octa-hedral environment whereas, bismuth is present in a distorted capped octahedron of chlorine and oxygen atoms. The $OC_2H_4OCH_3$ group binds to vanadium in a bidentate fashion which contrasts the monodentate mode observed in homometallic 2-methoxy ethoxide derivatives of Pb^{II} [63] and Bi^{III} [64].

The single crystal X-ray diffraction analysis performed on $(C_5H_5)Sn(\mu\text{-}OBu^t)_2Ge(OBu^t)$ [51] (eq. 47) reveals (Fig. 39a) a nearly planar four-membered SnO_2Ge ring terminated at Sn^{II} by the cyclopentadienyl ring and at Ge^{II} by the OBu^t group. The two terminal ligands occupy *cis* positions with respect to the plane of the ring. The sum of the angles around Ge^{II} and Sn^{II} indicate a stereochemically active lone pair giving the two bivalent metal atoms a trigonal pyramidal configuration. Interestingly, a similar reaction between $(C_5H_5)SnCl$ and $KPb(OBu^t)_3$ afford an unanticipated product $(C_5H_5)Pb(\mu\text{-}OBu^t)_2Sn(OBu^t)$ [50] which involves a transfer of cyclopentadienyl group from tin to lead. However, the overall molecular framework remains the same. Owing to the presence of two NMR active metal nuclei, the solution spectral data were indicative of a transfer of the $C_5H_5^-$ ligand from tin to lead. The most interesting feature in the solid state structures of the two derivatives is the different hapticity of the $C_5H_5^-$ ligands toward the tin and lead atoms. The tin germanate shows a peripherally ($\eta^{1/3}$) bonded cyclopentadienyl ring (Fig. 39a) possessing a diene character whereas, a centrally bonded (η^5) cyclopentadienyl ring (Fig. 39b) is observed in the tin plumbate.

Out of the $[(C_5H_5)Sn\{M_2(OPr^i)_9\}]$ (M = Zr, Hf)

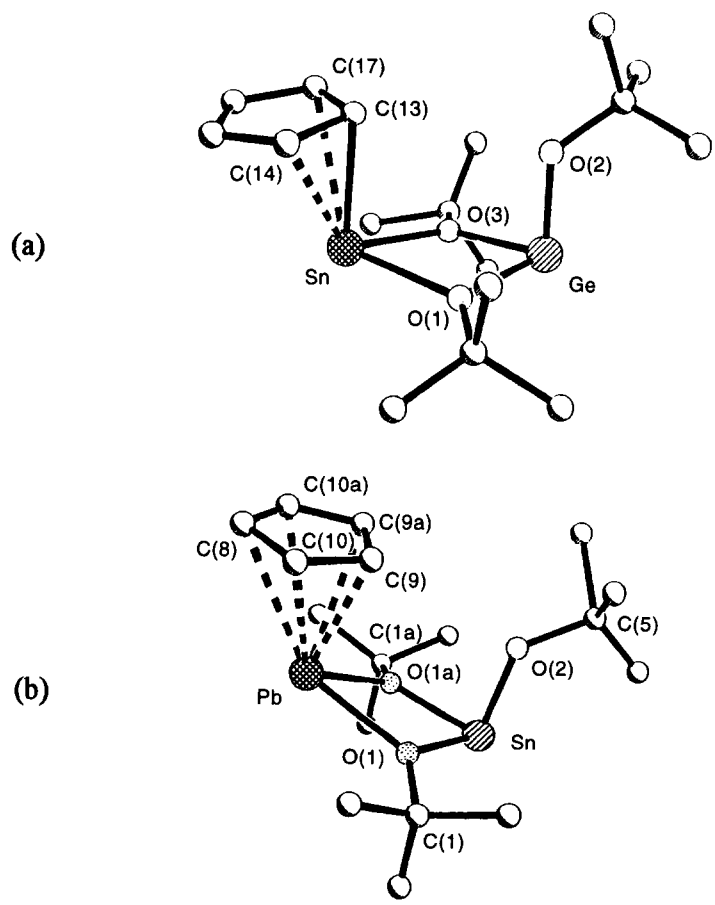

Fig. 39. Molecular structures of (a) $(C_5H_5)Sn(\mu\text{-}OBu^t)_2Ge(OBu^t)$ [51] and (b) $(C_5H_5)Pb(\mu\text{-}OBu^t)_2Sn(OBu^t)$ [50].

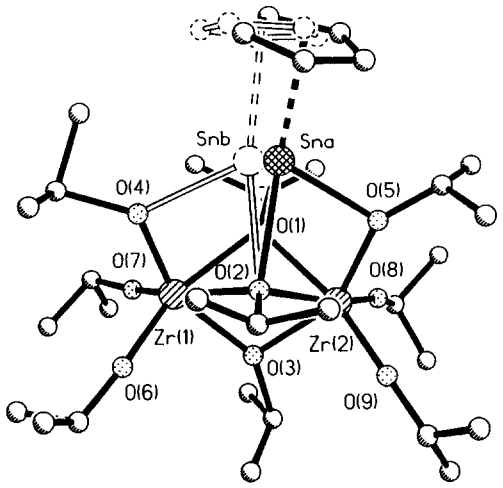

Fig. 40. Molecular structure of $[(C_5H_5)Sn\{Zr_2(OPr^i)_9\}]$ [50]. The unfilled line shows the partially occupied tin and cyclopentadienyl sites.

[50] derivatives (eq. 48), the zirconium compound characterized by X-ray crystallographic study (Fig. 40) features a $(C_5H_5)Sn^+$ fragment disordered with a 80:20 occupancy between the doubly bridging arms of the $Zr_2(OPr^i)_9^-$ unit. An interesting aspect of these heteroleptic ($C_5H_5^-/OR^-$) derivatives is their nuclearity with respect to that of the precursors. The substitution of chloride in dimeric $[ClSn\{M_2(OPr^i)_9\}]_2$ (M = Zr, Hf) complexes by a ligand (Cp^-) of higher bulk and denticity renders the product monomeric. This synthetic strategy can be used for obtaining more tractable heterometallic species as in contrast to the extraordinary bridging tendency of OR ligands, a cyclopentadienyl bridging would be thermodynamically disfavoured and can result in less associated heterometallic systems.

A recent study reports the formation of heteroleptic ($C_5HMe_4^-/OMe^-$) titanium(III)–magnesium (II) derivative $[(C_5HMe_4)_2Ti(\mu\text{-}OMe)_2]_2Mg$ [65] by the methanolysis of the hydride complex $[(C_5HMe_4)_2Ti(\mu\text{-}H_2)]_2Mg$. The molecule (Fig. 41) contains two non-equivalent octamethyl titanocene moieties each bonded through two bridging methoxy groups to the central magnesium atom.

2.2.3 *Reactions*

The halo-functionalised heterometal alkoxides are interesting synthons and the substitution of anionic halide ligand by an appropriate alkoxo, aryloxo, siloxo or cyclopentadienyl ligand results in a variety of heteroleptic heterometal alkoxy derivatives. Some typical reactions examined (eq. 51) are shown below.

$$XM\{M'_2(OR)_9\} + M''L \rightarrow LM\{M'_2(OR)_9\} + M''X \quad (51)$$

$M = Sn^{II}, Cd^{II}$; $M' = Ti, Zr, Hf$; $M'' = Na, K$

$L = OPr^i, OBu^t, OSiMe_3, OSiPH_3, C_5H_5$;

$X = Cl, I$

A controlled alcoholysis of $CpSn(OBu^t)_2Ge(OBu^t)$ gives a product devoid of cycopentadienyl group and shows only one single environment in the ^{119}Sn NMR spectrum which differs from the ^{119}Sn NMR chemical shift of $[Sn(OBu^t)_2]_2$ and suggests the formation of a tin–germanium heterobimetallic compound with 1:1 metal stoichiometry. However, no such product is formed on reacting $[Sn(OBu^t)_2]_2$ and $[Ge(OBu^t)_2]_2$ in equimolar ratio [18b]. Mixed ligand heterometal systems are of considerable interest as they provide access to metal stoichiometries not achievable by pure alkoxide constituent. Efforts to obtain definitive structural information about this compound by single crystal X-ray crystallography are currently underway.

$$(C_5H_5)Sn(\mu\text{-}OBu^t)_2Ge(OBu^t) + Bu^tOH \rightarrow {}' SnGe(OBu^t)_4{}' + C_5H_6 \quad (52)$$

In analogy to the heterobimetallic derivatives based on main group elements with ns^2 configuration, the novel cyclopentadienyl containing heterobimetallic alkoxides function as soft ligands too and have been used to synthesise elusive examples of heterotermetallic derivatives illustrated below (eq. 53) [66].

$$(C_5H_5)Sn(\mu\text{-}OBu^t)_2Ge(OBu^t) + Mo(CO)_6 \rightarrow (C_5H_5)Sn(OBu^t)_3Ge\text{-}Mo(CO)_5 + CO \quad (53)$$

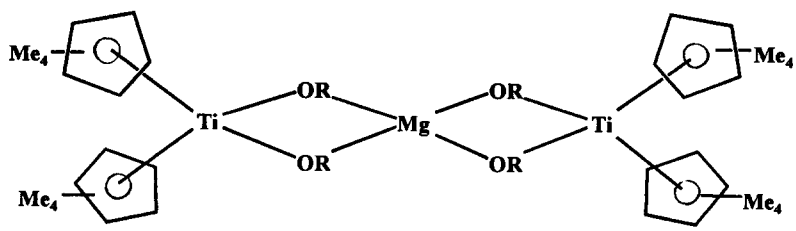

(R = Me)

Fig. 41. Representation of the molecular structure of $[(C_5HMe_4)_2Ti(\mu\text{-}OMe)_2]_2Mg$ [65].

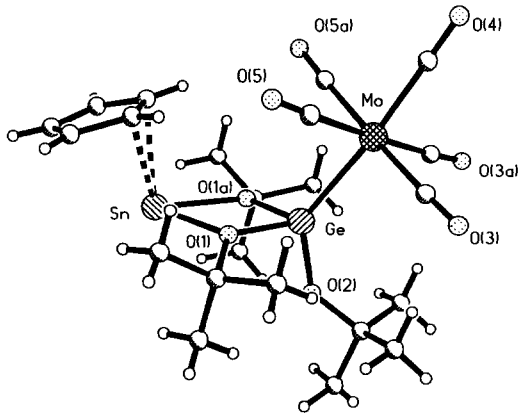

Fig. 42. Molecular structure of $[(C_5H_5)Sn(OBu^t)_3Ge\text{-}Mo(CO)_5]$ [66].

The X-ray structural study shows (Fig. 42) the selective coordination of metal carbonyl fragment at the Ge^{II} centre, protracted attempts to attach another $Mo(CO)_5$ unit at Sn^{II} were not successful. This observation is of considerable interest when compared with the high reactivity of Sn^{II} centre found in the heterobimetallic alkoxides of the type $Sn(\mu\text{-}OBu^t)_3M$ and $[Sn(\mu\text{-}OBu^t)_3]_2M'$ (see Section 2.1).

3. HETEROTERMETALLIC ALKOXIDES

Until recently the hetero*ter*metallic nature of the alkoxide clusters based on *three* different metals was considered ambiguous and the identity of the examples reported [67] mainly on the basis of elemental analysis and low resolution ^1H NMR data, in a few cases, was considered to be unreliable. This scepticism was supported by the fact that despite extensive investigations on metal alkoxide chemistry by various research groups, the existence of heterotermetallic alkoxides as discrete molecular species in solution and the solid state could not be unequivocally established. The reactive halide group in halo-functionalised heterobimetallic alkoxides, described in Section 2, can be replaced by a number of anionic alkoxometallate ligands to obtain new heterometal species containing three different metals. The elimination of salt (KCl, KI, etc.) as an insoluble product provides a thermodynamic assist and the yields are nearly quantitative in these reactions. The isolation and characterisation of novel heterotermetallic alkoxides demonstrate that salt elimination is not merely an ion-exchange phenomenon and if appropriate combinations of halide precursors and alkali reagents are chosen, it can prove to be an efficient strategy for the directed synthesis of heterometal alkoxide systems.

3.1 *Synthesis*

We have synthesised a large variety of heterotermetallic alkoxides employing both salt elimination and Lewis acid–base reactions (eqs 54–56) [6,13,14].

(i) Salt elimination reactions

$$ICd\{M_2(OPr^i)_9\} + KM'(OPr^i)_3 \rightarrow \tfrac{1}{2}[\{Cd(OPr^i)_3\}M'\{M_2(OPr^i)_9\}]_2 + KI \quad (54)$$

$M = Sn, Ti, Zr, Hf$; $M' = Ba, Sr, Ca$

$$1/2[IBa\{Zr_2(OPr^i)_9\}]_2 + KHf_2(OPr^i)_9 \rightarrow \{Hf_2(OPr^i)_9\}Ba\{Zr_2(OPr^i)_9\} + KI \quad (55)$$

$$1/2[IBa\{M_2(OPr^i)_9\}]_2 + KM'(OPr^i)_6 \rightarrow \{M'(OPr^i)_6\}Ba\{M_2(OPr^i)_9\} + KI \quad (56)$$

$M = Sn, Ti, Zr, Hf$; $M' = Nb, Ta$

(ii) Lewis acid–base reactions

The halide-free heterometallic alkoxides can also undergo Lewis acid–base reactions with another alkoxide to give novel heterotermetallic systems as illustrated in the following examples (eqs 57–60) [13].

$$\tfrac{1}{2}[BaTi_2(OPr^i)_{10}] + \tfrac{1}{2}M_2(OPr^i)_{10} \rightarrow \{M(OPr^i)_6\}Ba\{Ti_2(OPr^i)_9\} \quad (57)$$

$M = Nb, Ta$

$$\tfrac{1}{2}[BaTi_2(OPr^i)_{10}] + 2/n[Zr(OPr^i)_4]_n \rightarrow Ba_2Zr_2Ti_2(OPr^i)_{20} \quad (58)$$

$$(Pr^iO)Cd\{Hf_2(OPr^i)_9\} + Ti(OPr^i)_4 \rightarrow \{Ti(OPr^i)_5\}Cd\{Hf_2(OPr^i)_9\} \quad (59)$$

$$(Pr^iO)Cd\{Hf_2(OPr^i)_9\} + \tfrac{1}{2}[Ta(OPr^i)_5]_2 \rightarrow \{Ta(OPr^i)_6\}Cd\{Hf_2(OPr^i)_9\} \quad (60)$$

3.2 *Structural and spectral features*

Recently, we reported on the first synthesis and structural characterization of a series of novel heterotermetallic isopropoxides of general formula $[\{Cd(OPr^i)_3\}M'\{M'_2(OPr^i)_9\}]_2$ (M' = Ba, Sr, Ca; M = Sn, Ti, Zr, Hf) [6,13,14] (eq. 54). The most remarkable phenomenon encountered in the formation of these heterotermetallic derivatives is the exchange of the central atoms (Cd and Ba) between the precursors $ICd\{M_2(OPr^i)_9\}$ and $KM'(OPr^i)_3$. Astonishingly, no catastrophic breakdown or change in the structural features of the precursor complexes occurs and the $M_2(OR)_9^-$ sub-structure in the obtained heterotermetallic compounds binds to the alkaline earth metal atom rather than to the cadmium as anticipated in the targeted molecule. The rearrange-

ment of metallic elements in the formation of heterometallic framework is an unprecedented phenomenon in metal alkoxide chemistry and emphasises the need of single-crystal X-ray crystallographic studies in the complete characterization of heterometal alkoxides. The generality of the reaction has been examined for various $M_2(OR)_9^-$ ($M = Sn^{IV}$, Ti^{IV}, Zr^{IV}, Hf^{IV}) structures and alkaline earth metals (Ba, Sr, Ca). The mechanism for the observed switching of metals is not clear, however, it is possibly induced by the greater oxophilicity and tendency of larger alkaline earth metal cations to achieve higher coordination numbers. Another interesting aspect of this study is the role of multidentate $M_2(OPr^i)_9^-$ unit in the formation of heterotermetallic systems, which exhibit extraordinary versatility in binding the different metal atoms (Cd in the precursor and an alkaline earth element in the resulting complex) leading to the formation of a thermodynamically favoured heterotermetallic framework.

The $[\{Cd(OPr^i)_3\}M'\{M_2(OPr^i)_9\}]_2$ (M' = Ba, Sr, Ca; M = Sn, Ti, Zr, Hf) derivatives are isostructural and the heterotermetallic framework (Fig. 43) can be viewed as a combination of two triangular $BaM_2(\mu_3\text{-}OPr^i)_2(\mu_2\text{-}OPr^i)_3(OPr^i)_4^+$ units which are joined together by a $[(Pr^iO)_2Cd(\mu_2\text{-}OPr^i)_2Cd(OPr^i)_2]^{2-}$ unit. Alternatively, the structures can be described as a spirocyclic linking of two $Ba(OPr^i)_2L$ ($L = M_2(OPr^i)_9^-$) units to a four membered $Cd_2(OPr^i)_2$ ring. The novel potassium alkoxometallates $KM'(OPr^i)_3$ act as a source to generate coordinatively unsaturated '$M'(OPr^i)_3^-$' species which owing to the propensity of M'^{2+} to command higher coordination number initiates a rearrangement of metal atoms to form a stable heterotermetallic system that optimally fulfills the requirements of different metal atoms.

In contrast to the deceptively simply spectroscopic pattern generally exhibited by the heterometal derivatives, the solution ^1H and ^{13}C NMR spectra of $[\{Cd(OPr^i)_3\}M'\{M'_2(OPr^i)_9\}]_2$ [6,13,14] compounds are structurally informative. The retention of the dimeric structure (Fig. 43) in solution is indicated by the cryoscopic molecular weight measurements and is corroborated by the similar ^{113}Cd NMR chemical shifts observed in both solution and the solid state. In view of the wide dispersion and extreme sensitivity of the ^{113}Cd chemical shifts to the local coordination environments, the presence of cadmium in the heterobimetallic precursor and the resulting heterotermetallic species has proved a valuable tool in studying the structural behaviour of these derivatives.

Following the eq. 54, we have recently been able to characterise a novel heterotermetallic alkoxide of composition $Ba_2Zr_2Ti_2(OPr^i)_{20}$ [13] which represents the first example of a structurally characterised heterotrimetallic alkoxide based on 1 : 1 : 1 metal stoichiometry. The molecule is highly symmetrical and exhibits a 1 : 1 metal disorder of tetravalent elements [27]. Figure 44 shows one of the possible modes of disordering of Ti^{IV} and Zr^{IV}. The structural features are closely related to that of $[IBa\{M_2(OPr^i)_9\}]_2$ derivatives.

4. APPLICATIONS

The versatility of metal alkoxides as convenient precursors to advanced ceramic materials *via* sol–gel and MOCVD processes, is widely acclaimed, however, the use of well-characterised 'single source' precursors for these purposes remain extremely limited primarily due to the non-suitability of metal ratios present in the available molecules and that required in the desired ceramics. Among the useful heterometallic precursors,

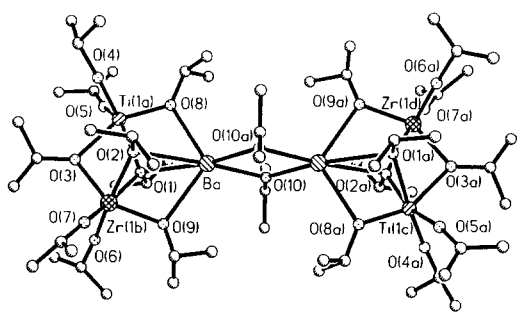

Fig. 44. Molecular structure of $[Ba_2Zr_2Ti_2(OPr^i)_{20}]$ [13].

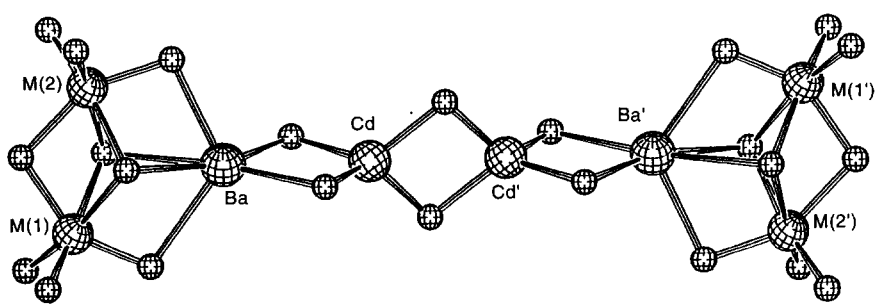

Fig. 43. Representation of the metal–oxygen skeleton observed in $[\{Cd(OPr^i)_3\}Ba\{M_2(OPr^i)_9\}]_2$ derivatives (M = Sn, Ti, Zr, Hf) [6,13].

$[LiNb(OEt)_6]_n$ [17] is a well-known example. Owing to the presence of Li/Nb atomic ratio corresponding to lithium niobate ceramic, useful for its ferro- and piezo-electric properties, $[LiNb(OEt)_6]_n$ has been used in numerous studies to obtain high quality $LiNbO_3$ films and powders [68].

Although volatile heterometal alkoxides are attractive precursors for the deposition of mixed-metal oxides by chemical vapour deposition technique, their use in obtaining multimetallic ceramics has not been pursued and lack of systematic studies make it a thrust area for research. In an attempt to develop new and effective routes to advanced ceramics, we have examined a number of homo- and hetero-metallic alkoxides to deposit new materials on a variety of substrates (quartz, silicon, copper, aluminium) by the MOCVD process. The *tert*-butoxides of bivalent Ge, Sn and Pb as well as their heterometal derivatives $M'M_2(OBu^t)_6$ ($M = Ge$, $M' = Sr$, Ba; $M = Sn$, $M' = Ca$, Sr, Ba; $M = Pb$, $M' = Ca$, Ba) when subjected to a single source chemical vapour deposition process produced biphasic metal/metal-oxide composites of the type M/MO_2 or $M/M'MO_3$ [69]. In all the cases, the uniform dispersion of metallic particles in a ceramic matrix (MO_2 or $M'MO_3$) has been confirmed by X-ray diffraction, electron spectroscopy, energy dispersion X-ray analysis (EDX) and photoelectron spectroscopy (XPS). The bivalent metal M^{II} ($M = Ge$, Sn, Pb) in the precursors undergo disproportionation (from +2 oxidation state) to give an elemental (M^0) phase and the phase containing formal M^{IV} cation. The composites consist of ball-shaped particles on which smaller particles are placed in a fractal manner. In the case of the composite $Sn.BaSnO_3$, the core of the ball-shaped particles has been analysed as pure elemental tin. The fundamental novel feature observed in the preparation of these composites is the chemically driven synthesis of two distinct phases with a regular dispersion of one (metallic phase) into another (ceramic phase). Further, on a hot substrate, all components are unified at the shortest distance possible which makes the adjustment of the physical parameters less important as the decomposition is predominantly chemical in nature.

Magnesium aluminium spinel ($MgAl_2O_4$) is a promising electronic material [70] and thin films of $MgAl_2O_4$ using single molecular precursors have been deposited *via* both sol–gel and MOCVD techniques. However, the higher carbon content in the resulting material or higher decomposition temperature for the precursor molecule are the intrinsic problems that persist. To design precursors with reduced organic part and enhanced volatility, we have synthesised new Mg–Al hydrido heterobimetallic alkoxides of the type $[Mg\{Al(OBu^t)_3H\}_2]$ [25] and $[Mg\{Al(OBu^t)_2H_2\}_2]$ [25]. The single crystal diffraction study performed in the case of mono-hydrido derivative reveals a molecular structure similar to that of $[Mg\{Al(OBu^t)_4\}_2]$ (Fig. 20) where one of the terminal OBu^t groups on each of the Al atoms has been replaced by a hydride ligand. The modified heterometallic derivatives have indeed proved to be extraordinary precursors for the deposition of $MgAl_2O_4$ thin films, on a variety of substrates, with significantly low decomposition temperatures and minimum carbon impurities [25].

5. CONCLUSIONS AND OUTLOOK

The present review outlines the recent research performed on heterometal alkoxides and emphasises the potential of halide heterobimetallic alkoxides as attractive synthons to heterotermetallic alkoxides and cyclopentadienyl containing heterobimetallic systems. The successful characterization of various stable and soluble heterotermetallic alkoxides is an exciting development which provides optimism, for the first time, for the synthesis of single source precursors to important ternary ceramics e.g., PZT [71] and PNM [72]. The stepwise chelation of a central metal atom by different alkoxometallate units, opens up new possibilities in the rational construction of heteropolymetallic ensemble, following a building block approach. However, the use of presently known alkoxometallate ligands towards various metal halides impose a limitation of fixed metal stoichiometries and the heterometal systems resulting from charge neutralisation principle, although of considerable academic interest can not serve as 'molecules of utility'.

The synthesis of single source precursors with desired combination of metallic elements require novel alkoxometallate anions based on metals present in unusual oxidation states or with inherent versatility in displaying different coordination numbers. The possibilities of modifying the heterometal alkoxides by introducing hetero-ligands such as a cyclopentadienyl, hydride, siloxide etc. can be advantageous in achieving new metal ratios and new type of reactivity. The sub-valent state of Group 14 elements in $M'M_2(OBu^t)_6$ (Section 2) play a key role in the chemical vapour decomposition process (Section 4) since the use of $[Ga(OBu^t)_3]_2$ as precursor in a CVD process gave only Ga_2O_3 and no elemental gallium was detected. However in cases where variable oxidation states of the metallic elements are not stable, a similar phenomenon could be induced by using hydride containing alkoxides [73]. The hydride modified alkoxides represent a promising class of heteroleptic alkoxide derivatives and it is relevant to add that using aluminium and gallium hydrido alkoxides of the type $[HM(OBu^t)_2]_2$ and $[H_2M(OBu^t)]_2$ ($M = Al$, Ga), we have obtained nanoscaled Al/Al_2O_3 and Ga/Ga_2O_3 composites, respectively [73]. We have recently shown that hydride containing Mg–Al heterobimetallic alkoxides are excellent precursors to pure $MgAl_2O_4$ ceramic. The emerging chemistry of polynuclear metal hydrido alkoxides and the potential for the development of new types of reactivity has recently been reviewed by Chisholm [74]. The hydrido alkoxides are highly reactive species and their reac-

tions with hydroxy reagents of the type $(C_6H_5)_3SiOH$ and $(C_6H_5)_2Si(OH)_2$ has led to novel molecular alumopolysiloxanes [75]. Also compounds involving siloxide ligands are attractive precursors for the dispersion of metallic elements in SiO_2 or Al_2O_3 matrices. We have reported on the new heterosiloxanes of bivalent Group 14 elements of the type $[Ph_3SiOM(\mu\text{-}OBu^t)]_2$ (M = Ge, Sn, Pb) [76]. This approach can be extended to mixed-metal systems. The reactivity studies on heterometal alkoxides are limited to a few reports. Ligand exchange or controlled hydrolysis reactions are of great importance in the context of sol–gel process where the precursor is often dissolved in an alcohol/protic reagent (of different pK_a and steric demands) used as solvent and the isolation and characterization of partially modified 'intermediate' molecules can throw light on the chemical transformation process taking place at molecular level.

In view of the inherent difficulties (e.g. twinning, plasticity, loss of crystallinity at ambient temperature) associated with the deceptively simple spectral patterns commonly observed in metal alkoxide chemistry, the structure determination by X-ray crystallography is often not straightforward and the unambiguous characterization of heterometal derivatives, in the absence of X-ray crystallographic data, requires an arsenal of complementary analytical techniques for instance multinuclear solution and solid state NMR studies, mass spectroscopy. The variable temperature NMR studies can provide useful information about the degree of aggregation of the complex, the coordination number at metal centres and the number of unique ligand environments present in the molecule. The use of NMR active nuclei can be of immense help in probing the solution structure and other associative-dissociative processes (monomer–dimer equilibrium) occurring in the solution especially in those cases where the single-crystal subjected to the X-ray diffraction analysis is not representative of the bulk material. Also, the molecular weight studies assume special significance in view of the tendency of heterometal alkoxides to dissociate in the solution.

Acknowledgements—The continuing support of the Deutsche Forschungsgemeinschaft (SFB-277) and Fonds der Chemischen Industrie, in accomplishing this work, is gratefully acknowledged. SM is thankful to the Alexander von Humboldt Foundation, Germany for a research fellowship.

REFERENCES

1. (a) Chisholm, M. H., *Inorganic Chemistry Toward the 21st Century*; p. 243. American Chemical Society: Washington DC. (1983); (b) Bradley, D. C., *Chem. Rev.*, 1989, **89,** 1317; (c) Chandler, C. D., Roger, C. and Hampden-Smith, M. J., *Chem. Rev.*, 1993, **93,** 4205 and refs therein; (d) Sanchez, C. and Ribot, F., *New J. Chem.*, 1994, **18,** 1107; (e) Hubert-Pfalzgraf, L. G., *Polyhedron*, 1994, **13,** 1181; (f) Bradley, D. C., *Polyhedron*, 1994, **13,** 1111; (g) Buhro, W. E., *Polyhedron*, 1994, **13,** 1131; (h) Judeinstein, P. and Sanchez, C., *J. Mater. Chem.*, 1996, **6,** 511; (i) Schubert, U., *J. Chem. Soc., Dalton Trans.*, 1996, 3343.
2. Rupich, M. W., Lagos, B. and Hachey, J. P., *Appl. Phys. Lett.*, 1989, **55,** 2447.
3. Putlin, S. N., Antipov, E. V., Chmaissen, O. and Marezio, M., *Nature*, 1993, **363,** 56.
4. Maeda, H., Tanaka, Y., Fukutomi, M. and Asane, T., *Jpn. J. Appl. Phys.*, 1988, **27,** L209.
5. (a) Veith, M., *Chem. Rev.*, 1990, **90,** 3; (b) Caulton, K. G. and Hubert-Pfalzgraf, L. G., *Chem. Rev.*, 1990, **90,** 969; (c) Mehrotra, R. C., Singh, A. and Sogani, S., *Chem. Rev.*, 1994, **94,** 1643; (d) Mehrotra, R. C., Singh, A. and Sogani, S., *Chem. Soc. Revs.*, 1994, 215; (e) Herrman, W. A., Huber, N. W. and Runte, O., *Angew. Chem.*, 1995, **107,** 2371; (f) Hubert-Pfalzgraf, L. G., *New J. Chem.*, 1995, **19,** 727; (g) Boyle, T. J. and Schwartz, R. W., *Comments Inorg. Chem.*, 1994, **16,** 243.
6. (a) Veith, M., Mathur, S. and Huch, V., *J. Am. Chem. Soc.*, 1996, **118,** 903; (b) Veith, M., Mathur, S. and Huch, V., *Inorg. Chem.*, 1996, **35,** 7295.
7. Bradley, D. C., Mehrotra, R. C. and Gaur, D. P., *Metal Alkoxides*. Academic Press, London (1978).
8. Veith, M. and Rösler, R., *Z. Naturforsch.*, 1986, **B41,** 1071.
9. Meese-Marktscheffel, J. A., Weimann, R., Schumann, H. and Gilje, J. W., *Inorg. Chem.*, 1993, **32,** 5894.
10. Veith, M., Yu, E. C. and Huch, V., *Chem. Eur. J.*, 1995, **1,** 1.
11. Hampden-Smith, M. J., Williams, D. S. and Rheingold, A. L., *Inorg. Chem.*, 1990, **29,** 4076.
12. Boyle, T. J., Bradley, D. C., Hampden-Smith, M. J., Patel, A. and Ziller, J. W., *Inorg. Chem.*, 1995, **34,** 5893.
13. Veith, M. and Mathur, S., unpublished results.
14. Veith, M., Mathur, S., Mathur, C. and Huch, V., *J. Chem. Soc., Dalton Trans.*, 1997, 2101.
15. Veith, M. and Reimers, R., *Chem. Ber.*, 1990, **123,** 1941.
16. Teff, D. J., Huffman, J. C. and Caulton, K. G., *Inorg. Chem.*, 1994, **33,** 6289.
17. Eichorst, D. J., Payne, D. A., Wilson, S. R. and Howard, K. E., *Inorg. Chem.*, 1990, **29,** 1458.
18. (a) Veith, M., Kaefer, D. and Huch, V., *Angew. Chem.*, 1986, **98,** 367; (b) Veith, M., Hans, J., Stahl, L., May, P. and Huch, V., *Z. Naturforsch.*, 1991, **46b,** 403.
19. (a) Teff, D. J., Huffman, J. C. and Caulton, K. G., *Inorg. Chem.*, 1995, **34,** 2491; (b) Teff, D. J., Huffman, J. C. and Caulton, K. G., *Inorg. Chem.*, 1996, **35,** 2981.
20. Veith, M., Mathur, S. and Huch, V., *Inorg. Chem.*, 1997, **36,** 2391.
21. Turevskaya, E. P., Berdyev, D. V., Turova, N. Ya., Starikova, Z. A., Yanovsky, A. I., Struchkov, Yu. T. and Belokon, A. I., *Polyhedron*, 1997, **16,** 663.
22. Turevskaya, E. P., Turova, N. Ya., Korolev, A. V., Yanovsky, A. I. and Struchkov, Yu. T., *Polyhedron*, 1995, **14,** 1531.

23. Veith, M., Käfer, D., Koch, J., May, P., Stahl, L. and Huch, V., *Chem. Ber.*, 1992, **125,** 1033.
24. Wijk, M., Norrestam, R., Nygren, M. and Westin, G., *Inorg. Chem.*, 1996, **35,** 1077.
25. Veith, M. and Wolfanger H., unpublished results.
26. (a) Gulliver, E. A., Wark, T. A., Garvey, J. G., Hampden-Smith, M. J. and Datye, A., *J. Am. Ceram. Soc.*, 1991, **74,** 1091; (b) Purdy, A. P., George, C. F. and Callahan, J. H., *Inorg. Chem.*, 1991, **30,** 2812; (c) Hampden-Smith, M. J., Smith, D. E. and Duesler, E. N., *Inorg. Chem.*, 1989, **28,** 3399.
27. Sassmannshausen, J., Riedel, R., Pflanz, K. B. and Chimiel, H., *Z. Naturforsch.*, 1993, **48B,** 7.
28. Turevskaya, E. P., Kessler, V. G., Turova, N. Ya., Pisarevsky, A. P., Yanovsky, A. I. and Struchkov, Y. T., *J. Chem. Soc., Chem. Commun.*, 1994, 2303.
29. Vaartstra, B. A., Huffman, J. C., Streib, W. E. and Caulton, K. G., *J. Chem. Soc., Chem. Commun.*, 1990, 1750.
30. Vaartstra, B. A., Samuels, J. A., Barash, E. H., Martin, J. D., Streib, W. E., Gasser, C. and Caulton, K. G., *J. Organomet. Chem.*, 1993, **449,** 191.
31. Vaartstra, B. A., Streib, W. E. and Caulton, K. G., *J. Am. Chem. Soc.*, 1990, **112,** 8593.
32. Borup, B., Streib, W. E. and Caulton, K. G., *Chem. Ber.*, 1996, **129,** 1003.
33. Evans, W. J., Denning, T. J., Olofson, J. M. and Ziller, W. J., *Inorg. Chem.*, 1989, **28,** 4027.
34. Veith, M., Weidner, S., Kunze, K., Hans, J. and Huch, V., *Coord. Chem. Revs.*, 1994, **137,** 297.
35. Tripathi, U. M., Singh, A., Mehrotra, R. C., Goel, S. C., Chiang, M. Y. and Buhro, W. E., *J. Chem. Soc., Chem. Commun.*, 1992, 152.
36. Lamotte, J., Oideberg, O., Dupont, L. and Durfut, P., *Cryst. Struct. Commun.*, 1981, **10,** 59.
37. Meese-Marktscheffel, J. A., Fukuchi, R., Kido, M., Tachhibana, G., Jensen, C. M. and Gilje, J. W., *Chem. Mater.*, 1993, **5,** 755.
38. Mehrotra, R. C. and Singh, J., *J. Ind. Chem. Soc.*, 1977, **54,** 109.
39. Veith, M. and Rösler, R., *Angew. Chem., Int. Ed. Engl.*, 1982, **21,** 858.
40. Folting, K., Streib, W. E., Caulton, K. G., Poncelet, O. and Hubert-Pfalzgraf, L. G., *Polyhedron*, 1991, **10,** 1639.
41. Rogova, T. V., Turova, N. Y. and Kozlova, N. I., *Sov. J. Coord. Chem.*, 1986, **12,** 440.
42. Turevskaya, E. P., Kessler, V. G., Turova, N. Y., Pisarevsky, A. P., Yanovsky, A. I. and Struchkov, Y. T., *J. Chem. Soc., Chem. Commun.*, 1994, 2303.
43. Vaartstra, B. A., Streib, W. E., Huffman, J. C. and Caulton, K. G., *Inorg. Chem.*, 1991, 30, 3068.
44. Clark, D. L. and Watkin, J. G., *Inorg. Chem.*, 1993, **32,** 1766.
45. Cotton, F. A., Marler, D. O. and Schwotzer, W., *Inorg. Chem.*, 1984, **23,** 4211.
46. Kuhlman, R., Vaartstra, B. A., Streib, W. E., Huffman, J. C. and Caulton, K. G., *Inorg. Chem.*, 1993, **32,** 1272.
47. Malpezzi, L., Zucchini, U. and Dall'Occo, T., *Inorg. Chem. Acta*, 1991, **180,** 245.
48. Sogani, S., Singh, A., Bohra, R., Mehrotra, R. C. and Noltemeyer, M., *J. Chem. Soc., Chem. Commun.*, 1991, 738.
49. Olmstead, M. M., Power, P. P. and Sigel, G., *Inorg. Chem.*, 1979, **17,** 1962.
50. Veith, M., Mathur, C., Mathur, S. and Huch, V., *Organometallics*, 1997, **16,** 1292.
51. Veith, M., Mathur, C. and Huch, V., *Organometallics*, 1996, **15,** 2858.
52. Veith, M., Mathur, S. and Huch, V., *J. Chem. Soc., Dalton Trans.*, 1996, 2485.
53. Pell, J. W., Davis, W. C. and zur Loye, H. C., *Inorg Chem.*, 1996, **35,** 5754.
54. Moulson, A. J. and Herbert, J. M., *Electroceramics: Materials, Properties and Applications*, Chapman and Hall, London (1990).
55. (a) Holland, G. F. and Stacy, A. M., *Acc. Chem. Res.*, 1988, **21,** 8; (b) Poole, C. P., *Copper Oxide Superconductors*, Wiley Inc., New York (1988).
56. Reinen, D. and Friebel, C., *Inorg. Chem.*, 1984, **23,** 791.
57. Blanchette, J. D. and Willett, R. D., *Inorg. Chem.*, 1988, **27,** 843.
58. Bradley, D. C., Chudzynska, H., Hursthouse, M. B. and Motevalli, M., *Polyhedron*, 1991, **10,** 1049.
59. (a) Evans, W. J., Sollberger, M. S. and Hanusa, T. P., *J. Am. Chem. Soc.*, 1988, **110,** 1841; (b) Evans, W. J., Olofson, J. M. and Ziller, J. W., *Inorg. Chem.*, 1989, **28,** 4308.
60. Evans, W. J., Sollberrger, M. S. and Ziller, J. W., *J. Am. Chem. Soc.*, 1993, **115,** 4120.
61. Hogerheide, M. P., Ringelberg, S. N., Grove, D. M., Jastrzebski, J. T. B. H., Boersma, J., Smeets, W. J. J., Spek, A. L. and Koten, G. V., *Inorg. Chem.*, 1996, **35,** 1185.
62. (a) Clark, D. L., Huffman, J. C. and Watkin, J. G., *Inorg. Chem.*, 1992, **31,** 1554; (b) Clark, D. L., Gordon, J. C., Huffman, J. C., Vincent-Hollis, R. L., Watkin, J. G. and Zwick, B. D., *Inorg. Chem.*, 1994, **33,** 5903.
63. Goel, S. C., Chiang, M. Y. and Buhro, W. E., *Inorg. Chem.*, 1990, **29,** 4640.
64. Matchett, M. A., Chiang, M. Y. and Buhro, W. E., *Inorg. Chem.*, 1990, **29,** 358.
65. Gyepes, R., Hiller, J., Thewalt, U., Polasek, M., Sindelar, P. and Mach, K., *J. Organomet. Chem.*, 1996, **516,** 177.
66. Veith, M. and Huch, V., *Phosphorous, Sulfur and Silicon*, 1997 (in press).
67. (a) Mathur, S., Singh, A. and Mehrotra, R. C., *Polyhedron*, 1992, **11,** 341; (b) Mathur, S., Singh, A. and Mehrotra, R. C., *Polyhedron*, 1993, **12,** 1073.
68. (a) Weis, R. S. and Gaylord, T. K., *Appl. Phys. A*, 1985, **37,** 191; (b) Eichorst, D. J. and Payne, D. A., *Mater. Res. Soc. Symp. Proc.*, 1988, **121,** 773.
69. (a) Veith, M. and Kneip, S., *J. Mater. Sci. Lett.*, 1994, **13,** 335; (b) Veith, M., Kneip, S. J., Jungmann, A. and Hüfner, S., *Z. Anorg. Allg. Chem.*, (in press).
70. (a) Jones, K., Davis, T. J., Emblenn, H. G. and Parks, P. B., *Ceramic through Chemistry (II)*, ed. C. J. Brinker, D. E. Klark and D. R. Ulrich, *Mater. Res. Soc. Symp.*, 1986, **73,** 111; (b) Hartnett, T. M. and Gentilman, R. L., *Proc. SPIE*, 1984, **505,** 15.
71. (a) Schwartz, R. W., Assink, R. A. and Headley, T. J., *J. Mater. Res. Soc. Symp. Proc.*, 1992, **243,**

245; (b) Schwartz, R. W., Bunker, B. C., Dimos, D. B., Assink, R. A., Tuttle, B. A., Tallant, D. R. and Weinstock, I. A., *Ferroelectrics*, 1992, **2,** 243.
72. (a) Okuwada, K., Imai, M. and Kakuno, K., *Jpn. J. Appl. Phys.*, 1989, **28,** 1271; (b) Okuwada, K., Nakamura, S.-I., Imai, M. and Kakuno, K., *Jpn. J. Appl. Phys.*, 1990, **29,** 1153.
73. (a) Veith, M., Faber, S., Wolfanger, H. and Huch, V., *Chem. Ber.*, 1996, **129,** 381; (b) Veith, M., Faber, S., Hempelmann, R., Janssen, S., Prewo, J. and Eckerlde, H., *J. Mater. Sci.*, 1996, **31,** 2009.
74. Chisholm, M. H., *Chem. Soc. Revs.*, 1995, 79.
75. Veith, M., Jarczyk, M. and Huch, V., *Angew. Chem.*, 1997, **109,** 140.
76. Veith, M., Mathur, C. and Huch, V., *J. Chem. Soc., Dalton Trans.*, 1997, 995.

Pergamon

Polyhedron Vol. 17, No. 7, p. 1035, 1998
© 1998 Elsevier Science Ltd
All rights reserved. Printed in Great Britain
0277–5387/98 $19.00+0.00

Preface

This Polyhedron Symposium-in-Print entitled "Recent Progress in Organometallic Chemistry" is dedicated to Professor Wolfgang A. Herrmann on the occasion of his 50th birthday. It is intended to reflect the various facets of the research endeavours that his former students, postdoctoral and other close associates are presently engaged in. We hope that the contributions collected here are also representative of the increased breadth and sophistication that organometallic chemistry has achieved over the last two decades. Since the late seventies organometallic chemistry has progressed in such way that it now encompasses not only the late transition metals, but also early transition metals and lanthanides as well as the radioactive element technetium. While structure determinations by X-ray diffraction and nuclear magnetic resonance spectroscopy helped improve substantially the understanding of the properties of the various metals, the design of novel ligand systems has opened up new applications in homogeneous catalysis, a discipline that has particularly benefited from the advances in organometallic chemistry.

MALCOLM H. CHISHOLM JUN OKUDA

Pergamon

PII: S0277-5387(97)00489-0

Polyhedron Vol. 17, No. 7, pp. 1037–1043, 1998
© 1998 Elsevier Science Ltd
All rights reserved. Printed in Great Britain
0277-5387/98 $19.00+0.00

Selective conversion of an ethylene to an ethylidene ligand in reactions of a hydrido(ethylene) complex of tantalum with iodofluorocarbons. Molecular structure of $[Ta(\eta^5\text{-}C_5H_5)_2(\eta^1\text{-}CHCH_3)I]$†

Russell P. Hughes,[a]* Susan M. Maddock,[a] Arnold L. Rheingold[b] and Ilia A. Guzei[b]

[a] Department of Chemistry, 6128 Burke Laboratory, Dartmouth College, Hanover, New Hampshire 03755, U.S.A.

[b] Department of Chemistry, University of Delaware, Newark, Delaware 19716, U.S.A.

(Received 30 September 1997; accepted 17 November 1997)

Abstract—Reactions of $[TaCp_2(C_2H_4)H]$ (**3**) with perfluoro-*n*-butyl iodide or perfluorobenzyl iodide cleanly yield the iodo(ethylene) complex $[TaCp_2(C_2H_4)I]$ (**4**) together with the hydrofluorocarbons $CF_3CF_2CF_2CF_2H$ and $C_6F_5CF_2H$, respectively. In sharp contrast, reactions of **3** with perfluoro-iso-propyl iodide or pentafluorophenyl iodide cleanly afford the isomeric iodo(ethylidene) complex $[TaCp_2(CHCH_3)I]$ (**5**). No interconversion of **4** and **5** is observed under these reaction conditions, indicating that each is formed under conditions of kinetic control. The structure of **5** has been confirmed by X-ray crystallography. Similar results to give much more thermally sensitive products are observed for the niobium analogues. Possible mechanisms for these highly selective reactions are discussed. © 1998 Elsevier Science Ltd. All rights reserved

Keywords: ethylene; ethylidene ligand; iodofluorocarbons.

For some time we have been interested in the introduction of fluoroalkyl groups into organometallic complexes as a means of enhancing their solubilities in saturated fluorocarbons and supercritical CO_2, thereby allowing stoichiometric and catalytic chemistry to be conducted in these unusual media [1]. In a number of cases we have shown that reactions of low valent organometallic complexes with fluoroalkyl iodides can lead to fluoroalkylation at the metal center or at cyclopentadienyl rings, depending on the ligands present on the metal, and the structure of the fluoroalkyl iodide [2,3].

Recently we described the chemistry of $[WCp_2(C_2H_4)]$ (**1**: Cp = η^5-C_5H_5) with the secondary fluoroalkyl iodide $(CF_3)_2CF$-I, in which *exo*-fluoroalkylation at the cyclopentadienyl ring was observed, followed by loss of ethylene and hydrogen migration to the metal to afford **2** [4]. Similar results were obtained using the molybdenum analogue of **1**. Evidence for a fluoroalkyl carbanion intermediate was obtained in this system [4]. The tertiary fluoroalkyl iodide $(CF_3)_3C$-I affords fluoroalkylation at the ethylene ligand [4], whereas the major products using primary fluoroalkyl and perfluorobenzyl iodides result from fluoroalkylation at the metal [5].

As a seemingly logical extension of this chemistry we chose to examine the corresponding reactions of fluoroalkyl iodides with $[TaCp_2(C_2H_4)H]$ (**3**), which is isoelectronic with **1**. In this paper we describe the results of these reactions, which unfortunately lead not to fluoroalkylated organometallic complexes, but which reveal a remarkably selective reaction leading to isomerization of coordinated ethylene to ethylidene. In hindsight it is fortunate that we chose to look at the secondary fluoroalkyl iodide $(CF_3)_2CF$-I

† Dedicated to Prof. Dr W. A. Herrmann on the occasion of his 50th birthday.

* Author to whom correspondence should be addressed.

first, since the results of corresponding reactions of primary fluoroalkyl iodides might be regarded as quite mundane.

RESULTS AND DISCUSSION

Reaction of **3** with perfluoro-*n*-butyl iodide, $CF_3CF_2CF_2CF_2$-I, in an NMR tube in C_6D_6 afforded clean and quantitative conversion to the known [6] iodo(ethylene) complex **4**, along with $CF_3CF_2CF_2CF_2H$. The presence of the hydrofluorocarbon was confirmed by both ^{19}F and ^1H NMR spectroscopy [7]; observation of the ^1H NMR resonance as a triplet of triplets at δ 4.82 ppm serves as a ready identification of this product. Similarly, reaction of **3** with perfluorobenzyl iodide, $C_6F_5CF_2$-I, under the same conditions generated **4** and the corresponding hydrofluorocarbon $C_6F_5CF_2$-H; once again the hydrofluorocarbon was readily identified by its characteristic proton resonance at δ 6.14 ppm, with strong triplet coupling to the adjacent CF_2, and the appropriate ^{19}F NMR resonances. Treatment of **3** with I_2 also led exclusively to **4**.

In sharp contrast, reaction of **3** with the secondary fluoroalkyl iodide, $(CF_3)_2CF$-I, afforded the expected hydrofluorocarbon product $(CF_3)_2CF$-H, identified by a characteristic doublet of septets at δ 3.54 ppm in the ^1H NMR spectrum, but none of the iodo(ethylene) complex **4** was observed. Instead the organometallic product exhibited two resonances for inequivalent cyclopentadienyl rings, together with a doublet CH_3 resonance at δ 5.14 ppm coupled by 9 Hz to a quartet CH resonance at δ 11.58 ppm. Observation of corresponding ^{13}C NMR resonances at δ 270.2 (CH) and 35.5 (CH_3) confirmed the presence of an ethylidene rather than an ethylene ligand, and allowed for-

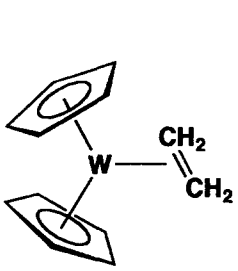

1

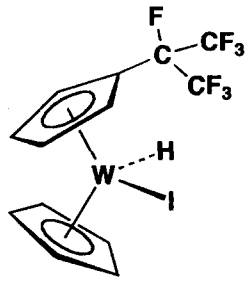

2

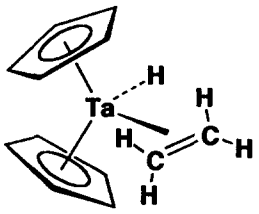

3

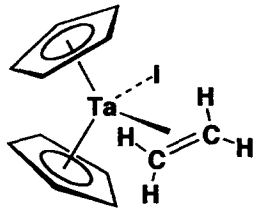

4

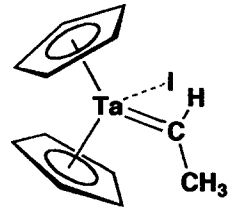

5

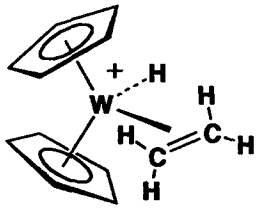

6

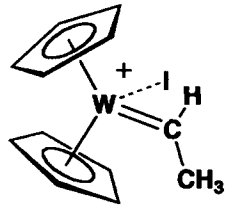

7

mulation of the product as complex **5**. Complex **5** was also the exclusive organometallic product formed on treatment of **3** with pentafluorophenyl iodide, C_6F_5I; C_6F_5H was readily identified as the hydrofluorocarbon product. Reaction of **3** with the tertiary iodide, $(CF_3)_3C\text{-}I$, led to extensive molecular demolition of both components, with no readily identifiable organometallic or organic fragments. The ethylene ligand in **4** and the ethylidene ligand in **5** showed no further reactivity on treatment with any of the fluorocarbon iodides, indicating that each product is formed under conditions of kinetic control.

While it is formed cleanly as determined by NMR spectroscopy, isolation of complex **5** as extremely air sensitive crystals could only be achieved in 44% yield. The crystals were subjected to a single crystal X-ray diffraction study. An ORTEP diagram is presented in Fig. 1. Details of the crystallographic determination are provided in Table 1, and some key bond distances and angles are presented in Table 2. The Ta=C(11) distance of 2.024(11) Å is identical within experimental error to that in the methylidene complex $[TaCp_2(CH_2)CH_3]$, [8]; a characteristically obtuse angle of 140.9(12)° is observed for Ta—C(11)—C(12). As observed in $[TaCp_2(CH_2)CH_3]$ [8] and related complexes [6], the plane of the alkylidene ligand lies perpendicular to the plane of I—Ta—C(11), with a high barrier to rotation about the Ta=C bond [9] leading to inequivalent

Table 1. Crystallographic data for $[Ta(C_5H_5)_2(=CHCH_3)I]$ (**5**)

Formula	$C_{12}H_{14}ITa$
Formula weight	466.08
Space group	*Pbca*
a (Å)	13.60180(10)
b (Å)	12.3154(3)
c (Å)	14.7533(2)
β (°)	—
V (Å^3)	2471.68(7)
Z	8
Crystal color, habit	brown block
D_{calc} (g cm^{-3})	2.505
μ(Mo–K$_\alpha$) (cm^{-1})	113.53
Temperature (K)	223(2)
Diffractor	Siemans P4/CCD
Radiation	Mo–K$_\alpha$ (λ = 0.71073 Å)
$R(F)$, %[a]	3.79
$R(wF^2)$, %[a]	13.52

[a] Quantity minimized = $R(wF^2) = \Sigma[w(F_o^2 - F_c^2)^2]/\Sigma[(wF_o^2)^2]^{1/2}$; $R = \Sigma\Delta/\Sigma(F_o)$, $\Delta = |(F_o - F_c)|$.

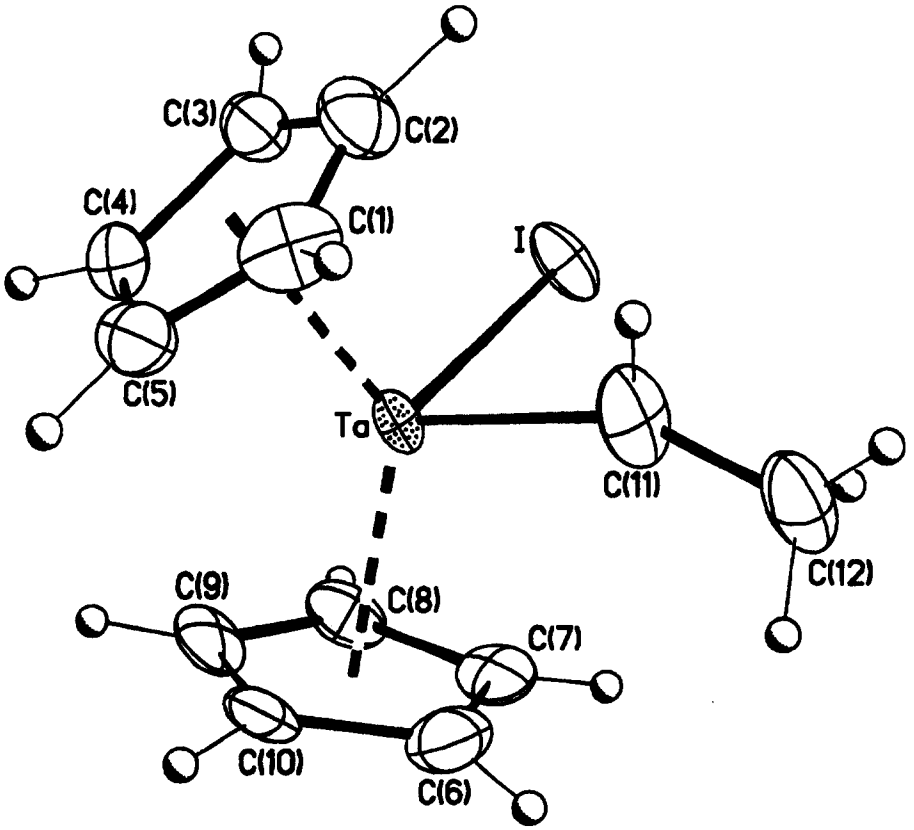

Fig. 1. Molecular Structure of **5**.

Table 2. Selected bond lengths (Å) and angles (°) for **5**

Ta—C(11)	2.024(11)	Ta—C(6)	2.411(11)
Ta—C(5)	2.412(12)	Ta—C(7)	2.399(10)
Ta—C(10)	2.416(9)	Ta—C(2)	2.424(12)
Ta—C(1)	2.432(13)	Ta—C(9)	2.440(9)
Ta—C(4)	2.449(12)	Ta—C(3)	2.445(13)
Ta—C(8)	2.453(11)	Ta—I	2.8840(7)
Ta—CEN(1)	2.122(13)	Ta—CEN(2)	2.101(13)
C(1)—C(2)	1.39(2)	C(1)—C(5)	1.41(2)
C(2)—C(3)	1.37(2)	C(3)—C(4)	1.44(2)
C(4)—C(5)	1.38(2)	C(6)—C(7)	1.39(2)
C(6)—C(10)	1.43(2)	C(7)—C(8)	1.47(2)
C(8)—C(9)	1.41(2)	C(9)—C(10)	1.40(2)
C(11)—C(12)	1.35(2)		
CEN(1)—Ta—CEN(2)	133.2(6)	CEN(1)—Ta—I	107.0(6)
CEN(2)—Ta—I	105.1(6)	CEN(1)—Ta—C(11)	104.5(6)
CEN(2)—Ta—C(11)	109.1(6)	C(12)—C(11)—Ta	140.9(12)
C(11)—Ta—I	89.2(3)		

resonances for the cyclopentadienyl rings in the ^1H and ^{13}C NMR spectra.

Examples of conversion of ethylene to ethylidene ligands are rare indeed; only two examples appear to have been observed. The only known example in tantalum chemistry has been reported by Schrock [10], in which the complex $[TaL(C_2H_4)]$ $\{L = N(CH_2CH_2NSiMe_3)_3\}$ is isomerized to its thermodynamically more stable isomer $[TaL(CHCH_3)]$ by the primary phosphine $PhPH_2$, in a series of α- and β-hydrogen elimination and addition reactions. However, the first such example, and that most relevant to our observations, was reported by Cooper, in which the tungsten complex **6** is converted to **7** on treatment with I_2 [11]. The mechanism suggested by Cooper is presented in Scheme 1, with isomerization of **6** to its ethylidene isomer **10** occurring via the ethyl intermediate **9**. Deuterium labeling studies could not distinguish whether the proposed hydrogen atom loss, with $I^\bullet$ as the acceptor, occurred directly from the α-carbon of intermediate **9**, or from the metal-hydride position of **10**. Numerous attempts on our part to selectively label the tantalum complex **3** with deuterium, by treatment of the iodo complex **4** with BD_4^- Et_3BD^-, or AlD_4^-, led to samples of **3** in which deuterium was scrambled between the metal position and the two ends of the coordinated olefin. This indicates that **3** is indeed in equilibrium with an ethyl isomer, analogous to **9**, but also that ethylene rotation in **3**, while known to be slow on the NMR timescale [12], is sufficiently rapid on the timescale required for reaction workup that complete deuterium scrambling occurs. In the absence of selectively labeled **3** it is clearly not possible to ascertain which H is lost to give **4** or **5**, and makes mechanistic discussion more speculative than would normally be desirable. However based on our previous results, and other observations from the chemistry of iodofluorocarbons, one possible mechanism can be suggested.

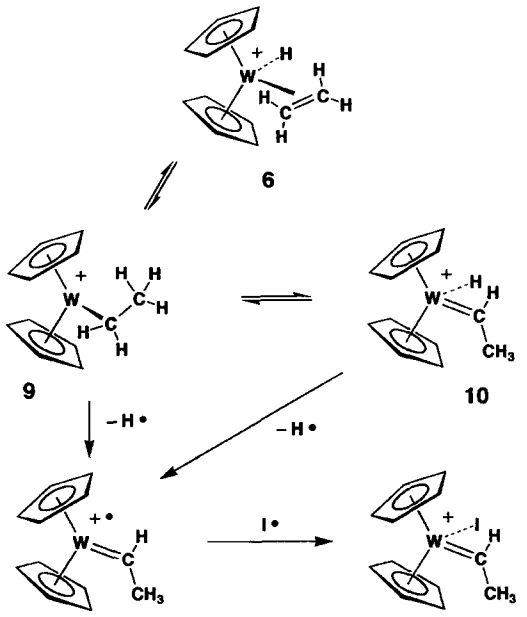

Scheme 1.

The chemistry of iodofluorocarbons is replete with examples in which the first step is electron transfer [13–15], with the radical anion thus generated, $[R_F\text{-}I]^{\bullet -}$, being known to give I^- and $R_F^\bullet$, at least when R_F is a primary fluoroalkyl [13]. Abstraction of the metal-bound H (the weakest bond to hydrogen in the intermediate radical cation intermediate **11**) can then occur when $R_F^\bullet$ is a relatively small primary or benzylic radical, as shown in Scheme 2, with final trapping by

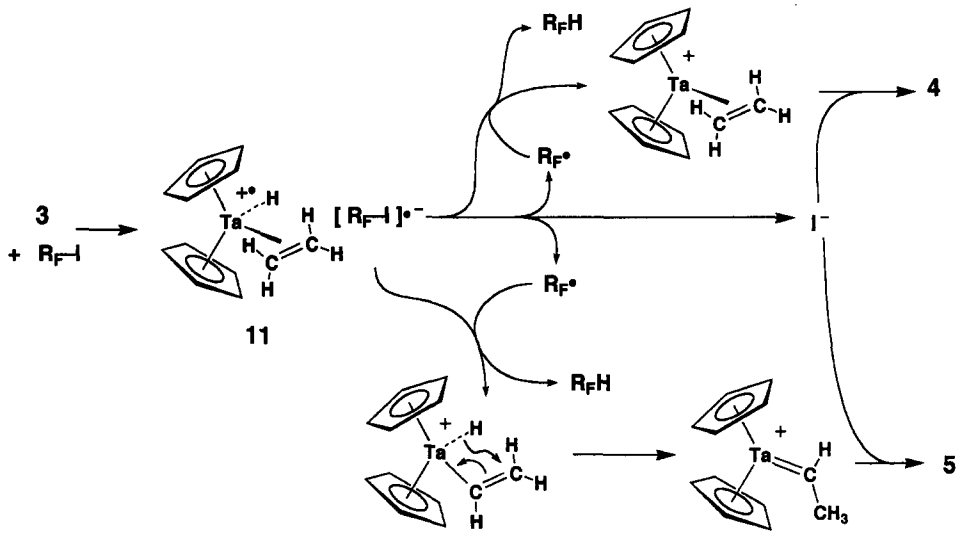

Scheme 2.

I^- completing the reaction to give **4**. An analogous pathway presumably occurs using I_2. But why then do the secondary iodides afford a different organometallic product? If the initial step of the mechanisms is the same, it is possible that the significantly more sterically demanding secondary radicals are too large to get close enough to abstract the metal bound hydrogen, and accordingly are restricted to abstracting a more peripheral hydrogen from the ethylene ligand. The resultant vinyl complex could rearrange to the ethylidene intermediate, which is then trapped by iodide to give **5**. Without the ability to selectively label the hydride or ethylene ligands we have no means of testing the required consequences of reaction scheme, and further discussion would be even more speculative. We should point out however that there may well be a completely different mechanism operating for primary or benzylic, versus secondary and aromatic iodofluorocarbons, as we [4,5] and others [13–15,17] have established in different systems. However we do not see any traces of $CF_3CF{=}CF_2$, the fluoroolefin signature of a fluorocarbanion intermediate [4], in any reactions using $(CF_3)_2CF$-I, and so it is certainly possible that the chemistry observed here really does represent different selective chemistry of fluoroalkyl radical intermediates.

Finally, we have carried out some reactions using the niobium analogue of **3**. Reaction of $[NbCp_2(C_2H_4)H]$ with perfluorobenzyl iodide affords $C_6F_5CF_2$-H and an organometallic product whose ^1H NMR spectrum showed a cyclopentadienyl singlet at δ 6.14 ppm, and two pseudo triplets at δ 2.14 and 1.16 ppm, consistent with formation of $[NbCp_2(C_2H_4)I]$. The product was sufficiently thermally unstable that we were unable to isolate it from the reaction mixture; this compound does not appear to have been prepared before, although the corresponding chloride has been reported [16]. In contrast, reaction of $[NbCp_2(C_2H_4)H]$ with perfluoro-iso-propyl iodide affords $(CF_3)_2CF$-H and the corresponding iodo-(ethylidene) niobium analogue of **5**, which was identified by NMR spectroscopy, but was so unstable that correct microanalysis results could not be obtained. Thus the corresponding niobium chemistry appears to parallel the tantalum results, except that the organometallic products are much more thermally sensitive and difficult to handle.

EXPERIMENTAL SECTION

General considerations

All reactions were performed in oven-dried glassware, using standard Schlenk techniques, under an atmosphere of dinitrogen which had been deoxygenated over BASF catalyst and dried over Aquasorb®, or in a Braun Drybox. Benzene was distilled from sodium immediately before use. IR spectra were recorded on a Perkin–Elmer FTIR 1600 Series spectrometer. NMR spectra were recorded on a Varian Unity Plus 300 FT spectrometer. ^1H and $^{13}C\{^1H\}$ NMR spectra are referenced as ppm downfield from TMS. ^{19}F NMR spectra were referenced to $CFCl_3$ (0.00 ppm). Microanalyses were performed by Schwarzkopf Microanalytical Laboratory, Woodside, NY. $I(CF_2)_3CF_3$ (Aldrich), C_6F_5I, $ICF(CF_3)_2$ and $ICF_2C_6F_5$ (PCR) were purified by washing with a solution of sodium thiosulfate to remove iodine, followed by washing with water and then drying over magnesium sulfate and deoxygenation by several cycles of freeze-evacuate-thaw. $[TaCp_2(C_2H_4)H]$ [12a] and $[NbCp_2(C_2H_4)H]$ [12b] were prepared according to literature procedures.

Reaction of $[TaCp_2(C_2H_4)H]$ *with* $(CF_3)_2CFI$; *preparation of* $[TaCp_2(CHCH_3)I]$ **(5)**

$[TaCp_2(C_2H_4)H]$ (**3**) (0.070 g, 0.206 mmol) was dissolved in benzene (6 ml). $(CF_3)_2CFI$ (0.035 ml, 0.206 mmol) was added and the solution turned orange-/brown. It was stirred for 15 min then filtered. The solvent was removed and the residue was dissolved in benzene (12 ml) and filtered. The solvent volume was reduced and hexane was added to precipitate the product. Recrystallization from benzene/hexane afforded $[TaCp_2(CHCH_3)I]$ (**5**) (0.040 g, 43.5%), as exceedingly air sensitive, deep orange brown crystals, m.p. 140–142°C. ^1H NMR (C_6D_6) δ 11.58 (q, $J_{HH} = 8.9$ Hz, 1H, =CH); 5.16 (s, 5H, C_5H_5); 5.12 (s, 5H, C_5H_5); 3.14 (d, $J_{HH} = 8.9$ Hz, 3H, CH_3). $^{13}C\{^1H\}$ NMR (C_6D_6) δ 270.2 (s, Ta=C); 102.5 (s, C_5H_5); 101.9 (s, C_5H_5); 35.5 (s, CH_3). Anal. calc. for $C_{12}H_{14}ITa$; %C 32.31, %H 3.16. Found: %C 31.91, %H 3.46.

The reaction was carried out on the same scale in an NMR tube using C_6D_6 as solvent, and showed essentially complete formation of **5** along with a stoichiometric amount of $(CF_3)_2CFH$; ^1H NMR (C_6D_6) δ 3.54 (1H, dsept, $^2J_{FH} = 43.0$, $^3J_{FH} = 5.3$ Hz). ^{19}F NMR (C_6D_6) δ −76.39 (6F, dd, $^3J_{FH} = 5.3$, $^3J_{FF} = 11.6$ Hz), −214.0 (1F, dsept, $^2J_{FH} = 43.0$, $^3J_{FF} = 11.6$ Hz). The reaction is not completely quantitative as there is always formation of small amounts of insoluble yellow solid which could not be characterized.

A similar NMR tube reaction using C_6F_5I afforded clean formation of **5** along with C_5F_5H.

Crystallographic structure determination of $[TaCp_2(CHCH_3)I]$ **(5)**

Crystal, data collection, and refinement parameters are given in Table 1. The systematic absences in the diffraction data of **5** were uniquely consistent for space group *Pbca* whose correctness was subsequently confirmed by chemically reasonable and computationally stable results of refinement. The structure was solved using direct methods, completed by subsequent difference Fourier synthesis and refined by full-matrix least-squares procedures. All non-hydrogen atoms were refined with anisotropic displacement coefficients, and all hydrogen atoms were treated as idealized contributions. Empirical absorption corrections were applied by using the program DIFABS. There are two high peaks (ca 2 e/Å^3) in the vicinity of the tantalum and iodine atoms respectively, that have no apparent chemical relevance.

All software and sources of the scattering factors are contained in the SHELXTL (version 5.03) program library (G. Sheldrick, Siemens XRD, Madison, WI). Program DIFABS is described by Walker and Stuart in *Acta Cryst.*, 1983, **A39,** 158.

Reaction of $[TaCp_2(C_2H_4)H]$ *with* $C_6F_5CF_2I$; *preparation of* $[TaCp_2(C_2H_4)I]$ **(4)**

As described above, reaction of $[TaCp_2(C_2H_4)H]$ with a stoichiometric amount of $C_6F_5CF_2I$ in C_6D_6 an NMR tube afforded clean conversion to $[TaCp_2(C_2H_4)I]$, whose ^1H NMR data matched those in the literature [12], and a stoichiometric amount of $C_6F_5CF_2H$; ^1H NMR (C_6D_6) δ 6.14 (1H, t, $^2J_{FH} = 52.5$ Hz). ^{19}F NMR (C_6D_6) δ −113.75 (2F, dtd, $^2J_{FH} = 52.5$, $^4J_{FF} = 8.5$, $^6J_{FF} = 2.3$ Hz, CF_2), −144.19 (2F, m, F_{ortho}), −149.92 (1F, m, F_{para}), −161.19 (2F, m, F_{meta}).

An analogous reaction with $CF_3CF_2CF_2CF_2$-I afforded **4** and a stoichiometric amount of $CF_3CF_2CF_2CF_2H$; ^1H NMR (C_6D_6) δ 4.82 (1H, tt, $^2J_{FH} = 51.3$, $^3J_{FH} = 4.8$ Hz). ^{19}F NMR (C_6D_6) δ −81.77 (3F, m, CF_3), −128.08 (2F, m, CF_2), −130.40 (2F, m, CF_2), −137.33 (2F, m, $^2J_{FH} = 51.3$, CF_2).

Reaction of $[NbCp_2(C_2H_4)H]$ *with* $(CF_3)_2CFI$; *preparation of* $[NbCp_2(CHCH_3)I]$

$NbCp_2(C_2H_4)H$ (0.065 g, 0.258 mmol) was dissolved in benzene (5 ml) and $(CF_3)_2CFI$ (0.038 ml, 0.270 mmol) was added giving a red/brown solution. This was stirred for 15 min then filtered. The solvent was removed giving a brown residue and a small amount of orange solid which was much less soluble in benzene. The brown residue was dissolved in benzene (5 ml) and filtered. The solvent volume as reduced to approximately 0.5 ml and hexane was added to complete precipitation of the product. It was recrystallized from benzene/hexane to afford the product as an extremely air sensitive solid (0.029 g, 29.8%); m.p. dec. 140°C, ^1H NMR (C_6D_6) δ 13.15 (q, $J_{HH} = 9.0$ Hz, 1H, =CH); 5.25 (s, 5H, C_5H_5); 5.17 (s, 5H, C_5H_5); 2.70 (d, $J_{HH} = 9.0$ Hz, 3H, CH_3); $^{13}C\{^1H\}$ NMR (C_6D_6) δ 102.3 (br s, C_5H_5); 36.9 (s, CH_3), the carbene carbon could not be observed, possibly due to quadrupolar broadening by the Nb nucleus. Anal. calc. for $C_{12}H_{14}INb$: %C 38.12, %H 3.73. Found, %C 36.85, %H 3.72. Due to the extreme air sensitive nature of this compound, these are the best microanalyses we could obtain. An analogous reaction carried out in an NMR tube showed clean formation of $[NbCp_2(CHCH_3)I]$ along with a stoichiometric amount of $(CF_3)_2CFH$.

Supplementary material—Details of the X-ray structure determinations, tables of atomic coordinates and anisotropic thermal parameters, bond lengths and bond angles, anisotropic displacement parameters, and hydrogen atom coordinates for **5** are available from author R.P.H. upon request.

Acknowledgments—R.P.H. acknowledges partial support of this research by the National Science Foundation and by the Donors of the Petroleum Research Fund, administered by

the American Chemical Society. Enlightening discussions with Prof. N. John Cooper are also gratefully acknowledged.

REFERENCES

1. Horváth, I. T. and Rábai, J., *Science*, 1994, **266,** 72. Gladysz, J. A., *Science*, 1994, **266,** 55. Hughes, R. P. and Trujillo, H. A., *Organometallics*, 1996, **15,** 286. Curran, D. P. and Hadida, S., *J. Am. Chem. Soc.*, 1996, **118,** 2531. DiMagno, S. G., Dussault, P. H. and Schultz, J. A., *J. Am. Chem. Soc.*, 1996, **118,** 5312. Curran, D. P., *Chemtracts-Org. Chem*, 1996, **9,** 75. Zhu, D.-W., *Synthesis*, 1993, 953. DeSimone, J. M., Guan, Z., Elsbernd, C. S., *Science*, 1992, **257,** 945. Studer, A., Hadida, S., Ferrito, R., Kim, S.-Y., Jeger, P., Wipf, P. and Curran, D. P., *Science*, 1997, **275,** 823.
2. Hughes, R. P., Husebo, T. L., Rheingold, A. P. and Yap, G. P. A., *Organometallics*, 1997, **16,** 5.
3. Hughes, R. P., Husebo, T. L., Holliday, B. J., Rheingold, A. L. and Liable-Sands, L. M., *J. Organomet. Chem.*, 1997, in press.
4. Hughes, R. P., Maddock, S. M., Rheingold, A. L. and Liable-Sands, L. M., *J. Am. Chem. Soc.*, 1997, **119,** 5988.
5. Hughes, R. P. and Maddock, S. M., unpublished results.
6. Schrock, R. R. and Sharp, P. R., *J. Am. Chem. Soc.*, 1978, **100,** 2389.
7. Andreades, S., *J. Am. Chem. Soc.*, 1964, **86,** 2003.
8. Guggenberger, L. J. and Schrock, R. R., *J. Am. Chem. Soc.*, 1975, **97,** 6578.
9. Lauher, J. W. and Hoffmann, R., *J. Am. Chem. Soc.*, 1976, **98,** 1729.
10. Freundlich, J. S., Schrock, R. R., Cummins, C. C. and Davis, W. M., *J. Am. Chem. Soc.*, 1994, **116,** 6476.
11. Miller, G. A. and Cooper, N. J., *J. Am. Chem. Soc.*, 1985, **107,** 709.
12. (a) Eichner, M. E., Alt, H. G. and Rausch, M. D., *J. Organomet. Chem.*, 1984, **264,** 309. (b) Yasuda, H., Arai, T., Okamoto, T. and Nakamura, A., *J. Organomet. Chem.*, 1988, **361,** 161.
13. Andrieux, C. P., Gélis, L., Medebielle, M., Pison, J. and Savéant, J.-M., *J. Am. Chem. Soc.*, 1990, **112,** 3509.
14. Wakselman, C., *J. Fluorine Chem.*, 1992, **59,** 367.
15. Feiring, A. E., *J. Org. Chem.*, 1985, **50,** 3269.
16. Fredericks, S. and Thomas, J. L., *J. Am. Chem. Soc.*, 1978, **100,** 350.
17. Wakselman, C. and Lantz, A., in *Organofluorine Chemistry; Principles and Commercial Applications*. ed. R. E. Banks, B. E. Smart and J. C. Tatlow. Plenum, New York, 1994.

Pergamon

PII: S0277-5387(97)00490-7

Polyhedron Vol. 17, No. 7, pp. 1045–1054, 1998
© 1998 Elsevier Science Ltd
All rights reserved. Printed in Great Britain
0277-5387/98 $19.00+0.00

Alkylidene dynamics in the cluster complex $Cp^*Rh(CpCo)_2(CO)_2(\mu\text{-}CH_2)$: Observation of an intermediate containing a μ_3-methylidene ligand†

Craig E. Barnes* and F. Holger Försterling§

Department of Chemistry, University of Tennessee, Knoxville, TN 37996-1600, U.S.A.
Email: cebarnes@utk.edu

(Received 2 November 1997; accepted 20 November 1997)

Abstract—The dynamic behaviour of the methylidene ligand in the triangular cluster complex, $Cp^*Rh(CpCo)_2(CO)_2(\mu\text{-}CH_2)$ **3**, has been investigated using multidimensional NMR techniques. Two distinct processes have been identified whereby the methylidene ligand moves between bridging different metal–metal bonds in the complex: (1) methylidene jumps from a Rh—Co bond to the Co—Co bond and (2) degenerate methylidene jumps between the two Rh—Co bonds of the metal triangle. An intermediate has been observed for the latter process. Based on ^1H and ^{13}C NMR data, we propose that the methylidene ligand in this intermediate occupies a triply-bridging coordination position above the metal triangle, simultaneously interacting with all three metal atoms in the complex. To our knowledge, this is the first observation of an intermediate involved in the dynamic behaviour of an alkylidene ligand. Furthermore, it is only the second example of a μ_3-methylidene ligand to be reported. The implications of these results in the areas of alkylidene mobility on metal surfaces and catalysis are discussed. © 1998 Elsevier Science Ltd

Keywords: alkylidene; cluster complex; μ_3-methylidene ligand.

C_1-based hydrocarbon fragments (alkyl, alkylidene and alkylidyne) form one of the most important sets of ligands in organometallic chemistry [1]. When present in discrete mononuclear or polynuclear metal complexes, the series of alkyl, alkylidene and alkylidyne ligands normally assumes one of three coordination modes: terminal, bridging two metal atoms (μ_2, or "μ") or bridging three metal atoms (μ_3 or triply-bridging) (Scheme 1). Within the coordination manifold for the alkylidene ligand, many examples are known for both the terminal and μ_2 geometries. In contrast, very few examples of complexes containing a triply-bridging alkylidene ligand have been reported [2].

Although similar to the ubiquitous carbon monoxide ligand in a number of respects [3], alkylidene ligands are, in general, less labile and exhibit a smaller range of coordination geometries in cluster complexes. While CO ligands may be found simultaneously in all three geometries in a cluster

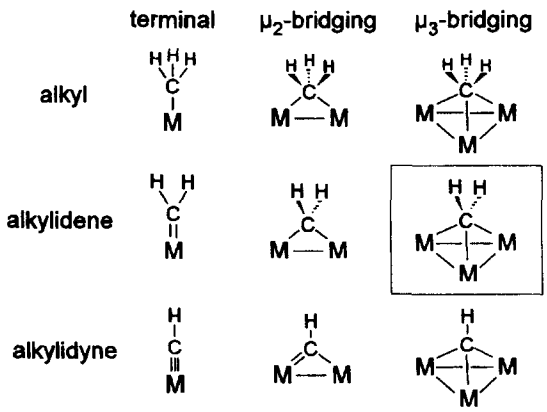

Scheme 1. η^1-Alkyl, alkylidene and alkylidyne coordination modes in organometallic chemistry.

† Dedicated to Prof Dr W. A. Herrmann on the occasion of his 50th birthday.

* Author to whom correspondence should be addressed.

§ Present address: Institut für Organische Chemie, Universität Frankfurt, Marie Curie Str. 11, D-60439 Frankfurt, Germany.

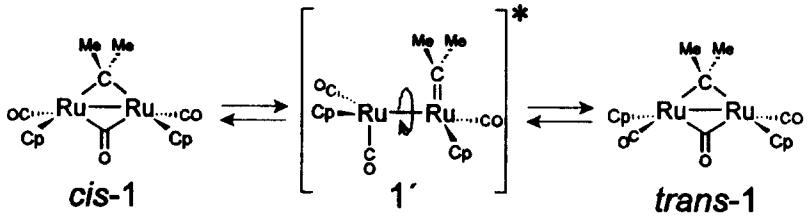

complex, the alkylidene ligand shows a marked preference for the bridging, μ_2, coordination mode [3,4]. Furthermore, CO ligands are frequently fluxional at room temperature in cluster complexes and rapidly exchange between two or all three coordination modes. Alkylidene ligands are rarely fluxional at room temperature and generally exhibit significantly larger barriers toward interchanging coordination positions or modes.

The first example of a $\mu_2 \rightleftarrows$ terminal geometry interchange for an alkylidene ligand was described by Knox and coworkers [5] for the complex $[Cp^*Ru(CO)]_2(\mu\text{-}CO)(\mu\text{-}CMe_2)$ **1**. The high barrier (80 kJ mole^{-1}) to inter-conversion of *cis* and *trans* isomers for **1** led Knox to propose that the intermediate/transition state for this process involved a terminally coordinated propylidene ligand (**1′**).

Theopold and Bergman [6] described a similar *cis/trans* isomerization for the mixed metal complex $CpRh(CpCo)_2(\mu\text{-}CH_2)(CO)_2$ **2**. Of interest with regard to the results described here is their observation of two fluxional processes for **2**; a low energy process ($\Delta G^{\neq} \approx 54$ kJ mole^{-1}) involving terminal $\rightleftarrows$ bridging inter-conversion of the CO ligands in the *trans* isomer and a high energy ($\Delta G^{\neq} \approx 75$ kJ mole^{-1}), *cis/trans* isomerization for which a mechanism involving bridge-to-terminal inter-conversion for the μ-CH_2 group was proposed. Finally, Holmgren and Shapley [7] described the first and only example of alkylidene fluxionality in a cluster complex. NMR spin saturation transfer experiments and a high $\Delta G^{\neq}$ (ca 73 kJ mole^{-1}) for the movement of a μ-methylidene ligand between Ru—Ru edges in the trinuclear complex $Ru_3(CO)_{10}(\mu\text{-}CH_2)$ led to the proposal of a mechanism again involving a species having a terminal methylidene ligand.

In the examples above and all other cases of alkylidene fluxionality no intermediates have been observed. A theoretical study [8] of the bonding and dynamics of C_1-hydrocarbon species on metal surfaces described the properties of terminal, μ_2- and μ_3-coordination geometries of a methylidene group on models for several different metal surfaces. An important conclusion of this study was that although M—C interactions increase in the more highly bridging geometries, the total energy of the system (metal surface + methylidene fragment) increased as well which lead to the prediction that the μ_3-coordination would be the least stable geometry of the three.

In this report we describe the dynamics of the μ-methylidene ligand in the trinuclear complex $Cp^*Rh(CpCo)_2(CO)_2(\mu\text{-}CH_2)$ **3**. Two distinct processes have been identified in the movement of the bridging methylidene ligand in **3**:methylidene jumps between Rh—Co and Co—Co bonds and degenerate methylidene jumps between the two Rh—Co bonds in the complex. An intermediate which exists in dynamic equilibrium with the two major isomers for the complex is observed for the latter process. The properties of the methylidene ligand in the intermediate have been studied via high field, multidimensional NMR techniques and are inconsistent with a terminal coordination geometry. We therefore propose that this intermediate involves a μ_3-methylidene ligand simultaneously interacting with the three metal atoms in the complex.

EXPERIMENTAL

General

All solvents were reagent grade and were further purified via distillation under nitrogen from Na/K alloy or CaH_2. Air sensitive complexes were handled under nitrogen using Schlenk techniques or under helium in a glove box. Anaerobic chromatography was performed using silica gel which had been degassed under dynamic vacuum overnight and thereafter stored under nitrogen. NMR samples were prepared by vacuum transfer of the deuterated solvent followed by flame sealing of the tube. $Cp^*Rh(CO)_2$ [9], $CpCo(C_2H_4)_2$ [10], $(CpCo)_2Cp^*Rh(CO)_2$ [11] were prepared according to literature procedures. Diazomethane, CH_2N_2 was prepared in ether solution ($\sim$1 M) from Diazald (Aldrich) following a literature procedure [12].

Caution! Diazomethane is toxic and potentially explosive in concentrated solution or when pure. All manipulations of diazomethane should be conducted in an adequately ventilated hood and care should be taken not to allow concentrated samples to develop.

$^{13}CH_2N_2$ enriched diazomethane was prepared via the same procedure using Diazald-99%-^{13}C (Aldrich).

$Cp^*Rh(^{13}CO)$

In a Schlenk vessel, 400 mg of the dicarbonyl complex were dissolved in methylene chloride. A separate

flask containing 1 L of ^{13}CO gas with a glass breakseal was connected to this vessel via an O-ring joint. The methylene chloride solution of the dicarbonyl was degassed via 4 freeze–pump–thaw cycles. With the two flasks isolated, the breakseal was broken and the solution stirred for 3 days. At 24 h intervals aliquots from the solution were analysed by mass spectrometry. After removing solvent, the residue was sublimed onto a cold finger under vacuum. The final enrichment was 81% (65% $Cp^*Rh(^{13}CO)_2$, 31.5% $Cp^*Rh(^{13}CO)(^{12}CO)$, 3.4% $Cp^*Rh(^{12}CO)_2$). This sample was used to prepare the doubly labelled alkylidene via the unsaturated cluster complex $(CpCo)_2Cp^*Rh(^{13}CO)_2$ and $^{13}CH_2N_2$ as described below.

$(CpCo)_2Cp^*Rh(CO)_2(CH_2)$ 3

In a glove box, between 200 and 500 mg of $(CpCo)_2Cp^*Rh(CO)_2$ were dissolved in degassed ether in a Schlenk flask. The solution was frozen and an ether solution of diazomethane at −78°C was added via cannula. The solutions were allowed to melt and were stirred together for 5–10 min whereupon all volatiles were removed under vacuum. The residue was chromatographed under nitrogen to give the alkylidene complex **3a** in 40% yield. Spectral data (IR, NMR) are summarized in the text and Table 1. Analysed (found) for $C_{23}H_{25}O_2Co_2Rh$; C: 49.66 (49.63) H: 4.85 (4.86).

NMR spectroscopy

Standard NMR experiments were performed on a Bruker AMX400WB spectrometer equipped with an QNP probehead. The $^1H\{^{13}C\}$ HMQC experiment was performed on an MAX600 spectrometer employing BIRD for suppression of the C-12 signal. The $^1H\{^{13}CO\}$ HMBC experiment was performed on a Bruker DRX600 spectrometer equipped with a *z*-axis gradient TBI probe. The gradient enhanced HMBC pulse sequence $90°(^1H)\text{-}d6\text{-}90°/(^{13}C)\text{-}d17\text{-}180°(^{13}C)\text{-}t_{1/2}\text{-}G_z(1)\text{-}180°(^1H)\text{-}G_z(2)\text{-}t_{1/2}\text{-}90°(^{13}C)\text{-}G_z(3)\text{-}$ acquire was used with the delay d6 set to 140 ms and d17 equals the total duration of the gradients $G_z(1)$ and $G_z(2)$ (2 ms). Selective excitation of the carbonyl ligands was accomplished by using Gaussian shaped pulses on the carbon channel with a bandwidth of 10 kHz centred at 250 ppm. 400 increments were acquired with 64 scans each, with phase sensitive detection in f1 using TPPI. Coherence selection was achieved by setting the gradient strength $G_z(1):G_z(2):G_z(3) = 50:30:40$ with a gradient length of 1 ms each.

RESULTS AND DISCUSSION

Reaction of the unsaturated cluster complex $Cp^*Rh(CpCo)_2(CO)_2$ [11] with diazomethane in ether solution gives two major products. The first involves the incorporation of the intact diazomethane molecule

Table 1. NMR Data for Complexes **3a**, **3b**, **3c** in CD_2Cl_2

	3a		**3b**		**3c**	
^1H NMR[a]	$\delta(^1H)$ (ppm)	J (Hz)	$\delta(^1H)$ (ppm)	J (Hz)	$\delta(^1H)$ (ppm)	J (Hz)
CH_2: H_{exo}	5.972	$^2J_{HH} = 0.5$ $^2J_{HRh} = 2.4$ $^1J_{HC} = 138.6$	7.12	$^2J_{HH} = 0.5$ $^2J_{HRh} = 0.6$ $^1J_{HC} = 137.14$	8.3	$^2J_{RhH} = 1.4$ $^1J_{HC} = 145.3$
H_{endo}	6.674	$^2J_{HH} = 0.5$ $^2J_{HRh} = 0.5$ $^1J_{HC} = 146.9$	7.02	$^2J_{HH} = 0.5$ $^2J_{HRh} < 0.2$ $^1J_{HC} = 138.6$		
Cp	4.73 4.79		4.82		4.57	
Cp*	1.80	$^2J_{HRh} = 0.5$	1.77	$^2J_{HRh} = 0.5$	1.62	$^2J_{RhH} = 0.6$
^{13}C NMR[b]	$\delta(^{13}C)$	J	$\delta(^{13}C)$	J	$\delta(^{13}C)$	J
CH_2	138.3	$^1J_{CRh} = 33$	135.1	—	145	$^1J_{CRh} = 29$
Cp	87.5 87.4		86.4		89.7	
Cp*: ring-C	101.8	$^1J_{CRh} = 4.0$	103.3		—	
Cp*: CH_3	9.8		11.4		10.6	
CO	250.0 262.7	$^1J_{CRh} = 50$	249.0	$^1J_{CRh} = 50$	257	$^1J_{CRh} = 39$

[a] 293 K;
[b] 170 K.

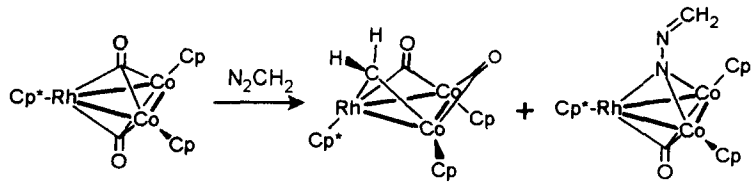

3a

into the complex in the form of a μ_3-hydrazone ligand. The properties of this complex will be described in a future publication. The second product is the methylidene complex **3a** wherein a methylidene and two CO ligands bridge the Rh—Co and Co—Co edges of the triangular cluster complex.

The structure of **3a** in the crystal [13] reveals that the μ_2-methylidene ligand is disordered between the two Rh—Co edges while the CO ligands occupy bridging positions on the remaining Rh—Co and Co—Co edges in the complex. All three bridging ligands are found on the same side of the plane of the metal atoms in a "crown" arrangement while the Cp and Cp* ligands all occupy positions beneath this plane (Fig. 1).

Spectroscopic data (Table 1) for **3a** are in accord with its structure in the solid state. IR spectra for **3a** both in solution and in the solid state, show two stretches at 1793 and 1829 cm^{-1} (KBr) consistent with the presence of edge-bridging CO ligands in the complex. In the proton NMR, two singlets are observed for the Cp ligand protons and one for the Cp* protons with the expected 1 : 1 : 3 intensity ratio. The methylidene protons are diastereotopic and two, non-identical doublet-of-doublets are observed for these protons (Fig. 2). Both signals show a geminal coupling between the two protons of 0.5 Hz ($^2J_{HH}$). Although small in comparison to what is observed in most other bridging methylidene systems [3] a similar value for geminal coupling has been reported for the related dinuclear system **2** [6]. Unequal two-bond coupling between the rhodium and each of the methylidene protons is also observed; ^2J = 0.5 and 2.4 Hz for the downfield and upfield signals, respectively.

NOESY spectra for **3a** show a large cross peak between the signals of the methylidene protons consistent with their close proximity. An additional cross peak is also observed between the down field methylidene proton resonance and the signals for the Cp* and one of the Cp ligands. Based on these data we assign the methylene proton resonance at 5.972 ppm to the "exo" proton that is directed out, away from the triangle of metal atoms and the resonance at 6.674 ppm to the "endo" proton which is above the metal triangle

The ^{13}C spectrum for **3a** is also consistent with its structure in the solid state. Two carbonyl ligand signals are observed at 250.0 and 262.7 ppm. The upfield signal is split into a doublet (J = 50 Hz) due to coupling to rhodium and may be assigned to the CO ligand bridging the Rh—Co edge. Both the CO ligand signals are significantly broadened at room temperature due to quadrupole interactions with the cobalt nuclei and can only be observed clearly at low temperature. The methylidene carbon signal is observed at 140.5 ppm. It is split into a doublet ($^1J_{RhC}$ = 33 Hz) due to coupling to rhodium. Un-decoupled spectra show additional, unequal coupling of this carbon to each of the methylidene protons which, based on the information above, may be specifically assigned to the exo ($^1J_{CH}$ = 146.9 Hz) and endo ($^1J_{CH}$ = 138.8 Hz) protons. The carbon signals for the Cp and Cp* ligands are observed in the usual ranges.

When **3a** is left in solution overnight a new set of

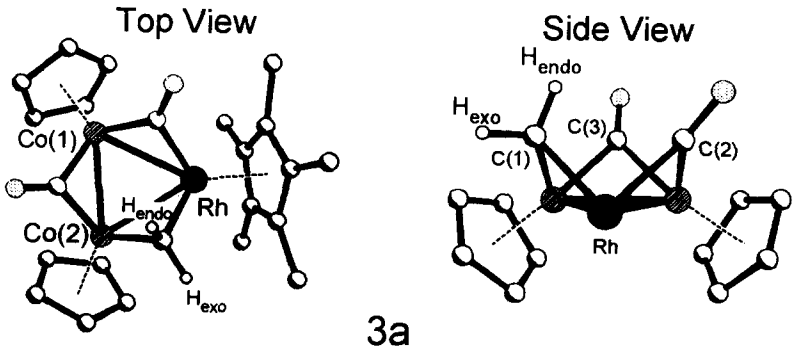

3a

Fig. 1. Two views of the molecular structure of **3a** in the solid state. In the side view the Cp* ligand coordinated to rhodium has been removed for clarity.

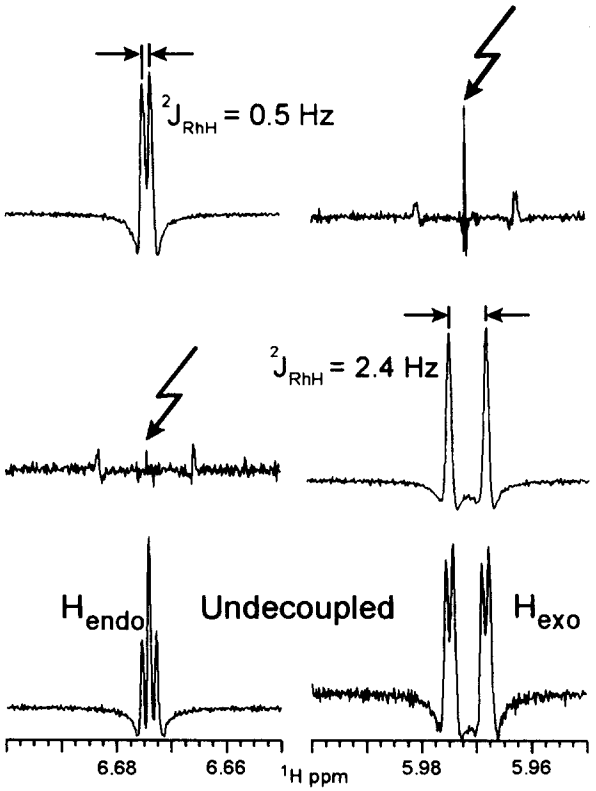

Fig. 2. Illustration of homonuclear ^1H decoupling experiments elucidating the proton–proton and rhodium–proton coupling for the methylidene ligand protons of **3a**.

signals appears at the expense of those assigned to **3a**. Analysis of this new set of NMR signals leads to the identification of a second isomer of **3** in which the methylidene ligand bridges the Co—Co bond with the two carbonyl ligands bridging Rh—Co bonds (**3b**). Both sets of CO and Cp ligands in **3b** each give rise to single signals reflecting mirror symmetry for the molecule. The methylidene carbon and two protons lie in the plane of symmetry through the molecule which bisects the Co—Co bond. As expected the two methylidene protons are again diastereotopic and give rise to two multiplets ($\delta(H_{endo}) = 7.02$; $\delta(H_{exo}) = 7.12$ ppm)). Surprisingly, the exo methylidene hydrogen couples to the rhodium ($J_{RhH} = 0.6$ Hz) whereas any rhodium coupling to the endo hydrogen is too small to be observed (>0.2 Hz). The ^{13}C resonance for the two CO ligands in **3b** exhibits the expected coupling to rhodium (50 Hz) and a chemical shift value almost identical to the analogous CO ligand in **3a** (249 vs 250 ppm, respectively). The methylidene ^{13}C shift in **3b** is 135.1 ppm. When the methylidene ligand bridges the Co—Co bond, however, no rhodium-to-carbon coupling is observed. A complete summary of the ^1H and ^{13}C data for isomers **3a** and **3b** is presented in Table 1.

The kinetics and thermodynamics for the equilibrium isomerization of **3a–3b** in toluene solution

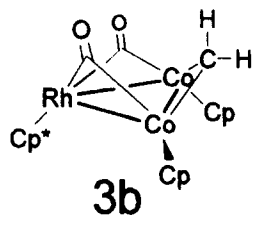

have been studied via a VT NMR. At 330 K the rate for the conversion of **3a** to **3b** is 1.8×10^{-4} s^{-1} with a free energy of activation of 104 kJ mol^{-1}. The equilibrium constant for the mixture at room temperature is 2.63 (favouring **3b** and statistically normalized for the presence of two enantiomers of **3a**) which corresponds to a free energy of -1.2 kJ mol^{-1}.

Having determined that methylidene migration occurs in **3a**, we were also interested in mapping the proton exchange pathways between the four magnetically distinct methylidene protons of **3a** and **3b**. Phase sensitive NOESY experiments offer an attractive method to address this question. At temperatures where exchange is slow, negatively phased cross peaks within the methylidene proton signal sets for **3a** and **3b** are observed. As the temperature is raised and

exchange of the methylidene ligand between the Rh—Co and Co—Co edges enters the time scale of the experiment, positively phased cross peaks should be observed between these sets of methylidene protons reflecting the mapping function for proton exchange and thus the stereochemistry involved in the methylidene ligand jump. Unfortunately, decomposition of **3a** ensues before temperatures high enough to bring the exchange rate into the time scale of the experiment could be reached. However, two new exchange phenomena are observed (Fig. 3). First, the NOE derived cross peak between the signals of the methylidene protons of **3a** became weaker, nulled and then grew again as a positively phased cross peak as the temperature was raised. This is clear evidence that an exchange pathway exists which equilibrates the two methylidene protons of **3a** and which does not involve a double jump mechanism involving **3b** as an intermediate (**3a** ⇄ **3b** ⇄ **3a**'). Furthermore, an additional exchange derived cross peak appeared between the protons of **3a** and a hitherto unobserved signal at 8.3 ppm. Subsequent 1 D spectra of **3a** confirmed that a small doublet (1.4 Hz) is present in spectra of **3a** at room temperature.

Further NOESY experiments optimized for the observation of cross peaks in the Cp region of the spectrum also gave rise to an exchange derived cross peak between the two Cp signals of **3a**. Quantitative analysis of cross peak intensity versus temperature for the three processes described above gave consistent results (350 K : $k_{rate} = 0.13\ s^{-1}$; $\Delta G^{\neq} = 92$ kJ/mole) indicating that a single process is involved in all of these processes: (1) exchange between the two methylidene proton signals; (2) exchange of the identities of the two Cp rings and (3) exchange of both methylidene proton signals of **3a** with a new signal in a species which we now refer to as **3c**.

Exchange of the identities of the Cp rings in **3a** rules out a mechanism in which the methylidene ligand remains bridging a single Rh—Co edge but rotates about an axis through the carbon and between the two protons. Furthermore, an intermediate in which the HCH plane of the methylidene is parallel to the Rh—Co bond (rotated 90° with respect to the orientation in **3a**) is not consistent with the observation of a single resonance for both protons nor is it likely based on the results of previous theoretical studies [8].

Further information concerning the identity of **3c** was clearly required. When crystals of **3a** are dissolved in deuterated methylene chloride at 0°C, no trace of the signal at 8.3 ppm was observed (Fig. 4). Upon warming the sample to room temperature this signal appears within a few minutes. Careful monitoring of the Cp and Cp* regions of the spectrum also reveals the emergence of one signal for each set of protons at 4.57 and 1.62 ppm, respectively. The maximum concentration of **3c** in the presence of **3a** and **3b** is ca 1% based on integrations of the methylidene protons signals. From these data we identify **3c** as a separate species in equilibrium with **3a** and **3b** which is involved

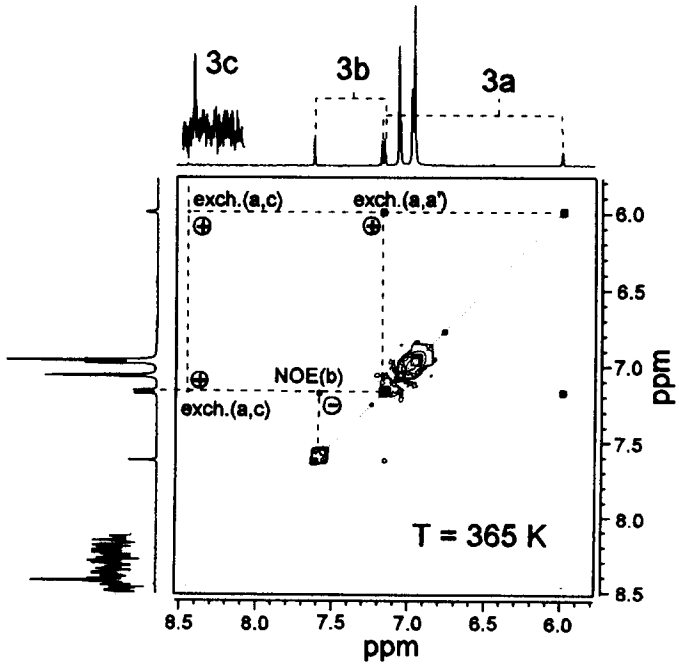

Fig. 3. Phase sensitive NOESY spectrum (methylidene region) for a mixture of **3a**, **3b** and **3c** in toluene-d_8 at 365 K. The cross peak labelled NOE(b) is derived from NOE interactions between the methylidene protons of **3b**. Cross peaks labelled exch(a,a') and exch(a,c) are derived from a dominant chemical exchange process involving the methylidene protons of **3a** and the methylidene protons of **3a** and **3c**, respectively.

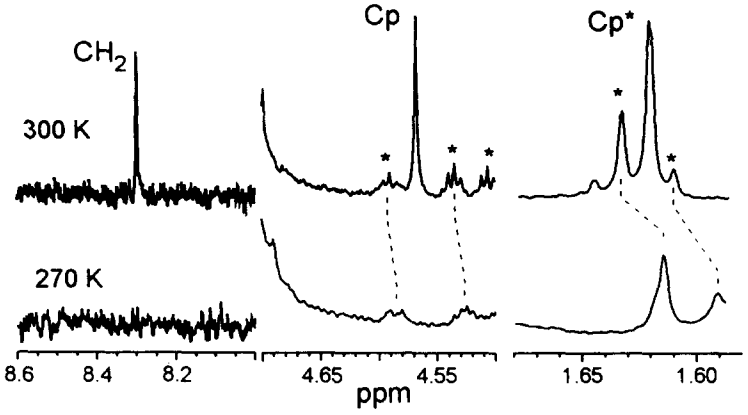

Fig. 4. Variable temperature ^1H NMR spectra illustrating the formation of the methylidene, Cp and Cp* signals of **3c** at 300 K. Signals marked with "*" are natural abundance ^{13}C satellites from the signals for the Cp and Cp* ligands of **3a**.

in the direct migration of the methylidene ligand between the Rh—Co edges of **3a**. To our knowledge, this is the first observation of an intermediate involved with alkylidene fluxionality where the ground-state structures involve μ_2-alkylidene coordination modes.

Our attention now focused on obtaining further spectroscopic data which would allow us to propose a more detailed picture for the structure of **3c**. ^{13}C NMR data were critical in these efforts for several reasons. First, the chemical shift of the alkylidene ligand is quite sensitive to its coordination mode. Herrmann has pointed out that the chemical shift ranges for the terminal vs μ_2-bridging coordination geometries are distinct with the terminal range considerably downfield (240–370 ppm) of that for the bridging mode (100–210 ppm) [3]. Furthermore, both the observation and magnitude of any Rh—C coupling for the methylidene ligand in **3c** can be used to distinguish between bridging and terminal coordination modes. The Rh—C coupling constant for a ligand terminally coordinated to rhodium should be roughly double that for the same ligand in a bridging mode [14]. Finally, the observation any C—C scalar coupling between the carbonyl and the alkylidene ligands would reveal possible bonding between these ligands in **3c**. For these reasons, ^{13}C enriched samples of **3a** were prepared in which only the alkylidene ligand or both the alkylidene and CO ligands were enriched (see Experimental).

In order to exclude mistaking signals from trace impurities for those of **3c**, multidimensional pulse techniques in which only ^{13}C signals correlated to proton chemical shifts and coupling constants already known for **3c** were considered in our assignments. Using an equilibrated sample of **3a**, 99% enriched in ^{13}C at the methylidene carbon, an inverse detected, ^1H $\{^{13}C\}$ correlation spectrum (HMQC pulse sequence) was obtained at $-50°C$ (Fig. 5). In addition to the expected cross peaks in the methylidene region for **3a** and **3b**, a cross peak correlating the methylidene proton resonance of **3c** to a carbon signal at 145.5 ppm was detected. Furthermore, Rh—C coupling of 29 Hz was observed for this cross peak. A second, identical experiment using doubly labelled **3a** (>80% enriched in both the methylidene and CO ligands) failed to show any extra coupling due to possible bond formation between the methylidene and CO ligands in **3c**.

Neither the chemical shift nor the Rh—C coupling constant observed for the methylidene-derived ^{13}C resonance of **3c** are consistent with a terminal coordination mode. Failure to observed additional C—C coupling in the double label experiment indicates that the methylidene remains independent of the CO ligands in **3c**. Both the observed rhodium–proton (1.4 Hz) and rhodium–carbon coupling (29 Hz) are similar to analogous couplings observed in **3a**. Therefore some type of geometry that maintains interaction with the rhodium is necessary. Although no ^{13}C NMR shifts for μ_3-alkylidene ligands have been reported, based on the trends observed for the carbonyl ligand in terminal, μ_2 and μ_3-geometries, the two bridging geometries should have similar and overlapping chemical shift ranges. These arguments, together with overall C_s symmetry in **3c** (single signals for the methylidene and Cp ligand protons) lead us to propose that **3c** contains a triply-bridging methylidene ligand as shown in the illustration of **3c**. Having the HCH plane parallel to the Co—Co bond vector in **3c** is also consistent with the chemical exchange of the exo and endo proton identities when **3c** functions as the intermediate in the movement of the methylidene ligand between Rh—Co edges in **3a**. We cannot, however, rule out the possibility that the methylidene ligand rotates freely in the triply-bridging geometry in **3c** as one theoretical study has predicted [8].

Having addressed the question of the coordination mode of the methylidene ligand in **3c** we conclude our initial investigations into the identity of this complex with a look at the disposition of the carbonyl ligands

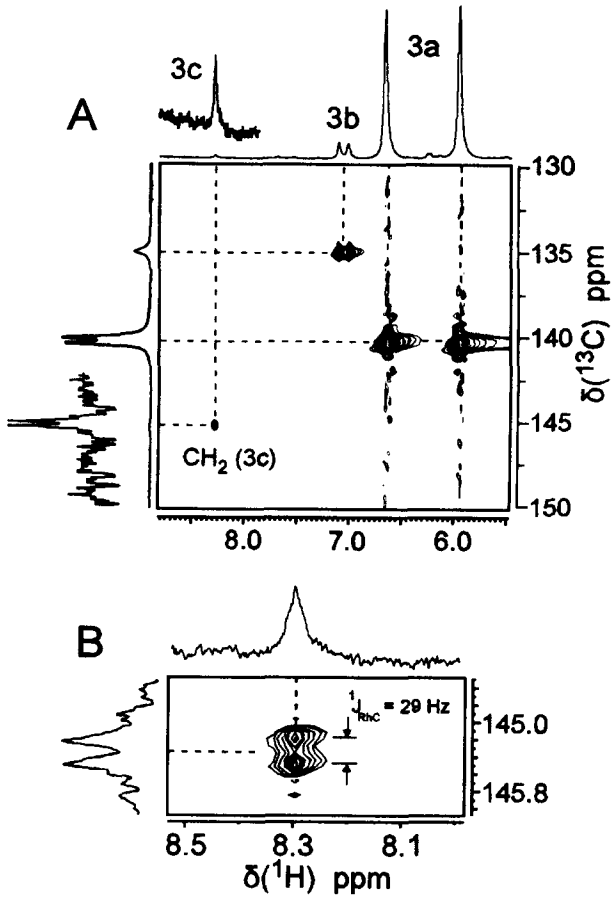

Fig. 5. Methylidene region of the HMQC spectrum of ^{13}C enriched (99%) **3a**, **3b** and **3c** (CD_2Cl_2, 300 K). A: Cross peaks relating the methylidene protons of each isomer with their respective carbon signals. B: Expansion of the cross peak for **3c** illustrating Rh—C coupling of 29 Hz.

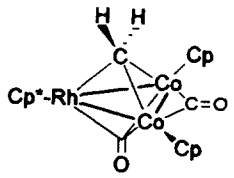

3c

in this complex. IR spectra of equilibrium mixtures of **3a–3c** exhibit an extra band at 1655 cm^{-1} which suggests the presence of a triply-bridging CO ligand in **3c**. Further evidence for a μ_3-CO ligand in **3c** comes from heteronuclear NMR experiments. Using the ^{13}C enriched sample described above, a heteronuclear multiple bond correlation (HMBC) experiment employing long range couplings gave rise to peak correlating the methyl group protons of the Cp* ligand with a shift at 257 ppm in the carbon spectrum (Fig. 6). A rhodium–carbon coupling constant of 39 Hz was observed for this signal.

Although the signal for the Cp* ligand in **3c** is not as distinctive as that for the methylidene ligand, we are confident of our assignment of the signal at 257 ppm to one of the CO ligands in **3c** through additional H/Rh correlations in which both the Cp* and methylidene signals give rise to cross peaks with the same rhodium chemical shift [15]. Our inability to observe coherence transfer between the methylidene protons and the CO ligand of **3c** may be due to the fact that only two protons are involved in this 3-bond coupling path while 15 protons are involved in the 4-bond path between the Cp* and carbonyl ligand. Although the coupling path involves more legs, the increase in intensity for the second mechanism due to the larger proton spin reservoir appears to facilitate a larger overall transfer of coherence between these two spin populations.

The observed chemical shift and Rh—C coupling constant for one of the CO ligands in **3c** is inconsistent with that expected for a terminal CO ligand. The shift

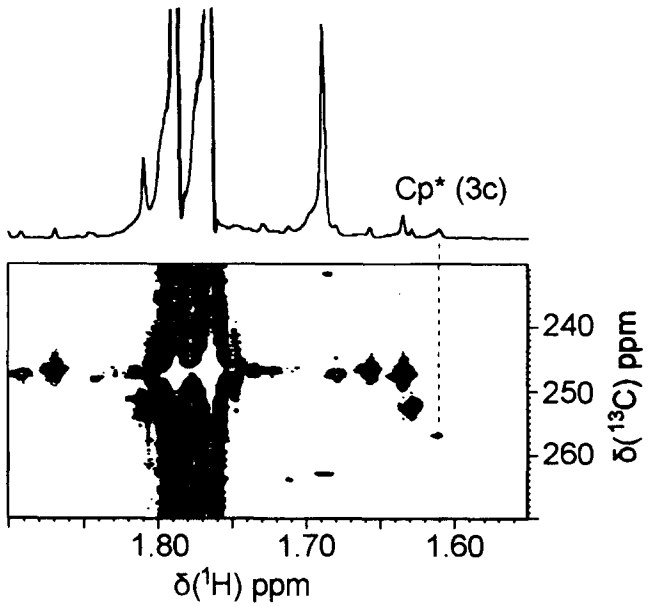

Fig. 6. HMBC spectrum for a sample containing doubly labelled (methylidene 99% ^{13}C); CO (80% ^{13}C) **3a**, **3b** and **3c** showing signal correlating the Cp* proton signal of **3c** with a shift at 257 ppm in the carbon spectrum.

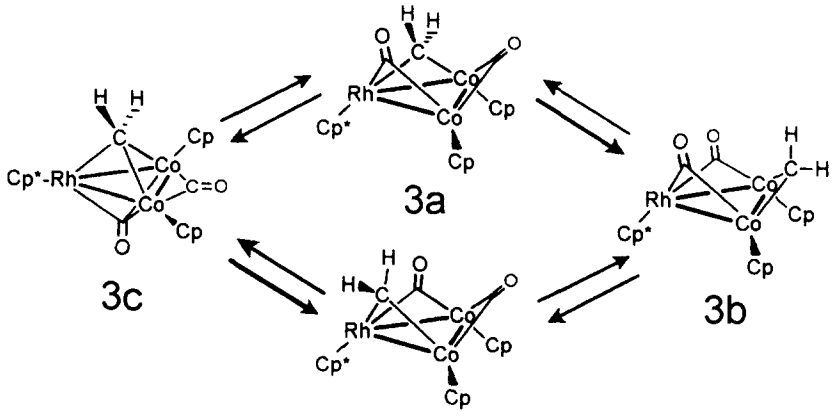

Scheme 2.

is intermediate between the values observed for the μ_2-CO ligands bridging either Rh—Co or Co—Co bonds in **3a** and **3b** and is therefore consistent with a bridging CO ligand interacting with both metals. These NMR data, together with the stretching frequency in the IR and C_s symmetry for the complex as a whole, support the assignment of one of the two CO ligands in **3c** as a triply-bridging ligand, presumably on the side opposite that of the μ_3-methylidene ligand. Unfortunately, it is not possible to describe in more detail the fluxional behaviour of the CO ligands without knowing whether the two distinct ligands exchange identities as the methylidene ligand jumps between Rh—Co edges. Our attempts to obtain these data have been thwarted to date by excessive broadening of the CO signals at temperatures where exchange could be monitored.

Our understanding of the methylidene dynamics in the isomer family **3a–3c** is summarized in Scheme 2. Two separate processes account for the movement of the methylidene ligand between the Rh—Co and Co—Co edges of this complex. The first is a "high" energy process involving the direct movement of the methylidene ligand from the Rh—Co (**3a**) to Co—Co edge (**3b**). The second process is degenerate and involves the movement of the methylidene between the two Rh—Co edges. An intermediate (**3c**) has been observed for the second process. Based on detailed NMR studies we propose that this intermediate is composed of the three metals interacting with a triply

bridging methylidene and a triply-bridging carbonyl ligand on opposite sides of the plane of the metals. The final CO ligand in **3c** presumably bridges the Co—Co edge.

These investigations have lead to the first observation and characterization of an intermediate in the movement of a methylidene ligand between metal–metal bonds in a cluster complex. Furthermore, this intermediate contains a triply-bridging methylidene ligand. In contrast to other coordination modes for the alkylidene ligand, the μ_3 geometry is very rare and until the present study no examples were known involving late transition metal cluster complexes. For this reason, it has not been seriously considered as a possible intermediate in alkylidene dynamics in cluster complexes and, more importantly, on the surfaces of metal crystals such as those frequently involved in heterogeneous catalysts [1,16] As catalyst scientists extend theoretical models for such systems, it is important that correct models for surface species and kinetic pathways are used. We suggest here that the triply-bridging coordination geometry be included among the models both as a viable coordination mode and for alkylidene dynamics on metal surfaces.

Acknowledgment—The authors would like to thank the Petroleum Research Fund administered by the American Chemical Society. We also wish to thank Dr Christian Griesinger for helpful discussions and the use of NMR instrumentation in his laboratories in obtaining HMBC spectral data.

REFERENCES

1. (a) Collman, J. P., Hegedus, L. S., Norton, J. R. and Finke, R. G., *Principles and Application of Organotransition Metal Chemistry*. University Science Books, Mill Valley, CA, 1987, Chapter 2; (b) Zaera, F., *Chem. Rev.*, 1995, **95,** 2651.
2. Herzog, A., Roesky, H. W., Jäeger, F., Steiner, A. and Noltemeyer, M., *Organometallics*, 1996, **15,** 909.
3. Herrmann, W. A., *Adv. Organometal. Chem.*, 1982, **20,** 160.
4. (a) Laws, W. J. and Puddephatt, R. J., *J. Chem. Soc., Chem. Comm.*, 1983, 1020; (b) Akita, M., Hua, R., Oku, T. and Moro-oka, Y., *Organometallics*, 1996, **15,** 2548; (c) Hsu, G., Wilson, S. R. and Shapely, J. R., *Organometallics*, 1994, **13,** 4159.
5. Dyke, A. F., Knox, S. A. R., Mead, K. A. and Woodward, P., *J. Chem. Soc., Chem. Comm.*, 1981, 861.
6. Theopold, K. H. and Bergman, R. G., *J. Am. Chem. Soc.*, 1983, **105,** 464.
7. Holmgren, J. S. and Shapley, J. R., *Organometallics*, 1985, **4,** 793.
8. Zheng, C., Apeloig, Y. and Hoffmann, R., *J. Am. Chem. Soc.*, 1978, **100,** 7726.
9. Plank, J., Riedel, D. and Herrmann, W. A., *Angew. Chem. Int. Ed., Eng.*, 1980, **19,** 937.
10. Jonas, K, Deffense, E. and Habermann, D., *Angew. Chem. Suppl. Ed.*, 1983, 1005.
11. Barnes, C. E., Dial, M. R., Orvis, J. A., Staley, D. L. and Rheingold, A. L., *Organometallics*, 1990, **9,** 1021.
12. Black, T. H., *Aldrichemica Acta*, 1983, **16,** 3.
13. Försterling, F. H. and Barnes, C. E., *J. Am. Chem. Soc.*, 1997, **119,** 7585.
14. Mann, B. E. and Taylor, B. F., *^{13}C NMR data for Organometallic Compounds*. Academic Press, New York, 1981.
15. Försterling, F. H. and Barnes, C. E., manuscript in preparation.
16. (a) Sheppard, N., *Annu. Rev. Phys. Chem.*, 1988, **39,** 589; (b) Pines, H., *The Chemistry of Catalytic Hydrocarbon Conversions*. Academic Press, London, 1981; (c) Somorjai, G. A., *Introduction to Surface Chemistry and Catalysis*. Wiley, New York, 1994.

Pergamon

PII: S0277-5387(97)00491-9

Polyhedron Vol. 17, No. 7, pp. 1055–1064, 1998
© 1998 Elsevier Science Ltd
All rights reserved. Printed in Great Britain
0277–5387/98 $19.00+0.00

Silyl and siloxanediyl cyclopentadienyl titanium and zirconium complexes: synthesis and reactivity. X-ray molecular structure of $[Zr\{\eta^5\text{-}C_5H_4SiMe_2(\mu\text{-}OH)\}(\mu\text{-}Cl)Cl_2]_2$†

Santiago Ciruelos, Tomás Cuenca,* Rafael Gómez, Pilar Gómez-Sal,‡ Antonio Manzanero‡ and Pascual Royo

Departamento de Química Inorgánica, Universidad de Alcalá, Campus Universitario, 28871 Alcalá de Henares, Spain

(Received 7 October 1997; accepted 10 November 1997)

Abstract—Chloro(dimethyl)silyl-η^5-cyclopentadienyl group 4 metal complexes of the type $[M(\eta^5\text{-}C_5H_4SiMe_2Cl)Cl_3]$ (M = Ti **1**, Zr **2**) react with thallium salts $Tl(C_5H_4R)$ (R = H, $SiMe_3$) to give mixed dicyclopentadienyl derivatives $[M(\eta^5\text{-}C_5H_4R)(\eta^5\text{-}C_5H_4SiMe_2Cl)Cl_2]$, (M = Ti, R = H **3**, R = $SiMe_3$ **4**; M = Zr, R = H **5**, R = $SiMe_3$ **6**) in high yield. Hydrolysis of complexes **3** and **4** affords the dinuclear complexes $[Ti(\eta^5\text{-}C_5H_4R)Cl_2]_2\{\mu\text{-}[(\eta^5\text{-}C_5H_4SiMe_2)_2O]\}$ (R = H **7**, R = $SiMe_3$ **8**) containing a siloxanyl bridge, by elimination of two equivalents of HCl. Reactions of complexes **1** with hydroxo containing reagents such as anhydrous LiOH and $SiPh_2(OH)_2$ give the derivatives $[Ti(\eta^5\text{-}C_5H_4SiMe_2Cl)Cl_2]_2(\mu\text{-}O)]$, **9** and $Ti[\mu\text{-}(\eta^5\text{-}C_5H_4SiMe_2OSiPh_2\text{-}\eta^1\text{-}O)]Cl_2$, **10** identified by analytical, spectrometric and spectroscopic data. Treatment of analogous complex **2** with water produces the dimeric monocyclopentadienyl zirconium trichloride adduct $[Zr(\eta^5\text{-}C_5H_4SiMe_2OH)Cl_3]_2$, **11**. Compound **11** has been characterized by X-ray crystallography. © 1998 Elsevier Science Ltd. All rights reserved

Keywords: titanium; zirconium; siloxanediyl cyclopentadienyl; hydroxide.

Cyclopentadienyl transition metal complexes have been the subject of considerable interest for many years due to their synthetic and catalytic applications [1]. Particularly relevant has been the development of new dicyclopentadienyl group 4 metal derivatives because of their application as catalysts in homogeneous polymerization of α-olefins [2]. For this reason, a large number of such complexes with variously functionalised substituents on the cyclopentadienyl rings have been synthesized and spectroscopically and structurally characterized [3].

The aim of combining the properties of the homogeneous and heterogeneous catalysts [4], extending and improving the industrial applications of these compounds, has promoted a growing interest in the study of transition metal complexes based on functionalized cyclopentadienyl ligands allowing their attachment to organic polymers and inorganic surfaces. Several approaches have been studied. Polysiloxanes have been investigated as useful polymers for supporting organometallic complexes [5]. Metallocene derivatives containing silyl groups in the side chain of the cyclopentadienyl ligand have also been synthesized and used as models, either by anchoring them to organic or inorganic substrates, or by polymerising them to organometallic polymers [6].

Chlorosilyl-η^5-cyclopentadienyl group 4 metal complexes are good candidates to prepare supported catalysts using the Si—Cl bond as a reactive site [7]. We have previously reported chloro(dimethyl)silyl-η^5-cyclopentadienyl group 4 metal derivatives $M(\eta^5\text{-}C_5H_4SiMe_2Cl)Cl_3$ (M = Ti **1**, Zr **2**) [8] and their reactions with amines and amides. In this paper, we describe the synthesis and reactivity of these and other new dicyclopentadienyl complexes of titanium and zirconium with different hydroxo containing reagents

* Author to whom correspondence should be addressed.

† Dedicated to Prof. W. A. Herrmann on the occasion of his 50th birthday.

‡ X-ray diffraction studies.

as an important step in the investigation of suitable anchoring systems for the immobilization of the corresponding active metal centers.

RESULTS AND DISCUSSION

Synthesis of mixed dicyclopentadienyl derivatives and their reactions with water

The reaction of the trichloro metal compounds $M(\eta^5\text{-}C_5H_4SiMe_2Cl)Cl_3$ (M = Ti **1**; Zr **2**) with one equiv. of the thallium salts $Tl(C_5H_4R)$ (R = H, $SiMe_3$) afforded the corresponding mixed dicyclopentadienyl derivatives $M(\eta^5\text{-}C_5H_4R)(\eta^5\text{-}C_5H_4SiMe_2Cl)Cl_2$, (M = Ti, R = H **3**, R = $SiMe_3$ **4**; M = Zr, R = H **5**, R = $SiMe_3$ **6**) in high yield (80–90%), by modification of the procedure previously described [9]. Complexes **3** and **6** have been recently mentioned in the literature, although not fully characterized [10].

All these complexes show the characteristic thermal stability of group 4 dicyclopentadienyl derivatives [1b] but are moisture sensitive due to the hydrolysis of the $SiMe_2Cl$ moiety. They are insoluble in hydrocarbons, and soluble in toluene and chlorinated solvents.

Reactions of titanium complexes **3** and **4** with one equiv. of water yielded the corresponding dinuclear complexes $[Ti(\eta^5\text{-}C_5H_4R)Cl_2]_2\{\mu\text{-}[(\eta^5\text{-}C_5H_4SiMe_2)_2O]\}$ (R = H **7**, R = $SiMe_3$ **8**) in 50% yield based on titanium, by means of the intermolecular hydrolysis of the Si—Cl bonds to give the siloxanediyl fragment $[(\eta^5\text{-}C_5H_4SiMe_2)_2O]^{2-}$ binding both titanium centres with evolution of HCl. This behaviour, which reveals that a selective reaction of the Si—Cl bonds without modification of the Ti—Cl bonds takes place, is different from that observed for the monocyclopentadienyl derivatives $Ti(\eta^5\text{-}C_5H_4SiMe_2Cl)Cl_3$ [8] for which simultaneous unselective reaction of both Si—Cl and the more covalent Ti—Cl bonds was observed. The reaction is also different from that observed [8] for the bis[chloro(dimethyl)silyl-η^5-cyclopentadienyl]zirconium complex $Zr(\eta^5\text{-}C_5H_4SiMe_2Cl)_2Cl_2$ in which the same selective hydrolysis of the Si—Cl bonds led to the mononuclear *ansa*-derivative $Zr[\mu\text{-}\{(\eta^5\text{-}C_5H_4SiMe_2)_2O\}]Cl_2$ in an intramolecular reaction. Complexes **7** and **8** show physical and spectroscopic properties similar to those observed for the related derivatives $[Ti(C_5H_5)Cl_2]_2\{\mu\text{-}[(\eta^5\text{-}C_5H_4)_2E]\}$ (E = $SiMe_2$; $(SiMe_2O)_2SiMe_2$; $SiMe_2(CH_2)_nSiMe_2$, n = 1 or 2) with variable interannular bridge lengths [11]. Complexes **7** and **8** are air and moisture stable, soluble in chlorinated solvents, but sparingly soluble in toluene and insoluble in hydrocarbons.

The spectroscopic and analytical data for compounds **3**–**8** and all of the other complexes described in this paper, are given in the Experimental Section and will not be discussed, except where appropriate. ^{1}H NMR spectra of complexes **3**–**8** show the expected resonances of the cyclopentadienyl ring protons as two sets of pseudotriplets due to an AA′BB′ spin system [11]. The value of $\Delta\delta = \delta_d - \delta_p$ for complex **7** (δ_d and δ_p being the chemical shifts of the distal and proximal protons of the bridged cyclopentadienyl rings respectively) is 0.30 ppm, slightly smaller than the value observed for the *ansa*-compound $Ti[\mu\text{-}\{(\eta^5\text{-}C_5H_4SiMe_2)_2O\}]Cl_2$ ($\Delta\delta$ = 0.41 ppm) [6a,12], where the ligand is acting as a chelating group. Such a value has been used as a spectroscopic parameter for dis-

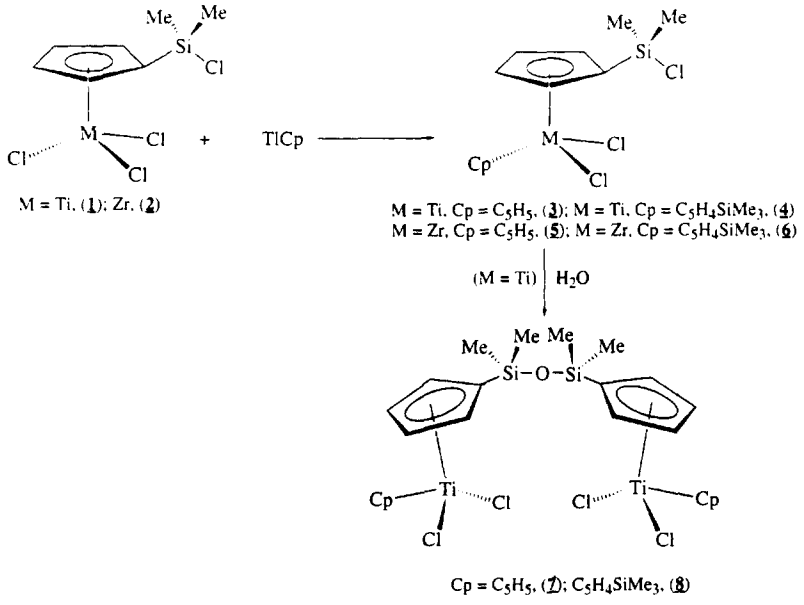

Scheme 1.

tinguishing the chelating and the bridging coordination modes of the cyclopentadienyl ligands bridged by silyl groups [13,14]. The lower value of $\Delta\delta$ observed for $Ti[\mu\text{-}\{(\eta^5\text{-}C_5H_4SiMe_2)_2O\}]Cl_2$ can be attributed to the large interannular bridge angle formed by the two cyclopentadienyl rings and the metal centre, which induces a relaxation of the constrained environment of the metal [13]. These electronic and steric dispositions shown by the *ansa*-derivatives having large interannular bridges are similar to those found for the unbridged counterparts with substituted cyclopentadienyl ligands. In both types of complexes similar values of $\Delta\delta$ have been obtained indicating, in this case, that this spectroscopic parameter cannot be used to distinguish between the chelating and the bridging disposition of the dicyclopentadienyl ligand. However, the relative chemical shifts of the bridgehead carbon of the cyclopentadienyl rings could be used to distinguish between the two types of coordination. It has been observed that in chelating compounds, this resonance appeared at fields higher than the proximal and distal carbon resonances of the same ring [13], while for a bridging coordination mode, in dinuclear derivatives [11a,14] or for unbridged mononuclear substituted metallocene analogues [15], the reverse was observed. This feature has been explained as the result of a redistribution of the π-electron density of the ring in the *ansa*-metallocene caused by the bridge and the presence of the silicon atom [13a], resulting in shielding the C_{ipso} atom but deshielding the remaining ring carbon atoms. In contrast, complexes with an interannular hydrocarbon link do not present this spectroscopic behaviour for the C_{ipso} atom [16]. The ^{13}C NMR spectrum of complex **7** exhibits two signals at δ 121.0 and 129.2 assigned to the distal and proximal carbons of the bridging cyclopentadienyl rings and one resonance of lower intensity at δ 129.3 attributed to the C_{ipso}. These data are in agreement with a bridging coordination mode of the $[(\eta^5\text{-}C_5H_4SiMe_2)O]^{2-}$ fragment in **7**. An analogous result was observed for complex **8**. The same spectroscopic characteristics [11a] have been found in other complexes containing shorter bridges like those with the $[(\eta^5\text{-}C_5H_4)_2SiMe_2]^{2-}$ fragment. The IR spectra for complexes **7** and **8** show no absorptions due to hydroxo groups or Ti—O—Ti linkage. In addition, the mass spectra of the two compounds are in agreement with their dinuclear formulation.

Reactions of monocyclopentadienyl derivatives with hydroxo containing reagents

We have previously reported that both Si—Cl and Ti—Cl bonds in compound **1** are simultaneously involved in reactions with water and amines, whereas reactions with nucleophilic Grignard reagents or highly polar lithium amides take place selectively at the Ti—Cl bond [8,17]. In order to obtain additional information about this different reactivity we have studied the reaction of **1** with $SiPh_2(OH)_2$ and LiOH.

Complex **1** reacts with one equiv. of $SiPh_2(OH)_2$ in the presence of two equiv. of NEt_3 to afford the mononuclear derivative $Ti[\mu\text{-}(\eta^5\text{-}C_5H_4SiMe_2OSiPh_2\text{-}\eta^1\text{-}O)]Cl_2$ **10,** characterized by its analytical and spectroscopic data. This reaction involves both Si—Cl and Ti—Cl bonds as does the similar reaction with water. Treatment of **1** with anhydrous LiOH in a 1 : 1 molar ratio in the presence of one equiv. of dry NEt_3 gives the new oxo derivative $[Ti(\eta^5\text{-}C_5H_4SiMe_2Cl)Cl_2]_2(\mu\text{-}O)$, **9** as yellow crystals in a 42% yield and a white precipitate of $HCl\cdot NEt_3$, on the basis of their analytical and spectroscopic data.

The formation of the dinuclear complex $[Ti\{(\eta^5\text{-}C_5H_4SiMe_2\text{-}\eta^1\text{-}O)\}Cl_2]_2$ obtained by hydrolysis of **1** [8] or the recently reported compound $(TiCl_2)_2(\mu\text{-}O)\{\mu\text{-}[(\eta^5\text{-}C_5H_4SiMe_2)_2O]\}$ [12] is not detected in this reaction. The synthesis of the dinuclear complex **9** suggests that the reaction of **1** with LiOH proceeds with intermolecular elimination of HCl from the Ti—Cl bonds. In contrast, the mononuclear "constrained geometry derivatives" $Ti[\mu\text{-}(\eta^5\text{-}C_5H_4SiMe_2\text{-}\eta^1\text{-}NR)]Cl_2$ [17] are obtained in the reaction of **1** with LiNHR, involving the formation of the amidotitanium derivative $[Ti(\eta^5\text{-}C_5H_4SiMe_2Cl)(Cl_2)(NHR)]$ and further intramolecular HCl elimination from the silicon-bonded chlorine of the same molecule. In addition, the IR spectrum of **9** shows a broad absorption band at 798 cm^{-1} attributed to a Ti—O—Ti fragment [18] and its mass spectrum is consistent with a dinuclear structure.

However, the reaction of the zirconium complex **2** with one equiv. of water under the same conditions has been decribed to give a white solid, insoluble in all common solvents [8]. The IR spectrum for this substance shows an absorption band at 3604 cm^{-1} attributed to the presence of a Si—OH group [19] and the NMR data are not reported because of its lack of solubility in the most common deuterated solvents. By using the method described in the experimental section we were successful in isolating single crystals of this compound suitable for definitive characterization by diffraction methods. The structure corresponds to a dimer of the monocyclopentadienyl zirconium trichloride unit $[Zr\{\eta^5\text{-}C_5H_4SiMe_2(\mu\text{-}OH)\}(\mu\text{-}Cl)Cl_2]_2$, **11** with both zirconium atoms bridged by two chlorines and the OH groups. This result confirms that the Si—Cl bonds of the chlorodimethylsilyl cyclopentadienyl substituted zirconium complex **2** react selectively with water, in contrast with the unselective hydrolysis observed for complex **1** [8].

Description of the crystal structure of $[Zr\{\eta^5\text{-}C_5H_4SiMe_2(\mu\text{-}OH)\}(\mu\text{-}Cl)Cl_2]_2$, **11**

Figure 1 shows an ORTEP view of **11** along with the numbering scheme used. Selected bond lengths and angles with their standard deviations are listed in Table 1. The X-ray determination shows **11** as a dimer of two $[Zr(\eta^5\text{-}C_5H_4SiMe_2OH)Cl_3]$ units. The metal

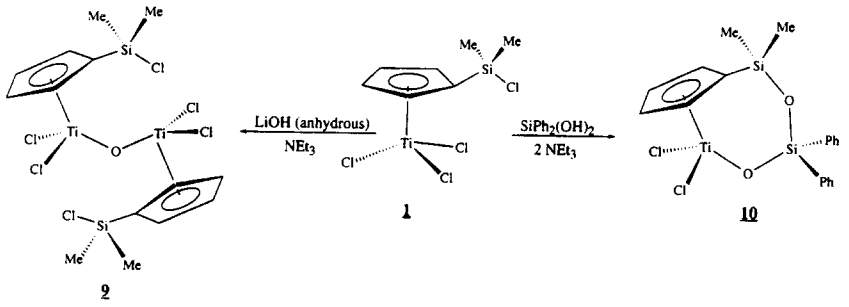

Scheme 2.

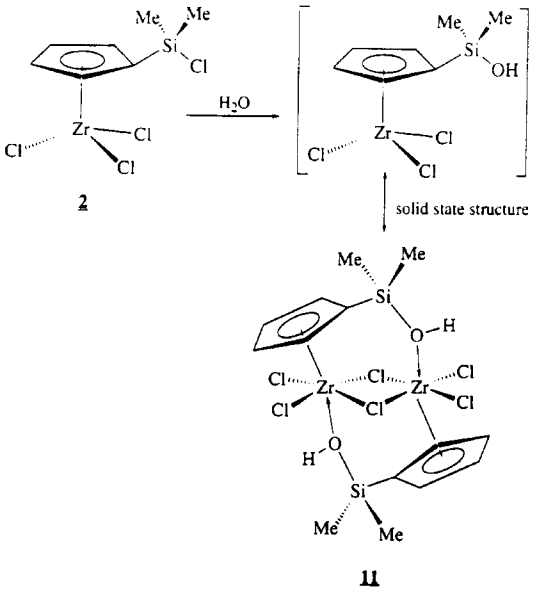

Scheme 3.

centre can be considered as having a distorted octahedral environment, surrounded by a silyl substituted cyclopentadienyl ligand that occupies one coordination site, four chlorine atoms defining the equatorial positions (two of which act as terminal atoms and the other two bridging the adjacent zirconium atoms) and a hydroxy group bound to the silicon of the neighbouring silyl group of the other cyclopentadienyl unit in a *trans* position with respect to the ring. The metal atom is located above the plane defined by its chloride substituents (0.5785 Å). The Zr—Cl terminal distances are slightly different (Zr(1)—Cl(2), 2.435(2) Å and Zr(1)—Cl(3), 2.456 (2) Å) despite the symmetry of the molecule. The dimer is centrosymmetric and exhibits the trapezoidal $[Zr_2(\mu\text{-}Cl)_2]$ fragment found in analogous monocyclopentadienyl zirconium derivatives [20] and other related cyclopentadienyl free ligand complexes [21]. The two Zr—Cl bridging distances are longer than the terminal Zr—Cl bonds and remain inequivalent (Zr(1)—Cl(1), 2.612(1) Å and Zr(1)—Cl(1a), 2.646(1) Å).

The Zr—Cp(centroid) bond distance of 2.216 Å can be compared to the values reported for other similar complexes such as 2.19 Å for $Zr(C_5H_5)Cl_3$ [20a] or 2.20 Å for $Zr(\eta^5\text{-}C_5H_5)_2Cl_2$ [22] but is smaller than in the related complex $Zr[\eta^5\text{-}C_5H_3\text{-}1,3\text{-}(SiMe_2CH_2P^iPr_2)_2]Cl_3$ (2.260 Å) [23]. The loss of the polymeric structure found in $Zr(\eta^5\text{-}C_5H_5)Cl_3$ must be attributed to the formation of the hydroxo adduct, *trans* to the cyclopentadienyl group. The Zr(1)—O(1) bond distance of 2.321(4) Å is comparable to that found in other monocyclopentadienyl zirconium adduct complexes such as $Zr(\eta^5\text{-}C_5H_5)Cl_3 \cdot 2THF$ (2.393 and 2.314 Å) or $Zr(\eta^5\text{-}C_5H_4Me)Cl_3 \cdot 2THF$ (2.377 and 2.310 Å) [24], although higher than that observed for terminal hydroxo complexes such as $Zr(\eta^5\text{-}C_5Me_5)_2(OH)_2$ (1.982 and 1.975 Å) [25] or $Zr(\eta^5\text{-}C_5Me_5)_2(OH)Cl$ (1.950 Å) [25].

If the centroid of the silyl-substituted ring is considered as a coordination site bonded to zirconium, the structure of **11** can be viewed as showing an eight-membered ring $(Zr—O—Si—Cp)_2$ with two interanular Zr—Cl—Zr connections (Fig. 2*A*). This eight-membered core has also been observed in other titanium and zirconium compounds: $[TiCl_2\{\mu\text{-}(\eta^5\text{-}\eta^1\text{-}C_5H_4SiMe_2O)\}]_2$ [8] (Fig. 2*B*) and $[Zr\{\eta^5\text{-}C_5H_4SiMe_2(\mu\text{-}O)\}Cl_2\{H_2NCH(Me)Ph\}]_2$ [17] (Fig. 2*C*). The zirconium derivative (*A*) exhibits a "chair conformation" similar to that found in the titanium compound (*B*), with the main plane of this chair conformation perpendicular to the plane defined by the zirconium and the bridged chlorine atoms (Fig. 3). The zirconium compound (*C*) shows a planar disposition for the cycle. The difference between the $(M—O—Si—Cp)_2$ cores displayed in *A* and *B* is a variation in those atoms located out of the plane. In compound **11** (*A*), the silicon atoms are located at ±0.6101 Å from the plane defined by the rest of the atoms, whereas in the structure *B* the cyclopentadienyl rings are located out of the plane. The structure *C* can also be considered as two lateral Zr—Cp—Si—O "oxazirconacycle" rings connected by a central $[Zr(\mu\text{-}O)]_2$ ring with the angle values substantialy away from linearity ($\alpha = 141.6$ and $\beta = 108.2°$). The

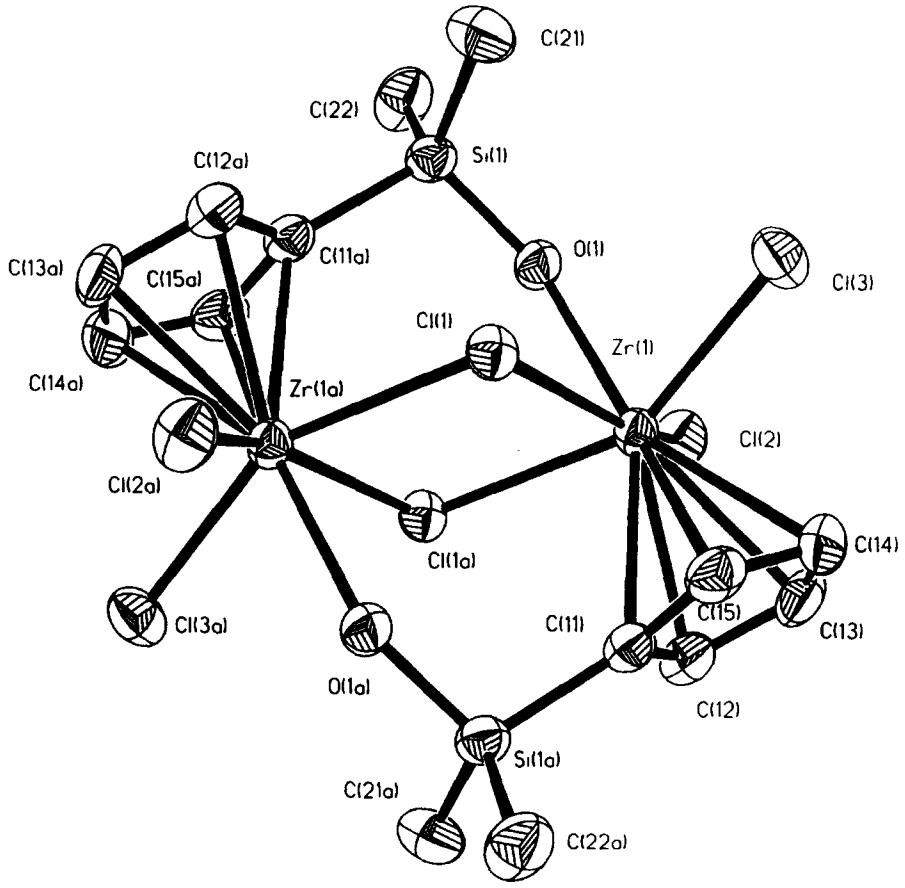

Fig. 1. ORTEP view of the molecular structure of $[Zr\{\eta^5\text{-}C_5H_4SiMe_2(\mu\text{-}OH)\}(\mu\text{-}Cl)Cl_2]_2$ **11** with the atom-numbering scheme.

Table 1. Selected bond lengths [Å] and angles [°] for **11**

Zr(1)—O(1)	2.321(4)	Zr(1)—Cl(2)	2.435(2)
Zr(1)—Cl(3)	2.456(2)	Zr(1)—C(12)	2.489(6)
Zr(1)—C(11)	2.506(5)	Zr(1)—C(13)	2.520(6)
Zr(1)—C(15)	2.525(6)	Zr(1)—C(14)	2.548(6)
Zr(1)—Cl(1)	2.612(1)	Zr(1)—Cl(1a)	2.646(1)
Cl(1)—Zr(1a)	2.646(1)	Si(1)—O(1)	1.697(4)
Si(1)—C(22)	1.846(6)	Si(1)—C(21)	1.838(7)
Si(1)—C(11a)	1.868(6)	C(11)—C(12)	1.419(8)
C(11)—C(15)	1.413(8)	C(11)—Si(1a)	1.868(6)
C(12)—C(13)	1.405(8)	C(13)—C(14)	1.382(10)
C(15)—C(14)	1.404(9)	Zr(1)—Cp(1)	2.216

O(1)—Zr(1)—Cl(2)	76.39(10)	O(1)—Zr(1)—Cl(3)	77.79(10)
Cl(2)—Zr(1)—Cl(3)	96.99(6)	O(1)—Zr(1)—Cl(1)	77.03(10)
Cl(2)—Zr(1)—Cl(1)	151.60(5)	Cl(3)—Zr(1)—Cl(1)	87.00(5)
O(1)—Zr(1)—Cl(1a)	75.67(10)	Cl(2)—Zr(1)—Cl(1a)	85.72(5)
Cl(3)—Zr(1)—Cl(1a)	151.87(5)	Cl(1)—Zr(1)—Cl(1a)	78.17(4)
Zr(1)—Cl(1)—Zr(1a)	101.83(4)	O(1)—Si(1)—C(22)	106.0(3)
O(1)—Si(1)—C(21)	110.9(3)	C(22)—Si(1)—C(21)	112.3(3)
Si(1)—O(1)—Zr(1)	141.4(2)	O(1)—Zr(1)—Cp(1)	178.76
Cl(1)—Zr(1)—Cp(1)	103.09	Cl(1a)—Zr(1)—Cp(1)	103.13
Cl(2)—Zr(1)—Cp(1)	103.27	Cl(3)—Zr(1)—Cp(1)	103.45

Symmetry transformations used to generate equivalent atoms: $-x$, $-y+2$, $-z+1$.
Cp(1) is the centroid of C11 C12 C13 C14 C15.

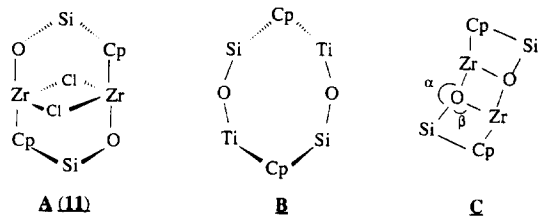

Fig. 2. Comparison of the eight-membered cores defined in the compounds $[Zr\{\eta^5\text{-}C_5H_4SiMe_2(\mu\text{-}OH)\}(\mu\text{-}Cl)Cl_2]_2$ (*A*, **11**). $[TiCl_2\{\mu\text{-}(\eta^5\text{-}\eta^1\text{-}C_5H_4SiMe_2O)\}]_2$ (*B*) and $[Zr\{\eta^5\text{-}C_5H_4SiMe_2(\mu\text{-}O)\}Cl_2\{H_2NCH(Me)Ph\}]_2$ (*C*).

O(1)—Zr(1)—Cp(1) angle in *A* is almost linear (178.76°) whereas the value of the Si(1)—O(1)—Zr(1) and C(11a)—Si(1)—O(1) angles are 141.4(2) and 108.4(6)° respectively. The Zr(1)—Zr(1a) distance in compound **11** is 4.081 Å, larger than that found in the compound *C* (3.597 Å). The Ti—O—Si angle in the titanium compound *B* is larger (160.2°) than that found in *C* but smaller than that found in *A*. The metallic environment has a direct influence on the difference between these structures. Whereas the coordination around the titanium atom in *B* is pseudotetrahedral, the zirconium atom in *A* and *C* shows a pseudooctahedral environment and they adopt a disposition which allows their connection through the chlorine or oxygen bridges.

The formation of the adduct in complex **11** is related to the structure of the starting material **2**, in which the hydroxo group has probably been replaced by a chlorine atom. Therefore, we tentatively assume a dimeric structure in the solid state for complex **2**, instead of a polymeric structure that may be envisaged for less hindered substituted cyclopentadienyl ligands.

EXPERIMENTAL

All manipulations were performed under argon using Schlenk and high-vacuum line techniques or a glove box model HE-63. Solvents were purified by distillation under argon from an appropriate drying agent (sodium for toluene, sodium-potassium alloy for hexane and P_2O_5 for dichloromethane). $SiPh_2(OH)_2$ (Aldrich) and anhydrous LiOH (Ventron) were commercially obtained and used without further purification. NEt_3 (Fluka) was distilled from sodium before use and stored over 4 Å molecular sieves. $Ti[\eta^5\text{-}C_5H_4SiMe_2Cl]Cl_3$, **1** [8], $Zr[\eta^5\text{-}C_5H_4SiMe_2Cl]Cl_3$, **2** [8], $Tl(C_5H_5)$ [26] and $Tl(C_5H_4SiMe_3)$ [27] were prepared by known procedures. C, H and N microanalyses were performed on a Perkin–Elmer 240B and/or Heraeus CHN-O-Rapid microanalyzer. Electron impact (EI) mass spectra were recorded at 70 eV on a Hewlett-Packard 5988A spectrometer. IR spectra were recorded on a Perkin–Elmer 883 spectrophotometer using KBr pellets; only selected MS and IR data are reported. NMR spectra, measured at 25°C, were recorded on a Varian Unity FT-300 (^{1}H

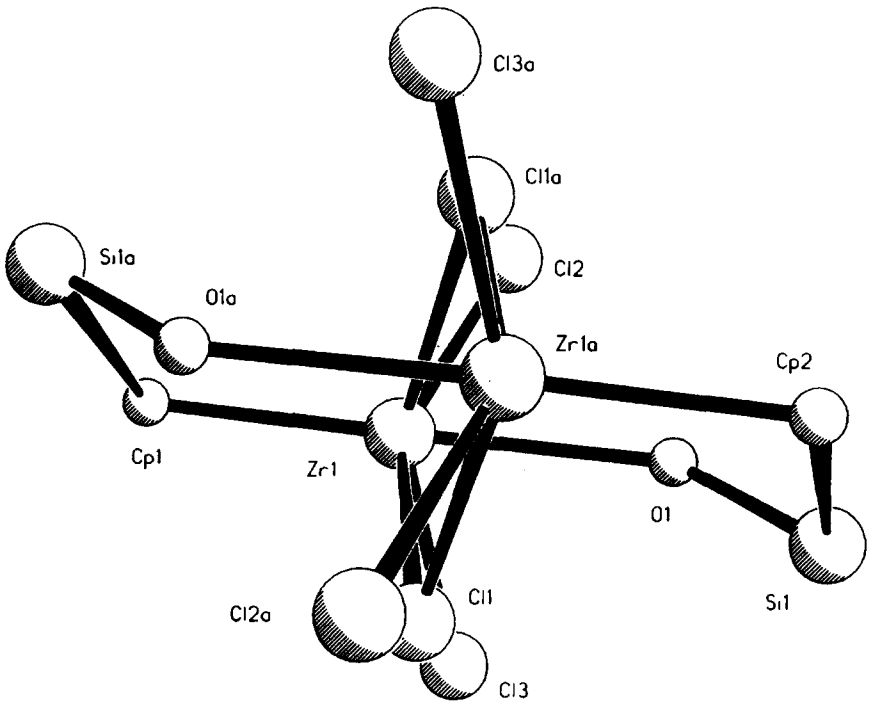

Fig. 3. "Chair-conformation" view of the eight-membered core found in compound **11**.

NMR at 300MHz, ^{13}C NMR at 75 MHz) spectrometer and chemical shifts are referenced to TMS via residual protons (^{1}H) or the carbon resonances (^{13}C) of the solvent.

Synthesis of $Ti(\eta^5\text{-}C_5H_5)(\eta^5\text{-}C_5H_4SiMe_2Cl)Cl_2$ (**3**)

A mixture of **1** (4.7 g, 15.1 mmol) and $Tl(C_5H_5)$ (4.1 g, 15.2 mmol) in 100 ml of toluene was refluxed for 5 h. A deep red solution was formed. The reaction mixture was filtered and the residue washed with dichloromethane (2 × 25 ml). The solutions were combined and solvent was removed *in vacuo*. The resulting crystalline solid was washed with cold hexane (2 × 50 ml) and dried under vacuum to obtain a red powder identified as **3** (4.2 g, 12.3 mmol, 82% yield). Anal. cald. for $C_{12}H_{15}Cl_3SiTi$: C: 42.20; H: 4.43. Found: C: 42.84; H: 4.36. ^{1}H NMR ($CDCl_3$): δ 0.74 (s, 6H, $SiMe_2$); 6.59 (s, 5H, C_5H_5); 6.61 (m, 2H, C_5H_4); 6.89 (m, 2H, C_5H_4). ^{1}H NMR (C_6D_6): δ 0.76 (s, 6H, $SiMe_2$): 5.65 (m, 2H, C_5H_4); 5.92 (s, 5H, C_5H_5) 6.42 (m, 2H, C_5H_4). $^{13}C\{^{1}H\}$ NMR ($CDCl_3$): δ 3.2 ($SiMe_2$); 119.7, 129.0 ($C_{2\text{-}5}$, C_5H_4); 120.6 (C_5H_5); 128.0 (C_{ipso}, C_5H_4). MS: *m/z* [assignment, R_{int} (%)]: 342 [M^+, 2]; 327 [$(M\text{-}CH_3)^+$, 1]; 305 [$(M\text{-}Cl)^+$, 12]; 277 [$(M\text{-}C_5H_5)^+$, 100]; 122 [$(C_5H_4SiMe_2)^+$, 92].

Synthesis of $Ti(\eta^5\text{-}C_5H_4SiMe_3)(\eta^5\text{-}C_5H_4SiMe_2Cl)Cl_2$ (**4**)

The same procedure described to prepare complex **3** using **1** (3.8 g, 12.2 mmol) and $Tl(C_5H_4SiMe_3)$ (4.2 g, 12.3 mmol) gave **4** as a reddish-brown powder (4.5 g, 10.9 mmol, 89% yield). Anal. cald. for $C_{15}H_{23}Cl_3Si_2Ti$: C: 43.54; H: 5.60. Found: C: 43.41; H: 5.50. ^{1}H NMR ($CDCl_3$): δ 0.27 (s, 9H, $SiMe_3$); 0.75 (s, 6H, $SiMe_2$); 6.56 (m, 2H, C_5H_4); 6.60 (m, 2H, C_5H_4); 6.81 (m, 4H, C_5H_4). ^{1}H NMR (C_6D_6): δ 0.28 (s, 9H, $SiMe_3$); 0.80 (s, 6H, $SiMe_2$); 5.74 (m, 2H, C_5H_4); 5.84 (m, 2H, C_5H_4); 6.37 (m, 2H, C_5H_4); 6.47 (m, 2H, C_5H_4). $^{13}C\{^{1}H\}$ NMR ($CDCl_3$): δ 0.0 ($SiMe_3$); 3.3 ($SiMe_2$); 118.2, 120.3, 129.8, 130.0 ($C_{2\text{-}5}$, C_5H_4); 128.3, 133.6 (C_{ipso}, C_5H_4). MS: *m/z* [assignment, R_{int} (%)]: 414 [M^+, 3]; 399 [$(M\text{-}CH_3)^+$, 8]; 377 [$(M\text{-}Cl)^+$, 6]; 277 [$(M\text{-}C_5H_4SiMe_3)^+$, 100]; 122 [$(C_5H_4SiMe_2)^+$, 58].

Synthesis of $Zr(\eta^5\text{-}C_5H_5)(\eta^5\text{-}C_5H_4SiMe_2Cl)Cl_2$ (**5**)

A mixture of **2** (10.6 g, 29.8 mmol) and $Tl(C_5H_5)$ (8.1 g, 30 mmol) in 200 ml of toluene was refluxed for 5 h. A colourless solution was formed. After filtration, the residue was washed with dichloromethane (2 × 75 ml). The solutions were combined and solvent was removed *in vacuo*. The resulting crystalline solid was washed with cold hexane (2 × 75 ml) and dried under vacuum to obtain an off-white powder identified as **5** (9.6 g, 27 mmol, 84% yield). Anal. cald. for $C_{12}H_{15}Cl_3SiZr$: C: 37.45; H: 3.93. Found: C: 37.30; H: 3.98. ^{1}H NMR ($CDCl_3$): δ 0.73 (s, 6H, $SiMe_2$); 6.49 (s, 5H, C_5H_5); 6.57 (m, 2H, C_5H_4); 6.79 (m, 2H, C_5H_4). ^{1}H NMR (C_6D_6): δ 0.67 (s, 6H, $SiMe_2$); 5.77 (m, 2H, C_5H_4); 5.91 (s, 5H, C_5H_5) 6.34 (m, 2H, C_5H_4). $^{13}C\{^{1}H\}$ NMR ($CDCl_3$): δ 3.1 ($SiMe_2$); 116.3 (C_5H_5); 117.0, 125.2 ($C_{2\text{-}5}$, C_5H_4); 121.7 (C_{ipso}, C_5H_4). MS: *m/z* [assignment, R_{int} (%)]: 384 [M^+, 4]; 369 [$(M\text{-}CH_3)^+$, 1]; 349 [$(M\text{-}Cl)^+$, 9]; 319 [$(M\text{-}C_5H_5)^+$, 100]; 122 [$(C_5H_4SiMe_2)^+$, 67].

Synthesis of $Zr(\eta^5\text{-}C_5H_4SiMe_3)(\eta^5\text{-}C_5H_4SiMe_2Cl)Cl_2$ (**6**)

The same procedure described to prepare complex **5** using **2** (5.3 g, 14.9 mmol) and $Tl(C_5H_4SiMe_3)$ (5.1 g, 14.9 mmol) gave **6** as an off-white powder (5.7 g, 12.4 mmol, 84% yield). Anal. cald. for $C_{15}H_{23}Cl_3Si_2Zr$: C: 39.41; H: 5.07. Found: C: 39.84; H: 5.19. ^{1}H NMR ($CDCl_3$): δ 0.28 (s, 9H, $SiMe_3$); 0.73 (s, 6H, $SiMe_2$); 6.53 (m, 4H, C_5H_4); 6.69 (m, 2H, C_5H_4); 6.74 (m, 2H, C_5H_4). ^{1}H NMR (C_6D_6): δ 0.28 (s, 9H, $SiMe_3$); 0.73 (s, 6H, $SiMe_2$); 5.83 (m, 2H, C_5H_4); 5.90 (m, 2H, C_5H_4); 6.34 (m, 2H, C_5H_4); 6.41 (m, 2H, C_5H_4). $^{13}C\{^{1}H\}$ NMR ($CDCl_3$): δ 0.0 ($SiMe_3$); 3.1($SiMe_2$); 115.8, 116.5, 125.8, 126.1 ($C_{2\text{-}5}$, C_5H_4); 121.7, 127.1 (C_{ipso}, C_5H_4). MS: *m/z* [assignment, R_{int} (%)]: 456 [M^+, 1]; 441 [$(M\text{-}CH_3)^-$, 30]; 421 [$(M\text{-}Cl)^+$, 4]; 319 [$(M\text{-}C_5H_4SiMe_3)^+$, 41]; 122 [$(C_5H_4SiMe_2)^+$, 100].

Synthesis of $[Ti(\eta^5\text{-}C_5H_5)Cl_2]_2[(\mu\text{-}\eta^5\text{-}\eta^5\text{-}C_5H_4SiMe_2)_2O]$ (**7**)

Distilled water (174 μl, 9.7 mmol) was added to 150 ml of dry toluene. This mixture was stirred for 15 h and then **3** (3.3 g, 9.7 mmol) was dissolved in portions. The reaction mixture was stirred at room temperature for 3 days. During the course of the reaction, a red crystalline solid formed which was collected by filtration, washed with both cold toluene (15 ml) and hexane (2 × 30 ml) and dried under vacuum at 110°C for 2 h to give **7** (1.6 g, 2.5 mmol, 53% yield based on starting complex **3**). Anal. cald. for $C_{24}H_{30}Cl_4OSi_2Ti_2$: C: 45.88; H: 4.81. Found: C: 46.42; H: 4.77. ^{1}H NMR ($CDCl_3$): δ 0.35 (s, 12H, $SiMe_2$); 6.56 (s, 10H, C_5H_5); 6.58 (m, 4H, C_5H_4); 6.88 (m, 4H, C_5H_4). $^{13}C\{^{1}H\}$ NMR ($CDCl_3$): δ 2.0 ($SiMe_2$); 120.4 (C_5H_5); 121.0, 129.2 ($C_{2\text{-}5}$, C_5H_4); 129.3 (C_{ipso}, C_5H_4). MS: *m/z* [assignment, R_{int} (%)]: 628 [M^+, not observed]; 378 [$(M\text{-}Cp_2TiCl_2)^+$, 14]; 343 [$(M\text{-}Cp_2TiCl_2\text{-}Cl)^+$, 9]; 248 [$(Cp_2TiCl_2)^+$, 23]; 183 [$(CpTiCl_2)^+$, 100]; 122 [$(C_5H_4SiMe_2)^+$, 41].

Synthesis of $[Ti(\eta^5\text{-}C_5H_4SiMe_3)Cl_2]_2[(\mu\text{-}[\eta^5\text{-}\eta^5\text{-}C_5H_4SiMe_2)_2O]$ (**8**)

The same procedure described to prepare complex **7** using **4** (2.9 g, 7.0 mmol) and distilled water (126 μl,

7.0 mmol) gave **8** as a microcrystalline red solid (1.3 g, 1.7 mmol, 49% yield based on starting complex **4**). Anal. cald. for $C_{30}H_{46}Cl_4OSi_4Ti_2$: C: 46.63; H: 6.00. Found: C: 46.23; H: 5.79. ^{1}H NMR ($CDCl_3$): δ 0.27 (s, 18H, $SiMe_3$); 0.35 (s, 12H, $SiMe_2$); 6.52 (m, 4H, C_5H_4); 6.58 (m, 4H, C_5H_4); 6.77 (m, 4H, C_5H_4); 6.81 (m, 4H, C_5H_4). ^{1}H NMR (CD_2Cl_2): δ 0.28 (s, 18H, $SiMe_3$); 0.36 (s, 12H, $SiMe_2$); 6.55 (m, 4H, C_5H_4); 6.60 (m, 4H, C_5H_4); 6.77 (m, 4H, C_5H_4); 6.80 (m, 4H, C_5H_4). $^{13}C\{^1H\}$ NMR ($CDCl_3$): δ 0.0 ($SiMe_3$); 2.1 ($SiMe_2$); 119.7, 120.0, 129.8, 130.2 (C_{2-5}, C_5H_4); 129.3, 133.2 (C_{ipso}, C_5H_4). MS: *m/z* [assignment, R_{int} (%)]: 772 [M^+, not observed]; 392 {[($C_5H_4SiMe_3)_2TiCl_2]^+$, 2}; 378 {[M-($C_5H_4SiMe_3)_2TiCl_2]^+$, 100}; 343 {[M-($C_5H_4SiMe_3)_2TiCl_2$-Cl]$^+$, 26}; 255 [($C_5H_4SiMe_3$)$TiCl_2^+$, 36]; 122 [($C_5H_4SiMe_2$)$^+$, 38].

Synthesis of [Ti(η^5-$C_5H_4SiMe_2Cl$)Cl_2]$_2$(μ-O) (**9**)

A suspension of anhydrous LiOH (93 mg, 3.8 mmol) and NEt_3 (0.53 ml, 3.8 mmol) was added to a solution of **1** (1.2 g, 3.8 mmol) in 50 ml of toluene. The reaction mixture was allowed to stir at room temperature for 20 h and then filtered. Solvent was completely removed from the resulting orange-yellow solution *in vacuo* to give **10** as a yellow solid which was further purified by recrystallization from a mixture of toluene (20 ml) and hexane (40 ml) at -40°C (0.46 g, 0.8 mmol, 42% yield based on starting complex **1**). Anal. cald. for $C_{14}H_{20}Cl_6OSi_2Ti_2$: C: 29.55; H: 3.54. Found: C: 29.90; H: 3.52. ^{1}H NMR ($CDCl_3$): δ 0.46 (s, 12H, $SiMe_2$); 7.06 (m, 4H, C_5H_4); 7.22 (m, 4H, C_5H_4). ^{1}H NMR (C_6D_6): δ 0.29 (s, 12H, $SiMe_2$); 6.22 (m, 4H, C_5H_4); 6.64 (m, 4H, C_5H_4). $^{13}C\{^1H\}$ NMR ($CDCl_3$): δ 1.3 ($SiMe_2$); 126.4, 129.1 (C_{2-5}, C_5H_4); 139.3 (C_{ipso}, C_5H_4). MS: *m/z* [assignment, R_{int} (%)]: 568 [M^+, not observed]; 553 [(M-CH_3)$^+$, 3]; 277 [($C_5H_4SiMe_2TiCl_2$)$^+$, 75]; 122 [($C_5H_4SiMe_2$)$^+$, 100]. IR (KBr, cm^{-1}): ν(Ti—O—Ti) = 798.

Synthesis of Ti($\eta^5C_5H_4SiMe_2OSiPh_2$-$\eta^1$-O)$Cl_2$ (**10**)

To a cooled (-60°C) suspension of **1** (2.0 g, 6.4 mmol) in 100 ml of hexane, a suspension of $SiPh_2(OH)_2$ (1.39 g, 6.4 mmol) and NEt_3 (1.77 ml, 12.8 mmol) was added. The cold bath was allowed to warm to room temperature and the reaction mixture was stirred overnight and then filtered. The resulting solution was concentrated *in vacuo* to 10 ml and stored overnight at -30°C to obtain yellow needles identified as **9**. The product was further purified by recrystallization from hexane (1.3 g, 2.9 mmol, 45% yield). Anal. cald. for $C_{19}H_{20}Cl_2O_2Si_2Ti$: C: 50.12; H: 4.43. Found: C: 50.14; H: 4.75. ^{1}H NMR ($CDCl_3$): δ 0.48 (s, 6H, $SiMe_2$); 6.75 (m, 2H, C_5H_4); 7.13 (m, 2H, C_5H_4); 7.37–7.41 (m, 6H, Ph); 7.62–7.65 (m, 4H, Ph). ^{1}H NMR (C_6D_6): δ 0.17 (s, 6H, $SiMe_2$); 6.26 (m, 2H, C_5H_4); 6.50 (m, 2H, C_5H_4); 7.13–7.15 (m, 6H, Ph); 7.76–7.80 (m, 4H, Ph). $^{13}C\{^1H\}$ NMR ($CDCl_3$): δ 0.1 ($SiMe_2$); 125.3, 125.6 ($C_{2\ 5}$, C_5H_4); 128.0, 130.8, 134.2 (C_{ortho}, C_{meta}, C_{para}, Ph); 130.3 (C_{ipso}, C_5H_4); 133.0 (C_{ipso}, Ph). MS: *m/z* [assignment, R_{int} (%)]: 454 [M^+, 13]; 439 [(M-CH_3)$^+$, 23]; 377 [(M-Ph)$^+$, 50]; 300 [(M-2Ph)$^+$, 52].

Synthesis of [Zr{η^5-$C_5H_4SiMe_2$(μ-OH)}(μ-Cl)Cl_2]$_2$ (**11**)

Distilled water (0.1 ml, 5.6 mmol) was added to 50 ml of dry toluene. This mixture was stirred for 15 h and after this time this solution was added dropwise over a period of 2 h to a solution of **2** (2.0 g, 5.6 mmol) in 200 ml of dry toluene cooled to 0°C. The reaction mixture was stirred at room temperature overnight. During the course of the reaction, off-white crystals formed (some of them suitable for X-ray crystallographic analysis) which were collected by filtration, washed with dichloromethane (50 ml) and hexane (2 × 50 ml) and dried under vacuum to give **11** (0.9 g, 1.3 mmol, 47% yield). Anal. cald. for $C_{14}H_{22}Cl_6O_2Si_2Zr_2$: C: 24.96; H: 3.29. Found: C: 24.49; H: 3.32. IR (KBr, cm^{-1}): ν(Si—OH) = 3604. NMR data are not reported because the product was insoluble in common deuterated solvents.

Crystal structure determination of [Zr{η^5-C_5H_4Si Me_2(μ-OH)}(μ-Cl)Cl_2]$_2$ (**11**)

Off-white crystals of compound **11** were obtained by crystallization from dry toluene and a suitable sized crystal was mounted in a Lindemann tube and mounted in an Enraf-Nonius CAD 4 automatic four-circle difractometer with graphite monochromated Mo–K_α radiation (λ = 0.71073 Å). Crystallographic and experimental details are summarized in Table 2. Data were collected at room temperature. Intensities were corrected for Lorentz and polarization effects in the usual manner. No absorption or extintion correction were made. The structure was solved by direct methods (SHELXL 90) [28] and refined by least squares against F^2 (SHELXL 93) [29]. All non-hydrogen atoms were refined anisotropically, and the hydrogen atoms were introduced from geometrical calculations and refined using a riding model with thermal parameters equivalent to those of the atoms to which they are bonded. The hydrogen atom of the hydroxo group was not included. Calculations were carried out on an ALPHA AXP(Digital) workstation.

Supplementary material—A list of the positional parameters and their standard deviations, a complete list of bond lengths and angles, anisotropic displacement parameters, the calculated fractional coordinates of the hydrogen atoms and a list of observed and calculated structure factors are available from author T. C. upon request.

Acknowledgments—We are grateful to the DGICYT (Project PB-92-0178-C) and University of Alcalá for financial support

Table 2. Crystal, experimental data and structure refinement procedures for compound **11**

Formula	$C_{14}H_{22}Cl_6O_2Si_2Zr_2$
Crystal habit	Prismatic
Color	white
Crystal size	$0.25 \times 0.30 \times 0.35$mm
Symmetry	Monoclinic, $P2_1/a$
Unit cell dimensions	
a (Å)	8.767(1)
b (Å)	16.115(1)
c (Å)	9.1480(1)
β (°)	115.71(1)
V, Å^3	1164.4(2)
Z	4
D_{calc}, g cm^{-3}	1.915
M_w	335.82
$F(000)$	660
μ, cm^{-1}	16.946
Scan mode	$\omega/2\theta$ $2.47 < \theta < 28.18$
No. of reflections	
Measured	3095
Independent observed	2863 ($R_{int} = 0.0190$)
Range of h, k, l	$-11 < h < 0, -21 < k < 0, -12 < l < 12$
Standard reflections	3 every 200 refl.
Refinement method	Full matrix least squares on F^2.
Final R indices ($I > 2\sigma(I)$)[a]	$R_1 = 0.0330, wR_2 = 0.0749$
R indices (all data)	$R_1 = 0.0514, wR_2 = 0.1117$
Weighting scheme	calc. $\omega = 1/[\sigma^2(F_o^2) + (0.0846P)^2 + 10.1458P]'$ where $P = (F_o^2 + 2F_c^2)/3$
Max peak in final diff. map (e/Å3)	0.975
Min peak in final diff. map (e/Å3)	−0.753
Goodness-of-fit on F^2	0.537

[a] $R_1 = \Sigma\|F_o| - |F_c|/\Sigma|F_o|$; $wR_2 = \{[\Sigma\omega(F_o^2 - F_c^2)]/[\Sigma\omega(F_o^2)^2]\}^{1/2}$.

of this research. S.C. acknowledges the MEC for providing a fellowship. A.M. is grateful to the Consejería Educación (CAM) for a fellowship.

REFERENCES

1. (a) Davies, S. G., *Organotransition Metal Chemistry: Applications to Organic Syhthesis.* Pergamon Press, 1989. (b) ed. Abel, E. W., Stone F. G. A., Wilkinson G., *Comprehensive Organometallic Chemistry II. A Review of the Literature* (1982–1994). Vol 4, p. 213–632, 1994.
2. (a) Kaminsky, W., Sinn, H. (Eds.) *Transition Metals and Organometallics as Catalysts for Olefin Polymerization.* Springer New York, 1988. (b) Möhring, P. C. and Coville, N. J., *J. Organomet. Chem.*, 1994, **479,** 1. (c) Brintzinger, H. H., Fischer, D., Mülhaupt, R., Rieger, B. and Waymouth, R. M., *Angew. Chem., Int. Ed. Engl.*, 1995, **34,** 1143. (d) Bochmann, M., *J. Chem. Soc., Dalton Trans.*, 1996, 225.
3. (a) Okuda, J., *Comments Inorg. Chem.*, 1994, **16,** 185. (b) Jutzi, P. and Siemeling, U., *J. Organomet. Chem.*, 1995, **500,** 175 and references therein.
4. (a) Allum, K. G., Hancock, R. D., Howell, I. V., McKenzie, S., Pitkethly, R. C. and Robinson, P. J., *J. Organomet. Chem.*, 1975, **87,** 203. (b) Lau, C. P., Chang, B. H., Grubbs, R. H. and Brubaker, C. H., *J. Organomet. Chem.*, 1981, **214,** 325. (c) Booth, B. L., Ofunne, G. C., Stacey, C. and Tait, P. J. T., *J. Organomet. Chem.*, 1986, **315,** 143. (d) Antberg, M., Lüker, H. and Böhm, L., *Eur. Pat. Appl.*, EP 293,815, 1988, Hoechst A.-G. (*Chem Abstr.*, 1989, **111,** 195585).
5. (a) Cermak, J., Kvicalova, M., Blechta, V., Capka, M. and Bastl, Z., *J. Organomet. Chem.*, 1996, **509,** 77 and references therein.
6. (a) Curtis, M. D., D'Errico, J. J., Duffy, D. N., Epstein, P. S. and Bell, L. G., *Organometallics*, 1983, **2,** 1808. (b) Manners, I., *Angew. Chem., Int. Ed. Engl.*, 1996, **35,** 1602.
7. Reissova, A., Bastl, Z. and Capka, M., *Collect. Czech., Chem. Commun.*, 1986, **51,** 1430.
8. Ciruelos, S., Cuenca, T., Gómez-Sal, P., Manzanero, A. and Royo, P., *Organometallics*, 1995, **14,** 177.
9. (a) Rogers, R. D., Benning, M. M., Kurihara, L. K., Moriarty, K. J. and Rausch, M. D., *J. Organomet. Chem.*, 1985, **293,** 51. (b) Osaga, M., Mallin, D. T., Macomber, D. W., Rausch, M. D., Rogers, R. D. and Rollins, A. N., *J. Organomet. Chem.*, 1991, **405,** 41.
10. (a) Churakov, A. V., Lemenovskii, D. A. and Kuz'mina, L. G., *J. Organomet. Chem.*, 1995, **489,** C81. (b) Deck, P. A., Fisher, T. S. and Downey,

J. S., *Organometallics*, 1997, **16,** 1193. (c) Lisowsky, R., *Eur. Pat. Appl.*, EP 760,374, 1997, Witco. (*Chem. Abstr.*, 1997, **126,** 225413).
11. (a) Cuenca, T., Flores, J. C., Gómez, R., Gómez-Sal, P., Parra-Hake, M. and Royo, P., *Inorg. Chem.*, 1993, **32,** 3608. (b) Lee, D.-H, Yoon, K.-B, Lee, E.-H., Noh, S.-K., Buyn, G. G. and Lee, C.-S., *Macromol. Rapid Commun.*, 1995, **16,** 265. (c) Huhmann, J. L., Corey, J. Y., Rath, N. P., *J. Organomet. Chem.*, 1997, **533,** 61.
12. Noh, S. K., Byun, G.-G., Lee, C.-S., Lee, D., Yoon, K.-B. and Kang, K. S., *J. Organomet. Chem.*, 1996, **518,** 1.
13. (a) Bajgur, C. S., Tikkanen, W. R. and Petersen, J. L., *Inorg. Chem.*, 1985, **24,** 2539. (b) Gómez, R., Cuenca, T., Royo, P., Herrmann, W.A. and Herdtweck, E., *J. Organomet. Chem.*, 1990, **382,** 103. (c) Gómez, R., Cuenca, T., Royo, P. and Hovestreydt, E., *Organometallics*, 1991, **10,** 2516.
14. (a) Reddy, K. P. and Petersen, J. L., *Organometallics*, 1989, **8,** 2107. (b) Ciruelo, G., Cuenca, T., Gómez-Sal, P., Martín, A. and Royo, P., *J. Chem. Soc., Dalton Trans.*, 1995, 231.
15. Lappert, M. F., Pickett, C. J., Riley, P. I. and Yarrow, P. I. W., *J. Chem. Soc., Dalton Trans.*, 1981, 805.
16. (a) Hughes, A. K., Meetsma, A. and Teuben, J. H., *Organometallics*, 1993, **12,** 1936. (b) Trouve, G., Laske, D.A., Meetsma, A. and Teuben, J. H., *J. Organomet. Chem.*, 1996, **511,** 255.
17. Ciruelos, S., Cuenca, T., Gómez, R., Gómez-Sal, P., Manzanero, A. and Royo, P., *Organometallics*, 1996, **15,** 5577.
18. (a) Palacios, F., Royo, P., Serrano, R., Balcázar, J. L., Fonseca, I. and Florencio, F., *J. Organomet. Chem.*, 1989, **375,** 51. (b) Babcock, L. M., Day, V. W. and Klemperer, W. G., *J. Chem. Soc., Chem. Commun.*, 1987, 858.
19. Liu, F. Q., Roesky, H. W., Schmidt, H. G. and Noltemeyer, M., *Organometallics*, 1992, **11,** 2965.
20. (a) Engelhardt, L. M., Papasergio, R. I., Raston, C. L. and White, A. H., *Organometallics*, 1984, **3,** 18. (b) Martín, M., Mena, M. and Palacios, F., *J. Organomet. Chem.*, 1994, **480,** C10. (c) Arnold, J., Engeler, M. P., Elsner, F. H., Heyn, R. H. and Tilley, T. D., *Organometallics*, 1989, **8,** 2284.
21. (a) Herrmann, W. A., Huber, N. W. and Behm, J., *Chem. Ber.*, 1992, 125, 1405. (b) Fenske, D., Hartmann, E. and Dehnicke, K., *Naturforsch*, 1988, **43B,** 1611.
22. Prout, K., Cameron, T. S., Forder, R. A., Critchley, S. R., Denton, B. and Rees, G. V., *Acta Crystallogr., Sect.B*, 1974, **30B,** 2290.
23. Fryzuk, M. D., Mao, S. S. H., Duval, P. B. and Rettig, S. J., *Polyhedron*, 1995, **14,** 11.
24. Erker, G., Sarter, C., Albrecht, M., Dehnicke, S., Kruger, C., Raabe, E., Schlund, R., Benn, R. and Rufinska, A., *J. Organomet. Chem.*, 1990, **382,** 89.
25. Bortolin, R., Pavel, V., Munday, J., Taylor, N. J. and Carty, A. J., *J. Chem. Soc., Chem. Commun.*, 1985, 456.
26. Brauer, H. G., *Handbuch der Präparativen Anorganischen Chemie.*, F. Enke Verlag, Stuttgart, 1981, Vol III, p 1811.
27. Harvey, S., Raston, C. L., Skelton, B. W., White, A. H., Lappert, M. F. and Srivastava, G., *J. Organomet. Chem.*, 1987, **328,** C1.
28. Sheldrick, G. M., *Acta Crystallogr. Sect. A*, 1990, **46,** 467.
29. Sheldrick, G. M. SHELXL 93, University of Gottingen, Gottingen, Germany, 1993.

Pergamon

PII: S0277-5387(97)00492-0

Polyhedron Vol. 17, No. 7, pp. 1065–1071, 1998
© 1998 Elsevier Science Ltd
All rights reserved. Printed in Great Britain
0277-5387/98 $19.00+0.00

Cationic monocyclooctatetraenyl-lanthanoid complexes derived from metallic lanthanoid: crystal structures of $[Sm(\eta^8\text{-}C_8H_8)(hmpa)_3]I$ and $[Sm(\eta^8\text{-}C_8H_8)(hmpa)_3][Sm(\eta^8\text{-}C_8H_8)_2]$ (HMPA = hexamethylphosphoric triamide)†

Kazushi Mashima,[a]* Hiroki Fukumoto,[a] Yuushou Nakayama,[b] Kazuhide Tani,[a] and Akira Nakamura[b]

[a] Department of Chemistry, Graduate School of Engineering Science, Osaka University, Toyonaka, Osaka 560, Japan

[b] Department of Macromolecular Science, Graduate School of Science, Osaka University, Toyonaka, Osaka 560, Japan

(Received 15 October 1997; accepted 14 November 1997)

Abstract—Addition of an excess hexamethylphosphoric triamide (abbr. HMPA) to a neutral complex $SmI(\eta^8\text{-}C_8H_8)(thf)$ (**1**) (C_8H_8 = 1,3,5,7-cyclooctatetraene), which was prepared by a direct reaction of metallic samarium with C_8H_8 in the presence of iodine in THF, afforded a cationic samarium complex $[Sm(\eta^8\text{-}C_8H_8)(hmpa)_3]I$ (**2**). Complex **2** can also be prepared by a simple one-pot reaction of stoichiometric amounts of metallic samarium, cyclooctatetraene, and iodine in the presence of an excess HMPA at 50°C. With a catalytic amount of iodine, ionic complexes of general formula $[Ln(\eta^8\text{-}C_8H_8)(hmpa)_n][Ln(\eta^8\text{-}C_8H_8)_2]$ [Ln = La and n = 4 (**6**); Ln = Sm and n = 3 (**7**)] were obtained by treating metallic lanthanum or samarium, respectively, with cyclooctatetraene in the presence of HMPA. The structure of the diamagnetic complex **6** as well as the paramagnetic complexes **2** and **7** was determined by ^1H NMR spectroscopy. Crystal structures of **2** and **7** were revealed by X-ray analyses, indicating that these complexes comprised of a cationic $[Sm(\eta^8\text{-}C_8H_8)(hmpa)_3]^+$ and an anionic part; for **2** and **7** being I^- and $[Sm(\eta^8\text{-}C_8H_8)_2]^-$, respectively. © 1998 Elsevier Science Ltd. All rights reserved

Keywords: lanthanum; samarium; cyclooctatetraene; hexamethylphosphoric triamide; cationic complex; anionic complex; sandwich complex; half-sandwich complex.

Dianion of 1,3,5,7-cyclooctatetraene ($C_8H_8^{2-}$) is one of the aromatic cyclic hydrocarbons. This dianion has attracted less interest as the unique π-conjugated multicenter ligand for organometallic complexes, though cyclopentadienyl ligand ($C_5H_5^-$) and its derivatives have been utilized as the unique and versatile ligands for a wide variety of organometallic complexes including organolanthanoid complexes [1]. The size of the dianion ligand is larger than that of cyclopentadienyl, and thus this ligand is expected to have the capability of suitably coordinating to highly electropositive lanthanide elements, producing various mono- and bis-cyclooctatetraenyl-lanthanoid complexes [2–4]. These complexes have so far been classified into three categories (1) the half sandwich type $Ln(\eta^8\text{-}C_8H_8)XL_n$, (2) the cationic half sandwich type $[Ln(\eta^8\text{-}C_8H_8)L_n]^+$, and (3) the anionic sandwich type $[Ln(\eta^8\text{-}C_8H_8)_2]^-$. These complexes have been mostly prepared by the metathesis reaction of lanthanoid halides with alkali compounds such as $K_2(C_8H_8)$. The isolation of the product from the resulting salt has been difficult and hampered due to the strong interaction between the salt and the organolanthanoid complexes. The salt-

† Dedicated to Prof. Dr W. A. Herrmann on the occasion of his 50th birthday.

* Author to whom correspondence should be addressed.

free method (oxidative reaction of low-valent organolanthanoid complexes [5–11], the reaction of metallic lanthanoid with organomercury compounds [12–16], and so on) has been developed recently by several research groups. We have developed a more convenient synthetic method, i.e., the reaction of metallic lanthanoid with oxidant which gives simple crystallization affording pure compounds in modest yields [17–23].

As an extension of our synthetic strategy, we report on the synthesis of a cationic monocyclooctatetraenyl lanthanoid complex $[Sm(\eta^8\text{-}C_8H_8)(hmpa)_3]I$ (**2**) and ionic complexes of general formula $[Ln(\eta^8\text{-}C_8H_8)(hmpa)_n][Ln(\eta^8\text{-}C_8H_8)_2]$, [Ln = La and $n = 4$ (**6**); Ln = Sm and $n = 3$ (**7**)] which were derived from metallic lanthanoids and cyclooctatetraene in the presence of HMPA with a stoichiometric or a catalytic amount of iodine. Crystal structures of **2** and **7** comprised of a cationic $[Sm(\eta^8\text{-}C_8H_8)(hmpa)_3]^+$ and an anionic part; and for **2** and **7**, I^- and $[Sm(\eta^8\text{-}C_8H_8)_2]^-$, respectively, were characterized crystallographically.

RESULTS AND DISCUSSION

Synthesis of cationic cyclooctatetraenyl-lanthanoid complexes

We have previously reported that the reaction of metallic samarium with equimolar amounts of cyclooctatetraene and iodine in THF resulted in the quantitative formation of a violet complex, which became opaque under the flow of argon, indicating that the THF ligand is labile, and readily released under reduced pressure to give $(\eta^8\text{-}C_8H_8)SmI(thf)$ (**1**) (eqn (1)) [17,19]; in accordance with the lability of the THF ligand of a samarocene complex $Cp^*_2Sm(thf)_2$ which gives Cp^*_2Sm in high vacuum [24]. Hexamethylphosphoric triamide (= HMPA) is known to be much stronger donor ligand and sometimes causes the cleavage of the Ln—X bond to give a cationic lanthanoid complexes; e.g., $[Yb(hmpa)_4(thf)_2]I_2$ [25], $[\{Yb(hmpa)_3\}(\mu\text{-}SPh)_3\{Yb(hmpa)_3\}][SPh]$ [23], and $[Ln(Spy)_2(hmpa)_3]I$ (Ln = Pr, Nd, Sm, Eu, Er, Yb) [22]. Thus, addition of HMPA to a THF solution of **1** gave rise to a cationic complex $[(\eta^8\text{-}C_8H_8)Sm(hmpa)_3]^+I^-$ (**2**) (eqn (2)). It is tempting to speculate that the reactions depicted in eqns (1) and (2) proceeded in one-pot; this was the case that a reaction mixture involving equimolar amounts of metallic samarium, cyclooctatetraene, and iodine in the presence of an excess HMPA, resulted in the formation of **2** in 34% yield.

$$\mathrm{Sm\,(metal)} + C_8H_8 + 1/2\,I_2 \xrightarrow[\mathrm{THF}]{} (\eta^8\text{-}C_8H_8)SI(thf) \quad \textbf{(1)}$$

1

$$\mathbf{1} + \mathrm{ex.\ HMPA} \xrightarrow[\mathrm{THF}]{} [(\eta^8\text{-}C_8H_8)Sm(hmpa)_3]I \quad (2)$$

2

The ^1H NMR spectrum of **2** in THF-d_8 displayed a singlet at δ 10.7 due to a dianionic C_8H_8 ligand together with a broad resonance around δ 2.58 assignable to the HMPA ligand. Although chemical shift values of paramagnetic lanthanide complexes depend on the condition, especially the concentration and the temperature, the chemical shift value of $\eta^8\text{-}C_8H_8$ of **2** is comparable to that found for Sm(III)—C_8H_8 complexes such as **1** (δ 12.4) [17,19], $([Sm(\mu\text{-}SC_6H_5)(\eta^8\text{-}C_8H_8)(thf)_2]_2$ (**3**) (δ 11.2) [18,19], $[Sm(\mu\text{-}SeC_6H_5)(\eta^8\text{-}C_8H_8)(thf)_2]_2$ (**4**) (δ 11.5) [18], and $[Sm(\mu\text{-}SC_6H_2Pr^i_3\text{-}2,4,6)(\eta^8\text{-}C_8H_8)(thf)]_2$ (**5**) (δ 11.3) [18,19].

These Sm(III)-calcogenolate complexes **3** and **4** together with $[(\eta^8\text{-}C_8H_8)CeCl(thf)_2]_2$ [26], $(\eta^8\text{-}C_8H_8)CeI(thf)_3$ [19], and $(\eta^8\text{-}C_8H_8)Sm(Spy)(hmpa)_2$ [27] adopt four-legged piano-stool geometry, whereas **5** [18,19] and $(\eta^8\text{-}C_8H_8)Yb(py)_3$ [28] have been crystallographically determined to have three-legged piano-stool geometry. On the basis of integration ratio (approximately 8 : 54) of protons due to one $\eta^8\text{-}C_8H_8$ and three HMPA ligands, respectively, three HMPA ligands presumably coordinated to the samarium center, corresponding to the neutral formulation of $(\eta^8\text{-}C_8H_8)SmI(hmpa)_3$ as opposed to a cationic formulation of **2**, which ultimately determined by X-ray crystallography (*vide infra*), it thus was difficult to assign the ^1H NMR spectrum of **2** to a cationic HMPA complex of Sm(III).

Cationic lanthanide(III) complexes of general formula $[Ln(\eta^8\text{-}C_8H_8)(hmpa)_n][Ln(\eta^8\text{-}C_8H_8)_2]$ [Ln = La and $n = 4$ (**6**); Ln = Sm and $n = 3$ (**7**)] were prepared in modest yields by the direct reaction of metallic lanthanoid with C_8H_8 in the presence of catalytic amounts of iodine (for activating lanthanide metal) and an excess HMPA at 50°C for several days (eqn (3)). Once isolated as crystals, complexes **6** and **7** have very low solubility in common organic solvents such as toluene or THF.

$$2\,\mathrm{Ln\,(metal)} + 3\,C_8H_8 + \mathrm{ex.\ HMPA} \xrightarrow[\mathrm{THF}]{} [Ln(\eta^8\text{-}C_8H_8)(hmpa)_n][Ln(\eta^8\text{-}C_8H_8)_2] \quad (3)$$

6 Ln = La; $n = 4$

7 Ln = Sm; $n = 3$

Structure of **6** made of a cationic $[La(\eta^8\text{-}C_8H_8)(hmpa)_4]^+$ and an anionic $[La(\eta^8\text{-}C_8H_8)_2]^-$ can be determined on the basis of ^1H NMR spectroscopy, while that of complex **7** comprised of a cationic $[Sm(\eta^8\text{-}C_8H_8)(hmpa)_3]^+$ and an anionic $[Sm(\eta^8\text{-}C_8H_8)_2]^-$ was characterized by ^1H NMR spectroscopy together with an X-ray crystallographic study (*vide infra*). The ^1H NMR spectrum of **6** in THF-d_8 displayed two singlet resonances due to two kinds of C_8H_8 ligands at δ 6.17 and 5.74 in the ratio of 1 : 2; thus these corresponded to the cationic and anionic parts, respectively. In addition to the signals of the C_8H_8 ligands, a broad singlet was observed at δ 2.44 due to the four HMPA molecules coordinated to the

lanthanum center of the cationic part. In contrast to the formulation of the complex **6**, the cationic center of the complex **7** has three HMPA ligands; the ^{1}H NMR spectrum of **7** in THF-d_8 exhibited a rather broad singlet of the HMPA ligands around δ 2.28 together with two singlets at δ 13.2 and 10.1 due to two kinds of C_8H_8 protons. The different number of the coordinated HMPA ligands between **6** and **7** might be attributed to the difference of ionic radii; larger lanthanum(III) center (1.061 Å) [29] can accept four HMPA ligands but smaller samarium(III) center (0.964 Å) [29] favors a three-legged piano-stool geometry as determined by X-ray analysis (*vide infra*).

Molecular structures of $[Sm(\eta^8\text{-}C_8H_8)(hmpa)_3]I$ **(2)** *and* $[Sm(\eta^8\text{-}C_8H_8)(hmpa)_3][Sm(\eta^8\text{-}C_8H_8)_2]$ **(7)**

The molecular structures of **2** and **7** are shown in Figs 1 and 2, and the selected bond distances and angles are listed in Table 2. Complexes **2** and **7** have the ionic structure composed of a cationic $[Sm(\eta^8\text{-}C_8H_8)(hmpa)_3]^+$ and an anionic part, I^- for **2** and $[Sm(\eta^8\text{-}C_8H_8)_2]^-$ for **7**. There is no significant interaction between the cationic and the anionic moieties in both of **2** and **7**. To the best of our knowledge, these are the first examples of the discrete cationic monocyclooctatetraenyl-lanthanoid complexes. though a unique dimeric complex of $[Nd(\eta^8\text{-}C_8H_8)(thf)_2]^+(\mu\text{-}\eta^2:\eta^8\text{-}(C_8H_8))[Nd(\eta^8\text{-}C_8H_8)]^-$, in which two carbon atoms of one cyclooctatetraenyl ligand of $[Nd((\eta^8\text{-}C_8H_8)_2]^-$ coordinates to the neighboring cationic monocyclooctatetraenyl Nd center in $[Nd(\eta^8\text{-}C_8H_8)(thf)_2]^+$, has been reported previously [30,31].

In each cationic part of **2** and **7**, the dianionic planar C_8H_8 rings coordinate to the samarium in η^8 fashion, and thus each samarium metal adopts the three-legged piano-stool geometry surrounded with three HMPA molecules. The distance (1.95 Å for both of **2** and **7**) between samarium and the centroid of the C_8H_8 ring is not exceptional; being comparable to that of monocyclooctatetraenyl-Sm(III) complexes such as **3** (1.97 Å) [19], **4** (1.94 Å) [19], **5** (1.90 Å) [19], $Sm(\eta^5\text{-}NC_4H_2Bu^t_2\text{-}2,5)(\eta^8\text{-}C_8H_8)(thf)$ (1.913(3) Å) [32], and $Sm(\eta^8\text{-}C_8H_8)(\eta^5\text{-}C_5H_4PPh_2)$ (1.984 Å) [33]. As normal as expected for ionic complexes, the average distance (1.975 Å) between samarium metal and the centroid of the C_8H_8 ring in the anionic part of **7** is comparable to that found in the cationic part of **7** (1.95 Å) and a samarium(III) complex $[Li(thf)_2\{\mu\text{-}(\eta^2:\eta^8\text{-}C_8H_8)\}Sm\{CH(SiMe_3)_2\}_2]$ (1.969(1) Å) [34],

Table 1. Crystal and refinement data for complexes **2** and **7**

Complex	**2**	**7**
Formula	$C_{26}H_{62}O_3N_9ISmP_3$	$C_{42}H_{78}O_3N_9Sm_2P_3$
Formula weight	919.06	1150.74
Crystal system	Orthorhombic	Monoclinic
Space group	*Pbca* (#61)	$P2_1/n$ (#14)
a (Å)	20.648(4)	11.790(6)
b (Å)	20.487(6)	24.918(8)
c (Å)	19.61(4)	18.766(7)
β (°)	–	106.66(4)
Z	8	4
V (Å^3)	8295(21)	5282(4)
D_{calc} (g cm^{-3})	1.472	1.447
Radiation	Mo–K$_\alpha$ (λ = 0.71069 Å)	Mo–K$_\alpha$ (λ = 0.71069 Å)
Crystal size (mm)	0.2 × 0.2 × 0.2	0.5 × 0.4 × 0.3
Abs. coeff (cm^{-1})	23.15	23.35
Scan mode	ω–2θ	ω–2θ
Temperature (°C)	23	20
$2\theta_{max}$ (°)	55.0	55.0
$T_{min,max}$	0.8063, 1.0000	0.4515, 0.9416
Data collected	9650	13,031
No. of observation	2384 ($I > 3.00\sigma(I)$)	12,149 (all)
Refinement on	F	F^2
No. of variables	363	532
R^a, Rw^b	0.054, 0.059	–
R^a, wR^c	–	0.0506, 0.1222
GOF	1.49	0.999
$\Delta\rho_{min,max}$ (eÅ^{-3})	−0.72, 0.96	−0.88, 0.57
Δ/σ_{max}	0.09	−0.001

$^a R = \Sigma\|F_o|-|F_c\|/\Sigma|F_o|$.
$^b Rw = [\Sigma w(|F_o|-|F_c|)^2/\Sigma wF_o^2]^{1/2}$; $w = 1/\sigma^2(F_o)$; function minimized; $\Sigma\, w(|F_o|-|F_c|)^2$.
$^c wR = [\Sigma w(F_o^2-F_c^2)^2/\Sigma wF_o^4]^{1/2}$; $w = 1/[\sigma^2(F_o^2)+0.0745P^2+0.0000P]$ where $P = (F_o^2+2F_c^2)/3$.

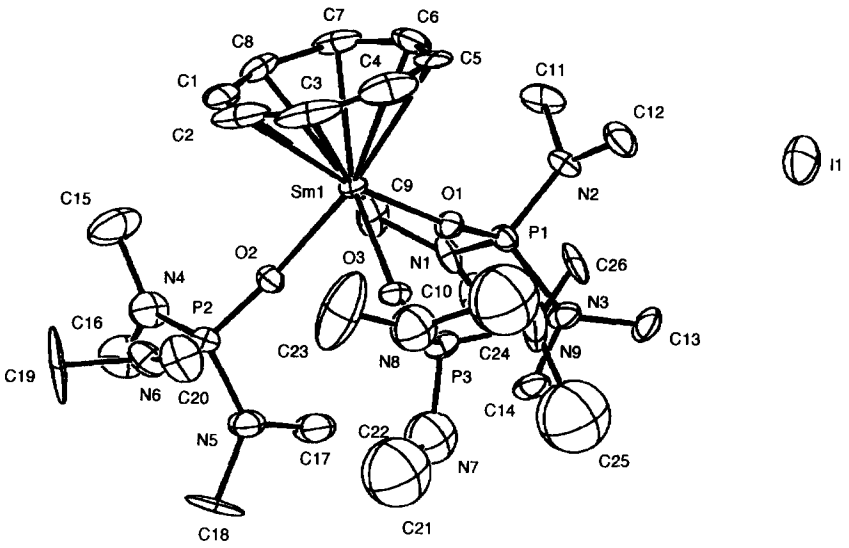

Fig. 1. ORTEP drawing of complex **2** with the atom numbering scheme.

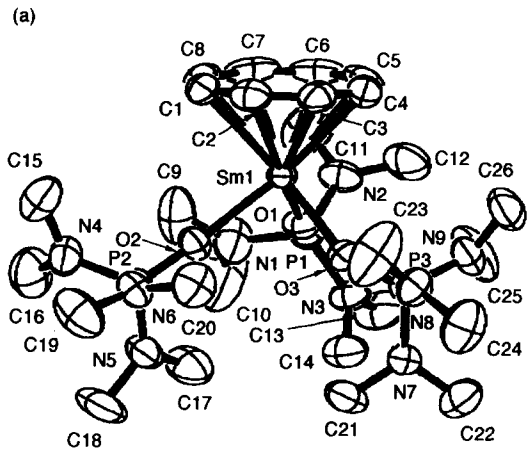

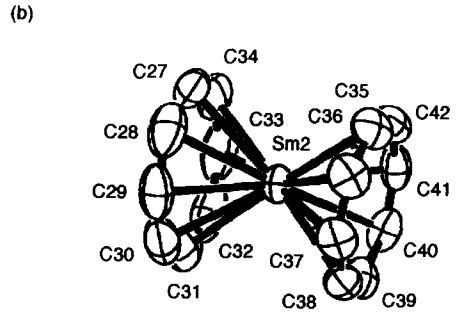

Fig. 2. ORTEP drawings of complex **7** with the atom numbering scheme. The cationic part of **7** (a: top); the anionic part of **7** (b: bottom).

and also is comparable to that found for anionic sandwich complexes of formula $[Ln(\eta^8\text{-}C_8H_8)_2]^-$ such as $[Li(thf)_4][Ce(III)(\eta^8\text{-}C_8H_8)_2]$, (2.043 Å) [35], $[(\eta^8\text{-}C_8H_8)Er(\mu\text{-}\eta^8\text{-}C_8H_8)K(\mu\text{-}\eta^8\text{-}C_8H_8)Er(\mu\text{-}\eta^8\text{-}C_8H_8)K(thf)_4]$ [36], and $[K(C_4H_{10}O_2)][Yb(II)(\eta^8\text{-}C_8H_8)_2]^-$ (2.03 Å) ($C_4H_{10}O_2$ = dimethoxyethane) [37,38], which are characterized crystallographically, on taking into account the difference of ionic radii of Ln metal.

The Sm—O(hmpa) distances of **2** (av 2.31(1) Å) and **7** (av 2.331(4) Å) are comparable to that of HMPA-samarium(III) complexes, e.g., $Sm(SPh)_3(hmpa)_3$ (av 2.299(4) Å) [23], $SmI_3(hmpa)_2(H_2O)_5$ (av 2.253(4) Å) [39], and $SmI_3(hmpa)_3(H_2O)_4$ (av 2.297(4) Å) [39], but shorter than that found for a HMPA-Sm(II) complex $SmI_2(hmpa)_4$ (av 2.500(6) Å) [[25]; the observed different distances found for Sm(II) and Sm(III) complexes can be explained on taking account the difference of ionic radii of Sm(II) and Sm(III) (0.19–0.20 Å for Sm(II/III)) [40].

CONCLUSION

In this paper, we have demonstrated that the reactions of metallic lanthanum and samarium with cyclooctatetraene in the presence of an excess HMPA afforded cationic complexes **6** and **7**, respectively. Reaction of metallic samarium with stoichiometric amounts of cyclooctatetraene and iodine in the presence of an excess HMPA gave a cationic complex **2**. Both of the reactions are very convenient and rationally selective routes for the preparation of the corresponding cationic monocyclooctatetraenyl–lanthanoid compounds.

Table 2. Selected bond distances (Å) and angles (°) of **2** and **7**

Complex	**2**	**7**
Cationic part		
Sm(1)—C(1)	2.65(2)	2.667(7)
Sm(1)—C(2)	2.67(3)	2.691(7)
Sm(1)—C(3)	2.69(3)	2.683(7)
Sm(1)—C(4)	2.63(3)	2.676(8)
Sm(1)—C(5)	2.66(2)	2.664(7)
Sm(1)—C(6)	2.64(2)	2.670(7)
Sm(1)—C(7)	2.67(2)	2.658(7)
Sm(1)—C(8)	2.64(2)	2.648(7)
Sm(1)—C(av.)	2.66	2.670
Sm(1)—C_8H_8(1)	1.95	1.95
Sm(1)—O(1)	2.31(1)	2.313(4)
Sm(1)—O(2)	2.32(1)	2.338(4)
Sm(1)—O(3)	2.31(1)	2.341(4)
Sm(1)—O(av.)	2.31	2.331
P(1)—O(1)	1.48(1)	1.489(5)
P(2)—O(2)	1.48(1)	1.494(5)
P(3)—O(3)	1.49(1)	1.494(4)
P(1)—N(1)	1.64(2)	1.632(7)
P(1)—N(2)	1.62(2)	1.625(6)
P(1)—N(3)	1.63(1)	1.622(6)
P(2)—N(4)	1.64(2)	1.636(6)
P(2)—N(5)	1.60(2)	1.618(7)
P(2)—N(6)	1.64(2)	1.630(6)
P(3)—N(7)	1.58(3)	1.624(6)
P(3)—N(8)	1.63(3)	1.643(6)
P(3)—N(9)	1.58(2)	1.629(6)
Anionic part		
Sm(2)—C(27)	—	2.691(10)
Sm(2)—C(28)	—	2.682(10)
Sm(2)—C(29)	—	2.678(9)
Sm(2)—C(30)	—	2.691(10)
Sm(2)—C(31)	—	2.654(9)
Sm(2)—C(32)	—	2.669(10)
Sm(2)—C(33)	—	2.673(9)
Sm(2)—C(34)	—	2.673(10)
Sm(2)—C_8H_8(2)	—	1.97
Sm(2)—C(35)	—	2.694(8)
Sm(2)—C(36)	—	2.701(7)
Sm(2)—C(37)	—	2.690(7)
Sm(2)—C(38)	—	2.712(8)
Sm(2)—C(39)	—	2.686(8)
Sm(2)—C(40)	—	2.681(8)
Sm(2)—C(41)	—	2.664(8)
Sm(2)—C(42)	—	2.706(8)
Sm(2)—C_8H_8(3)	—	1.98
Cationic part		
Sm(1)—O(1)—P(1)	169.5(8)	160.0(3)
Sm(1)—O(2)—P(2)	163.9(8)	171.5(3)
Sm(1)—O(3)—P(3)	162.3(8)	152.8(3)
O(1)—Sm(1)—O(2)	84.8(8)	87.6(2)
O(2)—Sm(1)—O(3)	86.6(4)	85.9(2)
O(3)—Sm(1)—O(1)	87.7(4)	87.1(2)
O(1)—P(1)—N(1)	107.1(8)	107.0(3)
O(1)—P(1)—N(2)	115.1(8)	115.4(3)
O(1)—P(1)—N(3)	111.1(7)	108.8(3)
O(2)—P(2)—N(4)	111.2(9)	116.7(3)
O(2)—P(2)—N(5)	110.1(9)	108.6(3)
O(2)—P(2)—N(6)	111.3(8)	108.7(3)
O(3)—P(3)—N(7)	112(1)	110.1(3)
O(3)—P(3)—N(8)	111(1)	108.0(3)
O(3)—P(3)—N(9)	111(1)	115.9(3)
Anionic part		
C_8H_8(2)—Sm—C_8H_8(3)	—	175.6

C_8H_8 presents the centroid of a cyclooctatetraenyl ligand.

EXPERIMENTAL

General procedures

All manipulations involving air- and moisture-sensitive organometallic compounds were carried out by using the standard Schlenk techniques under an argon atmosphere. THF was dried over sodium benzophenone ketyl. Hexamethylphosphoric triamide was purified by distillation after drying over CaH_2. 1,3,5,7-Cyclooctatetraene was purchased from Aldrich Chemical, Co. Inc. and used without further purification. SmI(η^8-C_8H_8)(thf) was prepared according to the literature procedure [17,19].

Nuclear magnetic resonance [^{1}H (270 MHz)] spectra were measured on a JEOL JNM-EX270 spectrometer. Elemental analyses were performed at Elemental Analysis Center, Faculty of Science, Osaka University. All melting points were measured in sealed tubes and were not corrected.

Addition of HMPA to SmI(η^8-C_8H_8)(thf) (**1**)

To a violet solution of **1** (0.17 g, 0.36 mmol) in THF (5 ml) was added HMPA (0.26 ml, 1.5 mmol) at room temperature. Rapid reaction occurred and red solids were precipitated. Recrystallization of red precipitation from THF afforded a cationic complex [Sm(η^8-C_8H_8)(hmpa)$_3$]I (**2**) (0.16 g, 49% yield) as red crystals, mp > 300°C (decomp). ^{1}H NMR (THF-d_8, 35°C): δ 10.7 (s, 8H, C_8H_8), 2.58 (brs, 54H, Me(hmpa)). Anal. Calc. for $C_{26}H_{62}IN_9O_3P_3Sm$: C, 33.98, H, 6.80, N, 13.73. Found: C, 33.82, H, 6.83, N, 13.73.

Preparation of [Sm(η^8-C_8H_8)(hmpa)$_3$]I (**2**) *from metallic samarium*

A reaction mixture of samarium metal (0.30 g, 2.0 mmol), C_8H_8 (0.22 ml, 2.0 mmol), HMPA (1.0 ml, 5.7 mmol), iodide (0.25 g, 1.0 mmol) in THF (40 ml) was stirred at room temperature for 12 h to give a red solution. Removal of insoluble impurities by centrifugation and followed by concentration afforded **2** (0.62 g, 34% yield) as red microcrystals.

Preparation of [La(η^8-C_8H_8)(hmpa)$_4$][La(η^8-C_8H_8)$_2$] (**6**)

A reaction mixture of lanthanum metal (0.42 g, 3.0 mmol), C_8H_8 (0.50 ml, 4.4 mmol), HMPA (3.0 ml, 17 mmol) and a catalytic amount of iodine in THF (40 ml) was stirred at 50°C for a period of 10 days. After removal of insoluble impurities, the resulting pale yellow solution was concentrated and then cooled to −20°C to give **6** as pale yellow crystals in a quantitative yield. ^{1}H NMR (THF-d_8, 35°C): δ 6.17 (s, 8H, C_8H_8 of a cationic part), 5.74 (s, 16H, C_8H_8 of an

anionic part), 2.44 (brs, 72H, Me(hmpa)). Complex **6** is highly air- and moisture-sensitive, and thereby the elemental analysis of **6** did not give a satisfactory result.

Preparation of $[Sm(\eta^8\text{-}C_8H_8)(hmpa)_3][Sm(\eta^8\text{-}C_8H_8)_2]$ (**7**)

A reaction mixture of samarium metal (0.30 g, 2.00 mmol), C_8H_8 (0.40 ml, 3.55 mmol), HMPA (3.0 ml, 17.2 mmol) and a catalytic amount of iodine in THF (40 ml) was stirred at 50°C for a period of 5 days to give a deep red-purple solution. Removal of insoluble impurities followed by concentration and cooling to −20°C afforded the deep red crystals of **7** (0.54 g, 47% yield), mp > 300°C (decomp). ^{1}H NMR (THF-d_8, 35°C): δ 13.2 (s, 16H, C_8H_8 of an anionic part), 10.1 (s, 8H, C_8H_8 of a cationic part), 2.28 (brs, 54H, Me(hmpa)). Complex **7** is highly air- and moisture-sensitive, and the elemental analysis of **7** did not give a satisfactory result.

Crystallographic data collections and structure determinations of **2** *and* **7**

Data collections. The crystals of **2** and **7** suitable for X-ray diffraction studies were sealed in glass capillaries under argon atmosphere, and then each crystal of the two complexes was mounted on four-circle data collection instruments (Rigaku AFC-5R for **2** and Rigaku AFC-7R for **7**) using Mo–K_α radiation (λ = 0.71069 Å). The units cell parameters at 23°C were determined by a least-squares fit to 2θ values of 25 strong higher reflections for both of the two complexes. For each complex, three standard reflections were chosen and monitored every 150 reflections. No decay correction was applied for complex **2**, while a linear correction factor was applied to the raw data (6.89% decay) for **7**. Empirical absorption corrections for both of the two complexes were carried out based on azimuthal scans. All data were corrected for Lorentz and polarization effects.

Structure determination of **2**. Measured non-equivalent reflections with $I > 3.0\sigma(I)$ were used for the structure determination. The systematic absences of $(0kl)$ with k = odd, $(h0l)$ with l = odd, and $(hk0)$ with h = odd uniquely determined the space group to be *Pbca*. The structure was solved by a heavy atom Patterson method and expanded using Fourier techniques, and refined by the full-matrix least squares method. Three carbon atoms and two nitrogen atoms of one HMPA ligand were refined isotropically, and the remaining carbon and nitrogen atoms as well as samarium, oxygen, and phosphorus atoms were refined anisotropically. In the final refinement cycle (full-matrix), hydrogen atom coordinates were included at idealized positions, and the hydrogen atoms were given the same temperature factor as that of the carbon atoms to which they were bonded. All calculations were performed using the TEXSAN crystallographic software package.

Structure determination of **7**. The systematic absences of $(h0l)$ with $h0l$ = odd and $(0k0)$ with k = odd for non-equivalent reflections with $I > 2.0\sigma(I)$ resulted in the specification to the space group $P2_1/n$. The structure was solved by a direct method (SHELX86) [41] and expanded using Fourier techniques, and refined by the full-matrix least squares method. All non-hydrogen atoms (carbon, nitrogen, oxygen, phosphorus and samarium atoms) were refined anisotropically. In the final refinement cycle (full-matrix), the H-atoms of C_8H_8 and HMPA were included in the refinement on calculated positions riding on their atoms (C—H_{sp2} = 0.93 Å, C—H_{sp3} = 0.96 Å, U_{iso} = 1.2 U_{eq} (e) Å^2).

Supplementary material—Final positional parameters, final thermal parameters, bond distances, angles, and torsion angles for the complexes **2** and **7** (45 pages) are available from author K.M. upon request.

Acknowledgment—This work was supported by Grant-in-Aid for Scientific Research on Priority Areas (No. 283, "Innovative Synthetic Reactions") from the Ministry of Education, Science, Sports and Culture of Japan. This work was also supported by Asahi Glass Foundation. We appreciate Dr T. Yamagata (Osaka University) for his kind guidance on the X-ray diffraction study of **7**.

REFERENCES

1. Schumann, H., *Angew. Chem., Int. Ed. Engl.*, 1984, **23,** 474.
2. Edelmann, F. T., Scandium Yttrium, and the Lanthanide and Actinide Elements, in *Comprehensive Organometallic Chemistry II*, ed. E. W. Abel, F. G. A. Stone and G. Wilkinson. Pergamon, 1995, p. 98.
3. Edelmann, F. T., *New J. Chem.*, 1995, **19,** 535.
4. Edelmann, F. T., *Angew. Chem., Int. Ed. Engl.*, 1995, **34,** 2466.
5. Berg, D. J., Andersen, R. A. and Zalkin, A., *Organometallics*, 1988, **7,** 1858.
6. Berg, D. J., Burns, C. J., Andersen, R. A. and Zalkin, A., *Organometallics*, 1989, **8,** 1865.
7. Nolan, S. P., Stern, D. and Marks, T. J., *J. Am. Chem. Soc.*, 1989, **111,** 7844.
8. Edelmann, F. T., Rieckhoff, M., Haidue, I. and Silaghi-Dumitrescu, I., *J. Organomet. Chem.*, 1993, **447,** 203.
9. Wedler, M., Recknagel, A., Gilje, J. W., Nottemeyer, M. and Edelmann, F. T., *J. Organomet. Chem.*, 1992, **426,** 295.
10. Recknagel, A., Moltemeyer, M., Stalke, D., Pieper, U., Schmidt, H.-G. and Edelmann, F. T., *J. Organomet. Chem.*, 1991, **411,** 347.
11. Recknagel, A. and Edelmann, F. T., *Angew. Chem., Int. Ed. Engl.*, 1991, **30,** 693.
12. Deacon, G. B., Forsyth, C. M. and Newham, R. H., *Polyhedron*, 1987, **6,** 1143.
13. Deacon, G. B., Hitchcock, P. B., Holmes, S. A.,

Lappert, M. F., MacKinnon, P. and Newnham, R. H., *J. Chem. Soc., Chem. Commun.*, 1989, 935.
14. Deacon, G. B., Tuong, T. D. and Wilkinson, D. L., *Inorg. Synth.*, 1990, **28,** 286.
15. Deacon, G. B., Forsyth, C. M., Gatehouse, B. M. and White, P. A., *Aust. J. Chem.*, 1990, **43,** 795.
16. Deacon, G. B., Tuong, T. D. and Wilkinson, D. L., *Inorg. Synth.*, 1990, **27,** 136.
17. Mashima, K. and Takaya, H., *Tetrahedron Lett.*, 1989, **30,** 3697.
18. Mashima, K., Nakayama, Y., Kanehisa, N., Kai, Y. and Nakamura, A., *J. Chem. Soc., Chem. Commun.*, 1993, 1847.
19. Mashima, K., Nakayama, Y., Nakamura, A., Kanehisa, N., Kai, Y. and Takaya, H., *J. Organomet. Chem.*, 1994, **473,** 85.
20. Mashima, K., Nakayama, Y., Fukumoto, H., Kanehisa, N., Kai, Y. and Nakamura, A., *J. Chem. Soc., Chem. Commun.*, 1994, 2523.
21. Mashima, K., Sugiyama, H. and Nakamura, A., *J. Chem. Soc., Chem. Commun.*, 1994, 1581.
22. Mashima, K., Shibahara, T., Nakayama, Y. and Nakamura, A., *J. Organomet. Chem.*, 1995, **501,** 263.
23. Mashima, K., Nakayama, Y., Shibahara, T., Fukumoto, H. and Nakamura, A., *Inorg. Chem.*, 1996, **35,** 93.
24. Evans, W. J., Hughes, L. A. and Hanusa, T. P., *J. Am. Chem. Soc.*, 1984, **106,** 4270.
25. Hou, Z. and Wakatsuki, Y., *J. Chem. Soc., Chem. Commun.*, 1994, 1205.
26. Hodgson, K. O. and Raymond, K. N., *Inorg. Chem.*, 1972, **11,** 171.
27. Shibahara, T. and Mashima, K., unpublished result.
28. Wayda, A. L., Mukerji, I., Dye, J. L. and Rogers, R. D., *Organometallics*, 1987, **6,** 1328.
29. Marks, T. J., *Prog. Inorg. Chem.*, 1978, **24,** 51.
30. Ely, S. R., Hopkins, T. E. and DeKock, C. W., *J. Am. Chem. Soc.*, 1976, **98,** 1624.
31. DeKock, C. W., Ely, S. R., Hopkins, T. E. and Brault, M. A., *Inorg. Chem.*, 1978, **17,** 625.
32. Schumann, H., Rosenthal, E. C. E., Winterfeld, J., Weimann, R. and Demtschuk, J., *J. Organomet. Chem.*, 1996, **507,** 287.
33. Visseaux, M., Dormond, A., Kubicki, M. M., Moïse, C., Baudry, D. and Ephritikhine, M., *J. Organomet. Chem.*, 1992, **433,** 95.
34. Schumann, H., Winterfeld, J., Görlitz, F. H. and Pickardt, J., *J. Chem. Soc., Chem. Commun.*, 1993, 623.
35. Kilimann, U., Scafer, M., Herbst-Irmer, R. and Edelmann, F. T., *J. Organomet. Chem.*, 1994, **469,** C15.
36. Xia, J., Jin, Z. and Chen, W., *J. Chem. Soc., Chem. Commun.*, 1991, 1214.
37. Kinsley, S. A., Streitwieser, A. Jr, and Zalkin, A., *Organometallics*, 1985, **4,** 52.
38. Boussie, T. R., Eisenberg, D. C., Rigsbee, J., Streitwieser, A. and Zalkin, A., *Organometallics*, 1991, **10,** 1922.
39. Imamoto, T., Yamamori, Y., Tsuruta, H., Yamaguchi, K., Yamazaki, M. and Inanaga, J., *Chem. Lett.*, 1995, 949.
40. Shannon, R. D., *Acta Crystallogr.*, 1976, **A32,** 751.
41. Sheldrick, G. M., *Crystallographic Computing* 3, ed. G. M. Sheldrick, C. Krüger and R. Goddard. Oxford University Press, 1985, p. 179.

Pergamon

PII: S0277-5387(97)00493-2

Polyhedron Vol. 17, No. 7, pp. 1073–1080, 1998
© 1998 Elsevier Science Ltd
All rights reserved. Printed in Great Britain
0277-5387/98 $19.00+0.00

Zirconium, hafnium and yttrium complexes containing two linked amido–tetramethylcyclopentadienyl ligands: Synthesis, reactivity and molecular structure of $Hf(\eta^5:\eta^1\text{-}C_5Me_4SiMe_2NiPr)_2$†

Jun Okuda,* Francisco Amor, Karen E. du Plooy, Thomas Eberle, Kai C. Hultzsch and Thomas P. Spaniol

Institut für Anorganische Chemie und Analytische Chemie, Johannes Gutenberg-Universität, J.-J.-Becher-Weg 24, D-55099 Mainz, Germany

(Received 1 November 1997; accepted 24 November 1997)

Abstract—Zirconium and hafnium complexes $M(\eta^5:\eta^1\text{-}C_5Me_4SiMe_2NR')_xCl_{(4-2x)}$ (M = Zr, Hf; x = 1, 2; R′ = *i*Pr, *t*Bu) containing one or two linked amido–tetramethylcyclopentadienyl ligands $C_5Me_4SiMe_2NR'$ have been synthesized by the reaction of the dilithium derivative $Li_2(C_5Me_4SiMe_2NR')$ with $MCl_4(THF)_2$. The crystal structure of the hafnium complex $Hf(\eta^5:\eta^1\text{-}C_5Me_4SiMe_2NiPr)_2$ has been determined by a single-crystal X-ray diffraction study and shows a C_2-symmetric helical metallocene, in which the amido ligands are bonded as π-donor ligands with Hf—N bond lengths of 2.115(2) Å. The isoelectronic heterobimetallic yttrium complex $Li[Y(\eta^5:\eta^1\text{-}C_5Me_4SiMe_2NCH_2CH_2OMe)_2]$ reacts with phenylacetylene to give the bis(phenylacetylide) derivative $Li[Y\{\eta^5\text{-}C_5Me_4SiMe_2NH(CH_2CH_2OMe)\}_2(C{\equiv}CPh)_2]$. © 1998 Elsevier Science Ltd. All rights reserved

Keywords: zirconium; hafnium; yttrium; amido–cyclopentadienyl; alkynyl complex.

Homogeneous α-olefin polymerization catalysts based on titanium complexes that contain the linked amido–cyclopentadienyl ligand $C_5Me_4SiMe_2NR'$ (R′ = alkyl, aryl) have recently gained considerable technological importance through the efficient synthesis of new types of polyethylenes and copolymers with comonomers such as 1-octene and styrene [1]. The linked amido–cyclopentadienyl ligand was introduced by Bercaw and Shapiro to successfully develop the first single-component catalysts $[Sc(\eta^5:\eta^1\text{-}C_5Me_4SiMe_2NtBu)R'']$ (R″ = H, alkyl) for the living polymerization of propylene [2]. Compared with Brintzinger-type *ansa*-metallocenes, the increased Lewis acidity together with a sterically open ligand sphere [3,4] appear to accommodate the bulkier comonomers better. In the course of synthetic and structural studies on group 4 metal complexes of general formula $M(\eta^5:\eta^1\text{-}C_5R_4SiMe_2NR')X_2$ (M = Ti, Zr, Hf; X = halide, amido, alkyl) [3,4] we have isolated and characterized several complexes containing two linked amido–cyclopentadienyl ligands with different amido and cyclopentadienyl substituents $M(\eta^5:\eta^1\text{-}C_5R_4SiMe_2NR')_2$ [3c,d]. Such compounds have attracted some attention as C_2-symmetric metallocenes and were also shown to form by aminolysis reactions [5], sometimes more reproducibly than by the salt metathesis reactions using the dianion of the ligand [6]. More recently, we have discovered that isoelectronic heterobimetallics of the general type $Li[Ln(\eta^5:\eta^1\text{-}C_5R_4SiMe_2NCH_2CH_2X)_2]$ (Ln = Y, Lu; C_5R_4 = C_5Me_4, C_5H_4, C_5H_3tBu; X = OMe, NMe_2) can be obtained when a tridentate linked amido–cyclopentadienyl ligand is used [7]. Here we describe the preparation and characterization of zirconium, hafnium, and yttrium complexes containing two amido-functionalized tetramethylcyclopentadienyl ligands $C_5Me_4SiMe_2NR'$ along with some reactivity studies.

* Author to whom correspondence should be addressed.

† Dedicated to Prof. Dr. W. A. Herrmann on the occasion of his 50th birthday.

RESULTS AND DISCUSSION

As was independently noted by other authors [4–6], we too have occasionally observed the formation of group 4 metal complexes of the type $M(\eta^5:\eta^1\text{-}C_5R_4SiMe_2NR')_2$ containing two amido-functionalized cyclopentadienyl ligands $C_5Me_4SiMe_2NR'$. Generally, the larger metals, zirconium and hafnium, have a greater tendency to form such complexes than titanium. For example, for R′ = allyl and M = Zr the metallocene derivative $Zr(\eta^5:\eta^1\text{-}C_5Me_4SiMe_2NCH_2CH{=}CH_2)_2$ is exclusively formed in the reaction of $Li(C_5Me_4SiMe_2NCH_2CH{=}CH_2)$ with $ZrCl_4(THF)_2$, whilst the reaction with $TiCl_3(THF)_3$, followed by oxidative chlorination with $PbCl_2$ results in the expected formation of the mono(ligand) complex $Ti(\eta^5:\eta^1\text{-}C_5Me_4SiMe_2NCH_2CH{=}CH_2)Cl_2$ [3c,d]. We suspected that the nature of the amido substituent R′ may play a decisive role, and in fact, we observe no formation of the metallocene for R′ = *t*Bu, even when an excess of the dilithium salt is employed. Thus in the reaction of $Li_2(C_5Me_4SiMe_2N\textit{t}Bu)$ under various conditions and independently of the solvent only the mono(ligand) complexes $M(\eta^5:\eta^1\text{-}C_5Me_4SiMe_2N\,\textit{t}Bu)Cl_2$ (**1**) (**a** = Zr, **b** = Hf) are detected and isolated as colourless crystals in good to moderate yields. The synthesis of the zirconium complex **1a** was previously described by Petersen *et al.* [4c]. These findings may suggest that the complexation of the amido group precedes that of the cyclopentadienyl moiety.

On the other hand, when the *iso*-propylamido ligand $Li_2(C_5Me_4SiMe_2N\textit{i}Pr)$ is employed in the complexation reaction with $MCl_4(THF)_2$, a mixture of the mono(ligand) and metallocene are formed under a variety of conditions for M = Zr. For M = Hf, the mono(ligand) complex $Hf(\eta^5:\eta^1\text{-}C_5Me_4SiMe_2N\textit{i}Pr)Cl_2$ (**2b**) can be prepared only in toluene, whereas in THF, the metallocene $Hf(\eta^5:\eta^1\text{-}C_5Me_4SiMe_2N\textit{i}Pr)_2$ (**3b**) is formed in moderate yields. We suspected therefore that the higher solubility of the dilithium derivative would cause higher local concentrations of the dianion leading to the preferred formation of the bis(ligand) complex. In fact, reactions in THF tend to increase the yield of the metallocene over that of the mono(ligand) complex. However, it is remarkable that the latter does not react with an excess of the dilithium derivative to give the metallocene complex, suggesting different intermediates on the way to both products. Evidently, the situation is more complicated and no conclusive explanation can be given at this time.

The significantly more soluble, C_2-symmetric metallocenes $M(\eta^5:\eta^1\text{-}C_5R_4SiMe_2NR')_2$ are easily distinguished from the C_s-symmetric mono(ligand) complexes $M(\eta^5:\eta^1\text{-}C_5R_4SiMe_2NR')Cl_2$ by the chirality which results in pairs of diastereotopic methyl resonances. One remarkable feature is the low-field shift for the methine proton that is recorded as a multiplet at δ = 4.13 and 3.99 for **3a** and **3b**, respectively. Preliminary studies reveal that the formally 20-electron metallocene $M(\eta^5:\eta^1\text{-}C_5R_4SiMe_2NR')_2$ **3a** and **b** are capable of initiating the polymerization of ε-caprolactone, albeit at much slower rates than the isolelectronic rare earth complexes $Li[Ln(\eta^5:\eta^1\text{-}C_5R_4SiMe_2NCH_2CH_2X)_2]$ also mentioned below [7].

An ORTEP diagram of the molecular structure of complex **3b** is depicted in Fig. 1. Crystallographic data are compiled in Table 1, selected bond distances and angles are listed in Table 2. The compound residing on a crystallographic C_2-axis adopts the typical bent metallocene configuration in agreement with the solution structure. The angle between the two cyclopentadienyl rings is 127.9°, similar to the values found in the literature for non-linked hafnocenes such as

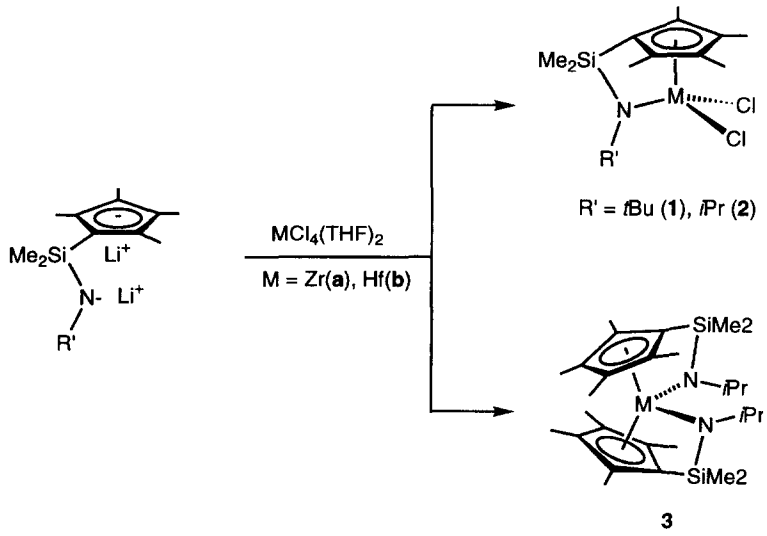

Scheme 1.

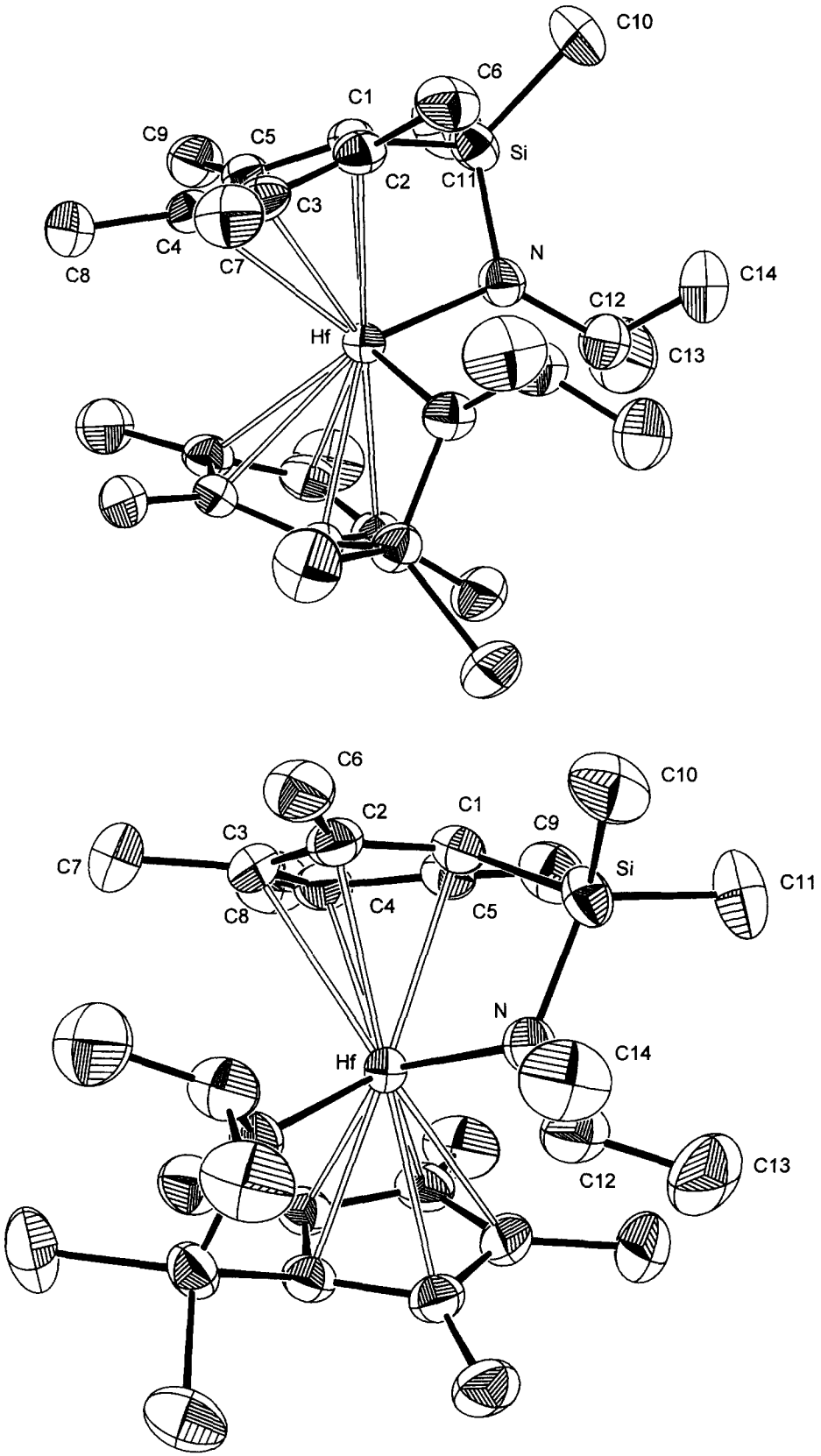

Fig. 1. (a) ORTEP diagram of the molecular structure of $Hf(\eta^5:\eta^1\text{-}C_5Me_4SiMe_2N\text{i}Pr)_2$ (**3b**). (b) Alternative view from the front. Thermal ellipsoids are drawn at a 50% probability level. Hydrogen atoms are omitted for the sake of clarity.

Table 1. Crystallographic data for $Hf(\eta^5:\eta^1\text{-}C_5Me_4SiMe_2NiPr)_2$ (**3b**)

Empirical formula	$C_{28}H_{50}HfN_2Si_2$
Formula weight	649.37
Crystal colour	Colourless
Crystal size mm	$0.50 \times 0.28 \times 0.23$
Crystal system	Monoclinic
Space group	$C2/c$ (No. 15)
a (Å)	17.456(2)
b (Å)	12.128(2)
c (Å)	14.272(1)
β (°)	100.245(8)
Volume (Å^3)	2973.3(6)
Z	8/2
D_{calc}, Mg/m^3	1.451
Abs. coeff. (mm^{-1})	3.607
$F(000)$	1328
Temperature (K)	296(2)
Radiation	Mo–K_α (λ = 0.71070 Å)
θ range	3.4–29.9°
Reflns measd	$-21 \leqslant h \leqslant 24$; $0 \leqslant k \leqslant 17$; $-20 \leqslant l \leqslant 19$
Refinement	
No. reflns measd	7235
No. indep. reflns	4310 [R_{int} = 0.0192]
No. obsd reflns	3854 ($I > 2\sigma(I)$)
Goodness-of-fit	1.097
R	0.0182
wR_2	0.0360
Extinction coefficient	0.00051(8)
Largest e-max, e-min (e Å^{-3})	0.703, −0.513

Table 2. Selected bond lengths (Å) and angles (°) for $Hf(\eta^5:\eta^1\text{-}C_5Me_4SiMe_2NiPr)_2$ (**3b**)

Hf—N	2.115(2)	Cp_{cent}—Hf—N	97.9
Hf—C(1)	2.476(2)	Cp_{cent}—Hf—N′	116.7
Hf—C(2)	2.535(2)	Cp_{cent}—Hf—Cp_{cent}′	127.9
Hf—C(3)	2.644(2)	Cp_{cent}′—Hf—N	116.7
Hf—C(4)	2.698(2)	N—Hf—N′	96.2(1)
Hf—C(5)	2.595(2)	N—Si—C(10)	118.7(1)
Si—N	1.721(2)	N—Si—C(11)	114.6(2)
Si—C(1)	1.864(2)	N—Si—C(1)	93.60(9)
N—C(12)	1.483(3)	C(10)—Si—C(11)	103.4(2)
		Hf—N—C(12)	128.8(2)
		Si—N—C(12)	124.8(2)
		Hf—N—Si	106.47(9)
		N—C(12)—C(13)	112.8(3)
		N—C(12)—C(14)	113.0(2)
		C(13)—C(12)—C(14)	109.4(3)

$Hf(\eta^5\text{-}C_5H_5)_2(CH_2Ph)_2$ (128.2°) [8a] and $Hf(\eta^5\text{-}C_5Me_5)(\eta^5\text{-}C_5H_5)Cl_2$ (130.6°) [8b], but significantly smaller than in the decamethylhafnocene derivative $Hf(\eta^5\text{-}C_5Me_5)_2(H)(NMe_2)$ (139.1°) [9]. The distances between the hafnium center and the centroid of each five-membered ring of 2.29 Å are somewhat longer than those observed in comparable hafnocene complexes (about 2.2 Å) [8,9]. The tetramethylcyclopentadienyl ligands are bonded in a pentahapto fashion as judged by the sum of the angles at the ring (540°) and the metal to ring-carbon distances ranging from 2.476(2) to 2.698(2) Å. The angle at hafnium N—Hf—N′ is 96.2(1)°, significantly smaller than that found in $Zr(\eta^5:\eta^1\text{-}C_5H_4SiMe_2NPh)_2$ (106.5(8)°) [5a]. This can be accounted for by the presence of the bulkier phenyl rings on the amido nitrogen atoms and the possibility of gear meshing of the two *iso*-propyl groups in **3b**.

The Hf—N bond length of 2.115(2) Å is slightly longer than the Hf—N distances observed in amido complexes where the amido ligand acts as a 3-electron ligand (2.027(8) Å in $Hf(\eta^5\text{-}C_5Me_5)_2(H)(NMe_2)$ [9], 2.041(4), 2.065(3) in $Hf(\eta^5\text{-}C_5Me_5)(NiPr_2)_3$ [10a], 2.065(3) in $Hf(\eta^5:\eta^1\text{-}C_{13}Me_8SiMe_2CH_2NtBu)Cl_2$ [10b]). However, the nitrogen atom is trigonal planar, the sum of the angles at the nitrogen atom being 360°. These observations support the view that the π-electrons are delocalized over both nitrogen atoms, a feature found in the only other structurally authenticated derivative $Zr(\eta^5:\eta^1\text{-}C_5H_4SiMe_2NPh)_2$ (Zr—N bond length 2.137(2), 2.127(2) Å) [5a]. In the isoelectronic yttrium complex $Li[Y(\eta^5:\eta^1\text{-}C_5Me_4SiMe_2NCH_2CH_2OMe)_2]$ (**5**) pyramidalization of the amido nitrogen atoms are detectable, but not particularly pronounced [7a]. According to the theoretical model by Lauher and Hoffmann for d^0-metallocenes Cp_2MX_2 containing two potential π-donors such as amido or alkoxo ligands [11], only one lone pair of electrons can be accommodated in the empty a_1 orbital of the Cp_2MX_2 unit. In some d^0-Cp_2MX_2 complexes, structural evidence for the localization of a single and double bond can be found [11,12].

Reaction of two equivalents of $Li_2(C_5R_4SiMe_2NCH_2CH_2X)$ (C_5R_4 = C_5Me_4, C_5H_4, C_5H_3tBu; X = OMe, NMe_2) with anhydrous $LnCl_3$ (Ln = Y, Lu) has been shown to give the C_2-symmetric heterobimetallic lanthanocenes $Li[Ln(\eta^5:\eta^1\text{-}C_5R_4SiMe_2NCH_2CH_2X)_2]$ in high yield, whereas in the presence of one equivalent of the dilithium salt, inseparable product mixtures are formed [7]. In order to investigate the influence of the length of the amido side chain, an additional methylene carbon was introduced. The reaction of anhydrous YCl_3 with $Li_2(C_5Me_4SiMe_2NCH_2CH_2CH_2OMe)$ gives colourless crystals of $Li[Y(\eta^5:\eta^1\text{-}C_5Me_4SiMe_2NCH_2CH_2CH_2OMe)_2]$ (**4**) for which a C_2-symmetric heterobimetallic structure analogous to that of $Li[Y(\eta^5:\eta^1\text{-}C_5Me_4SiMe_2NCH_2CH_2OMe)_2]$ (**5**) can be assumed based on the NMR spectroscopic data and elemental analysis.

The electronically "oversaturated" metallocene unit $[Ln(\eta^5:\eta^1\text{-}C_5R_4SiMe_2NCH_2CH_2X)_2]^-$ incorporates two π-donating amido ligands and can be assumed to show nucleophilic behaviour toward electrophiles. All heterobimetallic complexes have been

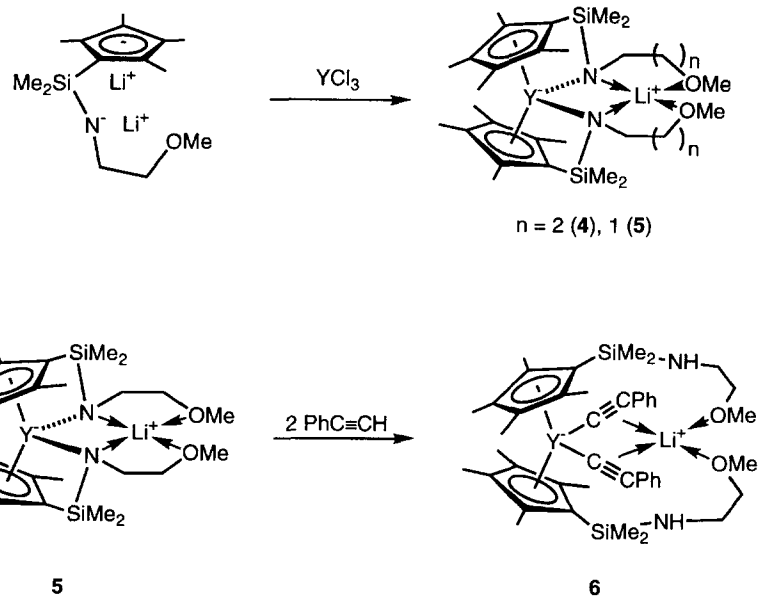

Scheme 2.

shown to be active catalysts for the polymerization of ε-caprolactone [7]. In order to prove the nucleophilicity of the amido substituents, the reaction with a weak Brönsted acid has been studied. Thus, the reaction of Li[Y(η^5 : η^1-$C_5Me_4SiMe_2NCH_2CH_2OMe)_2$] with two equivalents of phenylacetylene leads to the formation of colourless crystals of the bis (acetylide) complex Li[Y{η^5-$C_5Me_4SiMe_2NH(CH_2CH_2O$-Me)}$_2$(C≡CPh)$_2$] (**6**) with the structure proposed in Scheme 2. The ^{1}H NMR and ^{13}C NMR spectrum of **6** consists of only one signal for the methyl groups on the silicon and two signals for the methyl groups on the cyclopentadienyl ring. Additional evidence for the loss of the helical chiral structure of the starting material is the observation of an AA′XX′ instead of the ABCD pattern for the four methylene protons of the ligand side-chain. The methylene protons next to the oxygen of the side chain give rise to a triplet, whereas a doublet of triplets are observed for the methylene protons attached to the $NHSiMe_2$ group due to the coupling to the amine proton. The latter is recorded at δ 1.40 as a triplet with $^3J_{HH}$ = 7.8 Hz. The coordination of the acetylide ligand to both yttrium and lithium in solution is obvious from the ^{13}C NMR spectrum that shows a doublet of a quartet for the α-carbon of the acetylide ligand at δ 141.2 ($^1J_{YC}$ = 49.9 Hz, $I(^{89}Y) = \frac{1}{2}$; $^1J_{LiC}$ = 7.3 Hz, $I(^7Li) = \frac{3}{2}$) (Fig. 2), whereas a doublet at δ 114.9 ($^2J_{YC}$ = 10.1 Hz) is found for the β-carbon. A similar bridging coordination of the acetylide ligands to yttrium and lithium atom was found in the crystallographically confirmed structure of $Cp^*_2Y(\mu$-C≡$CCMe_3)_2$ Li(THF) [13]. However no coupling of lithium to carbon was observed in the ^{13}C NMR spectrum of this complex. A bridging mode of two acetylide ligands are quite common in dimeric

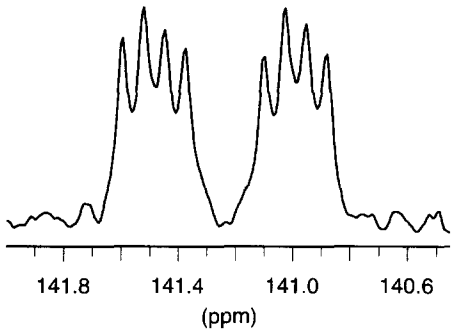

Fig. 2. ^{13}C NMR signal for the acetylide α-carbon atom in Li[Y{η^5-$C_5Me_4SiMe_2NH(CH_2CH_2OMe)$}$_2$(C≡CPh)$_2$] (**6**).

lanthanocenes of the type [Ln(η^5-$C_5R_5)_2(\mu$-C≡$CR')_2$] [14]. The chemical shifts and coupling constants for the sp-hybridized α-carbon atom of the acetylide ligand are in the normal range for terminal acetylide complexes, such as $Cp^*_2Y(\mu$-C≡$CCMe_3)_2$Li(THF) (δ 127.0, $^1J_{YC}$ = 46 Hz) [13], Cp^*_2Y(C≡CPh)(OEt_2) (δ 146.95, $^1J_{YC}$ = 70.9 Hz) [15], (DAC)Y(C≡CPh) (THF) (DAC = 4,13-Diaza-18-crown-6; δ 149.1, $^1J_{YC}$ = 46.9 Hz) [16]. The ^{13}C–^{7}Li coupling constant is slightly smaller than that observed in LiC≡C*t*Bu ($^1J_{LiC}$ = 16 Hz in THF at −90°C) [17a] and Li*t*Bu ($^1J_{LiC}$ = ca 10 Hz in toluene at room temperature) [17b].

In conclusion, we have shown that the apparent 20-electron configuration in the metallocenes of the type [M(η^5 : η^1-$C_5R_4SiMe_2NR')_2$] (M = Zr, Hf, Ln^+) results in some nucleophilic behaviour, the polymerization activity toward ε-caprolactone being one

example. It will be interesting to see whether this type of metallocene complexes exhibits further novel reactivities. One principal drawback, however, would be the loss of the helical chirality upon modification of the amido function.

EXPERIMENTAL

General considerations

All operations were performed under an inert atmosphere of argon using standard Schlenk or glovebox techniques. THF, toluene and hexane were purified by distillation from sodium/benzophenone ketyl. $MCl_4(THF)_2$ (M = Zr, Hf) [18], $Li_2(C_5Me_4SiMe_2NiPr)$ [3j], $Li_2(C_5Me_4SiMe_2NtBu)$ [2a] and $Li_2(C_5Me_4SiMe_2NCH_2CH_2CH_2OMe)$ [7c] were synthesized according to published procedures. YCl_3 (ALFA) was used as received. Li*n*Bu was used as received and titrated prior to use [19]. NMR spectra were recorded on a Bruker DRX 400 spectrometer at 25°C, mass spectra on a Finnigan 8230 spectrometer. Elemental analyses were performed by the Microanalytical Laboratory of this department.

$Zr(\eta^5:\eta^1\text{-}C_5Me_4SiMe_2NtBu)Cl_2$ (**1a**) [4c]

A mixture of $ZrCl_4(THF)_2$ (2.61 g, 6.92 mmol) and $Li_2(C_5Me_4SiMe_2NtBu)$ (1.82 g, 6.92 mmol), obtained by double deprotonation of $(C_5Me_4H)SiMe_2NHtBu$ using Li*n*Bu in hexane, was treated dropwise with 35 ml of toluene at −60°C and stirred for 3 days at room temperature. Filtration of the reaction mixture through glass fibre, followed by concentrating the filtrate and recrystallization at −20°C afforded 2.11 g (74% yield) of colourless crystals. ^1H NMR (C_6D_6): δ 0.53 (s, 6 H, $SiCH_3$), 1.44 (s, 9 H, $C(CH_3)_3$), 2.07 (s, 6 H, ring CH_3), 2.13 (s, 6 H, ring CH_3). $^{13}C\{^1H\}$ NMR (C_6D_6): δ 6.0 ($SiCH_3$), 11.9, 14.7 (ring CH_3), 33.1 ($C(CH_3)_3$), 56.6 ($C(CH_3)_3$), 101.2 (ring C attached to Si), 131.5, 134.2 (ring C). EI MS: *m/z* 410 (3%, M^+), 395 (51%, M^+-CH_3), 340 (5%, M^+-2Cl). Anal. calc. for $C_{15}H_{27}Cl_2NSiZr$: C, 43.77; H, 6.61; N, 3.40. Found C, 43.33, H, 6.84, N, 3.54.

$Hf(\eta^5:\eta^1\text{-}C_5Me_4SiMe_2NtBu)Cl_2$ (**1b**)

Following a procedure analogous to that described for the preparation of **1a**, $Li_2(C_5Me_4SiMe_2NtBu)$ (1.00 g, 3.80 mmol) was reacted with $HfCl_4(THF)_2$ (1.76 g, 3.80 mmol) to give **1b** (0.50 g, 38% yield) as colourless microcrystals. ^1H NMR (C_6D_6): δ 0.44 (s, 6 H, $SiCH_3$), 1.29 (s, 9 H, $C(CH_3)_3$), 1.98, 2.08 (s, 6 H, ring CH_3). $^{13}C\{^1H\}$ NMR (C_6D_6): δ 6.2 ($SiCH_3$), 11.5, 14.4 (ring CH_3), 33.9 ($C(CH_3)_3$), 55.3 ($C(CH_3)_3$), 100.7 (ring C attached to Si), 130.1, 131.8 (ring C). EI MS: *m/z* 500 (9%, M^+), 464 (18%, M^+-Cl), 429 (7%, M^+-2Cl). Anal. calc. for $C_{15}H_{27}NSiCl_2Hf$: C, 36.12; H, 5.41; N, 2.80. Found: C, 36.68; H, 6.97; N, 3.05.

$Zr(\eta^5:\eta^1\text{-}C_5Me_4SiMe_2NiPr)Cl_2$ (**2a**)

This compound can only be prepared as an inseparable mixture with $Zr(\eta^5:\eta^1\text{-}C_5Me_4SiMe_2NiPr)_2$ (**3a**) (*vide infra*). ^1H NMR (C_6D_6): δ 0.15 (s, 6 H, $SiCH_3$), 1.08 (d, $^3J_{HH}$ = 6.3 Hz, 6 H, $CH(CH_3)_2$), 1.97, 2.12 (s, 6 H, ring CH_3), 3.03 (sept, $^3J_{HH}$ = 6.6 Hz, 1 H, $CH(CH_3)_2$).

$Hf(\eta^5:\eta^1\text{-}C_5Me_4SiMe_2NiPr)Cl_2$ (**2b**)

Toluene (30 ml) was added to a solid mixture of $Li_2(C_5Me_4SiMe_2NiPr)$ (1.50 g, 6.02 mmol) and $HfCl_4(THF)_2$ (2.80 g, 6.02 mmol) at −78°C. The mixture was stirred overnight, the solution was filtered, concentrated and cooled to −30°C to give a white solid. Extraction with hexane (2 × 10 ml) followed by filtration and cooling afforded 0.58 g (20% yield) of **2b** as colourless microcrystals. ^1H NMR (C_6D_6): δ 0.26 (s, 6 H, $SiCH_3$), 0.85 (d, $^3J_{HH}$ = 6.6 Hz, 6 H, $CH(CH_3)_2$), 2.14, 2.19 (s, 6 H, ring CH_3), 3.05 (sept, $^3J_{HH}$ = 6.6 Hz, 1 H, $CH(CH_3)_2$). $^{13}C\{^1H\}$ NMR (C_6D_6): δ 1.0 ($SiCH_3$), 12.3, 15.9 (ring CH_3), 26.1 ($CH(CH_3)_2$), 48.8 ($CH(CH_3)_2$), 107.9 (ring C attached to Si), 131.4, 133.4 (ring C). EI MS: *m/z* (%) 450 (3%, M^+-Cl), 415 (6%, M^+-2Cl).

$Zr(\eta^5:\eta^1\text{-}C_5Me_4SiMe_2NiPr)_2$ (**3a**)

A mixture of $ZrCl_4(THF)_2$ (0.62 g, 1.64 mmol) and $Li_2(C_5Me_4SiMe_2NiPr)$ (0.82 g, 3.29 mmol) was treated dropwise with 35 ml of toluene at −60°C and stirred for 2 days at room temperature. Filtration of the extracts, followed by concentrating the filtrate and cooling to −50°C afforded 0.30 g of pale yellow crystals, yield: 33%. ^1H NMR (C_6D_6): δ 0.65, 0.78 (s, 3 H, $SiCH_3$), 1.29 (d, $^3J_{HH}$ = 6.3 Hz, 3 H, $CH(CH_3)_2$), 1.35 (d, $^3J_{HH}$ = 6.6 Hz, 3 H, $CH(CH_3)_2$), 1.96 (s, 6H, ring CH_3), 2.09, 2.42 (s, 3 H, ring CH_3), 4.13 (m, 1 H, $CH(CH_3)_2$). $^{13}C\{^1H\}$ NMR (C_6D_6): δ 8.6, 8.9 ($SiCH_3$), 11.4, 12.1, 13.6, 15.3 (ring CH_3), 28.8, 29.6 ($CH(CH_3)_2$), 52.7 ($CH(CH_3)_2$), 107.3 (ring C attached to Si), 122.9, 124.5, 125.9, 128.6 (ring C). EI MS: *m/z* 560 (24%, M^+), 545 (39%, M^+-CH_3) 517 (17%, M^+-CHMe_2), 501 (100%, $M^+-NH_2CHMe_2$), 460 (25%, $M^+-CHMe_2-NCHMe_2$), 387 (27%, $M^+-Me_2SiNHCHMe_2-NCHMe_2$). Anal. calc. for $C_{28}H_{50}N_2Si_2Zr$: C, 59.83; H, 8.83; N, 4.98. Found: C, 62.37; H, 9.34; N, 6.10.

$Hf(\eta^5:\eta^1\text{-}C_5Me_4SiMe_2NiPr)_2$ (**3b**)

Following a similar procedure described for the preparation of **2b**, $Li_2(C_5Me_4SiMe_2NiPr)$ (1.00 g, 4.01 mmol) was reacted with $HfCl_4(THF)_2$ (1.86 g, 4.01

mmol) in THF to obtain $Hf(\eta^5:\eta^1\text{-}C_5Me_4SiMe_2NiPr)_2$ (**3b**) (0.65 g, 25% yield) as colourless crystals, suitable for X-ray diffraction studies. ^1H NMR (C_6D_6): δ 0.53, 0.64 (s, 3 H, $SiCH_3$), 1.18, 1.23 (d, $^3J_{HH}$ = 6.4 Hz, 3 H, $CH(CH_3)_2$), 1.88, 1.90, 2.02, 2.30 (s, 3 H, ring CH_3), 3.99 (m, 1 H, $CH(CH_3)_2$). $^{13}C\{^1H\}$ NMR (C_6D_6): δ 8.6, 8.7 ($SiCH_3$), 11.5, 12.2, 13.6, 15.3 (ring CH_3), 28.9, 30.0 ($CH(CH_3)_2$), 52.1 ($CH(CH_3)_2$), 106.4 (ring C attached to Si), 121.6, 124.6, 125.0, 127.2 (ring C). EI MS: *m/z* 650 (52%, M^+), 591 (13%, $M^+ - NH_2CHMe_2$), 534 (20%, $M^+ - Me_2SiNHCHMe_2$), 505 (97%, $M^+ - Me_2SiNHCHMe_2 - 2\,CH_3$). Anal. calc. for $C_{28}H_{50}N_2Si_2Hf$: C, 51.81; H, 7.82; N, 4.31. Found: C, 47.80; H, 7.82; N, 3.79.

$Li[Y(\eta^5:\eta^1\text{-}C_5Me_4SiMe_2NCH_2CH_2CH_2OMe)_2]$ (**4**)

YCl_3 (223 mg, 1.14 mmol) and $Li_2(C_5Me_4SiMe_2NCH_2CH_2CH_2OMe)$ (638 mg, 2.28 mmol) were combined in a flask and pre-cooled THF (15 ml) was added at −78°C with stirring. The resulting mixture was allowed to warm to room temperature and stirred for 13 h. The solvent was removed *in vacuo* and the crude product extracted with 2 × 10 ml of toluene. LiCl was filtered off and the clear solution was concentrated to 2 ml. After crystallization at −25°C for 24 h, the mother liquor was decanted off and the crystals were dried *in vacuo* to yield 605 mg (85%) of **4** as pale yellow microcrystals. ^1H NMR (C_6D_6): δ 0.52, 0.64 (s, 6 H, $SiCH_3$), 1.50 (m, 4 H, $NCH_2CH_2CH_2O$), 2.08, 2.17, 2.21, 2.32 (s, 6 H, ring CH_3), 2.81 (s, 6 H, OCH_3), 2.92, 3.09 (m, 2 H, CH_2O), 3.38 (m, 4 H, NCH_2); ^{13}C NMR (C_6D_6): δ 2.3, 9.3 ($SiCH_3$), 10.8, 12.0, 13.4, 15.7 (ring CH_3), 37.2 ($NCH_2CH_2CH_2O$), 46.9 (NCH_2), 58.9 (OCH_3), 74.8 (CH_2O), 105.8 (ring C attached to Si), 120.0, 121.3, 121.4, 124.3 (ring C). Anal. calc. for $C_{30}H_{54}LiN_2O_2Si_2Y$: C, 57.49; H, 8.68; N, 4.47. Found: C, 51.06; H, 8.28; N, 4.42.

$Li[Y\{\eta^5\text{-}C_5Me_4SiMe_2NH(CH_2CH_2OMe)\}_2(C{\equiv}CPh)_2]$ (**6**)

$Li[Y(\eta^5:\eta^1\text{-}C_5Me_4SiMe_2NCH_2CH_2OMe)_2]$ (**5**) (57 mg, 95 μmol) was dissolved in C_6D_6 (0.5 ml) and phenylacetylene (20 mg, 196 μmol) was added at room temperature. The solution was kept at 5°C overnight, before the NMR spectra were recorded. The compound was isolated by removal of the solvent *in vacuo* and the crude product recrystallized from hexane at −30°C to yield 63 mg (83%) of **6** as colourless microcrystals. ^1H NMR (C_6D_6): δ 0.54 (s, 12 H, $SiCH_3$), 1.40 (t, $^3J_{HH}$ = 7.8 Hz, 2 H, NH), 2.21, 2.52 (s, 12 H, ring CH_3), 2.67 (dt, $^3J_{HH}$ = 7.8 Hz, $^3J_{HH}$ = 5.5 Hz, 4 H, NCH_2), 2.83 (s, 6 H, OCH_3), 2.89 (t, 4 H, $^3J_{HH}$ = 5.5 Hz, CH_2O), 6.99 (m, 2 H, 4-C_6H_5), 7.07 (m, 4 H, 3-C_6H_5), 7.49 (m, 4 H, 2-C_6H_5); ^{13}C NMR (C_6D_6): δ 1.8 ($SiCH_3$), 11.9, 15.6 (ring CH_3), 41.5 (NCH_2), 58.3 (OCH_3), 75.0 (CH_2O), 111.7 (ring C attached to Si), 114.9 (d, $^2J_{YC}$ = 10.1 Hz, C≡*C*Ph), 121.4, 125.3 (ring C), 126.5 (*ipso*-C_6H_5), 126.9 (*para*-C_6H_5), 128.4 (*meta*-C_6H_5), 131.7 (*ortho*-C_6H_5), 141.2 (dq, $^1J_{YC}$ = 49.9 Hz, $^1J_{LiC}$ = 7.3 Hz, *C*≡CPh). Anal. calc. for $C_{44}H_{62}LiN_2O_2Si_2Y$: C, 65.81; H, 7.78; N, 3.49. Found: C, 65.86; H, 8.50; N, 4.56.

X-ray crystal structure analysis of **3b**

Crystal data for **3b** are summarized in Table 1. The compound, obtained as colourless crystals by cooling a concentrated pentane solution, crystallizes in the monoclinic space group *C*2/*c* (No. 15). Data collection in the range $3.4° < \theta < 29.9°$ was performed using ω-scans on an Enraf-Nonius CAD-4 diffractometer with graphite-monochromated Mo-K_α radiation. Data correction for Lorentz polarization and absorption (empirically using PSI-scans) was carried out using the program system MolEN [20a]. From 7235 measured reflections, all 4310 independent reflections were used and 251 parameters were refined by full-matrix least-squares against all F_o^2 data (SHELXL-93) [20b]. The structure was solved using direct methods (SHELXS-86) [20c] and difference Fourier syntheses and refined with anisotropic thermal parameters for non-hydrogen atoms. All hydrogen atoms were refined with isotropic thermal parameters. The refinement converged with $R = 0.0182$, $wR_2 = 0.0360$ for all observed F_o data, goodness-of-fit 1.097. Listings of all crystal data and refinement parameters, atomic parameters including hydrogen atoms, thermal parameters, and bond lengths and angles have been deposited at the Cambridge Crystallographic Centre.

Acknowledgements—This work was supported by the Fonds der Chemischen Industrie, the Volkswagen-Foundation and the BASF AG (Kunsstofflaboratorium). F.A. is indebted to the European Community (TMR program) and K.E.d.P. to the Alexander-von-Humboldt Foundation for a post-doctoral fellowship. K.C.H. thanks the Fonds der Chemischen Industrie for a doctoral scholarship.

REFERENCES

1. (a) Canich, J. M., Hlatky, G. G. and Turner, H. W., PCT Appl. WO 92-00333 1992, Canich, J. M., Eur. Patent Appl. EP 420 436-A1, 1991, (Exxon Chemical Co.); (b) Stevens, P. N., Timmers, F. J., Wilson, D. R., Schmidt, G. F., Nickias, P. N., Rosen, R. K., Knight, G. W. and Lai, S., Eur. Patent Appl. EP 416 815-A2, 1991, (Dow Chemical Co.); (c) Sernetz, F. G., Mülhaupt, R., Amor, F., Eberle, T. and Okuda, J., *J. Polym. Sci., Part A*, 1997, **35,** 1571; Sernetz, F. G., Mülhaupt, R. and Waymouth, R. M., *Macromol. Chem. Phys.*, 1996, **197,** 1071; Sernetz, F. G., Mülhaupt, R. and Waymouth, R. M., *Polymer Bulletin*, 1997, **38,** 141; (d) McKnight, A. L., Masood, Md. A. and Waymouth, R. M., *Organometallics*, 1997, **16,** 2879; (e) Shiomura, T., Asanuma, T. and

Inoue, N., *Macromol. Rapid Commun.*, 1996, **17,** 9; Shiomura, T., Asanuma, T. and Sunaga, T., *Macromol. Rapid Commun.*, 1997, **18,** 169; (f) Soga, K., Uozumi, T., Nakamura, S., Toneri, T., Teranishi, T., Sano, T. and Arai, T., *Macromol. Chem. Phys.*, 1996, **197,** 4237; (g) Hagihara, H., Shiono, T. and Ikeda, T., *Macromolecules*, 1997, **30,** 4783.

2. (a) Shapiro, P. J., Bunel, E. E., Schaefer, W. P. and Bercaw, J. E., *Organometallics*, 1990, **9,** 867; (b) Shapiro, P. J., Cotter, W. D., Schaefer, W. P., Labinger, J. A. and Bercaw, J. E., *J. Am. Chem. Soc.*, 1994, **116,** 4623; (c) Piers, W. E., Shapiro, P. J., Bunel, E. E. and Bercaw, J. E., *Synlett*, 1994, **2,** 74.
3. (a) Okuda, J., *Chem. Ber.*, 1990, **123,** 1649; (b) Okuda, J., Schattenmann, F. J., Wocadlo, S. and Massa, W., *Organometallics*, 1995, **14,** 789; (c) du Plooy, K. E., Moll, U., Wocadlo, S., Massa, W. and Okuda, J., *Organometallics*, 1995, **14,** 3129; (d) Okuda, J. du Plooy, K. E., Massa, W., Kang, H. C. and Rose, U., *Chem. Ber.*, 1996, **129,** 275; (e) Amor, F., Okuda, J., *J. Organomet. Chem.*, 1996, **520,** 245; (f) Okuda, J., Verch, S., Spaniol, T. P. and Stürmer, R., *Chem. Ber.*, 1996, **129,** 1429; (g) Okuda, J., Eberle, T. and Spaniol, T. P., *Chem. Ber.*, 1997, **130,** 209; (h) Amor, F., Spaniol, T. P. and Okuda, J., *Organometallics*, 1997, **16,** 4765; (i) Amor, F., Spaniol, T. P. and Okuda, J., *J. Organomet. Chem.*, in press; (j) Eberle, T., Spaniol, T. P. and Okuda, J., *Chem. Ber.*, in press.
4. (a) Devore, D. D., Timmers, F. J., Hasha, D. L., Rosen, R. K., Marks, T. J., Deck, P. A. and Stern, C. L. *Organometallics*, 1995, **14,** 3132; (b) Kloppenburg, L. and Peterson, J. L., *Organometallics*, 1996, **15,** 7; (c) Carpenetti, D. W., Kloppenburg, L., Kupec, J. T. and Petersen, J. L., *Organometallics*, **15,** 1996, 1572; (d) Kloppenburg, L. and Peterson, J. L., *Organometallics*, 1997, **16,** 3548; (e) Ciruelos, S., Cuenca, T., Gomez-Sal, P., Manzanero, A. and Royo, P., *Organometallics*, 1995, **14,** 177; (f) Ciruelos, S., Cuenca, T., Gomez, R., Gomez-Sal, P., Manzanero, A. and Royo, P., *Organometallics*, 1996, **15,** 5577; (g) Dias, H. V. R., Wang, Z. and Bott, S. G., *J. Organomet. Chem.*, 1996, **508,** 91.
5. (a) Herrmann, W. A., Morawietz, M. J. A. and Priermeier, T., *Angew. Chem., Int. Ed. Engl.*, 1994, **33,** 1946; (b) Herrmann, W. A. and Morawietz, M. J. A., *J. Organomet. Chem.*, 1994, **482,** 169.
6. Böhme, U. and Thiele, K. H., *J. Organomet. Chem.*, 1994, **472,** 39.
7. (a) Hultzsch, K. C., Spaniol, T. P. and Okuda, J., *Organometallics*, 1997, **16,** 4845. (b) Hultzsch, K. C. and Okuda, J., *Macromol. Rapid Commun*, 1997, **18,** 809. (c) Hultzsch, K. C., Spaniol, T. P. and Okuda, J., *Organometallics*, in press.
8. (a) Atwood, J. L., Barker, G. K., Holton, J., Hunter, W. E., Lappert, M. F. and Pearce, R., *J. Am. Chem. Soc.*, 1977, **99,** 6645; (b) Rogers, R. D., Benning, M. M., Kurihara, L. K., Moriarty, K. J. and Rausch, M. D., *J. Organomet. Chem.*, 1985, **293,** 51.
9. Hillhouse, G. L., Bulls, A. R., Santarsiero, B. D. and Bercaw, J. E., *Organometallics*, 1988, **7,** 1309.
10. (a) Bai, Y., Roesky, H. W., Noltemeyer, M. and Witt, M. *Chem. Ber.*, 1992, **125,** 825; (b) Dias, H. V. R., Wang, Z. and Bott, S. G., *J. Organomet. Chem.*, 1996, **508,** 91; (c) Fryzuk, M. D., Haddad, T. S. and Pettig, S. J., *Organometallics*, 1989, **8,** 1723; (d) Bol, J. E., Hessen, B., Teuben, J. H., Smeets, W. J. J. and Spek, A. L., *Organometallics*, 1992, **11,** 1981.
11. Lauher, J. W. and Hoffmann, R., *J. Am. Chem. Soc.*, 1976, **98,** 1729.
12. Baker, R. T., Whitney, J. F. and Wreford, S. S., *Organometallics*, 1983, **2,** 1049. According to the MLX formalism developed by M. L. H. Green, the amido ligands are classified as LX type ligands: Green, M. L. H., *J. Organomet. Chem.*, 1995, **500,** 127.
13. Evans, W. J., Drummond, D. K., Hanusa, T. P. and Olofson, J. M., *J. Organomet. Chem.*, 1989, **376,** 311.
14. (a) Evans, W. J. and Wayda, A. L., *J. Organomet. Chem.*, 1980, **202,** C6; (b) Atwood, J. L., Hunter, W. E., Wayda, A. L. and Evans, W. J., *Inorg. Chem.*, 1981, **20,** 4115; (c) Evans, W. J., Bloom, I., Hunter, W. E. and Atwood, J. L., *Organometallics*, **2,** 1983, 709; (d) Shen, Q., Zheng, D., Lin, L. and Lin, Y., *J. Organomet. Chem.*, 1990, **391,** 307; (e) Forsyth, C. M., Nolan, S. P., Stern, C. L. and Marks, T. J., *Organometallics*, 1993, **12,** 3618; (f) Ren, J., Hu, J., Lin, Y. and Xing, Y., *Polyhedron*, 1996, **15,** 2165.
15. den Haan, K. H., Wielstra, Y. and Teuben, J. H., *Organometallics*, 1987, **6,** 2053.
16. Lee, L., Berg, D. J. and Bushnell, G. W. *Organometallics*, **14,** 1995, 5021.
17. (a) Fraenkel, G. and Pramanik, P., *J. Chem. Soc., Chem. Commun.*, 1983, 1527; (b) McKeever, D. and Waack, R., *J. Chem. Soc., Chem. Commun.*, 1969, 750.
18. Manzer, L. E., *Inorg. Synth.*, 1982, **21,** 135.
19. Suffert, J., *J. Org. Chem.*, 1989, **54,** 509.
20. (a) Fair, C. K., MolEN, An Interactive Structure Solution Procedure, Enraf-Nonius, Delft, 1990; (b) Sheldrick, G. M., SHELXL-93, Program for the Refinement of Crystal Structures, University of Göttingen, Germany, 1993; (c) Sheldrick, G. M., SHELXS-86, Program for the Solution of Crystal Structures, University of Göttingen, Germany, 1986.

Pergamon

PII: S0277-5387(97)00494-4

Polyhedron Vol. 17, No. 7, pp. 1081–1089, 1998
© 1998 Elsevier Science Ltd
All rights reserved. Printed in Great Britain
0277-5387/98 $19.00+0.00

Heterodinuclear TiMo and TiW complexes bridged by the (dimethylsilanediyl) dicyclopentadienyl ligand†

Mercedes Calvo, Pilar Gómez-Sal,‡ Antonio Manzanero‡ and Pascual Royo*

Departamento de Química Inorgánica, Facultad de Ciencias, Universidad de Alcalá de Henares, 28871-Alcalá de Henares, Spain

(Received 7 October 1997; accepted 24 October 1997)

Abstract—Reactions of the tricarbonyl-molybdenum and -tungsten complexes $[M(CO)_3(MeCN)_3]$ (M = Mo, W) or $[Mo(CO)_3(mesitylene)]$ with equimolar amounts of $[Ti(\eta^5\text{-}Cp')\{(\eta^5\text{-}C_5H_3)(SiMe_2)_2(C_5H_4)\}Cl_2]$ ($Cp' = C_5H_5$, C_5Me_5) lead to the heterodinuclear compounds $[Ti(\eta^5\text{-}Cp')Cl_2\{\mu\text{-}[(SiMe_2)_2(\eta^5\text{-}C_5H_3)_2]\}MH(CO)_3]$. These dinuclear complexes are isolated as single *cis*- and *trans*-isomers or as mixtures of both depending on the starting complex and the reaction conditions. The molar ratio of the two resulting isomers is controlled by thermodynamic and kinetic factors which prevent the application of stereoselective methods for some of the products. Reaction of the hydrido *cis*- and *trans*-complexes with CCl_4 in CH_2Cl_2 allows the isolation of chloro complexes $[Ti(\eta^5\text{-}Cp')Cl_2\{\mu\text{-}[(SiMe_2)_2(\eta^5\text{-}C_5H_3)_2]\}MCl(CO)_3]$ of the same configuration. All of the new heterodinuclear compounds reported were characterized by their analytical composition, IR and NMR spectroscopy and the molecular structure of *cis*-$[Ti(\eta^5\text{-}C_5Me_5)Cl_2\{\mu\text{-}[(SiMe_2)_2(\eta^5\text{-}C_5H_3)_2]\}WH(CO)_3]$ was studied by X-ray diffraction methods. © 1998 Elsevier Science Ltd. All rights reserved

Keywords: heterodinuclear complexes; titanium-molybdenum; titanium-tungsten; cyclopentadienyl

Heterodinuclear organometallic complexes containing two metals with very different reactivity in close proximity have received considerable attention [1] because they may produce cooperative effects and new reactivity patterns when used in stoichiometric and catalytic reactions. Particular efforts have focused on complexes containing both early electron-deficient and middle or late electron-rich transition metals. Several strategies using different bridging groups have been used to prepare complexes of this type with and without metal–metal bonds. On of the most intensively studied [2] groups of compounds is that formed by using cyclopentadienylphosphine systems as bridging groups which are η^5-coordinated to the early or middle group 4–6 transition metal and phosphorus-coordinated to the late transition metal. However most of the reported heterodinuclear compounds involving group 4 metals are phosphido- [3a–c] and carbonyl- [3d–g] bridged complexes.

In recent years many dinuclear complexes containing bridging cyclopentadienyl systems have been described. They include fulvalene [4a–e] derivatives and those containing cyclopentadienyl rings singly bridged by different alkyl [5] and silyl [6] groups. Some similar trinuclear compounds have also been reported [7]. Although numerous homodimetallic complexes of this type have been synthesized and investigated, the range of synthetic methods available to isolate heterodinuclear compounds is limited mainly to the late transition metal derivatives.

We reported [8] the use of dilithium or dithallium salts of the [{1,1′:2,2′-bis(dimethylsilanediyl)}bis(η^5-cyclopentadienyl)] ($CpSi_2Cp$) dianion to prepare homodinuclear group 4 and 6 metal complexes containing the dicyclopentadienyl system as a bridging ligand. Related reactions using the monolithium salt of the ligand prepared as reported elsewhere [9] gives access to complexes containing only one of the cyclopentadienyl rings η^5-coordinated to the group 4 metal center, leading to mono- and mainly mixed dicyclo-

* Author to whom correspondence should be addressed.

† Dedicated to Prof. Dr W. A. Herrmann on the occasion of his 50th birthday.

‡ X-ray diffraction studies.

pentadienyl-type derivatives $[M(\eta^5Cp')(\eta^5\text{-}CpSi_2C_5H_4)Cl_2]$ [10]. In these complexes the other cyclopentadiene moiety remains available for further reactions with a second different metal complex. Herein we report the application of this strategy to study migration reactions of the acidic cyclopentadiene ring proton to molybdenum and tungsten carbonyls as a method to prepare heterodinuclear compounds of the type *cis*- and *trans*-$[TiCp'Cl_2\{\mu\text{-}(CpSi_2Cp)\}MH(CO)_3]$ ($Cp' = C_5H_5$, C_5Me_5; $CpSi_2Cp = (SiMe_2)_2(\eta^5\text{-}C_5H_3)_2$) containing one titanium and one group 6 metal fragment. Conversion of the hydrido into the chloro complexes and the structural characterization of all these compounds is also reported.

RESULTS AND DISCUSSION

Reactions of the mixed dicyclopentadienyl titanium complexes $[Ti(\eta^5\text{-}Cp')\{(\eta^5\text{-}C_5H_3)(SiMe_2)_2(C_5H_4)\}Cl_2]$ [$Cp' = C_5H_5$ (**1**), C_5Me_5 (**2**)] with equimolar amounts of $[M(CO)_3(MeCN)_3]$ (M = Mo, W) or $[Mo(CO)_3$(mesitylene)] resulted in migration of the acidic ring hydrogen of the cyclopentadiene moiety to the group 6 metal with elimination of the acetonitrile or mesitylene ligands, which were replaced by the η^5-coordinated cyclopentadienyl ring to give the hydrido tricarbonyl complexes $[TiCp'Cl_2\{\mu\text{-}(CpSi_2Cp)\}MH(CO)_3]$ [$Cp' = C_5H_5$, M = Mo (**3**), W (**4**); $Cp' = C_5Me_5$, M = Mo (**5**), W (**6**)], as shown in Scheme 1.

The rigidity of the bridging dicyclopentadienyl ligand is responsible for the formation of different stereoisomers in this type of dinuclear compound for which six different structural dispositions have been found in the solid by X-ray diffraction studies. Two were reported [11] to belong to a *trans*-configuration of the two metal centers with the central six-membered ring of the ligand exhibiting either a boat or an essentially planar conformation, and the other two show the metal fragments in a *cis*-disposition occupying either the internal or the external faces of the boat configuration of the central ring of the ligand. In addition we have recently reported [8f] two new configurations: one *cis*-configuration showing an almost planar disposition of the central ring of the ligand and a *trans*-configuration with the ligand exhibiting a chair disposition. It is not easy to explain the preferential formation of one of these structures when the two metals are not connected either by metal–metal bonds or through additional ligand bridges, because it results from the contribution of many different factors including the conformation of the starting complex and the mechanism followed by the reaction leading to the final product.

It has been reported [9] that the monoalkali-metal derivatives of the ligand exist at low temperature as a mixture of two stable enantiomers which show fluxional behavior being interconverted at higher temperatures through a silatropic rearrangement. Solutions of the starting titanium complexes **1** and **2** may contain an enantiomeric mixture of two stereoisomers, showing the cyclopentadiene proton in *cis*- and *trans*-disposition with respect to the metal fragment in variable molar ratios of both stereoisomers at different temperatures. It must be expected that hydrogen transfer to the group 6 metal in the *cis*- and *trans*-isomers should lead, respectively, to the heterodinuclear complex with the same *cis*- or *trans*-disposition of the metal fragments. However this transformation which is thermodynamically and kinetically controlled may give different molar ratios of the resulting stereoisomers for each reaction and under different conditions even assuming that the hydrogen transfer process follows the same mechanism. For these reasons, using the pure solid complexes **1** and **2**, we observed that the *cis*- or *trans*-configuration of the resulting final heterodimetallic product depends on the solvent, the temperature and time of reaction and the nature of the carbonyl derivative $M(CO)_3(MeCN)_3$ or $Mo(CO)_3$(mesitylene) used as the starting compound. Both *cis*- and *trans*-isomers can be easily distinguished by ^1H NMR spectroscopy because, although both show the same pattern of resonances due to an ABB′ spin system for both nonequivalent cyclopentadienyl rings bonded to the different metal fragments, the difference between the chemical shifts of the two nonequivalent silyl-methyl singlets is larger for the *cis*- than for the *trans*-isomer (see Experimental).

Reaction of complex $[Ti(\eta^5\text{-}C_5H_5)\{(\eta^5\text{-}C_5H_3)(SiMe_2)_2(C_5H_4)\}Cl_2]$ (**1**) with $[Mo(CO)_3$(mesitylene)] in THF at room temperature for 6 h led to *cis*-$[Ti(\eta^5\text{-}C_5H_5)Cl_2\{\mu\text{-}[(SiMe_2)_2(\eta^5\text{-}C_5H_3)_2]\}MoH(CO)_3]$ (*cis*-**3**) isolated as a red solid in 95% yield whereas the same reaction carried out with $[Mo(CO)_3(MeCN)_3]$ under the same conditions led to mixtures of *cis*-**3** and *trans*-**3** in different molar ratios, the *trans*-isomer always being the main component. Separation of the isomers was not possible. The reaction of complex **1** with $[W(CO)_3(MeCN)_3]$ at 50°C for 4 h led to the stereoselective formation of *cis*-$[Ti(\eta^5\text{-}C_5H_5)Cl_2\{\mu\text{-}[(SiMe_2)(\eta^5\text{-}C_5H_3)_2]WH(CO)_3]$ (*cis*-**4**) isolated as a red solid in 95% yield. In contrast, reaction of $[Ti(\eta^5\text{-}C_5Me_5)\{(\eta^5\text{-}C_5H_3)(SiMe_2)_2(C_5H_4)\}Cl_2]$ (**2**) with $[Mo(CO)_3$(mesitylene)] in THF at room temperature gave a mixture of *cis*-**5** and *trans*-**5** with the *cis*-isomer being the main product, whereas use of $[Mo(CO)_3(MeCN)_3]$ under the same conditions resulted in the stereoselective formation of *trans*-$[Ti(\eta^5\text{-}C_5Me_5)Cl_2\{\mu\text{-}[(SiMe_2)(\eta^5\text{-}C_5H_3)_2]MoH(CO)_3]$ (*trans*-**5**), isolated as a red solid in 85% yield. In the reaction of $[W(CO)_3(MeCN)_3]$ with compound **2** we sometimes obtained *cis*-**6** and sometimes a mixture of *cis*-**6** and *trans*-**6**, *cis*-**6** being the main product. This reaction was carried out under various conditions: in THF or dichloromethane at room temperature for 24 h or in THF at 50°C for 4 h but the results of the reactions were unpredictable.

Complexes **3**–**6** are air stable for short periods, insoluble in alkanes but soluble in aromatic solvents,

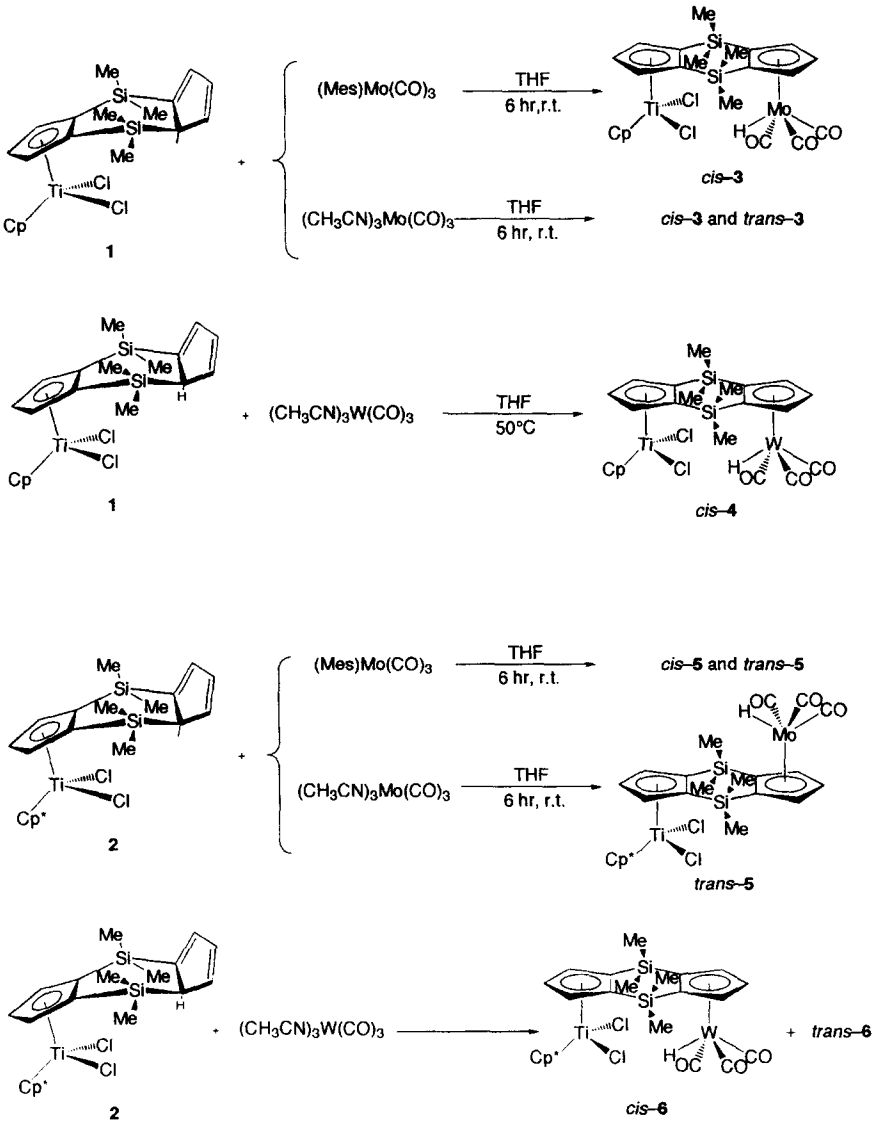

Scheme 1.

ethers and dichloromethane. They react with CCl_4 (see Scheme 2) at room temperature to be transformed into the related chlorotricarbonyl derivatives *cis*-$[TiCp'Cl_2\{\mu\text{-}Si_2(\eta^5\text{-}Cp)_2\}MCl(CO)_3]$ (Cp′ = Cp, M = Mo *cis*-**7**, W *cis*-**8**, Cp′ = Cp*, M = Mo *trans*-**9**, Cp′ = Cp*, M = W *cis*-**10**) in yields higher than 90%. These compounds are air stable red solids insoluble in alkanes and in toluene but soluble in ethers and dichloromethane.

All of the new heterodinuclear complexes were identified by elemental analysis and IR, ^1H and ^{13}C NMR spectroscopy. All of the compounds show the presence of one dicyclopentadienyl-type titanium fragment and one pseudo-square pyramidal hydrido or chloro tricarbonyl group 6 metal fragment, each bonded to one of the two cyclopentadienyl rings of the bridging ligand, with no interaction between the metal centers. The IR spectra of all the complexes show the expected two absorption bands between 2054 and 1914 cm^{-1}. The high field resonance due to the hydrido ligand in complexes **3**–**6** was observed between δ −4.86 and δ −7.48 ppm. The ^1H NMR spectra of all of the complexes show the presence of two nonequivalent cyclopentadienyl rings each with the expected ABB′ spin system proton resonances. Two pairs of nonequivalent silyl–methyl groups provide two additional singlets with a difference in their chemical shifts for the *cis*-isomers (0.25 ppm) larger than that observed for the *trans*-isomers (less than 0.06 ppm). The ^{13}C NMR spectra show the expected two singlets for the silyl–methyl carbon atoms and six resonances due to the nonequivalent two C_β and two pairs of C_{ipso} and C_α ring atoms, together with one or two singlets for the additional cyclopentadienyl or

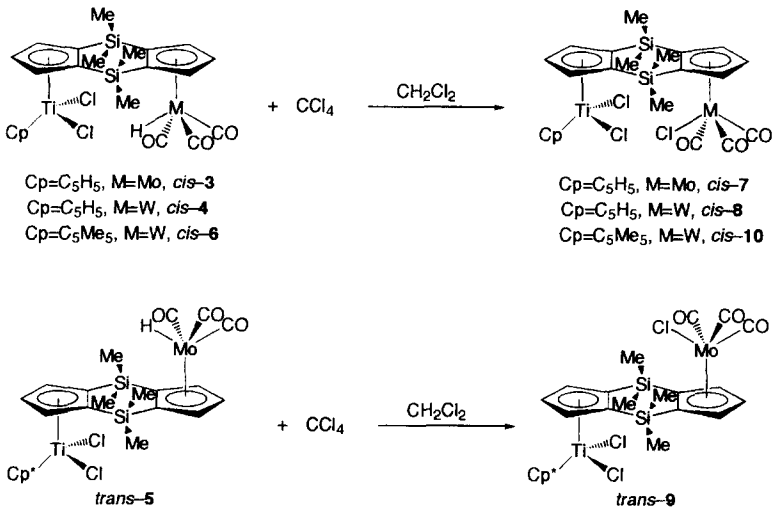

Scheme 2.

pentamethylcyclopentadienyl ring carbons respectively and two low field resonances due to the CO ligands, which could not be observed for some of the complexes (see Experimental).

Crystals suitable for X-ray study were obtained for complex *cis*-**6** whose molecular structure is shown in Fig. 1 together with the atomic labeling scheme. Selected bond distances and angles are given in Table 1.

The structure of **6** shows a *cis*-disposition of the two metal fragments bonded to the external faces of the cyclopentadienyl rings in order to place the two metal centers farther apart (6.298 Å), in the asymmetric molecule. Both cyclopentadienyl rings are planar and bound to the titanium and tungsten atoms in a slightly asymmetric η^5-fashion [the W—C distances range from 2.327(9) to 2.340(8) Å with a W—Cp(centroid) distance of 1.99 Å; the Ti—C distances range from 2.347(8) to 2.496(8) Å]. The dihedral angle between the two bridging cyclopentadienyl rings is 37.7(3)°. The central ring formed by the two silicon and the four carbon-ipso atoms is not planar in such a way that the dihedral angles between the mean planes containing Si(1), Si(2), C(11), C(12) and Si(1), Si(2), C(21), C(22) and the corresponding cyclopentadienyl ring are 13.7(3)° and 12.3(2)°, respectively, and the Si(1) and Si(2) atoms

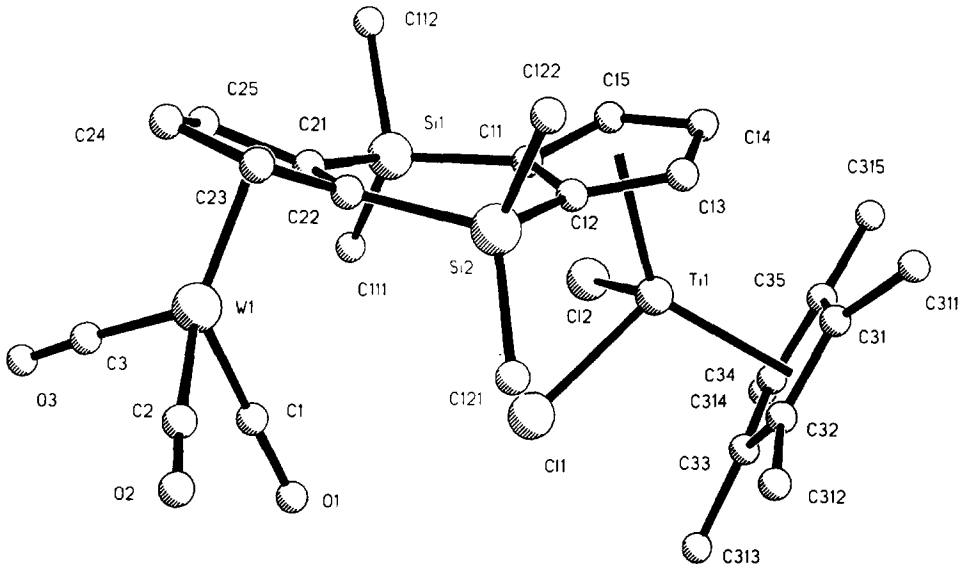

Fig. 1. Perspective view of complex *cis*-**6** with the atomic labeling scheme.

Table 1. Selected bond lengths (Å) and angles (°) for *cis*-**6**

W(1)—C(3A)	1.88(4)	W(1)—C(1)	1.89(2)
W(1)—C(3)	1.89(3)	W(1)—C(1A)	1.91(4)
W(1)—C(2A)	1.92(4)	W(1)—C(2)	2.01(3)
W(1)—C(23)	2.327(9)	W(1)—C(25)	2.331(9)
W(1)—C(24)	2.333(9)	W(1)—C(21)	2.339(8)
W(1)—C(22)	2.340(8)	Ti(1)—Cl(1)	2.324(3)
Ti(1)—C(14)	2.347(8)	Ti(1)—Cl(2)	2.355(3)
Ti(1)—C(13)	2.367(8)	Ti(1)—C(32)	2.386(8)
Ti(1)—C(15)	2.400(8)	Ti(1)—C(35)	2.400(8)
Ti(1)—C(31)	2.411(8)	Ti(1)—C(33)	2.421(8)
Ti(1)—C(34)	2.456(8)	Ti(1)—C(11)	2.486(8)
Ti(1)—C(12)	2.496(8)	Si(1)—C(111)	1.844(8)
Si(1)—C(11)	1.866(8)	Si(1)—C(112)	1.874(9)
Si(1)—C(21)	1.878(8)	Si(2)—C(121)	1.843(9)
Si(2)—C(122)	1.873(9)	Si(2)—C(12)	1.874(8)
Si(2)—C(22)	1.875(8)	C(11)—C(15)	1.424(11)
C(11)—C(12)	1.442(10)	C(12)—C(13)	1.396(11)
C(13)—C(14)	1.386(11)	C(14)—C(15)	1.411(11)
C(21)—C(25)	1.416(11)	C(21)—C(22)	1.452(11)
C(22)—C(23)	1.422(11)	C(23)—C(24)	1.383(12)
C(24)—C(25)	1.432(12)	C(31)—C(35)	1.412(12)
C(31)—C(32)	1.415(12)	C(31)—C(311)	1.499(11)
C(32)—C(33)	1.432(11)	C(32)—C(312)	1.507(12)
C(33)—C(34)	1.394(11)	C(33)—C(313)	1.491(12)
C(34)—C(35)	1.410(11)	C(34)—C(314)	1.496(11)
C(35)—C(315)	1.504(12)	C(1A)—C(1)	0.70(3)
C(1A)—O(1A)	1.22(4)	C(1A)—O(1)	1.43(4)
C(1A)—C(3)	2.03(4)	O(1A)—O(1)	1.02(3)
O(1A)—C(1)	1.50(3)	C(2A)—C(2)	0.66(4)
C(2A)—O(2A)	1.13(4)	C(2A)—O(2)	1.47(4)
O(2A)—O(2)	0.91(3)	O(2A)—C(2)	1.20(3)
C(3A)—C(3)	1.13(4)	C(3A)—(3A)	1.23(4)
C(3A)—O(3)	1.93(4)	O(3A)—O(3)	1.38(3)
O(3A)—C(3)	1.52(4)	C(1)—O(1)	1.17(2)
C(2)—O(2)	1.08(3)	C(3)—O(3)	1.20(3)
C(1)—W(1)—C(3)	82.4(10)	C(1)—W(1)—C(2)	75.2(9)
C(3)—W(1)—C(2)	109.6(10)	Cl(1)—Ti(1)—Cl(2)	94.57(10)
C(111)—Si(1)—C(11)	116.8(4)	C(111)—Si(1)—C(112)	109.0(4)
C(11)—Si(1)—C(112)	106.5(4)	C(111)—Si(1)—C(21)	113.1(4)
C(11)—Si(1)—C(21)	105.6(4)	C(112)—Si(1)—C(21)	105.2(4)
C(121)—Si(2)—C(122)	108.3(5)	C(121)—Si(2)—C(12)	117.9(4)
C(122)—Si(2)—C(12)	104.9(4)	C(121)—Si(2)—C(22)	113.7(4)
C(122)—Si(2)—C(22)	105.9(4)	C(12)—Si(2)—C(22)	105.3(3)
O(1A)—C(1A)—W(1)	177(3)	O(3A)—C(2A)—W(1)	166(4)
O(3A)—C(3A)—W(1)	153(3)	O(1)—C(1)—W(1)	177(2)
O(2)—C(2)—W(1)	173(3)	O(3)—C(3)—W(1)	176(3)

lie 0.348(2) Å and 0.291(2) Å, respectively, above the plane of the ring bonded to tungsten, and 0.195(2) Å and 0.479(2) Å above the plane of the ring bonded to titanium.

The titanium fragment shows the typical disposition of a bent dicyclopentadienyl system with an angle between the rings of 52.9(3)° with normal Ti—Cl distances [average 2.341(3) Å]. The tungsten fragment shows a pseudo-square pyramidal coordination in which the hydrido ligand, which could not be localized, presumably occupies the fourth position between the two C(2)O(2) and C(3)O(3) carbonyl ligands for which the C(2)—W(1)—C(3) angle is more open [109(1)°] than the other two [C(1)—W(1)—C(2) of 82(1)° and C(1)—W(1)—C(3) of 75(1)°] although the disorder found for the positions occupied by the carbonyl ligands prevents a rigorous assignment of their bonding situation.

EXPERIMENTAL

Reagents and general techniques

All reactions were carried out in dried Schlenk tubes under argon or nitrogen, and the manipulations were carried out using syringes or cannulas through Subaseals. Solvents were dried and distilled under nitrogen: tetrahydrofuran from sodium benzophenone ketyl; hexane and pentane from sodium and potassium amalgam; dichloromethane from P_2O_5 and carbon tetrachloride from $CaCl_2$. Unless otherwise stated, reagents were obtained from commercial sources and used as received. IR spectra were recorded in Nujol mulls for solids over the range 4000–200 cm^{-1} or in solution over the range 2500–1500 cm^{-1} on a Perkin–Elmer 583 spectrophotometer. IR data are given in cm^{-1}. The ^1H and ^{13}C NMR spectra were recorded at 200 and 50 MHz respectively on a Gemini 200 spectrometer, at 299.95 and 75.43 MHz respectively on a Varian Unity 300 spectrometer and at 499.85 and 125.7 MHz on a Varian Unity 500 Plus spectrometer; chemical shifts, in ppm, are positive downfield relative to external $SiMe_4$, and coupling constants are in Hz. C, H, and N analyses were performed with a Perkin–Elmer 240-B instrument.

The compounds $[Ti(\eta^5\text{-}C_5H_5)Cl_2\{(\eta^5\text{-}C_5H_3)[Si(CH_3)_2]_2(C_5H_4)\}]$ and $[Ti(\eta^5\text{-}C_5Me_5)Cl_2\{(\eta^5\text{-}C_5H_3)[Si(CH_3)_2]_2(C_5H_4)\}]$ were prepared as reported elsewhere [10b].

Synthesis of cis-$[Ti(\eta^5\text{-}C_5H_5)Cl_2\{(\eta^5\text{-}C_5H_3)_2[Si(CH_3)_2]_2\}MoH(CO)_3]$ (*cis*-**3**)

THF (50 ml) was added to a mixture of $[Ti(\eta^5\text{-}C_5H_5)Cl_2\{(\eta^5\text{-}C_5H_3)[Si(CH_3)_2]_2(C_5H_4)\}]$ (1.43 g, 3.35 mmol) and $[Mo(CO)_3(mesitylene)]$ (1.01 g, 3.35 mmol). After stirring for 6 h at room temperature the resulting red solution was concentrated to dryness *in vacuo* leaving a red solid which was washed with pentane and identified as complex *cis*-**3** (1.93 g, 95%). Anal. calc. for $C_{22}H_{24}Cl_2MoO_3Si_2Ti$: C, 43.51; H, 3.98. Found: C, 43.87; H, 4.06. ^1H NMR (300 MHz, C_6D_6): δ −4.91 (s, 1H, Mo-*H*), 0.10 (s, 6H, Si-*Me*), 0.61 (s, 6H, Si-*Me*), 4.98 (d, J = 2.4 Hz, 2H, $C_\alpha C_5H_3$), 5.10 (t, J = 2.4 Hz, 1H, $C_\beta C_5H_3$), 5.44 (t, J = 2.4 Hz, 1H, $C_\beta C_5H_3$), 5.94 (s, 5H, C_5H_5), 6.52 (d, J = 2.4 Hz, 2H, $C_\alpha C_5H_3$). $^{13}C\{^1H\}$ NMR (125 MHz, C_6D_6): 3.1 (Si-*C*H_3), 3.4 (Si-*C*H_3), 95.9 (C_β *C*$_5H_3$), 96.8 (C_α *C*$_5H_3$), 109.1 (C_{ipso} *C*$_5H_3$), 113.3 (C_β *C*$_5H_3$), 119.8 (*C*$_5H_5$), 133.2 (C_α *C*$_5H_3$), 138.7 (C_{ipso} *C*$_5H_3$), 223.8 (*C*O). IR (nujol): ν_{CO} 2015, 1915 cm^{-1}. IR (THF): ν_{CO} 2020, 1928 cm^{-1}.

When the reaction was carried out under the same experimental conditions using the equimolar amount of $[Mo(CO)_3(MeCN)_3]$ a mixture of *cis*-**3** and *trans*-**3** was obtained after concentrating the resulting red solution to dryness. The complex *trans*-**3** could not be isolated. ^1H NMR (300 MHz, C_6D_6): δ −5.43 (s, 1H, Mo-*H*), 0.40 (s, 6H, Si-*Me*), 0.44 (s, 6H, Si-*Me*), 5.06 (t, J = 2.4 Hz, 1H, $C_\beta C_5H_3$), 5.09 (d, J = 2.4 Hz, 2H, $C_\alpha C_5H_3$), 5.45 (t, J = 2.4 Hz, 1H, $C_\beta C_5H_3$), 5.92 (s, 5H, C_5H_5), 6.48 (d, J = 2.4 Hz, 2H, $C_\alpha C_5H_3$).

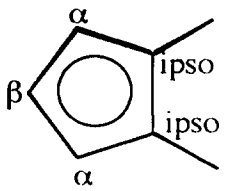

Synthesis of cis-$[Ti(\eta^5\text{-}C_5H_5)Cl_2\{(\eta^5\text{-}C_5H_3)_2[Si(CH_3)_2]_2\}WH(CO)_3]$ (*cis*-**4**)

THF (50 ml) was added to a mixture of $[Ti(\eta^5\text{-}C_5H_5)Cl_2\{(\eta^5\text{-}C_5H_3)[Si(CH_3)_2]_2(C_5H_4)\}]$ (1.14 g, 2.91 mmol) and $[W(CO)_3(MeCN)_3]$ (1.24 g, 2.91 mmol). After stirring for 4 h at 50°C the resulting red solution was concentrated to dryness *in vacuo* leaving a red solid which was washed with pentane and identified as complex *cis*-**4** (1.91 g, 94%). Anal. calc. for $C_{22}H_{24}Cl_2O_3Si_2TiW$: C, 38.01; H, 3.48. Found: C, 37.74; H, 3.55. ^1H NMR (300 MHz, $CDCl_3$): δ −6.82 (s, 1H, W-*H*), 0.32 (s, 6H, Si-*Me*), 0.57 (s, 6H, Si-*Me*), 5.58 (d, J = 2.4 Hz, 2H, $C_\alpha C_5H_3$), 5.74 (t, J = 2.4 Hz, 1H, $C_\beta C_5H_3$), 6.40 (t, J = 2.4 Hz, 1H, $C_\beta C_5H_3$), 6.54 (s, 5H, C_5H_5), 7.10 (d, J = 2.4 Hz, 2H, $C_\alpha C_5H_3$). $^{13}C\{^1H\}$ NMR (75 MHz, $CDCl_3$): 3.1 (Si-*C*H_3), 3.6 (Si-*C*H_{38}), 94.7 ($C_\beta C_5H_3$), 95.6 ($C_\alpha C_5H_3$), 106.2 (C_{ipso} *C*$_5H_3$), 113.8 (C_β *C*$_5H_3$), 120.1 (*C*$_5H_5$), 133.4 (C_α *C*$_5H_3$), 139.2 (C_{ipso} *C*$_5H_3$), *C*O was not observed. IR (nujol): ν_{CO} 2012, 1914 cm^{-1}; IR(THF): ν_{CO} 2016, 1920 cm^{-1}.

Synthesis of trans-$[Ti(\eta^5\text{-}C_5Me_5)Cl_2\{(\eta^5\text{-}C_5H_3)_2[Si(CH_3)_2]_2\}MoH(CO)_3]$ (*trans*-**5**)

THF (50 ml) was added to a mixture of $[Ti(\eta^5\text{-}C_5Me_5)Cl_2\{(\eta^5\text{-}C_5H_3)[Si(CH_3)_2]_2(C_5H_4)\}]$ (1.48 g, 2.97 mmol) and $[Mo(CO)_3(MeCN)_3]$ (0.9 g, 2.97 mmol). After stirring for a night at room temperature the resulting red solution was concentrated to dryness *in vacuo* leaving a red solid which was washed with pentane and identified as complex *trans*-**5** (1.88 g, 93%). Anal. calc. for $C_{27}H_{34}Cl_2MoO_3Si_2Ti$: C, 47.87; H, 5.06. Found: C, 47.59; H, 5.25. ^1H NMR (300 MHz, C_6D_6): δ −5.54 (s, 1H, Mo-*H*), 0.47 (s, 6H, Si-*Me*), 0.59 (s, 6H, Si-*Me*), 1.70 (s, 15H, C_5Me_5), 5.05 (m, 3H, $C_\alpha C_5H_3 + C_\beta C_5H_3$), 5.68 (t, J = 2.4 Hz, 1H, $C_\beta C_5H_3$), 6.48 (d, J = 2.4 Hz, 2H, $C_\alpha C_5H_3$). $^{13}C\{^1H\}$ NMR (50 MHz, C_6D_6): 2.5 (Si-*C*H_3), 4.7 (Si-*C*H_3), 13.5 (C_5Me_5), 97.5 ($C_\beta C_5H_3$), 98.8 ($C_\alpha C_5H_3$), 105.2 (C_{ipso} *C*$_5H_3$), 117.4 (C_β *C*$_5H_3$), 129.6 (*C*$_5$Me$_5$), 131.5 (C_α *C*$_5H_3$), 137.7 (C_{ipso} *C*$_5H_3$), 227.9 and 228.0 (*C*O).

IR (nujol): ν_{CO} 2016, 1920 cm^{-1}; IR(THF): ν_{CO} 2018, 1928 cm^{-1}.

When the reaction was carried out with $Mo(CO)_3$ (mesitylene) in the same conditions, a mixture of *cis*-**5** and *trans*-**5** was obtained after concentrating to dryness and washing with pentane. Complex *cis*-**5** could not be isolated. ^1H NMR (300 MHz, C_6D_6): δ −4.86 (s, 1H, Mo-*H*), 0.20 (s, 6H, Si-*Me*), 0.73 (s, 6H, Si-*Me*), 1.73 (s, 15H, C_5Me_5), 5.02 (d, J = 2.4 Hz, 2H, C_α C_5H_3), 5.11 (t, J = 2.4 Hz, 1H, C_β C_5H_3), 6.65 (t, J = 2.4 Hz, 1H, C_β C_5H_3), 6.51 (d, J = 2.4 Hz, 2H, C_α C_5H_3).

Synthesis of cis-[Ti(η^5-C_5Me_5)Cl_2\{(η^5-C_5H_3)$_2$ [Si$(CH_3)_2]_2$\}WH$(CO)_3$] (*cis*-**6**)

THF (50 ml) was added to a mixture of [Ti(η^5-C_5Me_5)Cl_2 \{(η^5-C_5H_3)[Si$(CH_3)_2]_2(C_5H_4)$\}] (1.38 g, 2.77 mmol) and [$W(CO)_3(MeCN)_3$] (1.08 g, 2.77 mmol). After stirring for 4 h at 50°C the resulting red solution was concentrated to dryness *in vacuo* leaving a red solid which was washed with pentane and identified as complex *cis*-**6** (1.95 g, 92%). Anal. calc. for $C_{27}H_{34}Cl_2O_3Si_2TiW$: C, 42.37; H, 4.48. Found: C, 42.59; H, 4.59. ^1H NMR (300 MHz, $CDCl_3$): δ −6.78 (s, 1H, W-*H*), 0.31 (s, 6H, Si-*Me*), 0.55 (s, 6H, Si-*Me*), 2.04 (s, 15H, C_5Me_5), 5.56 (d, J = 2.4 Hz, 2H, C_α C_5H_3), 5.71 (t, J = 2.4 Hz, 1H, C_β C_5H_3), 6.09 (t, J = 2.4 Hz, 1H, C_β C_5H_3), 6.66 (d, J = 2.4 Hz, 2H, C_a C_5H_3). $^{13}C\{^1H\}$ NMR (75 MHz, $CDCl_3$): 2.8 (Si-*C*H_3), 4.9 (Si-*C*H_3), 13.8 (C_5Me_5), 95.0 (C_β C_5H_3), 95.7 (C_α C_5H_3), 106.0 (C_{ipso} C_5H_3), 116.0 (C_β C_5H_3), 130.1 (C_5Me_5), 131.8 (C_α C_5H_3), 139.0 (C_{ipso} C_5H_3), *C*O was not observed. IR (nujol): ν_{CO} 2012, 1920 cm^{-1}; IR(THF): ν_{CO}: 2016, 1922 cm^{-1}.

When the reaction yielded a mixture of isomers, we were unable to isolate complex *trans*-**6**. ^1H NMR (300 MHz, $CDCl_3$): δ −7.48 (s, 1H, W-*H*), 0.43 (s, 6H, Si-*Me*), 0.48 (s, 6H, Si-*Me*), 2.02 (s, 15H, C_5Me_5), 5.62 (d, J = 2.4 Hz, 2H, C_α C_5H_3), 5.76 (t, J = 2.4 Hz, 1H, C_β C_5H_3), 6.18 (t, J = 2.4 Hz, 1H, C_β C_5H_3), 6.63 (d, J = 2.4 Hz, 2H, C_α C_5H_3).

Synthesis of cis-[Ti(η^5-C_5H_5)Cl_2\{(η^5-C_5H_3)$_2$[Si$(CH_3)_2]_2$\}MoCl$(CO)_3$] (*cis*-**7**)

CCl_4 (2 ml) was added to a solution of complex *cis*-**3** (1 g, 1.65 mmol) in CH_2Cl_2 (40 ml). After stirring for a night, the solution was concentrated to dryness *in vacuo* leaving a red solid which was washed with pentane and recrystallized from a mixture CH_2Cl_2: pentane 1 : 1 at −40°C to give *cis*-**7** as a red solid (0.95 g, 90%). Anal. calc. $C_{22}H_{23}Cl_3MoO_3Si_2Ti$: C, 41.17; H, 3.61. Found: C, 41.69; H, 4.19. ^1H NMR (300 MHz, $CDCl_3$): 0.33 (s, 6H, Si-*Me*), 0.57 (s, 6H, Si-*Me*), 5.55 (d, J = 2.4 Hz, 2H, C_α C_5H_3), 6.25 (t, J = 2.4 Hz, 1H, C_β C_5H_3), 6.40 (t, J = 2.4 Hz, 1H, C_β C_5H_3), 6.56 (s, 5H, C_5H_5), 7.13 (d, J = 2.4 Hz, 2H, C_α C_5H_3). $^{13}C\{^1H\}$ NMR (75 MHz, $CDCl_3$): 1.8 (Si-*C*H_3), 3.0 (Si-*C*H_3), 96.7 (C_β C_5H_3), 105.8 (C_{ipso} C_5H_3), 111.6 (C_α C_5H_3), 113.9 (C_β C_5H_3), 120.3 (C_5H_5), 133.5 (C_α C_5H_3), 139.1 (C_{ipso} C_5H_3), 222.8 and 242.5 (*C*O). IR (nujol): ν_{CO} 2045, 1946 cm^{-1}; IR(CH_2Cl_2): ν_{CO} 2054, 1976 cm^{-1}.

Synthesis of cis-[Ti(η^5-C_5H_5)Cl_2\{(η^5-C_5H_3)$_2$[Si$(CH_3)_2]_2$\}WCl$(CO)_3$] (*cis*-**8**)

This complex was obtained by the same procedure described for *cis*-**7** starting from *cis*-**4** (1 g, 1.44 mmol) as a red solid (1 g, 95%). Anal. calc. for $C_{22}H_{23}Cl_3O_3Si_2TiW$: C, 36.21; H, 3.18. Found: C, 35.84; H, 3.15. ^1H NMR (300 MHz, $CDCl_3$): δ 0.36 (s, 6H, Si-*Me*), 0.60 (s, 6H, Si-*Me*), 5.57 (d, J = 2.4 Hz, 2H, C_α C_5H_3), 6.41 (m, 2H, 2C_β C_5H_3), 6.57 (s, 5H, C_5H_5), 7.13 (d, J = 2.4 Hz, 2H, C_α C_5H_3). $^{13}C\{^1H\}$ NMR (75 MHz, $CDCl_3$): 2.0 (Si-*C*H_3), 3.2 (Si-*C*H_3), 96.4 (C_β C_5H_3), 102.7 (C_{ipso} C_5H_3), 110.0 (C_α C_5H_3), 113.9 (C_β C_5H_3), 120.4 (C_5H_5), 133.4 (C_α C_5H_3), 139.2 (C_{ipso} C_5H_3), 214.2 and 232.4 (*C*O). IR (nujol): ν_{CO} 2013, 1952 cm^{-1}; IR(CH_2Cl_2): ν_{CO} 2046, 1958 cm^{-1}.

Synthesis of trans-[Ti(η^5-C_5Me_5)Cl_2\{(η^5-C_5H_3)$_2$[Si$(CH_3)_2]_2$\}MoCl$(CO)_3$] (*trans*-**9**)

This complex was obtained by the same procedure described for *cis*-**7** starting from *trans*-**5** (1 g, 1.47 mmol) as a red solid (0.97 g, 93%). Anal. calc. for $C_{27}H_{33}Cl_3O_3Si_2TiMo$: C, 45.55; H, 4.67. Found: C, 44.65; H, 4.47. ^1H NMR (300 MHz, $CDCl_3$): δ 0.42 (s, 6H, Si-*Me*), 0.46 (s, 6H, Si-*Me*), 2.01 (s, 15H, C_5Me_5), 5.57 (d, J = 2.4 Hz, 2H, C_α C_5H_3), 6.21 (t, J = 2.4 Hz, 1H, C_β C_5H_3), 6.24 (t, J = 2.4 Hz, 1H, C_β C_5H_3), 6.58 (d, J = 2.4 Hz, 2H, C_α C_5H_3). $^{13}C\{^1H\}$ NMR (50 MHz, $CDCl_3$): 0.5 (Si-*C*H_3), 3.5 (Si-*C*H_3), 13.7 (C_5Me_5), 103.3 (C_β C_5H_3), 104.4 (C_{ipso} C_5H_3), 108.8 (C_α C_5H_3), 118.2 (C_β C_5H_3), 129.5 (C_5Me_5). 130.4 (C_α C_5H_3), 137.0 (C_{ipso} C_5H_3), 224.7 and 243.4 (*C*O). IR (nujol): ν_{CO} 2039, 1956 cm^{-1}; IR(CH_2Cl_2): ν_{CO} 2050, 1970 cm^{-1}.

Synthesis of cis-[Ti(η^5-C_5Me_5)Cl_2\{(η^5-C_5H_3)$_2$[Si$(CH_3)_2]_2$\}WCl$(CO)_3$ (*cis*-**10**)

This complex was obtained by the same procedure described for *cis*-**7** starting from *cis*-**6** (1 g, 1.30 mmol) as a red solid (0.94 g, 90%). Anal. calc. for $C_{27}H_{33}Cl_3O_3Si_2TiW$: C, 40.55; H, 4.16. Found: C, 40.22; H, 4.05. ^1H NMR (300 MHz, $CDCl_3$): δ 0.35 (s, 6H, Si-*Me*), 0.62 (s, 6H, Si-*Me*), 2.06 (s, 15H, C_5Me_5), 5.49 (d, J = 2.4 Hz, 2H, C_α C_5H_3), 6.10 (t, J = 2.4 Hz, 1H, C_β C_5H_3), 6.37 (t, J = 2.4 Hz, 1H, C_β C_5H_3), 6.68 (d, J = 3 Hz, 2H, C_α C_5H_3). $^{13}C\{^1H\}$ NMR (75 MHz, $CDCl_3$): 2.5 (Si-*C*H_3), 2.7 (Si-*C*H_3), 13.8 (C_5Me_5), 97.1 (C_β C_5H_3), 103.1 (C_{ipso} C_5H_3), 109.2 (C_α C_5H_3), 116.2 (C_β C_5H_3), 130.4 (C_5Me_5), 131.9 (C_α C_5H_3), 138.8 (C_{ipso} C_5H_3), 214.9 (*C*O), 232.9 (*C*O). IR

Table 2. Crystal, experimental data and structure refinement procedures for compound *cis*-**6**

Formula	$C_{27}H_{34}Cl_2O_3Si_2TiW$
Crystal habit	Prismatic
Color	Red
Crystal size	$0.20 \times 0.25 \times 0.30$ mm
Symmetry	Monoclinic, $P2_1/a$
Unit cell dimensions	
a (Å)	16.150(10)
b (Å)	12.021(3)
c (Å)	17.04(2)
β (°)	112.87(4)
V (Å^3)	3048(4)
Z	4
D_{calc} (g cm^{-3})	1.668
M_w	765.37
$F(000)$	1512
μ(cm^{-1})	43.13
Scan mode	$\omega/2\theta$ $2.13 < \theta < 24.01$
No. of reflections	
Measured	4783
Independent observed	3297
Range of h, k, l	$-18 < h < 16$, $0 < k < 13$, $0 < l < 19$
Standard reflections	3 every 200 refl.
Refinement method	Full matrix least squares on F^2
Final R indices ($I > 2\sigma(I)$)[a]	$R_1 = 0.0419$, $wR_2 = 0.0902$
R indices (all data)	$R_1 = 0.1019$, $WR_2 = 0.1288$
Weighting scheme	Calc. $\omega = 1/[\sigma^2(F_o^2) + (0.0352P)^2 + 14.9107P]$ where $P = (F_o^2 + 2F_c^2)/3$
Maximum peak in final diff. map (e/Å^3)	0.826
Minimum peak in final diff. map (e/Å^3)	−0.851
Goodness of fit on F^2	1.107

[a] $R_1 = \Sigma\|F_o| - |F_c|/\Sigma|F_o|$; $wR_2 = \{[\Sigma\omega((F_o^2 - F_c^2]/[\Sigma\omega(F_o^2)^2]\}^{1/2}$.

(nujol): ν_{CO} 2039, 1952 cm^{-1}. IR(CH_2Cl_2): ν_{CO} 2046, 1958 cm^{-1}.

X-ray structural determination for **6**

Red crystals of compound **6** were obtained by crystallization from THF and a suitable sized crystal in a Lindemann tube was mounted in an Enraf-Nonius CAD 4 automatic four-circle diffractometer with graphite monochromated Mo–K_α radiation ($\lambda = 0.71069$ Å). Crystallographic and experimental details are summarized in Table 2. Data were collected at room temperature. Intensities were corrected for Lorentz and polarization effects in the usual manner. No absorption or extinction corrections were made. The structure was solved by direct methods (SHELXL 90) [12] and refined by least squares against F^2 (SHELXL 93) [13]. A severe disorder appeared in the coordination sphere of the W atom and two different sets of carbonyl groups with similar occupancies were found. Unfortunately the second set shows the angle of one carbonyl group with an important deviation from linearity. All non-hydrogen atoms were refined anisotropically and the hydrogen atoms were introduced from geometrical calculations and refined using a riding model with thermal parameters equivalent to those of the atoms to which they are bonded. It was not possible to find the hydrogen atom bonded to W due to the disorder and this atom could not be included in any way. Calculations were carried out on an ALPHA AXP (Digital) workstation.

Supplementary material—Tables of positional parameters and their estimated standard deviations (Table 1), full list of bond lengths (Å) and angles (°) (Table 2), anisotropic displacement parameters (Table 3), hydrogen coordinates and isotropic displacement parameters (Table 4), and structure factors (Table 5) are available from author P.R. upon request.

Acknowledgment—The authors are grateful to DGICYT (Project PB-920178C) and CAM (I + D 0033/94) for financial support. A.M. is grateful to CAM for fellowship.

REFERENCES

1. (a) Chetcuti, M., *J. Comprehensive Organometallics Chemistry II*, **10**, 23, ed. E. W. Abel, A. Stone and G. Wilkinson. Pergamon, Oxford, U.K., 1995; (b) Stephan, D. W., *Coord. Chem.*

Rev., 1989, **95,** 41; (c) Bruce, M. I., *J. Organomet. Chem.*, 1983, **242,** 147.

2. (a) Rigny, S., Bakhmutov, V. I., Nuber, B., Leblanc, J.-C. and Moïse, C., *Inorg. Chem.*, 1996, **35,** 3202; (b) He, X. D., Maisonnat, A., Dahan, F. and Poilblanc, R., *Organometallics*, 1989, **8,** 2618; (c) Baker, R. T., Fultz, W. C., Marder, T. B. and Williams, I. D., *Organometallics*, 1990, **9,** 2357.
3. (a) Ara, I., Delgado, E., Forniés, J., Hernández, E., Lalindo, E., Mansilla, N. and Moreno, M. T., *J. Chem. Soc., Dalton Trans.*, 1996, 3201; (b) Kool, L. B., Ogasa, M., Rausch, M. D. and Roger, R. D., *Organometallics*, 1989, **8,** 1785; (c) Tikkanen, W., Fujita, Y. and Petersen, J. L., *Organometallics*, 1986, **5,** 888; (d) Longato, B., Norton, J. R., Huffman, J. C., Masella, J. A. and Caulton, B. G., *J. Am. Chem. Soc.*, 1981, 209; (e) Dick, D. G. and Stephan, D. W., *Organometallics*, 1990, **9,** 1910; (f) Longato, B., Martin, B. D., Norton, J. R. and Anderson, O. P., *Inorg. Chem.*, 1985, **24,** 1389; (g) Galakhov, M., Martín, A., Mena, M. and Yélamos, C., *J. Organomet. Chem.*, 1995, **496,** 217.
4. (a) Begley, M. J., Mountford, P., Stewart, P. J., Swallow, D. and Wan, S., *J. Chem. Soc., Dalton Trans.*, 1996, 1323; (b) Cuenca, T., Gómez, R., Gómez-Sal, P., Rodríguez, G. M. and Royo, P., *Organometallics*, 1992, **11,** 1229; (c) Alvaro, L. M., Cuenca, T., Flores, J. C., Royo, P., Pellinghelli, M. A. and Tiripicchio, A., *Organometallics*, 1992, **11,** 330; (d) Cano, A., Cuenca, T., Rodríguez, G., Royo, P., Cardin, C. and Wilcock, D. J., *J. Organomet. Chem.*, 1993, **447,** 51; (e) Cano, A., Cuenca, T., Galakhov, M., Rodríguez, G. M., Royo, P., Cardin, C. J. and Convery, M. A., *J. Organomet. Chem.*, 1995, **493,** 17.
5. (a) Buzinkai, J. F. and Schrock, R. R., *Organometallics*, 1987, **6,** 1447; (b) Schneider, D. and Werner, H., *J. Organomet. Chem.*, 1990, **384,** C33; (c) Storzo, C. L. and Stille, J. K., *Organometallics*, 1990, **9,** 687; (d) Diamond, G. M., Chernega, A. N., Mountford, P. and Green, M. L. H., *J. Chem. Soc., Dalton Trans.*, 1996, 921.
6. (a) Nifant'ev, I. E., Borzov, M. V., Churakov, A. V., Mkoyan, S. G. and Atovmyan, L. O., *Organometallics*, 1992, **11,** 3942; (b) Ciruelos, S., Cuenca, T., Flores, J. C., Gómez, R., Gómez-Sal, P. and Royo, P., *Organometallics*, 1993, **12,** 944; (c) Cuenca, T., Flores, J. C., Gómez, R., Gómez-Sal, P., Parra-Hake, M. and Royo, P., *Inorg. Chem.*, 1993, **32,** 3608; (d) Gómez-Sal, P., de Jesús, E., Pérez, A. I. and Royo, P., *Organometallics*, 1993, **12,** 4633; (e) Ciruelo, G., Cuenca, T., Gómez-Sal, P., Martín, A. and Royo, P., *J. Chem. Soc., Dalton Trans.*, 1995, **231**; (f) Cuenca, T., Padilla, A., Royo, P., Parra-Hake, M., Pellinghelli, M. A. and Tiripicchio, A., *Organometallics*, 1995, **14,** 848; (g) Amor, F., Gómez-Sal, P., de Jesús, E., Martín, A., Pérez, A. I., Royo, P. and Vázquez de Miguel, A., *Organometallics*, 1996, **15,** 2103; (h) Mieling, I., Ph. D. Dissertation, Univ. Bielefeld, 1993.
7. (a) Siemeling, U. and Jutzi, P., *Chem. Ber.*, 1992, **125,** 31; (b) Bergerat, P., Blümel, J., Fritz, M., Hiermeier, J., Hudeczek, P., Kahn, O. and Köhler, F. H., *Angew. Chem. Int. Ed. Engl.*, 1992, **31,** 1258; (c) Fritz, M., Hiermeier, J., Hertkorn, N., Köhler, F. H., Müller, G., Reber, G. and Steigelmann, O., *Chem. Ber.*, 1991, **124,** 1531.
8. (a) Cano, A., Cuenca, T., Gómez-Sal, P., Royo, B. and Royo, P., *Organometallics*, 1994, **13,** 1688; (b) Amor, F., Gómez-Sal, P., de Jesús, E., Royo, P. and Vázquez de Miguel, A., *Organometallics*, 1994, **13,** 4322; (c) Galakhov, M. H., Gil, A., de Jesús, E. and Royo, P., *Organometallics*, 1995, **14,** 3746; (d) Amor, F., de Jesús, E., Pérez, A. I., Royo, P. and Vázquez de Miguel, A., *Organometallics*, 1996, **15,** 365; (e) Amor, F., de Jesús, E., Royo, P. and Vázquez de Miguel, A., *Inorg. Chem.*, 1996, **35,** 3440; (f) Calvo, M., Galakhov, M. V., Gómez-García, R., Gómez-Sal, P., Martín, A., Royo, P. and Vázquez de Miguel, A., *J. Organomet. Chem.*, 1997, **548,** 157.
9. Hiermeier, J., Köhler, F. H. and Müller, G., *Organometallics*, 1991, **10,** 1787.
10. (a) Lang, H., Blau, S., Muth, A., Weiss, K. and Neugebauer, U., *J. Organomet. Chem.*, 1995, **490,** C32; (b) Gómez-García, R. and Royo, P., unpublished results.
11. Corey, J. Y., Huhmann, J. L. and Rath, N. P., *Inorg. Chem.*, 1995, **34,** 3203.
12. Sheldrick, G. M., *Acta Crystallogr. Sect. A*, 1990, **46,** 467.
13. Sheldrick, G. M., SHELXL 93; University of Göttingen, Göttingen, Germany, 1993.

Pergamon

PII: S0277-5387(97)00495-6

Polyhedron Vol. 17, No. 7, pp. 1091–1102, 1998
© 1998 Elsevier Science Ltd
All rights reserved. Printed in Great Britain
0277-5387/98 S19.00+0.00

Synthesis and spectroscopic characterisation of binuclear molybdenum–rhenium complexes

Michael G. B. Drew,[a] Vitor Félix,[b,c] Isabel S. Gonçalves,[b,c] Fritz E. Kühn,[d] André D. Lopes[b] and Carlos C. Romão[b]*

[a] Department of Chemistry, University of Reading, Whiteknights, Reading, RG6 6AD, U.K.

[b] Instituto de Tecnologia Química e Biológica, Quinta do Marquês, EAN, Apartado 127, 2780 Oeiras, Portugal

[c] Departamento de Química, Universidade de Aveiro, Campus de Santiago, 3800 Aveiro

[d] Anorganisch-chemisches Institut der Technischen Universität München, Lichtenbergstraße 4, D-85747 Garching bei München, Germany

(Received 8 October 1997; accepted 10 November 1997)

Abstract—Protonation of $CpMo(\eta^3\text{-}C_3H_5)(CO)_2$ followed by reactions with several diazole ligands produce the molybdenum half-sandwich complexes $[CpMo(CO)_2L_2]^+$ (L_2 = Bisimidazole (H_2Biim), pyrazole $(Hpz)_2$, Cpz_4, and $[Bpz_4]^-$) in good yields. Deprotonation of $[CpMo(CO)_2(H_2Biim)]^+$ gives the anionic complex $[CpMo(CO)_2(Biim)]^-$.

The structure of $[CpMo(CO)_2(H_2Biim)][ReO_4]$ was determined by X-ray single crystal analysis. The coordination geometry around the molybdenum atom in the complex cation $[CpMo(CO)_2(H_2Biim)]^+$ can be described as a distorted square pyramid. The basal plane is defined by two nitrogen atoms of H_2Biim bidentate ligand and two carbon atoms of carbonyl groups. The apical position is occupied by five carbon atoms of the $\eta^5\text{-}C_5H_5$ ligand. The Mo centre lies at 0.94(1) Å from the basal plane in the apical direction.

$[CpMo(CO)_2(Biim)]^-$ reacts with $ClReO_3$ or $MeReO_3$ (MTO) to give binuclear complexes of the formula $[\{CpMo(CO)_2\}(\mu\text{-}Biim)\{Re(X)O_3\}]Na$ (X = Cl, CH_3) in quantitative yields. $[CpMo(CO)_2(\mu\text{-}Cpz_4)][BF_4]$ reacts with $ClReO_3$ to yield $[\{CpMo(CO)_2\}(\mu\text{-}Cpz_4)\{Re(Cl)O_3\}][BF_4]$. The corresponding adduct $[\{CpMo(CO)_2\}(\mu\text{-}Cpz_4)\{Re(Cl)O_3\}][BF_4]$ can not be obtained in a pure form. The reaction of $[Bpz_4]^-$ with $ClReO_3$ yields the known Bpz_4ReO_3, with $MeReO_3$ the sensitive $[Bpz_4\{Re(CH_3)O_3\}]K$ is obtained. Deprotonation of the molybdenocene complex $[Cp_2Mo(H_2Biim)]^{2+}$ leads to the neutral compound $Cp_2Mo(Biim)$. The latter compound can be reacted with CH_3ReO_3 or $ClReO_3$ to form $[\{Cp_2Mo\}(\mu\text{-}Biim)\{Re(X)O_3\}]$ (X = CH_3, Cl). A ^{95}Mo NMR investigation shows the influence of the overall charge of the complex and the electron donor capability on the Mo centre. It is shown by ^{95}Mo, ^{17}O, ^1H NMR, and IR spectroscopy that the donor capability of the molybdenocene to the rhenium(VII) centre in the binuclear complexes is not very pronounced and can be compared to the strength of organic nitrogen donor complexes, e.g. 2,2′-bipyridyl. In donor solvents temperature dependent, rapid dynamic exchange processes can be observed. © 1998 Elsevier Science Ltd. All rights reserved

Keywords: Re(VII) oxides; Mo/Re binuclear complexes; bisimidazole and polypyrazolyl ligands.

The interaction of metal centres through ligand bridges is a very important aspect of coordination chemistry which is present in many ligand substitution and electron transfer mechanisms and is widely used by nature in metalloenzymes [1a]. The elaborate design and assembling of appropriate interacting centres has produced novel molecular magnets [1b] and the search for cooperative effects in catalysis has led to an extensive study of early-late heterobimetallic complexes [2,3]. On the other hand, interactions between bridged metals in high and low oxidation states has been scarcely studied. Since its own discovery of the multigram synthesis of CH_3ReO_3,

* Author to whom correspondence should be addressed.

trivially nicknamed MTO [4], Herrmann *et al.* have intensively explored the chemistry of Re(VII) oxides and produced a variety of organic and inorganic $XReO_3$ complexes. These form adducts of the general formula $XReO_3 \cdot L_n$ ($n = 1, 2$), mainly with *N* donor ligands which modulate the electronic and reactivity characteristics of the oxo ligands [5]. In this respect, organometallic ligands can play an important role inasmuch as their electronic properties may be further tuned by the manipulation of variables absent in organic ligands, e.g. net charge, metal oxidation state and metal spin.

Following these ideas, the present work describes the synthesis and characterization of binuclear adducts formed between high-oxidation state $XReO_3$ complexes and organometallic ligands bearing bridges with *N* donors like bisimidazole (H_2Biim), pyrazole (Hpz), tetrapyrazolyborate [Bpz_4^-] and tetrapyrazolylmethane (Cpz_4). Molybdenocene, Mo(IV), and $[CpMo(CO)_2]^+$, Mo(II), derivatives were chosen for their high thermodynamic and kinetic stability. $ClReO_3$ was used because if forms more stable complexes with electron donors than most organorhenium(VII) oxides [5]. Being the most stable organorhenium(VII) derivative known to date and by far the most thoroughly examined Re(VII) complex, MTO provides a probe to evaluate the bonding characteristics of these organometallic ligands [4,5].

RESULTS AND DISCUSSION

Synthesis and characterization of the organometallic ligands

The molybdenum based organometallic ligands used in this work are of two types. Type I ligands comprise a variety of half-sandwich complexes, derived from $CpMo(\eta^3\text{-}C_3H_5)(CO)_2$ (**1**) of the general formula $[CpMo(CO)_2L_2]^+$ (L_2 = bisimidazole (H_2Biim) (**2**), pyrazole $(Hpz)_2$ (**3**), Cpz_4 (**4**) and $[Bpz_4]^-$ (**5**)) (**I**) whereas type II ligands are confined to the molybdenocene derivative $Cp_2Mo(Biim)$ (**7**), derived from $[Cp_2Mo(H_2Biim)]^{2+}$ (**6**).

Table 1 summarizes ^{95}Mo data, selected ^1H shifts and selected IR vibrations for these molecules and their adducts with $XReO_3$ compounds. Type I molecules are prepared as depicted in Scheme 1, following the method first used by Cutler *et al.* [6] and later by Romão *et al.* [3c–g,i] to prepare a wide range of cyclopentadienyl and indenyl cations of the general formula $[(\eta^5\text{-}Cp')M(CO)_2L_2]BF_4$ (L = N, P, S, and O ligands) [3a,b].

The starting complex **1** [3c,d] is protonated with $HBF_4 \cdot OEt_2$ in CH_2Cl_2 at room temperature and the resulting red solution treated with the diazole ligand L to give the products **2**–**4** in yields of ca 80–90%. The crystal structure of the $[ReO_4]^-$ salt of $\mathbf{2}^+$ (**2a**) is described below. In the case of the $[Bpz_4]^-$ ligand it was not possible to isolate the known complex ligand $[CpMo(CO)_2(k^2\text{-}Bpz_4)]$ [7] and the binuclear species $[\{CpMo(CO)_2\}_2(\mu\text{-}Bpz_4)][BF_4]$ (**5**) was formed instead. The ^1H-NMR spectrum of this complex shows only one singlet for the Cp groups and six singlets belonging to pyrazol-protons of $[Bpz_4]^-$. The ^{95}Mo-NMR shows one signal at 108 ppm. Two ν(CO) IR vibrations can be observed. In keeping with these data we propose the structure of **5** as depicted below with both equivalent Cp rings and Mo atoms.

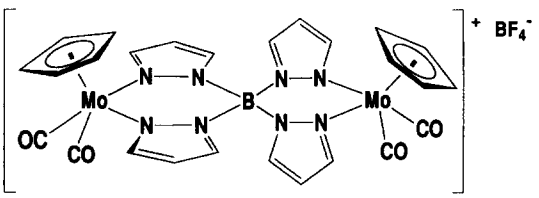

5

In order to prepare the organometallic ligand with the bisimidazole bridge the cation **2** was deprotonated by reaction with excess NaH in THF. The resulting anionic complex $[CpMo(CO)_2(Biim)]Na$ (**8**) was isolated in good yield. It is a very hygroscopic and air sensitive species freely soluble in Et_2O, THF and CH_2Cl_2. The similar deprotonation of the bispyrazole cation **3** was attempted but the expected anionic complex $[CpMo(CO)_2(pz)_2]^-$ could not be isolated pure. The alternative preparation from [CpMo-

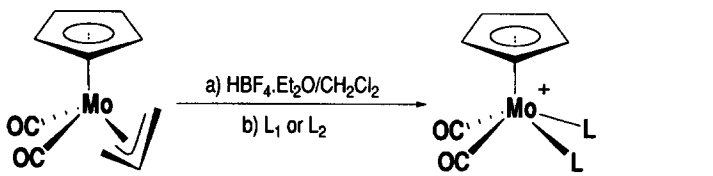

1 L_1 or L_2 = H_2Biim (**2**), H pz (**3**), Cpz_4 (**4**)

Scheme. 1.

Table 1. Selected IR [ν(C≡O), cm^{-1}], ^1H, and ^{95}Mo NMR data [ppm].

Compound		δ (^1H) Cp	ν(C≡O)	δ (^{95}Mo)
$[CpMo(CO)_2(H_2Biim)][BF_4]$	**2**	5.63	1965, 1875	−119
$[CpMo(CO)_2(Hpz)_2][BF_4]$	**3**	5.77	1979, 1875	−45
$[CpMo(CO)_2(Cpz_4)][BF_4]$	**4**	6.00	1979, 1890	+150
$[\{CpMo(CO)_2\}_2(\mu\text{-}Bpz_4)][BF_4]$	**5**	5.70	1964, 1873	+108
$[CpMo(CO)_2(Biim)]Na$	**8**	5.65	1954, 1871	−239
$[\{CpMo(CO)_2\}(\mu\text{-}Biim)\{Re(CH_3)O_3\}]Na$	**10**	5.40	1958, 1863	−212
$[\{CpMo(CO)_2\}(\mu\text{-}Biim)\{Re(Cl)O_3\}]Na$	**11**	5.62	1962, 1965	−208
$[\{CpMo(CO)_2\}(\mu\text{-}Cpz_4)\{Re(Cl)O_3\}][BF_4]$	**12**	6.01	1979, 1894	+151
$[Cp_2Mo(H_2Biim)][BF_4]_2$	**6**	5.83	—	−175
$Cp_2Mo(Biim)$	**7**	5.50	—	−390
$[\{Cp_2Mo\}(\mu\text{-}Biim)\{Re(CH_3)O_3\}]$	**16**	5.61	—	−48
$[\{Cp_2Mo\}(\mu\text{-}Biim)\{Re(Cl)O_3\}]$	**17**	5.65	—	−40

All the ^{95}Mo spectra were recorded in NCMe at room temperature, the spectra of **16, 17** in nitromethane.

$(CO)_2(NCCH_3)_2]^+$ and Kpz gave similarly disappointing results.

The spectroscopic data in Table 1 allows for some comparisons between the properties of the organometallic ligands **4** and **8** to be made assuming that they correlate with the electronic richness of the metal in these structurally very similar species. In agreement with the expected trend, **8** which bears the more electron rich anionic ligand has the lower values of ν(CO). This general trend is paralleled by the values of the chemical shifts of the Cp rings in the ^1H-NMR spectra where **8** presents the more shielded resonance at $\delta(^1H) = 5.65$ ppm. However, these criteria do not seem very sensitive to the variations which occur upon coordination of the free *N* donor atoms. The comparison of the ν(CO) and δ Cp (^1H-NMR) resonances between **2** and **8** is illustrative of the small differences found suggesting that most of the electron density gained upon deprotonation of **2** remains on the bisimidazole ring of **8** while the electron density of the other ligands (Cp and CO) is not influenced significantly. This point will be again found upon coordination of **4** and **8** to $XReO_3$ complexes (see below). A much more sensitive measure of the differences felt in the environment of the Mo atom of all these complexes is given by the ^{95}Mo-NMR chemical shifts which, however, are not so straightforward to interpret [8]. Indeed, the comparison of the ^{95}Mo-NMR chemical shift of the precursor compound $CpMo(\eta^3\text{-}C_3H_5)(CO)_2$ ($\delta(^{95}Mo) = -1625/-1804$ ppm (endo/exo isomer)) [3i], with those of **2–5** and **8** reveals the vast dissimilarity of bonding environments at the molybdenum in both types of compounds with the same formal oxidation state and built upon the same fragment $[CpMo(CO)_2]^+$. However, the similar chemical and structural environments of the Mo in complexes **2–5** and **8** allows for some conclusions to be drawn. The chemical shift of compounds **2–5** and **8** differs significantly and should reflect the donor capability of the ligand L, a better donor producing a more shielded resonance. Accordingly, the capability of electron donation to the Mo centre measured by the value of the ^{95}Mo NMR chemical shifts decreases in the order $(Biim)^{2-}$ (**8**) > H_2Biim (**2**) > $(Hpz)_2$ (**3**) > Cpz_4 (**4**). The Cpz_4 ligand is the weakest donor of the series, leading to a difference of ca 390 ppm between the ^{95}Mo NMR chemical shifts of **4** and **8**. This order of decreasing donation to the central Mo parallels that predicted on the basis on the respective ν(CO) frequencies $(Biim)^{2-} > H_2Biim > (Hpz)_2 > Cpz_4$ and is very similar to the one based on the values of δ Cp (^1H-NMR) chemical shifts $H_2Biim \geqslant (Biim)^{2-} > (Hpz)_2 > Cpz_4$.

The first attempted synthesis of the metallocene ligand (type II) introduced the novel preparation of Cp_2MoI_2 (**9**) from $[Cp_2Mo(CO)I][BF_4]$ and $(n\text{Bu})_4NI$ in CH_2Cl_2. The reaction of **9** with $TlBF_4$ and H_2Biim leads to the known $[Cp_2Mo(H_2Biim)][BF_4]_2$ (**6**) [9]. However, this complex is best prepared from $[Cp_2Mo(NCCH_3)_2][BF_4]_2$ and H_2Biim in boiling *N*-methylformamide/aceton. Complex **6** can be deprotonated with an excess of NaH to form the new organometallic ligand $Cp_2Mo(Biim)$ (**7**). This very reactive complex which was fully characterized, displays a ^{95}Mo-NMR signal at −390 ppm which is an upfield shift of 215 ppm relative to **6**. This shift is due to the higher electron density of the neutral molecule and is almost twice the one observed in the closely related transformation of **2** to **8**.

Molecular and crystal structure of $[CpMo(CO)_2(H_2Biim)][ReO_4]$ (**2a**)

The structure of the complex (**2a**) which was unexpectedly obtained from very slow decomposition of

[{CpMo(CO)$_2$}(μ-Biim){Re(CH$_3$)O$_3$}]Na (**10**) was established by X-ray single crystal diffraction analysis. The asymmetric unit is composed by one discrete [CpMo(CO)$_2$(H$_2$Biim)]$^+$ cation and one discrete [ReO$_4$]$^-$ anion. Figure 1 shows the X-ray single crystal structure of [CpMo(CO)$_2$(H$_2$Biim)][ReO$_4$] with the labelling scheme adopted.

The complex cation and complex anion are close to each other leading to intermolecular interactions N—H···O between one oxygen of the anion with both uncoordinated nitrogen atoms of H$_2$Biim ligand [N(24)—H(24)···O(1) 2.119 Å, 145.2° and N(27)—H(27)···O(1) 2.188 Å, 139.2°]. In the crystal structure these donor atoms still establish hydrogen bonds with two other oxygen atoms of the anion. [N(24)—H(24)···O(3) 2.458 Å, 126.6° ($-x+1$, $-y$, $-z$) and N(27)—H(27)···O(4) 2.211 Å, 131.6° ($-x+1$, $-y+1$, $-z$)].

Table 2 lists selected bond lengths and angles for the complex cation. The coordination geometry around the molybdenum centre can be described as a distorted square pyramid. Two nitrogen atoms of the bisimidazole ligand, and two carbons from carbonyl groups define the basal plane. The η^5-C$_5$H$_5$ ring occupies the apical position. The Mo atom lies at 0.94(1) Å from the least square plane, through N(21), N(30), C(41) and C(51), in the apical direction. The vector Mo–Cp (Cp = centroid of the Cp ring) is perpendicular to the plane of the Cp ring; the dihedral angle between them is 90.1°. The subtended angles at the Mo centre range from 72.8(6)° to 126.3(9)°. Similar geometric arrangements, with comparable structural parameters, have been found for other derivatives of the type [CpMo(CO)$_2$LL'] [10]. The Mo—C—O angles of 175(3)° and 179(2)° show that the carbonyl ligands are bonded linearly to molybdenum centre. The average bond lengths Mo—N 2.19(2) Å and Mo—C 1.94(2) Å fall in the expected range of 2.118–2.239 Å and of 1.906–1.986 Å for Mo—C for Mo—N bond lengths, respectively. These ranges were obtained with structural data available from Crystallographic Cambridge Data Base for com-

Table 2. Selected bond lengths (Å) and angles (°) for [CpMo(CO)$_2$(H$_2$Biim)]$^+$

Mo—Cp	1.981
Mo—C(41)	1.92(2)
Mo—C(51)	1.97(3)
Mo—N(30)	2.171(19)
Mo—N(21)	2.208(15)
C(41)—Mo—Cp	118.1
C(51)—Mo—Cp	120.1
N(30)—Mo—Cp	114.7
N(21)—Mo—Cp	115.7
C(41)—Mo—C(51)	76.4(11)
C(41)—Mo—N(30)	83.4(10)
C(51)—Mo—N(30)	124.9(10)
C(41)—Mo—N(21)	126.3(9)
C(51)—Mo—N(21)	79.2(8)
N(30)—Mo—N(21)	72.8(6)
O(42)—C(41)—Mo	175(3)
O(52)—C(51)—Mo	179(2)

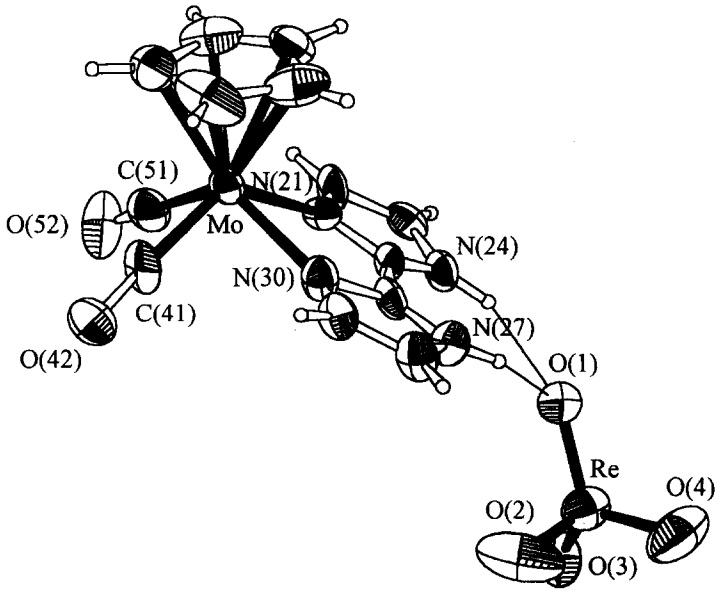

Fig. 1. Single crystal X-ray structure of [CpMo(CO)$_2$(H$_2$Biim)][ReO$_4$] (**2a**). Thermal ellipsoids are drawn at the 30% probability level.

pounds related with the complex cation under study [11].

Synthesis and characterization of the binuclear complexes with $XReO_3$

Reaction of the complexes **4** and **8** with CH_3ReO_3 and $ClReO_3$, respectively, leads to immediate formation of the complexes $[\{CpMo(CO)_2\}(\mu\text{-Biim})\{Re(CH_3)O_3\}]Na$ (**10**), $[\{CpMo(CO)_2\}(\mu\text{-Biim})\{Re(Cl)O_3\}]Na$ (**11**), and $[\{CpMo(CO)_2\}(\mu\text{-Cpz}_4)\{Re(Cl)O_3\}][BF_4]$ (**12**) according to Schemes 2 and 3. $ClReO_3$ was prepared *in situ* from $ClSiMe_3$ and Re_2O_7 for these reactions as reported before [5b].

A clean compound of composition $[\{CpMo(CO)_2\}(\mu\text{-Cpz}_4)\{Re(CH_3)O_3\}][BF_4]$ (**13**), however, could not be obtained. Several by products were formed which we were not able to remove in appropriate manner. The analogous reaction between $KBpz_4$ and $ClReO_3$ yielded neither the adduct $[Re(Cl)O_3(k^2\text{-Bpz}_4)]K$ nor the dimer $[\{Re(Cl)O_3\}_2(\mu\text{-Bpz}_4)]$ but the already known $(k^3\text{-Bpz}_4)(ReO_3)$ (**14**) [12] and KCl (Scheme 4). Obviously, the Cl—Re bond is weak enough to be split to form the neutral Re complex and the salt KCl. Reaction of $KBpz_4$ with CH_3ReO_3 leads to a very sensitive, yellow complex of formula $[Bpz_4(CH_3)ReO_3]K$ (**15**).

IR spectrum of this compound at room temperature show ligand fragments, $KReO_4$ and ReO_3. The formation of $KReO_4$ can also be observed by ^{17}O-NMR. If the reaction is performed at $-45°C$ the product is more stable. A proton NMR of compound **15** displays the signal for the Re—CH_3 group at $\delta(^1H) = 1.83$ ppm in acetone, compared to free MTO at 2.63 ppm in the same solvent. This shift difference clearly indicates the formation of a donor adduct of MTO with the $[Bpz_4]^-$ anion. However, even with excess of MTO

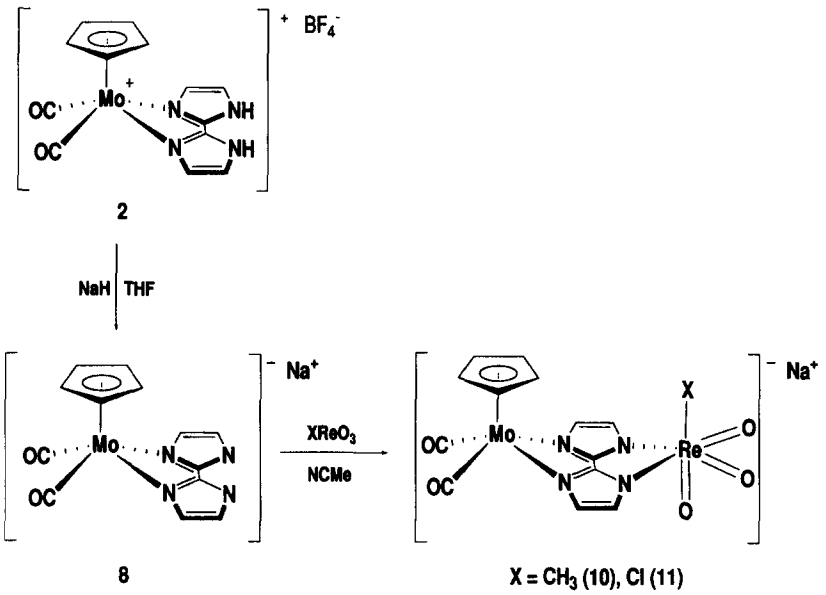

Scheme. 2.

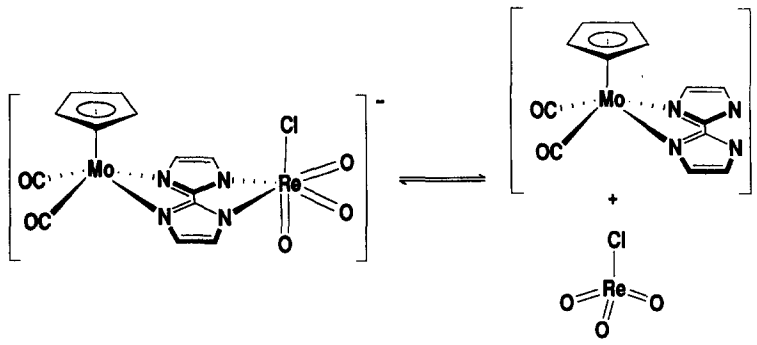

Scheme. 3.

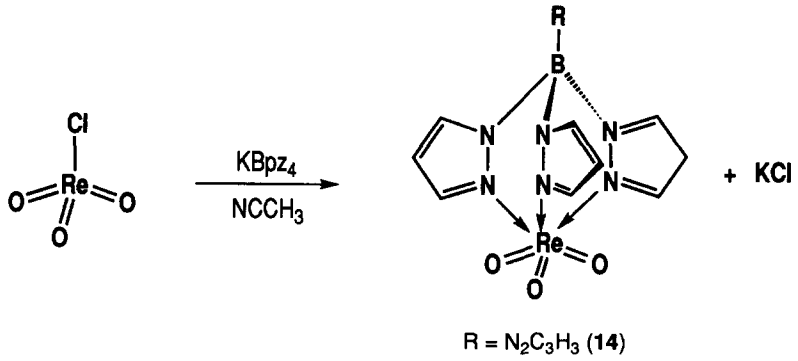

R = $N_2C_3H_3$ (**14**)

Scheme. 4.

a complex of the composition [{$Re(CH_3)O_3$}(μ-Bpz_4)]K could not be obtained. Complex **15** changed its colour during slow warming up to room temperature from yellow to black, yielding the same decomposition products as mentioned above.

The stability of all these adducts in solution is relatively limited and thwarted all attempts of growing crystals suitable for X-ray crystallography. The crystals of **2a** were obtained during the prolonged attempted crystallization of **10** from CH_2Cl_2/Et_2O. Decomposition of **10** by adventitious water, eventually induced by light, is the most plausible explanation for the observed transformation. In fact, it is well known that MTO decomposes to $[ReO_4]^-$ and CH_4 upon reaction with OH^- [4]. The rather basic character of **8** and the easy dissociation of **10** in solution (discussed below) create the conditions for this decomposition pathway. A similar process is certainly operative in the decomposition of the adducts with $ClReO_3$ all of which are very moisture sensitive decomposing with formation of $[ReO_4]^-$(IR evidence). It is known that the adduct $ClReO_3 \cdot$ bipy [5b], although originally reported as air stable, decomposes in air to the also colourless $[Hbipy]^+[ReO_4]^-$ like ('Bubipy)$Re(CH_3)O_3$ [5].

The original ^{95}Mo-NMR signal of **8** is shifted ca 25 ppm downfield after the addition of $(CH_3)ReO_3$ to form **10**. The original ^{95}Mo-NMR signal of **4** is also influenced by the addition of $(CH_3)ReO_3$ and $ClReO_3$, respectively: in both cases a downfield shift of ca 20 ppm is observed, indicating the electron withdrawing influence of the Re(VII) fragment. In keeping with the previously mentioned lack of sensitivity of the ν(CO) and δ Cp (^{1}H-NMR) chemical shifts these values remain almost constant for **10–12**. ^{17}O-NMR experiments performed in CD_3CN indicate a relatively weak Re–N interaction because the chemical shift of the Re bound oxo groups is only insignificantly different from that of free CH_3ReO_3 ($\delta(^{17}O) = 824$ ppm) and $ClReO_3$ ($\delta(^{17}O) = 825$ ppm) in the same solvent at room temperature and above. Despite the octahedral coordination of the Re centre in **10–12** only one ^{17}O-NMR signal can be observed at room temperature and above. In an octahedrally coordinated complex one would expect two oxygen signals in a 1:2 ratio due to the chemically different oxo groups in apical and equatorial positions. However, this result is not unexpected as it is known that in donor solvents, e.g. CH_3CN and THF, rapid solvent/ligand exchange takes place at the Re(VII) centre at room temperature leading only to one "mediated" signal [13]. In the case of **10–12** cooling down the solution leads only to a significant broadening, but not to separation into two signals. The explanation for such an exchange process is based on Scheme 3. In our experience with related complexes this broadening is not mainly caused by the natural line broadening of the ^{17}O-core during cooling but by the slowing down of the exchange processes. It is not possible, however, to separate the signals into two distinct peaks with the temperature range available in the solvents CD_3CN and THF. This indicates a relatively weak Re–N interaction in the examined complexes **10–12**. From the ν(ReO) vibrations the force constants of the Re=O vibrations were calculated (see Table 3) according to Ref. [14]. The results show that the Re=O force constants in the the solid state (IR measurements were performed in KBr) are of an equal order of magnitude to those in complexes of $ClReO_3$ and CH_3ReO_3 with organic donor ligands, e.g. 2,2′-bipyridyl [5b]. It is known that these complexes also undergo exchange equilibria with donor solvents in solution [13]. Unfortunately, such good strong donors are the only solvents capable of dissolving such ionic adducts and limit the scope of our studies. Therefore the study of neutral adducts formed from neutral organometallic ligands and $XReO_3$ complexes was considered as a possibility of avoiding such problems. It should be noted in this context that it has been tried before to link CH_3ReO_3 with other organo transition metal complexes with bipyrimidine (bpm) to generate neutral products. However, this approach did not lead to stable products. Only CH_3ReO_3(bpm) could be isolated [5i].

Reaction of **7** with CH_3ReO_3 leads to [{Cp_2Mo}(μ-Biim){$Re(CH_3)O_3$}] (**16**) which is well soluble in ace-

Table 3. Force constants F(ReO) and symmetric and asymmetric stretching vibrations ν(Re=O) of selected Re(VII)O_3 complexes

Compound		F(ReO) [mdyn/Å]	ν(Re=O) [cm^{-1}]
[{CpMo(CO)$_2$}(μ-Biim){Re(CH_3)O_3}]Na	**10**	7.48	949, 920
[{CpMo(CO)$_2$}(μ-Biim){Re(Cl)O_3}]Na	**11**	7.38	935, 918
[{CpMo(CO)$_2$}(μ-Cpz$_4$){Re(Cl)O_3}][BF_4]	**12**	7.38	935, 918
[(Bpz$_4$){Re(CH_3)O_3}]K	**15**	7.39	934, 920
[{Cp_2Mo}(μ-Biim){Re(CH_3)O_3}]	**16**	7.55	953, 924
[{Cp_2Mo}(μ-Biim){Re(Cl)O_3}]	**17**	7.35	931, 918
$ClReO_3$ · (bipy)[a]		7.40	946, 912
Ch_3ReO_3 · (bipy)[a]		7.29	934, 908

[a] see Ref. [5b].

tone (Scheme 5). The ^{1}H-NMR signal of the CH_3-Re group appears at 1.39 ppm which is more than 1.2 ppm low field shifted relative to free CH_3ReO_3 (δ(^{1}H) = 2.63 ppm) [5]. Shifts of this magnitude are usually caused by strong Lewis bases fixed to the Re(VII) centre. The ^{95}Mo signal of **16** is observed at −48 ppm representing a much higher shift than the one observed between the neutral and the protonated form of the ligand, **7** and **6** respectively. This good agreement between the ^{1}H and ^{95}Mo-NMR data point to the strongly electron withdrawing nature of the Re(VII) fragment which obviously leads to considerable deshielding of the Mo(IV) core. The ^{17}O-NMR spectrum in nitromethane as a solvent shows one signal at 828 ppm. This is only a minor shift difference to free CH_3ReO_3 (δ(^{17}O) = 818 ppm in nitromethane) but clearly shows a shift change caused by the reaction of the Re(VII)trioxo moiety with an electron donor. A similar shift is observed upon coordination of MTO to methoxyanilins [13a]. The chemical shift of the cyclopentadienyl ligands also reflects the lower electron density around the Mo core in **16** relative to **7**. In the cationic complex **6** the Cp groups show up at δ (^{1}H) = 5.83 ppm. Removal of two protons leads to a shift of the Cp signal of about 0.3 ppm to higher field. Addition of the electron withdrawing CH_3ReO_3 causes a downfield shift of ca 0.1 ppm. The data obtained for the adduct [{Cp_2Mo}(μ-Biim){Re(Cl)O_3}] (**17**) closely resemble the data of compound **16**. However, following the general trend already noted above, **17** is less stable and decomposes relatively quickly in air and is also less soluble in most solvents preventing the obtention of ^{17}O-NMR data of sufficient quality.

EXPERIMENTAL

All preparations and manipulations were done with standard Schlenk techniques under an oxygen-free and water-free argon atmosphere. Solvents were dried by standard procedure THF, Et_2O, pentane, and hexane over Na/benzophenone ketyl; acetonitrile and dichloromethane were distilled after refluxing several hours over P_2O_5. Acetone was distilled over K_2CO_3 and kept over 4 Å molecular sieves. Microanalyses were performed at the TUM (Garching) and at the ITQB (Oeiras). ^{1}H NMR spectra were obtained with a Bruker CXP 300 spectrometer. Infrared spectra were recorded on a Unican Mattson Mod 7000 FTIR spectrophotometer using KBr pellets and/or in solution. ^{17}O-NMR and ^{95}Mo-NMR spectra were measured at 54.14 MHz on a JEOL JNM and a GX-400 BRUKER ADVANCED DPX-400. ^{17}O labelled Re_2O_7 and CH_3ReO_3 were prepared according to the literature [13a,15]. CpMo(η^3-C_3H_5)(CO)$_2$ [3], [Cp_2Mo(CO)I][BF_4] [3i], KBpz$_4$ [16], H_2Biim [9], Cpz$_4$ [17], were prepared as described previously.

Preparation of [CpMo(CO)$_2$(H_2Biim)][BF_4] (**2**)

A solution of CpMo(η^3-C_3H_5)(CO)$_2$ (0.50 g, 1.94 mmol) in CH_2Cl_2 (15 ml) was treated with HBF_4 · Et_2O (1 equivalent). After 10 min, H_2Biim was added (0.33 g, 2.50 mmol) and the reaction left for 4 h at room temperature. The resulting orange solution was filtered, evaporated to dryness, extracted with acetone. After concentration to ca 5 ml and addition of ether, an orange microcrystalline product precipitated. The mother liquor was filtered off and the remaining precipitate was washed with ether and dried in an oil vacuum pump. Yield, 90%. Found: C, 35.76; H, 2.39; N, 12.63, Mo 22.28. Calc. for $C_{13}H_{11}BF_4N_4O_2Mo$: C, 35.65; H, 2.53; N, 12.79, Mo 21.90%. Selected IR (KBr, ν cm^{-1}): 3457 s, 3105 m, 1965 vs (C≡O), 1875 vs (C≡O), 1526 m, 1421 m, 1086 vs, 760 s. ^{1}H NMR ($NCCD_3$, 300 MHz, r.t., δ ppm): 7.52 (d, 2H, H_2Biim); 7.41 (d, 2H, H_2Biim); 5.63 (s, 5H, Cp).

X-ray analysis of [CpMo(CO)$_2$(H_2Biim)][ReO_4] (**2a**)

Crystal data [CpMo(CO)$_2$(H_2Biim)][ReO_4], $C_{13}H_{11}MoN_4O_6Re$, M = 601.40, triclinic a = 6.537

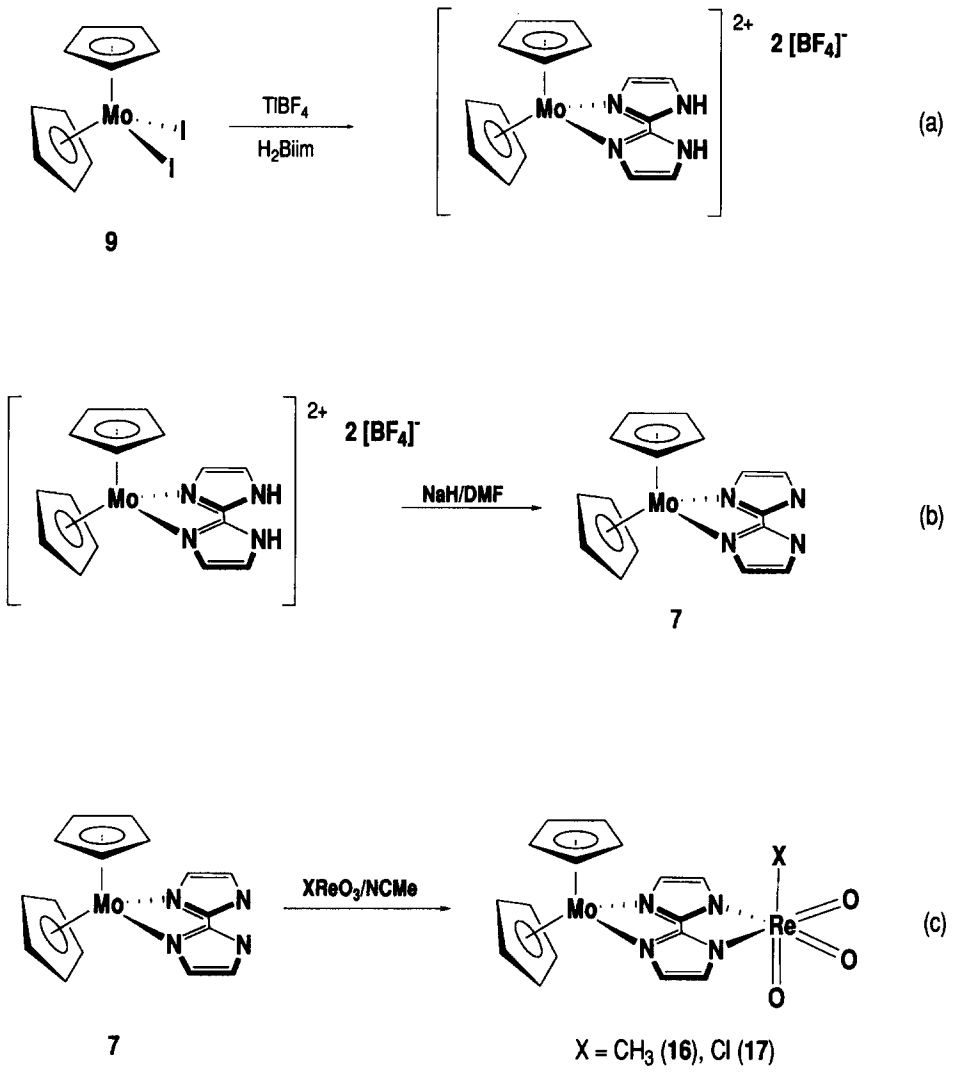

Scheme. 5.

(7), $b = 8.340(8)$, $c = 16.966(18)$ Å, $\alpha = 96.40(1)$, $\beta = 100.29(1)$, $\delta = 105.42(1)°$, $V = 865(2)$ Å, space group $P_{\bar{1}}$, $Z = 2$, $D_c = 2.309$ g cm^{-3}, $F(000) = 564$, $\mu = 7.753$ mm^{-1}.

X-ray data were collected with graphite monochromated Mo–K_α radiation (0.71073 Å) on a Mar-research image plate system in Reading University. The crystal was positioned at 75 mm from the plate. An exposure time of 2 min was used per 2° frame collected. Data analysis was carried out with XDS program [18].

The coordinates of the molybdenum and rhenium atoms were determined by direct methods, and the positions of the remaining non-hydrogen atoms were subsequently found by successive difference Fourier syntheses.

The structure refinement was carried out by full matrix least square method on F^2. Some cycles with isotropic temperature factors for all non hydrogen atoms gave R value of 0.2413 for all *hkl* data. At this point refinement an empirical absorption was applied to the data, using a version of DIFABS program [19], modified for Mar-research image plate system geometry. The R value then lowered to 0.2021. Anisotropic parameters were used for all non hydrogen atoms. Hydrogen atoms were included in the refinement in geometric positions giving thermal parameters equivalents to 1.2 times those of the atom to which they were attached. The final refinement of 227 parameters converged R values of 0.0907 for 1918 reflections with $I > 2\sigma(I)$ and 0.1235 for 2594 unique reflections and GOF of 1.180. A weighting scheme with the form $w = 1/[\sigma^2(F_o^2) + (0.1372P)^2 + 15.70P]$, and $P = [\max(F_o^2) + F_o^2]/3$ was used. In the last difference Fourier map the residual electronic density was in the range 3.048 to -5.501 e Å^{-3}. The highest

peak and deepest hole were both situated within 0.89 Å of the rhenium atom.

All calculations required to solve and to refine the structure were carried out with SHELXS and SHELXL within the SHELX97 package [20]. The molecular diagram was drawn with ORTEP II [21].

Additional material is available from the Cambridge Crystallographic Data Centre and comprises atomic co-ordinates, thermal parameters and all bond lengths and angles.

Preparation of $[CpMo(CO)_2(Hpz)_2][BF_4]$ **(3)**

A solution of $CpMo(\eta^3\text{-}C_3H_5)(CO)_2$ (0.50 g, 1.94 mmol) in CH_2Cl_2 (15 ml) was treated with $HBF_4 \cdot Et_2O$ (1 equivalent). After 10 min, pyrazole was added (0.29 g, 4.25 mmol) and the reaction left for 3 h at room temperature. After concentration to ca 5 ml and addition of ether, a violet product precipitated mixtd with a dark oil. Upon addition of pentane an oily residue separated which was solidified after repeated washings and scratching with pentane. Yield, 83%. Found: C, 35.42; H, 2.74; N, 13.05. Mo, 21.51. Calc. for $C_{13}H_{13}BF_4N_4O_2Mo$: C, 35.49; H, 2.98; N, 12.73 Mo, 21.80%. Selected IR (KBr, ν cm^{-1}): 3352 s, 3119 m, 1979 vs (C≡O), 1875 vs (C≡O), 1528 m, 1476 vs, 1406 m, 1355 m, 1084 vs, 1049 vs, 771 s, 606 m. ^1H NMR ($NCCD_3$, 300 MHz, r.t., δ ppm): 7.79 (s, 2H, Hpz); 7.47 (s, 2H, Hpz); 6.49 (s, 2H, Hpz); 5.77 (s, 5H, Cp).

Preparation of $[CpMo(CO)_2(Cpz_4)][BF_4]$ **(4)**

A solution of $CpMo(\eta^3\text{-}C_3H_5)(CO)_2$ (0.50 g, 1.94 mmol) in CH_2Cl_2 (20 ml) was treated with $HBF_4 \cdot Et_2O$ (1 equivalent). After 10 min, Cpz_4 was added (0.54 g, 1.93 mmol) and the reaction left for 6 h at room temperature. The resulting solution was filtered and taken to dryness. The residue was washed with ether (10 ml). Further recrystallization from CH_2Cl_2/Et_2O gave the violet compound in 91%. Found: C, 41.93; H, 3.36; N, 19.01. Calc. for $C_{20}H_{17}F_4N_8O_2Mo$: C, 41.12; H, 2.93; N, 19.18%. Selected IR (KBr, ν cm^{-1}): 3130 m, 1979 vs (C≡O), 1890, vs (C≡O), 1410 s, 1321 s, 1051 vs, 1029 vs, 874 s, 762 s, 602 m. ^1H NMR ($NCCD_3$, 300 MHz, r.t., δ ppm): 8.97 (s, Cpz_4); 8.68 (s, Cpz_4); 8.38 (s, Cpz_4); 8.29 (s, Cpz_4); 7.45 (s, Cpz_4); 6.78 (s, Cpz_4); 6.00 (s, Cp).

Preparation of $[\{CpMo(CO)_2\}_2(\mu\text{-}Bpz_4)][BF_4]$ **(5)**

A solution of $CpMo(\eta^3\text{-}C_3H_5)(CO)_2$ (0.50 g, 1.94 mmol) in CH_2Cl_2 (20 ml) was treated with $HBF_4 \cdot Et_2O$ (1 equivalent). After 10 min, $KBpz_4$ was added (0.61 g, 1.94 mmol) and the reaction left for 2 h at room temperature. The resulting solution was filtered and taken to dryness. The residue was washed with ether (10 ml). Further recrystallization from CH_2Cl_2/Et_2O gave the compound in 96% yield. Found: C, 39.34; H, 2.70; N, 13.63; Mo, 24.27. Calc. for $C_{26}H_{22}B_2F_4N_8O_4Mo_2$: C, 39.04; H, 2.77; N, 14.01; Mo, 23.98%. Selected IR (KBr, ν cm^{-1}): 3117 m, 1964 vs (C≡O), 1873; vs (C≡O), 1389 s, 1292 s, 1070 vs, 826 s, 762 s. ^1H NMR ($NCCD_3$, 300 MHz, r.t., δ ppm): 8.14 (s, 2H, Bpz_4); 7.87 (s, 2H, Bpz_4); 7.79 (s, 2H, Bpz_4); 6.81 (s, 2H, Bpz_4); 6.73 (s, 2H, Bpz_4); 6.39 (s, 2H, Bpz_4); 5.70 (s, 10H, Cp).

Preparation of $[Cp_2Mo(H_2Biim)][BF_4]_2$ **(6)**

Method (a). A solution of $[Cp_2Mo(NCCH_3)_2][BF_4]_2$ (1.20 g, 2.50 mmol) in acetone/*N*-methylformamide (NMF), (20/10 ml) was treated with H_2Biim (0.33 g, 2.50 mmol) and refluxed for 12 h. The resulting orange solution was concentrated and a mixture of pentane/ether was added until precipitation of the orange product occurred. The complex obtained was washed with Et_2O and dried in vacuum. Yield 90%.

Method (b). A mixture of solid Cp_2MoI_2 (1.00 g, 2.08 mmol), H_2Biim (0.28 g, 2.08 mmol) and $TlBF_4$ (1.21 g, 4.16 mmol) was weighed in a Schlenk tube. Acetone and *N*-methylformamide (NMF) was added and refluxed for 12 h. The resulting orange solution was filtered, taken to the dryness, washed with Et_2O and dried in vacuum. Yield 87%. EA and IR (KBr) data are in agreement with Ref. [9].

Preparation of $Cp_2Mo(Biim)$ **(7)**

A solution of $[Cp_2Mo(H_2Biim)(CO)_2][BF_4]_2$ (0.50 g; 0.93 mmol) in DMF (15 ml) was treated with an excess NaH (2.50 mmol) for 2 h with vigorous stirring. The resulting yellow-orange solution was filtered and evaporated to dryness. The product was recrystallized from CH_2Cl_2/Et_2O. Yield, 85%. Found: C, 53.38; H, 3.81; N, 15.43. Calc. for $C_{16}H_{14}N_4Mo$: C, 53.64; H, 3.94; N, 15.64%. IR (KBr, ν cm^{-1}): 3107 m, 1383 vs, 1195 s, 1138 s, 1096 vs, 995 m, 841 s, 741 s, 708 m; ^1H NMR (CD_3NO_2, 400 MHz, r.t., δ ppm): 7.41 (s, 2H, Biim); 6.70 (s, 2H, Biim); 5.50 (s, 10H, Cp).

Preparation of $[CpMo(CO)_2(Biim)]Na$ **(8)**

A suspension of $[CpMo(H_2Biim)(CO)_2][BF_4]$ (0.50 g; 1.14 mmol) in THF (20 ml) was treated with excess NaH for 1 h with vigorous stirring. The resulting orange solution was filtered and evaporated to dryness. The residue was extracted with dichloromethane and taken to dryness to give a powder in 79% yield. Found: C, 41.97; H, 2.59; N, 14.82; Mo, 25.79. Calc. for $C_{13}H_9N_4NaO_2Mo$: C, 41.96; H, 2.44; N, 15.05; Mo, 25.78%. Selected IR (KBr, ν cm^{-1}): 3113 m, 1954 vs (C≡O), 1871 vs (C≡O), 1406 s, 1134 m, 812 m, 756 m, 542 m. ^1H NMR ($Me_2CO\text{-}d_6$, 300 MHz, r.t., δ ppm): 7.42 (d, 2H, H_2Biim); 7.36 (d, 2H, H_2Biim); 5.65 (s, 5H, Cp).

Preparation of Cp_2MoI_2 (**9**)

A solution of $[Cp_2Mo(CO)I][BF_4]$ (1.0 g, 2.10 mmol) in dichloromethane (20 ml) was treated with excess of $(nBu)_4NI$ (0.92 g, 2.50 mmol). The solution was irradiated and refluxed for 8 h. A green precipitate formed slowly, and the solution became almost colorless. After being concentrated and cooled the precipitate was filtered, and washed CH_2Cl_2/Et_2O. Yield, 87%. EA, IR (KBr) and ^1H NMR data are in agreement with Ref. [22].

Preparation of $[\{CpMo(CO)_2\}(\mu\text{-Biim})\{Re(CH_3)O_3\}]Na$ (**10**)

A solution of $MeReO_3$ (0.23 g; 0.91 mmol) in NCMe (5 ml), was added to a solution of 0.91 mmol of the deprotonated ligand $[CpMo(CO)_2(Biim)]Na$. A violet solution formed after a few seconds. The reaction mixture was stirred for 15 min. After concentration to ca 5 ml and addition of ether, a microcrystalline product precipitated. The mother liquor was filtered off and the remaining precipitate was washed with Et_2O/pentane and dried in vacuum. Yield 85%. Found: C, 26.86; H, 2.19; N, 8.87, Re, 30.10. Calc. for $C_{14}H_{11}N_4NaO_5MoRe$: C, 27.06; H, 1.95; N, 9.02, Re 29.97%. Selected IR (KBr, ν cm^{-1}): 3115 m, 1958 vs (C≡O), 1863, vs (C≡O), 1599 m, 1404 s, 1011 m, 959 s, 949 s (sym (Re=O)), 920 vs (asym (Re=O)), 815 m, 754 s, 538 m. ^1H NMR (CD_2Cl_2, 300 MHz, r.t., δ ppm): 7.19 (s, 2H, Biim); 7.09 (s, 2H, Biim); 5.40 (s, 5H, Cp); 1.83 (s, 3H, Me).

Preparation of $[\{CpMo(CO)_2\}(\mu\text{-Biim})\{Re(Cl)O_3\}]Na$ (**11**)

A solution of Re_2O_7 (0.20 g, 0.41 mmol) in NCMe (5 ml), was treated with 0.82 mmol of Me_3SiCl. After 5 min, 0.82 mmol of the ligand $[CpMo(CO)_2(Biim)]Na$ was added to the solution. A pale yellow-brown solution formed after a few seconds. The reaction mixture was stirred for 15 min. After concentration and addition of ether, an orange microcrystalline product precipitated. The mother liquor was filtered off and the remaining precipitate was washed with Et_2O/pentane and dried under oil pump vacuum. Yield 82%. Found: C, 24.55; H, 1.50; N, 8.29, Re, 28.70. Calc. for $C_{13}H_9ClN_4NaO_5MoRe$: C, 24.33; H, 1.41; N, 8.73, Re, 29.01%. Selected IR (KBr, ν cm^{-1}): 3117 m, 1962 vs (C≡O), 1865, vs (C≡O), 1516 m, 1408 s, 935 s (sym (Re=O)), 918 vs (asym (Re=O)), 908 s, 820 m, 758 s, 540 m. ^1H NMR ($NCCD_3$, 300 MHz, r.t., δ ppm): 7.50 (d, 2H, Biim); 7.39 (d, 2H, Biim); 5.62 (s, 5H, Cp).

Preparation of $[\{CpMo(CO)_2\}(\mu\text{-}Cpz_4)\{Re(Cl)O_3\}][BF_4]$ (**12**)

A solution of Re_2O_7 (0.15 g, 0.31 mmol) in THF (5 ml), was treated with 0.62 mmol of Me_3SiCl. After 5 min, 0.62 mmol of the ligand $[CpMo(CO)_2(Cpz_4)][BF_4]$ was added to the solution. A violet solution formed after a few seconds. The reaction mixture was stirred for 15 min. After concentration and addition of ether, a violet product precipitated. The mother liquor was filtered off and the remaining precipitate was washed with Et_2O/pentane and dried under oil pump vacuum. Recrystallization from $NCMe/Et_2O$ gave the compound in 81% yield. Found: C, 27.71; H, 2.20; N, 12.84. Calc. for $C_{20}H_{17}BClF_4N_8O_5MoRe$: C, 28.14; H, 2.01; N, 13.12%. Selected IR (KBr, ν cm^{-1}): 3123 m, 1979 vs (C≡O), 1894 vs (C≡O), 1408 s, 1321 s, 1087 s, 1049 s, 935 s (sym (Re=O)), 918 vs (asym (Re=O)), 908 vs, 876 s, 764 s, 598 m. ^1H NMR ($NCCD_3$, 300 MHz, r.t., δ ppm): 8.99 (s, Cpz_4); 8.68 (s, Cpz_4); 8.38 (s, Cpz_4); 8.28 (s, Cpz_4); 7.47 (s, Cpz_4) 6.78 (s, Cpz_4); 6.01 (s, Cp).

Attempted preparation of $[\{CpMo(CO)_2\}(\mu\text{-}Cpz_4)\{Re(CH_3)O_3\}][BF_4]$ (**13**)

A solution of CH_3ReO_3 (0.15 g, 0.62 mmol) in THF (5 ml), was treated with 0.62 mmol of the ligand $[CpMo(CO)_2(Cpz_4)][BF_4]$. A brownish-yellow solution formed after a few seconds. The reaction mixture was stirred for 15 min. After concentration and addition of ether, a brown product precipitated. The mother liquor was filtered off and the remaining precipitate was washed with Et_2O/pentane and dried under oil pump vacuum. However, the product turned out to be impure and despite several attempts it was not possible to remove the impurities satisfactorily. The impurities could be observed in both the NMR and the IR spectra and prevented a proper characterization of this complex.

Preparation of Bpz_4ReO_3 (**14**)

A solution of Re_2O_7 (0.20 g, 0.41 mmol) in NCMe (5 ml), was treated with 0.82 mmol of Me_3SiCl. After 5 min, 0.82 mmol of the $KBpz_4$ was added to the solution. A pale yellow solution formed after a few seconds. The reaction mixture was stirred for 15 min and then taken to dryness. The residue was extracted with dichloromethane (20 ml) taken to dryness and dried in oil pump vacuum. Yield, 86%. EA, IR (KBr) and ^1H NMR data are in agreement with Ref. [12].

Preparation of $Bpz_4(CH_3)ReO_3$ (**15**)

A cooled solution of CH_3ReO_3 (0.10 g, 0.42 mmol) in NCMe (5 ml, −45°C), was treated with 0.42 mmol of $KBpz_4$. A pale yellow solution formed after a few seconds. The reaction mixture was stirred for 15 min and then taken to dryness. The residue was extracted with cold dichloromethane (20 ml), again taken to dryness and dried in oil pump vacuum at −20°C.

Yield, 56%. Found: C, 27.39; H, 2.35; N, 19.40. Calc. for $C_{13}H_{15}BN_8O_3Re$: C, 27.57; H, 2.66; N, 19.75%; IR (KBr, ν cm^{-1}): 3148 m, 1661 m, 1505 m, 1416 m, 1391 s, 1290 s, 1217 m, 1190 m, 1098 vs, 1051 s, 920 m (Re=O), 855 m, 822 s, 779 m, 752 m, 581 m, 625 m; ^{1}H NMR (Me_2CO-d_6, 400 MHz, r.t., δ ppm): 7.48 (s, 4H, pz), 7.18 (s, 4H, pz), 6.07 (s, 4H, pz), 1.83 (s, 3H, Re-CH_3).

Preparation of [{Cp_2Mo}(μ-Biim){$Re(CH_3)O_3$}] (**16**)

A solution of $MeReO_3$ (0.30 g, 1.20 mmol) in NCMe (15 ml), was treated with 1.20 mmol of the ligand Cp_2Mo(Biim). An orange precipitate formed after a few seconds. The reaction mixture was stirred for 15 min. After addition of ether (5 ml), all the microcrystalline product precipitated. It was filtered and washed with Et_2O/pentane and dried in vacuum. Yield 96%. Found: C, 33.38; H, 2.74; N, 9.23. Calc. for $C_{17}H_{17}N_4O_3MoRe$: C, 33.61; H, 2.82; N, 9.22%. Selected IR (KBr, ν cm^{-1}): 3113 m, 2287 s, 1576 m, 1393 s, 1132 s, 953 s, (sym (Re=O)), 924 vs (asym (Re=O)), 841 m, 748 s, 698 m. ^{1}H NMR (Me_2CO-d_6, 300 MHz, r.t., δ ppm): 7.46 (s, 2H, Biim); 6.86 (s, 2H, Biim); 5.61 (s, 10H, Cp); 1.39 (s, 3H, Me).

Preparation of [{Cp_2Mo}(μ-Biim){$Re(Cl)O_3$}] (**17**)

A solution of Re_2O_7 (0.60 g, 1.24 mmol) in NCMe (5 ml), was treated with 2.48 mmol of Me_3SiCl. After 5 min 1.20 mmol of the ligand Cp_2Mo(Biim) were added to the solution. An orange precipitate formed after a few seconds. The reaction mixture was stirred for 15 min. After addition of ether (5 ml), all the microcrystalline product precipitated. It was filtered and washed with Et_2O/pentane and dried in vacuum. Yield 91%. Found: C, 30.85; H, 2.35; N, 9.03. Calc. for $C_{16}H_{14}N_4ClO_3MoRe$: C, 30.61; H, 2.25; N, 8.92%. Selected IR (KBr, ν cm^{-1}): 3103 m, 2855 s, 1543 m, 1422 s, 1140 s, 931 s, (sym (Re=O)), 918 vs (asym (Re=O)), 870 m, 744 s, 623 m. ^{1}H NMR (Me_2CO-d_6, 300 MHz, r.t., δ ppm): 7.32 (s, 2H, Biim); 6.94 (s, 2H, Biim); 5.65 (s, 10H, Cp).

CONCLUSIONS

Organomolybdenum ligands of the type [CpMo-$(CO)_2L_2$] are easily prepared and coordinate Re(VII) trioxo complexes to yield binuclear Mo/Re systems with bridging pyrazolyl type ligands. The Re—N bond in these complexes is relatively weak when compared to certain Lewis base adducts of organohenium oxides or rheniumoxo halides with related heterocyclic ligands. In donor solvents these complexes undergo rapid exchange reactions of the $XReO_3$ fragment with the solvent. This exchange can be avoided by use of neutral ligands which, like Cp_2Mo(Biim), give adducts soluble in apolar, non-coordinating solvents. In these cases a strong Re–N interaction can be preserved, for exchange equilibria in solution play only a minor role. In general, the results obtained with the neutral Mo/Re complexes show relevant spectroscopic changes in both metal fragments which result from the combination of molecules in a high and in a low oxidation state. This has given further impetus to the synthesis of appropriate ligands of this type and the study of their adducts with group VI and VII oxides which is currently being undertaken in our laboratories.

Supplementary material—Full tables of bond distances and bond angles, a table of the general displacement parameter expressions and a listing of structure factors are available from author C.C.R. upon request.

Acknowledgement—This work was partially supported by PRAXIS XXI, Projects (2/2.1/QUI/316/94 and 2./2.1/QUI/419/94). The authors want to thank the DAAD (Acções Integradas programme), the BMFT/JNICT Protokoll and Prof. W. A. Herrmann (TU München) for generous support. I.S.G (BPD) and A.D.L (BD) thank PRAXIS XXI for grants, F.E.K. thanks the Alexander von Humboldt-foundation for a fellowship.

REFERENCES

1. (a) Lippard, S. J. and Berg, J. M., *Principles of Bioinorganic Chemistry*. University Science books, Mill Valley, California, 1994; (b) Kahn, O., *Molecular Magnetism*. Verlag Chemie, Weinheim, 1993.
2. Stephan, D. W., *Coord. Chem. Rev.*, 1989, **95,** 41.
3. (a) Ascenso, J. R., Gonçalves, I. S., Herdtweck, E. and Romão, C. C., *J. Organomet. Chem.*, 1996, **508,** 169; (b) Calhorda, M. J., Gamelas, C. A., Gonçalves, I. S., Herdtweck, E. and Romão, C. C., L. Veiros, in press, 1997; (c) Ascenso, J. R., De Azevedo, C. G., Gonçalves, I. S., Herdtweck, E., Moreno, D. S., Pessanha, M. and Romão, C. C., *Organometallics.*, 1995, **14,** 3901; (d) Ascenso, J. R., Azevedo, C. G., Gonçalves, I. S., Herdtweck, E., Moreno, D. S., Romão, C. C. and Zühlke, J., *Organometallics*, 1994, **13,** 429; (e) Gonçalves, I. S. and Romão, C. C., *J. Organomet. Chem.*, 1995, **48,** 155; (f) Almeida, J. M., Gonçalves, I. S. and Romão, C. C., *Anales de Química Int. Ed.*, 1997, **93,** 8; (g) de Azevedo, C. G., Calhorda, M. J., de C. T. Carrondo, M. A. A. F., Dias, A. R., Duarte, M. T., Galvão, A. M., Gamelas, C. A., Gonçalves, I. S., da Piedade, F. M. and Romão, C. C., *J. Organomet. Chem.*, in press, 1997; (h) Félix, V., Calhorda, M. J., Drew, M. G. B., Gonçalves, I. S. and Romão, C. C., in press, 1997; (i) Gonçalves, *PhD Dissertation*, Technical University of Lisbon, 1996.
4. Recent reviews: (a) Herrmann, W. A. and Kühn, F. E., *Acc. Chem. Res.*, 1997, **130,** 169; (b) Romão, C. C., Kühn, F. E. and Herrmann, W. A., *Chem. Rev.*, 1997, **97,** 3197; (c) Herrmann, W. A., *J. Organomet. Chem.*, 1995, **500,** 149.
5. (a) Kühn, F. E., Haider, J. J., Herdtweck, E.,

Herrmann, W. A., Lopes, A. D., Pillinger, M. and Romão, C. C., *Inorg. Chim. Acta*, 1998, in press; (b) Herrmann, W. A., Kühn, F. E., Romão, C. C., Kleine, M. and Mink, J., *Chem. Ber.*, 1994, **127,** 47; (c) Herrmann, W. A., Kühn, F. E., Mattner, M. R., Artus, G. R. J., Geisberger, M. R. and Correia, J. D. G., *J. Organomet. Chem.*, 1997, **539,** 203; (d) Herrmann, W. A., Correia, J. D. G., Rauch, M. U., Artus, G. R. J., Kühn, F. E., *J. Mol. Catal.*, 1997, **118,** 33; (e) Herrmann, W. A., Kuchler, J. G., Weichselbaumer, G., Herdtweck, E. and Kiprof, P., *J. Organomet. Chem.*, 1989, **372,** 351; (f) Herrmann, W. A., Weichselbaumer, G. and Herdtweck, E., *J. Organomet. Chem.*, 1989, **372,** 371; (g) Herrmann, W. A., Kuchler, J. G., Kiprof, P. and Riede, J., *J. Organomet. Chem.*, 1990, **395,** 55; (i) Herrmann, W. A., Roesky, P. W., Alberto, R. and Artus, G. R. J., unpublished results.

6. Markham, J., Menard, K. and Cutlef, A., *Inorg. Chem.*, 1985, **24,** 1581.
7. (a) Calderon, J. L., Cotton, F. A. and Shaver, A., *J. Organomet. Chem.*, 1972, **37,** 127; (b) Holt, E. M. and Holt, S. L., *J. C. S. Dalton*, 1973, 1893.
8. (a) Le Gall, J. Y., Kubicki, M. M. and Petillon, F. Y., *J. Organomet. Chem.*, 1981, **221,** 287; (b) Masters, A. F., Brownlee, R. T. C., O'Connor, M. J. and Wedd, A. G., *Inorg. Chem.*, 1981, **20,** 4183; (c) Minelli, M., Enemark, J. H., Brownlee, R. T. C., O'Connor, M. J. and Wedd, A. G., *Coord. Chem. Rev.*, 1985, **86,** 169; (d) Grieves, R. A. and Mason, J., *Polyhedron*, 1986, **5,** 415; (e) Green, J. C., Grieves, R. A. and Mason, J., *J. Chem. Soc. Dalton Trans.*, 1986, 1313; (f) Faller, J. W. and Whitmore, B. C., *Organometallics*, 1986, **5,** 752; Mason, J., *Chem. Rev.*, 1987, **87,** 1299; (g) Alyea, E. C., Malito, J., Ernst, S. D., Kaim, W. and Kohlmann, S. J., *Polyhedron*, 1989, **8,** 921; (h) Nakatsuji, H. and Sugimoto, M., *Inorg. Chem.*, 1990, **29,** 1221.
9. Calhorda, M. J. and Dias, A. R., *J. Organomet. Chem.*, 1980, **197,** 291.
10. (a) Bernal, I., Laplaca, S. J., Korp, J., Brunner, H. and Herrmann, W. A., *Inorg. Chem.*, 1978, **17,** 382; (b) Creswik, M. W. and Bernal, I. *Inorg. Chim. Acta*, 1983, **74,** 241; (c) Bruner, H., Agrifoglio, G., Bernal, I. and Creswick, M. W., *Angew. Chem. Int. Ed. Engl.*, 1980, **19,** 641.
11. Allen, F. H., Davies, J. E., Galloy, J. J., Johnson, O., Kennard, O., Macrae, C. F. and Watson, D. G., *J. Chem. Inf. Comp. Sci.*, 1991, **31,** 204.
12. (a) Domingos, A., Marçalo, J., Paulo, A., de Matos, A. P. and Santos, I., *Inorg. Chem.*, 1993, **32,** 5114; (b) Paulo, A., Domingos, A., Marçalo, J., de Matos, A. P. and Santos, I., *Inorg. Chem.*, 1995, **34,** 2113; (c) Paulo, A., Domingos, A. and Santos, I., *Inorg. Chem.*, 1996, **35,** 1798.
13. (a) Herrmann, W. A., Kühn, F. E. and Roesky, P. W., *J. Organomet. Chem.*, 1995, **485,** 243; (b) Herrmann, W. A., Kühn, F. E., Rauch, M. U., Correia, J. D. G. and Artus, G. R. J., *Inorg. Chem.*, 1995, **24,** 2914; (c) Herrmann, W. A., Wojtczak, W. A., Artus, G. R. J., Kühn, F. E. and Mattner, M. R., *Inorg. Chem.*, 1997, **36,** 465.
14. (a) Mink, J., Keresztury, A., Stirling, A. and Herrmann, W. A., *Spectrochimica Acta*, 1994, **50A,** 2039, (b) Kühn, F. E., *Ph. D. Thesis*, Technische Universität München, 1994, pp. 194–204.
15. Herrmann, W. A., Kühn, F. E., Fischer, R. W., Thiel, W. R. and Romão, C. C., *Inorg. Chem.*, 1992, **31,** 4431.
16. Trofimenko, S., *J. Am. Chem. Soc.*, 1967, **89,** 3170.
17. (a) Trofimenko, S., *J. Am. Chem. Soc.*, 1970, **92,** 5118; (b) Juliá, S., del Mazo, J. M., Avila, L. and Elguero, J., *Org. Prep. Proc. Int.*, 1984, **16,** 299.
18. Kabsch, W., *J. Appl. Crystallogr.*, 1988, **21,** 916.
19. Walker, N. and Stuart, D., *DIFABS, Acta Cryst. Sect. A*, 1983, **39,** 158.
20. Sheldrick, G. M., *SHELX*-97, University of Göttingen, 1997.
21. Johnson, K., *ORTEP II*, A Fortram Thermal-ellipsoid, Plot Program for Crystal Structure Illustrations, Report ORNL-513, Oak Ridge National Laboratory, Oak Ridge, TN, 1976.
22. Nakamura, A. and Otsuka, S., *J. Am. Chem. Soc.*, 1972, **94,** 1886.

Pergamon

PII: S0277-5387(97)00498-1

Polyhedron Vol. 17, No. 7, pp. 1103–1114, 1998
© 1998 Elsevier Science Ltd
All rights reserved. Printed in Great Britain
0277-5387/98 $19.00+0.00

Trichlorogermyl complexes of molybdenum and tungsten bearing cyclopentadienyl ligands: Synthesis, structure and isomerization studies†

Alexander C. Filippou,* Johannes G. Winter, Michael Feist, Gabriele Kociok-Köhn and Isolde Hinz

Institut für Anorganische und Allgemeine Chemie, Humboldt-Universität zu Berlin, Hessische Strasse 1–2, D-10115 Berlin, Germany

(Received 17 October 1997; accepted 14 November 1997)

Abstract—Molybdenum and tungsten trichlorogermyl complexes of the type *cis*-(η^5-C_5R_5)M(CO)$_2$ (PMe_3)$GeCl_3$ (**2b–2d**) (**2b**: M = W; R = H; **2c**: M = Mo; R = Me; **2d**: M = W; R = Me) were obtained by the stereoselective insertion reaction of $GeCl_2$ into the metal-chlorine bond of *cis*-(η^5-C_5R_5)M(CO)$_2$(PMe_3)Cl (**1b–1d**). Simultaneous thermal analysis (TG-DTA) of **2b–2d** revealed an exothermic solid-state isomerization of **2b–2d** to *trans*-(η^5-C_5R_5)M(CO)$_2$(PMe_3)$GeCl_3$ (**3b–3d**) and the thermoanalytical results were used to prepare the *trans* isomers **3b–3d** in large scale. In comparison, the trichlorogermyl complex *cis*-CpW(CO)$_2$(CNEt)$GeCl_3$ (**5**) was found to undergo an endothermic isomerization in the melt to afford a mixture of **5** and *trans*-CpW(CO)$_2$(CNEt)$GeCl_3$ (**6**) in a 1 : 1.2 ratio. The complexes **2b–2d, 3b–3d** and **6** were fully characterized and the solid-state structures of the isomers **2d** and **3d** were determined by single-crystal X-ray diffraction analyses.
© 1998 Elsevier Science Ltd. All rights reserved

Keywords: germylene; insertion; isomerization; molybdenum; tungsten.

In recent years germylenes (germanediyls) were used as versatile precursors in the synthesis of new organogermanium compounds, like Ando's 1,2-digermacyclobutane [$CH_2Ge[CH(SiMe_3)_2]_2]_2$ [1], Egorov's germylene radical anion $Ge[CH(SiMe_3)_2]_2^-$ [2], Sekiguchi's cyclotrigermene $Ge_3(Si^tBu_3)_4$ [3] and cyclotrigermenium cation $[Ge_3(Si^tBu_3)_3]^+$ [4], Wiberg's tetrahedrotetragermane $Ge_4(Si^tBu_3)_4$ [5], and Power's transition-metal germylyne complex $Cp(CO)_2Mo{\equiv}GeC_6H_3$-2,6-$Mes_2$ [6]. In this context several new germylenes were prepared and their fascinating chemistry is currently in rapid progress [7]. One of the oldest known divalent germanium compounds is $GeCl_2$, which is not stable under normal conditions [8]. Stabilization of $GeCl_2$ is achieved upon complexation with cyclic ethers [9], nitrogen bases [10], phosphanes [11] and arsanes [12] to give $GeCl_2$(Do) adducts (Do = donor). Among these adducts the $GeCl_2$(1,4-dioxane) complex [9] has been used mostly as $GeCl_2$ source and has been shown to insert readily into σ-bonds [13,14]. Using this reactivity of $GeCl_2$(1,4-dioxane) we have prepared recently several Mo^{II} and W^{II} trichlorogermyl and dichlorogermyl complexes of the general formula (η^5-C_5R_5)M-(CO)$_{3-m}$(L)$_m$$GeCl_{3-n}H_n$ (R = H, Me; M = Mo, W; L = EtNC, PMe_3; m, n = 0, 1) starting from the corresponding M^{II} chloro and hydrido complexes [15]. Interestingly, the trimethylphosphine derivative *cis*-CpMo(CO)$_2$(PMe_3)$GeCl_3$ (**2a**) was found to isomerize in CH_2Cl_2 solution at room temperature to *trans*-CpMo(CO)$_2$(PMe_3)$GeCl_3$ (**3a**), whereas the ethylisocyanide derivative *cis*-CpW(CO)$_2$(EtNC)$GeCl_3$ (**5**) retained its configuration under the same conditions [15a]. *Cis-trans* isomerism of "four-legged piano-stool" complexes containing a cyclopentadienyl ligand [16] have been observed for various transition metals in solution under thermal or photochemical conditions [17]. In comparison, *cis-trans* isomerization reactions of "four-legged piano-stool" complexes occurring in the solid state are rare [18]. The observed *cis-trans* isomerization of **2a** to **3a** [15a]

† Dedicated to Prof. Dr. W. A. Herrmann on the occasion of his 50th birthday.

* Author to whom correspondence should be addressed.

prompted us to prepare the related trichlorogermyl complexes *cis*-(η^5-C_5R_5)M(CO)$_2$(PMe$_3$)GeCl$_3$ (**2b–2d**) (**2b**: M = W; R = H; **2c**: M = Mo; R = Me; **2d**: M = W; R = Me) and to study their structure and isomerization reactions to *trans*-(η^5-C_5R_5)M(CO)$_2$(PMe$_3$)GeCl$_3$ (**3b–3d**).

RESULTS AND DISCUSSION

Starting materials for the reactions described below were the Mo^{II} and W^{II} chloro complexes *cis*-(η^5-C_5R_5)M(CO)$_2$(PMe$_3$)Cl (**1b–1d**) (**1b**: M = W; R = H; **1c**: M = Mo; R = Me; **1d**: M = W; R = Me). Treatment of these compounds with one equivalent of GeCl$_2$(1,4-dioxane) in CH$_2$Cl$_2$ at −78°C, and subsequent warming of the reaction solutions to ambient temperature, resulted in a rapid and clean insertion of GeCl$_2$ into the metal-chlorine bond of **1b–1d** to give the trichlorogermyl complexes *cis*-(η^5-C_5R_5)M(CO)$_2$(PMe$_3$)GeCl$_3$ (**2b–2d**) (eqn (1)).

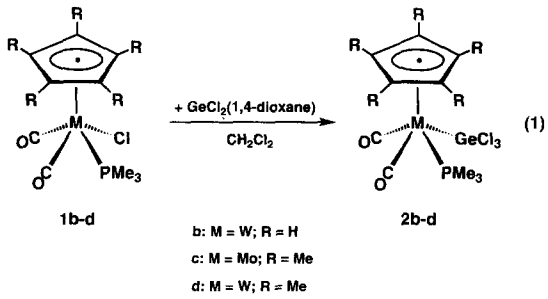

(1)

Evidence for the selective formation of **2b–2d** was given by the IR spectra of the reaction solutions, which showed that the two ν(CO) absorptions of the starting materials at 1949 and 1848 cm^{-1} (**1b**), 1944 and 1850 cm^{-1} (**1c**) and 1931 and 1837 cm^{-1} (**1d**) had been replaced at the end of the reactions by those of the products at 1967 and 1892 cm^{-1} (**2b**), 1961 and 1892 cm^{-1} (**2c**) and 1953 and 1878 cm^{-1} (**2d**), respectively. Working up of the reaction solutions afforded the trichlorogermyl complexes **2b–2d** as yellow, microcrystalline solids in high yields. The new complexes are soluble in CH$_2$Cl$_2$ and THF, but sparingly soluble in Et$_2$O and *n*-pentane and were fully characterized. Thus, the IR spectra of **2b–2d** show in the region of 2200–1500 cm^{-1} two ν(CO) absorption bands (Table 1).

The higher energy absorption of the symmetric ν(CO) vibration is more intense than the lower energy absorption of the antisymmetric ν(CO) vibration indicating the presence of the *cis*-isomer [15,19]. Both ν(CO) absorptions of **2b–2d** appear at higher wavenumbers than those of the chloro complexes **1b–1d** showing that insertion of GeCl$_2$ into the metal–chlorine bond reduces the electron density at the metal center and weakens thereby the metal ($d\pi$)—CO(π^*) back bonding (Table 1). Furthermore, the ν(CO) absorptions of the Cp derivatives **2a** [ν(CO) in CH$_2$Cl$_2$: 1976 and 1907 cm^{-1}] [15] and **2b** are observed at higher frequency than those of the Cp* derivatives **2c** and **2d**, respectively, indicating the weaker electron donating properties of the Cp ligand compared with the Cp* ligand (Cp* = C_5Me_5).

The ^{1}H, ^{31}P{^{1}H} and ^{13}C{^{1}H} NMR spectra also support the structures proposed for **1b–1d** and for **2b–2d** (Tables 2 and 3).

Thus, the ^{1}H NMR spectra of **1b–1d** and **2b–2d** display a doublet resonance for the methyl protons of the PMe$_3$ ligand and a singlet or doublet resonance for the Cp and Cp* ring protons (Table 2). The ^{13}C{^{1}H} NMR spectra of **1b–1d** and **2b–2d** display two resonances for the inequivalent carbonyl ligands, indicating in agreement with the IR spectra the pres-

Table 1. ν(C≡NEt) and ν(CO) absorptions of the complexes **1b–6** in cm^{-1}; solvent: CH$_2$Cl$_2$

Complex	ν(C≡NEt)	ν(CO)
cis-CpW(CO)$_2$(PMe$_3$)Cl (**1b**)	—	1949 vs, 1848 s
cis-Cp*Mo(CO)$_2$(PMe$_3$)Cl (**1c**)	—	1944 vs, 1850 s
cis-Cp*W(CO)$_2$(PMe$_3$)Cl (**1d**)	—	1931 vs, 1837 s
cis-CpW(CO)$_2$(PMe$_3$)GeCl$_3$ (**2b**)	—	1967 vs, 1892 s
cis-Cp*Mo(CO)$_2$(PMe$_3$)GeCl$_3$ (**2c**)	—	1961 vs, 1892 s
cis-Cp*W(CO)$_2$(PMe$_3$)GeCl$_3$ (**2d**)	—	1953 vs, 1878 s
trans-CpW(CO)$_2$(PMe$_3$)GeCl$_3$ (**3b**)	—	1955 m, 1877 vs
trans-Cp*Mo(CO)$_2$(PMe$_3$)GeCl$_3$ (**3c**)	—	1955 m, 1881 vs
trans-Cp*W(CO)$_2$(PMe$_3$)GeCl$_3$ (**3d**)	—	1943 m, 1866 vs
cis-CpW(CO)$_2$(CNEt)Cl	2172 s	1967 vs, 1888 s
cis-CpW(CO)$_2$(CNEt)GeCl$_3$ (**5**)	2166 m	1984 vs, 1916 s
cis/*trans*-CpW(CO)$_2$(CNEt)GeCl$_3$ (**5**/**6**)	2177 m[a]	1984 s[a], 1912 vs[a]

[a] The indicated ν(CNEt) and ν(CO) absorptions are those recorded for the mixture of the two isomers **5** and **6** in the ratio 1 : 1.2.

Table 2. ^{1}H NMR and ^{31}P{^{1}H} NMR data of the complexes **1b–3d, 5** and **6** in CD_2Cl_2 at 20°C; relative intensities and multiplicities of the signals in parentheses, coupling constants in Hz

Complex	$P(CH_3)_3$; CH_3CH_2NC	$C_5(CH_3)_5$	C_5H_5	δ_P
1b	1.65(9, d), ^2J(PH) = 9.8	—	5.55(5, s)	−20.3, ^1J(WP) = 256.4
1c	1.40(9, d), ^2J(PH) = 9.2	1.85(15, s)	—	5.5
1d	1.48(9, d), ^2J(PH) = 9.3	1.95(15, s)	—	−21.1, ^1J(WP) = 256.8
2b	1.83(9, d), ^2J(PH) = 9.8	—	5.54(5, d), ^3J(PH) = 0.6	−30.9, ^1J(WP) = 221.2
2c	1.64(9, d), ^2J(PH) = 9.1	2.01(15, s)	—	0.1
2d	1.75(9, d), ^2J(PH) = 9.3	2.13(15, s)	—	−32.2, ^1J(WP) = 231.9
3b	1.79(9, d), ^2J(PH) = 9.9	—	5.42(5, d), ^3J(PH) = 1.3	−17.3, ^1J(WP) = 214.1
3c	1.62(9, d), ^2J(PH) = 9.4	1.99(15, d), ^4J(PH) = 0.6	—	18.0
3d	1.72(9, d), ^2J(PH) = 9.6	2.11(15, d), ^4J(PH) = 0.5	—	−18.2, ^1J(WP) = 235.8
5	1.46(3, t), ^3J(HH) = 7.2[a] 4.03(2, q), ^3J(HH) = 7.2[a]	—	5.61(5, s)	—
6	1.46(3, t), ^3J(HH) = 7.2[a] 4.03(2, q), ^3J(HH) = 7.2[a]	—	5.51(5, s)	—

[a] The methyl and methylene protons of the isomers **5** and **6** have by accident the same chemical shifts.

Table 3. ^{13}C{^{1}H} NMR data of the complexes **1b–3d, 5** and **6** in CD_2Cl_2 at 20°C; signal multiplicities in parentheses, coupling constants in Hz

Complex	$C_5(CH_3)_5$	$P(CH_3)_3$; CH_3CH_2NC	C_5H_5	$C_5(CH_3)_5$	EtNC	CO
1b	—	17.2(d), ^1J(PC) = 34.3	92.8	—	—	238.9(d), ^2J(PC) = 9.1; 250.9(d), ^2J(PC) = 23.2
1c	10.9	15.8(d), ^1J(PC) = 28.5	—	106.4	—	248.0(d), ^2J(PC) = 7.7; 262.1(d), ^2J(PC) = 32.0
1d	11.1	15.8(d), ^1J(PC) = 33.0	—	104.6	—	241.6(d), ^2J(PC) = 10.9; 255.5(d), ^2J(PC) = 22.3
2b	—	22.6(d), ^1J(PC) = 35.9	90.7	—	—	226.7; 229.4(d), ^2J(PC) = 23.4
2c	11.1	20.7(d), ^1J(PC) = 30.3	—	105.7	—	239.2; 242.8(d), ^2J(PC) = 31.3
2d	11.3	21.2(d), ^1J(PC) = 34.2	—	104.1	—	229.8; 233.0(d), ^2J(PC) = 23.8
3b	—	21.0(d), ^1J(PC) = 37.4	90.5	—	—	223.1(d), ^2J(PC) = 21.7
3c	11.4	19.3(d), ^1J(PC) = 31.9	—	105.5	—	238.0(d), ^2J(PC) = 31.9
3d	11.5	19.4(d), ^1J(PC) = 36.5	—	104.0	—	231.0(d), ^2J(PC) = 25.2
5	—	14.9; 42.1	91.0	—	142.5	222.5; 224.5
6	—	15.5; 41.8	90.5	—	—[a]	218.6

[a] The isocyanide carbon resonance of **6** was not observed.

ence of the *cis* isomer (Table 3). The carbonyl resonances of the chloro complexes **1b–1d** appear as doublets due to ^{13}C–^{31}P coupling. In comparison, only the lower-field carbonyl resonance of the trichlorogermyl complexes **2b–2d** is split to a doublet, the ^{13}C–^{31}P coupling of the higher-field carbonyl–carbon resonance being too small to be resolved. The lower field carbonyl–carbon resonance of **1b–1d** and **2b–2d** with the large ^2J(PC) coupling constant is assigned to the CO ligand, which is disposed in *cis* position relative to the PMe_3 ligand [15]. Finally, the carbonyl resonances of the trichlorogermyl complexes **2b–2d** are found at higher field than those of the chloro complexes **1b–1d**. This is in full agreement with previous NMR studies on Group VI transition metal carbonyl complexes, which have shown that a weaker metal–carbonyl back bonding causes a shielding of the carbonyl–carbon nucleus [20].

The solid state structure of **2d** was determined by a single-crystal X-ray diffraction study. Suitable crystals were obtained after slow evaporation of a CH_2Cl_2 solution of **2d** at room temperature. A ZORTEP drawing of the molecular structure of **2d** with the atom-labeling scheme adopted is shown in Fig. 1. Selected bond lengths and angles of **2d** are listed in Table 4.

Complex **2d** has the expected square pyramidal coordination geometry of a "four-legged piano-stool" complex with a *cis* disposition of the trichlorogermyl and the trimethylphosphine ligand. The W—C(ring) bond lengths range from 228.6(5) to 238.6(5) pm and have an average value of 233.6 pm, which is close to

Table 4. Selected bond lengths (pm) and bond angles (°) with estimated standard deviations for **2d**

W—C(1)	228.6(5)	Ge—W—P	81.71(3)
W—C(2)	232.3(5)	Ge—W—C(9)	125.1(2)
W—C(3)	238.6(5)	Ge—W—C(10)	74.23(14)
W—C(4)	237.7(5)	P—W—C(9)	75.5(2)
W—C(5)	231.0(5)	P—W—C(10)	120.6(2)
W—C(9)	195.5(5)	C(9)—W—C(10)	75.9(2)
W—C(10)	195.4(6)	W—Ge—Cl(1)	122.97(5)
W—Ge	255.90(5)	W—Ge—Cl(2)	120.71(4)
W—P	251.33(12)	W—Ge—Cl(3)	114.14(4)
Ge—Cl(1)	220.8(2)	Cl(1)—Ge—Cl(2)	98.52(6)
Ge—Cl(2)	221.1(2)	Cl(2)—Ge—Cl(3)	98.35(6)
Ge—Cl(3)	219.92(14)	Cl(1)—Ge—Cl(3)	97.16(6)

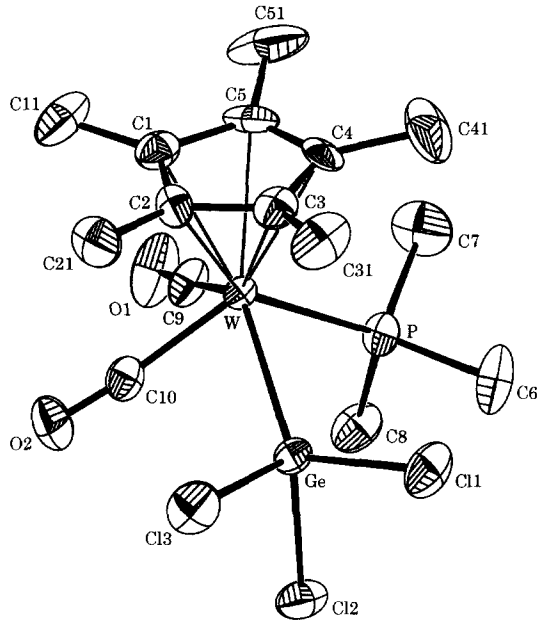

Fig. 1. ZORTEP plot of the molecular structure of **2d** with thermal ellipsoids drawn at the 50% probability level.

that of $Cp^*W(CO)_3GeCl_3$ [$(W—C_{ring})_{av.}$ = 232.6 pm] [15]. The tungsten–carbonyl groups are approximately linear, with the W—C—O bond angles being 174.8(5) and 174.9(5)°, respectively. The W—CO bonds of **2d** [$(W—CO)_{av.}$ = 195.4 pm] are shorter than those of $Cp^*W(CO)_3GeCl_3$ [$(W—CO)_{av.}$ = 199.5 pm] indicating in full agreement with the IR and NMR spectroscopic data a stronger $M(d\pi)—CO(\pi^*)$ back bonding in **2d** than in $Cp^*W(CO)_3GeCl_3$ [15a].

The major focus of interest is on the structural features of the trichlorogermyl ligand. The tetrahedral coordination of the germanium atom in **2d** is strongly distorted as shown by the Cl—Ge—Cl bond angles with an average value of 98.01° and the W—Ge—Cl bond angles with an average value of 119.27° (Table 4). Furthermore, a comparison of the compounds $GeCl_4$, $Cp^*W(CO)_3GeCl_3$, *cis*-$Cp^*W(CO)_2(EtNC)GeCl_3$ and *cis*-$Cp^*W(CO)_2(PMe_3)GeCl_3$ (**2d**) reveals a continous increase of the Ge—Cl bond lengths [$GeCl_4$: $(Ge—Cl)_{av.}$ = 211.3 pm; $Cp^*W(CO)_3GeCl_3$: $(Ge—Cl)_{av.}$ = 217.9 pm; *cis*-$Cp^*W(CO)_2(EtNC)GeCl_3$: $(Ge—Cl)_{av.}$ = 219.6 pm; **2d**: $(Ge—Cl)_{av.}$ = 220.6 pm] and a continuous decrease of the Cl—Ge—Cl bond angles [$GeCl_4$: (Cl—Ge—Cl) = 109.5°; $Cp^*W(CO)_3GeCl_3$: $(Cl—Ge—Cl)_{av.}$ = 100.2°; *cis*-$Cp^*W(CO)_2(EtNC)GeCl_3$: $(Cl—Ge—Cl)_{av.}$ = 99.1°; **2d**: $(Cl—Ge—Cl)_{av.}$ = 98.01°] as one chloro substituent in $GeCl_4$ is replaced by a more and more electropositive metal carbonyl fragment [15a,21]. These trends can be explained, if one suggests a stronger hyperconjugation between the metal carbonyl fragment and the trichlorogermyl ligand, as the electron density at the metal center is enhanced [22]. Alternatively, the observed trends can be explained using the atom rehybridization model of Bent [23]. Using this model one would also predict in the absence of any steric effects an elongation of the W—Ge bond in the series **2d** < *cis*-$Cp^*W(CO)_2(EtNC)GeCl_3$ < $Cp^*W(CO)_3GeCl_3$. In fact, the W—Ge bond of $Cp^*W(CO)_3GeCl_3$ [$(W—Ge)_{av.}$ = 256.2(2) pm] is longer than that of *cis*-$Cp^*W(CO)_2(EtNC)GeCl_3$ (W—Ge = 254.4(2) pm), but similar in length to that of **2d** [W—Ge = 255.90(5) pm]. This suggests an opposing steric to the electronic effect of the PMe_3 ligand on the W—Ge bond length of **2d**. Experimental evidence for an increased steric repulsion between the trimethylphosphane and the trichlorogermyl ligand in **2d** is given by the larger Ge—W—P angle of 81.71(3)° compared with the Ge—W—$C_{isonitrile}$ bond angle of *cis*-$Cp^*W(CO)_2(C-NEt)GeCl_3$ [75.2(4)°] and the Ge—W—$C_{CO(cis)}$ bond angles of $Cp^*W(CO)_3GeCl_3$ [$(Ge—W—C)_{av.}$ = 74.1°] [15a].

The tungsten complex **2b** isomerizes in CH_2Cl_2 solution at ambient temperature to the thermodynamically more stable isomer *trans*-$CpW(CO)_2(PMe_3)GeCl_3$ (**3b**) (eqn (2)).

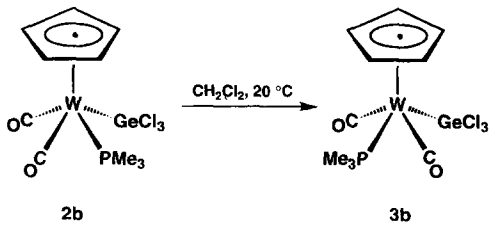

2b 3b (2)

This indicates that insertion of $GeCl_2$ into the W—Cl of **1b** to give **2b** is a stereoselective reaction. *cis-trans* isomerization of **2b** was monitored by IR and NMR spectroscopy to be complete after 2 days and to be slightly slower than that of the analogous molybdenum complex *cis*-$CpMo(CO)_2(PMe_3)GeCl_3$ (**2a**) [15a]. In comparison, the related Cp* derivatives *cis*-$Cp^*M(CO)_2(PMe_3)GeCl_3$ (**2c**: M = Mo; **2d**: M = W) were found to be stable with respect to isomerization under the same conditions. Thus, no evidence for the formation of the *trans* isomers could be found even after 15 days in CH_2Cl_2 solution at ambient temperature. However, complexes **2c** and **2d** undergo as **2b** a selective isomerization to *trans*-$Cp^*M(CO)_2(PMe_3)GeCl_3$ (**3c**: M = Mo; **3d**: M = W), when heated in the solid-state. This was shown by simultaneous thermal analysis (STA), the results of which are summarized in Table 5.

The STA curves (T, TG, DTG and DTA) of the tungsten complex **2d** are depicted in Fig. 2 and the DTA curves of **2b–3d** are shown in Fig. 3. When complex **2d** was heated two DTA effects were recorded, for which no considerable mass loss was observed (Fig. 2).

The first transition occurs at $T_e = 182°C$, is exothermic ($\Delta H_{iso} = -17$ kJ/mol) and corresponds to the solid-state isomerization of *cis*-$Cp^*W(CO)_2(PMe_3)GeCl_3$ (**2d**) to the thermodynamically more stable isomer *trans*-$Cp^*W(CO)_2(PMe_3)GeCl_3$ (**3d**). Evidence for this was given by a separate STA run, in which **2d** was heated under the same conditions to

Table 5. Thermal analysis data of **2b–3d** and **5** obtained from STA curves (T, TG, DTG, DTA), visual inspection and IR spectroscopic characterization after various thermal treatments from 20°C to T_{max} (heating rate: 5°C/min, purge gas: argon; for further details of the STA experiments see experimental section); used abbreviations: m.p.: melting, dec.: decomposition, iso.: *cis-trans* isomerization, ph.: phase transition

Complex	Run	Thermal effects I T/°C; ΔH/kJ·mol^{-1}	II T/°C; ΔH/kJ·mol^{-1}	III T/°C	T_{max} (°C)	Sample state	Complex configuration
cis-$CpW(CO)_2(PMe_3)GeCl_3$ (**2b**)	1	89(T_i); −12 (iso.)	246(T_e) +9 (m.p.)	333 (dec.)	340	Molten	—[a]
	2				270	Molten	*trans*
	3				120	Solid	*trans*
trans-$CpW(CO)_2(PMe_3)GeCl_3$ (**3b**)	1	204(T_e); +7 (ph.)	250(T_e); +6 (m.p.)	—	270	Molten	*trans*
	2				220	Solid	*trans*
cis-$Cp^*Mo(CO)_2(PMe_3)GeCl_3$ (**2c**)	1	199(T_p); −54 (iso.)	—	—	220	Solid	*trans*
trans-$Cp^*Mo(CO)_2(PMe_3)GeCl_3$ (**3c**)	1	237(T_e); +81 (dec.)	—	—	285	Molten	—[a]
cis-$Cp^*W(CO)_2(PMe_3)GeCl_3$ (**2d**)	1	182(T_e); −17 (iso.)	257(T_e); +18 (m.p.)	—	270	Molten	*trans*
	2				245	Solid	*trans*
trans-$Cp^*W(CO)_2(PMe_3)GeCl_3$ (**3d**)	1	256(T_e); +20 (m.p.)	—	—	270	Molten	*trans*
cis-$CpW(CO)_2(EtNC)GeCl_3$ (**5**)	1	96(T_e); +17 (m.p.)	123(T_i); +4 (iso.)	301 (dec.)	340	Molten	—[a]
	2				145	Molten	*cis/trans*
	3				115	Molten	*cis*

[a] Thermal decomposition of the complex was observed.

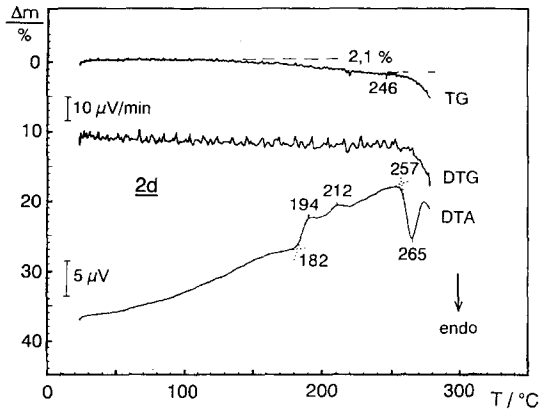

Fig. 2. STA curves (T, TG, DTG and DTA) of **2d**.

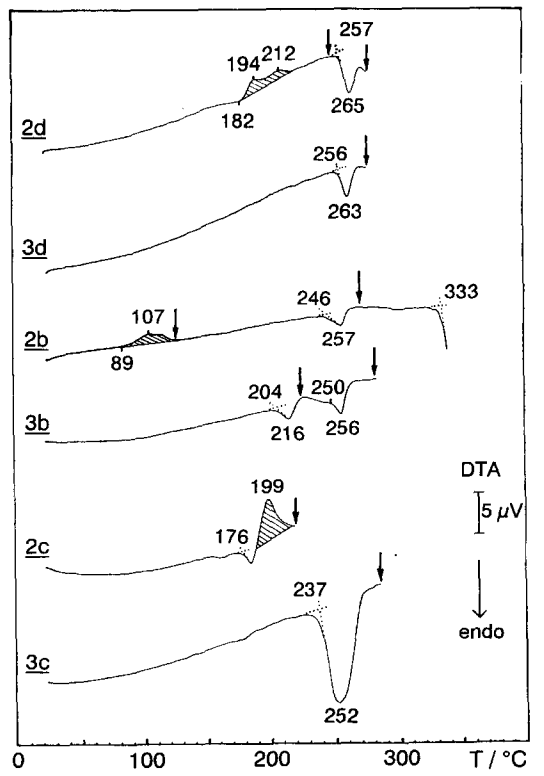

Fig. 3. DTA curves of the *cis* isomers **2b–2d** and the *trans* isomers **3b–3d**. The arrows indicate T_{max} of the separate STA runs carried out for sample characterization (Table 5, Experimental). Hatched areas were used for the calculation of the isomerization enthalpy.

245°C (Table 5). The resulting pale-yellow solid was identified by its characteristic ν(CO) absorptions in CH_2Cl_2 at 1943 (m) and 1866 (vs) cm^{-1} to be the *trans* isomer **3d** (Table 1). The exothermic isomerization of **2d** to **3d** is followed by an endothermic transition, which occurs at $T_e = 257$°C (Fig. 2) and corresponds to the melting of the *trans* isomer **3d** with almost the same enthalpy of fusion ($\Delta H_f = 18$ kJ/mol) as that determined separately for the *trans* isomer **3d** ($\Delta H_f = 20$ kJ/mol) (Fig. 3, Table 5).

Similarly, the molybdenum complex **2c** was found to undergo an exothermic solid-state *cis-trans* isomerization to **3c** at $T_p = 199$°C ($\Delta H = -54$ kJ/mol) (Fig. 3, Table 5). After heating to 220°C (T_{max}) the sample was allowed to cool to room temperature and the obtained pale-yellow solid was identified by its characteristic ν(CO) absorptions in CH_2Cl_2 at 1955 (m) and 1881 (vs) cm^{-1} to be the *trans* isomer **3c** (Tables 1 and 5). The solid-state isomerization of **2c** shows a small endothermal pre-effect at $T_e = 176$°C that was not studied any further (Fig. 3). In a separate run the *trans*-isomer **3c** was observed to melt at $T_e = 237$°C (Fig. 3, Table 5). Melting of **3c** was accompanied by a considerable mass loss of 8.3% indicating the concomitant decomposition of **3c**.

Finally, the STA of the cyclopentadienyl derivative **2b** shows three processes (Fig. 3, Table 5). The first transition at $T_i = 89$°C is exothermic ($\Delta H = -12$ kJ/mol), is not accompanied by a mass loss and corresponds to the solid-state isomerization of **2b** to the *trans* isomer **3b**. This was verified by a separate STA experiment, in which complex **2b** was heated under the same conditions to $T_{max} = 120$°C and the resulting pale-yellow solid was identified by IR spectroscopy to be the *trans* isomer **3b** (Table 1, Table 5). The solid-state isomerization of the cyclopentadienyl derivative **2b** occurs at a much lower temperature than that of the pentamethylcyclopentadienyl derivatives **2c** and **2d** (Table 5) suggesting a smaller activation barrier for the *cis-trans* transformation of **2b**. This is in full agreement with the observations in CH_2Cl_2 solution (eqn (2)).

The second transition in the DTA curve of **2b** is endothermic and corresponds to the melting of the *trans* isomer **3b** ($T_e = 246$°C) with almost the same enthalpy of fusion as that determined for the *trans* isomer **3b** ($\Delta H_f = 6$–9 kJ/mol) (Fig. 3). After melting the slight accompanying mass loss accelerates considerably and shows the complete decomposition of molten **3b** above 300°C (Fig. 3, Table 5). Surprisingly, the DTA curve of a pure sample of the *trans* isomer **3b**, prepared by isomerization of **2b** in solution, shows a further endothermic transition ($\Delta H = 7$ kJ/mol), which occurs at $T_e = 204$°C before melting (Fig. 3, Table 5). Heating of **3b** in a separate STA experiment to $T_{max} = 220$°C followed by visual inspection and IR spectroscopic characterization did not show any change of the sample suggesting that the endotherm at $T_e = 204$°C might correspond to a phase transition. No evident explanation can be proposed, why this endotherm is not observed in the DTA curve of **2b**. Possibly the *trans* isomer **3b** formed upon heating of **2b** is amorphous so that crystallinity and/or ordering phenomena do not occur as in the case for the separately prepared *trans* isomer **3b**.

Two mechanisms can be envisaged for the solid-state isomerization of **2b–2d** to **3b–3d**. The first one

involves a rearrangement of **2b–2d** via a Cp(Cp*) capped trigonal bipyramidal intermediate and has been suggested for the most thermal *cis-trans* isomerizations of "four-legged piano-stool complexes" in solution (intramolecular mechanism) [17]. The second mechanism involves a ligand dissociation from the *cis* isomer to give a 16e-complex intermediate followed by rearrangement and ligand association to generate the *trans* isomer. This mechanism has been suggested for some photochemically-induced *cis-trans* isomerizations of "four legged piano-stool complexes" (intermolecular mechanism) [17m,18a]. Dissociation of a carbonyl or trimethylphosphane ligand is unlikely to be the initial step of the solid-state *cis-trans* isomerization of **2b–2d,** because the volatile ligands would be expected to be removed by the purge gas leading to considerable decomposition during isomerization. However, an intermolecular mechanism involving an ionic 16e-intermediate formed from **2b–2d** after heterolytic cleavage of the metal–halogen bond cannot be excluded on the basis of the present results. Such a mechanism has been proposed for the photochemical *trans-cis* isomerization of the rhenium complexes $(\eta^5\text{-}C_5H_4R)Re(CO)(L)(X)_2$ (R = H, alkyl; L = CO, $P(OR)_3$; X = Br, I) on the surface of silica gel [18c].

The thermoanalytical results of **2b–3d** were used to prepare the *trans* isomers in large scale. For this purpose 100–400 mg of the *cis* isomers **2b, 2c** and **2d** were weighted under argon in Schlenk tubes, which then were evacuated and heated in an oven for 20–30 min at 130, 205 and 230°C respectively (eqn (3)). In order to achieve a reasonable reaction time the oven temperature was chosen about 20–40°C higher than the temperature obtained in the STA experiments for the solid-state isomerization of **2b, 2c** and **2d**. Heating was accompanied by a color change of the solids from yellow to pale-yellow. After cooling the Schlenk tubes to room temperature the *trans*-isomers **3b, 3c** and **3d** were isolated as air-stable, pale-yellow solids in high yields.

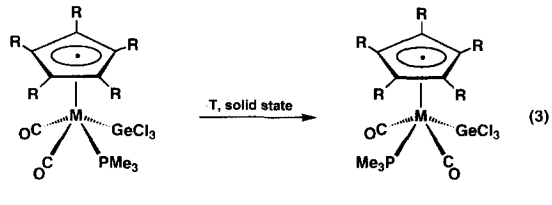

(3)

The IR and NMR spectroscopic data of **3b–3d** show unequivocally the *trans* arrangement of the carbonyl ligands in these compounds (Tables 1–3). Thus, two ν(CO) absorptions are observed in the IR spectra at 1955 and 1877 cm^{-1} (**3b**), 1955 and 1881 cm^{-1} (**3c**) and 1943 and 1866 cm^{-1} (**3d**) (Table 1). For all three compounds the higher energy absorption of the symmetric ν(CO) vibration is less intense than the lower energy absorption of the antisymmetric ν(CO) vibration as expected for a *trans* disposition of two carbonyl ligands in a "four-legged piano-stool complex" [15,19]. The ν(CO) absorptions of the trichlorogermyl complexes **3b** and **3d** appear at higher wavenumbers than those of the chloro complexes *trans*-$CpW(CO)_2(PMe_3)Cl$ [ν(CO) in CH_2Cl_2: 1961 and 1865 cm^{-1}] and *trans*-$Cp^*W(CO)_2(PMe_3)Cl$ [ν(CO) in CH_2Cl_2: 1943 and 1846 cm^{-1}], respectively [24]. This suggests as in the case of the *cis* isomers that insertion of $GeCl_2$ into the W—Cl bond causes a reduction of the electron density at the metal center and thereby weakens the metal ($d\pi$)—CO(π^*) back bonding. Additional support for the *trans* arrangement of the carbonyl ligands in **3b–3d** is given by the ^{13}C NMR spectra, which display besides the expected resonances for the PMe_3 and Cp/Cp* ligands only one resonance for the equivalent carbonyl–carbon nuclei at δ 223.1 (**3b**), 238.0 (**3c**) and 231.0 (**3d**) (Table 3). This resonance is split to a doublet due to ^{13}C–^{31}P-coupling, the magnitude of the coupling constant (21.7–31.9 Hz) being indicative of a *cis* disposition of the CO ligands relative to the PMe_3 ligand [15]. The carbonyl–carbon signals of the trichlorogermyl complexes **3b** and **3d** appear at higher field than those of the chloro complexes *trans*-$CpW(CO)_2(PMe_3)Cl$ [δ(CO) = 232.4, ^2J(PC) = 18.1 Hz (CD_2Cl_2, 20°C)] and *trans*-$Cp^*W(CO)_2(PMe_3)Cl$ [δ(CO) = 240.3, ^2J(PC) = 20.3 Hz (CD_2Cl_2, 20°C)], respectively [24]. This indicates in agreement with the IR spectra that the metal ($d\pi$)—CO(π^*) back bonding in the trichlorogermyl complexes is weaker than that in the chloro complexes.

The solid state structure of **3d** was determined by a single-crystal X-ray diffraction study. Suitable single crystals were obtained after slow evaporation of a CH_2Cl_2 solution of **3d** at ambient temperature. A ZORTEP plot of the molecular structure of **3d** with the atom-labeling scheme adopted is shown in Fig. 4. Selected bond lengths and angles of **3d** are listed in Table 6.

The *trans* isomer **3d** shows like the *cis* isomer **2d** the expected square pyramidal coordination geometry of a "four-legged piano stool" complex with similar bonding parameters of the Cp* ligand [**3d**: $(W—C_{ring})_{av.}$ = 234.5 pm, W—Cp* = 200.0 pm; **2d**: $(W—C_{ring})_{av.}$ = 233.6 pm, W—Cp* = 199.9 pm] (Cp* denotes the center of the pentamethylcyclopentadienyl ring) and the carbonyl ligands [**3d**: $(W—CO)_{av.}$ = 197.4 pm; **2d**: $(W—CO)_{av.}$ = 195.5 pm]. The tetrahedral coordination geometry of the germanium atom is in **3d** as in the *cis* isomer **2d** strongly distorted. Thus, the Cl—Ge—Cl bond angles of **3d** are more acute than that of an ideal tetrahedron having an average value of 98.6°, which is similar to that of the *cis* isomer **2d** [$(Cl—Ge—Cl)_{av.}$ = 98.01°]. Consequently, the W—Ge—Cl bond angles of **3d** are more obtuse than

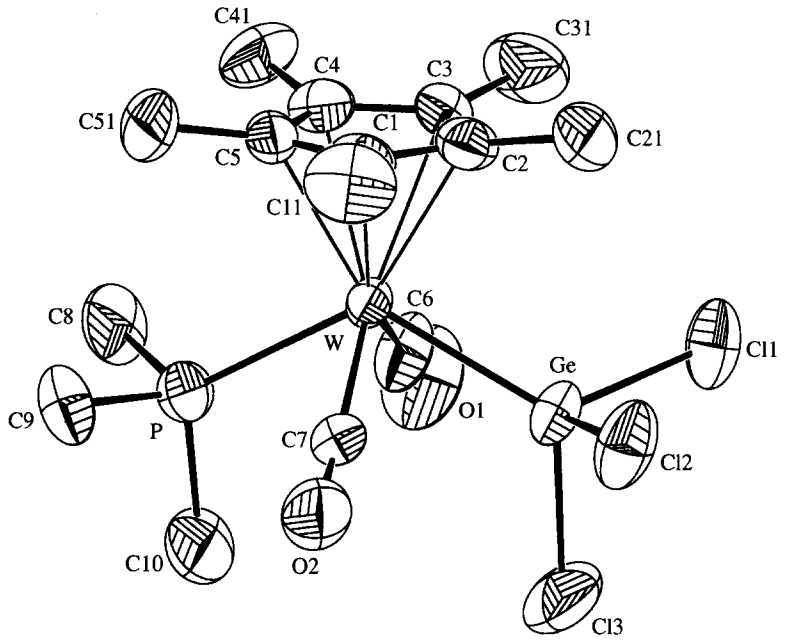

Fig. 4. ZORTEP plot of the molecular structure of **3d** with thermal ellipsoids drawn at the 50% probability level.

Table 6. Selected bond lengths (pm) and bond angles (°) with estimated standard deviations for **3d**

W—C(1)	236.6(9)	Ge—W—P	124.65(6)
W—C(2)	236.4(7)	Ge—W—C(6)	76.2(3)
W—C(3)	233.6(10)	Ge—W—C(7)	73.3(3)
W—C(4)	231.9(10)	P—W—C(6)	76.4(3)
W—C(5)	234.2(9)	P—W—C(7)	74.3(3)
W—C(6)	196.7(11)	C(6)—W—C(7)	112.4(4)
W—C(7)	198.1(9)	W—Ge—Cl(1)	120.03(12)
W—Ge	251.59(14)	W—Ge—Cl(2)	118.64(9)
W—P	248.7(3)	W—Ge—Cl(3)	117.94(11)
Ge—Cl(1)	220.9(3)	Cl(1)—Ge—Cl(2)	98.69(13)
Ge—Cl(2)	219.7(3)	Cl(2)—Ge—Cl(3)	99.0(2)
Ge—Cl(3)	219.1(3)	Cl(1)—Ge—Cl(3)	98.2(2)

that of an ideal tetrahedron and have an average value of 118.87°, which is also similar to that of the *cis* isomer **2d** [(W—Ge—Cl)$_{av.}$ = 119.27°]. Furthermore, the Ge—Cl bond lengths of both isomers are similar [**3d**: (Ge—Cl)$_{av.}$ = 219.9 pm; **2d**: (Ge—Cl)$_{av.}$ = 220.6 pm] and considerably longer than that of $GeCl_4$ [(Ge—Cl)$_{av.}$ = 211.3(3) pm] (see discussion of the structure of **2d** for interpretation). However, the W—Ge bond of **3d** is with 251.59(14) pm considerably shorter than that of the *cis* isomer **2d** with 255.90(5) pm. This shortening can be attributed to the weaker *trans* influence of the PMe_3 ligand compared with the carbonyl ligand and the reduction of steric repulsion between the trichlorogermyl and the trimethylphosphane ligand in the *trans* isomer **3d**. The strong *trans* influence of the carbonyl ligand is also reflected in the longer W—P bond of **2d** [251.33(12) pm] compared with that of **3d** [248.7(3) pm] [25].

Furthermore, we wanted to elucidate the influence of other 2e-donor ligands than PMe_3 on the thermal behavior of the half-sandwich trichlorogermyl complexes and therefore studied the ethyl isocyanide derivative *cis*-$CpW(CO)_2(EtNC)GeCl_3$ (**5**) by STA (Fig. 5).

Three endothermal DTA effects were observed upon heating of **5**. The first transition occurring at T_e = 96°C corresponds to the melting of **5** (ΔH_f = +17 kJ/mol) (Fig. 5) [15a]. This was verified by a separate STA run in which **5** was heated under the same conditions to T_{max} = 115°C (Table 5). The resulting red melt solidified upon cooling to room temperature to a glass-like mass, that was identified

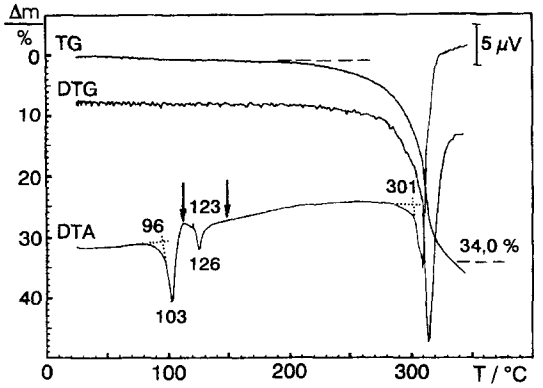

Fig. 5. STA curves (T, TG, DTG and DTA) of **5**. The arrows indicate T_{max} of the separate STA runs carried out for sample characterization (Table 5, Experimental).

by IR spectroscopy to be the *cis* isomer **5** (Table 1). Molten **5** undergoes at $T_i = 123°C$ an endothermic transition ($\Delta H = +4$ kJ/mol), which is not accompanied by a mass loss and corresponds to a *cis-trans* isomerization process leading to an equilibrium mixture of **5** and **6** (ratio **5**/**6** = 1 : 1.2) (Fig. 5, Table 5) (eqn (4)).

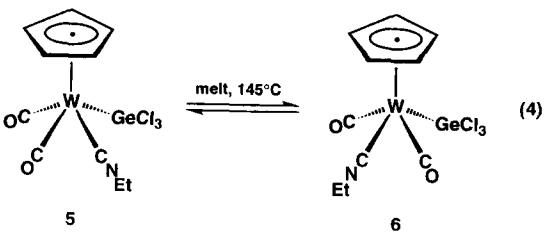

This was evidenced by a separate STA run, in which after heating of **5** to $T_{max} = 145°C$ the red melt was allowed to cool to room temperature and the resulting solid was shown by IR and ^1H NMR spectroscopy to be the above mentioned mixture of isomers (Tables 1 and 2). In addition, this transformation was carried out in preparative scale and the mixture of **5** and **6** was fully characterized (see Experimental). Complex **5** isomerizes also in CH_2Cl_2 solution at ambient temperature. Isomerization is however very slow, leading only after several weeks to the thermodynamic equilibrium between **5** and **6**, that favors slightly the *cis* isomer (**5**/**6** ratio : 1.1 : 1).

Finally, a third endotherm is observed in the DTA curve of **5** at $T_e = 301°C$ and is accompanied by a total mass loss of 34% indicating extensive decomposition of the sample.

The observed *cis-trans* isomerizations of **2b**, **2c** and **2d** are rare examples of solid-state reactions in organometallic chemistry that need further attention. Preliminary studies show that also other molybdenum and tungsten trichlorogermyl complexes containing cyclopentadienyl ligands undergo an isomerization in the solid-state.

EXPERIMENTAL

Standard inert-atmosphere techniques were used for all syntheses and sample manipulations. The solvents were dried by standard methods (pentane over CaH_2, Et_2O over Na/benzophenone, CH_2Cl_2 over P_2O_5 and Na/Pb alloy), distilled under argon and stored over 4 Å molecular sieves prior to use. Elemental analyses were obtained from the Zentrale Analytische Gruppe des Instituts für Chemie der Humboldt Universität zu Berlin. IR spectra were recorded on a Bruker IFS-55 spectrometer. ^1H, $^{13}C\{^1H\}$ and $^{31}P\{^1H\}$ NMR spectra were recorded on a Bruker AM 300 spectrometer in dry deoxygenated methylene-d_2-chloride. The ^1H and $^{13}C\{^1H\}$ NMR spectra were calibrated against the solvent signals (methylene-d_2-chloride, δ_H 5.32 and δ_C 53.8 ppm) and the $^{31}P\{^1H\}$-NMR spectra against an external 85% H_3PO_4 aqueous solution. Mass spectra were obtained with a HP 5995A spectrometer; *m/z* values are given relative to the ^{98}Mo, ^{184}W, ^{74}Ge and ^{35}Cl isotopes. Melting points were determined using a Büchi 530 melting point apparatus and are not corrected. The samples used for the determination of the melting points were sealed in capillary tubes under argon.

The complexes *cis*-(η^5-C_5R_5)M(CO)$_2$(PMe_3)Cl (**1b**–**1d**) (**1b**: M = W; R = H; **1c**: M = Mo; R = Me; **1d**: M = W; R = Me) were obtained by chlorination of the hydrido complexes *cis*/*trans*-(η^5-C_5R_5)M(CO)$_2$(PMe_3)H [26] with CCl_4. Chlorination of *cis*/*trans*-(η^5-C_5R_5)M(CO)$_2$(PMe_3)H afforded first *cis*-/*trans*-mixtures of the chloro complexes (η^5-C_5R_5)M(CO)$_2$(PMe_3)Cl. The *trans* isomer isomerized then in solution at room temperature to the *cis* isomer [24]. $GeCl_2$(1,4-dioxane) was prepared following the procedure reported by Nefedov *et al.* [27]. Complex **5** was prepared as described previously [15a].

The simultaneous thermal analysis (STA) curves (T, DTA, TG, DTG) were obtained with a Netzsch-Thermoanalyser STA 429 using the mini sample holder system (platinum crucibles, sample mass 6–12 mg, Pt/PtRh10 thermoelements, α-Al_2O_3 as reference, heating rate 5°C/min, purge gas: argon, flow rate 100 ml/min). Determination of the characteristic temperatures in the STA curves (T_i, initial; T_e, extrapolated onset; T_p, peak) was carried out following international recommendations [28]. A caloric calibration of the measuring system using appropriate standard substances [29] preceded the enthalpimetric evaluation of the DTA curves and yielded at best values with an accuracy of 10–12%. In order to give a meaningful interpretation of the processes observed during thermal analysis, separate STA runs were carried out under identical conditions (sample mass, heating rate). In these runs the samples were heated to the relevant temperatures obtained from the overview

STA experiments and then were cooled under argon to room temperature. The obtained samples were compared with authentic samples by visual inspection and were characterized by IR spectroscopy and/or ^1H NMR spectroscopy. The arrows on the DTA curves (Figs 3 and 5) indicate these distinguished temperatures of characterization. The control STA experiments of the *cis* isomers **2b–2d** and **5** were reproduced in a preparative scale to obtain the *trans* isomers **3b–3d** and a mixture of **5** and **6**, respectively (see synthesis of **3b–3d** and **5/6** below).

cis-$CpW(CO)_2(PMe_3)GeCl_3$(**2b**)

A mixture of 84 mg (0.20 mmol) of **1b** and 49 mg (0.21 mmol) of $GeCl_2$(1,4-dioxane) was suspended at −78°C in 30 ml of CH_2Cl_2 and the suspension was allowed to warm to room temperature and stirred for 1 h. During this time the red solution brightened. Completion of the reaction was confirmed by IR spectroscopy. The solution was then filtered from some insoluble gray material through a filter canula and the filtrate was evaporated to dryness. The residue was washed twice with 5 ml of an Et_2O/pentane (1/3) mixture to afford complex **2b** as a yellow, microcrystalline solid. Yield: 106 mg (95%). Found: C, 21.23; H, 2.64; Cl, 20.12; P, 4.99; $C_{10}H_{14}Cl_3GeO_2PW$ (559.99). Calc.: C, 21.45; H, 2.52; Cl, 18.99; P, 5.53%. EI-MS (70 eV): *m/z* 560 $[M]^+$, 525 $[M—Cl]^+$, 388 $[M—CO—GeCl_2]^+$, 360 $[M—2\ CO—GeCl_2]^+$ (base peak).

cis-$Cp^*Mo(CO)_2(PMe_3)GeCl_3$ (**2c**)

Following the procedure described above for the synthesis of **2b**, complex **2c** was isolated as a yellow, microcrystalline solid after treatment of 204 mg (0.51 mmol) of **1c** with 118 mg (0.51 mmol) of $GeCl_2$(1,4-dioxane) in 40 ml of CH_2Cl_2 for 3 h at room temperature. Yield: 271 mg (98%). Found: C, 32.64; H, 4.65; Cl, 20.15; $C_{15}H_{24}Cl_3GeMoO_2P$ (542.22). Calc.: C, 33.23; H, 4.46; Cl, 19.61%. EI-MS (70 eV): *m/z* 544 $[M]^+$, 509 $[M—Cl]^+$, 453 $[M—Cl—2\ CO]^+$, 400 $[M—GeCl_2]^+$, 372 $[M—GeCl_2—CO]^+$, 344 $[M—GeCl_2—2CO]^+$, 268 $[M—GeCl_2—2\ CO—PMe_3]^+$ (base peak).

cis-$Cp^*W(CO)_2(PMe_3)GeCl_3$ (**2d**)

Following the procedure described above for the synthesis of **2b**, complex **2d** was obtained as a yellow, microcrystalline solid after treatment of 234 mg (0.48 mmol) of **1d** with 109 mg (0.47 mmol) of $GeCl_2$(1,4-dioxane) in 40 ml of CH_2Cl_2 for 3 h at room temperature. Yield 244 mg (81%). Found: C, 28.06; H, 3.77; Cl, 16.93; P, 4.42; $C_{15}H_{24}Cl_3GeO_2PW$ (630.13). Calc.: C, 28.59; H, 3.84; Cl, 16.88; P, 4.92%. EI-MS (70 eV): *m/z* 630 $[M]^+$, 595 $[M—Cl]^+$, 519 $[M—Cl—PMe_3]^+$, 486 $[M—GeCl_2]^+$, 458 $[M—GeCl_2—CO]^+$, 430 $[M—GeCl_2—2\ CO]^+$ (base peak).

trans-$CpW(CO)_2(PMe_3)GeCl_3$ (**3b**)

A 100 ml Schlenk tube was charged with 151 mg (0.27 mmol) of **2b** and tightly closed with a glass stopper. The Schlenk tube was evacuated and placed in an oven at 130°C for 20 min. During this time the color of the yellow solid changed to pale yellow. Subsequently, the Schlenk tube was slowly cooled to room temperature and filled with argon. Selective formation of **3b** was revealed by an IR spectrum of a small sample of the pale-yellow, microcrystalline solid in CH_2Cl_2. Yield: quantitative. M.p.: 246°C. Found: C, 21.30; H, 2.44; Cl, 18.41; P, 5.52; $C_{10}H_{14}Cl_3GeO_2PW$ (559.99). Calc.: C, 21.45; H, 2.52; Cl, 18.99; P, 5.53%.

trans-$Cp^*Mo(CO)_2(PMe_3)GeCl_3$ (**3c**)

Following the procedure described above for the synthesis of **3b**, complex **3c** was obtained as a pale-yellow, microcrystalline solid after heating 344 mg (0.63 mmol) of **2c** at 205°C for 20 min. M.p.: 237°C (dec.). Yield: quantitative. Found: C, 32.88; H, 4.82; Cl, 19.81; P, 5.39; $C_{15}H_{24}Cl_3GeMoO_2P$ (542.22). Calc.: C, 33.23; H, 4.46; Cl, 19.61; P, 5.71%. EI-MS (70 eV): *m/z* 544 $[M]^+$, 509 $[M—Cl]^+$, 453 $[M—Cl—CO]^+$, 433 $[M—Cl—PMe_3]^+$, 372 $[M—GeCl_2—CO]^+$, 344 $[M—GeCl_2—2CO]^+$, 268 $[M—GeCl_2—2\ CO—PMe_3]^+$ (base peak).

trans-$Cp^*W(CO)_2(PMe_3)GeCl_3$ (**3d**)

Following the procedure described above for the synthesis of **3b**, complex **3d** was obtained as a pale-yellow, microcrystalline solid after heating of 104 mg (0.17 mmol) of **2d** at 230°C for 15 min. M.p.: 256°C. Yield: quantitative. Found: C, 28.07; H, 4.09; Cl, 15.66; $C_{15}H_{24}Cl_3GeO_2PW$ (630.13). Calc.: C, 28.59; H, 3.84; Cl, 16.88%. EI-MS (70 eV): *m/z* 630 $[M]^+$, 595 $[M—Cl]^+$, 519 $[M—Cl—PMe_3]^+$, 486 $[M—GeCl_2]^+$, 458 $[M—GeCl_2—CO]^+$, 430 $[M—GeCl_2—2\ CO]^+$.

cis/trans-$CpW(CO)_2(CNEt)GeCl_3$ (**5/6**)

A Schlenk tube was charged with 230 mg (0.42 mmol) of *cis*-$CpW(CO)_2(CNEt)GeCl_3$ (**5**), then evacuated and heated at 145°C for 15 min. During this time the sample molt to give a dark-red melt. After cooling the Schlenk tube to room temperature the melt solidified to a glassy red residue, which was dissolved in 20 ml of CH_2Cl_2. The solution was then filtered from some insoluble material through a filter canula and the filtrate was concentrated to ca 2 ml and treated with 20 ml of pentane. The resulting yellow

Table 7. Summary of X-ray diffraction data

Compound	**2d**	**3d**
Molecular formula	$C_{15}H_{24}Cl_3GeO_2PW$	$C_{15}H_{24}Cl_3GeO_2PW$
Crystal color	Orange	Yellow
Crystal size (mm)	$0.38 \times 0.19 \times 0.15$	$0.76 \times 0.30 \times 0.15$
Crystal system	Monoclinic	Orthorhombic
Space group	$P2_1/c$ (No. 14)	$Pna2_1$ (No. 33)
a (Å)	14.752(2)	22.471(2)
b (Å)	8.951(2)	9.686(3)
c (Å)	16.151(2)	10.1170(7)
β (°)	98.760(11)	
V (Å^3)	2107.8(5)	2202.0(7)
Z	4	4
D_{calc} (g cm^{-3})	1.986	1.901
μ(Mo–K_α) (mm^{-1})	7.071	6.768
Radiation (Mo–K_α) (Å)	0.71073	0.71073
T (K)	200(2)	293(2)
2θ range (°)	2.7–26.1	1.8–25.0
Total data	14501	4500
Data unique	4111 ($R_{(int)} = 0.0961$)	2060 ($R_{(int)} = 0.0380$)
No. of reflections	4101 ($I > 2\sigma I$)	1997 ($I > 2\sigma I$)
No. of refined param.	208	208
Absorption correction, min/max		Ψ-scan, 0.068/0.159
min/max density (e Å^{-3})	−0.864/1.156	−1.673/0.657
R_1[a]	0.0267	0.0252
wR_2[b]	0.0535	0.0604

[a] $R_1 = \Sigma||F_o| - |F_c||/\Sigma|F_o|$.
[b] $wR_2 = [\Sigma[w(F_o^2 - F_c^2)^2]/\Sigma[w(F_o^2)^2]]^{1/2}$.

precipitate was allowed to settle and the supernatant solution was removed. The precipitate was washed once with 10 ml of pentane and dried *in vacuo* to give the mixture of the two isomers **5** and **6** as a yellow, microcrystalline solid. Yield: 212 mg (92%).

Crystal structure determination of **2d** *and* **3d**

A summary of the crystal data, data collection and refinement for **2d** and **3d** is given in Table 7. Data collection for **2d** was performed on a STOE IPDS area detector equipped with a low temperature device and for **3d** on a STOE STADI4 four circle diffractometer. Lattice parameters derived from the setting angles of 28 reflections in the range of $27° \leqslant 2\theta \leqslant 33°$ for **3d** and from 5000 reflections after data collection for **2d**. Data for **3d** were collected in the ω-2θ scan mode. The crystal of **2d** was oscillated in 1.4° steps to yield 129 exposures and each of them was exposed for 4 min. Intensity data were integrated and converted into a SHELX *hkl*-file with the STOE IPDS software [30]. The input files for the SHELX programs were prepared with the program UTILITY [31]. Structure solution was performed with Patterson methods for **3d** and direct methods for **2d** (SHELXS-86) [32] and subsequent difference-Fourier synthesis (SHELXL-93) [33]. Refinement on F^2 was carried out by full-matrix least squares techniques (SHELXL-93). Non hydrogen atoms were refined with anisotropic thermal parameters. Hydrogen atoms were included using a riding model with $d_{CH} = 0.96$ Å and $U_{iso} = 0.08$ Å^2. Neutral atom scattering factors were taken from Cromer and Mann [34]. Illustrations were performed with ZORTEP [35].

REFERENCES

1. Ohgaki, H., Kabe, Y. and Ando, W., *Organometallics*, 1995, **14,** 2139.
2. Egorov, M. P., Nefedov, O. M., Lin, T.-S. and Gaspar, P. P., *Organometallics*, 1995, **14,** 1539.
3. Sekiguchi, A., Yamazaki, H., Kabuto, C. and Sakurai, H., *J. Am. Chem. Soc.*, 1995, **117,** 8025.
4. Sekiguchi, A., Tsukamoto, M. and Ichinohe, M., *Science*, 1997, **275,** 60.
5. Wiberg, N., Hochmuth, W., Nöth, H., Appel, A. and Schmidt-Amelunxen, M., *Angew. Chem.*, 1996, **108,** 1437; *Angew. Chem. Int. Ed. Engl.*, 1996, **35,** 1333.
6. Simons, R. S. and Power, P. P., *J. Am. Chem. Soc.*, 1996, **118,** 11966.
7. (a) Jutzi, P., Becker, A., Stammler, H. G. and Neumann, B., *Organometallics*, 1991, **10,** 1647; (b) Jutzi, P., Becker, A., Leue, C., Stammler, H.-G., Neumann, B., Hursthouse, M. B. and Karaulov, A., *Organometallics*, 1991, **10,** 3838; (c) Herrmann, W. A., Denk, M., Behm, J., Scherer,

W., Klingan, F.-R., Bock, H., Solouki, B. and Wagner, M., *Angew. Chem.*, 1992, **104,** 1489; *Angew. Chem. Int. Ed. Engl.*, 1992, **31,** 1485; (d) Driess, M., Janoschek, R., Pritzkow, H., Rell, S. and Winkler, U., *Angew. Chem.*, 1995, **107,** 1746; *Angew. Chem. Int. Ed. Engl.*, 1995, **34,** 1614; (e) Jutzi, P., Schmidt, H., Neumann, B. and Stammler, H.-G., *J. Organomet. Chem.*, 1995, **499,** 7.

8. (a) Brewer, F. M. and Dennis, L. M., *J. Phys. Chem.*, 1927, **31,** 1526; (b) Dennis, L. M. and Hunter, H. L., *J. Am. Chem. Soc.*, 1929, **51,** 1151; (c) Moulton, C. W. and Miller, J. G., *J. Am. Chem. Soc.*, 1956, **78,** 2702.
9. (a) Kolesnikov, S. P., Shiryaev, V. I. and Nefedov, O. M., *Izv. Akad. Nauk. SSSR, Ser. Khim.*, 1966, **584**; (b) Kulishov, V. I., Bokii, N. G., Struchkov, Y. T., Nefedov, O. M., Kolesnikov, S. P. and Perl'mutter, B. L., *Zh. Strukt. Khim.*, 1970, **11,** 71.
10. (a) Jutzi, P., Hoffmann, H. J., Brauer, D. J. and Krüger, C., *Angew. Chem.*, 1973, **85,** 1116; *Angew. Chem. Int. Ed. Engl.*, 1973, **12,** 1002.
11. (a) du Mont, W.-W., Neudert, B., Rudolph, G. and Schumann, H., *Angew. Chem.*, 1976, **88,** 303; *Angew. Chem. Int. Ed. Engl.*, 1976, **15,** 308; (b) du Mont, W.-W. and Rudolph, G., *Chem. Ber.*, 1976, **109,** 3419.
12. (a) Nefedov, O. M., Kolesnikov, S. P. and Rogozhin, I. S., *Izv. Akad. Nauk. SSSR, Ser. Khim.*, 1973, 2824; (b) du Mont, W.-W. and Rudolph, G., *Z. Naturforsch.*, 1981, **36b,** 1215.
13. Satgé, J., Massol, M. and Rivière, P., *J. Organomet. Chem.*, 1973, **56,** 1.
14. Recent examples of $GeCl_2$ insertion reactions: (a) Bauer, A., Schier, A. and Schmidbaur, H., *J. Chem. Soc., Dalton trans.*, 1995, 2919; (b) Bauer, A. and Schmidbaur, H., *J. Am. Chem. Soc.*, 1996, **118,** 5324; (c) Bauer, A. and Schmidbaur, H., *J. Chem. Soc., Dalton Trans.*, 1997, 1115.
15. (a) Filippou, A. C., Winter, J. G., Kociok-Köhn, G. and Hinz, I., *J. Organomet. Chem.*, 1997, **542,** 35; (b) Filippou, A. C., Winter, J. G., Kociok-Köhn, G. and Hinz, I., *J. Organomet. Chem.*, 1997, **544,** 225.
16. Kubácek, P., Hoffmann, R. and Havlas, Z., *Organometallics*, 1982, **1,** 180.
17. (a) Faller, J. W. and Anderson, A. S., *J. Am. Chem. Soc.*, 1969, **91,** 1550; (b) Faller, J. W. and Anderson, A. S., *J. Am. Chem. Soc.*, 1970, **92,** 5852; (c) Kalck, P., Pince, R., Poilblanc, R. and Roussel, J., *J. Organomet. Chem.*, 1970, **24,** 445; (d) Wright, G. and Mawby, R. J., *J. Organomet. Chem.*, 1971, **29,** C29; (e) Barnett, K. W. and Slocum, D. W., *J. Organomet. Chem.*, 1972, **44,** 1; (f) Brunner, H. and Herrmann, W. A., *Chem. Ber.*, 1973, **106,** 632; (g) Brunner, H. and Herrmann, W. A., *J. Organomet. Chem.*, 1974, **74,** 423; (h) King, R. B. and Reimann, R. H., *Inorg. Chem.*, 1976, **15,** 179; (i) Flood, T. C., Rosenberg, E. and Sarhangi, A., *J. Am. Chem. Soc.*, 1977, **99,** 4334; (j) Pfeiffer, E., Vrieze, K. and McLeverty, J. A., *J. Organomet. Chem.*, 1979, **174,** 183; (k) Alway, D. G. and Barnett, K. W., *Inorg. Chem.*, 1980, **19,** 1533; (l) Einstein, F. W. B., Klahn-Oliva, A. H., Sutton, D. and Tyers, K. G., *Organometallics*, 1986, **5,** 53; (m) Hill, R. H. and Palmer, B. J., *Organometallics*, 1989, **8,** 1651; (n) Debad, J. D. and Hill, R. H., *Can. J. Chem.*, 1990, **68,** 2216.
18. (a) Palmer, B. J., Becalska, A., Hader, R. and Hill, R. H., *Polyhedron*, 1991, **10,** 877; (b) Cheng, L. and Coville, N. J., *Organometallics*, 1996, **15,** 867; (c) Cheng, L. and Coville, N. J., *Organometallics*, 1997, **16,** 591.
19. (a) Manning, A. R., *J. Chem. Soc. A*, 1967, 1984; (b) King, R. B., Reimann, R. H. and Darensbourg, D. J., *J. Organomet. Chem.*, 1975, **93,** C23; (c) Beach, D. L. and Barnett, K. W., *J. Organomet. Chem.*, 1975, **97,** C27; (d) Beach, D. L., Dattilo, M. and Barnett, K. W., *J. Organomet. Chem.*, 1977, **140,** 47; (e) Filippou, A. C., Lungwitz, B., Kociok-Köhn, G. and Hinz, I., *J. Organomet. Chem.*, 1996, **524,** 133.
20. (a) Todd, L. J. and Wilkinson, J. R., *J. Organomet. Chem.*, 1974, **77,** 1; (b) Filippou, A. C., Wanninger, K. and Mehnert, C., *J. Organomet. Chem.*, 1993, **461,** 99; (c) Lungwitz, B. and Filippou, A. C., *J. Organomet. Chem.*, 1995, **498,** 91.
21. Morino, Y., Nakamura, Y. and Iijima, T., *J. Chem. Phys.*, 1960, **32,** 643.
22. Pauling, L., Die Natur der chemischen Bindung, Verlag Chemie, 1968.
23. Bent, H. A., *Chem. Rev.*, 1961, **61,** 275.
24. Filippou, A. C., Winter, J. G., Troll, C. and Hinz, I., unpublished results.
25. Pidcock, A., Richards, R. E. and Venanzi, L. M., *J. Chem. Soc. A*, 1966, 1707.
26. (a) Alt, H. G., Engelhardt, H. E., Kläui, W. and Müller, A., *J. Organomet. Chem.*, 1987, **331,** 317; (b) Tudoret, M.-J., Robo, M.-L. and Lapinte, C., *Organometallics*, 1992, **11,** 1419.
27. (a) Kolesnikov, S. P., Rogozhin, I. S. and Nefedov, O. M., *Izv. Akad. Nauk. SSSR, Ser. Khim.*, 1974, **10,** 2379; (b) Kolesnikov, S. P., Rogozhin, I. S. and Nefedov, O. M., *Chem. Abstr.*, 1975, **82,** 25328u.
28. Hill, J. O. (ed.), For Better Thermal Analysis, Special Edition of the International Confederation for Thermal Analysis (ICTA), 3rd Edition, 1991.
29. Hemminger, W. and Cammenga, H. K., Methoden der Thermischen Analyse, Springer-Verlag, Heidelberg, 1989.
30. STOE IPDS, Darmstadt, 1996.
31. Pickardt, J., UTILITY, Technische Universität Berlin, FRG, 1994.
32. Sheldrick, G. M., SHELXS-86, Program for Crystal Structure Solution, Universität Göttingen, FRG, 1986.
33. Sheldrick, G. M., SHELXL-93, Program for Crystal Structure Determination, Universität Göttingen, FRG, 1993.
34. Cromer, D. T. and Mann, J. B., *Acta Crystallogr.*, 1968, **24A,** 321.
35. Zsolnai, L. and Pritzkow, H., ZORTEP, ORTEP program for PC, Universität Heidelberg, 1994.

Pergamon

PII: S0277-5387(97)00496-8

Polyhedron Vol. 17, No. 7, pp. 1115–1119, 1998
© 1998 Elsevier Science Ltd
All rights reserved. Printed in Great Britain
0277-5387/98 $19.00+0.00

New $CpCrCl_2(PR_3)$ complexes: physical properties and reduction chemistry†

Matthieu Bender-Gresse,[a] Edmond Collange,[a] Rinaldo Poli[a]* and Sundeep Mattamana[b]

[a] Laboratoire de Synthèse et d'Electrosynthèse Organométallique, Université de Bourgogne, Faculté de Sciences "Gabriel", 6 Boulevard Gabriel, 21100 Dijon Cedex

[b] Department of Chemistry and Biochemistry, University of Maryland, College Park, Maryland 20742

(Received 25 September 1997; accepted 24 October 1997)

Abstract—Compounds $CpCrCl_2L$ (L = PMe_2Ph, **1**; $PMePh_2$, **2**; PPh_3, **3**) have been prepared. Their magnetic moment is in accord with the presence of three unpaired electron and a variable temperature ^1H NMR investigation of **1** shows Curie–Weiss behavior. The ^1H NMR, EPR and UV-visible spectra are in agreement with those of other previously reported compounds of the same family. An electrochemical investigation shows the accessibility of an irreversible reduction process. A parallel sodium reduction investigation of complexes $CpCrCl_2L$ (L = PMe_3 and η^1-dppe) suggests that the reduction process is followed by immediate chloride loss, and then by a ligand redistribution process to afford chromocene and unstable inorganic phosphine complexes of Cr(II). © 1998 Elsevier Science Ltd. All rights reserved

Keywords: $CpCrCl_2$; reduction chemistry; Curie-Weiss behavior.

We have investigated in some detail a class of stable organometallic radicals based on the $CpMoCl_2(PR_3)_2$ stoichiometry and have shown that they undergo a dissociative phosphine exchange process [1]. The supposed 15-electron $CpMoCl_2(PR_3)$ intermediate is probably favored by the release of pairing energy, since it is calculated to adopt a spin quartet ground state [2,3], while the associative path is disfavored by sterics and the high energy HOMO of the precursor. Attempts to stabilize and isolate such an intermediate, which is isostructural and isoelectronic with stable Cr(III) complexes, have been to date unfruitful [4,5]. The relative stability of the 17-electron $S = 1/2$ structure for CpMo(III) complexes and of the 15-electron $S = 3/2$ structure for CpCr(III) complexes have been rationalized on a theoretical standpoint by differences in M—PR_3 bonding and electron pairing energy [2,3].

We have thus become interested in examining the corresponding phosphine exchange process on the 15-electron Cr(III) compounds. For this purpose, a larger number of complexes was required than previously available and an exchange reaction that would be amenable to a kinetic study. We report here the synthesis of these complexes, a study of their physical properties to complement those already available in the literature, and an electrochemical and chemical reduction study. The phosphine exchange kinetic studies are in progress and will be presented in a later contribution.

EXPERIMENTAL

All operations were carried out under an atmosphere of dinitrogen. Solvents were dehydrated by conventional methods and distilled directly from the dehydrating agent prior to use (THF and Et_2O from Na/benzophenone, hexane from Na/K, heptane and toluene from Na, and CH_2Cl_2 from P_2O_5). NMR spectra were recorded on a Bruker AC200 spectrometer; the peak positions are reported with positive shifts downfield of TMS as calculated from the residual solvent peaks (^1H) or downfield of external 85% H_3PO_4 (^{31}P). For each ^{31}P-NMR spectrum, a sealed capillary containing H_3PO_4 was immersed in the same NMR solvent used for the measurement and this was

† Herrn Prof. Dr. h.c. mutt. W. A. Herrmann zurn 50. Geburstag geuidmet.

* Author to whom correspondence should be addressed.

used as the external reference. Visible spectra were recorded on a Kontron Uvikon 810/820 spectrophotometer. EPR spectra were recorded on a Bruker ESP300 spectrometer equipped with an X-band microwave generator. The cyclic voltammograms were obtained with a Radiometer analog potentiostats (model PRT30-01) or with a Radiometer digital electrochemical analyzer (model DEA332). The electrochemical cell was a locally modified Schlenk tube with fittings for a platinum disk working electrode, a Pt wire counterelectrode, an SCE reference electrode, and a nitrogen inlet. Bu_4NBF_4 (ca 0.1 M) was used as supporting electrolyte. All potentials are reported relative to the ferrocene standard, which was added to each solution and measured at the end of the experiments. The magnetic susceptibility measurements were carried out with a Johnson Matthey magnetic balance, which operates by a modified Gouy method. The molar susceptibilities for the calculation of the magnetic moments were corrected for the diamagnetism of the ligands by using Pascal's constants. The elemental analyses were by M-H-W Laboratories, Phoenix, Arizona or were carried out at the Université de Bourgogne with a Fisons Instruments EA1108 analyzer. $CrCl_3(THF)_3$ was prepared according to the literature from $CrCl_3 \cdot 6H_2O$ and $SOCl_2$ in THF [6]. Solid $CpNa(THF)_x$ was prepared from Na and freshly cracked CpH in THF, followed by evaporation, precipitation by addition of hexane, filtration, and vacuum drying. The amount of residual THF was determined by acid-base titration after quenching with degassed water. Compounds $CpCrCl_2L$ (L = PMe_3, PEt_3, η^1-dppe) were prepared as previously described [7,8]. PMe_2Ph (Aldrich), $PMePh_2$ (Strem) and PPh_3 (Aldrich) were used as received without further purification.

Synthesis of $CpCrCl_2(PMe_2Ph)$, **1**

A blue solution of $CpCrCl_2(THF)$ was prepared *in situ* from $CrCl_3(THF)_3$ (0.496 mg, 1.325 mmol) and $NaCp(THF)_{0.46}$ (0.17 g, 1.4 mmol) in THF (20 ml). The ligand PMe_2Ph (0.2 ml, 1.4 mmol) was added, causing an immediate change of color to a deeper blue. The mixture was evaporated to dryness and the residue is extracted with CH_2Cl_2 (2 ml). After filtration, the slow diffusion of a hexane layer (15 ml) produced 0.364 g of blue crystals of **1** (84% yield). Elemental analysis: calculated for $C_{13}H_{16}Cl_2CrP$: C, 47.88; H, 4.94. Found: C, 47.92; H, 4.83. ^1H NMR ($CDCl_3$ δ/ppm ($w_{1/2}$/Hz)): 250 (3600) (Cp), 11.4 (49) (p-Ph), 5.28 (61) (m-Ph), −27 (740) (Me). $\mu_{eff} = 3.81$ μ_B ($\chi_g = 18.6 \cdot 10^{-6}$ cgsu, molar diamagnetic correction: $5.6 \cdot 10^{-2}$ cgsu). EPR (toluene, 105 K): $g_x = 4.480$; $g_y = 3.590$; $g_z = 1.990$. Visible (CH_2Cl_2, λ_{max}/nm (ε/cm^{-1} M^{-1})): 458 (394), 620 (666).

Synthesis of $CpCrCl_2(PMePh_2)$, **2**

A blue solution of $CpCrCl_2(THF)$ was prepared *in situ* from $CrCl_3(THF)_3$ (0.740 mg, 1.97 mmol) and $NaCp(THF)_{0.46}$ (0.24 g, 2.0 mmol) in THF (30 ml). The ligand $PMePh_2$ (0.28 ml, 2.0 mmol) is added, causing an immediate change of color to a deeper blue. The mixture was evaporated to dryness and the residue was extracted with CH_2Cl_2 (2 ml). After filtration, the slow diffusion of a hexane layer (20 ml) produced 0.598 g of blue crystals of **2** (78% yield). Elemental analysis: calculated for $C_{18}H_{18}Cl_2CrP$: C, 55.69; H, 4.67. Found: C, 55.90; H, 4.65. ^1H NMR (acetone-d^6, δ/ppm ($w_{1/2}$/Hz)): 255 (2700) (Cp), 9.75 (48) (p-Ph), 7.13 (70) (m-Ph), −21 (600) (Me). $\mu_{eff} = 3.73$ μ_B ($\chi_g = 14.7 \cdot 10^{-6}$ cgsu, molar diamagnetic correction: $7 \cdot 10^{-2}$ cgsu). EPR (toluene, 105 K): $g_x = 4.489$; $g_y = 3.590$; $g_z = 1.994$. Visible (CH_2Cl_2, λ_{max}/nm (ε/cm^{-1} M^{-1})): 480 (230), 666 (926).

Synthesis of $CpCrCl_2(PPh_3)$, **3**

A blue solution of $CpCrCl_2(THF)$ was prepared *in situ* from $CrCl_3(THF)_3$ (0.493 mg, 1.31 mmol) and $NaCp(THF)_{0.46}$ (0.17 g, 1.4 mmol) in THF (30 ml). The ligand PPh_3 (0.378 g, 1.44 mmol) was added, causing an immediate change of color to a deeper blue. The mixture evaporated to dryness and the residue is extracted with CH_2Cl_2 (2 ml). After filtration, the slow diffusion of a hexane layer (20 ml) produced blue crystals of **3**. These were recrystallized several times by the same procedure, until the ^1H and ^{31}P NMR spectra indicated the complete elimination of free PPh_3. Yield 0.204 g, 34%. Elemental analysis: calculated for $C_{23}H_{20}Cl_2CrP$: C, 61.35; H, 4.48. Found: C, 60.64; H, 4.43. ^1H NMR ($CDCl_3$, δ/ppm ($w_{1/2}$)): 260 (4500) (Cp), 9.32 (46) (p-Ph), 7.97 (73) (m-Ph). $\mu_{eff} = 3.76$ μ_B ($\chi_g = 12.77 \cdot 10^{-6}$ cgsu, molar diamagnetic correction: $2.32 \cdot 10^{-2}$ cgsu). EPR (toluene, 105 K): $g_x = 4.306$; $g_y = 3.635$; $g_z = 1.989$. Visible (CH_2Cl_2, λ_{max}/nm (ε/cm^{-1} M^{-1})): 518 (135), 662 (461).

Sodium reduction of $CpCrCl_2(PMe_3)$

Compound $CpCrCl_2(PMe_3)$ (0.689 g, 2.62 mmol) was dissolved in THF (60 ml) and the resulting blue solution was transferred into a Schlenk where 1% sodium amalgam (64 mg, 2.8 mmol of Na) had previously been prepared. The resulting mixture was stirred at room temperature for 12 h to afford rapid precipitation of a white solid, presumably NaCl. The final solution had a dark color. After filtration through Celite, the dark solution was evaporated to dryness and the residue was extracted with hexane and filtered. Cooling the resulting yellow-brown solution to −80°C afforded brown crystals, which were identified as Cp_2Cr by elemental analysis and comparison of the ^1H NMR ($\delta_{Cp} = 320$ ppm) and cyclic voltammetric properties (rev. oxidation at $E_{1/2} = -1.1$ V vs Cp_2Fe) with those reported in the literature [9]. Further work-up of the residue of the

hexane extraction did not lead to other soluble products.

Sodium reduction of $CpCrCl_2(\eta^1$-dppe)

Compound $CpCrCl_2(\eta^1$-dppe) (2.039 g, 3.48 mmol) was dissolved in THF (30 ml) and the resulting blue solution was transferred into a Schlenk where 1% sodium amalgam (80 mg, 3.5 mmol of Na) had previously been prepared. The resulting mixture was stirred at room temperature for 12 h to afford a brown suspension with precipitation of a white solid. After filtration through Celite, the solution was evaporated to dryness and the residue was extracted with hexane and filtered. Cooling the resulting yellow-brown solution to −80 C afforded brown crystals of Cp_2Cr (see previous section). The residue of the extraction is a beige solid which is soluble in THF. Its ^1H and ^{31}P NMR spectrum in C_6D_6 shows only the presence of free dppe. After nitric acid attack, the solution gives a positive test for the chloride ion.

A solid identical in appearance and solubility properties to this beige residue is obtained by sodium amalgam reduction of $CrCl_3(THF)_3$. Treatment of this solid with dppe in THF does not lead to any observable change.

RESULTS AND DISCUSSION

The new compounds $CpCrCl_2L$ (L = PMe_2Ph, **1**; $PMePh_2$, **2**; PPh_3, **3**) have been prepared by following the same protocol previously used for the analogous compounds where L = PMe_3, PEt_3, η^1-dmpm, η^1-dmpe, and η^1-dppe [7,8]. This consists of exchange of THF by the appropriate phosphine on compound $CpCrCl_2(THF)$, which is obtained *in situ* from $CrCl_3(THF)_3$ and NaCp.

The spin quartet ground state for the class of 15-electron CpCr(III) compounds has previously been established [10]. In accordance with previous findings, the measured magnetic moments for compounds **1–3** is close to the spin-only value expected for three unpaired electrons. The ^1H-NMR properties of compounds **1–3** are also in accord with those reported for similar compounds [7,8]. The relatively short electronic relaxation times for the magnetic states of the spin quartet compounds are responsible for the observation of paramagnetically shifted but relatively sharp NMR resonances for the protons. Only the resonance of the *ortho* phenyl protons could not be clearly identified. Furthermore, the coordinated P nucleus does not lead to the observation of any resonance in the ^{31}P NMR spectrum. The short electronic relaxation times are also responsible for the absence of an EPR spectrum at room temperature for these complexes. A rhombic spectrum, however, can be observed in the glassy state at low temperature, in conformity with previous analogues [8,11].

A variable temperature magnetic study had apparently not been carried out on any of the previously reported complexes of this class. Compound **1** has been investigated in detail in $CDCl_3$. The position of the ^1H NMR resonances for the various observed protons as a function of the inverse temperature gives straight lines (see Fig. 1), in accordance with the expected Curie–Weiss behavior of the magnetically diluted complex.

Complexes **1–3,** like the previously reported analogues, are blue. Visible absorption bands are therefore expected. Indeed, compounds **1–3** show a strong (ε = 500–1000 cm^{-1} M^{-1}) and broad absorption in the 600–750 nm region, which is probably the overlap of two or more transitions, in addition to a weaker (ε = 150–500) and more blue-shifted (450–500 nm) absorption. These spectra are similar to those previously reported for $CpCrCl_2(L)$ (L = η^1-dmpm, -dmpe, and -dppe) [8]. Although qualitatively similar, the spectra of the various compounds show significant differences, with the more methyl-substituted derivatives showing slightly blue shifted and more intense absorption bands relative to more phenyl-substituted derivatives. This feature is being exploited for the determination of the ligand exchange kinetics by stopped-flow with visible monitoring. A preliminary ^1H NMR investigation shows that the $CpCrCl_2(PMe_3)/PMe_3$ self-exchange process is too slow for accurate kinetics to be determined by the line-broadening technique, while the use of PMe_3-d^9 shows that it is too fast for a classic mixing and monitoring study.

To the best of our knowledge, an electrochemical

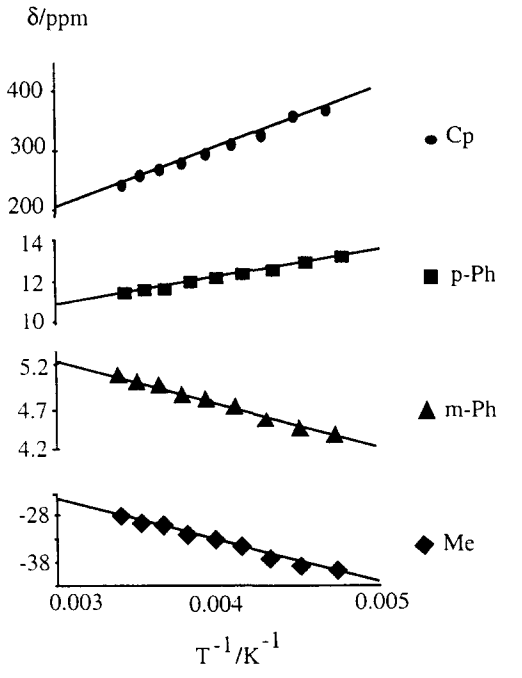

Fig. 1. Chemical shifts for compound **1** as a function of temperature. Solvent = $CDCl_3$.

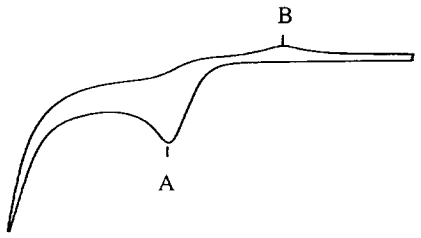

Fig. 2. A typical cyclic voltammogram for compounds $CpCrCl_2L$ in CH_2Cl_2 (see Table 1 for the list of L ligands and potentials for waves A and B).

Table 1. Cyclic voltammetric parameters for the study of compounds $CpCrCl_2L$ in CH_2Cl_2 at room temperature[a]

L	$E_{p,c}$ (A)[b] V	$E_{p,a}$ (B)[b] V
PMe_3	−1.60	−1.10
PMe_2Ph	−1.58	−1.06
$PMePh_2$	−1.51	−0.89
PPh_3	−1.61	−1.02
PEt_3	−1.72	−1.08
η^1-dppe	−1.58	−1.14

[a] Values of potentials are relative to the ferrocene internal standard.

[b] See Fig. 2 for the definition of waves A and B.

investigation has never been reported for dichloride CpCr(III) complexes of this stoichiometry. On the other hand, coordination compounds of Cr(III) are known to afford, by reduction, related complexes of Cr(II). The related alkyl derivative $[Cp^*CrMe(dmpe)]^+$ has been shown to undergo a reversible electrochemical and chemical reduction to the neutral Cr(II) complex [12]. We have therefore carried out a cyclic voltammetric investigation on compounds **1**–**3**, as well as on the previously reported analogous complexes with PMe_3, PEt_3, and η^1-dppe ligands. As expected, a reduction process takes place (wave A in Fig. 2). This, however, is irreversible and is followed by a smaller intensity, irreversible oxidation wave at a more positive potential (wave B in Fig. 2). The spectrum is qualitatively identical for all compounds investigated, with the related potentials being collected in Table 1. The voltammogram of compound $CpCrCl_2(\eta^1$-dppe) is characterized also by a second reduction wave at $E_{p,c} = -1.98$ V.

The results of a chemical reduction study suggest a possible explanation for the cyclic voltammetric results. A sodium amalgam reduction was carried out on compounds $CpCrCl_2(PMe_3)$ and $CpCrCl_2(\eta^1$-dppe). The PMe_3 complex gave rise to a mixture of Cp_2Cr and uncharacterized inorganic species. The dppe complexes analogously gave rise to Cp_2Cr and free dppe, accompanied by a beige solid that contains chloride and that appears identical to a solid obtained by sodium amalgam reduction of $CrCl_3(THF)_3$. Therefore, we propose the mechanism shown in Scheme 1 for both the electrochemical and chemical reductions.

Following the reduction process to the 16-electron Cr(II) anion, a fast chemical process must occur according to the electrochemical study. This is likely to be loss of the chloride ion, since the chemical reduction study shows rapid precipitation of a white solid, presumably NaCl. The presumed CpCrClL intermediate is not susceptible to oxidation at accessible potentials, since the oxidation scan of the voltammogram does not show oxidation waves of the same intensity as the initial reduction wave. Given that this complex is electron deficient (14-electron), it is reasonable to imagine that its oxidation might be difficult. This proposed intermediate proceeds to an apparent ligand redistribution reaction, since chromocene has been identified as one of the products for the reduction of both PMe_3 and dppe complexes. Isolated chromocene shows an oxidation process at a potential corresponding to process B in Fig. 2.

The stoichiometry of the ligand redistribution process in Scheme 1 allows a second product of stoichiometry $CrCl_2L_2$. However, a $CrCl_2(PMe_3)_2$ complex is not known and our attempts to characterize the inorganic material produced by the reduction of the PMe_3 complex have been unfruitful. The same ligand redistribution process occurs for the reduction of the dppe complex. In this case, a 6-coordinate $CrCl_2(dppe)_2$ complex might be obtained. This would be similar to the reported $CrCl_2(LL)_2$ complexes with LL = dmpe [13] and dippe [14]. However, a previous report shows that the $CrCl_2(dppe)_x$ complex is rather unstable and easily loses dppe [15]. Our

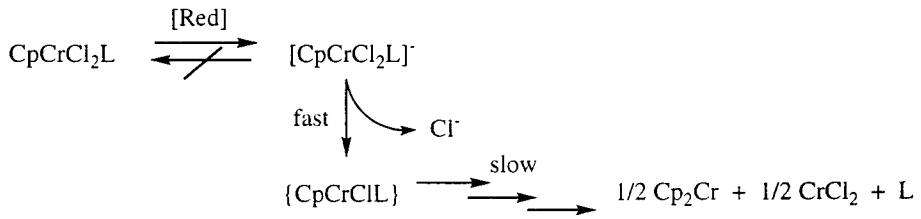

Scheme 1.

observations are fully consistent with these previous findings.

It is to be noted that, while a 14-electron $CpCrCl(PMe_3)$ intermediate is likely to gain stability by formation of a di-μ-chloro bridged dimer, opening the way to ligand scrambling with formation of the proposed products of Scheme 1, the corresponding $CpCrCl(\eta^1$-dppe) intermediate also has the possibility of stabilizing itself by chelation and formation of a mononuclear 16-electron $CpCrCl(\eta^2$-dppe). The result of the electrochemical and chemical reduction studies clearly indicate that either this does not occur, or the phosphine chelation process must be a fast and reversible process. Interestingly, however, the analogous 16-electron $Cp^*Cr(CH_3)$(dmpe) complex is stable [12]. This difference could be attributed to the ability of the chloride ligand to bridge the two metals and/or to the greater ionic character of the Cr—Cl bond relative to the Cr—CH_3 bond, also favoring the ligand exchange process.

In conclusion, we have synthesized a greater number of 15-electron complexes of the $CpCrCl_2L$ family and thoroughly investigated their physical and spectroscopic properties. A preliminary investigation shows that a study of the phosphine exchange kinetics is accessible by fast mixing methods. The reduction of these derivatives to the Cr(II) state triggers a ligand redistribution reaction with formation of chromocene and unstable inorganic Cr(II)-phosphine complexes.

Acknowledgements—We are grateful to the National Science Foundation (grant CHE-9508521) and to the Région Bourgogne for support of this work.

REFERENCES

1. Cole, A. A., Fettinger, J. C., Keogh, D. W. and Poli, R., *Inorg. Chim. Acta*, 1995, **240,** 355–366.
2. Cacelli, I., Keogh, D. W., Poli, R. and Rizzo, A., *New J. Chem.*, 1997, **21,** 133–135.
3. Cacelli, I., Keogh, D. W., Poli, R. and Rizzo, A., *J. Phys. Chem.*, 1997, **101,** 9801–9812.
4. Abugideiri, F., Keogh, D. W., Kraatz, H.-B., Poli, R. and Pearson, W., *J. Organomet. Chem.*, 1995, **488,** 29–38.
5. Fettinger, J. C., Keogh, D.W. and Poli, R., *J. Am. Chem. Soc.*, 1996, **118,** 3617–3625.
6. Herwig, W. and Zeiss, H. H., *J. Org. Chem.*, 1958, **23,** 1404.
7. Grohmann, A., Köhler, F. H., Müller, G. and Zeh, H., *Chem. Ber.*, 1989, **122,** 897–899.
8. Fettinger, J. C., Mattamana, S. P., Poli, R. and Rogers, R. D., *Organometallics*, 1996, **15,** 4211–4222.
9. Robbins, J. L., Edelstein, N., Spencer, B. and Smart, J. C., *J. Am. Chem. Soc.*, 1982, **104,** 1882–1893.
10. Fischer, E. O., Ulm, K. and Kuzel, P., *Z. Anorg. Allg. Chem.*, 1963, **319,** 253–265.
11. Barrera, J. A. and Wilcox, D. E., *Inorg. Chem.*, 1992, **31,** 1745–1752.
12. Thomas, B. J., Noh, S. K., Schulte, G. K., Sendlinger, S. C. and Theopold, K. H., *J. Am. Chem. Soc.*, 1991, **113,** 893–902.
13. Girolami, G. S., Salt, J. E., Wilkinson, G., Thornton-Pett, M. and Hursthouse, M. B., *J. Am. Chem. Soc.*, 1983, **105,** 5954–5956.
14. Hermes, A. R., Morris, R. J. and Girolami, G. S., *Organometallics*, 1988, **7,** 2372–2379.
15. Ellermann, J., Hagen, K. and Krauss, H. L., *Z. Anorg. Allg. Chem.*, 1982, **487,** 130–140.

Pergamon

PII: S0277-5387(97)00499-3

Polyhedron Vol. 17, No. 7, pp. 1121–1131, 1998
© 1998 Elsevier Science Ltd
All rights reserved. Printed in Great Britain
0277-5387/98 $19.00+0.00

Cycloalkanes as ligand backbones part 5 [1] coordination chemistry of *trans*-2-pyrazol-1-ylcyclohexan-1-ol and derivatives: synthesis, spectroscopic features and solid state structures of first and second row transition metal complexes†

M. Barz, E. Herdtweck and W. R. Thiel*

Anorganisch-chemisches Institut der Technischen Universität München, Lichtenbergstr. 4, D-85747 Garching, Germany

(Received 25 September 1997; accepted 22 October 1997)

Abstract—The synthesis and spectroscopic and structure chemical properties of complexes with the ligands *trans*-2-pyrazol-1-ylcyclohexan-1-ol (**1**), *cis*-(1-amino)(2-pyrazol-1-yl)cyclohexane (**2**) and 2-pyrazol-1-ylcyclohexanonoxime (**4**) coordinated to a variety of first and second row transition metals are described. These new systems bear cycloalkane backbones, which give rise to rigid ligand arrangements at the metal centre. X-ray crystallographic investigations of the copper(II) complexes $CuCl_2(\mathbf{1})_2 \cdot (H_2O)_2$ (**5e**) and $[Cu(\mathbf{1})_2](CuCl_4)$ (**5f**) proved the coordination of two different enantiomers of ligand **1** to one copper centre. Owing to their d^9 configuration, both octahedrally coordinated metal centres show typical Jahn-Teller distortions with either loosely bound chloro ligands or bridging $CuCl_4^{2-}$ anions occupying the apical positions. The copper(II) complex $[CuCl_2(\mathbf{2})]_2 \cdot$ (**6**) forms dimers in the solid state, wherein the trigonal bipyramidally coordinated Cu centres are linked by bridging chloro ligands. © 1998 Elsevier Science Ltd. All rights reserved

Keywords: chiral ligands; amino alcohols; transition metal complexes; crystal structure.

During the last years, complexes of 1,2-amino alcohols have been applied for MOCVD [2] and, in the case of chiral systems, as catalysts for enantioselective transformations [3]. While the coordination chemistry of aliphatic 1,2-amino alcohols is well established [4], relatively few transition and main group element complexes bearing chelating 1,3-amino alcohols [5] or 1,2-amino alcohols with aromatic *N*-donor sites [6], have been structurally investigated. We are interested in 1,3-amino alcohols with aromatic pyrazolyl *N*-donor fragments, where both donor sites are attached to a rigid cyclolkane backbone. These ligands can be obtained easily and in high yields by nucleophilic attack of a pyrazole derivative to an epoxicycloalkane. The reaction leads, under opening of the oxirane ring, to the corresponding 1,2-*trans* configurated cycloalkanols, with both substituents in equatorial orientation (Scheme 1).

Since we are interested in these compounds as chiral ligands for enantioselective catalysis, we worked out a route for kinetic resolution of the resulting racemates. In the presence of lipase B from *candida antarctica*, the esterification of the (*R*,*R*)-enantiomers is performed with enantiomeric excesses of more than 95% [7]. The resulting esters can be separated from the alcohols by crystallization or preparative MPLC. Following this procedure, both enantiomers of the chelate ligands are available in amounts of several grams in high stereochemical purity. These new chiral compounds are also versatile starting materials for the synthesis of enantiomerically pure multidentate ligand systems. In this paper, we report the coordination chemistry of *trans*-2-pyrazol-1-ylcyclohexan-1-ol (**1**)

* Author to whom correspondence should be addressed.

† Dedicated to Prof. Dr. Drs. h. c. W. A. Herrmann on the occassion of his 50th birthday.

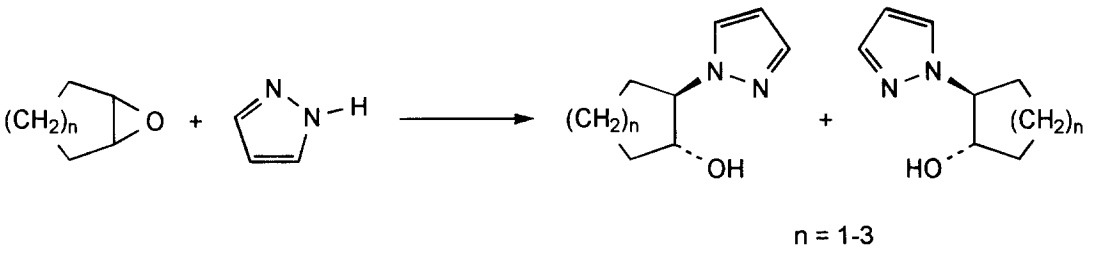

Scheme 1.

and two other new pyrazolylcyclohexane derivatives, chelated to first and second row transition metals.

EXPERIMENTAL

General

trans-2-Pyrazol-1-ylcyclohexan-1-ol (**1**), *cis*-(1-amino)(2-pyrazol-1-yl)cyclohexane (**2**) and $(C_6H_5CN)_2PdCl_2$ were synthesized according to published procedures [7a, 7c, 8]. All other starting materials were purchased from Aldrich. The NMR (Bruker DPX 400), infrared (Perkin–Elmer 1600 Series FTIR) and mass spectra (GC–MS: Hewlett-Packard gaschromatograph HP 5890 and mass selective detector HP 5970) and all elemental analyses were carried out at the *Anorganisch-chemisches Institut der TU München*. The NMR spectra are assigned according to Scheme 2.

rac-2-Pyrazol-1-ylcyclohexanone (**3**)

DMSO (22 ml, 330 mmol) is added to a solution of **1** (22.6 g, 138 mmol) in CH_2Cl_2 (100 ml) stirred at $-60°C$ and kept under nitrogen. After 30 min, oxalic chloride (12.2 ml, 152 mmol) is added dropwise, with keeping the temperature carefully at $-60°C$. After 1 h, triethylamine (89 ml, 640 mmol) is added. The reaction mixture is stirred for 1 h at $-60°C$ and then quenched by the addition of water (100 ml). The aqueous layer is separated and extracted with CH_2Cl_2 (4×30 ml), the combined organic phases are washed with brine and dried over $MgSO_4$. Removing the solvent and sublimation *in vacuo* yields **3** (15.5 g, 95 mmol, 69%) as a colourless solid. IR (KBr): ν (C=O) 1714 vs, cm^{-1}; ^1H NMR δ_H (400.13 MHz, 25°C, $CDCl_3$) ppm: 7.52 (d, 1H, $^3J_{1,2}$ 2.0 Hz, 1-H), 7.40 (d, 1H, $^3J_{2,3}$ 2.5 Hz, 3-H), 6.31 (t, 1H, 2-H), 5.01 (dd, 1H, $^3J_{4,5\text{-eq}}$ 5.5 Hz, $^3J_{4,5\text{-ax}}$ 13.0 Hz, 4-H), 2.61–1.70 (m, 8H, CH_2); $^{13}C\{^1H\}$ NMR δ_C (100.25 MHz, 25°C, $CDCl_3$) ppm: 204.9 (C-9), 139.0 (C-1), 128.7 (C-3), 105.8 (C-2), 69.0 (C-4), 41.0 (C-8), 34.3 (C-5), 27.1 (C-7), 24.6 (C-6); MS (EI) m/z (%): 164 (19) [M^+], 136 (35) [$(M—CO)^+$], 107 (27) [$C_8H_{11}^+$], 95 (38) [$C_3H_3N_2$-$C_2H_4^+$], 81 (53) [$C_3H_3N_2$-CH_2^+], 69 (100) [$C_3H_5N_2^+$], 55 (14) [$C_4H_7^+$], 41 (34) [$C_3H_5^+$].

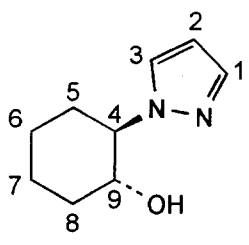

Scheme 2.

rac-2-Pyrazol-1-ylcyclohexanonoxime (**4**)

1.0 M NaOH (30 ml) is added dropwise to a solution of **3** (4.59 g, 28 mmol) and $[NH_3OH]Cl$ (1.93 g, 28 mmol) in H_2O (100 ml). After 12 h of stirring, the resulting precipitate is filtered off, washed with H_2O and dried *in vacuo*, yielding **4** (4.5 g, 25 mmol, 90%) as a colourless microcrystalline solid. Found: C, 60.28; H, 7.29; N, 23.55. Calc. for $C_9H_{13}N_3O$: C, 60.32; H, 7.31; N, 23.45%. IR (KBr): ν (O—H) 3261 s, ν (C=N) 1672 w, cm^{-1}. ^1H NMR δ_H (400.13 MHz, 25°C, $CDCl_3$) ppm: 7.59 (s, 1-H), 7.47 (s, 3-H), 6.29 (s, 2-H), 4.86 (m, 2H, 4-H, OH), 2.59–1.65 (m, 8H, CH_2). $^{13}C\{^1H\}$ NMR δ_C (100.25 MHz, 25°C, $CDCl_3$) ppm: 157.5 (C-9), 139.7 (C-1), 130.6 (C-3), 106.4 (C-2), 62.9 (C-4), 33.5 (C-8), 26.1 (C-5), 23.7 (C-7), 23.6 (C-6). MS (EI) m/z (%): 179 (12) [M^+], 162 (14) [$(M—HO)^+$], 147 (1) [$(M—NH_2O)^+$], 110 (6) [$(M—C_3H_5N_2)^+$], 81 (54) [$C_6H_9^+$], 69 (100) [$C_3H_5N_2^+$], 32 (4) [NH_2O^+].

Synthesis of transition metal complexes, general procedure

10 mmol of the ligand and 5 mmol of the corresponding metal salt are dissolved in MeOH and heated under reflux conditions for 6 h. After removal of the solvent *in vacuo*, the resulting microcrystalline solids are washed with diethylether and dried *in vacuo*. Recrystallization from MeOH gives crystalline materials.

[Dichlorobis(2-pyrazol-1-ylcyclohexan-1-ol)chromium(III)]chloride (**5a**)

From $[Cr(H_2O)_6]Cl_3$; yield: 52%, green microcrystalline solid. Found: C, 43.74; H, 6.13; N, 11.32. Calc. for $C_{18}H_{28}Cl_3CrN_4O_2$: C, 44.05; H, 5.75; N, 11.42%. IR (KBr): ν (O—H) 3413 vs, 3131 s, cm^{-1}.

Dichlorobis(2-pyrazol-1-ylcyclohexan-1-ol)iron(II) (**5b**)

From $[Fe(H_2O)_6]Cl_2$; yield: 56%, yellow microcrystalline solid. Found: C, 46.94; H, 6.18; Cl, 15.42; Fe, 12.12; N, 12.25. Calc. for $C_{18}H_{28}Cl_2FeN_4O_2$: C, 47.08; H, 6.15; Cl, 15.44; Fe, 12.16; N, 12.20%. IR (KBr): ν (O—H) 3152 vs, cm^{-1}.

Dichlorobis(2-pyrazol-1-ylcyclohexan-1-ol)cobalt(II) (**5c**)

From $[Co(H_2O)_6]Cl_2$; yield: 82%, violet microcrystalline solid. Found: C, 46.61; H, 6.15; N, 12.05. Calc. for $C_{18}H_{28}Cl_2CoN_4O_2$: C, 46.77; H, 6.10; N, 12.12%. IR (KBr): ν (O—H) 3138 vs, cm^{-1}.

Dichlorobis(2-pyrazol-1-ylcyclohexan-1-ol)nickel(II) (**5d**)

From $[Ni(H_2O)_6]Cl_2$; yield: 92%, pale green microcrystalline solid. Found: C, 46.43; H, 6.25; Cl, 15.25; N, 12.44; Ni, 13.02. Calc. for $C_{18}H_{28}Cl_2N_4NiO_2$: C, 46.79; H, 6.11; Cl, 15.35; N, 12.13; Ni, 12.70%. IR (KBr): ν (O—H) 3121 vs, cm^{-1}.

Dichlorobis(2-pyrazol-1-ylcyclohexan-1-ol)copper(II) dihydrate (**5e**) *and* [bis(2-pyrazol-1-ylcyclohexan-1-ol)copper(II)]tetrachlorocuprate(II) (**5f**)

From $Cu(H_2O)_2Cl_2$; yield: 54%. Recrystallization from MeOH results first in the formation of blue crystals of **5e** and finally in the formation of a small amount (< 10%) of green crystals of **5f**. Analytical data of **5e**: Found: C, 42.77; H, 6.41; Cl, 14.15; Cu, 12.50; N, 11.35. Calcd. for $C_{18}H_{28}Cl_2CuN_4O_2 \cdot (H_2O)_2$: C; 42.98, H, 6.41; Cl, 14.10; Cu, 12.63; N, 11.14%. IR (KBr): ν (O—H) 3287 vs, 3142 vs, cm^{-1}. Analytical data of **5f**: Found: C, 35.80; H, 4.75; Cl, 23.67; Cu, 21.00; N, 9.43. Calc. for $C_{18}H_{28}Cl_4Cu_2N_4O_2$: C, 35.96; H, 4.69; Cl, 23.59; Cu, 20.11; N, 9.32%. IR (KBr): ν (O—H) 3133 s, cm^{-1}.

[Bis(2-pyrazol-1-ylcyclohexan-1-ol)zinc(II)] tetranitratozincate(II) (**5g**)

From $[Zn(H_2O)_6](NO_3)_2$; yield: 90%, colourless microcrystalline solid. Found: C, 30.00; H, 4.43; N, 15.28. Calc. for $C_{18}H_{28}N_8O_{14}Zn_2$: C, 30.40; H, 3.97; N, 15.76%. IR (KBr): ν (O—H) 3484 s, ν (NO_3) 1386, 1353, cm^{-1}. ^1H NMR δ_H (400.13 MHz, 25°C, CDCl3) ppm: 7.87 (d, 1H, $^3J_{1,2}$ 2.5 Hz, 1-H), 7.75 (d, 1H, $^3J_{2,3}$ 2.5 Hz, 3-H), 6.53 (t, 1H, 2-H), 4.18 (ddd, 1H, $^3J_{8,9ax}$ 4.0 Hz, $^3J_{8,9eq}$ 9.8 Hz, $^3J_{4,9}$ 12.0 Hz, 9-H), 3.79 (ddd, 1H, $^3J_{4,5ax}$ 4.5 Hz, $^3J_{4,5eq}$ 8.2 Hz, 4-H), 2.72 (br, 1H, OH), 2.26–1.31 (m, 8H, CH_2). ^{13}C NMR δ_C (100.13 MHz, 25°C, CDCl3) ppm: 141.0 (C-1), 131.0 (C-3), 106.8 (C-2), 75.2 (C-9), 64.4 (C-4), 34.2 (C-8), 29.5 (C-5), 24.4 (C-6), 23.5 (C-7).

(Acetylacetonato)(*cis*-dioxo)(*rac-trans*-2-pyrazol-1-ylcyclohexyloxy)molybdenum(VI) (**5h**)

A solution of **1** (0.83 g, 5.00 mmol) in absolute ethanol (10 ml) is added within a period of 5 min to a solution of $MoO_2(acac)_2$ (0.82 g, 2.50 mmol) in absolute ethanol (20 ml). After stirring at room temperature for 2 d, the solvent is removed *in vacuo* and the resulting pale orange residue is washed several times with diethylether and dried *in vacuo*. Yield: 72%, colourless microcrystalline, air and moisture sensitive solid. Found: C, 42.65; H, 5.12; N, 7.18; Mo, 24.30. Calc. for $C_{14}H_{20}MoN_2O_5$: C, 42.87; H, 5.14; N, 7.14; Mo, 24.46%. IR (KBr) ν (C=O) 1615 s, 1517 vs, ν (Mo=O) 924 vs, 904 vs, cm^{-1}. ^1H NMR δ_H (400.13 MHz, 25°C, $CDCl_3$) ppm: 7.59 (d, 1H, $^3J_{1,2}$ 2.5 Hz, 1-H), 7.28 (d, 1H, $^3J_{2,3}$ 2.5, 3-H), 6.31 (t, 1H, 2-H), 5.70 (s, 1H, CO-CH-CO), 4.47 (br, 2H, 4-H, 9-H), 2.14 (s, 3H, CH_3), 2.05 (s, 3H, CH_3), 2.52–1.29 (m, 8H, CH_2). $^{13}C\{^1H\}$ NMR δ_C (100.25 MHz, 25°C, $CDCl_3$) ppm: 190.6 (2 × CO), 139.4 (C-1), 128.3 (C-3), 105.6 (C-2), 104.0 (CO—*C*H—CO), 85.4 (C-9), 63.7 (C-4), 33.5 (C-8), 29.5 (C-5), 27.8 (C-6), 26.2 (C-7), 24.1 (2 × CH_3).

(1-Amino-2-pyrazol-1-ylcyclohexan)dichlorocopper(II) (**6**)

From $Cu(H_2O)_2Cl_2$; yield: 38%, turquoise microcrystalline solid. Found: C, 36.12; H, 4.95; Cl, 23.28; Cu, 20.10; N, 14.02. Calc. for $C_9H_{15}Cl_2CuN_3$: C, 34.68; H, 4.85; Cl, 22.75; Cu, 20.39; N, 13.48%. IR (KBr): ν (N—H) 3443 s, 3249 s, 3202 s, cm^{-1}.

Dichloro(2-pyrazol-1-yl-cyclohexanonoxime)palladium(II) (**7**)

$PdCl_2(C_6H_5CN)_2$ (0.38 g, 1.00 mmol) is added to a slurry of **4** (0.18 g, 1.00 mmol) in CH_2Cl_2 (15 ml). The resulting orange coloured clear solution is stirred for 30 min, filtered to remove traces of elemental pal-

ladium and added dropwise to *n*-pentane (50 ml). **7** precipitates as a bright orange coloured microcrystalline solid, which is washed with diethylether (2 × 50 ml) to remove benzonitrile and dried *in vacuo*. Yield: 92%. Found: C, 30.41; H, 3.70; N, 11.87. Calc. for $C_9H_{13}Cl_2N_3OPd$: C, 30.32; H, 3.68; N, 11.79%. IR (KBr): *v* (O—H) 3136 s, 3118 s, 3100 s, *v* (C=N) 1652 w, cm^{-1}. ^1H NMR δ_H (400.13 MHz, 25°C, DMSO-d_6) ppm: 8.04 (s, 1-H), 7.66 (s, 3-H), 6.38 (s, 2-H), 5.55 (m, 2H, 4-H, OH), 2.59–1.65 (m, 8H, CH_2). $^{13}C\{^1H\}$ NMR δ_C (100.25 MHz, 25°C, DMSO-d_6) ppm: 162.3 (C-9), 142.0 (C-1), 132.9 (C-3), 107.4 (C-2), 59.7 (C-4), 28.4 (C-8), 26.0 (C-5), 21.4 (C-7), 20.2 (C-6).

Crystallographic structure determination of the copper complexes **5e**, **5f** *and* **6**

Crystals were fixed inside a Lindemann class capillary. The intensity data were obtained at 293 K (**5e**, **5f**) and 193K(**6**) with graphite monochromated Mo-K_α radiation on an Enraf Nonius CAD4 diffractometer (**5e**), an Enraf-Nonius MACH3 diffractometer (**5f**) and on a STOE IPDS (**6**). Preliminary positions of heavy atoms were found by direct methods (SIR92 [9]), while positions of the other non-hydrogen atoms were determined from successive Fourier difference maps coupled with an initially isotropic least squares refinement (SHELXL93 [10]) in the program system STRUX-V [11]. The hydrogen atoms of **5e** and **5f** were located in the difference Fourier maps and refined with isotropic temperature parameters. For **6**, hydrogen atoms were placed in calculated positions and included in the structure factor calculations but not refined. Additional crystal data, data collection and refinement parameters are presented in Table 1.

Crystallographic data (excluding structure factors) for the structures reported in this paper have been deposited with the Fachinformationszentrum Karlsruhe as supplementary publication with the CSD numbers 408002 (**5e**), 408003 (**5f**) and 408004 (**6**).

RESULTS AND DISCUSSION

Ligand synthesis

In the case of the amino alcohol **1**, obtained by reaction of epoxycyclohexane and pyrazole, the 1,2-*trans*-substitution pattern at the cycloalkane ring leads to an equatorial arrangement of the substituents and therefore to a chelate system with low steric demand, which should not cause severe problems of steric repulsion when coordinated to a transition metal centre. However, the steric demand of this type of ligands can be increased by a stereochemical inversion of the CH—OH carbon atom, leading to a 1,2-*cis* substituted cyclohexane. This type of substitution pattern will give rise to an almost perpendicular orientation of the cyclohexane fragment with respect to the plane defined by the metal atom and both donor centres of the chelate ligand. We thoroughly investigated the transformation of the hydroxy compound **1** into the corresponding amine **2**, which proceeds under inversion of the configuration [1] and which can either be achieved by tosylation, reaction with NaN_3 and reduction of the resulting azide or by a so-called Mitsunobu amination [12] (Scheme 3). Another way to influence the stereochemical properties of the chelate ligand is to oxidize the alcohol to the corresponding ketone **3**. Reaction of **3** with hydroxylammonium chloride leads to the oxime **4** (Scheme 3).

The molecular geometry of **3** and **4** is proved by their spectroscopic properties. While a broad absorption at 3245 cm^{-1} in the infrared spectrum of **1**, characteristic for a OH function included in hydrogen bonding, this absorption is no longer observed for **3**. However, an intense C=O absorption at 1714 cm^{-1} appears. In the infrared spectrum of the oxime **4**, a new absorption at 3261 cm^{-1} can be assigned to the O—H vibration of the N—OH fragment and a weak absorption at 1672 cm^{-1} is characteristic for the C=N vibration of oximes. The ^1H NMR and ^{13}C spectra of **3** and **4** differ only marginally. A large coupling constant ($^3J_{HH}$ = 13 Hz) of the proton of the CH-pz (pz = pyrazolyl) group proves the equatorial orientation of the pyrazole fragment at the six-membered aliphatic ring system. ^{13}C NMR resonances at 204.9 and 157.5 ppm are characteristic for aliphatic ketones and oximes, respectively.

Transition metal complexes

trans-2-Pyrazol-1-ylcyclohexan-1-ol (**1**) dissolved in methanol reacts with a variety of two- and trivalent first row transition metal halides in a 2 : 1 ratio, giving the chelate complexes **5a–g** (Scheme 4). However, the reaction of two equivalents of **1** with $MoO_2(acac)_2$ does not lead to the corresponding bischelate complex $MoO_2(\mathbf{1})_2$ but stops at the mono adduct $MoO_2(acac)(\mathbf{1})$ (**5h**).

This result is in contrast to observations of Herrmann *et al.*, who investigated ligand exchange reactions of $MoO_2(acac)_2$ in the presence of a series of 2-pyridinylmethanols. They found molybdenum complexes of the type $MoO_2(L—L)_2$ (L—L = 1-pyridinylmethanolato ligand) [13]. Only when the pyridine ring of the chelate ligand is *ortho* substituted, the steric demand of the ligand gives rise to the formation of a dinuclear molybdenum(VI) derivative of the type $[MoO_2(L—L)]_2(\mu\text{-}O)$. In our case, the reaction stops at the mono adduct **5h**, presumably for steric reasons. The second acetylacetonato ligand is not split off the metal centre to allow further nucleation. Owing to the strong Lewis-acidic Mo(VI) centre, the hydroxy function of the chelate ligand is deprotonated, forming a hydroxo donor moiety, manifested by the absence of an OH absorption in the infrared spectrum of **5h**. The oxo ligands are coor-

Table 1. Crystal data and summary of intensity data collection and structure refinement of **5e**, **5f** and **6**

Compound	**5e**	**5f**	**6**
Mol. formula	$C_{18}H_{32}Cl_2CuN_4O_4$	$C_{18}H_{28}Cl_4Cu_2N_4O_2$	$C_{18}H_{30}Cl_4Cu_2N_6$
Formula weight	502.94	601.36	599.38
Colour/shape	blue prisms	green prisms	turquoise prisms
Crystal size (mm^3)	0.75·0.64·0.53	0.46·0.38·0.30	0.51·0.38·0.31
Crystal system	monoclinic	monoclinic	monoclinic
Space group (Int. Tab. Nr.)	$P2_1/n$ (14)	C2/c (15)	$P2_1/c$ (14)
T (C)	20±1	20±1	−80±1
a (Å)	9.181(2)	13.522(3)	6.518(1)
b (Å)	14.891(1)	11.289(2)	13.593(1)
c (Å)	9.221(2)	15.069(3)	13.042(1)
α ( )	90	90	90
β ( )	117.58(1)	93.80(2)	90.80(1)
γ ( )	90	90	90
V ($Å^3$)	1117.4(4)	2295.2(8)	1155.4(1)
D_{calc} (g cm^{-3})	1.495	1.740	1.723
Z	2	4	2
$F(000)$	526	1224	612
μ_{calc} (cm^{-1})	12.5	23.4	23.2
Diffractometer	Enraf-Nonius CAD4	Enraf-Nonius Mach3	STOE IPDS
Scan type	ω-scan	ω-scan	oscillation
Radiation,graphite	Mo-K_α	Mo-K_α	Mo-K_α
Θ range ( )	$2.59 \leqslant \Theta \leqslant 29.96$	$2.35 \leqslant \Theta \leqslant 29.96$	$2.38 \leqslant \Theta \leqslant 27.66$
Range of h, k, l	0/12, 0/20, −12/11	−18/18, 0/15, −21/0	−8/8, −17/17, −11/17
Reflexions measured	3144	3240	6185
Independent reflexions	2985	3128	2580
Refl. observed $F_0 > 2 \cdot \sigma(I)$	2638	2917	2289
Refined parameters	197	194	136
R^a (obs. data)	0.0382	0.0223	0.0269
ωR_2^b (obs. data)	0.0928	0.0602	0.0711
GOF^c	1.075	1.109	1.107
Largest features final diff. map ($eÅ^{-3}$)	0.18/−0.20	0.44/−0.62	0.42/−0.45

$^a R = \Sigma||F_o|-|F_c||/\Sigma|F_o|$.
$^b \omega R_2 = [\Sigma\omega(F_o^2 - F_c^2)^2/\Sigma\omega F_o^2]^{1/2}$.
^{c} GOF $= [\Sigma\omega(F_o^2 - F_c^2)^2/(NO\text{-}NV)]^{1/2}$.

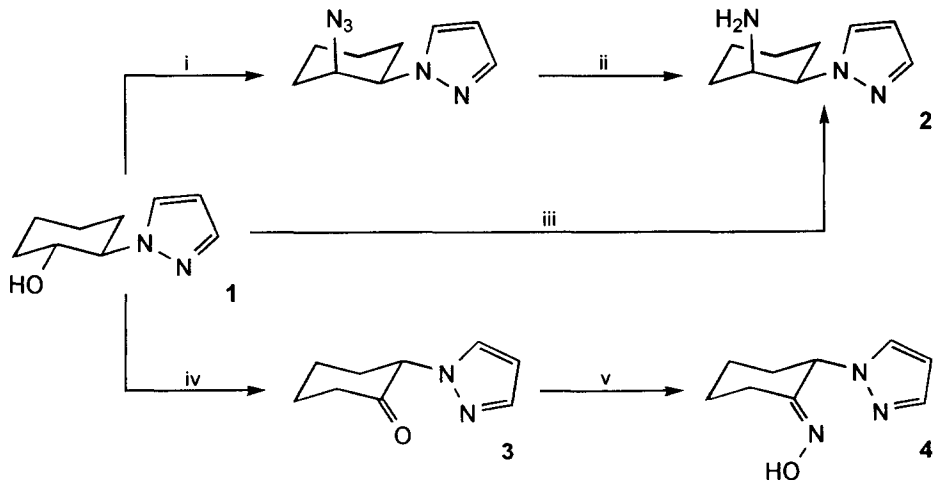

Scheme 3. (i) 1. TsCl, pyridine, room temp., 48 h, 2. NaN_3, dmf, 160°C, 3 h; (ii) $LiAlH_4$, diethylether, refl., 3 h; (iii) 1. EtOOC—N=N—COOEt, PPh_3, thf, 24 h, room temp., 2. N_2H_4, methanol, HCl, refl., 14 h; (iv) 1. DMSO, CH_2Cl_2, −60°C, 30 min, 2. $C_2O_2Cl_2$, −60°C, 1 h, 3. NEt_3, 1 h, −60°C; (v) NaOH, $[NH_3OH]Cl$, room temp.

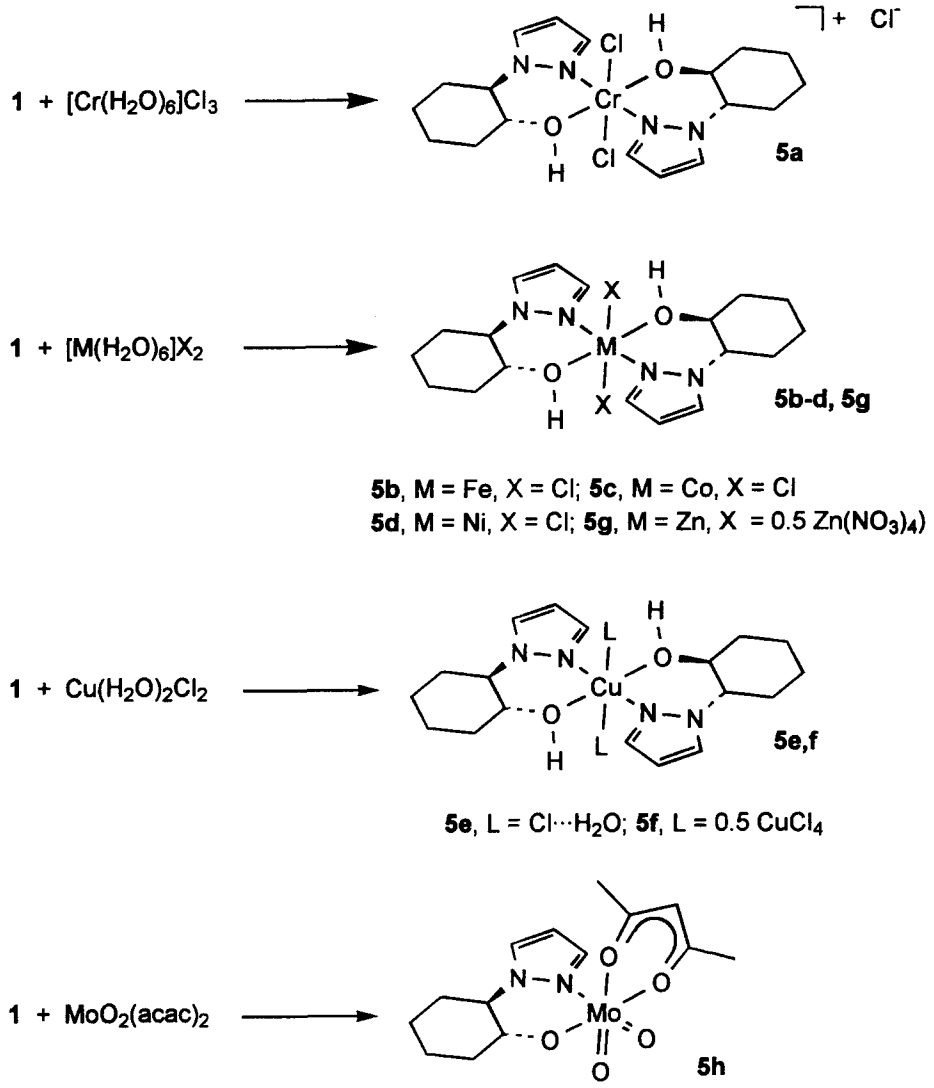

Scheme 4.

dinated in *cis* geometry, resulting in two Mo=O absorptions (924 vs and 904 vs cm^{-1}). Coordination shifts the ^1H NMR resonances of the protons at the substituted carbon atoms of the cyclohexane ring for about 0.67 ppm and the ^{13}C NMR resonance of the *C*H—OH group for about 12.3 ppm to lower field with respect to the free ligand **1**. In contrast to **5h**, the chelate ligands of the complexes **5a–g**, bearing two- and trivalent first row transition metal centres, are not deprotonated at the OH group, which is proved by elemental analysis as well as by infrared spectroscopy. The IR spectra show intense absorptions at 3150–3120 cm^{-1}, characteristic for coordinated hydroxy functions.

Reacting two equivalents of **1** with $Cu(H_2O)_2Cl_2$ in methanol gives $CuCl_2(\mathbf{1})_2 \cdot (H_2O)_2$ (**5e**), which should be comparable in its structure chemical features with the complexes **5a–d**. $[Cu(\mathbf{1})_2](CuCl_4)$ (**5f**), which is structurally comparable to **5g** and bears two differently coordinated copper(II) centres, was obtained as a side product in less than 10% yield. The solid state structures of both copper complexes were determined by means of X-ray structure analysis and will be discussed later on.

The amine **2** reacts with $Cu(H_2O)_2Cl_2$ in methanolic solution to yield the chelate complex $CuCl_2(\mathbf{2})$ (**6**) (Scheme 5). Since four-coordination by two amino and two chloro ligands is not observed for copper(II) centres, a bridging coordination of chloro ligands leads to the formation of a dinuclear complexes in the solid state, as it was found in a variety of Cu(II) complexes bearing chelating amines [14]. The solid state structure of the copper complex **6** was determined by means of X-ray structure analysis and will be discussed later on.

Reaction of the chelating oxime **4** with $(C_6H_5CN)_2PdCl_2$ gives, under exchange of the labile benzonitrile ligands, the palladium oxime complex **7** in almost quantitative yield (Scheme 6).

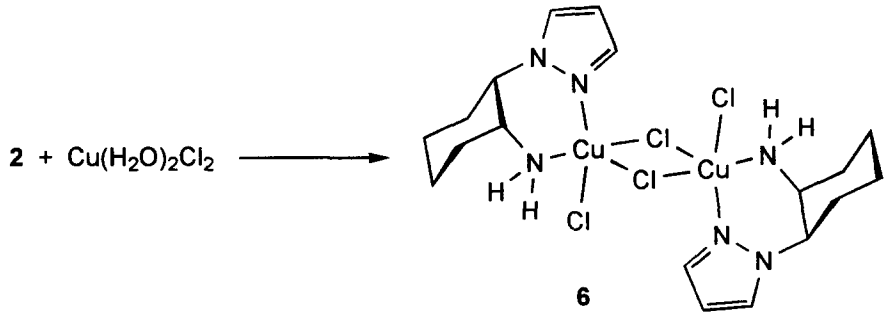

Scheme 5.

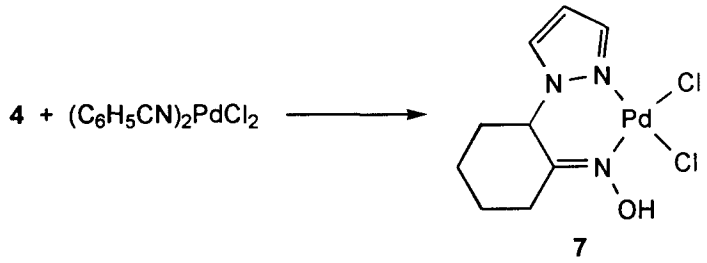

Scheme 6.

The chelating complexation of the Pd(II) centre by two nitrogen donors is proved by both infrared and NMR spectroscopic data of **7**. While the C=N stretching frequency shifts from 1672 (**4**) to 1652 cm^{-1} (**7**), the ν(O—H) shifts about 140 cm^{-1} to lower wavenumbers, indicating both, reduced C=N and O—H bond strengths. The coordination of the pyrazolyl moiety in **7** is manifested by a shift of the aromatic ^1H and ^{13}C NMR resonances to lower field, as well as a low-field shift of the ^{13}C resonance of the oxime carbon atom proves the coordination of the C=NOH group.

X-ray structure analysis

Figure 1 shows the coordination geometry of the metal centre of **5e**, which crystallizes from methanol as deep blue prisms in the monoclinic space group $P2_1/n$. The copper(II) ion, which is a centre of inversion, is coordinated in a distorted octahedral mode with long axial copper chlorine interactions and two chelate ligands occupying the equatorial positions of the polyhedron. All bond angles between the donor sites and the metal centre are close to 90°. Characteristic bond lengths and angles are presented in table 2.

Owing to the symmetry of **5e**, both enantiomers of **1** are found to coordinate one copper(II) ion, with the cyclohexane ring occupying a chair conformation. We suppose this mode of coordination to be the thermodynamically favoured one, since **5f** shows the same geometry and since we do not find any indications for the formation of diastereomers in the NMR spectra of the diamagnetic zinc complex **5g**. The Cu—N and Cu—O distances of **5e** are observed as expected [17]. The electronic configuration (d^9) of the copper centre leads to a typical Jahn-Teller distortion, with long Cu—Cl distances of 2.962(1) Å. For that reason, two additional molecules of water are included in the solid state structure of **5e**, forming stabilizing hydrogen bonds to the chloro ligands. The analogous complexes **5a–d** crystallize without adduct formation with water or methanol. Hydrogen bonding finally results in a two dimensional network shown in Figure 2.

In the complex **5f**, the weak coordination of the axial chloro ligands to the d^9 configurated copper(II) centre is not stabilized by hydrogen bonding but by involving an excess of $CuCl_2$ to form $CuCl_4^{2-}$ anions, which act as linkers between $[Cu(\mathbf{1})_2]^{2+}$ cations. **5f** crystallizes as green prisms in the monoclinic space group C2/c. Figure 3 shows a plot of the resulting chains parallel to the crystallographic c-axis, characteristic bond parameters are given in Table 2. This mode of chain formation by $CuCl_4^{2-}$ anions linking two transition metal centres has been observed only in two cases before [18].

Cu(1) is coordinated in a distorted octahedral mode with a Cu(1)—Cl(1) distance being about 0.14 Å shorter than in **5e**. The reason for this finding is a hydrogen bridge between OH and Cl(2) of the $CuCl_4^{2-}$ anion, which leads to the formation of a six-membered ring consistent of Cu(1), O(1), H(10), Cl(2), Cu(2), and

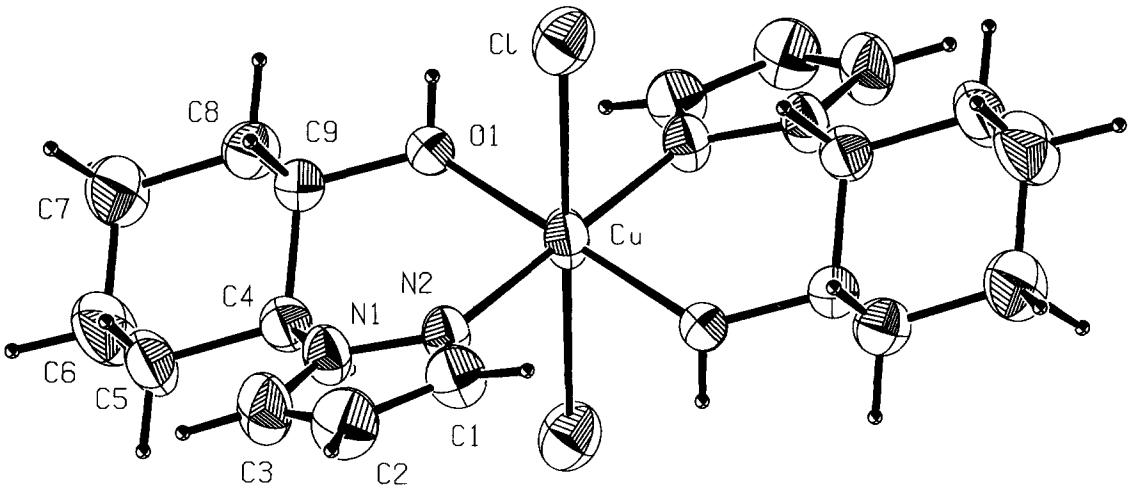

Fig. 1. PLATON plot [15] of the coordination sphere around the copper(II) centre of **5e**. Thermal ellipsoids are at the 50% level.

Table 2. Selected bond lengths (Å) and angles (°) of the copper complexes **5e** and **5f**

	5e		**5f**
	bond lengths [Å]		
Cu—O(1)	1.978(2)	Cu(1)—O	2.008(1)
Cu—N(2)	1.961(2)	Cu(1)—N(2)	1.957(1)
Cu—Cl	2.962(1)	Cu(1)—Cl(1)	2.822(1)
O(1)—H(10)	0.81(4)	O—H(10)	0.74(2)
O(2)—H(2A)	0.77(3)	Cu(2)—Cl(1)	2.233(1)
O(2)—H(2B)	0.80(5)	Cu(2)—Cl(2)	2.267(1)
O(2)—H(10)	1.80(3)	Cl(2)···H(10)[a]	2.29(2)
Cl···H(2A)[a]	2.40(3)	Cu(1)···Cu(2)[a]	4.293(1)
Cl···H(2B)[a]	2.34(5)		
	bond angles [°]		
O(1)—Cu—N(2)	90.08(7)	O—Cu(1)—N(2)	90.54(5)
O(1)—Cu—Cl	88.40(5)	O—Cu(1)—Cl(1)	94.39(4)
N(2)—Cu—Cl	89.95(6)	N(2)—Cu(1)—Cl(1)	97.88(4)
Cu—O(1)—C(9)	127.58(13)	Cu(1)—O—C(9)	128.13(9)
Cu—N(2)—N(1)	124.73(13)	Cu(1)—N(2)—N(1)	123.37(10)
Cu—O(1)—H(10)	112(2)	Cu(1)—O—H(10)	108(2)
C(9)—O(1)—H(10)	106(3)	C(9)—O—H(10)	110(2)
H(2A)—O(2)—H(2B)	113(4)	Cl(1)—Cu(2)—Cl(2)	97.07(3)
O(1)—H(10)···O(2)	171(3)	Cl(1)—Cu(2)—Cl(1A)	93.83(3)
O(2)—H(2A)···Cl	155(3)	Cl(2)—Cu(2)—Cl(2A)	94.89(3)
O(2)—H(2B)···Cl	168(4)	Cu(1)—Cl(1)—Cu(2)	115.77(3)
		O—H(10)···Cl(2)	177(2)

[a] Sum of van der Waals radii: $r^{vdw}(H)+r^{vdw}(Cl) = 1.20+1.80 = 3.00$ Å [17]

Cl(1). Cu(2) is coordinated in a distorted tetrahedral mode with short Cu(2)—Cl(1) and Cu(2)—Cl(2) distances of 2.233(1) and 2.267(1) Å. The interatomic distance between Cu(1) and Cu(2) is 4.293(1) Å.

The X-ray structure analysis of **6** shows a dinuclear Cu(II) complex, with the copper centres linked by bridging chloro ligands. These chloro ligands occupy two of the equatorial positions at the trigonal bipyramidally coordinated copper ions, while the 1,2-*cis*-substituted chelate ligands occupies the third equatorial (pyrazole) and one of the axial (NH_2) positions. Intra- and intermolecular hydrogen bondings of the NH_2 protons not only stabilize the dinuclear structures but also lead to the formation of infinite chains along the crystallographic a-axis. Figure 4 shows a plot of the one dimensional network of the hydrogen

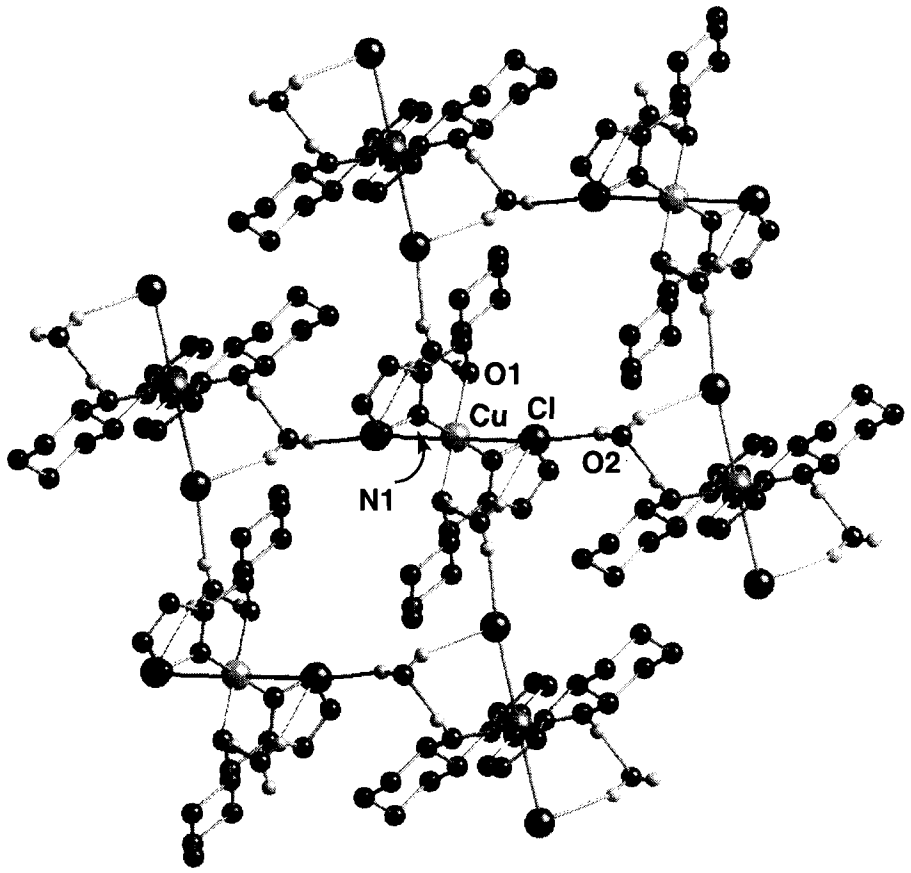

Fig. 2. Plot of the two dimensional network of hydrogen bondings in the solid state structure of **5e**.

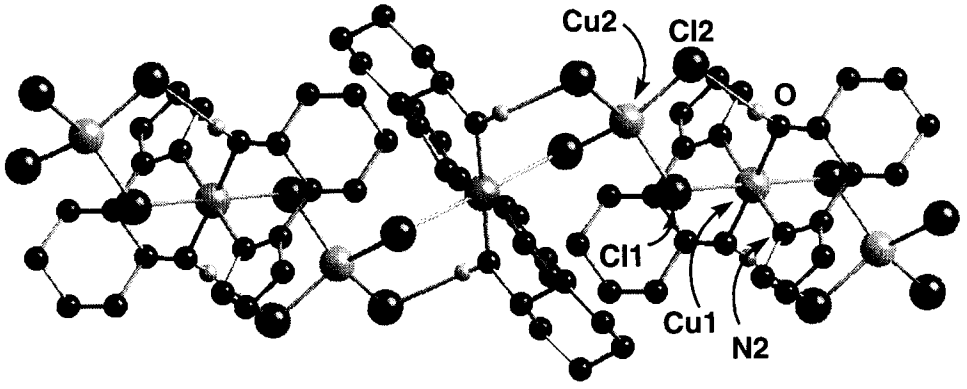

Fig. 3. Plot of the chain building the solid state structure of **5f**.

bondings in the solid state structure of **6**, characteristic bond parameters are given in Table 3.

As predicted, the 1,2-*cis* substituted cyclohexane ring of the *N,N'*-chelate ligand, which is again observed in the energetically favourable chair conformation, is orientated almost perpendicular to the plane defined by Cu, N(2) and N(3).

CONCLUSION

The special requirements of 1,2-disubstituted cyclohexane backbones (either *trans* or *cis*) open an access to chelate ligand with completely different stereochemical properties, which may be of interest for applications in enantioselective catalysis. We were

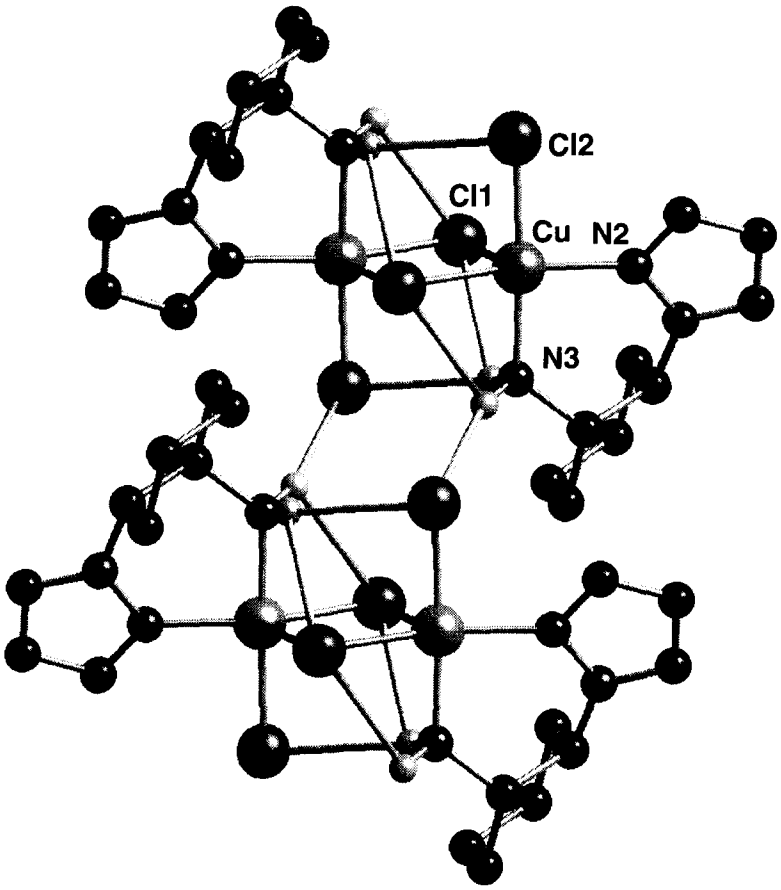

Fig. 4. Plot of the chain building the solid state structure of **6**.

Table 3. Selected bond lengths [Å] and angles [°] of the copper complex **6**

		bond lengths [Å]	
Cu—Cl(1)	2.2859(5)	Cu—N(2)	2.000(2)
Cu—Cl(2)	2.2601(5)	Cu—N(3)	2.004(1)
Cu—Cl(1a)	2.8950(5)	H(3A)···Cl(2)	2.717(2)
		H(3B)···Cl(2)	2.557(2)
		bond angles [°]	
Cl(1)—Cu—Cl(2)	91.63(2)	Cl(1a)—Cu—Cl(2)	91.45(2)
Cl(1)—Cu—Cl(1a)	92.91(2)	Cl(1a)—Cu—N(3)	83.59(5)
Cl(1)—Cu—N(3)	87.10(5)	Cl(1a)—Cu—N(2)	108.46(5)
Cl(1)—Cu—N(2)	158.24(5)	N(2)—Cu—N(3)	91.12(6)
Cl(2)—Cu—N(3)	174.81(5)	Cu—Cl(1)—Cu(a)	87.09(2)
Cl(2)—Cu—N(2)	91.92(4)		

[a] Sum of van der Waals radii: $r^{vdw}(H)+r^{vdw}(Cl) = 1.20+1.80 = 3.00$ Å [17]

able to show that 1,3-amino alcohols of the type **1**, form stable complexes with a whole series of first and second row transition metal complexes and that they are versatile starting materials for the generation of new chelate ligands, possessing centres of chirality.

Acknowledgements—Financial support by the Deutsche Forschungsgemeinschaft and the Fonds der Chemischen Industrie is gratefully acknowledged.

REFERENCES

1. Part 4. Thurner, C. L., Barz, M., Spiegler, M. and Thiel, W. R., *Acta Crystallogr. C*, in press.
2. Herrmann, W. A., Runte, O. and Huber, N., *Angew. Chem.*, 1995, **107,** 2371; *Angew. Chem. Int. Ed. Engl.*, 1995, **34,** 2187.
3. (a) Noyori, R., *Asymmetric catalysis in Organic Synthesis*, John Wiley & Sons, New York, 1994; (b) Noyori, R. and Kitamura, M., *Angew. Chem.*, 1995, **102,** 34; *Angew. Chem. Int. Ed. Engl.*, 1991, **30,** 49.
4. Vagg, R. S., in *Comprehensive Coordination Chemistry*, Vol. 2, ed. G. Wilkinson, Pergamon Press, London, 1987, pp. 793.
5. (a) Berg, J. M. and Holm, R. H., *J. Am. Chem. Soc.*, 1985, **107,** 917; (b) Sanni, S. B., Lenstra, A. T. H. and Patel, V. C., *Acta Crystallogr., C*, 1985, **41,** 199; (c) Walz, L., Paulus, H. and Haase, W., *J. Chem. Soc., Dalton Trans.*, 1985, 913; (d) Myllyviita, S. and Sillanpää, R., *J. Chem. Soc., Dalton Trans.*, 1994, 2125; (e) Kaptein, B., Barf, G., Kellogg, R. M. and van Bolhuis, F., *J. Org. Chem.*, 1990, **55,** 1890; (f) Li, Z.-Y., Yu, W.-Y., Che, C.-M., Poon, C.-K., Wang, R.-J. and Mak, T. C. W., *J. Chem. Soc. Dalton Trans.*, 1992, 1657.
6. (a) Darensbourg, D. J., Fontal, B., Chojnacki, S. S., Klausmeyer, K. K. and Reibenspies, J. H., *Inorg. Chem.*, 1994, **33,** 3526; (b) Hoang, N. N., Valach, F., Dunaj-Jurčo, M. and Melník, M., *Acta Crystallogr., C*, 1992, **48,** 443; (c) Schultz, B. E., Gheller, S. F., Muetterties, M. C., Scott, M. J. and Holm, R. H., *J. Am. Chem. Soc.*, 1993, **115,** 2714; (d) Hawkins, J. M., Dewan, J. C. and Sharpless, K. B., *Inorg. Chem.*, 1986, **25,** 1501; (e) Sommerer, S. O., Baker, J. D., Jensen, W. P., Hamza, A. and Jacobson, R. A., *Inorg. Chim. Acta*, 1993, **210,** 173; (f) Gerber, T. I. A., Kemp, H. J., Du Preez, J. G. H. and Bandoli, G., *J. Coord. Chem.*, 1993, **28,** 329.
7. (a) Barz, M., Herdtweck, E. and Thiel, W. R., *Tetrahedron: Asymmetry*, 1996, **7,** 1717; (b) Glas, H., Spiegler, M. and Thiel, W. R., *Eur. J. Inorg. Chem.*, 1998, **1,** 275; (c) Barz, M., Rauch, M. U. and Thiel, W. R., *J. Chem. Soc. Dalton. Trans.*, 1997, 2155.
8. Anderson, G. K. and Lin, M., *Inorganic Synthesis*, Vol. 28, ed. R. J., Angelici, John Wiley & Sons, New York, 1990, pp. 61,.
9. Altomare, A., Cascarano, G., Giacovazzo, C. and Guagliardi, A., *J. Appl. Cryst.*, 1993, **26,** 343.
10. Sheldrick, G. M., *SHELXL-93: Program for Crystal Structure Determination*, University of Göttingen, 1993.
11. Artus, G., Scherer W., Priermeier, T., Herdtweck, E., *STRUX-V, ein Programmsystem zur Verarbeitung von Röntgenstrukturdaten*, Technische Universität München, 1994.
12. Mitsunobu, O., *Synthesis*, 1981, 1.
13. Herrmann, W. A., Lobmaier, G. M., Priermeier, T., Mattner, M. R., and Schabert, B., *J. Mol. Catal. A: Chemical*, 1997, **117,** 455. (b) Herrmann, W. A. and Lobmaier, G. M., personal communication.
14. (a) Beckingsale, P. G., Morcom, A. T., Rickard, C. E. F. and Waters, T. N., *J. Chem. Soc., Dalton Trans.*, 1977, 2135; (b) Marsh, W. E., Patel, K. C., Hatfield, W. E. and Hodgson, D. J., *Inorg. Chem.*, 1983, **22,** 511; (c) Bream, R. A., Estes, E. D. and Hodgson, D. J., *Inorg. Chem.*, 1975, **14,** 1672; (d) Plakatouras, J. C., Hadjiliadis, N., Perlepes, S. P., Albinati, A. and Kalkanis, G., *Polyhedron*, 1993, **12,** 2069; (e) Bakalbassis, E. G., Mrozinski, J., Perlepes, S. P., Hadjiliadis, N., Lianza, F. and Albinati, A., *Polyhedron*, 1994, **13,** 3209; (f) Chang, W.-K., Lee, G.-H., Wang, Y., Ho, T.-I., Su, Y. O. and Lin, Y.-C., *Inorg. Chim. Acta*, 1994, **223,** 139; (g) Chiari, B., Piovesana, O., Tarantelli, T. and Zanazzi, P. F., *Inorg. Chem.*, 1990, **29,** 1172; (h) Phelps, D. W., Goodman, W. H. and Hodgson, D. J., *Inorg. Chem.*, 1976, **15,** 2266; (i) Wahnon, D., Keith, C., Chin, J. and Hynes, R. C., *Acta Crystallogr., C*, 1996, **52,** 1877; Latour, J.-M., Tandon, S. S. and Povey, D. C., *Acta Crystallogr., C*, 1989, **45,** 7.
15. Spek, A. L., *Acta Crystallogr., A*, 1990, **46,** C34.
16. Wells, A. F., *Structural Inorganic Chemistry*, Clarendon Press, 1987.
17. (a) Gou, S.-H., Xu, Z., You, X.-Z., Zheng, P.-J. and Dong, J., *Chin. J. Chem.*, 1992, **10,** 232; (b) Herceg, M. and Weiss, R., *Acta Crystallogr., Sect. B*, 1973, **29,** 542.
18. (a) Kharitonov, Y. Y., Tabidze, E. I., Tsintsadze, G. V. and Nikolaev, V. P., *Koord. Khim.*, 1986, **12,** 425; (b) Studer, M., Riesen, A. and Kaden, T. A., *Helv. Chim. Acta*, 1989, **72,** 1253.

Pergamon

PII: S0277-5387(97)00500-7

Polyhedron Vol. 17, No. 7, pp. 1133–1140, 1998
© 1998 Elsevier Science Ltd
All rights reserved. Printed in Great Britain
0277 5387/98 $19.00+0.00

Steps towards $[(C_5Me_5)TcO_3]$: Novel synthesis of $[(C_5Me_5)Tc(CO)_3]$ from $[\{Tc(\mu_3\text{-}OH)(CO)_3\}_4]$ and oxidation of $[(C_5Me_5)M(CO)_3]$ (M = Tc, Re) with Br_2

Roger Alberto,[a]* Roger Schibli,[a] André Egli,[a] Ulrich Abram,[b] Sonja Abram,[b] Thomas A. Kaden[c] and P. August Schubiger[a]

[a] Division of Radiopharmacy, Paul Scherrer Institute, CH-5232 Villigen, Switzerland

[b] Institute of Inorganic Chemistry, University of Tübingen, D-72076 Tübingen, Germany

[c] Institute of Inorganic Chemistry, University of Basel, CH-5067 Basel, Switzerland

(Received 6 October 1997; accepted 10 November 1997)

Abstract—$[NEt_4]_2[Tc(Cl)_3(CO)_3]$ was prepared directly from $[NBu_4][TcO_4]$. Dissolution of $[NEt_4]_2[Tc(Cl)_3(CO)_3]$ in water yielded the aqua ion $[Tc(OH_2)_3(CO)_3]^+$ which, upon titration with 1 eq. of OH^-, gave the tetranuclear complex $[\{Tc(\mu_3\text{-}OH)(CO)_3\}_4]$ in quantitative yield and of which the structure could be elucidated. Reaction of $[\{Tc(\mu_3\text{-}OH)(CO)_3\}_4]$ with HC_5Me_5 gave the important starting material $[(C_5Me_5)M(CO)_3]$ (M = Tc, Re). To achieve complexes in higher oxidation states with the $C_5Me_5^-$ ligand, oxidation was performed with $[Br_2]$ for the rhenium and the corresponding technetium complex. Oxidation in trifluoroacetic acid yielded *cis/trans*-$[(C_5Me_5)M(Br)_2(CO)_2]$ (M = Tc, Re). Oxidation in dichloromethane gave in both cases the seven co-ordinate, $18e^-$ M(III) complex $[(C_5Me_5)MBr(CO)_3]^+$. The structure of the rhenium complex was elucidated. It was found that oxidation took place at the metal centre and the $C_5Me_5^-$ ring to yield $[(CO)_3M(\mu\text{-}Br)_3M(CO)_3]$ as the counterion. © 1998 Elsevier Science Ltd. All rights reserved

Keywords: Technetium; carbonyls; oxidation; halogenation; titration.

During the past decade, the organometallic chemistry of metal complexes in the high oxidation states has received enormous attention. This widespread interest has been initialized by the synthesis of several novel organometallic rhenium complexes in its highest possible valency of +VII. These compounds were in particular $[(C_5Me_5)ReO_3]$ and $[CH_3ReO_3]$ [1–9]. The chemistry of these compounds, gave an insight into their various properties, ranging from fundamentally novel compounds and mechanisms to application in catalytic processes [10–12]. The question arose, would the lower homologues parallel the corresponding rhenium chemistry or differ principally as found within group 8 transition metals. Far less is known of the organometallic chemistry of technetium in the lower valencies and practically nothing is known in the high valencies [13,14].

The reasons for this fact, which are three-fold, have to be explained. (i) During the period of exploration of pure organometallic chemistry 30–40 years ago, the artificial element technetium was very rare and not at all readily available. Nevertheless, a few fundamental complexes have been synthesized and characterized during this time [15–17]. (ii) One of the isotopes, Tc-99(m), possesses interesting decay characteristics for application in nuclear medicine. Consequently, coordination chemistry in aqueous systems was investigated thoroughly with the goal of yielding compounds to be applied in life sciences. Obviously, the main focus was put onto classical Werner type complexes rather than on organometallics. (iii) In addition, the gap in behaviour between organometallic complexes of technetium and those of rhenium was so small that investigations in this field of technetium chemistry was not encouraged.

It is known in particular from the group 8 elements,

* Author to whom correspondence should be addressed.

that analogue compounds in high oxidation states display fundamentally different behaviour. The question arose again, would the small gap in low valent 7 complexes become that large when going from oxidation states +I to +VII, thus, resulting in principally different reactivity. Indeed, the answer was found to be "yes" for the complex $[CH_3TcO_3]$ compared to $[CH_3ReO_3]$ [18]. The former is able to oxidize alkenes stereospecifically without additional oxidants, whereas the latter acts as oxidation catalyst only in the presence of additional agents.

Consequently, similar investigations were intended for $[(C_5Me_5)TcO_3]$. $[(C_5Me_5)ReO_3]$ can be prepared conveniently by several methods, whereas the analogues Tc compound resisted all preparative attempts to date (Scheme 1) [19]. A polymeric complex of composition $[Tc(\mu\text{-}O)_3Tc(C_5Me_5)]_n$ has been described as the product of H_2O_2 oxidation of $[(C_5Me_5)Tc(CO)_3]$ in tiny amounts [20]. We doubted this formulation for spectroscopic reasons [18] and it was recently suggested from analysis of X-ray data, that the complex was in fact $[(C_5Me_5)ReO_3]$ [19]. It seemed that not only the higher oxidation potential of Tc was responsible, since, even with highly oxidizing agents such as $[Mn_2O_7]$ or dioxirane, no reactions were found. We concluded from our own attempts to oxidize $[(C_5Me_5)Tc(CO)_3]$ with any of these oxidants, that catalytic decomposition, particularly of dioxirane and Mn_2O_7, took place. Vigorous O_2 evolution was observed at $-78°C$, when adding the oxidant to $[(C_5Me_5)Tc(CO)_3]$ or *vice versa*. $[(C_5Me_5)Tc(CO)_3]$ was usually re-isolated quantitatively. Nevertheless, it can be concluded from theoretical calculations, that $[(C_5Me_5)TcO_3]$ should exist [21,22] and, thus, different approaches are demanded.

Nowadays, enough technetium is available, an interest in high valent organometallic chemistry emerged, but now, for safety reasons, it is relatively difficult to synthesize synthons of technetium, i.e. $[Tc_2(CO)_{10}]$, on which organometallic chemistry is ultimately based. The motivation for this study was, thus, to bypass $[Tc_2(CO)_{10}]$ and to find a convenient pathway to $[(C_5Me_5)Tc(CO)_3]$ as a source for attempted preparations of $[(C_5Me_5)TcO_3]$, starting finally from $[TcO_4]^-$ under laboratory conditions.

We have developed a strategy to the quantitative preparation of $[TcCl_3(CO)_3]^{2-}$ [23] which can be treated as an analogue of $[TcCl(CO)_5]$, giving access to almost any complex containing the "*fac*-$Tc(CO)_3$" moiety including the important $[(C_5H_5)Tc(CO)_3]$ and $[(C_5Me_5)Tc(CO)_3]$.

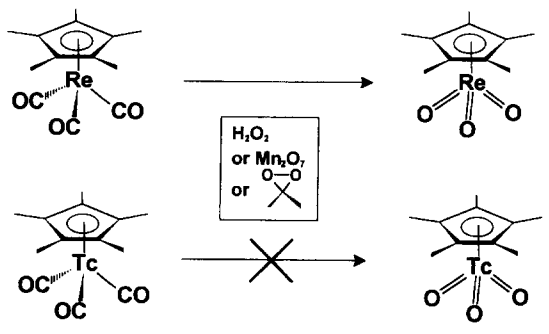

Scheme 1. Literature preparations of $[(C_5Me_5)ReO_3]$ from $[(C_5Me_5)Re(CO)_3]$ and unsuccessful attempts in case of the analogues technetium compound.

EXPERIMENTAL

All chemicals have been purchased from Fluka AG Buchs and used without further purification. Since none of the complexes is sensitive against water, no special drying of solvents was required. The starting materials have been prepared as described earlier, however the modified protocol given below allowed a better isolated yield. IR spectra have been recorded on a Perkin–Elmer 16PC instrument, NMR spectra on Gemini 2000 system running at 300 MHz. The titration experiments were performed using a Metrohm 665 potentiometer and a Metrohm 615 automatic dispenser.

Synthesis of $[NEt_4]_2[TcCl_3(CO)_3]$ (1)

A 1 M solution of BH_3 in tetrahydrofurane (THF) (7 cm^3, 7 mmol) was added to a solution of $[NB_4]Cl$ (0.61 g, 2.2 mmol) in THF (17 cm^3). H_2 evolved from H_2O present in $[NB_4]Cl$. A slow stream of CO was bubbled through this solution for 10 min. A solution of $[NB_4][TcO_4]$ (0.3 g, 0.74 mmol) dissolved in THF (5 cm^3) was dropped over a 10 min period into the solution. After each addition the colour changed to yellow and then back to colourless. After addition was finished, CO bubbling was continued for 3 h at r.t. or 1 h at 50–60°C. After this period the solution was colourless. Excess BH_3 was then neutralized by the addition of 1 M HCl (1 cm^3). H_2 should be generated thereby indicating the presence of excess BH_3. THF was evaporated and ethanole (7 cm^3) added. To the clear solution $[NEt_4]Cl$ (0.6 g, 3.7 mmol) was added and stirred over night. A white powder precipitated, which was filtered. Washing with cold EtOH and drying *in vacuo* gave an analytically pure product of **1** (0.35 g, 87 %). IR (cm^{-1}): 2989 w, 2028 vs, 1902 vs, 1458 m, 1184 w, 798 w, 668 w, 638 w, 500 w. ^{99}Tc NMR (δ, D_2O): −876 (s, $\Delta_{1/2}$ = 67 Hz). Anal. Calc. for $C_{19}H_{40}Cl_3O_3Tc$: Tc, 17.7%. Found 18.0%.

Synthesis of $[\{Tc(\mu_3\text{-}OH)(CO)_3\}_4]$ (3)

1 (0.17 g, 0.31 mmol) was dissolved in water (5 cm^3) and a 1 M solution of NaOH (310 μl) added. The solution turned turbid and was overlayered with 30 cm^3 of diethylether (Et_2O) and stirred over night. Et_2O was separated and the aqueous layer again washed

with Et_2O. The combined Et_2O phases were dried over Mg_2SO_4, separated and evaporated, leaving **3** as a white powder in analytically pure form (0.065 g, 98%). IR (KBr, cm^{-1}): 3611 s, 3599 s, 2044 vs, 1919 vs, 835 w, 792 m, 668 m, 639 m, 535 m. ^{99}Tc NMR (δ, D_2O): -565 (s, $\Delta_{1/2} = 130$ Hz).

Synthesis of $[(C_5H_5)Tc(CO)_3]$

1 (0.25 g, 0.45 mmol) was slurried in THF (5 cm^3) in a round bottom flask and $Ag[PF_6]$ (0.23 g, 0.9 mmol) dissolved in THF was added. AgCl and most of $[NEt_4][PF_6]$ precipitated immediately. Freshly sublimed $Tl[C_5H_5]$ (0.125 g, 0.46 mmol) was added and the mixture heated to 60°C for a few hours. The reaction was cooled to -20°C and filtered cold to remove TlCl, $[NEt_4][PF_6]$ and AgCl. THF was evaporated, the residue dissolved in Et_2O and, upon cooling to -30°C, colourless crystals of the product were collected (0.085 g, 77%). The synthesis for the rhenium complex was performed identically. IR (KBr, cm^{-1}): 2029 vs, 1949 vs. 1H NMR (δ, $CDCl_3$): 4.45. ^{99}Tc NMR (δ, $CDCl_3$): -1716 (s, $\Delta_{1/2} = 180$ Hz).

Synthesis of $[(C_5Me_5)Tc(CO)_3]$ (**4**)

3 (0.08 g, 0.1 mmol) was mixed in a small Schlenk tube with $[HC_5Me_5]$ (65 μl, 0.48 mmol). The mixture was brought to 150°C for 30 min during which period it became a colourless solution. On cooling to r.t., the contents solidified. Recrystallization from hexane at -30°C or column chromatography (silica gel, hexane) yielded **3** as a white powder (0.12 g, 95 %). The proceeding of the reaction and the radiochemical purity could be monitored by TLC on silica gel using hexane as a mobile phase, $R_f = 0.3$. IR (KBr, cm^{-1}): 2989 w, 2007 vs, 1904 vs, 1458 m, 1184 w, 798 w, 668 w, 638 w, 500 w. ^{99}Tc NMR (δ, D_2O): -1874. ^1H NMR (δ, $CDCl_3$): 2.07 (s, CH_3). ^{13}C NMR (δ, $CDCl_3$): 11.7 (CH_3).

Synthesis of $[(C_5Me_5)Tc(CO)_3Br][(CO)_3Tc(\mu\text{-}Br)_3Tc(CO)_3]$ (**5**)

4 (0.12 g, 0.38 mmol) was dissolved in dichloromethane (CH_2Cl_2) and Br_2 (40 μl, 0.75 mmol) was dropped to the solution. The colour turned to red–brown and then after a few hours to deep blue–green. The solvent was evaporated and the residue extracted with Et_2O to remove unreacted **4** and organic decomposition products. The brown–yellow residue was dissolved in CH_2Cl_2 and overlayered with hexane. After several days brown–yellow crystals of X-ray quality (in case of rhenium) were collected (0.062, 48% relative to Tc). Synthetic conditions were identical when the reaction was performed with the corresponding rhenium complex. IR (KBr, cm^{-1}): 2108 s, 2062 s, 2048 s, 2018 s, 1914 vs,br, 1896 vs,br. ^1H NMR (δ, $CDCl_3$): 2.27 (s, CH_3). ^{13}C NMR (δ, $CDCl_3$): 15.7 (CH_3).

Table 1. Crystallographic data, data collection and structure refinement parameters for $[\{Tc(OH)(CO)_3\}_4]$ **3**, $[(C_5Me_5)Re(CO)_3Br][(CO)_3Re(\mu\text{-}Br)_3Re(CO)_3]$ **5**

	3	**5**
Empirical formula	$C_{12}H_{12}O_{20}Tc_4$	$C_{19}H_{15}Br_4O_9Re_3$
Molecular weight	868.22	1265.55
Space group	$I(-)4$	$P2_1/n$
a (Å)	11.675(1)	10.283(3)
b (Å)	11.675(1)	17.853(4)
c (Å)	8.975(1)	15.792(6)
α (°)	90	90
β (°)	90	91.69(1)
γ (°)	90	90
V (Å^3)	1223.6(2)	2897.8(14)
Z	2	4
D_c, g/cm^3	2.357	2.901
μ, mm^{-1}	2.301	18.058
$F(000)$	832	2264
R_1, %	2.14	4.99
wR_2, %	6.4	11.16

X-ray crystallography

Unit cell parameters and intensity data for compounds **3** and **5** were obtained on a CAD-4 diffractometer. The unit cell parameters were determined by least square refinement of the setting angles of 25 centred reflections with $6.7 < \theta < 15.9°$ (**3**) and $8.3 < \theta < 13.4°$ (**5**) respectively. Crystallographic data and final R indices for both complexes are summarized in Table 1. Both structures were solved using the Patterson methode (SHELXS86) and refined on F^2 using SHELXL93 [24]. Literature values were taken for atomic scattering factors [25]. All non-hydrogen atoms were refined anisotropically. The hydrogen atoms could be localized in compound **3**, were introduced at calculated positions in **5** and refined isotropically for both compounds. Psi-scan absorption correction was applied in both compounds. ZORTEP was used for drawings [26]. Presentations of the complexes are depicted in Figs 2 and 3. Important bond lengths and angles are given in Tables 2 and 3.

RESULTS AND DISCUSSION

Synthesis of $[(C_5H_5)Tc(CO)_3]$ and $[(C_5Me_5)Tc(CO)_3]$ *from* $[TcCl_3(CO)_3]^{2-}$

Common approaches to cyclopentadienyl complexes are usually performed either by oxidative addition to the homoleptic carbonyls or by sub-

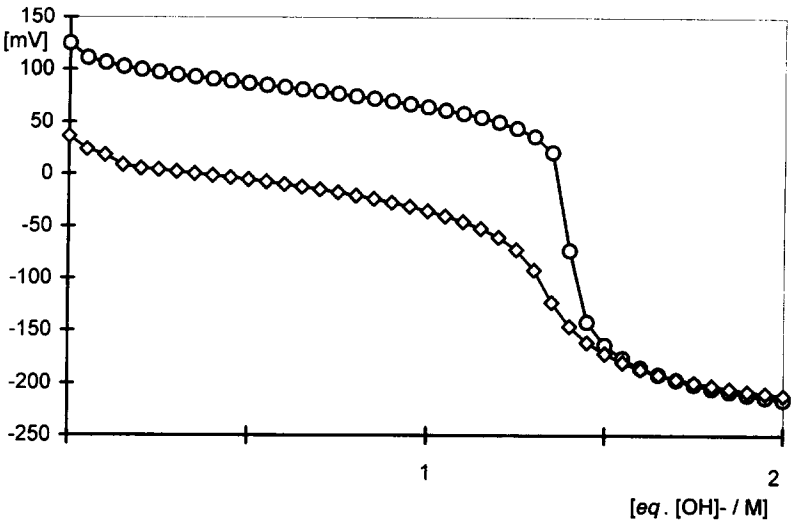

Fig. 1. Titration curves of $[Re(OH_2)_3(CO)_3]^+$ (above) and $[Tc(OH_2)_3(CO)_3]^+$ (below) with 0.01 M NaOH. "[M]" = 1.15 10^{-3} M, I = 0.1 (KNO_3).

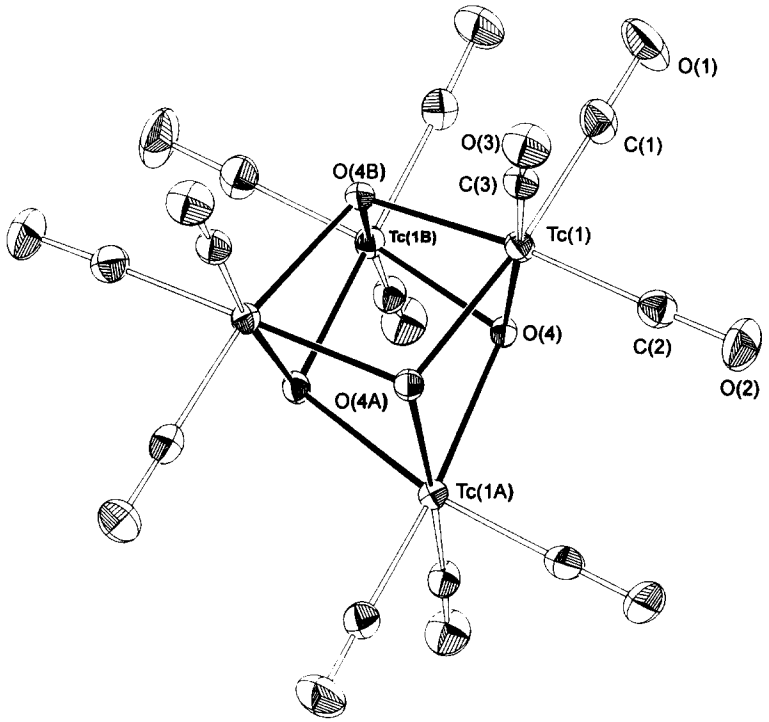

Fig. 2. ORTEP presentation of the complex molecule $[\{Tc(\mu_3\text{-}OH)(CO)_3\}_4]$. Ellipsoids are drawn on the 30% probability level.

stitution of a halide and two other ligands, mostly CO's, with the corresponding cyclopentadienyl salts of mono-cations. In the case of Tc, $[Tc_2(CO)_{10}]$ is applied to the former and $[TcCl(CO)_5]$ to the latter process [27,28]. Both compounds are prepared by high pressure approaches, thus, it was important to use $[TcCl_3(CO)_3]^{2-}$ as the starting material for both compounds by a more convenient pathway. Different attempts to use directly $[TcCl_3(CO)_3]^{2-}$ (**1**) as a precursor failed. Thus, precipitation of two halides with $Ag[PF_6]$ led to the formation of $[TcCl(THF)_2(CO)_3]$. Both, AgCl and $[NEt_4][PF_6]$, readily precipitated from THF. Subsequent reaction with $Tl[C_5H_5]$ led straight forward and in very good yield to $[(C_5H_5)Tc(CO)_3]$.

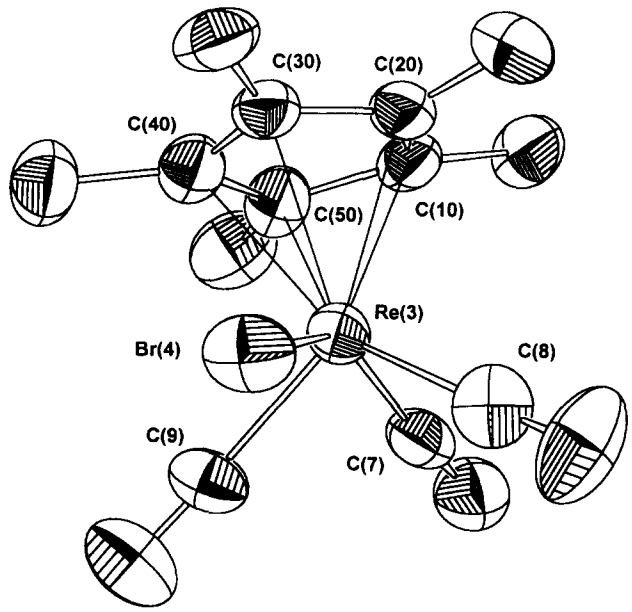

Fig. 3. ORTEP presentation of the complex cation $[(C_5Me_5)Re(Br)(CO)_3]^+$. Ellipsoids are drawn on the 30% probability level.

Table 2. Selected bond lengths (Å) and angles (°) for $[\{Tc(OH)(CO)_3\}_4]$

Tc—C(1)	1.886(4)
Tc—C(2)	1.899(4)
Tc—C(3)	1.905(4)
Tc—O(4)	2.180(3)
Tc—O(4A)	2.185(3)
Tc—O(4B)	2.191(3)
C(1)—O(1)	1.145(5)
C(2)—O(2)	1.146(6)
C(3)—O(3)	1.135(5)
O(4)—Tc(B)	2.185(3)
O(4)—Tc(A)	2.191(3)
C(1)—Tc—C(2)	86.4(2)
C(1)—Tc—C(3)	87.6(2)
C(2)—Tc—C(3)	87.1(2)
C(1)—Tc—O(4)	98.3(2)
C(2)—Tc—O(4)	95.3(2)
C(3)—Tc—O(4)	173.79(14)
O(4A)—Tc—O(4B)	73.82(10)
O(4)—Tc—O(4A)	75.68(12)
O(4)—Tc—O(4B)	75.55(12)
Tc—O(4)—Tc(B)	102.28(12)
Tc—O(4)—Tc(A)	102.08(12)
Tc(B)—O(4)—Tc(A)	105.08(10)

Table 3. Selected bond lengths (Å) and angles (°) for the complex cation $[(C_5Me_5)Re(CO)_3Br]^+$

Re(3)—C(7)	1.971(14)
Re(3)—C(9)	1.972(12)
Re(3)—C(8)	1.992(14)
Re(3)—C(50)	2.252(10)
Re(3)—C(10)	2.266(11)
Re(3)—C(40)	2.298(11)
Re(3)—C(20)	2.334(11)
Re(3)—C(30)	2.391(12)
Re(3)—Br(4)	2.5720(14)
C(7)—Re(3)—C(9)	80.9(5)
C(7)—Re(3)—C(8)	81.6(5)
C(9)—Re(3)—C(8)	106.6(6)
C(7)—Re(3)—C(50)	82.1(5)
C(8)—Re(3)—C(50)	144.6(5)
C(9)—Re(3)—C(50)	101.6(5)
C(7)—Re(3)—C(10)	81.3(5)
C(8)—Re(3)—C(10)	108.6(5)
C(9)—Re(3)—C(10)	137.5(5)
C(7)—Re(3)—C(40)	117.0(4)
C(8)—Re(3)—C(40)	154.0(5)
C(9)—Re(3)—C(40)	94.8(5)
C(7)—Re(3)—C(20)	113.4(4)
C(8)—Re(3)—C(20)	97.2(5)
C(9)—Re(3)—C(20)	154.0(5)
C(7)—Re(3)—C(30)	137.5(4)
C(8)—Re(3)—C(30)	120.0(5)
C(9)—Re(3)—C(30)	120.3(5)
C(7)—Re(3)—Br(4)	142.7(3)
C(8)—Re(3)—Br(4)	76.9(4)
C(9)—Re(3)—Br(4)	76.6(4)

The corresponding salts of HC_5Me_5 are difficult to prepare and even more difficult to handle with tiny amounts of Tc-complexes. An alternative approach had to be developed, that allowed a more general

approach to complexes of differently substituted cyclopentadienyl derivatives.

Dissolution of **1** in water yielded readily the stable organometallic aqua ion $[Tc(OH_2)_3(CO)_3]^+$ (**2**). The complete substitution of Cl^- by H_2O could be confirmed by IR spectroscopy in the νCO region but also by the more sensitive ^{99}Tc NMR spectroscopy. Aqueous solutions show one single signal at −876 ppm (relative to $[TcO_4]^-$). Considering the nuclear spin of 9/2 would expect a rather broad line, however in a relatively symmetric complex, small half line width of 67 Hz were found. On precipitating the Cl^- with Ag^+ salts of weakly coordinating anions, the position of the resonance remained essentially unchanged.

2 can be considered as a Broenstedt acid, undergoing deprotonation upon titration with OH^-. Recently, we reported about the determination of the pK_a values of the corresponding complex $[Re(OH_2)_3(CO)_3]^+$ which was found to be a relatively strong mono-cationic acid [29,30]. The species $[Re(OH)(OH_2)_2(CO)_3]$ and $[Re_2(OH)_2(OH_2)_4(CO)_6]$ were derived from a mechanistic model but could not be observed directly due to oligomerization to anionic di- and tri-nuclear complexes. $[Tc(OH_2)_3(CO)_3]^+$ was found to obey the same mechanistic pathway, the formation constants however being significantly lower than those of rhenium (Fig. 1). From identical calculations, the mono-deprotonated intermediate $[Tc(OH)(OH_2)_2(CO)_3]$ should be present in very low concentrations but could be isolated as its tetranuclear complex $[\{Tc(\mu_3\text{-}OH)(CO)_3\}_4]$ (**3**) by extraction into diethylether in quantitative yields. $[Tc(OH)(OH_2)_2(CO)_3]$ is obviously not able to accept the high electron density provided by a terminal OH^- group but tends to bridge two different Tc-centres with concerted loss of a water ligand (Scheme 2). The formation is reversible, therefore **3** can be considered as a Broenstedt acid.

Protonation of **3** in a non-coordinating solvent would easily generate an electronically unsaturated 14 e^- or 16 e^- species. It could reasonably be expected that such an intermediate coordinates to any potential ligand present in solution. HC_5Me_5 can act as both, as a weak acid and as a ligand system occupying the free sites generated upon protonation.

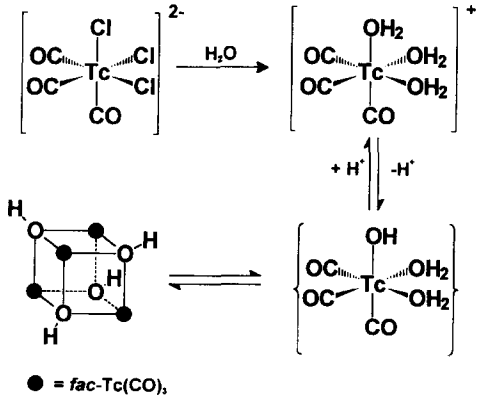

Scheme 2. Aquatization of $[TcCl_3(CO)_3]^{2-}$ and subsequent formation of $[\{Tc(\mu_3\text{-}OH)(CO)_3\}_4]$ by titration with 1 eq. of OH^-.

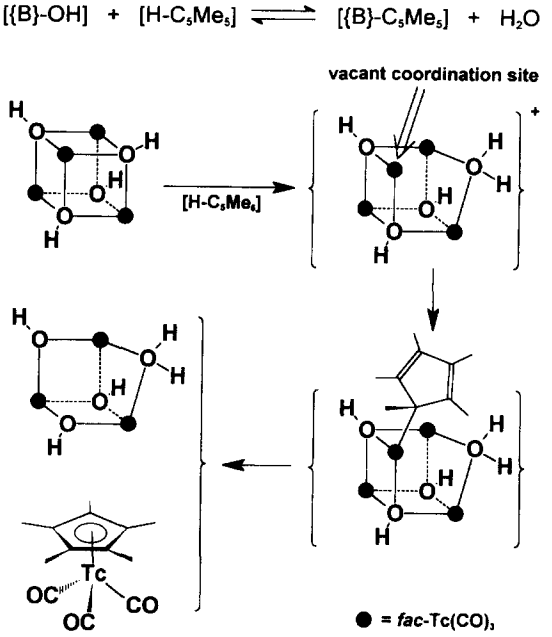

Scheme 3. Acid-base reaction between $[H\text{-}C_5Me_5]$ and "$[(CO)_3Tc]$-OH" leading to the formation of $[(C_5Me_5)Tc(CO)_3]$.

These two properties of HC_5Me_5 coupled with the basicity of **3** make the important synthon $[(C_5Me_5)Tc(CO)_3]$ (**4**) easily accessible by an acid-base reaction with subsequent coordination of the conjugated base to the coordinatively unsaturated metal centre. The thermodynamically favoured η^5-coordination led to the cleavage of the remaining "μ_3-OH" bridges and generated further terminal OH ligands which are more susceptible for protonation and cleavage (Scheme 3).

The overall process allows the preparation of **4**, directly from $[TcO_4]^-$ in two steps without applying high pressure conditions. Thus, by the presented methodology, a useful base is given for the exploration of organometallic technetium chemistry in low and, probably, also for high oxidation states finally.

Oxidation of $[(C_5Me_5)M(CO)_3]$ (*M = Tc, Re*) *with* Br_2

The original reaction conditions for the preparation of $[(C_5Me_5)ReO_3]$ were straight forward in that $[(C_5Me_5)Re(CO)_3]$ could be oxidized by a number of oxidizing agents such as H_2O_2, Mn_2O_7 or dioxirane [31,32]. Other low valent organometallic complexes of i.e. molybdenum could be oxidized in a similar way.

However, all these attempts failed in the case of the analogous technetium complexes. No reaction was found with H_2O_2 and even under vigorous conditions, the educt $[(C_5Me_5)Tc(CO)_3]$ could be isolated at the end of the "reaction" almost quantitatively. The very powerful agent Mn_2O_7 readily decomposed into MnO_2 and O_2 when dropped into a solution of **4** at temperatures of $-78°C$ or higher. No traces of any oxidized technetium compounds could be detected. The same behaviour was also observed for dioxirane. The decomposition rate of these oxidizing agents and the fact that the technetium compound could be reisolated, resembled a catalytic decomposition process. This assumption was partly supported by the observation, that small amounts of **4**, dropped into solutions of either of these oxidants, resulted readily in their decomposition. These qualitative results led to a strategy of initial oxidation by elemental halogens and, subsequently, further oxidation with oxygen transfer agents (Scheme 4).

One of these intermediates achieved by oxidative addition reaction should be $[(C_5Me_5)Tc(Br)_2(CO)_2]$. The *cis* and *trans* isomers have been described and are easily prepared by a literature protocol for rhenium and technetium [28].

It was intended to modify the described protocol in order to increase yield and distribution ratio between *cis*- and *trans*-isomers. Instead, oxidation in CH_2Cl_2 with Br_2 lead to quantitative isolation of the cation $[(C_5Me_5)MBr(CO)_3]^+$ (M = Re, Tc) with the dinuclear complex $[(CO)_3M(\mu\text{-}Br)_3M(CO)_3]^-$ as a counterion (**5**). The cation has been prepared for rhenium but in a different way [33,34]. Under these conditions and even at low temperatures, only trace amounts of $[(C_5Me_5)M(Br)_2(CO)_2]$ could be detected by chromatographic methods. Obviously, halogen attack does not occur exclusively at the metal centre but also at the $C_5Me_5^-$ ring. This ring oxidation lead to cleavage and release as it is known from other reactions. The unusually stable dimer $[(CO)_3M(\mu\text{-}Br)_3M(CO)_3]^-$ was then built up, resisting in its pure form attack from halogens. In parallel to the oxidation of the $C_5Me_5^-$ ring system, oxidative addition took also place at the metal centre to yield the M(III) complex cation $[(C_5Me_5)MBr(CO)_3]^+$. It is interesting to note, that the principal differences found in attempts to oxidize with potential oxygen transfer reagents is not found with the halogens. Rate of oxidation and product distributions could well be monitored by chromatography or by NMR spectroscopy and were found to be essentially the same for both elements.

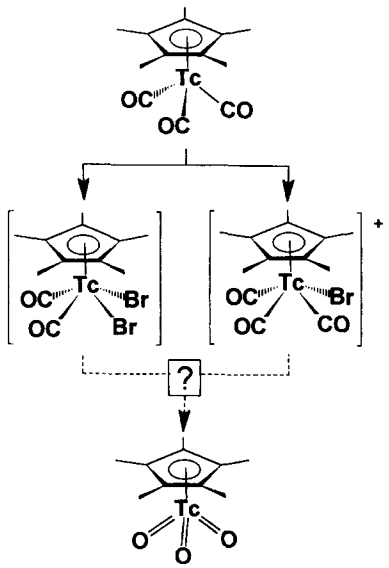

Scheme 4. Oxidative addition of $[(C_5Me_5)Tc(CO)_3]$ with Br_2 as the gate to $[(C_5Me_5)TcO_3]$?

SUMMARY AND CONCLUSION

The question of the preparation of high valent organometallic technetium compounds is inherently coupled to the question of how to prepare conveniently low valent technetium compounds. The problem could be solved by the synthesis of $[NEt_4]_2[TcCl_3(CO)_3]$ directly from $[TcO_4]^-$ with the oxophilic, non coordinating reducing agent BH_3·THF at 1 atm of CO. $[NEt_4]_2[Tc(Cl)_3(CO)_3]$ can be considered as a starting material for Tc(I) chemistry comparable to $[TcX(CO)_5]$. Addition of 1 eq. of OH^- to an aqueous solution of **1** yielded the important synthon $[\{Tc(\mu_3\text{-}OH)(CO)_3\}_4]$. Protonation of the *in situ* base OH^- generates unsaturated complexes, able to adopt even weakly coordinating ligands. This behaviour was used to overcome the difficulties in preparing $[(C_5Me_5)Tc(CO)_3]$. The simple acid base reaction between $[\{Tc(OH)(CO)_3\}_4]$ and HC_5Me_5 made $[(C_5Me_5)Tc(CO)_3]$ quantitatively accessible and open the further development of Tc(I) chemistry with η^5-coordinating ligands. Finally, since all attempts to oxidize $[(C_5Me_5)Tc(CO)_3]$ to higher valencies failed to date, halogenation might be an alternative initial step. Reaction with Br_2 yielded the two compounds *cis*/*trans*-$[(C_5Me_5)M(Br)_2(CO)_2]$ and $[(C_5Me_5)MBr(CO)_3]^+$ (M = Tc, Re). $[(C_5Me_5)TcBr(CO)_3]^+$ is the first Tc(III) complex containing three CO ligands bound to the metal centre.

Both complexes can be considered as intermediates in the preparation of $[(C_5Me_5)TcO_3]$.

Acknowledgements—The first author wishes to express his honest gratitude to Prof. W. A. Herrmann for the education, the reliance and the possibilities for independent research given to him during his post doctoral fellowship.

REFERENCES

1. Herrmann, W. A., Serrano, R. and Bock, H., *Angew. Chem. Int. Ed. Engl.*, 1984, **23**, 383.

2. Klahn-Oliva, A. H. and Sutton, D., *Organometallics*, 1984, **3,** 1313.
3 Herrmann, W. A., *Comments Inorg. Chem.*, 1988, **7,** 73.
4. Herrmann, W. A., *Angew. Chem. Int. Ed. Engl.* 1988, **27,** 1297.
5. Herrmann, W. A., Kuchler, J. G., Felixberger, J. K., Herdtweck, E. and Wagner, W., *Angew. Chem. Int. Ed. Engl.*, 1988, **27,** 394.
6. Herrmann, W. A., Ladwig, M., Kiprof, P. and Riede, J., *J. Organomet. Chem.*, 1989, **C13,** 371.
7. Herrmann, W. A., Kühn, F. E. and Roesky, P. W., *J. Organomet. Chem.*, 1995, **485,** 243.
8. Herrmann, W. A., Taillefer, M., Bellefon, C. M. and Behm, J., *Inorg. Chem.*, 1991, **30,** 3247.
9. Beattie, I. R. and Jones, P. J., *Inorg. Chem.* 1979, **18,** 2318.
10. Herrmann, W. A., Fischer, R. W. and Marz, D., *Angew. Chem. Int. Ed. Engl.*, 1991, **30,** 1638.
11. Herrmann, W. A., Fischer, R. W., Rauch, M. U. and Scherer, W., *J. Mol. Catal.*, 1994, **86,** 243.
12. Rudolph, J., Reddy, K. L., Chiang, J. P. and Sharpless, K. B., *J. Am. Chem. Soc.*, 1997, **119,** 6189.
13. Alberto, R., *Topics Current Chem.*, 1996, **196,** 149.
14. Baldas, J., *Adv. Inorg. Chem.*, 1994, **41**.
15. Hileman, J. C., Huggins, D. K. and Kaesz, H. D., *J. Am. Chem. Soc.*, 1961, **83,** 2953.
16. Baumgärtner, F., Fischer, E. O and Zahn, U., *Naturwissenschaften*, 1962, **49,** 156.
17. Hileman, J. C., Huggins, D. K. and Kaesz, H. D., *Inorg. Chem.*, 1962, **1,** 933.
18. Herrmann, W. A., Alberto, R., Kiprof, P. and Baumgärtner, F., *Angew. Chem. Int. Ed. Engl.*, 1990, **29,** 189.
19. Burell, A. K., Cotton, F. A., Daniels, L. M. and Petricek, V., *Inorg. Chem.*, 1995, **34,** 4253.
20. Kanellakopoulos, B., Nuber, B., Raptis, K. and Ziegler, M. L., *Angew. Chem.*, 1989, **101,** 1055.
21. Szyperski, T. and Schwertfeger, P., *Angew. Chem.*, 1991, **101,** 1271.
22. Chan, A. W. E. and Hoffmann, R., *Inorg. Chem.*, 1991, **30,** 1086.
23. Alberto, R., Schibli, R., Egli, A., Schubiger, P. A., Herrmann, W. A., Artus, A., Abram, U. and Kaden, Th. A., *J. Organomet. Chem.*, 1995, **493,** 119.
24. Sheldrick, G., *SHELXL*93, *Program for structure refinement*, University of Göttingen, Germany, 1993.
25. Cromer, D. T. and Waber, J. T., *International Tables for X-ray crystqallography*, Vol. 4. The Kynoch Press, Birmingham, 1974.
26. Zsolnai, L. and Pritzkow, H., *ZORTEP. ORTEP original programm modified for PC*, University of Heidelberg, Germany, 1994.
27. Palm, C., Fischer, E. O. and Baumgärtner, F., *Naturwissenschaften*, 1962, **49,** 279.
28. Knight Castro, H. H., Meetsma, A., Teuben, J. H. and Vaalburg, W., *J. Organomet. Chem.*, 1991, **410,** 63.
29. Alberto, R., Egli, A., Abram, U., Hegetschweiler, K., Gramlich, V. and Schubiger, P. A., *J. Chem. Soc. Dalton Trans.*, 1994, 2815.
30. Egli, A., Hegetschweiler, K., Alberto, R., Abram, U., Schibli, R., Hedinger, R., Gramlich, V., Kissner, R. and Schubiger, P. A., *Organometallics*, 1997, **16,** 1833.
31. Herrmann, W. A., Kiprof, P., Rypdal, K., Tremmel, J., Blom, R., Alberto, R., Behm, J., Albach, R. W., Bock, H., Solouki, B., Mink, J., Lichtenberger, D. and Gruhn, N. E., *J. Am. Chem. Soc.*, 1991, **113,** 6527.
32. Wolowiec, S. and Kuchi, J., *Inorg. Chem.*, 1991, **30,** 1215.
33. Patton, A. P., Strouse, C. E., Knobler, C. B. and Gladysz, J. A., *J. Am. Chem. Soc.*, 1983, **105,** 5804.
34. Einstein, F. W. B., Klahn-Oliva, A. H., Sutton, D. and Tyers, K. G., *Organometallics*, 1986, **5,** 53.

Pergamon

PII: S0277-5387(97)00501-9

Polyhedron Vol. 17, No. 7, pp. 1141–1148, 1998
© 1998 Elsevier Science Ltd
All rights reserved. Printed in Great Britain
0277-5387/98 $19.00+0.00

Migration of the ferrocenyl moiety during the McMurry coupling of ferrocenyl ketones†

Peter Härter,* Klaus Latzel, Michael Spiegler and Eberhardt Herdtweck

Anorgan.-chem. Institut der Technischen Universität München, Lichtenbergstr. 4, 85747 Garching

(Received 2 October 1997; accepted 31 October 1997)

Abstract—The coupling of [3]-ferrocenophan-1-one **1** with McMurry type reagents to yield olefins *E,Z*-bis([3]-ferrocenophane-1-ylidene) **2a,b** is described. In the case of the $TiCl_3$/Zn reagent only pinacol rearrangement to complex **3** subsequent to coupling takes place in high yield. In contrast, upon addition of pyridine the reaction proceeds to the olefins in high yield. The X-ray structure of **3** and the electrochemistry of the olefins **2a,b** is described. © 1998 Elsevier Science Ltd. All rights reserved

Keywords: McMurry coupling; pinacol rearrangement; ferrocenyl ketones; biferrocenes; electrochemistry; crystal structure.

The reductive coupling of organic carbonyls by low valent transition metal compounds is a valuable tool for the preparation of diols and olefins [1]. Recently Fürstner and his group have established a reliable system based on the couple $TiCl_3$/Zn [2], which also exists as a catalytic version [3]. There are several reports on the possible mechanism of the McMurry reaction showing the course of the coupling being strongly dependent on the nature of the reagent used [4]. In the field of ferrocene chemistry several coupling reactions of ferrocenyl ketones to the corresponding olefins have been reported [5]. We are interested in the self exchange electron transfer of biferrocenes and therefore pursued the preparation of olefins **2a,b**, in which the ferrocene moieties have a fixed orientation relative to one another. We herein describe the preparation of compounds **2a,b** by using the McMurry reaction starting from ferrocenophanone **1**, as well as preliminary results on the electrochemistry of **2a,b**.

RESULTS

Preparation of E,Z-Bis([3]-ferrocenophane-1-ylidene) **2a,b**

Since the coupling of organic carbonyls with low valent metals very much depends on the system in use, we initially set out to synthesize compounds **2a,b** by coupling ferrocenophanone **1** with the classical McMurry reagent $TiCl_3/LiAlH_4$ [6]. As expected the coupling results in a mixture of the *E*- and *Z*-isomers with a ratio of $E/Z = 2:1$, but the yields are poor (37% overall yield), because of the hydrogenation of a considerable amount of ketone **1** to [3]-ferrocenophane under the reaction conditions. Recently Fürstner and his group [2] published the so called "instant method" which leads to excellent yields for the coupling of organic carbonyls. Therefore, in a second attempt, complex **1** was treated with a mixture of $TiCl_3$ and Zn (Ti/Zn = 2:5) in refluxing dimethoxyethane. After 24 h the starting material vanished and a new compound **3** had been formed. As shown by tlc this new compound was not identical with the olefins **2a,b**. After purification of the reaction mixture by flash chromatography on silica, a pale-yellow compound **3** was isolated in 70–80% yield.

Under conditions of the catalytic variant of the "instant method" [3], i.e. using $(CH_3)_3SiCl$ as oxygen scavenger, the main product again is complex **3** (30%). Additionally, the silylated diol **4** also forms in 12% yield. The synthesis of olefins **2a,b** under conditions of the "instant method" could eventually be achieved by adding 2 equiv. of pyridine to the reaction mixture. In this case the olefins **2a,b** are obtained in 70% overall yield with varying ratios of *E*- and *Z*-isomer. Up untill now we are not able to find a clear trend in the variation of the *E/Z*-ratio but in a few runs we noticed a higher amount of *Z*-isomer, when the reaction was conducted only to low conversion.

* Author to whom correspondence should be addressed.

† Dedicated to Prof. Dr W. A. Herrmann on occasion of his 50th birthday.

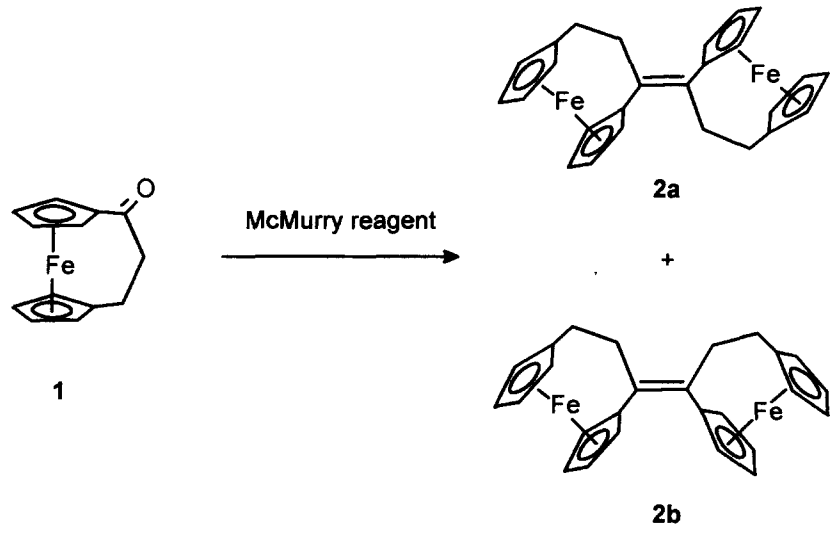

Scheme 1.

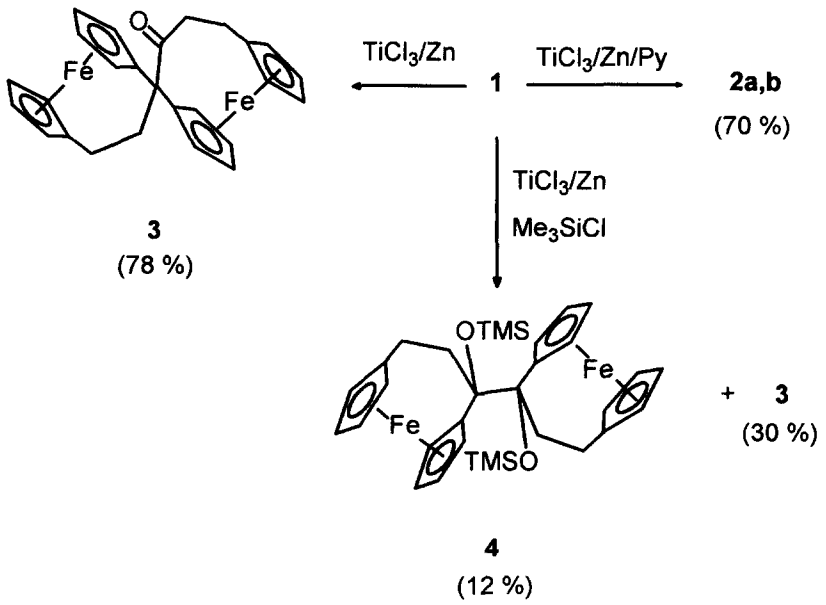

Scheme 2.

Spectroscopic characterization of compounds **2a,b** *and* **3**

The ^{1}H-MNR spectrum of **3** is temperature dependent exhibiting several coalescence transitions due to inversion of the transannular bridges which is typical for ferrocenophanes of this kind [7]. The ^{13}C-NMR spectrum shows a signal at $\delta = 206$ ppm for a keto function. This is also detected in the IR-spectrum by a CO-stretching mode at ν (CO) = 1697 cm^{-1}. The olefins **2a,b** exhibit clear olefinic signals in the ^{13}C-NMR spectra at $\delta = 134$ and 136 ppm, respectively. Due to their symmetric constitution no IR signals were recorded in the olefinic C–C vibrational region, whereas in the Raman spectrum absorptions are found at ν(C=C) = 1620 and 1628 cm^{-1}. A distinction between the *E*- and *Z*-isomers **2a,b** can be made on the basis of the ^{1}H-NMR signals of the cyclopentadienyl (cp) ligands. In the case of the *E*-isomer three multiplets at $\delta = 4.17$ (8H), 4.13 (4H) and 4.02 (4H) ppm are found, whilst the *Z*-isomer exhibits four signals with $\delta = 4.15$ (4H), 4.01 (4H), 3.98 (4H) and 3.93 (4H) ppm. The difference in the appearance of the cp-ring protons may be due to anisotropy effects. In fact, protons in α-position of the

ipso-carbon atom of the cyclopentadienyl ring which is bonded to the olefin moiety, may be within the ring current area of the other cyclopentadienyl ring bound to the olefin moiety. Such a situation can only be found in the *Z*-isomer which then leads to an upfield shift of these protons (ca 0.2 ppm).

X-ray diffraction studies on complex **3**

Orange-red crystals of **3** suitable for X-ray structure determination were grown from a mixture of *n*-hexane/methylenechloride at −30°C. The crystallographic data are shown in Table 1 and the characteristic bond parameters are given in Table 2. The molecular structure of **3** is depicted in Fig. 1. It shows two ferrocenophane molecules tied together by a spiro-carbon atom, which is part of transannular trimethylene- and tetramethylene-2-on-bridges. It is further directly connected to a cyclopentadienyl ligand at each ferrocene moiety. According to the asymmetric surrounding of the spiro carbon atom C1, the tetrahedral angles range from 105 to 114°. In general, the distances and angles are very similar to corresponding mononuclear complexes. For instance, the aperture gap in the [3]-ferrocenophane part (cp1/cp1′) is ca 11° with an opening of the wedge opposite to the *ansa*-bridge. In the [4]-ferrocenophan-2-on (cp2/cp2′) moiety the opening of the aperture gap (ca 5°) is directed towards the interannular C_4-bridge. These values are more or less identical to that found in [3]- and [4]-ferrocenophanes [7,8] indicating that there is no steric strain within the molecule. The cyclopentadienyl rings in [3]-ferrocenophane part are coordinated in an eclipsed conformation, whereas in the [4]-ferrocenophane part, the cp rings are slightly rotated (ca 11°) towards a staggered conformation.

Electrochemistry of **2a,b** *and* **3**

The original impetus of this work was the preparation of the olefins **2a,b** in order to generate mixed valence biferrocenes with a rigid spacer. It was of interest therefore to investigate the electrochemical behaviour of these complexes. The cyclovoltammetric measurements for **2a,b** are depicted in Fig. 2 and the data are listed in Table 3.

They show **2a** having only one oxidation step. The wide separation of the reduction and oxidation wave (Δ = 113 mV) and their broadened wave forms imply that the second electron transfer step may be very close to the first one. In the *Z*-isomer **2b** two clear oxidation waves are present with narrow separations of the reduction and oxidation waves (Δ = 67 mV), which is typical for reversible one-electron transfer processes [10]. Compound **3**, not surprisingly, exhibits two reversible oxidation waves. Similar effects have

Table 1. Crystallographic data of complex **3**

Empirical formula	$C_{26}H_{24}Fe_2O$
Formula weight	464.17
Temperature (K)	193(1)
Wavelength (Å)	0.71073
Crystal system	Orthorhombic
Space group	$P2_12_12_1$
a (Å)	7.340(1)
b (Å)	11.426(1)
c (Å)	23.278(3)
V (Å^3)	1952.3(4)
Z	4
Density (calculated) (Mg/m^3)	1.579
Absorption coefficient (cm^{-1})	15.0
F(000)	960
Crystal size (mm)	0.2 × 0.2 × 0.2
θ range (°)	$1.99 \leqslant \theta \leqslant 24.92$
Index ranges	$-8 \leqslant h \leqslant 8, -13 \leqslant k \leqslant 13, -27 \leqslant l \leqslant 27$
Reflections collected	27,517
Independent reflections	3343
Refinement method	Full-matrix least-squares on F^2
Data/restraints/parameters	3343/0/359
Goodness-of-fit on F^2	1.087
Final R_1 indices [$I > 2\sigma(I)$]	0.0247
wR_2 indices (all data)	0.0592
Largest diff. peak and hole (e Å^{-3})	0.298 and −0.295

Table 2. Selected atomic distances (pm) and angles (°) of complex **3** [9]

Fe1—(C111—C115)	202.0–205.9(3)	C11—C1—C111	111.7(2)
Fe1—(C121 —C125)	201.4–206.7(3)	C11—C1—C211	110.1(2)
Fe1—cp1	163.9	C11—C1—C21	108.4(2)
Fe1—cp1′	164.3	C111—C1—C21	106.8(2)
Fe2—(C211—C215)	203.3–209.3(3)	C211—C1—C21	105.6(2)
Fe2—(C221—C225)	204.0–207.0(3)	C111—C1—C211	113.9(2)
Fe2—cp2	165.1	C1—C11—C12	115.0(2)
Fe2—cp2′	166.4	C1—C21—C22	118.2(2)
Fe1—Fe2	610.9	C1—C21—O	121.6(2)
C21—O	121.4(3)	O—C21—C22	120.2(3)

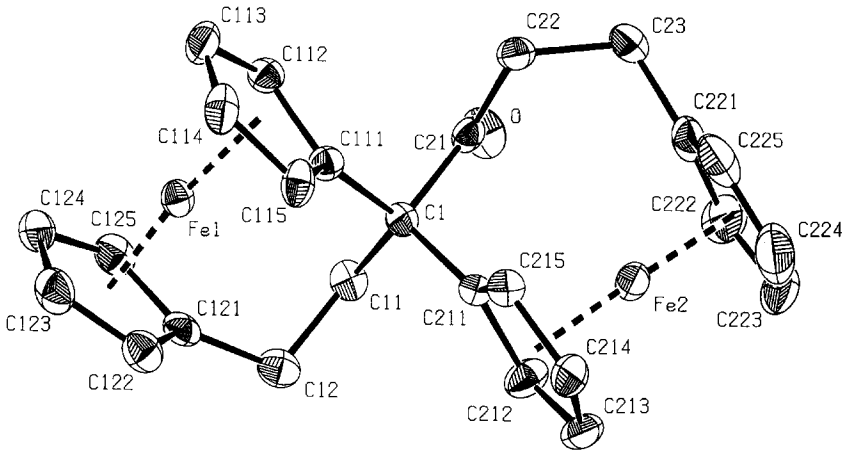

Fig. 1. X-ray structure of complex **3**.

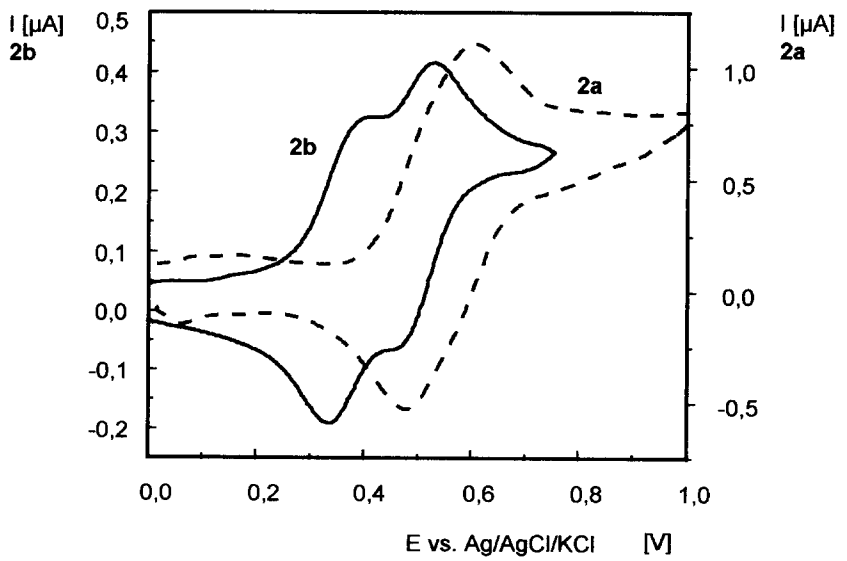

Fig. 2. Cyclovoltammograms of **2a,b**.

Table 3. Cyclic voltammetric formal potentials of compounds **2a,b**, **3** at 298 K in CH_2Cl_2 (0.1 M Bu_4NPF_6) at a Pt electrode, scan rate 100 mV/s

Compound	$E_{1/2}$, (mV) vs Ag/AgCl/KCl ($\Delta = E_{pc} - E_{pa}$, mV)
2a	+530(113)
2b	+380(67)
	+516(67)
3	+466(66)
	+643(66)

been found recently by Bildstein and his coworkers in the case of di- and tetraferrocenyl substituted ethylene [5c].

DISCUSSION

The reactions described above show that the C-C-coupling step of ferrocenophanone **1** takes place with any McMurry reagent. This rules out stereochemical reasons for the different performances of the various coupling reagents. The results can be best interpreted using the mechanistic schemes introduced by Bogdanović and his coworkers [4c]. These mechanisms show indeed, that formation of the diolate state can be reached with any low valent Ti reagent, but the formation of the olefin is strongly dependent on the oxidation state of the Ti centres of the intermediates. In the case of the classical McMurry reagent $TiCl_3$/Li-AlH_4 the active species is a dinuclear hydridotitaniumchloride where the metal centres have the formal oxidation state +II. Elimination of H_2 leads to Ti(I). Reaction with ketones first leads to a dimeric diolate complex were the +II oxidation state of the Ti-centres has been restored. From this dinuclear intermediate the olefin can be liberated by formation of TiOCl.

This +I/+III change in oxidation states is not present in the "instant method". Here the active intermediate is the dinuclear diolate complex **A** with Ti-centres exhibiting oxidation state +III. This species is in a disproportional equilibrium with the mononuclear diolate complex **B** and $TiCl_2ZnCl_2(DME)_2$ **C**, which is only slightly soluble. According to Bogdanović, elimination of the olefin takes place at the dinuclear intermediate **A**.

This requires a second reduction step with Zn. Since the equilibrium is mainly on the side of the mononuclear diolate **B** only a low concentration of **A** will be formed, which could be responsible for the high yields of olefin formed with the "instant method".

In the case of the coupling of ferrocenophanon **1** the second reduction step is hindered by a fast pinacol rearrangement starting from mononuclear diolate **B** to forming complex **3**. The reason for this rearrangement to **3** may be the Lewis acidity of $ZnCl_2$ which forms during the course of the reaction and which is able to open the mononuclear diolate. This is supported by the strong ability of the ferrocene moiety to stabilize carbenium ions [11], which should be formed during the pinacol rearrangement. It should be noted at this point that trying to bring about the coupling without Ti-reagent but using elemental Zn in form of a Clemmensen type reaction no reaction takes place at all. A similar behaviour has been found very recently by Bildstein and his coworkers [5c,12]. They found that Clemmensen reduction of ferrocenyl ketones takes place only when small traces of protons are present. In order to find out if the pinacol rearrangement was peculiar to ferrocenophanone **1**, we treated acetylferrocene under conditions of the "instant method". Here a pinacol rearrangement also takes place, albeit in a reduced yield of 3,3-bis(ferrocenyl)butan-2-one **5** and some formation of the corresponding olefins *E,Z*-2,3-bis(ferrocenyl)but-2-en **6a,b** (olefin 8%, pinacolon 31%). Further support for the view of $ZnCl_2$ being the Lewis acid needed for the rearrangement comes from the fact, that upon addition of pyridine the reaction is reversed. Therefore, no pinacol rearrangement but formation of the olefins **2a,b** in good yields is detected. The fact that the *Z*-isomer **2b** is formed in variable yields by using the "instant method" could be due to **2b** being thermally not stable under the reaction conditions. This could be ruled out, since refluxing **2b** in dimethoxyethane for a prolonged time does not lead to the formation of *E*-isomer **2a**, nor does it detectably decompose.

The electrochemistry as studied so far is surprising. If one considers the Fe—Fe distances in the *E*- and *Z*-isomer being not very different, one would expect an influence of the positive charge created by the first

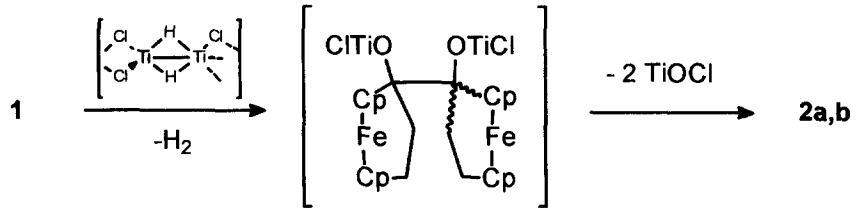

Scheme 3.

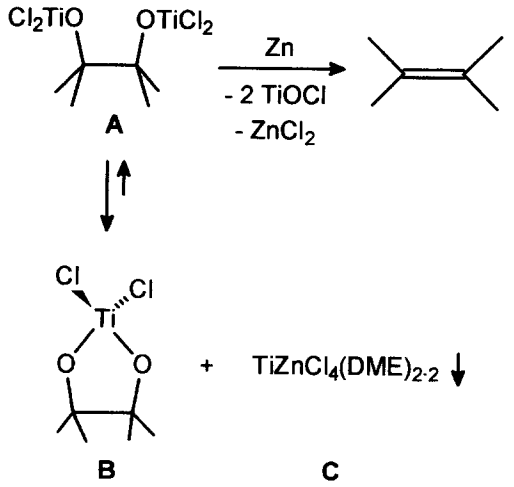

Scheme 4.

oxidation on the second oxidation step. This is only present in the case of the *Z*-isomer. In the *E*-isomer the two Fe-centres seem to be independent, thus showing only a very weak coupling. The difference between the two structures is that in the case of the *Z*-isomer two cyclopentadienyl rings can be positioned face-to-face. This opens up an electron transition through the π-system of the cyclopentadienyl ligands. Such an electron transfer has been favoured by Newton upon theoretical considerations [13]. In order to find out if such a mechanism is feasible in such systems, the preparation and structural investigation of similar derivates is pursued.

EXPERIMENTAL

All reactions were performed with standard Schlenk techniques with dried solvents under an argon atmosphere. Solvents were dried by standard methods and distilled under N_2. Pyridine and TMEDA were dried over Na and distilled prior to use. $TiCl_3$ was purchased from Strem Chemicals. $TiCl_3/LiAlH_4$ (2:1), acetylferrocene were purchased from Aldrich. All commercial reagents were used without further purification. [3]-Ferrocenophan-1-one was prepared according to the literature [15]. Flash column chromatography was done using silica 60 (230–400 mesh), purchased from Aldrich.

Infrared spectra were recorded on a Perkin–Elmer 1600. Raman spectra were recorded on a Riber Jobin Yvon Instruments S.A. spectrometer coupled with a Kr-laser unit from Coherent Innova 301, excitation wave length 647.1 nm. ^{1}H-NMR and ^{13}C-NMR spectra were recorded on a Bruker DPX-400 or JEOL JNM-GX-400 instrument and calibrated against residual protons of the deuterated solvents. The mass spectra were conducted on a double focusing Finnigan MAT 90 instrument. Cyclovoltammograms were recorded on a HEKA potentiostat PG 28. Elemental analysis were carried out at the microanalytical laboratory of the Technische Universität München.

Reaction of [3]-ferrocenophan-1-one **1** *with* $TiCl_3/LiAlH_4$

A mixture of 2.145 g (12.4 mmol $TiCl_3$) $TiCl_3/LiAlH_4$ (2:1) was suspended in 30 ml dry THF at −78°C. The stirred suspension was allowed to warm to room temperature during 16 h. After the dropwise addition of 1.2 g (5.0 mmol) [3]-ferrocenophan-1-one **1** in 20 ml dry THF the reaction mixture was stirred at room temperature until the evolution of H_2 was finished, then the reaction was quenched with 10 ml 2 M HCl. After extraction with CH_2Cl_2 the organic layer was washed with saturated $NaHCO_3$ solution and dried over anhydrous $MgSO_4$. After removal of the solvent the products were seperated by flash column chromatography (eluent *n*-hexane/ethylacetate 10:1 → 1:1). The first orange band eluted from the column yielded 0.169 g (0.75 mmol, 15%) [3]-ferrocenophane. The second band gave 0.416 g (0.93 mmol, 37%) of the desired olefins **2a,b**. The *E*- and *Z*-olefins (*E*/*Z* 2:1) were obtained as pale-yellow crystals after crystallisation from CH_2Cl_2/*n*-hexane.

2a. ^{1}H-NMR ($CDCl_3$, 400.13 MHz, ppm): δ = 4.17 (m, 8H), 4.13 (t, 4H), 4.02 (t, 4H), 2.72 (m, 4H), 2.17 (m, 4H). ^{13}C-NMR ($CDCl_3$, 100.63 MHz, ppm): δ = 134.0, 86.9, 83.6, 70.2, 69.6, 68.6, 68.4, 40.5, 27.8. Raman: ν(C=C) = 1620 cm^{-1}. MS (CI): *m*/*z* = 448 [M$^+$]. Found: C, 67.43; H, 5.46. Calc. for $C_{26}H_{24}Fe_2 \cdot 1/5CH_2Cl_2$: C 67.65; H, 5.29.

2b. ^{1}H-NMR ($CDCl_3$, 400.13 MHz, ppm): δ = 4.15 (t, 4H), 4.01 (t, 4H), 3.98 (t, 4H), 3.93 (t, 4H), 2.71 (m, 4H), 2.24 (m, 4H). ^{13}C-NMR ($CDCl_3$, 100.63 MHz, ppm): δ = 133.2, 86.6, 83.1, 70.6, 70.2, 68.6, 68.1, 37.8, 27.5. Raman: ν(C=C) = 1628 cm^{-1}. MS (CI): *m*/*z* = 448 [M$^+$]. Found: C, 69.09; H, 5.61; Fe, 23.74. Calc. for $C_{26}H_{24}Fe_2$: C, 69.68; H, 5.40; Fe, 24.92.

Reaction of [3]-ferrocenophan-1-one **1** *with* $TiCl_3/Zn$ (1:2:5)

A suspension of 2.458 g (10.2 mmol) [3]-ferrocenophan-1-one **1**, 3.275 g (21.0 mmol, 2 equiv.) $TiCl_3$, 3.267 g (50.0 mmol, 5 eq) Zn dust in 100 ml dry DME was refluxed for 20 h. The reaction mixture was cooled to room temperature and filtered through a short pad of silica. After washing the silica with CH_2Cl_2 the combined filtrates were evaporated. The purification of the residue by flash column chromatography (eluent *n*-hexane/ethylacetate 1:0 → 10:1) yielded 1.879 g (4.0 mmol, 78%) of the pinacolone **3** after crystallization from CH_2Cl_2/*n*-hexane. Only a trace of olefins **2a,b** could be detected.

3. ^{1}H-NMR (C_6D_6, 400.13 MHz, *T* = 70°C, ppm): δ = 4.1–3.5 (m, 16H), 2.93 (ddd, 1H, ^2J = 12 Hz,

$^3J_{cis}$ = 11 Hz, $^3J_{trans}$ = 3 Hz), 2.67 (ddd, 1H, ^2J = 12 Hz, $^3J_{cis}$ = 11 Hz, $^3J_{trans}$ = 3 Hz), 2.44 (ddd, 1H, ^2J = 11 Hz, $^3J_{cis}$ = 9 Hz, $^3J_{trans}$ = 2 Hz), 2.20 (ddd, 1H, ^2J = 11 Hz, $^3J_{cis}$ = 9 Hz, $^3J_{trans}$ = 2 Hz), 2.11 (m, 2H, ^2J = 6 Hz, $^3J_{cis}$ = 11, $^3J_{trans}$ = 3 Hz), 1.90 (ddd, 1H, ^2J = 15 Hz, $^3J_{cis}$ = 9 Hz, $^3J_{trans}$ = 2 Hz), 1.76 (ddd, 1H, ^2J = 15 Hz, $^3J_{cis}$ = 9 Hz, $^3J_{trans}$ = 2 Hz). ^{13}C-NMR ($CDCl_3$, 100.63 MHz, ppm): δ = 206.0, 91.6, 88.5, 87.2, 71.5–67 (cp), 54.8, 44.2, 41.4, 26.9, 21.5. IR (CH_2Cl_2): ν(CO) = 1697 (s). MS(CI, %): m/z = 464 (100) [M^+], 436 (14) [$M^+ - CO$]. Found: C, 66.85; H, 5.28; Fe, 23.47. Calc. for $C_{26}H_{24}Fe_2O$: C, 67.28; H, 5.21; Fe, 24.06.

Reaction of [3]-ferrocenophan-1-one **1** *with* $TiCl_3$/Zn/Pyridine (1 : 2 : 5 : 2)

This reaction was carried out under the same conditions according to the preceeding procedure. No pinacolone **3** could be obtained. After purification the desired olefins **2a,b** obtained as a pale-yellow mixture of crystals with a yield of 70% (variable E/Z ratios).

Reaction of [3]-ferrocenophan-1-one **1** *with* $TiCl_3$/Zn/$(CH_3)_3SiCl$ (1 : 0.1 : 5 : 5)

To a suspension of 3.123 g (13 mmol) [3]-ferrocenophan-1-one **1,** 0.203 g (1.3 mmol, 0.1 equiv.) $TiCl_3$, 4.241 g (65 mmol, 5 equiv.) Zn dust in 55 ml dried MeCN was added dropwise 8.4 ml (65 mmol, 5 equiv.) $(CH_3)_3SiCl$. The reaction mixture was refluxed for 2 h according to Fürstners procedure. After cooling with an ice bath the suspension was filtered through silica. The silica layer was washed with ethylacetate and the combined filtrates were freed from solvent. Purification by flash column chromatography (eluent *n*-hexane/ethylacetate 10 : 1 → 1 : 1) gave as the first zone 0.52 g (0.54 mmol, 12%) of the yellow silylated diol-4 which was recrystalized from CH_2Cl_2/*n*-hexane. The second zone contained 0.895 g (1.9 mmol, 30%) of pinacolone 3. ^{1}H-NMR ($CDCl_3$, 400.13 MHz, ppm): δ = 4.09 (t, 2H), 4.00 (t, 2H), 3.95 (t, 2H), 3.94 (t, 2H), 3.92 (t, 2H), 3.88 (t, 2H), 3.75 (t, 2H), 3.73 (t, 2H), 2.39 (m, 6H), 2.16 (m, 2H), 0.35 (s, 18H). ^{13}C-NMR ($CDCl_3$, 100.63 MHz, ppm): δ = 92.3, 84.4, 81.5, 71.0, 69.3, 69.0, 68.0, 67.3, 66.4, 66.2, 66.0, 41.5, 21.3, 3.4. MS (CI, %): m/z = 626 (46) [M^+], 313 (27) [M^{2+}], 241 (42), 154 (100). Found: C, 60.91; H, 6.71; Fe,17.57; Si, 9.07. Calc. for $C_{32}H_{42}Fe_2O_2Si_2$: C, 61.34; H, 6.76; Fe, 17.83; Si, 8.97.

Reaction of acetylferrocene with $TiCl_3$/Zn (1 : 2 : 5)

Acetylferrocene reacts under the conditions of formation of compound **3** to yield 0.34 g (0.77 mmol, 31%) pinacolone **5** and 0.09 g (0.21 mmol, 8%) olefins **6a,b** starting from 1.15 g (5.0 mmol) acetylferrocene.

5. ^{1}H-NMR ($CDCl_3$, 400.13 MHz, ppm): δ = 4.16 (t, 4H), 4.08 (t, 4H), 4.07 (s, 10H), 2.04 (s, 3H), 1.86 (s, 3H). ^{13}C-NMR ($CDCl_3$, 100.63 MHz, ppm): δ = 264.5, 93.5, 68.8, 67.7, 67.0, 50.7, 27.6, 24.1. IR (CH_2Cl_2, cm^{-1}) ν(CO) = 1702. MS (CI, %): m/z = 440 (100) [M^+], 397 (17) [$M^+ - COCH_3$], 255 (10) [$M^+ - Fc$]. Found: C, 65.67; H, 5.62. Calc. for $C_{24}H_{24}Fe_2O$: C, 65.48 H, 5.50.

6a. ^{1}H-NMR ($CDCl_3$, 400.13 MHz, ppm): δ = 4.04 (s, 10H), 4.02 (t, 4H), 3.87 (t, 4H), 2.09 (s, 6H). ^{13}C-NMR ($CDCl_3$, 100.63 MHz, ppm): δ = 127.7, 90.4, 69.4, 68.6, 66.7, 22.6.

6b. ^{1}H-NMR ($CDCl_3$, 400.13 MHz, ppm): δ = 4.29 (t, 4H), 4.20 (t, 4H), 4.14 (s, 10H), 2.13 (s, 6H). ^{13}C-NMR ($CDCl_3$, 100.63 MHz, ppm): δ = 127.8, 90.6, 69.0, 68.9, 67.5, 22.0.

CONCLUSION

We have shown to our knowledge for the first time that in Ti based McMurry type coupling reactions of ferrocenyl ketones, pinacol rearrangement reactions can be the main reaction path. Since this behaviour of the ferrocenyl moiety is dependant on the reagent used, it could help to detect mononuclear diolate intermediates in other McMurry systems and thus distinguish between mechanisms proved by Bogdanovic and mechanisms which may be similar to that found by Ephritikhine [14].

Acknowledgement—We thank Prof. B. Bogdanovic and Dr A. Fürstner for helpful discussions. We also thank the staff of the microanalytical laboratorium of the Technische Universität München under supervision of Mr M. Barth, as well as Mrs R. Dumitrescu and Dr G. Raudaschl-Sieber for recording the mass and the Raman spectra. Financial support of this work by the Deutsche Forschungsgemeinschaft (SFB 377) and the Fonds der Chemischen Industrie is gratefully acknowledged.

REFERENCES

1. (a) McMurry, J. E., *Chem. Rev.*, 1989, **89,** 1513. (b) Betschart, C. and Seebach, D., *Chimia*, 1989, **43,** 39. (c) Dang, Y. and Geise, H. Y., *J. Organomet. Chem.*, 1991, **405,** 1. (d) Lenoir, D., *Synthesis*, 1989, 883. (e) Fürstner, A. and Bogdanovic, B., *Angew. Chem.*, 1996, **108,** 2582.
2. Fürstner, A., Hupperts, A., Ptock, A. and Jannsen, E., *J. Org. Chem.*, 1994, **59,** 5215.
3. Fürstner, A. and Hupperts, A., *J. Am. Chem. Soc.*, 1995, **117,** 4468.
4. (a) Aleandri, L. E., Bogdanović, B., Gaidies, A., Jones, D. J., Liao, S., Michalowicz, A., Rozière, J. and Schott, A., *J. Organomet. Chem.*, 1993, **459,** 87. (b) Aleandri, L. E., Becke, S., Bogdanović, B. and Rozière, J., *J. Organomet. Chem.*, 1994, **472,** 97. (c) Bogdanović, B. and Bolte, A., *J. Organomet. Chem.*, 1995, **502,** 109. (d) Dams, R., Malinowski, M., Westdorp, I. and Geise, H. Y., *J. Org. Chem.*, 1982, **47,** 248.
5. (a) Dong, T.-Y., Ke, T.-J., Peng, S.-M. and Yeh,

S.-K., *Inorg. Chem.*, 1989, **28,** 2103. (b) Kasahara, A. and Izumi, T., *Chem. Lett.*, 1978, 21. (c) Bildstein, B., Denifl, P., Wurst, K., André, M., Baumgarten, M., Friedrich, J. and Ellmerer-Müller, E., *Organometallics*, 1995, **14,** 4334.
6. McMurry, J. E. and Fleming, M. P., *J. Am. Chem. Soc.*, 1974, **96,** 4708.
7. Hillman, M., Fujita, E., Dauplaise, H., Kvick, A. and Kerber, R. C., *Organometallics*, 1984, **3,** 1170.
8. (a) Hillmann, M. and Austin, J. D., *Organometallics*, 1987, **6,** 1737. (b) Hisatome, M., Kawajiri, Y., Yamakawa, K., Kozawa, K. and Uchida, T., *J. Organomet. Chem.*, 1982, **236,** 359.
9. Further details of the crystal structure investigation are available on request from the Fachinformationszentrum Karlsruhe, Gesellschaft für wissenschaftlich-technische Information mbH, D-76344 Eggenstein-Leopoldshafen 2, on quoting the depository number CSD-408272, the names of the authors and the journal citation, or from the author E.H.
10. Kissinger, P. T. and Heineman, W. R. (Eds.), *Laboratory Techniques in Electroanalytical Chemistry*. Dekker, NY, 1984.
11. Watts, W. E., in *Comprehensive Organometallic Chemistry*, Vol. 8, Chapter 59, ed. G., Wilkinson, F. G. A., Stone and E. W., Abel. Pergammon Press, Oxford, 1982, p. 1051.
12. Denifl, P., Hradsky, A., Bildstein, B. and Wurst, K., *J. Organomet. Chem.*, 1996, **523,** 79.
13. Newton, M. D., Ohta, K. and Zhong, E., *J. Phys. Chem.*, 1991, **95,** 2317.
14. Maury, O., Villiers, C. and Ephritikhine, M., *Angew. Chem. Int. Ed. Engl.*, 1996, **35,** 1129.
15. Turbitt, T. D. and Watts, W. E., *J. Organomet. Chem.*, 1972, **46,** 109.

Pergamon

PII: S0277-5387(97)00502-0

Polyhedron Vol. 17, No. 7, pp. 1149–1157, 1998
© 1998 Elsevier Science Ltd
All rights reserved. Printed in Great Britain
0277-5387/98 $19.00+0.00

Sterically demanding ferrocene-based *tris*(1-pyrazolyl)borate ligands†

Eberhardt Herdtweck, Frank Peters, Wolfgang Scherer and Matthias Wagner*

Anorganisch-chemisches Institut der Technischen Universität München, Lichtenbergstr. 4, D-85747 Garching, Germany.

(Received 6 October 1997; accepted 10 November 1997)

Abstract—Ferrocene-based mono- and bifunctional *tris*(1-pyrazolyl)borates bearing either methyl or phenyl substituents at the 3-positions of their pyrazolyl rings have been obtained from $FcB(NMe_2)_2$ and 1,1′-$fc[B(NMe_2)_2]_2$ (Fc: ferrocenyl; fc: ferrocenylene) and the corresponding pyrazole derivatives via a transamination reaction. All novel ligands have been characterized as their thallium(I) complexes, and the molecular structure of $FcB(pz^{Ph})_3Tl$ (pz^{Ph}: 3-phenylpyrazolyl) has been determined by X-ray crystallography. The compound features monomeric units with tridentate $[FcB(pz^{Ph})_3]^-$ ligands in the crystal lattice, which is in striking contrast to the sterically less congested complex $FcB(pz)_3Tl$, that forms polymeric rods in the solid state. For the purpose of comparison, the single crystal X-ray structure of the ferrocene-free parent compound $HB(pz)_3Tl$ (pz: pyrazolyl) has also been investigated, which again revealed the conventional structural motif of monomeric complexes. © 1998 Elsevier Science Ltd. All rights reserved

Keywords: ferrocene; tris(1-pyrazolyl)borates; thallium complexes.

Tris(1-pyrazolyl)borate (scorpionate) ligands [1,2] have found extensive use in numerous different areas of coordination chemistry. Although a large variety of scorpionates $[R'B(pz^R)_3]^-$ (R′ = H, alkyl, aryl; pz^R = pyrazolyl, substituted pyrazolyl) has been prepared until today, examples of redox-active derivatives [3] as well as of ligands bearing more than one $[R'B(pz^R)_3]^-$ unit are still surprisingly scarce [4].

For this reason, we became interested in the design and synthesis of novel ferrocene-based mono-(**[1H]**$^-$; Fig. 1) and bifunctional (**[2H]**$^{2-}$; Fig. 1) *tris*(1-pyrazolyl)borates [5,6]. The investigation of their corresponding metal complexes revealed structural motifs that are unprecedented in the coordination chemistry of this class of ligands.

The molybdenum complex $FcB(pz)_3Mo(CO)_2(\eta^3\text{-}CH_2C(CH_3)CH_2)$, **1H-Mo**, (Fig. 2) preferentially adopts a chiral conformation with the ferrocenyl unit and the allyl substituent occupying two different segments of the scorpionate moiety, as has been shown both in the solid state (crystal structure determination) and in solution (low-temperature NMR spectroscopy) [6]. The thallium(I) derivative $FcB(pz)_3Tl$ **1H-Tl**, (Fig. 2) provided the first example of a *tris*(1-pyrazolyl)borate complex featuring a polymeric structure in the crystal lattice. Each thallium atom binds to two pyrazolyl rings of one scorpionate ligand and to one pyrazolyl ring of another ligand, thereby deviating from the usually observed tridentate coordination mode [5]. These cited observations already suggest the steric demands of the ferrocenyl substituent to have an influence on the pending scorpionate fragment. It is the purpose of this paper

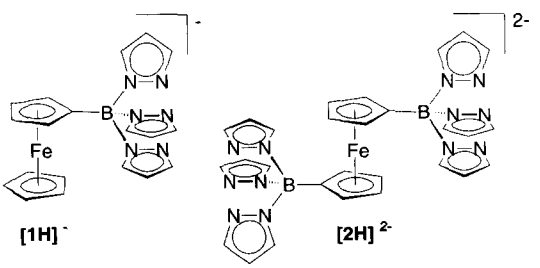

Fig. 1. Ferrocene-based mono- and bifunctional *tris*(1-pyrazolyl)borate ligands.

† Dedicated to Prof. Dr. W. A. Herrmann on the occasion of his 50th birthday.

* Author to whom correspondence should be addressed.

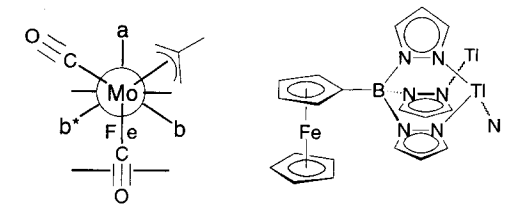

Fig. 2. The chiral molybdenum complex **1H-Mo** and polymeric **1H-Tl**.

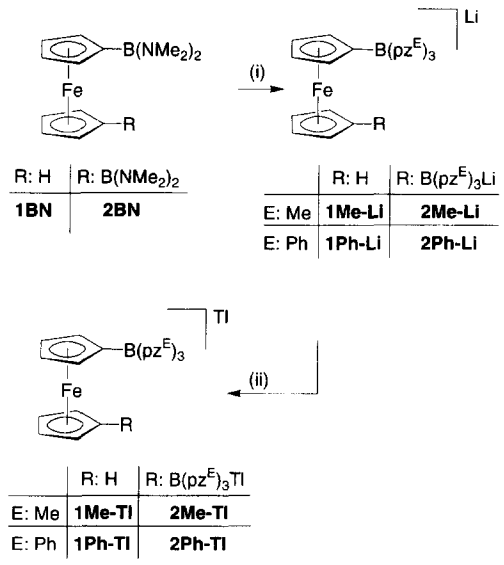

Scheme 1. Preparation of sterically demanding ferrocene-based *tris*(1-pyrazolyl)borate ligands and their thallium complexes. (i) R = H: +1 $Lipz^E$, +2 Hpz^E, toluene/THF, 12 h reflux; R = $B(NMe_2)_2$: +2 $Lipz^E$, +4 Hpz^E, toluene/THF, 12 h reflux. (ii) R = H: +1 $TlNO_3$, THF/H_2O; R = $B(pz^E)_3Li$: +2 $TlNO_3$, THF/H_2O.

to gather more definite evidence on this point. Special emphasis will be put on identifying those factors, that are responsible for the polymerisation of **1H-Tl**.

Apart from **1H-Tl** there are 11 structurally characterized thallium(I) scorpionate complexes currently available from the Cambridge Crystal Structure File (Release 5.10) [7]. All of them are monomeric and share two common features: (i) Sterically demanding substituents occupy the 3-positions of the pyrazolyl rings. (ii) In addition to the three pz^R moieties, the boron centre bears a small hydrogen atom. In contrast, **1H-Tl** offers a largely unrestricted access space to the metal on one hand and possesses a bulky and pronounced non-symmetric ferrocenyl group at boron on the other. Either of these two peculiarities may lead to the unique polymeric solid state structure of **1H-Tl** and thus requires more detailed examination. To be able to study both effects independently, we have prepared the sterically demanding ferrocene-based scorpionate complexes **1Me-Tl** to **2Ph-Tl** (Scheme 1) and the uncongested ferrocene-free compound $HB(pz)_3Tl$, **3H-Tl** (Fig. 3). **1Ph-Tl** and **3H-Tl** have been investigated by X-ray crystallography. Apart from the structural problems discussed so far, sterically demanding scorpionates L are generally required to support monomeric ML(X) species of the first-row transition metals (X = e.g. alkyl, hydride, hydroxide, halide) [8,9] and to stabilize highly reactive metal complexes kinetically [2].

Henceforth, the abbreviation Fc will be used for the monosubstituted ferrocenyl unit $(C_5H_5)Fe(C_5H_4)$, while fc stands for the 1,1′-disubstituted moiety $(C_5H_4)Fe(C_5H_4)$. The 3-substituent at the pyrazolyl (pz) rings is denoted by a superscript; thus HPz^{Me} is 3-methylpyrazole and Hpz^{Ph} is 3-phenylpyrazole.

RESULTS AND DISCUSSION

Syntheses

The lithium salts **1Me-Li** and **1Ph-Li** of the monofunctional scorpionates are synthesized from $FcB(NMe_2)_2$ [5,6], **1BN**, with 1 equiv. of $Lipz^E$ and 2 equiv. of Hpz^E in refluxing toluene/THF (**1Me-Li**: E = Me, **1Ph-Li**: E = Ph; Scheme 1). Without further purification the crude products are converted to the respective Tl(I) complexes **1Me-Tl** and **1Ph-Tl** by metathesis with $TlNO_3$ in THF/H_2O. The same method was applied to transform the commercially available sodium salt $HB(pz)_3Na$, **3H-Na**, into **3H-Tl**.

The bifunctional lithium scorpionates **2Me-Li** and **2Ph-Li** are accessible from 1,1′-fc$[B(NMe_2)_2]_2$ [5,6], **2BN**, 2 equiv. of $Lipz^E$ and 4 equiv. of Hpz^E (**2Me-Li**: E = Me, **2Ph-Li**: E = Ph; Scheme 1). The synthesis of **2Me-Li** suffered from only moderate yield, and the compound was contaminated with small amounts of Hpz^{Me} even after several purification steps. However,

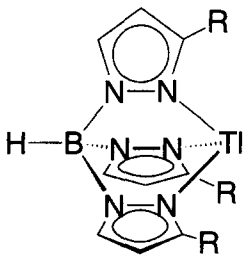

3H-Tl : R = H
3Tol-Tl : R = p-tolyl

Fig. 3. Ferrocene-free *tris*(1-pyrazolyl)borato thallium(I) reference complexes.

analytically pure thallium complexes **2Me-Tl** and **2Ph-Tl** are readily obtained upon reaction of **2Me-Li** and **2Ph-Li** with $TlNO_3$.

All compounds **1Me-Li** to **2Ph-Tl** are stable towards air and moisture even for extended periods of time.

Spectroscopic properties

The ^{11}B NMR signals of **1Me-Li** to **2Ph-Tl** appear in the range between -1 and $+2$ ppm, thereby testifying to the presence of tetracoordinated boron nuclei.

The Fc substituents of **1Me-Li** to **1Ph-Tl** give rise to three resonances, while two resonances are found for the disubstituted fc backbones of **2Me-Li** to **2Ph-Tl** both in the ^1H- and the ^{13}C NMR spectra. In all cases only one set of signals is observed for the pyrazolyl units of the scorpionate ligands. On the basis of these NMR patterns it is obvious, that the methyl (phenyl) substituents of each derivative **1Me-Li** to **2Ph-Tl** are attached either only at the 3- or only at the 5-positions of the scorpionate fragments, and the formation of isomeric products can consequently be ruled out. Since bulky substituents are well-known to have a strong tendency to occupy the 3-positions of *tris*(1-pyrazolyl)borate ligands [2,7], it can be safely assumed, that this holds for **1Me-Li** to **2Ph-Tl**, too. This view is also supported by the X-ray crystal structure determination of **1Ph-Tl** (see below).

The ^1H and ^{13}C NMR shift values of **1Me-Li** to **2Ph-Tl** all appear in the expected regions and thus do not merit further discussion. The NMR spectra of the lithium salts are rather similar to those of the thallium complexes, with the exception of the proton resonances of the methyl substituents, which are shifted to lower field by 0.85 ppm upon going from **1Me-Li** to **1Me-Tl**.

X-ray crystallography

Orange crystals of **1Ph-Tl** were obtained by layering its CH_2Cl_2 solution with benzene. The compound crystallizes together with 0.5 equiv. of benzene (triclinic; space group $P\bar{1}$; Table 1). Large colourless crystals of **3H-Tl** (monoclinic; space group $P2_1$; Table 1) were grown from toluene by slow evaporation of the solvent.

In contrast to polymeric **1H-Tl** [5], the more crowded derivative **1Ph-Tl**, as well as the ferrocene-free parent compound **3H-Tl**, feature the common structural motif of monomeric units in the solid state (Figs 4, 5). Thallium coordination occurs in a tridentate fashion in both molecules.

Similar to **1H-Mo** (Fig. 2), the ferrocenyl substituent in **1Ph-Tl** is located in the uncongested cleft between two pyrazolyl rings, thereby placing the third pz^{Ph} substituent (N(1) to C(3)) in a unique position almost perpendicular to the cyclopentadienyl ring. The $B(pz^{Ph})_3Tl$ fragment deviates significantly from an ideal C_3-symmetry, since its individual Tl—N bond lengths differ by as much as 0.083 Å (Tl—N(2): 2.519(5) Å, Tl—N(4): 2.563(5) Å, Tl—N(6): 2.602(5) Å; Table 2).

The mean value Tl—N = 2.561 Å in ferrocene-based **1Ph-Tl** is almost identical to that found in the related ferrocene-free **3Tol-Tl** (Fig. 3; Tl—N = 2.576 Å) [10], but is considerably shorter than that of polymeric **1H-Tl** (Tl—N = 2.698 Å) [5]. The difference Δ(Tl—N) between the mean Tl—N values of **1H-Tl** and **1Ph-Tl** amounts to Δ(Tl—N) = 0.137 Å. In **1Ph-Tl**, the bond angles at Tl (N(2)—Tl—N(4) = 74.9(2)°, N(2)—Tl—N(6) = 70.6(2)°, N(4)—Tl—N(6) = 75.2(2)°) fall in the usually observed range for thallium(I) scorpionate complexes [9], and surprisingly similar values are found even in the polymeric congener **1H-Tl** (N(2)—Tl—N(4) = 70.9(2)°, N(2)—Tl—N(6A) = 83.2(1)°, N(4)—Tl—N(6A) = 92.4(1)°; Tl—N(6A) is the intermolecular bond).

The ferrocene-free **3H-Tl** crystallizes with two crystallographically independent molecules (**3H-Tla**, **3H-Tlb**) in the asymmetric unit (Fig. 5). While **3H-Tla** possesses three Tl—N bonds of similar length (2.603(7) Å, 2.605(7) Å, 2.621(7) Å), one shorter and two significantly longer Tl—N bonds are found in **3H-Tlb** (2.549(7) Å, 2.667(7) Å, 2.668(7) Å). The mean values Tl—N in **3H-Tla** (2.610 Å) and **3H-Tlb** (2.628 Å) are, however, very close, but still larger than in the sterically congested congener **3Tol-Tl** (Tl—N = 2.576 Å). Consequently, even though sterically demanding substituents at the 3-positions of the pyrazolyl rings are known to efficiently protect scorpionate complexes from intermolecular attack, there appears to be no major intramolecular repulsion between the three phenyl groups both in **3Tol-Tl** and in **1Ph-Tl**.

CONCLUSION

Tl—N bonds in thallium scorpionate complexes are not very strong, and the corresponding potential energy minima appear to be rather shallow. The actual coordination geometry of the Tl centres is therefore likely to be influenced by crystal packing forces which, however, are difficult to estimate quantitatively. Nevertheless, on the basis of the structural data available, we suggest the following qualitative interpretation of factors leading to polymeric or non-polymeric thallium *tris*(1-pyrazolyl)borate complexes in the solid state.

From the molecular structure of **3H-Tl** it is evident, that the absence of bulky substituents at the 3-positions of the pyrazolyl rings does not by itself lead to the generation of a polymeric thallium(I) scorpionate. A comparison of **3H-Tl** with **1H-Tl** indicates the Fc group to be required to induce polymerization, and the critical factor appears to be the degree of steric crowding at boron. In the hypothetical tridentate

Table 1. Summary of crystallographic data of complexes **1Ph-Tl** and **3H-Tl**

Compound	**1Ph-Tl**	**3H-Tl**
Formula	$C_{37}H_{30}BFeN_6Tl \cdot 0.5\ C_6H_6$	$C_9H_{10}BN_6Tl$
fw	868.76	417.41
Crystal dimension (mm)	$0.41 \times 0.28 \times 0.13$	$0.20 \times 0.20 \times 0.10$
Crystal system	Triclinic	Monoclinic
Space group	$P\bar{1}$ (No. 2)	$P2_1$ (No. 4)
Temperature (K)	163(2)	173(2)
a (Å)	10.5622(6)	7.7812(3)
b (Å)	13.3208(9)	9.3364(4)
c (Å)	14.0361(9)	16.9680(6)
α ( )	62.057(6)	90
β ( )	80.559(6)	91.761(4)
γ ( )	72.687(6)	90
V (Å^3)	1664.8(2)	1232.1(1)
ρ_{calc} (g cm^{-3})	1.733	2.250
Z	2	4
Radiation	Mo–K_α, 0.71073 Å	Mo–K_α, 0.71073 Å
No. of total reflections	10,403	15,671
No. of unique reflections	5835	5762
No. of observed reflections ($>2\sigma$)	5197	5556
No. of parameters	421	306
μ(cm^{-1})	53.1	130.9
Final R_1[a]	0.0490 [all data]	0.0353 [all data]
Final wR_2[b]	0.1155 [all data]	0.0870 [all data]
GOOF[c]	1.027 [all data]	1.043 [all data]

[a] $R_1 = \Sigma(||F_o| - |F_c||)/\Sigma|F_o|$.
[b] $wR_2 = [\Sigma w(F_o^2 - F_c^2)^2/\Sigma w(F_o^2)^2]^{1/2}$.
[c] GOOF $= [\Sigma w(F_o^2 - F_c^2)^2/(NO-NV)]^{1/2}$.

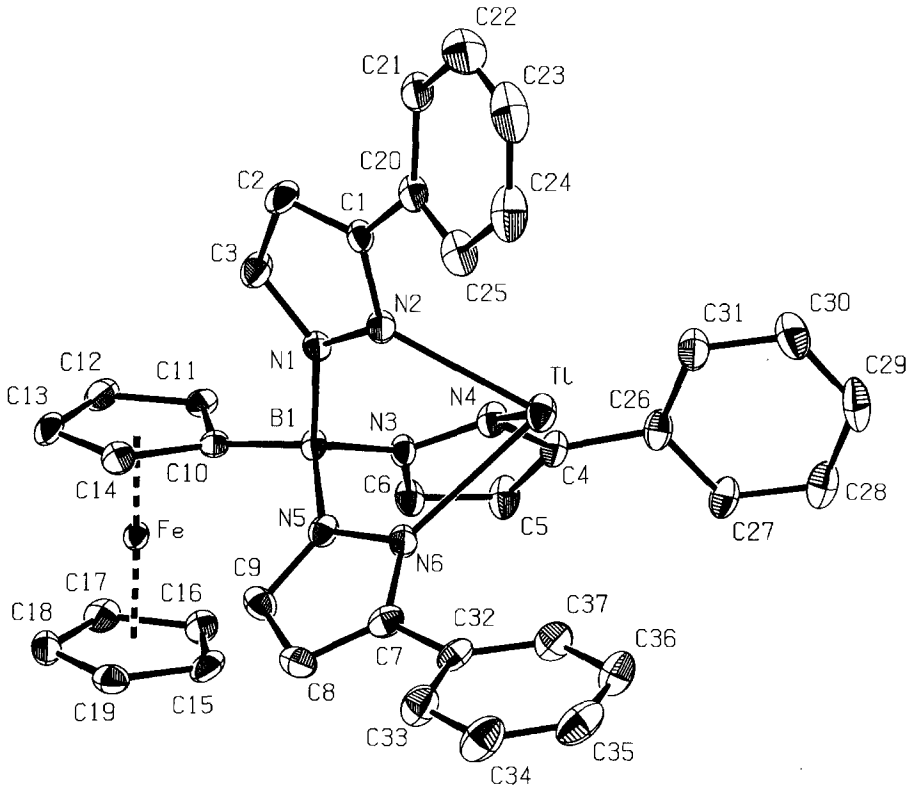

Fig. 4. PLATON-plot of **1Ph-Tl**; thermal ellipsoids are drawn at the 50% probability level.

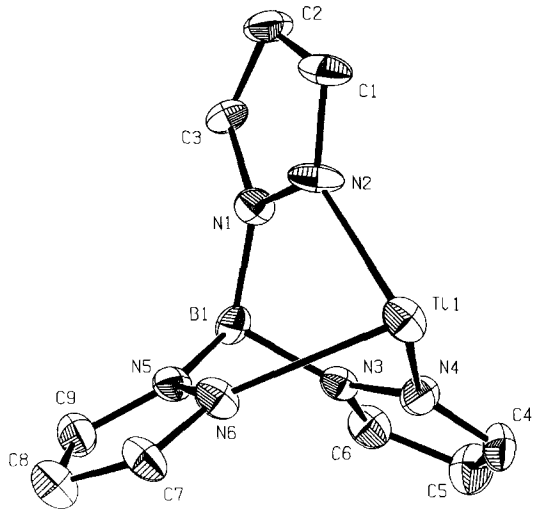

Fig. 5. PLATON-plot of **3H-Tla**; thermal ellipsoids are drawn at the 50% probability level.

Table 2. Selected bond distances (Å) and angles (°) of compounds **1Ph-Tl** and **3H-Tl**

	1Ph-Tl	**3H-Tla** **3H-Tlb**
B(1)—C(10)	1.601(9)	— —
B(1)—N(1)	1.563(8)	1.533(10) 1.544(10)
B(1)—N(3)	1.556(9)	1.538(10) 1.547(10)
B(1)—N(5)	1.569(9)	1.550(11) 1.544(10)
N(1)—N(2)	1.360(7)	1.377(9) 1.361(10)
N(1)—B(1)—N(3)	109.7(5)	110.1(6) 111.0(6)
N(1)—B(1)—N(5)	108.2(5)	111.1(6) 108.6(6)
N(3)—B(1)—N(5)	106.5(4)	110.6(6) 111.1(5)
N(3)—N(4)	1.366(7)	1.364(9) 1.358(9)
N(5)—N(6)	1.370(7)	1.360(9) 1.359(9)
Tl—N(2)	2.519(5)	2.603(7) 2.667(7)
Tl—N(4)	2.563(5)	2.621(7) 2.549(7)
Tl—N(6)	2.602(5)	2.605(7) 2.668(7)
N(2)—Tl—N(4)	74.9(2)	72.7(2) 72.5(2)
N(2)—Tl—N(6)	70.6(2)	73.8(2) 72.8(2)
N(4)—Tl—N(6)	75.2(2)	72.4(2) 74.0(2)

coordination mode, both the C(6)—H(6) and the C(9)—H(9) vector would point towards the Fc backbone (cf. **1Ph-Tl**). This sterically congested arrangement can be improved by rotating one of the two pyrazolyl rings by ca 90° about the B—N axis. The scorpionate fragment now still acts as a chelating ligand, and on the other hand establishes only one unfavourable short distance to the ferrocene backbone (Fig. 6; marked with an asterisk). The dangling pyrazolyl donor, which can only act as a bridging ligand, consequently induces the formation of polymeric rods. In **1H-Tl**, short intermolecular distances of about 4 Å are found between adjacent ligands (Fig. 6; short distances are marked with a "#"). It is obvious that, for example, a phenyl ring occupying the 3-positions of the scorpionate ligands will not fit into this limited space, and consequently **1Ph-Tl** is forced to adopt a different (monomeric) solid state structure.

The conclusion which asserts itself in view of the facts just summarized is that steric congestion due to an Fc substituent at boron, facilitates the formation of thallium(I) *tris*(1-pyrazolyl)borate coordination polymers (**1H-Tl**). However, this effect may be outweighed by (i) the steric demands of bulky substituents in the 3-positions of the pyrazolyl rings (**1Ph-Tl**) and (ii) the use of metal complex fragments with a high affinity to strongly coordinating chelate ligands (**1H-Mo**). In both cases, a tridentate coordination mode leading to monomeric units is strongly favoured.

EXPERIMENTAL

All reactions and manipulations of air-sensitive compounds were carried out in dry, oxygen-free argon using standard Schlenk ware or in an argon-filled drybox. Solvents were freshly distilled under N_2 from Na/K alloy-benzophenone (toluene, hexane, THF) or from CaH_2 (CH_2Cl_2) prior to use. NMR: Jeol JMN-GX 400 and Bruker DPX 400 (abbreviations: s = singlet, d = doublet, tr = triplet, vtr = virtual triplet, q = quartet, n.r. = multiplet expected but not resolved, br = broad, n.o. = not observed, Fc = $(C_5H_5)Fe(C_5H_4)$, fc = 1,1′-$(C_5H_4)Fe(C_5H_4)$, Ph = C_6H_5, *i* = ipso, *o* = ortho, *m* = meta, *p* = para, pz = pyrazolyl fragment in pz^{Me} and in pz^{Ph}). NMR spectra were recorded at ambient temperature. ^{11}B NMR shifts are given relative to external $BF_3 \cdot Et_2O$. MS (CI, FAB mode): Finnigan MAT 90. Elemental analyses: Microanalytical laboratory of the Technische Universität München.

The compounds $FcB(NMe_2)_2$ (**1BN**) [5,6], 1,1′-$fc[B(NMe_2)_2]_2$ (**2BN**) [5,6], and Hpz^{Ph} [8] were synthesized according to literature procedures. The lith-

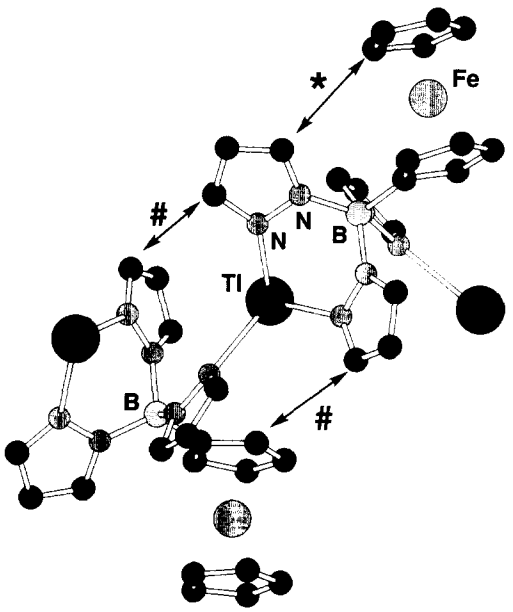

Fig. 6. Section of a polymeric rod of **1H-Tl**; short inter- (#) and intramolecular (*) contacts are marked.

ium pyrazolides $Lipz^{Me}$ and $Lipz^{Ph}$ were obtained from the respective pyrazoles (Hpz^{Me}, Hpz^{Ph}) and *n*-butyl lithium in toluene.

Synthesis of $FcB(pz^{Me})_3Li$ (**1Me-Li**)

1BN (2.91 g, 10.25 mmol) in toluene (100 ml) was treated dropwise with stirring at ambient temperature with a solution of $Lipz^{Me}$ (0.99 g, 11.25 mmol) in THF (30 ml). Hpz^{Me} (1.85 g, 22.53 mmol) in toluene (20 ml) was added and the red-orange solution refluxed for 12 h. The clear solution was allowed to cool to ambient temperature and concentrated *in vacuo* to a volume of 50 ml, whereupon an orange precipitate formed, which was collected on a frit (G3), triturated with toluene (10 ml) and hexane (30 ml) and dried *in vacuo*. Yield: 3.88 g (85%).

^{11}B NMR (128.3 MHz, $CDCl_3$): δ 0.2 ($h_{1/2}$ = 320 Hz). ^1H NMR (400 MHz, $CDCl_3$): δ 1.50 (very br, 9H, CH_3), 4.05 (br, 2H, C_5H_4), 4.35 (s, 5H, C_5H_5), 4.44 (br, 2H, C_5H_4), 5.85 (br, 3H, pz-H4), 8.3 (very br, 3H, pz-H5). ^{13}C NMR (100.5 MHz, $CDCl_3$): δ 12.2 (br, CH_3), 69.2 (C_5H_5), 69.7, 75.3 (C_5H_4), n.o. (C_5H_4-*i*), 103.8 (pz-C4), 137.4 (pz-C5), 150.0 (br, pz-C3). Found: C, 59.63; H, 5.75; N, 18.73. Calc. for $C_{22}H_{24}BFeLiN_6$ [446.07]: C, 59.24; H, 5.42; N, 18.84%.

Synthesis of $FcB(pz^{Me})_3Tl$ (**1Me-Tl**)

1Me-Li (0.69 g, 1.55 mmol) in THF (20 ml) was treated dropwise with stirring at ambient temperature with a solution of $TlNO_3$ (0.45 g, 1.69 mmol) in deionized and degassed water (10 ml), whereupon a yellow precipitate formed. The slurry was stirred for 1 h, and filtered through a frit (G3). The insoluble material was triturated with water (10 ml) and hexane (20 ml) and dried *in vacuo*. Yield: 0.93 g (94%).

^{11}B NMR (128.3 MHz, $CDCl_3$): δ 0.4 ($h_{1/2}$ = 120 Hz). ^1H NMR (400 MHz, $CDCl_3$): δ 2.35 (s, 9H, CH_3), 4.21 (s, 5H, C_5H_5), 4.26, 4.46 (2 × vtr, 2 × 2H, J(HH) = 1.8 Hz, C_5H_4), 5.92 (d, 3H, J(HH) = 2.0 Hz, pz-H4), 7.97 (n.r., 3H, pz-H5). ^{13}C NMR (100.5 MHz, $CDCl_3$): δ 13.4 (br, CH_3), 69.0 (C_5H_5), 69.9, 75.4 (C_5H_4), n.o. (C_5H_4-*i*), 104.0 (pz-C4), 136.1 (pz-C5), 148.4 (pz-C3). CI-MS: *m/z* 644 [M^+; 100%]; 358 [$M^+ - Tlpz^{Me}$; 60%]. Found: C, 41.63; H, 3.85; N, 13.16. Calc. for $C_{22}H_{24}BFeN_6Tl$ [643.51]: C, 41.06; H, 3.76; N, 13.06%.

Synthesis of $FcB(pz^{Ph})_3Li$ (**1Ph-Li**)

1Ph-Li was synthesized similar to **1Me-Li** from **1BN** (1.46 g, 5.14 mmol), $Lipz^{Ph}$ (0.85 g, 5.66 mmol) and Hpz^{Ph} (1.63 g, 11.31 mmol). Yield: 2.93 g (81%).

^{11}B NMR (128.3 MHz, $CDCl_3$): δ 0.3 ($h_{1/2}$ = 260 Hz). ^1H NMR (400 MHz, $CDCl_3$): δ 4.34 (s, 5H, C_5H_5), 4.45, 4.56 (2 × vtr, 2 × 2H, J(HH) = 1.5 Hz, C_5H_4), 6.32 (d, 3H, J(HH) = 2.0 Hz, pz-H4), 7.21 (tr, 3H, J(HH) = 7.5 Hz, Ph-*p*), 7.29 (vtr, 6H, J(HH) = 7.5 Hz, Ph-*m*), 7.61 (d, 6H, J(HH) = 7.5 Hz, Ph-*o*), 8.18 (br, 3H, pz-H5). ^{13}C NMR (100.5 MHz, $CDCl_3$): δ 69.1 (C_5H_5), 70.1, 75.6 (C_5H_4), n.o. (C_5H_4-*i*), 101.9 (pz-C4), 126.9 (Ph-*o*), 127.1 (Ph-*p*), 128.2 (Ph-*m*), 135.0 (Ph-*i*), 136.1 (pz-C5), 152.6 (br, pz-C3). Found: C, 69.64; H, 5.21; N, 12.33. Calc. for $C_{37}H_{30}BFeLiN_6$ [632.29] × 1.0 THF [72.11]: C, 69.91; H, 5.44; N, 11.93%.

Synthesis of $FcB(pz^{Ph})_3Tl$ (**1Ph-Tl**)

1Ph-Tl was synthesized similar to **1Me-Tl** from **1Ph-Li** × 1 THF (0.59 g, 0.84 mmol) and $TlNO_3$ (0.25 g, 0.94 mmol). X-ray quality crystals were obtained from benzene/CH_2Cl_2. Yield: 0.64 g (88%).

^{11}B NMR (128.3 MHz, $CDCl_3$): δ 1.2 ($h_{1/2}$ = 250 Hz). ^1H NMR (400 MHz, $CDCl_3$): δ 4.21 (s, 5H, C_5H_5), 4.31, 4.48 (2 × vtr, 2 × 2H, J(HH) = 1.8 Hz, C_5H_4), 6.54 (d, 3H, J(HH) = 2.5 Hz, pz-H4), 7.29 (tr, 3H, J(HH) = 7.5 Hz, Ph-*p*), 7.36 (vtr, 6H, J(HH) = 7.5 Hz, Ph-*m*), 7.60 (d, 6H, J(HH) = 7.5 Hz, Ph-*o*), 8.11 (d, 3H, J(HH) = 2.5 Hz, pz-H5). ^{13}C NMR (100.5 MHz, $CDCl_3$): δ 68.9 (C_5H_5), 70.0, 74.9 (C_5H_4), n.o. (C_5H_4-*i*), 103.2 (pz-C4), 126.6 (Ph-*o*), 127.6 (Ph-*p*), 128.8 (Ph-*m*), 133.7 (Ph-*i*), 137.1 (pz-C5), 152.6 (br, pz-C3). CI-MS: *m/z* 830 [M^+; 100%]; 482 [$M^+ - Tlpz^{Ph}$; 70%]. Found: C, 54.08; H, 4.07; N, 9.67. Calc. for $C_{37}H_{30}BFeN_6Tl$ [829.72] × 0.5 THF [72.11]: C, 54.10; H, 3.96; N, 9.70%.

Synthesis of 1,1′-fc[B(pz^{Me})$_3$Tl]$_2$ (**2Me-Tl**)

2BN (2.96 g, 7.73 mmol) in toluene (80 ml) was treated dropwise with stirring at ambient temperature with a solution of $Lipz^{Me}$ (1.36 g, 15.45 mmol) in THF (30 ml). Hpz^{Me} (2.55 g, 31.06 mmol) in toluene (20 ml) was added and the orange solution refluxed for 12 h, whereupon an orange precipitate gradually formed. The slurry was allowed to cool to ambient temperature, all insolubles were separated by filtration and extracted with toluene (2 × 10 ml). The combined filtrates were concentrated *in vacuo* to a volume of 10 ml, and stored at −30°C for 12 h. A yellow microcrystalline solid of 1,1′-fc[B(pz^{Me})$_3$Li]$_2$ was obtained, which was collected on a frit (G3), triturated with hexane (10 ml) and dried *in vacuo*. The crude product still contained small amounts of Hpz^{Me}, but could be purified by conversion into the thallium(I) complex.

2Me-Li (0.65 g, 0.92 mmol) in THF (40 ml) was treated dropwise with stirring at ambient temperature with a solution of $TlNO_3$ (0.54 g, 2.03 mmol) in deionized and degassed water (10 ml), whereupon a yellow precipitate immediately formed. The slurry was stirred for 1 h and filtered through a frit (G3). The insoluble material was triturated with water (2 × 10 ml) and hexane (5 ml) and dried *in vacuo*. Yield: 0.53 g (52%).

^{11}B NMR (128.3 MHz, $CDCl_3$): δ 0.4 ($h_{1/2}$ = 270 Hz). ^{1}H NMR (400 MHz, $CDCl_3$): δ 2.37 (s, 18H, CH_3), 4.38, 4.39 (n.r., 2 × 4H, C_5H_4), 5.95 (d, 6H, *J*(HH) = 1.8 Hz, pz-H4), 8.03 (n.r., 6H, pz-H5). ^{13}C NMR (100.5 MHz, $CDCl_3$): δ 13.5 (br, CH_3), 72.0, 76.0 (C_5H_4), n.o. (C_5H_4-*i*), 104.2 (pz-C4), 136.1 (pz-C5), 148.5 (pz-C3). FAB-MS: *m/z* 1102 [M^+; 5%], 530 [$M^+ - 2$ $Tlpz^{Me}$; 85%], 449 [$M^+ - 2$ $Tlpz^{Me} - pz^{Me}$; 100%]. Found: C, 37.09; H, 3.59; N 15.13. Calc. for $C_{34}H_{38}B_2FeN_{12}Tl_2$ [1100.97]: C, 37.09; H, 3.48; N, 15.27%.

Synthesis of 1,1′fc[B(pz^{Ph})$_3$Li]$_2$ (**2Ph-Li**)

2BN (1.97 g, 5.14 mmol) in toluene (100 ml) was treated dropwise with stirring at ambient temperature with a solution of $Lipz^{Ph}$ (1.56 g, 10.39 mmol) in THF (25 ml). Neat solid Hpz^{Ph} (3.00 g, 20.81 mmol) was added through a powder funnel and the orange mixture refluxed for 12 h, whereupon a yellow precipitate gradually formed. The slurry was allowed to cool to ambient temperature. All insolubles were collected on a frit (G3), triturated with toluene (2 × 10 ml) and hexane (10 ml) and dried *in vacuo*. The combined filtrates were slowly concentrated *in vacuo* to yield a second crop of **2Ph-Li**. Yield: 5.00 g (90%).

^{11}B NMR (128.3 MHz, $CDCl_3$): δ −0.1 ($h_{1/2}$ = 300 Hz). ^{1}H NMR (400 MHz, $CDCl_3$): δ 4.67, 4.69 (2 × n.r., 2 × 4H, C_5H_4), 6.36 (d, 6H, *J*(HH) = 1.5 Hz, pz-H4), 7.26 (tr, 6H, *J*(HH) = 7.5 Hz, Ph-*p*), 7.34 (vtr, 12H, *J*(HH) = 7.5 Hz, Ph-*m*), 7.64 (d, 12H, *J*(HH) = 7.5 Hz, Ph-*o*), 8.3 (very br, 6H, pz-H5). ^{13}C NMR (100.5 MHz, $CDCl_3$): δ 72.2, 76.3 (C_5H_4), n.o. (C_5H_4-*i*), 102.1 (pz-C4), 126.9 (Ph-*o*), 127.1 (Ph-*p*), 128.2 (Ph-*m*), 134.9 (Ph-*i*), 136.3 (pz-C5), 152.8 (br, pz-C3). Found: C, 70.70; H, 4.29; N, 15.91. Calc. for $C_{64}H_{50}B_2FeLi_2N_{12}$ [1078.54]: C, 71.27; H, 4.64; N, 15.58%.

Synthesis of 1,1′-fc[B(pz^{Ph})$_3$Tl]$_2$ (**2Ph-Tl**)

2Ph-Li (1.06 g, 0.98 mmol) in THF (60 ml) was treated dropwise with stirring at ambient temperature with a solution of $TlNO_3$ (0.58 g, 2.18 mmol) in deionized and degassed water (15 ml), whereupon a yellow precipitate formed. The slurry was stirred for 1 h, and filtered through a frit (G3). The insoluble material was triturated with water (5 ml) and hexane (10 ml) and dried *in vacuo*. Yield: 1.24 g (82%).

^{11}B NMR (128.3 MHz, $CDCl_3$): δ 0.7 ($h_{1/2}$ = 300 Hz). ^{1}H NMR (400 MHz, $CDCl_3$): δ 4.40, 4.43 (2 × n.r., 2 × 4H, C_5H_4), 6.56 (d, 6H, *J*(HH) = 2.0 Hz, pz-H4), 7.29 (tr, 6H, *J*(HH) = 7.5 Hz, Ph-*p*), 7.36 (vtr, 12H, *J*(HH) = 7.5 Hz, Ph-*m*), 7.60 (d, 12H, *J*(HH) = 7.5 Hz, Ph-*o*), 8.16 (n.r., 6H, pz-H5). ^{13}C NMR (100.5 MHz, $CDCl_3$): δ 72.0, 75.3 (C_5H_4), n.o. (C_5H_4-*i*), 103.3 (pz-C4), 126.6 (br, Ph-*o*), 127.7 (Ph-*p*), 128.9 (Ph-*m*), 133.7 (Ph-*i*), 137.2 (pz-C5), 152.7 (br, pz-C3). FAB-MS: *m/z* 1474 [M^+; 5%], 778 [$M^+ - 2$ $Tlpz^{Ph}$; 100%], 635 [$M^+ - 2$ $Tlpz^{Ph} - pz^{Ph}$; 90%]. Found: C, 52.99; H, 4.10; N 10.91. Calc. for $C_{64}H_{50}B_2FeN_{12}Tl_2$ [1473.40] × 1.0 THF [72.11]: C, 52.85; H, 3.78; N, 10.88%.

Synthesis of HB(pz)$_3$Tl (**3H-Tl**)

3H-Na (0.53 g, 2.25 mmol) in THF (30 ml) was treated dropwise with stirring at ambient temperature with a solution of $TlNO_3$ (0.66 g, 2.48 mmol) in deionized and degassed water (15 ml) and stirred for 2 h. The clear colourless solution was slowly concentrated under reduced pressure, whereupon a colourless precipitate formed, which was collected on a frit (G3), triturated with H_2O (2 × 10 ml) and dried *in vacuo*. Yield: 0.86 g (92%). X-ray quality crystals of **3H-Tl** were grown by slow evaporation of its toluene solution at ambient temperature.

^{11}B NMR (128.3 MHz, $CDCl_3$): δ −2.1 ($h_{1/2}$ = 220 Hz). ^{1}H NMR (400 MHz, $CDCl_3$): δ 4.65 (q, 1H, *J*(HH) = 105 Hz, BH), 6.19 (vtr, 3H, *J*(HH) = 1.6 Hz, pz-H4), 7.53, 7.72 (2 × d, 2 × 3H, *J*(HH) = 1.6 Hz, pz-H3,5). ^{13}C NMR (100.5 MHz, $CDCl_3$): δ 104.1 (pz-C4), 135.6, 139.2 (pz-C3,5). Found: C, 25.90; H, 2.59; N, 20.20. Calc. for $C_9H_{10}BN_6Tl$ [417.40]: C, 25.90; H, 2.41; N, 20.13%.

Crystal structure determination of **1Ph-Tl**

Suitable crystals were grown by layering a CH_2Cl_2 solution of **1Ph-Tl** with benzene at ambient temperature. The compound crystallizes together with 0.5

equiv. of benzene, $C_{37}H_{30}BFeN_6Tl \cdot 0.5\ C_6H_6$, $fw = 868.76$; crystal size $0.41 \times 0.28 \times 0.13$ mm, triclinic space group $P\bar{1}$ (I.T. No. 2), $a = 10.5622(6)$ Å, $b = 13.3208(9)$ Å, $c = 14.0361(9)$ Å, $\alpha = 62.057(6)°$, $\beta = 80.559(6)°$, $\gamma = 72.687(6)°$, $V = 1664.8(2)$ Å^3, $Z = 2$; $\rho_{calc} = 1.733$ g cm^{-3}; $F000 = 854$; $\mu = 53.1$ cm^{-1}. Crystal data, together with details of the data collection and structure refinement, are listed in Table 1. Preliminary examination and data collection were carried out on an imaging plate diffraction system (IPDS; STOE&CIE) equipped with a rotating anode (ENRAF NONIUS FR591; 50 kV; 80 mA; 4.0 kW) and graphite monochromated Mo–K_α radiation ($\lambda = 0.71073$). The data collection was performed at 163(2) K within the θ-range of $2.0° < \theta < 25.6°$ with an exposure time of 2.5 min per image (rotating scan modus from $\varphi = 0°$ to 164° with $\Delta\varphi = 1°$). A total number of 10,403 reflections were collected, from which a sum of 5835 independent reflections remained and were used for all calculations. Data were corrected for Lorentz and polarization effects [11]. Corrections for intensity decay and absorption effects are based on the program DECAY (SF = 4) [11]. The unit cell parameters were obtained by least squares refinements of 4557 reflections with the program CELL [11,12]. The structure was solved by direct methods and refined by full-matrix least squares calculations with anisotropic thermal parameters for all non-hydrogen atoms of **3Ph-Tl** and isotropic thermal parameters for benzene. All hydrogen atoms were calculated in ideal positions. Full matrix least squares refinements were carried out by minimizing $\Sigma w(F_o^2 - F_c^2)^2$ with SHELXL weighting scheme $(w = 1/[\sigma^2(F_o^2) + (0.090 \cdot P)^2 + 0.0000 \cdot P]$ where $P = (F_o^2 + 2 \cdot F_c^2)/3)$ and stopped at shift/err < 0.001, $wR_2 = 0.1155$, and $R_1 = 0.0490$ for all data; GOOF = 1.027, 421 parameters, residual electron density +3.20 e Å^{-3}, −3.64 e Å^{-3} (Tl residual). Neutral atom scattering factors for all atoms and anomalous dispersion corrections for the non-hydrogen atoms were taken from the *International Tables for X-Ray Crystallography* [13]. All calculations were performed on a DEC 3000 AXP workstation with the STRUX-V system [14], including the programs PLATON-92 [15], PLUTON-92 [15], SIR-92 [16], and SHELXL-93 [17].

Atomic coordinates have been deposited with the Cambridge Crystallographic Data Centre.

Crystal structure determination of **3H-Tl**

Suitable crystals of **3H-Tl** were grown by slow evaporation of its toluene solution at ambient temperature. There are two crystallographically independent molecules in the asymmetric unit (**3H-Tla, 3H-Tlb**), $C_9H_{10}BN_6Tl$, $fw = 417.41$; crystal size $0.20 \times 0.20 \times 0.10$ mm, monoclinic space group $P21$ (I.T. No. 4); $a = 7.7812(3)$ Å, $b = 9.3364(4)$ Å, $c = 16.9680(6)$ Å, $\beta = 91.761(4)°$, $V = 1232.1(1)$ Å^3, $Z = 4$; $\rho_{calc} = 2.250$ g cm^{-3}; $F000 = 768$; $\mu = 130.9$ cm^{-1}. Crystal data together with details of the data collection and structure refinement are listed in Table 1. Preliminary examination and data collection were carried out on an imaging plate diffraction system (IPDS; STOE&CIE) equipped with a rotating anode (ENRAF NONIUS FR591; 50 kV; 80 mA; 4.0 kW) and graphite monochromated Mo–K_α radiation ($\lambda = 0.71073$). The data collection was performed at 173(2) K within the θ-range of $2.5° < \theta < 27.8°$ with an exposure time of 3 min per image (rotating scan modus from $\varphi = 0.0°$ to 270.0° with $\Delta\varphi = 1°$). A total number of 15,671 reflections were collected, from which a sum of 5762 independent reflections remained and were used for all calculations (12 systematically absent reflections rejected). Data were corrected for Lorentz and polarization effects [11]. Corrections for intensity decay and absorption effects are based on the program DECAY (SF = 3) [11]. The unit cell parameters were obtained by least squares refinements of 5000 reflections with the program CELL [11,12]. The structure was solved by the Patterson method and refined by full-matrix least squares calculations with anisotropic thermal parameters for all non-hydrogen atoms. All hydrogen atoms were calculated in ideal positions. Full matrix least squares refinements were carried out by minimizing $\Sigma w(F_o^2 - F_c^2)^2$ with SHELXL weighting scheme $(w = 1/[\sigma^2(F_o^2) + (0.0510 \cdot P)^2 + 0.0000 \cdot P]$ where $P = (F_o^2 + 2 \cdot F_c^2)/3)$ and stopped at shift/err < 0.001, $wR_2 = 0.0870$, and $R_1 = 0.0353$ for all data; GOOF = 1.043, 306 parameters, residual electron density +4.35 e Å^{-3}, −1.64 e Å^{-3} (Tl residual), Flack parameter = −0.0032 (0.0108). (Structure refinement of the enantiomorphic model gave values $wR_2 = 0.134$, and $R_1 = 0.0498$ for all data; GOOF = 1.052, Flack parameter = 1.0529 (0.0196).) Neutral atom scattering factors for all atoms and anomalous dispersion corrections for the non-hydrogen atoms were taken from the *International Tables for X-Ray Crystallography* [13]. All calculations were performed on a DEC 3000 AXP workstation with the STRUX-V system [14], including the programs PLATON-92 [15], PLUTON-92 [15], SIR-92 [16] and SHELXL-93 [17].

Atomic coordinates have been deposited with the Cambridge Crystallographic Data Centre.

Acknowledgement—Financial funding by the "Deutsche Forschungsgemeinschaft" and the "Fonds der Chemischen Industrie" is gratefully acknowledged.

REFERENCES

1. Trofimenko, S., *J. Am. Chem. Soc.*, 1967, **89,** 3170.
2. Trofimenko, S., *Chem. Rev.*, 1993, **93,** 943.
3. Niedenzu, K., Serwatowski, J. and Trofimenko, S., *Inorg. Chem.*, 1991, **30,** 524.
4. Brock, C. P., Das, M. K., Minton, R. P. and Niedenzu, K., *J. Am. Chem. Soc.*, 1988, **110,** 817.

5. Jäkle, F., Polborn, K. and Wagner, M., *Chem. Ber.*, 1996, **129,** 603.
6. de Biani, F. F., Jäkle, F., Spiegler, M., Wagner, M. and Zanello, P., *Inorg. Chem.*, 1997, **36,** 2103. Note: Figure 1 of this paper contains a structural formula with wrong connectivity (compound B). For the right connectivity see Ref. [3].
7. Allen, F. H., Kennard, O. and Taylor, R., *Acc. Chem. Res.*, 1983, **16,** 146.
8. Trofimenko, S., Calabrese, J. C. and Thompson, J. S., *Inorg. Chem.*, 1987, **26,** 1507.
9. Parkin, G., *Adv. Inorg. Chem.*, 1995, **42,** 291.
10. Ferguson, G., Jennings, M. C., Lalor, F. J. and Shanahan, C., *Acta Crystallogr.*, 1991, **C47,** 2079.
11. *IPDS Operating System*, Version 2.6. STOE &CIE. GmbH: Darmstadt, Germany, 1995.
12. Schütt, W., Herdtweck, E., Hahn, F. and Kreißl, F. R., *J. Organomet. Chem.*, 1993, **443,** C33, and references cited therein.
13. *International Tables for X-ray Crystallography*, ed. A. J. C. Wilson. Kluwer Academic Publishers: Dordrecht, 1992, Vol. C, Tables 4.2.4.2 (pp. 193–199), 4.2.6.8 (pp. 219–222) and 6.1.1.4 (pp. 500–502).
14. Artus, G., Scherer, W., Priermeier, T. and Herdtweck, E., *"STRUX-V", A Program System to Handle X-ray Data.* TU München: Germany, 1994.
15. Spek, A. L., *Acta Crystallogr.*, 1990, **A46,** C34.
16. Altomare, A., Cascarano, G., Giacovazzo, C., Guagliardi, A., Burla, M. C., Polidori, G. and Camalli, M., *SIR*-92; University of Bari, Italy.
17. Sheldrick, G. M., *J. Appl. Cryst.*, 1993, in press.

Pergamon

PII: S0277-5387(97)00503-2

Polyhedron Vol. 17, No. 7, pp. 1159–1164, 1998
© 1998 Elsevier Science Ltd
All rights reserved. Printed in Great Britain
0277-5387/98 $19.00+0.00

Chiral and achiral phosphine–phosphite ligands in Pd(II)-catalyzed alternating copolymerization of propene with CO†

Kyoko Nozaki,* Masako Yasutomi, Koji Nakamoto, and Tamejiro Hiyama

Department of Material Chemistry, Graduate School of Engineering, Kyoto University, Yoshida, Sakyo-ku, Kyoto 606-01, Japan

(Received 13 October 1997; accepted 31 October 1997)

Abstract—In addition to (*R*,*S*)-BINAPHOS, several related phosphine-phosphite ligands have been prepared and their use in Pd(II) catalyzed asymmetric alternating copolymerization of propene with carbon monoxide was examined. Small changes of the ligand substituents caused drastic changes of the stereo regularity of the product, which reveals that not only the electronic bias of (*R*,*S*)-BINAPHOS but also its steric demand is essential to produce completely isotactic copolymer from propene and CO in highly enantioselective fashion.
© 1998 Elsevier Science Ltd. All rights reserved

Keywords: palladium; phosphine-phosphite; propene; carbon monoxide; asymmetric copolymerization.

The alternating copolymerization of olefins with carbon monoxide is of great interest due to the potential use of the resulting polymer as a new material [1]. When α-olefins such as propene and styrene are used, control of regio- and enantioselectivities of the olefin insertion becomes a problematic issue for obtaining stereoregular polyketones. Thus, asymmetric copolymerization using chiral catalysts is now attracting much attention. Most of the successful reports on this subject deal with C_2 symmetrical bidentate ligands [2]. Recently, we have demonstrated that a cationic Pd(II) complex of unsymmetrical chiral bidentate phosphine–phosphite, (*R*,*S*)-BINAPHOS (=(*R*)-2-diphenylphosphino-1,1′-binaphthalen-2′-yl (*S*)-1,1′-binaphthalen-2,2′-diyl phosphite) [3], serves as an efficient catalyst for the asymmetric copolymerization of propene with carbon monoxide [4]. Highly isotactic polyketone was obtained with high enantioselectivity. The unique unsymmetrical character of this ligand attracted our attention, and thus we further investigated the catalytic activities of Pd(II) complexes bearing related phosphine–phosphite ligands. Here we report the synthesis of some chiral and achiral phosphine–phosphite ligands and their use in the copolymerization.

EXPERIMENTAL

Phosphine–phosphite ligands were prepared as follows. Detailed procedures have been reported elsewhere [3]. (*R*)-2-Diarylphosphino-2′-hydroxy-1,1′-binaphthyls or their analogs were prepared according to the literature procedure [10]. These phosphine parts were combined with 1,1′-binaphthyl-2,2′-diyl chlorophosphite in the presence of triethylamine in ether. After aqueous work up, the crude products were purified by silica-gel column chromatography. ^{31}P NMR of the products are summarized in Table 1. Other spectroscopic data are as follows. (*R*,*S*)-$(Me_2C_6H_3)_2$-Et_2-BINAPHOS: ^{1}H NMR ($CDCl_3$) δ 1.99 (s, 6H, $ArCH_3$), 2.07 (s, 6H, $ArCH_3$), 6.00 (d, J = 9.0 Hz, 1H, aromatic), 6.72–8.00 (m, aromatic, 29H). Found: C, 80.37; H, 5.32. Calcd for $C_{56}H_{42}P_2O_3$: C, 81.54; H, 5.13. (*R*,*S*)-(*c*-Pen)$_2$-BINAPHOS: ^{1}H NMR ($CDCl_3$) δ 0.50–2.20 (m, aliphatic, 18H), 6.71–8.04 (m, aromatic, 24H). Found: C, 79.61; H, 5.63. Calcd for $C_{50}H_{42}P_2O_3$: C, 79.77; H, 5.62. (*R*,*S*)-BINAPHOS: ^{1}H NMR ($CDCl_3$) δ 0.57–0.78 (m, 6H, CH_2CH_3), 1.20–1.80 (m, 4H, CH_2CH_3), 6.16 (d, J = 8.6 Hz, 1H, aromatic), 7.00–8.10 (m, 23H). Found: C, 75.08; H,

* Author to whom correspondence should be addressed.

† This paper is dedicated to Professor Dr Wolfgang A. Herrmann on the occasion of his 50th birthday.

Table 1. ^{31}P NMR for phosphine–phosphite ligands and their neutral and cationic Pd(II) complexes

L	L δ (ppm), (J_{P-P}, Hz)	$Pd(CH_3)(Cl)(L)$[a] δ (ppm), ($J_{P\ P}$, Hz)	$[Pd(CH_3)(CH_3CN)(L)]\cdot[B\{3,5\text{-}(CF_3)_2C_6H_3\}4]$[d] δ (ppm), ($J_{P\ P}$, Hz)
(*R,S*)-BINAPHOS	δ 1447, −14.6 (29.0)	Major: δ 149.4, 12.2 (64.0)[b] Minor: δ 154.1, 33.1 (54.9)	δ 142.9, 13.0 (63.4)
(*R,S*)-($Me_2C_6H_3$)-BINAPHOS	δ 145.5, −12.4 (30.50)	Major: δ 148.2, 12.9 (63.4)[c] Minor: δ 153.9, 34.3 (55.7)	δ 141.8, 13.6 (63.3)
(*R,S*)-(*c*-Pen)$_2$-BINAPHOS	δ 146.4, −10.6 (4.6)	δ 148.9, 16.7 (64.8)	δ 144.2, 18.0 (61.8)
(*R,S*)-Et_2-BINAPHOS	δ 146.5; −26.5 (24.7)	δ 150.4, 11.8 (65.6)	δ 145.7, 7.4 (67.1)
(*R,S*)-H_8-BINAPHOS	δ 146.7, −15.0 (41.2)	δ 147.9, 10.6 (65.6)	δ 141.4, 11.7 (64.0)
o-$C_6H_4(PPh_2)\{OP(OPh)_2\}$ (**1**)	δ 127.5, −15.9 (12.2)	δ 160.5, 11.0 (19.0)	Complex mixture
o-$C_6H_4(PPh_2)\{CH_2OP(OPh)_2\}$ (**2**)	δ 129.1, −15.8 (0.0)	δ 128.1, 9.7 (61.0)	δ 115.8, 6.9 (65.0)

[a] *SP*-4-2-isomers were obtained as exclusive products if otherwise stated.
[b] Obtained as a 5 : 1 mixture of *SP*-4-2- and *SP*-4-3-isomers.
[c] Obtained as a 3 : 1 mixture of *SP*-4-2- and *SP*-4-3-isomers.
[d] *SP*-4-3-isomers were obtained as exclusive products.

5.01. Calcd for $C_{44}H_{34}P_2O_3\cdot 0.2\ (CHCl_3)$: C, 76.21; H, 4.95. (*R,S*)-H_8-BINAPHOS: ^1H NMR ($CDCl_3$) δ 0.70–0.80 (m, 2H), 1.10–2.00 (m, 10H), 2.57 (m, 2H), 2.90 (m, 2H), 6.18 (d, $J = 9.0$ Hz, 1H, aromatic), 6.90–7.90 (m, aromatic, 25H). Found: C, 80.29; H, 5.69. Calcd for $C_{52}H_{42}P_2O_3$: C, 80.40; H, 5.45.

The ligands were allowed to react with $Pd(CH_3)(Cl)(COD)$ [11] in benzene to form neutral methylpalladium complexes [4b]. Pd(Me)(Cl){(*R,S*)-($Me_2C_6H_3$)$_2$-BINAPHOS}: Major product: ^1H NMR ($CDCl_3$) δ 1.47 (dd, $J_{P-H} = 8.3$, 2.6 Hz, 3H, PdCH_3), 1.89 (s, 6H, ArCH_3), 2.16 (s, 6H, ArCH_3), 4.75 (d, $J = 9.0$ Hz, 1H, aromatic), 6.40–8.20 (m, aromatic, 29H). Minor product: ^1H NMR ($CDCl_3$) δ 0.52 (dd, $J_{P-H} = 4.0$, 11.5 Hz, 3H, PdCH_3), 1.92 (s, 6H, ArCH_3), 2.19 (s, 6H, ArCH_3), 4.65 (d, $J = 9.0$ Hz, 1H, aromatic), 6.40–8.20 (m, aromatic 29H). Pd(Me)(Cl){(*R,S*)-(*c*-Pen)$_2$-BINAPHOS}: ^1H NMR ($CDCl_3$) δ 0.20–0.40 (m, 1H), 0.80–2.00 (m, 16H), 1.42 (dd, $J_{P-H} = 7.8$, 2.1 Hz, 3H, PdCH_3), 2.70–2.95 (m, 1H), 4.60 (d, $J = 9.0$ Hz, 1H, aromatic), 6.75–8.20 (m, 23H). Pd(Me)(Cl){(*R,S*)-Et_2-BINAPHOS}: ^1H NMR ($CDCl_3$) δ 1.40–2.00 (m, 10H, aliphatic), 1.55 (dd, $J_{P-H} = 8.0$, 2.0 Hz, 3H, PdCH_3), 7.02–8.50 (m, 24H, aromatic). Pd(Me)(Cl){(*R,S*)-H_8-BINAPHOS}: ^1H NMR ($CDCl_3$) δ 0.20–2.00 (m, 12H), 1.34 (dd, $J_{P-H} = 7.9$, 2.3 Hz, 3H, PdCH_3), 2.57 (m, 2H), 3.05 (m, 2H), 5.33 (d, $J = 9.0$ Hz, 1H, aromatic), 7.00–8.00 (m, 25H, aromatic).

The neutral complexes were mixed with equimolar amount of $NaB(3,5\text{-}(CF_3)_2C_6H_3)_4$ in CH_2Cl_2–CH_3CN to give cationic Pd complexes [4b]. [Pd(Me)(MeCN){(*R,S*)-($Me_2C_6H_3$)$_2$-BINAPHOS}]·[B{3,5-$(CF_3)_2C_6H_3$}$_4$]: ^1H NMR ($CDCl_3$) δ 1.26 (bd, $J_{P-H} = 7.6$ Hz, 3H, PdCH_3), 1.80 (bs, 3H, CH_3CN), 1.89 (s, 6H, ArCH_3), 2.21 (s, 6H, ArCH_3), 4.77 (d, $J = 9.0$ Hz, 1H, aromatic), 6.10 (d, $J = 9.0$ Hz, 1H, aromatic), 6.40–8.25 (m, 28H, aromatic). [Pd(Me)(MeCN){(*R,S*)-(*c*-Pen)$_2$-BINAPHOS}]·[B{3,5-$(CF_3)_2C_6H_3$}$_4$]: ^1H NMR ($CDCl_3$) δ 0.80–2.10 (m, 16H, aliphatic), 1.24 (bd, $J_{P-H} = 6.9$ Hz, 3H, PdCH_3), 2.02 (bs, 3H, CH_3CN), 2.85 (m, 2H, aliphatic), 4.59 (d, $J = 9.0$ Hz, 1H, aromatic), 6.77–8.30 (m, 23H, aromatic). [Pd(Me)(MeCN){(*R,S*)-Et_2-BINAPHOS}]·[B{3,5-$(CF_3)_2C_6H_3$}$_4$]: ^1H NMR ($CDCl_3$) δ 0.50–2.25 (m, 13H, aliphatic), 2.02 (bs, 3H, CH_3CN), 5.24 (d, $J = 9.0$ Hz, 1H, aromatic), 7.02–8.50 (m, 23H, aromatic). [Pd(Me)(MeCN){(*R,S*)-H_8-BINAPHOS}]·[B{3,5-$(CF_3)_2C_6H_3$}$_4$]: ^1H NMR ($CDCl_3$) δ 0.42 (m, 1H, aliphatic), 0.65 (m, 1H, aliphatic), 1.00–2.00 (m, 10H, aliphatic), 1.12 (bd, $J_{P-H} = 7.3$ Hz, 3H, PdCH_3), 2.38 (m, 1H), 2.56 (m, 1H), 3.01 (m, 2H), 2.30 (bs, 3H, CH_3CN), 5.30 (d, $J = 9.0$ H, 1H, aromatic), 6.95–7.98 (m, 25H).

Asymmetric copolymerization of propene (3 atm) with CO (20 atm) was carried out in CH_2Cl_2 (2 mmol) using cationic Pd complexes (0.011 mmol) as catalysts in a 100-mL auto-clave at 20°C. The detailed procedure has been reported in our previous report [4].

RESULTS AND DISCUSSIONS

Ligand synthesis

The phosphine–phosphite ligands employed here are summarized in Chart 1. In (*R,S*)-($Me_2C_6H_3$)$_2$-BINAPHOS, two methyl groups are placed at 3- and 5-position in each of the phenyl groups of the parent (*R,S*)-BINAPHOS. The phenyl groups of (*R,S*)-BINAPHOS are replaced by cyclopentyl and ethyl groups in (*R,S*)-(*c*-Pen)$_2$-BINAPHOS and (*R,S*)-Et_2-BINAPHOS, respectively. Instead of 2,2′-dihy-

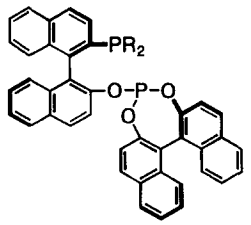

R = Ph: (*R,S*)-BINAPHOS

R = 3,5-$Me_2C_6H_3$: (*R,S*)-$(Me_2C_6H_3)_2$-BINAPHOS

R = *cyclo*-C_5H_9: (*R,S*)-(*c*-Pen)$_2$-BINAPHOS

R = Et: (*R,S*)-Et_2-BINAPHOS

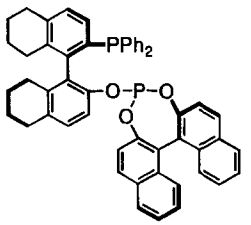

(*R,S*)-H_8-BINAPHOS

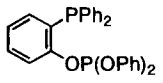

1

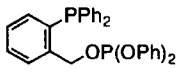

2

Chart 1

droxy-1,1′-binaphthyl, 5,5′,6,6′,7,7′,8,8′-octahydro-2,2′-dihydroxy-1,1′-binaphthyl was used to construct the phosphine site in (*R,S*)-H_8-BINAPHOS [5]. In addition to the BINAPHOS derivatives, achiral phosphine–phosphites **1** and **2** were prepared. The ^{31}P NMR data for the ligands are all listed in Table 1.

Preparation of Pd(II)-complexes

Neutral complexes Pd(Me)(Cl)(ligand) were prepared by admixture of the ligands with Pd(Me)(Cl)(cod). In Table 1, ^{31}P NMR data for the neutral complexes are summarized. A 5 : 1 mixture of isomers was obtained for Pd(Me)(Cl){(*R,S*)-BINAPHOS} and we previously determined the structures of the major and the minor complexes to be *SP*-4-2 and *SP*-4-3, respectively [4b]. Theoretical studies also suggested that the methyl group is stable at trans to a phosphine (corresponding to SP-4-2) than at trans to a phosphite (corresponding to *SP*-4-3) [4b]. Hence we tentatively determine the structure of the major complexes to be *SP*-4-2.

The neutral complexes were converted into the corresponding cationic complexes by treatment with $NaBAr_4$ (Ar = 3,5-$(CF_3)_2C_6H_3$). With BINAPHOS derivatives and **2**, single species were obtained, their ^{31}P NMR data are also shown in Table 1. Their structures were analogously assigned to be *SP*-4-3 on the basis of [*SP*-4-3-Pd(Me)(MeCN){(*R,S*)-BINAPHOS}]·[BAr_4] [4b]. From neutral complex Pd(Me)(Cl) (**1**), the corresponding cationic species was not formed and a complex mixture resulted. BINAPHOS derivatives form 8-membered palladacycle when they coordinate to Pd(II), whereas phosphine–phosphite **1** and **2** give 6- and 7-membered ring, respectively. The less stability of [Pd(Me) (MeCN)(**1**)]·[BAr_4] may be attributed to its smallest chelation-ring size.

Alternating copolymerization of propene with CO catalyzed by cationic Pd(II) complexes

Propene was copolymerized with carbon monoxide using the cationic Pd(II)-complexes as catalysts. The

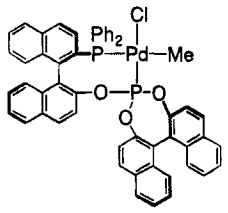

SP-4-2-Pd(Me)(Cl) {(*R,S*)-BINAPHOS}

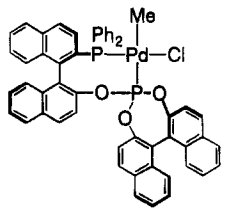

SP-4-3-Pd(Me)(Cl) {(*R,S*)-BINAPHOS}

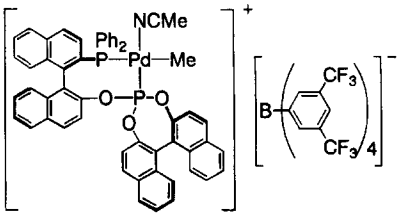

SP-4-3-[Pd(Me)(MeCN){(*R,S*)-BINAPHOS}]·[B{3,5-$(CF_3)_2C_6H_3$}$_4$]

complexes bearing BINAPHOS derivatives were all active for the copolymerization and completely alternating copolymers were obtained. The head-to-tail selectivity and isotacticity of the copolymers were determined by ^1H and ^{13}C NMR spectroscopy. When (*R*,*S*)-($Me_2C_6H_3$)$_2$- and (*R*,*S*)-(*c*-Pen)$_2$-BINAPHOS were used as a ligand, highly isotactic polyketone was obtained in a manner similar to the reaction with (*R*,*S*)-BINAPHOS. With (*R*,*S*)-Et_2-BINAPHOS, however, polyketone was formed with lower regioselectivity. The presence of head-to-head and tail-to-tail structures were suggested by ^{13}C NMR. Three peaks were observed for the carbonyl carbon at 208, 212, 215 ppm and their ratio was roughly estimated to be 1 : 6.5 : 1. The peaks were assigned to tail-to-tail, head-to-tail, and head-to-head structures, respectively, according to the literature values [6]. Comparison of the result with (*R*,*S*)-(*c*-Pen)$_2$- and that with (*R*,*S*)-Et_2-BINAPHOS suggests that the different steric demand in the phosphine site substantially affects the regioselectivity. We previously proposed a model in which propene insertion to an acyl-palladium bond takes place via propene coordination to Pd at a cis site to a phosphine than to a phosphite in a Pd–phosphine–phosphite complex (Scheme 1) [4]. In this model, 1,2-insertion of propene is favored over 2,1-insertion, probably due to the steric repulsion between one of the phenyl groups in the phosphine and the methyl group of propene. This model is consistent with the present considerable substituent-effect. That is, the phosphine site located cis to the coordination site of propene, most effectively, controls the regio- and enantioselectivities of the propene insertion. The use of achiral phosphine–phosphite **2** gave a polyketone with even lower regioselectivity, the ratio of tail-to-tail, head-to-tail, and head-to-head being 1 : 3.6 : 1. The low regio regularity should be attributed to either the absence of chirality or the less steric demand in the phosphite site.

The yield and molecular weight of the copolymers were compared by quenching the polymerization after 6 h as described in Table 2. Among the BINAPHOS derivatives, Pd(II)-(*R*,*S*)-H_8-BINAPHOS complex showed the highest yield and molecular weight. The propene conversion to the copolymer is plotted against the reaction time in Fig. 1 in order to compare the two ligands, (*R*,*S*)-BINAPHOS and (*R*,*S*)-H_8-BINAPHOS. With (*R*,*S*)-H_8-BINAPHOS, the initial

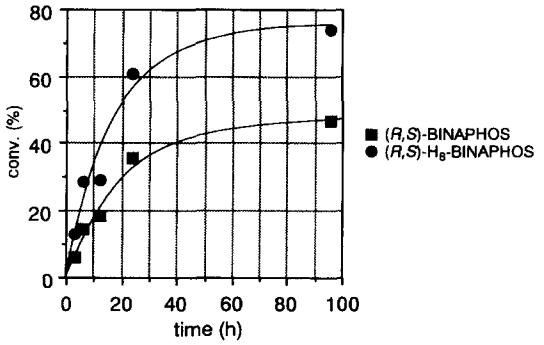

Fig. 1.

reaction rate is almost twice as high as with (*R*,*S*)-BINAPHOS. The living nature of the Pd(II)-(*R*,*S*)-H_8-BINAPHOS-catalyzed copolymerization has been disclosed as shown in Fig. 2. Prolonged reaction time with (*R*,*S*)-H_8-BINAPHOS, however, resulted in a molecular weight (96 h, Mn = 49,000, Mw/Mn = 1.57) similar to that with (*R*,*S*)-H_8-BINAPHOS (96 h, Mn = 65,000; Mw/Mn = 1.60). Most probably, the deposition of polymer in this solvent inhibits further growth of the polymer.

We previously reported that higher enantioselectivity was achieved with H_8-BINAP (5,5′,6,6′,7,7′,8,8′) - octahydro-2,2′ - diphenylphos - phino-1,1′-binaphthyl) than with BINAP (2,2′-diphenylphosphino-1,1′-binaphthyl) in Rh(I)-catalyzed asymmetric hydrogenation of α,β-unsaturated carboxylic acids [5a]. The larger bite angle, P–Rh–P, is suggested to cause stronger steric demand around the reaction site of Rh(I) center. Here in this study, (*R*,*S*)-H_8-BINAPHOS should chelate to the Pd(II) center with larger P–Pd–P angle than (*R*,*S*)-BINAPHOS and thus the Pd(II) is less exposed in the (*R*,*S*)-H_8-BINAPHOS complex. Recently, Leitner and his coworkers reported that a ligand with a larger steric block around

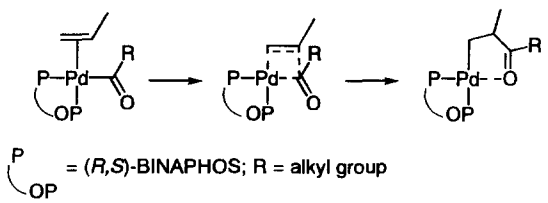

Scheme 1.

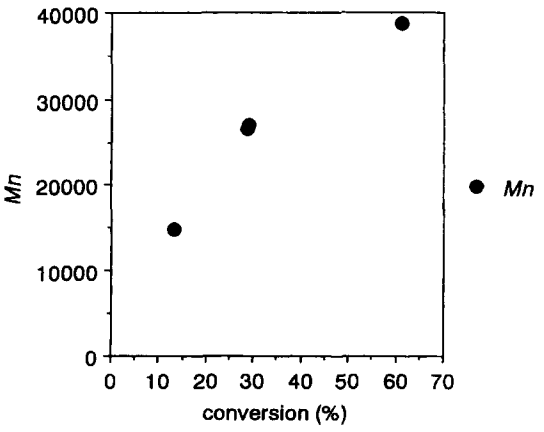

Fig. 2.

Table 2. Copolymerization of propene with CO catalyzed by cationic Pd(II)–phosphine–phosphite complexes[a]

L	Yield (%)	Tacticity	Mn	Mw/Mn	UV[b] λ_{max} (nm)	UV[b] ε_{max}	CD[b] λ_{max} (nm)	CD[b] $\Delta\varepsilon$	CD[b] g $\Delta\varepsilon/\varepsilon_{max}$
(*R*,*S*)-BINAPHOS	15	Isotactic	16,400	1.07	273	55.8	276	−1.66	-2.97×10^{-2}
(*R*,*S*)-($Me_2C_6H_3$)-BINAPHOS	11	Isotactic	13,700	1.07	272	59.8	276	−1.56	-2.61×10^{-2}
(*R*,*S*)-(*c*-Pen)$_2$-BINAPHOS	20	Isotactic	15,900	1.24	272	58.8	276	+2.06	-2.97×10^{-2}
(*R*,*S*)-Et_2-BINAPHOS	7[c]	Atactic[d]	1300	1.04	—[e]	—[e]	—[e]	—[e]	—[e]
(*R*,*S*)-H_8-BINAPHOS	29	Isotactic	26,600	1.07	272	56.0	275	−1.64	-2.93×10^{-2}
o-$C_6H_4(PPh_2)\{OP(OPh)_2\}$ (1)[f]	0[g]	—	—	—	—	—	—	—	—
o-$C_6H_4(PPh_2)$ $\{CH_2OP(OPh)_2\}$ (2)	5[h]	Atactic[d]	4800	1.11	—[e]	—[e]	—	—	—

[a] The reaction was stopped after 6 h, if otherwise stated, in order to compare the catalytic activity.
[b] 0.01 M in $(CF_3)_2CHOH$.
[c] The reaction was stopped after 24 h.
[d] Regio irregular and atactic polyketone was obtained.
[e] Not determined.
[f] Cationic complex was not obtained as a single species. A complex mixture was used as a catalyst.
[g] The reaction was stopped after 58 h.
[h] The reaction was stopped after 96 h.

the metal center resulted in higher catalytic activity in the Rh(I)-catalyzed reduction of carbon dioxide to formic acid [7]. They explained this phenomenon that the less solvation due to the steric hindrance caused the higher catalytic activity. A parallel interpretation is applicable for the present result that a favorable approach of monomers, propene and carbon monoxide, than of solvents, e.g. acetonitrile and CH_2Cl_2, has been realized in the (*R*,*S*)-H_8-BINAPHOS complex.

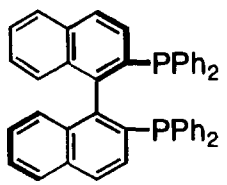

(*R*)-BINAP

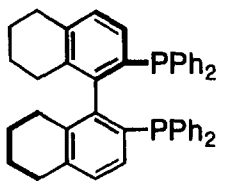

(*R*)-H_8-BINAP

CD spectra of the polyketones

The UV and CD spectra of the polyketones obtained with (*R*,*S*)-BINAPHOS, (*R*,*S*)-($Me_2C_6H_3$)$_2$-BINAPHOS, and (*R*,*S*)-H_8-BINAPHOS exhibit the absorption due to the carbonyl group at essentially the same wave length (λ_{max} = 272–276 nm). The agreement of λ_{max} between UV and CD suggests that the UV absorption corresponds to the single CD absorption but not to a sum of multiple ones. The dissymmetry factor g was calculated in such a way as $g = (\Delta\varepsilon)/(\varepsilon)$ [8]. For the copolymers obtained with (*R*,*S*)-BINAPHOS, (*R*,*S*)-($Me_2C_6H_3$)$_2$-BINAPHOS, and (*R*,*S*)-H_8-BINAPHOS, the g values were substantially the same, suggesting that the enantiometric homogeneity of the polymers is essentially the same [9]. We previously determined the enantiomeric excess of the chirotopic carbons to be at least 95% *ee* (*S*) in the propene-CO copolymer obtained with (*R*,*S*)-BINAPHOS [4b]. Hence it is suggested that the copolymers produced with (*R*,*S*)-($Me_2C_6H_3$)$_2$-BINAPHOS and (*R*,*S*)-H_8-BINAPHOS have almost complete enantiomerical purity, too. It is noteworthy that (*R*,*S*)-(*c*-Pen)$_2$-BINAPHOS gave a polyketone with the opposite sign of CD absorption to the one with BINAPHOSs bearing diarylphosphino groups. This means that the chirotopic carbons in this copolymer have *R* absolute configuration. Thus the study reveals that the enantiofacial selection for propene by a ligand heavily depends on the structure and the electronic circumstance of the phosphine site.

CONCLUSION

The present study reveals that a Pd(II) complex of (*R*,*S*)-H_8-BINAPHOS is a more active catalyst compared to that of (*R*,*S*)-BINAPHOS for alternating copolymerization of propene with carbon monoxide. Completely isotactic copolymer was obtained in high optical purity with (*R*,*S*)-H_8-BINAPHOS, (*R*,*S*)-($Me_2C_6H_3$)$_2$-BINAPHOS, and (*R*,*S*)-(*c*-Pen)$_2$-BINAPHOS. The opposite enantioface of propene was selected by (*R*,*S*)-(*c*-Pen)$_2$-BINAPHOS. Copolymer with low regio regularity was obtained with (*R*,*S*)-Et_2-BINAPHOS. Thus slight change around the phos-

phine site strongly affects the stereo regularity of the polyketone. The use of achiral phosphine–phosphites **1** and **2** resulted in no reaction and formation of stereo irregular polyketone, respectively. Therefore, we conclude that not only the electronic bias of (*R,S*)-BINAPHOS but also its steric demand is essential to produce completely isotactic copolymer from propene and CO in highly enantioselective fashion.

Acknowledgement—This work was supported by NEDO for the project on Technology for Novel High-Functional Materials in Industrial Science and Technology Frontier Program, AIST.

REFERENCES

1. (a) Drent, E. and Budzelaar, P. H. M. *Chem. Rev.*, 1996, **96,** 663; (b) Drent, E., van Broekhoven, J. A. M. and Budzelaar, P. H. M. *Recl. Trav. Chim. Pays-Bas*, 1996, **115,** 263; (c) Sen, A., *Acc. Chem. Res.*, 1993, **26,** 303; (d) Drent, E., van Broekhoven, J. A. M. and Doyle, M. J., *J. Organomet. Chem.*, 1991, **417,** 235; (e) Drent, E., *Pure Appl. Chem.*, 1990, **62,** 661; (f) Sen, A., *Adv. Polym. Sci.*, 1986, **73/74,** 125; (g) Sen, A., *Chemtech*, 1986, 48.
2. Asymmetric synthesis: (a) Barsacchi, M., Batistini, A., Consiglio, G. and Suter, U. W., *Macromolecules*, 1992, **25,** 3604; (b) Jiang, Z., Adams, S. E. and Sen, A., *Macromolecules*, 1994, **27,** 2694; (c) Bronco, S., Consiglio, G., Hutter, R., Batistini, A. and Suter, U. W., *Macromolecules*, 1994, **27,** 4436; (d) Jiang, Z. and Sen, A., *J. Am. Chem. Soc.*, 1995, **117,** 4455; (e) Sperrie, M. and Consiglio, G., *J. Am. Chem. Soc.*, 1995, **117,** 12,130; (f) Kacker, S., Jiang, Z. and Sen, A., *Macromolecules*, 1996, **29,** 5852; (g) Brookhart, M., Wagner, M. I., Balavoine, G. G. A. and Haddou, H. A., *J. Am. Chem. Soc.*, 1994, **116,** 3641; (h) Bartolini, S., Carfagna, C. and Musco, A., *Macromol. Rapid Commun.*, 1995, **16,** 9.
3. For the synthesis of (*R,S*)-BINAPHOS, Nozaki, K., Sakai, N., Nanno, T., Higashijima, T., Mano, S., Horiuchi, T. and Takaya, H., *J. Am. Chem. Soc.*, 1997, **119,** 4413.
4. (a) Nozaki, K., Sato, N. and Takaya, H., *J. Am. Chem. Soc.*, 1995, **117,** 9911; (b) Nozaki, K., Sato, N., Tonomura, Y., Yasutomi, M., Takaya, H. and Hiyama, T., *J. Am. Chem. Soc.*, in press.
5. (a) Uemura, T., Zhang, X., Matsumura, K., Sayo, N., Kumobayashi, H., Ohta, T., Nozaki, K. and Takaya, H. J. *Org. Chem.*, 1996, **61,** 5510; (b) Zhang, X., Mashima, K., Koyano, K., Sayo, N., Kumobayashi, H., Akutagawa, S. and Takaya, H., *J. Chem. Soc., Perkin Trans.* 1, 1994, 2309.
6. Batistini, A., Consiglio, G. and Suter, U. W., *Angew Chem., Int. Ed. Engl.*, 1992, **31,** 303.
7. Angermund, K., Baumann, W., Dinjus, E., Fornika, R., Görls, H., Kessler, M., Krügger, C., Leitner, W. and Lutz, F., *Chem. Eur. J.*, 1997, **3,** 755.
8. Nakanishi, K., Berova, N. and Woody, R. W. (eds) in *Circular Dichroism. Principles and Applications*. VCH: New York, 1994.
9. The influence of molecular weight on the *g* value was negligible. Copolymers in molecular weight range of Mn = 6000–60,000 showed the same level of *g* when they were prepared by (*R,S*)-BINAPHOS–Pd(II).
10. (a) Kurz, L., Lee, G., Morgans, D., Jr., Waldyke, M. J. and Ward, T., *Tetrahedron Lett.*, 1990, **31,** 6321; (b) Uozumi, Y., Tanahashi, A., Lee, S.-Y. and Hayashi, T. *J. Org. Chem.*, 1993, **58,** 1945.
11. Rülke, R. E., Ernsting, J. M., Spek, A. L., Elsevier, C. J., van Leeuwen, P. W. N. M. and Vrieze, K. *Inorg. Chem.*, 1993, **32,** 5769.

Pergamon

PII: S0277-5387(97)00504-4

Polyhedron Vol. 17, No. 7, pp. 1165–1176, 1998
© 1998 Elsevier Science Ltd
All rights reserved. Printed in Great Britain
0277-5387/98 $19.00+0.00

Chemistry of chelate-stabilized aryloxopalladium(II) complexes: syntheses, X-ray crystal structures and formation of C—H···O hydrogen-bonds*

M. Beller,† T. H. Riermeier, W. Mägerlein, T. E. Müller and W. Scherer

Anorganisch-chemisches Institut der Technischen Universität München, Lichtenbergstraße 4, D-85747 Garching, Germany

(Received 4 November 1997; accepted 18 November 1997)

Abstract—In this paper the synthesis, characterization and properties of various Pd(II) complexes with 2-acylphenolates as chelating ligands are reported. The compounds are easily accessible by stirring 2-acylphenoles with Pd(II) complexes in the presence of potassium *tert*-butoxide. Cyclometallated tri(*o*-tolyl)phosphine derivatives and allyl palladium complexes were chosen as palladium precursor. The solid state structures of the complexes 2-acetylphenolato-[*o*-(di-*o*-tolylphosphino)benzyl]palladium(II) (**2**), 2-benzoylphenolato-[*o*-(di-*o*-tolylphosphino)benzyl]palladium(II) (**4**) and 2-acetyl-1-naphtholato-[*o*-(di-*o*-tolylphosphino)benzyl] palladium(II) (**6**) were further studied by X-ray diffraction analyses. In all complexes the palladium center is coordinated in a square planar fashion. Interestingly, coordination of the 2-acylphenolates to palladium results in a significant perturbation of the delocalization within the aromatic ring. The strong hydrogen-bond acceptor behavior of the phenolic oxygen as well as the *cis*/*trans*-isomerisation is discussed in terms of the solid structure (**2, 4** and **6**) and the NMR shifts observed in various solvents. © 1998 Elsevier Science Ltd. All rights reserved

Keywords: palladacycles; π-allylpalladium complexes; hydrogen bonds

The chemistry of late transition metal alkoxide complexes has recently attracted much attention [1]. Such complexes are important intermediates in various transition metal-catalyzed reactions [2], including the palladium-catalyzed formation of carbon-oxygen bonds [3] and the rhodium and palladium mediated activation of C—O single bonds [4]. During the last few years important aspects of the chemistry of palladium(II) alkoxide and aryloxide complexes were established elegantly by van Koten *et al.* and others [5–8]. However, there are only few reports of palladium alkoxide complexes containing an additional donor group (usually nitrogen or phosphorus) [7,8]. Pd(II)-complexes with easily accessible 2-acylphenolates and related ligands are surprisingly rare in the literature and, to the best of our knowledge, there is no structural characterization of such compounds [9]. An interesting feature of palladium and other late transition metal alkoxides is the formation of intermolecular O—H···O hydrogen bonds to an aditional alcohol [10]. The formation of O—H···O hydrogen bonding has important effects on the properties and self organization of the corresponding metal complexes [11]. In addition to an O—H···O interaction there are few examples known with C—H···O hydrogen bonds [6,8,12]. Here the carbon atom participating in the C—H···O hydrogen bond is attached to a heteroatom (O,N), which coordinates to a metal center. Thus, this interaction is a model of the initial stage of a base-assisted β-hydride elimination.

In cooperation with Herrmann *et al.* we have been engaged in the synthesis of cyclometallated palladium complexes of tri(*o*-tolyl)phosphine, e.g. **1**, as efficient catalysts or catalyst-precursors for important C—C coupling reactions [13]. Recently, we have shown that cyclometallated palladium complexes are also suitable

* Dedicated to Prof. Dr. Drs. h. c. W. A. Herrmann on the occasion of his 50th birthday.

† Author to whom correspondence should be addressed.

for C—N coupling processes [14]. In order to synthesize model complexes for similar C—O coupling reactions, as well as to study the behavior of 2-acylphenolates as ligand, we were interested in the preparation of cyclometallated palladium complexes containing the 2-acylphenolate ligand.

Herein, we report for the first time on the synthesis and properties of this class of complexes. The synthesis and characterisation of π-allylpalladium complexes containing 2-acylphenolate ligands is presented. These π-allylpalladium complexes with additional coordination of a phenoxide ligand are interesting as model compounds for the palladium-catalyzed *O*-arylation and phenoxycarbonylation of allylic substrates leading to allyl–aryl ethers and unsaturated esters, respectively [15].

RESULTS AND DISCUSSION

Preparation of the aryloxopalladium(II) complexes

The palladium phenolate complexes **2–6** were readily prepared by stirring a solution of the palladacycle **1** [13] and 2 equiv. of the corresponding 2-acylphenol together with 2 equiv. of potassium *tert*-butoxide in toluene at room temperature (Scheme 1). Good to very good yields (76%–92%) were obtained after crystallization from toluene/pentane.

The addition of a strong base is crucial for the success of the reaction. Only starting material was isolated from the reaction mixture of **1** and 2-acylphenol if sodium acetate was used as base. Using 2-hydroxybenzophenone as ligand, the synthesis is succesful if performed under reflux conditions. However, in case of 2-hydroxyacetophenone as ligand, palladium black is formed under such reaction conditions. This may be due to formation of enolates from the acetophenone.

The palladium(II) phenolate complexes **9–12**, which contain an η^3-allyl unit, were prepared in a similar way to compounds **2–6**. Addition of 2 equiv. of the 2-acylphenol and 2 equiv. of potassium *tert*-butoxide to a toluene solution of the corresponding π-allylpalladium chloride dimer and stirring the mixture for approximately 7 h at ambient temperature yielded the desired products (Scheme 2). When weak bases, such as sodium acetate, were employed, starting material was recovered unchanged. Though precipitation of palladium black seems to be inevitable during the course of the reaction, the allylic complexes **9–12** were isolated in reasonable yields of 73–88% as yellow solids.

The allylic complexes **9–12** are less stable than the corresponding phosphapalladacycles **2–6**. Toluene solutions of **9–12** decomposed slowly with metal deposition at room temperature. In the solid state (room temperature) their yellow color darkens within a few days due to formation of elemental palladium. In the case of **9**, the *O*-allylated ligand could be detected (^{1}H NMR) as a decomposition product resulting from reductive elimination.

Molecular structures of the complexes **2**, **4** *and* **6**

Compounds **2**, **4** and **6** were characterized by X-ray diffraction analysis. Selected bond distances and angles are given in Table 1.

The molecular structure of **2** is depicted in Fig. 1. The structure consists of a palladium atom which is coordinated in a square planar fashion by a cyclometallated tri(*o*-tolyl)phosphine and a chelating 2-acetyl phenolate ligand. Two geometric isomers are possible with the phenolic oxygen located *cis* or *trans* to the phosphorus atom and both were observed in solution (*vide infra*). In complex **2** O31, the phenolic oxygen and O11, the carbonyl oxygen of the parent 2-acetyl phenol ligand, are located *trans* to the phosphorus atom P and C27 of the phosphine ligand, respectively. The principal coordination sphere is close to planar, the maximum deviation being 0.047(2) Å. The distances Pd—P = 2.223(1) Å and Pd—C27 = 2.010(4) Å compare favorably with those observed in **1** (2.216(1) Å and 2.021(5) Å, respectively) [16].

The phenolic oxygen palladium bond Pd—O31 = 2.042(2) Å was significantly shorter than

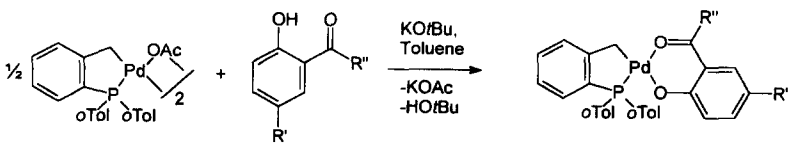

1

	R'	R"	yield
2	H	CH_3	86 %
3	F	CH_3	92 %
4	H	C_6H_5	77 %
5	CH_3	C_6H_5	76 %
6	2-Acetyl-1-naphtholate		79 %

Scheme 1.

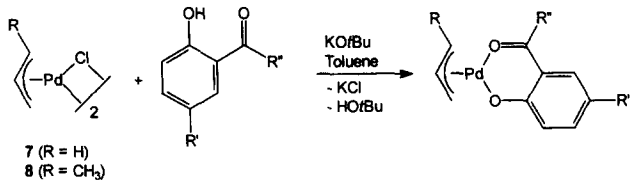

7 (R = H)
8 (R = CH_3)

	R	R'	R''	yield
9	H	H	C_6H_5	88 %
10	CH_3	F	CH_3	74 %
11	CH_3	H	C_6H_5	73 %
12	CH_3	2-Acetyl-1-naphtholate		81 %

Scheme 2.

the carbonyl oxygen palladium bond Pd—O11 = 2.110(2) Å and associated with this effect are different C—O bond distances (C3—O31 = 1.302(4) Å, C1—O11 = 1.254(4) Å). However, the difference is not as much as one would expect for a purely phenolic C—O single and a C=O double bond. The distances for C1—C2 = 1.427(5) Å and C2—C3 = 1.427(5) Å are equal, which is surprising as these are an aromatic and a single bond in the parent ligand, respectively, and should therefore differ more. Distances within the fused benzene ring deviate from the normal sixfold symmetry with short bonds for C6—C7 and C4—C5 (1.335(8) Å and 1.356(7) Å, respectively). The significant differences in the two Pd—O and the two C—O bond lengths indicate that the presence of the fused benzene ring has attenuated the resonance system in the chelate ring, of the type found in most metal complexes with β-diketones, such as acylacetonato complexes.

The interpretation of these results in terms of resonance structures is in line with the assumption that the delocalisation within the aromatic ring (Scheme 3, A) is less significant and that the acac-type delocalization (Scheme 3, B) makes an important contribution to the overall structure and reactivity of this molecule. Analogous effects have been observed in the complexes $Ni(C_9H_9O_2)_2$ [17], $C_9H_9O_2$ = 2-acetyl-4-methyl-phenol and $Cu(C_8H_7O_2)_2py$ [18], $C_8H_7O_2$ = 2-aceto-phenol, py = pyridine.

Regarding hydrogen bonds of the coordinated oxygen atoms there is a short contact between O11 and the methyl group C47. The non-bonded distance O11 · · · C47 = 3.13 Å is considerably shorter than the sum of the van-der-Waals radii of oxygen and an averaged radius for the methyl group indicating a weak hydrogen bond between C47—H · · · O11. Recent studies of such C—H · · · O contacts show their importance as secondary interactions and in determining the crystal packing [11].

The molecular structure of complex **4** is similar to the structure of complex **2** except that in **4** the carbonyl oxygen O11 is located *trans* to the phosphorus atom and the phenolic oxygen O31 is *trans* to C27 (Fig. 2). This geometry avoids steric conflict between the phenyl group attached to C1 and the *o*-tolyl groups attached to the phosphorus atom. The distances Pd—P = 2.198(1) Å, Pd—C27 = 2.022(2) Å in **4** are comparable to those observed in **2**. However, the distances of palladium to the oxygen atoms are different with Pd—O31 = 2.092(1)Å longer and Pd—O11 = 2.087(1) Å slightly shorter than in compound **2**, probably reflecting the different *trans*-influence of phosphorus and carbon. As expected, the phenolic C3—O31 bond (1.290(3) Å) is longer than the C1—O11 bond (1.244(2) Å), but again the difference is less pronounced compared to a localized C—O single and a C=O double bond. The asymmetry in the aromatic ring is more pronounced than in complex **2** with C4—C5 and C6—C7 being short (1.361(3) Å and 1.367(3) Å, respectively) and C2—C3 being long (1.441(3) Å). Again, this effect can be explained in terms of resonance structure B. The phenyl ring attached to C1 is not conjugated with the chelate ring being twisted by 52° to the plane defined by Pd, O31, O11, C1, C2, C3.

There are short contacts between O31 and the methyl groups of the *o*-tolyl rings. The non-bonded distances C · · · O are longer than those observed in **2**, however, there are two weak contacts with methyl groups (O31 · · · C37 = 3.31Å; O31 · · · C47 = 3.40 Å). The hydrogen atoms of the methyl groups were clearly located in the difference map and allow to further characterize the geometry around O31. The distance of H37a to O31 is 2.40 Å (H37a—C37 = 0.91 Å) and the angle O31 · · · H37a—C37 is 176°. The distance of H47b to O31 is 2.59 Å (H47b—C47 = 0.86 Å) and the angle O31 · · · H47b—C47 is 155°. The oxygen atom is in a pseudotetrahedral environment with an angle H37a · · · O31 · · · H47b = 98°. This arrangement is clearly indicative of C—H · · · O interactions.

The X-ray structure of the complex **6** is shown in Fig. 3. The overall geometry of **6** is very similar to that observed in **2** (Fig. 1). The steric requirement of the naphthyl group favors the position of the phenolic oxygen *trans* to phosphorus. Bond distances to palladium (Pd—P = 2.221(1) Å, Pd—C27 = 2.017(2) Å,

Table 1. Selected bond lengths (Å) and angles (°)

Complex	**2**	Complex	**4**	Complex	**6**
Pd—C(27)	2.010(4)	Pd—C(27)	2.022(2)	Pd—C(27)	2.017(2)
Pd—O(11)	2.110(2)	Pd—O(11)	2.0871(13)	Pd—O(11)	2.104(2)
Pd—O(31)	2.042(2)	Pd—O(31)	2.0915(13)	Pd—O(31)	2.057(2)
Pd—P	2.2225(9)	Pd—P	2.1982(5)	Pd—P	2.2209(6)
P—C(21)	1.811(3)	C(1)—O(11)	1.244(2)	P—C(21)	1.811(2)
P—C(31)	1.822(3)	C(1)—C(2)	1.451(2)	P—C(31)	1.832(2)
P—C(41)	1.824(3)	C(1)—C(11)	1.495(3)	P—C(41)	1.835(2)
C(1)—O(11)	1.254(4)	C(2)—C(7)	1.412(3)	C(1)—O(11)	1.254(3)
C(1)—C(2)	1.427(5)	C(2)—C(3)	1.441(3)	C(1)—C(2)	1.435(3)
C(1)—C(11)	1.513(6)	C(3)—O(31)	1.290(3)	C(1)—C(11)	1.515(3)
C(2)—C(7)	1.423(5)	C(3)—C(4)	1.428(3)	C(2)—C(3)	1.423(3)
C(2)—C(3)	1.427(5)	C(4)—C(5)	1.361(3)	C(2)—C(7)	1.443(3)
C(3)—O(31)	1.302(4)	C(5)—C(6)	1.403(3)	C(3)—O(31)	1.293(3)
C(3)—C(4)	1.413(5)	C(6)—C(7)	1.367(3)	C(3)—C(4)	1.457(3)
C(4)—C(5)	1.356(7)	P—C(21)	1.816(2)	C(4)—C(5)	1.409(3)
C(5)—C(6)	1.374(8)	P—C(41)	1.820(2)	C(4)—C(4A)	1.414(4)
C(6)—C(7)	1.335(8)	P—C(31)	1.831(2)	C(4A)—C(4B)	1.375(4)
				C(4B)—C(5B)	1.394(5)
				C(5)—C(5A)	1.417(4)
				C(5)—C(6)	1.425(4)
				C(5A)—C(5B)	1.358(5)
				C(6)—C(7)	1.336(4)
O(31)—Pd—O(11)	86.59(9)	O(11)—Pd—O(31)	86.95(5)	O(31)—Pd—O(11)	86.00(6)
C(27)—Pd—P	83.87(13)	C(27)—Pd—P	82.85(7)	C(27)—Pd—P	83.94(7)
C(21)—P—Pd	104.26(13)	O(11)—C(1)—C(2)	125.2(2)	C(21)—P—Pd	104.82(8)
C(31)—P—Pd	121.85(11)	O(11)—C(1)—C(11)	114.7(2)	C(31)—P—Pd	123.55(7)
C(41)—P—Pd	113.25(11)	C(2)—C(1)—C(11)	120.1(2)	C(41)—P—Pd	112.27(7)
O(11)—C(1)—C(2)	124.8(3)	C(1)—O(11)—Pd	128.18(12)	O(11)—C(1)—C(2)	124.9(2)
O(11)—C(1)—C(11)	114.9(4)	C(7)—C(2)—C(3)	119.0(2)	O(11)—C(1)—C(11)	114.8(2)
C(2)—C(1)—C(11)	120.4(4)	C(7)—C(2)—C(1)	118.4(2)	C(2)—C(1)—C(11)	120.3(2)
C(1)—O(11)—Pd	129.7(3)	C(3)—C(2)—C(1)	122.6(2)	C(1)—O(11)—Pd	129.7(2)
C(7)—C(2)—C(1)	118.7(4)	O(31)—C(3)—C(4)	117.9(2)	C(3)—C(2)—C(1)	123.7(2)
C(7)—C(2)—C(3)	117.2(4)	O(31)—C(3)—C(2)	125.6(2)	C(3)—C(2)—C(7)	117.7(2)
C(1)—C(2)—C(3)	124.0(3)	C(4)—C(3)—C(2)	116.5(2)	C(1)—C(2)—C(7)	118.6(2)
O(31)—C(3)—C(4)	116.9(4)	C(3)—O(31)—Pd	123.31(12)	O(31)—C(3)—C(2)	125.7(2)
O(31)—C(3)—C(2)	125.8(3)	C(5)—C(4)—C(3)	122.4(2)	O(31)—C(3)—C(4)	115.8(2)
C(4)—C(3)—C(2)	117.3(4)	C(4)—C(5)—C(6)	120.8(2)	C(2)—C(3)—C(4)	118.5(2)
C(3)—O(31)—Pd	129.0(2)	C(7)—C(6)—C(5)	119.0(2)	C(3)—O(31)—Pd	129.2(2)
C(5)—C(4)—C(3)	122.0(5)	C(6)—C(7)—C(2)	122.4(2)	C(5)—C(4)—C(3)	120.8(2)
C(4)—C(5)—C(6)	120.9(5)	C(21)—P—Pd	105.08(6)	C(4)—C(5)—C(6)	119.0(2)
C(7)—C(6)—C(5)	119.4(5)	C(41)—P—Pd	121.51(6)	C(7)—C(6)—C(5)	120.6(2)
C(6)—C(7)—C(2)	123.2(5)	C(31)—P—Pd	113.74(6)	C(6)—C(7)—C(2)	123.4(2)
C(26)—C(27)—Pd	118.8(3)	C(26)—C(27)—Pd	118.42(13)	C(26)—C(27)—Pd	119.3(2)

Pd—O31 = 2.057(2) Å and Pd—O11 = 2.104(2) Å) as well as the carbon-oxygen distances (C3—O31 = 1.293(3) Å and C1—O11 = 1.254(3) Å) are nearly identical to those observed in **2**. The naphthyl ring has a short bond C6—C7 = 1.336(4) Å, relatively short bonds for C5a—C5b = 1.358(5) Å and C4a—C4b = 1.375(4) Å and long bonds for C2—C7 = 1.443(3) Å and C3—C4 = 1.457(3) Å indicating partially localized double bonds. A similar asymmetry of the naphthyl ring has been detected in the complex $Cd(C_{12}H_8O_2)_2bpy$, $C_{12}H_8O_2$ = 2-acetyl-1-hydroxy-naphthalene, bpy = 2,2′-bipyridine [25]. As observed in **2**, there is a short contact between O11 and the protons of the methyl group C47 with a non-bonded distance O11 ··· C47 = 3.17 Å.

Solution studies

Obviously, the complexes **2–6** can exist as two isomers, with the phenolic oxygen *cis* or *trans* towards

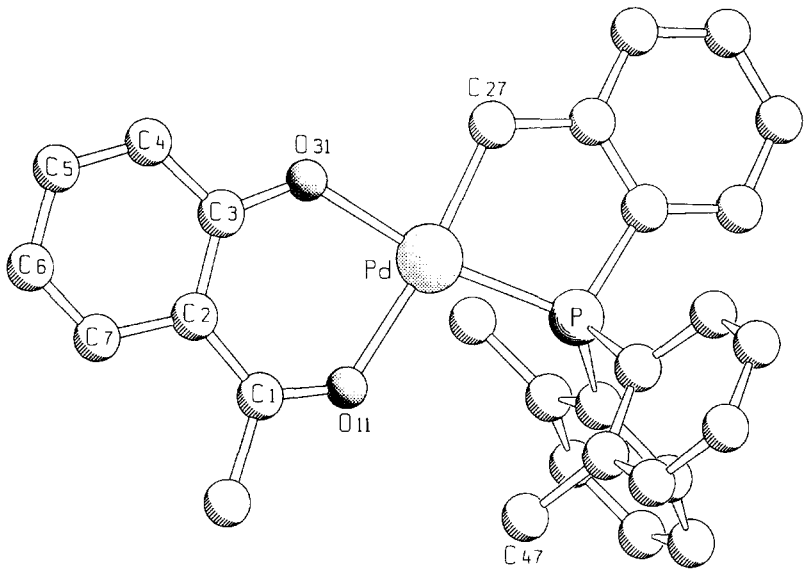

Fig. 1.

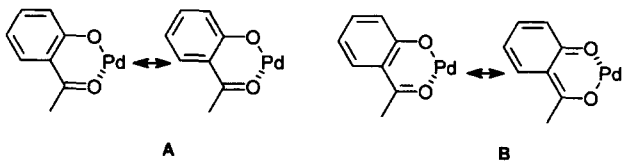

Scheme 3.

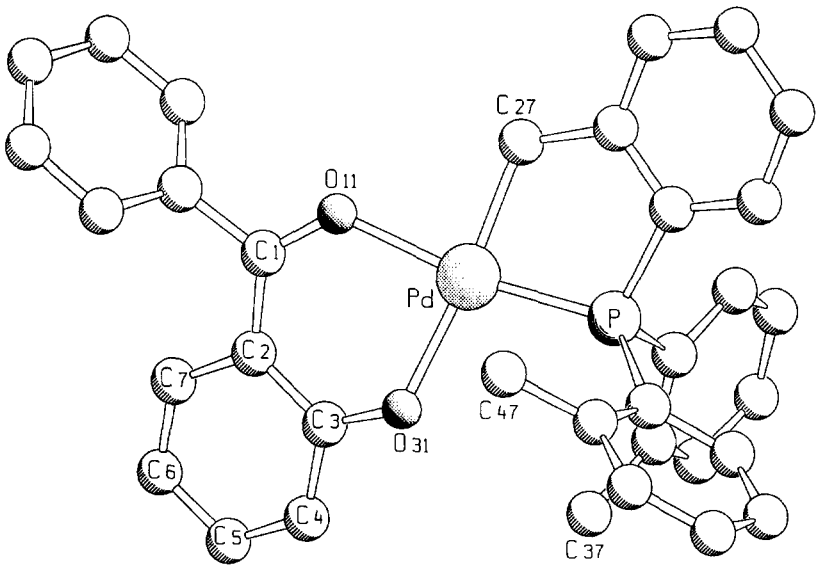

Fig. 2.

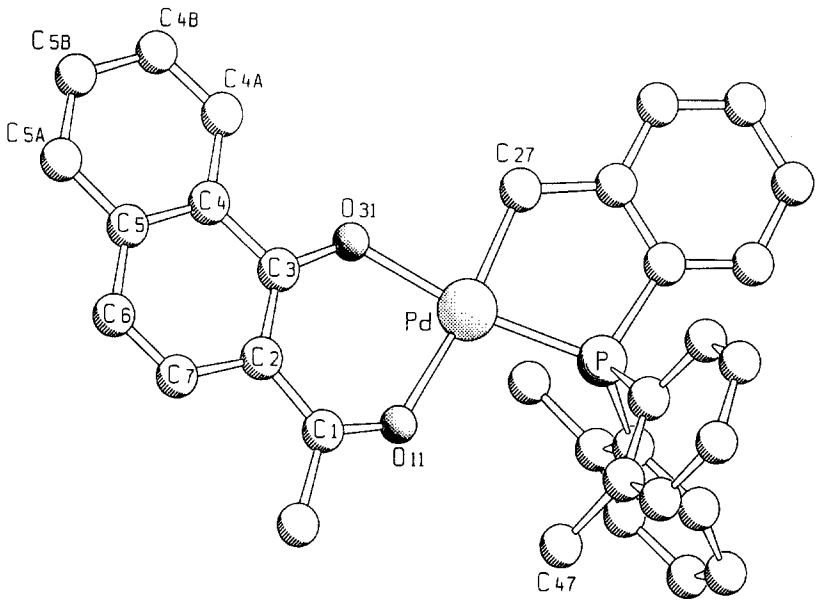

Fig. 3.

the phosphorus atom (Scheme 4). Depending on the substituent R″ the *cis*- or *trans*-isomer can be preferred. This was exemplified by the geometry of complexes **2, 4,** and **6** in the solid state. To further investigate isomerization processes and the ratio between the two isomers, NMR experiments were performed in various solvents. For each of the two geometric isomers of **2–6** distinct $^{31}P\{^1H\}$NMR signals were observed.

We provisionally assign the high field $^{31}P\{^1H\}$NMR signal to **D** and the low field signal to **C**. The intensity of the high field signal is always higher than that of the low field signal for each of the compounds **2–6**.

Taking into account the ability of the oxygen atoms in **2–6** to participate in hydrogen bonding, the *cis*-/*trans*-isomerization should be affected by the solvent. To study the isomerization phenomenon in further detail, the $^{31}P\{^1H\}$NMR spectrum of **2** was recorded in 10 different solvents. In $CDCl_3$, two signals were observed at 35.7 ppm and 34.2 ppm. The ratio of the intensities of the two signals (K) changed slightly upon warming. It changes from 0.11 (25°C) to 0.14 (50°C) reversibly. A similar effect was observed in toluene-d_8 as solvent: K changes from 0.44 (25°C) to 0.50 (50°C). As expected, the nature of the solvent has a dramatic effect on K (Table 2).

As shown in Table 2, K can vary from 0 to 0.5. There seems to be no correlation between K and either

Table 2. K values of **2** in different solvents (K = intensity of the ^{31}P NMR low field signal to the intensity of the high field signal)

Solvent	Ratio of ^{31}P NMR intensities	K
MeOD/2-BuOH	0:100	0
$CDCl_3$	10:90	0.11
CD_2Cl_2	14:86	0.16
DMSO-d_6	17:83	0.21
C_6H_5Cl	22:78	0.29
Sulfolane	22:78	0.29
thf-d_8	27:73	0.37
Benzene-d_6	29:71	0.40
Toluene-d_8	31:69	0.44
CCl_4	33:67	0.48

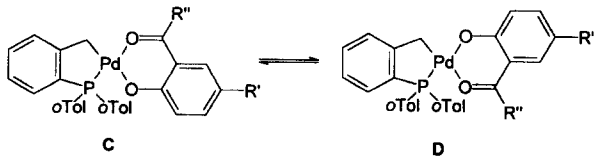

Scheme 4.

the E_T^N-values as empirical parameter of solvent polarity [20] or the π^*-scale of solvent dipolarity/polarity [21]. Obviously, K is affected by other properties of the solvent. As mentioned earlier, phenolate complexes usually behave as strong hydrogen bond acceptors (HBA). In the solid state even hydrogen bonds from the benzylic protons of the *o*-tolyl substituents are formed (stabilizing **C**). An interaction of the phenolic oxygen with the solvent would be easier in form **D** because of minor sterical hindrance. Since hydrogen bond acceptors usually are also electron-pair donors, K should be affected by both the ability of the solvent to act as hydrogen bond donor (HBD) α and the solvent acceptor number AN [22].

This argumentation is in good agreement with the observed data. Alcohols and chloroform are good HBD solvents and therefore K is low, leading to **D** as the predominant species in solution. On the other hand, tetrachloromethane or toluene are not able to form hydrogen bonds. Thus high values are observed for K. The same tendency is observed if correlating K with the acceptor number A [22].

The ^{1}H and ^{13}C NMR spectra of the allylic complexes exhibit some interesting features concerning the dynamic solution behavior of the η^3-allyl unit. In the case of **9** the ^{13}C NMR (room temperature) shows a broad signal at 55.2 ppm similar to a doublet which is assigned to C1/C3 of the η^3-allyl ligand. Apparently, the absorptions for these carbon atoms almost coalescence, indicating a rotation of the allyl group. The ^{1}H NMR of **9** exhibits only one absorption each for the *syn* and *anti* hydrogens.

In contrast, in the ^{13}C NMR spectrum of **12** each of the signals for C1, C3 of the crotyl moiety and CH_3 of the phenolate ligand consists of two sharp peaks (C1: 51.39 ppm, 50.35 ppm; C3: 72.60 ppm, 71.48 ppm; CH_3: 27.71 ppm, 27.16 ppm), arising from the stereoisomers **12a** and **12b** (Scheme 5). Therefore the rotation of the allyl unit is slow compared to the NMR time scale. The resonances of the aromatic carbon atoms of the 2-acylphenolate-ligand are not influenced by the orientation of the crotyl ligand; only one peak per carbon atom is observed for both stereoisomers.

The ratio of the *cis*/*trans* isomers of **12** can be determined from the ^{1}H NMR spectrum (25°C, $CDCl_3$; 63:37).

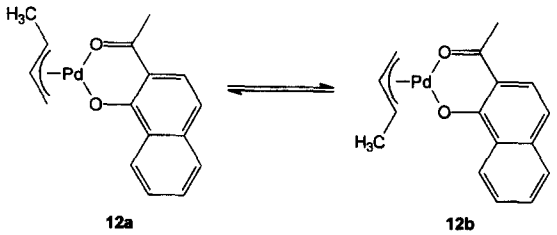

12a **12b**

Scheme 5.

In the ^{1}H and ^{13}C NMR spectra of compounds **10** and **11** there is no evidence for a hindered rotation of the allyl moiety as only one absorption appears for each atom. However, this may be due to very similar chemical environments in both stereoisomers.

EXPERIMENTAL

General comments

NMR spectra (^{1}H, ^{13}C, ^{31}P) were recorded on a Jeol JMX-GX 400 instrument. FAB-MS spectra were recorded on a Varian MAT 311a. Elemental analyses were carried out by the Microanalytical Laboratory at the TU München. IR spectra were recorded on a Perkin–Elmer 1600.

The palladacycle **1** was prepared as reported previously [13]. Bis(η^3-allyl)di(μ-chloro)dipalladium(II) (**7**) and bis[(1,2,3-η)-2-butenyl]di(μ-chloro)palladium (II) (**8**) were prepared from the corresponding allylic chlorides according to the literature [23].

The substituted phenoles and 2-acetyl-1-naphthole were obtained from Aldrich and were used without further purification. All operations were carried out under an atmosphere of argon using standard Schlenk techniques. All solvents were dried according to standard procedures.

X-ray crystal structure determination

Suitable single crystals of **2** and **4** for the X-ray diffraction studies were grown by slow diffusion of pentane into the sample solution in toluene. Suitable crystals of **6** were obtained by recrystallization of the compound from chloroform. The structures were solved by a combination of direct methods, difference-Fourier syntheses and least-squares methods. Neutral atom scattering factors for all atoms and anomalous dispersion corrections for the non-hydrogen atoms were taken from the *International Tables for X-Ray Crystallography* [24]. All calculations were performed on a DEC 3000 AXP workstation with the STRUX-V [25] system, including the programs PLATON-92 [26], PLUTON-92 [26], SIR-92 [27] and SHELXL-93 [28].

Data collection

A summary of the crystal and experimental data is reported in Table 3. Preliminary examination and data collection were carried out on an imaging plate diffraction system (IPDS; STOE&CIE) (**2, 4**) or a CCD system (KappaCCD; NONIUS) equipped with a rotating anode (NONIUS FR591; 50 kV; 80 (**2, 4**)/60 (**6**) mA) and graphite monochromated Mo–K_α radiation. Data collection were performed at 293 (193 and 293) K within the θ-range of $3.1° < 2\theta < 50.2°$ ($4.1° < 2\theta < 51.2°$; $6.8° < 2\theta < 61.7°$) with an

Table 3. Crystallographic data for **2, 4** and **6**

Complex	**2**	**4**	**6**
Formula	$C_{29}H_{27}O_2PPd \cdot 0.5C_7H_8$	$C_{34}H_{29}O_2PPd$	$C_{33}H_{29}O_2PPd \cdot CHCl_3$
Fw	590.94	606.94	714.30
T (K)	293(1)	193(1)	293(1)
Wavelength	0.71073 Å	0.71073 Å	0.71073 Å
Crystal system	Triclinic	Triclinic	Triclinic
Space group	$P\bar{1}$	$P\bar{1}$	$P\bar{1}$
a (Å)	8.8819(4)	9.9178(6)	9.0148(1)
b (Å)	9.7722(6)	10.2461(6)	12.5287(3)
c (Å)	17.2956(10)	14.5783(9)	14.5763(4)
α (°)	99.535(7)	78.342(6)	100.7739(9)
β (°)	101.262(6)	70.273(6)	102.641(2)
γ (°)	101.511(6)	78.925(6)	91.721(2)
V (Å^3)	1409.58(13)	1353.33(14)	1573.75(6)
Z	2	2	2
d_c (g cm^{-3})	1.392	1.489	1.507
μ (mm^{-1})	0.742	0.775	0.925
$F(000)$	606	620	724
Crystal size (mm)	$0.125 \times 0.125 \times 0.1$	$0.30 \times 0.24 \times 0.13$	$0.25 \times 0.20 \times 0.20$
Theta range (°)	1.5 to 25.1	2.05 to 25.61	3.4 to 30.85
Index ranges	$-10 \leqslant h \leqslant 10$, $-11 \leqslant k \leqslant 11$, $-20 \leqslant l \leqslant 20$	$-1 \leqslant h \leqslant 12$, $-12 \leqslant k \leqslant 12$, $-17 \leqslant l \leqslant 17$	$0 \leqslant h \leqslant 9$, $-16 \leqslant k \leqslant 16$, $-19 \leqslant l \leqslant 18$
Total data collected	14,253	11,358	19,521
Total unique data	4487	4724	7528
No. of data used	4335	4721	7526
Parameters	408	459	398
G.O.F	0.910	1.027	1.087
R_1[a]	0.0295	0.0234	0.0345
wR_2[b]	0.0634	0.0581	0.0938
Largest diff. peak and hole (e Å^{-3})	0.354 and −0.412	0.360 and −0.398	0.367 and −0.574

[a] $(R_1 = \Sigma(\|F_o\| - \|F_c\|)/\Sigma|F_o|)$, for $F^2 > 2\sigma(F^2)$.
[b] $wR_2 = [\Sigma[w(F_o^2 - F_c^2)^2]/\Sigma[w(F_o^2)^2]]^{1/2}$.

exposure time of 5.0 min (5.0 min; 25 s) per image (rotation scan modus from $\phi = 0.0°$ (75°; 0°) to 290° (293°; 360°) with $\Delta\phi = 1°$). A total number of 14,253 (11,358; 19,521) reflections were collected. After merging a sum of 4487 (4724; 7528) independent reflections remained and were used for all calculations (2, 3, 2 reflections were suppressed during refinements on compounds **2, 4, 6,** respectively). Data were corrected for Lorentz and polarization effects. The unit cell parameters were obtained by full-matrix least-squares refinements of 4813 (4815; 15,927) reflections with the program Cell [29a] (DENZO-SMN [29b]).

The structures were solved using the heavy atom method. In **2** additional toluene as solvent is disordered over two positions which are related by a center of symmetry. In **6** the $CHCl_3$ is disordered over two positions which are related by a rotation around the C—H axis. For **4** all hydrogen atoms were located, for **2** all hydrogen atoms with exception of the toluene hydrogen atoms were located and refined. The hydrogen atoms of toluene in **2** and the hydrogen atoms in **6** were generated geometrically and allowed to ride on their respective parent carbon atoms. In **2** and **6** the hydrogen atoms were assigned fixed isotropic temperature factors (1.2 $U_{equiv.}$ and 1.5 $U_{equiv.}$ of the parent carbon atom for aromatic and other CH groups, respectively). Full matrix least squares refinement of all non-hydrogen atoms with anisotropic temperature factors led to convergence. Owing to the high disorder of $CHCl_3$ in **6,** the R values are higher.

General procedure for the synthesis of complexes **2–6**

0.10 g (0.21 mmol) of the palladacycle **1** is stirred together with 2.0 equiv. of the corresponding 2-acylphenole and 47 mg (0.42 mmol) potassium *tert*-butoxide in 10 ml toluene. After approximately 12 h the reaction mixture is filtered and the solvent is removed *in vacuo*. Analytically pure samples of the phenolate complexes are obtained by crystallization from toluene/pentane.

2-Acetylphenolato-[*o*-(di-*o*-tolylphosphino)benzyl] palladium(II) (**2**) (*yellow needles, 86% yield*)

^{1}H NMR ($CDCl_3$, 20°C, 400 MHz): δ = 7.58–6.82 (15H, m, H_{Ar}); 6.44 (1H, m, H_{Ar}); 3.65 (2H, s, broad, CH_2); 2.85 (3H, s, broad, $CH_{3\,(Benzyl)}$); 2.50 (3H, s, broad, $CH_{3\,(Benzyl)}$); 2.42 (3H, s, $CH_{3\,(Acetyl)}$). $^{31}P\{^1H\}$ NMR ($CDCl_3$, 20°C, 161.85 MHz, with integral *I*): δ = 35.7 (s, *I* = 10%); 34.2 (s, *I* = 90%). IR (cm^{-1}, KBr): 3054 m, 3005 m, 2953 m, 2910 m, 2869 m, 1593 s, 1523 s, 1469 m, 1431 s, 1374 m, 1354 m, 1338 m, 1283 w, 1250 w, 1219 s, 1157 w, 1135 m, 1085 w, 966 m, 861 m, 804 w, 760 s, 755 s, 714 m, 585 m, 561 m, 472 m. MS (FAB): *m/z* = 544 [M^+], 409 [M^+ – phenolate ligand]. $C_{29}H_{27}O_2PPd$ (544.93): calc. (+0.5 toluene) C 66.05, H 5.28, P 5.24; found C 65.82, H 5.60, P 5.27.

2-Acetyl-4-fluorophenolato-[*o*-(di-*o*-tolylphosphino) benzyl]palladium(II) (**3**) (*yellow needles, 92% yield*)

^{1}H NMR ($CDCl_3$, 20°C, 400 MHz): δ = 7.44–6.83 (15H, m, H_{Ar}); 3.66 (2H, s, broad, CH_2); 2.85 (3H, s, broad, $CH_{3\,(Benzyl)}$); 2.49 (3H, s, broad, $CH_{3\,(Benzyl)}$); 2.37 (3H, s, $CH_{3\,(Acetyl)}$). $^{31}P\{^1H\}$ NMR (CDC_{l3}, 20°C, 161.85 MHz, with integral *I*): δ = 35.8 (s, *I* = 12%); 34.3 (s, *I* = 88%). IR (cm^{-1}, KBr): 3056 m, 3011 w, 2967 w, 2889 w, 1602 s, 1523 s, 1469 m, 1444 s, 1375 m, 1324 s, 1284 w, 1241 w, 1201 s, 1186 m, 1119 w, 967 m, 914 m, 811 s, 749 s, 560 m, 527 w, 479 m. MS (FAB): *m/z* = 562 [M^+], 409 [M^+ – phenolate ligand]. $C_{29}H_{26}FO_2PPd$ (562.91): calc. C 61.88, H 4.65, P 5.50; found C 61.84, H 4.87, P 5.50.

2-Benzoylphenolato-[*o*-(di-*o*-tolylphosphino)benzyl] palladium(II) (**4**) (*yellow needles, 77% yield*)

^{1}H NMR ($CDCl_3$, 20°C, 400 MHz): δ = 7.66–6.85 (20H, m, H_{Ar}); 6.37 (1H, m, H_{Ar}); 3.72 (2H, s, broad, CH_2); 2.80 (3H, s, broad, $CH_{3\,(Benzyl)}$); 2.47 (3H, s, broad, $CH_{3\,(Benzyl)}$). $^{31}P\{^1H\}$ NMR (toluene-d_8, 20°C, 161.85 MHz, with integral *I*): δ = 35.6 (s, *I* = 34%); 33.9 (s, *I* = 66%). IR (cm^{-1}, KBr): 3047 w, 2962 w, 2868 w, 1613 s, 1579 s, 1561 s, 1515 s, 1466 m, 1452 m, 1442 m, 1415 s, 1351 s, 1261 m, 1228 m, 1203 w, 1177 w, 1141 m, 1078 s, 1025 m, 939 m, 913 w, 854 m, 802 s, 751 s, 713 m, 751 s, 699 s, 674 w, 643 m, 586 m, 559 m, 521 m. MS (FAB): *m/z* = 605 [M^+ – H], 409 [M^+ – phenolate ligand]. $C_{34}H_{29}O_2PPd$ (606.99): calc. C 67.28, H 4.82, P 5.10; found C 66.78, H 4.81, P 4.99.

2-Benzoyl-4-methylphenolato-[*o*-(di-*o*-tolylphosphino)benzyl]palladium(II) (**5**) (*orange needles, 76% yield*)

^{1}H NMR ($CDCl_3$, 20°C, 400 MHz): δ = 7.58–6.88 (20H, m, H_{Ar}); 3.73 (2H, s, broad, CH_2); 2.82 (3H, s, broad, $CH_{3(P\text{-}Benzyl)}$); 2.49 (3H, s, broad, $CH_{3(P\text{-}Benzyl)}$); 2.12 (3H, s, $CH_{3(Benzyl)}$). $^{31}P\{^1H\}$ NMR ($CDCl_3$, 20°C, 161.85 MHz, with integral *I*): δ = 35.6 (s, *I* = 10%); 34.5 (s, *I* = 90%). IR (cm^{-1}, KBr): 3054 w, 2920 w, 2855 w, 1624 m, 1581 s, 1557 s, 1508 s, 1445 s, 1401 m, 1374 m, 1336 m, 1284 w, 1233 s, 1199 m, 1143 m, 1073 w, 953 w, 824 m, 814 m, 756 s, 733 m, 707 m, 561 w, 521 w. MS (FAB): *m/z* = 620 [M^+ – H], 409 [M^+ – phenolate ligand]. $C_{35}H_{31}O_2PPd$ (621.02): calc. (+0.5 toluene) C 69.32, H 5.29, P 4.79; found C 69.06, H 5.44, P 4.40.

2-Acetyl-1-naphtholato-[*o*-(di-*o*-tolylphosphino) benzyl]palladium(II) (**6**) (*yellow needles, 79% yield*)

^{1}H NMR ($CDCl_3$, 20°C, 400 MHz): δ = 7.66–6.70 (22H, m, H_{Ar}); 3.82 (2H, s, broad, CH_2); 2.90 (3H, s, broad, $CH_{3\,(P\text{-}Benzyl)}$); 2.55 (3H, s, broad, $CH_{3(P\text{-}Benzyl)}$); 2.45 (3H, s, $CH_{3\,(Acetyl)}$). $^{31}P\{^1H\}$ NMR ($CDCl_3$, 20°C, 161.85 MHz, with integral *I*): δ = 35.6 (s, *I* = 38%); 34.5 (s, *I* = 62%). IR (cm^{-1}, KBr): 3052 w, 2989 w, 2933 w, 2878 w, 1616 m, 1578 s, 1528 s, 1490 w, 1454 w, 1424 w, 1387 s, 1280 w, 1248 m, 1238 m, 1203 m, 1160 m, 1128 m, 1080 w, 1023 w, 989 w, 896 w, 787 m, 765 s, 749 m, 737 m, 713 m, 688 w, 585 w, 560 w, 527 w, 479 w, 471 m. MS (FAB): *m/z* = 594 [M^+], 409 [M^+ – naphtholate ligand]. $C_{33}H_{29}O_2PPd$ (594.98): calc. C 66.62, H 4.91; found C 66.81, H 4.88.

General procedure for the synthesis of complexes **9**–**12**

0.30 g (0.82 mmol) of the π-allylpalladium chloride complex (**7**) (0.32 g (0.82 mmol) of the π-(1-methylallyl)palladium chloride complex (**8**)) are stirred together with 2.0 equiv. of the protonated ligand and 184 mg (1.64 mmol) potassium *tert*-butoxide in 13 ml toluene at ambient temperature. After some hours the initially orange solution turns black due to precipitated palladium-metal which is removed by filtration (celite) to obtain a yellow solution. The solvent is removed *in vacuo* and the yellow residue is washed with two 15 ml portions of pentane. The allyl complexes can be recrystallized from toluene/pentane at −78°C. The numeration of the atoms of the ligands are similar to the X-ray studies of the aforementioned compounds.

η^3-Allyl-(2-benzoylphenolato)palladium(II) (**9**) (*yellow needles, 88% yield*)

^{1}H NMR ($CDCl_3$, 25°C, 300 MHz): δ = 7.50 (1H, m, $H_{Ar\text{-}2'}$); 7.44 (1H, m, $H_{Ar\text{-}4'}$); 7.35 (1H, m, $H_{Ar\text{-}3'}$); 7.27 (1H, ddd, $^3J_1$(H,H) = 6.4 Hz, $^3J_2$(H,H) = 8.6 Hz, ^4J(H,H) = 2.0 Hz, $H_{Ar\text{-}5}$); 7.20 (1H, dd, ^3J(H,H) = 8.2 Hz, ^4J(H,H) = 1.8 Hz, $H_{Ar\text{-}7}$); 6.89 (1H, dd, ^3J(H,H) = 8.4 Hz, ^4J(H,H) = 1.4 Hz, $H_{Ar\text{-}4}$); 6.34 (1H, ddd, $^3J_1$(H,H) = 8.0 Hz, $^3J_2$(H,H) = 6.6

Hz, ^4J(H,H) = 1.4 Hz, $H_{Ar\text{-}6}$); 5.48 (1H, m, $H_{Allyl\text{-}2}$); 3.91 (2H, d, ^3J(H,H) = 6.8 Hz, $H_{Allyl\text{-}syn}$); 2.90 (2H, d, ^3J(H,H) = 12.0 Hz, $H_{Allyl\text{-}anti}$). $^{13}C\{^1H\}$ NMR ($CDCl_3$, 25°C, 75 MHz): δ = 196.02 (C=O); 171.55 ($C_{Ar\text{-}3}$); 139.21 ($C_{Ar\text{-}1'}$); 135.63 ($C_{Ar\text{-}5}$); 135.21 ($C_{Ar\text{-}7}$); 129.94 ($C_{Ar\text{-}4'}$); 128.53 ($C_{Ar\text{-}2'}$); 127.00 ($C_{Ar\text{-}3'}$); 123.64 ($C_{Ar\text{-}4}$); 120.01 ($C_{Ar\text{-}2}$); 112.64 ($C_{Ar\text{-}6}$); 110.95 ($C_{Allyl\text{-}2}$); 55.2 ($C_{Allyl\text{-}1,3}$, broad). IR (cm^{-1}, KBr): 3053 w, 1605 s, 1582 s, 1560 s, 1518 s, 1456 m, 1421 m, 1385 w, 1365 m, 1351 m, 1254 w, 1235 m, 1201 w, 1169 w, 1142 m, 1117 w, 1033 w, 999 w, 944 w, 933 w, 838 w, 761 m, 718 w, 705 m, 644 w, 596 w, 522 w. MS (FAB): m/z = 344 [M^+], 302 [M^+ − allyl − H]. $C_{16}H_{14}O_2Pd$ (344.71): calc. C 55.7, H 4.1, O 9.3; found C 54.2, H 4.1, O 8.9.

2-Acetyl-4-fluorophenolato-[(1,2,3-η)-2-butenyl]palladium(II) (**10**) (*yellow crystals, 74% yield*)

^1H NMR ($CDCl_3$, 25°C, 300 MHz): δ = 7.13 (1H, dd, ^3J(H,F) = 10.2 Hz, ^4J(H,H) = 3.0 Hz, $H_{Ar\text{-}7}$); 7.01 (1H, ddd, ^3J(H,F) = 9.6 Hz, ^3J(H,H) = 7.4 Hz, ^4J(H,H) = 3.4 Hz, $H_{Ar\text{-}5}$); 6.75 (1H, dd, broad, ^3J(H,H) = 9.0 Hz, ^4J(H,F) = 5.0 Hz, $H_{Ar\text{-}4}$); 5.23 (1H, m, $H_{Allyl\text{-}2}$); 3.66 (1H, d, ^3J(H,H) = 6.4 Hz, $H_{Allyl\text{-}1,syn}$); 3.65 (1H, m, broad, $H_{Allyl\text{-}3}$); 2.63 (1H, d, ^3J(H,H) = 11.4 Hz, $H_{Allyl\text{-}1,anti}$); 2.46 (3H, s, $CH_{3\,(Acetyl)}$); 1.28 (3H, d, ^3J(H,H) = 6.2 Hz, $CH_{3\,(Allyl)}$). $^{13}C\{^1H\}$ NMR ($CDCl_3$, 25°C, 75 MHz): δ = 197.00 (C=O); 167.00 ($C_{Ar\text{-}3}$); 150.34 (d, ^1J(CF) = 232 Hz, $C_{Ar\text{-}6}$); 126.04 ($C_{Ar\text{-}4}$); 124.57 (d, ^2J(CF) = 25 Hz, $C_{Ar\text{-}5/7}$); 118.17 ($C_{Ar\text{-}2}$); 114.21 (d, ^2J(CF) = 22 Hz, $C_{Ar\text{-}5/7}$); 110.66 ($C_{Allyl\text{-}2}$); 73.85 ($C_{Allyl\text{-}3}$); 49.76 ($C_{Allyl\text{-}1}$); 27.29 ($CH_{3\,(Acetyl)}$); 15.92 ($CH_{3\,(Allyl)}$). IR (cm^{-1}, KBr): 2958 w, 2918 w, 1649 m, 1628 m, 1605 s, 1526 s, 1486 m, 1447 s, 1429 s, 1374 m, 1324 s, 1281 m, 1243 m, 1206 s, 1181 s, 1124 m, 1059 w, 1026 w, 970 m, 913 m, 864 m, 832 w, 807 s, 782 m, 698 w, 667 w, 638 w, 581 w, 523 w. MS (FAB): m/z = 314 [M^+]. $C_{12}H_{13}FO_2Pd$ (314.65): calc. C 45.8, H 4.2, O 10.2; found C 45.2, H 4.2, O 9.9.

2-Benzoylphenolato-[(1,2,3-η)-2-butenyl]palladium(II) (**11**) (*yellow crystals, 73% yield*)

^1H NMR ($CDCl_3$, 25°C, 300 MHz): δ = 7.58–7.18 (7H, m, H_{Ar}); 6.89 (1H, m, $H_{Ar\text{-}4}$); 6.33 (1H, m, $H_{Ar\text{-}6}$); 5.26 (1H, m, $H_{Allyl\text{-}2}$); 3.73 (1H, d, ^{3}J(H,H) = 6.6 Hz, $H_{Allyl\text{-}1,syn}$); 3.72 (1H, m, $H_{Allyl\text{-}3}$); 2.68 (1H, d, ^3J(H,H) = 11.0 Hz, $H_{Allyl\text{-}1,anti}$); 1.33 (3H, d, ^3J(H,H) = 6.0 Hz, $CH_{3\,(Allyl)}$). $^{13}C\{^1H\}$ NMR ($CDCl_3$, 25°C, 75 MHz): δ = 196.07 (C=O); 172.06 ($C_{Ar\text{-}3}$); 139.40 ($C_{Ar\text{-}1'}$); 135.40 ($C_{Ar\text{-}5}$); 135.12 ($C_{Ar\text{-}7}$); 129.93 ($C_{Ar\text{-}4l}$); 128.66 ($C_{Ar\text{-}2'}$); 126.94 ($C_{Ar\text{-}3'}$); 123.94 ($C_{Ar\text{-}4}$); 120.33 ($C_{Ar\text{-}2}$); 112.14 ($C_{Ar\text{-}6}$); 110.52 ($C_{Allyl\text{-}2}$); 74 ($C_{Allyl\text{-}3}$, broad); 50 ($C_{Allyl\text{-}1}$, broad); 16.05 ($CH_{3\,(Allyl)}$). IR (cm^{-1}, KBr): 3051 w, 2945 w, 1603 s, 1581 m, 1552 s, 1517 s, 1454 m, 1446 m, 1413 s, 1348 s, 1249 m, 1228 s, 1180 m, 1164 w, 1141 s, 1114 m, 1077 w, 1028 m, 997 w, 976 w, 945 m, 928 w, 854 w, 836 m, 803 w, 764 m, 757 m, 718 w, 702 s, 642 m, 598 w, 533 w, 520 w, 457 w. MS (FAB): m/z = 358 [M^+], 304 [M^+ − crotyl + H]. $C_{17}H_{16}O_2Pd$ (358.73): calc. C 56.9, H 4.5, O 8.9; found C 55.6, H 4.6, O 8.2.

2-Acetyl-1-naphtholato-[(1,2,3-η)-2-butenyl]palladium(II) (**12**) (*yellow powder, 81% yield*)

^1H NMR ($CDCl_3$, 25°C, 300 MHz): δ = 8.48 (1H, d, ^3J(H,H) = 8.0 Hz, $H_{Ar\text{-}4}$); 7.52–7.26 (4H, m, H_{Ar}); 6.72 (1H, d, ^3J(H,H) = 9.0 Hz, $H_{Ar\text{-}8}$); 5.29 (1H, m, $H_{Allyl\text{-}2}$); 3.75–3.62 (2H, m, $H_{Allyl\text{-}1,syn}$ and $H_{Allyl\text{-}3}$); 2.69 (1H, d, ^3J(H,H) = 12.0 Hz, $H_{Allyl\text{-}1,anti}$); 2.53 (3H, s, $CH_{3\,(Acetyl)}$); 1.42 (d, ^3J(H,H) = 6.2 Hz, I = 63%, $CH_{3\,(Allyl)}$); 1.33 (d, ^3J(H,H) = 6.2 Hz, I = 37%, $CH_{3\,(Allyl)}$). $^{13}C\{^1H\}$ NMR ($CDCl_3$, 25°C, 75 MHz): δ = 194.69 (C=O); 170.27 ($C_{Ar\text{-}3}$); 136,73, 130.10 ($C_{Ar\text{-}3a/7a}$); 128.75; 127.23; 125.82; 125.60; 123.76 (all C_{Ar}); 113.36 ($C_{Ar\text{-}2}$); 112.56 ($C_{Ar\text{-}8}$); 110.82 ($C_{Allyl\text{-}2}$); 72.60, 71.48 (both $C_{Allyl\text{-}3}$); 51.39, 50.35 (both $C_{Allyl\text{-}1}$); 27.71, 27.16 (both $CH_{3\,(Acetyl)}$); 16.00 ($CH_{3\,(Allyl)}$). IR (cm^{-1}, KBr): 2962 w, 1614 m, 1602 w, 1576 s, 1527 s, 1489 m, 1449 m, 1427 m, 1408 w, 1388 m, 1349 w, 1279 w, 1240 m, 1205 w, 1151 w, 1130 w, 1023 w, 992 w, 937 w, 895 w, 856 w, 806 w, 792 m, 756 w, 735 w, 690 w, 609 w, 579 w, 532 w, 513 w, 447 w. MS (FAB): m/z = 346 [M^+], 289 [M^+ − crotyl − 2H]. $C_{16}H_{16}O_2Pd$ (346.72): calc. C 55.4, H 4.7; found C 54.9, H 4.7.

CONCLUSION

Pd(II)-complexes with chelating 2-acylphenolate ligands and cyclometallated tri(*o*-tolyl)phosphine or allyl units, respectively, are easily available in good yields by treatment of an appropriate Pd(II)-precursor with the corresponding 2-acylphenole and a strong base such as potassium *tert*-butoxide. X-ray diffraction analyses of **2, 4** and **6** show that the coordination sphere of palladium is close to square planar. The conjugated aromatic system of the free ligands is partially disrupted through coordination to the metal. The different *cis*-/*trans*-stereochemistry observed for compounds **2, 6** and **4** can be correlated with the steric requirement of the 2-acylphenolate ligand. All structures exhibit short $CH_3 \cdots O$ distances which is indicative of C—H···O interactions. This phenomena was further studied in solution using complex **2**. The ratio of **C** to **D** depends on the ability of the solvent to act as a hydrogen donor, replacing a $CH_3 \cdots O$ by a H-solvent···O interaction. The NMR spectra of the allyl and crotyl complexes displayed that the former one is highly dynamic at room temperature while the latter ones exist as two stable isomers in solution.

Acknowledgements—This work has been supported by the Bayerischer Forschungsverbund Katalyse (ForKat). Dr. E. Herdtweck is thanked for the X-ray diffraction analysis of **2**

and A. Zapf for his contributions to the crystal structure determinations.

REFERENCES

1. Recent reviews: Mehrotra, R. C., Agarwal, S. K. and Singh, Y. P., *Coord. Chem. Rev.*, 1985, **68,** 101; Wills, C. J., *Coord. Chem. Rev.*, 1988, **88,** 133; Bryndza, H. E. and Tam, W., *Chem. Rev.*, 1988, **88,** 1163.
2. Tsuji, J. and Minami, I., *Acc. Chem. Res.*, 1987, **20,** 140; Alper, H. and Ali, B., *J. Mol. Catal.*, 1991, **67,** 29; Barbaro, P., Bianchini, C., Frediani, P., Meli, A. and Vizza, F., *Inorg. Chem.*, 1992, **31,** 1523; Sen, A., Lin, M., Kao, L.-C. and Hutson, A. C., *J. Am. Chem. Soc.*, 1992, **114,** 6385; Carpentier, J. F., Castanet, Y., Mortreux, A. and Petit, F., *J. Organomet. Chem.*, 1994, **482,** 31; Drent, E., van Broekhoven, J. A. M. and Doyle, M. J., *J. Organomet. Chem.*, 1991, **417,** 235; Drent, E., Arnoldy, P. and Budzelaar, P. H. M., *J. Organomet. Chem.*, 1994, **475,** 57.
3. Palucki, M., Wolfe, J. P. and Buchwald, S. L., *J. Am. Chem. Soc.*, 1996, **118,** 10333; Mann, G. and Hartwig, J. F., *J. Am. Chem. Soc.*, 1996, **118,** 13109; Palucki, M., Wolfe, J. P. and Buchwald, S. L., *J. Am. Chem. Soc.*, 1997, **119,** 3395; Widenhoefer, R. A., Zhong, H. A. and Buchwald, S. L., *J. Am. Chem. Soc.*, 1997, **119,** 6787.
4. van der Boom, M. E., Liou, S.-Y., Ben-David, Y., Vigalok, A. and Milstein, D., *Angew. Chem.*, 1997, **109,** 637; *Angew. Chem. Int. Ed. Engl.*, 1997, **36,** 626.
5. Kim, K.-Y., Osakada, K., Takenaka, A. and Yamamoto, A., *J. Am. Chem. Soc.*, 1990, **112,** 1096; Seligson, A. L., Cowan, R. L. and Trogler, W. C., *Inorg. Chem.*, 1991, **30,** 3371; Kim, Y.-J., Choi, J.-C. and Osakada, K., *J. Organomet. Chem.*, 1995, **491,** 97; Hunter, C. A., Lu, X.-J., Kapteijn, G. M. and van Koten, G., *J. Chem. Soc., Faraday Trans.*, 1995, **91,** 2009; Alsters, P. L., Baesjou, P. J., Janssen, M. D., Kooijman, H., Sicherer-Roetman, A., Spek, A. L. and van Koten, G., *Organometallics*, 1992, **11,** 4124.
6. Kapteijn, G. M., Grove, D. M., Smeets, W. J. J., Spek, A. L. and van Koten, G., *Inorg. Chim. Acta* 1993, **207,** 131; Kapteijn, G. M., Dervisi, A., Grove, D. M., Kooijman, H., Lakin, M. T., Spek, A. L. and van Koten, G., *J. Am. Chem. Soc.*, 1995, **117,** 10939; Kapteijn, G. M., Grove, D. M., Kooijman, H., Smeets, W. J. J., Spek, A. L. and van Koten, G., *Inorg. Chem.*, 1996, **35,** 526; Kapteijn, G. M., Spee, M. P. R., Grove, D. M., Kooijman, H., Spek, A. L. and van Koten, G., *Organometallics*, 1996, **15,** 1405.
7. Platt, A. W. G. and Pringle, P. G., *J. Chem. Soc., Dalton Trans.*, 1989, 1193.
8. Kapteijn, G. M., Baesjou, P. J., Alsters, P. L., Grove, D. M., Smeets, W. J. J., Kooijman, H., Spek, A. L. and van Koten, G., *Chem. Ber. Recueil*, 1997, **130,** 35.
9. Rogachev, B. G., Astarkhova, A. S., Roshchupkina, O. S. and Khidekel, A. L., *Izv. Akad. Nauk SSSR, Ser. Khim.*, 1972, **8,** 1855; Kawato, T., *Polyhedron*, 1983, **2,** 339; Rao, T. S., Reddy, K. L. and Lingaiah, P., *Ind. J. Chem.*, 1988, **27A,** 510.
10. Kegley, S. E., Schaverien, C. J., Freudenberger, J. H., Bergman, R. G., Nolan, S. P. and Hoff, C. D., *J. Am. Chem. Soc.*, 1987, **109,** 6563; Koelle, U., Wang, M. H. and Raabe, G., *Organometallics*, 1991, **10,** 2573; Osakada, K., Oshiro, K. and Yamamoto, A., *Organometallics*, 1991, **10,** 404; Sone, T., Iwata, M., Kasuga, N. and Komiya, S., *Chem. Lett.*, 1991, 1949; Osakada, K., Kim, K.-Y. and Yamamoto, A., *J. Organomet. Chem.*, 1990, **382,** 303; Simpson, R. D. and Bergmann, R. G., *Organometallics*, 1993, **12,** 781; Ozawa, F., Yamagami, I. and Yamamoto, A., *J. Organomet. Chem.*, 1994, **473,** 265.
11. Vögtle, F., *Supramolecular Chemistry*. Wiley, Chichester, 1991; Brammer, L., Zhao, D., Ladipo, F. T. and Braddock-Wilking, J., *Acta Cryst.*, 1995, **B51,** 632.
12. For reviews on C—H···O hydrogen bonds see: Desiraju, G. R., *Acc. Chem. Res.*, 1991, **24,** 290; Steiner, T., *Chem. Commun.*, 1997, 727.
13. Herrmann, W. A., Broßmer, C., Öfele, K., Reisinger, C.-P., Priermeier, T., Beller, M. and Fischer, H., *Angew. Chem.*, 1995, **107,** 1989; *Angew. Chem. Int. Ed. Engl.*, 1995, **34,** 1844; Beller, M. and Riermeier, T. H., *Tetrahedron Lett.*, 1996, **37,** 6535; Beller, M., Fischer, H., Herrmann, W. A., Öfele, K. and Broßmer, C., *Angew. Chem.*, 1995, **107,** 1992; *Angew. Chem. Int. Ed. Engl.*, 1995, **34,** 1848; Herrmann, W. A., Broßmer, C., Reisinger, C.-P., Riermeier, T. H., Öfele, K. and Beller, M., *Chem. Eur. J.*, 1997, **3,** 1357.
14. Beller, M., Riermeier, T. H., Reisinger, C.-P. and Herrmann, W. A., *Tetrahedron Lett.*, 1997, **38,** 2073.
15. Iourtchenko, A. and Sinou, D., *J. Mol. Catal.*, 1997, **122,** 91; Goux, C., Lhoste, P., Sinou, D. and Masdeu, A., *J. Organomet. Chem.*, 1996, **511,** 139.
16. Broßmer, C. M., Ph.D. Thesis, TU München, 1994.
17. Mounts, R. D. and Fernando, Q., *Acta Cryst.*, 1974, **B30,** 542.
18. Duckworth, V. F. and Stephenson, N. C., *Acta Cryst.*, 1969, **B25,** 2245.
19. Annan, T. A., Peppe, C. and Tuck, D. G., *Can. J. Chem.*, 1990, **68,** 423.
20. Reichardt, C., *Chem. Rev.*, 1994, **94,** 2319.
21. Laurence, C., Nicolet, P. and Dalati, M. T., *J. Phys. Chem.*, 1994, **98,** 5807.
22. Reichardt, C., *Solvents and Solvent Effects in Organic Chemistry*, 2nd edn VCH, Weinheim, Germany, 1988.
23. Tatsuno, Y. and Yoshida, T., in *Inorganic Synthesis*, ed. D. F. Shriver. Wiley, New York, 1979, p. 220.
24. *International Tables for Crystallography*, Vol. C, Tables 6.1.1.4 , 4.2.6.8 and 4.2.4.2 , ed. A. J. C. Wilson. Kluwer Academic Publishers, Dordrecht, The Netherlands, 1992, pp. 500–502, pp. 219–222, pp. 193–199.
25. Artus, G., Scherer, W., Priermeier, T. and Herdtweck, E., *"STRUX-V", A Program System to*

Handle X-ray Data, TU München, Germany, 1994.
26. Spek, A. L., "PLATON-92"–"PLUTON-92", An Integrated Tool for the Analysis of the Results of a Single Crystal Structure Determination, *Acta Crystallogr.*, 1990, **A46,** C34.
27. (a) Altomare, A., Cascarano, G., Giacovazzo, C., Guagliardi, A., Burla, M. C., Polidori, G. and Camalli, M., "SIR-92", University Bari, Italy, 1992. (b) Sheldrick, G. M., "SHELXS-86", A Program for the Solution of Crystal Structures from Diffraction Data, *Acta Crystallogr.*, 1990, **A46,** 467.
28. Sheldrick, G. M., *J. Appl. Cryst.* (in press) *Programm "SHELXL-93"*. Universität Göttingen, Deutschland, 1993.
29. (a) IPDS Operating System, Version 2.7. STOE-&CIE. GmbH, Darmstadt, Deutschland, 1996. (b) DENZO-SMN, Version 1.8.0. Zbyszek Otwinowski, U.S.A., 1998–1993.

Pergamon

PII: S0277-5387(97)00505-6

Polyhedron Vol. 17, No. 7, pp. 1177–1181, 1998
© 1998 Elsevier Science Ltd
All rights reserved. Printed in Great Britain
0277-5387/98 $19.00+0.00

Reactions of methyl iridium complexes with H_2, CO or O_2 in H_2O and DMSO†

David P. Paterniti and Jim D. Atwood*

Department of Chemistry, University at Buffalo, State University of New York, Buffalo NY 14260-3000, U.S.A.

(Received 17 October 1997; accepted 10 November 1997)

Abstract—New water soluble alkyl iridium(I) complexes were synthesized and their reaction with small molecules (H_2, CO and O_2) in DMSO or H_2O examined. Hydrogenation of *trans*-Ir$(CH_3)(CO)(TPPMSK)_2$ [TPPMSK = $(P(C_6H_5)_2(m\text{-}C_6H_4SO_3K))_2$] in DMSO produced CH_4 and Ir$(CO)(H)(TPPMSK)_3$ as major products. Carbonylation of *trans*-Ir$(CH_3)(CO)L_2$ (L = TPPMSK or TPPMS [TPPMS = $P(C_6H_5)_2(m\text{-}C_6H_4SO_3Na)$]), in DMSO, produced Ir$(C(O)CH_3)(CO)_2L_2$. Reactions in water were complicated by rapid hydrolysis of the Ir—CH_3 bond forming CH_4 and *trans*-Ir$(CO)(OH)L_2$. The hydrolysis was inhibited by excess L allowing the reactions to be studied in water. © 1998 Elsevier Science Ltd. All rights reserved

Keywords: water soluble; TPPMS; iridium; hydrolysis; carbonylation

Recent needs for environmentally-friendly catalytic systems that generate less hazardous waste, easier product separation, decreased price, increased safety and catalyst recycling led to the development of water-soluble catalysts, where hydrophilic ligands make an organometallic complex soluble in water [1–8]. The use of water-soluble organometallic complexes as catalysts for hydroformylation [2–4] continues to increase [7], in part, due to the success of the Ruhrchemie/Rhône-Poulenc process [8], where propylene is converted to butanal using a Rh(CO)$H(TPPTS)_3$ catalyst. While no mechanistic information pertaining to the carbonylation of a water-soluble rhodium alkyl complex has been reported, a water-soluble methyl iridium(I) complex offers an excellent opportunity to model carbonylation in water. We report here the synthesis of *trans*-Ir$(CO)(CH_3)(TPPMS)_2$; the attempted synthesis of *trans*-Ir$(CO)(CH_3)(TPPTS)_2$; carbonylation of *trans*-Ir$(CO)(CH_3)L_2$ (L = PPh_3, TPPMSK or TPPMS) in DMSO; the hydrolysis of the CH_3—Ir bond from *trans*-Ir$(CO)(CH_3)(TPPMS)_2$; and carbonylation of *trans*-Ir$(CO)(CH_3)(TPPMS)_2$ in H_2O with 5% excess TPPMS (TPPMS = $PPh_2(m\text{-}C_6H_4SO_3Na)$, TPPMSK = $PPh_2(m\text{-}C_6H_4SO_3K)$, TPPTS = $P(m\text{-}C_6H_4SO_3Na)_3$).

EXPERIMENTAL

Materials

$IrCl_3 \cdot 3H_2O$ was purchased or borrowed from Johnson Matthey. Triphenylphosphine, *n*-octylamine, fuming sulfuric acid (20% and 30% SO_3 w/w) and CH_3Li were purchased from Aldrich Chemical Co. Deuterated solvents were purchased from Cambridge Isotope Labs, Aldrich Chemical Co. or MSD Labs and were used as received, unless otherwise noted. CO was obtained from Matheson. Solvents used outside the glove-box were used as received without further drying or purification unless otherwise noted. Water was triply distilled and deionized while D_2O and d_6-DMSO were degassed on a high-vacuum line (three freeze-pump-thaw cycles) in a tube fitted with a Teflon stopcock. Solvents used within the glove-box were dried and degassed. The compounds: *trans*-Ir$(CO)(CH_3)(PPh_3)_2$ [9], *trans*-Ir$(CO)(CH_3)(TPPMSK)_2$ [10], $[Ir(CO)_3(PPh_3)_2]ClO_4$ [11], $[Ir(CO)_2(PPh_3)_3]ClO_4$ [11], TPPMS [12] and TPPMSK [10] were prepared as previously described.

Instrumental measurements

Infrared spectra were obtained on a Perkin–Elmer Paragon 1000 FT-IR using 0.5 mm NaCl or 0.1 mm CaF_2 (DMSO or H_2O) cells while solid-state spectra

* Author to whom correspondence should be addressed.

† Dedicated to Prof. Dr W. A. Herrmann on the occasion of his 50th birthday.

were recorded as KBr disks. All spectra are reported in wavenumbers (cm^{-1}). UV-visible spectra were obtained on a Hewlett Packard 8452A diode array spectrophotometer employing a quartz cuvette of 1 cm path length. All UV-visible data are reported in nanometers.

^1H and ^{31}P NMR spectra were recorded on Varian VXR-400 or 500 MHz spectrometers. ^1H NMR spectra were referenced to the deuterated solvent and all NMR spectra contained resonances corresponding to aromatic protons, but these resonances were not assigned. ^{31}P NMR spectra were referenced to an external sample of 85% H_3PO_4 in D_2O (reference was set to 0.0 ppm) and were proton decoupled. For ^1H and ^{31}P NMR spectra that were recorded in H_2O, a sealed D_2O reference was placed into the sample for signal locking. Solvent suppression techniques were utilized during the acquisition of ^1H NMR spectra in water. All chemical shifts (δ) are reported in ppm and all coupling constants (J) are reported in Hz.

trans-Ir(CO)(CH_3)(TPPMS)$_2$

93 mg of *trans*-Ir(CO)$(CH_3)(PPh_3)_2$ and 90 mg of TPPMS were suspended in 10 ml of THF. The solution was stirred for 3 days before collecting the product on a fine sintered glass filter where it was washed sequentially with THF, ether and hexane, yield 54 mg or 46%. ^{13}C NMR(DMSO-d_6) δ 1.2(s) ppm (decoupled). Elemental analysis found: C(46.51), H(3.68), P(5.76) and S(6.60) error limit $\pm$0.3%. Requires: C(46.43), H(3.39), P(6.31) and S(6.51) for a formula of *trans*-Ir(CO)$(CH_3)(P(C_6H_5)_2(C_6H_4SO_3Na\cdot\frac{1}{2}H_2O))_2$. The infrared and NMR properties of *trans*-Ir(CO)(CH_3)(TPPMS)$_2$ were consistent with PPh_3 [9] and TPPMSK [10] analogues (Table 1).

trans-Ir(CO)$(CH_3)L_2$ (L = TPPMSK *or* TPPMS) *with* O_2 *in DMSO*-d_6

NMR-scale solutions of *trans*-Ir(CO)$(CH_3)L_2$ (L = TPPMSK or TPPMS) in DMSO-d_6 were reacted with O_2 overnight to produce dioxygen complexes Ir(CO)$(CH_3)(O_2)L_2$. The dioxygen complexes could not be deoxygenated under nitrogen. The spectral characteristics of Ir(CO)$(CH_3)(O_2)L_2$ (L = TPPMSK or TPPMS) (Table 1) were similar to Ir(CO)$(CH_3)(O_2)(PPh_3)_2$ [9].

trans-Ir(CO)(CH_3)(TPPMS)$_2$ *in water as a function of time*

Using the method previously described for preparing NMR scale samples, a 0.02 molar aqueous chilled solution of *trans*-Ir(CO)(CH_3)(TPPMS)$_2$ was flame sealed while under vacuum. ^{31}P and ^1H NMR spectra were recorded over time at 50°C. Almost immediately after sealing the NMR tube, CH_4 was observed. Analysis of the solution shortly after, revealed *trans*-Ir(CO)(OH)(TPPMS)$_2$ [13] and CH_4 with no *trans*-Ir(CO)(CH_3)(TPPMS)$_2$ present.

Analyses conducted 1.25 h, 2 h and 3 days later revealed no new products. The NMR tube was opened and the infrared spectrum and pH were recorded (pH = 8.6). To complete the characterization of the iridium product, the water was removed by vacuum and the residue dissolved in DMSO-d_6 and combined with 10 mg of *trans*-Ir(CO)(CH_3)(TPPMS)$_2$ for NMR characterization. The ^1H NMR and ^{31}P NMR spectra clearly showed equal quantities of *trans*-Ir(CO)(OH)(TPPMS)$_2$ and *trans*-Ir(CO)(CH_3)(TPPMS)$_2$. The pH and spectral characteristics of *trans*-Ir(CO)(CH_3)(TPPMS)$_2$ in H_2O were identical to *trans*-Ir(CO)(OH)(TPPMS)$_2$ [10].

Kinetic investigations for reactions of *trans*-Ir(CO)(CH_3)(TPPMS)$_2$ *with* H_2O *and with* D_2O

In a 25 ml Schlenk flask, a 5×10^{-3} M stock solution of *trans*-Ir(CO)(CH_3)(TPPMS)$_2$ in DMSO was prepared, sealed with a rubber septum and removed from the glove-box. With the aid of a 250 μl Hamilton syringe, a 200 μl aliquot of stock metal solution was withdrawn from the sealed Schlenk flask and mixed with 3800 μl of degassed H_2O (or D_2O) in a 1-cm quartz cell adapted for air-sensitive work. Utilizing conventional UV-visible spectroscopic techniques, absorption changes were monitored at 404 nm [14] for the disappearance of *trans*-Ir(CO)(CH_3)(TPPMS)$_2$ as a function of time for at least five half-lives.

The following rate constants were measured: $k_{obs} = 0.083 \pm 0.003$ s^{-1} (H_2O reaction) and $k_{obs} = 0.081 \pm 0.005$ s^{-1} (D_2O reaction).

trans-Ir(CO)$(CH_3)L_2$ (L = PPh_3, TPPMSK *or* TPPMS) *with* CO *in DMSO*-d_6

Solutions of *trans*-Ir(CO)$(CH_3)L_2$ (L = PPh_3, TPPMSK or TPPMS) were prepared in DMSO. Bubbling CO through the solutions for at least 2 h produced Ir$(C(O)CH_3)(CO)_2L_2$, Ir$(C(O)CH_3)(CO)_3L$ and L. Subjecting the mixture of Ir$(C(O)CH_3)(CO)_2L_2$, Ir$(C(O)CH_3)(CO)_3L$ and L to a N_2 purge for at least 1 h resulted in the disappearance of Ir$(C(O)CH_3)(CO)_3L$ and L, reduction in the amount of Ir$(C(O)CH_3)(CO)_2L_2$ and the appearance of Ir$(CO)_2(CH_3)L_2$ and *trans*-Ir(CO)$(CH_3)L_2$. The products from carbonylation and decarbonylation reactions (Table 1) were identical for analogous reactions involving PPh_3 and P(*p*-tolyl)$_3$ analogues reported in non-polar solvents [9,15].

Attempted carbonylation of impure *trans*-Ir(CO)(CH_3)(TPPTS)$_2$ *in* H_2O

Using NMR scale procedures, an aqueous solution containing 23% *trans*-Ir(CO)(OH)(TPPTS)$_2$, 51%

Table 1. IR and NMR data for iridium complexes

Complex	ν_{CI} (cm^{-1})	$\nu_{C=O}$ (cm^{-1})	^{31}P (ppm)	^{1}H δ (ppm)
trans-$Ir(CO)(CH_3)(PPh_3)_2$	1935[a]	—	31.2(s)[b]	−0.4(t), J_{PH} = 8.5 Hz[b]
trans-$Ir(CO)(CH_3)$(TPPMSK)$_2$	1937[a]	—	31.5(s)[b]	−0.4(t), J_{PH} = 8.9 Hz[b]
trans-$Ir(CO)(CH_3)$(TPPMS)$_2$	1937[a]	—	31.6(s)[b]	−0.4(t), J_{PH} = 8.5 Hz[b]
			30.7(br)[c,d]	−0.4(br)[c,d]
trans-$Ir(CO)(CH_3)$(TPPTS)$_2$[e]	n/a	—	28.4(s)[b]	−0.8(br)[b]
			31(br)[f]	−0.8(br)[f]
trans-$Ir(CO)(OH)$(TPPMS)$_2$	1953[c]	—	28.4(s)[c]	n/a
			26.8(s)[b]	0.2(t), J_{PH} = 6.5 Hz[b]
trans-$Ir(CO)(OH)$(TPPTS)$_2$[e]	1961[c]	—	28.3(s)[b]	−0.01(m)[b]
			28.5(br)[f]	
$Ir(C(O)CH_3)(CO)_2(PPh_3)_2$	1923, 1976[a]	1621[a]	−1.0(br)[b]	2.0(s)[b]
$Ir(C(O)CH_3)(CO)_2$(TPPMSK)$_2$	1924, 1976[a]	1622[a]	−0.4(br)[b]	2.1(s)[b]
$Ir(C(O)CH_3)(CO)_2$(TPPMS)$_2$	1924, 1979[a]	1624[a]	−0.5(br)[b]	2.1(s)[b]
	1940, 1992[c,g]	n/a	−0.4(br)[c,g]	2.0(s)[c,g]
$Ir(C(O)CH_3)(CO)_2$(TPPTS)$_2$[f]	1941, 1987[c]	1626[c]	−0.4(s)[c]	2.1(s)[c]
$Ir(C(O)CH_3)(CO)_3(PPh_3)$	2045(w)[a] [23]	1645[a]	−8.0(s)[b]	2.6(s)[b]
$Ir(C(O)CH_3)(CO)_3$(TPPMSK)	2046(w)[a] [23]	1645[a]	−7.6(s)[b]	2.6(s)[b]
$Ir(C(O)CH_3)(CO)_3$(TPPMS)	1968, 2045(w)[a]	1648[a]	−7.6(s)[b]	2.6(s)[b]
$[Ir(CO)_3$(TPPTS)$_2]OH$[f]	2032(sh)[c]	—	0.4(s)[c]	n/a
$Ir(CO)_2(CH_3)(PPh_3)_2$	1908, 1962[a]	—	5.1(s)[b]	0.05(br)[b]
$Ir(CO)_2(CH_3)$(TPPMSK)$_2$	1910, 1964[a]	—	5.0(s)[b]	0.02(br)[b]
$Ir(CO)_2(CH_3)$(TPPMS)$_2$	1909, 1963[a]	—	5.2(s)[b]	0.04(br)[b]
	1914, 1965[c,h]	6.1(s)[c,h]	−0.1(br)[c,h]	
$Ir(CO)(CH_3)O_2$(TPPMSK)$_2$	1970[b]	—	8.6(s)[b]	0.6(t), J_{PH} = 4.5 Hz[b]
$Ir(CO)(CH_3)O_2$(TPPMS)$_2$	n/a	—	8.7(s)[b]	0.7(t), J_{PH} = 4.8 Hz[b]

[a] DMSO; [b] DMSO-d_6; [c] H_2O; [d] solution contained 44.8% *trans*-$Ir(CO)(CH_3)$(TPPMS)$_2$, 25.2% *trans*-$Ir(CO)(OH)$(TPPMS)$_2$, 17.1% $[Ir(CO)_2$(TPPTS)$_3]OH$, 12.8% $Ir(CO)_2(CH_3)$(TPPMS)$_2$ and initially 5% TPPMS added; [e] solution contained 23.3% *trans*-$Ir(CO)(OH)$(TPPTS)$_2$, 50.9% *trans*-$Ir(CO)(CH_3)$(TPPTS)$_2$ and initially 17.4% TPPTS; [f] D_2O; [g] solution contained 79% $Ir(C(O)CH_3)(CO)_2$(TPPMS)$_2$, 21% $[Ir(CO)_2$(TPPMS)$_3]OH$ and initially 5% TPPMS added; [h] solution contained 41% $Ir(CO)_2(CH_3)$(TPPMS)$_2$, 33% $Ir(C(O)CH_3)(CO)_2$(TPPMS)$_2$, 26% $[Ir(CO)_2$(TPPMS)$_3]OH$ and initially 5% TPPMS added; [i] solution contained 51.3% $[Ir(CO)_2$(TPPTS)$_3]OH$, 28.3% $Ir(CO)_2H$(TPPTS)$_2$, 10.8% $Ir(C(O)CH_3)(CO)_2$(TPPTS)$_2$, 9.5% $[Ir(CO)_3$(TPPTS)$_2]OH$ and 17% TPPTS (initially).

trans-$Ir(CH_3)(CO)$(TPPTS)$_2$ and 17% TPPTS (obtained by TPPTS exchange for PPh_3 on *trans*-$Ir(CO)(CH_3)(PPh_3)_2$ in a biphasic reaction) was subjected to a CO atmosphere. Analysis of the product after 2 h showed $[Ir(CO)_2$(TPPTS)$_3]^+OH^-$ (51%), $Ir(CO)_2H$(TPPTS)$_2$ (28%), $Ir(C(O)CH_3)(CO)_2$(TPPTS)$_2$ (11%) and $[Ir(CO)_3$(TPPTS)$_2]^+OH^-$ (9%). The spectroscopic properties of $[Ir(CO)_2$(TPPTS)$_3]^+OH^-$, $[Ir(CO)_3$(TPPTS)$_2]^+OH^-$, $Ir(CO)_2H$(TPPTS)$_2$ and $Ir(C(O)CH_3)(CO)_2$(TPPTS)$_2$ correlated well with those of their PPh_3 analogues (Table 1).

trans-$Ir(CO)(CH_3)$(TPPMS)$_2$ *with 5% added* TPPMS *and excess* CO *in* H_2O

An aqueous solution of *trans*-$Ir(CO)(CH_3)$(TPPMS)$_2$ containing 5% TPPMS (prepared using NMR-scale procedures) was subjected to a CO purge for 2 h. Solution analysis revealed $Ir(C(O)CH_3)(CO)_2$(TPPMS)$_2$ (79%) and $[Ir(CO)_2$(TPPMS)$_3]^+OH$ (21%). The infrared and NMR properties of $Ir(C(O)CH_3)(CO)_2$(TPPMS)$_2$ in H_2O (Table 1) were similar to $Ir(C(O)CH_3)(CO)_2(PPh_3)_2$ [9], $Ir(C(O)CH_3)(CO)_2(P(p\text{-tolyl})_3)_2$ [9] and nearly identical to $Ir(C(O)CH_3)(CO)_2L_2$ (TPPMSK and TPPMS) in DMSO-d_6 (Table 1). Subjecting the product mixture to a N_2 purge for 2.5 h resulted in some decarbonylation ($Ir(CO)_2(CH_3)$(TPPMS)$_2$ (40%), $Ir(C(O)CH_3)(CO)_2$(TPPMS)$_2$ (32%), $[Ir(CO)_2$(TPPMS)$_3]OH$ (25%), *trans*-$Ir(CO)(CH_3)$(TPPMS)$_2$ (2%) and a trace of *trans*-$Ir(CO)(OH)$(TPPMS)$_2$). The spectral characteristics of $Ir(CO)_2(CH_3)$(TPPMS)$_2$ were consistent with the PPh_3 and P(*p*-tolyl)$_3$ analogues [9,15] and corresponding analogues in DMSO-d_6 from Table 1.

RESULTS AND DISCUSSION

Synthesis

The methyl complex of TPPMS (*trans*-$Ir(CO)(CH_3)$(TPPMS)$_2$) is prepared by ligand exchange on

trans-$Ir(CO)(CH_3)(PPh_3)_2$ (eqn (1)), using stoichiometric amounts of

$$\textit{trans}\text{-}Ir(CO)(CH_3)(PPh_3)_2 + 2L \xrightarrow{THF} \textit{trans}\text{-}Ir(CO)(CH_3)L_2(\downarrow) + 2PPh_3L = TPPMS \quad (1)$$

TPPMS and *trans*-$Ir(CO)(CH_3)(PPh_3)_2$, where *trans*-$Ir(CO)(CH_3)(TPPMS)_2$ precipitates slowly in THF. The characterization data shown in Table 1 confirm the product formulation.

In DMSO the reactions of *trans*-$Ir(CO)(CH_3)(TPPMS)_2$ with CO, H_2 and O_2 are completely analogous to the reactions of *trans*-$Ir(CO)(CH_3)(PPh_3)_2$ in organic solvents. Studies of reactions of *trans*-$Ir(CO)(CH_3)(TPPMS)_2$ in water are impeded by rapid hydrolysis [18].

$$\textit{trans}\text{-}Ir(CO)(CH_3)L_2 + H_2O \rightarrow \textit{trans}\text{-}Ir(CO)(OH)L_2 + CH_4$$
$$L = TPPMS \quad (2)$$

The presence of free TPPMS slows the hydrolysis such that the complex can be characterized in water and carbonylation can be examined. Rate studies on the hydrolysis in the absence of TPPMS give a rate constant of $(1.5 \pm 0.2) \times 10^{-3}\ s^{-1}\ M^{-1}$ and do not show a large deuterium isotope effect from D_2O. Attempts to prepare *trans*-$Ir(CO)(CH_3)(TPPTS)_2$ from *trans*-$Ir(CO)(CH_3)(PPh_3)_2$ by biphasic exchange in toluene/H_2O produced a mixture of the hydroxy and methyl complexes. However, previous characterization of the hydroxy complex allowed spectroscopic characterization of *trans*-$Ir(CO)(CH_3)(TPPTS)_2$ (see Table 1).

Carbonylation of *trans*-$Ir(CO)(CH_3)(TPPMS)_2$ containing a 5% excess of TPPMS shows competition between hydrolysis ($Ir(CO)_2(TPPMS)_3^+$ in 21% yield) and carbonylation with $Ir(C(O)CH_3)(CO)_2(TPPMS)_2$ formed in 79% yield. This experiment demonstrates that carbonylation of an iridium alkyl occurs in water giving the acyl which is not hydrolyzed, consistent with the effectiveness of hydroformylation in water with $HRh(CO)(TPPTS)_3$ with a large excess of TPPTS[2–4].

Purging the mixture of $Ir(C(O)CH_3)(CO)_2(TPPMS)_2$ and $Ir(CO)_2(TPPMS)_3^+$ in water with N_2 for 2.5 h leaves the cationic complex unchanged and forms some $Ir(CO)_2(CH_3)(TPPMS)_2$. While neither $Ir(C(O)CH_3)(CO)_2(TPPMS)_2$ or $Ir(CO)_2(CH_3)(TPPMS)_2$ were isolated the spectroscopic characterizations are very similar to the reactions in DMSO and analogous reactions of PPh_3 complexes in organic solvents (see Table 1) [9]. Indeed, except for hydrolysis of *trans*-$Ir(CO)(CH_3)(TPPMS)_2$, the carbonylation of *trans*-$Ir(CO)(CH_3)L_2$ (L = TPPMS, P(*p*-tolyl)$_3$ and PPh_3) is unchanged from solvents such as toluene to DMSO and water. Figure 1 shows a ^{31}P spectrum of carbonylation of *trans*-$Ir(CO)(CH_3)(TPPMS)_2$ in an NMR tube (limited CO).

Two aspects of the hydrolysis of *trans*-$Ir(CO)(CH_3)(TPPMS)_2$ are quite interesting. First, the reaction is inhibited by TPPMS and second, the five-coordinate methyl complex, $Ir(CO)_2(CH_3)(TPPMS)_2$ does not appear to hydrolyze. We have previously suggested that square-planar iridium complexes exist in H_2O with a hydrogen bond along the *z* axis [19]. If such hydrogen bonding provides the route to hydrolysis of *trans*-$Ir(CO)(CH_3)(TPPMS)_2$ then excess TPPMS could block the site and slow hydrolysis. Such hydrogen bonding does not exist for five-coordinate iridium complexes [19]. A similar protonated square-planar platinum intermediate was suggested for reductive elimination of CH_4 from reaction of HCl with $Pt(Cl)(CH_3)(PEt_3)_2$ in CH_3OH [20–22]

In reactions with O_2 and H_2 in DMSO, *trans*-$Ir(CO)$

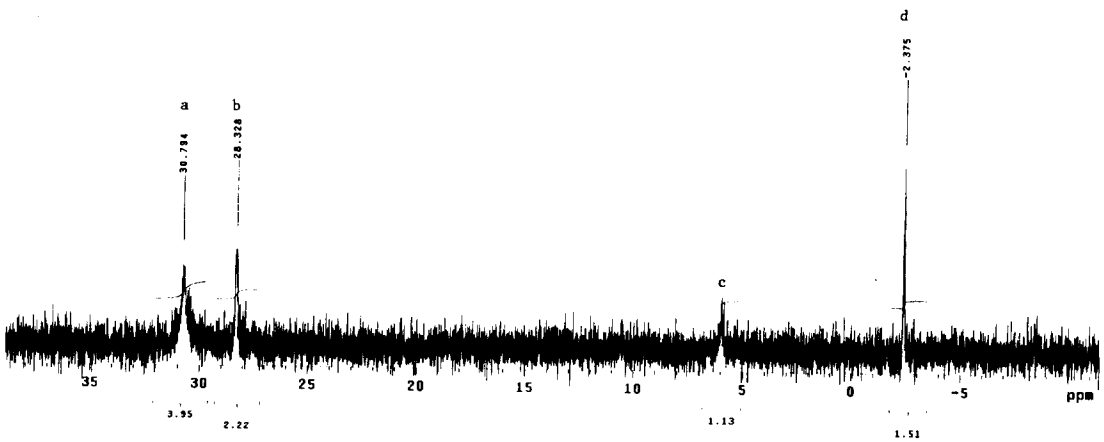

Fig. 1. A ^{31}P NMR spectrum of *trans*-$Ir(CO)(CH_3)(TPPMS)_2$ in D_2O with 5% added TPPMS in the presence of 0.74 atm of CO. The peak labeled (a) is *trans*-$Ir(CO)(CH_3)(TPPMS)_2$, (b) is *trans*-$Ir(CO)(OH)(TPPMS)_2$, (c) is $Ir(CO)_2(CH_3)(TPPMS)_2$ and (d) is $[Ir(CO)_3(TPPMS)_2^+][OH^-]$.

$(CH_3)(TPPMS)_2$ behaves just as the PPh_3 analogues with $Ir(CO)(CH_3)(O_2)(TPPMS)_2$ (Table 1) formed irreversibly with O_2 and methane eliminated from reaction with H_2. With the concentration of H_2 significantly lower, the *fac*- and *mer*-$Ir(CO)(H)_3(TPPMS)_2$ complexes are accompanied by $Ir(CO)(H)(TPPMS)_3$.

CONCLUSION

Methyl iridium complexes containing water-soluble phosphine ligands react with H_2, CO and O_2 much like their PPh_3 analogues, but have the additional complication in H_2O of hydrolysis of the Ir—CH_3 bond. The hydrolysis is inhibited by excess ligand and apparently occurs only for the square-planar complex.

Acknowledgment—J.D.A. enjoyed his collaboration with Wolfgang Herrmann, sponsored by the Humboldt Foundation and acknowledges support of the research reported in this manuscript by the Department of Energy, Grant No. ER13775.

REFERENCES

1. Herrmann, W. A. and Christian, W. K., *J. Mol. Catal.*, 1992, **73,** 191.
2. Joó, F. and Tóth, Z., *J. Mol. Catal.*, 1980, **8,** 369.
3. (a) Kalck, P. and Monteil, F., *Advances in Organometallic Chemistry*, 1992, **34,** 219; (b) Li, C. J., *Chem. Rev.*, 1993, **93,** 2023.
4. Kuntz, E. G., *CHEMTECH*, 1987, **17,** 570.
5. Herrmann, W. A. and Christian, W. K., *Angew. Chem. Int. Ed. Engl.*, 1993, **32,** 1524.
6. Barton, M. and Atwood, J. D., *J. Coord. Chem.*, 1991, **24,** 43.
7. (a) Beller, M., Cornils, B., Frohning, C. D. and Kohlpaintner, C. W., *J. Mol. Cat. A*, 1995, **104,** 17; (b) Herrmann, W. and Kohlpaintner, C. W., *Angew. Chem. Int. Ed. Engl.*, 1993, **32,** 1524.
8. (a) Morel, D. and Jenck, J., Fr. Patent 2,550,202 to Rhône-Polenc Recherches (08-03-1983); (b) Cornils, B. and Kuntz, E. G., *J. Organomet. Chem.*, 1995, **502,** 177.
9. Rees, W. M., Churchill, M. R., Li, Y. J. and Atwood, J. D., *Organometallics*, 1985, **4,** 1162.
10. Roman Jr., P. J., Paterniti, D. P., See, R. F., Churchill, M. R. and Atwood, J. D., *Organometallics*, 1997, **16,** 1484.
11. Malatesta, L., Caglio, G. and Angoletta, M., *J. Chem. Soc.*, 1965, 6974.
12. Ahland, S., Chatt, J., Davies, N. R. and Williams, A. A., *J. Chem. Soc.*, 1958, 264.
13. The ^{31}P NMR resonance of *trans*-$Ir(CO)(OH)(TPPMS)_2$ was similar to *trans*-$Ir(CO)(OH)(PPh_3)_2$ (δ 26(s) ppm in $CDCl_3$) [10].
14. Since *trans*-$Ir(CO)(CH_3)(TPPMS)_2$ was too reactive in H_2O to obtain its UV-visible spectrum, the decision to use 404 nm instead of 414 nm (the absorption band observed for *trans*-$Ir(CO)(CH_3)(TPPMS)_2$ in DMSO) was based on UV-visible spectral absorption shifts observed for *trans*-$Ir(CO)Cl(TPPMS)_2$ in H_2O vs DMSO.
15. Randall, S. L., Miller, C. A., See, R. F., Churchill, M. R., Janik, T. S., Lake, C. H. and Atwood, J. D., *Organometallics*, 1994, **13,** 5088.
16. Yagupsky, G. and Wilkinson, G., *J. Chem. Soc.(A)*, 1969, 725.
17. (a) Levison, J. J. and Robinson, S. D., *J. Chem. Soc. (A)*, 1970, 2947; (b) Roman Jr, P. J., Ph.D. Dissertation, State University of New York at Buffalo, 1997.
18. Paterniti, D.P. and Atwood, J. D., *Chem. Comm.*, 1997, 1665.
19. Paterniti, D. P., Roman Jr., P. J. and Atwood, J. D., *Organometallics*, 1997, **16,** 3371.
20. Stahl, S. S., Labinger, J. A. and Bercaw, J. E., *J. Am. Chem. Soc.*, 1996, **118,** 5961.
21. Belluco, U., Giustiniani, M. and Graziani, M., *J. Am. Chem. Soc.*, 1967, **89,** 6494.
22. Alibrandi, G., Minniti, D., Romeo, R., Uguagliati, P., Calligoro, Li., Belluco, U. and Crociani, B., *Inorg. Chim. Acta*, 1985, **100,** 107.
23. The ν_{CO} at around 1970 cm^{-1} for $Ir(C(O)CH_3)(CO)_3L$ (L = PPh_3 or TPPMSK) was buried beneath the more intense ν_{CO} of $Ir(C(O)CH_3)(CO)_2L_2$, which was the major product.

Pergamon

PII: S0277-5387(97)00497-X

Polyhedron Vol. 17, No. 7, pp. 1183–1193, 1998
© 1998 Elsevier Science Ltd
All rights reserved. Printed in Great Britain
0277-5387/98 $19.00+0.00

Synthesis of 2,6-bis(diphenylphosphinomethyl) pyridine-monoligand-rhodium(I) complexes [Rh(PNP)L]X with L = pyridine, CH_3CN, DMSO and X = CF_3SO_3, BF_4 from the corresponding ethylene complex and comparison of the structures to the piperidine complex (L = piperidine, X = BF_4)†

Christine Hahn,[a] Joachim Sieler[b] and Rudolf Taube[c]*

[a] Universität Würzburg, Institut für Anorganische Chemie, Am Hubland, D-97074 Würzburg, Germany

[b] Universität Leipzig, Institut für Anorganische Chemie, Linnéstr. 3, D-04103 Leipzig, Germany

[c] Technische Universität München, Anorganisch-Chemisches Institut, Lichtenbergstrae 4, D-85747 Garching, Germany

(Received 13 August 1997; accepted 26 November 1997)

Abstract—Investigation of the coordination conditions at the 2,6-bis(diphenylphosphinomethyl)pyridine-rhodium(I) fragment $[Rh(PNP)]^+$ by X-ray crystallography showed a square planar geometry of the neutral chloro and the cationic piperidine complexes, [Rh(PNP)Cl] (**1**) and $[Rh(PNP)(pip)]BF_4$ (**2**). New cationic rhodium(I) complexes [Rh(PNP)L]X (L = pyridine, X = SO_3CF_3 **3**; L = CH_3CN, X = SO_3CF_3 **4a**, X = BF_4 **4b**; L = DMSO, X = SO_3CF_3 **5**) have been synthesized from the ethylene complexes $[Rh(PNP)(C_2H_4)]X$ by substitution of the ethylene by the ligand L (L = py, CH_3CN, or DMSO). The complexes **3–5** were characterized by IR spectroscopy, ^1H-, ^{13}C-, and ^{31}P-NMR spectroscopy and X-ray crystallography. The influence of the ligands on the structure of the complexes was investigated. The *cis* influence was determined by measurement of the coupling constant J_{P-Rh} and the average length of the Rh—P bonds and the *trans* influence by the length of the Rh—N(1) bond. © 1998 Elsevier Science Ltd. All rights reserved.

Keywords: cationic rhodium(I) complexes; 2,6-bis(diphenylphosphinomethyl)pyridine; X-ray crystal structure analyses; ethylene substitution; *cis* and *trans* influence.

The hydroamination of olefins, that is the N–H addition at the C–C double bond represents the simplest amine synthesis. It is especially interesting from the point of view of atom economy, since no by-product is formed (cf. eqn (1)). Although during the last decades several catalytic routes have been discovered using structurally different catalysts, until now no convenient catalyst for the hydroamination of olefins is known [1].

We have found that the cationic ethylene rhodium(I) complex $[Rh(C_2H_4)(PPh_3)_2(Me_2CO)]PF_6$, is the first complex which catalyzes the addition of secondary amines such as piperidine to the ethylene at

(1)

† Dedicated to Prof. Dr W. A. Herrmann on the occasion of his 50th birthday.

* Author to whom correspondence should be addressed.

room temperature and under normal pressure [2,3], but only a low productivity is reached.

Using the tridentate ligand 2,6-bis(diphenylphosphinomethyl)pyridine (PNP) [4] cationic olefin rhodium(I) complexes [Rh(PNP)(olefin)]X (olefin = ethylene, styrene; X = BF_4, PF_6, CF_3SO_3) have been synthesized and characterized as model compounds for the catalyst complex [5]. The corresponding amine complexes [Rh(PNP)(HNR_2)]X (HNR_2 = piperidine, $HNMe_2$, $HNEt_2$) were obtained from the olefin complexes and secondary amines by substitution of the olefin without attack at the C–C double bond [5]. These Rh(PNP) complexes have been used as models to study the course and mechanism of the catalytic reaction.

In this paper we present the X-ray structure analyses of the neutral chloro-complex [Rh(PNP)Cl] [6] and the cationic piperidine complex [Rh(PNP)(pip)]BF_4 [5], report the synthesis and characterization of further monoligand complexes [Rh(PNP)L]X, and give a comparison of the structure of Rh(PNP) complexes as they change with the ligand variation.

EXPERIMENTAL

General

All reactions were carried out under dry argon. Ethanol, acetone and acetone-d_6 were refluxed over 4 Å molecular sieves and degassed by bubbling argon. Toluene, THF and diethyl ether were refluxed over Na/benzophenone and toluene-d_8 over K/Na alloy. Pyridine, acetonitrile and DMSO were dried over 4 Å molecular sieves and distilled before use.

Infrared spectra were recorded in nujol ([Rh(PNP)Cl] **1**) or as KBr pellets (cationic complexes **2**–**5**) on a Perkin-Elmer FT-IR 16 spectrometer. The ^{1}H-, ^{13}C-{^{1}H}, and ^{31}P{^{1}H}-NMR spectra were recorded at 300, 75, and 121 MHz respectively, on a Varian Gemini 300 NMR spectrometer. The ^{1}H- and ^{13}C-NMR shifts were referenced to the resonance of the residual protons of the solvents. The ^{31}P-NMR shifts were referenced to an external reference of 85% H_3PO_4. Elemental analyses of C, H and N were carried out on a LECO CHN 932 analyzer and Rh was determined using a photometric method [7].

The complex [{RhCl(COT)$_2$}$_2$] (COT = cyclooctene) was prepared according to the procedure in [8].

Synthesis of [Rh(PNP)Cl] (**1**)

The procedure described in [6] was slightly modified: A solution of 4.1 g (8.6 mmol) of 2,6-bis(diphenylphosphinomethyl)pyridine in 200 ml of toluene was added dropwise to a solution of 3.1 g (8.6 mmol) of [{RhCl(COT)$_2$}$_2$] in 200 ml of toluene over 5 hours. The resulting suspension was stirred overnight. The mixture of yellow and red solids which precipitated was filtered off and washed with 30 ml of ethanol to obtain the crude red product. Another fraction was obtained crystallized by concentration of the mother liquor (toluene solution) to 30 ml under reduced pressure. Both fractions were collected and recrystallized from refluxing toluene.

Yield: 2.6 g (4.3 mmol, 50%). M.p.: 230°C. ^{31}P-NMR δ (ppm) in toluene-d_8: 21.4, ($J_{P\text{-}Rh}$ = 152 Hz).

Synthesis of [Rh(PNP)(pip)]BF_4 (**2**)

The complex **2** was obtained from the reaction of [Rh(PNP)(C_2H_4)]BF_4 with an excess of piperidine according to the procedure in [5].

Synthesis of [Rh(PNP)[(py)]SO_3CF_3 (**3**)

1 ml (12 mmol) of pyridine was added to a suspension of 926 mg (1.2 mmol) of [Rh(PNP)(C_2H_4)]-SO_3CF_3 [5] in 15 ml of THF. The solid dissolved with evolution of gas and the solution changed in colour to orange. After stirring for 1 h the reaction mixture was filtered and the crude product was precipitated by dropwise addition diethyl ether to the filtrate. The orange-yellow solid was collected by filtration, washed with diethyl ether and dried in vacuum. The crude product was recrystallized from refluxing THF.

Yield: 716 mg (0.89 mmol, 74%). M.p.: 191°C. Found: C, 55.31; H, 3.80; N, 3.64; Rh 13.07. Calc. for $C_{37}H_{32}F_3N_2O_3P_2RhS$: C, 55.10; H, 3.99; N, 3.47; Rh, 12.76%. IR ν (cm^{-1}): 1604, 1564 (py); 1266, 1224, 1154, 1030, 638, 572 (CF_3SO_3). ^{1}H-NMR: δ (ppm): 4.36 (vt, N = 4.4 Hz, 4H, CH_2P), 7.15 (t, $J_{H\text{-}H}$ = 7.5 Hz, 2H, py), 7.49–7.38 (m, 14H, py[PNP], Ph), 7.65–7.60 (m, 9H, py[PNP], Ph), 7.74 (t, $J_{H\text{-}H}$ = 7.9 Hz, 1H, py), 8.75 (d, $J_{H\text{-}H}$ = 5.0 Hz, 2H, py). ^{13}C-NMR: δ (ppm): 43.6 (vt, N = 12.7 Hz, CH_2P), 122.7 (vt, N = 5.8 Hz, 3,5-py[PNP]), 126.0 (s, 3,5-py), 129.8 (vt, N = 4.8 Hz, PC_{meta}), 131.3 (s, PC_{para}), 133.3 (vt, N = 7.2 Hz, PC_{ortho}), 137.3 (s, 4-py[PNP]), 137.4 (s, 4-py), 155.3 (s, 2-py), 163.8 (vt, N < 3 Hz, 2,6-py[PNP]).

Syntheses of [Rh(PNP)(CH_3CN)]X (X = SO_3CF_3 **4a**, X = BF_4 **4b**) *and* [Rh(PNP)(DMSO)]SO_3CF_3 (**5**)

The complex **4a** was prepared from the reaction of 862 mg (1.14 mmol) of [Rh(PNP)(C_2H_4)]SO_3CF_3 and 5 ml of acetonitrile and complex **4b** from 693.3 mg (1.00 mmol) of [Rh(PNP)(C_2H_4)]BF_4 and 5 ml of acetonitrile in 15 ml of THF respectively. The complex **5** was prepared from 805 mg (1.06 mmol) of [Rh(PNP)(C_2H_4)]SO_3CF_3 and 1 ml of DMSO in 15 ml of THF. The complexes **4a**, **4b** and **5** were isolated in the same manner described for the complex **3**, except that the crude products precipitated as oils upon dropwise addition of diethyl ether to the reaction solution.

The oils crystallized after several hours. The crude products were recrystallized from refluxing THF.

4a: Yellow-brown crystalline solid, yield: 779 mg (0.89 mmol, 78%). M.p.: 126–130°C. Found: C, 52.92; H, 3.89: N, 4.04; Rh, 13.04. Calc. for $C_{34}H_{30}F_3N_2O_3P_2RhS$: C, 53.14; H, 4.21; N, 3.64; Rh, 13.39%. IR ν (cm^{-1}): 1602, 1566, (py); 1268, 1224, 1154, 1030, 638, 572 (CF_3SO_3); 2279, 2325 (CH_3CN). ^{1}H-NMR δ (ppm): 4.29 (vt, N = 4.4 Hz, 4H, CH_2P), 2.40 (s, 3H, CH_3), 7.53 (m, 14H, py, Ph), 7.79 (t, J_{H-H} = 7.9 Hz, 1H, py), 7.89–7.86 (m, 8H, Ph). ^{13}C-NMR δ (ppm): 3.8 (s, CH_3), 42.9 (vt, N = 11.6 Hz, CH_2P), 122.8 (vt, N = 5.1 Hz, 3,5-py), 129.9 (vt, N = 5.1 Hz, PC_{meta}), 131.5 (s, PC_{para}), 133.5 (vt, N = 7.3 Hz, PC_{ortho}), 138.0 (s, 4-py), 164.0 (vt, N < 3 Hz, 2,6-py).

4b: Yellow-brown crystalline solid, yield: 572 mg (0.81 mmol, 81%). IR ν (cm^{-1}): 1596, 1562 (py): 1268, 1062, (BF_4); 2283, 2330 (CH_3CN). ^{1}H-NMR δ (ppm): 2.41 (s, 3H, CH_3), 4.33 (vt, N = 4.4 Hz, 4H, CH_2P), 7.53 (m, 14H, py, Ph), 7.81 (t, J_{H-H} = 7.9 Hz, 1H, py), 7.86–7.90 (m, 8H, Ph). ^{13}C-NMR δ (ppm): 3.4 (s, CH_3), 42.5 (vt, N = 11.6 Hz, CH_2P), 122.5 (vt, N = 5.1 Hz, 3,5-py), 129.6 (vt, N = 5.1 Hz, PC_{meta}), 131.3 (s, PC_{para}), 133.3 (vt, N = 7.3 Hz, PC_{ortho}), 137.8 (s, 4-py), 163.8 (vt, N < 3 Hz, 2,6-py).

5: Yellow crystalline solid, yield: 763 mg (0.97 mmol, 91%). M.p.: 138–142°C. Found: C, 51.57; H, 4.34: N, 2.05; Rh, 12.18. Calc. for $C_{34}H_{33}F_3NO_4P_2RhS_2 \cdot 1/2\ (CH_3)_2CO$: C, 51.37; H, 4.43; N. 1.66; Rh, 12.22%. IR ν (cm^{-1}): 1600, 1562, (py); 1272, 1224, 1162, 1028, 636, 572 (CF_3SO_3); 1100 (DMSO). ^{1}H-NMR δ (ppm): 2.68 (s, 6H, CH_3), 4.51 (vt, N = 4.4 Hz, 4H, CH_2P), 7.59–7.54 (m, 14H, py, Ph), 7.86 (t, J_{H-H} = 7.8 Hz, 1H, py), 7.99–7.94 (m, 8H, Ph). ^{13}C-NMR δ (ppm): 44.2 (vt, N = 12.4 Hz, CH_2P), 50.6 (s, CH_3), 123.1 (vt, N = 5.3 Hz, 3,5-py), 130.1 (vt, N = 5.0 Hz, PC_{meta}), 132.2 (s, PC_{para}), 134.3 (vt, N = 6.8 Hz, PC_{ortho}), 140.5 (s, 4-py), 162.8 (vt, N < 3 Hz, 2,6-py).

X-ray structural analyses

A data collection and structure determination summary for the compounds **1**–**5** is given in Table 1. An empirical absorption correction for **1** and **5** (Ψ-scan, 10 reflections) and **2**, **3** and **4b** (SADABAS [9]) was applied. The structures were solved by Patterson methods and refined with a full matrix least-squares algorithm using the programs SHELXS-86 [10] and SHELXL-93 [11], respectively. Anisotropic displacement parameters for all nonhydrogen atoms were used. For compounds **1** and **5** the hydrogen atoms were placed in calculated positions and refined isotropically. The hydrogen atoms for the compounds **2**, **3** and **4b** could be located in difference Fourier syntheses and were included in the final cyclus of the refinement with isotropic displacement parameters. The numbering of the atoms for the 2,6-bis (diphenylphosphinomethyl)pyridine-rhodium(I) fragment $[Rh(PNP)]^+$ is the same for compounds **1**–**5**.

Further details of the crystal structure determination are deposited at the Fachinformationszentrum Karlsruhe, D-76344 Leopoldshafen-Eggenstein, and may be obtained by quoting the depository numbers CSD 407975 (**1**), CSD 407974 (**2**), CSD 407973 (**3**), CSD 407972 (**4b**), CSD 407971 (**5**).

RESULTS AND DISCUSSION

X-ray structure analysis of [Rh(PNP)Cl] (**1**) *and* [Rh(PNP)(pip)]BF_4 (**2**)

The structure of the chloro-PNP-rhodium(I) complex [Rh(PNP)Cl] (**1**) [6] represents the origin for further ligand variation at the $[Rh(PNP)]^+$ fragment. Therefore the characterization of **1** by X-ray crystallography is a contribution of fundamental importance for our model studies.

The chloro-complex **1** was prepared according to the literature procedure [6], except that toluene was used as a solvent. When the PNP ligand solution was added dropwise to the solution of $[\{RhCl(COT)_2\}_2]$ the yellow dinuclear complex $[Rh_2(PNP)_3]Cl_2$ as well as the red chloro-complex precipitated. The dinuclear complex could be separated by extraction of the mixture with ethanol, leaving the red chloro-complex **1** as a solid. Further concentration of the mother liquor (toluene solution) gave a further preciptate of **1**, from which X-ray quality single crystals could also be obtained. The melting point of 230°C and the characteristic IR bands for the pyridine ring vibrations at 1550 and 1586 cm^{-1} of **1** are in good agreement with the literature data [6]. In the ^{31}P-NMR spectrum a doublet appears at 21.4 ppm ($J_{P\ Rh}$ = 152 Hz). The molecular structure of the chloro-complex is shown in Fig. 1. The PNP ligand atoms and Cl are coordinated to the rhodium atom in a nearly square planar geometry. The N(1)–Rh–Cl(1) angle (178.10(12)°) is not significantly distorted from the linearity whereas the P(1)–Rh–P(2) (163.53(5)°) is relatively small due to the steric constraints of two five-membered rings formed by coordination of the PNP ligand at the rhodium atom. The Rh–Cl(1) distance (2.344(2) Å) is significantly shorter than that found, for example, in $[RhCl(PPh_3)_3]$ (red allotrope, 2.376(4) Å) [12].

As reported in [5], the X-ray crystal structure analysis of the cationic olefin complexes [Rh(PNP)(olefin)]BF_4 show a square planar coordination geometry of the complex cation without any close interaction of the Rh with the BF_4^- ion. The related piperidine complex [Rh(PNP)(pip)]BF_4 **2**, obtained from the reaction of the ethylene complex [Rh(PNP)(C_2H_4)]BF_4 with an excess of piperidine [5] is also without coordination interaction between the central atom and the anion. Single crystals suitable for X-ray crystal structure analysis were obtained from a solution of **2** in acetone overlayered with diethyl ether. The molecular structure of the complex cation of **2** is shown in Fig. 2. The Rh–N(2) distance (2.122(3)Å) is

Table 1. Crystallographic data and parameters of X—ray data collection and refinement

Compound	**1**	**2**	**3**	**4b**	**5**
Formula	$C_{31}H_{27}ClNP_2Ph$	$C_{36}H_{38}BF_4N_2P_2Rh \cdot 0.5CH_3OCH_3$	$C_{37}H_{32}F_3N_2O_3P_2RhS$	$C_{36}H_{36}BF_4N_2OP_2Rh$	$C_{34}H_{33}F_3NO_4P_2RhS_2 \cdot 0.5\ CH_3COCH_3$
Formula weight [g · mol^{-1}]	613.84	766.34	806.56	764.33	834.62
Crystal	Prism ; red	Prism ; yellow	Needles ; orange	Prism ; yellow	Needles ; yellow
Crystal size [mm]	0.28 × 0.26 × 0.22	0.24 × 0.22 × 0.20	0.32 × 0.26 × 0.22	0.22 × 0.18 × 0.18	0.32 × 0.15 × 0.12
Crystal system	Monoclinic	Monoclinic	Monoclinic	Monoclinic	Monoclinic
Space group ; Z	$P2_1/c$; 4	$C2/c$	$P2_1/c$	$C2/c$	$C2/c$
a [Å]	10.431(2)	18.2124(11)	11.040(2)	17.0796(9)	30.749(5)
b [Å]	15.767(5)	14.9278(9)	17.239(3)	15.0508(8)	11.0650(10)
c [Å]	17.210(1)	26.136(2)	18.250(4)	27.450(2)	21.653(2)
α [°]	90.0(0)	90.0(0)	90.0(0)	90.0(0)	90.0(0)
β [°]	104.18(3)	96.8760(10)	97.40(3)	97.2270(10)	100.280(10)
γ [°]	90.0(0)	90.0(0)	90.0(0)	90.0(0)	90.0(0)
Volume [Å^3]	2744(2)	7054.5(7)	3444.4(12)	7000.4(6)	7249(2)
Density (calc.) [Mg · m^{-3}]	1.486	1.443	1.555	1.450	1.530
Absorption coeff. [mm^{-1}]	0.857	0.627	0.706	0.632	0.731
Diffractometer	STADI4 (Stoe)	CCD-System (Siemens)	CCD-System (Siemens)	CCD-System (Siemens)	STADI4 (Stoe)
θ range [°]	1.78–27.00	1.57–23.24	1.63–23.26	1.50–26.18	1.91–25.01
Reflections/R_{int}	5975/0.072	5009/0.0281	4916/0.0483	6170/0.0242	6393/0.0143
Data/parameters	5294/347	5009/558	4916/570	6170/16/527	6393/446
Goof on F^{f2}	0.984	1.190	1.132	0.774	1.038
R_1/wR_2 [$I > 2\sigma(I)$]	0.0386/0.0962	0.0356/0.1012	0.0437/0.1006	0.0356/0.0851	0.0336/0.0842
R_1/wR_2 [all data]	0.1125/0.1212	0.0412/0.1036	0.0542/0.1066	0.0443/0.0924	0.0440/0.0917
Largest diff. peak [e · $^{-3}$]	0.965	1.344	0.403	0.512	1.268

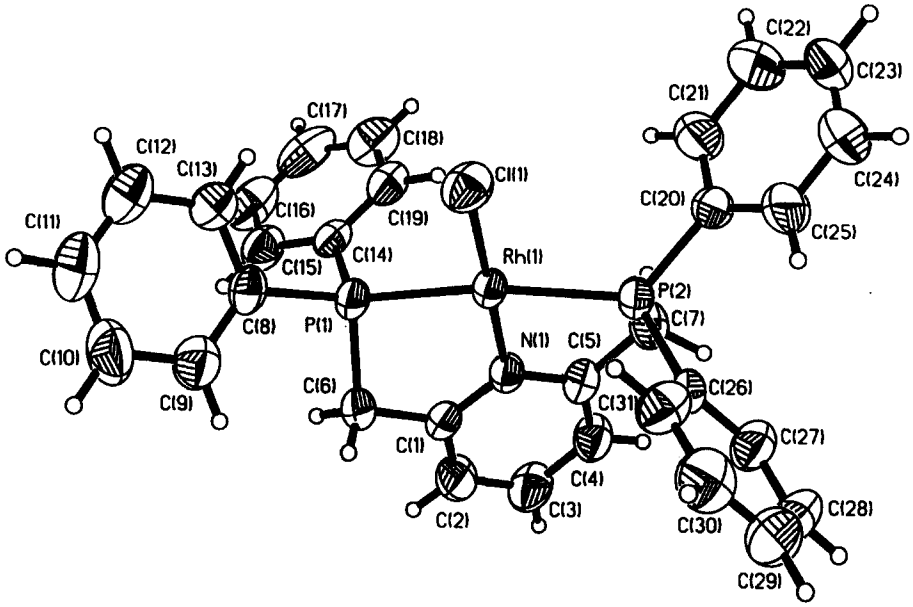

Fig. 1. ORTEP drawing structure of [Rh(PNP)Cl] **1**. Selected bond lengths [Å] and angles [°]: Rh—N(1) 2.040(4), Rh—Cl(1) 2.344(2), Rh—P(1) 2.263(2), Rh—P(2) 2.260(2), P(1)—C(6) 1.833(5), P(2)—C(1) 1.847(7), P(1)—Rh—P(2) 163.53(5), N(1)—Rh—P(1) 81.67(12), N(1)—Rh—P(2) 82.20(12), N(1)—Rh—Cl(1) 178.10(12).

comparable to those found in $[RhCl(C_2H_4)(pip)_2]$ (A form, 2.085(3) and 2.220(3) Å) [13].

Synthesis and characterization of [Rh(PNP)L]X (L = py, X = SO_3CF_3 **3**; L = CH_3CN, X = SO_3CF_3 **4a**, X = BF_4 **4b**)

To investigate the variation of the *N*-bonding conditions ($Nsp^3 \rightarrow Nsp^2 \rightarrow Nsp$) at the $[Rh(PNP)]^+$ fragment the pyridine and acetonitrile complexes [Rh(PNP)L]X (L = py, X = SO_3CF_3 **3**; L = CH_3CN, X = SO_3CF_3 **4a**, X = BF_4 **4b**) were synthesized. The complexes $[Rh(PNP)(C_2H_4)]X$ (X = SO_3CF_3, BF_4) were used as starting compounds since they are easily accessible [5]. When an excess of the respective ligand L was added to a suspension of the ethylene complex in THF at room temperature it reacted immediately by displacement of ethylene, cf. eqn. (2).

The complexes **3**, **4a** and **4b** were obtained in good yields as crystalline solids which are stable in air and are soluble in acetone, THF, and ethanol and insoluble in diethyl ether and hydrocarbons such as toluene or hexane. In the IR spectrum of **3**, **4a** and **4b** the bands observed at about $\nu = 1603$ cm^{-1} and 1565 cm^{-1} indicate coordination of the pyridine ring of the tridentate PNP-ligand [4]. The different absorption bands for the $CF_3SO_3^-$ anion (see Experimental section) found in the spectra of the complexes **3** and **4a** as well the band at 1062 cm^{-1} found for the BF_4^- anion, suggest that these anions are not coordinated to rhodium [14,15], as was also found for the ethylene and piperidine complexes [Rh(PNP)L]X (L = C_2H_4, piperidine; X = SO_3CF_3, BF_4) [5]. The complexes **4a** and **4b** show the characteristic bands of coordinated acetonitrile at about 2280 and 2330 cm^{-1} [16].

The complexes **3**, **4a** and **4b** were further characterized by ^{31}P-, ^1H-, and ^{13}C-NMR spectroscopy. In

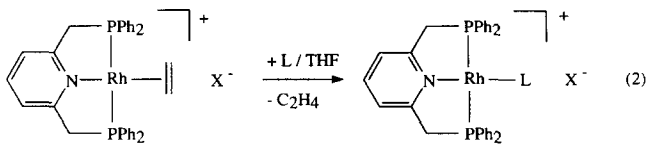

L = pyridine, X = CF_3SO_3 **3**
L = CH_3CN, X = CF_3SO_3 **4a**
X = BF_4 **4b**

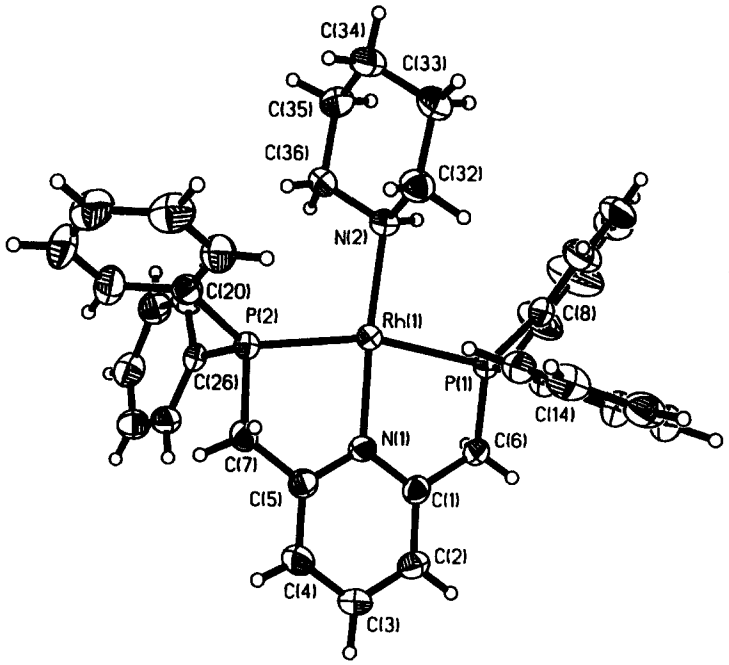

Fig. 2. ORTEP drawing structure of the cation of $[Rh(PNP)(pip)]BF_4$ **2**. Selected bond lengths [Å] and angles [°]: Rh—N(1) 2.062(3), Rh—N(2) 2.122(3), Rh—P(1) 2.2512(10), Rh—P(2) 2.3051(10), P(1)—C(6) 1.837(4), P(2)—C(7) 1.835(4), P(1)—Rh—P(2) 163.43(4), N(1)—Rh—P(1) 81.25(9), N(1)—Rh—P(2) 82.33(9), N(1)—Rh—N(2) 175.57(12), C(32)—N(2)—Rh 112.6(3), C(36)—N(2)—Rh 116.4(2).

the ^{31}P-NMR spectrum a doublet was found at 30.9 ppm ($J_{P\text{-}Rh}$ = 152 Hz) for **3**, 31.7 ppm ($J_{P\text{-}Rh}$ = 142 Hz) for **4a** and 30.6 ppm ($J_{P\text{-}Rh}$ = 143 Hz) for **4b**. The ^{1}H- and ^{13}C-NMR chemical shifts of the coordinated ligands (pyridine, acetonitrile) were shifted down field in comparison to the free ligand, as presented in Table 2.

Suitable single crystals of the pyridine complex **3** were obtained from a solution of the complex in acetone overlayered with diethyl ether while single crystals of **4b** were obtained from a concentrated solution of **4b** in acetone. The molecular structures of the complex cations $[Rh(PNP)(py)]^+$ and $[Rh(PNP)(CH_3CN)]^+$ are shown in Figs 3 and 4, respectively. Both exhibit a square planar coordination geometry. The X-ray crystal structure analyses of **3** and **4b** confirms the non-coordination of the $CF_3SO_3^-$ as well as the BF_4^- ions. The pyridine ligand in the complex **3** is nearly perpendicularly orientated to the coordination plane. An almost linear arrangement of Rh–N(2)–C(33)–C(32) is generated by the end-on coordination of the acetonitrile in the complex **4b** (C(33)–N(2)–Rh 173.7(3)°, N(2)–C(33)–C(32) 177.1(5)°) similar to that found for the structurally related cationic acetonitrile complex $[Rh(PPh_3)_3(CH_3CN)]BF_4$ (C–N–Rh 169.5(11)°, N–C–C 177.2(14)°) [17].

Table 2. ^{1}H- and ^{13}C-NMR chemical shifts of the free and coordinated ligands L (pyridine, acetonitrile) in **3** and **4a**

	^{1}H-NMR		^{13}C-NMR	
Ligand	Free	Coordn	Free	Coordn
Pyridine (**3**)	8.62, 7.69, 7.29	8.75, 7.74, 7.15	149.9, 136.2, 124.2	155.3, 137.4, 126.0
CH_3CN (**4a**)	1.93	2.40	118.2, 1.3	130.7 ($J_{C\text{-}Rh}$ = 11.4 Hz), 3.8

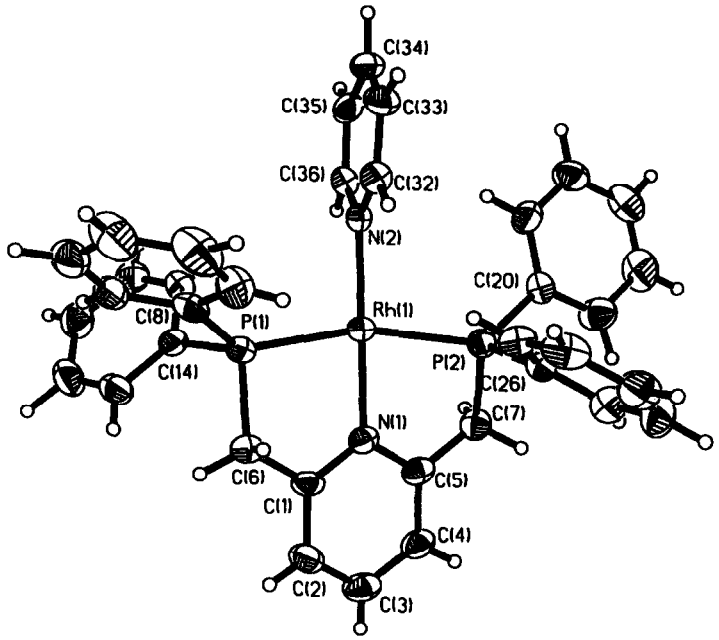

Fig. 3. ORTEP drawing structure of the cation of $[Rh(PNP)(py)]SO_3CF_3$ **3**. Selected bond lengths [Å] and angles [°]: Rh—N(1) 2.068(4), Rh—N(2) 2.063(4), Rh—P(1) 2.2705(12), Rh—P(2) 2.2819(13), P(1)—C(6) 1.835(5), P(2)—C(7) 1.836(5), P(1)—Rh—P(2) 163.06(4), N(1)—Rh—P(1) 83.12(10), N(1)—Rh—P(2) 81.20(10), N(1)—Rh—N(2) 177.37(14), C(32)—N(2)—Rh 122.9(3), C(36)—N(2)—Rh 120.3(3).

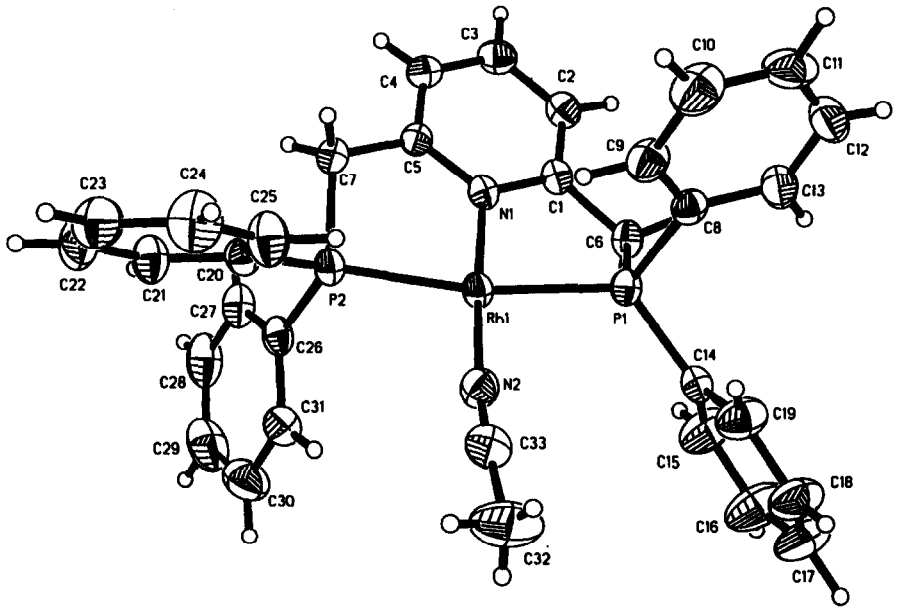

Fig. 4. ORTEP drawing structure of the cation of $[Rh(PNP)(CH_3CN)]BF_4$ **4b**. Selected bond lengths [Å] and angles [°]: Rh—N(1) 2.045(3), Rh—N(2) 1.984(3), Rh—P(1) 2.2648(8), Rh—P(2) 2.2770(8), P(1)—C(6) 1.828(3), P(2)—C(7) 1.838(4), P(1)—Rh—P(2) 166.34(4), N(1)—Rh—P(1) 82.82(7), N(1)—Rh—P(2) 83.54(7), N(1)—Rh—N(2) 175.53(14), C(33)—N(2)—Rh 173.7(3), N(2)—C(33)—C(32) 177.1(5).

Comparing the Rh–N(2) distances in the *N*-donor ligand complexes [Rh(PNP)L]X (L = piperidine, pyridine, acetonitrile) a significant shortening of this bond length is observed according to the hybridization of the nitrogen atom ($Nsp^3 \rightarrow Nsp^2 \rightarrow Nsp$): 2.122(3) for **2**, 2.063(4) for **3** and 1.984(3) for **4b**.

Attempts at the preparation of O-donor ligand complexes

In a manner analogous to the synthesis of the *N*-donor complexes **2–4**, attempts were made to prepare complexes with strong *O*-donor ligands such as HMPT, DMSO and DMF from the ethylene complex $[Rh(PNP)(C_2H_4)]SO_3CF_3$. However, the ethylene could not be substituted by HMPT and DMF. Even after refluxing of the ethylene complex with an excess of HMPT or DMF in THF over several hours, only the starting complex could be isolated. Also acetone and THF both showed no tendency to coordinate. This is in contrast to the coordination of *O*-donor ligands to the rhodium(I) in the complexes $[Rh(C_2H_4)_2(solv)_2]^+$ (solv = THF, acetone) [18] or in the catalyst complex $[Rh(C_2H_4)(PPh_3)_2(Me_2CO)]PF_6$. This indicates the weak affinity of the rhodium(I) in the PNP-complex toward *O*-donor ligands, which are not able to compete with the coordinated ethylene. With HMPT the coordination may be additionally suppressed by steric hindrance as similarly observed for the sterically comparable di-*iso*-propylamine which also did not react with the ethylene complex [5].

DMSO, however, reacts immediately when it is added dropwise to a suspension of the ethylene complex in THF at room temperature. The reaction solution changed in colour to yellow and the evolution of gas was observed. However, the isolated complex proved to be an *S*-donor ligand complex (cf. eqn (3)) as shown by IR spectroscopy and X-ray crystal structure analysis (*vide infra*), cf. Fig. 5.

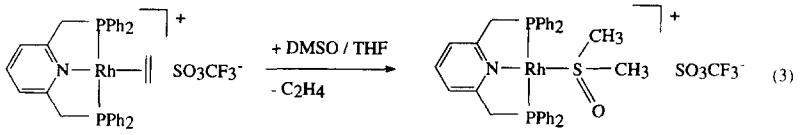

(3)

5

The complex $[Rh(PNP)(DMSO)]SO_3CF_3$ (**5**) is a yellow air stable crystalline solid. The complex was characterized by IR, ^{31}P-, ^1H-, and ^{13}C-NMR spectroscopy. In the IR spectrum of **5** the bands at 1600 and 1562 cm^{-1} indicate the coordination of the PNP pyridine ring while those of the triflate ion indicate its non-coordination as was observed for **3** and **4**. The band at 1100 cm^{-1}, assigned as $\nu(S{=}O)$, lies in the expected range for *S*-coordinated DMSO [19,20]. The ^{31}P-NMR spectrum exhibits a doublet at 36.7 ppm (J_{P-Rh} = 145 Hz). The ^1H-NMR signal of CH_3 of the coordinated DMSO at 2.68 ppm is shifted down field in comparison with the free molecule (2.49 ppm) as but not so far as it is expected for an *S*-bonded mode of DMSO [19].

X-ray quality single crystals were obtained from a solution of the complex in acetone overlayered with diethyl ether. The molecular structure of the complex cation of **5** is shown in Fig. 5. The Rh–S distance (2.1873(10) Å) is comparable to the Ru–S distance (2.188(3) Å) found in the Ru(II) complex $[Ru(NH_3)_3(DMSO)][PF_6]_2$ [21] which was described as particularly short. This may be an indication of a partial double bond character arising from d_π–p_π back donation from the metal to the sulfur. However, the S–O distance (1.473(3) Å) is not lengthened but lies within the range of the average bond length of *S*-coordinated sulfoxides [20].

Structural influences of L on the $[Rh(PNP)]^+$ fragment

In both ^{31}P NMR spectroscopy and the solid state structure, as determind by X-ray crystallography, of complexes of the type $[Rh(PNP)L]^+$ (L = Cl, py, CH_3CN, DMSO, olefin amine) the influence of different ligands on the Rh–P (*cis*) and Rh–N (*trans*) could be seen.

In Table 3 the ^{31}P-NMR results of the new cationic monoligand complexes **3–5** are assembled together with those of the chloro-, olefin, and amine PNP–rhodium(I) complexes. These are arranged in order of decreasing phosphorus–rhodium coupling constant J_{P-Rh}. Although in general the *cis* influence of a ligand is expected to be relatively small compared to its *trans* influence [22, 23] and the coupling constant J_{P-Rh} reflects only one aspect of the phosphorus–rhodium bond (primarily the s-orbital contribution to the bond order) the principal trend concerning the donor/acceptor strength can be seen in this series of the ligands. While for the σ-donor ligands (amines, chloride, and pyridine) relatively high values of J_{P-Rh} between 149 and 157 Hz were observed the phosphorus–rhodium coupling constant decreases with the increasing π-acceptor strength of the other ligands in the order: $DMSO \approx CH_3CN < C_2H_4 <$ styrene.

The influence of the negative charge of the chloro ligand can be seen in the significant up field shift to

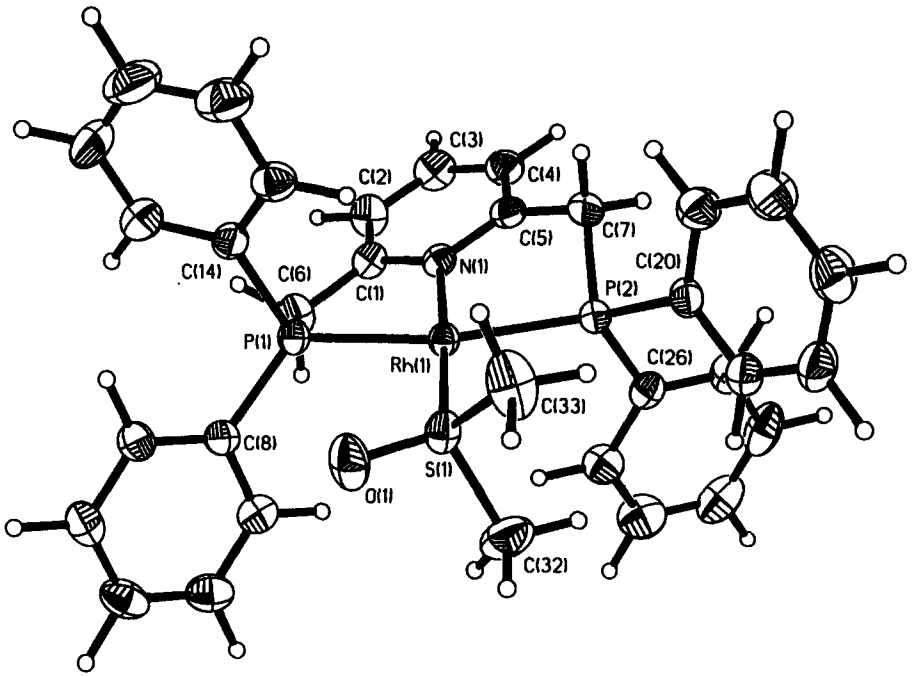

Fig. 5. ORTEP drawing structure of the cation of $[Rh(PNP)(DMSO)]SO_3CF_3 \cdot \frac{1}{2}(CH_3)_2CO$ **3**. Selected bond lengths [Å] and angles [°]: Rh—N(1) 2.093(2), Rh—S(1) 2.1870(9), Rh—P(1) 2.2696(8), Rh—P(2) 2.2884(8), S(1)—O(1) 1.474(3), S(1)—C(32) 1.786(4), P(1)—C(6) 1.839(3), P(2)—C(7) 1.841(3), P(1)—Rh—P(2) 163.76(3), N(1)—Rh—P(1) 81.84(7), N(1)—Rh—P(2) 81.91(7), N(1)—Rh—S(1) 177.48(7), O(1)—S(1)—Rh 118.76(10), C(33)—S(1)—Rh(1) 113.3(2), C(32)—S(1)—C(33) 100.5(2), O(1)—S(1)—C(32) 106.4(2).

Table 3. ^{31}P–NMR data of the PNP–rhodium(I) complexes

Complex		δ ppm	J_{P-Rh}[Hz]	Solvent
$[Rh(PNP)(HNMe_2)]BF_4$	[5]	34.3	157	Acetone-d_6
$[Rh(PNP)(HNEt_2)]BF_4$	[5]	38.9	156	Acetone-d_6
[Rh(PNP)Cl]	**1**	21.4	152	Toluene-d_8
$Rh(PNP)(py)]SO_3CF_3$	**3**	30.9	152	Acetone-d_6
$[Rh(PNP)(pip)]BF_4$	**2**	34.9	149	Acetone-d_6
$[Rh(PNP)(DMSO)]$-SO_3CF_3	**5**	36.7	145	Acetone-d_6
$[Rh(PNP)(CH_3CN)]BF_4$	**4b**	30.6	143	Acetone-d_6
$[Rh(PNP)(C_2H_4)]SO_3CF_3$	[5]	38.2	131	Acetone-d_6
$[Rh(PNP)(styrene)]BF_4$	[5]	41.7	126	Acetone-d_6

21.4 ppm. This is in contrast to the cationic complexes which are all observed at a lower field than 30 ppm. Since different structural and electronic factors of the neutral ligands have to be take into consideration it is difficult to explain completely the ordering of the ^{31}P-NMR shifts of the corresponding PNP complexes. However, comparing for example the pyridine and the styrene complexes (30.9 and 41.7 ppm, resp.) the main features of their bonding character are distinguishable, the strong σ-donating of the pyridine and the strong π-accepting property of the styrene, which seem to have an unambiguous effect on the total electron density of the $[Rh(PNP)]^+$ fragment.

Further information about the extent of the influence of the ligands on the structure of the complex fragment is obtained from the X-ray crystal structures of these complexes. In each of these complexes the PNP and the respective ligand L generates a nearly square planar coordination geometry (cf. Figs 1–5). In all cases a P(1)–Rh–P(2) angle of 163° was observed (cf. Table 4) comparable to that found in the olefin complexes of 161° [5]. Presumably, the geometric strain by the two five-membered rings formed by the coordination of the chelate PNP ligand at the rhodium atom does not allow any appreciable variation of the coordination geometry in the $[Rh(PNP)]^+$ moiety.

No significant distortion of the N(1)–Rh–L angle from linearity was observed with variation of the ligand L ranging from 178.10(12)° (Cl) to 175.55(14)° (pip). It is to be noted that in rhodium(I) complexes of the analogous type [Rh(ttp)(L)]X with the tridentate triphosphine ligand $PhP(CH_2CH_2CH_2PPh_2)_2$ (ttp), which forms two six-membered rings in the chelate structure, significant *trans* influence and steric distortion effects of a series of σ-donor and π-acceptor ligands L were distinguishable [24].

While the influence of the ligands L on the distortion from the planar coordination geometry is not pronounced in the Rh(PNP) complexes an influence

Table 4. Structural data of the X-ray crystal structure analyses of [Rh(PNP)Cl] and [Rh(PNP)L]X complexes (X = BF_4, SO_3CF_3)

Complex	Rh—N(1)	Rh—P(1) Rh—P(2)	Rh—L	N(1)—Rh—L	P(1)—Rh—P(2)
[Rh(PNP)Cl]	2.040(4)	2.263(2) 2.260(13)	2.344(2)	178.10(12)	163.53(5)
[Rh(PNP)(pip)]BF_4	2.062(3)	2.2512(10) 2.3051(10)	2.1212(3)	175.57(12)	163.43(4)
[Rh(PNP)(py)]SO_3CF_3	2.068(4)	2.2705(12) 2.2819(13)	2.063(4)	177.37(14)	163.06(4)
[Rh(PNP)(CH_3CN)]BF_4	2.045(3)	2.2648(8) 2.2770(8)	1.9884(3)	175.53(14)	166.34(4)
[Rh(PNP)(DMSO)]SO_3CF_3	2.093(2)	2.2696(8) 2.2884(8)	2.1873(10)	177.48(7)	163.76(3)
[Rh(PNP)(C_2H_4)]BF_4	2.092(4)	2.2690(13) 2.3001(13)	Rh—C(32) 2.142(6) Rh—C(33) 2.157(6)	N—Rh—C(32) 156.3(3) N—Rh—C(33) 166.8(2)	161.39(5)
[Rh(PNP)(styrene)]BF_4	2.102(3)	2.2916(10) 2.3004(11)	Rh—C(32) 2.144(5) Rh—C(33) 2.201(4)	N—Rh—C(32) 157.0(2) N—Rh—C(33) 165.8(2)	161.96(4)

on the Rh–N(1) and Rh–P bond length could be detected. An examination of the Rh–P bond length shows that in complexes bearing more bulky ligands such as piperidine or DMSO the bond length are significantly different. This feature is also found in the PEt_3 complex [Rh(ttp)(PEt_3)]AsF_6 [24] caused by intramolecular interaction between the ligand moiety and the phenyl rings of the diphenylphosphino groups.

However, on the ^{31}P-NMR time scale in each case the both phosphorus atoms of the PNP complexes are equivalent, and comparing the ordering of $J_{P\text{-}Rh}$ to the average of the Rh–P(1) and Rh–P(2) distances (2.261 Å Cl, 2.271 Å CH_3CN, 2.276 Å py, 2.278 Å pip, 2.279 Å DMSO, 2.284 Å C_2H_4, 2.296 Å styrene) a good agreement exists, reflecting the expected *cis* influence of the ligands.

The order of increasing Rh–N(1) bond length is also consistent with the expected strength of the *trans* influence of these ligands. The shortest Rh–N(1) bond length (2.040 Å), is found in the case of Cl^-, the σ-donor ligand with the highest electronegativity. On the other hand significant Rh–N(1) bond lengthening occurs with the *S*- and *C*-ligands with the lowest electro-negativity: 2.092 Å for DMSO, 2.092 Å for C_2H_4, and 2.102 Å for styrene. In general, however, the *trans* influence of these ligands observed in the Rh(PNP) complexes is scarcely larger than the *cis* influence.

CONCLUSION

In a manner analogous to the secondary amines it was shown that also the *N*-donor ligands pyridine and acetonitrile and the DMSO, as an *S*-donor ligand, can liberate the ethylene from [Rh(PNP)(C_2H_4)]X by the formation of the respective ligand complexes [Rh(PNP)L]X (L = py, CH_3CN, DMSO) which were fully characterized by ^{1}H-, ^{13}C-, and ^{31}P-NMR spectroscopy. On the other hand HMPT, DMF, THF and acetone are not able to displace the ethylene, indicating the weak affinity of the $[Rh(PNP)]^+$ fragment toward *O*-donor molecules. The results of the ^{31}P-NMR spectroscopy and X-ray crystal structure analyses of the chloro, amine, and olefin complexes allowed a *cis* and *trans* influence series to be established. The order Cl ≈ piperidine ≈ py < DMSO–CH_3CN < C_2H_4 < styrene observed from $J_{P\text{-}Rh}$ and the average Rh–P bond lengths in the Rh(PNP) complexes characterizing the *cis* influence is in good agreement with that of the *trans* influence on the Rh–N(1) bond length which is slightly pronounced. Both *cis* and *trans* influence of these ligands are obviously consistent with in general the expected order concerning their electronegativity. However, the $[Rh(PNP)]^+$ fragment must be characterized as a rigid complex moiety which is rather insensitive toward a variety of ligands.

Since the formation and the cleavage of a Rh–C σ-bond play an essential role in the catalytic cycle of the hydroamination of ethylene it is of interest to investigate its nature in the related organo–PNP–rhodium(I) complexes, which we have already prepared as further model compounds in this complex series which will be reported in another paper.

Acknowledgements—We thank the Deutsche Forschungsgemeinschaft (Sonderforschungsbereich 347 of the University Würzburg) for financial support.

REFERENCES

1. (a) Taube, R., in *Applied Homogeneous Catalysis with Organometallic Compounds*, Vol. 1, ed. B. Cornils and W. A. Herrmann. Verlag Chemie, Weinheim, 1996, pp. 507; (b) Steinborn, D. and Taube, R., *Z. Chem.*, 1986, **26,** 349; (c) Brunet, J.-J., Neibecker, D. and Niedercorn, F. J., *J. Mol. Catal.*, 1989, **49,** 235; (d) Brunet, J.-J., *Gazz. Chim. Ital.*, 1997, **127,** 111.
2. Krukowka, E., Dissertation, TH Merseburg, 1985.
3. Krukowka, E., Taube, R. and Steinborn, D., DD 296 909 A5 (10.11.88) 1988, C. A. 1992, **116,** 2139936.
4. Dahlhoff, W. V. and Nelson, S. M., *J. Chem. Soc. (A)*, 1971, 2184.
5. Hahn, C., Sieler, J. and Taube, R., *Chem. Ber.*, 1997, **130,** 939.
6. Vasapollo, G., Giannoccaro, P., Nobile, C. F. and Sacco, A., *Inorg. Chim. Acta*, 1981, **48,** 125.
7. Lange, B. and Vejdelek, Z. J., *Kolorimetrische Analyse*. Verlag Chemie, 1982, p. 232.
8. v. d. Ent, A. and Onderdelinden, A. L., *Inorg. Synth.*, 1968, **14,** 92.
9. Sheldrick, G. M., SADABAS, Program for Empirical Absorption Correction, University of Göttingen, 1996.
10. Sheldrick, G. M., SHELXS-86, Program for Crystal Structure Solution, University of Göttingen, 1986.
11. Sheldrick, G. M., SHELXL-93, Program for Crystal Structure Determination, University of Göttingen, 1993.
12. Bennett, M. J. and Donaldson, P. B., *Inorg. Chem.*, 1977, **16,** 655.
13. Selent, D., Scharfenberg-Pfeiffer, D., Reck, G. and Taube, R., *J. Organomet. Chem.*, 1991, **415,** 417.
14. Aresta, M. and Quaranta, E., *Organomet.*, 1993, **12,** 2032.
15. Beck, W. and Sünkel, K., *Chem. Rev.*, 1988, **88,** 1405.
16. Storhoff, B. N. and Lewis, H. C., *Coord. Chem. Rev.*, 1977, **23,** 1.
17. Pimblettt, G., Garner, C. D. and Clegg, W., *J. Chem. Soc., Dalton Trans.*, 1985, 1977.
18. Schrock, R. R. and Osborn, J. A., *J. Am. Chem. Soc.*, 1971, **93,** 3089.
19. Davies, J. A., *Adv. Inorg. Chem. Radiochem.*, 1981, **24,** 115.
20. Calligaris, M. and Carugo, O., *Coord. Chem. Rev.*, 1996, **153,** 83.
21. March, F. C. and Ferguson, G., *Can. J. Chem.*, 1971, **49,** 3590.
22. Hartley, F. R., *Chem. Soc. Rev.*, 1973, **2,** 163.
23. Burdett, J. K. and Albright, T. A., *Inorg. Chem.*, 1979, **18,** 2112.
24. Christoph, G. G., Blum, P., Liu, W. C., Elia, A. and Meek, D. W., *Inorg. Chem.*, 1979, **18,** 894.

Pergamon

PII: S0277-5387(97)00506-8

Polyhedron Vol. 17, No. 7, pp. 1195–1201, 1998
© 1998 Elsevier Science Ltd
All rights reserved. Printed in Great Britain
0277-5387/98 $19.00+0.00

Synthesis and characterisation of alkali metal bis(dimethylsilyl) amides: infinite all-planar laddering in the unsolvated sodium derivative

Jörg Eppinger,[a] Eberhardt Herdtweck[a] and Reiner Anwander*[b]

[a] Anorganisch-chemisches Institut, Technische Universität München, Lichtenbergstrasse 4, D-85747 Garching, Germany

[b] Institut für Technische Chemie I, Universität Stuttgart, Pfaffenwaldring 55, D-70569 Stuttgart, Germany

(Received 13 November, 1997; accepted 24 November 1997)

Abstract—The synthesis of the bis(dimethylsilyl)amide complexes $[MN(SiHMe_2)_2]$ (M = Li (**1**), Na (**2**), K (**3**)) was accomplished in high yield (>95%) by various standard procedures. Additionally, a novel trans-silylamination reaction has been applied to synthesize the sodium derivative **2**. The alkali metal amide complexes which are readily soluble in aliphatic hydrocarbons were characterised by means of IR and ^1H, ^{13}C and ^{29}Si NMR spectroscopy. A single crystal X-ray diffraction study of the sodium derivative **2** revealed the formation of an infinite, all-planar ladder structure. Compound **2** crystallizes from *n*-hexane at −35°C in the orthorhombic space group *Pnma* with $a = 5.4439(2)$ Å, $b = 15.7268(9)$ Å, $c = 10.9751(6)$ Å, $V = 939.63(8)$ Å^3 and $Z = 4$. Least squares refinement of the model based on 873 reflections converged to a final $\omega R_2 = 0.1124$. © 1998 Elsevier Science Ltd. All rights reserved

Keywords: alkali metal; bis(dimethylsilyl) amide; sodium; X-ray structure; laddering

INTRODUCTION

Alkali metal silylamide complexes are convenient amide transfer reagents [1]. This synthetic approach has been thoroughly studied in the case of the $[N(SiMe_3)_2]$ group to isolate low-coordinated main group and transition monometallic complexes [2]. Compared to the dialkyl congeners, in particular LDA (lithium diisopropylamide) [3], their utilization in deprotonation reactions is limited. However, the changed nucleophilicity/basicity makes them still promising reagents in proton abstraction reactions involving substrates carrying valuable functional groups [4] and for the isolation of reaction intermediates [5]. The solid state chemistry of both solvent-free and solvated alkali metal amides not only revealed intriguing structural features such as ring-laddering [6], but often is an important parameter in terms of evaluating complex reactivity [7]. The solid state structures of $CMN(SiMe_3)_2]$, the most utilized silylamide complexes, have been studied in detail and their structural patterns as depicted in Fig. 1 seem to reflect not only ionic size effects [8–11]. Both the sodium and potassium derivative form close intramolecular $M\cdots CH_3$ contacts often termed agostic interactions [12].

Very recently we introduced the sterically reduced bis(dimethylsilyl)amide ligand, $N(SiHMe_2)_2$ [13], as a kinetically less restricted and spectroscopically prolific moiety into organo-f-element chemistry [14]. A detailed synthetic study on $La[N(SiHMe_2)_2]_3(thf)_2$

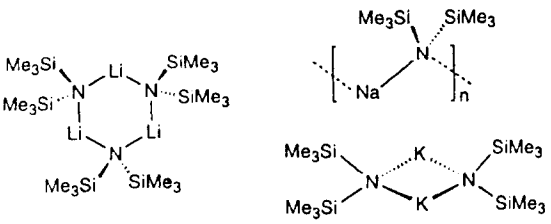

Fig. 1. Structural motifs of solvent-free alkali metal bis(trimethylsilyl)amides.

* Author to whom correspondence should be addressed.

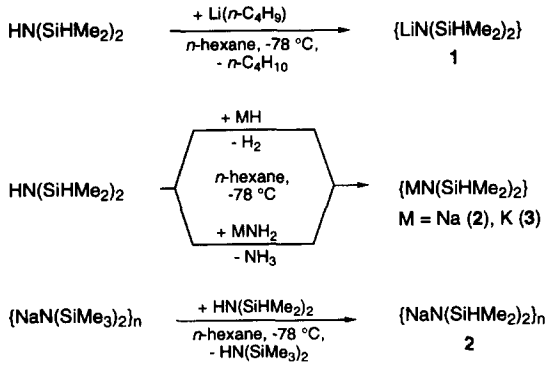

Scheme 1. Synthesis of compounds $[MN(SiHMe_2)_2]$.

revealed that product formation is markedly affected by the nature and solvation of the alkali metal of the amide precursor [15], a fact well-known in salt elimination and proton abstraction applications [16]. Herein, we present synthetic, spectroscopic, and structural details of these novel alkali metal silylamide compounds.

RESULTS AND DISCUSSION

Synthesis and spectroscopy

The synthesis of the alkali metal amide complexes $[MN(SiHMe_2)_2]$ (M = Li (**1**), Na (**2**), K (**3**)) was accomplished according to well established procedures [3] as comprised in Scheme 1. In addition, a novel transsilylamination reaction was applied to prepare the sodium derivative **2**. The pK_a discrepancy of the parent silylamines [(pK_a(THF): 25.8 ($HN(SiMe_3)_2$), 22.6 ($HN(SiHMe_2)_2$)] [17] and the low Lewis acidity of the alkali metal cation facilitate such a transamination reaction [18]. Compounds **1**, **2** and **3** were obtained in almost quantitative yield and characterized by IR and NMR spectroscopy and elemental analysis. Compound **2** slowly dissolves in *n*-hexane, whereas the lithium and potassium derivative are readily soluble in aliphatic hydrocarbons, a behaviour which was previously ascribed to a strong ion-pairing interaction between the metal cation and the amide anion [10]. The melting points decrease in the order **3** (139–141°C) > **1** (127–129°C) > **2** (116–120°C). Upon melting all three silylamides decompose into a white solid which does not melt until 320°C.

The spectroscopic details of the silylamide ligands of a homologous series are known to reflect the extent of the ionic character of the M—N bonding [19]. Both the Si—H and Si—CH_3 magnetic resonances are shifted upfield in the case of the more ionic M—N bond of the larger alkali metal (Table 1). The decreased Si—H coupling, observed for the more ionic complex, is in accord with a weaker Si—H bonding and can be explained by an increased $p_\pi(N)$–$d_\pi(Si)$ back donation. This trend is further emphasized by the $\nu_{as}(NSi_2)$ vibration frequency within the homologous series (**1** (1060), **2** (1048), **3** (1098 cm^{-1}); solid state). The Si—H stretch vibration is often used as a meaningful probe for metal···(Si—H) agostic interactions [14,20]. The lithium and potassium silylamide **1** and **3** show a Si—H stretch vibration in the non-interacting range both in the solid state and in solution (Table 1) [21]. However, compound **2** shows a considerable shift to lower energy (1960 cm^{-1}) and the presence of a still lower energy shoulder at approximately 1930 cm^{-1} in the solid state, while only a very strong SiH stretch vibration at 2004 cm^{-1} appears in benzene solution. This supports the presence of Na···(Si—H) agostic interactions in the solid state. The non-agostic behaviour of **2** in solution is also consistent with the normal ^1J(Si,H) coupling constant of 164 Hz. Very recently Li···(Si—H) agostic interactions were reported for $[(SiHMe_2)_2CC(SiHMe_2)_2][Li(OEt_2)]_2$ and shown to be stable even in solution (ν(SiH) = 1937 cm^{-1}; ^1J(Si,H) = 141 Hz) [22]. Na···(Si—H) interactions have been noted earlier for the cage compound $[Na_B(O_3C_5H_{11})_6(SiH_3)_2]$ [23].

Table 1. Spectroscopic data for alkali metal bis(dimethylsilyl)amide complexes

Compound	IR[a] ν(SiH)	^{1}H NMR[b] δ(SiH)	^{1}H NMR[b] $\delta(SiCH_3)$	^{29}Si NMR[b] $\delta_{Si}(^1J_{SiH})$	Ref.
$HN(SiHMe_2)_2$	2118	4.40		−11.1	15
$[LiN(SiHMe_2)_2]$ (**1**)	1990 s [1996 s][c]	4.65	0.23	−21.6 (168)	[d]
$[LiN(SiHMe_2)_2(THF)]$	2025 s	5.15	0.42	−23.5 (170)	15
$[NaN(SiHMe_2)_2]_n$ (**2**)	1961 s, 1926(sh) m [2004 s][c]	4.82	0.26	−23.5 (164)	[d]
$[KN(SiHMe_2)_2]$ (**3**)	1980 s [1979 s][c]	4.94	0.26	−29.5 (162)	[d]

[a] IR spectra recorded as nujol mulls (cm^{-1}).
[b] NMR spectra recorded in benzene-d_6 solution at 20°C (ppm).
[c] IR spectra [ ] recorded in benzene solution.
[d] This work.

Solid state structure of $[NaN(SiHMe_2)_2]_n$ **(2)**

Due to the limited solubility of **2** in aliphatic hydrocarbons single crystals could be successfully grown from a saturated *n*-hexane solution at −35°C. The X-ray structure analysis revealed the formation of an all-planar, infinite ladder structure. Figures 2 and 3 show structure diagrams of a ladder segment arrangement and the long range packing, respectively. Tables 2 and 3 list selected bond lengths and angles and crystallographic parameters. The unit cell consists of two independent ladder segments, displaying no intermolecular interaction (distance >4 Å).

The core features, comprising a distorted rope ladder pattern, are emphasized in Fig. 2. Each ladder segment is composed of antiparallel Na—N rungs of equal lengths (2.456(2) Å) and parallel Na—N edges which deviate markedly in lengths. This indicates alternating covalent (2.449(3) Å) and donor bonding (3.115(3) Å), according to a vertical Na—N ··· Na—N ··· edge. The Na—N bond distances compare well with those of other sodium silylamides [24], as exemplified by the 2.355(3) Å in polymeric $[NaN(SiMe_3)_2]_n$ [9] or the 2.509(4) Å in dinuclear [LiNa $\{N(SiMe_3)_2\}_2(THF)_3$] [24f]. The long Na—N edge is longer than previously reported Na—N donor bond lengths (e.g., 2.54 Å in $[Na_{10}(NMe_2)_{10}(tmeda)_4]$) [25]

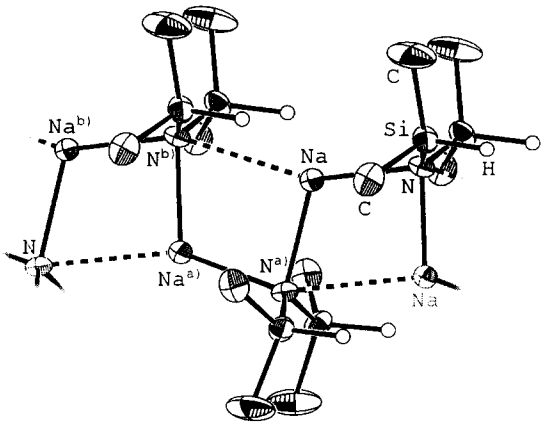

Fig. 2. Representative ORTEP style plot of polymeric $[NaN(SiHMe_2)_2]_n$ **(2)**. Thermal ellipsoids are drawn at the 50% probability level.

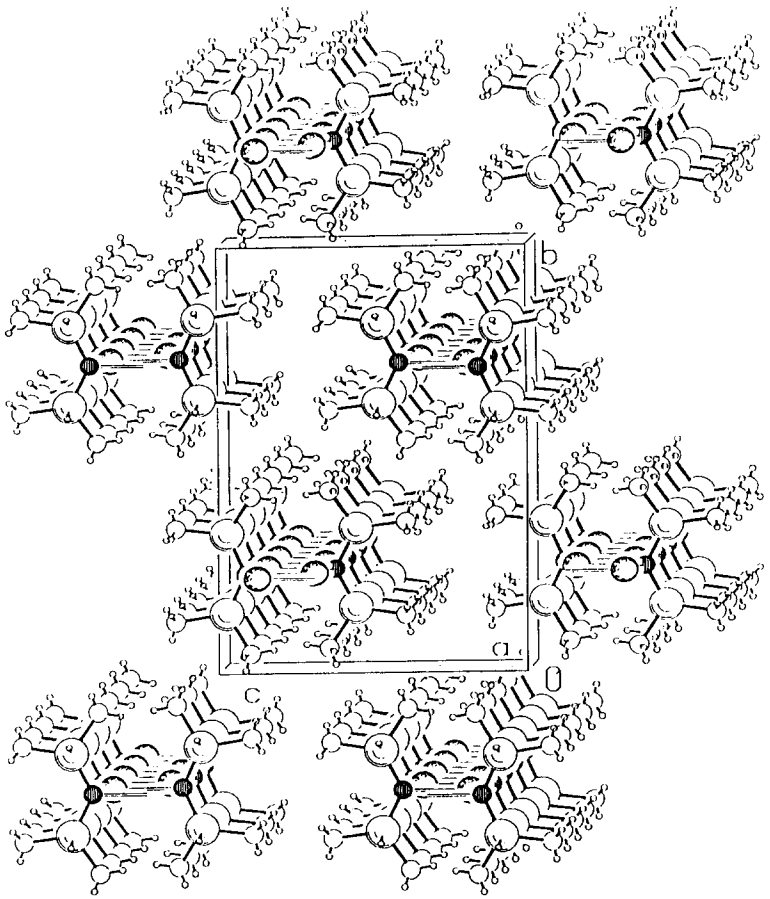

Fig. 3. Unit cell plot of polymeric $[NaN(SiHMe_2)_2]_n$ **(2)** along the crystallographic *a*-axis, showing the all-planar, all-stacked laddered structure.

Table 2. Selected bond lengths (Å), interatomic contacts (Å) and bond angles (°) for $[NaN(SiHMe_2)_2]_n$ (**2**)

Si—N(1)	1.694(1)
Si—C(1)	1.853(4)
Si—C(2)	1.856(3)
Si—C(3)	1.62(2)
Na—N	2.449(3)
Na—N^a	2.456(2)
Na···N^b	3.115(3)
Na···N^b—Na^a	71.5(1)
Na—N^b—Na^a	84.5(1)
Na^a···N^b—Na^b	156.0(1)
N—Na—N^a	111.4(1)
N—Na···N^b	156.0(1)
N^a—Na···N^b	92.6(1)
Na—N^b—Si^b	112.0(1)
Na—N^b—Si^c	112.0(1)
Na^a···N^b—Si^b	80.7(1)
Na^a···N^b—Si^c	80.7(1)
Na^b—N^b—Si^b	109.3(1)
Na^b—N^b—Si^c	109.3(1)
Si^b—N^b—Si^c	123.0(1)

Symmetry operations: $^a 0.5+x, 0.5-y, 1.5-z$; $^b 1+x, y, z$; $^c 0.5+x, y, 1.5-z$.

Table 3. Crystallographic data for $[NaN(SiHMe_2)_2]_n$ (**2**)

Formula	$C_4H_{14}NNaSi_2$
Fw	155.32
Space group	*Pnma*
a	5.4439(2) Å
b	15.7268(9) Å
c	10.9751(6) Å
V	939.63(8) Å^3
Z	4
T	163 K
λ	0.71073 Å
ρ_{calc}	1.098 g cm^{-3}
μ	3.4 cm^{-1}
$R_1{}^a$	0.0490
$\omega R_2{}^b$	0.1124

$^a R_1 = \Sigma(||F_o|-|F_c||)/\Sigma|F_o|$;
$^b \omega R_2 = [\Sigma\omega(F_o^2-F_c^2)^2/\Sigma\omega(F_o^2)^2]^{1/2}$ where $\omega \equiv$ SHELXL-93 weights.

and causes the significantly differing internal bridge angles NaN^bNa^a/N^a NaN^b and $NaN^bNa^a/NNaN^a$ of 84.5/92.6° and 71.5/111.4°, respectively (Fig. 2). The sodium and nitrogen core atoms are 3- and 5-coordinated, respectively, affording a T-shape coordination geometry at the sodium. Each two $SiHMe_2$ groups of the μ_3-amide moieties extend out of the all-planar arrangement in an all-transoid and all-stacked fashion (Fig. 3) which certainly minimizes the intramolecular steric hindrance. Simultaneously, this conformation allows for a perfect shielding of each side of the ladder core and brings the silicon hydrides pairwise within bonding distance of the donor-attached sodium cations. The $SiHMe_2$ groups are disordered with respect to the Si–N bond and could be resolved such that the positions near the donor-attached sodium cation are alternatively occupied by hydrogen atoms (82%) and methyl groups (18%) [26].

The observed $SiHMe_2$ orientation may be governed both by steric and electronic factors. On the one hand, location of the H atom at the disordered site results in a reasonably short Na···H distance of 2.51 Å, while methyl population affords improbably short Na···C distances (2.51(1) Å). This certainly argues in favour of steric restriction.

On the other hand, according to the solid state IR spectrum the formation of close $Na(\delta+)\cdots SiH(\delta-)$ contacts seems to be plausible, and therefore, might affect the orientation of the amide substituents, perhaps even direct the ladder arrangement. Close Si—H contacts with electron-deficient metal centers are meanwhile well-established and were shown to be very stable in the case of a diagostic interaction [14d]. Also low-coordinated alkali metal centers were often shown to extend their coordination sphere by, e.g., close $Na(\delta+)\cdots CH_3(\delta-)$ contacts [27]. Figure 4 emphasizes both the SiH positions and a possible diagostic interaction with the sodium atom, resulting in a formally 5-coordinated metal centre. However, the proposed Na···(Si—H) contacts should be considered as a loose diagostic interaction due to the spectroscopic results. A distinct widening of the Si—N—Si angle is not observed. Interestingly, the same overall structural features were found in $[Na(NC_4Me_4)]_n$ (**4**), a polymeric 2,3,4,5-tetramethyl-1-sodiopyrrole, which crystallizes in the monoclinic space group $P2_1/n$ [28]. A detail of the laddering in complex **4** is schematically redrawn in Fig. 4, representing that the electronically and sterically unsaturated sodium atoms are additionally coordinated by the π-system of the pyrrole rings.

The lateral connection of the planar trapezium-like ladder segments afford the all-planar band structure of **2**. In general, laddering is a well-known structural motif for alkali metal salts, bearing organic counter ligands such as alkyls, amides, alkoxides and phosphides [6,29,30]. Factors such as the size of the organic

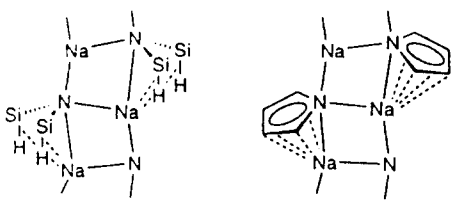

Fig. 4. Structural details of the laddering motifs of $[NaN(SiHMe_2)_2]_n$ (**2**) and $[Na(NC_4Me_4)]_n$ (**4**) [26]. The methyl groups at the silicon atoms are omitted for clarity.

counter ligand, the presence and type of coordinating coligands (chelating/non-chelating), and the presence of different alkali metal ions direct the formation and extent of laddering. Two previous contributions, featuring complex **4** [28] and an intermetallic ladder in $[LiNa\{N(CH_2Ph)_2\}_2(OEt_2)_2]$ (Na—N: rung, 2.398(3) Å; edge 2.539(3) Å) [31], revealed that sodium amides also tend to associate laterally. In contrast, the more bulky $SiMe_3$ substituents in $[NaN(SiMe_3)_2]_n$ counteract additional close Na—N donor bonding (Na···N, 5.297(3) Å) and the laddering motif is replaced at the expense of an infinite chain structure (Na—Na—Na, 141.98°; N—Na—N, 150.22°; Na—N—Na, 101.99°) [9]. However, the formally 2-coordinated sodium atoms in $[NaN(SiMe_3)_2]_n$ probably also form additional close intramolecular contacts to methyl groups as crystallographically evidenced for the isostructural $[Na\{CH(SiMe_3)_2\}]_n$ (Na···H, 2.40–2.65 Å) [32]. Comparison can also be drawn to the solid state structure of the most important amide derivative, LDA. The infinite helical arrangement of LDA shows nearly linear N—Li—N units (average 176°), exhibiting 2-coordinate lithium atoms [3]. Although the changed basicity of the $N(CHMe_2)_2$ and $N(SiHMe_2)_2$ ligands may affect the aggregation/bridging of the "$M(NR_2)$" monomers, these ligands are similarly sized and display similar coordination behavior, as evidenced by, e.g., M···(E—H) agostic interactions [33]. However, the smaller lithium metal sterically disfavours any N—Li—N bending and hence prevents laddering.

CONCLUSION

The bis(dimethylsilyl)amide ligand provides alkali metal complexes $[MN(SiHMe_2)_2]$ (M = Li, Na, K) which are readily soluble in aliphatic hydrocarbons. X-ray structure analysis revealed the formation of a rare infinite all-planar ladder structure of the sodium derivative. The existing all-stacked orientation of the $SiHMe_2$ in the solid state can be rationalized on the basis of steric and electronic considerations. The presence of an agostic Na···(Si—H) interaction is supported by the solid state IR spectrum of $[NaN(SiHMe_2)_2]_n$. We are currently exploiting the coordination behaviour of the $N(SiHMe_2)_2$ ligand towards other sterically and electronically unsaturated metal centres.

EXPERIMENTAL SECTION

The alkali metal amide complexes described below were handled under nitrogen using standard Schlenk, vacuum line and glovebox techniques. NaH and KH (Aldrich) were subsequently washed with toluene and *n*-hexane and dried *in vacuo*. $NaNH_2$, KNH_2 and $[NaN(SiMe_3)_2]$ were prepared according to the literature [34]. Physical measurements have been described previously [35]. Elemental analyses were performed by the microanalytical laboratory in Munich.

Bis(dimethylsilyl)amido lithium, **1**

1,1,3,3-Tetramethyldisilazane (20.00 g, 150.0 mmol) was placed in a 500 ml flask, dissolved in *n*-hexane (150 ml) and cooled to −78°C. Then a 1.6 molar solution of *n*-butyllithium in *n*-hexane (90.0 ml, 144 mmol) was added over a period of 30 min under vigorous stirring. After complete addition, the white suspension was allowed to warm up to ambient temperature, stirred for another 2 h and evaporated to dryness, leaving **1** (19.78 g, 142.0 mmol, 99%) as a voluminous white powder. IR (Nujol, cm^{-1}): 1990(br) vs, 1254 s, 1240 m, 1090 s, 1060 s, 948 m, 897 s, 820 m, 780 m, 749 m, 739 m, 696 w, 678 w, 644 w, 629 m, 600 w, 508 m; ^1H NMR (400 MHz, C_6D_6, 25°C): δ 4.65 (sp, $^1J(Si,H) = 168$ Hz, $^3J(H,H) = 2.8$ Hz, 2 H, SiH), 0.23 (d, $^3J(H,H) = 3.0$ Hz, 12 H, $SiCH_3$); $^{13}C\{^1H\}$ NMR (100.5 MHz, C_6D_6, 25°C): δ 3.60 (s, $SiCH_3$); $^{29}Si\{^1H\}$ NMR (79.5 MHz, C_6D_6): δ 28.64. $^{15}N\{^1H\}$ NMR (14.9 MHz, C_6D_6): δ—136. Anal. Calc. for $C_4H_{14}LiNSi_2$: C, 34.5; H, 10.1; N, 10.1. Found: C, 35.5; H, 9.7; N, 9.5.

Bis(dimethylsilyl)amido sodium, **2**

Method A. NaH (0.348 g, 14.50 mmol) was placed in a 50 ml flask, dispersed in *n*-hexane (10 ml) and cooled to −78°C. Then a solution of 1,1,3,3-tetramethyldisilazane (2.000 g, 15.00 mmol) in 15 ml of *n*-hexane was added over a period of 30 min under vigorous stirring, while gas evolution indicates the reaction. After complete addition, the white suspension is allowed to warm up to ambient temperature, stirred for another 2 h and evaporated to dryness, leaving **2** (2.207 g, 14.21 mmol, 98%) as a voluminous white powder.

Method B. According to method A with $NaNH_2$ (0.566 g, 14.50 mmol) instead of NaH. **2** is obtained as a white powder (2.196 g, 14.14 mmol, 98%).

Method C. According to method A with $[NaN(SiMe_3)_2]$ (2.659 g, 14.50 mmol) instead of NaH. **2** is obtained as a white powder (2.210 g, 14.22 mmol, 98%) and can be crystallized from *n*-hexane at −35°C as long needles. IR (Nujol, cm^{-1}) 2924 vs, 2853 vs, 2724 m, 1961 brm, 1926 (br)m, (2 × (Si—H)), 1460 vs, 1377 s, 1304 w, 1251 m, 1152 m, 1048 brs, 969 m, 889 s, 833 m, 782 m, 762 m, 722 s, 668 m, 629 w, 594 w; ^1H-NMR (400 MHz, C_6D_6, 25°C) 4.82 (br, s, 2 H, SiH), 0.26 (br, d, $^3J(H,H) = 22.2$ Hz, 12 H, $SiCH_3$); $^{13}C\{^1H\}$ NMR (100.5 MHz, C_6D_6, 25°C) 5.63 (s, $SiCH_3$); Anal. Calc. for $C_4H_{14}NNaSi_2$: C, 30.9; H, 9.1; N, 9.0. Found: C, 30.85; H, 8.8; N, 10.8.

Bis(dimethylsilyl)amido potassium, **3**

Method A. KH (0.582 g, 14.50 mmol) was placed in a 50 ml flask, dispersed in *n*-hexane (10 ml) and

cooled to −78°C. Then a solution of 1,1,3,3-tetramethyldisilazane (2.000 g, 15.00 mmol) in 15 ml of *n*-hexane was added over a period of 30 min under vigorous stirring, while gas evolution indicates the reaction. After complete addition, the white suspension was allowed to warm up to ambient temperature, stirred for another 2 h and evaporated to dryness, leaving **3** (2.477 g, 14.2 mmol, 98%) as a voluminous white powder.

Method B. According to method A with KNH_2 (0.799 g, 14.50 mmol) instead of KH. **3** is obtained as a white powder (2.458 g, 14.10 mmol, 98%). IR (Nujol, cm^{-1}): 1980 vs, 1308 w, 1254 s, 1149 sh, 1098(br) vs, 956 m, 930 s, 886 vs, 828 m, 813 m, 772 m, 752 m, 669 m, 638 w, 618 m, 580 w; ^1H NMR (400 MHz, C_6D_6, 25°C): δ 4.94 (sp, $^1J(Si,H) = 162$ Hz, $^3J(H,H) = 2.8$ Hz, 2 H, SiH), 0.26 (br, $^3J(H,H) = 2.6$ Hz, 12 H, $SiCH_3$); $^{13}C\{^1H\}$ NMR (100.5 MHz, C_6D_6, 25°C): δ 5.5 (s, $SiCH_3$); Anal. Calc. for $C_4H_{14}KNSi_2$: C, 28.0; H, 8.2; N, 8.2. Found: C, 28.3; H, 7.8; N, 8.25.

X-ray data collection, structure determination, and refinement for $[NaN(SiHMe_2)_2]_n$, **2**

Suitable single crystals of complex **2** were obtained from a saturated *n*-hexane solution at −35°C. The structure was solved by a combination of direct methods, difference-Fourier syntheses and least-squares refinements. Neutral atom scattering factors for all atoms and anomalous dispersion corrections for the non-hydrogen atoms were taken from the *International Tables for X-Ray Crystallograpy*. All calculations were performed on a DEC 3000 AXP workstation with the STRUX-V system, including the programs PLATON-92, PLUTON-92, SIR-92 and SHELXL-93 [36].

A brief summary of the crystallographic data are reported in Table 3. Preliminary examination and data collection were carried out on an imaging plate diffraction system (IPDS; Stoe & Cie) equipped with a rotating anode (ENRAF NONIUS FR591; 50 kV; 60 mA) and graphite monochromated MoK_α radiation. The data collection was performed at 163 K within the θ-range of $4.18° < \theta < 25.58°$ with an exposure time of 7.5 min per image (oscillation scan modus from $\phi = 0.0°$ to 264° with $\Delta\phi = 1°$). A total number of 9555 reflections were collected. 873 systematic absent reflections were rejected from the original data set. After merging a sum of 873 independent reflections remained and were used for all calculations. Data were corrected for Lorentz and polarization effects. A correction for intensity decay effects (icing) with the program DECAY [36a] was applied. The unit cell parameters were obtained by least-squares refinements of 3804 reflections with the program CELL [36a]. All "heavy atoms" of the asymmetric unit were anisotropically refined. The methyl hydrogen atoms at C(1) and C(2) were refined free with one but fixed thermal parameter ($B_H = 1.2 \cdot B_C$). Hydrogen atoms at the silicon atom and the disordered (18%) carbon atoms were calculated in ideal positions (riding model; $d_{Si,H} = 1.50$ Å; $d_{C-H} = 0.98$ Å; $B_H = 1.2 \cdot B_{Si,C}$). Full-matrix least-squares refinements were carried out by minimizing $\Sigma\omega(F_o^2 - F_c^2)^2$ with SHELXL-93 weighting scheme and stopped at shift/err < 0.001. Further details of the crystal structure investigations are available on request from the Fachinformationszentrum Karlsruhe, Gesellschaft für wissenschaftlich-technische Information mbH, D-76344 Eggenstein-Leopoldshafen 2, on quoting the depository number CSD-380 the names of the authors and the journal citation.

Acknowledgement—We thank the Deutsche Forschungsgemeinschaft for the award of a DFG fellowship to R.A.

REFERENCES

1. Lappert, M. F., Power, P. P., Sanger, A. R. and Srivastava, R. C., *Metal And Metalloid Amides*, Ellis Horwood, Chichester, 1980.
2. (a) Harris, D. H. and Lappert, M. F. in *Organometallic Chemistry Reviews: Organosilicon Reviews*, Elsevier Scientific Publishing Company, Amsterdam, 1976, p. 13. (b) Bradley, D. C. and Chisholm, M. H., *Acc. Chem. Res.*, 1976, **9,** 273.
3. Barnett, N. D. R., Mulvey, R. E., Clegg, W. and O'Neil, P. A., *J. Am. Chem. Soc.*, 1991, **113,** 8187.
4. Armstrong, D. R., Davidson, M. G., Davies, R. P., Mitchell, H. J., Oakley, R. M., Raithby, P. R., Snaith, R. and Warren, S., *Angew. Chem. Int. Ed. Engl.*, 1996, **35,** 1942.
5. (a) Ihara, M., Suzuki, S., Tokunaga, Y., Takeshita, H. and Fukomoto, K., *Chem. Commun.*, 1996, 1801. (b) Mukerji, I., Wayda, A. L., Dabbagh, G. and Bertz, S. H., *Angew. Chem. Int. Ed. Engl.*, 1986, **25,** 760.
6. (a) Mulvey, R. E., *Chem. Soc. Rev.*, 1991, **20,** 167. (b) Gregory, K., Schleyer, P. von R. and Snaith, R. *Adv. Inorg. Chem.*, 1991, **37,** 47.
7. Kottke, T. and Stalke, D., *Organometallics*, 1996, **15,** 4552.
8. (a) Mootz, D., Zinnius, A. and Böttcher, B., *Angew. Chem.*, 1969, **81,** 398. (b) Rogers, R. D., Atwood, J. L. and Grüning, R., *J. Organomet. Chem.*, 1978, **157,** 229.
9. Grüning, R. and Atwood, J. L., *J. Organomet. Chem.*, 1977, **137,** 101.
10. (a) Williard, P. G., *Acta Cryst.*, 1988, **C44,** 270. (b) Tesh, K. F., Hanusa, T. P., Huffman, J. C., *Inorg. Chem.*, 1990, **29,** 1584.
11. Tesh, K. F., Jones, B. D., Hanusa, T. P. and Huffman, J. C., *J. Am. Chem. Soc.*, 1992, **114,** 6590.
12. Brookhart, M. and Green, M. L. H., *J. Organomet. Chem.*, 1983, **250,** 395.
13. Mainz, V. V. and Andersen, R. A., *Inorg. Chem.*, 1980, **19,** 2165.
14. (a) Herrmann, W. A., Anwander, R., Munck, F. C., Scherer, W., Dufaud, V., Huber, N. W. and Artus, G. R. J., *Z. Naturforsch. Teil B*, 1994, **49,**

1789. (b) Runte, O., Priermeier, T. and Anwander, R., *Chem. Commun.*, 1996, 1385. (c) Herrmann, W. A., Munck, F. C., Artus, G. R. J., Runte, O. and Anwander, R., *Organometallics*, 1997, **16,** 682. (d) Herrmann, W. A., Eppinger, J., Spiegler, M., Runte, O. and Anwander, R., *Organometallics*, 1997, **16,** 1813.

15. Anwander, R., Runte, O., Eppinger, J., Gerstberger, G., Herdtweck, E. and Spiegler, M., in press.
16. Andrews, P. C., Barnett, N. D. R., Mulvey, R. E., Clegg, W., O'Neil, P. A., Barr, D., Cowton, L., Dawson, A. J. and Wakefield, B. J., *J. Organomet. Chem.*, 1996, **518,** 85.
17. (a) Fraser R. R., Mansour, T. S. and Savard, S., *J. Org. Chem.*, 1985, **50,** 3232. (b) Herrmann, W. A., Eppinger, J., Spiegler, M. and Anwander, R. unpublished results.
18. More Lewis acidic metal cations such as B^{3+} or Al^{3+} disrupt the N—Si bonds under the prevailing reaction conditions: (a) Schmidbaur, H. and Schmidt, M., *Angew. Chem. Int. Ed. Engl.*, 1962, **1,** 327. (b) Riedel, R., Schaible, S., Klingebiel, U., Noltemeyer, M. and Werner, E., *Z. Anorg. Allg. Chem.*, 1991, **603,** 119. (c) Gerstberger, G., Herdtweck, E. and Anwander, R., unpublished results.
19. Eller, P. G., Bradley, D. C., Hursthouse, M. B. and Meek, D. W., *Coord. Chem. Rev.*, 1977, **24,** 1.
20. (a) Herrmann, W. A., Huber, N. W. and Behm, J., *Chem. Ber.*, 1992, **125,** 1405. (b) Procopio, L. J., Carroll, P. J. and Berry, D. H., *J. Am. Chem. Soc.*, 1994, **116,** 177.
21. Lukevics, E., Pudowa, O. and Sturkovich, R., *Molecular Structure of Organosilicon Compounds.* Silicon hydrides generally display $^1J_{Si,H}$ coupling constants in the range 160–200 Hz. Ellis-Horwood, Chichester, England, 1989.
22. Sekiguchi, A., Ichinohe, M., Takahashi, M., Kabuto, C. and Sakurai, H., *Angew. Chem. Int. Ed. Engl.*, 1997, **36** 109, 1577.
23. Pritzkow, H., Lobreyer, T., Sundermeyer, W., von Eikemma Hommes, N. J. R. and von R. Schleyer, P., *Angew. Chem. Int. Ed. Engl.*, 1994, **33,** 216.
24. (a) Brauer, D. J., Bürger, H., Geschwandtner, W., Liewald, G. R. and Kruger, C., *J. Organomet. Chem.*, 1983, **248,** 1. (b) Tilley, T. D., Andersen, R. A. and Zalkin, A., *Inorg. Chem.*, 1984, **23,** 2271. (c) Veith, M., Böhnlein, J. and Huch, V., *Chem. Ber.*, 1989, **122,** 841. (d) Dippel, K., Klingebiel, U., Kottke, T., Pauer, F., Sheldrick, G. M. and Stalke, D., *Chem. Ber.*, 1990, **123,** 237. (e) Pieper, U., Stalke, D., Vollbrecht, S. and Klingebiel, U., *Chem. Ber.*, 1990, **123,** 1039. (f) Williard, P. G. and Nichols, M. A., *J. Am. Chem. Soc.*, 1991, **113,** 9671. (g) Niemeyer, M. and Power, P. P., *Organometallics*, 1996, **15,** 4107.
25. Lorenzen, N. P., Kopf, J., Olbrich, F., Schümann, U. and Weiss, E., *Angew. Chem. Int. Ed. Engl.*, 1990, **29,** 1441.
26. A final decision whether the disordering is based on a rotation around the Si—N bond in the solid state or a statistcal (82/18) distribution of the hydrogen (82%) and methyl (18%) sites can be reached by a variable temperature X-ray diffraction measurement. Unfortunately, we were not able to perform such a study.
27. (a) Schade, C. and Schleyer, P. von R., *Adv. Organomet. Chem.*, 1987, **27,** 169. (b) Weiss, E., *Angew. Chem. Int. Ed. Engl.*, 1993, **32,** 1501.
28. Kuhn, N., Henkel, G. and Kreutzberg, J., *Angew. Chem. Int. Ed. Engl.*, 1990, **29,** 1143.
29. For examples featuring a finite ladder structure, see: (a) Williard, P. G. and Carpenter, G. B., *J. Am. Chem. Soc.*, 1986, **108,** 462. (b) Williard, P. G. and Hintze, M. J., *J. Am. Chem. Soc.*, 1987, **109,** 5539. (c) Armstrong, D. R., Barr, D., Clegg, W., Hodgson, S. M., Mulvey, R. E., Reed, D., Snaith, R. and Wright, D. S., *J. Am. Chem. Soc.*, 1989, **111,** 4719. (d) Barnett, N. D. R., Clegg, W., Horsburgh, L., Lindsay, D. M., Liu, Q.-Y., Mackenzie, F. M., Mulvey, R. E. and Williard, P. G., *Chem. Commun.*, 1996, 2321. (e) Hey-Hawkins, E. and Sattler, E., *J. Chem. Soc., Chem. Commun.*, 1992, 775.
30. For examples featuring an infinite ladder structure, see: (a) Andrews, P. C., Clegg, W., Mulvey, R. E., O'Neil, P. A. and Wilson, H. M. M., *J. Chem. Soc., Chem. Commun.*, 1993, 1142. (b) Rabe, G. W., Yap, G. P. A. and Rheingold, A. L., *Inorg. Chem.*, 1997, **36,** 1990.
31. Baker, D. R., Mulvey, R. E., Clegg, W. and O'Neil, P. A., *J. Am. Chem. Soc.*, 1993, **115,** 6472.
32. Hitchcock, P. B., Lappert, M. F., Leung, W.-P., Diansheng, L. and Shun, T., *J. Chem. Soc., Chem. Commun.*, 1993, 1386.
33. (a) Aspinall, H., Moore, S. R. and Smith, A. K., *J. Chem. Soc., Chem. Commun.*, 1993, 993. (b) Evans, W. J., Anwander, R., Ziller, J. W. and Khan, S. I., *Inorg. Chem.*, 1995, **34,** 5927.
34. Krüger, C. R. and Niederprüm, H., *Inorg. Synth.*, 1966, **8,** 15.
35. Anwander, R., Munck, F. C., Priermeier, T., Scherer, W., Runte, O. and Herrmann, W. A., *Inorg. Chem.*, 1997, **36,** 3545.
36. (a) IPDS Operating System Version 2.8. Stoe & Cie. GmbH, Darmstadt, Deutschland, (1997). (b) Altomare, A., Cascarano, G., Giacovazzo, C., Guagliardi, A., Burla, M. C., Polidori, G. and Camalli M. "SIR-92", University Bari, Italy. (1992). (c) *International Tables for Crystallography, Vol.* C, Tables 6.1.1.4 (pp. 500–502), 4.2.6.8 (pp. 219–222), and 4.2.4.2 (pp. 193–199), Ed. A. J. C. Wilson. Kluwer Academic Publishers, Dordrecht, The Netherlands, 1992. (d) Sheldrick, G. M. "SHELXL-93", in *Crystallographic Computing* 3, ed. G. M. Sheldrick, C. Krüger and R. Goddard, Oxford University Press, U.K., pp. 175–189, 1993. (e) Spek, A. L. "PLATON-92" – "PLUTON-92", An Integrated Tool for the Analysis of the Results of a Single Crystal Structure Determination, *Acta Crystallogr. Sect. A*, 1990, **46,** C34. (f) Artus, G., Scherer, W., Priermeier, T. and Herdtweck, E. "STRUX-*V*", A Program System to Handle X-ray Data, TU München, Germany, 1997.

Pergamon

PII: S0277-5387(98)00507-X

Polyhedron Vol. 17, No. 7, pp. 1203–1210, 1998
© 1998 Elsevier Science Ltd
All rights reserved. Printed in Great Britain
0277-5387/98 $19.00+0.00

Organometallic chemical vapour deposition of cobalt/indium thin films using the single-molecule precursors $[(CO)_4Co]_aInR_{3-a}$ ($R = CH_2CH_2CH_2NMe_2$; $a = 1$–3)

Roland A. Fischer*, Jurij Weiß and Wolfram Rogge

Lehrstuhl für Anorganische Chemie II, Ruhr-Universität Bochum, D-44780 Bochum

(Received 30 October 1997; accepted 27 November 1997)

Abstract—Pure cobalt indium alloy thin films of the nominal compositions $Co_{0.50}In_{0.50}$, $Co_{0.66}In_{0.33}$ and $Co_{0.75}In_{0.25}$ were grown by OMCVD using volatile organometallic precursors of the general formula $[(CO)_4Co]_a$-InR_{3-a} [$R = CH_2CH_2CH_2N(CH_3)_2$; **1**: $a = 1$; **2**: $a = 2$; **3**: $a = 3$]. These organometallic compounds contain direct Co—In bonds and allow molecular control of the metal ratio of the grown films. The distribution of the metals were uniform throughout the films. The films were examined by AES depth profiling, SEM-EDX and X-ray diffraction. The phase composition of the films follows the phase diagram of the Co/In system, e.g. reflections of the crystalline phases Co, $CoIn_2$ and $CoIn_3$ were detected. Due to the multi-phase nature of the films, the coatings were unstable with respect to interfacial reactions with InP, e.g. the formation of CoP was observed by X-ray diffraction. © 1998 Elsevier Science Ltd. All rights reserved

Keywords: OMCVD; cobalt; indium; thin alloy films.

The deposition of mixed metal thin alloy films is usually achieved by physical techniques like sputtering or evaporation. Chemical deposition methods, in particular organometallic chemical vapour deposition, offer among other benefits the possibility to use molecular precursors of low thermodynamic stability to deposit the material at comparably mild conditions. At low substrate temperatures (200–400°C) OMCVD processes are typically controlled by the kinetics of the surface reactions, relevant for the decomposition of the molecular precursors to yield the thin solid coating. Some examples exist showing, that specifically tailored so-called single molecule precursors may lead to metastable phases [1] or even novel materials, which cannot be made by traditional methods [2]. In extension of our ongoing studies of OMCVD of transition metal aluminides [3] and gallides [4,5] we selected the Co/In system for the studies presented here, because the binary Co/In system exhibits a large immiscibility gap.

Cobalt and indium peritectally form two crystallographically characterized intermetallic phases: $CoIn_2$ at 550°C (monoclinic; $a = 5.393$ Å, $b = 17.845$ Å, $c = 9.218$ Å, $\beta = 88.73°$), and $CoIn_3$ at 490°C (tetragonal; $a = 6.832$ Å, $c = 7.098$ Å) [6]. A phase Co_1In_1 described by A. N. Khalpova does not exist [7]. The phase diagram exhibits an immiscibility gap (from 23 to 75 At.-% indium) at the monotectical temperature of 1286°C [8,9]. Small single crystals of $CoIn_2$ and $CoIn_3$ were grown at the surface of solid cobalt grains disperged into molten indium at 400°C [10]. These cobalt indides can also be synthesized by rapid arc melting. We were interested to investigate the phase composition of Co/In films grown from organometallic single molecule precursors at even lower temperatures of 200–250°C. The precursor molecules employed in this study, $(CO)_4Co$-$In[(CH_2)_3NMe_2]_2$ **1** [11], $[(CO)_4Co]_2In[(CH_2)_3NMe_2]_2$ **2** [12] and $[(CO)_4Co]_3In$ **3** [13] contain a covalent direct Co—In bond (Scheme 1). By using this molecular approach the constituents of the alloy are already mixed together in an atomic scale. The precursors were synthesized by methods described elsewhere [11–13].

* Author to whom correspondence should be addressed.

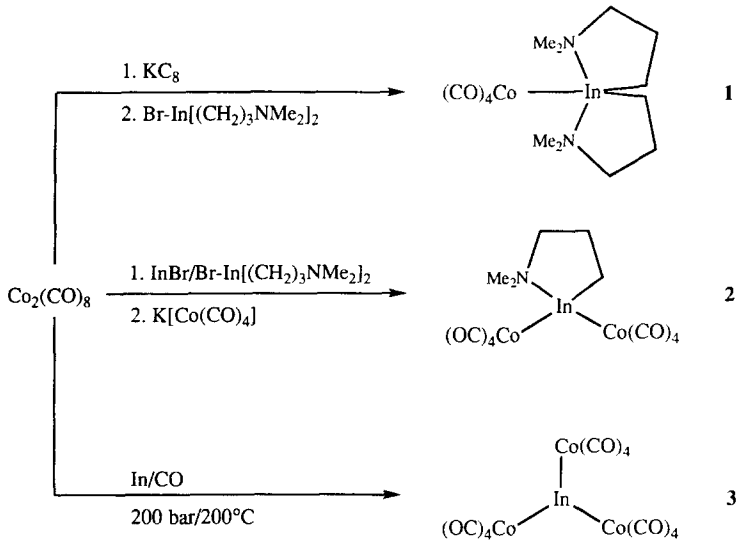

Scheme 1. Chemical synthesis of the precursors **1–3**.

RESULTS AND DISCUSSION

Precise molecular control of the thin film composition

The deposition experiments were carried out using a common horizontal isothermal hot wall tube reactor filled with various substrates, typically with microscope slides made of borosilicate glass. The respective precursor (**1–3**) was sublimed through the heated tube *in vacuo* and the deposited coatings on the substrates were characterized analytically ex situ after the deposition *ex-situ*. Very pure (C, N, O < 1 at.-% by AES) mixed metal thin films representing the *exact* metal ratio Co:In of the organometallic precursor compound, e.g. 1:1, 2:1 and 3:1 (by AAS), were obtained independently from the settings of the OMCVD apparatus (see Tables 1 and 2, e.g. temperature of the oven and the precursor reservoir; pressure). The precursor compound quantitatively decomposes to yield the metallic coatings. Such an exact reproduction of the metal stoichiometry of the precursor in the films is not necessarily observed, when so-called mixed-metal single molecule precursors are used for OMCVD experiments. In the related cases of the deposition of β-CoGa films using $(CO)_4Co$-$Ga(C_2H_5)_2[N(CH_3)_3]$ [4] or ε-NiIn films using [η^5-C_5H_5](CO)Ni-In[$(CH_2)_3NMe_2$]$_2$ [14] thermally comparably stable organometallic fragments of low molecular weight, e.g. $Ga(C_2H_5)_3$ or (η^5-C_5H_5)In, are produced at the surface via the decomposition of the precursors and desorb before further fragmentation. This mechanism explains the formation of transition metal rich films M_1E_{1-x} (M = Co, Ni; E = Ga, In). In the case of the CoIn-precursors **1–3** however, a related mechanism which allows the "escape" of the indium as stable alkylindium compound, e.g. In[$(CH_2)_3NMe_2$]$_3$ [15], does not exist. The In—C_{alkyl} bond energy is rather low (ca 47 kcal mol^{-1}) and the splitting of the alkyl group is kinetically favoured by facile β-hydrogen elimination (Scheme 2). For example, when BrIn[$(CH_2)_3NMe_2$]$_2$ is passed through a hot quartz tube at 250°C *in vacuo*, InBr collects at the colder parts outside the tube quantitatively. Also, the azide derivative (N_3)In[$(CH_2)_3NMe_2$]$_2$ serves as low temperature single-molecule precursor for stoichiometric, polycrystalline InN [16]. These examples show, that the organometallic fragments {In[$(CH_2)_3NMe_2$]$_2$} as well as {In[$(CH_2)_3NMe_2$]} are ideally suited to release the In atom at low substrate temperatures, even below 250°C. The cobalt fragment, $\{(CO)_4Co\}$, is known to be thermally quite labile and splits off the CO-groups easily, releasing the Co atom. Under the quoted experimental conditions, there exists no mechanism to convert the transition metal constituent into a organometallic compound which is stable against further fragmentation. This explains why the metal ratios of the molecular precursors **1–3** are perfectly retained in the grown mixed-metal thin films.

Chemical purity

Thin films grown with precursor **1** were studied with respect to chemical purity in some detail. Table 1 contains the results of the chemical and spectroscopic thin film analysis. The level of impurities (C, H, N, O) is below 1 atom-% by elemental analysis of the collected macroscopic quantities (50–100 mg) of the alloy, which peeled off from the wall of the reactor upon rapid cooling. AES and depth profiling [Fig. 1(a), (b)] revealed that the signals for C, N and O were below the detection limits throughout the bulk of the

Table 1. Analytical data for $Co_{0.50}In_{0.50}$ films grown using precursor **1**, $(CO)_4CoIn[(CH_2), NMe_2]_2$ *in vacuo* [$p = 0.010(5)$ Torr]. Entries marked with * refer to quantitive AES analysis. The notation ** refers to quantitive SEM-EDX analysis. Entries marked with refer to combustion analysis

T [°C]	250	250	250	280	300	350
$(CO)_4CoInR_2$	CoIn#1	CoIn#2	CoIn#3	CoIn#4	CoIn#5	CoIn#6
Co [μg] (by AAS)	1623(5)	1254(5)	1254(5)	1323(5)	1008(5)	555(5)
In [μg] (by AAS)	3125(5)	2430(5)	2430(5)	2838(5)	1852(5)	1058(5)
Co/In (by AAS)	1.0	1.0	1.0	1.0	1.0	1.0
Co [%] (±2)	46*	50**	47*	47*	49*	51
In [%] (±2)	45*	44**	50*	50*	51*	49
C [%] (±1)	1	≪1**	≪1*	≪1*	≪1*	—
H [%] (±1)	4	—	—	—	—	—
C/H	0.25	—	—	—	—	—
O [%] (±1)	4	5**	3*	3*	≪1*	—
N [%] (±1)	—	≪1**	≪1*	—	—	—

Table 2. Analytical data for $Co_{0.66}In_{0.33}$ and $Co_{0.75}In_{0.25}$ films grown using precursor **2**, $[Co(CO)_4]_2InR$ ($R = (CH_2)_3NMe_2$) and **3**, $[Co(CO)_4]_3In$ *in vacuo*

T [°C]	250
$[Co(CO)_4]_2InR$	$Co_{0.66}In_{0.33}$
Co [μg] (by AAS)	268(1)
In [μg] (by AAS)	263(1)
Co/In (by AAS)	1.99
Co [%] (by EDX)	63(2)
In [%] (by EDX)	37(2)
Co/In (by EDX)	1.7
T [°C]	280
$[Co(CO)_4]_3In$	$Co_{0.75}In_{0.25}$
Co [%] (by EDX)	74(2)
In [%] (by EDX)	25(2)
Co/In (by EDX)	3.0

deposited coatings. The same was observed by EDX and WDX spectroscopy. A SIMS analysis of film #2 showed only the background signal for C and N throughout the bulk of the film [Fig. 1(c)]. A primary beam of oxygen ions was used for the SIMS experiment. Therefore Fig. 1(c) does not tell the contents of O-impurities in the film. The concentration of the impurities arising from the alkyl ligands (C and N) are thus certainly far below 1 atom-%. The occurrence of oxygen impurities in the AES spectra may be due to impure precursor samples as well as caused by the leaking rate of the OMCVD apparatus.

The use of carbonyl group (CO) containing precursors for OMCVD applications is still a matter of controversial discussion. In principle, CO molecules can dissociatively chemisorb at metal surfaces, which ultimatively will lead to a more or less severe incorporation of carbidic carbon and oxygen atoms into the growing film. This autocatalytic mechanism is very important for the growth of "early" transition metals, e.g. Ti, Cr or Mo, from carbonyl compounds [17]. In the case of "late" transition metals (Co, Ni), this mechanism is much less a problem [18]. Nothing is known to date about the chemisorption of CO on a mixed phase polycrystalline CoIn surface. But our results may at least indicate that the residual carbon impurities are likely to be graphitic or hydrocarbons (C : H ~ 1, by combustion analysis, see Experimental) but are not essentially carbidic. Firstly, high carbon contents never occur combined with high oxygen contents, but are accompanied with rather high hydrogen levels (measured by combustion analysis; see C/H ratios of Table 1). This situation is very similar to the case of the growth of β-CoGa films or mixed phase CoAs films using tetracarbonylcobaltato substituted alkylgallanes [4] or amidoarsanes, e.g. $(CO)_4CoAs[\eta^2$-$(^tBuNCH_2CH_2N^tBu)]$, respectively [19]. In summary the obtained Co/In films proved to be rather pure when compared to other metal films deposited from organometallic precursors under similar conditions [20].

Thin film morphology

Figure 2 shows SEM images of some representative but thick Co/In films of about 2 μm. A uniform coverage of the surface with dendritic grains of about 1 μm length and ca. 0.2–0.3 μm thickness can be seen. These grains proved to be of uniform composition using SEM-EDX (resolution: 300 × 300 nm) and AES (resolution: 50 × 50 nm). The growth of the films follows the model of Movchan and Demchishin [21] which

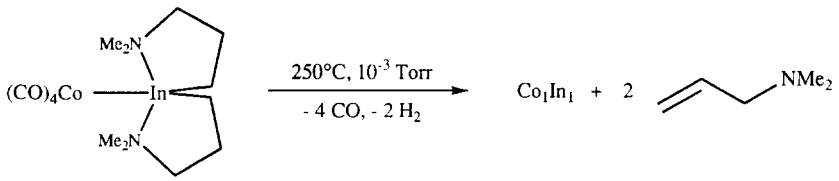

1

Scheme 2. Decomposition of precursor **1** during film growth.

explains the dendritic morphology as seen in the cross sectional view of the $Co_{0.75}In_{0.25}$ film [Fig. 2(c)]. The specific resistivity for the $Co_{0.75}In_{0.25}$ films were checked at room temperature with a standard four point probe (FP 2000 Fa. Veeco; AC current). Depending on the impurities and the size of the crystallites, resistivities ranging from 170–1000 $\mu\Omega$ cm were measured.

Crystallinity, phase identity and thin film reactions

The X-ray powder diffraction pattern of film $Co_{0.50}In_{0.50}$ [Fig. 3(a)] of Table 1 (sample #2) exhibits the characteristic reflections for the two stable intermetallic compounds of the Co/In systems $CoIn_2$ and $CoIn_3$. According to the Co/In phase diagram the 1 : 1 composition of the film requires elemental cobalt as the third phase. However, reflections due to crystalline Co could not be detected. Probably the respective reflections due to Co were too broad (very small crystallites) to be observed. For the cobalt rich films ($Co_{0.66}In_{0.33}$ and $Co_{0.75}In_{0.25}$) of Table 2 the X-ray diffraction patterns [Fig. 3(b), (c)] show evidence for $CoIn_2$ and $CoIn_3$ besides α-Co. Heating of the Co_3In alloy at 400°C in hydrogen atmosphere and the so achieved recrystallization results in sharpened XRD reflections as one would expect (larger crystallites). There was no indication for any other reflections arising from some novel, probably metastable CoIn phase. For the grown films an estimation of the typical crystallite size of about 1 μm length and 0.2–0.3 μm width was made based on the diffraction patterns and using Scherrer's formula [22].

Co/In films of a 1 : 1 metal ratio were deposited at 250°C on InP(100). The AES depth profile of such a $Co_{0.50}In_{0.50}$ film grown on InP showed the presence of a significant and constant concentration of P throughout the film and a ratio for Co : In of 0.67 rather than the expected 1.0. The presence of the crystalline phases CoP, $CoIn_2$ and $CoIn_3$ were affirmed by X-ray diffraction. As deduced from thermodynamics, the pure phases $CoIn_2$ and $CoIn_3$ should be rather stable with respect to chemical reaction at the interface [23,24]. The driving force of the segregation of large amounts of In and P into the growing film is the presence of "excess" metallic cobalt, which forms CoP and additional amounts of $CoIn_2$ and $CoIn_3$.

CONCLUSION

It was demonstrated that comparably pure Co/In films can be easily grown using the single molecule precursors **1**–**3**. These organometallic compounds contain direct Co—In bonds and labile bonded ancillary ligands. They allow unusually precise molecular control of the metal ratio of the grown films. The distribution of the metals were uniform throughout the films. The phase composition of the films follows the phase diagram of the Co/In system. No new Co/In phase could be detected. Due to the multi-phase nature of the films, e.g. the presence of excess Co, the coatings are unstable with respect to interfacial reactions with InP. An atomically abrupt interface CoIn/InP, which would be necessary for the construction of thermodynamically stable Schottky barriers useful for microelectronic devices and similar to related CoGa/GaAs heterostructures [21,22], cannot be formed with these films. The results however show, that related organometallic alkylindium derivatives of cobalt carbonyl complexes with a $CoIn_2$ stoichiometry may well be suited to yield sufficiently chemically pure single phased $CoIn_2$ films which should be stable on InP surfaces and may be interesting as metal contacts.

EXPERIMENTAL

Precursor preparation, characterization and handling

All manipulations were carried out under dry and oxygen-free nitrogen or argon atmosphere using oven-dried glassware. Solvents were freshly distilled from Na/K alloy. The synthesis of $[(CO)_4Co]_aInR_{3-a}$ [R = $CH_2CH_2CH_2N(CH_3)_2$; **1**: $a = 1$; **2**: $a = 2$; **3**: $a = 3$] on a typical scale of 10–20 mmol (5–10 g) has been described in detail elsewhere (see Scheme 1) [11–13]. The compounds sublime quantitatively without decomposition at 50–90°C and 0.1–10 Pa with practical rates up to 1–2 $g \cdot h^{-1}$. All manipulations with the precursor compounds should be carried out by a skilled person using inert-gas techniques and a closed apparatus (e.g. Schlenk-line or glove box) in combination with a good ventilated hood. Due to the significant volatility of the compounds, and their partial hydrolysis in air to yield volatile toxic $(CO)_4CoH$, care must be taken to avoid inhalation. The com-

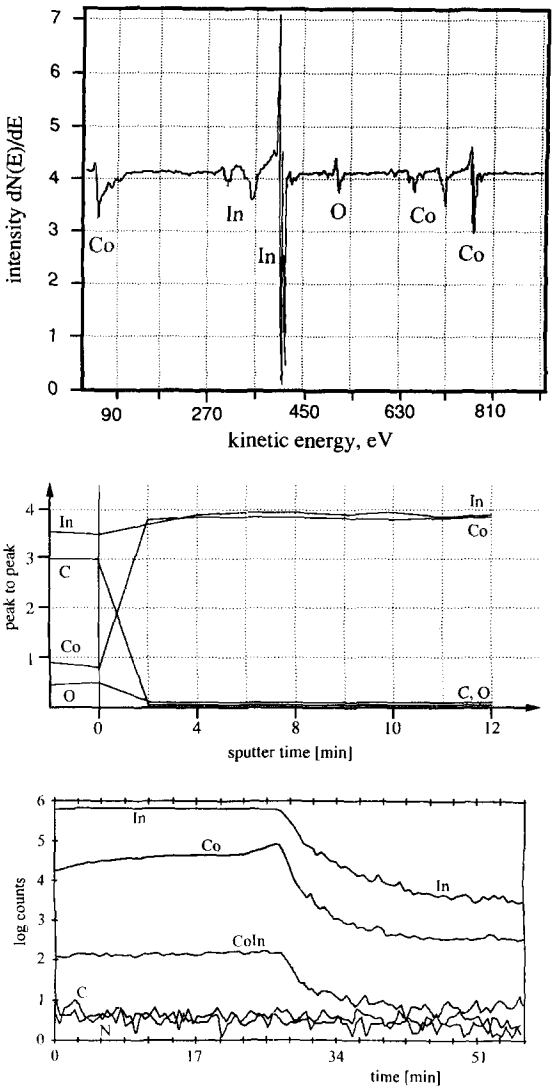

Fig. 1. (a) AES survey plot for a typical $Co_{0.50}In_{0.50}$ thin film grown at 250°C, 10 mTorr (sputter cleaned film #2, Table 1) ⟨1⟩. (b) AES depth profile of the same film ⟨on a quartz substrate⟩. The surface of the grown films was always covered with high hydrocarbon and oxygen impurities, which is probably caused by the condensation of non fragmented precursor molecules and hydrolysis of those upon exposition of the films to the air by opening the reactor after the experiment was finished. Those impurities are removed by a 1–2 min of initial sputter cleaning (Ar ions) of the surface. (c) SIMS depth profile analysis of the same film for the secondary ions Co^+, In^+, $CoIn^+$, C^+ and N^+, giving qualitative evidence for very low C and N contaminations.

pounds are not pyrophoric and can be stored under inert gas atmosphere with cooling (−10°C) for an unlimited period of time. Any residues of the precursors can be safely destroyed either by careful oxidative acid hydrolysis with dilute H_2O_2/H_2SO_4 (with cooling to 0°C) or by dissolution into isopropanol/KOH. NMR spectra were recorded using a JEOL GMX 400 spectrometer (C_6D_6, 20°C). Elemental analysis were obtained from the Microanalytic Laboratory of the Technical University Munich. Mass spectra were recorded on Finnigan MAT 90 (EI, 70 eV) and Varian MAT 311a (FI and CI with isobutene) spectrometers. Gas chromatographic analyses were performed using a HP 5890 equipped with a mass selective detector system (HP 5970B). A fused silica capillary column (HP-1, # 19091Z-102) with 100% methylpolysiloxane ($l = 50$ m, $\phi = 0.2$ mm, film thickness 0.33 μm) was used. The molar fractions of the observed gaseous constituents are reported on the bases of non-calibrated total ion currents.

Film deposition by OMCVD

The vacuum OMCVD experiments were carried out in an isothermal horizontal hot wall quartz tube reactor described in detail elsewhere [14]. The substrates for CVD studies consisted of borosilicate microscope slides, quartz, silicon(111) slides and InP(100) slides, which were cleaned by degreasing in trichloroethylene, isopropanol/acetone, rinsing with deionized water and treated by usual etching procedures. After charging the reactor with various substrates the system was evacuated to a base pressure of $< 10^{-4}$ Pa (turbo molecular pump, Edwards EXT 150) and heated to 350°C for several hours. The precursor reservoir was loaded under an inert gas atmosphere with 1–2 g of the precursor compound and cooled to −30°C. Then the valve to the reactor was opened and the system was evacuated again to 10^{-4} Pa for several hours. The temperature of the furnace was set at the desired value and was allowed to stabilize. The temperature of the precursor reservoir was then adjusted to 35–80°C allowing the precursors to sublime through the hot zone at pressures of 0.1–10 Pa. Reflective metallic depositions formed on the wall of the tube and on the substrates. Carrier gases were not used in these experiments.

Thin film characterization

The films obtained were examined *ex situ* by various surface analytic tools (SIMS, AES and SEM-EDX) and X-ray powder diffraction. The metal ratio was determined independently by AAS after quantitative dissolution of representative films in aqueous nitric acid (p.a.; 6.5 weight-%). Thick films were grown on the walls of the reaction tube, which peeled of by rapid cooling of the tube (10°C · sec^{-1}). After collecting typical quantities of 50–100 mg of the deposited material, classical combustion analysis was performed (C, H, and N). The compositions of the films were uniform over the plated areas of typically ~3 cm^2 (AES mapping and profiling). The EDX-spectra were recorded using a scanning electron microscope JEOL JSM-35C equipped with an EG&G Ortec System 5000 X-ray analysator system. A typical standardless program for quantitative analysis "AUTOZAP" 3.08 ("ZAF"-

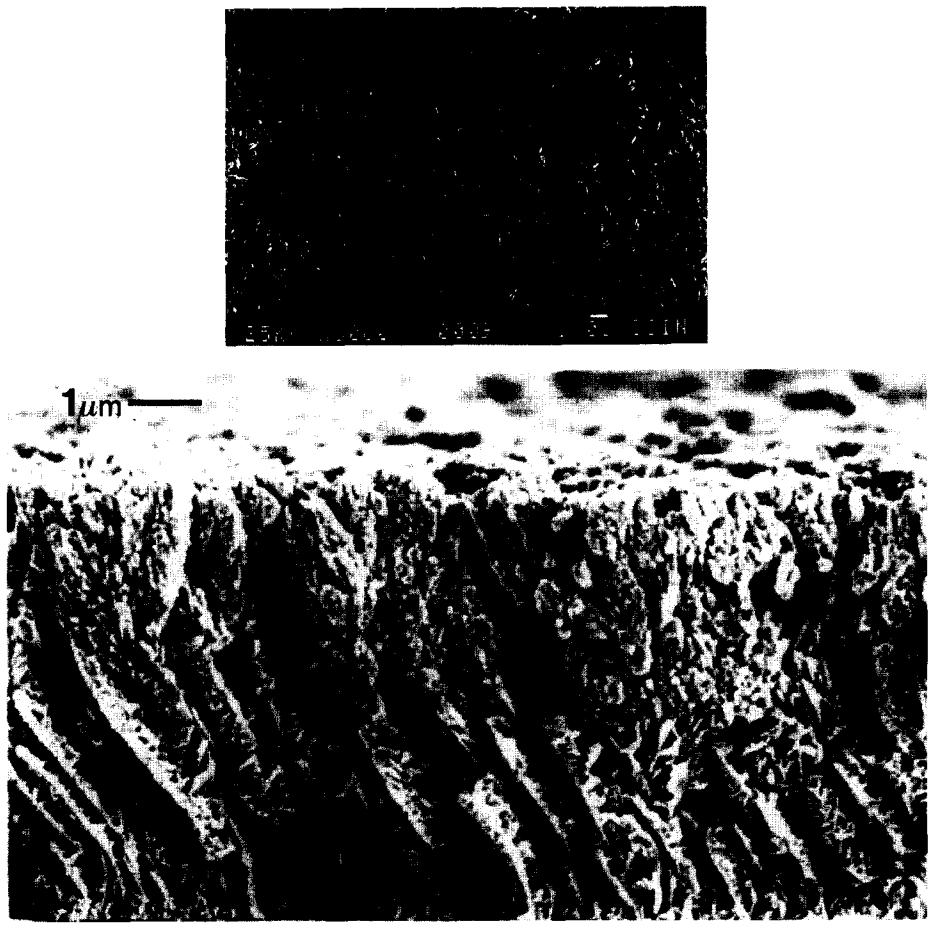

Fig. 2. (a) SEM image of the $Co_{0.50}In_{0.50}$ film #2 of Table 1 grown from **1** on borosilicate glass. (b) SEM image (cross section) of a $Co_{0.75}In_{0.25}$ film grown from **3**.

correction) was employed. The obtained values for the Co and In contents were found to be valid within a relative error of $\pm 10\%$ (comparison with AAS values). AUGER electron spectra were recorded using a PHI 595 spectrometer with a base pressure of 2–4×10^{-7} Pa and a working pressure of 2–5×10^{-6} Pe with a standard cylindrical mirror analyzer (3 keV primary beam energy, 0.2 μA primary beam intensity, a maximum of 500 Å lateral resolution; rate of argon ion sputtering 300 Å sec^{-1} on Ta_2O_5 for an area of 1×1 mm). Typical data collection time was 30 min for 1 keV scan width. The films were cleaned first by 5 min of argon ion (Ar^+, 3 keV) sputtering (5×5 mm area) at a pressure of 5×10^{-4} Pa. The quantitative analysis was based on differentiated spectra and accepted standard sensitivity factors for C (0.18), N (0.32), O (0.50) and Co (0.27). The usual sensitivity factor for In of 1.0 however had to be corrected to 0.30 in our case, on the basis of the AAS and EDX values. This may probably be due to the effect of preferential sputtering of In. The specific resistivity of the deposited metallic coatings were routinely checked by a usual commercial four point probe system at room temperature with an AC current (FPP-5000, Veeco). The analytical data are compiled in Tables 1 and 2.

Structural characterization

The X-ray diffraction patterns were recorded on a Huber-Guinier-Diffractometer 653; Ge-monochromated Cu $K_{\alpha 1}$ ($\lambda = 1.54059$ Å) using the step scanning method with an angle of incidence of 3°, a scan width of 0.005° (counting time of 10 s) and a rotating probe head. The X-ray diffraction patterns of $Co_{0.75}In_{0.25}$ were recorded on a Siemens-D500-Diffractometer, graphite secondary monochromator, Cu $K_{\alpha 1,2}$ ($\lambda_1 = 1.54059$ Å, $\lambda_2 = 1.54443$ Å), using step scanning method (C 0.02°, 2Θ) with beam divergence of 0.3° (counting time 14 s). The measured d-values were calibrated against polycrystalline Si powder.

By-product analysis

The exhaust gases of the vacuum OMCVD experiments were monitored *in situ* by a quadrupolar mass

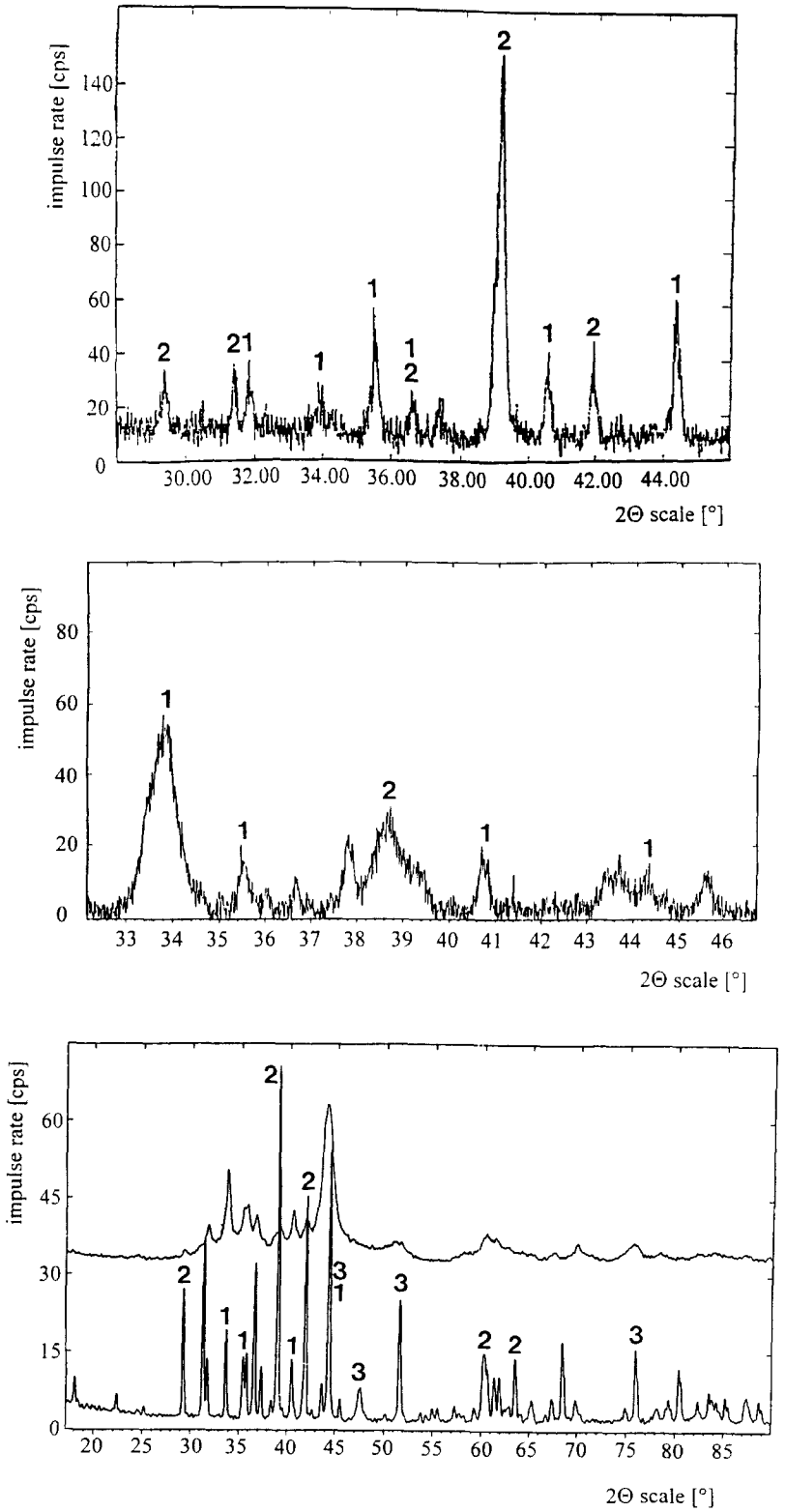

Fig. 3. (a) XRD pattern of the $Co_{0.50}In_{0.50}$ film #2 of Table 1. (b) XRD pattern of the $Co_{0.66}In_{0.33}$ film (Table 2). (c) XRD pattern of the $Co_{0.75}In_{0.25}$ film (Table 2). The observed reflections are denoted as follows: **1** = $CoIn_2$, **2** = $CoIn_3$, **3** = Co [6,10,25].

spectrometer (gas analysis system HPR30-HAL/3F, 1–510 a.m.u.; HIDEN) which was connected to the apparatus by a gas sampling unit with a pin-hole ($\emptyset = 0.7$ mm). The condensables were collected in cold trap attached to the reactor chamber. After the deposition experiment was completed, the cold trap was isolated from the remaining apparatus and the contents were vacuum-transferred into a NMR-tube. C_6D_6 was added and the NMR tube was sealed. The tube contents were analyzed by ^1H NMR and ^{13}C NMR spectroscopy. Subsequently the NMR tube was opened again and the contents were characterized by a GC-MS analysis system. The results of a typical experiment with **1** as precursor (#2 of Table 1) are as follows. The predominant species ($\Sigma > 99$mol.%; GC/MS) of the collected condensable effluent were identified as $Me_2C{=}CH_2$, $H_2C{=}CHCH_2NEt_2$, *cis*-/*trans*-$CH_3CH{=}CHNEt_2$ and $CH_3CH_2CH_2NEt_2$. The ratio of unsaturated to saturated amines was calculated to 4 : 1. The metal content of the condensables was measured in various experiments after aqueous work up (hydrolysis with HNO_3, 6.5 wt.-%) using AAS showing only negligible traces of Co and In.

Acknowledgement—This research was supported by the Alfried Krupp Prize for Young University Teachers of the Krupp Foundation. One of the authors is very much indebted to Prof. Dr. Drs. hc. W. A. Herrmann for generous support, in every respect, during the years 1990–1995 (habilitation of R.A.F.) at the Technische Universität München, at which place parts of the above work have been accomplished.

REFERENCES

1. Fix, R. M., Gordon, G. and Huffmann, D. M., *J. Am. Chem. Soc.*, 1990, **112,** 7833.
2. Cleaver, W. M., Späth, M., Hnyk, D., McMurdo, G., Power, M. B., Stuke, M., Rankin, D. W. H. and Barron, A. R., *Organometallics*, 1995, **14,** 690.
3. Fischer, R. A. and Priermeier, T., *Organometallics*, 1994, **13,** 4306.
4. Fischer, R. A. and Miehr, A., *Chem. Mater.*, 1996, **8,** 497.
5. Miehr, A., Fischer, R. A., Schulte, M. M. and Herdtweck, E., *J. Chem. Soc. Chem. Commun.*, 1995, 337.
6. Ellner, M. and Bhan, S., *J. Less-Common Met.*, 1981, **79,** P1.
7. Khalopova, A. N., *Khim. Redkikh Elementov*, 1954, **1,** 115.
8. Köster, W. and Horn, E., *Z. Metallkd.*, 1952, **43,** 333.
9. Dasarathy, C., *Z. Metallkd.*, 1968, **58,** 829.
10. Schöbel, J.-D. and Stadelmeier, H. H., *Z. Metallkd.*, 1970, **61,** 342.
11. Fischer, R. A., Behm, J., Priermeier, T. and Scherer, W., *Angew. Chem.*, 1993, **105,** 776.
12. Weiß, J., Frank, A., Herdtweck, E., Nlate, S. and Fischer, R. A., *Chem. Ber.*, 1995, **129,** 297.
13. Hieber, W. and Teller, U., *Z. Anorg. Allg. Chem.*, 1942, **249,** 43.
14. Fischer, R. A. and Kleine, M., *Chem. Mater.*, 1995, **7,** 1863.
15. Schumann, H., Seuss, T. D. and Hemling, H., *Eur. J. Solid State Inorg. Chem.*, 1992, **29,** 81.
16. Fischer, R. A., Miehr, A., Metzger, T., Born, E., Ambacher, O., Angerer, H. and Dimitrov, R., *Chem. Mater.*, 1996, **8,** 1356.
17. Singmaster, K. A., Houle, F. A. and Wilson, R. J., *J. Phys. Chem.*, 1990, **94,** 6864.
18. Hampden-Smith, M. J. and Kodas, T. T., *The Chemistry of Metal CVD.* Verlag Chemie, Weinheim, 1996.
19. Herrmann, W. A., Fischer, R. A., Klingan, F. R. and Miehr, A., *Appl. Phys. Lett.*, 1995, **67,** 822.
20. Hampden-Smith, M. J. and Kodas, T. T., *The Chemistry of Metals CVD.* Verlag Chemie, Weinheim, 1994.
21. Frey, H. and Kinel, G., *Dünnschichttechnologie.* VDI-Verlag, Düsseldorf, 1987; p. 176.
22. Scherrer, P., *Göttinger Nachr.*, 1918, **2,** 98.
23. Williams, R. S., *Appl. Surf. Sci*, 1992, **60/61,** 613.
24. Kaesz, H. D., Williams, R. S., Hicks, R. F., Zink, J. I., Chen, Y.-J., Müller, H.-J., Xue, Z., Xu, D., Shuh, D. K. and Kim, Y. Y., *New J. Chem.*, 1990, **14,** 527.
25. Stadelmaier, H. H. and Manaktala, H. K., *Acta Cryst.*, 1975, **B31,** 374.
26. *Natl. Bur. Stand. (U.S.) Monogr.* 25, 1996, **4,** 10.
27. Hofer, L. J. E. and Peebles, W. C., *J. Am. Chem. Soc.*, 1947, **69,** 893.

Pergamon

PII: S0277-5387(97)00406-3

Polyhedron Vol. 17, No. 8, pp. 1211–1216, 1998
© 1998 Elsevier Science Ltd
All rights reserved. Printed in Great Britain
0277-5387/98 $19.00+0.00

Synthesis and spectral studies on $Ru_3(CO)_{12-n}$ (μ-$Ph_2AsCH_2AsPh_2$)(L) ($n = 3$, L: PPh_3, PCy_2Ph, $P(OCH_3)_3$); $n = 4$, L = $Ph_2PCH_2PPh_2$): crystal and molecular structures of $Ru_3(CO)_9$ (μ-$Ph_2AsCH_2AsPh_2$)(PCy_2Ph) and $Ru_3(CO)_8$ (μ-$Ph_2AsCH_2AsPh_2$)(μ-$Ph_2PCH_2PPh_2$)

Omar bin Shawkataly,[a]* K. Ramalingam,[a,c] S. T. Lee,[a] M. Parameswary,[a] H. K. Fun[b] and K. Sivakumar[b,d]

[a]Chemical Sciences Programme, Centre for Distance Education, Universiti Sains Malaysia, Minden, 11800 Penang, Malaysia

[b]X-ray Crystallography Laboratory, School of Physics, Universiti Sains Malaysia, Minden, 11800 Penang, Malaysia

(Received 4 August 1997; accepted 2 October 1997)

Abstract—Mixed ligand triangulotriruthenium cluster carbonyls, $Ru_3(CO)_9(\mu\text{-}Ph_2AsCH_2AsPh_2)(L)$ (L = PPh_3, PCy_2Ph, $P(OCH_3)_3$) and $Ru_3(CO)_8(\mu\text{-}Ph_2AsCH_2AsPh_2)(\mu\text{-}Ph_2PCH_2PPh_2)$ were synthesised and characterised by microanalysis, IR, ^1H, ^{13}C and ^{31}P NMR spectrometry. Single crystal X-ray structure determination of $Ru_3(CO)_9(\mu\text{-}Ph_2AsCH_2AsPh_2)(PCy_2Ph)$ and $Ru_3(CO)_8(\mu\text{-}Ph_2AsCH_2AsPh_2)(\mu\text{-}Ph_2PCH_2PPh_2)$ are reported. In both the clusters, the triruthenium framework is planar. In $Ru_3(CO)_9(\mu\text{-}Ph_2AsCH_2AsPh_2)(PCy_2Ph)$, the monodentate phosphine occupies an equatorial position for steric reasons. The effect of trisubstitution is explicit in the highly significant differences observed in Ru—Ru distances (2.8301(6), 2.8653(7) and 2.8873(7) Å) in the present compound compared to $Ru_3(CO)_{10}(\mu\text{-}Ph_2AsCH_2AsPh_2)$. The observed Ru—As distances are 2.4508(7) and 2.4331(7) Å respectively and the Ru—P distance is 2.362(1) Å. In the case of $Ru_3(CO)_8(\mu\text{-}Ph_2AsCH_2AsPh_2)(\mu\text{-}Ph_2PCH_2PPh_2)$, the chelating ligands occupy four equatorial positions. Two of the Ru—Ru distances are similar in length (2.848(2), 2.850(2) and 2.828(2) Å). However, positional disorder is associated with As and P atoms. Other bond parameters are normal. © 1998 Elsevier Science Ltd. All rights reserved

Keywords: crystal structure; steric effect; triruthenium; carbonyl cluster; phosphine substitution.

Synthetic and structural reports on substituted triangulotriruthenium clusters have always been on the rise for their interesting structural variations and related catalytic activity [1]. The metal–metal bond rupture in clusters under catalytic reaction conditions is of concern [2]. The stability of the clusters have been ensured by the presence of a bridging or a capping ligand. Identification of a new radical initiation synthetic route by the Adelaide group has enabled a host of new substituted triangulotriruthenium clusters to be identified and characterised [3,4]. A large number of substituted derivatives, $Ru_3(CO)_{12-n}L_n$ (L = group 15 ligand) have been reported [5–7]. The effect of substitution on the triruthenium clusters manifests itself in many ways [8] with a decrease in the molecular symmetry. Also, introduction of a non-CO ligand, in general results in the lengthening of M—M bonds and only smaller molecules, such as isocyanides, occupy axial positions. However, the

* Author to whom correspondence should be addressed.

[c] Post-Doctoral Fellow on leave from: Department of Chemistry, Annamalai University, Annamalainagar 608 002, Tamilnadu, India.

[d] Present address: Department of Physics, Anna University, Madras 600 025, India.

trend in increase of M—M bond distances is only marginal. The group 15 ligands allow a degree of tuning of the reactivity of mixed ligand clusters [7]. In the case of a chelating ligand substituted cluster viz, $Ru_3(CO)_{10}(\mu\text{-}Ph_2PCH_2PPh_2)$, only the equatorial position gets activated for subsequent substitution [8]. A number of substituted carbonyls such as $Ru_3(CO)_9(\mu\text{-}Ph_2PCH_2PPh_2)L$ (L: $P(OCH_3)_3$) have been reported from our laboratory [9]. In continuation of our interest in the substituted clusters, we report the synthesis and characterisation of $Ru_3(CO)_9(\mu\text{-}Ph_2AsCH_2AsPh_2)(L)$ [L = PPh_3, PCy_2Ph (Cy: cyclohexyl), $P(OCH_3)_3$] and X-ray structures of $Ru_3(CO)_9(\mu\text{-}Ph_2AsCH_2AsPh_2)(PCy_2Ph)$ and $Ru_3(CO)_8(\mu\text{-}Ph_2AsCH_2AsPh_2)(\mu\text{-}Ph_2PCH_2PPh_2)$.

EXPERIMENTAL

Materials

$Ru_3(CO)_{12}$ (Aldrich), $Ph_2AsCH_2AsPh_2$(dpam), $Ph_2PCH_2PPh_2$(dppm), PCy_2Ph (Press Chemical Co) and $P(OCH_3)_3$ (BDH) were used as received. Kieselgel $60GF_{254}$ was used for TLC separations. The THF solvent was dried over sodium wire and freshly distilled for every reaction. Oxygen free nitrogen was used to maintain an inert atmosphere. Microanalysis was performed using a model 240 × A from Control Equipment Corporation. IR spectra were recorded with a Mattson 1000 FTIR spectrometer in a NaCl solution cell (0.1 mm). NMR spectra were recorded in $CDCl_3$ with a Bruker B2H 300/52.

(Bis(diphenylarsino)methane)decacarbonylruthenium(0), $Ru_3(CO)_{10}(\mu\text{-}Ph_2AsCH_2AsPh_2)$. The compound was prepared by using the phenylketyl initiator route as previously reported [4].

(Bis(diphenylarsino)methane)nonacarbonyl(triphenylphosphino)ruthenium(0), $Ru_3(CO)_9(\mu\text{-}Ph_2AsCH_2AsPh_2)(PPh_3)$. $Ru_3(CO)_{10}(\mu\text{-}Ph_2AsCH_2AsPh_2)$ (100 mg, 0.0947 mmol) and PPh_3 (26 mg, 0.0995 mmol) were stirred THF (25 ml) under nitrogen. About 0.2 ml of diphenylketyl radical anion initiator was introduced into the reaction mixture under a current of nitrogen. The reaction mixture turned intense red. After 2 h of stirring, the solvent was removed under vacuum. The reaction mixture was separated using TLC (cyclohexane: acetone, 80:20). Three bands appeared including a minor quantity of the starting material. The major band (red) $R_f = 0.85$, was separated and characterised. Yield = 47.5 mg, 38.9 %, m.p. 223–225° C. (Found: C, 48.40 ; H, 2.90; Calc.: C, 48.42; H, 2.89). IR (cyclohexane), ν(CO) 2054 w, 1994 vs, 1976 vs, 1943 sh cm^{-1}. ^1H NMR ($CDCl_3$) δ 7.3–7.7 (m, 25 H, Ph), δ 4.0 (s, 2H, CH_2), ^{13}C NMR($CDCl_3$) δ 129.0–137.0 (m, Ph), δ 198.6 (m, CO), ^{31}P NMR($CDCl_3$) δ 35.5 (s, PPh_3).

(Bis(diphenylarsino)methane)nonacarbonyl(trimethylphosphite)ruthenium(0), $Ru_3(CO)_9(\mu\text{-}Ph_2AsCH_2AsPh_2)P(OCH_3)_3$. $Ru_3(CO)_{10}(\mu\text{-}Ph_2AsCH_2AsPh_2)$ (100 mg, 0.0947 mmol) and $P(OCH_3)_3$ (12mg, 0.094 mmol) in THF (25 ml) was added with 0.2 ml of initiator solution. The resultant mixture was stirred for 30 min and then the solvent was removed under vacuum. The products were separated using TLC. Three bands appeared including a very small quantity of the starting material and the major band was separated ($R_f = 0.50$, benzene: ethanol; 90:10). Yield: 31.1 mg, 28.5%, m.p. 219°C (Found: C, 38.50; H, 2.72; Calc.: C, 38.49; H, 2.71). IR (cyclohexane) ν(CO) 2083 w, 2067 w, 2040 w, 1988 s, 1967 vs, 1925 sh, 1912 sh cm^{-1}. ^1H NMR ($CDCl_3$) δ 7.2–7.4 (m, 20H, Ph); δ 4.0 (s, 2H, CH_2); δ 3.6–3.8 (m, 9H, CH_3). ^{13}C NMR ($CDCl_3$) δ 30.0 (s, CH_3) δ 198.6 (m, CO); ^{31}P NMR ($CDCl_3$) δ 55.5–57.5 (d, P).

(Dicyclohexyl)phenylphosphino)(bis(diphenylarsino)methane) nonacarbonylruthenium(0), $Ru_3(CO)_9(\mu\text{-}Ph_2AsCH_2AsPh_2)(PCy_2Ph)$. $Ru_3(CO)_{10}(\mu\text{-}Ph_2AsCH_2AsPh_2)$ (100 mg, 0.0947 mmol) and PCy_2Ph(27.3 mg, 0.0995 mmol) in dry THF (25 ml) were added with 0.1 ml initiator and stirred for 4 h. The product as a major band was separated by TLC which contained four bands in all with a very minor quantity of the starting material; dichloromethane: ethanol; 90:10; $R_f = 0.26$; yield, 53.0 mg., 43.2%; m.p. 214–216°C. Found, C, 47.95; H, 3.77; Calc., 47.97; H,3.79. IR (cyclohexane) ν(CO) 2052 w, 1989 vs, 1973 vs, 1938 m cm^{-1}. ^1H NMR ($CDCl_3$) δ 7.25–7.45 (m, 25H, Ph); δ 4.0 (s, 2H, CH_2); δ 1.52 (s, 22H, Cy). ^{13}C NMR ($CDCl_3$) δ 128.5–130.0 (d, Ph), δ 199.0 (m, CO); ^{31}P NMR ($CDCl_3$) δ 41.5 (s, P).

(Bis(diphenylarsino)methane)(bis(diphenylphosphino)methane)octacarbonylruthenium(0), $Ru_3(CO)_8(\mu\text{-}Ph_2AsCH_2AsPh_2)(\mu\text{-}Ph_2PCH_2PPh_2)$. $Ru_3(CO)_{10}(\mu\text{-}Ph_2AsCH_2AsPh_2)$ (100 mg, 0.0947 mmol) and $Ph_2PCH_2PPh_2$ (38.22 mg, 0.0994 mmol) in THF (25 ml) under dry nitrogen was added with 0.1 ml initiator and stirred for 6 h. The product as a major band was separated by TLC which contained five bands including trace amounts of the starting material; hexane: acetone; 80:20; $R_f = 0.50$; yield, 44.2 mg, 35.5%, m.p. 240°C. IR (cyclohexane) ν(CO) 2081 w, 2040 w, 2013 w, 1981 sh, 1963 vs, 1896 w cm^{-1}. ^1H NMR ($CDCl_3$) δ 7.1–7.4(m, 40H, Ph); δ 5.85 (s, 2H, CH_2); δ 3.6–3.8 (q, 2H, CH_2). ^{13}C NMR ($CDCl_3$) δ 124.0–128 (m, Ph), δ 198.8 (m, CO); ^{31}P NMR ($CDCl_3$) δ 18.0–24.0 (dd, P).

X-ray data collection

Determination of cell constants and data collection were carried out at room temperature (293 K) with Mo–K_α radiation on a Siemens P4 diffractometer equipped with a graphite monochromator. Data were recorded by $\theta/2\theta$ scan technique and were corrected for Lorentz and polarisation effects. The structure was solved by direct methods with SHELXTL-PC [11] and refined by full-matrix least squares technique on F^2 with SHELXL93 [12]. All the hydrogens were fixed

Table 1. Crystallographic data collection and refinement parameters. **1**: $Ru_3(CO)_9(\mu\text{-}Ph_2AsCH_2AsPh_2)(PCy_2Ph)$. **2**: $Ru_3(CO)_8(\mu\text{-}Ph_2AsCH_2AsPh_2)(\mu\text{-}Ph_2PCH_2PPh_2)$

	1	**2**
Empirical formula	$C_{52}H_{49}As_2O_9PRu_3$	$C_{58}H_{44}As_2O_8P_2Ru_3$
M	1301.9	1383.7
Crystal system	triclinic; P-1	orthorhombic; Pca21
a (Å)	12.570(1)	21.586(2)
b (Å)	12.902(1)	15.839(2)
c (Å)	16.949(2)	18.383(1)
α (°)	92.07(1)	90
β (°)	110.50(1)	90
γ (°)	98.14(1)	90
U (Å)	2537.8(4)	6285.2(1)
D_c/(Mg m^{-3})	1.704	1.453
Z	2	4
μ (Mo-K_α) (cm^{-1})	22.61	23.21
Scan mode	$\theta/2\theta$	$\theta/2\theta$
T (°K)	293(2)	293(2)
θ range (°)	1.60–27.50	1.59–27.58
Recorded reflections	11,868	8573
Independent reflections $[I > 2\sigma(I)]$	10,382 [R(int) = 0.0288]	7574 [R(int) = 0.0336]
Residual R, Rw	0.0360, 0.0941	0.0549, 0.1700

geometrically with the HADD utility [11]. The relevant data collection and refinement parameters are given in Table 1.

RESULTS AND DISCUSSION

Microanalysis of the compounds agreed well with the proposed molecular formulae for all the reported compounds within the experimental errors.

IR spectra

Isolation of a number of specifically substituted derivatives of $Ru_3(CO)_{12}$ has enabled a definitive ν(CO) spectral information possible on different entities [4,6]. As the number of substituents increases, the frequencies of the bands decrease in magnitude in general. Similarly, as the basicity of the ligand increases, the frequencies of the bands show a decrease. In the present study, trisubstituted, $Ru_3(CO)_9(\mu\text{-}Ph_2AsCH_2AsPh_2)(L)$ clusters show two strong bands of almost equal intensities characteristically, one band at $\sim$ 1960 and the other at $\sim$ 2000 cm^{-1}. In the case of the tetra-substituted cluster, six bands were observed, of which the one at 1963 cm^{-1} was the strongest and appears to be the characteristic band similar to earlier observations [4].

NMR spectra

^{1}H NMR spectra of all the compounds showed a multiplet around δ 7.0 characteristic of the phenyl groups. Other than that, the signal at δ 4.0 is due to the CH_2 protons. For the methoxy protons, the signal appeared at δ 3.6–3.8. In the case of the dicyclohexylphenylphosphine-cluster the signal at 1.52 ppm corresponds to the cyclohexyl protons. ^{13}C NMR spectra of all the substituted clusters showed a prominent signal around δ 128.5–130.0 ppm characteristic of the phenyl carbons. The carbonyl carbons in all the clusters showed as a multiplet at $\delta \sim$ 198.6 ppm. In addition, the methoxy carbons appeared at δ 30.0 ppm for the corresponding cluster. ^{31}P NMR spectra showed signals at δ values 35.5, 41.5 and 55.5–57.5 ppm for PPh_3, PCy_2Ph and $P(OCH_3)_3$ substituted clusters respectively. The observed trend is in keeping with their relative basicities. In the case of $Ru_3(CO)_8$ $(\mu\text{-}Ph_2AsCH_2AsPh_2)(\mu\text{-}Ph_2PCH_2PPh_2)$, ^{1}H NMR showed signals corresponding to phenyl and methylene protons at δ values 7.1–7.4, 5.85 ($Ph_2AsCH_2AsPh_2$) and 3.6–3.8($Ph_2PCH_2PPh_2$) respectively. In the range of δ: 124.0–128.0, ^{13}C NMR spectrum showed signal due to phenyl carbons and ^{31}P NMR spectrum showed signals due to the P atoms at 18.0–24.0 ppm split by by the methylene protons.

X-ray crystal structures

The ORTEP plot of $Ru_3(CO)_9(\mu\text{-}Ph_2AsCH_2AsPh_2)(PCy_2Ph)$ is shown in Fig. 1. The selected bond parameters are given in Table 2. The triangulotriruthenium framework is planar. The three Ru—Ru distances are 2.8301(6), 2.8653(7) and 2.8873(7) Å. All three distances are significantly different from each other. A comparison of the

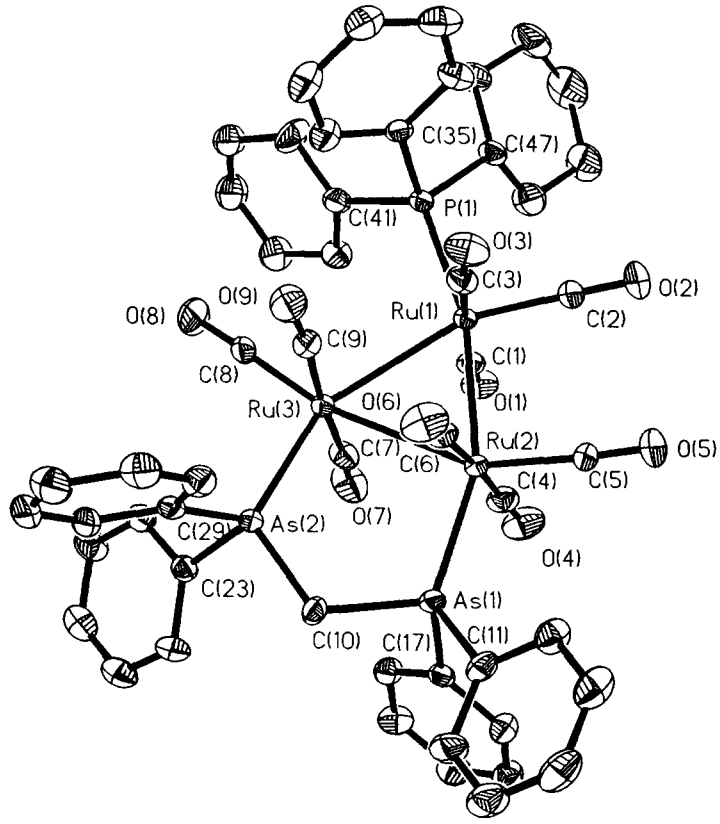

Fig. 1. ORTEP plot of $Ru_3(CO)_9(\mu\text{-}Ph_2AsCH_2AsPh_2)(PCy_2Ph)$.

Ru—Ru distances of $Ru_3(CO)_{10}(\mu\text{-}Ph_2AsCH_2AsPh_2)$ [10] (2.817(1), 2.845(1), 2.840(1) Å) clearly shows that the dissimilarities have increased as a consequence of further substitution. Relatively, significant lengthening observed in Ru(1)—Ru(3) bond reflects itself in the shortening of the Ru(3)—Ru(2) bond. The equatorial Ru—C bond distances (mean: 1.853(6) Å) are shorter than the axial (mean: 1.922(6) Å) as observed in the parent $Ru_3(CO)_{12}$ cluster [13]. The Ceq—Ru—Cax angles are close to 90° and Cax—Ru—Cax angles are close to 180° excepting the ones associated with Ru(1) which show considerable deviations due to the bulky monodentate PCy_2Ph. The Ru—P distance in the compound is 2.362(1) Å. The Ru—As distances in the present compound are 2.4508(7) and 2.4331(7) Å; which are asymmetric clearly compared to the distances observed in $Ru_3(CO)_{10}(\mu\text{-}Ph_2AsCH_2AsPh_2)$ (2.430(1), 2.422(1) Å) [10]. The substituent, (PCy_2Ph) on Ru(1) is on an equatorial position for steric reasons and Ru—P-(Cy_2Ph) bond is *trans* to the Ru_3As_2 plane. The cyclohexyl rings are in the preferred chair conformation. The bond parameters associated with the phenyl rings are normal.

The ORTEP plot of $Ru_3(CO)_8(\mu\text{-}Ph_2AsCH_2AsPh_2)(\mu\text{-}Ph_2PCH_2PPh_2)$ is shown in Fig. 2 and selected bond parameters are given in Table 3. The triangulotriruthenium frame work is planar as observed in the other structure. Two of the Ru—Ru distances are similar, viz. 2.850(2) and 2.848(2) Å whereas the third bond is significantly shorter (2.828(2) Å) than the other two. The two chelating ligands occupy equatorial positions. However, unlike the case of the PCy_2Ph analogue, the bond distances are not affected to a greater extent compared to the $Ru_3(CO)_{12}$ [13], $Ru_3(CO)_{10}(dppm)$ [14] and $Ru_3(CO)_{10}(dpam)$ [10]. The equatorial Ru—C bonds are shorter (mean: 1.83(2) Å) and the axial Ru—C bonds are longer (mean: 1.90(2) Å). Positional disorder associated with arsenic and phosporous atoms in the present structure excludes a rigorous comparison of the bond parameters. The distances corresponding to As(1) and As(2) on the basis of a higher site occupancies (site occupancies: As(1): 0.6333, As(2): 0.6333) from the metal centre are 2.394(2) and 2.404(2) Å. Similarly, Ru—P distances correponding to higher site occupancies are 2.359(3) and 2.345(3) Å. The bond parameters associated with the phenyl rings are normal.

Therefore, the steric effects due to the presence of

Table 2. Selected bond distances (Å) and angles (°) for $Ru_3(CO)_9(\mu\text{-}Ph_2AsCH_2AsPh_2)(PCy_2Ph)$

Ru(1)—C(2)	1.861(6)	Ru(1)—C(3)	1.924(6)
Ru(1)—C(1)	1.923(6)	Ru(1)—P(1)	2.3622(14)
Ru(1)—Ru(2)	2.8301(6)	Ru(1)—Ru(3)	2.8873(7)
Ru(2)—C(5)	1.875(6)	Ru(2)—C(4)	1.926(7)
Ru(2)—C(6)	1.933(7)	Ru(2)—As(1)	2.4331(7)
Ru(2)—Ru(3)	2.8653(7)	Ru(3)—C(8)	1.859(6)
Ru(3)—As(2)	2.4508(7)	As(1)—C(17)	1.941(5)
As(1)—C(11)	1.950(5)	As(1)—C(10)	1.974(6)
As(2)—C(23)	1.940(6)	As(2)—C(29)	1.952(5)
As(2)—C(10)	1.983(5)	P(1)—C(35)	1.838(6)
P(1)—C(41)	1.838(6)	P(1)—C(47)	1.852(6)

C(2)—Ru(1)—P(1)	96.3(2)	C(3)—Ru(1)—P(1)	91.7(2)
C(1)—Ru(1)—P(1)	93.7(2)	C(2)—Ru(1)—Ru(2)	98.0(2)
C(3)—Ru(1)—Ru(2)	82.3(2)	C(1)—Ru(1)—Ru(2)	92.4(2)
P(1)—Ru(1)—Ru(2)	164.24(4)	C(2)—Ru(1)—Ru(3)	158.1(2)
C(3)—Ru(1)—Ru(3)	87.8(2)	C(1)—Ru(1)—Ru(3)	90.4(2)
P(1)—Ru(1)—Ru(3)	105.24(4)	Ru(2)—Ru(1)—Ru(3)	60.14(2)
C(5)—Ru(2)—As(1)	108.1(2)	C(4)—Ru(2)—As(1)	88.0(2)
C(6)—Ru(2)—As(1)	88.6(2)	C(5)—Ru(2)—Ru(1)	95.7(2)
C(4)—Ru(2)—Ru(1)	85.6(2)	C(6)—Ru(2)—Ru(1)	96.8(2)
As(1)—Ru(2)—Ru(1)	155.55(2)	C(5)—Ru(2)—Ru(3)	154.1(2)
C(4)—Ru(2)—Ru(3)	96.8(2)	C(6)—Ru(2)—Ru(3)	81.8(2)
As(1)—Ru(2)—Ru(3)	96.58(2)	Ru(1)—Ru(2)—Ru(3)	60.92(2)
C(8)—Ru(3)—As(2)	102.1(2)	C(7)—Ru(3)—As(2)	92.0(2)
C(9)—Ru(3)—As(2)	93.7(2)	C(8)—Ru(3)—Ru(2)	164.8(2)
C(7)—Ru(3)—Ru(2)	84.7(2)	C(9)—Ru(3)—Ru(2)	94.3(2)
As(2)—Ru(3)—Ru(2)	92.84(2)	C(8)—Ru(3)—Ru(1)	106.2(2)
C(7)—Ru(3)—Ru(1)	87.6(2)	C(9)—Ru(3)—Ru(1)	87.0(2)
As(2)—Ru(3)—Ru(1)	151.70(2)	Ru(2)—Ru(3)—Ru(1)	58.94(2)
As(1)—C(10)—As(2)	113.4(3)		

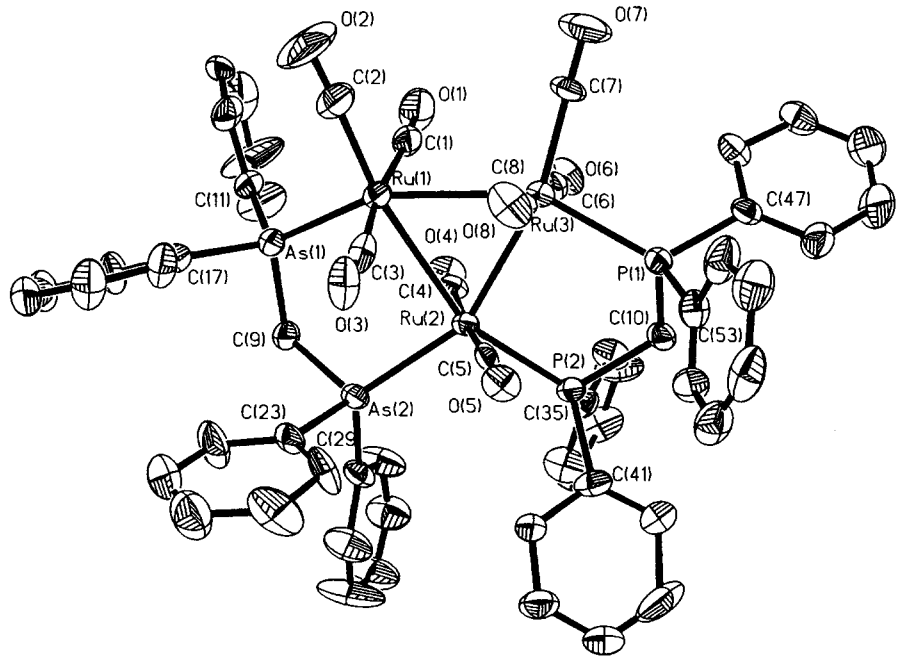

Fig. 2. ORTEP plot of $Ru_3(CO)_8(\mu\text{-}Ph_2AsCH_2AsPh_2)(\mu\text{-}Ph_2PCH_2PPh_2)$.

Table 3. Selected bond distances (Å) and angles (°)[a] for $Ru_3(CO)_8(\mu—Ph_2AsCH_2AsPh_2)(\mu—Ph_2PCH_2PPh_2)$

Ru(1)—C(2)	1.82(2)	Ru(1)—C(1)	1.90(2)
Ru(1)—C(3)	1.90(2)	Ru(1)—As(1)	2.394(2)
Ru(1)—P(1)	2.394(2)	Ru(1)—Ru(3)	2.848(2)
Ru(1)—Ru(2)	2.850(2)	Ru(2)—P(3)	2.345(3)
Ru(2)—As(3)	2.345(3)	Ru(2)—As(2)	2.404(2)
Ru(2)—P(2)	2.404(2)	Ru(2)—Ru(3)	2.828(2)
Ru(3)—As(4)	2.359(3)	Ru(3)—P(4)	2.359(3)
C(2)—Ru(1)—P(1)	100.6(7)	C(1)—Ru(1)—P(1)	91.4(6)
C(3)—Ru(1)—P(1)	97.7(6)	C(2)—Ru(1)—Ru(3)	108.5(7)
C(1)—Ru(1)—Ru(3)	79.8(6)	C(3)—Ru(1)—Ru(3)	90.6(7)
As(1)—Ru(1)—Ru(3)	149.27(7)	P(1)—Ru(1)—Ru(3)	149.27(7)
C(2)—Ru(1)—Ru(2)	165.7(7)	C(1)—Ru(1)—Ru(2)	96.0(6)
C(3)—Ru(1)—Ru(2)	80.0(6)	As(1)—Ru(1)—Ru(2)	92.76(6)
P(1)—Ru(1)—Ru(2)	92.76(6)	Ru(3)—Ru(1)—Ru(2)	59.50(4)
P(3)—Ru(2)—As(2)	110.28(9)	As(3)—Ru(2)—As(2)	110.28(9)
P(3)—Ru(2)—P(2)	110.28(9)	As(3)—Ru(2)—P(2)	110.28(9)
P(3)—Ru(2)—Ru(3)	97.86(8)	As(3)—Ru(2)—Ru(3)	97.86(8)
As(2)—Ru(2)—Ru(3)	151.61(7)	P(2)—Ru(2)—Ru(3)	151.61(7)
P(3)—Ru(2)—Ru(1)	156.58(8)	As(3)—Ru(2)—Ru(1)	156.58(8)
As(2)—Ru(2)—Ru(1)	92.33(7)	P(2)—Ru(2)—Ru(1)	92.33(7)
Ru(3)—Ru(2)—Ru(1)	60.22(4)	As(4)—Ru(3)—Ru(2)	90.80(7)
C(7)—Ru(3)—Ru(1)	105.5(6)	C(6)—Ru(3)—Ru(1)	92.8(5)
As(4)—Ru(3)—Ru(1)	150.16(8)	P(4)—Ru(3)—Ru(1)	150.16(8)
Ru(2)—Ru(3)—Ru(1)	60.28(4)	P(4)—Ru(3)—Ru(2)	90.80(7)

[a] Positional disorder is associated with As and P atoms and hence four Ru—As and four Ru—P bonds and related bond angles are listed.

PCy_2Ph in the strucure very clearly manifests itself in the dissimilarities associated with the Ru—Ru bonds but such a dissimilarity is reduced to a larger extent in the cluster with two chelating ligands, however disorder associated with the latter precludes a detailed comparison.

Acknowledgement—O.b.S, acknowledges a research grant from the Malaysian Toray Science Foundation.

REFERENCES

1. Marko, L. and Vizi-Orosz, in *Metal Clusters in Catalysis*, ed. Gates, B. C., Guczi, L., Knozinger, H. Elsevier, Amsterdam, 1986.
2. Doyle, M. J., Kouvenhoven, A. P., Shaap, C. A. and van Oort, B., *J. Organomet. Chem.*, 1975, **174,** C55.
3. Bruce, M. I., Kehoe, D. C., Matisons, J. G., Nicholson, B. K, Rieger, P. H. and Williams, M. L., *J. Chem. Soc., Chem. Commun.*, 1982, 442.
4. Bruce, M. I., Matisons, J. G. and Nicholson, B. K., *J. Organomet. Chem.*, 1983, **247,** 321.
5. Bruce, M. I., Liddel, M. J., Hughes, C. A., Patrick, J. M., Skelton, B. W. and White, A. H., *J. Organomet. Chem.*, 1988, **347,** 181.
6. Bruce, M. I., Liddel, M. J., Shawkataly, O. B., Hughes, C. A., Skelton, B. W. and White, A. H., *J. Organomet. Chem.*, 1988, **347,** 207.
7. Bruce, M. I., Shawkataly, O. B. and Williams, M. L., *J. Organomet. Chem.*, 1985, **287,** 127.
8. Bruce, M. I., Liddel, M. J., Shawkataly, O. B., Bytheway, I., Skelton, B. W. and White, A. H., *J. Organomet. Chem.*, 1989, **369,** 217.
9. Shawkataly, O. B., Ramalingam, K., Dewiyana, M. A., Fun, H. K. and Razak, I. A., *Acta Crystallogr.*, 1997, **C54,** submitted for publication.
10. Teoh, S. G., Fun, H. K. and Shawkataly, O. B., *Z. Kristallogr.*, 1990, **190,** 287.
11. Sheldrick, G. M., SHELXTL-PC, *Structure Determination Software Programmes*, Siemens Analytical X-ray Instruments Inc., Madison, Wisconsin, U.S.A., 1990.
12. Sheldrick, G. M., SHELXL-93, *Programme for Crystal Structure Refinement*, Universitat Göttingen, Germany, 1993.
13. Churchill, M. R., Hollander, F. J. and Hutchinson, J. P., *Inorg. Chem.*, 1976, **16,** 2655.
14. Coleman. A. W, Jones, D. F., Dixneuf, P. H., Brisson, C., Bonnet, J. J. and Lavigne, G., *Inorg. Chem.*, 1984, **23,** 952.

Pergamon

PII: S0277-5387(97)00404-X

Polyhedron Vol. 17, No. 8, pp. 1217–1221, 1998
© 1998 Elsevier Science Ltd
All rights reserved. Printed in Great Britain
0277-5387/98 $19.00+0.00

Structural exploration of hydroxo bridged triamine complexes of zinc(II)

Arunendu Mondal,[a] Golam Mostafa,[b] Ashutosh Ghosh,[c] N. Ray Chaudhuri[a]* and Wing-Tak Wong[d]

[a] Department of Inorganic Chemistry, Indian Association for the Cultivation of Science, Calcutta 700 032, India

[b] X-ray Crystallography Laboratory, Department of Solid State Physics, Indian Association for the Cultivation of Science, Calcutta 700 032, India

[c] Department of Chemistry, Bidhan Nagar College, Calcutta 700 064, India

[d] Department of Chemistry, The University of Hong Kong, Pokfulam Road, Hong Kong

(Received 4 August 1997; accepted 2 October 1997)

Abstract—Single crystal structure of $[Zn_2(dpt)_2(\mu\text{-}OH)](ClO_4)_3$ (dpt = bis(3-aminopropyl) amine) shows that two units of Zn(dpt) are bridged by oxygen atom of the hydroxo group. Each Zn-atom possesses distorted tetrahedral geometry. Analogous complexes $[Zn_2L_2(\mu\text{-}OH)](ClO_4)_3$ [L = bis(3-aminopropyl) methylamine(medpt), bis(2-aminoethyl)methylamine(medien)] have been synthesised. © 1998 Elsevier Science Ltd. All rights reserved

Keywords: hydroxo bridged zinc(II); triamine; zinc(II) triamine complex; single crystal structure.

The synthesis and structural characterisation of classical Werner type coordination compounds of zinc(II) with *N*- and *O*-donor ligands have in the past few years experienced a dramatic resurgence [1]. This is undoubtedly triggered by the rapidly growing knowledge of the structures of zinc-containing active sites of a variety of enzymes. In the active centre of zinc containing enzymes, the zinc ion is mostly attached in a tetrahedral fashion to three aminoacid side chains while a water molecule or a OH group occupies the fourth coordination site. This basic L_3ZnX arrangement has been found in several protein crystal structure determinations [2,3]. So triamine complexes of zinc have been widely used for model studies to elucidate the role of zinc(II) ion and the detailed reaction mechanism in zinc containing enzymes [4–12]. Because of the lability of zinc complexes and the diverse coordination possibilities for zinc, it is unexpectedly difficult to obtain this simple coordination pattern, L_3ZnX in model complexes [1]. With the simple linear chain triamines such as bis(3-aminopropyl) amine(dpt), (2-aminoethyl)(3-aminopropyl)amine (aepn), and bis(2-aminoethyl)amine (dien) number of studies have been reported [13–16]. The stability as well as C^{13}-NMR spectral studies on $[Zn(dpt)(OH)]^+$ and $[Zn(aepn)(OH)]^+$ are documented [13–15]. Curtis *et al.* [16] isolated $[Zn_2(dpt)_2(OH)](ClO_4)_3$ in the solid state owing to its high stability constant. Recently number of single crystal structure analyses of linear chain triamine complexes of zinc are reported [17,18], but hydroxo bridged triamine complexes of zinc lacks single crystal structural information. Here we report the syntheses and characterisation of $[Zn_2(medpt)_2(\mu\text{-}OH)]^{3+}$ and $[Zn_2(medien)_2(\mu\text{-}OH)]^{3+}$ [medpt = bis(3-aminopropyl)methylamine and medien = bis(2-aminoethyl)methylamine] and also single crystal structure of $[Zn_2(dpt)_2(\mu\text{-}OH)](ClO_4)_3$.

EXPERIMENTAL

Materials

Bis(3-aminopropyl)amine(dpt), bis(3-aminopropyl)methylamine(medpt) and bis(2-aminoethyl)

* Author to whom correspondence should be addressed.

methylamine(medien) were purchased from Aldrich Chemical Company Inc. and used as received. All other chemicals used were of AR grade.

Physical measurements

Elemental analysis, IR spectrum (halocarbon mull/KBr disc at ambient temperature) have been carried out in Perkin–Elmer 2400 Series(II) CHN Analyser, Perkin–Elmer 783 Infrared Spectrophotometer, respectively.

Synthesis of $[Zn_2(dpt)_2(\mu\text{-}OH)](ClO_4)_3$ (**1**)

Synthesised according to the procedure described by Curtis *et al.* [16]. Yield: 75%. Found: C, 20.2; H, 4.9; N, 11.8; O, 29.2; Cl, 15.1; Zn, 18.5. Calc. for $C_{12}H_{35}N_6O_{13}Cl_3Zn_2$ (**1**): C, 20.3; H, 4.9; N, 11.8; O, 29.3; Cl, 15.0; Zn, 18.4. IR spectra (cm^{-1}): 3530 (s) (νOH); 3320 (s) (sym νNH_2); 3270 (s) (assym νNH_2); 2940 (s) (νCH_2); 1590 (s) (δNH_2); 1470 (s), 1430 (w), 1380 (w) (δCH_2); 1325 (w), 1290 (br), 1260 (m) ($\rho_w CH_2$).

Synthesis of $[Zn_2(medpt)_2(\mu\text{-}OH)](ClO_4)_3$ (**2**)

Medpt(1.5 mmol, 0.217 gm) in ethanol (5 cm^3) was added slowly with stirring to $Zn(ClO_4)_2 \cdot 6H_2O$ (1 mmol, 0.372 g) in ethanol and 2,2-dimethoxypropane mixture (1 : 1) (5 cm^3). The resulting mixture digested on a steam-bath for 10 mins. The white crystals separated were filtered off and washed with ethanol and dried in a $CaCl_2$-desiccator. Yield: 50%. Found: C, 22.8; H, 5.3; N, 11.3; O, 28.2; Cl, 14.5; Zn, 17.6. Calc. for $C_{14}H_{39}N_6O_{13}Cl_3Zn_2$ (**2**): C, 22.8; H, 5.3; N, 11.4; O, 28.2; Cl, 14.4; Zn, 17.7. IR spectra (cm^{-1}): 3530 (s) (νOH); 3320 (s) (sym νNH_2); 3265 (s) (assym νNH_2); 2940 (m) (νCH_2); 1590 (s) (δNH_2); 1470 (s), 1445 (m), 1385 (w) (δCH_2); 1335 (w), 1315 (m) 1290 (w), 1275 (s) ($\rho_w CH_2$).

Synthesis of $[Zn_2(medien)_2(\mu\text{-}OH)](ClO_4)_3$ (**3**)

Medien (1.5 mmol, 0.176 g) in ethanol (5 cm^3) was added slowly with stirring to $Zn(ClO_4)_2 \cdot 6H_2O$ (1 mmol, 0.372 g) in ethanol and 2,2-dimethoxypropane mixture (1 : 1) (5 cm^3). The resulting mixture digested on a steam-bath for 10 mins. The white crystals separated were filtered off and washed with ethanol and dried in a $CaCl_2$-desiccator. Yield: 40%. Found: C, 17.6; H, 4.4; N, 12.2; O, 30.4; Cl, 15.6; Zn, 19.1. Calc. for $C_{10}H_{31}N_6O_{13}Cl_3Zn_2$ (**3**): C, 17.6; H, 4.5; N, 12.3; O, 30.5; Cl, 15.6; Zn, 19.2. IR spectra (cm^{-1}): 3510 (s) (νOH); 3325 (m) (sym νNH_2); 3280 (s) (assym νNH_2); 2950 (w) (νCH_2); 1590 (s) (δNH_2); 1465 (s), 1420 (w), 1380 (w) (δCH_2); 1360 (w), 1315 (s) 1290 (w), 1270 (w) ($\rho_w CH_2$).

X-ray diffraction structural study

Colourless crystal suitable for X-ray data collection were obtained by recrystallisation of **1** from acetonitrile solution. The block shaped crystals used for X-ray data collection having dimensions of 0.22 mm × 0.22 mm × 0.29 mm was mounted in a glass capillary. The unit cell parameter and the orientation matrix were determined by least squares refinement using the setting angles of 25 centred reflections ($12^\circ < 2\theta < 22.5^\circ$) measured on an Enraf-Nonious diffractometer with graphite monochromated Mo–K_α radiation. Intensity data were collected at 298 K using a ω-2θ scan technique up to a maximum 2θ of 50°. The weak reflections ($I < 6.0\sigma(I)$) were rescanned and the counts were accumulated to ensure good counting statistics. Crystal and instruments stabilities were monitored with a set of three standard reflections measured every 97 minutes of X-ray exposure time; in all cases no significant variation was found. 5246 reflections were measured ($h \rightarrow 0$ to 16, $K \rightarrow 0$ to 14, $l \rightarrow -19$ to 19) which after data reduction ($R_{int} = 0.0451$) gave 2499 unique reflections. The data were corrected for Lorentz and polarisation effects [19]. An empirical absorption correction based on ψ-scans was also applied resulting in transmission factors ranging from 0.63 to 1.00. Crystal data are summarised in Table 1.

The structure was solved by Patterson method followed by successive Fourier synthesis and refined through full-matrix block least-squares on F^2 with anisotropic thermal parameters for all non-hydrogen atoms. Hydrogen atoms were constrained to ride on the respective carbon or nitrogen atoms (C—H 0.97 Å, N—H 0.900 Å) with an isotropic displacement parameter equal to 1.2 the equivalent isotropic displacement parameter of their parent atom. During last stage of refinement seven reflections (042; 031; 044; 055; 017; 405; 687) were omitted for refinement procedure due to extinction effect. At convergence (maximum parameter shift/esd 0.070), the final residuals were $R1 = 0.0659$; $wR2 = 0.1755$; for 2492 reflections with $I > 2\sigma(I)$, goodness of fit (GoF) = 1.027. Final difference Fourier map showed the maximum and minimum peak hights at 0.97 $eÅ^{-3}$ and -1.02 $eÅ^{-3}$, respectively. The largest one being within 0.91 Å of Zn atom, and having no chemical significance. The perchlorate ion shows symmetry imposed disorder, deviations from tetrahedral geometry and could not be modelled satisfactorily. The high displacement parameters for perchlorate anions are typical for this group for a refinement on room temperature data. Complex neutral-atom scattering factors were used [20]. All calculations were carried out using SHELXS-86 [21], SHELXL-93 [22], PARST [23] and ZORTEP [24] programs. Selected bond lengths [Å] and bond angles [°] are listed in Table 2.

RESULTS AND DISCUSSION

A ZORTEP view of **1** with atom numbering scheme is shown in Fig. 1. Solution of crystal structure reveals

Table 1. Crystallographic data for complex **1**

Empirical formula	$C_{12}H_{35}Cl_3N_6O_{13}Zn_2$
Colour	Colourless
Formula weight	708.55
Temperature	293(2) K
Wavelength, λ (Å)	0.71073
Crystal system	Orthorhombic
Space group	*Pnma*
a (Å)	13.652(1)
b (Å)	12.049(1)
c (Å)	16.455(2)
α (°)	90
β (°)	90
γ (°)	90
V (Å^3)	2706.8(4)
Z	4
ρ_{calcd} (g cm^{-3})	1.739
Absorption coefficient, μ (mm^{-1})	2.136
$F(000)$	1456
Crystal size (mm)	0.22 mm × 0.22 mm × 0.29 mm
Scan mode	ω-2θ
Scan width	$(0.55+0.35\tan\theta)^\circ$
$2\theta_{max}$	50°
Absorption correction	Empirical
T_{max}	1.0000
T_{min}	0.6256
No of reflections used and θ range (°) used for cell parameter	25, $12^\circ < 2\theta < 22.5^\circ$
Reflections collected	5246
Independent reflections	2499
Refinement on	F^2
Data/Restraints/Parameters	2492/0/247
Final R [$I > 2\sigma(I)$]	$R_1 = 0.0659$[a], $wR_2 = 0.1755$[b]
Final R (all data)	$R_1 = 0.1236$, $wR_2 = 0.2143$
Weighting parameters (A, B)[c]	0.1347, 1.3284
Goodness-of-fit on (S)[d]	1.027
Maximum Δ/σ	0.022
ρ_{max} (e Å^{-3})	0.97
ρ_{min} (e Å^{-3})	−1.02

[a] $R_1 = \Sigma\|F_o|-|F_c\|/\Sigma|F_o|$.
[b] $wR = [\Sigma\{w(F_o^2-F_c^2)^2\}/\Sigma\{w(F_o^2)^2\}]^{1/2}$.
[c] $w = 1/[\sigma^2(F_o^2)+(AP)^2+BP]$, where $P = (F_o^2+F_c^2)/3$,
[d] $S = [\Sigma\{(F_o^2-F_c^2)^2\}/(N-P)]^{1/2}$, where N is the number of data and P is the total number of parameters refined.

Table 2. Selected bond lengths [Å] and angles [°] for **1**

Zn—O	1.889(3)
Zn—N(1)	1.979(6)
Zn—N(3)	2.012(7)
Zn—N(2)	2.043(6)
O—Zn 1	1.889(3)
N(1)—C(1)	1.442(10)
N(2)—C(3)	1.402(11)
N(2)—C(4)	1.498(11)
N(3)—C(6)	1.397(10)
C(1)—C(2)	1.445(13)
C(2)—C(3)	1.542(13)
C(4)—C(5)	1.406(13)
C(5)—C(6)	1.484(12)
O—Zn—N(1)	109.7(3)
O—Zn—N(3)	113.0(4)
N(1)—Zn—N(3)	121.2(4)
O—Zn—N(2)	112.5(2)
N(1)—Zn—N(2)	99.3(3)
N(3)—Zn—N(2)	99.8(3)
Zn 1—O—Zn	134.3(4)
C(1)—N(1)—Zn	113.3(5)
C(3)—N(2)—C(4)	112.0(8)
C(3)—N(2)—Zn	115.0(6)
C(4)—N(2)—Zn	109.8(5)
C(6)—N(3)—Zn	119.0(6)
N(1)—C(1)—C(2)	117.7(7)
C(1)—C(2)—C(3)	120.6(9)
N(2)—C(3)—C(2)	118.2(7)
C(5)—C(4)—N(2)	117.9(8)
C(4)—C(5)—C(6)	121.3(8)
N(3)—C(6)—C(5)	118.7(8)

Symmetry transformations used to generate equivalent atoms: #1 x, $-y+1/2$, z.

that two units of Zn(dpt) are bridged by one oxygen atom. The bridging angle is 134.3(4)°. Each Zn possesses distorted tetrahedral geometry. The degrees of distortion from an ideal tetrahedral geometry are reflected in the valence angle around zinc [range: 99.3(3)° to 121.2(4)°]. The average angles of O—Zn—N and N—Zn—N are 111.7° and 106.8° respectively which are close to that of $[Zn([12]aneN_3)OH]^+$ [7] (([12]aneN$_3$) = 1,5,9-triazacyclododecane). The Zn atom is 0.74 Å above the plane of the three nitrogen atom. The six membered chelate ring Zn—N1—C1—C2—C3—N2 adopts a stable chair conformation with Zn and C2 atom lying 0.705 Å and 0.553 Å respectively on opposite side of the least square plane through remaining endocyclic atoms, the maximum in plane atom deviation being 0.040 Å for C3 atom. The other six membered chelate ring Zn—N2—C4—C5—C6—N3 also adopts chair conformation with Zn and C5 atom lying 0.58 and 0.53 Å respectively on opposite side of the least square plane (maximum deviation C4 0.09 Å). The Zn—O distance is 1.889(3) Å. The Zn—N (primary) distances are 1.979(6) Å and 2.012(7) Å and the Zn—N (secondary) distance is 2.043(6) Å. The Zn···Zn distance in this complex is 3.481 Å. The Zn···O bond lengths, the bridging angles and the Zn···Zn closest distance in analogous hydroxo bridged zinc complexes are listed in Table 3. The solid state packing of complex **1** is mainly governed by several hydrogen bonding between perchlorate anion, amine nitrogen and bridging oxygen. IR spectrum of complex **1** gives strong absorption band at 3530 cm^{-1} corresponding to ν_{O-H} stretching vibration. Similar strong band corresponding to ν_{O-H} stretching vibration has also been

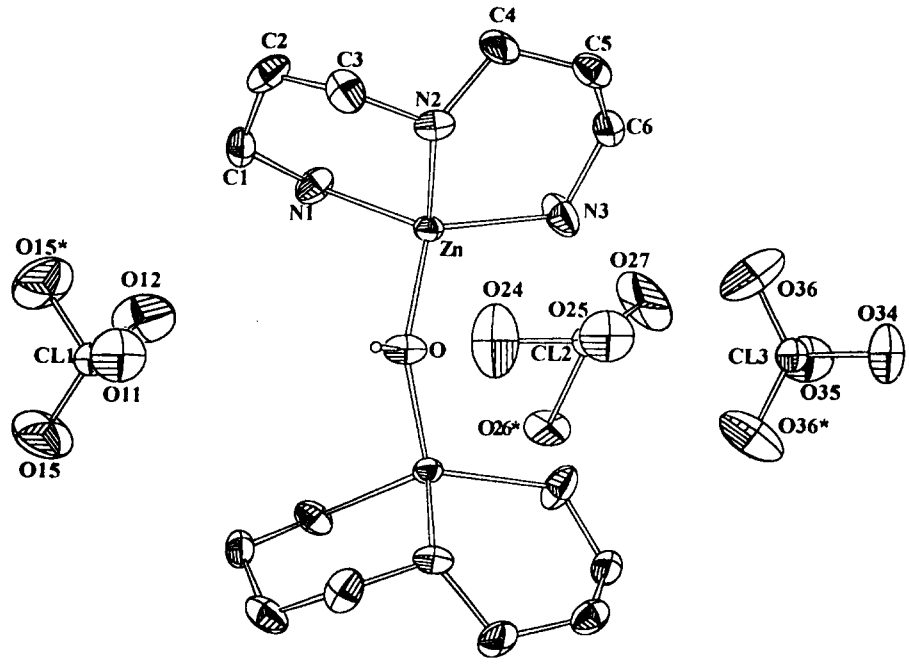

Fig. 1. ZORTEP view of complex **1** showing thermal ellipsoides of the 50% probability level ("*" marked atoms are symmetry related atoms).

Table 3. Some structural parameters of zinc complexes with OH bridge

Complex	Zn···Zn Å	Zn···O Å	Zn—O—Zn	C.N.	Ref.
$[L^1_6Zn_2(\mu\text{-}OH)](ClO_4)_3$	3.54	1.91*	137°	4	[25]
$[L^2_2Zn_2(\mu\text{-}OH)_2](ClO_4)_2$	3.02	1.96*	100.2°	5	[12]
$[L^3_2Zn_2(\mu\text{-}OH)_2]$	2.96	1.89	102.3°	3	[26]
$[L^4_2Zn_2(OH)(\mu\text{-}OH)]_2$	2.71	2.32	71.4°	4	[27]
$[L^2_2Zn_2(\mu\text{-}OH)(\mu\text{-}CH_3CO_2)_2]$ $(ClO_4)\cdot H_2O$	3.31	1.99	112.1°	6	[12]
$[L^5Zn(\mu\text{-}OH)]_3$		1.93*	136.6°	4	[28]
$[(dpt)_2Zn_2(\mu\text{-}OH)](ClO_4)_3$	3.48	1.89	134.3°	4	This work

* Average Zn—O distance; C.N.—Coordination number.

L^1 = 3-tert-butylpyrazole; L^2 = 1,4,7-trimethyl-1,4,7-triazacyclononane; L^3 = tris(dimethylphenylsilyl) methyl; L^4 = tertiary butyl phosphate; L^5 = bis(3-tert-butylpyrazolyl)hydroborate.

observed for **2** and **3** at 3530 and 3510 cm^{-1} respectively.

We tried to synthesise single crystals of **2** and **3** as well but failed. However, comparison study of elemental analysis and IR spectroscopy lead us to assume that **2** and **3** also possess similar structure as **1**. Parameters shown in Table 3. are comparable to that of **1** signifying its possibility to act as a model compound for hydroxo bridged zinc containing enzymes.

Acknowledgment—Funding for the work described was provided by the Council of Scientific and Industrial Research (New Delhi) Grants Scheme is gratefully acknowledged.

REFERENCES

1. Prince, R. H., in *Comprehensive Coordination Chemistry*, Vol. 5, ed. G. Wilkinson. Pergamon, Oxford, 1987, p. 926.
2. Sigel, H., (ed.), Zinc and its role in Biology and Nutrition, in *Metal ions in Biological systems*, Vol. 15. Marcel Dekker, New York, 1983.
3. Spiro, T., (ed.), *Zinc Enzymes*, Wiley, New York, 1983.
4. Dunn, M. F., *Struct. Bonding, (Berlin)*, 1975, **23,** 61.
5. Prince, R. H., *Adv. Inorg. Chem. Radiochem.*, 1979, **22,** 349.

6. Brown, R. S., Huguet, J. and Curtis, N. J., in *Zinc Enzymes*, ed. T. Spiro. Wiley, New York, 1988, p. 55
7. Kimura, E., Shiota, T., Koike, T., Shiro, M. and Kodama, M., *J. Am. Chem. Soc.*, 1990, **112,** 5805.
8. Koike, T. and Kimura, E., *J. Am. Chem. Soc.*, 1991, **113,** 8935.
9. Zhang, X., van Eldic, R., Koike, T. and Kimura, E., *Inorg. Chem.*, 1993, **32,** 5749.
10. Kimura, E., Nakamura, I., Koike, T., Shionoya, M., Kodama, Y., Ikeda, T. and Shiro, M., *J. Am. Chem. Soc.*, 1994, **116,** 4764.
11. Brown, R. S., Curtis, N. J. and Huguet, J., *J. Am. Chem. Soc.*, 1981, **103,** 6953.
12. Chaudhuri, P., Stockheim, C., Wieghardt, K., Deck, W., Gregorzik, R., Vahrenkamp, H., Nuber, B. and Weiss, J., *Inorg. Chem.*, 1992, **31,** 1451.
13. Vacca, A., Arenare, D. and Paoletti, P., *Inorg. Chem.*, 1966, **5,** 1384.
14. Hague, D. N. and Moreton, A. D., *J. Chem. Soc., Dalton. Trans.*, 1987, 2889.
15. Dagnall, S. P., Hague, D. N. and Moreton, A. D., *J. Chem. Soc., Dalton. Trans.*, 1988, 1989.
16. Curtis, N. F., Hay, R. W. and Curtis, Y. M., *J. Chem. Soc. (A)*, 1968, 182.
17. Curtis, N. F., McCormick, I. R. N. and Waters, T. N., *J. Chem. Soc., Dalton. Trans.*, 1973, 1537.
18. Itoh, T., Fujii, Y., Tada, T., Yoshikawa, Y. and Hisada, H., *Bull. Chem. Soc. Jpn*, 1996, **69,** 1265.
19. North, A. C. T., Philips, D. C. and Mathews, F. S., *Acta Cryst.*, 1968, **A24,** 351.
20. *International Tables for Crystallography*, Vol. C, Tables 4.2.6.8 and 6.1.1.4, 1992.
21. Sheldrick, G. M., SHELXS 86. *Program for the Solution of Crystal Structures.* University of Gottingen, Germany 1985.
22. Sheldrick, G. M., SHELXL 93. *Program for the Solution of Crystal Structure.* University of Gottingen, Germany 1993.
23. Nardelli, M., *Comput. Chem.*, 1983, **7,** 1995.
24. Zsolnai, L., ZORTEP. *A program for the presentation of thermal ellipsoids.* University of Heildelberg, Germany, 1994.
25. Alsafasser, R., Powell, A. K. and Vahrenkamp, H., *Angew. Chem., Int. Ed. Engl.*, 1990, **29,** 898.
26. Al-Juaid, S. S., Buttrus, N. H., Eaborn, C., Hitchcock, P. B., Roberts, A. T. L., Smith, J. D. and Sullivan, A. C., *J. Chem. Soc. Chem. Commun.*, 1986, 908.
27. Arif, A. M., Cowley, A. H., Jones, R. A. and Koschmieder, S. U., *J. Chem. Soc. Chem. Commun.*, 1987, 1319.
28. Gorrell, I. B., Looney, A. and Parkin, G., *J. Am. Chem. Soc.*, 1990, **112,** 4068.

Pergamon

PII: S0277-5387(97)00403-8

Polyhedron Vol. 17, No. 8, pp. 1223–1229, 1998
© 1998 Elsevier Science Ltd
All rights reserved. Printed in Great Britain
0277-5387/98 $19.00 + 0.00

Protonation and stability constants for Co^{2+}, Ni^{2+}, Cu^{2+} and Zn^{2+} of two open-chain hexadentate N_6 ligands containing two pyridyl groups: Crystal structures of their Ni(II) complexes

Sun-Deuk Kim,[a]* Jun-Kwang Kim[a] and Woo-Sik Jung[b]

[a] Department of Chemistry, Taegu University, Kyongsan 713-714, South Korea

[b] School of Chemical Engineering and Technology, Yeungnam University, Kyongsan 712-749, South Korea

(Received 16 July 1997; accepted 2 October 1997)

Abstract—Two open-chain hexadentate N_6 ligands containing two pyridyl groups, 1,13-bis(2-pyridyl)-2,5,9,12-tetraazatridecane (bpytd) and 1,14-bis(2-pyridyl)-2,6,9,13-tetraazatetradecane (bpytt), have been synthesized as their tetrahydrochloride salts and their proton association constants and stability constants of Co(II), Ni(II), Cu(II) and Zn(II) chelates have been determined by potentiometry. The stability constants are higher than those for analogous hexadentate N_6 ligands containing one pyridyl moiety, which are in turn higher than those for analogous aliphatic N_6 ligands. The Ni(II) complexes $[Ni(bpytd)](ClO_4)_2 \cdot H_2O$ (**1**) and $[Ni(bpytt)](ClO_4)_2$ (**2**) have been synthesized and their structures have been determined by three-dimensional X-ray diffraction methods. Their geometries at nickel are six-coordinate pseudo-octahedra, with pyridyl nitrogen atoms being mutually *cis* for **1** and *trans* for **2**. © 1998 Elsevier Science Ltd. All rights reserved

Keywords: protonation; stability; structure; complexes.

Our recent interest has been in the development of new open-chain saturated polyamine ligands containing pyridyl or imidazoyl groups and the investigation on their interactions with first-row transition metal ions [1,2]. The stability constants of the ligands with the metal ions are higher than those of the analogous aliphatic polyamines [1–6]. The saturated polyamines, which are soluble and stable in water, have been synthesized by hydrogenation of aldimino groups in parent Schiff bases [1,2,7].

This paper describes the preparation of two new potentially hexadentate N_6 ligands, 1,13-bis(2-pyridyl)-2,5,9,12-tetraazatridecane (bpytd) and 1,14-bis(2-pyridyl)-2,6,9,13-tetraazatetradecane (bpytt) by hydrogenation of —C=N bonds of parent Schiff bases and their protonation constants and stability constants of metal chelates. These ligands contain one or two propylenic spacers, which make six-membered chelate rings, between the aliphatic nitrogen atoms. In a previous paper we reported the preparation of 1,12-bis(2-pyridyl)-2,5,8,11-tetraazadodecane (pytrien) with all ethylenic spacers, which make five-membered chelate rings, between the aliphatic nitrogen atoms [1]. It is our intention to establish whether or not the presence of propylenic spacers has an effect on the equilibrium constants and the structure of metal complexes coordinated with the ligands. Structures of the nickel(II) complexes $[Ni(bpytd)](ClO_4)_2 \cdot H_2O$ (**1**) and $[Ni(bpytt)](ClO_4)_2$ (**2**) are reported and compared with the structure of $[Ni(pytrien)](ClO_4)_2$ [7].

* Author to whom correspondence should be addressed.

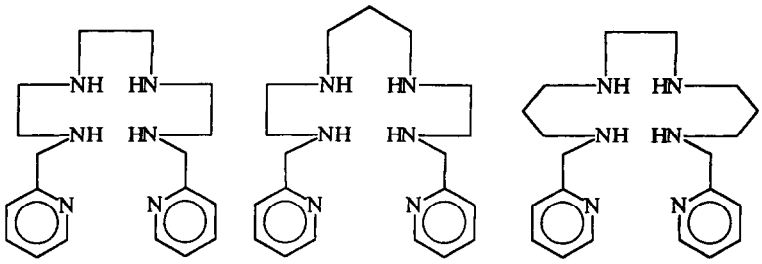

pytrien bpytd bpytt

EXPERIMENTAL

Preparation

1,13-*Bis*(2-*pyridyl*)-2,5,9,12-*tetraazatridecane* · *tetrahydrochloride*(*bpytd*·4*HCl*). To a solution of pyridine-2-carboxaldhyde (2.14 g, 0.02 mol) in absolute methanol (25 ml) was added *N*,*N*′-bis(2-aminoethyl)-1,3-propane diamine (1.80 g, 0.01 mol), and the solution was refluxed overnight under dinitrogen atmosphere. Sodium borohydride (1.51 g, 0.04 mol) was added in small parts to the solution, and the mixture was neutralized to pH 7.0–7.5 with concentrated hydrochloric acid in an ice bath and filtered to remove the white solid formed. The filtrate was further acidified to pH 2 and allowed to stand at 4°C for 6 h. The white crystals formed were filtered off, washed with H_2O/methanol (5/95, v/v) and air-dried. Yield: 3.3 g (68%). Anal. Found: C, 46.9; H, 7.0; N, 17.0. Calc. for $C_{19}H_{34}N_6Cl_4$: C, 46.7; H, 7.0; N, 17.2. ^{1}H NMR (D_2O-DMSO-d_6): 8.50 (2H, d, *J*(CH) 7.35 Hz, pyridine H), 7.91 (2H, t, *J*(CH) 8.57, 14.25 Hz, pyridine H), 7.47 (4H, m, pyridine H), 4.33 (4H, s, pyridylmethyl), 3.40 (8H, s, ethylene), 3.50 (4H, t, *J*(CH) 11.61, 12 Hz, propylene), 2.10 (2H, m, propylene); ^{13}C NMR (D_2O-DMSO-d_6): 147.3, 145.4, 137.2, 122.2, 121.6, 48.1, 42.0, 40.9, 40.3, 19.9. IR (cm^{-1}): 2940 (s), 2755 (vs), 2705 (vs), 2555 (s), 2405 (s), 1590 (s), 1465 (s), 1435 (s), 1040 (s), 805 (w), 758 (s).

1,14-*Bis*(2-*pyridyl*)-2,6,9,13-*tetraazatetradecane tetrahydrochloride* (*bpytt*·4*HCl*). *N*,*N*′-bis(3-aminopropyl)ethylenediamine (1.95, 0.01 mol) and 5 ml of triethylorthoformate were slowly added to a solution of pyridine-2-carboxaldehyde (2.14 g, 0.02 mol) in absolute methanol (20 ml). The yellow solution was concentrated with a rotary evaporator and the remaining yellow oil was subsequently dissolved in methanol (40 ml). Sodium borohydride (1.51 g, 0.04 mol) was added in small portions to the solution, and the mixture was neutralized to pH 7.0–7.5 with concentrated hydrochloric acid in an ice bath and filtered to remove the white solid formed. The white filtrate was further acidified to pH 2 and allowed to stand at 4°C for 6 h. The white crystals formed were filtered off, washed with H_2O: methanol (5:95, v/v) and air-dried. Yield: 4.0 g (79%). Anal. Found: C, 48.0; H, 7.5; N, 16.5. Calc. for $C_{20}H_{36}N_6Cl_4$: C, 47.8; H, 7.2; N, 16.7; ^{1}H NMR (D_2O-DMSO-d_6): 8.52 (2H, d, *J*(CH) 7.35 Hz, pyridine H), 7.90 (2H, t, *J*(CH) 3.48, 10.77 Hz, pyridine H), 7.47 (2H, m, pyridine H), 4.34 (4H, s, pyridylmethyl), 3.38 (4H, s, ethylene), 3.14 (8H, m, propylene), 2.10 (4H, m, propylene); ^{13}C NMR (D_2O-DMSO-d_6): 146.5, 146.0, 136.6, 122.1, 121.6, 47.7, 42.3, 41.5, 40.2, 19.8. IR (cm^{-1}): 2947 (vs), 2700 (vs), 2400 (vs), 1490 (s), 1461 (s), 1432 (s), 1267 (w), 1032 (w), 1019 (w), 763 (s). Mass: 355 $[MP\text{-}4HCl]^+$.

[Ni(bpytd)]$(ClO_4)_2 \cdot H_2O$ (**1**) *and* [Ni(bpytt)]$(ClO_4)_2$ (**2**). The complex **1** was prepared by the following method. A mixture of sodium acetate trihydrate (0.54 g, 4 mmol) and bpytd · 4HCl (0.48 g, 1 mmol) in absolute methanol (30 ml) was stirred for 30 min and filtered. Nickel acetate tetrahydrate (0.24 g, 1 mmol) was added to the filtrate. Excess sodium perchlorate (0.50 g, 4 mmol) dissolved in methanol was added to the resulting pink solution and then the mixture was stored at room temperature during 2 days. The pink parallelepiped crystals formed were filtered off, washed with a small amount of cold methanol, and air-dried. Recrystallization from methanol: CH_3CN (1 : 1, v/v) afforded crystals suitable for X-ray crystallographic analysis. Yield: 53% (0.32 g) Anal. Found: C, 37.2; H, 4.9; N, 13.6. Calc. for $NiC_{19}H_{32}N_6O_9Cl_2$: C, 37.2; H, 4.6; N, 13.7; λ_{max} (CH_3CN) = 535 nm (ε = 13 M^{-1} cm^{-1}); molar conductance (CH_3CN) = 285 Ω^{-1} M^{-1} cm^{-2}; IR (cm^{-1}): 3304 (s), 3270 (s), 3200 (s), 2920 (s), 2880 (s), 1600 (s), 1430 (s), 1230 (w), 1090 (vs), 762 (s), 622 (vs).

The complex **2** was synthesized by the method given for **1** except that it was isolated in a refrigerator. Yield: 60% (0.36 g) Anal. Found: C, 39.3; H, 4.9; N, 13.6. Calc. for $NiC_{20}H_{32}N_6O_8Cl_2$: C, 39.4; H, 4.6; N, 13.8; λ_{max}(CH_3CN) = 524 nm (ε = 42 M^{-1} cm^{-1}); molar conductance (CH_3CN) = 279 Ω^{-1} M^{-1} cm^{-2}; IR (cm^{-1}): 3290 (s), 3170 (w), 2940 (s), 1650 (s), 1481

(w), 1431 (s), 1284 (w), 1092 (vs), 955 (s), 903 (w), 764 (s), 624 (vs).

Equilibrium constant determinations

All titrations were carried out in aqueous solution under dinitrogen atmosphere on a Metrohm 605 pH meter. In all cases, the ligand was present at 1.00×10^{-3} M. Solutions were adjusted to 0.10 M ionic strength by the addition of KNO_3 at 25.0 ± 0.1°C. The proton association constants (K_H^n) of the ligand (L), which are defined by $[H_nL]/[H][H_{n-1}L]$, were determined by titration of the protonated ligand with standardized KOH in absence of complexing metal ions and then by calculation of the results by the aid of a computer program of PUKAS [8].

The stability constants (K_{ML}) of metal (M) chelates, which are defined by [ML]/[M][L], were determined by titration of the protonated ligand with KOH in the presence of metal ions. The titrations were performed on 1 : 1 molar ratios of the ligand with the metal ions. Titration curves were calculated using a computer program of BESTA [8].

Physical measurements

UV-vis electronic absorption spectra were recorded on a Shimadzu UV-160A spectrophotometer. ^{1}H- and ^{13}C-NMR spectra were recorded with a Bruker AM-300 spectrometer and reported as δ in ppm relative to DMSO-d_6 (2.64 ppm for ^{1}H and 39.7 ppm for ^{13}C). Infrared spectra of the powdered samples (KBr discs for ligands and mulls for complexes) were taken using a Shimadzu IR 440 spectrophotometer. Mass spectra were obtained with a Kratos 25-RFA GC-Mass spectrometer and elemental analysis were performed on a Carlo Erba Model 1160.

Crystal structure determination

A selected crystal was set up on an automatic diffractometer. Unit cell dimensions with estimated standard deviations were obtained from least-squares refinements of the setting angles of 25 well centered reflections. Two standard reflections were monitored periodically; they showed no change during data collection. Corrections were made for Lorentz and polarization effects. Empirical absorption correction (DIFABS) [9] and an extinction correction were applied. Computations were performed by using the PC version of CRYSTALS [10]. Atomic form factors for neutral Ni, Cl, O, N, C and H were taken from Ref. 11. Real and imaginary parts of anomalous dispersion were taken into account. The structure was solved by direct methods (SHELXS) [12] and successive Fourier maps. Some hydrogens could be found on difference maps and the other hydrogens were geometrically located. They were all given an overall isotropic thermal parameter. All non-hydrogen atoms were anisotropically refined. Full matrix least-square refinements were carried out by minimizing the function $\Sigma w(F_0 - |F_c|)^2$ where F_0 and F_c are the observed and calculated structure factors, respectively. Models reached convergence with $R = \Sigma(|F_0 - |F_c||)/\Sigma w\ F_0$ and $Rw = [\Sigma w(F_0 - |F_c|)^2/\Sigma w(F_0)^2]^{1/2}$, each reflection being assigned a weight unity. Criteria for a satisfactory complete analysis were the ratios of rms shift to standard deviations being less than 0.1 and no significant features in the last difference map.

RESULTS AND DISCUSSION

Syntheses and characterization

The ligands, 1,13-bis(2-pyridyl)-2,5,9,12-tetraazatridecane (bpytd) and 1,14-bis(2-pyridyl)-2,6,9,13-tetraazatetradecane (bpytt), were isolated as tetrahydrochloride salts by hydrogenation of C=N bonds of the Schiff bases obtained from condensation reactions of pyridine-2-carboxyaldehyde with *N,N'*-bis(2-aminoethyl)-1,3-propanediamine and *N,N'*-bis(3-aminopropyl)-1,3-ethylenediamine, respectively. For the case of bpytt, H_2O which was formed by the condensation reaction was removed by addition of triethylorthoformate. The ligands were characterized by elemental analysis, IR, ^{1}H- and ^{13}C-NMR and mass spectra (see Experimental section).

The complexes **1** and **2** were synthesized by the reactions of methanolic solution of 1 equiv. of the respective ligand with 4 equiv. of sodium acetate and 1 equiv. of nickel acetate, followed by the addition of sodium perchlorate. The values of molar conductance of **1** and **2** in CH_3CN indicate that the complexes are 1 : 2 electrolytes. The perchlorate anions in the complexes were identified by their IR spectra.

Equilibrium constants

Protonation constants of bpytd and bpytt have been studied in 0.10 M KNO_3 in aqueous solution at 25.0°C. Their stepwise protonation constants were calculated from potentiometric equilibrium curves and are listed in Table 1, together with the corresponding values for 1,12-bis(2-pyridyl)-2,5,8,11-tetraazadodecane (pytrien). The constants from K_H^1 to K_H^4 correspond to those of protonation of aliphatic amine groups and the constant K_H^5 corresponds to that of protonation on one of nitrogen atoms in pyridyl moieties, considering that the nitrogen atom on the pyridyl moiety is less basic than those on aliphatic amines [13]. Each stepwise protonation constant for bpytt is similar to that for bpytd but is higher than for pytrien. The results are expected from the fact that the electrostatic repulsions between protonated aliphatic nitrogen atoms are mitigated for the ligands having propylenic spacers between the aliphatic nitrogen atoms [14].

Table 1. Ligand protonation constants for pytrien, bpytd and bpytt at 298.1 K in 0.10 M KNO_3

Ligand	log K_H^1	log K_H^2	log K_H^3	log K_H^4	log K_H^5	Reference
pytrien	9.08	8.78	7.51	5.42	2.99	1
bpytd	9.68	9.24	7.79	5.64	3.48	This work
bpytt	9.62	9.31	7.88	6.03	3.20	This work

Table 2. Logarithms of stability constants for Co^{2+}, Ni^{2+}, Cu^{2+} and Zn^{2+} chelates of N_6-containing ligands at 298.1 K in 0.10 M KNO_3

Ligand	Co^{2+}	Ni^{2+}	Cu^{2+}	Zn^{2+}	Reference
aptatd	18.00	21.31	23.62	15.60	2
Me_2linpen[a]	14.8	18.2	21.6	14.0	15
pytrien	17.02	23.03	24.15	16.03	1
bpytd	20.75	25.16	27.72	17.89	This work
bpytt	17.75	23.84	26.54	16.33	This work

[a] In 0.15 M $NaClO_4$.

Table 3. Selected bond lengths (Å) and angles (°) for the non-hydrogen atoms of **1**

Ni(1)—N(1)	2.10(1)	Ni(1)—N(2)	2.14(1)
Ni(1)—N(3)	2.09(1)	Ni(1)—N(4)	2.14(1)
Ni(1)—N(5)	2.12(1)	Ni(1)—N(6)	2.10(1)
N(1)—Ni(1)—N(2)	79.9(4)	N(1)—Ni(1)—N(3)	93.2(4)
N(2)—Ni(1)—N(3)	83.9(4)	N(1)—Ni(1)—N(4)	99.0(4)
N(2)—Ni(1)—N(4)	177.0(5)	N(3)—Ni(1)—N(4)	93.4(4)
N(1)—Ni(1)—N(5)	171.6(5)	N(2)—Ni(1)—N(5)	96.3(4)
N(3)—Ni(1)—N(5)	93.8(4)	N(4)—Ni(1)—N(5)	85.2(4)
N(1)—Ni(1)—N(6)	92.8(4)	N(2)—Ni(1)—N(6)	92.9(4)
N(3)—Ni(1)—N(6)	172.6(5)	N(4)—Ni(1)—N(6)	90.0(4)
N(5)—Ni(1)—N(6)	79.9(5)	Ni(1)—N(1)—C(1)	127.6(10)

Table 4. Selected bond lengths (Å) and angles (°) for the non-hydrogen atoms of **2**

Ni(1)—N(1)	2.133(5)	Ni(1)—N(2)	2.112(5)
Ni(1)—N(3)	2.120(5)	Ni(1)—N(4)	2.113(5)
Ni(1)—N(5)	2.118(5)	Ni(1)—N(6)	2.116(5)
N(1)—Ni(1)—N(2)	80.7(2)	N(1)—Ni(1)—N(3)	88.4(2)
N(2)—Ni(1)—N(3)	91.8(2)	N(1)—Ni(1)—N(4)	103.5(2)
N(2)—Ni(1)—N(4)	171.8(2)	N(3)—Ni(1)—N(4)	81.4(2)
N(1)—Ni(1)—N(5)	90.0(2)	N(2)—Ni(1)—N(5)	93.9(2)
N(3)—Ni(1)—N(5)	173.8(2)	N(4)—Ni(1)—N(5)	93.1(2)
N(1)—Ni(1)—N(6)	166.3(2)	N(2)—Ni(1)—N(6)	90.5(2)
N(3)—Ni(1)—N(6)	102.3(2)	N(4)—Ni(1)—N(6)	86.6(2)
N(5)—Ni(1)—N(6)	80.1(2)		

Titrations of bpytd·4HCl in the presence of the ions Co(II), Ni(II), Cu(II) and Zn(II) with KOH yield neutralization curves. The chelate stability constants (K_{ML}) obtained from the curves are listed in Table 2, along with those of bpytt, pytrien, 1-amino-13-(2-pyridyl)-3,6,9,12-tetraazatridecane (aptatd) and *N,N'*-dimethyl-3,6,9,12-tetraazatetradecane-1,14-diamine(Me_2linpen). As expected on the basis of the general Irving–Williams order, the stability constants for all ligands given follow the order: $Co^{2+} < Ni^{2+} < Cu^{2+} > Zn^{2+}$. The stability constants for the ligands (e.g. pytrien, bpytd and bpytt) carrying two pyridyl moieties increase in the order: pytrien < bpytt < bpytd. The order might be explained to some extent by taking account of two factors, i.e. the size of chelate rings and the steric strain, even though the factors are hard to be evaluated quantitatively.

The stability constants for ligands used in this study are higher for each metal chelate than those for ligands (e.g. aptatd) carrying one pyridyl moiety, which are in turn higher than those for the aliphatic N_6 ligands (e.g. Me_2linpen) [15]. The results are in agreement with the general trend that the stability constants for first-row transition metal ions of pyridyl-containing ligands are higher than those of analogous polyamines [1–6]. This enhanced stability is partially attributed to π bonding between the pyridyl π or π^* orbitals and *d* orbitals of appropriate metal ions. But the π bonding alone is not likely to offer sufficient explanation of the enhanced stability of Zn(II) ion with the d^{10} electronic configuration because the *d* orbitals of zinc are too low in energy to overlap strongly with ligand orbitals. As explained by Martell *et al.* [6], there are entropic and enthalpic differences between chelation by an aliphatic amine and chelation by nitrogen bound in a more rigid pyridyl ring. The aliphatic amines must sacrifice rotational freedom about the C—N bonds in order to chelate a metal ion, leading to the less favorable entropies.

X-ray crystal structures of $[Ni(bpytd)](ClO_4)_2 \cdot H_2O$ *and* $[Ni(bpytt)](ClO_4)_2$

Cations in these complexes have distorted octahedral coordination geometry, as shown in Figs 1 and 2. Selected bond distances and angles for each cation are listed in Tables 3 and 4. In both cations the ligands are coordinated to nickel atom through six nitrogen atoms involving two pyridyl (N1 and N6) and four secondary amine nitrogen atoms (N2, N3, N4 and N5). The bond lengths between Ni and pyridyl nitro-

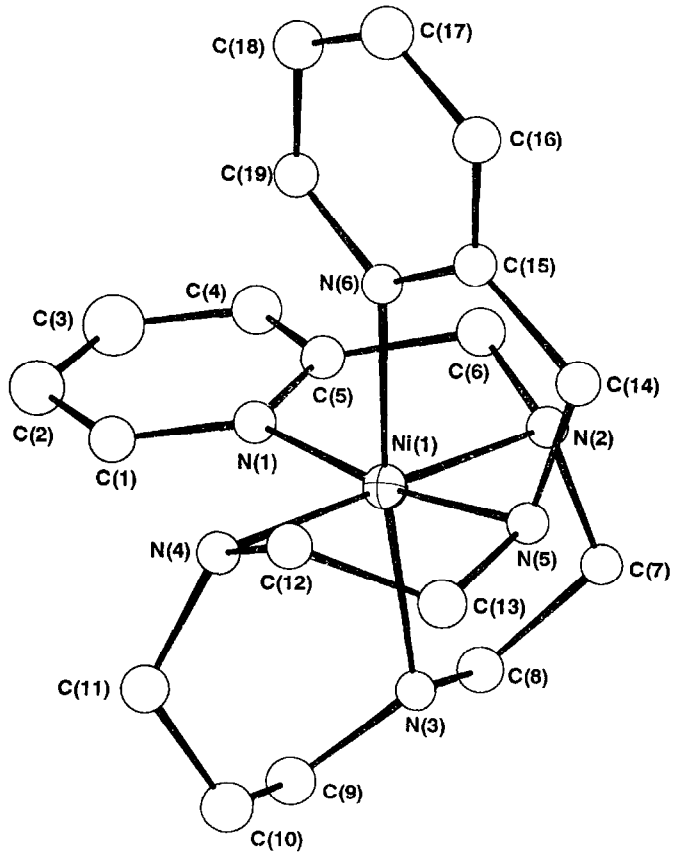

Fig. 1. CAMERON drawing of the molecular structure of $[Ni(bpytd)]^{2+}$ cation showing 30% probability thermal ellipsoids.

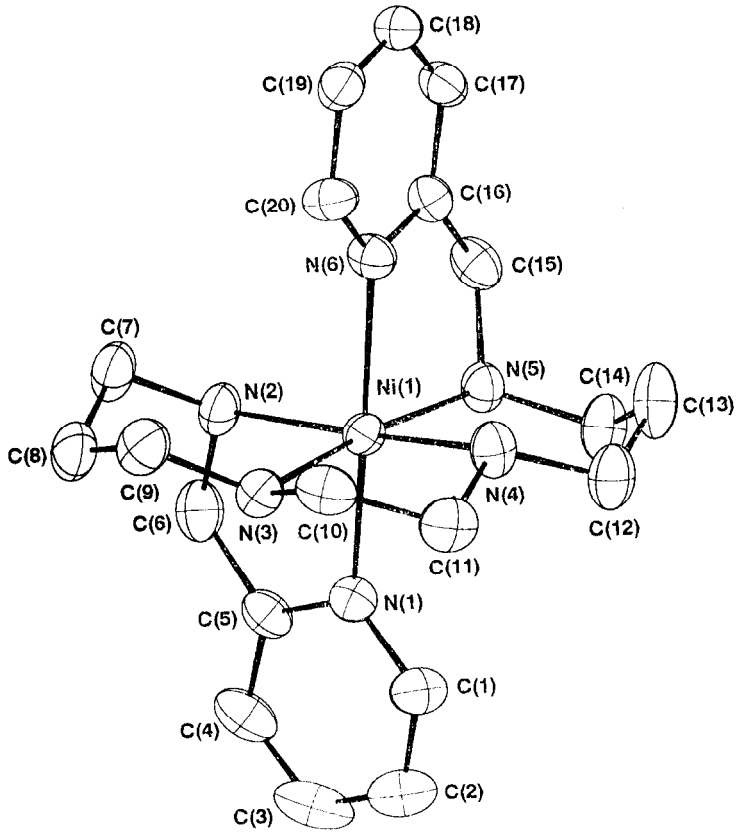

Fig. 2. CAMERON drawing of the molecular structure of $[Ni(bpytt)]^{2+}$ cation showing 30% probability thermal ellipsoids.

gen atoms are not really different from those between Ni and amine nitrogen atoms. The structure of $[Ni(bpytd)]^{2+}$ cation is similar to that [7] of $[Ni(pytrien)]^{2+}$ cation in that the pyridyl nitrogen atoms are mutually *cis*. In both cations four chelate bond angles subtended by each ligand at the nickel atom are similar to each other but one chelate bond angle N(3)—Ni(1)—N(4) for the former cation is closer to 90° than the corresponding angle for the latter cation, because of the presence of the propylenic space. In the structure of $[Ni(bpytt)]^{2+}$ cation the pyridyl nitrogen atoms are mutually *trans*. The bond angles are more deviated from those in an octahedral geometry in the order: $[Ni(bpytt)]^{2+} < [Ni(bpytd)]^{2+} < [Ni(pytrien)]^{2+}$. For example, bond angles such as N(2)—Ni(1)—N(3) and N(4)—Ni(1)—N(5) for $[Ni(bpytt)]^{2+}$ are almost rectangular because of the presence of two propylenic spacers between aliphatic nitrogen atoms. The deviation in the bond angles seems to result in decreasing the stability of metal complexes.

Supplementary material. Tables (Tables S1-1–5 for **1** and S2-1–5 for **2**) of X-ray crystallographic data, including complete refined positional parameters, anisotropic thermal parameters, bond distances, bond angles and observed/calculated structure factors are available from the authors upon request.

Acknowledgements—We are grateful to Professor Pierre Gouzerh and Dr Claudette Bois, Laboratoire de Chimie des Métaux de Transition, Université Pierre et Marie Curie for X-ray structure determination. This research was supported by the Taegu University Research Grant, 1997.

REFERENCES

1. Kim, S.-D., Kim, J.-K. and Jung, W.-S., *Bull. Kor. Chem. Soc.*, 1996, **17**, 80.
2. Kim, S.-D., Kim, J.-K. and Jung, W.-S., *Bull. Kor. Chem. Soc.*, 1997, **18**, 653.
3. Lacoste, R. G. and Martell, A. E., *Inorg. Chem.*, 1964, **3**, 881.
4. Harris, W. R., Murase, I., Timmons, J. H. and Martell, A. E., *Inorg. Chem.*, 1978, **17**, 889.
5. Timmons, J. H., Harris, W. R., Murase, I. and Martell, A. E., *Inorg. Chem.*, 1978, **17**, 2192.
6. Timmons, J. H., Martell, A. E., Harris, W. R. and Murase, I., *Inorg. Chem.*, 1982, **21**, 1525.
7. Arulsamy, N., Glerup, J. and Hodgson, D. J., *Inorg. Chem.*, 1994, **33**, 3043.
8. Motekaitis, R. J. and Martell, A. E., *Determination and Use of Stability Constants*, VCH, U.S.A., 1992.
9. Walker, N. and Stuart, D., *Acta Crystallogr.*, 1983, **A39**, 158.
10. Watkin, D. J., Carruthers, J. R. and Betteridge,

P. W., *Crystals User Guide*, *Chemical Crystallography Laboratory*, Oxford, 1988.
11. *International Tables for X-ray Crystallography*, Vol. IV, Kynoch Press, Birmingham, England, 1974.
12. Sheldrick, G. M., *SHELXS* 86, *Program for Crystal Structure Solution*, University of Göttingen, Göttingen, 1986.
13. Huheey, J. E., *Inorganic Chemistry*, 3rd edn, Harper, Cambridge, U.K., 1983, p. 150.
14. Aguilar, J. A., Bianchi, A., García-España, E., Luis, S. V., Llinares, J. M., Ramírez, J. A. and Soriano, C., *J. Chem. Soc., Dalton Trans.*, 1994, 637.
15. (a) Aragó, J., Bencini, A., Bianchi, A., García-España, E., Micheloni, M., Paoletti, P., Ramírez, J. A. and Paoli, P., *Inorg. Chem.*, 1991, **30,** 1843; (b) Aragó, J., Bencini, A., Bianchi, A., García-España, E., Micheloni, M., Paoletti, P., Ramírez, J. A. and Rodriguez, A., *J. Chem. Soc., Dalton Trans.*, 1991, 3077; (c) Bencini, A., Bianchi, A., Fusi, V., Paoletti, P., Valtancoli, B., Andrés, A., Aragó, J. and García-España, E., *Inorg. Chim. Acta*, 1993, **204,** 221.

Pergamon

PII: S0277-5387(97)00399-9

Polyhedron Vol. 17, No. 8, pp. 1231–1240, 1998
© 1998 Elsevier Science Ltd
All rights reserved. Printed in Great Britain
0277-5387/98 $19.00+0.00

Synthesis and characterization of nickel(II), copper(II), manganese(III) and iron(III) complexes with new chiral salen-type ligand {N,N′-bis(3,5-di-*tert*-butylsalicylidene)-(1*R*,3*S*)-1,3-diamine-1,2,2-trimethylcyclopentane}

Andrzej Vogt,[a]* Stanisław Wołowiec,[a] Ram L. Prasad,[b]† Anil Gupta,[b] and Jacek Skarżewski,[b]*

[a] Department of Chemistry, University of Wrocław, 50-383 Wrocław, Poland;

[b] Institute of Organic Chemistry, Biochemistry and Biotechnology, Technical University, 50-370 Wrocław, Poland

(Received 8 August 1997; accepted 24 September 1997)

Abstract—The title Schiff base (^{tBu}SalcamH$_2$) obtained by condensation of enantiomerically pure (1*R*,3*S*)-1,2,2-trimethyl-1,3-cyclopentanediamine with 3,5-di-*tert*-butylsalicylic aldehyde was used as a ligand to prepare Ni(II), Cu(II), Mn(III), and Fe(III) 1 : 1 complexes. The compounds were characterized by physicochemical methods. Catalytic activity of (^{tBu}Salcam)MnCl complex was tested in the reactions of single oxygen atom transfer. © 1998 Elsevier Science Ltd. All rights reserved

Keywords: chiral salen type complexes; nickel complex; copper complex; manganese complex; iron complex.

INTRODUCTION

Transition metal complexes with Schiff bases derived from diamines (salen-type ligands) have been studied broadly in view of their significance as biomimetic catalysts. During the last decade increasing interest in the catalyzed asymmetric synthesis has brought much attention to the chiral metal complexes of this class [1]. So far, the chiral salen-type ligands used, including the most spectacular Jacobsen catalyst, (^{tBu}Salchl)MnCl designed for enantioselective epoxidation were obtained from optically active 1,2-diamines and rather little is known about the corresponding 1,3-diamine derivatives [2].

The outstanding catalytic activity of (^{tBu}Salchl)MnCl based on chiral 1,2-cyclohexanediamine prompted us to study other salen-type transition metal complexes. Previously, we have investigated the catalytic role played by the achiral (^{tBu}Salen)Mn(III) complex in the epoxidation of olefins in the presence of 4-alkoxypyridine 1-oxides [3]. Now, we attempt to modify the spatial relations within a ligand by introducing chiral, conformationally affixed 1,3-cyclopentanediamine instead of 1,2-cyclohexanediamine used in (^{tBu}Salchl)MnCl. Such a modification renders two faces of the complexes unequivalent. This may lead to the new conditions for chirality transfer in the catalyzed reaction.

In this paper we report the synthesis and physicochemical characterization of new homochiral ligand: N,N′-bis(3,5-di-*tert*-butylsalicylidene)-(1*R*,3*S*)-1,3-diamine-1,2,2-trimethylcyclopentane (^{tBu}SalcamH$_2$) and their complexes with Ni(II), Cu(II), Mn(III), and Fe(III) ions. We studied their

* Author to whom correspondence should be addressed.
† Visiting scholar from NERIST, Nirjuli, India.

stereochemistry by 2D NMR and other spectral methods. Additionally, catalytic activity of the respective manganese(III) complex in the oxidation reactions was examined and its performance was compared with that for Jacobsen catalyst.

EXPERIMENTAL

FT IR spectra in KBr pellets were performed on a Perkin-Elmer 1725X instrument. Electronic spectra were recorded on a Cary-5 or Beckman UV 5240 spectrophotometer. The circular dichroism spectra were taken with a JASCO 600 J instrument. EPR spectra were recorded with Bruker 100TT instrument. Magnetic susceptibility measurements were carried out using the Gouy method at the temperature range of 77–300 K. Mass spectra were obtained at a Finnigan MAT TSQ 700 spectrometer by the Electro-Spray Ionization method at 4.5 kV ionisation potential and 250°C capillary temperature in acetonitrile solvent. ^{1}H NMR spectra were obtained with a Bruker AMX300 spectrometer using standard procedures for COSY and NOESY measurements and fast-pulse sequence (repetition time 0.1 s) for paramagnetic manganese(III) and iron(III) complexes. The chloroform-d was the solvent in all cases. The residual solvent peak at 7.24 ppm was used as internal chemical shift standard. Cyclic voltammograms were taken on an Electrochemical Analysis Software analyser, model 270 using a solution of metal complex (5.0 mM) in methylene dichloride containing tetrabutylammonium chloride (0.10 M) as a supporting electrolyte at 0.5 $Vsec^{-1}$ scan rate. GC/MS spectra were determined on a Hewlett-Packard 5890 II gas chromatograph (25 m capillary column) with a Hewlett Packard mass spectrometer 5971 A operating on the electron impact mode (70 eV). Separations of products by chromatography were performed on silica gel 60 (230–400 mesh) purchased from Merck or florisil from Fluka. Thin layer chromatography analyses were performed using silica gel 60 precoated plates (Merck).

Syntheses of ligands

Preparation of the known chiral diamine **1** used for the Schiff base synthesis was carried out as described by Sato and coworkers [4]. GC: over 98% purity. $[\alpha]^{578} = +30.5°$ (c 1.0, ethanol). Yield 94%.

N,N'-bis(3,5-*di*-tert-*butylsalicylidene*)-(1R,3S)-1,3-*diamine*-1,2,2-*trimethylcyclopentane*, (**2**), ((^{tBu}*Salcam*)H_2). To a solution of chiral diamine **1** (0.290 g, 2.04 mmol) in abs. ethanol (10 ml) 3,5-di-*tert*-butylsalicyl aldehyde (0.955 g, 4.08 mmol) was added and the mixture was refluxed for 1 h. After ethanol was evaporated, the crude product was purified by chromatography on florisil (eluent: *n*-hexane + 6% di-isopropyl ether). Thus obtained oily product has solidified after standing for a few days at room temperature. M.p. 186–186.5°C; 84% yield; $[\alpha]^{578} = +10.4°$ (c 0.996, CCl_4); IR (film, cm^{-1}): $\gamma_{C=N}$ 1633, γ_{C-O} 1480, γ_{C-N} 2872, 2888, 2964; ^{1}H NMR ($CDCl_3$, δ, ppm, the assignments based on COSY and NOESY experiments, for numbering, see: scheme 1): 1.30, 1.29 (two *s*, 18H, *t*-Bu_9 and *t*-Bu_{16}); 1.30 (*s*, 3H, Me_1); 1.43, 1.42 (two *s*, 18H, *t*-Bu_{11} and *t*-Bu_{18}); 0.97, 0.95 (two *s*, 6H, $2Me_2$); 2.35–1.97 (m, 4H, H_4 and H_5); 3.55 (*t*, 1H, $J = 9.4$ Hz, H_3); 7.20, 7.09 (two *d*, 2H, H_8 and H_{15}); 7.37, 7.36 (two overlapping doublets, 2H, $J = 2.8$ Hz $H_{10} + H_{17}$); 8.34 (*s*, 2H, H_6 and H_{13}); 13.83, 14.20 (two *s*, 2 × 1H, two O*H* 12 and 19). UV-Vis {λ [nm] (ε)}: 230 (5.26×10^4); 265 (4.03×10^4); 330 (1.07×10^4); 425 (150). Anal. Calc. for $C_{38}H_{58}N_2O_2$: C 79.39; H 10.17; N 4.87. Found: C 79.55; H 10.09; N 4.47.

N,N'-bis(*salicylidene*)-(1R,3S)-1,3-*diamine*-1,2,2-*trimethylcyclopentane*, (**3**) (*SalcamH*$_2$). The synthesis and purification of ligand **3** was done according to the same procedure as in case of ligand **2** (see scheme 1). The product was recrystallized from toluene/hexane. Yield 54%, m.p. 159.5–160°C, $[\alpha]^{578} = +27.7°$ (1.02 mol × dm^{-3} in CCl_4), $\gamma_{C=N}$ 1630, γ_{C-O} 14..., γ_{C-H} 2872, 2900, 2988. ^{1}H NMR ($CDCl_3$): 0.94, 0.95 and 1.30 (three *s*, 3 × 3H) 2 × Me_2 and Me_1 1.75–2.35 (m, 4H, $H_4 + H_5$); 3.58 (*t*, 1H, $J = 9.4$ Hz, H_3); 6.84–7.32 (multiplets, 8H, aromatic H); 8.33 (*s*, 2H, $H_6 + H_{13}$); 13.58–14.09 (two *s*, 2 × 1H, two O*H* 12 and 19). Anal. Calc. $C_{22}H_{26}N_2O_2$: C 75.36; H 7.47; N 8.02. Found: C 75.20; H 7.22; N 7.94. MS 351 {$(SalcamH_3)^+$}.

Syntheses of complexes

(^{tBu}*Salcam*)*Ni*. The nickel(II) complex of **2** was obtained by dropwise addition of 0.175 g $Ni(CH_3COO)_2 \cdot 4H_2O$ (0.703 mmol) dissolved in 10 ml ethanol into stirred mixture containing 0.403 g (0.701 mmol) **2** in 4 ml methylene dichloride, 6 ml ethanol and 5 ml water, containing 0.056 g sodium hydroxide under reflux. The heating was continued 1 h and then the product (^{tBu}Salcam)Ni was extracted with petroleum ether. Organic phase was dried over sodium sulphate and the solvents were evaporated. The crude product was purified by chromatography on silica gel with 90 : 9 : 1 hexane : chloroform : ethanol mixture with increasing gradient of ethanol. Yield 33%.

(^{tBu}Salcam)Ni Anal. Calc. $C_{38}H_{56}N_2O_2Ni$: C 72.26; H 8.94; N 4.44. Found: C 72.11; H 8.94; N 4.17, MS 632 {(^{tBu}Salcam)Ni^+}, IR $\gamma_{C=N}$ 1612 cm^{-1}, ^{1}H NMR (see results and discussion). UV-Vis{λ [nm] (ε)}: intraligand: 233 (2.98×10^4); 280 (2.90×10^4); 338 (5.0×10^3); 357 (*sh*, 4.57×10^3); CT bands: 251 (3.85×10^4); 427 (6.3×10^3); 413 (*sh*, 5.95×10^3); *d–d* transitions: 525 (*sh*, 287); 637 (102). CD (λ_{max} [nm], ($\Delta\varepsilon$)): 512 (+0.41); 610 (+0.19); 700 (−0.63).

(^{tBu}*Salcam*)*Cu*. The copper(II) complex was prepared similarly as the nickel(II) one. The $CuSO_4$ dissolved in 4 ml H_2O was used for metal insertion. Yield 37%.

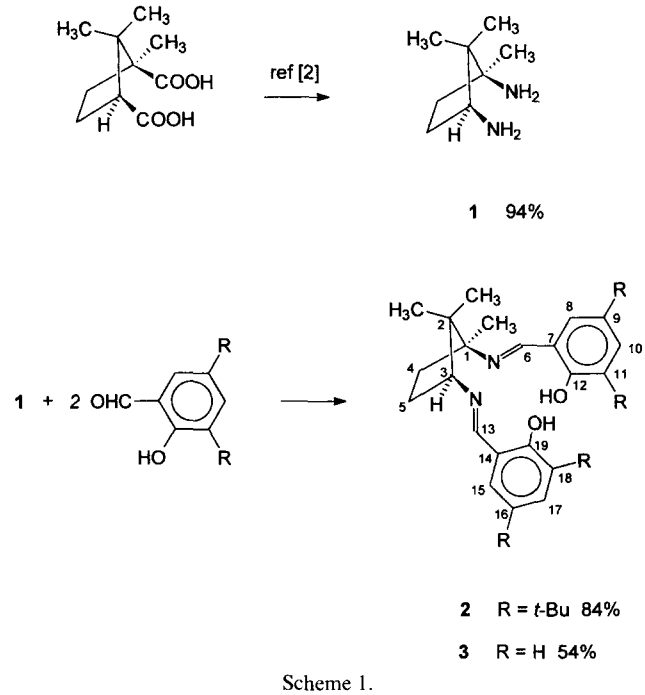

Scheme 1.

(*t-Bu*Salcam)Cu Anal. Calc. $C_{38}H_{56}N_2O_2Cu$: C 71.72; H 8.87; N 4.40. Found: C 71.72; H 9.05; N 4.21, MS 636 {(*t-Bu*Salcam)Cu^+}, IR $\gamma_{C=N}$ 1617 cm^{-1}, UV-Vis{λ [nm] (ε)}: intraligand: 238 (5.97×10^4); 282 (3.79×10^4); 315 (1.13×10^4); CT bands: 251 (4.91×10^4); 389 (1.41×10^4); 413 (*sh*, 1.02×10^4); *d–d* transition: 627 (490). CD (λ_{max} [nm], ($\Delta\varepsilon$)): 530 (+1.61); 640 (−2.74). Magnetic moment. 1.77 BM, EPR (methylene dichloride solution, 77 K): $g_{iso}=2.204$, $A_{\perp}=199\times10^{-4}$ cm^{-1}; (room temperature): $g_{iso}=2.204$, $A_{iso}=81\times10^{-4}$ cm^{-1}.

(*t-Bu*Salcam)*MnCl*. To a refluxing solution of **2** (0.408 g, 0.710 mmol) and $Mn(CH_3COO)_2\cdot4H_2O$ (0.174 g, 0.710 mmol) in 13.5 ml ethanol aqueous potassium hydroxide solution (0.130 g, 5 ml H_2O) was added dropwise and heating was continued until all solids dissolved. Then the saturated ethanolic solution of lithium chloride was added and refluxing was continued over next 0.5 h. The solvents were evaporated and the solid residue was extracted with methylene dichloride, the solution was dried over sodium sulfate and then chromatographed twice on silica gel with the mixture 1:1 chloroform:hexane and then 3:1 chloroform:acetonitrile solvents. The crystals of (*t-Bu*Salcam)MnCl·CH_2Cl_2 (as found by thermogravimetric analysis) were grown from methylene dichloride:hexane solution. Yield 30%.

(*t-Bu*Salcam)MnCl (solvent removed under vacuum) Anal. Calc. $C_{38}H_{56}N_2O_2MnCl$: C 68.81; H 8.51; N 4.22; Cl 5.34 Found: C 71.72; H 9.05; N 4.21, MS 628 {$(C_{38}H_{56}N_2O_2Mn)^+$}, IR $\gamma_{C=N}$ 1611 cm^{-1}, UV-Vis{λ [nm] (ε)} (in solution): intraligand: 225 (3.22×10^4); 280 (2.80×10^4); 357 (6.7×10^3); CT bands: 242 (3.10×10^4); 418 (5.64×10^3); *d–d* transitions: 525 (1.25×10^3); 740 (324). (in solid state); *d–d* transitions (λ [nm]): 525, 725, 815. CD (λ_{max} [nm], ($\Delta\varepsilon$)): 555 (+0.77); 660 (+0.90). Magnetic moment 4.52 BM. ^{1}H NMR: −294; −155 ppm (intensity ratio 2:1, total intensity 2H, H_6+H_{13}); −24.4; −19.8 ppm (aromatic C-H, 2H).

(*t-Bu*Salen)*MnX* (*X* = *Cl,Br*). The complexes have been prepared as described previously [3]. UV-Vis (λ [nm], *d–d* transitions only): (*t-Bu*Salen)MnCl (in solution): 505, 705, 822; (in solid state): 500, 715, 800 (*t-Bu*Salen)MnBr (in solid state): 505, 700, 800.

(*Salcam*)*MnCl*. The synthetic procedure to obtain the manganese complex of **3** was the same as that in case of (*t-Bu*Salen)MnX.[3] MS 403 {$(C_{22}H_{26}N_2O_2Mn^+$}, IR $\gamma_{C=N}$ 1611 cm^{-1}, UV-Vis{λ [nm] (ε)} (in solution): *intraligand*: 314 (8.02×10^3); 393 (4.60×10^3); 417 (3.65×10^3); 488 (1.02×10^3); *d–d* transition: 728 (2.33×10^2). CD (λ_{max} [nm], ($\Delta\varepsilon$)): 251 (−2.27); 266 (+0.42); 286 (−2.94); 310 (+0.97); 323 (−0.25); 346 (−1.26); 382 (+3.28); 425 (−2.02); 470 (−0.25); 535 (+0.84); 650 (+0.081). Magnetic moment 4.52 BM. ^{1}H NMR: −250; −200 ppm (intensity ratio 2:1, total intensity 2H, H_6+H_{13}); −26.9, −20.2, −17.7, −16.6 (aromatic C-H, 4H).

(*t-Bu*Salcam)*FeCl*. In a typical procedure the iron(III) complex was obtained on 1 mmolar scale by dissolving iron(III) chloride and **2** in ethanol followed by solvent removal and extraction (*t-Bu*Salcam)FeCl with methylene dichloride. The product was purified by chromatography on silica gel with chloroform:ethyl acetate eluent with increasing gradient of ethyl acet-

ate. Finally the violet complex was eluted with 9:1 ethyl acetate:acetonitrile eluent. Pure (^{tBu}Salcam)FeCl was recrystallized from mixture of methylene dichloride and hexane. The solid violet (^{tBu}Salcam)FeCl cocrystallized with one molecule of hexane per two molecules of (^{tBu}Salcam)FeCl ($C_{38}H_{56}N_2O_2FeCl \cdot 1/2\ C_6H_{14}$).

(^{tBu}Salcam)FeCl · 1/2 C_6H_{14}: Anal. Calc. $C_{41}H_{63}N_2O_2FeCl$: C 69.93; H 8.98; N 3.96; Found: C 69.73; H 9.17; N 3.99; MS (for hexane-free complex) 628 {(^{tBu}Salcam)Fe^+}, IR $\gamma_{C=N}$ 1610, UV-Vis{λ [nm] (ε)}: intraligand: 232 (2.59×10^4); 290 (1.13×10^4); 324 (1.00×10^4); CT bands: 263 (2.74×10^4); 389 (1.41×10^4); 413 (*sh*, 1.02×10^4); *d–d* transition: 627 (490). Magnetic moment 5.70 BM, EPR (solid sample): $g = 1.87, 2.31, 4.42$. ^{1}H NMR: 103.6; 100.5 ppm (2H, $H_6 + H_{13}$); 65.0; 58.6 ppm (H_{10} and H_{17}); 41.0; 31.0 ppm (H_8 and H_{15}).

Catalytic oxidations

Oxidation of thioanisole. A solution of thioanisole, $C_6H_5SCH_3$ in CH_2Cl_2 (2 ml 1.0 M) containing 4-phenylpyridine N-oxide (0.4 mmol), Bu_4NCl (0.1 mmol), and (^{tBu}Salcam)MnCl (0.1 mmol) was vigorously stirred with 2.28 ml 1.0 M NaOCl(aq) for 4 h at 0°C. The reaction mixture was washed with water, brine, and dried over anh. Na_2SO_4. The methylene dichloride phase was filtered through the short pad of silica gel. The fractions obtained were evaporated, weighted and subjected to GC/MS analysis, which indicated that 69% of starting material was recovered and the sulfoxide yield was 18%. The enantioselectivity was estimated by two independent methods: the observed specific rotation $[\alpha]_D - 14.6°$ (Polarimeter AA-5, Optical Activity Ltd.) and the gas chromatography on Chirasil-val column (Alltech) gave the same value of $10 \pm 0.5\%$ ee.

Oxidation of styrene. Analogous conditions as previously described [3] were used to test the two-phase epoxidation of styrene with aqueous sodium hypochlorite in the catalytic presence of (^{tBu}Salcam)MnCl. The reaction proceeded 6 h. Products were analyzed by GC/MS. It was found that 8% of epoxide and 2% of phenylacetic acid were formed, with $\leqslant 12\%$ ee for epoxide (by specific rotation).

Oxidation of norbornene with dimethyldioxirane (DMDO). The epoxidation of norbornene into exo-2,3-epoxynorbornane with dimethyldioxirane in the presence or absence of complex was monitored by ^{1}H NMR spectroscopy by disappearance of resonance at 6.0 ppm (protons 2 and 3 of norbornene) and growing of resonance at 3.0 ppm (from exo-epoxide). In a typical procedure the manganese complex was dissolved in deuterated acetone (concentration was variable within 1–8 mM region) containing 0.01 M norbornene, the solutions were frozen at liquid nitrogen, then the DMDO (as 0.2 M solution in acetone-d_6) was added to the reaction mixture in NMR tube and the solution was warmed up quickly to 233 K in the cavity of NMR spectrometer. The reaction was then followed by sampling every 2 min. The results are collected as a graph at Fig. 5.

RESULTS AND DISCUSSION

Synthesis

Recently Sato *et al.*, have reported the successful preparation of enantiomerically pure (1*R*,3*S*)-1,2,2-trimethyl-1,3-cyclopentanediamine (**1**) and application of its N,N-dimethyl derivatives as chiral ligands for asymmetric reaction [4]. On the other hand, the striking catalytic activity of chiral manganese(III) complex with Schiff base derived from optically active 1,2-cyclohexyldiamine and sterically hindered 3,5-di-*tert*-butylsalicylaldehyde (^{tBu}Salchl)MnCl in enantioselective epoxidation of olefins [1] prompted us to study the properties of similar Schiff base containing **1** as a structural element. Thus we prepared the ligand **2** in 84% yield reaction of **1** with 3,5-di-*tert*-butylsalicylaldehyde. It has been demonstrated that the presence of bulky substituents at the 3,3′- and 5,5′-positions of the salen-type ligand had a marked effect on the selectivity of catalyzed reaction [5]. For the purpose of comparison we also synthesized the ligand **3** (SalcamH_2)—the Schiff base derived from **1** and unsubstituted salicyl aldehyde. The complexes were prepared by heating the equimolar amounts of **2** and corresponding metal ion salts in ethanol in alkaline conditions, followed by chromatographic purification. The satisfactory elemental analyses and mass spectral data confirmed the simple 1:1 ligand to metal stoichiometry of nickel(II) and copper(II) complexes and 1:1:1 ligand:metal ion:chloride stoichiometry of manganese(III) and iron(III) complexes. The coordination compounds were then characterized by spectral methods, magnetic susceptibility measurements, and electrochemical measurements (in case of manganese(III) complex).

Magnetic, electrochemical and spectral (UV-Vis, CD, IR, EPR) studies

Magnetic susceptibility measurements indicated that expected diamagnetic nickel(II) is formed, and in the series of copper(II), manganese(III), and iron(III) complexes the mononuclear compounds are formed with the values of magnetic moments corresponding to one unpaired electron in the case of Cu(II) complex and a high-spin electronic configuration for manganese(III) and iron(III) complexes (see: Experimental). The linear $(\chi)^{-1}$ vs T relationship demonstrated that no intermolecular magnetic exchange was present in either of the complexes studied. The EPR spectrum of copper(II) complex showed a hyperfine structure corresponding to N_2O_2 coordination mode in square planar complexes [6]. The

EPR spectrum of iron(III) complex is typical for that type of electronic configuration. Also the *d–d* transitions observed in UV-Vis spectra correspond to high-spin configuration of manganese(III) and iron(III) five-coordinated square-pyramidal complexes. The CD spectra obtained for the same *n*-hexane solutions revealed the Cotton effects observed for the respective electronic absorptions. A comparison of these effects for the *d–d* bands in (^{t}Bu-Salcam)MnCl and (*R,R*)-(^{t}BuSalchl)MnCl shows that in both cases the coordination sphere of Mn(III) bears the chirality of ligands [7]. The observed relay of chirality to the metal can be potentially extended to the reactant in a catalytic process.

The examination of infrared absorption spectra revealed 21–23 cm^{-1} shift of $\gamma_{C=N}$ upon coordination of Fe(III), Mn(III), and Ni(II), and only 16 cm^{-1} shift in the Cu(II) complex [8]. This difference correlates with the energy of CT band (mainly $d_{xy} \rightarrow \pi^*$) localized on the azomethine group which is shifted 30–44 nm to higher energy for Cu(II) complex in comparison with the corresponding bands for the other three complexes. In the contrary, the shift of phenolic ν_{C-O} to the larger wavelengths is the smallest in case of Cu(II) complex. These two tendencies reflect the relative strength of the coordination bonds; in the case of Cu(II) complex, Cu(II)—N bond seems to be relatively the strongest of all the complexes studied.

Cyclic voltammetry indicated that (^{t}Bu-Salcam)MnCl, unlike its achiral analogue (^{t}Bu-Salen)MnCl [3] is oxidizable reversibly in a one-electron process at a platinum electrode. The difference in peak potentials of 53 mV ($E_{1/2}$ 1.004 V vs AgCl/Ag), the peak current ratio near unity, and the identity of both single and multiple scan cyclic voltammograms demonstrated the reversibility and simplicity of electron transfer. Coulommetric experiment showed that one electron was transferred and the EPR spectrum of oxidized sample confirmed the presence of Mn(IV) complex (eight-line hyperfine structure, g_{iso} 2.068, A_{iso} 80.2 Gs). The same EPR spectrum was obtained when (^{t}BuSalcam)MnCl in methylene dichloride was oxidized with aqueous sodium hypochlorite. It seems that the observed redox behavior of (^{t}BuSalcam)MnCl and its low catalytic activity (vide infra) are caused by strong stabilization of Mn(IV) species, thus unfavorably shifting an equilibrium from Mn(V)=O to Mn(IV) species [3]. Moreover, both chemical and electrochemical oxidations of this complex were unaffected by the presence of additional ligand (4-dodecyloxypyridine N-oxide). Because this ligand strongly activated the catalytic action of (^{t}Bu-Salen)MnCl [3], we suppose that a steric hindrance imposed by 1,3-cyclopentanediimine bridge prevents the complexation of additional, axial ligand.

^{1}*H NMR Studies*

The ^{1}H NMR spectrum of **2** (Fig. 1) indicated that two substituted salicyl rings are almost magnetically equivalent. Similarly the slight chemical shift difference between two methyl groups at carbon-2 indicated that they are only slightly diastereotopic. Consequently, free rotation around C_1—N and C_3—N bonds of free ligand can be assumed. It is not the case in the diamagnetic nickel(II) complex, for which total assignment was based on the 2D COSY and NOESY techniques. The spectra were taken at room temperature and the relevant fragments of COSY and NOESY spectra together with connectivity pattern are shown at Figs 2–4.

The scalar cross-peak in COSY map allowed to assign four doublets in the aromatic region of spectrum into the corresponding pair of C—H coupled pairs, i.e. H_8—H_{10} and H_{15}—H_{17} ones. By default two singlets at 7.16 and 7.04 ppm were assigned to azomethine protons H_6 and H_{13}. The singlet resonances in the region 1.7–0.8 ppm belong to *tert*-butyl and methyl protons. Two singlets at 1.60 and 0.87 ppm are scalary coupled and they originate from methyl substituents at C_2. Those cross-peaks are not labelled on the COSY map presented at Fig. 2a, 2b presents the expanded region of COSY spectrum containing the multiplet pattern of resonances corresponding to protons at C_1-C_3. Every of five protons resonates at different field. The resonances from axial protons are shifted upfield. The most intense cross-peaks are observed between geminal protons (H_{4a}—H_{4b}—cross-peak 2 and H_{5a}—H_{5b}—cross-peak 4) and vicinal protons H_3—H_{4a}—cross-peak 1. The weaker cross-peaks 3 and 5 illustrate the vicinal coupling between equatorial H_{4b} and H_{5b} and axial H_{4a} and H_{5a}, respectively. The cross-peak 6 originate from weak vicinal coupling between H_{5a} and H_{4b}. The doublet at 2.82 ppm has been identified as originate from H_3 based on NOESY experiment.

The crucial starting point of spectral assignments are two pairs of cross-peaks observed in NOESY experiment, i.e. those corresponding to spatial interaction between azomethine and aromatic protons: H_{13} vs H_{15} and H_6 vs H_8 (cross-peaks *a* and *b* at Fig. 3a, respectively). The sequence of NOE cross-peaks: *c* (between H_8 and *t*-Bu_9), *d* (between *t*-Bu_9 and H_{10}), *e* (between H_{10} and *t*-Bu_{11}) combine the resonances within one part of the ligand, whereas those labelled as *f* (between H_{15} and *t*-Bu_{16}-Fig. 3b), *g* (between *t*-Bu_{16} and H_{17}), and *h* (between H_{17} and *t*-Bu_{18}) give the total assignment of all aromatic and azomethine protons (Fig. 3b). The observed NOE cross-peak *i* (Fig. 3c) between azomethine proton H_{13} and H_3 allowed to unambiguously complete the assignment. Furthermore, the spatial contacts between: H_3 and Me_{2a} (cross-peak *j*), vicinal methyls 1 and 2a and 2b (cross-peaks *k* and *l*, respectively) were observed (Fig. 3d). The connectivity pattern with the arrowed NOE cross-peaks is presented at Fig. 4 for clarity.

The ^{1}H NMR spectrum of (^{t}BuSalcam)FeCl complex at room temperature is typical for high-spin Fe(III) complexes with Schiff bases [9a,b]. The doubled resonances from azomethine protons are the most shifted

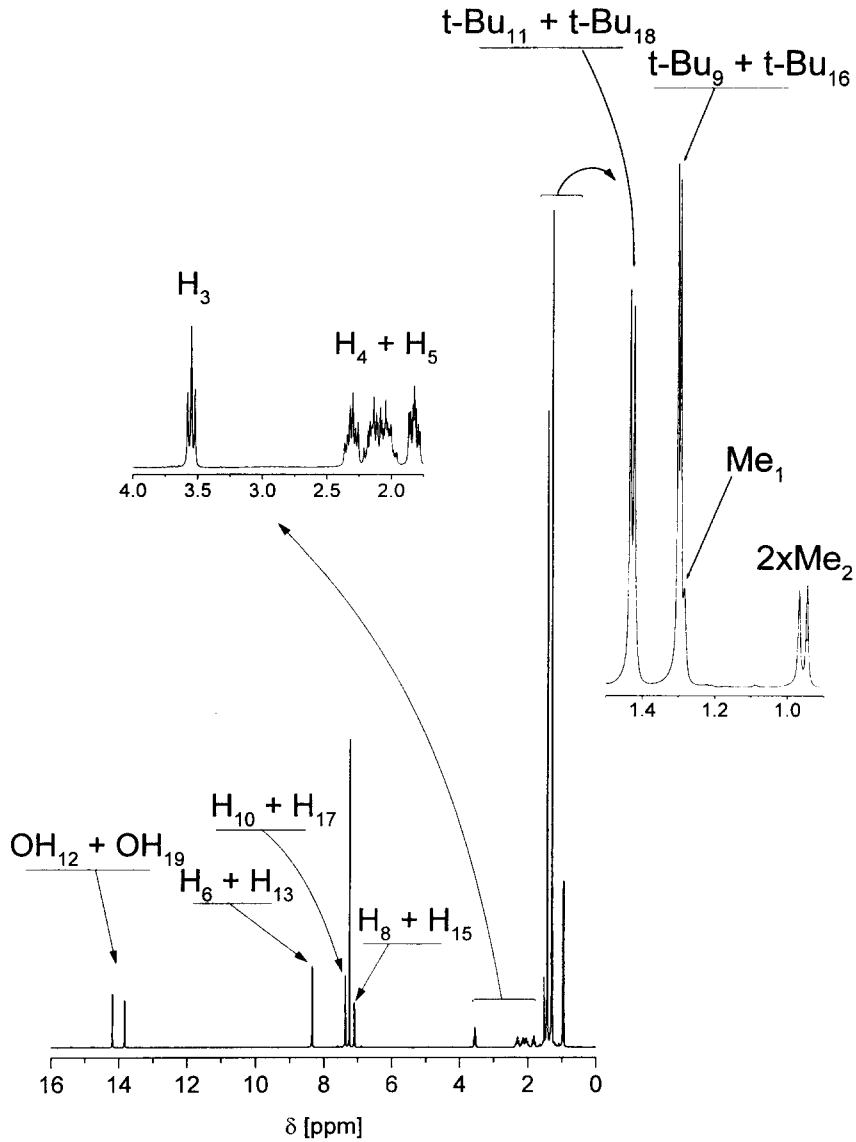

Fig. 1. ^{1}H NMR spectrum of ^{tBu}SalcamH$_2$ in chloroform-*d* at 293 K. Resonance assignment according to Scheme I.

downfield (100 ppm). Also the chemical shift of H_{10} and H_{17} phenyl protons are within the expected region. The resonances between 15 and 0 ppm can be assigned based upon integral intensity, whereas those at around 40 and 30 ppm arise from H_8 and H_{15} protons. The (^{tBu}Salcam)FeCl complex is easily convertible into binuclear μ-oxo species by shaking the chloroform solution of (^{tBu}Salcam)FeCl with KOH-saturated D_2O. The spectrum changes dramatically and all resonances are then present in the region of 15–0 ppm. (14.3 ppm for H_{10} and H_{17} and 10.3 ppm for H_8 and H_{15}) [9c].

The ^{1}H NMR spectrum of (^{tBu}Salcam)MnCl complex is well-resolved due to short electronic relaxation time of manganese(III) complexes in high-spin configuration (10^{-10}–10^{-11} s [9d] and spread over wide range of chemical shift. Phenyl proton resonances are located within the region $-15 \div -30$ ppm (assignment based on comparison with Mn(Salcam)Cl). The azomethine protons are shifted upfield to -150 and -300 ppm for Mn(^{tBu}Salcam)Cl and -200 and -250 ppm for the Mn(Salcam)Cl. For comparison the azomethine resonance in case of mononuclear [Mn(salpn)(H_2O)](ClO_4) complex is shifted upfield to -94.2 ppm [9e]. Two azomethine resonances of (^{tBu}Salcam)MnCl have different intensity: The integral intensity ratio of lower to higher shifted resonances is about 2:1 and arise from two different

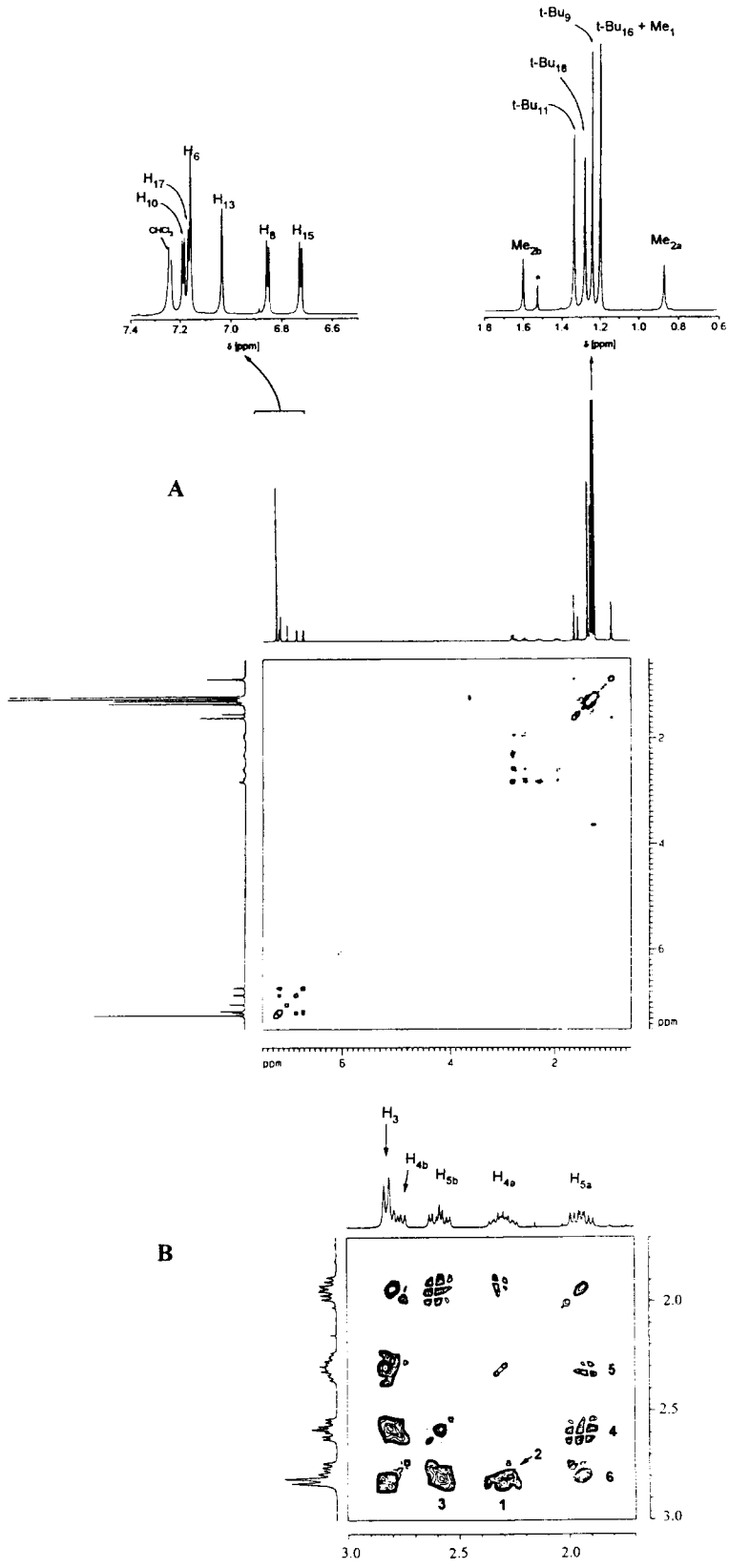

Fig. 2. (A) 2-D ^{1}H NMR COSY spectrum of ($^{t\text{-}Bu}$Salcham)Ni(II) complex in chloroform-*d* at 293 K. Two upper insets represent the expanded region of 1-D projection. The labelling of resonances was made according to Scheme I. (B) The expended region of the COSY map demonstrating the scalar couplings within aliphatic proton region.

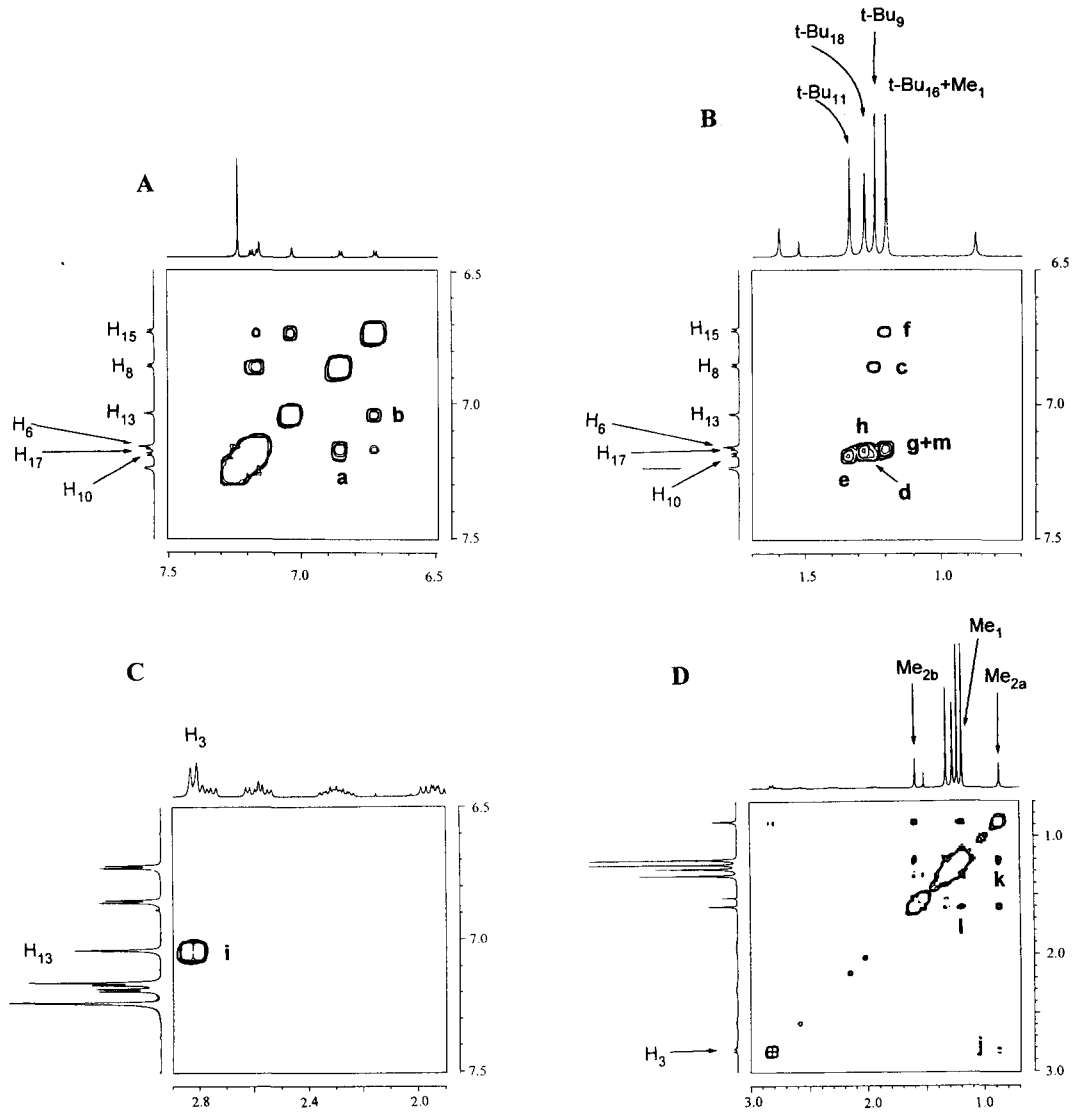

Fig. 3. The relevant fragments of 2D ^{1}H NMR NOESY spectrum of (^{tBu}Salcam)Ni(II) complex in chloroform-*d* at 293 K. The resonance and cross-peak assignments follows those used in text.

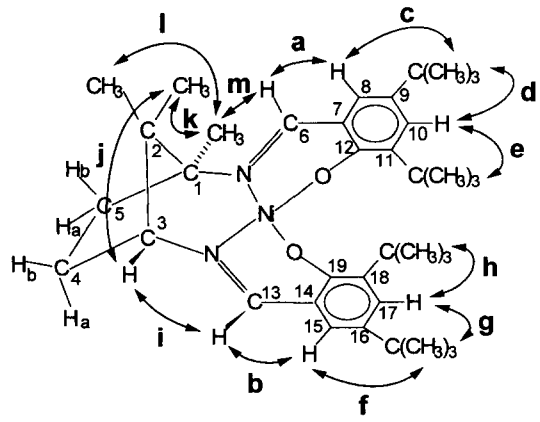

Fig. 4. Connectivity scheme demonstrating observed spatial contacts for (^{tBu}Salcam)Ni(II).

complexes, bearing axial chloride bound at opposite sides of the complex plane. Interestingly, the solid complex, isolated from the methylene dichloride/hexane solvent mixture has the chloride ion coordinated on the opposite side in respect to C_3 [10].

Catalytic studies

The examination of catalytic activity of (^{tBu}Salcam)MnCl complex in oxidation of methyl phenyl sulfide with sodium hypochlorite in methylene dichloride/water system in the presence of 4-phenylpyridine N-oxide and Bu_4NCl indicated rather low catalytic performance with slight enantioselectivity (10% ee). Similar result was obtained in the two-phase catalytic epoxidation of styrene ($\leqslant$ 12% ee).

A series of manganese(III) complexes with salen-

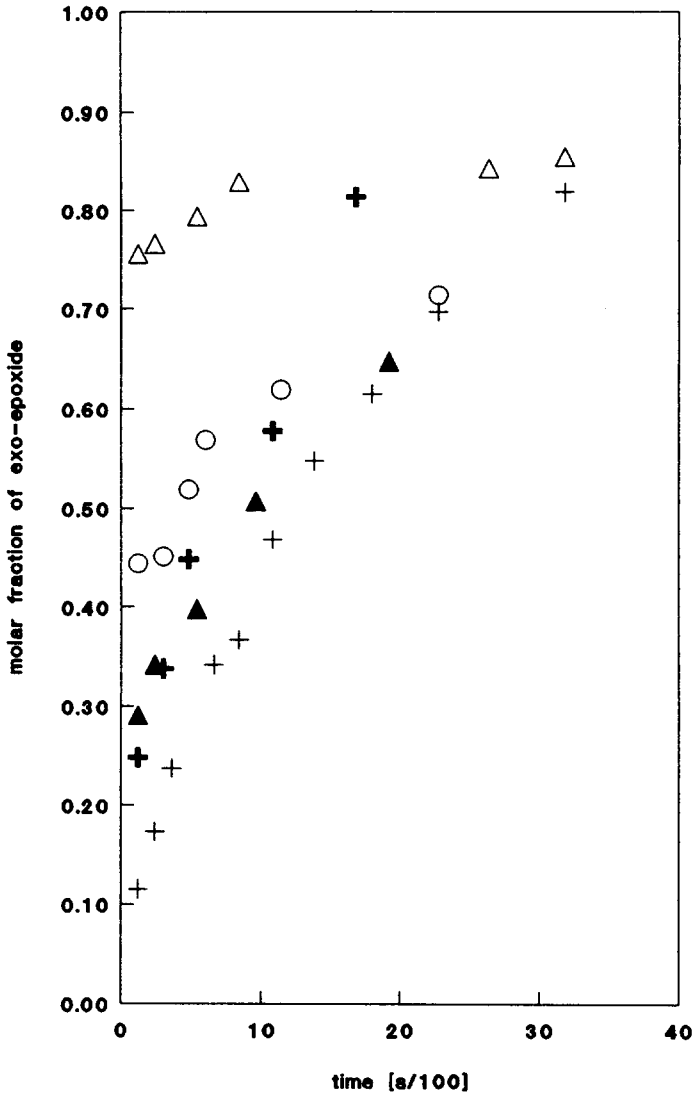

Fig. 5. The time course of catalytic oxidation of norbornene with dimethyldioxirane in presence of (^{tBu}Salchl)Mn(III)Cl (c = 7.9 mM—open triangles, c = 1.4 mM—open circles), (^{tBu}Salcam)Mn(III)Cl (c = 3.7 mM—bold crosses), (Salcam)Mn(III)Cl (c = 3.9 mM—solid triangles), and blank (light crosses).

type ligands were tested for catalytic activity in the homogenous epoxidation of olefin using dimethyldioxirane in acetone. Dioxiranes are strong oxidants and single oxygen transfer agents [11]. It has been demonstrated that they are able to stereoselectively oxidise many organic [11] and inorganic [12] substrates. Manganese(III)-porphyrin has been reported as efficient catalyst in epoxidation of uracil derivatives with dimethyldioxirane (DMDO) [13]. Here the reaction of epoxidation of norbornene into exo-2,3-epoxynorbornane with dimethyldioxirane has been chosen to test the catalytic activity of (^{tBu}Salcam)MnCl, (Salcam)MnCl, and (^{tBu}Salchl)MnCl. The results are collected as a graph at Fig. 5. All the studied complexes indicated some activity in the testing reaction. However, only the (^{tBu}Salchl)MnCl complex was substantially active catalyst (75% conversion in 10 min, blank–12%). Both (^{tBu}Salcam)MnCl and (Salcam)MnCl showed limited catalytic activity (50% and 40% conversion in 10 min, respectively). Moreover, the (^{tBu}Salcam)MnCl and (^{tBu}Salchl)MnCl complexes presumably persist untouched (they remain catalytic activity after 20 min) whereas the non-protected with t-butyl substituents (Salcam)MnCl looses its activity within 20 min. While the catalytic activity of the title compound is rather

low, it is noteworthy that high activity of (^{t}Bu-Salchl)MnCl complex is confirmed in the DMDO/norbornane test.

CONCLUSIONS

It seems probable that the low activity of (^{t}Bu-Salcam)MnCl and (Salcam)MnCl is due to steric hindrance imposed by 1,3-cyclopentanediimine moiety around the metal center and marginal stereoselectivity is consistent with the fact that both faces of the complexes are involved in binding single oxygen (the starting chloride species bears chloride ions coordinated axially on both sides, although the opposite sides in case of (^{t}Bu Salcam)MnCl are less equivalent than those in case of (Salcam)MnCl (as it demonstrated by large differences of the chemical shift of azomethine protons of two isomers in NMR spectra). Presumably in the former complex the metal ion is more sterically crowded and that induces large dipolar contributions of opposite sign into isotropic shift experienced by azomethine protons. Indeed, the molecule of (^{t}Bu-Salcam)MnCl complex is substantially tetrahedrally distorted from square planar geometry as it was indicated by X-ray crystallographic studies of solvent-free crystals [10].

Acknowledgements—The authors thank the Polish Committee for Scientific Research for financial support (KBN Grant No 3 TO9A 028 12). R.L.P. thanks for a fellowship under the Polish Academy of Sciences-INSA (India) exchange programme. We are grateful to Dr J. Jezierska and Prof. M. Wilgocki for performing the EPR and CV measurements, respectively.

REFERENCES

1. For the review see (a) Balavoine, G. G. A. and Manoury, E., *Appl. Organomet. Chem.*, 1995, **9,** 199; (b) Nishinaga, A., Yamato, H., Abe, T. and Maruyama, T., *Tetrahedron Lett.*, 1988, **29,** 6309; (c) Zhang, W., Leobach, J. W., Wilson, S. R. and Jacobsen, E. N., *J. Am. Chem. Soc.*, 1990, **112,** 2801; (d) Irie, R., Noda, K., Ito, Y., Matsumoto, T. and Katsuki, T., *Tetrahedron Lett.*, 1990, **31,** 7345; (e) Zhang, W. and Jacobsen, E. N., *J. Org. Chem.*, 1991, **56,** 2296; (f) Jacobsen, E. N., Zhang, W., Muci, A. R., Ecker, J. R. and Deng. L., *J. Am. Chem. Soc.*, 1991, **113,** 7063; (g) O'Connor, K. J., Wey, S.-J. and Burrows, C. J., *Tetrahedron Lett.*, 1992, **33,** 1001; (h) Reddy, D. R. and Thronton, E. R., *J. Chem. Soc., Chem. Comm.*, 1992, 172; (i) Yamada, T., Imagaea, K., Nagata, T. and Mukaiyama, T., *Chem. Lett.*, 1992, 2231; (j) Wey, S.-J., O'Connor, K. J. and Burrows, C. J., *Tetrahedron Lett.*, 1993, **34,** 905; (k) Hosoya, N., Irie, R. and Katsuki, T., *Synlett*, 1993, 261; (l) Sasaki, H., Irie, R. and Katsuki, T., *Synlett*, 1993, 300; (m) Hosoya, N., Hatayama, A., Irie, R., Sasaki, H. and Katsuki, T., *Tetrahedron*, 1994, **50,** 4311; (n) Sasaki, H., Irie, R., Hamada, T., Suzuki, K. and Katsuki, T., *Tetrahedron*, 1994, **50,** 11827; (p) Chang, S., Galvin, J. M. and Jacobsen, E. N., *J. Am. Chem. Soc.*, 1994, **116,** 6937; (q) Fukuda, T., Irie, R. and Katsuki, T., *Synlett*, 1995, 197; (r) Bernardo, K. D. S., Robert, A. and Meunier, B., *New J. Chem.*, 1995, **19,** 129; (s) Kuroki, T., Hamada, T. and Katsuki, T., *Chem. Lett.*, 1995, 339.
2. Togni, A. and Venanzi, L. M., *Angew. Chem. Int. Ed. Engl.*, 1994, **33,** 497.
3. Skarżewski, J., Gupta, A. and Vogt, A., *J. Mol. Catal.*, 1995, **103,** 63.
4. Urabe, H., Yamakawa, T. and Sato, F., *Tetrahedron: Asymmetry*, 1992, **3,** 5.
5. Katsuki, T., *Coord. Chem. Rev.*, 1995, **140,** 189 and refs cited therein.
6. Jezierska, J. and Jeżowska-Trzebiatowska, B., *Bull. Pol. Acad. Sci., Ser. Sci. Chim.*, 1985, **33,** 227.
7. Bosnich, B., *J. Am. Chem. Soc.*, 1968, **90,** 627.
8. (a) Gluvchinsky, P., Mockler, G. M. and Sinn, E., *Spectrochim. Acta*, 1977, **33A,** 1073; (b) Jeżowska-Trzebiatowska, B., Lisowski, J., Vogt, A. and Chmielewski, P., *Polyhedron*, 1988, **7,** 337.
9. (a) Bertini, I. and Luchinat, C., in *NMR of Paramagnetic Molecules in Bilogical Systems*, Physical Bioinorganic Chemistry Series, ed. A. B. P. Lever, H. B. Gray. The Benjamin/Cummings Publ. Co., Inc., 1986, p 219; (b) Heistand II, R. H., Lauffer, R. B., Fikrig, E. and Que Jr, L., *J. Am. Chem Soc.*, 1982, **104,** 2789; (c) LaMar, G. N., Eaton, G. N., Holm, R. H. and Walker, F. A., *J. Am. Chem. Soc.*, 1973, **95,** 63; (d) Bertini, I. and Luchinat, C., in *NMR of Paramagnetic Molecules in Biological Systems*, Physical Bioinorganic Chemistry Series, ed. A. B. P. Lever, H. B. Gray. The Benjamin/Cummings Publ. Co., Inc., 1986, p. 77, p. 231; (e) Gohdes, J. W. and Armstrong, W. H., *Inorg. Chem.*, 1992, **31,** 368.
10. Lis, T., Olejnik, A. Z., Vogt, J. and Skarżewski, in preparation.
11. (a) Jeyaraman, R. and Murray, R. W., *J. Am. Chem. Soc.*, 1984, **106,** 106 and references cited therein; (b) Murray, R. W., *Chem. Rev.*, 1989, **89,** 1187.
12. (a) Wołowiec, S. and Kochi, J. K., *J. Chem. Soc., Chem. Commun.*, 1990, 1782; (b) Wołowiec, S. and Kochi, J. K., *Inorg. Chem.*, 1991, **30,** 1215.
13. Saladino, R., Bernini, R., Mincione, E., Tagliatesta, P. and Boschi, T., *Tetrahedron Lett.*, 1996, **37,** 2647.

Pergamon

PII: S0277-5387(97)00393-8

Polyhedron Vol. 17, No. 8, pp. 1241–1246, 1998
© 1998 Elsevier Science Ltd
All rights reserved. Printed in Great Britain
0277-5387/98 $19.00+0.00

Axial additions in nickel(II) complexes of 3,14-dimethyl-2,6,13,17-tetraazatricyclo[14,4,$0^{1,18}$,$0^{7,12}$]docosane: syntheses and crystal structures of the octahedral nickel(II) complexes

Ki-Young Choi*[a], Haiil Ryu[b] and Il-Hwan Suh[c]

[a] Department of Chemistry, Mokwon University, Taejeon 301-729, Korea

[b] Department of Chemical Education, Kongju National University, Kongju 314–701, Korea

[c] Department of Physics, Chungnam Nation University, Taejeon 305–764, Korea

(Received 21 July 1997; accepted 19 September 1997)

Abstract—The complex $[NiL]Cl_2 \cdot 2H_2O$ (L = 3,14-dimethyl-2,6,13,17-tetraazatricyclo[14,4,$0^{1,18}$,$0^{7,12}$]docosane) undergoes axial additions with monodentate ligands ($X = N_3^-$, NCS^-). The octahedral $[NiLX_2]$ complexes have been characterised and structures established by X-ray crystallography. The crystal structures of $[NiL(N_3)_2]$ **1** and $[NiL(NCS)_2]$ **2** show that both structures are centrosymmetric and the nickel centre has an axially elongated octahedral geometry with two nitrogen atoms of the axial ligands. Electronic spectra and redox potentials of the complexes also reveal a high-spin octahedral geometry, which is reflected by the nature of the axial ligands. © 1998 Elsevier Science Ltd. All rights reserved

Keywords: octahedral nickel(II) complexes with 14-membered tetraaza macrocyle.

Macrocyclic polyamines with C-alkyl substituents of the macrocyclic ring and their metal complexes have attracted considerable attention because of their structural and chemical properties, which are often quite different from those of the unalkylated macrocyclic ligands [1–14]. Several factors influence the chemical properties and structures of metal complexes of macrocylic ligands [1]. These factors are the metal ion, ring size, degree of unsaturation and types and number of substituents on the macrocyclic ring. Difference in kinetic stability of two isomers of 5,12-dialkylcyclam (cyclam = 1,4,8,11-tetraazacyclotetradecane) nickel (II) complexes have been reported by McAuley *et al.* [4]. It is evident that the stereochemistry of the ligands contributes in an important way to the electron-transfer processes of the macrocyclic nickel complexes. Comparable work on the 5,7,7,12,14,14-hexamethylcyclam complexes is hindered by the large numbers of isomers that contribute further to the steric effects [2]. We recently reported the preparation and X-ray structure of $[NiL]Cl_2 \cdot 2H_2O$ [10]. In addition, Mochizuki *et al.* [15] showed that *trans*-[Ni(cyclam)$(OH_2)_2$]$Cl_2 \cdot 4H_2O$ has the octahedral geometry and longer Ni—N (secondary amine) bond distances (2.065 and 2.072 Å) when compared with that of square-planar $[NiL]Cl_2 \cdot 2H_2O$ (1.941 and 1.954 Å) [10]. Furthermore, the spectrochemical study of a series of high-spin $[NiAX_2]$ (A = tetraaza macrocyclic ligands; $X = Br^-$, Cl^-, N_3^- and NCS^-) was reported by Busch *et al.* [16]. In this study, it was found that the ligand field strengths for axial ligands reflect the normal spectrochemical series. Redox potentials for these complexes are also consistent with the spectral results.

In the present study, we report the syntheses and properties of $[NiLX_2]$ (L = 3,14-dimethyl-2,6,13,17-tetraazatricyclo[14,4,$0^{1,18}$,$0^{7,12}$]docosane; $X = N_3^-$ and NCS^-). To understand the nature of the axial ligands, the solid state X-ray crystal structures of

* Author to whom correspondence should be addressed.

$[NiLX_2]$ complexes are determined and compared to their solution structures by the electronic absorption spectroscopy and cyclic voltammetry.

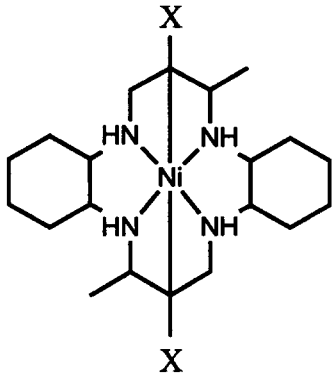

(X: N_3^-, NCS^-)

EXPERIMENTAL

Materials

All solvents were reagent grade and purified according to the literature [17]. All chemicals used in syntheses were of reagent grade and were used without further purification. The macrocyclic ligand L and complex $[NiL]Cl_2 \cdot 2H_2O$ were prepared as described previously [10,18].

Measurements

Infrared spectra were recorded as KBr pellets on a Perkin–Elmer Paragon 1000 FT–IR spectrophotometer, electronic spectra with a Jasco Uvidec-610 spectrophotometer. High-resolution fast atom bombardment mass spectrometry (FAB mass) were performed by using a Jeol JMS-HA 110A/110A instrument. Elemental analyses were carried out by the Korea Research Institute of Chemical Technology, Taejeon, Korea. Cyclic voltammograms were obtained by using a BAS 100BW electrochemical system. All measurements were made on 0.01 M tetraethylammonium perchlorate–dichloromethane solution at 20°C. A hanging mercury dropping electrode for cathodic voltammetry and a platinum disc electrode of about 2 mm diameter for anodic voltammetry were used as the working electrodes. The counter electrode was a coiled platinum wire and a saturated calomel electrode was used as a reference electrode. The solution was degassed with high purity nitrogen prior to carrying out the electrochemical measurements.

Synthesis of $[NiL(N_3)_2]$ (1)

To a methanol solution (20 cm^3) of $[NiL]Cl_2 \cdot 2H_2O$ (251 mg, 0.5 mmol) was added NaN_3 (65 mg, 1 mmol) and the mixture was heated for 30 min on a steam bath. The solution was filtered to remove the sodium chloride. The solution was then evaporated to dryness. The resulting solid was extracted into chloroform and recrystallized by adding acetonitrile. The violet crystals were collected by filtration and dried *in vacuo* (yield: 187 mg, 78%). Calc. (found) for $NiC_{20}H_{40}N_{10}$: C, 50.1 (49.9); H, 8.4 (8.5); N, 29.2 (29.1)%. IR (KBr, cm^{-1}): 3218 s (ν NH), 2036 vs (ν N_3). Electronic spectra ($CHCl_3$): λ_{max}, nm (ε, M^{-1} cm^{-1}): 528 (10.7), 317 (2133) and 244 (5770). FAB mass (CH_2Cl_2, m/z): 479 $(M)^+$.

Synthesis of $[NiL(NCS)_2]$ (2)

To a methanol solution (20 cm^3) of $[NiL]Cl_2 \cdot 2H_2O$ (251 mg, 0.5 mmol) was added KSCN (97 mg, 1 mmol) and the mixture was heated for 30 min on a steam bath. The solution was filtered to remove the potassium chloride. The solution was then taken to dryness and the resulting solid dissolved in acetonitrile/water (1:1, 10 cm^3). When this mixture was allowed to stand for a few days, a quantity of violet crystals precipitated. These were filtered off, washed with diethyl ether and dried *in vacuo* (yield: 192 mg, 75%). Calc. (found) for $NiC_{22}H_{40}N_6S_2$ C, 51.7 (51.5); H, 7.9 (8.0); N, 16.4 (16.4)%. IR (KBr, cm^{-1}): 3212 s (ν NH) and 2062 vs (ν SCN). Electronic spectra ($CHCl_3$): λ_{max} nm (ε, M^{-1} cm^{-1}): 510 (9.9), 323 (20) and 245 (5398). FAB mass (CH_2Cl_2, m/z): 511 $(M)^+$.

Crystallography

Analyses on single crystals of $[NiL(N_3)_2]$ (1) and $[NiL(NCS)_2]$ (2) were carried out with an Enraf–Nonius CAD4 diffractometer. A summary of the data collection and details of the structure refinement is given in Table 1. The violet crystals of **1** and **2** were mounted on the diffractometer and used for data collections with graphite-monochromated Mo–K_α radiation (0.71069 Å). Unit-cell parameters and a crystal orientation matrix were determined by least-squares fit of 25 reflections. An asymmetric unit of intensity data were collected in the ω-2θ scan mode. A total of 2265 and 2451 unique reflections of **1** and **2** were measured, of which 2086 and 1980 with $[F_o > 3\sigma(F_o)]$ were used in the structure determination. The intensity data were collected for Lorentz and polarization effects. No absorption correction was applied. The structure was solved by direct methods and refined by full matrix least-squares refinement (NRCVAX and SHELXL-93) [19,20]. All non-hydrogen atoms were placed with a combination of difference Fourier and least-squares calculations. Hydrogen atoms in methyl groups were located from difference Fourier maps,

Table 1. Crystallographic data

	$[NiL(N_3)_2]$ (**1**)	$[NiL(NCS)_2]$ (**2**)
Formula	$NiC_{20}H_{40}N_{10}$	$NiC_{22}H_{40}N_6S_2$
Formula weight	479.31	511.42
Crystal system	Triclinic	Triclinic
Space group	$P\bar{1}$	$P\bar{1}$
a (Å)	8.976(1)	9.303(1)
b (Å)	9.647(1)	9.738(1)
c (Å)	7.945(2)	8.606(2)
α (°)	65.91(2)	108.63(2)
β (°)	77.49(1)	117.07(2)
γ (°)	101.49(1)	65.43(1)
V (Å^3)	580.3(2)	623.1(2)
Z	1	1
$F(000)$	258	274
T(K)	293	293
D_c(Mg m^{-3})	1.372	1.363
λ (Mo-K$_\alpha$) (Å)	0.71069	0.71069
μ (mm^{-1})	0.87	0.96
Crystal size (mm)	$0.3 \times 0.25 \times 0.2$	$0.26 \times 0.30 \times 0.12$
2θ range (°)	51.82	51.82
Index ranges	$-11 \leqslant h \leqslant 10$	$-10 \leqslant h \leqslant 11$
	$0 \leqslant k \leqslant 11$	$0 \leqslant k \leqslant 11$
	$-8 \leqslant l \leqslant 9$	$-10 \leqslant l \leqslant 10$
No. unique reflections	2265	2451
No. observed reflections $[F_o > 3\sigma(F_o)]$	2086	1980
No. parameters	222	222
R^a	0.028	0.041
Rw^b	0.036	0.043
GoF^c	0.68	0.65

$^a R = \Sigma\|F_o| - |F_c\|/\Sigma|F_o|$.
$^b Rw = [\Sigma w(|F_o - F_c|)^2/\Sigma w(|F_o|)^2]^{1/2}$.
^{c} GoF $= [\Sigma w(|F_o - F_c|)^2/(\text{no. reflns} - \text{no. params})]^{1/2}$.

other hydrogen atoms were placed in calculated positions. Anisotropic thermal parameters were used for all non-hydrogen atoms and isotropic thermal parameters were used with the hydrogen atoms. The positions of hydrogen atoms were fixed during the least-squares process. Full crystallographic details, atomic coordinates, interatomic distance and angles, hydrogen atom coordinates, anisotropic displacement parameters and structure factor tables for **1** and **2** have been deposited with the editor as supplementary material.

RESULTS AND DISCUSSION

Crystal structures of complexes

The ligand skeleton of the present compounds contains the most stable *trans*-III conformation with two gauche five-membered and two chair six-membered chelate rings. Two methyl groups on the six-membered chelate rings are *anti* with respect to the N_4 plane. The N—Ni—N angles of the six-membered chelate rings are longer than those of the five-membered chelate rings. An inversion centre of these complexes exists on the central nickel(II) ion.

An ORTEP drawing of $[NiL(N_3)_2]$ (**1**) with atomic labelling scheme is shown in Fig. 1 and selected bond lengths and angles in Table 2. The crystal structure of **1** shows that the nickel(II) ion is coordinated by the secondary amines of the macrocycle and that the axial positions are bonded by two nitrogen atoms of the azide ligands. The average Ni—N (secondary amines) distance [2.085(2) Å] is significantly longer than in the square-planar geometry of $[NiL]Cl_2 \cdot 2H_2O$ [1.948(4) Å] [10], but is similar to that observed for high-spin octahedral nickel(II) complexes with 14-membered tetraaza macrocyclic ligands [15,21–25]. However, the four Ni—N distances in NiN_4 plane are shorter than the axial Ni—N(3) distance of 2.175(2) Å, indicating an axially elongated octahedral geometry. The axial Ni—N(3) linkages are bent slightly off the perpendicular to the NiN_4 plane by 1.0–4.6°. The axial Ni—N(3) bond distance and Ni—N(3)—N(4) angle [119.8(2)°] are similar to those observed for catena-(μ-N_3) $[Ni(cyclam)](ClO_4) \cdot H_2O$ [26]. Furthermore,

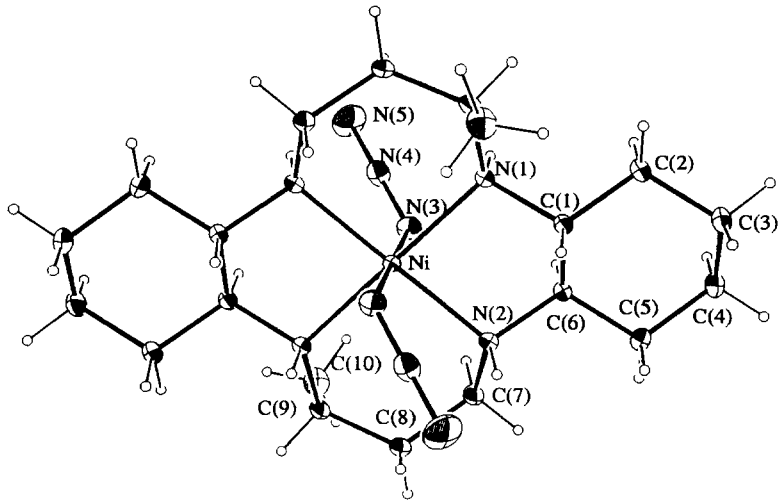

Fig. 1. An ORTEP drawing of $[NiL(N_3)_2]$ (**1**) with the atomic labelling scheme.

Table 2. Selected bond lengths (Å) and angles ( ) for $[NiL(N_3)_2]$ (**1**)

Ni—N(1)	2.098(2)	Ni—N(2)	2.072(2)
Ni—N(3)	2.175(2)	N(3)—N(4)	1.172(3)
N(4)—N(5)	1.161(4)	N(1)—C(1)	1.487(3)
N(1)—C(9′)	1.498(3)	N(2)—C(6)	1.493(3)
N(2)—C(7)	1.483(3)		
N(1)—Ni—N(2)	84.3(1)	N(1)—Ni—(2′)	95.7(1)
N(1)—Ni—N(3)	94.6(1)	N(2)—Ni—(3)	91.0(1)
Ni—N(3)—N(4)	119.8(2)	Ni—N(1)—C(1)	107.1(1)
Ni—N(1)—C(9′)	120.7(1)	Ni—N(2)—C(6)	106.6(1)
Ni—N(2)—C(7)	112.4(2)	N(3)—N(4)—N(5)	179.2(3)

Primes denote the symmetry equivalent $-x, -y, -z$.

Table 3. Selected bond lengths (Å) and angles (°) for $[NiL(NCS)_2]$ (**2**)

Ni—N(1)	2.085(3)	Ni—N(2)	2.080(3)
Ni—N(3)	2.115(3)	N(3)—C	1.156(5)
C—S	1.621(4)	N(1)—C(1)	1.490(4)
N(1)—C(9′)	1.502(5)	N(2)—C(6)	1.468(5)
N(2)—C(7)	1.477(5)		
N(1)—Ni—N(2)	83.9(1)	N(1)—Ni—N(2′)	96.1(1)
N(1)—Ni—N(3)	86.1(1)	N(2)—Ni—N(3)	92.5(1)
Ni—N(3)—C	143.7(3)	Ni—N(1)—C(1)	108.3(2)
Ni—N(1)—C(9′)	121.1(2)	Ni—N(2)—C(6)	107.7(2)
Ni—N(2)—C(7)	112.5(2)	N(3)—C—S	177.2(3)

Primes denote the symmetry equivalent $-x, -y, -z$.

the azido group is slightly asymmetric [N(3)—N(4) = 1.172(3) and N(4)—N(5) = 1.161(4) Å] and linear [N(3)—N(4)—N(5) angle = 179.2(3)], as found for monodentate azido ligands in complex **1**.

An ORTEP diagram of $[NiL(NCS)_2]$ (**2**) with atomic labelling scheme is shown in Fig. 2 and selected bond lengths and angles in Table 3. The coordination environment around nickel(II) ion shows a six-coordinated octahedron with two nitrogen atoms of thiocyanate ligands and four nitrogen atoms of the macrocyclic ligand. The average Ni—N (secondary amines) distance [2.083(3) Å] is similar to that found in **1** and shorter than the axial Ni—N(3) distance of 2.115(3) Å, giving an axially elongated octahedral geometry. Also, the axial Ni—N(3) bond is not perpendicular to the NiN_4 plane with N(3)—Ni—N(1) and N(3)—Ni—N(2) angles of 86.1(1) and 92.5(1)°. The Ni—N(3)—C and N(3)—C—S angles related to the thiocyanate ligand are 143.7(3) and 177.2(3)°, respectively.

Spectra and properties of the complexes

The complexes **1** and **2** are stable in the solid state and are soluble in water, acetonitrile, nitromethane, methylene chloride and chloroform. The infrared spectra of the complexes **1** and **2** are listed in Table 4. The infrared spectra of these complexes show a band at *ca.* 3200 cm^{-1}, which is assigned to the ν (NH) of the coordinated secondary amines. That the spectrum of **1** contains only a single very strong broad band at 2036 cm^{-1} associated with the azide stretching mode is consistent with the crystal structure of **1**. For complex **2** the infrared data are consistent with the N-bonded thiocyanato structure as a strong broad band at 2062 cm^{-1} is characteristic of Ni—N bonding [27] which shows the crystal structure of **2**. The electronic absorption spectra (Table 4) of complexes **1** and **2** in chloroform solution show maximum absorptions at 528–510, 317–323 and 244–245 nm. The wavelengths of the *d–d* bands for the present complexes are 65–47

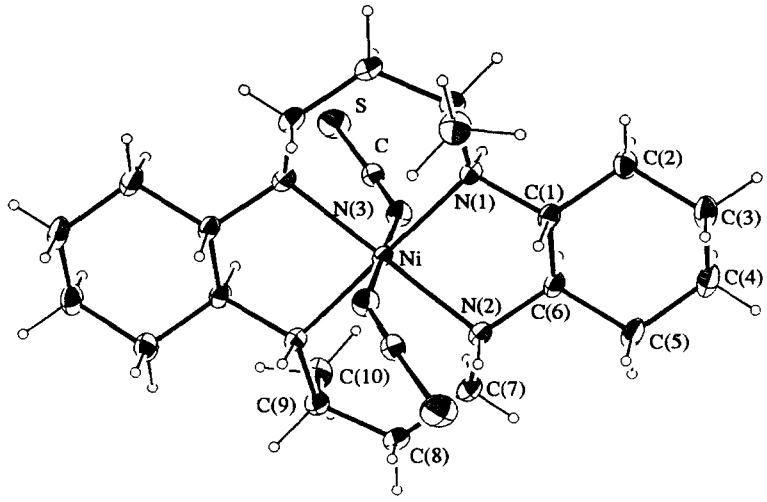

Fig. 2. An ORTEP drawing of $[NiL(NCS)_2]$ (**2**) with the atomic labelling scheme.

Table 4. Infrared and electronic spectral data

Complex	IR (cm^{-1}) ν (NH)	ν (N_3)	ν (SCN)	Electronic, λ_{max}, nm (ε, M^{-1} cm^{-1})[a]
$[NiL][ClO_4]_2$[b]	3185 (s)			463(73)[c]
$[NiL(N_3)_2]$ (**1**)	3218 (s)	2036 (vs)		528(10.7), 317(2133), 244(5770)
$[NiL(NCS)_2]$ (**2**)	3212 (s)		2062 (vs)	510(9.9), 323(20), 245(5398)

[a] In chloroform solution at 25°C.
[b] Reference 18.
[c] In nitromethane solution.

nm longer than that of $[NiL][ClO_4]_2$ (463 nm) [18], indicating that the complexes **1** and **2** have a six-coordinated octahedral geometry. However, the wavelength of the *d–d* band of **1** is somewhat longer than that of **2** in spite of the similar average Ni—N (secondary amines) bond distance. This fact can be reasonably explained by the spectrochemical series ($N_3^- < NCS^-$). A similar result was observed for related octahedral nickel(II) complexes of 14-membered tetraaza macrocyclic ligands [16].

Cyclic voltammetry data for nickel(II) complexes in 0.01 M TEAP-CH_2Cl_2 solution are given in Table 5. The complexes **1** and **2** exhibit two one-electron waves corresponding to Ni(II)/Ni(III) and Ni(II)/Ni(I) processes. The more negative potentials for **1** and **2**, compared with $[NiL][ClO_4]_2$, are resulted from the structural geometry (high-spin octahedral vs low-spin square-plane), which makes the oxidation of Ni(II) to Ni(III) easier and the reduction to Ni(I) difficult. Meanwhile, although complexes **1** and **2** have a similar average Ni—N (secondary amines) bond distance, the redox potentials for **2** are slightly more positive than those for **1** indicating that those of complex **2** are difficult to oxidize and easier to reduce. This result can be reflected by the π-donor ability of the axial ligands as observed in the visible spectra of these complexes.

Table 5. Cyclic voltammetric data for the nickel(II) complexes[a]

Complex	Potentials (V) vs Ag/AgCl Ni(II)/Ni(III)	Ni(II)/Ni(I)
$[NiL][ClO_4]_2$[b]	+1.08	−1.28
$[NiL(N_3)_2]$ (**1**)	+0.66	−1.54
$[NiL(NCS)_2]$ (**2**)	+0.79	−1.30

[a] Measured in 0.01 M TEAP-CH_2Cl_2 solution at 20°C.
[b] Reference 18.

Acknowledgements—This study was supported by the Basic Science Research Institute Program, Ministry of Education of Korea, Project No. BSRI-97-3435 and the Research Fund of Mokwon University, 1977.

REFERENCES

1. Lovecchio, F. V., Gore, E. S. and Busch, D. H., *J. Am. Chem. Soc.*, 1974, **24,** 2639.
2. Zeigerson, E., Ginzburg, G., Becker, J. Y., Kirschenbaum, L. J., Cohen, H. and Meyerstein, D., *Inorg. Chem.*, 1981, **20,** 3988.
3. Hay, R. W., Jeragh, B., Ferguson, G., Kaither, B. and Ruhl, B. L., *J. Chem. Soc., Dalton Trans.*, 1982, 1531.
4. Fairbank, M. G., Norman, P. R. and McAuley, A., *Inorg. Chem.*, 1985, **24,** 2639.
5. Hay, R. W. and Pujari, M. P., *J. Chem. Soc., Dalton Trans.*, 1986, 1485.
6. Kang, S.-G., Kim, M.-S., Choi, J.-S. and Cho, M. H., *Polyhedron*, 1995, **14,** 781.
7. Kang, S.-G., Kim, M.-S., Choi, J.-S., Whang, D. and Kim, K., *J. Chem. Soc., Dalton Trans.*, 1995, 363.
8. Kang, S.-G., Kim, S.-J., Kwak, C.-H. and Kim, J., *J. Chem. Soc., Dalton Trans.*, 1996, 2809.
9. Black, D. G., Jordan, R. F. and Rogers, R. D., *Inorg. Chem.*, 1997, **36,** 103.
10. Choi, K.-Y., Kim, J. C., Jensen, W. P., Suh, I.-H. and Choi, S.-S., *Acta Crystallogr., Sect. C*, 1996, **52,** 2166.
11. Choi, K.-Y., Oh, M.-R. and Suh, I.-H., *Chem. Lett.*, 1997, 141.
12. Choi, K.-Y., *Polyhedron*, 1997, **16,** 2073.
13. Choi, K.-Y., Suh, I.-H. and Kim, J. C., *Polyhedron*, 1997, **16,** 1783.
14. Choi, K.-Y. and Suh, I.-H., *Polyhedron*, 1997, **16,** 2393.
15. Mochizuki, K. and Kondo, T., *Inorg. Chem.*, 1995, **34,** 6241.
16. Martin, L. Y., Sperati, C. R. and Busch, D. H., *J. Am. Chem. Soc.*, 1977, **99,** 2968.
17. Perrin, D. D., Armarego, W. L. F. and Perrin, D. R., *Purification of Laboratory Chemicals*, 2nd edn. Pergamon Press, New York, 1985.
18. Kang, S.-G., Kweon, J. K. and Jung, S.-K., *Bull. Korean Chem. Soc.*, 1991, **12,** 483.
19. Gabe, E. J., Page, Y. L., Charland, J. P., Lee, F. L. and White, P. S., *J. Appl. Crystallogr.*, 1989, **22,** 384.
20. Sheldrick, G. M., SHELXL 93, University of Göttingen, 1993.
21. Riesen, A., Zehnder, M. and Kaden, T. A., *Helv. Chim. Acta.*, 1986, **69,** 2067.
22. Hay, R. W., Pujari, M. P., Moodie, W. T., Craig, S., Richens, D. T., Perotti, A. and Ungaretti, L., *J. Chem. Soc., Dalton Trans.*, 1987, 2605.
23. Jide, X., Shisheng, N. and Yuguan, L., *Inorg. Chem.*, 1988, **27,** 4651.
24. Fallis, I. A., Farrugia, L. J., Macdonald, N. M. and Peacock, R. D., *J. Chem. Soc., Dalton Trans.*, 1993, 2759.
25. Satate, Y., Ihara, Y., Senda, H., Suzuki, M. and Uehara, A., *Inorg. Chem.*, 1992, **31,** 3248.
26. Escuer, A., Vicente, R., Ribas, J., El Fallah, M. S. and Solans, X., *Inorg. Chem.*, 1993, **32,** 1033.
27. Nakamoto, K., *Infrared and Raman Spectra of Inorganic and Coordination Compounds*, 4th edn. John Wiley & Sons, New York, 1986.

Pergamon

PII: S0277-5387(97)00390-2

Polyhedron Vol. 17, No. 8, pp. 1247–1255, 1998
© 1998 Elsevier Science Ltd
All rights reserved. Printed in Great Britain
0277-5387/98 $19.00+0.00

tert-Butylammonium silicododecamolybdate. Synthesis, vibrational study, crystal structure, thermal behaviour and electrochemical properties

Ana S. J. Wery,[a] Juan M. Gutiérrez-Zorrilla,[a]* Antonio Luque,[a] Pablo Vitoria,[a] Pascual Román[a] and Martín Martínez-Ripoll[b]

[a] Departamento de Química Inorgánica, Universidad del País Vasco, Apartado 644, 48080 Bilbao, Spain

[b] Departamento de Cristalografía, Instituto de Química-Física Rocasolano, CSIC, Serrano 119, 28006 Madrid, Spain

(Received 16 July 1997; accepted 19 September 1997)

Abstract—The compound $[(CH_3)_3CNH_3]_4[SiMo_{12}O_{40}] \cdot 2H_2O$ has been synthesized and characterized chemically by means of FT-IR and Raman spectroscopy, microanalyses and thermal analyses. The X-ray diffraction crystal analysis reveals the presence of the Keggin cluster, *t*-butylammonium cations and water molecules joined by means of electrostatic interactions and hydrogen contacts. On the other hand, an electrochemical study using cyclic voltammetry was carried out, showing reversible cathodic redox processes. © 1998 Elsevier Science Ltd. All rights reserved

Keywords: silicododecamolybdate; *tert*-butylammonium cation; crystal structure.

The chemistry of Mo(VI), W(VI) and V(V) in aqueous solution is dominated by the formation of iso- and heteropolyoxometalates that can be viewed as discrete fragments of close-packed extended oxide structure [1].

During the last two decades this class of compounds has aroused increasing interest due to their unique properties including size, electron transfer abilities, thermal stability and lability of lattice oxygen [2]. In addition, some of these compounds have found applications in analytical and clinical chemistry [3], as well as in the fields of catalysis [4], photochemistry [5], medicine and biology [6] and material science [7]. The most active area of applications is catalysis, being the Keggin type anions [8] the most widely employed as homogeneous and heterogeneous catalysts [9]. The Keggin polyanion can be formulated as $[X^{n+}M_{12}O_{40}]^{(8-n)-}$ (M = Mo, W; X = Si, P, Ge, S, B, ...). Their structure result from the association of four M_3O_{13} units tetrahedrally disposed around the central atom X. According to Baker and Figgis [10], there are five possible isomers, α, β, γ, δ and ε, which differ by rotation of one, two, three of four M_3O_{13} groups by $\pi/3$. Until now, only the α and β isomers are known as isolated polyanions [11]. Other isomers, such as ε, are known as polycations $\{[Al_{13}O_4(OH)_{24}(H_2O)_{12}]^{7+}$ [12] and as part of larger structures [13].

Several structures containing the $[\alpha\text{-}SiMo_{12}O_{40}]^{4-}$ anion are known from the literature: $H_4[SiMo_{12}O_{40}] \cdot 13H_2O$ [14], $(CH_6N_3)_4[SiMo_{12}O_{40}] \cdot H_2O$ [15], $(NH_4)_3[(C_4H_9)_2NH_2][SiMo_{12}O_{40}] \cdot 2H_2O$ [16], $(TTF)_2^0$ $(TTF_4)^{2+}(H^+)(Et_4N)^+[SiMo_{12}O_{40}]$ [17], $[Fe(C_5Me_5)_2]_4[SiMo_{12}O_{40}] \cdot DMF$ [18] and $(DMNP)_2(MNP)_2[SiMo_{12}O_{40}] \cdot 2DMF$ [19].

In the present paper, we report the synthesis, vibrational study, crystal structure, thermal behaviour and electrochemical properties of $[(CH_3)_3NH_3]_4[SiMo_{12}O_{40}] \cdot 2H_2O$.

* Author to whom correspondence should be addressed.

EXPERIMENTAL

General and instrument

All chemicals were procured commercially and used without subsequent purification. Microanalyses of carbon, nitrogen and hydrogen were performed on a Perkin-Elmer 240 C-, H-, N-analyser and silicon and molybdenum were determined thermogravimetrically as $SiO_2 + MoO_3$ after thermal decomposition of the samples in an argon–oxygen atmosphere.

IR spectra were recorded on a Nicolet 740 FT-IR spectrometer as KBr pellets in the spectral region 4000–400 cm^{-1}. Raman spectra were made on a Nicolet 950 FT Raman spectrometer equipped with a Spectra Physics $Nd:YVO_4$ laser (1064 nm, 1.5 W) as static powder samples. A Setaram TAG 24S 16 thermobalance was used to obtain simultaneously the differential thermal analysis (DTA) and thermogravimetric analysis (TGA) curves, in a synthetic air atmosphere and in an inert atmosphere of argon with a heating rate of 5°C min^{-1}.

The electrochemical study was carried on by means of cyclic voltammetry in a polargraph PAR 174A coupled to a register X-Y Houston 2000. The cell of measurement consists of three electrodes: Ag/AgCl(s)/KCl as reference electrode, a Pt wire as auxiliary electrode and an electrode of glassy C METROHM (diameter = 3 mm) as working electrode. KCl 1 M was used as electrolyte and the concentration of the electroactive specie was of the order of 10^{-3} M. All the solutions were deoxygenated passing a current of nitrogen before the measurement. The potential scan was done at a speed of 20 $mV \cdot s^{-1}$ in the range from 1.0 V to −2.0 V.

Synthesis of $[(CH_3)_3CNH_3]_4[SiMo_{12}O_{40}] \cdot 2H_2O$

To a solution of $[(CH_3)_3CNH_3]_4[Mo_8O_{26}] \cdot 6H_2O$ [20] (1.15 g, 0.72 mmol) in 50 ml of water were added 5 ml of Na_2SiO_3(aq) (0.31 M, 1.55 mmol SiO_2) and the solution was acidified with HCl (3 M) up to pH = 1 (yellow solution). Crystals of the compound appeared after two weeks. Found: C, 8.9; H, 2.4; N, 2.6; ($MoO_3 + SiO_2$) 83.08. Calc. for $C_{16}H_{52}Mo_{12}N_3O_{42}Si$: C, 8.89; H, 2.46; N, 2.62; ($MoO_3 + SiO_2$) 83.84%.

X-ray diffraction

Single crystals suitable for X-ray analysis of the compound were obtained as described above. Structural measurements were performed on a Philips PW1100 diffractometer (graphite monochromated MoKα radiation, $\lambda = 0.71069$ Å). The data were collected at 295 K using ω–2θ scan technique up to 50° in 2θ. The intensities were corrected for Lorentz and polarization effects. Neutral atoms scattering factors and anomalous dispersion factors were taken from the literature [21].

The structure has been solved using the program DIRDIF92 [22] finding the anion $[SiMo_{12}O_{40}]^{4-}$ and three of the *t*-butylammonium cations. The last *t*-butylammonium cation and the position of the water molecules were located on successive Fourier maps. An empirical absorption correction (DIFABS) [23] was applied when all the non-hydrogen atoms had been located. The crystal structure was then refined with anisotropic thermal parameters for all the non-hydrogen atoms by full-matrix least-squares analysis. The hydrogen atoms were generated at geometrically fixed positions. Most calculations were carried out using the XRAY 76 [24] system running on a Micro VAXII computer. Table 1 summarizes crystal data and data collection procedures for this compound.

Table 1. Crystallographic data for compound $[C_4H_{12}N)]_4[SiMo_{12}O_{40}] \cdot 2H_2O$

Formula	$C_{16}H_{52}Mo_{12}N_4O_{42}Si$
Mr	2151.96
Space group	$P\bar{1}$ (no. 2)
a (Å)	21.005(2)
b (Å)	11.968(1)
c (Å)	11.685(1)
α (°)	110.625(1)
β (°)	103.774(1)
γ (°)	81.000(2)
V (Å^3)	2661.6(4)
Z	2
F(000)	2060
D_0 (Mg m^{-3})	2.70(1)
D_x (Mg m^{-3})	2.685
μ (MoKα) (cm^{-1})	27.88
Form	Prism
Dimensions (mm)	0.26 × 0.36 × 0.55
Colour	Yellow
Diffractometer	Philips PW 1100
Temperature (K)	295(1)
Radiation (A[faAn]	0.71069
Monochromator	Oriented graphite
Scan mode	ω–2θ
θ range	1–25
hkl	$0 \rightarrow 24$; $-14 \rightarrow 14$; $-13 \rightarrow 13$
Controls	Intensity and orientation
−Reflections	8 0 0; $\bar{8}$ 0 0
−Periodicity	5400 s
Independent reflections	9335
Observed reflections	8394 [$I \geqslant 3\sigma(I)$]
No. of variables	677
$\Delta\rho_{max}$ (e Å^{-3})	0.86
Absorption correction	DIFABS; $T_{min} = 0.912$; $T_{max} = 1.175$
R	0.026
R_w	0.037

RESULTS AND DISCUSSION

Thermal decomposition

The thermal decomposition of $[(CH_3)_3CNH_3]_4[SiMo_{12}O_{40}] \cdot 2H_2O$ starts with the loss of the water molecules in both atmospheres yielding the anhydrous salt that is stable up to 240°C approximately. This stability range is similar to the one observed for the compound tris(*tert*-butylammonium)phosphododecamolybdate(VI) dihydrate [25]. Then, the decomposition of the anhydrous salt takes place in both atmospheres without stable intermediate products (Table 2). In oxidant atmosphere it occurs in three exothermic steps finishing at 440°C in a stable residue that corresponds to $MoO_3/SiO_2 = 12:1$, but only the existence of MoO_3 could be confirmed by means of Powder Diffraction Data. While in inert atmosphere, the decomposition of the anhydrous salt takes place in two overlapping steps followed by a progressive mass loss, the process finishes at 600°C. The presence of Mo(V) in the black final residue has been confirmed by means of EPR.

Figure 2 shows the TG, DTG and DTA curves corresponding to the thermal decomposition in synthetic air and argon atmospheres of the compound.

Vibrational spectroscopy

The infrared and Raman spectra of the title compound are shown in Fig. 3. A systematic study of the cation-size effect on the vibrational spectra of Keggin polyanions has been performed by Rochcchiccioli-Deltcheff [26]. The anion–anion electrostatic interactions are responsible for a strong increase in the stretching frequencies. These interactions can be considered as perturbations on the charge-density distribution, on the geometry of the anion and on the vibrational spectra with respect to isolated anion. Table 3 lists the values of the frequencies of the stretching modes for the compound together with the $H_4[SiMo_{12}O_{40}]$ (higher anion–anion interactions) and $(TBA)_4[SiMo_{12}O_{40}]$ (neglected anion–anion interactions) for comparison.

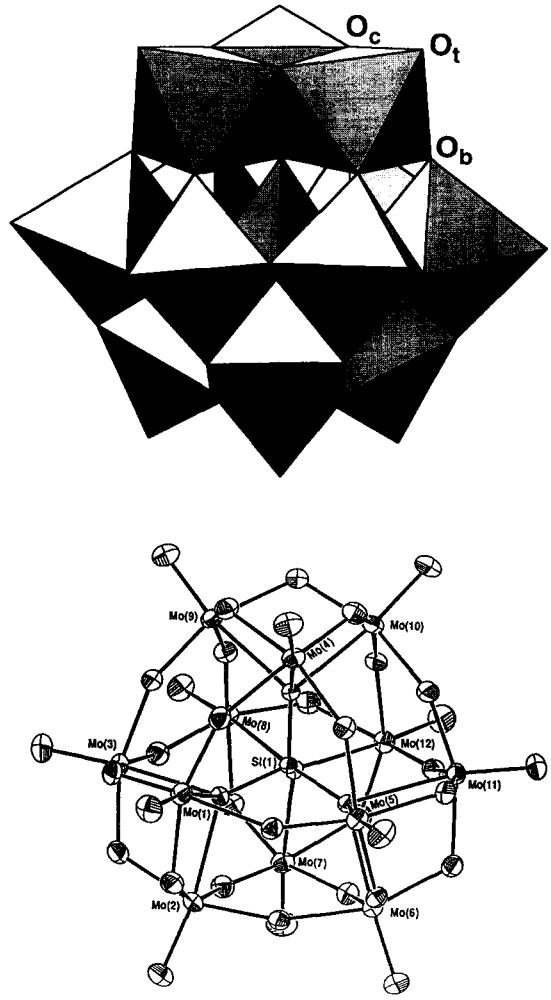

Fig. 1. Keggin polyanion: (top) polyhedral representation, along with the designation of the oxygen atoms; (bottom) ORTEP view displaying Mo labelling.

Table 2. Steps, initial, final and maximum peak temperature (°C), partial and total weight loss (%), during the thermal decomposition of the compound in synthetic air and argon atmospheres

Step	$T_i - T_f$	T_m	ΔH	% Δm
		Synthetic air		
1	80–125	110	Endo	1.66
2	240–285	265	Exo	3.79
3	285–360	285	Exo	3.16
4	360–440	390	Exo	7.57
			Σ% Δm	16.16
			Calc.	16.92
		Argon		
1	65–120	100	Endo	1.68
2	245–295	275	Endo	7.69
3	295–330	295	Endo	2.33
4a	330–600			7.92
			Σ% Δm	19.57

[a] Progressive weight loss

Crystal structure of $[(CH_3)_3CNH_3]_4[SiMo_{12}O_{40}] \cdot 2H_2O$

The asymmetric unit consists of a $[SiMo_{12}O_{40}]^{4-}$ anion, four *t*-butylammonium cations and two water molecules. The silicododecamolybdate(VI) anion adopts the α-Keggin structure in which a central tetrahedron SiO_4 is surrounded by twelve MoO_6 octahedra that are disposed in four groups Mo_3O_{13} of three edge-sharing octahedra, each group is joined to the adjacent

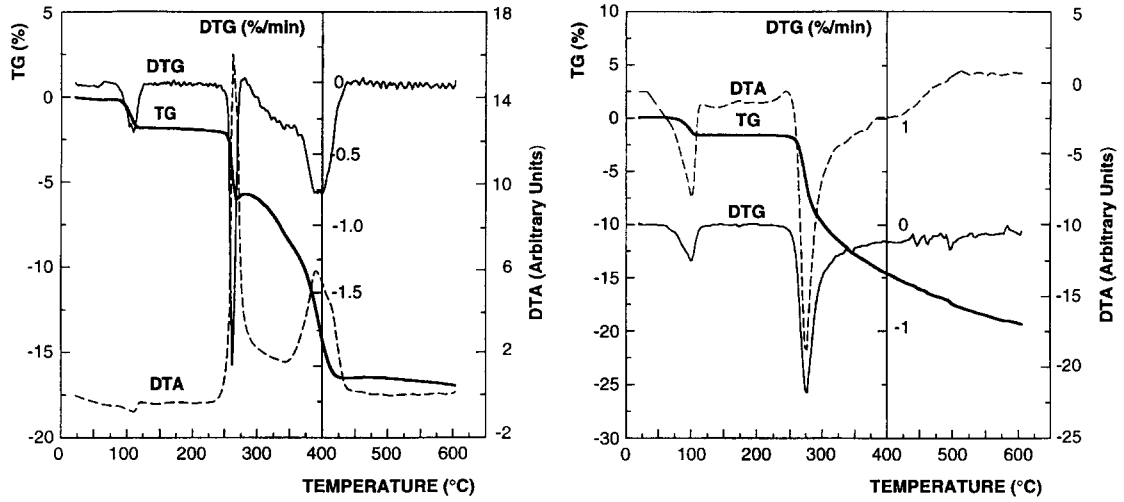

Fig. 2. Thermal decompositions in an oxidant atmosphere (left) and an inert atmosphere (right).

Table 3. Some assignments in the vibrational spectra of some α-Keggin $[SiMo_{12}O_{40}]^{4-}$ anions

Cation[a] assignment	H^+	$(C_4H_{12}N)^+$	$[(n\text{-}C_4H_9)_4N]^+$
IR bands			
	995 (sh)	991 (vw)	985 (w)
ν_{as} (Mo—O_t)	957 (s)	957 (sh)	945 (sh)
		948 (s)	
ν_{as} (Si—O_a)	904 (vs)	903 (vs)	899 (vs)
ν_{as} (Mo—O_b—Mo)	855 (m)	865 (m)	868 (s)
ν_{as} (Mo—O_c—Mo)	770 (vs)	790 (vs)	795 (vs)
			735 (sh)
		635 (w)	635 (w)
	535 (m)	534 (m)	532 (w)
		510 (m)	
	422 (w)	499 (m)	
Raman bands			
ν_s (Mo—O_t)	988 (vs)	976 (vs)	967.5 (vs)
ν_{as} (Mo—O_t)	963.5 (m)	959 (s)	941.5 (m)
	907 (w)	942 (m)	
ν (Mo—O_b—Mo)	875 (vw)	884 (w)	883.5 (w)
		729 (w)	
	682 (sh)	670 (sh)	686 (w)
ν_s (Mo—O_c—Mo)	632 (m)	629 (m)	620.5 (m)
	451 (vw)	464 (w)	465 (w)
	368 (vw)	368 (w)	371 (w)
	290 (vw)	288 (vw)	290 (vw)
ν_s (Mo—O_a)	250.5 (s)	248 (s)	246.5 (s)
	220 (m)	208 (m)	208.5 (m)
	162 (m)	165 (m)	167 (w)
	111 (s)	119 (m)	109.5 (s)

[a] Data for H^+ and TBA salts were taken from ref. 26

groups and to the central tetrahedron sharing corners. Figure 1 shows a polyhedral representation and an ORTEP view of the silicododecamolybdate anion. There are four types of oxygen atoms in the Keggin

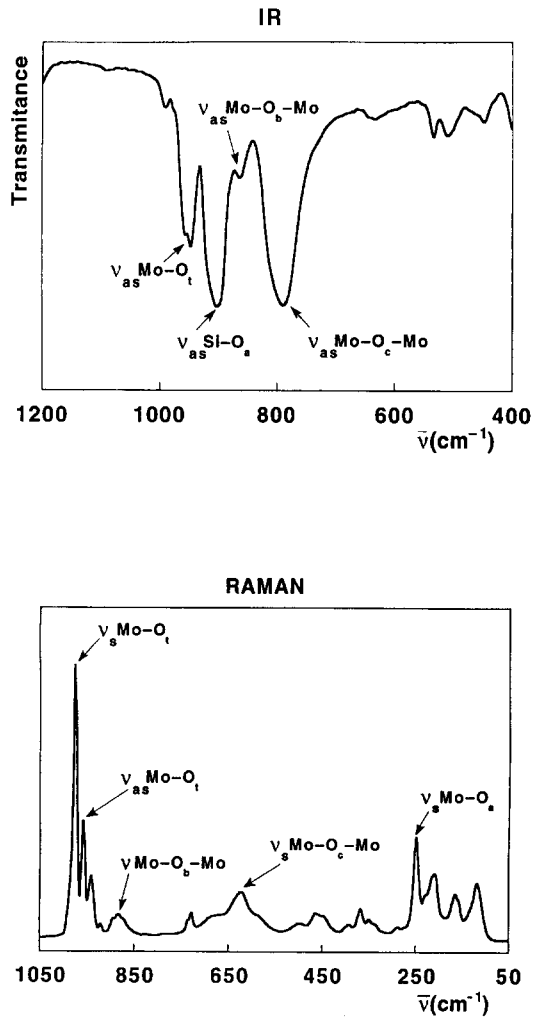

Fig. 3. IR and Raman spectra for $[SiMo_{12}O_{40}]^{4-}$ polyanion.

Table 4. Bond distances Mo—O, Si—O and O···O (Å) and bond angles O—Mo—O and O—Si—O (°)

	Mo(1)	O(1)	O(13)	O(15)	O(16)	O(17)	O(37)
O(1)	1.692(5)		95.0(3)	103.1(2)	104.1(3)	97.4(2)	167.6(3)
O(13)	2.024(6)	2.748(7)		88.8(2)	156.3(2)	79.0(2)	72.6(2)
O(15)	1.815(5)	2.747(7)	2.691(6)		100.2(2)	157.0(2)	76.7(2)
O(16)	1.822(6)	2.771(8)		2.791(8)		84.6(2)	88.1(2)
O(17)	2.056(4)	2.825(6)	2.596(8)		2.614(6)		81.0(2)
O(37)	2.323(4)		2.586(7)*	2.600(6)	2.904(7)	2.852(6)	
	Mo(2)	O(2)	O(13)	O(14)	O(18)	O(19)	O(37)
O(2)	1.685(7)		102.8(3)	97.7(2)	102.8(2)	99.0(2)	170.2(2)
O(13)	1.830(5)	2.749(8)		89.2(2)	97.5(2)	157.3(2)	75.5(2)
O(14)	1.998(4)	2.780(7)	2.690(7)		156.5(2)	81.6(2)	72.7(2)
O(18)	1.847(4)	2.762(8)	2.764(6)			83.7(2)	87.1(2)
O(19)	2.037(5)	2.840(8)		2.637(6)	2.595(6)		81.9(2)
O(37)	2.341(5)		2.586(7)*	2.586(8)	2.907(6)	2.877(7)	
	Mo(3)	O(3)	O(14)	O(15)	O(20)	O(21)	O(37)
O(3)	1.679(5)		100.9(3)	97.8(2)	103.1(2)	101.1(3)	168.9(2)
O(14)	1.873(6)	2.741(6)		86.0(2)	97.0(2)	156.1(2)	74.3(2)
O(15)	2.029(5)	2.804(7)	2.663(7)		157.9(2)	82.0(2)	72.1(2)
O(20)	1.814(5)	2.737(7)	2.761(8)			86.9(2)	87.5(2)
O(21)	1.996(5)	2.844(9)		2.642(7)	2.622(7)		82.4(2)
O(37)	2.362(4)		2.586(8)	2.599(6)	2.914(6)	2.884(6)	
	Mo(4)	O(4)	O(16)	O(22)	O(27)	O(28)	O(38)
O(4)	1.701(5)		99.2(3)	101.4(2)	98.9(2)	102.6(3)	171.5(2)
O(16)	2.011(6)	2.833(9)		84.9(2)	81.2(2)	157.4(2)	81.7(2)
O(22)	1.870(4)	2.765(6)	2.623(7)		157.0(2)	96.5(2)	87.2(2)
O(27)	1.992(4)	2.811(7)	2.605(7)			89.5(2)	72.8(2)
O(28)	1.806(6)	2.738(7)		2.743(7)	2.678(7)		75.9(2)
O(38)	2.353(5)		2.867(6)	2.932(6)	2.595(6)	2.592(8)	
	Mo(5)	O(5)	O(17)	O(22)	O(23)	O(29)	O(39)
O(5)	1.676(5)		104.0(2)	100.0(2)	99.9(2)	96.0(2)	167.3(2)
O(17)	1.801(5)	2.742(7)		88.5(2)	97.3(2)	159.0(2)	88.0(2)
O(22)	1.994(5)	2.818(7)	2.651(8)		157.2(2)	81.8(2)	84.0(2)
O(23)	1.887(5)	2.732(7)	2.768(5)			85.3(2)	74.2(2)
O(29)	2.040(5)	2.773(7)		2.640(6)	2.663(8)		72.5(2)
O(39)	2.330(4)		2.895(6)	2.905(7)	2.569(6)	2.594(7)	
	Mo(6)	O(6)	O(18)	O(23)	O(24)	O(30)	O(39)
O(6)	1.682(5)		99.6(2)	96.2(2)	102.8(2)	101.2(2)	167.8(2)
O(18)	2.003(5)	2.821(6)		82.1(2)	85.9(2)	157.7(2)	82.3(2)
O(23)	2.008(4)	2.755(7)	2.634(7)		159.0(2)	87.6(2)	72.0(2)
O(24)	1.825(4)	2.742(6)	2.611(6)			97.4(2)	89.3(2)
O(30)	1.868(6)	2.745(8)		2.685(6)	2.775(7)		75.7(2)
O(39)	2.336(4)		2.866(8)	2.569(6)	2.948(7)	2.607(5)	
	Mo(7)	O(7)	O(19)	O(24)	O(25)	O(31)	O(40)
O(7)	1.696(6)		101.9(3)	99.8(2)	101.4(2)	98.8(3)	170.8(2)
O(19)	1.807(5)	2.721(6)		86.6(2)	96.7(2)	157.4(2)	87.1(2)
O(24)	1.992(4)	2.827(7)	2.609(7)		157.3(2)	81.0(2)	82.5(2)
O(25)	1.856(4)	2.751(7)	2.737(7)			87.9(2)	75.3(2)
O(31)	2.015(6)	2.826(9)		2.602(7)	2.690(7)		72.6(2)
O(40)	2.360(5)		2.899(8)	2.882(6)	2.606(7)	2.604(6)	
	Mo(8)	O(8)	O(20)	O(25)	O(26)	O(32)	O(40)
O(8)	1.671(5)		98.0(2)	96.9(2)	102.6(2)	102.9(2)	169.8(2)
O(20)	2.030(5)	2.803(7)		80.3(2)	84.7(2)	157.5(2)	82.2(2)
O(25)	2.026(5)	2.778(6)	2.616(6)		156.8(2)	88.9(2)	73.0(2)
O(26)	1.845(5)	2.746(7)	2.614(8)			98.7(2)	87.6(2)
O(32)	1.831(5)	2.740(7)		2.704(8)	2.789(6)		75.8(2)
O(40)	2.334(4)		2.879(6)	2.606(7)	2.913(6)	2.589(6)	

Continued overleaf

Table 4—*Continued.*

	Mo(9)	O(9)	O(21)	O(26)	O(27)	O(33)	O(38)
O(9)	1.689(4)		102.7(3)	100.0(2)	102.1(2)	97.2(2)	169.3(3)
O(21)	1.836(6)	2.755(8)		85.1(2)	96.2(2)	158.3(2)	87.9(2)
O(26)	1.987(4)	2.823(6)	2.588(6)		156.9(2)	83.3(2)	81.6(1)
O(27)	1.840(5)	2.747(6)	2.735(8)			87.6(2)	75.5(2)
O(33)	1.997(6)	2.774(7)		2.649(8)	2.658(7)		72.4(2)
O(38)	2.349(4)		2.923(6)	2.846(6)	2.595(6)	2.582(7)	
	Mo(10)	O(10)	O(28)	O(33)	O(34)	O(36)	O(38)
O(10)	1.689(7)		95.0(2)	100.4(2)	99.8(2)	105.1(2)	166.1(2)
O(28)	2.079(4)	2.791(7)		84.1(2)	81.2(2)	158.5(2)	71.7(2)
O(33)	1.872(4)	2.738(8)	2.652(6)		155.9(2)	99.4(2)	74.9(2)
O(34)	1.977(4)	2.811(7)	2.641(6)			87.8(2)	82.4(2)
O(36)	1.798(5)	2.769(9)		2.799(6)	2.620(6)		88.6(2)
O(38)	2.332(5)		2.592(8)	2.582(7)	2.851(7)	2.910(6)	
	Mo(11)	O(11)	O(29)	O(30)	O(34)	O(35)	O(39)
O(11)	1.690(5)		103.0(2)	95.8(2)	103.9(2)	98.2(2)	168.5(2)
O(29)	1.818(4)	2.747(7)		88.9(2)	98.3(2)	157.0(2)	75.9(2)
O(30)	2.028(5)	2.768(9)	2.697(7)		156.8(2)	80.1(2)	72.8(2)
O(34)	1.843(5)	2.783(6)	2.770(6)			85.0(2)	87.6(2)
O(35)	2.033(4)	2.823(7)		2.614(6)	2.623(7)		81.5(2)
O(39)	2.346(5)		2.594(7)	2.607(5)	2.921(8)	2.870(6)	
	Mo(12)	O(12)	O(31)	O(32)	O(35)	O(36)	O(40)
O(12)	1.687(5)		102.0(2)	98.3(2)	102.0(2)	99.4(2)	170.5(2)
O(31)	1.837(6)	2.741(9)		88.5(2)	99.7(2)	157.0(2)	75.9(2)
O(32)	2.004(4)	2.800(7)	2.683(6)		155.9(2)	80.1(2)	72.5(2)
O(35)	1.812(4)	2.721(7)	2.790(8)			83.9(2)	87.4(2)
O(36)	2.063(5)	2.870(6)		2.618(8)	2.597(6)		81.6(2)
O(40)	2.348(4)		2.604(6)	2.589(6)	2.900(6)	2.890(8)	
	Si(1)	O(37)	O(38)	O(39)	O(40)		
O(37)	1.638(5)		109.6(2)	109.5(2)	109.4(3)		
O(38)	1.638(5)	2.677(8)		109.4(3)	109.8(2)		
O(39)	1.630(4)	1.668(6)	2.668(6)		109.1(2)		
O(40)	1.624(4)	2.662(6)	2.669(6)	2.651(6)			

polyanion: four O_a atoms which connect Si and Mo atoms; twelve bridging O_b atoms, located in the shared corners between two Mo_3O_{13} units; twelve O_c atoms, which connect edge-sharing MoO_6 octahedra in Mo_3O_{13} units, and twelve terminal oxygen atoms, O_t.

The Mo atoms are not at the centre of the octahedron but located towards the terminal oxygen atom giving the following distribution of distances: Mo—O_t (short): 1.671–1.701 Å; Mo—O_{b-c} (medium): 1.801–2.063 Å; Mo—O_a (long): 2.323–2.362 Å. The Si—O distances are in the range 1.624–1.638 Å (Table 4).

Figure 4 shows the projections onto the plane (011). The anions and water molecules are placed in shells parallel to the plane (100) at two different x levels ($x = \frac{1}{4}$ and $x = \frac{3}{4}$). The *t*-butylammonium cations are located between the shells of polyanions forming an extended network of hydrogen contacts of the types N—H···O, N—H···O_w, O_w—H···O, C—H···O and C—H···O_w, however, hydrogen contacts between the water molecules are not observed (Table 5). Cations **1** and **2** are joined to three different polyanions and to the water molecule $O(41)_w$ while cations **3** and **4** form hydrogen contacts with oxygen atoms from two different silicododecamolybdate(VI) anions and with the water molecule $O(42)_w$.

Electrochemical studies

Table 6 summarizes the cathodic and anodic peak potentials (mV) as well as the difference potential for the tetrakis(*tert*-butylammonium)silicododecamolybdate(VI) dihydrate. Figure 5(a) shows the voltamperogram for this compound done at a sensitivity of 20 μA. Three reversible processes that involve one e^- are observed. If the measurement is done at a sensitivity of 100 mA, three more cathodic processes are observed but only the last two are revers-

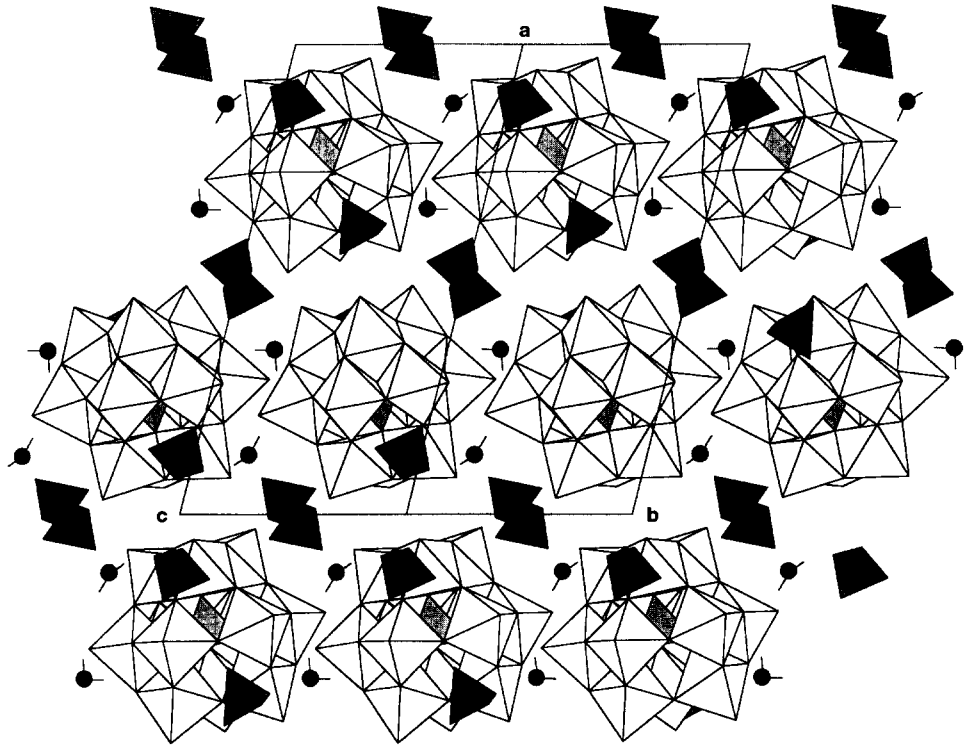

Fig. 4. View along the [0 1 1] direction. *tert*-Butylammonium cations are represented by tetrahedra for clarity.

Table 5. Hydrogen-contacts (Å)

Bond type	X···O	Bond type	X···O
N(11)—H(111)···O(23)[1]	2.801(7)	O(41)w—H(411)w···O(18)[1]	2.948(7)
N(11)—H(112)···O(4)[2]	3.025(7)	O(41)w—H(412)w···O(33)[3]	2.936(9)
N(11)—H(113)···O(10)[3]	2.92(1)	O(42)w—H(421)w···O(14)[2]	2.68(1)
N(21)—H(211)···O(41)$_w$[4]	2.906(9)	O(42)w—H(422)w···O(12)[5]	3.027(8)
N(21)—H(212)···O(22)[5]	3.09(1)	O(42)w—H(422)w···O(35)	3.196(8)
N(21)—H(213)···O(1)	3.101(8)	C(13)—H(132)···O(5)[5]	3.49(1)
N(31)—H(311)···O(9)[6]	3.103(8)	C(15)—H(153)···O(9)[6]	3.49(1)
N(31)—H(312)···O(30)[1]	2.867(7)	C(23)—H(231)···O(28)[5]	3.52(1)
N(31)—H(313)···O(42)$_w$[2]	3.15(1)	C(23)—H(232)···O(27)[6]	3.21(1)
N(41)—H(411)···O(42)$_w$	2.91(1)	C(44)—H(442)···O(8)[2]	3.46(1)
N(41)—H(412)···O(7)[7]	2.94(1)		
N(41)—H(413)···O(25)[2]	3.02(1)		

Symmetry codes
[1] y, x, −1+z
[2] 1−y, 1−x, −z
[3] −1+y, x, z
[4] x, y, −1+z
[5] 1−x, 1−y, −z
[6] x, −1+y, z
[7] 1+x, y, 1+z.

ible [Fig. 5(b)]. The first of them corresponds to a process of 2 e^- ($\Delta Ep = 40$ mV) and the second one to a process of 1 e− ($\Delta Ep = 60$ mV). The peaks at −1310 mV and −1070 mV are wide and asymmetric, fact that could be due to the existence of two overlapping processes. The reversibility criteria used was $\Delta E_p = E_c - E_a = 59/n$ mV (n = number of electrons).

Table 6. Cathodic and anodic peak potential (E_c) and (E_{pa}) (mV), difference of potential for the cyclic voltamperogram of the compound at a sensitivity of 20 μA and 100 mA, respectively

Sensitivity 20 μA			Sensitivity 100 μA		
E_c	E_a	ΔE_p	E_c	E_a	ΔE_p
110(h)	210	100	−1000 (h)		
20	110	90	−1110	−1070	40
−200	−80	120	−1310	−1250	60

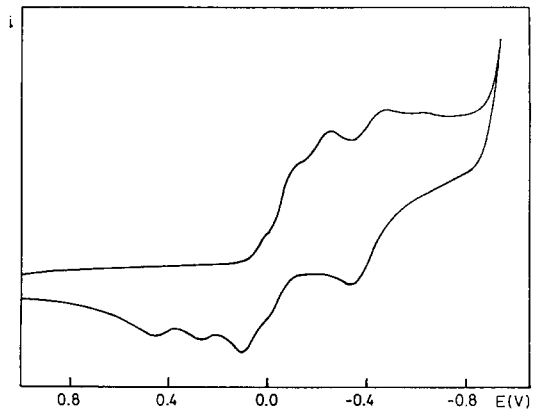

(a)

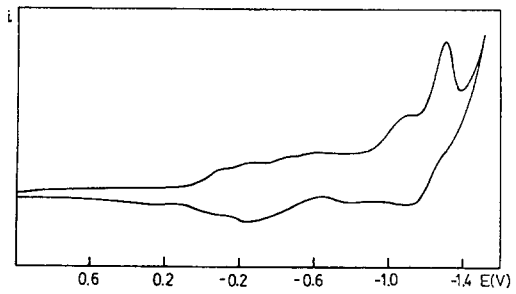

(b)

Fig. 5. CV of title compound in KCl (1 M), (a) sensitivity 20 μA, V = 20 mV s^{-1}. (b) sensitivity 100 μA, V = 20 mV s^{-1}.

Acknowledgements—This work was supported by Gobierno Vasco (Grant PI-96/69). A.S.J.W. acknowledges financial support from European Union S&T Fellowship Program in Japan, ERB CIPI CT950003.

REFERENCES

1. Pope, M. T. and Müller, A., ed. *Polyoxometalates: From Platonic Solids to Antiretrovial Activity*. Kluwer, Dordrecht, The Netherlands, 1994; Pope, M. T., In *Progress in Inorganic Chemistry*, ed. S. J. Lippard. John Wiley and Sons, New York, 1991, p. 181; Baker, L. C. W., *Advances in the Chemistry of Coordination Compounds*. MacMillan, New York, 1961, p. 604.
2. Pope, M. T. and Müller, A., *Angew. Chem. Int. Ed. Engl.*, 1991, **30,** 34.
3. Osmond, F., *Bull. Soc. Chim. Fr.*, 1887, **47,** 745; Keana, J. F. W., Wu, Y. and Wu, G., *J. Org. Chem.*, 1987, **52,** 2571; Parker, G. A., *Analytical Chemistry of Molybdenum*. Springer-Verlag, New York, 1983.
4. Misono, M., *Catal. Rev. Sci. Eng.*, 1988, **30,** 339; Mizuno, M. and Misono, M., *J. Phys. Chem.*, 1990, **94,** 890; Misono, M. and Nojiri, N., *Appl. Catal.*, 1990, **64,** 1; Lee, K. Y., Arai, T., Nakata, S., Asaoka, S., Okuhara, T. and Misono, M., *J. Am. Chem. Soc.*, 1992, **114,** 2836; Kozhevnikov, I. V. and Matveev, K. O., *Appl. Catal.*, 1983, **5,** 135; Belanger, R. and Moffat, J. B., *J. Catal.*, 1995, **152,** 171; Corma, A., *Chem. Rev.*, 1995, **95,** 559; Hill, C. L. and Prosser-Mccartha, M., *Coord. Chem. Rev.*, 1995, **143,** 407.
5. Naruke, H. and Yamase, T., *J. Lumin.*, 1991, **50,** 50; Papaconstantinou, E., *Chem. Soc. Rev.*, 1989, **18,** 1; Hill, C. L. and Prosser-Mccartha, M. In *Photosensitization and Photocatalysis Using Inorganic and Organometalic Complexes*, ed. K. Kalyanasundaran and M. Grätzel. Kluwer, Dordrecht, 1993, p. 307.
6. Hill, C. L., Weeks, M. S. and Schinazu, R. F., *J. Med. Chem.*, 1990, **33,** 2767; Inouye, Y., Tale, Y., Tokutake, Y., Yoshida, T., Yamamoto, A., Yamase, T. and Nakamura, S., *Chem. Pharm. Bull.*, 1990, **38,** 285.
7. Baker, C. W., Simmons, V., Wasfi, S. H., Candela, G. and Kahn, A. H., *J. Am. Chem. Soc.*, 1972, **94,** 5499; Gómez-García, C. J., Coronado, E., Ouahab, L., *Angew. Chem. Int. Edn. Eng.*, 1992, **31,** 240; Coronado, E., Gómez-García, C. J., *Comments Inorg. Chem.*, 1995, **17,** 255.
8. Keggin, J. F., *Proc. Royal Soc.*, 1934, **A144,** 75.
9. Stobbe-Kreemers, A. W., Dielis, R. B., Makkee, M. and Scholten, J. J. F., *J. Catal.*, 1995, **154,** 175; Hamamoto, M., Nakayama, K., Nishiyama, Y. and Ishii, Y., *J. Org. Chem.*, 1993, **58,** 6421.
10. Baker, L. C. W. and Figgis, J. S., *J. Am. Chem. Soc.*, 1970, **92,** 3794.
11. Pope, M. T., *Heteropoly and Isopoly Oxometalates*. Springer-Verlag, New York, 1983.
12. Johansson, G., *Ark. Kemi*, 1963, **20,** 305–319.
13. Khan, M. I., Müller, A., Dillinger, S., Bögge, H., Chen, Q. and Zubieta, J., *Angew. Chem.*, 1993, **105,** 1811–1814.
14. Feist, M., Molchanov, V. N., Kazanoskii, L. P. and Torchenkova, E. A., *Zhurnal Neorganisch. Khimii.*, 1980, **25,** 733.
15. Ichida, H., Kobayashi, A. and Sasaki, Y., *Acta Cryst.*, 1980, **B36,** 1382.
16. Yu, L., Wang, J. and Chen, H., *J. Solid State Chem.*, 1992, **97,** 239–242.
17. Ouahab, L., Bencharif, M., Mhanni, A., Pelloquin, D., Halet, J. F., Pena, O., Padiou, J. and Grandjean, D., *Chem. Mater.*, 1992, **4,** 666–674.
18. Le Magueres, P., Ouahab, L., Golhen, S., Grand-

jean, D., Peña, O., Jegaden, J. C., Gómez-García, C. J. and Delhaes, P., *Inorg. Chem.*, 1994, **33,** 5187.
19. Zhang, X.-M., Shan, B.-Z. and You, X.-Z., *Polyhedron*, 1997, **16,** 95–102.
20. Román, P., San José, A., Luque, A. and Gutiérrez-Zorrilla, J. M., *Z. Kristallogr.*, 1993, **204,** 179.
21. *International Tables for X-ray Crystallography*, Vol. IV. Kynoch Press, Birmingham, England, 1974.
22. Beurkens, P. T., Admiraal, G., Beurkens, G., Bosman, W. P., Garcia-Granda, S., Gould, R. O., Smits, J. M. M. and Smykalla, C., The DIRDIF program system. Technical Report of the Crystallography Laboratory, University of Nijmegen, The Netherlands, 1992.
23. Walker, N. and Stuart, D., *Acta Crystallogr.*, 1983, **A39,** 158.
24. Stewart, J. M., Machin, P. A., Dickinson, C. W., Ammon, H. L., Heck, H., and Flack, H., The X-RAY76 System. Technical Report TR-446. Computer Science Center, University of Maryland, College Park, Maryland, U.S.A., 1976.
25. Wery, A. S. J., Gutiérrez-Zorrilla, J. M., Luque, A., Ugalde, M. and Román P., *Polyhedron*, 1997, **16,** 2589.
26. Rocchiccioli-Deltcheff, C., Fournier, M., Franck, M. and Thouvenot, R., *Inorg. Chem.*, 1983, **22,** 207.

Pergamon

PII: S0277-5387(97)00386-0

Polyhedron Vol. 17, No. 8, pp. 1257–1266, 1998
© 1998 Elsevier Science Ltd
All rights reserved. Printed in Great Britain
0277-5387/98 $19.00+0.00

The synthesis and characterisation of $[Pd(S_2CNEt_2)(Ph_2PCH_2CH_2PPh_2)]^+$ salts of some chloro- and bromo-metallate anions—X-ray crystal structures of $[Pd(S_2CNEt_2)(Ph_2PCH_2CH_2PPh_2)]^+[MCl_2]^-$ (M = Cu, Ag)

George Exarchos, Stanley C. Nyburg and Stephen D. Robinson

Department of Chemistry, King's College London, Strand, London WC2R 2LS, U.K.

(Received 5 May 1997; accepted 15 September 1997)

Abstract—The palladium complex $[PdCl_2(PhCN)_2]$ reacts readily with metal bis(dialkyl dithiocarbamates) $[M(S_2CNR_2)_2]$ (M = Pb, Zn, Cd, Hg, Cu, Ni, MoO_2, VO; R = Et, Bu^n), in refluxing dichloromethane, to afford the known complexes $[\{PdCl(S_2CNR_2)\}_2]$ in virtually quantitative yield. In boiling acetonitrile the diphosphine complexes $[PdX_2(Ph_2PCH_2CH_2PPh_2)]$ (X = Cl, Br) react readily with bi- and trivalent metal diethyl dithiocarbamates $[M(S_2CNEt_2)_n]$ (M = Pb, Zn, Cd, Hg, Ni, MoO_2, VO $n = 2$; M = Co, Fe, Mn, $n = 3$) to afford salts of the general form $[Pd(S_2CNEt_2)(Ph_2PCH_2CH_2PPh_2)]_2^+[MX_4]^{2-}$. Diethyl dithiocarbamates of copper(II) and silver(I) form salts of the $[Pd(S_2CNEt_2)(Ph_2PCH_2CH_2PPh_2)]^+$ cation containing linear $[CuX_2]^-$ and $[AgX_2]^-$ anions respectively (X = Cl, Br). The X-ray crystal structures of $[Pd(S_2CNEt_2)(Ph_2PCH_2CH_2PPh_2)][CuCl_2]$ and $[Pd(S_2CNEt_2)(Ph_2PCH_2CH_2PPh_2)][AgCl_2]\cdot 0.5CH_2Cl_2$ are reported. © 1998 Elsevier Science Ltd. All rights reserved

Keywords: palladium; dithiocarbamate halometallate anions; crystal structure.

Dithiocarbamate ligands display a rich and varied coordination chemistry providing a wide range of transition and main group metal complexes, many of which have important chemical and biological properties [1–4]. Most transition metals form bis-and/or tris-(dithiocarbamato) complexes in which the sulfur atoms of the chelate dithiocarbamate ligands possess nonbonding lone pairs. Such complexes should in principle be capable of acting as S-donor ligands to other metal centres and thereby generating homo- or hetero-polynuclear complexes. This behaviour pattern is commonly encountered with transition metal aminothiolate complexes *cis*-$[M(N–S)_2]$ and *fac*-$[M(N–S)_3]$ (N–S = 2-aminoethane thiolate or L-cysteinate) which form S-bridged polynuclear species by acting as bidentate or tridentate S-donor ligands respectively towards a variety of class b metal ions [5]. However, it is a relatively rare phenomenon in dithiocarbamate coordination chemistry. The few structurally characterised homonuclear examples in which the chelate dithiocarbamate ligands bridge through sulfur to a second metal centre include the ruthenium complexes $[Ru_2(Et_2NCS_2)_5][BF_4]$ [6], $[\{Ru(CO)(S_2CNEt_2)_2\}_2]$ and $[Ru_3(CO)_3Cl_2(S_2CNEt_2)_4]$ [7], the cobalt complex $[Co_2(S_2CNEt_2)_5][BF_4]$ [8] and the rhodium complex $[Rh_2(S_2CNMe_2)_5][BF_4]\cdot 0.5CH_2Cl_2$ [9]. In addition several bis(dithiocarbamato) complexes exist in the solid state as dimers (e.g. $[Cu(S_2CNEt_2)_2]_2$ [10], $[Zn(S_2CNEt_2)_2]_2$ [11]) or polymers (e.g. $[Mn(S_2CNEt_2)_2]_n$ [12]), with chelate dithiocarbamate ligands bridging through sulfur to a second metal atom. Structurally characterised examples of heteronuclear complexes in which chelate dithiocarbamate ligands bridge through sulfur to a second metal atom are even less common. The best established examples are the iron/zinc species $[(p\text{-}ClPhNC)_2Fe(S_2CNEt_2)_2ZnI_2]$ [13], and some adducts of copper(I) halides with tris(dithiocarbamato) complexes $[M(S_2CNR_2)_3]$ (M = Co, Rh, Cr) [14–18]. Finally, several authors have reported "het-

erobimetallic" dithiocarbamato bridged complexes "$MM'_2(S_2CNR_2)_6$" and "$[MM'(S_2CNR_2)_4]_n$" (M = Zn, Cd, Hg; M′ = VO, Mn, Fe, Co, Ni, Cu, Zn) formed by adding stoichiometric amounts of simple metal salts MX_2 (X = $MeCO_2$, NO_3) and M^IY_2 (Y = NO_3, Cl, $1/2SO_4$) to a solution of sodium dithiocarbamate in 4:1 acetone:water. However, our investigations show that the products are simple mixtures of mononuclear bis- or tris(dithiocarbamato) complexes [19]. In an attempt to synthesise further examples of heteropolynuclear complexes containing S-bridging dithiocarbamate ligands we are investigating the reactions of bis- and tris(dithiocarbamato) complexes $[M(S_2CNR_2)_n]$ (n = 2, 3) with a range of soft (class b) metal ions. In the present paper we describe the reactions of dithiocarbamato complexes with the palladium species $[PdCl_2(PhCN)_2]$ and $[PdX_2(Ph_2PCH_2CH_2PPh_2)]$ (X = Cl, Br), and the characterisation of products isolated therefrom.

EXPERIMENTAL

All solvents used were dried over molecular sieves prior to use. 1,2-bis(diphenylphosphino)ethane was purchased from Lancaster Synthesis, palladium chloride and bromide from Johnson Matthey. Metal dithiocarbamates were prepared from the metal nitrates and the sodium salt of the ligand in aqueous media and recrystallised from dichloromethane/petroleum spirit 60–80°C. Dichloro[bis(benzonitrile)]palladium(II) was prepared by dissolving palladium(II) chloride in benzonitrile on a steam bath over a period of 5 h, cooling to room temperature and filtering off the precipitated product. Dichloro- and dibromo[1,2-bis(diphenylphosphino)ethane]palladium(II) were prepared by dissolving the relevant palladium halide in acetonitrile under reflux and adding the stoichiometric amount of diphosphine to the filtered solution thus obtained. Both complexes were recrystallised from dichloromethane. Infrared spectra were recorded using Perkin–Elmer 983G (4000–500 cm^{-1}) and Perkin–Elmer FTIR System 2000 (500–100 cm^{-1}) as cesium iodide pellets. NMR spectra were recorded using a Bruker AM360 spectrometer at 360 MHz (^1H) and 145 MHz (^{31}P) in $CDCl_3$ solutions and were referenced to $SiMe_4$ and external H_3PO_4 85% respectively. Melting points were recorded in sealed tubes under nitrogen using an Electrothermal apparatus. Elemental analyses were performed at the Microanalytical Laboratory, University College London.

Di-μ-chlorobis(N,N-*di*-n-*butyldithiocarbamato*) *dipalladium(II)*

Dichloro[bis(benzonitrile)] palladium (0.384 g, 1.00 mmol) and bis(*N*,*N*-di-*n*-butyldithiocarbamato) copper (0.236 g, 0.50 mmol) were refluxed in dichloromethane (60 ml) for 30 min. The solution obtained was filtered from an insoluble brown precipitate and evaporated to dryness under reduced pressure. The residue was washed with diethyl ether (2 × 10 ml) and dried *in vacuo* for 3 h. Slow evaporation of a benzene solution of the product afforded dark orange–red crystals. Yield: 0.312 g, 90%; m.p. 118–120°C. [Reaction with other bis-dithiocarbamato complexes $M(S_2CNR_2)_2$ (M = Pb, Zn, Cd, Hg, Ni, MoO_2, VO) on a similar scale using the same method afforded the same product (R = Bu^n) or an analogous product (R = Et).]

(N,N-*diethyldithiocarbamato*)[1,2 - *bis*(*diphenylphosphino*)*ethane*]*palladium(II) tetrachlorozincate* 0.5 *dichloromethane*

Dichloro[1,2-bis(diphenylphosphino)ethane]palladium (0.230 g, 0.40 mmol) and bis(*N*,*N*-diethyldithiocarbamato)zinc (0.072 g, 0.20 mmol) were refluxed in acetonitrile (60 cm^3) with stirring for 1 h. The solution obtained was filtered and evaporated to dryness under reduced pressure. The oily residue that formed was dissolved in dichloromethane (5 cm^3) and the complex reprecipitated by the addition of diethyl ether (60 cm^3). The fine yellowish–white powder obtained was filtered off, washed with diethyl ether and dried *in vacuo*. Yield: 0.278 g, 92%; m.p. 149–151°C.

The following complexes were obtained on a similar scale by the same method:

(*N*,*N*-diethyldithiocarbamato)[1,2-bis(diphenylphosphino)ethane]palladium(II) tetrabromozincate 0.5 dichloromethane as yellowish–white fine powder. Yield: 93%; m.p. 142–144°C.

(*N*,*N*-diethyldithiocarbamato)[1,2-bis(diphenylphosphino)ethane]palladium(II) tetrachlorocadmate dichloromethane(1/2) as yellowish–white fine powder. Yield: 92%; m.p. 140–142°C.

(*N*,*N*-diethyldithiocarbamato)[1,2-bis(diphenylphosphino)ethane]palladium(II) tetrabromocadmate as yellowish–white fine powder. Yield: 93%; m.p. 135–137°C.

(*N*,*N*-diethyldithiocarbamato)[1,2-bis(diphenylphosphino)ethane]palladium(II) tetrachloromercurate(II) as yellowish–white fine powder. Yield: 93%; m.p. 163–165°C.

(*N*,*N*-diethyldithiocarbamato)[1,2-bis(diphenylphosphino)ethane]palladium(II) tetrabromomercurate(II) as yellowish–white fine powder obtained using chloroform (8 cm^3) instead of dichloromethane. Yield: 92%; m.p. 140–142°C.

(*N*,*N*-diethyldithiocarbamato)[1,2-bis(diphenylphosphino)ethane]palladium(II) tetrachloroplumbate 1.0 chloroform as yellowish–white fine powder obtained using chloroform (8 cm^3) instead of dichloromethane. Yield: 93%; m.p. 104–106°C.

(*N*,*N*-diethyldithiocarbamato)[1,2-bis(diphenylphosphino)ethane]palladium(II) tetrabromoplumbate 0.5 dichloromethane as yellowish–white fine powder. Yield: 95%; m.p. 116–118°C.

(*N,N*-diethyldithiocarbamato)[1,2-bis(diphenylphosphino)ethane]palladium(II) tetrachloronickelate as light green fine powder. Yield: 91%; m.p. 144–146°C.

(N,N-*diethyldithiocarbamato*)[1,2 - *bis*(*diphenylphosphino*)*ethane*]*palladium*(*II*) "*trichloroargentate*(*I*)" 0.5 *dichloromethane*

Dichloro[1,2 - bis(diphenylphosphino)ethane]palladium (0.230 g, 0.40 mmol) and (*N,N*-diethyldithiocarbamato)silver (0.102 g, 0.40 mmol) were refluxed in acetonitrile (60 cm^3) for 1 h. The solution obtained was filtered through celite to remove the fine greyish–white precipitate of silver chloride formed and evaporated to dryness under reduced pressure. The oily residue obtained was dissolved in dichloromethane (10 cm^3) and the complex was reprecipitated by the addition of diethyl ether (75 cm^3). The fine yellowish–white powder obtained was filtered off, washed with diethyl ether and dried *in vacuo*. Yield: 91%; m.p. 166–168°C.

(*N,N* - diethyldithiocarbamato)[1,2 - bis(diphenylphosphino)ethane]palladium(II) "tribromoargentate(I)" 1.0 chloroform was similarly obtained as yellowish–white fine powder using chloroform (12 cm^3) instead of dichloromethane. Yield: 90%; m.p. 122–124°C. (See the Discussion section for a statement concerning the nature of the "trichloroargentate" and "tribromoargentate" anions.)

(N,N - *diethyldithiocarbamato*)[1,2-*bis*(*diphenylphosphino*)*ethane*]*palladium*(*II*) *dichlorocuprate*(*I*)

Dichloro[1,2 - bis(diphenylphosphino)ethane]palladium (0.230 g, 0.40 mmol) and bis(*N,N*-diethyldithiocarbamato)copper (0.072 g, 0.20 mmol) were refluxed in acetonitrile (60 cm^3) for 1 h. The solution obtained was filtered and evaporated to dryness under reduced pressure. The oily residue that formed was dissolved in dichloromethane (10 cm^3) and the complex was reprecipitated by the addition of diethyl ether (75 cm^3). The fine light green powder obtained was filtered off, washed several times with diethyl ether to remove all the tetraethylthiuram disulfide byproduct, and dried *in vacuo*. Yield: 90%; m.p. 173–175°C.

The following complex was obtained on a similar scale by the same method:

(*N,N*-diethyldithiocarbamato)[1,2-bis(diphenylphosphino)ethane]palladium(II) dibromocuprate(I) as brownish–green fine powder. Yield: 93%; m.p. 160–162°C.

(N,N - *diethyldithiocarbamato*)[1,2 - *bis*(*diphenylphosphino*)*ethane*]*palladium*(*II*) *tetrachlorocobaltate*(*II*) 0.5 *dichloromethane*

Dichloro[1,2 - bis(diphenylphosphino)ethane]palladium (0.230 g, 0.40 mmol) and tris(*N,N*-diethyldithiocarbamato)cobalt (0.101 g, 0.20 mmol) were refluxed in acetonitrile (70 cm^3) for 10 h. The solution obtained was filtered and evaporated to dryness under reduced pressure. The oily residue that formed was dissolved in dichloromethane (10 cm^3) and reprecipitated by the addition of diethyl ether (75 cm^3). The fine green powder obtained was filtered off, washed several times with diethyl ether to remove all the tetraethylthiuram disulfide byproduct, and dried *in vacuo*. Yield: 90%; m.p. 100–102°C.

The following complex was obtained on a similar scale by the same method:

(*N,N*-diethyldithiocarbamato)[1,2-bis(diphenylphos-phino)ethane]palladium(II) tetrabromocobaltate(II) as green fine powder. Yield: 89%; m.p. 143–145°C.

(N,N-*diethyldithiocarbamato*)[1,2-*bis*(*diphenylphosphino*)*ethane*]*palladium*(*II*) *tetrachloroferrate*(*II*) 0.5 *chloroform*

Dichloro[1,2-bis(diphenylphosphino)ethane]palladium (0.230 g, 0.40 mmol) and tris(*N,N*-diethyldithiocarbamato)iron (0.100 g, 0.20 mmol) were refluxed in acetonitrile (70 cm^3) for 1 h under nitrogen. The solution obtained was filtered and evaporated to dryness under reduced pressure. The oily residue that formed was dissolved in chloroform (12 cm^3) and the complex reprecipitated by the addition of diethyl ether (75 cm^3). The slightly air sensitive olive green powder obtained was filtered off, washed several times with diethyl ether to remove all the tetraethylthiuram disulfide byproduct, and dried *in vacuo*. Yield: 92%; m.p 130–132°C.

The following complexes were obtained on a similar scale by the same method:

(*N,N*-diethyldithiocarbamato)[1,2-bis(diphenylphosphino)ethane]palladium(II) tetrabromoferrate(II) 0.5 dichloromethane as air sensitive dark olive green fine powder obtained using dichloromethane (10 cm^3) instead of chloroform. Yield: 92%; m.p. 116–118°C.
(*N,N*-diethyldithiocarbamato)[1,2-bis(diphenylphosphino)ethane]palladium(II) tetrachloromanganate (II) as light yellow fine powder. Yield: 89%; m.p. 147–149°C.
(*N,N*-diethyldithiocarbamato)[1,2-bis(diphenylphosphino)ethane]palladium(II) tetrabromomanganate(II) as light yellow fine powder. Yield: 93%; m.p. 139–141°C.

(N,N - *diethyldithiocarbamato*)[1,2 - *bis*(*diphenylphos - phino*)*ethane*]*palladium*(*II*) *tetrachlorodioxomolybdate*(*VI*) 0.5 *dichloromethane*

Dichloro[1,2-bis(diphenylphosphino)ethane]palladium (0.230 g, 0.40 mmol) and bis(*N,N*-diethyldithiocarbamato)dioxomolybdenum(VI) (0.085 g, 0.20 mmol) were refluxed in acetonitrile (60 cm^3) for

1 hour. The solution obtained was filtered and evaporated to dryness under reduced pressure. The oily residue that formed was dissolved in dichloromethane (10 cm^3) and the complex reprecipitated by the addition of diethyl ether (75 cm^3). The yellowish white powder obtained was filtered off, washed with diethyl ether and dried *in vacuo*. Yield: 94%; m.p. 118–120°C.

The following complexes were obtained on a similar scale by the same method:

(*N*,*N*-diethyldithiocarbamato)[1,2-bis(diphenylphosphino)ethane]palladium(II) tetrachlorooxovanadate(IV) as light green fine powder. Yield: 93%; m.p. 126–128°C.

(*N*,*N*-diethyldithiocarbamato)[1,2-bis(diphenylphosphino)ethane]palladium(II) tetrabromooxovanadate(IV) as light green fine powder. Yield: 89%; m.p. 135–137°C.

Crystallography. X-ray crystal structures have been determined for $[Pd(S_2CNEt_2)(Ph_2PCH_2CH_2PPh_2)]^+[CuCl_2]^-$ (**1**) and $[Pd(S_2CNEt_2)(Ph_2PCH_2CH_2PPh_2)]^+[AgCl_2]^- \cdot 0.5CH_2Cl_2$ (**2**). In each case crystals were obtained from the powdered product by slow crystallisation from a mixture of $CH_2Cl_2/C_6H_5CH_3$.Crystal data were collected on a four-cycle automated Picker diffractometer using Ni filtered Cu—Kα and zirconium filtered Mo—Kα radiation, respectively, with pulse-height analysis. Data reduction and all computations were carried out with the NRCVAX package [20]. Crystal data for compounds (**1**) and (**2**) are set out in Table 1. Atomic coordinates, thermal parameters and bond lengths and angles have been deposited at the Cambridge Crystallographic Data Centre (CCDC).

RESULTS AND DISCUSSION

Initial attempts to prepare heteronuclear complexes involved the reaction of bis(dithiocarbamato) complexes $M(S_2CNR_2)_2$ (M = Pb, Zn, Cd, Hg, Cu, Ni, MoO_2, VO; R = Et, Bu^n) with $PdCl_2(PhCN)_2$. As anticipated, the labile weakly bound PhCN ligands are readily displaced. However the "$PdCl_2$" residues, instead of coordinating to the intact $M(S_2CNR_2)_2$ complexes through the sulfur atoms, underwent a ligand exchange process leading to formation of the known complexes $[PdCl(S_2CNR_2)]_2$ [21]. When the ratio of reagents was adjusted to take account of the new reaction stoichiometry the yield of the palladium complex became almost quantitative. An X-ray crystal structure determination of $[PdCl(S_2CNBu^n_2)]_2$, by one of us (S.C.N.), has been reported elsewhere [22].

The reactions of the palladium(II) diphosphine complex $PdCl_2(Ph_2PCH_2CH_2PPh_2)$ with bis(dithiocarbamate) complexes were then investigated in an attempt to displace the chloride ligands from the soft "$Pd(Ph_2PCH_2CH_2PPh_2)^{2+}$" moiety and generate cationic complexes of the general form $[\{(Ph_2PCH_2CH_2PPh_2)Pd\}_2M(S_2CNEt_2)_2]^{4+}$. Once again, ligand exchange was the preferred reaction pathway and chlorometallate salts of the general form $[Pd(S_2CNEt_2)(Ph_2PCH_2CH_2PPh_2)]_2[MCl_4]$ were obtained in good yield. When the corresponding reactions were attempted with the tris(dithiocarbamato) complexes

Table 1. Crystal data and refinement for complexes **1** and **2**

	1	**2**
Empirical formula	$C_{31}H_{34}Cl_2CuNP_2PdS_2$	$C_{31}H_{34}Cl_2AgNP_2PdS_2 \cdot 0.5CH_2Cl_2$
Crystal system	Orthorhombic	Monoclinic
Space group	Pbna	$P2_1/n$
a/Å	17.002(7)	9.977(9)
b/Å	17.237(15)	24.501(12)
c/Å	23.25(3)	15.153(5)
β/°	—	97.53(6)
v/Å^3	6813.5	3672
Z	8	4
D_c/gcm^{-3}	1.535	1.580
μ/nm^{-1}	(Cu—K_α)8.82	(Mo—K_α)1.37
F(000)	3183	1616
10^2 crystal size/mm	25 × 60 × 60	20 × 20 × 20
Crystal colour	Pale green	Pale yellow
θ range/°	3–45	3–20
$h\ k\ l$ ranges	0–15, 0–15, 0–21	±9, 0–14, 0–23
No. of reflections collected	2739	3393
No. of reflections with $I_{net} > 2.5\sigma(I_{net})$	2230	2734
No. of parameters	243	383
R	0.058 [$I > 2.5\sigma$(I)]	0.075 [$I > 2.5\sigma$(I)]

$M(S_2CNEt_2)_3$ (M = Mn, Fe, Co) the facile ligand exchange reactions were accompanied by concomitant reduction of the trivalent metal to the divalent state. Thus the products were again salts of the general form $[Pd(S_2CNEt_2)(Ph_2PCH_2CH_2PPh_2)]_2[MCl_4]$. The reaction of $Cu(S_2CNEt_2)_2$ with $PdCl_2(Ph_2PCH_2CH_2PPh_2)$ was also accompanied by reduction, this time to afford copper(I) in the form of the dichlorocuprate(I) salt $[Pd(S_2CNEt_2)(Ph_2PCH_2CH_2PPh_2)][CuCl_2]$. An attempt to prepare the analogous silver(I) complex $[Pd(S_2CNEt_2)(Ph_2PCH_2CH_2PPh_2)][AgCl_2]$ from the silver(I) dithiocarbamate afforded a complex which gave elemental analyses corresponding to the stoichiometry $[Pd(S_2CNEt_2)(Ph_2PCH_2CH_2PPh_2)]_2[AgCl_3]$. However, a crystal selected for X-ray diffraction study was found to have the stoichiometry $[Pd(S_2CNEt_2)(Ph_2PCH_2CH_2PPh_2)][AgCl_2]\cdot 0.5CH_2Cl_2$. Closer examination of the bulk sample revealed evidence for the presence of two crystal forms. We therefore conclude that the elemental analyses data reflect the presence of a ca 50/50 mixture of $[Pd(S_2CNEt_2)(Ph_2PCH_2CH_2PPh_2)][AgCl_2]$ and $[Pd(S_2CNEt_2)(Ph_2PCH_2CH_2PPh_2)][Cl]$. Formation of a silver chloride precipitate, corresponding to 91% of the calculated mass, is consistent with reaction sequence given in Scheme 1. However, on the basis of the available evidence it is not possible to determine whether the dissociation of the $AgCl_3^{2-}$ anion to form $AgCl_2^-$ and Cl^- occurred during the initial synthesis or in the course of the procedure used to grow crystals for the X-ray structure determination.

An essentially similar set of reactions involving the dibromopalladium complex $PdBr_2(Ph_2PCH_2CH_2PPh_2)$ gave the corresponding bromometallate complexes $[Pd(S_2CNEt_2)(Ph_2PCH_2CH_2PPh_2)]_2[MBr_4]$ (M = Pb, Zn, Cd, Hg, Co, Fe, Mn, MoO_2, VO) and $[Pd(S_2CNEt_2)(Ph_2PCH_2CH_2PPh_2)][M'Br_2]$ (M' = Cu, Ag) in good yield. Again the elemental analyses data for the silver(I) product were consistent with the presence of ca 50% of the simple halide salt $[Pd(S_2CNEt_2)(Ph_2PCH_2CH_2PPh_2)][Br]$.

The complex salts were characterised by elemental analyses (Table 2), infrared spectroscopy (Table 3) and ^1H and $^{31}P\{^1H\}$ NMR.The dichlorocuprate(I) and dichloroargentate(I) salts were also structurally characterised by X-ray diffraction methods. The elemental analyses data indicated the presence of

$$2PdCl_2(Ph_2PCH_2CH_2PPh_2) + 2Ag(S_2CNEt_2) \rightarrow [Pd(S_2CNEt_2)(Ph_2PCH_2CH_2PPh_2)]_2[AgCl_3] + AgCl$$

$$[Pd(S_2CNEt_2)(Ph_2PCH_2CH_2PPh_2)]_2[AgCl_3] \rightarrow [Pd(S_2CNEt_2)(Ph_2PCH_2CH_2PPh_2)][AgCl_2] + [Pd(S_2CNEt_2)(Ph_2PCH_2CH_2PPh_2)][Cl]$$

Scheme 1.

Table 2. Analytical data [a] for halometallate salts of the $[Pd(S_2CNEt_2)(Ph_2PCH_2CH_2PPh_2)]^+$ cation

Anion	Solvent	%C	%H	%N
$PbCl_4^{2-}$	[b]	42.85(42.65)	3.95(3.95)	1.50(1.60)
$ZnCl_4^{2-}$	[c]	48.70(48.25)	4.45(4.50)	1.85(1.80)
$CdCl_4^{2-}$	[c]	46.60(46.80)	4.30(4.35)	1.75(1.75)
$HgCl_4^{2-}$	—	44.80(45.15)	4.00(4.15)	1.60(1.70)
$CuCl_2^-$	—	47.50(47.30)	4.30(4.35)	1.65(1.80)
$AgCl_2^-/Cl^-$	[c]	48.25(48.05)	4.50(4.45)	1.55(1.80)
$NiCl_4^{2-}$	—	49.70(49.40)	4.45(4.55)	1.70(1.85)
$CoCl_4^{2-}$	[c]	48.15(48.45)	4.35(4.50)	1.55(1.80)
$FeCl_4^{2-}$	[d]	48.00(48.00)	4.60(4.45)	1.95(1.80)
$MnCl_4^{2-}$	—	49.35(49.55)	4.40(4.55)	1.70(1.85)
$MoO_2Cl_4^{2-}$	[c]	46.50(46.40)	4.35(4.30)	1.70(1.75)
$VOCl_4^{2-}$	—	48.80(49.20)	4.20(4.55)	1.30(1.85)
$PbBr_4^{2-}$	[c]	39.05(39.45)	3.60(3.70)	1.50(1.45)
$ZnBr_4^{2-}$	[c]	43.30(43.30)	3.90(4.00)	1.55(1.60)
$CdBr_4^{2-}$	—	42.20(42.85)	3.80(3.95)	1.60(1.60)
$HgBr_4^{2-}$	—	40.90(40.75)	3.75(3.75)	1.40(1.55)
$CuBr_2^-$	—	42.45(42.45)	3.80(3.90)	1.80(1.60)
$AgBr_2^-/Br^-$	[b]	42.40(42.65)	3.70(3.90)	1.50(1.60)
$CoBr_4^{2-}$	—	43.85(44.20)	3.70(4.10)	0.90(1.65)
$FeBr_4^{2-}$	[c]	43.25(43.55)	3.95(4.05)	1.90(1.65)
$MnBr_4^{2-}$	—	45.00(44.30)	4.10(4.10)	1.40(1.65)
$VOBr_4^{2-}$	—	44.50(44.05)	3.80(4.05)	1.00(1.65)

[a] Calculated figures in parentheses.
[b] Solvated with 1.0 $CHCl_3$ per anion.
[c] Solvated with 0.5 CH_2Cl_2 per anion.
[d] Solvated with 0.5 $CHCl_3$ per anion.

Table 3. Infrared spectroscopic data for halometallate salts of the $[Pd(S_2CNEt_2)(Ph_2PCH_2CH_2PPh_2)]^+$ cation

Anion	ν(C—N)	ν(C—S)	ν(Pd—P)	ν(Pd—S)	ν(M—X)
Cl^-	1526s	1027, 998s	391w	371m	—
$PbCl_4^{2-}$	1526s	1027, 998s	391w	369m	203vw[b]
$ZnCl_4^{2-}$	1525s	1027, 998s	393w	370m	277s
$CdCl_4^{2-}$	1526s	1027, 998s	394w	370m	249m
$HgCl_4^{2-}$	1525s	1027, 998s	391w	369m	220m
$CuCl_2^-$	1526s	1026, 998s	394w	373m	410w
$AgCl_2^-/Cl^-$	1525s	1027, 998s	394w	371m	291vw[b]
$NiCl_4^{2-}$	1527s	1027, 998s	394w	370m	291m
$CoCl_4^{2-}$	1526s	1027, 998s	393w	371m	290m
$FeCl_4^{2-}$	1522s	1027, 998s	[a]	374m	282m
$MnCl_4^{2-}$	1525s	1027, 998s	394w	371m	281m
$MoO_2Cl_4^{2-}$[c]	1526s	1027, 998s	391w	368m	331m, 263m
$VOCl_4^{2-}$[d]	1525s	1027, 998s	391w	371m	311m, 284m
$PbBr_4^{2-}$	1525s	1027, 998s	392w	371m	142vw[b]
$ZnBr_4^{2-}$	1526s	1027, 998s	392w	370m	206m
$CdBr_4^{2-}$	1527s	1027, 998s	391w	369m	178m
$HgBr_4^{2-}$	1526s	1027, 998s	392w	370m	152m
$CuBr_2^-$	1526s	1027, 998s	393w	372m	328w
$AgBr_2^-/Br^-$	1526s	1027, 998s	393w	370m	251vw[b]
$CoBr_4^{2-}$	1525s	1027, 998s	393w	368m	235m
$FeBr_4^{2-}$	1525s	1027, 998s	393w	369m	216m
$MnBr_4^{2-}$	1525s	1027, 998s	393w	371m	218m
$VOBr_4^{2-}$[d]	1525s	1027, 999s	391w	367m	241w, 217w

[a] Not observed.
[b] Tentative assignment.
[c] ν(Mo=O) at 912 and 878 cm^{-1} (both m), indicating *cis* oxygen ligands.
[d] ν(V=O) at 954 cm^{-1} ($VOCl_4^{2-}$, s) and 956 cm^{-1} ($VOBr_4^{2-}$, m).
vw, Very weak.
w, Weak.
m, Medium.
s, Strong.

CH_2Cl_2 or $CHCl_3$ of solvation in many instances. This was confirmed for the dichloroargentate(I) salt by X-ray diffraction and, for the other complexes, by detection of a ^1H NMR signal (δCH_2Cl_2 5.3 ppm, $\delta CHCl_3$ 7.27 ppm). The infrared spectra showed bands attributable to coordinated S_2CNEt_2 and $Ph_2PCH_2CH_2PPh_2$ ligands but were mainly employed to characterise the halometallate anions. With the exception of the $PbCl_4^{2-}$, $PbBr_4^{2-}$, $AgCl_2^-$, $AgBr_2^-$ anions, for which we were unable to find reliable data, the infrared spectra recorded agreed well with the literature values for the anions concerned. All the salts, save those containing paramagnetic anions, displayed essentially identical ^1H and $^{31}P\{^1H\}$ NMR data consistent with the presence of the $[Pd(S_2CNEt_2)(Ph_2PCH_2CH_2PPh_2)]^+$ cation. A typical data set is as follows: $^1H\delta$1.3(t), CH_3CH_2N; 3.80(q) CH_3CH_2N; 3.1(d $^2J_{HP}$ 22.3 Hz) PCH_2CH_2P; 7.55 (m) and 7.75 (m), C_6H_5. $^{31}P\{^1H\}$ δ59.5 (s). Changes associated with variations in the nature of the anion present are $\pm$0.05 ppm and $\pm$0.5 ppm for ^1H and $^{31}P\{^1H\}$ resonances respectively.

Two aspects of these reactions need further comment. First, the dithiocarbamate ligands transferred quantitatively to the "$Pd(Ph_2PCH_2CH_2PPh_2)^{2+}$" moiety even when the other metal involved was relatively soft in character, i.e. Hg^{2+}, Pb^{2+}. This suggests that soft palladium(II) further softened by the presence of the coordinated diphosphine ligand has a particularly high affinity for the dithiocarbamate anion. Second, in the reaction involving tris(dithiocarbamato) complexes, the ligand exchange and the accompanying redox reactions occurred readily even when the relatively inert low spin d^6 cobalt(III) dithiocarbamate was involved. This behaviour contrasts sharply with that of the corresponding cobalt(III) 2-aminoethane thiolate complex *fac*-$[Co(SCH_2CH_2NH_2)_3]$ which binds intact to soft metal centres as a tridentate S-donor ligand [5].

The halometallate salts, though obtained in high yield and purity, did not readily afford crystals for X-ray crystallography. However crystals of adequate size and quality were obtained for the dichlorocuprate(I) and dichloroargentate(I) salts. Their crystal structures were therefore determined in order to confirm the nature of the cation and more importantly, given the absence of unambiguous spectroscopic data, to establish the stoichiometry and structure of the chlo-

roargentate anion present. The crystal structures of the dichlorocuprate(I) and dichloroargentate(I) salts are illustrated in PLUTO plots (Figs 1 and 2, respectively). The atomic labelling scheme employed for the $[Pd(S_2CNEt_2)(Ph_2PCH_2CH_2PPh_2)]^+$ cations is given in Fig. 3. Selected bond lengths and bond angles for both salts are presented in Table 4.

The dichlorocuprate(I) salt contains eight molecules per unit cell, only two of which are shown in Fig. 1. The geometry of the Pd complex cation is essentially square planar, however, the bond angles subtended at the palladium atom reflect the narrow bites of the diphosphine and diethyldithiocarbamate chelate ligands. The central coordination of the diphosphine and the S_2CN part of the diethyl dithiocarbamate moiety are closely coplanar with the Pd atom. The plane of C(4)—N—C(6) is however twisted 8.1(8)° from the coordination plane due, presumably, to packing forces. The copper atoms of the two independent $[CuCl_2]^-$ ions lie in the $z = 0$ plane on different two-fold special positions (four of each per unit cell). Whereas Cu(2) lies on the centre of symmetry at the origin and thus the ion is linear symmetric: Cu(2)—Cl(2) = 2.085(9) Å, Cu(1) lies on a diad axis with Cu(1)—Cl(1) = 2.055(6) Å and with the angle Cl(1)—Cu(1)—$Cl(1)_a$ = 1.7(3)°. The data found for the $[CuCl_2]^-$ anion are in good agreement with those previously reported for a range of dichlorocuprate(I) salts containing a variety of counter cations [23].

The dichloroargenate(I) salt contains four molecules per unit cell, two of which are shown in Fig. 2. The geometry of the cation is essentially the same as in the dichlorocuprate(I) salt. In contrast to the $[CuCl_2]^-$ ion the $[AgCl_2]^-$ anion has, to the best of our knowledge, been characterised by X-ray diffraction methods only in the complex salt [K(Crypt 2,2,2)][$AgCl_2$] [24]. The dimensions recorded for the $[AgCl_2]^-$ ion in the present study (Table 4) agree well with those previously reported for [K(Crypt 2,2,2)][$AgCl_2$]. The anion is essentially linear and the Ag atom does not lie on a special position. The crystal also contains two molecules of dichloromethane of crystallisation per unit cell. These lie too close to the centre of symmetry for both motifs to be present sim-

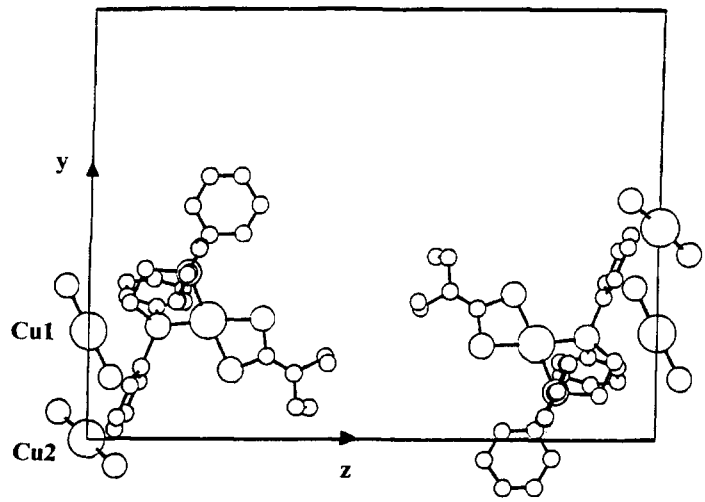

Fig. 1. PLUTO Diagram for $[Pd(S_2CNEt_2)(Ph_2PCH_2CH_2PPh_2)]^+[CuCl_2]^-$ (**1**).

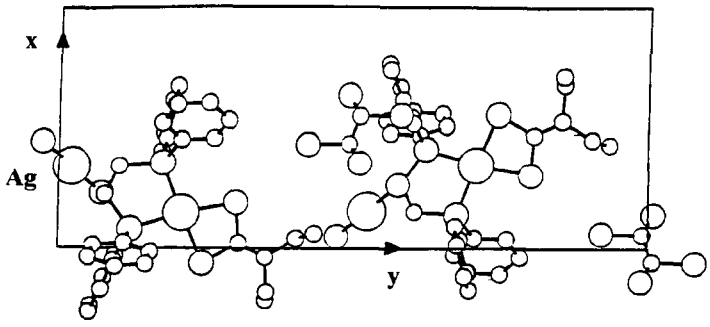

Fig. 2. PLUTO Diagram for $[Pd(S_2CNEt_2)(Ph_2PCH_2CH_2PPh_2)]^+[AgCl_2]^- \cdot 0.5CH_2Cl_2$ (**2**).

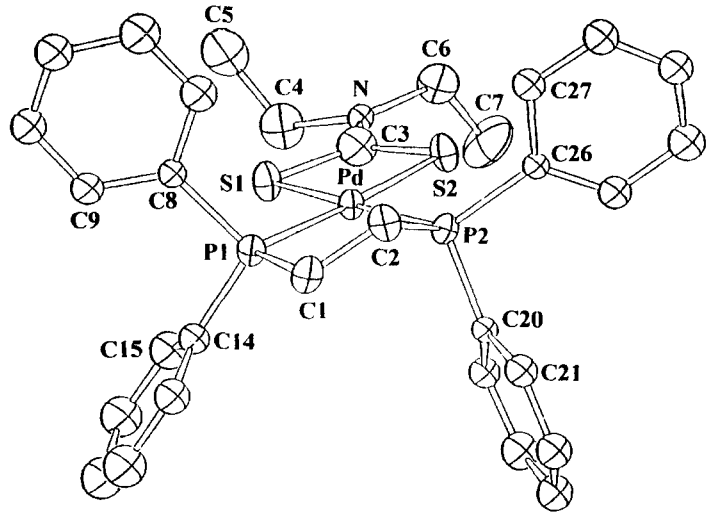

Fig. 3. ORTEP Diagram for $[Pd(S_2CNEt_2)(Ph_2PCH_2CH_2PPh_2)]^+$ cation showing atom labelling scheme.

Table 4. Selected bond distances (Å) and bond angles ( ) for compounds (**1**) and (**2**)

	(1) M = Cu	(2) M = Ag
Pd—S1	2.334(4)	2.338(3)
Pd—S2	2.331(4)	2.339(4)
Pd—P1	2.280(4)	2.285(4)
Pd—P2	2.249(4)	2.248(3)
S1—C3	1.745(15)	1.705(13)
S2—C3	1.705(14)	1.721(13)
C3—N	1.329(20)	1.329(17)
P1—C1	1.865(14)	1.838(13)
P2—C2	1.850(13)	1.813(12)
C1—C2	1.507(22)	1.507(18)
M(1)—Cl(1)	2.055(6)	2.304(1)
M(2)—Cl(2)	2.085(9)	2.306(4)
P1—Pd—P2	85.60(15)	85.86(12)
S1—Pd—S2	75.73(15)	75.75(13)
C1—P1—Pd	107.6(5)	108.1(4)
C2—P2—Pd	106.5(5)	106.1(4)
Cl(1)—M—Cl(1)a	174.9(3)	177.6(2)
Cl(2)—M—Cl(2)a	179.4	—

ultaneously and are thus given half occupancy. The two Cl atoms refined anisotropically but the carbon would not.

Finally the crystal structures of the complexes (**1**) and (**2**) reveal the presence of a number of short contact distances between the chloride ligands of the MCl_2^- anions and the phenyl hydrogens of the complex cations (Table 5, Figs 4 and 5) which we attribute to H-bonding interactions. Hydrogen bonding between C—H moieties and chloride anions [25,28] or chloride ligands [25–27] is now a well established phenomenon. The H···Cl distances and C—H···Cl angles found for complexes (**1**) and (**2**) are well within the range of values associated with this type of interaction (H···Cl = 2.569–2.944 Å; C—H···Cl = 119.3–169.2°) [25]. Indeed the H···Cl distances are all at the lower end of the range, and suggest the presence of relatively strong C—H···Cl interactions. There is also a short interatomic distance (see Table 5) between a phenyl proton and one of the chlorine atoms of the disordered CH_2Cl_2 solvent molecule, which we take to indicate the presence of a $ClCH_2$—Cl···H—C hydrogen bonding interaction.

Acknowledgements—We thank Dr C. A. Koh for the use of the Perkin–Elmer FTIR System 2000 instrument.

Table 5. C—H···Cl Hydrogen bonding interactions in complexes **1** and **2**

Complex	Interaction	H···Cl Distance (Å)	Angle (°)
1	C(27)—H(27)···Cl(1)	2.553	147.0
	C(23)—H(23)···Cl(2)	2.681	150.3
	C(30)—H(30)···Cl(2)	2.603	165.4
2	C(19)—H(19)···Cl(1)	2.698	152.9
	C(29)—H(29)···Cl(4)[a]	2.55	148.1

[a] Cl(4) is chlorine atom of solvent molecule (CH_2Cl_2).

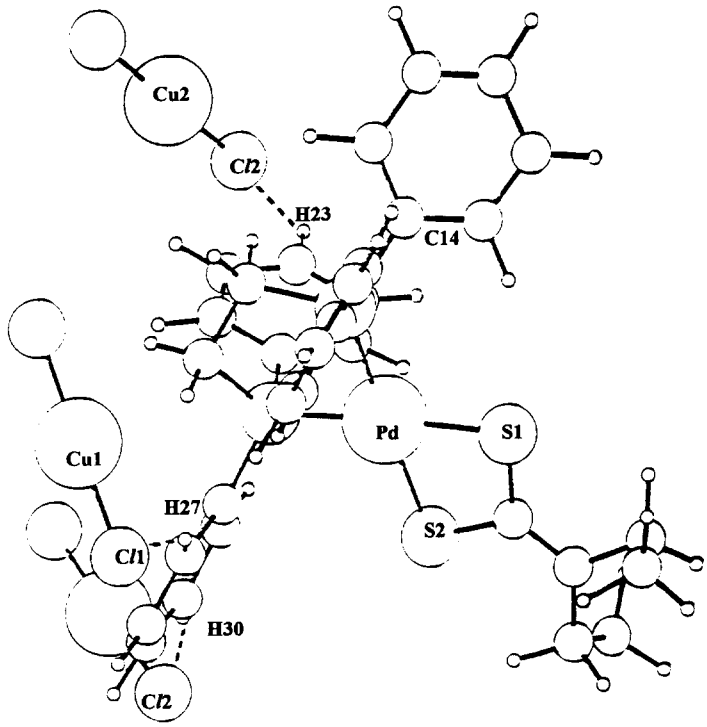

Fig. 4. Molecular structure for $[Pd(S_2CNEt_2)(Ph_2PCH_2CH_2PPh_2)]^+[CuCl_2[CuCl_2]^-$ (**1**) showing C—H···Cl interactions.

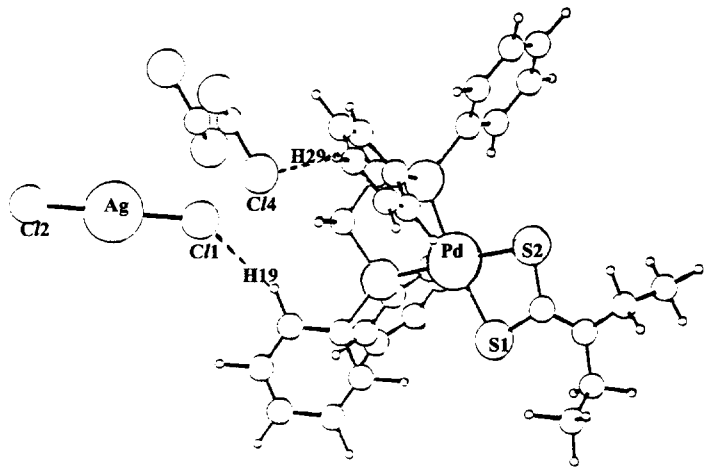

Fig. 5. Molecular structure for $[Pd(S_2CNEt_2)(Ph_2PCH_2CH_2PPh_2)]^+[AgCl_2]^- \cdot 0.5CH_2Cl_2$ (**2**) showing C—H···Cl interactions.

REFERENCES

1. Coucouvanis, D., *Progr. Inorg. Chem.*, 1970, **11,** 234; 1979, **26,** 301.
2. Eisenberg, R., *Progr. Inorg. Chem.*, 1970, **12,** 295.
3. Burns, R. P., McCullough F. P. and McAuliffe, C. A., *Adv. Inorg. Radiochem.*, 1980, **23,** 211.
4. Bond, A. M., *Coord. Chem. Rev.*, 1984, **54,** 23.
5. Konno, T. and Okamoto, K.-I., *Inorg. Chem.*, 1997, **36,** 1403, and references therein.
6. Mattson, B. M., Heiman, J. R. and Pignolet, L. H., *Inorg. Chem.*, 1976, **15,** 564.
7. Raston, C. L. and White, A. H., *J. Chem. Soc. Dalton Trans.*, 1975, 2418.
8. Hendrickson, A. R., Martin, R. L. and Taylor, D., *J. Chem. Soc. Dalton Trans.*, 1975, 2182.
9. Hendrickson, A. R., Martin, R. H. and Taylor, D., *Aust. J. Chem.*, 1976, **29,** 269.
10. Bonamico, M., Dessy, G., Magnoli, A., Vaciago, A. and Zambonelli, L., *Acta Cryst.*, 1965, **19,** 886.
11. Bonamico, M., Mazzone, G., Vaciago, A. and Zambonelli, L., *Acta Cryst.*, 1965, **19,** 898.
12. Ciampolini, M., Mengozzi, C. and Orioli, P., *J. Chem. Soc. Dalton Trans.*, 1975, 2051.
13. McCleverty, J. A., McLuckie, S., Morrison, N. J., Bailey N. A. and Walker, N. W., *J. Chem. Soc. Dalton Trans.*, 1977, 359.
14. Engelhardt, L. M., Healy, P. C., Papasergio, R. I. and White, A. H., *Inorg. Chem.*, 1988, **24,** 382.
15. Engelhardt, L. M., Healy, P. C., Skelton, B. W. and White, A. H., *Aust. J. Chem.*, 1988, **41,** 839.
16. Engelhardt, L. M., Healy, P. C., Shephard, R. M., Skelton B. W. and White, A. H., *Inorg. Chem.*, 1988, **27,** 2371.
17. Engelhardt, L. M., Healy, P. C., Skelton, B. W. and White, A. H., *Aust. J. Chem.*, 1989, **42,** 885.
18. Healy, P. C., Skelton, B. W. and White, A. H., *J. Chem. Soc. Dalton Trans.*, 1989, 971.
19. Exarchos, G. and Robinson, S. D., *Polyhedron*, 1997, **16,** 1573.
20. Gabe, E. J., Le Page, Y., Charland, J.-P., Lee, F. L. and White, P. S., *J. Appl. Cryst.*, 1988, **22,** 384.
21. Cornock, M. C., Davis, R. C., Leaver, D. and Stephenson, T. A., *J. Organomet. Chem.*, 1976, **107,** C43.
22. Nyburg, S. C., *Acta Cryst.*, 1996, **B52,** 328.
23. Jagner, S. and Helgesson, G., *Adv. Inorg. Chem.*, 1991, **37,** 1.
24. Helgesson, G. and Jagner, S., *Inorg. Chem.*, 1991, **30,** 2574.
25. Taylor, R. and Kennard, O., *J. Amer. Chem. Soc.*, 1982, **104,** 5063.
26. Bailey, R. D. and Benning, W. T., *Polyhedron*, 1997, **16,** 417, and references therein.
27. Hitchcock, P. B., Seddon, K. R. and Welton, T., *J. Chem. Soc. Dalton Trans.*, 1993, 2639, and references therein.
28. Askerby, C. B. and Seddon, K. R., *Z. Naturforsch*, 1993, **48B,** 1023, and references therein.

Pergamon

PII: S0277-5387(97)00396-3

Polyhedron Vol. 17, No. 8, pp. 1267–1273, 1998
© 1998 Elsevier Science Ltd
All rights reserved. Printed in Great Britain
0277-5387/98 $19.00+0.00

Theoretical investigation of the π-bonding ability of P-, S-, and N-containing ligands in group 6 transition metal complexes

S.-H. Park,† M. C. Milletti* and N. Gardner

Department of Chemistry, Eastern Michigan University, Ypsilanti, Michigan 48197, U.S.A.

(Received 28 March 1997; accepted 12 September 1997)

Abstract—The π-bonding ability of several ligands bonding through N, P, and S to group 6 transition metals was studied via non-empirical molecular orbital calculations. The ability of the ligands to donate or accept π electrons to or from the metal was compared in 1,2-$Mo_2[P(t\text{-}Bu)_2]_2[NMe_2]_4$ **[I]** and 1,2-$W_2[P(t\text{-}Bu)_2]_2[NMe_2]_4$ **[II]**; $(PSO)Cr(CO)_4$ **[III]** and $(PSO)W(CO)_4$ **[IV]** (PSO = 2-diphenyl phosphino methyl-2-phenylthiomethyl-1-methoxy propane); and $[W(2\text{-}Spy)(CO)_4]^-$ **[V]** and $[Mo(2\text{-}Spy)(CO)_4]^-$ **[VI]** (2-Spy = 2-thiol pyridine). Mulliken population analyses were used to study how two different atoms compete for π-bonding with the metal. Both NMe_2 and PMe_2 are π donors to the metal in complexes **[I]** and **[II]**. Overall, the phosphido ligand is a better π donor than the amido ligand. The PSO ligand in complexes **[III]** and **[IV]** is a good π acceptor and phosphorus is a better π acceptor than sulfur in both complexes. The 2-Spy ligand in the two anionic complexes, **[V]** and **[VI]**, is a good π acceptor. π back-donation from the metal *d* orbitals to the ligand is mostly through the nitrogen of the pyridine ring rather than the sulfur external to the pyridine ring. The electron density withdrawn from the metal through the nitrogen is delocalized throughout the π-conjugated ring. The π-accepting ability of the 2-Spy ligand in the two complexes is about the same.

The observed differences in the π-bonding ability of the ligands are explained in terms of the accessibility of the ligand molecular oribitals and the geometry of the complexes. A comparison of π-bonding between the two linking atoms in the same bidentate ligand is also made in terms of the type and energy of ligand orbitals (compound **[III]** vs **[IV]** and **[V]** vs **[VI]**). A direct comparison is made between electron density distribution and crystallographic bond lengths. © 1998 Elsevier Science Ltd. All rights reserved

Keywords: π-bonding; ligands; molecular orbitals.

One of the most common areas of inquiry involving transition metal complexes concerns the bonding of the ligands to the metal centers, be it by examining structures or spectroscopic data. Due to the rapid development of computer systems and the success of many semiempirical molecular orbital models in explaining bonding behavior of large systems, it is possible to investigate bonding in complex transition metal systems using easy-to-interpret molecular orbital calculations.

The main objective of this work is to study the π-bonding ability of ligands bonding via N-, P-, and S-atoms to group 6 transition metals, Cr, Mo, and W. The investigation was carried out by performing Fenske-Hall [1] molecular orbital calculations on three pairs of related transition metal complexes: 1,2-$Mo_2[P(t\text{-}Bu)_2]_2[NMe_2]_4$ **[I]** and 1,2-$W_2[P(t\text{-}Bu)_2]_2[NMe_2]_4$ **[II]** [2]; $(PSO)Cr(CO)_4$ **[III]** and $(PSO(W(CO)_4$ **[IV]**, PSO = 2-diphenylphosphino-methyl-2-phenylthiomethyl-1-methoxy propane [3a]; $[Mo(2\text{-}Spy)(CO)_4]^-$ **[V]** and $[W(2\text{-}Spy)(CO)_4]^-$ **[VI]**, 2-Spy = 2-thiol pyridine [4].

The first pair of complexes contains ligands of the type PR_2 and NR_2. These ligands are good electron donors to metals because the bonding atoms have unshared electron pairs. In the Mo and W dimers, the ligands are bonded to the same metal center and therefore compete for the same metal *d* orbitals to overlap with their readily accessible lone pairs in π-fashion. This pair of complexes, therefore, affords the opportunity of comparing the electron-donating

* Author to whom correspondence should be addressed.

† Current address: Department of Chemistry, Loyola University of Chicago, Chicago, Illinois 60626, U.S.A.

ability of PR_2 and NR_2 ligands. Furthermore, the two dimers enable a comparison of π-donating ability to differing metal centers: Mo and W.

In complexes **[III]** to **[VI]**, the PSO and $[2\text{-Spy}]^-$ ligands are bidentate to Cr or W and Mo or W, respectively. These ligands are expected to donate electron density from filled σ orbitals and to accept electron density from the filled $d\pi$ orbitals on the metal centers into their empty $p\pi$ orbitals. In this process, they compete with CO ligands, which are also known to be good π acceptors. Complexes **[III]**–**[VI]**, therefore, provide a comparison of π-accepting ability among P-, S-, and N-containing ligands when they bond with Cr, W, and Mo.

From the results of the calculations, conclusions will be drawn about the efficacy of PR_2, NR_2, 2-Spy, and PSO ligands as π acceptors or π donors to metal centers as a function of metal identity. The results will be analyzed in terms of electron density distribution and energies of molecular orbitals.

COMPUTATIONAL PROCEDURE

All molecular orbital calculations were carried out using the Fenske-Hall nonempirical method [1]. The atomic basis sets for carbon, nitrogen, oxygen, phosphorus, and sulfur were constructed according to Clementi's specifications for ground state atomic functions [5]. The $2p$ and $3p$ orbitals of these atoms were double-ξ, in which two different sets of coefficients and exponents are used to describe a single atomic basis function. Basis sets for P- and S-atoms included single-ξ $3d$ functions. The hydrogen exponent was set to 1.16 [6].

The basic functions employed for the metals were obtained from atomic X-α calculations on sets of optimized, orthonormal Slater-type orbitals (STOs) [7]. The exponents for these valence atomic orbitals were set to prevent the outer valence orbitals from being too diffuse [8,9]. The chromium $4s$ and $4p$ exponents were set to 2.0; the molybdenum $5s$ and $5p$ exponents were set to 2.2; and the tungsten $6s$ and $6p$ exponents were set to 2.4.

1,2-$Mo_2[P(t\text{-}Bu)_2]_2[NMe_2]_4$ *and* 1,2-$W_2[P(t\text{-}Bu)_2]_2[NMe_2]_4$

The structure of complexes **[I]** and **[II]** was obtained from structural data given in the literature [2]. The butyl groups on the phosphine ligands were substituted with methyl groups to facilitate analysis of the results. Such substitutions have been shown not to affect Mulliken population significantly [6]. The geometry of both complexes is shown in Fig. 1.

$(PSO)Cr(CO)_4$ *and* $(PSO)W(CO)_4$

X-ray crystal structures of **[III]** and **[IV]** were taken from the literature [3b]. The coordinates derived from the X-ray data for these molecules were idealized to an octahedral geometry in order to simplify analysis of the molecular orbitals (see Fig. 2). The phenyl groups

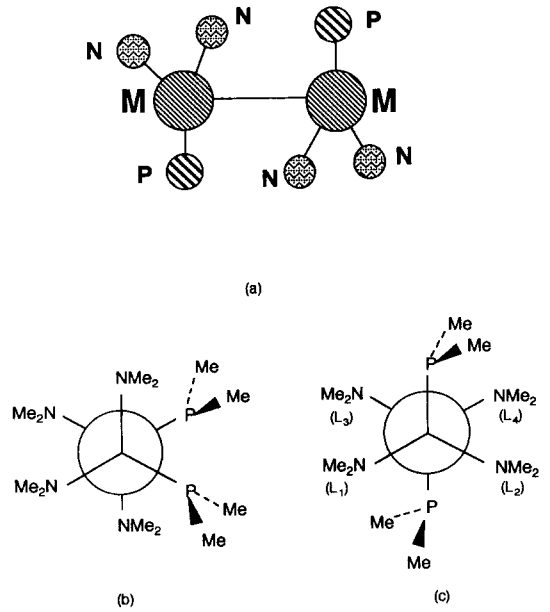

Fig. 1. (a) The molecular structure of 1,2-$M_2[PMe_2]_2[NMe_2]_4$, where M = Mo or W. (b) *gauche* conformation of the W dimer and (c) *anti* conformation of the Mo dimer.

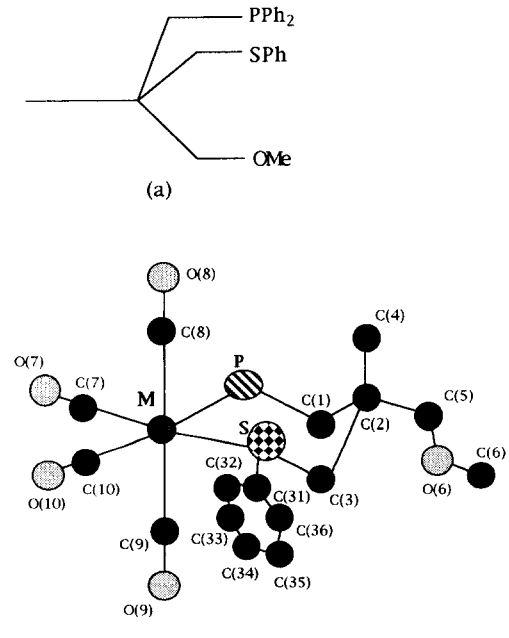

Fig. 2. Conformations of (a) the PSO ligand and (b) the metal complex, $(PSO)M(CO)_4$, where M is Cr or W. Two phenyl groups on P are omitted for clarity.

attached to both phosphorus and sulfur atoms were substituted by hydrides for simplicity of interpretation and greater ease in the computation.

$[W(2\text{-Spy})(CO)_4]^-$ *and* $[Mo(2\text{-Spy})(CO)_4]^-$

Since crystal structure data for these two molecules was not available, the energy minimization procedure of the Spartan software package [10] that employs the empirical molecular mechanics method based on the SYBYL force field [11] was used to obtain the geometry of $[Mo(2\text{-Spy})(CO)_4]^-$. This procedure was used to refine the preliminary structures constructed by using known bond lengths and angles from related compounds [12,13]. For the calculation of $[W(2\text{-Spy})(CO)_4]^-$, tungsten was substituted into the position of molybdenum and all other atom coordinates were unchanged. The structures of $[W(2\text{-Spy})(CO)_4]^-$ and $[Mo(2\text{-Spy})(CO)_4]^-$ are shown in Fig. 3. From this result, the position of the four carbonyl ligands bonded to the metal was idealized to an octahedral geometry. The difference in atomic coordinates between the preliminary structure and the optimized structure using molecular mechanics was minimal. For example, the ∠NMS angle obtained by the molecular mechanics optimization is 68.7°, which compares favorably to the value (67.0°) from the crystal structure data of a related complex [12].

RESULTS AND DISCUSSION

The study of π-bonding patterns in the metal complexes of interest in this work was accomplished mainly through the analysis of molecular orbital (MO) diagrams. From the MO diagram of the ligand in a specific metal complex, information regarding its function in the compound was obtained: specifically, whether the ligand is a π donor or a π acceptor. If the ligand MO diagram shows low-lying, unoccupied π orbitals, the ligand will function as a good π acceptor. If the ligand has high-energy, filled valence π orbitals, it can act as a π donor to the metal. In either type of ligand, the presence of a high-lying σ-orbital suggests it can form a σ bond with the metal. The quantitative analysis of π-bonding in the metal complexes was accomplished by using a Mulliken population analysis [14].

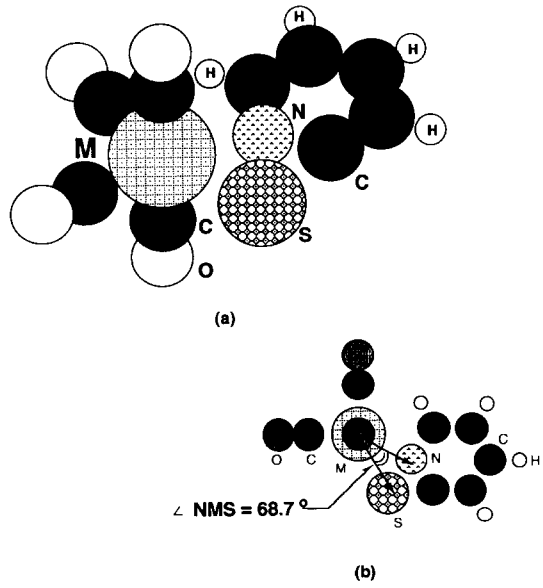

Fig. 3. (a) The structure of $[M(Spy)(CO)_4]^-$, M = W or Mo; (b) the nitrogen–metal–sulfur angle obtained from the geometry optimization.

Relative π-donating ability of amido and phosphido ligands in [I] *and* [II]

The relative π-donating ability of ligands such as OR, SR, NR_2, and PR_2 is currently not well understood. Two of the transition metal dimers under study, [I] and [II], allowed an analysis of the relative π-donating ability of an amido and a phosphido ligands, $N(CH_3)_2$ and $P(CH_3)_2$, to transition metal centers. These compounds also allowed a comparative analysis of π donation to a second row transition metal, Mo, vs a third row metal, W. The tungsten and molybdenum complexes have identical valence electron counts and the same ligands bonded to the metal. However, the two compounds have different conformations when they crystallize, anti and gauche respectively, as shown in Fig. 1.

An analysis of the MO diagram for [I] shows that the HOMO and SHOMO (second highest occupied molecular orbital) of the complex are mainly W—NR_2 π in character, while the occupied MOs at lower energy are PR_2 π and W—NR_2 π. In these molecular orbitals, the filled π orbitals of the phosphido and amido ligands donate electron density into empty metal *d* orbitals. Therefore, both phosphido and amido ligands are π donors in this complex.

The MO diagram for [II] is qualitatively similar to that of [I]. The HOMO is mainly Mo—NR_2 π in character while the SHOMO is mainly Mo—PR_2 π. At lower energy, again the orbitals are a mixture of Mo—PR_2 and Mo—NR_2 π bonds as in the case of the tungsten dimer. However, in the molybdenum dimer the mixing of orbitals is much more extensive, due in part to the lower symmetry of the complex.

A Mulliken population analysis is given in Table 1. The relative π-donating ability of the ligands, PMe_2 and NMe_2, to the two metal centers, W and Mo, may be inferred from these results. PMe_2 loses more π-electron density in both of the metal complexes (in [I] 0.1 e^- and in [II] 0.1–0.2 e^-), and therefore is a better π donor than NMe_2. This can be explained by the fact that, in both complexes, the energy of the PR_2 π orbital is closer than that of the NR_2 π orbital to the energy of the metal *d* orbitals. In other words, PR_2 is better

Table 1. Mulliken population analysis for 1,2-$W_2[PMe_2]_2[NMe_2]_4$, [I], and 1,2-$Mo_2[PMe_2]_2[NMe_2]_4$, [II]

	$P(CH_3)_2$	$N(CH_3)_2$
Free ligand	$(\sigma)^2(\pi^b)^2(\pi^*)^0$	$(\sigma)^2(\pi^b)^2(\pi^*)^0$
Ligand in W complex	$(\sigma)^{1.5}(\pi^b)^{1.3}(\pi^*)^{0.2}$	$(\sigma)^{1.5}(\pi^b)^{1.6}(\pi^*)^0$
Ligand in Mo complex L_1, L_4	$(\sigma)^{1.59}(\pi^b)^{1.37}(\pi^*)^{0.04}$	$(\sigma)^{1.57}(\pi^b)^{1.64}(\pi^*)^0$
Ligand in Mo complex L_2, L_3		$(\sigma)^{1.56}(\pi^b)^{1.5}(\pi^*)^0$

able to form a bonding molecular orbital with metal *d* orbitals than NR_2. Furthermore, the π-donating ability of the PMe_2 ligand and that of two of the NME_2 ligands (L_2 and L_3) decreases in going from molybdenum to tungsten. On the other hand, π-electron donation from the NR_2 L_1, L_4 ligands increases slightly in going from Mo to W.

Relative π-accepting ability of the PSO ligand in [III] *and* [IV]

Polydentate ligands have been studied extensively [15–18]. The synthesis of a tripodal phosphine ligand with two different π acceptor atoms (P and S) and its complexation to tungsten and chromium have been reported by Liu *et al.* [3]. The geometry of this ligand, 2-diphenyl-phosphinomethyl-2-phenylthiomethyl-1-methoxypropane, whose name will be abbreviated as PSO, is shown in Fig. 2(a). A theoretical investigation of the bonding in the complexes (PSO)$Cr(CO)_4$ and (PSO)$W(CO)_4$, shown in Fig. 2(b), will allow a comparison of P and S π-accepting ability between first and third row transition metals.

The MO diagram for the PSO ligand shows that the HOMO and the SHOMO are both σ with respect to the position of the metal center. The presence of a set of three low-lying virtual π orbitals indicates that PSO may fulfill the requirement of a good π acceptor.

The MO diagram for (PSO)$Cr(CO)_4$ is shown in Fig. 4. A fairly large gap separates the third highest occupied molecular orbital from the next set of occupied orbitals, which represent σ-bonding between the PSO ligand and the metal center. The HOMO and SHOMO and the third highest occupied MO are mainly bonding combinations of metal and CO π^* orbitals while the LUMO and unoccupied MOs at higher energy are anti-bonding combinations between the metal center and the PSO π orbitals. In conclusion, the PSO ligand acts both as a σ donor and a π acceptor in this complex.

The MO diagram for the (PSO)$W(CO)_4$ complex shows that the LUMO and MOs at higher energy have the same characteristics as in the chromium complex, indicating that there is π-back bonding from the tungsten *d* orbitals to the empty π orbitals of the PSO ligand.

A more quantitative description of the amount of electron donation from the metal to the ligand was

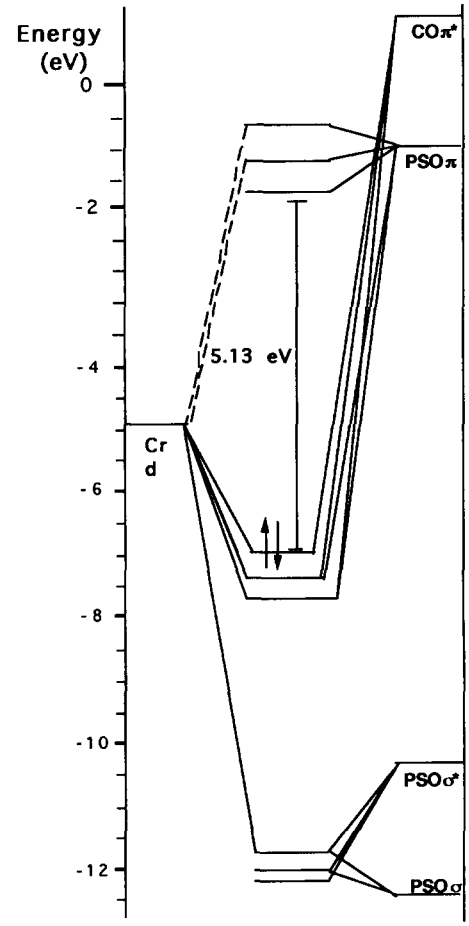

Fig. 4. MO diagram for (PSO)$Cr(CO)_4$.

obtained through a Mulliken population analysis. The data (shown in Table 2) indicates that the amount of π back donation from tungsten is greater than that from chromium. It is also of interest to differentiate between P and S in terms of the amount of back donation. This is done by looking at contributions from individual atoms to the electron density population of the ligand π orbitals participating in bonding with the metal.

More specifically, the PSO ligand receives electrons through the 3*p* and 3*d* orbitals of P and S. The combination of 3*p* and 3*d* is of π symmetry with respect

Table 2. Amount of π back donation to the PSO ligand in the complexes $W(CO)_4(PSO)$ and $Cr(CO)_4(PSO)$

	Orbital occupation of PSO orbitals	Total π back donation
PSO	$(\pi)^0(\pi^{nb})^0(\pi^*)^0$	
$W(CO)_4(PSO)$	$(\pi^b)^{0.31}(\pi^{nb})^{0.23}(\pi^*)^{0.01}$	0.55
$Cr(CO)_4(PSO)$	$(\pi^b)^{0.28}(\pi^{nb})^{0.22}(\pi^*)^{0.01}$	0.50

to the electron rich metal *d* orbital. Hence, a Mulliken population analysis has been employed at the atomic level to investigate how π-electron density is apportioned between P and S in the atomic orbitals specified above. The amount of π back donation to the individual P and S atoms in the tungsten complex are $0.33e^-$ and $0.16e^-$, respectively. In the case of the Cr complex, P withdraws $0.34e^-$ and S withdraws $0.13e^-$ (see Table 3).

As it is shown in Table 3, phosphorus is a better π acceptor than sulfur in both **[III]** and **[IV]**. In both metal complexes, the amount of π back donation to P ($0.33–0.34e^-$) is approximately two times greater than that to S ($0.13–0.16e^-$). As it was already shown in Table 2, the total π back donation to the PSO ligand was greater in the tungsten complex than in the chromium complex when we consider that π electrons were mainly back donated to empty *p* and *d* orbitals on P and S.*

The strength or amount of π acceptance of sulfur and phosphorus in an octahedral metal carbonyl complex can also be analyzed by inspecting the metal–carbonyl distance. Since the amount of π back donation to phosphorus is greater than that to sulfur, the competition in π back donation between phosphorus and sulfur should be evident from differences in the corresponding metal to carbonyl (M-C) distances [19]. The $W—C_{trans\ to\ sulfur}$ distance (1.88 Å) and $W—C_{trans\ to\ phosphorus}$ distance (1.94 Å) from the crystallographic data [3a] are consistent with our results. The same is true for the $Cr—C_{trans\ to\ sulfur}$ distance (1.806 Å) and $C—C_{trans\ to\ phosphorus}$ distance (1.820 Å) [3a]. The shorter distance between the carbonyl *trans* to the sulfur and the metal can be attributed to the fact that the amount of π back donation from the metal to sulfur is less than that to phosphorus. Consequently, the carbonyl ligand *trans* to S receives more π-electron density than another CO *trans* to P. Since the M—C bond becomes stronger as the amount of M to CO back-bonding increases, a carbonyl ligand *trans* to a sulfur atom will have a shorter M—C bond than one *trans* to phosphorus.

The results of the calculations are also confirmed when comparing the two equatorial carbonyls: the one *trans* to P has a longer M—C bond length in both complexes, since our data shows that P is a better π acceptor than S in the PSO ligand.

Relative π-bonding ability of S and N in the 2-Spy ligand in complexes **[V]** *and* **[VI]**

The relative π-bonding ability of sulfur and nitrogen bonded to group 6 transition metals in the two anionic complexes $[Mo(2\text{-}Spy)(CO)_4]^-$ and $[W(2\text{-}Spy)(CO)_4]^-$ was also investigated. The synthesis of these compounds has been carried out by Sanchez-Palaez *et al.* [4]. These compounds are of interest because π-accepting properties of N and S in this kind of bidentate ligand have never been studied.

The MO diagram of the bidentate ligand pyridine-2-thiol (2-Spy) shows that the highest occupied molecular orbital is σ with respect to the metal and it is predominantly localized on the sulfur atom (67% of the electron density in the MO). The diagram therefore suggests that the 2-Spy ligand can donate σ-electron density to the metal using the lone pair of electrons localized on the sulfur. The LUMO is π in character and localized on the nitrogen. The next highest molecular orbital is also π but it is mainly localized on the sulfur atom. Nitrogen also has lone pair electrons but it lies at a much lower energy (−6.13 eV) than the lone pair on sulfur (at −2.43 eV) which

* The sum of π back donation to P and S in Table 4 is less than the total amount of π back-donation shown in Table 3 because the numbers in Table 4 do not take into account π electron density that is delocalized onto the rest of the PSO ring.

Table 3. Comparison of π-back bonding to phosphorus and sulfur in the two metal complexes, $W(CO)_4(PSO)$ and $Cr(CO)_4(PSO)$

	AO occupations of P and S	π back donation to P	π back donation to S
Free PSO ligand	$(P\ 3p,\ 3d)^{1.74}\ (S\ 3p,\ 3d)^{2.64}$		
$W(CO)_4(PSO)$	$(P\ 3p,\ 3d)^{2.07}\ (S\ 3p,\ 3d)^{2.80}$	0.33	0.16
$Cr(CO)_4(PSO)$	$(P\ 3p,\ 3d)^{2.08}\ (S\ 3p,\ 3d)^{2.77}$	0.34	0.13

Table 4. Total π back donation to the 2-Spy ligand in the two anionic metal complexes, $[W(2\text{-Spy})(CO)_4]^-$ and $[Mo(2\text{-Spy})(CO)_4]^-$

	Orbital occupation of [2-Spy]$^-$ orbitals[a]	Total π back donation
2-Spy	$(\pi^N)^0(\pi^S)^0$	
$[W(2\text{-Spy})(CO)_4]^-$	$(\pi^N)^{0.49}(\pi^S)^{0.05}$	0.54
$[Mo(2\text{-Spy})(CO)_4]^-$	$(\pi^N)^{0.48}(\pi^S)^{0.04}$	0.52

[a] π^N is for the π orbitals of [2-Spy]$^-$ ligand localized on phosphorus and π^S is for the π orbitals of [2-Spy]$^-$ ligand localized on sulfur.

is involved in the HOMO. Consequently, S and N are in a position to be good π acceptors.

The MO diagrams based on our calculations for $[W(2\text{-Spy})(CO)_4]^-$ and $[Mo(2\text{-Spy})(CO)_4]^-$ confirm the π-back bonding characteristics predicted above. In Fig. 5, the LUMO of the ligand is stabilized by bonding with one of the W *d* orbitals. This represents the metal-to-ligand π-back bonding interaction through nitrogen in this molecule. The molybdenum complex shows a similar pattern of π-back bonding. The π donation from the ligand to the metal expected from the ligand MO diagram is also confirmed by the MO diagrams of the complexes. That is, the SHOMO of the ligand, which is a π orbital localized on sulfur, donates π electrons to the empty metal *d* orbitals in the SHOMO of the complex.

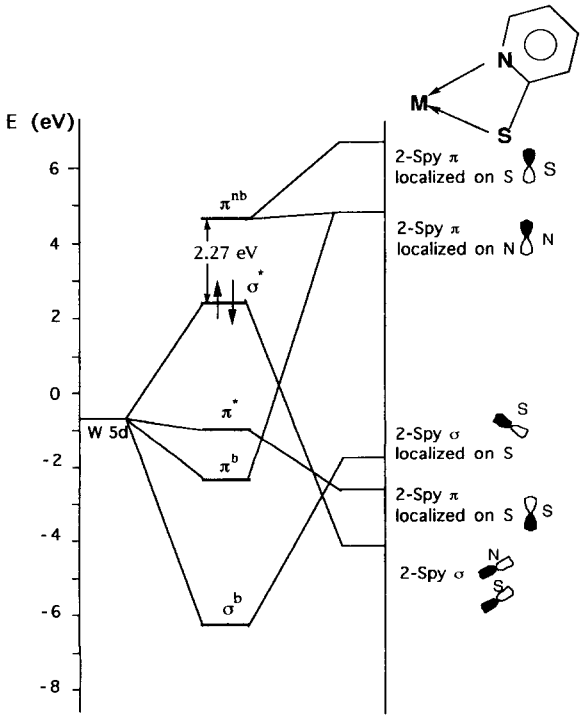

Fig. 5. MO diagram for the $[W(2\text{-Spy})(CO)_4]^-$ complex.

The π-electron density populations of the [2-Spy]$^-$ ligand before and after complexation with W and Mo are shown in Table 4. The amount of π back donation to the ligand is greater in the tungsten complex than in the molybdenum complex. Therefore the 2-Spy ligand acts as a better π acceptor in the tungsten complex than in the molybdenum complex. This can be explained by considering the energy differences between metal atomic orbitals and ligand molecular orbitals. The W *d* orbitals are closer in energy to the ligand LUMO than the Mo *d* orbitals and are therefore better able to donate π-electron density to the LUMO. The amount of π back donation to the 2-Spy ligand in both the tungsten and molybdenum complexes is not negligible (0.52–0.54e$^-$). However most of these electrons are transferred through nitrogen (0.48–0.49e$^-$): the empty ligand orbital localized on nitrogen is more accessible by the metal *d* electrons in terms of energy than that localized on sulfur.

The main channel for σ-bonding from the 2-Spy ligand to the metal is through sulfur, as explained earlier, but π electron back donation occurs mostly through nitrogen. These are consistent with the energy levels of the molecular orbitals localized on sulfur and nitrogen in the case of both σ-donation and π back donation. However, if the Mulliken populations for individual atomic orbitals are investigated, Table 5 shows that the π-electron density population on the nitrogen atom is negligibly small (0.02e$^-$ for the W complex and 0.01e$^-$ for the Mo complex). This may be attributed to π conjugation in the 2-Spy ligand. That is, the π-electron density taken from the metal through nitrogen is now delocalized through the pyridine ring via conjugated π orbitals.

CONCLUSIONS

Non-empirical Fenske-Hall molecular orbital calculations have been used to study the π-bonding ability of ligands bonding through N, S, and P to the metals Cr, Mo, and W. A qualitative description of the π-bonding pattern was obtained in each of the metal complexes through an analysis of the molecular orbital diagram. The relative amount of π-bonding in ligands bonding through N vs P; P vs S; and N vs S

Table 5. Comparison of π-electron density at nitrogen and sulfur as a result of π back donation from the metal in two anionic metal complexes, $[W(2\text{-Spy})(CO)_4]^-$ and $[Mo(2\text{-Spy})(CO)_4]^-$

	AO occupations of N and S	π density at N	π density at S
Free ligand	$(N\,2p_z)^{1.19}$ $(S\,3p_z)^{1.77}$		
$[W(2\text{-Spy})(CO)_4]^-$	$(N\,2p_z)^{1.21}$ $(S\,3p_z)^{1.82}$	0.02	0.05
$[Mo(2\text{-Spy})(CO)_4]^-$	$(N\,2p_z)^{1.20}$ $(S\,3p_z)^{1.82}$	0.01	0.05

to the same metal was obtained through Mulliken population analyses, as was the amount of π-bonding of the same ligand to different metal atoms. The results are summarized below.

The amido (NMe_2) and the phosphido (PMe_2) ligands in the dimers $1,2\text{-}Mo_2[P(t\text{-}Bu)_2]_2[NMe_2]_4$ and $1,2\text{-}W_2[P(t\text{-}Bu)_2]_2[NMe_2]_4$ are π donors to the metal. Overall, the phosphido ligand is a better π donor than the amido ligand in both metal complexes. The π-donating ability of the PMe_2 groups is greater toward molybdenum than towards tungsten. On the other hand, the π-donating ability of the NMe_2 ligand in the L_1 and L_4 positions in the molybdenum dimer is poorer than in the tungsten dimer.

The PSO ligand in $(PSO)Cr(CO)_4$ and $(PSO)W(CO)_4$ is a good π acceptor and also a ligand-to-metal σ donor. The π-accepting ability of the PSO ligand in $(PSO)W(CO)_4$ is greater than that in $(PSO)Cr(CO)_4$. In addition, phosphorus is a better π acceptor than sulfur in both complexes but the difference in π-bonding between the two metal complexes is negligible.

The 2-Spy ligand in the two anionic complexes $[Mo(2\text{-Spy})(CO)_4]^-$ and $[W(2\text{-Spy})(CO)_4]^-$ is a good σ donor as well as a good π acceptor. It also has some ability to donate π-electron density to the metal through ligand molecular orbitals localized on nitrogen. The π-accepting ability of the 2-Spy ligand in $[Mo(2\text{-Spy})(CO)_4]^-$ and $[W(2\text{-Spy})(CO)_4]^-$ is about the same. The ligand to metal σ-donation is from the lone pair of electrons on sulfur, and most of the metal to ligand π-accepting occurs through nitrogen. A Mulliken population analysis performed on the 2-Spy ligand's atomic orbitals shows a negligibly small π-electron density on N and S. This is attributed to the delocalization of the π electrons through the conjugated bonds in the pyridine ring.

In conclusion, the relative π-bonding ability of different ligands to group 6 metals was successfully investigated at the non-empirical level. By studying bidentate or polydentate ligands which bond through N, S, and P atoms in group 6 transition metal complexes, we were able to obtain relative order (or magnitude) of π-bonding ability.

REFERENCES

1. Fenske, R. F. and Hall, M. B., *Inorg. Chem.*, 1972, **11,** 768.
2. Buhro, W. E., Chisholm, M. H., Folting, K. and Huffman, H. C., *J. Am. Chem. Soc.*, 1987, **109,** 905.
3. (a) Liu, S.-T., Tsao, C.-L., Cheng, M.-C. and Peng, S.-M., *Polyhedron*, 1990, **9,** 2579–2584. (b) Liu, S.-T., National Taiwan University, Taipei, Taiwan, personal communication, 1991.
4. Sanchez-Palaez, A. E., Perpinan, M. F., Gutierrez-Puebla, E., Monge, A. and Ruiz-Valero, C., *J. Organomet. Chem.*, 1990, **384,** 79.
5. Clementi, E., *J. Chem. Phys.*, 1964, **40,** 1944.
6. Fenske, R. F. and Milletti, M. C., *Organometallics*, 1986, **5,** 1244.
7. Herman, S. and Skillman, S., *Atomic Structure Calculations*. Prentice-Hall, Englewood Cliffs, NJ, 1963.
8. Watson, R. E., *Phys. Rev.*, 1960, **119,** 1934.
9. Gianturco, F. A., *J. Chem. Soc.*, 1969, **A,** 23.
10. *Spartan 2.1*; Wavefunction, Irvine, CA, 1992.
11. Clark, M, Cramer III, R. D. and van Opdensch, N., *J. Comp. Chem.*, 1989, **10,** 982.
12. Darensbourg, D. J., Wiegreffe, H. P. and Reibenspies, J. H., *Organometallics*, 1991, **10,** 6.
13. Tseng, T.-W., Wu, I.-Y., Lin, Y.-C., Chen, C.-T., Chen, M.-C., Tsai, Y.-J., Chen, M.-C. and Wang, Y., *Organometallics*, 1991, **10,** 43.
14. Mulliken, R. S., *J. Chem. Phys.*, 1995, **23,** 1841.
15. Mabad, B., Cassoux, P., Tuchagues, J.-P. and Hendrickson, D. N., *Inorg. Chem.*, 1986, **25,** 1420.
16. Grim, S. O., Sangokoya, S. A., Colquhoun, I. J., McFarlane, W. and Khanna, R. K., *Inorg. Chem.*, 1986, **25,** 2699.
17. Grim, S. O., Sangokoya, S. A., Rheingold, A. L., Colquhoun, I. J., McFarlane, W. and Gilardi, R. D., *Inorg. Chem.*, 1991, **30,** 2519.
18. Modder, J. F., Vrieze, K., Spek, A. L., Challa, G. and Koten, G., *Inorg. Chem.*, 1992, **31,** 1238.
19. Cotton, F. A and Wilkinson, G., *Advanced Inorganic Chemistry*, 5th edn. John Wiley & Sons, New York, 1988, p. 59.

Pergamon

PII: S0277-5387(97)00378-1

Polyhedron Vol. 17, No. 8, pp. 1275–1279, 1998
© 1998 Elsevier Science Ltd
All rights reserved. Printed in Great Britain
0277-5387/98 $19.00+0.00

Synthesis and characterization of β-alkoxycarbonylethyltin trichloride complexes with dibutylsulfoxide. Crystal structure of $CH_3CH_2OCOCH_2CH_2SnCl_3 \cdot (n\text{-}C_4H_9)_2SO$

Laijin Tian,[a]* Zhengyu Zhou,[a] Bin Zhao[a] and Wentao Yu[b]

[a] Department of Chemistry, Qufu Normal University, Qufu, Shandong, 273165, P.R. China
[b] Institute of Crystal Material, Shandong University, Jinan, Shandong, 250100, P.R. China

(Received 2 July 1997; accepted 11 September 1997)

Abstract—The organotin(IV) complexes, $ROCOCH_2CH_2SnCl_3 \cdot nL$ (R = Me, Et, *n*-Pr, Allyl, *n*-Bu, *i*-Bu; $n = 1, 2$; L = dibutylsulfoxide) have been synthesized and characterized. The spectral data (IR, ^1H and ^{13}C NMR) indicate that the 1 : 1 ($n = 1$) and 1 : 2 ($n = 2$) complexes are all hexa-coordinated tin compounds, and the carbonyl oxygen is coordinated to intramolecular tin atom in 1 : 1 complexes and is free in 1 : 2 complexes. The crystal structure of $EtOCOCH_2CH_2SnCl_3 \cdot L$ shows that the tin atom adopts a distorted octahedral geometry via the oxygens of dibutylsulfoxide and intramolecular carbonyl group to tin coordination. © 1998 Elsevier Science Ltd. All rights reserved

Keywords: β-alkoxycarbonylethyltin trichloride; dibutylsulfoxide; complex; synthesis; characterization; crystal structure.

Since Hutton *et al* [1,2] developed a novel route to the preparation of β-alkoxycarbonylethyltin trichlorides, $ROCOCH_2CH_2SnCl_3$, these compounds have received considerable attention because of the variety of coordination geometries regarding the tin atom and also their applicability as a PVC stabilizer with low mammalian toxicities [3–10]. The crystal structure of $CH_3OCOCH_2CH_2SnCl_3$ [3] revealed that the central tin atom was penta-coordinated with the intramolecular carbonyl oxygen to tin atom coordination. However, the IR data indicated that the intramolecular coordination can be broken by external donor molecules, such as 2,2′-bipyridyl, 1,10-phenanthroline, etc. [4–8]. In order to go further into the coordinated chemistry of $ROCOCH_2CH_2SnCl_3$, we have synthesized and characterized the 1 : 1 and 1 : 2 complexes of the organotin compounds with monodentate ligand dibutylsulfoxide (L) and have determined the crystal structure of $EtOCOCH_2CH_2SnCl_3 \cdot L$.

* Author to whom correspondence should be addressed.

EXPERIMENTAL

All chemicals were of reagent grade and used without further purification. The solvents used were dried over $CaCl_2$ and distilled before use. Carbon and hydrogen analyses were carried out with a Perkin-Elmer 2400 elemental analyzer, and tin was determined gravimetrically as SnO_2. Melting points were measured on a WRS-1 melting point apparatus. IR spectra (4000–400 cm^{-1}) were recorded on an Alpha Centauri FT-IR spectrophotometer in KBr pellets. ^1H and ^{13}C NMR spectra in $CDCl_3$ against TMS as internal standard were recorded on a Bruker AC-80 FT-NMR spectrometer.

Preparation of $ROCOCH_2CH_2SnCl_3$

The compounds, $ROCOCH_2CH_2SnCl_3$ (R = Me, Et, *n*-Pr, Allyl, *n*-Bu, *i*-Bu), were prepared from $SnCl_2$, HCl and $CH_2{=}CHCO_2R$ by methods previously reported [2,8].

Preparation of $ROCOCH_2CH_2SnCl_3 \cdot L$

A solution of L (0.81 g, 5 mmol) dissolved in 40 cm^3 benzene was added dropwise to a stirred solution of

$ROCOCH_2CH_2SnCl_3$ (5 mmol) in 40 cm^3 benzene. The reaction mixture was refluxed for 1 h. The colourless crystals which formed in the concentrated solution were filtered off and recrystallized from benzene–petroleum ether (b.p. 70–90°C) (1 : 1, v/v). The yields, melting points, analysis, IR and NMR data of the complexes are listed in Tables 1 and 2.

Preparation of $ROCOCH_2CH_2SnCl_3 \cdot 2L$

An ether solution (30 cm^3) of $ROCOCH_2CH_2SnCl_3$ (5 mmol) was added slowly to a stirred solution of L (1.62 g, 10 mmol) in 30 cm^3 of ether. The reaction mixture was stirred continuously for 1 h at room temperature. The colourless semi-solids at the bottom were obtained by removing ether, and washed with ether and dried *in vacuo*. The results are listed in Tables 1 and 2.

Crystal structure determination of $EtOCOCH_2CH_2SnCl_3 \cdot (n\text{-}C_4H_9)_2SO$

Crystal data. $C_{13}H_{27}Cl_3O_3Sn$, M = 488.45, orthorhombic, space group $P2_12_12_1$, $a = 7.832(2)$, $b = 11.648(2)$, $c = 22.952(5)$ Å, $V = 2093.8(8)$ Å^3, $Z = 4$, $D_c = 1.59$ g cm^{-3}, $F(000) = 984$, $\mu(\text{Mo-}K_\alpha) = 1.708$ mm^{-1}, $\lambda = 0.71073$ Å, $T = 293(2)$ K.

Data collection and structure solution and refinement.

A colourless crystal with the dimensions $0.3 \times 0.2 \times 0.2$ mm was mounted on a Nicolet R3m/E four circle diffractometer. Graphite monochromated Mo-K_α radiation was used for the X-ray measurement. The unit-cell parameters were determined from a least-squares fit of the angular setting of 25 reflections in the range $2.5 < \theta < 13°$. The intensity of 2213 reflections were measured ($0 \leqslant h \leqslant 9$, $0 \leqslant k \leqslant 13$, $0 \leqslant l \leqslant 27$) by using the θ–2θ scan technique to $2\theta_{max} = 50°$. 2139 of these are independent reflections ($R_{int} = 0.0397$) and 1807 of these with $I \geqslant 2\sigma(I)$ were assumed to be observed reflections. Two standard reflections were remeasured every 50 reflections during the data collection and no significant intensity variation was observed (< 5%). The data were corrected for Lorentz and polarization effects and an empirical absorption correction based on ψ scans was applied, with transmission factors from 0.772 to 0.992. These

Table 1. M.p., yield, analysis and IR data of $ROCOCH_2CH_2SnCl_3 \cdot nL$

Compound		M.p.	Yield	Analysis (%), Found (Calc.)			IR (ν, cm^{-1})	
R	*n*	(°C)	(%)	C	H	Sn	C=O	S=O
Me	1	115.7–116.7	88	30.30(30.37)	5.17(5.31)	24.88(25.02)	1658	958
Et	1	102.1–102.7	87	32.08(31.08)	5.42(5.57)	24.35(24.30)	1654	960
n-Pr	1	88.1–88.7	84	33.12(33.46)	5.87(5.82)	23.48(23.62)	1650	962
Allyl	1	61.8–62.4	78	33.57(33.60)	5.22(5.44)	24.12(23.73)	1658	966
n-Bu	1	74.0–74.8	88	34.83(34.88)	6.14(6.05)	22.56(22.98)	1660	964
i-Bu	1	77.2–77.6	70	34.64(34.88)	5.92(6.05)	23.40(22.98)	1664	964
Me	2	semi-solid	83	37.34(37.73)	6.50(6.81)	18.53(18.64)	1728	948
Et	2	semi-solid	77	38.53(38.76)	6.84(6.97)	17.76(18.24)	1730	950
n-Bu	2	semi-solid	68	40.78(40.69)	7.33(7.28)	17.58(18.24)	1732	957

Table 2. NMR data of $ROCOCH_2CH_2SnCl_3 \cdot nL$

Compound		^{1}H NMR (δ, ppm)			^{13}C NMR (δ, ppm)				
R	*n*	CH_2O	CH_2	CH_2Sn	CH_2O	CO	CH_2	CH_2Sn	C—S
Me	1	4.00(s)	2.94(t)	1.96(t)	55.53	183.23	29.21	32.58	49.81
Et	1	4.41(q)	2.87(t)	1.92(t)	64.94	182.37	28.82	31.87	49.34
n-Pr	1	4.34(t)	2.88(t)	1.86(t)	68.90	182.48	28.70	32.42	49.27
Allyl	1	4.80(d)	2.84(t)	1.90(t)					
n-Bu	1	4.33(t)	2.84(t)	1.84(t)	68.68	182.36	28.70	32.12	49.27
i-Bu	1	4.14(d)	2.87(t)	1.90(t)					
Me	2	3.82(s)	2.82(t)	1.88(t)	54.30	180.62	29.72	34.16	50.30
Et	2	4.30(q)	2.81(t)	1.89(t)	64.23	181.28	29.23	32.90	50.10
n-Bu	2	4.18(t)	2.81(t)	1.83(t)	67.35	180.66	29.43	33.20	50.14

calculations were performed using program package SHELXTL [11]. The systematic extinction conditions $h00$, $h = 2n+1$; $0k0$, $k = 2n+1$; $00l$, $l = 2n+1$ are compatible with $P2_12_12_1$ space group. The structure was solved in this space group by direct methods in SHELXTL program [11] and refinement on F^2 was performed using SHELXL-93 program [12] by full-matrix least squares, with anisotropic displacement parameters for all non-H atoms. All H-atoms positions were located in calculated positions and isotopically refined. The weighing scheme was $w = 1/[\sigma^2(F_o^2)+(0.0409P)^2+0.6286P]$ where $P = (F_o^2+2F_c^2)/3$; an isotropic extinction correction was applied with $F_{corr} = F_c/k[1+0.001xF_c^2\lambda^3/\sin 2\theta]^{0.25}$ [x refined to 0.005(4)]. The refinement converged to final $R[F^2 > 2\sigma(F^2)] = 0.0362$. $wR(F^2) = 0.0785$, for 1807 unique observed reflections, $S = 1.081$. The maximum and minimum heights of 0.438 and -0.333 e Å^{-3}, respectively. The maximum Δ/σ in the last refinement cycle was 0.0. Atomic scattering factors were taken from the programs mentioned [11,13]. Molecular graphics were drawn with the program package SHELXTL [11].

RESULTS AND DISCUSSION

The complexes, $ROCOCH_2CH_2SnCl_3 \cdot nL$ were obtained by the reaction of $ROCOCH_2CH_2SnCl_3$ with dibutylsulfoxide ligand in appropriate molar ratios (1 : 1 or 1 : 2).

$$ROCOCH_2CH_2SnCl_3 + nL \rightarrow ROCOCH_2CH_2SnCl_3 \cdot nL.$$

The 1 : 1 complexes ($n = 1$) are colourless crystals with sharp melting points and the 1 : 2 complexes ($n = 2$) are colourless semi-solids. They are soluble in benzene, ethanol and chloroform, but insoluble in ethyl ether and petroleum ether. The observed molar conductances of the complexes in nitrobenzene at room temperature are in the range 3.96–5.27 ohm^{-1} cm^2 mol^{-1}, indicating that the compounds are non-electrolytes [14].

Spectroscopic properties of the complexes

The characteristic IR bands of the complexes relevant to their molecular structures are listed in Table 1. Among the stretching modes, the ν(C=O) band in the 1640–1740 cm^{-1} region is known to depend on the nature of coordination of the carbonyl oxygen to metal atom [4,5]. The ν(C=O) bonds of the 1 : 2 complexes (~1730 cm^{-1}) are in the same region as that of the free fatty acid ester (~1740 cm^{-1}), in which the carbonyl group is not coordinated to the tin atom, whereas the ν(C=O) bands of the 1 : 1 complexes (1650–1664 cm^{-1}) exhibit remarkable red shift from that of the free fatty acid ester. Such results clearly indicate that the coordination of the carbonyl oxygen to tin is maintained in the 1 : 1 complexes, but such a coordination is broken to accommodate two dibutylsulfoxide ligands. Compared with ν(S=O) of free dibutylsulfoxide (1038 cm^{-1}), the ν(S=O) of the complexes shifts to a lower frequency (948–966 cm^{-1}), confirming its coordination to tin via oxygen [15]. Thus, it may be seen that all the complexes are hexa-coordinated to tin.

The ^{1}H and ^{13}C NMR data listed in Table 2 also support the presence of carbonyl oxygen to tin coordination in the 1 : 1 complexes. $\delta(^1H)$ of CH_2O in the 1 : 1 complexes shows a downfield shift by 0.11–0.18 ppm compared to that of the corresponding 1 : 2 complexes, and the $\delta(^{13}C)$ values of C=O and CH_2O in the 1 : 1 complexes are deshielded by 1.09–2.61 ppm (C=O) and 0.71–1.33 ppm (CH_2O), respectively, relative to those of the corresponding 1 : 2 complexes. The coordination of carbonyl oxygen to tin in the 1 : 1 complexes causes the deshielding of CH_2OCO. However, when the coordination is broken by an external ligand, the shielding of CH_2OCO is recovered again.

Crystal structure of $EtOCOCH_2CH_2SnCl_3 \cdot L$

The molecular geometry and the atomic numbering scheme for $EtOCOCH_2CH_2SnCl_3 \cdot L$ are shown in Fig. 1. Bond lengths and bond angles are given in Table 3. The complex exists as a discrete molecule which contains a five-membered chelate ring, formed via ester carbonyl oxygen to tin coordination. The tin atom is hexa-coordinated with the coordinating atoms C(1), Cl(1), Cl(2), Cl(3), O(1) and O(2) in a distorted octahedral arrangement. The bond angles of C(1)—Sn(1)—Cl(1), O(1)—Sn(1)—Cl(3) and O(3)—Sn(1)—Cl(2) are 158.3(2), 170.4(2) and 174.3(2)°, respectively. The bond distances Sn(1)—O(1) (2.350(6) Å), Sn(1)—Cl(1) (2.372(2) Å), Sn(1)—Cl(2) (2.421(2) Å), Sn(1)—Cl(3) (2.401(2) Å), Sn(1)—C(1) (2.146(8) Å) are slightly longer than those (2.347(5), 2.303(2), 2.357(2), 2.317(2), 2.139(9) Å, respectively) in $CH_3OCOCH_2CH_2SnCl_3$ [3]. This indicates that the dibutylsulfoxide oxygen atom to tin coordination weakens the coordination of the other five atoms, compared with penta-coordinate compounds $ROCOCH_2CH_2SnCl_3$. The bond length Sn(1)—O(1) (2.350(6) Å) is longer than Sn(1)—O(3) (2.225(5) Å), and shows that O(3) coordination to tin is stronger than O(1). Thus, when L/EtOCO $CH_2CH_2SnCl_3$ is beyond a 1 : 1 mole ratio, the intramolecular coordination Sn—O(1) is replaced by the oxygen atom of L and the 1 : 2 complex is formed.

Acknowledgements—The authors wish to thank the National Natural Science Foundation of China (29673025) and the State Key Laboratory of Crystal Materials in Shandong University for their support of this project.

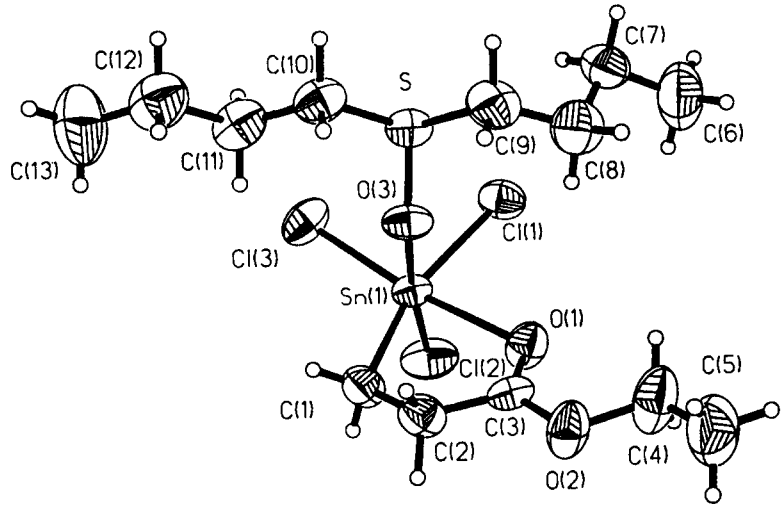

Fig. 1. Molecular structure and atomic numbering scheme.

Table 3. Bond lengths (Å) and angles (°) for $EtOCOCH_2CH_2SnCl_3 \cdot L$

Sn(1)—C(1)	2.146(8)	O(2)—C(4)	1.482(12)
Sn(1)—O(3)	2.225(5)	C(1)—C(2)	1.507(11)
Sn(1)—O(1)	2.350(6)	C(2)—C(3)	1.497(12)
Sn(1)—Cl(1)	2.372(2)	C(4)—C(5)	1.424(13)
Sn(1)—Cl(3)	2.401(2)	C(6)—C(7)	1.522(14)
Sn(1)—Cl(2)	2.421(2)	C(7)—C(8)	1.524(13)
S—O(3)	1.533(5)	C(8)—C(9)	1.502(13)
S—C(10)	1.805(9)	C(10)—C(11)	1.511(12)
S—C(9)	1.811(9)	C(11)—C(12)	1.505(12)
O(1)—C(3)	1.224(9)	C(12)—C(13)	1.50(2)
O(2)—C(3)	1.305(9)		

C(1)—Sn(1)—O(3)	83.2(3)	C(10)—S—C(9)	97.1(4)
C(1)—Sn(1)—O(1)	77.0(3)	C(3)—O(1)—Sn(1)	110.8(5)
O(3)—Sn(1)—O(1)	81.3(2)	C(3)—O(2)—C(4)	116.9(7)
C(1)—Sn(1)—Cl(1)	158.3(2)	S—O(3)—Sn(1)	128.2(3)
O(3)—Sn(1)—Cl(1)	87.0(2)	C(2)—C(1)—Sn(1)	110.4(5)
O(1)—Sn(1)—Cl(1)	82.4(2)	C(3)—C(2)—C(1)	114.0(7)
C(1)—Sn(1)—Cl(3)	104.7(2)	O(1)—C(3)—O(2)	122.9(8)
O(3)—Sn(1)—Cl(3)	89.48(14)	O(1)—C(3)—C(2)	114.4(7)
O(1)—Sn(1)—Cl(3)	170.4(2)	C(5)—C(4)—O(2)	109.3(9)
Cl(1)—Sn(1)—Cl(3)	94.50(9)	C(6)—C(7)—C(8)	111.9(8)
C(1)—Sn(1)—Cl(2)	97.9(2)	C(9)—C(8)—C(7)	114.2(8)
O(3)—Sn(1)—Cl(2)	174.3(2)	C(8)—C(9)—S	111.1(7)
Cl(1)—Sn(1)—Cl(2)	90.12(9)	C(11)—C(10)—S	112.7(6)
Cl(3)—Sn(1)—Cl(2)	95.63(9)	C(12)—C(11)—C(10)	112.0(8)
O(3)—S—C(10)	104.7(4)	C(13)—C(12)—C(11)	114.1(10)
O(3)—S—C(9)	104.1(4)		

REFERENCES

1. Burley, J. W., Hutton, R. E. and Oakes, V., *J. Chem. Soc., Chem. Commun.*, 1976, 803.
2. Hutton, R. E., Burley, J. W. and Oakes, V., *J. Organomet. Chem.*, 1978, **156**, 369.
3. Harrison, P. G., King, T. J. and Healy, M. A., *J. Organomet. Chem.*, 1979, **182**, 17.
4. Maughan, D., Wardell, J. L. and Burly, J. W., *J. Organomet. Chem.* 1981, **212**, 59.
5. Howie, R. A., Paterson, E. S., Wardell, J. L. and Burley, J. W., *J. Organomet. Chem.*, 1986, **304**, 301.

6. Deb, B. K. and Ghosh, A. K., *Polyhedron*, 1986, **5**, 863.
7. Fu, F., Tian, L., Pan, H., Willem, R. and Gielen, M., *Bull. Soc. Chim. Belg.*, 1990, **99**, 789.
8. Tian, L., Liu, S., Bi, S. and Fu, F., *Synth. React. Inorg. Met.-Org. Chem.*, 1997, **27**, 127.
9. Tian, L., Fu, F. and Pan, H., *Chin. Chem. Lett.*, 1995, **6**, 805; *Chem. Abstr.*, 1996, **124**, 87182m.
10. Kugele, T. G., *Belg. Pat.* 864, 976 (1978); *Chem. Abstr.* 1979, **90**, 104943j.
11. Nicolet XRD Corporation, SHELXTL User's Manual, Revision 4.1, Nicolet XRD Corporation, Madison, Wisconsin, U.S.A., 1985.
12. Sheldrick, G. M., SHELXL93. Program for the Refinement of Crystal Structure, University of Göttingen, Germany, 1993.
13. Shedrick, G. M., *Acta Cryst.*, 1990, **A46**, 467.
14. Gesry, W. J., *Coord. Chem. Rev.*, 1971, **7**, 81.
15. Kumar Das, V. G. and Kitching, W., *J. Organomet. Chem.*, 1968, **13**, 523.

Pergamon

PII: S0277-5387(97)00375-6

Polyhedron Vol. 17, No. 8, pp. 1281–1288, 1998
© 1998 Elsevier Science Ltd
All rights reserved. Printed in Great Britain
0277-5387/98 $19.00+0.00

Preparation and characterization of the dinuclear complexes $[Fe_2Cl_4L_2]$ and $[Fe_2Cl_4L_2]Cl_2$ (L = 2-(2′-pyridyl)quinoxaline)

Spyridoula Kasselouri,[a] Achilleas Garoufis,[a] Spyros P. Perlepes,[b] Frank Lutz,[c] Robert Bau,[c] Sotiris Gourbatsis[d] and Nick Hadjiliadis*[d]

[a] Department of Chemistry, Physics and Materials Technology, Technological Institution of Athens, Egaleo, Athens, Greece

[b] Department of Chemistry, University of Patras, 26500 Patras, Greece

[c] Department of Chemistry, University of Southern California, Los Angeles, CA 90089-0744, U.S.A.

[d] Laboratory of Inorganic and General Chemistry, Department of Chemistry, University of Ioannina, 451 10 Ioannina, Greece

(Received 19 June 1997; accepted 1 September 1997)

Abstract—The 1:1 reactions of $FeCl_2 \cdot 4H_2O$ and $FeCl_3$ with the biheteroaromatic ligand 2-(2′-pyridyl)quinoxaline (L) were studied in methanol. The new complexes $[Fe_2Cl_4L_2]$ (**1**) and $[Fe_2Cl_4L_2]Cl_2$ (**2**) were isolated and characterized by elemental analyses, conductivity measurements, magnetic susceptibilities at room temperature and spectroscopic (IR, far-IR, ligand field, ^{57}Fe Mössbauer) techniques. The X-ray crystal structure of **1** consists of two Fe^{II} centres bridged by two chloro ligands, with a terminal chloride and a chelating molecule of L completing five-coordination at each metal. The geometry at iron is distorted trigonal bipyramidal with the bridging chlorides occupying apical and equatorial sites of each Fe^{II} atom. A five-coordinate dinuclear structure is also assigned for the cation of complex **2**. All data are discussed in terms of the nature of bonding and known or assigned structures. © 1998 Elsevier Science Ltd. All rights reserved

Keywords: crystal structures; iron complexes; 2-(2-pyridyl)quinoxaline complexes; ^{57}Fe Mössbauer spectroscopy.

A unifying theme in some of our recent work has been the desire to establish the products from the reaction of the biheteroaromatic ligand 2-(2′-pyridyl) quinoxaline (L) with metal salts, mainly halides, as it has become apparent that this chemistry is rich in structural types, reactivity characteristics and ligand's coordination modes [1–9]. Ligand L, which can potentially combine the chelating properties of 2,2-bipyridine [10] with the bridging behaviour of quinoxaline [11], belongs to a family of heteroaromatic nitrogen heterocycles whose coordination chemistry is currently a subject of intense research efforts [12–17]. The study of complexes of these ligands is important in understanding electron transfer processes, mixed-valent complexes, excited-state acid-base properties of inorganic systems and magnetic coupling interactions; moreover, it finds applications in catalysis, bioinorganic materials chemistry.

Our work to-date has been concentrated on complexes with $3d^7$ (Co^{II}), d^8 (Ni^{II}, Pd^{II}, Pt^{II}), $3d^9$ (Cu^{II}) and d^{10} (Cu^{I}, Zn^{II}, Cd^{II}, Hg^{II}) metal ions. It thus seemed natural to seek to extend this chemistry further to d^5 and d^6 metal ions, and allow comparisons and contrasts to be made concerning the influence of the electronic structure of the metal on the structure of the products and on the coordination mode of L. In this report, we describe the identity of the solid products obtained from the 1:1 reactions of iron(II) and iron(III) chlorides with L and their study with a number or physical techniques. The iron(II) complex has

* Author to whom correspondence should be addressed.

been structurally characterized by single-crystal X-ray crystallography.

EXPERIMENTAL

All manipulations were performed under aerobic conditions using materials and solvents as received. L was synthesized as described previously [1]. Elemental analyses, physicochemical measurements and spectroscopic techniques were carried out by published methods [4,18–20].

Preparation of $[Fe_2Cl_4L_2]$ (1)

To a stirred pale green solution of $FeCl_2 \cdot 4H_2O$ (0.2 g, 1.0 mmol) in MeOH (10 ml) was added a solution of L (0.21 g, 1.0 mmol) in the same solvent (10 ml) to give a pale brown solution. The flask was stored at ambient temperature for 2 days, and the resulting brown crystals of **1** were collected by filtration, washed with cold MeOH (2 × 5 ml) and Et_2O (2 × 5 ml) and dried *in vacuo* over silica gel. The yield was 0.22 g (66%). Some crystals were suitable for X-ray crystallography. Anal. Calc. for $C_{26}H_{18}N_6Cl_4Fe_2$: C, 46.74; H, 2.72; N, 12.58; Cl, 21.23. Found: C, 46.98; H, 2.65; N, 12.70; Cl, 20.74%.

Preparation of $[Fe_2Cl_4L_2]Cl_2$ (2)

Solutions of $FeCl_3$ (0.16 g, 1.0 mmol) in MeOH (10 ml) and of L (0.21 g, 1.0 mmol) in the same solvent (10 ml) were combined, and the homogeneous solution obtained was stirred at ambient temperature overnight. The resultant red solution was then concentrated *in vacuo* to about 8 ml and kept at 0°C. After a few hours, a brown-red powder of **2** formed, which was filtered off, washed with cold MeOH (5 ml) and Et_2O (2 × 5 ml), and dried in air. Further concentration of the filtrate, and washings and storage at 0°C gave a further quantity of the complex. The total yield was 0.28 g (75%). Anal. Calc. for $C_{26}H_{18}N_6Cl_6Fe_2$: C, 42.26; H, 2.46; N, 11.38; Cl, 28.79. Found: C, 42.40; H, 2.31; N, 11.12; Cl, 29.60%.

X-ray crystallography and structure solution

Crystal data and details of the data collection and data processing are listed in Table 1. A crystal of **1** of approximate dimensions 0.3 × 0.3 × 0.2 mm was selected and X-ray diffraction data were collected at 20°C on a Siemens $P2_1$ automated diffractometer using graphite-monochromated Mo–K_α radiation (λ = 0.71073 Å). Unit cell parameters were derived by least-squares fit of 15 centred reflections. Throughout the data collection, three standard reflections were monitored periodically and no decay was observed.

The structure was solved by direct methods using SHELXS-85 [21] and refined by full-matrix least-squares techniques on F^2 with SHELXL-93 [22]. All non-hydrogen atoms were readily located and refined with anisotropic thermal parameters. All hydrogen atoms were placed in fixed, calculate positions. Selected bond lengths and angles of **1** are given in Table 2.

Table 1. Summary of crystal and intensity collection data for $[Fe_2Cl_4L_2]$ (**1**)

Parameter	**1**
Formula	$C_{26}H_{18}Cl_4Fe_2N_6$
M_r (g mol^{-1})	667.96
Crystal colour	brown
Crystal size (mm)	0.3 × 0.3 × 0.2
Crystal system	monoclinic
Space group	$P2_1/n$
a (Å)	7.773(2)
b (Å)	15.345(3)
c (Å)	10.750(2)
β (°)	91.45(3)
V (Å^3)	1281.8(5)
Z	2
D_{calc} (g cm^{-3})	1.731
$F(000)$	672
μ (mm^{-1})	1.579
Radiation, λ (Å)	Mo-K_α, 0.71073
θ range (°)	2.3–22.5
Range h	−1 to 8
Range k	−1 to 16
Range l	−11 to 11
Reflections collected	2302
Reflections unique	1678 (R_{int} = 0.0286)
Reflections used ($I > 2\sigma(I)$)	1485
Paramaters refined	172
Final R indices ($I > 2\sigma(I)$)	$R_1{}^a$ = 0.0265, $wR_2{}^b$ = 0.0637
R indices (all data)	$R_1{}^a$ = 0.0321, $wR_2{}^b$ = 0.0650
GOF[c]	1.585
Weighting scheme[d]	$w = 1/[\sigma^2(F^2) + (0.0000P)^2 + 0.0000P]$
$(\Delta\rho)_{max}$, $(\Delta\rho)_{min}$ (e Å^{-3})	0.24, −0.28

[a] $R_1 = \Sigma\|F_o| - |F_c\|/\Sigma|F_o|$.
[b] $wR_2 = \{\Sigma[w(F_o^2 - f_c^2)^2]/\Sigma[w(F_o^2)^2]\}^{1/2}$.
[c] Based on F^2.
[d] $P = (F_o^2 + 2F_c^2)/3$.

RESULTS AND DISCUSSION

Preparation and physical properties of the complexes

The preparation of the iron complexes is summarized in eqns (1) and (2).

$$2FeCl_2 \cdot 4H_2O + 2L \xrightarrow[\text{r.t.}]{MeOH} [Fe_2Cl_4L_2] + 8H_2O \quad (1)$$

1

Table 2. Selected bond distances (Å) and angles (°) for **1**[a]

Bond distances			
Fe(1)—N(1)	2.115(2)	N(1)—C(1)	1.349(3)
Fe(1)—N(2)	2.206(2)	N(1)—C(5)	1.349(4)
Fe(1)—Cl(2)	2.279(1)	C(5)—C(6)	1.488(4)
Fe(1)—Cl(1)	2.391(1)	N(2)—C(6)	1.322(3)
Fe(1)—Cl(1*)	2.511(1)	N(2)—C(9)	1.378(3)
Fe(1)—Fe(1*)	3.680(1)	C(8)—C(9)	1.408(4)
Bond angles			
N(1)—Fe(1)—N(2)	75.8(1)	Cl(2)—Fe(1)—Cl(1)	133.9(1)
N(1)—Fe(1)—Cl(2)	113.4(1)	Cl(2)—Fe(1)—Cl(1*)	99.3(1)
N(1)—Fe(1)—Cl(1)	112.1(1)	Cl(1)—Fe(1)—Cl(1*)	82.6(1)
N(1)—Fe(1)—Cl(1*)	96.3(1)	Fe(1)—Cl(1)—Fe(1*)	97.3(1)
N(2)—Fe(1)—Cl(2)	96.5(1)	Fe(1)—N(1)—C(1)	124.5(2)
N(2)—Fe(1)—Cl(1)	87.6(1)	Fe(1)—N(2)—C(6)	114.3(2)
N(2)—Fe(1)—Cl(1*)	164.1(1)	C(5)—C(6)—C(7)	12.2(3)

[a] Stars are used for the symmetry-related atoms.

$$2FeCl_3 + 2L \xrightarrow[\text{r.t.}]{\text{MeOH}} [Fe_2Cl_4L_2]Cl_2 \qquad (2)$$

2

Although 2-(2′-pyridyl)quinoxaline(L) was reacted with iron chlorides in mole ratios of 1 : 1, 2 : 1 and 3 : 1, complexes of 1 : 1 stoichiometry (**1**, **2**) were obtained in all cases. This behaviour contrasts with that of nickel(II), palladium(II), copper(II) and cadmium(II) [1–3,5,9], all of which form a complete set of 1 : 1 and 1 : 2 chloro complexes with L. [6,9].

The complexes are microcrystalline (**1**) or powder-like (**2**) and stable in the normal laboratory atmosphere; the iron(II) complex is stable to aerial oxidation so that L is capable of stabilizing iron(II). Complex **1** is insoluble in all common organic solvents, except MeOH, DMF and DMSO. For this compound the molar conductivity values in DMF (Λ_M = 43 S cm^2 mol^{-1}) and DMSO (Λ_M = 10 S cm^2 mol^{-1}) are intermediate to the values for a non-electrolyte and a 1 : 1 electrolyte [23], suggesting decomposition. The iron(III) complex **2**, on the other hand, is soluble in a variety of polar or relatively polar organic solvents, supporting an ionic formulation. Conductivity measurements for $\sim 10^{-3}$ M solutions (assuming a dimer formulation) of **2** at 25°C indicated this complex to be [23] a 1 : 2 electrolyte in Me_2CO (Λ_M = 191 S cm^2 mol^{-1}), MeOH (Λ_M = 177 S cm^2 mol^{-1}), MeCN (Λ_M = 262 S cm^2 mol^{-1}), DMF (Λ_M = 154 S cm^2 mol^{-1}) and DMSO (Λ_M = 72 S cm^2 mol^{-1}).

Description of structure

The molecular structure of $[Fe_2Cl_4L_2]$ (**1**) is shown in Fig. 1. The two iron(II) centres are bridged by two chloro ligands; in addition to the bridging chloro atoms, each Fe^{II} atom is coordinated to a chelating L molecule and a terminal chloride giving five-coordinate N_2Cl_3 ligand donor sets. The two metal centres are related by a crystallographically imposed centre of symmetry and, thus, the bridging Fe_2Cl_2 unit is strictly planar.

In contrast to the conformation of free L [4], in the coordinated L molecule the pyridine nitrogen and the nearest quinoxaline nitrogen are located on the same side of the carbon–carbon bond (C(5)—C(6)) which connects the two moieties; this is a consequence of the chelate effect. The two individually planar portions of L in **1**—the pyridine and the quinoxaline ring—are slightly twisted our of coplanarity, the angle between their best planes being 8.7°. In the free ligand the two planar moieties are more coplanar, planes making an angle of 3.4°. This slight, but significant, bending of L in **1** is illustrated in Fig. 2.

The Fe—Cl bond lengths are normal for iron(II) complexes with chloro ligands [24]. The iron-bridging chloro distances (2.391(1), 2.511(1) Å) are longer than the iron-terminal chloro distance (2.279(1) Å) as expected. There is a difference (ca 0.1 Å) in bond between the two Fe—N bonds, with the metal to pyridine-nitrogen (N(1)) distance being shorter; this may reflect a difference in donor strength of the respective nitrogen atoms. The same trend has been observed in complexes of L with Pd^{II} [9], Cu^{I} [6], Zn^{II} [5] and Hg^{II} [4,7,8]. In $[Cu_2Cl_4L_2]$ [2,3], however, the copper(II) to pyridine-nitrogen distance (2.106(5) Å) is longer than the copper(II) to quinoxaline-nitrogen distance (2.021(5) Å), emphasizing the importance of the metal ion in determining the relative donor strength of the two nitrogen atoms.

The coordination geometry about iron(II) is distorted trigonal bipyramidal. The atoms Cl(1), Cl(2) and N(1) form the equatorial plane with Fe(1) being displaced 0.100 Å from the plane toward the bridging

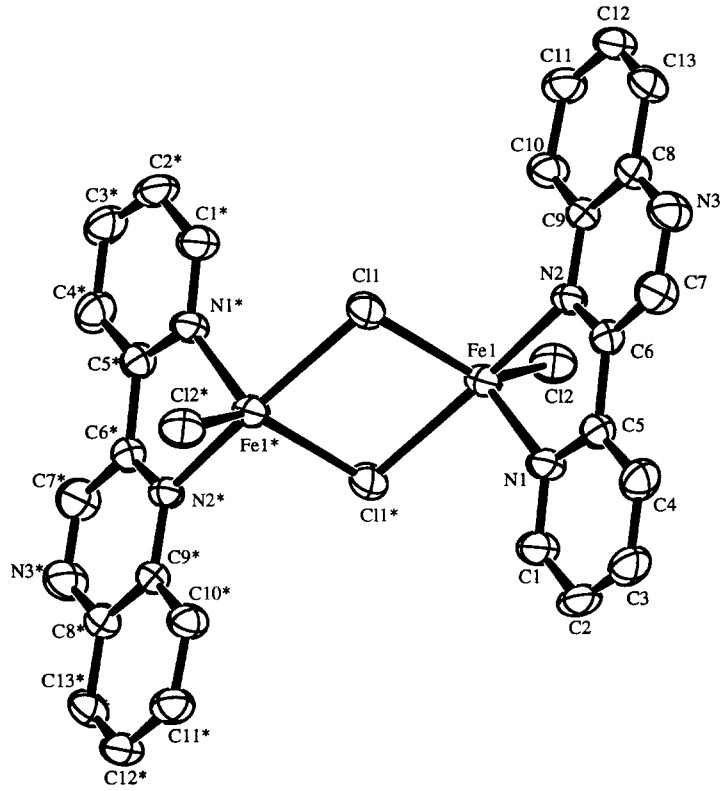

Fig. 1. Molecular structure of **1** with the atom labelling scheme.

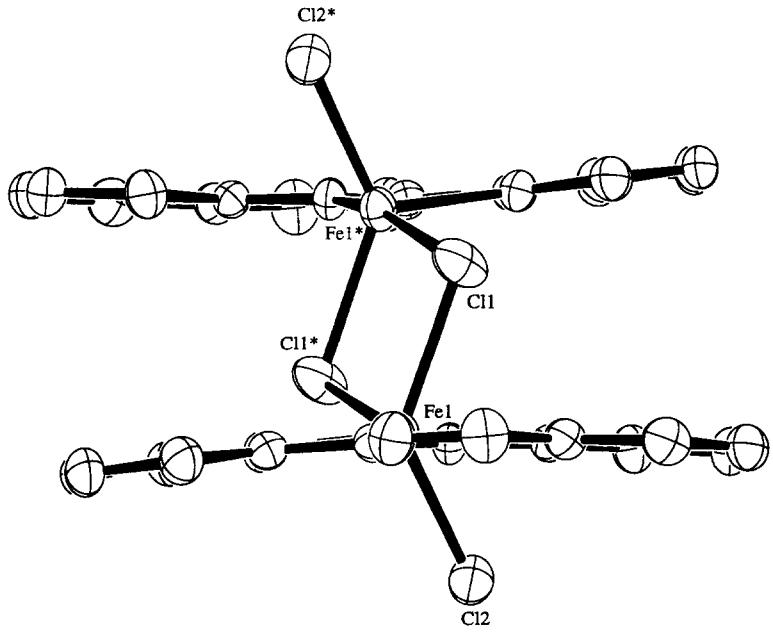

Fig. 2. A view of the molecular structure of **1** emphasizing the slight bending of **L**.

chloride Cl(1*). Thus, in the ligand arrangement encountered in **1**, the two Fe^{II} coordination spheres share a common edge involving equatorial and axial chloro atoms. The N(2)—Fe(1)—Cl(1*) axis is not linear, 164.1(1)°, deviating from perpendicularity to the equatorial plane. The bond angles in the equatorial plane of **1** are 112.1(1), 113.4(1) and 133.9(1)°. The effect of the chelate ring is mainly observed in the N(1)—Fe(1)—N(2) bond angle which deviates (4.2° from the idealized value. The chelating nature of L and the presence of the bridging chlorides affect significantly the details of the coordination sphere about the metal and presumably are responsible for the observed distortion. The axial Fe(1)—N(2) and Fe(1)—Cl(1*) bonds are longer than the respective equatorial bonds. This observation parallels the results reported for other high-spin trigonal iron(II) complexes [25]. Complex **1** joins a handful [25,26] of structurally characterized diferrous complexes with each iron(II) atom being in a trigonal bipyramidal coordination environment; to our knowledge, this is the first such complex with a Fe_2^{II} $(\mu\text{-Cl})_2$ core.

The structure of $[Fe_2Cl_4L_2]$, as detailed in the discussion above, shows remarkable similarity to the molecular structures of $[Cu_2Cl_4L_2]$ [2,3], $[Hg_2Cl_4L_2]$ [4], $[Hg_2Br_4L_2]$ [5] and $[Hg_2I_4L_2]$ [7].

Room-temperature magnetic moments and electronic spectra

The effective magnetic moment of **1** at 25°C (μ_{eff}) is 5.28 BM per iron(II). This value is typical of a high-spin Fe^{II} complex with both a spin contribution and a classic orbital contribution and it appears to exclude very strong ferro- or antiferromagnetic coupling; however, it is difficult to rule out weaker interactions.

The solid-state electronic (diffuse reflectance) spectrum of **1** exhibits one maximum at 9.1 kK and the tail of another band whose maximum is centred somewhere between 4.5 and 5.5 kK, assigned to the one-electron *d-d* transitions $^5E'' \rightarrow {}^5A_1'$, $^5E'' \rightarrow {}^5E'$ under D_{3h} symmetry, respectively [27]. The bond positions are consistent with the high-spin, five-coordinate Fe^{II} N_2Cl_3 chromophore [28], established by the X-ray study. The spectrum also exhibits two charge-transfer bands at 17.2 and 26.2 kK predominantly of the metal to ligand class [27,29].

The effective magnetic moment of **2** at 25°C is 4.90 BM per iron(III). This value is somewhat reduced from the normal high-spin Fe^{III} value of 5.92 BM and shows evidence of weak to moderate antiferromagnetic coupling, indicating a dimeric or polymeric structure [30].

The diffuse reflectance spectrum of the iron(III) complex exhibits several very weak, spin-forbidden *d-d* bands between 12.5 and 23.5 kK and two intense presumed ligand-to-metal charge-transfer absorptions at 26.2 and 28.1 kK [27].

IR and far-IR spectra

The mid-IR spectra of complexes **1** and **2** are similar to those of the 1:1 and 1:2 complexes in which L behaves as a bidentate chelate [1–9]. The characteristic in-plane and out-of-plane pyridine-ring bands at 620 and 401 cm^{-1} respectively, are shifted upwards in **1** (648 and 416 cm^{-1}) and **2** (651 and 419 cm^{-1}), showing the involvement of the pyridine nitrogen in bonding to iron [31]. The ca 960 cm^{-1} region is viewed as the key to differentiate between monodentate terminal and bidentate bridging coordination of the quinoxaline ring [32,33]. The spectrum of the free ligand shows a strong band at 960 cm^{-1}. The appearance of a single, sharp band at 969 and 967 cm^{-1} in the spectra of **1** and **2**, respectively, i.e. the fact that this band does not split on complexation, is typical of the monodentate quinoxaline coordination [32].

The far-IR data of the prepared complexes give an insight into the structure and bonding in the solid state. Assignments of metal-ligand stretching vibrations in Table 3 have been carefully given by considering the frequencies of the internal modes of L, the variation in band frequency with changing the oxidation state of iron and literature reports [28,34–36]. The far-IR spectra of both complexes show one clear terminal Fe—Cl stretch, two bands in the Fe—Cl bridging region and two Fe—N stretching modes. Thus, the data seem incompatible with a monomeric skeleton, but they can be explained on the basis of chloro-bridged structures (dimeric or polymeric), while the complexes still contain terminal Fe—Cl bonds. This spectroscopic behaviour is consistent with the X-ray structure of **1** and suggests a similar structure for the iron(III) complex. Our proposal for a dinuclear $[Fe_2(\mu\text{-Cl})_2Cl_2L_2]Cl_2$ structural type in **2** is further supported by the fact that one of the ν(Fe—Cl) bands appears at 348 cm^{-1}; this frequency is characteristic of terminal chlorides in pentacoordinate Fe^{III} species [35]. The observed wavenumbers of the (Fe—N) modes agree well with the literature data for other iron(II) and iron(III) complexes with chelating N-donor heterocycles [36].

^{57}Fe-Mössbauer spectroscopy studies

Zero-field Mössbauer spectra of polycrystalline samples of **1** and **2** were measured at 4.2 and 298 K. The spectra measured at 4.2 K are shown in Figs 3 and 4. Mössbauer spectral parameters obtained from least-squares fit to the experimental points assuming Lorentzian absorption lines are summarized in Table 4.

The spectrum of **1** consists of a single quadrupole-split doublet. The isomer shift δ is in the range expected for a high-spin Fe^{II} cation surrounded by a mixture of aromatic imine nitrogen atoms and chloro ligands [37]. The slight increase in the quadrupole splitting ΔE_Q as the temperature is decreased is typical

Table 3. IR[a] metal-ligand stretching frequencies (cm^{-1}) for the iron(II) and iron(III) complexes of L

Complex	$\nu(Fe—Cl)_t$	$\nu(FeCl)_b$	$\nu(Fe—N)$
$[Fe_2Cl_4L_2]$ (**1**)	273 s	230 wb, 212 m	281 m,[b] 266 m
$[Fe_2Cl_4L_2]Cl_2$ (**2**)	348 b	269 m, 249 m	290 mb

[a] Fourier-transform spectra.
[b] Overlapping with a vibration of L.
Abbreviations: b = broad; M = medium; $\nu(Fe—Cl)_t$ = the stretching vibration of the terminal Fe—Cl bond; $\nu(FeCl)_b$ = bridging FeCl stretching frequencies; s = strong; w = weak.

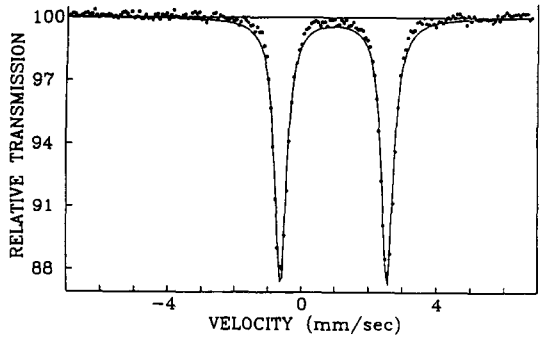

Fig. 3. Mössbauer spectrum of polycrystalline **1** at 4.2 K. The solid line is the best fit to the data with the spectral parameters listed in Table 5.

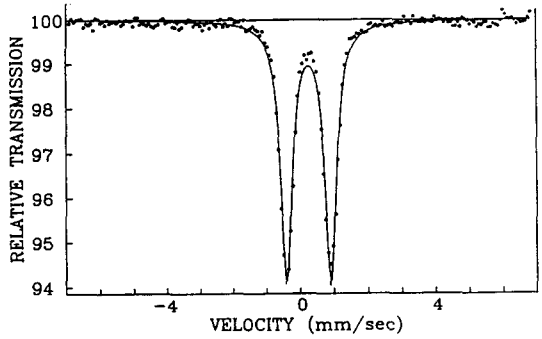

Fig. 4. Mössbauer spectrum of polycrystalline **2** at 4.2 K. The solid line is the best fit to the data with the spectral parameters listed in Table 5.

for high-spin ferrous systems [25,28], due to changes in the Boltzman populations of the low-lying electronic states that form as a consequence of spin-orbit and low-symmetry crystal field perturbations. It is interesting to note that the ΔE_Q value for **1** is significantly larger than reported quadrupole splitting values for six-coordinate dinuclear ferrous centres, but similar to those reported for five-coordinate dinuclear ferrous sites [25]; such differences are ascribed to the inherently less symmetric five-coordinate ligand

Table 4. ^{57}Fe-Mössbauer spectral parameters (mm s^{-1}) for the prepared complexes

Complex	T(K)	δ^a	ΔE_Q	Γ^b
1	298	0.92	3.00	0.21
	4.2	1.08	3.16	0.21
2	298	0.21	1.24	0.20
	4.2	0.35	1.31	0.21

[a] Isomer shift relative to iron foil at room temperature.
[b] Full width at half peak height.

environments compared to the more symmetric octahedral iron(II) sites [38]. The observed line width (full width at half maximum: $\Gamma_{298\ K} = \Gamma_{4.2\ K} = 0.21$ mm s^{-1}) is consistent with equivalent iron sites. Observations that the two sites have equivalent ΔE_Q values with similar temperature dependencies suggest that the two ferrous centres experience equivalent environments [25], consistent with the centrosymmetric structure of **1**.

The spectrum of **2** consists of only a single quadrupole-split doublet at both temperatures with no evidence of iron contaminants. No magnetic hyperfine interactions were observed in zero applied field. The isomer shift value is within the range expected for high-spin iron(III) in non-sulfur environments [20,26,39,40]. The relatively low δ value may indicate a five-coordinate iron(III) complex [35,40,41]. The temperature dependence of δ is that expected for a second-order Doppler shift [42]. The large value of the quadrupole splitting parameter (ca 1.3 mm s) indicates a highly unsymmetrical electric field [43]. A relatively narrow half-line width (ca 0.2 mm s) is observed for **2** indicating that only one type of iron site is present [42].

CONCLUSIONS

The present work has shown that the reactions of iron(II) and iron(III) chlorides with 2-(2′-pyr-

idyl)quinoxaline (L) in MeOH lead to the 1 : 1 complexes as the only products. The dimeric molecular structure of $[Fe_2Cl_4L_2]$ (**1**) reflects the great tendency of L to give dinuclear, doubly halogen-bridged, five-coordinate complexes [2–5,7].

Several molecular structures are possible for a product with the empirical formula $FeCl_3L$. These include (i) a neutral monomeric, five-coordinate complex, $[FeCl_3L]$; (ii) an ionic pseudotetrahedral monomer, $[FeCl_2L]Cl$; (iii) a neutral dimeric, six-coordinate complex, $[Fe_2(\mu\text{-}Cl)_2Cl_4L_2]$; (iv) a cationic dinuclear, five-coordinate species, $[Fe_2(\mu\text{-}Cl)_2Cl_2L_2]Cl_2$; (v) an ionic $[FeCl_2L_2][FeCl_4]$ product containing a six-coordinate cation and a tetrahedral anion; (vi) a neutral six-coordinate polymer, $[Fe(\mu\text{-}Cl)Cl_2L]_n$; (vii) a polymer consisting of cationic chains of five-coordinate Fe^{II} centres and single chloro bridges, $[Fe(\mu\text{-}Cl)ClL]_n(Cl)_n$; (viii) structures based on the mixed bidentate-monodentate bridging coordination [1,5,9] of L. The physical and spectroscopic study of **2**, presented above, leaves us with possibility (iv). If our proposal is correct, this means that the electronic configuration ($3d^5$ vs sd^6) and the size of the metal ion have little structural consequence.

Although the adducts formed between $FeCl_3$ and bidentate aromatic nitrogen bases, particularly 1,10-phenanthroline (phen) and 2,2′-bipyridine (bpy), have been widely studied in the older literature by way of a variety of synthetic and physical procedures, structural studies in this area in the last 15 years cast some doubt on the adequacy and validity of characterization of a number of these. It has been shown that complexes may be formed with a variety of stoichiometries and that, depending on the nature of the recrystallization solvent, these may be covalent or ionic in nature, with varying and variable solvation stages. For example, the structurally characterized Fe^{III}/Cl/phen complexes are $[FeCl_2(phen)_2][FeCl_4]$ [44,55], *fac*-$[FeCl_3(phen)(MeOH)]\cdot MeOH$ [46], *fac*-$[FeCl_3(phen)(H_2O)]$ [46], $[(phenH)[FeCl_4(phen)]\cdot 1^1/_2H_2O$ [46,47], *mer*-$[FeCl_3(phen)(DMF)]$ [48], $[FeCl_2(phen)_2][FeCl_4(phen)]\cdot MeCN$ [45] and $[Fe_2OCl_2(phen)_4]Cl_2\cdot 4.5H_2O$ [49].

SUPPLEMENTARY MATERIAL

Tables of atomic coordinates and anisotropic thermal parameters of non-hydrogen atoms, complete lists of bond lengths and angles, least-squares planes and dihedral angles, a crystal packing diagram, and observed and calculated structure factors for **1** are available from the authors on request.

Acknowledgements—The far-IR spectra of complexes **1** and **2** were obtained at the Laboratorium Anorganische Scheikunde, Rijksuniversitair Centrum Antwerpen, Belgium; we wish to thank Professor H. O. Desseyn for this convenience. The ^{57}Fe-Mössbauer spectra were recorded at the Institut of Materials Science, NRCPS "Demokritos", Aghia Paraskevi Attikis; we thank Dr A. Simopoulos for this convenience and for helpful discussions.

REFERENCES

1. Kasselouri, S., Garoufis, A., Katehanakis, A., Kalkanis, G., Perlepes, S. P. and Hadjiliadis, N., *Inorg. Chim. Acta*, 1993, **207,** 255.
2. Plakatouras, J. C., Hadjiliadis, N., Perlepes, S. P., Albinati, A. and Kalkanis, G., *Polyhedron*, 1993, **12,** 2069.
3. Bakalbassis, E. G., Mrozinski, J., Perlepes, S. P., Hadjiliadis, N., Lianza, F. and Albinati, A., *Polyhedron*, 1994, **13,** 3209.
4. Kasselouri, S., Garoufis, A., Paschalidou, S., Perlepes, S. P., Butler, I. S. and Hadjiliadis, N., *Inorg. Chim. Acta*, 1994, **227,** 129.
5. Perlepes, S. P., Kasselouri, S., Garoufis, A., Lutz, F., Bau, R. and Hadjiliadis, N., *Polyhedron*, 1995, **14,** 1461.
6. Garoufis, A., Perlepes, S. P., Vreugdenhil, A., Butler, I. and Hadjiliadis, N., *Inorg. Chim. Acta*, 1995, **240,** 673.
7. Garoufis, A., Perlepes, S. P., Schreiber, A., Bau, R. and Hadjiliadis, N., *Polyhedron*, 1996, **15,** 177.
8. Garoufis, A., Perlepes, S. P., Froystein, A. A., Sletten, J. and Hadjiliadis, N., *Polyhedron*, 1966, **15,** 1035.
9. Perlepes, S. P., Garoufis, A., Sletten, J., Bakalbassis, E. G., Katsarou, E., Plakatouras, J. C. and Hadjiliadis, N., *Inorg. Chim. Acta*, in press.
10. Constable, E. C., *Adv. Inorg. Chem.*, 1989, **34,** 1
11. Kaim, W., *Angew. Chem., Int. Edn. Engl.*, 1983, **22,** 171.
12. Constable, E. C. and Steel, P. J., *Coord. Chem. Rev.*, 1989, **93,** 205.
13. Steel, P. J., *Coord. Chem. Rev.*, 1990, **106,** 227.
14. Reedijk, J. In *Comprehensive Coordination Chemistry*, Vol. 2, ed. G. Wilkinson, R. D. Gillard and J. A. McCleverty. Pergamon, Oxford, 1987, Ch. 13.2, p. 73.
15. Vos, J. G., *Polyhedron*, 1992, **11,** 2285.
16. Masood, Md. A. and Hodgson, D. J., *Inorg. Chem.*, 1993, **32,** 4839, and refs therein.
17. Denti, G., Serroni, S., Campagna, S., Ricevuto, V., Juris, A., Ciano, M. and Balzani, V., *Inorg. Chim. Acta*, 1992, **198–200,** 507.
18. Louloudi, M., Hadjiliadis, N., Feng, J. A., Sukumar, S. and Bau, R., *J. Am. Chem. Soc.*, 1990, **112,** 7233.
19. Plakatouras, J. C., Perlepes, S. P., Mentzafos, D., Terzis, A., Bakas, T. and Papaefthymiou, V., *Polyhedron*, 1992, **11,** 2657.
20. Kamariotaki, M., Karaliota, A., Stabaki, D., Bakas, T., Papaefthymiou, V., Perlepes, S. P. and Hadjiliadis, N., *Transition Met. Chem.*, 1994, **19,** 241.
21. Sheldrick, G. M., *SHELXS*-86, structure solving program, University of Göttingen, Germany, 1986.
22. Sheldrick, G. M., *SHELXL*-93, program for the refinement of crystal structures, University of Göttingen, Germany, 1993.
23. Geary, W. J., *Coord. Chem. Rev.*, 1971, **7,** 81.

24. Cotton, F. A., Luck, R. L. and Son, K.-A., *Inorg. Chim. Acta*, 1991, **184,** 177.
25. Stassinopoulos, A., Schulte, G., Papaefthymiou, G. C. and Caradonna, J. P., *J. Am. Chem. Soc.*, 1991, **113,** 8686, and refs. therein.
26. Menage, S., Brennan, B. A., Juarez-Garcia, C., Münck, E. and Que, L., Jr., *J. Am. Chem. Soc.*, 1990, **112,** 6423.
27. Lever, A. B. P., *Inorganic Electronic Spectroscopy*. Elsevier, Amsterdam, 2nd edn., 1984, pp. 230–233, 329–339, 452, 453, 458–472.
28. Reiff, W. M., Dockum, B., Weber, M. A. and Frankel, R. B., *Inorg. Chem.*, 1975, **14,** 800.
29. Borovik, A. S., Hendrich, M. P., Holman T. R., Münck, E., Papaefthymiou, V. and Que, L., Jr., *J. Am. Chem. Soc.*, 1990, **112,** 6031.
30. Murch, B. P., Bradley, F. C., Boyle, P. D., Papaefthymiou, V. and Que, L., Jr., *J. Am. Chem. Soc.*, 1987, **109,** 7993.
31. Clark, R. J. and Williams, C. S., *Inorg. Chem.*, 1965, **4,** 350.
32. Lumme, P., Lindroos, S. and Lindell, E., *Inorg. Chim. Acta*, 1988, **144,** 75.
33. Lumme, P., Lindroos, S. and Lindell, E., *Acta Cryst., Sect. C*, 1987, **43,** 2053.
34. Perlepes, S. P., Kovala-Demertzi, D., Skaribas, S., Nicholls, D. and Paraskevas, S., *Thermochim. Acta*, 1989, **147,** 153.
35. Campbell, M. J. M., Grzeskowiak, R. and Juneja, G. S., *J. Inorg. Nucl. Chem.*, 1978, **40,** 1507.
36. Nakamoto, K., *Infrared and Raman Spectra of Inorganic and Coordination Compounds*. Wiley, New York, 4th edn., 1986, pp. 206–213, 324–331.
37. Charron, F. F., Jr. and Reiff, W. M., *Inorg. Chem.*, 1986, **25,** 2786.
38. Dickson, D. P. E. and Berry, F. J., *Mössbauer Spectroscopy*. Cambridge University Press, Cambridge, U.K., 1986.
39. Taft, K. L., Delfs, C. D., Papaefthymiou, G. C., Foner, S., Gatteschi, D. and Lippard, S. J., *J. Am. Chem. Soc.*, 1994, **116,** 823.
40. Greenwood, N. N. and Gibb, T. C., *Mössbauer Spectroscopy*. Chapman and Hall, London, 1971, Chap. 6.
41. Kurtz, D. M., Jr., *Chem. Rev.*, 1990, **90,** 585.
42. Lynch, M. W., Valentine, M. and Hendrickson, D. N., *J. Am. Chem. Soc.*, 1982, **104,** 6982.
43. McCusker, J. K., Vincent, J. B., Schmitt, E. A., Mino, M. L., Shin, K., Coggin, D. K., Hagen, P. M., Huffman, J. C., Christou, G. and Hendrickson, D. N., *J. Am. Chem. Soc.*, 1991, **113,** 3012.
44. Goodwin, H. J., McPartlin, M. and Goodwin, H. A., *Inorg. Chim. Acta*, 1977, **25,** L74.
45. Figgis, B. N., Patrick, J. M., Reynolds, P. A., Skelton, B. W., White, A. H. and Healy, P. C., *Aust. J. Chem.*, 1983, **36,** 2043.
46. Healy, P. C., Patrick, J. M., Skelton, B. W. and White, A. H., *Aust. J. Chem.*, 1983, **36,** 2031.
47. Veidis, M. F., Whitten, E. H., Reiff, W. M., Garafalo, A. and Brennan. T. F., *Inorg. Chim. Acta*, 1981, **53,** L237.
48. Reiff, W. M., Whitten, E. H., Mottle, K., Brennan, T. F. and Garafalo, A. R., *Inorg. Chim. Acta*, 1983, **77,** L27.
49. Healy, P. C., Skelton, B. W. and White, A. H., *Aust. J. Chem.*, 1983, **36,** 2057.

Pergamon

PII: S0277-5387(97)00380-X

Polyhedron Vol. 17, No. 8, pp. 1289–1294, 1998
© 1998 Elsevier Science Ltd
All rights reserved. Printed in Great Britain
0277-5387/98 $19.00+0.00

Probing the catalytic properties of copper(II) complexes of appended cyclams: correlations between catalysis and stability constants or electrochemical properties

Mitchell R. Malachowski,*[a] Brian T. Dorsey,[a] Michael J. Parker,[a] Mark E. Adams[a] and Richard S. Kelly[b]

[a]Chemistry Department, University of San Diego, San Diego, CA 92110, U.S.A.

[b]Department of Chemistry, Merrimack College, North Andover, MA 01845, U.S.A.

(Received 27 May 1997; accepted 28 August 1997)

Abstract—Copper(II) complexes were prepared from the dinucleating octadentate ligand tetra-1,4,8,11-(2-pyridylmethyl)-1,4,8,11-tetraazacyclotetradecane (tpmc). The five-coordinate complexes $[Cu_2(tpmc)X](ClO_4)_3$ (with X = F, Cl, Br, or I) were characterized by chemical analysis, absorption spectroscopy and cyclic voltammetry. The data show the dinculear Cu(II) complexes to be five-coordinate with a bridging halide donor. All display chemically reversible redox behavior, with two one-electron reductions observed in acetonitrile at glassy carbon. The values for $E^{0'}$ range from 118 to −126 mV vs SCE for the first reduction, and from −122 to −241 mV for the second reduction. Catalysis of the oxidation of 3,5-di-*tert*-butylcatechol to 3,5-di-*tert*-butylquinone using these complexes was studied. Correlations among reactivity, binding constants, and reduction potentials were determined. These correlations show that the rate of the oxidation reaction is linearly correlated to the binding of the halide bridge; the most reactive complex ($[Cu_2(tpmc)I](ClO_4)_3$) is the one with the smallest binding constant while the least reactive ($[Cu_2(tpmc)Cl](ClO_4)_3$) has the largest binding constant. Electrochemical data showed a non-linear relationship between the complexes' ability to oxidize 3,5-di-*tert*-butylcatechol and their reduction potentials. Comparisons to the naturally occurring enzyme tyrosinase are made. © 1998 Elsevier Science Ltd. All rights reserved

Keywords: copper(II) complexes; appended cyclams; catalysis.

Macrocyclic ligands with additional donor atoms appended to the ring have generated considerable interest because of their capacity to bind and transport metal ions, for the potential to prepare and study their mixed-valence forms, and as models for metalloproteins [1]. We particularly are interested in using transition metal complexes of appended macrocycles as models for copper-containing proteins. Copper is a component of a variety of proteins which function as mono-oxygenases, dioxygenases, in dioxygen transport, and in electron-transfer systems [2–3]. Due to their intriguing structural, spectroscopic and reactivity properties, we are involved in studying the protein hemocyanin and the related enzyme tyrosinase. Hemocyanins are found in the hemolymph of molluscs and arthropods and are responsible for binding and transporting oxygen while tyrosinase is found widely in mammals, plants, bacteria, and fungi and is responsible for the browning of fruits and vegetables and in melanin pigment formation [4–6]. It functions by catalyzing the oxidation of phenol to catechol (creolase activity) and the subsequent oxidation of catechol to quinone (catecholase activity).

Considerable chemical and spectroscopic evidence indicated that the active site of tyrosinases were virtually identical to the hemocyanins with the enhanced accessibility of tyrosinase to binding substrate molecules being the only difference [7–10]. However, recent data suggests that the two coppers of tyrosinase

* Author to whom correspondence should be addressed.

are found in different chemical environments with only one of the coppers being identical to the coppers found in hemocyanin [11–13].

We have been engaged in a project to systematically study the ability of Cu(II) complexes to catalyze the air oxidation of catechols in a fashion similar to that found for tyrosinase [14–16]. Our earlier work showed that modifications in the geometry, donor atoms, exogeneous donors, bridging groups, and mononuclear vs dinuclear systems all play a role in the reactivity of the complexes. Additionally, the electrochemical features of the complexes have been shown to be of considerable importance in modulating their reactivity.

Macrocyclic ligands derived from the 1,4,8,11-tetraazacyclotetradecane (cyclam) ring are of considerable utility because of the existence of hard nitrogen donors in the cavity of the ring and the potential to build binding sites from arms appended to the ring nitrogens. We recently reported the synthesis of a novel appended cyclam, tetra-1,4,8,11-(3,5-dimethylpyrazoylmethyl)-1,4,8,11-tetraazacyclotetradecane and a preliminary report of the catalytic properties of its Cu(II) complexes [17]. In this paper, we report the synthesis of a series of Cu(II) complexes with the formula $[Cu_2(tpmc)X](ClO_4)_3$ with (X = F, Cl, Br, or I) derived from the octadentate ligand tetra-1,4,8,11-(2-pyridylmethyl)-1,4,8,11-tetraazacyclotetradecane. This ligand contains cyclam in the backbone with pyridylmethyl arms attached to each of the four hard nitrogens (Fig. 1). The electrochemical features of the complexes have been determined, the reactivity of these complexes towards 3,5-di-*tert*-butylcatechol was assessed, and comparisons between the catalytic properties and their equilibrium binding constants and/or reduction potentials drawn.

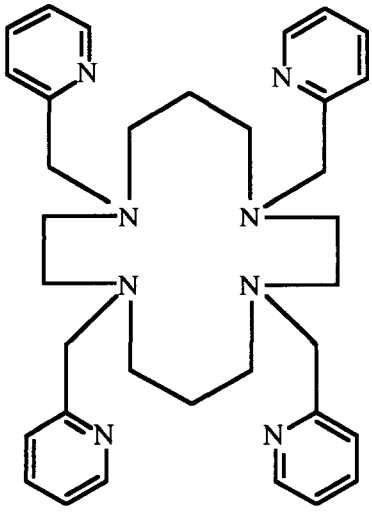

Fig. 1. Tpmc ligand.

EXPERIMENTAL

All reagents and solvents were purchased from commercial sources and used as received unless noted otherwise. Tetra-1,4,8,11-(2-pyridylmethyl)-1,4,8,11-tetraazacyclotetradecane, $[Cu_2(tpmc)F](ClO_4)_3$, $[Cu_2(tpmc)Cl](ClO_4)_3$, $[Cu_2(tpmc)Br](ClO_4)_3$ and $[Cu_2(tpmc)I](ClO_4)_3$ were prepared by the literature methods [18,19]. Melting points were obtained with the use of a Fisher-Johns apparatus and are uncorrected. C, H, and N chemical analyses were performed at Desert Analytical, Tucson, AZ. Metal contents were determined complexometrically by indirect titration with Na_2H_2edta and zinc acetate after destruction of the sample with concentrated nitric acid [20]. Halogen contents were determined by potentiometric titration with silver nitrate. IR spectra were recorded on a Nicolet 5ZDX instrument.

Kinetics were followed spectrophotometrically on a Uvikon 860 spectrophotometer by following the appearance of 3,5-di-*tert*-butylquinone over time using the 390 nm peak. The metal complex (0.3 cm^3 of a 1×10^{-3} M methanol/acetonitrile (7 : 3 solution)) and a 2.0 cm^3 solution (1.0×10^{-1} M methanol solution) of 3,5-di-*tert*-butylcatechol were equilibrated separately to 25°C and then added together in a spectrophotometric cell at 25°C.

Cyclic voltammetric data were collected using an IBM EC/225 voltammetric analyzer and a Soltec Model VP-6415S X–Y recorder. All scans were done at 0.050 V/s with glassy carbon electrodes (3 mm diameter; BAS, West Lafayette, IN) in acetonitrile (Burdick and Jackson, spectrophotometric grade) that contained 0.10 M tetrabutylammonium perchlorate (Eastman 99%) or tetraethylammonium tetrafluoroborate (Aldrich 99%) as the supporting electrolyte. In all cases, the concentration of the metal complex was 1×10^{-3} M. The glassy carbon electrodes were polished with 0.3- and 0.05-μm alumina on microcloth pads (Buehler, Lake Bluff, IL) and sonicated in distilled water for 30 s before use to remove alumina particles.

A three-electrode system was used in all the measurements, with potentials in acetonitrile recorded vs a Ag/Ag^+ non-aqueous reference electrode. The fill solution for this reference electrode was acetonitrile containing 0.01 M $AgNO_3$ and 0.1 M tetrabutylammonium perchlorate. The potential of this reference was measured daily vs an aqueous saturated calomel electrode (SCE) and an appropriate correction made (typically ca 300 mV) so that the $E^{0'}$ values for each complex could be reported vs SCE. Aqueous voltammetry was done in 0.1 M TRIS buffer adjusted to pH 7.00 with HCl. Potentials in TRIS were recorded vs an aqueous Ag/AgCl reference. A platinum wire served as the auxiliary electrode. The glass cell consisted of a vial of ca 5.0 cm^3 volume with a fitted Teflon cap. All solutions were purged with dry nitrogen prior to data collection.

Caution. Although there were no incidents in our

laboratory, transition metal perchlorates may explode violently. They should be prepared in small quantities and handled with care.

RESULTS

Synthesis

The ligand tetra-1,4,8,11-(2-pyridylmethyl)-1,4,8,11-tetraazacyclotetradecane was designed to allow for the binding of two copper ions in a dinuclear arrangement. The ligand was prepared with cyclam and 2-picolychloride serving as the starting materials [18].

The Cu(II) complexes were prepared either by mixing a solution of the ligand with Cu(II) perchlorate hexahydrate and the appropriate sodium salt (NaBr, NaF) or by adding the sodium salt (NaCl, NaI) to $[Cu_2(tpmc)](ClO_4)_4$. The complexes were analyzed by elemental analyses, absorption spectroscopy and infra-red spectroscopy. In all cases, the complexes are dinuclear with each five-coordinate Cu(II) bound to two aliphatic nitrogens, two pyridyl nitrogens and a bridging halide donor.

Electrochemistry

In the catalysis of 3,5-di-*tert*-butylcatechol to 3,5-di-*tert*-butylquinone, the Cu(II) complex is reduced to Cu(I). For this reason, we have studied the electrochemical properties of the complexes **1–4** to determine whether there is a correlation between their reduction potentials and catalytic abilities. The reduction potentials for complexes **1–4** were measured by cyclic voltammetry at a glassy carbon electrode in acetonitrile. The cyclic voltammetry data are shown in Table 1 and the cyclic voltammograms for the representative $[Cu_2(tpmc)Br](ClO_4)_3$ and $[Cu_2(tpmc)Cl](ClO_4)_3$ complexes are shown in Fig. 2. The average of the peak potentials from the cyclic voltammetry is taken as an approximation of the formal potential, $E^{0'}$. In all cases, the Cu(II) metal centers are reduced to Cu(I) in two successive one electron reductions.

In all cases, the reduced form of the complex displays high chemical stability on the time scale of the

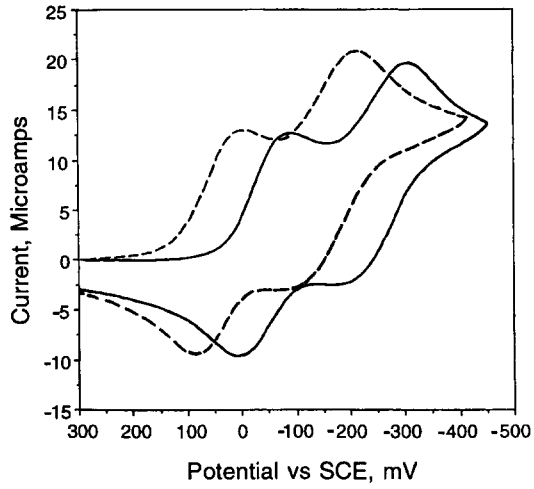

Fig. 2. Cyclic voltammograms recorded at a glassy carbon electrode in acetonitrile: (--) 1.0 mM solution of $[Cu_2(tpmc)Cl](ClO_4)_3$ (**1**); $E^{0'} = -27$ mV, $\Delta E_p = 96$ mV for first reduction; $E^{0'} = -241$, $\Delta E_p = 114$ mV for second reduction. (---) 1.0 mM solution of $[Cu_2(tpmc)Br](ClO_4)_3$ (**2**); $E^{0'} = +35$ mV, $\Delta E_p = 81$ mV for first reduction; $E^{0'} = -185$, $\Delta E_p = 140$ mV for second reduction. The scan rate was 50 mV/s and the supporting electrolyte was 0.1 M tetrabutylammonium perchlorate in both cases.

Table 1. Cyclic voltammetry,[a] binding constants, and kinetic data[b] for the oxidation of 3,5-di-*tert*-butylcatechol for $[Cu_2(tpmc)X](ClO_4)_3$ complexes

Complex	$E^{0'}$ (mV)[c] first wave	$E^{0'}$ (mV)[c] second wave	Binding constants [19]	Activity (μmol substrate/mg catalyst per min)
$[Cu_2(tpmc)Cl](ClO_4)_3$ (**1**)	−27	−241	4.80	0.0005
$[Cu_2(tpmc)Br](ClO_4)_3$ (**2**)	35	−185	3.77	0.264
$[Cu_2(tpmc)F](ClO_4)_3$ (**3**)	−126	—	3.03	0.274
$[Cu_2(tpmc)I](ClO_4)_3$ (**4**)	118	−122	2.76	0.362

[a]Electrochemistry was performed in an acetonitrile solution that contained 0.10 M tetrabutylammonium perchlorate or tetraethylammonium tetrafluoroborate as the supporting electrolyte. The concentration of the metal complex was 1×10^{-3} M. All complexes undergo chemically reversible oxidation-reduction reactions at a glassy carbon electrode with a Ag/Ag^+ non-aqueous reference electrode and a platinum wire as the auxiliary electrode. Scans were done at 0.050 V/s.

[b]Kinetics were performed spectrophotometrically at 25°C with 0.3 cm^3 of a 1.0×10^{-3} M methanol solution of metal complex and 2.0 cm^3 of a 1.0×10^{-1} M methanol solution of 3,5-di-*tert*-butylcatechol.

[c]The average of the peak potentials is taken as an approximation of the formal potential $E^{0'}$. All potentials are reported vs the aqueous saturated calomel reference (SCE). See the text for details.

cyclic voltammetry experiment; ratios of reverse to forward currents (i_{pa}/i_{pc}) are close to 1.0 for all complexes at a scan rate of 0.050 V/s.

A number of inferences can be drawn from the electrochemical data. First, although the complexes are symmetrical, the two copper(II) ions are not reduced at the same potential. There are other examples of this type of behavior for dinuclear Cu(II) complexes [21]. Secondly, as would be expected, the electrochemical data show that the reduction potentials of the copper(II) complexes are dependent on the nature of the halide bridging donors. The $E^{0'}$ values for the first reduction range from a low of 118 mV for $[Cu_2(tpmc)I](ClO_4)_3$ to a high of -126 mV for $[Cu_2(tpmc)F](ClO_4)_3$ For complexes **1–4**, there is a fairly smooth decrease in the reduction potential as the size of the bridging group increases. These values are displayed in Table 1. The data suggests that $[Cu_2(tpmc)F](ClO_4)_3$ is best able to stabilize the Cu(II) form at the expense of the copper(I) form in the copper(II)/(I) couple, while $[Cu_2(tpmc)I](ClO_4)_3$ is more likely to exist in the copper(I) form. For the second wave, there is also a smooth decrease in the values of $E^{0'}$ as the size of the bridging anion increases (the second wave could not be measured for the $[Cu_2(tpmc)F](ClO_4)_3$ complex).

In contrast to the results obtained in acetonitrile, all of the complexes display the same reduction potentials for both the first and second waves when dissolved in pH 7.00 TRIS buffer. The first reduction peak potential occurs at -200 mV (± 3 mV) vs Ag/AgCl and the second peak potential occurs at -310 mV (± 10 mV) for all complexes. It is possible that in this solvent system, H_2O replaces the bridging donor resulting in formation of the same complex in all cases.

Catalytic properties

The reactivity of the Cu(II) complexes, **1–4**, towards 3,5-di-*tert*-butylcatechol under catalytic conditions (0.3 cm^3 of a 1.0×10^{-3} M methanol–acetonitrile (7 : 3) solution of catalyst and 2.0 cm^3 of a 0.1 M methanolic solution of 3,5-di-*tert*-butylcatechol) in the presence of atmospheric O_2 was studied using electronic spectroscopy by following the appearance of the absorption maximum of the quinone at 390 nm over time. Our previous kinetic studies were performed in methanol but solubility constraints forced us to use this solvent mix. The results of the oxidations are presented in Fig. 3 and the data compiled in Table 1. All of the complexes are catalytically active in the oxidation of 3,5-di-*tert*-butylcatechol to 3,5-di-*tert*-butylquinone, however, it can be seen that the chloride complex is exceedingly slow in its ability to catalyze the oxidation reaction. We have seen similar results where varying the nature of a bridging or exogeneous donor greatly affects the rate of oxidation [14–16].

The activities of the complexes range from a high

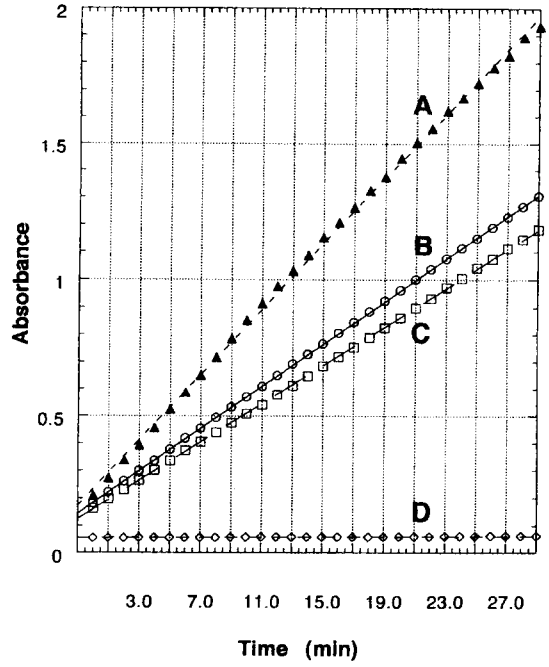

Fig. 3. Plot of absorbance vs time for $[Cu_2(tpmc)X](ClO_4)_3$ catalyzed oxidation of 3,5-di-*tert*-butylcatechol. Performed at 25°C in a CH_3OH solution of 1×10^{-1} M 3,5-di-*tert*-butylcatechol and 1×10^{-3} M metal complex: (A) $[Cu_2(tpmc)I](ClO_4)_3$; (B) $[Cu_2(tpmc)F](ClO_4)_3$; (C) $[Cu_2(tpmc)Br](ClO_4)_3$; (D) $[Cu_2(tpmc)Cl](ClO_4)_3$.

of 0.191 μmol substrate/mg catalyst per min for the $[Cu_2(tpmc)I](ClO_4)_3$ complex to a low of 0.00085 μmol substrate/mg catalyst per min for the $[Cu_2(tpmc)Cl](ClO_4)_3$ complex. Tyrosinase, the enzyme that catalyzes this reaction in nature, has two coppers per active site and it is thought that the binding of catechol involves simultaneous binding of the catechol by the two coppers with the transfer of two electrons to the coppers. Therefore, it is surprising that the values are so low for the dinuclear complexes **1–4** since we have seen more robust catalysis by a number of mononuclear species [14].

DISCUSSION

The two-electron oxidation of substituted *o*-catechols to quinones is one of the reactions that the copper-containing enzyme tyrosinase catalyzes. We previously have shown that changing the nature of the fifth donor atom, the counterion, or any bridging group bound to the copper ions has an effect on the rate of catalysis [14–16]. Others have also studied the oxidation reaction to try to determine the factors responsible for effective catalysis to occur [22–37]. In addition, it has been shown that electron transfer from catechol to the Cu(II) can begin only after catechol and the Cu(II) species form a Cu(II) catecholate intermediate [38]; this situation would require a vacant

coordination site on the metal so that complexation of the catechol can occur. Our premise is that the ease of dissociation of the halide bridge would greatly affect the ability of the complexes to catalyze this oxidation process. Therefore, in this work we are attempting to determine if there is a correlation between the ability of the complexes to catalyze the oxidation with the magnitude of their binding constants. In addition, since we have shown that reduction potentials are an important contributor to the catalytic properties of Cu(II) complexes [14], we have also compared the reactivity to the ease of reduction of the complexes.

Correlation with binding constants

The specific complexes, **1–4,** studied here were chosen because formation constants for the reaction:

$$[Cu_2(tpmc)]^4 + X \rightleftharpoons [Cu_2X(tpmc)]^{3+}$$

have been previously determined [19]. The binding constants (as determined by Vuckovic and co-workers) are displayed in Table 1. As shown, $[Cu_2(tpmc)I](ClO_4)_3$ is the least stable (binding constant = 2.76) while the $[Cu_2(tpmc)Cl](ClO_4)_3$ is the most stable complex (binding constant = 4.80). We assume that prior to oxidation, dissociation of the bridging donor will occur so that a vacant coordination site will be available for the binding of the catechol. Therefore, the larger the binding constant for the association of the bridging group, the slower the reaction will proceed if this step is part of the rate determining step of the reaction. In comparing the binding constants to catalytic rates, a reasonable straight line which correlates binding constants with activities can be seen (Fig. 4). This is consistent with a dissociative mechanism where the halogen bridge must leave prior to the complexation of the catechol and subsequent oxidation. Dissociation of the halide will leave two vacant coordination sites (one on each copper) so binding to the catechol should be readily attainable. However, since the Cu–Cu distance [19] in complex **1** is 4.47 Å and for complex **3** is 3.99 Å (and we would expect this value to increase after dissociation of the halide), the coppers could be too far apart for effective simultaneous binding of the two oxygens of the catechol. This would severely limit the rate of the reaction, a result that is borne out by our catalytic results.

Correlations with reduction potentials

In the oxidation of catechol to quinone, the Cu(II) ions are reduced to Cu(I). The reduction potentials of complexes **1–4** have been obtained in order to determine if there is also a correlation between the ease of reduction of the coppers and the rate of oxidation of 3,5-di-*tert*-butylcatechol. We have shown previously

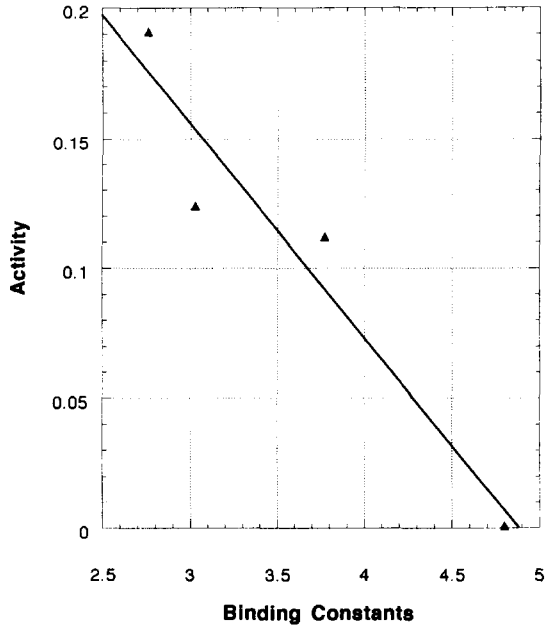

Fig. 4. Plot of binding constants vs activities for catalyzed oxidation of 3,5-di-*tert*-butylcatechol by $[Cu_2(tpmc)X](ClO_4)_3$ complexes.

that electrochemical potentials play a role in determining the reactivity properties of copper(II) complexes (although steric features of the ligands seem to be more important factors) [14].

In assessing whether there is a correlation between redox potentials and catalytic properties, a lack of a trend in these values is evident. Although the complex with the most positive potential (**4**) is the most catalytically active, the second most active complex (**3**) is the one with the most negative potential. Indeed, complex **1,** which has an intermediate value for its reduction potential, is essentially non-catalytic. For this series of Cu(II) complexes, it appears that the redox properties are secondary in importance to the binding constants in determining the catalytic properties of the complexes.

It is also worthwhile to consider whether the complexes' reduction potentials correlate with their binding constants. From the electrochemical values, it can be seen that the complex which is easiest to reduce ($[Cu_2(tpmc)I](ClO_4)_3$) is also the one whose halide bridge most easily dissociates. However, this trend does not hold throughout the series. For example, **3** has the second lowest binding constant but has the most negative reduction potential.

CONCLUSIONS

We have studied the air oxidation of 3,5-di-*tert*-butylcatechol to 3,5-di-*tert*-butylquinone by a series of dinuclear copper(II) complexes formed from a macrocyclic ligand. It is clear that the binding con-

stant between the copper(II) ion and the halogen bridge directly influences the redox properties of the complexes. However, there is no direct correlation between the reduction potentials and the ease of oxidation, a result which affirms earlier work that we performed on mononuclear copper(II) complexes [14–15].

It is also clear that the nature of the bridging group has profound effects on the capability of the complexes to perform the oxidation. As the magnitude of the binding constant decreases, the ability of the complex to bind to the substrate increases and the oxidation becomes more efficient. The positive correlation between the magnitude of the binding constant and the rate of oxidation for the complexes suggests that a dissociative mechanism is at work with the loss of the halogen bridge preceding the binding of the catechol. This confirms the results of Rogic [38] in which he shows that a vacant coordination site on the metal must be attained so that complexation of the catechol can occur. Work on related complexes which have bridging groups that are capable of dissociating is on-going.

Acknowledgements—This work was supported by a Cottrell College Science award of Research Corporation (M.R.M.).

REFERENCES

1. Dietrich, B., Viout, P. and Lehn, J. M., *Macrocyclic Chemistry: Aspects of Organic and Inorganic Supramolecular Chemistry*. VCH, New York, 1993.
2. Karlin, K. D. and Tyeklar, Z., *Bioinorganic Chemistry of Copper*. Chapman and Hall, New York, NY, 1993.
3. Reedijk, J. (ed.), *Bioinorganic Catalysis*. Marcel Dekker, Inc., New York, 1993.
4. Solomon, E. I., Baldwin, M. J. and Lowery, M. D., *Chem. Rev.*, 1992, **92,** 521.
5. Kitajima, N. and Mora-oka, Y., *Chem. Rev.*, 1994, **94,** 737.
6. Magnus, K. A., Ton-That, H., Carpenter, J., *Chem. Rev.*, 1994, **94,** 727.
7. Robb, D. A., In *Copper Proteins and Copper Enzymes*, Vol 2, ed. R. Lontie. CRC Press, Boca Raton, FL, 1984, p. 207.
8. Solomon, E. I. and Lowery, M. D., *Science*, 1993, **259,** 1575.
9. Wilcox, D. E., Porras, A. G., Lerch, K., Winkler, M. E. and Solomon, E. I., *J. Am. Chem. Soc.*, 1985, **103,** 4015.
10. Ross, P. K. and Solomon, E. I., *J. Am. Chem. Soc.*, 1991, **113,** 3246.
11. Lang, W. H. and Van Hold, K. E., *Proc. Natl Acad. Sci. U.S.A.*, 1991, **88,** 244.
12. Himmelwright, R. S., Eickman, N. and Solomon, E. I., *Biochem. Biophys. Res. Commun.*, 1978, **81,** 243.
13. Lubben, M., Hage, R., Meetsma, A., Byma, K. and Feringa, B. L., *Inorg. Chem.*, 1995, **34,** 2217.
14. Malachowski, M. R., Huynh, H. B., Tomlinson, L. J. and Kelly, R. S., *J. Chem. Soc., Dalton Trans.*, 1995, p. 31.
15. Malachowski, M. R., Dorsey, B., Sackett, J. G., Kelly, R. S., Ferko, A. L. and Hardin, R. N., *Inorg. Chim. Acta*, 1996, **249,** 85.
16. Malachowski, M. R., Tomlinson, L. J., Davidson, M. G. and Hall, M. J., *J. Coord. Chem.*, 1992, **25,** 171.
17. Malachowski, M. R., Tomlinson, L. J., Parker, M. J. and Davis, J. D., *Tetrahedron Lett.*, 1992, **33,** 1395.
18. Asato, E., Toftlund, H., Kida, S., Mikuriya, A. and Murray, K., *Inorg. Chim. Acta*, 1989, **165,** 207.
19. Vuckovic, G., Asato, E., Matsumoto, N. and Kida, S., *Inorg. Chim. Acta*, 1990, **171,** 45.
20. Vogel, A. I., *Quantitative Inorganic Analysis*. Longmans, London, 1961.
21. Gagne, R. R., Kreh, R. P. and Dodge, J. A., *J. Am. Chem. Soc.*, 1979, **101,** 6917.
22. Kida, S., Okawa, H. and Nishida, Y., In *Copper Coordination Chemistry: Biochemical and Inorganic Perspectives*, ed. K. D. Karlin and J. Zubieta. Adenine, Guilderland, NY, 1983, p. 425.
23. Thompson, J. S. and Calabrese, J. C., *Inorg. Chem.*, 1985, **24,** 3167.
24. Srinivas, B., Arulsamy, N. and Zacharias, P. S., *Polyhedron*, 1991, **10,** 731.
25. Abuhijleh, A. L., Woods, C., Bogas, E. and LeGuenniou, G., *Inorg. Chim. Acta*, 1992, **195,** 67.
26. Oishi, N., Nishida, Y., Ida, K. and Kida, S., *Bull. Chem. Soc. Jpn*, 1980, **53,** 2847.
27. Cabras, M. A. and Zoroddu, M. A., *Inorg. Chim. Acta*, 1987, **135,** L19.
28. Moore, K. and Vigee, G. S., *Inorg. Chim. Acta*, 1982, **66,** 125.
29. Lever, A. B. P., Ramaswamy, B. S. and Pickens, S. R., *Inorg. Chim. Acta*, 1980, **46,** L59.
30. Casellato, S., Tamburini, S., Vigato, P. A., DeStefani, A., Vidali, M. and Fenton, D. E., *Inorg. Chim. Acta*, 1983, **69,** 45.
31. Chyn, J. and Urbach, F. L., *Inorg. Chim. Acta*, 1991, **189,** 157.
32. Abuhijleh, A. L. and Woods, C., *J. Inorg. Biochem.*, 1996, **64,** 55.
33. Abuhijleh, A. L. and Woods, C., *Inorg. Chim. Acta*, 1993, **209,** 187.
34. Abuhijleh, A. L. and Woods, C., *Inorg. Chim. Acta*, 1994, **215,** 131.
35. Abuhijleh, A. L., *J. Inorg. Biochem.*, 1994, **55,** 255.
36. Abuhijleh, A. L. and Woods, C., *Inorg. Chim. Acta*, 1993, **209,** 187.
37. Abuhijleh, A. L., *Polyhedron*, 1996, **15,** 285.
38. Rogic, M. M., Swerdloff, M. D. and Demmin, T. R., In *Copper Coordination Chemistry: Biochemical and Inorganic Perspectives*, ed. K. D. Karlin and J. Zubieta. Adenine, Guilderland, NY, 1983, p. 167.

Pergamon

PII: S0277-5387(97)00391-4

Polyhedron Vol. 17, No. 8, pp. 1295–1301, 1998
© 1998 Elsevier Science Ltd
All rights reserved. Printed in Great Britain
0277–5387/98 $19.00+0.00

2-D COSY and NOESY ^{1}H NMR spectral studies on pyrazine-bridged dizinc(II)diporphyrin complex

Stanisław Wołowiec*

Department of Chemistry, University of Wrocław 14 Joliot-Curie 14, 50-383 Wrocław, Poland

(Received 5 June 1997; accepted 26 August 1997)

Abstract—The dinuclear [Zn(TTP-*m*-O-(CH_2)–)]$_2(CH_2)$ complex **1** (where TTP-*m*-O = 5-(*meta*-hydroxyphenyl)-10,15,20-tritolylporphyrin dianion) coordinates axially nitrogen bases; pyrazine (Py) and pyrimidine. The solid 1 : 1 Py : **1** adduct has been isolated and identified as dinuclear complex (μ-Py) [Zn(TTP-*m*-O-$(CH_2)-]_2(CH_2)$ **2** with pyrazine base bridging intramolecularly two zinc(II) metal ions based upon variable temperature 1-D and 2-D ^{1}H NMR spectral measurements. © 1998 Elsevier Science Ltd. All rights reserved

Keywords: dizinc(II)diporphyrin; pyrazine bridging; 2-D ^{1}H NMR spectroscopy.

In the previous papers of the series, dealing with dinuclear complexes of diporphyrins linked via flexible spacer, the coordination properties of diiron(III) and iron(III)/copper(II) diporphyrins with cyanide in organic solvents have been studied [1,2]. It has been found that the two proximal metal ions promote the formation of μ-cyanide dinuclear complexes in CN^--deficient solutions.

The dimetallic complexes of diporphyrins were studied extensively from the viewpoint of their catalytic activity [1,2] and references cited therein. The dicobalt(II) and dicopper(II) complexes of diporphyrins with flexible polyhydrocarbon spacer attached to the *meso*-phenyl ring of porphyrin showed high catalytic activity in two-electron oxidation of 3,5-di-*t*-butyl catechol with dioxygen in contrast to mononuclear porphynatocobalt(II) complexes [3]. The coordination of nitrogen bases to dizinc(II) complexes of *meso*-(tetraryl)porphyrin-based diporphyrins with the polyhydrocarbon spacer of variable length attached to *ortho*-, *meta*-, or *para*- *meso*-phenyl were studied in detail [3,4]. It has been found that the dizinc(II) complex of diporphyrin with a three-carbon spacer attached to *ortho*-phenyl Zn^{II}TTP*o*-O$(CH_2)_3$O-*o*TPPZn^{II}, coordinated two molecules of lutidine with $K_1/K_2 = 160$ while for its analogue Zn^{II}TTP*p*-O$(CH_2)_3$O-*p*TTPZn^{II} the ratio $K_1/K_2 = 1$. The low value of K_2 for the former is due to the steric hindrance from the second *ortho*-appended Zn(II)porphyrin half, which makes one face of Zn(II)porphyrin moiety less accessible for coordination of the second monodentate axial nitrogen base [4]. When a suitable heteroaromatic base with two nitrogen atoms (1,*n*-bis(4-pyridyl)alkane, where $n = 0$, 2, or 3) was applied as a ligand for dizinc(II) complex with face–face diporphyrin, with two diamido-type spacers attached to *ortho*- position of 5,15-*meso*-phenyls, and strapped on the opposite porphyrin face by another diamido substituent attached to 10,20-*meso*-phenyls, the intramolecular bridging of the nitrogen base was found to be dependent on the geometric factors of the studied systems [5]. In those rigid host–guest systems the best tuning between interporphyrin distance and the length of guest was achieved in the case of phenylenediamido spacer and 4,4′-bipyridyl as a guest [5]. The affinity of 4,4′-bipyridyl and other nitrogen bases to coordinate to zinc(II)porphyrin has been utilized in ligand-templated synthesis of cyclic and linear porphyrin oligomers [6,7]. A number of papers have been published in which di- and oligoporphyrins were assembled to study the energy transfer and photoinduced electron transfer in dizinc(II)diporphyrins adjacent together by means of coordinated, bridging axial nitrogen base [8,9].

Here the spontaneous conformational adjustment between the dizinc(II) diporphyrin with single, flexible spacer adjacent into *meso*-aryl substituents on both

* E-mail: sw@wchuwr.chem.uni.wroc.pl

porphyrin halves and pyrazine (and not pyrimidine) led to the isolation of pyrazine:Zn^{II}TTP*m*-O$(CH_2)_3$O-*m*TPPZn^{II} 1:1 adduct. The complex was studied by means of the ^{1}H NMR 2D COSY and NOESY spectral methods.

EXPERIMENTAL

Syntheses

Synthesis of [Zn(TPP-*m*-O-(CH_2)–)]$_2(CH_2)$ (**1**). The diporphyrin (H_2TTP-*m*-O-$(CH_2)_3$-O-*m*-$TPPH_2$) was synthesized according to the modified method of Little [10,1]. Zinc(II) ion was inserted by dropwise addition of 20-fold excess of zinc(II) chloride in methanol into the chloroform solution of (H_2TTP-*m*-O-$(CH_2)_3$-*O*-*m*-$TPPH_2$) under reflux in the presence of solid zinc(II) carbonate. The complex was separated chromatographically from impurities and solid materials on basic alumina (methylene dichloride eluent).

^{1}H NMR (the assignments based on ^{1}H 2D COSY and NOESY experiments, for numbering see Scheme 1): 8.90 ppm (8H, AB system, J_{AB} = 4.8 Hz, δ_A = 8.91 ppm, δ_B = 8.89 ppm, pyrrole β-H, 12,13(17,18)), 8.87 ppm (8H, AB system, J_{AB} = 4.8 Hz, δ_A = 8.90 ppm, δ_B = 8.85 ppm, pyrrole β-H, 2,3(7,8)), 8.05 ppm (4H, doublet, J_{om} = 7.9 Hz, o_3+o_4), 8.00 ppm (4H, doublet, J_{om} = 7.9 Hz, o_1), 7.96 ppm (4H, doublet, J_{om} = 7.9 Hz, o_2), 7.74 ppm (2H, singlet, o_6), 7.73 ppm (2H, doublet, J_{om} = 7.2 Hz, o_5), 7.53 ppm, (2H, doublet of doublets, J_{om} = 7.2 Hz, J_{mp} = 7.7 Hz, m_5), 7.50 ppm (4H, doublet, J_{om} = 7.9 Hz, m_3+m_4) 7.43 ppm (4H, doublet, J_{om} = 7.9 Hz, m_1), 7.39 ppm (4H, doublet, J_{om} = 7.9 Hz, m_2), 7.26 ppm (2H, doublet, J_{pm} = 7.7 Hz, p), 4.33 ppm (4H, triplet, $J_{\alpha\beta}$ = 6.1 Hz, $CH_{2(\alpha)}$), 2.66 ppm (6H, singlet, methyl at 15-*meso*-phenyl), 2.60 ppm (12H, singlet, methyls at 10- and 20-*meso*-phenyls), 2.36 (2H, quintet, $CH_{2(\beta)}$). UV–Vis (λ[nm], (ε [mol^{-1} × dm^3])): 423 (6.57×10^6); 552 (1.24×10^5); 594 (1.15×10^5).

Synthesis of (Py){[Zn(TTP-*m*-O-(CH_2)–)]$_2(CH_2)$} (**2**) Equimolar amounts of **1** and pyrazine were dissolved in chloroform (0.2 M) and hexane was carefully layered over the chloroform solution. The mixture was left for slow codiffusion of solvents at 0°C. Large, purple crystals were formed after 2 days. The crystals contained three molecules of solvent per one molecule of (Py){[Zn(TTP-*m*-O-(CH_2)–)]$_2(CH_2)$} (determined by integration of resonances in the ^{1}H NMR spectrum of $2 \times 3CHCl_3$). The crystals were too fragile to be mounted in X-ray diffractometer and therefore the weakly bound chloroform molecules were removed from the solid by a high vacuum applied overnight to the isolated crystals. Inspection of the ^{1}H NMR spectrum indicated that solvent molecules were no longer present. The crystals turned into powder after evaporation of the solvent.

Methods and reagents

^{1}H NMR spectra were obtained with a Bruker AMX300 spectrometer operating in the quadrature mode at 300 MHz. The 2-D COSY and NOESY spectra were collected by use of 1024 points in t_2 over desired bandwidth and 512 t_1 blocks with 16 scans per block in which four dummy scans were included. Repetition time was 2 s in all cases, the mixing time was 0.6 s for NOESY measurements. The NOESY spectra were processed in the phase-sensitive or magnitude modes. The deuterated solvents used were obtained from Glaser AG. The residual chloroform peak at 7.24 ppm was used as the internal chemical shift standard in presented spectra. The UV–Vis spectra were taken with HP 8453 diode-array spectrophotometer.

The equilibrium constant for the reaction:

$$Zn/Zn + py \rightleftharpoons Zn(\mu\text{-py})Zn$$

has been determined by both UV–Vis and ^{1}H NMR spectral titration at 295 K.

In the UV–Vis titration procedure 4.2×10^{-6} M solution of **1** in chloroform has been titrated with pyrazine stock solutions to achieve variable concentration of pyrazine within $2.15 \times 10^{-6} \div 0.2$ M region. A slight shift of Soret band into 422 nm and red shift of the Q-bands into 560 and 600 nm upon pyrazine coordination were found. Well resolved isosbestic points at 557 and 598 nm in the region of Q-bands up to 9.4×10^{-3} M pyrazine concentration were observed. The UV–Vis data were worked up at two wavelengths: 552 nm (corresponding to starting complex **1**) and 600 nm (corresponding to the maximum of the pyrazine adduct). Putting the two-parameter fitting procedure (equilibrium constant K and absorbance of the pyrazine adduct A_∞) into the equation:

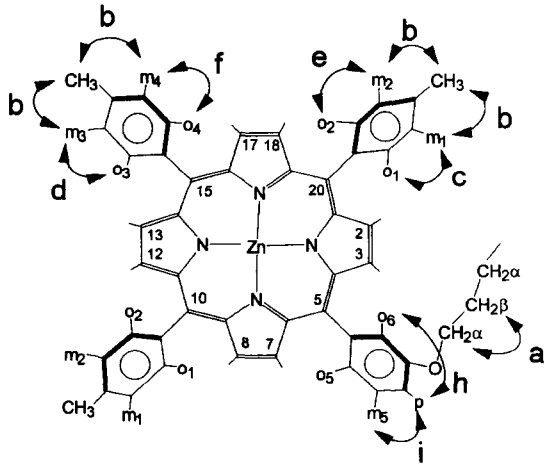

Scheme 1.

$$K = \frac{(A - A_0)}{(A_0 - A_\infty) \cdot [\text{py}]}$$

gave the averaged value of $K = 2.0(\pm 0.3) \times 10^4\ \text{M}^{-1}$.

In the ^{1}H NMR titration, 0.0038 M solution of **1** in $CDCl_3$ has been titrated with 0.2 M stock solution of pyrazine using the microsyringe technique. The pyrrole β-H resonances shifted from 8.93 ppm (δ_f) into 8.58 ppm (δ_c, the final chemical shift achievable upon the increase of pyrazine concentration above 0.005 M). The pairs of data, observed averaged chemical shift vs total pyrazine concentration, were fitted into the equation obtained by combination of the equations:

$$\delta = \delta_f \cdot p_f + \delta_c \cdot p_c,$$

where p_f and p_c are the populations (molar contributions) of free and pyrazine-coordinated dizinc(II)diporphyrin, respectively, and δ is observed chemical shift in titration procedure,

$$p_f + p_c = 1, K = \frac{p_c}{p_f \cdot [\text{py}]_f}$$

where $[\text{py}]_f$ is the concentration of free pyrazine. The solution of the resulting quadratic equation leads to the final relationship:

$$\delta = \frac{(\delta_f - \delta_c) \cdot \{C_0 \cdot \text{K} - [\text{py}]_0 \cdot \text{K}}{2 \cdot \text{C}_0 \cdot \text{K}} + \\ + \frac{\sqrt{[(1 + [\text{py}]_0 \cdot \text{K} - \text{C}_0 \cdot \text{K})2 + 4 \cdot \text{C}_0 \cdot \text{K}]}\}}{2 \cdot \text{C}_0 \cdot \text{K}} + \delta_c$$

where C_0 = the concentration of **1** and $[\text{py}]_0$ = the total concentration of pyrazine.

One-parameter fitting procedure resulted in the value of $K = 1.2(\pm 0.5) \times 10^4\ \text{M}^{-1}$.

Molecular mechanics calculations using the HyperChem software (Autodesk) were carried out and displayed on a PC 486 computer. The standard MM+ force field, with the constrains set on coordination bonds to achieve the geometry around the zinc(II) central ion were adapted from the published X-ray crystallographic data on pentacoordinate pyridine Zn(II)porphyrin complexes [11,12].

RESULTS AND DISCUSSION

The 1-D ^{1}H NMR *spectral results on coordination of pyrazine and pyrimidine to* **1**

Previously we have examined the ^{1}H NMR spectra of (H_2TTP-*x*-O-$(CH_2)_n$-O-*x*-TPPH_2) diporphyrin (n = 2,3, x = *o*-, *m*-, and *p*-) in detail [1]. In case of *ortho*-appended diporphyrins the ring current originated from neighbouring porphyrin macrocycle induced large upfield shifts of spacer-attached phenyl ring protons. It was not the case for the diporphyrin used here and consequently all resonances from aromatic *meso*-phenyls were grouped within the region of: 8.08–7.76 ppm (*ortho*); 7.58–7.40 ppm (*meta*); and 7.30 ppm (*para*). Nevertheless, the asymmetry imposed by one different *meso*-substituent (5-*meso*-substituted phenyl versus three *p*-methylphenyls) resulted in non-equivalence of β-pyrrole resonances, which gave one AB spectrum (2,3(7,8)) and a singlet (12,13(17,18)). Also, the presence of large aromatic porphyrin macrocycle appended at the *meta* position of *meso*-phenyl induced substantial up and down non-equivalence of *ortho* and *meta* 10- and 20-*meso*-phenyl protons. Both of these tendencies are even more pronounced in the case of dizinc(II) complex **1**, where all the β-pyrrole rings bear non-equivalent pairs of protons (two AB spectra, see Experimental).

The coordination of heteroaromatic bases: pyrazine and pyrimidine has been monitored by titration of **1** with these ligands. It was found that the system was in fast exchange on the ^{1}H NMR timescale. The chemical shift of ligands was always ligand concentration dependent. However, the isolation of solid **2** of fixed stoichiometry (1 : 1 of **1** : pyrazine) indicated that the complex of that stoichiometry is particularly stable in solid state. The crystal structure of **2** was not available. Thus it was necessary to find the method to determine if pyrazine bridges two Zn(II) intra- or intermolecularly in **2**. Neither mass spectrometric nor osmometric measurement results gave a definite answer to that question, due to the fast exchange between free and coordinated axial ligand processes taking place in solution **2**. However, an inspection of the ^{1}H NMR spectra showed that the chemical shift of **2** measured at three different solvents (chloroform, methylene dichloride and toluene), at four different temperatures (between 190 and 273 K), was only slightly dependent on concentration of **2**. Considering the possible routes leading to the formation of intramolecularly bridged dizinc(II) species (sequence of reactions (1) and (2)) and an intermolecularly bridged complex (sequence of reactions (1), (3), and (4)):

$$\text{Zn/Zn} + \text{py} \rightleftharpoons \text{pyZn/Zn} \quad (1)$$

$$\text{pyZn/Zn} \rightleftharpoons \text{Zn}(\mu\text{-py})\text{Zn} \quad (2)$$

$$\text{pyZn/Zn} + \text{py} \rightleftharpoons \text{pyZn/Znpy} \quad (3)$$

$$2\text{pyZn/Znpy} \rightleftharpoons \{\text{pyZn/Znpy})\}_2 \quad (4)$$

where Zn/Zn represents the starting complex **1**, pyZn/Zn corresponds to the species containing monodentate coordinate pyrazine, Zn(μ-py)Zn represents intramolecularly bridged dinuclear complex, pyZn/Znpy corresponds to the dinuclear complex containing two pyrazine coordinated via one nitrogen donor, and $\{\text{pyZn/Znpy})\}_2$ represents tetranuclear species with two pyrazine ligands bridging two dizinc(II)diporphyrin molecules), one may expect that in the case of intermolecular bridging, the chemical shift of pyrazine resonance or any porphyrin proton (the o_6 resonance was monitored as the most sensitive to pyrazine coordination) should substantially depend on [2] due to associative character of reaction (4). In

fact, within the concentration range used (0.01–0.5 M) the chemical shift of both pyrazine and o_6 protons are almost independent of concentration of **2**. Thus, it was assumed that **2** is a dizinc(II) complex bridged intramolecularly with pyrazine ligand. This conclusion was then strongly supported by the fact that when pyrimidine was used instead of pyrazine, the ligand resonances were considerably less shifted upon coordination if compared to **2**. The coordination shift in the latter case was comparable with that for TTPZn(II) mononuclear analogue (Table 1). The downfield coordination shift of 2-H of axial ligand (pyrmidine and pyridine), due to porphyrin ring current effect, was comparable (4.2 and 4.9 ppm, respectively) in both cases, suggesting the monodentate binding mode of pyrmidine into **1**. Intramolecular bridging of two zinc(II) centres of pyrazine in **2** leads to a larger coordination shift ($\Delta = 7.9$ ppm) due to additive ring current shifts from two porphyrin macrocycles.

The estimation of the equilibrium constant for the reaction of the formation of **2** (reactions (1)+(2)) based on UV–Vis and ^{1}H NMR spectral titrations gave the values 2.0 (± 0.3) $\times 10^4$ and 1.2 (± 0.5) $\times 10^4$ M^{-1}, respectively, which are in fair agreement despite the fact that three orders of magnitude of different concentrations were used in those two experiments. The value of $\log K = 4.3$ found for **1** is larger than that for binding of pyridine or bipyridyl to monomeric zinc(II)porphyrins and comparable to those found for bridging coordination to rigid dizinc(II)diporphyrins which are not well-suited to adopt the ligand due to steric reasons [5,6]. In some cases of face-to-face dizinc(II)diporphyrins the cooperative coordination led to $\log K$ as large as 7.4 [5] and 8.8 [6]. Here the cooperative effect is not large due to the fact that two porphyrins are adjacent together with flexible spacer.

The ^{1}H NMR spectrum of **2** in chloroform at room temperature consists of broad resonances both from the phenyl ring of diporphyrin macrocycle and from the pyrazine ligand. The spectrum changes remarkably at lower temperatures (Fig. 1). The pyrazine res-

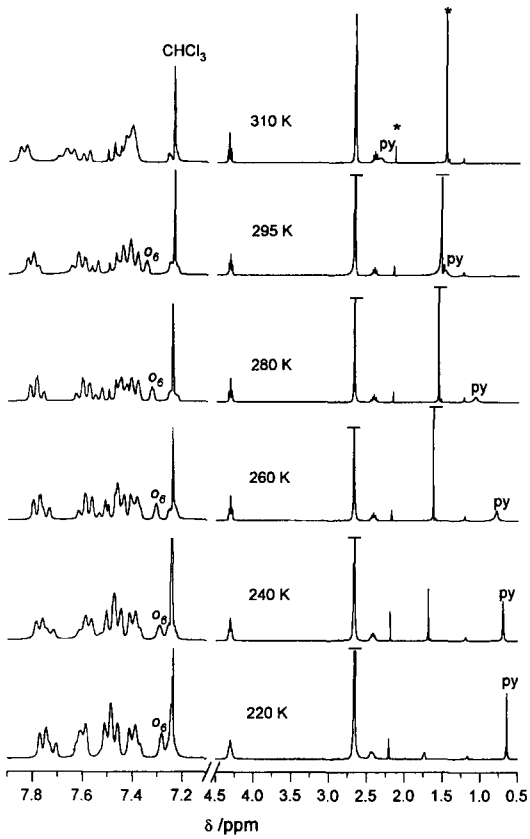

Fig. 1. The variable temperature ^{1}H NMR spectra of **2** in chloroform-*d*. The pyrazine hydrogen resonance is labelled as py, the impurity and residual water at 1.75 ppm resonances are labelled with asterisk.

Table 1. The ^{1}H NMR chemical shifts δ and coordination shift Δ (in parentheses) of pyrazine and pyrimidine protons for free and coordinated ligands (measured for 0.04 M $CDCl_3$ solutions)

	Temperature	pyrimidine			pyrazine
Composition of solution	[K]	δ 2 (Δ)	δ 4,6 (Δ)	δ 5 (Δ)	δ (Δ)
	295	9.2	9.71	7.3	8.6
	220	9.2	8.74	7.4	8.6
1 : *1* **1** : pyrimidine	310	6.25	6.82	6.37	
	295	5.76	6.51	6.23	
	280	5.37	6.27	6.13	
	260	4.98	6.04	6.04	
	240	4.83	6.03	5.91	
	220	4.80 (4.2)	6.05 (2.7)	5.90 (1.3)	
1 : *1* **1** TTPZn(II) : pyrazine	220				3.67 (4.93)
2	220				0.69 (7.91)

onance shifts 1.7 ppm upfield upon lowering temperature by 90° and further temperature decrease (down to 180 K in methylene dichloride-d_2 solvent) does not cause either the chemical shift changes or splitting of pyrazine or aliphatic resonances. Obviously, even in methylene dichloride solvent, at 180 K the rotation of pyrazine ligand around coordination bonds remains fast on NMR scale. Simultaneously the resonances from aliphatic spacer broaden and some changes are observed within an aromatic region of spectrum. Total assignment of resonances of **2** could provide some detailed information on the molecular structure of **2**. Therefore, 2-D ^{1}H NMR measurements were performed, particularly to analyze the crowded aromatic part of the ^{1}H NMR spectrum. The standard 2D ^{1}H NMR COSY and NOESY methods were used.

The total assignments of ^{1}H NMR *resonances based on* 2-D COSY *and* NOESY *results*

At 280 K the aromatic resonances in the region of 7–8 ppm are sharp and well-resolved and the COSY experiment allows to assign the resonances of *meso*-phenyls. The COSY map is presented in Fig. 2(A) and (B). The cross-peak **a** between α and β methylene protons of spacer was obvious and the cross-peak **b** between *p*-methylphenyl protons and the protons in aromatic region (Fig. 2(A)) allowed to identify the *meta*-phenyl proton resonances and provided a suitable starting point to analyze the cross-peaks within the aromatic region (Fig. 2(B)). Thus, two overlapping doublets of doublets of the relative intensity 2 : 1 at 7.8 ppm were assigned to the *ortho*-protons o_1 and o_3 (see the connectivity pattern at Scheme 1) located at the opposite side of porphyrin macrocycle plane to the appended second porphyrin ring. They were combined with the *meta* protons m_1 and m_3 via cross-peaks **c** and **d** (Fig. 2(B)). Two overlapping doublets of doublets of relative intensity 1 : 2 centred at 7.6 ppm belong to o_4 and o_2 protons, respectively and were coupled with the m_4 and m_2 resonances via cross-peaks **f** and **e**, respectively. It was assumed that *ortho* protons located at the same side of porphyrin plane as appended porphyrin ring (o_2 and o_4) should resonate at higher fields than o_1 and o_3. Corresponding pairs of *otho* protons are weakly coupled (cross-peak **g**). The 5-*meso*-phenyl ring protons gave the cross-peak pattern consistent with the couplings between *para* proton (overlapped with chloroform residual resonance at 7.24 ppm) and *meta* proton (triplet centred at 7.50 ppm at this temperature) by cross-peak **i** and *ortho*- proton o_6 located at the appended porphyrin side) by cross-peak **h**. The remaining cross-peak (not marked) corresponds to the vicinal coupling between o_5 (the resonance at 7.55) and m_5. As expected, the magnetic non-equivalence between *ortho* protons at the 5-*meso*-phenyl ring, attached via spacer to the second porphyrin was the largest of all *meso*-phenyls. The resonance of o_6 was the most upfield shifted of all

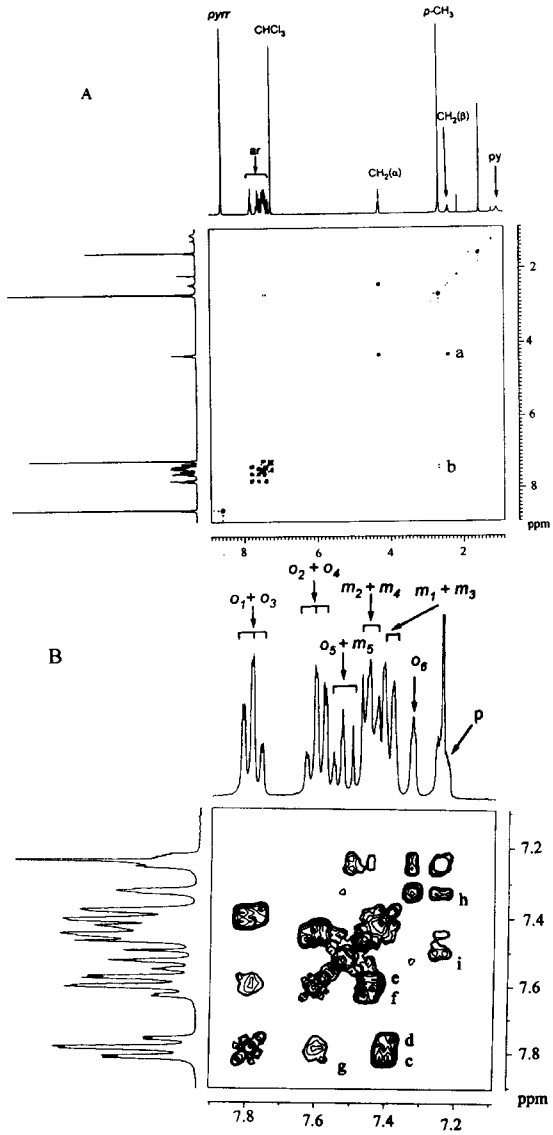

Fig. 2. The COSY map of **2**: (A), full spectrum taken at 280 K; (B), the expanded aromatic region. The abbreviations used are: *pyrr*: β-H pyrrole resonances; ar: the resonances of *meso*-phenyl protons; other labels follow those used in Scheme 1.

aromatic *ortho* and *meta* protons and it was located at a very fortunate position between other aromatic resonances from the downfield side and residual chloroform plus *para* proton resonance from the high-field side.

This connectivity pattern (presented at Scheme 1) was then confirmed by NOE cross-peaks obtained in NOESY experiment performed at 230 K. At this temperature the resonance from pyrazine protons is sharp and that provided a good opportunity to observe the spatial proximity of that proton with the porphyrin protons. The relevant fragments of NOESY map are presented in Fig. 3(A) and (B).

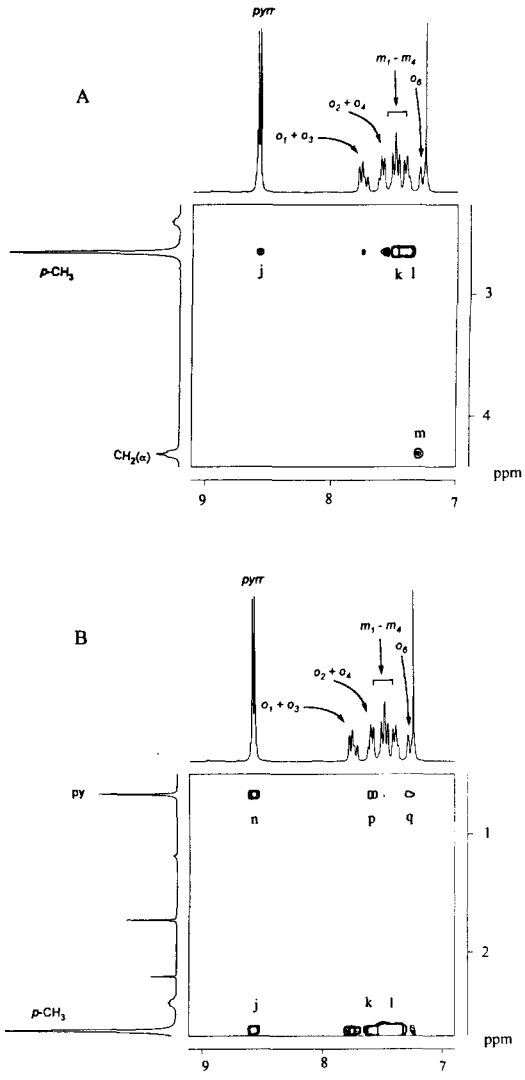

Fig. 3. The relevant fragments of NOESY spectrum of **2** taken at 230 K.

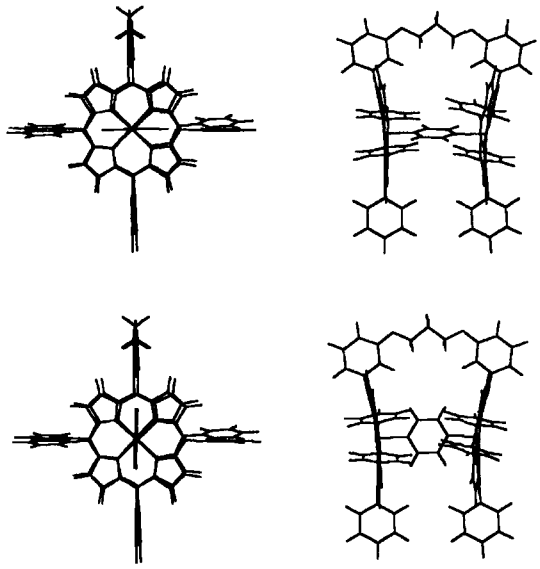

Fig. 4. Two projections of isomer **A** (upper pair) and **B** (lower pair) of **2** as obtained by MM+ calculations (using HyperChem program).

The observed cross-peaks: **j** between β-pyrrole and *p*-methyl protons, cross-peaks **k** and **l** between *p*-methyl and *meta* protons within porphyrin macrocycle were expected. The cross-peak **m** between α-methylene protons and o_6 confirmed the assignment of the latter unambiguously. The NOE cross-peaks **n, p,** and **q** indicated the spatial proximity of pyrazine protons to the β-pyrrole, o_2 o_4, and o_6, respectively (Fig. 3(B)) proving the proper assignment of o_2 and o_4 protons as those located at the same side of porphyrin macrocycle as appended porphyrin and bridging aromatic pyrazine ring.

The conformation of **2** *based on molecular model and* ^{1}H NMR *chemical shift*

In order to analyze details of confirmation of the intramolecularly bridged dinuclear complex the molecular model of **2** was constructed by means of HyperChem program. The set of constraints was imposed, in particular the Zn(II)—N(pyrrole) = 2.06 and Zn(II)—N(axial) = 2.14 Å bond lengths based on mean values taken from crystallographically established structures of pyridine pentacoordinate complexes of Zn(TPyP) and Zn(TPP–C_3Py) [11,12]. The resultant two conformations of **2** are presented in Fig. 4. The bridging pyrazine ring is located in the cavity along the C_{10}–C_{20} in case of rotational isomer **A,** whereas the isomer **B** bears the pyrazine ring rotated 90° along the coordination bonds. Although the free rotation of pyrazine can be reasonably assumed due to observation of NOE effects between pyrazine protons and all *ortho* phenyl protons located at the same side of porphyrin macrocycles as the bridging pyrazine, the analysis of chemical shift changes of *ortho* protons upon coordination indicates that the larger effect reveal o_6 (0.49 ppm upfield at 220 K) and o_4 (0.43 ppm upfield) protons in comparison with o_2 (0.35 ppm upfield). This suggests the larger contribution of rotational isomer **A,** for which the closest through-space contact estimated from molecular model between pyrazine proton and o_2 equals 2.81 Å whereas the distances between pyrazine protons and o_6 and o_4 are 3.16 and 2.91 Å, respectively, in isomer **B.**

Thus the dominating conformation of **2** can be represented by isomer **A** in Fig. 4. The pyrazine-bridged, diamagnetic dizinc(II) diporphyrin complex obtained as crystalline adduct serves a good standard for estimation of the isotropic shift for paramagnetic complexes with bridging pyrazine [13].

REFERENCES

1. Wołowiec, S. and Latos-Grażyński, L., *Inorg Chem.*, 1994, **33,** 3576.
2. Wołowiec, S., *Polyhedron*, 1997, **21**, 3779.
3. Okamoto, M., Oishi, N., Nishida, Y. and Kida, S., *Inorg. Chim. Acta*, 1982, **64,** L217.
4. Krausz, P. and Giannotti, C., *J. Chim. Phys.*, 1983, **80,** 299.
5. Yemori, Y., Nakatsubo, A., Imai, H., Nakagawa, S. and Kyuno, E., *Inorg. Chem.*, 1992, **31,** 5164.
6. Anderson, H. L. and Sanders, J. K. M., *Angew. Chemie Int. Ed. Engl.*, 1990, **29,** 1400.
7. Anderson, S., Anderson, H. L. and Sanders, J. K. M., *Angew. Chemie Int. Ed. Engl.*, 1992, **31,** 907.
8. Imahori, H., Yamada, K., Yoshizawa, E., Hagiwara, K., Okada, T. and Sakata, Y., *J. Porphyrins Phthalocyanines*, 1997, **1,** 55 and references 6–13 cited therein.
9. Vaijayanthimala, G. and Krishnan, V., *J. Porphyrins Phthalocyanines*, 1997, **1,** 17.
10. Little, R. G., *J. Heterocycl. Chem.*, 1978, **15,** 203.
11. Collins, D. M. and Hoard, J. L., *J. Am. Chem. Soc.*, 1970, **92,** 3761.
12. Bobrik, M. A. and Walker, F. A., *Inorg. Chem.*, 1980, **19,** 3383.
13. Wołowiec, S. The data on cyanide and pyrazine mixed ligand complexes of diiron(III)diporphyrin will be presented elsewhere.

Pergamon

PII: S0277-5387(97)00344-6

Polyhedron Vol. 17, No. 8, pp. 1303–1309, 1998
© 1998 Elsevier Science Ltd
All rights reserved. Printed in Great Britain
0277-5387/98 $19.00+0.00

Synthesis and structures of technetium(I) and rhenium(I) tricarbonyl complexes with bis(diphenylthiophosphoryl)amide, $\{M(CO)_3[(Ph_2PS)_2N](CH_3CN)\}$ (M = Tc, Re)

Ulrich Abram[a] *, Sonja Abram[a], Roger Schibli[b], Roger Alberto[b] and Jonathan R. Dilworth[c]

[a] Forschungszentrum Rossendorf, Institute of Radiochemistry, c/o Dresden University of Technology, Institute of Analytical Chemistry, D-01062 Dresden, Germany

[b] Paul Scherrer-Institute, Division of Radiopharmacy, CH-5232 Villigen, Switzerland

[c] University of Essex, Department of Biological and Chemical Sciences, Wivenhoe Park, Colchester, CO4 2SQ, U.K.

(Received 27 May 1997; accepted 8 August 1997)

Abstract—Complexes of the general formula $\{M(CO)_3[(Ph_2PS)_2N](CH_3CN)\}$ (M = Tc, Re) have been prepared by the reaction of $(Et_4N)_2[M(CO)_3X_3]$ (M = Tc, Re; X = Cl, Br) with sodium bis(diphenylthiophosphoryl)amide, $Na[(Ph_2PS)_2N]$, in acetonitrile. The metal is six-coordinate with facially arranged carbonyl ligands. Bis(diphenylthiophosphoryl)amide is deprotonated and bonded as S,S′-chelate with Tc—S distances of 2.526(3) and 2.546(3) Å. Acetonitrile occupies the sixth coordination position. The rhenium compound is isomorphous and the bonding situation in $\{Re(CO)_3[(Ph_2PS)_2N](CH_3CN)\}$ is similar to that in its technetium analogue. $(Et_4N)[Re(CO)_3Br_2(CH_3CN)]$ crystallizes from a hot acetonitrile solution of $(Et_4N)_2[Re(CO)_3Br_3]$ despite the fact that in solution only $[Re(CO)_3(CH_3CN)_3]^+$ can be detected spectroscopically. It has a facial arrangement of CO groups in an octahedral co-ordination geometry. © 1998 Elsevier Science Ltd. All rights reserved

Keywords: technetium; rhenium; carbonyl complexes; sulphur donor ligands; X-ray structures.

Bis(dialkylthiophosphoryl)amides and bis(diarylthiophosphoryl)amides (**I**) have been shown to be a versatile class of ligands which can easily be substituted to meet the specific requirements of the metals to be co-ordinated or of potential applications of the products [1,2]. Complexes with the tetraphenyl substituted amide have been discussed as models for the co-ordination sites of metalloenzymes [1]. Tetrahedral bis-co-ordinated complexes with divalent metal ions have been confirmed for Ni^{II} and Cu^{II} by X-ray crystallography and EPR spectroscopy [3,4].

The capabilities of the ligands to adopt the specific

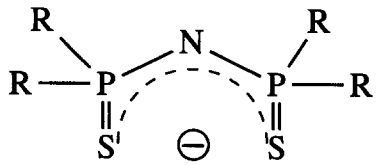

I

co-ordination requirements of the metals makes them interesting for the chemistry of technetium and rhenium which is of interest for diagnostic (^{99m}Tc: γ-emitter, half-life: 6 h) or therapeutic (^{186}Re, β^--emitter) nuclear medicine [5,6]. Rossi *et al.* [7,8] studied the co-ordination behaviour of $Ph_2P(X)NH(X)PPh_2$

* Author to whom correspondence should be addressed.

(X = O or S) and $K[Ph_2P(Se)N(Se)PPh_2]$ towards the $[ReO]^{3+}$ core and reported a considerable tendency for the products to decompose with loss of chalcogen donor atoms. It has been found more recently that the nitrogen containing $[ReN]^{2+}$ and $[ReNMe]^{3+}$ cores are more suitable to stabilize complexes with the "soft" sulphur donor sites of $[(Ph_2PS)_2N]^-$ than the oxorhenium(V) centre [9,10]

In the present paper, synthesis and structures of technetium(I) (using the long-lived isotope ^{99}Tc which is a weak β^--emitter with $t_{1/2} = 2.12 \times 10^5$ years) and rhenium(I) tricarbonyl complexes are described which demostrate that bis(diphenylthiophosphoryl)amide is also able to stabilize monomeric, low-valent metal complexes.

EXPERIMENTAL

The starting complexes $(Et_4N)_2[Tc(CO)_3Cl_3]$ and $(Et_4N)_2[Re(CO)_3Br_3]$ have been prepared by procedures reported previously [11,12]. $(Ph_2PS)_2NH$ was prepared from PPh_2Cl, $NH(SiMe_3)_2$ and sulphur as outlined in ref. 13 and converted into the sodium salt by the reaction with NaOMe. IR spectra were recorded as KBr pellets on a Perkin-Elmer Specord 75 IR. Mass spectra were recorded on a MAT TSQ-70 spectrometer (Finnigan). For FAB measurements xenon was used as primary beam gas. The ion gun was operated at 8 kV and 100 μA (probe temperature: 30°C) nitrobenzylalcohol was used as the matrix. ^{99}Tc and ^{31}P NMR spectra were recorded on Varian Gemini 2000 (300 MHz) and JEOL EX-270 spectrometers with H_3PO_4 and NH_4TcO_4 as references.

CAUTION! ^{99}Tc is a weak β-emitter. Although radiation from small amounts of material is completely absorbed by the glass walls, all operations have been carried out in a specially equipped laboratory under well ventilated hoods to avoid contamination or ingestion.

$\{Tc(CO)_3[(Ph_2PS)_2N](CH_3CN)\}$

55 mg (0.1 mmol) $(Et_4N)_2[Tc(CO)_3Cl_3]$ were dissolved in 10 ml acetonitrile and a solution of 51 mg (0.11 mmol) $Na[(Ph_2PS)_2N]$ in 5 ml CH_3CN was added dropwise. The colourless reaction mixture was heated under reflux for 1.5 h and the volume was reduced to about 3 ml. After standing overnight, colourless crystals formed which were filtered off and washed with a small amount of cold methanol. Recrystallization from CH_3CN. Yield: 80%. Found: Tc, 15.7%; $C_{29}H_{23}N_2O_3P_2S_2Tc$ requires: Tc, 15.3%. IR: ν(CO) 1925, 1953, 2035 cm^{-1} (st), ν(CN) 2362 cm^{-1} (w). ^{99}Tc-NMR: −1266 ppm (s).

$\{Re(CO)_3[(Ph_2PS)_2N](CH_3CN)\}$

The complex was prepared as the technetium analogue starting from 77 mg (0.1 mmol) $(Et_4N)_2[Re(CO)_3Br_3]$ and 51 mg (0.11 mmol) $Na[(Ph_2PS)_2N]$ in acetonitrile. Colourless crystals. Yield: 75%. Found: C, 44.65; H, 3.23; N, 3.91; S, 8.15%; $C_{29}H_{23}N_2O_3P_2S_2Re$ requires: C, 45.79; H, 3.03; N, 3.68; S, 8.42%. IR: ν(CO) 1919, 1948, 2043 cm^{-1} (st), ν(CN) 2362 cm^{-1} (w). ^{31}P-NMR: 38.7 ppm (s). FAB^+ MS: $m/z = 760$ ($[M]^+$, 5% B), $m/z = 719$ $\{(Re(CO)_3[(Ph_2PS)_2N]\}^+$, 100% B), $m/z = 691$ $\{(Re(CO)_2[(Ph_2PS)_2N]\}^+$, 45% B), $m/z = 663$ $\{(Re(CO)[(Ph_2PS)_2N]\}^+$, 20% B).

$\{Re(CO)_3[(Ph_2PS)_2N](py)\}$

76 mg (0.1 mmol) $\{Re(CO)_3[(Ph_2PS)_2](CH_3CN)\}$ were dissolved in 10 ml $CHCl_3$ and a few drops of pyridine were added. The mixture was heated on reflux for 10 min and allowed to cool to room temperature. Upon slow evaporation of the solvent a colourless solid precipitated which was removed by filtration and rinsed with a minimum amount of cold methanol. Yield 65%. Found: C, 47.92; H, 3.10; N, 3.19%; $C_{32}H_{25}N_2O_3P_2S_2Re$ requires C, 48.12; H, 3.13; N, 3.51%. IR: ν(CO) 1924, 1962, 2020 cm^{-1} (st). ^{31}P-NMR: 38.5 ppm (s). FAB^+ MS: $m/z = 798$ ($[M]^+$, 5% B), $m/z = 719$ ($\{Re(CO)_3[(Ph_2PS)_2N]\}^+$, 100% B), $m/z = 691$ ($\{Re(CO)_2[(Ph_2PS)_2N]\}^+$, 25% B), $m/z = 663$ ($\{Re(CO)[(Ph_2PS)_2N]\}^+$, 20% B).

$(Et_4N)[Re(CO)_3Br_2(CH_3CN)]$

77 mg (0.1 mmol) $(Et_4N)_2[Re(CO)_3Br_3]$ were dissolved in 10 ml acetonitrile and refluxed for 1 h. Upon slow evaporation of the solvent colourless crystals formed which were collected and rinsed with a minimum amount of cold water to remove $(Et_4N)Br$. Yield: almost quantitative. Found: C, 25.85; H, 3.91; N, 4.31%; $C_{13}H_{23}N_2O_3Br_2Re$ requires: C, 25.91; H, 3.82; N, 4.65%. IR: ν(CO) 1945, 1971, 2055 cm^{-1} (st), ν(CN) 2360 cm^{-1} (w). FAB^- MS: $m/z = 472$ ($[M]^-$, 7% B), $m/z = 431$ ($[Re(CO)_3Br_2]^-$, 100% B), $m/z = 403$ ($[Re(CO)_2Br_2]^-$, 15% B), $m/z = 475$ ($[Re(CO)Br_2]^-$, 20% B), $m/z = 350$ ($[Re(CO)_3Br]^-$, 60% B).

X-Ray structure determinations

The intensities for the X-ray determinations were collected on an automated single crystal diffractometer of the type CAD4 (Enraf-Nonius, Delft) using Mo-K_α radiation with ω-scans. The unit cell dimensions were determined from the angular settings of 25 high-angle reflections. The structures were solved by Patterson synthesis using SHELXS86 [14]. Subsequent Fourier-difference map analyses yielded the positions of the non-hydrogen atoms. Refinement was performed using SHELXL93 [15]. The hydrogen atoms were included at calculated positions and refined using the "riding model" option of

SHELXL93. Crystal data and more details of the data collections and refinements are contained in Table 1. Additional information on the structure determinations has been deposited at the Cambridge Crystallographic Data Centre.

RESULTS AND DISCUSSION

Recently, we reported on the synthesis of $(Et_4N)_2[M(CO)_3X_3]$ complexes (M = Tc, Re; X = Cl, Br) starting directly from the tetrabutylammonium permetallates and applying 1 atm of CO [11,12]. Dissolution of the complexes in co-ordinating solvents results in the replacement of only the weakly bound halide ligands and the formation of solvent complexes of the composition $[M(CO)_3(solv)_3]^+$. The course of the ligand exchange can easily be followed by IR spectroscopy [11]. After removing X^- by silver ions the addition of PF_6^- results in precipitation of the solvent complexes. Thus, the dissolution of $(Et_4N)_2[Re(CO)_3Br_3]$ or $(Et_4N)_2[Tc(CO)_3Cl_3]$ in acetonitrile and addition of $AgPF_6$ represents high yield syntheses of the well known complexes $[M(CO)_3(CH_3CN)_3]PF_6$. For further ligand exchange reactions, however, the readily soluble solvent complexes can be used without isolation. In particular, chelating ligands and good π-acceptors easily replace the weakly bound solvent ligands from the electron-rich metal centre. Upon dissolution of $(Et_4N)_2[Re(CO)_3Br_3]$ in acetonitrile and slow evaporation of the solution without removing the bromide anions $(Et_4N)[Re(CO)_3Br_2(CH_3CN)]$ can be isolated.

The reactions of the *in situ* generated $[M(CO)_3(CH_3CN)_3]^+$ cations with approximately equimolar amounts of sodium bis(diphenylthiophosphoryl) amide (**I**) in acetonitrile, give the neutral complexes $\{M(CO)_3[(Ph_2PS)_2N](CH_3CN)\}$ in good yields. Co-ordination of a second molecule $(Ph_2PS)_2N^-$ could not be observed, even when a large excess of ligand was used. In the latter case, however, the formation of considerable amounts of $(Ph_2PS)_2NH$ is observed when the solvent has not been tried very carefully prior to use. This causes serious problems in the isolation of pure $\{M(CO)_3[(Ph_2PS)_2N](CH_3CN)\}$ complexes and can be avoided by an $(Et_4N)_2[M(CO)_3X_3]/Na[(Ph_2PS)_2N]$ ratio not exceeding 1 : 1.1.

$\{Tc(CO)_3[(Ph_2PS)_2N](CH_3CN)\}$ is a colourless solid which crystallizes as large plates directly from the reaction mixture. The compound is soluble in warm acetonitrile, only sparingly soluble in alcohols and nearly insoluble in hydrocarbons. No decomposition could be detected in the solid state over a period of 4 weeks. In coordinating solvents (e.g. thf or pyridine), however, a ligand exchange acetonitrile vs solvent can be observed. This is a route for the synthesis of further derivatives containing the $\{Tc(CO)_3[(Ph_2PS)_2N]\}$ moiety.

The infrared spectrum of $\{Tc(CO)_3[(Ph_2PS)_2N](CH_3CN)\}$ in KBr shows a typical "*fac*-$Tc(CO)_3$" pattern for a slightly distorted C_{3v} symmetry with intense bands at 2035 (A_1), 1953 and 1925 (E) cm^{-1}. The coordinated acetonitrile shows a weak band at 2362 cm^{-1}. The ^{99}Tc resonance of the diamagnetic technetium(I) complex ($4d^6$) can be observed at -1266 ppm vs TcO_4^-. This value agrees well with those found for other neutral technetium(I) tricarbonyls. Cationic compounds of comparable structures show significantly highfield shifted ^{99}Tc NMR signals [18–20].

$\{Tc(CO)_3[(Ph_2PS)_2N](CH_3CN)\}$ crystallizes triclinic in the space group $P\bar{1}$. An ORTEP representation [21] of the molecular structure along with the atomic numbering scheme is given in Fig. 1. Selected bond lengths and angles are summarized in Table 2. The metal has a distorted octahedral coordination sphere with facially arranged carbonyls. The Tc—S bond lengths of 2.526(3) and 2.546(2) Å are longer by about 0.1 Å than those in the five-coordinate bis-chelate $\{Tc^VN[(Ph_2PS)_2N]_2\}$ [10]. This can easily be understood by the strong *trans* influence of the carbonyls. A similar tendency has been observed at Tc^V complexes when phosphines are co-ordinated *trans* to $(Ph_2PS)_2N^-$ [22]. The P—S distances are lengthened by a mean value of 0.07 Å and the P—N distances shortened by 0.09 Å with regard to the pro-ligand [23]. This relates to delocalization of electron density in the chelate rings although the six-membered ring is not planar. The pairs of P—S and P—N distances are almost equal as is expected for a chelate ring with delocalized electron density. The same situation has been observed in the structures of Re^V with $[(Ph_2PS)_2N]^-$ [7–10]. In contrast to that, the indium(III) complex $\{In[(Ph_2PS)_2N]_2Cl\}$ shows a "non-symmetric" co-ordination of the ligand with different S—P and P—N bond lengths in the chelate rings suggesting co-ordination with distinct "thiolate" and "phosphorus sulphide" donor sites [24].

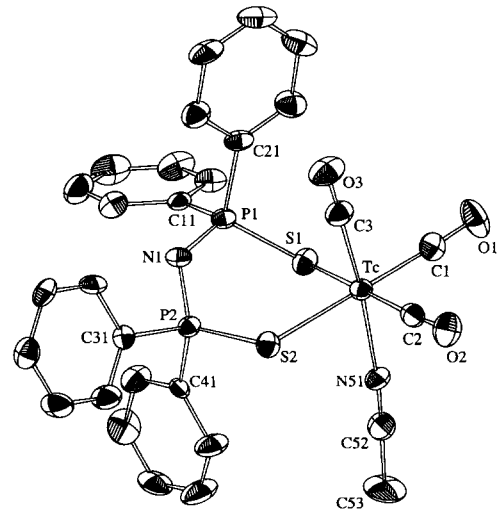

Fig. 1. Molecular structure [21] of $\{Tc(CO)_3[(Ph_2PS)_2N](CH_3CN)\}$ along with the atomic numbering scheme.

Table 1. X-ray structure data collection and refinement parameters

	$\{Tc(CO)_3[(Ph_2PS)_2N](CH_3CN)\}$	$\{Re(CO)_3[(Ph_2PS)_2N](CH_3CN)\}$	$(Et_4N)[Re(CO)_3Br_2(CH_3CN)]$
Crystal dimensions (mm^3)	0.3 · 0.1 · 0.1	0.25 · 0.15 · 0.05	0.5 · 0.3 · 0.2
Formula	$C_{29}H_{23}N_2O_3P_2S_2Tc$	$C_{29}H_{23}N_2O_3P_2S_2Re$	$C_{13}H_{23}N_2O_3Br_2Re$
M	671.55	759.75	601.35
Crystal system	triclinic	triclinic	triclinic
Space group	$P\bar{1}$	$P\bar{1}$	$P\bar{1}$
Unit cell	a = 10.693(9) Å	a = 10.709(4) Å	a = 8.440(4) Å
	b = 11.18(1) Å	b = 11.176(4) Å	b = 10.177(5) Å
	c = 12.96(1) Å	c = 12.901(4) Å	c = 11.740(7) Å
	α = 76.19(7)°	α = 76.34(3)°	α = 91.87(3)°
	β = 75.11(7)°	β = 75.33(3)°	β = 111.04(3)°
	γ = 86.95(6)°	γ = 87.45(2)°	γ = 91.69(3)°
V (Å^3)	1454(2)	1451.3(9)	939.8(9)
Z	2	2	2
D_c (g cm^{-3})	1.533	1.739	2.125
Linear absorption coefficient (mm^{-1})	0.782	4.475	10.726
Absorption correction	None	DIFABS [16]	DIFABS [16]
T_{min}		0.417	0.402
T_{max}		1.000	1.000
Weighting scheme ($P = (F_o^2 + 2F_c^2)/3$)	$w = 1/[\sigma^2(F_o^2) + (0.0272P)^2]$	$w = 1/[\sigma^2(F_o^2) + (0.0635P)^2]$	$w = 1/[\sigma^2(F_o^2) + (0.0677P)^2 + 3.6223P]$
Measured reflections	6017	5368	3879
Independent reflections	5119	4548	3283
Independent reflections ($I > 2\sigma(I)$)	3114	3841	2975
Refined parameters	352	352	202
$R_1(F)/wR2(F^2)$	0.055/0.0857	0.039/0.093	0.034/0.093
GooF	1.002	1.038	1.038
Programs used	SHELXS86 [14], SHELXL93 [15], PLATON, HELENA [17]	SHELXS86 [14], SHELXL93 [15], PLATON, HELENA [17]	SHELXS86 [14], SHELXL93 [15], PLATON, HELENA [17]

Table 2. Selected bond lengths and angles in $\{Tc(CO)_3[Ph_2PS)_2N](CH_3CN)\}$ and $\{Re(CO)_3[Ph_2PS)_2N](CH_3CN)\}$

	$\{Tc(CO)_3[Ph_2PS)_2N](CH_3CN)\}$	$\{Re(CO)_3[Ph_2PS)_2N](CH_3CN)\}$
M—C(1)	1.893(7)	1.913(9)
M—C(2)	1.900(7)	1.914(8)
M—C(3)	1.920(7)	1.933(7)
M—S(1)	2.546(3)	2.528(2)
M—S(2)	2.526(3)	2.544(2)
M—N(51)	2.155(6)	2.147(6)
N(51)—C(52)	1.124(7)	1.125(10)
C(1)—O(1)	1.147(7)	1.145(9)
C(2)—O(2)	1.155(7)	1.126(9)
C(3)—O(3)	1.142(7)	1.133(9)
S(1)—P(1)	2.012(3)	2.021(3)
P(1)—N(1)	1.590(5)	1.600(6)
P(2)—N(1)	1.592(5)	1.582(6)
S(2)—P(2)	2.013(3)	2.017(3)
C(1)—M—C(2)	88.8(3)	88.9(3)
C(1)—M—C(3)	90.5(3)	88.3(3)
C(1)—M—S(1)	85.9(2)	89.6(2)
C(1)—M—S(2)	177.3(2)	170.6(2)
C(1)—M—N(51)	95.6(2)	91.7(3)
C(2)—M—C(3)	88.0(3)	90.4(3)
C(2)—M—S(1)	171.3(2)	178.3(2)
C(2)—M—S(2)	88.9(2)	85.7(2)
C(3)—M—S(1)	98.9(2)	88.9(2)
C(3)—M—S(2)	87.9(2)	99.5(2)
C(3)—M—N(51)	173.9(3)	173.9(3)
S(1)—M—S(2)	96.52(9)	95.87(7)
S(1)—M—N(51)	82.0(2)	85.0(2)
S(2)—M—N(51)	85.9(2)	81.1(2)
M—C(1)—O(1)	176.8(6)	176.7(6)
M—C(2)—O(2)	175.8(6)	177.5(7)
M—C(3)—O(3)	174.9(6)	174.8(8)
M—S(1)—P(1)	104.7(1)	109.2(1)
S(1)—P(1)—N(1)	117.6(2)	119.2(3)
N(1)—P(2)—S(2)	119.7(2)	117.5(2)
M—S(2)—P(2)	108.8(1)	104.72(9)
M—N(51)—C(52)	173.6(5)	174.0(7)

Deviations from an idealized octahedron can be observed for the first co-ordination sphere of technetium in $\{Tc(CO)_3[(Ph_2PS)_2N](CH_3CN)\}$ (*cis* angles between 82.0 and 98.9°). The Tc—C bond *trans* to CH_3CN is slightly longer than the others suggesting a somewhat stronger *trans* influence of the acetonitrile ligand compared with the sulphur donor sites.

The bonding situation in $\{Re(CO)_3[(Ph_2PS)_2N](CH_3CN)\}$ is very similar to that in the technetium analogue. Therefore, the corresponding bond lengths and angles are compared in Table 2. An ellipsoid representation of the rhenium complex is given in Fig. 2. In both complexes M—N bond to the acetonitrile ligand is long by 2.155(6) and 2.147(6) Å, respectively. The suggested lability of this position is confirmed by the chemical behaviour of the complexes.

Dissolution of $\{Re(CO)_3[(Ph_2PS)_2N](CH_3CN)\}$ in $CHCl_3$ and addition of pyridine results in the for-

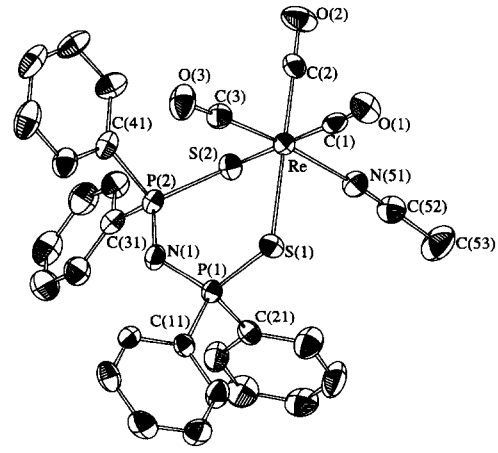

Fig. 2. Molecular structure [21] of $\{Re(CO)_3[(Ph_2PS)2N](CH_3CN)\}$ along with the atomic numbering scheme.

mation of $\{Re(CO)_3[(Ph_2PS)_2N](py)\}$ which can be isolated upon evaporation of the solvent. The colourless solid has been characterized spectroscopically.

The lability of acetonitrile ligands in rhenium tricarbonyl complexes can also be demonstrated by evaporation of a CH_3CN solution of $[Re(CO)_3(CH_3CN)_3]^+$ which has been prepared by dissolution of $[Re(CO)_3Br_3]^{2-}$ without removing the bromide ions by addition of a silver salt. Despite the infrared spectrum of such a solution, it is clearly identical to those of isolated $[Re(CO)_3(CH_3CN)_3]^+$ and solutions from which Br^- has been completely removed [11] and a ligand re-exchange CH_3CN vs Br^- can be observed upon concentration and colourless crystals of the $(Et_4N)[Re(CO)_3Br_2(CH_3CN)]$ deposit.

$(Et_4N)[Re(CO)_3Br_2(CH_3CN)]$ crystallizes triclinic in the space group $P\bar{1}$. Figure 3 shows an ORTEP plot of the complex anion. Table 3 contains selected bond lengths and angles. The facially arranged carbonyl ligands induce long Re—Br bond lengths of 2.623(2) and 2.632(2) Å, respectively. These values are in agreement with other Re—Br bonds in rhenium(I) complexes and in *trans* position to CO (2.633(1) – 2.662(1) Å in $[Re(CO)_3Br_3]^{2-}$ [12], 2.638(1) Å in [Re2(CO) $6Br_2$(tetraphos)] [12], 2.624(1) – 2.647(2) Å in rhenium(I) tricarbonyl complexes with thiourea derivatives [25]), but longer than in the rhenium(III) complex *cis*-$[Re(CO)_2Br4]^-$, where the Re—Br bond *trans* to CO is 2.542(1) Å [26]. As observed in the $\{Re(CO)_3[(Ph_2PS)_2N](CH_3CN)\}$ complexes, the Re—(CO) bond *trans* to acetonitrile is slightly longer than the others (0.04 Å in $[Re(CO)_3Br_2(CH_3CN)]^-$). The co-ordination geometry of rhenium comes close to an idealized octahedron with *cis* angles between 86.1(2) and 93.6(2)° and *trans* angles between 177.2(2) and 179.1(3)°.

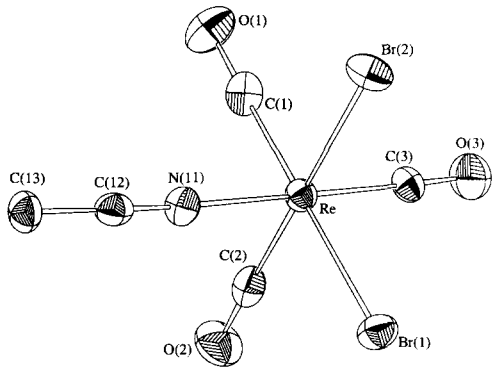

Fig. 3. Structure [21] of the complex anion in $(Et_4N)[Re(CO)_3Br_2(CH_3CN)]$ along with the atomic numbering scheme.

CONCLUSIONS

$[M(CO)_3X_3]^{2-}$ complexes (M=Tc, Re; X=Cl, Br) can be used as reactive starting materials for the synthesis of further rhenium(I) and technetium(I) tricarbonyl complexes. The halide ligands are only weakly bound and readily substituted by co-ordinating solvents. Addition of chelating ligands like $[(Ph_2PS)_2N]^-$ results in neutral, monomeric metal(I) tricarbonyl complexes with one remaining co-ordinated solvent molecule. The *in situ* produced $[Re(CO)_3(solvent)_3]^+$ complexes show a ligand rearrangement (solvent vs halide) upon concentration of their solutions.

Acknowledgement—The work was financially supported by the Deutsche Forschungsgemeinschaft and the Fonds der Chemischen Industrie. We thank Hermann Starck AG (Goslar) for generously providing rhenium metal, the DAAD and the British Council for supporting the collaboration between

Table 3. Selected bond lengths and angles in $(Et_4N)[Re(CO)_3Br_2(CH_3CN)]$

Re—C(1)	1.881(8)	N(11)—C(12)	1.14(1)
Re—C(2)	1.884(8)	C(12)—C(13)	1.45(1)
Re—C(3)	1.922(7)	C(1)—O(1)	1.17(1)
Re—Br(1)	2.623(2)	C(2)—O(2)	1.17(1)
Re—Br(2)	2.632(2)	C(3)—O(3)	1.124(9)
Re—N(11)	2.150(6)		

C(1)—Re—C(2)	91.6(2)	C(3)—Re—Br(2)	93.1(2)
C(1)—Re—C(3)	88.0(3)	C(3)—Re—N(11)	179.1(3)
C(1)—Re—Br(1)	177.4(2)	Br(1)—Re—Br(2)	87.89(5)
C(1)—Re—Br(2)	90.0(2)	Br(1)—Re—N(11)	86.1(2)
C(1)—Re—N(11)	92.2(3)	Br(2)—Re—N(11)	86.1(2)
C(2)—Re—C(3)	89.2(3)	Re—C(1)—O(1)	179.5(7)
C(2)—Re—Br(1)	90.4(2)	Re—C(2)—O(2)	178.5(7)
C(2)—Re—Br(2)	177.2(2)	Re—C(3)—O(3)	178.7(7)
C(2)—Re—N(11)	91.7(3)	Re—N(11)—C(12)	173.6(6)
C(3)—Re—Br(1)	93.6(2)		

the German and British groups. U.A. thanks Prof. J. Strähle (Tübingen) for his kind hospitality in Tübingen.

REFERENCES

1. Bereman, R. D., Wang, F. T., Najdzionek, J. and Braitsch, D. M., *J. Am. Chem. Soc.*, 1976, **98,** 7266.
2. Woolins, J. D., *J. Chem. Soc., Dalton Trans.* 1996, 2893.
3. Churchill, M. R., Cooke, J., Fennessey, J. P. and Wormald, J., *Inorg. Chem.*, 1971, **10,** 1031.
4. Haiduc, I. and Silahi-Dumitrescu, I., *Coord. Chem. Rev.*, 1986, **74,** 127.
5. Deutsch, E., Libson, K., Jurisson, S. and Lindoy, L., *Prog. Inorg. Chem.*, 1983, **30,** 75.
6. Volkert, W. A., Goeckeler, G. J. and Ketring, A. R., *J. Nucl. Med.*, 1991, **32,** 174.
7. Rossi, R., Marchi, A., Magon, L., Casellato, U., Tzamburrini, S. and Graziani, R., *J. Chem. Soc., Dalton Trans.*, 1991, 263.
8. Rossi, R., Marchi, A., Marvelli, L., Peruzzini, M., Casellato, U. and Graziani, R., *J. Chem. Soc., Dalton Trans.*, 1992, 435.
9. Rossi, R., Marchi, A., Marvelli, L., Magon, L., Peruzzini, M., Casellato, U. and Graziani, R., *J. Chem. Soc., Dalton Trans.*, 1993, 723.
10. Abram, U., Schulz Lang, E., Abram, S., Wegmann, J., Dilworth, J. R., Kirmse, R. and Woolins, J. D., *J. Chem. Soc., Dalton Trans.*, 1997, 623.
11. Alberto, R., Schibli, R., Schubiger, P. A., Abram, U. and Kaden, T. A., *Polyhedron*, 1996, **15,** 1079.
12. Alberto, R., Schibli, R., Egli, A., Schubiger, P. A., Herrmann, W. A., Artus, G., Abram, U. and Kaden, T. A., *J. Organomet. Chem.*, 1995, **493,** 119.
13. Wang, F. T., Najdzionek, J., Leneker, K. A., Wassermann, H. and Braitsch, D. M., *Synth. Inorg. Metal-Org. Chem.*, 1978, **8,** 20.
14. Sheldrick, G. M., SHELXS86—A program for the solution of X-ray structures, University of Göttingen, 1986.
15. Sheldrick, G. M., SHELXL93—A program for the refinement of X-ray structures, University of Göttingen, 1993.
16. Walker, N. and Stuart, D., *Acta Crystallogr.*, 1983, **A39,** 158.
17. Spek, A., PLATON, HELENA—Programs for data reduction and calculation on X-ray data, University of Utrecht, 1994.
18. Lorenz, B., Findeisen, M., Olk, B. and Schmidt, K., *Z. anorg. allg. Chem.*, 1988, **566,** 160.
19. Findeisen, M., Kaden, L., Lorenz, B., Rummel, S. and Wahren, M., *Inorg. Chim. Acta*, 1987, **128,** L15.
20. Findeisen, M., Kaden, L., Lorenz, B. and Wahren, M., *Inorg. Chim. Acta*, 1988, **142,** 3.
21. Zsolnai, L., ZORTEP—A program for the ellisoid presentation of X-ray structure results, University of Heidelberg, 1994.
22. Abram, U., Schulz Lang, E. and Dilworth, J. R., *Acta Cryst.*, 1997, **C53,** 289.
23. Hitchcock, P. B., Nixon, J. F., Silaghi-Dumitrescu, I. and Haiduc, I., *Inorg. Chim. Acta*, 1985, **96,** 77.
24. Abram, S. and Abram, U., unpublished results.
25. Abram, U., Abram, S., Alberto, R. and Schibli, R., *Inorg. Chim. Acta*, 1996, **248,** 193.
26. Abram, U., Hübener, R., Alberto, R. and Schibli, R., *Z. anorg. allg. Chem.*, 1996, **622,** 813.

Pergamon

PII: S0277-5387(97)00334-3

Polyhedron Vol. 17, No. 8, pp. 1311–1316, 1998
© 1998 Elsevier Science Ltd
All rights reserved. Printed in Great Britain
0277-5387/98 $19.00+0.00

Synthesis and magnetic studies of oxamido-bridged heterobinuclear copper(II)-iron(II) complexes

Cui-Wei Yan,[a] Yan-Tuan Li,*[b] Yu-Zhen Su[b] and Dai-Zheng Liao[c]

[a] Department of Biology, Qufu Normal University, Qufu Shandong, 273165, P.R. China

[b] Department of Chemistry, Qufu Normal University, Qufu Shandong, 273165, P.R. China

[c] Department of Chemistry, Nankai University, Tianjin, 300071, P.R. China

(Received 6 May 1997; accepted 8 August 1997)

Abstract—Six new μ-oxamido heterobinuclear complexes have been synthesized and identified as $[Cu(oxae)Fe(L)_2]SO_4$, where oxae denotes the N,N′-bis(2-aminoethyl)oxamido dianion and L represents 1,10-phenanthroline(phen); 5-nitro-1,10-phenanthroline (NO_2-phen); 5-chloro-1,10-phenanthroline (Cl-phen); 5-methyl-1,10-phenanthroline (CH_3-phen); 2,2′-bipyridine (bpy) and 4,4′-dimethyl-2,2′-bipyridine (Me_2bpy). Based on the elemental analyses, spectroscopic studies, magnetic moments at room temperature and molar conductivity measurements, extended oxamido-bridged structures consisting of a copper(II) and an iron(II) ions, which have a square planar environment and an octahedral environment, respectively, are proposed for these complexes. The $[Cu(oxae)Fe(bpy)_2]SO_4$ (**1**) and $[Cu(oxae)Fe(phen)_2]SO_4$ (**2**) complexes have been characterized by variable temperature magnetic susceptibility (4.2–300 K) and the observed data were least-squares fitted to the susceptibility equation derived from the spin Hamiltonian including single-ion zero-field interaction for the iron(II) ion, $\hat{H} = -2J\hat{S}_1 \cdot \hat{S}_2 - D\hat{S}_{z1}^2$, giving the exchange integrals $J = -30.6$ cm^{-1} for (**1**) and $J = -31.8$ cm^{-1} for (**2**). These results are commensurate with antiferromagnetic interactions between adjacent metal ions within each molecule. © 1998 Elsevier Science Ltd. All rights reserved

Keywords: μ-oxamido; copper(II); iron(II); heterobinuclear complex; synthesis; magnetism.

The synthesis and magnetic investigations of heterobinuclear transition-metal complexes propagated by multi-atom bridges are of current interest, not only for gaining some insight into the pathways of electron transfers in biological systems [1–3], but also for obtaining information about designing and synthesizing molecule-based magnets [4,5] and for investigating the spin-exchange mechanism between paramagnetic metal ions [5–7]. It is known that the mononuclear complexes *N,N′*-bis(alkylaminoalkyl) oxamidocopper(II) act as bidentate chelating ligands toward a second metal to form binuclear complexes [8–15]. The effective bridging function of μ-oxamido has been revealed by X-ray analysis for some of these complexes [9,11,12,13,16,17]. Quite recently, we utilized *N,N′*-bis(2-aminopropyl)oxamidocopper(II), [Cu(oxap)], as a bidentate mononuclear fragment to prepare the heterobinuclear complexes [18] $[Cu(oxap)Fe(L)_2]SO_4$ (L = bpy, Me_2bpy, phen, CH_3-phen, NO_2-phen, Cl-phen) and to study their magnetic properties. In order to provide more examples of oxamido-bridged heterobinuclear Cu(II)–Fe(II) complexes to investigate further the structural variation effects upon spin-coupling, in this paper, six new heterometal binuclear complexes, $[Cu(oxae)Fe(L)_2]SO_4$ (L = bpy, Me_2bpy, phen, NO_2-phen, CH_3-phen, Cl-phen) have been synthesized by using *N,N′*-bis(2-aminoethyl)oxamidocopper(II) (abbreviated as Cu(oxae)) as bridging ligand and the magnetic properties of the $[Cu(oxae)Fe(bpy)_2]SO_4$ (**1**) and $[Cu(oxae)Fe(phen)_2]SO_4$ (**2**) complexes have also been studied.

* Author to whom correspondence should be addressed.

EXPERIMENTAL

Materials

All the reagents used in the synthesis were analytical grade. $FeSO_4 \cdot 7H_2O$ was recrystallized by a general method before use. The terminal ligands 1,10-phenanthroline(phen); 5-nitro-1,10-phenanthroline (NO_2-phen); 5-chloro-1,10-phenanthroline (Cl-phen); 5-methyl-1,10-phenanthroline (CH_3-phen); 2,2′-bipyridine (bpy) and 4,4′-dimethyl-2,2′-bipyridine (Me_2bpy) (analytical grade) were purchased from Perking Chemical Company. The starting material Cu(oxae) was synthesized as previously described [19].

Synthesis of new heterobinuclear Cu(II)–Fe(II) *complexes*

The methods used to prepare the complexes are virtually identical and are exemplified by [Cu(oxae)Fe(bpy)$_2$]SO_4. To a suspension of Cu(oxae) (94.2 mg, 0.4 mmol) stirred in methanol (5 cm^3) was added successively a solution of $FeSO_4 \cdot 7H_2O$ (111.2 mg, 0.4 mmol) in methanol (10 cm^3) and a solution of bpy (125 mg, 0.8 mmol) in methanol (10 cm^3) under N_2 at room temperature. After stirring for 2 h, the solution was filtered. Greenish microcrystals were obtained, washed several times with methanol, water and diethyl ether and dried over P_2O_5 under reduced pressure.

All analytical data, colors, yields and melting points of the complexes are collected in Table 1. In the solid state all the complexes are fairly stable in air, in order to facilitate physical measurements.

Physical measurements

Carbon, hydrogen and nitrogen elemental analyses were performed with a Perkin–Elmer elemental analyzer Model 240. The metal contents were determined by EDTA titration. IR spectra were recorded with a NICOLET FT-IR 5DX spectrometer using KBr pellets. Electronic spectra (in DMF solutions) were measured on a Varian Cary, Model 219, spectrophotometer. Molar conductances were measured with a DDS-11A conductometer. The magnetic susceptibility measurements at room temperature were carried out by Gouy's method using Hg[Co(SCN)$_4$] as the calibrant. Variable-temperature magnetic susceptibilities (4.2–300 K) were performed at the Institute of Physics, Chinese Academy of Sciences, China, using a vibrating sample magnetometer Model CF-1. Diamagnetic corrections were made with Pascal's constants [20] for all the constituent atoms. The effective magnetic moments were calculated by the equation $\mu_{eff} = 2.828\ (\chi_M T)^{1/2}$, where χ_M is the molar magnetic susceptibility corrected for diamagnetisms of the constituting atoms.

RESULTS AND DISCUSSION

Synthetic route and molar conductance of the complexes

One strategy for the synthesis of heterobinuclear complexes is to use the reaction of a simple metal salt with a mononuclear fragment that can function as ligands to a second metal ion [12–15, 21–24]. In this study, our purpose was to obtain Cu(II)–Fe(II) heterobinuclear complexes, therefore, this synthetic

Table 1. Elemental analysis, yield, color and melting point (M.P.) of the complexes

Complex	Color	Yield (%)	M.P. (°C)	Elemental analyses (Calc.) (%)				
				C	H	N	Cu	Fe
(1)	Greenish	58	308	44.6 (44.6)	4.1 (4.0)	15.8 (16.0)	9.0 (9.1)	7.8 (8.0)
(2)	Greenish-black	76	296	48.1 (48.2)	3.8 (3.8)	14.9 (15.0)	8.3 (8.5)	7.4 (7.5)
(3)	Greenish-brown	60	317	47.6 (47.7)	4.7 (4.8)	14.6 (14.8)	8.3 (8.4)	7.2 (7.4)
(4)	Orange-yellow	85	325	43.1 (43.0)	3.0 (3.1)	16.5 (16.7)	7.5 (7.6)	6.5 (6.7)
(5)	Blue-violet	88	282	44.0 (44.1)	3.0 (3.2)	13.5 (13.7)	7.6 (7.8)	6.7 (6.8)
(6)	Dark-blue	76	311	49.5 (49.5)	4.4 (4.2)	14.2 (14.4)	8.0 (8.2)	7.1 (7.2)

(1) = [Cu(oxae)Fe(bpy)$_2$]SO_4, (2) = [Cu(oxae)Fe(phen)$_2$]SO_4, (3) = [Cu(oxae)Fe(Me_2bpy)$_2$]SO_4, (4) = [Cu(oxae)Fe(NO_2-phen)$_2$]SO_4, (5) = [Cu(oxae)Fe(Cl-phen)$_2$]SO_4, (6) = [Cu(oxae)Fe(CH_3-phen)$_2$]SO_4.

method was adopted and *N,N'*-bis(2-aminoethyl)oxamidocopper(II), [Cu(oxae)] was chosen as a bidentate mononuclear fragment, simultaneously, 1,10-phenanthroline (phen); 5-nitro-1,10-phenanthroline (NO_2-phen); 5-chloro-1,10-phenanthroline (Cl-phen); 5-methyl-1,10-phenanthroline (CH_3-phen); 2,2'-bipyridine (bpy) and 4,4'-dimethyl-2,2'-bipyridine (Me_2bpy) were used as terminal ligands, respectively. Indeed, elemental analyses indicate that the reaction of Cu(oxae) with $FeSO_4 \cdot 7H_2O$ and L (L = bpy, Me_2bpy, phen, NO_2-phen, Cl-phen, CH_3-phen) yielded the heterobinuclear complexes of the general formula $[Cu(oxae)Fe(L)_2]SO_4$. All the Cu(II)–Fe(II) binuclear complexes are sparingly soluble in water, ethanol, carbon tetrachloride, chloroform and benzene, but soluble in acetonitrile, DMF and DMSO to give stable solutions at room temperature. The $[Cu(oxae)Fe(bpy)_2]SO_4$ and $[Cu(oxae)Fe(phen)_2]SO_4$ complexes can be recrystallized in an acetonitrile/ethanol (1:2) mixture. In spite of our many efforts, single crystals suitable for X-ray crystallography have not yet been obtained for these complexes. For the six Cu(II)–Fe(II) binuclear complexes, the molar conductance values (10^{-3} mol·L^{-1} acetonitrile solution) fall in the expected range for 1:1 electrolytes [25] (see Table 2), indicting that the sulfate anion is situated outside the metal coordination sphere.

The binuclear complexes were further characterized on the basis of the following result.

Infrared spectra

The bonding mode of the iron(II) ion to the mononuclear fragment [Cu(oxae)] was investigated by IR spectroscopy. The most relevant IR absorption bands from the IR spectra of the complexes along with their assignments are shown in Table 2. Only the selected infrared bands will be discussed here. The carbonyl stretching vibration at 1615 cm^{-1} for Cu(oxae) is considerably shifted towards higher frequencies (ca 20–40 cm^{-1}) in the binuclear complexes. Therefore, in general, when the deprotonated amide nitrogen is coordinated to the metal ion, its amide I band shifts considerably towards lower wavenumbers. In the case of an oxamide dianion coordinated to two metal ions as a bridging ligands, the amide I band reverts to near its original position (in the protonated species) [8]. Although the amide I band is due to a composite N—C=O vibration, it can essentially be seen as $\nu_{C=O}$; it is likely that the bond order of C=O (carbonyl) in the binuclear complexes is higher than in the corresponding mononuclear complex Cu(oxae). This shift has often been used as a diagnostic indicator for oxamido-bridged structures [8]. On the other band, the C=O deformation at 720 cm^{-1} of the ligand complex, [Cu(oxae)], disappeared in the spectra of the binuclear complexes. This fact may be attributed to the coordination of the carbonyl oxygens to the Fe(II) ion [26]. In addition, the $-NH_2$ vibration at 3250 cm^{-1} for Cu(oxae) and —N=C— stretching vibration at 1530–1540 cm^{-1} for terminal ligand (bpy, Me_2bpy, phen, NO_2-phen, Cl-phen, CH_3-phen) were present for all the binuclear complexes and a broad band was observed at about 1120 cm^{-1}, which is typical for a non-coordinated sulphate anion [27].

Electronic spectra

The electronic absorption spectral data for these complexes (DMF solutions) are given in Table 2). As shown in Table 2, the electronic spectra of the six

Table 2. Physical data for the complexes

Complex	μ_{eff} (B.M.)	Λ_M[a] (Ω^{-1} cm^2 mol^{-1})	IR (cm^{-1})				UV ν(10^3 cm^{-1})/ε_{max}(mol^{-1} cm^{-1} L)		
			—NH_2	C=O	—N=C—	SO_4^{2-}	*d–d*		CT
Cu(oxae)	1.82		3250	1615			18.7		
$[Cu(oxae)Fe(bpy)_2]SO_4$	4.75	135	3250	1640	1530	1120	18.5 (190)	11 (10)	28.6 (19300)
$[Cu(oxae)Fe(phen)_2]SO_4$	4.70	145	3250	1635	1530	1120	18.4 (210)	11 (12)	28.2 (18600)
$[Cu(oxae)Fe(Me_2bpy)_2]SO_4$	4.76	130	3250	1650	1540	1125	18.4 (198)	11.2 (11)	28.8 (24000)
$[Cu(oxae)Fe(NO_2\text{-}phen)_2]SO_4$	4.85	150	3250	1648	1540	1120	18.3 (200)	11.1 (12)	27.5 (21500)
$[Cu(oxae)Fe(Cl\text{-}phen)_2]SO_4$	4.82	145	3250	1650	1545	1120	18.4 (220)	11.2 (15)	28.5 (19000)
$[Cu(oxae)Fe(CH_3\text{-}phen)_2]SO_4$	4.78	138	3250	1655	1540	1125	18.2 (188)	11.2 (15)	27.6 (17000)

[a] Values for 1×10^{-3} mol·l^{-1} acetonitrile solution.

complexes are similar to each other. Two *d–d* bands centered at $(11.2–11.0)\times10^3$ cm^{-1} and $(18.5–18.0)\times10^3$ cm^{-1} are observed. The weak band $(11.2–11.0)\times10^3$ cm^{-1} is due to the $^5T_{2g}\rightarrow{}^5E_g$ transition and is characteristic of a high spin octahedral configuration around iron(II) [28], whilst the strong band $(18.5–18.0)\times10^3$ cm^{-1} may be attributed to the *d–d* transition of the "inside" copper(II) in a square-planar environment. The frequency is lower than that for the mononuclear copper(II) complex $(18.7\times10^3$ $cm^{-1})$. Such a red shift of the *d–d* band may be attributed to the decreased planarity of the (CuN_4) chromophore on forming a binuclear complex with an iron(II) ion [29]. In addition, a stronger absorption in the short wavelength range (see Table 2) may be attributable to the charge-transfer absorption bands, which may be due to the spin-exchange interaction between the copper(II) and iron(II) ions through the π-path orbital set up by an oxamido bridge [8]. Further investigation of these and similar systems is required in order to obtain more detailed assignment for charge transfer.

Based on the composition of these complexes, their IR and electronic spectra, conductivity measurements, magnetic characterization (*vide infra*) and the crystal structure of the analogous complexes [11–13], these complexes are proposed to have extended oxamido-bridged structures and to consist of the iron(II) ion in an octahedral environment and the copper(II) ion in a square-planar environment, as shown in Fig. 1.

Magnetic properties

The observed magnetic moment per binuclear complex at room temperature shown in Table 2 is considerably less than the spin-only value (5.20 B.M.) for heterobinuclear complexes of Cu(II)–Fe(II) in the absence of exchange interaction. This suggests the operation of an antiferromagnetic spin-exchange interaction in these complexes [30]. In order to obtain further information on the structure of the complexes, variable-temperature susceptibility (4.2–300 K) data were collected for complexes (**1**) and (**2**), the temperature dependences of the susceptibilities (χ_M) and magnetic moments (μ_{eff}) for both binuclear complexes are shown in Fig. 2. From Fig. 2 it is evident that the magnetic moments decrease steadily with decreasing temperature, implying the existence of an antiferromagnetic spin-exchange interaction within each molecule [31]. This is consistent with the room-temperature magnetic moments of the complexes.

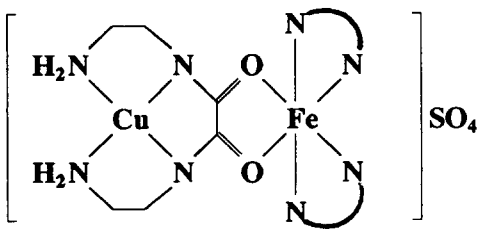

Fig. 1. Plausible coordination environments of the complexes (NN = bpy, Me_2bpy, phen, NO_2-phen, Cl-phen, CH_3-phen)

In order to understand quantitatively the magnitudes of spin-exchange interaction, the magnetic analysis for the complexes was initially carried out with the susceptibility eqn (1) based on the Heisenberg spin-exchange operator $(\hat{H}=-2J\hat{S}_1\cdot\hat{S}_2)$ for the Cu(II)–Fe(II) binuclear cluster:

$$\chi_M=\frac{N\beta^2g^2}{4kT}\left[\frac{10+35\exp(5J/kT)}{2+3\exp(5J/kT)}\right] \quad (1)$$

where χ_M denotes the susceptibility per binuclear complex and the other symbols have their usual meanings. The best fit parameters are $J=-28.5$ cm^{-1}, $g=2.04$ for (**1**); $J=-29.6$ cm^{-1}, $g=2.01$ for (**2**). The agreement factors F, defined here as $F=\Sigma[(\chi_M)_{obs}-(\chi_M)_{calc}]^2/\Sigma(\chi_M)_{obs}$ are then equal to 8.9×10^{-3} (**1**), 7.7×10^{-3} (**2**), respectively. However, the observed and calculated values do not satisfactorily fit this equation, especially at low temperature, because it neglects the single ion zero-field interaction of the iron(II) ion [30]. Considering the zero-field splitting of iron(II), a susceptibility equation was adopted based on the modified Heisenberg operator, $\hat{H}=-2J\hat{S}_1\cdot\hat{S}_2-D\hat{S}_{z1}^2$, where D is axial zero-field splitting parameter for the Fe(II) ion. In this case, the expression for the molar susceptibility (χ_M) is given by eqn (2)

$$\chi_M=\frac{N\beta^2g^2}{4kT}\left[\frac{25\exp(A)+9\exp(B)+\exp(C)+9\exp(G)+\exp(E)}{\exp(A)+\exp(B)+\exp(C)+\exp(G)+\exp(E)}\right] \quad (2)$$

$A=(35J/4+4D)/kT$
$B=(25J/4+5D/2+(25J^2/4-9DJ/2+9D^2/4)^{1/2})/kT$
$C=(25J/4+D/2+(25J^2/4-DJ/2+D^2/4)^{1/2})/kT$
$G=(25J/4+5D/2-(25J^2/4-9DJ/2+9D^2/4)^{1/2})/kT$
$E=(25J/4+D/2-(25J^2/4-DJ/2+D^2/4)^{1/2})/kT$

As shown in Fig. 2, good least-squares fits to the experimental data were attained with eqn (2) for the present case. The agreement factors are given in Table 3. Compared with a simple model $(\hat{H}=-2J\hat{S}_1\cdot\hat{S}_2$, $F\approx10^{-3})$, a much better fit was obtained with the operator including zero-field splitting. The magnetic parameters thus determined are $J=-30.6$ cm^{-1}, $g=2.06$, $D=-1.8$ cm^{-1} for $(Cu(oxae)Fe(bpy)_2)SO_4$ (**1**) and $J=-31.8$ cm^{-1}, $g=2.04$, $D=-2.0$ cm^{-1} for $(Cu(oxae)Fe(phen)_2)SO_4$ (**2**). The results indicated that the complexes showed an antiferromagnetic spin-exchange interaction within each binuclear unit. The weak antiferromagnetic spin-exchange interaction between iron(II) and copper(II) ions within each molecule may be explained by several models which have so far been proposed [32–34]. According to these mod-

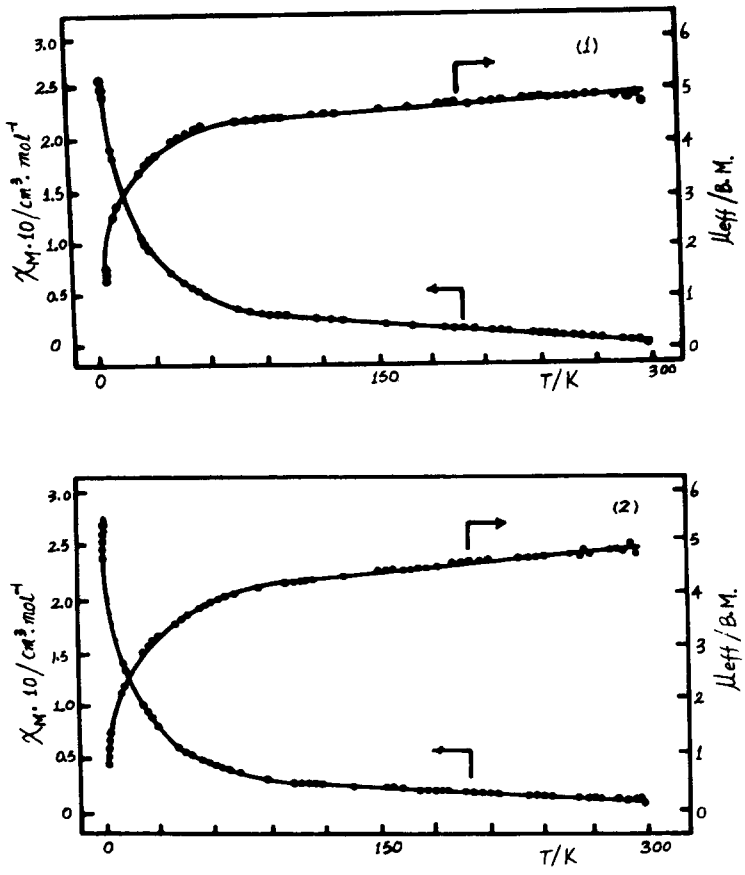

Fig. 2. Variable temperature magnetic susceptibility for $[Cu(oxae)Fe(bpy)_2]SO_4$ (**1**) and $[Cu(oxae)Fe(phen)_2]SO_4$ (**2**). The solid line represents the results of the least-squares fitting of the parameter of eqn (2) with experimental data.

Table 3. Magnetic data of the complexes

Complex	$-J$ (cm^{-1})	g	$-D$ (cm^{-1})	10^5F	Ref.
$[Cu(oxap)Fe(bpy)_2]SO_4$	20.9	2.08	1.6	3.8	18
$[Cu(oxap)Fe(phen)_2]SO_4$	22.5	2.04	2.4	3.5	18
$[Cu(oxae)Fe(bpy)_2]SO_4$	30.6	2.06	1.8	6.5	This work
$[Cu(oxae)Fe(phen)_2]SO_4$	31.8	2.04	2.0	3.2	This work

els, strict orbital orthogonality results in ferromagnetism ($J > 0$), otherwise an antiferromagnetic coupling ($J < 0$) should be involved in the system. On the basis of the crystal structure of a complex [12] that is analogous to the present complexes, if the whole molecular symmetry is considered to be C_{2v}, the 3d metallic orbitals of copper(II) and iron(II) ions transform [35] as $a_1(d_{z^2}$ and $d_{x^2-y^2})$, $a_2(d_{yz})$, $b_1(d_{xy})$ and $b_2(d_{zx})$. Around the copper(II) ion, there is just one unpaired electron which occupies the b_1 orbital, and around iron(II) there are four unpaired electrons which populate the a_1, a_2, b_1 and b_2 orbitals. Because there is no orthogonality between b_1(Cu) and b_1(Fe), namely $S = \langle b_1(Cu)|b_1(Fe)\rangle \neq 0$, antiferromagnetic exchange interactions should be observed in these complexes.

If we compare the present magnetic data with those previously reported for the analogous μ-oxamido copper(II)–iron(II) binuclear complexes [18] $[Cu(oxap)Fe(L)_2]SO_4$ (where oxap = *N*,*N*′-bis(2-aminopropyl) oxamido dianion, L = bpy and phen), which are given in Table 3, we can obtain the following results for the magnetic interaction: $[Cu(oxae)Fe(bpy)_2]SO_4$ ($J = -30.6$ cm^{-1}) > $[Cu(oxap)Fe(bpy)_2]SO_4$ ($J = -20.9$ cm^{-1}); $[Cu(oxae)Fe(phen)_2]SO_4$ ($J = -31.8$ cm^{-1}) > $[Cu(oxap)Fe$

$(phen)_2]SO_4$ ($J = -22.5$ cm^{-1}). In fact, these complexes have essentially the same skeletal structure and their IR and electronic spectra are also similar. The only difference between $[Cu(oxap)Fe(L)_2]SO_4$ and $[Cu(oxae)Fe(L)_2]SO_4$ (L = bpy and phen) is that there are two methyl ($-CH_3$) substituents in the former. Its presence may have effects on both electronic and molecular structures [36]. However, the electronic influence of the methyl groups on overlap between the magnetic orbitals should be small in view of its remoteness from the bridging site. On the other hand, the presence of this substituent will cause a decrease in coplanarity between the coordination environment of the copper(II) and that of the adjacent iron(II) ion, resulting in a decrease in overlap between the two magnetic orbitals. This would explain the differences in J values for these complexes.

Further investigations on this and similar systems are still required in order to get a deeper insight into the influence of the substituents in terminal ligands on magnetic interactions.

Acknowledgements—This project was supported by the Natural Science Foundation of Shandong Province and the National Natural Science Foundation of China.

REFERENCES

1. Richardson, J. S. R., Thomas, K. A., Rubin, B. H. and Richardson, D. C., *Natl. Acad. Sci. USA*, 1976, **73,** 2206.
2. Gambarotta, S., Arena, A., Florian, C. and Zanazzi, P. F., *J. Am. Chem. Soc.*, 1982, **104,** 5082.
3. Arena, F., Floriani, C., Chiesi-Villa, A. and Guastini, C., *Inorg. Chem.*, 1986, **25,** 4589.
4. Willett, R. D., Gatteschi, D. and Kahn, O. (Eds), *Magneto-Structural Correlation in Exchange Coupled Systems*, NATO ASI Series. Reidel, Dordrecht, Holland, 1985.
5. Kahn, O., *Struct. Bond. (Berlin)*, 1987, **68,** 89.
6. Cairns, C. J. and Busch, D. H., *Coord. Chem. Rev.*, 1986, **69,** 1.
7. Baron, V., Gillon, B., Plantevin, O., Cousson, A., Mathoniere, C., Kahn, O., Grand, A., Ohrstrom, L. and Delley, B., *J. Am. Chem. Soc.*, 1996, **118,** 11822.
8. Ojima, H. and Nonoyama, K., *Coord. Chem. Rev.*, 1988, **92,** 85.
9. Journaux, Y., Sletten, J. and Kahn, O., *Inorg. Chem.*, 1985, **24,** 4063.
10. Li, Y. T., Liao, D. Z., Jiang, Z. H. and Wang, G. L., *Polyhedron*, 1995, **14,** 2209.
11. Zhang, Z. Y., Liao, D. Z., Jiang, Z. H., Hao, S. Q., Yao, X. K., Wang, H. G. and Wang, G. L., *Inorg. Chim. Acta*, 1990, **173,** 201.
12. Liao, D. Z., Li, L. C., Jiang, Z. H., Yan, S. P., Cheng, P. and Wang, G. L., *Trans. Met. Chem.*, 1992, **17,** 356.
13. Mathoniere, C., Kahn, O., Daran, J.-C., Hilbig, H. and Kohler, F. H., *Inorg. Chem.*, 1993, **32,** 4057.
14. Li, Y. T., Jiang, Z. H., Ma, S. L., Li, X. Y., Liao, D. Z., Yan, S. P. and Wang, G. L., *Polyhedron*, 1994, **13,** 475.
15. Ma, S. L., Liao, D. Z., Jiang, Z. H., Yan, S. P. and Wang, G. L., *Polyhedron*, 1994, **13,** 1647.
16. Benelli, C., Fabrett, A. C. and Giusti, A., *J. Chem. Soc., Dalton Trans.*, 1993, **3,** 409.
17. Sanz, J. L., Ruiz, R., Gleizes, A., Lloret, F., Faus, J., Julve, M., Borras-Almenar, J. J. and Journaux, Y., *Inorg. Chem.*, 1996, **35,** 7384.
18. Li, Y. T., Yan, C. W. and Liao, D. Z., *Trans. Met. Chem.*, in press.
19. Ma, S. L., Jiang, Z. H., Liao, D. Z., Yan, S. P. and Wang, G. L., *Polyhedron*, 1993, **12,** 1523.
20. Selwood, P. W., *Magnetochemistry*, pp. 78–79, Interscience, New York, 1956.
21. Coucouvanis, D. J., *J. Am. Chem. Soc.*, 1970, **92,** 707.
22. Okawa, H. and Kida, S., *Inorg. Chim. Acta*, 1997, **33,** 253.
23. Liao, D. Z., Zhao, Q. H., Zhang, Z. Y. and Wang, G. L., *Trans. Met. Chem.*, 1991, **16,** 209.
24. Zhong, Z. J., Okawa, H., Matsumoto, N., Sakiyama, H. and Kida, S., *J. Chem. Soc., Dalton Trans.*, 1991, 497.
25. Geary, W. J., *Coord. Chem. Rev.*, 1971, **7,** 81.
26. Lioret, E., Journau, Y., Julve, M., *Inorg. Chem.*, 1990, **29,** 3967.
27. Nakamoto, K., *Infrared and Raman Spectra of Inorganic and Coordination Compounds*, 4th Edn., Wiley, New York, 1986.
28. Thimmaiah, K. N., Lloyd, W. D. and Chandrappa, G. T., *Inorg. Chim. Acta*, 1985, **106,** 81.
29. Sakamoto, M., Takagi, M., Ishimori, T. and Okawa, H., *Bull. Chem. Soc. Japan*, 1988, **61,** 1613.
30. Lambert, S. L., Spiro, C. L., Gagne, R. R. and Hendrickson, D. N., *Inorg. Chem.*, 1986, **21,** 118.
31. Liao, D. Z., Zhuang, J. Z., Okawa, H. and Kida, S., *Inorg. Chim. Acta*, 1986, **21,** 118.
32. Dance, I. G., *Inorg. Chim. Acta*, 1974, **9,** 77.
33. Hay, P. J., Thibeault, J. C. and Hoffmann, R., *J. Am. Chem. Soc.*, 1975, **97,** 4884.
34. Kahn, O. and Charlot, M. F., *Nouv. J. Chem.*, 1980, **4,** 567.
35. Morgenstern-Badarau, I., Rerat, M., Kahn, O., Jaud, J. and Galy, J., *Inorg. Chem.*, 1982, **21,** 3050.
36. Brewer, G. A. and Sinn, E., *Inorg. Chem.*, 1987, **26,** 1529.

Pergamon

PII: S0277-5387(97)00336-7

Polyhedron Vol. 17, No. 8, pp. 1317–1322, 1998
© 1998 Elsevier Science Ltd
All rights reserved. Printed in Great Britain
0277-5387/98 $19.00+0.00

Synthesis and structure of binuclear complexes of palladium and platinum containing bridging diphenylphosphinate ligand

Vimal K. Jain[a]* and Ray J. Butcher[b]

[a] Chemistry Division, Bhabha Atomic Research Centre, Trombay, Mumbai 400 085, India

[b] Department of Chemistry, Howard University, Washington, DC 20059, U.S.A.

(Received 18 April 1997; accepted 6 August 1997)

Abstract—Treatment of $[M_2Cl_2(\mu\text{-}Cl)_2(PR_3)_2]$ (M/PR_3=Pt/PEt_3, Pt/PBu_3, Pt/PMe_2Ph, Pt/$PMePh_2$, Pd/PMe_2Ph) with AgO_2PPh_2 at room temperature, gave diphenylphosphinato-bridged binuclear complexes $[M_2Cl_2(\mu\text{-}O_2PPh_2)_2(PR_3)_2]$. These complexes were characterized by NMR spectroscopy and elemental analysis. Crystal and molecular structure of $[Pt_2Cl_2(\mu\text{-}O_2PPh_2)_2(PMe_2Ph)_2]$ has been determined by single crystal X-ray diffraction. The eight-membered metallocyclic ring "$Pt_2(O_2P)_2$" has a boat conformation with Pt···Pt separation of 3.2212(6) Å. © 1998 Elsevier Science Ltd. All rights reserved

Keywords: palladium; platinum; NMR; diphenylphosphinate; X-ray.

Recently, we have isolated and characterized a series of binuclear palladium and platinum complexes of the type $[M_2X_2(\mu\text{-}Y)_2(PR_3)_2]$ containing anionic 1-, 2-, and 3-atom bridging ligands [1,2,3–6]. The latter family of ligands showed unusual behaviour. With certain ligands, such as dithiophosphate, only mononuclear complexes were formed exclusively [7] while others, such as 2-mercaptopyridinate, showed monomer⇌dimer equilibrium in solution [8]. However, ligands with smaller "bite" gave binuclear complexes with (e.g. carboxylate, triazenide) [3,4] or without (e.g. amidine, 2-hydroxypyridinate) [5,6] M—M interactions in a d^8 metal ion configuration. This has motivated us to examine molecules containing anionic 3-atom bridging ligands with different bite.

Diphenylphosphinic acid is isostructural and isoelectronic to carboxylic acids and is known to behave in a bridging fashion [9]. However, the ligand bites for two series of ligands are different, which may assist in stabilizing different structural forms. Indeed this is the case. For example, $[Pd_2Ph_2(\mu\text{-}OAc)_2(PPh_3)_2]$ has a "boat" conformation [10] with Pd···Pd distance of 3.079 Å while $[Pd_2Ph_2(\mu\text{-}O_2PPh_2)_2(PPh_3)_2]$ has a "chair" conformation [11] with Pd···Pd separation of 5.35 Å.

In view of the above and as part of our ongoing programme, we have synthesized and characterized binuclear complexes of palladium and platinum containing the bridging Ph_2PO_2-group.

RESULTS AND DISCUSSION

Treatment of $[M_2Cl_2(\mu\text{-}Cl_2)(PR_3)_2]$ with silver salt of diphenylphosphinic acid in 1 : 2 molar ratio readily gave diphenylphosphinato-bridged binuclear palladium and platinum complexes $[M_2Cl_2(\mu\text{-}O_2PPh_2)_2(PR_3)_2]$ **(I)** (M=Pt, PR_3=PEt_3, PBu_3, PMe_2Ph or $PMePh_2$; M=Pd, PR_3=PMe_2Ph) as cream coloured crystalline solids. When these samples were left in solution ($CDCl_3$ or C_6D_6) at room temperature for a few hours, some new species were formed (see Experimental). The ^1H NMR spectra of these complexes exhibited expected integration and peak multiplicities. The ^{31}P NMR spectra of these complexes displayed a single resonance for tertiary phosphine with platinum satellites (Table 1). The magnitude of ^1J(Pt–P) can be compared with the analogous acetato-bridged platinum complexes [3]. The bridging diphenylphosphinato group, in ^{31}P NMR spectra, also gave a single resonance which did not

* Author to whom correspondence should be addressed. Fax: 91-22-556 0750.

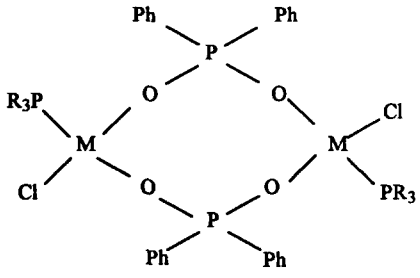

(M = Pd or Pt)

I

show ^2J platinum-phosphorus coupling. The $^{195}Pt\{^1H\}$ NMR spectrum of $[Pt_2Cl_2(\mu\text{-}O_2PPh_2)_2(PEt_3)_2]$ in C_6D_6 exhibited a doublet at δ −2988 ppm with ^1J(Pt–P) 4193 Hz. Unlike the spectra of acetato-bridged binuclear platinum complexes [3], the ^{31}P and ^{195}Pt NMR spectra for diphenylphosphinato-bridged molecules did not show any ^nJ(Pt···Pt) couplings. Absence of such couplings may be interpreted as increased platinum–platinum separation in these complexes due to increased ligand bite. In order to ascertain this conclusion structure of at least one complex, $[Pt_2Cl_2(\mu\text{-}O_2PPh_2)_2(PMe_2Ph)_2]$ has been established by X-ray diffraction.

The molecular structure of $[Pt_2Cl_2(\mu\text{-}O_2PPh_2)_2(PMe_2Ph)_2]$ together with the crystallographic numbering scheme is shown in Fig. 1. Selected bond lengths and angles are given in Table 2. The molecule consists of two square planar platinum atoms each coordinated with two *cis* oxygen atoms, a chloride group and a phosphine ligand. The two platinum atoms in the molecule are held together by two diphenylphosphinate bridges. The eight-membered central metallocyclic ring "$Pt_2(O_2P)_2$" has a boat-like conformation similar to the one reported for a number of acetato-bridged binuclear complexes, such as $[Pt_2(OAc)_2(\mu\text{-}OAc)_2(PPh_3)_2]$ (Pt···Pt = 3.10 Å) [12], $[Pd_2Cl_2(\mu\text{-}OAc)_2(PMe_2Ph)_2]$ (Pd···Pd = 2.946(2) Å) [13], $[Pd_2Ph_2(\mu\text{-}OAc)_2(PPh_3)_2]$ (Pd···Pd = 3.079(4) Å [10], $[Pd_2(\mu\text{-}OAc)_2(\eta^3\text{-}C_3H_5)_2]$ (Pd···Pd = 2.94 Å) [14]. It is noteworthy that the eight-membered metallocyclic ring in $[Pd_2Ph_2(\mu\text{-}O_2PPh_2)_2(PPh_3)_2]$ adopts a chair-like conformation with mean Pd···Pd distance of 5.35 Å [11].

The increased bite distance of O_2PPh_2 group as compared to acetate is reflected in lengthening of Pt···Pt separation [3.2212(6) Å]. The two Pt–P and Pt–Cl distances are essentially identical and compare well with the reported values [15]. There are distinctly two types of Pt–O distances [16], owing to different *trans* influence of the chloride and phosphine ligand. The Pt–O distances *trans* to chloride are shorter (~0.1 Å) than those *trans* to the phosphine.

EXPERIMENTAL

Diphenylphosphinic acid [17] and $[M_2Cl_2(\mu\text{-}Cl)_2(PR_3)_2]$ (M=Pd or Pt) [18] were prepared according to literature methods. All reactions were carried out in dried and distilled analytical grade solvents under a nitrogen atmosphere. ^1H, $^{31}P\{^1H\}$ and $^{195}Pt\{^1H\}$ NMR spectra were recorded on a Bruker DPX-300 spectrometer in freshly prepared $CDCl_3$ solutions unless otherwise specified. Chemical shifts are referred to internal chloroform peak (δ 7.26 ppm) for ^1H, external 85% H_3PO_4 for ^{31}P and external Na_2PtCl_6 solution in D_2O for ^{195}Pt. Elemental analysis were carried out by the Analytical Chemistry Division of this research centre.

Preparation of $[Pt_2Cl_2(\mu\text{-}O_2PPh_2)_2(PMe_2Ph)_2]$

To a stirred dichloromethane solution (15 cm^3) of $[Pt_2Cl_2(\mu\text{-}Cl)_2(PMe_2Ph)_2]$ (114 mg, 0.14 mmol) was added solid AgO_2PPh_2 (98 mg, 0.30 mmol). Colour faded immediately. The whole was stirred vigorously at room temperature for 3 h, and then centrifuged. Solution was filtered and the filtrate was concentrated *in vacuo*. The residue was recrystallized from dichloromethane–hexane mixture at 0°C. Yellow crystals thus obtained were separated, washed with hexane and dried in vacuum (yield 101 mg, 62%). Similarly all other complexes were prepared and the pertinent data are given in Table 1. When solutions of these complexes were left at room temperature for a few hours, an equilibrium between the parent species and a mixture of new species was established as revealed by ^{31}P and ^{195}Pt NMR spectroscopy. For example, spectra of a 24 h old benzene solution of $[Pt_2Cl_2(\mu\text{-}O_2PPh_2)_2(PEt_3)_2]$ showed a number of peaks which remained unchanged even after 3 days [δ ^{31}P: 42.8, 40.5 (parent complex), 38.2, 36.4 (O_2PPh_2); 8.6 (^1J(Pt–P) = 4122 Hz), 1.0 (d, 14 Hz), 0.78, 0.4, −0.1,

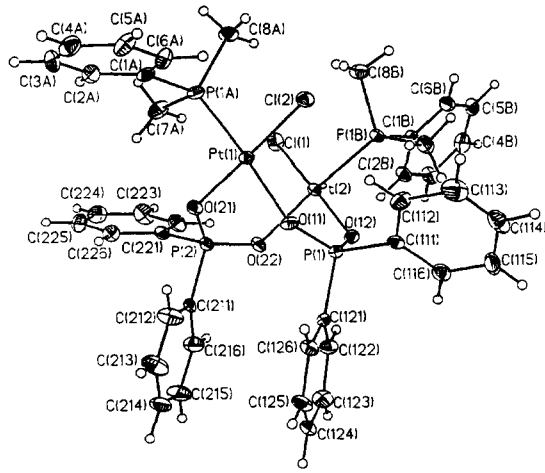

Fig. 1.

Table 1. M.P., analytical and NMR (^{1}H and ^{31}P) data for $[M_2Cl_2(\mu\text{-}O_2PPh_2)_2(PR_3)_2]$ complexes

Complex	m.p., °C	% Found (calc)		^{31}P NMR data			^{1}H NMR data
		C	H	δ O_2PPh_2	δ PR_3	^1J(Pt–P) in Hz	
$[Pt_2Cl_2(\mu\text{-}O_2PPh_2)_2(PEt_3)_2]^a$	169–170	38.9 (38.2)	4.3 (4.4)	40.3	−0.7	4152	1.10 (m, P–C–CH_3), 1.67 (m, PCH_2-); 7.16–7.30 (m), 7.68–7.74 (m)(Ph)
$[Pt_2Cl_2(\mu\text{-}O_2PPh_2)_2(PBu_3)_2]^b$	126–128	44.8 (44.3)	5.9 (5.7)	37.2	−11.4	4136	0.87 (m, PCCC–CH_3); 1.30 (m), 1.54 (m, br) ($PCH_2CH_2CH_2$-), 7.21–7.31 (m), 7.76–7.80 (m)(Ph)
$[Pt_2Cl_2(\mu\text{-}O_2PPh_2)_2(PMe_2Ph)_2]^a$	176–178[c]	40.3 (41.0)	3.2 (3.6)	41.5	−28.6	4286	1.57 (d, 12.5 Hz, PMe_2); 7.01–7.15 (m), 7.40–7.50 (m), 7.93–7.97 (m)(Ph)
$[Pt_2Cl_2(\mu\text{-}O_2PPh_2)_2(PMePh_2)_2]^a$	172–174[c]	46.8 (46.3)	3.5 (3.6)	38.4	−18.5	4336	1.87 (d, 12.0 Hz, PMe); 6.99–7.36 (m), 7.81–7.85 (m)(Ph)
$[Pd_2Cl_2(\mu\text{-}O_2PPh_2)_2(PMe_2Ph)_2]^a$	155–156[c]	47.3 (48.0)	3.8 (4.2)	36.8	9.8	–	1.56 (d, 13.5 Hz, PMe_2); 6.99–7.14 (m), 7.44–7.51 (m), 7.89–7.95 (m)(Ph)

[a] Recrystallized from CH_2Cl_2-hexane mixture in 60–70% yield.
[b] Recrystallized from hexane in 61% yield.
[c] Decompose or melts with decomposition.

Table 2. Selected bond distances (Å) and angles (°) for $[Pt_2Cl_2(\mu\text{-}O_2PPh_2)_2(PMe_2Ph)_2]$

Pt(1)—Pt(2)	3.2212(6)	P(2)—O(21)	1.538(6)
Pt(1)—P(1A)	2.205(2)	P(2)—O(22)	1.510(6)
Pt(2)—P(1B)	2.195(2)	P(1)—C(111)	1.807(9)
Pt(1)—Cl(2)	2.282(2)	P(1)—C(121)	1.795(8)
Pt(2)—Cl(1)	2.284(2)	P(2)—C(211)	1.799(9)
Pt(1)—O(21)	2.033(5)	P(2)—C(221)	1.798(9)
Pt(1)—O(11)	2.137(5)	P(1A)—C(7A)	1.806(10)
Pt(2)—O(22)	2.136(5)	P(1A)—C(8A)	1.796(9)
Pt(2)—O(12)	2.036(5)	P(1A)—C(1A)	1.835(9)
P(1)—O(11)	1.510(6)	P(1B)—C(7B)	1.794(9)
P(1)—O(12)	1.533(6)	P(1B)—C(8B)	1.799(9)
		P(1B)—C(1B)	1.822(8)
O(21)—Pt(1)—O(11)	87.6(2)	O(12)—Pt(2)—O(22)	85.1(2)
O(11)—Pt(1)—P(1A)	174.4(2)	O(22)—Pt(2)—P(1B)	176.4(2)
O(11)—Pt(1)—Cl(2)	90.3(2)	O(22)—Pt(2)—Cl(1)	93.5(2)
O(21)—Pt(1)—P(1A)	89.7(2)	O(12)—Pt(2)—P(1B)	91.9(2)
O(21)—Pt(1)—Cl(2)	176.3(2)	O(12)—Pt(2)—Cl(1)	176.9(2)
P(1A)—Pt(1)—Cl(2)	92.05(9)	P(1B)—Pt(2)—Cl(1)	89.37(9)
P(1)—O(11)—Pt(1)	134.0(3)	P(1)—O(12)—Pt(2)	124.4(3)
P(2)—O(21)—Pt(1)	127.5(4)	P(2)—O(22)—Pt(2)	128.8(3)
C(7A)—P(1A)—Pt(1)	113.7(3)	C(7B)—P(1B)—Pt(2)	113.5(3)
C(8A)—P(1A)—Pt(1)	116.3(4)	C(8B)—P(1B)—Pt(2)	114.8(4)
C(1A)—P(1A)—Pt(1)	109.8(3)	C(1B)—P(1B)—Pt(2)	114.2(3)
O(11)—P(1)—O(12)	117.4(3)	O(22)—P(2)—O(21)	117.7(3)
O(12)—P(1)—C(111)	105.9(4)	O(21)—P(2)—C(211)	105.9(4)
O(12)—P(1)—C(121)	107.9(3)	O(21)—P(2)—C(221)	107.8(4)
O(11)—P(1)—C(111)	110.0(4)	O(22)—P(2)—C(211)	110.1(4)
O(11)—P(1)—C(121)	109.6(3)	O(22)—P(2)—C(221)	109.8(4)
C(121)—P(1)—C(111)	105.3(4)	C(221)—P(2)—C(211)	104.7(4)
C(8A)—P(1A)—C(7A)	104.6(6)	C(7B)—P(1B)—C(8B)	103.9(5)
C(7A)—P(1A)—C(1A)	105.8(5)	C(8B)—P(1B)—C(1B)	105.3(4)
C(8A)—P(1A)—C(1A)	105.8(5)	C(7B)—P(1B)—C(1B)	104.0(5)

-0.4, -0.7 (^1J(Pt–P) = 4155 Hz, parent complex), -2.0 (PEt_3). δ ^{195}Pt: -2983 (d, ^1J(Pt–P) = 4190 Hz; parent complex, major component); -3022 (d, ^1J(Pt–P) = 3949 Hz); -3026 (d, ^1J(Pt–P) = 4123 Hz); -3054 (d, ^1J(Pt–P) = 4200 Hz); -3138 (d, ^1J(Pt–P) = 4136 Hz].

X-ray crystallography

All measurements were made at 20 ± 2°C on a Rigaku AFC6S diffractometer using graphite monocromated Mo–K_α radiation (λ = 0.71073 Å). Crystal data and data collection details are given in Table 3. The data were corrected for Lorentz and polarization effects. The structure was solved by a combination of the Patterson method and direct methods [19] and refined by full-matrix least-squares on F^2. Neutral atom factors were taken from Cromer and Waber [20]. Anomalous dispersion effects were included in F_{calc} [21]. All calculations were performed using the TEXSAN [23] crystallographic software package of the Molecular Structure Corporation. The numbering scheme employed is shown in Fig. 1, drawn with the ORTEP program [24].

Table 3. Crystal data and structure refinement details for $[Pt_2Cl_2(\mu\text{-}O_2PPh_2)_2(PMe_2Ph)_2]$

Empirical formula	$C_{40}H_{42}Cl_2O_4P_4Pt_2$
Formula weight	1171.70
Temperature	293(2) K
Wavelength	0.71073 Å
Crystal system	Monoclinic
Space group	$P2_1/n$
Unit cell dimensions	a = 16.953(3) Å
	b = 11.850(2) Å
	c = 20.831(3) Å
	β = 97.662(8)°
Volume	4147.7(1) Å^3
Z	4
Density (calculated)	1.876 Mg/m^3
Absorption coefficient	7.061 mm^{-1}
F(000)	2256
Crystal size	0.09 × 0.6 × 0.22 mm
θ range for data collection	2.10 to 27.50°
Index ranges	$0 \leqslant h \leqslant 19$, $0 \leqslant k \leqslant 15$, $-27 \leqslant l \leqslant 26$
Reflections collected	9446
Independent reflections	9112 (R_{int} = 0.0429)
Absorption correction	Semi-empirical from Ψ-scans
Max. and min. transmission	0.6564 and 0.2609
Refinement method	Full-matrix least-squares on F^2
Data/restraints/parameters	9108/0/516
Goodness-of-fit on F^2	1.037
Final R indices [$I > 2\sigma(I)$]	$R1$ = 0.0461, $wR2$ = 0.0901
R indices (all data)	$R1$ = 0.0884, $wR2$ = 0.1073
Extinction coefficient	0.00005(3)
Largest diff. peak and hole	1.498 and -1.135 eÅ^{-3}

Acknowledgements—We thank Drs J. P. Mittal and C. Gopinathan for their interest in this work. We also thank the Analytical Chemistry Division, Bhabha Atomic Research Centre, Mumbai for microanalyses.

REFERENCES

1. Jain, V. K., Kannan, S. and Bohra, R., *Polyhedron*, 1992, **11,** 155; Jain, V. K. and Kannan, S., *J. Organomet. Chem.*, 1992, **439,** 231; Jain, V. K., Kannan, S., Butcher, R. J. and Jasinski, J. P., *J. Chem. Soc., Dalton Trans.*, 1993, 1509; Singhal, A. and Jain, V. K., *J. Chem. Soc., Dalton Trans.*, 1993, 1515; Singhal, A. and Jain, V. K., *J. Organomet. Chem.*, 1995, **494,** 74.
2. Jain, V. K., Kannan, S. and Tiekink, E. R. T., *J. Chem. Soc., Dalton Trans.*, 1992, 2231; Jain, V. K., Kannan, S. and Tiekink, E. R. T., *J. Chem. Soc., Dalton Trans.*, 1993, 3625; Singhal, A., Jain, V. K. and Kannan, S., *J. Organomet. Chem.*, 1993, **447,** 317.
3. Kannan, S. and Jain, V. K., *Mag. Res. Chem.*, 1990, **28,** 1007.
4. Singhal, A. and Jain, V. K., *Polyhedron*, 1995, **14,** 285.
5. Singhal, A. and Jain, V. K., *Can. J. Chem.*, 1996, **74,** 2018.
6. Jain, V. K., *Trans. Met. Chem.*, 1996, **21,** 494.
7. Jain, V. K. and Chaudhury, S., *J. Organomet. Chem.*, 1994, **468,** 279; Jain, V. K., Chaudhury, S., Vyas, A. and Bohra, R., *J. Chem. Soc., Dalton Trans.*, 1994, 1207.
8. Gupta, M., Cramer, R. E., Ho, K., Pettersen, C., Mishina, S., Belli, J. and Jensen, C. M., *Inorg. Chem.*, 1995, **34,** 60.
9. Jain, V. K., *Coord. Chem. Rev.*, 1994, **135/136,** 809.
10. Hursthouse, M. B., Sloan, O. D., Thornton, P. and Walker, N. P. C., *Polyhedron*, 1986, **5,** 1475.
11. Kozitsyna, N. Yu., Ellern, A. M., Antipin, M. Yu., Struchkov, Yu. T. and Moiseev, I. I., *Mendeleev Commun.*, 1991, **3,** 92.
12. Kozitsyna, N. Yu., Surashskaya, M. V., Larina, T. B., Kozmin, P. A., Kotelnikova, A. C. and Moiseev, I. I., *Izv. Akad. Nauk SSSR, Ser. Khim.*, 1989, **8,** 1894.
13. Wong-Ng, W., Cheng, P. T., Kocman, V., Lüth, H. and Nyburg, S. C., *Inorg. Chem.*, 1979, **18,** 2620.
14. Churchill, M. R. and Mason, R., *Nature*, 1964, **204,** 777.
15. Clark, H. C., Ferguson, G., Jain, V. K. and Parvez, M., *Inorg. Chem.*, 1985, **24,** 1477; *Inorg. Chem.*, 1986, **25,** 3808.
16. Tan, A. L., Low, P. M. N., Zhou, Z. Y., Zheng, W., Wu, B. M., Mak, T. C. W. and Hor, T. S. A., *J. Chem. Soc., Dalton Trans.*, 1996, 2207.
17. Kosolapoff, G. M., "Organophosphorus Compounds", J. Wiley, New York, 1950.
18. Hartley, F. R., *The Chemistry of platinum and palladium*, Applied Science Publishers Ltd, London, 1973.
19. Calabrese, J. C., Ph.D. Thesis, University of Wisconsin, Madison (1972); Beurskens, P. T., Tech-

nical Report 1984/1 Crystallography Laboratory, Toernoolveld 6225 Ed, Nijmegen, The Netherlands.
20. Cromer, D. T. and Waber, J. T., International Tables for X-ray Crystallography, Kynoch Press, Birmingham, 1974, Vol. 4, Table 2.2 A.
21. Ibers, J. A. and Hamilton, W. C., *Acta Cryst.*, 1964, **17,** 781.
22. Cromer, D. T., International Tables for X-ray Crystallography, Kynoch Press, Birmingham, 1974, Vol. 4, Table 2.3.1.
23. TEXSAN, Structure Analysis Package, Molecule Structure Corporation, 1985.
24. Johnson, C. K., ORTEP II, Report ORNL-5138, Oak Ridge National Laboratory, Oak Ridge, TN, 1996.

Pergamon

PII: S0277-5387(97)00314-8

Polyhedron Vol. 17, No. 8, pp. 1323–1328, 1998
© 1998 Elsevier Science Ltd
All rights reserved. Printed in Great Britain
0277-5387/98 $19.00+0.00

Silver, copper and nickel complexes of 1-oxa-4,7-dithiacyclononane and 1-oxa-4,8-dithiacyclodecane

Weimin Liang,† Shuang Liu,‡ C. Robert Lucas* and David O. Miller

Department of Chemistry, Memorial University of Newfoundland, St. John's, Newfoundland, Canada, A1B 3X7

(Received 6 June 1997: accepted 15 July 1997)

Abstract—The complexes $[Ag(L1)(PPh_3)][CF_3SO_3]$, $[Cu(L1)(PPh_3)][ClO_4]$ and $[Ni(L2)_2][ClO_4]_2$ have been prepared. L1 = 1-oxa-4,7-dithiacyclononane and L2 = 1-oxa-4,8-dithiacyclodecane. NMR, conductance and electrochemical properties are described. © 1998 Elsevier Science Ltd. All rights reserved

Keywords: macrocycles; thioethers; metal complexes; X-ray structures.

The appearance in 1981 of Murray and Hartley's review [1] of the coordination chemistry of thioethers provoked considerable interest in them as monodentate and eventually as polydentate donors. Since that time, a substantial body of knowledge has been accumulated concerning these donors in both cyclic and acyclic ligands and this knowledge has begun to appear in current reviews [2,3]. More recently, interest in modification of complex properties by incorporation of other donors, in particular nitrogen, has become apparent [4–7] but little effort has been devoted to ethereal oxygen as a modifier [8,9]. As part of our long term interest in complexes of thioether [10] and modified thioether ligands [11], we have examined the structures and a few properties of nickel, copper and silver complexes of L1 and L2 that contain both ether and thioether donors as well as phosphine donors in some cases. The results are compared to those from studies of other related N,S-donor macrocyclic ligand complexes.

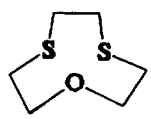

L1

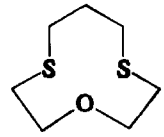

L2

EXPERIMENTAL

Commercially available reagents were obtained from the Aldrich Chemical Co. Inc., or from Morton Thiokol Alfa Products Inc. and were used without further purification. Preparations for ligands L1 and L2 have been reported previously [10,12]. NMR data were obtained by using a General Electric 300-NB instrument. Magnetic susceptibility data were obtained at room temperature by the Faraday method. The calibrant was $HgCo(NCS)_4$. Electrochemical measurements were carried out under a nitrogen atmosphere at room temperature by using a Cypress Systems, Inc., CS-1087 computer-controlled potentiostat. Solution concentrations were 10^{-3} mol/L in complex and 0.1 mol/L in supporting electrolyte (tetraethylammonium perchlorate). Voltammograms were recorded in acetonitrile by using a glassy carbon working electrode that was pre-polished with 0.3 μm Al_2O_3, a platinum counter electrode and an aqueous saturated calomel reference electrode checked periodically relative to a 1.0×10^{-3} mol/L solution of ferrocene in acetonitrile containing 0.1 mol/L tetraethylammonium perchlorate for which the ferrocene/ferrocenium reduction potential was 400 mV. The ref-

* Author to whom correspondence should be addressed.

† Present address: Department of Computer Science, The Technical University of Nova Scotia, Halifax, N.S., Canada, B3J 2X4.

‡ Present address: Dupont Merck Pharmaceutical Company, Radiopharmaceutical Division, 331 Treble Cove Rd., N. Billerica, MA 01862, U.S.A.

erence electrode was separated from the bulk of the solution by a porous Vycor tube. Junction potential corrections were not used. Conductance data were obtained by using a General Radio Co. Type 1605-AH bridge with impedance comparator and a constant-temperature bath adjusted to 25°C. X-ray diffraction data were collected by using a Rigaku AFC6S diffractometer. Analyses were performed by Canadian Microanalytical Service Ltd.

Preparation

$[Ag(L1)(PPh_3)][CF_3SO_3]$. Solutions of L1 (66 mg, 0.40 mmol) in methanol (5 cm^3) and $AgCF_3SO_3$ (103 mg, 0.400 mmol) in methanol (5 cm^3) were mixed and stirred for 5 min. To this solution was added $P(C_6H_5)_3$ (105 mg, 0.400 mmol) in methanol (10 cm^3). The resulting solution was allowed to evaporate slowly to a final volume of ~ 2 cm^3 when colourless crystals formed that were collected and washed with a little cold methanol and dried in air. Yield: 129 mg (47%). Anal. calcd for $C_{25}H_{27}AgF_3O_4PS_3$: C, 43.93; H, 3.98. Found: C, 43.54; H, 3.80. NMR ($CDCl_3$, in ppm from TMS int. std.), ^1H; 7.47 (m, 15H) C_6H_5, 3.68 (t, $J = 5.1$ Hz, 4H) $—CH_2OCH_2—$, 3.09 (s, 4H) $—SCH_2CH_2S—$, 2.84 (t, $J = 5.1$ Hz, 4H) $—CH_2SCH_2CH_2SCH_2—$.

$[Cu(L1)(PPh_3)][ClO_4]$. Solutions of L1 (82 mg, 0.50 mmol) in acetonitrile (10 cm^3) and $[Cu(CH_3CN)_4][ClO_4]$ (164 mg, 0.500 mmol) in acetonitrile (10 cm^3) were mixed and refluxed with stirring for 2 h before being cooled to room temperature. To the solution was added $P(C_6H_5)_3$ (131 mg, 0.500 mmol) in acetonitrile (5 cm^3). The solution was allowed to evaporate slowly to a final volume of ~ 4 cm^3 when colourless crystals formed that were separated, washed with a small amount of acetronitrile and dried in air. Yield: 215 mg (73%). Anal. calcd for $C_{24}H_{27}ClCuO_5PS_2$: C, 48.89; H, 4.62. Found: C, 48.70; H, 4.65.

$[Ni(L2)_2][ClO_4]_2$. A solution of $Ni(ClO_4)_2 \cdot 6H_2O$ (180 mg, 0.492 mmol) in methanol (5 cm^3) to which was added nitromethane (20 cm^3) was mixed with a solution of L2 (178 mg, 1.00 mmol) in nitromethane (10 cm^3). The deep blue solution that formed was filtered and left standing to evaporate solvent slowly until blue needle-like crystals formed. These were collected, washed with small amounts of dichloromethane, acetone and finally diethyl ether and dried in air. Yield: 212 mg (69%). Anal. calcd for $C_{14}H_{28}Cl_2NiO_{10}S_4$: C, 27.38; H, 4.59; S, 20.88; Ni, 9.56. Found: C, 27.29; H, 4.59; S, 20.39; Ni, 9.06. $\mu_{eff} = 2.98$ B.M. (22°C). ($\Lambda_M = 230$ ohm^{-1} cm^2 mol^{-1} in nitromethane at 4.6×10^{-4} mol/L).

X-ray studies

A summary of crystallographic data for $[Ag(L1)(PPh_3)][CF_3SO_3]$, $[Cu(L1)(PPh_3)][ClO_4]$ and $[Ni(L2)_2][ClO_4]_2$ is in Table 1. The diffraction intensities were collected at 299 K by the ω–2θ scan technique at a scan speed of 8°/min to a maximum 2θ value of 50.1°. Three standards were measured after every 150 reflections and no significant crystal decay was detected. The space groups were determined by systematic absences, packing considerations, a statistical analysis of intensity distribution and the successful solution and refinement of the structures. Unit cell parameters (Table 1) were determined by a least squares refinement of the setting angles for 19 reflections in the range $41.68 \leqslant 2\theta \leqslant 44.82°$ ($[Ag(L1)(PPh_3)][CF_3SO_3]$), 20 reflections in the range $38.43 \leqslant 2\theta \leqslant 43.35°$ ($[Cu(L1)(PPh_3)][ClO_4]$) and 18 reflections in the range $25.86 \leqslant 2\theta \leqslant 38.34°$ ($[Ni(L2)_2][ClO_4]_2$). Lorentz and polarization factors were applied and corrections were made for absorption. The structures were solved by direct methods [13,14] and refined by full matrix least-squares [15] with counting statistics weights. H-atom positions were calculated then refined and the hydrogens were assigned isotropic thermal parameters 20% greater than those of their bonding partners but the thermal parameters were not refined. H-atom positions were fixed for the final round of least squares refinement. Non-hydrogen atoms were refined anisotropically except in the structure of $[Cu(L1)(PPh_3)][ClO_4]$ where the ClO_4^- ion was refined isotropically and in the structure of $[Ni(L2)_2][ClO_4]_2$ where the disordered carbon, C(6), and most of the perchlorate oxygens were refined isotropically. The final cycle of refinement was based on 4032 observed reflections [$I > 2.00\sigma(I)$] and 380 variables ($[Ag(L1)(PPh_3)][CF_3SO_3]$), 1232 observed reflections [$I > 2.00\sigma(I)$] and 105 variables ($[Cu(L1)(PPh_3)][ClO_4]$) and 1348 observed reflections [$I > 2.00\sigma(I)$] and 139 variables ($[Ni(L2)_2][ClO_4]_2$) and converged. All calculations were performed with the TEXSAN crystallographic software package [16] of Molecular Structure Corporation. Scattering factors were taken from the usual source [17].

RESULTS AND DISCUSSION

The structure of $[Ag(L1)(PPh_3)][CF_3SO_3]$ is shown in Fig. 1 while selected bond lengths and angles are in Table 2.

There is a distorted pseudo-tetrahedral array of donor atoms about the silver with bond angles that lie in the range 85.41(4)–140.31(3)°. Angles at silver also involving atoms within the heterocyclic ring are all less than 86° due to formation of chelate rings whereas those between ring donors and the phosphorus atom are all greater than 113° and one [P—Ag—S1 = 140.31(3)°] is much greater. The range and magnitude of these angles are not unlike those reported for $[Ag_2L_2]^{2+}$ (L = 2,5,8,11-tetrathia[12](2,5)thiophenophane) [18]. The Ag—S bond lengths in $[Ag(L1)(PPh_3)][CF_3SO_3]$ [2.552(1), 2.572(1) Å] can be compared with those in $[Ag_2L_2]^{2+}$ (L = 2,5,8,11-

Table 1. Crystallographic data for $[Ag(L1)(PPh_3)][CF_3SO_3]$, $[Cu(L1)(PPh_3)][ClO_4]$ and $[Ni(L2)_2][ClO_4]_2$

	$[Ag(L1)(PPh_3)][CF_3SO_3]$	$[Cu(L1)(PPh_3)][ClO_4]$	$[Ni(L2)_2][ClO_4]_2$
Chem formula	$C_{25}H_{27}AgF_3O_4PS_3$	$C_{24}H_{27}ClCuO_5PS_2$	$C_{14}H_{28}Cl_2NiO_{10}S_4$
Fw		589.28	614.22
Space group	$P\bar{1}$ (#2)	$R\bar{3}$(h) (#148)	$R\bar{3}$c(h) (#167)
a (Å)	10.888(2)	11.044(4)	18.204(3)
b (Å)	14.529(3)		
c (Å)	10.247(4)	36.869(2)	38.023(9)
α (°)	108.47(2)		
β (°)	93.89(3)		
γ (°)	109.83(2)		
ρ_{calcd} (g cm^{-3})		1.507	1.682
V (Å^3)		3894(3)	10913(4)
Z		6	18
λ (Å)	0.71069	0.71069	0.71069
μ (cm^{-1})		12.28	14.01
R^a (%)		0.048	0.062
$R_w{}^b$ (%)		0.055	0.056

$^a R = \Sigma\|F_o| - |F_c\|/\Sigma|F_o|$.
$^b R_w = [(\Sigma w(|F_o| - |F_c|)^2/\Sigma wF_o^2)]^{1/2}$.

Table 2. Selected bond lengths (Å) and angles (°) in $[Ag(L1)(PPh_3)][CF_3SO_3]$

Ag—S(1)	2.552(1)	Ag—S(2)	2.572(1)
Ag—P(1)	2.3697(9)	Ag—O(1)	2.640(3)
S(1)—Ag—S(2)	85.41(4)	S(1)—Ag—P(1)	140.31(3)
S(2)—Ag—P(1)	134.24(3)	P(1)—Ag—O(1)	113.85(6)
S(1)—Ag—O(1)	72.94(7)	S(2)—Ag—O(1)	74.31(6)

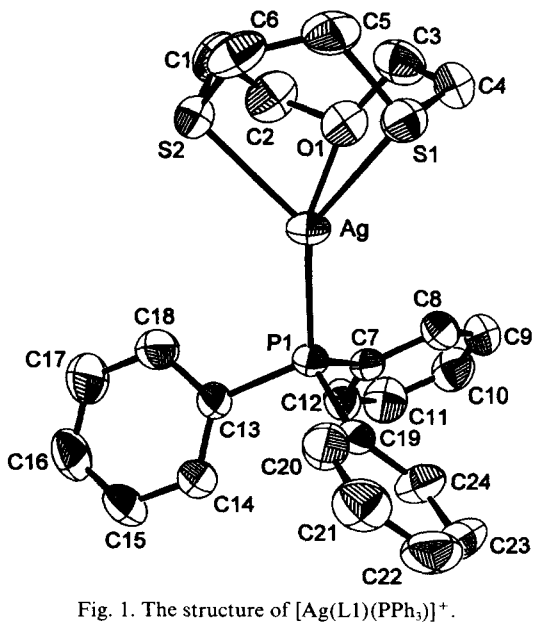

Fig. 1. The structure of $[Ag(L1)(PPh_3)]^+$.

tetrathia[12](2,5)thiophenophane) [18] which have an average length of 2.695 Å and a range of 2.564–2.995 Å. The Ag—P length [2.3697(9) Å] can be compared with that in *anti*-$[Ag_2(L')(PPh_3)_2]^{+2}$ (L' = 2,5,8,17, 20,23-hexathia[9](1,2)[9](4,5)cyclophane) [19] which is 2.407(3) Å and the Ag—O distance [2.640(3) Å] with that in $[(CH_2O)_6Ag_2][Ag][AsF_6]_3$ [2.458(5) Å] [20] or those in $[Ag([15]aneS_2O_3)]^+$ [2.667(5), 2.690(4), 2.492(4) Å] [21]. The conformation adopted by the ligand is [3,3,3] as a result of the interaction of the ether oxygen with the silver atom.

The structure of $[Cu(L1)(PPh_3)][ClO_4]$ is shown in Fig. 2 and selected bond lengths and angles are in Table 3.

The heterocyclic ligand is disordered about a three-fold axis with a chalcogen and two carbon atoms in the asymmetric unit. It was not possible to model the fragments separately so 'S(1)' represents 2/3 of a sulfur atom and 1/3 of an oxygen atom modelled with a 5/6 sulfur occupancy. Similarly C(7) and C(8) are a 2/3–1/3 superposition of two different methylene carbons which is reflected in the high thermal parameters of the two 'atoms'. The coordination geometry around copper is pseudo-tetrahedral with

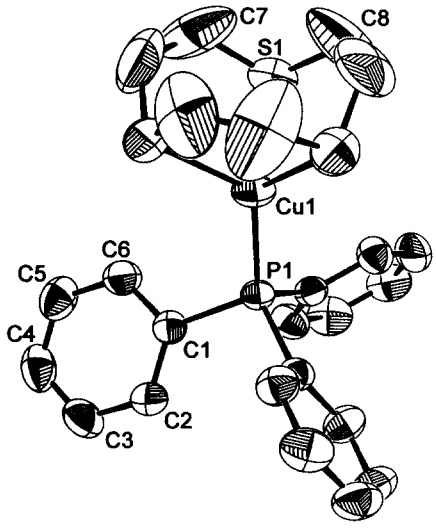

Fig. 2. The structure of $[Cu(L1)(PPh_3)]^+$.

bond angles at copper of 89.01(6)° for those within chelate rings while those involving the phosphorus atom are 125.96°. The bond lengths for all three Cu–L1 bonds have been determined to be the same [2.334(2) Å] while the Cu—P distance is found to be 2.188(2) Å. These may be compared to the Cu—S distances in $[Cu(3,6\text{-dithiaoctane})_2]^+$ which vary from 2.280(4) to 2.318(5) with an average of 2.303 Å [22] and to those in $[Cu(L)_2]^+$ (L = 2,5,8-trithia[9](2,5)thiophenophane) [23] which range from 2.301(3) to 2.392(3) with an average of 2.340 Å. Likewise, the Cu—P distance can be compared to those of 2.262(9) and 2.272(6) Å in $[(Cy_3P)_2(pzH)Cu]ClO_4 \cdot CH_3OH$ [24] or 2.190(2), 2.252(3) and 2.260(3) Å in $[Cu_2Br_2(PPh_3)_3]$ [25]. In the latter, one Ph_3P is in a sterically unencumbered position much like that in $[Cu(L1)(PPh_3)][ClO_4]$ and the corresponding Cu—P distances [2.190(2) and 2.188(2) Å] are very similar. Apparently, the change from two bridging bromines (as in $[Cu_2Br_2(PPh_3)_3]$) to two thioether and one ether (as in $[Cu(L1)(PPh_3)][ClO_4]$) as additional ligands has almost no influence on the Cu—P distance. There are few examples of Cu^I—O bond lengths in the literature but the Cu—O distance of 2.334(2) Å in $[Cu(L1)(PPh_3)][ClO_4]$ is longer than observed distances to carboxylate oxygens [1.923(5), 2.134(5), 1.945(6) and 2.107(6) Å] [26] and shorter than those to ether oxygens [27] [2.510(11) and 2.432(8) Å]. The Cu—O distance in $[Cu(L1)(PPh_3)][ClO_4]$ is also longer than those of 1.917(9) and 2.015(11) Å in the mixed-valence compound $[Cu_3Br_4(DMF)_2(H_2O)]_n$ in which the formal oxidation state of the copper atoms is on average 1.33 [28]. In fact, this distance is not unlike that in the Cu^{II} complex $CuCl_2 \cdot L$ (L = 1,9-bis(2-thienyl)-5-oxa-2,8-dithianonane) [11] [2.30(1) Å] which illustrates the ability of Cu to accommodate changes in oxidation state with or without a change in bond length in a manner reminiscent of its accommodating behaviour noted above with respect to bonds to phosphorus. The conformation of the ligand in this structure is [3,3,3], similar to that found in the analogous silver complex (*vide supra*) as a result of interaction between the oxygen atom of the ligand and the copper atom.

The structure of $[Ni(L2)_2][ClO_4]_2$ is shown in Fig. 3 and selected bond lengths and angles are in Table 4. The Ni—S lengths in pseudo-octahedral $[Ni(L2)_2][ClO_4]_2$ are 2.353(2) and 2.390(2) Å. The Ni—O bonds, which are not mutually *trans*, are 2.115(5) Å long. The larger Ni—S distance is typical of those in

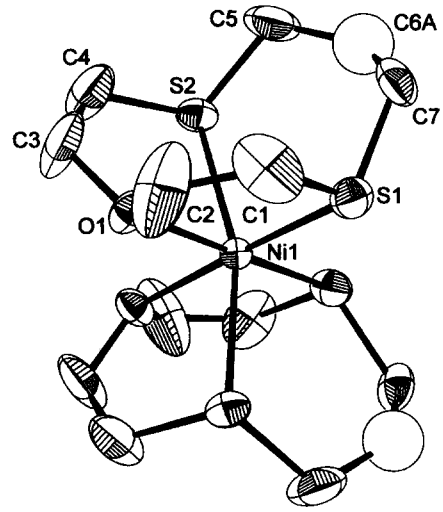

Fig. 3. The structure of $[Ni(L2)_2]^{2+}$.

Table 3. Selected bond lengths (Å) and angles (°) in $[Cu(L1)(PPh_3)][ClO_4]$

S(1)—Cu—S(2)	89.01(6)	S(1)—Cu—S(2)	89.01(6)
S(1)—Cu—O	89.01(6)	S(1)—Cu—P(1)	125.96(4)
S(2)—Cu—O	89.01(6)	S(2)—Cu—P(1)	125.96(4)
O—Cu—P(1)	125.96(4)		
Cu—S(1)	2.334(2)	Cu—S(2)	2.334(2)
Cu—O	2.334(2)	Cu—P(1)	2.188(2)

Table 4. Selected bond lengths (Å) and angles (°) in $[Ni(L2)_2][ClO_4]_2$

Ni—S(1)	2.353(2)	Ni—S(2)	2.390(2)
Ni—O(1)	2.115(5)		
S(1)—Ni—S(1)*	100.8(1)	O(1)—Ni—S(1)*	173.2(2)
S(2)—Ni—O(1)*	84.98(8)	O(1)—Ni—O(1)*	91.0(3)
S(2)—Ni—S(1)*	91.41(6)	S(2)—Ni—S(2)*	163.2(1)
S(1)—Ni—S(2)	99.34(8)	S(2)—Ni—O(1)*	85.0(2)
S(1)—Ni—O(1)	84.3(2)	S(2)—Ni—O(1)	83.2(2)

both linear [29] and cyclic [10] polythioether complexes. The smaller, however, is significantly shorter than the average length (2.43 Å) [1] of Ni—S bonds found in octahedral monodentate ligand complexes and slightly shorter than the usual range of lengths in cyclic ligand complexes as, for example, in $[Ni(9S3)_2]^{2+}$ [2.375(3)–2.400(5) Å] (9S3 = 1,4,7-trithiacyclononane) [30]. The general shortening is probably due to compression caused by use of a cyclic ligand while the extreme shortening may arise from the fact that the bond involved [Ni—S(1)] is *trans* to an ether oxygen. If thioethers participate in π-acid bonding whereas ethers do not, this would be the result expected. The Ni—O distance is unremarkable [29,31]. Bond angles range from 83.2(2) to 99.34(8)° and the greatest deviation from linearity across the Ni atom involves the angle S(2)—Ni—S(2) which is 163.2(1)°.

Coordination of L1 to Ag in $[Ag(L1)(PPh_3)][CF_3SO_3]$ produces a negligible (0.02, 0.04 ppm) shift in the nmr resonance frequencies (compared to the free ligand) [12] of hydrogens adjacent to the metal-bound thioether sites but a much larger (0.27 ppm) shift for hydrogens adjacent to the ethereal oxygen. This confirms the indication in the X-ray study that the oxygen atom is interacting with the silver atom. Coordination of the ligand also changes the coupling constants in the apparent triplet signals from 9.6 Hz in the free ligand to 5.1 Hz in the complex.

The cyclic voltammetric response of $[Ni(L2)_2][ClO_4]_2$ is very similar to that of its analogue with [20]aneO_2S_4 [10], the dimer of L2. That ligand supplies the same O_2S_4 donor set as two equivalents of L2 but in a single ring. Thus, $[Ni(L2)_2][ClO_4]_2$ is electrochemically silent between -0.7 and $+0.7$ V *vs* SCE unless the initial potential is set at less than -0.7 V or a scan into that region precedes a scan to $> +0.7$ V. Under the latter conditions, a wave at $+0.23$ V *vs* SCE occurs followed by a reduction wave at -1.06 V and then a minor return wave at -0.75 V and finally the major wave at $+0.23$ V *vs* SCE. On the basis of these observations, metal-based oxidation seems relatively unfavourable and the observed reduction is irreversible.

The conductivity of $[Ni(L2)_2][ClO_4]_2$ is roughly that of the 1:2 electrolytes, $[Ni(L)(H_2O)][ClO_4]_2 \cdot CH_3OH$, ($\Lambda_M$ = 205 ohm^{-1} cm^2 mol^{-1} in acetonitrile at 5.0×10^{-4} mol/L) (L = 1,9-bis(2-pyridyl)-2,5,8-trithianonane) [29] and $[Co(L')][ClO_4]_2$ (Λ_M = 199 ohm^{-1} cm^2 mol^{-1}) (nitromethane; 2.5×10^{-4} mol/L) (L′ = 1,12-bis(2-pyridyl)-2,5,8,11-tetrathiadodecane) [32] the structures and properties of which we have reported previously.

CONCLUSIONS

The ligand 1-oxa-4,7-dithiacyclononane (L1) adopts a [3,3,3] conformation in both the Ag^I and Cu^I complexes examined in this study and in this respect it resembles other [9]aneX_3 (X = N,S) ligands [33,34]. The interaction of ethereal oxygen with Cu^I and Ag^I by L1 is also observed in the behaviour of L2 with nickel. Thus, addition of an extra methylene to the ring does not alter substantially the ligands' coordination behaviour. In the literature, there are few X-ray structures of Cu^I or Ag^I involving ether or phosphine ligands and fewer still that have thioether donors as well, and it is usually argued that Cu^I and Ag^I being 'soft' acids should have little affinity for the 'hard' base oxygen. The present results are therefore significant in the sense that they show both thioether and ether donors coordinated to Cu^I and Ag^I. The X-ray structure of $[Ni(L2)_2][ClO_4]_2$ provides further evidence of the π-bonding capability of thioether sulfur through the observation of its short Ni—S bond *trans* to —O— compared to the longer Ni—S distance *trans* to —S—.

Acknowledgements—Financial support by the Natural Sciences and Engineering Research Council of Canada is acknowledged as is the assistance of Dr J. N. Bridson with the X-ray crystallography.

REFERENCES

1. Murray, S. G. and Hartley, F. R., *Chem. Rev.* 1981, **81,** 365.
2. Blake, A. J. and Schröder, M., *Adv. Inorg. Chem.* 1990, **35,** 1.
3. Reid, G. and Schröder, M., *Chem. Soc. Rev.* 1990, **19,** 239.
4. Bernardo, M. M., Heeg, M. J., Schroeder, R.

R., Ochrymowycz, L. A. and Rorabacher, D. B., *Inorg. Chem.* 1992, **31,** 191.
5. Chandrasekhar, S. and McAuley, A., *J. Chem. Soc., Dalton Trans.* 1992, 2967.
6. de Vries, N. and Reedijk, J., *Inorg. Chem.* 1991, **30,** 3700.
7. Blake, A. J., Reid, G. and Schröder, M., *J. Chem. Soc., Dalton Trans.* 1994, 3291.
8. Robinson, G. H., *Coord. Chem. Rev.* 1992, **112,** 227.
9. Adam, K. R., Antolovich, M., Baldwin, D. S., Duckworth, P. A., Leong, A. J., Lindoy, L. F., McPartlin, M. and Tasker, P. A., *J. Chem. Soc., Dalton Trans.* 1993, 1013.
10. Lucas, C. R., Liu, S. and Bridson, J. N., *Can. J. Chem.* 1995, **73,** 1023.
11. Wu, H. and Lucas, C. R., *Inorg. Chem.* 1993, **32,** 526.
12. Lucas, C. R. and Liang, W., *Inorg. Chem.*, submitted.
13. Gilmore, C. J., *J. Appl. Cryst.* 1984, **17,** 42.
14. Beurskens, P. T., in *Technical Report 1984/1*, Crystallographic Laboratory, Toernooiveld, 6525 Ed, Nijmegen, Netherlands (1984).
15. Function minimized: $\Sigma w(|F_o|-|F_c|)^2$ where $w = 4F_o^2/\sigma_2(F_o^2)$; $\sigma^2(F_o^2) = [S^2(C+R^2B)+(pF_o^2)^2]/Lp^2$ and S = scan rate; C = total integrated peak count; R = ratio of scan time to background counting time; B = total background count; Lp = Lorentz-polarization factor; p = p factor.
16. TEXSAN-TEXRAY Molecular Structure Package, Molecular Structure Corporation, Woodlands, TX, 1985.
17. International Tables for X-ray Crystallography, Vol. IV, Table 2.2A. Kynoch Press, Birmingham, England (1974).
18. Lucas, C. R., Liu, S., Newlands, M. J., Charland, J. P. and Gabe, E. J., *Can. J. Chem.* 1990, **68,** 644.
19. Loeb, S. J. and Shimizu, G. K. H., *Inorg. Chem.* 1993, **32,** 1001.
20. Roesky, H. W., Peymann, E., Schimkowiak, J., Noltemeyer, M., Pinkert, W. and Sheldrick, G. M., *Chem. Commun.* 1983, 981.
21. Blake, A. J., Reid, G. and Schröder, M., *Chem. Commun.* 1992, 1074.
22. Baker, E. N. and Norris, G. E., *J. Chem. Soc., Dalton Trans.* 1977, 877.
23. Lucas, C. R., Liu, S., Newlands, M. J., Charland, J. P. and Gabe, E. J., *Can. J. Chem.* 1988, **66,** 1506.
24. Pettinari, C., Marchetti, F., Polimante, R., Cingolani, A., Portalone, G. and Colapietro, M., *Inorg. Chim. Acta* 1996, **249,** 215.
25. Negita, H., Hiara, M., Kushi, Y., Kuramoto, M. and Okuda, T., *Bull. Chem. Soc. Jpn.* 1981, **54,** 1247.
26. Aalten, H. L., van Koten, G., Tromp, J., Stam, C. H., Goubitz, K., Mak, A. N. S. and van der Kerk-van Hoof, A., *Recl. Trav. Chim. Pays-Bas* 1989, **108,** 295.
27. Drew, M. G. B., Lavery, A., McKee, V. and Nelson, S. M., *J. Chem. Soc., Dalton Trans.* 1985, 1771.
28. Blake, A. J., Dorse, R. L., Rawson, J. M. and Winpenny, R. E. P., *Polyhedron* 1994, **13,** 2793.
29. Adhikary, B., Liu, S. and Lucas, C. R., *Inorg. Chem.* 1993, **32,** 5957.
30. Setzer, W. N., Ogle, C. A., Wilson, G. S. and Glass, R. S., *Inorg. Chem.* 1983, **22,** 266.
31. Blake, A. J., Halcrow, M. A. and Schröder, M., *J. Chem. Soc., Dalton Trans.* 1992, 2803.
32. Adhikary, B., Liu, S. and Lucas, C. R., *Inorg. Chim. Acta* 1997, in press.
33. Boeyens, J. C. A. and Dobson, S. M., in *Stereochemistry of Organometallic and Inorganic Compounds*, Vol. 2. Elsevier, Amsterdam (1982).
34. Hancock, R. D., Dobson, S. M. and Boeyens, J. C. A., *Inorg. Chim. Acta* 1987, **133,** 221.

Pergamon

PII: S0277-5387(97)00304-5

Polyhedron Vol. 17, No. 8, pp. 1329–1341, 1998
© 1998 Elsevier Science Ltd. All rights reserved
Printed in Great Britain
0277-5387/98 $19.00+0.00

The synthesis and characterisation of some stable Ce^{III} β-diketonate compounds; X-ray crystal structures of $[Ce_2(etbd)_6(tetraglyme)]$ and $[NH_4][Ce(etbd)_4]$ [etbd = 1-ethoxy-4,4,4-trifluorobutane-1,3-dionate and tetraglyme = $CH_3O(CH_2CH_2O)_4CH_3$]

Ian Baxter,[a] Jawwad A. Darr,[b]† Michael B. Hursthouse,[a]* K. M. Abdul Malik,[a] John McAleese,[b] and D. Michael P. Mingos[b]*

[a]Department of Chemistry, University of Wales Cardiff, P.O. Box 912, Park Place, Cardiff CF1 3TB, U.K.

[b]Department of Chemistry, Imperial College of Science, Technology and Medicine, South Kensington, London SW7 2AY, U.K.

(Received 12 June 1997; accepted 10 July 1997)

Abstract—The cerium(III) β-diketonate compounds $[Ce_2(\beta\text{-diket})_6(tetraglyme)]$ [β-diket = etbd (1-ethoxy-4,4,4-trifluorobutane-1,3-dionate) **1**, hfpd (1,1,1,5,5,5-hexafluoropentane-2,5-dionate) **2** and hfod (1,1,1,2,2,3,3-heptafluoro-7,7-dimethyloctane-4,6-dionate) **3** and tetraglyme = $CH_3O(CH_2CH_2O)_4CH_3$] were synthesised from the reaction of $CeCl_3 \cdot 7H_2O$ and tetraglyme with an aqueous ethanolic solution of Na(β-diket). The unusual reaction of cerium ammonium nitrate, $[Ce(NH_4)_2(NO_3)_6]$, and Hetbd in an ammoniacal mixture of dimethoxyethane resulted in the ammonium cerium(III) salt, $[NH_4][Ce(etbd)_4]$ **4**, rather than the expected cerium(IV) species. All compounds were characterised by spectroscopic methods and in the cases of **1** and **4**, also by X-ray crystallography. The structure of $[Ce_2(etbd)_6(tetraglyme)]$ **1** consists of two $Ce(etbd)_3$ moieties bridged by a tetraglyme molecule. The two Ce atoms in this molecule are eight and nine coordinate respectively with distorted docahedral and monocapped square antiprismatic geometries. The crystal structure of **4** is stabilised by an extensive hydrogen bonding network involving the NH_4^+ cation and one oxygen atom from each of the four etbd ligands belonging to the $[Ce(etbd)_4]^-$ anion, with additional $NH_4^+ \cdots F_3C(etbd)$ interactions. The Ce atom in the $[Ce(etbd)_4]^-$ anion is eight coordinate with a distorted square antisprismatic geometry. All the complexes are air and moisture stable, and some compounds have good volatilities and thermal stabilities, as demonstrated by sublimation and TGA/DSC studies. © 1998 Elsevier Science Ltd. All rights reserved

Keywords: cerium(III) β-diketonates; tetraglyme; chemical vapour deposition (CVD); X-ray structure.

Ceria supported gadolinia with the composition $Ce_{0.9}Gd_{0.1}O_{1.95}$ (CSG) is an attractive material for low temperature solid oxide fuel cells (SOFCs) [1]. These materials can operate satisfactorily at substantially lower temperatures (ca 400–600°C) compared to present SOFC electrolytes. The preparation of thin films of ceria (CeO_2) from chemical vapour deposition (CVD) has led to a number of recent reports of volatile molecular precursors [2]. Previous reports of cerium alkoxides resulted in either large, involatile oligomers or extremely air and thermally sensitive compounds which were unsuitable for CVD [3]. The thermal properties and stability of some cerium(IV) β-dike-

* Authors to whom correspondence should be addressed. E-mail: malikka@cardiff.ac.uk.

† Current Postal Address; Department of Chemistry, University Park, Nottingham, NG7 2RD, U.K. E-mail: pczjad@unix.ccc.nottingham.ac.uk.

tonates make them more suitable as CVD precursors for ceria films and examples of these type of species include compounds where β-diketonate = pd (pentane-2,4-dionate) [4,5] tmhd (2,2,6,6-tetramethylheptane-2,4-dionate) [6] and dppd (1,3-diphenylpropane-1,3-dionate) [7]. In contrast, there are hardly any known examples of well characterised eight coordinate cerium(III) β-diketonates which have been evaluated as CVD precursors to thin films of ceria, and this is despite the fact that they have been shown to give films of ceria (CeO_2) rather than the expected cerous oxide (Ce_2O_3).

It has been shown that volatilities and thermal stabilities of many homoleptic lanthanide(III) β-diketonates are often improved by chelation to multidentate glyme(s) despite the increase in molecular weight [8,9]. Examples in which glyme moieties are observed to bridge between two [Ln(tmhd)$_3$] molecules include; [Ln$_2$(tmhd)$_6$(tetraglyme)] (Ln = Er [8] Gd [9]), [Ln$_2$(tmhd)$_6$(triglyme)] (Ln = Y [10], Eu [11], Tb [11] or Tm [12]), [EuY(tmhd)$_6$(triglyme)] [12] and [Gd$_2$(tmhd)$_6$(heptaglyme)] [9]. The saturation of available metal coordination sites via multidentate chelates often result in lower melting points and increased volatility and air and moisture stability with respect to the homoleptic analogues. Furthermore, fluorinated β-diketonates generally give more volatile compounds than their non-fluorinated structural analogues, because of the reduced van der Waals' interactions between molecules. Such precursors can often produce CeO_2 films which contain significant amounts of fluoride contamination; this may, however, be reduced by using water vapour in conjunction with inert carrier gases [2]. The present work is a continuation of our investigations to study the volatility characteristics of lanthanide(III) β-diketonate compounds which may be potential MOCVD precursors to their metal oxides [8]. Several cerium(III) β-diketonates were investigated for thermal stability and volatility by sublimation studies and by simultaneous thermogravimetric analysis (TGA) and differential scanning calorimetry (DSC). The X-ray structures of two of the complexes are also reported.

EXPERIMENTAL

General procedures

All reactions were conducted in round bottom flasks without any special precautions to exclude air. Elemental analyses were performed by the microanalytical department at Imperial College. The melting points were measured under nitrogen in capillaries and are uncorrected. Infrared spectra were recorded on a Perkin Elmer FTIR 1720 spectrometer as Nujol results between 25 × 4 mm^2 KBr plates. The Nujol was pre-dried with 4Å molecular sieves prior to use and the samples were protected from the atmosphere by an O-ring sealed Presslock™ holder (Aldrich Chemicals). The NMR solution samples were prepared in the glove-box, using 5 mm NMR tubes fitted with Young's valves. Solution NMR spectra were recorded on a Jeol GS 270 NMR spectrometer. ^{1}H NMR spectra were recorded at 270.16 MHz. Chemical shifts were referenced to the *protio* impurities of the deuterated solvent. Mass spectra were run on a VG Autospec. instrument at the Mass Spectrometry Department at Imperial College (FAB$^+$ mode). Controlled TGA and DSC measurements were done using a Polymer Laboratories 1500H simultaneous thermal analyzer, controlled by an Omni Pro 486DX-33 PC. The weight of the samples investigated was between 14–27 mg. The measurements were carried out in alumina crucibles under an atmosphere of flowing (25 cm^3 min^{-1}) nitrogen gas, using heating rates of 15°C min^{-1}.

Starting materials

All hydrocarbon solvents (BDH), gaseous ammonia (BOC) and NaOH (BDH) pellets were used as obtained. $CeCl_3 \cdot 7H_2O$ was obtained from Janssen Chemica, Hhfpd (Inorgtech) was obtained as a gift, whilst Hetbd, Hhfod and tetraglyme were purchased from Aldrich. All ligands were used as obtained. **CAUTION**: care should be taken when using ammonia gas by performing all ammoniation reactions in a well-ventilated fume cupboard.

Synthesis of [Ce$_2$(etbd)$_6$(tetraglyme)] **1**

NaOH pellets (0.93 g, 23.2 mmol) were dissolved in distilled water (5.0 cm^3) and 95% EtOH (50.0 cm^3), and to this solution was added Hetbd (4.27 g, 23.2 mmol) with stirring. Separately, $CeCl_3 \cdot 7H_2O$ (2.98 g, 8.0 mmol) was dissolved in a mixture of EtOH (10.0 cm^3), distilled water (5.0 cm^3) and tetraglyme (0.89 g, 4.0 mmol). The Na-etbd solution was then added dropwise via a dropping funnel to the cerium chloride solution over a period of 20 min. The mixture was filtered to remove a white precipitate, the volume of the filtrate reduced to ca 10.0 cm^3 and the mixture redissolved in CH_2Cl_2 (50.0 cm^3). Removal of the organic layer by decantation and reducing the volume to ca 15 cm^3, resulted in the precipitation of a white solid. The mixture was filtered and the solvent removed to give a red oil, which on standing yielded an orange coloured crystalline product. Yield: 5.20 g (81%), m.p. 103–106°C. (Found: C, 35.1; H, 3.7. Calc. for $Ce_2C_{46}H_{58}O_{23}F_{18}$: C, 34.5; H, 3.6%.) IR: 1719, 1676 (br), 1562, 1450, 1366, 1285, 1217, 1183, 1133, 1095, 1035, 923, 847, 796, 741, 676, 582, 520 cm^{-1}.

Synthesis of [Ce$_2$(hfpd)$_6$(tetraglyme)] **2**

Compound **2** was prepared by following similar procedure as employed for **1**, using Hhfpd (5.20 g,

25.0 mmol) rather than Hetbd. The product was obtained as orange needles. Yield: 4.81 g (66%); m.p. 125–128°C (Found: C, 26.9; H, 1.7. Calc. for $Ce_2C_{40}H_{28}O_{17}F_{36}$: C, 27.5; H, 1.6%.) IR: 1656, 1645, 1557, 1537, 1376, 1255, 1203, 1143, 1085, 944, 870, 800, 740, 659, 527, 462 cm^{-1}.

Synthesis of $[Ce_2(hfod)_6(tetraglyme)]$ **3**

The procedure adopted for **1** was also used for the preparation of **3**, using the diketone Hhfod (7.40 g, 25.0 mmol) rather than Hetbd. Removal of all volatiles yielded a red viscous oil. Yield: 7.79 g (82%). (Found: C, 37.2; H, 3.7. Calc. for $Ce_2C_{70}H_{82}O_{17}F_{42}$: C 37.0, H, 3.6%.) IR: 1625, 1535, 1393, 1346, 1280, 1239, 1120, 1067, 1021, 967, 938, 909, 832, 791, 754, 687, 476 cm^{-1}: ^1H NMR ($CDCl_3$, 270 MHz, 20°C), δ −14.66 (s, 4H, CH_2-glyme), −9.95 (s, 4H, CH_2-glyme), −9.20 (s, br, 6H, CH_3-glyme), −5.56 (s, 4H, CH_2-glyme), −5.17 (s, 4H, CH_2-glyme), 0.42 (s, 54H, Bu^t of hfod), 13.23 (s, 6H, CH of hfod).

Synthesis of $[NH_4][Ce(etbd)_4]$ **4**

CAN, $[Ce(NH_4)_2(NO_3)_6]$, (3.43 g, 6.26 mmol) was dissolved in a mixture of dimethoxyethane (DME) (50.0 cm^3) and Hetbd (4.60 g, 25.0 mmol). Gaseous ammonia was then introduced into the mixture for 45 min, giving an exothermic reaction and an orange colour after ca 5 min. The solution was stirred for a further hour, filtered and then washed with petroleum ether (2×5.0 cm^3). Removal of all volatiles yielded an orange oil which gave dark orange crystals upon standing. Yield: 4.56 g (81%); m.p. decomposes slowly above 145°C (Found: C, 33.1; H, 3.2; N, 1.5. Calc. for $CeC_{24}H_{28}O_{12}NF_{12}$: C, 32.4; H, 3.1; N, 1.6%.) IR: 3199 (br), 1654, 1577, 1491, 1448, 1366, 1285, 1217, 1182, 1131, 1035, 915, 796, 677, 581, 419 cm^{-1}.

X-ray crystallography

Single crystals of $[Ce_2(etbd)_6(tetraglyme)]$ **1** and $[NH_4][Ce(etbd)_4]$ **4**, suitable for X-ray work, were mounted using silicone oil and then transferred to the goniostat. Crystallographic measurements for both compounds were made at 150 K using Mo-K_α radiation ($\lambda = 0.71069$ Å, graphite monochromator) on a Delft instruments FAST TV area detector diffractometer equipped with a rotating anode generator (50 kV, 50 mA), a buffer board, a DEP image intensifier, and an Oxford Cryostream low temperature cooling system by following previously described procedures [13]. The unit cell parameters were obtained by least squares refinement of the diffractometer angles for 250 reflections within the θ ranges 1.80–25.03° (**1**) and 1.78–25.10° (**4**). The intensity data were collected within the same θ ranges from volumes corresponding to slightly more than a hemisphere of reciprocal space; both data sets were corrected for Lorentz and polarisation factors and also for absorption effects using the program DIFABS [14].

The structures were solved by direct methods (SHELXS86) [15] and difference electron density syntheses, and refined on F^2 by full matrix least-squares (SHELXL93) [16] using all unique data with intensities greater than 0. The non-hydrogen atoms were anisotropic. The hydrogen atoms belonging to the NH_4 group in compound **4** were experimentally located and refined isotropically with the four N—H distances constrained to remain the same [final value 0.94(2) Å]. Other hydrogens in the structures were included in calculated positions (riding model) with $U_{iso} = n \times U_{eq}$ of the parent carbon ($n = 1.2$ for CH and CH_2, and 1.5 for CH_3 groups). The maximum residual electron densities in the final difference maps were very close to the cerium atoms [2.018 e $Å^{-3}$ (**1**) and 1.227 e $Å^{-3}$ (**4**)] and indicated no features of stereochemical significance. The final R (on F)/R_w (on F^2) values were 0.0608/0.1179 for **1** and 0.0638/0.0880 for **4** for all unique data and 810 and 468 parameters respectively. The corresponding R-values for 6069 (**1**) and 3619 (**4**) data with $I > 2\sigma(I)$ were 0.0460/0.1152 and 0.0382/0.0848 respectively. Sources of scattering factors as in [15]. The diagrams were drawn with the program SNOOPI [17]. The calculations were done on a Pentium P5-90 personal computer. The crystal data and details of data collection and structure refinement are presented in Table 1. Fractional atom co-ordinates, thermal coefficients, hydrogen atom parameters, and full lists of bond lengths and angles are available as supplementary data.

RESULTS AND DISCUSSION

Synthesis

The reaction of $CeCl_3 \cdot 7H_2O$ in the presence of half an equivalent of tetraglyme with an aqueous ethanolic solution of ca three molar equivalents of [Na(etbd)] yielded the product $[Ce_2(etbd)_6(tetraglyme)]$ **1**. Similar reactions with the sodium salts of Hhfpd and Hhfod (ca three molar equivalents with respect to Ce metal) produced the corresponding glyme adducted complexes $[Ce_2(\beta\text{-diket})_6(tetraglyme)]$ [β-diket = hfpd (**2**) and hfod (**3**)]. Water was effectively removed from these compounds by dissolving them in chloroform and separating the aqueous and organic layers.

$$2CeCl_3 \cdot 7H_2O + 6Na(hfpd) + tetraglyme \xrightarrow{\text{(i) } H_2O/EtOH,\ \text{(ii) } CH_2Cl_2} [Ce_2(hfpd)_6(tetraglyme)]\,\mathbf{3} + 6NaCl + 14H_2O$$

Cerium ammonium nitrate (CAN), $[Ce(NH_4)_2(NO_3)_6]$, has been shown to be a versatile reagent for the synthesis of monomeric cerium(IV) β-diketonates [12]

Table 1. Crystal data and refinement results for $[Ce_2(etbd)_6(tetraglyme)]$ **1** and $[NH_4][Ce(etbd)_4]$ **4**[a]

	1	**4**
Chem. formula	$C_{46}H_{58}Ce_2F_{18}O_{23}$	$C_{24}H_{28}CeF_{12}NO_{12}$
fw	1601.16	890.59
Space group	$P\bar{1}$ (No. 2)	$P2_1/n$ (No. 14)
a (Å)	9.590(3)	12.679(2)
b (Å)	13.677(4)	20.087(3)
c (Å)	25.316(4)	14.951(2)
α (°)	89.73(2)	90
β (°)	98.97(2)	114.050(7)
γ (°)	108.34(2)	90
V (Å^3)	3109.8(14)	3477.2(9)
Z	2	4
D_c (g cm^{-3})	1.710	1.701
μ (Mo-K_α) (cm^{-1})	15.72	14.29
F(000)	1592	1764
Crystal size (mm)	$0.20 \times 0.10 \times 0.08$	$0.25 \times 0.08 \times 0.06$
θ range (°)	1.80–25.03	1.78–25.10
Index range	$-10 \leqslant h \leqslant 7$	$-14 \leqslant h \leqslant 13$
	$-15 \leqslant k \leqslant 15$	$-23 \leqslant k \leqslant 15$
	$-25 \leqslant l \leqslant 30$	$-17 \leqslant l \leqslant 16$
Reflections collected	11,556	13,123
Independent reflections	8088	5298
R_{int}	0.0636	0.0750
Absorption correc. factors	0.882–1.022	0.889–1.038
Data/restraints/parameters	8088/0/810	5298/4/468
Goodness-of-fit on F^2	1.003	0.856
ρ_{max} and ρ_{min} (e Å^{-3})	2.018 and −0.734	1.227 and −0.465
R^b	0.0608 (0.0460)[c]	0.0638 (0.0382)[c]
R_w	0.1179 (0.1152)[c]	0.0880 (0.0848)[c]

[a] Details in common: X-radiation, Mo-K_α, $\lambda = 0.71069$ Å, $T = 150(2)$ K.

[b] $R = \Sigma[(F_o)-(F_c)]/\Sigma(F_o)$; $R_w = [\Sigma\{w(F_o^2-F_c^2)^2\}/\Sigma\{w(F_o^2)^2\}]^{1/2}$; $w = [\sigma^2(F_o)^2+(aP)^2]$, where $P = [(F_o)^2+2(F_c)^2]/3$, and $a = 0.0535$ (**1**) and 0.0212 (**4**).

[c] The *R*-values for observed data only $[I > 2\sigma(I)]$ are given in parentheses.

alkoxides [18], and siloxides [19]. In the present work, we aimed at synthesising a *tetrakis*(β-diketonate)Ce^{IV} derivative by reacting CAN with four molar equivalents of the β-diketone, Hetbd, using ammonia as a base to facilitate deprotonation of the β-diketone, however, we obtained the ammonium *tetrakis*(β-diketonate)cerium(III) salt, $[NH_4][Ce(etbd)_4]$ **4**. Clearly, ammonia has acted as a reducing agent during the reaction. The reduction of the Ce^{IV} to Ce^{III} has been observed previously and may be attributed to the excellent oxidizing potential of CAN [20]. Compound **3** was obtained as red oil, whilst **1**, **2** and **4** were orange crystalline solids. All the compounds were stable in air and moisture.

Spectroscopic characterisation

The IR spectra of complexes **1**–**4** (Nujol mulls) show several bands characteristic of the coordinated β-diketonate ligands, with strong absorptions between 1577 and 1535 cm^{-1} corresponding to C⋯O and C⋯C vibrational stretches [11]. In complexes **1**–**3**, the ν(C—O) stretching modes due to coordinated tetraglyme are located in the range 1095–1067 cm^{-1}, whilst M—O (metal–oxygen) stretches involving the β-diketonate ligands are observed in the range 419–520 cm^{-1}. In compound **4**, a broad peak centered at 3199 cm^{-1} is attributed to the ν(N—H) stretches of the ammonium cation (broadness caused by hydrogen bonding), and is comparable to similar bands in other ammonium compounds [13].

NMR spectra for all the complexes gave broad and shifted peaks due to their paramagnetism. In the case of compound **2**, however, the peaks have been tentatively assigned previously [21] (also given in the Experimental section).

Thermal analyses and mass spectrometry

Simultaneous TGA and DSC studies were undertaken for the three glyme-bridged compounds **1**–**3** and the ammonium salt **4** to evaluate their suitability as CVD precursors. $[Ce_2(etbd)_6(tetraglyme)]$ **1** melts between ca 103–106°C in a capillary, whilst a sharp

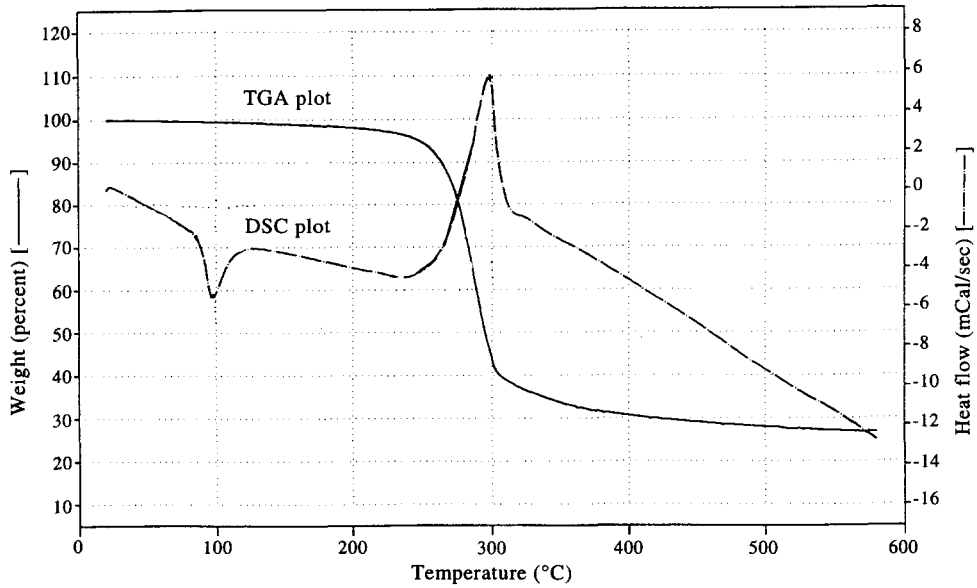

Fig. 1. The TGA plot for $[Ce_2(etbd)_6(tetraglyme)]$ **1**.

endotherm is observed for this process at 98.0°C (−4.79 mcal mg^{-1}) in the DSC curve. Sublimation studies revealed that this compound decomposes without sublimation at 255°C/10^{-2} Torr to give a black oil at the bottom of the sublimation vessel. The TGA plot for this compound (Fig. 1) shows a residue of ca 27% at 550°C, which is much higher than expected for CeO_2 (calc. 21.5%) but very close to that expected for CeF_4 (calc. 27.0%). In comparison, $[Ce_2(hfod)_6$ (tetraglyme)] **3** sublimes quantitatively (ca 235°C) at 0.1 Torr, whilst the TGA studies show the loss of over 87% of the material between ca 200–350°C to give a final residue of ca 9% by 500°C [21]. This is in contrast with $[Ce_2(hfpd)_6(tetraglyme)]$ **2**, which sublimes with substantial decomposition at 249°C (10^{-2} Torr). The TGA plot for this compound shows a weight loss of ca 80% by 340°C due to sublimation, followed by a further weight loss process up to 600°C (residue of 4.7%) due most probably to a combination of decomposition and sublimation. The DSC curves of compounds **2** and **3** show broad exotherms corresponding to the sublimation reactions. The TGA plot for the complex salt $[NH_4][Ce(etbd)_4]$ **4** shows that the compound decomposes slowly over the temperature range 90–700°C, with at least two overlapping weight loss processes. The residue left at 700°C is ca 35% of the original weight, which is much higher than that expected for either CeO_2 (calc. 19.3%) or CeF_4 (calc. 24.3%) and probably contains a substantial amount of carboneceous products. The corresponding DSC curve is complicated showing a very broad endotherm centred at ca 159.3°C due to several overlapping reactions. The compound decomposes (without sublimation) at ca 240°C/10^{-2} Torr to give a black solid of unknown composition.

Mass spectroscopic studies for the complexes **1**–

Table 2. Assignments for selected molecular ions in the mass spectra of complexes **1**–**4**

	1	**2**	**3**	**4**
$[Ce_2(L)_2(F)_2(4g)]^+$	—	—	1425(trace)	—
$[Ce(L)_3]^+$	—	—	—	689(45)
$[Ce(L)_2(4g)]^+$	728(100)	776(100)	952(100)	—
$[Ce(L)_2(4g)-CF_3]^+$	590(12)	—	—	—
$[Ce(L)(F)(4g)]^+$	—	558(22)	676(15)	—
$[Ce(L)_2]^+$	506(2)	553(8)	730(10)	506(62)
$[Ce(L)(F)]^+$	—	366(8)	454(12)	342(28)
$[Ce(F)_2(4g)]^+$	400(4)	400(10)	400(8)	—
$[Ce(F)_2]^+$	—	178(8)	178(16)	—

Key: L = β-diketonate; 4g = tetraglyme.

4 (Table 2) are consistent with the stoichiometries suggested for the compounds. The FAB^+ spectra for all the tetraglyme hemi-adducted compounds **1–3** show $[Ce(L)_2(tetraglyme)]^+$, $[Ce(L)_2]^+$, (L = corresponding β-diketonate) or similar fragments and a peak at 400 amu corresponding to $[CeF_2(tetraglyme)]^+$. A trace peak in the mass spectrum of **3** at 1425 amu was also assigned as the glyme bridged ion $[Ce(L)_3(F)_2(4g)]^+$.

Crystal structure of $[Ce_2(etbd)_6(tetraglyme)]$ **1**

A single crystal X-ray study was undertaken for $[Ce_2(etbd)_6(tetraglyme)]$ **1** to unambiguously identify the bonding modes of the glyme ligand. A SNOOPI plot of the structure is shown in Fig. 2 and selected bond lengths and angles are given in Table 3. The structure of the complex consists of two $Ce(etbd)_3$ moieties unsymmetrically bridged by a tetraglyme molecule. Ce(1) is eight coordinated with six oxygens from three chelating etbd ligands and with two chelating oxygens from one end of the tetraglyme molecule, whilst Ce(2) is nine co-ordinated with six oxygens from three chelating etfa ligands and with the remaining three oxygens from the tetraglyme. In the case of $[Er_2(tmhd)_6(tetraglyme)]$ [8], the glyme ligand was observed to bind via two of the oxygen atoms from each end of the polyether (the middle oxygen uncoordinated). However, in the gadolinium analogue $[Gd_2(tmhd)_6(tetraglyme)]$ [9], the two moieties are bridged in an asymmetric manner resulting in an uncoordinated oxygen at one end of the polyether chain [9]. This suggests that a lanthanide cation larger than Gd^{3+} should be able to bind additionally to the third outer oxygen of the polyether chain and indeed, this phenomenon has been observed in the structure of compound **1**. The coordination polyhedra around the cerium atoms show considerable distortions from idealised geometries (Fig. 3); that around Ce(1)

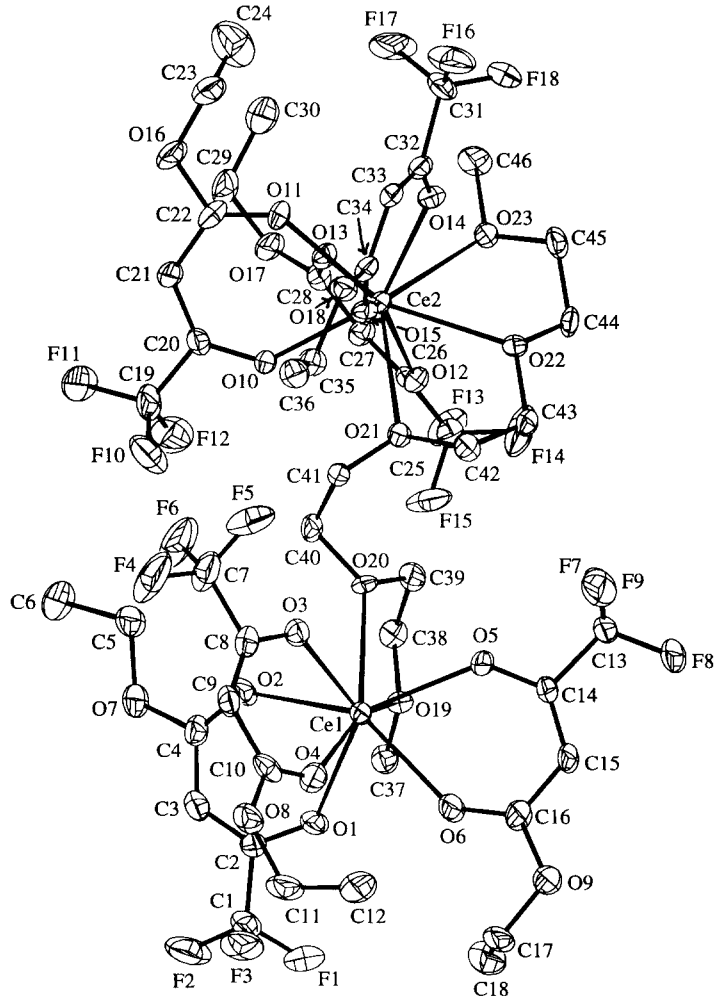

Fig. 2. Molecular structure of $[Ce_2(etbd)_6(tetraglyme)]$ **1** showing the atom numbering scheme. The hydrogen atoms have been omitted for clarity.

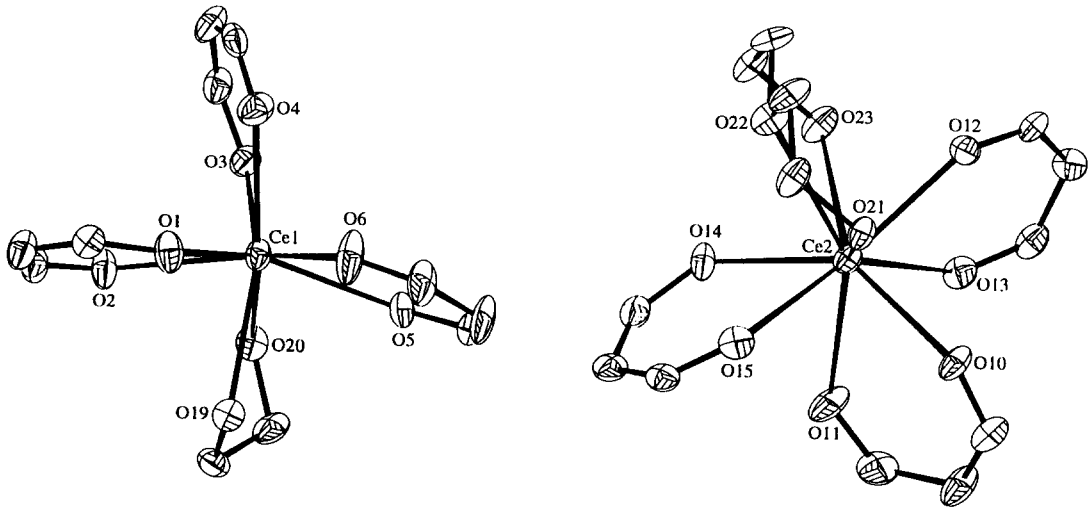

Fig. 3. Illustration of the coordination polyhedra around Ce(1) (distorted dodecahedron) and Ce(2) (distorted monocapped square antiprism) in $[Ce_2(etbd)_6(tetraglyme)]$ **1**.

approximates to a distorted dodecahedron and that around Ce(2) may be described as monocapped square antiprism. In the latter case, the capping atom O(21) lies on the face defined by O(10), O(12), O(15) and O(22).

The Ce—O bond lengths for each cerium atom fall into three distinct categories. The longest Ce—O bonds are associated with the glyme ligands; Ce—O bonds with the β-diketonate ligands are much shorter, but these can be clearly subdivided into two groups. It is also observed that the bonds to Ce(2) are in general longer than the corresponding bonds with Ce(1); this is however expected on the basis of the increase in coordination number of Ce(2) compared with Ce(1) [nine vs eight]. The Ce(1)—O(glyme) bonds are 2.623(5) and 2.586(5) Å (average 2.605 Å), the Ce(2)—O(glyme) bonds are 2.650(5), 2.633(5) and 2.702(5) Å (average 2.662 Å), the longest bond is associated with the terminal oxygen. This lengthening of the Ce—O bonds with the two terminal oxygens may be attributed to the steric crowding due to the methyl groups on these oxygens.

Examination of the Ce—O(etbd) distances reveal several interesting features which merit discussion in somewhat greater detail. Thus, the effect of varying the coordination numbers for the two metals as well as the asymmetry in the Ce—O bonds for each β-diketonate ligand are clearly reflected in the Ce—O bonds. These points are best illustrated in Fig. 4, which shows the average values of the relevant bond lengths associated with the $Ce(O_2C_3)$ chelates for each cerium. For both the metal centres, the Ce—O(etbd) chelate distances are clearly asymmetric and fall into two narrow ranges: 2.390(5)–2.444(5), average 2.408 Å and 2.464(5)–2.488(5), average 2.472 Å for Ce(1), and 2.384(5)–2.452(5), average 2.420 Å and 2.476(5)–2.508(5), average 2.496 Å for Ce(2). The variations for these two sets of values (between **a** and **a′** in Fig. 4) reflecting the asymmetry in the Ce—O(etbd) chelates bonds are 0.064 Å for Ce(1) and 0.076 Å for Ce(2). The effect of increased coordination number for Ce(2) is also reflected in these bonds being slightly but systematically longer by ~0.02 Å than the corresponding bonds with Ce(1). Another feature relates to the C—C distances within the O_2C_3 fragment of the chelates; it is observed that for each β-diketonate, the two C—O bond lengths (**b** and **b′** in Fig. 4) are always different [1.277(9)–1.292(9), average 1.296 Å and 1.228(10)–1.239(9), average 1.234 Å for Ce(1) and 1.274(9)–1.283(9), average 1.278 Å and 1.208(9)–1.243(9), average 1.229 Å for Ce(2)], with the longer distances being associated with those oxygens having shorter bonds with cerium. Similarly, the two C—C distances in each chelate (**c** and **c′** in Fig. 4) are also different [1.341(11)–1.347(11), average 1.344 Å and 1.418(12)–1.456(12), average 1.433 Å for Ce(1) and 1.352(11)–1.361(10), average 1.357 Å and 1.427(12)–1.441(11), average 1.434 Å for Ce(2)]. These variations in the C—O and C—C bonds (by ca 0.05 and 0.09 Å respectively) are systematic and consistent with the suggestion that the O_2C_3 moieties in this structure are not completely delocalised as commonly observed in metal β-diketonate chelate structures, but one canonical form (**A** rather than **A′** in Fig. 4) predominates. This is an interesting situation and may be correlated with the effects of the substituents on the chelate ring, i.e. electron withdrawing CF_3 and electron donating EtO groups on the two carbons C_α and C_β respectively in Fig. 4. The Ce-etbd chelate rings show slight folding about the O···O axis [4.6(5)–15.2(2)° for Ce(1) and 1.9(3)–14.7(3)° for Ce(2)]. The O—Ce—O chelate angles for the etbd ligands lie in a very narrow range,

Table 3. Selected bond lengths (Å) and angles (°) for $[Ce_2(etbd)_6(tetraglyme)]$ **1**

Ce(1)—O(1)	2.390(5)	Ce(1)—O(2)	2.488(5)
Ce(1)—O(3)	2.390(5)	Ce(1)—O(4)	2.464(6)
Ce(1)—O(5)	2.444(5)	Ce(1)—O(6)	2.463(5)
Ce(1)—O(19)	2.623(5)	Ce(1)—O(20)	2.586(5)
Ce(2)—O(10)	2.384(5)	Ce(2)—O(11)	2.508(5)
Ce(2)—O(12)	2.452(5)	Ce(2)—O(13)	2.476(5)
Ce(2)—O(14)	2.423(5)	Ce(2)—O(15)	2.503(5)
Ce(2)—O(21)	2.650(5)	Ce(2)—O(22)	2.633(5)
Ce(2)—O(23)	2.702(5)		
O(1)—C(2)	1.277(9)	O(2)—C(4)	1.236(9)
O(3)—C(8)	1.288(9)	O(4)—C(10)	1.228(10)
O(5)—C(14)	1.292(9)	O(6)—C(16)	1.239(9)
O(7)—C(4)	1.339(9)	O(7)—C(5)	1.478(10)
O(8)—C(10)	1.334(9)	O(8)—C(11)	1.464(10)
O(9)—C(16)	1.326(10)	O(9)—C(17)	1.434(10)
O(10)—C(20)	1.283(9)	O(11)—C(22)	1.236(9)
O(12)—C(26)	1.277(9)	O(13)—C(28)	1.208(9)
O(14)—C(32)	1.274(9)	O(15)—C(34)	1.243(9)
O(16)—C(22)	1.343(9)	O(16)—C(23)	1.463(11)
O(17)—C(28)	1.352(9)	O(17)—C(29)	1.453(10)
O(18)—C(34)	1.337(9)	O(18)—C(35)	1.474(9)
O(19)—C(37)	1.426(9)	O(19)—C(38)	1.430(9)
O(20)—C(39)	1.411(9)	O(20)—C(40)	1.435(8)
O(21)—C(41)	1.426(8)	O(21)—C(42)	1.444(8)
O(22)—C(44)	1.444(9)	O(22)—C(43)	1.473(9)
O(23)—C(46)	1.437(9)	O(23)—C(45)	1.447(8)

O(1)—Ce(1)—O(3)	125.4(2)	O(1)—Ce(1)—O(5)	134.8(2)
O(3)—Ce(1)—O(5)	97.3(2)	O(1)—Ce(1)—O(6)	70.8(2)
O(3)—Ce(1)—O(6)	133.3(2)	O(5)—Ce(1)—O(6)	68.8(2)
O(1)—Ce(1)—O(4)	74.1(2)	O(3)—Ce(1)—O(4)	69.5(2)
O(5)—Ce(1)—O(4)	114.0(2)	O(6)—Ce(1)—O(4)	76.2(2)
O(1)—Ce(1)—O(2)	69.7(2)	O(3)—Ce(1)—O(2)	77.8(2)
O(5)—Ce(1)—O(2)	142.2(2)	O(6)—Ce(1)—O(2)	139.8(2)
O(4)—Ce(1)—O(2)	99.5(2)	O(1)—Ce(1)—O(20)	131.8(2)
O(3)—Ce(1)—O(20)	71.6(2)	O(5)—Ce(1)—O(20)	70.9(2)
O(6)—Ce(1)—O(20)	134.6(2)	O(4)—Ce(1)—O(20)	141.2(2)
O(2)—Ce(1)—O(20)	72.0(2)	O(1)—Ce(1)—O(19)	79.9(2)
O(3)—Ce(1)—O(19)	132.5(2)	O(5)—Ce(1)—O(19)	81.2(2)
O(6)—Ce(1)—O(19)	90.7(2)	O(4)—Ce(1)—O(19)	153.4(2)
O(2)—Ce(1)—O(19)	75.7(2)	O(20)—Ce(1)—O(19)	63.0(2)
O(10)—Ce(2)—O(14)	137.8(2)	O(10)—Ce(2)—O(12)	85.2(2)
O(14)—Ce(2)—O(12)	135.8(2)	O(10)—Ce(2)—O(13)	74.7(2)
O(14)—Ce(2)—O(13)	105.9(2)	O(12)—Ce(2)—O(13)	70.2(2)
O(10)—Ce(2)—O(15)	85.9(2)	O(14)—Ce(2)—O(15)	69.2(2)
O(12)—Ce(2)—O(15)	138.8(2)	O(13)—Ce(2)—O(15)	144.1(2)
O(10)—Ce(2)—O(11)	69.9(2)	O(14)—Ce(2)—O(11)	70.8(2)
O(12)—Ce(2)—O(11)	137.8(2)	O(13)—Ce(2)—O(11)	70.6(2)
O(15)—Ce(2)—O(11)	74.4(2)	O(10)—Ce(2)—O(22)	134.5(2)
O(14)—Ce(2)—O(22)	78.4(2)	O(12)—Ce(2)—O(22)	73.1(2)
O(13)—Ce(2)—O(22)	129.7(2)	O(15)—Ce(2)—O(22)	85.3(2)
O(11)—Ce(2)—O(22)	147.5(2)	O(10)—Ce(2)—O(21)	73.2(2)
O(14)—Ce(2)—O(21)	121.3(2)	O(12)—Ce(2)—O(21)	73.2(2)
O(13)—Ce(2)—O(21)	132.6(2)	O(15)—Ce(2)—O(21)	65.8(2)
O(11)—Ce(2)—O(21)	126.7(2)	O(22)—Ce(2)—O(21)	62.5(2)
O(10)—Ce(2)—O(23)	144.6(2)	O(14)—Ce(2)—O(23)	66.1(2)
O(12)—Ce(2)—O(23)	71.1(2)	O(13)—Ce(2)—O(23)	72.7(2)
O(15)—Ce(2)—O(23)	129.2(2)	O(11)—Ce(2)—O(23)	110.9(2)
O(22)—Ce(2)—O(23)	63.5(2)	O(21)—Ce(2)—O(23)	121.4(2)
C(2)—O(1)—Ce(1)	136.1(5)	C(4)—O(2)—Ce(1)	135.8(5)
C(8)—O(3)—Ce(1)	133.5(5)	C(10)—O(4)—Ce(1)	137.0(5)
C(14)—O(5)—Ce(1)	135.3(5)	C(16)—O(6)—Ce(1)	139.7(6)
C(4)—O(7)—C(5)	115.9(6)	C(10)—O(8)—C(11)	116.2(7)
C(16)—O(9)—C(17)	117.7(6)	C(20)—O(10)—Ce(2)	135.5(5)

Table 3. *Continued.*

C(22)—O(11)—Ce(2)	134.0(5)	C(26)—O(12)—Ce(2)	134.8(5)
C(28)—O(13)—Ce(2)	136.6(5)	C(32)—O(14)—Ce(2)	133.8(5)
C(34)—O(15)—Ce(2)	136.0(5)	C(22)—O(16)—C(23)	117.6(7)
C(28)—O(17)—C(29)	116.6(6)	C(34)—O(18)—C(35)	115.2(6)
C(37)—O(19)—C(38)	111.2(6)	C(37)—O(19)—Ce(1)	120.1(5)
C(38)—O(19)—Ce(1)	118.4(4)	C(39)—O(20)—C(40)	117.5(6)
C(39)—O(20)—Ce(1)	114.7(4)	C(40)—O(20)—Ce(1)	125.7(4)
C(41)—O(21)—C(42)	114.5(5)	C(41)—O(21)—Ce(2)	120.4(4)
C(42)—O(21)—Ce(2)	115.5(4)	C(44)—O(22)—C(43)	109.6(5)
C(44)—O(22)—Ce(2)	116.6(4)	C(43)—O(22)—Ce(2)	117.9(4)
C(46)—O(23)—C(45)	109.9(6)	C(46)—O(23)—Ce(2)	118.6(4)
C(45)—O(23)—Ce(2)	112.0(4)		

68.8(2)–70.2(2), average 69.6°, and those with tetraglyme in the range 62.5(2)–63.5(2), average 63.0°; these values are comparable with the corresponding values in other polyether adducts of lanthanide β-diketonate complexes [8,9]. It is also noted that in contrast with structure **4** (see later), the two types of Ce—O—C_α and Ce—O—O_β angles (Fig. 4) have nearly similar values [133.5(5)–136.1(5), average 135.0° and 135.8(5)–139.7(6), average 137.5° for Ce(1); 133.8(5)–135.5(5), average 134.7° and 134.0(5)–136.6(5), average 135.5° for Ce(2)]. The C—F, C—C and C—O bond lengths involving the CF_3 and ethoxide substituents on the β-diketonate and the tetraglyme ligands have normal values; the C—O—C angles involving the ethoxides lie in the narrow range 115.2(6)–117.7(6)°, whilst those in the tetraglyme molecule show larger variations 109.6(5)–117.5(6)°, most probably due to the chelating/bridging bonding modes of the glyme ligand. Other geometry parameters associated with the structure are as expected. The dimeric molecules are held together in the crystal by weak H···F/O interactions (≥2.51 Å) and van der Waals' forces.

Crystal structure of $[NH_4][Ce(etbd)_4]$ **4**

The structure of the complex anion $[Ce(etbd)_4]^-$ in **4** is shown in Fig. 5 and selected bond distances and

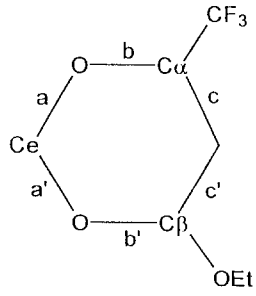

	Complex **1**		Complex **4**
	Ce(1)	Ce(2)	Ce(1)
a =	2.408	2.420	2.454
a′ =	2.472	2.496	2.468
b =	1.286	1.278	1.293
b′ =	1.234	1.229	1.234
c =	1.344	1.357	1.352
c′ =	1.433	1.434	1.432

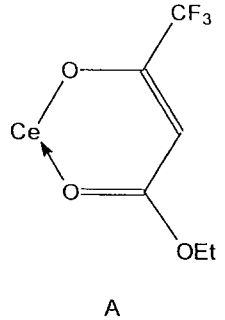

A

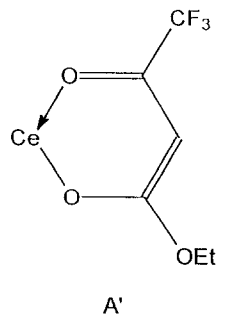

A'

Fig. 4. Average bond lengths (Å) in the $Ce(O_2C_3)$ chelate in **1**, and the two possible cannonical forms **A** and **A′**.

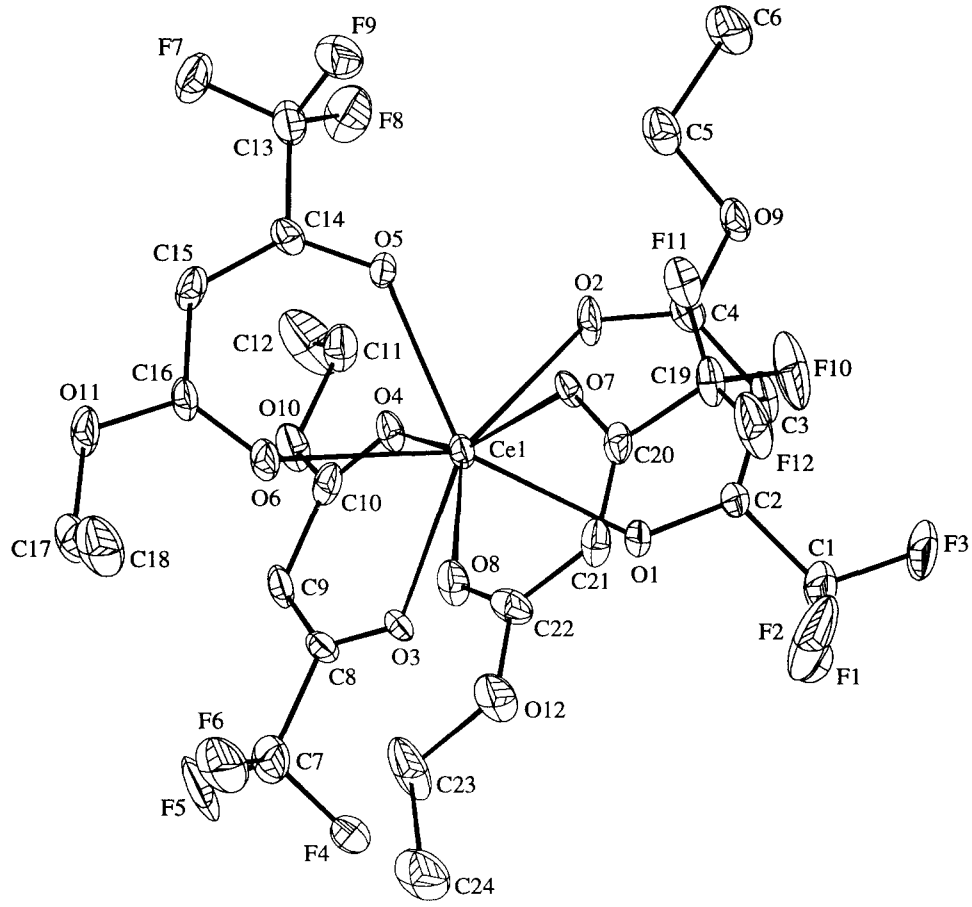

Fig. 5. Structure of the $[Ce(etbd)_4]^-$ anion in **4**, showing the atom numbering scheme. The hydrogen atoms have been omitted for clarity.

angles in the anion are presented in Table 4. All four β-diketonate ligands are chelated to the eight coordinate cerium ion, as shown in Fig. 6, in a distorted square antiprismatic arrangement. In fact, the distortion from ideal geometry is large enough to approximate the coordination geometry even as a bicapped trigonal prism.

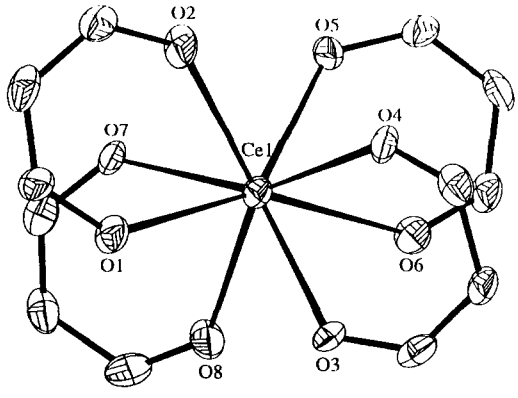

Fig. 6. Illustration of the coordination geometry (distorted square antiprism) of the $[Ce(etbd)_4]^-$ anion in **4**.

The two types of Ce—O distances in the present complex ion (**a** and **a**′ in Fig. 4) lie in the ranges 2.444(4)–2.460(4), average 2.454 Å, and 2.457(4)–2.477(4), average 2.468 Å respectively (average of all eight Ce—O distances 2.461 Å). The difference in the values for **a** and **a**′ in **4** (Fig. 4) is very small (0.014 Å) compared with 0.064 Å (for the eight coordinate Ce) and 0.076 Å for (nine coordinate Ce) in compound **1**. Nevertheless, we feel that these differences suggest asymmetry in the Ce—O chelate bonds. Certainly, the asymmetry in both the C—O and C—C bonds in the chelate rings 1.275(7)–1.300(7), average 1.293 Å (**a**), 1.223(6)–1.247(7), average 1.234 Å (**a**′), [Δ(**a**–**a**′) = 0.059 Å] and 1.345(8)–1.361(8) average 1.352 Å (**c**), 1.419(8)–1.448(8), average 1.432 Å (**c**′), [Δ(**c**–**c**′) = 0.080 Å] follow the same trend as observed in other structures [12], and therefore it may be concluded that the canonical form **A** is predominant in this complex anion also. The situation is again explained in terms of the electron withdrawing or electron

Table 4. Selected bond lengths (Å) and angles (°) for $[NH_4][Ce(etbd)_4]$ **4**

Ce(1)—O(1)	2.457(4)	Ce(1)—O(2)	2.470(4)
Ce(1)—O(3)	2.456(3)	Ce(1)—O(4)	2.467(4)
Ce(1)—O(5)	2.444(4)	Ce(1)—O(6)	2.477(4)
Ce(1)—O(7)	2.460(4)	Ce(1)—O(8)	2.457(4)
O(1)—C(2)	1.300(7)	O(2)—C(4)	1.228(7)
O(3)—C(8)	1.275(7)	O(4)—C(10)	1.223(6)
O(5)—C(14)	1.292(7)	O(6)—C(16)	1.239(7)
O(7)—C(20)	1.303(7)	O(8)—C(22)	1.247(7)
O(9)—C(4)	1.330(7)	O(9)—C(5)	1.442(7)
O(10)—C(10)	1.342(7)	O(10)—C(11)	1.453(7)
O(11)—C(16)	1.314(7)	O(11)—C(17)	1.433(7)
O(12)—C(22)	1.329(7)	O(12)—C(23)	1.468(7)
C(2)—C(3)	1.361(8)	C(3)—C(4)	1.428(8)
C(8)—C(9)	1.353(8)	C(9)—C(10)	1.431(8)
C(14)—C(15)	1.348(8)	C(15)—C(16)	1.448(8)
C(20)—C(21)	1.345(8)	C(21)—C(22)	1.419(8)

O(5)—Ce(1)—O(3)	134.85(13)	O(5)—Ce(1)—O(8)	123.23(14)
O(3)—Ce(1)—O(8)	69.83(13)	O(5)—Ce(1)—O(1)	139.54(13)
O(3)—Ce(1)—O(1)	81.01(12)	O(8)—Ce(1)—O(1)	81.74(14)
O(5)—Ce(1)—O(7)	83.12(12)	O(3)—Ce(1)—O(7)	135.76(13)
O(8)—Ce(1)—O(7)	69.43(13)	O(1)—Ce(1)—O(7)	76.85(12)
O(5)—Ce(1)—O(4)	79.86(13)	O(3)—Ce(1)—O(4)	69.86(12)
O(8)—Ce(1)—O(4)	138.08(12)	O(1)—Ce(1)—O(4)	102.82(13)
O(7)—Ce(1)—O(4)	152.48(12)	O(5)—Ce(1)—O(2)	71.20(13)
O(3)—Ce(1)—O(2)	130.21(13)	O(8)—Ce(1)—O(2)	139.44(13)
O(1)—Ce(1)—O(2)	70.02(13)	O(7)—Ce(1)—O(2)	76.05(13)
O(4)—Ce(1)—O(2)	78.05(13)	O(5)—Ce(1)—O(6)	68.90(13)
O(3)—Ce(1)—O(6)	73.46(12)	O(8)—Ce(1)—O(6)	77.87(13)
O(1)—Ce(1)—O(6)	151.54(13)	O(7)—Ce(1)—O(6)	113.42(13)
O(4)—Ce(1)—O(6)	80.20(13)	O(2)—Ce(1)—O(6)	137.15(13)
C(2)—O(1)—Ce(1)	132.5(3)	C(4)—O(2)—Ce(1)	136.5(4)
C(8)—O(3)—Ce(1)	129.5(3)	C(10)—O(4)—Ce(1)	133.6(4)
C(14)—O(5)—Ce(1)	130.0(3)	C(16)—O(6)—Ce(1)	136.5(4)
C(20)—O(7)—Ce(1)	130.6(3)	C(22)—O(8)—Ce(1)	135.7(4)
C(4)—O(9)—C(5)	115.3(5)	C(10)—O(10)—C(11)	117.2(4)
C(16)—O(11)—C(17)	117.0(5)	C(22)—O(12)—C(23)	117.4(5)

releasing effects of the substituents (CF_3 and OEt groups respectively) on the C_α and C_β atoms in Fig. 4. The Ce-etbd chelate rings are non-planar and are folded by 14.0(3)–22.5(1)° about the O···O axis. The O—Ce—O chelate angles lie in the narrow range 68.90(13)–70.02(13), average 69.6° and these are comparable with the corresponding values in **1** and other β-diketonate complexes [12]. The C—O—C angles involving the ethoxide substituents on the β-diketonate ligands are 115.3(5)–117.4(5)° and comparable with the corresponding values in **1**.

The gross crystal structure of $[NH_4][Ce(etbd)_4]$ **4** consists of $[NH_4]^+$ cations and $[Ce(etbd)_4]^-$ anions held together by an extensive network of N—H···O/F hydrogen bonds and short interactions. The dimensions of hydrogen bonds and other important short contacts are presented in Table 5. It is observed that all four hydrogen atoms of the $[NH_4]^+$ cation are involved in fairly strong hydrogen bonds (H···O ≥ 2.30 Å) with the chemically equivalent oxygen atoms O(1), O(3), O(5) and O(7) on the four etbd ligands which are all bonded to C_α (Fig. 4). One effect of these hydrogen bonds is manifested in the fact that the Ce—O(1)/O(3)/O(5)/O(7)—C_α angles [129.5(3)–132.5(3), average 130.7°] are narrowed down by ca 5° compared with the Ce—O(2)/O(4)/O(6)/O(8)—C_β angles [133.6(4)–136.5(4), average 135.6°]. In the absence of similar hydrogen bonds, no such differences in the corresponding Ce—O—C angles are observed in **1**.

The structures of compounds **1** and **4** may be compared with several other related lanthanide complexes. In eight coordinate complexes of the type MX_4, where X is a bidentate ligand such as β-diketonate, the coordination geometry is predominantly either square antiprismatic or dodecahedral [22], but small potential energy differences between these two forms often lead to considerable distortions from the idealised geometries and intermediate forms are also found. It is difficult to predict *a priori* the particular geometry

Table 5. Dimensions of the hydrogen bonds and short interactions in $[NH_4][Ce(etbd)_4]$ **4**. Distances in (Å) and angles in (°)

A—H···B	A—H	H···B	A···B	<A—H···B
N(1)—H(3N)···O(7)^{i}	0.94	1.86	2.794	173
N(1)—N(4N)···O(5)	0.94	1.94	2.800	152
N(1)—H(2N)···O(3)^{ii}	0.94	1.85	2.770	166
N(1)—H(1N)···O(1)^{ii}	0.94	2.03	2.839	143
N(1)—H(1N)···F(1)^{ii}	0.94	2.36	3.107	137
N(1)—H(4N)···F(9)^{i}	0.94	2.51	3.219	133
C(3)—H(3)···F(3)^{i}	0.95	2.36	2.734	103
C(9)—H(9)···F(5)^{i}	0.95	2.36	2.728	102
C(15)—H(15)···F(7)^{i}	0.95	2.39	2.745	102
C(21)—H(21)···F(12)^{i}	0.95	2.35	2.727	103
C(17)—H(17B)···F(10)^{iii}	0.99	2.56	3.387	141

Symmetry code: (i) (x, y, z); (ii) $(-0.5+x, 0.5-y, -0.5+z)$; (iii) $(-0.5+x, 0.5-y, 0.5+z)$.

adopted in a given compound since it depends on a number of factors such as the nature and bulk of the ligands, the oxidation state and ionic radii of the central metal, and inter-ligand and intermolecular interactions including any hydrogen bonding. In the Ce^{III} complex **1**, the two different Ce^{III} centres have different coordination numbers (eight and nine) and different geometries (dodecahedral and monocapped square antiprismatic) with large distortions from idealised polyhedra, due mainly to the bonding of the metal centres with the polyether molecule. In the Ce^{III} complex **4**, where all the four chelating ligands are the same, the observed geometry is best described as square antiprismatic. Similar coordination type was also reported for the homoleptic Ce^{IV} complexes [α-$Ce(pd)_4$] [4], [β-$Ce(pd)_4$] [5], α-[$Ce(tmhd)_4$] [6], [$Ce(dppd)_4$] [7] and [$Ce(pmhd)_4$] (pmhd = 1-phenyl-6-methylhexane-1,3-dionate) [23]. This situation is in contrast with a number of salt like compounds, e.g., $[C_9H_8N][Ce(ttbd)_4]$ {ttbd = 4,4,4-trifluoro-1-(2-thienyl)butane-1,3-dionato} [24], $[NH_4][Pr(ttbd)_4]\cdot H_2O$ [25] and [Cs][$Y(hfpd)_4$] [26], where the metal atoms are all in +3 oxidation state, but the coordination geometry is distorted dodecahedral. Distorted dodecahedral geometry was also observed in the Ce^{IV} complex β-[$Ce(tmhd)_4$] [23].

CONCLUSIONS

Our work has emphasised once more that the presence/strength of intermolecular interactions in β-diketonate compounds has a great influence on the volatility characteristics and hence on their potential as CVD precursors for ceria (CeO_2). The physical and structural properties of compound **4** appear to suggest that the extensive hydrogen bonding between the NH_4^+ cation and the β-diketonate ligands in the $[Ce(etbd)_4]^-$ anion are responsible for its low volatility (decomposes on attempted sublimation), and this makes this complex unsuitable as a CVD precursor for the preparation of ceria. Compound **1** decomposes without sublimation at 255°C, whilst **2** sublimes with substantial decomposition at 249°C, suggesting that both these tetraglyme adducted products are of only marginal importance as CVD precursors. However, the other tetraglyme adduct, $[Ce_2(hfod)_6(tetraglyme)]$ (also known as CFT), is an air and moisture stable compound with excellent thermal stability and volatility and it sublimes quantitatively at ca 220°C/10^{-2} Torr. This compound was obtained as a viscous oil and preliminary results have shown that uniform carry-over rates are obtained in our CVD apparatus compared to the solid precursors. Unlike other cerium precursors to ceria which are currently in use, such as [$Ce(tmhd)_4$] and [$Ce(hfod)_4$], CFT does not appear to undergo any pyrolysis from prolonged heating at ca 250°C in a CVD bubbler [2]. Indeed, thin films of ceria have been grown on a variety of substrates using CFT and the results have been reported recently [21].

Acknowledgements—The authors would like to thank the E.S.P.R.C. (M.B.H., K.M.A.M. and J.A.D.) for support, the Leverhulme Trust (J. McA.), and B.P. for endowing D.M.P.M.'s chair. Thanks to Hilary O'Callaghan and Patrick Barrie who performed some of the spectroscopic/analytical measurements. We would also like to thank Inorgtech Chemicals for gifts of chemicals.

REFERENCES

1. Steel, B. C. H., *Mat. Sci. and Eng.*, 1992, **B13**, 79; U.K. Pat. Application 9,125,012.6, 25 November 1991.
2. Becht, M., Gerfin, T. and Dahmen, K.-H., *Chem. Mater.*, 1993, **5**, 137; Plakatouras, J. C., McAleese, J. and Steele, B. C. H. *Thin Solid Films*, 1996, **280**, 152.
3. Bradley, D. C., Chatterjee, A. K. and Wardlaw, W., *J. Chem. Soc. (London)*, 1957, 2601.
4. Matkovic, B. and Grdenic, D., *Acta Cryst.*, 1963,

16, 456; Matkovic, B. and Grdenic, D., *Acta Cryst.*, 1959, **12**, 817.
5. Titze, H., *Acta Chem. Scand.*, 1969, **23**, 399.
6. Leskela, M., Sillanpaa, R., Niinsto, L. and Tiitta, M., *Acta Chem. Scand.*, 1991, **45**, 1006.
7. Wolf Von L. and Barnighausen, H., *Acta Cryst.*, 1960, **13**, 778; Keppert, D. L., Patrick, J. M. and White, A. H., *J. Chem. Soc., Dalton Trans.*, 1983, 567.
8. Hibbs, D. E., Darr, J. A., Hursthouse, M. B., Malik, K. M. A. and Mingos, D. M. P., *Polyhedron*, 1996, **15**, 3225.
9. Baxter, I., Drake, S. R., Hursthouse, M. B., Malik, K. M. A., McAleese, J., Otway, D. J. and Plakatouras, J. C., *Inorg. Chem.*, 1995, **34**, 1384.
10. Drake, S. R., Hursthouse, M. B., Malik, K. M. A., Miller, S. A. S. and Otway, D. J., *Inorg. Chem.*, 1993, **32**, 4464.
11. Drake, S. R., Lyons, A., Otway, D. J., Slawin, A. M. Z. and Williams, D. J., *J. Chem. Soc., Dalton Trans.*, 1993, 2379.
12. Baxter, I., Darr, J. A., Hursthouse, M. B., Malik, K. M. A., Miller, S. A. S., Mingos, D. M. P. and Otway, D. J., unpublished results.
13. Darr, J. A., Drake, S. R., Hursthouse, M. B. and Malik, K. M. A., *Inorg. Chem.*, 1993, **32**, 5704.
14. Walker, N. P. C. and Stuart, D., *Acta Crystallogr.*, 1983, **A39**, 158; adapted for FAST geometry by A. I. Karaulov, University of Wales, Cardiff, 1991.
15. Sheldrick, G. M., *Acta Crystallogr.*, 1990, **A46**, 467.
16. Sheldrick, G. M., *SHELXL*93 *Program for Crystal Structure Refinement*, University of Gottingen, Germany, 1993.
17. Davies, K., *SNOOPI Program for Structural Drawing*, University of Oxford, U.K., 1983.
18. Gradeff, P. S., Schreiber, F. G., Brooks, K. C. and Sievers, R. E., *Inorg. Chem.*, 1985, **24**, 1110; Gradeff, P. S., Yunlu, K., Deming, T. J., Olofson, J. M., Doedens, R. J. and Evans, W. J., *Inorg. Chem.*, 1990, **29**, 420.
19. Galy, J., Gradeff, P. S., Gleizes, A. and Yunlu, K., *Polyhedron*, 1989, **8**, 1001.
20. Kalsotra, B. L., Multani, R. K. and Jain, B. D., *Inorg. Nucl. Chem.*, 1973, **35**, 311; Kalsotra, B. L., Multani, R. K. and Jain, B. D., *Isr. J. Chem.*, 1971, **9**, 567; Evans, W. J., Deming, T. J. and Ziller, J. W., *Organometallics*, 1989, **8**, 1581.
21. Darr, J. A., McAleese, J. and Steele, B. C. H., *Chem. Vap. Deposition*, 1996, **2**, 244.
22. Hoard, L. and Silverton, J. V., *Inorg. Chem.*, 1963, **2**, 235; Lippard, S. J., *Progr. Inorg. Chem.*, 1967, **8**, 109; Muetterties, E. L. and Wright, C. M., *Qurt. Rev.*, 1967, **21**, 109.
23. Baxter, I., Darr, J. A., Hursthouse, M. B., Malik, K. M. A., McAleese, J. and Mingos, D. M. P., *J. Chem. Cryst* accepted for publication.
24. McPhail, A. T. and Tschang, P.-S. W., *J. Chem. Soc., Dalton Trans.*, 1974, 1165.
25. Lalancette, R. A., Cefola, M., Hamilton, W. C. and La Placa, S. J., *Inorg. Chem.*, 1967, **6**, 2127.
26. Bennet, M. J., Cotton, F. A., Legzdins, P. and Lippard, S. J., *Inorg. Chem.*, 1968, **7**, 1770.

Pergamon

PII: S0277-5387(97)00300-8

Polyhedron Vol. 17, No. 8, pp. 1343–1354, 1998
© 1998 Elsevier Science Ltd
All rights reserved. Printed in Great Britain
0277-5387/98 $19.00+0.00

The chemistry of cobalt acetate—IV.† The isolation and crystal structure of the symmetric cubane, tetrakis[(μ-acetato)(μ_3-oxo)(pyridine)cobalt(III)] · chloroform solvate, $[Co_4(\mu_3\text{-}O)_4(\mu\text{-}CH_3CO_2)_4(C_5H_5N)_4] \cdot 5CHCl_3$ and of the dicationic partial cubane, trimeric, [(μ-acetato)(acetato)tris(μ-hydroxy)(μ_3-oxo)hexakispyridinetricobalt(III)]hexafluorophosphate · water solvate, $[Co_3(\mu_3\text{-}O)(\mu\text{-}OH)_3(\mu\text{-}CH_3CO_2)(CH_3CO_2)(C_5H_5N)_6][PF_6]_2 \cdot 2H_2O$

James K. Beattie,* Trevor W. Hambley, John A. Klepetko, Anthony F. Masters* and Peter Turner

School of Chemistry, The University of Sydney, NSW 2006, Australia

(Received 13 January 1997; accepted 2 July 1997)

Abstract—The isolation from "cobalt(III) acetate" and characterisation by single crystal X-ray diffraction (refined to $R = 0.087$, $R_w = 0.084$) of the symmetric neutral cubane, $[Co_4(\mu_3\text{-}O)_4(\mu\text{-}CH_3CO_2)_4(C_5H_5N)_4]$, and of the hexafluorophosphate salt (refined to $R = 0.078$, $R_w = 0.073$) of the trimeric dication, the partial cubane, $[Co_3(\mu_3\text{-}O)(\mu\text{-}OH)_3(\mu\text{-}CH_3CO_2)(CH_3CO_2)(C_5H_5N)_6]^{2+}$, are reported. The cubane crystallises as its chloroform solvate, $[Co_4(\mu_3\text{-}O)_4(\mu\text{-}CH_3CO_2)_4(C_5H_5N)_4] \cdot 5CHCl_3$, whilst the partial cubane crystallises as its water solvate, $[Co_3(\mu_3\text{-}O)(\mu\text{-}OH)_3(\mu\text{-}CH_3CO_2)(CH_3CO_2)(C_5H_5N)_6][PF_6]_2 \cdot 2H_2O$. The cubane and partial cubane dication have average Co···Co distances of 2.818(8), 2.683(6) and 2.918(6), 2.767(5) Å, respectively, and average Co—μ_3-O distances of 1.86 and 1.91 Å, respectively. © 1998 Elsevier Science Ltd. All rights reserved

Keywords: cobalt acetate; cubane; trimeric.

Metal carboxylates have attracted extensive study because of the range of structural types and magnetic, bonding, catalytic, etc. properties which they exhibit. Thus, for example, a trimeric iron species of the basic acetate, oxo-centred type has been isolated from solutions which oxidise alkanes, and copper acetate and chromium acetate were the first compounds for which δ- and quadruple metal–metal bonding were postulated [1–4].

Cobalt carboxylates are of particular practical interest as they are the most widely used industrial homogeneous catalysts, predominantly for the oxidations of a variety of hydrocarbons [5–11]. Paradoxically, however, the structure and composition of "$[Co(OAc)_3]$" (OAc = CH_3COO^-) are incompletely established [12–22]. Although "well defined green octahedrons" were reported in 1924 and a trimeric structure was proposed in 1929 [13,14], amorphous materials are generally produced from the variety of preparative methods developed by various workers [13–15,22–26]. Thus, "$[Co(OAc)_3]$" has been postulated to consist of various combinations of monomers, dimers, trimers and mixed valence trimers.

* Authors to whom correspondence should be addressed.

† Part III. Beattie, J. K., Hambley, T. W., Klepetko, J. A., Masters, A. F. and Turner, P., *Polyhedron*, 1997, in press.

Analogous triangular, homo- and heteronuclear, single and mixed valence, oxo-centred basic acetate derivatives have long been known for many transition metals, whilst related dimeric, hydroxy-bridged cobalt(III) amine cations were prepared by Werner [27–29].

A significant breakthrough in the structural chemistry of "cobalt(III) acetate" was reported in 1973 by Uemura *et al.*, who showed that crystalline derivatives could be isolated from "cobalt(III) acetate" by the addition of aromatic nitrogen bases as co-ligands [26]. Thus, for example, addition of pyridine and $NaClO_4 \cdot H_2O$ to a methanolic solution of "cobalt(III) acetate", prepared by ozonolysis of cobalt(II) acetate tetrahydrate in acetic acid, produced $[Co_3O(OAc)_6(py)_3][ClO_4]$ (py = C_5H_5N), formulated, on the basis of solid state infra-red spectra and powder X-ray diffraction, to contain the cation (**1**). Solid $[Co_3O(OAc)_6(py)_3][ClO_4]$ was obtained in less than quantitative yield. However, structural characterisation of "cobalt(III) acetate", its constituents or its derivatives was still lacking. Subsequently, Sumner reported the crystallographic characterisation of salts of the symmetric, dinuclear, hydroxy-bridged cation, $[Co_2(\mu\text{-}OH)_2(\mu\text{-}OAc)(OAc)_2(py)_4]^+$, (**2**), and the trinuclear, oxo-centred cations, $[Co_3(\mu_3\text{-}O)(\mu\text{-}OH)_2(\mu\text{-}OAc)_3(py)_5]^{2+}$, (**3**) and $[Co_3(\mu_3\text{-}O)(\mu\text{-}OR)(\mu\text{-}OAc)_5(py)_3]^+$, (**4**), using the strategy used by Uemura to obtain crystalline, pyridine-containing derivatives [30,31,34].

We have recently shown that dimeric cations such as (**5**) and (**6**) can also be isolated from "cobalt(III) acetate" solutions using pyridine as a co-ligand [32]. The cations (**5**) and (**6**) are formally derived from (**2**) by the successive interchange on each cobalt atom of a pyridine ligand with the non-hydrogen bonded acetate oxygen atom.

Recently, we reported the structure of the "parent", symmetric cation $[Co_3(\mu_3\text{-}O)(\mu\text{-}OAc)_6(py)_3]^+$, (**7**) [33], previously isolated by Sumner and Steinmetz from metal-catalysed autoxidation reactions, and prepared by them from the reaction of $[Co_3(\mu_3\text{-}O)(\mu\text{-}OH)(\mu\text{-}OAc)_5(py)_3]^+$, (**4a**), with acetic acid/acetic anhydride [34].

$$[Co_3O(OH)(OAc)_5(py)_3]^+ + HOAc \xrightarrow{Ac_2O,\,-H_2O} [Co_3O(OAc)_6(py)_3]^+$$

(**4a**) (**7**)

Trinuclear $[Co_3(\mu_3\text{-}O)(\mu\text{-}OH)(\mu\text{-}OAc)_5(py)_3]^+$, (**4a**), was itself prepared in 81% yield as its PF_6^- salt by the addition of aqueous NH_4PF_6 to a solution obtained from the peracetic acid oxidation of cobalt(II) acetate in warm aqueous acetic acid in the presence of pyridine.

In attempting to produce stable analogues of potential models of the photosynthetic water oxidation centre in plants and bacteria, Dimitrou *et al.* prepared in good (69%) yield, $[Co_2(\mu\text{-}OH)_2(\mu\text{-}OAc)(OAc)_2(bpy)_2][ClO_4]$, (**8**, bpy = bipyridyl), the bipyridyl analogue of (**2**), by H_2O_2 (3 equivalents) oxidation of $[Co(OAc)_2(H_2O)_4]$ in methanol/water at 50°C in the presence of bipyridine, followed by the addition of $LiClO_4$ [35]. A similar reaction at room temperature in ethanol/water with a deficiency of bipyridine and excess (10 equivalents) of H_2O_2 yielded (51% as the ClO_4^- salt) the partial cubane dication $[Co_3(\mu_3\text{-}O)(\mu\text{-}OH)_3(\mu\text{-}OAc)(OAc)(bpy)_3]^{2+}$ (**9**). Reaction of (**8**) with Li_2O_2 in hot dimethylsulfoxide generated the ClO_4^- salt of the dicationic cubane, $[Co_4(\mu_3\text{-}O)_4(\mu\text{-}OAc)_2(bpy)_4]^{2+}$, (**10**), in 64% yield. Although not isolated from, nor hitherto observed in, typical "cobalt(III) acetate" solutions, structures of the types (**9**) and (**10**) are clearly of interest in the examination of the constitution of "cobalt(III) acetate".

Similarly, oxidation of $[Co(PhCO_2)_2]$ with aqueous H_2O_2 in dimethylformamide or acetonitrile leads to the mixed-valence octanuclear $[Co_8(\mu_4\text{-}O)_4$

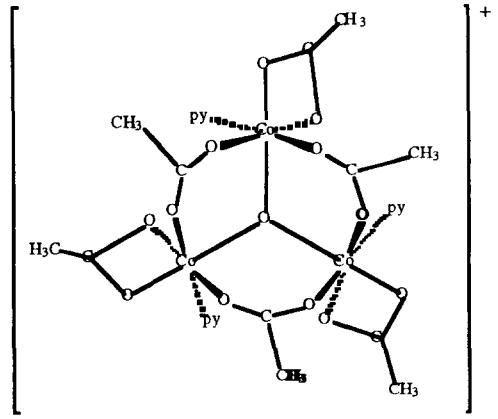

(**1**)

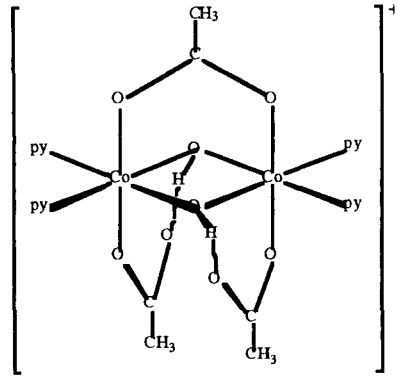

(**2**)

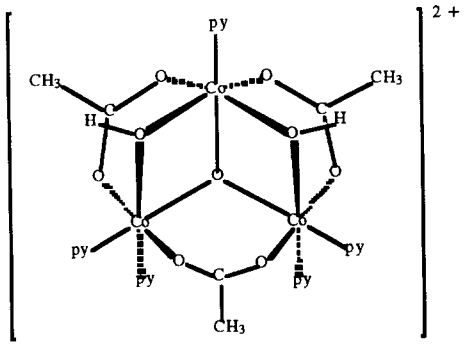

(3)

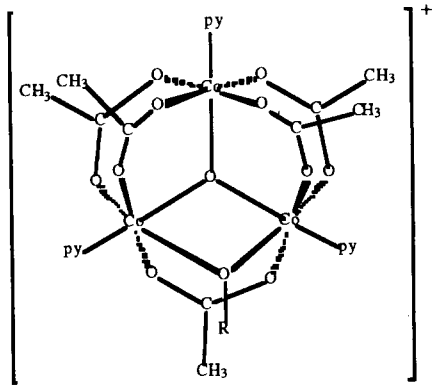

(4a R = H, 4b R = 3-phenylpropyl)

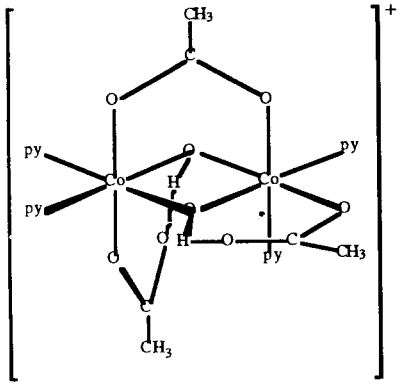

(5)

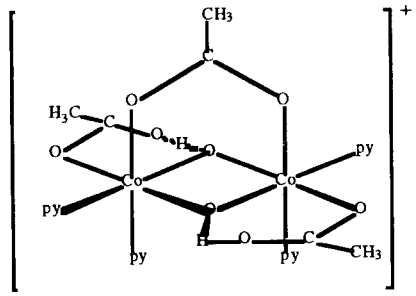

(6)

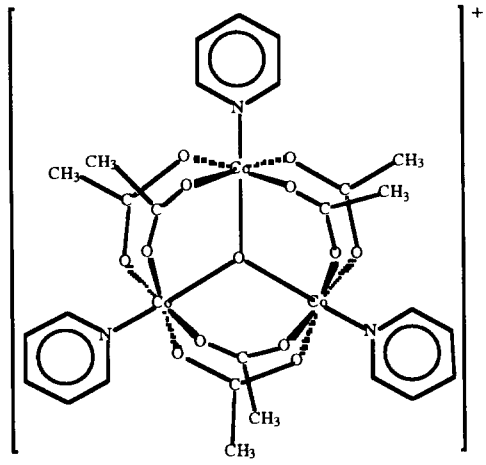

(7)

$(PhCO_2)_{12}(L)_3(H_2O)]$ (L = DMF, MeCN, H_2O) [36, 37]. We have recently shown that the mixed valence octanuclear $[Co_8(\mu_4\text{-}O)_4(\mu\text{-}OAc)_6(\mu\text{-}OMe)_4(Cl)_4(OH_n)_4]$ (n = 1 or 2) is produced in good yield during the recrystallisation of "cobalt(III) acetate" from methanol over several months in the presence of a halide source such as CH_2Cl_2 or AX (A = H^+, Li^+, NH_4^+; X = Cl^-) [38].

In continuation of our studies on the constitution of "cobalt(III) acetate" we report here the isolation

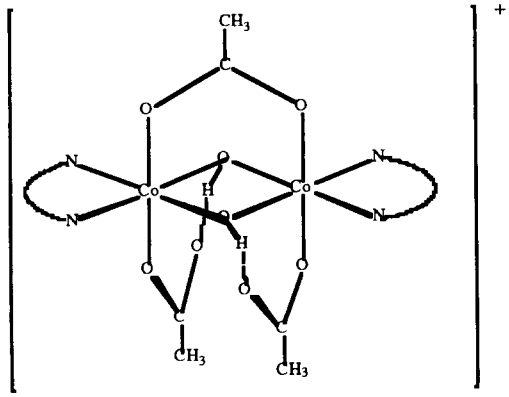

(8)

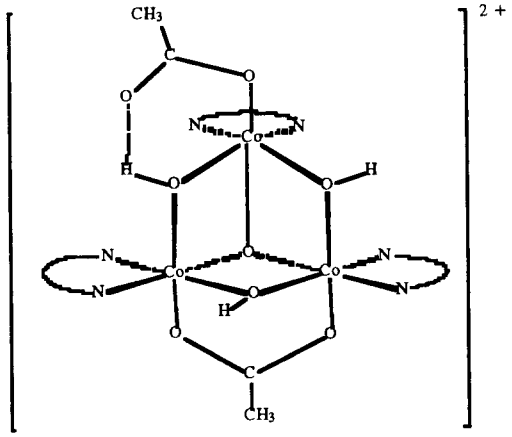

(9)

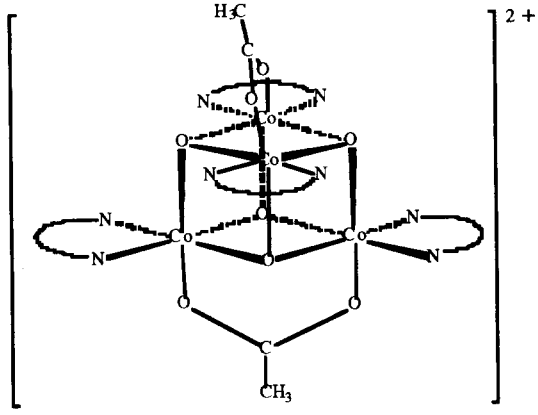

(10)

from "cobalt(III) acetate"/pyridine of the neutral cubane, $[Co_4(\mu_3\text{-}O)_4(\mu\text{-}OAc)_4(py)_4]$, (**11**), the synthesis of the partial cubane, the trinuclear dication, $[Co_3(\mu_3\text{-}O)(\mu\text{-}OH)_3(\mu\text{-}OAc)(OAc)(py)_6]^{2+}$, (**12**), as its hexafluorophosphate salt, and the structural characterisation of these compounds.

EXPERIMENTAL

WARNING: perchlorate salts are potentially explosive and must be treated with care.

Chemicals

Cobalt(II) acetate tetrahydrate and lithium peroxide (both Aldrich), acetic acid (Biolab), light petroleum (BDH), acetic anhydride, ammonium hexafluorophosphate, dichloromethane, dimethylformamide, dimethylsulfoxide, ethanol, methanol and sodium perchlorate hydrate (all Merck), acetonitrile, chloroform, pyridine (all Ajax) and hydrogen peroxide (27.5%, Pacific) were of analytical reagent grade and were used as received. Dimethylsulfoxide was dried over molecular sieves (4A) for several days before use.

The compounds $[Co_2(\mu\text{-}OH)_2(\mu\text{-}OAc)(OAc)_2(py)_4][PF_6]$, (**2**)$[PF_6]$ and (**5**)$[PF_6]$, $[Co_3(\mu_3\text{-}O)(\mu\text{-}OAc)_6(py)_3][PF_6]$, (**7**)$[PF_6]$, and $[Co_3(\mu_3\text{-}O)(\mu\text{-}OH)(\mu\text{-}OAc)_5(py)_3][PF_6]$, (**4a**)$[PF_6]$, were prepared by published methods [32,34]. "Cobalt(III) acetate" was prepared using the following adaptation of a reported method [26]. Cobalt(II) acetate tetrahydrate (12.5 g, 0.05 mol) was stirred overnight in acetic acid (125 cm^3) precipitating anhydrous pink cobalt(II) acetate with some pink cobalt(II) acetate remaining dissolved. The mixture was then ozonated (20 l (O_2)/h) with a

Wallace and Tiernan laboratory ozonator (model BA-023012) ("250 V") for 19 h. The solution turned from pink to dark brown within several minutes. The resulting green solution was evaporated *in vacuo* at $< 20°C$ to give dark green crude "cobalt(III) acetate" (11.0 g). Crude "cobalt(III) acetate" (10.0 g) was then crushed and dissolved in chloroform (~ 200 cm^3) and the solution filtered. Light petroleum (60–80°C; ~ 500 cm^3) was then added to the filtrate and the green "pure" "cobalt(III) acetate" isolated by filtration and dried *in vacuo* (8.1 g, 69% as "$Co(OAc)_3$"). Selected IR data (KBr): ν_{max}/cm^{-1}. 1576 (vs), 1420 (vs), 1347 (w), 1044 (w), 1030 (w), 957 (w), 890 (w), 805 (w), 747 (vw), 720 (vw), 698 (s), 631 (m), 581 (vw), 496 (w), 414 (w).

Tetrakis[(*μ-acetato-κO*: *κO′*)-*μ*$_3$-*oxo*-(*pyridine*)*cobalt* (*III*)], $[Co_4(\mu_3\text{-}O)_4(\mu\text{-}OAc)_4(py)_4]$ (**11**)

Method A—Formation from "cobalt(III) acetate". In a sealed vessel, pyridine (0.4 g, 5 mmol) and $NaClO_4 \cdot nH_2O$ (0.2 g, $\sim$ 1 mmol) were added to a dark green solution of "pure" "cobalt(III) acetate" (1.0 g, 4.2 mmol as "$Co(OAc)_3$") in methanol (10 cm^3) and the mixture stirred briefly. The mixture was left at room temperature for 1 h and filtered. Small brown crystals were collected by filtration, washed with diethyl ether and dried in air (0.01 g). The solid was identified by ESI/MS and solution ^{1}H NMR in CD_3CN and CD_2Cl_2 as a mixture of mainly $[Co_3(\mu_3\text{-}O)(\mu\text{-}OMe)(\mu\text{-}OAc)_5(py)_3][ClO_4]$, a smaller amount of (**4a**)$[ClO_4]$ and another species not readily identified. The filtrate was left for another 10 h, precipitating more solid (0.3 g) which was collected by filtration and dried over silica gel. The ^{1}H NMR in CD_3CN and CD_2Cl_2 showed the material also consisted of (**4a**)$[ClO_4]$ and $[Co_3(\mu_3\text{-}O)(\mu\text{-}OMe)(\mu\text{-}OAc)_5(py)_3][ClO_4]$, as well as other products not easily identified by ^{1}H NMR. After removal of the solvent *in vacuo*, a dark brown paramagnetic solid was obtained (0.58 g). The solid was washed through alumina with acetonitrile, to give an olive/green solution. The solvent was removed and the solid dried *in vacuo*. ^{1}H NMR in CD_3CN showed the solid to contain a mixture of species including the cubane, (**11**), (**5**), (**2**), (**3**) and other species not easily or previously identified by 200 MHz ^{1}H NMR. Selected IR data (KBr): ν_{max}/cm^{-1} 3110 (w), 3071 (w), 3046 (w), 3005 (w), 2926 (w), 1606 (w), 1550 (sh, s), 1540 (vs), 1485 (m), 1451 (m), 1414 (s), 1338 (m), 1214 (m), 1152 (w), 1073 (w), 1048 (w), 1019 (vw), 761 (m), 694 (s), 647 (sh), 632 (s), 585 (m), 572 (m). UV/Vis (CH_2Cl_2): 604 (sh) nm ($\varepsilon_M = 509\ M^{-1}\ cm^{-1}$), 484 (sh) nm ($\varepsilon_M = 893\ M^{-1}\ cm^{-1}$), 364 nm ($\varepsilon_M = 9342\ M^{-1}\ cm^{-1}$). ^{1}H NMR (200 MHz; CD_3Cl): δ 8.37 (d, 8H), δ 7.59 (t, 4H), δ 7.16 (t, 8H), δ 1.99 (s, 12H). ^{13}C NMR (200 MHz; CD_3Cl): δ 186.86, δ 153.47, δ 124.46, δ 138.62, δ 26.63. ESI/MS: 853 ($[M+H]^+$), 774 ($[M+H\text{-}py]^+$), 695 ($[M+H\text{-}2py]^+$).

Method B—Direct ozonation oxidation method. Cobalt(II) acetate tetrahydrate (3.125 g, 12.5 mmol) was dissolved in water (25 cm^3). Acetic acid (10 cm^3, 18 M) and pyridine (1.00 g, 12.6 mmol) were then added to the mixture and stirred (1 h). The reaction mixture was then ozonated (2 h) during which the solution changed colour from pink/red to dark olive/brown. After ozonolysis the reaction mixture was immediately and quickly heated ($\sim 65°C$) and ammonium hexafluorophosphate (1.36 g, 8.3 mmol) dissolved in water (5 cm^3) was added. The resulting mixture was allowed to cool to room temperature and subsequently kept at low temperature (5d, $< 5°C$). The product mixture of small crystals (2.6 g) was collected by filtration, washed with water, and dried over silica gel overnight. ^{1}H NMR indicated that the solid contained a mixture of mainly (**4a**)$[PF_6]$ with smaller amounts of (**3**)$[PF_6]_2$ and a material formulated as $[Co(\mu\text{-}OH)_2(\mu\text{-}OAc)(OAc)_2(py)_3(solvent)][PF_6]$ [32] and trace amounts of the dimeric species (**2**)$[PF_6]$. The filtrate was again kept at low temperature for several days after which a second crop of solid material was filtered, washed with a little water and dried (0.02 g). The remaining filtrate was extracted into methylene chloride (3×50 cm^3), the combined methylene chloride extracts washed with water, hydrogen carbonate solution and finally sodium chloride solution and the solvent removed by rotary evaporation at room temperature. The resulting brown solid was finally dried *in vacuo* (0.55 g). The solid obtained from the methylene chloride extract was found to contain a mixture of mainly the oxo-centred trimers (**7**)$[PF_6]$, (**4a**)$[PF_6]$, (**3**)$[PF_6]_2$ and the cubane (**11**) as observed by solution ^{1}H NMR and TLC. The cubane, (**11**), can be isolated from the mixture using column chromatography.

Method C—Preparation from $[Co_2(\mu\text{-}OH)_2(\mu\text{-}OAc)(OAc)_2(py)_4][PF_6]$. A procedure similar to that reported [35] for the preparation of $[Co_4(\mu_3\text{-}O)_4(\mu_2\text{-}OAc)_2(bpy)_4]^{2+}$ was used to synthesise $[Co_4(\mu_3\text{-}O)_4(\mu_2\text{-}OAc)_4(py)_4]$. Crystals suitable for X-ray crystallographic analysis were obtained by this method. Under nitrogen, $[Co_2(\mu\text{-}OH)_2(\mu\text{-}OAc)(OAc)_2(py)_4][PF_6]$ ((**2**)$[PF_6]$) (0.079 g, 0.1 mmol) and lithium peroxide (0.023 g, 0.5 mmol) were stirred and heated to 55°C (15 min) in dimethylsulphoxide (5 cm^3). The original red solution changed colour to olive/brown during the reaction and after cooling the reaction mixture was filtered. Chloroform (25 cm^3) was added to the filtrate and the mixture left stoppered ($< 5°C$). Over one week large dark olive crystals formed and were subsequently filtered, dried in air and identified as pure (**11**) (0.01 g, 23%) by using solution ^{1}H NMR and IR. The salts (**5**)$[PF_6]$, (**7**)$[PF_6]$, (**4a**)$[PF_6]$, or (**12**)$[PF_6]_2$ can be used in place of (**2**)$[PF_6]$, with yields of 21, 27, 48 and 8%, respectively, depending on the crystallisation time and temperature. Similarly, (**4a**)$[PF_6]$ can be reacted with Li_2O_2 as above, but in DMF, rather than in DMSO to produce predominantly (**11**). Alternatively, (**4a**)$[PF_6]$ can be

reacted as above with DMSO in the presence or absence of KOH (in place of Li_2O_2) to give (**11**) in yields of 23 and 58%, respectively.

Acetato(μ-acetato-κO: κO′)-tris(μ$_3$-hydroxo)-μ$_3$-oxo-hexakis(pyridine)tricobalt(III) hexafluorophosphate, $[Co_3(\mu_3\text{-}O)(\mu\text{-}OH)_3(\mu\text{-}OAc)(OAc)(py)_6][PF_6]_2$, (**12**)$[PF_6]_2$

Method A—Direct ozonation oxidation method. Cobalt(II) acetate tetrahydrate (3.125 g, 12.5 mmol) dissolved in water (25 cm^3) was stirred with pyridine (2.00 g, 25.3 mmol) and the pink/red solution ozonated (2 h). The resulting dark brown solution was quickly heated (~70°C) and added to an aqueous solution of ammonium hexafluorophosphate (1.36 g, 8.3 mmol in 5 cm^3). After cooling to room temperature a brown solid was collected by filtration, washed with water, and dried over silica gel overnight (3.7 g). Solution ^{1}H NMR in CD_3CN showed the solid to contain a mixture of species including (**5**), (**3**), (**2**), (**12**), (**6**) and trace amounts of other species. The filtrate was extracted into methylene chloride (3 × 100 cm^3), the combined methylene chloride extracts evaporated to 5 cm^3 and layered with diethylether. After 24 h a brown solid was filtered (0.6 g) and was found to consist of a mixture of (**2**), (**5**), (**12**), (**6**), (**3**) and trace amounts of other species as identified by solution ^{1}H NMR in CD_3CN.

Method B. The synthesis of $[Co_3(\mu_3\text{-}O)(\mu\text{-}OH)_3(\mu\text{-}OAc)(OAc)(py)_6][PF_6]_2$ was adapted from that reported for $[Co_3(\mu_3\text{-}O)(\mu\text{-}OH)_3(\mu\text{-}OAc)(OAc)(bpy)_3][ClO_4]_2$ [35]. Cobalt(II) acetate tetrahydrate (1.24 g, 5.0 mmol) was dissolved in water (4 cm^3) and subsequently stirred (15 min) with ethanol (24 cm^3) and pyridine (0.8 g, 10.1 mmol) to form a purple solution. The stirred cobalt(II) solution was treated dropwise with hydrogen peroxide (5.8 cm^3) over ~45 min. The solution changed colour to dark brown and increased in temperature to 37°C during the addition of hydrogen peroxide. Ammonium hexafluorophosphate (0.55 g, 3.4 mmol) dissolved in ethanol (2 cm^3) and water (1 cm^3) was then added and the solution was stirred briefly (5 min) and then left covered at room temperature. After one week a microcrystalline solid (typically ~0.22 g) was separated by filtration, the filtrate was retained and the solid was dried over silica gel. The crude dried solid was extracted into acetonitrile and a small amount of purple paramagnetic material was removed by filtration. The acetonitrile was evaporated and the resulting brown solid was found to contain mainly (**12**)$[PF_6]_2$ with trace amounts of (**5**)$[PF_6]$ and (**3**)$[PF_6]_2$ as identified by ^{1}H NMR in CD_3CN. The remaining original reaction mixture filtrate was cooled (<5°C) for one week and then filtered. A brown precipitate (0.15 g) was obtained from the supernatant and found (^{1}H NMR) to contain a mixture of species including (**5**)$[PF_6]$, (**3**)$[PF_6]_2$, (**12**)$[PF_6]_2$ with others as yet unidentified. The remaining dark brown filtrate was evaporated to dryness *in vacuo* to give a dark brown solid (1.42 g). ^{1}H NMR in CD_3CN, after filtration through alumina, revealed the extract contained a mixture of pyridine containing species including (**2**)$[PF_6]$, (**5**)$[PF_6]$, (**3**)$[PF_6]_2$, and others as yet unidentified. Pure brown/orange (**12**)$[PF_6]_2$ ($Rf \simeq 0.24$) was obtained by chromatographing small amounts of the first microcrystalline material through a short column of flash silica using 4 : 1 methylene chloride : acetonitrile as eluent after examination by TLC ((**5**)$[PF_6]$, $Rf \simeq 0.35$ and (**3**)$[PF_6]_2$, $Rf \simeq 0.43$). Anal. $[Co^{III}_3(\mu_3\text{-}O)(\mu\text{-}OH)_3(\mu\text{-}OAc)_2(py)_6][PF_6]_2$ (**12**)$[PF_6]_2$. Selected IR data (KBr): ν_{max}/cm^{-1} 1609 (w), 1490 (w), 1451 (m), 1385 (w), 1331 (w), 1218 (w), 1074 (w), 1049 (w), 1021 (w), 880 (m), 844 (vs), 765 (w), 700 (m), 693 (m), 600 (br), 558 (s). Selected ^{1}H NMR (200 MHz; CD_3CN, TMS): −2.75 (s, 1H), −0.36 (s, 1H), 0.88 (s, 3H), 2.15 (s, 3H), 5.17 (s, 1H). ^{13}C NMR (200 MHz; CD_3CN, TMS): 24.73, 25.61, 156.5, 151.93, 152.79, 153.84, 155.31, 155.48, 125.43, 126.16, 126.25, 126.45, 126.74, 140.43, 140.66, 140.92, 141.06, 185.02, 189.85. ESI/MS: 981.0 ($[M\text{-}PF_6]^+$), 418 ($[M\text{-}2PF_6]^{2+}$).

Structure determinations

Discrete single dark green-olive crystals of the cubane, $[Co_4(\mu_3\text{-}O)_4(\mu\text{-}OAc)_4(py)_4]\cdot 5CHCl_3$, ((**11**)·$5CHCl_3$), were obtained as the $CHCl_3$ solvate by leaving a DMSO solution in contact with $CHCl_3$ for several weeks below 5°C. Crystals of (**11**)·$5CHCl_3$ lost solvent readily. Accordingly a green plate was quickly mounted and cooled to −50°C. Small prismatic red crystals of the PF_6^- salt of the partial cubane, $[Co_3(\mu_3\text{-}O)(\mu\text{-}OH)_3(\mu\text{-}OAc)(OAc)(py)_6][PF_6]_2 \cdot 2H_2O$, ((**12**)$[PF_6]_2\cdot 2H_2O$), were obtained by slow crystallisation from the mother liquor over two weeks. X-ray diffraction measurements were made with a Rigaku AFC7R diffractometer employing graphite monochromated Cu-K_α radiation generated with a 12 kW direct drive rotating anode. Primitive cell constants were obtained from a least-squares refinement using the setting angles of 22(25) (for the cubane, ((**11**)·$5CHCl_3$), and (in parentheses) partial cubane, ((**12**)$[PF_6]_2\cdot 2H_2O$), respectively) reflections in the range $41.15(18.40) < 2\theta < 69.80(23.78)°$. The data were collected at $-50(21) \pm 1$°C using ω–2θ scans to a maximum 2θ value of 110.1(100.1)°. Omega scans of several intense reflections, made prior to data collection, had an average width at half-height of 0.19(0.34)°. The data were collected with scans of $(1.47(1.21) + 0.35 \tan\theta)°$ at a speed of 32.0(16.0)°/min (in omega). The weak reflections ($I < 15.0\sigma(I)$) were rescanned up to 10 scans, and the counts were accumulated. Stationary background counts were recorded on each side of the reflection. The ratio of peak counting time to background counting time was 2 : 1. Over the course of data collection, the intensities of three

representative reflections, measured every 150 reflections, decreased by 3.2(3.8)%. Empirical absorption corrections based on azimuthal scans of three reflections were applied to each set of data, with transmission factors ranging from 0.33(0.73) to 1.00. The data were also corrected for Lorentz and polarisation effects.

All calculations were performed using the teXsan crystallographic software package [39]. The structures were solved by direct methods and expanded using Fourier techniques [40,41]. The solution of the cubane structure in Pnma (#62), revealed a $[Co_4(\mu_3\text{-}O)_4(\mu\text{-}OAc)_4(py)_4]$ cluster bisected by a mirror plane and surrounded by five chloroform molecules distributed over six sites (a chloroform on a general site was assigned half occupancy). Two chloroform molecules straddle the same mirror that splits the complex, and one of these has a two-fold rotational disorder about the mirror plane. Not all of the non-hydrogen atoms could be refined anisotropically. Hydrogen atoms were included in the full matrix refinement at calculated positions with group temperature factors. Hydrogen atoms were not attached to four of the five chloroform molecules. In the case of the partial cubane salt, $[Co_3(\mu_3\text{-}O)(\mu\text{-}OH)_3(\mu\text{-}OAc)(OAc)(py)_6][PF_6]_2$, the limited data obtained from the small crystal, (1765 observed reflections, $(I > 1.5\sigma(I))$ precluded the anisotropic refinement of all of the non-hydrogen atoms. Hydrogen atoms were included in the full matrix refinement at calculated positions with group temperature factors. The hydroxyl and water hydrogen atoms could not be located and were not included at calculated positions in the refinement model. One of the hexafluorophosphate counterions was found to be severely disordered.

The residual weighting scheme for each solution was based on counting statistics and included a statistical uncertainty factor ($p = 0.003$). Neutral atom scattering factors were taken from Cromer and Waber [42]. Anomalous dispersion effects were included in the structure factor calculation [43], and the values for $\Delta f'$ and $\Delta f''$ were those of Creagh and McAuley [44]. The values for the mass attenuation coefficients are those of Creagh and Hubbell [45].

Full tables of bond lengths and angles, listings of atomic coordinates, observed and calculated structure factors and anisotropic thermal parameters are available as supplementary material (Tables S1–S16). Selected interatomic bond lengths and bond angles are given in Tables 2–5.

Crystal data

$C_{33}H_{34}Cl_{15}Co_4N_4O_{12}$, $M = 1446.18$, orthorhombic, space group, *Pnma*, (62), $a = 10.181(4)$, $b = 21.655(2)$, $c = 27.407(6)$ Å, $U = 6043(2)$ Å^3, D_c $(Z = 4) = 1.590$ g cm^{-3}, $F(000) = 2876.00$, λ(Cu-K_α) = 1.54178 cm^{-1}, μ(Cu-K_α) = 150.00 cm^{-1}. Specimen: green blade, $0.52 \times 0.17 \times 0.05$ mm. $N = 3978$, N_0 $(I > 2.0\sigma(I)) = 1292$, range of *hkl* 0–23, 0–29, 0–10, $R = 0.087$, $R_w = 0.084$, residual extrema +0.76, −0.70 e Å^{-3}.

$C_{34}H_{36}Co_3O_{10}P_2F_{12}N_6$, $M = 1155.42$, monoclinic, space group, $P2_{1/c}$, (14), $a = 20.340(4)$, $b = 12.730(2)$, $c = 20.585(4)$ Å, $\beta = 114.80(1)$, $U = 4839(2)$ Å^3, D_c $(Z = 4) = 1.586$ g cm^{-3}, $F(000) = 2324.00$, λ(Cu-K_α) = 1.54178 cm^{-1}, μ(Cu-K_α) = 95.20 cm^{-1}. Specimen: red prism, $0.20 \times 0.10 \times 0.08$ mm. $N = 5465$, N_0 $(I > 1.5\sigma(I)) = 1765$, range of *hkl* 0–20, 0–12, −20–20, $R = 0.078$, $R_w = 0.073$, residual extrema +0.66, −0.40 e Å^{-3}.

RESULTS AND DISCUSSION

Following the procedure of Uemura *et al.*, the known trimers, $[Co_3(\mu_3\text{-}O)(\mu\text{-}OR)(\mu\text{-}OAc)_5(py)_3]^+$ (R = H, Me), were isolated as their brown ClO_4^- or PF_6^- salts from methanol solutions of "cobalt(III) acetate" and pyridine. These materials were not known at the time of the work of Uemura *et al.* who correctly predicted that the structure of the solid first precipitated by this method differs from that of the $[M_3(\mu_3\text{-}O)(OAc)_6(solvent)_3]^{n+}$ species known at that time. Small amounts of additional, as yet unidentified, species were also precipitated in the present work, the total amount of characterised and uncharacterised precipitated salts accounting for approximately half of the "cobalt(III) acetate". Removal of the solvent left a dark brown paramagnetic solid, found to consist of the neutral diamagnetic tetramer $[Co_4(\mu_3\text{-}O)_4(\mu\text{-}OAc)_4(py)_4]$, (**11**), in a mixture of other species, some previously identified, others currently unidentified. The tetramer was characterised by vibrational, electronic, ^{1}H and ^{13}C NMR and electrospray mass spectroscopies. The single ^{1}H NMR resonance due to the acetate protons (δ 1.99 ppm in CD_3CN) and the simple set of pyridine resonances suggested a species of high symmetry in solution, whilst the mass spectrum indicated a tetramer. This structure was confirmed as a cubane by single X-ray diffraction and is illustrated in Fig. 1.

The cubane, $[Co_4(\mu_3\text{-}O)_4(\mu\text{-}OAc)_4(py)_4]$, (**11**), can also be isolated by direct ozonolysis of $[Co(OAc)_2(H_2O)_4]$ in water/acetic acid/pyridine (25/10/1 v/v), followed by precipitation of (**4a**), (**3**) and (**2**) with NH_4PF_6, extraction into dichloromethane and chromatographic separation from (**7**), (**4a**) and (**3**), or by reaction of Li_2O_2 with the dimers (**2**) or (**5**) or with the trimers (**7**), (**4a**) or with the trinuclear partial cubane (**12**) in dimethylsulfoxide or with the trinuclear (**4a**) in dimethylformamide. Alternatively, trimeric (**4a**) can be heated in dimethylsulfoxide in the presence or absence of KOH. The reaction of (**2**) with Li_2O_2 in DMSO is analogous to the preparation of $[Co_4(\mu_3\text{-}O)_4(\mu\text{-}OAc)_2(bipy)_4]^{2+}$ by Dimitrou *et al.* [35]. Interestingly, the neutral cubane, $[Co_4(\mu_3\text{-}O)_4(\mu\text{-}OAc)_4(py)_4]$, is formed, rather than

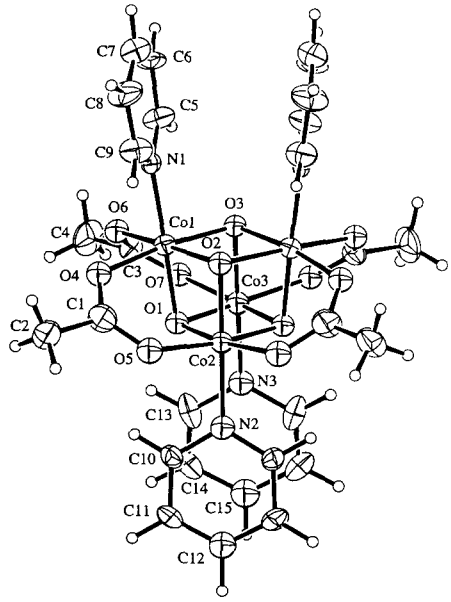

Fig. 1. ORTEP [46] illustration of the cubane, $[Co_4(\mu_3\text{-}O)_4(\mu\text{-}OAc)_4(py)_4]$, (**11**), showing the atom numbering scheme.

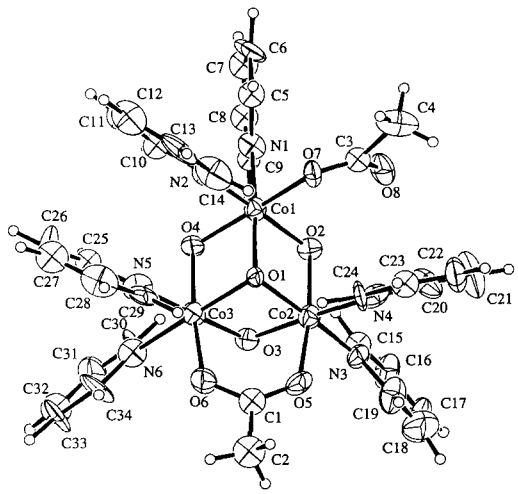

Fig. 2. ORTEP [46] illustration of the trimeric partial cubane dication, $[Co_3(\mu_3\text{-}O)(\mu\text{-}OH)_3(\mu\text{-}OAc)(OAc)(py)_6]^{2+}$, (**12**), showing the atom numbering scheme.

$[Co_4(\mu_3\text{-}O)_4(\mu\text{-}OAc)_2(py)_8]^{2+}$, the analogue of the known bipyridyl derivative.

Ozonation of $[Co(OAc)_2(H_2O)_4]$ in water/pyridine (13/1 v/v), followed by brief heating results in a mixture of products. The partial cubane dication, $[Co_3(\mu_3\text{-}O)(\mu\text{-}OH)_3(\mu\text{-}OAc)(OAc)(py)_6]^{2+}$, (**12**), can be isolated from this mixture as its PF_6^- salt. Alternatively, oxidation of $[Co(OAc)_2(H_2O)_4]$ by H_2O_2 in water/ethanol/pyridine (4/24/1 v/v) followed by treatment with NH_4PF_6 generates an unidentified paramagnetic purple solid from which (**12**)$[PF_6]_2$ can be chromatographically separated from salts of the dimeric cations (**2**) and (**5**) and of the trimeric cation (**3**). The compound was characterised spectroscopically (vibrational, ^1H NMR, ^{13}C NMR and electrospray mass spectra). A trinuclear formulation is suggested by the mass spectrum, whilst the ^1H NMR indicates two different acetate and three different hydroxyl (one of which is involved in hydrogen bonding) environments in solution. Restricted rotation of some of the pyridine ligands about the Co–N axes is also suggested by the ^1H NMR spectrum. The trinuclear structure of the cation was confirmed by single crystal X-ray crystallography and is illustrated in Fig. 2. Salient NMR data of these compounds are collected in Table 1.

The cubane has possibly previously escaped notice as a "constituent" or derivative of "cobalt(III) acetate" because of its high solubility in the solvents used, its colour and lack of charge. Indeed, the formation of the cubane from salts of any of (**2**), (**5**), (**12**), (**4a**) or (**7**) in d^6-DMSO can be monitored by ^1H NMR. The predominant species is invariably the cubane (**11**) with some free pyridine and trace amounts of other, at present unidentified, species. The variable yields of cubane from the different preparations are thus mainly due to the high solubility of this neutral species. Solution ^1H NMR spectra in CD_2Cl_2, D_2O, CD_3CN, CD_3OD and $(CD_3)_2SO$ at room temperature are consistent with the solid state structure and retention of T_d symmetry in these solvents. However, a different ^1H NMR spectrum is obtained in CD_3CO_2D at room temperature. Two pyridine environments are apparent, consistent with the formation of the diprotonated species, $[Co_4(\mu_3\text{-}O)_2(\mu\text{-}OH)_2(\mu\text{-}OAc)_4(py)_4]^{2+}$. After further rearrangements over several weeks at room temperature, the oxo-centred trimers, (**2**) and (**7**) were observed as the predominant species. However, in CD_3OD at room temperature, ^1H NMR shows the cubane (**11**) to be stable for several months, unlike (**4a**), for example, which slowly converts to other species in this solvent.

X-ray crystallographic analysis of (**11**)

Single crystals of (**11**) are composed of discrete $[Co_4(\mu_3\text{-}O)_4(\mu\text{-}OAc)_4(py)_4]$ molecules with the five chloroform molecules of crystallisation per tetramer located in large channels in the crystal lattice between the tetramers. The tetranuclear species contains four cobalt atoms and four oxygen atoms located at alternate corners of a slightly distorted cube in a typical $[M_4(\mu_3\text{-}O)_4]$ cubane type arrangement. Every cobalt atom is surrounded by a slightly distorted octahedron of two oxygen atoms from bridging acetate ligands, a nitrogen atom of a pyridine ligand and three neighbouring $[Co_4(\mu_3\text{-}O)_4]$ core oxygen atoms.

Each $[Co_4(\mu_3\text{-}O)_4(\mu\text{-}OAc)_4(py)_4]$ molecule is bisected by a crystallographic mirror plane. Consequently, two Co···Co distances are observed, that (average 2.818 Å) bridged by two oxo ligands only, and that (average 2.683 Å) bridged by two oxo ligands

Table 1. Selected spectrophotometric data for selected polynuclear cobalt(III) carboxylate species. ^{1}H NMR chemical shifts (ppm) of the acetate, hydroxy and pyridine protons in some cobalt complexes (200 MHz)

Complex	Solvent (ref.)	Methyl protons	Hydroxyl and methoxy proton(s)	Pyridine protons
$[Co_3O(OAc)_6(py)_3][PF_6]$	CD_3CN (TMS)	2.07 (s, 18H)		8.90 (d, 6H), 8.15 (t, 3H), 7.74 (t, 6H)
$[Co_3O(OMe)(OAc)_5(py)][PF_6]$	CD_3CN (TMS)	2.15 (s, 3H), 2.15 (s, 6H), 1.87 (s, 6H)	0.73 (s, 3H)	9.27 (d, 2H), 8.68 (d, 4H), 8.31 (t, 1H), 8.21 (t, 2H), 7.93 (t, 2H), 7.79 (t, 4H)
$[Co_3O(OH)(OAc)_5(py)][PF_6]$	CD_3CN (TMS)	2.08 (s, 3H), 2.05 (s, 6H), 1.95 (s, 6H)	−3.09 (s, 1H)	9.26 (d, 2H), 8.83 (d, 4H), 8.31 (t, 1H), 8.18 (t, 2H), 7.92 (t, 2H), 7.76 (t, 4H)
$[Co_4O_4(OAc)_4(py)_4]$	CD_3CN (TMS)	1.99 (s, 12H)		8.37 (d, 8H), 7.58 (t, 4H), 7.09 (t, 8H)
$[Co_3O(OH)_3(OAc)_2(py)_6][PF_6]_2$	CD_3CN (TMS)	0.88 (s, 3H), 2.15 (s, 3H)	−2.75 (s, 1H), −0.36 (s, 1H), 5.17 (s, 1H)	9.5 −6.85 (multiplets & broad peaks)

Table 2. Selected intramolecular distances (Å) involving the nonhydrogen atoms for $[Co_4O_4(OAc)_4(py)_4]\cdot 5CHCl_3$, (**11**) $\cdot 5CHCl_3$

Co(1)—Co(1)	2.817(7)	Co(2)—O(1)	1.86(1)
Co(1)—Co(2)	2.685(6)	Co(2)—O(2)	1.83(2)
Co(1)—Co(3)	2.680(6)	Co(2)—O(5)	1.96(2)
Co(2)—Co(3)	2.818(8)	Co(2)—O(5)	1.96(2)
Co(1)—O(1)	1.86(1)	Co(2)—N(2)	1.97(3)
Co(1)—O(2)	1.91(1)	Co(3)—O(1)	1.83(1)
Co(1)—O(3)	1.88(1)	Co(3)—O(1)	1.83(1)
Co(1)—O(4)	1.94(2)	Co(3)—O(3)	1.89(2)
Co(1)—O(6)	1.95(2)	Co(3)—O(7)	1.98(2)
Co(1)—N(1)	1.97(2)	Co(3)—O(7)	1.98(2)
Co(2)—O(1)	1.86(1)	Co(3)—N(3)	1.98(3)

Estimated standard deviations in the least significant figure are given in parentheses.

and a bidentate acetate ligand. These distances are marginally shorter (oxo bridged) and longer (carboxylate bridged) than the corresponding distances (average 2.852(2) and 2.665(2) Å) in $[Co_4(\mu_3\text{-}O)_4(\mu\text{-}OAc)_2(bpy)_4]^{2+}$, (**10**) [35]. The bis-oxo bridged Co···Co distances have no exact parallel in the known structures of tri- and tetranuclear pyridine-ligated basic cobalt(III) acetate complexes; however, the oxo/carboxylate bridged Co···Co distances are the shortest yet reported in these species. The pyridine planes containing N(2) and N(3) are inclined at 18.3(8)° and those containing N(1) and N(1*) are inclined at 16.4(8)°. The N(1) to N(1*) contact is 3.37(4) Å and that between N(2) and N(3) is 3.26(4) Å.

Each cobalt-centred octahedron is tilted slightly into the cubane core presumably because of steric interactions between the pyridine ligands which are oriented perpendicular to the cube faces bridged by two oxo ligands only and because of the bridging acetate arrangement around the $[Co_4(\mu_3\text{-}O)_4]$ core. The core μ_3-oxygen atoms are on average 1.01(1) Å out of their respective trimeric Co_3 planes.

Other structural parameters of (**11**) are similar to those of species containing the $[Co_4(\mu_3\text{-}O)_4]^{4+}$ (or $[Co_4(\mu_4\text{-}O)_4]^{4+}$) core; $[Co_4(\mu_3\text{-}O)_4(\mu\text{-}O_2CC_6H_4\text{-}p\text{-}Me)_2(bpy)_4]^{2+}$, $[Co_4(\mu_3\text{-}O)_3(\mu_3\text{-}OH)(\mu\text{-}O_2CC_6H_4\text{-}p\text{-}Me)_2(bpy)_4]^{3+}$, $[Co_4(\mu_4\text{-}O)_4(\mu\text{-}O_2CPh)_{12}(MeCN)_3(H_2O)]$ and $[Co_8(\mu_4\text{-}O)_4(\mu_3\text{-}OMe)_4(\mu\text{-}O_2CMe)_6(O)_4(Cl)_4]$ [35–38].

X-ray crystallographic analysis of (**12**) $[PF_6]_2$

The dication of $[Co_3(\mu_3\text{-}O)(\mu\text{-}OH)_3(\mu\text{-}OAc)(OAc)(py)_6][PF_6]_2\cdot 2H_2O$ is an oxo-centred trinuclear cobalt(III) cluster containing six pyridine, one bidentate bridging acetate, one monodentate acetate, and three bridging hydroxyl ligands. Each cobalt atom is situated in a slightly distorted octahedral environment. The $[Co_3(\mu_3\text{-}O)(\mu\text{-}OH)_3]$ core can be considered as a partial cubane, lacking the fourth cobalt atom to

Table 3. Selected intramolecular bond angles (°) involving the nonhydrogen atoms for $[Co_4O_4(OAc)_4(py)_4]\cdot 5CHCl_3$, (**11**)$\cdot 5CHCl_3$

O(1)—Co(1)—O(2)	86.3(7)	O(5)—Co(2)—O(5)	95(1)
O(1)—Co(1)—O(3)	87.3(7)	O(5)—Co(2)—N(2)	91.6(8)
O(1)—Co(1)—O(4)	87.5(6)	O(5)—Co(2)—N(2)	91.6(8)
O(1)—Co(1)—O(6)	88.6(7)	O(1)—Co(3)—O(1)	81.2(9)
O(1)—Co(1)—N(1)	178.6(7)	O(1)—Co(3)—O(3)	87.7(7)
O(2)—Co(1)—O(3)	83.7(6)	O(1)—Co(3)—O(7)	91.2(6)
O(2)—Co(1)—O(4)	90.5(7)	O(1)—Co(3)—O(7)	171.2(7)
O(2)—Co(1)—O(6)	172.2(7)	O(1)—Co(3)—N(3)	93.6(8)
O(2)—Co(1)—N(1)	94.7(8)	O(1)—Co(3)—O(3)	87.7(7)
O(3)—Co(1)—O(4)	172.5(8)	O(1)—Co(3)—O(7)	171.2(7)
O(3)—Co(1)—O(6)	90.1(7)	O(1)—Co(3)—O(7)	91.2(6)
O(3)—Co(1)—N(1)	93.8(9)	O(1)—Co(3)—N(3)	93.6(8)
O(4)—Co(1)—O(6)	95.2(7)	O(3)—Co(3)—O(7)	87.7(6)
O(4)—Co(1)—N(1)	91.5(8)	O(3)—Co(3)—O(7)	87.7(6)
O(6)—Co(1)—N(1)	90.4(7)	O(3)—Co(3)—N(3)	178(1)
O(1)—Co(2)—O(1)	79.6(9)	O(7)—Co(3)—O(7)	96.1(9)
O(1)—Co(2)—O(2)	88.5(7)	O(7)—Co(3)—N(3)	91.2(7)
O(1)—Co(2)—O(5)	92.6(7)	O(7)—Co(3)—N(3)	91.2(7)
O(1)—Co(2)—O(5)	171.1(8)	Co(1)—O(1)—Co(2)	92.4(7)
O(1)—Co(2)—N(2)	93.1(8)	Co(1)—O(1)—Co(3)	93.2(7)
O(1)—Co(2)—O(2)	88.5(7)	Co(2)—O(1)—Co(3)	99.5(6)
O(1)—Co(2)—O(5)	171.1(8)	Co(1)—O(2)—Co(1)	95.0(9)
O(1)—Co(2)—O(5)	92.6(7)	Co(1)—O(2)—Co(2)	91.7(8)
O(1)—Co(2)—N(2)	93.1(8)	Co(1)—O(2)—Co(2)	91.7(8)
O(2)—Co(2)—O(5)	87.0(7)	Co(1)—O(3)—Co(1)	97.3(9)
O(2)—Co(2)—O(5)	87.0(7)	Co(1)—O(3)—Co(3)	90.7(7)
O(2)—Co(2)—N(2)	178(1)	Co(1)—O(3)—Co(3)	90.7(7)

Estimated standard deviations in the least significant figure are given in parentheses.

achieve a full cubane ($[Co_4(\mu_3\text{-}O)_4]$) configuration. Alternatively the molecule can be viewed as consisting of three edge sharing octahedra sharing a central μ_3-oxygen atom at a common vertex.

Each pair of cobalt atoms is bridged by a hydroxyl ligand. The atoms Co(2) and Co(3) are also bridged by a bidentate acetate ligand. Atom Co(1) is coordinated to the oxygen of a monodentate acetate ligand. This monodentate acetate ligand is hydrogen bonded to the hydroxyl ligand bridging Co(1) and Co(2). Two pyridine ligands complete the coordination about each cobalt atom.

Table 4. Selected intramolecular distances (Å) involving the nonhydrogen atoms for $[Co_3O(OH)_3(OAc)_2(py)_6][PF_6]_2\cdot 2H_2O$, (**12**)$[PF_6]_2\cdot 2H_2O$

Co(1)—Co(2)	2.900(5)	Co(2)—O(3)	1.92(1)
Co(1)—Co(3)	2.935(6)	Co(2)—O(5)	1.95(2)
Co(2)—Co(3)	2.767(5)	Co(2)—N(3)	1.95(2)
Co(1)—O(1)	1.92(1)	Co(2)—N(4)	1.99(3)
Co(1)—O(2)	1.93(1)	Co(3)—O(1)	1.92(1)
Co(1)—O(4)	1.94(1)	Co(3)—O(3)	1.88(1)
Co(1)—O(7)	1.91(2)	Co(3)—O(4)	1.93(1)
Co(1)—N(1)	1.99(2)	Co(3)—O(6)	1.92(2)
Co(1)—N(2)	1.88(2)	Co(3)—N(5)	1.95(2)
Co(2)—O(1)	1.90(1)	Co(3)—N(6)	1.97(2)
Co(2)—O(2)	1.93(1)		

Estimated standard deviations in the least significant figure are given in parentheses.

The μ_3-O atom is approximately 0.96 Å out of the Co_3 plane, a displacement similar to that (0.97 Å) in the bipyridine-containing partial cubane, $[Co_3(\mu_3\text{-}O)(\mu\text{-}OH)_3(\mu\text{-}OAc)(OAc)(bpy)_3]^{2+}$, (**9**) [35].

The hydrogen bonding distance between the acceptor monodentate acetate carbonyl oxygen atom and the hydroxyl oxygen donor atom is approximately 2.63(2) Å, typical of distances involved in similar bridging hydroxyl/monodentate acetate hydrogen bonding interactions observed within the dimeric species (**2**), (**5**) and (**6**) [32]. $[Co_3(\mu_3\text{-}O)(\mu\text{-}OH)_3(\mu\text{-}OAc)(OAc)(py)_6][PF_6]_2\cdot 2H_2O$ crystallises in the centrosymmetric space group $P2_1/c$ (#14); therefore both enantiomers of the molecule are present in the unit cell. The structural parameters of (**11**) and (**12**) may be compared with those of related polynuclear basic acetate cobalt(III) species collected recently [33].

CONCLUSIONS

To our knowledge isolation of a cubane ($[Co_4(\mu_3\text{-}O)_4]$) type moiety from "cobalt(III) acetate" chem-

Table 5. Selected intramolecular bond angles (°) involving the nonhydrogen atoms for $[Co_3O(OH)_3(OAc)_2(py)_6][PF_6]_2 \cdot 2H_2O$, (**12**)$[PF_6]_2 \cdot 2H_2O$

O(1)—Co(1)—O(2)	81.5(6)	Co(1)—O(1)—Co(2)	98.9(6)
O(1)—Co(1)—O(4)	80.6(6)	Co(1)—O(1)—Co(3)	99.8(6)
O(1)—Co(1)—O(7)	95.8(6)	Co(2)—O(1)—Co(3)	92.9(6)
O(1)—Co(1)—N(1)	171.1(8)	Co(1)—O(2)—Co(2)	97.5(6)
O(1)—Co(1)—N(2)	94.4(8)	Co(2)—O(3)—Co(3)	93.3(6)
O(2)—Co(1)—O(4)	92.4(6)	Co(1)—O(4)—Co(3)	98.8(6)
O(2)—Co(1)—O(7)	91.5(6)	O(3)—Co(2)—N(4)	178(1)
O(2)—Co(1)—N(1)	93.6(7)	O(5)—Co(2)—N(3)	92.6(8)
O(2)—Co(1)—N(2)	175.1(8)	O(5)—Co(2)—N(4)	89.0(9)
O(4)—Co(1)—O(7)	174.2(7)	N(3)—Co(2)—N(4)	92(1)
O(4)—Co(1)—N(1)	92.2(7)	O(1)—Co(3)—O(3)	85.6(6)
O(4)—Co(1)—N(2)	89.6(8)	O(1)—Co(3)—O(4)	80.9(6)
O(7)—Co(1)—N(1)	91.8(7)	O(1)—Co(3)—O(6)	93.1(6)
O(7)—Co(1)—N(2)	86.2(8)	O(1)—Co(3)—N(5)	94.7(8)
N(1)—Co(1)—N(2)	90.8(9)	O(1)—Co(3)—N(6)	177.4(9)
O(1)—Co(2)—O(2)	82.1(6)	O(3)—Co(3)—O(4)	85.3(6)
O(1)—Co(2)—O(3)	85.2(6)	O(3)—Co(3)—O(6)	90.9(7)
O(1)—Co(2)—O(5)	91.4(7)	O(3)—Co(3)—N(5)	179.1(8)
O(1)—Co(2)—N(3)	171.7(9)	O(3)—Co(3)—N(6)	91.8(9)
O(1)—Co(2)—N(4)	95.0(9)	O(4)—Co(3)—O(6)	173.1(7)
O(2)—Co(2)—O(3)	86.7(6)	O(4)—Co(3)—N(5)	94.0(7)
O(2)—Co(2)—O(5)	172.6(7)	O(4)—Co(3)—N(6)	98.8(9)
O(2)—Co(2)—N(3)	93.4(8)	O(6)—Co(3)—N(5)	89.8(8)
O(2)—Co(2)—N(4)	95.0(9)	O(6)—Co(3)—N(6)	87(1)
O(3)—Co(2)—O(5)	89.2(7)	N(5)—Co(3)—N(6)	88(1)
O(3)—Co(2)—N(3)	87.6(8)		

Estimated standard deviations in the least significant figure are given in parentheses.

istry is unprecedented with the exception of the octameric cobalt acetate species $[Co_8(\mu_4\text{-}O)_4(\mu\text{-}OAc)_6(\mu_3\text{-}OMe)_4(Cl)_4(OH_n)_4]$ ($n = 1$ or 2) which contains the "$[Co_4(\mu_3\text{-}O)_4]$" unit "capped" by two $[Co_2(\mu_3\text{-}OMe)_2]$ dimers [38].

The presence of cubane and partial cubane type structures in "cobalt(III) acetate" formed from the ozonation oxidation of cobalt(II) acetate tetrahydrate in acetic acid has not been suggested previously, despite much investigation on this system. This unusual neutral pyridine-containing cobalt(III) acetate cubane $[Co_4(\mu_3\text{-}O)_4(\mu\text{-}OAc)_4(py)_4]$ was isolated from solutions of cobalt(III) acetate in methanol after the addition of pyridine. The cubane has also been synthesised from the ozone oxidation of cobalt(II) acetate solutions containing pyridine and directly from various pyridine containing cobalt(III) acetates. The isolation of the cubane and of the mixed valence octameric cobalt acetate species from cobalt acetate solutions, suggests that cobalt cubanes and related structures may be significant in the chemistry of cobalt acetates. Similar species with acetic acid in place of pyridine may be constituents of "cobalt(III) acetate". Thus, for example, the possibility that pyridine ligands simply took the place of solvent acetic acid or water ligands without substantially altering the reaction chemistry was suggested by the report that the cobalt(III) clusters, $[Co_3(\mu_3\text{-}O)(\mu\text{-}OH)_n(OAc)_{6-n}(py)_3][PF_6]$ ($n = 0, 1$), are catalyst precursors for the autoxidation of aromatic hydrocarbons [30].

We have noted previously that the μ_3-oxygen atom is located in the Co_3 plane of the symmetric trimer, $[Co_3(\mu_3\text{-}O)(\mu\text{-}OAc)_6(py)_3]^+$, (**7**), and that as the bidentate bridging carboxylate ligands are successively replaced by monodentate bridging ligands, the μ_3-oxygen atom is displaced from the Co_3 plane [33]. A change in the hybridization of the μ_3-oxygen atom from sp^2 to sp^3 and a corresponding change in reactivity accompanies this displacement from the Co_3 plane. The present pair of complexes complete the series of pyridine ligated acetate derivatives with the μ_3-oxygen atom displacement being 0.04, ~0.35, 0.71, 0.96 and 1.01 Å for $[Co_3(\mu_3\text{-}O)(\mu\text{-}OAc)_6(py)_3]^+$, (**7**), $[Co_3(\mu_3\text{-}O)(\mu\text{-}OR)(\mu\text{-}OAc)_5(py)_3]^+$, (**4**), $[Co_3(\mu_3\text{-}O)(\mu\text{-}OH)_2(\mu\text{-}OAc)_3(py)_5]^{2+}$, (**3**), $[Co_3(\mu_3\text{-}O)(\mu\text{-}OH)_3(\mu\text{-}OAc)(OAc)(py)_6]^{2+}$, (**12**) and $[Co_4(\mu_3\text{-}O)_4(\mu\text{-}OAc)_4(py)_4]$, (**11**), respectively. The Co···Co separations in these pyridine ligated "cobalt(III) acetate" derivatives vary over about 0.5 Å, from ~3.2 Å when the cobalt atoms have a $(\mu\text{-}O)(\mu\text{-}OAc)_2$ bridge, to ~2.7 Å for a $(\mu\text{-}O)_2(\mu\text{-}OAc)$ bridge. In all these derivatives, the Co—N and Co—O (acetate) distances are relatively constant at 1.96–1.99 Å and 1.87–1.99 Å, respectively, and the Co—$(\mu_3\text{-}O)$ distances vary between 1.80 and 1.92 Å [33].

Protonation of the cubane core has been achieved

and may be possible to a greater extent than with the bipyridine containing cubane where charge build-up was suggested to inhibit further protonation. The demonstration of the $[Co_4(\mu_3\text{-}O)_4]^{n+}$ core within the mixed valence octanuclear, $[Co_8(\mu_4\text{-}O)_4(\mu\text{-}OAc)_6(\mu_3\text{-}OMe)_4(Cl)_4(OH_n)_4]$ ($n = 1$ or 2), and of the ready synthesis of $[Co_4(\mu_3\text{-}O)_4(\mu\text{-}OAc)_4(py)_4]$, (**11**) in solution suggests a hitherto unexpected importance of this $[Co_4(\mu_3\text{-}O)_4]^{n+}$ unit in cobalt acetate chemistry.

Acknowledgments—We thank the Australian Research Council for financial support and Professor L. A. P. Kane Maguire of the University of Wollongong for the electrospray mass spectra. JAK thanks the University of Sydney for a Postgraduate Scholarship.

REFERENCES

1. Barton, D. H. R., Gastiger, M. J. and Motherwell, W. B., *J. Chem. Soc., Chem. Commun.*, 1983, 731.
2. Figgis, B. N. and Martin, R. L., *J. Chem. Soc.*, 1956, 3837.
3. Adams, R. W., Barraclough, C. G., Martin, R. L. and Winter, G., *Inorg. Chem.*, 1966, **5,** 346.
4. Dubicki, L. and Day, P., *Inorg. Chem.*, 1972, **11,** 1868.
5. Shilov, A. E., *Activation of Saturated Hydrocarbons by Transition Metal Complexes*. D. Reidel, Dordrecht, 1984.
6. Tolman, C. A., Druliner, J. D., Nappa, M. J. and Herron, N., in *Activation and Functionalization of Alkanes*, ed. C. L. Hill. Wiley-Interscience, New York, 1989, p. 303.
7. Sheldon, R. A. and Kochi, J. K., *Oxidation and Combustion Reviews*, 1973, **5,** 226.
8. Sheldon, R. A. and Kochi, J. K., *Adv. Catal.*, 1976, **25,** 272.
9. Zeile Krevor, J. V., in *Selective Hydrocarbon Activation Principles and Progress*, ed. J. A. Davies, P. L. Watson, A. Greenberg and J. F. Liebman. VCH, New York, 1990, p. 19.
10. Gates, B. C., *Catalytic Chemistry*. Wiley-Interscience, New York, 1992.
11. Parshall, G. W. and Ittel, S. D., *Homogeneous Catalysis*. Wiley-Interscience, New York, 1992.
12. Copaux, *Ann. Chim. Phys.*, 1905, **6,** 548.
13. Schall, C. and Markgraf, H., *Trans. Am. Electrochem. Soc.* (*Chem. Abstracts*, 1924, **18,** 944) 1924, **45,** 161.
14. Schall, C. and Thieme-Weidtmarkter, C., *Z. Electrochem.* (*Chem. Abstracts*, 1929, **23,** 4412) 1929, **35,** 337.
15. Sharp, J. A. and White, A. G., *J. Chem. Soc.*, 1952, 110.
16. Mori, M., Kyumo, K. and Shibata, M., *Nippon Kagaku Zasshi*, 1956, **77,** 1434.
17. Koubek, E. and Edwards, J., *J. Inorg. Nucl. Chem.*, 1963, **25,** 1401.
18. Lande, S. S., Falk, C. D. and Kochi, J. K., *J. Inorg. Nucl. Chem.*, 1971, **33,** 4101.
19. Ziolkowski, J. J., Pruchnik, F. and Szymanska-Buzar, T., *Inorg. Chim. Acta*, 1973, **7,** 473.
20. Jones, G. H., *J. Chem. Soc., Chem. Commun.*, 1979, 536.
21. Jones, G. H., *J. Chem. Res.* (*M*), 1981, 2801.
22. Blake, A. B., Chipperfield, J. R., Lau, S. and Webster, D. E., *J. Chem. Soc., Dalton Trans.*, 1990, 3719.
23. Kopsch, U. and Walker, W. O., Canada Patent, 367,728, 1937.
24. Heiba, E. I., Dessau, R. M. and Koehl, W. J. J., *J. Am. Chem. Soc.*, 1969, **91,** 6830.
25. Koubek, E. and Edwards, J. O., *J. Inorg. Nucl. Chem.*, 1963, **25,** 1401.
26. Uemura, S., Spencer, A. and Wilkinson, G., *J. Chem. Soc., Dalton Trans.*, 1973, 2565.
27. Werner, A., *Liebigs Ann.*, 1910, **375,** 1.
28. Mandel, G. S., Marsh, R. E., Schaefer, W. P., Mandel, N. S. and Wang, B.-C., *Acta Cryst. B*, 1977, **33,** 3185.
29. Maas, G., *Z. anorg. allg. Chem.*, 1977, **432,** 203.
30. Sumner, C. E., Jr and Steinmetz, G. R., *J. Am. Chem. Soc.*, 1985, **107,** 6124.
31. Sumner, C. E., Jr, *Inorg. Chem.*, 1988, **27,** 1320.
32. Beattie, J. K., Hambley, T. W., Klepetko, J. A., Masters, A. F. and Turner, P., in preparation.
33. Beattie, J. K., Hambley, T. W., Klepetko, J. A., Masters, A. F. and Turner, P., *Polyhedron*, 1996, **15,** 2141.
34. Sumner, C. E., Jr and Steinmetz, G. R., *Inorg. Chem.*, 1989, **28,** 4290.
35. Dimitrou, K., Folting, K., Streib, W. E. and Christou, G., *J. Am. Chem. Soc.*, 1993, **115,** 6432.
36. Dimitrou, K., Folting, K., Streib, W. E. and Christou, G., *J. Chem. Soc., Chem. Commun.*, 1994, 1385.
37. Dimitrou, K., Sun, J.-S., Folting, K. and Christou, G., *Inorg. Chem.*, 1995, **34,** 4160.
38. Beattie, J. K., Hambley, T. W., Klepetko, J. A., Masters, A. F. and Turner, P., *Polyhedron*, 1997, **16,** 2109.
39. *teXsan*: *Single Crystal Structure Analysis Software*, Molecular Structure Corporation, The Woodlands, TX, 1993.
40. Altomare, A., Burla, M. C., Camalli, M., Cascarano, M., Giacovazzo, C., Guagliardi, A. and Polidori, G., *J. Appl. Cryst.*, 1993, **26,** 343.
41. Beurskens, P. T., Admiraal, G., Beurskens, G., Bosman, W. P., de Gelder, R., Israel, R. and Smits, J. M. M., The DIRDIF-94 program system. Technical Report of the Crystallography Laboratory, University of Nijmegen, The Netherlands, Nijmegen, 1994.
42. Cromer, D. T. and Waber, J. T., in *International Tables for X-Ray Crystallography*, ed. J. A. Ibers and W. C. Hamilton), Vol. IV. Kynoch Press, Birmingham, England, 1974, p. 71.
43. Ibers, J. A. and Hamilton, W. C., *Acta Crystallogr.*, 1964, **17,** 781.
44. Creagh, D. C. and McAuley, W. J. in *International Tables for Crystallography*, ed. A. J. C. Wilson, Vol. C. Kluwer Academic Publishers, Boston, 1992, p. 219.
45. Creagh, D. C. and Hubbell, J. H. in *International Tables for Crystallography*, ed. A. J. C. Wilson, Vol. C. Kluwer Academic Publishers, Boston, 1992, p. 200.
46. Johnson, C. K., *ORTEP, a Thermal Ellipsoid Plotting Program*, Oak Ridge National Laboratories, Oak Ridge TN, 1976.

Pergamon

PII: S0277-5387(97)00296-9

Polyhedron Vol. 17, No. 8, pp. 1355–1361, 1998
© 1998 Elsevier Science Ltd
All rights reserved. Printed in Great Britain
0277-5387/98 $19.00+0.00

Axial ligational properties of macrocyclic cobalt complexes

M. Radhakrishna Reddy, K. Hussain Reddy* and K. Mohana Raju

Department of Chemistry, Sri Krishnadevaraya University, Anantapur 515 003, India

(Received 20 February 1997; accepted 27 June 1997)

Abstract—Macrocyclic cobalt complexes have been prepared by template synthesis using acetylacetone and different aromatic diamines *viz.* 1,2-diaminobenzene and 3,4-diaminotoluene for the first time. These complexes have been alkylated using CH_3I and/or C_2H_5Br in the presence of pyridine and/or imidazole to obtain corresponding macrocyclic organocobalt complexes. The parent cobalt complexes and their alkyl derivatives have been characterized by elemental analyses, conductivity data, magnetic susceptibility measurements, electronic, infrared and ^1H NMR spectral data. Various ligand field parameters have been calculated. Electrochemical behaviour of these complexes has been studied by cyclic voltammetry. Axial ligation properties of parent cobalt complexes are supported by syntheses, electronic spectra and cyclic voltammetric studies. © 1998 Elsevier Science Ltd. All rights reserved

Keywords: macrocyclic cobalt complexes; ascial ligation; template synthesis; electronic spectra; cyclic voltammetry.

The cobaloximes [1] prepared using dimethylglyoxime ligand have been used as models for many B_{12} reactions. Subsequently cobalt complexes of SALEN [2,3] ACACEN [4] and oxime-schiff base ligands [5] have been derived as models for vitamin B_{12}. There has been considerable interest in the chemistry of macrocyclic metal complexes [6] which are considered as better model compounds for metalloporphyrins and metallocorrins for their intrinsic structural properties.

Spontaneous self-assembly reactions have been considered as vehicles for reliable and economical preparation of macrocyclic complexes. Although macrocyclic nickel(II) and copper(II) complexes derived using substituted acetylacetone and unsubstituted aromatic diamines have been synthesized and characterized to demonstrate the advantages of template synthesis by Jaeger [7–11] and Chipperfield [12], the corresponding macrocyclic cobalt complexes are not investigated. Recently, we have reported [13–15] macrocyclic nickel(II) and copper(II) complexes of acetylacetone buckled with different diamines. In the light of lacuna identified and in continuation of our earlier studies herein we report the synthesis, characterization, spectral studies and electrochemistry of macrocyclic cobalt complexes (**I**) and (**VI**) derived using acetylacetone and different diamines *viz.* 1,2-diaminobenzene and 3,4-diaminotoluene. Studies on corresponding alkylated derivatives are also carried out in support of axial ligational properties.

* Author to whom correspondence should be addressed.

EXPERIMENTAL

All the solvents used were of AR grade. Cobalt(II) chloride hexahydrate (Qualigens): 1,2-diaminobenzene and 3,4-diaminotoluene (Fluka AG); and iodomethane (Merck), bromoethane (Merck), pyridine (Qualigens) and Imidazole (spectrochem) were used in the present study.

Synthesis of complexes **I** *and* **VI**

A 250 cm^3 Erlenmeyer flask was charged with spinbar, cobalt(II) chloride hexahydrate (2.298 g, 0.0097 mol) aromatic diamine (0.0194 mol), dry butanol (30 cm^3) and acetylacetone (2.0 cm^3, 0.0194 mol) added by syringe. The flask was set upon a hot plate stirrer and equipped with a reflux condenser. The mixture was brought to a brisk reflux and continued for 8 h. The flask was removed from the hot source and allowed to cool. Then methanol (15 cm^3) was added and the mixture was cooled on ice–salt bath for at

least 15 min. Then an oily layer was separated out. The oily layer was treated with water and stirred vigorously to obtain black coloured substance. It was collected, washed with hot water, then with cold methanol and dried *in vacuo*.

Synthesis of alkyl derivatives

In a Schlenk tube, a saturated methanolic solution of macrocyclic cobalt complex (**I**) and (**VI**) (0.0042 mol) was taken and stirred under nitrogen atmosphere. Sodium hydroxide (0.0042 moles) and pyridine/imidazole (0.0021 mol) were added to the contents of the tube. The stirred suspension was then cooled to -5°C and stirred for 15 min. Then solid $NaBH_4$ (0.0042 mol) followed by alkylating agent (CH_3I or C_2H_5Br, 0.0021 mol) were added. The solution was gradually warmed to 20°C and stirred for a further 30 min. The solution was evaporated to half the volume and stirred with 20 cm^3 of water and filtered. It was collected washed with aqueous methanol and ether and then dried *in vacuo*. The yield, colour and melting points for all the complexes are given in Table 1.

Physical measurements

The elemental analyses were performed by the HERAEUS (Mikro standard 8304071) Carbon and Hydrogen Analyzer. The magnetic susceptibility measurements were made using a vibrating sample magnetometer (VSM) operating at a field strength of 2–8 KG. The electrical conductivity measurements were made in dimethylformamide (DMF) (*ca* 10^{-3} M) at room temperature (27 ± 2°C) using a Systronic 303 direct reading conductivity bridge. The electronic spectra for all complexes in the UV–vis region (180–1100 nm) were recorded with Schimadzu UV-160A spectrophotometer. The IR spectra were recorded in the ranges 4000–400 cm^{-1} (in KBr) and 450–50 cm^{-1} (in polyethylene) using Bruker IFS 66V FT-IR Spectrophotometer. ^1H NMR spectra were recorded on an

Table 1. Colour, partial elemental analyses and conductivities of the cobalt complexes

Complex	Molecular Formula	Colour (M.P., °C)	Found (Calc.) % C	H	N	Molar conductance (cm^2 Ohm^{-1} mol^{-1})
I	$[Co(C_{22}H_{22}N_4)]$	Blackish brown (250 D)	65.98 (65.85)	5.56 (5.49)	14.02 (13.97)	4.1
II	$[CH_3Co(C_{22}H_{22}N_4)C_5H_5N]$	Black (>300)	67.49 (67.88)	6.01 (6.06)	11.61 (11.31)	6.1
III	$[CH_3Co(C_{22}H_{22}N_4)C_3H_4N_2]$	Black (>300)	64.40 (64.47)	5.92 (5.99)	11.41 (11.57)	8.3
IV	$[C_2H_5Co(C_{22}H_{22}N_4)C_5H_5N]$	Blackish brown (289 D)	68.98 (68.36)	6.30 (6.29)	11.12 (11.00)	2.0
V	$[C_2H_5Co(C_{22}H_{22}N_4)C_3H_4N_2]$	Brown (>300)	65.05 (65.07)	6.11 (6.23)	11.15 (11.24)	4.2
VI	$[Co(C_{24}H_{26}N_4]$	Blackish brown (193 D)	67.20 (67.15)	6.03 (6.06)	13.03 (13.06)	2.3
VII	$[CH_3Co(C_{24}H_{26}N_4)C_5H_5N]$	Blackish brown (>300)	68.76 (68.97)	6.49 (6.51)	10.58 (10.71)	12.0
VIII	$[CH_3Co(C_{24}H_{26}N_4)C_3H_4N_2]$	Brown (292 D)	65.59 (65.64)	6.52 (6.45)	10.95 (10.93)	8.1
IX	$[C_2H_5Co(C_{24}H_{26}N_4)C_5H_5N]$ (>300)	Brown 69.18 (69.27)	69.18 (69.27)	6.66 (6.70)	10.44 (10.43)	16.0
X	$[C_2H_5Co(C_{24}H_{26}N_4)C_3H_4N_2]$	Brown (>300)	66.19 (66.17)	6.61 (6.65)	10.61 (10.65)	6.3

AMX-400 MHz high resolution NMR instrument in DMSO-d_6 solvent at room temperature. The cyclic voltammetry was performed with a BAS model CV-27 controller and a conventional three electrode, Ag/AgCl reference electrode, glassy carbon working electrode and platinum counter electrode. Nitrogen was used as a purge gas and all solutions were 0.1 M concentration in $TBAClO_4$.

RESULTS AND DISCUSSION

Attempts to isolate free ligands using acetylacetone and aromatic diamines were, however, unsuccessful. Hence the corresponding macrocyclic complexes were prepared by using the template method.

All the complexes are insoluble in water but readily soluble in methanol dimethylformamide and dimethylsulfoxide. The conductivity measurements show their non-electrolytic nature and the molecular weights of cobalt complexes are consistent with monomers.

Magnetic susceptibility and electronic spectra

The magnetic moment values of parent macrocyclic cobalt complexes are found to be in the 2.1–2.7 BM range as expected for low spin cobalt(II) complexes [16]. All alkyl derivatives (**II, III, IV, V, VII, VIII, IX** and **X**) are found to be diamagnetic.

In the electronic spectra of macrocyclic cobalt complexes (**I** and **VI**) (in DMF), two bands are observed in 16,103–16,530 (ν_2) and 22,371–22,936 cm^{-1} (ν_3) assigned to $^4T_{1g}(F) \rightarrow {}^4A_{2g}(F)$ and $^4T_{1g}(F) \rightarrow {}^4T_{1g}(P)$ transitions respectively in favour of an octahedral geometry [17]. The ν_1 values are calculated using the following equation.

$$\nu_1 = 5\,Dq - 7.5\,B + 1/2(225\,B^2 + 100\,Dq^2 + 180\,Dq\,B)^{1/2}$$

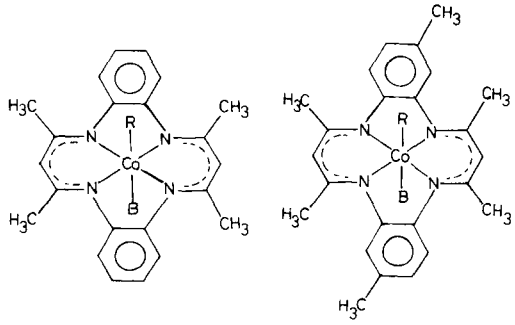

I. R and B absent
II. R=CH_3; B = Py
III. R=CH_3; B = Im
IV. R= C_2H_5; B= Py
V. R= C_2H_5; B = Im
VI. R and B absent
VII. R= CH_3; B= Py
VIII. R = CH_3; B= Im
IX. R = C_2H_5; B = Py
X. R = C_2H_5; B = Im

The interelectronic repulsion (B) and 10 Dq for all cobalt complexes are found to be in the range of 916–940 and 8074–8359, respectively. The ratio of observed ν_2 to calculated ν_1 lie between 2.22 and 2.36 as required for an octahedral cobalt complex [18]. The values of Dq, B, B_{35} and ν_2/ν_3 are given in Table 2. The electronic spectral data suggests an octahedral geometry for the present cobalt complexes facilitated by axial coordination of solvent (DMF) molecules.

Electronic spectral data of alkyl complexes are given in Table 3. The most intense bands in the highest energy region have been assigned [19] to $\pi \rightarrow \pi^*$ transition of equatorial ligand. The lowest energy band found in 21,000–25,000 cm^{-1} has been assigned to Co—C charge transfer transition. This band shifts to longer wavelength with increasing electron donating ability of alkyl groups and axial bases.

IR spectra

In the IR spectra of the complexes, the stretching and deformation vibrations of NH_2 are absent suggesting the formation of parent macrocyclic cobalt complexes (**I**) and (**VI**). Strong bands appearing in the range 1614–1634 cm^{-1} are assigned [20–23] to the stretching vibration of coordinated and conjugated ν(C=N) group present in all the complexes. Bands characteristic of acetylacetone moiety are observed in the 1450–1456 [ν_{asy}(C—CH_3)] and 1372–1394 cm^{-1} [ν_{sym}(C—CH_3)] regions in the IR spectra of all complexes. Characteristic bands are observed in the far IR spectra of complexes. Bands in the 432–466 cm^{-1} region are assigned to ν(Co—N) vibrations [24–27] suggesting the participation of conjugated (and equatorial) nitrogen in coordination. In organocobalt complexes bands observed in 312–341 and 235–269 cm^{-1} regions are tentatively assigned [19] to Co—C and Co—N (axial base) vibration, respectively.

^1H NMR spectra

All complexes are characterized by high resolution (400 MHz) ^{1}H NMR spectra. These spectral data incorporating chemical shifts (δ), multiplicity and the proton assignment are presented in Table 4. Broad multiplets centered between 6.6–7.1 ppm are observed in low field strength regions of spectra due to aromatic protons. As expected, methyl protons of the equatorial ligand resonate at high field strength (2.09–2.38 ppm). The spectra of methyl cobalt complexes show a singlet in 0.68–0.88 ppm range, where as the spectra of the ethylcobalamins exhibit two signals corresponding to methylene and methyl protons in 1.56–1.77 and 0.68–0.93 ppm, respectively. The signals due to the coordinated pyridine and Imidazole in the present complexes gave broad multiplets. However, the signals due to α and β protons of the pyridine are obscured by the signals due to aromatic protons of equatorial ligand.

Table 2. Electronic spectral data and ligand field parameters of non-alkylated cobalt complexes

Complex	ν_1[a] (cm^{-1})	ν_2 (cm^{-1})	ν_3 (cm^{-1})	B	B_{35}[b]	10 Dq	ν_2-ν_1	ν_2/ν_1	LFSE
I	7265	16103	22371	916	0.94	8359	8838	2.22	23.88
VI	6995	16529	22936	940	0.97	8074	9534	2.36	23.07

[a] Calculated value.
[b] B_{35} = B/971.

Table 3. Electronic spectral data (cm^{-1}) of alkyl derivatives

Complex	$\pi \rightarrow \pi^*$ (equatorial)	Co—C (Charge transfer)
II	32895 28986	22523
III	32787 28986	22989
IV	33222 28818	21598
V	32787 28818	22624
VII	33112 28571	22371
VIII	33003 28653	24938
IX	32680 28901	21834
X	33003 28818	22573

Electrochemical studies

The CV data of all the complexes are given in Table 5. The cyclic voltammograms of unalkylated complexes (**I**) and (**VI**) have cathodic peaks in the range -0.71 to -0.79 V, corresponding to Co^{III}/Co^{II} reduction couple which is irreversible. These non-alkylated complexes have reversible one electron [$Co^{II} \rightarrow Co^{I}$] couple with $E_{1/2}$ in the range -1.12 to 1.17 V. The $E_{1/2}$ values of (**I**) may be compared with interest. Complex **VI** has macrocyclic ligand containing two methyl groups. It is reduced at more negative potentials in comparison with complex **I**. This suggests that the complexes with less electron donating ligands have less negative $E_{1/2}$ values than those of ligands containing electron donating groups.

In general, CV of alkylcobalt complexes show two one electron reduction corresponding to $Co^{III} \rightarrow Co^{II}$ and a further $Co^{II} \rightarrow Co^{I}$ reduction. Except for **II, III, IV** and **V** complexes, all other alkyl cobalt complexes show reversible one electron reduction. The complexes of **II, III, IV** and **V** shows an irreversible reduction at E_{pc} in the range -1.00 to 1.38 V which corresponds to the $Co^{II} \rightarrow Co^{I}$ couple.

It is interesting to compare the half wave potentials of present complexes containing different axial bases. It is observed that the imidazole coordinated complexes are reduced at less negative potentials [29].

The second reduction wave (cathodic peak) which is irreversible is present in the CV of all alkylated complexes that correspond to Co^{II}/Co^{I} reduction couple.

Inspection of the data reveals that the nature of alkyl groups have profound effect [30] on the first

Table 4. ^{1}H NMR Spectral data of alkyl cobalt complexes

Complex	Chemical Shift (δ)	Multiplicity[a] (n)	No. of Protons	Assignment
II	6.6–6.93	d	8H	Phen H
	7.1–8.25	m	5H	Py H
	4.32	s	2H	Methine H
	2.38	s	12H	(CH_3—C=N) H
	0.87	s	3H	(CH_3—Co) H
III	6.6–6.93	d	8H	Phen H
	7.4–8.23	m	4H	Im H
	4.21	s	2H	Methine H
	2.37	s	12H	(CH_3—C=N) H
	0.86	s	3H	(CH_3—Co) H
IV	6.5–6.93	d	8H	Phen H
	7.1–7.98	m	5H	Py H
	4.22	s	2H	Methine H
	2.38	t	12H	(CH_3—C=N) H
	1.77	s	2H	CH_2 of ethyl H
	0.88	s	3H	CH_3 of ethyl H
V	6.6–9.4	d	8H	Phen H
	7.1–8.24	m	4H	Im H
	4.66	s	2H	Methine H
	2.23	s	12H	(CH_3—C=N) H
	1.56	s	2H	CH_2 of ethyl H
	0.86	s	3H	CH_3 of ethyl H
VII	6.94–7.0	m	6H	Phen H
	7.18–8.32	m	5H	Py H
	4.23	s	2H	Methine H
	2.39–2.45	t	12H	(CH_3—C=N) H
	2.51	s	3H	Ar—CH_3 H
	0.88	s	3H	(CH_3—Co) H
VIII	6.92–7.00	m	6H	Phen H
	7.2–8.1	m	4H	Im H
	4.03	s	2H	Methine H
	2.15–2.38	m	12H	(CH_3—C=N) H
	2.54	s	3H	Ar—CH_3 H
	0.68	s	3H	(CH_3—Co) H
IX	6.96–7.11	m	6H	Phen H
	7.21–8.28	m	5H	Py H
	4.16	s	2H	Methine H
	2.21–2.32	m	12H	(CH_3—C=N) H
	2.50	s	3H	Ar—CH_3 H
	1.65	s	2H	CH_2 of ethyl H
	0.72	s	3H	CH_3 of ethyl H
X	6.9–7.1	m	6H	Phen H
	7.1–8.1	m	4H	Im H
	4.51	s	2H	Methine H
	2.09–2.38	t	12H	(CH_3—C=N) H
	2.56	s	3H	Ar—CH_3 H
	1.77	s	3H	CH_2 of ethyl H
	0.93	s	2H	CH_3 of ethyl H

[a] d = doublet; m = multiplet; s = singlet; t = triplet.

reduction potential. For example, complex **VIII** is reduced at more negative potential in comparison with complex **X**.

Thus axial ligation properties of present macrocyclic cobalt complexes are evidenced by (i) the synthesis and characterization of alkyl derivatives, (ii) electronic and infrared spectra and (iii) electrochemical studies.

Acknowledgements—The authors thank the Department of Science and Technology, Government of India, New Delhi (SP/S1/F-07/92) for financial support. The authors also

Table 5. Cyclic voltammetric data of cobalt complexes (10^{-3} M) in DMF containing 0.1 M $TBAClO_4$ at 1.0 V/s at glassy carbon electrode, temp. 26°C

Complex	Gain	Redox couple	$E_{pc}V$	$E_{pa}V$	$E_{1/2}$	ΔE
I	0.05	**III/II**	−0.71	—	—	—
		II/I	−1.20	−1.03	−1.12	170
	0.10	**III/II**	−0.76	—	—	—
		II/I	−1.20	−1.04	−1.12	160
II	0.02	**III/II**	−0.95	—	—	—
III	0.01 &	**III/II**	—	−0.51	—	—
	0.02	**II/I**	−1.07	—	—	—
IV	0.01 &	**III/II**	—	−0.45	—	—
	0.02					
V	0.01	**III/II**	—	−0.50	—	—
		II/I	−1.38	—	—	—
VI	0.05	**III/II**	−0.79	—	—	—
		II/I	−1.21	−1.09	−1.15	120
	0.10	**II/I**	−1.21	−1.12	−1.17	90
VII	0.01 &	**III/II**	—	−0.38	—	—
	0.02	**II/I**	−1.23	—	—	—
VIII	0.02	**III/II**	−0.60	−0.43	−0.52	170
		II/I	−1.27	—	—	—
IX	0.01	**III/II**	−0.40	−0.45	−0.43	50
		II/I	−1.28	—	—	—
X	0.02	**III/II**	−0.51	−0.39	−0.45	120
		II/I	−1.35	—	—	—

thank the RSIC, Madras and SIF, Bangalore for providing IR and ^1H NMR spectral data, respectively.

REFERENCES

1. Schrauzer, G. N., *Acc. Chem. Res.*, 1968, **1,** 97.
2. Costa, G., Mestroni, G. and Pellizer, G., *J. Organomet. Chem.*, 1968, **11,** 333.
3. Biggotto, A., Costa, G., Mestroni, G., Pellizer, G., Puxeddu, A., Reisenhofer, E., Stefani, L. and Tauzer, G., *Inorg. Chimica Acta Rev.*, 1970, **4,** 41.
4. Costa, G., Mestroni, G., Tauzer, G. and Stefani, L., *J. Organomet. Chem.*, 1966, **6,** 181.
5. Darbien, D. H., Dahan, F., Costes, J. P., Laurent, J. P. and Cros, G., *J. Chem. Soc., Dalton Trans.*, 1988, 219.
6. Lindoy, L.F., *The Chemistry of Macrocyclic Ligand Complexes.* Cambridge University Press, Cambridge (1989).
7. Jaeger, E. G., *Z. Chem.*, 1964, **4,** 437.
8. Jaeger, E. G., *Z. Chem.*, 1967, **7,** 63.
9. Jaeger, E. G., *Z. Chem.*, 1968, **8,** 30.
10. Jaeger, E. G., *Z. Chem.*, 1968, **8,** 470.
11. Jaeger, E. G., *Z. Anorg. Allg. Chem.*, 1969, **364,** 177.
12. Chipperfield, J. R. and Woodward, S., *J. Chem. Ed.*, 1994, **71,** 175.
13. Hussain Reddy, K., Krishnaiah, G. and Sreenivasulu, Y., *Polyhedron*, 1991, **10,** 2785.
14. Radhakrishna Reddy, M., Mohana Raju, K. and Hussain Reddy, K., *Ind. J. Chem.*, 1996, **35A** 677.
15. Hussain Reddy, K., Radhakrishna Reddy, M. and Mohana Raju, K., *Polyhedron*, 1997, **16,** 2673.
16. Cotton, F. A. and Wilkinson, G., *Advanced Inorganic Chemistry*, p. 772, John Wiley, New York (1980).
17. Konig, E., *Structure and Bonding*, p. 175, Springer, New York (1971).
18. Lever, A. B. P., *Inorganic Electronic Spectroscopy*, pp. 199–332, Elsevier, Amsterdam (1965).
19. Toscano, P. J. and Marzilli, L. G., *Progress in Inorganic Chemistry* (Ed. S. J. Lippard), **31,** pp. 140 & 142. John Wiley, New York (1984).
20. Eggleston, D. S. and Jackels, S. C., *Inorg. Chem.*, 1980, **19,** 1953.
21. Coltrain, B. K. and Jackels, S. C., *Inorg. Chem.*, 1981, **20,** 2932.

22. Baldwin, D. A., Peiffer, R. M., Richgott, D. W. and Rose, N. J., *J. Am. Chem. Soc.*, 1975, **95,** 515.
23. Jakels, S. C., Farmery, K., Barefield, E. K., Rose, N. J. and Busch, D. H., *Inorg. Chem.*, 1972, **11,** 2893.
24. Nakamoto, K., *Infrared Spectra of Inorganic and Coordination Compounds.* Wiley, New York (1970).
25. Ferraro, J. R., *Low Frequency Vibrations of Inorganic and Coordination Compounds*, Plenum Press, New York (1972).
26. Rana, V. B., Singh, D. P., Singh, P. and Teotia, M. P., *Trans. Met. Chem.*, 1981, **6,** 36.
27. Malik, W. U., Bembi, R. and Singh, R., *Polyhedron*, 1983, **2,** 369.
28. Christodoulou, D., Kanatzidis, M. G. and Couconvanis, D., *Inorg. Chem.*, 1990, **29,** 191.
29. Hogenkamp, H. P. C. and Holmes, S., *Biochem.*, 1970, **9,** 1886.
30. Costa, G., Puxeddu, A. and Tauzher, G., *Inorg. Nucl. Chem. Lett.*, 1968, **4,** 319.

Pergamon

PII: S0277-5387(97)00283-0

Polyhedron Vol. 17, No. 8, pp. 1363–1368, 1998
© 1998 Elsevier Science Ltd
All rights reserved. Printed in Great Britain
0277-5387/98 $19.00+0.00

Syntheses and characterization of *N,N'*-dipropyl/diisopropylethane-1,2-diamine complexes of nickel(II) nitrate: thermal studies and X-ray single crystal structure analysis of *cis*-nitratobis (*N,N'*-dipropylethane-1,2-diamine)nickel(II) nitrate

Inamur Rahaman Laskar,[a] Debasis Das,[a] Nirmalendu Ray Chaudhuri,[a]* Golam Mostafa[b] and Alan J. Welch[c]

[a] Department of Inorganic Chemistry, Indian Association for the Cultivation of Science, Calcutta-700 032, India

[b] X-ray Laboratory, Department of Solid State Physics, Indian Association for the Cultivation of Science, Calcutta-700 032, India

[c] Department of Chemistry, Heriot-Watt University, Edinburgh, Edinburgh EH14 4AS, U.K.

(Received 27 March 97; accepted 25 June 97)

Abstract—The blue complex *cis*-$[Ni(dipren)_2(NO_3)](NO_3)$ **1** and the greenish blue *cis*-$[Ni(dipren)_2(H_2O)_2](NO_3)_2 \cdot 2H_2O$ **2** (dpren/dpren = dipropyl/diisopropylethane-1,2-diamine) have been synthesized. Complex **2** upon heating loses four water molecules in a single step and undergoes melting accompanied with colour change, greenish blue to deep green, **2a**. Configuration of the complexes **1, 2** and **2a** have been proposed to be *cis*-octahedral on the basis of magnetic, IR and electronic spectroscopic studies and confirmed in case of complex **1** by X-ray single crystal structure analysis. The role of steric factor of the alkyl groups on the selectivity of coordinating mode of nitrate ion is studied. © 1998 Elsevier Science Ltd. All rights reserved.

Keywords: *N,N'*-dipropylethane-1,2-diamine; *N,N'*-diisopropylethane-1,2-diamine; nitratobis(*N,N'*-dipropylethane-1,2-diamine)nickel(II) nitrate; *cis*-octahedral geometry of nickel(II); nickel(II) diamine complex; thermochromism.

N,N/N,N'-dialkyl (where alkyl groups are methyl/ethyl) substituted ethane-1,2-diamine complexes of Ni^{II} nitrate were reported by Goodgame *et al.* in 1963 [1,2]. Later on Ihara *et al.* carried out thermal studies of these complexes and showed novel deaquation–anation reaction in the solid state [3,4]. Ray Chaudhuri *et al.* also studied such type of complexes where they observed thermally induced phase transition phenomena besides deaquation–anation reaction and the study reveals that nitrate anion plays an interesting role in the formation of configuration depending on the nature of the diamines, solvents, temperature etc. [5,6]. For example *N,N'*-dimethylethane-1,2-diamine produces both *cis*-and *trans*-isomer on changing the solvent, propan-2-ol to methanol, and the *cis*-isomerises to *trans* on thermal excitation in the solid state [5], whereas, *N,N'*-diethylethane-1,2-diamine yields only *cis*-complex which does not isomerise to *trans* [6]. However, studies with symmetrically substituted diamines with alkyl groups having longer chain length are not yet reported. The present paper reports the syntheses and characterization of *N,N'*-dipropylethane-1,2-diamine (dpren) and *N,N'*-diisopropylethane-1,2-diamine (dipren) complexes of nickel(II) nitrate, their thermal studies in the solid state and X-

† Author to whom correspondence should be addressed.

ray single crystal structure analysis of *cis*-nitratobis(dpren)nickel(II) nitrate.

EXPERIMENTAL

Materials

High purity *N,N'*-dipropylethane-1,2-diamine (dpren) and *N,N'*-diisopropylethane-1,2-diamine (dipren) were purchased from Aldrich Chemical Company Inc. and used as received. All other chemicals used were of analytical reagent grade.

Physical measurements

Thermal analysis (TG-DTA) were carried out using a Shimadzu DT-30 thermal analyser under a flow of dinitrogen (flow rate: 30 cm^3 min^{-1}). The sample (particle size of 150–200 mesh) was heated in a platinum crucible at a rate of 10°C min^{-1} with inert alumina as a reference. Elemental analyses were performed using a Perkin-Elmer 240C elemental analyser. IR-spectra (4000–400 cm^{-1}) were taken at 27°C using a Perkin-Elmer IR 783 where KBr/Nujol was used as medium/reference material. Electronic spectra (1400–200 nm) were obtained at 27°C using a Hitachi UV-VIS-NIR model U-3410 where Nujol was used as a medium as well as a reference. The magnetic susceptibility was measured at 27°C using an EG and G PAR 155 vibrating sample magnetometer, where $[HgCo(SCN)_4]$ was used as a reference material and diamagnetic corrections were made using Pascal's constants. Molar conductances were measured using a Systronics 304 conductivity meter, where cell constant was calibrated with 0.02 M KCl solution and dry methanol was used as solvent.

Preparation of the complexes

Cis-$[Ni(dpren)_2(NO_3)](NO_3)$ **1** was synthesized by adding the acetonitrilic solution (5 cm^3) of the diamine (2 mmol) to the acetonitrilic solution (10 cm^3) of nickel(II) nitrate hexahydrate (1 mmol). The resulting blue coloured solution was kept in a $CaCl_2$-desiccator. After a few days fine blue crystals were separated out, which were filtered and washed with propan-2-ol and dried in a $CaCl_2$-desiccator (yield, 73%). Single crystals suitable for X-ray analysis were obtained by recrystallisation of the complex from acetonitrile-butanol (1 : 1) mixture. (Found: C, 40.7; H, 8.4; N, 17.8; Ni, 12.5. Calc. for $NiC_{16}H_{40}N_6O_6$: C, 40.7; H, 8.5; N, 17.8; Ni, 12.5%. $\mu_\beta = 3.1$; λ_{max}(Nujol) = 924, 575 and 364 nm; $\Lambda = 92\ \Omega^{-1}\ cm^2\ dm^{-3}$).

Cis-$[Ni(dipren)_2(H_2O)_2](NO_3)_2 \cdot 2H_2O$ **2** was prepared by adding dry acetonitrilic solution (5 cm^3) of the diamine (2 mmol) to the dry butanolic solution (10 cm^3) of anhydrous nickel(II) nitrate (1 mmol), obtained by refluxing $Ni(NO_3)_2 \cdot 6H_2O$ in 2,2-dimethoxypropan. The resulting mixture was refluxed for 10–15 min and was kept in a $CaCl_2$-desiccator. After a few days greenish blue complex was separated out, which was filtered and washed with dry butanol and dried in a $CaCl_2$-desiccator (yield, 62%). (Found: C, 35.4; H, 8.9; N, 10.3; Ni, 10.8. Calc. for $NiC_{16}H_{48}N_6O_{10}$: C, 35.4; H, 8.8; N, 10.3; Ni, 10.8%. $\mu_\beta = 3.1$; λ_{max}(Nujol) = 1034, 625 and 382 nm; $\Lambda = 105\ \Omega^{-1}\ cm^2\ dm^{-3}$). Preparation of single crystals suitable for X-ray analysis was unsuccessful.

X-ray diffraction structural study

A single crystal of complex **1** was mounted on a Siemens P4 diffractometer. Lattice parameters were determined by least squares refinement of the angular settings ($5.15 < \theta < 12.47$) of 26 well-centered reflections. Intensity data were collected using graphite monochromated Mo-K_α radiation ($\lambda = 0.71073$ Å) using ω-scan mode. The stability of the crystals were measured during X-ray exposure by monitoring three standard reflections after every 97 reflections. Intensity data were corrected for Lorentz and polarisation effects [7]. An empirical absorption correction was applied (T_{min}/T_{max} 0.645/0.762). The structure was solved by the Patterson method followed by Fourier syntheses and refined through full-matrix least squares calculations. Anisotropic full-matrix refinements based on F^2 were carried out for all non-hydrogen atoms. During the refinements the crystal structure was found to be disordered. The carbon atoms [C(9), C(10), C(15), C(16)] were found to occupy [C(9), C(10), C(15), C(16) with site occupancy factor 0.6 and C(9′), C(10′), C(15′), C(16′) with site occupancy factor 0.4] two positions. The hydrogen atoms, except those attached to disordered atoms, were clearly visible in the difference map. The located hydrogen atoms, with isotropic thermal parameters 1.2 times U_{eq} of the atom to which the respective hydrogen atom attached to the final structure factors calculations, were treated as fixed contributors. Complex neutral atom scattering factors [8] were used throughout the refinement. All calculations were carried out using SHELXS 86 [9], SHELXL 93 [10], PARST [11] and ORTEP II [12] programs. Crystallographic data are summarised in Table 1. Selected bond distances and angles are listed in Table 2.

RESULTS AND DISCUSSION

N,N'-dipropylethane-1,2-diamine (dpren) and *N,N'*-diisopropylethane 1,2-diamine (dipren) yielded complexes with nickel(II) nitrate having composition, $Ni(dpren)_2(NO_3)_2$ **1** and $Ni(dipren)_2(NO_3)_2 \cdot 4H_2O$ **2** respectively, as is evident from their elemental analyses. The former one is blue whereas the latter one is greenish blue. Magnetic susceptibility data of both the complexes correspond to octahedral nickel(II). Electronic spectral study also corroborates this. The

Table 1. Crystallographic data for $[Ni(dpren)_2(NO_3)](NO_3)$ **1**

Empirical formula	$NiC_{16}H_{40}N_6O_6$
Colour	Blue
Formula weight	471.25
Temperature (K)	293(2) K
Wavelength, λ (Å)	0.71073
Crystal system	Monoclinic
Space group	$P2_1/c$
a (Å)	12.561(1)
b (Å)	14.319(1)
c (Å)	14.547(2)
β (°)	101.049(8)
V (Å^3)	2567.9(4)
ρ_{calc} (g cm^{-3})	1.219
Z	4
Absorption coefficient, μ (mm^{-1})	0.793
$F(000)$	1016
Crystal size	$0.76 \times 0.60 \times 0.42$ mm
Diffractometer	Siemens P4
Scan mode	ω scan
Absorption correction	Empirical
T_{max}	0.645
T_{min}	0.762
No of reflections used and θ range (°) used for cell parameter	26, $5.15 < \theta < 12.47$
Reflections collected	5815
Independent reflections	4479 [$R_{int} = 0.0238$]
Refinement on	F^2
No of parameters	298
Final R [$I > 2\sigma(I)$]	$R1^a = 0.0418$, $wR2^b = 0.0914$
Final R (all data)	$R1 = 0.0777$, $wR2 = 0.1104$
Weighting parameters $(A,B)^c$	0.0442, 0.1047
Goodness-of-fit $(S)^d$	1.016
Maximum Δ/σ	0.566
ρ_{max} (eÅ^{-3})	0.19
ρ_{min} (eÅ^{-3})	−0.17

$^a R1 = \Sigma\|F_o| - |F_c\|/\Sigma|F_o|$.
$^b wR2 = [\Sigma\{w(F_o^2 - F_c^2)^2\}/\Sigma\{w(F_o^2)^2\}]^{1/2}$.
$^c w = 1/[\sigma^2(F_o^2) + (AP)^2 + BP]$, where $P = (F_o^2 + 2F_c^2)/3$.
$^d S = [\Sigma\{w(F_o^2 - F_c^2)^2\}/(N-P)]^{1/2}$, where N is the number of data and P is the total number of parameters refined.

complexes exhibit IR-bands due to $\nu(NH_2)$ and $\nu(CH_2)$, are comparable to those of similar diamine systems, where the chelate character of the diamines have been established by X-ray single crystal analyses [13,14]. In complex **1** either both the nitrate groups are coordinated or one of them coordinated in a bidentate fashion to maintain its octahedral geometry. Thus, it is now essential to know the exact mode of coordination of the nitrate ions so that the actual configuration of the complex can be assigned. IR spectra have been studied to determine the mode of coordination of the NO_3^- ion at the region of 1700–1800 cm^{-1}, where the combination band of ν_1-symmetric stretching and the double degenerate in-plane bending mode (ν_4) of coordination of nitrate ions in metal complexes have been assigned [15,16]. Complex **1** exhibits IR-bands at 1778, 1740 and 1708 cm^{-1} (Fig. 1). The peak at ~1740 cm^{-1} suggests the presence of free NO_3^- ion. The large separation (70 cm^{-1}) between the other two peaks indicates that the other NO_3^- ion is acting as bidentate ligand. Thus, in complex **1**, one of the nitrate ions is coordinated in a bidentate fashion and the remaining one is uncoordinated which is corroborated by its molar conductance datum (*vide supra*). The complex **1** exhibits no splitting of d–d band in its electronic spectrum (Nujol) at near-IR region and thereby suggesting its *cis*-configuration (Fig. 2) [17]. On the other hand, complex **2** shows only one very sharp and strong IR band at ~1763 cm^{-1} (Fig. 1) which indicates the presence of free nitrate ions in the complex and molar conductance datum of the complex is typical to 1:2 electrolyte suggesting noncoordination of nitrate ions. All these, indirectly suggest the coordination of two water molecules in complex **2** and the IR-band at ~700 cm^{-1} corroborates this. These two water molecules may be either in *cis* or in *trans*-positions. Electronic spectrum in the near-IR region shows no splitting in d–d bands

Table 2. Selected bond lengths [Å] and angles [°] for complex **1**

Ni—N(3)	2.083(3)
Ni—N(1)	2.084(3)
Ni—N(4)	2.123(3)
Ni—N(2)	2.132(3)
Ni—O(1)	2.149(2)
Ni—O(2)	2.152(3)
O(1)—N(5)	1.266(4)
O(2)—N(5)	1.268(4)
O(3)—N(5)	1.213(4)
N(1)—C(5)	1.470(5)
N(1)—C(1)	1.485(5)
N(2)—C(2)	1.468(5)
N(2)—C(8)	1.475(5)
N(3)—C(11)	1.469(5)
N(3)—C(3)	1.482(6)
N(4)—C(4)	1.470(6)
N(4)—C(14)	1.484(6)
C(1)—C(2)	1.499(6)
C(3)—C(4)	1.476(7)
N(3)—Ni—N(1)	103.2(1)
N(3)—Ni—N(4)	83.3(2)
N(1)—Ni—N(4)	93.2(1)
N(3)—Ni—N(2)	94.0(1)
N(1)—Ni—N(2)	83.8(1)
N(4)—Ni—N(2)	175.4(1)
N(3)—Ni—O(1)	98.7(1)
N(1)—Ni—O(1)	158.0(1)
N(4)—Ni—O(1)	89.2(1)
N(2)—Ni—O(1)	94.9(1)
N(3)—Ni—O(2)	158.6(1)
N(1)—Ni—O(2)	98.1(1)
N(4)—Ni—O(2)	95.0(1)
N(2)—Ni—O(2)	88.9(1)
O(1)—Ni—O(2)	59.9(1)
N(5)—O(1)—Ni	92.2(2)
N(5)—O(2)—Ni	92.0(2)
C(5)—N(1)—C(1)	112.8(3)
C(5)—N(1)—Ni	113.0(2)
C(1)—N(1)—Ni	107.2(2)
C(2)—N(2)—C(8)	111.4(4)
C(2)—N(2)—Ni	104.1(2)
C(8)—N(2)—Ni	120.3(3)
C(11)—N(3)—C(3)	113.1(3)
C(11)—N(3)—Ni	113.5(3)
C(3)—N(3)—Ni	107.8(3)
C(4)—N(4)—C(14)	113.1(4)
C(4)—N(4)—Ni	104.5(3)
C(14)—N(4)—Ni	118.2(3)
O(3)—N(5)—O(1)	121.6(4)
O(3)—N(5)—O(2)	122.5(4)
O(1)—N(5)—O(2)	115.9(3)
N(1)—C(1)—C(2)	109.8(3)
N(2)—C(2)—C(1)	108.6(3)
C(4)—C(3)—N(3)	110.5(4)
N(4)—C(4)—C(3)	108.9(4)
O(6)—N(6)—O(5)	121.7(3)
O(6)—N(6)—O(4)	119.2(3)
O(5)—N(6)—O(4)	119.0(3)

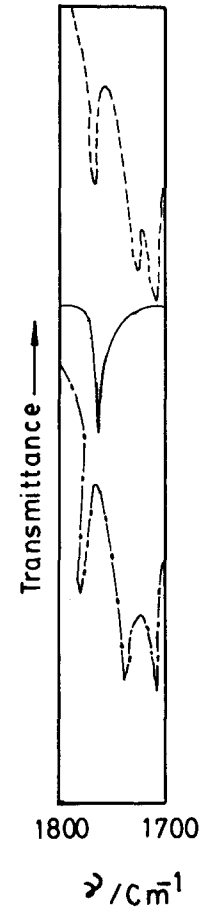

Fig. 1. IR spectra (Nujol) of *cis*-[Ni(dpren)$_2$(NO$_3$)](NO$_3$) **1** (–·–·–); *cis*-[Ni(dipren)$_2$(H$_2$O)$_2$](NO$_3$)$_2$·2H$_2$O **2** (—) and *cis*-[Ni(dipren)$_2$(NO$_3$)](NO$_3$) **2a** (– – –).

indicating *cis*-configuration and thereby the water molecules are in *cis*-positions.

The complex **1** upon heating starts to decompose at ~245°C, whereas, complex **2** starts to lose water at ~145°C and becomes dehydrated accompanied by melting at ~180°C with change in colour, greenish-blue to deep green. The molten species, **2a** undergoes solidification on cooling to ambient temperature. Magnetic susceptibility (3.1 μ_β at 27°C) and electronic spectrum [λ_{max}(Nujol) = 1015, 621 and 380 nm] of **2a** suggest it possesses an octahedral geometry. It can be stored in a desiccator but it reverts in humid atmosphere (90% or above). However, it exhibits IR-spectrum similar to that of complex **1** at the region of 1700–1800 cm^{-1} (1765, 1730 and 1708 cm^{-1}) which indicates that the coordinating mode of nitrate ions in this complex is alike to that of complex **1** and near-IR spectrum also corroborates this. It is interesting to note that the chromophore around nickel(II) does not alter on deaquation–anation reaction. The cause of colour change is proposed to be due to change in ligand field strength.

Table 3. Hydrogen bonding geometry

D—H···A	D—H	D···A	H···A	<D—H···A
N1—HN1···O4^{i}	0.936(3)	2.983(4)	2.057(3)	170.2(2)
N4—HN4···O5^{i}	0.913(3)	3.221(5)	2.355(3)	158.3(2)
C3—H3B···O4^{i}	0.970(5)	3.399(5)	2.496(3)	154.9(3)
C16—H16C···O5^{i}	0.96(3)	3.43(2)	2.47(2)	174(2)
N3—HN3···O4^{ii}	0.847(3)	3.015(5)	2.173(3)	172.4(2)
N2—HN2···O6^{ii}	0.941(3)	3.147(5)	2.227(4)	165.5(2)
C5—H5A···O6^{iii}	1.039(4)	3.441(5)	2.438(3)	161.9(2)

Symmetry code: (i) x, y, z; (ii) $-x+1, -y, -z$; (iii) $-x+1, +y+1/2, -z+1/2$.

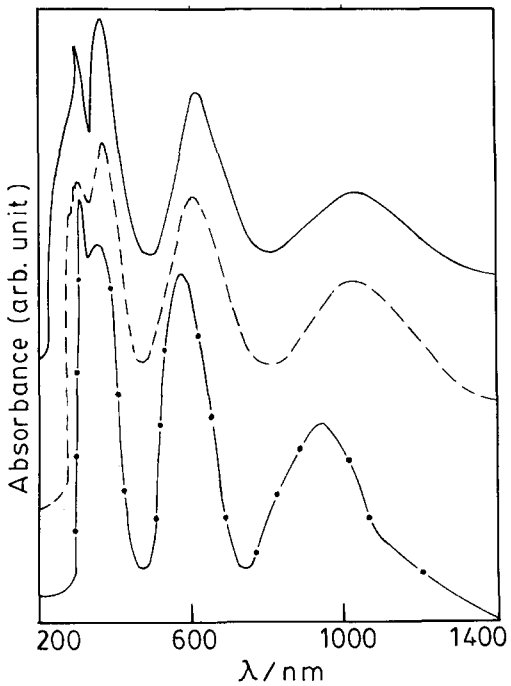

Fig. 2. Electronic spectra (Nujol) of *cis*-[Ni(dpren)$_2$(NO$_3$)](NO$_3$) **1** (–·–); *cis*-[Ni(dipren)$_2$(H$_2$O)$_2$](NO$_3$)$_2$·2H$_2$O **2** (– – –) and *cis*-[Ni(dipren)$_2$(NO$_3$)](NO$_3$) **2a** (—).

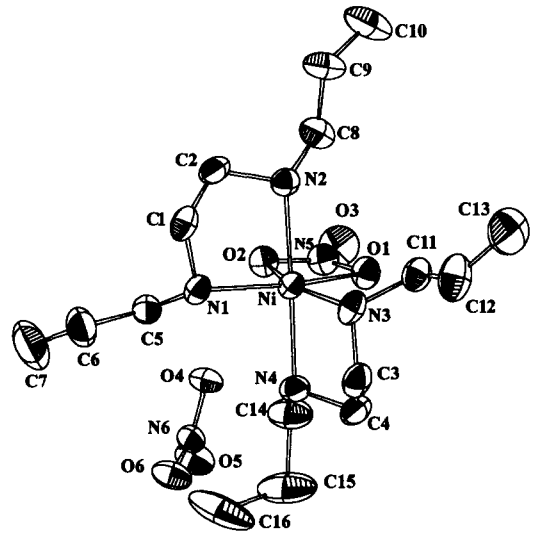

Fig. 3. ORTEP-plot, *cis*-[Ni(dpren)$_2$(NO$_3$)](NO$_3$) **1** with atom numbering scheme.

An ORTEP view of the complex **1** with the atom numbering scheme is shown in Fig. 3. The crystal structure consists of discrete [Ni(dpren)$_2$NO$_3$] cation and NO$_3$ anion. The ligand moieties [dpren and NO$_3$] are monometallic and bidentate. The coordination polyhedron around the metal is best described as a distorted octahedron. The two nitrogen atoms (N1, N3) of the diamines and two oxygen atoms (O1, O2) of the *cis*-bidentate nitrate group define the equatorial plane and the remaining-two N atoms (N2, N4) of the diamine ligands are in axial position [N2—Ni—N4 175.4(1)°]. The N2—Ni—N4 axis is nearly orthogonal to the equatorial plane [angle ranges from 83.3(2)° to 98.1(1)°]. The cluster of complex **1** has a two-fold axis that passes through the metal atom and the mid point of two oxygen atoms (O1, O2) of the coordinating nitrate group and the equatorial plane, containing the two fold axis, serves as a mirror. So the molecule has approximate C_{2v} symmetry. The five membered chelate rings, Ni—N1—C1—C2—N2 and Ni—N3—C3—C4—N4 display open envelope geometries with the flap atoms C2 and C4 0.602 Å and 0.595 Å, respectively, away from the least squares planes through the remaining endocyclic atoms. The dihedral angle between the planar parts of the chelate rings is 100.6(2)°. The Ni—N, Ni—O distances are consistent with the corresponding nickel(II) diamine/nitrato-diamine complexes [14, 18]. Complex **1** is stabilised mainly by intermolecular and intramolecular hydrogen bonds which control overall chelate ring conformations. The crystal packing is dominated by the strings of molecules which are held together by an extensive intermolecular hydrogen bonding network. These are given in Table 3.

From the report presented above it may be inferred

that as the chain length of the alkyl group increases, nickel(II) nitrate prefers to form *cis*-octahedral bis (diamine) species over its *trans*-isomer. If the steric effect is increased as is exerted by isopropyl group, nitrate ion coordination becomes difficult. Thus, the mode of coordination of nitrate ions may selectively be controlled by using appropriate diamine. Here, it may be mentioned that for higher alkyl substituted diamines, solvent and temperature have little effect on the overall configuration of the complex.

Acknowledgements—The authors wish to thank Professor A. K. Pal, Department of Material Science, IACS, for near-IR spectra and Council of Scientific and Industrial Research (Grant to N. R. C.), New Delhi, for financial support.

REFERENCES

1. Goodgame, D. M. L. and Venanzi, L. M., *J. Chem. Soc.*, 1963, 616.
2. Goodgame, D. M. L. and Venanzi, L. M., *J. Chem. Soc.*, 1963, 5909.
3. Ihara, Y., Izumi, E., Uehara, A., Tsuchiya, R., Nakagawa, S. and Kyuno, E., *Bull. Chem. Soc. Jpn*, 1982, **55,** 1028.
4. Ihara, Y., Saiaki, Y., Suzuki, M. and Uehara, A., *Bull. Chem. Soc. Jpn*, 1991, **64,** 3647.
5. Koner, S., Ghosh, A. and Ray Chaudhuri, N., *J. Chem. Soc., Dalton Trans.*, 1990, 1563.
6. Pariya, C., Ghosh, A. and Ray Chaudhuri, N., *Thermochim. Acta*, 1996, **273,** 185.
7. North, A. C. T., Philips, D. C. and Mathews, F. S., *Acta Cryst.*, 1968, **A24,** 351.
8. *International Tables for Crystallography*, Vol. C, Tables 4.2.6.8 and 6.1.1.4, 1992.
9. Sheldrick, G. M., *SHELXS* 86. *Program for the Solution of Crystal Structures*. University of Gottingen, Germany, 1985.
10. Sheldrick, G. M., *SHELXL* 93. *Program for the Solution of Crystal Structure*. University of Gottingen, Germany, 1993.
11. Nardelli, M., *Comput. Chem.*, 1983, **7,** 1995.
12. Johnson, C. K., ORTEPII, Report ORNL-5138, Oak Ridge National Laboratory, Tennessee, 1976.
13. Mukherjee, A. K., Mukherjee, M., Welch, A. J., Ghosh, A. and Ray Chaudhuri, N., *J. Chem. Soc., Dalton Trans*, 1987, 997.
14. Das, D., Nayak, N. P., Mukherjee, A. K., Ghosh, A. and Ray Chaudhuri, N., *Polyhedron*, 1997, **16,** 2361.
15. Curtis, N. F. and Curtis, Y. M., *Inorg. Chem.*, 1965, **4,** 804.
16. Lever, A. B. P., Mantovani, E. and Ramaswamy, B. S., *Can. J. Chem.*, 1971, **49,** 1957.
17. Lever, A. B. P., *Inorganic Electronic Spectroscopy*, 2nd edn. Elsevier, Amsterdam, 1984, pp. 507–520.
18. Soriano-Garcia, M., Pandiyan, T. and Druan de Bazua, C., *Acta Cryst.*, 1995, **C51,** 1107.

Pergamon

PII: S0277-5387(97)00282-9

Polyhedron Vol. 17, No. 8, pp. 1369–1374, 1998
© 1998 Elsevier Science Ltd
All rights reserved. Printed in Great Britain
0277-5387/98 $19.00+0.00

A structural and electrochemical study of some oxovanadium(IV) heterochelate complexes

Madhumita Chatterjee,[a] Saktiprosad Ghosh,[a]* Bo-Mu Wu[b] and Thomas C. W. Mak[b]

[a] Department of Inorganic Chemistry, Indian Association for the Cultivation of Science, Calcutta 700 032, India

[b] Department of Chemistry, The Chinese University of Hong Kong, Shatin, New Territories, Hong Kong

(Received 17 March 1997; accepted 25 June 1997)

Abstract—Physicochemical studies on two oxovanadium(IV) heterochelates involving the biologically active ONO donor ligand, dipicolinic acid (DPA) is reported. Structure of the complex $[VO(DPA)(ophen)]\cdot 3H_2O$ has been determined and this led to the understanding of the geometry of the donor sites around the oxovanadium(IV) centre of other related complexes. Electrochemical behavior of the complexes were explored by cyclic voltammetry. © 1998 Elsevier Science Ltd. All rights reserved

Keywords: oxovanadium(IV) heterochelates; structural study; dipicolinic acid ligand; electrochemical investigation.

Design and synthesis of heterochelate complexes are generally intended to study the effect of unsymmetrical ligand fields on transition metal acceptor centres. This effect is expected to be revealed in their electronic, IR spectra, magnetic moment values, electrochemical activity, chemical reactivity and of course in their structures.

A host of mixed ligand oxovanadium(IV) complexes including some heterochelates involving the biologically active versatile ligand dipicolinic acid (DPA) has been reported [1,2]. It is surprising that no structural study of any of them has been reported to date. This paper deals mainly with the X-ray crystallographic study of the heterochelate $[VO(DPA)(ophen)]\cdot 3H_2O$ which may be considered as the representative of the class [VO(DPA)(B—B)] where B—B is a neutral bidentate chelating ligand. The crystal structure of this complex allowed us to predict the disposition of the donor sites of the mother complex $[VO(DPA)(H_2O)_2]H_2O$ (**1**) from which the heterochelates are prepared. Electronic, infrared spectra, magnetic moment values and electrochemical behavior of these complexes are also reported and discussed here.

* Author to whom correspondence should be addressed.

EXPERIMENTAL

All chemicals were of reagent grade and used without further purification. Tetraethylammonium perchlorate (TEAP) used for electrochemical work was prepared as reported in literature [3]. All operations were performed under purified dinitrogen.

Physical measurement

IR spectra were recorded at room temperature on a Perkin Elmer 783 spectrophotometer as KBr pellets. Magnetic moments of solid complexes at 298 K were determined using a PAR model 155 vibrating sample magnetometer with $Hg[Co(SCN)_4]$ as the calibrant. Electronic spectra were recorded in DMF solution with Shimadzu Model UV-2100 spectrophotometer and cyclic voltammetric experiments were performed using BAS CV-27 electrochemical analyser and a BAS XY recorder at 298 K. The electrodes used were glassy carbon working electrode, Pt wire counter electrode and a Ag/AgCl reference electrode separated from the working compartment by a salt bridge fitted with a medium glass frit. Under identical conditions the value of the $E_{1/2}$ of the ferrocene/ferrocenium couple is found to be ± 0.59 V ($\Delta E = 250$ mV). Electrical

conductivity in solution was measured by a Philips PR 9500 conductivity bridge. C, H and N were analysed by Perkin Elmer 2400 CHNS/O analyser.

Synthesis of complexes

$[VO(DPA)(H_2O)_2]H_2O$ (**1**): 0.5 gm (1.75 mmole) of $VOSO_4$ and 0.4 gm (2.45 mmole) of dipicolinic acid were dissolved in hot water (20 cm^3) when a bright green solution was obtained. It was then cooled to 5°C, the precipitated excess acid was filtered off and the filtrate kept overnight in a refrigerator. Shiny blue crystals were filtered, washed with rectified spirit and dried in air for a few hours (yield 60%). Found: C, 29.32; H, 3.18; N, 4.70. Calc. for $[VO(DPA)(H_2O)_2]H_2O$: C, 29.37 H, 3.15; N, 4.89%.

$[VO(DPA)(ophen)]\cdot 3H_2O$ (**2**): 0.3 gm (1.04 mmole) of blue $[VO(DPA)(H_2O)_2]H_2O$ reacts readily in aqueous solution with a 0.25 gm (1.25 mmole) alcoholic solution of o-phenanthroline to provide a chocolate brown crystalline product, which was washed with alcohol and dried over anhydrous $CaCl_2$ (yield 65%). Found: C, 48.32; H, 3.80; N, 7.60. Calc. for $[VO(DPA)(ophen)]3H_2O$: C, 48.93; H, 3.65; N, 7.73%.

$[VO(DPA)(bipy)]H_2O$ (**3**): The same method was employed with bipyridine in place of phenanthroline to provide yellowish brown crystals (yield 60%). Found: C, 49.82; H, 3.18; N, 10.10. Calc. for $[VO(DPA)(bipy)]H_2O$: C, 50.25; H, 3.20; N, 10.34%.

Crystal structure determination

A brown prismatic crystal of $0.30 \times 0.40 \times 1.0$ mm^3 was chosen for diffraction study. The compound crystallised in the monoclinic space group $P2_1/c$. The unit cell dimensions and cell volume are given in Table 1. Intensity data were collected on a MSC/Rigaku Raxis-

Table 1. Data collection and processing parameters

Molecular formula	$C_{19}H_{17}N_3O_8V$
Molecular weight	466.3
Color and habit	Brown prism
Crystal size	$0.30 \times 0.40 \times 1.0$ mm^3
Crystal system	Monoclinic
Space group	$P2_1/c$ (No. 14)
$a = 13.978(1)$ (Å)	
$b = 13.554(1)$ (Å)	
$c = 10.521(1)$ (Å)	
$\beta = 101.22(1)°$	
$V = 1955.2(10)$ (Å^3)	
$Z = 4$	
$F(000) = 956$	
Density (calc.) (g cm^{-3})	1.584
Radiation	Graphite-monochromatized Mo-K_α, $\lambda = 0.71073$ Å
R_{int} (from merging of equiv. reflections)	0.018
Absorption coefficient (mm^{-1})	0.562
Mean μr	0.168
Scan type and rate	take oscillation IP photos; 30 frames in total, $\phi = 0-180°$, $\Delta\phi = 6.0°$ 8 mins per frame
Crystal to detector distance (mm)	69.465
Background level	−50
Collection range	$-17 \leqslant h \leqslant 17$, $-17 \leqslant k \leqslant 17$, $0 \leqslant l \leqslant 13$
Reflections collected	6980
Independent reflections	3799 ($R_{int} = 1.84\%$)
Obs. data with $\|F_o\| \geqslant 6\sigma(\|F_o\|)$, n	3188
No. of variables, p	291
Extinction correction	$\chi = 0.0010(3)$, where $F^* = F[1 + 0.002\chi F^2/\sin(2\theta)]^{-1/4}$
Weighting scheme	$w = [\sigma^2\|F_o\| + 0.0001\|F_o\|^2]^{-1}$
$R_F = \Sigma\|\|F_o\| - \|F_o\|\|/\Sigma\|F_o\|$	0.056
$wR = [\Sigma w(\|F_o\| - \|F_c\|)^2/\Sigma w\|F_o\|^2]^{1/2}$	0.071
$s = [\Sigma w(\|F_o\| - \|F_c\|)^2/(n-p)]^{1/2}$	3.32
Largest and mean Δ/σ	0.013, 0.001
Residual extrema in final difference map (e Å^{-3})	+0.91 to −0.85

Table 2. Selected bond lengths (Å) and bond angles (°)

V(1)—N(1)	2.021(2)	O(3)—C(6)	1.297(3)
V(1)—N(3)	2.126(2)	C(6)—C(1)	1.509(4)
V(1)—O(4)	2.031(2)	C(1)—N(1)	1.331(4)
V(1)—N(2)	2.312(3)	N(1)—C(5)	1.336(4)
V(1)—O(3)	2.037(2)	C(5)—C(7)	1.509(4)
V(1)—O(5)	1.581(3)	C(7)—O(4)	1.296(3)
N(3)—C(18)	1.378(4)	C(6)—O(1)	1.224(4)
C(18)—C(19)	1.425(4)	C(7)—O(2)	1.221(4)
C(19)—N(2)	1.358(3)	O(3w)···O(2w)	2.960(6)
O(2w)···O(1w)	2.741(5)	O(1'w)···O(2w)	2.395(6)
O(1w)···O(1)	2.785(6)	O(1'w)···O(1)	2.878(6)
N(1)—V(1)—N(2)	88.3(1)	N(1)—V(1)—N(3)	161.9(1)
N(2)—V(1)—N(3)	73.9(1)	N(1)—V(1)—O(3)	76.8(1)
N(2)—V(1)—O(3)	85.2(1)	N(3)—V(1)—O(3)	104.2(1)
N(1)—V(1)—O(4)	77.0(1)	N(2)—V(1)—O(4)	82.6(1)
N(3)—V(1)—O(4)	97.1(1)	O(3)—V(1)—O(4)	151.3(1)
N(1)—V(1)—O(5)	106.7(1)	N(2)—V(1)—O(5)	165.0(1)
N(3)—V(1)—O(5)	91.2(1)	O(3)—V(1)—O(5)	97.7(1)
O(4)—V(1)—O(5)	100.8(1)	O(1)···O(1'w)···O(2w)	135.0(3)

IIC imaging plate diffractometer using graphite monochromatised Mo-K_α radiation ($\lambda = 0.71073$ Å) from a rotating anode generator powered at 60 KV and 90 mA. A total of 6980 reflections were collected, with 3799 independent reflections ($R_{int} = 1.84\%$), covering indices $-17 \leqslant h \leqslant 17$, $-17 \leqslant k \leqslant 17$; $0 \leqslant l \leqslant 13$, by oscillation photographs (30 frames in total), with $\phi = 0-180°$, $\Delta\phi = 6.0°$ at a scan rate of 8 minutes per frame [4,5]. The intensities were corrected for Lorentz and polarization effects and for absorption using the ABSCOR program. The structure was solved by direct method. All non-hydrogen atoms were refined anisotropically by full matrix least squares, with riding model for hydrogen atoms, using the SHELXTL-PC package [6]. For 3188 observed reflections ($|F_o| \geqslant 6\sigma(|F_o|)$), refinement converged ($\Delta/\sigma = 0.001$) with $R_F = 0.056$ and $wR = 0.071$. The weighing scheme was $w = [\sigma^2|F_o| + 0.0001\,|F_o|^2]^{-1}$. Goodness of fit $S = 3.32$. Selected bond lengths and bond angles are given in Table 2. Figure 1 shows the ORTEP diagram and atom numbering scheme of (**2**) and Fig. 2 its packing diagram.

Description of the structure

The deprotonated dipicolinic acid acting as a tridentate chelating agent coordinates to the VO^{+2} centre through the heterocyclic ring nitrogen N(1) and the carboxylate oxygens O(3) and O(4). All three of them occupy three positions of a distorted square plane (Fig. 1), the fourth position being occupied by one of the ophen nitrogen atoms N(3). The oxygen atom of the vanadyl moiety lie above the plane defined by O(3)—N(1)—O(4)—N(3), while the position *trans* to the vanadyl oxygen is occupied by the N(2) nitrogen atom of the coordinated ophen. The V—O(5) distance of 1.581(3) Å is a little shorter than is generally found in most VO^{+2} complexes with a nitrogen donor attached to its trans position [7–9]. Of the two V—N bonds generated by the coordinated ophen, the V—N(2) bond *trans* to the V=O bond is longer (2.312 Å) than the other V—N(3) bond (2.126 Å). Thus the vanadium(IV) centre exists in a distorted octahedral donor environment. The deviation of the vanadium atom from the plane defined by O(3)—N(1)—O(4)—N(3) is 0.2910 Å and the dihedral angle between the mean planes defined by the aromatic ligands is 93.90°. Figure 1 shows that O(1w), O(2w) and O(3w) form part of the asymmetric unit. O(1w) is directly H-bonded with O(1) of the molecule. Each of the O(1w), O(2w) and O(3w) are connected to the symmetry generated O(1b), O(2a) and O(4c) respectively with transformation codes *a*(x, $1+y$, z); *b*($1-x$, $1-y$, $-z$); *c*(x, $0.5-y$, $-0.5-z$). Two of the oxygens O(1w) and O(2w) form three hydrogen bonds whereas O(3w) is connected by only two hydrogen bonds. Molecules are packed within the lattice through this type of hydrogen bonds. O(1w) exhibits two-fold disorder and accordingly atom O(1w) and O(1'w) are assigned 0.7 and 0.3 occupancy respectively.

RESULTS AND DISCUSSION

The complex $[VO(DPA)(ophen)]\cdot 3H_2O$ is expected to be 6-coordinated with the vanadyl oxygen occupying one coordination position and it may exist in the following two forms:

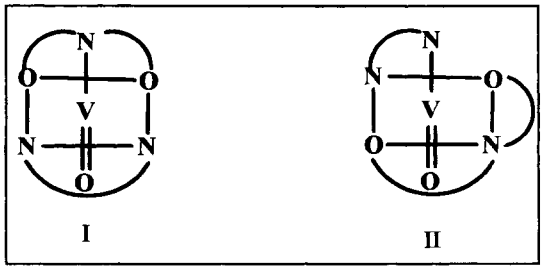

Only crystal and molecular structure determination can identify the form in which it actually exists. From the preceding description of the structure it is clear that the form II is the actual disposition of the coordination sites. It leads to an interesting observation that one of the two nitrogen atoms [N(2)] of the ophen moiety has manifested its weaker donor character, compared to the other, through its larger V(1)—N(2) bond length (Table 2). It also corroborates the previous observation that in many oxovanadium(IV) complexes of N—O donors, the weakest donor is generally found to occupy the position trans to the vanadyl oxygen [10]. From the structure of this compound it is clear that the dianionic tridentate DPA moiety behaves as a planar tridentate chelating ligand. This finding allows us to formulate the structure of (3) in which the coordinated ophen of (2) is replaced by a very similar ligand bipy. It also helps us to make a logical guess about the geometry of the coordination environment of the oxovanadium(IV) moiety of the complex $VO(DPA)(H_2O)_2]H_2O$ (1) from which the complex (2) was first prepared. Facile reaction of ophen on (1) at even a low temperature of 2–5°C indicates that the two coordinated water molecules are *cis* to each other, which is consistent with the planar disposition of DPA as well as the placement of the weakest ligand in a position trans to the V=O oxygen. The conclusion may be extended to other complexes of the type [VO(DPA)(B—B)] and [VO(DPA)X_2] where B—B is a neutral bidentate chelating ligand and X is a neutral monodentate donor. The structure of the other reported compound [VO(DPA)(bipy)]H_2O should also be similar so far as the disposition of the donor sites around the VO^{+2} acceptor centre are concerned. Structure determination of one compound of a related series of compounds, in this case, has been of much help in understanding the geometry of the donor sites around the central metal ion of a host of structurally related complexes.

Infrared spectra. The ν(V=O) mode is an accepted

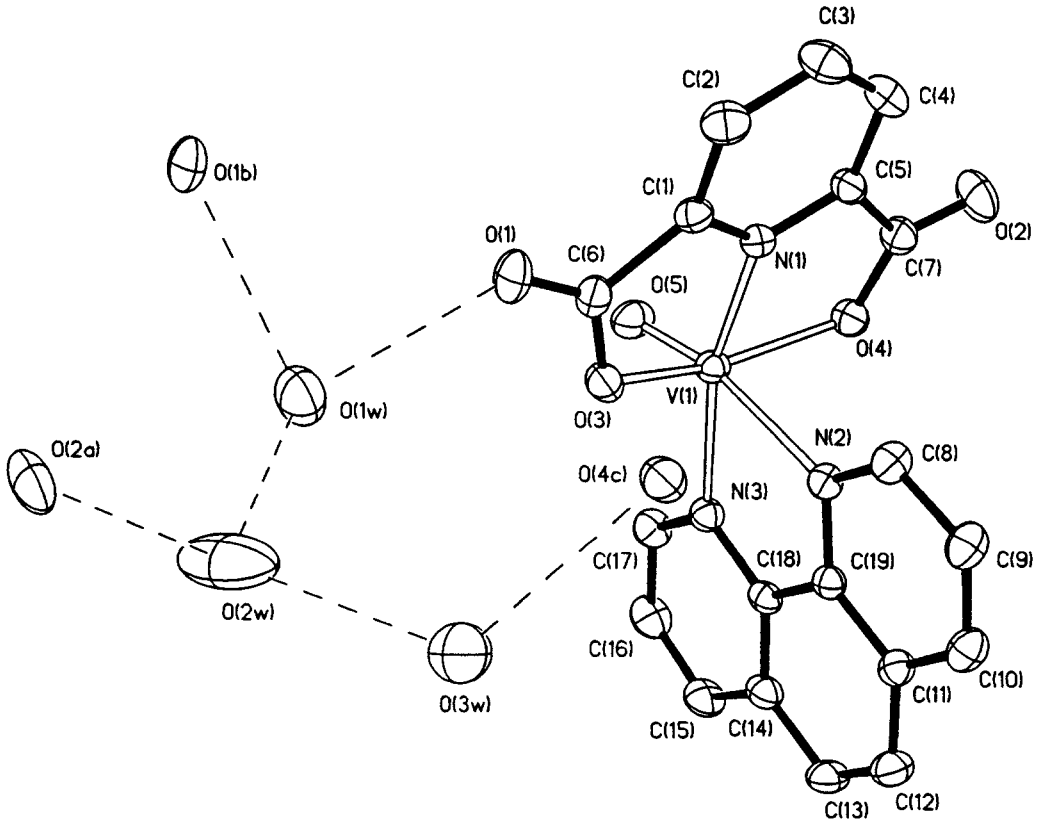

Fig. 1. ORTEP diagram and atom numbering scheme of $[VO(DPA)(ophen)]3H_2O$ (2).

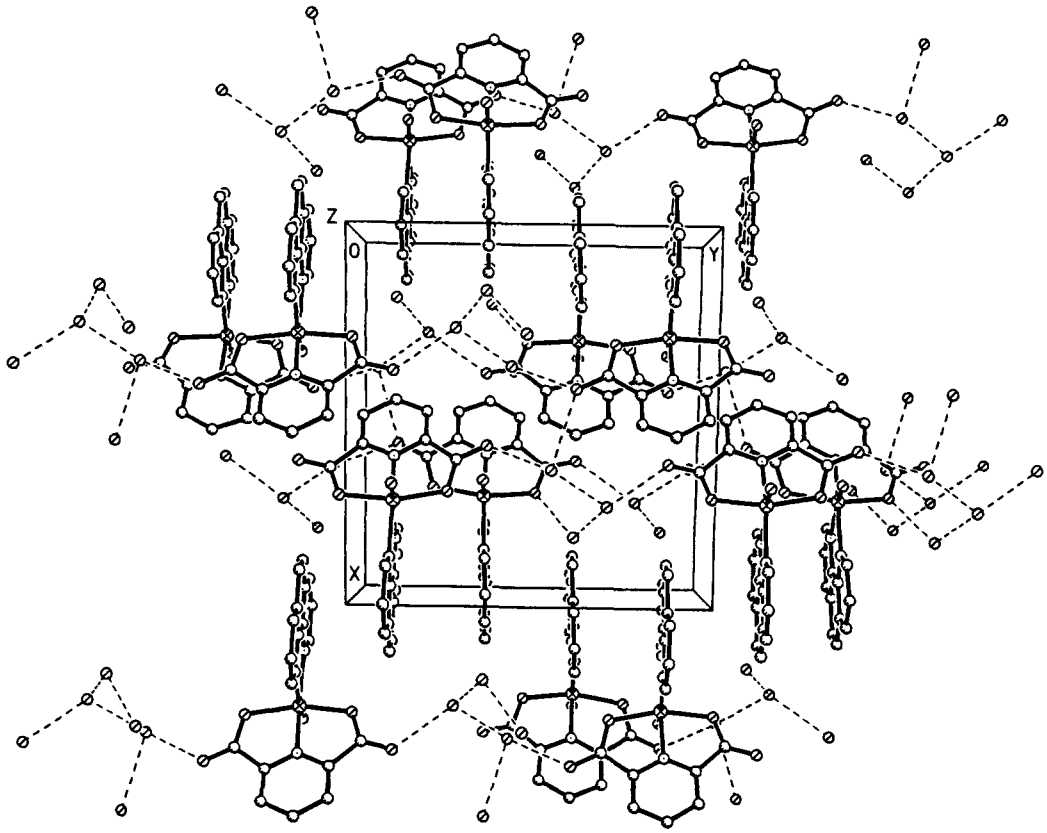

Fig. 2. Packing diagram of [VO(DPA)(ophen)]3H_2O (**2**).

leverage [11–13] which can be utilised for recognising the relative σ-donor capacity of the donor *trans* to the vanadyl oxygen Greater the σ-donor capacity of the ligand lesser is the ν(V=O). The values of ν(V=O) of the complexes (**1**), (**2**) and (**3**) are given in Table 3. It is seen that the ν(V=O) in (**1**) is observed at 980 cm^{-1} while those of (**2**) and (**3**) are at 978 cm^{-1}. These values indicate that both ophen and bipy are a little stronger σ-donors than the two water molecules and there is no difference between ophen and bipy in this respect. But it is well known that ophen and bipy are much higher up in the spectrochemical series than

Table 3. IR, magnetic moment, UV and electrochemical results

	$\nu_{V=O}$ (cm^{-1})	μ (BM)	λ_{max} (cm^{-1})	$E_{1/2}$,[a] V (ΔE_p,[b] mV)
[VO(DPA)(H_2O)$_2$]H_2O (**1**)	980	1.78	11,800 16,342 20,035	−1.04(180); +0.988
[VO(DPA)(ophen)]3H_2O (**2**)	978	1.83	13,333 18,767 22,005	−1.08(70); +0.85
[VO(DPA)(bipy)]H_2O (**3**)	978	1.83	12,856 18,576 21,978	−1.08(78); +0.84

[a] Condition: Solvent, DMF; supporting electrolyte, TEAP (0.1 M); working electrode, platinum; reference electrode, SCE; solute concentration, 10^{-3} M; scan rate, 0.4 V/sec; and temperature, 298 K. $E_{1/2}$ is calculated as the average of anodic (E_{pa}) and cathodic (E_{pc}) peak potential.

[b] $\Delta E = E_p - E_{pc}$.

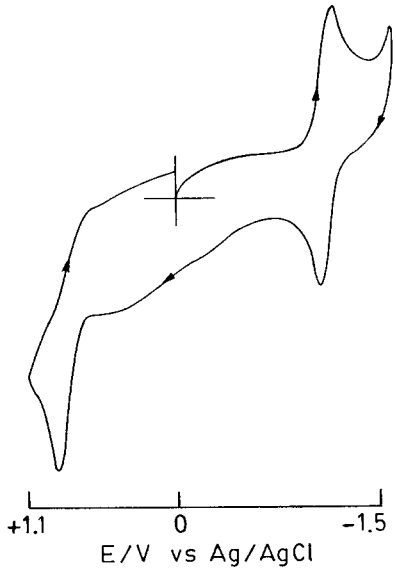

Fig. 3. Cyclic voltammogram of [VO(DPA)(ophen)]$3H_2O$ (**2**) in DMF at 298 K with scan rate 0.4 V/sec.

water yet the difference observed here is marginal. This opens up an interesting question, is the frequency of the ν(V=O) regulated solely by the ligand *trans* to the vanadyl oxygen atom, or is it the nature of the main ligand that exerts significant control on the change? From our study it appears that the second factor is more important. Magnetic moment values corresponds to the presence of one unpaired d-electron in all the three complexes.

Electronic spectra. UV spectra of VO^{+2} complexes are well documented and discussed [14–17]. Electronic spectra of the compounds (**1**), (**2**) and (**3**) (Table 3) both in solid state and in DMF solution exhibit three bands in the 11,800–22,005 cm^{-1} region. The bands in the 11,800–13,400 cm^{-1} (Band I), 16,300–18,800 cm^{-1} (Band II) and 20,000–22,050 cm^{-1} (Band III) are attributed to the transition $b_2 \rightarrow e_{\pi}^{*}$, $b_2 \rightarrow b_1^{*}$ and $b_2 \rightarrow a_1^{*}$ respectively. The position of the λ_{max} in both (**2**) and (**3**) is almost identical.

Electrochemistry. The results of the cyclic voltammetric studies are listed in Table 3 and the cyclic voltammogram of (**2**) is shown as the representative (Fig. 3). Potential separation between the anodic and the cathodic waves (ΔE) for the process V(IV)/V(III) (Table 3) indicates that the process is irreversible for (**1**) and reversible for both (**2**) and (**3**)—the slightly higher values compared to the ideal Nernstial value of 59 mV may be attributed to uncompensated solution resistance [18]. On the oxidation side, however, only the oxidation step V(IV)/V(V) could be observed for all the three complexes. It is clear that the differences between the V(IV)/V(III) and V(IV)/V(V) potentials of the three compounds are quite small. Such small differences point to the fact that keeping in line with the closely similar spectral and magnetic moment data, the electrochemical properties of (**1**), (**2**) and (**3**) are quite comparable. The basic reason behind such similarities is the presence of the same principal ligand in the same disposition of its donor points in all the three complexes and the consequent structural similarity. Otherwise the spectral, magnetic and electrochemical properties of the compound (**1**) which contains two water molecules in place of the ophen in (**2**) and bipy in (**3**) could not exhibit such close similarity.

CONCLUSION

This work may be regarded as a useful example where the structure determination of one key member of a related series of compounds can lead to a general idea of the geometry of the donor sites present in other related complexes. It also illustrates that if the major ligand of a related series of heterochelates behaves similarly, the nature of the secondary ligand belonging to the same class does not significantly affect the properties as well as the coordination geometry of the resultant heterochelates.

REFERENCES

1. Dutta, R. L. and Ghosh, S., *J. Inorg. Nucl. Chem.*, 1966, **28,** 247.
2. Selbin, J., *Coord. Chem. Rev.*, 1966, **1,** 293.
3. Sawyer, D. T. and Roberts, J. L., *Experimental Electrochemistry for Chemists*; Wiley, New York, 1974, p. 212.
4. Sato, M., Yamamoto, M., Imada, K., Katsube, Y., Tanaka, N. and Higashi, T., *J. Appl. Crystallogr.*, 1992, **25,** 348.
5. Kraus, K. L., Jr and Phillips, G. N., *J. Appl. Crystallogr.*, 1992, **25,** 146.
6. Sheldrick, G. M., *Computational Crystallography*, ed. D. Sayre. Oxford University Press, New York, 1982, p. 506.
7. Ghosh, M. and Ray, S., *Acta Cryst. C.*, 1983, **39,** 1367.
8. Cornman, C. R., Kampf, J., Soo Lah, M. and Pecoraro, V. L., *Inorg. Chem.*, 1992, **31,** 2035.
9. Cotton, F. A., Czuchajowska, J. and Feng, X., *Inorg. Chem.*, 1991, **30,** 349.
10. Kabanos, T. A., Keramides, A. D., Papaioannou, A. and Terzis, A., *Inorg. Chem.*, 1994, **33,** 845.
11. Selbin, J., Holmes, L. H. Jr and McGlynn, S. P., *J. Inorg. Nucl. Chem.*, 1963, **25,** 1359.
12. Selbin, J., Holmes, L. H. Jr and McGlynn, S. P., *Chem. Ind. (London)*, 1961, 746.
13. Maity, A. and Ghosh, S., *Proc. Indian Acad. Sci. (Chem. Sci.)*, 1992, **104,** 369.
14. Ballhausen, C. J. and Gray, H. B., *Inorg. Chem.*, 1962, **1,** 111.
15. Lever, A. B. P., *Inorganic Electronic Spectroscopy*, Second Ed. Elsevier, Amsterdam, 1984, p. 173.
16. Ballhausen, C. J., Djuvinsky, B. F. and Watson, K. J., *J. Am. Chem. Soc.*, 1968, **90,** 3305.
17. Ghosh, S. and Maity, A., *Indian J. Chem.*, 1987, **A26,** 44.
18. Callahan, R. W., Keene, F. R., Meyer, T. J. and Salmon, D. J., *J. Am. Chem. Soc.*, 1977, **99,** 1064.

Pergamon

PII: 50277-5387(97)00278-7

Polyhedron Vol. 17, No. 8, pp. 1375–1380, 1998
© 1998 Elsevier Science Ltd
All rights reserved. Printed in Great Britain
0277-5387/98 $19.00+0.00

Synthesis, crystal structure and properties of a new dinuclear manganese(II) complex bridged by butane 1,4-dicarboxylic acid: $[Mn_2(BIPY)_4(BTD)(H_2O)_2] \cdot (ClO_4)_2 \cdot 2H_2O$

Dao Feng Xiang,[a] Xiang Shi Tan,[a] Wen Xia Tang,[a]* Feng Xue[b] and Thomas C. W. Mak[b]*

[a] State Key Laboratory of Coordination Chemistry, Coordination Chemistry Institute, Nanjing University, Nanjing 210093, P. R. China

[b] Department of Chemistry, The Chinese University of Hong Kong, Shatin, New Territories, Hong Kong

(Received 29 April 1997; accepted 20 June 1997)

Abstract—A new dinuclear manganese(II) complex bridged by bridging ligand butane 1,4-dicarboxylic acid, $[Mn_2(BIPY)_4(BTD)(H_2O)_2] \cdot (ClO_4)_2 \cdot 2H_2O$ has been prepared and structurally characterized by X-ray crystallography. The crystal structure comprises a dinuclear cation, perchlorate anions and lattice water molecules. Each Mn^{II} dimer unit is linked to its neighbours by the two noncoordinating carboxylate oxygens of BTD^{2-} ligand, the bound water and two bridging water molecules through double hydrogen bonds, forming an infinite chain running parallel to the crystallographic *b*-axis. The electrochemical properties of the complex was studied in CH_3CN by cyclic voltammetry (CV). The temperature-dependent magnetic susceptibility data (75–300 K) were fitted based on $H = -2Js_1s_2$, yielding the intramolecular coupling constant J value of $-0.137\ cm^{-1}$. Besides, the complex shows a catalase-like activity in pyridine. © 1998 Elsevier Science Ltd. All rights reserved

Keywords: manganese complexes; dinuclear complexes; crystal structures; magnetism; butane 1,4-dicarboxylic acid; 2,2′-bipyridine.

In recent years there has been considerable interest in coordination chemistry of manganese complexes with carboxylate ligands, due to the fact that polynuclear metal carboxylates are good candidates for the investigation of exchange-coupling interactions between adjacent metal ions [1,2], and at the same time the interest has been fuelled by the identification of a number of Mn-containing enzymes [3]. In addition to the tetra-Mn photosynthetic water-oxidizing complex, several Mn-containing non-haem catalases have also been isolated and characterised [4-6]. Manganese catalases catalyse the disproportionation of hydrogen peroxide into water and molecular oxygen and this process is important for cell detoxification. The Mn catalases are known to contain two manganese ions at their active center [7] and the enzyme can exist in at least four different oxidation states: a reduced Mn^{II}/Mn^{II} form, a mixed-valence Mn^{II}/Mn^{III} form, an oxidized Mn^{III}/Mn^{III} form, and an inactive superoxidized Mn^{III}/Mn^{IV} form [8]. It is generally believed that the disproportionation reaction is catalysed by the interconversion of the two oxidation states Mn^{III} Mn^{III} and Mn^{II} Mn^{II} [8–10]. However, the active-site structure is not proven and the H_2O_2 proportionation mechanism remains unclear [8]. Accordingly at this stage it is of value to use simple model complexes to gain insight into the structure and catalytic mechanism of Mn catalase and much effort has been made [11–14]. As part of our ongoing studies into the coordination chemistry of dicarboxylic acid [15,16], we succeeded in preparing the title complex, $Mn_2(BIPY)_4(BTD)(H_2O)_2] \cdot (ClO_4)_2 \cdot 2H_2O$. To our knowledge the title complex is the first structurally characterized dinuclear manganese complex with extended bridging BTD^{2-} ligand [17]. The complex is also interesting for its novel hydrogen bonding character. Here the synthesis, crystal structure, magnetic

* Authors to whom correspondence should be addressed.

properties and electrochemical properties of the title complex are described, together with its catalytic activity towards the disproportionation of H_2O_2.

EXPERIMENTAL

Preparations

All reagents were reagent grade and used as received. Piperidinium salt of butane 1,4-dicarboxylic acid was prepared in a similar method to piperidinium salt of terephthalic acid [18].

A methanolic solution (20 cm^3) of bipyridine (0.8 mmol) and piperidinium salt of butane 1,4-dicarboxylic acid (0.2 mmol) was slowly added to a solution (20 cm^3) of manganese(II) perchlorate hexahydrate (0.4 mmol) in the same solvent with continuous stirring. The yellow powder separated during the addition was filtered off. Light yellow prismatic single crystals of the title complex suitable for X-ray analysis were obtained in a 64% yield after two weeks by slow evaporation of the mother-liquor at room temperature. Anal: Calc. for $C_{11}H_{11.5}Cl_{0.5}Mn_{0.5}N_2O_4$: C, 47.03; H, 4.13; N, 9.98; Mn, 9.78. Found: C, 47.25; H, 4.16; N, 10.12; Mn, 9.98%. IR (KBr matrix) cm^{-1}: ν_a(COO), 1580; ν_s(COO), 1410 (the results suggested the unidentate coordination mode of the dicarboxylate).

Caution: Metal perchlorate salts containing organic ligands are potentially explosive and should be handled with great care.

Physical measurements

Magnetic susceptibility data on powder samples were measured over a temperature range of 75–300 K at 6000 G by using a CAHN-2000 Faraday-type magnetometer. The apparatus was calibrated with $[Ni(en)_3]S_2O_3$ (en = ethylenediamine). Diamagnetic corrections were made using Pascal's constants.

X-ray crystallography

A summary of the crystal data, intensity collection and structure refinement is given in Table 1. The intensities were collected at 294 K on a Rigaku RAXIS IIC imaging-plate diffractometer using Mo-K_α radiation ($\lambda = 0.71073$ Å) from a rotating-anode generator operating at 50 kV and 90 mA ($2\theta_{max} = 55.2°$); 60 oscillation frames in the range of 0–180° [19], exposure 8 min per frame for the title complex.

The structure of the title complex was solved by direct methods. All non-hydrogen atoms were refined anisotropically by full-matrix least squares (on F). Hydrogen atoms of the ligand and the solvent molecules were placed in calculated positions (C—H 0.96 Å), assigned fixed isotropic thermal parameters, and allowed to ride on their respective parent atoms. The contributions of these hydrogen atoms were included in the structure-factor calculations.

Table 1. Crystal data for title complex

Formula	$C_{22}H_{23}ClMnN_4O_8$
Formula weight	561.8
Colour/habit	light brown prism
Crystal size (mm)	$0.10 \times 0.15 \times 0.30$
Crystal system	Triclinic
Space group	$P\bar{1}$
a (Å)	8.681(1)
b (Å)	10.849(1)
c (Å)	14.365(2)
α (°)	97.89(1)
β (°)	107.08(1)
γ(°)	101.02(1)
V (Å^3)	1242.1(6)
Z	2
F(000)	578
d_{calc}, (g cm^{-3})	1.502
Radiation (Mo K_α, Å)	0.71073
μ (mm^{-1})	0.693
No. of total data	4348
No. of unique data	4348
No. of obs. data [$F > 8.0\sigma(F)$]	2553
R, wR (obs. data)	0.0428, 0.0479
Goodness of fit	1.25
$\Delta\rho_{max}$, $\Delta\rho_{min}$ (eÅ^{-3})	0.27, −0.59
w^{-1}	$\sigma^2(F) + 0.0000F^2$

All computations were carried out on a PC-486 computer, using the SHELXTL-PC program package [20]. Analytical expressions of neutral-atom scattering factors were employed, and anomalous dispersion corrections were incorporated [21].

RESULTS AND DISCUSSION

Structure description

Selected bond lengths and angles are listed in Table 2. The labelled molecular structure and the packing arrangement of molecules in a unit cell are depicted in Figs 1 and 2, respectively.

The complex crystallizes in the triclinic space group $P\bar{1}$ and possess a dinuclear structure bridged by adianion of butane 1,4-dicarboxylic acid, which acts as a bidentate ligand and each carboxy group of the dicarboxylate is coordinated to a manganese atom unidentately (using O1). Each of the two symmetry related Mn^{II} atoms has a distorted octahedral N_4O_2 coordination geometry. Each metal is surrounded by two chelating bipy groups, one carboxylate oxygen atom [O1] from the bridging BTD^{2-} ligand and the oxygen atom [O1w] of a water molecule which is in a syn-position with respect to the coordinated carboxylate oxygen [O1] of the bridging TBD^{2-} ligand. The Mn—N (bipy) average bond length is 2.255(4)

Table 2. Selected bond distances (Å) and angles (°) for title complex

Mn(1)—N(1)	2.247(4)	Mn(1)—N(2)	2.265(3)
Mn(1)—N(3)	2.250(4)	Mn(1)—N(4)	2.259(4)
Mn(1)—O(1)	2.118(3)	Mn(1)—O(1w)	2.148(4)
N(1)—Mn(1)—N(2)	72.7(1)	N(1)—Mn(1)—N(3)	91.8(1)
N(2)—Mn(1)—N(3)	102.9(1)	N(1)—Mn(1)—N(4)	98.5(1)
N(2)—Mn(1)—N(4)	170.2(2)	N(3)—Mn(1)—N(4)	72.4(1)
N(1)—Mn(1)—O(1)	88.4(1)	N(2)—Mn(1)—O(1)	90.8(1)
N(3)—Mn(1)—O(1)	165.7(1)	N(4)—Mn(1)—O(1)	93.4(1)
N(1)—Mn(1)—O(1w)	167.3(1)	N(2)—Mn(1)—O(1w)	95.1(1)
N(3)—Mn(1)—O(1w)	94.5(1)	N(4)—Mn(1)—O(1w)	93.9(1)
O(1)—Mn(1)—O(1)	88.2(1)		
Hydrogen bonding parameters			
O(1w)···O(2w)	2.676(10)	O(1w)···O(2w)···O(2)	114.4(6)
O(1w)···O(2w)···O(5)	106.1(6)	O(1w)···O(2w)···O(5)	106.1(6)
O(2)···O(2w)···O(5)	104.9(6)	O(2)···O(2w)···O(5)	104.9(6)

Symmetry codes: (a) $-x, -y, -z$.

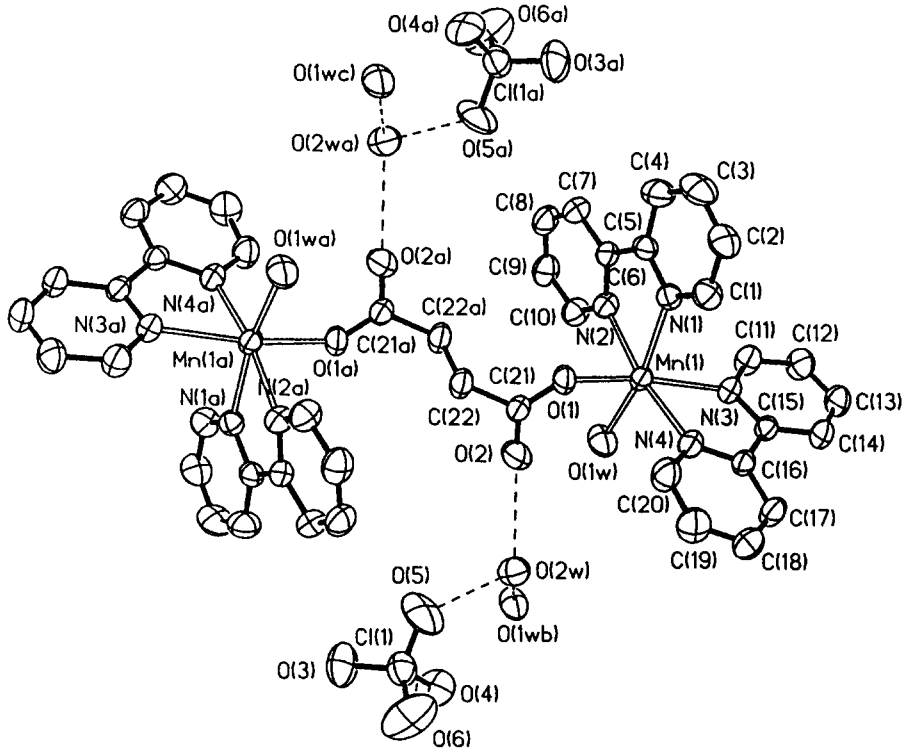

Fig. 1. Molecular structure of the title complex. Hydrogen atoms are omitted for clarity.

Å, the bond lengths of Mn—O1 (carboxylate) and Mn—O1w (water) are 2.118(3) and 2.148(4) Å, respectively. These bond lengths are similar to those reported for other manganese(II) complexes [16]. Large deviations of bond angle from 90° of the idealized octahedral geometry are found for angle N1—Mn1—N2 [72.7(1)] and angle N3—Mn1—N4 [72.4(1)] which are restricted by the bipy five-membered chelate ring. So the Mn ion has a distorted-octahedral coordination geometry. The best equatorial plane is defined by atoms O1w, N1, N2 and N4. The largest deviation from the mean plane is 0.0818 Å for N2 and the Mn atom is 0.0116 Å out of this plane. The Mn···Mn separation is 8.717 Å. Each of

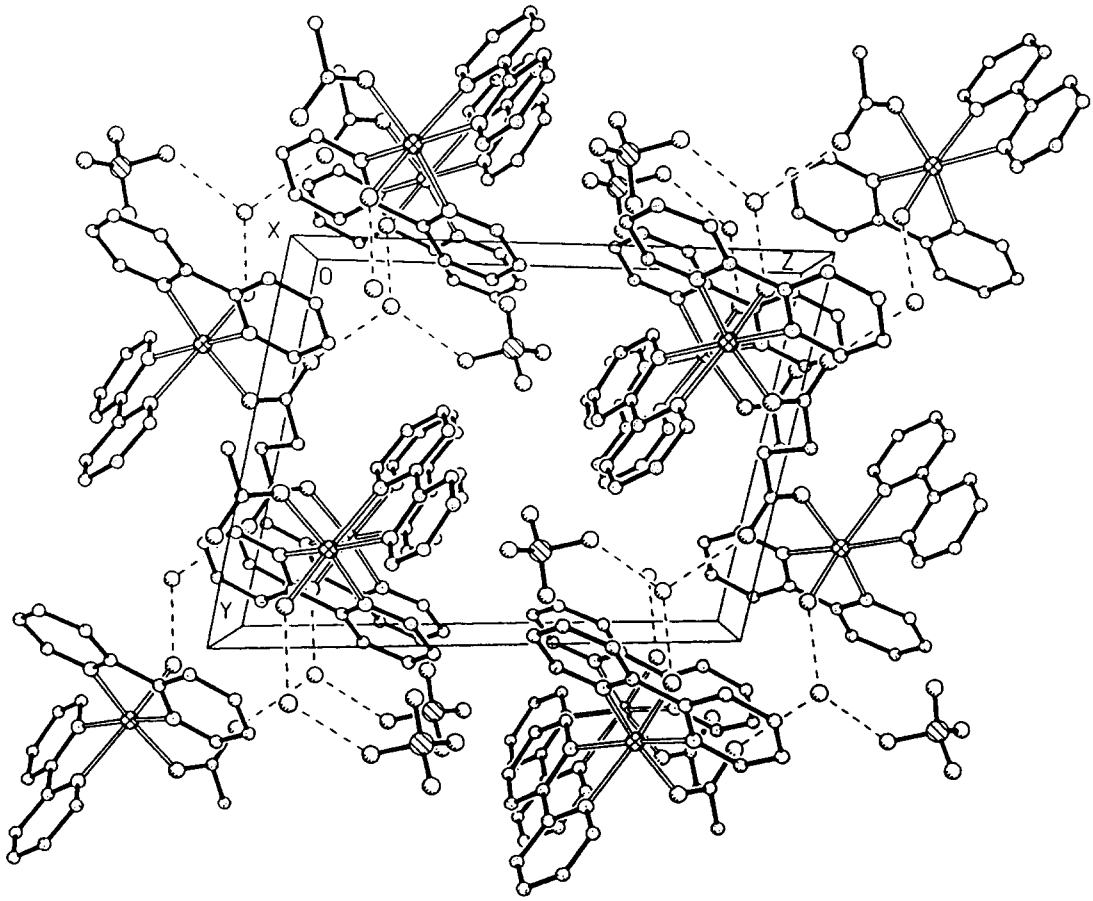

Fig. 2. Packing arrangement of molecules in the unit cell.

the bipy ligands is coplanar. The perchlorate groups have their expected tetrahedral geometry.

There is significant intermolecular association between two adjacent molecules of the complex caused by the presence of two bridging water molecules (O2w). Each of the two bridging water molecules is hydrogen bonded to the uncoordinated carboxylate oxygen (O2) in one molecule and the oxygen (O1w) of the coordinated water in another molecule, respectively, forming two hydrogen-bonding bridges between two molecules (Fig. 2). Furthermore, a perchlorate is also hydrogen bonded to each of the bridging water oxygens (O2w). All the hydrogen bonding parameters are listed in Table 2.

Magnetic properties

The temperature dependence of the magnetic susceptibility for the title complex in the form of χ_M vs T is shown in Fig. 3. The effective magnetic moment at 300.20 K is 8.29 B.M. which is slightly lower than the spin-only value of 8.36 B.M. expected for two uncoupled high-spin Mn^{II} ions. Upon cooling, the magnetic moment value decreases slowly from 8.29 B.M. at 300.2 K to 7.84 B.M. at 75 K, showing the presence of extremely weak antiferromagnetic exchange interaction. Assuming isotropic exchange, the exchange Hamiltonian is $H = -2JS_1S_2$ with

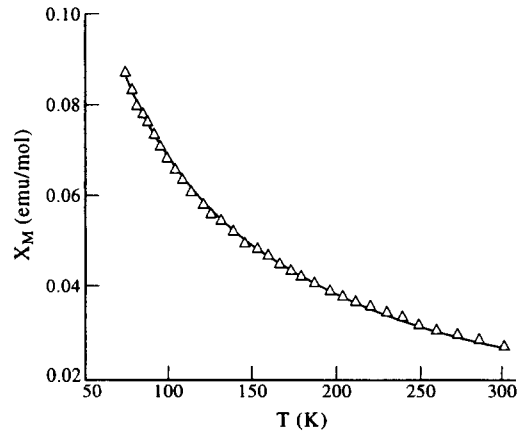

Fig. 3. The plot of χ_M/T for the title complex. The solid line represents best fit of data according to eq. (2).

$S_1 = S_2 = 5/2$, and the magnetic susceptibility per dinuclear molecule is given by eq. (1) [22] where N, g, β, x are Avogadro's constant, g factor, Bohr magneton, and $x = J/kT$, respectively, and J is the exchange coupling constant for the dinuclear molecule.

$$\chi_M = 2Ng^2\beta^2/kT[(e^x + 5e^{3x} + 14e^{6x} + 30e^{10x} + 55e^{15x})/(1 + 3e^x + 5e^{3x} + 7e^{6x} + 9e^{10x} + 11e^{15x})] \quad (1)$$

Improving on the calculated expression, a molecular field (zJ') [23] was added so as to describe the inter-dimer Mn^{II} unit exchange interactions. The expression for the magnetic susceptibility of the title complex becomes:

$$\chi_M = \chi_M/[1 - 2zJ'\chi_M/Ng^2\beta^2] \quad (2)$$

Using eq. (2), the least-squares fitting with an assumed g value of 2.00 gives the parameters: $J = -0.137$ cm^{-1}, $zJ' = -0.05$ cm^{-1} and $R = 2.35 \times 10^{-4}$ [$R = \Sigma(\chi_{calc} - \chi_{obs})^2]/\Sigma(\chi_{obs})^2]$. The magnetic susceptibility calculated by using the fit parameters is shown as the solid line in Fig. 3.

The magnetic exchange interaction through bridging BTD ligands is very weak. The J is slightly smaller than those of other Mn^{II} complexes bridged by terephthalate, isophthalate or *trans* butene diacid salt ligands ($J = -1.04 - -0.53$) [15,24].

Electrode process

The cyclic voltammogram of the title complex in CH_3CN containing 0.1 mol dm^{-3} TBAP is shown in Fig. 4. The oxidation of $[Mn_2(BIPY)_4(BTD)(H_2O)_2] \cdot (ClO_4)_2 \cdot 2H_2O$ at +0.14 V is assigned to two concident one-electron processes ($Mn_2^{III}/Mn^{III}\,Mn^{II}$ and $Mn^{III}\,Mn^{II}/Mn_2^{II}$) which is quasi-reversible. This is based on the following observations: the ratio of the cathodic-to-anodic peak currents, i_{pa}/i_{pc}, is not unity, the separation between the anodic and cathodic peak potentials, ΔE_p (125 mV), remains constant with increase of scan rate from 0.05 to 0.2 V/s, and the ratio of (peak current)/(scan rate)$^{1/2}$, $i_p/V^{1/2}$, is independent of the scan rate (0.05–0.2 V/s) [25].

Hydrogen peroxide disproportionation studies

Into a closed vessel containing the title complex (10 mg) and pyridine (1 cm^3), aqueous hydrogen peroxide (2.90 M, 1 cm^3, 2.90 mmol) was added and the mixture was stirred and thermostated at 13°C, and the O_2 evolved was measured volumetrically. The title complex in pyridine vigorously catalyze the disproportionation of H_2O_2. The time courses of the dioxygen evolution are shown in Fig. 5(a). During the first 30 s of the reaction, each molecular of the title complex on average disproportionated 250 molecules of H_2O_2. In addition we also examined the catalase activity of a mononuclear Mn^{III} complex, $[Mn^{III}(sal)(bipy)(H_2O)_2] \cdot (ClO_4) \cdot H_2O$, which was reported by us earlier [26] under the identical conditions and the results are shown in Fig. 5(b). During the first 30 s of the reaction, each molecule of the mononuclear complex on average disproportionated 22 molecules of H_2O_2. Obviously the title complex shows much higher catalase activity than the mononuclear complex. However, the reaction of either of the two complexes alone with H_2O_2 were very sluggish. As

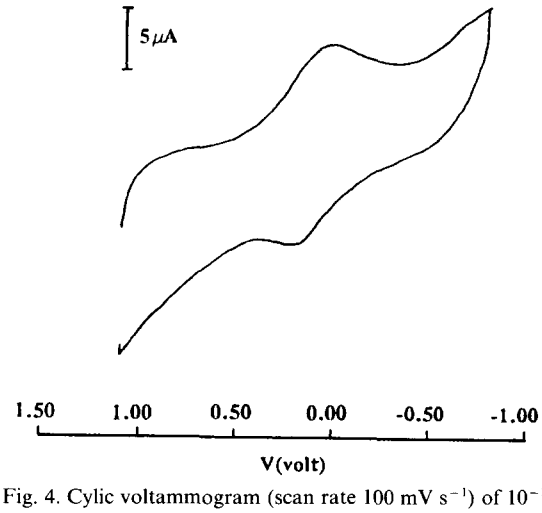

Fig. 4. Cylic voltammogram (scan rate 100 mV s^{-1}) of 10^{-3} M solutions of the title complex in CH_3CN (0.1 M TBAP) at a glassy-carbon electrode (298 K), and Ag/AgCl as a reference electrode.

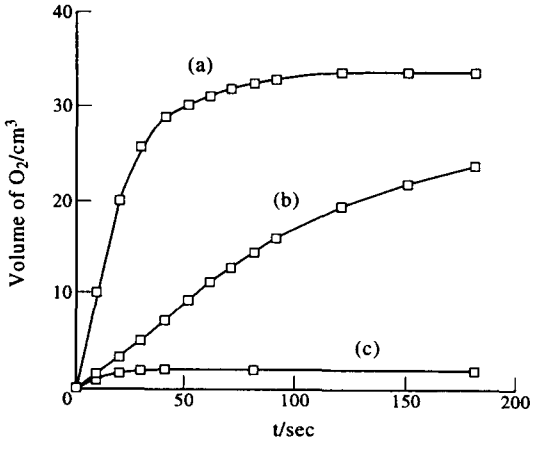

Fig. 5. Time course of O_2 evolution in H_2O_2 disproportionation by the title complex. (a) The title complex (10 mg, 8.9×10^{-3} mmol), with added pyridine (1 cm^{-3}); (b) the mononuclear complex (10 mg, 1.9×10^{-2} mmol), with added pyridine (1 cm^{-3}); (c) pyridine only. Conditions: H_2O_2 (2.9 M, 1 cm^3, 2.9 mmol), at 13°.

expected, the base pyridine by itself did not react with H_2O_2 (Fig. 5(c)). The above results show that the catalase-like activity of the two manganese complexes was greatly enhanced in the presence of pyridine base, and it is in agreement with literature reports [27]. Although the effects of added pyridine on the rate of disproportionation of H_2O_2 in the manganese-containing systems are indeed quite marked the exact role of the heterocyclic base in these catalytic reactions is unclear [28].

REFERENCES

1. *Magneto-structural Correlations in Exchange Coupled Systems*, eds R. D. Willet, D. Gatteschi and O. Kahn. NATO ASI Series, Reidel, Dordrecht, 1985.
2. Andruh, M., Roesky, H. W., Noltemeyer, M. and Schmidt, H.-G., *Polyhedron*, 1993, **12,** 2901.
3. Larson, E. J. and Pecoraro, V. L., in *Manganese Redox Enzymes*, ed. V. L. Pecoraro, VCH, New York, 1992, ch. 1.
4. Khangulov, S. V., Barynin, V. V., and Antonyuk, B. S. V., *Biochim. Biophys. Acta*, 1990, **25–33,** 1020.
5. Algood, G. S. and Perry, J. J., *J. Bacteriol.*, 1986, **168,** 563.
6. Kono, Y. and Fridovich, I., *J. Biol. Chem.*, 1983, **285,** 6015.
7. Pecoraro, V. L., Baldwin, M. J. and Gelasco, A., *Chem. Rev.*, 1994, **94,** 807.
8. Waldo, G. S. and Penner-Hahn, J. E., *Biochemistry*, 1995, **34,** 1507.
9. Pessiki, P. J., Khangulov, S. V., Ho, D. M. and Dismukes, G. C., *J. Am. Chem. Soc.*, 1994, **116,** 891.
10. Pessiki, P. J. and Dismukes, G. C., *J. Am. Chem. Soc.*, 1994, **116,** 898.
11. Fronko, R. M. and Penner-Hahn, J. E., *J. Am. Chem. Soc.*, 1988, **110,** 7554.
12. Waldo, G. S., Yu, S. and Penner-Hahn, J. E., *J. Am. Chem. Soc.*, 1992, **114,** 5869.
13. Casey, M. T., McCann, M., Devereux, M., Curran, M., Cardin, C., Convery, M., Cuillet, V. and Harding, C., *J. Chem. Soc., Chem. Commun.*, 1994, 2643.
14. Higuchi, C., Sakiyama, H., Okawa, H. and Fenton, D. E., *J. Chem. Soc., Dalton Trans.*, 1995, 4015.
15. Xiang Shi Tan, Dao Feng Xiang, Wen Xia Tang and Jie Sun, *Polyhedron*, 1997, **16,** 689.
16. Xiang Shi Tan, Dao Feng Xiang, Wen Xia Tang and Kai Bei Yu, *Polyhedron*, 1997, **16,** 1411.
17. Zhorzholiani, N. B., Shvelashvili, A. E., Sobolev, A. N., Vardosanidze, T. O., Sokol, V. I. C., *Inst. Fiz. Org. Khim. im. Khim.*, 1984, **13,** 102 (in Russian).
18. Verdaguer, M., Gouterson, J., Jeannin, S., Jeannin, Y. and Kahn, O., *Inorg. Chem.*, 1984, **23,** 4291.
19. (a) Tanner, J. and Krause, K., *The Rigaku J.*, 1994, **11,** 4; 1990, **70,** 28; (b) Kraus, K. L. and Phillips, G. N., *J. Appl. Crystallogr.*, 1992, **25,** 146; (c) Higashi, T., ABSCOR, Rigaku Corporation, Tokyo, 1995.
20. Sheldrick, G. M., in *Computational Crystallography*, ed. D. Sayre, Oxford University Press, New York, 1982, pp. 506–514.
21. *International Tables for X-ray Crystallography*, Vol. 4, Kynoch Press, Birmingham (now distributed by Kluwer Academic Press, Dordrecht), 1974, pp. 55, 99, 149.
22. Kahn, O., *Molecular Magnetism*. VCH, Inc., New York, 1993.
23. Ginsberg, A. P. and Lines, M. E., *Inorg. Chem.*, 1972, **11,** 2289.
24. Cano, J., Munno, G. D., Sanz, J., Ruizm, R., Lloret, F., Faus, J. and Julve, M., *J. Chem. Soc., Dalton. Trans.*, 1994, 3465.
25. Pessiki, P. J., Khangulov, S. V., Ho, D. M. and Dismukes, G. C., *J. Am. Chem. Soc.*, 1994, **116,** 891.
26. Xiang Shi Tan, Jian Chen, Pei Ju Zheng and Wen Xia Tang, *Acta Cryst.*, 1995, **C51,** 1268.
27. Devereux, M., McCann, M., Casey, M. T., Curran, M., Ferguson, G., Cardin, C., Convery, M. and Quillet, V., *J. Chem. Soc., Dalton Trans.*, 1995, 771.
28. Larson, E. J. and Pecoraro, V. L., *J. Am. Chem. Soc.*, 1991, **113,** 3810.

Pergamon

PII: S0277-5387(97)00280-5

Polyhedron Vol. 17, No. 8, pp. 1381–1385, 1998
© 1998 Elsevier Science Ltd
All rights reserved. Printed in Great Britain
0277-5387/98 $19.00+0.00

Synthesis and characterization of some hydrous TPPTS · Ln complexes (Ln = Sc, Y, La, Nd, Sm, Gd, Ho; and TPPTS = TRIS (m-sulfonatophenyl) phosphine)

Xin-Lan Chen,[a]* Peng Lei,[a] Qin-lin Qiao,[a] Lun Zhan[a] and Shi-yan Yan[b]

[a] Department of Chemistry, Wuhan University, Wuhan, 430072 P.R. China

[b] Lanzhou Institute of Chemical Physics, Chinese Academy of Science, Lanzhou, 730000 P.R. China

(Received 23 April 1997; accepted 20 June 1997)

Abstract—The TPPTS · Ln (Ln = Sc, Y, La, Nd, Sm, Gd, Ho; and TPPTS = tris (m-(sulfonatophenyl) phosphine) were synthesized from the precursor TPPTS · Na_3 and oxides of rare earth. The chemical composition of TPPTS · Ln was determined by elemental analysis and ICP-AES. The XPS showed that the sulfonate group in the complexes was coordinated with rare earth in a bridging tridentate manner. IR, Raman, ^{31}P NMR and TG-DTA graphs were recorded and discussed. © 1998 Elsevier Science Ltd. All rights reserved

Keywords: synthesis; rare earth; water-soluble phosphine; TPPTS · Ln complex.

The use of trisulfonated triphenylphosphine trisodium salt P-(m-$C_6H_4SO_3$)Na_3 (TPPTS · Na_3) for the development of a water-soluble homogeneous catalyst has attracted a great deal of attention in recent years [1–6]. The well known aqueous-phase hydroformylation catalyst HRh(CO)(TPPTS · Na_3)$_3$, as reported by Kuntz [2], was utilized in industrial process [7]. Some other metal complexes based on TPPTS · Na_3 ligand as catalyst in various chemical process are also reported, such as the hydrogenation [8], the catalytic substitution of allylic substrates [9] and alkylation [10]. The water-soluble catalysts solved the problem of separating catalyst from the reaction media. Notably, a wide variety of coordination compounds with TPPTSNa_3 as a ligand has been reported by Herrmann *et al.* [1]. The cations of water-soluble phosphine (TPPTS) which were reported were Na^+, K^+ and R_4N^+ [11]. No literature about corresponding compounds which contained Ln^{3+} have been published up to now according to our knowledge. The trivalent rare earth metal ion (Sc^{3+}) can enhance the catalytic activity of the transition metal in formylation [12]. It is therefore considered that TPPTS can be used as a bridging ligand because the oxygen atoms of three sulfonic groups can coordinate with rare earths while the phosphorus atom can coordinate with transition metal. The complexes with bridging ligands TPPTS modified with rare earth ion (III) may be both water-soluble and highly active in some water-organic catalytic process.

More recently we have synthesized TPPTS · Ln · xH_2O compounds. The TPPTS · Ln with $NiCl_2$, $PdCl_2$, $RhCl_3$, respectively as a catalytic system were also investigated in the hydroformylation of 1-heptene. The TPPTS · Y with $RhCl_3$ and TPPTS · Ho with $NiCl_2$ demonstrated the more satisfactory results than TPPTS · Na_3 [13].

As a part of our series of works, this paper described the synthesis and properties of TPPTS · Ln · $8H_2O$ (Ln = Sc, Y, La, Sm, Nd, Ho). The composition of these complexes was characterized by elemental analysis, ICP-AES. The IR and Raman spectroscopes, XPS, TG-DTA and molar conductivity were also discussed.

EXPERIMENTAL

Starting materials

The rare earth oxides were obtained from Rare Earth Research Institute, Hunan, China. The purity

* Author to whom correspondence should be addressed.

of rare earth oxides is greater than 99.9%. TPPTS·Na_3 was synthesized according to the patent with some changes [2(a)]. 30 g triphenylphosphine (TPP) (0.113 mol) was added to the 250 ml fuming sulfuric acid (50 wt% SO_3) in an ice bath under argon and stirred vigorously. The reaction temperature was slowly allowed to increase to 20°C for 1 h. After 24 h at 22°C, the reaction solution was added slowly to 300 cm^3 chilled degassed water. The aqueous solution was neutralized by 50% NaOH with vigorous stirring under ice temperature. TPPTS·Na_3 was separated and purified according to the literature [14(a)]. The formula of TPPTS·Na_3 was P-(m-$C_6H_4SO_3Na)_3$·$4H_2O$. The yield of highly pure product was about 35%. IR spectra was consistent with the literature [3(a)]. The ^{31}P NMR appeared at −5.25 ppm. This confirms that the compound contained no corresponding oxide (^{31}P NMR, 34.8 ppm) [14].

Synthesis of the complexes

Air-sensitive materials were manipulated in an inert atmosphere using Schlenk techniques. TPPTS·Na_3 5 g was dissolved in about 10 cm^3 degassed water. The solution after treated with the acidic cationic-exchange column (80–120 mesh, $\phi 2 \times 40$ cm) was concentrated under vacuum to 25 cm^3. The concentrated solution stirred with rare earth oxides *ca* 1.5 g (excesses) at room temperature until the pH of the mixture was about 6–7 and filtered. The filtrate was evaporated under the vacuum. The residual solid was refluxed with 40 cm^3 absolute ethanol for 2 h under nitrogen. The mixture was filtered and the solid dried under vacuum. Yield is around 75%.

Chemical analysis

In order to avoid the interference between P and S, the contents of P, S and rare-earth cation were readily determined by ICP-AES (Inductively Coupled Plasma-Atomic Emission Spectrum), and the contents of C and H were obtained by the typical elemental analysis.

Spectroscopic and structural analysis

For IR analysis, a Nicolet 60 SXB FT-IR spectrometer was used (as KBr disks). The samples for Raman were analyzed in the solid state using the Nicolet 910 FT-Raman spectrometer fitted with a Nd : YAG 1.064 μm laser. The samples of TPPTS·Sc and TPPTS·Ho for XPS was dehydrated under dynamic vacuum at 190–200°C for 6 h and cooled to the room temperature under nitrogen. The XPS spectra were recorded on KRATOS (XSAM 800). ^{31}P NMR spectra were recorded on a JEDL JNM-90G spectrometer using 85% H_3PO_4 as internal standard. Shimadzu DT-40 was used for TG-DTA.

RESULTS AND DISCUSSION

Synthesis and properties

The formation of the TPPTS·Ln complexes by the reaction of the rare earth oxides with aqueous $TPPTSH_3$ occurs according to the following equation:

$$1/2Ln_2O_3 + TPPTSH_3 \xrightarrow[20\text{–}25^\circ C]{} TPPTS \cdot Ln + 3/2\,H_2O$$

$$Ln = Sc, Y, La, Nd, Sm, Gd, Ho$$

$$TPPTSH_3 = P\text{-}(m\text{-}C_6H_4SO_3H)_3$$

The tris(m-sulfonatophenyl) phosphine acid ($TTPTSH_3$) can be obtained from two methods. One is from the unneutralized aqueous reaction mixture of TPP with oleum. The other is from the pure TPPTS·Na_3 treated with acidic cation-exchange column. The acid $TPPTSH_3$ which was separated according to the first method was always a phosphonium sulfate with the formula $[HP\text{-}(m\text{-}C_6H_4SO_3H)_3]_2SO_4$ [15]. It cannot be adapted to prepare the corresponding rare earth complex because $Ln_2(SO_4)_3$ which formed due to an extra sulfate in the phosphonium sulfate was difficult to remove. The $TPPTSH_3$ from the second method was not thermally stable and readily oxidized, the temperature of reaction should not exceed 50°C and all manipulation must be carried out in an inert atmosphere.

The TPPTS·Ln·xH_2O complexes are more thermally stable as shown by DTA analysis. These complexes were pale yellow powders except that the TPPTS·Nd was pale violet and very soluble in water. The results of chemical analysis were given in Table 1. From these results the formula of these complexes were determined as P-(m-C_6H_4-$SO_3)_3$Ln·$8H_2O$. The water content in TPPTS·Ln complexes was higher than in usual rare earth complexes because of the highly hydrophilic properties of TPPTS·Ln. It was possible that these complexes absorbed water from air before chemical analysis.

Vibrational spectroscopy

Since these complexes had similar IR and Raman spectra, this indicated that TPPTS·Ln has a similar manner of coordination. The possible assignments of TPPTS·Na_3, TPPTS·Y and TPPTS·Sm which were chosen as representatives were given in Table 2.

The broad band at 3287 ~ 3454 cm^{-1} and the strong band near 1640 cm^{-1} in IR spectra of all complexes were assigned to ν_{OH} and δ_{HOH}, respectively. Comparison of IR and Raman spectra of TPPTS·Ln complexes with those of TPPTS·Na_3 showed that the stretching frequency of S—O in TPPTS·Na_3 appeared at 1206 cm^{-1} with a very strong band and at 1040 cm^{-1} with a broad band and deforming frequency at 623 cm^{-1} [14], while these bands of TPPTS·Ln were observed at 1170, 1037 and 617 cm^{-1}

Table 1. Chemical analysis for TPPTS · Ln complexes[a]

Complexes	C%	H%	Ln%	S%	P%
TPPTS · Sc · H_2O	31.14 (31.40)	3.89 (4.07)	6.70 (6.54)	13.42 (13.95)	4.09 (4.59)
TPPTS · Y · $8H_2O$	29.33 (29.51)	3.79 (3.83)	12.22 (12.16)	13.04 (12.94)	4.29 (4.23)
TPPTS · La · $8H_2O$	27.81 (27.62)	3.91 (3.83)	17.79 (17.77)	12.31 (12.28)	3.89 (3.96)
TPPTS · Nd · $8H_2O$	27.23 (27.45)	3.63 (3.56)	18.32 (18.30)	12.02 (12.20)	4.01 (3.94)
TPPTS · Sm · $8H_2O$	27.55 (27.24)	3.78 (3.54)	17.81 (18.16)	12.33 (12.10)	4.05 (3.91)
TPPTS · Gd · $8H_2O$	26.74 (27.00)	3.89 (3.50)	20.10 (19.65)	11.87 (12.00)	4.11 (3.87)
TPPTS · Ho · $8H_2O$	26.34 (26.73)	3.26 (3.47)	20.60 (20.42)	12.12 (11.88)	3.98 (3.84)

[a] Required values (%) given in parentheses.

Table 2. Typical IR, Raman data and assignments for TPPTS · Ln, TPPTS · Na_3 complexes[a]

TPPTS · Na_3		TPPTS · Y		TPPTS.Sm		
IR	Raman	IR	Raman	IR	Raman	Assignments
	246(m)		253(m)		253(m)	ν(Ln—O)
	342(m)		335(m)		335(m)	νs(C—S)
404(sh)		404(sh)		406(vw)		δ(C—C)
463(w)	465(w)	462(sh)	462(w)	460(sh)	480(w)	δas(SO_3)
538(s)		535(s)		535(w)		δas(SO_3)
623(s)		617(s)		616(s)		δs(S—O)
	678(m)		674(m)		673(s)	δs(SO_3)
691(s)		688(s)		688(s)		δ(C—C)
799(m)	799(sh)	801(m)	810(sh)	801(m)	809(sh)	νs(C—S) + δ(C—H)
994(m)	995(vs)	993(m)	995(vs)	993(m)	995(vs)	P-ring breathing
1040(vs)	1049(m)	1037(vs)	1044(m)	1037(vs)	1043(m)	νas(SO_3) + δ(C—H)
	1081(m)		1085(m)		1085(m)	νas(SO_3) + δ(C—H)
1101(s)		1102(s)		1102(s)		δ(C—H)
		1130(s)		1129(sh)		νas(SO_3)
	1178(m)	1170(vs)	1176(s)	1169(vs)	1174(s)	νas(SO_3)
1206(sh)		1230(s)		1229(s)		νas(SO_3)
1402(m)	1408(w)	1404(m)	1402(w)	1404(m)	1403(w)	ν(C—C) aromatic
1467(m)		1468(m)		1468(m)		ν(C—C) aromatic
1588(w)	1587(s)	1589(w)	1587(vs)	1589(m)	1585(vs)	ν(C—C) aromatic
1637(m)		1640(m)		1640(m)		δ(O—H) H_2O
3068(w)	3069(vs)	3063(m)	3066(vs)	3063(m)	3064(s)	δ(C—H)
3230 ~ 3455(vs)		3230 ~ 3426(vs)		3284 ~ 3454(vs)		ν(O—H) H_2O

[a] ν, stretch; δ, deformation; w, weak; m, medium; s, strong; sh, shoulder; v, very.

respectively. The stretching frequency of C—S shifted from 799 cm^{-1} (in TPPTS · Na_3) to 810 cm^{-1}. It was clear that comparing with TPPTS · Na_3 the frequencies of $\nu_{S\text{-}O}$ and $\delta_{S\text{-}O}$ in TPPTS · Ln shifted to the lower frequencies and $\nu_{C\text{-}S}$ moved to the higher frequency. The asymmetric stretching peak of SO_3 groups in IR spectra of the TPPTS · Na_3 at around 1200 cm^{-1} split into 4 shoulder peaks and widened in TPPTS · Ln. All these shifts and changes of IR and Raman spectra as noted previously corroborated the geometric deformation brought about by coordination and are similar to those of $M(ClO_4)_3$ (M = Mn, Co, Ni ...) [16] and $Ln(CF_3SO_3)_3$ [17] complexes, in which ClO_4 and CF_3SO_3 are bridging tridentate. Namely the coordination of SO_3 induced a lengthening of the S—O bond and a shorting of the C—S bond.

The ^{31}P NMR spectra of TPPTS · La and TPPTS · Sm which were chosen as representatives were recorded. The single peak appeared at δ-6.20 ppm and δ-5.60 ppm, respectively. This indicated no corresponding oxides.

TG-DTA and molar conductivity

All complexes showed the similar TG-DTA graphs as typically given in Fig. 1 for TPPTS · $Sm8H_2O$. The TG curve indicated TPPTS · $Sm8H_2O$ weight-loss stages. TPPTS · $Sm8H_2O$ completely dehydrated at

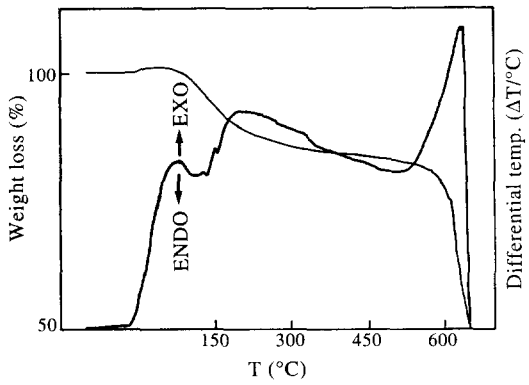

Fig. 1. Typical TG-DTA curves of TPPTS · Sm.

about 322°C (found: 18.32%; theo: 18.16%). This was consistent with the results of elemental analysis and ICP-AES. TG curve also indicated that TPPTS · Sm8H_2O lost five moles of crystalline water from 40 to 150°C (found 12.54%; theo: 12.18%), then lost three moles of coordinated water from 150 to 322°C. Therefore it was evident that only three moles of water are coordinated with the central rare earth ion. The TG-DTA showed that these complexes are stable to 425°C.

The molar conductivity of these complexes which were measured in water or in methanol were 3.0 ~ 4.5 S cm^{-2} mol^{-1} at 25°C. The very low conductivity indicated these complexes were non-electrolytes [18].

XPS studies

To get further insight into the nature of bonding, XPS of the TPPTS · Sc and TPPTS · Ho were recorded in powder form at room temperature. The results of XPS of TPPTS · Sc, TPPTS · Ho, TPPTS · Na_3 and Ln_2O_3 are given in Table 3. TPPTS · Sc (533.16 eV) and TPPTS · Ho (533.12 eV) with that of TPPTS · Na_3 (532.02 eV) showed that the oxygen in TPPTS · Sc and TPPTS · Ho tends to lose electron as a donator because of increase of the binding energy, and that Sc in TPPTS · Sc and Ho in TPPTS · Ho meanwhile tends to accept the electron as an acceptor because the binding energy of Sc^{2P} in TPPTS · Sc decreased from 401.9 eV (Sc^{2P} in Sc_2O_3) to 400.09 eV and Ho^{4d} in TPPTS · Ho decreased from 164.4 eV (in Ho_2O_3) to 162.87 eV. The oxygen 1 s peaks of the TPPTS · Sc is symmetric, which showed the oxygen atoms of TPPTS · Ln coordinated with the lanthanide ion in an identical form.

Table 3. Binding energy (eV) for TPPTS · Na_3, TPPTS · Sc, TPPTS · Ho and Ln in Ln_2O_3

Complexes	O^{1s}	S^{2p}	Ln in complexes	Ln in oxides
TPPTS · Na_3	532.02	168.45	—	—
TPPTS · Sc	533.16	168.63	400.09[a]	401.9[a]
TPPTS · Ho	533.12	168.76	162.87[b]	164.4[b]

[a] Sc^{2p}.
[b] Ho^{4d}.

From the results and previous analysis, it was proposed that the SO_3 groups in TPPRS · Ln complexes are bridging tridentate and that coordinating number of rare earth is 12 which contained three molecular coordinated water. The coordinating manner in TPPTS · Ln as we suggested previously is shown in following formula:

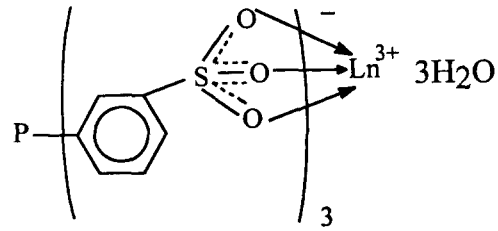

Acknowledgements—This project was financially supported by the State Key Lab OSSO (Oxo Synthesis and Selectively Oxide) in Lanzhou Institute of Chemical Physics, Chinese Academy. The authors also thank Dr Mo Shao-bo for recording XPS spectra and helpful discussions.

REFERENCES

1. Hermann, W. A., Kellnar, J. and Ripel, H., *J. Organomet. Chem.*, 1990, **389,** 103.
2. (a) Kuntz, E. G., U. S. Patent 4,248,802, 1981; (b) Kuntz, E. G., *Chemtech*, 1987, **22,** 570.
3. (a) Bartik, T., Bartik, B., Hanson, B. E., Glass, T. E. and Babout, W. E., *Inorg. Chem.*, 1992, **31,** 2667; (b) *ibid*, 1993, **32,** 5833.
4. Larpent, G., Dabard, R. and Patin, H., *Inorg. Chem.*, 1987, **26,** 2922.
5. Fache, E., Santini, C., Senocq, F. and Basset, J. M., *J. Mol. Catal.*, 1992, **72,** 331.
6. Guo, I., Hanson, B. E., Toth, I. and Davis, M. E., *J. Organomet. Chem.*, 1991, **403,** 231.
7. Kuntz, E. G., Rhone-Poulenc Industry, French Patent 2,314,910, 1975.
8. (a) Larpent, C., Dbard, R. and Patin, H., *Tetrahedron Lett.*, 1987, **28,** 2507; (b) Grosselin, J. M., Mercier, C., Alimang, G. and Grass, F., *Organometall.*, 1991, **10,** 2126.
9. Blant, E., Geuet, J. P., Safi, M., Savignac, M. and Sinoub, D., *Tetrahedron*, 1994, **50,** 505.
10. Casalnuovo, A. L. and Calabrese, J. C., *J. Am. Chem. Soc.*, 1990, **112,** 4224.
11. Bahrmann, H., Cornils, B., Lipps, W., Lappe, P. and Spinger, H., Canadian Patent CA 1,247,642, 1988.
12. Mitamura Shuichi, Kawado Atsushi and Kobayashi Ossm, Japanese Patent 94 157 39, 1994.

13. Lei Ping, M.S. Thesis, Wuhan University, 1997.
14. (a) Kalck, P. and Monteil, F., *Adv. Organomet. Chem.*, 1993, **34,** 219; (b) Larpent, C., Patin, H., Thilmont, N. and Valdor, J. F., *Synthetic Communications*, 1991, **21,** 327.
15. Arhancet, J. P. and Davis, M. C., *J. Catal.*, 1990, **121,** 327.
16. Favier, F. and Pascal, J. L., *J. Chem. Soc., Dalton Trans.*, 1992, 1997.
17. (a) Hamidi, M. H. and Pascal, J. L., *Polyhedron*, 1994, **13,** 1797; (b) Boumizane, K., Herzog-Cance, M. H., Jones, D. J., Pascal, J. L., Potier, J. and Roziere, J., *Polyhedron*, 1991, **10,** 2757.
18. Geary, W. J., *Coord. Chem. Rev.*, 1971, **7,** 81.

Pergamon

PII: S0277-5387(97)00277-5

Polyhedron Vol. 17, No. 8, pp. 1387–1396, 1998
© 1998 Elsevier Science Ltd
All rights reserved. Printed in Great Britain
0277-5387/98 $19.00+0.00

Ruthenium(II) bipyridine complexes with modified phenolic Schiff base ligands. Synthesis, spectroscopic characterization and Redox properties

Kripa Devi Keerthi, Bidyut Kumar Santra and Goutam Kumar Lahiri*

Department of Chemistry, Indian Institute of Technology, Powai, Bombay—400 076, India

(Received 14 April 1997; accepted 20 June 1997)

Abstract—A group of stable new ruthenium(II) mixed-ligand tris-chelated complexes of the type $[Ru(bpy)_2L]ClO_4$ (**1–6**), (bpy = 2,2′-bipyridine; L = deprotonated form of the HL ligands, *o*-(HO)—C_6H_3(R)C(R′)=N—CH_2—C_6H_5 or *o*-(HO)—C_6H_3(R)C(R′)=N—NH—C_6H_5; where R = H, *p*-NO_2 and R′ = H, CH_3) have been synthesized and characterized. The complexes are essentially diamagnetic and behave as 1 : 1 electrolytes in acetonitrile solution. They display two metal-to-ligand-charge-transfer (MLCT) transitions near 500 and 400 nm respectively and intra ligand π–π^* transitions in the UV-region. In acetonitrile solution the complexes exhibit weak emission from the lowest energy MLCT band at room-temperature. The quantum yields of the complexes are found to be in the range 0.0004–0.01. In acetonitrile solution the complexes show quasi-reversible ruthenium(II)–ruthenium(III) oxidation couples in the range 0.33 → 0.70 V and irreversible ruthenium(III)–ruthenium(IV) oxidations in the range 1.53 → 1.95 V vs SCE. Two successive reversible bipyridine reductions are observed for each complex in the ranges −1.4 → −1.62 V and −1.59 → −1.85 V vs SCE respectively. The presence of trivalent ruthenium in the oxidized solution for one complex **5** is evidenced by the rhombic EPR spectrum with *g* values, $g_1 = 2.389$, $g_2 = 2.081$ and $g_3 = 1.810$. The EPR spectrum of the coulometrically oxidized species, $\mathbf{5}^+$ has been analyzed to furnish values of axial ($\Delta = 4745\ cm^{-1}$) and rhombic ($V = 3692\ cm^{-1}$) distortion parameters as well as the energies of the two expected ligand field transitions ($v_1 = 3071\ cm^{-1}$ and $v_2 = 6819\ cm^{-1}$) within the t_2 shell. One of the ligand field transitions has been observed experimentally at 6578 cm^{-1} by near-IR spectrum which is close to the computed v_2 value. © 1998 Elsevier Science Ltd. All rights reserved

Keywords: ruthenium; synthesis; spectra; redox; electronic structure.

The chemistry of ruthenium-bipyridine complexes has been the focus of continuous research activity since the discovery of their important redox, photophysical and photochemical properties [1]. Several ruthenium-bipyridine complexes have been exploited in solar energy schemes [2], in the oxidation of water to dioxygen [3], in the conversion of chloride ion to chlorine [4] and in the electrochemical reduction of acetylene to ethylene and ethane [5]. This has also been used to investigate photochemically induced charge-transfer [6], ligand substitution [7], stereochemical isomerization processes [8], and finally to probe important metal–ligand interactions [9]. In fact these properties have spurred the development of newer ruthenium bipyridine systems either by incorporating desired groups within the bipyridine moiety itself or by using other types of donor sites along with the $[Ru(bpy)_2]$ core to form mixed ligand tris-chelates to modulate the photo-redox activities of this class of complexes.

The present work originates from our interest to introduce phenolic Schiff base ligands (HL) having CH_2 or NH spacer [OH—C_6H_3(R)C(R′)=N—CH_2—C_6H_5 or OH—C_6H_3(R)C(R′)=N—NH—C_6H_5, Scheme 1] as a third ligand in the $[Ru(bpy)_2]$ core to prepare new mixed ligand ruthenium-bipyridine complexes of type $[Ru(bpy)_2L]$ to understand the

* Author to whom correspondence should be addressed.

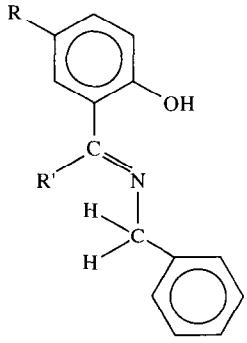

A

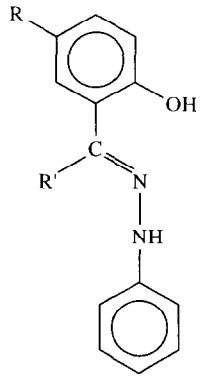

B

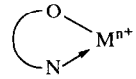

ML

R = H, R' = H ⟶ HL^1
R = H, R' = CH_3 ⟶ HL^2
R = NO_2, R' = H ⟶ HL^3

R = H, R' = H ⟶ HL^4
R = H, R' = CH_3 ⟶ HL^5
R = NO_2, R' = H ⟶ HL^6

Scheme 1.

effect of newly inducted groups on the redox and spectroscopic properties of the $[Ru(bpy)_2]$ core system.

Herein we report the synthesis of six complexes of the kind having RuN_5O chromophore, their redox properties, spectroelectrochemical correlation, preliminary photophysical aspects and electronic structure of one of the electrogenerated trivalent congeners.

RESULTS AND DISCUSSION

Synthesis

Six phenolic Schiff base ligands used for the present study are abbreviated HL^1–HL^6 respectively. The ligands are primarily classified into two groups, HL^1–HL^3 (**A**) and HL^4–HL^6 (**B**) depending on the nature of the spacer (CH_2 or NH) present in between the imine nitrogen and phenyl ring and within each group the three ligands differing with respect to substituents present either on the phenolic ring or on the imine fragment (Scheme 1). The anionic form of the ligands (L^-) bind to the metal ion as bidentate N, O coordinators forming six membered chelate ring (**ML**) systems.

The complexes, $[Ru(bpy)_2(L)]^+$ (**1–6**) (bpy = 2,2′-bipyridine) have been synthesized from $[Ru(bpy)_2CO_3]$ following the general decarbonation synthetic route shown in eqn (1):

$$Ru(bpy)_2CO_3 + HL \xrightarrow[\Delta]{MeOH} [Ru(bpy)_2L]^+ + HCO_3^- \quad (1)$$

Ligand Complex

$L^1 \rightarrow$ **1**

$L^2 \rightarrow$ **2**

$L^3 \rightarrow$ **3**

$L^4 \rightarrow$ **4**

$L^5 \rightarrow$ **5**

$L^6 \rightarrow$ **6**

The red colored cationic complexes have been isolated as perchlorate salts and the crude products were purified by column chromatography using a silica gel column.

The microanalytical data of the complexes are shown in Table 1. The results are in very good agreement with the calculated values thus confirming the gross composition of the mixed ligand tris chelates $[Ru(bpy)_2L]ClO_4$ (**1–6**). The complexes exhibit 1 : 1 conductivity in acetonitrile solution (Π_M, 140–155 Ω^{-1} cm^2 M^{-1}). Solid state magnetic moment measurements at room temperature indicate that all the monocations (**1–6**) are essentially diamagnetic (t_{2g}^6, idealized, S = 0).

Spectral study

IR spectra. FTIR spectra of the complexes were recorded as KBr discs. The $\nu_{(C=N)}$ stretching frequency of the free ligands (HL) appears near 1630 cm^{-1} which has been shifted to 1600 cm^{-1} in accordance with the coordination of the azomethine function to the metal

Table 1. Microanalytical and electronic spectral data

Compound	Elemental analysis (%)[a] C	H	N	Electronic spectral data[b] λ_{max} (nm) (ε[c], $M^{-1}\,cm^{-1}$)
1	56.65	3.93	9.77	580 (2554)[d], 510 (5108), 460 (4561)[d], 379 (7297), 330 (5472)[d], 294 (27000), 233 (24333), 212 (24446)
	(56.47)	(3.88)	(9.69)	
2	57.19	4.02	9.41	586 (1600)[d], 508 (4060), 381 (6350), 297 (29710), 245 (25790), 217 (24190)
	(57.02)	(4.07)	(9.50)	
3	53.33	3.45	11.11	480 (14030), 389 (13310), 328 (14040), 293 (48030) 241 (40670)
	(53.16)	(3.52)	(10.94)	
4	54.68	3.67	11.58	591 (2570)[d], 504 (5210), 374 (8000), 331 (6980)[d], 296 (36420), 233 (36150)
	(54.73)	(3.73)	(11.61)	
5	55.45	3.84	11.47	599 (2520)[d], 511 (4960), 375 (7980), 297 (31710), 244 (25870), 218 (23680)
	(55.32)	(3.93)	(11.38)	
6	51.67	3.32	12.87	478 (16060), 390 (14830), 323 (13810)[d], 293 (50000) 244 (37330), 215 (33280)
	(51.53)	(3.38)	(12.75)	

[a] Calculated values are in parentheses.
[b] In acetonitrile solution.
[c] Extinction coefficient.
[d] Shoulder.

ion [10]. The O—H stretch in the free ligands is observed as a prominent bond near 3400 cm^{-1}. This band is absent in the complexes as expected. A very strong and broad band near 1100 cm^{-1} and a strong and sharp vibration band near 630 cm^{-1} are observed for all the complexes due to the presence of ionic perchlorate.

^1H NMR spectra. ^1H NMR spectra of the complexes were recorded in $CDCl_3$ solvent using a 300 MHz instrument. The representative spectra of complexes **3** and **6** are shown in Fig. 1. The O—H proton of the free ligands appears as a broad peak near 14 ppm as expected [11]. The absence of OH proton of the free ligand (HL) in the spectra of the complexes suggests coordination through the phenolato oxygen. The methylene protons (—CH_2) appear as a singlet near 4.8 ppm for the free ligands (HL^1–HL^3), the same protons are observed for the corresponding complexes (**1–3**) as a doublet of doublet near 4.9 ppm (Fig. 1(a)). The —NH proton for the free ligands (HL^4–HL^6) appears near 5.5 ppm as a broad peak, whereas for the corresponding complexes (**4–6**) the same is observed as a triplet near 6.0 ppm due to the nitrogen nuclear spin ($I = 1$) (Fig. 1(b)).

The presence of asymmetric ligands L in the complexes make all the six aromatic rings inequivalent. The complexes **1, 2, 4, 5** and **3, 6** thus possess twenty-five and twenty-four non-equivalent aromatic protons respectively. Since the electronic environment of many aromatic hydrogen atoms are similar, their signals may appear in a narrow chemical shift range. In fact aromatic regions of the spectra are complicated due to the overlapping of several signals which has precluded the identification of individual resonances. However, the direct comparison of the intensity of the aromatic region proton signals with that of the clearly observable —CH_2 protons (δ, 4.9 ppm) for the complexes **1–3** reveal the presence of the expected twenty-five aromatic protons and one azomethine (CH=N) proton for the complex **1**, twenty-five aromatic protons for the complex **2** and twenty-four aromatic protons and one azomethine proton for the complex **3** (Fig. 1(a)).

Similarly the direct comparison of the intensity of the aromatic protons with that of the clearly observable —NH proton (δ, 5.8 ppm) reveals the presence of the calculated number of protons in the aromatic region for the complexes **3–6** (Fig. 1(b)).

Methyl (CH_3) protons for the complexes **2** and **5** have appeared as a singlet at 2.51 and 2.49 ppm respectively.

Electronic spectra. Solution electronic spectra of the complexes were recorded in acetonitrile solvent in the UV-visible region (200–700 nm). The spectral data are listed in Table 1 and the representative spectra are shown in Fig. 2. The presence of different acceptor levels in the complexes may be responsible for the observed multiple absorptions [12]. The complexes exhibit primarily two bands in the visible region near 500 nm and 400 nm respectively (Table 1).

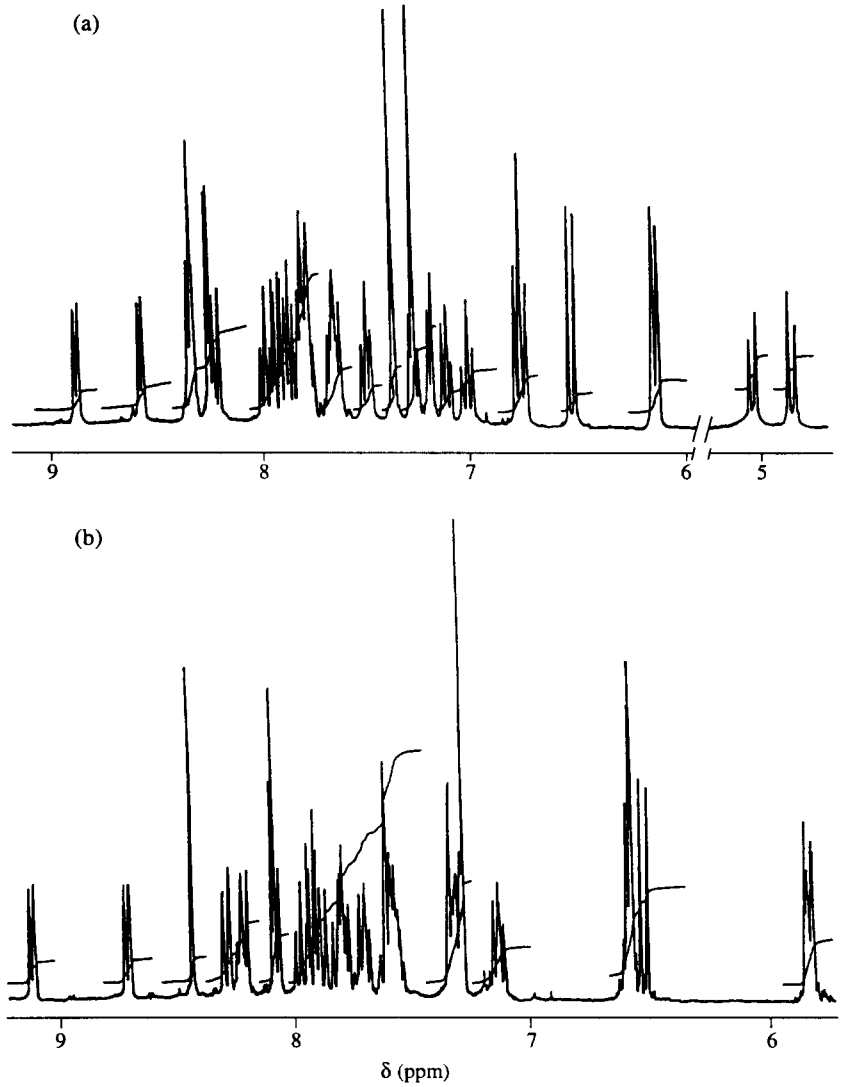

Fig. 1. ^{1}H NMR spectra of (a) $[Ru^{II}(bpy)_2L^3]ClO_4$, **3** and (b) $[Ru^{II}(bpy)_2L^6]ClO_4$, **6** in $CDCl_3$.

The origin of these two bands in the visible region has been assigned on the basis of reported spectra of $Ru(bpy)_2^{2+}$ complexes having other kinds of chelating third ligands [13]. Two different kinds of bipyridine acceptor levels, one symmetric (χ) and one antisymmetric (ψ) have developed with respect to the C_2 axis of bipyridine ligand and the transitions from metal filled $d\pi$ orbital to those two π^* orbitals result in the observed two MLCT bands. The lower energy band near 500 nm is considered to be $\pi(Ru) \rightarrow \pi^*(\psi)$ and the higher energy band near 400 nm may be due to $d\pi(Ru) \rightarrow \pi^*(\chi)$ transitions.

The higher energy bands in the UV-region are of intra-ligand (π–π^*) type or charge-transfer transitions involving energy levels which are higher in energy than the ligand lowest unoccupied molecular orbital (LUMO).

The lowest energy MLCT band of $[Ru(bpy)_3]^{2+}$ appears at 450 nm in acetonitrile solution [14]. Thus the replacement of one strong π-acidic symmetric bipyridine ligand by an asymmetric phenolato Schiff base ligand (L) in the complexes (**1–6**) decreases the energy of the same transition. Lower ligand field strength of the ligands L compared to the bipyridine ligand and the overall lowering of the molecular symmetry while going from $[Ru(bpy)_3]^{2+}$ to complexes **1–6** might be the probable reasons for the observed shift of MLCT band. The observed red shifts of the lowest energy MLCT bands for the complexes **3** and **6** (where nitro group is present in the ligands L^3 and L^4) as compared to $[Ru(bpy)_3]^{2+}$ are not as much as that of the other four complexes (**1, 2, 4, 5**) (Table 1).

Room temperature emission spectra. Emission properties of the complexes have been studied in acetonitrile solvent at room temperature. Excitations of the complexes in acetonitrile solution, at the top of

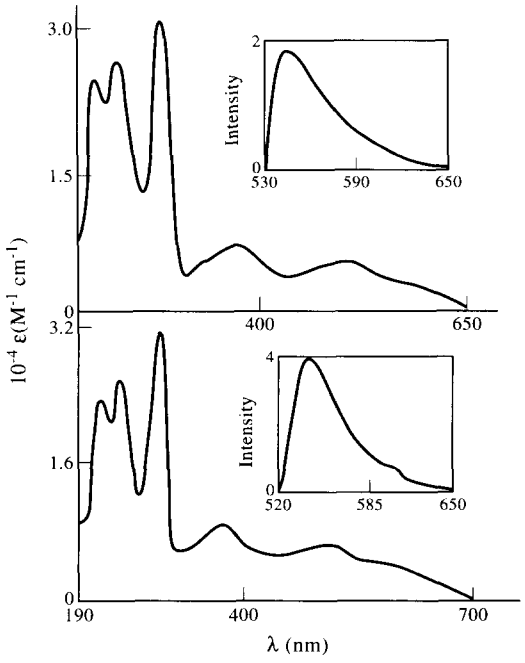

Fig. 2. Electronic spectra of (a) $[Ru^{II}(bpy)_2L^2]ClO_4$, **2** and (b) $[Ru^{II}(bpy)_2L^5]ClO_4$, **5** in acetonitrile. The insets show the emission spectra of the corresponding complexes at 298 K in acetonitrile.

the lowest energy MLCT bands (λ_{max}, near 500 nm for the complexes **1, 2, 4, 5** and near 480 nm for the complexes **3** and **6**) exhibit weak emissions near 550 nm (Table 2, Fig. 2). The origin of these emission spectra are further confirmed by the excitation spectra of the corresponding same solutions. Intensity of the observed emission spectra of the complexes under each class of ligands L, **A** and **B** follows the order **3** < **1** < **2** and **6** < **4** < **5** respectively. The complexes having keto based Schiff base ligands, **2** and **5** are exhibiting the strongest emissions and within the two classes of ligands, **A** and **B**, the complexes having ligands of type **B** (phenyl hydrazine derived Schiff base) are more effective from an emission point of view.

The quantum yields of the complexes are determined by comparison with the reported quantum yield of $[Ru(bpy)_3][PF_6]_2$ complex in acetonitrile solution ($\phi_{em,r} = 0.062$) [15]. For the calculation of quantum yield of the complexes, the excitation wave lengths are chosen such that the standard reference and sample absorptions are equal. The quantum yield of the emission process is calculated by following the reported method, eqn (2), where A_s, A_r are the absorption values of sample and reference, I_s, I_r are the emission intensities of sample and reference and n_s, n_r are the refractive indices of sample and reference.

$$\phi_{em,s} = \phi_{em,r}(A_r/A_s)(I_s/I_r)(n_s/n_r)^2 \quad (2)$$

Since A_s and A_r are equal and the refractive indices are assumed to be similar, eqn (2) can then be modified to eqn (3).

$$\phi_{em,s} = \phi_{em,r}(I_s/I_r) \quad (3)$$

The calculated quantum yields for the complexes are listed in Table 2. The quantum yields for the complexes **2** and **5** are much higher than the rest (Table 2).

Redox properties

Redox properties of the complexes have been studied in acetonitrile solution by cyclic voltammetry (CV) using a platinum working electrode. Complexes are electroactive with respect to metal as well as ligand centers and display four redox processes in the potential range +2 V vs saturated calomel electrode (SCE). Representative voltammograms are shown in Fig. 3 and the reduction potentials data are depicted in Table 3. The assignments of the responses to specific couples in Table 3 are based on the following considerations.

The ruthenium(III)–ruthenium(II) couple. All the complexes display one reversible oxidation process (Fig. 3) which is assigned to the metal oxidation, eqn (4). The one-electron nature of the responses is estab-

Table 2. Emission data[a]

Compound	λ_{max} (excitation) (nm)	λ_{max} (emission) (nm)	Relative intensity	Quantum yield[b]
1	510	556	1.5×10^2	0.0004
2	508	547	1.8×10^3	0.005
3	480	541	0.4×10^2	0.0001
4	504	554	1.7×10^3	0.005
5	511	548	4.0×10^3	0.01
6	478	547	0.5×10^3	0.002

[a] In acetonitrile.
[b] Calculated by using eqn (3).

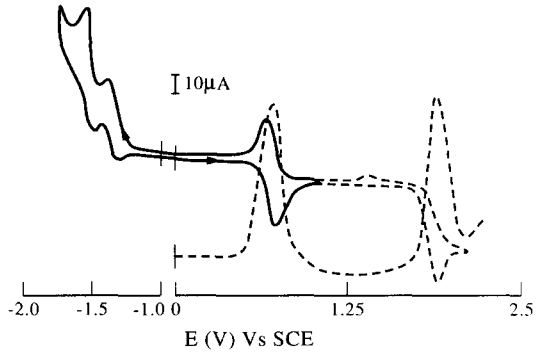

Fig. 3. Cyclic voltammograms of $\sim 10^{-3}$ M solution of the complex **3** in acetonitrile at 298 K.

lished by current height and constant potential coulometry data.

$$[Ru^{III}(bpy)_2L]^{2+} + e^- \rightleftharpoons [Ru^{II}(bpy)_2L]^+ \quad (4)$$

The presence of trivalent ruthenium in the oxidized solution is confirmed by characteristic rhombic EPR spectrum of the ruthenium(III) congener (see later). The formal potential of the couple (eqn 4) varies depending on the nature of ligands L. The complexes having phenyl hydrazine derived ligands L (**4–6**) are exhibiting lower reduction potentials compared to the corresponding complexes derived from benzylamine based ligands L (**1–3**) and within each class the reduction potential follows the order **3** > **1** > **2** and **6** > **4** > **5** respectively as expected. Thus a potential shift of maximum 300 mV has been observed in each class depending on the substituents present (Table 3), which implies the stability of the bivalent ruthenium in the case of NO_2 substituted ligand (L^3 or L^6) is more as compared to the others.

Under identical experimental conditions, the ruthenium(III)–ruthenium(II) reduction potential of $[Ru(bpy)_3]^{2+}$ appears at 1.29 V [13,14]. Thus substitution of one bipyridine ligand from the $[Ru(bpy)_3]^{2+}$ by a σ-donating phenolato Schiff base ligand, L, results in a decrease of ruthenium(III)–ruthenium(II) potential by 0.6–1 V depending on the particular R and R′ groups present in the ligands L. The reduction of overall charge of the complex cation from +2 in $[Ru(bpy)_3]^{2+}$ to +1 in the present complexes provides further electrostatic stabilization of the oxidized trivalent Ru^{III}—L species which has possibly originated from the σ-donor character of the phenolato group [16]. This decrease of metal oxidation potential (Ru^{II}–Ru^{III}) while going from $[Ru(bpy)_3]^{2+}$ to $[Ru(bpy)_2L]^+$ complexes and the reversible nature of the voltammograms (Fig. 3) suggests the possibility of isolating trivalent congeners of the complexes under the present mixed ligand tris chelated environment.

Although the ruthenium(II)–ruthenium(III) oxidation potentials for the present complexes are reasonably low, the oxidized trivalent congeners are not too stable to isolate (see later section).

Table 3. Electrochemical data at 298 K[a]

Compound	Ru^{III}–Ru^{II} couple E^0_{298} (V) (ΔE_p (mV)	n^b	Ru^{III}–Ru^{IV} E^c_{pa} (V)	Ligand reduction E^0_{298} (V) (ΔE_p (mV))	ΔE^0 (V)[d]	ν_{MLCT} (cm^{-1}) Cal.[e]	Obs.[f]
1	0.43 (80)	1.02	1.60	−1.58 (80) −1.85 (90)	2.01	19210	19608
2	0.38 (70)	1.04	1.55	−1.57 (70) −1.81 (90)	1.92	18726	19685
3	0.70 (70)	0.98	1.91	−1.40 (80) −1.59 (80)	2.10	19936	20833
4	0.39 (70)	0.95	1.55	−1.59 (80) −1.79 (90)	1.98	18968	19685
5	0.33 (70)	1.01	1.53	−1.62 (80) −1.80 (90)	1.95	18726	19569
6	0.62 (90)	0.97	1.75	−1.49 (70) −1.68 (80)	2.11	20017	20920

[a] Condition: solvent acetonitrile; supporting electrolyte, TEAP; reference electrode, SCE; solute concentration, $\sim 10^{-3}$ M; working electrode, platinum wire.

[b] $n = Q/Q'$, where Q' is the calculated coulomb count for 1 e^- transfer and Q is the coulomb count found after exhaustive electrolysis of $\sim 10^{-2}$ M solution of the complex.

[c] E_{pa} values are considered due to the irreversible nature of the voltammograms.

[d] Calculated by using eqn (8) of text.

[e] Calculated by using eqn (7) of text.

[f] In acetonitrile solution.

Search for ruthenium(IV)–ruthenium(III) couple. The complexes exhibit a second irreversible oxidation process in the range 1.5–1.9 V vs SCE (Fig. 3). Although the current height of this irreversible process is ~1.5 times more than the previous one-electron process ($Ru^{III} \rightleftharpoons Ru^{II}$), the one-electron nature of this second oxidation process has been established with the help of the differential pulse voltammetry (Fig. 3). This second oxidation process could be due to either $Ru^{III} \rightarrow Ru^{IV}$ oxidation or oxidation of the coordinated ligand L. The potential difference between the two successive processes, in the range ~1.1–1.2 V, is comparable well with the reported observed potential difference between the two successive redox processes for the ruthenium center ($Ru^{II/III}$–$Ru^{III/IV}$) in mononuclear systems [17,10,16]. Since the free ligands (HL) do not show any redox activity within the specified potential range (±2 V), therefore it may be reasonable to consider the second irreversible oxidative process as ruthenium(III) → ruthenium(IV) oxidation.

Ligand reductions. The complexes display two successive reductions in the ranges −1.40 → −1.62 V and −1.57 → −1.85 V (Table 3, Fig. 3). The one-electron nature of these couples has been established by current height consideration. The observed two reductions are assigned to be due to the reductions of the coordinated bipyridine ligands. 2,2′-bipyridine is a well known potential electron-transfer center and each bipyridine can accept two electrons in one electrochemically accessible LUMO [18]. Since the complexes (**1**–**6**) have two bipyridine units, four one-electron reductions are therefore expected. However, in practice we have observed two reductions corresponding to eqns (5) and (6) within the ±2 V potential range.

$$[Ru^{II}(bpy)_2(L)]^+ + e^- \rightleftharpoons [Ru^{II}(bpy)(b\bar{p}y)(L)] \quad (5)$$

$$[Ru(bpy)(b\bar{p}y)(L)] + e^- \rightleftharpoons [Ru(b\bar{p}y)(b\bar{p}y)(L)]^- \quad (6)$$

The other expected two reductions could not be seen possibly due to solvent cut-off.

Spectroelectrochemical correlation. The lowest energy metal to ligand charge-transfer (MLCT) bands of the complexes (**1**–**6**) are observed in the range 510–475 nm (Table 1). The reduction potentials of the reversible ruthenium(III)–ruthenium(II) couple for the complexes and the first ligand reduction (reduction of the diimine fragment) have been detected in the ranges 0.33 → 0.70 V and −1.40 → −1.62 V vs SCE respectively. The lowest energy MLCT transition involves excitation of the electron from the filled t_{2g}^6 orbital of ruthenium(II) to the lowest π^* orbital of the bipyridine ligand (dominated by the diimine, —N=C—C=N— fragment). Now the associated energy of the MLCT band for each complex can be predicted from the experimentally observed electrochemical data by considering the following eqns (7) and (8) [19].

$$\nu_{MLCT} = 8065(\Delta E^0) + 3000 \quad (7)$$

$$\Delta E^0 = E^0_{298}(Ru^{III}/Ru^{II}) - E^0_{298}(L) \quad (8)$$

Here, E^0_{298} (Ru^{III}/Ru^{II}) and E^0_{298} (L) are the formal potentials (in V) of the ruthenium(III)–ruthenium(II) couple and the first ligand reduction respectively. The ν_{MLCT} is the frequency of the lowest energy MLCT transition (in cm^{-1}). The factor 8065 in eqn (7) is used to convert potential difference, ΔE from volt to cm^{-1} and the term 3000 cm^{-1} is of empirical origin. The calculated and experimentally observed ν_{MLCT} transition frequencies for the complexes are depicted in Table 3 and there is a linear relationship between the ν_{MLCT} and ΔE (Fig. 4). Here, the calculated values for all the complexes lie within the 900 cm^{-1} of the experimentally observed MLCT energies which are in very good agreement with the previously observed correlation in the other mixed ligand ruthenium bipyridine and other related systems [20].

Electrogeneration of trivalent ruthenium congener and distortion parameters. Chemical oxidation of the complexes (**1**–**6**) in acetonitrile solvent by aqueous cerric ammonium sulfate or cerrium(IV) in 0.1 M aqueous $HClO_4$ resulted initially in a green solution corresponding to the trivalent congener of the complexes and which then eventually decomposed to an unidentified product even at 273 K.

In order to trap the trivalent analogues of (**1**–**6**) we have tried to oxidize the complexes by a constant potential coulometric technique. Coulometric oxidations of the complexes at a potential 200 mV positive to the corresponding E_{pa} of Ru^{II}/Ru^{III} couple in acetonitrile solution at 273 K produced a green solution in all cases. The observed coulomb count corresponds to 1 e^- transfer for all the complexes (Table 3). The coulometrically oxidized species ($\mathbf{1}^+$–$\mathbf{6}^+$) are not stable enough to be isolated in pure solid state and this has precluded its further characterization.

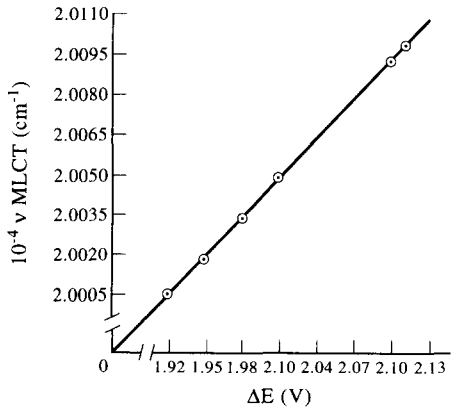

Fig. 4. Least squares plot of the lowest energy metal-to-ligand charge-transfer band (ν_{MLCT}, cm^{-1}) vs the difference in potential (ΔE, (V)) between the $Ru^{II/III}$ couple and the first bipyridine reduction.

However, in the case of complex 5^+ the situation is better to some extent which has allowed us to record the EPR and electronic spectrum of the oxidized species (5^+). X-band EPR spectrum of 5^+ is recorded by quickly freezing the green solution (liquid N_2). The rhombic nature of the spectrum (Fig. 5) at 77 K ($g_1 = 2.389$, $g_2 = 2.081$ and $g_3 = 1.810$) is characteristic of trivalent ruthenium(III) in a distorted octahedral environment (low-spin Ru^{III}, t_{2g}^5, $S = 1/2$) [21]. In the UV-visible region electronic spectrum of the oxidized complex, 5^+ shows one broad ligand to metal charge transfer (LMCT) band at 774 nm [11] and ligand based transitions in the UV region (Fig. 6).

The theory of EPR spectra of distorted octahedral low-spin d^5 (idealized t_{2g}^5, ground term $^2T_{2g}$) complexes are documented in literature [22,10,16,17,21]. The distortion of pseudo-octahedral complexes is expressed as the sum of axial (Δ) and rhombic (V) components. The t_2 orbital consists of the components $t_2(xy)$, $t_2^+(xz)$ and $t_2^-(yz)$. The degeneracy of t_2 orbital is partially removed by axial distortion (Δ), which placed t_2^0 (b) above t_2^+/t_2^- (e). The superimposed rhombic distortion (V) then further splits (e) into t_2^+ and t_2^-.

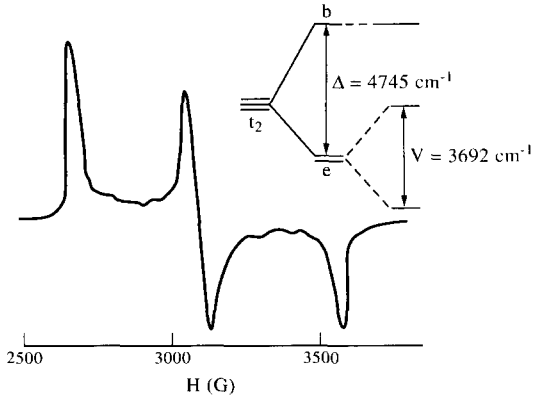

Fig. 5. X-band EPR spectrum and t_2 splittings of the coulometrically oxidized complex $[Ru^{III}(bpy)_2L^5]^{2+}$, 5^+ in acetonitrile solution at 77 K.

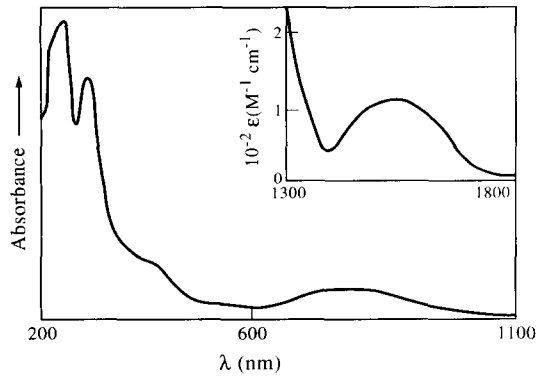

Fig. 6. Electronic spectrum of the coloumetrically oxidized complex $[Ru^{III}(bpy)_2L^5]^{2+}$, 5^+ in acetonitrile. The inset shows the electronic spectrum of 5^+ in the range 1300–1800 nm.

The distortion parameter (Δ and V) and the energies of two optical transitions (ν_1 and ν_2) from ground to upper Kramers doublets can be obtained from the analysis of EPR spectrum using the g tensor theory of low-spin d^5 ions.

The EPR spectrum provides only the absolute g values and so neither their signs nor the correspondence of g_1, g_2 and g_3 to g_x, g_y and g_z are known. There are forty-eight possible combinations based on the labelling (x, y, z) and signs chosen for the experimentally observed g values. For the present case we have chosen the combination $-g_1 > -g_2 > g_3$ as this particular set gives the reasonable value of orbital reduction factor, ($k < 1.0$). The value of k for all other combinations of g parameters does not fall within the limit ($k < 1.0$) and hence is rejected. The computed values of orbital reduction factor (k), axial distortion (Δ), rhombic distortion (V) and the two optical transitions (ν_1 and ν_2) for the complex, 5^+ are 0.606 cm^{-1}, 4745 cm^{-1}, 3692 cm^{-1}, 3071 cm^{-1} and 6819 cm^{-1} respectively. The spin-orbit coupling constant (λ) of the ruthenium(III) is taken as 1000 cm^{-1} [22].

The computed ν_2 band has been observed experimentally by near IR spectrum in the expected position, 6578 cm^{-1} (ε, M^{-1} cm^{-1}, 110) (Fig. 6). In view of the involved approximation in the theory, the agreement between the experimentally observed ν_2 and the calculated ν_2 band value is excellent [23]. Due to instrumental limitation (maximum wavelength scan up to 2200 nm) it has not been possible to compare the ν_1 band. Here axial distortion (Δ) is ~ 1.3 times more than the rhombic (V) distortion.

CONCLUSIONS

We have thus observed the effect of the presence of phenolic Schiff base ligands having CH_2 or NH spacer (**A** or **B**) as a third ligand in the $[Ru(bpy)_2]$ core with respect to redox and photophysical aspects. The presence of both the classes of ligands (**A** and **B**) in the complexes (**1**–**6**) facilitate the successive ruthenium(II) $\rightleftharpoons$ ruthenium(III) and ruthenium(III) $\rightarrow$ ruthenium(IV) oxidations and make the complex environment susceptible to undergo room temperature emission from the lowest energy metal-to-ligand-charge-transfer (MLCT) band. In general, the complexes (**4**–**6**) having the third ligand with NH spacer (Class **B**), are more effective than the ligands with CH_2 spacer (Class **A**) from the emission point of view and in particular ketone based third ligands (L^2 and L^5) in both the classes (**A** and **B**) are more suitable with respect to emission efficiency. In addition, correlations between the energies of the lowest MLCT absorption bands and the electrochemical redox potentials of the complexes follow an excellent linear

relationship in accordance with the other $Ru(bpy)_2L$ systems.

EXPERIMENTAL

Materials

Commercial ruthenium trichloride (S.D. Fine Chemicals, Bombay, India) was converted to $RuCl_3 \cdot 3H_2O$ by repeated evaporation to dryness with concentrated hydrochloric acid. The *cis*-$[Ru(bpy)_2CO_3]$ was prepared according to the reported procedure [24]. 2-hydroxy-5-nitrobenzaldehyde, benzylamine and 2-hydroxyacetophenone were obtained from Aldrich, U.S.A. Other chemicals and solvents were reagent grade and used as received. Silica gel (60–120 mesh) used for chromatography was purchased from S.D. Fine Chemicals, Bombay, India. For spectroscopic and electrochemical studies HPLC grade solvents were used. Commercial tetraethylammonium bromide was converted to pure tetraethyl ammonium perchlorate (TEAP) by following an available procedure [25].

Physical measurements

Solution electrical conductivity was checked using a Systronic conductivity bridge, 305. Electronic spectra (700–200 nm) were recorded using a Shimadzu UV 265 spectrophotometer. Near IR spectrum was recorded by using a Hitachi 330 spectrophotometer. Infrared (4000–400 cm^{-1}) spectra were taken on a Nicolet spectrophotometer with samples prepared as KBr pellets. Magnetic susceptibility was checked with a PAR vibrating sample magnetometer. ^1H NMR spectra were obtained with the use of a 300 MHz Varian FT-NMR spectrometer. Cyclic voltammetric measurements were carried out using a PAR model 362 scanning potentiostat electrochemistry system. A platinum wire working electrode, a platinum wire auxiliary electrode, and an aqueous saturated calomel reference electrode (SCE) were used in a three-electrode configuration. TEAP was the supporting electrolyte and the solute concentration was $\sim 10^{-3}$ M. The half wave potential E^0_{298} was set equal to 0.5 $(E_{pa} + E_{pc})$, where E_{pa} and E_{pc} are anodic and cathodic cyclic voltammetric peak potentials respectively. The scan rate used was 50 mV s^{-1}. The coulometric experiments were done with a PAR model 370-4 electrochemistry apparatus incorporating a 179, digital coulometer. A platinum wire gauze working electrode was used in coulometric experiments. All experiments were carried out under dinitrogen atmosphere and are uncorrected for junction potentials. EPR measurement was made with a Varian model 109 E-line X-band spectrometer fitted with a quartz dewar for measurements at 77 K (liquid nitrogen). The spectrum was calibrated by using tetracyanoethylene (TCNE) ($g = 2.0037$). The elemental analyses were carried out with a Carlo Erba (Italy) elemental analyzer. Solution emission properties were checked using a SPEX-fluorolog spectrofluorometer.

CAUTION! Perchlorate salts of metal complexes are generally explosive. Care should be taken while handling such complexes.

Treatment of EPR data

An outline of the procedure can be found in our recent publications [16].

Synthesis of ligands and complexes

The ligands HL^1–HL^3 and HL^4–HL^6 were prepared by condensing benzylamine and phenylhydrazine respectively with appropriate 2-hydroxyaldehydes and ketone at 273 K in methanol solvent.

The complexes (**1–6**) were achieved using general methods. Yields varied in the range 70–75%. Specific details are given for one representative case.

Bis(2,2′-bipyridine)(N-benzyl salicylideneimine) ruthenium(II) perchlorate $[Ru(bpy)_2L^1]ClO_4$ (**1**). $Ru(bpy)_2CO_3$ (200 mg, 0.42 mmol) was dissolved in 20 cm^3 of methanol and heated to reflux for 10 min. To this solution the ligand HL^1 (173 mg, 0.84 mmol) was added. The resulting mixture was heated to reflux over a period of 5 h. The initial violet solution gradually turned to a red color. The progress of the reaction was monitored periodically by TLC. The volume of the solvent was then reduced under reduced pressure and the concentrated solution was treated with an excess of saturated aqueous sodium perchlorate solution. The dark red colored precipitate thus obtained was collected by filtration and washed thoroughly with cold methanol and a little ice-cold water. The solid mass was then dried *in vacuo* over P_4O_{10}.

The crude product was then purified by column chromatography on a silica gel (60–120 mesh) column. Unreacted excess ligand was eluted first with benzene and was rejected. The pure complex was eluted with a 2:1 ratio of benzene and acetonitrile solvents. On removal of the solvent mixture under reduced pressure fine crystalline complex $[Ru(bpy)_2(L^1)]ClO_4$ was obtained. Yield: 75%.

Acknowledgements—Financial support received from the Department of Science and Technology, New Delhi, India is gratefully acknowledged. We are grateful to Professor A. Q. Contractor and Ms Sukeerthi, IIT Bombay for assistance with electrochemical measurements. Special acknowledgement is made to the Regional Sophisticated Instrumental Center, RSIC, IIT Bombay for providing NMR and EPR facilities.

REFERENCES

1. Coe, B. J., Friessen, D. A., Thompson, D. W. and Meyer, T. J., *Inorg. Chem.*, 1996, **35,** 4575;

Milkevitch, M., Brauns, E. and Brewer, K. J., *Inorg. Chem.*, 1996, **35,** 1737; Ward, M. D., *Inorg. Chem.*, 1996, **35,** 1712; Rasmussen, S. C., Thompson, D. W., Singh, V. and Petersen, J. D., *Inorg. Chem.*, 1996, **35,** 3449; Cargill Thompson, A. M. W., Jeffery, J. C., Liard, D. J. and Ward, M. D., *J. Chem. Soc., Dalton Trans.*, 1996, 879; Greaney, M. A., Coyle, C. L., Harmer, A. J. and Stiefel, E. I., *Inorg. Chem.*, 1989, **28,** 912; Kroner, R., Heeg, M. J. and Deutsch, E., *Inorg. Chem.*, 1988, **27,** 558; Thakur, G. A., Narayanaswamy, K. and Lahiri, G. K., *Indian J. Chem.*, 1996, **35A,** 379; Rao, P. S., Thakur, G. A. and Lahiri, G. K., *Indian J. Chem.*, 1996, **35A,** 946; Santra, B. K., Menon, M., Pal, C. K. and Lahiri, G. K., *J. Chem. Soc., Dalton Trans.*, 1997, 1387; Mukherjee, R. N. and Chakravorty, A., *J. Chem. Soc., Dalton Trans.*, 1983, 2197.

2. Sprintschnik, G., Sprintschnik, H. W., Kirsch, P. P. and Whitten, D. G. J., *J. Am. Chem. Soc.*, 1976, **98,** 2337.
3. Gilbert, J. A., Eggleston, D. S., Murphy, W. R. Jr., Gaselowitz, D. A., Gersten, S. W., Hodgson, D. J. and Meyer, T. J., *J. Am. Chem. Soc.*, 1985, **107,** 3855; Gersten, S. W., Samuels, G. J. and Meyer, T. J., *ibid.*, 1982, **104,** 4029; Gilbert, J. A., Geselowitz, D. and Meyer, T. J., *ibid.*, 1986, **108,** 1493; Honda, K. and Frank, A. J., *J. Chem. Soc., Chem. Commun.*, 1984, 1635.
4. Ellis, C. D., Gilbert, J. A., Murphy, W. R. Jr. and Meyer, T. J., *J. Am. Chem. Soc.*, 1983, **105,** 4842; Vining, W. and Meyer, T. J., *J. Electroanal. Chem. Interfacial Electrochem.*, 1985, **195,** 183.
5. Tanaka, K., Morimoto, M. and Tanaka, T., *Inorg. Chim. Acta*, 1981, **56,** L61.
6. Rillema, D. P., Dressick, W. J. and Meyer, T. J., *J. Chem. Soc., Chem. Commun.*, 1980, 247; Durham, B., Dressick, W. J. and Meyer, T. J., *ibid.*, 1979, 381; Dressick, W. J., Meyer, T. J., Durham, B. and Rillema, D. P., *Inorg. Chem.*, 1982, **21,** 345.
7. Gleria, M., Minto, F., Beggiato, G. and Bortolus, P. J., *J. Chem. Soc., Chem. Commun.*, 1978, 285; Durham, B., Caspar, J. V., Nagle, J. K. and Meyer, T. J., *J. Am. Chem. Soc.*, 1982, **104,** 4803.
8. Durham, B., Wilson, S. R., Hodgson, D. J. and Meyer, T. J., *J. Am. Chem. Soc.*, 1980, **102,** 600.
9. Sullivan, B. P., Salmon, D. J. and Meyer, T. J., *Inorg. Chem.*, 1978, **17,** 3334; Casper, J. V. and Meyer, T. J., *ibid.*, 1983, **22,** 2444.
10. Ghosh, P., Pramanik, A., Bag, N., Lahiri, G. K. and Chakravorty, A., *J. Organomet. Chem.*, 1993, **454,** 273.
11. Hariram, R., Santra, B. K. and Lahiri, G. K., *J. Organomet. Chem.*, 1997, **540,** 155.
12. Juris, A., Balzani, V., Barigelletti, F., Campagna, S., Belser, P. and Zelewsky, A. V., *Coord. Chem. Rev.*, 1988, **84,** 85.
13. Ceulemansm, A. and Vanquickenborne, L. G., *J. Am. Chem. Soc.*, 1981, **103,** 2238; Root, M. J. and Deutsch, E., *Inorg. Chem.*, 1985, **14,** 1464; Alsfasser, R. and Eldik, R. V., *Inorg. Chem.*, 1996, **35,** 628; Coe, B. J., Meyer, T. J. and White, P. C., *Inorg. Chem.*, 1995, **34,** 593.
14. Brown, G. M., Weaver, T. R., Keene, F. R. and Meyer, T. J., *Inorg. Chem.*, 1976, **15,** 190.
15. Godefroi, E. F. and Little, E. L., *J. Org. Chem.*, 1956, **21,** 1163; Chem, P., Duesing, R., Graff, D. K. and Meyer, T. J., *J. Phys. Chem.*, 1991, **95,** 5850.
16. Lahiri, G. K., Bhattacharya, S., Ghosh, B. K. and Chakravorty, A., *Inorg. Chem.*, 1987, **26,** 4324.
17. Santra, B. K. and Lahiri, G. K., *J. Chem. Soc., Dalton Trans.*, 1997, 129; Bag, N., Lahiri, G. K., Bhattacharya, S., Falvello, L. R. and Chakravorty, A., *Inorg. Chem.*, 1988, **27,** 4396; Lahiri, G. K., Bhattacharya, S., Mukherjee, M., Mukherjee, A. K. and Chakravorty, A., *Inorg. Chem.*, 1987, **26,** 3359.
18. Bhattacharya, S., *Polyhedron*, 1993, **12,** 235; Elliott, C. M., *J. Chem. Soc., Chem. Commun.*, 1980, 261; Tokel-Takvoryan, N. E., Hemingway, R. E. and Bard, A. J., *J. Am. Chem. Soc.*, 1973, **95,** 6583; Morris, D. E., Hanck, K. W. and DeArmond, M. K., *Inorg. Chem.*, 1985, **24,** 977.
19. Goswami, S., Mukherjee, R. N. and Chakravorty, A., *Inorg. Chem.*, 1983, **22,** 2825; Ghosh, B. K. and Chakravorty, A., *Coord. Chem. Rev.*, 1989, **95,** 239.
20. Sullivan, B. P., Caspar, J. V., Johnson, S. R. and Meyer, T. J., *Organometallics*, 1984, **3,** 1241; Dodsworth, E. S. and Lever, A. B. P., *Chem. Phys. Lett.*, 1986, **124,** 152; Greaney, M. A., Coyle, C. L., Harmer, M. A., Jordan, A. and Stiefel, E. I., *Inorg. Chem.*, 1989, **28,** 912.
21. Chattopadhyay, S., Bag, N., Basu, P., Lahiri, G. K. and Chakravorty, A., *J. Chem. Soc., Dalton Trans.*, 1990, 3389; Pramanik, A., Bag, N., Lahiri, G. K. and Chakravorty, A., *J. Chem. Soc., Dalton Trans.*, 1990, 3823.
22. Hill, N. J., *J. Chem. Soc., Faraday Trans.*, 1972, **2,** 427; Bleaney, B. and O'Brien, M. C. M., *Proc. Phys. Soc. London, B*, 1956, **69,** 1216; Griffith, J. S., *The Theory of Transition Metal Ions*, Cambridge University Press, London, 1972, p. 364; Daul, C. and Goursot, A., *Inorg. Chem.*, 1985, **24,** 3554; Mahapatra, A. K., Datta, S., Goswami, S., Mukherjee, M., Mukherjee, A. K. and Chakravorty, A., *Inorg. Chem.*, 1986, **25,** 1715.
23. Pramanik, A., Bag, N. and Chakravorty, A., *Inorg. Chem.*, 1993, **32,** 811.
24. Johnson, E. C., Sullivan, B. P., Salmon, D. J., Adeyemi, S. A. and Meyer, T. J., *Inorg. Chem.*, 1978, **17,** 2211.
25. Sawyer, D. T., Sobkowiak, A. and Roberts, J. L., Jr, *Electrochemistry for Chemists*, 2nd ed., Wiley, New York, 1995.

Pergamon

PII: S0277-5387(97)00276-3

Polyhedron Vol. 17, No. 8, pp. 1397–1405, 1998
© 1998 Elsevier Science Ltd
All rights reserved. Printed in Great Britain
0277-5387/98 $19.00+0.00

Synthesis and characterisation of copper(II) complexes derived from methylene bridged bis(tridentate) ligands

P. Kamatchi and M. Kandaswamy*

Department of Inorganic Chemistry, School of Chemistry, University of Madras, Madras-25, India

(Received 23 April 1997; accepted 19 June 1997)

Abstract—New methylene bridged bis(tridentate) binucleating ligands, bis[2-hydroxy-5-chloro{(4-methyl-piperazin-1-yl)methyl} phenyl]methane (L^1H_2), bis[2-hydroxy-3-{(1-imino-*N*,*N*-dimethyl aminopropyl)ethyl}-5-chlorophenyl]methane (L^2H_2) and bis[2-hydroxy-3-{(1-imino-*N*,*N*-diethylaminopropyl)ethyl}-5-chloro-phenyl] methane (L^3H_2) and their copper(II) complexes have been synthesised and reported. These complexes have been characterised by elemental analysis, electronic and ESR spectroscopy. The binuclearity of these complexes were confirmed by FAB mass spectroscopy. Electrochemical studies of the complexes suggested that the reduction processes are quasi-reversible single step two electron transfer $Cu^{II}Cu^{II}/Cu^{I}Cu^{I}$ at negative potentials (−0.2 to −0.6 V). The magnetic moment μ_{eff} (per Cu) for these complexes at 298 K are found in the range 1.71 to 1.83 B.M. Variable temperature magnetic susceptibility measurements revealed the absence of exchange coupling between Cu^{II} centres. ESR spectra of these complexes at liquid nitrogen temperature (77 K) are similar to mononuclear copper(II) complex with nuclear spin 3/2. © 1998 Elsevier Science Ltd. All rights reserved

Keywords: binucleating ligands; bistridentate ligands; copper(II) complexes; hexadentate ligands; binuclear copper(II) complexes; electrochemical studies.

The synthesis of multidentate ligands have attracted considerable attention in recent years [1–7]. This interest has arisen because such ligands can accommodate two metal centres and thus may provide the basis of models for the active sites of biological systems [8–10], and serve as multi-metal-centred catalysts [7d,11]. The development of multidentate ligands [12–15] through various approaches has led to the successful synthesis of homo and heterobinuclear metal complexes [7c,d,16,17].

Several series of complexes utilise ligands that hold the metals in close fixed arrangements, as in the case of molecular A-frames [18], cofacial diporphyrins [19], side-by-side macrocycles [20], and macrocyclic inclusion complexes [14,21]. A different series of complexes utilise more flexible ligands, which provide a less restricted environment for a second metal centre relative to the first metal. Examples for this series of complexes include wishbone complexes [22], earmuff complexes [23] and other similar complexes [24]. The ligands containing two remote multidentate donor sets separated by rigid [22a] or flexible [2,4,25] bridges form binuclear complexes. In these complexes metal ions are held at a sufficiently long distance such that the two sets of donor groups could not coordinate to the same metal ion. Earlier reports on binuclear Cu^{II} complexes of remote donor set ligands linked *via* phenyl, biphenyl [26,27] and pyrazine [6,7a] groups show a considerable amount of antiferromagnetic interaction between the two Cu^{II} centres.

In this paper we report the syntheses of bis(tridentate) binucleating ligands by introducing sp^3 carbon (—CH_2— group) between the 1,1′sp^2 carbons of the phenyl rings containing the tridentate moieties. The binuclear copper(II) complexes using these ligands were synthesised and characterised. The elec-

* Author to whom correspondence should be addressed.

tro-chemical and magnetic properties of these complexes were investigated.

EXPERIMENTAL

Physical measurements

Elemental analyses were carried out with a Heraeus-CHN-Rapid Analyser, ^{1}H NMR spectra were recorded using a 90 MHz spectrometer (model EM 390) and IR spectra were recorded on a Shimadzu IR-408 spectrometer using KBr discs. Electronic spectra were recorded on a Hitachi-320 spectrophotometer. The FAB mass spectra were recorded on a Jeol SX 102/DA-6000 mass spectrometer. The X-ray diffraction study of the ligand L^1H_2 was carried out on an Enraf-Nonius CAD-4 diffractometer using graphite-monochromatised Cu-K_α radiation in the range $0 < 2\theta < 140$. Variable temperature (77–298 K) magnetic susceptibility measurements were performed on the Princeton Applied Research Model-155 vibrating sample magnetometer operating at 5000 gauss and calibrated with metallic nickel supplied with the instrument. ESR measurements were carried out using a Bruker ER-200D-SRC spectrometer. Electrochemical measurements were carried out using an apparatus comprising of a PAR model-175 universal programmer, model-173 potentiostat/galvanostat, Model-176 current follower and Model-179 coulomb/ampere hour meter (EG & G Ltd.) and Hitachi (057) Perkin-Elmer X–Y recorder. Platinum foil was used both as working and counter electrodes and Ag/AgCl as the reference electrode. TBAP was used as the supporting electrolyte (0.1 M) and all the solutions were around 10^{-3} M concentration.

Materials

Methanol (AR) and DMF (HPLC grade) were obtained from SD Fine Chemicals. Tetrabutylammonium perchlorate was obtained from Fluka and was recrystallised from methanol. 2,2′-dihydroxy-5,5′-dichlorodiphenylmethane was synthesised by the literature method [25]. All other chemicals and solvents were of reagent grade and were used as received. Distilled ethanol was used for the syntheses.

1. *Synthesis of bis*[2-*hydroxy*-5-*chloro*{(4-*methylpiperazin*-1-*yl*)*methyl*}*phenyl*]*methane* (L^1H_2). The ligand, L^1H_2, was synthesised by mixing 2,2′-dihydroxy-5,5′-dichlorodiphenylmethane (6.725 g, 0.025 mol) and *N*-methyl piperazine (5.75 g, 0.057 mol) in 75 cm^3 ethanol. Formaldehyde (35%, 6.25 ml, 0.066 mol) was added slowly with stirring (Scheme 1). The mixture was then heated to reflux on a water bath for 24 h with 1 cm^3 addition of formaldehyde at each 8 h interval. Finally, ethanol was removed *in vacuo* and the resulting oil was washed with saturated aqueous sodium carbonate solution, extracted with diethyl

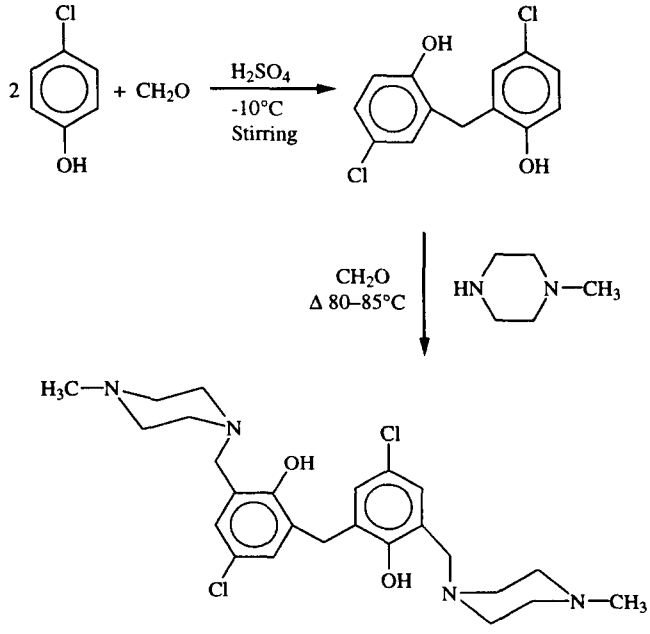

L^1H_2 Bis [2-hydroxy-5-chloro {(4-methylpiperazin-1-yl) methyl} phenyl] methane

Scheme 1.

ether and evaporated at room temperature. The white product obtained was recrystallised from hot methanol. Yield: 9 g (73%), m.p.: 162°C. (Found: C, 60.79; H, 6.92; N, 11.40. Calc. for $C_{25}H_{34}N_4O_2Cl_2$: C, 60.85; H, 6.90; N, 11.36%.) ^{1}H NMR spectrum ($CDCl_3$): δ 6.7–6.9 (d, 4H, aromatic CH), δ 3.9 (s, 2H, Ar—CH_2—Ar), δ 3.6 (s, 4H, benzylic CH_2), δ 2.5 (s, 16H, NCH_2) and δ 2.2 (s, 6H, NCH_3); IR spectrum (KBr disc): 3050 cm^{-1} (phenolic OH), 2850 cm^{-1} (NCH_2) and 1450 cm^{-1} (aromatic skeleton); mass spectrum: m/z 494 ($m+1$).

Synthesis of precursor compounds

2. *Synthesis of 2,2′-diacetoxy-5,5′-dichlorodiphenylmethane.* The compound 2,2′-dihydroxy-5,5′-dichlorodiphenylmethane (10 g) was dissolved in 100 cm^3 of acetic anhydride and a catalytic amount of conc. H_2SO_4 was added. The solution was refluxed in an oil bath for 1 h, poured into ice-cold water and extracted with diethyl ether. The ethereal phase was washed with sodium bicarbonate solution (5%, 200 cm^3) and distilled water (100 cm^3), treated with active charcoal and dried over anhydrous sodium sulphate. By evaporation of the filtrate to dryness a white solid was obtained. The crude was recrystallised from hot ethanol. Yield: 8.5 g (65%), m.p.: 100°C.

3. *Synthesis of 2,2′-dihydroxy-3,3′-diacetyl-5,5′-dichloro diphenylmethane* (P.C.−1). Anhydrous aluminium trichloride (15 g, 0.112 mol) was heated in an oil bath at 140°C for 5 min and the compound 2,2′-diacetoxy-5,5′-dichlorodiphenylmethane (5 g, 0.02 mol) was added with stirring. The temperature was allowed to rise to 170–180°C and maintained for 20 min. After cooling, the compound was added to 200 cm^3 of 2N HCl. The insoluble material was filtered, washed with water and dried. The crude product was recrystallised from hot ethanol to give pale green needle shaped crystals. Yield: 3.5 g (70%), m.p.: 203°C. ^{1}H NMR spectrum: δ 7.6–7.4 (d, 4H, aromatic CH), δ 4 (s, 2H, Ar—CH_2—Ar), δ 2.62 (s, 6H, acetyl CH_3). IR spectrum (KBr disc): 3150 cm^{-1} (phenolic OH), 1640 cm^{-1} (C=O), 1450 cm^{-1} (aromatic skeleton).

Synthesis of copper(II) complexes

Synthesis of complexes (**1a–1d**). *Synthesis of* $[Cu_2L^1(ClO_4)_2]\cdot 2H_2O$ (**1a**). The ligand L^1H_2 (1.64 g, 3.3 mmol) and lithium hydroxide (0.28 g, 6.6 mmol) was dissolved in ethanol. Two equivalents of $Cu(ClO_4)_2\cdot 6H_2O$ (2.5 g, 6.6 mmol) in ethanol was added to the above solution and refluxed. The solution was filtered when hot, allowed to cool to room temperature and left as such. After a few days the dark green colour product formed was filtered, washed with water, dried and recrystallised from ethanol. Yield: 2 g (70%).

The same procedure was adopted to prepare other complexes (**1b–1d**) by varying the copper(II) salts.

Synthesis of complexes (**2a–3d**). *Synthesis of* $[Cu_2L^2(ClO_4)_2]\cdot 2H_2O$ (**2a**). The mixture of 2,2′-dihydroxy-3,3′-diacetyl-5,5′-dichlorodiphenylmethane (0.624 g, 2 mmol) with 3-di-methylamino-1-propylamine (0.7 cm^3, 4 mmol) in ethanol was refluxed for 1 h to obtain a clear yellow-orange solution. Then two equivalents of copper perchlorate hexahydrate (1.55 g, 4.2 mmol) in ethanol was added and refluxed for 6 h and filtered. The green colour product was filtered and washed with chloroform to remove unreacted ketones. The solid was recrystallised from ethanol. Yield: 1 g (62%).

The above procedure was adopted to prepare other complexes (**2b–3d**) by varying the amine as well as copper(II) salts (Scheme 2).

RESULTS AND DISCUSSION

The ligand L^1H_2 is made by the Mannich reaction of one equivalent of 2,2′-dihydroxy-5,5′-dichlorodiphenylmethane, two equivalents of *N*-methylpiperazine in the presence of formaldehyde (35%) in ethanol medium. The ligand was characterised by elemental analysis, ^{1}H NMR, IR, mass spectroscopy and X-ray crystallographic methods. The orientation of two tridentate moieties bridged through the methylene group has been identified from the ORTEP diagram [28] of Fig. 1.

Copper(II) complexes

The syntheses of copper(II) complexes (**1a–1d**) were achieved by the reaction of one equivalent of ligand L^1H_2 and two equivalents of copper salts in ethanol medium. To synthesise the complexes (**2a–3d**), first the ligands L^2H_2 and L^3H_2 were prepared *in situ* by condensation of one equivalent 2,2′-dihydroxy-3,3′-diacetyl-5,5′-dichlorodiphenylmethane and two equivalents of 3-dialkylamino-1-propylamine in ethanol, followed by the addition of two equivalent of copper(II) salts in ethanol to the reaction mixture.

Elemental analysis of these compounds are consistent with the theoretical values (Table 1). These complexes were found to have the composition $[Cu_2L(X_2)]\cdot nH_2O$ where X = ClO_4, OAc, Cl, Br and L = binucleating ligands.

FAB mass spectra

The positive-ion FAB mass spectra of complexes **1b, 2a** and **3b** show peaks corresponding to dipositive binuclear core $[Cu_2L]^{2+}$. Peaks corresponding to various mass units are given in Table 2. The FAB mass spectrum of complex **2a** is given in Fig. 2.

Spectral and magnetic studies

The IR spectra of these complexes show that a broad band around 3300–3500 cm^{-1} can be attributed

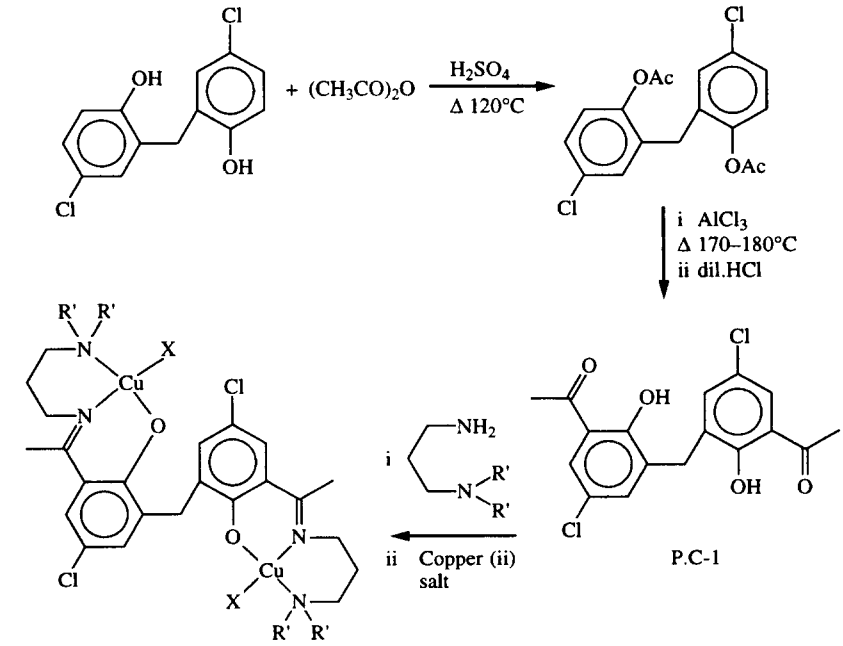

$[Cu_2L^2X_2]$; R', R' = CH_3

$[Cu_2L^3X_2]$; R', R' = C_2H_5

X = ClO_4, OAc, Cl, Br

P.C-1 2, 2'-dihydroxy-3, 3'-diacetyl-5, 5'-dichlorodiphenylmethane

Scheme 2.

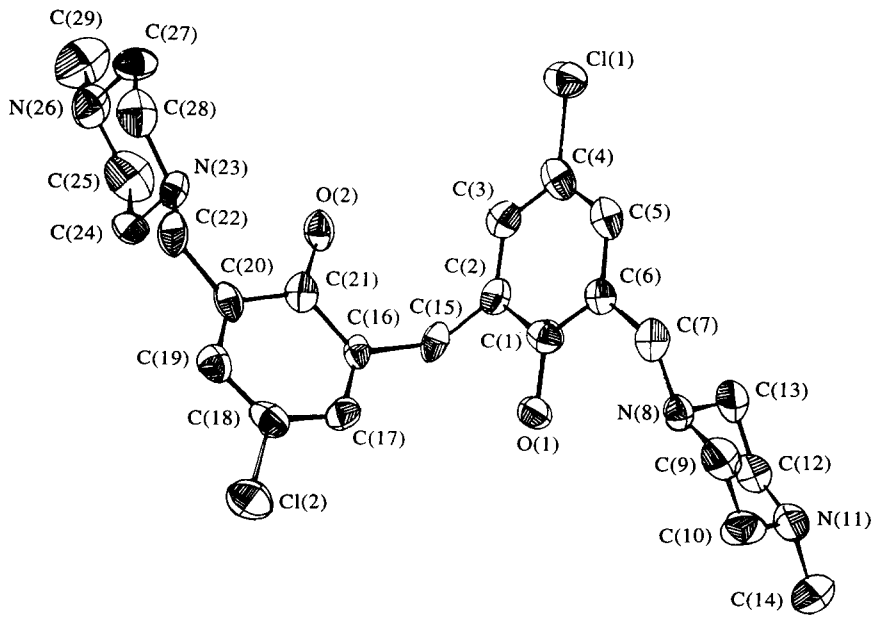

Fig. 1. ORTEP diagram of the ligand L^1H_2.

Table 1. Analytical data for the complexes

Name of the Complexes	Experimental (%) C	H	N	Cu	Theoretical (%) C	H	N	Cu
1a $[Cu_2L^1(ClO_4)_2]\cdot 2H_2O$	35.2	4.2	6.6	14.9	35.3	4.2	6.4	14.9
1b $[Cu_2L^1(OAc)_2]\cdot 2H_2O$	45.1	5.4	7.3	16.5	45.1	5.5	7.4	16.5
1c $[Cu_2L^1Cl_2]\cdot 2H_2O$	41.4	4.8	7.7	17.4	41.3	4.9	7.7	17.5
1d $[Cu_2L^1Br_2]\cdot 2H_2O$	36.9	4.4	6.8	15.6	36.8	4.4	6.8	15.6
2a $[Cu_2L^2(ClO_4)_2]\cdot 2H_2O$	36.6	4.2	6.1	14.3	36.7	4.5	6.3	14.4
2b $[Cu_2L^2(OAc)_2]\cdot 2H_2O$	40.3	5.2	7.0	15.9	40.5	5.0	7.0	15.8
2c $[Cu_2L^2Cl_2]\cdot 2H_2O$	43.0	5.4	7.5	16.7	43.0	5.3	7.4	16.8
2d $[Cu_2L^2Br_2]\cdot 2H_2O$	38.4	4.6	6.4	15.2	38.4	4.7	6.6	15.0
3a $[CuL^3(ClO_4)_2]\cdot 2H_2O$	39.7	5.1	5.9	13.5	39.7	5.1	5.9	13.5
3b $[Cu_2L^3(OAc)_2]\cdot 2H_2O$	43.2	5.7	6.5	14.8	43.4	5.6	6.5	14.8
3c $[Cu_2L^3Cl_2]\cdot 2H_2O$	45.9	5.9	6.9	15.7	45.9	5.9	6.9	15.7
3d $[Cu_2L^3Br_2]\cdot 2H_2O$	41.4	5.3	6.2	14.2	41.4	5.3	6.2	14.1

Table 2. Positive-ion FAB mass spectra of the binuclear complexes

Name of the complexes	[Fragment]	*m/z* (% intensity)[a]
1b	$[Cu_2L^1(H_2O)_2]^{2+}$	655 (75)
	$[Cu_2L^1(H_2O)]^{2+}$	636 (70)
	L^1	493 (25)
2a	$[Cu_2L^2(H_2O)_2(ClO_4)]^+$	781 (60)
	$[Cu_2L^2(H_2O)_2]^{2+}$	679 (30)
	$[CuL^2]$	580 (10)
	L^2	518 (75)
3b	$[Cu_2L^3(OAc)]^+$	761 (35)
	$[Cu_2L^3]^{2+}$	701 (30)
	$[CuL^3]$	639 (50)
	L^3	577 (15)

[a] Relative to base peak.

to the coordinated water molecules present in the complexes. The formation of the Schiff base is confirmed [29,30] from the band around 1580–1600 cm^{-1} corresponding to the C=N stretching vibration and is lower than the vibrational frequency of the C=O group of the precursor compound for which the stretching vibration is observed at 1640 cm^{-1}. The IR spectra of perchlorato complexes show splitting of ν_3 mode at 1100 cm^{-1} corresponding to weakly coordinated ClO_4^- anion in the solid state [31,32]. For acetato complexes the stretching vibration observed around 1615–1620 cm^{-1} is due to the acetate anion [33]. The band observed around 1520–1540 cm^{-1} for all the complexes (**2a–3d**) has been assigned to (C⋯O) of phenol [34].

Electronic spectra of these complexes were recorded in DMF solvent. The UV-vis spectral data for the complexes are given in Table 3. The d–d transitions are observed for perchlorato complexes around 630–660 nm, acetato complexes around 640–660 nm, chloro complexes around 660–740 nm and bromo complexes around 660–750 nm. On comparing with perchlorato and acetato complexes the corresponding chloro or bromo complexes exhibit λ_{max} at lower energy regions. This may be due to the deviation of metal ions from their square-basal coordination plane upon halide ion coordination [35]. The high energy transition located around 350–460 nm are attributed to ligand-to-metal charge transfer transition. The other high energy transition observed in the range 260–290 nm is assigned to the intraligand transition [36].

The ESR spectrum of complex (**1b**) was recorded in frozen DMF solution at liquid nitrogen temperature (77 K) and is shown in Fig. 3. This ESR spectrum is similar to a mononuclear Cu^{II} complex [37,38] with nuclear spin 3/2 ($g_\perp = 2.03$, $A_\parallel = 175$ G (1 G = 1×10^{-4} T) and $g_\parallel = 2.2$); three of four expected hyperfine signals are seen, with the fourth being hidden under the $g_\perp$ line. The effective magnetic moments, μ_{eff} (per Cu), of these complexes were measured and found in the range 1.71–1.83 B.M. at 298 K. Variable temperature magnetic susceptibility measurements (77–298 K) show absence of exchange coupling between Cu^{II} centres. This is due to the discontinuity in the electron delocalisation of two phenyl rings by the sp^3 carbon of the methylene group [5,27].

Cyclic voltammetric studies

The electrochemical property of all the complexes (**1a–3d**) were studied by cyclic voltammetry. The electrochemical data such as cathodic peak potential (E_{pc}), anodic peak potential (E_{pa}), peak separation (ΔE_p) and redox potential $E_{1/2}$ are given in Table 4. Cyclic voltammogram of complexes **1b** and **3d** recorded in dmf are given in Fig. 4.

In the cathodic potential range 0 to −1.3 V all the

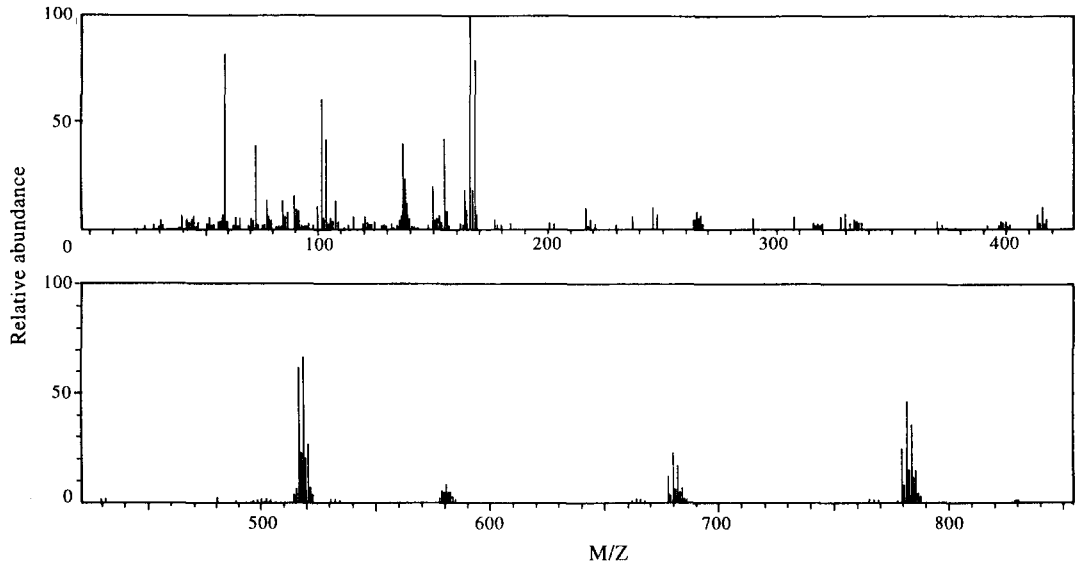

Fig. 2. Positive-ion FAB mass spectrum of complex $[Cu_2L^2(ClO_4)_2] \cdot 2H_2O$ (**2a**) in m-Nitrobenzyl alcohol at room temperature with accelerating voltage 10 kV.

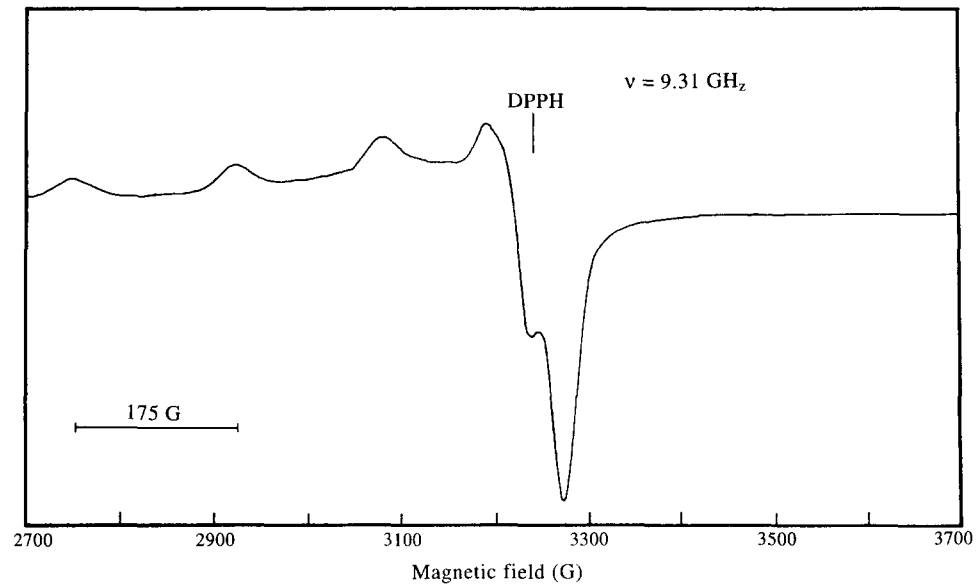

Fig. 3. ESR spectra of complex $[CuL^1(OAc)_2] \cdot 2HO$ (**1b**) determined in DMF at 77 K.

complexes exhibit two quasi-reversible charge transfer steps at different potentials. The quasi-reversible reduction of the complexes is evident from the following observations; $E_{1/2}$ values were independent of scan rate, ΔE_p values vary with the scan rate and these values were found to be more than 60 mV/sec and the ratio of cathodic and anodic currents were not equal. In all the complexes the well defined peaks, observed in the potential range -0.2 to -0.6 V were due to the reduction of $Cu^{II}Cu^{II}$ to $Cu^{I}Cu^{I}$. Coulometric experiments conducted at constant potentials (-0.62 V; slightly higher than the first reduction potential) indicate the consumption of two electrons per molecule. The second ill-defined waves observed in the potential range -0.7 to -1.2 V are due to the reduction of $Cu^{I}Cu^{I}$ to $Cu^{0}Cu^{0}$. This is evident from the deposition of reduced copper on the electrode surface. Based on the observations, it is reasonable to suggest that the reduction process may involve the following steps:

Table 3. Electronic spectral data for the complexes (in dmf)

Name of the complexes	λ_{max}(nm) (ε, $dm^3\ mol^{-1}\ cm^{-1}$) Charge transfer band	d–d band
1a	290 (13780), 438 (1510)	640 (260)
1b	290 (11435), 430 (900) sh	644 (200)
1c	290 (12410), 440 (1260)	740 (266)
1d	290 (12190), 444 (1315)	750 (350)
2a	280 (14800), 395 (5810), 440 (1300) sh	630 (213)
2b	280 (13540) sh, 420 (3230) sh, 460 (1200)	640 (274)
2c	280 (11200), 390 (4235), 460 (1220)	660 (140)
2d	290 (11610), 400 (4380), 460 (1300)	660 (140)
3a	270 (14935), 360 (5655), 440 (1440)	660 (350)
3b	270 (13860), 350 (5780), 460 (1570)	660 (340)
3c	270 (13820), 350 (7220), 460 (1490)	680 (280)
3d	270 (14200), 350 (6690), 460 (13300)	680 (295)

Table 4. Electrochemical data[a] for the complexes (in dmf)

Name of the complexes	E^1_{pc}	E^1_{pa}	$E^1_{1/2}(\Delta E_P)$	E^2_{pc}	E^2_{pa}	$E^2_{1/2}(\Delta E_P)$
1a	−0.27	−0.1	−0.17 (171)	−1.02	−0.71	−0.86 (313)
1b	−0.23	−0.13	−0.18 (103)	−0.89	−0.73	−0.81 (164)
1c	−0.58	−0.30	−0.44 (280)	−0.94	−0.81	−0.88 (128)
1d	−0.53	−0.22	−0.37 (310)	−0.77	−0.67	−0.72 (100)
2a	−0.26	−0.06	−0.16 (194)	−1.03	−0.83	−0.93 (204)
2b	−0.36	−0.17	−0.26 (190)	−1.13	−1.01	−1.09 (80)
2c	−0.44	−0.3	−0.37 (140)	−1.13	—	—
2d	−0.46	−0.25	−0.35 (210)	−1.08	−0.87	−0.97 (210)
3a	−0.29	−0.08	−0.18 (205)	−1.01	—	—
3b	−0.33	−0.09	−0.21 (239)	−1.15	−1.02	−1.087 (127)
3c	−0.50	−0.27	−0.39 (230)	−1.15	−1.09	−1.12 (60)
3d	−0.49	−0.25	−0.37 (236)	−0.74	−0.68	−0.71 (60)

[a] Potentials are given in V vs (Ag/AgCl); $\Delta E_P = E_{pc} - E_{pa}$ in mV.

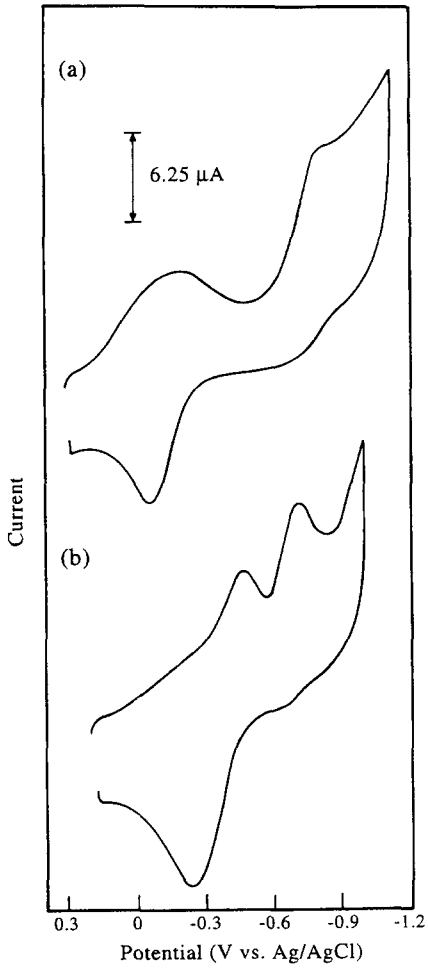

Fig. 4. Cyclic voltammogram of complexes in DMF at scan rate of 50 mV/sec. (a) $[Cu_2L^1(OAc)_2]\cdot 2H_2O$ (**1b**) and (b) $[Cu_2L^3Br_2]\cdot 2H_2O$ (**3d**).

$$Cu^{II}Cu^{II} \underset{E^1_{pa}}{\overset{E^1_{pc}}{\rightleftharpoons}} Cu^{I}Cu^{I} \underset{E^2_{pa}}{\overset{E^2_{pc}}{\rightleftharpoons}} Cu^{0}Cu^{0}$$

For perchlorato complexes the first reduction takes place in the potential range −0.26 to −0.29 V, acetato complexes in the range −0.23 to −0.36 V, chloro complexes in the range −0.44 to −0.58 V and bromo complexes in the range of −0.46 to −0.53 V. For perchlorato and acetato complexes the observed first reduction potentials are in the range −0.23 to −0.36 V and for chloro and bromo complexes −0.44 to −0.53 V. The higher reduction potential for chloro and bromo complexes are due to the change in the nature and number of coordinating atoms [38–40].

SUMMARY

Binucleating bis(tridentate) ligands and their copper(II) complexes were synthesised. These complexes were characterised by elemental analysis, IR, and UV-vis spectroscopy. ESR spectra of these complexes are similar to the mononuclear Cu^{II} complex with nuclear spin 3/2. The magnetic moment μ_{eff} (per Cu) of these complexes were measured and found in the range 1.71–1.83 B.M. at 298 K. In the potential range −0.2 to −0.6 V all these complexes undergo quasi-reversible two-electron single-step reductions ($Cu^{II}Cu^{II}/Cu^{I}Cu^{I}$) at the same potential.

Acknowledgement—We thank the University Grants Commission, New Delhi, Government of India, for the financial support to one of the authors, Mrs P.K.

REFERENCES

1. (a) Sessler, J. L., Sibert, J. W. and Lynch, V., *Inorg. Chem.*, 1990, **29,** 4143; (b) Sessler, J. L., Sibert, J. W., Lynch, V., Markert, J. T. and Wooten, C. L., *Inorg. Chem.*, 1993, **32,** 621; (c) Brudenell, S. J., Spiccia, L. and Tiekink, E. R. T., *Inorg. Chem.*, 1996, **35,** 1974.
2. Wieghardt, K., Tolksdorf, I. and Herrmann, W., *Inorg. Chem.*, 1985, **24,** 1230.
3. Lee, D. H., Murthy, N. N. and Karlin, K. D., *Inorg. Chem.*, 1996, **35,** 804.
4. Whitmore, B. C. and Eisenberg, R., *Inorg. Chem.*, 1983, **22,** 1.
5. Zacharias, P. S. and Ramachandraiah, A., *Polyhedron*, 1985, **4,** 1013.
6. Villa, J. F. and Hatfield, W. E., *J. Am. Chem. Soc.*, 1971, **93,** 4081.
7. (a) Inman, G. W., Jr. and Hatfield, W. E., *Inorg. Chem.*, 1972, **11,** 3085; (b) Lindoy, L. F., *The Chemistry of Macrocyclic Ligands.* Cambridge University Press, Cambridge, 1989; (c) Zanello, P., Tamburini, S., Vigato, P. A. and Mazzocchin, G. A., *Coord. Chem. Rev.*, 1987, **77,** 165; (d) Vigato, P. A., Tamburini, S. and Fenton, D. E., *Coord. Chem. Rev.*, 1990, **106,** 25.
8. Solomon, E. I., Baldwin, M. J. and Lowery, M. D., *Chem. Rev.*, 1992, **92,** 521.
9. Kitajima, N. and Moro-oka, Y., *Chem. Rev.*, 1994, **94,** 737.
10. *Copper Coordination Chemistry*; *Biological and Inorganic Perspectives*, ed. K. D. Karlin and J. Zubieta. Adenine Press, New York, 1983, pp. 1–22.
11. (a) Muetterties, E. L., *Bull. Chem. Chim. Belg.*, 1975, **84,** 959; (b) Zippel, F., Ahlers, F., Werner, R., Haase, W., Nolting, H. F. and Krebs, B., *Inorg. Chem.*, 1996, **35,** 3409; (c) Mahoney, W. S. and Stryker, J. M., *J. Am. Chem. Soc.*, 1989, **111,** 8818.
12. Casellato, U., Vigato, P. A., Fenton, D. E. and Vidali, M., *Chem. Soc. Rev.*, 1979, **8,** 199.
13. Collman, J. P., Elliott, C. M., Halberg, T. R. and Tovrog, B. S., *Proc. Natn. Acad. Sci. U.S.A.*, 1977, **74,** 8.
14. Alberts, A. H., Annunziata, R. and Lehn, J. M., *J. Am. Chem. Soc.*, 1977, **99,** 8502.
15. Nishida, Y., Takahashi, K., Kuramoto, H. and Kida, S., *Inorg. Chim. Acta*, 1981, **54,** L103.
16. (a) Carlisle, W. D., Fenton, D. E., Roberts, P. B., Casellato, U., Vigato, P. A. and Graziani, R.,

Transition Met. Chem., 1986, **11,** 292; (b) Ikawa, Y., Nagata, T. and Maruyama, K., *Chem. Lett.*, 1993, 1049.
17. (a) Aono, T., Wada, H., Aratake, Y., Matsumoto, N., Okawa, H. and Matstuda, Y., *J. Chem. Soc., Dalton Trans.*, 1996, 25; (b) Timken, M. D., Marrit, W. A., Hendrickson, D. N., Gagne, R. R. and Sinn, E., *Inorg. Chem.*, 1985, **24,** 4202.
18. (a) Kubiak, C. P. and Eisenberg, R., *J. Am. Chem. Soc.*, 1977, **99,** 6129; (b) Brown, M. P., Puddephatt, R. J., Rashidi, M., Manojlovic'-Muir, Lj., Muir, K. W., Solomun, T. and Seddon, K. R., *Inorg. Chim. Acta*, 1977, **23,** L33.
19. (a) Ogoshi, H., Sugimoto, H. and Yoshida, Z., *Tetrahedron Lett.*, 1977, 169; (b) Chang, C. K., *J. Chem. Soc., Chem. Commun.*, 1977, 800.
20. (a) Guerriero, P., Tamburini, S. and Vigato, P. A., *Coord. Chem. Rev.*, 1995, **139,** 17; (b) Pilkington, N. H. and Robson, R., *Aust. J. Chem.*, 1970, **23,** 2225.
21. Louis, R., Agnus, Y. and Weiss, R., *J. Am. Chem. Soc.*, 1978, **100,** 3604.
22. (a) Ng, C. Y., Motekaitis, R. J. and Martell, A. E., *Inorg. Chem.*, 1979, **18,** 2982; (b) Ng, C. Y., Martell, A. E. and Motekaitis, R. J., *J. Coord. Chem.*, 1979, **9,** 255.
23. Bulkowski, J. E., Burk, P. L., Ludmann, M. F. and Osborn, J. A., *J. Chem. Soc., Chem. Commun.*, 1977, 498.
24. Karlin, K. D., Dahlstrom, P. L., Cozzette, S. N., Scensny, P. M. and Zubieta, J., *J. Chem. Soc., Chem. Commun.*, 1981, 881.
25. Russo, U., Zarli, B., Zanonato, P. and Vidali, M., *Polyhedron*, 1991, **10,** 1353.
26. Hasty, E. F., Wilson, L. T. and Hendrickson, D. N., *Inorg. Chem.*, 1978, **17,** 1834.
27. Hasty, E. F., Colburn, T. J. and Hendrickson, D. N., *Inorg. Chem.*, 1973, **12,** 2414.
28. Velmurugan, D., Gunasekaran, K., Kamatchi, P. and Kandaswamy, M., accepted for publication in *Acta Crystallographica-C*, 1997.
29. Mandal, S. K. and Nag, K., *J. Chem. Soc., Dalton Trans.*, 1983, 2429.
30. Thompson, L. K., Mandal, S. K., Tandon, S. S., Bridson, J. N. and Park, M. K., *Inorg. Chem.*, 1996, **35,** 3117.
31. Drew, M. G. B., Nelson, J., Esho, F., McKee, V. and Nelson, S. M., *J. Chem. Soc., Dalton Trans.*, 1982, 1837.
32. Bautista, D. V., Dewan, J. C. and Thompson, L. K., *Can. J. Chem.*, 1982, **60,** 2583.
33. Thompson, L. K., Chacko, V. T., Elvidge, J. A., Lever, A. B. P. and Parish, R. V., *Can. J. Chem.*, 1969, **47,** 4141.
34. Mandal, S. K., Adhikary, B. and Nag, K., *J. Chem. Soc., Dalton Trans.*, 1986, 1175.
35. (a) Mandal, S. K., Thompson, L. K., Newlands, M. J., Biswas, A. K., Adhikary, B., Nag, K., Gabe, E. J. and Lee, F. L., *Can. J. Chem.*, 1989, **67,** 662; (b) Hoskins, B. F., McLeod, N. J. and Schaap, H. A., *Aust. J. Chem.*, 1976, **29,** 515.
36. (a) Okawa, H., Kakimoto, M., Izumitani, T., Nakamura, M. and Kida, S., *Bull. Chem. Soc. Japan*, 1983, **56,** 149; (b) Izumitani, T., Nakamura, M., Okawa, H. and Kida, S., *Bull. Chem. Soc. Japan*, 1982, **55,** 2122.
37. McLachlan, G. A., Fallon, G. D., Martin, R. L. and Spiccia, L., *Inorg. Chem.*, 1995, **34,** 254.
38. Fraser, C. and Bosnich, B., *Inorg. Chem.*, 1994, **33,** 338.
39. Karunakaran, S. and Kandaswamy, M., *J. Chem. Soc., Dalton Trans.*, 1994, 1595.
40. Karunakaran, S. and Kandaswamy, M., *J. Chem. Soc., Dalton Trans.*, 1995, 1851.

Pergamon

PII: S0277-5387(97)00423-3

Polyhedron Vol. 17, No. 9, pp. 1407–1413, 1998
© 1998 Elsevier Science Ltd
All rights reserved. Printed in Great Britain
0277-5387/98 $19.00+0.00

Seven-coordinate bromocarbonyl complexes of molybdenum(II) and tungsten(II) containing neutral sulfur donor ligands: crystal structure of $[WBr_2(CO)_3\{PhS(CH_2)_2SPh\text{-}S,S'\}]$

Paul K. Baker,*[a] Alec I. Clark,[a] Michael G. B. Drew,[c] Marcus C. Durrant,[b] and Raymond L. Richards[b]

[a] Department of Chemistry, University of Wales, Bangor, Gwynedd, LL57 2UW

[b] Nitrogen Fixation Laboratory, John Innes Centre, Norwich Research Park, Colney Lane, Norwich, NR4 7UH

[c] Department of Chemistry, University of Reading, Whiteknights, Reading, RG6 6AD

(Received 21 July 1997; accepted 17 October 1997)

Abstract—Treatment of $[MBr_2(CO)_3(NCMe)_2]$ (M = Mo or W) with a slight excess of $RS(CH_2)_2SR$ (R = Ph, C_6H_4F-4) in CH_2Cl_2 at room temperature gave the acetonitrile displaced products $[MBr_2(CO)_3\{RS(CH_2)_2SR\text{-}S,S'\}]$. The complex with M = W, R = Ph was crystallographically characterised and has a distorted capped octahedral geometry with one carbonyl group in the capping position, two carbonyls and one sulfur atom in the capped face, and one sulfur and two bromines in the uncapped face. Reaction of $[WBr_2(CO)_3(NCMe)_2]$ with two equivalents of $RS(CH_2)_2SR$ in CH_2Cl_2 at room temperature gives the cationic complexes $[WBr(CO)_3\{RS(CH_2)_2SR\text{-}S\}\{RS(CH_2)_2SR\text{-}S,S'\}]Br$. Similarly, treatment of $[WBr_2(CO)_3(NCMe)_2]$ with one and two equivalents of $Ph_2P(S)CH_2P(S)Ph_2$ in CH_2Cl_2 at room temperature afforded $[WBr_2(CO)_3\{Ph_2P(S)CH_2P(S)Ph_2\text{-}S,S'\}]$ and $[WBr(CO)_3\{Ph_2P(S)CH_2P(S)Ph_2\text{-}S\}\{Ph_2P(S)CH_2P(S)Ph_2\text{-}S,S'\}]Br$ respectively. Reaction of $[MBr_2(CO)_3(NCMe)_2]$ with one equivalent of $MeS(CH_2)_2S(CH_2)_2SMe$ in CH_2Cl_2 at room temperature gave $[MoBr_2(CO)_2\{MeS(CH_2)_2S(CH_2)_2SMe\text{-}S,S',S''\}]$ and $[WBr_2(CO)_3\{MeS(CH_2)_2S(CH_2)_2SMe\text{-}S,S'\}]$ respectively. Finally, reaction of equimolar quantities of $[MoBr_2(CO)_2(NCMe)_2]$ and ttob (ttob = 2,5,8-trithia[9]-*o*-benzenophane) gives the S_3 bonded complex $[MoBr_2(CO)_2(ttob\text{-}S,S',S'')]$. © 1998 Elsevier Science Ltd. All rights reserved

Keywords: seven-coordinate; molybdenum(II); thioether; tungsten(II); crystal structure; sulfur donor ligands.

Molybdenum and tungsten complexes containing sulfur donor ligands are important for a number of reasons, including, for example, the fact that the active site of the nitrogenase enzyme contains molybdenum with attached sulfur donor ligands [1–3]. A number of iodocarbonyl complexes containing neutral sulfur donor ligands have been described. Over the years we have reported the reactions of $[MI_2(CO)_3(NCMe)_2]$ with thioureas [4,5], thioacetamide [5,6], $SPPh_3$ [7], S_2CPCy_3 [8], $RS(CH_2)_2SR$ [9], $MeS(CH_2)_2S(CH_2)_2SMe$ [9], $Ph_2P(S)CH_2P(S)Ph_2$ [10], trithiamacrocyclic ligands [11] and tetrathiamacrocyclic ligands [12]. However, apart from the 2,5-dithiahexane complexes $[MX_2(CO)_3(2,5\text{-dithiahexane})]$ (M = Mo or W; X = Br or I) reported by Mannerskantz and Wilkinson [13] in 1962 and our crystallographically characterised complex $[MoBr(CO)_2\{Me_8[16]aneS_4\text{-}S,S',S'',S'''\}][MoBr_3(CO)_4]$ [12,14] very few bromocarbonyl seven-coordinate complexes of molybdenum(II) and tungsten(II) containing neutral sulfur donor ligands have been described.

In our initial report of the synthesis of the highly versatile seven-coordinate complexes $[MX_2(CO)_3(NCMe)_2]$ (M = Mo or W; X = Br or I) in 1986 [15] it was suggested that the dibromo complexes were considerably less stable than their diiodo counter-

* Author to whom correspondence should be addressed.

parts. However, more recently in 1994 [16] we have described an improved synthesis of the dibromotricarbonyl complexes $[MBr_2(CO)_3(NCMe)_2]$, by reacting *fac*-$[M(CO)_3(NCMe)_3]$ (prepared *in situ* [17]) with an equimolar amount of Br_2 at $-78°C$. In this paper, we describe the reactions of the dibromo complexes $[MBr_2(CO)_3(NCMe)_2]$ (M = Mo or W) with the neutral sulfur donor ligands, $RS(CH_2)_2SR$ (R = Ph or $C_6H_4CF_3$-4), $Ph_2P(S)CH_2P(S)Ph_2$, $MeS(CH_2)_2S(CH_2)_2SMe$ and ttob (ttob = 2,5,8-trithia[9]-*o*-benzenophane). The X-ray crystal structure of $[WBr_2(CO)_3\{PhS(CH_2)_2SPh\text{-}S,S'\}]$ is also discussed.

EXPERIMENTAL

All reactions described in this paper were carried out using standard Schlenk line techniques. The starting materials $[MBr_2(CO)_3(NCMe)_2]$ (M = Mo or W) [15,16], $RS(CH_2)_2SR$ (R = Ph or $C_6H_4CF_3$-4) [18], $Ph_2P(S)CH_2P(S)Ph_2$ [19], $MeS(CH_2)_2S(CH_2)_2SMe$ [9] and ttob [20] were prepared by published methods. All chemicals used were purchased from commercial sources, and CH_2Cl_2 was dried over phosphorus pentoxide and distilled before use.

Elemental analyses (C, H and S) were obtained using a Carlo Erba Elemental Analyser MOD 1108 (using helium as a carrier gas). IR spectra were recorded on a Perkin–Elmer 1600 FT IR spectrophotometer. The ^1H NMR spectra were recorded on a Bruker AC 250 MHz NMR spectrometer at the University of Wales, Bangor, and referenced to $SiMe_4$.

$[WBr_2(CO)_3\{PhS(CH_2)_2SPh\text{-}S,S'\}]$ (2)

To a stirred solution of $[WBr_2(CO)_3(NCMe)_2]$ (0.21 g, 0.41 mmol) in CH_2Cl_2 (15 cm^3) under a stream of dry nitrogen was added $PhS(CH_2)_2SPh$ (0.11 g, 0.45 mmol). The resulting solution was stirred for 2 h before filtering over a fine frit and the solvent was removed *in vacuo* to produce an orange brown powder. The powder was dissolved in a minimum of CH_2Cl_2 and cooled to $-15°C$ to give orange crystals of $[WBr_2(CO)_3\{PhS(CH_2)_2SPh\text{-}S,S'\}]$ (**2**) (0.12 g, 0.19 mmol, 45%), one of which was suitable for X-ray crystallography.

A similar reaction of $[MoBr_2(CO)_3(NCMe)_2]$ (0.19 g, 0.45 mmol) with $PhS(CH_2)_2SPh$ (0.12 g, 0.46 mmol) followed by recrystallisation from CH_2Cl_2 gave the brown complex $[MoBr_2(CO)_3\{PhS(CH_2)_2SPh\text{-}S,S'\}]$ (**1**) (0.11 g, 0.18 mmol, 40%).

$[WBr_2(CO)_3\{4\text{-}FC_6H_4S(CH_2)_2C_6H_4F\text{-}4\text{-}S,S'\}]$ (4)

To a stirred solution of $[WBr_2(CO)_3(NCMe)_2]$ (0.25 g, 0.49 mmol) in CH_2Cl_2 (20 cm^3) under a stream of dry nitrogen was added $4\text{-}FC_6H_4S(CH_2)_2SC_6H_4F$-4 (0.15 g, 0.51 mmol). The resulting solution was stirred for 23 h before filtering over a fine frit and the solvent was removed *in vacuo* to produce an orange brown powder. The powder was dissolved in a minimum of CH_2Cl_2 and cooled to $-15°C$ to give the orange complex $[WBr_2(CO)_3\{4\text{-}FC_6H_4S(CH_2)_2SC_6H_4F\text{-}4\text{-}S,S'\}]$ (**4**)(0.15 g, 0.22 mmol, 44%).

A similar reaction of $[MoBr_2(CO)_3(NCMe)_2]$ (0.19 g, 0.45 mmol) with $4\text{-}FC_6H_4S(CH_2)_2SC_6H_4F$-4 (0.13 g, 0.45 mmol) in CH_2Cl_2 for 4 h followed by recrystallisation from CH_2Cl_2 gave the brown complex $[MoBr_2(CO)_3\{4\text{-}FC_6H_4S(CH_2)_2SC_6H_4F\text{-}4\text{-}S,S'\}]$ (**3**) (0.13 g, 0.21 mmol, 46%).

$[WBr(CO)_3\{PhS(CH_2)_2SPh\text{-}S\}\{PhS(CH_2)_2SPh\text{-}S,S'\}]Br$ (5)

To a stirred solution of $[WBr_2(CO)_3(NCMe)_2]$ (0.21 g, 0.41 mmol) in CH_2Cl_2 (15 cm^3) under a stream of dry nitrogen was added $PhS(CH_2)_2SPh$ (0.21 g, 0.83 mmol). The resulting solution was stirred for 17 h before filtering over a fine frit and the solvent was removed *in vacuo* to produce an orange brown powder. The powder was dissolved in a minimum of CH_2Cl_2 and cooled to $-15°C$ to give the brown complex $[WBr(CO)_3\{PhS(CH_2)_2SPh\text{-}S\}\{PhS(CH_2)_2SPh\text{-}S,S'\}]Br$ (**5**) (0.15 g, 0.17 mmol, 41%).

A similar reaction of $[WBr_2(CO)_3(NCMe)_2]$ (0.19 g, 0.37 mmol) with $4\text{-}FC_6H_4S(CH_2)_2SC_6H_4F$-4 (0.21 g, 0.75 mmol) followed by recrystallisation from CH_2Cl_2 gave the brown complex $[WBr(CO)_3\{4\text{-}FC_6H_4S(CH_2)_2SC_6H_4F\text{-}4\text{-}S\}\{4\text{-}FC_6H_4S(CH_2)_2SC_6H_4F\text{-}4\text{-}S,S'\}]Br$ (**6**) (0.17 g, 0.18 mmol, 47%).

$[WBr_2(CO)_3\{Ph_2P(S)CH_2P(S)Ph_2\text{-}S,S'\}]$ (7)

To a stirred solution of $[WBr_2(CO)_3(NCMe)_2]$ (0.07 g, 0.14 mmol) in CH_2Cl_2 (15 cm^3) under a stream of dry nitrogen was added $Ph_2P(S)CH_2P(S)Ph_2$ (0.07 g, 0.15 mmol). The resulting solution was stirred for 4 h before filtering over a fine frit and the solvent was removed *in vacuo* to produce a green sticky oil. The oil was washed with hexane and then dissolved in a minimum of CH_2Cl_2 and cooled to $-15°C$ to give the green complex $[WBr_2(CO)_3\{Ph_2P(S)CH_2P(S)Ph_2\text{-}S,S'\}]$ (**7**) (0.08 g, 0.09 mmol, 60%).

A similar reaction of $[WBr_2(CO)_3(NCMe)_2]$ (0.07 g, 0.14 mmol) with $Ph_2P(S)CH_2P(S)Ph_2$ (0.14 g, 0.29 mmol) in CH_2Cl_2 gave the green complex $[WBr(CO)_3\{Ph_2P(S)CH_2P(S)Ph_2\text{-}S\}\{Ph_2P(S)CH_2P(S)Ph_2\text{-}S,S'\}]Br$ (**8**) (0.08 g, 0.06 mmol, 45%).

$[MoBr_2(CO)_2\{MeS(CH_2)_2S(CH_2)_2SMe\text{-}S,S',S''\}]$ (9)

To a stirred solution of $[MoBr_2(CO)_3(NCMe)_2]$ (0.30 g, 0.72 mmol) in CH_2Cl_2 (15 cm^3) under a stream of dry nitrogen was added $MeS(CH_2)_2S(CH_2)_2SMe$ (0.13 g, 0.73 mmol). The resulting solution was stirred for 5 h before filtering over cellite and the solvent was removed *in vacuo* to produce a red oily solid. The

oil was washed with hexane and then dissolved in a minimum of CH_2Cl_2 and cooled to $-15°C$ to give the red brown complex $[MoBr_2(CO)_2\{MeS(CH_2)_2S(CH_2)_2SMe\text{-}S,S',S''\}]$ (**9**) (0.20 g, 0.40 mmol, 55%).

A similar reaction of $[WBr_2(CO)_3(NCMe)_2]$ (0.29 g, 0.57 mmol) with $MeS(CH_2)_2S(CH_2)_2SMe$ (0.11 g, 0.575 mmol) in CH_2Cl_2 (15 cm^3) for 12 h followed by washing with hexane and recrystallisation from CH_2Cl_2 gave the green complex $[WBr_2(CO)_3\{MeS(CH_2)_2S(CH_2)_2SMe\text{-}S,S'\}]$ (**10**) (0.19 g, 0.31 mmol, 54%).

$[MoBr_2(CO)_2\{ttob\text{-}S,S',S''\}]$ (**11**)

To a stirred solution of $[MoBr_2(CO)_3(NCMe)_2]$ (0.41 g, 0.99 mmol) in CH_2Cl_2 (15 cm^3) under a stream of dry nitrogen was added ttob (0.26 g, 1.00 mmol). The resulting solution was stirred for 4 h before filtering over cellite and the solvent was removed *in vacuo* to produce a brown solid. The solid was washed with hexane and then dissolved in a minimum of CH_2Cl_2 and cooled to $-15°C$ to give the brown complex $[MoBr_2(CO)_2\{ttob\text{-}S,S',S''\}]$ (**11**) (0.34 g, 0.59 mmol, 60%).

Crystallography. Crystal data for **2** are given in Table 1, together with refinement details. Data were collected with Mo-K_α radiation using the MAR Research Image Plate System. The crystal was positioned at 80 mm from the Image Plate. 95 Frames were measured at 2° intervals with a counting time of 2 min. Data analysis was carried out with the XDS program [21]. The structure was solved using direct methods with the Shelx86 program [22]. Apart from the carbon atoms in the carbonyl groups, the non-hydrogen atoms were refined with anisotropic thermal parameters. The hydrogen atoms were included in geometric positions and given thermal parameters equivalent to 1.2 times those of the atom to which they were attached. An absorption correction was applied using DIFABS [23]. The structure was then refined using Shelx1 [24]. All calculations were carried out on a Silicon Graphics R4000 Workstation at the University of Reading. Bond lengths and angles in the metal coordination sphere are given in Table 2.

RESULTS AND DISCUSSION

The reaction of $[MBr_2(CO)_3(NCMe)_2]$ (M = Mo or W) with a slight excess of $RS(CH_2)_2SR$ (R = Ph or C_6H_4F-4) in CH_2Cl_2 at room temperature gave the seven-coordinate complexes $[MBr_2(CO)_3\{RS(CH_2)_2SR\text{-}S,S'\}]$ (**1–4**) in reasonable yields. Complexes **1–4** were characterised by elemental analysis C, H and S (Table 3), IR spectroscopy (Table 4) and ^1H NMR spectroscopy (Table 5). All four complexes are soluble in dichloromethane and DMSO, but are totally insoluble in diethyl ether, the molybdenum com-

Table 1. Crystal data and structure refinement for **2**

Empirical formula	$C_{17}H_{14}Br_2O_3S_2W$
Formula weight	674.07
Temperature (K)	293(2)
Wavelength Å	0.71073
Crystal system	monoclinic
Space group	$P2_1/c$
a (Å)	12.438(12)
b (Å)	13.162(12)
c (Å)	12.728(12)
β (°)	106.11(1)
V (Å^3)	2002(3)
Z	4
D_{calc} (g cm^{-3})	2.237
Absorption coefficient mm^{-1}	9.984
$F(000)$	1264
Crystal size (mm)	$0.25 \times 0.25 \times 0.30$
θ range for data collection (°)	2.30 to 23.61
Index ranges	$0 \leqslant h \leqslant 13$, $-14 \leqslant k \leqslant 14$, $-14 \leqslant l \leqslant 13$
Reflections collected	3661
Independent reflections	2503 [$R_{int} = 0.0831$]
Weighting Scheme (a,b)[a]	0.059, 52.08
Data/restraints/parameters	2503/0/212
Goodness-of-fit on F^2	1.079
Final R indices [$I > 2\sigma(I)$]	$R_1 = 0.0819$, $wR_2 = 0.1941$
R indices (all data)	$R_1 = 0.1124$, $wR_2 = 0.2063$
Largest diff. peak and hole (e Å^{-3})	0.792 and -1.071

[a] Weighting scheme $w = 1/(\sigma^2(F_o^2) + (aP)^2 + bP)$, where $P = (F_o^2 + 2F_c^2)/3$

Table 2. Bond lengths (Å) and angles (°) in the metal coordination sphere for **2**

W(1)—C(300)	1.81(2)
W(1)—C(100)	1.96(4)
W(1)—C(200)	2.01(3)
W(1)—S(2)	2.557(7)
W(1)—S(1)	2.573(7)
W(1)—Br(2)	2.626(3)
W(1)—Br(1)	2.659(4)
C(300)—W(1)—C(100)	71.9(12)
C(300)—W(1)—C(200)	106.0(10)
C(100)—W(1)—C(200)	75.4(13)
C(300)—W(1)—S(2)	113.0(7)
C(100)—W(1)—S(2)	74.2(11)
C(200)—W(1)—S(2)	118.7(7)
C(300)—W(1)—S(1)	87.0(7)
C(100)—W(1)—S(1)	134.8(11)
C(200)—W(1)—S(1)	149.7(7)
S(2)—W(1)—S(1)	78.4(2)
C(300)—W(1)—Br(2)	80.1(6)
C(100)—W(1)—Br(2)	129.2(11)
C(200)—W(1)—Br(2)	72.7(7)
S(2)—W(1)—Br(2)	156.5(2)
S(1)—W(1)—Br(2)	83.1(2)
C(300)—W(1)—Br(1)	164.4(6)
C(100)—W(1)—Br(1)	123.6(10)
C(200)—W(1)—Br(1)	79.0(7)
S(2)—W(1)—Br(1)	75.6(2)
S(1)—W(1)—Br(1)	82.0(2)
Br(2)—W(1)—Br(1)	87.58(11)

plexes being more soluble than their tungsten analogues. Complexes **1**–**4** are all very air-sensitive in solution and only slightly less so in the solid state, and much less stable than their diiodo analogues. Hence, the complexes were handled in air only for very short periods of time and decomposed very rapidly in solution. Conductivity measurements in acetone showed complexes **1**–**4** to be non-electrolytes as was expected.

The IR spectra of complexes **1**–**4** were recorded as KBr disks. No solution infrared spectra were obtained due to the extremely air-sensitive nature of the complexes. Three carbonyl stretching bands were observed for all of the four complexes (Table 4). This is consistent with the complexes being seven-coordinate tricarbonyl complexes and having one conformation in the solid-state. The ^{1}H NMR spectra (Table 5) showed the coordinated thioether resonances to be shifted slightly downfield compared to the free thioether ligands.

The solid-state structure of the tungsten complex **2** has been solved by X-ray crystallography and is shown in Fig. 1, together with atomic numbering scheme. It is likely that the three other complexes **1, 3** and **4** will have similar geometries in the solid state. The structure can best be considered as a distorted capped octahedron with one carbonyl C(100) in the capping position, two carbonyls C(200), C(300) and one sulfur S(2) in the capped face and the two bromides and the other sulfur S(1) in the uncapped face. The structure is very similar to that previously found for $[WI_2(CO)_3\{4\text{-}MeC_6H_4S(CH_2)_2SC_6H_4Me\text{-}4\text{-}S,S'\}]$ [9] both in the details of their metal coordination spheres and in the conformation of the Ph—S—CH_2—CH_2—S—Ph moiety. In the present structure one bromine atom Br(1) is *trans* to the carbonyl group C(300) at 2.659(4) Å while the other Br(2) is *trans* to S(2) at 2.626(3) Å. The two W—S(1) distances are equivalent within experimental error despite their different positions in the coordination sphere {2.557(7), 2.573(7) Å}. More variation is obtained for $[WI_2(CO)_3\{4\text{-}MeC_6H_4S(CH_2)_2SC_6H_4Me\text{-}4\text{-}S,S'\}]$ [9] where the mutually *trans* W—S and W—I are shorter at 2.54(3), 2.836(1) Å than those *trans* to carbonyl 2.59(3), 2.875(1) Å.

The reactions of $[WBr_2(CO)_3(NCMe)_2]$ with two equivalents of $RS(CH_2)_2SR$ (R = Ph or C_6H_4F-4) gave the cationic complexes $[WBr(CO)_3\{RS(CH_2)_2SR\text{-}S\}\{RS(CH_2)_2SR\text{-}S,S'\}]Br$ (R = Ph or 4-FC_6H_4) (**5** and **6**) respectively in good yield. Complexes **5** and **6** were characterised by elemental analysis C, H and S (Table 3), IR spectroscopy (Table 4) and ^{1}H NMR spectroscopy (Table 5). The found sulfur analysis for complex **5** is low, and is most likely to be due to the instability of this complex when exposed to air. Both complexes were soluble in dichloromethane and DMSO, but are totally insoluble in diethyl ether. They are very air-sensitive in solution, and only slightly less so in the solid state. Conductivity measurements in acetone showed both complexes to be typical 1 : 1 electrolytes (Λ_m = 123 and 126 S cm^2 mol^{-1}). These data suggest that one of the sulfur atoms from the second thioether ligand has displaced one of the bromide groups from the starting material.

The IR spectra of both complexes are recorded as KBr disks. Three carbonyl stretching bands were observed for both complexes (Table 4). This is consistent with the complexes being seven-coordinate and having one conformation in the solid-state. The ^{1}H NMR spectra (Table 5) again showed the coordinated thioether resonances to be shifted downfield compared to those of the free thioethers. In these cases, however, resonances are also observed for the uncoordinated end of the monodentately bound thioether ligand. It may be likely that given the similarities in spectroscopic data between complexes **5** and **6** and the crystallographically characterised product **2**, they will have similar solid-state structures, i.e. capped octahedral (Fig. 2). Several unsuccessful attempts were made to obtain ^{31}P NMR spectra for complexes **5** and **6**. These very weak spectra showed a number of resonances due to rapid decomposition of the complexes in solution.

Treatment of $[WBr_2(CO)_3(NCMe)_2]$ with one or two equivalents of $Ph_2P(S)CH_2P(S)Ph_2$ gave the green seven-coordinate complexes $[WBr_2(CO)_3\{Ph_2P(S)CH_2P(S)Ph_2\text{-}S,S'\}]$ (**7**) and $[WBr(CO)_3\{Ph_2P(S)CH_2P(S)Ph_2\text{-}S\}\{Ph_2P(S)CH_2P(S)Ph_2\text{-}S,S'\}]Br$ (**8**)

Table 3. Physical and analytical data[a] for thioether and diphosphine disulfide dibromocarbonyl seven-coordinate complexes of molybdenum(II) and tungsten(II)

Complex	Yield (%)	Colour	C(%)	H(%)	S(%)
1 $[MoBr_2(CO)_3\{PhS(CH_2)_2SPh\text{-}S,S'\}]$	40	brown	34.6 (34.8)	2.9 (2.4)	10.5 (10.9)
2 $[WBr_2(CO)_3\{PhS(CH_2)_2SPh\text{-}S,S'\}]$	45	orange	30.1 (30.3)	2.7 (2.1)	10.3 (9.5)
3 $[MoBr_2(CO)_3\{4\text{-}FC_6H_4S(CH_2)_2SC_6H_4F\text{-}4\text{-}S,S'\}]$	46	brown	32.7 (32.8)	1.8 (1.9)	10.0 (10.3)
4 $[WBr_2(CO)_3\{4\text{-}F\text{-}C_6H_4S(CH_2)_2SC_6H_4F\text{-}4\text{-}S,S'\}]$	44	orange	28.0 (28.8)	1.9 (1.7)	9.2 (9.0)
5 $[WBr(CO)_3\{PhS(CH_2)_2SPh\text{-}S\}\{PhS(CH_2)_2SPh\text{-}S,S'\}]Br$	41	brown	40.1 (40.5)	3.6 (3.1)	12.4 (13.9)
6 $[WBr(CO)_3\{4\text{-}FC_6H_4S(CH_2)_2SC_6H_4F\text{-}4\text{-}S\}\{4\text{-}FC_6H_4S(CH_2)_2SC_6H_4F\text{-}4\text{-}S,S'\}]Br$	47	brown	37.5 (37.5)	2.0 (2.4)	12.4 (12.9)
7 $[WBr_2(CO)_3\{Ph_2P(S)CH_2P(S)Ph_2\text{-}S,S'\}]$	60	green	38.3 (38.4)	2.6 (2.5)	7.8 (7.3)
8 $[WBr(CO)_3\{Ph_2P(S)CH_2P(S)Ph_2\text{-}S\}\{Ph_2P(S)CH_2P(S)Ph_2\text{-}S,S'\}]Br$	45	green	48.2 (48.8)	3.5 (3.6)	8.0 (9.5)
9 $[MoBr_2(CO)_2\{MeS(CH_2)_2S(CH_2)_2SMe\text{-}S,S',S''\}]$	55	red brown	18.9 (19.5)	2.4 (2.9)	19.1 (19.5)
10 $[WBr_2(CO)_3\{MeS(CH_2)_2S(CH_2)_2SMe\text{-}S,S'\}]$	54	green	16.8 (16.5)	1.9 (2.4)	16.2 (16.5)
11 $[MoBr_2(CO)_2\{ttob\text{-}S,S',S''\}]$	60	brown	30.1 (29.6)	2.7 (2.8)	16.0 (16.9)

[a] Calculated values in parentheses.

Table 4. IR data[a] for thioether and diphosphine disulfide bromocarbonyl seven-coordinate complexes of molybdenum(II) and tungsten(II)

Complex	$\nu(C{\equiv}O)$ (cm^{-1})
1	2042 (s), 1959 (s), 1901 (s)
2	2035 (s), 1965 (s), 1908 (s)
3	2022 (s), 1968 (s), 1915 (sh)
4	2025 (s), 1965 (s), 1908 (sh)
5	2043 (s), 1960 (s), 1896 (s)
6	2047 (s), 1965 (s), 1905 (s)
7	2034 (s), 1960 (s), 1892 (s)
8	2037 (s), 1961 (s), 1893 (s)
9	1962 (s), 1862 (s)
10	2036 (s), 1950 (s), 1905 (s)
11	1951 (s), 1871 (s)

[a] Spectra recorded as KBr disks.

respectively in good yield. Both complexes were characterised by elemental analysis C, H and S (Table 3), IR spectroscopy (Table 4) and ^1H NMR spectroscopy (Table 5). Both complexes are soluble in dichloromethane and DMSO, but are totally insoluble in diethyl ether. The complexes are very air-sensitive in solution and only slightly less so in the solid state.

Table 5. ^1H NMR data[a] for thioether and diphosphine disulfide bromocarbonyl seven-coordinate complexes of molybdenum(II) and tungsten(II)

Complex	^1H (δ) (ppm)
1	7.4 (m, 10H, Ph), 3.55 (s, 4H, CH_2)
2	7.5 (m, 10H, Ph), 3.55 (s, 4H, CH_2)
3	7.4 (m, 4H, C_6H_4), 7.2 (m, 4H, C_6H_4), 3.1 (s, 4H, CH_2)
4	7.35 (m, 4H, C_6H_4), 7.1 (m, 4H, C_6H_4), 3.1 (s, 4H, CH_2)
5	7.3 (m, 15H, Ph, coord), 7.1 (m, 5H, Ph, uncoord), 3.2 (s, 8H, CH_2)
6	7.4 (m, 8H, C_6H_4), 7.2 (m, 8H, C_6H_4), 3.1 (s, 8H, CH_2)
7	8.0 (m, 8H, Ph-ortho), 7.5 (m, 12H, Ph-meta+para), 4.6 (t, J_{PH} = 15 Hz, 2H, CH_2)
8	7.9 (m, 16H, Ph-ortho), 7.4 (m, 24H, Ph-m and p), 4.6 (brdd, 4H, CH_2)
9	3.1 (m, 8H, CH_2), 2.3 (s, 6H, CH_3)
10	3.76 (m, 4H, CH_2SCH_2, coord), 3.66 (m, 2H, CH_2SCH_3, coord), 2.9 (s, 3H, SCH_3, coord), 2.5 (m, 2H, CH_2SCH_3, uncoord), 2.2 (s, 3H, SCH_3, uncoord)
11	7.51 (m, 4H, Ph-H), 4.2 (m, 4H, $PhCH_2S$), 2.75 (m, 8H, SCH_2CH_2S)

[a] Spectra recorded in dimethylsulfoxide at 25°C and referenced to $SiMe_4$.

Hence, the complexes were handled in air only for very short periods and were used very quickly in order to avoid decomposition. Conductivity measurements of complex **7** showed the complex to be a non-electrolyte in acetone, however, complex **8** was shown to be a typical 1 : 1 electrolyte (Λ_m = 128 S cm^2 mol^{-1}) in acetone. The conductivity data suggests that in complex **8** one of the sulfur atoms from the second diphosphine disulfide ligand has displaced one of the bromide ligands from the starting material.

The IR spectra of both complexes were recorded as KBr disks. Three carbonyl stretching bands were observed for both complexes (Table 4). This is consistent with the complexes being seven-coordinate and having one conformation in the solid-state. The ^{1}H NMR spectra (Table 5) again showed the coordinated diphosphine disulfide resonances to be shifted slightly downfield compared to those of the free ligand. Similar reactions were attempted with the molybdenum complex $[MoBr_2(CO)_3(NCMe)_2]$, however no pure products could be isolated, which is probably due to their greater instability.

The reaction of $[MBr_2(CO)_3(NCMe)_2]$ with an equimolar amount of $MeS(CH_2)_2S(CH_2)_2SMe$ in CH_2Cl_2 at room temperature gave the seven-coordinate dicarbonyl complex $[MoBr_2(CO)_2\{MeS(CH_2)_2S(CH_2)_2SMe\text{-}S,S',S''\}]$ (**9**) and the tricarbonyl complex $[WBr_2(CO)_3\{MeS(CH_2)_2S(CH_2)_2SMe\text{-}S,S'\}]$ (**10**), respectively in high yield. Complexes **9** and **10** were characterised by elemental analysis C, H and S (Table 3), IR spectroscopy (Table 4) and ^{1}H NMR spectroscopy (Table 5). Both complexes are soluble in dichloromethane and DMSO but are totally insoluble in diethyl ether; the molybdenum complex is less soluble than its tungsten analogue. Both complexes are very air-sensitive in solution and only slightly less sensitive in the solid state. Conductivity measurements in acetone showed both complexes to be non-electrolytes. The IR spectra of both complexes were recorded as KBr disks (Table 4). Complex **9** showed two carbonyl stretching bands suggesting a dicarbonyl complex while three carbonyl stretching bands were observed for complex **10**.

The ^{1}H NMR spectra (Table 5) of both complexes showed the coordinated thioether resonances to be shifted downfield compared to those of the free thioethers. However, in the case of complex **10** a resonance

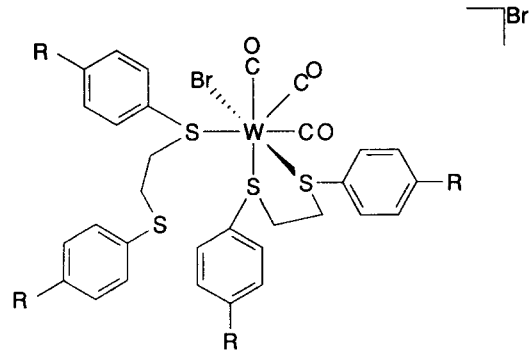

Fig. 2. Proposed structure of $[WBr(CO)_3\{RS(CH_2)_2SR\text{-}S\}\{RS(CH_2)_2SR\text{-}S,S'\}]Br$ (**5** and **6**) (R = Ph or $C_6H_4CF_3$-4).

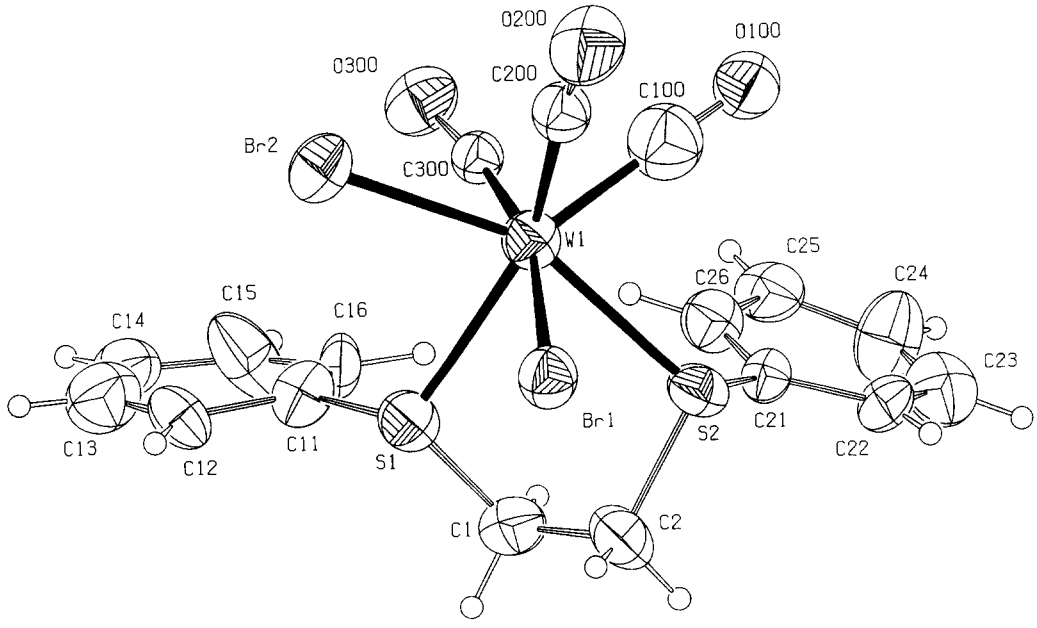

Fig. 1. The structure of **2**, together with the atom numbering scheme. Ellipsoids are shown at 30% probability. Hydrogen atoms are drawn with small arbitrary radii.

can be assigned to the methyl group of the uncoordinated sulfur atom. The geometry for complex **9** may be a capped octahedron (Fig. 3) for the dicarbonyl molybdenum complex $[MoBr_2(CO)_2\{MeS(CH_2)_2S(CH_2)_2SMe\text{-}S,S',S''\}]$ (**9**) since the previously confirmed crystallographically determined structure of the diiodo-complex $[WI_2(CO)_2\{MeS(CH_2)_2S(CH_2)_2SMe\text{-}S,S',S''\}]$ [9], is capped octahedral, and their spectral properties are also very similar. Several unsuccessful attempts to prepare the analogous tungsten complex $[WBr_2(CO)_2\{MeS(CH_2)_2S(CH_2)_2SMe\text{-}S,S',S''\}]$ were made by using longer reaction times. The greater lability of molybdenum carbonyl complexes compared to tungsten carbonyl complexes is well known [25].

Treatment of $[MoBr_2(CO)_3(NCMe)_2]$ with an equimolar amount of 2,5,8-trithia[9]-*o*-benzeneophane (ttob) gave the seven-coordinate dicarbonyl complex $[MoBr_2(CO)_2\{ttob\text{-}S,S',S''\}]$ (**11**) in high yield. Complex (**11**) was light brown in colour and was characterised by elemental analysis C, H and S (Table 3), IR spectroscopy (Table 4) and ^1H NMR spectroscopy (Table 5). The complex was soluble in dichloromethane and DMSO but was totally insoluble in diethyl ether. As expected the complex was very air-sensitive in both solution and in the solid state and hence was handled accordingly. Conductivity measurements in acetone showed the complex to be a non-electrolyte. The IR spectrum was recorded as a KBr disk (Table 4). The complex showed two carbonyl stretching bands suggesting a dicarbonyl complex similar to that of previously described complex (**9**). Similar reactions of $[WBr_2(CO)_3(NCMe)_2]$ with an equimolar amount of 2,5,8-trithia[9]-*o*-benzeneophane (ttob) were attempted, but resulted in a mixture of unstable products. Attempts to separate the products were unsuccessful due to decomposition occurring while recrystallisation was attempted.

In conclusion, the results described in this paper closely mimic those previously observed for the related reactions of the diiodo complexes, $[MI_2(CO)_3(NCMe)_2]$ with neutral sulfur donor ligands previously described.

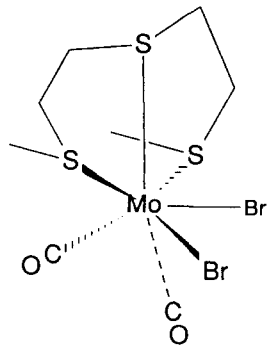

Fig. 3. Proposed structure of $[MoBr_2(CO)_2\{MeS(CH_2)_2S(CH_2)_2SMe\text{-}S,S',S''\}]$ (**9**).

Acknowledgements—A.I.C. thanks the BBSRC for support. We also thank the EPSRC for support and together with the University of Reading for funds towards the purchase of the image plate system.

REFERENCES

1. Kim, J. and Rees, D. C., *Science*, 1992, **257,** 1677.
2. Orme-Johnson, W. H., *Science*, 1992, **257,** 1639.
3. Kim, J. and Rees, D. C., *Nature* (*London*), 1992, **360,** 553.
4. Baker, P. K. and Fraser, S. G., *Polyhedron*, 1987, **6,** 2081.
5. Baker, P. K., Flower, K. R. and Thompson, S. M. L., *Transition-Met. Chem.*, 1987, **12,** 349.
6. Baker, P. K. and Fraser, S. G., *Inorg. Chim. Acta*, 1988, **142,** 219.
7. Baker, P. K. and ap Kendrick, D., *Inorg. Chim. Acta*, 1990, **174,** 119.
8. Baker, P. K. and ap Kendrick, D., *J. Organomet. Chem.*, 1991, **411,** 215.
9. Baker, P. K., Harris, S. D., Durrant, M. C., Hughes, D. L. and Richards, R. L., *J. Chem. Soc., Dalton Trans.*, 1994, 1401.
10. Baker, P. K., Harris, S. D., Durrant, M. C. and Richards, R. L., *Polyhedron*, 1996, **15,** 3595.
11. Baker, P. K., Coles, S. J., Durrant, M. D., Harris, S. D., Hughes, D. L., Hursthouse, M. B. and Richards, R. L., *J. Chem. Soc., Dalton Trans.*, 1996, 4003.
12. Baker, P. K., Durrant, M. C., Harris, S. D., Hughes, D. L. and Richards, R. L., *J. Chem. Soc., Dalton Trans.*, 1997, 509.
13. Mannerskantz, H. C. E. and Wilkinson, G., *J. Chem. Soc.*, 1962, 4454.
14. Durrant, M. C., Hughes, D. L., Richards, R. L., Baker, P. K. and Harris, S. D., *J. Chem. Soc., Dalton Trans.*, 1992, 3399.
15. Baker, P. K., Fraser, S. G. and Keys, E. M., *J. Organomet. Chem.*, 1986, **309,** 319.
16. Baker, P. K., Hursthouse, M. B., Karaulov, A. I., Lavery, A. J., Malik, K. M. A., Muldoon, D. J. and Shawcross, A., *J. Chem. Soc., Dalton Trans.*, 1994, 3493.
17. Tate, D. P., Knipple, W. R. and Augl, J. M., *Inorg. Chem.*, 1962, **1,** 433.
18. Bell, E. and Bennett, G., *J. Chem. Soc.*, 1928, 3189.
19. Davison, A. and Reger, D. L., *Inorg. Chem.*, 1971, **10,** 1967.
20. de Groot, B., Giesbrecht, G. R., Loeb, S. J. and Shimizu, G. K. H., *Inorg. Chem.*, 1991, **30,** 177.
21. Kabsch, W., *J. Appl. Cryst.*, 1988, **21,** 916.
22. Shelx86, Sheldrick, G. M., *Acta Cryst.*, 1990, **A46,** 467.
23. Walker, N. and Stuart, D., *Acta Cryst., Sect. A*, 1983, **39,** 158.
24. Shelx1, Sheldrick, G. M., 1993, program for crystal structure refinement. University of Göttingen, Germany.
25. Baker, P. K., *Adv. Organomet. Chem.*, 1996, **40,** 45, and references cited therein.

Pergamon

PII: S0277-5387(97)00425-7

Polyhedron Vol. 17, No. 9, pp. 1415–1422, 1998
© 1998 Elsevier Science Ltd
All rights reserved. Printed in Great Britain
0277-5387/98 $19.00+0.00

Syntheses, properties and X-ray crystal structures of the octahedral nickel(II) complexes of 2,5,9,12-tetramethyl-1,4,8,11-tetraazacyclotetradecane

Ki-Young Choi,*[a] Suk Nam Choi[b] and Il-Hwan Suh[c]

[a] Department of Chemistry, Mokwon University, Taejeon 301-729, Korea

[b] Department of Chemistry, Kongju National University, Kongju 314-701, Korea

[c] Department of Physics, Chungnam National University, Taejeon 305-764, Korea

(Received 1 September 1997; accepted 16 October 1997)

Abstract—The syntheses and structural characterization of $NiLX_2$ (X = H_2O (**1**), N_3^- (**2**) and NCS^- (**3**); L = 2,5,9,12-tetramethyl-1,4,8,11-tetrazacyclotetradecane) complexes are reported. The crystal structures of $NiLX_2$ complexes have an axially elongated octahedral geometry with two axial ligands and adopt the *trans*-III conformation. The equilibrium of **1** $NiL^{2+} + 2H_2O \rightleftarrows NiL(H_2O)_2^{2+}$ has been studied in aqueous solution over a temperature range, yielding $\Delta H^\circ = -7.1 \pm 0.1$ kJ mol^{-1} and $\Delta S^\circ = -18.7 \pm 0.3$ J K^{-1} mol^{-1}. Electronic absorption spectra of $NiLX_2$ complexes show that two absorption bands ($^3B_{1g} \rightarrow {}^3E_g^c$ and $^3B_{1g} \rightarrow {}^3E_g^b$) reflect the normal spectrochemical series for axial ligands but one absorption band ($^3B_{1g} \rightarrow {}^3B_{2g}$) depends in reciprocal fashion in the range 300–800 nm. Cyclic voltammetry of $NiLX_2$ complexes exhibit two one-electron waves corresponding to Ni(II)/Ni(III) and Ni(II)/Ni(I) processes. The redox potentials of the complexes are influenced significantly by the nature of the axial ligands. © 1998 Elsevier Science Ltd. All rights reserved

Keywords: octahedral nickel(II) complexes; tetramethyl tetraaza macrocycle.

Macrocyclic polyamine complexes of bivalent transition metals have been of great interest due to their importance as an essential metalloenzyme active site [1]. Typically the 14-membered tetraamine macrocycle cyclam (1,4,8,11-tetraazacyclotetradecane) is well recognized as an example among the macrocyclic polyamines in coordination chemistry [2]. Since the physical and chemical properties of the metal complexes are closely related to the structural features of the corresponding macrocyclic ligands, numerous efforts in this area have been directed toward the synthesis of new types of cyclam analogs. These include the variation of the ring size [3,4], functionalization of the cyclam skeleton [5], attachment of pendant donors to tetraamines [6], introduction of variable degrees of unsaturation [7] and introduction of substituents to the methylene carbon skeleton [6–12]. There have been reported that the modified cyclam complexes show considerable changes in physical and chemical properties, structures and catalytic efficiency [5,13,14]. Among the previously reported scope of cyclam analogs, few examples which possess additional groups at the carbon atoms of dimethylene linkages are known. Recently, the nontemplate condensation reaction of methyl vinyl ketone, 1,2-diaminopropane and perchloric acid followed by reduction with $NaBH_4$, resulting 2,5,9,12-tetramethyl-1,4,8,11-tetraazacyclotetradecane which contains four *anti* methyl groups on the macrocyclic ring, has been described [15,16]. Of much interest with this ligand is the effect on structures of metal complexes, oxidation states of the inserted metal ions and stabilities of metal complexes.

In this paper we report the syntheses and characterization of $NiLX_2$ (X = H_2O (**1**) N_3^- (**2**) and NCS^- (**3**); L = 2,5,9,12-tetramethyl-1,4,8,11-tetraazacyclotetradecane) complexes. We have investigated the

* Author to whom correspondence should be addressed.

equilibrium, spectroscopic and electrochemical properties of these complexes. Furthermore to understand the nature of the axial ligands the solid state X-ray crystal structures of $NiLX_2$ complexes are determined and compared to their solution structures by electronic absorption spectroscopy and cyclic voltametry.

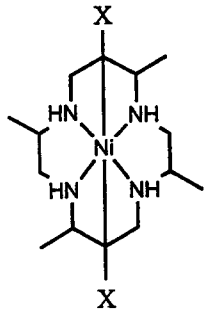

(X: OH_2 (1), N_3^-(2), NCS^-(3))

EXPERIMENTAL

Materials

All solvents were reagent grade and purified according to the literature [17]. Distilled water was used for all reactions. Reagent grade $NiCl_2 \cdot 6H_2O$, methyl vinyl ketone, 1,2-diaminopropane, perchloric acid and $NaBH_4$ were purchased from Aldrich. All other reagents were reagent grade.

Analytical methods

Infrared spectra were recorded as KBr pellets on a Perkin–Elmer Paragon 1000 FT-IR spectrophotometer. Electronic absorption spectra were obtained on a Jasco Uvidec-610 spectrophotometer. High-resolution fast atom bombardment mass spectrometry (FAB mass) were performed by using a Jeol JMS-HA 110A/110A instrument. Element analyses were carried out by the Korea Research Institute of Chemical Technology Taejeon, Korea.

Preparation of ligand (L)

The ligand L was prepared according to previously published procedures [15,16]. Calc. (found) for $C_{14}H_{32}N_4$: C, 65.6 (65.7); H, 12.6; H, 12.6 (12.6); N, 21.9 (21.7)%. IR (KBr, cm^{-1}): 3248 (ν NH), 3212 (ν NH), 2962, 2918, 2874, 2732, 1473, 1452, 1382, 1163, 1121, 1093, 941, 834, 831, 781, 621, 568 and 506. FAB mass (CH_2Cl_2 m/z): 256.4 $(M)^+$.

Preparation of $[NiL(H_2O)_2]Cl_2$ (1)

A methanol solution (20 cm^3) of L (256 mg, 1 mmol) and $NiCl_2 \cdot 6H_2O$ (238 mg, 1 mmol) was heated at reflux for 2 h. The solution was cooled to room temperature and the solvent was removed. The crude product was dissolved in 10 cm^3 of water, filtered and recrystallized by adding 10 cm^3 of acetonitrile. Violet crystals of **1** were collected by filtration and dried *in vacuo* (Yield: 300 mg, 71%). Calc. (found) for $NiC_{14}H_{36}N_4O_2Cl_2$: C, 39.8 (39.6); H, 8.6 (8.5); N, 13.3 (13.5)%. IR (KBr, cm^{-1}) 3239 (ν NH), 2967, 2878, 1659 (ν HOH), 1452, 1382, 1113, 1066, 1001, 947 and 741. Electronic spectra ($CHCl_3$): λ_{max} nm (ε, M^{-1} cm^{-1}): 352 (15.6), 534 (8.2) and 685 (4.0). FAB mass (CH_2Cl_2 m/z): 422.1 $(M)^+$.

Preparation of $[NiL(N_3)_2]$ (2)

To a methanol solution (20 cm^3) of **1** (127 mg. 0.3 mmol) was added NaN_3 (39 mg, 0.6 mmol) and the mixture was heated for 30 min on a steam bath. The solution was filtered to remove the sodium chloride. The solution was then evaporated to dryness. The resulting mauve solid was extracted into chloroform and recrystallized by adding 10 cm^3 of acetonitrile. Light brown crystals of **2** were collected by filtration and dried *in vacuo* (Yield: 91 mg, 76%). Calc. (found) for $NiC_{14}H_{32}N_{10}$: C, 42.1 (42.3); H, 8.1 (8.0); N, 35.1 (35.0)%. IR (KBr, cm^{-1}): 3192 (ν NH), 2964, 2910, 2870, 2032 (ν N_3), 1443, 1378, 1336, 1178, 1115, 1024, 988, 961, 942, 903, 836 and 615. Electronic spectra ($CHCl_3$): λ_{max}, nm (ε, M^{-1} cm^{-1}): 343 (17.6), 528 (10.3) and 712 (2.9). FAB mass (CH_2Cl_2, m/z): 399.2 $(M)^+$.

Preparation of $[NiL(NCS)_2] \cdot H_2O$ (3)

To methanol solution (20 cm^3) of **1** (127 mg, 0.3 mmol) was added KSCN (58 mg, 0.6 mmol) and the mixture was heated for 30 min on a steam bath. The solution was filtered to remove the potassium chloride. The solution was then evaporated to dryness and the resulting solid dissolved in acetonitrile/water (1 : 1, 10 cm^3). When this mixture was allowed to stand for a few days, a quantity of violet crystals precipitated. These were filtered off, washed with diethyl ether and dried *in vacuo* (Yield: 105 mg, 78%). Calc. (found) for $NiC_{16}H_{32}N_6S_2 \cdot H_2O$: C, 42.8 (42.6); H, 7.6 (7.7); N, 18.7 (18.8)%. IR (KBr, cm^{-1}): 3215 (ν NH), 2929, 2873, 2064 (ν SCN), 1447, 1379, 1114, 1060, 1009, 934, 899, 833, 784 and 480. Electronic spectra ($CHCl_3$): λ_{max}, nm (ε, M^{-1} cm^{-1}): 332 (15.1), 508 (9.7) and 735 (2.5). FAB mass (CH_2Cl_2, m/z): 449.3 $(M)^+$.

Equilibrium measurements

Measurements were carried out on a Uvidec-610 spectrophotometer with 1 cm quartz cell. The cell

containing solution was maintained in a temperature-controlled air-bath. The temperature of the solution was determined by the resistance of a calibrated thermistor. The concentration of **1** in an ionic strength of 0.10 M $NaClO_4$ was 6.04×10^{-3} M.

Electrochemical measurements

Cyclic voltammograms were recorded using a BAS 100BW electrochemical system. All measurements were made on 0.01 M tetraethylammonium perchloratedichloromethane solution at 20.0 ± 0.1°C. A hanging mercury dropping electrode for cathodic voltammetry and platinum disc electrode of about 2 mm diameter for anodic voltammetry were used as the working electrode. The counter electrode was a coiled platinum wire and a saturated calomel electrode was used as a reference electrode. The solution was degassed with high purity nitrogen prior to carrying out the electrochemical measurements.

X-ray structure analysis

Analyses on single crystals of $[NiL(H_2O)_2]Cl_2$ (**1**), $[NiL(N_3)]$ (**2**) and $[NiL(NCS)_2] \cdot H_2O$ (**3**) were carried out with an Enraf-Nonius CAD4 X-ray diffractometer. A summary of crystal data, data collection, and refinement for all crystallographically characterized compounds are given in Table 1. Violet crystal of **1**, light brown crystal of **2** and violet crystal of **3** (approximated dimensions $0.2 \times 0.2 \times 0.2$, $0.2 \times 0.3 \times 0.2$ and $0.4 \times 0.3 \times 0.1$ mm^3) were mounted on the diffractometer, and used for data collections at room temperature with graphite-monochromated Mo–K_α radiation ($\lambda = 0.71069$ Å). Accurate cell parameters and a crystal orientation matrix were determined by least-squares fit of 25 reflections. An asymmetric unit of intensity data were collected in the ω-2θ scan mode. Intensity data were corrected for Lorentz and polarization effects. No absorption correction was applied. The structure was solved by direct methods and refined by full matrix least-squares refinement (NRCVAX and SHELXL-93) [18,19]. All non-hydrogen atoms were placed with a combination of difference Fourier and least-squares calculations. Hydrogen atoms in methyl group were located from different Fourier maps, other hydrogen atoms were placed in calculated positions. Anisotropic thermal parameters were used for all non-hydrogen atoms and isotropic thermal parameters were used with the hydrogen atoms. The positions of hydrogen atoms

Table 1. Crystallographic data

	1	**2**	**3**
Chemical Formula	$NiC_{14}H_{36}O_2N_4Cl_2$	$NiC_{14}H_{32}N_{10}$	$NiC_{16}H_{32}N_6S_2 \cdot H_2O$
Formula weight	422.08	399.18	449.31
Crystal system	Triclinic	Triclinic	Triclinic
Space group	$P\bar{1}$	$P\bar{1}$	$P\bar{1}$
a (Å)	7.947(3)	7.828(2)	10.307(1)
b (Å)	9.618(1)	9.074(1)	14.277(4)
c (Å)	7.447(1)	7.242(1)	8.235(4)
α (°)	109.97(1)	94.86(1)	90.43(3)
β (°)	75.26(1)	97.73(2)	77.52(2)
γ (°)	95.63(2)	111.16(1)	111.07(2)
V (Å^3)	517.3(2)	470.4(2)	1100.8(6)
Z	1	1	2
$F(000)$	227	214	477
D_{calc} (g cm^{-3})	1.355	1.409	1.355
λ (Mo–K_α) (Å)	0.71069	0.71069	0.71069
μ (mm^{-1})	1.21	1.05	1.08
T (K)	288	288	288
Index range	$-9 \leqslant h \leqslant 9, 0 \leqslant k \leqslant 11,$ $-9 \leqslant l \leqslant 8$	$-9 \leqslant h \leqslant 8, 0 \leqslant k \leqslant 11,$ $-8 \leqslant l \leqslant 8$	$-12 \leqslant h \leqslant 11, 0 \leqslant k \leqslant 16$ $-9 \leqslant l \leqslant 9$
2θ range (°)	51.84	51.82	49.84
No. of unique reflections	2027	1838	3853
No. of observed reflections $[F_o > 3\sigma(F_o)]$	1684	1677	1680
R^a	0.035	0.039	0.041
Rw^b	0.037	0.042	0.046
GoF^c	0.57	0.67	0.43

[a] $R = \Sigma(|F_o| - |F_c|)/\Sigma|F_o|$.
[b] $Rw = [\Sigma w(|F_o| - |F_c|)^2/\Sigma w(|F_o|)^2]^{1/2}$.
[c] $\text{GoF} = [\Sigma w(|F_o| - |F_c|)^2/(\text{No. of rflns} - \text{No. of params})]^{1/2}$.

were fixed during the least-squares process. Full crystallographic details, atomic coordinates, ineratomic distances and angles, hydrogen atom coordinates, anisotropic displacement parameters and structure factor tables for **1**, **2** and **3** have been deposited with the Editor as supplementary material.

RESULTS AND DISCUSSION

Structural descriptions

The ligand skeleton of the present compounds take the most stable *trans*-III conformation with two chair form six-membered and two gauche five-membered chelate rings. An inversion center of these complexes exits on the central nickel(II) ion. The N—Ni—N angles of the six-membered chelate rings are larger than those of the five-membered chelate rings.

An ORTEP diagram of $[NiL(H_2O)_2]Cl_2$ (**1**) with the atomic numbering scheme is shown in Fig. 1 and selected bond lengths and angles in Table 2. The crystal structure of **1** consists of $[NiL(H_2O)_2]^{2+}$ cation and two Cl^- anions which is very similar to that of *trans*-$[Ni(cyclam)(H_2O)_2]Cl_2 \cdot 4H_2O$ [20]. Two water molecules axially coordinate to the central nickel(II) ion, which is six-coordinate in the high-spin octahedral geometry. The average bond distance of Ni—N is 2.074(3) Å, which is comparable to those found in *trans*-$[Ni(cyclam)(H_2O)_2]Cl_2 \cdot H_2O$ [2.069(7) Å] [20] and $[Ni(cyclam)Cl_2]$ [2.058(8) [21] and 2.067(2) Å [22]]. The Ni—O distance of 2.194(2) Å is slightly longer than those of the cyclam complexes [2.176(2) [20] and 2.16 Å [23]]. Substitution of the methyl groups on the macrocyclic chelate rings may have detrimental effect on the coordination of water molecules to the central nickel(II) ion. Figure 2 shows the four hydrogen-bonding chelate rings involving the chlorides, water molecule, secondary amines of macrocycle and the central nickel(II) ion (Table 3).

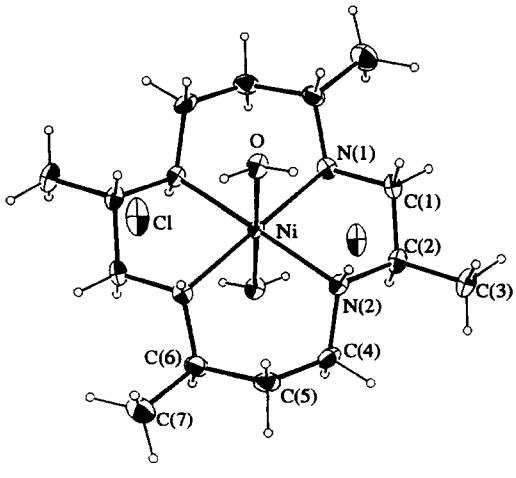

Fig. 1. ORTEP diagram of **1** with the atom-numbering scheme.

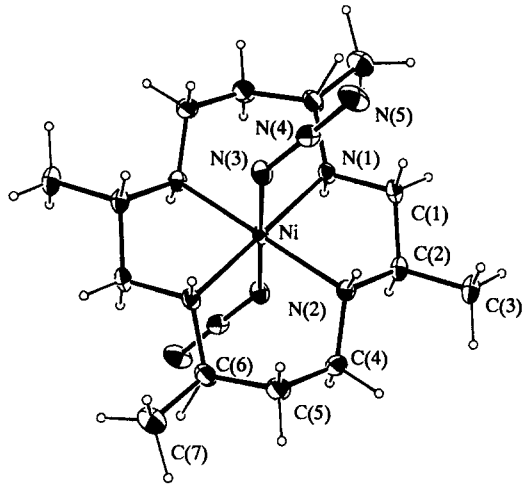

Fig. 2. Hydrogen-bond system of **1**.

An ORTEP diagram of $[NiL(N_3)_2]$ (**2**) with atomic numbering scheme is shown in Fig. 3 and selected bond lengths and angles in Table 2. The crystal structure of **2** reveals a six-coordinated octahedral geometry with bonds from the nickel(II) ion to the secondary amine nitrogens of the macrocycle and to the two axial azide ligands. The Ni—N(3) linkage is bent slightly off the perpendicular to the NiN_4 plane by 0.45–5.43°. The average bond distance of 2.075(3) Å, between nickel and secondary nitrogen, which is close to that found for **1** and shorter than the Ni—N(3) distance of 2.161 Å indicates an axially elongated octahedral geometry. The apical Ni—N(3) bond distance and Ni—N(3)—N(4) angle [128.2(2)°] are similar to the observed for catena-(μ-N_3)[Ni(cyclam)]$(ClO_4) \cdot H_2O$ [24] and [(Ni(Me_2[14]-1,3-dieneN$_4$)(μ-N(3)$_n$)]$(ClO_4)_n$ [25]. Both azido groups which act monodentate ligands are slightly asymmetric [N(3)—N(4) = 1.177(4) and N(4)—N(5) = 1.161(4) Å] and linear within the experimental error [N(3)—N(4)—N(5) angles = 179.0(3)°].

An ORTEP diagram of $[NiL(NCS)_2] \cdot H_2O$ (**3**) with the atomic numbering scheme is shown in Fig. 4 and selected bond lengths and angles in Table 2. There are two crystallographically independent $[NiL(NCS)_2]$ complexes, in each of which resides at a center of symmetry. The crystal structure of **3** confirms a six-coordinated octahedral geometry with bonds from the nickel(II) ion to the secondary amine nitrogens of the macrocycle and to the two axial thiocyanate ligands. The total stereochemistry of the ligands in **3** is essentially the same and very similar to that found for $[Ni(cyclam)(NCS)_2]$ [22]. The two axial Ni—N-(thiocyanato) distances are similar (2.109(7) and 2.100(7) Å) and longer than the average distance of Ni(1)—N_4 and Ni(2)—N_4 plane [2.094(6) and 2.080(6) Å], giving an axially elongated octahedral

Table 2. Selected bond lengths (Å) and angles (°)

		1	
Ni—O	2.194(2)	Ni—N(2)	2.073(3)
Ni—N(1)	2.074(3)		
O—Ni—N(1)	90.3(1)	Ni—N(1)—C(1)	106.3(2)
O—Ni—N(2)	89.8(1)	Ni—N(1)—C(6)[a]	116.8(2)
N(1)—Ni—N(2)	84.6(1)	Ni—N(2)—C(2)	107.1(2)
N(1)—Ni—N(2)[a]	95.4(1)	Ni—N(2)—C(4)	114.6(2)
		2	
Ni—N(1)	2.074(3)	N(3)—N(4)	1.177(4)
Ni—N(2)	2.075(3)	N(4)—N(5)	1.161(4)
Ni—N(3)	2.161(3)		
N(1)—Ni—N(3)	84.6(1)	Ni—N(1)—C(1)	106.1(2)
N(2)—Ni—N(3)	89.6(1)	Ni—N(1)—C(6)[a]	117.8(2)
N(1)—Ni—N(2)	85.3(1)	Ni—N(2)—C(2)	105.9(2)
N(1)—Ni—N(2)[a]	94.7(1)	Ni—N(2)—C(4)[a]	114.3(2)
Ni—N(3)—N(4)	128.2(2)	N(3)—N(4)—N(5)	179.0(3)
		3	
Ni(1)—N(1)	2.109(7)	Ni(2)—N(2)	2.100(7)
Ni(1)—N(11)	2.112(6)	Ni(2)—N(21)	2.076(6)
Ni(1)—N(12)	2.076(6)	N(2)—N(22)	2.084(5)
N(1)—C(1)	1.144(10)	N(2)—C(2)	1.164(10)
C(1)—S(1)	1.628(8)	C(2)—S(2)	1.631(8)
N(1)—Ni(1)—N(11)	92.7(2)	N(2)—Ni(2)—N(21)	91.5(3)
N(1)—Ni(1)—N(12)	86.9(3)	N(2)—Ni(2)—N(22)	86.7(2)
N(11)—Ni(1)—N(12)	84.6(3)	N(21)—Ni(2)—N(22)	85.2(2)
N(11)—Ni(1)—N(12)[a]	95.4(3)	N(21)—Ni(2)—N(22)[b]	94.8(2)
Ni(1)—N(1)—C(1)	154.6(6)	Ni(2)—N(2)—C(2)	162.2(5)
Ni(1)—N(11)—C(11)	104.7(5)	Ni(2)—N(21)—C(21)	105.2(4)
Ni(1)—N(11)—C(16)[a]	114.4(5)	Ni(2)—N(21)—C(26)[b]	118.1(5)
Ni(1)—N(12)—C(12)	105.7(4)	Ni(2)—N(22)—C(22)	106.8(4)
Ni(1)—N(12)—C(14)	114.3(5)	Ni(2)—N(22)—C(24)	114.4(4)
Ni(1)—C(1)—S(1)	179.4(7)	N(2)—C(2)—S(2)	179.1(6)

[a] $-x, -y, -z$.
[b] $-x, 1-y, -z$.

Table 3. Hydrogen-bond parameters (Å,°) for **1**

D—H···A	D—H	H···A	D—A	D—H···A
O—H(O1)—Cl[i]	0.83(4) Å	2.31(4) Å	3.124(3) Å	167(4)°
O—H(O2)—Cl	0.78(5) Å	2.33(5) Å	3.103(3) Å	172(5)°
N(1)—HN(1)—Cl	0.68(3) Å	2.73(3) Å	3.374(3) Å	160(4)°
N(2)—HN(2)—Cl[i]	0.85(4) Å	2.54(4) Å	3.382(3) Å	174(3)°

[i] $x, -y, 1-z$.

geometry. Of particular interest is the wide variety of orientation modes of the thiocyanate ligands. The Ni(1)—N(1) and Ni(2)—N(2) linkage is bent slightly off the perpendicular to the NiN_4 plane by 2.7–3.1° and 1.5–3.3°, respectively. The two Ni—N—C angles related to the thiocyanate ligands are Ni(1)—N(1)—C(1) [154.6(6)°] and Ni(2)—N(2)—C(2) [162.2(5)°]. The thiocyanate sulfur atom

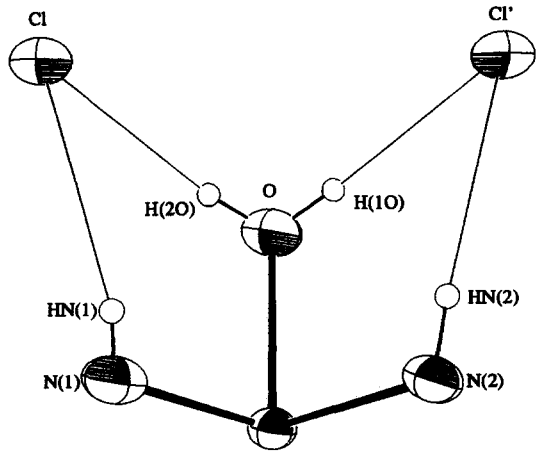

Fig. 3. ORTEP diagram of **2** with the atom-numbering scheme.

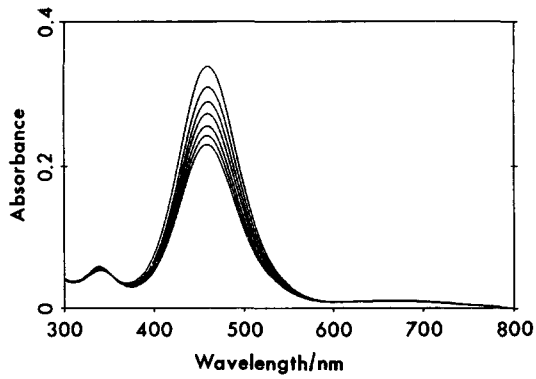

Fig. 5. Electronic absorption spectra of **1** in aqueous 0.10 M $NaClO_4$. [**1**] = 6.04×10^{-3} M. The spectra were determined (in terms of increasing absorbance) at 8.2, 15.2, 24.7, 34.0, 43.8, 58.8 and 77.8°C.

forms two hydrogen bonding O···S(2) [3.371(14) Å] and O···S(1)^{i} [$1+x$, $1+y$, z, 3.532(12) Å] with adjacent water molecule.

Equilibrium studies of **1**

Complex **1** exists in aqueous solution as an equilibrium mixture of a yellow, square-planar, low-spin species and a violet, octahedral, high-spin species according to eqn (1) [4,28]. The equilibrium was studied over a temperature range as shown in Fig. 5.

$$[NiL]^{2+} + 2H_2O \overset{K}{\rightleftarrows} [NiL(H_2O)_2]^{2+} \qquad (1)$$

The yellow square-planar species has a single d-d band in aqueous solution at 460 nm. This band is due exclusively to the square-planar species, and the proportion of the square-planar species was found to increase with increasing temperature. On addition of 7.2 M $NaClO_4$, the absorption coefficient of the band at 460

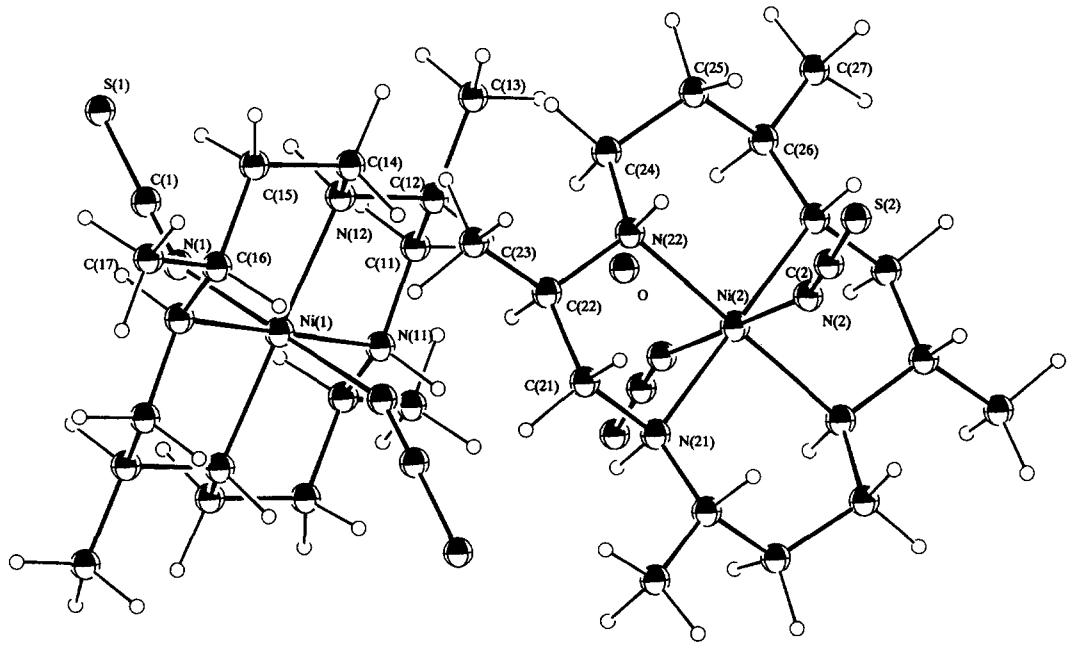

Fig. 4. ORTEP diagram of **3** with the atom-numbering scheme.

Table 4. Thermodynamic parameters for the square-planar to octahedral conversion of nickel(II) complexes with macrocyclic tetraamines in aqueous 0.10 M $NaClO_4$

Ligand	λ_{max} (nm)	ΔH° (kJ mol^{-1})	ΔS° (J K^{-1} mol^{-1})
L	460	-7.1 ± 0.1[a]	-18.7 ± 0.3[a]
Cyclam[b]	444	-22.6	-83.7
Isocyclam[c]	463	-22.2 ± 0.4	-78.2 ± 2

[a] Calculated from the ln K vs $1/T$ plot: 8.2°C ln K = 0.788; 15.2°C, 0.713; 24.7°C, 0.626; 34.0°C, 0.548; 43.8°C, 0.451; 58.8°C, 0.329; 77.8°C, 0.182.
[b] Ref. [28].
[c] Ref. [4].

nm eventually reaches a limiting value ($\varepsilon = 121.8$ M^{-1} cm^{-1}) which is taken as the molar absorption coefficient of the square-planar chromophore. Moreover, heating this solution does not increase the absorbance any further indicating that the ε value is not temperature-dependent. The equilibrium constant of the square-planar to octahedral conversion K ($K = \varepsilon/\varepsilon_{lim} - \varepsilon$) was determined at different temperatures in the range 8.2–77.8°C for the solution of **1** in 0.10 M $NaClO_4$. A plot of ln K against $1/T$ makes ΔH° and ΔS° values available. Thermodynamic parameters shown in Table 4 for the square-planar to octahedral conversion of $[NiL]^{2+}$ are compared with those for corresponding complexes of macrocycles. The reactions are exothermic due to the formation of two axial Ni—OH_2 bonds in the octahedral species. However, this effect is counterbalanced to some degree by the weaker Ni—N bond in the octahedral species, where the Ni—N bonds are somewhat longer [2.074(3) Å] than those observed in the square-planar species [Ni—N 1.90–1.91 Å] [26,27]. Constriction of two water molecules also leads to a negative entropy change. The entropy change of **1** is considerably lower than those observed in cyclam [28] and isocyclam [4]. This may be attributed to the elongation of the axial Ni—OH_2 bond by the substitution of the tetramethyl groups on the macrocycle.

Spectroscopic studies

The electronic absorption bands of $NiLX_2$ complexes in $CHCl_3$ solution are summarized in Table 5. All complexes investigated in this study show three absorption bands [$^3B_{1g} \rightarrow {}^3E_g^c$, $^3B_{1g} \rightarrow {}^3E_g^b$, and $^3B_{1g} \rightarrow {}^3B_{2g}$] [29] in the range 300–800 nm. Two absorption bands [$^3B_{1g} \rightarrow {}^3E_g^c$ and $^3B_{1g} \rightarrow {}^3E_g^b$] of complexes increase toward higher energies in the order of $H_2O < N_3^- < NCS^-$, which is reasonably explained by the spectrochemical series, but one absorption band [$^3B_{1g} \rightarrow {}^3B_{2g}$] depends in a reciprocal fashion. This observation is consistent with previously reported work for the spectrochemical properties of nickel(II) macrocyclic complexes [29]. The electronic spectra of **1** in the solid state (KBr pellet) was observed at 531 and 348 nm, which are similar to those of $CHCl_3$ solution. One pertinent feature of **1** in parallel with the solid state X-ray structural result is the dominant population of octahedral species in $CHCl_3$ solution. This is an evidence by the presence in the absorption band centered at 534 nm (high-spin chromophore) compared to band centered at 460 nm (low-spin chromophore) in aqueous solution. It is well understood that **1** exists in equilibrium mixture of the square planar (low-spin) and octahedral (high-spin) species aqueous solution as shown eqn (1).

The prominent IR bands in $NiLX_2$ complexes are also listed in Table 5. The IR spectra of the complexes show a band at ca 3200 cm^{-1}, which is assigned to the ν(NH) of the coordinated secondary amines. An absorption band at 1659 cm^{-1} for in **1** was assigned to HOH bending vibration of coordinated water [30], which is agreed with the crystal data of **1**. A single very strong band at 2032 cm^{-1} of **2** was associated with the azide stretching mode is consistent with the crystal structure of **2**. For **3** the IR data are in accordance with the N-bonded thiocyanato structure as a strong broad band at 2064 cm^{-1} is characteristic of Ni—N bonding [30] which reveals the crystal structure of **3**.

Electrochemistry

Cyclic voltametry data for $NiLX_2$ complexes in 0.01 M TEAP-CH_2Cl_2 solution are given in Table 6. The

Table 5. Spectral data for nickel(II) complexes

	Electronic,[a] λ_{max}, nm (ε, M^{-1} cm^{-1})			IR (cm^{-1})			
Complex	$^3B_{1g} \rightarrow {}^3E_g^c$	$\rightarrow {}^3E_g^b$	$\rightarrow {}^3B_{2g}$	ν(NH)	ν(HOH)	$\nu(N_3)$	ν(SCN)
1	352(15.6)	534(8.2)	685(4.0)	3239 (s)	1659 (vs)		
2	343(17.6)	528(10.3)	712(2.9)	3192 (s)		2032 (vs)	
3	332(15.1)	508(9.7)	735(2.5)	3215 (s)			2064 (vs)

[a] In $CHCl_3$.

Table 6. Cyclic voltammetric data for nickel(II) complexes[a]

Complex	Potentials (V) vs Ag/AgCl	
	Ni(II)/Ni(III)	Ni(II)/Ni(I)
1	+0.66	−1.53
2	+0.67	−1.47
3	+0.80	−1.44

[a]Measured in 0.01 M TEAP-CH_2Cl_2 solution at 20.0±0.1°C.

complexes exhibit two one-electron waves corresponding to Ni(II)/Ni(III) and Ni(II)/Ni(I) processes. It is of interest to compare the redox potentials for $NiLX_2$ complexes with the axial ligands. The electron density on the nickel atom of these complexes is decreased with the axial ligands in the order of **1** > **2** > **3**. This fact indicates that the oxidation process is unfavorable but the reduction process if favorable. The order of series reflects the π-donor ability of the axial ligands, stabilizing the Ni(III) and Ni(I) center in the order of $NCS^- > N_3^- > H_2O$. This is consistent with the spectral results discussed previously.

Acknowledgements—This work was supported by the Basic Science Research Institute Program of Education of Korea, Project No. BSRI-97-3435 and the Research Fund of Mokwon University, 1997.

REFERENCES

1. Bertini, I. and Luchinat, C., in *Bioinorganic Chemistry*, ed. I. Bertini, H. B. Gray, S. J. Lippard and J. Valentine. University Science Books, Mill Valley, CA, U.S.A., 1994.
2. Curtis, N. F., In *Coordination Chemistry of Macrocylic Compounds*, ed. G. A. Melson. Plenum, New York, 1979.
3. Miyoshi, K., Tanaka, H., Kimura, E., Tsuboyama, S., Shimizu, H. and Ishizu, K., *Inorg. Chim. Acta*, 1983, **78,** 23.
4. Sabatini, L. and Fabbrizzi, L., *Inorg. Chem.*, 1979, **18,** 438.
5. Kimura, E., Kotake, Y., Koike, T., Shionoya, M. and Shiro, M., *Inorg. Chem.*, 1990, **29,** 4991.
6. Kang, S.-G., Kim, M.-S., Choi, J.-S., Whang, D. and Kim, K., *J. Chem. Soc., Dalton Trans.*, 1995, 363.
7. Lovecchio, F. V., Gore, E. S. and Busch, D. H., *J. Am. Chem. Soc.*, 1974, **96,** 3109.
8. Choi, K.-Y., Kim, J. C., Jensen, W. P., Suh, I.-H. and Choi, S.-S., *Acta Cryst.*, 1996, **C52,** 2166.
9. Choi, K.-Y., Oh, M.-R. and Suh, I.-H., *Chem. Lett.*, 1997, 147.
10. Choi, K.-Y., Suh, I.-H. and Kim, J. C., *Polyhedron*, 1997, **16,** 1783.
11. Choi, K.-Y., *Polyhedron*, 1997, **16,** 2073.
12. Choi, K.-Y. and Suh, I.-H., *Polyhedron*, 1997, **16,** 2396.
13. Shionoya, M., Kimura, E. and Iitaka, Y., *J. Am. Chem. Soc.*, 1990, **112,** 9237.
14. Fujita, E., Haff, J., Sanzenbacher, R. and Elias, H., *Inorg. Chem.*, 1994, **33,** 4627.
15. Kolinsk, R. A., Korybut-Daszkiewicz, B., Kubaj, Z. and Mrozinski, J., *Inorg. Chim. Acta*, 1982, **57,** 269.
16. Kang, S.-G., Kweon, J. K. and Jung, S.-K., *Bull. Kor. Chem. Soc.*, 1991, **12,** 483.
17. Perrin, D. D., Armarego, W. L. F. and Perrin, D. R., *Purification of Laboratory Chemicals*, 2nd edn. Pergamon Press, New York, 1985.
18. Gabe, E. J., Page, Y. L., Charland, J. P., Lee, F. L. and White, P. S., *J. Appl. Cryst.*, 1989, **22,** 384.
19. Sheldrick, G. M., *SHELXL* 93. *Program for the Crystal Structure Refinement.*, University of Göttingen, Göttingen, Germany, 1993.
20. Mochizuki, K. and Kondo, T., *Inorg. Chem.*, 1995, **34,** 6241.
21. Bosnich, B., Mason, M., Pauling, P. J., Robertson, G. B. and Tobe, M. L., *J. Chem. Soc., Chem. Commun.*, 1965, 97.
22. Ito, T., Kato, M. and Ito, H., *Bull. Chem. Soc. Jpn*, 1984, **57,** 2641.
23. Thom, V. J., Fox, C. C., Boeynes, J. C. A. and Hancock, R. D., *J. Am. Chem. Soc.*, 1984, **106,** 5947.
24. Escuer, A., Vicente, R., Ribas, J., El Fallah, M. S. and Solaus, X., *Inorg. Chem.*, 1993, **32,** 1033.
25. Vicente, R., Escuer, A., Ribas, J., El Fallah, M. S., Solaus, X. and Font-Bardia, M., *Inorg. Chem.*, 1995, **34,** 1278.
26. Nyburg, S. C. and Wood, J. S., *Inorg. Chem.*, 1964, **3,** 468.
27. McPherson, A., Rossmann, J. M. G., Margerum, D. W. and James, M. R., *J. Coord. Chem.*, 1971, **1,** 39.
28. Anichini, A., Fabbrizzi, L., Paoletti, P. and Clay, R. M., *Inorg. Chim. Acta*, 1977, **24,** L21.
29. Martin, L. Y., Sperati, C. R. and Busch, D. H., *J. Am. Chem. Soc.*, 1977, **99,** 2968.
30. Nakamoto, K., *Infrared and Raman Spectra of Inorganic and Coordination Compounds*, 4th edn. John Wiley & Sons, New York, 1986.

Pergamon

PII: S0277-5387(97)00424-5

Polyhedron Vol. 17, No. 9, pp. 1423–1427, 1998
© 1998 Elsevier Science Ltd
All rights reserved. Printed in Great Britain
0277-5387/98 $19.00+0.00

Synthesis and magnetic properties of μ-chloranilato iron(III) binuclear complexes

Yan-Tuan Li,*[a] Cui-Wei Yan,[b] Yong-Jun Zheng[a] and Dai-Zheng Liao[c]

[a] Department of Chemistry, Qufu Normal University, Qufu Shandong, 273165, P.R. China

[b] Department of Biology, Qufu Normal University, Qufu Shandong, 273165, P.R. China

[c] Department of Chemistry, Nankai University, Tianjin, 300071, P.R. China

(Received 18 August 1997; accepted 16 October 1997)

Abstract—Six new iron(III) binuclear complexes have been synthesized and characterized, namely $[Fe_2(CA)L_4](ClO_4)_4$ [L denotes 2,2′-bipyridine (bpy); 1,10-phenanthroline (phen); 4,4′-dimethyl-2,2′-bipyridine (Me_2bpy); 5-methyl-1,10-phenanthroline (Me-phen); 5-chloro-1,10-phenanthroline (Cl-phen) and 5-nitro-1,10-phenanthroline (NO_2-phen)], where CA represents the dianion of chloranilic acid. Based on elemental analyses, molar conductivity and magnetic moment measurements, and spectroscopic studies, it is proposed that these complexes have CA-bridged structures and consist of two iron(III) ions in a distorted octahedral environment. The complexes $[Fe_2(CA)(bpy)_4](ClO_4)_4$ (**1**) and $[Fe_2(CA)(phen)_4](ClO_4)_4$ (**2**) were characterized by variable temperature magnetic susceptibility measurements (4–300 K) and the observed data were successfully simulated by the equation based on the spin Hamiltonian operator, $\hat{H} = -2J\hat{S}_1 \cdot \hat{S}_2$, giving the exchange integral $J = -2.1$ cm^{-1} for (**1**) and $J = -5.8$ cm^{-1} for (**2**). This result indicates that there is a weak antiferromagnetic spin-exchange interaction between two of the Fe(III) ions within each molecule. © 1998 Elsevier Science Ltd. All rights reserved

Keywords: μ-chloranilato; iron(III); binuclear complex; magnetism; synthesis; characterization.

Chloranilate dianions (abbreviated as CA), due to their peculiar structure, could be good candidates in supporting long-distance magnetic exchange interactions. Many works have been published on binuclear copper(II) complexes containing the μ-chloranilato ligand [1–5]. The effective bridging function of μ-chloranilato and the long-distance antiferromagnetic exchange interactions of these complexes have been revealed by single-crystal X-ray and magnetic analyses. However, to our knowledge no binuclear iron(III) complex bridged by a chloranilate group of this kind has so far been reported. In order to provide more examples of chloranilato-bridged binuclear complexes and to understand better the magnetic properties of this kind of complexes, this paper deals with the synthesis, characterization and magnetism of six new iron(III) binuclear complexes using the dianion of chloranilic acid as bridging ligand: $[Fe_2(CA)L_4](ClO_4)_4$ [where CA = dianion of chloranilic acid; L = 2,2′-bipyridine (bpy); 1,10-phenanthroline (phen); 4,4′-dimethyl-2,2′-bipyridine (Me_2bpy); 5-methyl-1,10-phenanthroline (Me-phen); 5-chloro-1,10-phenanthroline (Cl-phen) and 5-nitro-1,10-phenanthroline (NO_2-phen), respectively].

EXPERIMENTAL

Materials

All the reagents used in the synthesis were analytical grade. Hydrated iron(III) perchlorate was prepared and purified by the literature method [6]. Chloranilic acid (H_2CA), 2,2′-bipyridine (bpy); 1,10-phenanthroline (phen); 4,4′-dimethyl-2,2′-bipyridine (Me_2bpy); 5-methyl-1,10-phenanthroline (Me-phen); 5-chloro-1,10-phenanthroline (Cl-phen) and 5-nitro-

* Author to whom correspondence should be addressed.

1,10-phenanthroline (NO_2-phen) were analytical grade and used as commercially obtained.

Synthesis of iron(III) binuclear complexes

All six complexes were prepared in a similar fashion as typified by $[(Fe_2(CA)(bpy)_4](ClO_4)_4$. To an absolute methanol solution (10 cm^3) of chloranilic acid (0.2 mmol, 41.8 mg) was successively added dropwise an acetonitrile solution (10 cm^3) of $Fe(ClO_4)_3 \cdot 6H_2O$ (0.4 mmol, 186.2 mg) and a solution of bpy (0.8 mmol, 125.0 mg) in 10 cm^3 of methanol with stirring. The mixture was refluxed for 3 h to yield dark-brown microcrystals, which were filtered, washed with methanol and diethyl ether several times and dried over P_2O_5 under reduced pressure. All the analytical data, yields, colors and melting points of the complexes are collected in Table 1. In the solid state all the complexes are fairly stable in air so as to allow physical measurements.

Measurements

Analysis for C, H and N were carried out on a Perkin–Elmer elemental analyser model 240. Metal contents were determined by EDTA titration. The infrared spectra were measured on a Shimadzu infrared spectrometer model 810 in KBr pellets. The electronic spectra (DMF solution) were measured on a Perkin–Elmer Hitachi-240 spectrophotometer. Molar conductances were measured (DMF solution) with a DDS-11A conductometer. Magnetic susceptibility measurements at room temperature were carried out by Gouy's method using $Hg[Co(SCN)_4]$ as the calibrant. Variable temperature magnetic susceptibilities were measured at the Institute of Physics, Chinese Academy of Sciences, using a vibrating magnetometer Model CF-1 (sensitivity $m = 10^{-4}$ emu). Diamagnetic corrections were made with Pascal's constants [7] for all the constituent atoms and effective magnetic moments were calculated by the equation $\mu_{eff} = 2.828 (\chi_M T)^{1/2}$, where χ_M is the molar magnetic susceptibility corrected for diamagnetisms of the constituting atoms.

RESULTS AND DISCUSSION

Composition of the complexes

On the basis of elemental analyses and physical data listed in Table 2 it is reasonable to conclude that the reaction of chloranilic acid (H_2CA) with $Fe(ClO_4)_3 \cdot 6H_2O$ and L (L = bpy, phen, Me_2bpy, NO_2-phen, Cl-phen, Me-phen) in 1:2:4 mole ratio yielded the binuclear complexes of the general formula $[Fe_2(CA)L_4](ClO_4)_4$, as expected. All the Fe(III)—Fe(III) binuclear complexes are sparingly soluble in water, ethanol, carbon tetrachloride, chloroform and benzene, but soluble in DMF and DMSO to give stable solutions at room temperature. For the six complexes, the molar conductance values in DMF solution at 25°C (see Table 2) fall in the expected range for 1:4 electrolytes [8], indicating that the four perchlorate anions are situated outside the metal coordination sphere.

In spite of our many efforts, single crystals suitable for X-ray crystallography have not yet been obtained for these complexes. However, the binuclear structures are supported by the following results.

Infrared spectra

In order to clarify the mode of bonding, the IR spectra of the free ligand (H_2CA) and binuclear iron(III) complexes were studied and assigned on the basis of a careful comparison of the latter with the free ligand. The most relevant IR absorption bands due to the complexes along with their assignments are shown in Table 2. We will only discuss the selected infrared bands. In the IR spectra of the six complexes, a very strong peak at 1520–1530 cm^{-1} and a medium peak at 1385–1380 cm^{-1} is observed due to C=O stretching vibrations of the CA ligand. This agrees with D_{2h} symmetry for the CA ligand and suggests a

Table 1. Elemental analyses, yields, colours and melting points (M.p.) of the complexes

Complex	Color	Yield (%)	M.p. (°C)	Found (Calcd) (%) C	H	N	Fe
(1)	dark-brown	70	298	41.1 (41.2)	2.3 (2.4)	8.3 (8.4)	8.2 (8.3)
(2)	brown	86	312	45.0 (45.1)	2.1 (2.2)	7.7 (7.8)	7.6 (7.8)
(3)	dark-blue	72	331	44.4 (44.6)	3.0 (3.3)	7.6 (7.7)	7.5 (7.7)
(4)	yellow	88	315	40.0 (40.1)	1.6 (1.7)	10.2 (10.4)	6.8 (6.9)
(5)	black	78	319	41.0 (41.2)	1.6 (1.8)	6.9 (7.1)	7.0 (7.1)
(6)	dark-green	81	301	46.5 (46.7)	2.6 (2.7)	7.2 (7.5)	7.4 (7.5)

(1) = $[Fe_2(CA)(bpy)_4](ClO_4)_4$, (2) = $[Fe_2(CA)(phen)_4](ClO_4)_4$, (3) = $[Fe_2(CA)(Me_2bpy)_4](ClO_4)_4$, (4) = $[Fe_2(CA)(NO_2\text{-phen})_4](ClO_4)_4$, (5) = $[Fe_2(CA)(Cl\text{-phen})_4](ClO_4)_4$, (6) = $[Fe_2(CA)(Me\text{-phen})_4](ClO_4)_4$.

Table 2. Physical data for the complexes

Complex	Λ_M (S cm^2 mol^{-1})	IR (cm^{-1}) ν (C=O)	ν (ClO_4^-)	ν (N=C)	μ_{eff} (B.M.)
(1)	305	1380, 1525	1100, 625	1550	8.30
(2)	300	1386, 1530	1095, 630	1565	8.28
(3)	302	1385, 1520	1100, 630	1560	8.25
(4)	308	1380, 1520	1085, 630	1555	8.20
(5)	310	1380, 1525	1100, 625	1550	8.21
(6)	301	1380, 1530	1100, 630	1560	8.26

bridging *bis*-bidentate coordination mode [3]. The *bis*-bidentate coordination modes of the bridging ligand have been revealed by X-ray diffraction analyses of analogous complexes [1,2]. On the other hand, the —N=C— vibrations for the terminal ligands (bpy, phen, Me_2bpy, NO_2-phen, Cl-phen, Me-phen) were shifted to higher frequencies in their binuclear complexes (see Table 2) suggesting that the N atoms of the terminal ligands coordinate with the metal ion. In addition, a broad intense band centered at ca 1100 cm^{-1} and a strong sharp band at ca 630 cm^{-1}, typical for a non-coordinated perchlorate group [9,10], were present for all binuclear complexes. This is consistent with the conductance data of the complexes.

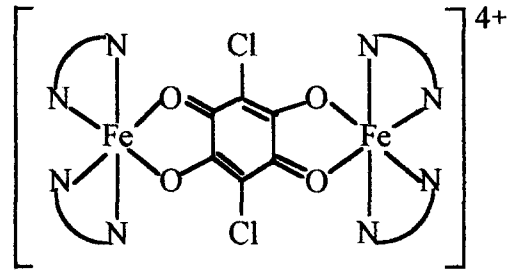

Fig. 1. Coordination environments of the complexes (N $\widehat{\text{N}}$ = bpy, phen, Me_2bpy, Me-phen, NO_2-phen, Cl-phen).

Electronic spectra

As shown in Table 3, the electronic spectra of the six complexes in DMF solutions are similar. Three very weak absorptions ($\varepsilon < 0.1$) were observed. The assignments (see Table 3) of these d-d bands are commensurate with a six-coordinated octahedral geometry [11]. In addition, a broad band at about 500–510 nm was observed in the electronic spectra of the complexes. It is attributed to charge-transfer bands arising from CA ligand, as expected for *p*-benzoquinones [12], further supporting a bridging *bis*-bidentate coordination proposed for CA.

Based on the composition of these complexes, their infrared spectra, electronic spectra, conductivity measurements and magnetic data (*vide infra*), these complexes are proposed to have an extended CA-bridged structure and to contain two Fe(III) ions bridged by the CA ligand in a *bis*-bidentate fashion and each iron(III) ion has an octahedral coordinated environment, as shown in Fig. 1.

Magnetic properties

The observed magnetic moment per binuclear complex at room temperature shown in Table 2 is less than

Table 3. Electronic spectral bands and assignments of the complexes

Complex	UV (nm) CT	^6A_1g–^4T_1g(G)	^6A_1g–^4T_2g(G)	^6A_1g–^4E_g(G)
(1)	500	858	535	390
(2)	505	850	530	395
(3)	508	850	535	385
(4)	500	855	525	390
(5)	510	850	530	390
(6)	500	850	535	380

the spin-only value (8.37 B.M.). This suggests the operation of an antiferromagnetic spin-exchange interaction in these complexes [13]. Being interested in the magnetic behavior of the complexes, variable-temperature (4–300 K) magnetic susceptibility data were further collected for complexes $[Fe_2(CA)(bpy)_4](ClO_4)_4$ (**1**) and $[Fe_2(CA)(phen)_4](ClO_4)_4$ (**2**) and are shown in Fig. 2 in the form of the χ_M, μ_{eff} versus T plot, χ_M being the molar magnetic susceptibility, μ_{eff} the effective moment and T the absolute temperature. From Fig. 2 it is evident that the magnetic behaviors of the two complexes are similar. When the temperature is lowered, the effective magnetic moments values decrease steadily from 8.30 B.M. for (**1**) and 8.28 B.M. for (**2**) at 300 K to 7.01 B.M. (**1**) and 6.98 B.M. (**2**) at 27.15 K and to 3.45 B.M. (**1**) and 3.38 B.M. (**2**) at 4.50 K. Thus, the observed magnetic behavior clearly demonstrates the operation of a weak intramolecular antiferromagnetic spin-exchange interactions between high-spin iron(III) ions through the CA-bridge within each binuclear unit [14,15]. This is consistent with the room temperature magnetic moment data of the complexes. The rapid decrease of the magnetic moment below 4.50 K may be attributed to an intermolecular antiferromagnetic interaction and/or a zero-field splitting of the iron(III) ion. As can be seen in other cases [16–18], the contribution of the intermolecular interaction and the zero-field

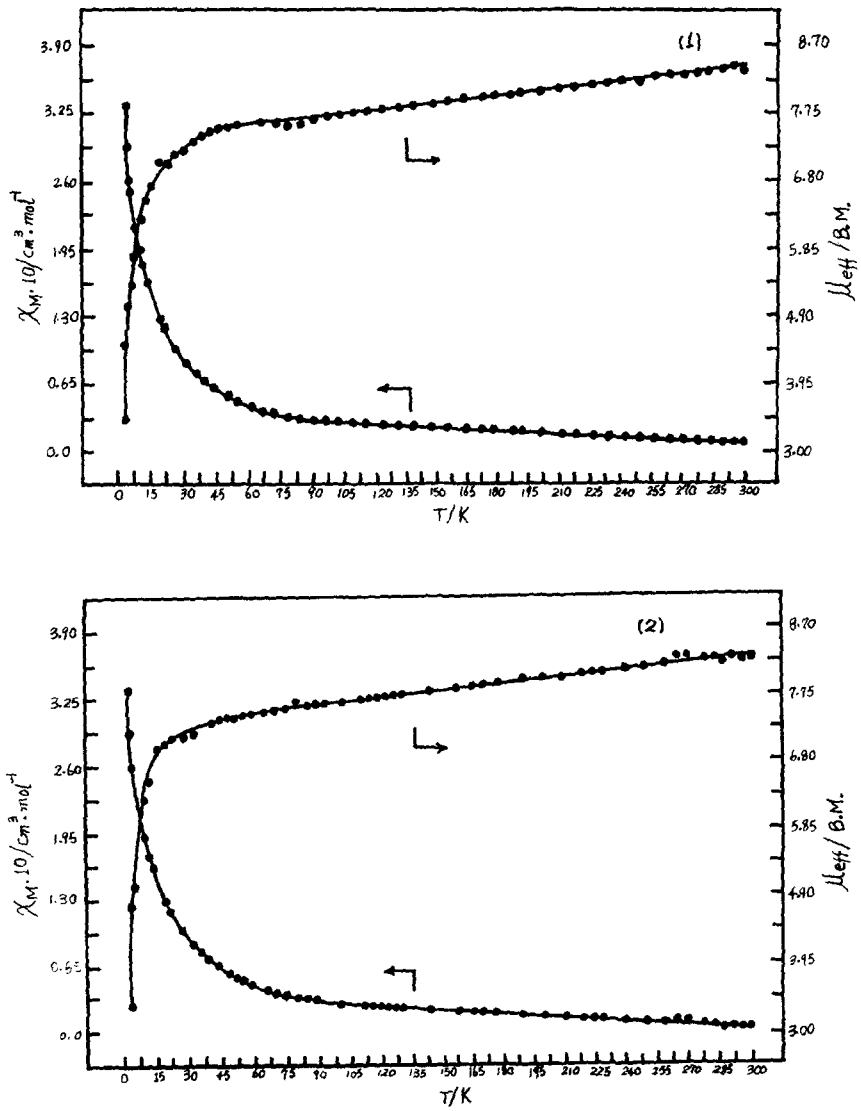

Fig. 2. Temperature variation of χ_M (lower curve) and μ_{eff} (upper curve) for the complexes $[Fe_2(CA)(bpy)_4](ClO_4)_4$ (**1**) and $[Fe_2(CA)(phen)_4](ClO_4)_4$ (**2**). The curve is based on equation (1) using the magnetic parameters given in the text (•), experimental data, (—), calculated curve as described in text.

splitting are evidently weaker than the intramolecular spin exchange and can be negligible. In order to understand quantitatively the magnitude of the spin-exchange interaction, the magnetic analysis was carried out using the susceptibility equation (1) which includes the fraction of a small amount of uncoupled iron(III) impurity (ρ) based on the Heisenberg operator ($\hat{H} = -2J\hat{S}_1 \cdot \hat{S}_2, S_1 = S_2 = 5/2$):

$$\chi_M = (2N\beta^2 g^2/kT)[A/B](1-\rho) + (2.19g^2/T)\rho \quad (1)$$

where

$$A = \exp(2J/kT) + 5\exp(6J/kT + 14\exp(12J/kT) + 30\exp(20J/kT) + 55\exp(30J/kT)$$

$$B = 1 + 3\exp(2J/kT) + 5\exp(6J/kT) + 7\exp(12J/kT) + 9\exp(20J/T)) + 11\exp(30J/kT)$$

and χ_M denotes the molecular susceptibility per binuclear complex, and the remaining symbols have their usual meanings. As shown in Fig. 2, good least-squares fit to the experimental data were obtained with equation (1) for complexes (**1**) and (**2**). This also indicates that the effect of the intermolecular interaction and the zero-field splitting in this case is nominal. The magnetic parameters thus determined and the agreement factor F, defined here as $F = \Sigma[(\chi_M)_{calc} - (\chi_M)_{obs}]^2/\Sigma(\chi_M)_{obs}$ are: $J = -2.1$ cm^{-1}, $g = 2.00$, $\rho = 0.002$, $F = 1.5 \times 10^{-5}$ for (**1**); $J = -5.8$ cm^{-1}, $g = 2.01$, $\rho = 0.004$, $F = 2.1 \times 10^{-5}$ for (**2**). These results indicate that the complexes are essentially binuclear and undergo weak antiferromagnetic spin-exchange interaction between the iron(III) ions within each molecule. The J values of the present complexes are very similar with those of related chloranilato-bridged copper(II) binuclear complexes previously reported [1,2]. The weak antiferromagnetic behavior for these systems may be explained as follows. (i) The distance between metal ions in chloranilato-bridged complexes is rather long [7.843 Å for Cu(II)—Cu(II)] [3]. (ii) Two substituents (Cl) on hydranilic acid may influence the electronic structure of the bridged group. It is well known that the delocalization of the d electrons of the metal towards the bridging atom is one of the main factors affecting the magnetic exchange interaction, while the delocalization extent is determined by the energy gap between the d orbital and bridged atom orbital [19]. Since the chlorine atoms are electron-withdrawing groups which cause decreases in the electron density of the bridged group. The reduction of electron density on the bridged group decreases the electron-electron repulsion and reduced the bridged orbital levels. This will in turn lead to a larger energy gap between the metal and the highest occupied molecular orbitals of the bridge [20] and lower delocalization of the metal orbitals towards the oxygen atoms of bridge, so as to decrease the antiferromagnetic interaction [19].

Acknowledgements—This project was supported by the Natural Science Foundation of Shandong Province and the National Natural Science Foundation of China.

REFERENCES

1. Tinti, F., Verdaguer, M., Kahn, O. and Savariault, J. M., *Inorg. Chem.*, 1987, **26,** 230.
2. Folgado, J. V., Ibanez, R., Coronodo, E., Beltran, D., Savariault, J. M. and Galy, J., *Inorg. Chem.*, 1988, **27,** 19.
3. Deng, C. L., Jiang, Z. H., Liao, D. Z., Yan, S. P. and Wang, G. L., *Synth. React. Inorg. Met.-Org. Chem.*, 1993, **23,** 247.
4. Kawata, S., Kitagawa, S., Konodo, M., Furuchi, I. and Munakata, M., *Angew. Chem., Int. Ed. Engl.*, 1994, **33,** 1759.
5. Kawata, S., Kitagawa, S., Kumagai, H., Kudo, C., Kamesaki, H., Ishiyama, T., Suzuki, R., Konodo, M. and Katado, M., *Inorg. Chem.*, 1996, **35,** 4449.
6. Lindstrand, F., *Z. Anorg. Chem.*, 1936, **230,** 187.
7. Selwood, P. W., *Magnetochemistry*, Intersciences, New York, 1956, p. 78.
8. Geary, W. J., *Coord. Chem. Rev.*, 1971, **7,** 81.
9. Radecka-Paryzek, W., *Inorg. Chim. Acta*, 1979, **34,** 5.
10. Nakamoto, K., *Infrared and Raman Spectra of Inorganic and Coordination Compounds*, 3rd. edn, Wiley Interscience, New York, 1978.
11. Lever, A. B. P., *Inorganic Electronic Spectroscopy*, Elsevier Science Publishers, B. V., Amsterdam, Oxford, New York, Tokyo, 1984.
12. Morton, R. A., In *Biochemistry of Quinones*, ed. R. A. Morton, Academic, London, 1965.
13. Lambert, S. D., Spiro, C. L., Gagne, R. R. and Hendrickson, D. N., *Inorg. Chem.*, 1982, **21,** 68.
14. Dutta, K., Werner, R., Floke, U., Mohanta, S., Nanada, K. K., Haase, W. and Nag, K., *Inorg. Chem.*, 1996, **35,** 2292.
15. Liao, D. Z., Zhung, J. Z., Okawa, H. and Kida, S., *Inorg. Chim. Acta*, 1986, **118,** 21.
16. Kodera, M., Shimakoshi, H., Nishimura, M., Okawa, H., Iijima, S. and Kano, K., *Inorg. Chem.*, 1996, **35,** 4967.
17. Chang, S. H., Jinkwon, K., Nam, H. H. and Youngkyu, D., *Inorg. Chem.*, 1996, **35,** 5110.
18. Ademir, N., Marcos, A. B., Ivo, V., Valderes, D., Klaus, G. and Wolfgang, H., *Inorg. Chem.*, 1996, **35,** 2360.
19. Kahn, O., *Angew. Chem., Int. Ed. Engl.*, 1985, **24,** 834.
20. Ward, M. D., *Inorg. Chem.*, 1996, **35,** 1712.

Pergamon

PII: S0277-5387(97)00400-2

Polyhedron Vol. 17, No. 9, pp. 1429–1433, 1998
© 1998 Elsevier Science Ltd
All rights reserved. Printed in Great Britain
0277-5387/98 $19.00+0.00

Complexes of cobalt(II), nickel(II) and copper(II) with *ortho*- and *para*-phenylenediamine derivatives

Issam J. Sallomi* and Amera J. Shaheen

Department of Chemistry, College of Education, University of Mosul, Mosul, Iraq

(Received 12 July 1995, accepted 8 October 1997)

Abstract—Cobalt(II), nickel(II) and copper(II) complexes with BOP-H_2 (dibenzoinlidene-*o*-phenylenediamine) and BPP-H_2 (dibenzoinlidene-*p*-phenylenediamine) of general formulae $[M(H_2L)X_2]$, $[M_2(H_2L)_2X_4]$, $[M(L)]$ and $[M_2(L)_2]$ (where M = Co, Ni, Cu; X = Cl or NO_3; H_2L and L are the neutral and dibasic forms of the ligands) have been prepared by the reaction of the corresponding metal salts with the two ligands in neutral and basic media. The complexes were characterised by elemental analysis, electrical conductance, magnetic susceptibility and spectral measurements. The studies revealed two different actions of the ligands, neutral tetradentate in neutral medium giving hexacoordinated metal atoms with octahedral geometry and dibasic tetradentate in alkaline solution giving tetrahedral and square planar structures © 1998 Elsevier Science Ltd. All rights reserved

Keywords: cobalt(II); nickel(II); copper(II); phenylene diamine derivatives.

A great deal of work has been reported on the synthesis and structural investigation of different types of Schiff bases and their complexes with transition and non-transition elements [1–6]. The importance of Schiff bases in their action as ligands is due to the ease and flexibility of their synthetic procedures as well as the sensitivity towards the central metal atom [7–9]. The majority of Schiff bases that give stable complexes usually act as multidentate N—N and N—O donors with the formation of mononuclear complexes. In some cases stable oxygen-bridges polynuclear complexes have been reported [6,10,11]. Aside from the interesting ligational properties, these Schiff bases have important biological activity [12–14].

We have reported previously the synthesis of many Schiff bases derived from the reactions of benzoin with acid hydrazides [5,6] or aminophenol [15]. In these complexes the ligands act as tri- and tetradentates forming mononuclear and oxygen-bridged binuclear complexes. In this paper we report the synthesis of Schiff bases derived from the reaction of benzoin with *o*- and *p*-phenylenediamine and the study of their complexes with cobalt(II), nickel(II) and copper(II).

* Author to whom correspondence should be addressed.

EXPERIMENTAL

Analysis and physical measurements

The complexes and the ligands were analysed for carbon, hydrogen and nitrogen using a 1106 CE microanalyser. Conductivity measurements were carried out using a 10^{-3} M solution in dimethylformamide on a LF-42 digital conductivity meter at 25°C. The magnetic susceptibility measurements were made by the Faraday method at room temperature using a Bruker BM6 instrument.

Diamagnetic corrections for the ligands were calculated using Pascal's constants [16]. Infrared absorption spectra were recorded on Pye-Unicam Sp-2000 and Sp-1100 spectrophotometers (200–4000 cm^{-1}) as KBr discs. The electronic spectra were recorded on a Shimadzu UV-160 spectrophotometer for 10^{-3} M solution of the compounds in DMF at 25°C, using a 1 cm quartz cell.

MATERIALS AND METHODS

All the chemicals were of AnalaR. B.D.H., Aldrich or Fluka grade used without further purification. Synthesis of the ligands: the Schiff base ligands, BOP-

H_2 and BPP-H_2, were prepared by the reaction of *o*- or *p*-phenylenediamine with benzoin (in 1:2 molar ratio) in absolute ethanol following the standard procedure reported for similar compounds [6].

Preparation of the complexes

The complexes were prepared by the following general procedure using the appropriate stoichiometries for the metal salt and ligand. A warm ethanolic solution of the metal salt (0.01 mol in 15 cm^3) was added to a warm stirred ethanolic solution of the ligand (0.01 mol in 20 cm^3). The resulting mixture was then treated in two different ways. In the first, the mixture was refluxed on a water bath for about 5–6 h. The solution was then evaporated to about half its volume and on cooling a crystalline product separated out. In the second method, 0.1 M potassium hydroxide was added slowly, with constant stirring, to the mixture till pH 8–8.5. At this pH complete precipitation occurred and the mixture was digested on a water bath for about 10 min and then cooled. The separated complexes from both methods were filtered off, washed with cold ethanol, diethylether and dried *in vacuo*.

RESULTS AND DISCUSSION

The new complexes were synthesized in good yield by the reaction of the metal salts with the two ligands in neutral and basic media according to the following equations:

$$MX_2 + \text{BOP-}H_2 \rightarrow [M(\text{BOP-}H_2)X_2]$$

$$2MX_2 + 2\text{BPP-}H_2 \rightarrow [M_2(\text{BPP-}H_2)_2X_4] \quad (1)$$

$$MX_2 + \text{BOP-}H_2 + 2KOH \rightarrow [M(BOP)] + 2KCl + 2H_2O$$

$$2MX_2 + 2\text{BPP-}H_2 + 4KOH \rightarrow [M_2(BPP)_2] + 4KX + 4H_2O \quad (2)$$

where M = Co, Ni, Cu; X = Cl or NO_3; BOP-H_2 BPP-H_2 are the neutral forms of the ligands derived from *o*- and *p*-phenylenediamine, respectively, and BOP, BPP are the dibasic form of the same ligands. The complexes gave satisfactory analytical data (Table 1) indicating 1:1 metal-to-ligand stoichiometry for all of them. The complexes are air stable at room temperature but they decompose without melting at temperatures above 250°C. All the complexes are insoluble in water but they are soluble to a limited extent in methanol, ethanol, DMF and DMSO. Their low electrical conductances in DMF are consistent with the given formulation (Table 1) indicating non-electrolytic nature [17]. The active sites of the ligands and their coordination to the metal atoms as well as the structure of the resulting complexes were inferred by spectral and magnetic measurements.

Infrared spectra

The bonding of the ligands to the metal atom was characterised by comparison of the main infrared absorption bands of the free ligands and their complexes. Each ligand contains two symmetrical benzoinlidene groups (HO—C—C=N—) which show OH and C=N function in the same infrared region. The important bands of the free ligands and their complexes are given in Table 2.

For complexes formed in neutral medium (**1**), $[M(\text{BOP-}H_2)X_2]$ and $[M_2(\text{BPP-}H_2)_2X_4]$, the bands due to ν(OH) and δ(OH) vibrations showed negative shift of about 100–130 and 30–40 cm^{-1}, respectively, suggesting the involvement of alcoholic hydroxyle in coordination through their oxygen atoms.

The observation of a ν(C—O) band at lower frequency by 30–40 cm^{-1} and its splitting into two peaks (due to C—O—H) was considered to be further support for the coordinate of alcohol groups without deprotonation (Fig. 1) as observed in similar complexes [6]. The shifting of ν(C=N) band to lower values by 25–30 cm^{-1} indicates the participation of the two azomethine nitrogen atoms in bonding [8,9,18]. Additional bands, not observed in the free ligands' spectra located at about 1530, 1280 and 930 cm^{-1} are attributed to νN—O of unidentate coordination of nitrato groups [19]. The chloro complexes exhibit bands in the range 280–290 cm^{-1} and are assigned to the stretching frequency of coordinated chloride ions [20].

For **2** complexes formed in basic solution, [(BOP)] and $[M_2(BPP)_2]$, the disappearance of OH-stretching and deformation bands indicates the action of the ligands in their dibasic forms. This coordination was confirmed by the negative shift of the single ν(C—O) band by 30–35 cm^{-1}. Furthermore, the C=N stretching bands in their complexes were lowered by 25–30 cm^{-1} and thus suggesting bond formation through azomethine groups similar to that observed in **1** complexes [8].

In both types, new bands were noticed in the infrared spectra at 440–450 and 480–485 cm^{-1} and assigned to stretching modes of M—N and M—O, respectively [21,22].

Electronic spectra and magnetic moments

The μ_{eff} values and the positions of the electronic spectral bands together with the proposed geometries are given in Table 3. The electronic spectra of the complexes in DMF indicate two different structural configurations. For cobalt(II) complexes of **1**, two bands were observed and assigned to $^4T_1g(F) \rightarrow {}^4T_2g(F)(\nu_1)$ and $^4T_1g(F) \rightarrow {}^4T_1g(P)(\nu_3)$ transitions, respectively, in an octahedral environment [23]. The

Table 1. Analytical data and some physical properties

No.	Complex	Colour	% Yield	Λ_M (cm^2 ohm^{-1} mol^{-1})	Found (calc.) % C	H	N
1	BOP-H_2	Yellow-brown	96	—	82.6(82.3)	5.4(5.6)	5.3(5.6)
2	BPP-H_2	Deep yellow	94	—	82.5(82.3)	5.8(5.6)	5.3(5.6)
3	$[Co(BOP\text{-}H_2)Cl_2]$	Brown	78	14	65.6(65.2)	4.3(4.5)	4.4(5.5)
4	$[Ni(BOP\text{-}H_2)NO_2)_2]$	Brown	76	6	60.3(60.1)	4.3(4.1)	8.4(8.2)
5	$[Cu(BOP\text{-}H_2)Cl_2]$	Deep yellow	80	10	65.1(64.7)	4.6(4.4)	4.4(4.4)
6	$[Co_2(BPP\text{-}H_2)_2Cl_4]$	Pale brown	68	12	65.5(65.2)	4.4(4.5)	4.6(4.5)
7	$[Ni_2(BPP\text{-}H_2)(NO_3)_4]$	Brown	74	7	60.5(60.1)	4.0(4.1)	8.3(8.2)
8	$[Cu_2(BPP\text{-}H_2)_2Cl_4]$	Pale brown	70	4	64.2(64.7)	4.1(4.4)	4.2(4.4)
9	[Co(BOP)][a]	Deep yellow	86	3	74.1(73.8)	4.6(4.7)	4.8(5.1)
10	[Ni(BOP)][a]	Light brown	84	8	73.5(73.8)	4.5(4.7)	4.7(5.1)
11	[Cu(BOP)][a]	Light brown	84	5	72.9(73.2)	4.8(4.7)	5.2(5.0)
12	$[Co_2(BPP)_2]$[a]	Brown	80	10	73.4(73.8)	4.3(4.7)	5.3(5.1)
13	$[Ni_2(BPP)_2]$[a]	Deep yellow	87	6	74.2(73.8)	4.6(4.7)	5.2(5.1)
14	$[Cu_2(BPP)_2]$[a]	Pale brown	81	5	73.5(73.2)	4.9(4.7)	5.4(5.0)

[a] The same compound was obtained by using different metal salts.

Table 2. Important IR spectral data (cm^{-1})

Compound No.	ν (OH)	ν (C=N)	δ (OH)	ν (C—O)	ν (M—N)	ν (M—O)	ν (M—X)[b]
1	3500	1635	1310	1240	—	—	—
2	3500	1635	1320	1240	—	—	—
3	3380	1610	1280	1200 1205	440	485	285
4	3385	1605	1275	1200 1205	440	485	1530, 1280, 930
5	3400	1605	1280	1200 1210	445	485	285
6	3385	1610	1280	1205 1210	450	480	290
7	3390	1605	1285	1200 1210	450	485	1525, 1280, 935
8	3390	1605	1280	1200 1205	445	485	280
9	—	1610	—	1210	440	480	—
10	—	1610	—	1210	440	480	—
11	—	1605	—	1210	440	485	—
12	—	1610	—	1205	440	485	—
13	—	1610	—	1205	450	485	—
14	—	1605	—	1210	450	485	—

[a] As in Table 1.
[b] X = Cl or NO_3.

ν_2 band due to $^4T_1g(F) \rightarrow {}^4A_2g(F)$ transition could not be observed, as it is a two electron process and is much weaker than the other two transitions [24]. Therefore the ν_2 transition remain almost unobserved because of its weakness and proximity to a strong ν_3 transition [25]. However the values of ν_2 bands have been calculated and the results are in good agreement with Tanabe–Sugano diagram for a d^7 ion in an octahedral environment where ν_2 and ν_3 transitions are predicted to lie almost at the same position [26]. The electronic spectra of nickel(II) complexes of **1** exhibit three bands attributed to ν_1, ν_2 and ν_3 which correspond to the transitions $^3A_2g(F) \rightarrow {}^3T_2g(F)$, $^3A_2g(F) \rightarrow {}^3T_1g(F)$ and $^3A_2g(F) \rightarrow {}^3T_1g(P)$, respectively. The spectra of both nickel(II) complexes referred to considerable distortion for octahedral symmetry (not observed for

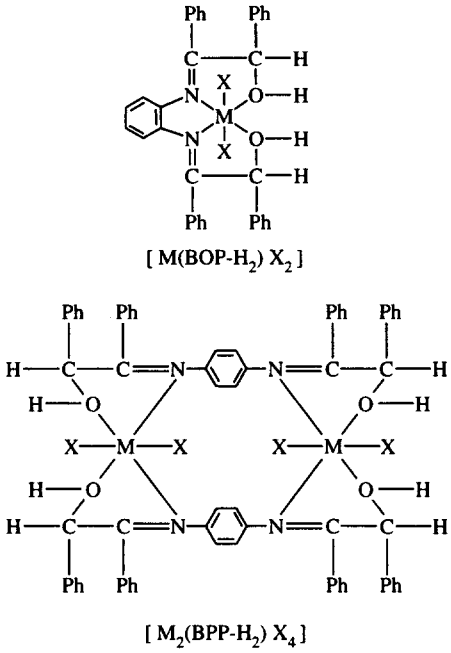

[M(BOP-H_2) X_2]

[M_2(BPP-H_2) X_4]

Fig. 1.

cobalt(II) complexes) since the calculated energy difference between $^3T_1g(P)$ and $^3T_1g(F)$ levels (14,500 cm^{-1}) is greater by about 5200 cm^{-1} than the difference ν_3–ν_2 (~9300 cm^{-1}). This is presumably due to interligand interaction and repulsion causing elongation of metal–ligand bonds and thus leading to distortion of the octahedron [27]. In the case of copper(II) **1** complexes a broad asymmetric band was observed and assigned to the three combined transitions $^2B_1g \rightarrow {}^2A_1g$, $^2B_1g \rightarrow {}^1B_2g$ and $^2B_1g \rightarrow {}^2Eg$ of tetragonally distorted octahedral environment around copper(II) ion due to the Jahn–Teller effect [28–30].

The effective magnetic moments for BOP-H_2 complexes measured at room temperature fall in the range expected for high-spin octahedral geometries [31] for cobalt(II), d^7, nickel(II), d^8, and copper(II), d^9, systems consistent with the presence of three, two and one unpaired electrons, respectively. On the other hand, the μ_{eff} values for BPP-H_2 complexes were less than those expected. The lower values may be attributed to binuclear dimeric structure as observed for similar complexes and ascribed as antiferromagnetic coupling of the unpaired electrons on the adjacent metal ions [32].

The complexes of **2** exhibit two different geometries as found from the electronic spectra and magnetic moments. Cobalt(II) and nickel(II) complexes exhibit two bands due to $^4A_2(F) \rightarrow {}^4T_2(P)$. $^4A_2(F) \rightarrow {}^4T_1(F)$ and $^3T_1(F) \rightarrow {}^3A_2(F)$, $^3T_1(F) \rightarrow {}^3T_1(P)$ transitions and assigned to ν_2 and ν_3, respectively. The low energy transition $^4T_2(F) \rightarrow {}^4T_2(F)$ and $^3T_1(F) \rightarrow {}^3T_2(F)$ of the unobserved band ν_1 was theoretically calculated [24]. The positions and intensity of these bands are consistent with tetrahedral geometry for the tetracoordinated cobalt(II) and nickel(II) complexes [23]. For copper(II) complexes, only one broad band was observed in their electronic spectra. This band is attributed to the $^2B_1g \rightarrow {}^2Eg$ transition which is consistent with square planar geometry around the copper(II) ion [33]. Once again, all the complexes were found to be paramagnetic with magnetic moments (Table 3), for BOP-complexes consistent with three, two and one unpaired electron, while for BPP-complexes lower μ_{eff} values were observed (as in **1**) and attributed to superexchange mechanism.

From the above discussion and on the bases of the data given in Tables 1–3, the following conclusion can be drawn. Both ligands act as tetradentate forming hexacoordinate complexes (in neutral medium) with most probable octahedral or distorted octahedral

Table 3. Magnetic moments, electronic spectral data and proposed geometries

Compound No.[a]	Electronic bands (cm^{-1}) ν_1	ν_2	ν_3	Magnetic moments (BM)	Geometry
3	9240	18,800[b]	19,600	4.0	Octahedral
4	8900	15,850	25,150	3.11	Distorted octahedral
5	13,800	—	—	1.95	Distorted octahedral
6	9260	18,820[b]	19,650	3.58	Octahedral
7	8950	15,988	25220	1.66	Distorted octahedral
8	14,100	—	—	1.58	Distorted octahedral
9	3250[b]	6500	14,500	3.95	Tetrahedral
10	3950[b]	7100	13,950	3.10	Tetrahedral
11	24,100	—	—	1.95	Square planar
12	3280[b]	6550	14,550	3.65	Tetrahedral
13	4000[b]	7150	14,000	2.60	Tetrahedral
14	24,300	—	—	1.65	Square planar

[a] As in Table 1.
[b] Calculated values.

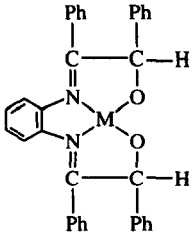

[M(BOP)]

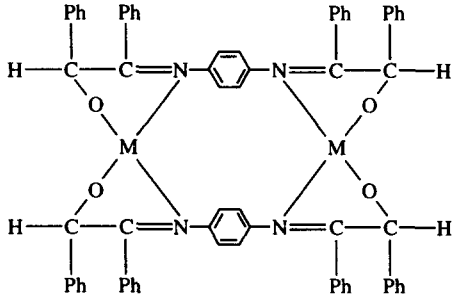

[$M_2(BPP)_2$]

Fig. 2.

structures. In basic medium, they act as dibasic tetradentate forming tetrahedral and probably distorted planar [for cobalt(II) and nickel(II)] and square planar [for copper(II)] complexes. Mononuclear complexes were obtained with BOP ligand, while BPP acts as bridging ligand forming dinuclear complexes as shown in Figs 1 and 2.

REFERENCES

1. Yamada, S., *Coord. Chem. Rev.*, 1966, **1,** 415; 1967, **2,** 83.
2. Kahwa, I. A., Hsieh, T. C. Y., Laine, R. A. and Selbin, J., *Inorg. Chim. Acta*, 1986, **118,** 179.
3. Golonka, M. C. and Bartecki, A., *Coord. Chem. Rev.*, 1979, **31,** 251.
4. O'Conner, C. J., Romananch, R. J., Robertson, D. M. Edudk, E. E. and Fronczek, F. F., *Inorg. Chem.*, 1983, **22,** 449.
5. Sallomi, I. J. and Shaheen, A. J., *Iraqi J. Chem.*, 1990, **15,** 129.
6. Sallomi, I. J. and Shaheen, A. J., *Trans. Met. Chem.*, 1994, **19,** 275 and refs therein.
7. Bomlneri, G., Benetoilo, F., Pollo, A., De Cola, L., Smales, D. L. and Vallarino, I. M., *Inorg. Chem.*, 1986, **25,** 1127.
8. Dey, K., Ray, S., Bhattacharyya, P. K., Gangopadhyay, A., Bhasin, K. K. and Verma, R. D., *J. Indian Chem. Soc.*, 1985, **62,** 809.
9. Sallomi, I. J. and Shaheen, A. J., *J. Iraqi Chem. Soc.*, 1987, **12,** 159.
10. Padhye, S. and Kauffman, G. B., *Coord. Chem. Rev.*, 1985, **63,** 127.
11. Sinn, E. and Harris, C. M., *Coord. Chem. Rev.*, 1969, **4,** 391.
12. Hodnett, E. M. and Dunn, W. J., *J. Med. Chem.*, 1970, **12,** 768.
13. Hodnett, E. M. and Moony, P. D., *J. Med. Chem.*, 1970, **13,** 786.
14. Billman, H. J. and Schrmidgall, R. L., *J. Pharm. Sci.*, 1970, **59,** 1191.
15. Sallomi, I. J., *Trans. Met. Chem.*, in press.
16. Selwood, P. W., *Magnetochemistry*. Interscience, New York, 1956.
17. Geary, W. J., *Coord. Chem. Rev.*, 1971, **7,** 81.
18. Taylor, L. T. and Patton, R. D., *Inorg. Chim. Acta.*, 1974, **8,** 191.
19. Gatehouse, B. M., Livingston, S. E. and Nyholm, R. S., *J. Chem. Soc.*, 1957, p. 4222; *J. Inorg. Nucl. Chem.*, 1958, **8,** 75.
20. Nakamoto, K., *Infrared Spectra of Inorganic and Coordination Compounds*. New York, 1983.
21. Madan, S. K. and Donohus, A. M., *J. Inorg. Nucl. Chem.*, 1969, **28,** 1303.
22. Fay, R. C. and Pinnavaia, T. J., *Inorg. Chem.*, 1968, **7,** 502.
23. Lever, A. B. P., *Inorganic Electronic Spectroscopy*. Elsevier, Amsterdam, 1968.
24. Lever, A. B. P., *J. Chem. Ed.*, 1968, **45,** 711.
25. Ram Rao, N., Surya Rao, D. and Ganorkar, M. C., *Indian J. Chem. Sect. A.*, 1982, **21,** 839.
26. Lever, A. B. P., *J. Chem. Soc., A*, 1967, p. 241.
27. Sallomi, I. J., *J. Indian Chem. Soc.*, 1995, **72,** 327.
28. Jahn, H. A. and Teller, E., *Proc. Roy. Soc. (London)*, 1937, **161,** 220.
29. Duff, E. J., Hughes, M. N., and Rutt, K. J., *J. Chem. Soc.*, 1969, p. 2126.
30. Satyanarayana, D. and Mahapatra, B. K., *Indian J. Chem.*, 1975, **13,** 414.
31. Figgis, B. N. and Lewis, J., *Prog. Inorg. Chem.*, 1964, **6,** 37.
32. McLellan, A. W. and Melson, G. A., *J. Chem. Soc., A*, 1967, p. 137.
33. Ferguson, J., *Theor. Chim. Acta.*, 1965, **3,** 287.

Pergamon

PII: S0277-5387(97)00415-4

Polyhedron Vol. 17, No. 9, pp. 1435–1438, 1998
© 1998 Published by Elsevier Science Ltd
All rights reserved. Printed in Great Britain
0277-5387/98 $19.00+0.00

EPR studies on irradiated group VI tetrachalconide ions

Tim Ecclestone, Stuart H. Laurie,* Martyn C. R. Symons and Fatai A. Taiwo

Department of Chemistry, De Montfort University, The Gateway, Leicester LE1 9BH, U.K.

(Received 21 July 1997; accepted 7 October 1997)

Abstract—EPR measurements have been made at X-band frequency and at 77 K on γ-irradiated glassy solutions of salts of the d^0 chalconide anions MX_4^{2-} (M = Cr, X = O; M = Mo, X = O or S; M = W, X = O or S). Annealing of the irradiated solutions revealed broad high-field spectral features attributable to one-electron addition to the anions. The exception being WS_4^{2-}, for which no EPR signal was detectable at 77 K or above. The results point to the added electron being predominantly located on the metal centre (d^1). The g-shifts are interpreted in terms of a distorted T_d geometry with a $d_{x^2-y^2}$ configuration. © 1998 Elsevier Science Ltd. All rights reserved

Keywords: EPR; γ-irradiation; tetrachalconides; group VI.

INTRODUCTION

Early work by one of us demonstrated that conversion of MnO_4^- into MnO_4^{2-} and MnO_4^{3-} occurred in alkaline solutions [1–3], similarly CrO_4^{2-} was observed to convert to CrO_4^{3-} simply by dissolution in concentrated aqueous alkali at room temperature [3]. It was also shown that exposure of potassium chromate crystals to ionizing radiation gave an EPR spectrum assignable to CrO_4^{3-} ions [4]. EPR spectra were also obtained [5,6] for MnO_4^{2-}, MnO_4^{3-} and FeO_4^{2-}. These early studies have been summarised in a review [7]. At about the same time Banks *et al.* [8] showed that CrO_4^{3-} ions formed at very high temperatures in Ca_3PO_4Cl doped with chromate, the Cr(V) centres were characterised by EPR and optical spectroscopy. It is also worth noting that the concentrated alkaline solutions referred to above evolve oxygen, formed from the solvent water [9]. It was suggested that this reaction involved an initial electron transfer from OH^- ions [1,2,9]. So far as we know this novel source of ·OH (·O$^-$) radicals has never been exploited or refuted.

We know of no comparable studies for d^1 Mo or W tetraoxides or tetrasulphides. A report [10] on irradiated calcium tungstate describes a centre with g values greater than the free spin value (2.0023) which, in our view, seems to arise from the electron-loss centre $O_3W—O^{\circ-}$ and not the expected d^1 derivative WO_4^{3-}. The lowest orbitals available for an added electron in these tetrahedral anions are the $e_2 d_{x^2-y^2}$ and d_{z^2} pair and the $p(\pi)$ orbitals of the ligands. The orbital degeneracy is strongly lifted by distortions to give either $d^1_{z^2}$ or $d^1_{x^2-y^2}$ ground-states, both these have g tensor components less than the free-spin value.

The aim of the present work was to prepare and contrast the CrO_4^{3-}, MoX_4^{3-} and WX_4^{3-} d^1 complex ions (X = O or S). One particular reason for this arose from the finding of Mo(V) and W(V) centres in some new ternary metal sulphides prepared from the d^0 MoS_4^{2-} and WS_4^{2-} ions [11,12] and the need to prepare and characterise simple MS_4^{3-} centres for comparison. This can readily be achieved using ionizing radiation coupled with matrix isolation. By selecting suitable solvents in which the substrate (Su) is soluble and which freezes to a glassy solid without phase separation, only electron addition to give Su^- centres occurs initially [13]. Hence, we set out to add one electron only to the d^0 CrO_4^{2-}, MoO_4^{2-}, WO_4^{2-}, MoS_4^{2-} and WS_4^{2-} anions. Recently there has been a strong revival of interest in the high-valence states of transition metals. This is in part because of the realisation that anions such as CrO_4^{2-} are potential carcinogens, and in part because of the recognition that high-valence states, especially of iron, are of potential importance in biological redox processes [14].

* Author to whom correspondence should be addressed.

EXPERIMENTAL

Ammonium or potassium salts of the tetraoxo ions of AnalaR or Puriss grade were used (the cation was found to have no influence in the dilute systems used). $(NH_4)_2MoS_4$ and $(NH_4)_2WS_4$ were prepared by standard literature methods and their purities verified by their UV/VIS and IR spectra [15,16].

For irradiation the compounds were dissolved in de-gassed deuterated water–methanol (D_2O–CD_3OD) mixtures which formed glassy solids on freezing at 77 K. Frozen pellets were irradiated at 77 K in a Vickrad ^{60}Co gamma source at doses between 10^3 and 10^4 Gy.

First derivative EPR spectra were measured at 77 K using a Bruker EMX 6/1 X-band spectrometer set at a frequency of ca 9.7 GHz using 100 KHz modulation in a T_{102} rectangular cavity. Operating conditions were 10 mW microwave power, 7G modulation amplitude, centre field 3488G, sweep width 3000G, time constant 20.48 min and scan time 41.94 s with multiple accumulations to enhance the signal-to-noise ratio. Qualitative assignment of spin Hamiltonian parameters was by simulation using the Simfonia program (Bruker). After the first measurements the samples were subsequently annealed by warming above 77 K to eliminate solvent radicals, and re-cooling rapidly back to 77 K for further EPR measurements. This annealing cycle was continued until no further changes were observed apart from some loss in the solute-radical spectra.

RESULTS AND DISCUSSION

In all cases, except for WS_4^{2-} solutions, broad high-field features were observed in addition to the signals from solvent radicals in the free-spin region. The broad features can be assigned to electron capture species. That electron capture species had formed rather than trapped electrons was indicated by the absence of any narrow ESR singlet and the absence of any intense (purple-black) colouration. In all cases these high-field features were broad and ill defined at 77 K but narrowed irreversibly on annealing. Clear parallel ($\parallel$) and perpendicular ($\perp$) features were then resolved (see, for example, Figs 1 and 2).

Only WS_4^{2-} failed to give any detectable EPR spectrum after irradiation. The EPR spectrum of any electron capture species in this case is most likely to be too broad to be detected at 77 K. This is not unexpected; in fact, it is more surprising that we were able to detect the WO_4^{3-} species, despite the very large g-shifts (see Table 1). Weak features observed on either side of the main peaks are assignable to the presence of low abundant magnetic nuclei, i.e., ^{53}Cr (9.5%, $I = 3/2$), ^{95}Mo (15.9%, $I = 5/2$) and ^{97}Mo (9.55%,

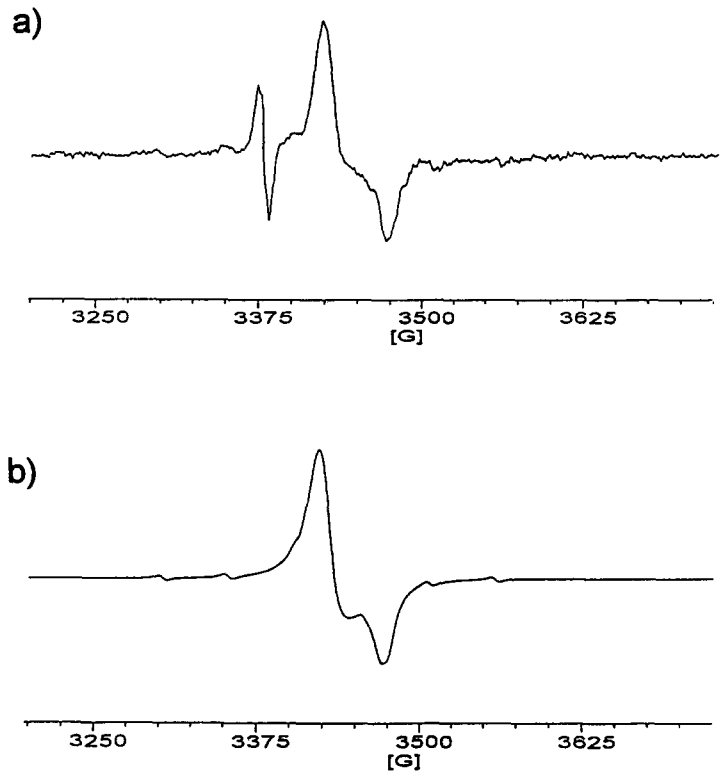

Fig. 1. (a) First derivative X-band EPR spectrum for a dilute solution of $(NH_4)_2MoS_4$ in CD_3OD after exposure to ^{60}Co γ-rays at 77K; (b) Simulation using the data in Table 1. The narrow feature at $g = 2.0023$ is assigned to solvent radicals.

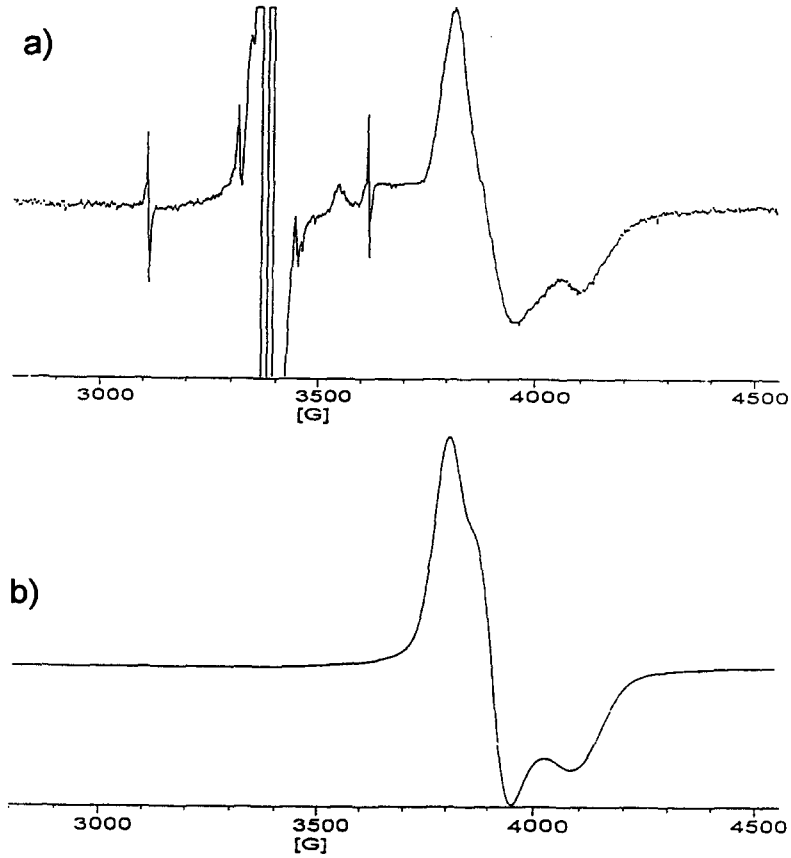

Fig. 2. First derivative X-band EPR spectrum for a dilute solution of $(NH_4)_2 WO_4$ in CD_3OD after exposure to ^{60}Co γ-rays at 77 K; (b) Simulation using the data in Table 1.

Table 1. Experimental EPR parameters assigned to the electron adducts

Anion	g-Values		Hyperfine coupling/G[a]	
	$g_\parallel$	$g\perp$	$A_\parallel$	$A_\perp$
CrO_4^{3-} [b]	1.930	1.983	+60	+24
CrO_4^{3-} [c]	1.990	1.950	A_x 8.2,	A_y 24.9, A_z 21.0
MoO_4^{3-}	1.912	1.937	+77	+39
WO_4^{3-}	1.65	1.75	+30	+71
MoS_4^{3-}	1.953	1.973	+51.2	+30
WS_4^{3-}	[d]			

[a] $G = 10^{-4}T$,
[b] This work,
[c] Ref. [9],
[d] Spectrum not detected.

$I = 5/2$) (Fig. 1). The hyperfine features from the two Mo isotopes were not separately resolved. Unfortunately, the main features for WO_4^{3-} were always so broad that the expected satellite features from ^{183}W (14.28%, $I = 1/2$) were not resolvable (see Fig. 2).

Interpretation of spectra

The observed g-shifts suggest that the (T_d) e_2 d orbitals of the central metal ion must have been extensively split as a result of marked deviations from the pure T_d symmetry of the parent di-anions. In the present examples these distortions appear to place the $d_{x^2-y^2}$ level below the d_{z^2} level in contrast, for example, with the results reported by McGarvey and co-workers [8] for CrO_4^{3-}. For the $d^1_{x^2-y^2}$ systems the order $g_\parallel < g_\perp < FS$ is expected, whilst for the d_{z^2} configuration the order is $g_\perp < g_\parallel \approx FS$ (FS = the free spin value of 2.0023), see Table 1.

The form of the hyperfine splitting for ^{53}Cr and $^{95/97}Mo$ also accord with expectation for a $d^1_{x^2-y^2}$ configuration. Both $A_\parallel$ and $A_\perp$ are assigned "positive" values in order to obtain data of the expected form [we note that all the magnetic nuclei have negative moments so that signs are reversed compared with

those for the more usual positive nuclei]. This choice of signs results in "positive" values for both A_{iso} and 2B (Table 2), where 2B is the purely anisotropic dipolar interaction term. The "positive" signs with A_{iso} and 2B and their magnitude are in accord of the assignment of the $d_{x^2-y^2}$ orbital as the singly occupied molecular orbital (SOMO).

It is of interest to compare these results for the CrO_4^{3-} anion with those of McGarvey and co-workers [8]. Their d^1 anion was generated thermally in a phosphate lattice. In this case, the mode of distortion from T_d symmetry would be strongly influenced by lattice requirements, this would explain the inversion of g values compared with our results. Furthermore, the spin Hamiltonians clearly show that their Cr (V) nuclei are not purely axial in symmetry; $|A_x| \neq |A_y|$, (see Table 1). The estimated spin density on the metal ion in this case is ~50%, a strong indication of less charge transfer from the oxo-ligands to the metal than in our system with a metal spin density of ~94%. The form of the ^{53}Cr hyperfine components fit nicely with a $d_{z^2}^1$ assignment. It was earlier suggested that for d^1 systems with $|A| > |B|$ the ground-state would be consistent with a $d_{z^2-y^2}^1$ configurations, whilst if $|A| < |B|$ it should be $d_{z^2}^1$. Reported experimental data do not support this as a general rule; so we prefer to argue from the relative g-values as above. It seems clear from the CrO_4^{3-} results that small changes in symmetry induced by the environment, can switch the system between $d_{x^2-y^2}^1$ and $d_{z^2}^1$ configurations.

For the present study, a further strong possibility, especially on annealing, would be protonation of the anions. The parent anions would already be strongly solvated so that movement of H^+ within such units would be facile. However, there was no direct evidence of protonation having occurred.

Table 2. Estimated spin-densities on Mo and W centres

Complex	A_{iso}/G[a]	2B/G	Spin-densities on metal
CrO_4^{3-} [b]	+38.0	+19.9	94%
CrO_4^{3-} [c]	+18.0	+10.0	50%
MoO_4^{3-}	+50.7	+23.3	90%
MoS_4^{3-}	+43.0	+28.0	91%
WO_4^{3-}	[d]		

[a] G = 10^4T.
[b] From Ref. [9],
[c] From Ref. [8],
[d] No hyperfine features resolved.

CONCLUSIONS

This study underlines the utility and simplicity of the use of ionizing radiation coupled with dilute glassy media for generating one-electron addition at low temperatures. These systems are ideal for study by EPR spectroscopy. From this work it appears that the d^1 anions CrO_4^{3-}, MoO_4^{3-} and WO_4^{3-} have very similar structures, the larger g-value shifts for WO_4^{3-} being a reflection of the large spin-orbit coupling constant for tungsten. The similarity in magnetic parameters of MoO_4^{3-} and MoS_4^{3-} is consistent with the electron being predominantly located on the metal centre (d^1), this is further supported by the spin-density values shown in Table 1. [Although these estimated values are regarded as approximations only our experience has always been that the method does give qualitatively meaningful values of spin-densities.]

REFERENCES

1. Symons, M. C. R., *J. Chem. Soc.*, 1953, 3956.
2. Carrington, A. and Symons, M. C. R., *J. Chem. Soc.*, 1956, 3372.
3. Bailey, N. and Symons, M. C. R., *J. Chem. Soc.*, 1957, 203.
4. Carrington, A., Ingram, D. J. E., Schonland, D. and Symons, M. C. R., *J. Chem. Soc.*, 1956, 4710.
5. Lister, D. H. and Symons, M. C. R., *J. Chem. Soc.*, 1970, 782.
6. Carrington, A., Ingram, D. J. E., Lott, K. A. K., Schonland, D. and Symons, M. C. R., *Proc. Roy. Soc. A.*, 1960, **254,** 101.
7. Carrington, A. and Symons, M. C. R., *Chem. Rev.*, 1963, **63,** 443.
8. Banks, E., Greenblatt, M. and McGarvey, B. R., *J. Chem. Phys.*, 1967, **47,** 3772.
9. Symons, M. C. R., *J. Chem. Soc.*, 1954, 3676.
10. Zeldes, H. and Livingston, R., *J. Chem. Phys.*, 1961, **34,** 247.
11. Laurie, S. H., Pratt, D. E. and Raynor, J. B., *Inorg. Chim. Acta*, 1986, **123,** 193.
12. Ecclestone, T. and Laurie, S. H., unpublished observations.
13. Symons, M. C. R., *Pure and Applied Chem.*, 1981, **53,** 223.
14. Bielski, B. H. J., Sharma, V. K. and Czaski, G., *Radiat. Phys. Chem.*, 1994, **44,** 479.
15. Mellor, J. W., *A Comprehensive Treatise on Inorganic and Theoretical Chemistry*, Vol. 11, Longmans, London, 1943, p. 650.
16. Clarke, N. J. and Laurie, S. H., *Inorg. Chim. Acta.*, 1982, **66,** L135.

Pergamon

PII: S0277-5387(97)00421-X

Polyhedron Vol. 17, No. 9, pp. 1439–1448, 1998
© 1998 Elsevier Science Ltd
All rights reserved. Printed in Great Britain
0277-5387/98 $19.00+0.00

Interaction of the polyfunctional 2-mercaptonicotinic acid with the ruthenium(III)-edta complex

Francisca N. Rein and Henrique E. Toma*

Instituto de Química, Universidade de São Paulo, C. Postal 26077, CEP 05599–970, São Paulo, SP, Brazil

(Received 18 May 1997; accepted 6 October 1997)

Abstract—Ruthenium(III)-edta reacts with the 2-mercaptonicotinic ligand in aqueous solution yielding a red product (λ_{max} = 530 nm) coordinated at the S atom. This species undergoes deprotonation with an apparent pK_a = 3.80, generating a blue complex in which the ligand is (*S,N*)-bidentate. In the presence of two times excess of ruthenium(III)-edta a binuclear species is formed, involving two bidentate (*N,S*) and (*S,O*) coordination modes for the bridging ligand. The corresponding mixed-valence species exhibits a strong intervalence band at 8000 cm^{-1}, involving an electronic coupling energy of 990 cm^{-1}. An extensive investigation is reported for the complexes, based on kinetics, cyclic voltammetry and spectroelectrochemistry. © 1998 Elsevier Science Ltd. All rights reserved

Keywords: ruthenium-edta; mixed-valence complex; polyfunctional ligand.

The coordination chemistry of polyfunctional ligands can be particularly interesting from the point of view of their selective binding to transition metal ions and formation of extended structures. As a matter of fact, polyfunctional ligands are widespread in biological systems, including the aminoacids and nucleic acids, and in addition, the properties of their metal derivatives can be exploited in the area of molecular materials [1], and in supramolecular chemistry and devices [2].

In this work we focused on the reaction of the 2-mercaptonicotinic acid (H_2mnic) with the ruthenium-(III)-edta complex in aqueous solution. This polyfunctional molecule exhibits three potential binding sites for transition metal ions, and can act as a monodentate, bidentate and bridging ligand, as illustrated in Scheme (1).

In fact, all these species can be generated, under controlled conditions, in the presence of the $[Ru^{III}(edta)]^-$ complex. The investigation of their kinetics, redox and spectroelectrochemical properties, is reported herein.

* Author to whom correspondence should be addressed.
E-mail: henetoma@quim.iq.usp.br

EXPERIMENTAL

The $[Ru^{III}(Hedta)H_2O]\cdot 4H_2O$ complex, here denoted $Ru^{III}A$, was obtained according to the procedures previously reported in the literature [3,4]. Found: C, 25.4; H, 4.0; N, 5.9. Calc. for $RuC_{10}H_{23}N_2O_{13}$: C, 25.0; H, 4.8; N, 5.8. The blue complex $Na_3[Ru^{III}(edta)(mnic)]\cdot 8H_2O$ was prepared by reacting 0.070 g (0.15 mmol) of $Ru^{III}A$ with 0.024 g (0.15 mmol) of mnic (Aldrich), in 10 cm^3 of water, under an argon atmosphere. After 10 min the pH was raised up to 6.50 by adding a 0.1 mol dm^{-3} NaOH solution, and the mixture was evaporated to dryness using a rotary evaporator. The dark solid was dissolved in 10 cm^3 of methanol, and precipitated by adding 15 cm^3 of diethyl ether. The blue complex was colleted on a filter, washed with ether and dried under vacuum. Found: C, 25.6; H, 3.8; N, 5.3. Calc. for $Na_3RuC_{16}H_{31}N_3O_{18}S$: C, 25.4; H, 4.1; N, 5.5.

The electronic spectra of the complexes were recorded on a Hewlett-Packard model 8452-A diode-array spectrophotometer, or on a Guided-Wave model 260 fiber-optics instrument. Cyclic voltammetry was carried out using a Princeton Applied Research Corp. (PARC) model 173 potentiostat and

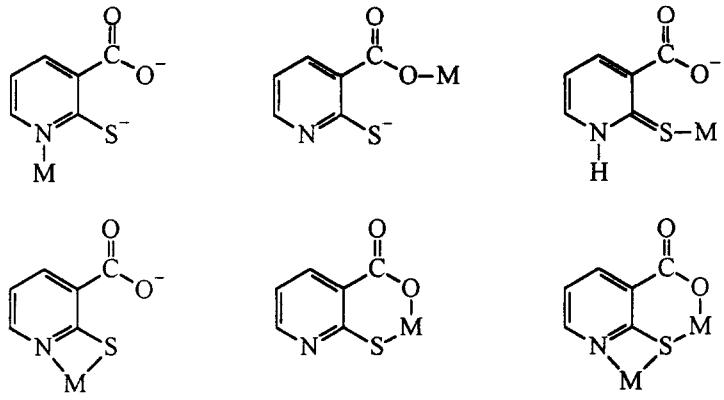

Scheme 1.

model 175 universal programmer. A glassy carbon working electrode and a platinum wire auxiliary electrode were employed for the measurements vs the Ag/AgCl (1 M KCl) reference electrode ($E^{\circ} = 0.222$ V vs SHE). The reversible behavior of the voltammetric waves has been evaluated, considering, simultaneously, the separation of the anodic and cathodic peaks (typically in the 60–70 mV range), their similar intensities; and the linear response of the peak currents vs the square root of the scan rates.

Spectroelectrochemical measurements were carried out using the PARC 173 potentiostat in parallel with the diode-array or Guided Wave spectrophotometer. A three-electrode system was designed for a rectangular quartz cell of 0.025 cm internal path length. A gold minigrid was used as a transparent working electrode, in the presence of a small Ag/AgCl reference electrode and of a platinum auxiliary electrode. The kinetics of the substitution reactions involving $Ru^{III}A$ and $Hmnic^{-}$ were investigated using an Applied Photophysics stopped-flow instrument.

Molecular modeling and semiempirical calculations were carried out using the ZINDO/1 method, at a refinement level of 1×10^{-5} kcal.

RESULTS AND DISCUSSION

The 2-mercaptonicotinic acid undergoes three successive acid-base equilibria, leading to characteristic changes in the UV spectra, as shown in Fig. 1. a–c.

The electronic spectrum of the neutral H_2mnic species (pH 2.00) consists of three bands at 224 ($\varepsilon = 5100$ mol^{-1} dm^3 cm^{-1}), 296 (11,400) and 362 nm (3100), which can be compared with the $\pi \rightarrow \pi^*$ bands observed at 230, 247 and 324 nm for the 2-mercaptopyridine compound [5]. Analogously to the related examples reported in the literature [5–7], 2-mercaptonicotinic acid can be better represented by a tautomeric structure exhibiting a protonated N-atom and a thione group, as in Scheme (2).

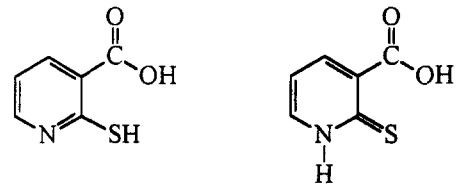

Scheme 2.

In the pH range from 2–7, the $\pi \rightarrow \pi^*$ bands are shifted to lower wavelengths. The calculated pK_a from the spectrophotometric measurements was 3.68, corresponding to the deprotonation of the carboxylic group. Above pH 7 there is a decay in $\pi \rightarrow \pi^*$ band around 360 nm, and the absorption spectra approach those of typical aromatic N-heterocyclic compounds. The calculated pK_a was 9.75, in comparison with 9.81 for 2-mercaptopyridine [5], corresponding to the deprotonation of the N—H group. The H_2mnic compound can be protonated below pH 0 at the C=S group, leading to dramatic changes in the electronic spectra, as shown in Fig. 1 A. The calculated pK_a was -0.71 in comparison with -1.38 for the 2-mercatopyridine [5].

The reaction of $Ru^{III}A$ with H_2mnic below pH 4 leads to a red product absorbing at 530 nm ($\varepsilon_{max} = 2400$ mol^{-1} dm^3 cm^{-1}), while above this pH, a deep blue ($\lambda_{max} = 616$ nm, $\varepsilon_{max} = 2100$ mol^{-1} dm^3 cm^{-1}) complex is formed. As a matter of fact, the red and blue species coexist in equilibrium in the 3–6 pH range, as shown in Fig. 2, with an apparent $pK_a = 3.80$. A similar behavior has already been observed for the reaction of $Ru^{III}A$ with 2-mercaptopyridine [8], with an apparent $pK_a = 4.35$.

According to the previous work [8], the red complex can be ascribed to the coordination of the thione (C=S) group to the $[Ru^{III}(edta)]^{-}$ complex, as in Scheme (3).

The characteristic band in the visible corresponds to a charge-transfer transition from the ligand C=S donor group to the d_{π} orbitals of Ru^{III} [8,9].

The blue complex results from the deprotonation

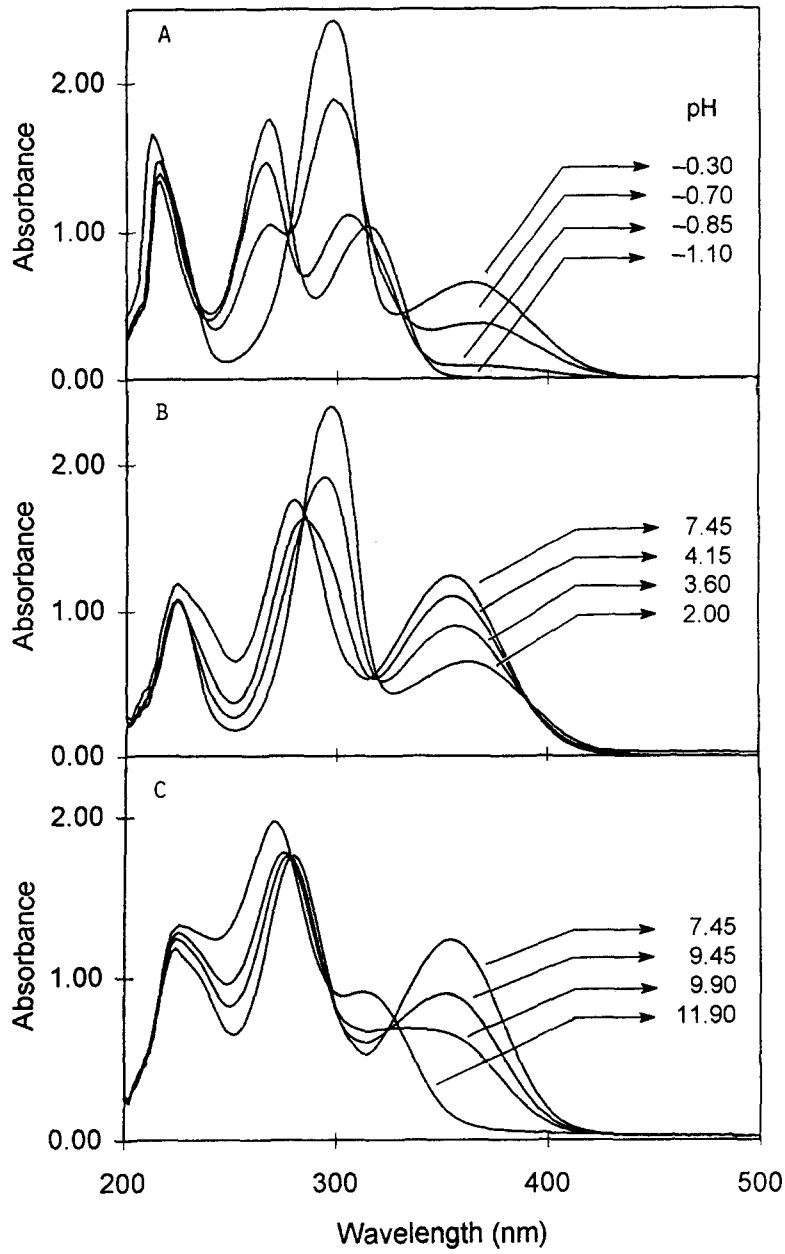

Fig. 1. Electronic spectra of the 2-mercaptonicotinic acid in aqueous solution (pH 2.00) showing the changes due to (a) protonation ($pK_a = -0.71$), and (b, c) successive deprotonation ($pK_a = 3.68$ and 9.75) equilibria.

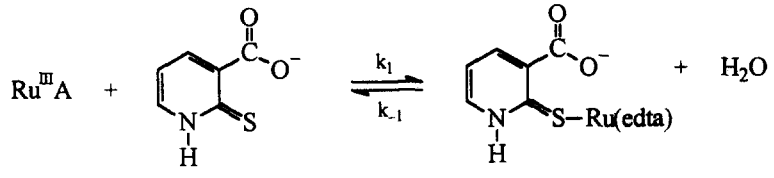

Scheme 3.

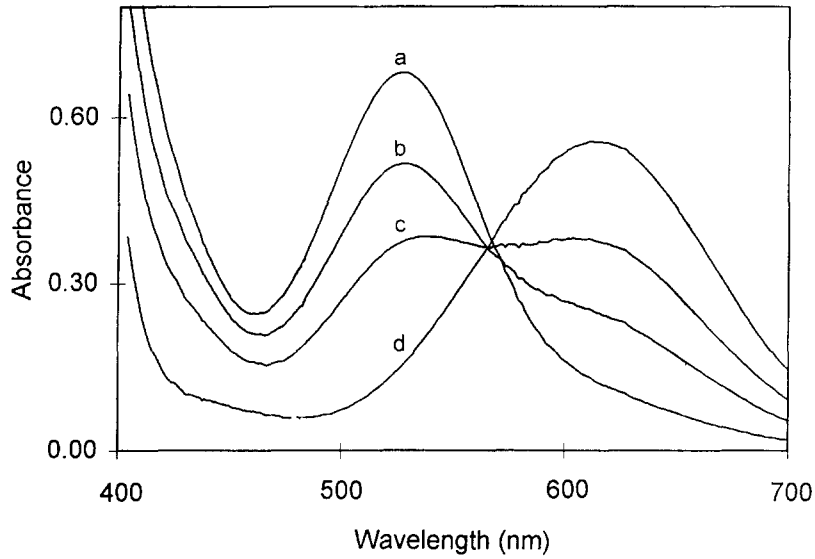

Fig. 2. Electronic spectra of the $[Ru^{III}(edta)(mnic)]^{3-}$ complex, at pH (a) 2.00, (b) 3.50, (c) 4.00 and (d) 6.60, showing the interconversion of the red and blue species.

of the N—H site, and formation of a bidentate structure, as shown in Scheme (4).

Its blue color arises from a ligand-to-metal charge-transfer transition involving the deprotonated —N=C—S^- group and the Ru^{III} d_π orbitals [8].

The decrease of the pK_a of the N—H group from 9.75 in the $Hmnic^-$ ligand to 3.80 in the $[Ru^{III}(edta)(Hmnic)]^{2-}$ complex can be explained considering the Lewis acidity of the Ru^{III} ion and the additional stabilization provided by the chelate ring in the product.

Formation kinetics

The formation of the red complex and its conversion into the blue complex can be monitored by using stopped-flow techniques, according to two well separated consecutive steps, proceeding at time scales of 100 ms and 100 s, respectively, as shown in Fig. 3. For both steps, the kinetics were typically of first order. The observed rate constants for the formation of the red complex were 11, 15 and 18 s^{-1} for $[Hmnic^-] = 0.9$, 1.3 and 1.7 mmol dm^{-3}, respectively, leading to a second order kinetic constant (k_1) of $1.2 \pm 0.1 \times 10^4$ mol^{-1} dm^3 s^{-1} ($T = 25°C$, [KCl] = 0.10 mol dm^{-3}, 0.01 mol dm^{-3} acetate buffer). This step

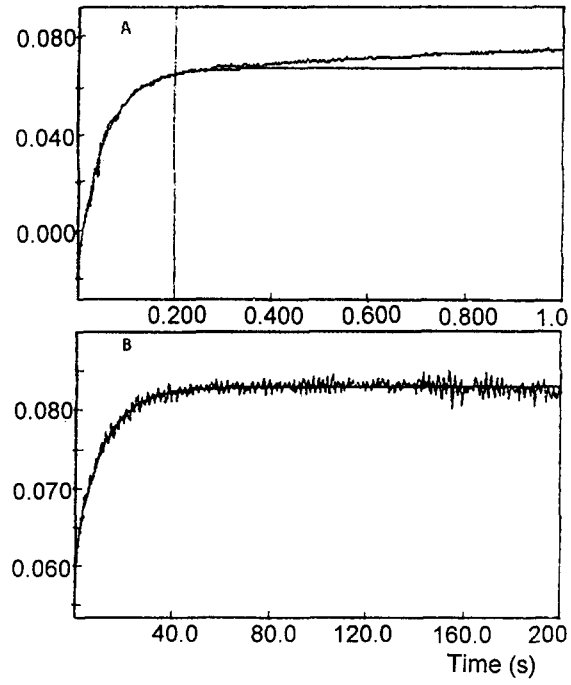

Fig. 3. Stopped-flow kinetic plots for the reaction of $[Ru^{III}(edta)]^-$ with $Hmnic^-$, showing (a) the rapid formation of the red complex, and (b) its conversion to the blue species (pH 3.80, 0.01 mol dm^{-3} acetate buffer, $I = 0.10$ mol dm^{-3} KCl).

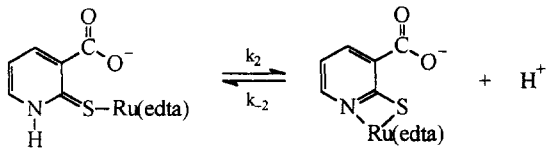

Scheme 4.

involves the substitution of the labile water molecule in $[Ru(edta)H_2O]^-$, which is known to proceed via an associative mechanism in aqueous solution [10,11].

The conversion of the red complex to the blue species proceeds to the equilibrium at pH 3.80, with an observed rate constant of $0.094 \pm 0.002\ s^{-1}$ which does not depend on the concentration of the 2-mercaptonicotinic ligand. As for a typical equilibrium kinetics, the observed rate constants should be expressed in terms of the forward and reverse rate constants, i.e., $k_{obs} = k_{forward} + k_{reverse}$.

Since $k_{obs} = k_2 + k_{-2}[H^+]$ and $K_2 = (k_2/k_{-2}) = 1.6 \times 10^{-4}$ mol dm^{-3}, one can calculate $k_2 = 0.048\ s^{-1}$ and $k_{-2} = 3.0 \times 10^2$ mol^{-1} dm^3 s^{-1}.

Dissociation kinetics

The dissociation of the blue $[Ru^{III}(edta)(mnic)]^{3-}$ complex proceeds very slowly even in the presence of a high excess of pyridine as the entering ligand, leading to the decay of the characteristic charge-transfer bands in the visible region. The kinetics were typically of first order, with $k_{obs} = 6.3 \pm 0.2 \times 10^{-4}\ s^{-1}$, independently of the concentration of pyridine above 0.1 mol dm^{-3}, [KCl] = 0.1 mol dm^{-3}, pH 5.50.

Based on the microscopic reversibility principle, the following Scheme (5) can be proposed for the substitution kinetics:

$$Ru^{III}(NS\text{-}mnic) + H^+ \overset{K_2^{-1}}{\rightleftharpoons} Ru^{III}(S\text{-}Hmnic)$$

$$Ru^{III}(S\text{-}Hmnic) + H_2O \underset{k_1}{\overset{k_{-1}}{\rightleftharpoons}} Ru^{III}A + Hmnic$$

$$Ru^{III}A + py \overset{k_{py}}{\rightleftharpoons} Ru^{III}py + H_2O \qquad (5)$$

Assuming a steady state approximation for $[Ru^{III}A]^-$

$$-\frac{d[Ru^{III}(NS-mnic)]}{dt} = k_{obs}[Ru^{III}(NS-mnic)]$$

where

$$k_{obs} = \frac{k_{py}k_{-1}K_2^{-1}[H^+][py]}{k_1[Snic] + k_{py}[py]}$$

Since [py] ≫ [mnic], and k_1 is of the same magnitude as k_{py} [10], the expression for k_{obs} reduces to

$$k_{obs} = k_{-1}K_2^{-1}[H^+]$$

Therefore, considering that $[H^+] = 3.2 \times 10^{-6}$ mol dm^{-3}, and $K_2^{-1} = 6.3 \times 10^3$ mol^{-1} dm^3, one can calculate $k_{-1} = 3.2 \times 10^{-2}\ s^{-1}$, from the observed rate constants, and

$$K_1 = \frac{k_1}{k_{-1}} = \frac{1.1 \times 10^4}{3.2 \times 10^{-2}} = 3.4 \times 10^5 \text{ mol}^{-1} \text{ dm}^3$$

Cyclic voltammetry and spectroelectrochemistry

The electrochemical behavior of the $[Ru(edta)(mnic)]^{3-}$ complex in aqueous solution is typically reversible, as shown in Fig. 4. The $E_{1/2}$ values for

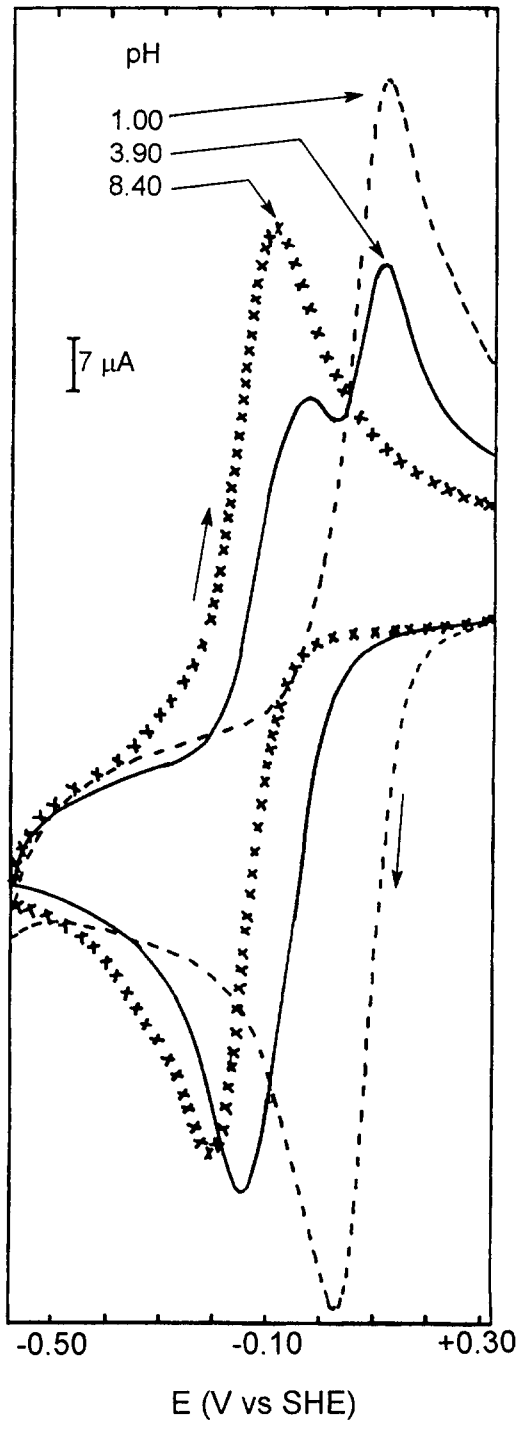

Fig. 4. Cyclic voltammograms of the $[Ru^{III}(edta)(mnic)]^{3-}$ complex at several pHs, scan rate = 100 mV s^{-1}, $I = 0.10$ mol dm^{-3} KCl.

the red and blue species can be evaluated from the measurements below pH 2 and above pH 5, as 0.080 and −0.150 V, respectively. At intermediate pHs the interconversion of the two species in the reduced form proceeds slow enough to be detected by cyclic voltammetry. The kinetic constant for the conversion of $[Ru^{II}(edta)(NS\text{-}mnic)]^{4-}$ into $[Ru^{II}(edta)(S\text{-}Hmnic)]^{3-}$ can be calculated from the cyclic voltammograms obtained at several scan rates using Nicholson and Shain equation [12], as previously reported for the 2-mercaptopyridine complex [8]. The calculated constant was $0.104 \pm 0.002\ s^{-1}$, in comparison with $1.9\ s^{-1}$ for the 2-mercaptopyridine analogue.

Typical spectroelectrochemical results are shown in Fig 5. The reduction of the red complex proceeds in a reversible way, leading to rise of a strong band at 460 nm (4500) ascribed to a ruthenium(II)-to-mnic^{2-} $d_\pi \rightarrow p_\pi^*$ charge transfer transition. In the case of the blue complex the reduction leads to the decay of the typical band at 616 nm (2100) and to the rise of a strong metal-to-ligand charge-transfer band at 425 nm (2100). The E° values obtained spectroelectrochemically for the red and blue complexes were 0.080 and −0.150 V, respectively, in excellent agreement with those estimated by cyclic voltammetry.

Based on the redox potentials and equilibrium con-

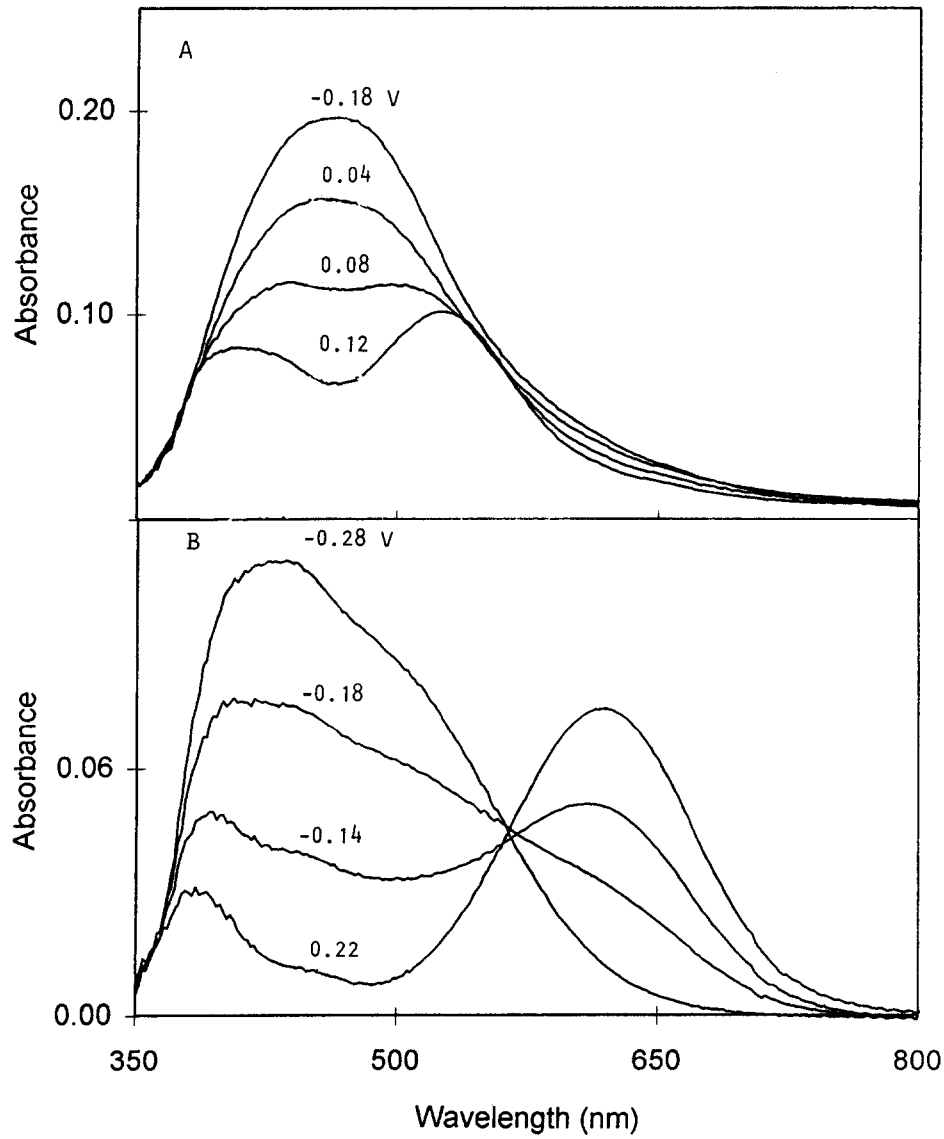

Fig. 5. Spectroelectrochemical behavior of the (a) red and (b) blue forms of the $[Ru^{III}(edta)(mnic)]^{3-}$ complex, at pH 2.0 and 7.0 respectively.

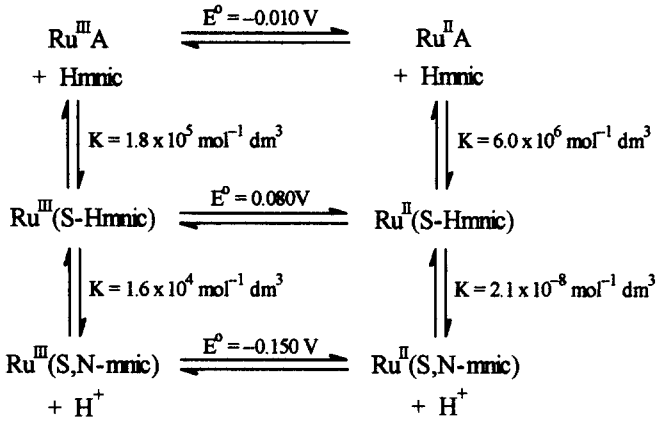

Scheme 6.

stants for the formation of the red and blue complexes, a square thermodynamic cycle can be solved, as previously described [8], in order to calculate the corresponding constants for the reduced species. The complete data are summarized in Scheme (6).

Binuclear complex

The formation of binuclear species was investigated by reacting the mononuclear blue complex with an equivalent amount of $[Ru^{III}A]^-$. The experiments were performed using relatively high concentrations of the complexes, e.g. 50 mmol dm^{-3}, in order to minimize the dissociation of the product. Under such conditions, the reaction led to an intensification and broadening of the characteristic charge transfer band at 600 nm, suggesting the involvement of the thiolate group in the new chromophore group. It should be noticed that ruthenium(III)-carboxylate complexes do not display charge-transfer bands in the visible region.

Typical cyclic voltammograms for the 1 : 1 mixture of the $[Ru^{III}(edta)(mnic)]^{3-}$ and $[Ru^{III}A]^-$ complexes are shown in Fig. 6. Their broad shape reflects composite waves which can be deconvoluted in terms of two reversible peaks exhibiting $E_{1/2} = -0.120$ and -0.040 V. In contrast, the simulation of the composite voltammograms in terms of the starting $[Ru^{III}(edta)(mnic)]^{3-}$ and $[Ru^{III}A]^-$ complexes ($E_{1/2} = -0.150$ and -0.010 V), showed two well resolved peaks, departing from the observed results.

In addition to the spectroscopic and electrochemical results, a definite evidence for the formation of the binuclear complex was obtained spectroelectrochemically, as shown in Fig. 7.

When the applied potential was close to the first $E^\circ = -0.040$ V, a new, strong absorption band appeared in the near infrared region, at 1200 nm. The intensity of this band reached its maximum in the mixed valence region (-0.040 to -0.120 V), decaying completely after the second $E^\circ = -0.120$ V, due to the formation of the totally reduced species. A careful treatment of the spectroelectrochemical data, as shown in Fig. 7 (inset), was consistent with a composite Nernst behavior involving two reversible, monoelectronic redox processes with $E^\circ = -0.040$ and -0.120 V, in excellent agreement with the cyclic voltammetry.

The absorption band in the near infrared region is characteristic of the mixed valence binuclear species, and its high intensity ($\varepsilon = 1200$ mol^{-1} dm^3 cm^{-1}) indicates a substantial electronic coupling between the two metal ions. The binding of the second ruthenium complex by means of the carboxylate group is not favored kinetic and thermodynamically in this case. As a matter of fact, most of the reactions of $[Ru(edta)]^-$ complexes have been carried out in acetate buffer, with no evidence of binding interactions [10]. On the other hand, coordination at the carboxylate group would increase the metal–metal separation, decreasing the extent of the electronic coupling. In contrast, the thiolate group is a strong nucleophile and its binding to $[Ru^{III}(edta)]^-$ would facilitate the formation of a bidentate structure, involving the vicinal carboxylate group. Therefore, the bidentate binuclear complex is expected to exhibit two types of ruthenium centers, represented, in terms of their binding modes, as $Ru^{III}(N,S)$ and $Ru^{III}(S,O)$, or as in Scheme (7).

The simulated structure for the binuclear complex, based on ZINDO/1 calculations, is illustrated in Fig. 8. As one can see, the two metal complexes are not located in the molecular plane of the 2-mercaptonicotinic ligand. The distortion from coplanarity, due to steric reasons, shortens the metal-metal distance to only 4.5 Å.

The electronic coupling, expressed by H_{ab}, can be calculated according to the equation

$$H_{ab} = 2.05 \times 10^{-2} \frac{(\varepsilon_{max} \nu_{max} \Delta\nu_{1/2})^{1/2}}{R}$$

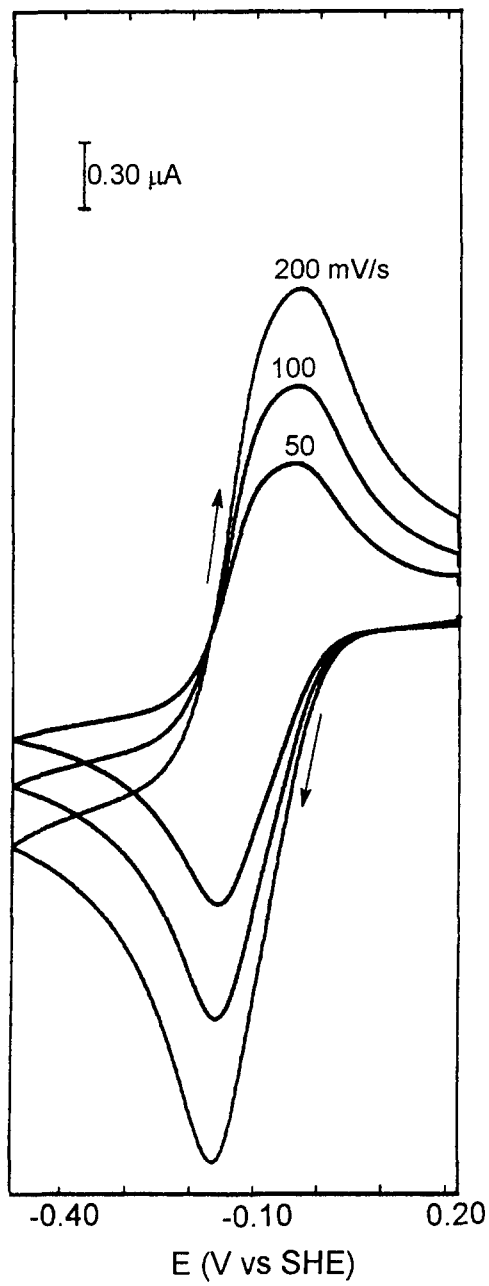

Fig. 6. Cyclic voltammetry of the binuclear $[\{Ru^{III}(edta)\}_2(mnic)]^{4-}$ complex, 50 mmol dm^{-3}, in D_2O, $pD = 6.5$, $I = 1$ mol dm^{-3} KCl.

where, R is the metal–metal distance, and ε_{max}, ν_{max} and $\Delta\nu_{1/2}$ are the extinction coefficient (1200 mol^{-1} dm^3 cm^{-1}), maximum wavenumber (8000 cm^{-1}) and half bandwidth of the intervalence band. In this way, $H_{ab} = 990$ cm^{-1}, indicating a substantial interaction between the two metal centers via the bridging ligand. This value is considerably higher than those observed for typical binuclear mixed valence complexes [13].

The involvement of a common thiolate group in the bridged complex is probably responsible for the increase in the electronic coupling between the two ruthenium centers. The importance of this group becomes evident by comparing the properties of the 2-mercaptonicotinic species with those of the nicotinic analogue. As a matter of fact, the results obtained in this work for the nicotinic ligand indicated that only the mononuclear, N-(pyridine) coordinated complex is formed with $[Ru^{III}(edta)]$. In addition, the spectroelectrochemical measurements carried out under identical conditions for the 2-mercaptonicotinic complex, provided no evidence for intervalence transitions in the near-infrared region.

It is interesting to note that the substantial intervalence coupling, as suggested by the optical data, is not apparent in the electrochemistry of the binuclear complex. As a matter of fact, in most typical, symmetric mixed valence complexes, a high degree of electronic coupling is reflected in the electrochemical behavior by an increase in the separation between the redox potentials. However, it should be mentioned that the electrochemical criterion applies well to most conventional mixed valence complexes where the σ-bond strength is nearly constant for the several redox states involved, so that the E° splitting arises mainly from the π-electron delocalization effects.

In the present case, the binuclear complex is quite asymmetric, and each metal center exhibits a typical E° value. Therefore, in contrast to the symmetrical systems, the two E° values reflect the contrasting metal ion environments, rather than the splitting associated with the stabilization of the mixed-valence complex. On the other hand, the E° values are also related to the metal–ligand affinities, as expressed by the ratio of the equilibrium constants for the $Ru^{II}L$ and $Ru^{III}L$ complexes, i.e., $\log K^{II}/K^{III}$. In this way, the changes in the metal–ligand affinities can shift the redox waves in any direction, depending on the nature of the complex, complicating the interpretation of the electrochemical data.

In order to evaluate this point, the closely related 2-mercaptobenzoic ligand, containing a bidentate (S,O) group, was employed to simulate the $Ru(S,O)$ moiety in the binuclear complex. In fact, the reaction of the 2-mercaptobenzoic ligand with $[Ru^{III}(edta)]^-$ led to a blue complex ($\lambda_{max} = 598$ nm), exhibiting an absorption spectrum coinciding with that proposed for the $Ru(S,O)$ moiety in the binuclear complex. However, the $E_{1/2}$ for the 2-mercaptobenzoic complex was -0.36 V, in contrast to -0.12 V observed for the corresponding center in the binuclear species. This result is consistent with the decrease of the σ-donor strength of the bridging sulfur atom in the mixed valence complex, as a consequence of the electron withdrawing effects from the coordinated metal ions.

A similar conclusion was obtained by comparing the E° value for the 2-mercaptopyridine complex, e.g. -0.105 V [8], with that for the corresponding $Ru(N,S)$ center in the binuclear complex ($E^\circ = -0.040$ V). Again, reflecting the decrease in the σ-donor strength of the bridging sulfur atom, there is

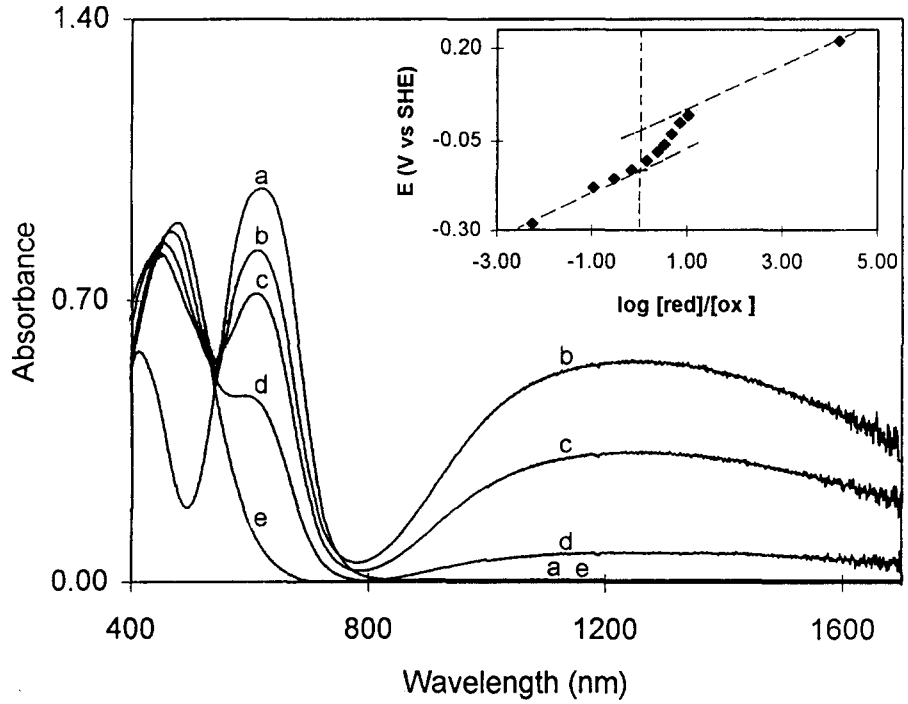

Fig. 7. Spectroelectrochemical behavior of the binuclear $[\{Ru^{III}(edta)\}_2(mnic)]^{4-}$ complex, 50 mmol dm^{-3}, in D_2O, $pD = 6.5$, $I = 1$ mol dm^{-3} KCl, at (a) 0.20, (b) −0.08, (c) −0.13, (d) −0.18 and (e) −0.33 V, showing the intervalence band at 1200 nm for the mixed valence species. Inset: Nerst plot, indicating two redox couples at $E^{\circ} = -0.040$ ($Ru^{III,III}/Ru^{III,II}$) and −0.120 V ($Ru^{III,II}/Ru^{II,II}$), respectively.

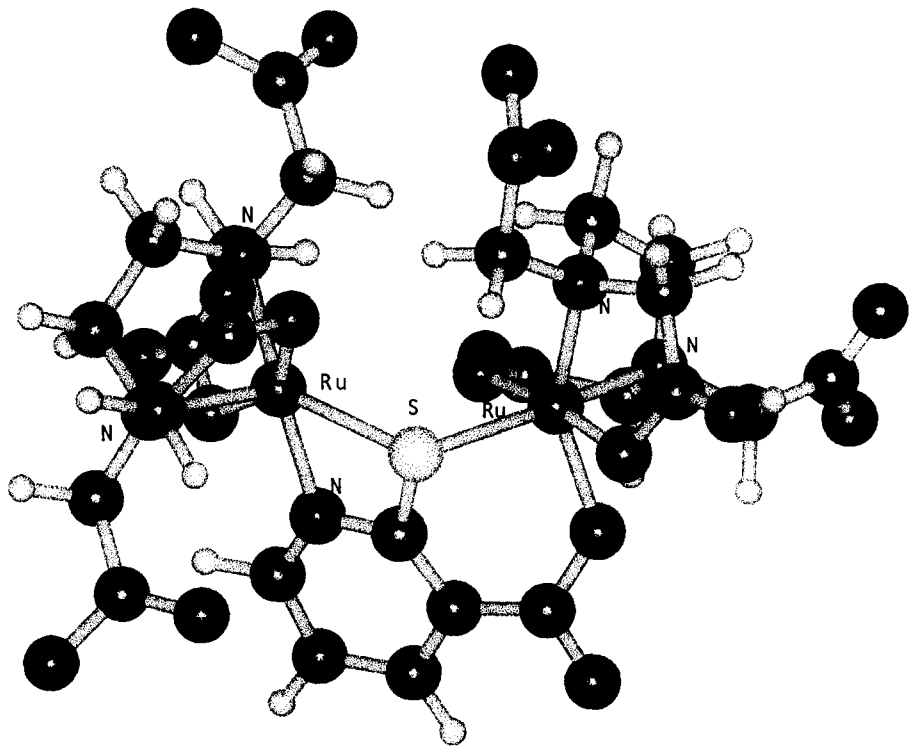

Fig. 8. ZINDO/1 structural simulation for the the binuclear $[\{Ru^{III}(edta)\}_2(mnic)]^{4-}$ complex, showing the close proximity of the metal centers (4.5 Å).

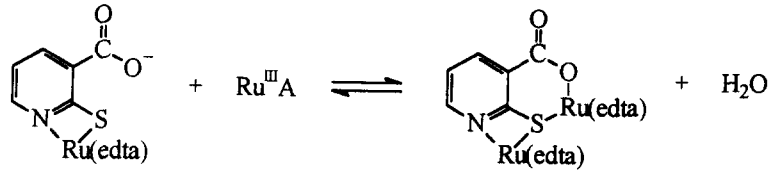

Scheme 7.

an increase of E° for the $Ru^{III/II}(S,N)$ center in the binuclear complex.

Acknowledgements—We thank FAPESP, CNPq and PADCT for a fellowship (F.N.R.) and financial support; and Dr R. C. Rocha, for his help in the theoretical calculations.

REFERENCES

1. Bruce, D. W. and O'Hare, D., *Inorganic Materials*. John Wiley, New York, 1992.
2. Vögte, F., *Supramolecular Chemistry*. John Wiley, New York, 1991.
3. Mukaida, M., Okuno, H. and Ishimori, T., *Nippon Kakagu Sasshi*, 1965, **86,** 589.
4. Oshino, Y., Uehiro, T. and Saito, M., *Bull. Chem. Soc. Jpn*, 1979, **52,** 1060.
5. Jones, R. A. and Katrizky, A. R., *J. Chem. Soc.*, 1958, 3610.
6. Spinner, E., *J. Chem. Soc.*, 1960, 1237.
7. Kennedy, B. F. and Lever, A. B. P., *Can. J. Chem.*, 1972, **50,** 3488.
8. Toma, H. E., Santos, P. S., Mattioli, M. P. D. and Oliveira, L. A. A., *Polyhedron*, 1987, **6,** 603.
9. Araki, K., Rein, F. N., Camera, S. G. and Toma, H. E., *Trans. Metal Chem.*, 1992, **17,** 535.
10. Matsubara, T. and Creutz, C., *Inorg. Chem.*, 1979, **18,** 1956.
11. Bajaj, H. C. and van Eldik, R., *Inorg. Chem.*, 1990, **29,** 2855.
12. Nicholson, R. S. and Shain, I., *Anal. Chem.*, 1964, **36,** 706.
13. Creutz, C., *Progr. Inorg. Chem.*, 1983, **30,** 1.

Pergamon

PII: S0277-5387(97)00414-2

Polyhedron Vol. 17, No. 9, pp. 1449–1461, 1998
© 1998 Elsevier Science Ltd
All rights reserved. Printed in Great Britain
0277-5387/98 $19.00+0.00

Acid-catalysed hydrolysis kinetics of carbonato cobalt(III) complexes with nonlabile tripodal quadridentate ligands

Y. Kitamura,* S. Murakami and A. Shibata

Department of Chemistry, Faculty of Science, Ehime University, Matsuyama 790, Japan

(Received 4 August 1997; accepted 3 October 1997)

Abstract—Acid-catalysed hydrolysis reaction velocity was studied by the stopped-flow method at 25°C, ionic strength (I) of 2.0 ($NaClO_4$) and $[H^+] = 0.02$–1.0 M (M = mol dm^{-3}) for seven cobalt(III) bidentate carbonato complexes $[CoL(O_2CO)]^{n+}$ with a uninegative or a dinegative tripodal quadridentate ligand L of *fac*(*N*)-5-dptma, *mer*(*N*)-5-dptma, *fac*(*N*)-i-dtma, *mer*(*N*)-i-dtma, *mer*(*N*)-i-2,3-ma, *cis*(*O*)-aeida and *trans*(*O*)-aeida where 5-dptma stands for *N*,*N*-bis(3-aminopropyl)glycinato, i-dtma for *N*,*N*-bis(2-aminoethyl)glycinato, i-2,3-ma for *N*-(2-aminoethyl)-*N*-(3-aminopropyl)glycinato, and aeida for *N*-(2-aminoethyl)-*N*-(carboxymethyl)glycinato. The time course of the absorbance of the acidic aqueous solution of the reactant complex was followed at relevant wavelength in the UV region and was analysed according to a program for the consecutive first-order reactions with two experimental rate constants k_{fast} and k_{slow}. In the cases of L = *fac*(*N*)-5-dptma, *mer*(*N*)-i-dtma and *trans*(*O*)-aeida, both the k_{fast} and the k_{slow} increase with the increasing acidity of the solution. These results are incompatible with the current mechanism predicting one acidity dependent and the other acidity independent rate constants. Therefore, we have assumed additionally the deprotonation equilibrium from the intermediate complex *cis*-$[CoL(OH_2)(O_2COH)]^{n+1}$ giving rise to an inert monodentate carbonato complex *cis*-$[CoL(OH_2)(O_2CO)]^{n+}$ and derived from the acidity dependences of the k_{fast} and the k_{slow} the relevant equilibrium and rate constants. In the case of L = *mer*(*N*)-5-dptma, the k_{slow} changes slightly with the acidity attaining a flat maximum around $[H^+] = 0.2$ M, which we have interpreted by assuming an amphoteric character of the *mer*(*N*)-$[Co(5\text{-dptma})(OH_2)(O_2COH)]^+$. © 1998 Elsevier Science Ltd. All rights reserved

Keywords: carbonato cobalt(III) complex; acid hydrolysis velocity; tripodal quadridentate ligand.

The acid-catalysed hydrolysis reaction of a cobalt(III) complex with a bidentate carbonato ligand has been studied for about 40 years.

$$\underset{\mathbf{1}}{[CoL(O_2CO)]^{n+}} + 2H^+ + H_2O \rightarrow \underset{\mathbf{4}}{[CoL(OH_2)_2]^{n+2}} + CO_2 \quad (1)$$

where L is the nonlabile ligand occupying the residual four coordination sites of the coordination octahedron. The interesting features of this reaction are that with L = $(NH_3)_4$ one water oxygen in the product diaqua complex **4** stems from the reactant complex **1** [1] and that with L = $(en)_2$ the velocity accelerates in D_2O, where en stands for ethylenediamine [2]. In accordance with these features the current mechanism is shown in Scheme 1. A preprotonation to the bidentate carbonato ligand in **1** occurs with the equilibrium constant K; one of the Co—O(bicarbonato) bonds in the bidentate bicarbonato complex **2** cleaves with the first order rate constant $k_{Co\text{-}O}$; and the O—C bond in the monodentate bicarbonato complex **3** cleaves with the first-order rate constant $k_{O\text{-}C}$ [3].

In this mechanism, the time course of the absorbance in the UV-vis region is given by eqn (2).

$$|A_t - A\infty| = M\exp\left(-\frac{k_{Co\text{-}O}K[H^+]}{1+K[H^+]}t\right) + N\exp(-k_{O\text{-}C}t) \quad (2)$$

where A_t and $A\infty$ are the absorbances of the reacting solution at reaction time t and at infinity. M and N

* Author to whom correspondence should be addressed.

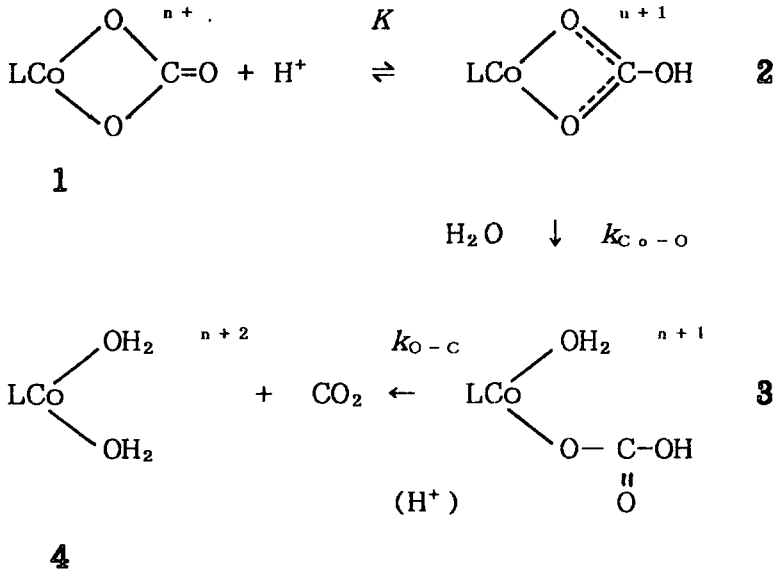

Scheme 1. Current mechanism for reaction 1.

are constants independent of t, which are given by the M'' (eqn (11)) and the N'' (eqn (12)) to be mentioned later respectively with neglection of the K_a nor the K_b value. The velocity of reaction 1 has been studied with various L ligands. The results up to 1982 have been summarized in a review [4]. It was considered that the experimental first-order rate constant k_{obs} is composed of two components

$$k_{obs} = k_0 + Kk_{Co\text{-}O}[H^+]$$

where k_0 is the spontaneous hydrolysis rate constant of the reactant complex **1**. The magnitudes of k_0 and $Kk_{Co\text{-}O}$ were experimentally determined and it was demonstrated that the magnitude of $Kk_{Co\ O}$ depends significantly on the variation of the L ligand. However, the magnitude of K was not experimentally determined and therefore the magnitude of $k_{Co\text{-}O}$ was not explicitly known. The magnitudes of $k_{O\ C}$ was experimentally determined only at limited acidity for several L ligands: $k_{O\text{-}C} = 0.4\text{–}60\ s^{-1}$ at 25°C [4]. Recently, we have studied reaction 1 with certain L ligands and pointed out that the experimentally estimated magnitudes at 25°C of K differ significantly from the assumed value $10^{-6}\ M^{-1}$: with L = (methylamine)$_4$ $K = 0.7\ M^{-1}$ at $I = 2.0$ ($NaClO_4$); with L = (ethylamine)$_4$ $K = 0.8\ M^{-1}$ at $I = 2.0$ ($NaClO_4$); with L = (propylamine)$_4$ $K = 1.3\ M^{-1}$ at $I = 1.0$ ($NaClO_4$) [5]. Buckingham *et al.* studied reaction 1 with nine L ligands at $[H^+] = 0.1\text{–}1.0$ M. $I = 1.0$ ($NaClO_4$) and 25°C [3,6]. They have shown that the k_0 is negligibly small and have analysed the time course of the absorbance in the visible region of the reacting solution according to the non-linear least-squares-fitting routine for consecutive first-order reactions.

$$|A_t - A\infty| = m\exp(-k_{fast}t) + n\exp(-k_{slow}t) \qquad (3)$$

where k_{fast} and k_{slow} are the faster and the slower experimental first-order rate constants with m and n being constants independent of t. They have obtained one acidity dependent and the other acidity independent experimental first-order rate constants and assigned them to the $k_{Co\text{-}O}K[H^+]/(1+K[H^+])$ and the $k_{O\text{-}C}$ in eqn (2), respectively. They have shown that the magnitudes of K (0.4–1.5 M^{-1}) and $k_{O\text{-}C}$ (0.3–4.1 s^{-1}) are rather independent of the kind of L, whereas the magnitude of $k_{Co\text{-}O}$ (0.008–85 s^{-1}) depends significantly on the variation of L and pointed out that the great variation of the $k_{Co\text{-}O}$ may be ascribable to the differing abilities to transfer the *exo*-O proton to the *endo*-O ring oxygen in the intermediate **2**.

In the present report, we are interested in reaction 1 with further variation of L ligand. We have studied reaction 1 with four tripodal quadridentate ligands: *N,N*-bis(3-aminopropyl)glycinato $H_2NCH_2CH_2CH_2N(CH_2COO^-)CH_2CH_2CH_2NH_2$ (5-dptma); *N,N*-bis (2-aminoethyl)glycinato $H_2NCH_2CH_2N(CH_2COO^-)CH_2CH_2NH_2$ (i-dtma); *N*-(2-aminoethyl)-*N*-(3-aminopropyl)glycinato $H_2NCH_2CH_2CH_2N(CH_2COO^-)CH_2CH_2NH_2$ (i-2,3-ma) and *N*-(2-aminoethyl)-*N*-(carboxymethyl)glycinato $H_2NCH_2CH_2N(CH_2COO^-)_2$ (aeida). As shown in Fig. 1, the 5-dptma, i-dtma and i-2,3-ma ligands coordinate to cobalt(III) with three nitrogen and one oxygen atoms in the *fac*(*N*) or the *mer*(*N*) mode; the aeida ligand with two nitrogen and two oxygen atoms in the *cis*(*O*) or the *trans*(*O*) mode. We have treated seven among eight possible bidentate carbonato complexes bearing these quadridentate ligands, since we have obtained only one isomer of the i-2,3-ma carbonato complex. Thus, our reactant complexes are nonelectrolyte or of uninegative charge, whereas most of the carbonato cobalt(III) complexes studied hitherto are of unipositive charge [3,6]. We have analysed the time course of the UV absorbance of the reacting solution accord-

Fac(N)- [Co(CO_3)(5-dptma)] *Mer(N)*- [Co(CO_3)(5-dptma)]

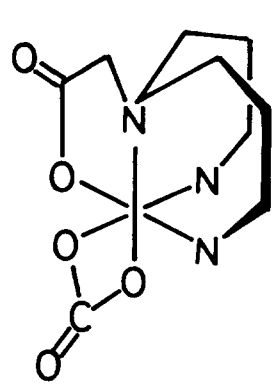

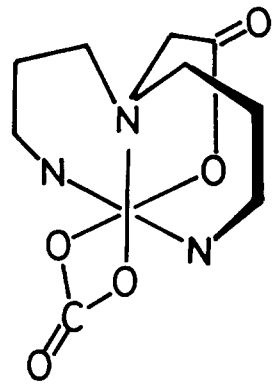

Cis(O)- [Co(aeida)(CO_3)]$^-$ *Trans(O)*- [Co(aeida)(CO_3)]$^-$

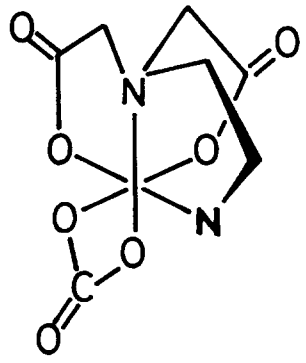

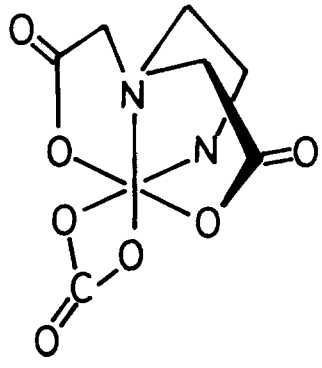

Fig. 1. Structures of the reactant carbonato complexes.

ing to eqn (3) and have found that for certain carbonato complexes both the k_{fast} and the k_{slow} increase with the increasing acidity of the solution. These results are incompatible with the current mechanism predicting one acidity dependent pseudo first-order rate constant $k_{Co\text{-}O}K[H^+]/(1+K[H^+])$ and the other acidity independent first-order rate constant $k_{O\text{-}C}$ as given by eqn (2). Therefore, we interpret our results assuming an additional deprotonation equilibrium from the species **3** giving rise to an inert monodentate carbonato complex.

EXPERIMENTAL

Materials

Analytical grade reagents and distilled water were used. The concentration $[H^+]$ of the hydronium ion in the solution was determined by titration against NaOH, where potassium hydrogen phthalate was used as a primary standard. The preparations of *fac*(*N*)-[Co(CO_3)(5-dptma)]·$2H_2O$ and *mer*(*N*)-[Co(CO_3)(5-dptma)]·$5H_2O$ have been described in a previous report [7]. The other bidentate carbonato complex samples were derived from relevant precursors and were isolated by the fractional precipitation technique. The isomeric purity was checked by the glycinato ring proton resonance spectra (Table 1). In the case of [Co(CO_3)(i-dtma)], the AB quartet pattern corresponds to the *fac*(*N*)-isomer, where the two glycinato protons exist in different environments and the singlet to the *mer*(*N*) isomer, where the two glycinato protons exist in a similar environment. In the case of [Co(aeida)(CO_3)]$^-$, one AB quartet pattern with 4H intensity corresponds to the *trans*(*O*)-isomer where the two glycinato rings are equivalent and two AB quartet patterns each with 2H intensity

Table 1. Glycinato ring proton resonance and UV-vis absorption spectra of the relevant complexes

Complex	δ/ppm[a]	intensity	J/Hz	λ_{max}/nm (ε)
fac(*N*)-[Co(CO_3)(i-dtma)]	3.01, 2.95, 2.58, 2.52	2H	16.5	526 (144), 364 (141)
fac(*N*)-[Co(i-dtma)(H_2O)$_2$]$^{2+}$[b]	2.98, 2.91, 2.35, 2.29	2H	17.1	518 (152), 369 (123)
mer(*N*)-[Co(CO_3)(i-dtma)]	2.53	2H		514 (126), 405$_{sh}$, 365 (91)
mer(*N*)-[Co(i-dtma)(H_2O)$_2$]$^{2+}$[b]	2.68	2H		511 (95), 370 (109)
mer(*N*)-[CoCl(i-2,3-ma)(H_2O)]$^+$	2.73, 2.66, 1.90, 1.83	2H	18.6	591 (52), 379 (71)
mer(*N*)-[Co(CO_3)(i-2,3-ma)]	2.68, 2.61, 1.93, 1.86	2H	18.3	522 (86), 360 (62)
mer(*N*)-[Co(i-2,3-ma)(H_2O)$_2$]$^{2+}$[b]	2.79, 2.72, 2.01, 1.94	2H	18.2	521 (56), 362 (61)
cis(*O*)-[Co(aeida)(CO_3)]$^-$	2.93, 2.87, 2.73, 2.67	2H	15.9	534 (159), 376 (125)
	2.61[c]	2H		
cis(*O*)-[Co(aeida)(H_2O)$_2$]$^+$[b]	2.91, 2.85, 2.38, 2.32	2H	16.2	
	2.80, 2.74, 2.72, 2.66	2H	18.5	
trans(*O*)-[Co(aeida)(CO_3)]$^-$	3.23, 3.17, 2.75, 2.69	4H	16.8	572 (159), 490$_{sh}$, 377 (184)
trans(*O*)-[Co(aeida)(H_2O)$_2$]$^+$[b]	3.18, 3.12, 2.47, 2.41	4H	16.6	538 (185), 382 (178)

[a] δ = 0 ppm for 2-methyl-2-propanol.
[b] Prepared in the corresponding carbonato complex solution by addition of a drop of 60% aqueous $HClO_4$.
[c] Collapsed quartet.

to the *cis*(*O*)-isomer, where the two glycinato rings are inequivalent. In the case of [Co(CO_3)(i-2,3-ma)], we cannot assign the isomerism on the AB quartet pattern, since both the *fac*(*N*) and the *mer*(*N*) isomers of this complex will show such pattern. We examined the UV-vis absorption spectra of the aquachloro precursor and of the diaqua hydrolysis product and assigned them to the *mer*(*N*) isomers (Table 1). On this base we presume the *mer*(*N*) structure of our [Co(CO_3)(i-2,3-ma)]. The broad half widths of the first bands 180 nm of [CoCl(i-2,3-ma)(H_2O)]$^+$ and 152 nm of [Co(i-2,3-ma)(H_2O)$_2$]$^{2+}$ are also reported for the *mer*(*N*) isomers of similar Co(III) complexes. For example, half widths 180, 180, 146 and 135 nm have been reported for the first bands of *mer*(*N*)-[Co(Cl)(5-dptma)(H_2O)]$^+$, *mer*(*N*)-[Co(Cl)(i-dtma)(H_2O)]$^+$, *mer*(*N*)-[Co(5-dptma)(H_2O)$_2$]$^{2+}$ and *mer*(*N*)-[Co(i-dtma)(H_2O)$_2$]$^{2+}$, respectively [7].

Fac(*N*)-[Co(CO_3)(i-dtma)]. A mixture of *mer*(*N*)-[Co(Cl)(i-dtma)(H_2O)]ClO_4 (18.6 g), $NaHCO_3$ (8.5 g) and water (30 cm^3) was stirred at 50°C for 2 h [8]. After the filtration, the filtrate was combined with two volumes of ethanol. Resultant oily lower layer was separated by decantation. It was warmed, while the container wall was rubbed with a glass rod. Resultant precipitates of the carbonato complex were collected and dissolved in minimum amount of water. It was evaporated and the resultant violet crystals were collected from the hot solution. They were washed with methanol and recrystallized from hot water. Yield: 2 g. Found: C, 30.1; H, 5.0; N, 14.8%. Calcd for $CoC_7H_{14}O_5N_3$: C, 30.1; H, 5.1; N, 15.1%.

Mer(*N*)-[Co(CO_3)(i-dtma)]·H_2O. The filtrate in the above procedure for the *fac*(*N*) isomer was combined with equal volume of ethanol. Pink crystals separated on rubbing the container wall. They were collected prior to contamination with the violet crystals of the *fac*(*N*) isomer. They were washed with ethanol and recrystallized from the minimum amount of water by addition of two volumes of ethanol. Yield: 4 g. Found: C, 28.1; H, 5.5; N, 13.7%. Calcd for $CoC_7H_{16}O_6N_3$: C, 28.3; H, 5.4; N, 14.1%.

Mer(*N*)-[CoCl(i-2,3-ma)(H_2O)]ClO_4. *Mer*(*N*)-[Co(i-2,3-ma)(NO_2)$_2$]·H_2O (20 g) was treated with conc. HCl (100 cm^3) and warmed until the gas evolution cease [9]. It was filtered and the filtrate was evaporated to near dryness. The resulting green precipitates (18 g) presumably of [$CoCl_2$(i-2,3-ma)] were collected and washed with ethanol. These (5 g) were dissolved in water (20 cm^3) and drops of $HClO_4$ (60%) were added to the solution. The resulting blue precipitates (4 g) were recrystallized from water and washed with methanol and ether. Found: C, 21.9; H, 4.7; N, 10.9%. Calcd for $CoC_7H_{18}O_7N_3Cl_2$: C, 21.8; H, 4.7; N, 10.9%.

Mer(*N*)-[Co(CO_3)(i-2,3-ma)]·4H_2O. A mixture of *mer*(*N*)-[CoCl(i-2,3-ma)(H_2O)] ClO_4 (2.6 g), $NaHCO_3$ (1.5 g) and water (8 cm^3) was stirred at 50°C for 2 h. After the filtration, ethanol was added to the filtrate. The resultant pink precipitates were collected and washed with methanol and ether. Found: C, 26.2; H, 4.8; N, 11.1%. Calcd for $CoC_8H_{24}O_9N_3$: C, 26.3; H, 4.4; N, 11.5%. The same substance was obtained from the latter filtrate left for some while.

Trans(*O*)-Na[Co(aeida)(CO_3)]·4H_2O. *Trans*(*O*)-[Co(aeida)(H_2O)$_2$]NO_3 (10 g) and $NaHCO_3$ (5.1 g) were dissolved in hot water (30 cm^3) [10]. After filtration the filtrate was combined with ethanol (80 cm^3) and kept in a refrigerator overnight. Resultant violet precipitates were collected and washed with ethanol. Yield: 7 g. Found: C, 21.8; H, 3.9; N, 7.2%. Calcd for $CoC_7H_{18}O_{11}N_2Na$: C, 21.7; H, 4.7; N, 7.2%. We assume that the water of crystallization of this complex is removed during the pre-drying treatment for the elemental analysis.

Cis(*O*)-Na[Co(aeida)(CO_3)]·H_2O. The latter fil-

trate in the above procedure for the *trans(O)* isomer was concentrated to 5 cm^3 and filtered. The filtrate was combined with ethanol (10 cm^3) and warmed slightly. Resultant red–violet precipitates were aged in a refrigerator overnight. They were collected; washed with 70% methanol and methanol; and were recrystallized from minimum amount of water by the addition of two volumes of ethanol. Yield: 1 g. Found: C, 25.1; H, 3.6; N, 8.3%. Calcd for $CoC_7H_{12}O_8N_2Na$: 25.2; H, 3.6; N, 8.4%.

CAUTION! Although we have experienced no difficulty with the cobalt(III) complexes reported here, these should be regarded as potentially explosive and be handled accordingly.

Kinetic measurements

A Unisoku RS-450 stopped-flow apparatus was used for the kinetic measurements. The reaction temperature was controlled at 25.0±0.1°C. Equal volumes of the complex solution (I = 2.0, $NaClO_4$) and of the perchloric acid solution (I = 2.0, $NaClO_4$) were mixed in a cell (path length = 1 cm). The time course of the absorbance was checked at several wavelengths in the UV-vis region and was recorded at relevant wavelength where substantial change of the absorbance can be observed. It was analyzed using a computing routine the Unisoku kinetic analysis program version 1.1 according to eqn (3) through the following procedures. Certain latter part of the trace was regarded as a curve for the single first order process and treated with the Guggenheim's method. The magnitude of k_{slow} was estimated from the gradient of the linear relation between $\ln|A_{t+\Delta t}-A_t|$ and t with Δt being a half of the relevant time interval. The constant n was so selected as to make the resultant term $n\exp(-k_{slow}t)$ reproduce the part of the trace. The difference between the original trace and thus calculated trace $n\exp(-k_{slow}t)$ was treated with the Guggenheim's method and the magnitude of k_{fast} was estimated. This operation was repeated a few times. Finally, k_{slow} was estimated on the original trace after six half lives of the fast process ($4.14/k_{fast}$s) and k_{fast} on the difference trace from t = 0 to five half lives of the fast process ($3.45/k_{fast}$s). The reliability of k_{fast} or k_{slow} was checked by the correlation coefficient (generally 0.999) of the Guggenheim's linear plot. Thus, in some cases, both k_{fast} and k_{slow} were reliable enough, whereas in other cases only one of them was reliable. Alternatively, the whole trace was well approximated as a curve for a single first-order process. This occurs in the cases of *mer(N)*-[$Co(CO_3)$(5-dptma)] at 306.8 or 290 nm; of *mer(N)*-[$Co(CO_3)$(i-2,3-ma)] at 301.6 or 290 nm; of *trans(O)*-[Co(aeida)$(CO_3)]^-$ at 280 nm. Four independent runs were performed and the average values of the k_{fast} or the k_{slow} are given in Table 2. In the case of *trans(O)*-[Co(aeida)$(CO_3)]^-$ ($[H^+]$ = 0.151–0.504 M), the traces were alternatively analyzed using the Unisoku nonlinear least-squares-fitting routine *ANALYSIS EXE* according to eqn (3). The resultant values of the k_{fast} and the k_{slow} by this method (not given in this report) were essentially the same as the corresponding ones obtained by the above mentioned method.

Spectral determination of K.

The zero-time absorbance (A_{obs}) of the reacting solution was estimated by the extrapolation of the A_t to t = 0 over the mixing dead time 2 ms (Table 2). The absorbance A_1 due to the species **1** was measured by the stopped-flow mixing of the complex solution (I = 2.0, $NaClO_4$) with 2 M $NaClO_4$ solution and is given in Table 2 as the A_{obs} at $[H^+]$ = 0 M. Value of K was calculated therefrom by the linear plot between $1/(A_1-A_{obs})$ and $1/[H^+]$ as described by Buckingham *et al.* [3].

$$\frac{1}{(A_1-A_{obs})}=\frac{1}{K(A_1-A_2)[H^+]}+\frac{1}{(A_1-A_2)} \quad (4)$$

where A_2 represents the absorbance of the species **2**.

Apparatus

A JEOL-GSX-270-FT-NMR instrument and a Shimadzu UV-2200 UV-vis spectrophotometer were used.

RESULTS AND DISCUSSION

Isomerization of the diaqua hydrolysis product

The NMR spectra were measured for the D_2O solutions of the carbonato complex after about 30 min from the treatment by $HClO_4$ (Table 1.b). In the cases of *mer(N)*-[$Co(CO_3)$(i-dtma)] and *mer(N)*-[$Co(CO_3)$(i-2,3-ma)] the resultant solutions contain only the corresponding *mer(N)* diaqua product and in other cases the solutions are more or less contaminated with the isomeric diaqua product; 4% *mer(N)* isomer from *fac(N)*-[$Co(CO_3)$(i-dtma)], 2% *cis(O)* isomer from *trans(O)*-[Co(aeida)$(CO_3)]^-$ and 20% *trans(O)* isomer from *cis(O)*-[Co(aeida)$(CO_3)]^-$. In similar experiments for *fac(N)*- and *mer(N)*-[$Co(CO_3)$(5-dptma)], complete retention of the isomeric configuration has been demonstrated during the acid-catalysed hydrolysis [7]. Assuming that the mechanism is common for the seven carbonato complexes treated here, we consider that the acid-catalysed hydrolysis (eqn (1)) proceeds with retention of the isomeric configuration and that the diaqua product isomerizes subsequently more or less. In the cases of *fac(N)*-[$Co(CO_3)$(i-dtma)] and *trans(O)*-[Co(aeida)$(CO_3)]^-$ the isomerization extent may be negligible. The isomerization velocity was followed spectrophotometrically at 540 nm for the solution of *cis(O)*-[Co(aeida)$(CO_3)]^-$ (7 mM) in 2 M $HClO_4$.

Table 2. Experimental rate constants, zero-time absorbances and the equilibrium or rate constants derived therefrom for the acid-catalyzed hydrolyses of carbonato cobalt(III) complexes at 25°C and $I = 2.0$ ($NaClO_4$)

fac(*N*)-[Co(CO_3)(5-dptma)]					
λ/nm[a]	293		293		293
$[Co]_T$/mM	0.3		0.3		0.3
$[H^+]$/M	k_{fast}/s^{-1}	k_{calc}/s^{-1}[b]	k_{slow}/s^{-1}	k_{calc}/s^{-1}[c]	A_{obs}
0					0.831
0.021			0.0080[d]	0.0091	
0.040			0.0160[d]	0.0171	
0.061			0.0233	0.0247	
0.081			0.0307	0.0318	
0.101			0.0377	0.0382	
0.151			0.0529	0.0524	0.761[d]
0.256	0.300	0.296	0.0746	0.0757	0.735
0.357	0.329	0.331	0.090	0.0924	0.709
0.509	0.350	0.363	0.105	0.109	0.684
0.760	0.399	0.393	0.123	0.131	0.648
1.02	0.418	0.410	0.130	0.145	0.627
K/M^{-1}			2.2±0.2		1.6±0.1
k_{Co-O}/s^{-1}			0.21±0.01		
K_a/M	0.15±0.02				
k_{O-C}/s^{-1}	0.47±0.02				

mer(*N*)-[Co(CO_3)(5-dptma)]						
λ/nm[a]	306.8	290		310		290
$[Co]_T$/mM	0.8	0.2		1.1		0.2
$[H^+]$/M	k_{fast}/s^{-1}	k_{fast}/s^{-1}	k_{calc}/s^{-1}[e]	k_{slow}/s^{-1}	k_{calc}/s^{-1}[f]	A_{obs}
0						0.921
0.021	2.15		1.91			
0.040	3.94		3.70	0.161	0.156	
0.061	5.57		5.47	0.166	0.163	
0.081	7.20		7.22	0.167	0.166	
0.101	8.81		8.87	0.170	0.168	0.844
0.151		12.7	12.8	0.172	0.170	0.817
0.253		19.9	20.1	0.172	0.171	0.777
0.355		26.7	26.5	0.170	0.170	0.744
0.508		35.3	34.8	0.167	0.168	0.712
0.764		47.3	45.9	0.164	0.163	0.682
1.02		57.3	54.6	0.160	0.160	0.665
K/M^{-1}	0.75±0.06					1.0±0.1
k_{Co-O}/s^{-1}	126±10					
K_a/M				0.006		
$(K_h/K_w)/M^{-1}$				0.12		
k_{O-C}/s^{-1}				0.18		

fac(*N*)-[Co(CO_3)(i-dtma)]				
λ/nm[a]	280		280	280
$[Co]_T$/mM	0.37		0.37	0.37
$[H^+]$/M	k_{fast}/s^{-1}	k_{calc}/s^{-1}[e]	k_{slow}/s^{-1}	A_{obs}
0				0.905
0.251				0.811
0.352	1.96	1.97	0.976	0.789
0.504	2.40	2.32	1.10	0.756
0.755	2.74	2.68	1.12	0.713
1.00	2.85	2.90	1.03	0.676
K/M^{-1}	2.9±0.5			1.2±0.2
k_{Co-O}/s^{-1}	3.9±0.3			
k_{O-C}/s^{-1}			~1	

Table 2—*Continued.*

mer(*N*)-[Co(CO_3)(i-dtma)]					
λ/nm[a]	330		330		280
$[Co]_T$/mM	11.7		11.7		0.26
$[H^+]$/M	k_{fast}/s^{-1}	k_{calc}/s^{-1}[b]	k_{slow}/s^{-1}	k_{calc}/s^{-1}[c]	A_{obs}
0					1.047
0.151	0.951	0.936	0.316	0.328	0.981
0.253	1.14	1.22	0.430	0.430	0.948
0.355	1.30	1.40	0.497	0.496	0.924
0.508	1.49	1.57	0.555	0.560	0.893
0.755					0.851
0.764	1.76	1.74	0.603	0.623	
1.02	1.98	1.83	0.621	0.659	0.820
K/M^{-1}			4.6 ± 0.3		1.4 ± 0.1
k_{Co-O}/s^{-1}			0.8 ± 0.0		
K_a/M	0.2 ± 0.0				
k_{O-C}/s^{-1}	2.2 ± 0.2				
mer(*N*)-[Co(CO_3)(i-2,3-ma)]					
λ/nm[a]	301.6	290		290	290
$[Co]_T$/mM	0.4	0.4		0.4	0.4
$[H^+]$/M	k_{fast}/s^{-1}	k_{fast}/s^{-1}	k_{calc}/s^{-1}[e]	k_{slow}/s^{-1}	A_{obs}
0					0.955
0.020	0.111[d]		0.123		
0.040	0.229[d]		0.242		
0.061	0.357		0.360		
0.081	0.481		0.477		
0.101	0.601		0.588		
0.152	0.883		0.863		
0.256		1.41	1.39		0.877
0.357		1.87	1.85		0.854
0.509		2.43	2.47	0.25[g]	0.826
0.760		3.20	3.35	0.24[g]	0.784
1.02		3.82	4.11	0.25[g]	0.756
K/M^{-1}	0.51 ± 0.08				0.91 ± 0.05
k_{Co-O}/s^{-1}	12 ± 2				
k_{O-C}/s^{-1}				~0.3	
cis(*O*)-[Co(aeida)(CO_3)]$^-$					
λ/nm[a]	280	280			280
$[Co]_T$/mM	0.25	0.25			0.25
$[H^+]$/M	k_{fast}/s^{-1}	k_{slow}/s^{-1}	k_{calc}/s^{-1}[c]		A_{obs}
0					1.106
0.020		0.0315	0.0330		
0.041		0.0655	0.0650		
0.061		0.0986	0.0969		
0.081		0.131	0.128		
0.101		0.163	0.157		
0.151		0.237	0.230		
0.251		0.377	0.366		1.020
0.352		0.495	0.491		0.995
0.504		0.636	0.662		0.971
0.755					0.930
1.00	2.02	0.954	1.03		
K/M^{-1}		0.48 ± 0.1			1.3 ± 0.2
k_{Co-O}/s^{-1}		3.4 ± 0.7			
k_{O-C}/s^{-1}	~2				

Table 2—*Continued.*

trans(*O*)-[Co(aeida)(CO_3)]$^-$					
λ/nm[a]	280		280		280
$[Co]_T$/mM	0.3		0.3		0.3
$[H^+]$/M	k_{fast}/s^{-1}	k_{calc}/s^{-1}[b]	k_{slow}/s^{-1}	k_{calc}/s^{-1}[c]	A_{obs}
0					1.064
0.020	0.275[d]	0.289			
0.041	0.541	0.540			
0.061	0.767	0.765			
0.081	0.956	0.962			
0.101	1.13	1.13			
0.151	1.47	1.50	0.245	0.248	
0.251	2.01	2.04	0.400	0.389	0.998
0.352	2.42	2.40	0.534	0.516	0.978
0.504	2.92	2.78	0.702	0.683	0.956
0.755			0.898	0.911	0.922
1.00			0.997	1.09	0.899
K/M^{-1}			0.7±0.1		1.0±0.1
k_{Co-O}/s^{-1}			2.8±0.4		
K_a/M	0.3±0.0				
k_{O-C}/s^{-1}	4.4±0.1				

[a] Reaction was followed at this wavelength.
[b] Calculated by eqn (9).
[c] Calculated by eqn (8).
[d] This datum was not used for the derivation.
[e] Calculated by eqn (6).
[f] Calculated by eqn (13).
[g] Correlation coefficient was 0.995 or 0.996.

Rate constant of 7.7×10^{-4} s^{-1} was estimated at 25°C for the isomerization

cis(*O*)-[Co(aeida)$(H_2O)_2$]$^+$ ⇌ *trans*(*O*)-[Co(aeida)$(H_2O)_2$]$^+$

This velocity is slow enough compared with the hydrolysis velocity. Thus, we consider that the isomerization of the diaqua product does not interfere with the kinetic course of the acid hydrolysis of *cis*(*O*)-[Co(aeida)(CO_3)]$^-$.

Spontaneous hydrolysis

Absorption spectrum (300–600 nm) of the neutral aqueous solution of each of our seven carbonato complexes remained unchanged during 1 h with the total concentration ~5 mM of the cobalt(III) complex at I = 2.0 ($NaClO_4$) and 25°C. Therefore, we neglect the contribution of the spontaneous hydrolysis.

Acid-catalyzed hydrolysis

The experimental rate constants k_{fast} and k_{slow} and the zero-time absorbance data A_{obs} are summarized in Table 2 with the equilibrium or the rate constants derived therefrom. The values of the k_{fast} or the k_{slow} are calculated according to eqn (6), (8), (9) or (13) to be mentioned later, using the derived values of the constants and are given as k_{calc} in Table 2. These k_{calc}'s agree satisfactorily with the corresponding values of the k_{fast} or the k_{slow} and justify the treatments by these equations. In the cases of *fac*(*N*)-[Co(CO_3)(5-dptma)], *mer*(*N*)-[Co(CO_3)(i-dtma)] and *trans*(*O*)-[Co(aeida)(CO_3)]$^-$, both the k_{fast} and the k_{slow} increase with the increasing acidity of the solution as illustrated in Fig. 2. These results are incompatible with the current mechanism that predicts one acidity dependent and the other acidity independent rate constants as given by eqn (2). Therefore, we propose the modification I for the current mechanism: a deprotonation equilibrium from the species **3** giving rise to an inert monodentate carbonato complex **5**. According to this modified mechanism I (Scheme 2), the time course of the absorbance is given by eqn (5).

$$|A_t - A\infty| = M' \exp\left(-\frac{k_{Co-O}K[H^+]}{1+K[H^+]}t\right) + N' \exp\left(-\frac{k_{O-C}[H^+]}{[H^+]+K_a}t\right) \quad (5)$$

M' and N' are constants independent of t, which are

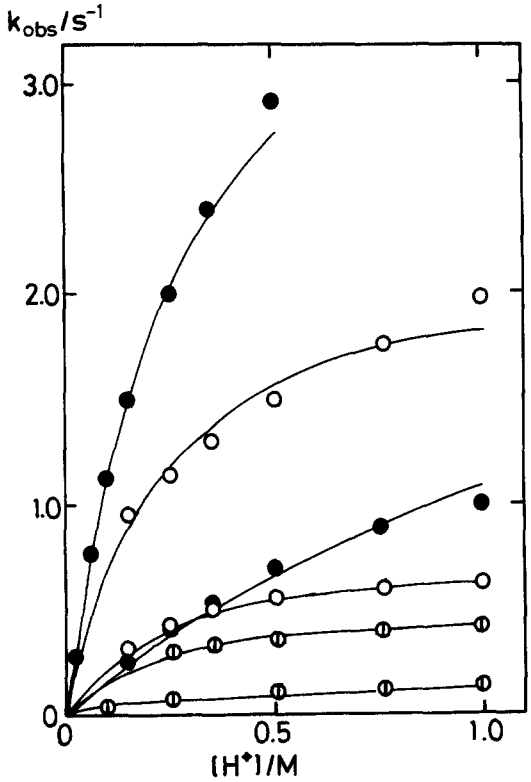

Fig. 2. Plots of k_{obs} (k_{fast} and k_{slow}) versus [H$^+$] for the acid hydrolysis of *fac*(*N*)-[Co(CO$_3$)(5-dptma)] (Φ), *mer*(*N*)-[Co(CO$_3$)(i-dtma)] (○) and *trans*(*O*)-[Co(aeida)(CO$_3$)]$^-$ (●) in aqueous solutions at 25°C and I = 2.0 (NaClO$_4$). The lines show the k_{calc} (see text).

given by the M'' (eqn (11)) and N'' (eqn(12)) to be mentioned later respectively with the neglection of the K_b value. K_a is the acidic dissociation constant of the species **3**. Eqn (5) involves two acidity dependent pseudo first-order rate constants, but the correspondence between these and the k_{fast} or the k_{slow} is not a priori clear. Therefore, we consider two possible correspondences: one with eqns (6) and (7); and the other with eqns (8) and (9).

$$k_{fast} = \frac{k_{Co\text{-}O}K[H^+]}{1+K[H^+]} \tag{6}$$

$$k_{slow} = \frac{k_{O\text{-}C}[H^+]}{[H^+]+K_a} \tag{7}$$

$$k_{slow} = \frac{k_{Co\text{-}O}K[H^+]}{1+K[H^+]} \tag{8}$$

$$k_{fast} = \frac{k_{O\text{-}C}[H^+]}{[H^+]+K_a} \tag{9}$$

We derive the magnitudes of $k_{Co\text{-}O}$, K, $k_{O\text{-}C}$ or K_a according to these equations: the linear relations between the $1/k_{fast}$ or the $1/k_{slow}$ and the $1/[H^+]$. In the case of *fac*(*N*)-[Co(CO$_3$)(5-dptma)], K is derived as 6.7 and 2.2 M^{-1} by eqns (6) and (8), respectively. The latter value agrees satisfactorily with the K = 1.6 M^{-1} alternatively derived by eqn (4). Therefore, we prefer eqn (8) and derive K_a = 0.15 M by eqn (9). In the case of *mer*(*N*)-[Co(CO$_3$)(5-dptma)], K is derived as 0.75 M^{-1} by eqn (6). This value agrees well with the K = 1.0 M^{-1} by eqn (4). The k_{slow} is approximately constant and we cannot estimate the K_a value by eqn (7). In the case of *fac*(*N*)-[Co(CO$_3$)(i-dtma)], the K = 2.9 M^{-1} by eqn (6) agrees well with the K = 1.2 M^{-1} by eqn (4). The k_{slow} is again approximately constant and we cannot estimate the K_a value. In the case of *mer*(*N*)-[Co(CO$_3$)(i-dtma)], both the K = 4.9 M^{-1} by eqn (6) and the K = 4.6 M^{-1} by eqn (8) are comparable to the K = 1.4 M^{-1} by eqn (4). We tentatively prefer eqn (8) and derive K_a = 0.2 M by eqn (9). In the case of *mer*(*N*)-[Co(CO$_3$)(i-2,3-ma)], the K = 0.51 M^{-1} by eqn (6) agrees well with the K = 0.91 M^{-1} by eqn (4). The k_{slow} is again approximately constant and

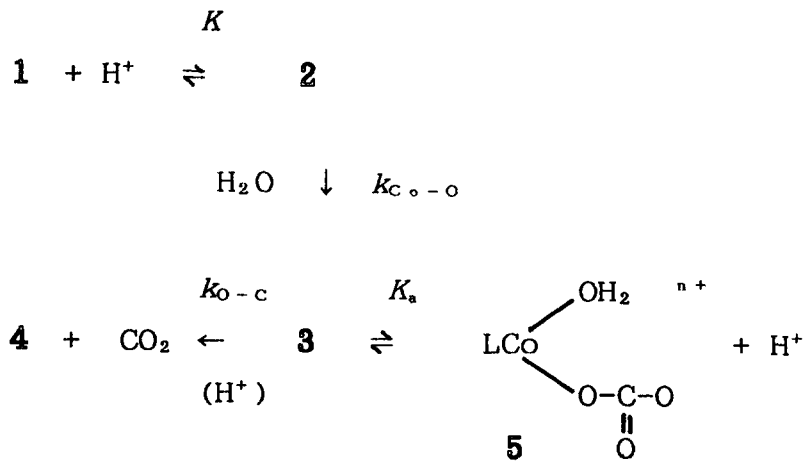

Scheme 2. Modified mechanism I for reaction 1.

we cannot estimate the K_a value. In the case of *cis*(*O*)-[Co(aeida)(CO_3)]$^-$, the $K = 0.48$ M^{-1} by eqn (8) agrees well with the $K = 1.3$ M^{-1} by eqn (4) and we tentatively estimate $k_{O\text{-}C} \fallingdotseq 2$ s^{-1}. In the case of *trans*(*O*)-[Co(aeida)(CO_3)]$^-$ the K is derived as 3.5 M^{-1} by eqn (6) and as 0.7 M^{-1} by eqn (8). The latter value agrees well with the $K = 1.0$ M^{-1} by eqn (4). We derive $K_a = 0.3$ M by eqn (9). In the case of *mer*(*N*)-[Co(CO_3)(5-dptma)], the k_{slow} is approximately independent of the acidity as mentioned above. However, this case cannot be explained by the current mechanism (Scheme 1) on account of the following observation. In certain limited acidity range, the whole trace of the absorbance at 306.8 or 290 nm is well approximated as a curve for a single first-order process, whereas it deviates from this beyond such acidity range. In the current mechanism, the K_a is negligibly small and the whole trace should reduce to a curve for a single first-order process at the isosbestic wavelength between the species **3** and **4** irrespective of the acidity. On close examination, it can be noticed that the k_{slow} for this complex changes slightly with the acidity and attains a flat maximum around $[H^+] = 0.2$ M. This suggests an amphoteric character of the species **3**; a deprotonation from **3** giving rise to the inert complex **5** and a protonation to **3** giving rise to the inert carbonic acid complex **6** as shown in Scheme 3. According to this modified mechanism II (Scheme 3), the time course of the absorbance is given by eqns (10)–(12).

$$|A_t - A\infty| = M'' \exp\left(-\frac{k_{Co\text{-}O}K[H^+]}{1+K[H^+]}t\right) + N'' \exp\left(-\frac{k_{O\text{-}C}[H^+]}{(K_h/K_w)[H^+]^2+[H^+]+K_a}t\right) \quad (10)$$

$$M''/[Co]_T = \frac{\varepsilon_1 - \varepsilon_4 + K[H^+](\varepsilon_2 - \varepsilon_4)}{1+K[H^+]} + \beta\left\{\frac{K_a(\varepsilon_5 - \varepsilon_4)}{[H^+]} + \varepsilon_3 - \varepsilon_4 + (K_h/K_w)[H^+](\varepsilon_6 - \varepsilon_4)\right\} \quad (11)$$

$$N''/[Co]_T = \beta\left\{\frac{K_a(\varepsilon_4 - \varepsilon_5)}{[H^+]} + \varepsilon_4 - \varepsilon_3 + (K_h/K_w)[H^+](\varepsilon_4 - \varepsilon_6)\right\} \quad (12)$$

$$\beta \equiv \frac{k_{Co\text{-}O}\alpha K[H^+]}{k_{O\text{-}C}\alpha(1+K[H^+]) - k_{Co\text{-}O}K[H^+]}$$

$$\alpha \equiv \frac{[H^+]}{(K_h/K_w)[H^+]^2+[H^+]+K_a}$$

The ε_1, ε_2, ε_3, ε_4, ε_5 and ε_6 are the extinction coefficients at the relevant wavelength due to the complex species **1**, **2**, **3**, **4**, **5** and **6**, respectively. $[Co]_T$ is the total concentration of the Co(III) complex in the solution. K_h is the equilibrium constant for

$$\mathbf{3} + H_2O \rightleftharpoons \mathbf{6} + OH^-$$

and K_w is the autoprotolysis constant of water. Comparing eqn (3) with eqn (10), we interpret the k_{slow} for *mer*(*N*)-[Co(CO_3)(5-dptma)] by eqn (13)

$$k_{slow} = \frac{k_{O\text{-}C}[H^+]}{(K_h/K_w)[H^+]^2+[H^+]+K_a} \quad (13)$$

and estimate the relevant constants by the quadratic relation between the $[H^+]/k_{slow}$ and the $[H^+]$ (Table 2). In the case of *fac*(*N*)-[Co(CO_3)(i-dtma)], the k_{slow} also changes slightly with the acidity with a flat maximum at $[H^+] \sim 0.7$ M. This may also be explained by the modified mechanism II, but we keep from the estimation of the constants because of the scarcity of the k_{slow} data. We assume that for this complex the $k_{O\text{-}C}$ is close to the mean k_{slow} value on account of the proximity between the estimated value of $k_{O\text{-}C}$ and the mean k_{slow} for *mer*(*N*)-[Co(CO_3)(5-dptma)]. Similarly, we assume that for *mer*(*N*)-[Co(CO_3)(i-2,3-ma)] $k_{O\text{-}C}$ is close to the mean k_{slow} value. The equilibrium and the rate constants thus derived for our seven carbonato complexes are summarized in Table 3 with those given previously by Buckingham *et al.* for nine carbonato complexes [3,6]. In Table 3, the following may be noticed. The K values are surprisingly independent of the variation of the L ligand and are about 1 M^{-1} for these sixteen carbonato complexes. This may be explained that the protonation occurs at a site well removed from the Co(III) center and therefore not influenced by the coordination environment around the Co(III). This magnitude of the K remarkably differs from the previously presumed magnitude 10^{-6} M [4]. In contrast, the values of $k_{Co\text{-}O}$ depend significantly on the variation of the L ligand and cover a reactivity range of 10^4. The $k_{Co\text{-}O} = 126$ s^{-1} with L = *mer*(*N*)-5-dptma is the greatest among hitherto reported $k_{Co\text{-}O}$ values. This may be explained that this bond cleavage occurs between the LCo(III) moiety and the bicarbonato ligand and therefore is much influenced by the variation of the L or the coordination environment around the Co(II). However, we cannot find any general trend between the magnitude of the $k_{Co\text{-}O}$ and the charge or the constitution of the L ligand. It ranges 0.008–9.7 s^{-1} for the neutral L; 0.2–126 s^{-1} for the uninegative L; and 3–4.1 s^{-1} for the dinegative L. The *mer*(*N*)-[Co(5-dptma)(O_2COH)]$^+$ ring-opens much faster than the *fac*(*N*) congener, whereas the *mer*(*N*)-[Co(i-dtma)(O_2COH)]$^+$ ring-opens rather slower than its *fac*(*N*) congener. The *cis*(*O*) and the *trans*(*O*)-[Co(aeida)(O_2COH)] ring-open with essentially the same half life. In this bond cleavage, the trans-effect should be operative. As can be understood in Fig. 1, the two Co—O(bicarbonato) bonds in the bidentate bicarbonato complex **2** are inequivalent and the weaker

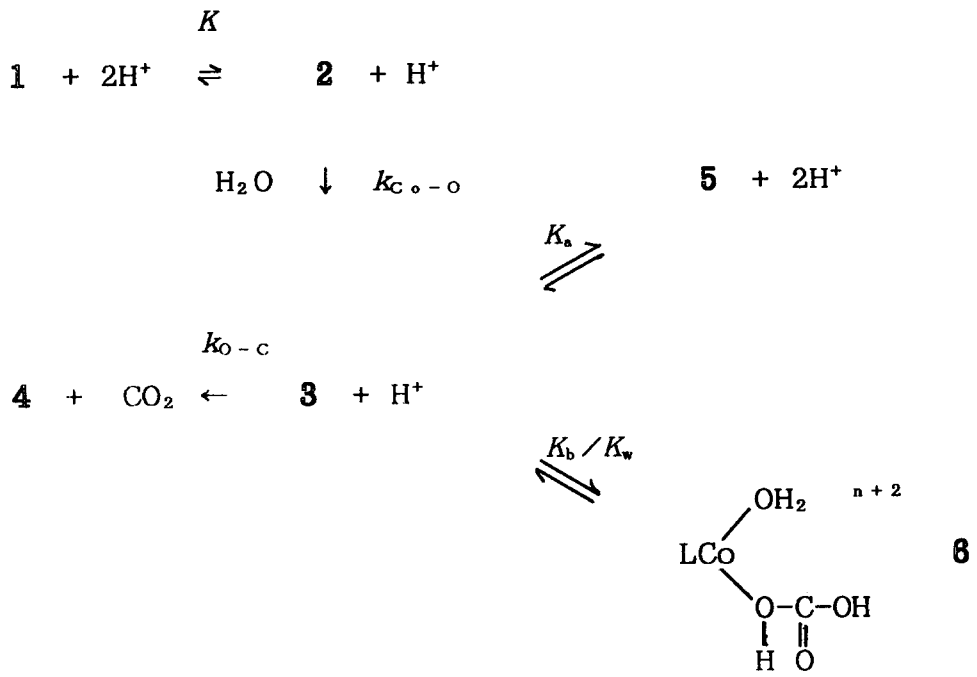

Scheme 3. Modified mechanism II for reaction 1.

Table 3. Equilibrium and rate constants for the acid-catalysed hydrolysis of $[CoL(O_2CO)]^{n+}$ at 25°C

L	K/M^{-1}[d]	$k_{Co\text{-}O}$/s^{-1}	$k_{O\text{-}C}$/s^{-1}	K_a/M[e]	(K_h/K_w)/M^{-1}[e]
$(NH_3)_4$[a]	1.0[e]	1.7	1.5	—	—
$(en)_2$[b]	0.9	0.9	0.9	0.23	—
α-trien[a]	0.7[e]	9.7	0.6	0.06	1.6
β-trien[a]	0.8[e]	0.3	0.5	—	—
tren[a]	0.6[e]	4.3	0.3	—	—
cyclen[a]	2.4	0.01	—	—	—
N-mecyclen[a]	0.4[e]	0.008	—	—	—
fac(*N*)-5-dptma[c]	1.6	0.21	0.47	0.15	—
mer(*N*)-5-dptma[c]	1.0	126	0.18	0.006	0.12
fac(*N*)-i-dtma[c]	1.2	3.9	~1	—	—
mer(*N*)-i-dtma[c]	1.4	0.8	2.2	0.2	—
mer(*N*)-i-2,3-ma[c]	0.9	12	~0.3	—	—
cis(*O*)-aeida[c]	1.3	3.4	~2	—	—
trans(*O*)-aeida[c]	1.0	2.8	4.4	0.3	—
$(gly)_2$[d]	1.5	4.1	4.1	—	—
nta[a]	0.9	85	2.0	—	—

[a] Ref. [6]. I = 1.0 ($NaClO_4$).
[b] Ref. [3]. I = 1.0 ($NaClO_4$).
[c] This work. I = 2.0 ($NaClO_4$).
[d] Determined from zero-time absorbance data unless otherwise indicated.
[e] Kinetically determined.
trien = 1,8-diamino-3,6-diazaoctane; tren = tris(2-aminoethyl)amine; cyclen = 1,4,7,10-tetraazacyclododecane; *N*-mecyclen = 1-methyl-1,4,7,10-tetraazacyclododecane; H(gly) = glycine; H_3(nta) = nitrilotriacetic acid.

one should cleave. The most interest point may be that we have found in the case of certain our carbonato complexes that both of the k_{fast} and the k_{slow} depend on the acidity, whereas Buckingham *et al.* have considered that in the case of their carbonato complexes one between the k_{fast} and the k_{slow} is independent of the acidity [3,6]. In this connection, we have reinvestigated reaction 1 with L of $(en)_2$ or α-trien at 25°C

and $I = 2.0$ ($NaClO_4$) [11]. With L = $(en)_2$, Buckingham *et al.* have assumed the acidity independent $k_{fast} = 0.93\ s^{-1}$ at lower acidity [3], whereas we have found that the k_{fast} increases significantly with the increasing acidity, for example with $[Co]_T = 0.7$ mM and $\lambda = 278$ or 280 nm; $k_{fast} = 0.51\ s^{-1}$ at $[H^+] = 0.15$ M and $1.08\ s^{-1}$ at $[H^+] = 1.00$ M, we have estimated that $k_{O\text{-}C} = 1.3\ s^{-1}$ and $K_a = 0.23\ M^{-1}$ according to eqn (9). With L = α-trien, Buckingham *et al.* have reported essentially acidity independent $k_{slow} = 0.62\ s^{-1}$ at $[H^+] = 0.2$–1.0 M [6], whereas we have found that the k_{slow} changes with the acidity with a maximum around $[H^+] = 0.2$ M. For example, with $[Co]_T = 0.8$ mM and $\lambda = 284$ nm; $k_{slow} = 0.16\ s^{-1}$ at $[H^+] = 0.02$ M, $0.81\ s^{-1}$ at $[H^+] = 0.20$ M and $0.57\ s^{-1}$ at $[H^+] = 1.00$ M, we have estimated that $k_{O\text{-}C} = 0.94\ s^{-1}$ and $K_a = 0.06$ M and $K_b/K_w = 1.6\ M^{-1}$ according to eqn (13). We consider that the acidity independent k_{slow} or k_{fast} reported by Buckingham *et al.* for reaction 1 with L = $(NH_3)_4$, β-trien, tren $(gly)_2$ and nta may also be explained by the amphoteric character of the complex **3** with the $k_{O\text{-}C}$ value close to the mean value of the corresponding k_{slow} or k_{fast} [6]. Thus, the $k_{O\text{-}C} = 0.2$–$4\ s^{-1}$ in Table 3 are again almost independent of the variation of the L ligand. This may be explained that the O—C bond cleavage occurs at the bicarbonato ligand coordinating to Co(III) and therefore is not influenced by the variation of the coordination environment around the Co(III). The $K_a = 0.006$–0.3 M for *cis*-$[CoL(OH_2)(O_2COH)]^{n+1}$ (**3**) are somewhat dependent on the variation of the L ligand, which is rather unexpected in consideration of the deprotonation site apart from the Co(III) center. These K_a values are incompatible with the reported equilibrium constant 4×10^{-7} M (25°C, $I = 0.5$) for an analogous acid dissociation eqn (14) from the pentaammine-bicarbonatocobalt(III) complex [12].

$$(H_3N)_5Co\,O{-}\overset{\overset{O}{\|}}{C}{-}OH^{2+} \rightleftharpoons (H_3N)_5Co\,O{-}\overset{\overset{O}{\|}}{C}{-}O^{+} + H^{+} \quad (14)$$

However, considering that the metal center moiety $CoL(OH_2)$ may correspond to a proton, the acid dissociation from *cis*-$[CoL(OH_2)(O_2COH)]^{n+1}$ may be reasonably compared with the first dissociation from carbonic acid.

$$HO{-}\overset{\overset{O}{\|}}{C}{-}OH \rightleftharpoons HO{-}\overset{\overset{O}{\|}}{C}{-}O^{-} + H^{+}$$

Our $K_a = 0.006$–0.3 M do not differ so drastically from the equilibrium constant 1.7×10^{-4} M (25°C, $I = 0$) of the latter [4]. The $K_b/K_w = 0.12$ and $1.6\ M^{-1}$ means very weak basicity $K_b = 10^{-15}$–10^{-14} M of *mer*(*N*)-$[Co(5\text{-dptma})(OH_2)(O_2COH)]^+$ or of α-$[Co(trien)(OH_2)(O_2COH)]^{2+}$. Since we have no precedent value of the equilibrium constant for this type of basicity, we have studied the acid hydrolysis of the monodentate carbonato complex $[Co(CO_3)(NH_3)_5]^+$ at 25°C and $I = 2.0$ ($NaClO_4$); with $[H^+] = 0.02$–1.01 M, $[Co]_T = 1.9$ mM and $\lambda = 278$ nm [11]. The whole trace was well regarded as a curve for a single first-order process with the experimental rate constant decreasing monotonically with the increasing acidity: for example $1.28\ s^{-1}$ at $[H^+] = 0.02$ M and $0.99\ s^{-1}$ at $[H^+] = 1.01$ M. From this result, we can estimate the equilibrium constant $0.3\ M^{-1}$ for the equilibrium

$$(H_3N)_5Co{-}O{-}\overset{\overset{O}{\|}}{C}{-}OH^{2+} + H^{+} \rightleftharpoons (H_3N)_5Co{-}\underset{\underset{H}{|}}{O}{-}\overset{\overset{O}{\|}}{C}{-}OH^{3+} \quad (15)$$

although we cannot estimate a reliable equilibrium constant for the above mentioned equilibrium 14. Equilibrium 15 is analogous to our proposed equilibrium

$$\mathbf{3} + H^+ \rightleftharpoons \mathbf{6}$$

and the proximity of the above estimated constant $0.3\ M^{-1}$ for equilibrium 15 to the $K_b/K_w = 0.12$ or $1.6\ M^{-1}$ for the latter is quite reasonable. In conclusion, we consider that the general mechanism of reaction 1 is given by our modified mechanism II (Scheme 3) with the magnitudes of K_a being rather dependent on the variation of the L ligand. In the cases of *fac*(*N*)-$[Co(CO_3)(5\text{-dptma})]$, *mer*(*N*)-$[Co(CO_3)(i\text{-dtma})]$ and *trans*(*O*)-$[Co(aeida)(CO_3)]^-$, we cannot estimate reliable K_b/K_w values from our kinetic data, since in our acidity range the k_{fast} increases monotonically with the increasing acidity or the effect of the basicity is dormant.

REFERENCES

1. Posey, F. A. and Taube, H., *J. Am. Chem. Soc.*, 1953, **75,** 4099.
2. Harris, G. M. and Hyde, K. E., *Inorg. Chem.*, 1978, **17,** 1892.
3. Buckingham, D. A. and Clark, C. R., *Inorg. Chem.*, 1993, **32,** 5405.
4. Palmer, D. A. and van Eldik, R., *Chem. Rev.*, 1983, **83,** 651.
5. Hashimoto, K., Yamao, S. and Kitamura, Y., Presented at the *15th Symposium on Solution Chemistry of Japan* (*Matsuyama*, 1992), p. 30.
6. Buckingham, D. A. and Clark, C. R., *Inorg. Chem.*, 1994, **33,** 6171.
7. Shibata, A., Kitamura, Y. and Tanabe, Y., *Polyhedron*, 1996, **15,** 1225.
8. Kitamura, Y., Shibata, A., Azuma, N. and Ozawa, T., *Polyhedron*, 1994, **13,** 2477.

9. Kitamura, Y., Azuma, N., Minamoto, K., Murakami, S. and Tanabe, Y., *Polyhedron*, 1997, **16,** 3757.
10. Kitamura, Y. and Shibata, A., *Polyhedron*, 1993, **12,** 2143.
11. Kitamura, Y. *et al.*, to be published.
12. Dasgupta, T. P. and Harris, G. M., *J. Am. Chem. Soc.*, 1968, **90,** 6360.

Pergamon

PII: S0277-5387(97)00405-1

Polyhedron Vol. 17, No. 9, pp. 1463–1470, 1998
© 1998 Elsevier Science Ltd
All rights reserved. Printed in Great Britain
0277-5387/98 $19.00+0.00

Preparation and spectral properties of nickel(II) and copper(II) complexes with two isomeric cyclohexylcyclams

Kazunori Sakata,[a]* Takeharu Odamura,[a] Yumie Kanbara,[a] Tamami Nibu,[a] Mamoru Hashimoto,[a] Akihiko Tsuge[a] and Yoshiki Moriguchi[b]

[a] Department of Chemistry, Faculty of Engineering, Kyushu Institute of Technology, Tobata-ku, Kitakyushu 804, Japan

[b] Department of Chemistry, Fukuoka University of Education, Akama, Munakata 811-41, Japan

(Received 25 August 1997; accepted 2 October 1997)

Abstract—The nickel(II) complexes of two isomeric cyclohexylcyclams were prepared by employing a nickel template reaction. The cyclohexylcyclams were synthesized from the nickel(II) complexes and then the copper(II) complexes were prepared from the free ligands and copper(II) perchlorate. The nickel(II) and copper(II) complexes exhibit clusters of ions corresponding to $[M-ClO_4]^+$ and $[M-2ClO_4+2H]^+$ which is the base peak in FAB mass spectra. A strong band observed at ca 3200 cm^{-1} is assigned to the N—H stretching mode and the band is slightly shifted to lower frequency on metal coordination, indicating freshly strong bands due to ClO_4^- stretching mode at ca 1090 and ca 620 cm^{-1}. The molar conductances for the complexes are 1:2 electrolytes in *N,N*-dimethylformamide and the perchlorate anions are ionized on dissolution in the solvent. The nickel(II) and copper(II) complexes of the two isomers are subjected to the square-planar ligand-field, but the ligand-field band for the nickel(II) complex of isomer L_t^3, *trans*-cyclohexylcyclam, shows the distorted octahedral form in coordinating solvent. ESR spectra for the copper(II) complexes of the two isomers also give the spin Hamiltonian parameters of the square-planar coordination. ^{13}C-NMR spectral results are comparable with those of another spectra. © 1998 Elsevier Science Ltd. All rights reserved

Keywords: macrocycle; cyclohexylcyclam; two isomers; nickel(II) complex; copper(II) complex; spectrum.

Substantial effort has been expended on the investigation of cyclam (1,4,8,11-tetraazacyclotetradecane) complexes and *N*-substituted cyclam complexes [1]. These are rare examples of cyclam complexes substituted by cyclohexyl groups at the 2-, 3-, 9- and 10-positions. Since the complexes have been synthesized on the basis of the structural interest, the spectral research has not been advanced satisfactorily. Kobiro *et al.* presented only the synthesis and molecular structures of nickel(II) complexes with cyclohexylcyclams and dicyclohexylcyclams (1,2,3,4,5,6,7,8,9,10,11,12,13,14,15,16,17,18,19,20,21,22-docosahydrodibenzo[*b,i*]-[1,4,8,11]tetraazacyclotetradecine) without the study of the spectral properties [2]. We have already reported the syntheses, the spectral properties and the kinetic data of cobalt(III), nickel(II), copper(II) and zinc(II) complexes with dicyclohexylcyclams [3].

In the present work, we employed the nickel(II) and copper(II) complexes with cyclohexylcyclams, namely

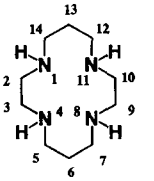

cyclam

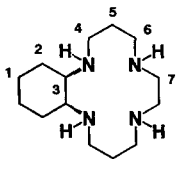

L_c^3

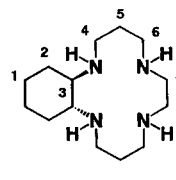

L_c^3

cyclohexylcyclam

* Author to whom correspondence should be addressed.

2,3-*cis*-cyclohexano-1,4,8,11-tetraazacyclotetradecane (L_c^3, *cis*-cyclohexylcyclam) and 2,3-*trans*-cyclohexano-1,4,8,11-tetraazacyclotetradecane (L_t^3, *trans*-cyclohexylcyclam), to make a further exploration into the influence on the cyclohexyl group in the dicyclohexylcyclam complexes. We report here the spectral properties and characterization of the nickel(II) and copper(II) complexes of cyclohexylcyclams, as examined by electronic, vibrational, mass, NMR and ESR spectroscopy. The characteristic behavior of the cyclohexylcyclam complexes is discussed by reference to that of cyclam and dicyclohexylcyclam complexes.

EXPERIMENTAL

Physical measurements

All melting points were observed on a Yanaco MP-500D micro melting point apparatus (hot-plate type). Elemental analyses were determined with a Yanaco CHN corder MT3. EI mass spectra (at 70 eV) for cyclohexylcyclams and their intermediates and FAB mass spectra (in a matrix of 3-nitrobenzyl alcohol) for the complexes were carried out with a JEOL JMS-DX 300 gas chromatograph-mass spectrometer. Conductivity measurements were made on *N,N*-dimethylformamide solutions of the complexes kept at 25.0 ± 0.1°C with a Coolnics Thermo-Bath (model CTE-310). Conductivities were measured with a TOA Electronics Ltd, CM-20E. Infrared spectra covering the 400–4000 cm^{-1} range were obtained on a Hitachi 260-30 spectrophotometer at room temperature with neats and potassium bromide disks. Electronic spectra were taken on a Shimadzu UV 200S double beam spectrophotometer for *N,N*-dimethylformamide solutions at room temperature in the range 12,500–37,000 cm^{-1}. Proton and carbon-13 NMR spectra were recorded on a JEOL JNM-A500 spectrometer in chloroform-*d*, methanol-d_4, dimethyl sulfoxide-d_6 and/or trifluoroacetic acid-*d* at room temperature and the chemical shifts are reported in ppm relative to tetramethylsilane as an internal reference standard. ESR spectra were measured on a JEOL JES-RE2X X-band spectrometer equipped with a 100 kHz field modulation unit. The copper(II) complexes were run in *N,N*-dimethylformamide at room temperature with a capillary tube and at 77 K. The manganese ions diffused into magnesium oxide were utilized to gain the standard reference signals for measurements.

Separation of cis-*cyclohexane*-1,2-*diamine* (cis-*dac*) *and* trans-*cyclohexane*-1,2-*diamine* (trans-*dac*)

The method of Saito and Kidani was modified for the separation of *cis*-dac and *trans*-dac [4]. To a solution of cyclohexane-1,2-diamine (*cis*- and *trans*-mixtures) (Aldrich Chemical Co. Inc., 25.0 g, 0.22 mol) in methanol (160 ml) was added in limited amounts a solution of nickel(II) chloride hexahydrate (26.0 g, 0.11 mol) in methanol (440 ml) at room temperature with stirring. After 3 h, the precipitates deposited were separated by filtration, washed sufficiently with methanol, and vacuum dried to give 11.9 g (30%) of fine yellow crystals (*cis*-dac nickel(II) complex). The yellow crystals (7.90 g, 0.022 mol) were decomposed by adding 6 N sulfuric acid (15 ml). The solution was evaporated under reduced pressure and ethanol (80 ml) was added to the oil residue. The colorless precipitates deposited were collected by filtration and recrystallized from water to obtain colorless plates (*cis*-dac H_2SO_4 salt). The yield was 8.72 g (93%) (lit. [5] mp 304–309°C), mp 308–311°C (dec). IR (KBr): 3100–2000 (N—H), 1610, 1530 (N—H), 1150, 620 (S—O) cm^{-1}.

After the separation procedure of the above yellow *cis*-dac nickel(II) complex, water (100 ml) was added to the filtrate, which was allowed to stand for a week in a refrigerator. The resulting deposits were isolated by filtration and washed with water to afford 22.5 g (52%) of violet needles (*trans*-dac nickel(II) complex). The reaction of the violet needles (8.6 g, 0.022 mol) with 6 N hydrochloric acid (15 ml), following the above procedure, gave colorless prisms (*trans*-dac 2HCl salt). The yield was 6.54 g (80%) (lit. [4] mp 321–326°C), mp 318–323°C (dec). IR (KBr): 3000–2100 (N—H), 1610, 1520 (N—H) cm^{-1}.

Preparation of cyclohexylcyclams and their complexes

N,N′-*Bis*(2-*cyanoethyl*)-cis-1,2-*diaminocyclohexane* (1c). After sodium (1.07 g, 46.8 mmol) was dissolved in methanol (200 ml), *cis*-dac H_2SO_4 salt (5.15 g, 24.3 mmol) was added to it at room temperature with stirring. To the reaction solution was added dropwise at 0°C a solution of freshly distilled acrylonitrile (2.23 g, 42.1 mmol) in methanol (3.0 ml). The reaction mixture was stirred for 1 h at 0°C and heated under reflux for 5 h with stirring. After being cooled down at room temperature, the excess acrylonitrile was evaporated *in vacuo* to yield 4.76 g (89%) of a colorless viscous liquid (1c). An analytical sample was recrystallized from *n*-hexane-ethyl ether at −60°C to obtain colorless prisms. IR (KBr): 3320, 3270 (N—H), 2230 (C≡N) cm^{-1}. EIMS *m/z* (relative intensity): 221 (21.9), 220 (95.8), 180 (69.6), 166 (23.5), 151 (45.1), 150 (60.4).

N,N′-*Bis*(2-*cyanoethyl*)-trans-1,2-*diaminocyclohexane* (1t). The reaction of *trans*-dac 2HCl salt (4.08 g, 24.3 mmol), sodium (1.07 g, 46.8 mmol) and acrylonitrile (2.08 g, 39.2 mmol) in methanol (200 ml), following the above procedure, gave colorless prisms (1t) using tetrahydrofuran instead of ethyl ether. The yield was 4.18 g (87%). IR (KBr): 3315, 3280 (N—H), 2230 (C≡N) cm^{-1}. EIMS *m/z* (relative intensity): 221 (10.1), 220 (100), 180 (68.8), 166 (20.2).

5,6-cis-*Cyclohexano*-4,7-*diazadecane*-1,10-*diamine* (L_c^1). To a mixture of lithium aluminum hydride (1.51

g, 39.8 mmol) and anhydrous ethyl ether (40 ml) was added a solution of aluminum chloride (5.31 g, 39.8 mmol) in anhydrous ethyl ether (40 ml) at room temperature with stirring under argon atmosphere. To the mixture was added anhydrous tetrahydrofuran (70 ml) and to it was added a solution of 1c (3.52 g, 15.9 mmol) in anhydrous tetrahydrofuran (10 ml) at 40°C over 20 min with stirring. After being refluxed for 2 h and being cooled at room temperature, methanol (10 ml) was added dropwise to the reaction mixture and then a 20% aqueous potassium sodium tartrate solution (100 ml) was added. The organic solvent was taken off by diminished pressure and a 25% aqueous sodium hydroxide solution (100 ml) was added to the residue. The aqueous mixture was extracted three times with dichloromethane (100 ml). The organic layer was dried over anhydrous sodium sulfate overnight and distilled under nitrogen atmosphere at 150°C (1 torr) to give a colorless viscous liquid (L_c^1) (lit. [2b] bp 152°C (1 torr)). The yield was 3.10 g (86%). IR (neat): 3260 (N—H), 1600 (N—H) cm^{-1}. EIMS *m/z* (relative intensity): 228 (13.3), 182 (12.9), 155 (27.7), 154 (100). ^{1}H-NMR (chloroform-*d*): δ 1.0–2.0 (m, 18H), 2.5–3.0 (m, 10H).

5,6-trans-*Cyclohexano*-4,7-*diazadecane*-1,10-*diamine*(L_t^1). The reaction of 1t (3.51 g, 15.9 mmol) and lithium aluminum hydride (1.51 g, 39.8 mmol) in an anhydrous mixed solvent composed of ethyl ether (65 ml) and tetrahydrofuran (70 ml), following the above procedure, gave a colorless viscous liquid of bp 157°C (2 torr) (lit. [2b] bp 159°C (2 torr)). The yield was 3.13 g (86%). IR (neat): 3265 (N—H), 1600 (N—H) cm^{-1}. EIMS *m/z* (relative intensity): 228 (32.0), 156 (21.6), 155 (100). ^{1}H-NMR (chloroform-*d*): δ 1.13 (q, 4H, J = 8.9 Hz), 1.5–1.9 (m, 12H), 2.1 (s, 4H), 2.3–3.0 (m, 8H).

(5, 6-cis-*Cyclohexano*-4, 7-*diazadecane*-1, 10-*diamine*) *nickel(II) diperchlorate* ($NiL_c^1(ClO_4)_2$). A mixture of L_c^1 (3.02 g, 13.2 mmol) and methanol (5.0 ml) was added into nickel(II) perchlorate hexahydrate (4.83 g, 13.2 mmol), which was dissolved in methanol (10 ml), at room temperature for 3 h with stirring. The precipitates deposited were collected by filtration and vacuum dried to give 3.13 g (49%) of fine orange crystals; mp 207.7–208.2°C (dec). IR (KBr): 3280, 3220 (N—H), 1610 (N—H), 1090, 615 (Cl—O) cm^{-1}. FABMS *m/z* (relative intensity): 487 (1.55), 485 (1.64), 387 (66.6), 385 (90.9), 286 (100).

(5,6-trans-*Cyclohexano*-4,7-*diazadecane*-1,10-*diamine*)*nickel(II) diperchlorate* ($NiL_t^1(ClO_4)_2$. The reaction of L_t^1 (2.81 g, 12.3 mmol) and nickel(II) perchlorate hexahydrate (4.49 g, 12.3 mmol) in methanol (15 ml), following the above procedure, gave fine orange crystals. The yield was 1.85 g (31%); mp 224.8–226.7°C (dec). IR (KBr): 3320, 3235 (N—H), 1595 (N—H), 1100, 610 (Cl—O) cm^{-1}. FABMS *m/z* (relative intensity): 487 (1.73), 485 (1.83), 387 (85.3), 385 (100), 286 (100).

(2,3 - cis - *Cyclohexano* - 1,4,8,11 - *tetraazacyclotetradecane*)*nickel(II) diperchlorate* ($NiL_c^3(ClO_4)_2$). To a stirred solution of $NiL_c^1(ClO_4)_2$ (0.51 g, 1.06 mmol) in water (50 ml) was added to a 40% glyoxal solution (0.27 g, 1.72 mmol) during 10 min and then the mixture was heated at 50°C for 5 h with stirring. The resulting slurry was cooled to 5°C and treated with sodium borohydride (0.08 g, 2.12 mmol), which was added in small portions over 1 h. The reaction mixture was heated at 90°C for 30 min, and then the hot solution was filtered rapidly through a glass filter. The filtrate was acidified with a 60% perchloric acid and permitted to stand overnight at room temperature. The product deposited was separated by filtration and recrystallized from water to afford fine orange crystals. The yield was 0.41 g (75%); (lit. [2b] mp > 290°C) mp 225.6–226.1°C (dec). IR (KBr): 3205 (N—H), 1605 (N—H), 1090, 615 (Cl—O) cm^{-1}. FABMS *m/z* (relative intensity): 510 (2.94), 411 (29.9), 312 (36.7), 311 (42.4), 277 (100).

(2,3 - trans - *Cyclohexano* - 1,4,8,11 - *tetraazacyclotetradecane*)*nickel(II) diperchlorate* ($Ni_t^3(ClO_4)_2$). The reaction of $Ni_t^1(ClO_4)_2$ (0.51 g, 1.06 mmol), 40% glyoxal (0.25 g, 1.70 mmol) and sodium borohydride (0.08 g, 2.12 mmol) in water (50 ml), following the above procedure, gave fine orange crystals. The yield was 0.34 g (63%); (lit. [2b] mp > 275°C (dec)), mp 237.8–239.1°C (dec). IR (KBr): 3200 (N—H), 1610 (N—H), 1100, 620 (Cl—O) cm^{-1}. FABMS *m/z* (relative intensity): 510 (7.61), 411 (100), 312 (47.2), 311 (88.3).

2,3 - cis - *Cyclohexano* - 1,4,8,11 - *tetraazacyclotetradecane*(cis-*Cyclohexylcyclam*, L_c^3). The method of Kobiro *et al.* was modified for the preparation of *cis*-Cyclohexylcyclam [2b]. To a stirred solution of $Ni_c^3(ClO_4)_2$ (1.47 g, 2.87 mmol) in water (10 ml) was added sodium cyanide (0.94 g, 14.4 mmol) over 10 min at room temperature. The mixture was kept under reflux for 3 h with stirring. After the resulting mixture was cooled to room temperature, sodium hydroxide (100 mg, 2.5 mmol) was added and the reaction mixture was extracted three times with dichloromethane (10 ml). The organic layer was separated and dried over anhydrous sodium sulfate overnight. The solvent was evaporated *in vacuo*, and then the resulting crude solid was recrystallized from acetonitrile to give fine white crystals. The yield was 0.44 g (61%), (lit. [2b] mp 137.5–138°C), mp 133.2–134.7°C (dec). IR (KBr): 3250, 3180 (N—H), 2900, 2800 (C—H) cm^{-1}. FABMS *m/z* (relative intensity): 255 (5.88), 254 (39.4), 253 (7.16), 210 (15.3), 196 (18.5), 182 (28.5), 180 (41.6), 168 (35.7), 167 (100).

2,3 - trans - *Cyclohexano* - 1,4,8,11 - *tetraazacyclotetradecane* (trans-*Cyclohexylcyclam*, L_t^3). The reaction of $Ni_t^3(ClO_4)_2$ (0.70 g, 1.37 mmol) and sodium cyanide (0.45 g, 6.85 mmol) in water (10 ml), following the above procedure, was obtained as fine white crystals which was recrystallized from a blended solvent of chloroform and ethyl ether. The yield was 0.24 g (69%) (lit. [2b] mp 218–219°C), mp 216.0–217.9°C. IR (KBr): 3260, 3170 (N—H), 2920, 2800 (C—H) cm^{-1}. FABMS *m/z* (relative intensity): 255 (10.2), 254

(80.8), 253 (8.91), 210 (13.4), 196 (21.3), 182 (43.9), 180 (51.2), 168 (49.2), 167 (100).

(2,3 - cis - *Cyclohexano* - 1,4,8,11 - *tetraazacyclotetradecane)copper(II) diperchlorate* ($CuL_c^3(ClO_4)_2$). To a stirred solution of L_c^3 (0.09 g, 0.36 mmol) in methanol (3.0 ml) was added a solution of copper(II) perchlorate hexahydrate (0.14 g, 0.36 mmol) in methanol (1.0 ml) at room temperature. The reaction mixture was heated at 50°C for 2 h and cooled to room temperature. The precipitates deposited were isolated by filtration and recrystallized from water to obtain claret prisms. The yield was 0.14 g (73%), mp 285–288°C (dec). IR (KBr): 3220 (N—H), 2940, 2860 (C—H), 1610 (N—H) 1100, 610 (Cl—O) cm^{-1}. FABMS *m/z* (relative intensity): 518 (1.54), 515 (0.53), 418 (77.2), 416 (100), 317 (45.6), 315 (58.0), 254 (51.5).

(2,3 - trans - *Cyclohexano* - 1,4,8,11 - *tetraazacyclotetradecane)copper(II) diperchlorate* ($CuL_t^3(ClO_4)_2$). The reaction of L_t^3 (0.05 g, 0.21 mmol) and copper(II) perchlorate hexahydrate (0.08 g, 0.21 mmol) in methanol (4.0 ml), following the above procedure, gave claret needles. The yield was 0.07 g (65%), mp > 300°C. IR (KBr): 3240 (N—H), 2940, 2860 (C—H), 1600 (N—H), 1090, 620 (Cl—O) cm^{-1}. FABMS *m/z* (relative intensity): 518 (1.04), 515 (0.42), 418 (68.4), 416 (89.2), 317 (36.4), 315 (50.4), 259 (24.7).

RESULTS AND DISCUSSION

Synthesis of cyclohexylcyclams and their complexes

Cis-Cyclohexane-1,2-diamine (*cis*-dac) and *trans*-cyclohexane-1,2-diamine (*trans*-dac) were separated from a mixture according to a modification of the procedure reported by Saito and Kidani [4]. The cyclam with bulky substituents at *cis*-positions on one side of cyclam ring, namely *cis*-cyclohexylcyclam L_c^3, was synthesized according to a modification of the method described by Kobiro *et al.*, as shown in Scheme 1 [2b]. The *trans*-cyclohexylcyclam L_t^3 was also synthesized in a similar procedure as L_c^3. Reaction of diamine (*cis*-dac and *trans*-dac) and acrylonitrile followed by lithium aluminum hydride reduction gave tetraamine (L_c^1 and L_t^1). The nickel(II) templated reaction of the tetraamine with glyoxal followed by sodium borohydride reduction led to the cyclohexylcyclam nickel(II) complexes, $NiL_c^3(ClO_4)_2$ and $NiL_t^3(ClO_4)_2$. The template cyclization was achieved at 50°C, while the reduction was performed at 90°C. The nickel(II) complexes are obtained as fine orange crystals. Cyclohexylcyclams were liberated by the treatment of the nickel(II) complexes with sodium cyanide in water. *cis*-Cyclohexylcyclam and *trans*-cyclohexylcyclam were synthesized with a maximum overall yield of 28 and 15%, respectively. The cyclohexylcyclams easily yielded the claret copper(II) diperchlorate complexes by reaction with copper(II) perchlorate hexahydrate in methanol at 50°C. The analytical data for the cyclohexylcyclams and their complexes are summarized in Table 1. The elemental analyses of these crystalline samples were in good agreement with compounds of these expected compositions.

Mass spectra

The EI mass spectra of cyclohexylcyclams and their intermediates exhibit molecular ions, respectively. The nickel(II) and copper(II) complexes reveal clusters of ions corresponding to $[M-ClO_4]^+$ and $[M-2ClO_4+2H]^+$ which is the base peak in FAB

Table 1. Analytical data for cyclohexylcyclams and their complexes

Compound	Empirical formula	Elemental analyses Calc./Found (%)		
		C	H	N
$NiL_c^3(ClO_4)_2$	$C_{14}H_{30}Cl_2N_4NiO_8$	32.7	5.7	11.2
		32.8	5.9	10.9
$NiL_t^3(ClO_4)_2$	$C_{14}H_{30}Cl_2N_4NiO_8$	32.7	5.8	10.9
		32.8	5.9	10.9
L_c^3	$C_{14}H_{30}N_4$	66.2	12.0	21.8
		66.1	11.9	22.0
L_t^3	$C_{14}H_{30}N_4$	66.3	11.8	21.9
		66.1	11.9	22.0
$CuL_c^3(ClO_4)_2$	$C_{14}H_{30}Cl_2N_4CuO_8$	32.3	5.8	10.7
		32.5	5.9	10.8
$CuL_t^3(ClO_4)_2$	$C_{14}H_{30}Cl_2N_4CuO_8$	32.4	5.7	10.7
		32.5	5.9	10.8

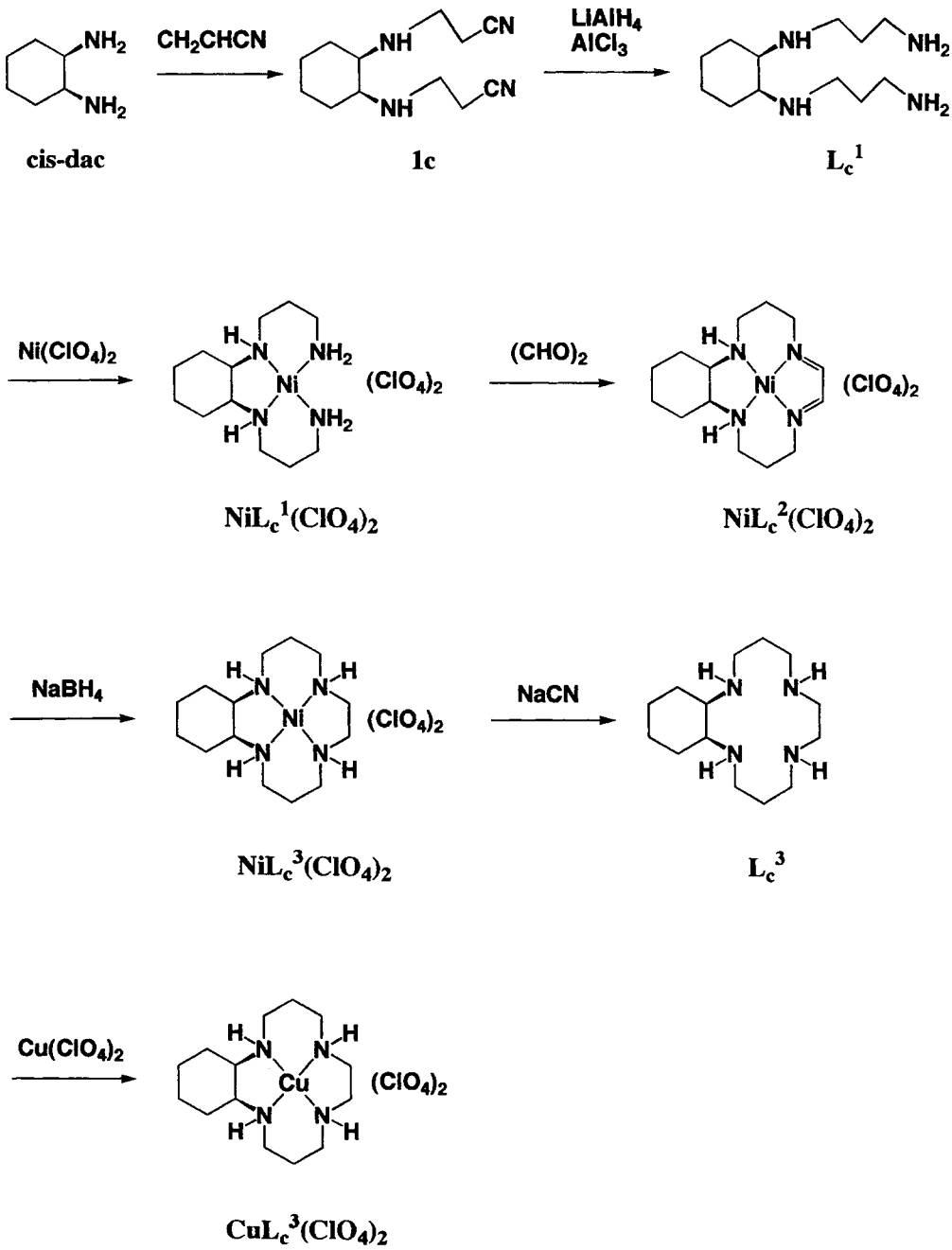

Scheme 1

mass spectra. When the complexes are analyzed with FAB and FD technique, the molecular ions are not observed.

Molar conductivity

The molar conductances for the nickel(II) and copper(II) complexes are listed in Table 2. The complexes, $[ML](ClO_4)_2$ (M = Ni(II) or Cu(II); L = L_c^3 or L_t^3), are 1 : 2 electrolyte in *N,N*-dimethylformamide (DMF) at 25°C and are tetra-coordinated in this solvent. Therefore, the perchlorate anions are ionized on dissolution in the solvent. This result is consistent with the corresponding infrared and electronic spectral behavior.

Infrared spectra

The characteristic IR bands for the present discussion are collected in the Experimental section. The

Table 2. Molar conductances for the complexes at 25°C in *N,N*-dimethylformamide[a]

Complex	$\Lambda_M(\Omega^{-1}\,cm^2\,mol^{-1})$	Type of electrolyte
$NiL_c^3(ClO_4)_2$	155	3 (1 : 2)
$NiL_t^3(ClO_4)_2$	161	3 (1 : 2)
$CuL_c^3(ClO_4)_2$	160	3 (1 : 2)
$CuL_t^3(ClO_4)_2$	153	3 (1 : 2)

[a] For ca 10^{-3} mol dm^{-3} solution. Assignment of the type of electrolyte presented in solution was made on the basis of the conductance data compiled by Geary [6].

metal-free cyclohexylcyclams show strong bands at ca 3250 cm^{-1} which are associated with N—H stretching modes. The nickel(II) and copper(II) complexes also indicate only one strong band near 3200 cm^{-1} owing to secondary amine stretching vibrations. It is clear that this vibrational modes shift slightly to lower frequency upon complex formation. Intense broad bands are newly observed in the 1090–1100 cm^{-1} region with the formation of the nickel(II) and copper(II) complexes and can be attributed to the stretching vibration modes of perchlorate ions [7]. This band is most sensitive to metal-coordination among the absorption peaks appearing in the NaCl range. The perchlorate group in these metal complexes may be present not as a coordinated group but as a simple isolated anion, judging from the vibrational frequency [8]. This result is supported by the conductance data. An other band based upon the perchlorate group is observed at about 620 cm^{-1} that may be attributable to its bending vibration [8].

Electronic spectra

The two copper(II) complexes, $CuL_c^3(ClO_4)_2$ and $CuL_t^3(ClO_4)_2$, show only one broad band in the range appearing below 34,000 cm^{-1} as shown in Fig. 1. The general feature of the spectra for the complexes is similar to each other. This suggests that the coordination structure of the copper(II) complexes is almost analogous. The absorption band observed at about 19,100 cm^{-1} is attributed to a ligand-field transition, because the molar extinction coefficient of the band is similar to that commonly assigned to a ligand-field transition [9]. The spectral behavior is comparable with that of square-planar copper(II) complexes [9] and with that of the copper(II) complexes derived from dicyclohexylcyclams [3a]. Hence, the copper(II) complexes are square-planar coordination.

The two nickel(II) complexes are different from each other on the ligand-field spectra in coordinating solvent. $NiL_c^3(ClO_4)_2$ complex exhibits only one broad ligand-field band at 22,400 cm^{-1} as shown in Fig. 2. Analogous ligand-field spectra have been observed for $Ni(DMG)_2$ and $Ni(4\text{-}N)(ClO_4)_2$ [3a,10]. This seems to

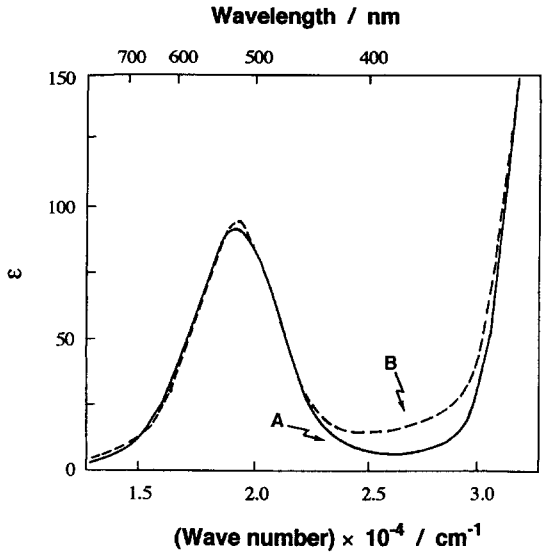

Fig. 1. Electronic spectra for the copper(II) complexes of cyclohexylcyclams at room temperature in *N,N*-dimethylformamide; A, $CuL_c^3(ClO_4)_2$; B, $CuL_t^3(ClO_4)_2$.

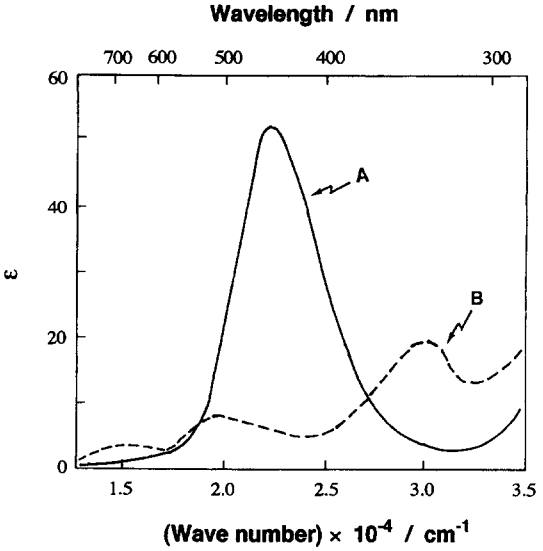

Fig. 2. Electronic spectra for the nickel(II) complexes of cyclohexylcyclams at room temperature in *N,N*-dimethylformamide; A, $NiL_c^3(ClO_4)_2$; B, $NiL_t^3(ClO_4)_2$.

indicate that the structure of $NiL_c^3(ClO_4)_2$ complex is a square-planar configuration [9]. On the other hand, $NiL_t^3(ClO_4)_2$ complex reveals three ligand-field bands in coordinating solvent such as DMF, as shown in Fig. 2. This spectrum suggests that the complex is an octahedral configuration [3a,9]. When the coordinating ability of the solvent is very poor, $NiL_t^3(ClO_4)_2$ complex assumes a square-planar configuration.

Table 3. Electronic absorption bands for the nickel(II) and copper(II) complexes of cyclohexylcyclams[a]

Complex	Ligand-field transition in cm^{-1} (ε)
$NiL_c^3(ClO_4)_2$	22300 (52)
$NiL_t^3(ClO_4)_2$	14800 (3.5), 19600 (8.0), 29700 (19)
$CuL_c^3(ClO_4)_2$	19100 (92)
$CuL_t^3(ClO_4)_2$	19200 (95)

[a] Measured in *N,N*-dimethylformamide at room temperature.

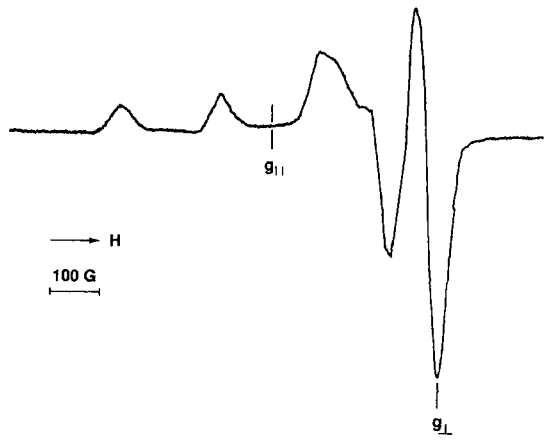

Fig. 3. ESR spectrum of the copper(II) complex, $CuL_c^3(ClO_4)_2$, in *N,N*-dimethylformamide at 77 K.

Hence, the coordination structure of the nickel(II) complexes is determined with their spectra in coordinating solvent. A similar phenomenon has been observed for $Ni(4\text{-}P)(ClO_4)_2$ complex [3a]. It is very interesting to note that $Ni(4\text{-}P)(ClO_4)_2$ complex containing two cyclohexyl groups, $NiL_t^3(ClO_4)_2$ complex bearing one cyclohexyl group and $Ni(cyclam)^{2+}$ complex having no cyclohexyl group show the distorted octahedral forms in coordinating solvent in contrast to square-planar forms of $Ni(4\text{-}N)(ClO_4)_2$ and $NiL_c^3(ClO_4)_2$ complexes [11]. Accordingly, the magnitude of ligand-field for $NiL_c^3(ClO_4)_2$ complex is approximately similar to that for $Ni(4\text{-}N)(ClO_4)_2$ complex. The ligand-field transition bands of the complexes are summarized in Table 3.

ESR spectra

In the ESR spectra of the copper(II) complexes measured in *N,N*-dimethylformamide at room temperature, a set of four hyperfine lines were observed by the magnetic interaction between an unpaired electron and a copper nucleus ($I = 3/2$), but superhyperfine lines based upon the nitrogen nuclei ($I = 1$) do not turn up. The ESR spectrum of $CuL_c^3(ClO_4)_2$ complex in *N,N*-dimethylformamide at 77 K is shown in Fig. 3. The general feature of the spectrum is in accord with that of square-planar coordination. A set of four copper hyperfine lines on the parallel component of the *g*-tensor ($g_{\parallel}$) in the low field region are observed, while such hyperfine lines are not obvious on the perpendicular component of the *g*-tensor ($g_{\perp}$) which lies in the higher field region. Superhyperfine lines based upon the nitrogen nuclei do not appear on the $g_{\parallel}$ and $g_{\perp}$ components. The general features of the spectra for $CuL_c^3(ClO_4)_2$ and $CuL_t^3(ClO_4)_2$ complexes are analogous to each other. The spin Hamiltonian parameters observed in this work are very similar to those for porphyrin, phthalocynaine, cyclam and dicyclohexylcyclam copper(II) complexes as given in Table 4 [3a,12,13,14]. Consequently, the present copper(II) complexes are of square-planar coordination.

NMR spectra

Definitive assignments for the cyclohexylcyclams (L_c^3, L_t^3) and their nickel(II) complexes are very difficult because of giving several peaks of a multiplet in the ^{1}H-NMR spectra. Therefore, ^{1}H-NMR spectra of these compounds cannot be utilized to distinguish between two isomers.

^{13}C-NMR data of *cis*-dac, *trans*-dac, L_c^3, L_t^3 and the nickel(II) complexes are compiled in Table 5. The carbon signals of L_c^3, L_t^3 and their nickel(II) complexes indicate seven lines, respectively. $NiL_t^3(ClO_4)_2$ complex do not give a well-resolved ^{13}C-NMR spectrum in dimethyl sulfoxide-d_6 and pyridine-d_5 which are strong coordinating solvents. This shows that these solvents coordinate the axial positions of the complex, which becomes an octahedral configuration in the solvents and is a paramagnetism. The ^{13}C-NMR spectra are scarcely susceptible to solvent effect in a solvent of which the coordinating power is very poor. The peaks of C(3), C(4) and C(6) positions adjacent to amines are shifted downfield by 1.8–7.7 ppm upon formation of the nickel(II) complexes. The magnitude of the downfield for $NiL_c^3(ClO_4)_2$ complex is larger than that for $NiL_t^3(ClO_4)_2$ complex. The downfield shift can be attributable to the deshielding effect due to the positive charge provided by the nickel ion in the complexes. The deshielding effect for $NiL_c^3(ClO_4)_2$ complex is greater than that for $NiL_t^3(ClO_4)_2$ complex. This seems to indicate that the coordinated structure of the two nickel(II) complexes is somewhat different. The magnitude of the shifts for C(1) and C(2) positions is smaller than that for C(3) and C(4) positions. This is mainly due to the fact that the C(1) and C(2) positions are placed further from the positive charge of the nickel(II) ion which affords the deshielding effect.

Acknowledgements—The authors are grateful to the Center

Table 4. Spin Hamiltonian parameters for the copper(II) complexes[a]

Ligand	Medium	Temperature	$\bar{g}$	$g_{\parallel}$	$g_{\perp}$	$\bar{A}^{Cu} \times 10^4$ (cm^{-1})	$A_{\parallel}^{Cu} \times 10^4$ (cm^{-1})	Reference
L_c^3	DMF	Room temperature	2.099			95.2		
L_c^3	DMF	77 K		2.198	2.069		209.2	
L_t^3	DMF	Room temperature	2.096			96.1		
L_t^3	DMF	77 K		2.196	2.060		209.8	
4-P	DMF	Room temperature	2.094			92.2		3(a)
4-P	DMF	77 K		2.193	2.066		208.1	3(a)
4-N	DMF	Room temperature	2.097			92.3		3(a)
4-N	DMF	77 K		2.183	2.061		204.8	3(a)
H_2TPP	$CHCl_3$	Room temperature	2.1073			97.7		12
H_2TPP	$CHCl_3$	77 K		2.187	2.067		218	12
TACM	H_2O	77 K		2.18	2.07		210	14
H_2PC	$CHCl_3$	77 K		2.1746	2.045		202	13

[a] 4-P, 4-N, isomers of 1,2,3,4,5,6,7,8,9,10,11,12,13,14,15,16,17,18,19,20,21,22-docosahydrodibenzo[*b*,*i*][1,4,8,11]tetraazacyclotetradecine; H_2TPP, 5,10,15,20-tetraphenylporphine: TACM, 1,4,8,11-tetraazacyclotetradecane-2-one; H_2PC, phthalocynaine.

Table 5. ^{13}C-NMR spectral data of cyclohexylcyclams, their nickel(II) complexes and their related compounds[a]

Compound	Solvent	C(1)	C(2)	C(3)	C(4)	C(5)	C(6)	C(7)
trans-dac	$CDCl_3$	25.4	35.5	57.7				
cis-dac	$CDCl_3$	21.9	31.0	51.9				
cyclam	$CDCl_3$					29.7	50.7	49.3
L_t^3	$CDCl_3$	25.2	31.3	62.2	50.8	29.7	49.4	48.0
L_c^3	$CDCl_3$	22.2	29.5	57.4	48.8	27.4	48.2	47.0
$NiL_t^3(ClO_4)_2$	CF_3COOD	26.0	31.6	67.8	53.2	27.9	51.2	47.7
$NiL_c^3(ClO_4)_2$	CF_3COOD	21.9	28.1	65.1	53.5	26.1	50.8	49.5

[a] *trans*-dac, *trans*-cyclohexane-1,2-diamine; *cis*-dac, *cis*-cyclohexane-1,2-diamine; cyclam, 1,4,8,11-tetraazacyclotetradecane; chemical shifts in ppm from internal TMS; measured at room temperature.

for Instrumental Analysis, Kyushu Institute of Technology for elemental analyses, mass spectra, ESR spectra and NMR spectra.

REFERENCES

1. (a) Wilkinson, G., Gillard, R. D. and McCleverty, J. A., *Comprehensive Coordination Chemistry*, Pergamon, Oxford, 1987; (b) Melson, G. A., *Coordination Chemistry of Macrocyclic Compounds*, Plenum, New York, 1979; (c) Bernal, I., *Stereochemical and Stereophysical Behaviour of Macrocycles*, Vol. 2, Elsevier, Amsterdam, 1987; (d) Izatt, R. M., Pawlak, K. and Bradshaw, J. S., *Chem. Rev.*, 1995, **95**, 2529.
2. (a) Kobiro, K., Nakayama, A., Hiro, T., Suwa, M., Kakiuchi, K., Tobe, Y. and Odaira, Y., *Chem. Lett.*, 1990, 1979; (b) Kobiro, K., Nakayama, A., Hiro, T., Suwa, M. and Tobe, Y., *Inorg. Chem.*, 1992, **31**, 676.
3. (a) Sakata, K., Wada, S., Sato, N., Kurisu, M., Hashimoto, M. and Kato, Y., *Inorg. Chim. Acta*, 1986, **119**, 111; (b) Moriguchi, Y. and Sakata, K., *J. Coord. Chem.*, 1991, **23**, 321.
4. Saito, R. and Kidani, Y., *Chem. Lett.*, 1976, 123.
5. Yashunskii, V. G., *Zh. Obsch. Khim.*, 1958, **28**, 1361; *Chem. Abstr.*, 1958, **52**, 19979.
6. Geary, W. J., *Coord. Chem. Rev.*, 1971, **7**, 81.
7. Nakamoto, K., *Infrared and Raman Spectra of Inorganic and Coordination Compounds*, 3rd edn, Wiley, New York, 1978.
8. Hathaway, B. J. and Underhill, A. E., *J. Chem. Soc.*, 1961, 3091.
9. (a) Lever, A. B. P., *Inorganic Electronic Spectroscopy*, 2nd edn, Elsevier, Amsterdam, 1984; (b) Figgis, B. N., *Introduction to Ligand Fields*, Wiley, New York, 1966.
10. Maki, G., *J. Chem. Phys.*, 1958, **29**, 1129.
11. Fabbrizzi, L., *Inorg. Chem.*, 1977, **16**, 2667.
12. Assour, J. M., *J. Chem. Phys.*, 1965, **43**, 2477.
13. Kivelson, D. and Neiman, R., *J. Chem. Phys.*, 1961, **35**, 149.
14. Kimura, E., Koike, T., Machida, R., Nagai, R. and Kodama, M., *Inorg. Chem.*, 1984, **23**, 4181.

Pergamon

PII: S0277-5387(97)00417-8

Polyhedron Vol. 17, No. 9, pp. 1471–1475, 1998
© 1998 Elsevier Science Ltd
All rights reserved. Printed in Great Britain
0277-5387/98 $19.00+0.00

A far-infrared study and investigation of the difference between the asymmetric and symmetric POO^- stretching frequencies in metal diphosphonate complexes‡

Albert W. Herlinger,[a]* John R. Ferraro,[b] Julie A. Garcia[a] and Renato Chiarizia[b]

[a] Department of Chemistry, Loyola University Chicago, Chicago, IL, 60626, U.S.A.

[b] Chemistry Division, Argonne National Laboratory, Argonne, IL, 60439, U.S.A.

(Received 4 August 1997; accepted 1 October 1997)

Abstract—Lanthanide complexes of P,P′-di(2-ethylhexyl) methanediphosphonic acid, $H_2DEH[MDP]$, were prepared and investigated by infrared spectroscopy. Qualitative information about the nature of the phosphonate binding in the complexes was obtained by measuring the asymmetric and symmetric POO^- stretching frequencies of the ligand. These vibrational modes appear at lower energy in the complexes than in the sodium salt. This indicates symmetrical coordination of the phosphonate groups through chelate and/or bridging interactions. The frequency difference between the POO^- stretching bands $\Delta\nu$ becomes smaller as the ionic potential e/r of the metal ion increases. The correlation is valid when both oxygen atoms are involved in the bonding and no other absorption bands interfere with the POO^- vibrations. The origin of this empirical correlation is the change in the P—O bond order which arises from a change in the strength of the metal–diphosphonate interaction. The far-infrared spectra of the lanthanide complexes, an ^{54}Fe-labelled compound, and the sodium salt of $H_2DEH[MDP]$ were measured to provide insight into the nature of the metal–ligand interaction. The appearance of metal–oxygen stretching bands in the iron compound indicates that the iron–diphosphonate interaction has a substantial covalent component whereas the absence of metal–oxygen stretching bands in the lanthanide complexes indicates the binding is predominantly ionic. © 1998 Elsevier Science Ltd. All rights reserved

Keywords: lanthanide complexes; metal diphosphonates; infrared stretching frequencies.

Alkyl-substituted diphosphonic acids are of considerable interest as solvent extraction reagents for metal ions [1–3]. These molecules are powerful complexing agents and the strong acidity of the diphosphonic acid functionality permits the formation of metal complexes of high stability under very acidic conditions [4–6]. We recently reported that qualitative information about the coordination mode of the phosphonate groups in metal complexes of P,P′-di(2-ethylhexyl) methanediphosphonic acid ($H_2DEH[MDP]$) may be obtained by comparing the energies of the asymmetric and symmetric POO^- stretching modes of the ligand in the complexes to their corresponding values in the sodium salt [7]. Interpretation of the vibrational data uses bonding arguments developed for analogous complexes of carboxylic acids where relationships between the COO^- stretching frequencies and the type of carboxylate coordination are well established [8].

While investigating the complexation chemistry of $H_2DEH[MDP]$, we observed that the frequency difference $\Delta\nu$ between the POO^- stretching bands in the metal compounds becomes smaller as the ionic potential e/r of the metal ion increases [7]. This type of correlation had been reported previously by Peppard and Ferraro for ionic complexes of organ-

‡ Work performed under the auspices of the Office of Basic Energy Sciences, Division of Chemical Sciences, U.S. Department of Energy, under contract number W-31-109-ENG-38.

* Author to whom correspondence should be addressed.

ophosphoric acids of the type $(RO)_2PO(OH)$ and $(RO)(R)PO(OH)$ [9,10] and was subsequently observed for metal complexes of P,P′-di(2-ethylhexyl) ethanediphosphonic acid, $H_2DEH[EDP]$ [11]. Similar correlations between the ionic potential of the metal ion and anion stretching vibrations have been demonstrated for nitrate [12,13] and carboxylate [14,15] compounds. In the present study, lanthanide complexes of $H_2DEH[MDP]$ were prepared and characterized to test the general validity of this correlation for diphosphonate complexes. The far-infrared spectra of the lanthanide complexes, an ^{54}Fe-labeled compound, and the sodium salt of $H_2DEH[MDP]$ were measured to provide information about the nature of the metal-diphosphonate interaction.

EXPERIMENTAL

Materials

Reagent grade $La(NO_3)_3 \cdot 6H_2O$, $Pr(NO_3)_3 \cdot 5H_2O$, $Gd(NO_3)_3 \cdot 5H_2O$, and $Yb(NO_3)_3 \cdot 5H_2O$ obtained from Aldrich Chemical Co. were used without further purification. Reagent grade $Nd(NO_3)_3 \cdot 6H_2O$ from GFS Chemical Co. was used as received. Iron-54 wire, 96.4% isotopically pure, was obtained from Cambridge Isotope Laboratories, Inc., dissolved in 1 M HNO_3, and used to prepare an ^{54}Fe-labeled $H_2DEH[MDP]$ complex. Aqueous solutions were prepared using Ultrex reagent nitric acid (J. T. Baker Chemical Co.) and water obtained from a Milli-Q2 purification system.

Measurements

Infrared spectra in the 4800–400 cm^{-1} region were obtained on a Nicolet 510P PC/IR Fourier transform spectrometer. Solid samples were run as KBr pellets with air as the background. The spectra were checked as nujol mulls supported on KBr plates. Spectra in the 650–150 cm^{-1} range were obtained by collecting 128 scans at 4 cm^{-1} resolution on a Bruker 98 vacuum FT-IR interferometer using a globar source, a DTGS detector, and a mylar beam splitter. Solid samples were run as CsI pellets referenced against a blank CsI pellet. The reproducibility of the spectra was checked by multiple scans on at least two different samples over the desired frequency range. The uncertainty in the measured frequencies for the absorption bands is 1 cm^{-1}.

Elemental analyses were performed by Galbraith Laboratories, Inc., Knoxville, TN. Metal ion analyses for the compounds were performed by the Analytical Chemistry Division of ANL using ICP-AES. Solid samples were weighed into a platinum crucible and ignited in air at 1100°C. The residue was fumed with concentrated H_2SO_4 and made up to the final volume with dilute nitric acid. The relative uncertainty in the metal ion analysis is estimated to be ~5%.

Preparation of compounds

P,P′-di(2-ethylhexyl) methanediphosphonic acid. $H_2(C_{17}H_{36}O_6P_2)$ was prepared by the reaction of two equivalents of 2-ethylhexanol with methanediphosphonic acid in dry THF as previously described [7]. $Na_2(DEH[MDP])$, $Fe_2(DEH[MDP])_3$, and $Eu_2(DEH[MDP])_3$ were prepared as reported earlier [7].

$La_2(C_{17}H_{36}O_6P_2)_3 \cdot 2H_2O$, $Pr_2(C_{17}H_{36}O_6P_2)_3 \cdot 3H_2O$, $Nd_2(C_{17}H_{36}O_6P_2)_3 \cdot 2H_2O$, $Gd_2(C_{17}H_{36}O_6P_2)_3 \cdot 5H_2O$, $Tb_2(C_{17}H_{36}O_6P_2)_3 \cdot 2H_2O$, and $Yb_2(C_{17}H_{36}O_6P_2)_3 \cdot 2H_2O$. The lanthanide complexes were prepared by slow addition of a methanol solution of $H_2DEH[MDP]$ to an equivalent amount of metal nitrate in methanol solution which had been acidified with 2 drops of 0.1 M HCl. The flocculent precipitate which formed upon concentrating the reaction mixture was collected by filtration, washed with water and methanol, and dried overnight at 60°C. Typical yields were in the 70–90% range. The infrared spectra of the solids indicated that the salts were isolated as hydrates. The stoichiometry of the hydrate was established by drying to constant weight at 120°C. Anal. for $La_2C_{51}H_{112}O_{20}P_6$. Found: C, 40.42, H, 7.79, La, 19.34, H_2O, 2.30; Calc. C, 40.59, H, 7.48, La, 18.41, H_2O, 2.39. Anal. for $Pr_2C_{51}H_{114}O_{21}P_6$. Found: C, 40.28, H, 7.88; Pr, 19.05, H_2O, 3.40. Calc. C, 40.04, H, 7.51, Pr, 18.32, H_2O, 3.53. Anal. For $Nd_2C_{51}H_{112}O_{20}P_6$. Found: C, 41.34, H, 7.22, Nd, 18.70, H_2O, 2.63. Calc. C, 40.31, H, 7.43, Nd, 18.98, H_2O, 2.37. Anal. for $Gd_2C_{51}H_{118}O_{23}P_6$. Found: C, 38.68, H, 7.32, P, 11.17, H_2O, 5.47. Calc. C, 38.73, H, 7.39, P, 11.62, H_2O, 5.62. Anal. for $Tb_2C_{51}H_{112}O_{20}P_6$. Found: C, 39.41, H, 7.55, P, 12.27, H_2O, 2.46. Calc. C, 40.01, H, 7.38, P, 12.00, H_2O, 2.32. Anal. for $Yb_2C_{51}H_{112}O_{20}P_6$. Found: C, 39.52, H, 7.33, P, 13.56, H_2O, 2.56. Calc. C, 38.83, H, 7.16, P, 11.78, H_2O, 2.28.

RESULTS AND DISCUSSION

The spectra of the lanthanide compounds prepared in this study in the mid-infrared region are very similar to the spectrum previously reported for the Eu(III)-$H_2DEH[MDP]$ complex [7]. In all cases, the compounds exhibit absorption bands in regions characteristic for water of hydration (*vide infra*). The stretching and bending vibrations of the 2-ethylhexyl group appear in conventional regions characteristic of alkyl groups. The frequencies and tentative assignments of the absorption bands in the 1250–950 cm^{-1} region are listed in Table 1. These assignments have been discussed in detail for the Eu(III) complex [7] and need no further explanation. The frequency of the asymmetric and symmetric POO^- stretching modes of the diphosphonate ligand are lower in the lanthanide compounds than in the sodium salt, i.e. 1246 and 1144 cm^{-1}, respectively. The shift of both $\nu_{asym}(POO^-)$ and $\nu_{sym}(POO^-)$ to lower energy in the lanthanide com-

Table 1. Absorption bands for the lanthanide complexes of $H_2DEH[MDP]$ in the P—O stretching region

La(III)	Pr(III)	Nd(III)	Eu(III)	Gd(III)	Tb(III)	Yb(III)	Assignments
1169 vs	1166 vs	1169 vs	1171 s	1171 vs	1171 vs	1170 s	asym POO^- str
1097 vs	1097 vs	1099 vs	1107 s	1113 vs	1008 vs	1112 m	sym POO^- str
1045 vs	1044 vs	1046 vs	1046 vs	1046 vs	1048 vs	1052 s	P—OR str
980 sh	978 sh	980 sh	980 sh	980 sh	983 sh	980 sh	C—C str
72	69	70	64	58	57	58	$\Delta\nu$ (cm^{-1})

plexes is similar to that observed for other $H_2DEH[MDP]$ compounds [7].

The decrease in $\nu_{asym}(POO^-)$ observed upon complexation essentially rules out monodentate coordination of the phosphonate groups. Coordination of a single oxygen of a $>PO_2^-$ group would result in considerably different P—O bond orders and increase the frequency of the asymmetric POO^- stretching vibration. The asymmetric COO^- stretching mode in analogous monodentate carboxylate complexes generally appears at frequencies that are significantly higher than values characteristic for ionic salts or bidentate and bridged complexes [8]. The separation between the COO^- stretching frequencies also generally is larger in monodentate carboxylate complexes than is characteristic for other types of bonding [8]. Symmetrical coordination of the $>PO_2^-$ groups on the other hand can reduce the bond order of both P—O bonds by the same amount and cause both stretching modes to decrease in energy. Symmetrical coordination of diphosphonate ligand can occur through chelation and/or bridging arrangements. Several recently reported lanthanide complexes of 1-hydroxyethane-1, 1-diphosphonic acid have structures in which both coordination modes are utilized by the ligand to complex the metal ion [16]. In the Nd(III) and Eu(III) complexes, the diphosphonate ligand simultaneously bridges two different metal ions through the $>PO_2^-$ groups and coordinates in a bidentate fashion to form 6-member chelate rings [16].

The frequency difference $[\nu_{asym}(POO^-)-\nu_{sym}(POO^-)]$ between the asymmetric and symmetric POO^- stretching modes of the phosphonate group are sensitive to the lanthanide ion present in the complex. The difference $\Delta\nu$ becomes progressively smaller as the ionic potential of the metal ion increases. Figure 1 shows a plot of the ionic potential, e/r (charge/ionic radius for coordination number 6) [17] vs $\Delta\nu$ for the complexes reported in this study. This correlation which was previously observed with other $H_2DEH[MDP]$ and $H_2DEH[EDP]$ compounds [7,11] thus appears to be generally valid for diphosphonate complexes when both oxygen atoms of the $>PO_2^-$ groups are involved in complexing the metal ion. The correlation should be useful for identifying changes in metal-ligand bonding across a series of complexes containing similar metal ions such as lanthanides [16] or actinides and with changes in metal oxidation state.

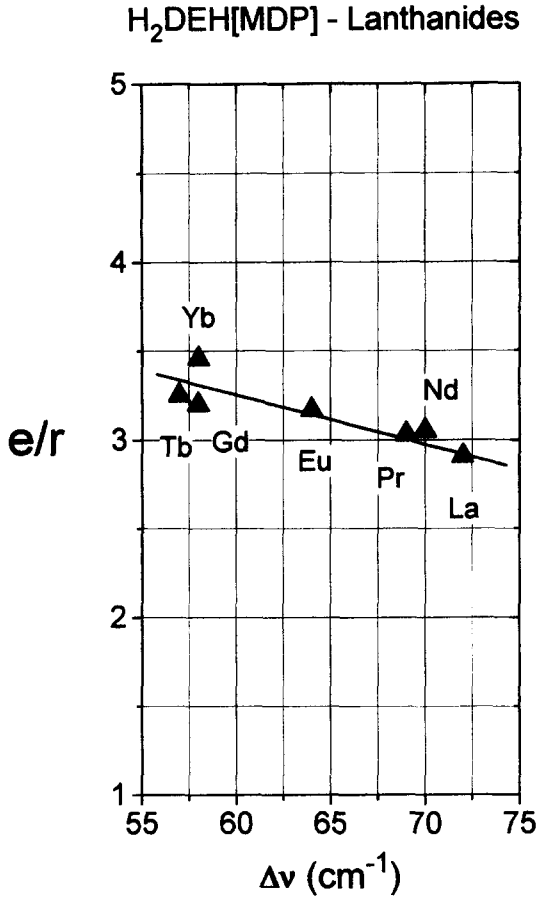

Fig. 1. A plot of e/r, the ionic potential of the metal ion, versus the difference $\Delta\nu$ between $\nu_{asym}(POO^-)$ and $\nu_{sym}(POO^-)$ for lanthanide complexes of $H_2DEH[MDP]$, where e = ion charge and r = Shannon ionic radius.

The frequency difference between the asymmetric and symmetric COO^- stretching bands in hydrated lanthanide acetates has been reported [15] to show a decrease with decreasing metal ion radius that is analogous to the correlation observed for the lan-

thanide diphosphonates in the present study. The crystal structure of $Er(CH_3COO)_3(H_2O)_4$ reveals that the carboxylate ion in this lanthanide complex is coordinated to the metal as a chelating ligand as well as in an arrangement involving both chelation and bridging [18]. Bands at 260 cm^{-1} and 196 cm^{-1} in the far-infrared spectrum of the erbium complex have been assigned to Er—O stretching modes on the basis of a normal coordinate analysis [19].

A vibrational analysis by Kumamoto indicates that the P—O bond order within alkyl-phosphate anions plays a major role in determining the frequency of the P—O stretching vibrations [20]. Since this is undoubtedly true for diphosphonate anions as well, the variation of $\Delta\nu$ with e/r is a reflection of a change in the P—O bond order which results from a change in the strength of metal–diphosphonate interaction [21]. Changes in the P—O bond order that result from changes in the metal–ligand bond strength could arise from P—O bond polarization due to purely electrostatic effects, covalence in the metal–oxygen interaction, or a combination of both effects. We suggested earlier that changes in the nature of the metal–ligand interaction might be involved since the smallest $\Delta\nu$ values are observed for the diphosphonate compounds where the metal–oxygen electronegativity difference is the least [11].

The far-infrared spectra of the lanthanide complexes prepared in this study, the iron complex, and the sodium salt of H_2DEH[MDP] were measured to provide insight into the nature of the metal-diphosphonate interaction. Figure 2 shows the spectra for Na_2(DEH[MDP]), Fe_2(DEH[MDP])$_3$, and Eu_2(DEH[MDP])$_3$. All of the compounds investigated have two bands in the 550–450 cm^{-1} region where the POO^- deformation, δ(POO), and POC deformation, δ(POC), modes generally appear [22,23]. The higher energy band in this region was tentatively assigned earlier as δ(POO) on the basis of its metal sensitivity [7]. The iron complex also has a strong absorption band at 256 cm^{-1} that is not present in the spectrum of H_2DEH[MDP] or any of the other compounds listed in Table 2. This band was initially assigned as a metal–oxygen stretching mode, ν(M—OP), by comparison with related iron(III) complexes [24]. A metal–oxygen stretching mode will become IR active if the metal–oxygen bond is sufficiently covalent. Depending upon the actual symmetry of the iron complex at least two Fe–O stretching bands are expected to be infrared active.

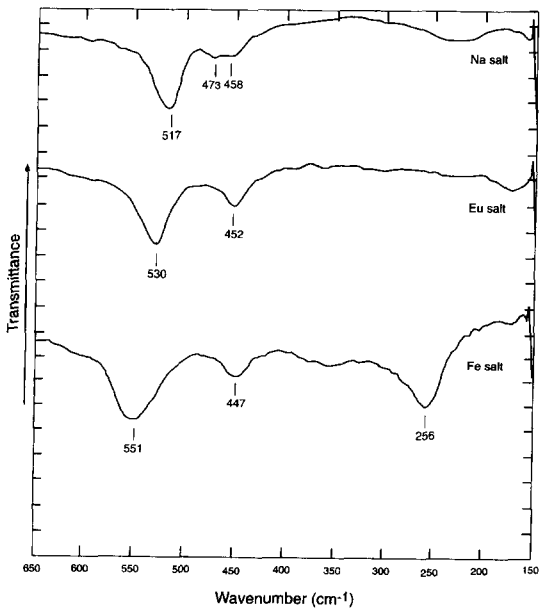

Fig. 2. The far-infrared spectra of the sodium-, europium-, and iron-H_2DEH[MDP] compounds in the 650–150 cm^{-1} region.

The metal isotope technique developed by Nakamoto [25] provides a unique method to identify metal–ligand vibrations since only vibrations involving motion of the metal atom are shifted by metal isotope substitution. The frequency of the absorption bands in the far-infrared for the ^{54}Fe-labeled H_2DEH[MDP] complex are compared in Table 2 with those for the compound prepared from the natural iron isotopic mixture, i.e. 91.5% ^{56}Fe. (The spectra for the two samples were identical in the mid-infrared region). The 256 cm^{-1} absorption band shifts to higher frequency upon substitution with the lighter isotope. The magnitude and direction of this isotopic shift are similar to that reported for Fe—O stretching modes in the tris(acetylacetonato)iron(III) complex [26].

The 551 cm^{-1} band also shifts to higher energy upon isotopic substitution. This band is relatively broad and asymmetric in the iron complex and most likely does not represent a pure vibrational mode. A small isotopic shift is expected for the δ(POO) band which is strongly metal sensitive since POO^- bending involves some metal motion and the vibration should be coupled with the metal–oxygen stretching mode [27]. The 4 cm^{-1} shift, however, is larger than expected. The large isotopic shift indicates that the 551 cm^{-1}

Table 2. Far-infrared absorption bands for metal-H_2DEH[MDP] compounds

Metal	δ(POO)	δ(POC)	ν(M—OP)
Na	517	473, 458	—
La	532	453	—
Nd	532	452	—
Eu	530	452	—
			—
^{56}Fe	551*	447	256
^{54}Fe	555	446	259

*This band has a substantial metal–oxygen stretching component, *vide infra*.

band has a substantial iron–oxygen stretching component. A band at nearly this frequency in the infrared spectrum of the tris(oxalato)ferrate(III) complex has been identified on the basis on a normal coordinate analysis as an iron–oxygen stretching mode [27]. The frequency of the δ(POC) mode is unaffected by isotopic substitution as expected.

The appearance of metal–oxygen stretching bands in the anhydrous iron-H_2DEH[MDP] complex indicates that the iron-diphosphonate interaction has a substantial covalent component. The absence of these bands in the lanthanide complexes indicates that the binding is predominantly ionic in these compounds. Thus, based on these findings, it appears that changes in the P—O bond order in metal-diphosphonate complexes arise from a combination of bond polarization and covalence effects. This conclusion is consistent with the physical properties of the compounds, the results from our solvent extraction and aggregation studies [1,7], and small angle neutron scattering measurements [28]. The absence of metal–oxygen stretching bands in the lanthanide complexes further indicates that the water in these ionic compounds is not coordinated to the metal ion. This inference is in agreement with the observed structural results for analogous lanthanide complexes of 1-hydroxyethane-1,1-diphosphonic acid [16].

Acknowledgements—The authors wish to thank Paul G. Rickert for preparing the P,P′-di(2-ethylhexyl) methanediphosphonic acid and Ken L. Nash for helpful discussions and suggestions. We also wish to thank Marcos H. Grimsditch and S. Uram for use of the Bruker 98 vacuum FT-IR interferrometer and help in recording the spectra. The support provided for this work by the Department of Energy, Office of Basic Energy Sciences (BES) is acknowledged. One of us (J.A.G.) also wishes to acknowledge support from the U.S. Department of Education under the GAANN Fellowship Program.

REFERENCES

1. Chiarizia, R., Horwitz, E. P., Rickert, P. G. and Herlinger, A. W., *Solvent Extr. Ion Exch.*, 1996, **14,** 773.
2. Chiarizia, R., Herlinger, A. W. and Horwitz, E. P., *Solvent Extr. Ion Exch.*, 1997, **15,** 417.
3. Chiarizia, R., Herlinger, A. W., Cheng, Y. D., Ferraro, J. R., Rickert, P. G. and Horwitz, E. P., *Solvent Extr. Ion Exch.*, 1998, in press.
4. Rizkalla, E. N., *Rev. Inorg. Chem.*, 1983, **5,** 223.
5. Nash, K. L. and Horwitz, E. P., *Inorg. Chim. Acta.*, 1990, **169,** 245.
6. Nash, K. L., *Radiochimica Acta*, 1991, **54,** 171.
7. Herlinger, A. W., Ferraro, J. R., Chiarizia, R. and Horwitz, E. P., *Polyhedron*, 1997, **16,** 1843.
8. Deacon, G. B. and Phillips, R. J., *Coord. Chem. Rev.*, 1980, **33,** 227 and references therein.
9. Peppard, D. F. and Ferraro, J. R., *J. Inorg. Nucl. Chem.*, 1959, **27,** 2055.
10. Ferraro, J. R. and Peppard, D. F., *Nucl. Sci. Eng.*, 1963, **16,** 389.
11. Herlinger, A. W., Chiarizia, R., Ferraro, J. R., Rickert, P. G. and Horwitz, E. P., *Solvent Extr. Ion Exch.*, 1997, **15,** 401.
12. Addison, C. C., Adams, D. W., Sutton, D. and Hoyle, W. H. H., *J. Chem. Soc.* (*A*), 1967, 808.
13. Choca, M., Ferraro, J. R. and Nakamoto, K., *J. Chem. Soc.* (*A*), 1972, 2297.
14. Kagarise, E., *J. Phys. Chem.*, 1955, **59,** 271.
15. Grigor'ev, A. I. and Maksimov, V. N., *Russ. J. Inorg. Chem.*, 1964, **9,** 580.
16. Nash, K. L., Rogers, R. D., Ferraro, J. R. and Zhang, J., *Inorg. Chim. Acta*, 1997, in press.
17. Shannon, R. D., *Acta Cryst.*, 1976, **A32,** 751.
18. Aslanov, L. A., Abdul'minev, I. K., Porai-Koshits, M. A. and Ivanov, V. I., *Dolk. Chem.*, 1972, **205,** 568.
19. Zaitseva, M. G., Stepanyan, S. A. and Kravchenko, V. V., *Russ. J. Inorg. Chem.*, 1976, **21,** 1820.
20. Kumamoto, J., *Spectrochim. Acta*, 1965, **21,** 345.
21. Munze, R., *J. Inorg. Nucl. Chem.*, 1972, **34,** 661.
22. Thomas, L. C., The identification of functional groups in organophosphorus compounds. In *Analysis of Organic Materials, An International Series of Monographs*, Vol. 7, ed. R. Belcher and D. M. W. Anderson, Academic Press, London, U.K., 1974.
23. Thomas, L. C., *Interpretation of the Infrared Spectra of Organophosphorus Compounds*. Heyden, London, 1974.
24. Nakamoto, K., *Infrared Spectra of Inorganic and Coordination Compounds*, 2nd ed. Wiley-Interscience, New York, 1970.
25. Nakamoto, K., Shobatake, K. and Hutchinson, B., *Chem. Commun.*, 1969, **00,** 1451.
26. Nakamoto, K., Udovich, C. and Takemoto, J., *J. Amer. Chem. Soc.*, 1970, **92,** 3973.
27. Mikami, M., Nakagawa, I. and Shimanouchi, T., *Spectrochim. Acta*, 1967, **23A,** 1037.
28. Urban, V., Chiarizia, R., Herlinger, A. W., Ku, C. Y. and Thiyagarajan, P., *Physica B—Condensed Matter*, 1998, in press.

Pergamon

PII: S0277-5387(97)00409-9

Polyhedron Vol. 17, No. 9, pp. 1477–1480, 1998
© 1998 Elsevier Science Ltd
All rights reserved. Printed in Great Britain
0277-5387/98 $19.00+0.00

The template synthesis and characterization of the yttrium and lanthanide complexes of new 19-membered pentadentate azaoxa macrocycle

Wanda Radecka-Paryzek,* Violetta Patroniak-Krzyminiewska and Hanna Litkowska

Faculty of Chemistry, Adam Mickiewicz University, 60-780 Poznań, Poland

(Received 21 July 1997; accepted 1 October 1997)

Abstract—The template reactions of 2,6-diacetylpyridine with 1,12-diamine-4,9-dioxadodecane in the presence of yttrium and lanthanide ions produce the pentadentate macrocyclic complexes with N_3O_2 set of donor atoms as a result of [1 + 1] Schiff base condensation. The complexes were characterized by spectral data (IR, UV–vis, ^{1}H NMR, FAB-MS), thermogravimetric and elemental analysis. © 1998 Elsevier Science Ltd. All rights reserved

Keywords: Schiff bases; Macrocyclic complexes; Template synthesis; Yttrium; Lanthanides.

The design and synthesis of macrocyclic lanthanide complexes is currently attracting considerable attention since they can be used as supramolecular devices and sensors [1,2], contrast agents in magnetic resonance imaging [3–5], potential radiopharmaceuticals [6], as possible bioinorganic models for the active sites in metallobiomolecules [7,8], as synthetic nucleases for *in vivo* application [9]. The conjugation of macrocyclic complexes of yttrium and lanthanide radioisotopes to monoclonal antibodies results in agents for radioimmunotherapy and other medical applications [10]. In all of these situations the metal complex must be sufficiently stable *in vivo*, inert to metal release under physiological conditions in order to avoid the damage to nontarget cells. The Schiff base macrocyclic yttrium and lanthanide complexes fulfill these requirements, because they are extremely inert with respect to release of the metal ion, whereas the exocyclic ligands (anion or water molecules) are labile and easy to change.

Many of the synthetic routes to macrocyclic ligands involve the use of the metal ion template to orient the reacting groups of the ligand in the desired conformation for optimum ring closure. The favorable enthalpy for the formation of the metal–ligand bonds overcomes the unfavorable entropy from the ordering of the multidentate ligand around the metal ion and thereby promotes the cyclization reaction [11–13].

In searching for new stable complexes of the rare earth elements in view of their potential applications and continuing our studies on the effectiveness of metal ions of varying radius and electron configuration in the synthesis of macrocyclic and macroacyclic compounds we have recently reported the template action of yttrium and heavier (smaller) lanthanide(III) ions (dysprosium, erbium, thulium and lutetium) in the synthesis of 15-membered pentadentate Schiff base macrocyclic ligand derived from 2,6-diacetylpyridine and 3,6-dioxaoctane-1,8-diamine [14,15]. The higher lanthanide(III) ions (lanthanum, samarium and europium) have been found to be ineffective as templates in the synthesis of this macrocycle under similar conditions. These results have prompted us to investigate the template action of the lanthanides in the synthesis of related macrocyclic ligand with greater ring size. The preparation and characterization of new 19-membered macrocyclic Schiff base complexes formed in the lanthanide-promoted condensation reactions between one molecule of 2,6-diacetylpyridine and one molecule of 1,12-diamine-4,9-dioxadodecane is the subject of this paper. We have also found that under different experimental conditions these ions may act as effective templates in the synthesis of the dinuclear octadentate macroacyclic complexes of podate type with terminal

* Author to whom correspondence should be addressed.

acetylpyridyl groups and N_4O_4 set of donor atoms as a result of [2+1] Schiff base partial condensation of two molecules of 2,6-diacetylpyridine with one molecule of 1,12-diamine-4,9-dioxadodecane [16].

EXPERIMENTAL

The hydrated lanthanide(III) salts were prepared by dissolving the 99.99% oxides (Fluka) in a slight excess of appropriate acid. The solutions were evaporated and precipitates recrystallized from methanol. 2,6-Diacetylpyridine and 1,12-diamine-4,9-dioxadodecane (Aldrich Chemical Company) were used without further purification.

Preparation of the complexes. General procedures

All complexes were performed under similar conditions. To a mixture of appropriate metal salt (0.1 mmol) in methanol (10 cm^3) and 2,6-diacetylpyridine (0.1 mmol) in methanol (10 cm^3), 1,12-diamine-4,9-dioxadodecane (0.1 mmol) in methanol (10 cm^3) was added dropwise with stirring. The reaction was carried out for 4 h. The solution volume was then reduced to 10 cm^3 by roto-evaporation and an orange precipitate formed on addition of a small amount of diethyl ether. This was filtered off, washed with ether, and dried *in vacuo*. Yields: 76–81%. The results of elemental analysis of the complexes are listed in Table 1.

Measurements

IR spectra were recorded using CsI pellets in the range 4000–200 cm^{-1} on a Perkin-Elmer 580 spectrophotometer. Electronic spectra were measured on a Shimadzu UV-160 spectrophotometer. ^1H NMR spectra were run in DMSO-d_6 on a Varian Gemini 300 spectrometer using TMS as an internal reference. FAB-mass spectra were obtained on a AMD-604 mass spectrometer with the glycerol as matrix. Thermogravimetric measurements were performed using Shimadzu TGA-50 derivatograph.

RESULTS AND DISCUSSION

The lanthanide(III) ion complexes of the new macrocyclic ligand **L**-product of a Schiff base cyclocondensation of one molecule of 2,6-diacetylpyridine with one molecule of 1,12-diamine-4,9-dioxadodecane were prepared by the reaction of appropriate metal salts acting as template agents with diketone and diamine in the 1 : 1 : 1 molar ratio of starting materials.

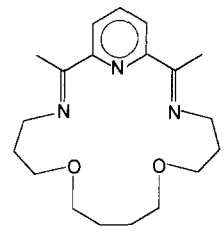

L

The formulations of these complexes as $LnL(H_2O)_nX_3 \cdot mH_2O$, where L is $Me_2pyo[19]triene\text{-}N_3O_2$, Ln = Y^{3+}, La^{3+}, Eu^{3+}, Gd^{3+}, Dy^{3+}, Ho^{3+}, Er^{3+}, Tm^{3+}, Yb^{3+}, Lu^{3+}, X = NO_3^- or Cl^-, n = 0–4, m = 0–4, follow from spectral data (IR, UV–vis, ^1H NMR, FAB-MS) and thermogravimetric and elemental analyses. The complexes are orange air stable solids, moderately soluble in CH_3CN and DMSO.

The infrared spectra of these complexes taken in the region 4000–200 cm^{-1} are all very similar except for anion vibrational modes (Table 2) and provide some information regarding the bonding in the complexes. They confirm the formation of the macrocyclic compounds by the absence of bands characteristic of

Table 1. Analytical data for the complexes of L

Compound	Found (%)			Calculated (%)		
	C	H	N	C	H	N
$YL(ClO_4)_3 \cdot 4H_2O$	30.8	4.5	5.1	28.9	4.7	5.3
$LaL(H_2O)_4(NO_3)_3 \cdot H_2O$	32.3	5.2	10.9	30.5	5.2	11.2
$EuL(H_2O)_3(NO_3)_3 \cdot H_2O$	31.9	4.7	10.7	30.8	5.0	11.3
$GdL(H_2O)(NO_3)_3 \cdot H_2O$	30.8	4.4	10.1	32.1	4.7	9.9
$GdL(H_2O)_3(ClO_4)_3 \cdot 2H_2O$	25.5	3.9	4.3	26.0	4.5	4.7
$DyL(H_2O)_2(ClO_4)_3 \cdot H_2O$	30.2	4.7	5.8	31.1	4.8	5.7
$HoL(H_2O)_2(ClO_4)_3$	28.8	3.9	4.8	27.5	4.0	5.0
$ErL(H_2O)(ClO_4)_3 \cdot 2H_2O$	27.7	4.1	4.8	26.8	4.1	4.9
$TmL(H_2O)(ClO_4)_3$	29.4	3.9	5.0	27.9	3.8	5.1
$TmL(H_2O)_4(NO_3)_3 \cdot H_2O$	30.7	5.4	10.5	29.4	5.1	10.8
$YbL(H_2O)_4(NO_3)_3 \cdot 2H_2O$	29.3	5.0	10.1	28.6	5.2	10.5
$LuL(H_2O)_3Cl_3 \cdot 3H_2O$	31.5	5.8	5.9	31.6	5.7	5.8

Table 2. Infrared spectral data (cm^{-1}) for the complexes of L

Compound	OH	C=N	py	C—O—C	X^-
$YL(ClO_4)_3 \cdot 4H_2O$	3440	1630	1580, 1020, 630		1200–970, 635
$LaL(H_2O)_4(NO_3)_3 \cdot H_2O$	3400, 855	1640	1585, 1030, 668	1095	1550–1300, 825, 818
$EuL(H_2O)_3(NO_3)_3 \cdot H_2O$	3420, 855	1640	1590, 1030, 660	1090	1550–1250, 820
$GdL(H_2O)(NO_3)_3 \cdot H_2O$	3440, 860	1650	1589, 1010, 620	1085	1490–1250, 820
$GdL(H_2O)_3(ClO_4)_3 \cdot 2H_2O$	3424, 858	1630	1598, 1027, 668		1200–900, 626
$DyL(H_2O)_2(ClO_4)_3 \cdot H_2O$	3420, 856	1660	1590, 1025, 660		1199–1000, 625
$HoL(H_2O)_2(ClO_4)_3$	3420, 820	1625	1590, 1010, 665		1165–930, 625
$ErL(H_2O)(ClO_4)_3 \cdot 2H_2O$	3420, 855	1653	1597, 1026, 668		1250–950, 625
$TmL(H_2O)(ClO_4)_3$	3440, 815	1625	1570, 1020, 665		1160–925, 625
$TmL(H_2O)_4(NO_3)_3 \cdot H_2O$	3407, 852	1635	1595, 1026, 668	1093	1500–1300, 825, 816
$YbL(H_2O)_4(NO_3)_3 \cdot 2H_2O$	3425	1630	1594, 1026, 664	1092	1500–1300, 825
$LuL(H_2O)_3Cl_3 \cdot 3H_2O$	3420, 855	1620	1595, 1030, 655	1095	225

carbonyl and amine groups of the starting materials. An important feature is the occurrence of a strong band at 1650–1620 cm^{-1} attributable to C=N stretching modes indicating the Schiff base condensation. The spectra exhibit medium to strong bands at 1598–1570 cm^{-1} as expected for the high energy ring vibrations of the coordinated pyridine. The bonding of the pyridine nitrogen atom is also shown by the presence of the band at 1030–1010 cm^{-1} and 668–630 cm^{-1} attributable to the ring breathing frequency and the low energy pyridine ring vibrations, respectively [17]. The C—O—C stretching mode occurs at 1095–1085 cm^{-1} indicating ether oxygen coordination [18]. The complexes show the broad diffuse band centered at ca 3450–3400 cm^{-1} due to the stretching and bending modes of lattice and/or coordinated water. In addition, weak bands are detectable at 860–815 cm^{-1} region (except for yttrium) which may be assigned to rocking or wagging modes of water molecules interacting with the metal ion [19]. The presence of water bound in two different ways is confirmed by the results of thermogravimetric analysis. The complexes lose the water molecules in two steps: below 100°C and/or above 150°C corresponding to the lattice and/or coordinated water molecules, respectively. The amount of these two kinds of water molecules per mol of metal ion was calculated from the weight loss observed for the complexes at these two temperature ranges. Information about the bonding mode of the counterions in these complexes may also be obtained from IR spectra [20]. In the spectra of the nitrate complexes ν(N—O) stretching frequency is observed as a very strong broad band centered at 1380 cm^{-1}. In addition medium bands at 825–816 cm^{-1} are also detectable. Comparison with the infrared spectral data of the various nitrate complexes with known X-ray crystal structures reveals that the broadening or splitting of these bands is characteristic of the presence of both coordinated and ionic nitrates [21–24]. The spectrum of the chloride complex shows medium absorption band at 225 cm^{-1} attributable to the M—Cl frequency indicating the interaction of at least part of the chloride counterions with the metal. The IR spectra of the perchlorate complexes exhibit the strong absorption band centered at 1080 cm^{-1} typical of the asymmetric Cl—O stretching mode and a weak band at 625 cm^{-1} associated with the asymmetric Cl—O bending mode. The considerable broadening (1200–900 cm^{-1}) of the higher energy band suggests, similarly to the nitrate complexes, that the perchlorate counterions are partially involved in the coordination sphere of the metal ion [20,21]. However the C—O—C stretching mode of the polyether chain also falls in this region.

The FAB mass spectrum of the lanthanum nitrate complex provides strong evidence for the formation of the macrocyclic complex with the ligand **L** as a product of the template condensation of one molecule of diketone with one molecule of diamine and confirms the presence of nitrate anions in both inner and outer spheres of the complex. The highest peak of the spectrum observed at m/z 599.1 corresponds to the $[LaL(NO_3)_2]^+$. This species loses the nitrate group resulting in the formation of the fragment $[LaL(NO_3)]^{2+}$ at m/z 536.0. The spectrum also exhibits a peak due to the free ligand at m/z 470.

The electronic spectra of the complexes for solutions in acetonitrile show similar features, containing intense and medium bands with maxima at 207–220 and 266–276 nm which may be assigned to the transition of the $\pi \rightarrow \pi^*$ type of the coordinated macrocycle.

The ^1H NMR spectra of DMSO-d_6 solution of the diamagnetic yttrium and lutetium complexes exhibit three multiplets in a ratio 1:1:2: the protons α to nitrogen give raise to a triplet (4H) at δ 2.85 ($J = 7.6$) for the yttrium complex and at δ 2.81 ($J = 6.9$) for the lutetium complex, the protons β to nitrogen to quintet (4H) at δ 1.77 ($J = 7.3$) for the yttrium complex and at δ 1.76 ($J = 6.2$) for the lutetium complex and the protons adjacent to the oxygen to the triplet (8H) at δ 3.43 ($J = 6.1$) for the yttrium complex and δ 3.42 ($J = 5.5$) for the lutetium complex. The remain-

ing protons of the —$OCH_2CH_2CH_2CH_2O$— chain (4H) occur at δ 1.54 and 1.52 for the yttrium and the lutetium complex, respectively. The pyridine protons are observed at δ 8.3–7.8 (6H) and the methyl protons of the two CH_3CN groups (6H) at δ 2.53 for the yttrium complex and at δ 2.51 for the lutetium complex. The integrated relative intensities of the above signals are in good agreement with the required ratios consistent with the proposed formulations of the complexes.

On the basis of available evidence it can be concluded that the yttrium and lanthanide ions are effective templates for the synthesis of new Schiff base macrocyclic complexes, in which the new ligand with N_3O_2 set of donor atoms acts as pentadentate chelator. The 19-membered macrocyclic product of the template process, contrary to the 15-membered coronand with similar set of donor atoms [14,15], appears to be large enough to encapsulate all the lanthanides irrespective of the ionic radius size of the central atoms. The high coordination number characteristic of these ions is achieved by the incorporation of water molecules and/or counterions in the coordination sphere of the complexes. Since there is no ligand field stabilization energy effect in the yttrium and lanthanide(III) ions (d^0 configuration) their coordination environment is determined mainly by the chelating power of the ligand (preferred conformation, nature and disposition of donor atoms). Thus these ions can be accommodated by the particular stereochemical constraints enforced by the template process. Efforts to prepare free macrocycle in the reaction of the 2,6-diacetylpyridine with 1,12-diamine-4,9-dioxadodecane in the absence of metal ion were unsuccessful and resulted in the formation of insoluble yellow compound of polymeric character terminated with carbonyl functions. The failure of this system to undergo complete condensation and cyclization confirms the importance of metal ion in directing the steric course of the condensation process, which ultimately ends with ring closure.

Acknowledgements—The partial financial support from the National Committee for Scientific Research (grant T09A 13109) is gratefully acknowledged.

REFERENCES

1. Sabbatini, N., Guargigli, M., Manet, I., Ungaro, R., Casnati, A., Ziessel, R., Ulrich, G., Asfari, Z. and Lehn, J.-M., *Pure Appl. Chem.*, 1995, **67,** 135 and refs therein.
2. Oude Wolbers, M. P., van Veggel, F. C. J. M., Snellick-Ruël, B. H. M., Hofstraat, J. W., Guerts, F. A. J. and Reinhoudt, D. N., *J. Am. Chem. Soc.*, 1997, **119,** 138 and refs therein.
3. Géze, C., Mouro, C., Hindré, F., Le Plouzennec, M., Moinet, C., Rolland, R., Alderighi, L., Vacca, A. and Simmonneaux, G., *Bull. Chem. Soc. Chim. Fr.*, 1996, **133,** 267.
4. Choppin, G. R. and Schaab, K. M., *Inorg. Chim. Acta,* 1996, **252,** 299 and refs therein.
5. Sessler, J. L., Moody, T. D., Hemmi, G. W., Lynch, V., Young, S. W. and Miller, R. A., *J. Am. Chem. Soc.*, 1993, **115,** 10368 and refs therein.
6. Jurisson, S., Berning, D., Jia Wei and Ma Dangshe, *Chem. Rev.*, 1994, **93,** 1137.
7. Evans, C. H., in *Biochemistry of Lanthanides*, ed. E. Frieden. Plenum Press, New York, 1990, Ch.9.
8. Tweedle, M. F., in *Lanthanide Probes in Life, Chemical and Earth Sciences*, ed. J.-C. Bünzli and G. R. Choppin. Elsevier, Amsterdam, 1989, Ch. 5.
9. Amin, S., Morrow, J. R., Lake, C. H. and Churchill, M. R., *Angew. Chem. Int. Ed. Engl.*, 1994, **33,** 773 and refs therein.
10. Parker, D. and Williams, J. A. G., *J. Chem. Soc., Dalton Trans.*, 1996, 3613.
11. Dietrich, B., Viout, P. and Lehn, J.-M., *Macrocyclic Chemistry.* VCH Verlagsgesellschaft, Weinheim, 1993.
12. Constable, E. C., *Metals and Ligand Reactivity.* VCH Verlagsgesellschaft, Weinheim, 1996.
13. Alexander, V., *Chem. Rev.*, 1995, **95,** 273 and refs therein.
14. Radecka-Paryzek, W. and Patroniak-Krzyminiewska, V., *Polyhedron*, 1995, **14,** 2059.
15. Patroniak-Krzyminiewska, V. and Radecka-Paryzek, W., *Coll. Czech. Chem. Comm.*, in press.
16. Patroniak-Krzyminiewska, V. and Radecka-Paryzek, W., *J. Alloys Comp.*, in press.
17. Radecka-Paryzek, W. and Patroniak, V., *Polyhedron*, 1994, **13,** 2125.
18. Bandin, R., Bastida, R., de Blas, A., Castro, P., Fenton, D. E., Macias, A., Rodriguez, A. and Rodriguez, T., *J. Chem. Soc. Dalton Trans.*, 1994, 1185.
19. Nakamoto, K., *Infrared and Raman Spectra of Inorganic and Coordination Compounds.* Wiley Interscience, New York, 1978.
20. Radecka-Paryzek, W., Jankowska, E. and Luks, E., *Polyhedron*, 1988, **7,** 439 and refs therein.
21. Bastida, R., de Blas, A., Castro, P., Fenton, D. E., Macias, A., Rial, R., Rodriguez, A. and Rodriguez-Blas, T., *J. Chem. Soc., Dalton Trans.*, 1996, 1493.
22. Radecka-Paryzek, W. and Gdaniec, M., *Polyhedron*, 1997, **16,** 3681.
23. Wieghardt, K., Kleine-Boymannn, M., Nuber, B., Weiss, J., Zsolnai, L. and Huttner, G., *Inorg. Chem.*, 1986, **25,** 1647.
24. Cramer, R. E., Mitchell, K. A., Hirazumi, A. Y. and Smith, S. L., *J. Chem. Soc., Dalton Trans.*, 1994, 563.

Pergamon

PII: S0277-5387(97)00408-7

Polyhedron Vol. 17, No. 9, pp. 1481–1493, 1998
© 1998 Elsevier Science Ltd
All rights reserved. Printed in Great Britain
0277-5387/98 $19.00+0.00

Palladium(II) coordination chemistry of monoethyl 2-quinolylmethylphosphonate

Ljerka Tušek-Božić[a]* and Martina D'Alpaos[b]

[a] Department of Chemistry, Ruđer Bošković Institute, Bijenička c. 54, 10000 Zagreb, Croatia

[b] Servizio di Spettrometria di Massa, Area di Ricerca del CNR, Corso Stati Uniti 4, 35100 Padova, Italy

(Received 17 July 1997; accepted 1 October 1997)

Abstract—The synthesis and some spectroscopic properties of the new palladium(II) complexes with monoethyl 2-quinolylmethylphosphonate (2-mqmp) have been reported. It was shown that the molecular or the ionic complexes could be isolated by reaction of 2-mqmp with PdX_4^{2-} (X = Cl, Br) depending on the acidity of the aqueous reaction solution. The square planar dihalide complexes *trans*-$Pd(2\text{-mqmp})_2X_2$ with monodentate N-bonded ligand through the quinoline nitrogen were obtained at pH ~ 3.5. Under acidic conditions at pH < 3 the ion-pair salt complexes [2-mqmp H^+][Pd(2-mqmp)X_3^-] containing the protonated quinoline ligand as cation and the quinoliniummethylphosphonatetrihalopalladate complex as anion were isolated. These ionic complexes by heating in methanol were decomposed: the chloro complex to the molecular dichloropalladium adduct $Pd(2\text{-mqmp})_2Cl_2$, while its bromo analogue gave a mixture of the dibromopalladium adduct $Pd(2\text{-mqmp})_2Br_2$ and the ion-pair hexabromodipalladium salt complex [2-mqmp H^+]$_2$[$Pd_2Br_6^{2-}$]. The chelate complex Pd(2-mqmp-H)$_2\cdot 2H_2O$ was isolated at pH > 6. In this compound 2-mqmp acts as a bidentate ligand through the quinoline nitrogen and the phosphonic acid oxygen. The new complexes were identified and characterized on the basis of elemental and thermogravimetric analysis, magnetic and conductance measurements, as well as by infrared and positive/negative-ion FAB-mass spectroscopic studies. © 1998 Elsevier Science Ltd. All rights reserved

Keywords: palladium(II) complexes; quinolylmethylphosphonate complexes; infrared study; mass spectroscopy.

Organophosphorus compounds such as derivatives of various aminophosphonic acids, have currently attracted considerable interest not only because of their complexation capability towards numerous metal ions that enable application of the selected derivatives as catalysts, extractants, ion-exchangers etc [1–6], but also of their occurrence in living organisms and bioactivity [7–9]. The investigation of their interaction with metal ions, both in the solid state and in solution, may contribute to a better understanding of the biological activity of these compounds which is mainly displayed through their metabolic regulation and ability to inhibit various metalloenzymes having an amino acid as substrate. The differences in size, shape and basicity of the carboxylate and phosphonate groups might reflect in differences in the enzyme-substrate interactions.

As a part of our systematic investigation on coordination behaviour of various aminophosphonic acid derivatives with respect to Pd(II) ion, especially of those derived from quinoline and aniline which might be of interest as anticancer and antiviral agents [10–12], we describe here the preparation and characterization of new palladium complexes with monoethyl 2-quinolylmethylphosphonate (2-mqmp). In our earlier papers we studied Pd(II) halide complexes with diethyl 2-quinolylmethylphosphonate (2-dqmp), the ligand which appeared to coordinate metal ion in a monodentate and bidentate manner via only the quinoline nitrogen or both the quinoline nitrogen and the phosphoryl oxygen atoms [10,13]. Monoester 2-mqmp containing the phosphonic acid group has shown different complex-forming behaviour, since depending on the acidity of the reaction solution either the zwitterion, molecular or anionic form of this organophosphonate ligand can coordinate to the metal ion.

* Author to whom correspondence should be addressed.

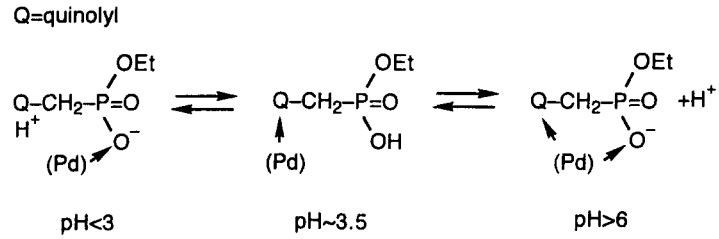

Dihalide adducts containing mutually *trans*-bonded ligand via the quinoline nitrogen are formed at pH ~ 3.5, at higher acidity this ligand acts in a zwitterion form yielding salt complexes with the protonated quinolylmethylphosphonate ligand as cation and the quinoliniummethylphosphonatetrihalopalladate complex as its counterion, while at lower acidity the phosphonate monoanion coordinates to metal through the quinoline nitrogen and the deprotonated phosphonic acid group. Ionic trihalopalladium salt complexes upon heating in methanol are decomposed to the molecular dihalopalladium complexes. The bromo complex along the dibromo adduct gave also the quinolinium salt of the hexabromodipalladate anionic complex without direct Pd-organophosphorus ligand bonding.

EXPERIMENTAL

Materials

Monoethyl 2-quinolylmethylphosphonate (2-mqmp) and sodium monoethyl 2-quinolylmethylphosphonate, prepared as previously described [14], were purified by recrystallization from absolute ethanol prior to use. Dichloro-bis(acetonitrile)-palladium(II) and dibromo-bis(benzonitrile)palladium(II) complexes were prepared according to literature methods [15]. All other reagents and solvents were analytical grade products and were used without purification.

Preparation of complexes

$Pd(2\text{-mqmp})_2Cl_2$ (**1**). For the preparation of this complex few general procedures could be used, either reaction of 2-mqmp with $K_2[PdCl_4]$ in aqueous solution, or with $Na_2[PdCl_4]$ in methanolic solution, reaction of 2-mqmp with dichloro-bis(acetonitrile) palladium(II) complex in dichloromethane, or it could be obtained from the ionic quinolinium trichloropalladium complex **3**.

(a) Addition of a concentrated aqueous solution of $K_2[PdCl_4]$ (0.135 g, 0.41 mmol) to a stirred solution of 2-mqmp (0.205 g, 0.82 mmol) in water (5 ml) gave a solution with pH ~ 3.5. The reaction mixture was continuously stirred for 24 h at room temperature. The yellow precipitate formed was filtered off, washed with cold water and methanol, and dried *in vacuo* over P_2O_5. Yield: 0.180 g (65%).

(b) A mixture of 2-mqmp (0.200 g, 0.80 mmol) and $Na_2[PdCl_4]$ (0.117 g, 0.40 mmol) in methanol (10 ml) was stirred for 12 h at r.t. The precipitate which formed was separated and dried as described. Yield 0.101 g (78%). Alternatively, refluxing the reaction mixture under a stream of N_2, complex **1** precipitated with the same yield after only 3 h of vigorous stirring.

(c) $Pd(CH_3CN)_2Cl_2$ (0.120 g, 0.45 mmol) was dissolved in hot dichloromethane (10 ml), filtered to remove any impurities, and added to a stirred solution of 2-mqmp (0.222 g, 0.88 mmol) in dichloromethane (5 ml). After heating the reaction mixture under reflux for 4 h with continuous stirring, the precipitate formed was separated by filtration of the hot suspension. Yield: 0.201 g (67%).

(d) Heating the trichloropalladium complex **3** in methanol at reflux temperature under inert atmosphere gave rise to the precipitation of **1** in an almost quantitative yield.

$Pd(2\text{-mqmp})_2Br_2$ (**2**). Efforts to prepare pure complex **2** according to the same synthetic procedures as that used for preparation of **1**, by reaction of 2-mqmp with $K_2[PdBr_4]$ either in aqueous or methanolic solution, were unsuccessful. A mixture of complexes **2** and **5** were obtained. However, two other methods could be used, the reaction of 2-mqmp with dibromo-bis(benzonitrile)palladium(II) complex and decomposition of the ionic quinolinium tribromopalladium complex **4** in the methanolic solution.

(a) A suspension of $Pd(PhCN)_2Br_2$ (0.150 g, 0.32 mmol) in hot dichloromethane (10 ml) was added to a stirred solution of 2-mqmp (0.150 g, 0.60 mmol) in the same solvent (5 ml). The reaction mixture was refluxed with vigorous stirring for 4 h. The orange precipitate formed was immediately separated by filtration, washed with cold dichloromethane and ether, and dried *in vacuo* overnight at r.t. Yield: 0.090 g (39%).

(b) By refluxing in methanol for 12 h under an inert atmosphere complex **4** was almost completely converted into complex **2**.

[2-mqmp H][Pd(2-mqmp)Cl_3] (**3**). To a concentrated solution of 2-mqmp (0.252 g, 1.0 mmol) in water under stirring was added dropwise a mixture of $K_2[PdCl_4]$ (0.165 g, 0.51 mmol) and 1 : 1 HCl (0.6 cm^3)

in water (3 ml). An addition constant stirring for 12 h at +4°C yielded a hazel precipitate (0.180 g, 50%) which was washed with the minimum ice-cold water and methanol, and dried *in vacuo* at r.t. This complex could be prepared also by reaction of 2-mqmp with a mixture of $PdCl_2$ and HCl under the similar reaction conditions.

[2-mqmp H][Pd(2-mqmp)Br_3] (**4**). This complex could be prepared by reaction of 2-mqmp with $K_2[PdBr_4]$ in water (pH ~3.5) or by reaction of the same reactants in the HBr acidic medium (pH <3).

(a) A concentrated aqueous solution of $K_2[PdBr_4]$ (0.210 g, 0.42 mmol) was added dropwise to a stirred solution of 2-mqmp (0.200 g, 0.80 mmol) in water (5 ml). The reaction mixture was continuously stirred for 6 h at r.t. Complex **4** obtained as a brown precipitate was separated by filtration, washed with ice-cold water and methanol, and dried in desicator over P_2O_5. Yield 0.140 g (42%). After long standing from the mother aqueous solution complex **2** was gradually formed as an ochre precipitate. Yield: 0.090 g (29%).

(b) A mixture of $K_2[PdBr_4]$ (0.267 g, 0.53 mmol) and concentrated HBr (0.5) in water (5 ml) was slowly added to a stirred solution of 2-mqmp (0.252 g, 1.0 mmol). After an additional stirring of 6 h at +4°C only complex **4** precipitated. Yield: 0.711 g (74%).

[2-mqmp H]$_2$[Pd_2Br_6] (**5**). The quinolinium tribromopalladium complex **4** was refluxed for 15 min in methanol under a stream of nitrogen. The hot solution was filtered to remove any impurities and the brown crystal precipitate obtained gradually on cooling was isolated, washed with cold methanol and dried overnight *in vacuo* at r.t. The longer heating afforded a mixture of the complexes **2** and **5**, which were separated under the microscope.

Pd(2-mqmp-H)$_2 \cdot 2H_2O$ (**6**). Two methods were applied for preparation of this complex.

(a) A concentrated aqueous solution of $K_2[PdCl_4]$ (0.125 g, 0.38 mmol) was added dropwise to a stirred solution of sodium salt of 2-mqmp (0.209 g, 0.77 mmol) in water (5 ml). The reaction mixture was continuously stirred for 48 h at r.t. The yellow precipitate formed was filtered off, washed with minimum cold water and absolute ethanol, and dried *in vacuo* over P_2O_5. Yield: 0.150 g (61%).

(b) A concentrated aqueous solution of $K_2[PdCl_4]$ (0.147 g, 0.45 mmol) was slowly added to a stirred solution of 2-mqmp (0.210 g, 0.84 mmol) in water (5 ml). The pH was adjusted to pH ~6 with dilute sodium hydroxide. An additional stirring of 48 h yielded a precipitate which was separated, washed and dried as described. Yield: 0.184 g (68%).

Physical measurements and analyses

Melting points were determined on a hot stage microscope and are uncorrected. Infrared spectra were recorded on a Perkin Elmer 580 B spectrophotometer using KBr pellets (4000–250 cm^{-1}) and Nujol mulls in polyethylene (400–200 cm^{-1}). Mass spectrometric measurements were performed on a double-focusing reverse-geometry VG ZAB 2F instrument operating under FAB conditions using the 8 keV Xe atoms. Glycerol or 3-nitrobenzyl alcohol were employed as the matrix for recording the positive-ion mass spectra. Negative-ion spectra were obtained with the 3-nitrobenzyl alcohol liquid matrix. Metastable transitions were detected by mass-analysed ion kinetic energy (MIKE) spectrometry [16]. Expected natural abundance isotope clusters patterns for various ion clusters were calculated with the Isotopic Distribution Program (IDS) contained in the FTMS 7.01 application program of the NICOS operating system using polynomial expansion based on natural abundances of the isotopes. Conductance measurements were carried out at room temperature using a CD 7A Tacussel conductance bridge for 10^{-3} mol l^{-1} solutions in methanol and dimethylformamide. Magnetic susceptibilities in the solid state were measured at r.t. by the standard Gouy method using a Cahn-Ventron RM-2 balance and $CuSO_4 \cdot 5H_2O$ as the susceptibility standard. Elemental analyses were performed by the standard analytical methods in the Ruđer Bošković Institute.

RESULTS AND DISCUSSION

Synthesis and properties

Investigations of the complex-forming behaviour of monoethyl 2-quinolylmethylphosphonate towards palladium(II) ion have shown that this ligand under different reaction conditions can act in a monodentate manner either through the quinoline nitrogen or the phosphonic acid oxygen, forming *trans*-square dihalide adducts (**1** and **2**) in the first case, and the ion-pair salt complexes with the protonated quinolylmethylphosphonate ligand as cation and the quinoliniummethylphosphonatetrihalopalladium(II) complex as anion (**3** and **4**) in the second one. The bonding mode of 2-mqmp also include the bidentate coordination through both the quinoline nitrogen and the deprotonated phosphonic acid group giving chelate complex Pd(L—H)$_2$ (**6**). It may be presumed that 2-mqmp in aqueous medium over a wide pH range exhibits either the molecular, zwitterion or the anionic form and therefore according to the acidity of the reaction solution three types of complexes have been obtained (Fig. 1).

The molecular dichloride complex **1** could be obtained either by reaction of 2-mqmp with K_2PdCl_4 in water or with Na_2PdCl_4 in methanol. Under the same reaction conditions 2-mqmp by reacting with K_2PdBr_4 gave a mixture of the corresponding bromo complex **2** and the ion-pair quinoliniumtribromopalladium salt complex **4**. In addition, dihalide adducts **1** and **2** could be obtained by reaction of

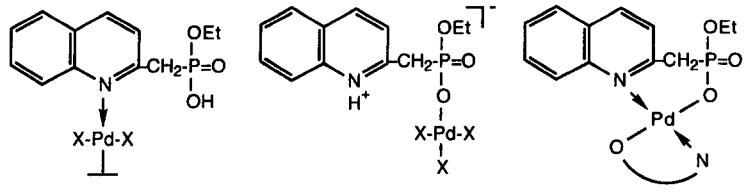

trans-Pd(2-mqmp)$_2$X$_2$ X=Cl (**1**); X=Br (**2**)

[2-mqmp H$^+$][Pd(2-mqmp)X$_3^-$] X=Cl (**3**); X=Br (**4**)

Pd(2-mqmp–H)$_2$ (**6**)

Fig. 1. Proposed chemical structures of palladium complexes with monoethyl 2-quinolylmethylphosphonate (2-mqmp).

2-mqmp with dichloro-bis(acetonitrile)palladium(II) and dibromo-bis(benzonitrile)palladium(II) complex, respectively, under refluxing in dichloromethane. In HX acidic medium (pH <3) 2-mqmp reacts in a zwitterion form with PdX_4^{2-} (X = Cl, Br) forming anionic complexes $PdLX_3^-$ with palladium ion bonded at the phosphonic acid moiety, while the quinoline nitrogen is remained protonated. The isolated quinolinium salt complexes $[LH^+][PdLX_3^-]$ are stable in the solid phase but unstable in solution. By heating in methanol the chloro complex **3** was converted into the dichloropalladium adduct **1**, while the corresponding bromo complex **4** gave a mixture of the dibromo adduct **2** and the quinolinium hexabromodipalladium salt complex **5** with two cationic quinolinium moieties and dimeric bromobridged dianionic complex $Pd_2Br_6^{2-}$. In neutral and basic media the phosphonate acid group is deprotonated and 2-mqmp acts as chelate ligand giving very stable complex **6** with two six-membered {N,O} chelate rings.

Physical properties, analytical and conductance data of the novel palladium complexes are reported in Table 1, while the most important spectral data (IR and FAB-mas) are summarized in Tables 2–4. The prepared complexes are microcrystalline, coloured yellow to red, and are stable under normal laboratory conditions. Their diamagnetic behaviour suggests the square-planar stereochemistry around the palladium(II) ion. The molar conductance measurements are consistent with the proposed structure of the complexes and their stoichiometry. The molar conductance of complexes **1** and **2** ($\Lambda_M = \sim 20$ S cm^2 mol^{-1} in dmf) corresponds to those of non-electrolyte compounds and is comparable with that obtained for the free monoester ligand, which confirms that these complexes are true molecular addition compounds. The ionic complexes **3** and **4** exhibit conductivities as expected for 1 : 1 electrolytes ($\Lambda_M = \sim 45$ in dmf), while complex **5** behaves as a 2 : 1 electrolyte in dimethylformamide and methanol solution ($\Lambda_M = 89.2$ and 189.2, respectively). The very low conductance value obtained for complex **6** ($\Lambda_M = 0.5$ in dmf) confirms the presence of deprotonated phosphonic acid groups in this chelate compound. In general, complexes are only slightly soluble or insoluble in all common solvents, and slightly soluble or soluble in dimethylformamide and dimethylsulfoxide. In general, palladium bromide complexes are more soluble than the corresponding chloride analogues, as are ionic complexes with respect to the molecular complexes. Because of the insolubility of the prepared complexes in suitable solvents or their instability, we could not grow crystals for the X-ray crystal analysis. The structures of the complexes were deduced mainly from their infrared and mass spectroscopic studies.

Infrared spectra

The IR frequencies associated with the main and characteristic functional groups of the free 2-mqmp and its palladium(II) complexes are summarized in Table 2. As a general remark we must emphasize that some vibrational modes are coupled giving rise to a great complexity of the spectra as was shown in Fig. 2. Infrared spectrum of the free 2-mqmp clearly indicates zwitterion structure of this organophosphorus ligand in the solid phase, similarly as was determined for a large number of various aminophosphonic acids and their monoesters both by infrared and X-ray crystallographic studies [17–20]. The absorption attributed to the protonated quinoline nitrogen appears as a strong band at 1652 cm^{-1} and two very broad bands of medium intensity around 2450 and 2000 cm^{-1} [10], while the ionized PO_2^- group gives strong absorption bands between 1245–1200 cm^{-1} characteristic of the antisymmetric stretching and between 1070–1025 cm^{-1} of the symmetric stretching vibration of this group [21]. In the latter frequency range the ν[P—O—(Et)] absorption is superimposed upon that of the symmetric PO_2^- vibration [22]. The position and complexity of the $\nu(NH^+)$ and $\nu(PO_2^-)$ bands indicate a strong hydrogen bonding in this organophosphorus compound. In going from the free ligand to the complexes the significant differences may be noticed in the bands arising from various modes of donor groups which are involved in bonding to palladium.

In dihalopalladium complexes **1** and **2** the ligand molecule is coordinated in a molecular form through the quinoline nitrogen what was supported by missing of the $\nu(NH^+)$ absorption as well as by changes

Table 1. Analytical[a] and physical data for the palladium complexes of 2-mqmp

Complex	Colour	Melting point (°C)	Analysis (%) Pd	C	H	N	P	Halogen	Λ_M[b] (S cm^2 mol^{-1})
1 $Pd(2\text{-mqmp})_2Cl_2$	Pale yellow	292–310 dec.	15.8 (15.7)	42.6 (42.4)	3.9 (4.2)	4.5 (4.2)	9.4 (9.1)	10.1 (10.4)	19.1[c]
2 $Pd(2\text{-mqmp})_2Br_2$	Ochre	268–269	13.6 (13.8)	37.5 (37.5)	3.5 (3.7)	3.6 (3.7)	8.2 (8.1)	20.6 (20.8)	22.0[c]
3 [2-mqmp H][Pd(2-mqmp)Cl_3]	Hazel	190–200 dec.	14.9 (14.9)	40.1 (40.3)	3.9 (4.1)	3.8 (3.9)	8.8 (8.7)	14.7 (14.9)	43.5[c]
4 [2-mqmp H][Pd(2-mqmp)Br_3]	Brown	192–210 dec.	12.6 (12.5)	33.9 (33.9)	3.0 (3.4)	3.4 (3.3)	7.4 (7.3)	28.1 (28.2)	48.7, 124.0 dec.
5 [2-mqmp H]$_2$[Pd_2Br_6]	Brown	198–200	17.9 (17.8)	24.2 (24.1)	2.6 (2.5)	2.5 (2.3)	5.0 (5.2)	40.3 (40.1)	89.2, 189.2
6 $Pd(2\text{-mqmp-H})_2 \cdot 2H_2O$[d]	Pale yellow	210–211	16.9 (16.6)	45.0 (44.8)	4.8 (4.7)	4.3 (4.4)	9.9 (9.6)	—	0.5[c]

[a] Calculated values are given in parenthesis.
[b] At room temperature for 1×10^{-3} mol l^{-1} dimethylformamide, methanol solutions.
[c] Too insoluble for measurements.
[d] Water content determined by TG analysis. Found: 5.3%. Calcd for $2H_2O$ 5.6%.

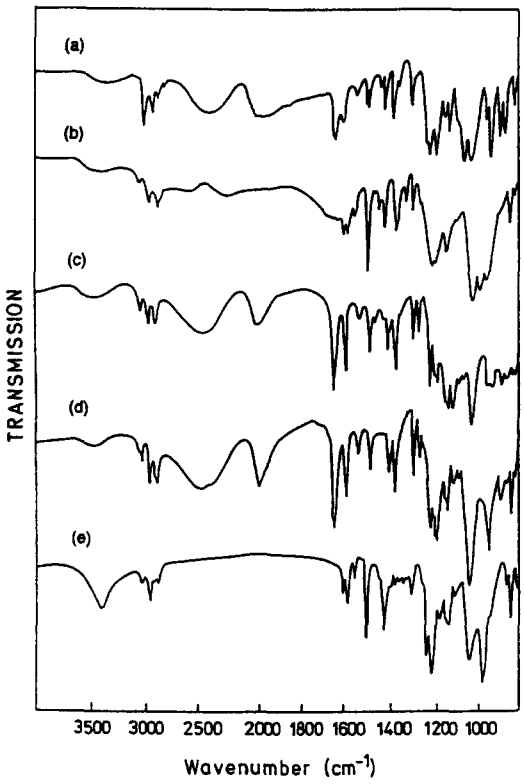

Fig. 2. The part of the infrared spectra of 2-mqmp and its complexes: (a) 2-mqmp, (b) **2**, (c) **4**, (d) **5** and (e) **6**.

noticed in the 1600–1500 cm^{-1} region where occur bands arising from the stretching modes of the C=C and C=N vibrations of the quinoline ring. These bands show a small higher frequency shift and the lowest band that appeared at 1514 cm^{-1} also marked an intensity increase with respect to the corresponding absorptions in the free 2-mqmp. Furthermore, these complexes show bands attributed to the (P)—O—H and P—O—(H) absorptions. There is no evidence of band at about 3500 cm^{-1} normally ascribed to the OH stretching because of the very strong hydrogen bonding between the P—O—H and the P=O group. There are instead three typical broad shallow bands in the 2800–1600 cm^{-1} region that are appeared to be characteristic of the P—OH group whole rather than of the OH group alone. The highest band at 2620 cm^{-1} could be assigned to an OH vibration perturbed by strong intermolecular hydrogen bonding, the second one at 2320 cm^{-1} is a combination band of the P—O—(H) stretching and O—H deformation vibrations, and the lowest band at 1660 cm^{-1} is also a combination band involving the P=O vibration. The similar bands were found for a number of various acidic phosphorus esters [21,23]. The P—O—(H) stretching vibration is superimposed on the P—O—(C) stretching vibration giving broad and complex bands around 1000 cm^{-1}. The ligand bands attributed to the ν[C—O—(P)] and ν[P—C] vibrations between 1160–1140 cm^{-1} and at 774 cm^{-1}, respectively, remain almost at the same position as in the free ligand.

The ionic complexes **3**, **4** and **5** similarly as the uncoordinated ligand show three characteristic bands for the protonated quinoline $\nu(NH^+)$ vibration. Because of the weaker hydrogen bonding in complexes than in the free ligand, these bands are displayed in spectra of complexes at higher frequencies. The presence of both the bonded and the non-bonded phosphonate acid group in complexes **3** and **4** gives rise to considerably complicated spectra in the region of

Table 2. Selected infrared spectroscopic data for 2-mqmp and its palladium(II) complexes (cm^{-1})[a]

Compound	ν(OH)[b]	$\nu(NH^+)$	ν[(P)—O—H]	ν(C=C) ν(C=N)	ν(P=O) $\nu_{as}(PO_2^-)$	ν(C—O—(P))	ν(P—O—(C)) $\nu_{sym}(PO_2^-)$ ν(P—O—(H))	ν(P—C)	ν(Pd—O)	ν(Pd—X)[c]	ν(Pd—N)
2-mqmp	—	2450 m, vbr 2000 m, vbr 1652 m–s	—	1615 w–m 1608 w–m 1553 w 1507 w	1245 m–s 1230 s 1200 s	1160 w–m 1142 m	1068 s 1042 s 1028 s	774 s	—	—	—
1	—	—	2620 w, vbr 2320 w, vbr 1660 w, vbr	1620 w–m 1602 w–m 1568 w 1514 s	1228 m 1210 m	1161 m 1140 w	1038 vs 1002 vs 972 s	774 s	—	358 m	272 w
2	—	—	2620 w, br 2320 w, br 1660 w, br	1620 w–m 1602 w–m 1568 w 1514 s	1229 s 1218 sh	1164 m	1039 vs 1002 vs 971 s	774 m–s	—	316 w	271 w
3	—	2560 w–m, vbr 2020 w–m, br 1660 s	—	1607 m 1552 w 1498 w–m	1240 s 1212 s 1185 s	1154 s 1130 s	1042 vs 980 m–s 956 s, br	769 s 763 s	409 w–m	310 sh 338 m 280 sh 220 w	—
4	—	2530 w–m, vbr 2020 w–m, br 1660 s	—	1607 m–s 1548 w 1500 m	1240 s 1214 s 1206 s	1151 s 1128 s	1042 vs 970 m–s 945 s, br	769 s 763 s	376 w–m	320 vw 259 w	—
5	—	2500 w–m, br 2008 w–m, br 1660 s	—	1607 m 1552 w 1502 w–m	1238 m–s 1218 s 1207 s	1164 m 1152 m	1050 vs, br 965 s	779 s	—	252 w	—
6	3420 m, br	—	—	1620 w–m 1598 m 1513 s	1230 vs 1218 vs	1151 s 1128 s	1052 s 998 vs	760 s	385 w	—	272 w, br

[a] Abbreviations: vs = very strong, s = strong, m = medium, w = weak, vbr = very broad, br = broad, sh = shoulder.
[b] From H_2O.
[c] X = Cl, Br.

1250–950 cm^{-1}, so the proposed assignments must be regarded as approximate description of the vibrations.

The spectrum of complex **6** is much simpler with respect to spectra of the other complexes. There is no evidence of the NH^+ and P—O—H bands what is consistent with the assumption that 2-mqmp in this complex is deprotonated and that acts as chelate ligand in the anionic form. This is confirmed by the characteristic changes in the stretching vibrations of the quinoline-ring caused by coordination of the quinoline nitrogen as well as by the presence of the $\nu(PO_2^-)$ absorption as two strong bands at 1230 and 1218 cm^{-1} for the asymmetric and a very strong band at 998 cm^{-1} for the symmetric mode of this vibration. The bands attributed to the P—O—C and P—C groups are slightly shifted to lower frequencies due to metal bonding through the deprotonated phosphonic acid group. The presence of the lattice water in this complex is indicated by the medium and very broad ν(OH) absorption around 3420 cm^{-1}.

The far-IR spectra of complexes give insight into the metal-ligand vibrations which are very useful for determining the modes of ligand coordination. Dihalide complexes PdL_2X_2 show one band for the Pd—X stretching in the expected range for terminal halides in a *trans*-square planar D_{2h} stereochemistry [24], and one band for the Pd—N stretching at about 270 cm^{-1} characteristic for the coordinated quinoline ring [10,25]. In the case of the ionic quinolinium trihalopalladium complexes the position and multiplicity of the palladium-halide stretching bands are in agreement with those obtained for complexes having the form $[Pd(Pt)LX_3^-]$, X = Cl, Br [26,27]. The C_{2v} symmetry is a reasonable approximation for this type complexes. The absorption at 409 cm^{-1} in complex **3** and that at 376 cm^{-1} in complex **4** may be attributed to ν(Pd—O) vibration. This band was found to increase in frequency with the decrease in the ionic radii of the halogen ion. The metal-oxygen bond is stronger when palladium(II) is bonded to chloride since it is more electronegative than bromide and the amount of positive charge on palladium(II) ion is greater [28]. The lower value obtained for the bromide complex also agrees with the *trans*-influence [29]. Only one ν(Pd—Br) band is found in the examined range for the hexabromodipalladium complex **5**, as the other bands for this complex containing both the terminal and bridged bromide ligands are expected to be below 200 cm^{-1} [30]. The {N,O} chelation in complex **6** of two ligand molecules in a *trans*-orientation is confirmed by the presence of one ν(Pd—O) and one ν(Pd—N) band.

Table 3. Major fragments in positive-ion mass spectra of Pd(II) complexes **1–6**[a]

Ionic species[b]	Compound *m/z* (rel. int. %)[c]					
	1	**2**	**3**	**4**	**5**	**6**
$[M+H]^+$	679 (0.5)	767 (—)	715 (—)	847 (—)	1191 (—)	607 (37)
$[(M+Na)-X]^+$	—	—	702 (1)	—	—	—
$[(M+H)-X]^+$	—	—	680 (0.5)	—	—	—
$[(M+Na)-HX]^+$	665 (2)	709 (1.5)	—	—	—	—
$[(M+H)-HX]^+$	643 (1)	—	—	—	—	—
$[(M+Na)-2X]^+$	—	—	667 (2)	—	—	—
$[(M+H)-2X]^+$	—	—	645 (3)	—	—	—
$[(M+Na)-2HX]^+$	629 (3)	629 (3)	—	—	—	—
$[(M+H)-2HX]^+$	607 (8)	607 (6)	—	—	—	—
$[(M+Na)-3X]^+$	—	—	632 (1)	—	—	—
$[(M+H)-3X]^+$	—	—	610 (2.5)	—	—	—
$[Pd(L-H)_2+H]^+$	[d]	[d]	607 (3)	607 (0.5)	6.07 (3)	[e]
$[(M+H)-PO(OEt)OH]^+$	569 (2)	657 (0.5)	—	—	—	498 (7)
$[(M+H)-(PO(OEt)OH)_2]^+$	[f]	549 (1)	—	—	—	—
$[Pd(QCH_2)_2]^+$	—	—	—	—	—	390 (6)
$[L_2+Na]^+$	525 (4)	525 (1.5)	525 (12)	525 (4)	525 (10)	—
$[L_2+H]^+$	503 (1)	503 (1.5)	503 (56)	503 (37)	503 (15)	503 (5)
$[Pd(L-H)+H]^+$	357 (7)	357 (7)	357 (10)	357 (2)	357 (7)	357 (44)
$[Pd(QCH_2PO_2OH]^+$	328 (5)	328 (20)	328 (4)	328 (1)	328 (9)	328 (10)
$[Pd(QCH_2)]^+$	248 (6)	248 (22)	248 (10)	248 (2)	248 (12)	248 (36)
$[PdQ]^+$	236 (4)	236 (6)	236 (4)	236 (2)	236 (7)	236 (11)
$[Q]_2^+$	260 (22)	260 (57)	260 (17)	260 (12)	260 (90)	260 (17)
$[L+Na]^+$	274 (66)	274 (100)	274 (63)	274 (44)	274 (95)	274 (20)
$[L+H]^+$	252 (100)	252 (86)	252 (100)	252 (100)	252 (100)	252 (100)
$[L+H-C_2H_4]^+$	224 (14)	224 (30)	224 (48)	224 (41)	224 (83)	224 (81)
$[L+H-EtOH]^+$	206 (15)	206 (26)	206 (70)	206 (50)	206 (36)	206 (75)

[a] FAB matrix 3-nitrobenzyl alcohol for complexes **1–5** and glycerol for complex **6**.
[b] X = Cl, Br; L = 2-mqmp.
[c] Ion masses referenced to isotopes ^{106}Pd, ^{35}Cl and ^{79}Br;
[d] See $[(M+H)-2HX]^+$ ion.
[e] See $[M+H]^+$ ion.
[f] Overlapped with $(3NBA+H)^+$ ion at *m/z* 460.

Mass spectra

The positive/negative fast atom bombardment mass spectrometric investigations of 2-quinolylmethylphosphonate (2-mqmp) and its palladium(II) complexes give valuable structural information of these compounds. Their fragmentation pathways including possible structures of fragment ions have been proposed on the basis of the accurate mass measurements, metastable ion studies and some high-resolution results. The fragment ions containing palladium and halide atoms are identified by the presence of the characteristic clusters of isotopic peaks corresponding to the relative abundances of the palladium and halide isotopes. The theoretical isotopic mass distributions of Pd and Pd_nX_m (X=Cl, Br; $n = 1, 2$; $m = 1$–6) clusters were also calculated to justify the ion assignments. The major structurally informative fragment ions observed in the positive-ion mode of complexes **1–6** are summarized in Table 3, while those obtained in the negative-ion mode of the ionic complexes **3–5** are given in Table 4. The *m/z* values of the mass ions are referred to ^{106}Pd, ^{35}Cl and ^{79}Br isotope-containing species. m-Nitrobenzyl alcohol (NBA) or glycerol (G) were used as matrix for recording the positive- and NBA for the negative-ion mass spectra.

The results related to decomposition behaviour of the free organophosphorus ligand provides a basis for interpreting its palladium neutral and ionic complexes. The predominant pathway for the ligand ion fragmentation is the dissociation or complete loss of the phosphonate ester group as is shown in Scheme 1. The dissociation mechanism is dominated by six-membered McLafferty-type rearrangement of the protonated molecular ion [31], which is the base peak at *m/z* 252, resulting in the protonated quinolylmethylphosphonic acid $[QCH_2P(OH)_3]^+$ at *m/z* 224.

The further loss of a water molecule yields the $[QCH_2PO(OH)]^+$ ion at *m/z* 206. The MIKE analysis of the protonated parent ligand shows that the initial

Table 4. Major ion fragments in negative-ion mass spectra of the ionic Pd(II) complexes

Ionic species[b]	Compound m/z (rel. int. %)[c] 3	4	5[d]	
$[M-H]^-$	713 (1)	845 (1)	1189 (—)	
$[(M-H)-X]^-$	678 (5)	766 (1)	—	
$[(M-H)-2X]^-$	643 (2)	687 (1.5)	—	
$[(M-H)-3X]^-$	608 (3)	608 (3)	—	
$[LPd_2X_6]^-$	—	—	935 (8)	A
$[LPd_2X_5]^-$	—	—	857 (6)	B
$[L_2PdX_3]^-$	—	—	844 (4)	C
$[Pd_2(L-H)_2]^-$	—	712 (4)	712 (22)	D
$[Pd_2X_6]^{-2}$	—	686 (2)	686 (6)	E
$[(L-H)Pd_2X_2]^-$	—	620 (3)	620 (23)	F
$[Pd_2X_5]^-$	—	607 (3)	607 (56)	G
$[Pd(L-H)_2-H]^-$	605 (2.5)	[e]	[e]	
$[LPdX_3]^-$	462 (7)	594 (2)	594 (20)	H
$[(L-H)PdX_2]^-$	426 (55)	514 (11)	514 (19)	I
$[(L-H)PdX]^-$	391 (27)	435 (2.5)	435 (11)	J
$[(L_2-H)]^-$	501 (13)	501 (5)	501 (37)	K
$[Pd_2X_4]^-$	—	528 (11)	528 (57)	L
$[Pd_2X_3]^-$	—	449 (12)	449 (55)	M
$[Pd_2X_2]^-$	—	370 (5)	370 (22)	N
$[PdX_3]^-$	211 (32)	343 (44)	343 (100)	O
$[PdX_2]^-$	176 (84)	264 (18)	264 (100)	P
$[L-H]^-$	250 (100)	250 (100)	250 (100)	R
$[(L-H)-H_2O]^-$	232 (6)	232 (16)	232 (10)	S
$[(L-H)-C_2H_4]^-$	222 (23)	222 (18)	222 (62)	T
$[(L-H)-EtOH]^-$	204 (42)	204 (12)	204 (43)	U

[a] FAB matrix 3-nitrobenzyl alcohol.
[b] X = Cl, Br, L = 2-mqmp.
[c] Ion masses referenced to isotopes ^{106}Pd, ^{35}Cl and ^{79}Br.
[d] In Fig. 5 the fragment ions are designated with the corresponding letters.
[e] Overlapped with $[Pd_2Br_5]^-$ ion.

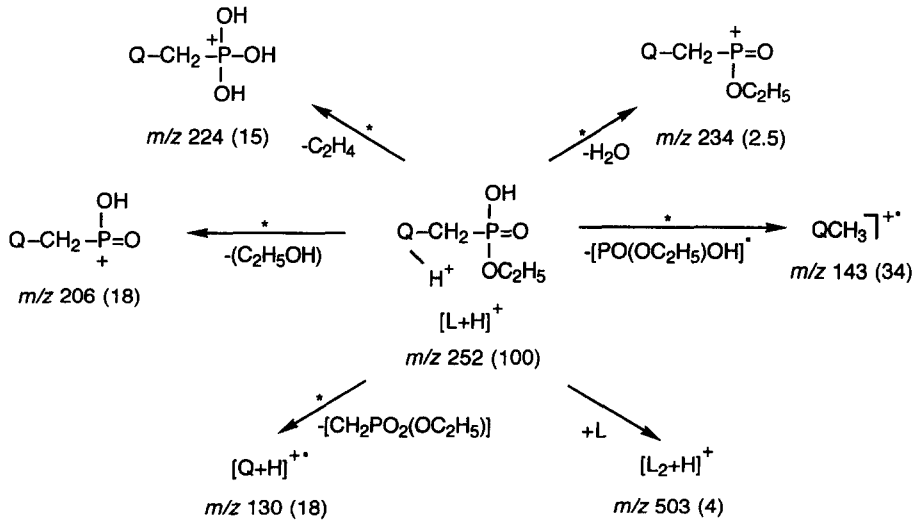

Q=quinolyl

*Verified by metastable transition

Scheme 1. FAB positive-ion fragmentation pathway for ligand 2-mqmp (L).

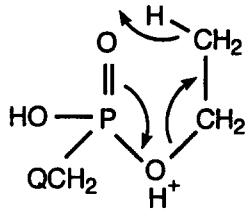

dissociation routes involve also a loss of a water molecule as well as the ethanol loss, a process often observed in mass spectrometry of the ethyl esters [32,33]. Further fragmentations include direct cleavage of the C—P and Q—C bonds giving ions at *m/z* 143 and *m/z* 130, respectively. In addition, FAB-induced dimerization of the organophosphorus ligand as well as of its quinolylmethyl fragment gives rise to ions at *m/z* 503 and *m/z* 284, respectively. In the high-mass region there are also few characteristic peaks obtained by interaction with the glycerole matrix [34]. The most abundant addition products of glycerol to ligand molecule or its fragments, ranged about 10%, are detected at *m/z* 292 $(PO_2(OEt)+2G)^+$, *m/z* 314 $(QH+2G)^+$ and *m/z* 344 $(MH+G)^+$.

In the positive-ion FAB mass study of the palladium complexes it has been found that the protonated ligand ion at *m/z* 252 represents the major fragment ion and that the other most intense fragment ions correspond to the fragments of the free non-coordinated ligand molecule. The ions based on organophosphorus or halide loss from the parent complex molecule as well as ligand exchange or addition of the matrix molecules could also be detected, which is in agreement with the FAB mass results obtained for various coordination compounds of transition metals [35–38]. The first point to be noted is that the relative abundance of the protonated molecular ion in the spectra of the halide complexes is either very small (<1% in complex **1**) or absent (in complexes **2**–**5**) and the highest mass ions in principle originate from the halide loss from the parent molecular ion. Only complex **6** exhibits the moderate intense protonated molecular ion indicating the great stability of this complex with ligand bonded in a bidentate manner forming six-membered chelate ring.

Decomposition of palladium dihalide complexes **1** and **2** goes under two fragmentation routes: those in which the parent molecular ion sequentially loses hydrogen halides and those corresponding to loss of the phosphonate ester group or its fragments. The most important fragmentation pathway is the loss of two HX molecules, which may be assumed to give rise to ion at *m/z* 607 corresponding to the protonated chelate complex **6** $[Pd(L—H)_2+H]^+$ (Scheme 2). This was supported by the presence of the identical fragmentation patterns to those obtained for complex **6** in the metastable ion studies (Fig. 3). The most important fragmentation reactions for this complex are outlined in Scheme 3. The initial decompositions are the same to those described for the free ligand related to losses of H_2O, C_2H_4, EtOH and PO(OEt)OH, respectively. The most interesting fragmentation pathways are the loss of the one or both phosphonate ester group giving mono- and dimetallated complexes at *m/z* 498 and *m/z* 390, respectively. Further fragmentation is considered to involve the loss of the whole quinolylmethylphosphonate ligand molecule accompanied by its fragmentation. The most abundant palladium containing fragment ions are those at *m/z* 357 and *m/z* 248. The former contains one bidentate N,O-bonded organophosphorus ligand, while in the latter the quinolylmethyl fragment undergoes palladation at the quinoline nitrogen and the quinolylmethyl carbon atom. The high stability of such metallated systems is in agreement with the general assumption of high stability of the cyclopalladated complexes with the nitrogen donor ligands [39,40]. Glycerine adducts are the same as in the spectrum of free ligand at *m/z* 266, 292, 314 and 344.

In the positive-ion mass spectra of all ionic complexes **3**–**5** it could be observed that the protonated ligand molecule as the intact cation is the major fragment ion and that the diagnostic fragment ions of the palladium halide complex anions are very poor. Only complex **3** contains structurally relevant fragment ions that allow also the anion characterization. Structure-specific fragment ions are formed by the successive losses of three chloride ions from the qui-

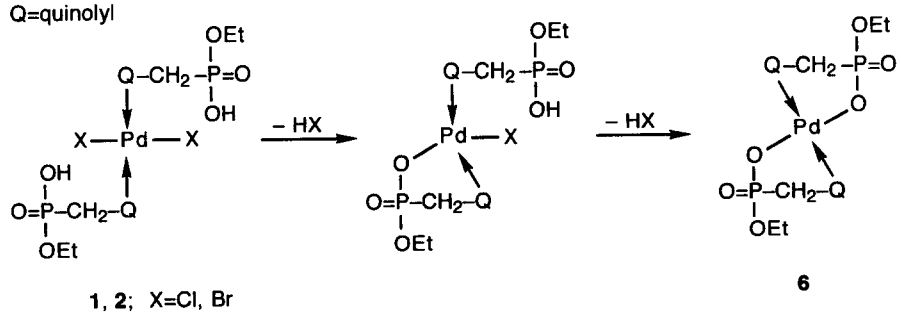

1, 2; X=Cl, Br

Scheme 2.

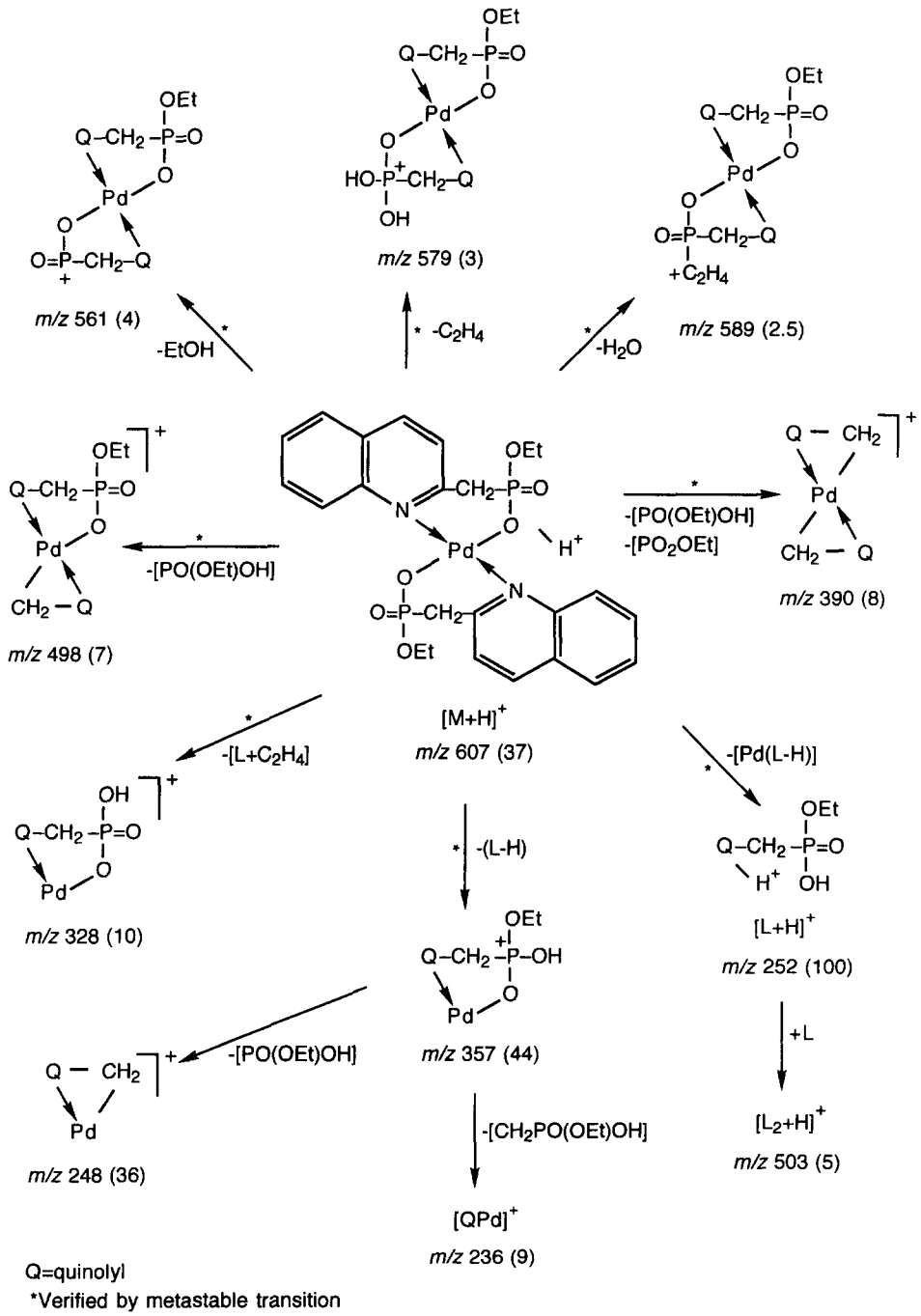

Scheme 3. FAB-induced fragmentation pathway for complex **6**.

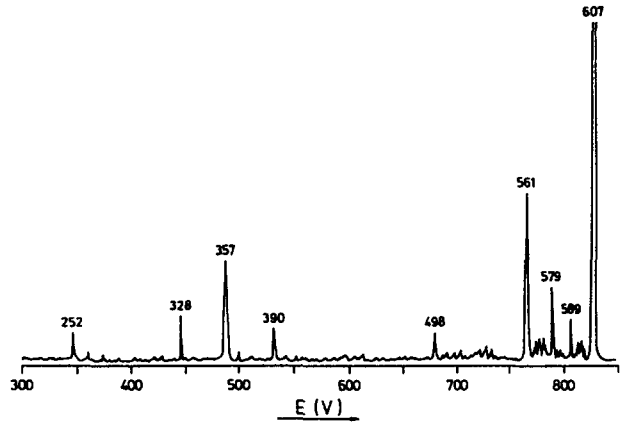

Fig. 3. MIKE spectrum of the ionic species at m/z 607 present in the FAB mass spectrum of complex **6**.

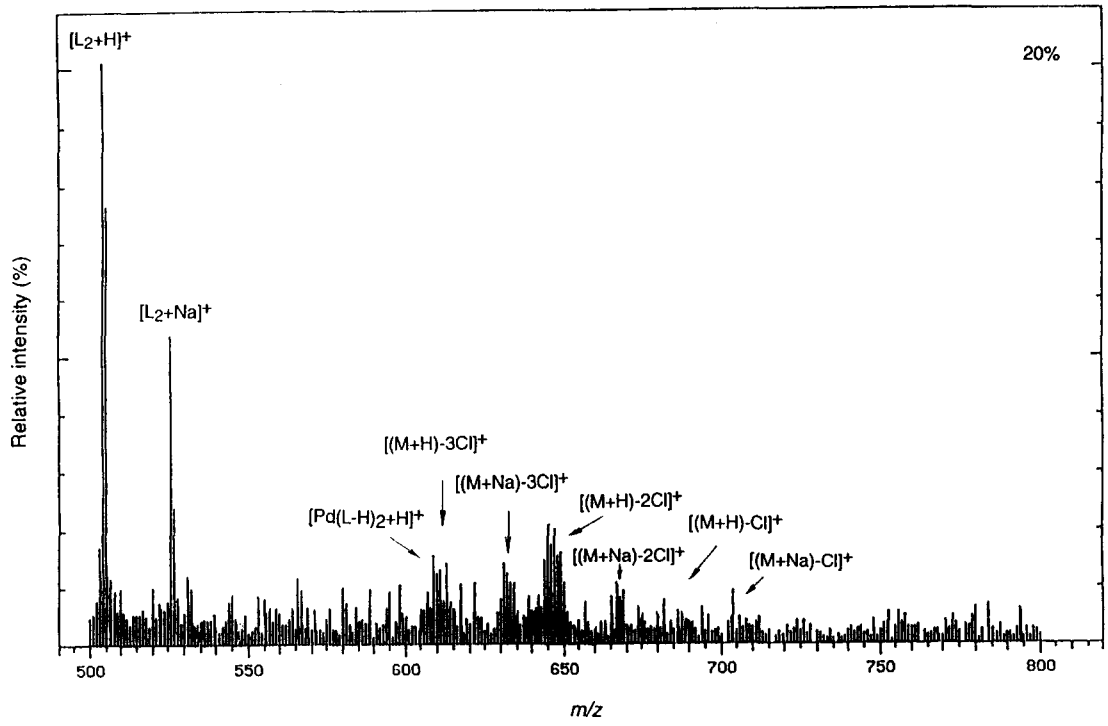

Fig. 4. The part of the positive-ion FAB mass spectrum of complex **3** with NBA as matrix.

noliniummethylphosphonatetripalladium complex, giving the small abundant fragment ions at m/z 680, m/z 645 and m/z 610, respectively, as is shown in Fig. 4. Increasing dehalogenation is evident specially in the case of bromide complexes which did not produce any palladium halide fragment ion. Predominant peaks corresponding to ions containing palladium are those with metal bonded to one or two ligand molecules or their fragments, identically as in the non-ionic complexes. It may be presumed that the very low stability of the palladium halide containing fragment ions in positive-ion mass spectroscopy in addition to high ligand abundance in the ionic source contribute to formation of these palladium adduct ions. Such reaction might occur in a matrix solution by the FAB-induced condensed phase reaction.

Mass spectra of halide complexes **1**–**5** were recorded by using matrix 3-nitrobenzyl alcohol (NBA) containing sodium chloride, which leads to more complex spectra because of incorporation of the Na^+ into some fragment ions. It is known that cations present with sample undergoing FAB perturb the distribution of desorbed molecular adduct ions [41]. Thus almost all halide containing fragments as well as ligand mono-

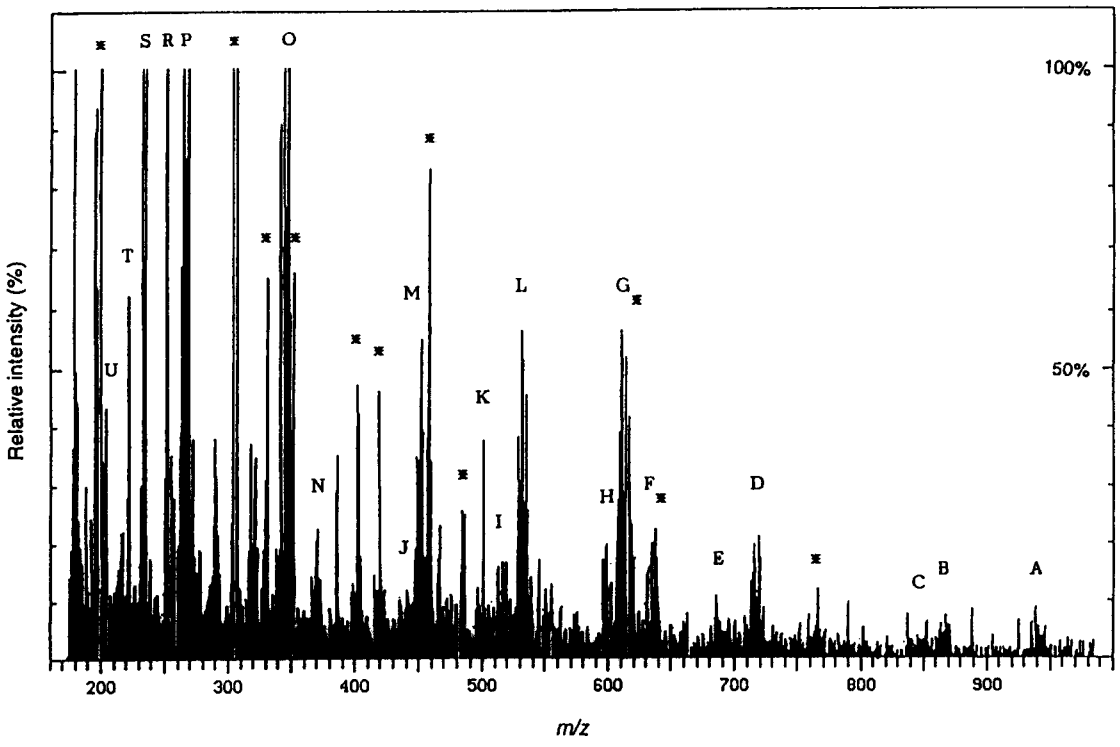

Fig. 5. Negative-ion FAB mass spectrum of complex **5** with NBA as matrix. Matrix ions are indicated by an asterix.

mer and ligand dimer molecules form sodium adduct ions as was shown in Table 3. The potential sites for binding of sodium ion are halides and phosphonate oxygen atoms. Furthermore, besides numerous matrix ions and their sodium adducts, in each spectrum there are also present adduct ions obtained by reaction with NBA matrix or its fragments (e.g. NO_2, N, O). Among them the most abundant are those at *m/z* 404 $(LH+NBA)^+$ and *m/z* 414 $(2Q+NBA+H)^+$.

In order to get more structural information of the ionic complexes **3**–**5**, especially of their anionic part, these compounds have been investigated also by spectrometric measurements carried out under negative-ion FAB conditions, Generally, in negative-ion mass spectrometry the palladium halide fragment ions are more stable and abundant than in the positive-ion mode [42]. The major fragment ions are summarized in Table 4. The initial fragmentation pathway of trihalide palladium complexes **3** and **4** is similar to that described for chloride complex **3** in the positive-ion mass study, consisting of sequential loss of three halide radicals from the deprotonated molecular ion. It should be pointed out that the most important fragment ions are those related to the intact complex anion $[PdLX_3]^-$ at *m/z* 462 and *m/z* 594, respectively, and those obtained by subtracting one and two halide radicals from these ionic species. In addition, simple palladium trihalide and dihalide adduct ions are present also in a high abundance. It is further noteworthy that bromide complex **4** shows a more complicated fragmentation pattern than its chloride analogue complex **3**. This is specially related to the presence of dipalladium bromide adduct ions $[Pd_2Br_n]^-$, $n = 2$–6, indicating that this complex is converted partly into the hexabromodipalladium complex **5** in the gas phase under FAB conditions, similarly as does also by heating in solution. The most abundant and extensive fragmentation patterns could be observed in the case of dimeric bromobridged complex **5**, where a spectrum with fragment ion assignation is presented in Fig. 5. All intense metal-containing peaks reveal multiplet structures corresponding to the relative abundances of the palladium and halide isotopes. The fragmentation pattern of the organophosphorus ligand in ionic complexes is similar to that obtained in the positive-ion mode including C_2H_4, H_2O, EtOH and PO(OEt)OH loss from the deprotonated ligand molecular ion. It could be concluded that a combination of the ion-positive/negative FAB mass spectrometry investigation gives a very useful information on either the stability of the product ions or the reactivity of the ionic species.

Acknowledgements—The financial support granted by the Ministry of Science, Technology and Informatics of the Republic of Croatia (Grant No. 009806-07) is gratefully acknowledged. The authors thank Prof. P. Traldi for valuable discussions.

REFERENCES

1. (a) Menke, G. and Walmsley, F., *Inorg. Chim. Acta*, 1976, **17,** 193; (b) Sahni, S. K., van Bennekom, R. and Reedijk, J., *Polyhedron*, 1985, **4,** 1643.
2. Appleton, T. G., Hall, J. R. and McMahon, I. J., *Inorg. Chem.*, 1986, **25,** 720.
3. (a) Radomska, B., Matczak-Jon, E. and Wojciechowski, W., *Inorg. Chim. Acta*, 1986, **124,** 83; (b) Matczak-Jon, E. and Wojciechowski, W., *Inorg. Chem. Acta*, 1990, **173,** 85.
4. Kiss, T., Balla, J., Nagy, G., Kozlowski, H. and Kowalik, K., *Inorg. Chem. Acta*, 1987, **138,** 25.
5. Ochocki, J., Kostka, K., Zurowska, B., Mrozinski, J., Galdecka, E., Galdecki, Z. and Reedijk, J., *J. Chem. Soc., Dalton. Trans.*, 1992, 2955.
6. Sawada, K., Kanda, T., Naganuma, Y. and Suzuki, T., *J. Chem. Soc., Dalton. Trans.*, 1993, 2557.
7. Horiguchi, M. and Kandatsu, M., *Nature (London)*, 1959, **184,** 901.
8. (a) Kittredge, J. S. and Hughes, R. R., *Biochemistry*, 1964, **3,** 991; (b) Kittredge, J. S. and Roberts, E., *Science*, 1969, **164,** 37.
9. Mastalerz, P., in ed. R. I. Zalewski and J. J. Skolik, *Natural Product Chemistry*, Elsevier, Amsterdam, 1984, p. 171.
10. Tušek-Božić, Lj., Matijašić, I., Bocelli, G., Calestani, G., Furlani, A., Scarcia, V. and Papaioannou, A., *J. Chem. Soc., Dalton Trans.*, 1991, 195.
11. Tušek-Božić, Lj., Matijašić, I., Bocelli, G., Sgarabotto, P., Furlani, A., Scarcia, V. and Papaioannou, A., *Inorg. Chim. Acta*, 1991, **185,** 229.
12. Ćurić, M., Tušek-Božić, Lj., Vikić-Topić, D., Scarcia, V., Furlani, A., Balzarini, J. and De Clercq, E., *J. Inorg. Biochem.*, 1996, **63,** 125.
13. (a) Tušek-Božić, Lj. and Trojko, R., *Thermochim. Acta*, 1991, **189,** 175; (b) Tušek-Božić, Lj., Matijašić, I. and Ćurić, M., *J. Mol. Struct.*, 1992, **267,** 87.
14. Jagodić, V., Božić, B., Tušek-Božić, Lj. and Herak, M. J., *J. Heterocycl. Chem.*, 1980, **17,** 1528.
15. Hartley, F. R., *The Chemistry of Platinum and Palladium*, J. Wiley and Sons, New York, 1993.
16. Cooks, R. G., Beynon, J. H., Caprioli, R. M. and Lester, G. R., *Metastable Ions*. Elsevier, Amsterdam, 1973.
17. Jagodić, V., *Croat. Chem. Acta*, 1977, **49,** 127.
18. Menke, G. and Walmsley, F., *Inorg. Chim. Acta*, 1976, **17,** 193.
19. Appleton, T. G., Hall, J. R. and McMahon, I. J., *Inorg. Chem.*, 1986, **25,** 720.
20. Galdecki, Z. and Wolf, W. M., *Acta Crystallogr., Sect. C*, 1990, **46,** 271; and refs therein.
21. Thomas, L. C., *Interpretation of the Infrared Spectra of Organophosphorus Compounds*. Plenum, New York, 1974.
22. Katcyuba, S. A., Monakhova, N. I., Ashrafullina, L. Kh. and Shagidulin, R. R., *J. Mol. Struct.*, 1992, **269,** 1.
23. Jagodić, V. and Tušek, Lj., *Croat. Chem. Acta*, 1972, **44,** 445.
24. Ferraro, J. R., *Low Frequency Vibrations of Inorganic and Coordination Compounds*. John Wiley, New York, 1971.
25. Gomez-Vaamonde, C., Alvarez-Valdes, A., Navarro-Ranninger, M. C. and Masaguer, J. R., *Transition Met. Chem.*, 1984, **9,** 52.
26. Brown, D. B., Khokhar, A. R., Hacker, M. P., McCormack, J. M. and Stalick, W. M., *Inorg. Chim. Acta*, 1982, **67,** 45.
27. Muir, M. M., Gomez, G. M., Cadiz, M. E. and Muir, J. A., *Inorg. Chim. Acta*, 1990, **168,** 47.
28. Kovala-Demertzi, D., Kyrkou, P. and Zakharoba, I., *Polyhedron*, 1991, **13,** 1507.
29. Nakamoto, K., *Infrared and Raman Spectra of Inorganic and Coordination Compounds*. John Wiley, New York, 1986.
30. Moreno-Vida, M. I., Colacio-Rodriguez, E., Moreno-Carretero, M. N. and Salas-Peregrin, J. M., *Inorg. Chim. Acta*, 1989, **157,** 201.
31. McLafferty, F. W., *Interpretation of Mass Spectra*, 3rd edn., p. 65. University Science Books, CA, 1980.
32. Caliceti, P., Veronese, F. M., Marsilio, F., Lora, S. and Traldi, P., *Org. Mass Spectrom.*, 1992, **27,** 1199.
33. Harden, C. H., Snyder, A. P. and Eiceman, G. A., *Org. Mass Spectrom.*, 1993, **28,** 585.
34. Clareboudt, J., Baeten, W., Geise, H. and Claeys, M., *Org. Mass Spectrom.*, 1993, **28,** 71.
35. (a) Bertani, R., Cecchetto, W., Polloni, R., Crociani, B., Seraglia, R. and Traldi, P., *Inorg. Chim. Acta*, 1990, **174,** 61; (b) Bertani, R., Mozzon, M., Michelin, R. A., Seraglia, R. and Traldi, P., *Org. Mass Spectrom.*, 1993, **27,** 1187.
36. Dieder, P., Jacquet, J., Kirsch-De Mesmaeker, A., Hueber, R. and van Dorsselaer, A., *Inorg. Chem.*, 1992, **31,** 4803.
37. Burrows, A., Machell, J. C., Michael, D., Mingos, P. and Powell, H. R., *J. Chem. Soc., Dalton Trans.*, 1992, 1521.
38. (a) Miller, J. M., *Mass Spectrom. Rev.*, 1989, **9,** 319; (b) Kemp, T. J., *Coord. Chem. Rev.*, 1993, **25,** 333.
39. Suton, D., *Chem. Rev.*, 1993, **193,** 995.
40. Tušek-Božić, Lj., Ćurić, M. and Traldi, P., *Inorg. Chim. Acta*, 1997, **254,** 49.
41. Mallis, M. and Russel, D. H., *Int. J. Mass Spectrom. Ion Processes*, 1987, **78,** 147.
42. Musser, S. M. and Kelley, J. A., *Org. Mass Spectrom.*, 1993, **28,** 672.

Pergamon

PII: S0277-5387(97)00412-9

Polyhedron Vol. 17, No. 9, pp. 1495–1501, 1998
© 1998 Elsevier Science Ltd
All rights reserved. Printed in Great Britain
0277-5387/98 $19.00+0.00

Crystal and molecular structure and electronic properties of $[Cu(phen)_2(HL)] \cdot (phen)_{0.5} \cdot 7H_2O$ (H_3L = 1,3,5-triazine-2,4,6(1H,3H,5H)-trione), a novel *N*-cyanurate(2-) derivative

Juan Server-Carrió,[a]* Emilio Escrivà[a] and José-Vicente Folgado[b]

[a] Departament de Química Inorgànica, Universitat de València, c/Vicent Andrés Estellés, s/n, 46100 Burjassot (València) Spain

[b] ICMUV, Universitat de València, c/ Dr. Moliner 50, 46100 Burjassot (València) Spain

(Received 21 July 1997; accepted 29 September 1997)

Abstract—The crystal and molecular structure of $[Cu(phen)_2(HL)] \cdot (phen)_{0.5} \cdot 7H_2O$ (H_3L = 1,3,5-triazine-2,4,6(1H,3H,5H)-trione) has been determined by X-ray diffraction methods. The structure is built up of neutral $[Cu(phen)_2(HL)]$ entities (which are associated to form dinuclear units through hydrogen bonds involving the cyanurate ions), uncoordinated phenanthroline and crystallisation water molecules. The copper atom is involved in a CuN_5 chromophore, with an stereochemistry near to a compressed trigonal bipyramid (TBP) but with a significant degree of distortion towards the square pyramidal (SP) topology. The EPR spectrum is indicative of a mixed $d_{z^2}/d_{x^2-y^2}$ ground state for the copper(II) ions in agreement with the structural data. No exchange coupling has been detected down to 4.2 K by means of magnetic susceptibility measurements. This feature is discussed on the basis of the bridging network. © 1998 Elsevier Science Ltd. All rights reserved

Keywords: crystal stucture; copper complexes; cyanurate; hydrogen bonds; epr spectroscopy.

A continuing effort has been focused in the last years towards the characterisation of binuclear and polynuclear transition metal complexes comprising two or more metal centres bridged by extended polyatomic ligands [1,2]. In such a context, the role played by nitrogen heterocyclic systems, both non-chelating (i.e. azines and azoles) and chelating as bridging ligands, has been recently investigated. In contrast, what occurs with azoles and the coordinating behaviour of higher azines (triazines and tetraazines) is relatively unexplored [3]. The cyanuric acid (1,3,5-triazine-2,4,6(1H,3H,5H)-trione, hereinafter H_3L), a related system, may be considered as a potential candidate to construct extended arrays involving metal centres. Therefore, the cyanurate(2-) anion could behave as a bridging ligand and simultaneously take part in stabilising interactions, such as hydrogen bonds, due to its functionality as both hydrogen-donor and acceptor [4]. By taking advantage of these features, the cyanurate(2-) ions could be used to synthesise metal complexes linked by hydrogen bonds. These types of system have been explored in the development of synthetic strategies for the construction of molecular precursor compounds [5] and ordered supramolecular aggregates [6].

In the last years, the preparation of several cyanurato complexes have been described [7–9] but only a few have been structurally characterised [4,10–13]. Therefore, the coordination behaviour of the cyanuarate anion is not sufficiently explored. In this paper we report the synthesis, crystal structure and electronic properties of a new phenanthroline-containing copper(II) cyanurate complex. As far we are aware, it is the first compound structurally characterised containing bisdeprotonated cyanuric acid as ligand.

* Author to whom correspondence should be addressed.

EXPERIMENTAL

Preparation of the complex

A solution of phenanthroline (2.2 mmol) in water–ethanol (25 ml) was added to an aqueous solution of copper(II) nitrate (1 mmol in 25 ml), then, an aqueous solution of Na_2HL (1 mmol in 20 ml) was added. The resultant blue-green solution (pH = 10.8) was left at room temperature and after two weeks prismatic blue crystals appeared, which were separated by filtration, washed and dried. Found C, 51.9; Cu 8,2; N 14.4; Calc. for $C_{33}H_{35}CuN_8O_{10}$: C, 51.6; Cu 8.3; N 14.6%.

Physical measurements

The IR spectrum (KBr pellets) was recorded on a Pye Unicam SP2000 spectrophotometer. Diffuse reflectance spectrum was obtained using a Perkin–Elmer Lambda 9 UV/VIS/IR spectrophotometer. Polycrystalline powder EPR spectra were recorded at room temperature on a Bruker ESP-300 spectrometer working at Q-band. Magnetic susceptibility measurements were carried out on polycrystalline samples with a pendulum-type apparatus equipped with a helium cryostat. The experimental susceptibilities were corrected both for the diamagnetic contributions using the Pascal constants [14] and for the temperature independent paramagnetism of the Cu(II) ion estimated to be 6×10^{-5} cm^3 mol^{-1} per copper(II) ion.

Crystal structure

A blue prismatic crystal of the title compound with approximate dimensions ($0.2 \times 0.3 \times 0.4$ mm^3) was mounted on a Enraf–Nonius CAD-4 diffractometer. Intensity data and the 25 reflections for the unit cell determination (least squares fit with $8° < \theta < 14°$) were measured at room temperature using Mo–K_α radiation with a graphite monochromator. The technique used was $\omega/2\theta$ scan, variable speed, width $(0.7 + 0.35 \tan\theta)°$ in ω, and θ limits $1° < \theta < 25°$ in the range $0 < h < 12$, $0 < k < 38$, $-12 < l < 12$. No intensity decay was detected. From the 6009 independent reflections 3319 with $I > 2\sigma(I)$ were considered to have been observed. Absorption correction was not applied.

The structure solution by direct methods with the program SIR92 [15] revealed the presence, in each asymmetric unit, of one complex unit, several water molecules and one half of non-copper-coordinated phenanthroline molecule, disordered across an inversion centre as shown in Scheme 1. C(34) and C(35) atoms were refined with occupancy factors of 0.5 and the atom pairs C(33)/N(33) and C(31)/N(31) included with 0.5 individual occupancy and linked parameters.

On the other hand, two water molecules—O(10) and O(11)— were also refined with 0.5 occupancy factors. The hydrogen atoms of the phenanthrolines were geometrically calculated and those of O(4) to O(9) water molecules and that of N(7)—from the cyanurate anion—were found in the Fourier map. We were not able to find the hydrogen atoms of the O(10) and O(11) water molecules. Once placed, all H-atoms were included in the refinement as isotropic fixed contributors with a common thermal parameter (those of C(34) and C(35) with a 0.5 occupancy factor). This chemical model—all non-hydrogen atoms with anisotropic thermal motion—was refined by least squares on F using the XRAY76 System [16] (487 parameters). In the final stages an empirical weighting scheme was chosen in order to give no trends in $\langle w\Delta^2 F \rangle$ vs $\langle F_o \rangle$

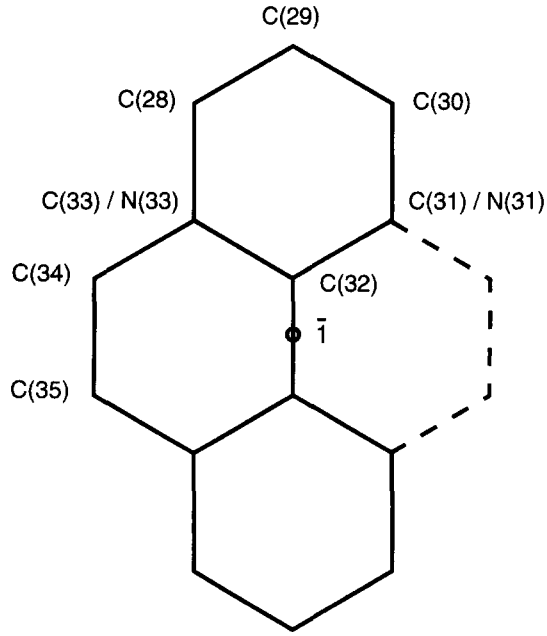

Scheme 1

Table 1. Crystal data

Chemical formula	$CuC_{33}H_{35}N_8O_{10}$
Symmetry	Monoclinic $P2_1/c$
a (Å)	10.471(1)
b (Å)	32.800(2)
c (Å)	10.504(1)
β (°)	108.29(1)
U (Å^3), Z	3425(1), 4
D_c (g cm^{-3}), M, $F(000)$	1.49, 767.3, 1592
μ (cm^{-1}), λ (Å), T (K)	7.08, 0.7107, 293
S, unit weight standard deviation	0.82
Final δF peak (e Å^{-3})	0.38
Final $R = \Sigma\|\Delta F\|/\Sigma\|F_o\|$	0.052
Final $R_w = [\Sigma w(\Delta F^2)]/[\Sigma w F_o^2]^{1/2}$	0.056

and vs $\langle \sin\theta/\lambda \rangle$ using the program PESOS [17]. Geometric calculations were made with PARST [18].

All calculations were done with a VAX6410 computer and atomic scattering factors, and anomalous dispersion corrections were taken from Ref. 19. Other relevant parameters of the crystal structure analysis are listed in Table 1.

RESULTS AND DISCUSSION

Crystal structure description

The crystal structure of the title compound is built up of neutral $[Cu(phen)_2(HL)]$ entities—which are associated to form dinuclear units through hydrogen bonds involving the cyanurate ions—uncoordinated phenanthroline molecules and molecules of water of crystallisation. Figure 1 shows a perspective view of the $[Cu(phen)_2(HL)]$ entity with the atomic numbering scheme and Fig. 2 shows a view of the unit cell contents. Selected bond distances and angles are listed in Table 2.

The structure of the molecule involves five-coordinated CuN_5 chromophores, which exhibit compressed trigonal bypiramid (TBP) coordination geometry, similar to those reported for several $[Cu(N—N)_2X]$ entities [20–22]. Such a stereochemistry for five-coordinated copper(II) systems is slightly stabilised if significant steric hindrances are present [23]. Three nitrogen atoms define the equatorial plane: one of each phenanthroline molecule—N(1) and N(3)—and the third, N(5), from the cyanurate anion. The deviation of the copper(II) ion from this plane is of ca 0.03 Å towards the N(2) atom. The angles in the equatorial plane are considerably distorted from the ideal trigonal angle of 120°, with one small angle of 99.4° between the Cu—N(phen) equatorial bonds. On the other hand, despite that the N(2) and N(4) atoms being slightly removed from the ideal axial positions (due to a small bite angle of the rigid bidentate phenanthroline ligands) none of the out-of-plane N_{ax}—Cu—N_{eq} angles can be considered as unusual ($90 \pm 10°$). The Cu—N_{ax} distances are shorter than Cu—N_{eq}(phen) which is usual for this type of system [19,20]. In the equatorial plane the two Cu—N(phen) bond distances are not significantly different (mean value of 2.130(5) Å) and larger (by ca 0.16 Å) than Cu—N(cyanurato) the latter being similar to those reported for other cyanurato-containing copper(II) complexes [10,13]. All these features clearly indicate a significant distortion in the

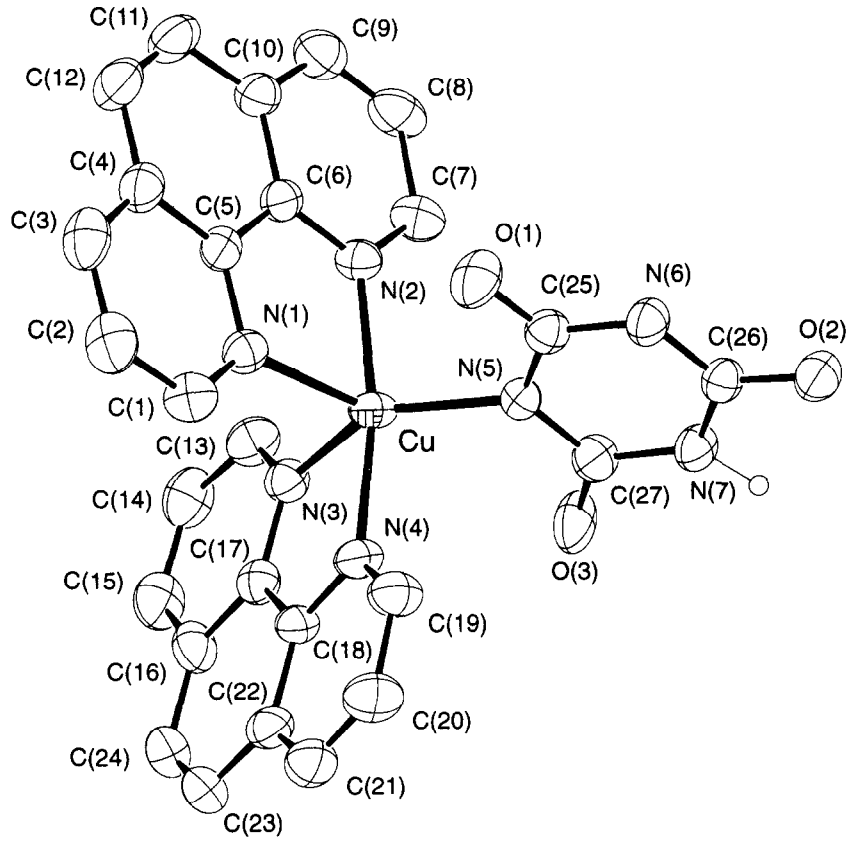

Fig. 1. View of the $[Cu(phen)_2(HL)]$ units, showing the atom labelling. For clarity, the hydrogen atoms of the phenanthroline molecules have been omitted.

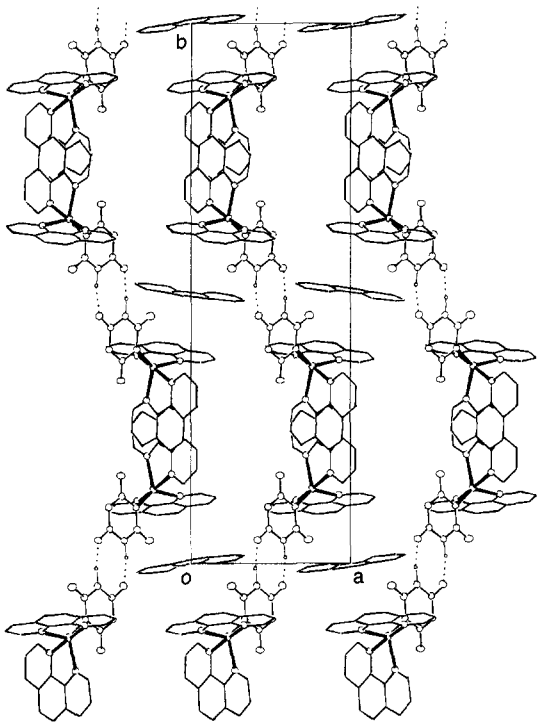

Fig. 2. Crystal packing as projected along *c* axis. Water molecules and hydrogen atoms of phenanthroline molecules have been omitted.

coordination polyhedron; we have quantified this distortion—from an ideal TBP geometry ($\Delta = 0$) towards a square pyramidal one (SP, $\Delta = 1$)—by application of the method of Muetterties and Guggemberger [24] using the analytical formula proposed by Galy [25]. The obtained value of $\Delta = 0.19$ indicates the predominance of the TBP form, but with a significant degree of distortion towards the SP topology.

Both coordinated phenanthroline molecules are essentially planar and are located nearly perpendicular to the equatorial plane (dihedral angles of 89.3 and 92.9°). On the other hand, the whole of bond distances and angles compares well with those reported for related $[Cu(phen)_2X]$ complexes [20,26].

The cyanurate ring is essentially planar and it is located nearly parallel to the equatorial plane (dihedral angle of 13.6°). The whole of angle and bond distances compares well with those reported for other cyanurato-complexes (see Table 3). As usual, the cyanurate ion coordinates through a nitrogen atom (in only a few cases has the presence of coordinated O-cyanurate ions been postulated, based on vibrational spectroscopic data [8b,8d] but no structural confirmation has been provided). The most striking feature is the low value of the δ parameter ($\delta = \Sigma|120-\alpha_i|$, being α_i the C—N—C and N—C—N angles in the C_3N_3 nucleus) compared with those calculated for other cyanurato-complexes as well as the cyanuric free molecule (see Table 3) making evident that in the title compound the ring is not greatly distorted from a regular hexagon. The all six C—N bonds are alike (see Table 2), the mean value indicating an appreciable double bond character. This mean value is similar to those observed in cyanuric acid as well as other cyanurate copper(II) compounds. On the other hand, the three C—O bond distances are also similar to those reported for related compounds and slightly longer than those in free cyanuric acid (see Table 4). With regard to the coordinating behaviour displayed by the cyanurate(2-) groups in this compound, it may be outlined that its potential functionality as a bridging ligand could be blocked by steric hindrance factors as well as by the propensity for aggregation of the cyanurate [4]. In this sense, it must be stressed that the nitrogen atom N(7) acts as protonic donor towards the oxygen atom O(2) of a centrosymmetrically related $[Cu(phen)_2(HL)]$ molecule, thus linking two complex units by means of double N—H···O interactions forming dimeric entities $[Cu(phen)_2(HL)]_2$ (intradimer Cu—Cu distance of ca 12.11 Å) which are aligned parallel to the *b* axis (see Fig. 2).

All water molecules are involved in moderate hydrogen bonds as indicated by the intermolecular O···X distances and the corresponding O—H···X angles (X = O, N) listed in Table 4. Molecules O(4), O(5), O(6) and O(9) connect two cyanurate ions of different dimeric entities forming infinite zig-zag chains along the *c* axis with a Cu—Cu distance of 9.13 Å. Finally, the free phenanthroline molecules are located along the *b* axis (see Fig. 2) stacked between two coordinated ones belonging to adjacent dimeric entities related by an inversion centre.

Vibrational and electronic spectra

The vibrational spectrum of $[Cu(phen)_2(HL)]\cdot(phen)_{0.5}\cdot 7H_2O$ shows several bands in the 4000–2000 cm^{-1} region, varying from 3600 to 2800 cm^{-1} assigned to stretching of the NH groups and water molecules implied in hydrogen bonds. In the 1700–400 cm^{-1} there are several bands from phenanthroline molecules and cyanurate anions. Despite its complexity, in comparing the spectra reported for several cyanurate derivatives [8–10], some absorptions were tentatively assigned. So, the set of bands observed between 1740 and 1600 cm^{-1} are assigned to ν(C=O) and ν(C=N) vibrations, the higher wavenumber corresponding to those of ν(C=O). On the other hand, the doublet observed at ca 420 cm^{-1} is tentatively attributed to the Cu—N stretching vibrations [10].

The electronic reflectance spectrum of the studied compound exhibits a broad absorption band centred at ca 14,500 cm^{-1} with a shoulder at ca 13,000 cm^{-1}. These features are in good agreement with the stereochemistry observed around the copper(II) ions [28]. If the non-equivalence of the bond lengths in the CuN_5 chromophores is neglected, the point group symmetry

Table 2. Selected bond lengths (Å) and angles (°)

Copper coordination sphere			
Cu—N(1)	2.152(4)	Cu—N(4)	2.002(4)
Cu—N(2)	2.005(4)	Cu—N(5)	1.969(5)
Cu—N(3)	2.125(5)		
N(1)—Cu—N(2)	80.4(2)	N(2)—Cu—N(4)	169.5(2)
N(1)—Cu—N(3)	99.4(2)	N(2)—Cu—N(5)	96.4(2)
N(1)—Cu—N(4)	92.4(2)	N(3)—Cu—N(4)	80.4(2)
N(1)—Cu—N(5)	125.0(2)	N(3)—Cu—N(5)	135.5(2)
N(2)—Cu—N(3)	93.2(2)	N(4)—Cu—N(5)	93.9(2)
Cianurate anion			
O(1)—C(25)	1.240(7)	N(6)—C(25)	1.359(9)
O(2)—C(26)	1.253(8)	N(6)—C(26)	1.333(9)
O(3)—C(27)	1.239(9)	N(7)—C(26)	1.381(8)
N(5)—C(25)	1.377(8)	N(7)—C(27)	1.369(9)
N(5)—C(27)	1.348(7)		
C(25)—N(5)—C(27)	120.0(5)	O(2)—C(26)—N(6)	123.4(5)
C(25)—N(6)—C(26)	119.4(5)	O(2)—C(26)—N(7)	117.3(5)
C(26)—N(7)—C(27)	122.0(5)	N(6)—C(26)—N(7)	119.3(5)
O(1)—C(25)—N(5)	117.8(5)	O(3)—C(27)—N(5)	122.7(6)
O(1)—C(25)—N(6)	120.8(5)	O(3)—C(27)—N(7)	119.5(6)
N(5)—C(25)—N(6)	121.4(5)	N(5)—C(27)—N(7)	117.9(5)

Table 3. Mean bond lengths and angles for the cyanurate group in several systems

Compound	C—N (Å)	C—O (Å)	N—C—N (°)	C—N—C (°)	δ (°)	Reference
H_3L	1.37±0.00	1.22±0.00	115±0	125±0	30.0	27
$[Cu(NH_3)_2(H_2L)_2]$	1.41±0.03	1.29±0.04	119±11	120±11	59.1	13
$Na_2[Cu(H_2L)_2(H_2O)_2]\cdot(H_2L)_2\cdot 4H_2O$						10
H_2L^- coordinated	1.36±0.02	1.23±0.02	117±3	124±3	21.0	
H_2L^- uncoordinated	1.36±0.01	1.24±0.02	118±4	122±4	19.0	
$[M(H_2L)(H_2O)_5]\cdot H_2L\cdot 2H_2O$						4
H_2L^- coordinated	1.37±0.02	1.23±0.01	116±3	123±3	22.4	
H_2L^- uncoordinated	1.36±0.01	1.23±0.01	117±3	123±2	16.7	
$[Cu(phen)_2(HL)]\cdot(phen)_{0.5}\cdot 7H_2O$	1.37±0.01	1.24±0.01	120±2	120±1	8.4	This work

Table 4. Hydrogen bonds in the $[Cu(phen)_2(HL)]\cdot(phen)_{0.5}\cdot 7(H_2O)$ crystal

X—H···Y (Å)	X—H (Å)	X···Y (Å)	H···Y (Å)	< X—H···Y (°)
O(4)—H(401)···O(1)	1.14	2.70(1)	1.59	160
O(4)—H(402)···O(5)	1.03	2.90(1)	1.89	163
O(5)—H(501)···O(6)	0.98	2.82(1)	1.83	173
O(6)—H(601)···O(9)	0.94	2.82(1)	2.01	143
O(7)—H(701)···O(5)	0.91	2.80(1)	1.91	171
O(8)—H(801)···O(7)	1.05	2.91(1)	1.95	151
O(9)—H(902)···O(10)	1.06	3.01(1)	2.00	162
O(6)—H(602)···N(6^{I})	0.68	2.79(1)	2.23	141
O(9)—H(901)···O(2^{I})	1.06	2.83(1)	1.79	169
N(7)—H(70)···O(2^{II})	1.04	2.84(1)	1.81	168

Symmetry operators: I $x, -y+1/2, z-1/2$; II $-x+1, -y, -z+1$.

of the coordination polyhedron is close to C_{2v}, with the shorter Cu—N bond defining the direction of the two-fold axis. Taking into account these considerations, it may be assumed that the *d–d* band structure arises from the overlap of the

$$^2B_2(d_{xy}) \rightarrow {}^2A_1(d_{z^2}/d_{x^2-y^2}),$$
$$^2A_2(d_{yz}) \rightarrow {}^2A_1(d_{z^2}/d_{x^2-y^2})$$
and
$$^2B_1(d_{xz}) \rightarrow {}^2A_1(d_{z^2}/d_{x^2-y^2})$$

transitions. In addition to the *d–d* band structure, the spectrum displays one more intense band centred at ca 22,500 cm^{-1}, assignable to metal ligand ($e_g \rightarrow \pi^*$) transitions [29].

EPR spectroscopy and magnetic behaviour

The room-temperature X-band EPR powder spectrum of the title compound shows wide features corresponding to orthorhombic symmetry with no possibility of extracting accurate g values. Hyperfine coupling is observed in the low field part of the spectrum with a line separation of 118 G. However, a clear signal corresponding to $\Delta Ms = \pm 2$ (at about 1600 G) is observed with increasing the gain of the spectrometer, indicating some degree of interaction between the different chromophores. In the Q-band spectrum three signals are clearly defined giving g values of 2.017, 2.125 and 2.235 ($g_{av} = 2.125$). Again, hyperfine coupling is well resolved on the largest g value giving $A = 124 \cdot 10^{-4}$ cm^{-1}. These values are very similar to those found in the complexes Cu(terpy)X_2 (X = Br, I, NCS) [30]—which contain pentacoordinate CuN_3X_2 chromophores having a coordination geometry close to C_{2v}—and $[Cu(bipy)_2(NH_3)](BF_4)_2$ (with CuN_5 chromophores intermediate between the ideal square pyramidal, C_{4v}, and trigonal bipyramidal, D_{3h}) [28]. As discussed above, in our compound the local symmetry is nearly C_{2v}. Following the vibrational model proposed by Reinen [23], the ground-state wave function of a five-coordinated copper(II) complex can be expressed as follows:

$$\varphi_g = (1+c^2)^{-1/2}[d_{z^2} + cd_{x^2-y^2}]$$

The mixing coefficient c is zero for the trigonal bipyramid (d_{z^2} ground state) and is $1/\sqrt{3}$ for the square pyramid ($d_{z^2-y^2}$ ground state). The corresponding expressions for the g values are:

$$g_z = g_o + 8[c^2/(1+c^2)]u_z$$
$$g_y = g_o + 2[c^2/(1+c^2)][1-\sqrt{3}/c]^2 u_y$$
$$g_x = g_o + 2[c^2/(1+c^2)][1+\sqrt{3}/c]^2 u_x$$

where u_i is the orbital contribution. Taking u_i as 0.032 ($g_{av} = g_o + 4u_i$), the experimental g values can be sufficiently reproduced with c values of 0.33 ± 0.03, and very close to that of 1/3 expected for an actual C_{2v} geometry, thus implying a ground state for the Cu(II) ions between d_{z^2} (TBP) and $d_{x^2-y^2}$ (SP). Hence, there is a full agreement between the structural and spectroscopic results. Moreover, from the well-resolved hyperfine coupling in the g_z component, we can estimate the mixing coefficient of the copper(II) ground state function in the whole molecular orbital containing the unpaired electron, by application of well known equations relating the MO and EPR parameters [31]. A value of 0.80 results, which is similar to that observed for other Cu—N bonded complexes indicating an important amount of covalency.

The magnetic study of the title compound shows that in the temperature range (4.2–300 K) the $\chi_M T$ product is nearly constant and the whole susceptibility data can be fitted to the Curie–Weiss expression $\chi_M = C/(T-\theta)$ affording $C = 0.429$ cm^3 mol^{-1} ($g = 2.14$) and $\theta = +0.35$ K. The small absolute value of the Weiss correction could suggest a very weak ferromagnetic interaction between the copper(II) ions. Notwithstanding, this interaction if present, could only be detected unambiguously at very low temperatures. Therefore, this result indicates that the copper(II) ions may be viewed as essentially magnetically non-coupled. In all cases, very small values of $|J|$ would be expected due the large exchange distance (both the intradimer and interdimer pathways). According to the limit function proposed by Coffman and Buetter [32] for long-range exchange interactions, $|J|$ values less than 10^{-2}–10^{-3} cm^{-1} would be expected for the title compound.

Acknowledgements—We thank Drs F. Lloret and L. Lezama for their assistance with susceptibility measurements and Q-band EPR experiences, respectively. We also thank Dr M. Martínez-Ripoll and the U.E. de Cristalografía at the Instituto Rocasolano (CSIC, Madrid) for providing access to computing facilities in the crystal structure determination.

REFERENCES

1. Hendrickson, D., in *Magneto-Structural Correlations in Exchange Coupled Systems*, D. Reidel, Dordrecht, The Netherlands, 1985, p. 523.
2. Petersen, J. D., Murphy, W. R., Sahai, R., Brewer, K. J. and Ruminski, R. R., *Coord. Chem. Rev.*, 1985, **64,** 261.
3. Steel, P. J., *Coord. Chem. Rev.*, 1990, **109,** 227.
4. Falvello, L. R., Pascual, I. and Tomás, M., *Inorg. Chim. Acta*, 1995, **229,** 135.
5. Breeze, S. R. and Wang, S., *Inorg. Chem.*, 1993, **32,** 5981.
6. Lehn, J. M., *Angew. Chem., Int. Ed. Engl.*, 1990, **29,** 1304 and references therein.
7. Taylor, R. M., *Z. Anorg. Allg. Chem.*, 1972, **390,** 85.
8. (a) Seifer, G. B., Chumaevskii, N. A., Minaeva, N. A. and Tarasova, Z. A., *Russ. J. Inorg. Chem.*, 1986, **31,** 791; (b) Seifer, G. B., Minaeva, N. A. and Tarasova, Z. A., *Russ. J. Inorg. Chem.*, 1987, **32,** 169; (c) Seifer, G. B., Chumaevskii, N. A., Minaeva, N. A. and Tarasova, Z. A., *Russ. J.*

Inorg. Chem., 1988, **33,** 1464; (d) Seifer, G. B., Chumaevskii, N. A., Minaeva, N. A. and Tarasova, Z. A., *Russ. J. Inorg. Chem.*, 1990, **35,** 1437; (e) Seifer, G. B. and Tarasova, Z. A., *Russ. J. Inorg. Chem.*, 1991, **36,** 957; (f) Seifer, G. B. and Tarasova, Z. A., *Russ. J. Inorg. Chem.*, 1995, **40,** 1303.

9. Gurevich, M. Z., Branzburg, M. Z. and Dyatlova, N. M., *Russ. J. Inorg. Chem.*, 1982, **27,** 398.
10. Slade, P. G., Raupach, M. and Radoslovich, E. W., *Acta Cryst.*, 1973, **B29,** 279.
11. Agre, V. M., Syosoeva, T. F., Trunov, V. K., Gurevich, M. Z. and Branzburg, M. Z., *Koord. Khim.*, 1986, **12,** 122.
12. Syosoeva, T. F., Starikova, Z. A., Gurevich, M. Z. and Branzburg, M. Z., *Koord. Khim.*, 1991, **17,** 17.
13. Hart, R. D., Skelton, B. and White, A. H., *Aust. J. Chem.*, 1992, **45,** 1927.
14. Kahn, O., *Molecular Magnetism*, VCH Publishers Ic., New York, 1993, p. 3.
15. Altomare, A., Burla, M. C., Camalli, M., Cascarano, G., Giacovazzo, G., Guagliardi, A. and Polidori, G., *J. Appl. Crystallogr.*, 1994, **27,** 435.
16. Stewart, J. M., Machin, P. A., Dickinson, C. W., Ammon, H. L., Heck, H. and Flack, H., *The X-RAY 76 System*, Technical Report TR-446, Computer Science Center, University of Maryland, College Park, Maryland, 1976.
17. Martínez-Ripoll, M. and Cano, F. H., *PESOS Computer Program*, Instituto Rocasolano, C.S.I.C., Madrid, Spain, 1975.
18. Nardelli, M., *Comput. Chem.*, 1983, **7,** 95.
19. *International Tables for X-Ray Crystallography*, Vol. 4, Kynoch Press, Birmingham, U.K., 1974, p. 71–79, 149.
20. Anderson, O. P., *Inorg. Chem.*, 1975, **14,** 730.
21. Carugo, O. and Castellani, C. B., *J. Chem. Soc., Dalton Trans.*, 1990, 2985 and references therein.
22. García-Lozano, J., Server-Carrió, J., Escrivà, E., Folgado, J. V., Molla, C. and Lezama, L., *Polyhedron*, 1997, **16,** 939.
23. Reinen, D. and Atanasov, M., *Chem. Phys.*, 1989, **136,** 27.
24. Muetterties, E. L. and Guggemberger, L. J., *J. Am. Chem. Soc.*, 1974, **96,** 1748.
25. Galy, J., Bonnet, J. J. and Anderson, S., *Acta Chem. Scand.*, 1979, **A33,** 383.
26. Fitgerald, W. and. Hathaway, B. J., *Acta Crystallogr.*, 1984, **C40,** 243 and references therein.
27. Verschoor, G. C. and Keulen, E., *Acta Crystallogr.*, 1971, **B27,** 134.
28. Tyagi, S., Hathaway, B. J., Kremer, S., Stratemeier, H. and Reinen, D., *J. Chem. Soc., Dalton Trans.*, 1984, 2087 and references therein.
29. Lever, A. B. P., *J. Chem. Ed.*, 1974, **51,** 612.
30. (a) Arriortua, M. I., Mesa, J. L., Rojo, T., Debaermaeker, T., Beltrán, D., Stratemeier, H. and Reinen, D., *Inorg. Chem.*, 1988, **27,** 2976; (b) Kutoglu, A., Allmann, R., Folgado, J. V., Atanasov, M. and Reinen, D., *Z. Naturforsch.*, 1991, **46b,** 1193.
31. Mabbs, F. E. and Collison, D., *Electron Paramagnetic Resonance of d Transition Metal Compounds*, Elsevier, Amsterdam, 1992.
32. Coffman, R. E. and Buettner, G. R., *J. Chem. Phys.*, 1979, **83,** 2387.

Pergamon

PII: S0277-5387(97)00411-7

Polyhedron Vol. 17, No. 9, pp. 1503–1509, 1998
© 1998 Elsevier Science Ltd
All rights reserved. Printed in Great Britain
0277–5387/98 $19.00+0.00

New aliphatic and aromatic thiolato-bridged complexes of palladium(II) and platinum(II)

José Ruiz, Consuelo Vicente, Venancio Rodríguez and Gregorio López*

Departamento de Química Inorgánica, Universidad de Murcia, 30071 Murcia, Spain

(Received 4 June 1997; accepted 29 September 1997)

Abstract—The hydroxo binuclear complexes $[NBu_4]_2[\{M(C_6F_5)_2(\mu\text{-}OH)\}_2]$ (M = Pd or Pt) react with thiols in methanol at room temperature to give the binuclear di-μ-thiolato complexes $[NBu_4]_2[\{M(C_6F_5)_2(\mu\text{-}SR)\}_2]$ (M = Pd, R = Et **1**, t-Bu **2**, C_6H_5 **3**, and *p*-MeC_6H_4 **4**; M = Pt, R = Et **5**, t-Bu **6**, C_6H_5 **7** or *p*-MeC_6H_4 **8**). The trinuclear palladium complexes $[NBu_4]_2[(C_6F_5)_2Pd(\mu\text{-}SEt)_2Pd(\mu\text{-}SEt)_2Pd(C_6F_5)_2]$ **9** or $[NBu_4]_2[(C_6F_5)_2Pd(\mu\text{-}1,2\text{-}S_2C_6H_4)Pd(\mu\text{-}1,2\text{-}S_2C_6H_4)Pd(C_6F_5)_2]$ **10** have been obtained by reaction of the binuclear hydroxo palladium complex $[NBu_4]_2[\{Pd(C_6F_5)_2(\mu\text{-}OH)\}_2]$ with an excess of EtSH in refluxing methanol or with an excess of $C_6H_4(SH)_2$-1,2 in methanol at room temperature, respectively. The mixed hydroxo-azolate bridged complexes $[\{M(C_6F_5)_2\}_2(\mu\text{-}OH)(\mu\text{-}L)]^{2-}$ [M = Pd, L = pyrazolate (pz); M = Pt, L = pyrazolate (pz) or 3,5-dimethylpyrazolate (dmpz)] react with thiols (1:1 molar ratio) in methanol to give the corresponding mixed thiolato-azolate bridged palladium or platinum complexes $[\{M(C_6F_5)_2\}_2(\mu\text{-}SR)(\mu\text{-}L)]^{2-}$ (M = Pd, L = dmpz, R = C_6H_5 **11**, *p*-MeC_6H_4 **12**; M = Pt, L = pz, R = C_6H_5 **13**, *p*-MeC_6H_4 **14**, Et **15**, t-Bu **16**; L = dmpz, R = C_6H_5 **17**, R = *p*-MeC_6H_4 **18**, Et **19**]. The complexes have been characterized by partial elemental analyses, conductance measurements and spectroscopic (IR and ^1H and ^{19}F NMR) methods. © 1998 Elsevier Science Ltd. All rights reserved

Keywords: palladium; platinum; thiolate complexes.

There has been recent interest in platinum and palladium μ-thiolato complexes due to their possible use in homogeneous catalysis [1–4]. Thus, for example, the systems of the type $[Pt_2(\mu\text{-}SR)(\mu\text{-}Cl)Cl_2(PR'_3)_2]/SnCl_2\cdot 2H_2O$ have a high catalytic activity in the hydrogenation of styrene [5].

We have reported on the synthesis of $[NBu_4]_2[\{M(C_6F_5)_2(\mu\text{-}OR)\}_2]$ (M = Ni, Pd and Pt; R = H, Me or Ph) and we have used them as precursors in synthetic work, based on the considerable nucleophility of the bridging OR groups [6–10]. Thus the hydroxo complexes react with protic acids HL to give mono- or bi-nuclear complexes [6–13] depending on the chelating or bridging nature of the L^- ligand. We report here the reactions of $[NBu_4]_2[\{M(C_6F_5)_2(\mu\text{-}OH)\}_2]$ (M = Pd or Pt) and $[NBu_4]_2[\{M(C_6F_5)_2\}_2(\mu\text{-}OH)(\mu\text{-}L)]$ (L = pyrazolate-type ligand) with aliphatic and aromatic thiols RSH. The synthesis of the related bi- and tri-nuclear nickel(II) complexes have been reported recently [14].

* Author to whom correspondence should be addressed.

EXPERIMENTAL

The C, H, N, S analyses were performed with a Carlo Erba model EA 1108 microanalyzer. Decomposition temperatures were determined with a Mettler TG-50 thermobalance at a heating rate of 5°C min^{-1} and the solid samples under nitrogen flow (100 ml min^{-1}). The NMR spectra were recorded on a Bruker AC 200E or Varian Unity 300 spectrometer. Infrared spectra were recorded on a Perkin–Elmer 16F PC FT-IR spectrophotometer using Nujol mulls between polyethylene sheets. Conductance measurements were performed with a Crison 525 conductimeter (solvent acetone; $c \approx 5\times10^{-4}$ mol l^{-1}). Solvents were dried by the usual methods. The precursors $[\{MC_6F_5)_2(\mu\text{-}OH)\}_2]^{2-}$ and $[\{M(C_6F_5)_2\}_2(\mu\text{-}OH)(\mu\text{-}L)]^{2-}$ (M = Pd or Pt; L = pz or dmpz) were prepared by procedures described elsewhere [6,8,9].

Preparation of the complexes

Complexes **1–4**. The appropriate thiol RSH (0.143 mmol) was added to a solution of $[NBu_4]_2$

$[\{Pd(C_6F_5)_2(\mu\text{-}OH)\}_2]$ (0.10 g, 0.071 mmol) in methanol (10 cm^3). The resulting solution was stirred at room temperature for 1 h and then concentrated under reduced pressure. Addition of water caused the precipitation of the title complexes as yellow solids, which were filtered off and air-dried.

Complexes **5–7**. The corresponding thiol RSH (0.127 mmol) was added to a solution of $[NBu_4]_2[\{Pt(C_6F_5)_2(\mu\text{-}OH)\}_2]$ (0.0635 mmol) in methanol (10 cm^3). The solution was boiled under reflux for 7 h and then concentrated under reduced pressure. Addition of water caused the precipitation of the complexes as yellow solids, which were filtered off and air-dried.

Complex **8**. *p*-MeC_6H_4SH (0.127 mmol) was added to a solution of $[NBu_4]_2[\{Pt(C_6F_5)_2(\mu\text{-}OH)\}_2]$ (0.0635 mmol) in benzene (8 cm^3). The solution was boiled under reflux for 7 h and then concentrated under reduced pressure. Addition of hexane caused the precipitation of complex **8** as a yellow solid which was filtered off and air-dried.

Complex **9**. EtSH (0.571 mmol) was added to a solution of $[NBu_4]_2[\{Pd(C_6F_5)_2(\mu\text{-}OH)\}_2]$ (0.10 g, 0.071 mmol) in methanol (12 cm^3). The solution was boiled under reflux for 6 h, whereupon the yellow complex **9** precipitated. It was collected by filtration and air-dried.

Complex **10**. To a solution of $[NBu_4]_2[\{Pd(C_6F_5)_2(\mu\text{-}OH)\}_2]$ (0.10 g, 0.071 mmol) in methanol (12 cm^3) was added $C_6H_4(SH)_2$-1,2 (0.286 mmol). The resulting deep yellow solution was stirred at room temperature for 1.5 h, whereupon the yellow complex **10** precipitated. The complex was collected by filtration and air-dried.

Complexes **11** *and* **12**. The appropriate thiol RSH (0.067 mmol) was added to a solution of $[NBu_4]_2[\{(C_6F_5)_2Pd\}_2(\mu\text{-}OH)(\mu\text{-dmpz})]$ (0.067 mmol) in methanol (6 cm^3). The resulting solution was stirred at room temperature for 1 h, during which time the white binuclear complexes precipitated spontaneously, and then the solvent was partly evaporated under reduced pressure. The complexes were collected by filtration and air-dried.

Complexes **13–19**. The corresponding thiol RSH (0.060 mmol) was added to a solution of $[NBu_4]_2[\{(C_6F_5)_2Pt\}_2(\mu\text{-}OH)(\mu\text{-L})]$ (L = pz or dmpz) (0.060 mmol) in methanol (8 cm^3). The solution was boiled under reflux for 7 h and then concentrated under reduced pressure until complexes **13, 14, 17** or **18** precipitated as white solids, which were filtered off and air-dried. For complexes **15, 16** and **19**, the resulting solutions were vacuum-evaporated to dryness and the residues treated with isopropanol. The complexes were collected by filtration and air-dried.

RESULTS AND DISCUSSION

The reactions of the hydroxo-complexes $[NBu_4]_2[\{M(C_6F_5)_2(\mu\text{-}OH)\}_2]$ (M = Pd and Pt) with thiols RSH in methanol at room temperature in the 1 : 2 molar ratio yield the new binuclear di-μ-thiolato complexes $[NBu_4]_2[\{M(C_6F_5)_2(\mu\text{-}SR)\}_2]$ **1–8** (Scheme 1). The acidic proton of the thiol is abstracted by the corresponding hydroxo-complex generating the

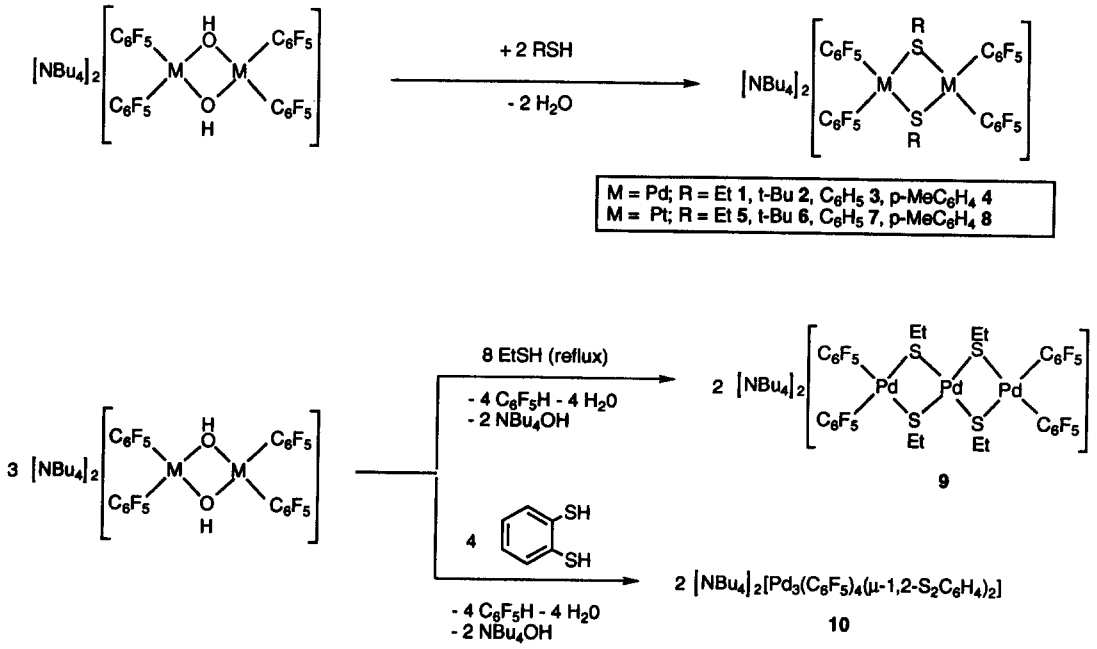

Scheme 1.

anionic ligand RS^- which is subsequently trapped by the organometallic moiety $M(C_6F_5)_2$ to form complexes **1–8** and the concomitant release of water.

Partial elemental analyses and decomposition temperatures for all the complexes are given in Table 1. In acetone solution, they behave as 2:1 electrolytes [15], in agreement with the proposed formulae. The new complexes show IR absorptions characteristic of the C_6F_5 group (1630 m, 1490 vs, 1050 s, 950 vs and 810–770 cm^{-1}) [16]. The IR absorption at approx. 800 cm^{-1} is a split band which is the so-called X-sensitive mode and is characteristic of the *cis* geometry of the $M(C_6F_5)_2$ fragment [17,18].

The ^1H and ^{19}F NMR spectra (Table 2) are consistent with the proposed formulae. The ^{19}F NMR spectra show the presence of four equivalent freely rotating C_6F_5 rings giving three resonances with relative intensities of 8:4:8 due to the *ortho*-, *para*-, and *meta*-F atoms, respectively. As expected, the *ortho*-F signals of complexes **5–8** are flanked by the satellites due to the coupling to ^{195}Pt.

The reaction of $[\{Pd(C_6F_5)_2(\mu\text{-}OH)\}_2]^{2-}$ with an

Table 1. Analytical data, yields and physical properties for the new complexes

Complex	Yield (%)	M.p.[a] (°C)	Analysis (%)[b] C	H	N	S	Λ_M[c]	Selected IR bands[d] X-sensitive
1	80	223	48.7 (48.4)	5.5 (5.6)	1.9 (1.9)	4.0 (4.3)	189	775, 760
2	75	242	49.7 (49.8)	6.0 (5.9)	1.8 (1.8)	4.3 (4.2)	175	775, 765
3	70	232	51.2 (51.6)	5.2 (5.2)	1.8 (1.8)	4.4 (4.1)	180	780, 770
4	72	227	52.0 (52.1)	5.1 (5.4)	1.7 (1.7)	3.9 (4.0)	174	780, 770
5	76	241	43.1 (43.3)	4.8 (5.0)	1.5 (1.7)	3.8 (3.9)	180	790, 780
6	75	249	44.3 (44.6)	5.0 (5.3)	1.6 (1.6)	3.6 (3.7)	185	790, 785
7	82	261	45.9 (46.1)	4.7 (4.7)	1.6 (1.6)	4.0 (3.6)	183	790, 780
8	79	259	46.8 (47.0)	4.5 (4.8)	1.2 (1.6)	3.6 (3.6)	186	790, 780
9	65	234	44.2 (44.5)	5.4 (5.4)	1.5 (1.6)	7.4 (7.5)	190	770, 760
10	60	238	46.7 (46.6)	4.7 (4.6)	1.6 (1.6)	7.4 (7.3)	192	770, 760
11	65	238	50.8 (51.2)	5.6 (5.4)	3.5 (3.6)	2.3 (2.0)	208	780, 770
12	55	234	50.9 (51.6)	5.7 (5.5)	3.5 (3.5)	2.2 (2.0)	199	785, 770
13	63	268	45.0 (45.4)	4.9 (4.7)	3.1 (3.3)	2.1 (1.9)	187	795, 780
14	47	264	45.2 (45.7)	4.9 (4.8)	3.4 (3.3)	1.9 (1.9)	208	795, 780
15	70	280	43.3 (43.8)	5.0 (4.8)	3.5 (3.4)	2.1 (1.9)	225	795, 780
16	91	267	44.1 (44.5)	5.2 (5.0)	3.4 (3.3)	1.6 (1.9)	188	790, 775
17	78	264	46.0 (46.0)	4.9 (4.8)	3.2 (3.2)	1.6 (1.8)	217	800, 785
18	76	221	45.9 (46.4)	5.1 (4.9)	3.1 (3.2)	2.1 (1.8)	221	795, 780
19	64	260	44.1 (44.4)	5.0 (5.0)	3.3 (3.3)	2.2 (1.9)	217	795, 775

[a] Decomposition temperatures.
[b] Calculated values in parentheses.
[c] In $ohm^{-1}\,cm^2\,mol^{-1}$.
[d] In Nujol mulls (cm^{-1}).

Table 2. NMR data (J in Hz) for the palladium and platinum complexes (in $(CD_3)_2CO$)

Complex	^1H $\delta(SiMe_4)$[a]	^{19}F $\delta(CFCl_3)$
1	1.77 (q, 4 *H*, CH_2S, *J* 7.4)	−110.8 (d, 8 F_o, *J* 31.6)
	0.51 (t, 6*H*, $\underline{CH_3}CH_2S$, *J* 7.4)	−166.8 (m, 8 F_m+4F_p)
2	1.11 (s, 18 *H*, CH_3)	−111.3 (d, 8 F_o, *J* 29.3)
		−167.2 (m, 8 F_m)
		−167.7 (t, 2 F_p, *J* 20.3)
3	7.59 (m, 4 H_o)	−111.6 (d, 8 F_o, *J* 28.5)
	6.73 (m, 4 H_m+2 H_p)	−167.1 (m, 8 F_m+4 F_p)
4[b]	7.11 (d, 2 H_o, *J* 8.0)	−113.1 (d, 8 F_o, *J* 28.3)
	6.50 (d, 2 H_m, *J* 8.0)	−166.2 (m, 8 F_m+4 F_p)
	2.10 (s, 6 *H*, CH_3)	
5	2.12 (q, 4 *H*, CH_2S, *J* 7.3)	−112.7 (d, 8 F_o, *J* 28.8, $J_{Pt}Fo$ 444.2)
	1.04 (t, 6 *H*, $\underline{CH_3}$ CH_2S, *J* 7.3)	−165.0 (m, 8 F_m)
		−165.8 (t, 4 F_p, *J* 19.2)
6	1.05 (s, 18 *H*, CH_3)	−114.9 (d, 8 F_o, *J* 28.2, $J_{Pt}Fo$ 443.3)
		−168.2 (m, 8 F_m)
		−169.2 (t, 4 F_p, *J* 20.3)
7	7.61 (m, 4 H_o)	−115.9 (d, 8 F_o, *J* 26.8, $J_{Pt}Fo$ 446.4)
	6.78 (m, 4 H_m+2 H_p)	−168.1 (m, 8 F_m)
		−168.6 (t, 4 F_p, *J* 20.0)
8	7.48 (d, 4 H_o, *J* 7.9)	−115.8 (d, 8 F_o, *J* 27.4, $J_{Pt}Fo$ 443.3)
	6.61 (d, 4 H_m, *J* 7.9)	−168.1 (m, 8 F_m)
	2.10 (s, 6 *H*, CH_3)	−168.8 (t, 4 F_p, *J* 20.0)
9	2.18 (q, 8 *H*, CH_2S, *J* 7.4)	−112.2 (d, 8 F_o, *J* 29.9)
	1.31 (t, 12 *H*, $\underline{CH_3}CH_2S$, *J* 7.4)	−166.2 (m, 8 F_m+2 F_p)
10	6.42 (m, 4 *H*, $C_6H_4S_2$)	−109.3 (br, 4 F_o)
	6.07 (m, 4 *H*, $C_6H_4S_2$)	−113.7 (d, 4 F_o, *J* 31.2)
		−165.5 (br, 4 F_m)
		−166.9 (t, 4 F_p, *J* 19.8)
		−168.1 (m, 4 F_m)
11	7.06 (d, 2 *H*, H_o, *J* 7.6)	−110.5 (br, 4 F_o)
	6.45 (m, 3 *H*, 2 H_m+H_p)	−112.5 (br, 4 F_o)
	5.20 (s, 1 *H*, H^4 of dmpz)	−166.9 (t, 2 F_p, *J* 20.0)
	1.62 (s, 6 *H*, CH_3 of dmpz)	−167.2 (br, 4 F_m)
		−168.2 (m, 2 F_p+4 F_m)
12	6.89 (d, 2 *H*, H_o, *J* 8.0)	−110.5 (br, 4 F_o)
	6.25 (d, 2 *H*, H_m, *J* 8.0)	−112.0 (br, 4 F_o)
	5.21 (s, 1 *H*, H_4 of dmpz)	−166.9 (t, 2 F_p, *J* 20.0)
	1.95 (s, 3 *H*, CH_3)	−167.2 (br, 4 F_m)
	1.62 (s, 6 *H*, CH_3 of dmpz)	−168.1 (m, 4 F_m)
		−168.6 (t, 2 F_p, *J* 19.8)
13	7.30 (d, 2 *H*, H_o, *J* 7.8)	−115.1 (d, 4 F_o, *J* 29.2, $J_{Pt}Fo$ 457)
	6.88 (d, 2 *H*, H^3, H^5 of pz, *J* 1.9)	−115.9 (d, 4 F_o, *J* 31.0 $J_{Pt}Fo$ 451)
	6.62 (m, 3 *H*, 2 H_m+H_p)	−167.0 (m, 2 F_p+4 F_m)
	5.68 (t, 1 *H*, H^4 of pz, *J* 1.9)	−168.8 (m, 4 F_m)
		−169.2 (t, 2 F_p, *J* 19.8)
14	7.18 (d, 2 *H*, H_o, *J* 7.8)	−115.1 (d, 4 F_o, *J* 27.9, $J_{Pt}Fo$ 463)
	6.88 (d, 2 *H*, H^3, H^5 of pz, *J* 1.8)	−115.9 (d, 4 F_o, *J* 28.2, $J_{Pt}Fo$ 446)
	6.44 (d, 2 *H*, H_m, *J* 7.8)	−167.1 (m, 2 F_p+4 F_m)
	5.67 (t, 1 *H*, H^4 of pz, *J* 1.8)	−168.9 (m, 4 F_m)
	2.03 (s, 3 *H*, CH_3)	−169.4 (t, 2 F_p, *J* 19.8)
15	6.92 (d, 2 *H*, H^3, H^5 of pz, *J* 2.1)	−115.5 (d, 4 F_o, *J* 27.9, $J_{Pt}Fo$ 427)
	5.64 (t, 1 *H*, H^4 of pz, *J* 2.1)	−115.6 (d, 4 F_o, *J* 31.0, $J_{Pt}Fo$ 418)
	1.40[c] (CH_2S)	−166.7 (m, 4 F_m)
	0.95[c] ($\underline{CH_3}CH_2S$)	−167.1 (t, 2 F_p, *J* 20.0)
		−168.3 (m, 4 F_m+2 F_p)
16	7.24 (d, 2 *H*, H^3, H^5 of pz, *J* 1.8)	−115.4 (d, 8 F_o, *J* 29.1, $J_{Pt}Fo$ 436)
	5.69 (t, 1 *H*, H^4 of pz, *J* 1.8)	−166.8 (m, 4 F_m)
	1.21 (s, 9 *H*, CH_3)	−167.7 (t, 2 F_p, *J* 19.8)
		−168.8 (m, 4 F_m)
		−169.5 (t, 2 F_p, *J* 19.8)

Table 2*Continued.*

Complex	^{1}H δ(SiMe$_4$)[a]	^{19}F δ(CFCl$_3$)
17	7.44 (d, 2 *H*, *J* 7.0)	−114.8 (br, 8 F_o)
	6.56 (m, 3 *H*)	−168.2 (m, 4 F_m)
	5.19 (s, 1 *H*, H^4 of dmpz)	−168.7 (t, 2 F_p, *J* 19.8)
	1.57 (s, 6 *H*, CH$_3$ of dmpz)	−169.3 (m, 4 F_m)
		−169.9 (t, 2 F_p, *J* 20.0)
18	7.26 (d, 2 *H*, *J* 7.6)	−114.8 (br, 8 F_o)
	6.37 (d, 2 *H*, *J* 7.6)	−168.2 (br, 4 F_m)
	5.20 (s, 1 *H*, H^4 of dmpz)	−168.7 (t, 2 F_p, *J* 20.0)
	2.01 (s, 3 *H*, CH$_3$)	−169.3 (br, 4 F_m)
	1.58 (s, 6 *H*, CH$_3$ of dmpz)	−170.3 (t, 2 F_p, *J* 20.0)
19	5.32 (s, 1 *H*, H^4 of dmpz)	−114.3 (br, 8 F_o)
	1.65 (s, 6 *H*, CH$_3$ of dmpz)	−168.2 (m, 4 F_m)
	1.40[c] (CH$_2$S)	−169.0 (m, 4 F_m + 2 F_p)
	0.95[c] (CH$_3$CH$_2$S)	−169.5 (t, 2 F_p, *J* 20.0)

[a] Additional peaks of $[NBu_4]^+$ are found at δ ca 3.43 (t, NCH_3), 1.80 (m, NCH_2CH_2), 1.40 (m, CH_2CH_3) and 0.95 (t, CH_3), the relative intensities being 16 : 16 : 16 : 24 respectively.

[b] In $CDCl_3$.

[c] Obscured by $[NBu_4]^+$ peaks.

excess of EtSH in refluxing methanol yields the formation of the tetrakis(μ-thiolato) tripalladium complex $[NBu_4]_2[(C_6F_5)_2Pd(\mu\text{-SEt})_2Pd(\mu\text{-SEt})_2Pd(C_6F_5)_2]$ **9** (Scheme 1). The analytical, conductance (Table 1) and ^{1}H NMR (2 $[NBu_4]^+$: 4 EtS^-) data for **9** are consistent with the proposed formula. This reaction implies cleavage of two Pd—C_6F_5 bonds leading to the likely formation of the homoleptic thiolato complex $[Pd(SEt)_4]^{2-}$, which in turn acts as a ligand to two $[Pd(C_6F_5)_2]$ moieties. The ^{1}H NMR spectrum of complex **9** indicates that the SEt groups are equivalent and the SEt resonances are found at lower field than in the spectrum of the binuclear complex **1**, as previously observed in the analogous trinuclear nickel complex $[NBu_4]_2[(C_6F_5)_2Ni(\mu\text{-SEt})_2Ni(\mu\text{-SEt})_2Ni(C_6F_5)_2]$, the structure of which was confirmed by X-ray diffraction [14]. The syntheses of pentafluorobenzenethiolato trinuclear palladium or platinum complexes $[(C_6F_5)_2M(\mu\text{-}SC_6F_5)_2M(\mu\text{-}SC_6F_5)_2M(C_6F_5)_2]^{2-}$, by reaction of $[M(C_6F_5)_2(thf)_2]$ (thf = tetrahydrofuran) with $[M(SC_6F_5)_4]^{2-}$ (M = Pd or Pt) [19], and the tetrakis (μ-thiolato) palladium complex $Pd_3(\mu\text{-SCy})_4Cl_2(PMe_3)_2$, from $[\{PdCl(PMe_3)(\mu\text{-Cl})\}_2]$ [1], have also been recently described.

On the other hand, the reaction of the binuclear hydroxo palladium complex $[NBu_4]_2[\{Pd(C_6F_5)_2(\mu\text{-OH})\}_2]$ with an excess of 1,2-benzenedithiol $C_6H_4(SH)_2$-1,2 in methanol at room temperature affords the trinuclear complex $[NBu_4]_2[Pd_3(C_6F_5)_4(\mu\text{-}1,2\text{-}S_2C_6H_4)_2]$ **10**. The ^{19}F NMR spectrum of complex **10** shows a single resonance for the *p*-fluorine atoms, in agreement with the presence of four equivalent C_6F_5 rings. The presence of two 1 : 1 resonances in the *o*-fluorine region, and two additional 1 : 1 resonances in the *m*-fluorine region, suggests restricted rotation around the Pd—C bonds. The NMR data of complex **10** are consistent with the structures A and B given below.

Examples of 1,2-dithiolate-bridged complexes such as $[Ru_2(CO)_4(\mu\text{-}1,2\text{-}S_2C_6H_4)(PPh_3)_2]$ [20] or $[Rh_2\{\mu\text{-}S(CH_2)_3S\}(cod)_2]$ (cod = cycloocta-1,5-diene) [21] are known in the literature. It is noteworthy that the

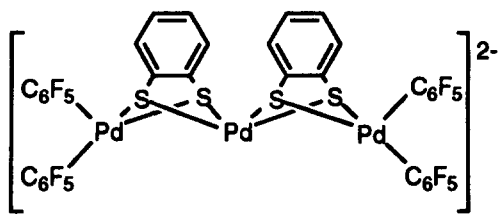

A

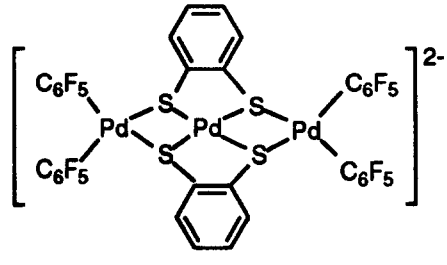

B

binuclear $[NBu_4]_2[(C_6F_5)_2Pd(\mu\text{-}1,2\text{-}S_2C_6H_4)Pd(C_6F_5)_2]$ was not obtained when the reaction of the binuclear hydroxo palladium complex $[NBu_4]_2[\{Pd(C_6F_5)_2(\mu\text{-}OH)\}_2]$ with 1,2 benzenedithiol $C_6H_4(SH)_2$-1,2 in a 1 : 1 molar ratio was tried, a mixture containing the trinuclear complex **10** together with starting material was detected instead.

The hydroxo-azolate bridged complexes $[\{(C_6F_5)_2M\}_2(\mu\text{-}OH)(\mu\text{-}L)]^{2-}$ (M = Pd or Pt, L = pyrazolate-type ligand) were also treated with thiols, RSH, in a 1 : 1 molar ratio to give the heterobridged complexes $[\{(C_6F_5)_2M\}_2(\mu\text{-}SR)(\eta\text{-}L)]^{2-}$ **11–19** (Scheme 2). These reactions imply protonation of the hydroxo group and replacement by μ-thiolates. Palladium and platinum heterobridged binuclear complexes containing the central core $[M_2(\mu\text{-}SR)(\mu\text{-}X)]$ (X = Br, O_2CMe or pyrazolato) have been reported [22–25].

The ^1H NMR spectra of complexes **11–19** are consistent with the proposed formulae. Thus the dimethylpyrazolate ligand (dmpz) in complexes **11, 12** and **17–19** gives one singlet (H^4) and another singlet (for the Me group), with relative intensities of 1 : 6, as expected for a bridging dmpz ligand [6,9,22]. For the pyrazolate ligand (pz) in complexes **13–16** one triplet (H^4) and one doublet (H^3 and H^5), with relative intensities of 1 : 2, are observed.

The ^{19}F NMR spectra of **11–19** (Table 2) should exhibit six resonances for the C_6F_5 rings, in accordance with the presence of two equivalent C_6F_5 rings *trans* to S and two equivalent C_6F_5 rings *trans* to N, but overlapping of some signals is observed in some cases. Furthermore, also in some cases, at room temperature some of the resonances of the *o*-F or *m*-F atoms are broad, which suggests some restriction on the rotation around the M—C bonds. For example, only a very broad resonance at 20°C is observed in the *o*-fluorine region of the NMR spectrum of **18** (δ −114.8 ppm), whereas the low temperature spectrum (−70°C) shows four 2 : 2 : 2 : 2 sharp resonances in the *o*-fluorine region (δ −113.2, −114.3, −116.9 and −117.0 ppm).

Acknowledgements—Financial support of this work by the DGICYT (project PB94-1157), Spain, is acknowledged. V.R. thanks the Dirección General de Educación y Universidad (Comunidad Autónoma de Murcia, Spain) for a research grant.

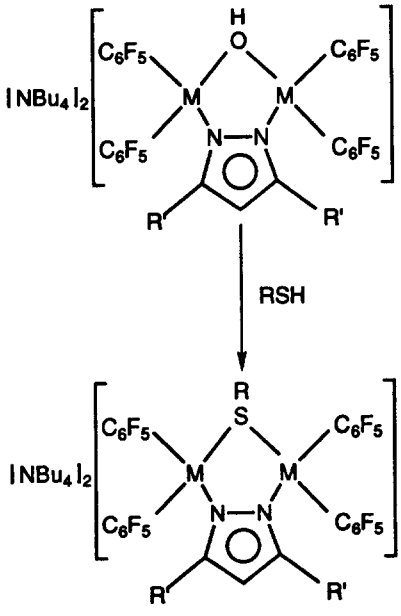

M = Pd, R = Me, R' =	C_6H_5	11
	p-MeC_6H_4	12
M = Pt, R = H, R' =	C_6H_5	13
	p-MeC_6H_4	14
	Et	15
	Bu^t	16
R = Me, R' =	C_6H_5	17
	p-MeC_6H_4	18
	Et	19

Scheme 2.

REFERENCES

1. Padilla, E. M. and Jensen, C. M., *Polyhedron*, 1991, **10,** 89.
2. Jim, Y. K., Osakada, K., Sugita, K., Yamamoto, T. and Yamamoto, A., *Organometallics*, 1988, **7,** 2182.
3. Jain, V. K. and Rao, G. S., *Inorg. Chim. Acta*, 1987, **127,** 161.
4. Singhal, A. and Jain, V. K., *J. Organomet. Chem.*, 1995, **494,** 75, and references cited therein.
5. Clark, H. C., Jain, V. K. and Rao, G. S., *J. Organomet. Chem.*, 1985, **279,** 181.
6. López, G., Ruiz, J., García, G., Vicente, C., Casabó, J., Molins, E. and Miravitlles, C., *Inorg. Chem.*, 1991, **30,** 2605.
7. López, G., García, G., Sánchez, G., García,J., Ruiz, J., Hermoso, J. A., Vegas, A. and Martínez Ripoll, M., *Inorg. Chem.*, 1992, **31,** 1518.
8. López, G., Ruiz, J., Garcí, G., Vicente, C., Martí, J. M., Hermoso, J. A., Vegas, A. and Martínez-Ripoll, M., *J. Chem. Soc., Dalton Trans.*, 1992, 53.
9. López, G., Ruiz, J., García, G., Vicente, C., Rodríguez, V., Sánchez, G., Hermoso, J. A. and Martínez Ripoll, M., *J. Chem. Soc., Dalton Trans.*, 1992, 1681.
10. Ruiz, J., Rodríguez, V., López, G., Chaloner, P. A. and Hitchcock, P. B., *Organometallics*, 1996, **15,** 1662.
11. López, G., Ruiz, J., García, G., Vicente, C., Martí, J. M. and Rodríguez, V., *J. Organomet. Chem.*, 1992, **436,** 121.
12. Ruiz, J., Martínez, M. T., Vicente, C., García, G., López, G., Chaloner, P. A. and Hitchcock, P. B., *Organometallics*, 1993, **12,** 4321.
13. López, G., Sánchez, G., García, G., Ruiz, J., Gar-

cía, J., Martínez Ripoll, M., Vegas, A. and Hermoso, J. A., *Angew. Chem. Int. Ed. Engl.*, 1991, **30,** 716.
14. Sánchez, G., Ruiz, F., Santana, M. D., García, G., López, G., Hermoso, J. A. and Martínez-Ripoll, M., *J. Chem. Soc., Dalton Trans.*, 1994, 19.
15. Geary, W. J., *Coord. Chem. Rev.*, 1971, **7,** 81.
16. Long, D. A. and Steele, D., *Spectrochim. Acta*, 1963, 1955.
17. Maslowski, E., *Vibrational Spectra of Organometallic Compounds*. Wiley, New York, 1977, p. 437.
18. López, G., Ruiz, J., Vicente, C., Martí, J. M., García, G., Chaloner, P. A., Hitchcock, P. B. and Harrison, R. M., *Organometallics*, 1991, **11,** 4090, and references cited therein.
19. Usón, R., Forniés, J., Usón, M. A., Tomás, M. and Ibáñez, M. A., *J. Chem. Soc., Dalton Trans.*, 1994, 19.
20. Shiu, K.-B., Li, C.-H., Chan, T.-J., Peng, S.-M., Cheng, M.-C., Wang, S.-L., Liao, F.-L. and Chiang, M. Y., *Organometallics*, 1995, **14,** 524.
21. Masdeu, A. M., Ruiz, A., Castillón, S., Claver, C., Hitchcock, P. B., Chaloner, P. A., Bó, C., Poblet, J. M. and Sarasa, P., *J. Chem. Soc., Dalton Trans.*, 1993, 2689.
22. Ruiz, J., Cutillas, N., Torregrosa, J., Garcí, G., López, G., Chaloner, P. A., Hitchcock, P. B. and Harrison, R. M., *J. Chem. Soc., Dalton Trans.*, 1994, 2353.
23. Ruiz, J., Cutillas, N., Sampedro, J., López, G., Hermoso, J. A. and Martínez-Ripoll, M., *J. Organomet. Chem.*, 1996, **526,** 67.
24. Jain, V. K. and Kannan, S., *J. Chem. Res. (S)*, 1992, 278.
25. Jain, V. K. and Kannan, S., *Polyhedron*, 1992, **11,** 27.
26. Carmona, D., Oro, L. A., Lamata, M. P., Puebla, M. P., Ruiz, J. and Maitlis, P. M., *J. Chem. Soc., Dalton Trans.*, 1987, 639.

Pergamon

PII: S0277-5387(97)00416-6

Polyhedron Vol. 17, No. 9, pp. 1511–1516, 1998
© 1998 Elsevier Science Ltd. All rights reserved
Printed in Great Britain
0277-5387/98 $19.00+0.00

Zigzag chain of hepta-coordinate manganese complexes

Ziming Sun, Peter K. Gantzel and David N. Hendrickson*

Department of Chemistry-0358, University of California at San Diego, La Jolla, California 92093-0358, U.S.A.

(Received 7 July 1997; accepted 26 September 1997)

Abstract—The preparation of the polymeric chain complex, $\{[Mn(bic)(H_2O)]_2 \cdot 2Br \cdot 2H_2O\}_n$ (**2**) is reported. Characterization is made by single X-ray structure, IR and magnetochemistry data. Each seven-coordinate manganese ion has a slightly distorted pentagonal bipyramidal coordination geometry. Bicine is a hexadentate ligand using one nitrogen, three oxygen and one μ_2-oxygen atom from the carboxylate group to coordinate to two Mn^{II} ions. The two hydroxyl groups are not deprotonated, and the μ_2-oxygen atom of the carboxylate moiety of the bic^- ligand is a bridge leading to a polymeric chain. One water molecule coordinates to the Mn^{II} ion, and also forms a strong hydrogen bond with other non-coordinated water molecules. Both non-coordinated water and counter Br^- ion are located between the zigzag chains. Weak pairwise antiferromagnetic exchange interactions ($J = -1.42\ cm^{-1}$) are found within the chain complex due to antiparallel geometry orientations of neighboring Mn^{II} centers. © 1998 Elsevier Science Ltd. All rights reserved.

Keywords: bicine; manganese; magnetic exchange; one-dimensional; polymer.

The use of polydentate ligands with deprotonatable hydroxyl groups as bridging ligands has led to the formation of Co_{24} [1], Fe_{19}, Fe_{17} [2], Fe_{10} [3], Fe_6 [4], Mn_{13} [5], Mn_{10} [6], Mn_7 [7] polynuclear metal complexes. Interesting structural and magnetic properties have been reported for several of these complexes. *N,N-bis*(2-hydroxyethylglycine) (bicine) is one of these polydentate ligands that is widely used as a buffer substance in biochemical studies [8]. In solution bicine reacts with various transition metal ions [9]; the X-ray structures of only a few of these bicinate metal complexes have been determined [10]. In the structurally characterized complexes it is found that bicine is a versatile ligand and functions either as a tetradentate ligand to form mononuclear metal complexes or as a pentadentate ligand to form polymeric chain complexes [9,10].

Recently we employed bicine as a ligand to prepare a polynuclear manganese complex. A linear polymeric complex of Mn^{II}, $\{[Mn(bic)Cl]_2 \cdot 2H_2O\}_n$ (**1**), was formed by the reaction of $MnCl_2 \cdot 6H_2O$ with bicine in a basic methanol solution [11]. Each Mn^{II} ion is six coordinate, the bicinate (bic) ligand is a pentadentate ligand, and the Cl^- ion is coordinated to the Mn^{II} ion. In this paper we report the synthesis and characterization of $\{[Mn(bic)(H_2O)]_2 \cdot 2Br \cdot 2H_2O\}_n$ (**2**), a zigzag chain of seven coordinate Mn^{II} ions that have pentagonal bipyramidal geometry.

EXPERIMENTAL

Instrumentation and materials

A room-temperature infrared spectrum was obtained on a Nicolet 550 Magna FTIR spectrophotometer. Variable-temperature magnetic susceptibility data were collected for a polycrystalline sample of complex **2** on a Quantum Design MPMS5 SQUID susceptometer equipped with a 55 kG magnet and operating in the range of 1.8–400 K. Diamagnetic corrections were estimated using Pascal's constants and were subtracted from the experimental molar susceptibility to obtain the paramagnetic molar susceptibilities [12]. Solvents and reagents were used as purchased.

Synthesis

Equal equivalents of $MnBr_2 \cdot 6H_2O$ (2.00 g, 8.25 mmol) and bicine (1.34 g, 8.25 mmol) were dissolved

* Author to whom correspondence should be addressed.

in 30 cm^3 deionized water. A 4.0 ml 25% methanolic solution of $[(CH_3)_4N]OH$ (9.50 mmol) was added dropwise to give a solution with pH $\approx$ 8. The solution was warmed to boiling for 10 mins, and the color of the solution gradually changed from colorless to brown. X-ray quality crystals were obtained by slow evaporation over several days. Found: C, 21.70; H, 4.64; N, 4.18; Calc. for $\{[Mn(bic)(H_2O)]_2 \cdot 2Br \cdot 2H_2O\}_n$ (**2**): C, 21.64; H, 4.84; N, 4.20. The yield was 68.80% based on $MnBr_2$.

X-ray crystallography

Data were collected at room temperature on a Siemens R3m/v four circle diffractometer, employing Mo K_α ($\lambda = 0.71073$ Å) radiation with a graphite crystal monochromator. Data were measured by using Wyckoff omega scans. Crystallographic data and other pertinent information are given in Table 1. Selected bond distances and angles are listed in Table 2. Lorentz and polarization corrections were applied and direct methods (SHELXTL PC) revealed the structure. The structure was refined in the monoclinic space group $C2/c$ system using anisotropic thermal parameters for all non-hydrogen atoms and isotropic ones for the hydrogen atoms. The positional parameters of all hydrogen atoms were included in the least-squares refinement cycles. The discrepancy indices $R = (\Sigma||F_o| - |F_c||)/\Sigma|F_o|$ and $R_w = [\Sigma w(|F_o| - |F_c|)^2/\Sigma w|F_o|^2]^{1/2}$ are listed in Table 1.

Table 1. Crystallographic data for complex **2**

Formula	$C_6H_{16}BrMnNO_6$
Formula weight	333.01
Temperature	188 K
Wavelength (Å)	0.71073
Crystal system	monoclinic
Space group	$C2/c$
a (Å)	19.048(9)
b (Å)	8.083(5)
c (Å)	15.571(11)
β (°)	98.440(0)
V (Å^3)	2371(2)
Z	8
Density (mg m^{-3})	1.832
Range of 2θ (°)	3–55
Absorption coefficient (mm^{-1})	4.490
F_{000}	1288
Crystal size (mm)	$0.5 \times 0.8 \times 0.9$
Index range	$-24 \leqslant h \leqslant 24$, $-10 \leqslant k \leqslant 0$, $-20 \leqslant l \leqslant 0$
No. unique data	2732
Data with $F_o^2 > 4(F_o^2)$	2307
Refinement method	full matrix least-squares on F
R	0.0353
R_w	0.0430
Largest diff. peak (e Å^{3-}) and hole (e Å^{3-})	0.76 −0.48

RESULTS AND DISCUSSION

Compound preparation

The goal of this research was to prepare a polynuclear manganese complex that incorporates Mn ions and the bicinate anion. In order to prepare a high nuclearity Mn complex, a *basic* aqueous solution containing Mn^{II} and bicine was allowed to react in air. It is clear that some of the Mn^{II} was oxidized, for the color of the solution changed from colorless to dark brown. Two products were isolated: light brown crystals that analyzed as $\{[Mn(bic)(H_2O)]_2 \cdot 2Br \cdot 2H_2O\}_n$ (**2**) and a dark brown solid. Efforts are continuing to characterize the dark brown solid. In the following is given a characterization of the light brown crystals of complex **2**.

Structural description

The polymeric structure of complex **2** is comprised of a dimeric $[Mn(bic)(H_2O)]_2^{2+}$ repeating unit with two counter bromide ions and two hydrogen bonded H_2O molecules. The one-dimensional structure is shown in Fig. 1 together with the atom-numbering scheme. The carboxylate moiety of the bicinate ligand acts as a tridentate group where one carboxylate oxygen atom bridges two Mn^{II} ions, yielding a chain that runs parallel to the b axis as depicted in Fig. 2. Each Mn^{II} ion is seven coordinate, and coordination geometry is that of a slightly distorted pentagonal bipyramid. Within the chain the dimeric units are arranged head to tail, and all pentagonal plane atoms of Mn^{II} are co-planar, making a *zigzag* chain. A water molecule is hydrogen bonded to the coordinated water, and each water molecule only forms one strong hydrogen bond: the distances and angles of the O(5)—H···O(6) interaction are 2.690 Å, 171.1°, respectively. The bromide ion is only 3.040 Å away from the O(3) atom of the bicinate ligand, and there is probably a weak Br···H—O hydrogen bond. Both non-coordinated water molecules and the bromide ions fill the void between the chains. There are two pairs of anti-parallel chains running through each unit cell. If one assumes the O(2) atom in Fig. 1 is the head of a chain, then in Fig. 2(a) the two top chains run out of the paper, whereas the two bottom chains run into the paper. The intra-chain distance between neighboring Mn^{II} ions are 7.87, 7.98, and 11.59 Å. The intra-chain distance between two neighboring Mn^{II} ions is 4.41(3) Å, and it is shorter than that in complex **1** (4.987 Å), because the bridge in complex **2** is a single oxygen atom, whereas in complex **1** the bridging is by a CO_2^-.

Each Mn^{II} ion in complex **2** has a distorted hepta coordination comprised of two hydroxyl-oxygen

Table 2. Selected bond distances (Å) and angles (°) for complex **2**

Mn(1)—O(1)	2.213(3)	N(1)—C(5)	1.482(4)
Mn(1)—O(3)	2.218(3)	O(1)—C(2)	1.270(3)
Mn(1)—O(4)	2.214(3)	O(2)—C(2)	1.255(4)
Mn(1)—O(5)	2.149(3)	O(3)—C(4)	1.427(5)
Mn(1)—O(1A)	2.346(3)	O(4)—C(6)	1.429(5)
Mn(1)—O(2A)	2.292(3)	C(1)—C(2)	1.510(5)
O(1)—Mn(1)—O(3)	87.9(1)	O(1)—Mn(1)—O(4)	145.6(1)
O(3)—Mn(1)—O(4)	94.7(1)	O(1)—Mn(1)—O(5)	88.3(1)
O(3)—Mn(1)—O(5)	169.3(1)	O(4)—Mn(1)—O(5)	83.0(1)
O(1)—Mn(1)—N(1)	73.9(1)	O(3)—Mn(1)—N(1)	75.2(1)
O(4)—Mn(1)—N(1)	73.7(1)	O(5)—Mn(1)—N(1)	94.2(1)
O(1)—Mn(1)—O(1A)	133.6(1)	O(3)—Mn(1)—O(1A)	85.9(1)
O(4)—Mn(1)—O(1A)	80.8(1)	O(5)—Mn(1)—O(1A)	103.9(1)
N(1)—Mn(1)—O(1A)	146.5(1)	O(1)—Mn(1)—O(2A)	78.8(1)
O(3)—Mn(1)—O(2A)	95.3(1)	O(4)—Mn(1)—O(2A)	134.8(1)
O(5)—Mn(1)—O(2A)	93.7(1)	N(1)—Mn(1)—O(2A)	151.3(1)
O(1A)—Mn(1)—O(2A)	56.2(1)	Mn(1)—O(1)—C(2)	118.0(2)
Mn(1)—O(1)—Mn(1A)	151.0(1)	C(2)—O(1)—Mn(1A)	90.5(2)
C(2)—O(2)—Mn(1A)	93.4(2)	Mn(1)—O(3)—C(4)	113.2(2)
Mn(1)—O(4)—C(6)	120.0(2)	Mn(1)—N(1)—C(1)	108.0(2)

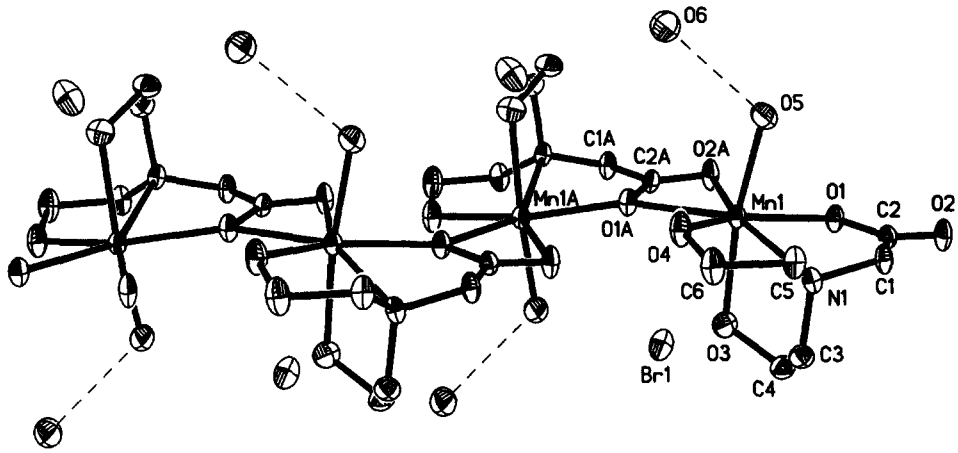

Fig. 1. X-ray structural representation of the linear chain in $\{[Mn(bic)(H_2O)]_2 \cdot 2Br \cdot 2H_2O\}_n$ (complex **2**). Atoms are represented by their 50% probability ellipsoids. Hydrogen atoms on carbon atoms are omitted for clarity. Hydrogen-bonding contacts between coordinated H_2O and uncoordinated H_2O molecules are indicated by dashed lines.

atoms O(3) and O(4), one nitrogen atom N(1), one oxygen atom O(5) from a water molecule, one carboxylate oxygen atom O(1) and another two oxygen atoms O(1A), O(2A) from a second bicinate ligand. The Mn—N bond length (2.356 Å) is significantly longer than the Mn—O bond distances to the carboxylate and hydroxyl oxygen atoms that are about 2.20 Å. This is different from what was found [10] in the bicinate copper complexes. For all copper complexes, at least one Cu—O bond (hydroxyl oxygen) is longer than Cu—N bond. This difference is likely the result of the different coordination geometry. In the case of complex **2**, since it is hepta-coordinate, this requires the five-membered chelate rings associated with the bic^- ligand to be more distorted from the conformation observed in the five-coordinate Cu^{II} complexes and in the six-coordinate complex **1**. There is an appreciable bond length difference for the μ_2-oxygen atom in the carboxylate coordinate to two Mn^{II} centers [2.213 and 2.346 Å for Mn(1)—O(1A), Mn(2)—O(1A), respectively]. The origin of these differences is probably due to the steric effects from the unusual bridging mode for the carboxylate ligand in complex **2**.

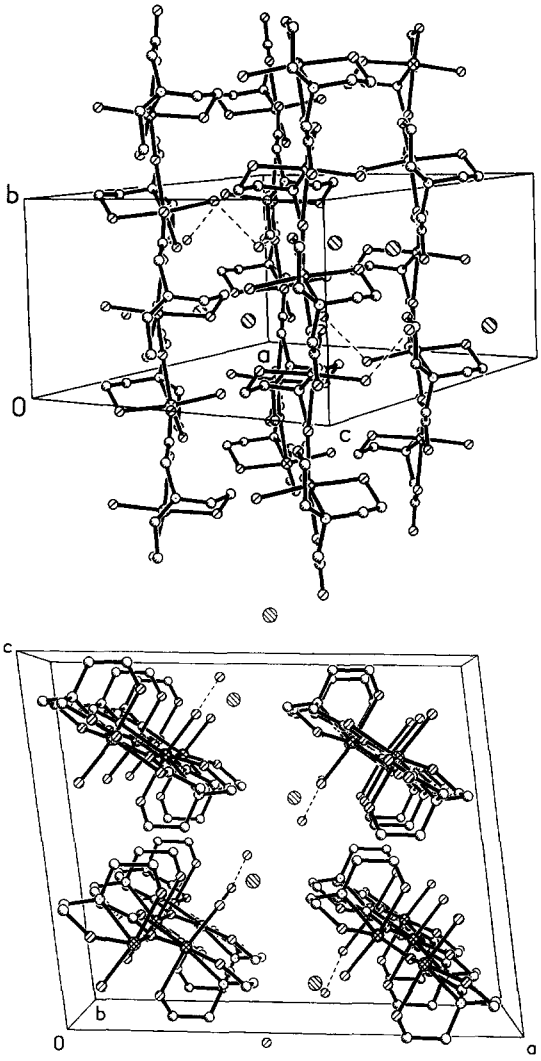

Fig. 2. Drawing showing the unit cell arrangement in two different views (a) and (b) of $\{[Mn(bic)(H_2O)]_2 \cdot 2Br \cdot 2H_2O\}_n$ (complex **2**).

A carboxylate moiety can bridge between metal ions in different ways. The most common bridging mode is shown in (I).

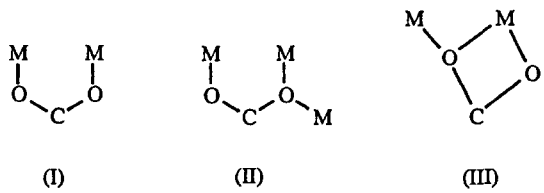

In bridging mode (II) one oxygen atom of the CO_2^- unit interacts with one metal ion, whereas the other oxygen atom bridges between two other metal ions. There have been several examples of carboxylate bridging mode (II) reported [13] for polynuclear manganese complexes. The less commonly encountered bridging mode (III) is found in complex **2**. Both O(1A) and O(2A) coordinate to Mn(1) forming an unusual four-membered ring. Steric effects keep these two oxygen atoms somewhat removed from the normal bond length of Mn—O (~2.20 Å) in manganese carboxylate complexes [13a].

Small deviations from an idealized pentagonal bipyramid are found at the Mn^{II} center. The best equatorial pentagonal plane is defined by atoms O(1), O(1A), O(2A), O(1), N(1), O(4) and Mn(1). The five angles in this plane are approximately evenly distributed, except for the small angle from the unusual four-membered ring of the carboxylate moiety [73.67(1), 73.94(1), 78.78(1), 56.18(1), 80.76(1)° for O(1)—Mn(1)—N(1), N(1)—Mn(1)—O(4), O(4)—Mn(1)—O(1A), O(1A)—Mn(1)—O(2A), O(2A)—Mn(1)—O(1), respectively]. The atoms O(3) and O(5) are found at apical sites with nearly equal bond lengths (Table 1); the O(3)—Mn(1)—O(5) angle is 168.34(1)°. The polydentate structure of the bicinate ligand and unusual coordination mode of the carboxylate moiety contribute to the distortion from pentagonal bipyramidal geometry.

A few hepta-coordinate manganese complexes have been reported [14–16]. Macrocyclic ligands or rigid, resonance-stabilized planar ligands have been employed to enforce pentagonal planar coordination. Bicine is neither macrocyclic nor rigid, however it can adopt a conformation in which it acts as hexadentate ligand with extremely unusual μ_2-bridging oxygen atom from the carboxylate moiety. The bicinate ligand uses four atoms to coordinate to the Mn^{II} ion to form three five-membered chelate rings, leaving appreciable space to accommodate three other atoms. Then, two oxygen atoms of a carboxylate from another bic^- insert to form a four-membered ring. The last position is taken by an H_2O molecule. The versatility of the bic^- ligand is fully manifested in complex **2** with three five-membered rings and one four-membered chelate ring.

Oxygen atoms from the deprotonated ethyl hydroxyl group in the ligand heidi [N(2-hydroxyethyl)iminodiacetic acid] serve as a μ_3-oxo bridge in the formation of Fe_{17} and Fe_{19} clusters [2]. Deprotonated hydroxy groups are not seen for bicine, even though both ligands are structurally similar. It is likely that the ethyl hydroxyl group of heidi is more acidic than that in bicine because the former has two strong electron withdraw carboxylic groups, and there is only one carboxylic group in bicine. In the case of complex **2**, the most remarkable structural features are the hepta coordination and the unusual coordination mode of the carboxylate moiety leading to the formation of the first chain complex with hepta coordinate metal centers.

Complexes **1** and **2** were obtained by the same reaction in different solvents. The formation of complex **1** could be related to the limited amount of water in methanol and the excess of Cl^- used in the reaction.

In this case the Cl^- ion coordinates to the Mn^{II} ion; each Mn^{II} has a distorted octahedral coordination geometry, and the bic^- ligand is pentadentate. Complex **2** was formed in aqueous solution. The Br^- ion is apparently too large to bind together with the bic^- ligand.

Infrared spectroscopy

Four strong broad bands are found in the KBr-pellet IR spectrum for complex **2** at energies above 3000 cm^{-1}; they are at 3470, 3411, 3369, and 3217 cm^{-1}. The two bands at 3369 and 3217 cm^{-1} are reasonably assigned to OH stretching vibrations [10d], and the two higher frequency bands (3470, 3411 cm^{-1}) are attributable to coordinated and non-coordinated H_2O molecules. That both bands appeared at lower frequencies than seen in complex **1** [11] could be due to the stronger hydrogen bonding between two water molecules present in complex **2**.

The bands at 1567 and 1446 cm^{-1} are assigned to the COO^- antisymmetric and symmetric stretching vibrations, respectively. The frequency separation of these two bands is only 121 cm^{-1}, which is much smaller than that of free ligand, and also smaller than in copper complexes which have carboxylate bonding mode I [10]. This could be attributed to the unusual coordination mode of the carboxylate group.

Magnetochemistry

Variable-temperature dc magnetic susceptibility data were collected in a 10 kG field for a powdered sample of complex **2** constrained in parafilm. A plot of the effective magnetic moment (μ_{eff}) per molecule or unit in the temperature range of 2.0–320 K is shown in Fig. 3 (circles). The effective magnetic moment per Mn decreases gradually from 5.65 μ_B at 320 K to 5.75 μ_B at 70.0 K, and then more rapidly to 0.96 μ_B at 2.00 K. A weak antiferromagnetic exchange interaction between Mn^{II} centers is evident.

The data were analyzed assuming an isotropic Heisenberg pairwise interaction between Mn^{II} ions in a linear chain. The spin Hamiltonian is given in eqn (1). Wagner and Friedberg [17] derived the equation for the magnetic susceptibility for a linear chain with S = 5/2 ions in

$$H = -2J \sum_{i=1}^{n} S_i \cdot S_{i-1} \quad (1)$$

$$\chi_M = \{Ng^2\mu_B^2 S(S+1)/3kT\}\{(1+U)/(1-U)\} \quad (2)$$

eqn (2), where $U = \coth(K - 1/K)$ and $K = 2JS(S+1)/kT$. The parameters are **J** for the magnetic exchange interaction and an isotropic g value. The solid curve (circles) in Fig. 3 represents the least-squares fit of the data to eqn (2) to give the parameters

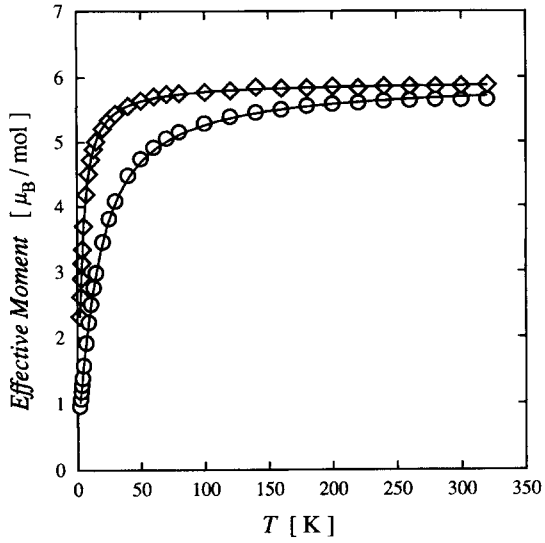

Fig. 3. Plot of the effective magnetic moment versus temperature for a powder sample of $\{[Mn(bic)Cl]_2 \cdot 2(H_2O)\}_n$ (**1**) and $\{[Mn(bic)(H_2O)]_2 \cdot 2Br \cdot 2H_2O)\}_n$ (**2**) (diamonds for complex **1** and circles for complex **2**). Data were collected in a 10.0 kG field. The solid lines represent the best fit of the data to eqn (2).

$J = -1.42(2)$ cm^{-1} and $g = 2.00(1)$. It can be seen that the agreement between the theory and experimental data is quite satisfactory.

The data and fitting results for complex **1** (diamonds) are also shown in Fig. 3. In this complex, the magnetic exchange coupling constant **J** was found to be $-0.30(1)$ cm^{-1}. The stronger antiferromagnetic interaction in complex **2** compared to that in complex **1** probably results from the fact that the magnetic exchange in complex **2** is supported by the μ_2-oxygen bridge atom from the carboxylate group, whereas in complex **1** it is supported by the three atoms of a bridging carboxylate group.

Much effort has been spent to synthesize and characterize Mn^{II} linear chain complexes [17–22]. Three types of bridging ligands have been found that support weak antiferromagnetic interactions: carboxylate, phosphinate and chloride ions. The magnetic exchange parameter **J** varies from -9.3 cm^{-1} for the chloro bridge to -0.2 cm^{-1} for the carboxylate and phosphinate bridges [17–22]. The **J** values for complexes **1** and **2** are within this range.

Acknowledgement—This work was supported by National Science Foundation grant CHE-94-20322 (D.N.H.).

REFERENCES

1. Brechin, E. K., Harris, S. G., Harrison, A., Parsons, S., Whittaker, A. G. and Winpenny, R. E. P., *J. Chem. Soc., Chem. Commun.*, 1997, 653.
2. (a) Powell, A. K., Heath, S. L., Gatteschi, D., Pardi, L., Sessoli, R., Spina, G., Del Giallo, F.

and Pieralli, F., *J. Am. Chem. Soc.*, 1995, **117,** 2491; (b) Heath, S. L. and Powell, A. K., *Angew. Chem. Int. Ed. Engl.*, 1992, **31,** 191.
3. Taft, K. L., Delfs, C. D., Papaefthymiou, G. C., Foner, S., Gatteschi, D. and Lippard, S. J., *J. Am. Chem. Soc.*, 1994, **116,** 823.
4. McCusker, J. K., Christmas, C. A., Hagen, P. M., Chadha, R. K., Harvey, D. F. and Hendrickson, D. N., *J. Am. Chem. Soc.*, 1991, **113,** 6115.
5. Sun, Z., Gatzel, P. K. and Hendrickson, D. N., *Inorg. Chem.*, 1996, **35,** 6640.
6. Goldberg, D. P., Caneschi, A., Delfs, C. D., Sessoli, R. and Lippard, S. J., *J. Am. Chem. Soc.*, 1995, **117,** 5789.
7. Bolcar, M. A., Aubin, S. M. J., Folting, K., Hendrickson, D. N. and Christou, G., *J. Chem. Soc., Chem. Commun.*, in press.
8. (a) Sigel, H., *Coord. Chem. Rev.*, 1993, **122,** 277; (b) Krishnamoorthy, C. R. and Nakon, R. J., *J. Coord. Chem.*, 1991, **23,** 233.
9. (a) Ji, L.-N., Corfu, N. A. and Sigel, H., *Inorg. Chim. Acta*, 1993, **206,** 215; (b) Curfu, N. A., Song, B. and Ji, L.-N., *Inorg. Chim. Acta*, 1992, **192,** 234.
10. (a) Yamaguchi, H., Nagase, M., Yukawa, Y., Inomata, Y. and Takeuchi, T., *Bull. Chem. Soc. Jpn.*, 1988, **61,** 2763; (b) Yamaguchi, H., Inomata, Y. and Takeuchi, T., *Inorg. Chim. Acta*, 1991, **B,** 31. (c) Yamaguchi, H., Inomata, Y. and Takeuchi, T., *Inorg. Chim. Acta*, 1989, **161,** 217; (d) Yamaguchi, H., Inomata, Y. and Takeuchi, T., *Inorg. Chim. Acta*, 1990, **172,** 105.
11. Sun, Z., Gantzel, P. K. and Hendrickson, D. N., *Polyhedron*, 1997, **16,** 3267.
12. Boudreaux, E. A. and Mulay, L. N., ed. *Theory and Applications of Molecular Paramagnetism.* John Wiley & Sons, New York, 1976.
13. (a) Halcrow, M. A., Streib, W. E., Folting, K. and Christou, G., *Acta Cryst.*, 1995, **C51,** 1263; (b) Schake, A. R., Vincent, J. B., Li, Q., Boyd, P. D. W., Folting, K., Huffman, J. C., Hendrickson, D. N. and Christou, G., *Inorg. Chem.*, 1989, **28,** 1915.
14. Gou, S., You, X., Yu, K. and Lu, J., *Inorg. Chem.*, 1993, **32,** 1883.
15. (a) Brooker, S. and McKee, V., *Acta Cryst.*, 1993, **C49,** 441; (b) Brooker, S. and McKee, V., *J. Chem. Soc., Dalton Trans.*, 1990, 2397.
16. Bencini, A., Bianchi, A., Dapporto, P., Garcia-Espana, E., Marcelino, V., Micheloni, M., Paoletti, P. and Paoli, P., *Inorg. Chem.*, 1990, **29,** 1716.
17. Wagner, G. R. and Friedberg, S. A., *Phys. Lett.*, 1964, **9,** 11.
18. Dingel, R., Lines, M. E. and Holts, S. L., *Phys. Rev.*, 1969, **187,** 643.
19. Weng, W., Bartik, T. and Gladysz, J. A., *Angew. Chem. Int. Ed. Engl.*, 1994, **33,** 2199.
20. (a) Cicha, W. V., Hayes, J. S., Oliver, K. W., Rettig, S. J., Thompson, R. C. and Trotter, J., *Can. J. Chem.*, 1985, **63,** 1055; (b) Du, J.-L. Rettig, S. J., Thompson, R. C. and Trotter, J., *Can. J. Chem.*, 1992, **70,** 73,217; (c) Bino, P. B. A., Du, J.-L., Lo, L. S.-M. and Thompson, R. C., *Inorg. Chim. Acta*, 1990, **170,** 45.
21. (a) Borras-Alamenar, J. J., Burriel, R., Coronado, E., Gatteschi, D., Gomez-Garcia, C. J. and Zanchini, C., *Inorg. Chem.*, 1991, **30,** 947; (b) Borras-Alamenar, J. J., Coronado, E., Gomez-Garcia, C. J., Gatteschi, D. and Zanchini, C., *J. Appl. Phys.*, 1990, **67,** 6006.
22. Biagini-Cingi, M., Manotti-Lanfredi, A. M., Ugozzoli, F., Haasnoot, J. G. and Reedijk, J., *Gazz. Chim. Ital.*, 1994, **124,** 509.

Pergamon

PII: S0277-5387(97)00413-0

Polyhedron Vol. 17, No. 9, pp. 1517–1523, 1998
© 1998 Elsevier Science Ltd
All rights reserved. Printed in Great Britain
0277-5387/98 $19.00+0.00

Spectroscopic and theoretical study of aromatic α–hydroxy hydrazones and their copper(II) complexes in dioxane–water mixtures

Gabriela N. Ledesma, Manuel Gonzalez Sierra and Graciela M. Escandar*

Facultad de Ciencias Bioquímicas y Farmacéuticas, Universidad Nacional de Rosario, Suipacha 531 (2000) Rosario, Argentina

(Received 12 April 1997; accepted 26 September 1997)

Abstract—Two aromatic α-hydroxy hydrazones, *N*-phenyl-*N'* (2-hydroxy-1-phenylmethylene hydrazine) and *N*-phenyl-*N'* (2-hydroxy-1-naphthylmethylene hydrazine), and their copper(II) complexes have been studied in both 30% and 70% dioxane–water (v/v) systems. Structural analysis of the anionic forms of the free compounds has been performed using ^{13}C NMR and electronic absorption spectroscopies and semiempirical MO calculations. The equilibrium constants for the deprotonation reactions of the hydrazones and for their coordination with Cu(II) ion were studied by spectrophotometric titration. Coordination binding sites and stereochemistry of the chelates were inferred from NMR spectroscopy. © 1998 Elsevier Science Ltd. All rights reserved

Keywords: spectroscopy; coordination chemistry; aromatic α-hydroxy hydrazones.

Hydrazones are compounds with wide applications in several areas such as organic, analytical and industrial chemistries. The electronic structure of certain hydrazones allows their use as hole-transporting agents in organic layered photoconductors, employed in the electrophotographic process in copiers and printers [1]. From a biological point of view, they have both herbicide and insecticide activities, and are components of several drugs for the treatment of diseases such as cancer and schizophrenia [2]. Pyridoxal hydrazone derivatives have been utilized as chelating agents for mobilizing iron during the therapy of iron overload, in order to replace the commonly used desferrioxamine [3]. At present, there is an increasing interest in the coordination chemistry of suitable ligands for biomedical objectives. However, little information is known in the literature about metal equilibrium constants and complexation behavior of hydrazones. The present investigation was undertaken in view of this and of the potential biological use of complexes formed with this type of ligand.

In the present work, we focus our study on the evaluation of the coordination ability of aromatic α-hydroxy hydrazones with copper(II) ion, as part of a general program devoted to the analysis of prototropic and binding properties of aromatic compounds containing conjugated heterocycles [4]. Specifically, the ligands studied are: *N*-phenyl-*N'*(2-hydroxy-1-phenylmethylene hydrazine) (PHPH) and *N*-phenyl-*N'*(2-hydroxy-1-naphthylmethylene hydrazine) (PHNH) (Scheme 1). These ligands and their metal complexes are not soluble in water but in mixtures of water with dioxane. The use of such solvent mixtures has the advantage of allowing the study of the metal–ligand interaction in a medium with a dielectric constant which is lower relative to pure water, resembling to a certain degree, the interaction in biological media (e.g. active-site cavities of enzymes) [5]. On the other hand, since water–dioxane mixtures are compatible with the membrane glass electrode, a simple relationship between the formed complexes and the pH of the media can be established. The studies are performed by a combination of spectroscopy and semiempirical-molecular mechanics calculations. The relationship of both the tautomeric and isomeric properties of the

* Author to whom correspondence should be addressed.

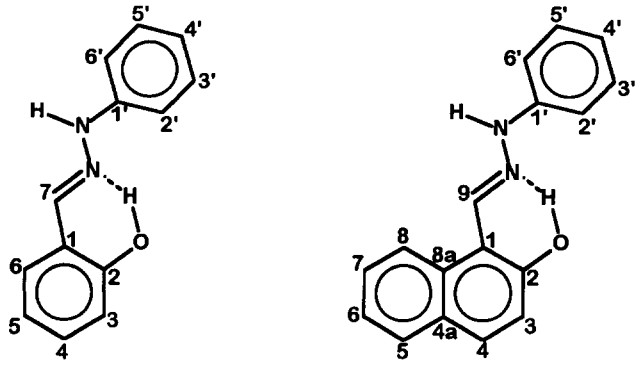

PHPH **PHNH**

Scheme 1.

studied compounds to their acid-base and chelating behaviors is investigated.

EXPERIMENTAL

Reagents and solvents

A stock solution of Cu(II) (0.010 M) was prepared from $Cu(NO_3)_2.3H_2O$ (Mallinckrodt) and the exact concentration was volumetrically determined with ethylenediaminetetraacetic acid and murexide as indicator [6]. Solutions of carbonate-free NaOH in 30% dioxane–70% water (v/v) and 70% dioxane–30% water (v/v) were standardized with the use of the Gran's plots [7]. 1,4-Dioxane (p.a.) was obtained from Merck. The water employed was purified by ion exchange and distilled.

Synthesis of the ligands

The ligands were prepared using standard procedures [8]. Briefly, an aqueous solution of phenylhydrazine hydrochloride was allowed to react with the corresponding ethanolic aldehyde solution (salicylaldehyde or 2-hydroxynaphthalene-1-carbaldehyde) in the presence of sodium acetate. This mixture was warmed and shaken. After cooling, the obtained solid was recrystallized from water/ethanol. Elemental analysis was performed by Atlantic Microlab Inc. for C, H and N, and was in agreement with the calculated values: for PHPH, found: C, 73.54; H, 5.73; N, 13.06; $C_{13}ON_2H_{12}$ requires C, 73.56; H, 5.70; N, 13.20%; for PHNH, found: C, 77.76; H, 5.37; N, 10.71; $C_{17}ON_2H_{14}$ requires C, 77.54; H, 5.36; N, 10.64%. The purity was also checked by thin layer chromatography using different solvent systems.

The stability of the ligands at both acid and alkaline pH was checked by chromatography and ^{13}C NMR, in the solvents and at usual concentrations.

pH determinations

pH values were obtained with a Metrohm 713 pH meter fitted with a glass and reference electrodes. In order to read $-\log [H^+]$, the pH meter–electrode system was calibrated with buffer solutions at 0.10 M ionic strength ($NaNO_3$). The effect of the solvent composition in the pH measurements was taken into account by correcting each meter reading with a conversion factor [9]. This factor was obtained, prior to each experiment, by titration of both 30% and 70% v/v dioxane–water solutions of standard HNO_3 with successive quantities of standard NaOH in the corresponding solvent mixture. In these latter titrations, the ionic strength was also adjusted to 0.10 M with $NaNO_3$ and the temperature was maintained at 20.0°C. The water hydrolysis constants, in our conditions of ionic strength and temperature, were found to be $10^{-14.2}$ and $10^{-15.7}$ for 30% and 70% v/v dioxane–water, respectively. The latter value is in accordance with that found by Motekaitis *et al.* [$K_w = 10^{-16.00}$, 25.00°C, $\mu = 0.100$ M (KCl)] [10].

Equilibrium constant determinations

Due to the low solubility of both ligands and their complexes, the equilibrium constant determinations were performed in diluted solutions using spectrophotometric techniques. The measurements were made at 20.0°C and $\mu = 0.10$ M ($NaNO_3$) using a Beckman DU640 spectrophotometer in 1.00 cm quartz microcells. Conformity to Beer's law in the concentration range used was verified prior the determinations. The initial concentrations of hydrazone in the experimental solutions were in the interval of $2–8 \times 10^{-5}$ M. The PHPH system could be evaluated in both solvent systems, whereas the PHNH system was only investigated in 70% v/v dioxane–water solvent for solubility reasons. Although 1:2 systems were

evaluated in addition to 1:1 metal–ligand systems, only 1:1 complexes were found. A typical spectrophotometric experiment was previously described in the literature [4]. Concisely, profiles of absorbances (at selected wavelengths) vs pH are obtained according to the following procedure: small increments of NaOH solution (made up in 30 or 70% v/v dioxane–water) are added to the solution containing hydrazone or hydrazone and metal in the corresponding solvent system. For each pH point (in the range 5–12.5) a known aliquot of solution is extracted and the absorption spectrum is read. Equilibrium conditions, determined by constant pH meter and absorbance readings, is obtained before proceeding with the next step. Each run was done in triplicate. The data processing for the computation of the equilibrium constants and of the species distribution diagram were performed using the EPSILON program [11].

^{13}C NMR measurements

Carbon-13 NMR spectra were recorded on a Bruker AC-200 NMR spectrometer operating at a nominal frequency of 50.3 MHz. The samples were ca 0.2 M in hydrazones, dissolved in acetone-d_6: water 90% v/v. This ratio of solvents was adequate to keep both the ligands and the complexes in solution at the high concentrations required in these experiments. The alkaline medium was obtained by adding 3 M NaOH. The metal ion was introduced as an appropriate aliquot of 0.1 M $Cu(NO_3)_2$ solution. Since increasing the Cu(II) ion concentration beyond 4×10^{-3} M causes complex precipitation, only a small metal concentration range was used (1×10^{-3}–4×10^{-3} M). The ^{13}C resonances were referenced against the CD_3 signal of acetone-d_6 (30.2 ppm) and converted to the TMS scale.

Molecular orbital and molecular mechanics calculations

Semiempirical MO (AM1) calculations (geometry optimization and calculation of heats of formation) and molecular mechanics (MM+) calculations were performed by using the Hyperchem package of programs on an Pentium-150 microcomputer.

RESULTS AND DISCUSSION

Structural analysis of the ligands

We have previously studied the proton transfer process in the ground state of PHPH and PHNH [12]. The results showed that the enolic tautomers (Scheme 1) are favored in both ligands, and that no aromaticity transfer occurs in the PHNH ligand from the ring containing the OH to the adjacent aromatic ring. In the present paper, structural information about the anionic forms of these compounds is obtained. When the −OH proton is released from the compounds, the C(7)—N(1) and C(9)—N(1) bonds in PHPH and PHNH respectively, are able to acquire single bond character. This may allow a rotation about these bonds, leading to the presence of two possible isomeric structures, A and B (Scheme 2). The heats of formation (ΔH_f°) calculated by AM1 indicate that B isomers are more stable than A forms (Table 1). Whereas in the protonated hydrazones the possibility of hydrogen bond between the OH group and N(1) stabilizes a six-membered ring structure (Scheme 1), in the anionic forms the hydrogen bond takes place between the oxygen and N(2)—H, favoring a structure with a seven membered-ring. Seven and eight membered hydrogen bonded rings have been previously characterized as being very stable [13].

Table 2 collects the complete ^{13}C NMR assignments for the studied compounds in alkaline media. These assignments were based on those previously reported for the protonated structures in $CDCl_3$ [12]. It should be noted that at the high concentration of hydrazones and due to their very low acidity constants in the solvent used, it is not possible to increase the alkali concentration to produce complete deprotonation with no undesirable side reactions. Therefore, the ^{13}C NMR spectra provide evidence for the behavior of deprotonated forms, albeit with a contribution of the protonated forms. The results show that there exist a contribution of the keto structures in the anions, as can be judged from the chemical shifts for the C—O carbon, which are displaced toward higher frequencies. Recall that the typical chemical shifts of C—O(H)

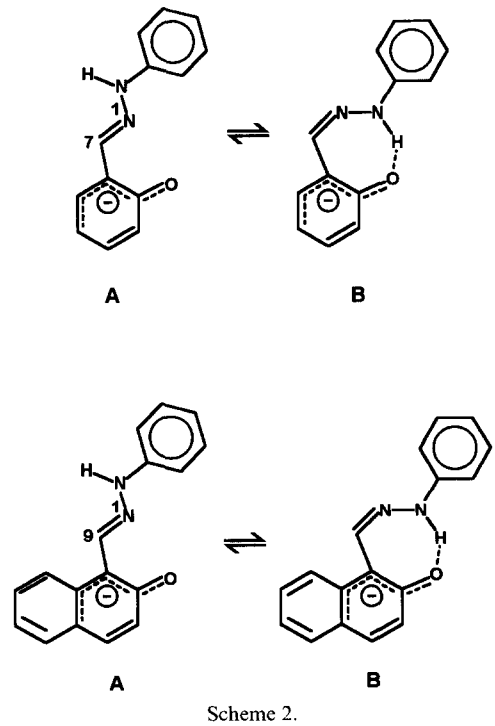

Scheme 2.

Table 1. Relevant AM1 results for the studied deprotonated ligands[a]

	PHPH		PHNH	
Parameter	A	B	A	B
ΔH_f°/kJ mol^{-1}	108.8	58.9	165.6	129.0
N—N—C—C—C—O portion				
N—N	1.358	1.333	1.357	1.341
N—C(7,9)[b]	1.312	1.304	1.309	1.307
C(7,9)[b]—C(1)	1.444	1.448	1.451	1.455
C(1)—C(2)	1.449	1.443	1.440	1.436
C(2)—O	1.258	1.269	1.257	1.263
Aromatic ring bearing the oxygen				
C(2)—C(3)	1.461	1.454	1.470	1.463
C(3)—C(4)	1.363	1.365	1.351	1.353
C(4)—C(5)	1.413	1.409		
C(5)—C(6)	1.380	1.381		
C(6)—C(1)	1.405	1.409		
C(4)—C(4a)			1.432	1.430
C(8a)—C(1)			1.411	1.410
Adjacent aromatic ring				
C(4a)—C(5)			1.406	1.408
C(5)—C(6)			1.381	1.379
C(6)—C(7)			1.408	1.410
C(7)—C(8)			1.375	1.374
C(8)—C(8a)			1.428	1.428

[a] Bond lengths are in Å

[b] C(7) applies to PHPH and C(9) to PHNH.

Table 2. ^{13}C NMR Chemical shift assignments for PHPH and PHNH in alkaline medium[a]

Carbon	PHPH	PHNH
1	126.4	111.6
2	169.2	161.2
3	115.8	120.2
4	132.5	131.7
4a		129.0
5	123.3	123.3
6	127.3	122.9
7	141.5	127.8
8		129.7
8a		133.4
9		140.2
1′	148.8	146.5
2′, 6′	114.6	113.2
3′, 5′	131.6	130.4
4′	120.8	121.8

[a] $C_{PHPH} = C_{PHNH} = 0.2$ M, $C_{OH} = 0.3$ M, solvent: CD_3COCD_3—H_2O 90% v/v.

moieties are in the range 150–155 ppm, whereas those corresponding to carbonylic groups are around 180 ppm.

Semiempirical MO (AM1) calculations (Table 1) are also in agreement with the NMR findings. Geometry optimization of the deprotonated ligands shows bond lengths about the N—N—C—C—C—O moiety corresponding to structures as shown in Scheme 2.

In contrast to the PHPH anion, the anionic form of PHNH is in principle able to suffer aromaticity transfer. However, the C—C bond lengths corresponding to the aromatic ring adjacent to that containing the oxygen show no significant aromaticity transfer, as in the case of the protonated hydrazone. As shown in Table 1, calculated bond lengths around the six-membered ring show alternation between formally double and single bonds. This result leads to the conclusion that the addition of an aromatic ring in going from PHPH to PHNH does not produce major structural changes. This differs from previous observations for related azo compounds and Schiff bases [4,14–16], and may have an influence on the values of deprotonation constants and complex formation.

Deprotonation constants

Tables 3 and 4 show, respectively, the spectral characteristics and deprotonation constant values of the ligands under study. Figure 1 shows the spectra of PHPH in 30% v/v dioxane–water at selected pH values (for clarity only some spectra are illustrated). As shown in this picture, the λ_{max} of 344 nm detected at acid pH, and in accordance with an enolic structure for the protonated ligand, shifts slightly towards a longer wavelength (366 nm) at high pH. This fact could indicate a contribution of the quinoid structure to the deprotonated ligand form. The comparability between the deprotonation constants (within experimental error) of both ligands in 70% dioxane–water could be attributed to the similar structures in both protonated and deprotonated forms, contrary to the case of related azocompounds [4]. The deprotonation constant values of PHPH in aqueous 30% and 70% dioxane could indicate that the solvent effect on the apparent acidity is significant.

Copper(II) complexes

The spectra of the complex solutions resemble those of the free compounds. Therefore, the determinations in the complex systems were performed at wavelengths similar to those used in the deprotonation constants calculations and keeping fixed the molar extinction coefficients and deprotonation constants of the free compounds. As an example of the spectrophotometric titration curves, Fig. 2 shows the profile for the Cu (II)—PHNH system in 70% dioxane–water solvent.

Table 3. Molar absorptivities ($\varepsilon/M^{-1}\,cm^{-1}$) of protonated (LH) and deprotonated (L) hydrazones and ($MH_{-n}L$) copper(II) complexes[a]

Species	PHPH (344 nm)[b]		PHNH (380 nm)[b]
	30% v/v dioxane	70% v/v dioxane	70% v/v dioxane
LH	20200 ± 300	23300 ± 100	23600 ± 200
L	6700 ± 300	19600 ± 700	3200 ± 200
MLH_{-1}	18800 ± 400	20700 ± 100	13200 ± 200
MLH_{-2}	3500 ± 300	See text	6600 ± 900

[a] Charges are omitted.
[b] wavelength values.

Table 4. Deprotonation constants of the studied hydrazones and their cupric complex equilibrium constants

Compound (LH)	Quotient	log K	
		30% v/v dioxane	70% v/v dioxane
PHPH	$[H^+][L^-]/[LH]$	−10.82 ± 0.04	−12.3 ± 0.2
		σ fit = 0.03	σ fit = 0.03
	$[H^+]^2[CuLH_{-1}]/[Cu^{2+}][LH]$	−7.5 ± 0.4	−6.9 ± 0.3
	$[H^+]^3[CuLH_{-2}]^-/[Cu^{2+}][LH]$	−17.5 ± 0.4	[a]
		σ fit = 0.008	σ fit = 0.01
PHNH	$[H^+][L^-]/[LH]$		−12.5 ± 0.3
			σ fit = 0.03
	$[H^+]^2[CuLH_{-1}]/[Cu^{2+}][LH]$		−6.5 ± 0.1
	$[H^+]^3[CuLH_{-2}]^-/[Cu^{2+}][LH]$		−17.5 ± 0.2
			σ fit = 0.02

[a] See text.

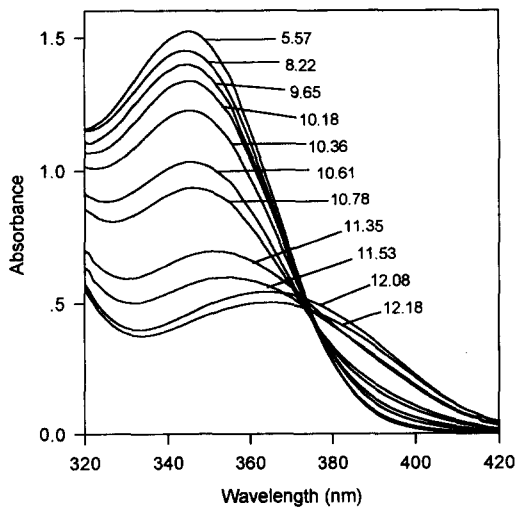

Fig. 1. Absorbance at different pH values of PHPH in 30% v/v dioxane–water; initial $C_{PHPH} = 7.37 \times 10^{-5}$ M, $\mu = 0.10$ M ($NaNO_3$), $t = 20.0$°C.

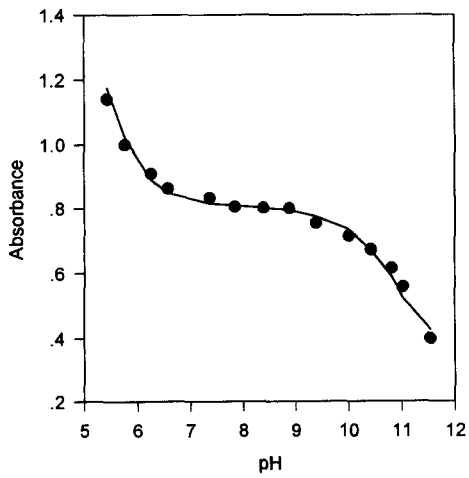

Fig. 2. Experimental (•) and calculated (—) absorbance values vs pH in the Cu(II)–PHNH system in 70% dioxane–water solvent; initial $C_{PHNH} = 6.14 \times 10^{-5}$ M, initial $C_{Cu} = 5.98 \times 10^{-5}$ M, $\mu = 0.10$ M ($NaNO_3$), $t = 20.0$°C.

The spectrophotometric curves of both ligand systems were processed and the best fit involved the formation of the $[CuLH_{-1}]$ and $[CuLH_{-2}]^-$ species. In the latter formula, L represents the ligands in their deprotonated forms and H_{-n} indicates the protons released in the complex formation, in addition to the ligand OH proton. The latter can be ascribed to the water molecules coordinated to the metal center. Hydrolytic species of the Cu(II) ion were not found.

The molar extinction coefficients and the equilibrium constant values for the Cu(II) complexes are listed in Tables 3 and 4, respectively. From the latter magnitudes the species distribution curves were calculated for each system. The species distribution diagram in Fig. 3 points out the interplay of the Cu (II)-containing species for the same system of Fig. 2.

Since no significant changes in the absorbance vs pH in the alkaline zone for the Cu(II)—PHPH system in 70% dioxane were observed, the equilibrium constant for the $[CuLH_{-2}]^-$ complex could not be determined. This fact is ascribed to the possible similarity between the molar extinction coefficients of the two equilibrating complexes.

The complex equilibrium constant values for both hydrazones are similar and this fact can be attributed to the absence of aromaticity transfer in the PHNH molecule, which leads both hydrazones to have similar electronic structures and therefore comparable abilities for coordination.

Structural analysis of complexes

Both A and B anionic forms of the studied hydrazones (Scheme 2) may coordinate the metal ion. In the first case, the donor groups of the ligands include the oxygen and N(1) (through its lone pair of electrons). Thus, six membered-ring chelates can be formed. On the other hand, with B anionic forms, the metal coordination may involve the lone pair electrons of N(2) and the oxygen atom, with seven membered-ring chelates formation. Due to the fact that a high coordination of the metal center would involve severe steric strain, a tetracoordinated copper(II) ion is suggested in both cases. The other binding positions could be fulfilled with hydroxyl groups. Both types of structures are represented in Scheme 3. Unfortunately, both the low concentrations of the complexes in the working solutions and the interference of the ligand's color prevented obtaining unambiguous conclusions from the *d-d* spectra of the complexes regarding the complex geometries.

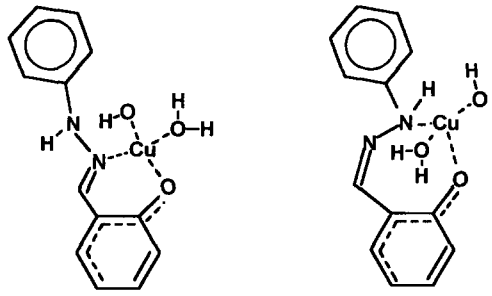

Scheme 3.

With the purpose of comparing the relative steric strain of the complexes involving the proposed spatial arrangements shown in Scheme 3, molecular mechanics calculations were carried out [17,18]. The obtained strain energies for the neutral $[CuLH_{-1}]$ complexes with either type of coordination (12.9 kcal mol^{-1} for both PHPH complexes with rings of six and seven members, and 13.6 and 13.1 kcal mol^{-1} for the PHNH complexes with rings of six and seven members, respectively) do not reflect significant differences. However, more rigorous structural information can be obtained from ^{13}C NMR experiments [19,20]. Upon addition of Cu(II) solution to an alkaline solution of PHPH dissolved in acetone-d_6, selective peak broadening in the ^{13}C NMR spectrum was observed. The affected signals in the complex spectrum are those corresponding to C(2) and C(7) (see Scheme 2). This result suggests that the more stable complex structure is that where the metal ion is bound to the oxygen of C(2) and to the lone pair electrons of N(1), forming a six-membered ring.

Since solid formation occurs even at very low metal ion concentration, the ^{13}C NMR spectrum corresponding to the Cu(II)–PHNH system could not be performed.

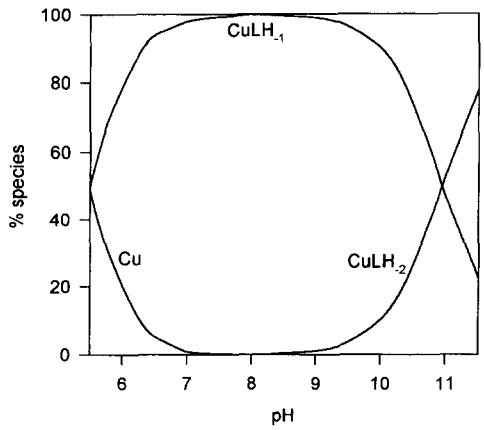

Fig. 3. Distribution of species as a function of pH in a Cu(II)–PHNH system in 70% dioxane–water solvent; initial $C_{PHNH} = 6.14 \times 10^{-5}$ M, initial $C_{Cu} = 5.98 \times 10^{-5}$ M, $\mu = 0.10$ M ($NaNO_3$), $t = 20.0$°C.

CONCLUSIONS

By using spectroscopic methods and semiempirical MO calculations the preferred isomeric and resonant forms of potential ligands as the anions of α-hydroxy hydrazones have been established. Thus, both the

anionic form of PHPH as well as that corresponding to PHNH have a contribution of the keto structures. These structures exist primarily as the isomers with hydrogen bond between the oxygen and the N(2) proton, forming a structure with a seven-membered-ring. No aromaticity transfer occurs in PHNH and this fact is related to the magnitude of the complex equilibrium constants. Both the deprotonation constants of the compounds and their copper(II) complexes were evaluated, confirming the existence of chelates with different degrees of deprotonation. The more probable complex structures would involve a metal coordination with the oxygen, nitrogen N(1) and hydroxyl groups.

Acknowledgements—We thank University of Rosario and CONICET for financial support. We are very grateful to Alejandro C. Olivieri for useful discussion.

REFERENCES

1. Pacansky, J., McLean, A. D. and Miller, M. D., *J. Phys Chem.*, 1990, **94,** 90.
2. Massarani, E., Nardi, D., Tajana, A. and Degen, L., *J. Med. Chem.*, 1971, **14,** 633.
3. Dubois, J. E., Fakhrayan, H., Doucet, J. P. and El Hage Chahine, J. M., *Inorg. Chem.*, 1992, **31,** 853.
4. Ibañez, G. A., Olivieri, A. C. and Escandar, G. M., *J. Chem. Soc., Faraday Trans.*, 1997, **93,** 545.
5. Sigel, H., *Coord. Chem. Rev.*, 1995, **144,** 287.
6. Schwarzenbach, G., *Complexometric Titrations.* Interscience, New York, 1960, p. 82.
7. Rossotti, F. J. C. and Rossotti, H. J., *J. Chem. Ed.*, 1965, **42,** 375.
8. Vogel, A. I., *Practical Organic Chemistry*, Longmans, London 1961, p. 722.
9. Van Uitert, L. G. and Haas, C. G., *J. Am. Chem. Soc.*, 1953, **75,** 451.
10. Motekaitis, R. J. and Martell, A. E., *Inorg. Chem.*, 1988, **27,** 2718.
11. Araujo, C. L., Ibañez, G. A., Ledesma, G. N., Escandar, G. M. and Olivieri, A. C., *Computers & Chem.*, in press.
12. Ledesma, G. N., Ibañez, G. A., Escandar, G. M. and Olivieri, A. C., *J. Mol. Struc.*, in press.
13. Olivieri, A. C., Sanz, D., Claramunt, R. M. and Elguero, J., *J. Chem. Soc., Perkin Trans.* 2, 1993, 1597.
14. Alarcón, S. H., Olivieri, A. C. and Gonzalez Sierra, M., *J. Chem. Soc., Perkin Trans.* 2, 1994, 1067.
15. Alarcón, S. H., Olivieri, A. C., Labadié, G. R., Cravero, R. M. and Gonzalez Sierra, M., *Tetrahedron*, 1995, **51,** 4619.
16. Alarcón, S. H., Olivieri, A. C., Labadié, G. R., Cravero, R. M. and Gonzalez Sierra, M., *Phys. Org. Chem.*, 1995, **8,** 713.
17. Brubaker, G. R. and Johnson, D. W., *Coord. Chem. Rev.*, 1984, **53,** 14.
18. Hancock, R. D. and Martell, A. E., *Chem. Rev.*, 1989, **89,** 1875.
19. Cook, I. B., Magee, R. J., Payne, R. and Ternai, B., *Aust. J. Chem.*, 1986, **39,** 1307.
20. Gyurcsik, B., Gajda, T., Nagy, L. and Burger, K., *J. Chem. Soc., Dalton Trans.*, 1992, 2787.

Pergamon

PII: S0277-5387(97)00401-4

Polyhedron Vol. 17, No. 9, pp. 1525–1534, 1998
© 1998 Elsevier Science Ltd
All rights reserved. Printed in Great Britain
0277-5387/98 $19.00+0.00

Chemistry of $[Ru(tpy)(pap)(L')]^{n+}$ (tpy = 2,2′,6′,2″-terpyridine; pap = 2-(phenylazo)pyridine; L′ = Cl^-, H_2O, CH_3CN, 4-picoline, N_3^-; n = 1, 2). X-ray crystal structure of $[Ru(tpy)(pap)(CH_3CN)](ClO_4)_2$ and catalytic oxidation of water to dioxygen by $[Ru(tpy)(pap)(H_2O)]^{2+}$

Nimai Chand Pramanik,[a] Kausikisankar Pramanik,[b] Prasanta Ghosh[b] and Samaresh Bhattacharya*[a]

[a] Department of Chemistry, Inorganic Chemistry Section, Jadavpur University, Calcutta 700032, India

[b] Department of Inorganic Chemistry, Indian Association for the Cultivation of Science, Calcutta 700032, India

(Received 5 June 1997; accepted 25 September 1997)

Abstract—The reaction of $[Ru(tpy)Cl_3]$ with pap has afforded $[Ru(tpy)(pap)Cl]^+$ which has been isolated and characterized as the perchlorate salt. Treatment of $[Ru(tpy)(pap)Cl]^+$ with Ag^+ in aqueous solution gives $[Ru(tpy)(pap)(H_2O)]^{2+}$. This aquo-complex has been reacted with three monodentate ligands (L′ = CH_3CN, 4-picoline and N_3^-) to afford complexes of type $[Ru(tpy)(pap)(L')]^{n+}$. Structure determination of $[Ru(tpy)(pap)(CH_3CN)](ClO_4)_2$ by X-ray crystallography shows that tpy is coordinated to ruthenium in the usual meridional fashion and the pap ligand is bound to ruthenium with the azo-nitrogen trans to CH_3CN. All these complexes except $[Ru(tpy)(pap)(H_2O)]^{2+}$ show a Ru(II)-Ru(III) oxidation in the range 1.11–1.50 V vs SCE and three ligand(pap/tpy)-based reductions on the negative side of SCE. The aquo-complex shows a $Ru^{II}—OH_2/Ru^{IV}=O$ couple in aqueous solution (pH = 1–4), the E° of this oxidation is estimated to be 0.82 V vs SCE. Attempt to chemically oxidize the aquo-complex by Ce^{4+} in aqueous solution (1 M $HClO_4$) results in the catalytic oxidation of water to dioxygen. © 1998 Elsevier Science Ltd. All rights reserved

Keywords: ruthenium; 2-(phenylazo)pyridine; synthesis; characterization; structure; reactivities.

There has been much current interest [1] in the chemistry of $[Ru(tpy)(L)Cl]^{n+}$ type of complexes (where tpy = 2,2′6′,2″-terpyridine, L = bidentate ligand, n = 0 or 1) primarily due to the dissociation of the Ru—Cl bond and the reactivities resulting thereof (Scheme 1). One particularly interesting aspect of this chemistry is the generation of oxo-ruthenium complex via the formation of aquo-complex. The oxo-ruthenium complexes are receiving continuous attention because of their usefulness as catalysts in different oxidation reactions [2]. As water is a rather labile ligand, the aquo-complexes are known to function as excellent staring materials for the synthesis of mixed ligand complexes and thus they can display quite interesting chemistry as well [3]. Efforts are being made to modulate the reactivities of such complexes by varying the nature of the ligand L. In the present study, we have chosen 2- (phenylazo)pyridine (pap, **1**) as the bidentate ligand. The 2-(phenylazo)pyridine ligand is a strong π-acid, stronger than 2,2′-bipyridine (bby) and other familiar N—N donor ligands, and is a recognized stabilizer of the lower oxidation states of ruthenium [4]. Oxo-ruthenium complexes containing

* Author to whom correspondence should be addressed.

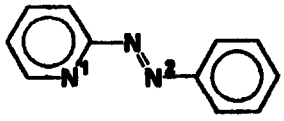

1

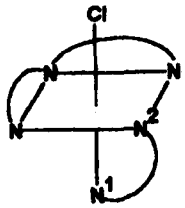

2

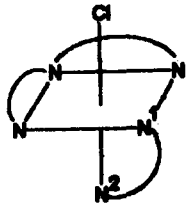

3

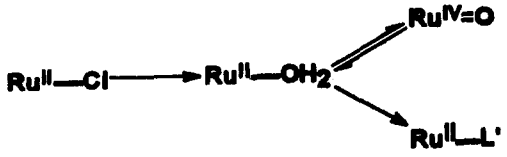

Scheme. 1.

the 2-(phenylazo)pyridine ligand are therefore expected to be strong oxidizing agents. We report here the chemistry of chloro-, aquo-, and oxo-complexes of ruthenium incorporating terpyridine and 2-(phenylazo)pyridine.

EXPERIMENTAL

Materials

Commercial ruthenium trichloride, purchased from Arora Matthey, Calcutta, India, was converted to $RuCl_3 \cdot 3H_2O$ by repeated evaporation to dryness with concentrated hydrochloric acid. [Ru(tpy)Cl_3] and 2-(phenylazo)pyridine were synthesized using literature procedures [5,6]. 4-Picoline (pic), sodium azide and sodium perchlorate were purchased from Aldrich. All other chemicals and solvents were reagent grade commercial materials and used as received. Purification of acetonitrile and preparation of tetraethylammonium perchlorate (TEAP) for electrochemical work were performed as reported in the literature [7].

Physical measurements

Microanalyses (C, H, N) were performed using a Perkin–Elmer 240C elemental analyser. IR spectra were obtained on a Perkin–Elmer 783 spectrometer with samples prepared as KBr pellets. Electronic spectra were recorded on a Hitachi U 3400 spectrophotometer. Magnetic susceptibilities were measured using a PAR 155 vibrating sample magnetometer. ^{1}H NMR spectra were obtained on a Varian Gemini 300 MHz NMR spectrometer using TMS as the internal standard. Solution electrical conductivities were measured using a Philips PR 9500 bridge with a solute concentration of 10^{-3} M. The pH measurements were made with a Systronics 361 pH meter. Electrochemical measurements were made using a PAR model 273 electrochemistry system. A platinum disc working electrode, a platinum wire auxiliary electrode and an aqueous saturated calomel reference electrode (SCE) were used in a three-electrode configuration. All electrochemical data were collected at 298 K and are uncorrected for junction potentials.

X-ray structure determination of [Ru(tpy) (pap) (CH_3CN)](ClO_4)$_2$ complex

Single crystals of the complex were grown at 298 K by slow diffusion of benzene into an acetonitrile solution of the complex. Selected crystal data and a data collection parameters are collected in Table 1. The unit cell parameters were determined by a least-squares fit of 30 machine-centered reflections ($14^\circ < 2\theta < 28^\circ$). Data were collected on a Siemens R3m/V diffractometer using graphite-monochromated Mo-K_α radiation ($\lambda = 0.71073$ Å) and were corrected for Lorentz and polarization factors. The data set was corrected for absorption emperically on the basis of azimuthal scans [8]. Two standard reflections monitored after 98 reflections showed no significant intensity variation.

Systematic absence led to the identification of space group $P2_1/c$. The structure was solved by the heavy-atom method, the positions of the metal ion being determined from a Patterson map and the remaining non-hydrogen atoms by successive Fourier-difference syntheses. The structure was then refined by full-matrix least-squares procedures. All non-hydrogen atoms excluding the disordered perchlorate oxygen atoms were refined anisotropically. Hydrogen atoms were included at their respective calculated positions with fixed isotropic thermal parameters (0.08 Å^2) at the final cycle of refinement. Final residuals are given in Table 1. All computations regarding data collection, structure solution and refinement were carried out on a Micro Vax II computer using the SHELXTL-PLUS programme package [9].

Preparation of the complexes

Warning: Perchlorate salts are hazardous because of the possibilities of explosion. They should be prepared in small amount and handled with care.

Table 1. Crystallographic data for $[Ru(tpy)(pap)(CH_3CN)](ClO_4)_2$

Formula	$C_{28}H_{23}Cl_2N_7O_8Ru$
Formula weight	757.5
Crystal system	Monoclinic
Crystal size (mm)	$0.2 \times 0.3 \times 0.4$
Space group	$P2_1/c$
a (Å)	12.934(4)
b (Å)	13.098(6)
c (Å)	18.655(7)
β (°)	101.08(3)
U (Å^3)	3101(2)
Z	4
F (000)	1528
D_{calc} (g cm^{-3})	1.622
μ (cm^{-1})	7.39
2θ range (°)	3–42
Temperature	295 K
λ (Mo-K_α)	0.71073 Å
Reflections collected	3789
Unique reflections	3347
Observed reflections [$I > 6\sigma(I)$]	2374
Min./Max. Transmission	0.7136/0.7669
Final R^a	0.0564
Final R_w^b	0.0708
GOF^c	1.38
Largest difference peak/e Å^{-3}	0.78

$^a R = \Sigma||F_o| - |F_c||/\Sigma|F_o|$.
$^b R_w = [\Sigma w(|F_o| - |F_c|)^2/\Sigma w|F_o|^2]^{1/2}$;
$w^{-1} = \sigma^2|F_o| + 0.0005|F_o|^2$.
^{c} The goodness of fit is defined as $[w(|F_o| - |F_c|)^2/(n_o - n_v)]^{1/2}$ where n_o and n_v denote the number of data and variables respectively.

$[Ru(tpy)(pap)Cl]ClO_4$

$[Ru(tpy)Cl_3]$ (200 mg, 0.45 mmol) and pap (125 mg, 0.68 mmol) were gently refluxed for 1 h in 30 cm^3 of 3 : 1 ethanol-water containing LiCl (200 mg) and triethylamine (0.06 cm^3). The hot solution was filtered to remove any insoluble material. The filtrate was cooled to room temperature and to it was added a saturated aqueous solution of $NaClO_4$ (10 cm^3). Upon standing pinkish-red microcrystalline solid separated out which was collected by filtration, washed with little cold water and dried *in vacuo* over P_4O_{10}, yield 230 mg, 78%.

$[Ru(tpy)(pap)(H_2O)](ClO_4)_2$

$[Ru(tpy)(pap)Cl]ClO_4$ (200 mg, 0.31 mmol) and $AgNO_3$ (53 mg, 0.31 mmol) were gently refluxed for 1 h in 30 cm^3 of 1 : 5 acetone-water. After being cooled to room temperature, the mixture was filtered to remove AgCl. To the filtrate was added a saturated aqueous solution of $NaClO_4$ (10 cm^3) and the solution was chilled overnight in a refrigerator to give microcrystalline red precipitate of $[Ru(tpy)(pap)(H_2O)](ClO_4)_2$ which was collected by filtration, washed with a minimum volume of cold water and dried *in vacuo* over P_4O_{10}, yield 157 mg, 70%.

$Ru(tpy)(pap)(CH_3CN)]ClO_4)_2$

$[Ru(tpy)(pap)(H_2O)](ClO_4)_2$ (200 mg, 0.27 mmol) was dissolved in acetonitrile (30 cm^3) and gently heated for 30 min with continuous stirring. The volume of the solution was then reduced to ~5 cm^3 and a saturated aqueous solution of $NaClO_4$ (10 cm^3) was added. Upon cooling the solution in an ice bath $[Ru(tpy)(pap)(CH_3CN)](ClO_4)_2$ precipitated as a dark crystalline solid. This was collected by filtration, washed with little cold water and dried *in vacuo* over P_4O_{10}, yield 175 mg, 85%.

$[Ru(tpy)(pap)(pic)](ClO_4)_2$

A solution of $[Ru(tpy)(pap)(H_2O)](ClO_4)_2$ (200 mg, 0.27 mmol) and pic (0.03 cm^3, 0.28 mmol) in 30 cm^3 of ethanol was gently refluxed for 2 h. The volume of the solution was reduced to ~5 cm^3 and a saturated aqueous solution of $NaClO_4$ (10 cm^3) was added to it. Upon cooling to 0°C a red microcrystalline precipitate separated out which was collected by filtration, washed with a little cold water and dried *in vacuo* over P_4O_{10}, yield 175 mg, 80%.

$[Ru(tpy)(pap)(N_3)]ClO_4$

$[Ru(tpy)(pap)(H_2O)](ClO_4)_2$ (200 mg, 0.27 mmol) was dissolved in 30 cm^3 of 3 : 1 methanol-water and to it was added NaN_3 (18 mg, 0.28 mmol). The solution was refluxed for 1 h on a water bath. The volume of the solution was reduced to ~10 cm^3. Upon cooling the solution in an ice-bath $[Ru(tpy)(pap)(N_3)]ClO_4$ separated out as a deep pink microcrystalline solid which was isolated by filtration, washed with little ice-cold water and dried *in vacuo* over P_4O_{10}, yield 147 mg, 82%.

RESULTS AND DISCUSSION

Synthesis and characterization

$[Ru(tpy)(pap)Cl]^+$ has been synthesized by the smooth reaction of pap with $[Ru(tpy)Cl_3]$ in refluxing ethanol in the presence of NEt_3 and LiCl. In this reaction NEt_3 functions as a reducing agent to help the dissociation of Cl^- from $[Ru(tpy)Cl_3]$, whereas LiCl is used to prevent any dissociation of Cl^- from the product. The complex cation has been isolated as perchlorate salt in the solid state and its composition has been confirmed by microanalytical data (Table 2). As pap is an unsymmetrical bidentate ligand, $[Ru(tpy)(pap)Cl]^+$ may exist in two geometrical isomeric

Table 2. Microanalytical, electronic spectral and molar conductivity data.

Complex	Microanalytical data[a] %C	%H	%N	Electronic spectral data[b] λ max/nm (ε/dm^3 mol^{-1} cm^{-1})	Molar conductivity data[c] (Λ_M)
[Ru(tpy)(pap)Cl]ClO_4	47.82(47.85)	2.98(3.07)	12.84(12.88)	680(360); 505(10,400); 325[e](25,300); 310(29,300)	138
[Ru(tpy)(pap)(H_2O)]$(ClO_4)_2$[d]	42.64(42.51)	3.02(3.00)	11.48(11.44)	650(500); 485(12,100); 350[e](9900); 320(25,400)	240
[Ru(tpy)(pap)(CH_3CN)]$(ClO_4)_2$	44.42(44.39)	3.14(3.04)	12.82(12.95)	660(500); 490(12,100); 350(11,300); 328(28,900)	245
[Ru(tpy(pap)(pic)]$(ClO_4)_2$	47.52(47.47)	3.40(3.34)	12.02(12.11)	650(490); 495(11,300); 360[e](8450); 320(20,900)	237
[Ru(tpy)(pap)(N_3)]ClO_4	47.30(47.38)	3.11(3.04)	19.02(19.13)	700(410); 514(10,600); 330[e](19,900); 312(26,200)	149

[a] Calculated values are in parentheses.
[b] In acetonitrile solution.
[c] In acetonitrile solution.
[d] In aqueous solution.
[e] Shoulder.

forms, **2** and **3**. We assign structure **3** to this complex in analogy to the structurally characterized [Ru(tpy)(pap)(CH_3CN)]$(ClO_4)_2$ complex (*vide infra*). Infrared spectrum of this complex shows many vibrations of different intensities below 1600 cm^{-1} and is therefore complex in nature. Attempts have not been made to assign each individual band. However, a sharp vibration observed at 325 cm^{-1} is assigned to ν(Ru—Cl) stretching mode. Another intense band at 1310 cm^{-1} is attributed to the ν(N=N) vibration [10]. Two intense vibrations are observed at 1100 cm^{-1} and 620 cm^{-1} due to the presence of ClO_4^-. Magnetic susceptibility measurement shows that [Ru(tpy)(pap)Cl]$^+$ is diamagnetic which is in accordance with the +2 state of ruthenium (low-spin d^6, S=0) in this complex. ^{1}H NMR spectrum of [Ru(tpy)(pap)Cl](ClO_4), recorded in CD_3CN solution, shows many sharp resonances (Fig. 1). In total thirteen resonances may be expected for the twenty hydrogens present in the [Ru(tpy)(pap)Cl]$^+$ complex, seven signals for the nine hydrogens of pap ligand and six signals for the eleven hydrogens of tpy ligand (because a plane of symmetry splits the tpy ligand into two equal halves). Actually eleven resonances are experimentally observed (Fig. 1) because of overlap of signals. Integration of the signals corresponds to the twenty hydrogens present in the complex. Assignment of all the observed signals to specific hydrogens has not been attempted. However, the two doublets (1-H each) observed at 9.86 and 8.73 ppm are respectively assigned to the 6-H and 3-H of the pyridine ring in the pap ligand.

Electronic spectrum of [Ru(tpy)(pap)Cl]ClO_4 recorded in acetonitrile solution, shows four absorptions in the visible region (Table 2). The low-intensity absorption observed at 680 nm is assigned to the *d-d* transition ($^1A_1 \rightarrow {}^1T_1$) ([11]. The other possible *d-d* transition ($^1A_1 \rightarrow {}^1T_2$) [11] could not be detected due to the presence of intense absorption at higher energies. The other three intense absorptions are probably due to allowed metal-to-ligand charge-transfer transitions. Multiple charge-transfer transitions in such complexes may result from lower symmetry splitting of the metal level, the presence of different acceptor orbitals and from the mixing of singlet and triplet configurations in the excited state through spin-orbit coupling [12]. Conductivity measurement in acetonitrile solution shows that [Ru(tpy)(pap)Cl]ClO_4 behaves as a 1 : 1 electrolyte (Table 2), as expected.

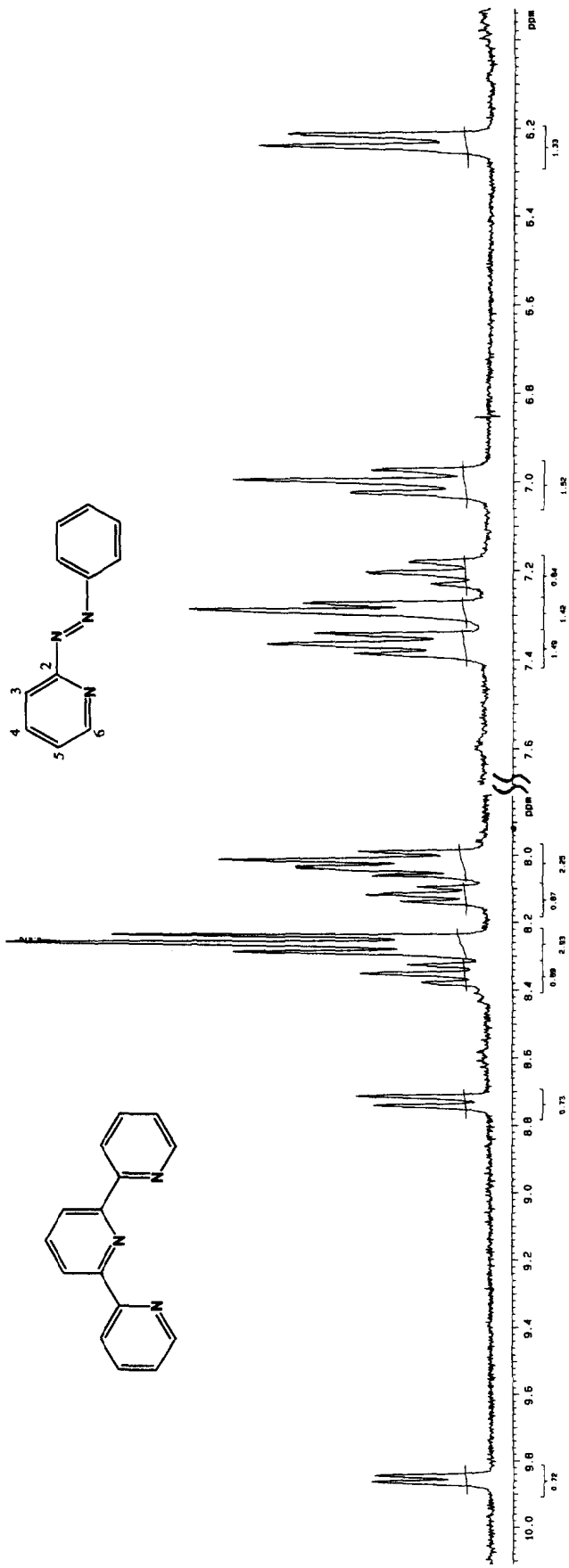

Fig. 1. ^{1}H NMR spectrum of [Ru(tpy)(pap)Cl]ClO_4 in CD_3CN solution.

Table 3. Selected bond distances (Å) and bond angles ( ) for [Ru(tpy)(pap) (CH_3CN)](ClO_4)$_2$

Ru—N(1)	2.084(9)	Ru—N(2)	1.987(8)
Ru—N(3)	2.075(8)	Ru—N(4)	2.062(7)
Ru—N(6)	1.971(7)	Ru—N(7)	2.057(7)
N(5)—N(6)	1.281(13)	N(7)—C(27)	1.123(11)
C(27)—C(28)	1.424(15)		
N(1)—Ru—N(2)	78.8(4)	N(1)—Ru—N(3)	157.7(4)
N(2)—Ru—N(3)	79.3(4)	N(1)—Ru—N(4)	100.4(4)
N(2)—Ru—N(4)	173.6(3)	N(3)—Ru—N(4)	101.8(3)
N(1)—Ru—N(6)	99.4(3)	N(2)—Ru—N(6)	97.5(3)
N(3)—Ru—N(6)	87.5(3)	N(4)—Ru—N(6)	76.3(3)
N(1)—Ru—N(7)	89.8(3)	N(2)—Ru—N(7)	90.6(3)
N(3)—Ru—N(7)	86.3(3)	N(4)—Ru—N(7)	95.8(3)
N(6)—Ru—N(7)	168.7(2)	Ru—N(7)—C(27)	171.4(9)
N(7)—C(27)—C(28)	178.5(13)		

Reaction of $[Ru(tpy)(pap)Cl]^+$ with Ag^+ in 1 : 5 acetone-water solution results in the deposition of AgCl leaving $[Ru(tpy)(pap)(H_2O)]^{2+}$ in solution, which has been subsequently precipitated as the red perchlorate salt. Elemental analytical data (Table 2) agree well with the composition of this complex. [Ru(tpy)(pap)(H_2O)](ClO_4)$_2$ is diamagnetic, as expected and is assumed to have a stereochemistry similar to **3** with H_2O replacing Cl^-. Infrared spectrum of this aquo-complex is very similar to that of the precursor chloro-complex, except that the ν(Ru—Cl) vibration, observed in the chloro-complex at 325 cm^{-1}, is absent in the aquo-complex. Besides that, an additional broad band centered around 3450 cm^{-1} is observed in the aquo-complex due to the coordinated water molecule. [Ru(tpy)(pap)(H_2O)](ClO_4)$_2$ behaves as a 1 : 2 electrolyte in aqueous solution (Table 2), as expected. Electronic spectrum recorded in aqueous solution shows two intense metal-to-ligand charge-transfer transitions at 485 nm and 350 nm together with a weak *d-d* ($^1A_1 \rightarrow {}^1T_1$) transition at 650 nm (Table 2).

Electronic spectrum of the aquo-complex is characteristically different in acetonitrile solution indicating coordination of CH_3CN. To investigate and utilize this lability of the aquo ligand, the aquo-complex has been reacted with three monodentate *N*-donor ligands [viz. acetonitrile, 4-picoline (pic) and azide (N_3^-)] and three complexes of type $[Ru(tpy)(pap)(L')]^{n+}$ are obtained in decent yields. Compositions of these three complexes have been verified by their elemental analytical data (Table 2). All three complexes are diamagnetic and show sharp ^1H NMR signals in $CDCl_3$ solution. These spectra are mostly similar to the spectrum of $[Ru(tpy)(pap)Cl]^+$, the differences observed are due only to the new ligand L′. For example in the acetonitrile complex (L′ = CH_3CN), the acetonitrile methyl signal is observed at 2.78 ppm. Infrared spectra of the $[Ru(tpy)(pap)(L')]^{n+}$ species are complex in nature, as expected, and they are very similar to one another with minor differences due to the difference in L′. Conductivity measurements of the three $[Ru(tpy)(pap)(L')]^{n+}$ complexes in acetonitrile solution show that the L′ = CH_3CN and pic complexes (n = 2) are 1 : 2 electrolytes and L′ = N_3^- (n = 1) complex is a 1 : 1 electrolyte (Table 2), as expected. Electronic spectra of these complexes in acetonitrile solution show several intense absorptions in the visible region (Table 2) which are probably due to metal-to-ligand charge-transfer transitions.

Crystal structure of [Ru(tpy)(pap)(CH_3CN)] (ClO_4)$_2$

A perspective view of the complex cation is shown in Fig. 2 and selected bond distances and angles are listed in Table 3. The coordination sphere around ruthenium is N_6 with varying Ru—N distances. The tpy ligand is coordinated in the usual fashion with the central nitrogen (N3) being closest to ruthenium [2(i),13]. The pap ligand is bound to ruthenium with the azo nitrogen (N6) *trans* to the coordinated CH_3CN. The Ru—N6 (azo) distance is much shorter than the Ru—N4 (py) distance which is attributed to the better π-backbonding [$d\pi$(Ru) $\rightarrow \pi^*$(azo)] power of the azo function [14]. Accordingly the azo N6-N5 distance is longer than that in the uncoordinated ligand [14]. The CH_3CN molecule is coordinated in the usual manner [13] with slight deviation from linearity around C27 and N7. The other three [Ru(tpy)(pap)(L′)]$^{n+}$ complexes are assumed to have similar structure with the L′ replacing CH_3CN.

Cyclic voltammetric studies

Cyclic voltammograms of all the complexes except $[Ru(tpy)(pap)(H_2O)]^{2+}$ have been recorded in acetonitrile solution. Voltammetric data are presented in Table 4 and selected voltammograms are shown in Fig. 3. All these complexes show a reversible one-electron oxidation in the range 1.1–1.5 V (all poten-

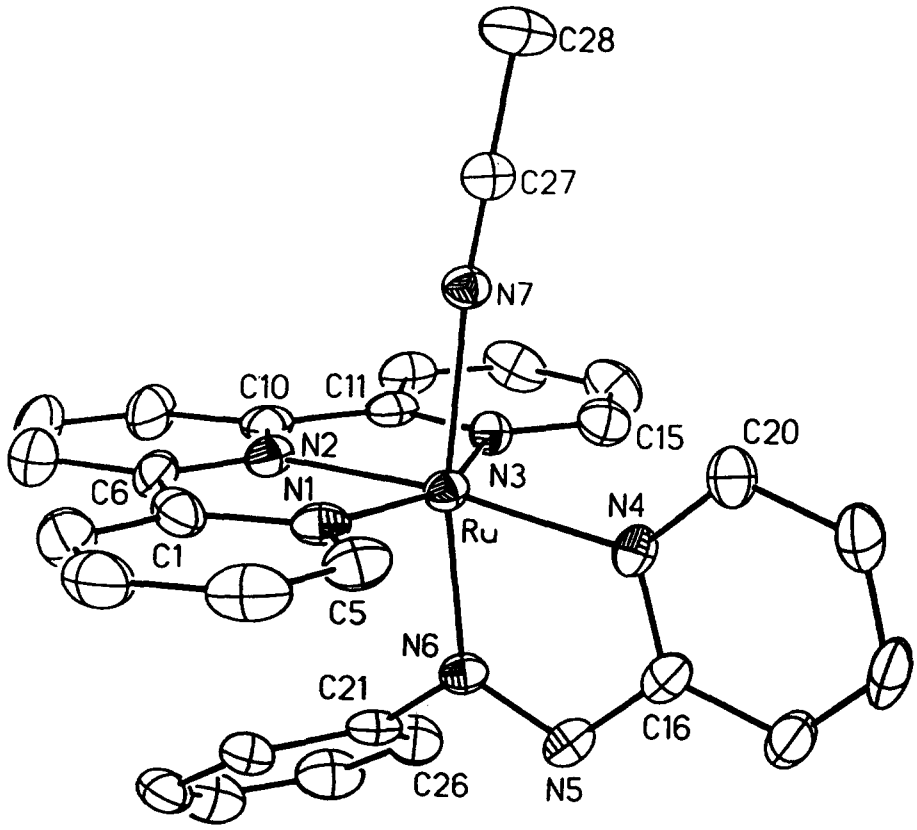

Fig. 2. An ORTEP plot and atom-labelling scheme for the cation of $[Ru(tpy)(pap)(CH_3CN)](ClO_4)_2$.

Table 4. Cyclic voltammetric data

Complex	Voltammetric data[a] Ru^{II}-Ru^{III}	E^0_{298}/V(ΔE_p/mV) Ligand reductions
$[Ru(tpy)(pap)Cl]ClO_4$	1.21(60)	−0.72(60); −1.21(100); −1.40(100)
$[Ru(tpy)(pap)(CH_3CN)](ClO_4)_2$	1.29(80)	−0.51(70); −1.29(60); −1.45(100)
$[Ru(tpy)(pap)(pic)](ClO_4)_2$	1.50(80)	−0.31(60); −1.04(80); −1.48(80)
$[Ru(tpy)(pap)(N_3)]ClO_4$	1.11(80)	−0.60(80); −1.27(80); −1.60(80)

[a] Condition: solvent, acetonitrile; supporting electrolyte, TEAP (0.1 M); working electrode, platinum; reference electrode, SCE; solute concentration, $\sim 10^{-3}$ M; $E^0_{298} = 0.5(E_{pa} + E_{pc})$, where E_{pa} and E_{pc} are anodic and cathodic peak potentials, $\Delta E_p = E_{pa} - E_{pc}$; scan rate, 50 mV s^{-1}.

tials are referenced to SCE) which is assigned to the ruthenium(II)-ruthenium(III) oxidation. The one-electron nature of this oxidation has been established by comparing its current height with that of standard ferrocene/ferrocenium couple under identical experimental condition. The ruthenium(II)-ruthenium(III) oxidation potential is ~400 mV more positive in $[Ru(tpy)(pap)Cl]^+$ than that in $[Ru(tpy)(bpy)Cl]^+$ [2(i)] which is due to the stronger π-acidity of pap than bpy. The ruthenium(II)-ruthenium(III) oxidation potential in $[Ru(tpy)(pap)Cl]^+$ appears to be the highest among the $[Ru(tpy)(N\text{-}N)Cl]^+$ complexes reported so far. The ruthenium(II)-ruthenium(III) oxidation potential in the other three $[Ru(tpy)(pap)(L')]^{n+}$ (L′ = CH_3CN, 4-picoline and N_3^-) complexes is observed to be sensitive to the nature of L′, as expected. For L′ = 4-picoline it is highest and lowest for L′ = N_3^- in this series.

Each complex shows three one-electron reductive responses on the negative side of SCE (Table 4). 2-(Phenylazo)pyridine is known to accept two electrons in its lowest unoccupied molecular orbital which is largely azo in nature [3(d)]. Polypyridine ligands are also capable of accepting electrons [13]. However it is

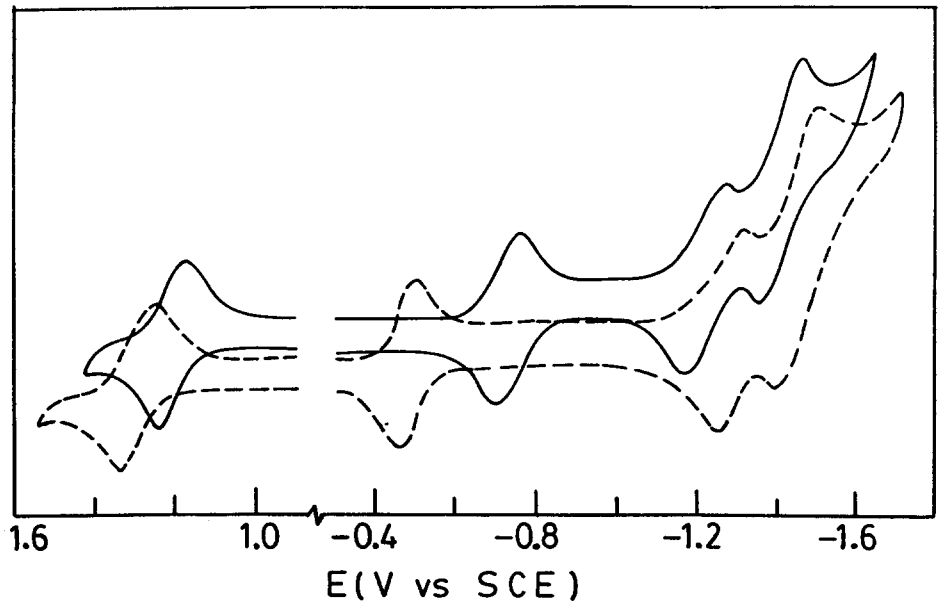

Fig. 3. Cyclic voltammograms of $[Ru(tpy)(pap)Cl]ClO_4$ (—) and $[Ru(tpy)(pap)(CH_3CN)](ClO_4)_2$ (- - -) in acetonitrile solution (0.1 M TEAP) at a scan rate of 50 mV s^{-1}. The solute concentration was $\sim 10^{-3}$ M.

well documented in literature that the azopyridine ligands are better acceptors and undergo easier reductions than the polypyridine ligands [3(d),15]. Hence the first two reductions observed in the $[Ru(tpy)(pap)(L')]^{n+}$ complexes are assigned to pap (eqn (1) and (2)) and the third one is assigned to tpy (eqn (3)).

$$[Ru^{II}(tpy)(pap)(L')]^{+/2+} + e^- \rightleftharpoons [Ru^{II}(tpy)(pap^{\bullet})(L')]^{0/+} \quad (1)$$

$$[Ru^{II}(tpy)(pap^{\bullet})(L')]^{0/+} + e^- \rightleftharpoons [Ru^{II}(tpy)(pap^{\bullet})(L')]^{-/0} \quad (2)$$

$$[Ru^{II}(tpy)(pap^{\bullet})L')]^{-/0} + e^- \rightleftharpoons [Ru^{II}(tpy^{\bullet})(pap^{\bullet})(L')]^{2-/-} \quad (3)$$

Cyclic voltammetry of $[Ru(tpy)(pap)(H_2O)]^{2+}$ in aqueous solution (pH 1–4) shows a single step two-electron oxidation (eqn 4). The two-electron nature of this oxidation has been established by comparing

$$[Ru^{II}(tpy)(pap)(H_2O)]^{2+} \rightarrow [Ru^{IV}(tpy)(pap)(O)]^{2+} + 2H^+ + 2e^- \quad (4)$$

its current height with that of $[Fe(CN)_6]^{4-}/[Fe(CN)_6]^{3-}$ couple under identical (pH = 7) experimental condition. This oxidation potential is sensitive to the pH of the solution and it decreases linearly with the increase in pH with a slope of 60 mV per unit pH. This, according to eqn 5

$$E = E^{\circ} - 0.059(m/n)pH \quad (5)$$

(where E = observed potential, E^0 = formal potential, m = number of proton transfer and n = number of electron transfer) [2(i)], indicates the loss of two protons along with two electrons. The formal potential of this oxidation, calculated from the intercept of the linear plot at pH = 0 (eqn 5), is found to be 0.82 V.

Synthesis of the oxo-ruthenium complex, $[Ru^{IV}(tpy)(pap)(O)]^{2+}$, has been attempted by chemical oxidation of the aquo-complex by Ce^{4+} in 1 M $HClO_4$. This reaction has been monitored spectrophotometrically and the results are shown in Fig. 4. Addition of a ten fold excess of Ce^{4+} to the aquo-complex initially brings about the expected oxidation (eqn 6), characterized by an instantaneous colour change from red to orange. Accordingly the intense absorption at 480 nm

$$[Ru^{II}(tpy)(pap)(H_2O)]^{2+} + 2Ce^{4+} \rightleftharpoons [Ru^{IV}(tpy)(pap)(=O)]^{2+} + 2Ce^{3+} + 2H^+ \quad (6)$$

(ε = 12 400 M^{-1} cm^{-1}) due to the aquo-complex disappears and a new absorption at 390 nm (ε = 11 700 M^{-1} cm^{-1}), characteristic of the oxo-complex, develops. However, with time this new absorption gradually disappears and the original absorption at 480 nm is restored slowly with an isosbestic point at 438 nm. This clearly indicates regeneration of the aquo-complex from the oxo-complex (eqn 7). This

$$[Ru^{II}(tpy)(pap)(O)]^{2+} + H_2O \rightarrow [Ru(tpy)(pap)(H_2O)]^{2+} + 1/2O_2 \quad (7)$$

reduction reaction is found to be pseudo-first-order

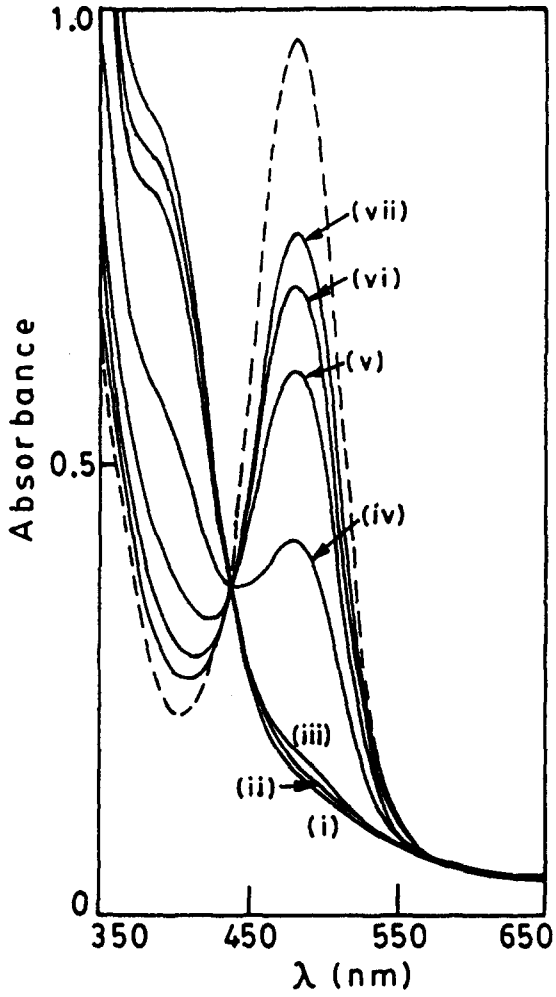

Fig. 4. Electronic spectrum of $[Ru(tpy)(pap)(H_2O)]^{2+}$ in 1 M $HClO_4$ (---) and the time dependent electronic spectra of $[Ru(tpy)(pap)(H_2O)]^{2+}$ with ten-fold excess of Ce^{4+} in 1 M $HClO_4$ (i–vii): (i) 5 min, (ii) 10 min, (iii) 15 min, (iv) 25 min, (v) 35 min, (vi) 45 min and (vii) 60 min.

with respect to the oxo-complex and the rate constant for this reaction has been found to be 4.6×10^{-4} sec^{-1}. If more Ce^{4+} is added to the reaction mixture, the same sequence of reactions is repeated. The net result is therefore the catalytic oxidation of water to dioxygen by $[Ru(tpy)(pap)(H_2O)]^{2+}$ in presence of Ce^{4+} (Scheme 2). The generation of dioxygen has been established by its characteristic cyclic voltammetric reduction at -0.3 V. Whether dioxygen is generated directly from water or via the formation of hydrogen peroxide is not known. Similar catalytic oxidation of water to dioxygen by aquo-complex of ruthenium is reported in the literature [16].

The pK_a of $[Ru(tpy)(pap)(H_2O)]^{2+}$, determined by pH-metric titration of the aquo-complex with standard alkali solution, is found to be 8.4. Comparison with the acidity of some similar $[Ru(tpy)(N\text{-}N)(H_2O)]^{2+}$ complexes (Table 5) shows that the *N-N* = pap complex is the strongest acid in this family, which is due to the better π-acidity of the pap than the other *N-N* ligands. The $[Ru(tpy)(pap)(H_2O)]^{2+}$ complex is the only example of its type which can catalyze the oxidation of water to dioxygen. The single-step two-electron two-proton transfer reaction (eqn 4) at high potential and the low pK_a of this aquo-complex are attributed to the observed catalytic activity. Utilization of the Ru^{II}—OH_2/Ru^{IV}=O couple for the catalytic oxidation of different organic substrates is under investigation.

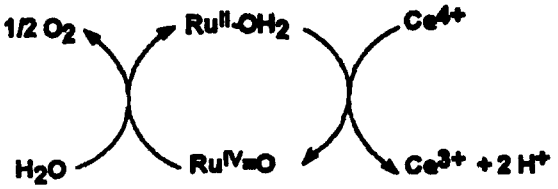

Scheme. 2.

Table 5. pK_a values of $[Ru(tpy)(N\text{-}N)(H_2O)]^{2+}$ complexes

N-N	pK_a
pap	8.4[a]
bpz	8.8[b]
pda	9.2[c]
bpy	9.7[b]
tmen	10.2[c]

[a] This work.
[b] Reference 2(i).
[c] Reference 2(h).

Acknowledgements—The crystal structure was determined at the National Single Crystal Diffractometer Facility, Department of Inorganic Chemistry, Indian Association for the Cultivation of Science, Calcutta. Financial support from the Council of Scientific and Industrial Research [Grant No. 01(1408)/96/EMR-II], New Delhi, India, is gratefully acknowledged. The authors thank the Third World Academy of Sciences for financial assistance for the purchase of electrochemical cell system. Thanks are also due to Dr Sreebrata Goswami, Indian Association for the Cultivation of Science, Calcutta, for many helpful discussions.

REFERENCES

1. (a) Constable, E. C. and Hannon, M. J., *Inorg. Chim. Acta*, 1993, **211**, 101; (b) Yu, W. Y., Chang, W. C., Che, C. M. and Wang, Y., *Polyhedron*, 1994, **13**, 2963; (c) Bhattacharya, S., *Polyhedron*, 1994, **13**, 451; (d) Coe, B. J., Thompson, D. W., Culbertson, C. T., Schoonover, J. R. and Meyer, T. J., *Inorg. Chem.*, 1995, **34**, 3385; (e) Bardwell,

D. A., Thompson, A. M. W. C., Jeffery, J. C., McCleverty, J. A. and Ward, M. D., *J. Chem. Soc., Dalton Trans.*, 1996, 873; (f) Dovletoglou, A., Adeyemi, S. A. and Meyer, T. J., *Inorg. Chem.*, 1996, **35,** 4120; (g) Sinha, P. K., Chakravarty, J. and Bhattacharya, S., *Polyhedron*, 1996, **15,** 2931.

2. (a) Llobet, A., Doppelt, P. and Meyer, T. J., *Inorg. Chem.*, 1988, **27,** 514; (b) Dengel, A. C., El-Hendawy, A. M., Griffith, W. P., O'Mahoney, C. A. and William, D. J., *J. Chem. Soc., Dalton Trans.*, 1990, 737; (c) Grover, N. and Thorp, H. H., *J. Am. Chem. Soc.*, 1991, **113,** 7030; (d) Griffith, W. P. and Jolliffe, J. M., *J. Chem. Soc., Dalton Trans.*, 1992, 3483; (e) Gupta, N., Grover N., Neyhart, G. A., Singh, P. and Thorp, H. H., *Inorg. Chem.*, 1993, **32,** 310; (f) Grover, N., Welch, T. W., Fairley, T. A., Cory, M. and Thorp, H. H., *Inorg. Chem.*, 1994, **33,** 3544; (g) Cheng, W. M., Yu, W. Y., Cheung, K. K. and Che, C. M., *J. Chem. Soc., Dalton Trans.*, 1994, 57; (h) Cheng, W. C., Yu, W. Y., Cheung, K. K. and Che, C. M., *J. Chem. Soc., Chem. Commun.*, 1994, 1063; (i) Gerli, A., Reedijk, J., Lakin, M. T. and Spec, A. L., *Inorg. Chem.*, 1995, **34,** 1863; (j) Maux, P. L., Bahri, H., Simmonneaux, G. and Toupet, L., *Inorg. Chem.*, 1995, **34,** 4691; (k) Hungko, P., Chen, T. Y., Zhu, J., Cheng, K. F., Peng, S. M. and Che, C. M., *J. Chem. Soc., Dalton Trans.*, 1995, 2215; (l) Bailey, A. J., Griffith, W. P. and Savage, P. W., *J. Chem. Soc., Dalton Trans.*, 1995, 3537; (m) Nararra, M., Galembeak, S. E., Romero, J. R. and Giovani, W. F. D., *Polyhedron*, 1996, **15,** 1531.
3. (a) Cheney, R. P. and Armor, J. N., *Inorg. Chem.*, 1977, **16,** 3338; (b) Bernhend, P., Lechmann, H. and Ludi, A., *J. Chem. Soc., Chem. Commun.*, 1981, 1216; (c) Goswami, S., Chakravarty, A. R. and Chakravorty, A., *Inorg. Chem.*, 1983, **22,** 602; (d) Goswami, S., Mukharjee, R. N. and Chakravorty, A., *Inorg. Chem.*, 1983, **22,** 2825.
4. Krause, R. A. and Krause, K., *Inorg. Chem.*, 1980, **19,** 2600; (b) Goswami, S., Chakravarty, A. R. and Chakravorty, A., *Inorg. Chem.*, 1981, **20,** 2246; (c) Krause, R. A. and Krause, K., *Inorg. Chem.*, 1982, **21,** 1714.
5. Sullivan, B. P., Calvert, J. M. and Meyer, T. J., *Inorg. Chem.*, 1980, **19,** 1404.
6. Campbell, N., Henderson, A. W. and Taylor, D., *J. Chem. Soc.*, 1953, 1281.
7. (a) Sawyer, D. T. and Roberts, J. L., *Jr. Experimental Electrochemistry for Chemists.* Wiley, New York, pp. 167–215.; (b) Walter, M. and Ramaley, L., *Anal. Chem.*, 1973, **45,** 165.
8. North, A. C. T., Philips, D. C. and Mathews, F. S., *Acta Crystallogr., Sect. A*, 1968, **24,** 351.
9. Sheldrick, G. M., SHELXTL-PLUS 90, Structure Determination Software Programs, Siemens Analytical X-Ray Instruments, Madison, WI, 1990.
10. Goswami, S., Chakravarty, A. R. and Chakravorty, A., *Inorg. Chem.*, 1982, **21,** 2737.
11. (a) Mercer, E. E. and Buckley, R. R., *Inorg. Chem.*, 1965, **4,** 1692; (b) El-Hendaway, A. E., Al-Kubaisi, A. H., El-Ghany, A., El-Kourashy and Shanab, M. M., *Polyhedron*, 1993, **12,** 2343; (c) Chakravarty, J. and Bhattacharya, S., *Polyhedron*, 1996, **15,** 257.
12. (a) Pankuch, B. J., Lacy, D. E., and Crosby, G. A., *J. Phys. Chem.*, 1980, **84,** 2061; (b) Ceulemans, A. and Vanquickenborne, L. G., *J. Am. Chem. Soc.*, 1981, **103,** 2238; (c) Decurtius, S., Felix, F., Ferguson, J., Gudel, H. U. and Ludi, A., *J. Am. Chem. Soc.*, 1980, **102,** 4102; (d) Kober, E. M. and Meyer, T. J., *Inorg. Chem.*, 1982, **21,** 3967.
13. Rasmussen, S. C., Ronco, S. E., Milsna, D. A., Billadeau, M. A., Pennington, W. T., Kolis, J. W. and Peterson, J. D., *Inorg. Chem.*, 1995, **34,** 821.
14. Seal, A. and Roy, S., *Acta Cryst.*, 1984, **C40,** 929.
15. Kelso, L. S., Reitsma, D. A. and Keene, F. R., *Inorg. Chem.*, 1996, **35,** 5144.
16. Goswami, S., Chakravarty, A. R. and Chakravorty, A., *J. Chem. Soc., Chem. Commun.*, 1982, 1288.

Pergamon

PII: S0277-5387(97)00392-6

Polyhedron Vol. 17, No. 9, pp. 1535–1540, 1998
© 1998 Elsevier Science Ltd
All rights reserved. Printed in Great Britain
0277-5387/98 $19.00+0.00

A trinuclear nickel(II) complex with alternating square-planar and octahedral geometries. Synthesis, crystal structure and magnetic properties of $[Ni_3(oxen)_2(en)][ClO_4]_2$

Zhong-Ning Chen,[a]* Hua-Xin Zhang,[a] Kai-Bei Yu,[b] Cheng-Yong Su[a] and Bei-Sheng Kang[a]

[a] Institute of Physical Chemistry, School of Chemistry and Chemical Engineering, Zhongshan University, Guangzhou, 510275 Guangdong, P.R. China

[b] Analysis Center, Chengdu Branch of Chinese Academy of Sciences, Chengdu 610041, Sichuan, P.R. China

(Received 28 April 1997; accepted 19 September 1997)

Abstract—The reaction of Ni(oxen) [oxen = *N*,*N*′-bis(2-aminoethyl)oxamido dianion], $NiCl_2$ and the disodium salt of EDTA (ethylenediamine tetraacetic acid) in 1 : 1 : 1 molar ratio gave the trinuclear complex $[Ni_3(oxen)_2(en)][ClO_4]_2$ (en = 1,2-ethylenediamine), where en came from the partial decomposition of oxen. The complex exhibits a curved Ni_3 metal arrangement with the angle Ni(2)—Ni(1)—Ni(2a) of 119.0°. The structure consists of a Ni_3^{II} unit with three nickel(II) atoms chelated and bridged by two oxamidato (oxen) groups in *cis*-conformation. The central nickel atom has a distorted octahedral geometry whereas the two on the sides have square-planar surroundings. The complex is paramagnetic and its magnetic behaviour can be interpreted by single-ion anisotropy with $D = 5.22\ cm^{-1}$ and $m_s = 0$ singlet ground state. © 1998 Elsevier Science Ltd

Keywords: crystal structure; magnetism; oxamidate; nickel(II) complex; trinuclear complex.

N,*N*′-disubstituted oxamides are multifunctional ligands which can chelate as well as bridge metal ions to form polynuclear and low-dimensional complexes. The versatility of these ligands (Scheme 1) is based on: (i) the variety of substituted derivatives, which can afford different numbers of chelate rings with different donor atoms [1], (ii) the bidentate character of the mononuclear compounds in *cis*-conformation which can chelate and bridge other metal ions to form polynuclear species [2–6] (Scheme 2), and (iii) the bisterdentate character of these ligands in the *trans*-conformation allowing the formation of *trans*-oxamidato-bridged metal dimers which can be linked by a second bridging ligand such as azide [7–9], cyanate [10], carboxylate [11–13], cyanide [14], pyrimidine [15,16], and 4,4′-bipyridine [15] to form 1D or 2D homo- or heterometallic complexes (Scheme 2).

The mononuclear nickel(II) compounds of oxamidates are diamagnetic due to the square-planar coordination with the strong-field amide N atoms [6], in contrast to the paramagnetic mononuclear copper(II) complexes, and polynuclear ones with oxamidate bridges which usually exhibit strong antiferromagnetic exchange interactions [7–17]. It is known that copper(II) complexes have been actively investigated due to the strong tendency of formation of *trans*-oxamidato-bridged copper(II) dimers which can be linked by a second bridging ligand to form low-dimensional magnetic coupling system [7–17], while the difficulty in the formation of nickel(II) analogues explains the lack of magnetic studies concerning these complexes. In an attempt to obtain oxamidato-bridged polynuclear [16] and low-dimensional nickel(II) complexes, a trinuclear nickel complex with *N*,*N*′-bis(2-aminoethyl)oxamide (H_2oxen) in *cis*-conformation was isolated and characterized by X-ray crystallography. We describe here the synthesis, structure together with its magnetic properties.

* Author to whom correspondence should be addressed.

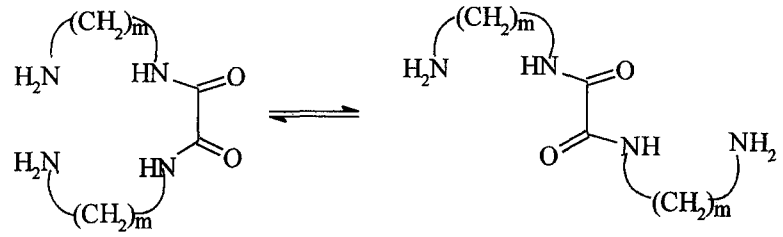

cis-Oxamidate *trans*-Oxamidate

m = 2; H_2oxen [N,N'-bis(2-aminoethyl)oxamide]

m = 3; H_2oxpn [N,N'-bis(3-aminopropyl)oxamide]

Scheme 1.

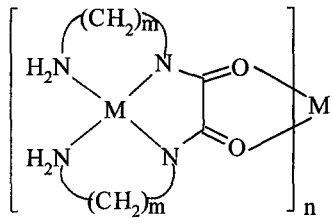

n = 1; binuclear complex
n = 2; trinuclear complex
n = 3; tetranuclear complex

M = Cu, Ni

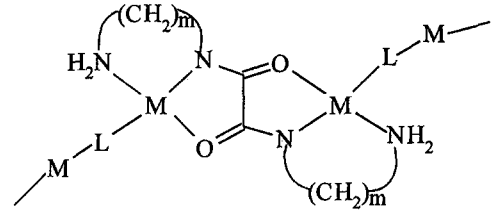

1D infinite chain complex

L = the second bridging ligand

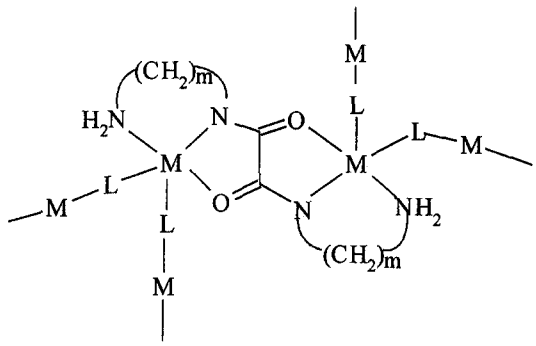

2D infinite sheet complex

Scheme 2.

EXPERIMENTAL

Preparation

The ligand H_2oxen and its mononuclear nickel(II) compound Ni(oxen) were obtained according to the literature [18].

$[Ni_3(oxen)_2(en)][ClO_4]_2$. To an aqueous solution of Ni(oxen) (1.0 mmol, 0.23 g) was added an aqueous solution of $NiCl_2 \cdot 2H_2O$ (1.0 mmol, 0.24 g) with stirring for 5 min to yield a yellow-green solution. An aqueous solution of disodium salt of EDTA (1.0 mmol, 0.37 g) was then added to the above solution to give a green solution which after standing at room temperature for two weeks gave well shaped green crystals. Yield: 42%. Found: C, 21.50; H, 4.08; N, 17.90. Calc. for $C_{14}H_{32}Cl_2N_{10}Ni_3O_{12}$: C, 21.56; H, 4.13; N, 17.96 %. IR (KBr, cm^{-1}): 3360 (m), 3318

(m), 3289 (m), 3149 (w), 2952 (w), 2896 (w), 2853 (w), 1672 (s), 1647 (s), 1574 (m), 1454 (m), 1377 (m), 1328 (w), 1284 (w), 1089 (s), 1011 (m), 969 (w), 871 (w), 723 (w), 660 (w), 625 (w), 540 (w), 470 (w), 435 (w). UV [λ_{max}, nm; (ε, $L \cdot mol^{-1} \cdot cm^{-1}$)]: 412.9 (255.5), 325.0 (2855.5), 300.1 (4759.1).

Crystal structure determination

A single crystal with suitable dimensions was mounted on a glass fiber and data collection was performed on a Siemens P4 diffractometer by ω-scan technique using graphite-monochromated Mo-K_α radiation ($\lambda = 0.71073$ Å). The crystal data, data collection and refinement parameters are summarized in Table 1.

The coordinates of the metal atoms were determined by direct methods and the remaining non-hydrogen atoms were located from successive Fourier difference syntheses. The structure was refined by full-matrix least-squares techniques with anisotropic thermal parameters for all the non-hydrogen atoms. The positions of the hydrogen atoms were isotropically added to the structure factor calculations but not refined. All calculations were performed on an IBM PC/486 computer with the Siemens SHELXTL-P4/PC program package [19].

Table 1. Summary of crystal data, data collection and refinement parameters for the complex

Formula	$C_{14}H_{32}Cl_2N_{10}Ni_3O_{12}$
Fomula weight	779.53
Temperature (K)	17
Crystal size (mm)	$0.56 \times 0.56 \times 0.50$
Crystal system	Tetragonal
Space group	$P\bar{4}2_1c$
a (Å)	13.460(1)
b (Å)	13.460(1)
c (Å)	14.981(2)
V (Å^3)	2714.1(5)
Z	4
D_{calc} (g cm^{-3})	1.908
Radiation (Mo-K_α) (Å)	0.71073
$F(000)$	1600
μ (cm^{-1})	23.33
θ range (°)	2–25.5
Range of hkl	0–16, 0–16, 0–18
Reflections measured	2779
Unique reflections	1437
Observed reflections with $I > 2\sigma(I)$	1244
No. of variables	187
R	0.0321
wR	0.0766
Goodness of fit	0.986
Largest Δ/σ	−0.003
Residual extrema (e Å^{-3})	0.328 to −0.352

Physical measurements

IR spectrum was obtained from a Perkin–Elmer 577 spectrophotometer as KBr pellets. UV spectrum was recorded on a Beckman DU-8B spectrophotometer with the sample dissolved in DMF. Variable-temperature magnetic susceptibilities in the temperature range 1.6–260 K were measured on a model CF-1 superconducting extracting sample magnetometer at a magnetic field of 5.0 T with the powdered sample kept in capsule for weighing. The temperature was raised gradually from 1.6 to 260 K. Data were recorded at an applied field gradient $H(dH/dX)$ of 1.4×10^7 Oe × Oe/cm. An interval of 30 s was kept between data collections and each measurement took 10 s.

RESULTS AND DISCUSSION

In an attempt to synthesize oxamidato-bridged polynuclear or low-dimensional nickel(II) complexes, the reaction of Ni(oxen), $NiCl_2 \cdot 6H_2O$ and Na_2EDTA was carried out in an equimolar ratio, on the assumption that oxamidato-bridged nickel(II) dimers can be connected via the carboxylate groups of EDTA to yield polymeric structure, where the oxamidato frequently changes conformation from *cis* into *trans* as observed in Cu(II) complexes [7–17]. Unexpectedly, the product isolated was a trinuclear complex bridged only by *cis*-oxamidate without involving EDTA. The co-ligand en may have been formed through the partial decomposition of oxen as that found in the reaction of Ni(oxen) with KSCN [6]. Ni(oxen) is more easily decomposed in aqueous solution as compared with Cu(oxen), especially when other acidic or basic reagents are present in the reaction system. The presence of nickel chloride and EDTA in the system may exert some influence on the decomposition, but it is believed that Ni(oxen) is stable enough in the absence of other acidic or basic species. Undoubtedly, Cu(oxen) is much more stable than Ni(oxen) as when Cu^{2+} is introduced into the aqueous solution of Ni(oxen), Cu(oxen) is formed immediately as the solution turned into violet-red from the yellow colour of Ni(oxen). Moreover, the *cis* conformation of the oxamidato-bridged nickel(II) dimer was unchanged even if a second bridging ligand was added. This behaviour is different from that of the copper(II) species in which *cis*-oxamidato-bridged dimers are easily linked by a second ligand to form *trans*-oxamidato-bridged polynuclear [17,20,21] or polymeric [7–17] structure.

The molecular structure with atom-labelling scheme and the packing in the unit cell are depicted in Figs 1 and 2, respectively. Selected atomic distances and bond angles are presented in Table 2. The structure consists of one cation $[Ni_3(oxen)_2(en)]^{2+}$ and two anions ClO_4^-. The trinuclear cation, which possesses a C_2 axis through atom Ni(1) and the

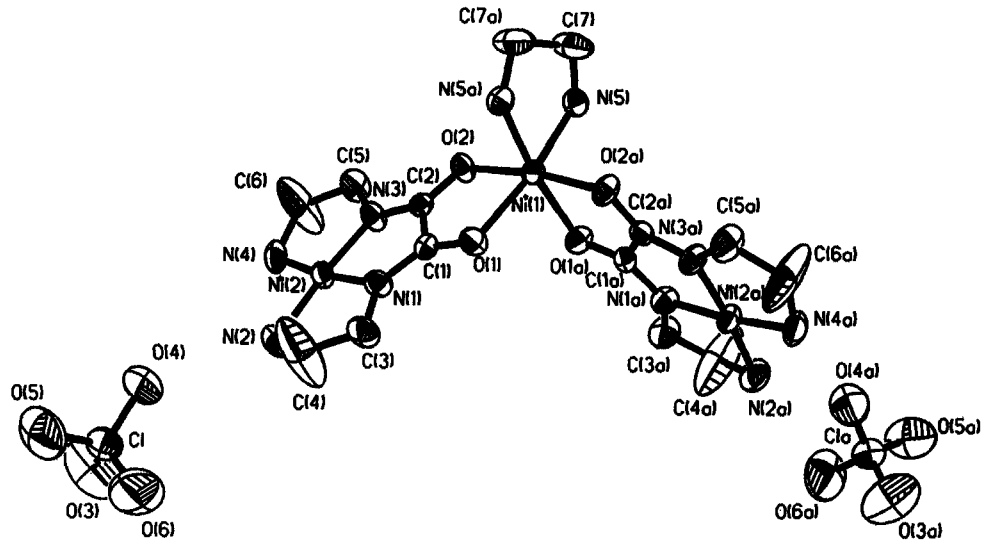

Fig. 1. Thermal ellipsoid plot (50%) showing the atom-labelling scheme of the complex $[Ni_3(oxen)_2(en)][ClO_4]_2$.

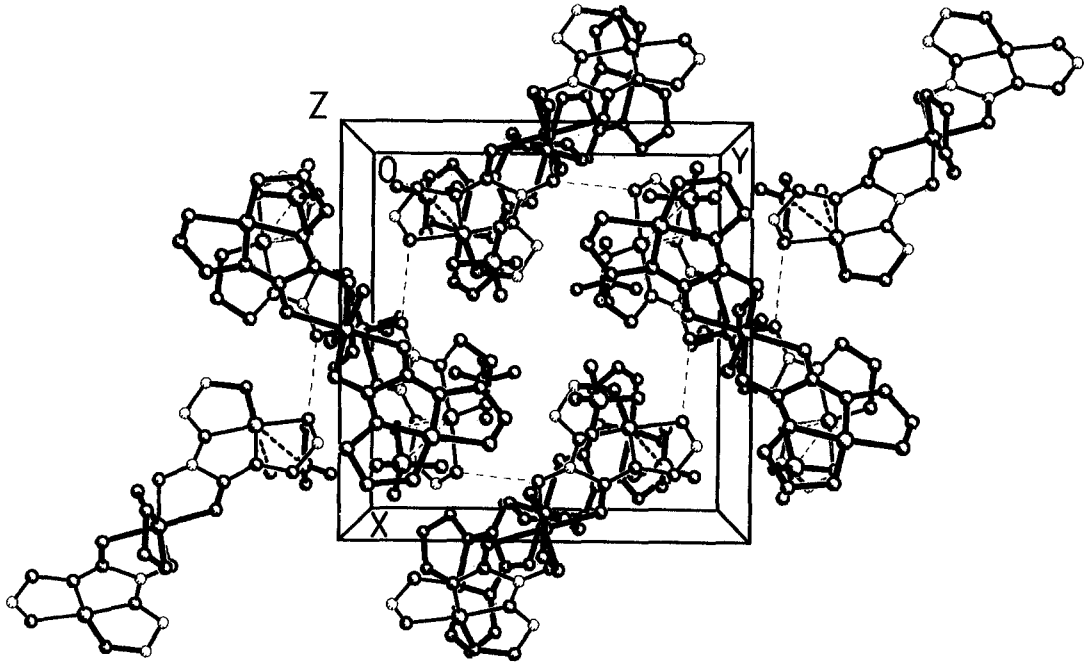

Fig. 2. The crystal packing of the complex $[Ni_3(oxen)_2(en)][ClO_4]_2$.

middle of the C(7)—C(7a) bond, can be viewed as a $Ni(en)^{2+}$ fragment, to which the two Ni(oxen) units with oxen in *cis* conformation are *cis* oriented. The arrangement of Ni_3 is curved with the angle of Ni(2)—Ni(1)—Ni(2a) being 119.0°, different from other Ni_3 complexes reported in literature with quasi-linear [22,23] or equilateral triangular [24,25] metal assembly.

The three metal centers exhibit alternating square-planar and octahedral coordination environments. The repeating asymmetric unit contains two nickel centers of non-identical geometries. Atom Ni(1) possesses a distorted octahedral environment with N_2O_4 core with the equatorial plane of Ni(1) defined by two N atoms of 1,2-ethenediamine and two O atoms from *cis*-oxen, while the axial coordination sites are occu-

Table 2. Selected atomic distances (Å) and bond angles (°) for the complex

Ni(1)—Ni(2)	5.248(2)	Ni(1)—O(1)	2.126(4)
Ni(1)—O(2)	2.055(4)	Ni(1)—N(5)	2.072(5)
Ni(2)—N(1)	1.844(4)	Ni(2)—N(2)	1.927(5)
Ni(2)—N(3)	1.834(5)	Ni(2)—N(4)	1.917(5)
O(1)—C(1)	1.258(6)	O(2)—C(2)	1.259(6)

O(2a)—Ni(1)—O(2)	172.4(2)	O(1)—Ni(1)—O(1a)	93.0(2)
O(2)—Ni(1)—N(5a)	95.6(2)	N(5)—Ni(1)—O(1)	170.5(2)
O(2)—Ni(1)—N(5)	90.1(2)	N(5a)—Ni(1)—N(5)	83.6(3)
O(2a)—Ni(1)—O(1)	93.0(2)	O(2)—Ni(1)—O(1)	81.70(14)
N(5a)—Ni(1)—O(1)	92.3(2)	N(3)—Ni(2)—N(1)	85.4(2)
N(3)—Ni(2)—N(4)	85.9(2)	N(1)—Ni(2)—N(4)	171.2(2)
N(3)—Ni(2)—N(2)	171.2(2)	N(1)—Ni(2)—N(2)	85.8(2)
N(4)—Ni(2)—N(2)	103.0(2)	C(1)—N(1)—Ni(2)	115.3(4)
C(1)—N(1)—C(3)	128.1(5)	C(3)—N(1)—Ni(2)	116.6(4)

pied by the other two O [O(2) and O(2a)] atoms from *cis*-oxen. Atom Ni(2) affords an approximately square-planar surroundings with N_4 donors [N(1), N(2), N(3) and N(4)] of amide and amine, and Ni(2) is displaced out of the plane by only 0.002 Å. There are only a few examples [22,26] of trinuclear nickel(II) complexes reported to date, in which three nickel(II) centers exhibit alternating square-planar and octahedral geometries.

The deprotonated oxen ligand in *cis* conformation forms one five-membered chelate ring for Ni(1) and three for Ni(2). The deprotonated amide N(1) and its symmetry-related N(1a) are sp^2-hybridized and the three atoms [Ni(2), C(1) and C(3)] around N(1) lie in a plane with the sum of the three angles C(1)—N(1)—Ni(2) [115.3(4)°], Ni(2)—N(1)—C(3) [116.6(4)°] and C(1)—N(1)—C(3) [128.1(5)°] close to 360°. The bridging group O(1)N(1)C(1)C(2)N(3)O(2) is planar within experimental error, with Ni(1) displaced by 0.045 Å and Ni(2) by 0.009 Å, from this plane. The dihedral angle between the five-membered chelate rings O(1)—C(1)—C(2)—O(2)—Ni(1) and O(1a)—C(1a)—C(2a)—O(2)—Ni(1a) is 88.0°. The Ni···Ni separation through the *cis*-oxamidate bridge is 5.25 Å.

The temperature-dependences of the molar magnetic susceptibility χ_M and of magnetic moment μ_{eff} are shown in Fig. 3. The susceptibility increases continuously down to the lowest measured temperature 1.6 K. However, fitting the experimental data with

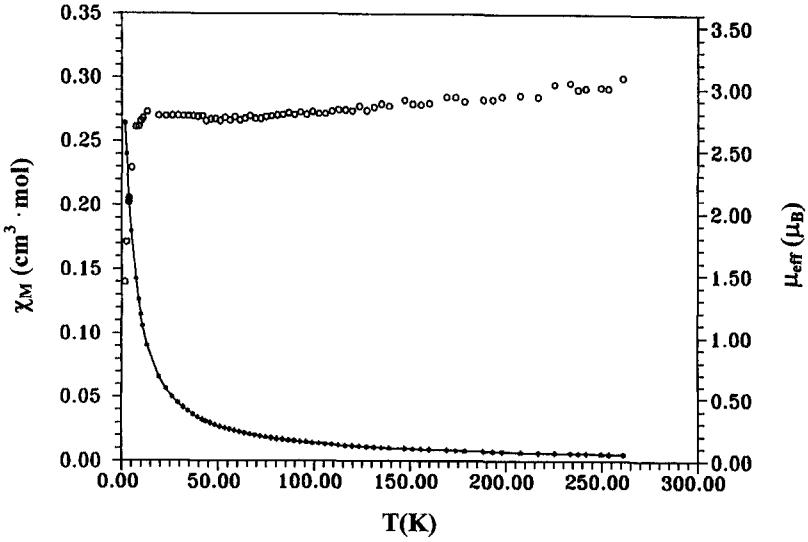

Fig. 3. Plots of the temperature dependences of the molar susceptibilities χ_M (*) and of the effective magnetic moments μ_{eff} (o) for the complex $[Ni_3(oxen)_2(en)][ClO_4]_2$. The solid line represent the best calculated curve.

the Curie–Weiss equation indicates that the deviation from Curie-like behaviour is obvious. The Curie–Weiss parameters are $C = 1.28\ cm^3 \cdot K \cdot mol^{-1}$ and $\theta = -3.2$ K. The value of the Curie constant shows the $g = 2.37$.

The effective magnetic moment μ_{eff} decreases slowly from 3.35 μ_B at 270 K to 3.04 μ_B at 8.7 K. Below this temperature, μ_{eff} drops rapidly to 2.58 μ_B at 4 K, and to 1.57 μ_B at 1.6 K. As shown in the trinuclear nickel(II) compound $[Ni_3(OC_6H_4S)_2(HOC_6H_4S)_2(PBu^n_3)_2]\cdot 2EtOH$ [22] with a similar structure, the slow decrease of μ_{eff} in the temperature range 270–9 K may originate from antiferromagnetic exchange and/or dipolar interaction between the nickel(II) ions, and the rapid decrease at very low temperature may result from single-ion anisotropy of octahedrally coordinated nickel(II) ion with the high-spin state S = 1. Hence, the experimental data can be fitted in terms of a model of single-ion zero-field splitting with the intermolecular exchange interaction in a molecular field approach. The expression of magnetic susceptibility [6,20] is shown as follows:

$$\chi_M = \frac{2Ng^2\mu_B^2}{3k(T-\theta)} \frac{2x^{-1} - 2e^{-x}x^{-1} + e^{-x}}{1 + 2e^{-x}} \qquad (1)$$

where $x = D/kT$. A least-squares fitting of the experimental data was carried out, allowing D, θ and g to vary. A set of the best fitting parameters gave $g = 2.37$, $D = 5.22\ cm^{-1}$ and $\theta = -1.45$ K with the deviation factor defined by $R = \Sigma(\chi_M^{obs} - \chi_M^{calc})^2/\Sigma(\chi_M^{obs})^2$ being 9.3×10^{-4}. A positive value of the parameter D means that the $m_s = 0$ state which lies below the $m_s = \pm 1$ state is the ground state.

Acknowledgments—The financial supports from the State Key Laboratory of Coordination Chemistry, Nanjing University, the NNSF of China and the NSF of Guangdong Province are greatly appreciated.

REFERENCES

1. Ojima, H. and Nonoyama, K., *Coord. Chem. Rev.*, 1988, **92,** 85.
2. Fabretti, A. C., Giusti, A., Albano, V. G., Castellari, C., Gatteschi, D. and Sessoli, R., *J. Chem. Soc., Dalton Trans.*, 1991, 2133.
3. Albano, V. G., Castellari, C., Fabretti, A. C. and Giusti, A., *Inorg. Chim. Acta*, 1992, **191,** 213.
4. Journaux, Y., Sletten, J. and Kahn, O., *Inorg. Chem.*, 1985, **24,** 4063.
5. Journaux, Y., Sletten, J. and Kahn, O., *Inorg. Chem.*, 1986, **25,** 439.
6. Chen, Z. N., Tang, W. X., Chen, J., Zheng, P. J., Chen, C. G. and Yu, K. B., *Polyhedron*, 1994, **13,** 873.
7. Lloret, F., Julve, M., Real, J. A., Faus, J., Ruiz, R., Mollar, M., Castro, I. and Bois, C., *Inorg. Chem.*, 1992, **31,** 2956.
8. Real, J. A., Ruiz, R., Faus, J., Lloret, F., Julve, M., Journaux, Y., Philoche-Levisalles, M. and Bois, C., *J. Chem. Soc., Dalton Trans.*, 1994, 3769.
9. Chen, Z. N., Qiu, J., Wu, Z. K., Fu, D. G., Yu, K. B. and Tang, W. X., *J. Chem. Soc., Dalton Trans.*, 1994, 1923.
10. Lloret, F., Julve, M., Faus, J., Ruiz, R., Castro, I., Mollar, M. and Philoche-Levisalles, M., *Inorg. Chem.*, 1992, **31,** 784.
11. Chen, Z. N., Liu, S. X., Qiu, J., Wang, Z. M., Huang, J. L. and Tang, W. X., *J. Chem. Soc., Dalton Trans.*, 1994, 2989.
12. Sanz, J. L., Cervera, B., Ruiz, R., Bois, C., Faus, J., Lloret, F., Julve, M., *J. Chem. Soc., Dalton Trans.*, 1996, 1359.
13. Bencini, A., Beneli, C., Fabretti, A. C., Franchini, G. and Gatteschi, D., *Inorg. Chem.*, 1986, **25,** 1063.
14. Chen, Z. N., Wang, J. L., Qiu, J., Miao, F. M. and Tang, W. X., *Inorg. Chem.*, 1995, **34,** 2255.
15. Chen, Z. N., Fu, D. G., Yu, K. B. and Tang, W. X., *J. Chem. Soc., Dalton Trans.*, 1994, 1917.
16. Chen, Z. N., Qiu, J., Tang, W. X. and Yu, K. B., *Inorg. Chim. Acta*, 1994, **224,** 171.
17. Dominguez-Vera, J. M., Galvez, N., Colacio, E., Cuesta, R., Costes, J. P. and Laurent, J. P., *J. Chem. Soc., Dalton Trans.*, 1996, 861.
18. Ojima, H. and Yamada, K., *Nippon Kagaku Zasshi*, 1968, **89,** 490.
19. Sheldrick, G. M., *SHELXTL-PC*. Siemens Analytical X-ray Instruments, Inc., Madison, WI, 1990.
20. Chen, Z. N., Tang, X. W and Yu, K. B., *Polyhedron*, 1994, **13,** 783.
21. Chen, Z. N., Qiu, J., Tang, W. X. and Yu, K. B., *Acta Cryst.*, 1995, **C51,** 1809.
22. Chen, Z. N., Kang, B. S., Lin, Z., Wu, B. M., Zhou, Z. Y., Mak, T. C. W., Chen, C. N. and Liu, H. Q., *J. Chem. Soc., Dalton Trans.*, 1996, 177.
23. Tremel, W., Kriege, M., Krebs, B. and Henkel, G., *Inorg. Chem.*, 1988, **27,** 3886.
24. Bosman, W. P. and van der Linden, *J. Chem. Soc., Chem. Commun.*, 1977, 714.
25. Matsumoto, K., Saiga, N., Tanaka, S. and Ooi, S., *J. Chem. Soc., Dalton Trans.*, 1991, 1265.
26. Brooker, S. and Croucher, P. D., *J. Chem. Soc., Chem. Commun.*, 1995, 1493.

Pergamon

PII: S0277-5387(97)00383-5

Polyhedron Vol. 17, No. 9, pp. 1541–1546, 1998
© 1998 Elsevier Science Ltd
All rights reserved. Printed in Great Britain
0277-5387/98 $19.00+0.00

Synthesis and characterization of novel heteropoly-tungstoarsenates containing lanthanides $[LnAs_4W_{40}O_{140}]^{25-}$ and their biological activity

Jing-Fu Liu,*[a] Ya-Guang Chen,[a] Lu Meng,[a] Jun Guo,[a] Ya Liu[b] and Michael T. Pope[c]

[a]Department of Chemistry Northeast Normal University, Changchun 130024, P.R. China

[b]Bethune Medical University, Changchun 130021, P.R. China

[c]Department of Chemistry, Georgetown University, Washington, DC 20057, U.S.A.

(Received 22 April 1997; accepted 18 September 1997)

Abstract—A series of lanthanide polyoxoanions $[LnAs_4W_{40}O_{140}]^{25-}$ (Ln = La, Ce, Pr, Nd, Sm, Eu, Gd, Tb, Dy or Yb) have been prepared from the cryptate anion $[NaAs_4W_{40}O_{140}]^{27-}$ and lanthanides and characterized by elemental analysis, ^{183}W NMR, emission spectra. A number of evidences indicate that the lanthanides occupy the central site in the complexes. The title complexes display anti-tumor activity *in vitro* and *in vivo*.
© 1998 Elsevier Science Ltd. All rights reserved

Keywords: polyoxometalates; lanthanide polyoxoanions; heteropoly-tungstoarsenates; antitumor activity.

A crystallographic investigation [1] of $[NaAs_4W_{40}O_{140}]^{27-}$ anion revealed it to be a cryptate containing an encapsulated central sodium cation. The close match between the ionic radii of Na^+ and Ln^{3+} suggested that the latter cations might be similarly incorporated into the polyanion skeleton. Because of their higher charge the lanthanide complexes would be expected to be even more stable than that of Na^+. This paper describes the synthesis and characterization of the novel polyanions $[LnAs_4W_{40}O_{140}]^{25-}$ (Ln = La, Ce, Pr, Nd, Sm, Eu, Gd, Tb, Dy or Yb) and their biological activity.

EXPERIMENTAL

Materials

The heteropolymetallates employed $Na_{27}[NaAs_4W_{40}O_{140}]\cdot XH_2O$, $K_{27}[KAs_4W_{40}O_{140}]\cdot XH_2O$ and $[K_{21/19}[KAs_4W_{40}O_{140}M_2]\cdot XH_2O$ ($M = Mn^{2+}$, Ni^{2+}, Cu^{2+} or Co^{2+}) (abbreviated as $NaAs_4W_{40}$ and $KAs_4W_{40}M_2$, respectively) were prepared according to literature method [2] and were identified by vis spectra, IR spectra and polarography. Other chemicals were reagent grade.

Preparation of $K_{23}H_2[LaAs_4W_{40}O_{140}]\cdot 45H_2O$

$Na_{27}[NaAs_4W_{40}O_{140}]$ (25 g, 2.2 mmol) was dissolved in water (100 cm^3) and to this solution a solution of $La(NO_3)_3$ (2.2 mmol) in H_2O (10 cm^3) was added dropwise with vigorous stirring. After the addition was complete stirring was continued for a further 30 min and solid KCl (4.5 g) was then added. Upon standing at 0°C an oil formed, which subsequently crystallized. The product was dissolved in water, which was passed through a cation exchange column (Dowex 50, potassium form, 20 mesh, flow rate 0.5 $cm^3\ min^{-1}$). The eluate was concentrated, producing a precipitate which was filtered off and recrystallized from hot water twice. Yield of the crude product was about 60% and the pure product was 30% (based on $NaAs_4W_{40}$).

* Author to whom correspondence should be addressed.

The other lanthanide complexes were prepared using a similar procedure as described above.

Preparation of $K_{21}[LaAs_4W_{40}O_{140}M_2]\cdot XH_2O$ ($M = Mn^{2+}$, Ni^{2+}, Cu^{2+} or Co^{2+})

$K_{23}H_2[LaAs_4W_{40}O_{140}]\cdot 45H_2O$ (12 g, ca 1 mmol) was dissolved in H_2O (50 cm^3) and to this solution a solution of $M(NO_3)_{2/3}$ (2.0×10^{-3} mol) in H_2O (10 cm^3) was slowly added, whilst stirring vigorously. After the addition was complete the mixture was then stirred for a further 30 min. Solid KCl (2.5 g, 3.3×10^{-2} mol) was then added to the mixture and the resulting precipitate, removed by filtration, was then dissolved and precipitated twice, in order to obtain a sodium-free potassium salt. The latter was recrystallized from warm H_2O. Yield ca 75%.

Analytical procedure

Tungsten was weighed as WO_3 after precipitation by 8-hydrooxyquinoline and ignition at 750°C. The lanthanides were determined volumetrically (back-titration of an excess of EDTA with $ZnSO_4$). Arsenic(III) was titrated with I_2. Potassium and transition metals were determined by atomic absorption spectroscopy. The water content was determined by thermogravimetry.

Elemental analyses of part samples were performed by E+R Microanalytical Laboratory, Inc., Corona, NY.

Physical measurements

UV–vis spectra were recorded on a Beckman DU-8B spectrophotometer. IR spectra were obtained on an Alpha Centauri IR Spectrometer with KCl pellets. Emission spectra were recorded with a P-E MPE-6 spectrofluorometer. Atomic absorptions were recorded with a P-E 1030 atomic absorption spectrometer. ^{183}W NMR spectra were recorded at 12.50 MHz on a Bruker WM 300 spectrometer using quadraphase detection.

RESULTS AND DISCUSSION

Analytical results and formulations

Chemical analyses of the potassium salts of the title anions leads to the formulae indicated in Table 1, showing that the lanthanides give $[LnAs_4W_{40}O_{140}]^{25-}$ type of complexes with $[NaAs_4W_{40}O_{140}]^{27-}$, while addition of transition metal cations to $[LaAs_4W_{40}O_{140}]^{25-}$ gave complexes of the type $[LaAs_4W_{40}O_{140}M_2]^{n-}$. ($M = Mn^{2+}$, Ni^{2+}, Cu^{2+} or Co^{2+}).

The magnetic susceptibilities of the complexed lanthanides were determined by the Faraday method at room temperature and from these data the effective magnetic moments were calculated; $K_{23}H_2[LaAs_4W_{40}O_{140}]$ was used for diamagnetic correction. The results are given in Table 2. The observed magnetic moments are very close to those given by Van Vleck, showing that the lanthanides in the complexes remain in the +3 oxidation state.

Emission spectrum

An X-ray structural investigation of $(NH_4)_{23}[NH_4As_4W_{40}O_{140}(CoOH_2)_2]\cdot$ca $20H_2O$ [1] revealed that the polytungstate is constructed from four B-type AsW_9O_{33} units and four WO_6 octahedra. The unshared oxygens of the latter defined an eight-coordinate site (S_1) occupied by an ammonium ion and four five-coordinate sites (S_2), each defined by four oxygen atoms and an arsenic central unshared electron pair.

In order to throw light on the coordination site problem for La in the complex the emission spectrum of $K_{21}H_4[EuAs_4W_{40}O_{140}]$ was recorded. Figure 2 shows the spectrum of the solid sample at 295 K; it consists of $^5D_0$—^7F_J bands split by the local crystal field, whose transition frequencies are listed in Table 3. It can be seen that the emission spectrum of $EuAs_4W_{40}$ is very similar to those of $Eu(SiW_{11})_2$, $Eu(GeW_{11})_2$ and $Eu(AsW_{11})_2$ in terms of both the number of peaks and transition frequencies, showing that they have similar local site symmetry. According to Blasse *et al.* [3], in $K_{13}[Eu(SiW_{11}O_{39})_2]$ structure. Eu is coordinated by eight oxygen atoms forming a distorted archimedean antiprism, like U in $[U(GeW_{11}O_{39})_2]^{12-}$ [4]. By comparing the emission spectra of these complexes we conclude that the Eu^{3+} ion is coordinated by eight oxygen atoms in the $[EuAs_4W_{40}O_{140}]^{25-}$ complex, i.e. the Eu^{3+} ion occupies the S_1 site in the complex.

^{183}W NMR spectra

The previously determined structure of $(NH_4)_{23}[NH_4As_4W_{40}O_{140}(CoOH_2)_2]\cdot$ca $20H_2O$ [1] revealed that the cobalt-free heteropolyanion had D_{2d} symmetry, and therefore contained six structurally distinct types of tungsten atoms. The ^{183}W NMR spectra of the lanthanide derivatives consist of six lines and similar to that of the sodium derivatives (Table 4).

From the emission spectrum of $EuAs_4W_{40}$ and the ^{183}W NMR spectra of $LaAs_4W_{40}$ or $EuAs_4W_{40}$ we conclude that the structure of both $NaAs_4W_{40}$ and $LnAs_4W_{40}$ are isostructural and that Ln^{3+} ion replaces Na^+ ion in the structure. This result is consistent with that of the other cryptate polyanions $[NaSb_9W_{21}O_{86}]^{18-}$ or $[NaP_5W_{30}O_{110}]^{14-}$, in which the Na^+ can be substituted by the lanthanide cation [7,8]. This conclusion is reinforced by strong similarities between reaction stoichiometry, IR spectra, visible spectra and redox properties.

Table 1. Analytical data

Compound	Found (calcd) % K	Ln	As	W	H_2O	M
$K_{23}H_2[LaX]^a \cdot 45H_2O$	7.56(7.64)	1.19(1.18)	2.24(2.56)	62.81(62.62)	7.03(6.90)	
$K_{21}H_4[CeX] \cdot 46H_2O$	6.81(7.01)	1.25(1.20)	2.16(2.57)	63.10(62.92)	7.08(7.09)	
$K_{22}H_3[PrX] \cdot 50H_2O$	7.15(7.28)	1.27(1.25)	2.14(2.54)	62.35(62.52)	7.52(7.63)	
$K_{23}H_2[NdX] \cdot 48H_2O$	7.55(7.61)	1.31(1.22)	2.10(2.54)	62.56(62.34)	7.08(7.33)	
$K_{21}H_4[SmX] \cdot 47H_2O$	7.04(7.02)	1.35(1.30)	2.28(2.57)	63.15(62.97)	7.45(7.23)	
$K_{21}H_4[EuX] \cdot 45H_2O$	7.26(6.99)	1.32(1.30)	2.20(2.56)	62.78(62.20)	7.17(6.94)	
$K_{21}H_4[GdX] \cdot 44H_2O$	7.04(7.02)	1.44(1.35)	2.31(2.57)	63.24(63.24)	6.90(6.79)	
$K_{21}H_4[TbX] \cdot 42H_2O$	7.12(7.01)	1.47(1.37)	2.25(2.58)	64.45(63.44)	6.54(6.53)	
$K_{22}H_3[DyX] \cdot 40H_2O$	7.12(7.45)	1.44(1.41)	2.20(2.60)	63.00(63.58)	6.40(6.23)	
$K_{23}H_2[YbX] \cdot 45H_2O$	7.48(7.62)	1.49(1.47)	2.25(2.55)	62.39(62.45)	6.71(6.83)	
$K_{21}[LaXMn_2]^a \cdot 45H_2O$	6.91(6.86)	1.24(1.19)	2.42(2.55)	63.08(62.48)	6.85(6.88)	0.95(0.93)
$K_{21}[LaXCo_2] \cdot 58H_2O$	6.90(6.82)	1.24(1.15)	2.37(2.49)	60.97(61.23)	8.25(8.69)	0.92(0.98)
$K_{21}[LaXNi_2] \cdot 50H_2O$	6.72(6.90)	1.17(1.16)	2.35(2.53)	62.08(61.98)	8.04(7.58)	1.00(0.99)
$K_{21}[LaXCu_2] \cdot 55H_2O$	6.75(6.84)	1.16(1.15)	2.40(2.51)	61.95(61.40)	7.95(8.27)	1.12(1.06)

[a] $K_{23}H_2[LaAs_4W_{40}O_{140}]$ and $K_{21}[LaAs_4W_{40}O_{140}Mn_2]$ were abbreviated as $K_{23}H_2[LaX]$ and $K_{21}[LaXMn_2]$, respectively.

Table 2. Magnetic measurement data

Compound	$Xg \times 10^6$	U_{eff} (B.M.)
$K_{23}H_2[LaAs_4W_{40}O_{140}] \cdot 45H_2O$	−0.149	0
$K_{22}H_3[PrAs_4W_{40}O_{140}] \cdot 50H_2O$	0.573	3.95(3.62)[a]
$K_{22}H_3[DyAs_4W_{40}O_{140}] \cdot 40H_2O$	3.875	10.48(10.60)

[a] Calculated in parentheses.

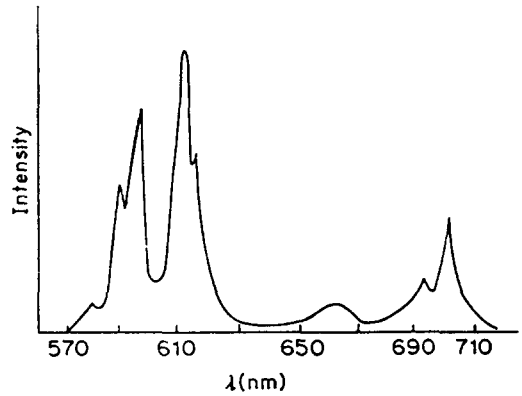

Fig. 2. Emission spectrum of $K_{21}H_4(EuAs_4W_{40}O_{140}) \cdot XH_2O$.

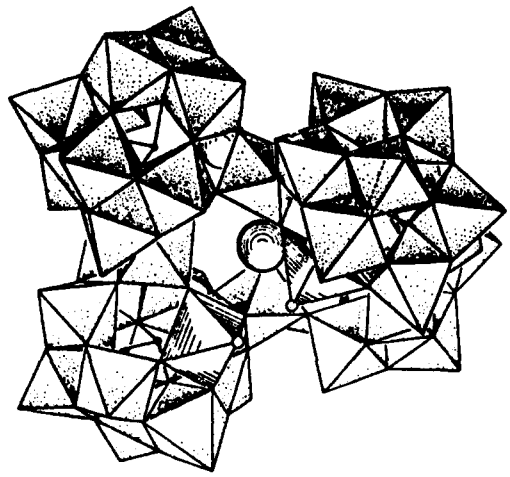

Fig. 1. $[(NH_4)As_4W_{40}O_{140}(CoOH_2)_2]^{23-}$. The aquocobalt ions, shown as shadowed square pyramide with small open circles (H_2O molecules), occupy two of the S_2 sites. A tightly bound ammonium ion (large circle) occupies the S_1 site at the center of the structure.

Reactions with transition metal ions

The stoichiometry for the $LaAs_4W_{40}$ and transition metal ion reactions were studied by conductivity measurements; the conductimetric titrations are shown in Fig. 3. Figure 3(a) shows an equivalent point for $M^{2+}/LaAs_4W_{40} = 2$(M = Co, Cu or Ni), corresponding to the reaction:

$$(LaAs_4W_{40}O_{140})^{25-} + 2M^{2+} \rightleftharpoons (LaAs_4W_{40}O_{140}M_2)^{21-}$$

Figure 3(b) shows an equivalent point for $Ag^+/LaAs_4W_{40}Co_2 = 2$. Since the visible spectrum of $LaAs_4W_{40}Co_2$ does not change during the titration, Ag^+ ions do not replace Co^{2+} ions, and therefore react according to:

Table 3. Transition frequencies in the emission spectra of some tungstoeuropates (nm)

Complex	$^5D_0$—$^7F_0$	—$^7F_1$	—$^7F_2$	—$^7F_3$	—$^7F_4$	Ref.
$K_{21}H_4(EuAs_4W_{40}O_{140})$	578 vw	588 s 594 vs	613 vs 616 s	662 w	690 ms 703 w	This work
$K_{13}Eu(SiW_{11}O_{39})_2$	579 vw	589 s 594 vs	614 vs 619 s	652 w	694 ms 700 s	3
$K_{13}Eu(GeW_{11}O_{39})_2$	579 vw	588 s 594 vs	613 vs 617 s	652 w	693 ms 698 vs	5

Table 4. ^{183}W NMR data

Anion	δ (ppm)						Ref.
$[NaAs_4W_{40}O_{140}]^{27-}$	−93.8	−103.7	−104.8	−118.6	−189.8	−196.8	6
$[NaAs_4W_{40}O_{140}]^{27-}$	−96.6	−108.6	−109.7	−123.0	−194.3	−201.5	This work
$[LaAs_4W_{40}O_{140}]^{25-}$	−109.3	−115.6	−119.8	−163.4	−187.6	−214.6	This work
$[EuAs_4W_{40}O_{140}]^{25-}$	−102.4	−112.0	−117.6	−147.8	−192.4	−198.1	This work

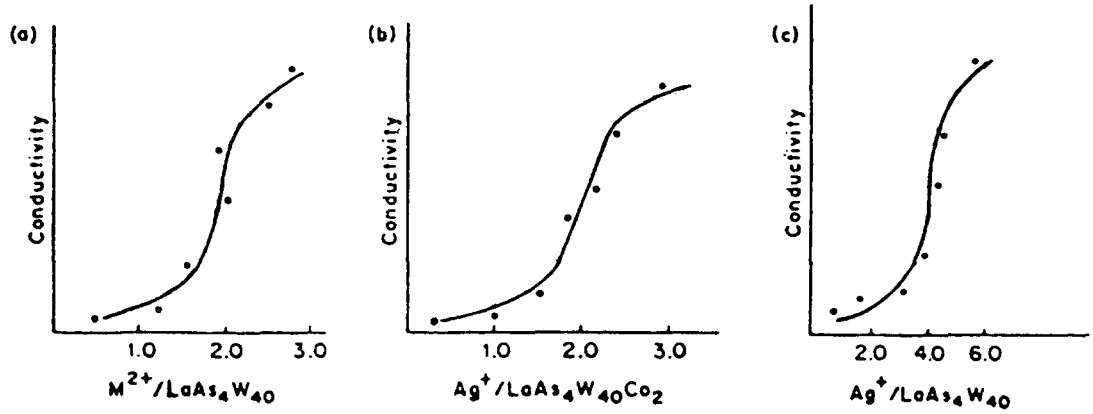

Fig. 3. Conductimetric titration of: (a) $LaAs_4W_{40}$ with Cu^{2+} ion; (b) $LaAs_4W_{40}Co_2$ with Ag^+ ion; (c) $LaAs_4W_{40}$ with Ag^+ ion.

$$(LaAs_4W_{40}O_{140}Co_2)^{21-} + 2Ag^+ \rightleftharpoons (LaAs_4W_{40}O_{140}Co_2Ag_2)^{19-}$$

Figure 3(c) shows an equivalent point for $Ag^+/LaAs_4W_{40} = 4$, corresponding to the reaction:

$$(LaAs_4W_{40}O_{140})^{25-} + 4Ag^+ \rightleftharpoons (LaAs_4W_{40}O_{140}Ag_4)^{21-}$$

The reaction stoichiometry of $LaAs_4W_{40}$ is similar to that of $NaAs_4W_{40}$ [2], giving further evidence that lanthanum occupies the S_1 site in the complex $LaAs_4W_{40}$.

Comparison between spectroscopic properties

Table 5 shows that the UV, IR and half-wave potentials of the $LnAs_4W_{40}$ anions closely resemble that of the $LaAs_4W_{40}$, indication that both have a similar

Table 5. UV, IR and polarographic half-potential for $LnAs_4W_{40}$

Compound	UV (nm) Ob/Oc → W	UV (nm) W—Od	IR (cm^{-1})[a] W—Ob	IR (cm^{-1})[a] As—Oa	IR (cm^{-1})[a] W—Oc	$E_{1/2}$ (V) $E_{1/2}$
$NaAs_4W_{40}$	240	950 ms	878 s	797 ms	707 s, 632 w	−1.67(6), −1.18(12)
$LaAs_4W_{40}$	240	951 ms	879 s	797 ms	712 s, 631 w	−1.08(6), −1.19(12)
$CeAs_4W_{40}$	240	950 ms	879 s	797 ms	711 s, 631 w	−1.07(6), −1.20(12)
$PrAs_4W_{40}$	240	951 ms	878 s	799 ms	711 s, 629 w	−1.06(6), −1.20(12)
$NdAs_4W_{40}$	240	952 ms	878 s	798 ms	712 s, 630 w	−1.08(6), −1.21(12)
$SmAs_4W_{40}$	240	953 ms	879 s	797 ms	710 s, 630 w	−1.08(6), −1.19(12)
$EuAs_4W_{40}$	240	954 ms	879 s	800 ms	710 s, 631 w	−1.08(6), −1.22(12)
$GdAs_4W_{40}$	240	951 ms	879 s	796 ms	710 s, 633 w	−1.08(6), −1.22(12)
$TbAs_4W_{40}$	240	953 ms	877 s	816 ms	715 s, 691 w	−1.08(6), −1.22(12)
$DyAs_4W_{40}$	240	953 ms	877 s	814 ms	713 s, 671 w	−1.07(6), −1.21(12)
$YbAs_4W_{40}$	240	952 ms	877 s	794 ms	707 s, 685 w	−1.07(6), −1.21(12)

[a] O_a = oxygen shared by WO_6 octahedra and the AsO_4 tetrahedron, Ob and Oc = oxygen linked to two different W atoms, Od = terminal unshared oxygen.

structure. A similar conclusion can be deduced from the fact that the visible spectra of $LaAs_4W_{40}M_2$ resemble those of the corresponding $KAs_4W_{40}M_2$ (Table 6).

Antitumor activity of $TbAs_4W_{40}$

The data summarized in Table 7 show that the $[TbAs_4W_{40}O_{140}]^{25-}$ displays inhibitory action to HL60 (leukemia), B_{16} (melanoma), H_{22} (liver cancer cell) cancers and rectum cancer vivicell as well as breast cancer vivicells.

Table 8 indicates that $TbAs_4W_{40}$ decreased substantially tumour weight and delayed survival time of mice bearing with S_{180} ascites cancer during animal tumor implantation test.

Acknowledgements—This work was supported by National

Table 6. Comparison of electronic absorption spectra for $LaAs_4W_{40}M_2$ and $KAs_4W_{40}M_2$ anions

Complex	Peak maxima (nm) (molar absorptivity)		
$KAs_4W_{40}Co_2$	595(118)	529(56)	475(42)
$LaAs_4W_{40}Co_2$	598(140)	532(74)	480(88)
$KAs_4W_{40}Ni_2$	810(30)	715(46)	425(135)
$LaAs_4W_{40}Ni_2$	804(42)	708(74)	418(215)
$KAs_4W_{40}Cu_2$	840(156)		
$LaAs_4W_{40}Cu_2$	830(170)		
$KAs_4W_{40}Mn_2$	Continuous		
$LaAs_4W_{40}Mn_2$	Continuous		

Table 7. Inhibitory effect of $TbAs_4W_{40}$ on some tumour cells *in vitro*

Tumor cell	Compound	Dose ($\mu g\ ml^{-1}$)	Inhibitory rate (%)
B_{16}	$TbAs_4W_{40}$	125	67.5
		62.5	40.4
H_{22}	$TbAs_4W_{40}$	125	71.4
		62.5	61.0
HL-60	$TbAs_4W_{40}$	20	35.0
Rectum cancer	$TbAs_4W_{40}$	20	65.0
Breast cancer	$EuAs_4W_{40}$	5	57.0

Table 8. Effect of $TbAs_4W_{40}$ on tumor weight and survival time of mice bearing with S_{180} ascites cancer

Compound	Dose ip × 10 (mg Kg^{-1} day^{-1})	Tumor weight[a] (g)	*P* value	Survival time (day)
Control		0.3130		
$TbAs_4W_{40}$	1.0	0.1967	<0.01	
Control				16
$TbAs_4W_{40}$	1.0			21
	0.5			20.5

[a]Mice were sacrificed on Day 11.

Natural Science Foundation of China and Laboratory of Rare Earth Chemistry and Physics, Changchun Institute of Applied Chemistry, Academia Sínica.

REFERENCES

1. Robert, F., Leyrie, M., Herve, G., Teze, A. and Jeann, Y., *Inorg. Chem.*, 1980, **19,** 1746.
2. Leyrie, M. and Herve, G., *Nouv. J. Chim.*, 1978, **2,** 233.
3. Blasse, G., Dirksen, G. J. and Zonnevijlle, F., *J. Inorg. Nucl. Chem.*, 1981, **43,** 2847.
4. Tourne, C. M., Tourne, G. F. and Prianso, M. C., *Acta Crystallogr.*, 1980, **36B,** 2012.
5. Liu, J., Zhu, Z., Zhao, B. and Liu, Z., *Inorg. Chim. Acta*, 1989, 179.
6. Herve, G. and Teze, A., *Inorg. Synth.*, 1990, **27,** 120.
7. Liu, J., Liu, S., Qu, L. and Pope, M. T., *Transition Met. Chem.*, 1992, **17,** 311.
8. Creaser, I., Heckel, M. C., Neitz, J. R. and Pope, M. T., *Inorg. Chem.*, 1993, **32,** 1573.

Pergamon

PII: S0277-5387(97)00376-8

Polyhedron Vol. 17, No. 9, pp. 1547–1552, 1998
© 1998 Elsevier Science Ltd
All rights reserved. Printed in Great Britain
0277-5387/98 $19.00+0.00

Electrochemical synthesis of metal (II) complexes of Schiff base 2-tosylamino (2′-pyridyl)aniline: the crystal structure of bis-[2-tosylamino(2′-pyridyl)anilinato]cobalt(II)

Jose A. Garcia-Vazquez,[a] Jaime Romero,[a] Maria L. Duran,[a] Antonio Sousa,[a,*] Alexander D. Garnovskii,[b,*] Anatolii S. Burlov[b] and Dimitrii A. Garnovskii[b]

[a] Departamento de Química Inorgánica, Universidad de Santiago de Compostela, 15706 Santiago de Compostela, Spain.

[b] Research Institute of Physical and Organic Chemistry, Rostov State University, Rostov on Don, 344090, Stahki av., 194/2, Russia

(Received 9 June 1997; accepted 10 September 1997)

Abstract—Complexes of cobalt(II), nickel(II), copper(II), zinc(II) and cadmium(II) with the anion of the Schiff base 2-tosylamino(2′-pyridyl)aniline (HL) have been prepared by using an electrochemical procedure. These compounds were characterized by elemental analysis, IR, UV and NMR spectroscopy, and in the case of $[CoL_2]$ by X-ray diffraction methods. In this compound the cobalt(II) atom is in a distorted tetrahedral environment, each Schiff base anion acting as a bidentate ligand with the pyridine nitrogen atom un-coordinated. © 1998 Elsevier Science Ltd. All rights reserved

Keywords: electrochemical synthesis; 2-tosylamino(2′-pyridyl)aniline; Schiff base complexes; crystal structure.

INTRODUCTION

This work continues studies of neutral complexes [1–11] of Schiff bases such as I and II where X = O, S, Se and Het = an heterocyclic ring. In these compounds, the pyridine nitrogen atom is un-coordinated although for the complexes of cobalt(II) [10] with ligand II (where X = S and Het = thiophene) and zinc(II) [11] with ligand I (where X = O) X-ray studies show a weak intramolecular secondary bond between the metallic atom and the $N_{pyridine}$ atoms.

We have now synthesized by an electrochemical procedure Co, Ni, Cu, Zn and Cd complexes containing the ligand L, derived from I with X = NHTs. The crystal structure of bis-[2-tosylamino(2′-pyridyl)anilinato]cobalt(II) is also reported.

EXPERIMENTAL

Materials

The metals (Ega Chemie) were used in the form of ca 2 × 2 cm plates. All solvents, 2-aminopyridine and other reagents except 2-tosylaminobenzaldehyde are commercially available and were used without further purification. 2-Tosylaminobenzaldehyde was prepared following a method previously described [12]. The Schiff base was prepared by addition of 10 ml of a solution of freshly distilled 2-aminopyridine (0.47 g, 0.005 mol) to a solution of 2-tosylaminobenzaldehyde (1.38 g, 0.005 mol) in 50 ml of dry toluene. The mix-

* Authors to whom correspondence should be addressed.

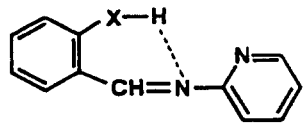

(I)

X = O, S, Se

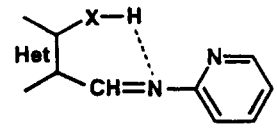

(II)

Het = Heterocyclic

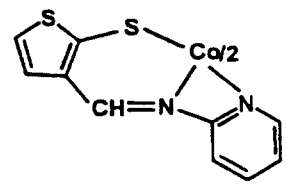

ture was heated in a Dean-Stark trap until the calculated amount of water was removed. After the reaction was completed, toluene was distilled off *in vacuo* on a water bath, and 30 ml of boiling methanol was added to the residue. The crystals precipitated upon cooling were filtered off, and washed twice with 5 ml of methanol. Recrystallized from a (1 : 1) methanol-benzene mixture, yielding light-yellow crystals with m.p. 112–113°. Anal: Calc. for $C_{19}H_{17}N_3O_2S$: C, 64.96; H, 4.84; N, 11.97; S, 9.12. Found: C, 64.71; H, 4.63; N, 11.89; S, 9.44.

Electrochemical synthesis

The electrochemical method used for the synthesis of the complexes was similar to that described by Tuck [13]. The cells were of the general type:

$$Pt_{(-)}/CH_3CN + HL/M_{(+)}$$

$$M = Co, Ni, Cu, Zn \text{ or } Cd$$

The solution was placed in a 100 ml tall form beaker, the anode was suspended into the solution by a platinum wire, and another platinum wire was used as the cathode. The ligand was dissolved in ca 50 ml of acetonitrile and a small amount of tetramethylammonium perchlorate (ca 10 mg) was added to the solution as the supporting electrolyte. **Caution!** Perchlorate salts solutions are potentially explosive. They should be handled in small quantity and with caution. As the electrolysis proceeded, hydrogen gas was evolved at the cathode. In the case of the zinc and cadmium complexes the yellow solids precipitated during the electrolysis; they were collected by filtration, washed twice with hot acetonitrile and diethylether and dried *in vacuo*. In the case of the nickel, cobalt and copper complexes, concentration of the reaction mixture by evaporation at room temperature was required to obtain solid products, which were purified as before. The crystals of $[CoL_2]$ obtained were suitable for X-ray diffraction studies. Details of the solution composition and the electrochemical conditions are given in Table 1.

Crystal structure determination

A yellow prismatic crystal of approximate dimensions $0.45 \times 0.20 \times 0.05$ mm was mounted on a glass fiber and used for data collection on a Nicolet P3 diffractometer. The monoclinic space group $P2_{1/c}$ was assumed due to extinctions observed. Data were collected at 293 K using Cu–K_α radiation ($\lambda = 1.54178$ Å) and the $\omega/2\theta$ scan technique. The data were corrected for Lorentz and polarization effects. An empirical absorption correction was made. The crystal data and a summary of the data collection and structure refinement for the compound are given in Table 2.

The structure was solved by direct methods [14] and refined on F^2 by full-matrix least squares method with unit weight and anisotropic displacement parameters for the non-hydrogen atoms. Hydrogen atoms were

Table 1. Experimental conditions for the electrochemical synthesis

Compound	Amount of H_2L_2(g)[a]	Initial Voltage (V)[b]	Time (h)	Metal dissolved (mg)	E_f (mol F^{-1})
$[CoL_2]$	0.20	15	4	88	0.51
$[NiL_2]$	0.17	25	4	96	0.53
$[CuL_2]$	0.25	15	2	96	1.00
$[ZnL_2]$	0.21	20	4	102	0.52
$[CdL_2]$	0.25	20	4	145	0.48

[a] Plus $[NMe_4]$ ClO_4 (ca 10 mg).
[b] Voltage to produce a current of 20 mA.

Table 2. Summary of crystal data for $[CoL_2]$

Formula	$C_{38}H_{32}CoN_6O_4S_2$
FW	759.75
Crystal system	Monoclinic
Space group	$P2_1/c$
a (Å)	11.668(3)
b (Å)	20.480(4)
c (Å)	30.075(7)
β (°)	100.85(2)
V (Å^3)	7058(3)
Z	8
D_{calc} (g cm^{-3})	1.430
$F(000)$	3144
Reflections collected	5299
Independent reflections (R_{int})	5299 (0.000)
No. of parameters	920
μ (mm^{-1})	5.331
R	0.1146
Rw	0.2919

located from geometrical considerations (C—H = 0.95 Å), and added to the structure factor calculations as fixed contributions (B_{iso} = 4.0 Å^2) and their positional parameters were not refined. The maximum difference density at final cycle 0.733; minimum −0.805. The crystal was strongly twinned, we managed to extract a correct lattice. That is the reason for the rather high R-factor and esd values. Two independent molecules differ in the region of p-tolylsulfonyl groups, one molecule has pseudosymmetry C_2, another is unsymmetrical.

Atomic scattering factors from International Tables for X-ray Crystallography [15]. Computations were performed on a DECMicroVAX 3500 computer. Atom positions, bond lengths and bond angles have been deposited as supplementary material.

RESULTS AND DISCUSSION

The anodic oxidation of the metal in an electrochemical cell containing a solution of the ligand LH in acetonitrile allows the isolation of compounds of composition $[ML_2]$, where L is the anion resulting of the deprotonation of the amide group of Schiff base.

For the cobalt, nickel, zinc and cadmium complexes, the electrochemical efficiency, defined as moles of metal dissolved per Faraday of charge, E_f, was close to 0.5 mol.F^{-1}, which is compatible with the following reaction scheme

$$\text{Cathode:}\quad 2HL + 2e^- \rightarrow H_{2(g)} + 2L^-$$

$$\text{Anode:}\quad 2L^- + M \rightarrow [ML_2] + 2e^-$$

$$M = Co, Ni, Zn \text{ or } Cd$$

For copper, E_f, was close to 1 mol.F^{-1}. This value shows that the anodic oxidation leads initially to Cu(I) species followed by further oxidation in solution to Cu(II).

$$\text{Cathode:}\quad HL + e^- \rightarrow 1/2H_{2(g)} + L^-$$

$$\text{Anode:}\quad L^- + Cu \rightarrow [CuL] + e^-$$

$$[CuL] + HL \rightarrow 1/2H_{2(g)} + [CuL_2]$$

The products obtained were characterized analitically and by IR, and NMR spectroscopies. The crystal structure of $[CoL_2]$ has been determined by X-ray diffraction.

Structure of $[CoL_2]$

The unit cell contains two crystallographically distinct but chemically equivalent molecules (molecules A and B). Figure 1 shows the structure of molecule A with the atom numbering system used. Selected bond distances and angles for both molecules are listed in Tables 4 and 5, respectively.

The complex consists of mononuclear units with a tetracoordinate cobalt atom bound to the nitrogen atoms of two bidentate monoanionic ligands. However, the two molecules A and B are slightly different and show some variation in bond distances and angles. Thus, A has N—Co—N angles in the range 93.6(5)–123.2(5)° and distances Co—N 1.981(13)–2.031(11) Å; in B the range of N—Co—N angles is 93.3(6)–131.9(6) and that of distances Co—N are 1.958(13)–1.999(13) Å. The tetrahedral environment of the cobalt atom is distorted due to the small bite required by N—Co—N = 93.0(6)–93.6(6)°, which also results in secondary deviation of the other perinuclear angles from the ideal values of 109°.

The Co—N_{imine} bond lengths [1.981(13), 2.000(12) Å] in A and [1.999(13) Å] in B are very similar between them, but they are shorter than the value found in another complex containing tetrahedral cobalt(II) and a Schiff base; for example, 2.066(8) Å in bis(tert-butylpyrrole-2-carboxaldimino)cobalt(II) [16]. However, the Co—N_{amide} bond lengths are substantially different in both molecules. Thus, whereas in the symmetric molecule B the Co—N_{amide} distance is 1.959(13) Å, in A those distances [1.982(12) and 2.031(11) Å] are different and larger than that of B.

The C—N bond length is in agreement with the value of 1.30 Å proposed for a C=N bond [17] and the pyridine nitrogen atom is not coordinated to the cobalt.

Spectroscopic and magnetic data

The ν(N—H) broad band of the free Schiff base in the 2800–3000 cm^{-1} region, characteristic of NH groups involved in intramolecular hydrogen bonds NH···N=C, is absent from the IR spectra of the complexes, consistent with the coordination of the

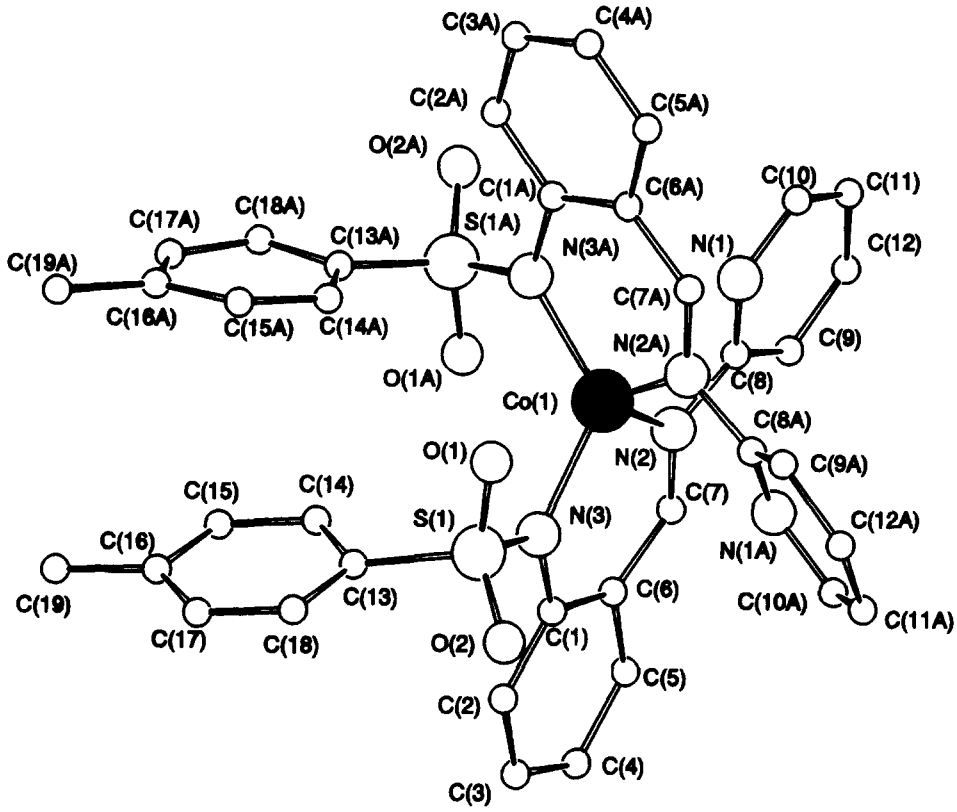

Fig. 1. The molecular structure of $[CoL_2]$.

Table 3. Analytical data for the complexes (%)[a]

Compound	Colour	m.p.	%C	%H	%N	%S
HL	Yellow	112	64.71(64.96)	4.63(4.84)	11.89(11.97)	9.44(9.12)
$[CoL_2]$	Brown	176	59.57(60.07)	4.21(4.25)	11.12(11.06)	7.69(8.44)
$[NiL_2]$	Brown	193	59.72(60.09)	4.06(4.25)	10.76(11.06)	7.69(8.44)
$[CuL_2]$	Brown	165	59.11(59.71)	3.74(4.22)	10.78(10.99)	8.54(8.39)
$[ZnL_2]$	Yellow	>250	58.64(59.57)	4.04(4.21)	10.64(10.97)	7.64(8.35)
$[CdL_2]$	Yellow	>250	55.59(56.12)	3.71(3.97)	10.20(10.33)	7.23(7.87)

[a] Calculated values in parentheses.

deprotonated ligand. The band attributable to ν(C=N) shifts to lower frequencies in all the complexes as a consequence of coordination through the imine nitrogen. On the other hand, the pyridine ring stretching band observed between 1600 and 1400 cm^{-1} and the ring deformation bands which appear at about 600 and 400 cm^{-1} are shifted to higher frequencies in the complexes. This behaviour has been proposed as a probe of pyridine nitrogen atom coordination to the metal. However, the structural data for $[CoL_2]$ show that the pyridine is not bound to the metal. We believe that the observed shift can be due to the change in the conjugation between the heterocyclic ring and the rest of the ligand as a result of the coordination of the imine nitrogen to the metal. This behaviour has been previously observed in other similar systems. Therefore, these results show that the Schiff base coordinates through the imine and amide nitrogen atoms in all complexes, with a coordination number of four for the metals, in agreement with the structure of $[CoL_2]$ elucidated by X-ray diffraction.

The proton NMR data of the zinc and cadmium complexes are in accord with the above conclusions. The spectrum of the free ligand shows a peak at 12.5

Table 4. Selected bond lengths (Å) for [CoL_2]

Co(1)—N(2)	1.981(13)	S(1C)—O(2C)	1.441(12)
Co(1)—N(3A)	1.982(12)	S(1C)—N(3C)	1.651(14)
Co(1)—N(2A)	2.000(12)	S(1C)—C(13C)	1.74(2)
Co(1)—N(3)	2.031(11)	N(1)—C(10)	1.35(3)
Co(2)—N(3B)	1.958(13)	N(1)—C(8)	1.36(2)
Co(2)—N(3C)	1.959(11)	N(2)—C(7)	1.30(2)
Co(2)—N(2B)	1.999(13)	N(2)—C(8)	1.40(2)
Co(2)—N(2C)	1.999(13)	N(3)—C(1)	1.42(2)
S(1)—O(2)	1.454(12)	N(1A)—C(8A)	1.34(2)
S(1)—O(1)	1.462(11)	N(1A)—C(10A)	1.41(2)
S(1)—N(3)	1.578(13)	N(2A)—C(7A)	1.33(2)
S(1)—C(13)	1.79(2)	N(2A)—C(8A)	1.44(2)
S(1A)—O(2A)	1.471(12)	N(3A)—C(1A)	1.46(2)
S(1A)—O(1A)	1.496(11)	N(1B)—C(12B)	1.32(2)
S(1A)—N(3A)	1.606(14)	N(1B)—C(8B)	1.34(2)
S(1A)—C(13A)	1.75(2)	N(2B)—C(7B)	1.28(2)
S(1B)—O(2B)	1.429(14)	N(2B)—C(8B)	1.42(2)
S(1B)—O(1B)	1.439(12)	N(3B)—C(1B)	1.43(2)
S(1B)—N(3B)	1.613(13)	N(1C)—C(8C)	1.31(2)
S(1B)—C(13B)	1.78(2)	N(1C)—C(12C)	1.34(3)
S(1C)—O(1C)	1.435(12)	N(2C)—C(7C)	1.30(2)
N(2C)—C(8C)	1.41(2)	N(3C)—C(1C)	1.40(2)

Table 5. Selected bond angles (deg) for [CoL_2]

N(2)—Co(1)—N(3A)	120.4(6)	O(2A)—S(1A)—C(13A)	107.5(7)
N(2)—Co(1)—N(2A)	114.1(5)	O(1A)—S(1A)—C(13A)	108.0(7)
N(3A)—Co(1)—N(2A)	93.6(6)	N(3A)—S(1A)—C(13A)	106.7(8)
N(2)—Co(1)—N(3)	93.6(5)	O(2B)—S(1B)—O(1B)	117.5(8)
N(3A)—Co(1)—N(3)	123.2(5)	O(2B)—S(1B)—N(3B)	114.6(8)
N(2A)—Co(1)—N(3)	113.5(5)	O(1B)—S(1B)—N(3B)	102.3(7)
N(3B)—Co(2)—N(3C)	119.1(5)	O(2B)—S(1B)—C(13B)	105.5(10)
N(3B)—Co(2)—N(2B)	93.3(6)	O(1B)—S(1B)—C(13B)	110.0(9)
N(3C)—Co(2)—N(2B)	119.0(5)	N(3B)—S(1B)—C(13B)	106.5(8)
N(3B)—Co(2)—N(2C)	131.9(6)	O(1C)—S(1C)—O(2C)	118.4(8)
N(3C)—Co(2)—N(2C)	93.0(6)	O(1C)—S(1C)—N(3C)	104.5(7)
N(2B)—Co(2)—N(2C)	101.4(6)	O(2C)—S(1C)—N(3C)	111.4(7)
O(2)—S(1)—O(1)	114.9(7)	O(1C)—S(1C)—C(13C)	107.4(8)
O(2)—S(1)—N(3)	114.0(7)	O(2C)—S(1C)—C(13C)	108.3(9)
O(1)—S(1)—N(3)	104.0(6)	N(3C)—S(1C)—C(13C)	106.1(8)
O(2)—S(1)—C(13)	106.4(8)	C(10)—N(1)—C(8)	119(2)
O(1)—S(1)—C(13)	108.1(7)	C(7)—N(2)—C(8)	117.3(14)
N(3)—S(1)—C(13)	109.3(8)	C(7)—N(2)—Co(1)	127.4(11)
O(2A)—S(1A)—O(1A)	116.9(7)	C(8)—N(2)—Co(1)	115.2(11)
O(2A)—S(1A)—N(3A)	114.4(7)	C(1)—N(3)—S(1)	121.2(10)
O(1A)—S(1A)—N(3A)	102.9(6)	C(1)—N(3)—Co(1)	125.5(10)
S(1)—N(3)—Co(1)	112.9(7)		

ppm, assignable to the amide hydrogen, which is absent in the spectra of the complexes. The peak for the imine hydrogen atom (9.3 ppm in the free ligand) undergoes a shift towards higher field in the compounds, 9.1 ppm, and the peak for the 6-hydrogen of the pyridine ring is practically at the same field in the spectra of complexes and free ligand.

The solid state electronic spectrum in the near IR-visible region of the cobalt(II) complex, shows two *d-d* transition bands, one at 16,800–18,800 cm^{-1} and the other in the range 6600–8400 cm^{-1}; of the type expected for distorted tetrahedral cobalt(II) compounds [18]. The band in the visible region has been assigned to a $^4T_1(P) \leftarrow {}^4A_2$ (ν_3) transition, and the multicomponent one in the near IR region to $^4T_1(F) \leftarrow {}^4A_2$ (ν_2) transition. The $^4T_2 \leftarrow {}^4A_2$ (ν_1) tran-

sition has not been observed, but its position at ca 4520 cm^{-1} has been calculated as described by Lever. The values obtained for 10 Dq (4520 cm^{-1}), β (0.83) and B (804 cm^{-1}) are also in the range expected for pseudotetrahedral cobalt(II) complexes. The magnetic moment for this complex is 4.65 B.M. is in the range expected for tetrahedral cobalt(II) compounds.

The value of the magnetic moment of the copper complex (1.8 B.M.) corresponds to one unpaired electron. The solid state electronic spectrum shows two bands at around 10,700 and 18,100 cm^{-1}, and is consistent with an approximately square-planar stereochemistry. The band that appears at 27,000 cm^{-1} may be assigned to a charge transfer transition. The magnetic moment of the nickel(II) complex (3.18 B.M.) and its solid reflectance spectrum are consistent with a tetrahedral geometry for the complex. The bands observed at ca 8200 and 14,200 cm^{-1} are assigned to the two highest of the three expected spin allowed transitions, $^3A_2 \leftarrow {}^3T_1$ (ν_2) and $^3T_1(P) \leftarrow {}^3T_1(F)$ (ν_3), respectively.

Acknowledgement—We thank the Russian Science Foundation N960332026a for financial support.

REFERENCES

1. Garnovskii, A. D., Nivorozhkin, A. L. and Minkin, V. I., *Coord. Chem. Rev.*, 1993, **126,** 1.
2. Yamada, S. and Yamanouchi, K., *Bull. Chem. Soc. Jap.*, 1969, **42,** 2562.
3. Garnovskii, A. D., Osipov, O. A. and Kogan, V. A., *Doklady AN SSR*, 1971, **198,** 341.
4. Drummond, J. and Woods, J. S., *J. Chem. Soc., Dalton Trans.*, 1972, 365.
5. Kolavole, G. A., *J. Coord. Chem.*, 1987, **16,** 67.
6. Parashar, R. K., Sharma, R. C., Kumar, A. and Mohan, G., *Inorg. Chim. Acta.*, 1988, **151,** 201.
7. Atherton, N. M., Fenton, D. E., Newson, C. J., McLean, C. H., Bastida, R., Romero, J., Sousa, A. and Castellano, E. E., *J. Chem. Soc., Dalton Trans.*, 1988, 1059.
8. Castiñeiras, A., Castro, J. A., Durán, M. L., García-Vázquez, J. A., Macías, A., Romero, J. and Sousa, A., *Polyhedron*, 1989, **8,** 1543.
9. Mistryukov, A. E., Vasilchenko, I. S., Sergienko, V. S., Nivorozhkin, A. L., Uraev, A. I. and Garnovski, A. D., *Mendeleev Commun.*, 1992, **2,** 30.
10. Shkolnikova, L. M., Zavodnivk, V. E. and Makarevich, S. S., *Koord. Chim. Rev.*, 1976, **2,** 115.
11. Garnovskii, A. D., Antsyshkina, A. S., Vasilchenko, I. S., Sergienko, V. S., Kochin, S. G., Nivorozhkin, A. L., Mistryukov, A. E., Uraev, A. I. and Garnovskii, D. A., *Russian J. Inorg. Chem.*, 1995, **40,** 67.
12. Chernova, N. I., Ryabokobylko, Y. S., Brudz, V. G. and Bolotin, B. M., *Zh. Neorg. Khim.*, 1971, 1680.
13. Oldham, C. and Tuck, D. G., *J. Chem. Ed.*, 1982, **59,** 420.
14. Sheldrick, G. M., SHELXTL-PLUS program package for the determination of crystal structures, Release 4.0, Siemens Analytical X-ray Instruments, Inc. Madison WI, 1990.
15. Cromer, D. T. and Waber, J. T., *International Tables for X-ray Crystallography*, Vol. IV, The Kynoch Press, Birmingham, England 1974, Table 2.2A.
16. Wei, C. H., *Inorg. Chem.*, 1972, **11,** 1100.
17. Allen, F. H., Kennard, O., Watson, D. G., Brammer, L., Orpen, A. G. and Taylor, R., *J. Chem. Soc., Perkin Trans. II*, 1987, S1.
18. Lever, A. B. P., *Inorganic Electronic Spectroscopy*, Elsevier, Amsterdam, 1984.

Pergamon

PII: S0277-5387(97)00368-9

Polyhedron Vol. 17, No. 9, pp. 1553–1559, 1998
© 1998 Elsevier Science Ltd
All rights reserved. Printed in Great Britain
0277-5387/98 $19.00+0.00

DNA degradation by the copper(II) complex with tripodal-ligands containing peptide group

Teruyuki Kobayashi,[a] Takashi Okuno,[a] Toshio Suzuki,[a] Mami Kunita,[a] Shigeru Ohba[b] and Yuzo Nishida*[a]

[a] Departments of Chemistry, Faculty of Science, Yamagata University, Yamagata 990, Japan

[b] Faculty of Science and Technology, Keio University, Yokohama 223, Japan

(Received 21 June 1997; accepted 3 September 1997)

Abstract—Copper-based transition metal complexes which perform single-strand scission of DNA in a site-specific manner have been designed. The complexes $Cu(dpg)^+$ and $Cu(dpgt)Cl^+$ (H(dpg) and (dpgt) represent bis(2-pyridylmethyl) derivatives of glycylglycine and glycylglycylglycine, respectively), were prepared in this study and its crystal structures were determined. We have found that $Cu(dpgt)Cl^+$ and $Cu(dpg)^+$ complexes convert supercoiled plasmid DNA into a mixture of nicked and linear forms in the presence of hydrogen peroxide, whereas related Cu(II) complexes, which lack a peptide group, produce complete degradation of DNA under the same experimental conditions. © 1998 Elsevier Science Ltd. All rights reserved

Keywords: DNA cleavage; copper(II) and hydrogen peroxide; tripodal-ligands containing peptide group; supercoiled DNA.

Reagents that bind sequence selectively to single- or double-strand DNA are of significant interest in molecular biology and medical chemistry as they may be developed into gene-targeted drugs for diagnostic and therapeutic application, and to provide tools for sequence specific modification of DNA [1,2]. Generally the metal complexes have at most a low level of specificity for different DNA sequence or structures, however one can transform them into probes for single sites on genomic DNA by tethering them to sequence-selective DNA binding moieties [3–5]. Recently copper(II) polypeptide complexes have been successfully used to functionalize sequence-specific DNA-binding molecules [6]. Functional metal complexes of polypeptides are an exciting area of research, especially in the generation of site-selective prove for DNA structure.

In this study we have prepared two copper(II) compounds with the ligands (H(dpg) and dpgt)) shown below, and determined the structures of the complexes, a polypeptide group is included in the ligand, (dpgt). We have examined the activities of these complexes for relaxation of supercoiled Form I DNA (pBR322) in the presence of hydrogen peroxide, in order to investigate the effect of the polypeptide group for site-specific degradation of DNA. Preparation and crystal structure of the $Cu(dpgs)ClClO_4$ was already reported by us [7].

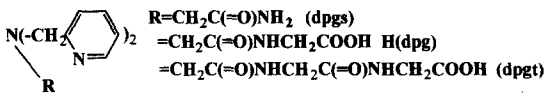

EXPERIMENTAL

Materials

The ligands, H(dpg) and (dpgt) were obtained according to the general methods as described in the previous paper [8]. Copper(II) compounds were obtained by mixing $CuCl_2 \cdot 2H_2O$ and methanol solution of the ligand, and also by the addition of $NaClO_4$ or NH_4PF_6. Yields of the compounds of $H(dpg)/ClO_4$, $H(dpg)/PF_6$, and (dpgt) complexes are 25, 30 and 60%, respectively. $Cu(dpgt)ClClO_4 \cdot 0.5H_2O$; Calcd C, 37.42; H, 3.66; N, 12.12%. Found: C, 37.34; H,

* Author to whom correspondence should be addressed.

3.49; N, 11.87%. Cu(dpg)PF_6; Calcd C, 36.83; H, 3.28; N, 10.74%. Found: C, 37.27; H, 3.46; N, 10.68%. Cu(dpg)$ClO_4 \cdot 3H_2O$; Calcd C, 36.23; H, 4.37; N, 10.56%. Found: C, 35.79; H, 4.10; N, 10.41%.

Crystal structure determination

The compounds used in the structure determination were recrystallized from a methanol/water mixture, and the crystal data of the compounds are listed in Table 1. X-ray diffraction intensities were measured up to $2\theta = 55^\circ$ using Mo–K_α radiation ($\lambda = 0.71073$ Å) on a Rigaku AFC-5 four-circle diffractometer, and absorption corrections were carried out by a numerical integration method. The structures were refined using CRYSTAN-GM software, and details have been deposited as Supplementary Materials.

Relaxation of pBR322 DNA

DNA (supercoiled pBR322) was purchased from Wako Chemicals. In a typical run, a copper(II) complex solution (4 μl of 0.1 mM solution), DNA (4 μl of 0.1 mg ml solution), Tris buffer (3 μl of 0.1 M solution, pH = 7.8) and hydrogen peroxide (4μl of 10 mM solution) were mixed and kept to stand for 1 h at 298 K. The extent of DNA cleavage was assessed by analysis on 0.9% agarose gel containing ethidium bromide [9]. The bands were photographed with Polaroid 667 film.

RESULTS AND DISCUSSION

Crystal structure

ORTEP drawing of two compounds illustrated in Figs 1 and 2, and the structural properties of Cu(dpgs)Cl^+ is also depicted in Fig. 3 [7]. In the Cu(dpgs)Cl^+ complex, the geometry around the copper(II) ion is that of a tetragonal pyramid with the oxygen atom of the amide-group at the apical position. Three nitrogen atoms (two pyridine nitrogen and one aliphatic amine) and the chloride ion are located in the basal plane of the complex. The structural properties of the Cu(dpgt)Cl^+ and Cu(dpg)$^+$ are essentially the same as those reported for the (dpgs)-complex, as shown in Figs 1–2 and Table 2, except for the polymeric structure of the (dpg)-complex in the solid state; in this case, carboxylic oxygen at the terminal peptide group (O(4), see Fig. 1) is also coordinating another copper(II) ion, forming a polymeric structure. However, the conductance data in the water solution indicates that this complex exists as a monomeric one in an aqueous solution, maybe Cu(dpg)$(H_2O)^+$ as illustrated below.

DNA scission chemistry

In this study, the copper(II) complex with (tpa), Cu(tpa)Cl^+ was also examined for DNA degradation, where (tpa) represents tris(2-pyridyl-methyl)amine. As shown in Fig. 4, it is clear that the degradation of

Table 1. Crystal data of the compounds

	Cu(dpg)$ClO_4 \cdot 3H_2O$	Cu(dpgt)$ClPF_6$
Formula	$CuC_{16}H_{23}O_{10}N_4Cl$	$CuC_{18}H_{21}N_5O_4ClPF_6$
FW	530.38	615.36
Crystal symmetry	monoclinic	triclinic
Space group	$P2_1/c$	$P\bar{1}$
a (Å)	12.335(2)	11.062(3)
b (Å)	9.440(2)	13.016(2)
c (Å)	19.284(1)	9.075(1)
α ( )	90	101.50(1)
β ( )	99.754(8)	93.56(1)
γ ( )	90	106.78(1)
V (Å^3)	2213.0(6)	1215.9(4)
Z	4	2
D_{calc} (Mg m^{-3})	1.592	1.681
μ (Mo–K_α) (mm^{-1})	1.168	1.156
Independent reflections	5076	5596
Observed reflections ($\|F_o\| > 3\sigma(\|F_o\|)$)	3384	3760
Scan	θ–2θ	ω
No. variables	306	346
$R(\omega R)$	0.063(0.056)	0.068(0.059)
$\Delta\rho_{max}$/eÅ^3	0.62	1.00
$\Delta\rho_{min}$/eÅ^3	−0.53	−0.63
Goodness of fit on F^2	1.45	1.33

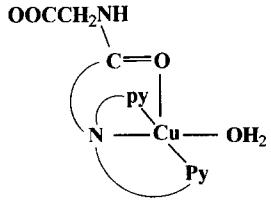

pBR322 DNA is highly dependent on the structure and concentration of the copper(II) compounds used.

In the concentration range of 0.5–1.0 mM of the copper(II) ion, all the complexes including (tpa) and compounds prepared in this study are competent to effect DNA strand scission. At 0.1 mM copper(II) ion concentration, the (dpgs)-complex gives Form II DNA, nicked from (relaxed circular) [9] (see lane 5), the (tpa)-complex gave both the Form II and Form III DNA (linear duplex) [9] (see lane 7 in Fig. 4), but the other two (dpg) and (dpgt)-compounds gave no effect for degradation (see lane 3, for example). At 0.5 mM, the (dpgs)-complex exhibited high efficiency for degradation, producing fragments with no supercoiled, nicked, and linear DNA (see lane 11). However, compounds with (dpg) and (dpgt) converted supercoiled plasmid to a mixture of nicked and linear DNA at 0.5 mM concentration, and even at 1.0 mM concentration (see lanes 9, 13, 15).

It is well known that metal complexes bind to DNA through both covalent and non-covalent modes. In the present cases, all the used copper(II) complexes with cationic charge may bind to the sugar-phosphate backbone electrostatically [10]. The high efficiency of DNA cleavage by the compounds with (dpgs) and (tpa) may indicate that these complexes bind to DNA with higher affinity than those of the (dpg) or (dpgt) complexes, however the details on this problem is unclear at present. Alternatively, it may be likely that the complexes with (dpg) and (dpgt) may bind to DNA in site-specific manner due to the presence of peptide group in the ligand.

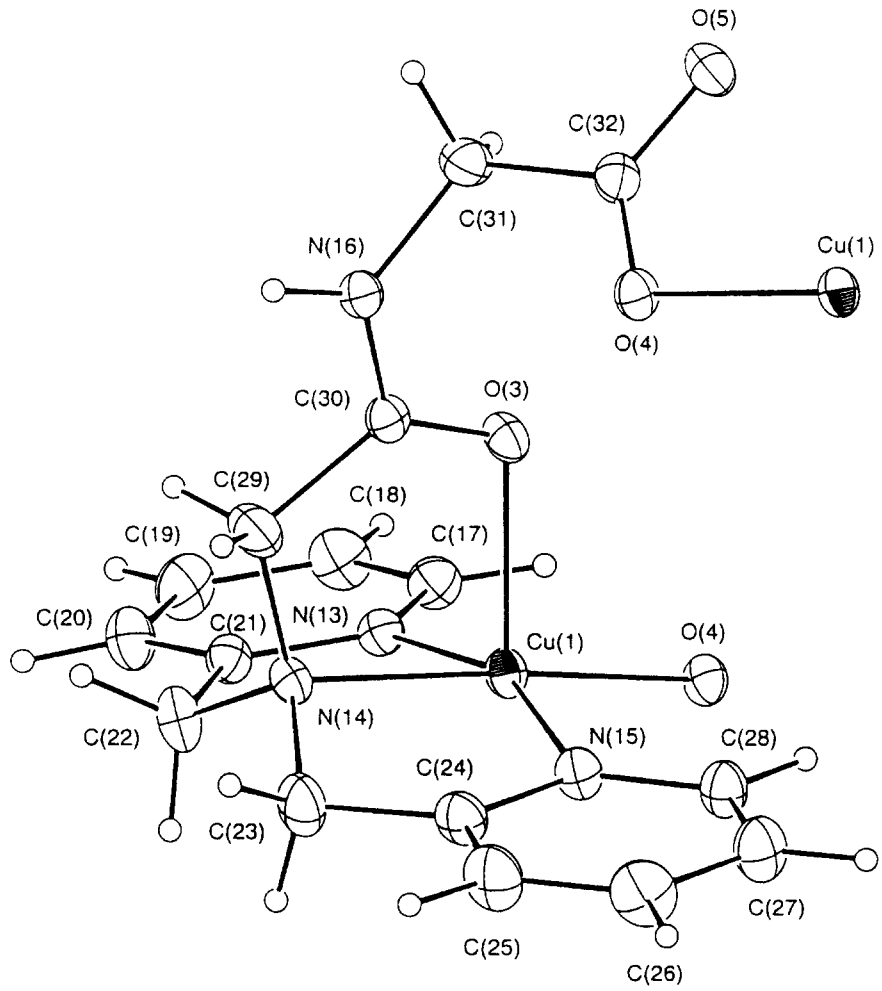

Fig. 1. ORTEP drawing of $Cu(dpg)^+$.

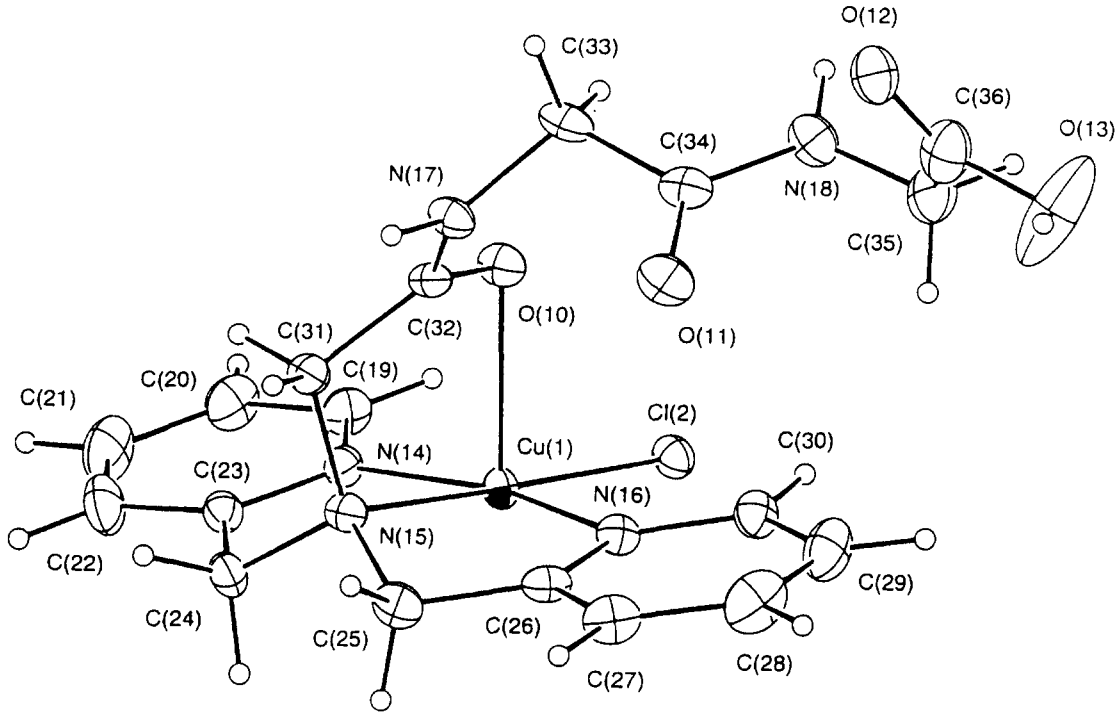

Fig. 2. ORTEP drawing of $Cu(dpgt)Cl^{+}$.

Table 2. Selected bond lengths (Å) and angles (°) of the compounds

$Cu(dpg)ClO_4$

Cu1—O3	2.227(3)	Cu1—N14	2.073(4)
Cu1—O4^{i}	1.944(3)	Cu1—N15	1.989(4)
Cu1—N13	1.973(4)		

O3—Cu1—O4^{i}	101.8(2)	O3—Cu1—N13	98.2(2)
O3—Cu1—O4^{i}	94.7(2)	O3—Cu1—N14	81.9(2)
N13—Cu1—O4^{i}	96.3(2)	N14—Cu1—O4^{i}	176.2(2)
N15—Cu1—O4^{i}	95.8(2)	N13—Cu1—N14	83.2(2)
N13—Cu1—N15	160.1(2)	N15—Cu1—N14	83.7(2)

$Cu(dpgt)ClPF_6$

Cu1—C12	2.267(2)	Cu1—N15	2.061(2)
Cu1—O10	2.383(4)	Cu1—N16	1.992(4)
Cu1—N14	1.993(4)		

C12—Cu1—O10	98.5(2)	C12—Cu1—N14	97.8(2)
C12—Cu1—N15	178.4(2)	C12—Cu1—N16	98.6(2)
N14—Cu1—O10	98.8(2)	N15—Cu1—O10	80.3(2)
N16—Cu1—O10	83.1(2)	N14—Cu1—N15	81.3(2)
N14—Cu1—N16	163.0(2)	N15—Cu1—N16	82.4(2)

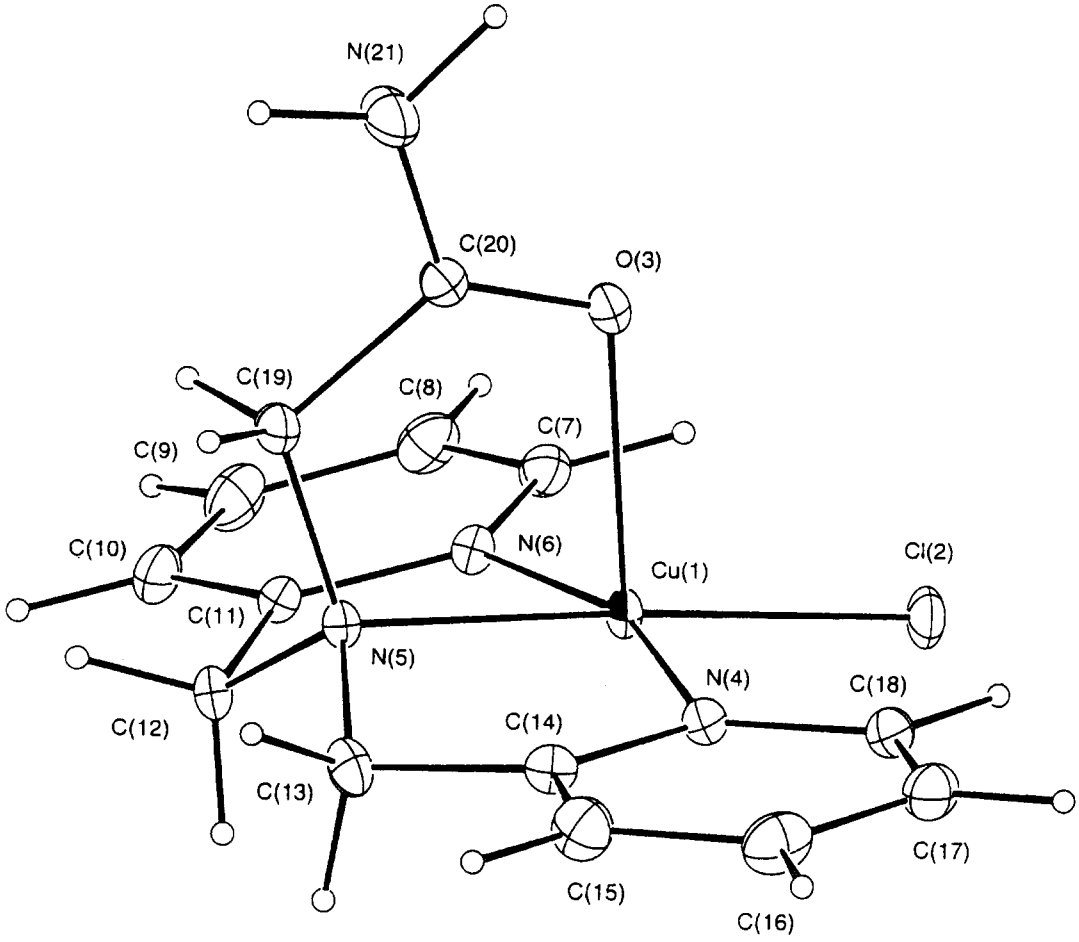

Fig. 3. Schematic illustration of $Cu(dpgs)Cl^+$ [7]

Cu(1)—Cl(2)	2.238(1)	Cu(1)—O(3)	2.288(3)
Cu(1)—N(4)	1.980(4)	Cu(1)—N(5)	2.072(4)
Cu(1)—N(6)	1.976(4) Å	Cl(2)—Cu(1)—O(3)	103.2(1)°

Active species for strand scission

In the previous paper, we have reported that a peroxide adduct formation occurs in the solution containing a copper(II) complex and hydrogen peroxide, as shown below [7];

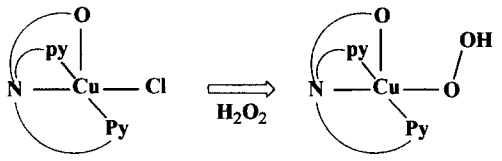

Copper, in the presence of oxygen donor species, is thought to be able to form different oxidative intermediates, depending on the specific complex and conditions. A nondiffusable copper-oxene intermediate has been invoked in some cleavage reactions, [11] while for others, Fenton-type chemistry, which involves release of diffusable hydroxyl radical, has been suggested [5]. The formation of the hydroxyl radical ($OH^\bullet$) has been investigated by the use of spin-trapping reagents, such as DMPO [13], however, its validity has been doubted by several authors [14–16]. Thus, at present it seems most likely that the most reliable method to produce and to detect $OH^\bullet$ should be the X-ray irradiation of N_2O-saturated aqueous solution, and evaluation of formation of 8-hydroxy derivative of guanosine or 2′-deoxyguanosine in the solution [17]. We already reported that formation of 8-hydroxydeoxyguanosine occurs in the solution of copper(II) chloride/hydrogen peroxide system in which no degradation of DNA was detected, however, little formation of 8-hydroxydeoxyguanosine was detected in the solutions of $Cu(tpa)Cl^+$/hydrogen peroxide and other copper(II) chelates used in this study [12]. We could not detect the formation of PBN—OH in the $Cu(tpa)Cl^+$ and $Cu(dpgs)Cl^+$/hydrogen peroxide solutions containing PBN(α-phenyl-N-*t*-butylnitrone), one of the

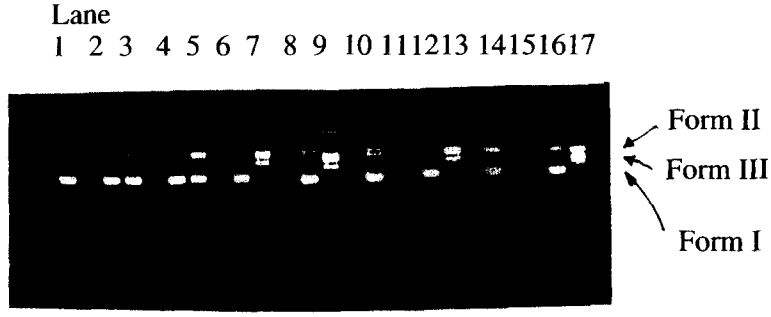

Fig. 4. Relaxation of pBR322 DNA by copper(II) complexes in the presence of hydrogen peroxide. Lane 1, DNA only; lane 2, DNA + (dpg)-complex; lane 3, DNA + (dpg)-complex (0.1 mM) + H_2O_2; lane 4, DNA + (dpgs)-complex (0.1 mM); lane 5, DNA + (dpgs)-complex (0.1 mM) + H_2O_2; lane 6, DNA + (tpa)-complex (0.1 mM); lane 7, DNA + (tpa)-complex (0.1 mM) + H_2O_2; lane 8, DNA + (dpg)-complex (0.5 mM); lane 9, DNA + (dpg)-complex (0.5 mM) + H_2O_2; lane 10, DNA + (dpgs)-complex (0.5 mM); lane 11, DNA + (dpgs)-complex (0.5 mM) + H_2O_2; lane 12, DNA + (dpgt)-complex (0.5 mM); lane 13, DNA + (dpgt)-complex (0.5 mM) + H_2O_2; lane 14, DNA + (dpgs)-complex (1.0 mM); lane 15, DNA + (dpgs)-complex (1.0 mM) + H_2O_2; lane 16, DNA + (dpg)-complex (1.0 mM); lane 17, DNA + (dpg)-complex (1.0 mM) + H_2O_2.

spin-trapping reagents [18]. Based on the above discussion, and also on the fact that the copper(II) complexes with (tpa) or (dpgs) have not activity for decomposition of hydrogen peroxide [7,19], i.e., a redox reaction between a copper(II) complex and hydrogen peroxide does not occur, it seems reasonable to assume that an active species for DNA cleavage is neither a hydroxy radical nor a copper-oxene species in the present cases. Above discussion may support the idea that an active species for DNA strand scission in the present cases should be a peroxide adduct as shown above.

Thus, we would like to propose that DNA strand scission by the copper(II) complexes should proceed via formation of a peroxide intermediate, as shown below; the peroxide adduct attacks the carbon atom of C4′-position, and activation of the peroxide ion in the intermediate is greatly enhanced as suggested [8], and this may induce degradation of the sugar ring, leading to facile strand scission of the DNA. Above proposal may be supported by the facts that (1) the copper(II)-peroxide adduct with end-on coordination mode exhibits an electrophilic nature, tending to interact with an organic moiety [7,8,20], and (2) the tetrahydrofuran-ring can facilely interact with a metal-peroxide ion [21,22].

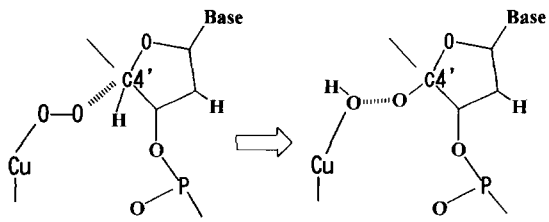

REFERENCES

1. Helene, C. and Toulme, J.-J., *Biochim. Biophys. Acta*, 1992, **1049,** 99.
2. Uhlemann, E. and Peyman, A., *Chem. Rev.*, 1990, **90,** 554.
3. Dreyer, G. B. and Dervan, P. B., *Proc. Natl. Acad. Sci. U.S.A.*, 1985, **82,** 968.
4. Moster, H. E. and Dervan, P. B., *Science*, 1987, **238,** 645.
5. Pamatong, F. V., Detner, C. A. and Bocarsly, J. F., *J. Am. Chem. Soc.*, 1996, **118,** 5339.
6. Back, D. P., Iverson, B. L. and Dervan P. B., *J. Am. Chem. Soc.*, 1988, **110,** 7572.
7. Okuno, T., Ohba, S. and Nishida, Y., *Polyhedron*, 1977, **16,** in press.
8. Ito, S., Okuno, T., Matsushima, H., Tokii, T. and Nishida, Y., *J. Chem. Soc., Dalton Trans.*, 1996, 4479.
9. Micklos, D. A. and Freyer, G. A., *DNA Science*. Cold Spring Harbor Laboratory Press, New York, 1990.
10. Pyle, A. M. and Barton, J. K., *Prog. Inorg. Chem.*, 1990, **38,** 413.
11. Sigmann, D. S. and Chen, C. B., *ACS Symp. Ser.*, 1989, **402,** 24.
12. Kobayashi, T., Ito, S., Hamazaki, H., Ohba, S. and Nishida, Y., *Chem. Lett.*, 1996, 347.
13. Halliwell, B. and Gutteridge, J. M. C., *Free radicals in Biology and Medicine*. Oxford University Press, London, 1985, Chapter 2.
14. Nishida, Y., Nasu, M. and Akamatsu, T., *J. Chem. Soc,. Chem. Commun.*, 1992, 93.
15. Nohn, H., Jordan, W. and Hegner, D., *FEBS Lett.*, 1981, **123,** 241.
16. Finkelstein, E., Rosen, G. M. and Rauckman, E. J., *Arch. Biochem. Biophys.*, 1980, **220,** 1.
17. Shiu, C. and Foote, C. S., *J. Am. Chem. Soc.*, 1995, **117,** 6439.
18. Jensen, E. G., Nutter, Jr., D. E. and Davis, E. R., *Can. J. Chem.*, 1978, **56,** 2237.

19. Nishida, Y., Takeuchi, M., Oishi, N. and Kida, S., *Inorg. Chim. Acta*, 1985, **96,** 81.
20. Ito, S., Suzuki, M., Kobayashi, T., Itoh, H., Harada, A., Ohba, S. and Nishida, Y., *J. Chem. Soc., Dalton Trans.*, 1996, 2579.
21. Liang, G., Gannett, P., Shi, X., Zhang, Y., Chen, F. and Gold, B., *J. Am. Chem. Soc.*, 1994, **116,** 1131.
22. Nishida, Y. and Ito, S., *J. Chem. Soc., Chem. Commun.*, 1995, 1211.

Pergamon

PII: S0277-5387(97)00364-1

Polyhedron Vol. 17, No. 9, pp. 1561–1570, 1998
© 1998 Elsevier Science Ltd
All rights reserved. Printed in Great Britain
0277-5387/98 $19.00+0.00

Synthesis, structural and spectral characterization of two polymeric complexes of 2-chloropyridine and 3-benzoylpyridine with copper(II) azide; $[Cu(2\text{-chloropyridine})(N_3)_2]_n$ and $[Cu(3\text{-benzoylpyridine})_2(N_3)_2]_n$

Mohamed A. S. Goher[a]* and Franz A. Mautner[b]

[a] Department of Chemistry, Faculty of Science, Kuwait University, P.O. Box 5969 Safat, 13060 Kuwait

[b] Institut für Physikalische und Theoretische Chemie, Technische Universität Graz, A-8010 Graz, Austria

(Received 6 June 1997; accepted 20 August 1997)

Abstract—Two new polymeric mixed ligand complexes of copper(II) azide with 2-chloropyridine (**1**) and 3-benzoylpyridine (**3**) have been prepared and characterized by crystallographic and spectroscopic methods. The 1:1 complex of 2-chloropyridine features penta-coordinate copper centers and two $\mu(1,1)$ bridging azido ligands forming chains of polyhedra along the *a*-axis of the unit cell. In the 1:2 complex, **2**, two copper atoms are located at different inversion centers. The coordination geometries of both copper atoms may be described as distorted tetragonal bipyramids and both azides serve as $\mu(1,3)$ bridging ligands giving rise to chains of polyhedra. The IR and Raman spectra are reported and vibrational bands of diagnostic values compared with those of parent ligands and correlated with the structures of the complexes. The solid and solution electronic spectra of **1** and **2** display strong absorptions due to $N_3^- \rightarrow Cu^{II}$ charge transfer transitions. The EPR spectra of powder samples and DMF solutions are recorded at both room temperature and 77 K. © 1998 Elsevier Science Ltd. All rights reserved

Keywords: copper(II) azide complexes; 2-chloropyridine; 3-benzoylpyridine; crystal structure; molecular vibrations; EPR spectra.

Copper(II) azide systems have been of considerable interest due to the broad range of their structural and magnetic properties [1]. In particular, azide can act as a bridging ligand giving rise to ferromagnetic exchange interactions and antiferromagnetic ones, depending upon its mode of coordination; $\mu(1,1)$ and $\mu(1,3)$, the Cu—N_3—Cu angle as well as the geometry of the copper center [2–8]. The azido ligand, therefore represents a good choice for the design of new magnetic systems. For this ligand, it is also important to note the great versatility in the coordination modes giving rise to high nuclearity systems [9, 10].

It has been reported that the interaction between copper(II) azide and pyridine produces different modifications of a polymeric 1:2 complex and the products described as brown, brownish-green or green [11–13]. X-ray structure determinations, however, have shown that while the green and brownish-green modifications contain distorted octahedral copper(II) atoms, the two azide groups are crystallographically distinct with different structural environments. In the green form of the 1:2 complex, one azide ligand is monodentate whereas the other coordinates asymmetrically to three different metal centers [14]. In the brownish-green form, each pair of copper atoms are simultaneously bridged by $\mu(1,1)$ and $\mu(1,3)$ azido ligands [15]. These different modifications reflect the versatile nature of the azido ligand. Such versatility manifests itself in the substantial array of copper(II)

* Author to whom correspondence should be addressed.

azide complexes of monosubstituted pyridine ligands that have been prepared, structurally characterized and shown to have a wide variety of stoichiometries, solid state stereochemistries and varying degrees of oligomerization [15–20]. In this paper we report the synthesis and characterization of two new polymeric complexes of copper(II) azide with 2-chloropyridine and 3-benzoylpyridine (hereafter abbreviated as 2-Clpy and 3-Bzpy, respectively), in order to appraise the influence of the substituent in the pyridine ring upon the mode of bonding of the azido ligand, as elucidated by X-ray crystallographic and spectroscopic methods.

EXPERIMENTAL

2-Chloropyridine and 3-benzoylpyridine were purchased from Aldrich company and other chemicals were of analytical grade quality.

Preparation of polymeric $[Cu(2\text{-chloropyridine})(N_3)_2]_n$ *complex* (**1**)

Copper(II) nitrate trihydrate (0.72 g, 3 mmol) dissolved in acetone (ca 40 cm^3) and 2-Clpy (1.13 g, 10 mmol) were mixed together, followed by addition of an aqueous solution of NaN_3 (0.52 g, 8 mmol). The green solution mixture was boiled for about 15 min and filtered. The filtrate was allowed to stand over three weeks in an open place, after which it separated into two layers. This final mixture was further allowed to stand over two months to produce black needles like crystals of the complex. Yield: 30%. Found: C, 23.1; H, 1.6; N, 37.4; Cu, 24.1. Calc.: C, 23.0; H, 1.55; N, 37.5; Cu, 24.3%.

Preparation of polymeric $[Cu(3\text{-benzoylpyridine})_2(N_3)_2]_n$ *complex* (**2**)

Copper(II) nitrate trihydrate (0.72 g, 3 mmol) and 3-benzoylpyridine (1.83 g, 10 mmol) were mixed together in 50 cm^3 acetone. To this mixture, an aqueous solution (ca 5 cm^3) of NaN_3 (0.48 g, 7.5 mmol) was added with continuous stirring. The green precipitate was filtered off and then dissolved in DMF. The final solution was filtered off and the filtrate boiled for ca 15 min, and allowed to stand in a refrigerator for ca two months until black crystals of the complex separated. Yield: 50%. Found: C, 56.3; H, 3.7; N, 21.6; Cu, 12.1. Calc.: C, 56.1; H, 3.5; N, 21.8; Cu, 12.4%.

Physical measurements

Raman spectra were obtained using a Perkin–Elmer System 2000 NIR FT-Raman spectrometer. Both compounds are very sensitive to the power of the laser beam. Below 100 mW, either no spectrum or a noisy spectrum obtained whereas above 100 mW the sample decomposed gradually and immediately at 200 mW. In order to obtain good spectrum the sample was ground with KBr and measured at a power of 200 mW. The experimental procedures and instruments used for other measurements are as described previously [20].

X-ray crystallography

A modified STOE four circle diffractometer was used for single crystal X-ray measurements. Orientation matrix and lattice parameters were obtained by least-squares refinement of the diffraction data from 28 (compound **1**) and 36 (compound **2**) reflections in the 2θ range 10–27°. Data were collected at 295(2) K using graphite crystal monochromatized Mo–K_α radiation ($\lambda = 0.71069$ Å) and the ω-scan technique. The intensities were corrected for Lorentz-polarization effects, intensity decay and for absorption [21]. Crystallographic data are collected in Table 1.

The structures were solved by heavy atom methods and subsequent Fourier analyses. Anisotropic displacement parameters were applied to the non-hydrogen atoms in full-matrix least-squares refinements based on F^2. The hydrogen atoms were assigned with common isotropic displacement factors and included in the final refinement cycles by use of geometrical restraints. Analytical expressions of neutral-atom scattering factors were employed, and anomalous dispersion corrections were incorporated. The programs DIFABS [21] and SHELXTX/PC [22], were used for computations. Selected bond distances and angles are given in Tables 2 and 3. Positional parameters, anisotropic displacement parameters, hydrogen atom coordinates, a full list of bond lengths and angles and F_o/F_c tables have been deposited as supplementary material.

Caution: Both compounds are very sensitive to grinding and explode upon heating and friction.

RESULTS AND DISCUSSION

The reaction of copper(II) ions and 2-chloropyridine and 3-benzoylpyridine in presence of azide ions in acetone media afforded the title complexes. In case of 2-Clpy, only 1 : 1 complex is formed whatever the ratio of the reactants. Indeed, all other 2-substituted pyridines, e.g. 2-picoline [17], 2-bromopyridine [19] and 2-aminopyridine [6], form only 1 : 1 complexes with copper(II) azide indicating that the steric hindrance of the substituent group in position 2 in pyridine ring plays the important role in the synthesis of their copper(II) azido complexes. Both complexes (**1**) and (**2**) are insoluble in many non-polar solvents as well some polar solvents, e.g. acetone, chloroform, methyl and ethyl alcohols indicating their polymeric nature. They are, however, quite soluble in DMSO and DMF giving rise to non-conducting solutions, although the color of complex (**2**) changes

Table 1. Crystallographic data and processing parameters

Compound	**1**	**2**
Molecular Formula	$C_5H_4ClCuN_7$	$C_{24}H_{18}CuN_8O_2$
Molecular weight	261.14	514.00
Color	black	deep green
System, Space group	Triclinic, *P*-1	Triclinic, *P*-1
a (Å)	5.775(2)	8.731(3)
b (Å)	8.443(3)	8.965(3)
c (Å)	10.006(4)	16.319(6)
α (°)	82.22(3)	95.40(3)
β (°)	76.84(3)	104.74(3)
γ (°)	88.30(3)	109.74(3)
V (Å^3)	407.7(3)	1139.7(7)
Z	2	2
μ(Mo–K$_\alpha$) (mm^{-1})	2.573	0.998
Normal. transmission factors	1.000–0.195	1.000–0.235
D_{calc}/D_{obs} (mg/m^3)	1.843/1.83(2)	1.498/1.50(2)
Approx. crystal size (mm)	$0.85 \times 0.12 \times 0.06$	$0.60 \times 0.18 \times 0.10$
θ range of data collection (°)	3.62–27.49	2.83–29.12
Reflections collected	2294	5677
Independ. refl. /R_{int}	1977/0.0402	5200/0.0335
Parameters	128	323
Goodness-of-Fit on F_o^2	1.043	1.041
R_1/wR_2	0.0689/0.1346	0.0662/0.1247
Weighting factors[a]: a/b	0.0758/0.0000	0.0617/0.0000
Largest peak/hole (e Å^{-3})	0.570/−1.067	0.348/−0.805

[a] $w^{-1} = [\sigma^2(F_o^2) + (aP)^2 + bP]$ and $P = (F_o^2 + 2F_c^2)/3$.

Table 2. Selected bond distances (Å) and angles (°) of **1**

Cu(1)···Cu(1b)	3.112(2)	Cu(1)···Cu(1a)	3.233(2)
Cu(1)—N(11a)	1.980(5)	Cu(1)—N(21)	1.978(5)
Cu(1)—N(21b)	2.019(5)	Cu(1)—N(1)	2.067(6)
Cu(1)—N(11)	2.270(5)	N(11)—N(12)	1.190(8)
N(11)—Cu(1a)	1.980(5)	N(12)—N(13)	1.145(8)
N(21)—N(22)	1.212(8)	N(21)—Cu(1b)	2.019(5)
N(22)—N(23)	1.123(9)	N(1)—C(1)	1.334(9)
N(1)—C(5)	1.340(8)	C(1)—C(2)	1.349(10)
C(1)—Cl(1)	1.732(7)	C(2)—C(3)	1.375(11)
C(3)—C(4)	1.361(12)	C(4)—C(5)	1.380(11)
N(11a)—Cu(1)—N(21)	170.4(2)	N(11a)—Cu(1)—N(21b)	94.6(2)
N(21)—Cu(1)—N(21b)	77.7(2)	N(11a)—Cu(1)—N(1)	93.9(2)
N(21)—Cu(1)—N(1)	95.7(2)	N(21b)—Cu(1)—N(1)	145.9(2)
N(11a)—Cu(1)—N(11)	81.2(2)	N(21)—Cu(1)—N(11)	96.6(2)
N(21b)—Cu(1)—N(11)	114.6(2)	N(1)—Cu(1)—N(11)	99.3(2)
Cu(1a)—Cu(1)—Cu(1b)	131.1(1)	N(12)—N(11)—Cu(1a)	124.1(4)
N(12)—N(11)—Cu(1)	129.1(4)	Cu(1a)—N(11)—Cu(1)	98.8(2)
N(13)—N(12)—N(11)	177.9(7)	N(22)—N(21)—Cu(1)	126.2(4)
N(22)—N(21)—Cu(1b)	125.8(5)	Cu(1)—N(21)—Cu(1b)	102.3(2)
N(23)—N(22)—N(21)	176.2(11)		

symmetry codes: (a) $-x+1, -y, -z$; (b) $-x, -y, -z$.

Table 3. Selected bond distances (Å) and angles (°) of **2**

Cu(1)···Cu(2)	5.092(2)	Cu(1)—N(21)	1.986(3)
Cu(1)—N(1)	2.007(3)	Cu(1)—N(13)	2.552(4)
Cu(2)—N(11)	1.981(4)	Cu(2)—N(2)	2.042(3)
Cu(2)—N(23)	2.552(4)	N(11)—N(12)	1.179(4)
N(12)—N(13)	1.148(4)	N(21)—N(22)	1.171(4)
N(22)—N(23)	1.151(5)	N(1)—C(5)	1.329(5)
N(1)—C(1)	1.341(5)	C(1)—C(2)	1.371(6)
C(2)—C(3)	1.387(6)	C(2)—C(6)	1.490(6)
C(3)—C(4)	1.362(6)	C(4)—C(5)	1.373(6)
C(6)—O(1)	1.221(5)	C(6)—C(7)	1.472(6)
C(7)—C(8)	1.387(6)	C(7)—C(12)	1.387(6)
C(8)—C(9)	1.362(7)	C(9)—C(10)	1.354(7)
C(10)—C(11)	1.372(7)	C(11)—C(12)	1.378(7)
N(2)—C(17)	1.325(5)	N(2)—C(13)	1.332(5)
C(13)—C(14)	1.376(6)	C(14)—C(15)	1.383(6)
C(14)—C(18)	1.499(6)	C(15)—C(16)	1.358(6)
C(16)—C(17)	1.375(6)	C(18)—O(2)	1.211(5)
C(18)—C(19)	1.490(6)	C(19)—C(24)	1.384(6)
C(19)—C(20)	1.393(6)	C(20)—C(21)	1.360(7)
C(21)—C(22)	1.372(8)	C(22)—C(23)	1.372(7)
C(23)—C(24)	1.358(6)		
N(21)—Cu(1)—N(1)	91.34(14)	N(21)—Cu(1)—N(13)	93.48(14)
N(1)—Cu(1)—N(13)	90.21(14)	N(11)—Cu(2)—N(2)	92.4(2)
N(11)—Cu(2)—N(23)	92.0(2)	N(2)—Cu(2)—N(23)	91.47(14)
N(12)—N(11)—Cu(2)	123.9(3)	N(13)—N(12)—N(11)	177.1(4)
N(22)—N(21)—Cu(1)	123.4(3)	N(23)—N(22)—N(21)	177.2(5)
Cu(1)—N(13)—N(12)	123.7(3)	Cu(2)—N(23)—N(22)	111.4(3)
O(1)—C(6)—C(7)	121.3(4)	O(1)—C(6)—C(2)	118.8(4)
O(2)—C(18)—C(19)	121.2(4)	O(2)—C(18)—C(14)	118.6(4)

to brown immediately in both solvents. The color change from green to brown in DMF and DMSO could be associated with the partial reduction of Cu(II) to Cu(I) leading to mixed-valence compounds which are well known to exhibit such brownish color.

Structure

Figures 1 and 2 illustrate the principle structural features of complex (**1**) for which selected bond lengths and bond angles are collected in Table 2. In the structure, $\mu(1,1)$ azido groups [N(11)—N(12)—N(13) and N(11a)—N(12a)—N(13a)] bridge a pair of copper centers, Cu(1) and Cu(1a), whereas $\mu(1,1)$ azido ligands [N(21)—N(22)—N(23) and N(21a)—N(22a)—N(23a)] bridge the pair of copper atoms, Cu(1) and Cu(1b), giving rise to chains of polyhedra along the *a*-axis of the unit cell. Each pair of copper centers is related by an inversion center forming a planar Cu_2N_2 ring. The coordination of copper(II) atom by 2-Clpy and azido ligands may be described as distorted trigonal bipyramid with N(21) and N(11a) at the axial sites and N(1), N(11) and N(21b) in the equatorial positions.

It is of interest to compare the structure of **1** with other 1 : 1 mixed ligand complexes of copper(II) azide with 2-substituted pyridines; 2-bromopyridine (**3**) [19], 2-methylpyridine (**4**) [17], 2-aminopyridine (monodentate and accompanied by H_2O) (**5**) [6] and 2-benzoylpyridine (**6**) [18]. Common structural features of this series of complexes are five coordination about the copper atom (trigonal bipyramidal in **1** and square pyramidal in the others) and a planar Cu_2N_2 ring. The dimeric nature of **6** arises from the fact that the three coordination sites around each metal atom are taken up by a terminal azide and a chelating bidentate 2-Bzpy molecule. Complex **5** is likewise binuclear, but the structure is further modified by the formation of intramolecular O···H—N (amine) acceptor and intermolecular O—H···N (terminal azide) donor hydrogen bonds [18]. The organic ligands is mondentate in **1**, **3** and **4**, and unsaturation in the copper(II) coordination sphere is satisfied by converting the remaining azide from terminal to $\mu(1,1)$ in **1** and **3** and $\mu(1,3)$ in **4**, thereby resulting in the formation of polymeric chains. The Cu—N(L) distance reported in these complexes is 2.076(8), 1.992(2) and 2.001(2) for **3**, **4** and **5**, respectively, and therefore it increases in the order 2-Mepy < 2-ampy < 2-Clpy < 2-Brpy.

A plot and atom numbering scheme of complex (**2**) are given in Fig. 3. In the asymmetric unit, two copper atoms are located at different inversion centers. Each

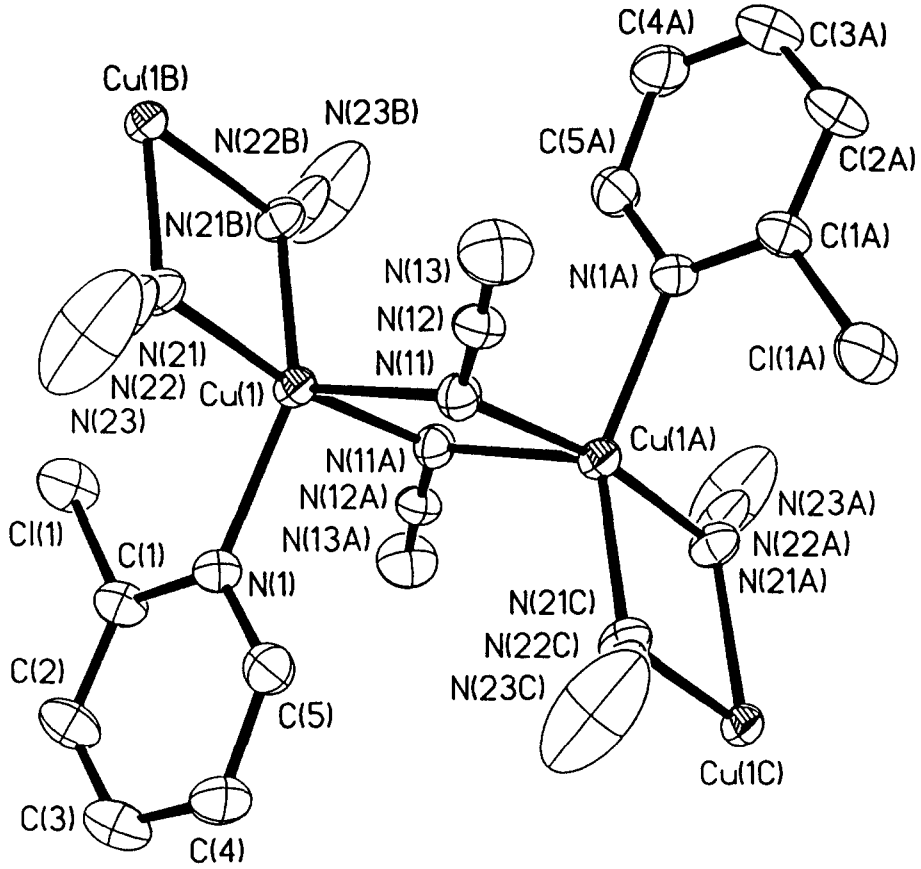

Fig. 1. Molecular geometry and atom labelling scheme of $[Cu(2\text{-chloropyridine})(N_3)_2]_n$, **1**. Hydrogen atoms are omitted.

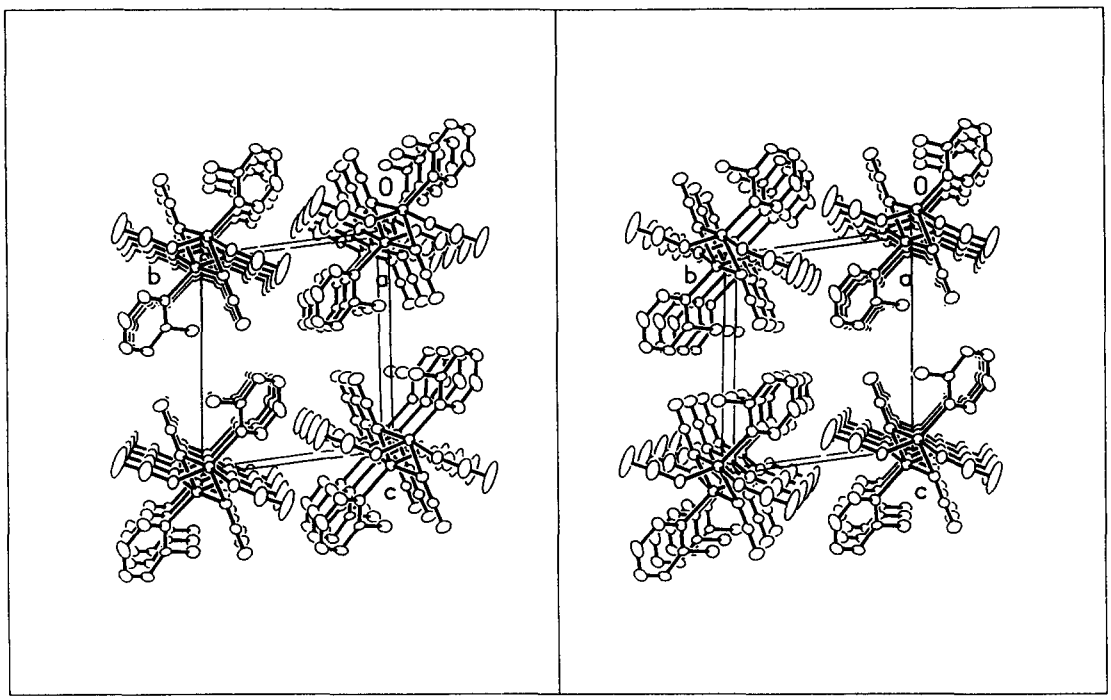

Fig. 2. Packing plot (stereo) of $[Cu(2\text{-chloropyridine})(N_3)_2]_n$, **1**, viewed along the *a*-axis of the unit cell.

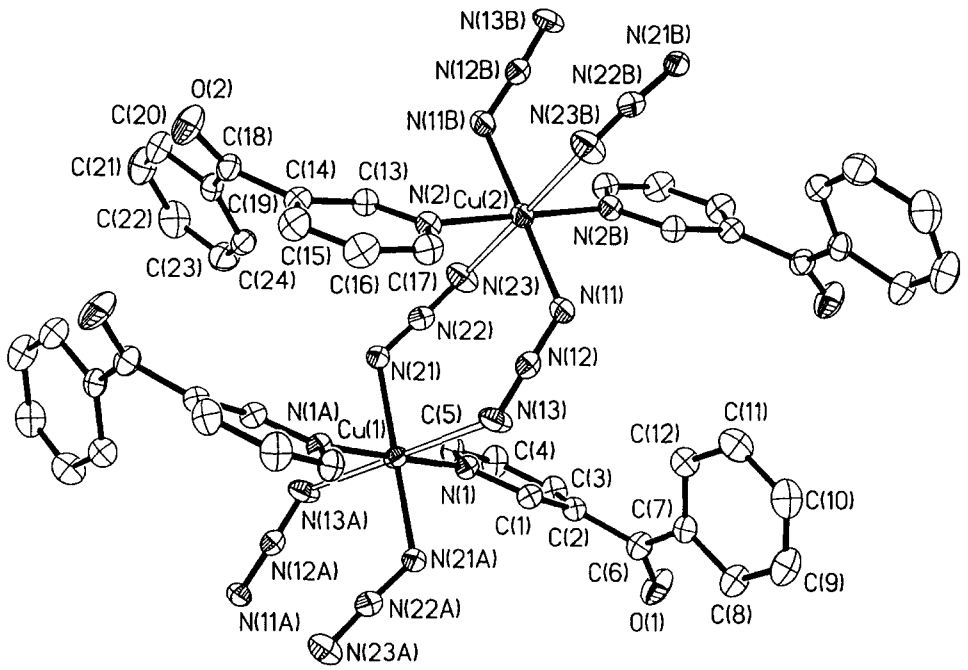

Fig. 3. Molecular geometry and atom labelling scheme of $[Cu(3\text{-benzoylpyridine})_2(N_3)_2]_n$, **2**. Hydrogen atoms are omitted for clarity.

copper center, however, is coordinated by two organic ligands and the end nitrogens of two di-$\mu(1,3)$ bridging azido groups. The coordination polyhedra of both copper atoms may be described as distorted tetragonal bipyramids with N(13) and N(13a) in case of Cu(1) and N(23) and N(23a) in case of Cu(2) at the axial site forming chains of polyhedra (Fig. 4). The Cu—$N(N_3)$ bond lengths vary from 1.981(4) to 2.552(4) Å, and the Cu—N(3-Bzpy) distances are 2.007(3) and 2.042(3) Å.

The di-$\mu(1,3)$ mode of azide bridging has previously been found in the discrete dinuclear complexes $[Cu(PPh_3)_2(N_3)_2]$ [23], $[Ni_2(tren)_2(N_3)_2]^{2+}$ where tren = tris(2-aminoethyl)amine [24], $[Cu(Me_4en)_2(N_3)_2]$ [25] and polymeric complex $[Cd(py)_2(N_3)_2]_n$ [26]. The structure of the title complex (**2**) differs from those of manganese(II) complexes of the same general formula $[MnL_2(N_3)_2]_n$ for L = ethyl isonicotinate [27], 3-acetyl pyridine [28], 4-cyanopyridine [28] and ethyl nicotinate [29]. In all of these complexes the manganese atom is located in a *trans*-octahedral environment and bonded to four azido ligands and two axial organic molecules. The four azido ligands behave differently; two azido groups are coordinated in the $\mu(1,1)$ fashion between two manganese atoms giving rise to a planar Mn_2N_2 units, and the other two azides bonded in the $\mu(1,3)$ mode.

The Cu···Cu distances of 3.112(2) and 3.233(2) within the cyclic Cu_2N_2 units in structure **1**, which are comparable with those found in the structure of $[Cu(2\text{-methyl-5-ethylpyridine})(N_3)_2]_n$ (3.131(1) and 3.236(1) Å) [30], are shorter than corresponding values found in $[Cu(3\text{-pic})(N_3)_2]_n$ (3.546(2) Å) [6] and $CuL'(N_3)_2$ (3.78 Å) L' = (2-aminoethyl)pyridine) [31], but longer than those found in $[Cu(py—NO)—(N_3)_2]_n$ (3.07 Å) [32]. The Cu···Cu distance of 5.092(2) Å, found in complex (**2**) within the eight-membered ring $Cu_2(N_3)_2$, are comparable with corresponding values of 5.004(2) Å and 5.227(7) Å reported in $[Cu(tmen)(N_3)_2]_2$ (tmen = tetramethylenediamine) [25] and $[Cu_2(Me_5\text{-dien})_2(N_3)_2]^{2+}$ [33], respectively.

IR and Raman spectra

The IR and Raman spectral results of the complexes are collected in Table 4. Raman spectra of good quality were obtained for free ligands and complex (**2**) only (see the experimental section). The IR spectrum of **1** exhibits two bands due to the $\nu_{as}(N_3)$ mode which are consistent with the presence of two azides of different degrees of asymmetry. Although the positions of these bands are not consistent with the $\nu_{as}(N_3)$ vs δd (δd is the difference between N—N distances in an azide group) relationship reported earlier [34], the higher frequency band may be assigned to the N(21)—N(22)—N(23) azide with δd of 0.089 Å whereas the 2020 cm^{-1} is related to the N(11)—N(12)—N(13) ligand with δd of 0.045 Å. The asymmetric nature of both azido ligands is strongly evidenced by the appearance of the $\nu_s(N_3)$ vibration bands in the range 1350–1270 cm^{-1}. For a symmetrical N_3^- ion, the ν_s mode (ν_1) is not IR active but

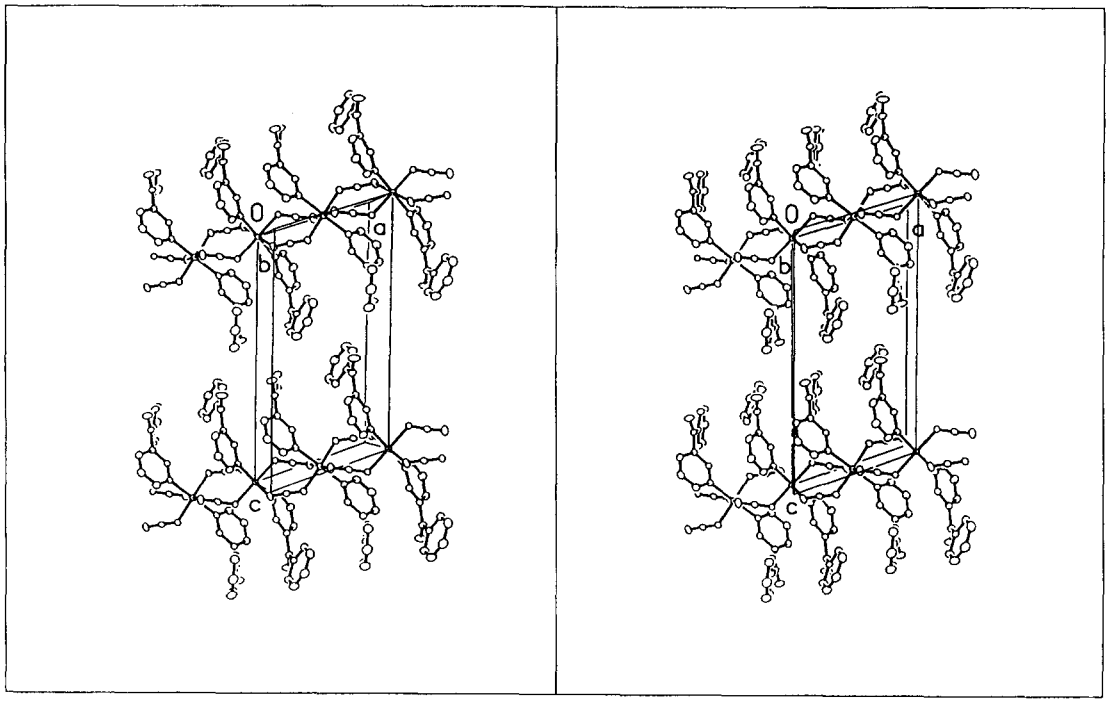

Fig. 4. Packing plot (stereo) of $[Cu(3\text{-benzoylpyridine})_2(N_3)_2]_n$, **2**, viewed along the *b*-axis of the unit cell.

Raman active, whereas $\nu_{as}(N_3)$ (ν_3) and $\delta(N_3)$ (ν_3) modes are IR active and Raman inactive. In accordance with this, the IR spectrum of **2** shows a very strong band at 2030 cm^{-1} due to ν_{as} and no band due to ν_s could be located in the range 1350–1270 cm^{-1}. This result strongly supports the symmetrical nature of both azido ligands in **2**. Other support comes from the Raman spectrum of **2**, which exhibits only a medium peak at 1327 cm^{-1} due to ν_s. The disappearance of the ν_{as} (N_3) and $\delta(N_3)$ vibration peaks suggests that the mutual exclusion rule is valid for such polymeric complex although it contains two metal atoms at two different inversion centers.

Electronic spectra

The electronic absorption spectra of complexes **1** and **2** measured as Nujol mulls are given in Table 5 and Fig. 5. These spectra exhibit *d–d* transitions as a broad band centered around 13888 cm^{-1} and 15870 cm^{-1}, suggesting five- and six-coordination geometries around metal atoms for **1** and **2**, respectively. The position of the *d–d* in **1** is very similar to that reported (See Fig. 1, ref. 5) for the polymeric 1 : 1 copper(II) azide complex of 3-picoline in which copper(II) atoms have a trigonal bipyramidal geometry. The spectrum of complex **1** also show a very strong band around 23,255 cm^{-1} along with a moderate band around 18,518 cm^{-1}. These bands are due to $N_3^- \rightarrow Cu^{II}$ LMCT transitions. While two and four azide-to-copper(II) CT transitions have been predicted on theoretical bases for terminal and (μ-1, 1) or (μ-1, 3) bridging azides, only one and two bands have been reported for monomers and $\mu(1,3)$ or $\mu(1,1)$ dimers, respectively [35]. Complex **2** which contains only $\mu(1,3)$ bridging azides shows a very broad and strong N_3^--MCT band around 21,300 cm^{-1}. As a distinct absorption band is usually observed in the range 17,000–21,000 cm^{-1} for copper(II) azide complexes containing di-$\mu(1,1)$ bridging azides, and as no band is observed in the above region of the spectrum of **2**, the 18,518 cm^{-1} band is evidently due to the di-$\mu(1,1)$ azide-to-copper CT transitions. The appearance of such a moderate band in copper(II) azido complexes, therefore may be taken as strong evidence for the presence of di-$\mu(1,1)$ azido system. In DMF and DMSO solution of **1**, however, only one broad and very strong band observed corresponds to the main $N_3^- \rightarrow$ MCT transition in the solid complex, whereas the *d–d* band remains at almost the same position. The DMF solution of **2** shows the CT band shifted to higher wave number whereas the *d–d* band appears at lower wave number suggesting five coordinate copper geometry in this solvent. It is possible that one of the two organic ligand molecules washed out and the solution contains only the 1 : 1 complex as the spectrum is very similar to that of **1**.

EPR spectra

The room temperature EPR spectrum of a polycrystalline sample of **1** is a well defined typical spec-

Table 4. Vibrational frequencies (cm^{-1}) in the IR and Raman spectra of the complexes

$[Cu(2\text{-}Clpy)(N_3)_2]_n$	3-Bzpy	$Cu(3\text{-}Bzpy)_2(N_3)_2]_n$		
IR	Raman	IR	Raman	Assignments
2070 vs		2030 vs, sp	—	$\nu_{as}(N_3)$
2020 vs				$\nu_{as}(N_3)$
	1648 s	1652 ms	1666 vs	$\nu_{C=O}$
1582 m	1579 ms	1585 m	1583 s	pyridine
1552 m	1585 vs	1570 sh	1576 m	pyridine
1446 m	1470 vw	1465 wm	1470 m	pyridine
1415 ms	1435 vw	1434 wm	1430 w	pyridine
1374 ms	1415 vvw	1409 wm	1412 w	pyridine
1330 m			1327 m	$\nu_s(N_3)$
1282 s				$\nu_s(N_3)$
1238 w	1287 w	1282 s	1282 s	2×630
1168 m	1201 w	1193 m	1200 w	
	1156 m	1156 m	1154 m	pyridine
1124 m		1115 wm	1120 m	
1084 m		1083 w	1080 w	pyridine
1045 m	1039 s	1045 w	1036 s	pyridine
1017 m	1028 s	1032 m	1025 w	
1017 m	1001 vs	1010 m	1001 ms	pyridine
	950 w	937 ms	930 w	
	923 w		881 ms	
	840 vw	823 m	825 w	pyridine
761 s	786 w	787 m	785 wm	pyridine + 2×370
728 m	745 m	702 wm	710 wm	pyridine
679 m	651 w	651 ms	651 m	pyridine
605 wm				$\delta(N_3)$
593 w				$\delta(N_3)$
473 m	432 w	450 wm	430 m	pyridine
437 m	408 w	415 w	418 wm	2×205
380 ms		350 m	315 m	$\nu Cu—N_3$
360 m				ν (Cu—N_3
270 ms		250 m	271 m	$\nu Cu—N(L)$
			203 m	
			182 m	

v = very, m = medium, s = strong, w = weak, sp = sharp, sh = shoulder.

Table 5. electronic spectral data[a]

Complex	Solvent	$N_3^- \rightarrow Cu^{II}CT$ (ξ)	d–d(ξ)
1	NM	23,255 vs, br 18,518 m	13,888 br
	DMF	23,529 (5400)	13,404 (15)
	DMSO	22,727 (6800)	12,853 (180)
2	NM	21,300 vs, vbr	15,870
	DMF	24,691 (6100)	13,947 (164)

[a] In cm^{-1}.
NM = Nujol mull.

trum of copper(II) system of axial type with $g_{\parallel} = 2.26$ and $g_{\perp} = 2.08$. At 77 K, the spectrum displays the same signals at 2.27 and 2.08, overlapped with a wide isotropic signal. In fact many 1 : 1 copper(II) azide solid complexes of similar ligands frequently exhibit such a broad isotropic signal [5,6]. In DMF, compound **1** is not freely soluble, and the room temperature spectrum of the filterate, however, consists of a half field signal at $g = 4.28$ (Fig. 6) indicating that dimeric units are present in this solution. The main signal at $g = 2.13$ is broad and poorly defined. At 77 K, the DMF solution does not show the half field signal. Instead, the spectrum shows very well hyperfine coupling with the copper nucleus of the g parallel, giving four peaks with hyperfine constant $A = 143$ G (average) and $g_{\perp} = 2.05$. The room temperature EPR spectrum of a polycrystalline sample of **2** is almost of axial type copper(II) systems, exhibiting a poor hyperfine coupling with the copper nucleus of the $g_{\parallel}$ with $A = 81$ G (average). At 77 K, the spectrum displays the same features except that the hyperfine constant A becomes 32.6 G (average).

Acknowledgements—Financial support by the Kuwait University Research Administration Project (No. SC 077) and

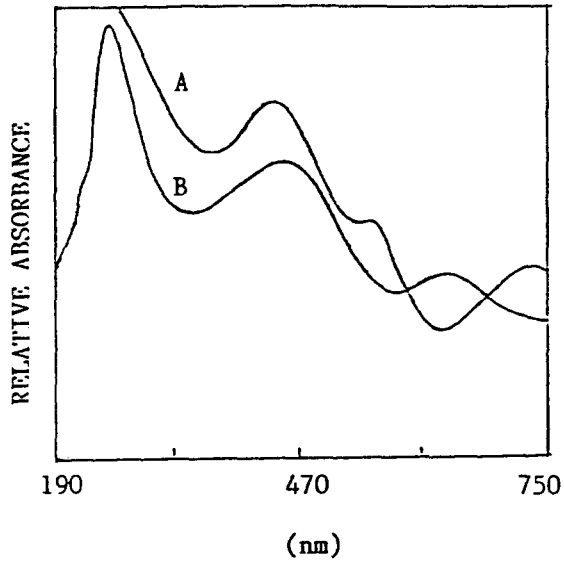

Fig. 5. Electronic absorption spectra of solid complexes; A-[Cu(2-chloropyridine)$(N_3)_2]_n$, B-[Cu(3-benzoylpyridine)$_2(N_3)_2]_n$.

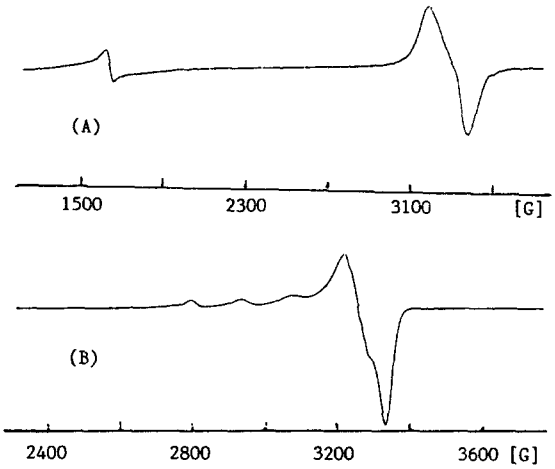

Fig. 6. EPR spectra of **1** in DMF solution; (A) at room temperature (B) at 77 K.

the Department of Chemistry General Facility Projects (Analab) are gratefully acknowledged. The authors thank Prof. Kratky for the use of the STOE diffractometer, and Prof. Escuer, Barcelona University, Spain, for the EPR measurements.

REFERENCES

1. Kahn, O., *Molecular Magnetism*, VCh Publishers, Weinheim, New York, 1993; Kahn, O. In *Magnetostructural Correlations in Exchange Coupled Systems*, ed. R. D. Willett, D. G. Gatteschi, O. Kahn. Reisel, Dordrecht, The Netherlands, 1985.
2. Sikorav, S., Bkouche-Waksman, K. and Kahn, O., *Inorg. Chem.*, 1984, **23,** 490.
3. Chaudhuri, P., Oder, K., Weighardt, K., Nuber, B. and Weiss, J., *Inorg. Chem.*, 1986, **25,** 2818.
4. Comarmond, J., Plumere, P., Lehn, J. M., Agnus, Y., Louis, R., Weiss, R., Kahn, O. and Morgenstern-Badarau, *J. Am. Chem. Soc.*, 1982, **104,** 6330.
5. Goher, M. A. S. and Mak, T. C. W., *Inorg. Chim. Acta*, 1984, **89,** 119.
6. Goher, M. A. S. and Mak, T. C. W., *Inorg. Chim. Acta*, 1984, **85,** 117.
7. Kahn, O., Sikorav, S., Gouteron, J., Jeannin, S. and Jeannin, Y., *Inorg. Chem.*, 1983, **22,** 2877; Tuczek, F. and Bensch, W., *Inorg. Chem.*, 1995, **34,** 1482.
8. Charlot, M. F., Kahn, O., Chaillet, M. and Larrieu, C., *J. Am. Chem. Soc.*, 1986, **108,** 2574.
9. Escuer, A., Vicente, R., Ribas, J., El-Fallah, M. S., Salonas, X. and Front-Bardia, M., *Inorg. Chem.*, 1993, **32,** 3727.
10. Cortes, R., Urtiaga, K., Lezama, L., Pizarro, J., Goni, A., Arriortua, M. I. and Rogo, T., *Inorg. Chem.*, 1994, **33,** 4009.
11. Dennis, L. M. and Isham, H. J., *J. Am. Chem. Soc.*, 1907, **29,** 19.
12. Strecker, W. and Schwinn, E., *J. Prakt. Chem.*, 1939, **152,** 210.
13. Cirulis, A. and Straumanis, M., *Z. Anorg. Allg. Chem.*, 1943, **251,** 349.
14. Agrell, I., *Acta Chem. Scand.*, 1969, **23,** 1667.
15. Mautner, F. A. and Goher, M. A. S., *Polyhedron*, 1995, **14,** 1809.
16. Goher, M. A. S., Wang, R. J. and Mak, T. C. W., *J. Mol. Struct.*, 1991, **243,** 179.
17. Goher, M. A. S. and Mautner, F. A., *Z. Naturforsch.*, 1991, **46b,** 687.
18. Goher, M. A. S. and Mak, T. C. W., *Inorg. Chem. Acta*, 1986, **117,** 17.
19. Mautner, F. A. and Goher, M. A. S., *Polyhedron*, 1992, **11,** 2537.
20. Goher, M. A. S. and Mautner, F. A., *Cryst. Res. Techn.*, 1992, **27,** 817; Goher, M. A. S., Al-Salem, N. A. and Mautner, F. A., *Polyhedron*, submitted.
21. Walker, N. and Stuart, D., *Acta Cryst.*, 1983, **A30,** 158.
22. SHELXTL/PC V 5.03, Siemens Analytical Automation Inc., Madison, WI, 1995.
23. Ziolo, R. F., Gaughan, A. P., Dori, Z., Pierpont, C. G. and Eisenberg, R., *Inorg. Chem.*, 1971, **10,** 1289.
24. Pierponf, C. G., Hindrickson, D. N., Duggan, D. M., Wagner, F. and Barefield, E. K., *Inorg. Chem.*, 1975, **14,** 604.
25. Bkoucho-Waksman, I., Sikorav, S. and Kahn, O., *J. Cryst. Spectr. Res.*, 1983, **13,** 303.
26. Agrell, I., *Acta Chem. Scand.*, 1970, **24,** 3575.
27. Escuer, A., Vicente, R., Goher, M. A. S. and Mautner, F. A., *Inorg. Chem.*, 1996, **35,** 6386.
28. Escuer, A., Vicente, R., Goher, M. A. S. and Mautner, F. A., *Inorg. Chem.*, Submitted.
29. Goher, M. A. S., Al-Salem, N. A. and Mautner, F. A., *J. Coord. Chem.*, submitted.
30. Goher, M. A. S., Al-Salem, N. A. and Mautner, F. A., *Polyhedron*, 1996, **15,** 4513.

31. Bailey, N. A., Fenton, D. E. and McLean, C. H., *Inorg. Chim. Acta*, 1991, **179,** 1.
32. Goher, M. A. S. and Mautner, F. A., *Polyhedron*, 1995, **14,** 1751.
33. Felthouse, T. R. and Hendrickson, D. N., *Inorg. Chem.*, 1978, **17,** 444.
34. Agrell, I., *Acta Chem. Scand.*, 1971, **25,** 2166; Goher, M. A. S., *Acta Chim. Hung.*, 1990, **127,** 213.
35. Pate, J. E., Ross, P. K., Thamann, T. J., Reed, G. A., Karlin, K. D., Sorrell, T. N. and Solomon, E. J., *J. Am. Chem. Soc.*, 1989, **111,** 5198.

Pergamon

PII: S0277-5387(97)00348-3

Polyhedron Vol. 17, No. 9, pp. 1571–1577, 1998
© 1998 Published by Elsevier Science Ltd
All rights reserved. Printed in Great Britain
0277-5387/98 $19.00+0.00

A new co-crystallised tri-metallic nickel(II) complex: bis(Δ,Λ-*bis*(ethylenediamine-*N*,*N*′)bis(thiocyanato)-nickel(II))-Δ,Λ-*tris*(ethylenediamine-*N*,*N*′)nickel(II)-hexafluorophosphate

Michael James,*† Hiroyuki Kawaguchi and Kazuyuki Tatsumi

Department of Chemistry, Faculty of Science, Nagoya University, Furo-cho, Chikusa-ku, Nagoya 464-01, Japan

(Received 23 June 1997; accepted 14 August 1997)

Abstract—The title compound, $[\Delta,\Lambda\text{-Ni(en)}_2(NCS)_2]_2[\Delta,\Lambda\text{-Ni(en)}_3][PF_6]_2$ (**1**) (en = ethylenediamine) has been synthesised via a molecular rearrangement reaction of *trans*-$Ni(en)_2(NCS)_2$. **1** consists of $[Ni(en)_2(NCS)_2]_2$ (**1a**), $[Ni(en)_3]^{2+}$ (**1b**) and $[PF_6]^-$ (**1c**) molecular units in a 2:1:2 ratio, such that both **1a** and **1b** crystallise in an ordered racemic sequence of Λ and Δ chiral units. Extensive intermolecular hydrogen bonding is observed between amine protons of the en chelate rings and the fluorine atoms of the $[PF_6]^-$ counteranions, as well as between the amine protons and sulfur atoms of the NCS ligands. The en chelates display ring conformations of $\Lambda\lambda\lambda$ for **1a** and $\Lambda\delta\delta\delta$ for **1b**. © 1998 Published by Elsevier Science Ltd. All rights reserved

Keywords: hydrogen bonding; amine protons; co-crystallisation.

The absolute configurations of optically active coordination compounds has been of long-standing interest to chemists. Since the structure and absolute configuration of the $[Co(en)_3]^{3+}$ (en = ethylenediamine) cation were determined in 1955 by Saito *et al.* [1], numerous studies of structurally related compounds have been made. Where such compounds contain five-membered chelating ethylenediamine (en) rings, two possible enantiomeric configurations (Δ or Λ) and two possible ring conformations (δ and λ) may be formed. In the case of the *tris*-chelating pseudo-octahedral complex, $[M(en)_3]^{n+}$, combination of these ring conformations and configurations leads to eight possible different isomers ($\Lambda\delta\delta\delta$, $\Lambda\delta\delta\lambda$, $\Lambda\delta\lambda\lambda$, $\Lambda\lambda\lambda\lambda$, $\Delta\delta\delta\delta$, $\Delta\delta\delta\lambda$, $\Delta\delta\lambda\lambda$ or $\Delta\lambda\lambda\lambda$); while for *bis*-chelating molecules, *cis*-$[M(en)_2]X_2$, there may be six different isomeric forms ($\Lambda\delta\delta$, $\Lambda\delta\lambda$, $\Lambda\lambda\lambda$, $\Delta\delta\delta$, $\Delta\delta\lambda$ or $\Delta\lambda\lambda$) [2]. In the solid state both complexes usually occur as racemic mixtures, crystallising in centrosymmetric space groups that lead to an equal number of Λ and Δ metal centres.

As part of a continuing study into polymetallic complexes of linearly coupled paramagnetic metal ions, we have focused on the synthesis and structural characterisation of systems based on the *trans*-$Ni(en)_2X_2$ monomeric unit; where X typically is a N- or O-donor ligand or a non-coordinated counteranion. More specifically, we have been investigating the reactivity of linear di-nitrogen bridging ligands such as pyrazine and 4,4′-bipyridine with *trans*-$Ni(en)_2(NCS)_2$. In the case of pyrazine, we observed that the bridging ligand was not sufficiently reactive under the conditions used to form a polymeric species. Rather, a molecular rearrangement reaction takes place whereby one monomer unit loses its thiocyanato ligands to another chelating en ligand and two other monomer units *trans*-/*cis*- isomerise. Together these three molecular units co-crystallise along with PF_6^- counterions to form a complex salt. Here we present the synthesis and structural analysis of this new tri-nickel complex salt: $[\Delta,\Lambda\text{-Ni(en)}_2(NCS)_2]_2[\Delta,\Lambda\text{-Ni(en)}_3](PF_6)_2$.

* Author to whom correspondence should be addressed.

† New Address: Neutron Scattering Group, ANSTO, Lucas Heights Research Laboratories, PMB1, Menai N.S.W. 2234, Australia.

EXPERIMENTAL

$Ni(NCS)_2^1/_2H_2O$, ethylenediamine, NH_4PF_6 and pyrazine were obtained from commercial sources and used as received. Methanol was of A.R. grade and was used without further purification.

Preparation of Δ,Λ-$[Ni(en)_2(NCS)_2]_2$-Δ,Λ-$[Ni(en)_3](PF_6)_2$

trans-$Ni(en)_2(NCS)_2$ was prepared from $Ni(NCS)_2^1/_2H_2O$ and ethylenediamine in the manner reported by Brown and Lingafelter [3]. The absolute configuration of this compound was confirmed as *trans*- by X-ray diffraction of a single crystal. To an aqueous solution of *trans*-$Ni(en)_2(NCS)_2$ (1 mmol, 30 ml) and NH_4PF_6 (2 mmol) was added a methanolic solution of pyrazine (1 mmol, 10 ml) with rapid stirring. No immediate precipitate resulted. Upon reducing the volume to ~20 ml on a hotplate and allowing the solution to stand in air for 3 weeks pale purple crystals of (**1**) suitable for X-ray diffraction were formed, along with a number of dark purple crystals of $[Ni(en)_2(\mu_{N,S}\text{-}NCS)]_2[PF_6]_2$ (**2**). The physical and structural characterisation of **2** is reported elsewhere [4].

Crystal structure determination

Measurements were made on Rigaku AFC7R diffractometer at ambient temperature using monochromated Mo-K_α radiation ($\lambda = 0.71069$ Å). A pale purple single crystal of **1** was placed at the end of a glass fibre. Cell constants were obtained by least-squares analysis of 25 strong reflections in the range $22.04° < 2\theta < 24.90°$. Details of crystal data, data collection and structure refinement are summarised in Table 1. The intensity data were corrected for Lorentz and polarisation effects and an empirical absorption correction based on azimuthal scans of several reflections was also applied. The structure of **1** was solved by direct methods and developed by alternating cycles of difference Fourier syntheses and full matrix least-squares refinements. The positions of the non-hydrogen atoms were determined unequivocally. The non-hydrogen atoms were refined anisotropically, while the hydrogen atoms were placed at calculated positions for the final refinement and their thermal parameters refined isotropically. Neutral atom scattering factors were taken from Ref. 5 and anomalous dispersion corrections were taken from Ref. 6. Crystallographic calculations were carried out with a teXsan crystallographic software package of Molecular Structure corporation (1985 & 1992).

Table 1. Summary of crystallographic data for **1**

Chemical formula	$Ni_3C_{18}H_{56}N_{18}S_4P_2F_{12}$
Formula weight	1119.026
Crystal system	Monoclinic
Space group	C_2/c (No. 15)
a (Å)	24.715(3)
b (Å)	12.806(2)
c (Å)	17.328(2)
α (°)	90
β (°)	124.532(6)
γ (°)	90
V (Å^3)	4518(1)
Z	4
μ (Mo–K_α) (cm^{-1})	22.02
Crystal size (mm)	$0.30 \times 0.10 \times 0.10$
D_{calc} (g cm^{-3})	1.645
Radiation (Å)	0.71069
$2\theta_{max}$ (°)	50.0
Reflections collected	3143
Reflections used	1738 ($I > 3\sigma(I)$)
Variables	260
$(\Delta/\sigma)_{max}$	0.01
ρ_{max}/ρ_{min} (e Å^{-3})	0.58/−0.38
R^a	0.049
R_w^b	0.056
GOF^c	1.60

$^a R = \Sigma\|F_o| - |F_c\|/\Sigma|F_o|$.
$^b R_w = [\Sigma w(|F_o| - |F_c|)^2/\Sigma w|F_o|^2]^{1/2}$.
^{c}GOF $= [\Sigma(|F_o| - |F_c|)^2/\Sigma(N_{reflns} - N_{params})]^{1/2}$.

RESULTS AND DISCUSSION

Molecular and crystal structure

The compound $[\Delta,\Lambda\text{-}Ni(en)_2(NCS)_2]_2[\Delta,\Lambda\text{-}Ni(en)_3](PF_6)_2$ (**1**) crystallises in the monoclinic space group C_2/c (No. 15) with $a = 24.715(3)$ Å, $b = 12.806(2)$ Å, $c = 17.328(2)$ Å, $\beta = 124.532(6)°$, $V = 4518(1)$ Å^3 and $Z = 4$. The arrangement of the three distinct molecules *cis*-$[Ni(en)_2(NCS)_2]$ (**1a**), $[Ni(en)_3]^{2+}$ (**1b**) and the counteranion $[PF_6]^-$ (**1c**) in the asymmetric unit of **1** is shown in Fig. 1. Selected bond lengths are given in Table 2 and selected bond angles in Table 3. The *bis*-chelate molecule (**1a**) is centred at a general (x,y,z) 8-fold crystallographic site; while the *tris*-chelate molecule (**1b**) and the counteranions (**1c**) occupy 4-fold sites at $(\frac{1}{2}, y, \frac{1}{4})$, $(0, y, \frac{1}{4})$ and $(\frac{1}{4}, \frac{1}{4}, 0)$ respectively, leading to a ratio of 2 : 1 : 2 in the unit cell. Numerous uni-metallic [7–19] complex salts containing the optically active $[Ni(en)_2X_2]$ or $[Ni(en_3)]^{2+}$ structural units have been studied; as have a number of di-nickel salts containing one or the other of these structural units [20–23]. To our knowledge, there has only been one other report of a co-crystallised salt containing both of these elements, notably $[Ni(en)_2(benzoyl\text{-}hydrazine)][Ni(en)_3]I_4 \cdot H_2O$ [24].

The $Ni(en)_2(NCS)_2$ *structural motif* (**1a**)

The structure of **1a** is in itself noteworthy. As an isolated molecule $Ni(en)_2(NCS)_2$ has only been detected in the solid state as a *trans*-isomer; although, two different structural modifications have been reported [3,25]. To our knowledge, this is the first

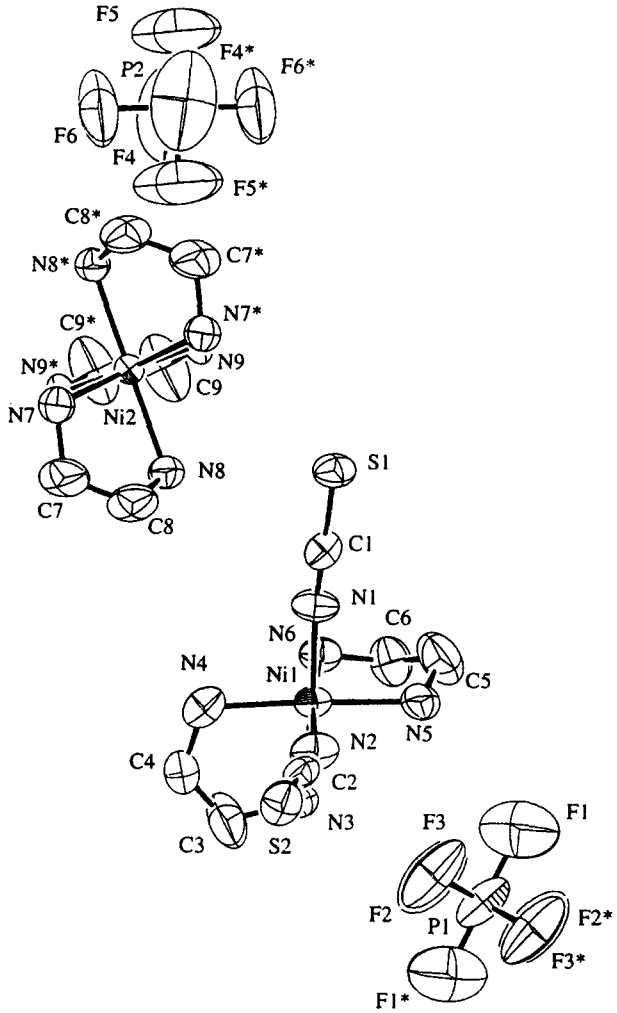

Fig. 1. An ORTEP drawing of the asymmetric unit of $[Ni(en)_2(NCS)_2]_2[Ni(en)_3](PF_6)_2$ (**1**). Hydrogen atoms have been omitted for clarity. All atoms are represented by the thermal ellipsoids at 50% probability.

Table 2. Selected bond lengths (Å) for **1a**, **1b** and **1c**

1a *cis*-$[Ni(en)_2(NCS)_2]$					
Ni(1)—N(1)	2.083(6)	N(1)—C(1)	1.142(8)	C(1)—S(1)	1.656(7)
Ni(1)—N(2)	2.070(6)	N(2)—C(2)	1.153(9)	C(2)—S(2)	1.635(8)
Ni(1)—N(3)	2.126(5)	N(3)—C(3)	1.45(1)	C(3)—C(4)	1.29(1)
N(4)—C(4)	1.42(1)	Ni(1)—N(4)	2.094(7)		
Ni(1)—N(5)	2.090(7)	N(5)—C(5)	1.46(1)	C(6)—C(5)	1.47(1)
N(6)—C(6)	1.44(1)	Ni(1)—N(6)	2.123(6)		
1b $[Ni(en)_3]^{2+}$					
Ni(2)—N(7)	2.135(6)	N(7)—C(7)	1.43(1)	C(7)—C(8)	1.43(1)
N(8)—C(8)	1.43(1)	Ni(2)—N(8)	2.133(6)		
Ni(2)—N(9)	2.117(6)	N(9)—C(9)	1.44(1)	C(9)—C(9)	1.37(2)
1c $[PF_6]^-$					
P—F(average)	1.528(7)				

Table 3. Selected bond angles (°) for **1a, 1b** and **1c**

1a *cis*-$[Ni(en)_2(NCS)_2]$					
N(1)—Ni(1)—N(2)	92.2(2)	N(1)—Ni(1)—N(3)	174.6(3)	N(1)—Ni(1)—N(4)	92.8(3)
N(1)—Ni(1)—N(5)	90.4(3)	N(1)—Ni(1)—N(6)	88.9(2)	N(2)—Ni(1)—N(3)	88.4(2)
N(2)—Ni(1)—N(4)	88.8(3)	N(2)—Ni(1)—N(5)	92.1(3)	N(2)—Ni(1)—N(6)	174.8(3)
N(3)—Ni(1)—N(4)	81.9(2)	N(3)—Ni(1)—N(5)	94.9(2)	N(3)—Ni(1)—N(6)	90.9(2)
N(4)—Ni(1)—N(5)	176.6(2)	N(4)—Ni(1)—N(6)	96.2(3)	N(5)—Ni(1)—N(6)	82.8(3)
Ni(1)—N(1)—C(1)	171.1(6)	N(1)—C(1)—S(1)	179.3(7)	Ni(1)—N(2)—C(2)	164.9(7)
N(2)—C(2)—S(2)	179.6(8)	Ni(1)—N(3)—C(3)	107.0(5)	N(3)—C(3)—C(4)	119.5(8)
C(3)—C(4)—N(4)	121.3(9)	C(4)—N(4)—Ni(1)	108.7(6)	Ni(1)—N(5)—C(5)	108.1(6)
N(5)—C(5)—C(6)	112.4(7)	C(5)—C(6)—N(6)	112.0(8)	C(6)—N(6)—Ni(1)	107.8(5)
1b $[Ni(en)_3]^{2+}$					
N(7)—Ni(2)—N(7)	170.7(3)	N(7)—Ni(2) N(8)	91.8(2)	N(7)—Ni(2)—N(8)	81.9(2)
N(7)—Ni(2)—N(9)	93.2(2)	N(7)—Ni(2)—N(9)	93.8(2)	N(8)—Ni(2)—N(8)	94.7(3)
N(8)—Ni(2)—N(9)	171.8(2)	N(8)—Ni(2)—N(9)	91.9(2)	N(9)—Ni(2)—N(9)	81.8(3)
Ni(2)—N(7)—C(7)	107.5(5)	N(7)—C(7)—C(8)	114.7(8)	C(7)—C(8)—N(8)	114.8(7)
C(8)—N(8)—Ni(2)	108.2(5)	Ni(2)—N(9)—C(9)	108.1(4)	N(9)—C(9)—C(9)	116.3(7)
1c $[PF_6]^-$					
F—P—F(range)	85.8(5)–93.6(5)	and	178.3(8)–178.7(3)		

report of an optically active Ni(II) centre containing *bis*-chelating en rings as well as two monodentate N-donor thiocyanato ligands in a *cis*-arrangement. Monomeric molecular structures of the type $Ni(en)_2(NCS)X$ have been reported where $X = Cl^-$, Br^- or NO_3^- [18]; while dimeric structures $[Ni(en)_2(\mu_{N,S}\text{-}NCS)]_2X_2$ have been characterised for $X = I^-$ or ClO_4^- [19]. As a part of our own study, the dimeric species $[Ni(en)_2(\mu_{N,S}\text{-}NCS)]_2[PF_6]_2$ (**2**) has also been isolated [4]. Recently, the 1-dimensional polymeric Ni(II) complex $\{catena\text{-}(\mu_{N,S}\text{-}NCS)[Ni(en)_2]\}(PF_6)$ has been reported [26]. Polymeric structures with bridging nitrito groups have also been noted for $\{catena\text{-}(\mu\text{-}NO_2)[Ni(en)_2]\}X$ where $X = BF_4^-$ [27], ClO_4^- [28], and I_3^- and PF_6^- [29].

The Ni1—N bond lengths of the thiocyanato ligands of **1a** (2.083(6) Å (Ni1 – N1) and 2.070(6) Å (Ni1 – N2)) are significantly shorter than that found in the case of the *trans*-isomer (2.15 Å) [3], and slightly longer than that reported for *cis*-$Ni(en)_2(NCS)Cl$ (2.01 Å) [18]. The N1—Ni1—N2 bond angle between the NCS ligands is 92.2(2)°, while the average bond angle between the Ni1—N(en) bonds and the Ni1—N(NCS) bonds are 90.2(3)° and 174.8(3)°. The average N—Ni1—N bond angle within the en rings of 82.4(3)° is characteristic of deviations away from regular octahedral geometry that have been observed for other chelating systems [7–13,20,21]. Ni1—N(en) bond lengths are typical of those found in other uni-metallic $Ni(en)_2(X)_2$ complexes; although in **1a**, a clear trans effect is observed relative to the thiocyanato ligands (Table 2). This feature has also been observed by Poraj-Kosic in the case of the compounds $Ni(en)_2(NCS)Cl$ and $Ni(en)_2(NCS)(NO_3)$ [18]. The bond lengths (Table 2) and bond angles (Table 3) of the en and NCS ligands of **1a** are characteristic of those found in other coordination complexes.

The ring pucker of the chelate rings in **1** can be quantified by the dihedral angle (ω) between the planes defined, for example, by N3—C3—C4 and C3—C4—N4. The values of ω for the N3—N4 and N5—N6 rings were found to be 14(1)° and 48(1)° respectively; the former being substantially smaller than usually found (~50°) in tri-chelating en complexes [9,11] This atypical ring pucker of the N3—N4 chelate may be a consequence of the strong hydrogen bonds that form between amine protons and acceptor sites on the counteranions (see below).

The $[Ni(en)_3]^{2+}$ *structural motif* (**1b**)

While the $[Ni(en)_3]^{2+}$ (**1b**) moiety displays C_3 pseudo-symmetry typical of *tris*-chelating molecular units, it is noteworthy that the true site symmetry in this crystal is C_2. The average Ni2—N bond length of 2.128(7) Å in **1b** is characteristic of those found in other uni-metallic $[Ni(en)_3]^{2+}$ complex salts [7–13]. N—Ni2—N bond angles within the en chelate rings of 81.9(3)° (N7—Ni2—N8) and 81.7(4)° (N9—Ni2—N9*) also show the usual deviations away from regular octahedral geometry that have been observed in other systems [7–13]. The average values for N—Ni2—N bond angles between adjacent chelate rings are 92.9(3)° and 171.5(3)°; being consistent with the above compounds. In general, the other bond lengths and bond angles within the chelate rings of **1b** are consonant with those observed in other

$[Ni(en)_3]^{2+}$ complex salts [7–13]. Dihedral angles (ω) of 43(1)° and 38(1)° for the N7—N8 and N9—N9* chelates indicate moderate ring pucker.

Hydrogen bonding

Extensive hydrogen bonding is observed in **1** between the amine protons and Lewis base (acceptor) sites. Table 4 contains selected intra- and intermolecular hydrogen bonding distances and angles. Figure 2 shows intermolecular hydrogen bonding (dashed lines) and partial packing of the unit cell, projected along the *b*-axis between $-0.28 \leqslant y \leqslant 0.28$. Both chiral elements **1a** and **1b** show strong intermolecular hydrogen bonding, particularly between amine donor protons and the fluorine atoms of **1c**; forming a 3-dimensional network within the crystal. In the case of **1a,** the majority of strong hydrogen bonds occur between amine protons that are parallel to the pseudo-C_3 axis. The converse is true in the case of **1b,** where strong hydrogen bonds are formed almost exclusively by amine protons that present oblique angles to the pseudo-C_3 axis of the molecule. Weaker intermolecular hydrogen bonds are also observed between amine protons and Lewis base sites at S atoms of the thiocyanato ligands and N atoms of other en groups.

Intermolecular hydrogen bonding is a feature commonly observed in compounds containing chelating en rings. In the case of *bis*-chelating molecules, strong intermolecular bonds have been observed between amine protons and coordinated NO_2 ligands [18], and ClO_4^- counteranions [28]. While not specifically mentioned by the authors Monfort *et al.* in the case of

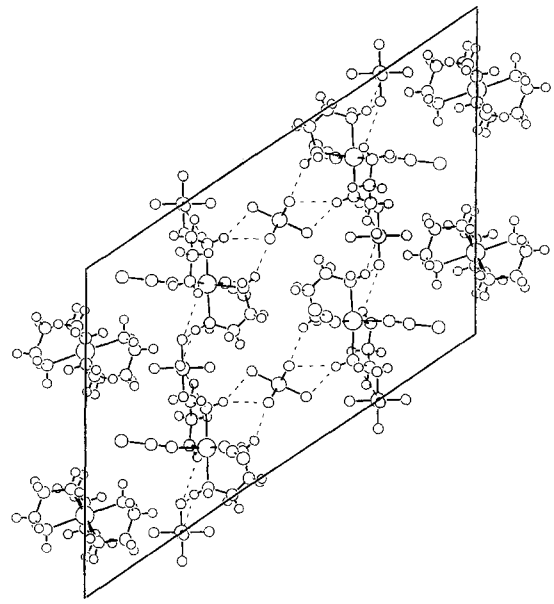

Fig. 2. Partial packing of the unit cell of **1** projected along the *b*-axis between $-0.28 \leqslant y \leqslant 0.28$.

Table 4. Selected intermolecular hydrogen bonds (distances (Å) and angles (°)) for **1**

D—H···A[a]	D···A	H···A	D—H···A	Symmetry[b]	Direction[c]
N3—H1···F2	3.32(1)	2.82	112.9	1	ob
N3—H2···F3	3.01(1)	2.15	148.5	1	pa
N3—H1···S1	3.72(1)	2.84	153.7	1	ob
N4—H7···F4	3.20(2)	2.43	136.1	1	pa
N4—H7···F6	3.22(1)	2.44	138.5	1	pa
N5—H9···F1	3.32(1)	2.44	152.0	1	pa
N5—H9···F3	3.29(1)	2.39	155.3	1	pa
N5—H10···F4	3.13(1)	2.24	157.4	2	ob
N6—H15···F6	3.21(1)	2.67	119.7	2	ob
N6—H16···S2	3.66(1)	2.78	153.7	1	pa
N7—H17···F2	3.18(1)	2.24	172.6	5	ob
N7—H17···N7	3.14(1)	2.93	93.5	4	ob
N8—H23···F5	3.51(1)	2.67	161.3	4	ob
N8—H23···N9	3.10(1)	2.88	94.5	4	ob
N8—H24···S2	3.66(1)	2.94	153.7	3	pa
N9—H25···S2	3.49(1)	2.60	155.2	3	pa
N9—H26···F5	3.29(1)	2.41	152.0	4	ob
N9—H26···N8	3.10(1)	2.87	95.0	4	ob

[a] D, hydrogen donor; A, hydrogen acceptor.

[b] Numbers refer to the following equivalent positions relative to the reference molecule at x, y, z: (1) x, y, z; (2) $x, -y, z+\frac{1}{2}$; (3) $-x+\frac{1}{2}, y+\frac{1}{2}, -z+\frac{1}{2}$; (4) $-x+1, y, -z+\frac{1}{2}$; (5) $x+\frac{1}{2}, y-\frac{1}{2}, z$.

[c] Direction of N—H bond relative to the pseudo-C_3 axis of the Ni centre: pa = parallel; ob = oblique.

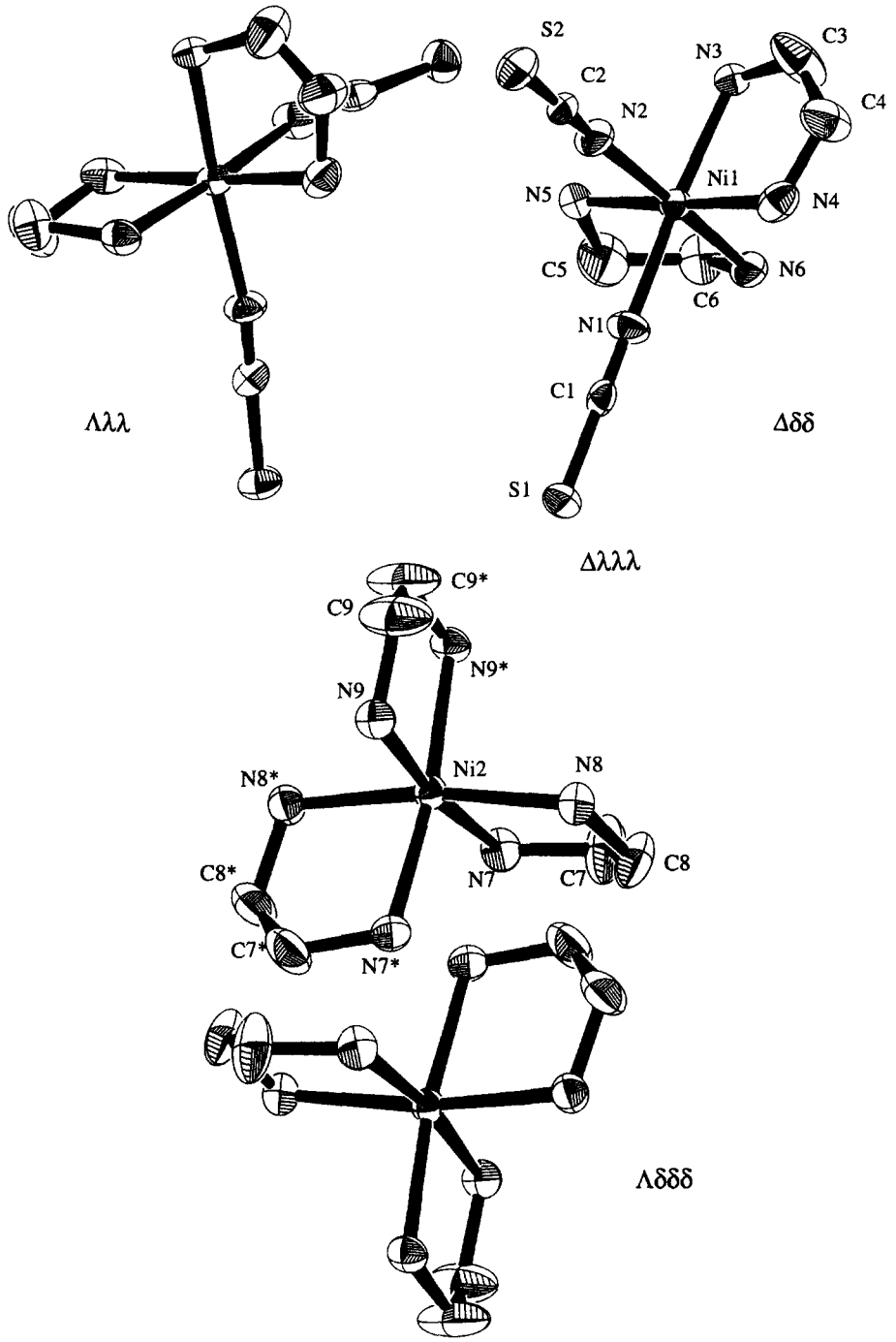

Fig. 3. Isomeric mirror image forms of (**a**) $\Lambda\lambda\lambda$ and $\Delta\delta\delta$ for **1a** and; (**b**) $\Lambda\delta\delta\delta$ and $\Delta\lambda\lambda\lambda$ for **1b**. Hydrogen atoms have been omitted for clarity.

{*catena*-($\mu_{N,S}$-NCS)[Ni(en)$_2$]}(PF_6) [26], it seems likely that hydrogen bonding interactions should also play a significant role in stabilising this compound. Strong intermolecular hydrogen bonding has also been observed in many *tris*-chelating molecules between amine protons and oxygen atoms of nitrate [7]; sulfate [9]; acetate [11] and tartrate [12] counterions.

Absolute configurations of **1a** *and* **1b**

Both molecular species **1a** and **1b** form chiral entities; however, due to the constraints of crystal symmetry presented by the centrosymmetric C_2/c space group, both Λ and Δ forms are present in equal quantities and ordered in the unit cell. The $\Lambda\lambda\lambda$ and $\Delta\delta\delta$ forms of **1a** are displayed in Fig. 3(a); while the $\Lambda\delta\delta\delta$

and $\Delta\lambda\lambda\lambda$ forms of **1b** are given in Fig. 3(b). The following discussion will relate to the Λ configuration only, keeping in mind that for racemic systems, these arguments hold equally true for their respective mirror images having the Δ configuration.

Much debate has centred around which chemical effects cause any of the four isomers ($\Lambda\delta\delta\delta$, $\Lambda\delta\delta\lambda$, $\Lambda\delta\lambda\lambda$, $\Lambda\lambda\lambda\lambda$) to be the most stable. Factors that have been considered include anion size [20], hydrogen bonding [30] and crystal packing forces [11]. Gollogly *et al.* [31] argued that entropy effects would cause the $\Lambda\delta\delta\lambda$ isomer to have the lowest free energy, and structural characterisation of compounds containing very few hydrogen bonds has lent weight to this proposal [13,32]. It has been observed that the most common configuration is $\Lambda\delta\delta\delta$, presumably because it is the one most easily stabilised by hydrogen bonds. Cramer and Huneke [13] proposed that this isomer should have the second lowest energy; while the rarely observed $\Lambda\lambda\lambda\lambda$ configuration which also has a strong tendency to from hydrogen bonds should be the isomer with the highest energy. As was observed for **1b**, Cramer and Huneke [13] found that in the case of the $\Lambda\delta\delta\delta$ configuration, the strongest or greatest number of hydrogen bonds were formed to amine protons that had oblique angles to the pseudo-C_3 axis. The converse was observed for λ rings; where a majority or the strongest bonds were formed with amine protons that were parallel to the pseudo-C_3 axis.

The conformations of *bis*-chelating en rings have received less attention; however, the absolute configuration of $\Lambda\lambda\lambda$ for **1a** is again consistent with a majority of strong hydrogen bonds being formed between counteranions and "parallel" amine protons.

REFERENCES

1. Saito, Y., Nakatsu, K., Shiro, M. and Kuroya, H., *Acta Cryst.*, 1955, **8,** 729.
2. *Inorg. Chem.*, 1970, **9,** 1.
3. Brown, B. W. and Lingafelter, E. C., *Acta Cryst.*, 1963, **16,** 753.
4. James, M., Kawaguchi, H. and Tatsumi, K., *Acta Crystallogr. C*, 1997 (In preparation).
5. Cromer, D. T. and Waber, J. T., *International Tables for X-ray Crystallography*, Vol. IV. ed. T. Hahn. Kynoch, Birmingham, England, 1974, Table 2.2A.
6. Ibers, J. A. and Hamilton, W. C., *Acta Crystallogr.*, 1964, **17,** 781.
7. Korp, J. D., Bernal, I., Palmer, R. A. and Robinson, J. C., *Acta Crystallogr.*, 1980, **B36,** 560.
8. Mazhar-Ul-Haque, Caughlan, C. N. and Emerson, K., *Inorg. Chem.*, 1970, **9,** 2421.
9. Cramer, R. E., *Inorg. Chem.*, 1972, **11,** 1019.
10. Raston, C. L., White, A. H. and Willis, A. C., *Aust. J. Chem.*, 1978, **31,** 415.
11. Cramer, R. E., van Doorne W. and Huneke, J. T., *Inorg. Chem.*, 1976, **15,** 529.
12. Mizuta, T., Yoneda, H. and Kushi, Y., *Inorg. Chim. Acta*, 1987, **132,** 11.
13. Cramer, R. E. and Huneke, J. T., *Inorg. Chem.*, 1978, **17,** 365.
14. Yu. I. Smolin, *J. Chem. Soc., D.*, 1969, 395.
15. Singh, R. and Gautam, R. K., *J. Indian Chem. Soc.*, 1987, **64,** 631.
16. Begum, N. S., Poojary, M. D. and Manohar, H., *J. Chem. Soc., Dalton Trans.*, 1988, 1303.
17. Tomlinson, A. A. G., Bonamico, M., Dessy, G., Fares, V. and Scaramuzza, L., *J. Chem. Soc., Dalton Trans.*, 1976, 1671.
18. Poraj-Kosic, M. A., *Acta Crystallogr.*, 1966, **21,** A149.
19. Svelasvili, A. E., *Acta Crystallogr.*, 1966, **21,** A153.
20. du Preez, J. G. H., Rohwer, H. E., Brecht, B. J. and Caira, M. R., *J. Chem. Soc., Dalton Trans.*, 1984, 975.
21. Chulmin Keum, Chonhan Kim, Chulsung Kim, Hyontae Kwak, Moonhee Kwon and Hae Namgung, *Bull. Korean Chem. Soc.*, 1992, **13,** 695.
22. Cernak, J., Potocnak, I. and Dunaj-Jurco, M., *Z. Kristallogr.*, 1994, **209,** 757.
23. Sisoeva, T. F., Arge, V. M., Trunov, V. K., Dyatlova, N. M. and Ya. Fridman, A., *Zh. Strukt. Khim.*, 1986, **27,** 108.
24. Shelvashvili, A. E., Vardosanidze, T. O., Sobolev, A. N., Beshkenadze, I. A. and Sokol, V. I., *Soob. Akad. Navak. Gruz. SSR*, 1983, **110,** 49.
25. Podberezskaya, N. V., Shakhshneider, T. P., Virovets, A. V. and Stabnikov, P. A., *Zh. Struk. Khim.*, 1991, **32,** 96–5.
26. Monfort, M., Bastos, C., Diaz, C. and Ribas, J., *Inorg. Chim. Acta*, 1994, **218,** 185.
27. Drew, M. G., Goodgame, D. M. L., Hitchman, M. A. and Rodgers, D., *Chem. Commun.*, 1965, 477.
28. Llewellyn, F. J. and Waters, J. M., *J. Chem. Soc.*, 1962, 3845.
29. Meyer, A., Gleizes, A., Girerd, J.-J., Verdaguer, M. and Kahn, O., *Inorg. Chem.*, 1982, **21,** 1729.
30. Raymond, K. N., Corfield, P. W. R. and Ibers, J. A., *Inorg. Chem.*, 1968, **7,** 842.
31. Gollogly, J. R., Hawkins, C. J. and Beattie, J. K., *Inorg. Chem.*, 1971, **10,** 317.
32. Raymond, K. N., Corfield, P. W. R. and Ibers, J. A., *Inorg. Chem.*, 1968, **7,** 1362.

Pergamon

PII: S0277-5387(97)00352-5

Polyhedron Vol. 17, No. 9, pp. 1579–1586, 1998
© 1998 Elsevier Science Ltd
All rights reserved. Printed in Great Britain
0277-5387/98 $19.00+0.00

Synthesis and structural characterization of the novel tetrahedral MNiFeS clusters containing functionally substituted cyclopentadienyl ligands $(\eta^5\text{-}RC_5H_4)(\eta^5\text{-}C_5H_5)MNiFeS(CO)_5$ (M = Mo, W; R = CHO, CH_3CO, CH_3O_2C, CH_2OH, $CH(OH)CH_3$, $(NO_2)_2C_6H_3NHN$). The crystal molecular structure of $(\eta^5\text{-}CHOC_5H_4)(\eta^5\text{-}C_5H_5)MoNiFeS(CO)_5$

Li-Cheng Song,[a]* Yu-Bin Dong,[a] Qing-Mei Hu,[a] Yan-Kun Li[a] and Jie Sun[b]

[a] Department of Chemistry, Nankai University, Tianjin 300071, China

[b] Laboratory of Organometallic Chemistry, Shanghai Institute of Organic Chemistry, Shanghai 200032, China

(Received 25 June 1997; accepted 14 August 1997)

Abstract—A series of functionally substituted cyclopentadienyl MNiFeS clusters $(\eta^5\text{-}RC_5H_4)(\eta^5\text{-}C_5H_5)MNiFeS(CO)_5$ (**1**, M = Mo, R = CHO; **2**, M = W, R = CHO; **3**, M = Mo, R = CH_3CO; **4**, M = W, R = CH_3CO; **5**, M = Mo, R = CH_3O_2C; **6**, M = W, R = CH_3O_2C) were successfully synthesized by isolobal displacement reactions of corresponding functional cyclopentadienyl MCoFeS clusters $\eta^5\text{-}RC_5H_4MCoFeS(CO)_8$ with nickelocene in THF at reflux. Further treatment of clusters **1**–**4** with reducing agent $NaBH_4$ at r.t. in MeOH yielded primary and secondary alcohol cluster derivatives (**7**, M = Mo, R = CH_2OH; **8**, M = W, R = CH_2OH; **9**, M = Mo, R = $CH(OH)CH_3$; **10**, M = W, R = $CH(OH)CH_3$), which could react with the alkylating reagent Et_3OBF_4 to give ether cluster derivatives (**11**, M = Mo, R = $CH(OC_2H_5)CH_3$; **12**, M = W, R = $CH(OC_2H_5)CH_3$). Although reactions of clusters **1** and **2** with an aqueous acid solution of 2,4-dinitrophenylhydrazine at r.t. led to almost complete decomposition of the starting clusters, the reactions of clusters **3** and **4** under similar conditions afforded phenylhydrazone cluster derivatives (**13**, M = Mo, R = 2,4-$(NO_2)_2C_6H_3NHN$; **14**, M = W, R = 2,4-$(NO_2)_2C_6H_3NHN$). All these novel cluster products have been characterized by elemental analysis and spectroscopic techniques, as well as for cluster **1** by X-ray crystallographic study. © 1998 Elsevier Science Ltd. All rights reserved

Keywords: functional cyclopentadienyl ligands; MoNiFeS clusters; WNiFeS clusters; isolobal displacement; crystal structure.

Transition metal clusters containing functionally substituted cyclopentadienyl ligands have been recently receiving considerable attention in our laboratory [1–9]. This is largely because (i) these can be potentially used as homogeneous catalysts or as models for adsorbed substrates or their fragments on the solid surface of heterogeneous catalytic processes [10–13]; (ii) the functionally substituted cyclopentadienyls of these clusters can undergo transformation reactions to give numerous novel transition metal cluster derivatives, which could be difficultly or even not prepared by other methods [2–5]. As a continuation of this project we undertook a study on the synthesis and structural characterization of tetrahedral MNiFeS clusters with a general formula $(\eta^5\text{-}RC_5H_4)(\eta^5\text{-}$

* Author to whom correspondence should be addressed.

C_5H_5)MNiFeS(CO)$_5$ (M = Mo, W; R = CHO, CH_3CO etc.) and herein report the interesting results concerning this study.

RESULTS AND DISCUSSION

It was found that the tetrahedral MCoFeS clusters containing functionally substituted cyclopentadienyl ligands η^5-$RC_5H_4MCoFeS(CO)_8$ [2,8,9] reacted with nickelocene in THF at reflux to give corresponding functionally substituted cyclopentadienyl MNiFeS clusters (η^5-RC_5H_4)(η^5-C_5H_5)MNiFeS(CO)$_5$ (**1–6**), as shown in Scheme 1.

Clusters **1–6** were actually derived from isolobal displacement of $Co(CO)_3(d^9ML_3)$ in starting clusters η^5-$RC_5H_4MCoFeS(CO)_8$ by η^5-$C_5H_5Ni(d^9ML_3)$ generated *in situ* from thermal decomposition of nickelocene [14,15]. Although η^5-$RC_5H_4M(CO)_2(d^5ML_5)$ is also isolobal with η^5-$C_5H_5Ni(d^9ML_3)$, no products derived from isolobal displacement of the former by η^5-C_5H_5Ni were found under such conditions. It follows that the isolobal fragment $Co(CO)_3$ is a much better leaving group than η^5-$RC_5H_4M(CO)_2$ in such isolobal displacement reactions. Among these products except **3** being previously reported [8], all are new and have been characterized by elemental analysis, IR, ^{1}H NMR and MS spectroscopy. IR spectra of these new clusters showed four absorption bands at 2065–1844 cm^{-1} and one absorption band at 1713–1631 cm^{-1}, characteristic of the CO ligands attached to transition metals and the carbonyl groups of the functional substituents, respectively. ^{1}H NMR spectra of these new clusters exhibited one singlet between 5.28–5.34 ppm and two multiplets between 5.40–6.20 ppm, which were assigned to five protons of the cyclopentadienyl ring and four protons of the substituted cyclopentadienyl ring, respectively. Since those functional substituents are electron-withdrawing, the upfield multiplet was attributed to H^3 and H^4 protons of the substituted cyclopentadienyl ring and the downfield multiplet attributed to H^2 and H^5 protons. In addition, for **1** and **2** the ^{1}H NMR spectra displayed one singlet at about 9.65 ppm for the proton of formyl group, whereas for **4–6** the ^{1}H NMR spectra showed one singlet at 2.36 ppm for the acyl proton and one singlet at about 3.87 ppm for carbomethoxy protons, respectively. The mass spectra of all new clusters exhibited not only their respective molecular ion (M^+) peaks, but also the corresponding fragment ion peaks such as those of $(M-nCO)^+$ and $MoNiFeS^+$ or $WNiFeS^+$.

Although reactions of the functional group of a cyclopentadienyl ring in mononuclear transition metal complexes, such as ferrocene derivatives [16] and group 6 monometallic compounds [17] have been extensively studied, the investigations of this kind of reactions involved in cluster systems are quite few [2,3]. In order to know the influence of the cluster core upon transformation reactions of the functional group of a cyclopentadienyl ring and to prepare a series of new functional cyclopentadienyl clusters, we explored some of functional transformation reactions of cluster **1–4**. It was found that clusters **1–4** could be reduced by $NaBH_4$ in methanol at room temperature to give primary and secondary alcohol cluster derivatives **7–10**. Further treatment of **9** and **10** with alkylating reagent Et_3OBF_4 in CH_2Cl_2 at room temperature gave rise to ether cluster derivatives **11** and **12**. It is worth noting that although clusters **1** and **2** reacted in ethanol with an aqueous acid solution of 2,4-dinitrophenylhydrazine at room temperature to lead almost complete decomposition of the clusters, the reactions with clusters **3** and **4** under similar conditions afforded the expected phenylhydrazone cluster derivatives **13** and **14**. All the reactions mentioned above are shown in Scheme 2.

The clusters **7–14** are all new functionalized cyclopentadienyl MNiFeS clusters, which have been char-

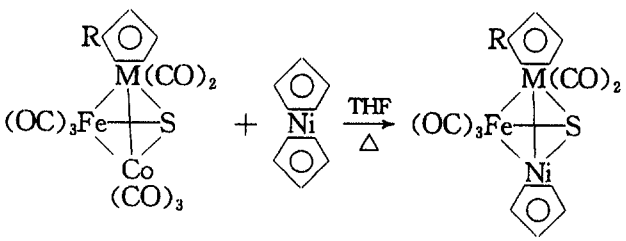

1—6

clusters	1	2	3	4	5	6
M	Mo	W	Mo	W	Mo	W
R	CHO	CHO	CH_3CO	CH_3CO	CH_3O_2C	CH_3O_2C

Scheme 1.

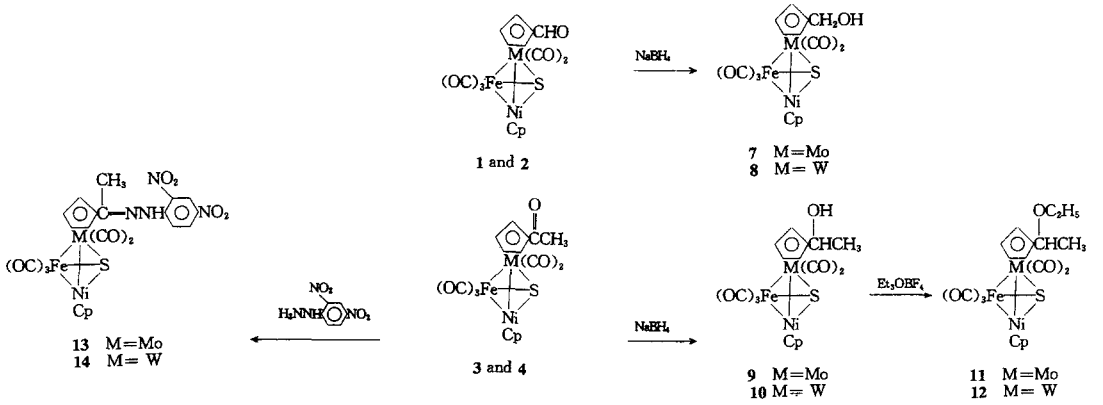

Scheme 2.

acterized by elemental analysis, IR and ^{1}H NMR spectroscopy. In IR spectra of **7–14** there were three to five absorption bands between 2065–1860 cm^{-1}, which are characteristic of the CO ligands bound to transition metals. In addition, IR spectra of **7–10** exhibited hydroxyl absorption bands between 3400–3440 cm^{-1}, whereas those of **11–12** showed C—O—C absorption bands at about 1021 cm^{-1} and those of **13–14** showed the C=N absorption bands at about 1612 cm^{-1}, respectively. ^{1}H NMR spectra of **7–14** indicated all their protons present in these molecules, such as the protons of hydroxyl groups of **7–10** between 1.46–2.14 ppm and imino groups of **13–14** at about 11.2 ppm. It is noteworthy that the four protons of the substituted cyclopentadienyl of **7–14** showed one or two multiplets in the range of 4.6–6.1 ppm. Except for **13** and **14**, the singlet for **7–12** caused by five protons of cyclopentadienyl ring coordinated to Ni atom were mingled together with their corresponding multiplets caused by four protons of the substituted cyclopentadienyl ring.

It is worth noting that during the separation of the products yielded from reactions mentioned above we usually observed several small continuous bands appeared on the TLC plates. The formation of these bands, which are difficult to be separated and might consist of both unreacted starting materials and some byproducts, causes the low yields of the isolated products.

In order to unambiguously confirm the structure of cluster **1**, an X-ray diffraction analysis was undertaken. The molecular structure of **1** is shown in Fig. 1. The selected bond lengths and angles are listed in Table 1. As shown in Fig. 1, cluster **1** consists of a distorted tetrahedral core MoNiFeS, which carries two carbonyls on Mo atom and three on Fe atom, one cyclopentadienyl ligand attached to the Ni atom and one formylcyclopentadienyl ligand coordinated to the Mo atom. For this molecule, the bond lengths involving the cluster core, the distance from Ni to centroid of cyclopentadienyl ring (denoted as Ni—Cp_{cent}), the distance from Mo to centroid of substituted cyclopentadienyl ring (Mo—Cp_{cent}) and the dihedral angle between two cyclopentadienyl rings (Z) are very close to the corresponding analog **3** [8], as shown in Table 2.

Finally, it should be noted that while the three carbonyls attached to Fe atom are terminal, one carbonyl bound to Mo atom C(12)—O(4) is terminal and the other C(13)—O(5) is semi-bridging. This is because the asymmetry parameter α (0.35) of C(13)—O(5) is well within the range for semi-bridging carbonyls, whereas that (0.61) of C(12)—O(4) falls out of the range [18]. The coexistence of both terminal and semi-bridging carbonyls are in good agreement with the IR spectrum of cluster **1** showing several strong absorption bands from 2032 cm^{-1} to 1844 cm^{-1}.

EXPERIMENTAL

All reactions were carried out under a prepurified nitrogen atmosphere using vacuum-line techniques. THF and diethyl ether were distilled from sodium benzophenone ketyl. Dichloromethane, methanol and ethanol were bubbled with nitrogen for 10 min prior to use. While $NaBH_4$ and 2,4-dinitrophenylhydrazine are of commercial origin, η^5-$RC_5H_4MCoFeS(CO)_8$ (M = Mo, W; R = CHO, CH_3CO, CH_3O_2C) [2,8,9], $(\eta^5$-$C_5H_5)_2Ni$ [19] and Et_3OBF_4 [20] were prepared according to literature methods. Preparative TLC was carried out on glass plates (26 × 19 cm) coated with silica gel G (10–40 μm). IR and ^{1}H NMR spectra were recorded on a Nicolet FT-5DX spectrophotometer and a Jeol FX 90Q spectrometer. C/H analyses, MS and melting points were performed by a Perkin–Elmer 240C analyzer, an HP 5988A spectrometer and a Yanaco MP-500 instrument, respectively.

Preparation of **1**

To a 100 cm^3 three-necked flask fitted with a magnetic stir-bar, a rubber septum and a reflux condenser

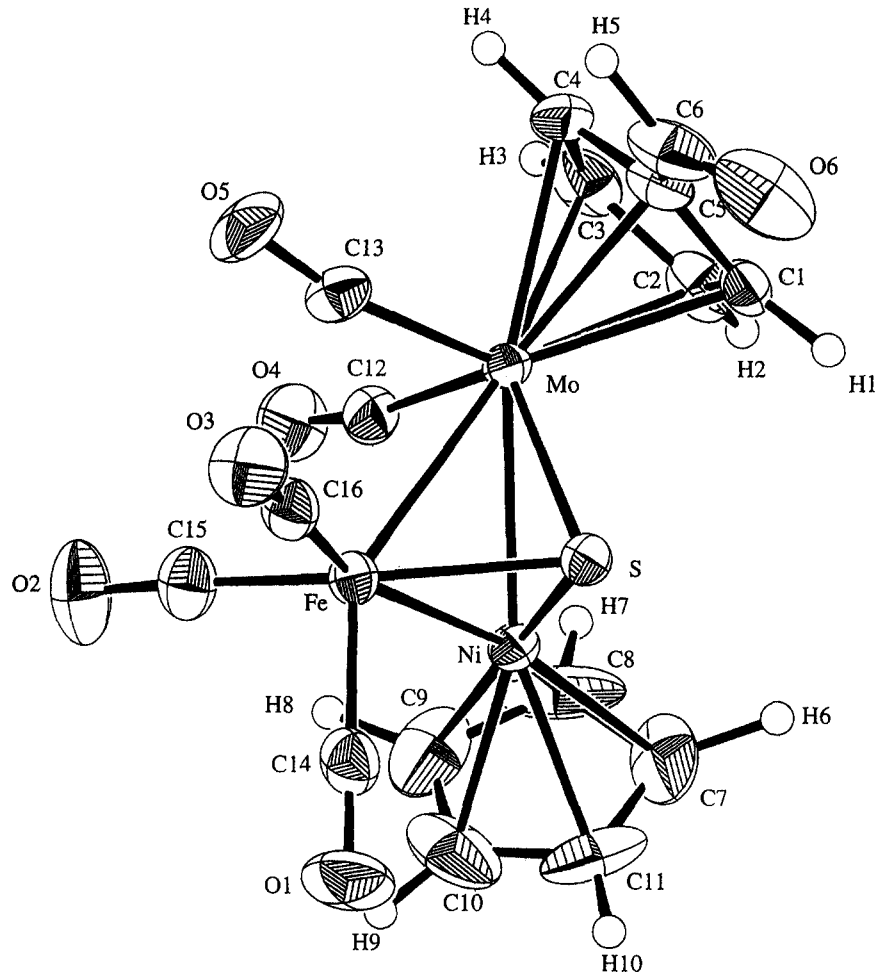

Fig. 1. Molecular structure of **1**.

Table 1. Selected bond lengths (Å) and bond angles (°) for **1**

Mo—Ni	2.658(1)	Mo—Fe	2.781(1)
Mo—S	2.346(2)	Ni—S	2.135(1)
Ni—Fe	2.482(2)	Fe—S	2.176(2)
Mo—C(1)	2.337(5)	Ni—C(7)	2.089(6)
Fe—C(14)	1.778(6)	Mo—C(12)	1.998(5)
Mo—C(13)	1.957(5)	C(14)—O(1)	1.143(7)
C(1)—C(2)	1.412(7)	C(7)—C(8)	1.41(1)

Ni—Mo—Fe	54.23(3)	Ni—Mo—S	50.03(4)
Ni—Mo—C(1)	106.1(1)	Fe—Mo—S	49.33(4)
Fe—Mo—C(1)	135.3(1)	Mo—Ni—S	57.39(5)
Mo—Ni—Fe	65.43(2)	Mo—Ni—C(7)	127.6(3)
Fe—Ni—S	55.64(4)	Mo—Fe—S	54.87(5)
Mo—Fe—C(14)	145.7(2)	Ni—Fe—S	54.08(5)
Ni—Fe—C(14)	88.7(2)	Mo—S—Ni	72.28(5)
Mo—S—Fe	75.80(4)	Ni—S—Fe	70.28(5)
Mo—C(13)—O(5)	167.6(5)	Mo—C(12)—O(4)	170.4(5)

Table 2. Comparison of some crystallographic data between **1** and **3**

Cluster	Mo—Fe	Mo—Ni	Fe—Ni	Mo—S	Fe—S	Ni—S	Ni—Cp_{cent}	Ni—Cp_{cent}	Z
1	2.78(1)	2.658(1)	2.482(2)	2.346(2)	2.176(2)	2.135(1)	1.725	1.996	105.57°
3	2.782(1)	2.652(1)	2.466(2)	2.362(3)	2.177(3)	2.131(3)	1.7149	2.006	102.88°

topped with a nitrogen inlet tube were added 0.560 g (1 mmol) of η^5-$CHOC_5H_4MoCoFeS(CO)_8$, 0.189 g (1 mmol) of Cp_2Ni and 30 cm^3 of THF. The mixture was refluxed for 5 h. Solvent was removed at reduced pressure and the residue was extracted with 2:1 CH_2Cl_2/petroleum ether. The extracts were subjected to TLC separation using 2:1 CH_2Cl_2/petroleum ether as eluent. Several small bands with a major one were developed. From the main green band was obtained 0.079 g (14.6%) of **1** as a deep-green solid. M.p. 157–158°C. Anal. Found: C, 35.58; H, 1.89. Calc. for $C_{16}H_{10}FeMoNiO_6S$: C, 35.54; H, 1.86%. IR (KBr, disk); $\nu_{(C\equiv O)}$ 2032 (s), 1967 (vs), 1926 (s), 1844 (s) cm^{-1}; $\nu_{(C=O)}$ 1680 (s) cm^{-1}. ^1H NMR ($CDCl_3$): δ 5.30 (s, 5H, C_5H_5), 5.56–5.76 (m, 2H, H^3, H^4), 6.00–6.20 (m, 2H, H^2, H^5), 9.69 (s, 1H, CHO) ppm. MS (EI, ^{98}Mo, ^{58}Ni), *m/z* (relative intensity): 542 (M^+, 10.7), 486 [$(M-2CO)^+$, 10.7], 458 [$(M-3CO)^+$, 30.5], 430 [$(M-4CO)^+$, 3.0], 402 [$(M-5CO)^+$, 100.0], 485 [$(M-CO-CHO)^+$, 5.6], 457 [$(M-2CO-CHO)^+$, 17.9], 429 [$(M-3CO-CHO)^+$, 1.9], 401 [$(M-4CO-CHO)^+$, 61.8], 373 [$(M-5CO-CHO)^+$, 24.1], 309 ($C_5H_5NiSFeMo^+$, 7.3), 308 ($C_5H_4NiSFeMo^+$, 9.4), 244 ($NiSFeMo^+$, 6.8).

Preparation of **2**

The same procedure as that for **1** was followed, but 0.627 g (1 mmol) of η^5-$CHOC_5H_4WCoFeS(CO)_8$ was used instead of η^5-$CHOC_5H_4MoCoFeS(CO)_8$ to give 0.113 g (18%) of **2** as a deep-green solid. M.p. 163–164°C. Anal. Found: C, 30.51; H, 1.86. Calc. for $C_{16}H_{10}FeNiO_6SW$; C, 30.57; H, 1.60%. IR (KBr, disk): $\nu_{(C\equiv O)}$ 2065 (m), 2032 (vs), 1959 (vs), 1868 (s) cm^{-1}; $\nu_{(C=O)}$ 1670 (m) cm^{-1}. ^1H NMR ($CDCl_3$): δ 5.30 (s, 5H, C_5H_5), 5.56–5.80 (m, 2H, H^3, H^4), 5.92–6.12 (m, 2H, H^2, H^5), 9.60 (s, 1H, CHO) ppm. MS (EI, ^{184}W, ^{58}Ni), *m/z* (relative intensity): 628 (M^+, 7.9), 572 [$(M-2CO)^+$, 8.6], 544 [$(M-3CO)^+$, 26.0], 488 [$(M-5CO)^+$, 100.0], 571 [$(M-CO-CHO)^+$, 5.2], 543 [$(M-2CO-CHO)^+$, 9.8], 487 [$(M-4CO-CHO)^+$, 43.3], 459 [$(M-5CO-CHO)^+$, 9.3], 395 ($C_5H_5NiSFeW^+$, 13.1), 394 ($C_5H_4NiSFeW^+$, 11.2), 330 ($NiSFeW^+$, 2.0).

Preparation of **3**

To the flask described above were added 1.00 g (1.70 mmol) of η^5-$CH_3COC_5H_4MoCoFeS(CO)_8$, 0.740 g (3.90 mmol) of Cp_2Ni and 20 cm^3 of THF. The mixture was refluxed for 10 h. Solvent was removed at reduced pressure and the residue was extracted with CH_2Cl_2. The extracts were subjected to TLC separation using 1:1 CH_2Cl_2/petroleum ether as eluent. Several small bands with a major one were developed. From the fourth main green band was obtained 0.385 g (40%) of **3** as a deep-green solid, which has been identified by comparison of its IR and ^1H NMR spectra with those of an authentic sample previously reported [8].

Preparation of **4**

To the flask described above were added 0.990 g (1.50 mmol) of η^5-$CH_3COC_5H_4WCoFeS(CO)_8$, 0.650 g (3.44 mmol) of Cp_2Ni and 20 cm^3 of THF. The mixture was refluxed for 30 h. The same workup as that for **3** was used to give 0.185 g (19.2%) of **4** as a black solid. M.p. 69–70°C. Anal. Found: C, 32.14; H, 1.85. Calc. for $C_{17}H_{12}FeNiO_6SW$: C, 31.77; H, 1.88%. IR (KBr, disk): $\nu_{(C\equiv O)}$ 2032 (vs), 1991 (s), 1959 (vs), 1852 (s) cm^{-1}; $\nu_{(C=O)}$, 1672 (s) cm^{-1}. ^1H NMR ($CDCl_3$): δ 2.36 (s, 3H, CH_3), 5.28 (s, 5H, C_5H_5), 5.44–5.80 (m, 2H, H^3, H^4), 5.88–6.16 (m, 2H, H^2, H^5) ppm. MS (EI, ^{184}W, ^{58}Ni), *m/z* (relative intensity): 642 (M^+, 9.6), 586 [$(M-2CO)^+$, 7.4], 558 [$(M-3CO)^+$, 22.0], 530 [$(M-4CO)^+$, 4.9], 502 [$(M-5CO)^+$, 100.0], 395 ($C_5H_5NiFeSW^+$, 7.1), 394 ($C_5H_4NiFeSW^+$, 11.2), 330 ($NiFeSW^+$, 4.3), 123 ($C_5H_5Ni^+$, 19.0).

Preparation of **5**

To the flask described above were added 1.160 g (1.97 mmol) of η^5-$CH_3O_2CC_5H_4MoCoFeS(CO)_8$, 0.840 g (4.43 mmol) of Cp_2Ni and 25 cm^3 of THF. The mixture was refluxed for 18 h. The same workup as that for **4** was used to give 0.330 g (29.4%) of **5** as a deep-green solid. M.p. 71–72°C. Anal. Found: C, 35.61; H, 2.12. Calc. for $C_{17}H_{12}FeMoNiO_7S$: C, 35.77; H, 2.12%. IR (KBr, disk): $\nu_{(C\equiv O)}$ 2041 (vs), 1991 (s), 1967 (vs), 1885 (s) cm^{-1}; $\nu_{(C=O)}$ 1713 (s) cm^{-1}. ^1H NMR ($CDCl_3$): δ 3.86 (s, 3H, CH_3), 5.28 (s, 5H, C_5H_5), 5.40–5.68 (m, 2H, H^3, H^4), 5.96–6.20 (m, 2H, H^2, H^5) ppm. MS (EI, ^{98}Mo, ^{58}Ni), *m/z* (relative intensity): 572 (M^+, 1.2), 516 [$(M-2CO)^+$, 0.9], 488 [$(M-3CO)^+$, 3.2], 460 [$(M-4CO)^+$, 1.0], 432 [$(M-5CO)^+$, 6.4], 373 ($C_5H_4MoFeSC_5H_5Ni^+$, 7.1), 309

($C_5H_5NiFeSMo^+$, 1.3), 308 ($C_5H_4MoFeSNi^+$, 1.8), 244 ($MoFeSNi^+$, 4.6), 123 ($C_5H_5Ni^+$, 6.8).

Preparation of **6**

To the flask described above were added 1.07 g (1.58 mmol) of η^5-$CH_3O_2CC_5H_4WCoFeS(CO)_8$, 0.650 g (3.44 mmol) of Cp_2Ni and 20 cm^3 of THF. The mixture was refluxed for 30 h. The same workup as that for **5** was used to give 0.130 g (12.5%) of **6** as a black solid. M.p. 75–76°C. Anal. Found: C, 31.28; H, 1.80. Calc. for $C_{17}H_{12}FeNiO_7SW$: C, 31.00; H, 1.84%. IR (KBr, disk): $\nu_{(C\equiv O)}$ 2032 (vs), 1991 (s), 1959 (vs), 1877 (s) cm^{-1}; $\nu_{(C\equiv O)}$ 1713 (s) cm^{-1}. ^1H NMR ($CDCl_3$): δ 3.88 (s, 3H, CH_3), 5.34 (s, 5H, C_5H_5), 5.50–5.76 (m, 2H, H^3, H^4), 5.92–6.20 (m, 2H, H^2, H^5) ppm. MS (EI, ^{184}W, ^{58}Ni), *m/z* (relative intensity): 658 (M^+, 4.2), 630 [$(M\text{-}CO)^+$, 0.7], 602 [$(M\text{-}2CO)^+$, 3.3], 574 [$(M\text{-}3CO)^+$, 11.6], 546 [$(M\text{-}4CO)^+$, 3.7], 518 [$(M\text{-}5CO)^+$, 21.5], 459 ($C_5H_4WFeS\text{-}C_5H_5Ni^+$, 13.5), 395 ($C_5H_5NiWFeS^+$, 4.7), 394 ($C_5H_4WFeSNi^+$, 4.7), 330 ($WFeSNi^+$, 1.2), 123 ($C_5H_5Ni^+$, 9.2).

Preparation of **7**

To a solution of 0.374 g (0.69 mmol) of **1** dissolved in 20 cm^3 of MeOH was added 0.026 g (0.69 mmol) of $NaBH_4$ and stirred for 20 min at room temperature. Solvent was removed at reduced pressure and the residue was extracted with CH_2Cl_2. The extracts were subjected to TLC separation using CH_2Cl_2 as eluent. Several small bands with a major one were developed. From the main green band was obtained 0.075 g (20.0%) of **7** as a deep-green solid. M.p. 128–129°C. Anal. Found: C, 36.02; H, 2.24. Calc. for $C_{16}H_{12}FeMoNiO_6S$: C, 35.40; H, 2.23%. IR (KBr, disk): $\nu_{(O\text{-}H)}$ 3400 (m) cm^{-1}; $\nu_{(C\equiv O)}$ 2032 (vs), 1983 (vs), 1950 (vs), 1918 (s), 1844 (s) cm^{-1}. ^1H NMR ($CDCl_3$): δ 1.46–1.88 (m, 1H, OH), 4.28–4.58 (m, 2H, CH_2), 5.12–5.72 (m, 9H, C_5H_5, C_5H_4) ppm.

Preparation of **8**

The same procedure as that for **7** was followed, but 0.434 g (0.69 mmol) of **2** instead of **1** to give 0.089 g (20.5%) of **8** as a deep-green solid. M.p. 133–134°C. Anal. Found: C, 30.80; H, 1.45. Calc. for $C_{16}H_{12}FeNiO_6SW$: C, 30.47; H, 1.92%. IR (KBr, disk): $\nu_{(O\text{-}H)}$ 3419 (m) cm^{-1}; $\nu_{(C\equiv O)}$ 2065 (m), 2032 (vs), 1959 (vs), 1860 (s) cm^{-1}. ^1H NMR ($CDCl_3$): δ 1.60–1.88 (s, 1H, OH), 4.20–4.60 (m, 2H, CH_2), 5.00–5.88 (m, 9H, C_5H_5, C_5H_4) ppm.

Preparation of **9**

To the flask described above were added 0.400 g (0.72 mmol) of **3**, 0.027 g (0.72 mmol) of $NaBH_4$ and 10 cm^3 of MeOH. The mixture was stirred overnight at room temperature. Solvent was removed at reduced pressure and the residue was extracted with 2:1 CH_2Cl_2/petroleum ether. The extracts were subjected to TLC separation using 2:1 CH_2Cl_2/petroleum ether as eluent. From the main blue band was obtained 0.300 g (75%) of **9** as a black oil. Anal. Found: C, 36.96; H, 2.39. Calc. For $C_{17}H_{14}FeMoNiO_6S$: C, 36.74; H, 2.36%. IR (KBr, disk): $\nu_{(O\text{-}H)}$ 3427 (m) cm^{-1}; $\nu_{(C\equiv O)}$ 2033 (vs), 1967 (vs), 1923 (s), 1860 (s) cm^{-1}. ^1H NMR ($CDCl_3$): δ 1.46 (d, J = 7.2 Hz, 3H, CH_3), 1.76–2.04 (m, 1H, OH), 4.48–4.80 (m, 1H, CH), 5.12–5.76 (m, 9H, C_5H_5, C_5H_4) ppm.

Preparation of **10**

The same procedure as that for **9** was followed, but 0.400 g (0.62 mmol) of **4** was added instead of **3** to give 0.311 g (78%) of **10** as a black oil. Anal. Found: C, 31.76; H, 1.79. Calc. For $C_{17}H_{14}FeNiO_6SW$: C, 31.72; H, 2.04%. IR (KBr, disk): $\nu_{(O\text{-}H)}$ 3440 (m) cm^{-1}: $\nu_{(C\equiv O)}$ 2020 (vs), 1950 (vs), 1860 (s) cm^{-1}. ^1H NMR ($CDCl_3$): δ 1.48 (d, 3H, J = 7.2 Hz, CH_3), 1.90–2.14 (m, 1H, OH), 4.50–4.92 (m, 1H, CH), 5.00–5.74 (m, 9H, C_5H_5, C_5H_4) ppm.

Preparation of **11**

To the flask described above were added 0.400 g (0.72 mmol) of **9**, 0.370 g (1.95 mmol) of Et_3OBF_4 and 15 cm^3 of CH_2Cl_2. The mixture was stirred at room temperature for 8 h. Solvent was removed at reduced pressure and the residue was extracted with 2:1 CH_2Cl_2/petroleum ether. The extracts were subjected to TLC separation using 2:1 CH_2Cl_2/petroleum ether as eluent. From the main blue band was obtained 0.054 g (13%) of **11** as a black solid. M.p. 144°C (dec.). Anal. Found: C, 39.07; H, 2.76. Calc. for $C_{19}H_{18}FeMoNiO_6S$: C, 39.08; H, 2.93%. IR (KBr, disk): $\nu_{(C\equiv O)}$ 2032 (vs), 1975 (vs), 1950 (vs), 1885 (s) cm^{-1}; $\nu_{(C\text{-}O)}$ 1023 (w) cm^{-1}. ^1H NMR ($CDCl_3$): δ 1.32–1.60 (m, 6H, $2CH_3$), 3.60–4.08 (m, 2H, CH_2), 4.60–5.52 (m, 10H, CH, C_5H_5, C_5H_4) ppm.

Preparation of **12**

The same procedure as that for **11** was followed, but 0.311 g (0.48 mmol) of **10** was used instead of **9** to give 0.048 g (15%) of **12** as a black solid. M.p. 170°C (dec.). Anal. Found: C, 34.19; H, 2.52. Calc. for $C_{19}H_{18}FeNiO_6SW$: C, 33.97; H, 2.55%. IR (KBr, disk): $\nu_{(C\equiv O)}$ 2068 (m), 2030 (vs), 1955 (vs), 1883 (vs) cm^{-1}; $\nu_{(C\text{-}O)}$ 1020 (m) cm^{-1}. ^1H NMR ($CDCl_3$): δ 1.31–1.60 (m, 6H, $2CH_3$), 3.80–4.20 (m, 2H, CH_2), 4.68–5.76 (m, 10H, CH, C_5H_5, C_5H_4) ppm.

Preparation of **13**

To the flask described above were added 0.300 g (0.54 mmol) of **3**, 10 cm^3 of ethanol and 3 cm^3 of 2,4-dinitrophenylhydrazine solution, prepared by dissolving 2.00 g (10.0 mmol) of 2,4-dinitrophenylhydrazine in 10 cm^3 of 98% concentrated H_2SO_4 followed by diluting with 14 cm^3 of distilled water and 46 cm^3 of 95% ethanol. The reaction mixture was stirred at room temperature for 3 h. The precipitate was filtered out and washed with ethanol. The washed precipitate was extracted with CH_2Cl_2. The extracts were subjected to TLC separation using 1 : 1 CH_2Cl_2/petroleum ether as eluent. From the main blue band was obtained 0.300 g (76%) of **13** as a black solid. M.p. 164°C (dec.). Anal. Found: C, 37.83; H, 2.26; N, 7.82. Calc. for $C_{23}H_{16}FeMoN_4NiO_9S$: C, 37.59; H, 2.19; N, 7.62%. IR (KBr, disk): $\nu_{(C\equiv O)}$ 2032 (vs), 1959 (vs), 1877 (s) cm^{-1}; $\nu_{(C=N)}$ 1614 (s) cm^{-1}. ^1H NMR ($CDCl_3$): δ 2.18 (s, 3H, CH_3), 5.23 (s, 5H, C_5H_5), 5.58 (t, 2H, H^3, H^4), 6.06 (t, 2H, H^2, H^5), 7.84–8.16 (m, 1H, H^6 of benzene ring), 8.24–8.56 (m, 1H, H^5 of benzene ring), 9.20 (s, 1H, H^3 of benzene ring), 11.29 (s, 1H, NH) ppm.

Preparation of **14**

The same procedure as that for **13** was followed, but 0.160 g (0.26 mmol) of **4** was used instead of **3** to give 0.080 g (37%) of **14** as a black solid. M.p. 105°C (dec.). Anal. Found: C, 33.35; H, 1.95; N, 6.84. Calc. For $C_{23}H_{16}FeN_4NiO_9SW$: C, 33.57; H, 1.96; N, 6.81%. IR (KBr, disk): $\nu_{(C\equiv O)}$ 2055 (w), 2020 (vs), 1955 (vs), 1868 (s) cm^{-1}; $\nu_{(C=N)}$ 1610 (s) cm^{-1}. ^1H NMR ($CDCl_3$): δ 2.20 (s, 3H, CH_3), 5.20 (s, 5H, C_5H_5), 5.44–5.76 (m, 2H, H^3 H^4), 5.84–6.08 (m, 2H, H^2, H^5), 7.76–8.00 (m, 1H, H^6 of benzene ring), 8.16–8.40 (m, 1H, H^5 of benzene ring), 9.04 (s, 1H, H^3 of benzene ring), 11.12 (s, 1H, NH) ppm.

Single-crystal structure determination of **1**

Crystals of **1** suitable for X-ray diffraction were obtained by slow evaporation of CH_2Cl_2/petroleum ether solution. A single-crystal measuring $0.20 \times 0.20 \times 0.50$ mm was mounted on a glass fiber and placed on a Rigaku AFC7R diffractometer with graphite monochromated Mo–K_α radiation and a 12 kW rotating anode generator. A total of 3006 independent reflections was collected at 293 K by ω-2θ scan mode, of which 2697 with $I \geqslant 3\sigma(I)$ were considered to be observed and used in subsequent refinement. The data was corrected for Lp factors. Details of crystal parameters, data collections and structure refinement of **1** are given in Table 3.

The structure was solved by direct methods and expanded using Fourier techniques. The non-hydrogen atoms were refined anisotropically. Hydrogen atoms were included but not refined. Final refinement by full-matrix least-squares method for non-hydrogen atoms converged to give the unweighted and weighted agreement factors R and Rw. The highest peak on the final difference Fourier map has a height of 1.15 $eÅ^{-3}$. All calculations were performed on Micro Vax II computer using the TEXSAN program system.

Table 3. Details of crystal parameters, data collections and structure refinements for **1**

Molecular formula	$C_{16}H_{10}FeMoNiO_5S$
Molecular weight	524.80
Color and habit	Black, prismatic
Crystal system	Triclinic
Space group	$P\bar{1}$(#2)
a (Å)	8.606(5)
b (Å)	15.054(5)
c (Å)	7.655(4)
α (°)	94.99(4)
β (°)	113.51(4)
γ (°)	96.88(4)
V ($Å^3$)	893.0(9)
Z	2
D_{calc} (g cm^{-3})	1.952
$F(000)$	516.00
μ (cm^{-1})	26.73
Diffractometer	Rigaku AFC7R
Temperature (K)	293
Radiation	Mo–K_α (λ = 0.71069 Å)
$2\theta_{max}$ (°)	50.0
Unique reflections measured	3006
R_{int}	0.065
No. observations, n	2697($I \geqslant 3.0\sigma(I)$)
No. variables, p	235
R	0.038
Rw	0.051
Maximum peak in final diff. map (e $Å^{-3}$)	1.15

Acknowledgements—We are grateful to the National Natural Science Foundation of China, State Key Laboratory of Structural Chemistry for financial support of this project.

REFERENCES

1. Song, L.-C., Shen, J.-Y., Hu, Q.-M., Wang, R.-J. and Wang, H.-G., *Organometallics*, 1993, **12**, 408.
2. Song, L.-C., Shen, J.-Y., Hu, Q.-M. and Huang, X.-Y., *Organometallics*, 1995, **14**, 98.
3. Song, L.-C., Shen, J.-Y., Hu, Q.-M. and Qin, X.-D., *Polyhedron*, 1995, **14**, 2079.
4. Song, L.-C., Shen, J.-Y., Hu, Q.-M., Han, B.-S., Wang, R.-J. and Wang, H.-G., *Inorg. Chim. Acta*, 1994, **219**, 93.
5. Song, L.-C., Shen, J.-Y., Hu, Q.-M., Liu, H. and Huang, X.-Y., *Polyhedron*, 1996, **15**, 2915.
6. Song, L.-C., Wang, J.-Q. and Hu, Q.-M., *Polyhedron*, 1995, **14**, 1101.

7. Song, L.-C., Wang, J.-Q., Hu, Q.-M. and Huang, X.-Y., *Polyhedron*, 1996, **15,** 2453.
8. Song, L.-C., Dong, Y.-B., Hu, Q.-M., Wu, B.-M. and Mak, T. C. W., *Chinese J. Struct. Chem.*, 1995, **14,** 393.
9. Song, L.-C., Li, Y.-K., Hu, Q.-M. and Sun, J., *J. Coord. Chem.*, In press.
10. Vahrenkamp, H., In *Transition Metal Chemistry—Current Problems of General, Biological and Catalytical Relevance*, ed. A. Müller and E. Diemann. Verlag Chemie, 1981, p. 35.
11. Muetterties, E. L. and Krause, M. J., *Angew. Chem., Int. Ed. Engl.*, 1983, **22,** 135.
12. Curtis, M. D., Penner-Hahn, J. E., Schwank, J., Baralt, O., McCabe, D. J., Thompson, L. and Waldo, G., *Polyhedron*, 1988, **7,** 2411.
13. Dobois, M. R., *Chem. Rev.*, 1989, **89,** 1.
14. Hoffmann, R., *Angew. Chem., Int. Ed. Engl.*, 1982, **21,** 711.
15. Vahrenkamp, H., Comments, *Inorg. Chem.*, 1985, **4,** 253.
16. Bublitz, D. E. and Rinehart, K. L. Jr., In *Organic Reactions*, Vol. 17, ed. W. G. Dauben. John Wiley & Sons, Inc., New York, 1969, pp. 1–154.
17. Macomber, D. W., Hart, W. P. and Rausch, M. D., *Advances in Organometallic Chemistry*, Vol. 21. Academic Press, Inc., New York, 1982, p. 1.
18. An asymmetric parameter α is defined as $\alpha = d_2 - d_1/d_1$ where d_1 and d_2 are the short and long distances of M—C(O), respectively. If $0.1 \leqslant \alpha \leqslant 0.6$, a semibridging carbonyl is designated according to Curtis' suggestion. Curtis, M. D., Han, K. R. and Butler, W. M., *Inorg. Chem.*, 1980, **19,** 2096.
19. Jolly, M. L. and Chazan, D. J., *Inorg. Synth.*, 1968, **11,** 22.
20. Meerwein, H., *Org. Synth.*, 1966, **46,** 113.

Pergamon

PII: SO277-5387(97)00349-5

Polyhedron Vol. 17, No. 9, pp. 1587–1590, 1998
© 1998 Elsevier Science Ltd
All rights reserved. Printed in Great Britain
0277-5387/98 $19.00+0.00

Synthesis and magnetic properties of copper(II)—cobalt(II) complexes of *N,N′*—oxamidobis (benzoato) cuprate(II)

Guang-Ming Yang, Juan Shi, Shi-Ping Yan, Dai-Zheng Liao,* Zong-Hui Jiang and Geng-Lin Wang

Department of Chemistry, Nankai University, Tianjin 300071, P. R. China

(Received 19 June 1997; accepted 14 August 1997)

Abstract—Four heteronuclear metal complexes $[Cu(obbz)Co(L)_2]\cdot nH_2O$ (L = 2,2′-bipyridine (bipy), 4,4′-dimethyl-2,2′-bipyridine (Me_2bipy), 1,10-phenanthroline (phen) or 5-nitro-1,10-phenanthroline (NO_2phen)), have been prepared by the reaction of sodium *N,N,′*-oxamidobis(benzoato)cuprate(II) quadrihydrate, $Na_2[Cu(obbz)]\cdot 4H_2O$, with a divalent metal ion and L. The complexes $[Cu(obbz)Co(bipy)_2]\cdot 5H_2O$ (**1**) and $[Cu(obbz)Co(phen)_2]\cdot 5H_2O$ (**3**) were characterized by variable-temperature magnetic susceptibility measurements, indicating that an antiferromagnetic spin-exchange interaction operates between the copper(II) and cobalt(II) ions. © 1998 Elsevier Science Ltd. All rights reserved

Keywords: binuclear complexes; copper(II)—cobalt(II); magnetic properties.

Binuclear metal complexes containing two different metal ions are of current interest in connection with spin-exchange and charge-transfer between metal ions and in the domain of metallo-enzymes and homogeneous catalysis [1]. Some years ago Kahn reported two alternating bimetallic chain compounds, of formula $MnCu(obbz)\cdot 5H_2O$ and $MnCu(obbz)\cdot H_2O$ and one binuclear compound, of formula $NiCu(obbz)\cdot 6H_2O$ where obbz stands oxamidobis(benzoato). These compounds were obtained by reaction of the copper(II) precursor $[Cu(obbz)]^{2-}$, shown below

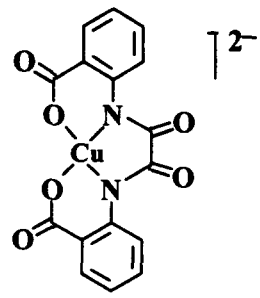

with the manganese(II) ion or nickel(II) ion [2]. However, to our knowledge, no other binuclear complexes of this kind have been reported till now. In this paper, we describe synthesis and magnetic properties of four novel heterobinuclear complexes $[Cu(obbz)]Co(L)_2]\cdot nH_2O$ (L = bipy, Me_2bipy, phen, NO_2phen).

EXPERIMENTAL

Materials

Oxalyl chloride and anthranilic acid were purchased from Aldrich and were of reagent grade. $Na_2[Cu(obbz)]\cdot 4H_2O$ was prepared by the literature method [2].

Synthesis of $[Cu(obbz)]Co(L)_2]\cdot nH_2O$ (L = *bipy, Me_2bipy, phen, NO_2phen*)

The methods used to prepare the four complexes $[Cu(obbz)]Co(L)_2]$ were virtually identical and are exemplified by $[Cu(obbz)Co(bipy)_2]\cdot 5H_2O$ (**1**). To a solution of bipy (62.4 mg, 0.4 mmol) and $Co(NO_3)_2\cdot 6H_2O$ (29.1 mg, 0.1 mmol) were stirred in H_2O (20 cm^3), was successively added a solution of $Na_2[Cu(obbz)]\cdot 4H_2O$ (51.0 mg, 0.1 mmol) in H_2O (20

* Author to whom correspondence should be addressed.

Table 1. Elemental analyses of complexes

Complex	Found (Calc.) %				
	C	H	N	Cu	Co
(1) $[Cu(obbz)Co(bipy)_2]\cdot 5H_2O$	50.93 (50.91)	3.53 (4.00)	9.99 (9.90)	7.66 (7.48)	7.57 (6.95)
(2) $[Cu(obbz)Co(Me_2bipy)_2]\cdot 5H_2O$	53.13 (53.07)	4.34 (4.64)	9.11 (9.29)	7.01 (7.02)	6.50 (6.52)
(3) $[Cu(obbz)Co(phen)_2]\cdot 5H_2O$	53.52 (53.54)	3.42 (3.79)	9.36 (9.37)	7.30 (7.08)	7.16 (6.58)
(4) $[Cu(obbz)Co(NO_2phen)_2]\cdot 4H_2O$	49.63 (49.50)	2.97 (3.10)	12.06 (11.56)	7.01 (6.56)	6.97 (6.69)

cm^3). After 12 h stirring the microcrystals thus obtained were filtered off, washed several times with H_2O and MeOH. The compounds were recrystallized from DMF, and dried *in vacuo*. Analytical data are given in Table 1.

Measurements

Elemental analyses of carbon, hydrogen and nitrogen were performed with a Perkin–Elmer Model 240 elemental analyser. Metal contents were determined by EDTA titration. IR spectra were measured on a Shimadzu Model 480 IR spectrophotometer, using KBr pellets. Variable temperature (77–300 K) magnetic susceptibility was measured on a Cahn 2000 microbalance. Diamagnetic correction were made with Pascal's constants for all the constituent atoms, and the magnetic moments were calculated using the equation $\mu = 2.828(X_M T)^{1/2}$.

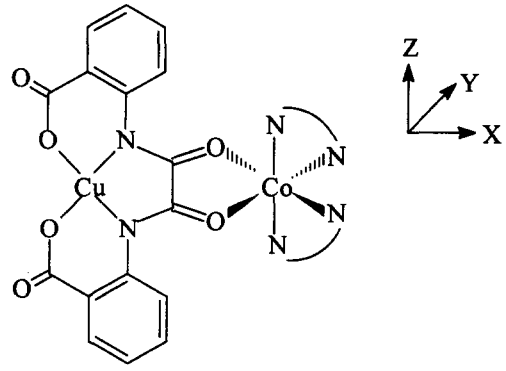

Fig. 1. Proposed chemical structures of complexes (L = bipy, Me_2bipy, phen, NO_2phen).

RESULTS AND DISCUSSION

General characterization

The elemental analysis (Table 1) and IR and magnetic measurements indicated that the reaction of $Na_2[Cu(obbz)]\cdot 4H_2O$ with $Co(NO_3)_2\cdot 6H_2O$ and bipy, Me_2bipy, phen or NO_2phen yielded the binuclear complexes, which are presumed to be chemical structures, as shown in Fig. 1. In the IR spectra, the characteristic bands attributed to the starting complex $Na_2[Cu(obbz)]\cdot 4H_2O$ and terminal ligands are present. The most characteristic features are the very strong and wide band centred at 1600 cm^{-1} and the strong and sharp band centred at ca. 800 cm^{-1}, due to the presence of oxamido group. On the other hand, a very strong and wide band attributable to water appears at 3400 cm^{-1}.

Magnetic properties

The temperature dependences of the susceptibility and magnetic moment for (1) and (3) are shown in Figs 2 and 3, the effective magnetic moments per molecule are 3.07 B.M (1) and 3.46 B.M. (3) at room temperature, respectively, which are slightly lower than the spin-only value 4.24 B.M., implying the operation of antiferromagnetic spin-exchange interaction. Variable temperature susceptibility data were collected for (1) and (3) (Figs 2 and 3). Cobalt(II) ion under O_h-symmetry possesses the $^4T_{1g}$ ground state. Therefore, the magnetic susceptibility for a copper(II)—cobalt(II) ($S = 3/2$) binuclear complex with cobalt(II) under O_h-symmetry is difficult to explain. However, for the present complexes the configuration around the cobalt(II) ion is somewhat distorted from O_h-symmetry. According to Sinn [3], it is likely that the Heisenberg model is applicable to the explanation for the magnetism of the present copper(II)—cobalt(II) complexes. Based on this model ($\hat{H} = -2J\hat{S}_1\hat{S}_2$), the molar magnetic susceptibility for a copper(II)—cobalt(II) ($S = 3/2$) binuclear complex is represented by eqn (1) [3].

$$X_M = \frac{2N\beta^2}{K(T-\theta)}\left[\frac{5g_2^2+g_1^2\exp(-4J/KT)}{5+3\exp(-4J/KT)}\right] \quad (1)$$

where $g_1 = (5g_{Co}-g_{Cu})/4$, $g_2 = (3g_{Co}+g_{Cu})/4$ and each symbol has its usual meaning.

As shown in Figs 2 and 3, good least-squares fits to the experimental data were attained with eqn (1). The magnetic parameters and the agreement factor $F = \Sigma[X_M)_{obs}-(X_M)_{calc}]^2/\Sigma((X_M)_{obs}$ thus determined

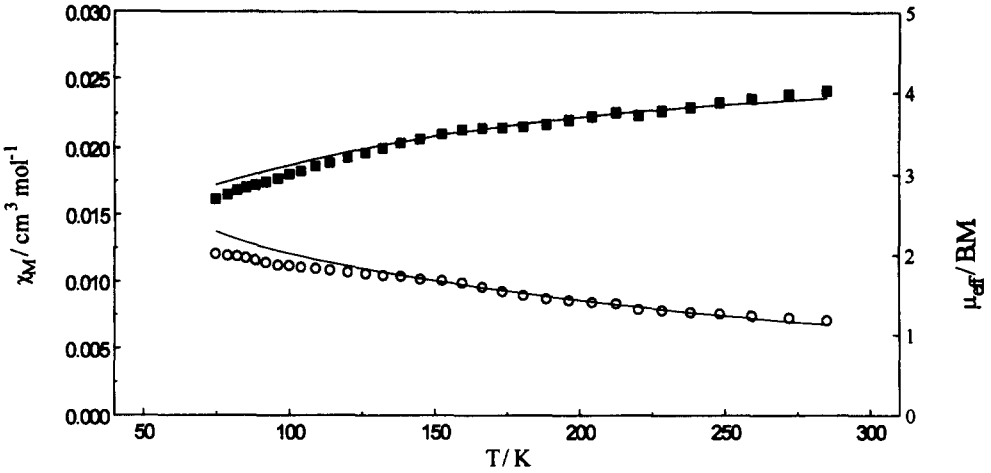

Fig. 2. X_M versus T plots for [Cu(obbz)Co(bipy)$_2$]. The curve is drawn based on eqn (1) with the magnetic parameter given in the text.

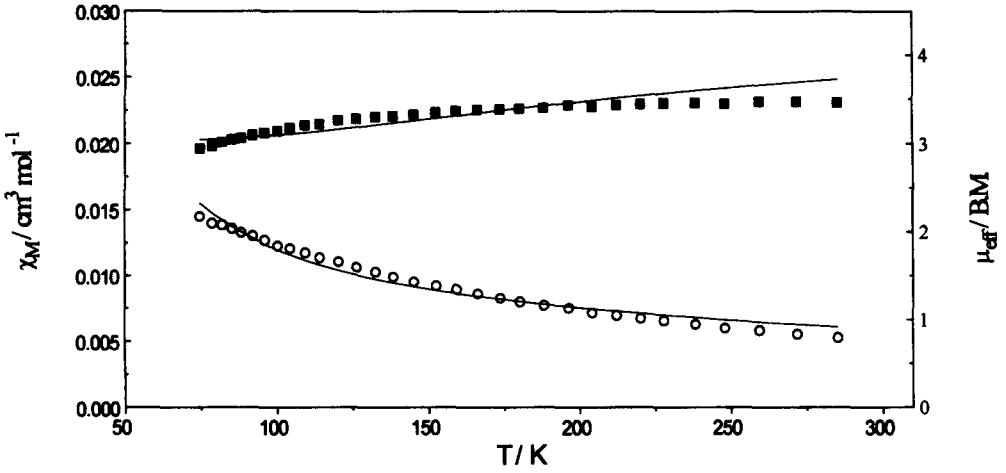

Fig. 3. X_M versus T plots for [Cu(obbz)Co(phen)$_2$]. The curve is drawn based on eqn (1) with the magnetic parameter given in the text.

are $\theta = -8$, $J = -48$ cm^{-1}, $g_{Cu} = 2.01$, $g_{Co} = 2.12$, $F = 2.8 \times 10^{-5}$ for (**1**) and $\theta = 0$, $J = -73$ cm^{-1}, $g_{Cu} = 2.01$, $g_{Co} = 2.11$, $F = 2.4 \times 10^{-5}$ for (**3**). These results ($J < 0$) indicate that the complexes undergo an antiferromagnetic spin-exchange interaction, between Cu(II) and Co(II) ions.

To describe the mechanism of the exchange interaction, several models have been proposed [4,5]. According to these models, strict orbital orthogonality results in ferromagnetism, otherwise an antiferromagnetic coupling should be expected. For the present complexes, if the whole molecular symmetry is considered to be C_{2v} and the coordinates used is shown by Fig. 1, the 3d metallic orbitals of copper(II) and cobalt(II) ions transform as $a_1(d_{z^2}, d_{x^2-y^2})$, $a_2(d_{yz})$, $b_1(d_{xy})$ and $b_2(d_{zx})$. Around the copper(II) ion there is just one unpaired electron which occupies the b_1(Cu) orbital. Around the cobalt(II) ion the unpaired electron has some distribution in b_1(Co) [6]. Because there is no orthogonality between the b_1 magnetic orbitals centred on the copper(II) and cobalt(II) ions, the antiferromagnetic interaction should be observed.

Acknowledgements—This project was supported by the National Natural Science Foundation of China and by grants from state Key Laboratory of Structural Chemistry of China.

REFERENCES

1. Willett, R. D., Gatteschi, D. and Kahn, O., ed. *Magneto-Structural Correlations in Exchange Coupled Systems*, NATO ASI Series, Vol. 140. Reidel, Dordrecht, 1985.

2. Nakatani, K., Carriat, J. Y., Journaux, Y., Kahn, O., Lloret, F., Renard, J. P., Pei, Y., Sletten, J. and Verdaguer, M., *J. Am. Chem. Soc.*, 1989, **111,** 5739.
3. Sinn, E., *Coord. Chem. Rev.*, 1970, **5,** 313.
4. Hay, P. J., Thibeault, J. C. and Hoffman, R., *J. Am. Chem. Soc.*, 1975, **97,** 4884.
5. Kahn, O. and Charlot, M. F., *Nouv. J. Chem.*, 1980, **4,** 567.
6. Kahn, O., Tola, P. and Coudanne, H., *Chem. Phys.*, 1979, **42,** 355.

Pergamon

PII: S0277-5387(97)00298-2

Polyhedron Vol. 17, No. 9, pp. 1591–1600, 1998
© 1998 Published by Elsevier Science Ltd
All rights reserved. Printed in Great Britain
0277-5387/98 $19.00+0.00

Reactions of mercury(II) with 2-pyridinecarboxylic and 6-methyl-2-pyridinecarboxylic acids and corresponding esters. Crystal structures of $[Hg(C_5H_4NCOO)_2]$, $[HgX_2(C_5H_4NCOOPr^i)]$, X = Br or I and $[HgCl_2(MeC_5H_3NCOOEt)]$

Pilar Gonzàlez-Duarte,[a]* Àngels Leiva,[a] Ricard March,[a] Josefina Pons,[a] William Clegg,[b] Xavier Solans,[c], Angel Álvarez-Larena[d] and Joan Francesc Piniella[d]

[a]Departament de Química, Unitat de Química Inorgànica, Universitat Autònoma de Barcelona, 08193-Bellaterra, Barcelona, Spain

[b]Department of Chemistry, University of Newcastle, Newcastle upon Tyne NE1 7RU, U.K.

[c]Departament de Cristal.lografia, Mineralogia i Dipòsits Minerals, Universitat de Barcelona, Martí i Franquès x/n, 08023-Barcelona, Spain

[d]Departament de Geologia, Unitat de Cristal.lografia, Universitat Autònoma de Barcelona, 08193-Bellaterra, Barcelona, Spain

(Received 8 April 1997; accepted 30 June 1997)

Abstract—Several mercury(II) complexes with 2-pyridinecarboxylic and 6-methyl-2-pyridinecarboxylic acids as well as with corresponding esters have been obtained and some of them structurally characterized by X-ray diffraction. $[HgC_5H_4NCOO)_2]$ consists of one-dimensional chains of octahedrally coordinated mercury atoms linked by means of the oxygen atoms of the carboxylate groups. The structure of the isomorphous complexes $[HgX_2(C_5H_4NCOOPr^i)]$, X = Br or I, consists of isolated centrosymmetric dimers with unsymmetrical μ-X bridges, where mercury atoms are in a distorted square pyramidal coordination. Complex $[Hg(Cl_2(Me-C_5H_3NCOOEt)]$ has a polymeric chain structure formed by loosely bound formula units through a unique non-planar bis(chloride) asymmetric $Hg(\mu\text{-}Cl)_2Hg$ bridge. In all cases picolinate ligands behave as chelates. The crystal structures are compared with those found for the related family $[HgCl_2(C_5H_4NCOOR)]$, R = Me, Et, Pr^n or Pr^i. © 1998 Published by Elsevier Science Ltd. All rights reserved

Keywords: mercury complexes; picolinate complexes; chelate complexes; crystal structures; FAB mass spectra.

A significant number of 1:1 adducts of mercury(II) halides, particularly with tertiary phosphines, have been structurally characterized [1,2]. Although the structure most frequently encountered consists of discrete centrosymmetric halide-bridged dimers, other more highly associated structures also occur [3]. However, the small amount and great diversity of structural data currently available thwart any attempt at a systematic catalogue.

We have recently reported the synthesis and X-ray crystal structure of $HgCl_2$ adducts with esters of 2-pyridinecarboxylic acid, which, unlike tertiary phosphines, behave as bidentate ligands. Accordingly, the structures of $[HgCl_2(C_5H_4NCOOR)]$ complexes have shown a great variety ranging from different one-dimensional chains for R = Me and Et, through well separated tetramers for R = Pr^i, to discrete dimers for

* Author to whom correspondence should be addressed.

R = Pr^n [4]. This remarkable diversity prompted us to extend the previous work to other halide ions and to ligands related to esters of 2-pyridinecarboxylic acid. As a result we now report the synthesis of $[HgX_2(C_5H_4NCOOPr^i)]$, X = Br (**5**), I (**6**), and $[HgCl_2(MeC_5H_3NCOOR)]$, R = Me (**7**), Et (**8**) complexes. The structural features observed for the isomorphous complexes **5** and **6** are similar to those already reported for $[HgCl_2(C_5H_4NCOOPr^n)]$, all three being discrete centrosymmetric dimers with unsymmetrical bis(μ-halide) bridges. Complex **8** consists of an infinite one-dimensional chain, which can be compared to that found in complex $[HgCl_2(C_5H_4NCOOEt)]$ [4], although the geometrical parameters of the linking —Hg(μ-Cl)$_2$Hg— units in both compounds are markedly different. Several mercury(II) complexes with 2-pyridinecarboxylic and 6-methyl-2-pyridinecarboxylic acids in anionic form are also reported. The X-ray structure of $[Hg(C_5H_4NCOO)_2]$ (**1**) shows that it consists of a one-dimensional chain where carboxylate groups bridge consecutive mercury atoms. A preliminary report on this structure has already been given [5].

EXPERIMENTAL

Preparations

The compound 6-methyl-2-pyridinecarboxylic acid was synthesized as previously described [6]. Its ester derivatives as well as the isopropyl ester of the commercially available 2-pyridinecarboxylic acid were obtained by the usual esterification procedure in acidic medium with an excess of the corresponding alcohol [7].

The same general procedure was used in all syntheses of complexes. A 4.10^{-2} M solution (25 cm^3) containing the mercury(II) salt was slowly added to the same volume of a solution of the ligand. In all cases a white solid formed after 30 min of stirring, which was filtered off, washed with diethyl ether and dried *in vacuo*. The solvent, the mercury(II) salt and the Hg^{II} to ligand molar ratio used in each synthesis, the yield of the reaction and the elemental analysis of each complex together with the corresponding label are given in Table 1. Transmission FT-IR were recorded from KBr discs at room temperature on a Perkin–Elmer 2000 spectrometer (2 cm^{-1} resolution) in the region 4000–400 cm^{-1}. The ^{1}H NMR spectra at room temperature were obtained in D_2O or CD_3OD solution in a Bruker AC-250 MHz instrument and externally referred to TMS. Positive-ion fast atom bombardment (FAB) mass spectra were obtained with a VG Quattro quadruple mass analyser.

Single crystals of **1** were obtained from a methanolic solution of $C_5H_4NCOOMe$ and $Hg(AcO)_2$ in a 1:1 molar ratio. Crystals of **5, 6** and **8** were obtained by recrystallization of the corresponding solid in ethanol for **5** and **6** and methanol for **8**.

X-ray crystallography

Crystal data and selected information on data collection and structure determination are given in Table 2. Data for **5** and **6** were collected on an Enraf–Nonius CAD4 diffractometer at room temperature; cell parameters were refined from an initially found set of reflections, and intensities were measured by $\omega/2\theta$ scan, using standard control software. Data for **8** were collected on a Siemens SMART CCD area detector diffractometer with nitrogen gas cooling; cell parameters were refined from the observed setting angles of all strong reflections in the complete data set, and intensities were integrated from series of narrow-frame exposures (0.3° in ω), using standard Siemens SMART and SAINT software. Graphite-monochromated Mo-$K\alpha$ radiation (λ = 0.71073 Å) was employed in all cases. Absorption corrections were applied semi-empirically, based on azimuthal scans and symmetry-equivalent reflections.

The structures were solved by direct methods [8] and refined by full-matrix least-squares on F^2 for all unique measured data [9], with weighting $w^{-1} = \sigma^2(F_0^2) + (aP)^2 + (bP)$, where $P = (F_0^2 + 2F_c^2)/3$. Hydrogen atoms were included with riding model constraints, and other atoms were refined anisotropically. In agreement with the ^{1}H-NMR spectrum, compound **8** was found to contain a disordered mixture of the ethyl and methyl ester ligands; the relative proportions are 0.47:0.53(3), and the terminal methyl group of the ethyl substituent is poorly defined.

Atomic coordinates, complete bond lengths and angles, and displacement parameters have been deposited as supplementary material at the Cambridge Crystallographic Data Centre.

RESULTS AND DISCUSSION

Synthesis, infrared and ^{1}H NMR results

Reactions of $Hg(AcO)_2$ with 2-pyridinecarboxylic acid at 1:2 or 1:1 metal to ligand molar ratio lead to complex **1**. However, the same reaction with 6-methyl-2-pyridinecarboxylic acid leads to complex **2** if the molar ratio used is 1:2 but to complex **3** if it is 1:1 (Table 1). Conductivity data for **2** and **3** indicate that none of them gives rise to ions in solution and thus it is likely that acetate ions in the solid are bound to mercury atoms. The slight solubility of **1** in most solvents has not allowed conductivity measurements and has precluded formation of single crystals from recrystallization of the corresponding solid. These have been obtained after leaving undisturbed for several weeks a methanolic solution of $Hg(AcO)_2$ and 2-pyridinecarboxylic acid methyl ester at 1:1 molar ratio.

According to infrared data, the pyridine nitrogen atom is coordinated to mercury in all the complexes, as shown by the two strong absorptions at 1350 and

Table 1. Physical and analytical data for the complexes **1–8**

Complex[a]	Hg^{II} salt[b]	Hg^{II} to ligand molar ratio	Yield (%)	Elemental analysis[c] C (%)	H (%)	N (%)	Conductivity[d] (Ω^{-1} cm^2 mol^{-1})
$[Hg(C_5H_4NCOO)_2]$ **1**	$Hg(AcO)_2$	1:2[e]	85	32.2 (32.4)	1.7 (1.8)	6.3 (6.3)	—
$[Hg(MeC_5H_3NCOO)_2]\cdot 2H_2O$ **2**	$Hg(AcO)_2$	1:2	72	35.2 (35.6)	2.5 (2.6)	5.8 (5.9)	2.06
$[Hg(MeC_5H_3NCOO)(CH_3COO)]$ **3**	$Hg(AcO)_2$	1:1	65	27.2 (27.3)	2.1 (2.3)	3.5 (3.5)	2.21
$[Hg(MeC_5H_3NCOOH)(MeC_5H_3NCOO)](NO_3)$ **4**	$Hg(NO_3)_2$	1:2	83	31.5 (31.4)	8.1 (7.8)	2.8 (2.5)	—
$[HgBr_2(C_5H_4NCOOPr^i)]$ **5**	$HgBr_2$	1:1[f]	69	20.3 (20.6)	2.1 (2.1)	2.7 (2.7)	1.30
$[HgI_2(C_5H_4NCOOPr^i)]$ **6**	HgI_2	1:1[f]	39	17.4 (17.5)	1.8 (1.8)	2.4 (2.3)	1.29
$[HgCl_2(MeC_5H_3NCOOMe)]$ **7**	$HgCl_2$	1:2[e]	36	22.7 (22.7)	2.2 (2.2)	3.2 (3.3)	3.40
$[HgCl_2(MeC_5H_3NCOOEt)]$ **8**	$HgCl_2$	1:2[e]	47	24.8 (24.7)	2.5 (2.5)	3.1 (3.2)	3.25

[a] The solvent used for the synthesis of complexes **1, 3, 7** and **8** was methanol, for complexes **2, 5** and **6,** ethanol and for complex **4,** a 1:1 MeOH/EtOH mixture.

[b] 4×10^{-2} M salt solutions have been used.

[c] Required values are given in parentheses.

[d] 10^{-3} M in methanol. Absence of data indicates insoluble complexes.

[e] A 1:1 ratio leads to the same complex.

[f] Synthesis are given in ref. [4]. As there reported, a 1:2 molar ratio affords the 1:1 adduct, $HgX_2(L)$, exclusively.

Table 2. Crystallographic data

Compound	**5**	**6**	**8**
Formula	$C_9H_{11}HgBr_2NO_2$	$C_9H_{11}HgI_2NO_2$	$C_9H_{11}Cl_2HgNO_2$
M	525.60	619.58	436.68
Crystal system	Triclinic	Triclinic	Monoclinic
Space group	$P\bar{1}$	$P\bar{1}$	$P2_1/c$
a (Å)	7.283(3)	7.460(4)	15.468(2)
b (Å)	9.370(3)	9.672(6)	9.6054(14)
c (Å)	10.295(9)	10.501(7)	7.6598(11)
α (°)	74.02(4)	75.48(4)	90
β (°)	77.47(5)	76.02(5)	90.444(4)
γ (°)	82.64(3)	84.37(5)	90
V (Å^3)	657.6(7)	711.2(8)	1138.0(3)
Z	2	2	4
D_c (g cm^{-3})	2.655	2.893	2.549
μ (mm^{-1})	17.76	15.15	13.97
F(000)	476	548	808
Temperature (K)	293	293	160
Crystal size (mm^3)	$0.1 \times 0.1 \times 0.2$	$0.3 \times 0.2 \times 0.2$	$0.4 \times 0.4 \times 0.2$
θ_{max} (°)	30.0	30.0	28.4
Maximum indices hkl	10, 13, 14	10, 13, 14	20, 12, 9
Reflections measured	3832	4134	6812
Unique reflections	3832	4134	2589
R_{int}	0	0	0.0713
Transmission	0.08–0.12	0.02–0.04	0.01–0.04
Weighting parameters a, b	0.0656, 0	0.1837, 3.4242	0.0576, 3.7873
Extinction coeff. x	0	0	0.0015(4)
No. of refined parameters	138	138	139
$R_w(F^2)$ (all data)	0.1227	0.1511	0.1072
$R(F)$ ('observed' data, $I > 2\sigma(I)$)	0.0450(2563)	0.0435(3234)	0.0380(2320)
Goodness of fit	0.997	0.991	1.087
Max., min. electron density (e Å^{-3})	3.21, −2.96	0.81, −0.43	2.29, −2.04

650 cm^{-1} [10,11]. Moreover, the difference between the symmetric and asymmetric stretching vibrations of the carboxylate group, $\Delta = [\nu(COO)_{as} - \nu(COO)_s]$, can provide information on the possible behaviour of anionic carboxylate ligands in complexes **1–4** as well as on that of the acetate group in complex **3**. Unfortunately, a Δ value cannot be easily established for complexes containing carboxylate groups of ester ligands. Comparison of the Δ values found for complexes **1–3** together with the proposed behaviour of the corresponding carboxylate group based on the literature data [12,13] is given in Table 3. A good agreement is found for complex **1** of known structure. According to the literature a Δ value in the range 200–270 is indicative of COO^- behaving as a unidentate ligand. For mercury–carboxylate complexes, this range would also be compatible with bidentate bridging carboxylate groups with two different mercury oxygen distances. This is the case for complex **1** of known structure (description of the structure below), where Hg—O bond lengths are 2.470 and 2.756 Å. Complexes **2** and **3** show essentially the same Δ value, which is close to that of **1** and thus the same behaviour of the COO^- group for 6-methyl-2-pyridinecarboxylate ligand in **2** and **3** as that of 2-pyridinecarboxylate in **1** could be proposed.

Overlapping of bands has not allowed prediction of the behaviour of carboxylate and nitrate groups in complex **4**. In this case the bands at 1720 and 1618 cm^{-1} can be assigned to the $\nu_{as}(COOH)$ and $\nu_{as}(COO)$ vibrations, respectively. The simultaneous presence of COOH and COO^- groups in metal complexes is not unusual; examples of complexes related to those reported here are: $[M(C_5H_4NCOOH)(C_5H_4NCOO)X]$, X = Cl, Br, SCN and M = Co, Ni, Cu [14,15] or X = Cl and M = Zn [16], $[Mn(C_5H_4NCOOH)(C_5H_4NCOO)Cl]_2$ [17] and $[Ag(C_5H_4NCOOH)(C_5H_4NCOO)]\cdot H_2O$ [18]. Although the X-ray structure for $[Ag(MeC_5H_3NCOOH)(MeC_5H_3NCOO)]$ is known, the correlation between infrared data and ligand behaviour remains difficult.

Table 3. Proposed behaviour of the carboxylate group in complexes **1–3**, based on infrared data

Complex	$\Delta = [\nu(COO)_{as} - \nu(COO)_s]$	Proposed behaviour for COO^- group[a]
1	196	Unidentate
2	205	Unidentate
3	206 ($MeC_5H_3NCOO^-$)	Unidentate
	167 ($MeCOO^-$)	Bidentate bridging or chelating[b]

[a] Literature data (ref. [12]) allow the following assignments: Δ = 200–270, unidentate; Δ = 160–172, chelating or bridging.

[b] In most examples (CSD, ref. [33]) of mercury complexes with acetate group, it behaves as bidentate bridging rather than chelating ligand.

The production of complexes **5–8** irrespective of the ester to metal molar ratio parallels the behaviour found for the series $[HgCl_2(C_5H_4NCOOR)]$, R = Me, Et, Pr^n and Pr^i, of known structure [4]. Conductivity and infrared data for complexes with esters of 2-pyridinecarboxylic acid (**5**, **6**) or 6-methyl-2-pyridinecarboxylic acid (**7**, **8**) are in good agreement with those observed for this series of $[HgCl_2(C_5H_4NCOOR)]$ complexes. This, together with the X-ray data for **5**, **6** and **8**, shows that the behaviour of chloride ions and ester ligand in complex **7** is probably similar to that in the other complexes.

^1H NMR spectra were recorded for all complexes except for **1** and **4** owing to their very low solubility in common solvents. Data for complexes **2**, **3** and **5–8** are shown in Table 4. The observed chemical shifts for the complexed ligands have very close values to those of the uncoordinated pyridinecarboxylate compounds. The spectrum of a solution of crystals of **8**, in contrast to those for complexes **5–7**, gave evidence that a partial trans-esterification reaction had occurred during its recrystallization from methanol. The X-ray crystal structure of **8** fully confirmed this observation. Integration of peaks for **3** indicated the presence of acetate and 6-methyl-2-pyridinecarboxylate anions in a 1:1 ratio.

FAB mass spectra

Positive-ion FAB mass spectra have been recorded for complexes **5** and **6** in glycerol and *p*-nitrobenzyl alcohol matrix, respectively. In both cases, the dinuclear nature of the corresponding complex species is fully confirmed by a molecular ion (MH^+) peak at *m/z* 1052 (**5**) and 1240 (**6**). Three most intense peaks can be attributed to the successive loss of one isopropyl group, then one halogen atom (Br for **5** and I for **6**) and finally one whole ester ligand. These peaks are observed at *m/z* 1018, 938 and 775 for complex **5** and 1204, 1077 and 912 for complex **6**. The spectrum of **6** is shown in Fig. 1 as representative of both complexes.

The molecular ion peak has not been observed in the FAB mass spectrum of complexes **1–4**, this is probably due to the low solubility of **2** and **3** and the practical insolubility of **1** and **4** in common organic solvents. The spectra of both **7** and **8**, feature fragmentation peaks corresponding to the breakdown of the complex with the loss of one chlorine atom.

Description of the structures of $[Hg(C_5H_4NCOO)_2]$ (**1**), $[HgBr_2(C_5H_4NCOOPr^i)]$ (**5**), $[HgI_2(C_5H_4NCOOPr^i)]$ (**6**) *and* $[HgCl_2(MeC_5H_3NCOOEt)]$ (**8**)

The structure of complex **1** consists of an infinite one-dimensional chain of mercury atoms linked by 2-pyridinecarboxylate ligands, which behave as chelates

Table 4. Proton NMR data for complexes **2, 3** in D_2O and **5–8** in CD_3OD[a]

Complexes with 6-methyl-2-pyridinecarboxylic acid and corresponding esters	signals of the 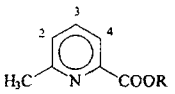 moiety			Signal of the CH_3 group	Signal of the AcO^- group	signals of the 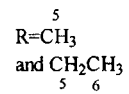 groups	
	H4	H3	H2			H5	H6
$[Hg(MeC_5H_3NCOO)_2]\cdot 2H_2O$ **2**	8.21 d	8.08 t ($J_{3-4}=8$)	7.74 d ($J_{2-3}=8$)	2.63 s	—	—	—
$[Hg(MeC_5H_3NCOO)(CH_3COO)]$ **3**	8.12 d	7.99 t ($J_{3-4}=8$)	7.75 d ($J_{2-3}=8$)	2.63 s	1.87 s	—	—
$[HgCl_2(MeC_5H_3NCOOMe)]$ **7**	7.98 d	7.89 t ($J_{3-4}=7$)	7.52 d ($J_{2-3}=7$)	2.62 s	—	3.98 s	—
$[HgCl_2(MeC_5H_3NCOOEt)]$ **8**	7.92 d	7.70 t ($J_{3-4}=7$)	7.33 d ($J_{2-3}=7$)	2.64 s	—	4.47 q ($J_{5-6}=7$)	1.42 t
Crystals of **8**[b]	7.86 d	7.78 t ($J_{3-4}=8$)	7.43 d ($J_{2-3}=8$)	2.53 s	—	4.37 q ($J_{5-6}=7$)/3.89 s	1.37 t

Complexes with isopropyl 2-pyridinecarboxylate	signals of the 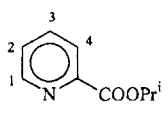 moiety				signals of the 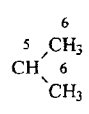 group	
	H1	H4	H3	H2	H5	H6
$[HgBr_2(C_5H_4NCOOPr^i)]$ **5**	8.58 d ($J_{1-2}=8$)	8.05 d	7.94 t ($J_{3-4}=8$)	7.53 t ($J_{2-3}=8$)	5.19 h ($J_{5-6}=7$)	1.30 d
$[HgI_2(C_5H_4NCOOPr^i)]$ **6**	8.57 d ($J_{1-2}=8$)	8.00 d	7.93 t ($J_{3-4}=8$)	7.50 t ($J_{2-3}=8$)	5.20 h ($J_{5-6}=7$)	1.29 d

[a] Chemical shifts δ are given in ppm; coupling constants J are in Hz; all integrations as expected. Abbreviations: s = singlet, d = doublet, t = triplet, q = quadruplet, h = heptuplet.
[b] In agreement with X-ray data and owing to a partial trans-esterification reaction, this compound includes two different R groups (see text).

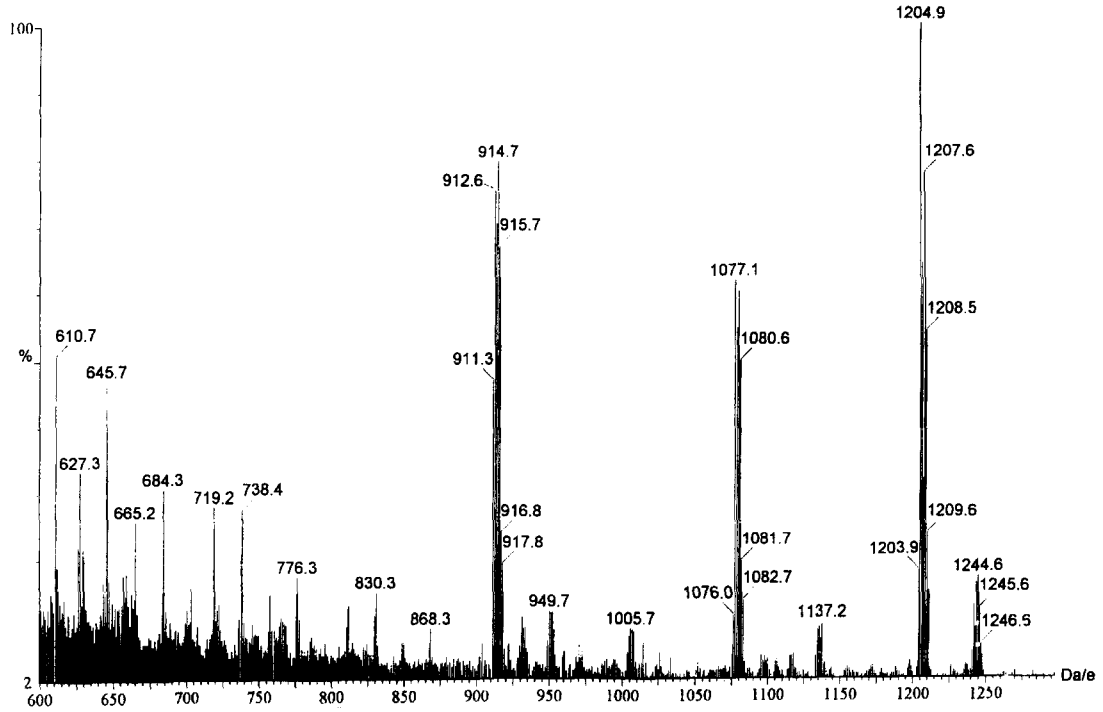

Fig. 1. Positive-ion FAB mass spectrum of $[HgI_2(C_5H_4NCOOPr^i)]$ **6** in *p*-nitrobenzyl alcohol matrix.

and simultaneously bridge two consecutive mercury atoms (Fig. 2). Selected bond lengths and angles are given in Table 5. The chain could be considered as formed by centrosymmetric units of formula $[Hg(C_5H_4NCOO)_2]$, where both ligands chelate the metal centre *via* the pyridine nitrogen and one carboxylate oxygen atom. The other oxygen of the same group is responsible for chain formation with the next mercury. The single crystallographically independent mercury atom completes the distorted octahedral coordination [73.15(14)–106.85(14)°] to the two chelating ligands with two additional oxygen atoms of neighbouring units. Because of the inversion centre on the mercury atom here are only one Hg—N and two different Hg—O distances; that within the chelating ligand [Hg—O(1), 2.470(5) Å] is significantly shorter than that with the oxygen atom of the neighbouring unit [Hg—O(2A), 2.756(4) Å], and both are greater than the sum of corresponding covalent radii, 2.22 Å [19]. Consistent with the two different Hg—O

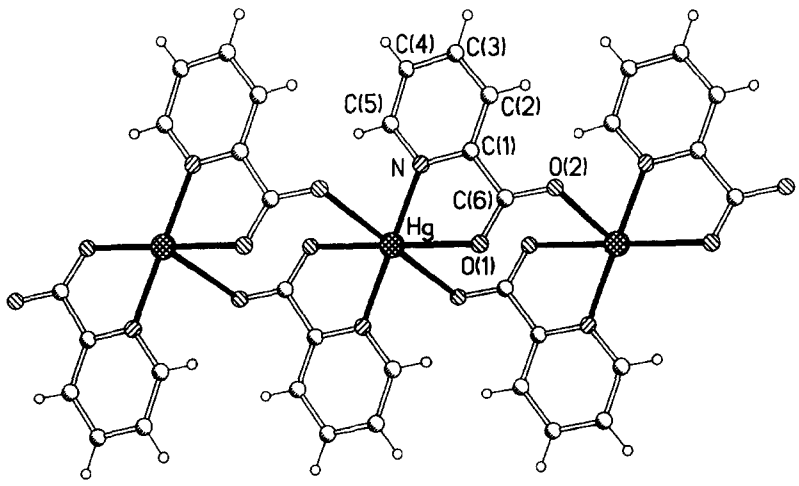

Fig. 2. Part of the polymeric chain structure of compound **1**, with unique atoms labelled.

Table 5. Selected bond lengths (Å) and angles (°) for [Hg(C_5H_4NCOO)] **1**

Hg—N	2.125(5)	Hg—O(1)	2.470(5)
Hg—O(2B)	2.756(4)	C(6)—O(1)	1.268(6)
C(6)—O(2)	1.232(7)	Hg—Hg(B)	5.662(1)
O(1)—Hg—N	73.15(14)	N—Hg—O(2B)	77.0(1)
O(1)—Hg—O(2B)	102.5(1)	N—Hg—O(1A)	106.85(14)

Symmetry operators: A, $-x, -y, -z$; B, $1+x, y, z$.

distances, the two C—O bond lengths in the carboxylate group also differ: C(6)—O(1) is 1.268(6) Å and C(6)—O(2) is 1.232(7) Å. The polymer chains run parallel to the *c* axis and are linked only by normal van der Waals interactions.

Mercury complexes with carboxylate ligands show for the COO^- group a wide variety of coordination modes. The one where each carboxylate oxygen is singly coordinated to a different mercury atom is the most common. However, with this restriction, complexes with carboxylate ligands containing an additional amine-nitrogen donor atom reduce to [MeHg($PhCH_2CH_2CH(NH_2)COO$)] [20], [MeHg($MeSCH_2CH_2CH(NH_2)COO$)] [21] and [$Hg_2\{Me_2NCH_2CH_2NMe_2CH_2CO_2\}_2Cl_4$] [22]. None of these three structures is comparable to that found for [Hg($C_5H_4NCOO)_2$], which has main structural features analogous to those observed in [Cu(C_5H_4N-$COO)_2$] [23].

The structure of complexes **5** and **6** consists of isolated centrosymmetric dimers with unsymmetrical μ-X bridges, X = Br or I, respectively; five-coordination at each mercury is completed by a terminal halogen and a chelating picolinate ester ligand, $C_5H_4NCOOPr^i$ (Fig. 3). The most significant bond lengths and angles are given in Table 6. The bridging Hg_2X_2 unit is strictly planar owing to a crystallographic inversion centre in the middle of the Hg(μ-X)$_2$Hg ring. The mercury-bridging halogen distances are, as expected, longer than the mercury-terminal halogen distances. They all are within the sum of the van der Waals radii and agree well with literature values for complexes containing centrosymmetric Hg(μ-X)$_2$Hg units in which the mercury atoms are pentacoordinated and linked by highly unsymmetric μ-bromo [24–27] and μ-iodo bridges [28–31]. Complexes **5** and **6** show a similar structure to that found in [$HgCl_2(C_5H_4NCOOPr^n)$] rather than that of [$HgCl_2(C_5H_4NCOOPr^i)$], which consists of isolated tetramers [4]. It is noteworthy that the angles about mercury in the first three vary over a wide range. Accordingly, the approach of Reedijk *et al.* [32] has been used to assign a specific coordination geometry. The values obtained for the trigonality index, τ (zero or one if the geometry is perfect square pyramidal or trigonal bipyramidal, respectively) are given in Table 7 and indicate that a distorted square-based pyramidal geometry should be assigned in the three complexes. Comparison with τ values for related complexes found in the literature is also included in the Table.

Complex **8** has a polymeric chain structure con-

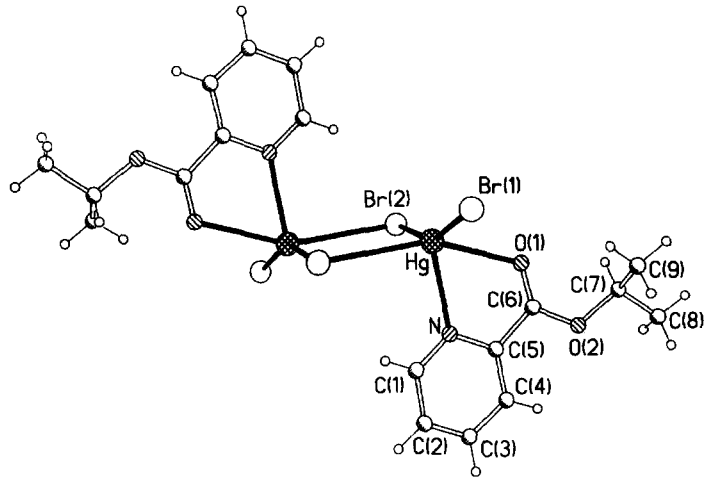

Fig. 3. The dimeric structure of compound **5**, with unique atoms labelled.

Table 6. Selected bond lengths (Å) and angles (°) for complexes $[HgBr_2(C_5H_4NCOOPr^i)]$ **5** and $[HgI_2(C_5H_4NCOOPr^i]$ **6**

	Complex **5**	Complex **6**		Complex **5**	Complex **6**
Hg—X(1)[a]	2.4351(13)	2.601(6)	Hg—O(1)	2.630(6)	2.658(6)
Hg—X(2)	2.4824(14)	2.638(2)	Hg—N	2.443(7)	2.455(6)
Hg—X(2A)	3.125(3)	3.411(2)	Hg···Hg(A)	4.0820(8)	4.363(1)
O(1)—Hg—N	65.4(2)	65.2(2)	N—Hg—X(2)	101.0(2)	102.55(14)
O(1)—Hg—X(1)	91.0(2)	89.6(2)	X(1)—Hg—X(2)	151.62(5)	150.62(3)
O(1)—Hg—X(2)	94.5(2)	97.2(2)	X(1)—Hg—N	106.6(2)	106.24(14)
X(1)—Hg—X(2A)	97.94(6)	96.3(2)	X(2)—Hg—X(2A)	87.27(6)	88.6(2)
N—Hg—X(2A)	92.4(2)	91.5(2)	O(1)—Hg—X(2A)	157.76(14)	156.7(2)
Hg—X(2)—Hg(A)	92.73(6)	91.4(2)			

[a] X = Br for complex **5** and X = I for complex **6**. Symmetry operator: A, $-x$, $-y+1$, $-z+1$ for **5** and A, $-x$, $-y+2$, $-z+1$ for **6**.

Table 7. Calculated trigonality index, τ, using Reedijk [32] approach for dimeric $HgX_2 \cdot L$ adducts, X = Br or I, with centrosymmetric but highly unsymmetrical $Hg(\mu\text{-}X)_2Hg$ units

Complex	τ	Ref.
$[HgBr_2(bipy)]$	0.07	[24]
$[HgBr_2\{C_5H_4NN(H)C(CH_3)O\}]$	0.13	[25]
$[Hg_2Br_4(C_{12}H_{24}S_6)]$	0.40	[26]
$[Hg_4Br_8(C_{10}H_{22}O_6)]$	0.10	[27]
$[Hg_2I_2(Et_2NCS_2)_2]$	0.05	[28]
$[HgI_2(C_3N_2Et)]$	0.77	[29]
$[HgI_2(C_5H_4NC_9H_6N)]$	0.28	[30]
$[HgI_2\{C_6H_5C(NH_2)S\}]$	0.72	[31]
$[HgCl_2(C_5H_4NCOOPr^n)]$	0.05	[4]
$[HgBr_2(C_5H_4NCOOPr^i)]$	0.10	This work
$[HgI_2(C_5H_4NCOOPr^i)]$	0.10	This work

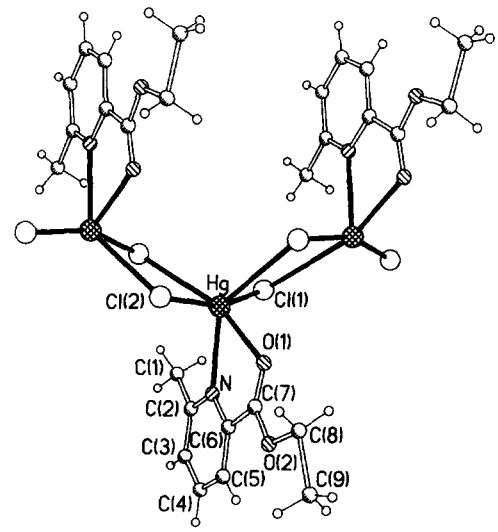

Fig. 4. Part of the polymeric chain structure of compound **8**, with unique atoms labelled.

sisting of $[HgCl_2(MeC_5H_3NCOOEt)]$ adducts, which are linked by means of secondary long range interactions between covalently bonded Hg–Cl pairs; the $Hg(\mu\text{-}Cl)_2Hg$ bridging unit thus formed is highly unsymmetrical (Fig. 4). Selected bond lengths and angles are given in Table 8. The primary coordination of the single crystallographically independent Hg atom is 4-fold by Cl(1), Cl(2) and one chelating ester ligand. On this basis the coordination geometry about mercury is very distorted with angles ranging between 158.72(7) and 64.86(19)°. Each $[HgCl_2(MeC_5H_3NCOOEt)]$ molecule links to two neighbouring units by means of a unique non-planar bis(chloride) asymmetric $Hg(\mu\text{-}Cl)_2Hg$ bridge with four different Hg—Cl distances varying from 2.3381(19) to 3.3844(19) Å and a dihedral angle between Hg—Cl(1)—Cl(2A) and Hg(A)—Cl(1)—Cl(2A) planes of 14.25°. Two of the four Hg—Cl distances are close and agree well with the expected value for mercury-terminal chlorine bonds; the sum of corresponding covalent radii is 2.43 Å. The other two are much longer but also close to each other and lie within the sum of van der Waals radii, 3.45 Å. Consideration of these long range interactions allows Hg to achieve an effective six coordination. The chain formed by the weak interaction of consecutive $[HgCl_2(MeC_5H_3NCOOEt)]$ units runs parallel to the c axis. Each unit is related to the next one by glide-plane symmetry, so that each unit is exactly one unit cell displaced from the next unit by one. Examination of the packing arrangements shows that the chains are well separated.

The X-ray structures of the series of adducts $[HgCl_2(C_5H_4NCOOR)]$, recently determined, have shown that complexes with R = Me and Et adopt polymeric chain structures, both different from complex **8**, while those with R = Pr^n or Pr^i comprise only discrete centrosymmetric dimers and tetramers,

Table 8. Selected bond lengths (Å) and angles (°) for $[HgCl_2(MeC_5H_3NCOOEt)]$ **8**

Hg—Cl(1)	2.3468(17)	Hg—O(1)	2.654(5)
Hg—Cl(2)	2.3381(19)	Hg—N	2.528(6)
Hg—Cl(2A)	3.201(2)	Hg—Cl(1B)	3.3844(19)
Hg···Hg(A)	4.3596(6)	Hg···Hg(B)	4.3596(6)
O(1)—Hg—N	64.86(19)	N—Hg—Cl(2)	100.18(15)
O(1)—Hg—Cl(1)	112.20(13)	Cl(1)—Hg—Cl(2)	158.72(7)
O(1)—Hg—Cl(2)	87.05(14)	Cl(1)—Hg—N	96.40(15)
Cl(1)—Hg—Cl(2A)	80.87(6)	Cl(2)—Hg—Cl(2A)	96.75(6)
N—Hg—Cl(2A)	134.14(15)	O(1)—Hg—Cl(2A)	73.90(13)
Cl(2)—Hg—Cl(1B)	77.02(6)	Cl(1)—Hg—Cl(1B)	85.23(5)
N—Hg—Cl(1B)	108.15(15)	O(1)—Hg—Cl(1B)	161.37(13)
Cl(2A)—Hg—Cl(1B)	117.11(5)	Hg—Cl(1)—Hg(A)	97.39(6)
Hg—Cl(2)—Hg(B)	102.72(7)		

Symmetry operators: A, x, $-y+\frac{1}{2}$, $z-\frac{1}{2}$; B, x, $-y+\frac{1}{2}$, $z+\frac{1}{2}$.

respectively [4]. Comparison of the one-dimensional chains found for the $[HgCl_2(C_5H_4NCOOR)]$, R = Me, Et, complexes with that of complex **8** indicates that the main difference lies in the geometric parameters of the corresponding $Hg(\mu\text{-}Cl)_2Hg$ building units. That of complex **8**, unlike the other two, allows a description of the chain as formed by loosely bound monomeric $[HgCl_2(MeC_5H_3NCOOEt)]$ molecules. These data indicate that not only the nature of the alkyl group R in $[HgCl_2(C_5H_4NCOOR)]$ complexes but an increase in the steric effects of the picolinate ester ligand, as happens in $[HgCl_2(MeC_5H_3NCOOEt)]$, have a strong influence on the geometry of the constituent $Hg(\mu\text{-}Cl)_2Hg$ bridging units, which probably play a significant role in influencing the structure of the corresponding $HgCl_2$ adducts. Moreover, while complexes **5** (X = Br) and **6** (X = I) of general formula $[HgX_2(C_5H_4NCOOPr^i)]$ are isostructural and consist of discrete dimers, the structure of the Cl analogue is formed by well separated tetramers. Thus, it is likely that the smaller size of the chlorine atom allows an increase in the nuclearity of the corresponding complex species.

Acknowledgments—We thank DGICYT (PB94-0695) and EPSRC for financial support. R.M. is grateful for a grant from Ministerio de Educación y Ciencia. Dr M. Seco is thanked for his help in recording the FAB mass spectra and for interesting discussions.

REFERENCES

1. Bell, N. A., Goldstein, M., Jones, T. and Nowell, I. W., *Inorg. Chim. Acta*, 1981, **48,** 185; Bell, N. A., Goldstein, M., Jones, T., March, L. A. and Nowell, I. W., *Inorg. Chim. Acta*, 1982, **61,** 83; Bell, N. A., Dee, T. D., Goldstein, M. and Nowell, I. W., *Inorg. Chim. Acta*, 1983, **70,** 215; Bell, N. A., March, L. A. and Nowell, I. W., *Inorg. Chim. Acta*, 1989, **156,** 201; **162,** 57.
2. Dean, P. A. W., *Prog. Inorg. Chem.*, 1978, **24,** 109.
3. Einstein, F. W. B., Jones, C. H., Jones, T. and Sharma, R. D., *Inorg. Chem.*, 1983, **22,** 3924.
4. Gonzàlez-Duarte, P., March, R., Pons, J., Clegg, W., Cucurull-Sánchez, L., Alvarez-Larena, A., Piniella, J. F. and Solans, X., *Inorg. Chim. Acta*, 1997, **266,** 81.
5. Alvarez-Larena, A., Piniella, J. F., Pons, J., March, R. and Casabó, J., *Z. Krist.*, 1994, **209,** 695.
6. Black, G., Depp, E. and Corson, B. B., *J. Org. Chem.*, 1949, **14,** 14.
7. Vogel, A. I., *Textbook of Practical Organic Chemistry*, 4th edn, London Longman, London, 1978.
8. Sheldrick, G. M., SHELXS-86, Program for crystal structure determination, University of Göttingen, Germany, 1986.
9. Sheldrick, G. M., SHELXL-93, Program for crystal structure refinement, University of Göttingen, Germany, 1993.
10. Paul, R. C., Chopra, R. S., Bhambri, R. K. and Singh, E., *J. Inorg. Nucl. Chem.*, 1974, **36,** 3703.
11. Nakamoto, K., *Infrared and Raman Spectra of Inorganic and Coordination Compounds*, 4th edn, Wiley-Interscience, New York, 1986.
12. Deacon, G. B. and Phyllips, R. J., *Coord. Chem. Rev.*, 1980, **38,** 3.
13. Robinson, S. D. and Uttley, M. F., *J. Chem. Soc., Dalton Trans.*, 1973, 1912.
14. Ellis, V. M., Vagg, R. S. and Watton, E. C., *J. Inorg. Nucl. Chem.*, 1974, **36,** 1031.
15. Ellis, V. M., Vagg, R. S. and Watton, E. C., *Aust. J. Chem.*, 1974, **27,** 1191.
16. Goher, M. A. S., Abu-Youssef, M. A. M. and Mautner, F. A., *Polyhedron*, 1996, **15,** 453.
17. Goher, M. A. S., Abu-Youssef, M. A. M., Mautner, F. A. and Popitsch, A., *Polyhedron*, 1993, **12,** 1751.
18. Deloume, J. P., Faure, R. and Loiseleur, H., *Acta Cryst. B.*, 1977, **33,** 2709.

19. Huheey, J. E., Keiter, E. A. and Keiter, R. L., *Inorganic Chemistry*, 4th edn. Harper Inter., 1993.
20. Alcock, N. W., Lampe, P. A. and Moore, P., *J. Chem. Soc., Dalton Trans.*, 1978, 1324.
21. Wong, Y. S., Carty, A. J. and Chieh, P. C., *J. Chem. Soc., Dalton Trans.*, 1977, 1157.
22. Wu, D. D. and Mak, T. C. W., *Acta Cryst.*, 1995, **C51,** 857.
23. Takenaka, A., Utsumi, H., Yamamoto, T., Furusaki, A. and Nitta, I., *J. Chem. Soc. Jpn*, 1970, **91,** 928.
24. Craig, D. C., Farhangi, Y., Graddon, D. P. and Stepherson, N. C., *Cryst. Struct. Commun.*, 1974, **3,** 155.
25. Lechat, J. R., Francisco, R. H. P. and Airoldi, C., *Acta Cryst.*, 1980, **B36,** 930.
26. Herceg, M. and Matkovic-Calogovic, D., *Acta Cryst.*, 1992, **C48,** 1779.
27. Rogers, R. D., Bond, A. H. and Wolff, J. L., *J. Coord. Chem.*, 1993, **29,** 187.
28. Chiech, C., *Can. J. Chem.*, 1977, **55,** 65.
29. Battaglia, L. P., Corradi, A. B., Biddau, M. and Ponticelli, G., *J. Cryst. Spectrosc.*, 1986, **16,** 721.
30. Garoufis, A., Perlepes, S. P., Schreiber, A., Bau, R. and Hadjiliadis, N., *Polyhedron*, 1996, **15,** 177.
31. Hiller, W., Castiñeiras, A., Arquero, A. and Masaguer, J. R., *Acta Cryst.*, 1986, **C42,** 151.
32. Addison, A. W., Rao, T. N., Reedijk, J., van Rijn, J. and Verschoor, G. C., *J. Chem. Soc., Dalton Trans.*, 1984, 1349.
33. Allen, F. H., Kennard, O. and Taylor, R., *Acc. Chem. Res.*, 1983, **16,** 146.

Pergamon

PII: S0277-5387(97)00471-3

Polyhedron Vol. 17, No. 10, pp. 1601–1610, 1998
© 1998 Elsevier Science Ltd
All rights reserved. Printed in Great Britain
0277-5387/98 $19.00+0.00

Cyclic voltammetric studies on *N,N*-disubstituted *N'*-ferrocenoylthioureas and their transition metal complexes

O. Seidelmann and L. Beyer*

Institute of Inorganic Chemistry, Department of Chemistry and Mineralogy, University of Leipzig, D-04103 Leipzig, Germany

(Received 7 October 1997; accepted 14 November 1997)

Abstract—The Fe(II)/Fe(III) redox potentials of *N,N*-disubstituted *N'*-ferrocenoylthioureas and the respective ferrocene-1,1'-dicarbonic acid-di- *N,N*-dialkyl-thioureids are shifted cathodically by complexation of Ni(II), Cu(II), Co(III), Mn(II), Pt(II) and Pd(II). The extent of the shift is more pronounced in the latter ligand class and reaches values up to −0.32 V. The *N,N*-disubstituted *N'*-ferrocenoylthioureas exhibit two redox processes in dichlormethane. A mechanistic scheme is proposed. Ferrocene-1,1'-dicarbonic acid-di- *N,N*-dialkyl-thioureids decompose after oxidation in dichlormethane. In contrast, complexes of both ligand types contain quasireversibly oxidisable ferrocene subunits. © 1998 Elsevier Science Ltd. All rights reserved

Keywords: ferrocene; thiourea; cyclic voltammetry; coordination compound; redox switch; transition metal.

Heterobimetallic compounds are being investigated intensively [1,2]. Their desired molecular features like catalysis, optical behaviour, conductivity and magnetism [3] are predominantly determined by the oxidation state of the metals involved and by metal–metal communication [4]. In order to increase this intermetal interaction, efforts are aimed to synthesise molecules in which metals are bound in close proximity and/or being connected by a conjugated pathway [5,6,7].

Ferrocene can be used as one part in heterobimetallic compounds. There is evidence that, owing to orbital geometry, interaction between the embedded iron and a second metal bound on sidechains of the cyclopentadienyl rings is poor [8]. Nevertheless, a rising number of ferrocene derivatives has been created capable of complexing additional metal ions. The ferrocene subunit itself meets a lot of basic requirements essential for a wide application like stability, large-scale availability, safe handling and ease of derivatisation. The reversible Fe(II)/Fe(III) redox behaviour may be the most useful feature of this compounds. On the one hand monitoring of these potential allows us to detect binding of an other (metal) ion [9–11], on the other hand the binding strength of this ion can be "tuned" by switching the ferrocene oxidation state [12–15].

Because of their biological importance, emphasis of many research activities has been placed on complexation of alkaline metals within ferrocene containing frameworks [16,17]. However, binding of transition metal ions on mainly nitrogen, nitrogen and oxygen or sulphur of ferrocenyl sidechains has been studied as well [18–20]. In many cases, electrochemical behaviour revealed a moderate anodic shift of the Fe(II)/Fe(III) redox couple after complexation [21].

N,N-disubstituted *N'*-acylthioureas are easily accessible, well investigated ligands [22] obtaining excellent chelating properties for a wide range of transition metal ions. They posses a hard and a softer donor atom and the possibility of compensating positive charges by deprotonation [23–25].

Introduction of the ferrocene moiety into this ligand class has been accomplished recently, heterobimetallic complexes have been synthesised [26,27]. In these compounds a conjugated link between the two metals is combined with their quite close proximity—especially concerning coordination compounds of the ferrocene-1,1'-dicarbonic acid-di- *N,N*-dialkyl-thi-

* Author to whom correspondence should be addressed.

oureids. Therefore, cyclic voltammetric studies should show distinct effects resulting from electronic changes by complexation of a second transition metal.

The following complex compounds have been employed.

EXPERIMENTAL

Synthesis of the compounds

Compounds **1**–**5**; (**1**–**4a**–**f**) and (**5**–**7**)**b** have been prepared according to literature methods [26,27]. Chelates (**5**–**7a**) have not been isolated but were only obtained in solution by mixing of stoichiometric amounts of ligand (dissolved in 20 cm^3 dichlormethane) and the respective metal acetate (dissolved in 0.5 cm^3 ethanol) at room temperature immediately prior voltammetric measurements.

Compounds **6** and **7** have been prepared as follows. The respective *N*,*N*-disubstituted thiourea (15 mmol = 1.95 g for **6**; 2.19 g for **7**) [28] was suspended in 30 cm^3 dry toluene and 15 mmol (1.2 g) dry pyridine under argon. At a temperature of 90°C 1,1′-ferrocene dicarbonylchloride (7.5 mmol = 2.33 g), dissolved in 30 cm^3 toluene, was added dropwise to the vigorously stirred suspension over a period of 45 min. After 5 h stirring at this temperature, the residue was filtered off and washed three times with 20 cm^3 hot toluene. The united dark brown toluene solution was washed twice with 20 cm^3 cold water, dried using sodium sulphate and evaporated to dryness. The dark paste was treated with hot *n*-hexane until it solidified. Recrystallisation in toluene yielded orange brown crystals.

Analytical data of the new compounds are to be found in Table 1.

Cyclic voltammetry

Cyclic voltammetry was performed using a conventional three-electrode system. The working electrode was a glassy carbon disc (Metrohm, number: 6.1204.000, ϕ = 3 mm), polished with an Al_2O_3 suspension prior every experiment. The counter electrode was a platinium disc (Sensortechnik Meinsberg, Germany). A double junction Ag/AgCl electrode was used as reference (Metrohm, number: 6.0726.110). The inner chamber was filled with a saturated solution of LiCl in ethanol, the outer chamber contained a 0.1 M TBAPC solution in dichlormethane. Dichlormethane was of p.a. grade and saturated with nitrogen. The concentration of supporting electrolyte (Bu_4NClO_4) was 0.1 M. The concentration of compounds investigated was 0.5 mM, 1 mM and 5 mM. The number of electrons involved in oxidation processes was determined by coulometry. All compounds were investigated at 25°C. Cyclic voltammograms of ligands **1**–**4** also were measured at 0°C. The estimated error of measured voltage is about 0.01 V. All data represent the average of five measurements.

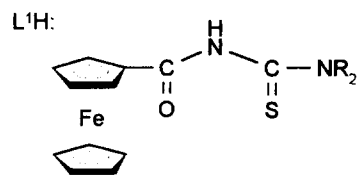

NR_2:		
	NEt_2	**1**
	$NBut_2$	**2**
	pyrrolidino	**3**
	morpholino	**4**

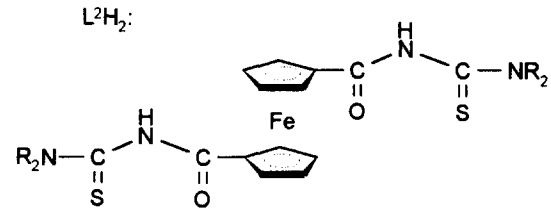

NR_2:		
	NEt_2	**5**
	pyrrolidino	**6**
	morpholino	**7**

O,S-coordinated bimetallic chelates:

$L^1_2Ni(II)$	**(1, 2, 3, 4) a**	$L^2Ni(II)$	**(5, 6, 7) a**
$L^1_2Cu(II)$	**(1, 2, 3, 4) b**	$L^2Cu(II)$	**(5, 6, 7) b**
$L^1_3Co(III)$	**(1, 2, 3, 4) c**		
$L^1_2Mn(II)$	**(1, 4) d**		
$L^1_2Pt(II)$	**(1, 2, 4) e**		
$L^1_2Pd(II)$	**(1, 4) f**		

Voltammograms (v = 1–50 mV s^{-1}) were recorded with the electrochemical interface (SI 1280, Solartron-Schlumberger) under application of the software CORRWARE (Scribner, Charlottesville VA). Voltammograms (v = 100–1000 mV s^{-1}) were recorded with a "AUTOLAB PGSTAT -10". "Digi Sim 2.0" by Bioanalytical Systems, Inc., was used to simulate cyclic voltammograms.

Potentiometric titration in dioxan/water 75 : 25 was employed to determine pK_s values.

RESULTS AND DISCUSSION

Ferrocenoyl-thioureas of the types L1H and L2H2

As an example of the ligand centred redox processes, the cyclic voltammogram (CV) of **4** in dichlormethane is shown in Fig. 1. Each CV recorded of **1–4** reveals the displayed shape. Two one-electron redox couples, the first at a potential of about 780 mV (I), the second at 900 mV (I), occur (Table 2). This is quite an unexpected result because the respective benzoylthiourea do not show any redox process without initial oxidation in a potential range of 1.1 V to −0.5 V [29] and the ferrocene subunit should only give rise to one such process (Fe(II)/Fe(III)). A third reduction peak occurs only at fast scan rates at about −0.2 V (III).

As side chain centred quasireversible redox processes are not expected, both redox couples should be caused by the ferrocene moiety. An anodic shift of the Fe(II)/Fe(III) couple compared with ferrocene/ferrocenium is expected because of the electron withdrawing effect of the carbonyl function attached to ferrocene in **1–4**. The shift extent of I (about +0.25 V) corresponds with comparable substituted compounds [21]. Therefore, we attribute this one electron step to this process. The redox potential is only slightly influenced by different -NR_2 (Table 2). Parallel to

Table 1. Analytical data of compounds **3**, **3a**, **3b**, **3c**, **6**, **7**

Compound	**3**	**3a**	**3b**	**3c**	**6**	**7**
yield (%) m.p. (°C) IR (cm^{-1}) (KBr)	71 131 3285 br 2977 w 2874 w 1776 m 1701 s 1660 s 1526 s 1463 s 1424 s 1247 m 1209 s 822 m 499 m	80 140 2924 w 2872 w 1769 m 1488 s 1440 s 1412 s 1329 s 1249 m 1003 m 823 m 500 m	86 180 2925 w 2872 w 1763 m 1490 s 1420 s 1312 s 1253 m 1010 m 830 m 505 m	64 234 2975 w 2925 w 2300 w 1630 br 1480 s 1460 s 1405 s 1348 s 1250 m 805 m 495 m	70 205 (dec.) 3210 br 2974 w 2875 w 1673 s 1535 s 1453 s 1430 s 1279 s 820 m 498 m	63 170 3208 m 2975 w 2874 w 1670 s 1541 s 1459 s 1430 s 1262 s 820 m 495 m
^{1}H-NMR ($CDCl_3$)	2.0 (m) 4H, CH_2 3.69 (t) J = 6.2 Hz, 2H, CH_2 3.85 (t) J = 6.4 Hz, 2H NCH_2 4.34 (s) 5H, Cp' 4.45 (pt) 2H, Cp 4.76 (pt) 2H, Cp 8.14 (s) 1H, NH	2.0 (br) 8H, CH_2 3.60 (s) 4H HCH_2 3.76 (s) 4H NCH_2 4.37 (s) 10H, Cp' 4.56 (s) 4H, Cp 4.90 (s) 4H, Cp		2.0 (br) 8H, CH_2 3.58 (br) 4H NCH_2 3.80 (br) 4H NCH_2 4.37 (s) 10H, Cp' 4.53 (s) 4H, Cp 4.92 (s) 4H, Cp	2.04 (m) 8H, CH_2 3.80 and 3.89 (m) together 8H NCH_2 4.59 (s) 4H, CpH 5.22 (s) 4H, CpH 9.44 (s) 2H, NH	3.79 (s) 4H NCH_2 3.82 (br) 8H OCH_2 4.28 4H NCH_2 4.61 (s) 4H, CpH 5.25 (s) 4H, CpH 9.51 (s) 2H, NH

Table 1. *Continued*

Compound	3	3a	3b	3c	6	7
^{13}C-NMR ($CDCl_3$)	25.1 and 26.7 (CH_2) 53.4 and 55.0 (NCH_2) 69.4 (CpH) 70.4 (Cp'H) 72.3 (CpH) 74.0 (Cp) 167.8 (CO) 176.3 (CS)	25.3 and 26.7 (CH_2) 52.9 and 54.7 (NCH_2) 70.7 (CpH) 71.2 (Cp'H) 71.4 (CpH) 73.2 (Cp) 171.9 (CO) 176.0 (CS)			25.3 and 26.7 (CH_2) 53.0 and 54.6 (NCH_2) 70.8 (CpH) 73.8 (CpH) 75.7 (Cp) 167.1 (CO) 177.0 (CS)	51.9 and 52.3 (NCH_2) 66.9 and 67.3 (OCH_2) 70.5 (CpH) 74.0 (CpH) 75.4 (Cp) 167.0 (CO) 179.5 (CS)
MS (% intensity)	(70 eV) 341.9 $(M)^+$ (35) 283 (43) 229 (32) 214 (33) 185 (41) 121 (100) 92 (42) 70 (55) 56 (45)	(FAB) 740.5 $(M)^+$ (17)	(FAB) 745 $(M)^+$ (9)	(FAB) 1082 $(M)^+$ (5)	(70 eV) 498 $(M)^+$ (2) 439 (5) 222 (12) 93 (50) 70 (99) 65 (100)	(70 eV) 530 $(M)^+$ (1) 412 (48) 384 (9) 292 (11) 179 (12) 121 (36) 92 (49) 59 (100)
C (%) (calc./fnd.)	56.15/56.20	51.90/52.01	51.56/51.60	53.28/53.29	53.01/53.55	49.81/49.70
H (%) (calc./fnd.)	5.30/5.42	4.63/4.61	4.60/4.52	4.75/4.82	5.26/5.21	4.94/5.02
N (%) (calc./fnd.)	8.18/8.13	7.56/7.74	7.51/7.54	7.76/7.95	11.24/11.08	10.57/10.56
O (%) (calc./fnd.)	4.68/4.34	4.32/4.34	4.29/4.19	4.44/4.91	6.42/6.46	12.07/12.10
S (%) (calc./fnd.)	9.35/9.80	8.64/8.51	8.59/8.86	8.87/8.91	12.84/12.30	12.07/12.13

our work, the redox behaviour of *N*-ferrocenoyl-*N'*-monosubstituted thiourea has been investigated [30]. A comparable influence of the amine substituents on the redox potential is attributed there to an intramolecular hydrogen bonding ring. As compounds **1**–**4** do not form hydrogen bridges, this effect cannot be explained in this way. The magnitude of the amine dependent redox shift corresponds with that of the experimental error. Therefore, we do not venture an explanation.

In order to investigate the nature of the redox processes, further CV experiments were carried out. They included repeated potential cycling, initial 200 s electrode polarisation at various potentials, varying of scan rate, temperature and concentration. The following results have been obtained.

(i) Adsorption could be excluded as a reason for one of the peaks because of their concentration independent height relation; (ii) Varying of concentration (0.5 up to 5 mmol l^{-1}) shows no effect on the redox potentials or CV shape; (iii) Oxidation peaks I and II are diffusion-controlled ($i \sim v^{1/2}$) (Fig. 2.); (iv) Reduction current III decreases to zero at scan rates < 10 mV s^{-1} (Fig. 1.); (v) Process III is only detectable after initial oxidation at II; (vi) During repeated potential cycling I disappears, the oxidation peak of II broadens, its reduction peak is shifted to more cathodic potentials and increases. Potential cycling within a potential window of 0.5 V and 0.9 V (redox couple I) results in quite reproducible CVs without any change of the peaks. Even an initial electrode polarisation at 0.9 V for 200 s does not affect the CV shape remarkably (Fig. 3.). This allows the conclusion of a comparatively stable oxidation product; (vii) Potential cycling beyond the anodic peak of I (0.75–1.2 V) covering both electrochemical processes of II leads to irreversible destruction of the chemical species involved. Similar effects are observable after

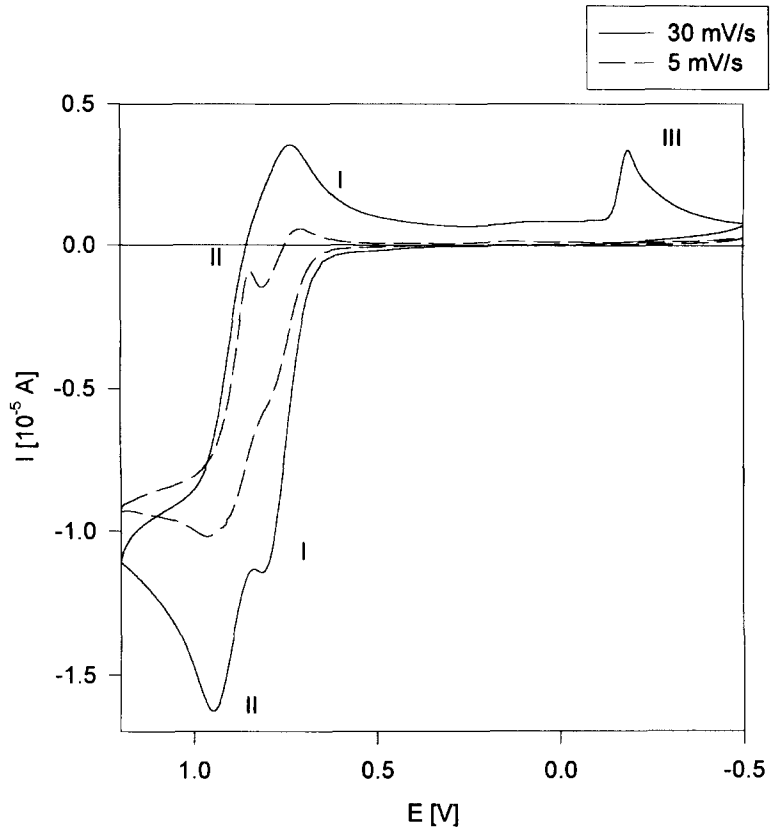

Fig. 1. Cyclic voltammogram of **4** (1 mM) in dichlormethane. Scan from 0 V to +1.2 V, −0.5 V and return. Scan rate: 30 mV s^{-1} and 5 mV s^{-1}.

Table 2. Redox data of ligands **1–7** (average of 5 measurements), 1 mM in dichlormethane, 0.1 M TBAPC. Scan rate 30 mV s^{-1}. Scans from 0 V to 1.4 V and return, 1st scan

Compound	E_{pa} (V)	E_{pc} (V)	ΔE_p[a] (V)	$E_{1/2}$[b] (V)
Ferrocene	0.59	0.47	0.12	0.53
1 process A	0.86	0.73	0.13	0.8
1 process B	1.05	0.89	0.16	0.97
2 process A	0.82	0.70	0.12	0.76
2 process B	1.02	0.88	0.14	0.95
3 process A	0.86	0.71	0.15	0.78
3 process B	1.06	0.88	0.18	0.97
4 process A	0.82	0.74	0.08	0.78
4 process B	0.95	0.87	0.08	0.91
5	1.05	—	—	0.95[c]
6	1.02	—	—	0.94[c]
7	1.09	0.85	0.24	0.97

[a] $\Delta E_p = |E_{pa} - E_{pc}|$.
[b] $E_{1/2} = \frac{1}{2}(E_{pa} + E_{pc})$.
[c] $E_{pa/2}$.

electrode polarisation beyond 0.95 V; (viii) Current of II is temperature dependent. At 0°C its magnitude is only 70% of that measured at 25°C while I seems to be unaffected.

These effects and the earlier drawn conclusion concerning the ferrocene centred character of II give rise to the assumption that this process involves the Fe (II)/Fe(III) couple of a product of I_{ox} which lost its positive charge by a chemical reaction. A similar CV behaviour has been observed recently [31]. There, the oxidised ferrocene subunit was immediately reduced by a phosphino substituent which led to a second Fe(II)/Fe(III) redox process. Here, the reaction following the first oxidation is supposed to be fast as well, because various v (1–1000 mV s^{-1}) do only have a slight effect on the current ratio II_{ox}/I_{ox}. Considering the weak but detectable acidity of ligands **1–4** [27] and its known enhancement by oxidation of ferrocene bearing acids [33]—due to the repulsive effect of positive charges—we propose to attribute II to the Fe (II)/Fe(III) redox couple of oxidised and deprotonated compounds **1–4**. The oxidation product of II seems to be chemically unstable and causes unidentified decomposition products. One of which gives rise to the reduction peak at −0.2 V if the scan rate is fast enough. The two broad redox peaks remaining after prolonged potential cycling and the increase of the reduction peak indicate an electrode surface coating which can also be seen visually.

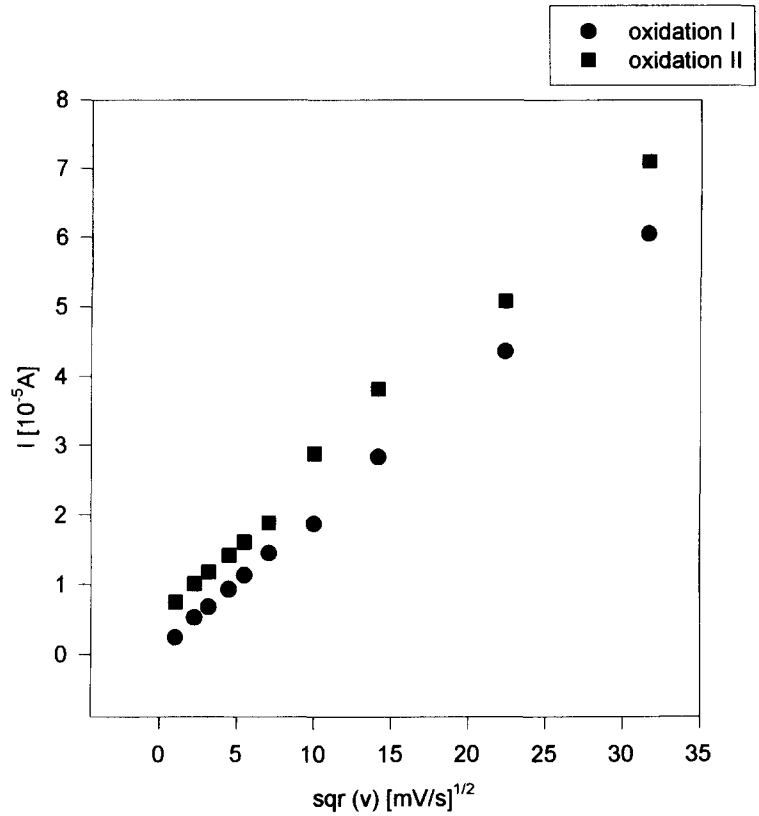

Fig. 2. Oxidation current of processes I and II vs sqr (v) (v: 1 mV s^{-1}–1000 mV s^{-1}, c = 1 mM).

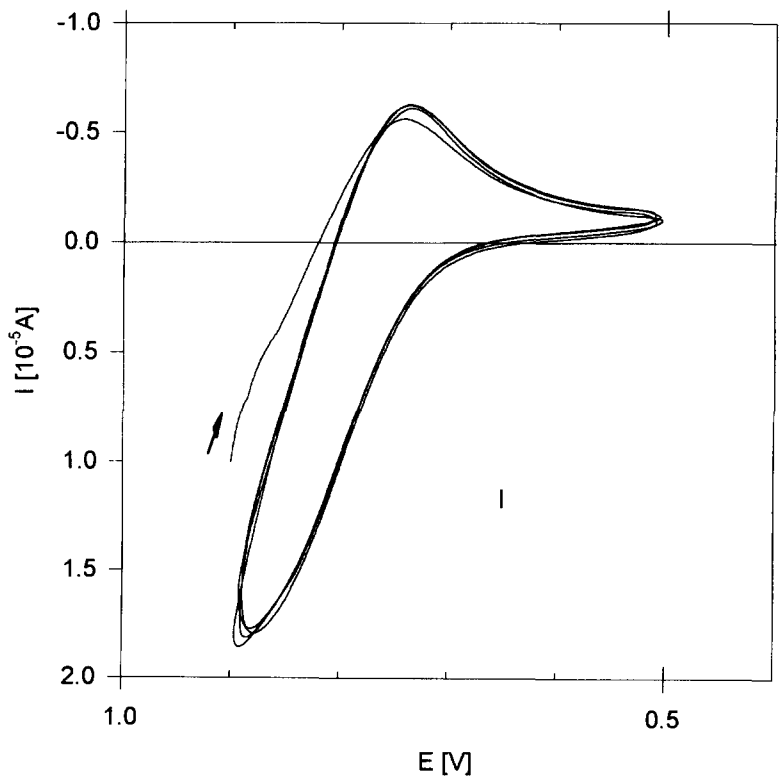

Fig. 3. Cyclic voltammogram of **4** (1 mM) in dichlormethane. Cycles without interim electrode polish. Scans: 200 s electrode polarisation at 0.9 V then 10 cycles, 0.9 V to 0.5 V and return.

The following scheme sums up chemical and electrochemical processes we assume to take place during CV studies on **1–4**.

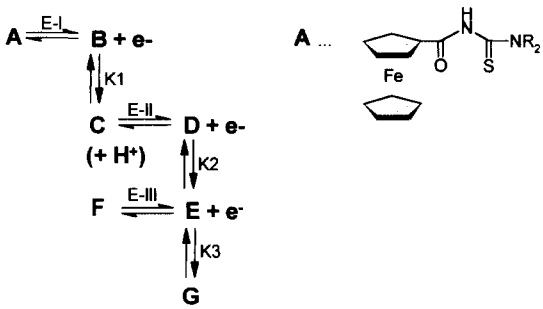

As indicated by the temperature dependence of II, a chemical reaction (K1) should be neccessary to form C. Reduction III is not detectable without initial oxidation II. Therefore, E should result from D and not from C. Obviously, stability of E is limited. Decomposition to the electrochemically inert G can be assumed.

To strengthen the theory of this mechanism the cyclic voltammograms were computer-simulated. According to the measured CVs, the curves were simulated for various scan rates and concentrations using one set of parameters. It cannot be expected that simulated CVs of such a complex mechanism resemble the measured ones in all characteristics. The mathematical software model is too simple to reflect the complex reality correctly. The estimation and variation of 23 independent parameters belonging to 8 mostly unknown species should give the true values only in exceptional cases. Nevertheless, one set of parameters yields CVs which resemble the experimentally recorded fairly well (Fig. 4). Accept from the absolute values of the current, the main charactristics are displayed correctly within a scan rate range of 1 mV s^{-1} to 1 V s^{-1}. Especially, the general shape and its relative changes are simulated adequately. At least, one can conclude from the simulations that there is no general contradiction between the proposed mechanism and the experimental data.

(Used parameter set: $E0_1 = 0.77$ V [$\alpha = 0.5$, $k_{s1} = 0.002$], $E0_2 = 0.97$ V [$\alpha = 0.5$, $k_{s2} = 0.01$], $E0_3 = -0.12$ V [$\alpha = 0.5$, $k_{s3} = 0.1$]; $K_{eq1} = 20$ [$k_f = 3$ s^{-1}, $k_b = 0.15\,s^{-1}$], $K_{eq2} = 50$ [$k_f = 100\,s^{-1}$, $k_b = 2\,s^{-1}$], $K_{eq3} = 60$ [$k_f = 0.01$ s^{-1}, $k_b = 0.000167$ s^{-1}]; D [cm^2 s^{-1}]: $D_A = 2 \cdot 10^{-5}$, $D_B = 0.0002$, $D_C = D_D = D_E = D_F = D_G = 1 \cdot 10^{-5}$.)

Ligands **5–7** show a different and less complex redox behaviour. Only one oxidation peak occurs in dichlormethane. As expected the extent of anodic shifting is about twice as large as measured at the monosubstituded ligands **1–4**, compared with ferrocene/ferrocenium. The influence of -NR_2 is negligible (Table 2). Repeated potential cycling reveals irreversibility of the oxidation process.

The two pK_s values of **5–7** lie in a narrow range around $pK_s1 = 11.1$ and $pK_s2 = 12.6$. So, compared with **1–4** [27], their first deprotonation step is slightly more enhanced. Therefore, a proton loss and further reactions following the oxidation is imaginable here as well. More probable, however, is a total destruction of the electron lacking ferrocene moiety which lost here the "electron buffer" capacity of the unsubstituted cyclopentadienyl ring [31].

Heterobimetallic coordination compounds

Cyclic voltammograms of (**1–4a–f**) reveal only one ferrocene centred redox couple representing a two electron transfer (Fig. 5). Hence, an interaction between the two ferrocenes can be excluded [21]. This redox process is shifted to more cathodic potentials compared with the free ligands (Table 3). Considering the positive charge of the coordinated metal ions, an anodic shift might be expected as it is reported in most papers dealing with comparable compounds. In [32] the first example of a cathodic shifted redox potential is reported. There and here deprotonation accompanies complexation and the entering transition metal has to "compensate" the electron withdrawing effect of the leaving, "hard" proton. This is done incompletely in general and means an increase in complex stability of the oxidised coordination compound compared with the neutral one [34]. As can be seen from the data of Table 3, the different metal ions investigated have only a modest metal specific influence on the Fe(II)/Fe(III) redox couple leading to comparable shifts of about −0.15 V with −0.05 V (**4d**) and −0.19 (**1c**) as most extreme values.

Whereas no general trend can be deduced from the data, the following order going parallel with increasing shift extents is valid within a compound class resulting from one ligand: Mn(II)Pd(II)Pt(II)Ni(II) Cu(II)Co(III). A reason for this order could be the charge/radius ratio. The smaller it is the more negative shifts should be detected. However, this approach does only apply to the order of Mn(II)—Ni(II)—Cu(II). Especially the large shift of the "hard" Co(III) can not be explained in this way. Therefore an other aspect should be taken into consideration. The cathodic shift could be caused by a a π-donation effect of the oxygen. Mn(II) is the best a π-acceptor of the ions mentioned above and Co(III) the worst. So the ferrocenium state is more stabilized by the a π-electron withdrawing Mn(II) ion than by Co(III).

In most cases the redox processes are more reversible here than those of the free ligands. A comparable repulsion of the bound metal ion followed by chemical reactions and compound destruction could not be observed during potential cycling. In all coordination compounds, except the palladium chelates, further electrochemical processes occur in addition to the ferrocene bound redox couple, especially the quasi reversible Cu(II)/Cu(I) is easily detectable (Fig. 5).

Nearly all CVs reveal another oxidation or redox process beyond 0.9 V. It does not show much metal

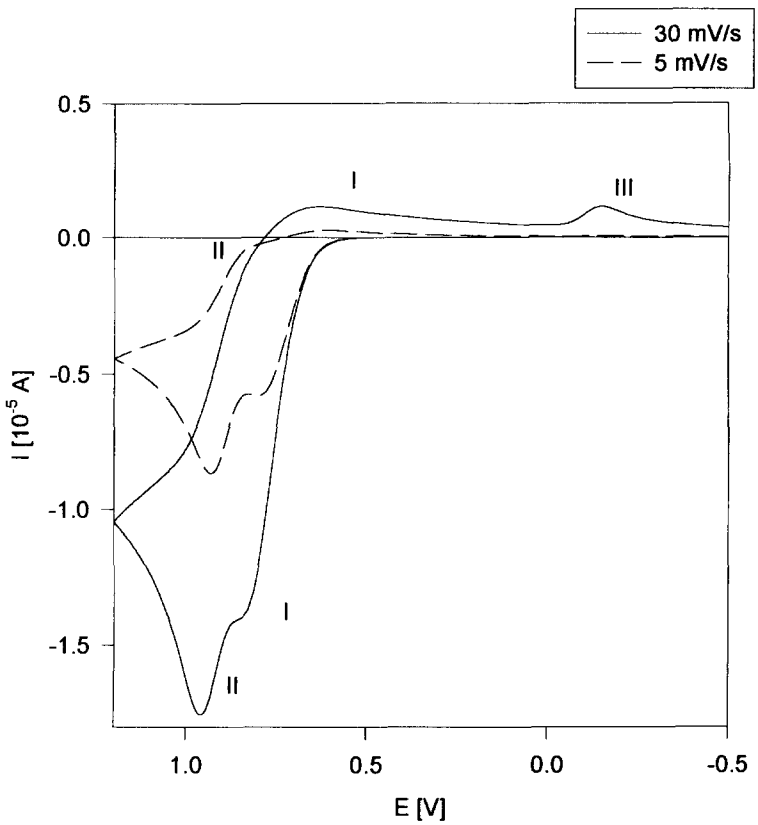

Fig. 4. Computer simulated cyclic voltammograms of ligands **1–4** (1 mM). Scan from 0 V to +1.2 V to −0.5 V. Scan rate: 30 mV s^{-1} and 5 mV s^{-1}.

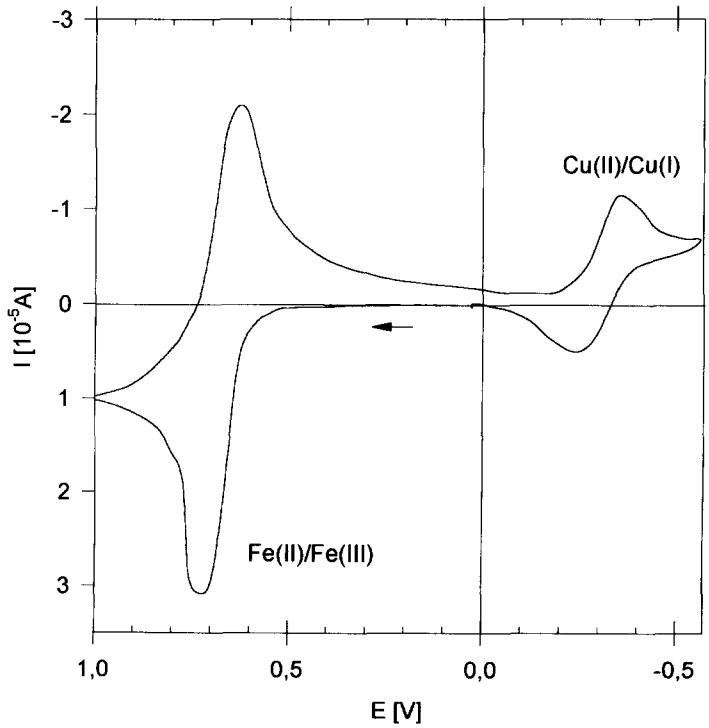

Fig. 5. Cyclic voltammogram of **4b** in dichlormethane. Scan from 0 V to 1 V to −0.6 V and return with a scan rate of 30 mV s^{-1}.

Table 3. Redox data of chelate (**1–7a–f**) (average of 5 measurements), 1 mM in dichlormethane, 0.1 M TBAPC. Scan rate 30 mV s^{-1}. Scans from 0 V to 1.6 V to −0.6 V and return, 1st scan

Compound	E_{pa} (V)	E_{pc} (V)	ΔE_p[a] (V)	$E_{1/2}$[b] (V)	$E_{1/2}$-shift compared with ligand[c] (V)
1a	0.72	0.65	0.07	0.68	−0.12
1b	0.69	0.55	0.14	0.62	−0.18
1c	0.70	0.51	0.19	0.61	−0.19
1d	0.75	0.63	0.12	0.69	−0.11
1e	0.69	0.60	0.09	0.64	−0.16
1f	0.77	0.69	0.08	0.73	−0.07
2a	0.69	0.59	0.10	0.64	−0.12
2b	0.69	0.57	0.12	0.63	−0.13
2c	0.70	0.48	0.22	0.59	−0.17
2e	0.70	0.60	0.10	0.65	−0.11
3a	0.67	0.61	0.06	0.64	−0.14
3b	0.66	0.60	0.06	0.63	−0.15
3c	0.66	0.56	0.10	0.61	−0.17
4a	0.71	0.63	0.12	0.67	−0.11
4b	0.72	0.62	0.10	0.67	−0.11
4c	0.75	0.52	0.23	0.64	−0.14
4d	0.83	0.62	0.21	0.73	−0.05
4e	0.73	0.62	0.11	0.68	−0.10
4f	0.72	0.63	0.09	0.68	−0.10
5a	0.78	0.71	0.07	0.74	−0.27 (−0.21)
5b	0.75	0.69	0.06	0.72	−0.30 (−0.23)
6a	0.74	0.68	0.06	0.71	−0.28 (−0.23)
6b	0.70	0.66	0.04	0.68	−0.32 (−0.26)
7a	0.81	0.70	0.11	0.76	−0.28 (−0.21)
7b	0.81	0.69	0.12	0.75	−0.28 (−0.22)

[a] $\Delta E_p = |E_{pa} - E_{pc}|$.
[b] $E_{1/2} = \frac{1}{2}(E_{pa} + E_{pc})$.
[c] $E_{1/2}$(ligand) − $E_{1/2}$(chelate); for (**5**, **6**, **7a**,**b**): E_{pa}(ligand) − E_{pa}(chelate) and in parentheses $E_{p/2}$(ligand) − $E_{1/2}$(chelate).

specificy. The lowest values are measured for manganese chelates (0.96 V), the highest for platinium complexes (1.5 V). They could be attributed to certain metal bound redox processes, i.e. Cu(II)/Cu(III) [35], Mn(II)/(III) or Ni(II)/Ni(III), but there is no certainty about it. Comparative measurements on benzoylthiourea revealed ligand oxidation beginning beyond 1.1 V [29].

Cyclic voltammograms of (**5–7a,b**) show at least one quasi reversible two electron redox step (Table 3). Compared with the free ligand it is shifted cathodically as well but more emphasised than observed at the monosubstituted ferrocene derivatives. A compound destruction does not occur during potential cycling. According to the cathodic shift, the complex stability is enhanced by oxidising the ligand. Obviously the extended conjugated chelate system is more capable of distributing the positive charge. Additionally the side chain electron withdrawing has been lowered by substitution the proton for "softer" metals.

As mentioned in [27] the nickel chelates **5–7** tend to polymerisation. Ten minutes after addition of the nickel acetate the CV peak began to decrease and the solution became clouded, indicating the beginning polymerisation process.

CONCLUSIONS

The Fe(II)/Fe(III) redox potential of *N,N*-disubstituted *N'*-ferrocenoylthioureas and the respective ferrocene-1,1'-dicarbonic acid-di- *N,N*-dialkylthioureids displays a distinct cathodic shift upon coordination of transition metal ions. Therefore they could be used as amperometric detectors or as pH-controlled "reversed" redox switches [36] as they tend to enhance metal bonding in their oxidised state by liberating protons. Limits are set by the low metal specificity and the polymerisation tendency of **5–7**—

chelates which up to now only allows to form definite copper complexes.

Ligand destruction following the oxidation step is generally avoided by complexation. Nevertheless, investigation of the destruction mechanism and its products might be promising in order to prove the proposed reaction scheme.

Acknowledgements—The authors wish to acknowledge financial support by the "Deutsche Forschungsgemeinschaft" (Project Be 1436/7-1) and the Freistaat Sachsen for a grant (O.S.). Helpful discussions with Dr K.-H. Lubert, Dr G. Wittstock and determination of the pK_s values by Dr F. Dietze are thankfully acknowledged. We would like to thank Dr R. Meier for supporting CV simulation.

REFERENCES

1. Nelson, S. M., *Pure Appl. Chem.*, 1980, **52,** 2461.
2. Sauvage, J.-P., Collin, J.-P., Chambron, J.-C., Guillerez, S., Coudret, C., Balzani, V., Barigelletti, F., De Cola, L. and Flamigui, L., *Chem. Rev.*, 1994, **94,** 1015.
3. Hay, P. J., Thibeault, J. C. and Hoffmann, R., *J. Am. Chem. Soc.*, 1975, **97,** 4884.
4. Strothkamp, K. G. and Lippard, S. J., *Acc. Chem. Res.*, 1982, **10,** 318.
5. Ferguson, G., Glidewell, C., Opromolla, G., Zakaria C. M. and Zanello, P., *J. Organomet. Chem.*, 1996, **517,** 183.
6. Beer, P. D. and Sikanyika, H., *Polyhedron*, 1990, **9,** 1091.
7. Andrews, M. P., Blackburn, C., McAleer, J. F. and Patel, V. D., *J. Chem. Soc., Chem. Commun.*, 1987, 1122.
8. Calabrese, J. C., Cheng, L.-T., Green, J. C., Marder, S. R. and Tam, W., *J. Am. Chem. Soc.*, 1991, **113,** 7227.
9. Beer, P. D., Chen, Z., Drew, M. G. B., Johnson, A. O. M., Smith, D. K. and Spencer, P., *Inorg. Chim. Acta*, 1996, **246,** 143.
10. Beer, P. D., *Chem. Soc. Rev.*, 1989, **18,** 409.
11. Tendero, M. J. L., Benito, A., Cano, J., Lloris, J. M., Martinez-Manes, R., Soto, J., Edwards, A. J., Raithby, P. R. and Rennie, M. A., *J. Chem. Soc., Chem. Commun.*, 1995, 1643.
12. DeSantis, G., Fabbrizzi, L., Licchelli, M. and Pallavicini, P., *Inorg. Chim. Acta*, 1994, **225,** 239.
13. Kotz, J. C. and Nivert, C. L., *J. Organomet. Chem.*, 1973, **52,** 387.
14. Plenio, H., Yang, J., Diodone, R. and Heinze, J., *Inorg. Chem.*, 1994, **33,** 4098.
15. Medina, J. C., Goodnow, T. T., Rojas, M. T., Atwood, J. L., Lynn, B. C., Kaifer, A. E. and Gokel, G. W., *J. Am. Chem. Soc.*, 1992, **114,** 10583.
16. Saji, T., *Chem. Lett.*, 1986, 275.
17. Plenio, H. and Diodone, R., *Inorg. Chem.*, 1995, **34,** 3964.
18. Yong-Min, L., Xiao-Li, W., Zhong-Lin, L., Xian-Min, L. and Yong-Xiang, M., *Bull. Soc. Chim. Belg.*, 1996, **105,** 1.
19. Izumi, T., Murakami, S. and Kasahara, A., *Bull. Chem. Soc. Jpn*, 1988, **61,** 3565.
20. Moriuchi, T., Ikeda, I. and Hirao, T., *Inorg. Chim. Acta*, 1996, **248,** 129.
21. Zanello, P., *Ferrocenes*. VCH Verlagsgesellschaft mbH, Weinheim, 1995, Chapt. 7.
22. Beyer, L., Hoyer, E., Hennig, H., Kirmse, R., Hartmann, H. and Liebscher, J., *J. Prakt. Chem.*, 1975, **317,** 829.
23. König, K. H., Schuster, M., Schneeweis, G. and Steinbrech, B., *Fresenius Z. Anal. Chem.*, 1984, **319,** 66.
24. Koch, K. R., du Troit, J., Caira, M. R. and Sacht, C. *J. Chem. Soc., Dalton Trans.*, 1994, 785.
25. Fitzl, G., Beyer, L., Sieler, J., Richter, R., Kaiser, J. and Hoyer, E., *Z. Anorg. Allg. Chem.*, 1977, **433,** 237.
26. Seidelmann, O., Beyer, L. and Richter, R., *Z. Naturforsch.*, 1995, **50b,** 1679.
27. Seidelmann, O., Beyer, L., Zdobinsky, G., Kirmse, R., Dietze, F. and Richter, R., *Z. Anorg. Allg. Chem.*, 1996, **622,** 692.
28. Hartmann, H. and Reuther, I., *J. Prakt. Chem.*, 1973, **315,** 144.
29. Hartung, J., Rosenbaum, K., Beyer, L., Losada, J. and Fernandez, V., *J. Prakt. Chem.*, 1991, **333,** 537.
30. Yuan, Y.-F., Zhang, L.-Y., Cheng, J.-P. and Wang, J.-T., *Transition Met. Chem.*, 1997, **22,** 281.
31. Podlaha, J., Stepnicka, P., Ludvik, J. and Cisarova, I., *Organometallics*, 1996, **15,** 543.
32. De Santis, G., Fabbrizzi, L., Licchelli, M. and Pallavicini, P., *Inorg. Chim. Acta*, 1994, **225,** 239.
33. De Santis, G., Fabbrizzi, L., Licchelli, M., Pallavicini, P. and Perotti, A., *J. Chem. Soc., Dalton Trans.*, 1992, 3283.
34. Miller, S. R., Gustowski, D. A., Chen, Z. C., Gokel, G. W., Echegoyen, L. and Kaifer, A. E., *Anal. Chem.*, 1988, **60,** 2021.
35. Mohamadou, A., Déchamps-Olivier, I. and Barbier, J.-P., *Polyhedron*, 1994, **13,** 3277.
36. Tendero, M. J. L., Benito, A., Martinez-Manez, R., Soto, J., Paya, J., Edwards, A. J. and Raithby, P., *J. Chem. Soc., Dalton Trans.*, 1996, 343.

Pergamon

PII: S0277-5387(97)00459-2

Polyhedron Vol. 17, No. 10, pp. 1611–1615, 1998
© 1998 Published by Elsevier Science Ltd
All rights reserved. Printed in Great Britain
0277-5387/98 $19.00+0.00

Copper(II), nickel(II), zinc(II) and cobalt(III) complexes of C-*meso*-5,12-diethyl-7,14-dimethyl-tetra-azacyclotetradeca-4,11-diene (C-*meso*-Me_2Et_2[14]dieneN_4)

Robert W. Hay,* Iain Fraser and Nicholas C. Owen

School of Chemistry, University of St Andrews, St Andrews KY16 9ST, U.K.

(Received 10 September 1997; accepted 11 November 1997)

Abstract—The dihydroperchlorate salt of the tetra-aza macrocycle C-*meso*-5,12-diethyl-7,14-dimethyl-tetra-azacyclotetradeca-4,11-diene (L) has been prepared by the reaction of ethylenediamine monohydroperchlorate with 4-hexen-3-one in methanol solution. A variety of *trans*-$[CoLX_2]^+$ complexes (X = Cl^-, Br^-, NCS^-, N_3^-, OAc^- and NO_2^-) have been prepared and characterised as their perchlorate salts. Infrared and visible spectra are reported. Copper(II), nickel(II) and zinc(II) complexes have also been prepared and characterised. © 1998 Published by Elsevier Science Ltd. All rights reserved

Keywords: tetra-azamacrocycle; synthesis; copper(II); nickel(II); cobalt(III); zinc(II) complexes.

The reaction of ethylenediamine monohydroperchlorate with α,β-unsaturated ketones gives a range of macrocyclic tetra-azacyclotetradecadienes (Scheme). The reaction involves Michael addition of the amine monohydroperchlorate to the α,β-unsaturated ketone to give the β-aminoketone; two moles of which can then cyclise to give the macrocyclic 14-membered diimine. The reaction appears to be stereospecific giving only the *trans*-diimine with no evidence for the *cis*-isomer. The present paper describes the reaction of ethylenediamine monohydroperchlorate with 4-hexen-3-one to give the dihydroperchlorate salt (**1**). Reduction of (**1**) with $NaBH_4$ gives the saturated ligand L_A. The crystal structure [1] of $[NiL_A](ClO_4)_2$ establishes that the complex has the C-*meso* configuration (**2**) with a *trans* III (RSSR) chiral *sec*-NH configuration, confirming that the macrocyclic diene does indeed have the expected *trans*-diimine stereochemistry.

In a previous paper [2] one of us has described the facile preparation of cobalt(III) complexes of a range of tetra-aza macrocyclic dienes using cobalt(II) precursor complexes and oxidation by dioxygen. We have now extended this synthetic approach to the preparation of a range of cobalt(III) complexes of the ligand (**1**) = L. Copper(II), nickel(II) and zinc(II) complexes of the ligand have also been prepared and characterised.

EXPERIMENTAL

Synthesis

C-*meso*-5,12-diethyl-7,14-dimethyl-tetra-azacyclotetradeca-4-11-diene dihydroperchlorate. Perchloric acid (72%, 8.3 cm^3, 0.102 mol) was added to a cooled 10% methanolic solution of ethylenediamine (6.12 g, 0.102 mol). The reaction mixture was cooled to −10°C and 4-hexen-3-one (10.0 g, 0.102 mol) in methanol (10 cm^3) added dropwise. After stirring for 30 min a white precipitate began to form. Stirring was continued for 3 h then the ligand dihydroperchlorate salt was filtered off, washed with methanol, then diethyl ether and dried *in vacuo*. A second crop was obtained by allowing the filtrate to stand at room temperature for several hours. The crude product was

* Author to whom correspondence should be addressed.

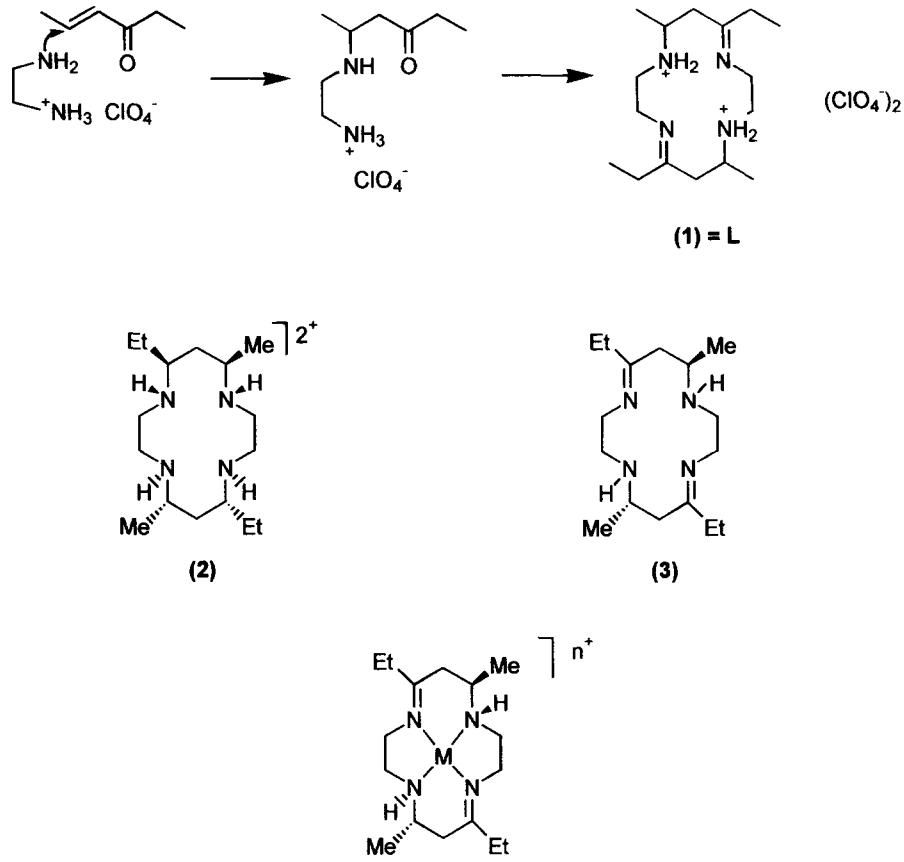

(1) = L

(2)

(3)

(4)

Scheme 1.

recrystallised from hot methanol. (**CARE!** *perchlorate salts of amines are hazardous materials and can explode on excessive heating.*) Yield: 15.1 g (61%), mp 108–109°C. Found: C, 40.0; H, 7.2; N, 11.7. Calc. for $C_{16}H_{34}Cl_2N_4O_8$, C, 39.9; H, 7.1; N, 11.6%. The infrared spectrum (KBr disc) has ν NH 3184, ν C=N 1668 and perchlorate bands at 1110 and 626 cm^{-1}.

$[CuL](ClO_4)_2$. An excess of basic copper(II) carbonate (0.36 g, 1.5 mmol) and the ligand dihydroperchlorate (0.5 g, 1.0 mmol) were slurried together in water and the mixture heated on a steam bath for 30 min. The unreacted carbonate was filtered off and the purple complex crystallised on cooling the filtrate. The complex was filtered off, washed with water then dried *in vacuo*. Yield: 0.20 g. Found: C, 35.5; H, 6.1; N, 10.3. Calc for $C_{16}H_{32}Cl_2CuN_4O_8$: C, 35.4; H, 5.9; N, 10.3%. The infrared spectrum (KBr disc) has ν NH 3238, ν C=N 1673 and perchlorate bands at 1103 and 635 cm^{-1}. The complex has λ_{max} 517 nm (ε = 87 $dm^3\ mol^{-1}\ cm^{-1}$) in aqueous solution.

$[NiL(H_2O)_2](ClO_4)_2$. This complex was prepared essentially as described above replacing basic copper(II) carbonate with nickel(II) carbonate. On cooling in ice the purple octahedral nickel(II) complex crystallised. The complex was filtered off, washed with water then dried *in vacuo*. Yield: (0.1 g). Found: C, 33.2; H, 6.3; N, 9.6. Calc. for $C_{16}H_{36}Cl_2NiN_4O_{10}$: C, 33.5; H, 6.3; N, 9.8%. The infrared spectrum (KBr disc) has ν NH bands at 3344, 3292 and 3254, ν C=N 1688 and perchlorate bands at 1089 and 624 cm^{-1}. The visible spectrum has λ_{max} at 550 and 870 nm (ε = 11 and 17 $dm^3\ mol^{-1}\ cm^{-1}$ respectively) in aqueous solution.

$[ZnL(H_2O)_2](ClO_4)_2$. Zinc(II) perchlorate hexahydrate (2.60 g, 7.0 mmol) and the ligand dihydroperchlorate salt (3.36 g, 7.0 mmol) were separately dissolved in water (ca 10 cm^3). The solutions were mixed and heated on a steam bath for 30 min. On cooling in ice very pale yellow crystals formed and were filtered off, washed with water and dried *in vacuo*. Yield: 0.95 g. Found: C, 33.1; H, 6.5; N, 9.6. Calc. for $C_{16}H_{36}Cl_2ZnN_4O_{10}$: C, 33.1; H, 6.25; N, 9.65%. The infrared spectrum has ν NH 3265; ν C=N 1670 and perchlorate bands at 1070 and 637 nm.

Trans-$[CoLCl_2]ClO_4 \cdot H_2O$. Cobalt(II) chloride hexahydrate (0.37 g, 1.55 mmol) and the ligand dihy-

droperchlorate (0.75 g, 1.56 mmol) were separately dissolved in hot methanol (10 cm^3). The solutions were mixed and heated on a steam bath for 10 min. During this time the colour changed from blue to green. On cooling in ice, the green complex crystallised and was filtered off, washed with methanol then diethyl ether and dried *in vacuo*. A second crop was obtained by reduction of the filtrate on a steam bath to ca 5 cm^3 followed by cooling in ice. Total yield: 0.75 g (91%). Found: C, 36.3; H, 6.5; N, 10.7. Calc. for $C_{16}H_{34}Cl_3CoN_4O_5$, C, 36.3; H, 6.9; N, 10.6%. Infrared spectrum ν H_2O 3418, ν NH 3205, ν C=N 1659 and perchlorate bands at 1090 and 623 cm^{-1}.

Trans-[CoLBr$_2$]ClO$_4$. Methanolic solutions of $CoBr_2 \cdot 6H_2O$ (0.51 g, 1.56 mmol) and the ligand dihydroperchlorate (0.75 g, 1.56 mmol) were treated as described above for the dichloro complex. Total yield of the green crystalline complex 0.8 g (86%). Found: C, 32.7; H, 5.6; N, 9.4. Calc. for $C_{16}H_{32}Br_2ClCoN_4O_4$: C, 33.0; H, 5.55; N, 9.6%. Infrared spectrum, ν NH 3196, ν C=N 1654 with perchlorate bands at 1084 and 623 cm^{-1}.

Trans-[CoL(NO$_2$)$_2$]ClO$_4 \cdot$ H$_2$O. *Trans*-[CoLCl$_2$]ClO$_4 \cdot H_2O$ (0.15 g, 0.28 mmol) was dissolved in hot methanol (10 cm^3). On addition of sodium nitrite (0.08 g, 1.16 mmol) dissolved in methanol (10 cm^3) the colour of the solution changed from green to yellow. After heating on a steam bath for 15 min, the solution was cooled to 4°C and diethyl ether (2 cm^3) added. On standing for several hours the yellow complex crystallised, and was filtered off, washed with diethyl ether and dried *in vacuo*. Yield: 0.10 g (65%). Found: C, 35.0; H, 5.9; N, 15.3. Calc. for $C_{16}H_{34}ClCoN_6O_9$: C, 35.0; H, 6.3; N, 15.3%. Infrared spectrum, ν H_2O 3458, ν NH 3202, ν C=N 1656, ν NO_2^- 1403, 1303, 821 and perchlorate bands at 1085 and 623 cm^{-1}.

Trans-[CoL(CH$_3$CO$_2$)$_2$]ClO$_4 \cdot$ 2H$_2$O. *Trans*-[CoLCl$_2$]ClO$_4 \cdot H_2O$ (0.10 g, 0.19 mmol) and sodium acetate (0.06 g, 0.73 mmol) were separately dissolved in hot methanol (10 cm^3). On addition of the sodium acetate solution to the cobalt complex the colour of the solution changed from green to wine red. The solution volume was reduced to ca 5 cm^3 on a steam bath and then allowed to stand for several days at 4°C. The red crystalline solid which precipitated was filtered off, washed with ethanol then diethyl ether and dried *in vacuo*. Yield: 0.8 g (71%). Found: C, 40.5; H, 6.5; N, 9.5. Calc. for $C_{20}H_{42}ClCoN_4O_{10}$: C, 40.50; H, 7.15; N, 9.45%. Infrared spectrum, ν H_2O 3440, ν C=N 1659, ν NH 3080, ν $CH_3CO_2^-$ 1577, 1388, 1329, 924, 685 with perchlorate bands at 1092 and 623 cm^{-1}.

Trans-[CoL(NCS)$_2$]ClO$_4 \cdot$ H$_2$O. *Trans*-[CoL(NCS)$_2$]ClO$_4 \cdot H_2O$ (0.15 g, 0.28 mmol) and sodium thiocyanate (0.09 g, 1.11 mmol) were separately dissolved in hot methanol (10 cm^3). On addition of the sodium thiocyanate solution the colour changed from green to deep red. The solution volume was reduced to ca 5 cm^3 and on cooling diethyl ether (2 cm^3) added. On standing for several days at 4°C a red crystalline solid deposited, which was filtered off, washed with cold methanol then diethyl ether and dried *in vacuo*. Yield: 0.07 g (44%). Found: C, 37.7; H, 6.5; N, 14.4. Calc. for $C_{18}H_{34}ClCoN_68O_5S_2$; C, 37.7; H, 6.3; N, 14.7%. Infrared spectrum, ν H_2O 3431, ν NH 3180, 3146, ν NCS^- 2103, ν C=N 1654 with perchlorate bands at 1087 and 623 cm^{-1}.

Trans-[CoL(N$_3$)$_2$]ClO$_4 \cdot$ O $\cdot$ 5H$_2$O. *Trans*-[CoLCl$_2$]ClO$_4 \cdot H_2O$ (0.10 g, 0.019 mmol) was dissolved in hot methanol (10 cm^3). To this solution was added sodium azide (0.05 g, 0.77 mmol) in water (5 cm^3). The colour of the solution changed immediately from green to purple. The solution was heated on a steam bath for 20 min, during which time the volume was reduced to ca 10 cm^3. On cooling to 4°C and standing for several

Table 1. Visible spectra of the metal complexes

Complex	λ_{max} (nm)	ε (dm^3 mol^{-1} cm^{-1})
[CuL](ClO$_2$)$_2$	517	87
[NiL(H$_2$O)$_2$](ClO$_4$)$_2$	550	11
	870	17
trans-[CoLCl$_2$]ClO$_4 \cdot$ H$_2$O	617	46
	440 (sh)	—
trans-[CoLBr$_2$]ClO$_4$	659	78
trans-[CoL(NO$_2$)$_2$]ClO$_4 \cdot$ H$_2$O	447	355
trans-[CoL(OAc)$_2$]ClO$_4 \cdot$ 2H$_2$O	552	42
	440	37
trans-[CoL(NCS)$_2$]ClO$_4 \cdot$ H$_2$O	542	233
trans-[CoL(N$_3$)$_2$]ClO$_4 \cdot$ O $\cdot$ 5H$_2$O	562	590

The spectrum of the cobalt(III) complexes was obtained using nitromethane solutions. The other spectra were obtained using aqueous solutions.

days a brown-purple solid precipitated which was filtered off, washed with diethyl ether and dried *in vacuo*. Yield: 0.05 g (50%). Found: C, 36.1; H, 6.1; N, 26.7. Calc. for $C_{16}H_{33}ClCoN_{10}O_{4.5}$; C, 36.1; H, 6.3; N, 26.3. Found: C, 36.12; H, 6.06; N, 26.67%. Infrared spectrum ν H_2O 3438, ν NH 3229, 3091, ν N_3^- 2017 with perchlorate bands at 1084 and 625 cm^{-1}.

Physical measurements

Infrared spectra were recorded as KBr discs on a Shimadzu IR-435 instrument. Electronic absorption spectra were obtained using a Perkin–Elmer Lambda 5 spectrophotometer. Magnetic susceptibility measurements were made using a Johnson Matthey magnetic susceptibility balance using $Hg[Co(NCS)_4]$ as calibrant.

RESULTS AND DISCUSSION

The reaction of ethylenediamine monohydroperchlorate with 4-hexen-3-one in methanol solution gives good yields (ca 60%) of the dihydroperchlorate salt of 5,12-diethyl-7,14-dimethyl-tetra-azacyclotetradeca-4,11-diene (**1**) which has the centrosymmetric C-*meso* configuration (**3**). The dihydroperchlorate salt reacts with cobalt(II) chloride in methanol solution in the presence of air to give the green *trans*-$[CoLCl_2]^+$ cation which can be crystallised in high yield as the perchlorate salt. The complex has an electronic spectrum typical [3,4] of a *trans*-$[CoN_4Cl_2]$ chromophore with bands at 617 nm (ε = 46 dm^3 mol^{-1}) with a shoulder on the charge transfer band at ca 440 nm, Table 1. Thus the trans-dichlorocobalt(III) complex of C-*meso*-5,12-Me_2 [14]diene has λ_{max} 624 nm (ε = 33) with a shoulder at 450 nm (ε = 39) [3].

The green bromo-complex can be similarly prepared by replacing cobalt(II) chloride by the bromide salt. Metal complexes of this type have two chiral *sec*-NH centres so that N-*meso* and N-*racemic* diastereoisomers can occur. This aspect of the stereochemistry was not investigated in detail, but the complexes normally have a single NH band suggesting that the N-*meso* stereochemistry (4) is preferred, Table 2.

Two bands are normally observed in the *d-d* spectra of cobalt(III) complexes the $^1A_{1g} \rightarrow {}^1T_{1g}$ and the $^1A_{1g} \rightarrow {}^1T_{2g}$. If the ligand field is sufficiently high the higher energy $^1A_{1g} \rightarrow {}^1T_{2g}$ transition is frequently obscured by the high intensity ligand-to-metal charge transfer band. As a result only the lower energy band is observed in the complexes $[CoLX_2]^+$ where X = NO_2^-, N_3^- and NCS^-. Two bands are observed in the dichloro complex and the diacetato complex due to the relatively weak ligand field exerted by these monodentate ligands. The spectrum of the acetato complex is shown in Fig. 1. The higher energy band in the bromo complex is obscured due to the lower energy of the Co^{III}–Br charge transfer transition which moves into the visible region.

The nickel(II) complex was obtained as the purple octahedral species $[NiL(H_2O)_2]^{2+}$ which was readily isolated as the perchlorate salt. The visible spectrum has λ_{max} 550 nm (ε = 11) and 870 nm (ε = 15 dm^3 mol^{-1} cm^{-1}) fully consistent with an octahedral stereochemistry. Normally such nickel(II) complexes are square planar and exhibit in some cases a planar $\rightleftharpoons$ octahedral equilibrium. It appears that the ligand field provided by this macrocycle is insufficient to lead to the square planar stereochemistry. The purple copper(II) complex has a single *d-d* band at 517 nm (ε = 87) which is quite characteristic of copper(II) complexes of tetra-aza macrocyclic dienes of this type. For example, the copper(II) complex of 5.6.12.13-tetramethyl-1,4,8,11-tetra-azacyclotetradeca-4,11-diene [4] has a *d-d* band at 513 nm (ε = 82).

The infrared spectra confirm that the complex $[CoL(NO_2)_2]$ has the isonitrito structure with N-bonded NO_2^- and the NCS^- derivative the N-bonded isothiocyanato structure. In isothiocyanato complexes the strength of the C—S bond increases while that of the N=C remains almost unchanged [5]. In the NCS^- ion ν C—S occurs at 749 cm^{-1} and ν C=N at 2049 cm^{-1}. In $[CoL(NCS)_2]ClO_4$ bands are seen at 2103 and 845 cm^{-1} fully consistent with the N-bonded structure. The acetato complex contains both monodentate acetate and anionic acetate and bands typical of these groups are seen in the spectrum.

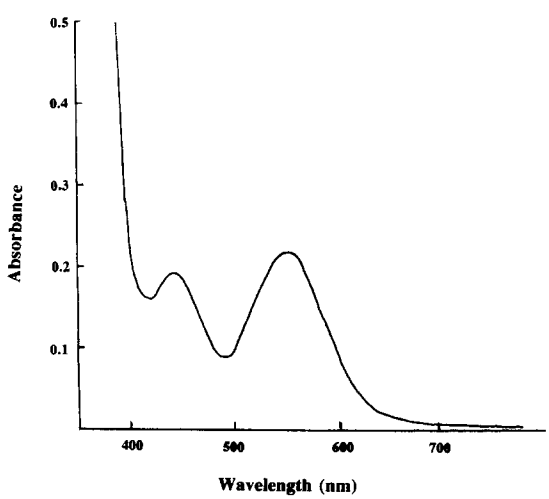

Fig. 1. The UV-vis spectrum of the complex $[CoL(OAc)_2]ClO_4 \cdot H_2O$ in nitromethane solution. The complex has λ_{max} 552 nm (ε = 42 dm^3 mol^{-1} cm^{-1}) and 440 nm (ε = 37 dm^3 mol^{-1} cm^{-1}).

Table 2. Infrared spectra of the cobalt(III) complexes of C-*meso*-Me_2Et_2[14]dieneN$_4$

Complex	(cm^{-1})	Assignment
$L \cdot 2HClO_4$	3184	ν NH
	1668	ν C=N
	1109	ν ClO_4^-
	626	ν ClO_4^-
$[CoLCl_2]ClO_4 \cdot H_2O$	3418	ν H_2O
	3205	ν NH
	1659	ν C=N
	1090	ν ClO_4^-
	623	ν ClO_4^-
$[CoLBr_2]ClO_4$	3196	ν NH
	1654	ν C=N
	1084	ν ClO_4^-
	623	ν ClO_4^-
$[CoL(NO_2)_2]ClO_4 \cdot H_2O$	3458	ν H_2O
	3202	ν NH
	1656	ν C=N
	1403	ν NO_2^-
	1303	ν NO_2^-
	1085	ν ClO_4^-
	821	ν NO_2^-
	623	ν ClO_4^-
$[CoL(CH_3CO_2)_2]ClO_4 \cdot 2H_2O$	3440	ν H_2O
	3080	ν NH
	1659	ν C=N
	1577	ν OAc^-
	1388	ν OAc^-
	1329	ν OAc^-
	1092	ν ClO_4^-
	924	ν OAc^-
	685	ν OAc^-
	623	ν ClO_4^-
$[CoL(NCS)_2](ClO_4 \cdot H_2O$	3431	ν H_2O
	3180	ν NH
	3146	ν NH
	2103	ν NCS^-
	1654	ν C=N
	1087	ν ClO_4^-
	623	ν ClO_4^-
$[CoL(N_3)_2]ClO_4$	3438	ν H_2O
	3229	ν NH
	3091	ν NH
	2017	ν N_3^-
	1084	ν ClO_4^-
	625	ν ClO_4^-

The infrared spectra were determined as KBr discs.

REFERENCES

1. Krajewski, J., Urbanczyk-Lipkowska, Z. and Gluzinski, P., *Bull. Pol. Acad. Sci.*, 1977, **25**, 939.
2. Hay, R. W. and Ali, M. A., *Inorg. Chim. Acta*, 1983, **76**, L47.
3. Hay, R. W. and Piplani, D. P., *J. Chem. Soc., Dalton Trans.*, 1977, 1956.
4. Hay, R. W., Piplani, D. P. and Jeragh, B., *J. Chem. Soc., Dalton Trans.*, 1977, 1951.
5. (a) Nakamoto, K., *Infrared Spectra of Inorganic and Coordination Compounds*. Wiley, New York, 1963; (b) Burger, K., *Coordination Chemistry: Experimental Methods*. Academiai Kiado, Budapest, 1973.

Pergamon

PII: S0277-5387(97)00466-X

Polyhedron Vol. 17, No. 10, pp. 1617–1620, 1998
© 1998 Elsevier Science Ltd
All rights reserved. Printed in Great Britain
0277-5387/98 $19.00+0.00

Electronic spectrum and crystal structure of *fac*-$MoOCl_3$(dppe)

Ralph A. Isovitsch, Frank R. Fronczek and Andrew W. Maverick*

Department of Chemistry, Louisiana State University, Baton Rouge, LA 70803-1804, U.S.A.

(Received 4 August 1997; accepted 10 November 1997)

Abstract—X-ray analysis of the oxomolybdenum(V) complex $MoOCl_3$(dppe) (dppe = 1,2-bis(diphenylphosphino)ethane) shows that it is the facial isomer. ($C_{26}H_{24}Cl_3MoOP_2$, space group $P2_1/n$, $a = 13.217(1)$, $b = 12.8935(8)$, $c = 16.0578(9)$ Å, $\beta = 99.967(5)°$, $V = 2695.1(6)$ Å^3, $Z = 4$, $R = 0.038$ for 6228 data with $I > 1\sigma(I)$.) The electronic absorption spectrum of the title compound is also compared with those of other oxomolybdenum(V) complexes. © 1998 Elsevier Science Ltd. All rights reserved

Keywords: crystal structure; molybdenum oxo complex; phosphine complex; electronic absorption spectrum.

Many oxomolybdenum(V) complexes are green in color; a simple example is *trans*-$MoOCl_4(H_2O)^-$, which shows maxima in its electronic absorption spectrum at 712 and 445 nm in HCl(aq.) [1]. Closely related species such as the square-pyramidal $MoOCl_4^-$ [2], and a variety of ligand-substitution products [3], are also green. We have recently studied the photochemistry of oxomolybdenum(V) in the presence of phosphines [4]. Although the initial solutions in these experiments, which are believed to contain $MoOCl_4L^-$ (L = PEt_2Ph, $PEtPh_2$, PPh_3), are also green, they turn deep red-brown on visible and near-UV irradiation. We proposed that this color is due to complexes of the type $MoOCl_3L_2$, but we were unable to isolate the products in pure form, and there are few data on this type of complex in the literature. We now report the identification of the dppe (dppe = $Ph_2PCH_2CH_2PPh_2$) example, $MoOCl_3$(dppe), as the facial isomer by X-ray crystallography; its electronic spectral properties are also discussed herein.

EXPERIMENTAL

Reagents and chemicals

$MoOCl_3$(dppe) was prepared as a microcrystalline brick-red powder according to the method used for the red form of the complex by Butcher and Chatt [6]. Wedge-shaped crystals suitable for X-ray analysis were isolated by layering a saturated CH_2Cl_2 solution of $MoOCl_3$(dppe) with diethyl ether. These crystals appeared orange-brown in transmitted light. Thinner crystals were deep red in one polarization and lighter orange-brown in the other polarization. IR: 944 cm^{-1} (ν_{MoO}). Anal: Calcd for $C_{26}H_{24}Cl_3OMoP_2$: C, 50.64; H, 3.92; Cl, 17.25. Found: C, 50.50; H, 4.18; Cl, 17.51.

Instrumentation

A Perkin–Elmer 1760X spectrometer was used to record FT-IR spectra; samples were thin films or KCl pellets. Electronic absorption spectra were recorded on an Aviv 14DS spectrophotometer. Fluorescence measurements utilized a Spex Fluorolog 2 Model F112X instrument, with Hamamatsu R406 (S-1) PMT.

X-ray crystallography

Diffraction data were collected on an Enraf-Nonius CAD4 diffractometer fitted with Mo-$K\alpha$ source and graphite monochromator, using the θ-2θ scan method. The intensities were corrected for absorption using ψ scan data for five reflections. The MoLEN [5] set of programs was used for structure solution and refinement. Selected bond distances and angles are presented in Table 1.

* Author to whom correspondence should be addressed.

Table 1. Selected bond lengths (Å) and angles (°) for $MoOCl_3(dppe)$

Mo1—P1	2.5839(7)	P1—C3	1.812(2)
Mo1—P2	2.5900(7)	P1—C9	1.815(3)
Mo1—Cl1	2.4790(6)	P2—C2	1.819(2)
Mo1—Cl2	2.3558(9)	P2—C15	1.816(2)
Mo1—Cl3	2.3567(8)	P2—C21	1.808(3)
Mo1—O1	1.674(2)	C1—C2	1.530(4)
P1—C1	1.827(3)		

P1—Mo1—P2	79.88(2)	P2—Mo1—O1	91.41(7)
P1—Mo1—Cl1	80.80(2)	Cl1—Mo1—Cl2	88.61(3)
P1—Mo1—Cl2	94.10(3)	Cl1—Mo1—Cl3	93.24(2)
P1—Mo1—Cl3	169.21(3)	Cl1—Mo1—O1	160.00(7)
P1—Mo1—O1	82.22(7)	Cl2—Mo1—Cl3	94.74(3)
P2—Mo1—Cl1	75.27(2)	Cl2—Mo1—O1	103.12(7)
P2—Mo1—Cl2	163.45(2)	Cl3—Mo1—O1	101.73(7)
P2—Mo1—Cl3	89.93(3)		

Crystal data: brown-orange wedge, $0.50 \times 0.42 \times 0.15$ mm; $C_{26}H_{24}Cl_3MoOP_2$; $a = 13.217(1)$, $b = 12.8935(8)$, $c = 16.0578(9)$ Å, $\beta = 99.967(5)^\circ$ (296 K); monoclinic, space group $P2_1/n$, $Z = 4$; 25 reflections ($12^\circ \leqslant \theta \leqslant 21^\circ$) used for unit cell definition; $-18 \leqslant h \leqslant 0$, $-18 \leqslant k \leqslant 0$, $-22 \leqslant l \leqslant 22$, $\theta_{max} = 30^\circ$; transmission factors 0.8102–0.9997 used for absorption correction; 9288 reflections measured, 7829 unique reflections ($R_{int} = 0.031$), 6228 reflections with $I > 1\sigma(I)$; $R = 0.038$, $R_w = 0.039$ for 299 parameters ($R = \Sigma\|F_o| - |F_c\|/\Sigma|F_o|$, $R_w = \sqrt{(\Sigma w(|F_o| - |F_c|)^2/\Sigma wF_o^2)}$; $w = 4F_o^2/(\sigma^2(I) + (0.02F_o^2)^2)$.

RESULTS AND DISCUSSION

$MoOCl_3(dppe)$ was first reported by Butcher and Chatt in 1971 [6]. Its magnetic moment was close to the value for one unpaired electron, suggesting a simple monomeric structure. They isolated red and brown forms of $MoOCl_3(dppe)$, with the red form turning brown on refluxing in 2-propanol for 3 h. The properties of these two forms were reported to be similar, the major difference being that the ν_{MoO} of the red isomer was 941 cm^{-1} and that of the brown was 952 cm^{-1}. Levason *et al.*, in their study of oxomolybdenum(IV) and -(V) complexes with diphosphine, diarsine and arsine-phosphine ligands, first reported the solution and solid state electronic absorption spectrum of the red form of $MoOCl_3(dppe)$ as well as those of other $MoOCl_3(L\text{-}L)$ complexes [7]. They did not prepare the brown form of $MoOCl_3(dppe)$, but they did isolate red and brown forms of a similar complex, $MoOCl_3(cis\text{-}Ph_2PCH{=}CHPPh_2)$, and noted that the differences in IR and electronic absorption spectra of these two forms were small. Herbowski reported an alternative procedure for the brown isomer of $MoOCl_3(dppe)$ and reported its IR and electronic absorption spectra [8]. His reported value for ν_{MoO} was in accord with that of Butcher and Chatt, but his electronic absorption data disagreed with those of Levason *et al.* [7]. Dziegielewski and Filipek [9] studied the red isomer of $MoOCl_3(dppe)$, but their electronic absorption data were also different from those of Levason *et al.* We find that the IR and UV-vis spectral properties of the compound agree closely with those originally reported by Levason and co-workers.

$MoOCl_3(dppe)$ is stable to dry air and light in the solid state and as a solution in CH_2Cl_2, $CHCl_3$ and CH_3CN. The infrared spectrum of this complex shows ν_{MoO} at 944 cm^{-1}, which corresponds well to the value reported by Butcher and Chatt [6] and Levason *et al.* [7] (941 cm^{-1}). We attempted to prepare the brown form of $MoOCl_3(dppe)$ by the literature method [6], but we obtained only material that was spectroscopically identical to that of the red form.

The deep red color of $MoOCl_3(dppe)$ in the solid and in solution is mainly due to an intense band in the middle of the visible region. Solutions in CH_3CN (Fig. 1) show this absorption at 495 nm ($\varepsilon = 1670$ M^{-1} cm^{-1}), and also a shoulder at ca 670 nm ($\varepsilon \sim 45$). The lower-energy band is likely to be due to a simple *d-d* transition similar to that in the "molybdenyl" ion [1]. The intensity of the 495-nm band suggests substantial charge-transfer character. For example, LMCT transitions are expected to occur at lower energy in Mo(V) than in Re(V), since the d_{xy} orbital in Mo(V) is half-occupied (vs fully occupied in Re(V)).

The distinctive absorption spectrum for $MoOCl_3(dppe)$ as compared to other oxomolybdenum(V) complexes, and discrepancies in the literature data for the compound, led us to an interest in confirming its structure. We were also interested in the compound as a model for the photochemical processes we were investigating in the Mo(V)/PR_3 systems. (Interestingly, although a number of other Mo(V) complexes $MoOCl_4L^-$ [L = H_2O and CH_3CN

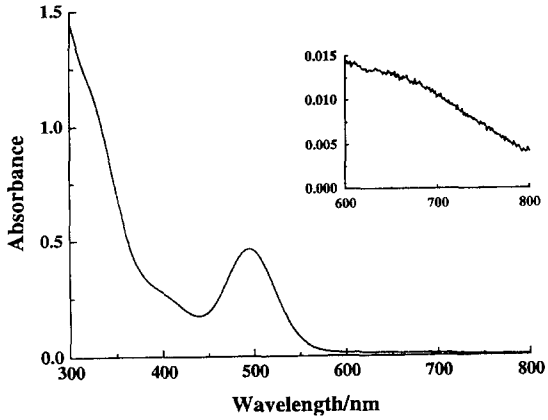

Fig. 1. Electronic absorption spectrum of a 0.0013 M solution of $MoOCl_3$ (dppe) in CH_3CN. Inset shows expanded view of 600–800 nm region.

[3a], and several phosphines [4] are fluorescent in solution at room temperature, we were unable to detect fluorescence from either solid $MoOCl_3$(dppe) or its solutions.)

Figure 2 is an ORTEP [10] drawing of $MoOCl_3$(dppe), which has the facial geometry. Molecules of $MoOCl_3$(dppe) show equatorial Mo—Cl bond lengths (see Table 1) that are indistinguishable from those observed in $(AsPh_4)[MoOCl_4(H_2O)]$ (2.359(3) Å) [11]. One of the characteristic features of metal-oxo complexes, a longer bond trans to the oxo group, is followed here (Mo—Cl1, 2.4790(6) Å). (For example, in the structure of $K_2[MoOCl_5]$, the axial Mo—Cl distance is ca 0.20 Å longer than the equatorial [12].) The two Mo—P bond lengths (Mo—P1 and Mo—P2) are similar. The Mo≡O bond length, 1.674(2) Å, falls into the normal range for terminal Mo≡O bonds in six-coordinate complexes (1.65–1.70 Å) [13].

As far as we are aware, only two *fac*-MOX_3L_2 (L = monodentate phosphine) complexes have been structurally characterized: *fac*-$ReOCl_3(PEt_2Ph)_2$ and the isostructural bromide. A search of the Cambridge Structural Database [15] yielded only one example of a MOX_3L_2 complex with M = group 6 metal: $WOCl_3(PEt_3)_2$, which has the *trans-mer* geometry [16]. The other examples are all rhenium complexes: *fac*-$ReOCl_3$(dppe) (which is isostructural with the present complex) [17], *trans-mer*-$ReOCl_3(PEt_2Ph)_2$ [18], *trans-mer*-$ReOCl_3(PPh_3)_2$ [19], and $ReOI_2Cl(PPh_3)_2$ (also *mer*, with I *trans* and PPh_3 *trans*) [20].

The present work establishes that $MoOCl_3$(dppe), like $ReOCl_3$(dppe), has the facial geometry. This is one of the two geometries that have been observed for analogous complexes $MOX_3(PR_3)_2$ of monodentate phosphines, the other being *trans-mer*. The product of the Mo(V)-PPh_3 photochemical reaction may be *fac*-$MoOCl_3(PPh_3)_2$, as suggested by the strong spectral similarities between it and $MoOCl_3$(dppe), but the *trans-mer* isomer cannot be ruled out. What is clear, on the other hand, is that simple substitution *trans* to the oxo group in *trans*-$MoOCl_4L^-$ cannot account for the formation of either *fac*- or *trans-mer*-$MoOCl_3(PPh_3)_2$. Instead, the phosphines in $MoOCl_3(PPh_3)_2$ are likely to be *cis* to the oxo group. This makes it likely that the initial photosubstitution reaction of Mo(V) with PPh_3 is also *cis*.

A structural comparison can be made between these MOX_3L_2 complexes and the quadrivalent MOX_2L_3 (L = phosphine) complexes. The only structurally characterized examples in the latter group appear to be of Mo(IV) and W(IV), all with the *cis-mer* geometry: $MoOCl_2(PMe_2Ph)_3$ [21], $MoOCl_2(PEt_2Ph)_3$ [22], $MoOCl_2(PMe_3)_3$ [23], and $MoOCl_2(PMePh_2)_3$ and $MoO(NCO)_2(PEt_2Ph)_3$ [24]; and $WOCl_2(PMe_3)_3$ [25], $WOCl_2(PMe_2Ph)_3$ [26], and $WOBr_2(PMe_2Ph)_3$ and $WOBr_2(PMePh_2)_3$ [27]. Although the nomenclature is different for the preferred products in $M^VOX_3L_2$ (*fac* and *trans-mer*) and

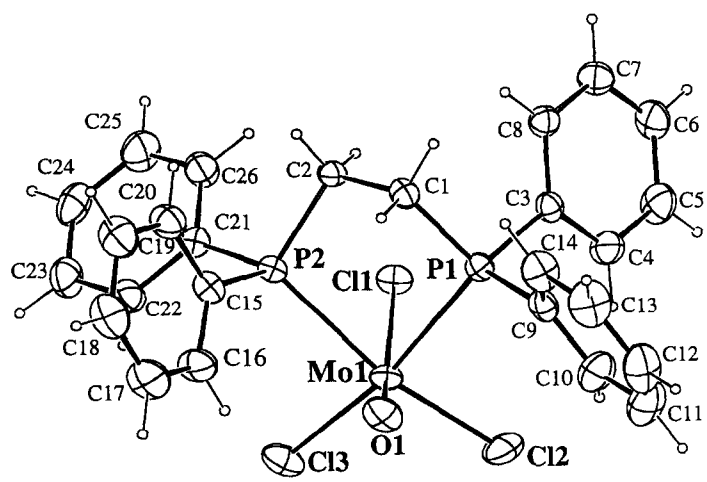

Fig. 2. ORTEP [10] drawing of $MoOCl_3$(dppe). Hydrogen atoms omitted for clarity.

$M^{IV}OX_2L_3$ (*cis-mer*), this is mainly because different ligands are used to identify the isomer (O and two L in M(V); O and two X in M(IV)). There is an important structural feature in common between the two oxidation states: in all of the crystallographically characterized examples so far, only the X ligand binds trans to the oxo group. (This is as expected if the best arrangement in both cases is with the stronger-field phosphine ligands *cis* to the oxo group, and a halide ligand in the *trans* position.)

Both the homogeneity of the title compound (as judged by its color and IR spectrum) and the previously published X-ray data (which include no examples of *cis-mer*-$M^{V}OX_3$(phosphine)$_2$ complexes) suggest that our samples of $MoOCl_3$(dppe) contain only the facial isomer.

Summary

The molybdenum(V) oxo complex $MoOCl_3$(dppe) has been determined by X-ray analysis to contain the facial isomer. Its electronic spectrum is very similar to that previously reported by Levason and co-workers [7] for the "red form" of the compound. It is also similar to those produced on irradiation of oxomolybdenum(V) in the presence of PEt_2Ph, $PEtPh_2$, and PPh_3 [4].

Acknowledgment—Improvements to the LSU X-ray Crystallography Facility were supported by Grant No. LEQSF(1996-97)-ENH-TR-10 administered by the Louisiana Board of Regents.

REFERENCES

1. (a) Jørgensen, C. K., *Acta Chem. Scand.*, 1957, **11,** 73–85; (b) Hare, C. R., Bernal, I and Gray, H. B., *Inorg. Chem.*, 1962, **1,** 831–835; (c) Carducci, M. D., Brown, C., Solomon, E. I. and Enemark, J. H., *J. Am. Chem. Soc.*, 1994, **116,** 11856–11868.
2. Garner, D., Hill, L. H., Mabbs, F. E., McFadden, D. L. and McPhail, A. T., *J. Chem. Soc., Dalton Trans.*, 1977, 853–858.
3. See, for example, (a) $MoOCl_4(CH_3CN)^-$: Mohammed, A. K. and Maverick, A. W., *Inorg. Chem.*, 1992, **31,** 4441–4443; (b) [(1,4,7-trimethyl-1,4,7-triazacyclononane)$MoOCl_2$]$^+$: Backes-Dahmann, G., Herrmann, W., Wieghardt, K. and Weiss, J., *Inorg. Chem.*, 1985, **24,** 485–491.
4. Isovitsch, R. A., Fronczek, F. R. and Maverick, A. W. submitted for publication.
5. Fair, C. K., *MolEN: An Interactive Structure Solution Procedure*. Enraf-Nonius, Delft, The Netherlands, 1990.
6. Butcher, A. V. and Chatt, J., *J. Chem. Soc. (A)*, 1971, 2356–2358.
7. Levason, W., Mcauliffe, C. A. and Sayle, B. J., *J. Chem. Soc., Dalton Trans.*, 1976, 1177–1181.
8. Herbowski, A., *Inorg. Chim. Acta*, 1981, **54,** L121–L122.
9. Dzięgielewski, J. O. and Filipek, K., *Polyhedron*, 1991, **10,** 1459–1463.
10. Johnson, C. K. *Ortep-II: A Fortran Thermal-Ellipsoid Plot Program for Crystal-Structure Illustrations*. Report ORNL-5138, National Technical Information Service, U.S. Department of Commerce, Springfield, VA, 1976.
11. Garner, C. D., Hill, L. H., Mabbs, F. E., McFadden, D. L. and McPhail, A. T., *J. Chem. Soc., Dalton Trans.*, 1977, 1202–1207.
12. Tkachev, V. V., Krasochka, O. N. and Atovmyan, L. O., *Zh. Strukt. Khim.*, 1976, **17,** 940–941.
13. Nugent, W. A. and Mayer, J. M., *Metal-Ligand Multiple Bonds*. John Wiley & Sons, New York, 1988.
14. Sergienko, V. S. and Porai-Koshits, M. A., *Doklady Phys. Chem.*, 1989, **309,** 978–981.
15. Allen, F. H., Kennard, O. and Taylor, R., *Acc. Chem. Res.*, 1983, **16,** 146–153.
16. Britton, D., Macomber, D. W. and Gassman, P. G., *Cryst. Struct. Commun.*, 1982, **11,** 1501–1505.
17. Sergienko, V. S., *Koord. Khim.*, 1994, **20,** 932–936; *Chem. Abstr.*, 1995, **123,** 213874h. Coordinates for this structure were obtained via the Cambridge Structural Database (Refcode BEZDOZ10) [15].
18. Ehrlich, H. W. W. and Owston, P. G., *J. Chem. Soc.*, 1963, 4368–4372.
19. Lebuis, A.-M. and Beauchamp, A. L., *Can. J. Chem.*, 1993, **71,** 441–449.
20. Rossi, S., Bélanger, S., Lebuis, A.-M. and Beauchamp, A. L., *Acta Crystallogr., Sect. C*, 1993, **C49,** 1498–1500.
21. (a) Manojlović-Muir, L., *J. Chem. Soc. (A)*, 1971, 2796–2800; (b) Yoon, K., Parkin, G., and Rheingold, A. L., *J. Am. Chem. Soc.*, 1991, **113,** 1437–1439; (c) Desrochers, P. J., Nebesny, K. W., LaBarre, M. J., Lincoln, S. E., Loehr, T. M. and Enemark, J. H., *J. Am. Chem. Soc.*, 1991, **113,** 9193–9200; (c) Yoon, K., Parkin, G. and Rheingold, A. L., *J. Am. Chem. Soc.*, 1992, **114,** 2210–2218.
22. Manojlović-Muir, L. and Muir, K. W., *J. Chem. Soc., Dalton Trans.*, 1972, 686–690.
23. Yoon, K., Parkin, G. and Rheingold, A. L., *J. Am. Chem. Soc.*, 1991, **113,** 1437–1438.
24. Cotton, F. A., Diebold, M. P. and Roth, W. J., *Inorg. Chem.*, 1987, **26,** 2848–2852.
25. Chiu, K. W., Lyons, D., Wilkinson, G., Thornton-Pett, M. and Hursthouse, M. B., *Polyhedron*, 1983, **2,** 803–810.
26. Yoon, K., Parkin, G., Hughes, D. L. and Leigh, G. J., *J. Chem. Soc., Dalton Trans.*, 1992, 769–773.
27. Cotton, F. A. and Mandal, S. K., *Inorg. Chim. Acta*, 1992, **194,** 179–187.

Pergamon

PII: S0277-5387(97)00465-8

Polyhedron Vol. 17, No. 10, pp. 1621–1625, 1998
© 1998 Elsevier Science Ltd
All rights reserved. Printed in Great Britain
0277-5387/98 $19.00+0.00

Homogeneous catalysis of the water-gas shift reaction by copper complexes in aqueous substituted pyridine solutions

Marta Mediavilla,[a] Doris Pineda,[a] Francisco Lopez,[b] Delfin Moronta,[c] Clementina Longo,[d] Sergio A. Moya,[e,*] Pablo J. Baricelli[b,*] and Alvaro J. Pardey[a,*]

[a] Escuela de Química, Facultad de Ciencias, Universidad Central de Venezuela, Apartado 47102, Caracas, Venezuela

[b] Centro de Investigaciones Químicas, Facultad de Ingeniería, Universidad de Carabobo, Valencia, Estado Carabobo, Venezuela

[c] Laboratorio de Paramagnetismo, Escuela de Física, Facultad de Ciencias, Universidad Central de Venezuela, Caracas, Venezuela

[d] Facultad de Farmacia, Universidad Central de Venezuela, Caracas, Venezuela

[e] Departamento de Química Aplicada, Facultad de Química y Biología, Universidad de Santiago de Chile, Casilla 40, Santiago 33, Chile

(Received 21 July 1997; accepted 10 November 1997)

Abstract—Homogeneous catalysis of the water-gas shift reaction has been accomplished by the use of solutions of $CuCl_2 \cdot 2H_2O$ in aqueous pyridine and other substituted pyridine (methyl pyridines or dimethylpyridine) solutions. This system is stable, low active catalyst displaying turnover frequencies for hydrogen production ($TF(H_2)$) of about 6 moles H_2 per mole Cu per day for [Cu] = 20 mM, P(CO) = 1.9 atm and $T = 120°C$.
© 1998 Elsevier Science Ltd. All rights reserved

Keywords: WGSR; homogeneous catalysis; copper complexes.

The water-gas shift reaction (WGSR, eqn (1)) $\Delta G^{\circ} = -28.5$ kJ mol^{-1} (298°K) is an important chemical transformation that find industrial applications in hydrogen production, carbon monoxide removal, and adjustment of CO : H_2 ratios in synthesis gas [1].

$$CO + H_2O \rightleftarrows CO_2 + H_2 \quad (1)$$

Previous studies by different groups have demonstrated WGSR catalysis by different soluble transition metal complexes [2–23]. For example $RhCl_3 \cdot 3H_2O$ dissolved in pyridine and other methylpyridines have been reported as stable and moderately active WGSR catalyst displaying turnover frequencies for hydrogen production ($TF(H_2)$) of about 10^2 moles of H_2 per mole Rh per day for [Rh] = 10 mM, P(CO) = 0.9 atm and $T = 100°C$ with Ea = value ~ 11.5 kcal mol^{-1} deg^{-1}. This studies was conducted in both, batch reactor [16,22] and continuous flow reactor [18]. In the course of continuing to explore similar system in these laboratories it became matter of interest to study an homogeneous copper system because is known that the most commercial active heterogeneous catalyst for the WGSR contained a mixture of copper and zinc oxide [1]. Described here is a study of the WGSR catalysis by a system formed by dissolving $CuCl_2 \cdot 2H_2O$ in aqueous solutions of pyridine and other substituted pyridines.

* Author to whom correspondence should be addressed. Fax: 58-41-673615 (PJB), apardey@strix.ciens.ucv.ve and smoya@lauca.usach.cl

EXPERIMENTAL

Materials

Pyridine, methylpyridines (4-picoline, 3-picoline and 2-picoline) and dimethylpyridine (2,6-lutidine) were obtained from Aldrich and distilled over KOH. Copper(II) dichloride was obtained from Merck. All gases and gas mixtures CO, N_2, He/H_2 (91.4/8.6%), CO/CH_4 (94/6%), $CO/CH_4/CO_2/H_2$ (84.8/5.1/5.3/4.8%) were purchased from BOC Gases and used as received. Water was doubly distilled.

Instrumentation

Infrared spectra were recorded on a Perkin–Elmer 1769X-FT spectrophotometer using NaCl for solutions samples. UV-visible spectra were recorded on a Perkin–Elmer 533 spectrophotometer in 1.0 cm (Precision) quartz cell. EPR experiments were carried out in a conventional Varian E-line X-band spectrometer, using a rectangular cavity operating in the TE 102 mode. Analysis of gaseous reactants and products were carried out on a Hewlett-Packard 5890 Series II programmable (ChemStation) gas chromatograph fitted with a thermal conductivity detector. The column used was Carbosieve-B, 80–10 mesh, (Hewlett-Packard). The column temperature was programmed from 60–175°C at a flow rate of 50 ml min^{-1} using a He/H_2 (91.4/8.6%) mixture as carrier gas. Calibration curves were prepared periodically for H_2, CO, CO_2, and CH_4. The individual analysis were found to be accurate and reproducible within $< \pm 10\%$.

Batch reactor procedures

Catalytic runs were conducted in all-glass reactor vessels consisting of round bottom flask (100–200 ml) connected to an "O" ring sealed joint to a two-way Rotoflow Teflon stopcock attached to the vacuum line [16,21]. In a typical catalytic run, copper salt and solvent system were added to the glass reactor vessel, then the solution was degassed by three freeze-pump-cycles. The reaction vessel was charged with CO/CH_4 (94/6%) mixture at the P(CO) = 1.5 atm at R.T. (equaled 1.9 atm at 120°C) and placed in a thermostatted glycerol oil bath at 120 ± 0.5°C. Gas samples of 1.0 ml were periodically removed from the reaction vessel at bath temperature, analyzed by gas chromatography and corrected for small background signals. Methane was used as internal standard, thus allowing the calculation of absolute quantities of consumed CO and produced H_2 and CO_2. The reaction vessel was periodically flushed and loaded with the CO/CH_4 mixture as described above.

RESULTS AND DISCUSSION

Catalysis studies of the WGSR

Catalysis runs were carried out for [Cu] = 20 mM prepared from $CuCl_2 \cdot 2H_2O$ with P(CO) = 1.9 atm in various aqueous/pyridine or substituted pyridine solutions (8/2 v/v amine/water) over temperature of 120°C. Quantitative analysis of gas samples taken after the reaction solution reached working temperature, indicated that production of H_2 and CO_2 and consumption of CO follow the stoichiometry shown in eqn (1). The active solutions have undergone some buffering owing to CO_2 produced and the subsequent formation of carbonates. The shift in basicity was probed by determining the resulting solution pH with a Denver model Acumet Basic pH-meter. A freshly prepared solution of $CuCl_2 \cdot 2H_2O$ in 80% aqueous 4-picoline gave a pH of 8.00 while aged catalytic solution gave lower pH value 7.48 ± 0.05. Figure 1 displays the production of H_2 for catalytic runs in different amines over a period of several hours. These plots show no discontinuities which means that catalytic activity is constant for the aged solutions. This activities defined as turnover frequency (TF = moles of product H_2 or CO_2/(g-atom. wt. of Cu)/(24 h)) are summarized in Table 1. The TF values for this copper/amine system proved to be dependent of the nature of the amine. The TF values were measured for different copper-substituted pyridine, in order to show the dependence of the catalytic activity on the nature of the organic cosolvent. Slight differences were noted for those pyridine monomethylated in β or γ positions and relative high differences were observed for the systems with α-substituted amine. A plot of log of $TF(H_2)$/day values vs pK_a of the protonated bases is shown in Fig. 2.

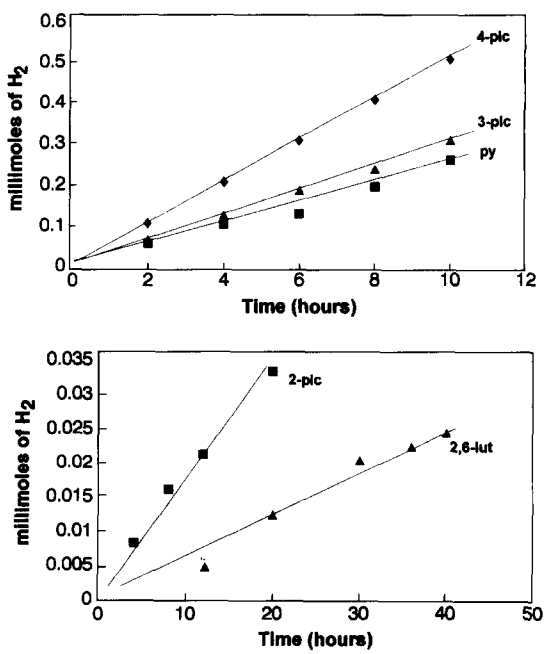

Fig. 1. Total H_2 produced as a function of time by a solution prepared from 0.2 mmol $CuCl_2 \cdot 2H_2O$ in 10 ml substituted pyridine/water solutions (8/2) under 1.9 atm CO at 120°C. Upper figure: reactions in sterically unhindered pyridines; lower figure: reactions in 2-picoline and 2,6-lutidine.

Table 1. WGSR activities by $CuCl_2 \cdot 2H_2O$ in aqueous pyridine and substituted pyridine[a]

Amine	pK_a[b]	TF(H_2)day[c]
4-picoline	6.00	6.1
3-picoline	5.52	4.1
pyridine	5.27	3.1
2-picoline	5.97	2.0
2,6-lutidine	6.75	1.2

[a] P(CO) = 1.9 atm, T = 120°C; [Cu] = 20 mM; 10 ml of solution amine/water, 8/2, v/v.

[b] From [24].

[c] Mol H_2/(g-atom. wt of Cu)/(24 h). Experimental uncertainty is about ± 10%.

Linearity is approximately followed in the case of nonhindered bases; also the slope indicates a minor basicity effects on catalytic activity. However, increasing steric effects effectively lower the reaction rates. Since methyl substitution in α position on the heterocyclic amine lowers the catalytic activity, coordination of the amine to the copper apparently plays an important role in determining the activity of these catalysts. Thus, it appears likely that in these media the hetero-aromatic amine behaves as a ligand as well as Brönsted base. These results suggest a critical steric parameter which can be viewed as the effects of competition for binding to the catalytic metal center, which is affected more by steric constraints than by electronic effects. The above observations are in agreement with earlier report on the depression of catalytic activity of $RhCl_3 \cdot 3H_2O$/amine system was depressed by the presence of a methyl substituent on the nitrogen of the amine.

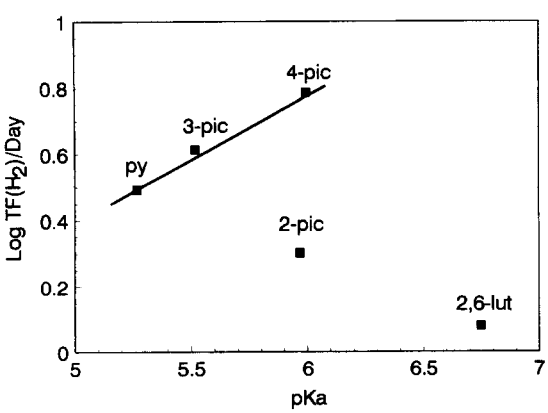

Fig. 2. Plot of log of TF(H_2)/day values vs pK_a of the protonated base for the sterically and nonsterically hindered pyridines.

Spectroscopic studies of catalyst solutions

Dissolution of $CuCl_2 \cdot 2H_2O$ (0.034 g, 0.20 mmol) in 10 ml of 80% aq. amine (amine = 4-picoline, 3-picoline, 2-picoline, pyridine or 2,6-lutidine) at room temperature leads to the gradual formation of a blue solution due to the formation of $CuCl_2(amine)_2$ and/or $CuCl_2(amine)_4$ [25,26]. After charging Cu/4-picoline blue solution with CO (1.5 atm) and heating the reaction vessel in a 120°C glycerol bath, this solution first changed to a green color, then (over 1–5 min) to a final red-brown color characteristic of a mature catalyst solution. Very similar color changes were seen when the solvent was 80% aqueous 2-picoline or 2,6-lutidine, but some differences were seen with pyridine or 3-picoline, which gave a final orange color solutions after similar treatment. For the Cu/aq. 4-picoline, the electronic absorption spectra of the red-brown solution noted above displayed a broad rinsing absorption from > 500 nm with a well defined shoulder at approximately 450 nm (Table 2). The electronic spectra of the red-brown solution of 2-picoline system displayed a similar shoulder shifted ~21 nm to longer wavelength, but also a weaker band at ~498 nm. The IR spectrum of the red-brown mature solution of the $CuCl_2 \cdot 2H_2O$/aq. 4-picoline or 2-picoline, systems displayed only a single peak in the CO stretching region, attributable to terminally coordinated CO (Table 2), indicating the presence of copper carbonyls complexes. These observations are similar to those of Gagne *et al.* [27]. who reported that IR spectra both in solution and in the solid state of the carbonyl adduct $Cu(LBF_2)(CO)$ (LBF = difluoro-3,3′-(trimethylenedinitrilo)*bis*(2-butanoneoximate)borate) show only one band in the ν_{CO} region (2080 cm^{-1}), characteristic of COs terminally coordinated to Cu. Similar observation was made for the compound $Cu(h^5\text{-}C_5H_5)(CO)$ which has a ν_{CO} at 2093 cm^{-1} [28]. Air exposure of the catalytic solution of the Cu/4-picoline system for several hours yields the formation of a blue color solid and a red-brown solution. The IR spectra of the blue solid and the remnant solution, each one showed no bands in the ν_{CO} region. These results reflect the non stability of the catalytic solutions to the air; that it, the copper carbonyls species present in the catalytic solutions are only stable in CO atmosphere. When the above heterogeneous system is charged with feed gases mixture, CO/CH_4, and heated to 120°C, it is observed the total dissolution of the blue solid and formation of the red-brown solution. However, catalytic activity of this recovered solution decreased by 50%. Figure 3 shows the EPR spectra of solution of $CuCl_2 \cdot 2H_2O$ in 95% aq. 4-picoline (A), and mature catalytic solution of the same system (B) in presence of CO. Calibration was made using the Varian Strong Pitch (g = 2.0028), and a diluted Mn^{2+} aq. solution. In both spectra, special care was taken in having the same amount of Cu atoms of the solutions in the cavity. The area of spectrum (A) is 4.0 times the area of (B). This indicates

Table 2. Infrared and visible spectra data of solutions resulting from reactions of $CuCl_2 \cdot 2H_2O$ in 80% aq. 4-picoline or 2-picoline solutions under CO[a]

Amine	Solution color	IR bands in the ν_{CO} region[b] (cm^{-1})	Electronic absorption bands[c] (nm)
4-picoline	red-brown	2067 (m)	451 (sh, 2343)
2-picoline	red-brown	2070 (m)	498 (sh, 72), 470 (sh,115)

[a] solvent = amine/water, 8/2, v/v, P(CO) = 1.5 atm, room temperature.
[b] (m) = medium.
[c] sh = shoulder, values in parentheses are approximate extinction coefficient in $M^{-1}\ cm^{-1}$.

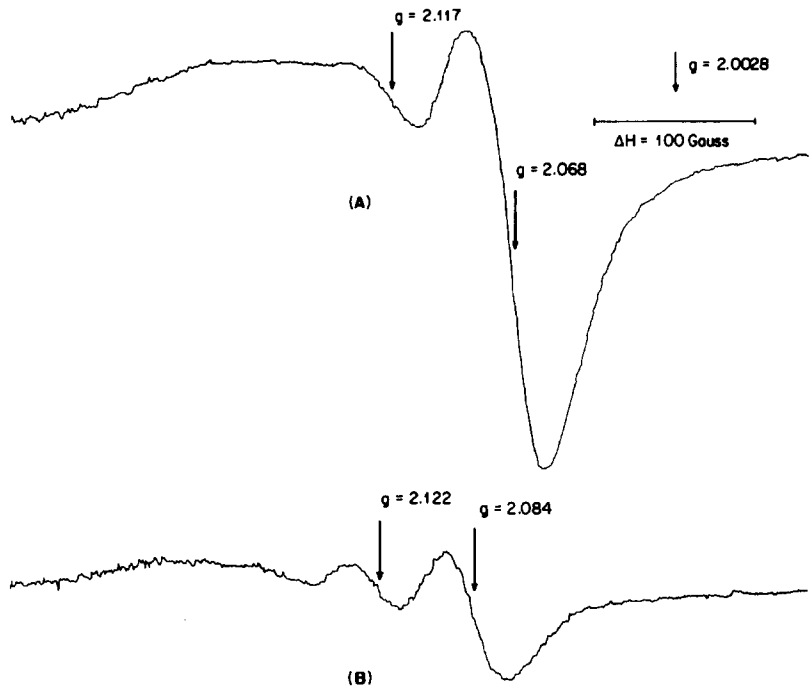

Fig. 3. EPR spectra for: (A) solution of 20 mM $CuCl_2 \cdot 2H_2O$ in 95% aq. 4-picoline (B) and mature catalytic solution of 20 mM of $CuCl_2 \cdot 2H_2O$ 95% aq. 4-picoline under P(CO) = 1.5 atm at 25°C.

the presence of copper(II) d^9 species in both solutions, but the copper(II) concentration is diminished in the mature solution. It is probably due to the reduction of Cu(II) to Cu(I) by the CO/H_2O couple. Similar results were observed for the other Cu/aq. amine systems mentioned above. Line shape and *g*-value differences between both spectra, are due to different molecular environments, and will be discussed in a forthcoming paper.

Summary

It was found that $CuCl_2 \cdot 2H_2O$ in 80% aq. amine under CO atmosphere formed a low active catalyst system for the WGSR. Among the catalyst systems studied, Cu/aq. 4-picoline was the most active. Finally the presence of terminal carbon monoxide indicated by the IR spectrum of $CuCl_2 \cdot 2H_2O$ in 80% aq. 4-picoline or 2-picoline solutions with CO under WGSR conditions as well as the EPR studies, provide strong experimental evidence of the formation of the Cu(I)—CO complex as a reaction intermediate.

Acknowledgments—The authors thanks to CONICIT-VENEZUELA (Proy. S1-2435), S.A.M. thanks to FONDECYT-CHILE, and P.J.B. thanks to CODECIHT-UC for financial support.

REFERENCES

1. Thomas, C. L., *Catalytic Processes and Proven Catalysts*. Academic Press, N.Y., 1970, p. 104.
2. Laine, R. M., Rinker, R. G. and Ford, P. C., *J. Am. Chem. Soc.*, 1977, **99**, 252.

3. Cheng, C. H., Hendriksen, D. E. and Eisenberg, R., *J. Am. Chem. Soc.*, 1977, **99,** 2791.
4. Kang, H., Mauldin, C. H., Cole, T., Slegeir, W., Cann, K. and Pettit, R., *J. Am. Chem. Soc.*, 1977, **99,** 8323.
5. Zudin, V. N., Liholobov, V. A., Yermakov, Yu. I. and Yeremenko, N. K., *Kinet. Katal.*, 1977, **18,** 524.
6. Kaneda, K., Hiraki, M., Sano, K., Imanaka, T. and Teranishi, S., *J. Mol. Catal.*, 1980, **9,** 227.
7. Ford, P. C., *Acc. Chem. Res.*, 1981, **14,** 31.
8. Laine, R. M. and Wilson, Jr., R. B., in *Aspects of Homogeneous Catalysis*, Vol. 5, ed. R. Ugo. Reidel, London, 1984, 217.
9. Collin, J. P., Ruppert, R. and Sauvaje, J. P., *Nouv. J. Chim.*, 1985, **9,** 395.
10. Mahajan, D., Creutz, C. and Sutin, N., *Inorg. Chem.*, 1985, **24,** 395.
11. Isida, H., Tanaka, K., Morimito, M. and Tanaka, T., *Organometallics*, 1986, **5,** 724.
12. Venalainen, T., Iiskola, E., Pakkanen, T. A. and Pakkanen, T. T., *J. Mol. Catal.*, 1986, **34,** 305.
13. Ford, P. C. and Rokicki, A., *Adv. Organometall. Chem.*, 1988, **28,** 139.
14. Taqui Khan, M., Halligudi, S. B. and Shukta, S., *Agnew. Chem. Int. Ed. Engl.*, 1988, **27,** 1735.
15. Laine, R. M. and Crawford, E. J., *J. Mol. Catal.*, 1988, **44,** 357.
16. Pardey, A. J. and Ford, P. C., *J. Mol. Catal.*, 1989, **53,** 247.
17. Taqui Khan, M., *Platinum Metals Rev.*, 1991, **35,** 70.
18. Lima Neto, B. S., Ford, K. H., Pardey, A. J., Rinker, R. G. and Ford, P. C., *Inorg. Chem.*, 1991, **30,** 3837.
19. Pruchnik, F. and Kluczewska-Patralek, G., *Rhodium Ex.*, 1994, **6,** 4.
20. Contreras, J., Pardey, A. and Baricelli, P., *Rhodium Ex.*, 1994, **6,** 11.
21. (a) Ungermann, C., Landis, V., Moya, S. A., Cohen, H., Walker, H., Pearson, R. G., Rinker, R. and Ford. P. C., *J. Am. Chem. Soc.*, 1979, **101,** 5922; (b) Mediavilla, M., Pardey, A. J., Baricelli, P., Longo-Pardey, C. and Moya, S. A., *Rhodium Ex.*, 1996, **15,** 9.
22. Fanchinetti, G., Fochi, G. and Funaioli. T., *Inorg. Chem.*, 1994, **33,** 1719.
23. Moya, S. A., Sariego, R., Aguirre, P., Sartori, R. and Dixneuf, P., *Bull. Soc. Chim. Belg.*, 1995, **104,** 19.
24. Schofield. K., *Hetero-Aromatic Nitrogen Compounds*. Plenum Press, New York, 1967, p. 146.
25. Frank, C. W. and Rogers, L. B., *Inorg. Chem.*, 1966, **5,** 617.
26. Van Oijen, J. A. C. and Reedijk. J., *Inorg. Chim. Acta*, 1977, **25,** 131.
27. Gagne, R. R., Allinson, J. L., Gall, R. S. and Koval, C. A., *J. Am. Chem. Soc.*, 1977, **99,** 7170.
28. Cotton, F. A. and Marks, T. J., *J. Am. Chem. Soc.*, 1970, **92,** 5114.

Pergamon

PII: S0277-5387(97)00467-1

Polyhedron Vol. 17, No. 10, pp. 1627–1630, 1998
© 1998 Elsevier Science Ltd
All rights reserved. Printed in Great Britain
0277-5387/98 $19.00+0.00

Evidence for formation of the $FeSbO_4$ phase at the surface of poreless silica

Edilson V. Benvenutti[a]* and Luci I. Zawislak[b]

[a]Instituto de Química, UFRGS, CP 15003, 91501-970, Porto Alegre, RS, Brazil

[b]Instituto de Física, UFRGS, CP 15051, 91501-970, Porto Alegre, RS, Brazil

(Received 27 May 1997; accepted 10 November 1997)

Abstract—A possible $FeSbO_4$ phase was detected at a poreless silica surface using Mossbauer spectroscopy and infrared absorption of pyridine adsorbed on the surface. The phase was obtained from $Fe(CO)_5$ as starting material, without calcination treatment. Attempts to synthesizing the $FeSbO_4$ phase using a porous silica gel, under these conditions failed. The influence of the pores on the support is discussed. © 1998 Elsevier Science Ltd. All rights reserved

Keywords: iron antimony; poreless silica; Mossbauer effect; infrared.

The $FeSbO_4$ phase produced by calcination of antimony and iron oxides at high temperatures is known to be very active in the allylic oxidation and ammoxidation of alkenes [1–8].

Recently, the synthesis and characterization of $FeSbO_4$ phases grafted onto a silica gel surface have been described as the product from an immersion of Sb/SiO_2 (antimony(V) oxide grafted onto a silica gel surface) in acid aqueous solution of iron III followed by heat treatment at 150°C [9,10], or an immersion of Sb/SiO_2 in a solution of $Fe(CO)_5$ in CCl_4 followed by hydrolysis and heat treatment at 800°C [10]. In the first case, the $FeSbO_4$ phase was formed at 150°C. This fact was explained by antimony(V) migration through the pores, from the internal to the external surface of the matrix, induced by acid medium. This mechanism was supported by XPS and Mossbauer analyses. The use of $Fe(CO)_5$ in CCl_4 has demonstrated that the $FeSbO_4$ phase is not detected at 150°C, but it appears after the heat treatment at 800°C. In this case, the high temperature treatment induces the Fe^{III} and Sb^{V} ions reaction.

In order to gain a better understanding of the mechanism involved in the $FeSbO_4$ phase formation on silica gel surface, the Sb/SiO_2 was synthesized using a poreless silica (aerosil). In this case, the $FeSbO_4$ phase formation will not depend on the migration mechanism of Sb^{V} ions through the pores, so this phase is expected to be formed from a solution of $Fe(CO)_5$ in CCl_4, at 150°C. Evidence for the formation of the $FeSbO_4$ phase were detected using FT-IR spectroscopy with pyridine as probe molecule, and by Mossbauer spectroscopy.

EXPERIMENTAL

Sb/SiO_2 (*Antimony oxide grafted on SiO_2*)

Fumed silica (aerosil) was activated at 150°C *in vacuo* (10^{-1} Pa). The $SbCl_5$ (Carlo Erba) (1 cm^3), previously distilled in a Schlenk apparatus, was dissolved in CCl_4 (Merck) (50 cm^3), dried above 0.4 nm molecular sieves. The activated silica (8.5 g) was then added. The mixture was stirred for 6 h under argon at solvent-reflux temperature. The resulting modified silica was filtered under argon in a Schlenk apparatus, washed with CCl_4 to eliminate unreacted $SbCl_5$ and trapped HCl, and finally degassed. The hydrolysis of the grafted $SbCl_5$ was carried out under a flux of wet air for 16 h, then washed with twice-distilled water and finally dried for 5 h under vacuum (10^{-1} Pa) at 150°C.

* Author to whom correspondence should be addressed.

The equations describing the reaction can be written as

$$n{\equiv}SiOH + SbCl_5 \rightarrow ({\equiv}SiO)_nSbCl_{5-n} + (5-n)HCl$$

$$({\equiv}SiO)_nSbCl_{5-n} + (5-n)H_2O \rightarrow ({\equiv}SiO)_nSb(OH)_{5-n} + (5-n)HCl,$$

where ≡SiOH represents a free silanol group on the silica surface. The resultant material $({\equiv}SiO)_n Sb(OH)_{5-n}$, obtained by this procedure was designated as Sb/SiO_2.

$Fe/Sb/SiO_2$ (*Iron^{III} oxide dispersed on* Sb/SiO_2). Approximately 4 g of Sb/SiO_2 and 0.5 cm^3 of $Fe(CO)_5$ were added to 30 cm^3 of CCl_4. The mixture was refluxed for 4 h under argon atmosphere. The subsequent solid was filtered off and washed with CCl_4 under argon atmosphere and degassed at 150°C. The resulting black material was exposed to water vapour from the air for 1 day giving the yellow Iron^{III} oxide dispersion and washed with water. The resulting material was dried 5 h at 150°C *in vacuo* (10^{-1} Pa).

IR analyses. The sorption of pyridine vapour by $Fe/Sb/SiO_2$ was studied by IR spectroscopy. Reagent-grade pyridine (Merck) was previously dried over 0.4 nm molecular sieves and submitted to various freeze–pump–thaw cycles. A self supporting disk of $Fe/Sb/SiO_2$ with an area of 5 cm^2 and weight of 50 mg, was prepared. The cell used was connected to a greaseless vacuum line and the system was pumped for 1 h at a pressure of 10^{-3} Pa at 150°C. After this treatment the pyridine was introduced into the cell at a pressure of 1.6 Pa at room temperature. The FT-IR equipment used was a Mattson, model 3020. The spectra were obtained after 100 scans, with a resolution of 4 cm^{-1}.

Mossbauer analyses The Mossbauer spectra were obtained in a standard transmission geometry, using a constant acceleration electromechanical drive system with a multichannel analyzer for collecting and storing the data. A source of ^{57}Co in a rhodium matrix was used at room temperature. The velocity scale and magnetic field were calibrated using metallic iron. Measurement at 4.2 K were done with the sample immersed in liquid helium.

Chemical analyses The antimony and iron analyses were carried out on a Rigaku RIX 2000 X-Ray Fluorescence Spectrometer. The quantities of Sb and Fe determined were (in wt%) Sb = 2.3% ; Fe = 3.0%.

RESULTS

IR analyses

The spectra of $Fe/Sb/SiO_2$ submitted to 1.6 kPa of pyridine are shown in Fig. 1. The bands at 1595 and 1444 cm^{-1} (Fig. 1a) are due to the 8a and 19b modes of pyridine bonded to the free silanol ≡SiOH groups through hydrogen bonds [11–13]. These bands were also observed in the pure silica and disappear after heating the disk *in vacuo*. Figure 1b shows the infrared spectrum after having pumped off the material for 1 h at 100°C with two bands at ca 1600 cm^{-1} (broad) and 1447 cm^{-1}, respectively, in consistency with the 8a and 19b modes of pyridine coordinated to Lewis acid sites in the $FeSbO_4$ phase supported on silica surface [10]. After further pumping (2 h) at the same temperature (100°C) it can be observed that the broad band at ca 1600 cm^{-1} resolves into two bands (1600 and 1612 cm^{-1}) (Fig. 1c). The band at 1612 cm^{-1} becomes more defined after heating the disk at 200°C *in vacuo* (10^{-3} Pa) for 1 h (Fig. 1d). The bands 1612 and 1451 cm^{-1} that remain in the spectrum (Fig. 1d), were assigned to the 8a and 19b modes of pyridine coordinated to iron^{III} oxide [14] (see Table 1). The band at ca 1489 cm^{-1} is due to the 19a mode and always present for all kinds of pyridine adsorption [15].

Mossbauer analyses

The Mossbauer spectrum of poreless $Fe/Sb/SiO_2$, obtained at room temperature, reveals a broadened quadrupole doublet, with an isomer shift, relative to α-Fe, of 0.38 mm s, a linewidth of 0.47 mm s and a quadrupole splitting of 0.74 mm s. These values are very close to the results already obtained for the $FeSbO_4$ phase [4,16–18].

At liquid helium temperature the Mossbauer spectrum shows two partially resolved hyperfine patterns. Site 1 with a hyperfine field of 469 (3) kOe and site 2 with 524 (3) kOe contributing with 70% and 30%, respectively, to the final spectrum. The hyperfine parameters obtained by a least-squares fit are shown in Table 2.

The site 1 data are comparable to the data for the $FeSbO_4$ phase, although the broad linewidth demonstrates the existence of hyperfine magnetic field distribution. This component of the spectrum was fitted to a field distribution with an average hyperfine field of 473 (3) kOe, a difference between the maximum and minimum values of 32 kOe and a linewidth fixed at 0.30 mm s^{-1}. The hyperfine parameters of site 1 fitted to a field distribution are quite similar to those published for the $FeSbO_4$ phase [10,17] (see Table 2).

The presence of two hyperfine fields (two sites) can be explained taking into account that the ratio Fe/Sb is 1.3, so there is an excess of iron on the sample that remains as iron^{III} oxide. The site 2 data are very close to the ones related to Fe^{III} oxide dispersed on silica surface [19] (531 kOe).

DISCUSSION

The Fe—Sb oxide system exhibits a behavior that strongly depends on the Sb/Fe ratio. The formation of α-Fe_2O_3 along with $FeSbO_4$ has been reported [4], even for the stoichiometric ratio of Sb/Fe = 1.0. In the Sb rich side (Sb/Fe ratio greater than one) $FeSb_2O_6$,

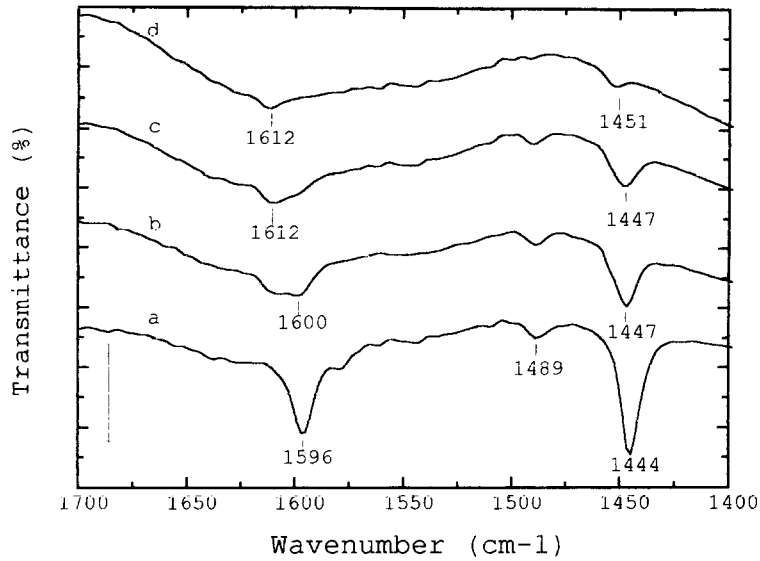

Fig. 1. Infrared spectra of poreless $Fe/Sb/SiO_2$ obtained at room temperature: (a) submitted to 1.6 kPa of pyridine; (b) after pumped off at 100°C for 1 h; (c) after pumped off at 100°C for 2 h; (d) after pumped off at 200°C for 2 h. The bar value is 8%.

Table 1. Wavenumbers for 8a and 19b modes of pyridine adsorbed on materials

Material	T[a]/°C	8a mode/cm^{-1}	19b mode/cm^{-1}
$Fe/Sb/SiO_2$ poreless	150	1600	1447
		1612	1451
$FeSbO_4/SiO_2$[b]		1600	1446
Fe/SiO_2[b]	150	1613	1451
Fe/SiO_2[c]		1613	1453

[a] Temperature of treatment.
[b] From Ref. 10.
[c] From Ref. 14.

Table 2. Mossbauer parameters obtained at liquid helium temperature

Sample	Site	H (kOe)[a]	ΔH (kOe)[b]	IS (mm s)[c]	Γ (mm s)[d]
$Fe/Sb/SiO_2$ poreless	1	469		0.49	0.90
	2	524		0.48	0.38
$Fe/Sb/SiO_2$ poreless	1	473	32	0.46	0.30
with field distribution	2	526		0.49	0.30
$FeSbO_4$[e]		487		0.46	
$FeSbO_4/SiO_2$[f]		461		0.45	

[a] Average effective magnetic field at the iron sites (±3 kOe).
[b] Difference between the maximum and the minimum values of H used in the field distribution.
[c] Isomer shift relative to α-Fe (±0.01 mm s).
[d] Linewidths at half-height.
[e] From Ref. 17.
[f] From Ref. 10.

$FeSb_2O_4$ or $Fe_2Sb_2O_7$ may be formed. However, in this case, Fe^{II} and Sb^{III} species would be present [1,4,16]. Our spectra do not exhibit traces of Fe^{II}.

The Mossbauer spectra at room temperature indicate that the only phases present are $FeSbO_4$ and α-Fe_2O_3. Both, values for isomer shift and for the quadrupole splitting at room temperature, indicating the existence of high spin Fe^{III} in distorted octahedral environment, are in very good agreement with those reported earlier for $FeSbO_4$ [4,16,18]. Moreover the spectrum recorded at liquid helium temperature exhibits the existence of hyperfine magnetic field distributions with hyperfine parameters similar to those published by F. J. Berry *et al.* [17]. The Sb/Fe ratio used in the preparation of the sample, minor than one, is also responsible for the non existence of Fe^{II}.

The hyperfine magnetic field of the Mossbauer spectrum at liquid helium temperature, shows unambiguously two sites of Fe^{III}, which we assign to α-Fe_2O_3 and $FeSbO_4$.

It is known [9–10], when the support is porous silica gel, that Sb^V ions prefer the internal position on the pores (internal surface), where the contact with iron-pentacarbonyl is very difficult. In this case, the reaction is possible only with calcination at 800°C. The $FeSbO_4$ phase is detected on the silica gel surface, at 150°C only, when the synthesis is carried out using $FeCl_3$ in acid medium.

In this work, the $FeSbO_4$ phase was evidenced before the calcination using $Fe(CO)_5$ as starting material, because the reaction was carried out on the fumed silica surface modified with antimony(V). The used support, has only external surface (poreless), so the Sb^V ions on the surface are directly exposed to iron and the possible $FeSbO_4$ phase can be detected at temperature of 150°C.

The $FeSbO_4$ phase formed on the surface in this condition consists in high dispersed form, and X-Ray Diffraction pattern is not possible to be obtained. However it is known [20] that monocrystals structures including two dimensional crystals for other systems has been obtained.

The synthesis carried out with low temperature treatment avoids agglomerates on the highly dispersed phase of the catalyst and changes in the morphology of support caused by calcination.

CONCLUSIONS

The important $FeSbO_4$ phase that is potentially a selective catalyst for oxidation and ammoxidation of alkenes might be obtained on poreless silica surfaces modified with antimony(V) ions at low temperatures (150°C) using $Fe(CO)_5$ deposition synthesis. This result confirms that, on the porous silica gel surface modified with antimony(V), this phase could be detected only if supported by the mechanism of migration of Sb^V ions by acid medium, in this case using acid aqueous solution of $iron^{III}$.

Acknowledgement—E.V.B. is indebted to FAPERGS for financial support.

REFERENCES

1. Aso, I., Furukawa, S., Yamazoe, N. and Seiyama, T., *J. Catal.*, 1980, **64,** 29.
2. Keulks, G. W. and Lo, M. Y., *J. Phys. Chem.*, 1990, **90,** 4768.
3. Weng, L. T., Spitaels, N., Yasse, B., Ladrière, J., Ruiz, P. and Delmon, B., *J. Catal.*, 1991, **132,** 319.
4. Burriesci, N., Garbassi, F., Petrera, M. and Petrini, G., *J. Chem. Soc., Faraday Trans.* 1, 1982, **78,** 817.
5. Teller, R. G., Brazdil, J. F. and Grasseli, R. K., *J. Chem. Soc., Farraday Trans.* 1, 1985, **81,** 1693.
6. Blangenois, N., Ruiz, P. and Delmon, B., Système catalytique pour l'oxidation de composé organique et procédé de préparation d'un tel système, B01J 23/84, Fr, 93870054.9, 24/03/93.
7. Bithell, E. G., Doole, R. C., Goringe, M. J., Allen, M. D. and Bowker, M., *Phys. Stat. Sol (a)*, 1994, **146,** 461.
8. Fattore, V., Fuhrmann, Z. A., Manara, G. and Notari, B., *J. Catal.*, 1975, **37,** 223.
9. Benvenutti, E. V., Gushikem, Y., Vasquez, A., de Castro, S. C. and Zaldivar, G. A. P., *J. Chem. Soc., Chem. Commun.*, 1991, 1325.
10. Davanzo, C. U., Gushikem, Y., de Castro, S. C., Benvenutti, E. V. and Vasquez, A., *J. Chem. Soc., Faraday Trans.*, 1996, **92,** 1569.
11. Benvenutti, E. V., Gushikem, Y. and Davanzo, C. U., *Appl. Spectrosc.*, 1992, **46,** 1474.
12. Pichat, P., Mathieu, M. V. and Imelik, B., *Bull. Soc. Chim. Fr.*, 1969, **8,** 2611.
13. Parry, E. P., *J. Catal.*, 1963, **2,** 371.
14. Connel, G. and Dumesic, J. A., *J. Catal.*, 1986, **101,** 103.
15. Benvenutti, E. V., Gushikem, Y., Davanzo, C. U., de Castro, S. C. and Torriani, I. L., *J. Chem. Soc., Faraday Trans.*, 1992, **88,** 3193.
16. Gadgil, M. M. and Kulshreshtha, S. K., *J. Mol. Catal. A: Chem.*, 1995, **95,** 211.
17. Berry, F. J., Labarta, A., Obradors, S., Rodriguez, R., Sarson, M. I. and Tejada, J., *Hyperfine Interact.*, 1988, **41,** 463.
18. Berry, F. J., Holden, J. G., Loretto, M. H. and Urch, D. S., *J. Chem. Soc., Dalton Trans.*, 1987, 1727.
19. Kündig, W. and Bömmel, H., *Phys. Rev.*, 1966, **142,** 327.
20. Zhang, J., Liu, J., Huang, J. L., Kim, P. and Lieber, C. M., *Science*, 1996, **274,** 757.

Pergamon

PII: S0277-5387(97)00456-7

Polyhedron Vol. 17, No. 10, pp. 1631–1635, 1998
© 1998 Elsevier Science Ltd
All rights reserved. Printed in Great Britain
0277-5387/98 $19.00+0.00

Synthesis and characterization of (μ-oxalato) copper(II) and nickel(II) complexes

Zdeněk Smékal,[a]* Peter Thornton,[b] Zdeněk Šindelář[a] and Roman Klička[a]

[a] Department of Inorganic and Physical Chemistry, Palacký University, Křížkovského 10, Olomouc 77147, Czech Republic

[b] Department of Chemistry, Queen Mary and Westfield College, Mile End Road, London E1 4NS, U.K.

(Received 24 September 1997; accepted 6 November 1997)

Abstract—Four new binuclear complexes of the type $[(Cu(L)_x)_2ox](ClO_4)_2$ (L = 1,3-diaminopropane (1,3-pn), $x = 1.5$ (**1**); L = 1,3-diaminopropane, $x = 1$ (**2**); L = *N*-(2-aminoethyl)-1,3-propanediamine (ept), $x = 1$ (**3**)) or $[(Ni(L)_2)_2ox](ClO_4)_2$ (L = 1,2-diaminopropane (1,2-pn) (**4**)) have been prepared and studied by elemental analysis, IR and electronic spectroscopies. Spectroscopic data are consistent with oxalate-bridged structures between five-coordinate (N_3O_2) Cu(II) (compounds **1** and **3**), four coordinate (N_2O_2) Cu(II) (**2**) and six-coordinate (N_4O_2) Ni(II) (**4**). Magnetochemical measurements (72–300 K) show (**2**) and (**4**) are antiferromagnetic ($J = -254$ and -33 cm^{-1} respectively ($H = -JS_1S_2$)). © 1998 Elsevier Science Ltd. All rights reserved

Keywords: copper(II) complexes; nickel(II) complex; μ-oxalato complexes; magnetic properties; antiferromagnetism.

Dinuclear oxalate-bridged copper(II) complexes are known in a range of metal coordination geometries from four to six [1–11]. Oxalate provides an efficient superexchange pathway to give antiferromagnetism of varying extents in these complexes. The theory initiated by Hoffmann and coworkers [12] and developed by Kahn and colleagues [13,14] has shown that there is a correlation between coordination geometry and magnitude of the singlet-triplet separation, $-J$. Values up to 400 cm^{-1} can be found. Indeed there is the above mentioned theory on the structure vs magnetism correlation of copper(II) binuclear compounds, but as it happens, the experimental verification came first, then theoretical work to rationalize the observations [15–18].

For nickel(II), oxalato bridging has been found with NiN_4O_2 octahedral chromophores [2,3,11–14,19–21]. The nitrogen donors are tetra-aza macrocycles, linear tetramines or two diamine molecules. Magnetostructural data concerning the oxalato-bridged nickel(II) complexes have revealed that the magnetic coupling J ($H = -JS_1S_2$), which varies from -22 to -40 cm^{-1}, is strongly dependent on the nature of the donor atoms of terminal ligands [22].

The aim of this work was the preparation and physicochemical study of new binuclear μ-oxalato complexes of copper(II) or nickel(II) with 1,3-diaminopropane (1,3-pn), *N*-(2-aminoethyl)-1,3-propanediamine (ept) or 1,2-diaminopropane (1,2-pn) of compositions $[(Cu(1,3\text{-pn})_{1.5})_2ox](ClO_4)_2$ (**1**), $[(Cu(1,3\text{-pn}))_2ox](ClO_4)_2$ (**2**), $[(Cu(ept))_2ox](ClO_4)_2$ (**3**) and $[(Ni(1,2\text{-pn})_2)_2ox](ClO_4)_2$ (**4**) and comparison with analogous known μ-oxalato complexes. Above mentioned three amines were chosen intentionally: 1,2-diaminopropane is an example of bidentate ligand which forms five-membered cycle in the complex, 1,3-diaminopropane as bidentate ligand forms six-membered cycle and *N*-(2-aminoethyl)-1,3-propanediamine is tridentate ligand which forms both five-membered cycle and six-membered cycle in the complex. The compounds prepared were characterized by elemental analysis, IR and UV-vis spectroscopies and variable temperature magnetic susceptibility measurements.

* Author to whom correspondence should be addressed.

EXPERIMENTAL

Chemicals and methods

The starting materials $Cu(ClO_4)_2 \cdot 6H_2O$ and $Ni(ClO_4)_2 \cdot 6H_2O$ were obtained by the reaction between basic copper and nickel carbonates and aqueous $HClO_4$. 1,3-Diaminopropane and 1,2-diaminopropane (racemic mixture) (Fluka), *N*-(2-aminoethyl)-1,3-propanediamine (Aldrich) and sodium oxalate (Lachema Brno) were used without further modification.

Elemental analyses of carbon, hydrogen and nitrogen were performed on a Fisons Instruments EA1108 CHN instrument. Nickel was determined gravimetrically using dimethylglyoxime. Electronic absorption spectra in water solution were run on a SPECORD M40. IR spectra were obtained as Nujol mulls on a SPECORD IR 80 using the Nujol technique. Temperature-dependent magnetochemical data were obtained by the Faraday method in the 72–300 K range as described previously [23]. Diamagnetic corrections were made with Pascal's constants for all the constituent atoms and magnetic moments were calculated using the equation $\mu_{eff} = 2.828(\chi_M T)^{1/2}$.

Syntheses

$[(Cu(1,3\text{-pn})_{1.5})_2ox](ClO_4)_2$ (**1**). A solution of 0.18 g (1.34 mmol) of sodium oxalate in 20 cm^3 water was added to a solution of 1.00 g (2.70 mmol) of $Cu(ClO_4)_2 \cdot 6H_2O$ and 0.34 cm^3 (4.10 mmol) of 1,3-diaminopropane in 30 cm^3 water. The reaction mixture was concentrated by heating to 15 cm^3 and then was allowed to stand overnight. The solid was filtered off and then recrystallized from water to give dark blue microcrystals. The crystals were filtered off, washed with small amount of water and dried at 40°C. The yield was 0.1 g (12%).

$[(Cu(1,3\text{-pn}))_2ox](ClO_4)_2$ (**2**). A solution of 0.18 g (1.34 mmol) of sodium oxalate in 20 cm^3 water was added to a solution of 1.00 g (2.70 mmol) of $Cu(ClO_4)_2 \cdot 6H_2O$ and 0.17 cm^3 (2.05 mmol) of 1,3-diaminopropane in 30 cm^3 water. A small amount of solid formed was discarded. The reaction mixture was concentrated by heating to 15 cm^3 and then was allowed to stand overnight. The solid was filtered off and then recrystallized from water to give light blue microcrystals. The crystals were filtered off, washed with a small amount of water and dried at 40°C. The yield was 0.1 g (13%).

$[(Cu(ept))_2ox](ClO_4)_2$ (**3**). A solution of 0.18 g (1.34 mmol) of sodium oxalate in 20 cm^3 water was added to a solution of 1.00 g (2.70 mmol) of $Cu(ClO_4)_2 \cdot 6H_2O$ and 0.34 cm^3 (2.70 mmol) of *N*-(2-aminoethyl)-1,3-propanediamine in 25 cm^3 water. The reaction mixture was concentrated by heating to 15 cm^3. After cooling a blue product was obtained. The solid was filtered off and then recrystallized from hot water to give blue microcrystals. The crystals were filtered off, washed with water and dried at 40°C. The yield was 0.60 g (68%).

$[(Ni(1,2\text{-pn})_2)_2ox](ClO_4)_2$ (**4**). A solution of 0.18 g (1.34 mmol) of sodium oxalate in 20 cm^3 water was added to a solution of 1.00 g (2.73 mmol) of $Ni(ClO_4)_2 \cdot 6H_2O$ and 0.47 cm^3 (5.51 mmol) of 1,2-diaminopropane in 25 cm^3 water. The reaction mixture was concentrated by heating to 20 cm^3. After cooling a violet product was obtained. The substance was filtered off and then recrystallized from hot water to give violet microcrystals. The product was filtered off, washed with water and dried at 40°C. The yield was 0.65 g (69%).

RESULTS AND DISCUSSION

The chemical composition of the complexes are given in Table 1. The data from physicochemical studies are given in Table 2 and 3 and Figs 1, 2, 3 and 4.

The new coordination compounds were prepared by the reaction of the metal perchlorate with the appropriate polyamine and sodium oxalate in aqueous solution.

The IR spectra were not studied in detail; only characteristic vibrations for $\nu_3(ClO_4)$, $\nu_4(ClO_4)$, $\nu_{asym}(CO_2)$, $\nu_{sym}(CO_2)$ and $\delta(CO_2)$ were interpreted. The values given in Table 2 are consistent with tetradentate oxalate [21,24] and perchlorate [25].

In the electronic absorption spectrum of Cu(II) complexes we can find a strong band corresponds to a *d-d* transition in the range 13,000–18,000 cm^{-1} [26]. In the present compounds bands at 16,300, 15,900 or 16,400 cm^{-1}, respectively, may be ascribed to *d-d* transitions of copper(II). In the octahedral complexes of Ni(II) we can find three bands which are due to a *d-d* transitions ($\nu_1 = {}^3T_{2g}(F) \Leftarrow {}^3A_{2g}(F)$, $\nu_2 = {}^3T_{1g}(F) \Leftarrow {}^3A_{2g}(F)$, $\nu_3 = {}^3T_{1g}(P) \Leftarrow {}^3A_{2g}(F)$); for $[Ni(en)_3]^{2+}$ $\nu_2 = 18{,}350$ cm^{-1}, $\nu_3 = 29{,}000$ cm^{-1}) [26]. In the present complex bands at 17,900 cm^{-1} and 28,700 cm^{-1}, respectively, may be assigned as ν_2 and ν_3, respectively.

The spectroscopic data described above are consistent with oxalate-bridged dimeric structures for all four complexes. Square planar four coordination is proposed for (**2**), and octahedral geometry for the nickel complex (**4**). For compounds (**1**) and (**3**) five-coordination is suggested, but there are various possibilities for isomerism, and we are not able to distinguish between the possibilities for the 5-coordinate structure.

A magnetochemical study of each compound has been made in the temperature range 70–300 K. The results are shown graphically in Figs 1–4. Complexes (**1**) and (**3**) are essentially magnetically dilute, with very little sign of antiferromagnetic exchange. It will be seen that for both these compounds the magnetic moment per copper dimer does not fall below the spin-only value. The slight falls in magnetic moment with

Table 1. Chemical composition of the complexes

Compound	Found (Calc.) (%) C	H	N	Ni
$[(Cu(1,3\text{-}pn)_{1.5})_2ox](ClO_4)_2$	20.9 (20.8)	5.1 (4.8)	13.1 (13.2)	—
$[(Cu(1,3\text{-}pn))_2ox](ClO_4)_2$	17.4 (17.1)	3.7 (3.6)	9.8 (10.0)	—
$[(Cu(ept))_2ox](ClO_4)_2$	22.6 (22.2)	5.0 (4.7)	12.9 (13.0)	—
$[(Ni(1,2\text{-}pn)_2)_2ox](ClO_4)_2$	24.6 (24.0)	5.9 (5.8)	15.5 (16.0)	16.6 (16.8)

Table 2. IR spectral data

Compound	IR (cm^{-1}) $\nu_3(ClO_4)$	$\nu_4(ClO_4)$	$\nu_{asym}(CO_2)$	$\nu_{sym}(CO_2)$	$\delta(CO_2)$
$[(Cu(1,3\text{-}pn)_{1.5})_2ox](ClO_4)_2$	1056 s	618 s	1664 s	1356 m	748 s
$[(Cu(1,3\text{-}pn))_2ox](ClO_4)_2$	1070 s	620 s	1672 s	1358 s	804 s
$[(Cu(ept))_2ox](ClO_4)_2$	1088 s	625 s	1630 s	1380 m	792 s
$[(Ni(1,2\text{-}pn)_2)_2ox](ClO_4)_2$	1084 s	622 s	1648 s	1356 m	794 s

Table 3. Magnetic and spectral properties of the complexes

Compound	μ_{eff} (μ_B)/T (K)	UV-vis (cm^{-1}) (ε_{max}($mol^{-1}\cdot dm^3\cdot cm^{-1}$))
$[(Cu(1,3\text{-}pn)_{1.5})_2ox](ClO_4)_2$	2.66/76.5–2.75/287.8	16,300 (130)
$[(Cu(1,3\text{-}pn))_2ox](ClO_4)_2$	0.76/93.8–2.05/302.1	15,900 (145)
$[(Cu(ept))_2ox](ClO_4)_2$	2.64/73.5–2.73/299.8	16,400 (134)
$[(Ni(1,2\text{-}pn)_2)_2ox](ClO_4)_2$	3.43/72.3–4.33/299.8	28,700 (13),17,900 (8)

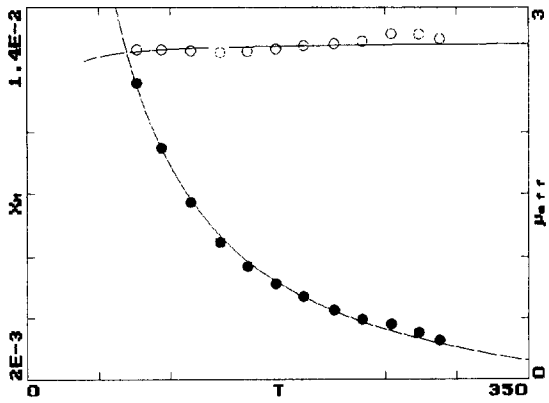

Fig. 1. The paramagnetic susceptibility (●-in cgs) and effective moment (○-μ_B) vs temperature curves for $[(Cu(1,3\text{-}pn)_{1.5})_2ox](ClO_4)_2$. The circles are the experimental points.

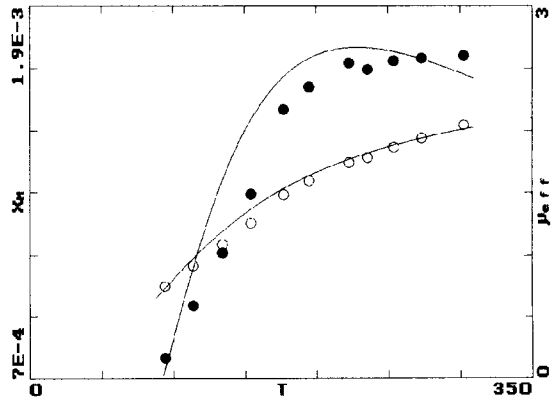

Fig. 2. The paramagnetic susceptibility (●-in cgs) and effective moment (○-μ_B) vs temperature curves for $[(Cu(1,3\text{-}pn))_2ox](ClO_4)_2$. The circles are the experimental points, the solid lines are theoretical lines.

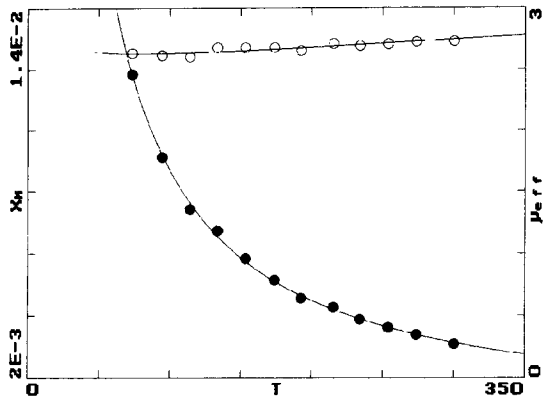

Fig. 3. The paramagnetic susceptibility (●-in cgs) and effective moment (○-μ_B) vs temperature curves for [(Cu(ept))$_2$ox](ClO$_4$)$_2$. The circles are the experimental points.

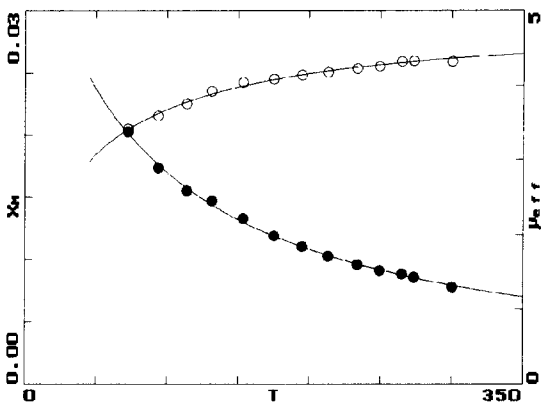

Fig. 4. The paramagnetic susceptibility (●-in cgs) and effective moment (○-μ_B) vs temperature curves for [(Ni(1,2-pn)$_2$)$_2$ox](ClO$_4$)$_2$. The circles are the experimental points, the solid lines are theoretical lines.

temperature are barely significantly outside the experimental error of +2% and +1.2% for compounds (**1**) and (**3**) respectively. Plots of reciprocal susceptibility against temperature give slightly antiferromagnetic Weiss constants of 16.4 and 11.1 K respectively. We conclude that it is not meaningful, for which a more extended temperature range of data is required. The analogous compound [(Cu(dien))$_2$ox](ClO$_4$)$_2$ (dien = diethylenetriamine) does not exhibit significant exchange down to 4 K [27].

Complex (**2**) behaves like a classical copper(II) dimer. The data follow the Bleaney-Bowers eqn [28]:

$$\chi_M = \left(\frac{2\mu_o N g^2 \beta^2}{kT}\right)[3+\exp[(-J)/(kT)]]^{-1} + N_\alpha \quad (1)$$

Using the usual value of the second order paramagnetic molar susceptibility N_α of 60 cgs units per copper and a fixed value of g, J is found [29] to be -254 cm^{-1} ($H = -JS_1S_2$, $S_1 = S_2 = 1/2$). If g is allowed to vary, the best fit to data is unrealistically found to be 1.85, with J equal to -234 cm^{-1}; if N_α is ignored, also unrealistically, the best value of g is 2.1, with $J = -260$ cm^{-1}. Because of the weak paramagnetism of this strongly coupled system there is a large experimental error of +4% on the data, which makes the fit of data to theory acceptable.

This strong antiferromagnetism can be explained by the proposed square planar coordination for copper. The [(1,3-pn)Cu(μ-ox)Cu(1,3-pn)] unit is planar, so that the x^2-y^2 magnetic orbitals on Cu will be ideally directed for overlap with the oxalate σ orbitals and the antiferromagnetic exchange will be maximized [13,14].

The effective magnetic moment of 3.06 μ_B at 299.8 K per Ni(II) ([Ni(1,2-pn)$_2$)$_2$ox](ClO$_4$)$_2$) is typical for octahedrally coordinated nickel(II). The variable-temperature magnetic moment and magnetic susceptibility in the range 72–300 K for a solid sample of the title compound is shown in Fig. 4. The magnetic moment is temperature dependent and decreases from 4.33 μ_B/mol (3.06 μ_B per Ni^{2+}) at 300 K to 3.43 μ_B at 72.3 K. This proves that there is antiferromagnetic coupling across the oxalate bridge (Weiss constant is 73.0 K). The magnetic behaviour of the title complex could be interpreted using isotropic spin Hamiltonian $H = -JS_1S_2$, where $S_1 = S_2 = 2/2$ and J is the exchange integral. The experimental data have been fitted to the expression [3]

$$\chi_M = \left(\frac{\mu_o N g^2 \beta^2}{3kT}\right)\frac{30\exp(3J/kT)+6\exp(J/kT)}{5\exp(3J/kT)+3\exp(J/kT)+1} + N_\alpha \quad (2)$$

by using of Klička's program [29] for HDVV-dimer model and using the usual value of the second order paramagnetic molar susceptibility N_α of 100 cgs units per nickel. The best fit parameters obtained are: $J = -33$ cm^{-1}, $g = 2.25$. ($H = -JS_1S_2$, $S_1 = S_2 = 2/2$) For Ni(II) complexes in octahedral geometry, the metal x^2-y^2 orbital is half occupied and is aligned to allow overlap with the oxalate σ-orbitals. For present complex, the observed J-value of -33 cm^{-1} is similar to those of [Ni$_2$(1,3-pn)$_4$ox](ClO$_4$)$_2$ [30] ($J = -36$ cm^{-1}) or [Ni$_2$en$_4$ox](NO$_3$)$_2$ (en = ethylenediamine) ($J = -32$ cm^{-1}) [19].

In conclusion, it can be seen that this group of four oxalate-brigded complexes clearly demonstrated the effect of varying coordination on the magnitude of exchange interactions.

Acknowledgement—This work was supported by the Grant Agency of the Czech Republic (Grant No. 203/96/0440).

REFERENCES

1. Curtis, N. F., *J. Chem. Soc.* (*A*), 1968, 1584.

2. Curtis, N. F., McCormick, J. R. N. and Waters, T. N., *J. Chem. Soc., Dalton Trans.*, 1973, 1537.
3. Duggan, D. M., Barefield, E. K. and Hendrickson, D. N., *Inorg. Chem.*, 1973, **12,** 985.
4. Nonoyama, M. and Nonoyama, K., *J. Inorg. Nucl. Chem.*, 1981, **43,** 2567.
5. Castro, I., Faus, J., Julve, M., Mollar, M., Monge, A. and Gutierrez-Puebla, E., *Inorg. Chim. Acta*, 1989, **161,** 97.
6. Bencini, A., Fabretti, A. C., Zanchini, C. and Zannini, P., *Inorg. Chem.*, 1987, **26,** 1445.
7. Nonoyama, K., Ojima, H., Ohki, K. and Nonoyama, M., *Inorg. Chim. Acta*, 1980, **41,** 155.
8. Julve, M., Faus, J., Verdaguer, M. and Gleizes, A., *J. Am. Chem. Soc.*, 1984, **106,** 8306.
9. Castro, I., Faus, J., Julve, M. and Gleizes, A., *J. Chem. Soc., Dalton Trans.*, 1991, 1937.
10. Tuero, L. S., Garcia-Lozano, J., Monto, E. E., Borja, M. B., Dahan, F., Tuchagues, J.-P. and Legros, J. P., *J. Chem. Soc., Dalton Trans.*, 1991, 2619.
11. Glerup, J., Goodson, P. A., Hodgson, D. J. and Michelsen, K., *Inorg. Chem.*, 1995, **34,** 6255 and references therein.
12. Hay, G. R., Thibeault, J. C. and Hoffmann, R., *J. Am. Chem. Soc.*, 1975, **97,** 4884.
13. Julve, M. Verdaguer, M., Kahn, O., Gleizes, A. and Philoche-Levisalles, M., *Inorg. Chem.*, 1983, **22,** 368.
14. Julve, M. Verdaguer, M., Gleizes, A., Philoche-Levisalles, M. and Kahn, O., *Inorg. Chem.*, 1984, **23,** 3808.
15. Harris, C. M., James, J. M., Milham, P. J. and Sinn, E., *Inorg. Chim. Acta*, 1969, **8,** 81.
16. Coles, R. B., Harris, C. M. and Sinn, E., *Inorg. Chem.*, 1969, **8,** 2607.
17. Gluvchinski, P., Mockler, G. M., Healy, P. C. and Sinn, E., *J. Chem. Soc., Dalton Trans.*, 1974, 1156.
18. Countryman, R. M., Robinson, W. T. and Sinn, E., *Inorg. Chem.*, 1974, **13,** 2013.
19. Ball, P. W. and Blake, A. B., *J. Chem. Soc. A.* 1969, 1415.
20. Escuer, A., Vicente, R., El Fallah, M. S. and Jaud, J., *Inorg. Chim. Acta*, 1995, **232,** 151 and references therein.
21. Březina, F., Smékal, Z., Trávníček, Z., Šindelář, Z., Pastorek, R. and Marek, J., *Polyhedron*, 1997, **16,** 1331.
22. Román, P., Guzmán-Miralles, Luque, A., Beitia, J. I., Cano, J., Lloret, F., Julve, M. and Alvarez, S., *Inorg. Chem.*, 1996, **35,** 3741.
23. Laffey, M. A. and Thornton, P., *J. Chem. Soc., Dalton Trans.*, 1982, 313.
24. Curtis, N. F., *J. Chem. Soc.*, 1963, 4109.
25. Hathaway, B. J. and Underhill, A. E., *J. Chem. Soc.*, 1961, 3091.
26. Greenwood, N. N. and Earnshaw, A., *Chemistry of the Elements.* Informatorium Prague, 1993, pp. 1433, 1479.
27. Duggan, D. M. and Hendrickson, D. N., *Inorg. Chem.*, 1973, **12,** 2422.
28. Bleaney, B. and Bowers, K. D., *Proc. R. Soc. London, Ser. A*, 1952, **214,** 451.
29. Klička, R. and Šindelář, Z., *Chem. listy*, 1993, **87,** 89.
30. Ribas, J., Monfort, M., Diaz, C. and Solans, X., *An. Quim.*, 1988, **84,** 186.

Pergamon

PII: S0277-5387(97)00458-0

Polyhedron Vol. 17, No. 10, pp. 1637–1642, 1998
© 1998 Elsevier Science Ltd
All rights reserved. Printed in Great Britain
0277-5387/98 $19.00+0.00

Copper(II) compound with long Cu(II)–phenolic oxygen atom bonding as galactose oxidase model

Sayo Ito,[a] Satoshi Nishino,[a] Hiroki Itoh,[a] Shigeru Ohba[b] and Yuzo Nishida*[a]

[a] Department of Chemistry, Faculty of Science, Yamagata University, Yamagata 990, Japan

[b] Department of Chemistry, Faculty of Science and Technology, Keio University, Yokohama 223, Japan

(Received 25 August 1997; accepted 6 November 1997)

Abstract—A crystal structure determination of $Cu(phpyH)ClClO_4 \cdot CH_3OH$ revealed that the protonated phenolic oxygen atom lies at the apex of a square pyramidal CuN_4O arrangement with Cu(II)—O(phenolic) distances of 2.46 and 2.57 Å; this is a novel copper(II) model compound for galactose oxidase where the Cu(II)–phenolic oxygen (Tyrosine-495) distance is rather long, 2.69 Å, and the present results may provide chemical evidence for possible participation of Tyrosine-495 in the oxidation of galactose. © 1998 Elsevier Science Ltd. All rights reserved

Keywords: long Cu(II)–phenol bond; galactose oxidase model; Tyrosine residue.

Galactose oxidase (GO) is a secreted mononuclear copper enzyme, which has been isolated from the cultured media of a number of fungal species [1]. Even though it contains only a single copper atom, the enzyme catalyzes the two-electron oxidation of the position-6 hydroxy group of galactose to the corresponding aldehyde, concurrent with the reduction of O_2 to H_2O_2 as follows.

$$RCH_2OH + O_2 \rightarrow RCHO + H_2O_2$$

An unusual property of GO, which distinguishes it from simple mononuclear copper enzymes, is that the protein has three well-defined and stable oxidation levels. Of these three, only the intermediate or one-electron oxidized from, shows a Cu(II) electron paramagnetic resonance (EPR) signal, and this is typical of the "Type-2" or normal class [2,3]. A recent X-ray absorption edge study by Clark *et al.* has established that galactose oxidase copper is cupric in the enzyme's highest oxidation level [4]. The fact that this form is EPR-silent indicates that the Cu(II) is anti-ferromagnetically coupled to a second $S = 1/2$ species. As GO contains no other metal besides the redox-active copper center, the paramagnetic species to which it is coupled is likely to be an organic radical, and that this organic radical should be phenol group of Tyrosine-495, or -272 [5], the possible participation of the latter (Tyr-272) being proposed by several authors [6].

Until now, many copper(II) complexes with phenolic oxygen atom are prepared and characterized; in almost all the cases, phenolic oxygen atom is located at the corner of the square plane containing the copper(II) ion; this situation corresponds to that of Tyr-272 in GO. There are few reports that phenoxo radical formation occurs in the reaction with dioxygen molecule for these compounds containing copper(I) or copper(II) ion [7], and this should be due to lowering of the occupied orbital energy of phenolic anion through coordination to a copper atom. Only in exceptional case, phenolic oxygen is at the apical position of the square pyramide in the complex with (2-hydroxy-5-nitrobenzyl)bis(2-pyridylmethyl)amine [8], however in this case copper(II)–phenolic oxygen atom is 2.268 Å, which is much shorter than that in the enzyme [5]. In this study we have succeeded in preparing the copper(II) complex with long copper(II)–phenolic oxygen distance, this may give useful information to elucidate origin and mechanism of radical formation in GO.

* Author to whom correspondence should be addressed.

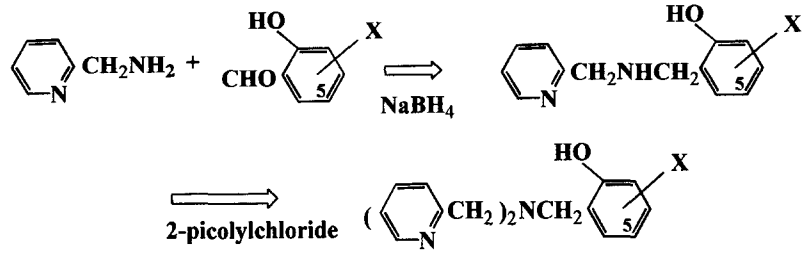

X=H, H(phpyH); X=5-Br, H(Br-phpyH)

Scheme 1

EXPERIMENTAL

Synthesis of copper(II) complexes

The schematic illustration of ligand synthesis is given above.

By adding $NaBH_4$ (2 g) to methanol solution (40 ml) containing 2-aminomethyl-pyridine (0.01 M) and salicylaldehyde (0.01 M), white *N*-(*o*-hydroxybenzyl)-2-aminomethylpyridine, **1** was obtained. Compound **1** was reacted with 2-picolychloride to give H(phpyH) (see scheme above) in an aqueous solution [9]. The aqueous solution was evaporated, and ligand, H(phpyH) was extracted by methanol, and the methanol solution was used for copper(II) complex synthesis without further purification. By adding $NaClO_4$ or NH_4PF_6 (500 mg) to a methanol solution (20 ml) containing a ligand, which was derived from **1** (0.004 M) and 2-picolychlorode (0.004 M), copper(II) chloride (0.004 M), the desired copper(II) compound was obtained as green crystals. The corresponding 5-Br derivative was synthesized according to the similar ways as described for the H(phpyH)-complex. Yields of the copper(II) compounds are in the range 50–60% based on the copper(II) chloride used. Anal: Calcd for Cu(phpyH)$ClClO_4$: C, 45.30; H, 3.80; N, 8.34. Found: C, 45.77; H, 4.31; N, 8.23%. Calc. for Cu (5-Br-phpyH)$ClClO_4 \cdot H_2O$: C, 38.96; H, 3.44; N, 717. Found: C, 38.74; H, 3.14; N, 7.11%.

Crystal structure determination

The compounds in the crystal structure determination were recrystalized from a methanol/water solution. The structures of two new compounds were determined in this study, and the crystal data of the complexes are summarized in Table 1. X-ray diffraction intensities were measured up to $2\theta = 55°$ using Mo-K_α radiation ($\lambda = 0.71073$ Å) on a Rigaku AFC-5 four-circle diffractometer, and the absorption corrections were carried out by a numerical integration method. The structures were refined using CRYSTAN-GM software, and the details have been deposited as a supplementary data.

Table 1. Crystallographic data of the copper(II) compounds

	Cu(phpyH)$ClClO_4 \cdot CH_3OH$	Cu(5-Br-phpyH)$PF_6 \cdot CH_3OH$
Formula	$C_{20}H_{23}Cl_2CuN_3O_6$	$C_{20}H_{22}ClBrCuN_3O_2PF_6$
FW	535.87	660.28
Crystal system	triclinic	monoclinic
Space group	$P\bar{1}$	$P2_1/c$
a (Å)	14.908(2)	12.188(3)
b (Å)	15.326(5)	9.326(2)
c (Å)	11.256(1)	22.351(2)
α (°)	109.78(1)	90
β (°)	98.90(1)	95.42(1)
γ (°)	97.93(1)	90
V (Å^3)	2340.3(6)	2529.2(7)
Z	4	4
D_{calc} (g cm^{-3})	1.521	1.734
Observed reflections ($F_o > 3\sigma(F_o)$)	6155	3562
R	0.068	0.069
ωR	0.056	0.059

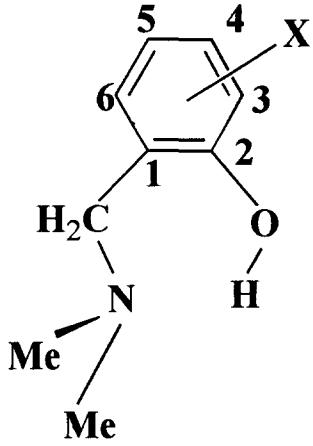

Scheme 2

Molecular orbital calculations

MO calculations for *N,N*-dimethyl-*o*-hydroxy-benzylamine and its 5-bromo derivative (neutral form, see the figure at the top of next page) were performed by the use of AM1 method [10].

RESULTS AND DISCUSSION

There are two independent molecules in unit cell of $Cu(phpyH)ClClO_4 \cdot CH_3OH$. In Fig. 1, the ORTEP drawing of one of the two $Cu(phpyH)Cl^+$ molecules is shown, and the projections along the Cl—Cu—N bonding are illustrated in Fig. 2, and the selected bond distances and angles are listed in Table 2. The structural property of the compound is essentially the same as that of the $Cu(mopy)Cl^+$ compound [10]. Copper(II) complex is of a square pyramid and square plane is occupied by three nitrogen atoms (two pyridine and one aliphatic amine) and chloride ion. It should be noted here that the apical position is occupied by the phenolic oxygen atom with protonated form, and the distances between copper and oxygen atom are 2.457(5) and 2.565(4) Å, which is much longer than that in the 5-nitro derivative [8], and is very similar to that in GO (2.69 Å) [5]. In Fig. 3 The ORTEP drawing of the corresponding 5-bromo-derivative is shown, and the selected bond distances and angles are also summarized in Table 3. The structural properties of the compound are essentially the same as that of the (phpyH)-complex, but the distance between the copper(II) ion and phenol oxygen is 2.363(5) Å, which is much shorter than that in the (phpyH)-ligand.

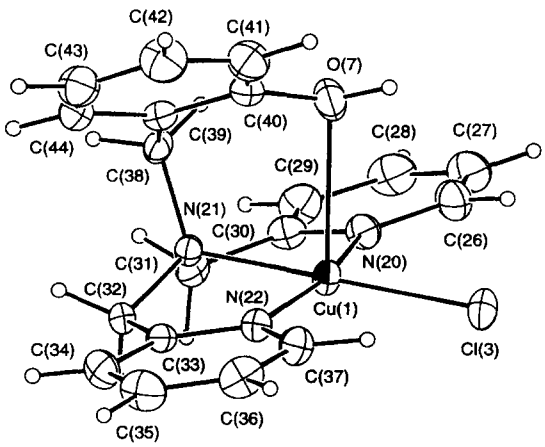

Fig. 1. ORTEP drawing of $Cu(phpyH)Cl^+$-(a), Cu(1) complex.

In Table 4, the energies of HOMO and LUMO of the two compounds, *N,N*-dimethyl-*o*-hydroxy-benzylamine and its 5-bromo-derivative are shown; it is clear that these two orbitals are consisted of *p*-orbitals of π-type, and that the energies of both HOMO and LUMO of the former compound are higher than those of the 5-bromo derivative. This suggests that the introduction of electron-withdrawing group on the phenolic ring induces the shortening of distances between the copper(II) ion and phenolic oxygen atom.

In the square pyramidal copper(II) compounds with (phpyH) and (5-Br-phpyH), HOMO of the ligand which contains *p*-orbital of phenol oxygen of π-type (see Table 4) approaches to a copper(II) atom along the *z*-axis (see Fig. 2 and Fig. 4 (A)), leading to interaction with d_{z^2}-orbital; angle between the phenol plane and the plane which contains the copper(II) coordination site is 39, 37, and 41° for Cu(1) and Cu(2) in the $Cu(phpyH)Cl^+$, and $Cu(5\text{-Br-phpyH})\,l^+$, respectively. In this case, since the d_{z^2}-orbital is doubly occupied (see Fig. 4 (B)), the interaction between the HOMO (π-type, containing phenolic oxygen) and the d_{z^2}-orbital does not contribute to the stabilization of the system, rather to induction of destabilization.

This may explain the shorter Cu(II)–oxygen atom distance observed for the corresponding 5-bromo derivative than that of the (phpyH)-complex. This may also support that radical formation (oxidation of phenolic ring) is more favorable for the system with long copper(II)–phenolic oxygen distance as observed in the native GO. Based on the above discussion, present results may suggest that the higher energy of HOMO of the phenolic group may lead to the longer the copper(II)–phenolic oxygen atom distance, and this makes the phenol ring to be more oxidizable, and that an ESR-silent state of GO (not necessarily diamagnetic) may be written as,

Cu(II)–phenoxo radical (Tyr 495)

and this may reacts as a two-electron acceptor in the reaction.

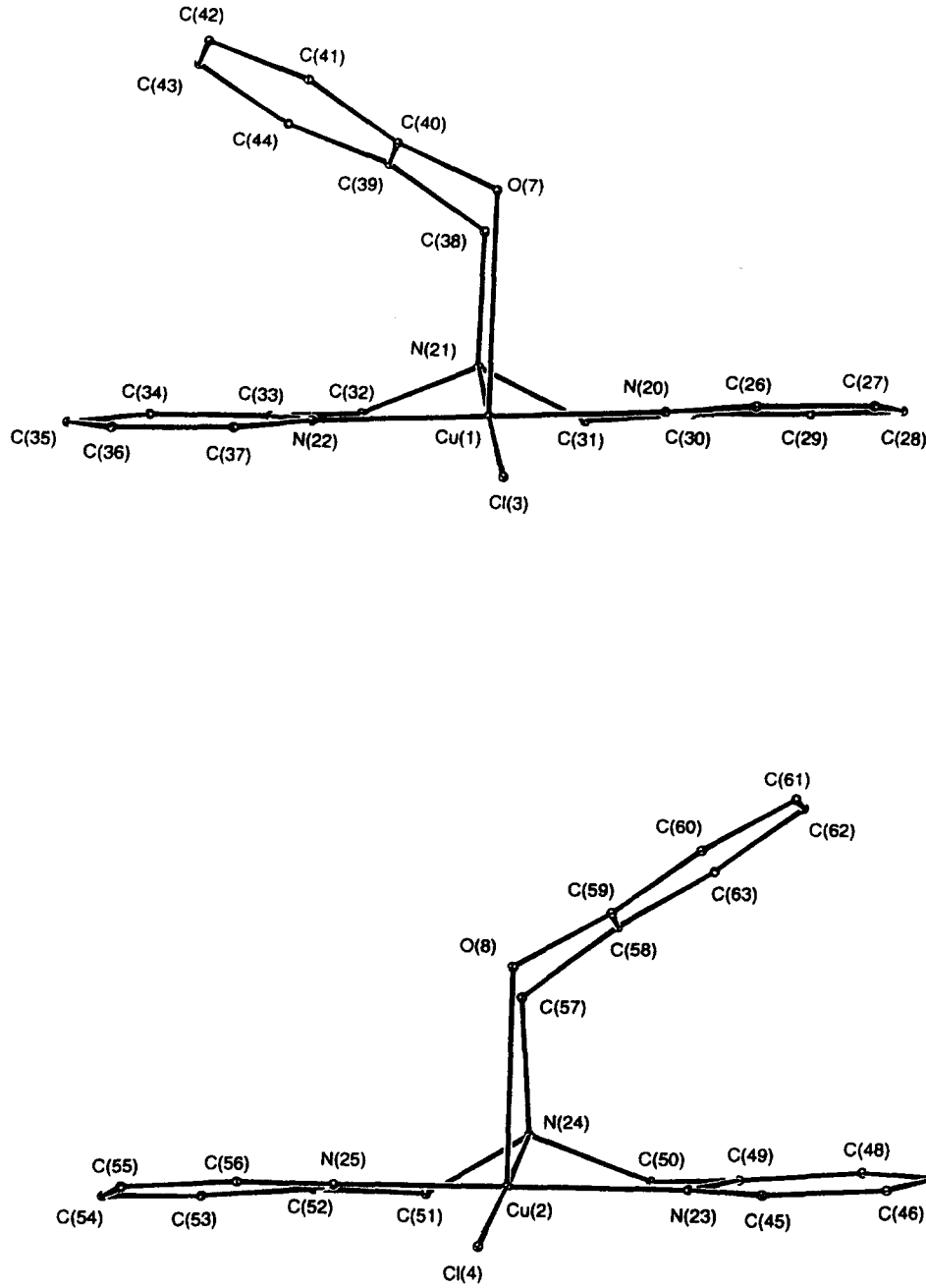

Fig. 2. Schematic illustration of copper(II) coordination site viewed from Cl—Cu—N bond-axes in Cu(phpyH)Cl^+ complex.

Table 2. Selected distances (Å) and angles (°) in $Cu(phpyH)ClClO_4$

Cu(1)—Cl(3)	2.238(2)	Cu(1)—O(7)	2.570(4)
Cu(1)—N(20)	1.987(5)	Cu(1)—N(21)	2.041(4)
Cu(1)—N(22)	1.978(5)	Cu(2)—Cl(4)	2.264(2)
Cu(2)—O(8)	2.457(5)	Cu(2)—N(23)	1.980(5)
Cu(2)—N(24)	2.059(4)	Cu(2)—N(25)	1.978(5)

Cl(3)—Cu(1)—N(20)	96.8(2)	Cl(4)—Cu(2)—N(23)	98.0(2)
Cl(3)—Cu(1)—N(21)	178.5(2)	Cl(4)—Cu(2)—N(24)	178.5(2)
Cl(3)—Cu(1)—N(22)	97.2(2)	Cl(4)—Cu(2)—N(25)	96.8(2)
O(7)—Cu(1)—N(20)	89.5(2)	O(8)—Cu(2)—N(23)	89.8(2)
O(7)—Cu(1)—N(21)	87.1(2)	O(8)—Cu(2)—N(24)	89.8(2)
O(7)—Cu(1)—N(22)	93.6(2)	O(8)—Cu(2)—N(24)	93.9(2)
N(20)—Cu(1)—N(21)	82.4(2)	N(23)—Cu(2)—N(24)	83.2(2)
N(20)—Cu(1)—N(22)	165.4(2)	N(23)—Cu(2)—N(25)	164.5(2)
N(21)—Cu(1)—N(22)	83.5(2)	N(24)—Cu(2)—N(25)	82.0(2)

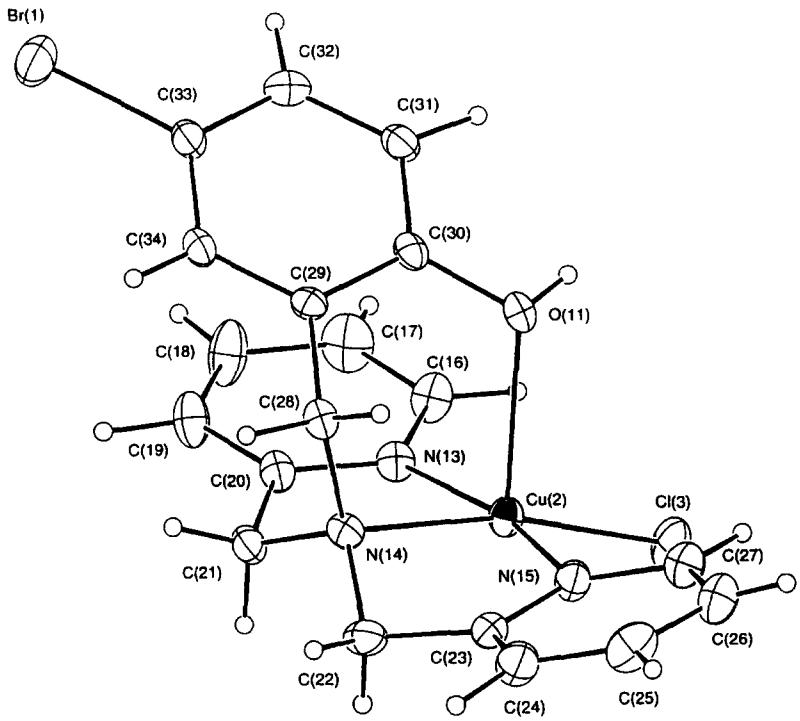

Fig. 3. ORTEP drawing of $Cu(5\text{-}Br\text{-}phpyH)Cl^+$.

Table 3. Selected bond distances (Å) and angles (°) in $Cu(5\text{-}Br\text{-}phpyH)ClPF_6$

Cu(2)—Cl(3)	2.242(2)	Cu(2)—O(11)	2.363(5)
Cu(2)—N(13)	1.983(6)	Cu(2)—N(14)	2.048(5)
Cu(2)—N(15)	1.962(6)		

Cl(13)—Cu(2)—O(11)	103.7(2)	Cl(3)—Cu(2)—N(13)	97.8(2)
Cl(3)—Cu(2)—N(14)	167.9(2)	Cl(3)—Cu(2)—N(15)	97.0(2)
O(11)—Cu(2)—N(13)	88.0(2)	O(11)—Cu(2)—N(14)	88.4(2)
O(11)—Cu(2)—N(15)	93.4(2)	N(13)—Cu(2)—N(14)	82.9(2)
N(13)—Cu(2)—N(15)	164.4(2)	N(14)—Cu(2)—N(15)	81.6(2)

Table 4. Energies of HOMO and LUMO of *N*,*N*-dimethyl-*o*-hydroxy benzylamine and its derivatives (in the calculation, benzene ring is placed in *x*-*y* plane)

	HOMO/eV	LUMO/eV
X = H	−8.94[a]	0.37[b]
5-Br	−9.02	0.07
3,5-Br_2	−9.17	−0.23
5-NO_2	−9.80	−0.94

[a] HOMO is written as $-0.39p_z(O)-0.21p_z(C6)-0.51p_z(C5)+0.33p_z(C4)-0.19p_z(C3)+0.47p_z(C2)+0.39p_z(C1)$.

[b] LUMO is written as $0.07p_z(O)+0.55p_z(C6)-0.13p_z(C5)-0.37p_z(C4)-0.41p_z(C3)-0.22p_z(C2)+0.53p_z(C1)$.

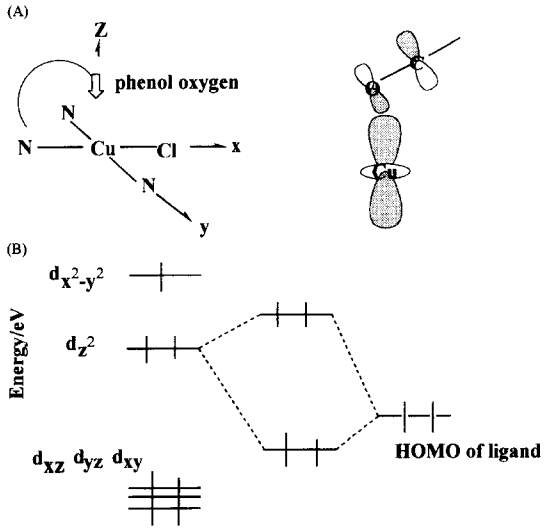

Fig. 4. (A) Interaction between HOMO of ligand and d_{z^2}-orbital of copper(II) ion. (B) Schematic illustration of relative energies of orbitals concerned. Bars (perpendicular) show an electron. As d_{z^2}-orbital is doubly occupied, this interaction induce destabilization of the complex, because HOMO of the ligand is also occupied by two electrons. Thus, the higher the energy of the HOMO, the longer the bond distance between copper(II) and phenol oxygen becomes.

REFERENCES

1. Avigad, G., Amaral, D., Asensio, C. and Hrecker, B., *J. Biol. Chem.*, 1962, **237,** 2736.
2. Ettinger, M. J. and Kosman, D. J. In *Copper Proteins*, ed. T. Spiro. Wiley Interscience, New York, 1982, pp. 193–218.
3. Whittaker, M. M. and Whittaker, J. W., *J. Biol. Chem.*, 1988, **263,** 6074.
4. Clark, K., P.-Hahn, J. E., Whittaker, M. M. and Whittaker, J. W., *J. Am. Chem. Soc.*, 1990, **112,** 6433.
5. Ito, N., Phillips, S. E. V., Stevens, C., Orgel, Z. B., McPherson, M. J., Keen, J. N., Yadav, K. D. S. and Knowles, P. F., *Nature*, 1991, **350,** 87.
6. Babcock, G. T., El.-Deeb, M. K., Sandusky, P. O., Whittaker, M. M. and Whittaker, J. W., *J. Am. Chem. Soc.*, 1992, **114,** 3727.
7. (a) Gagne, R. R., Coval, C. A., Smith, T. J. and Cimolino, M. C., *J. Am. Chem. Soc.*, 1979, **101,** 4571; (b) Karlin, K. D., Gultneh, Y., Nicholson, T. and Zubieta, J., *Inorg. Chem.*, 1985, **24,** 3725; (c) Nasir, M. S., Cohen, B. I. and Karlin, K. D., *J. Am. Chem. Soc.*, 1992, **114,** 2482; (d) Eisenstein, O., G.-Prettre, C., Maddaluno, J., Stussi, D. and Weber, J., *Arch. Biochem. Biophys.*, 1992, **296,** 247.
8. Uma, R., Viswanathan, R., Palaniandarev, M. and Lakshminarayanan, M., *J. Chem. Soc., Dalton Trans.*, 1994, 1219.
9. Toftlund, H. and Andersen, S. Y., *Acta Chim. Scand.*, 1981, **35A,** 575.
10. Kobayashi, T., Ito, S., Hamazaki, H., Ohba, S. and Nishida, Y., *Chem. Lett.*, 1996, 347.

Pergamon

PII: S00277-5387(97)00453-1

Polyhedron Vol. 17, No. 10, pp. 1643–1650, 1998
© 1998 Elsevier Science Ltd
All rights reserved. Printed in Great Britain
0277-5387/98 $19.00+0.00

Preparation of diaryl bimetallic compounds via nucleophilic substitution reactions of indenyl on tricarbonyl(η^6-4-fluorotoluene)chromium and tricarbonyl(η^6-4-fluoroanisole)chromium: molecular structure of 1-[tricarbonyl(η^6-4-toluene)chromium]-3-[tricarbonyl(η^6-4-anisole)chromium]-3-methylindene

Fung-E Hong,*[a] Shih-Ying Sun,[a] Sue-Lein Wang[b] and Fen-Ling Liao[b]

[a] Department of Chemistry, National Chung-Hsing University, Taichung 40227, Taiwan, R.O.C.

[b] Department of Chemistry, National Tsing-Hua University, Hsinchu 300, Taiwan, R.O.C.

(Received 21 July 1997; accepted 5 November 1997)

Abstract—1-[Tricarbonyl(η^6-4-toluene)chromium]-3-[tricarbonyl(η^6-4-anisole)chromium]indene (**7**) and 3-[tricarbonyl(η^6-4-toluene)chromium]-1-[tricarbonyl(η^6-4-anisole)chromium]indene (**7′**) were obtained as an isomeric mixture from the nucleophilic substitution of tricarbonyl(η^6-4-fluoroanisole)chromium (**6**) by deprotonated 3-[tricarbonyl(η^6-4-toluene)chromium]indene (**4**). Presumably, a 1,3-shift of a benzylic proton takes place during the formation of (**7**). The ratio of the two isomers is close to 1 : 1. 1-[Tricarbonyl(η^6-4-toluene)chromium]-3[tricarbonyl(η^6-4-anisole)chromium]-3-methylindene (**9**) was obtained as the only isolable product from the nucleophilic substitution of deprotonated 3-[tricarbonyl(η^6-4-toluene)chromium] methylindene (**8**) and 1-[tricarbonyl(η^6-4-toluene)chromium]methylindene (**8′**) with tricarbonyl(η^6-4-fluoroanisole)chromium (**6**). No proton shift was observed. Presumably, the nucleophilic substitutions take place directly on the fluorine-bearing carbon in all these cases. The new compounds were characterized by mass, infrared, ^{1}H, and ^{13}C NMR spectra. The molecular structure of (**9**) has been determined by an X-ray diffraction study. © 1998 Elsevier Science Ltd. All rights reserved

Keywords: nucleophilic substitution; hydride shift; diaryl bimetallic compounds.

The thermal, suprafacial vs antarafacial, sigmatropic 1,3- and 1,5-shifts of alkyl groups in geminally substituted cyclopentadienes is known to take place at elevated temperatures [1]. Our previous work provided some examples of 1,2- or 1,3-hydride migration around the cyclopentadienyl ring during the nucleophilic substitution of tricarbonyl (η^6-4-fluorotoluene)chromium (**1**) by cyclopentadienyl and related compounds at much lower reaction temperature (Schemes 1, 2) [2]. The reactions were carried out in tetrahydrofuran (THF) and hexamethylphosphoric triamide (HMPA) as cosolvent [3].

* Author to whom correspondence should be addressed.

It is known that the arene protons and the benzylic protons become more acidic in (arene)$Cr(CO)_3$, due to the strong electron-withdrawing ability of the $Cr(CO)_3$ fragment, and are thereby more easily removed [4]. Therefore, it was speculated that in the above reactions the benzylic protons of the presumably intermediates, (**2′**) or (**3′**) or (**4′**), were first pulled out by basic solvent forming their corresponding anionic species. Then, these anionic species abstracted protons from various sources and formed the corresponding neutral products, 1-tricarbonyl[(η^6-4-toluene)chromium]cyclopentadiene (**2**) or 1,4-bis[tricarbonyl(η^6-4-toluene)chromium] cyclopentadiene (**3**) or 3-[tricarbonyl(η^6-4-toluene)chromium]indene (**4**). The observed 1,2-

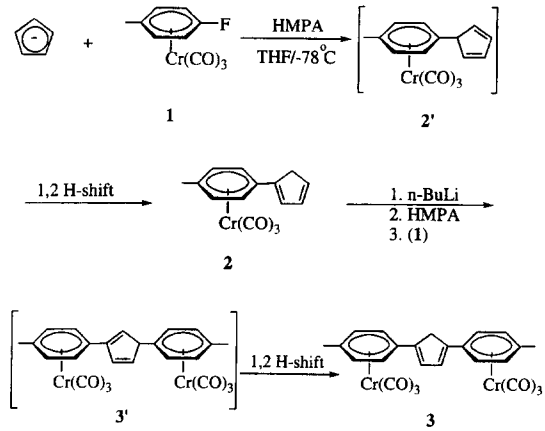

Scheme 1.

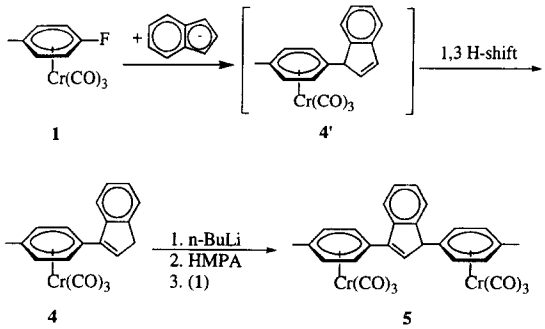

Scheme 2.

or 1,3-hydrogen shift at the end of the reaction resulted.

The fact that two distinct $-CH_3$ peaks were observed for 1,3-bis[tricarbonyl(η^6-4-toluene) chromium]indene (**5**) in one ^{1}H NMR spectrum is noteworthy (Scheme 2) [2b]. It implies that the benzylic proton does not become detached reversibly from compound **5** on the NMR timescale at room temperature as might be suggested. Otherwise, the molecule would be fluxional and it would not be possible to distinguish between the two $-CH_3$ groups [5]. It also suggests that the observed hydride shift must take place during the reaction not after it. It was therefore of interest to examine the factors which cause the hydrogen shift during the nucleophilic substitution reaction.

We also report the preparations and characterizations of some diaryl bimetallic compounds which have gained attention recently [6].

RESULTS AND DISCUSSION

The nucleophilic substitution of tricarbonyl(η^6-4-fluoroanisole)chromium (**6**) by deprotonated 3-[tricarbonyl(η^6-4-toluene)chromium] indene (**4**) was carried out in tetrahydrofuran first at $-78°C$ after which the reaction temperature was raised gradually to 25°C. A mixture of presumably 1-[tricarbonyl

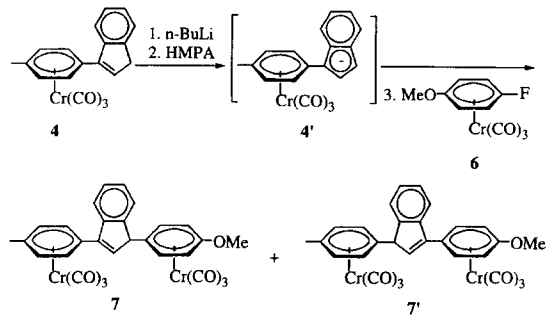

Scheme 3.

(η^6-4-toluene)chromium]-3-[tricarbonyl(η^6-4-anisole) chromium]indene (**7**) and 3-[tricarbonyl(η^6-4-toluene) chromium] - 1 - [tricarbonyl(η^6 - 4 - anisole)chromium] indene (**7′**) was yielded (Scheme 3). There were two sets of $-CH_3$ and $-OCH_3$ peaks observed in the ^{1}H NMR spectrum. Each set of peaks corresponds to one of the isomers, (**7**) or (**7′**). The ratio of these two isomers is close to 1 : 1 judging from the integration of their corresponding peaks in the ^{1}H NMR spectrum. It was further characterized by mass spectroscopy. Unfortunately, attempts to grow crystals were fruitless. The fact that two distinct sets of $-CH_3$ and $-OCH_3$ peaks were observed in the ^{1}H NMR spectrum was consistent with the previous observations on (**5**). It indicates that the conversion of these two isomers does not take place on the NMR timescale at room temperature.

A variable temperature ^{1}H NMR experiment was carried out for (**7**) and (**7′**) [7]. Since the structures of (**7**) and (**7′**) are very close and the benzylic proton is acidic, it was speculated that the conversion from (**7**) to (**7′**) or vice versa might be achieved simply by raising the temperature. The variable temperature ^{1}H NMR experiment for the isomers was conducted over the range 20°C to 70°C. Each measurement was taken at increments of 10°C. (Diagram 1). There was no significant change judging by the appearance of the spectra. This indicates that the conversion between (**7**) and (**7′**) on the NMR timescale cannot be achieved, at least below 70°C. The conversion did not happen when a small amount of THF, which was used as the solvent in the above reactions, was added to the solution.

A mixture of 3-[tricarbonyl(η^6-4-toluene)chromium] -1-methylindene (**8**) and its isomers, (**8′**) and (**8″**), was prepared by the procedures described in the Experimental Section (Scheme 5).

The nucleophilic substitution of tricarbonyl(η^6-4-fluoroanisole)chromium (**6**) by the deprotonated (**8**)

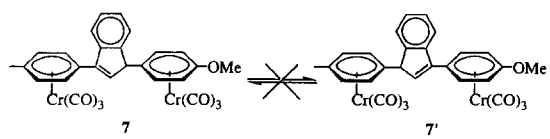

Scheme 4.

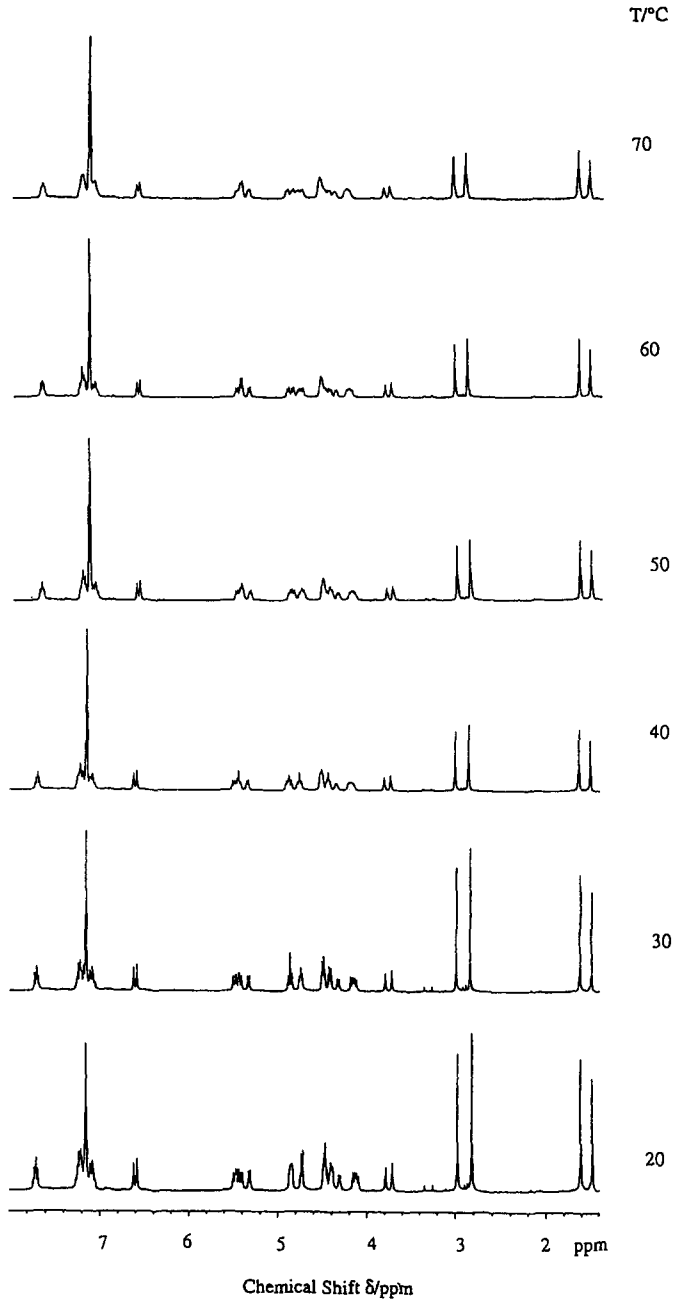

Diagram 1. Variable temperature ^{1}H NMR experiment for (**7**) and (**7′**)

and (**8′**) was carried out using similar reaction procedures to those described above (Scheme 6). Only one product, 1-[tricarbonyl(η^6-4-toluene)chromium]-3-[tricarbonyl(η^6-4-anisole)chromium]-1-methylindene (**9**), was obtained in this case.

Compound (**9**) was characterized by mass, infrared, and by ^{1}H and ^{13}C NMR spectra as well as by an X-ray crystal structure determination (Fig. 1). This shows that the two $Cr(CO)_3$ fragments are on opposite

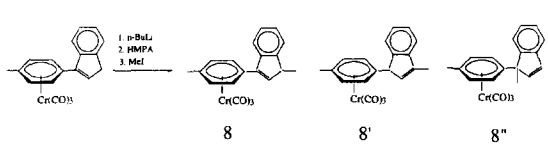

8 8′ 8″

Scheme 5.

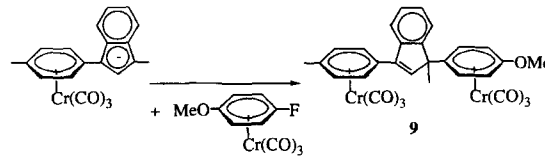

9

Scheme 6.

Table 1. Crystal data of **9**

Formula	$C_{30}H_{22}Cr_2O_7$
Formula weight	598.5
Crystal system	Monoclinic
Space group	$P2_1/c$
a (Å)	16.5315(2)
b (Å)	12.4787(1)
c (Å)	13.2708(1)
β (°)	101.981(1)
V (Å^3)	2678.0(7)
Z	4
D_{calc} (g cm^{-3})	1.484
λ (Mo–K$_\alpha$) (Å)	0.71073
μ (mm^{-1})	0.858
range (°)	2.5 to 57.8
Scan speed	10.00 seconds/frame
Scan range	0.30°/frame
Reflections collected	16,361
	($12{,}585 \geqslant 3.0\sigma(I)$)
Independent reflections	6323 ($R_{int} = 3.30\%$)
Observed reflections	($4712 \geqslant 3.0\sigma(I)$)
Refined parameters	353
[a] R_f for significant reflections	0.0386
[b] R_w for significant reflections	0.0507
[c] GOF	1.10

[a] $R_f = [\Sigma(F_o - F_c)/\Sigma F_o]$.
[b] $R_w = \Sigma w^{1/2}(F_o - F_c)/\Sigma w^{1/2} F_o$.
[c] GOF $= [\Sigma w(F_o - F_c)^2/(N_{rflns} - N_{params})]^{1/2}$.
$w^{-1} = \sigma^2(F) + 0.0010F^2$.

faces of the bridging ligand; this could be a result of packing effects in the solid state. The two (arene) $Cr(CO)_3$ fragments might actually rotate freely in solution. The bond lengths of C(21)—C(20) and C(21)—C(13) are 1.340 and 1.510 Å, respectively. Accordingly, the former is a typical double bond and the latter is a single bond (Table 2). The dihedral angles between the phenyl rings and the indenyl ring are 84° and 28°, respectively. The orientation of the $Cr(CO)_3$ in (arene)$Cr(CO)_3$ complexes has been the subject of extensive studies [8]. In our case, a staggered orientation was observed for the (methyl-arene) $Cr(CO)_3$ fragment, while an eclipsed orientation was observed for the (methoxy-arene)$Cr(CO)_3$ fragment.

The formation of (**9**) was a result of direct nucleophilic substitution. There was no alkyl group or 1,3-hydrogen shift observed after the substitution this contrasting with the result from the reaction shown in Scheme 2. Therefore, it is clear that the benzylic proton is necessary for the hydrogen shift. The methyl group could not be removed and further migration did not take place under these reaction conditions.

The organic moiety of (**9**), 1-(4-toluene)-3-(4-anisole)-1-methylindene, was obtained by exposing a CH_2Cl_2 solution of the complex to air. The metal free organic part was further purified and the conversion was shown to be almost quantitative. This demonstrates a pathway for making quaternary carbon which might be difficult to do in another way.

1-[Tricarbonyl(η^6-4-anisole)chromium]-3-[tricarbonyl(η^6-4-toluene)chromium]-1-methylindene, (**9′**), a structural isomer of (**9**), can be prepared and separated as the only product by the pathway shown in Scheme 7. However, an isomeric mixture of (**9**) and (**9′**) was obtained in a ratio of 1 : 1 from the reaction of deprotonated (**7**) and methyl iodide. This indicates that the observation of the single product (**9**) in Scheme 6 and (**9′**) in Scheme 7 is because of the different reaction pathways rather than being due to an energetic factor.

It seems reasonable to propose that the removal of the benzylic proton from the product of the nucleophilic substitution reaction is the key to the observed hydrogen shift. The reaction mechanism proposed is as follows. Firstly, the benzylic proton of the neutral product is removed by strong base(s) to form the anionic species. Then, this anionic species picks up a proton and forms the most stable structure(s). The end result is a hydrogen shift. There are, at least, two proton abstracting reagents capable of achieving the

Table 2. Selected bond distances (Å) and angles (°)

Cr(1)—C(7)	2.190(3)	Cr(1)—C(8)	2.241(3)
Cr(1)—C(9)	2.292(3)	Cr(1)—C(10)	2.237(3)
Cr(1)—C(11)	2.214(3)	Cr(1)—C(12)	2.241(3)
Cr(2)—C(22)	2.229(2)	Cr(2)—C(23)	2.217(3)
Cr(2)—C(24)	2.216(3)	Cr(2)—C(25)	2.237(3)
Cr(2)—C(26)	2.215(3)	Cr(2)—C(27)	2.210(2)
O(7)—C(9)	1.354(4)	O(7)—C(28)	1.439(4)
C(13)—C(14)	1.521(4)	C(13)—C(21)	1.510(4)
C(13)—C(29)	1.532(4)	C(14)—C(19)	1.400(4)
C(19)—C(20)	1.489(4)	C(20)—C(21)	1.340(3)
C(20)—C(22)	1.481(4)	C(25)—C(30)	1.505(5)

C(9)—O(7)—C(28)	117.3(3)	C(12)—C(13)—C(29)	112.6(2)
C(21)—C(13)—C(29)	110.8(2)	C(13)—C(14)—C(19)	110.3(2)
C(14)—C(13)—C(21)	101.0(2)	C(13)—C(21)—C(20)	112.4(2)
C(19)—C(20)—C(21)	108.9(2)		

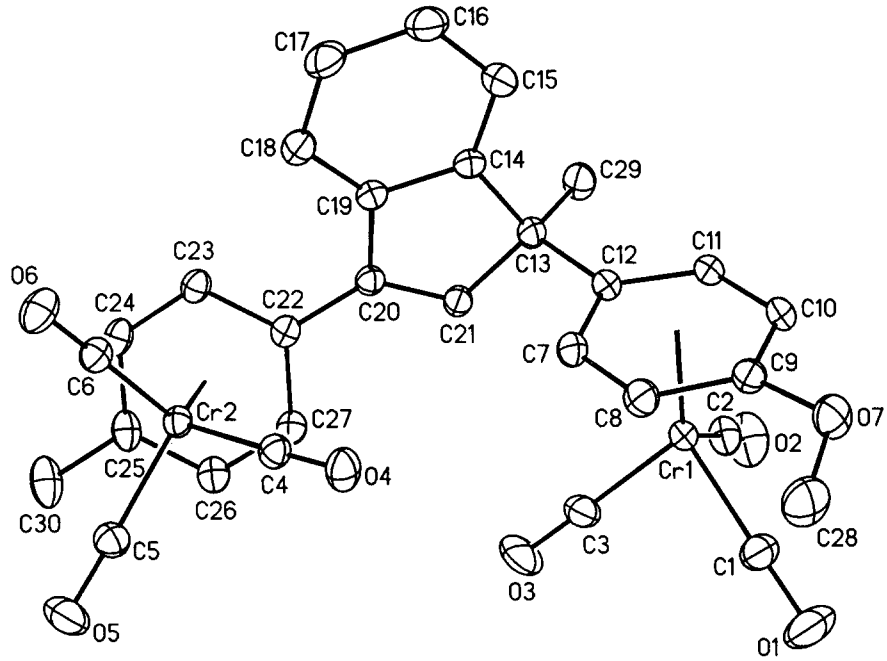

Fig. 1. ORTEP drawing with the numbering scheme of **9**. Hydrogen atoms are omitted for clarity.

deprotonation. The first one is *n*-BuLi. The benzylic proton might be abstracted by the excess *n*-BuLi. Secondly, the proton might be removed by an already deprotonated species such as deprotonated (**4**) or (**7**) in each case. The first possibility was examined as shown in Scheme 8. The isomeric mixture of (**7**) and (**7′**) was placed in a reaction flask this being followed by addition of *n*-BuLi and then by excess MeI [9]. The reaction mixture was allowed to stir for 2 h. The products, (**9**) and (**9′**), were characterized. It was shown that the benzylic proton had been replaced by a methyl group. This indicates that the *n*-BuLi is capable of removing the benzylic proton from the reactant(s). There was no reaction if *n*-BuLi was absent.

Another proton abstractor might be the deprotonated species obtained from the neutral species by addition of *n*-BuLi. This newly deprotonated species might abstract a benzylic proton from another neutral compound thereby forming a neutral species itself. This is demonstrated in Scheme 9. It shows that (**7a**), the deprotonated mixture of (**7**) and (**7′**), abstracts a benzylic proton from (**7**). The dissociated proton might attack (**7a**) at any available position and has an equal chance of forming (**7**) or (**7′**). This mechanism is capable of explaining why there are two isomers formed via the nucleophilic substitution reaction in Scheme 3 but only one product in Scheme 6.

The possibility that the deprotonated species is able to remove a benzylic proton is also supported by the following experiment (Scheme 10). In this experiment, the deprotonated (**4**) pulled out the benzylic proton of (**7**) and (**7′**) and resulted in the formation of (**9**) and (**9′**).

Another possible mechanism, modified from that proposed by Pauson and Brookhart, involving hydrogen migration via the metal would be consistent with our observed results, as demonstrated in Scheme 11

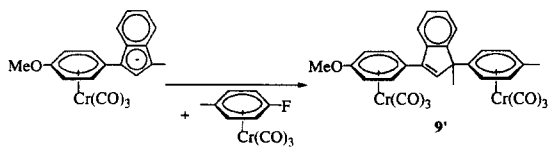

Scheme 7.

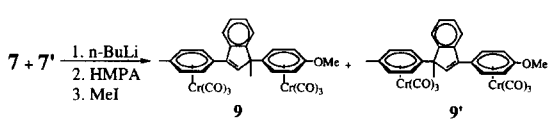

Scheme 8.

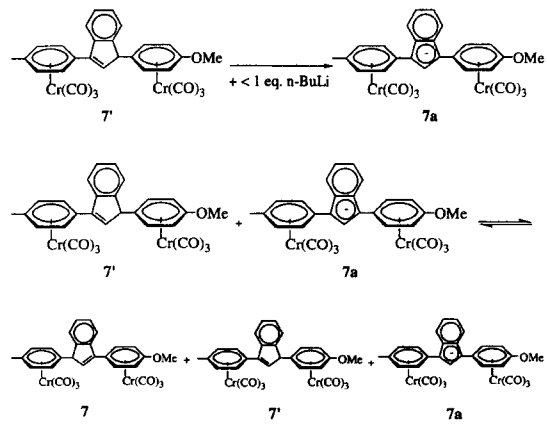

Scheme 9.

Table 3. Atomic coordinates ($\times 10^4$) and equivalent isotropic displacement coefficients ($Å^2 \times 10^3$)

	x	y	z	U(eq)
Cr(1)	1448(1)	5293(1)	2699(1)	40(1)
Cr(2)	4898(1)	2249(1)	2525(1)	41(1)
O(1)	1507(2)	7614(2)	3270(3)	108(1)
O(2)	538(2)	5964(3)	616(2)	100(1)
O(3)	2972(2)	5525(3)	1840(3)	97(1)
O(4)	4084(1)	3595(2)	3894(2)	62(1)
O(5)	6530(2)	3341(2)	3204(2)	82(1)
O(6)	5456(2)	604(2)	4166(2)	64(1)
O(7)	916(1)	5680(2)	4967(2)	61(1)
C(1)	1489(2)	6715(3)	3053(3)	63(1)
C(2)	873(2)	5689(3)	1418(3)	60(1)
C(3)	2390(2)	5445(3)	2178(3)	60(1)
C(4)	4421(2)	3070(2)	3398(2)	46(1)
C(5)	5894(2)	2927(2)	2959(2)	55(1)
C(6)	5238(2)	1236(2)	3539(2)	46(1)
C(7)	2003(2)	3850(2)	3494(2)	47(1)
C(8)	1901(2)	4589(2)	4268(2)	50(1)
C(9)	1107(2)	4991(2)	4264(2)	47(1)
C(10)	443(2)	4712(2)	3461(2)	47(1)
C(11)	559(2)	3966(2)	2699(2)	44(1)
C(12)	1341(2)	3503(2)	2720(2)	42(1)
C(13)	1485(2)	2597(2)	1984(2)	46(1)
C(14)	1754(2)	1622(2)	2659(2)	47(1)
C(15)	1331(2)	1096(3)	3316(3)	60(1)
C(16)	1724(3)	279(2)	3941(3)	69(1)
C(17)	2529(2)	15(3)	3923(3)	67(1)
C(18)	2962(2)	537(2)	3268(3)	57(1)
C(19)	2566(2)	1337(2)	2621(2)	45(1)
C(20)	2841(2)	2068(2)	1871(2)	42(1)
C(21)	2242(2)	2786(2)	1538(2)	44(1)
C(22)	3643(2)	2020(2)	1542(2)	43(1)
C(23)	4093(2)	1056(2)	1561(2)	47(1)
C(24)	4883(2)	1041(2)	1297(2)	52(1)
C(25)	5241(2)	1972(3)	1001(2)	55(1)
C(26)	4785(2)	2943(2)	965(2)	53(1)
C(27)	4008(2)	2969(2)	1228(2)	46(1)
C(28)	1589(3)	6101(3)	5729(3)	79(1)
C(29)	725(2)	2385(3)	1128(3)	61(1)
C(30)	6080(2)	1960(4)	729(3)	80(1)

* Equivalent isotropic U defined as one third of the trace of the orthogonalized U_{ij} tensor.

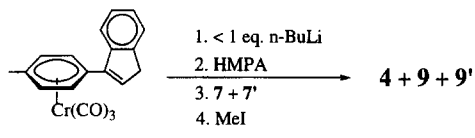

4

Scheme 10.

[10]. However, this is unlikely because of the long distance between the metal hydride and the positive charged carbon atom to be attacked.

In summary, it has been shown that both *n*-BuLi and the deprotonated product have the capacity to bring about the deprotonation which causes the

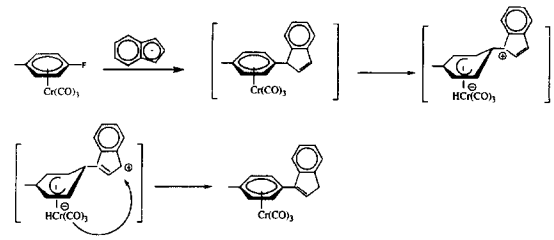

Scheme 11.

observed hydrogen shift. If *n*-BuLi is the only proton abstractor, the reaction will stop quickly after the total consumption of *n*-BuLi. It might not happen at all if the mole ratio of *n*-BuLi to the compound to be deprotonated is less than one mole equivalent. However, when less than one equivalent of *n*-BuLi was used in the reaction, the reaction still proceeded, even though, in lower yield. Therefore, it is very likely that the *n*-BuLi starts the reaction and the deprotonated species then takes over as the proton abstractor being itself converted to the product(s). Therefore, we propose that the deprotonated product abstracts the benzylic proton from the product of the direct nucleophilic substitution and itself forms the neutral compound(s). When the abstracted proton coordinates back to the deprotonated product forming the neutral product(s), it chooses to form the energetic favored structure(s). In this case, the favored structure(s) is the one with more and better conjugated double bonds in the molecule(s).

We have also been able to prepare diaryl bimetallic compounds through consecutive nucleophilic substitution and the structure of one of these compounds has been determined. We have also demonstrated that the organic moiety in the bimetallic compound (**9**), which might be difficult to make by a mere conventional method, can be obtained easily under mild oxidation conditions.

EXPERIMENTAL

Apparatus and materials

All operations were performed in a nitrogen-flushed glove box or in a vacuum system. Freshly distilled solvents were used. All processes of separation of the products were performed by Centrifugal Thin-Layer Chromatography (CTLC, Chromatotron, Harrison model 8924). ^1H and ^{13}C NMR spectra were recorded (Varian-300 spectrometer) at 300 and 75.46 MHz, respectively; chemical shifts are reported in ppm relative to internal TMS. IR spectra of solutions in $CHCl_3$ were recorded on a Hitachi 270-30 spectrometer. Mass spectra were recorded on a JOEL JMS-SX/SX 102A GC/MS/MS spectrometer.

Preparation of **7** *and* **7′**

Into a 40 cm^3 flask was placed (η^6-4-fluoroanisole)chromium (**4**) (0.214 g, 0.626 mmol), and the flask was then evacuated under reduced pressure for 10 min and finally filled with nitrogen. Anhydrous tetrahydrofuran (3 cm^3) was added to the reaction flask which was then cooled to −78°C (acetone-$N_{2(l)}$bath). Next, *n*-BuLi (1.6 M, 0.47 ml, 0.75 mmol) was added dropwise to the cold reaction flask. The deprotonation process was carried out at that temperature for 1.2 h and then HMPA (0.54 ml, 3.12 mmol) was added. Thirty minutes later, a solution of tricarbonyl(η^6-4-fluoroanisole)chromium (**6**) (0.20 g, 0.763 mmol) in 3 cm^3 of anhydrous THF was added slowly to the cold reaction mixture. The reaction was stirred at −78°C for another 3 h and gently warmed to 20°C during the next 16 h.

Subsequently, the resulting yellow solution was filtered through a small amount of silica gel. The filtrate was evaporated under reduced pressure to yield the crude product. On purification by centrifugal thin layer chromatography, a yellow band of 1-[tricarbonyl(η^6-4-anisole)chromium]-3-[tricarbonyl(η^6-4-toluene)chromium]indene (**7**) and 1-[tricarbonyl(η^6-4-toluene)chromium]-3-[tricarbonyl(η^6-4-anisole)chromium]indene (**7′**) was isolated (0.212 g, 58%).

Characterization of **7** *and* **7′**

^{1}H NMR($CDCl_3$): δ 2.17 (3H, —CH_3 in (toluene)$Cr(CO)_3$), 2.27 (3H, —CH_3 in (toluene)$Cr(CO)_3$), 3.69 (3H, —OCH_3 in (anisole)$Cr(CO)_3$), 3.78 (3H, —OCH_3 in (anisole)$Cr(CO)_3$), 4.25 (1H, indenyl), 4.30 (1H, indenyl), 5.05, 5.12, 5.33, 5.52, 5.68, 5.81, 5.95 (16H, arene in (toluene)$Cr(CO)_3$ and (anisole)$Cr(CO)_3$), 6.71 (2H, indenyl), 7.37, 7.67 (8H, arene in indenyl); ^{13}C NMR($CDCl_3$): δ 20.228, 20.358 (2C, Me), 51.965, 52.311 (2C, quaternary carbon in indenyl), 55.629, 55.770 (2C, —OCH_3), 77.222, 77.508, 77.977, 78.396, 92.292, 92.468, 92.860, 93.100, 93.244, 93.611, 93.692, 93.971, 95.194, 95.938, 102.190, 108.445, 109.594, 141.201, 141.325 (24C, (arene)$Cr(CO)_3$), 120.980, 121.146, 124.234, 126.678, 128.021, 129.005, 136.660, 137.242 (16C, indenyl), 233.163, 233.375, 233.674, 233.773 (3C, 3CO); IR(CH_2Cl_2): $\nu_{(CO)}$ 1886.6, 1965.7 cm^{-1}; MS *m/z* 584 (P^+).

Synthesis of **9**

The experimental procedures were similar to those given above. A mixture of **8** and **8′** (0.215 g, 0.604 mmol) was first deprotonated by *n*-BuLi (1.6 M, 0.45 ml, 0.72 mmol) then a solution of tricarbonyl(η^6-4-fluoroanisole)chromium (**6**) (0.190 g, 0.772 mmol) was added slowly to the reaction mixture. Purification of the resulting yellow solution was carried out on CTLC. A yellow band of 1-methyl-1-[tricarbonyl(η^6-4-anisole)chromium]-3-[tricarbonyl(η^6-4-toluene)chromium]indene (**9**) was isolated (0.125 g, 35%). In addition, a small amount of unreacted (**8**) and (**8′**) were recovered.

Characterization of **9**

^{1}H NMR ($CDCl_3$): δ 1.67 (3H, —CH_3 in indenyl), 2.27 (3H, —CH_3 in (toluene)$Cr(CO)_3$), 3.68 (3H, —OCH_3 in (anisole)$Cr(CO)_3$), 4.94, 5.08, 5.36, 5.82 (4H, (anisole)$Cr(CO)_3$), 5.36, 5.82 (4H, (toluene)$Cr(CO)_3$), 6.63 (1H, indenyl), 7.37, 7.62 (4H, arene in indenyl); ^{1}H NMR (C_6D_6): δ 1.39 (3H, —CH_3 in indenyl), 1.60 (3H, —CH_3 in (toluene)$Cr(CO)_3$), 2.81 (3H, —OCH_3 in (anisole)$Cr(CO)_3$), 4.13, 4.48, 5.34, 5.54 (4H, (anisole)$Cr(CO)_3$), 4.41, 5.16 (4H, (toluene)$Cr(CO)_3$), 6.53 (1H, indenyl), 7.71, 7.02 (4H, arene in indenyl); ^{13}C NMR ($CDCl_3$): δ 20.516 (1C, Me), 21.388 (1C, Me), 53.062 (1C, quaternary carbon in indenyl), 55.614 (1C, —OCH_3), 77.231, 93.549 (2C, (toluene)$Cr(CO)_3$), 92.659, 93.006, 93.237, 94.171 (4C, (anisole)$Cr(CO)_3$), 100.396, 105.838, 108.230 (3C, *ipso* of (arene)$Cr(CO)_3$), 121.417, 122.831, 126.859, 127.828, 138.544, 139.717, 143.585, 144.199 (8C, indenyl), 152.496 (1C, *ipso* of (anisole)$Cr(CO)_3$), 233.042, 233.495 (6CO); IR($CHCl_3$); $\nu_{(CO)}$ 1965.0, 1886.6 cm^{-1}; MS *m/z* 598 (P^+).

Characterization of **9′**

^{1}H NMR ($CDCl_3$): δ 1.69 (3H, —CH_3 in indenyl), 2.16 (3H, —CH_3 in (toluene)$Cr(CO)_3$), 3.77 (3H, —OCH_3 in (anisole)$Cr(CO)_3$), 4.94, 5.10, 5.33, 5.69 (4H, (toluene)$Cr(CO)_3$), 5.27, 5.98 (4H, (anisole)$Cr(CO)_3$), 6.67 (1H, indenyl), 7.36, 7.62 (4H, arene in indenyl); ^{13}C NMR ($CDCl_3$): δ 20.143 (1C, Me), 21.176 (1C, Me), 53.224 (1C, quaternary carbon in indenyl), 55.791 (1C, —OCH_3), 77.268, 79.031 (2C, (anisole)$Cr(CO)_3$), 91.090, 91.788, 93.530, 93.625 (4C, (toluene)$Cr(CO)_3$), 93.773, 94.186, 96.612 (3C, *ipso* of (arene)$Cr(CO)_3$), 110.194, 121.361, 122.954, 126.949, 127.951, 138.564, 142.400, 143.864 (8C, indenyl), 152.622 (1C, *ipso* of (anisole)$Cr(CO)_3$), 233.251, 234.048 (6CO); IR($CHCl_3$): $\nu_{(CO)}$ 1964.2, 1886.2 cm^{-1}; MS *m/z* 598 (P^+).

Preparation of **11** *and* **12**

Into a 50 cm^3 flask was placed (**9**) (0.10 g) and 20 cm^3 of CH_2Cl_2. The solution was exposed to air and sunlight for about 20 min. The green precipitate was separated and the filtrate was passed through a small amount of silica gel. The filtrate was evaporated under reduced pressure to yield the crude product. On purification by centrifugal thin-layer chromatography (eluent: hexane), a colorless band of (**11**) was isolated. The conversion to **11** from **9** is almost quantitative.

The experimental procedures for the preparation of **12** from **9′** were similar.

Characterization of **11**

^{1}H NMR ($CDCl_3$): δ 1.77 (3H, -CH_3 in indenyl), 2.41 (3H, —CH_3 in toluene), 3.77 (3H, —OCH_3 in anisole), 6.53 (1H, indenyl), 6.80, 7.24, 7.54 (m, 12H, arene in indenyl and toluene and anisole); ^{13}C NMR ($CDCl_3$): δ 21.290 (1C, Me), 23.068 (1C, Me), 54.894 (1C, quaternary carbon in indenyl), 55.223 (1C, —OCH_3), 113.725, 127.215, 127.544, 129.242 (8C toluene and anisole), 120.866, 123.026, 125.730, 126.503, 141.380, 142.100, 143.194, 154.603 (8C, indenyl), 132.684, 134.898, 137.485, 158.160 (4C, *ipso* of anisole and arene)); MS *m/z* 326 (P^+).

Characterization of **12**

^{1}H NMR ($CDCl_3$): δ 1.78 (3H, —CH_3 in indenyl), 2.30 (3H, —CH_3 in toluene), 3.87 (3H, —OCH_3 in anisole), 6.50 (1H, indenyl), 7.02–7.60 (m, 12H, arene in indenyl and toluene and anisole); ^{13}C NMR ($CDCl_3$): δ 20.785 (1C, Me), 22.848 (1C, Me), 55.075 (1C, quaternary carbon in indenyl), 55.266 (1C, —OCH_3), 114.065, 123.205, 126.188, 128.949 (8C, toluene and anisole), 113.589, 128.250, 140.147, 159.445 (4C, *ipso* of anisole and arene), 120.920, 125.89, 125.632, 129.231, 141.230, 142.436, 142.753, 154.681 (8C, indenyl); MS *m/z* 326 (P^+).

Crystal structure determination of **9**

A crystal of dimensions $0.21 \times 0.22 \times 0.45$ mm for $C_{30}H_{22}Cr_2O_7$ was selected for indexing and intensity data collection on a Seimens Smart-CCD diffractometer equipped with a normal focus, 3 kW sealed tube X-ray source. Intensity data were collected in 1271 frames with increasing ω (width of 0.3° per frame). Unit cell dimensions were determined by a least-squares fit of 8192 reflections with $5 < 2\theta < 50°$. Absorption correction was based on 10465 symmetry-equivalent reflections using the SHELTL-PC program package ($T_{min,max}$ = 0.821, 0.912). On the basis of systematic absence, statistics of intensity distribution, and successful solution and refinement of the structure, the space group was determined to be $P2_1/c$ (No. 14).

Acknowledgment—We thank the National Research Council of the Republic of China (Grant NSC-86-2113-M-005-004) for support.

REFERENCES

1. (a) Mironov, V. A., Sobolev, E. V. and Elizarova, A. N., *Tetrahedron*, 1963, **19,** 1939; (b) Roth, W. R., *Tetrahedron Lett.*, 1964, **17,** 1009; (c) McLean, S. and Haynes, P., *Tetrahedron Lett.*, 1964, **34,** 2385; (d) Ceccon, A., Gambaro, A., Gorttardi, F., Mannoli, F. and Venzo, A., *J. Organomet. Chem.*, 1989, **363,** 91; (e) Krekels, J. M. E., de Haan, J. W. and Kloosterziel, H., *Tetrahedron Lett.*, 1970, **32,** 2751.
2. (a) Hong, F.-E., Lo, S.-C., Liou, M.-W., Chou, L.-F. and Lin, C.-C., *J. Organomet. Chem.*, 1996, **516,** 123; (b) Hong, F.-E., Yang, Y.-C., Lo, S.-C. and Lin, C.-C., *Polyhedron*, 1977, **16,** 2005; (c) Ceccon, A., Gambaro, A., Gorttardi, F., Mannoli, F. and Venzo, A., *J. Organomet. Chem.*, 1989, **363,** 91.
3. Hong, F.-E., Lo, S.-C., Liou, M.-W., Chang, Y.-T. and Lin, C.-C., *J. Organomet. Chem.*, 1996, **506,** 101.
4. (a) Hegedus, L. S., *Transition Metals in the Synthesis of Complex Organic Molecules*. University Science Books, Mill Valley, CA, 1994; (b) Collman, J. P., Hegedus, L. S., Norton, J. R. and Finke, R. G., *Principles and Applications of Organotransition Metal Chemistry*. University Science Books, Mill Valley, CA, 1987; (c) Davis, R. and Kane-Maguire, L. A. P., *Comprehensive Organometallic Chemistry*, Vol. 3, ed. G. Wilkinson, F. G. A. Stone and E. W. Abel. Pergamon Press, Oxford, 1982, p. 953, and references cited therein; (d) Semmelhack, M. F. In *Comprehensive Organometallic Chemistry II*, Vol. 12, ed. E. W. Abel, F. G. A. Stone and G. Wilkinson. Elsevier Science Inc., New York, U.S.A., 1995, p 979.
5. Crabtree, R. H., *The Organometallic Chemistry of the Transition Metals*, 2nd edn. John Wiley & Sons, New York, 1994, Chap. 10.
6. Kang, Y. K., Chung, Y. K. and Lee, Soon W., *Organometallics*, 1995, **14,** 4905.
7. The sample tube was sealed. The variable temperature ^{1}H NMR spectra were recorded at 300 MHz in $CDCl_3$ solution.
8. (a) Albright, T. A., Hofmann, P. and Hoffmann, R., *J. Am. Chem. Soc.*, 1977, **99,** 7546; (b) Albright, T. A. and Carpenter, B. K., *Inorg. Chem.*, 1980, **19,** 3092.
9. The R_f values of (**7**) and (**7′**) in TLC are very close and separation of these two compounds is rather difficult.
10. (a) Davies, S. G., *Organotransition Metal Chemistry Applications to Organic Synthesis*, Vol. 2. Pergamon Press, 1982, p. 170 and references therein; (b) Lamanna, W. and Brookhart M., *J. Am. Chem. Soc.*, 1980, **102,** 3490; (c) Munro, G. A. M. and Pauson, P. L., *Chem. Comm.*, 1976, 134.

Pergamon

PII: S0277-5387(97)00452-X

Polyhedron Vol. 17, No. 10, pp. 1651–1657, 1998
© 1998 Elsevier Science Ltd
All rights reserved. Printed in Great Britain
0277–5387/98 $19.00+0.00

Cyclometallated platinum compounds with N-benzylidenebenzylamines bearing trifluoromethyl groups. Crystal structure of [PtMe{3-(CF_3)C_6H_3CH=NCH_2Ph}(PPh_3)]

Margarita Crespo,*[a] Xavier Solans[b] and Mercè Font-Bardía[b]

[a] Departament de Química Inorgànica, Universitat de Barcelona, Diagonal 647, 08028 Barcelona, Spain

[b] Departament de Cristal.lografia, Mineralogia i Dipòsits Minerals, Universitat de Barcelona, Martí i Franqués s/n. 08028 Barcelona, Spain

(Received 11 September 1997; accepted 3 November 1997)

Abstract—The reaction of [$Pt_2Me_4(\mu$-$SMe_2)_2$] (**1**) with the imine 3-(CF_3)C_6H_4CH=NCH_2Ph (**2a**) yields the cyclometallated compound [PtMe{3-(CF_3)C_6H_3CH=NCH_2Ph}(SMe_2)] (**3a**) by selective metallation at the less hindered of the two *ortho* positions of the aryl ring followed by loss of methane. A similar reaction for imine 2-(CF_3)C_6H_4CH=NCH_2Ph (**2c**) yields the cyclometallated compound [PtMe{2-(CF_3)C_6H_3CH=NCH_2Ph}(SMe_2)] (**3c**). The reactions of these compounds with triphenylphosphine in (1 : 1) ratio produce compounds [PtMe{3-(CF_3)C_6H_3CH=NCH_2Ph}(PPh_3)] (**4a**) and [PtMe{2-(CF_3)C_6H_3CH=NCH_2Ph}(PPh_3)] (**4c**). The X-ray structure of **4a** is reported. An excess of triphenylphosphine produces metallacycle cleavage and [PtMe{3-(CF_3)C_6H_3CH=NCH_2Ph}(PPh_3)$_2$] (**5a**) is formed with the imine acting as a [C^-] unidentate ligand. Oxidative addition of methyl iodide to compounds **4a** and **4c** gives cyclometallated platinum(IV) complexes. Imines 3,5-(CF_3)$_2C_6H_3$CH=NCH_2Ph (**2b**) and 2-F-6-(CF_3)C_6H_3CH=NCH_2Ph (**2d**) fail to react with [$Pt_2Me_4(\mu$-$SMe_2)_2$] (**1**). © 1998 Elsevier Science Ltd. All rights reserved

Keywords: selective metallation; N-benzylidenebenzylamine; trifluoromethyl.

There has been considerable interest in cyclometallated platinum(II) compounds due to their photochemical, photophysical and electrochemical properties [1]. The most convenient way to prepare cyclometallated compounds is the initial coordination of the heteroatom followed by metallation [2]. In particular, polyfunctional Schiff bases such as N-benzylidenebenzylamines, are suitable ligands to study these reactions, and the ease of such processes depends on the basicity of the N-donor atom and the nature of the substituents adjacent to the C-donor atom.

We are currently studying the influence of different substituents in the carbon atom adjacent to the metallation position on the formation of platinacycles from N-benzylidenebenzylamines. While metallation at the position adjacent to a small electron-withdrawing fluorine atom is favoured [3], electron-donating groups such as methyl or methoxy groups inhibit the metallation process [4]. For chlorinated N-benzylidenebenzylamines, metallation at a position adjacent to a chlorine atom has been achieved; however, metallation at the less hindered position is preferred for 3-ClC_6H_4CH=NCH_2Ph [5]. These results indicate a subtle balance between the favourable electron-withdrawing ability and the unfavourable size of the chlorine substituent.

We now report the results obtained for analogous imines bearing trifluoromethyl groups adjacent to the metallation positions such as 3-(CF_3)C_6H_4CH=NCH_2Ph (**2a**) and 3,5-(CF_3)$_2C_6H_4$CH=NCH_2Ph (**2b**). The trifluoromethyl group was chosen as a substituent because its approximate electronegativity (3.2) is similar to the electronegativities of chlorine (3.2) or flu-

* Author to whom correspondence should be addressed.

orine (4.0) [6] although it is considerably larger. A comparison of the stereo-electronic parameters of different substituents is presented in Table 1 [7].

Furthermore, the presence of CF_3 groups in the *ortho* positions of the aryl ring such as for ligands 2-$(CF_3)C_6H_4CH{=}NCH_2Ph$ (**2c**) and 2-F-6-$(CF_3)C_6H_3CH{=}NCH_2Ph$ (**2d**), may lead to activation of C(aliphatic)—F bonds upon reaction with the platinum substrate.

RESULTS AND DISCUSSION

The reactions of $[Pt_2Me_4(\mu\text{-}SMe_2)_2]$ (**1**) with iminic ligands $ArCH{=}NCH_2Ph$ containing trifluoromethyl groups (**2a–2d**) were carried out in acetone and the results are shown in Scheme 1.

For imine 3-$(CF_3)C_6H_4CH{=}NCH_2Ph$ (**2a**), formation of cyclometallated compound $[PtMe\{3\text{-}(CF_3)C_6H_3CH{=}NCH_2Ph\}(SMe_2)]$ (**3a**) by *ortho*-metallation with loss of methane was achieved. As we have reported for analogous imines 3-$XC_6H_4CH{=}NCH_2Ph$ (X = Me, OMe, Cl), metallation occurred selectively at the less hindered of the two non-equivalent *ortho* positions of the benzal ring.

When imine 3,5-$(CF_3)_2C_6H_3CH{=}NCH_2Ph$ (**2b**) was exposed to **1** no reaction occurred. Previous results for analogous imines with different substituents in the carbon atoms adjacent to the metallation positions indicate that, although formation of platinacycles is achieved for F [3] or Cl [5] substituents, no reaction takes place for Me or MeO groups [4]. The failure to produce metallation can be related to an unfavourable combination of steric and electronic effects. For the highly electron-withdrawing trifluoromethyl group, steric effects alone account for the results observed.

The reaction of imine 2-$(CF_3)C_6H_4CH{=}NCH_2Ph$ (**2c**) with **1** produced compound $[PtMe\{2\text{-}(CF_3)C_6H_3CH{=}NCH_2Ph\}(SMe_2)]$ (**3c**) by C—H bond activation with loss of methane. Activation of the C(aliphatic)—F bond to yield a six-membered metallacycle was not observed.

In order to attempt the activation of a C(aliphatic)—F bond, imine 2-F-6-$(CF_3)C_6H_3CH{=}NCH_2Ph$ (**2d**) was tested. Activation of the C(aliphatic)—F bond was not observed upon reaction with **1**. This result is not unexpected since it has been reported that imine 2,6-$F_2C_6H_3CH{=}NCH_2Ph$ fails to react, and C—F activation is less likely for an aliphatic than for an aromatic carbon atom.

In contrast to the results observed for imines containing methyl or methoxy groups, coordination of the imine ligand to platinum through the nitrogen atom was not detected when the reaction of imines **2a–2d** with **1** was monitored by ^1H NMR spectroscopy. This result suggests that the metallation step is fast for **2a** and **2c**; for **2b** and **2d**, the electron-withdrawing ability of the CF_3 groups decreases the basicity of the nitrogen atom and prevents the formation of coordination compounds.

The reaction of compound **3a** with one equivalent of triphenylphosphine in acetone yielded the cyclometallated compound $[PtMe\{3\text{-}(CF_3)C_6H_3CH{=}NCH_2Ph\}(PPh_3)]$ (**4a**). When the reaction was carried out using a large excess of triphenylphosphine, the displacement of both the SMe_2 and the iminic nitrogen for two PPh_3 produced the cleavage of the metallacycle and the formation of compound $[PtMe\{3\text{-}(CF_3)C_6H_3CH{=}NCH_2Ph\}(PPh_3)_2]$ (**5a**). The formation of analogous compounds with the imine acting as a $[C^-]$ unidentate ligand has been previously reported for compounds containing a chlorine [5] or a fluorine [8] atom at C^5, and this has been attributed to unfavourable steric effects between the halogen atom and the methyl group. However, the result obtained for compound **3a** could only be explained on electronic grounds by assuming that a weaker Pt—N bond in *cis* may result from the electron-withdrawing ability of the CF_3 group.

The reaction of compound **3c** with triphenylphosphine in acetone yielded the cyclometallated compound $[PtMe\{2\text{-}(CF_3)C_6H_3CH{=}NCH_2Ph\}(PPh_3)]$ (**4c**) and, in this case, cleavage of the metallacycle was not observed even when a large excess of PPh_3 was used.

The reactions of **4a** and **4c** with methyl iodide were also studied. Oxidative addition of alkyl halides to square-planar platinum(II) complexes is well documented; in particular, studies concerning compounds $[PtMe_2(NN)]$ (where NN is a bidentate nitrogen donor ligand) have been reported and experimental evidence points to *trans* stereochemistry in the resulting platinum compounds [9,10]. This process is inhibited by the presence of highly electron-withdrawing groups, as in $[Pt(4\text{-}CF_3C_6H_4)_2(bipy)]$ or by steric hindrance as in $[Pt(2\text{-}MeC_6H_4)_2(bipy)$ [11]. In the latter case, the presence of the *ortho*-substituent may prevent attack at the platinum by blocking the coordination sites above and below the plane.

Upon addition of an excess of methyl iodide to

Table 1. Electronic and steric parameters for several substituents[a]

	σ_I	σ_R	E_S
F	0.50	−0.31	−0.46
Me	−0.05	−0.13	−1.24
OMe	0.27	−0.42	−0.55
Cl	0.46	−0.18	−0.97
CF_3	0.42	0.08	−2.4

[a] σ_I, σ_R, and E_S are inductive (*para*), mesomeric (*para*) and steric parameters, respectively, taken from Ref. [7]. H is taken as a standard, with a value 0. Positive σ values indicate electron-withdrawing groups, negative σ values indicate electron-donating groups and negative E_S values indicate unfavourable steric effects.

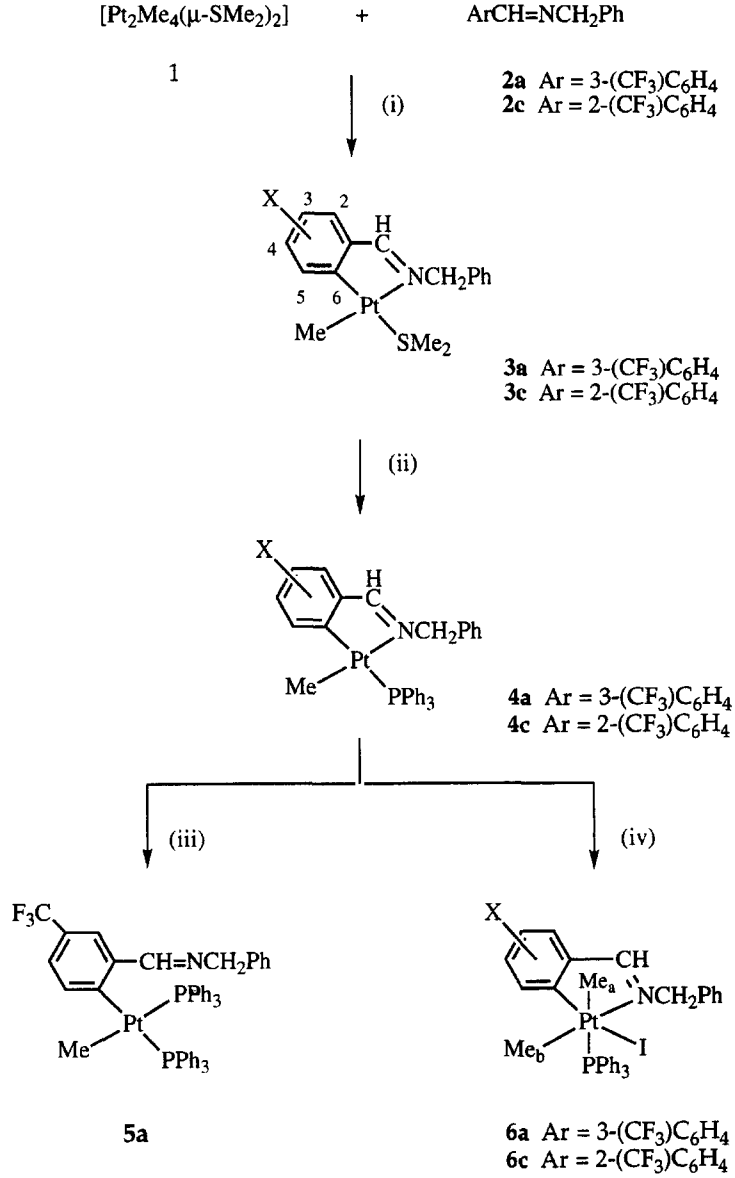

Scheme 1. (i) Acetone, room temperature, 16 h, C—CH_4 1 ; (ii) $+PPh_3$ (1 : 1), acetone, room temperature, 16 h ; (iii) $+PPh_3$ (5 : 1), acetone, room temperature, 16 h ; (iv) +HeI, acetone, room temperature, 2 h.

solutions of compounds **4** in acetone, the colour of the solution faded and compounds $[PtMe_2I\{(CF_3)C_6H_3CH{=}NCH_2Ph\}(PPh_3)]$ (**6**) were isolated. Thus, in this system, the presence of the electron-withdrawing group CF_3 does not prevent the oxidative addition; a similar result has been reported for fluorinated cyclometallated compounds [12]. Moreover, oxidative addition of methyl iodide takes place even when the bulky CF_3 group is in an *ortho* position of the aryl group as in **6c**.

Compounds **3a**, **3c**, **4a**, **4c**, **5a**, **6a** and **6c** were characterized by elemental analysis and ^1H and ^{19}F NMR spectra, together with ^{31}P NMR spectra for the phosphine derivatives. In the ^1H NMR spectra, the resonance for the methyl-platinum group, in all cases coupled to ^{195}Pt, appears as a singlet for compounds **3a** and **3c**, as a doublet due to coupling with one phosphorus atom for **4a** and **4c**, and as a doublet of doublets due to coupling with two non-equivalent phosphorus atoms for **5a**. For the latter compound, the coupling constant of the iminic hydrogen to platinum is much lower than that of cyclometallated compounds **3a** and **4a**. Two methyl-platinum resonances, coupled with ^{195}Pt and ^{31}P, appear for compounds **6**. The small value for the coupling constant of the axial methyl with platinum suggest a *trans* arrangement of

the axial methyl and the PPh_3, as previously observed for analogous compounds [13]. For all the compounds, the ^{19}F NMR spectra consist of a single resonance; the lack of platinum satellites for **3a** confirms that metallation occurred at position C^6. The ^{31}P NMR spectra consist of a single resonance for compounds **4** and **6**, and of a doublet of doublets for **5a**, in all cases with platinum satellites. Reduced coupling constants to platinum are observed for platinum(IV) compounds **6a** and **6c**.

Compound **4a** was also characterized crystallographically. Suitable crystals of **4a** were grown in acetone solution. The crystal structure is composed of discrete molecules separated by van der Waals distances. The structure is shown in Fig. 1 and the molecular dimensions are listed in Table 2. The coordination sphere of platinum is square-planar. The metallacycle is approximately planar; the largest deviation from the mean plane determined by the five atoms is 0.059 Å for C(6). The metallacycle is nearly coplanar with the coordination plane, the dihedral angle being 8.16°. The angles between adjacent atoms in the coordination sphere of platinum lie in the range 78.93(13)–98.97(9)°, the smallest angles corresponding to the metallacycle. Bond lengths in the coordination sphere of platinum are in the range expected for cyclometallated platinum compounds [4,8,13].

The results reported in this paper for N-benzylidenebenzylamines bearing trifluoromethyl groups indicate that the bulk of the CF_3 substituent inhibits the metallation at the adjacent positions. Thus, in contrast to the result obtained for chlorine substituents, the electron-withdrawing ability of the CF_3 group does not overcome its unfavourable steric effect. However, oxidative addition of methyl iodide to the obtained cyclometallated compounds is not prevented by the bulk of the CF_3 group due to the nearly coplanar arrangement of the metallacycle and the coordination plane.

EXPERIMENTAL

^1H and ^{31}P-$\{^1H\}$ NMR spectra were recorded by using Varian Gemini 200 (^1H, 200 MHz), Bruker WP80SY (^{31}P, 32.4 MHz), and Varian XL 300FT (^{19}F, 282.2 MHz; ^{31}P, 121.4 MHz) spectrometers, and referenced to $SiMe_4$ (^1H), H_3PO_4 (^{31}P) and CCl_3F (^{19}F). δ values are given in ppm and J values in Hz. Mic-

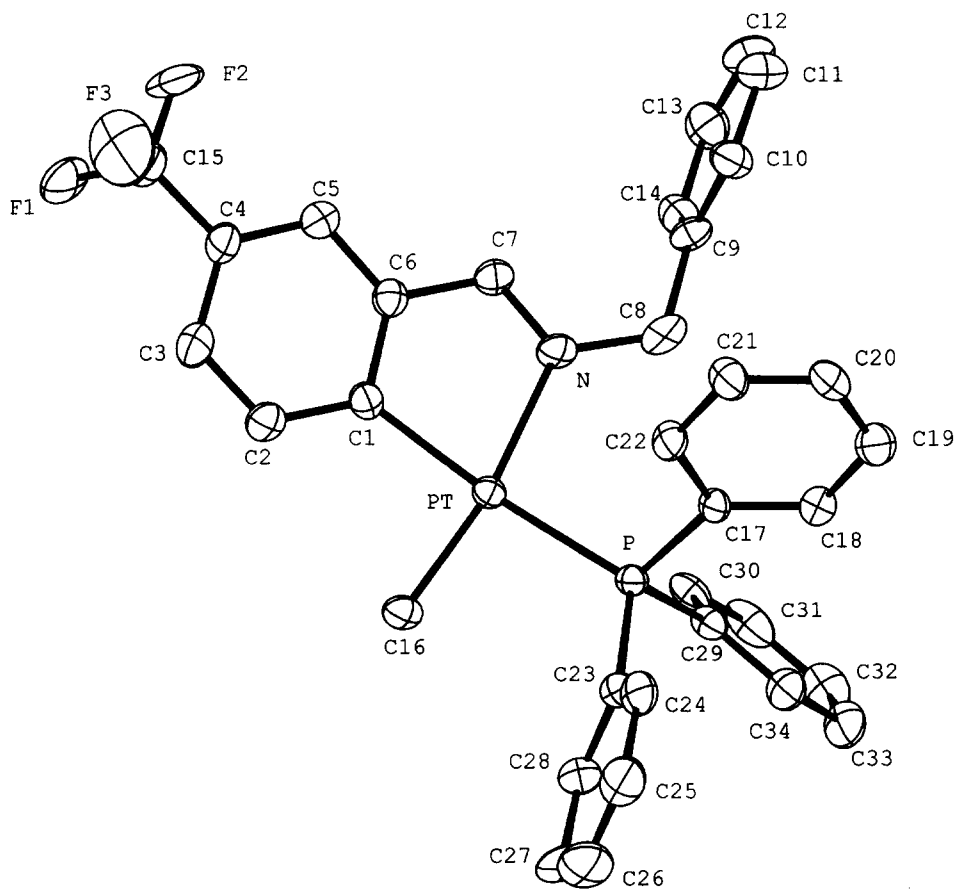

Fig. 1. Molecular structure of **4a**.

Table 2. Selected bond lengths (Å) and angles (°) for compound **4a** with estimated standard deviations in parentheses

Bond lengths			
Pt—C(1)	2.053(4)	N—C(7)	1.272(5)
Pt—C(16)	2.049(4)	N—C(8)	1.487(4)
Pt—N	2.148(3)	C(1)—C(6)	1.397(5)
Pt—P	2.2955(1)	C(4)—C(15)	1.491(6)
P—C(23)	1.822(3)	C(6)—C(7)	1.462(5)
P—C(29)	1.823(4)	C(8)—C(9)	1.488(5)
P—C(17)	1.828(3)	C(9)—C(10)	1.390(6)
Bond angles			
C(16)—Pt—C(1)	91.5(2)	C(23)—P—Pt	117.33(12)
C(16)—Pt—N	169.39(13)	C(29)—P—Pt	118.82(12)
C(1)—Pt—N	78.93(13)	C(17)—P—Pt	109.60(11)
C(16)—Pt—P	91.23(12)	C(7)—N—C(8)	120.3(2)
C(1)—Pt—P	170.04(10)	C(7)—N—Pt	113.5(2)
N—Pt—P	98.97(9)	C(8)—N—Pt	126.1(2)
N—C(7)—C(6)	118.3(3)	N—C(8)—C(9)	117.5(3)

roanalyses were performed by the Serveis Científico-Tècnics de la Universitat de Barcelona. Decomposition points were obtained with a Buchi 510 melting point instrument.

Preparation of the compounds

The complex $[Pt_2Me_4(\mu\text{-}SMe_2)_2]$ (**1**) was prepared by the method reported in the literature [14]. Compounds **2** were prepared by the reaction of 5 mmol of the corresponding aldehyde with 0.53 g (5 mmol) of the benzylamine in 25 ml of ethanol. The mixture was refluxed for 2 h and the solvent was removed in a rotary evaporator to yield yellow oils or white solids [15].

3-$(CF_3)C_6H_4CH{=}NCH_2Ph$ (**2a**). Yield: 1.0 g (76%). ^1H NMR ($CDCl_3$), $\delta = 4.86$ [s, CH_2], {7.35 [m], 7.56 [d, 1H], 7.66 [d, 1H], 7.96 [d, 1H], 8.07 [s], aromatics}, 8.43 [s, CHN]. ^{19}F NMR (acetone-d^6), $\delta = -69.29$ [s, CF_3].

3,5-$(CF_3)_2C_6H_3CH{=}NCH_2Ph$ (**2b**). Yield: 1.4 g (85%). ^1H NMR ($CDCl_3$), $\delta = 4.89$ [s, CH_2], {7.33 [m], 7.92 [s, 1H], 8.24 [s, 2H], aromatics}, 8.46 [s, CHN]. ^{19}F NMR (acetone-d^6), $\delta = -69.61$ [s, CF_3].

2-$(CF_3)C_6H_4CH{=}NCH_2Ph$ (**2c**). Yield: 1.1 g (84%). ^1H NMR ($CDCl_3$), $\delta = 4.87$ [s, CH_2], {7.34 [m], 7.53 [t, 1H], 7.66 [d, 1H], 8.26 [d, 1H], aromatics}, 8.77 [s, CHN]. ^{19}F NMR (acetone-d^6), $\delta = -63.82$ [s, CF_3].

2-F-6-$(CF_3)C_6H_3CH{=}NCH_2Ph$ (**2d**). Yield: 1.3 g (93%). ^1H NMR ($CDCl_3$), $\delta = 4.91$ [s, CH_2], {7.34 [m], 7.50 [m]}, 8.61 [s, CHN]. ^{19}F NMR (acetone-d^6), $\delta = -64.64$ [s, CF_3], -119.07 [s, F].

Compounds **3** were prepared by reaction of 100 mg (0.17 mmol) of $[Pt_2Me_4(\mu\text{-}SMe_2)_2]$ (**1**) with 0.35 mmol of the corresponding imine in acetone (25 ml). The mixture was stirred for 16 h and the solvent was removed in a rotary evaporator. The residue was washed with hexane (3 × 5 ml) and recrystallized in acetone (2 ml)/hexane (10 ml) to yield yellow-orange solids, which were filtered and washed with hexane (3 × 5 ml).

$[PtMe\{3\text{-}(CF_3)C_6H_3CH{=}NCH_2Ph\}(SMe_2)]$ (**3a**). Yield: 138 mg (74%) m.p. 115–118°C (d). Anal: calc. for $C_{18}H_{20}F_3NSPt$: C, 40.45; H, 3.77; N, 2.62. Found: C, 40.85; H, 3.93; N, 2.66. ^1H NMR (acetone-d^6), $\delta = 0.89$ [s, ^2J(HPt) = 83, Me], 1.97 [s, ^3J(HPt) = 27, SMe_2], 5.26 [s, ^3J(HPt) = 12, CH_2], {7.31 [m], 7.75 [m], aromatics}, 8.98 [s, ^3J(HPt) = 56, CHN]. ^{19}F NMR (acetone-d^6), $\delta = -63.96$ [s, CF_3].

$[PtMe\{2\text{-}(CF_3)C_6H_3CH{=}NCH_2Ph\}(SMe_2)]$ (**3c**). Yield: 140 mg (75%) m.p. 123–127°C (d). Anal: calc. for $C_{18}H_{20}F_3NSPt$: C, 40.45; H, 3.77; N, 2.62. Found: C, 40.85; H, 3.77; N, 2.62. ^1H NMR (acetone-d^6), $\delta = 0.89$ [s, ^2J(HPt) = 83, Me], 1.98 [s, ^3J(HPt) = 27, SMe_2], 5.38 [s, ^3J(HPt) = 10, CH_2], {7.32 [m], 7.90 [d, J(HPt) = 61, J(HH) = 8, 1H], aromatics}, 9.15 [s, ^3J(HPt) = 54, CHN]. ^{19}F NMR (acetone-d^6), $\delta = -59.97$ [s, ^5J(FPt) = 7, CF_3].

Compounds **4** were prepared by reaction of 50 mg (94 mmol) of the corresponding compound **3** with 25 mg (95 mmol) of PPh_3 in acetone (10 ml). The mixture was stirred at room temperature for 16 h. On addition of hexane (15 ml), yellow crystals were formed, and they were collected by filtration, washed with hexane (3 × 5 ml) and dried *in vacuo*.

$[PtMe\{3\text{-}(CF_3)C_6H_3CH{=}NCH_2Ph\}(PPh_3)]$ (**4a**). Yield: 50 mg (73%) m.p. 148°C (d). Anal: calc. for $C_{34}H_{29}F_3NPPt$: C, 55.59; H, 3.98; N, 1.91. Found: C, 55.72; H, 4.13; N, 2.12. ^1H NMR (acetone-d^6), $\delta = 0.74$ [d, ^2J(HPt) = 83, ^3J(HP) = 7, Me], 4.41 [s, ^3J(HPt) = 10, CH_2], {6.9 [m], 7.2 [m], 7.45 [m], 7.68 [m], aromatics}, 8.71 [s, ^3J(HPt) = 55, CHN]. ^{19}F

NMR (acetone-d^6), $\delta = -64.03$ [s, CF_3]. ^{31}P NMR (acetone), $\delta = 29.33$ [s, ^1J(PPt) = 2237].

[PtMe{2-(CF_3)C_6H_3CH=NCH_2Ph}(PPh_3)] (**4c**). Yield: 55 mg (80%) m.p. 145°C (d). Anal: calc. for $C_{34}H_{29}F_3NPPt$: C, 55.59; H, 3.98; N, 1.91. Found: C, 55.59; H, 4.01; N, 1.97. ^{1}H NMR (acetone-d^6), $\delta = 0.70$ [d, ^2J(HPt) = 82, ^3J(HP) = 7, Me], 4.47 [s, ^3J(HPt) = 9, CH_2], {6.8 [d, 2H], 7.21 [m], 7.43 [m], 7.61 [m], 8.05 [m, 1H], aromatics}, 8.83 [s, ^3J(HPt) = 58, CHN]. ^{19}F NMR (acetone-d^6), $\delta = -59.55$ [s, CF_3]. ^{31}P NMR (acetone), $\delta = 29.05$ [s, ^1J(PPt) = 2236].

Compound **5a** was prepared by reaction of 50 mg (94 mmol) of the corresponding compound **3a** with 120 mg (0.458 mol) of PPh_3 in acetone (10 ml). Within 1 h, the colour of the solution faded and a white precipitate was formed. After addition of hexane (10 ml), the white solid was collected by filtration, washed with hexane (3 × 5 ml) and dried *in vacuo*.

[PtMe{3-(CF_3)C_6H_3CH=NCH_2Ph}(PPh_3)$_2$] (**5a**). Yield: 80 mg (86%) m.p. 178°C (d). Anal: calc. for $C_{52}H_{44}F_3NP_2Pt$: C, 62.65; H, 4.45; N, 1.40. Found: C, 62.68; H, 4.62; N, 1.39. ^{1}H NMR (acetone-d^6), $\delta = 0.29$ [dd, ^2J(HPt) = 67, $^3J(HP_a)$ = 8, $^3J(HP_b)$ = 6, Me], {4.74 [d], 4.88 [d], ^2J(HH) = 13, *AB* pattern, CH_2], {6.5 [m], 6.7 [m], 7.2 [m], aromatics}, 9.52 [s, ^4J(HPt) = 10, CHN]. ^{19}F NMR (acetone-d^6), $\delta = -63.92$ [s, CF_3]. ^{31}P NMR (acetone), $\delta = 25.84$ [d, ^1J(PPt) = 1949, ^2J(PP) = 14], 26.18 [d, ^1J(PPt) = 1916, ^2J(PP) = 14].

Compounds **6** were prepared by reaction of 50 mg (68 mmol) of the corresponding compound **4** with an excess of methyl iodide (0.1 ml) in 10 ml of acetone. The mixture was stirred at room temperature for 2 h. On addition of hexane (15 ml), light yellow crystals were formed, and they were collected by filtration, washed with hexane (3 × 5 ml) and dried *in vacuo*.

[$PtMe_2$I{3-(CF_3)C_6H_3CH=NCH_2Ph}(PPh_3)] (**6a**). Yield: 50 mg (84%). Anal: calc. for $C_{35}H_{32}F_3INPPt$: C, 47.96; H, 3.68; N, 1.60. Found: C, 48.7; H, 4.0; N, 1.7. ^{1}H NMR (acetone-d^6), $\delta = 1.10$ [d, ^2J(HPt) = 60, ^3J(HP) = 8, Me_a], 1.59 [d, ^2J(HPt) = 70, ^3J(HP) = 8, Me_a], {4.74 [m], 5.65 [m], J(HH) = 16, *AB* system}, {6.7 [d, J(HH) = 8, J(HPt) = 43, 1H], 7.2 [m, 2H], 7.3 [m], 7.5 [m], aromatics}, 8.31 [s, ^3J(HPt) = 49, CHN]. ^{19}F NMR (acetone-d^6), $\delta = -65.18$ [s, CF_3]. ^{31}P NMR (acetone), $\delta = -9.63$ [s, ^1J(PPt) = 1021].

[$PtMe_2$I{2-(CF_3)C_6H_3CH=NCH_2Ph}(PPh_3)] (**6c**). Yield: 45 mg (75%). Anal: calc. for $C_{35}H_{32}F_3INPPt$: C, 47.96; H, 3.68; N, 1.60. Found: C, 47.9; H, 3.8; N, 1.7. ^{1}H NMR (acetone-d^6), $\delta = 1.08$ [d, ^2J(HPt) = 60, ^3J(HP) = 8, Me_a], 1.58 [d, ^2J(HPt) = 70, ^3J(HP) = 8, Me_a], {4.93 [m], 5.72 [m], J(HH) = 16, *AB* system}, {7.4 [m], 7.5 [m], aromatics}, 8.31 [s, ^3J(HPt) = 50, CHN]. ^{19}F NMR (acetone-d^6), $\delta = -61.02$ [s, CF_3]. ^{31}P NMR (acetone), $\delta = -9.85$ [s, ^1J(PPt) = 1015].

X-ray structure analysis, data collection

A prismatic crystal of **4a** was selected and mounted on an Enraf-Nonius CAD4 diffractometer. Unit cell parameters were determined from automatic centreing of 25 reflections ($12° < \theta < 21°$) and refined by least-squares method. Intensities were collected with graphite monochromatized Mo–K_α radiation, using $\omega/2\theta$ scan-technique. 8435 reflections were measured in the range $2.38° < \theta < 29.96°$, and 7202 were assumed as observed applying the condition $I > 2\sigma(I)$. Three reflections were measured every 2 h as orientation and intensity control, significant intensity decay was not observed. Lorentz-polarization and absorption corrections were made. Further details are given in Table 3.

Table 3. Crystallographic data and details of the refinements for compound **4a**

Formula	$C_{34}H_{29}F_3NPPt$
FW	734.64
Crystal system, Space group	triclinic, $P\bar{1}$
a, b, c (Å)	9.102(5), 12.162(2), 14.726(5)
α, β, γ (°)	108.90(2), 104.17(4), 98.31(3)
V (Å^3)	1450.1(10)
D_{calc} (g cm^{-3})	1.682
Z	2
F(000)	720
Crystal size (mm^3)	0.1 × 0.1 × 0.2
μ (Mo–K_α)	54.14
λ (Mo–K_α) (Å)	0.71069
Temperature (K)	293(2)
Reflections collected	8435
R	0.0297
$wR(F^2)$	0.0707
Refined parameters	469
Max. shift/esd	6.6
Max. and min. diff. peaks (e Å^{-3})	0.385 and −0.222

Structure solution and refinement

The structure was solved by direct methods, using SHELXS Computer Program [16], and refined by the full-matrix least-squares method, with the SHELX93 computer program [17] using 8435 reflections. The function minimized was $\Sigma w\|F_o|^2-|F_c|^2|^2$, where $w=[\sigma^2(I)+(0.0462P)^2]^{-1}$ and $P=(|F_o|^2+2|F_c|^2)/3$.f, f' and f'' were taken from International Tables of X-Ray Crystallography [18]. Fluorine atoms of CF_3 groups were located in disorder positions. An occupancy factor of 0.5 was assigned according to the height of Fourier synthesis. 19 hydrogen atoms were located from a difference synthesis and 10 hydrogen atoms were computed and refined with an overall isotropic temperature factor using a riding model. The final R factors, the number of refined parameters, and the maximum and minimum peaks in the final difference synthesis are given in Table 3.

Acknowledgments—We acknowledge financial support from the DGICYT (Dirección General de Investigación Científica y Técnica, Ministerio de Educación y Ciencia, Spain, PB 96-0164 project) and from the Generalitat de Catalunya (1995-SGR-0044 project).

REFERENCES

1. (a) Maestri, M., Deuschel-Cornioley, C. and von Zelewsky, A., *Coord. Chem. Rev.*, 1991, **111,** 117; (b) Minghetti, G., Pilo, M. I., Sanna, G., Seeber, R., Stoccoro, S. and Laschi, F., *J. Organomet. Chem.*, 1993, **452,** 257; (c) von Zelewsky, A., Suckling, A. P. and Stoeckli-Evans, H., *Inorg. Chem.*, 1993, **32,** 4585; (d) Mdleleni, M. M., Bridgewater, J. S., Watts, R. J. and Ford, P. C., *Inorg. Chem.*, 1995, **34,** 2334; (e) Kvam, P. I., Puzyk, M. V., Balashev, K. P. and Songstad, J., *Acta Chemica Scandinavica*, 1995, **49,** 335; (f) Gianini, M., Forster, A., Haag, P., von Zelewsky, A. and Stoeckli-Evans, H., *Inorg. Chem.*, 1996, **35,** 4889; (g) Jolliet, P., Gianini, M., von Zelewsky, A., Bernardinelli, G. and Stoeckli-Evans, H., *Inorg. Chem.*, 1996, **35,** 4883.
2. (a) Ryabov, A. D., *Chem. Rev.*, 1990, **90,** 403; (b) Omae, I., *Coord. Chem. Rev.*, 1988, **83,** 137.
3. Crespo, M., Martinez, M. and Sales, J., *Organometallics*, 1993, **12,** 4297.
4. Crespo, M., Solans, X. and Font-Bardía, M., *J. Organomet. Chem.*, 1996, **509,** 29.
5. Crespo, M., Solans, X. and Font-Bardía, M., *J. Organomet. Chem.*, 1996, **518,** 105.
6. Nyholm, R. S., *Quart. Rev.*, 1970, **24,** 1.
7. March, J., in *Advanced Organic Chemistry*, J. Wiley, New York, 1985, pp. 242–250.
8. Crespo, M., Solans, X. and Font-Bardía, M., *Organometallics*, 1995, **14,** 355.
9. (a) Scott, J. D. and Puddephatt, R. J., *Organometallics*, 1985, **4,** 1221; (b) Scott, J. D. and Puddephatt, R. J., *Organometallics*, 1986, **5,** 1538; (c) Crespo, M. and Puddephatt, R. J., *Organometallics*, 1987, **6,** 2548.
10. Crespo, M., *Polyhedron*, 1996, **15**(12), 1981.
11. Jawad, J. K. and Puddephatt, R. J., *J. Chem. Soc., Dalton Trans.*, 1977, 1466.
12. López, O., Crespo, M., Font-Bardía, M. and Solans, X., *Organometallics*, 1997, **16,** 1233.
13. Crespo, M., Solans, X. and Font-Bardía, M., *J. Organomet. Chem.*, 1994, **483,** 187.
14. Scott, J. D. and Puddephatt, R. J., *Organometallics*, 1983, **2,** 1643.
15. Bigelow, L. A. and Ealough, H., in *Organic Syntheses*, Vol. 1, ed. A. H. Blatt, J. Wiley. New York, 1944, Collect.
16. Sheldrick, G. M., *Acta Cryst.*, 1990, **A46,** 467.
17. Sheldrick, G. M., SHELX 93. *A computer program for crystal structure refinement.* University of Gottingen, Germany, 1993.
18. *International Tables of X-Ray Crystallography*, Vol. IV, Kynoch, Birmingham, 1974, pp. 99–100 and 149.

Pergamon

PII: S0277-5387(97)00451-8

Polyhedron Vol. 17, No. 10, pp. 1659–1675, 1998
© 1998 Elsevier Science Ltd
All rights reserved. Printed in Great Britain
0277-5387/98 $19.00+0.00

Synthesis and structural characterization of two interesting sandwich and double sandwich type mixed-valent tellurium-dithiocarbamate complexes; $[Te^{IV}\{S_2CN(C_2H_5)_2\}_3]_2[Te^{II}\{S_2CN(C_2H_5)_2\}_2](PF_6)_2$ and $[Te^{IV}\{S_2CN(C_2H_5)_2\}_3][Te^{II}\{S_2CN(C_2H_5)_2\}_2](ClO_4)$

R. Krishna Kumar,[a,*,‡] G. Aravamudan,[a,*] M. Seshasayee,[b] Kandasamy Sivakumar,[c,†] Hoong-Kun Fun[c] and Israel Goldberg[d]

[a] Department of Chemistry, Indian Institute of Technology, Madras 600036, India

[b] Department of Physics, Indian Institute of Technology, Madras 600036, India

[c] X-ray Crystallography Unit, School of Physics, Universiti Sains Malaysia, 11800 USM, Penang, Malaysia

[d] School of Chemistry, Tel Aviv University, 69978 Ramat Aviv, Israel

(Received 25 August 1997; accepted 3 November 1997)

Abstract—Two novel mixed-valent tellurium(II and IV) dithiocarbamate complexes have been prepared and their structures determined by X-ray diffraction studies. Complex **1**, $[Te^{IV}(S_2CNEt_2)_3]_2[Te^{II}(S_2CNEt_2)_2](PF_6)_2$, was obtained from the metathesis reaction of $[Te^{IV}(S_2CNEt_2)_3ClO_4]$ with KPF_6 due to the partial reduction of the primary product $[Te^{IV}(S_2CNEt_2)_3]PF_6$, which is thermodynamically unstable. The preparation of tellurium(IV) dithiocarbamate in dilute perchloric acid medium results in complex **2**, which has a composition $[Te^{IV}(S_2CNEt_2)_3][Te^{II}(S_2CNEt_2)_2](ClO_4)$. These two complexes represent the first examples of mixed valent complexes of tellurium consisting only the sulphur ligands. Their structural investigation shows that these complexes are stabilized primarily due to the supramolecular Te···Te interaction, the distance of which is shorter than the earlier known complex. While $Te^{II}(S_2CNEt_2)_2$ is sandwiched between two $Te^{IV}(S_2CNEt_2)_3$ molecules in **1**, two such Te(II) molecules are sandwiched in complex **2**. © 1998 Elsevier Science Ltd. All rights reserved

Keywords: tellurium-dithiocarbamate complexes; mixed-valent; supramolecular interactions; crystal structures.

One of the most interesting aspects in studies involving tellurium complexes with sulphur containing ligands, in both Te^{II} and Te^{IV} oxidation states, is their stereochemical activity and supramolecular associations [1]. Tellurium, in the aforementioned oxidation states, is known to exhibit a wide range of coordination geometries. Complexes with monodentate sulphur ligands, particularly thiourea and its derivatives, have been characterized structurally relatively well [2]. The geometry around tellurium in these complexes reflects the bonding ability of tellurium. However, bidentate 1,1-dithiolate ligands, such as dithiocarbamates, xan-

* Author to whom correspondence should be addressed.

† On leave from Department of Physics, Anna University, Madras 600025, India.

‡ Presently at School of Chemistry, Tel Aviv University.

thates and dithiophosphates exhibit a greater structural diversity in their tellurium coordination chemistry owing to their small bite. Apart from being excellent chelating agents, these ligands produce strong distortion in the coordination geometries around the central tellurium, compared to the monodentate ligands. Another important aspect which determines the coordination geometry in the tellurium complexes is presence of the lone pair(s) of electrons, which in some cases are stereochemically active, occupying the vertices of the coordination polyhedra, while in many other cases they are stereochemically inactive.

The neutral dithiocarbamate complexes of tellurium in both +II and +IV oxidation states are very well known [3]. Our earlier work in the mixed halide-dithiocarbamate complexes, combined with the results from other groups shows the diverse nature in the geometry exhibited by tellurium [4]. In mixed iodide-dithiocarbamate complexes of tellurium(II and IV), when the number of ligand atoms cannot satisfy the preferred coordination number, then bridging through the iodide results leadings to dimeric or polymeric structures [4a–c]. Despite the structural characterization of many tellurium complexes with sulphur ligands, their structures still remain largely unpredictable. Moreover, when the preferred coordination number of tellurium cannot be satisfied by the ligands of the specific molecular composition, then organization of the molecules in the crystal takes place in such a way as to have supramolecular interaction, which results in an extended coordination. This provides a strong motivation for our continuing studies in the chemistry of the dithiocarbamate complexes of tellurium.

Here we report the preparation and the characteristic structural features observed in two such complexes. In order to see what could be the geometrical features in the six-coordinated tris(dithiocarbamato)tellurium(IV) complex, if we are able to isolate that species with the non-coordinating PF_6^- anion, we obtained complex **1** of composition $[Te^{IV}\{(C_2H_5)_2NCS_2\}_3]_2Te^{II}\{(C_2H_5)_2NCS_2\}_2](PF_6)_2$. Complex **2** was obtained from the reaction of sodium tellurite with diethyldithiocarbamate in 4N perchloric acid.

RESULTS AND DISCUSSION

Syntheses and general properties

Complex **1** resulted from an attempted isolation of the $Te(S_2CNEt_2)_3PF_6$ species by reaction of $Te(S_2CNEt_2)_3ClO_4$ with KPF_6 in methanol–dichloromethane mixture. However the resultant compound, crystallized from dichloromethane with few drops of ethylacetate, conformed to the composition $[Te(S_2CNEt_2)_3]_2[Te(S_2CNEt_2)_2](PF_6)_2$. The reaction of sodium tellurite in 4N perchloric acid with sodium diethyldithiocarbamate resulted in **2**. Recrystallization in dichloromethane–ethylacetate mixture afforded black crystals. Both the compounds were characterized by elemental analyses. The infrared spectra exhibits the characteristic bands of the dithiocarbamate and that due to PF_6 and ClO_4 anions in their respective complexes. The complexes **1** and **2** are the first examples of a mixed-valent complex of tellurium containing only the sulphur ligands.

When a dichloromethane solution of $[Te(S_2CNEt_2)_3ClO_4]$ was reacted with the methanolic solution of KPF_6, immediate precipitation of $KClO_4$ takes place. The resultant $[Te(S_2CNEt_2)_3]PF_6$, due to its inherent instability undergoes a partial reduction and hydrolysis to yield **1** as one of the products. The most probable mechanistic pathway for such a reaction is given in Scheme 1.

$$2[Te^{IV}(S_2CNEt_2)_3]PF_6 \rightleftharpoons Te^{II}(S_2CNEt_2)_2 + [Te^{IV}(S_2CNEt_2)_2](PF_6)_2 + Et_2NC(S)SSC(S)NEt_2$$

$$[Te^{IV}(S_2CNEt_2)_2](PF_6)_2 + 2H_2O \rightarrow TeO_2 + 2(Et_2NCS_2)^- + 4H^+ + 2PF_6^-$$

$$[Te^{IV}(S_2CNEt_2)_2](PF_6)_2 + (Et_2NCS_2)^- \rightarrow [Te^{IV}(S_2CNEt_2)_3]PF_6 + PF_6^-$$

the overall reaction is,

$$10[Te^{IV}(S_2CNEt_2)_3]PF_6 + 2H_2O \rightarrow 3[Te^{IV}(S_2CNEt_2)_3]_2[Te^{II}(S_2CNEt_2)_2(PF_6)_2 + TeO_2 + 3Et_2NC(S)SSC(S)NEt_2 + 4HPF_6$$

Scheme 1.

The coordinatively unsaturated $[Te^{IV}(S_2CNEt_2)_3]PF_6$ first undergoes a partial autoreduction, as shown in Scheme 1, to $Te^{II}(S_2CNEt_2)_2$, tetraethylthiuramdisulphide, which is the oxidation product of the dithiocarbamate, and $[Te^{IV}(S_2CNEt_2)_2](PF_6)_2$. The resultant bis(diethyldithiocarbamato)tellurium(IV) dication is very unstable and as a result hydrolyzes slowly in the presence of water in methanol to tellurium oxide. The liberated dithiocarbamate combines with the dication and stabilizes it from further hydrolysis. The $Te^{II}(S_2CNEt_2)_2$ forms an adduct with tris(diethyldithiocarbamato)-tellurium(IV) cation, to give **1**. The final products formed are **1**, tellurium oxide, disulphide and HPF_6.

The reaction of aqueous sodium tellurite with the dithiocarbamate ligand in acidic conditions is used for the preparation of tetrakis(diethyldithiocarbamato)tellurium(IV). In 4N perchloric acid medium, and when methanol was used for dissolving the dithiocarbamate, $[Te^{IV}(S_2CNEt_2)_3(ClO_4)]$ was obtained as the sole product [5]. The structural study of this complex shows that the two oxygen atoms of the perchlorate anion are also coordinated to tellurium, so that the tellurium(IV) attains its pre-

ferred coordination number of 8, which is responsible for the stability of this complex. If water is used for dissolving the dithiocarbamate, the product obtained is **2**, representing an adduct of $[Te^{IV}(S_2CNEt_2)_3](ClO_4)$ and $Te^{II}(S_2CNEt_2)_2$ in 1:1 molar ratio. The tellurium(IV) is partially reduced by the dithiocarbamate to tellurium(II). This reduced tellurium(II) complexes with the dithiocarbamate and this complex stabilizes the already formed tris-(diethyldithiocarbamato)tellurium(IV) cation to yield adduct **2** as shown in equation 1.

$$2Na_2Te^{IV}O_3 + 12HClO_4 + 7NaS_2CNEt_2 \rightarrow \mathbf{2} + Et_2NC(S)SSC(S)NEt_2 + 11NaClO_4 + 6H_2O \quad (1)$$

Compound **2** undergoes hydrolytic decomposition very easily. In the presence of trace amount of water, the tellurium(IV) species undergoes hydrolysis to give tellurium oxide, while at the same time liberating the free dithiocarbamate. For each mole of $[Te^{IV}(S_2CNEt_2)_3]^+$ converting to TeO_2, three moles of the free dithiocarbamate are released, which in turn complexes with the unhydrolysed $[Te^{IV}(S_2CNEt_2)_3]^+$ to give $Te^{IV}(S_2CNEt_2)_4$. Thus the products of hydrolysis are $Te^{IV}(S_2CNEt_2)_4$, $Te^{II}(S_2CNEt_2)_2$ and TeO_2. This clearly shows that the driving force for the formation of the adduct is the presence of the coordinatively unsaturated $[Te^{IV}(S_2CNEt_2)_3]^+$ species. Once the saturation of coordination occurs by complexing with the fourth dithiocarbamate, the tellurium(II) complex is freed as shown in Scheme 2.

$$\mathbf{2} + H_2O \rightarrow [Te^{IV}(S_2CNEt_2)_3OH] + Te^{II}(S_2CNEt_2)_2 + HClO_4$$

$$[Te^{IV}(S_2CNEt_2)_3OH] + H_2O \rightarrow Te^{IV}O_2 + 3Et_2NCS_2^- + 3H^+$$

$$\mathbf{2} + (Et_2NCS_2)^- \rightarrow Te^{IV}(S_2CNEt_2)_4 + Te^{II}(S_2CNEt_2)_2 + ClO_4^-$$

the overall reaction is,

$$4[Te^{IV}(S_2CNEt_2)_3][Te^{II}(S_2CNEt_2)_2]ClO_4 + 2H_2O \rightarrow Te^{IV}O_2 + 3Te^{IV}(S_2CNEt_2)_4 + 4Te^{II}(S_2CNEt_2)_2 + 4HClO_4$$

Scheme 2.

In $[Te(S_2CNR_2)_3]X$ (where X = I, Br, Cl or SCN) [6], Te has a distorted pentagonal bipyramid geometry with the X atom occupying one of the axial positions, where the seventh coordination site is occupied by X. However, the isolation of the species, $[Te(S_2CNEt_2)_3]^+$, as such is difficult. In the perchlorate salt of this complex, the two oxygen atoms of the perchlorate are coordinated to Te, so that it was eight-coordinated with a distorted dodecahedron geometry. In the present instance the isolation of $[Te(S_2CNEt_2)_3]^+$ has become possible due to its adduct formation with $Te^{II}(S_2CNEt_2)_2$ through weak Te(II)···Te(IV) interaction. The complexes **1** and **2** differ only in the ratio of the Te(IV) and Te(II).

Structural characterization

The detailed structural study of title complexes show some very interesting features. The structure of **1** can be described as consisting of two independent tellurium complexes, $[Te^{IV}(S_2CNEt_2)_3]PF_6$ and $Te^{II}(S_2CNEt_2)_2$ in the ratio of 2:1 (Fig. 1), with the $Te^{II}(S_2CNEt)_2$ moiety sandwiched between two $Te^{IV}(S_2CNEt_2)_3$ molecules as shown in the crystal packing diagram (Fig. 2). This sandwich type structure is held together by means of short Te···Te and weak Te---S interactions. Each Te(IV) is seven-coordinated; six primary coordinations, by the S atoms of three dithiocarbamate ligands, and one secondary coordination, to Te(II), if the short Te···Te interaction is also taken into account. The Te(II), on the other hand, has a coordination number of six. It is coordinated by the four S atoms of the two dithiocarbamates and by the two Te(IV) atoms in the axial positions.

The tetravalent tellurium Te(1) is in a general position, whereas the divalent tellurium Te(2) sits on a two-fold axis (0, *y*, 1/4). The six primary coordination sites of Te(1) are occupied by the sulphur atoms of the three dithiocarbamate ligands. The Te—S bond distances ranges between 2.434–2.804 Å, with all the three dithiocarbamates bound in anisobidentate manner to the tellurium. The occurrence of such long distances Te—S bonds for these complexes have been explained on the basis of the three-centre four-electron bond concept [7]. All the Te—S distances and S—Te—S angles are similar to that observed in other $[Te(S_2CNR_2)_3]X$ compounds. In the $Te^{II}(S_2CNEt_2)_2$ moiety, the tellurium atom sits on a crystallographic special position and only one dithiocarbamate forms a part of the asymmetric unit. The two dithiocarbamates are coordinated in an anisobidentate manner (the Te—S distances being 2.487 and 2.859 Å) and the two axial positions are occupied by the Te(IV) atoms. In the previously known examples of $Te^{II}(S_2CNR_2)_2$ [8], the geometry around the tellurium atom is planar trapezoidal with one of the S—Te—S angles being very large (about 145°). Hence it could be interpreted as a planar pentagonal, with one of the corners missing. As Te(2) is on a two-fold axis, the $Te^{II}(S_2CNR_2)_2$ in **1** is symmetrically disposed. With two Te(1) atoms above and below, the geometry around Te(2) can be described as a distorted octahedron with the angle axial Te(1)—Te(2)—Te(1′) angle being 161.43°.

The shortest Te(IV)—S distance of 2.434 Å in the present instance, is incidentally, of that of axial sul-

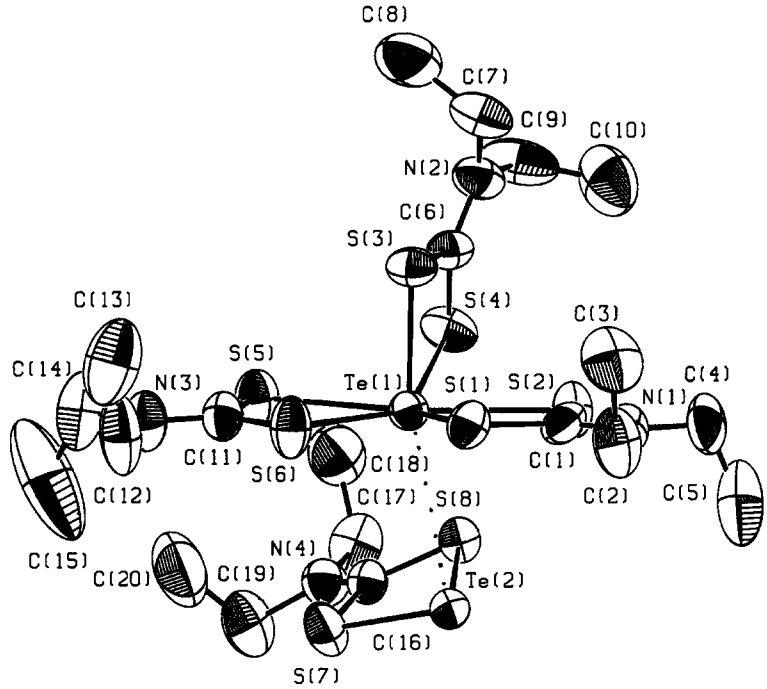

Fig. 1. An ORTEP plot of the cationic complex $\{[Te^{IV}\{S_2CN(C_2H_5)_2\}_3]\ 0.5[Te^{II}\{S_2CN(C_2H_5)_2\}_2]^+\}$ of **1** present in the asymmetric unit, drawn with 50% probability ellipsoids. Te^{II} is present on a crystallographic two-fold axis. The symmetry related half of the molecule and the hydrogen atoms are omitted for clarity.

phur atom (S3). This axial Te—S bond is *trans* to the Te···Te interaction and hence produces a *trans* bond lengthening effect on the Te—Te bond. The Te···Te distance of 3.390 Å is greater than the sum of the covalent radii of tellurium atoms (2.72 Å) [9] but close to the sum of the atomic radii of Te (3.28 Å), if the three-centre four-electron radii of Te is taken into account [7]. However in the latter case the radii was computed based on the square planar tellurium(II) complexes with monodentate ligands. This distance is also considerably shorter than the distance of 3.542 Å observed in the only previous known example [10] of a mixed valent Te(IV)—Te(II) complex $[I(Pr^i_2NCS_2)Te^{II}(\mu\text{-}I)Te^{IV}(S_2CNPr^i_2)_2I]$ containing the sulphur ligands. However in the already known example, iodide bridges the two tellurium atoms and the Te···Te interaction is only secondary. The one other known example [11] containing a Te—Te bond, with sulphur ligands coordinated to Te, is TeL_2-TeLSCN, and the distance observed there is 3.221 Å. However, both the telluriums here are in +II oxidation state.

Apart from the Te···Te interaction, the crystal structure is stabilized by Te---S secondary interactions. Te(1) has weak interaction with S(8), the sulphur atom bound to Te(2) at a distance of 3.500 Å. However, Te(II) has four such interactions, with

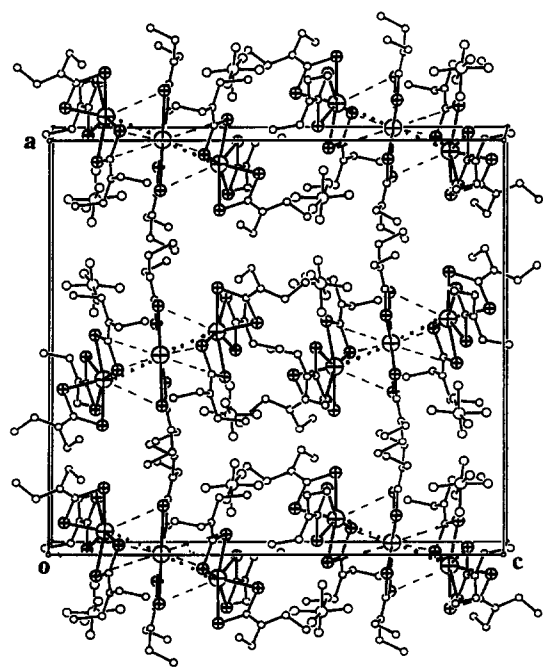

Fig. 2. The packing of the molecules of **1** in the unit cell illustrating the Te···Te interaction, the secondary Te---S interactions and the sandwich type arrangement.

two symmetry related S(1) and S(2) atoms at distances of 3.885 and 3.890 Å.

In complex **2** also there are two independent Te(IV) and Te(II) dithiocarbamate complexes $[Te^{IV}(S_2CNEt_2)_3]ClO_4$ and $Te^{II}(S_2CNEt_2)_2$ (Fig. 3), however in the ratio of 1 : 1. The structural difference with **1** arises basically due to the interleaving of another Te(II)-dithiocarbamate between the Te(II) and Te(IV) complexes, the two $Te^{II}(S_2CNEt_2)_2$ molecules being sandwiched between two $[Te^{IV}(S_2CNEt_2)_3]$ moieties as shown in Fig. 4.

The $Te^{IV}(S_2CNEt_2)_3$ moiety in this complex also is made of three anisobidentate dithiocarbamates and with almost similar geometrical features as that of **1** (Te—S distances ranges between 2.474–2.805 Å). Te(1) has six primary coordinations, with a pentagonal pyramidal geometry. When the secondary Te···Te interaction is also taken into account the geometry becomes pentagonal bipyramidal. The Te—S(3) bond distance (2.473 Å) in **2** is a bit longer than that in **1**, which again reflects in the Te···Te interaction, *viz.* shortening by almost similar magnitude. Thus, the Te···Te interaction of 3.347 Å is shorter than in **1**. There is a secondary interaction between Te(1) and S(8) of distance 3.601 Å, which essentially shows that the geometry around the Te(IV) centre is conserved as in **1**.

The main difference between the crystal structures of **1** and **2** lies around the Te(II) centre. The geometry around Te(2) in **2** is unlike in **1**. But it is similar to

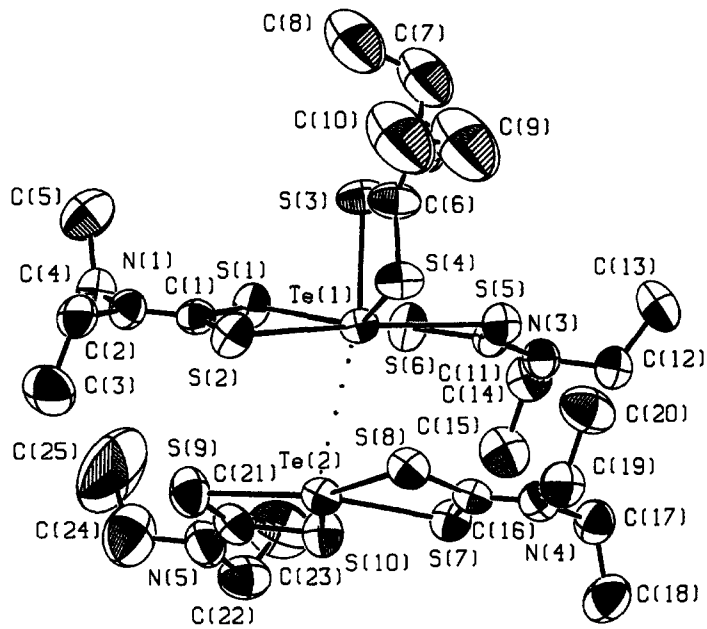

Fig. 3. An ORTEP plot of the cationic complex $\{[Te^{IV}\{S_2CN(C_2H_5)_2\}_3]\ [Te^{II}\{S_2CN(C_2H_5)_2\}_2]^+\}$ of **2** drawn with 50% probability ellipsoids. N(2) is hidden behind the atoms C(9) and C(10). The hydrogen atoms are omitted for the sake of clarity.

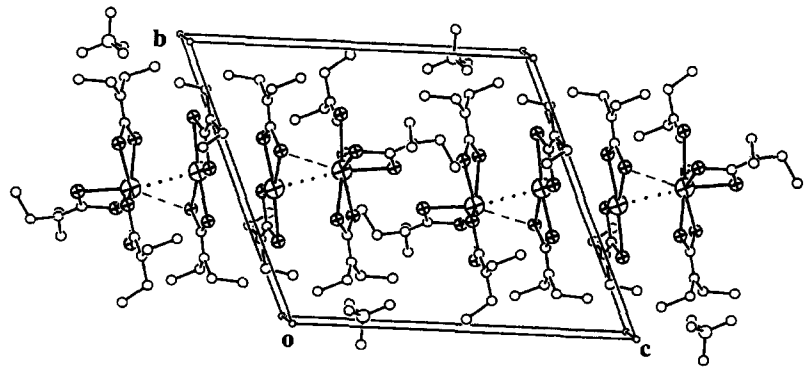

Fig. 4. The packing diagram of the molecules of **2** in the unit cell illustrating the Te···Te interaction, the secondary Te---S interactions and the double sandwich type arrangement.

that observed in the other structures, with one small and one large interligand S—Te—S angles (79.5 and 147.8°). If the Te···Te interaction is also taken into consideration, then the geometry becomes capped trapezoid. The Te(II)···Te(II) distance is rather large, and is close to the sum of the van der Waal's radii of the tellurium atoms (4.40 Å) [12], to be thus considered as a secondary interaction. There is just one more Te---S secondary interaction involving Te(II), which is with S(2) at a distance of 3.853 Å.

EXPERIMENTAL

Tellurium dioxide, sodium diethyldithiocarbamate and potassium hexafluorophosphate were used as obtained commercially. Dichloromethane, methanol and ethylacetate were distilled and stored over molecular sieves before use. The complex $Te\{(C_2H_5)_2NCS_2\}_3ClO_4$ was prepared as described previously [5]. The C, H and N analyses of the complexes were performed using a Heraeus CHN-O-RAPID analyser.

Preparation of $[Te^{IV}\{S_2CN(C_2H_5)_2\}_3]_2[Te^{II}\{S_2CN(C_2H_5)_2\}_2](PF_6)_2$ (**1**)

$Te\{(C_2H_5)_2NCS_2\}_3ClO_4$ (0.134 g, 0.2 mmol) was dissolved in dichloromethane (10 cm^3). A methanol solution (10 cm^3) of KPF_6 (0.076 g, 0.4 mmol) was then added to it with stirring. The white precipitate of $KClO_4$ was filtered off and the clear solution kept aside for solvent evaporation at room temperature. The gummy residue obtained was recrystallized in 10:1 *v/v* mixture of dichloromethane–ethylacetate, which yields small brown crystals of **1** (yield 70%). Found: C, 25.9; H, 4.2; N, 6.1. Calc. for $C_{40}H_{80}N_8S_{16}P_2F_{12}Te_3$: C, 25.9; H, 4.3; N, 6.0%.

Preparation of $[Te^{IV}\{S_2CN(C_2H_5)_2\}_3][Te^{II}\{S_2CN(C_2H_5)_2\}_2](ClO_4)$ (**2**)

Tellurium dioxide (0.040 g, 0.25 mmol) was dissolved in 1M NaOH (10 cm^3) in a beaker. This solution was then acidified by 4N perchloric acid (25 cm^3). To the clear solution, sodium diethyldithiocarbamate (0.281 g, 1.25 mmol) dissolved in water was added at room temperature with constant stirring. A red precipitate of **2** was formed and was filtered immediately. The precipitate was then air dried, dissolved in dichloromethane and washed thrice with 1N perchloric acid (10 cm^3). The clear red solution was then dried over anhydrous sodium sulphate to remove any moisture. The solvent was evaporated and the red residue washed repeatedly with CCl_4 (10 cm^3). Recrystallization in 10:1 *v/v* mixture of dichloromethane and ethylacetate yield dark black crystals of **2** (yield 60%). Found: C, 27.4; H, 4.7; N, 6.4. Calc. for $C_{25}H_{50}N_5S_{10}ClO_4Te_2$: C, 27.4; H, 4.6; N, 6.4%. The red gummy residue obtained along with it was identified as a mixture of $Te^{IV}\{S_2CN(C_2H_5)_2\}_4$ and $Te^{II}\{S_2CN(C_2H_5)_2\}_2$, formed as a result of hydrolysis of **2**. They were removed by a rapid washing with methanol. Small amounts of insoluble tellurium dioxide formed was discarded.

X-ray crystallography

The X-ray diffraction experiments were carried out at room temperature on automated Siemens P4 diffractometer (complex **1**) and Enraf-Nonius CAD4 (complex **2**) diffractometers with graphite monochromator. Cell constants and the orientation matrix for the data collection were obtained by least squares refinement of 25 carefully chosen high angle reflections. The crystal data and pertinent details of the experimental conditions are summarized in Table 1. The intensity data were collected by θ–2θ and ω–2θ scan modes, respectively, for **1** and **2**. Three standard reflections from different zones of the reciprocal space were measured periodically, with no significant variation in the intensity. Absorption correction based on ψ-scans was applied to the data of complex **1** ($T_{min} = 0.690$ and $T_{max} = 0.959$) while for data of complex **2** no corrections were employed.

The crystal structures were solved by direct methods (SHELXS-86) [13]. Their refinement were carried out by full-matrix least-squares method using SHELXL-93 [14]. The refinement calculations were based on F^2; the hydrogen atoms were introduced at calculated positions. In both the cases the refinements converged at a reasonably low *R*-value (Table 1), allowing a reliable description of the atomic parameters and of the intermolecular interactions involving tellurium and dithiocarbamate sulphurs. The weighting schemes employed during refinement were $w = 1/[\sigma^2|F_o| + (0.1517P)^2]$ and $1/[\sigma^2|F_o| + (0.0488P)^2 + 3.76P]$ where $P = [\max(F_o^2, 0) + 2|F_c|^2]/3$ for **1** and **2**, respectively. However some difficulties were encountered in the refinement procedure, similar to those typically observed in these types of compounds. The $(PF_6)^-$ anion of **1** was disordered and no correct model could be assigned for the disorder. All the fluorine atoms were refined isotropically and significant residual electron density was found around this anion, which does not in any way affect our observations in the positively charged tellurium complex. In **2**, the atoms N2, C7, C8, C9 and C10 of one of the dithiocarbamates was highly disordered, apart from the $(ClO_4)^-$ anion. No satisfactory model could be ascribed to the disorder and hence these atoms were refined isotropically. The highest residual electron density of 1.7 electrons per $Å^3$ in the final difference map is also around this disordered fragment with no apparent effect on the precise location of the other atoms.

The selected bond lengths and angles are given in Table 4. Complete sets of the atomic coordinates,

Table 1. Crystallographic data

Compound	**1**	**2**
Empirical formula	$C_{40}H_{80}F_{12}N_8P_2S_{16}Te_3$	$C_{25}H_{50}Cl\,N_5O_4S_{10}Te_2$
Formula weight	1858.8	1096.0
Temperature (K)	293(2)	293(2)
Crystal system	orthorhombic	triclinic
Space group	*P*bcn	$P\bar{1}$
a (Å)	22.671(7)	10.045(2)
b (Å)	14.127(5)	14.595(2)
c (Å)	24.625(7)	16.903(2)
α (°)	90.0	66.49(1)
β (°)	90.0	78.98(1)
γ (°)	90.0	87.09(1)
V (Å^3)	7887(4)	2229.6(6)
Z	4	2
D_{calc} (Mg m^{-3})	1.565	1.632
μ (mm^{-1})	1.628	1.872
F(000)	3704	1096
Crystal size (mm)	0.57 × 0.23 × 0.20	0.43 × 0.34 × 0.21
θ (°)	1.70–25.00	1.52–24.97
hkl ranges	−1–26, −1–13, −29–1	−11–11, −15–17, 0–20
Reflections collected	7608	7344
Reflections observed [$I > 2\sigma(I)$]	3495	6328
S	1.08	1.28
R	0.074	0.049
[a]*wR*2	0.201	0.135

[a]$[\Sigma w(F_o^2 - F_c^2)^2/\Sigma(wF_o^2)^2]^{1/2}$.

Table 2. Selected bond distances in **1** and **2**

	1	**2**
Te(1)—S(1)	2.577(3)	2.584(2)
Te(1)—S(2)	2.729(4)	2.772(2)
Te(1)—S(3)	2.435(3)	2.473(2)
Te(1)—S(4)	2.803(4)	2.805(2)
Te(1)—S(5)	2.783(4)	2.711(2)
Te(1)—S(6)	2.561(4)	2.581(2)
Te(2)—S(7)	2.486(4)	2.500(2)
Te(2)—S(8)	2.858(3)	2.899(2)
Te(2)—S(9)	—	2.807(2)
Te(2)—S(10)	—	2.479(2)
Te(1)···Te(2)	3.389(1)	3.347(1)

thermal parameters and bond lengths and angles have been deposited at the Cambridge Crystallographic Data Centre.

REFERENCES

1. Haiduc, I., King, R. B. and Newton, M. G., *Chem. Rev.*, 1994, **94,** 301.
2. (a) Foss, O., *Pure Appl. Chem.*, 1970, **24,** 31; (b) Husebye, S., *Phosphorus Sulfur*, 1988, **38,** 271.
3. (a) Foss, O., *Acta Chem. Scand.*, 1949, **3,** 708; (b) St. Nikolov, G., Jordanov, N. and Havezov, I., *J. Inorg. Nucl. Chem.*, 1971, **33,** 1055.
4. (a) Krishna Kumar, R., Aravamudan, G., Udupa, M. R., Seshasayee, M. and Hamor, T. A., *Acta Crystallogr.*, 1993, **C49,** 1328; (b) Krishna Kumar R., Aravamudan, G., Udupa, M. R., Seshasayee, M., Selvam, P. and Yvon, K., *Polyhedron*, 1996, **15,** 1453; (c) Krishna Kumar, R., Aravamudan, G., Udupa, M. R., Seshasayee, M. and Hamor, T. A., *Polyhedron*, 1993, **12,** 2201; (d) Schnabel, W., Von Deuten, K. and Klar, G., *Phosphorus Sulfur*, 1982, **13,** 345.
5. Chidambaram, S., Aravamudan, G., Seshasayee, M. and Shibanova, T. A., Simonov, V. I., *Polyhedron*, 1988, **7,** 1267.
6. (a) Rout, G. C., Seshasayee, M., Aravamudan, G. and Radha, K., *J. Crystallogr. Spectrosc. Res.*, 1984, **14,** 193; (b) Von Deuten, K., Schnabel, W. and Klar, G., *Phosphorus Sulfur*, 1980, **9,** 93; (c) Chidambaram, S., Aravamudan, G., Seshasayee, M., Snow, M. C. and Tiekink, E. R. T., *Aust. J. Chem.*, 1989, **42,** 969.
7. Foss, O., *Acta Chem. Scand.*, 1962, **16,** 779.
8. (a) Fabiani, C., Spagna, R., Vaciago, A. and Zambonelli, L., *Acta Crystallogr.*, 1971, **B27,** 1499; (b) Ganesh, V., Seshasayee, M., Chidambaram, S., Aravamudan, G., Goubitz, K. and Schenk, H., *Acta Crystallogr.*, 1989, **C45,** 1506.

9. Glidewell, C., *Inorg. Chem. Acta*, 1976, **20,** 113.
10. Ganesh, V., Seshasayee, M., Kumar, V., Chidambaram, S., Aravamudan, G., Goubitz, K. and Schenk, H., *J. Crystallogr. Spectrosc. Res.*, 1989, **19,** 745.
11. Radha, K., Aravamudan, G., Rajalakshmi, A., Rout, G. C. and Seshasayee, M., *Aust. J. Chem.*, 1986, **39,** 847.
12. Pauling, L., *The Nature of the Chemical Bond*, 3rd edn. Cornell University Press, Ithaca, NY, 1960.
13. Sheldrick, G. M., *Acta Crystallogr.*, 1990, **A46,** 467.
14. Sheldrick, G. M., SHELXL-93, a program for the refinement of crystal structures. University of Gottingen, 1993.

Table S1. Positional and equivalent isotropic thermal parameters of non-hydrogen atoms in **1**

atom	*x/a*	*y/b*	*z/c*	U_{eq}
Te(1)	0.0577(0)	0.9780(1)	0.1250(0)	0.045(0)
Te(2)	0.0000(0)	0.9394(1)	0.2500(0)	0.048(0)
S(1)	-0.0511(1)	1.0202(3)	0.1067(1)	0.056(1)
S(2)	0.0293(2)	1.1572(3)	0.1572(2)	0.069(1)
S(3)	0.0802(1)	1.0400(3)	0.0350(1)	0.058(1)
S(4)	0.1656(2)	1.0748(3)	0.1232(1)	0.067(1)
S(5)	0.1347(1)	0.8282(3)	0.1062(2)	0.068(1)
S(6)	0.0076(1)	0.8316(3)	0.0846(2)	0.071(1)
S(7)	0.0711(2)	0.8065(3)	0.2599(2)	0.071(2)
S(8)	0.1204(1)	0.9989(2)	0.2544(1)	0.054(1)
P(1)	0.1568(3)	0.5345(3)	0.4030(3)	0.113(2)
N(1)	-0.0863(5)	1.1903(8)	0.1389(4)	0.065(4)
N(2)	0.1660(5)	1.1656(8)	0.0268(5)	0.068(5)
N(3)	0.0724(5)	0.6812(8)	0.0669(6)	0.075(5)
N(4)	0.1850(5)	0.8449(8)	0.2731(5)	0.064(4)
C(1)	-0.0408(6)	1.1281(10)	0.1360(5)	0.060(5)
C(2)	-0.1454(6)	1.1627(12)	0.1216(7)	0.095(7)
C(3)	-0.1527(7)	1.1863(13)	0.0594(6)	0.105(8)
C(4)	-0.0788(9)	1.2864(11)	0.1601(7)	0.097(8)
C(5)	-0.0925(9)	1.2922(14)	0.2190(9)	0.134(11)
C(6)	0.1424(5)	1.1018(9)	0.0597(5)	0.055(4)
C(7)	0.1418(6)	1.1854(11)	-0.0268(6)	0.076(6)
C(8)	0.1799(8)	1.1313(14)	-0.0689(8)	0.112(9)
C(9)	0.2160(6)	1.2279(13)	0.0473(7)	0.095(8)
C(10)	0.1931(9)	1.3137(13)	0.0755(8)	0.118(9)
C(11)	0.0733(5)	0.7698(10)	0.0850(5)	0.061(5)
C(12)	0.0171(8)	0.6364(12)	0.0477(9)	0.116(10)
C(13)	0.0064(9)	0.6569(15)	-0.0120(9)	0.137(12)
C(14)	0.1251(8)	0.6224(13)	0.0657(9)	0.120(9)
C(15)	0.1409(12)	0.5639(16)	0.1086(13)	0.245(22)
C(16)	0.1324(5)	0.8818(8)	0.2632(5)	0.049(4)
C(17)	0.2373(6)	0.9028(11)	0.2761(6)	0.074(6)
C(18)	0.2652(7)	0.9179(13)	0.2240(8)	0.105(9)
C(19)	0.1921(7)	0.7434(11)	0.2859(7)	0.087(7)
C(20)	0.2160(3)	0.6931(5)	0.2401(3)	0.163(14)
*F(1)	0.1819(3)	0.4289(5)	0.4061(3)	0.196(6)
*F(2)	0.1219(3)	0.6351(5)	0.3903(3)	0.181(6)
*F(3)	0.1419(3)	0.5174(5)	0.3409(3)	0.180(6)
*F(4)	0.2219(3)	0.5634(5)	0.3837(3)	0.250(9)
*F(5)	0.1806(3)	0.5474(5)	0.4627(3)	0.324(13)
*F(6)	0.1019(3)	0.4884(5)	0.4141(3)	0.244(9)

*Atoms were isotropically refined.

Table S2. Positional parameters of hydrogen atoms in **1**

atom	*x/a*	*y/b*	*z/c*
H(2A)	-0.1751	1.1954	0.1421
H(2B)	-0.1507	1.0958	0.1266
H(3A)	-0.1909	1.1685	0.0460
H(3B)	-0.1474	1.2533	0.0550
H(3C)	-0.1228	1.1531	0.0394
H(4A)	-0.1029	1.3303	0.1403
H(4B)	-0.0382	1.3040	0.1556
H(5A)	-0.0868	1.3545	0.2337
H(5B)	-0.1332	1.2744	0.2229
H(5C)	-0.0681	1.2479	0.2383
H(7A)	0.1452	1.2523	-0.0331
H(7B)	0.1009	1.1684	-0.0289
H(8A)	0.1650	1.1463	-0.1043
H(8B)	0.2208	1.1490	-0.0667
H(8C)	0.1761	1.0645	-0.0625
H(9A)	0.2407	1.2459	0.0174
H(9B)	0.2396	1.1924	0.0725
H(10A)	0.2253	1.3518	0.0882
H(10B)	0.1699	1.3495	0.0501
H(10C)	0.1688	1.2955	0.1057
H(12A)	-0.0152	0.6625	0.0681
H(12B)	0.0181	0.5696	0.0548
H(13A)	-0.0302	0.6273	-0.0216
H(13B)	0.0041	0.7235	-0.0195
H(13C)	0.0378	0.6295	-0.0329
H(14A)	0.1584	0.6635	0.0611
H(14B)	0.1225	0.5826	0.0341
H(15A)	0.1764	0.5277	0.1043
H(15B)	0.1443	0.6035	0.1401
H(15C)	0.1080	0.5217	0.1129
H(17A)	0.2659	0.8733	0.2994
H(17B)	0.2270	0.9627	0.2918
H(18A)	0.2995	0.9572	0.2275
H(18B)	0.2763	0.8582	0.2084
H(18C)	0.2370	0.9485	0.2008
H(19A)	0.1541	0.7165	0.2934
H(19B)	0.2164	0.7348	0.3175
H(20A)	0.2200	0.6268	0.2480
H(20B)	0.1914	0.7012	0.2087
H(20C)	0.2542	0.7197	0.2330

Table S3. Anisotropic thermal parameters of non-hydrogen atoms in **1**

atom	U_{11}	U_{22}	U_{33}	U_{23}	U_{13}	U_{12}
Te(1)	0.044(0)	0.045(1)	0.045(0)	0.001(0)	0.000(0)	0.002(0)
Te(2)	0.050(1)	0.046(1)	0.049(1)	0.000(0)	0.004(1)	0.000(0)
S(1)	0.048(2)	0.059(2)	0.060(2)	-0.006(2)	-0.004(1)	0.009(2)
S(2)	0.072(2)	0.050(2)	0.085(3)	-0.014(2)	-0.015(2)	0.007(2)
S(3)	0.061(2)	0.070(2)	0.043(2)	0.008(2)	-0.004(1)	-0.008(2)
S(4)	0.059(2)	0.081(3)	0.062(2)	0.020(2)	-0.015(2)	-0.015(2)
S(5)	0.049(2)	0.059(2)	0.095(3)	-0.006(2)	-0.003(2)	0.006(2)
S(6)	0.051(2)	0.054(2)	0.107(3)	-0.021(2)	-0.013(2)	0.003(2)
S(7)	0.058(2)	0.044(2)	0.111(3)	0.007(2)	0.011(2)	-0.001(2)
S(8)	0.051(2)	0.050(2)	0.061(2)	-0.001(1)	-0.001(2)	0.000(1)
P(1)	0.140(4)	0.052(3)	0.146(5)	-0.010(3)	0.040(4)	-0.014(3)
N(1)	0.073(7)	0.064(8)	0.057(7)	0.000(6)	-0.012(5)	0.021(6)
N(2)	0.056(6)	0.069(8)	0.080(8)	0.018(7)	0.013(6)	0.002(6)
N(3)	0.066(7)	0.048(7)	0.112(10)	-0.007(7)	0.002(7)	0.014(6)
N(4)	0.061(7)	0.060(8)	0.073(7)	0.003(6)	-0.004(6)	0.009(6)
C(1)	0.063(8)	0.070(10)	0.047(8)	-0.010(6)	0.001(6)	0.016(7)
C(2)	0.062(9)	0.081(12)	0.142(16)	-0.007(11)	-0.007(10)	0.037(8)
C(3)	0.101(12)	0.121(15)	0.092(13)	0.023(11)	-0.047(10)	0.021(12)
C(4)	0.153(16)	0.056(11)	0.082(12)	-0.002(9)	-0.026(11)	0.040(11)
C(5)	0.159(19)	0.083(14)	0.160(21)	-0.035(14)	-0.030(16)	0.041(14)
C(6)	0.046(7)	0.073(9)	0.045(7)	0.011(7)	0.008(6)	0.006(6)
C(7)	0.069(9)	0.081(11)	0.078(10)	0.038(9)	-0.012(8)	-0.008(8)
C(8)	0.122(15)	0.119(16)	0.094(13)	0.014(12)	-0.007(12)	-0.032(13)
C(9)	0.071(10)	0.135(17)	0.080(11)	0.036(11)	-0.016(8)	-0.054(11)
C(10)	0.151(17)	0.082(13)	0.120(16)	-0.016(12)	-0.033(13)	-0.011(13)
C(11)	0.057(7)	0.058(9)	0.067(9)	-0.010(7)	-0.005(6)	0.011(6)
C(12)	0.088(12)	0.059(11)	0.200(25)	-0.052(14)	-0.010(14)	-0.002(9)
C(13)	0.138(18)	0.128(19)	0.146(21)	-0.068(16)	-0.023(16)	0.008(15)
C(14)	0.092(12)	0.093(14)	0.174(20)	-0.064(15)	-0.017(13)	0.015(11)
C(15)	0.245(33)	0.086(17)	0.404(53)	0.032(24)	-0.233(37)	0.012(19)
C(16)	0.057(7)	0.042(7)	0.049(7)	0.000(6)	0.003(6)	0.011(6)
C(17)	0.058(8)	0.092(12)	0.072(9)	-0.008(9)	-0.016(8)	0.005(8)
C(18)	0.075(11)	0.097(14)	0.144(17)	0.014(13)	-0.004(12)	0.008(10)
C(19)	0.071(9)	0.068(12)	0.122(15)	0.001(10)	-0.020(9)	0.031(8)
C(20)	0.268(32)	0.057(13)	0.165(23)	-0.003(14)	-0.050(22)	-0.001(17)

Table S4. Bond distances in (Å)

Te(1) - S(1)	2.577(3)	N(2) - C(9)	1.522(20)
Te(1) - S(2)	2.729(4)	N(3) - C(11)	1.329(18)
Te(1) - S(3)	2.435(3)	N(3) - C(12)	1.483(21)
Te(1) - S(4)	2.803(4)	N(3) - C(14)	1.454(21)
Te(1) - S(5)	2.783(4)	N(4) - C(16)	1.323(16)
Te(1) - S(6)	2.561(4)	N(4) - C(17)	1.443(18)
Te(2) - S(7)	2.486(4)	N(4) - C(19)	1.477(19)
Te(2) - S(8)	2.858(3)	C(2) - C(3)	1.576(23)
S(1) - C(1)	1.702(14)	C(4) - C(5)	1.486(28)
S(2) - C(1)	1.723(13)	C(7) - C(8)	1.551(24)
S(3) - C(6)	1.768(12)	C(9) - C(10)	1.491(26)
S(4) - C(6)	1.695(12)	C(12) - C(13)	1.520(32)
S(5) - C(11)	1.701(13)	C(14) - C(15)	1.389(36)
S(6) - C(11)	1.725(13)	C(17) - C(18)	1.447(23)
S(7) - C(16)	1.754(12)	C(19) - C(20)	1.440(18)
S(8) - C(16)	1.691(12)	P(1) - F(1)	1.598(9)
N(1) - C(1)	1.357(18)	P(1) - F(2)	1.657(9)
N(1) - C(2)	1.458(18)	P(1) - F(3)	1.585(10)
N(1) - C(4)	1.466(19)	P(1) - F(4)	1.604(10)
N(2) - C(6)	1.324(17)	P(1) - F(5)	1.578(10)
N(2) - C(7)	1.456(18)	P(1) - F(6)	1.431(10)

Table S5. Bond angles in **1** (°)

S(5)- Te(1)- S(6)	66.3(1)	S(2)- C(1)- N(1)	122.1(10)
S(4)- Te(1)- S(6)	140.8(1)	S(1)- C(1)- N(1)	119.8(10)
S(4)- Te(1)- S(5)	79.7(1)	S(1)- C(1)- S(2)	117.9(8)
S(3)- Te(1)- S(6)	91.7(1)	N(1)- C(2)- C(3)	108.9(12)
S(3)- Te(1)- S(5)	89.5(1)	N(1)- C(4)- C(5)	112.0(14)
S(3)- Te(1)- S(4)	68.2(1)	S(4)- C(6)- N(2)	126.3(10)
S(2)- Te(1)- S(6)	139.3(1)	S(3)- C(6)- N(2)	116.7(9)
S(2)- Te(1)- S(5)	154.4(1)	S(3)- C(6)- S(4)	117.0(7)
S(2)- Te(1)- S(4)	76.0(1)	N(2)- C(7)- C(8)	107.5(12)
S(2)- Te(1)- S(3)	88.9(1)	N(2)- C(9)- C(10)	111.4(14)
S(1)- Te(1)- S(6)	72.2(1)	S(6)- C(11)- N(3)	117.6(10)
S(1)- Te(1)- S(5)	138.4(1)	S(5)- C(11)- N(3)	124.8(10)
S(1)- Te(1)- S(4)	136.0(1)	S(5)- C(11)- S(6)	117.6(7)
S(1)- Te(1)- S(3)	87.6(1)	N(3)- C(12)- C(13)	111.2(16)
S(1)- Te(1)- S(2)	67.1(1)	N(3)- C(14)- C(15)	122.4(18)
S(7)- Te(2)- S(8)	66.4(1)	S(8)- C(16- N(4)	123.7(9)
Te(1)- S(1)- C(1)	90.1(4)	S(7)- C(16- N(4)	118.9(9)
Te(1)- S(2)- C(1)	84.7(5)	S(7)- C(16- S(8)	117.4(7)
Te(1)- S(3)- C(6)	91.8(4)	N(4)- C(17)- C(18)	113.4(12)
Te(1)- S(4)- C(6)	81.5(4)	N(4)- C(19)- C(20)	110.7(11)
Te(1)- S(5)- C(11)	84.6(4)	F(5)- P(1)- F(6)	99.9(5)
Te(1)- S(6)- C(11)	91.4(5)	F(4)- P(1)- F(6)	166.7(6)
Te(2)- S(7)- C(16)	93.5(4)	F(4)- P(1)- F(5)	86.1(5)
Te(2)- S(8)- C(16)	82.6(4)	F(3)- P(1)- F(6)	86.0(5)
C(2)- N(1)- C(4)	117.3(12)	F(3)- P(1)- F(5)	172.1(6)
C(1)- N(1)- C(4)	122.0(12)	F(3)- P(1)- F(4)	87.1(5)
C(1)- N(1)- C(2)	120.7(11)	F(2)- P(1)- F(6)	90.6(5)
C(7)- N(2)- C(9)	118.1(11)	F(2)- P(1)- F(5)	103.9(5)
C(6)- N(2)- C(9)	119.4(11)	F(2)- P(1)- F(4)	99.5(5)
C(6)- N(2)- C(7)	122.2(11)	F(2)- P(1)- F(3)	81.2(5)
C(12)- N(3)- C(14)	116.4(12)	F(1)- P(1)- F(6)	82.9(5)
C(11)- N(3)- C(14)	122.3(12)	F(1)- P(1)- F(5)	86.7(5)
C(11)- N(3)- C(12)	121.3(12)	F(1)- P(1)- F(4)	85.6(4)
C(17)- N(4)- C(19)	116.7(11)	F(1)- P(1)- F(3)	88.8(5)
C(16)- N(4)- C(19)	121.4(11)	F(1)- P(1)- F(2)	168.5(5)
C(16)- N(4)- C(17)	121.8(11)		

Table S6. Positional and equivalent isotropic thermal parameters of non-hydrogen atoms in **2**

atom	*x/a*	*y/b*	*z/c*	*Ueq*
Te(1)	0.4312(0)	0.4490(0)	0.3219(0)	0.045(0)
Te(2)	0.4551(0)	0.4759(0)	-0.1056(0)	0.052(0)
S(1)	0.5487(2)	0.6085(1)	0.3104(1)	0.058(1)
S(2)	0.2874(2)	0.6209(2)	0.2527(1)	0.063(1)
S(3)	0.3380(2)	0.4271(2)	0.4750(1)	0.064(1)
S(4)	0.1644(2)	0.3704(2)	0.3781(1)	0.061(1)
S(5)	0.4624(2)	0.2486(1)	0.3810(1)	0.057(1)
S(6)	0.6724(2)	0.3976(1)	0.3513(1)	0.061(1)
S(7)	0.3903(2)	0.6514(1)	-0.1299(1)	0.060(1)
S(8)	0.6836(2)	0.6150(1)	-0.1606(1)	0.059(1)
S(9)	0.3633(2)	0.2804(2)	-0.0627(2)	0.077(1)
S(10)	0.2042(2)	0.4577(2)	-0.0740(2)	0.066(1)
C(1)	0.4158(7)	0.6802(5)	0.2677(4)	0.052(3)
N(1)	0.4183(6)	0.7771(4)	0.2504(4)	0.058(3)
C(2)	0.3071(8)	0.8409(6)	0.2154(5)	0.068(4)
C(3)	0.3360(11)	0.8878(8)	0.1162(6)	0.100(5)
C(4)	0.5278(8)	0.8267(6)	0.2650(6)	0.068(4)
C(5)	0.5000(11)	0.8309(8)	0.3538(7)	0.101(6)
C(6)	0.1855(7)	0.3723(7)	0.4746(4)	0.069(4)
*N(2)	0.0993(8)	0.3301(6)	0.5495(4)	0.105(3)
*C(7)	0.1347(12)	0.3146(8)	0.6349(6)	0.109(3)
*C(8)	0.0902(13)	0.4075(8)	0.6489(9)	0.124(4)
*C(9)	-0.0032(13)	0.2539(9)	0.5614(12)	0.169(6)
*C(10)	-0.0982(17)	0.3393(12)	0.5391(12)	0.165(6)
N(3)	0.7279(6)	0.2129(4)	0.3688(4)	0.055(2)
C(11)	0.6317(6)	0.2766(5)	0.3676(4)	0.049(2)
C(12)	0.6964(9)	0.1082(6)	0.3837(5)	0.069(4)
C(13)	0.6958(12)	0.0382(7)	0.4773(6)	0.104(5)
C(14)	0.8726(7)	0.2413(6)	0.3480(6)	0.068(4)
C(15)	0.9242(8)	0.2871(7)	0.2500(6)	0.085(5)
N(4)	0.5785(6)	0.7916(4)	-0.1779(4)	0.057(3)
C(16)	0.5579(6)	0.6961(5)	-0.1585(4)	0.049(3)
C(17)	0.4651(8)	0.8611(6)	-0.1800(5)	0.069(4)
C(18)	0.4157(10)	0.8694(7)	-0.0934(7)	0.090(5)
C(19)	0.7164(8)	0.8355(6)	-0.1998(5)	0.070(4)
C(20)	0.7679(10)	0.8814(8)	-0.2975(6)	0.097(5)
N(5)	0.0923(7)	0.2800(5)	-0.0203(5)	0.076(3)
C(21)	0.2092(8)	0.3305(6)	-0.0495(5)	0.062(4)
C(22)	-0.0398(9)	0.3242(8)	-0.0016(6)	0.084(4)
C(23)	-0.1065(13)	0.3747(10)	-0.0774(8)	0.130(8)
C(24)	0.0875(14)	0.1726(9)	-0.0012(10)	0.131(8)
C(25)	0.0830(28)	0.1531(16)	-0.0744(17)	0.279(21)
Cl	0.9068(3)	0.9840(2)	0.2366(2)	0.090(1)
*O(1)	1.0266(10)	0.9463(7)	0.2112(7)	0.145(3)
*O(2)	0.8932(11)	1.0873(9)	0.1989(8)	0.168(4)
*O(3)	0.8481(16)	0.9378(12)	0.3232(11)	0.234(6)
*O(4)	0.8102(20)	0.9647(14)	0.1982(13)	0.274(8)

Table S7. Positional parameters of hydrogen in atoms in **2**

atom	*x/a*	*y/b*	*z/c*
H(2A)	0.2946	0.8932	0.2376
H(2B)	0.2235	0.8011	0.2356
H(3A)	0.2618	0.9288	0.0957
H(3B)	0.3468	0.8362	0.0940
H(3C)	0.4178	0.9283	0.0960
H(4A)	0.5413	0.8942	0.2203
H(4B)	0.6111	0.7914	0.2590
H(5A)	0.5748	0.8641	0.3602
H(5B)	0.4885	0.7642	0.3984
H(5C)	0.4188	0.8671	0.3597
H(12A)	0.7636	0.0874	0.3451
H(12B)	0.6083	0.1049	0.3693
H(13A)	0.6752	-0.0286	0.4848
H(13B)	0.6283	0.0580	0.5155
H(13C)	0.7834	0.0405	0.4914
H(14A)	0.9241	0.1826	0.3745
H(14B)	0.8861	0.2889	0.3728
H(15A)	1.0187	0.3048	0.2385
H(15B)	0.8743	0.3459	0.2237
H(15C)	0.9123	0.2397	0.2255
H(17A)	0.3902	0.8384	-0.1970
H(17B)	0.4946	0.9269	-0.2244
H(18A)	0.3427	0.9152	-0.0987
H(18B)	0.4887	0.8933	-0.0768
H(18C)	0.3843	0.8048	-0.0494
H(19A)	0.7774	0.7839	-0.1723
H(19B)	0.7159	0.8863	-0.1764
H(20A)	0.8576	0.9092	-0.3092
H(20B)	0.7086	0.9334	-0.3248
H(20C)	0.7701	0.8310	-0.3207
H(22A)	-0.1006	0.2716	0.0429
H(22B)	-0.0260	0.3721	0.0229
H(23A)	-0.1909	0.4008	-0.0591
H(23B)	-0.1235	0.3277	-0.1014
H(23C)	-0.0487	0.4284	-0.1214
H(24A)	0.1669	0.1421	0.0226
H(24B)	0.0080	0.1419	0.0432
H(25A)	0.0800	0.0822	-0.0582
H(25B)	0.1624	0.1819	-0.1183
H(25C)	0.0035	0.1818	-0.0976

Table S8. Anisotropic thermal parameters of non-hydrogen atoms in **2**

atom	U_{11}	U_{22}	U_{33}	U_{23}	U_{13}	U_{12}
Te(1)	0.036(0)	0.054(0)	0.047(0)	-0.023(0)	-0.010(0)	0.004(0)
Te(2)	0.044(0)	0.061(0)	0.049(0)	-0.017(0)	-0.009(0)	0.005(0)
S(1)	0.052(1)	0.055(1)	0.076(1)	-0.028(1)	-0.027(1)	0.008(1)
S(2)	0.048(1)	0.070(1)	0.081(1)	-0.037(1)	-0.025(1)	0.013(1)
S(3)	0.051(1)	0.098(2)	0.053(1)	-0.041(1)	-0.009(1)	-0.003(1)
S(4)	0.044(1)	0.088(1)	0.058(1)	-0.036(1)	-0.008(1)	-0.007(1)
S(5)	0.048(1)	0.057(1)	0.066(1)	-0.023(1)	-0.010(1)	-0.003(1)
S(6)	0.044(1)	0.057(1)	0.090(1)	-0.032(1)	-0.024(1)	0.006(1)
S(7)	0.042(1)	0.066(1)	0.071(1)	-0.029(1)	-0.006(1)	0.004(1)
S(8)	0.040(1)	0.068(1)	0.063(1)	-0.022(1)	-0.008(1)	0.003(1)
S(9)	0.067(1)	0.061(1)	0.090(2)	-0.020(1)	-0.009(1)	0.011(1)
S(10)	0.047(1)	0.062(1)	0.086(1)	-0.026(1)	-0.012(1)	0.004(1)
C(1)	0.047(4)	0.059(4)	0.049(4)	-0.024(3)	-0.007(3)	0.005(3)
N(1)	0.055(3)	0.054(3)	0.063(4)	-0.025(3)	-0.011(3)	0.010(3)
C(2)	0.067(5)	0.065(5)	0.074(5)	-0.031(4)	-0.017(4)	0.025(4)
C(3)	0.102(8)	0.101(7)	0.085(7)	-0.021(6)	-0.031(6)	0.032(6)
C(4)	0.063(5)	0.058(4)	0.084(6)	-0.028(4)	-0.016(4)	0.003(4)
C(5)	0.106(8)	0.108(8)	0.116(8)	-0.069(7)	-0.023(6)	0.001(6)
C(6)	0.051(4)	0.100(6)	0.054(4)	-0.032(4)	0.004(3)	-0.014(4)
N(3)	0.054(3)	0.054(3)	0.057(3)	-0.020(3)	-0.015(3)	0.011(3)
C(11)	0.045(3)	0.050(4)	0.050(4)	-0.019(3)	-0.010(3)	0.006(3)
C(12)	0.080(5)	0.057(4)	0.069(5)	-0.025(4)	-0.013(4)	0.012(4)
C(13)	0.140(10)	0.070(6)	0.078(6)	-0.002(5)	-0.021(6)	0.001(6)
C(14)	0.044(4)	0.079(5)	0.083(6)	-0.032(4)	-0.022(4)	0.017(4)
C(15)	0.055(5)	0.092(6)	0.095(7)	-0.028(5)	-0.005(4)	-0.003(4)
N(4)	0.057(3)	0.059(4)	0.056(3)	-0.021(3)	-0.017(3)	-0.002(3)
C(16)	0.042(3)	0.061(4)	0.041(3)	-0.016(3)	-0.008(3)	0.000(3)
C(17)	0.071(5)	0.066(5)	0.074(5)	-0.029(4)	-0.024(4)	0.008(4)
C(18)	0.088(6)	0.095(7)	0.099(7)	-0.052(6)	-0.022(5)	0.027(5)
C(19)	0.062(5)	0.071(5)	0.077(5)	-0.029(4)	-0.010(4)	-0.014(4)
C(20)	0.090(7)	0.111(8)	0.077(6)	-0.025(6)	-0.004(5)	-0.028(6)
N(5)	0.080(5)	0.061(4)	0.076(5)	-0.016(4)	-0.007(4)	-0.002(4)
C(21)	0.060(4)	0.058(4)	0.056(4)	-0.010(3)	-0.007(3)	-0.004(4)
C(22)	0.070(5)	0.103(7)	0.076(6)	-0.036(5)	0.002(4)	-0.018(5)
C(23)	0.117(10)	0.164(12)	0.115(10)	-0.048(9)	-0.056(8)	0.002(9)
C(24)	0.116(10)	0.103(9)	0.162(13)	-0.056(9)	0.015(9)	-0.025(7)
C(25)	0.450(41)	0.194(20)	0.305(30)	-0.182(22)	-0.145(28)	0.011(22)
Cl	0.076(1)	0.072(1)	0.115(2)	-0.040(1)	0.001(1)	0.016(1)

Table S9. Bond distances in **2** (Å)

Te(1) - S(1)	2.584(2)	N(2) - C(7)	1.481(13)
Te(1) - S(2)	2.772(2)	N(2) - C(9)	1.481(17)
Te(1) - S(3)	2.473(2)	N(2) - C(10)	2.018(19)
Te(1) - S(4)	2.805(2)	C(7) - C(8)	1.500(18)
Te(1) - S(5)	2.711(2)	C(9) - C(10)	1.499(20)
Te(1) - S(6)	2.581(2)	N(3) - C(11)	1.303(9)
Te(2) - S(7)	2.500(2)	N(3) - C(12)	1.486(11)
Te(2) - S(9)	2.807(2)	N(3) - C(14)	1.469(9)
Te(2) - S(10)	2.479(2)	C(12) - C(13)	1.501(12)
S(1) - C(1)	1.738(7)	C(14) - C(15)	1.511(12)
S(2) - C(1)	1.699(8)	N(4) - C(16)	1.316(10)
S(3) - C(6)	1.766(9)	N(4) - C(17)	1.482(10)
S(4) - C(6)	1.696(9)	N(4) - C(19)	1.474(10)
S(5) - C(11)	1.720(7)	C(17) - C(18)	1.504(15)
S(6) - C(11)	1.734(8)	C(19) - C(20)	1.507(12)
S(7) - C(16)	1.744(7)	N(5) - C(21)	1.320(10)
S(8) - C(16)	1.692(7)	N(5) - C(22)	1.481(12)
S(9) - C(21)	1.692(8)	N(5) - C(24)	1.470(15)
S(10) - C(21)	1.735(8)	C(22) - C(23)	1.470(16)
C(1) - N(1)	1.326(10)	C(24) - C(25)	1.384(37)
N(1) - C(2)	1.474(10)	Cl - O(1)	1.364(11)
N(1) - C(4)	1.458(12)	Cl - O(2)	1.393(12)
C(2) - C(3)	1.510(12)	Cl - O(3)	1.367(15)
C(4) - C(5)	1.498(16)	Cl - O(4)	1.363(24)
C(6) - N(2)	1.321(9)		

Table S10. Bond angles in **2** (°)

S(5) - Te(1) - S(6)	67.4(1)	C(6) - N(2) - C(9)	121.4(9)
S(4) - Te(1) - S(6)	139.8(1)	C(6) - N(2) - C(7)	122.0(6)
S(4) - Te(1) - S(5)	76.1(1)	C(9) - N(2) - C(10)	47.8(7)
S(3) - Te(1) - S(6)	94.3(1)	C(7) - N(2) - C(10)	118.6(8)
S(3) - Te(1) - S(5)	88.4(1)	C(7) - N(2) - C(9)	110.3(9)
S(3) - Te(1) - S(4)	67.7(1)	N(2) - C(7) - C(8)	104.6(9)
S(2) - Te(1) - S(6)	139.4(1)	N(2) - C(9) - C(10)	85.2(10)
S(2) - Te(1) - S(5)	152.9(1)	N(2) - C(10) - C(9)	47.0(7)
S(2) - Te(1) - S(4)	79.3(1)	C(12) - N(3) - C(14)	115.9(6)
S(2) - Te(1)- S(3)	92.8(1)	C(11) - N(3) - C(14)	122.9(6)
S(1) - Te(1) - S(6)	74.4(1)	C(11) - N(3) - C(12)	121.1(7)
S(1) - Te(1) - S(5)	140.5(1)	S(6) - C(11) - N(3)	119.6(6)
S(1) - Te(1) - S(4)	134.9(1)	S(5) - C(11) - N(3)	123.9(5)
S(1) - Te(1) - S(3)	85.0(1)	S(5) - C(11) - S(6)	116.5(4)
S(1) - Te(1) - S(2)	66.5(1)	N(3) - C(12) - C(13)	111.5(7)
S(9) - Te(2) - S(10)	67.0(1)	N(3) - C(14) - C(15)	111.4(6)
S(7) - Te(2) - S(10)	79.3(1)	C(17) - N(4) - C(19)	116.3(6)
S(7) - Te(2) - S(9)	146.4(1)	C(16) - N(4) - C(19)	121.6(7)
Te(1) - S(1) - C(1)	90.5(3)	C(16) - N(4) - C(17)	122.2(7)
Te(1) - S(2) - C(1)	85.2(3)	S(8) - C(16) - N(4)	124.0(6)
Te(1) - S(3) - C(6)	92.0(2)	S(7) - C(16) - N(4)	117.6(5)
Te(1) - S(4) - C(6)	82.8(3)	S(7) - C(16) - S(8)	118.4(4)
Te(1) - S(5) - C(11)	85.1(3)	N(4) - C(17) - C(18)	113.2(7)
Te(1) - S(6) - C(11)	89.0(2)	N(4) - C(19) - C(20)	111.8(7)
Te(2) - S(7) - C(16)	93.9(3)	C(22) - N(5) - C(24)	115.6(9)
Te(2) - S(9) - C(21)	82.7(3)	C(21) - N(5) - C(24)	120.5(9)
Te(2) - S(10) - C(21)	92.5(3)	C(21) - N5) - C(22)	123.8(7)
S(1)- C(1) - S(2)	117.7(4)	S(10) - C(21) - N(5)	117.2(6)
S(2) - C(1) - N(1)	123.6(6)	S(9) - C(21) - N(5)	125.2(6)
S(1) - C(1) - N(1)	118.6(6)	S(9) - C(21) - S(10)	117.6(5)
C(1) - N(1) - C(4)	123.1(7)	N(5) - C(22) - C(23)	115.4(9)
C(1) - N(1) - C(2)	120.8(7)	N(5) - C(24) - C(25)	113.1(15)
C(2) - N(1) - C(4)	116.1(6)	O(3) - Cl - O(4)	100.4(11)
N(1) - C(2) - C(3)	111.6(7)	O(2) - Cl - O(4)	94.1(10)
N(1) - C(4) - C(5)	112.7(8)	O(2) - Cl - O(3)	115.6(9)
S(3) - C(6) - S(4)	117.1(4)	O(1) - Cl - O(4)	108.9(10)
S(4) - C(6) - N(2)	124.0(5)	O(1) - Cl - O(3)	115.8(8)
S(3) - C(6) - N(2)	118.7(6)	O(1) - Cl - O(2)	117.5(7)
C(6) - N(2) - C(10)	115.1(7)		

Pergamon

PII: S0277-5387(97)00455-5

Polyhedron Vol. 17, No. 10, pp. 1677–1691, 1998
© 1998 Published by Elsevier Science Ltd
All rights reserved. Printed in Great Britain
0277-5387/98 $19.00+0.00

Ligation properties of N-substituted imidazoles: synthesis, spectroscopic and structural investigation, and behaviour in solution of zinc(II) and cadmium(II) complexes

C. Pettinari,[a]* F. Marchetti,[a] A. Cingolani,[a] S. I. Troyanov[b] and A. Drozdov[b]

[a] Dipartimento di Scienze Chimiche, Università degli Studi, via S. Agostino 1, 62032 Camerino, Italy

[b] Moscow State University, Chemistry Department, Vorobjevy Gory, 119899 Moscow, Russia

(Received 30 June 1997; accepted 31 October 1997)

Abstract—Novel zinc(II) and cadmium(II) derivatives of 1-methyl- (L′) and 1-benzyl-imidazole (L″) of the type 1 : 1 $[(L)MX_2]$ (L = L″, M = Zn, X = 4-acetyl-1-phenyl-3-methylpyrazolonato (Q″), 4-benzoyl-1-phenyl-3-methylpyrazol-5-onato (Q′) or 4-benzoyl-1,3-dimethylpyrazol-5-onato (Q*); L = L″, M = Cd, X = Q′ or Q*), 2 : 1 $[(L)_2MX_2]\cdot y(H_2O)$ (L = L′, M = Zn, X = Cl, Br, I, CH_3CO_2, Q′, Q″ or Q*; L = L′, M = Cd, X = I, CH_3CO_2, Q′ or Q*; L = L″, M = Zn, X = Cl, Br, I; L = L″, M = Cd, X = I or Q″), 3 : 1 $[(L'')_3MX_2]\cdot y(H_2O)$ (M = Zn, X = CF_3CO_2, NO_3 or BF_4; M = Cd, X = NO_3), 4 : 1 $[(L')_4Zn]X_2\cdot y(H_2O)$ (X = NO_3 or BF_4), 5 : 1 $[(L')_5Zn]X_2\cdot y(H_2O)$ (X = ClO_4 or CF_3CO_2) 6 : 1 $[(L')_6Zn]X_2\cdot y(H_2O)$ (L = L′, M = Zn, X = CF_3SO_3; L = L′, M = Cd, X = NO_3, ClO_4 or BF_4; L = L″, M = Cd, X = ClO_4 or BF_4), 4 : 3 $[(L'')_4(CdX_2)_3]$ (X = Cl or Br) and finally 5 : 3 $[(L')_5(CdBr_2)_3]$ have been prepared and characterized by IR and far-IR data, conductivity, ^1H NMR and in some cases also with ^{113}Cd NMR spectroscopy. The 4,7-dimethyl-1,10-phenanthroline (Me_2Phen) and 2,2′-bipyridine (Bipy) displace all the 1-methylimidazole donors from $[(L')_5Zn](ClO_4)_2\cdot H_2O$ or $[(L')_6Cd(ClO_4)_2$ diethyl ether suspension, yielding the trischelate complexes $[(Me_2Phen)_3M](ClO_4)_2$ and $[(Bipy)_3M](ClO_4)_2$ (M = Zn or Cd). On the other hand, 2-benzoylpyridine (Bzpy) and 4,7-diphenyl-1,10-phenanthroline (Ph_2Phen) react with $[(L')_5Zn](ClO_4)_2\cdot H_2O$ yielding the mixed ligands complexes $[(Bzpy)_2(L')_2Zn](ClO_4)_2$ and $[(Ph_2Phen)_2(L')Zn](ClO_4)_2$ respectively. From the reaction of Ph_2Phen with $[(L')_6Cd(ClO_4)_2$ the ionic compound $[(Ph_2Phen)_3Cd](ClO_4)_2$ is obtained. The structure of $[(L'')_3Cd(NO_3)_2]$ was determined by X-ray single crystal diffraction: the Cd atom exhibited a distorted trigonal bipyramidal geometry, involving two O-monodentate nitrato groups in axial position and three 1-benzylimidazole ligand in the equatorial positions. ^{113}Cd NMR solution data carried out on selected soluble pyrazolonato, carboxylato and nitrato derivatives indicated five- or six-coordinate N_3CdO_2, N_4CdO_2, N_2CdO_4 and $NCdO_4$ species in solution.
© 1998 Published by Elsevier Science Ltd. All rights reserved

Keywords: Zn(II) and Cd(II) complexes; imidazoles; phenanthroline; bipyridine; ^{113}Cd; crystal structure; pyrazolonate.

Imidazole is a molecule of considerable interest as versatile donor and potential fungicide [1] and also of great biochemical importance [2]: this five-membered nitrogen heterocycle in fact occurs in proteins as part of the side chain of the amino acid histidine [3], in nucleic acid structures as part of the purine moiety [4] of adenine and guanine, and in the vitamin B_{12} cohenzime as benzimidazole [5].

It has also been found that its conjugate base, the imidazolate ion (Im^-) acts as a bridging ligand between Cu(II) and Zn(II) centres in bovine heritrocyte superoxide dismutase (BESOD) [6].

Many studies have appeared in literature which describe the synthesis and characterization of imidazole-metal ion derivatives [7] as model compounds in order to obtain indirect knowledge of the nature of the interactions involved in a proposed enzyme-metal-ion-substrate complex, but generally the simple imidazole heterocycle has been employed.

* Author to whom correspondence should be addressed.

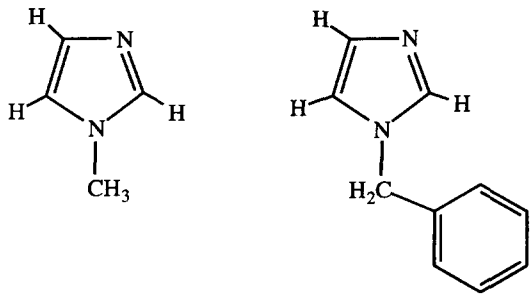

L' L''

Fig. 1. Structure of the imidazole donors employed in this work.

We have recently started to investigate the behaviour of variously substituted monoalkyl- and monoaryl-imidazoles with Hg(II) [8], Au(I) [9], Cu(I) [10] and Sn(IV) [11].

The purpose of this paper is to extend the knowledge of the modes of action of N-substituted imidazoles towards zinc and cadmium acceptors. In fact the presence of different R groups at the 1-position of the imidazolic ring may affect the coordination properties of the pyridinic nitrogen atom through steric and electronic effects. Here we report the synthesis and spectroscopic characterization of new zinc(II) and cadmium(II) derivatives of 1-methyl- (L') and 1-benzyl-imidazole (L'') (Fig. 1), two heterocyclic donors with different basicities [12]. The factors affecting the stoichiometry and the coordination number are discussed and rationalized on the basis of steric and electronic arguments. The X-ray crystal structure of $[(L'')_3Cd(NO_3)_2]$ has also been determined and compared with other imidazole complexes.

EXPERIMENTAL

The samples for microanalysis were dried *in vacuo* to constant weight (20°C, ca 0.1 Torr). Elemental analyses (CHNS) were carried out in the house with a Carlo Erba model 1106 instrument. IR spectra were recorded from 4000 to 100 cm^{-1} and from 4000 to 600 cm^{-1} with a Perkin–Elmer instrument System 2000 FT-IR and a 1600 Series FT-IR instrument, respectively. ^1H- and ^{113}Cd NMR spectra were recorded on a VX-300 Varian spectrometer operating at room temperature (300 MHz for ^1H and 66.55 MHz for ^{113}Cd). Melting points were taken on an IA 8100 Electrothermal instrument. The electric resistance of solutions was measured with a Crison CDTM 522 conductometer at room temperature. The osmometric measurements were carried out at 37° over a range of concentrations with a Knauer KNA0280 vapour pressure osmometer calibrated with benzil. The solvent was Baker Analyzed Spectrophotometric grade chloroform or acetone. The results were reproducible to ±2%.

Reagents

Preparation of the proligands 4-acetyl- *and* 4-benzoyl-1-phenyl-3-methylpyrazol-5-onato (HQ' *and* HQ''), *and* 1,3-dimethyl-4-benzoylpyrazol-5-onato (HQ*). The proligands 4-acetyl- and 4-benzoyl-1-phenyl-3-methylpyrazol-5-onato and 1,3-dimethyl-4-benzoylpyrazol-5-onato (HQ', HQ'' and HQ*) were prepared according to Jensen's procedure [13]. Their analytical and spectroscopic data are in accordance with those reported in literature [13,14].

Preparation of bis(1-methylimidazole)dichlorozinc(II) **1**. Compound **1** precipitated out upon mixing $ZnCl_2$ (1.0 mmol, 0.136 g) in diethyl ether (20 ml) with 1-methylimidazole (L') (2.0 mmol, 0.164 g) in the same solvent (20 ml) and recrystallized from chloroform/ether. Compounds **2–5** and **21–24** were prepared similarly, while EtOH was used for compounds **7–9, 13–17, 26** and **30–34**.

The adducts **18** and **35** (50% aqueous cadmium fluoroborate was employed), **6** and **25** were prepared by addition of an ether suspension of the salt to a stirred ether solution of the ligand.

Preparation of [*bis*(1-methylimidazole)*bis*(1-phenyl-3-methyl-4-benzoylpyrazol-5-onato)zinc(II)] **10**. An ethanolic solution (60 cm^3) of the proligand HQ' (2.0 mmol, 0.556 g) was added to an ethanolic solution (30 cm^3) of zinc(II) acetate dihydrate (1.0 mmol, 0.219 g). A pale-rose precipitate was formed immediately. The reaction mixture was set aside overnight and the solid product was filtered off, washed with ethanol, recrystallized with chloroform/diethyl ether and shown to be complex $[(Q')_2Zn(H_2O)]$ by analysis and spectral data. Furthermore, $[(Q')_2Zn(H_2O)]$ (1.0 mmol, 0.638 g) was added to a diethyl ether solution (50 cm^3) of L' (2.0 mmol, 0.163 g). The reaction mixture slowly changed to a clear yellow solution. This was refluxed for 6 h, then the volume was reduced on the rotary evaporator until formation of a yellow powder, which was filtered off, washed with diethyl ether (ca 20 cm^3) and shown to be compound **10** by analysis. Compounds **11, 12** and **27–29** were obtained similarly. Compounds **19, 20** and **36–38** were obtained similarly using Cd(II) acetate dihydrate as starting material.

Preparation of [(1-methylimidazole)*bis*(4,7-diphenyl-1,10-phenanthroline)zinc(II)]diperchlorate **40**. [Pentakis(1-methylimidazole)Zn(II)(aquo)]diperchlorate (1.0 mmol, 0.690 g) was added to a 1 : 1 diethyl ether/ethanol solution (60 cm^3) of 4,7-diphenyl-1,10-phenanthroline (2.0 mmol, 0.664 g).

The suspension was set aside for about 3 h. The colorless precipitate formed was filtered off, washed with diethyl ether and shown to be compound **40** by analysis. Compounds **39** and **41–45** were obtained similarly.

CAUTION. The perchlorate derivatives reported in this paper may explode by shock or heating when dry. Small quantities (≤0.5 g) of the dry products should be handled.

Table 1. Crystal data and structure refinement for **33**

Empirical formula	$C_{30}H_{30}CdN_8O_6$
Formula weight	711.02
Temperature (K)	293(2)
Wavelength (Å)	0.71073
Crystal system	Monoclinic
Space group	$P2_1/c$
a (Å)	13.352(3)
b (Å)	17.058(3)
c (Å)	15.064(3)
β (°)	114.23(3)
V (Å^3)	3128.7(11)
Z	4
D_{calc} (mg m^3)	1.509
Absorption coefficient (mm^{-1})	0.754
$F(000)$	1448
θ range for data collection (°)	1.67 to 26.97
Reflections collected	6813
Reflections observed [$I > 2\sigma(I)$]	5456
Number of parameters	406
Final R indice [$I > 2\sigma(I)$]	0.0371
wR_2	0.0814

Table 2. Bond lengths [Å] and angles (°) for **33**

Bond lengths	
Cd—N(3)	2.255(3)
Cd—N(5)	2.256(3)
Cd—N(7)	2.239(3)
Cd—O(1)	2.463(3)
Cd—O(2)	2.705(3)
Cd—O(4)	2.450(3)
Cd—O(5)	2.670(3)
N(1)—O(3)	1.224(3)
N(1)—O(2)	1.243(3)
N(1)—O(1)	1.253(3)
N(2)—O(6)	1.234(4)
N(2)—O(5)	1.235(4)
N(2)—O(4)	1.237(4)
N(3)—C(1)	1.314(4)
N(3)—C(3)	1.373(4)
N(4)—C(1)	1.329(4)
N(4)—C(2)	1.351(4)
N(4)—C(4)	1.471(4)
C(2)—C(3)	1.349(5)
Bond angles	
N(7)—Cd—N(3)	103.31(10)
N(7)—Cd—N(5)	147.24(10)
N(3)—Cd—N(5)	109.45(10)
N(7)—Cd—O(4)	90.96(10)
N(3)—Cd—O(4)	81.07(10)
N(5)—Cd—O(4)	94.15(10)
N(7)—Cd—O(1)	100.34(10)
N(3)—Cd—O(1)	79.96(9)
N(5)—Cd—O(1)	85.45(10)
O(4)—Cd—O(1)	159.71(9)
O(3)—N(1)—O(2)	121.9(3)
O(3)—N(1)—O(1)	120.1(3)
O(2)—N(1)—O(1)	118.1(3)
O(6)—N(2)—O(5)	120.9(3)
O(6)—N(2)—O(4)	119.9(3)
O(5)—N(2)—O(4)	119.1(3)
C(1)—N(3)—C(3)	105.4(3)
C(1)—N(3)—Cd	123.4(2)
C(3)—N(3)—Cd	131.1(2)
C(11)—N(5)—Cd	127.2(2)
C(13)—N(5)—Cd	127.7(2)
C(21)—N(7)—Cd	129.6(2)
C(23)—N(7)—Cd	124.9(2)
N(1)—O(1)—Cd	101.5(2)
N(2)—O(4)—Cd	101.1(2)

Crystal structure determination of $[(L'')_3Cd(NO)_3)_2]$ **33**.

Crystals of **33** were grown from ethanol/diethyl ether solution. A colorless crystal with dimension $0.6 \times 0.3 \times 0.2$ mm was mounted on a glass fibre. Diffraction data were collected on an Enraf-Nonius CAD-4 diffractometer using Mo–K_α radiation. To record the intensities of reflections θ–2θ scan method were used. The crystallographic calculations were performed using the SHELXS-86 for structure solution [15] and SHELXL-93 for structure refinement [16]. The position of cadmium atom was found by Patterson method. Successive Fourier syntheses gave the coordinates of other atoms. The structure was anisotropically refined by full-matrix least-squares for all non-hydrogen atom to $R = 0.037$. The hydrogen atoms were refined isotropically. The crystallographic data are given in Table 1, selected bond lengths and angles are presented in Table 2.

RESULTS AND DISCUSSION

Synthesis of 4-acyl-5-pyrazolonato-metal precursors $[(Q)_2M(H_2O)_x]$ ($x = 1$ or 2)

The β-diketones 4-acyl-5-pyrazolone proligands HQ (Fig. 2) (HQ′ = 1-phenyl-3-methyl-4-benzoyl-pyrazol-5-one, HQ″ = 1-phenyl-3-methyl-4-acetyl-pyrazol-5-one, HQ* = 1,3-dimethyl-4-benzoyl-pyrazol-5-one) react in ethanol with $[(CH_3CO_2)_2M]\cdot 2H_2O$ (M = Zn or Cd), giving the compounds $[(Q)_2M\cdot(H_2O)_y]$ in accordance with the following eqn (1):

$$2HQ + [(CH_3CO_2)_2M]\cdot 2H_2O \xrightarrow{EtOH/H_2O} 2CH_3COOH + [(Q)_2M\cdot(H_2O)_y]$$

(M = Cd or Zn; HQ = HQ′, HQ″ or HQ*, $y = 1$ or 2) (1)

These bis(β-diketonato) complexes are air and solution stable, generally soluble in acetone, DMSO and in chlorinate solvents, insoluble in alcohol, water and

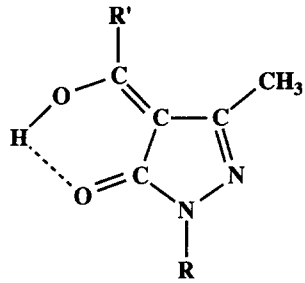

HQ': R = R' = Ph
HQ'': R = Ph, R' = Me
HQ*: R = Me, R' = Ph

Fig. 2. Structure of the proligands HQ', HQ'' and HQ*.

diethyl ether. According to literature [14a] and on the basis of spectral and analytical data [14b], the donors (Q) are coordinated to metal in the O_2-bidentate anionic form.

Synthesis of 1-methyl *and* 1-benzylimidazole *complexes*

1-Methylimidazole (L') and 1-benzylimidazole (L'') react in ethanol or diethyl ether solution/suspension with MX_2 acceptors (M = Zn, Cd; X = Cl, Br, I, NO_3, ClO_4, CF_3SO_3, BF_4, CH_3COO, CF_3COO, Q', Q'' or Q_M) affording the derivatives **1–38**:

$$nL + mMX_2(H_2O)_x \rightarrow (L)_n(MX_2)_m(H_2O)_x \quad (2)$$
$$\mathbf{1\text{–}38}$$

Some of the zinc(II) carboxylate, nitrate and perchlorate retain or absorb one or two water molecules. Derivatives **4, 5** and **6** are amorphous below 30°C and liquid up to 30°C, whereas all the other compounds are air stable microcrystalline solids with sharp melting points (Table 3). They are generally soluble in acetone and DMSO, insoluble in alcohols and diethyl ether. The derivatives of 1-methylimidazole show appreciable solubility also in chlorinated solvents.

The ligand/metal ratio $m:n$ has been found to vary in a wide range: 1 : 1 in the case of 4-acylpyrazolonato derivatives **27–29, 36** and **38** (Fig. 3a); 2 : 1 in the case of dihalide, *bis*(acetato) or *bis*(pyrazolonato) derivatives (Fig. 3b) **1–4, 10–12, 14, 15, 19–23, 32** and **37**; 3 : 1 in the case of nitrato, tetrafluoroborato e trifluoroacetato derivatives of L'' **24–26** and **33**; 4 : 1 in the case of $[(L')_4Zn(NO_3)_2]\cdot(H_2O)_2$ and $[(L')_4Zn(BF_4)_2]$ derivatives **6** and **8**; 5 : 1 in the case of derivatives $[(L')_5Zn](CF_3COO)_2\cdot(H_2O)$ **5** and $[(L')_5Zn](ClO_4)_2\cdot(H_2O)$ **9**; 6 : 1 in the case of derivatives **7, 16–18, 34** and **35**; finally from the reaction of dibromocadmium with L' and of dichloro- and dibromocadmium acceptors with L'' we have obtained poor soluble compounds with lower m/n ratio, i.e. 5 : 3 in **13** and 4 : 3 in **30** and **31**.

Several interesting trends emerge: in our conditions the dihalide give generally pseudotetrahedral 2 : 1 adducts. However, polynuclear 5 : 3 and 4 : 3 adducts were isolated when a sparingly soluble halo-bridged polymeric CdX_2 (X = Cl or Br) was employed as acceptor. 5 : 1 or 6 : 1 adducts are found only with good acceptors such as the perchlorate, tetrafluoroborate and trifluoroacetate and also with $Cd(NO_3)_2$, when the more basic and less hindered L' was employed as donor. No adduct has been isolated for zinc or cadmium cyanide, fluoride or cadmium sulphate, even when the reaction was performed under more forcing conditions, i.e. strong excess of the ligand and in refluxing solvents.

Reactivity of derivatives 1–3, 9, 14 *and* 17

The donor 4,7-dimethyl-1,10-phenanthroline and 2,2'-bipyridine react with compounds **9** and **17** yielding the *tris*-chelate complexes **39, 41, 44** and **45** upon complete displacement of the azole from the coordination sphere of the zinc, whereas the less basic 4,7-Ph_2-Phen and Bzpy displace respectively four and three molecules of the L' donor, yielding the mixed ligand derivatives $[(Ph_2Phen)_2(L')Zn](ClO_4)_2$ and $[(Bzpy)_2(L')_2Zn](ClO_4)_2$ **40** and **42** respectively. On the other hand 4,7-Ph_2-Phen and Bzpy are able to displace all the six molecules of L' from the adduct $[(L')_6Cd](ClO_4)_2$ **17**.

No reaction occurred in diethyl ether between the P-donors PR_3 (R = phenyl, benzyl or cyclohexyl) and the adducts **9** and **17**.

When the reaction between 4,7-Me_2-Phen, 4,7-Ph_2-Phen, Bipy or Bzpy and $[(L')_2ZnX_2]$ **(1–3)** or $[(L')_2CdI_2]$ **(14)** was carried out under the same conditions, the starting materials were always recovered.

Conductivity data

Conductivity measurements have been performed in dichloromethane or acetone solution for all the compounds **1–45** (Table 4).

Derivatives **1–5, 10–12, 15, 19, 20, 22, 27–29, 36–38** are non electrolytes. Derivatives **13, 14, 21, 23–25** and **30–32** for which a non-ionic structure has been observed in the solid state (see below the IR data section) show low conductance values in acetone, in accordance with ionic partial dissociation in this solvent. The dissociation seems to be dependent upon concentration of the solutions.

In the case of derivatives **6, 8, 9, 26** and **42,** which show conductance values typical of 1 : 1 electrolytes, an ionic structure in solution $[(L)_n(MX)_m(H_2O)]^+[X]^-$ can be hypothesized: on the basis of preliminar molecular weight determinations (r = ratio between experimental and theoretic molecular weight being in the range 0.50–0.70) carried out on selected derivatives we also suggest that these complexes undergo in solution ligand dissociation. The derivative

Table 3. Analytical data of compounds **1–45**

Compound	M.W.	No.	M.p. °C	Yield %	Elem. An. (found (calcd) %) C	H	N
$[(L')_2ZnCl_2]$	300.5	**1**	208–209	80	31.7	4.1	18.4
$C_8H_{12}Cl_2N_4Zn$					(32.0)	(4.0)	(18.6)
$[(L')_2ZnBr_2]$	389.4	**2**	188–189	92	24.8	3.2	14.2
$C_8H_{12}Br_2N_4Zn$					(24.7)	(3.1)	(14.4)
$[(L')_2ZnI_2]$	483.4	**3**	163–164	75	19.9	2.5	11.5
$C_8H_{12}I_2N_4Zn$					(19.9)	(2.5)	(11.6)
$[(L')_2Zn(CH_3COO)_2]\cdot(H_2O)_2$	383.7	**4**	oil	45	37.5	5.7	14.8
$C_{12}H_{22}N_4O_6Zn$					(37.6)	(5.8)	(14.6)
$[(L')_5Zn](CF_3COO)_2\cdot(H_2O)$	719.9	**5**	oil	49	40.2	4.3	19.6
$C_{24}H_{32}F_6N_{10}O_5Zn$					(40.0)	(4.5)	(19.4)
$[(L')_4Zn(NO_3)_2]\cdot(H_2O)_2$	553.0	**6**	oil	90	40.6	4.3	20.0
$C_{16}H_{28}N_{10}O_8Zn$					(41.0)	(4.3)	(19.9)
$[(L')_6Zn](CF_3SO_3)_2$	856.1	**7**	141–142	92	36.4	4.3	19.4
$C_{26}H_{36}F_6N_{12}O_6S_2Zn$					(36.5)	(4.2)	(19.6)
$[(L')_4Zn(BF_4)_2]$	567.4	**8**	157–159	89	33.9	4.3	19.8
$C_{16}H_{24}B_2F_8N_8Zn$					(33.9)	(4.3)	(19.7)
$[(L')_5Zn](ClO_4)_2\cdot(H_2O)$	692.8	**9**	190–191	85	34.4	4.6	19.1
$C_{20}H_{32}Cl_2N_{10}O_9Zn$					(34.7)	(4.7)	(20.2)
$[(L')_2Zn(Q')_2]$	784.2	**10**	134–136	93	64.1	4.8	14.4
$C_{42}H_{38}N_8O_4Zn$					(64.3)	(4.9)	(14.3)
$[(L')_2Zn(Q'')_2]$	660.1	**11**	259–262	75	58.2	5.2	17.0
$C_{32}H_{34}N_8O_4Zn$					(58.4)	(5.1)	(16.8)
$[(L')_2Zn(Q^*)_2]$	660.1	**12**	160 dec	43	58.1	5.3	17.1
$C_{32}H_{34}N_8O_4Zn$					(58.4)	(5.1)	(16.8)
$[(L')_5(CdBr_2)_3]$	1227.2	**13**	175–177	96	19.1	2.4	10.9
$C_{20}H_{36}Br_6Cd_3N_{10}$					(19.6)	(2.5)	(11.4)
$[(L')_2CdI_2]$	530.4	**14**	124–125	78	18.3	2.3	10.6
$C_8H_{12}CdI_2N_4$					(18.1)	(2.3)	(10.6)
$[(L')_2Cd(CH_3COO)_2]\cdot(H_2O)_2$	430.7	**15**	79 dec	38	33.3	5.0	12.8
$C_{12}H_{22}CdN_4O_6$					(33.5)	(5.1)	(13.0)
$[(L')_6Cd](NO_3)_2$	729.1	**16**	171–173	56	39.6	5.2	27.0
$C_{24}H_{36}CdN_{14}O_6$					(39.5)	(5.0)	(26.9)
$[(L')_6Cd](ClO_4)_2$	692.8	**17**	248 dec	88	35.9	4.7	20.9
$C_{24}H_{36}CdCl_2N_{12}O_8$					(35.9)	(4.5)	(20.9)
$[(L')_6Cd](BF_4)_2$	778.7	**18**	226–229	93	36.7	4.7	21.2
$C_{24}H_{36}B_2CdF_8N_{12}$					(37.0)	(4.7)	(21.6)
$[(L')_2Cd(Q')_2]$	831.2	**19**	192–193	62	60.9	4.7	13.4
$C_{42}H_{38}CdN_8O_4$					(60.7)	(4.6)	(13.5)
$[(L')_2Cd(Q^*)_2]$	707.1	**20**	195–198	93	54.6	4.8	15.9
$C_{32}H_{34}CdN_8O_4$					(54.4)	(4.8)	(15.8)
$[(L'')_2ZnCl_2]$	452.7	**21**	167–170	95	52.9	4.5	12.2
$C_{20}H_{20}Cl_2N_4Zn$					(53.1)	(4.5)	(12.4)
$[(L'')_2ZnBr_2]$	541.6	**22**	178–184	88	44.4	3.9	10.2
$C_{20}H_{20}Br_2N_4Zn$					(44.4)	(3.7)	(10.3)
$[(L'')_2ZnI_2]$	635.6	**23**	285–287	66	37.5	3.3	8.6
$C_{20}H_{20}I_2N_4Zn$					(37.8)	(3.2)	(8.8)
$[(L'')_3Zn(CF_3COO)_2]$	607.8	**24**	70–75	86	52.9	4.3	11.0
$C_{34}H_{30}F_6N_6O_4Zn$					(53.3)	(4.0)	(11.0)
$[(L'')_3Zn(NO_3)_2]\cdot(H_2O)$	682.0	**25**	108–109	88	53.0	4.8	16.4
$C_{30}H_{32}N_8O_7Zn$					(52.8)	(4.7)	(16.4)
$[(L'')_3Zn(BF_4)_2]$	713.6	**26**	131–134	56	50.6	3.9	11.8
$C_{30}H_{30}B_2F_8N_6Zn$					(50.5)	(4.2)	(11.8)
$[(L'')Zn(Q')_2]$	778.2	**27**	222–226	75	67.7	4.7	10.6
$C_{44}H_{36}N_6O_4Zn$					(67.9)	(4.7)	(10.8)
$[(L'')Zn(Q'')_2]$	654.0	**28**	144–146	55	62.8	5.2	13.1
$C_{34}H_{32}N_6O_4Zn$					(62.4)	(4.9)	(12.9)
$[(L'')Zn(Q^*)_2]$	654.0	**29**	182–185	53	61.9	5.2	12.8
$C_{34}H_{32}N_6O_4Zn$					(62.4)	(4.9)	(12.9)
$[(L'')_4(CdCl_2)_3]$	1182.7	**30**	202–205	54	40.2	3.5	9.3
$C_{40}H_{40}Cd_3Cl_6N_8$					(40.6)	(3.4)	(9.5)

Table 3—*Continued.*

Compound	M.W.	No.	M.p. °C	Yield %	Elem. An. (found (calcd) %) C	H	N
$[(L'')_4(CdBr_2)_3]$	1449.5	**31**	147 dec	48	33.6	2.9	7.7
$C_{40}H_{40}Br_6Cd_3N_8$					(33.2)	(2.8)	(7.7)
$[(L'')_2CdI_2]$	682.6	**32**	126 dec	50	34.8	3.0	7.9
$C_{20}H_{20}CdI_2N_4$					(35.2)	(3.0)	(8.2)
$[(L'')_3Cd(NO_3)_2]$	711.0	**33**	136–148	62	50.4	4.2	15.5
$C_{30}H_{30}CdN_8O_6$					(50.7)	(4.2)	(15.8)
$[(L'')_6Cd](ClO_4)_2$	1260.5	**34**	125–135	92	56.7	4.9	13.0
$C_{60}H_{60}CdCl_2N_{12}O_8$					(57.2)	(4.8)	(13.3)
$[(L'')_6Cd](BF_4)_2$	1235.2	**35**	136–146	93	57.1	5.0	13.3
$C_{60}H_{60}B_2CdF_8N_{12}$					(57.5)	(5.0)	(13.4)
$[(L'')Cd(Q')_2]$	833.3	**36**	159–160	67	63.5	4.7	10.9
$C_{44}H_{36}CdN_6O_4$					(63.0)	(4.5)	(10.5)
$[(L'')_2Cd(Q'')_2]$	859.3	**37**	166–169	72	61.2	5.0	12.8
$C_{44}H_{42}CdN_8O_4$					(61.5)	(4.9)	(13.0)
$[(L'')Cd(Q^*)_2]$	701.1	**38**	135–137	65	58.3	4.6	12.0
$C_{34}H_{32}CdN_6O_4$					(58.2)	(4.6)	(12.0)
$[(Me_2Phen)_3Zn](ClO_4)_2$	889.0	**39**	358–361	96	57.0	4.2	9.8
$C_{42}H_{36}Cl_2N_6O_8Zn$					(56.7)	(4.1)	(9.4)
$[(Ph_2Phen)_2(L')Zn](ClO_4)_2$	1011.2	**40**	394–396	65	61.5	3.9	8.1
$C_{52}H_{38}Cl_2N_6O_8Zn$					(61.8)	(3.8)	(8.3)
$[(Bipy)_3Zn](ClO_4)_2$	732.8	**41**	347–349	90	49.2	3.3	11.5
$C_{30}H_{24}Cl_2N_6O_4Zn$					(48.8)	(3.3)	(11.4)
$[(Bzpy)_2(L')_2Zn](ClO_4)_2$	794.9	**42**	134–137	89	48.6	3.9	10.6
$C_{32}H_{30}N_6Cl_2O_{10}Zn$					(48.3)	(3.8)	(10.8)
$[(Me_2Phen)_3Cd](ClO_4)_2$	936.1	**43**	374–376	86	53.4	4.0	8.9
$C_{42}H_{36}CdCl_2N_6O_8$					(53.9)	(3.9)	(9.0)
$[(Ph_2Phen)_3Cd](ClO_4)_2$	1308.5	**44**	370–373	75	66.3	3.7	6.4
$C_{72}H_{48}CdCl_2N_6O_8$					(66.4)	(3.9)	(6.5)
$[(Bipy)_3Cd](ClO_4)_2$	715.9	**45**	188–190	84	46.2	3.1	10.9
$C_{30}H_{24}CdCl_2N_6O_4$					(46.2)	(3.1)	(10.8)

$[(L')_6Zn](CF_3SO_3)_2$ **7,** which is ionic in the solid state, shows a value typical of a 1 : 1 electrolyte: in this case partial dissociation of the 1-methylimidazole donors and coordination of one CF_3SO_3 group is likely. However, in the case of compounds **7, 8, 9, 40** and **42** which show in dichloromethane a conductance value typical of a 1 : 1 electrolyte, we cannot exclude in this solvent the possibility of ion-pairing effects which cause a much lower value of conductivity with respect to that observed in acetone for analogous compounds.

Finally, in the case of derivatives **17, 18, 34, 35, 39–41** and **43–45,** 2 : 1 ionic species can be postulated in solution, with both the counterions (BF_4^- or ClO_4^-) out of the inner coordination sphere of the metal.

^1H NMR data

The proton NMR spectra of derivatives **1–45** have been recorded in deuterated chloroform or acetone (Table 5). The choice of the solvent was dictated by the solubility of the compounds. The signals of the azole ring protons of L′ and L″ have been found shifted to lower field upon coordination. The same trend has been observed for the proton signals of the R groups bonded to pyrrolic nitrogen (R = Me or Bz). However, the deshielding observed is attenuated at a position remote from the metal. The Δ observed is likely due to a σ-charge donation from the N-donor to zinc(II) or cadmium(II) acceptor and is evidence of the existence of the complexes in solution.

Also if one would expect in many of these compounds the existence in solution of more than one isomer, or the presence of non identical ligands, in all the ^1H NMR spectra of **1–45** we found only one set of signals for each equivalent proton group. This is likely due to a rapid exchange between free and bound ligand or between different metal coordination sites. This rapid exchange is operating also at low temperature: in fact the spectra of derivatives **1, 4, 7, 10** and **16** remain unchanged also at −70°C.

In the case of derivatives **4, 10–12, 15, 19, 20, 27–29** and **36–38** the integration of the absorptions due to the acetato groups or the acylpyrazolonato ligands

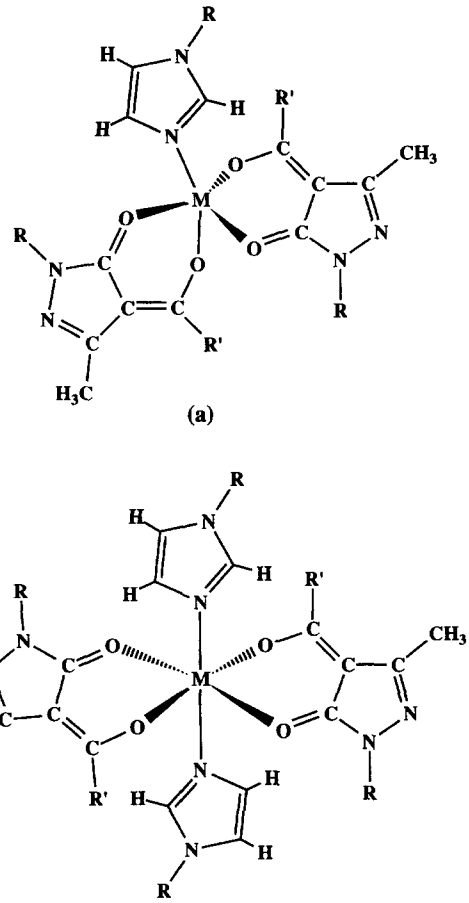

Fig. 3. Structures possible for the mixed ligand complexes 1 : 1 $[(L)M(Q)_2]$ and 2 : 1 $[(L)_2M(Q)_2]$.

and that of imidazoles is in accordance with the ligand/metal ratio *m*/*n* proposed in the empirical formula.

In the spectra of **39–45** all the expected signals of protons of bidentate and monodentate nitrogen donors have been detected. In the *tris*(chelate) derivatives the signals of the donor are generally downfield shifted upon coordination, whereas only a small displacement was observed in the mixed-ligand complexes.

^{113}*Cd NMR data*

We have carried out ^{113}Cd NMR spectra of deuterated acetone or chloroform solutions of several cadmium derivatives (Table 6). In the case of derivatives **15, 16, 19, 20, 33, 34** and **36–38** only a small resonance has been found in the range +59/+99 ppm, which is typical of five- or six-coordinate N_3CdO_2, N_4CdO_2, N_2CdO_4 and $NCdO_4$ species. Accordingly with the conductance value the derivative **16** likely possesses in solution an N_4CdO_2 core, differently from that observed in the solid state; it likely undergoes partial ligand L′ dissociation with consequent nitrato re-association. The presence in all the spectra of only a single absorbance is indicative of absence of isomers in solution or shows that a fluxional mechanism is operating at room temperature. It is well-known that ligands that bond to cadmium through oxygen cause increased shielding [17]. In fact the presence of only two oxygens bonded to cadmium in **15** and **16** is confirmed by their downfield shifted (+95.9 and +98.6 ppm, respectively) with respect to the other complexes containing four oxygens. In the case of derivatives **17** and **34** the absorption at ca +190/+200 ppm indicate a CdN_6 central core [18], as hypothesized also by conductance values. In the latter derivatives the cadmium nucleus is deshielded with respect to the former compounds due to the presence in the metal environment of only nitrogen atoms, poorer shielding donor than oxygens.

IR and far-IR data

Selected IR and far-IR data of derivatives **1–45** are reported in Table 7. The spectra are recorded in Nujol mull and some ones also in chloroform.

Besides the expected bands over 3000 cm^{-1}, due to ν(C—H) of the azoles, other absorptions in the range 1700–1500 cm^{-1} and below 600 cm^{-1} give additional information about the geometry of the derivatives.

In the case of di-halo-metal adducts **1–3, 14, 21–23** and **32** two M—N and two M—X stretching vibrations are expected to be IR active for pseudo-tetrahedral (C_{2v} symmetry) complexes. In our case, the assignments of the M-halogen symmetric and asymmetric stretching vibrations are unambiguous, well-distinguishable strong absorptions being present under 350 cm^{-1}, which are red-shifted on going from M—Cl (310–290 cm^{-1}) to M—Br (250–230 cm^{-1}) and to M—I (230–190 cm^{-1}) [19]. The medium absorptions in the range 230–250 cm^{-1} can be assigned to ν(M—N) stretching modes [19]: in the di-chloro- and di-iodo-zinc derivatives the ν(M—N) modes can be assigned without much ambiguity, but for the di-bromo-zinc derivatives they lie close to the ν(Zn—Br) region and coupling must be appreciable.

Derivatives **13, 30** and **31** likely possess a polynuclear nature, owing to their analytical formula and low solubility in all solvents. In fact the ν(M—X) vibrations are found at very low frequencies, in accordance with the presence of bridging metal-halogen bonds [20]. In these adducts the metal should be five- or six-coordinate, surrounded by four bridging halogens and one or two azoles.

Derivatives **7, 16–18, 34, 35, 39, 41** and **43–45** contain octahedral MN_6^{2+} ions. An ideally octahedral MN_6 species (O_h symmetry) should present only two asymmetric (M—N) modes (ν_3 and ν_4, whereas the symmetric ν_1 and ν_2 are Raman active) [20]. The existence of octahedral MN_6^{2+} species is supported by the

Table 4. Conductivity data of compounds **1–45**

Compound	No.	Solvent	Conc.[a]	Λ_m[b]
$[(L')_2ZnCl_2]$	**1**	CH_2Cl_2	$1.08\cdot10^{-3}$	0.33
$[(L')_2ZnBr_2]$	**2**	CH_2Cl_2	$1.16\cdot10^{-3}$	0.09
$[(L')_2ZnI_2]$	**3**	CH_2Cl_2	$1.03\cdot10^{-3}$	0.15
$[(L')_2Zn(CH_3COO)_2]\cdot(H_2O)_2$	**4**	CH_2Cl_2	$1.17\cdot10^{-3}$	0.27
$[(L')_5Zn](CF_3COO)_2\cdot(H_2O)$	**5**	CH_2Cl_2	$1.05\cdot10^{-3}$	1.88
$[(L')_4Zn(NO_3)_2]\cdot(H_2O)_2$	**6**	CH_2Cl_2	$1.34\cdot10^{-3}$	7.60
$[(L')_6Zn](CF_3SO_3)_2$	**7**	CH_2Cl_2	$1.06\cdot10^{-1}$	13.32
$[(L')_4Zn(BF_4)_2]$	**8**	CH_2Cl_2	$0.92\cdot10^{-3}$	13.64
$[(L')_5Zn](ClO_4)_2\cdot(H_2O)$	**9**	CH_2Cl_2	$0.99\cdot10^{-3}$	15.00
$[(L')_2Zn(Q')_2]$	**10**	CH_2Cl_2	$1.01\cdot10^{-3}$	1.60
$[(L')_2Zn(Q')_2]$	**11**	CH_2Cl_2	$0.81\cdot10^{-3}$	0.12
$[(L')_2Zn(Q^*)_2]$	**12**	CH_2Cl_2	$0.96\cdot10^{-3}$	0.23
$[(L')_5(CdBr_2)_3]$	**13**	Acetone	$0.94\cdot10^{-3}$	18.24
$[(L')_2CdI_2]$	**14**	Acetone	$0.62\cdot10^{-3}$	10.35
$[(L')_2Cd(CH_3COO)_2]\cdot(H_2O)_2$	**15**	Acetone	$1.16\cdot10^{-3}$	1.26
$[(L')_6Cd](NO_3)_2$	**16**	Acetone	$0.92\cdot10^{-3}$	16.85
$[(L')_6Cd](ClO_4)_2$	**17**	Acetone	$0.83\cdot10^{-3}$	175.06
$[(L')_6Cd](BF_4)_2$	**18**	Acetone	$0.96\cdot10^{-3}$	181.77
$[(L')_2Cd(Q')_2]$	**19**	CH_2Cl_2	$0.69\cdot10^{-3}$	0.05
$[(L')_2Cd(Q^*)_2]$	**20**	CH_2Cl_2	$0.72\cdot10^{-3}$	0.06
$[(L'')_2ZnCl_2]$	**21**	Acetone	$0.57\cdot10^{-3}$	21.89
$[(L'')_2ZnBr_2]$	**22**	Acetone	$0.82\cdot10^{-3}$	2.74
$[(L'')_2ZnI_2]$	**23**	Acetone	$0.84\cdot10^{-3}$	12.71
$[(L'')_3Zn(CF_3COO)_2]$	**24**	Acetone	$0.98\cdot10^{-3}$	12.06
$[(L'')_3Zn(NO_3)_2]\cdot(H_2O)$	**25**	Acetone	$0.97\cdot10^{-3}$	32.06
$[(L'')_3Zn(BF_4)_2]$	**26**	Acetone	$1.05\cdot10^{-3}$	140.03
$[(L'')Zn(Q')_2]$	**27**	CH_2Cl_2	$0.67\cdot10^{-3}$	0.15
$[(L'')Zn(Q'')_2]$	**28**	CH_2Cl_2	$0.81\cdot10^{-3}$	0.17
$[(L'')Zn(Q^*)_2]$	**29**	CH_2Cl_2	$0.59\cdot10^{-3}$	0.14
$[(L'')_4(CdCl_2)_3]$	**30**	Acetone	$0.45\cdot10^{-3}$	16.84
$[(L'')_4(CdBr_2)_3]$	**31**	Acetone	$0.38\cdot10^{-3}$	14.22
$[(L'')_2CdI_2]$	**32**	Acetone	$0.73\cdot10^{-3}$	6.23
$[(L'')_3Cd(NO_3)_2]$	**33**	Acetone	$1.11\cdot10^{-3}$	11.94
$[(L'')_6Cd](ClO_4)_2$	**34**	Acetone	$0.42\cdot10^{-3}$	197.14
$[(L'')_6Cd](BF_4)_2$	**35**	Acetone	$0.73\cdot10^{-3}$	187.67
$[(L'')Cd(Q')_2]$	**36**	CH_2Cl_2	$0.68\cdot10^{-3}$	0.15
$[(L'')_2Cd(Q'')_2]$	**37**	CH_2Cl_2	$0.83\cdot10^{-3}$	0.18
$[(L'')Cd(Q^*)_2]$	**38**	CH_2Cl_2	$0.43\cdot10^{-3}$	0.11
$[(Me_2Phen)_3Zn](ClO_4)_2$	**39**	CH_2Cl_2	$0.39\cdot10^{-3}$	37.05
$[(Ph_2Phen)_2(L')Zn](ClO_4)_2$	**40**	CH_2Cl_2	$0.95\cdot10^{-3}$	20.86
$[(Bipy)_3Zn](ClO_4)_2$	**41**	CH_2Cl_2	$0.64\cdot10^{-3}$	27.56
$[(Bzpy)_2(L')_2Zn](ClO_4)_2$	**42**	CH_2Cl_2	$1.00\cdot10^{-3}$	12.78
$[(Me_2Phen)_3Cd](ClO_4)_2$	**43**	CH_2Cl_2	$0.55\cdot10^{-3}$	35.64
$[(Ph_2Phen)_3Cd](ClO_4)_2$	**44**	CH_2Cl_2	$0.43\cdot10^{-3}$	33.56
$[(Bipy)_3Cd](ClO_4)_2$	**45**	CH_2Cl_2	$0.54\cdot10^{-3}$	29.44

[a] Conc. is molar concentration ($\times 10^3$).
[b] Λ_m in Ω^{-1} cm^2 mol^{-1}.

presence in these derivatives of two very strong absorptions in the range 150–220 cm^{-1} and by the spectroscopic behaviour of the respective counterions (ClO_4^-, BF_4^-, $CF_3SO_3^-$ and NO_3^-) which is typical of ionic outer-sphere groups: in the case of ionic ClO_4^- and BF_4^- (T_d geometry) only two vibrations (ν_3 and ν_4) are expected to be IR active [21], as in fact found at ca 1090 and ca 620 cm^{-1} in the spectra of perchlorates and at ca 1030 and ca 520 cm^{-1} in the spectra of tetrafluoroborates; the ionic $CF_3SO_3^-$ group has lower symmetry (C_{3v}), but the absence of splitting of the band at 1260 cm^{-1} (ν_3) should be indicative of ionic character; an ionic NO_3^- group (D_{3h} symmetry) should possess three IR active vibration modes (ν_2, ν_3

Table 5. ^{1}H NMR data[a] of compounds **1–45**

Compound	Solvent	Azole				Other data[b]
		H2	H4	H5	N—R	
L′	$CDCl_3$	7.38	6.99	6.84	3.63	
	Acetone	7.33	6.88	6.76	3.59	
1	$CDCl_3$	7.98	7.18	6.97	3.76	
2	$CDCl_3$	8.01	7.22	6.97	3.79	
3	$CDCl_3$	7.98	7.19	7.01	3.77	
4	$CDCl_3$	8.09	7.30	6.84	3.70	CH_3: 2.05
5	$CDCl_3$	7.96	7.14	6.88	3.70	H_2O: 2.9 br
6	$CDCl_3$	7.83	7.05	6.95	3.75	H_2O: 2.6 br
7	$CDCl_3$	8.07	7.05	7.03	3.82	H_2O: 2.9 br
8	$CDCl_3$	8.24	7.16	7.04	3.85	
9	$CDCl_3$	8.25	7.20	7.05	3.90	H_2O: 2.40 br
10	$CDCl_3$	7.70	7.19	6.90	3.68	CH_3: 1.75; Ph: 7.15 t, 7.32 t, 7.42 t, 7.45 t, 7.50 d, 8.05 d
11	$CDCl_3$	7.58	7.15	6.90	3.69	CH_3: 2.44, 2.46; Ph: 7.20 t, 7.36 t, 8.0 d
12	$CDCl_3$	7.60 br	7.20 br	6.90 br	3.80 br	CH_3: 3.40 br, 1.70 br; Ph: 7.30–7.40 br
13	Acetone	7.95	7.33	7.15	3.90	
14	Acetone	7.95	7.35	7.12	3.90	
15	Acetone	7.80	7.15	7.05	3.80	CH_3: 1.88; H_2O: 2.91
16	Acetone	7.68	7.12	6.93	3.77	
17	Acetone	7.80	7.25	6.90	3.80	
18	Acetone	7.80	7.30	6.90	3.80	
19	$CDCl_3$	7.72	6.84	7.13	3.64	CH_3: 1.67; Ph: 7.10 t, 7.20–7.40 m, 77.98 d
20	$CDCl_3$	7.73	6.85	7.16	3.68	CH_3: 3.40 br, 1.70 br; Ph: 7.30–7.40 m
L″	$CDCl_3$	7.47	6.84 pt	7.12 br	5.00	Ph: 6.95–7.40 m
	Acetone	7.82	7.10 pt	7.25 pt	5.39	Ph: 7.38–7.56 m
21	Acetone	8.18	7.15	—	5.41	Ph: 7.32–7.40
22	Acetone	8.22	7.20	—	5.44	Ph: 7.30–7.50
23	Acetone	8.25	7.20	—	5.44	Ph: 7.30–7.40; H_2O: 2.85
24	Acetone	8.10	7.15	7.30	5.38	Ph: 7.35–7.55
25	Acetone	8.45	7.20	7.38	5.45	Ph: 7.40–7.50 m; H_2O: 2.85
26	Acetone	8.60	7.28	7.60	5.45	Ph: 7.30–7.50 m
27	$CDCl_3$	7.50	7.18	7.35	5.08	CH_3: 1.80; Ph: 7.15 t, 8.05 d, 7.30–7.50 m
28	$CDCl_3$	7.70	6.90	7.18	5.10	CH_3: 2.43, 2.45; Ph: 7.10 m, 7.30–7.40 m, 8.05 d
29	$CDCl_3$	7.86	6.90	7.15	5.06	CH_3: 1.70, 3.48; Ph: 7.10 m, 7.30–7.50 m
30	Acetone	8.0 v br	7.10 v br	—	5.40	Ph: 7.30–7.40 br
31	Acetone	8.20	7.20	7.42	5.40	Ph: 7.40 br m
32	Acetone	8.15 br	7.15	7.42	5.40	Ph: 7.20–7.40 m
33	Acetone	7.95 br	7.00 br	7.30 br	5.40	Ph: 7.30–7.50 m
34	Acetone	7.95	6.90	—	5.35	Ph: 7.30–7.50 m
35	Acetone	7.90 br	6.85	7.30 br	5.32	Ph: 7.30–7.50 m
36	$CDCl_3$	7.80	6.82	7.15	5.00	CH_3: 1.68; Ph: 7.10 m, 7.20–7.40 m, 7.96 d
37	$CDCl_3$	7.80	6.82	7.30	5.00	CH_3: 2.30–2.38; Ph: 7.10 m, 7.30–7.40 m, 7.95 d
38	$CDCl_3$	7.82	6.83	7.20	5.00	CH_3: 1.60, 3.40; Ph: 7.10 m, 7.30–7.40 m
39	$CDCl_3$					Me-Phen: 2.90, 7.60 d, 8.10 d, 8.40
40	$CDCl_3$	7.95	6.90	7.10	3.70	Ph-Phen: 7.65 m, 8.05 d, 8.20, 8.80
41						Bipy: 7.75 t, 8.15 m, 8.28 t, 8.40 t
42	$CDCl_3$	8.05	6.98	7.20	3.80	Bzpy: 7.60 m, 7.88 t, 8.05 d, 8.74 d
43	$CDCl_3$					Me-Phen: 2.90, 7.92 d, 8.20, 8.84
44	$CDCl_3$					Ph-Phen: 7.60 m, 7.82 d, 8.05 d, 8.18, 9.55 d
45	$CDCl_3$					Bipy: 7.50 br, 7.90 br, 8.35 d, 8.60 br

[a] δ in ppm, all the signals are singlet, except where indicated: t = triplet, d = doublet, m = complex multiplet, br = broad, pt = pseudo triplet.

[b] H_2O and/or N_2-donor signals.

Table 6. ^{113}Cd NMR data

Compound	No.	Solvent	$\delta(^{113}Cd)$
$[(L')_2Cd(CH_3COO)_2]\cdot(H_2O)_2$	**15**	$CDCl_3$	98.6
$[(L')_6Cd(NO_3)_2]$	**16**	Acetone	95.9
$[(L')_2Cd(Q')_2]$	**19**	$CDCl_3$	77.1
$[(L')_2Cd(Q^*)_2]$	**20**	$CDCl_3$	82.1
$[(L'')_3Cd(NO_3)_2]$	**33**	Acetone	73.2
$[(L')_6Cd(ClO_4)_2]$	**34**	Acetone	192.1
$[(L'')Cd(Q')_2]$	**36**	$CDCl_3$	76.0
$[(L'')_2Cd(Q'')_2]$	**37**	$CDCl_3$	81.2
$[(L'')Cd(Q^*)_2]$	**38**	$CDCl_3$	59.1

and ν_4) [22], which have been found in the solid state spectrum of **16** at ca 1390, 830 and 720 cm^{-1}, together with an unsplitted $(\nu_1+\nu_4)$ combination band at 1740 cm^{-1}, in accordance with an ionic formulation of nitrato groups [23].

The β-diketonato derivatives **10, 11, 12, 19, 20, 27–29** and **36–38** show the typical ν(C···O) absorption bands in the range 1550–1650 cm^{-1} [24]. It can be noted that the higher frequency band shifts the blue of 10–20 cm^{-1} with respect to that of $(Q)_2M\cdot(H_2O)$ reactants, due to the lengthening of the M—O bonds upon increasing of the coordination number. They generally show two or three ν(M—O) absorptions between 370–440 cm^{-1} and one or two strong bands in the range 180–220 cm^{-1} due to ν(M—N). In the case of six-coordinate derivatives a *trans*-N_2MO_4 geometry (D_{4h} symmetry) is likely, whereas for five coordinate NMO_4 derivatives we are not able to indicate the preferred geometry.

In the case of carboxylate derivatives it is generally accepted [25] that it is possible to distinguish between ionic, unidentate, chelating bidentate or bridging bidentate groups on the basis of Δ value [where $\Delta = \nu_a(COO)—\nu_s(COO)$]. The following trend should be found:

$$\Delta_{unidentate} > \Delta_{ionic} > \Delta_{bridging\ bidentate} > \Delta_{chelating\ bidentate}$$

where Δ_{ionic} is ca 160–170 for acetates and ca 220–230 for trifluoroacetates [25]. In our 1-substituted imidazole derivatives **4, 5, 15** and **24** we predict a unidentate coordinating behaviour of $RCOO^-$: $\Delta = 213$ in derivative **4**, in accordance with a pseudo-tetrahedral geometry and an N_2ZnO_2 central core. Compound **15** is likely to be pseudo-tetrahedral, notwithstanding $\Delta = 165$ likely due to the possibility of H-bonded water to uncoordinated carbonyl, which should lower the $\nu_a(COO)$ [25]. Besides two strong absorptions at ca 170–190 cm^{-1} caused to ν(M—N) modes, we have also found a new band at ca 280 cm^{-1} likely due to ν(M—O). In the spectra of trifluoroacetates **5** and **24** the Δ value are 273 and 248 respectively, in accordance with a unidentate formulation of these groups. The derivative **5** could be hepta-coordinated while derivative **24** probably possesses a five-coordinate geometry. The difference in stoichiometry can be ascribed to the higher steric hindrance of L'' with respect to L'. A similar difference can also be observed between the nitrates **6** and **24** and tetrafluoroborates **8** and **26**. The electron-withdrawing power of CF_3 should be responsible for the higher coordination numbers found in the trifluoroacetates with respect to acetates. In the spectra of **5** and **24** we have also found a strong absorption at ca 280 cm^{-1} due to ν(M—O). No differences have been observed in the solution (chloroform) spectra of **4** and **5**, the $\Delta = [\nu_a(COO)—\nu_s(COO)]$ values being 209 and 260 cm^{-1}, respectively.

The zinc-nitrate derivative **6** should possess in the solid state a tetragonally distorted trans-octahedral N_4ZnO_2 central core: in fact two ν(Zn—N) and one ν(Zn—O) [26] have been identified in the far region. The nitrate behaviour is not well identified, due to the presence in the solid and in solution spectra of several overlapped absorptions in the region 1100–1500 cm^{-1}.

We assign a six-coordinate geometry to derivative **8** in the solid state, with both BF_4^- groups unidentate: in fact ν_3 mode is split into two broad bands (1100 and 1024 cm^{-1}). We observed also two bands at 775 and 521 cm^{-1} due to ν_1 and ν_4 respectively [27]. Moreover, the absorptions at 250–270 cm^{-1} could be tentatively assigned to ν(Zn—F) modes. In chloroform solution the derivative **8** shows a conductance value typical of 1:1 ionic species (see Conductivity data section), but in the IR spectrum in chloroform solution it is not possible to distinguish between the unidentate and the ionic BF_4^- group [28].

Derivative **9** should have a six-coordinate N_5ZnO core, both in the solid and in the solution state, in fact the spectra recorded in Nujol and in chloroform are almost identical and show several absorptions due to perchlorate groups: that centered at 1070 cm^{-1} (ν_3 mode) present a splitting likely due to lowering of symmetry from T_d (ionic) to C_{3v} (unidentate), together with bands at 959 (ν_1 mode, IR-inactive for ionic ClO_4^-), 654 and 622 cm^{-1} (ν_5 and ν_3 modes, respectively) [21].

Derivatives **25** and **26** possess a five-coordinate geometry in the solid state with both the counterions unidentate; in the case of derivative **33** the X-ray crystal structure (see below) shows a trigonal bipyramidal (or seven-coordinated) environment of cadmium: the IR data are in accordance with this evidence, in particular the combination band $\nu_1+\nu_4$ is split (1760 and 1744 cm^{-1}) with $\Delta = 16$, typical of unidentate or strongly asymmetric bidentate nitrates (C_s symmetry) [22,23]. A very similar spectroscopic behaviour has been found in the IR spectrum of compound $[(L'')_3Zn(NO_3)_2]\cdot(H_2O)$ **25**. In the spectrum of compound **26** the ν_3 band of BF_4^- is split into three absorptions (1100, 1055 and 1015 cm^{-1}) as expected for unidentate groups [21].

Finally, derivatives **40** and **42** possess ZnN_5^{2+} and

Table 7. Selected IR data (4000–100 cm^{-1})[a] of the donors and their derivatives **1–45**

Compound	No	ν(C—H)$_{azole}$	1650–1500	<600	Other data
L′		3106 s	1589 m, 1518 s	552 m, 354 m, 280 m, 227 w, 151 m, 119 m	$\nu(H_2O)$: 3378 br, $\delta(H_2O)$: 1676 m
$[(L')_2ZnCl_2]$	1	3117 m	1587 m, 1540 s, 1522 s	552 w, 371 m, 187 m, 160 m 143 s, 112 m	ν(Zn—Cl): 310 vs, 290 vs ν(Zn—N): 240 s, 220 m
$[(L')_2ZnBr_2]$	2	3111 w	1583 m, 1538 s, 1520 s	553 w, 370 m, 302 m, 279 w 187 m, 159 m, 137 m	ν(Zn—Br): 226 vs ν(Zn—N): 235 vs, 226 vs
$[(L')_2ZnI_2]$	3	3122 m 3040 w	1593 m, 1537 s, 1520 s	555 w, 366 s, 280 w, 169 m 139 m, 125 w	ν(Zn—I): 213 vs ν(Zn—N): 232 s, 225 s
$[(L')_2Zn(CH_3COO)_2]\cdot(H_2O)_2$	4	3129 m	1543 s, 1532 s	552 s, 421 w, 375 s, 354 w 246 w, 227 w, 151 w	ν(COO): 1591 sbr, 1378 sbr, $\nu(H_2O)$: 3411 br ν(Zn—O): 279 s, ν(Zn—N): 180 s, 171 m
	[b]	3140 m	1538 s, 1523 s	499 m, 373 s, 266 w, 240 m 118 w	ν(COO): 1610 vs, 1401 vs, $\nu(H_2O)$: 3358 br ν(Zn—O): 295 s, ν(Zn—N): 175 vs
$[(L')_2Zn(CF_3COO)_2]\cdot(H_2O)$	5	3106 m	1545 m, 1514 m	552 w, 517 w, 373 m, 352 m 303 w	ν(COO): 1694 sbr, 1421 sbr, ν(C—F): 1090 sbr $\nu(H_2O)$: 3428 br, ν(Zn—O): 261 s, ν(Zn—N): 181 vs
	[b]	3138 w	1595 m, 1543 s, 1518 s	520 m, 499 w, 417 w, 373 s 354 w, 250 w, 218 w, 194 w	ν(COO): 1682 vs, 1422 vs, ν(C—F): 1110 sbr, 179 sbr $\nu(H_2O)$: 3350 br, ν(Zn—O): 275 vs, 266 s, ν(Zn—N): 160 vs
$[(L')_4Zn(NO_3)_2]\cdot(H_2O)_2$	6	3120 m	1544 m, 1530 m, 1514 m	552 m, 419 w, 375 s, 355 m 279 w, 246 w, 227 w, 151 m	$\nu(NO_3)$: 1360 sbr, $\nu_1+\nu_4(NO_3)$: 1737 w, 1720 w, $\nu(H_2O)$: 3450 br $\delta(H_2O)$: 1644 m, ν(Zn—O): 278 m, ν(Zn—N): 181 s, 171 s
	[b]	3132 s	1599 s, 1548 vsbr	480 w, 416 w, 372 s, 354 w 117 w	$\nu(NO_3)$: 1370 vs br, $\nu_1+\nu_4(NO_3)$: 1749 w, 1731 w, $\nu(H_2O)$: 3393 br $\delta(H_2O)$: 1684 s, ν(Zn—O): 260 s, 245 m, ν(Zn—N): 162 s
$[(L')_6Zn(CF_3SO_3)_2]$	7	3127 m	1530 s, 1518 m	572 s, 552 sh, 373 m, 279 w 246 w, 227 w, 151 w, 121 w	$\nu(SO_3)$: 1263 vs, 636 s, 517 s ν(C—F): 1144 sbr, ν(Zn—N): 188 vs br
$[(L')_4Zn(BF_4)_2]$	8	3136 s 3087 w	1617 s, 1594 vs, 1530 vs	551 w, 373 m, 354 w, 153 w 121 w	$\nu(BF_4)$: 1100 sbr, 1024 sbr, 775 s, 521 vs ν(Zn—N): 170 sbr, ν(Zn—F): 272 s, 255 vs, 247 sh
	[b]	3138 w	1545 m, 1518 vs	470 w, 416 w, 372 s	$\nu(BF_4)$: 1112 m, 1099 m, 1945 vs, 798 vs, 521 m ν(Zn—N): 170 s, ν(Zn—F): 272 m, 262 m, 249 s
$[(L')_5Zn(ClO_4)_2]$	9	3128 s 3060 w	1622 s, 1545 s, 1516 m	554 w, 371 s, 152 w, 118 w	$\nu(ClO_4)$: 1145 sh, 1072 vs br, 1040 v, 959 m, 654 s, 629 s ν(Zn—O): 277 m, 259 s, ν(Zn—N): 189 vs, 172 s
	[b]	3034 s	1550 s, 1518 sbr	550 w, 373 s, 149 w, 115 w	$\nu(ClO_4)$: 1096 sh, 1048 sbr, 942 m, 627 sbr ν(Zn—O): 275 m, 248 m, ν(Zn—N): 180 sbr
$[(L')_2Zn(Q')_2]$	10	3127 m 3044 w	1636 vs, 1615 s, 1592 s 1579 m, 1531 s, 1519 m	549 w, 510 m, 355 w, 336 m 101 m	ν(Zn—O): 426 m, 395 m, 375 m ν(Zn—N): 209 sbr
$[(L')_2Zn(Q'')_2]$	11	3127 w 3045 w	1620 vs, 1594 s, 1560 sh 1528 m, 1506 s	591 w, 550 w, 512 s, 497 m 366 m, 326 m, 282 m, 173 m	ν(Zn—O): 424 m, 400 m, 381 m ν(Zn—N): 200 sbr

Table 7.*Continued.*

Compound	No	ν(C—H)$_{azole}$	1650–1500	<600	Other data
$[(L')_2Zn(Q^*)_2]$	12	3152 w 3121 w	1596 vs, 1577 sh, 1560 m 1540 w, 1526 m	598 m, 555 w, 526 m, 507 s 368 m, 297 m, 280 w, 180 w	ν(Zn—O) : 461 m, 409 s, 380 w ν(Zn—N) : 206 s
$[(L')_5(CdBr_2)_3]$	13	3106 w	1532 m, 1512 m	553 w, 398 w, 362 m, 302 w 280 w, 246 w, 226 w, 120 w	ν(Br—Cd—Br) : 101 s ν(Cd—N) : 199 m, 152 s
$[(L')_2CdI_2]$	14	3117 w	1534 m, 1514 m	554 w, 398 w, 360 m, 303 w 280 w, 246 w, 227 w, 151 w	ν(Cd—I) : 168 sbr ν(Cd—N) : 192 s
$[(L')_2Cd(CH_3COO)_2]\cdot(H_2O)_2$	15	3106 w	1512 m	554 w, 536 s, 466 m, 367 s 246 w, 227 w, 151 m, 120 w	ν(COO) : 1540 sbr, 1375 vs br, ν(H_2O) : 3425 br δ(H_2O) : 1653 m, ν(Cd—N) : 188 s, 172 s, ν(Cd—O) : 280 m
$[(L')_6Cd(NO_3)_2]$	16	3112 m	1531 m, 1514 m	553 m, 419 w, 398 w, 354 w 303 w, 246 w, 226 w, 202 w	ν(NO_3) : 1350 sbr, 832 m, 722 m, $\nu_1+\nu_4$(NO_3) : 1740 mbr ν(Cd—N) : 170 m, 151 vs, ν(Cd—O) : 278 m
$[(L')_6Cd(ClO_4)_2]$	17	3125 s	1624 s, 1600 m, 1529 s 1513 s	554 w, 363 m, 280 w, 246 w 227 w, 125 m	ν(ClO_4) : 1077 vs br, 620 sbr ν(Cd—N) : 165 s, 150 vs
$[(L')_6Cd(BF_4)_2]$	18	3129 s	1627 s, 1600 m, 1530 s 1514 s	551 w, 366 m, 279 w, 246 w 227 w	ν(CF_4) : 1033 vs br, 519 s ν(Cd—N) : 164 m, 150 vs
$[(L')_2Cd(Q')_2]$	19	3142 w	1613 vs, 1590 s, 1534 sh 1529 m	554 w, 508 m, 339 m, 254 w 227 w, 156 m	ν(Cd—O) : 410 m, 395 s ν(Cd—N) : 196 m, 183 m
$[(L')_2Cd(Q^*)_2]$	20	3144 w	1599 vs, 1558 m, 1527 m 1515 s	596 m, 554 w, 534 m, 460 m 361 m, 297 m, 223 w, 165 m	ν(Cd—O) : 404 s, 376 m ν(Cd—N) : 200 m, 180 m
L''			1601 m, 1585 m, 1503 s	579 m, 552 w, 465 s, 411 w 350 m, 280 w, 245 w, 203 m	ν(H_2O) : 3422 br δ(H_2O) : 1681 m
$[(L'')_2ZnCl_2]$	21	3115 m	1586 w, 1522 s	576 m, 553 w, 462 m, 359 w 327 w, 171 w, 150 m, 119 w	ν(Zn—Cl) : 303 vs, 291 m ν(Zn—N) : 229 s, 209 m
$[(L'')_2ZnBr_2]$	22	3116 m	1586 w, 1532 m, 1522 s	573 w, 553 w, 470 w, 352 w 328 w, 280 w, 151 m, 119 w	ν(Zn—Br) : 232 vs br ν(Zn—N) : 232 vs br, 209 m
$[(L'')_2ZnI_2]$	23	3121 m	1577 w, 1550 m, 1532 s 1521 s	576 w, 552 w, 456 m, 328 w 280 m, 246 w, 151 m, 120 w	ν(Zn—I) : 209 vs br ν(Zn—N) : 226 m, 209 vs br
$[(L'')_3Zn(CF_3COO)_2]$	24	3129 w	1590 m, 1560 m	572 w, 552 w, 460 s, 357 w 325 w, 246 w, 150 w, 119 w	ν(COO) : 1690 vs br, 1442 sbr, ν(C—F) : 1126 sbr ν(Zn—O) : 268 vs, ν(Zn—N) : 212 m, 176 s
$[(L'')_3Zn(NO_3)_2]\cdot(H_2O)$	25	3123 w	1587 w, 1522 s	577 w, 553 w, 473 m, 463 s 353 w, 246 w, 227 w, 151 m	ν(NO_3) : 1376 sbr, $\nu_1+\nu_4$(NO_3) : 1750 m, 1734 m, ν(H_2O) : 3416 br ν(Zn—O) : 281 s, 266 m, ν(Zn—N) : 203 s, 171 s
$[(L'')_3Zn(BF_4)_2]$	26	3133 s 3060 w	1607 m, 1597 m, 1537 s 1514 s	578 w, 552 w, 466 m, 375 m 358 w, 326 m, 280 m, 266 w	ν(BF_4) : 1100 sh, 1055 sbr, 1015 sh, 755 m, 520 s ν(Zn—N) : 195 s, ν(Zn—F) : 247 vs, 228 m
$[(L'')Zn(Q')_2]$	27	3127 w	1622 s, 1603 s, 1574 s 1532 m, 1523 sh, 1505 m	553 m, 511 s, 453 w, 350 s 280 w, 254 w, 151 w, 119 w	ν(Zn—O) : 440 m, 398 s ν(Zn—N) : 208 vs, 176 s

Table 7.*Continued.*

$[(L'')Zn(Q'')_2]$	28	3128 w	1623 s, 1593 s, 1540 m 1506 s	590 m, 512 s, 500 m, 463 m 324 m, 279 m, 226 w, 151 w	ν(Zn—O) : 420 m, 396 s, 379 m ν(Zn—N) : 194 vs, 171 s
$[(L'')Zn(Q^*)_2]$	29	3106 w	1616 s, 1591 s, 1528 s 1510 s	597 s, 538 s, 458 m, 369 m 304 w, 280 w, 151 w	ν(Zn—O) : 425 s, 409 m, 397 m ν(Zn—N) : 221 vs, 202 s
$[(L'')_4(CdCl_2)_3]$	30	3136 w 3114 m	1532 sh, 1513 s	576 m, 553 w, 466 m, 353 w 280 m, 233 w, 150 w	ν(Cl—Cd—Cl) : 170 s, 132 s ν(Cd—N) : 202 m, 189 s
$[(L'')_4(CdBr_2)_3]$	31	3113 w	1522 m, 1510 m	575 m, 465 m, 362 w, 313 w 278 w, 218 w, 157 w	ν(Cd—N) : 175 s
$[(L'')_2CdI_2]$	32	3106 w	1528 m, 1519 s	578 m, 460 s, 353 w, 280 m 253 w, 151 w	ν(Cd—I) : 158 s ν(Cd—N) : 178 s
$[(L'')_3Cd(NO_3)_2]$	33	3124 w	1534 sh, 1514 s	577 s, 467 s, 353 w, 280 m 222 w, 171 w, 151 w	$\nu(NO_3)$: 1428 s, 1307 s, 1030 m, 711 m, $\nu_1+\nu_4(NO_3)$: 1760 m, 1744 m ν(Cd—O) : 254 m, 247 m, ν(Cd—N) : 188 vs, 178 s
$[(L'')_6Cd(ClO_4)_2]$	34	3123 w	1602 m, 1586 s, 1557 m 1514 s	574 m, 460 s, 368 m, 313 w 272 m, 254 w, 203 m	$\nu(ClO_4)$: 1081 vs br, 620 s ν(Cd—N) : 161 s, 149 vs br
$[(L'')_6Cd(BF_4)_2]$	35	3123 w	1604 m, 1586 s, 1558 m 1514 s	573 m, 458 m, 370 m, 349 m 277 w, 254 w, 209 m	$\nu(BF_4)$: 1023 vs, 521 vs ν(Cd—N) : 158 sh, 150 vs
$[(L'')Cd(Q')_2]$	36	3123 w	1628 s, 1607 s, 1594 m 1577 m, 1514 s	545 m, 515 m, 505 m, 340 m 279 m, 254 w, 225 w, 173 w	ν(Cd—O) : 417 m, 408 m, 380 m ν(Cd—N) : 187 vs
$[(L'')_2Cd(Q'')_2]$	37	3119 w	1620 vs, 1592 s, 1538 m 1504 s	512 m, 494 w, 324 m, 279 w 226 w, 178 w	ν(Cd—O) : 412 m, 393 m ν(Cd—N) : 159 vs br
$[(L'')Cd(Q^*)_2]$	38	3088 w	1626 vs, 1597 s, 1560 m 1522 m, 1518 s	599 m, 533 m, 460 m, 326 m 303 m, 253 w, 226 w, 172 w	ν(Cd—O) : 418 m, 399 vs, 378 m ν(Cd—N) : 197 vs
$[(Me_2Phen)_3Zn(ClO_4)_2]$	39		1619 s, 1606 m, 1579 s 1523 vs	549 m, 539 s, 484 w, 418 w 354 w, 280 m	$\nu(ClO_4)$: 1094 vs br, 623 s ν(Sn—N) : 226 m, 209 vs
$[(Ph_2Phen)_2(L')Zn(ClO_4)_2]$	40	3104 w	1622 s, 1604 sh, 1597 m 1561 s, 1523 vs	550 m, 487 w, 390 w, 353 w 280 m, 254 m, 170 w, 151 w	$\nu(ClO_4)$: 1094 vs br, 623 s ν(Zn—N) : 227 s, 188 s, 181 m
$[(Bipy)_3Zn(ClO_4)_2]$	41	3090 w	1605 vs, 1600 sh, 1576 m 1564 m	552 w, 413 vs, 356 w, 280 w 254 w, 150 w	$\nu(ClO_4)$: 1087 vs br, 621 s ν(Zn—N) : 235 vs, 189 s
$[(Bzpy)_2(L')_2Zn(ClO_4)_2]$	42	3126 m	1614 m, 1599 w, 1568 w 1537 m, 1518 m	553 w, 427 w, 375 w, 254 w 151 m, 119 w	$\nu(ClO_4)$: 1080 vs br, 621 s ν(Zn—N) : 209 vs, 203 vs, 192 s, ν(Zn—O) : 280 vs
$[(Me_2Phen)_3Cd(ClO_4)_2]$	43	3121 w	1618 s, 1602 m, 1577 s 1520 vs	547 m, 533 s, 517 m, 354 w 280 m, 254 w, 151 m	$\nu(ClO_4)$: 1082 vs br, 623 s ν(Cd—N) : 202 sbr
$[(Ph_2Phen)_3Cd(ClO_4)_2]$	44	3099 w	1618 s, 1594 m, 1578 m 1560 s, 1522 m	594 m, 576 m, 548 s, 488 m 354 w, 280 m, 252 w, 157 m	$\nu(ClO_4)$: 1090 vs br, 621 s ν(Cd—N) : 232 s, 227 vs
$[(Bipy)_3Cd(ClO_4)_2]$	45	3122 w 3073 w	1603 s, 1594 s, 1577 m 1567 m, 1539 m, 1521 w	552 s, 485 w, 415 m, 354 w 280 m, 254 w, 150 m	$\nu(ClO_4)$: 1082 vs br, 623 s ν(Cd—N) : 209 s, 202 vs

[a] Nujol mull. [b] Chloroform solution.

$O_2ZnN_4^{2+}$ cations, respectively, with ionic perchlorate groups [21].

Structure description of derivative **33**

According to the X-ray analysis the compound $[(L'')_3Cd(NO_3)_2]$ **33** (Fig. 4) has a molecular structure. The cadmium atom is coordinated by three monodentate 1-benzylimidazole molecules and two unsymmetrically bidentate nitrate-groups situated in *trans* position (O(1)—Cd—(O4) = 159.7°). Taking into account two shortest Cd—O bonds, the coordination polyhedron could be described in a first approximation as a strongly distorted trigonal bipyramid, with two oxygen atoms situated in apexes and three nitrogen atoms of imidazoles occupying equatorial positions. The average Cd—N (imidazole) distance is 2.25 Å that corresponds to those in cadmium *bis*(1-ethylimidazole)thiolate (2.28 Å, [29]) and in $\{\eta^3$-HB(3-Bu^t-5-Mepz)$_3\}$Cd(η^2-O_2NO) (2.24 Å, [30]). In the crystal structures of hexakis (1-methylimidazole)cadmium nitrate [31] and [*tris*(3,5-dimethypyrazol-1-ylmethyl)-amine]Cd(η^2-O_2NO)(η^1-ONO_2) [32] average Cd—N (imidazole) distances are longer (2.35 Å and 2.36 Å, respectively) due to larger coordination number (CN) of Cd (CN = 6 and 7 respectively). The larger contrast between the molecular structure of derivative **33** and that of analogous $Cd(py)_3(NO_3)_2$ (py = pyridine [33]) lies in the difference of Cd—O(NO_3) distances within the same nitrate group: in our compound the shorter Cd—O distances (2.45, 2.46 Å) are in good accordance with the four bond distances found in $Cd(py)_3(NO_3)_2$ [33] (2.44, 2.49 Å) where the nitrate group acts as symmetrically bidentate ligand. Whereas the longer Cd—O distances (2.70 Å (O2) and 2.67 Å (O5)) are of the same order of magnitude as the longer one found (2.885(4) Å) in the derivative [*tris*(3,5-dimethypyrazol-1-ylmethyl)-amine]Cd(η^2-O_2NO)(η^1-ONO_2) [32]. The additional weak coordination of both nitrate group produces a marked distortion from the regular trigonal bipyramidal geometry: the O1—Cd—O4 angle is decreased to 159.7° (instead of 180°) and the N7—Cd—N5 is increased to 147.2° (instead of 120°) due to the repulsion from additional atoms O2 and O5. The bidentate coordination of the nitrate groups results in a slight distortion of O—N—O angles (118.1, 120.1, 121.9 for one NO_3 and 119.1, 119.9, 120.9° for the other) to compare with bidentate nitrate in $Cd(py)_3(NO_3)_2$ [33] (115.5, 121.9, 122.6°).

Bond distance and angles for 1-benzylimidazole are substantially similar to the values found in several N-alkylsubstituted imidazole derivatives of group 8–14 metals [34].

CONCLUSION

The combined evidence from measurements carried out in solid state and in solution (IR, molecular weight determinations, conductivity, NMR spectra, X-ray crystal structure determination) gives here a picture which is different from that obtained when other acceptors were considered.

The 1-R-imidazole (R = methyl or benzyl) seems to be a very good donor: in the derivatives here described the ligand/metal ratio, frequently a measure of the donating ability, is generally higher than 1 with the exception of sterically hindered derivatives **27–29**. The ratio is also higher than 4 with good acceptors such as MX_2 where X is a good leaving group such as ClO_4^-, NO_3^-, BF_4^-, $CF_3SO_3^-$ and $CF_3CO_2^-$. We have found a marked difference between the behaviour of 1-methyl and 1-benzylimidazole: the donating ability can be easily correlated to basicity and steric hindrance of the heterocyclic ring: the 1-methylimidazole which is more basic and less sterically hindered than 1-benzylimidazole, is also the best donor ligand.

Polynuclear derivatives are also possible in the case of cadmium halide acceptors: this behaviour is analogous to that found in the poly(pyrazolyl)alkane chemistry [35].

The 1-R-imidazole can be completely displaced

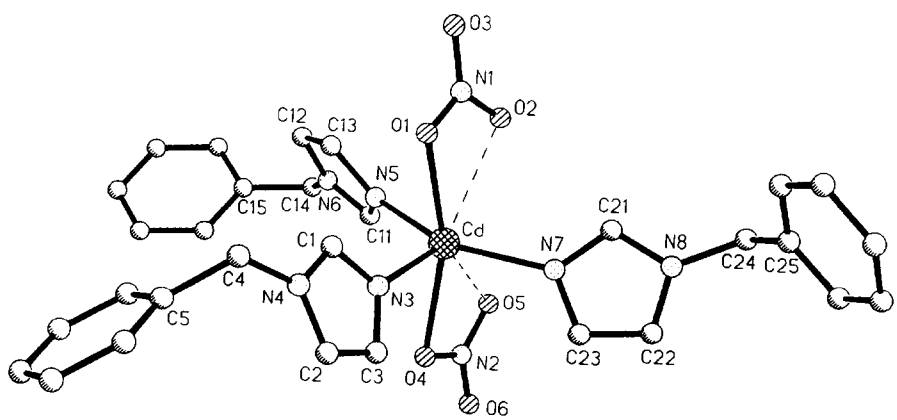

Fig. 4. Molecular structure of **33**, with H atoms omitted.

from the coordination environment of its zinc complexes only if very basic (such as 4,7-dimethylphenanthroline and 2,2′-bipyridil) chelating donors are employed (derivatives **39** and **41**). On the other hand when the less basic 2-benzoylpyridine and 4,7-diphenylphanthroline are used in the displacement reaction, mixed ligand complexes such as **40** and **42** are obtained.

Supplementary material— Tables of atomic coordinates and isotropic equivalent thermal parameters, tables of structure factors, a full list of bond lengths and angles, tables of anisotropic displacement parameters are available on request from one of the authors.

Acknowledgement—We thank the MURST, CNR-Rome and the University of Camerino for financial help.

REFERENCES

1. Mohapatra, K. C. and Dash, K. C., *J. Inorg. Nucl. Chem.*, 1977, **39,** 1253.
2. (a) Wardman, P., *Int. J. Radiat. Biol.*, 1975, **28,** 585; (b) Agscough, P. B., Elliot, A. J. and Salman, G. A., *Int. J. Radiat. Biol.*, 1975, **27,** 603.
3. Creighton, T. E., *Proteins, Structures and Molecular Properties*. W. H. Freeman, New York, 1984.
4. Saenger, W., *Principles of Nuclei Acid Structure*. Springer-Verlag, New York, 1984.
5. Pratt, J. M., *Inorganic Chemistry of Vitamin B_{12}*. Academic Press, New York, 1972.
6. Richardson, J. S., Thomas, K. A., Rubin, B. H., Richardson, D. C., *Proc. Natl. Acad. Sci., U.S.A.*, 1975, **72,** 1349.
7. There is a vast literature on this field, see for example: (a) Sheidt, W. R., Osvath, S. R. and Lee, Y. J., *J. Am. Chem. Soc.*, 1987, **109,** 1958; (b) Sheidt, W. R., Kirner, J. F., Hoard, J. L. and Reed, C. A., *J. Am. Chem. Soc.*, 1987, **109,** 1963; (c) Momenteau, M., Sheidt, W. R., Eigenbrot, C. W. and Reed, C. A., *J. Am. Chem. Soc.*, 1988, **110,** 1207, and references reported therein.
8. (a) Cingolani, A., Lorenzotti, A., Leonesi, D. and Bonati, F., *Gazz. Chim. Ital.*, 1981, **111,** 243; (b) Cingolani, A., Lorenzotti, A., Leonesi, D. and Bonati, F., *Inorg. Chim. Acta*, 1984, **81,** 127; (c) Cingolani, A., Lorenzotti, A., Leonesi, D. and Bonati, F., *Inorg. Chim. Acta*, 1984, **89,** 113.
9. Leonesi, D., Lorenzotti, A., Cingolani, A. and Bonati, F., *Gazz. Chim. Ital.*, 1981, **111,** 483.
10. (a) Pettinari, C., Gioia Lobbia, G., Sclavi, G., Leonesi, D., Colapietro, M. and Portalone, G., *Polyhedron*, 1995, **14,** 1709; (b) Pettinari, C., Marchetti, F., Polimante, R., Cingolani, A., Portalone, G. and Colapietro, M., *Inorg. Chim. Acta*, 1996, **249,** 215.
11. (a) Pettinari, C., Marchetti, F., Cingolani, A. and Bartolini, S., *Polyhedron*, 1996, **15,** 1263; (b) Pettinari, C., Marchetti, F., Pellei, M., Cingolani, A., Barba, L. and Cassetta, A., *J. Organomet. Chem.*, 1996, **515,** 119.
12. Catalàn, J., de Paz, J. L. G., Yanez, M., Claramunt, R. M., Lopez, C., Elguero, J., Anvia, F., Quian, J. H., Taagepera, M. and Taft, R. W., *J. Am. Chem. Soc.*, 1990, **112,** 1303, and references reported therein.
13. Jensen, B. S., *Acta Chem. Scand.*, 1959, **13,** 1347, 1668, 1890.
14. (a) Bovio, B., Cingolani, A., Marchetti, F. and Pettinari, C., *J. Organomet. Chem.*, 1993, **458,** 39; (b) Marchetti, F. and Pettinari, C., results to be published.
15. Sheldrick, G. M., SHELXS-86. Program for the Solution of Crystal Structures, University of Göttingen, Germany, 1986.
16. Sheldrick, G. M., SHELXS-93. Program for the Refinement of Crystal Structures, University of Göttingen, Germany, 1993.
17. Summers, M. F., *Coord. Chem. Rev.*, 1988, **86,** 43.
18. Reger, D. L., Mason, S. S., Rheingold, A. L. and Ostrander, R. L., *Inorg. Chem.*, 1996, **32,** 4904.
19. Cornilsen, B. C. and Nakamoto, K., *J. Inorg. Nucl. Chem.*, 1974, **36,** 2467.
20. Nakamoto, K., *Infrared and Raman Spectra of Inorganic and Coordination Compounds*, 4th edn. J. Wiley & Sons, U.S.A., 1986.
21. Rosenthal, M. R., *J. Chem. Ed.*, 1973, **50,** 331.
22. Addison, C. C., Logan, N., Wallwork, S. C. and Garner, C. D., *Quart. Rev.*, 1971, **25,** 289.
23. Lever, A. B. P., Mantovani, E., Ramaswamy, B. S., *Can. J. Chem.*, 1971, **49,** 1957.
24. Caruso, F., Leonesi, D., Marchetti, F., Rivarola, E., Rossi, M., Tomov, V. and Pettinari, C., *J. Organomet. Chem.*, 1996, **519,** 29.
25. Deacon, G. B. and Phillips, R. J., *Coord. Chem. Rev.*, 1980, **33,** 227.
26. Goodgame, D. M. L., Goodgame, M., Hayward, P. J. and Rayner-Canham, G. W., *Inorg. Chem.*, 1968, **7,** 2447.
27. Chebotarev, A. N., Shestakova, M. V., Shcherbakova, T. M., Khorunov, V. F. and Nikitin, V. I., *Russian J. Inorg. Chem.*, 1993, **38,** 253.
28. Tomlinson, A. A. G., Bonamico, M., Dessy, G., Fares, V. and Scaramuzza, L., *J. Chem. Soc., Dalton Trans.*, 1972, 1671.
29. Cowin, D. T. Jr, Gruff, E. S. and Kogh, S. A., *J. Chem. Soc, Chem. Comm.*, 1987, 966.
30. Looney, A., Saleh, A., Zhang, Y. and Parkin, G., *Inorg. Chem.*, 1994, **33,** 1158.
31. Rodesiler, P. F., Charles, N. G., Griffith, E. A. H., Lewinski, K. and Alma, E. L., *Acta Cryst.*, 1986, **C42,** 396.
32. Kleywegt, G. J., Wiesmeijer, W. G. R., Van Driel, G. J., Driessen, W. L., Reedijk, J. and Noordik, J. H., *J. Chem. Soc., Dalton Trans.*, 1985, 2177.
33. Cameron, A. F., Taylor, D. W. and Nuttall, R. H., *J. Chem. Soc., Dalton Trans.*, 1972, 1608.
34. Pettinari, C., Pellei, M., Miliani, M., Cingolani, A., Cassetta, A., Barba, L., Pifferi, A. and Rivarola, E., *J. Organomet. Chem.*, in press.
35. Pettinari, C., Lorenzotti, A., Pellei, M. and Santini, C., *Polyhedron*, 1997, **16,** 3435 and references therein.

Pergamon

PII: S0277-5387(97)00441-5

Polyhedron Vol. 17, No. 10, pp. 1693–1698, 1998
© 1998 Elsevier Science Ltd
All rights reserved. Printed in Great Britain
0277-5387/98 $19.00+0.00

Kinetics and mechanism of hydrazine oxidation by a tri-bridged manganese(IV,IV) dimer in weakly acidic media

Anath Bandhu Mondal, Anup Kumar Bhattacharya, Dilip Maji and Rupendranath Banerjee*

Department of Chemistry, Jadavpur University, Calcutta-700 032, India

(Received 23 July 1997; accepted 29 October 1997)

Abstract—The complex ion $[Mn_2^{IV}(\mu\text{-}O)_2(\mu\text{-}MeCO_2)(bipy)_2(H_2O)_2]^{+3}$ $\{\mathbf{1}\}^{3+}$ (bipy = 2,2′-bipyridine) and its aqua derivatives, $[Mn_2(\mu\text{-}O)_2(bipy)_2(H_2O)_4]^{+4}$ $\{\mathbf{2}\}^{4+}$ and $[Mn_2(\mu\text{-}O)_2(\mu\text{-}MeCO_2)(bipy)(H_2O)_4]^{+3}$ $\{\mathbf{3}\}^{3+}$ coexists in rapid equilibria in aqueous buffers ($MeCO_2^-$ + bipy; pH, 4.5–5.5). The solutions are reasonably stable and react with hydrazine to produce manganese(II) and N_2. The reactions follow simple first-order kinetics in the presence of excess hydrazine. The rate determining steps are one-electron reductions of $\{\mathbf{2}\}^{4+}$ and $\{\mathbf{3}\}^{3+}$ to $\{\mathbf{2}\}^{3+}$ and $\{\mathbf{3}\}^{2+}$ respectively. The 1e-reduced products rapidly produce $[(bipy)_2Mn^{III}(\mu\text{-}O)_2\text{-}Mn^{IV}(bipy)_2]^{3+}$ in the presence of excess bipy and deficit hydrazine. Kinetic activity of $\{\mathbf{1}\}^{3+}$ is insignificant compared to $\{\mathbf{2}\}^{4+}$ and $\{\mathbf{3}\}^{3+}$. Rate of reduction increased with increase in the concentration of hydrazine and ethanoate, but it decreased with increase in [bipy]. Increase in rate at higher pH indicates inner-sphere coordination and deprotonation of $N_2H_5^+$. The mild oxidising character of $\{\mathbf{2}\}^{4+}$ and $\{\mathbf{3}\}^{3+}$ along with major structural changes associated with one-electron oxidation of hydrazine disfavours an outer-sphere pathway. © 1998 Elsevier Science Ltd. All rights reserved

Keywords: manganese; hydrazine; binuclear complex; kinetics; redox.

A large number of multinuclear manganese complexes have been synthesised in the recent past [1]. They are well characterised and contain different types of ligands. These synthetic manganese complexes are quite attractive as biological models and as novel oxidants [2]. Their reactivity and kinetic studies, though limited in number, produced interesting results. The present kinetic investigation on the oxidation of hydrazine by the $[Mn_2^{IV}(\mu\text{-}O)_2(\mu\text{-}MeCO_2)(bipy)_2(H_2O)_2]^{+3}$ ion, [$\{\mathbf{1}\}^{3+}$; bipy = 2,2′-bipyridine] was initiated to further explore the reaction mechanism by which the multinuclear, high-valent manganese complexes are reduced. The dimanganese(IV,IV) complex, $\{\mathbf{1}\}(ClO_4)_3 \cdot H_2O$ is the first to include simultaneously a bridging ethanoate ligand, bis(μ-oxo) bridge and two water molecules, each coordinated to manganese(IV) ion [3]. Three of its structural features appear noteworthy: (1) a bending of the $Mn^{IV}(\mu\text{-}O)_2Mn^{IV}$ unit in the presence of ethanoate bridge, (2) elongation of the equatorial Mn—N bonds due to trans-influence of the bridging oxygen atom, and (3) presence of fully protonated water molecules in the coordination sphere of each manganese(IV). Features (1) and (2) significantly affects the solution chemistry of $\{\mathbf{1}\}^{3+}$. For example, the bridging ethanoate and one of the bipy ligands are labile and in solution $\{\mathbf{1}\}^{3+}$ coexists with its aqua derivatives. Spectrophotometric studies [4] indicated rapid solution equilibrium but no deprotonation of the coordinated water molecules at least up to pH 5.5. The rate-pH profile also suggested no kinetic contribution from any deprotonated $\{\mathbf{1}\}^{3+}$.

Though the facts are interesting, we could not so far ascertain whether the intimate mechanism of electron transfer is inner-sphere or outer-sphere. The present investigation attempts to explore this aspect.

EXPERIMENTAL

Materials

Hydrazinium nitrate was prepared by mixing dilute hydrazine hydrate (G.R., E. Merck) with dilute nitric

* Author to whom correspondence should be addressed.

acid in equivalent proportions. The resulting solution was standardised with KIO_3 in the presence of concentrated HCl [5]. Solutions of hydrazinium nitrate are stable [6] and did not loose in strength for at least a week at ~27°C. *p*-Dimethylamino benzaldehyde (G.R., E. Merck) was recrystallised from alcohol. All other materials including the complex $\{\mathbf{1}\}^{3+}$ and $[(bipy)_2Mn^{III}(\mu\text{-}O)_2Mn^{IV}(bipy)_2]^{+3}$ were described earlier [4,7b]. Doubly distilled water was used throughout.

Physical measurements and kinetics

Kinetics was determined spectrophotometrically at 420 nm [4b] in aqueous buffers (ethanoate + bipyridine; pH, 4.0–5.5) at $I = 1.0$ mol dm^{-3} ($NaNO_3$). Total concentration of 2,2′-bipyridine ($c_{bipy} = [bipy] + [Hbipy^+]$) and ethanoate ($c_{ea} = [MeCO_2^-] + [MeCO_2H]$) were in the ranges 5–35 and 5–20 mmol dm^{-3} respectively. Solution pH (Orion 710A pH meter), absorbance and electronic spectra (Shimadzu UV-1601 PC) were measured as stated earlier [4]. Pseudo first-order conditions were maintained with 20–50 times of hydrazine over total complex (0.1 mmol dm^{-3}). The first-order rate constant k_o was evaluated as usual from the least-squares slope of the ln $(A_t - A_\infty)$ vs time (t) data.

Stoichiometric measurements

Mixtures of hydrazine and the complex $\{\mathbf{1}\}^{3+}$ in different ratios (6.0–2.0) were allowed to react (pH, 4.0–5.5) until the solution turned colourless. Hydrazine content in the spent solution was estimated colorimetrically [8] at 458 nm, after developing a yellow colour with *p*-dimethylaminobenzaldehyde, dissolved in a mixture of ethanol and concentrated HCl. The final hydrazine concentrations used for calibration were $(2\text{–}85) \times 10^{-6}$ mol dm^{-3}. Gas evolved during the reaction was collected in a 5 ml microburette by downward displacement of water. The measured volume was corrected to NTP as usual. Stoichiometric measurements were carried out on a larger scale (total volume, 100 ml; complex, 1.0 mmol dm^{-3}) than used in kinetics. The very small volume of the gas evolved in the kinetic experiments had no effect on the absorbance, which did not change by time-to-time shaking of the spectrophotometer cell. Nessler's reagent [alkaline potassium iodomercurate(II)] was used to test qualitatively for ammonia. The test can detect 500 μg dm^{-3} of NH_3.

RESULTS AND DISCUSSION

Stoichiometry and reaction products

Measurements at different pH and different hydrazine : complex ratio yielded Δ[complex] : Δ[hydrazine] = 1.05 ± 0.1. Qualitative analysis of the reaction mixture for NH_3 gave negative results, though (0.98 ± 0.02) mole of a gas evolved per mole of the complex consumed. Hence, the most likely oxidation product of $N_2H_5^+$ is dinitrogen according to the stoichiometric eqn (1).

$$[Mn_2(\mu\text{-}O)_2(\mu\text{-}MeCO_2)(bipy)_2(H_2O)_2]^{3+} + N_2H_5^+ \rightarrow 2\,Mn^{II} + MeCO_2H + 2\,bipy + 4\,H_2O + N_2 \quad (1)$$

The reaction involves a net 4e-change and must be a multistep process. It is likely that all steps in (1) are 1e-changes and all manganese species except manganese(II) are binuclear in line with the evidences (a)–(c). (a) Electrochemical reduction of the (IV,IV) dimer $[Mn_2(\mu\text{-}O)_2(\mu\text{-}HPO_4)(bipy)_2(H_2PO_4)_2]$ yields the $Mn^{III}Mn^{IV}$ derivative, $[(bipy)_2Mn^{III}(\mu\text{-}O)_2Mn^{IV}(bipy)_2]^{+3}$. Electrochemical [9,10] and chemical [7] reduction of this and several other $Mn^{III}Mn^{IV}$ complexes with a $\{Mn_2O_2\}^{3+}$ core in turn, produce $(Mn^{III})_2$ dimer and then a mixture of Mn^{III} and Mn^{II} species. (b) Different oxidation-levels of the binuclear catalase enzyme models [11] preserve nuclearity. (c) The various oxidation levels (*S*-states) [12] of the manganese clusters in PS II [13] also apparently retain bond connectivity. (d) Manganese has a high tendency [14] for the generation and retention of the di(μ-oxo) bridged unit $\{Mn_2O_2\}^{n+}$.

In an attempt to detect any intermediate manganese complex, we mixed $\{\mathbf{1}\}^{3+}$ with less than stoichiometric amounts of hydrazine and recorded the spectra. Typically, with complex : hydrazine = 4 : 1; pH 4.5; c_{bipy}, 0.035 mol dm^{-3}; and $c_{ea} = 0.1$ mol dm^{-3}, we observed the growth and decay of a broad band at the longer wavelengths and a narrower band at 684 nm (Fig. 1). Both the bands are fingerprints [10c] for

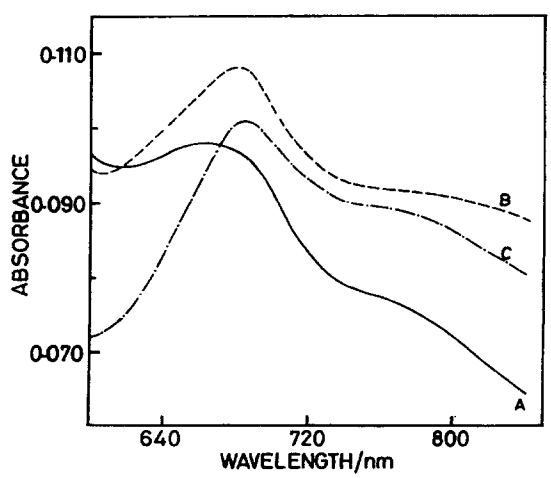

Fig. 1. (A): Spectra of 0.20 mmol dm^{-3} complex. Spectra of a mixture of (A) with hydrazine (4 : 1) after 2 min (B), and after 5 min (C) of mixing. (C) undergoes no further change with time. $c_{bipy} = 0.035$ mol dm^{-3}, $c_{ea} = 0.1$ mol dm^{-3}, pH = 4.50, $I = 1.0$ mol dm^{-3}, temp. = 25.0°C.

$[(bipy)_2Mn^{III}(\mu\text{-}O)_2Mn^{IV}(bipy)_2]^{3+}$, a complex which forms by 1e-reduction [4a] of $\{\mathbf{1}\}^{3+}$ by $S_2O_3^{2-}$ and in the electrochemical reduction [9] of $[Mn_2(\mu\text{-}O)_2(\mu\text{-}HPO_4)\text{-}(bipy)_2(H_2PO_4)_2]$. It appears very much likely that hydrazine also reduces complex $\{\mathbf{1}\}^{3+}$ by one-electron steps and that all the intermediates are binuclear.

Kinetics

At a fixed pH, c_{bipy} and c_{ea}, the first-order rate constant, k_o (Table 1) increases linearly with increase in hydrazine concentration. It also increases with increase in $[MeCO_2^-]$, but saturates at high $[MeCO_2^-]$ (>0.054 mol dm^{-3}) (Fig. 2A). Again at a fixed pH and c_{ea}, k_o decreased with increasing [bipy] and tends to a minimum value at high [bipy] (Fig. 2B). The results along with previous equilibrium studies [4a] indicate rapid ligand dissociation equilibria (2) and (3) and prominent kinetic activities for the hydrolytic derivatives $\{\mathbf{2}\}^{4+}$ and $\{\mathbf{3}\}^{3+}$.

$$[Mn_2(\mu\text{-}O)_2(\mu\text{-}MeCO_2)(bipy)_2(H_2O)_2]^{3+} \{\mathbf{1}\}^{3+} + 2H_2O \overset{K_{12}}{\rightleftharpoons} [Mn_2(\mu\text{-}O)_2(bipy)_2(H_2O)_4]^{4+} \{\mathbf{2}\}^{4+} + MeCO_2^- \quad (2)$$

$$\{\mathbf{1}\}^{3+} + 2H_2O \overset{K_{13}}{\rightleftharpoons} [Mn_2(\mu\text{-}O)_2(\mu\text{-}MeCO_2)(bipy)(H_2O)_4]^{3+} \{\mathbf{3}\}^{3+} + bipy \quad (3)$$

Increase in pH at fixed c_{bipy} and c_{ea} increases both [bipy] and $[MeCO_2^-]$. At $[MeCO_2^-] > 0.054$ mol dm^{-3} therefore one expects decrease in k_o with increasing pH provided only equilibria (2) and (3) are present. However, at all values of [bipy] and $[MeCO_2^-]$, k_o increases with increase in pH (Fig. 2C). It is necessary therefore that a deprotonation equilibrium involving either the reducing agent or the substrate complex

Table 1. First order rate constants[a]

pH	$10^2\,c_{bipy}$/mol dm^{-3}	$10^2\,c_{ea}$/mol dm^{-3}	$[N_2H_5^+]$/mmol dm^{-3}	$10^2\,k_o$/s^{-1}
4.50	3.50	10.00	2.00	1.72 (1.78)
4.60				2.12 (2.11)
4.71				2.56 (2.54)
4.82				3.08 (3.07)
5.00				4.22 (4.26)
5.20				6.43 (6.36)
5.36				8.76 (8.83)
5.50				11.8 (11.82)
4.50	0.50	20.00		12.9 (12.91)
	1.00			6.51 (6.49)
	1.50			4.38 (4.38)
	2.00			3.27 (3.30)
	2.20			2.97 (2.99)
	2.50			2.65 (2.66)
	2.70			2.49 (2.47)
	3.00			2.21 (2.24)
	3.50	0.50		0.82 (0.84)
		5.00		1.55 (1.59)
		7.00		1.70 (1.64)
		12.00		1.74 (1.73)
		15.00		1.82 (1.81)
		20.00		1.83 (1.83)
		10.00	2.50	2.25 (2.26)
			3.00	2.90 (2.70)
			3.50	3.15 (3.16)
			4.00	3.53 (3.63)
			4.50	3.92 (3.94)
			5.00	4.48 (4.50)

[a] Temp., 25.0°C; I, 1.0 mol dm^{-3}; [complex], 0.1 mmol dm^{-3}. The values were not affected significantly ($\leqslant 4\%$) by stray light, variation in complex concentration (0.05–0.3 mmol dm^{-3}) or when purified dinitrogen was passed through the solutions prior to kinetic measurements. Parenthetical values are k_o calculated using eqn (9).

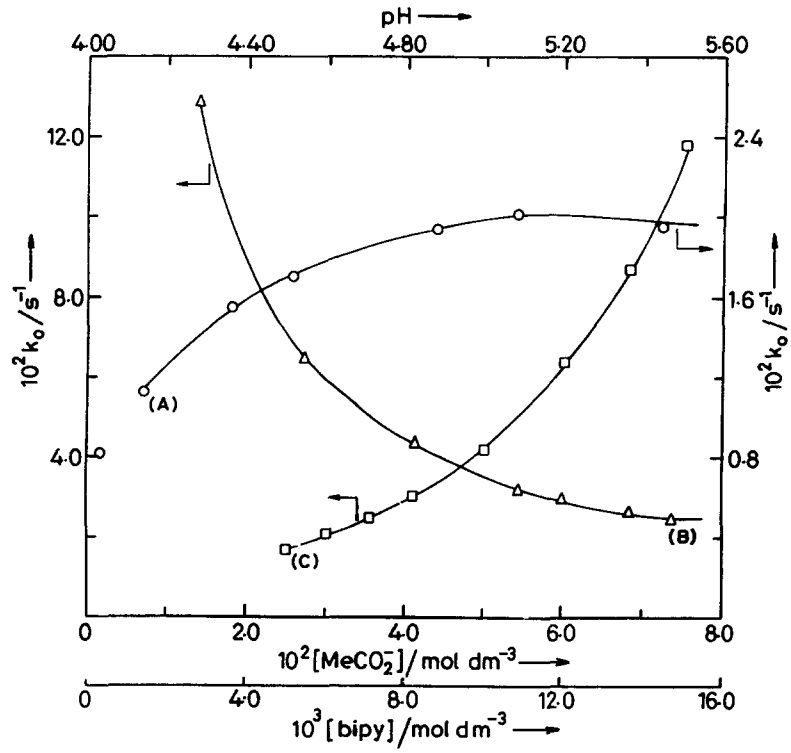

Fig. 2. Variation of k_o with $[MeCO_2^-]$ (A), [bipy] (B) and pH (C) at 25.0°C, I = 1.0 mol dm^{-3}. For (A): [bipy] = 0.0191 mol dm^{-3}, pH = 4.50. For (B): $[MeCO_2^-]$ = 0.073 mol dm^{-3}, pH = 4.50. For (C): c_{bipy} = 0.035 mol dm^{-3}, c_{ea} = 0.10 mol dm^{-3}.

must be considered in addition to equilibria (2) and (3). Previous equilibrium and kinetic studies [4] suggested inappreciable deprotonation of the oxidant. Hence deprotonation of the reducing agent seems logical. However, $N_2H_5^+$ is a weak acid (pK_a = 8.06) [15a] and, as such, an unlikely source for the observed proton dependence. We, therefore, presume that the deprotonation of $N_2H_5^+$ occurs after its coordination to a manganese(IV) centre (eqns (4) and (5)). A similar coordination of $N_2H_5^+$ to $[Mn(cydta)(H_2O)]^-$ (cydta is cyclohexyl-edta) and subsequent inner-sphere redox reaction is known [16]. Scheme 1 is therefore proposed.

The scheme presupposes a negligible kinetic activity for $\{\mathbf{1}\}^{3+}$ in line with our earlier kinetic observations. Analysis of observed dependence of k_o on different reagent concentrations supports this presumption (see later).

As discussed earlier, eqns (6) and (7) are likely to be multi-step, one-electron processes. Therefore, the immediate product of oxidation of N_2H_4 should be $N_2H_4^+$. This weak acid (pK_a = 7.1) [15b] is oxidized to N_2 via N_2H_2, detected [17] as an intermediate in the oxidation of $N_2H_5^+$ by $[IrCl_6]^{2-}$. The pathway for the conversion of N_2H_2 to N_2 is uncertain [18a] but in the present case the required oxidising equivalents are

$$\{\mathbf{2}\}^{4+} + N_2H_5^+ \overset{K_{2N}}{\rightleftharpoons} \underset{\mathbf{2N}}{[Mn_2(\mu\text{-}O)_2(bipy)_2(H_2O)_3(N_2H_4)]^{4+}} + H^+ + H_2O \quad (4)$$

$$\{\mathbf{3}\}^{3+} + N_2H_5^+ \overset{K_{3N}}{\rightleftharpoons} \underset{\mathbf{3N}}{[Mn_2(\mu\text{-}O)_2(\mu\text{-}MeCO_2)(bipy)(H_2O)_3(N_2H_4)]^{3+}} + H^+ + H_2O \quad (5)$$

$$\mathbf{2N} \overset{k_1}{\longrightarrow} \text{products } (Mn^{II}, N_2, \text{bipy}) \quad (6)$$

$$\mathbf{3N} \overset{k_2}{\longrightarrow} \text{products } (Mn^{II}, N_2, MeCO_2^-) \quad (7)$$

Scheme 1.

available from the high-valent manganese species. Dimerisation of N_2H_3 leads [18b] to NH_3, but this was absent in the present reactions. Presumably, $[N_2H_3]$ is very low and the rates of oxidation of $N_2H_4^+$ and its conjugate base N_2H_3 by the high-valent manganese species are very fast. Accumulation and dimerisation of N_2H_3 is thus disfavoured. The complex $[Mn_2(\mu\text{-}O)_2(\mu\text{-}HPO_4)(bipy)_2(H_2PO_4)_2]$ {**4**} is a close analogue of **3N**. Its electrochemical reactions [9] in phosphate buffer produces first the dimanganese(III,IV) complex $\{\mathbf{4}\}^-$. However, $\{\mathbf{4}\}^-$ is not stable and immediately changes to the dimer $[(bipy)_2Mn^{III}(\mu\text{-}O)_2\text{-}Mn^{IV}(bipy)_2]^{+3}$ $\{\mathbf{5}\}^{3+}$ (eqn (8)), which may undergo further reduction. We know that different reducing agents reduces $\{\mathbf{5}\}^{3+}$ to (Mn_2^{III}) and

$$\{\mathbf{4}\} + e \rightarrow \{\mathbf{4}\}^- \tag{8a}$$

$$\{\mathbf{4}\}^- + 2\,bipy + H^+ \rightarrow \{\mathbf{5}\}^{3+} + 3\,H_2PO_4^- \tag{8b}$$

subsequently to Mn^{II} under conditions similar to the present ones [7]. Equations (7a)–(7e) account for the reaction shown in eqn (7):

$$\mathbf{3N} \xrightarrow{k_3} \{\mathbf{3}\}^{2+} + N_2H_4 \tag{7a}$$

$$\{\mathbf{3}\}^{2+} + 3\,bipy \xrightarrow{fast} \{\mathbf{5}\}^{3+} \tag{7b}$$

$$\{\mathbf{5}\}^{3+} + R \xrightarrow{fast} (Mn_2^{III}) \tag{7c}$$

$$(Mn_2^{III}) + R \xrightarrow{fast} Mn^{II} + Mn^{III} \tag{7d}$$

$$Mn^{III} + R \xrightarrow{fast} Mn^{II} \tag{7e}$$

Here R represents a reducing equivalent, provided by $N_2H_5^+$ or any of its radicals.

A $[Mn^{III}Mn^{IV}(\mu\text{-}O)_2(\mu\text{-}MeCO_2)]^{2+}$ core analogous to that in $\{\mathbf{3}\}^{2+}$ has been isolated [19,20] and it is known that deaquation of $Mn^{III}Mn^{IV}$ dimers by bipy is fast in bipy-Hbipy$^+$ buffer [7b]. We also have verified that steps (7c) and (7d) are much faster compared to the step (7a). Pathways similar to (7a)–(7e) is expected for **2N** also.

Scheme 1 leads to eqn (9):

$$k_o = \left[\frac{k_1K_{2N}K_{12}[bipy]}{P[H^+]} + \frac{k_2K_{3N}K_{13}[MeCO_2^-]}{P[H^+]}\right] \tag{9}$$

The hydrazinium cation forms very weak complexes with metal ions and both K_{2N} and K_{3N} are likely to be very small. Therefore, from the known [4a] values of K_{12} $[(1.0\pm0.1)\times10^{-2}$ mol dm$^{-3}]$ and K_{13} $[(1.0\pm0.09)\times10^{-3}$ mol dm$^{-3}]$ one finds that under the experimental conditions,

$$P \approx [MeCO_2^-][bipy] + K_{12}[bipy] \tag{10}$$

Hence, eqn (9) transforms to (11):

$$(k_o\{[MeCO_2^-][bipy] + K_{12}[bipy]\}[H^+])/[N_2H_5^+] = k_1K_{2N}K_{12}[bipy] + k_2K_{3N}K_{13}[MeCO_2^-] \tag{11}$$

The known proton dissociation equilibrium constants for ethanoic acid ($K_{ea} = 1.8\times10^{-5}$) and Hbipy$^+$ ($K_{Hbipy} = 3.8\times10^{-5}$) give $[MeCO_2^-]$ and [bipy]:

$$[MeCO_2^-] = \frac{c_{ea}K_{ea}}{\{[H^+] + K_{ea}\}};$$

and

$$[bipy] = \frac{c_{bipy}K_{Hbipy}}{\{[H^+] + K_{Hbipy}\}}$$

Hence we get,

$$\frac{k_o(c_{ea}c_{bipy}K_{ea}K_{Hbipy} + K_{12}c_{bipy}K_{Hbipy}[H^+] + K_{12}c_{bipy}K_{Hbipy}K_{ea})[H^+]}{[N_2H_5^+]} = (k_1K_{2N}K_{12}K_{ea}c_{bipy}K_{Hbipy} + k_2K_{3N}K_{13}c_{ea}K_{ea}K_{Hbipy}) + (k_1K_{2N}K_{12}c_{bipy}K_{Hbipy} + k_2K_{3N}K_{13}c_{ea}K_{ea})[H^+] \tag{12}$$

Plots of left hand side of eqn (11) vs $[MeCO_2^-]$ at constant [bipy], and vs [bipy] at constant $[MeCO_2^-]$ were excellent straight lines. Their slopes yielded $k_1K_{2N} = (1.11\pm0.14)\times10^{-4}$ s^{-1} and $k_2K_{3N} = (6.33\pm0.23)\times10^{-3}$ s^{-1} at 25.0°C, $I = 1.0$ mol dm^{-3} using known K_{12} and K_{13} values. Excellent linear plots of left hand side of eqn (12) vs $[H^+]$ further supports the scheme. The k_1K_{2N} and k_2K_{3N} values can reproduce the k_o data within 5% (parenthetical values in Table 1). The agreement justifies exclusion of $\{\mathbf{1}\}^{3+}$ from the kinetic scheme, and the order of kinetic activity appears as: $\{\mathbf{1}\}^{3+} \ll \{\mathbf{2}\}^{4+} < \{\mathbf{3}\}^{3+}$. A similar order was observed earlier in the reactions of the complex $\{\mathbf{1}\}^{3+}$ with nitrite and thiosulphate and one finds that the rate of oxidation increases with increasing number of aqua ligands attached to a manganese centre. This trend is, however, not a speciality for the binuclear complexes, it is also well documented for higher valent mononuclear manganese complexes [21]. The probable reasons have been discussed earlier in details [4,7(a–c)].

The constants k_1K_{2N} and k_2K_{3N} should be replaced by k_1K_a and k_2K_a respectively, in case the reactions involve outer-sphere electron transfer with N_2H_4. Using the proton dissociation constant for $N_2H_5^+$, $K_a = 8.7\times10^{-9}$ mol dm^{-3} [15a], the outer-sphere rate constants are, $k_1 = 1.3\times10^4$ dm^3 mol^{-1} s^{-1} and $k_2 = 7.3\times10^5$ dm^3 mol^{-1} s^{-1}. Of these k_1 is comparable to the rate constant, 2.01×10^4 dm^3 mol^{-1} s^{-1} for the outer-sphere oxidation [22] of hydrazine by $[IrCl_6]^{2-}$ while k_2 exceeds it. The E° value for the $[IrCl_6]^{2-/3-}$ couple is 0.892 vs NHE [23]; its self exchange rate (2×10^5 dm^3 mol^{-1} s^{-1}) [24] is expected to

exceed those for the more rigid molecules, $\{2\}^{4+}$ and $\{3\}^{3+}$. Again, an estimated upper limit for the self-exchange rate constant for the $N_2H_4/N_2H_4^+$ couple is $k_{22} = 0.3$ mol^{-1} dm^3 s^{-1}. Its $E^\circ \sim (-0.73$ V). Assuming simple Marcus relation (13) for outer-sphere reactions, [25] and the same self exchange rates for $\{2\}^{4+}$, $\{3\}^{3+}$ and

$$k_{12} = (k_{11}k_{22}K_{12})^{1/2} \quad (13)$$

$[IrCl_6]^{2-}$, one can calculate a lower limit of E° for $\{2\}^{4+}$ and $\{3\}^{3+}$ as ~ 1 V. However, cyclic voltametry of $\{1\}^{3+}$ in CH_3CN shows an irreversible wave at 0.33 V vs SCE corresponding to the (IV,IV)/(III,III) reduction [3b]. Hence, the high E° value calculated from eqn (13) speaks against an outer-sphere mechanism. Stated simply, the low self-exchange rate of the $N_2H_4^+/N_2H_4$ couple and a moderately weak reducing character of $N_2H_5^+$ in weakly acidic solution disfavours outer-sphere reactions. In the present case, an additional barrier to outer-sphere reactions may be present. The highest occupied orbital of manganese ions in $\{2\}^{3+}$ and $\{3\}^{3+}$ is π^* but that in the reducing agent is σ. An outer-sphere electron transfer would thus be expected to be slow.

Acknowledgement—Financial assistance from the Department of Science and Technology (New Delhi) and the award of a fellowship to D.M. by the same agency are gratefully acknowledged.

REFERENCES

1. (a) Manchanda, R., Brudvig, G. W. and Crabtree, R. H., *Coord. Chem. Rev.*, 1995, **144,** 1; (b) Wieghardt, K., *Angew. Chem., Int. Ed. Engl.*, 1989, **28,** 1153; (c) Reddy, K. R., Rajasekharan, M. V., Arulsany, N. and Hodgson, D. J., *Inorg. Chem.*, 1996, **35,** 2283; (d) Kock, J. H., Russel, S. W., van der Wolf, L., Warnarr, J. B., Spek, A. L., Kerschner, J. and DelPizzo, L., *J. Chem. Soc., Dalton Trans.*, 1996, 353.
2. (a) Renger, G., *Angew. Chem., Int. Ed. Eng.*, 1987, **26,** 643; (b) Dismukes, G. C., *Chem. Rev.*, 1996, **96,** 2909; (c) Yachandra, V. K., Sauer, K. and Klein, M. P., *Chem. Rev.*, 1996, **96,** 2927.
3. (a) Reddy, K. R., Rajasekharan, M. V., Padhye, S., Dahan, F. and Tuchagues, J. P., *Inorg. Chem.*, 1994, **33,** 428; (b) Dave, B. C., Czernusewicz, R. S., Bond, M. C. and Carrano, J. C., *Inorg. Chem.*, 1993, **32,** 3593.
4. (a) Bhattacharya, A. K., Mondal, A. B. and Banerjee, R., *J. Chem. Soc., Dalton Trans.*, 1997, 2351; (b) Chaudhuri, S. and Banerjee, R., *Polyhedron*, 1997, **16,** 3493.
5. Andrews, L. W., *J. Am. Chem. Soc.*, 1903, **25,** 76.
6. Cotton, F. A. and Wilkinson, G., *Advanced Inorganic Chemistry*, 3rd edn, Wiley Eastern Ltd., New Delhi, 1976, pp. 351, 353.
7. (a) Kundu, S., Bhattacharya, A. K. and Banerjee, R., *J. Chem. Soc., Dalton Trans.*, 1996, 3951; (b) Chaudhuri, S., Mukhopadhyay, S. and Banerjee, R., *J. Chem. Soc., Dalton Trans.*, 1996, 3951; (c) Mondal, B., Kundu, S. and Banerjee, R., *Polyhedron*, 1997, **16,** 2199; (d) Ghosh, M. C., Reed, J. W., Bose, R. N. and Gould, E. S., *Inorg. Chem.*, 1994, **33,** 73.
8. Watt, G. W. and Ghrisp, J. D., *Anal. Chem.*, 1952, **24,** 2006.
9. Sarneski, J. E., Brzezinski, L. J., Anderson, B., Didiuk, M., Manchanda, R., Crabtree, R. H., Brudvig, G. W. and Shulte, G. K., *Inorg. Chem.*, 1993, **32,** 3265.
10. (a) Manchanda, R., Thorp, H. H., Brudvig, G. W. and Crabtree, R. H., *Inorg. Chem.*, 1991, **30,** 494; (b) Manchanda, R., Thorp,, H. H., Brudvig, G. W. and Crabtree, R. H., *Inorg. Chem.*, 1992, **31,** 4040; (c) Cooper, S. R. and Calvin, M., *J. Am. Chem. Soc.*, 1977, **99,** 6623; (d) Pal, S., Chan, M. K. and Armstrong, W. H., *J. Am. Chem. Soc.*, 1992, **114,** 6398.
11. Wieghardt, K., Bossek, U., Nuber, B., Weiss, J., Bonvoisim, J., Corbella, M., Vitols, S. E. and Girerd, J. J., *J. Am. Chem. Soc.*, 1988, **110,** 7398.
12. Kok, B., Forhush, B. and McGloin, M., *Photochem. Photobiol.*, 1970, **11,** 457.
13. Hiller, W., Lukins, P., Seibort, M. and Wydrzynski, T., *Biochemistry*, 1997, **36,** 76.
14. Brewer, K. J., Calvin, M., Lumpkin, R. S., Otvos, J. W. and Spreer, L. O., *Inorg. Chem.*, 1989, **28,** 4446.
15. (a) Smith, R. M. and Martel, A. E., *Critical stability Constants*, Plenum Press, New York, 1976, Vol. 4, p. 43; (b) Inbar, S. and Colen, S. G., *J. Am. Chem. Soc.*, 1978, **100,** 4490.
16. Arselli, P. and Mentasti, E., *J. Chem. Soc., Dalton Trans.*, 1983, 689.
17. Morris, D. F. C. and Ritter, T. J., *J. Chem. Soc., Dalton Trans.*, 1980, 216.
18. (a) Stedman, G., *Adv. Inorg. Chem. Radiochem.*, 1979, **22,** 113; (b) Sutherland, J. W., *J. Phys. Chem.*, 1979, **83,** 789.
19. Bashkin, J. S., Schake, A. R., Vincent, J. B., Chang, H. R., Li, Q., Huffman, J. C., Christou, G. and Hendrickson, D. N., *J. Chem. Soc., Chem. Commun.*, 1988, 700.
20. Bossek, U., Sahar, M., Weyhermuller, T. and Wieghardt, K., *J. Chem. Soc., Chem. Commun.*, 1992, 1780.
21. (a) Banerjee, R., Das, R. and Chakraburtty, A. K., *J. Chem. Soc., Dalton Trans.*, 1990, 3277; (b) Mukhopadhyay, S. and Banerjee, R., *J. Chem. Soc., Dalton Trans.*, 1993, 933; (c) Mukhopadhyay, S., Chaudhuri, S. and Banerjee, R., *Canad. J. Chem.*, 1993, **71,** 2155.
22. Stanbury, D. M., *Inorg. Chem.*, 1984, **23,** 2879.
23. Margerum, D. W., Chellappa, K. L., Bossu, F. P. and Bruce, G. L., *J. Am. Chem. Soc.*, 1975, **95,** 6894.
24. Stanbury, D. M., Wilmarth, W. K., Khalaf, S., Po, H. N. and Byrd, J. E., *Inorg. Chem.*, 1980, **19,** 2715.
25. (a) Marcus, R. A., *Annu. Rev. Phys. Chem.*, 1964, **15,** 155; (b) Marcus, R. A. and Sutin, N., *Inorg. Chem.*, 1975, **14,** 213.

Pergamon

PII: S0277-5387(97)00446-4

Polyhedron Vol. 17, No. 10, pp. 1699–1703, 1998
© 1998 Elsevier Science Ltd
All rights reserved. Printed in Great Britain
0277-5387/98 $19.00+0.00

Synthesis of high surface area silica by solvent exchange in alkoxy derived silica gels

S. Rajesh Kumar, P. Krishna Pillai and K. G. K. Warrier*

Structural Ceramics Unit, Regional Research Laboratory (CSIR), Trivandrum—695019, India

(Received 25 August 1997; accepted 28 October 1997)

Abstract—Silica gels have been prepared by the hydrolysis of tetraethyl orthosilicate at pH 9.5 with a high water: TEOS ratio. The gels were exchanged with different solvents such as ethanol, methanol, isopropanol and acetone. The resultant gels were calcined at 500°C for 3 h at heating rate of 3°C min^{-1}. The surface area and total pore volume of the calcined gels measured using nitrogen adsorption show much dependence with the nature of the liquid used for the exchange. The gel washed with ethanol under the conditions of present investigation shows maximum surface area. The adsorption isotherm of this gel also shows the characteristics of Type IV behaviour. Other gels usually show Type II behaviour. Solvents of low vapour pressure and high molecular volume favour the formation of gels with high pore volume. The method of exchange of solvents also influences the characteristics of the final gel precursor in terms of surface area and pore volume. Repeated washing of the gels with solvents and subsequent removal result in high surface area, while evaporating the gels with solvents results in relatively less porous gels. © 1998 Elsevier Science Ltd. All rights reserved

Keywords: solvent exchange; silica; surface area.

High purity silica is well known for a variety of industrial applications. It is used as catalytic supports, fillers, fused silicawares, optical glasses and waveguides [1]. Silica gels are also used as thermal and accoustic insulators. One of the methods for obtaining pure silica is by the controlled hydrolysis of silicon alkoxides [2–4]. Sol gel silica has been used as membranes, coatings and also to prepare low temperature glasses [5,6]. When the alcogels are dried at ambient pressures under moderate temperatures, xerogels are obtained. Supercritical conditions of drying result in aerogels which are characterised by low densities and extremely high porosities [7–8]. However, the porosities and other characteristics of the resultant silica gel depend primarily on the conditions of hydrolysis of the alkoxides, such as the nature of catalysts [9], the alkoxide/alcohol and alkoxide/water ratio [10], pH [9], presence of other solvents [11] and interaction with additives as well as gel modifiers [12]. Use of surfactant media involving inverse micelle and lamellar phase systems resulted in silica gels having cylindrical pores of controlled size [13]. Once a precursor gel having a desired structure is arrived at, the most important step for obtaining a porous ceramic is the removal of the solvent and volatiles. Usual drying methods lead to considerable shrinkage of the gel and this introduces stresses which result in the collapse of the gel structure. A gel having small pore radius containing solvent of high surface tension undergoes considerable shrinkage on drying. The capillary pressure exerted during drying by solvent evaporation is counteracted by the bulk modulus of gel which in turn is related to its skeletal strength. One of the solutions is to strengthen the gel walls or to allow the escape of the solvents with least disturbance which has been well achieved by drying under supercritical conditions [14]. However alternative simpler methods are being looked for in view of the expensive nature of this technique. Recently a few novel methods are reported to prepare aerogel like materials at ambient pressures. Smith *et al.* [15] achieved this by introducing hydrophobic groups in the gel network. Brinker *et al.* reported the silation technique by introduction of $Si(CH_3)_3$—O group in place of surface hydroxyl groups of the gel for preparing aerogel membranes [16]. Recently yet another simple method has been reported based on strengthening the gel structure by aging and using *n*-heptane as the liquid for drying [17].

* Author to whom correspondence should be addressed.

Therefore in the present investigation silica gels with identical skeletal strength are synthesised and have been exchanged with liquids of different chain lengths and molecular sizes and subsequently dried under identical conditions. The resultant gels are then calcined at 500°C and are characterised by specific surface area and pore volume data measured using BET nitrogen adsorption technique.

EXPERIMENTAL PROCEDURE

The gels were prepared by the hydrolysis of the tetraethyl orthosilicate (TEOS, Alfa chemicals, U.S.A., 99% purity). 15 ml of TEOS was mixed slowly with 60 ml of ethanol kept under stirring and this solution was added dropwise to 75 ml of double distilled water, pH being maintained at 9.5 by adding dilute ammonia [Qualigens, India]. The mixture was kept under stirring for 24 h. Further, this mixture was heated at refluxing conditions and then aged for 24 h before drying in an air oven at 50°C and designated as NS. To another batch of the above gel 20 ml ethanol was added, refluxed at 50°C for 3 h, cooled and the solvent was separated by filtration. The process was repeated 5 times. The gel was then dried in air oven at 50°C over a period of 3 h and designated as WE. The same procedure was adopted with other liquids such as methanol, isopropanol, acetone and are designated as WM, WI, WA respectively.

Another set of studies were done on similar precursor gel by adding 20 ml methanol and refluxing for 3 h at 50°C. The free methanol was evaporated by heating the gel at 50°C for 10 min. Such steps were repeated 5 times. The same procedure was also followed with isopropanol. The gels treated with methanol and isopropanol were designated as EM and EI respectively. All dried gels were calcined at 500°C for 3 h at heating rate of 3°C min^{-1}. The BET specific surface area and pore volume of the calcined gels were measured at liquid nitrogen temperature after degassing for 5 h at 200°C in flowing nitrogen in BET surface area analyser (Micromeritics, U.S.A., Model No. 2360). The dehydroxylation patterns of selected gel samples were studied using Schimadzu TGA 50H Thermogravimetric Analyser.

RESULTS AND DISCUSSION

In the present investigation, the silica gels were prepared under high water/alkoxide ratio in order to result in porous silica gels having high surface area. A high pH of 9.5 was maintained for the medium in order to achieve a gel with high permeability. The gels were also aged under refluxing conditions in order to enhance the skeletal strength. Since all the conditions of formation of the gels are kept constant, the gel structure is assumed to be similar. The dehydroxylation patterns presented in Fig. 1. indicate two steps of weight loss, one less than 100°C and the other at higher temperatures. The weight loss associated with the removal of free solvent as well as the dehydroxylation step of WM is found to be the least. In the dehydroxylation pattern of WE there are two distinct regions of weight loss. The treatment with solvents appears to effect the initial weight loss considerably. However, the second dehydroxylation step is more influenced only in the case of ethanol, the effective total loss increased considerably. This indicates that all the solvents are not influencing the gel structure.

The surface areas and pore volumes of the calcined gels are presented in Table 1. The surface area values of the gels treated with solvents and calcined follow the order WM < NS < WA < WI < WE. The pore volumes are in the order WM < WA < NS < WE < WI. On the other hand the surface areas of the evaporated samples are in general, much less than the corresponding washed samples. The surface area and pore volume values of both methanol washed and evaporated gels are much lower than others. In general WI and WE appear to be most promising in terms of specific surface area and also pore size distribution. The nitrogen adsorption isotherms of calcined gels are represented in Figs 2 and 3. The adsorption behaviour of the gels is highly influenced by the nature of the solvent used for exchange. However, the gels evaporated with solvents show considerable non porous behaviour.

Earlier studies [11] reported that the solvents present during hydrolysis of alkoxides have much importance on the final properties of the precursor gels especially on the surface area and pore volume. Effect of diols, drying control chemical additives, long chain alcohols and branched alcohols were studied in detail [11–13]. Alcohols with long hydrocarbon chains having very low vapour pressure as solvent for the hydrolysis medium of alkoxides give gels with high surface area and porosity. In the present study, exchange of water and ethanol mixture from the gel skeleton by extraction with different liquids and subsequently using them as drying liquids give large specific surface area and porosity.

Figure 4 shows the relation between the vapour pressure of the drying liquid and resultant properties such as surface area and pore volume of the calcined gels. Earlier studies show that as the vapour pressure of the liquid used in the hydrolysis of silicon alkoxides increases the surface area and pore volume of the resultant gel decreases. In the present case out of the many solvents used, methanol having the higher vapour pressure probably results in gels having least porosity. Acetone, with vapour presssure higher than methanol results in gel having higher surface area and pore volume than methanol counterpart. Probably factors other than vapour pressure of the drying liquid also influence these properties. Figure 5 relates the surface area and pore volume values of the calcined gel with the relative dielectric constants of the liquids

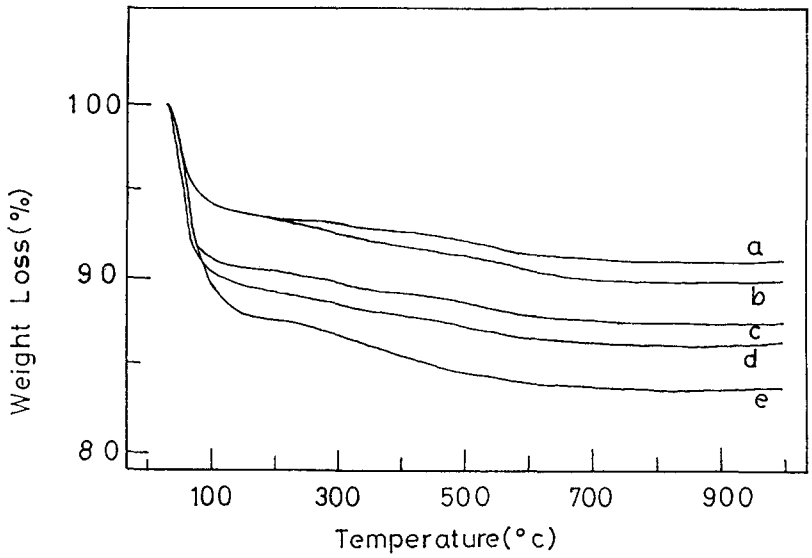

Fig. 1. TGA curves of silica samples; (a) WM, (b) WI, (c) NS, (d) WA and (e) WE.

Table 1. Surface area and total pore volume values of the gels calcined at 500°C

Sample	Surface area ($m^2 g^{-1}$)	Pore volume ($cm^3 g^{-1}$)
WA	518	0.651
WI	540	0.764
WM	345	0.578
WE	601	0.715
EI	282	0.583
EM	234	0.543
NS	396	0.683

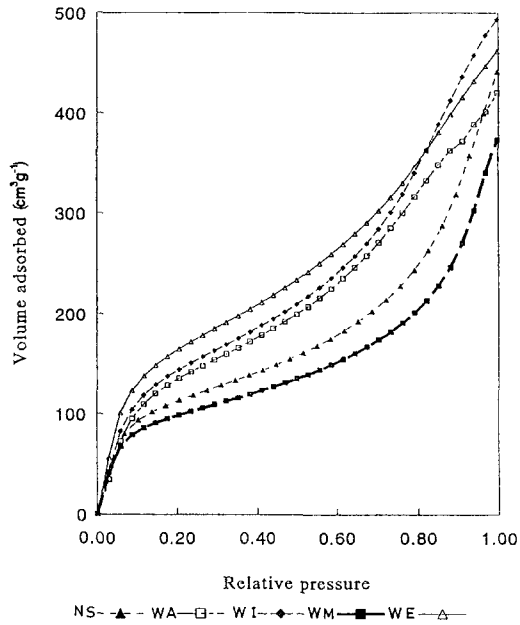

Fig. 2. Adsorption isotherms of silica gel samples washed with different solvents and calcined at 500°C for 3 h.

with which the gels were washed. Dielectric constant is frequently used as a measure of the reactions involving solvents, and it is accepted that ions are present more stably in a solvent having a higher dielectric constant [11]. Therefore with increase in relative dielectric constant of the drying liquids the surface area and pore volume values of the resultant gel decrease. This trend is followed generally in the present case with exception to ethanol. Figure 6 relates the surface area and pore volume values of the calcined gels with molecular volumes of the liquids used. Alcohols of long hydrocarbon chains are indicated to result in high surface area and pore volume in precursor gels. Generaly a similar trend is followed in the present case also. Acetone is an exception and might be due to its high vapour pressure.

The shrinkage in the gel is related much on the surface tension of the drying liquid as evidenced from the equation: $P_c = -2\gamma_{LV}/(r_p - t)$ [17] where P_c is the capillary pressure which causes the shrinkage. γ_{LV} = surface tension of the pore liquid, r_p = pore radius and t = thickness of the adsorbed layer. Here in the present work, the gels were prepared at identical conditions and hence we can take all the parameters constants except γ_{LV} for all the gels. The surface tension values of the drying liquids are in the order: isopropanol < ethanol < acetone < methanol. The pore volume values of the resultant gels are just in the reverse order i.e. as the surface tension of the pore liquid increases shrinkage also increases and hence

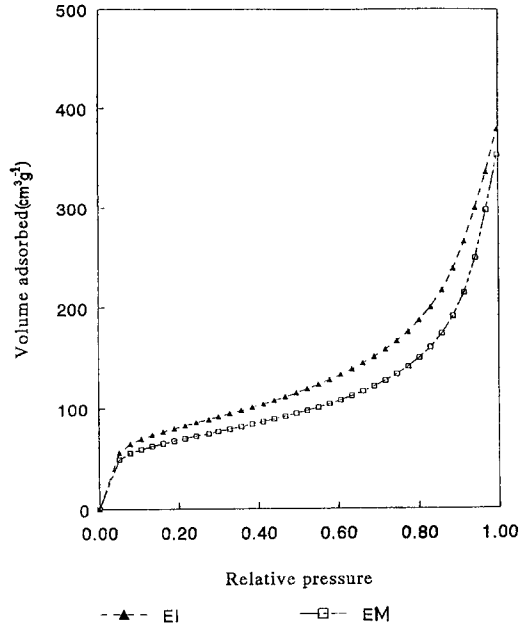

Fig. 3. Adsorption isotherms of silica gel samples evaporated with different solvents and calcined at 500°C for 3 h.

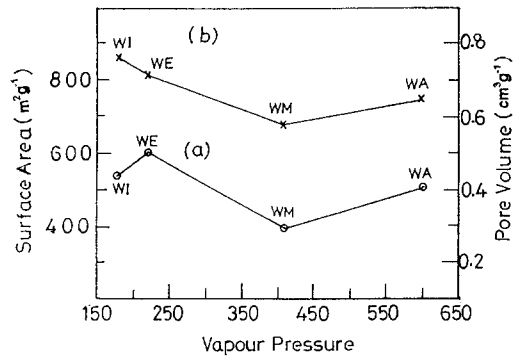

Fig. 4. Relation between (a) surface area and (b) pore volume values of the calcined silica gels (500°C for 3 h) and vapour pressure of the solvents used.

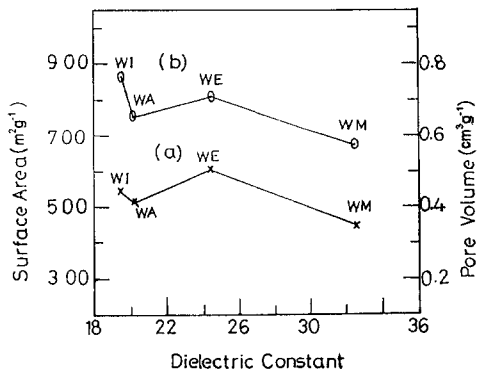

Fig. 5. Relation between (a) surface area and (b) pore volume values of the calcined silica gels (500°C for 3 h) and relative dielectric constants of the solvents used.

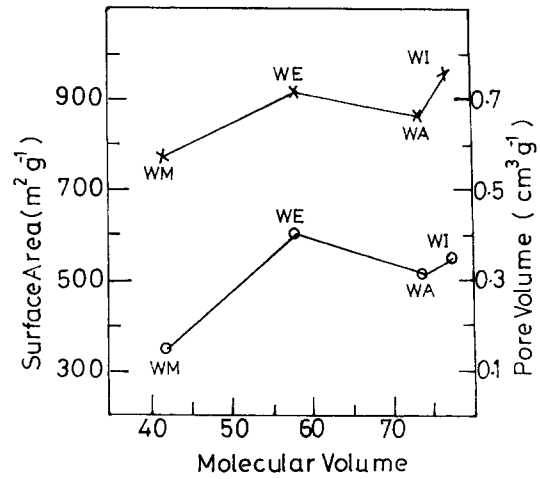

Fig. 6. Relation between (a) surface area and (b) pore volume values of the calcined silica gels (500°C for 3 h) and molecular volumes of the solvents used.

lower pore volumes for the resultant gels. Surface area of the gels are also in the same order except in the case of ethanol. It appears therefore that solvents with low values of vapour pressure, surface tension, relative dielectric constant, and higher molecular volumes as the drying liquids favour high porosity in the resultant xerogels.

The surface area and pore volume of methanol washed gel are found to be much lower than even that of the parent gel NS. Methanol has high vapour pressure, high dielectric constant, high surface tension and low molecular volume and is indicated to produce gels of low surface area and pore volume. The surface tension of 50% methyl alcohol with water at 50°C (32.95 dynes cm^{-1}) is much higher than that of ethyl alcohol-water mixture. On washing and drying, methanol evaporates much faster leaving behind residual water in the gel structure, hence causes high shrinkage and collapse of the gel structure during drying. On the contrary ethanol and isopropanol form azeotropic mixtures with water and carry increasing quantity of water on drying.

The procedure adopted for exchange of liquids is also an important criterion which determines the final properties of the dried gel. The method based on repeated washing does not disturb the gel structure or skeletal strength appreciably and hence higher surface area and pore volume values result. On the other hand the evaporation with solvents weakens the gel structure. The process appears to be promising with isopropanol, which forms an azeotropic mixture with water.

The adsorption isotherms of the gels generally show Type II behaviour. However, the patterns differ much from the starting gel to that washed with different solvents. Gels washed repeatedly with acetone and methanol are fairly non porous in nature compared

to other gels as evidenced from the Fig. 2. The gel washed with ethanol shows higher adsorption at low relative pressures is more microporous than the other gels. At higher relative pressures the gel washed with isopropanol shows more adsorption. The starting gel with micropores might have changed to macropores due to washing with isopropanol is reflected in the lower surface area and higher pore volume than the one washed with ethanol. This can be attributed to the larger molecular volume of isopropanol than ethanol. The volume of nitrogen adsorbed by these two gels in the partial pressure range 0.4–0.8 is much higher than the other gels which shows the mesoporous nature of the gels. These two gels appear to possess a combination are having some characteristics of Type II and IV adsorption isotherms. Fig. 2 shows the adsorption isotherms of the gels evaporated with isopropanol and methanol. Both show non-porous nature.

CONCLUSION

The present investigation ascertains that the nature of pore liquid in precursor gels is one of the major factors which decides the pore structure during drying. Liquids of low surface tension, low vapour pressure, low dielectric constant and high molecular volume favour the production of gels having high surface area and pore volume. Out of the various solvents investigated for solvent exchange ethanol and isopropanol appear to be most interesting and this method is simple. The exchange of solvents by other methods such as evaporation after soaking the gel with solvents has not been effective. As a result of repeated exchange it has further been possible to convert micropore-rich precursor to one having mesopore structure. In any case, in order to obtain porous gel, the gel structure has to be strengthened prior to solvent exchange.

Acknowledgement—One of the authors, (S.R.K.) acknowledges CSIR for Research Fellowship.

REFERENCES

1. Hoppener, R. H. and Bowen, H. K., *Adv. Ceram. Mat.*, 1988, **3**(6), 595.
2. Brinker, E. J., Keeffer, K. D., Schaefer, D. W and Ashley, C. S., *J. Non. Cryst. Solids*, 1982, **48,** 47.
3. Toghe, N., Moore, G. S. and Mackenzie, J. D., *J. Non. Cryst. Solids*, 1984, **63,** 95.
4. Butler, M. A., James, P. F. and Jackson, J. D., *J. Mat. Sci.*, 1996, **31,** 1675.
5. Matsuda, A., Kogure, T., Matsuno, Y., Katayama, S., Tsuno, T., Toghe, N. and Minami, T., *J. Am. Ceram. Soc.*, 1993, **76**(11), 2899.
6. Mukherjee, S. P., *J. Non. Cryst. Solids*, 1984, **63,** 35.
7. Kistler, S. S., *Nature*, 1931, **127,** 741.
8. Fricke, J., *J. Non. Cryst. Solids*, 1987, **95,** 1135.
9. Pope, E. J. A. and Mackenzie, J. D., *J. Non. Cryst. Solids*, 1986, **87,** 185.
10. Buckley, A. M. and Greenblatt, M., *J. Non. Cryst. Solids*, 1992, **143,** 1.
11. Hayashi, F., Takei, K., Machii, Y. and Shimazaki, T., *J. Ceram. Soc. Jpn. Int. Edn.*, 1990, **98,** 670.
12. Adachi, T., Sakka, S., *J. Mater. Sci.*, 1987, **22,** 4407.
13. Auvray, L., Ayral, A., Dabadie, T., Cot, L., Guizard, C. L. and Ramsay, J. D. F., *Far. Dis.*, 1995, 100.
14. Frick, J., ed. Aerogels. Springer Proceedings, Vol. 6, 1986.
15. Smith, D. M., Deshpande, R. and Brinker, C. J., in *Proc. Mater. Res. Soc. Symp.*, ed. Hampdsen, M. Smith, W. G. Klemperer and C. J. Brinker. Mater. Res. Soc., Pittsburgh, 1992, **271,** 567.
16. Prakash, S. S., Brinker, C. J., Hurd, A. J. and Rao, S. M., *Nature*, 1995, **374,** 439.
17. Haereid, S., Nilsen, E. and Einarsrud, M. A., *J. Por. Mat.*, 1996, **2,** 315.

Pergamon

PII: S0277-5387(97)00449-X

Polyhedron Vol. 17, No. 10, pp. 1705–1714, 1998
© 1998 Elsevier Science Ltd
All rights reserved. Printed in Great Britain
0277-5387/98 $19.00+0.00

Preparation of the new podand ligand S=P(pzpy)$_3$ [pzpy = 3-(2-pyridyl)-pyrazol-1-yl], and the syntheses and crystal structures of copper(II) and copper(I) complexes of its hydrolysis product $[OSP(pzpy)_2]^-$, and a double helical copper(I) complex of $[O_2P(pzpy)_2]^-$

James S. Fleming, Elefteria Psillakis, John C. Jeffery, Karen L. V. Mann, Jon A. McCleverty and Michael D. Ward*

School of Chemistry, University of Bristol, Cantock's Close, Bristol BS8 1TS, U.K.

(Received 25 August 1997; accepted 28 October 1997)

Abstract—The new podand ligand S=P(pzpy)$_3$ [L^1; pzpy = 3-(2-pyridyl)-pyrazol-1-yl], containing three bidentate pyrazolyl-pyridine arms linked to an apical P=S group via the pyrazolyl N^1 atoms, was prepared and crystallographically characterised. Reaction with Cu(II) or Cu(I) resulted in complexes of the partially-hydrolysed ligand $[OSP(pzpy)_2]^-$ (L^2), containing two bidentate chelating arms linked by a thiophosphinate fragment. $[Cu_2(L^2)_2(\mu\text{-pzpy})_2]$ contains a planar dinuclear copper(II) core with two pyrazolate bridges linking the metal centres, and one L^2 ligand attached to each metal by one bidentate arm with the other arm pendant. In $[Cu_2(L^2)_2]$ each ligand L^2 acts as an *N,N*-donor to one metal ion and an *N,S*-donor to the other with a non-coordinated pyridyl group, such that each metal ion has an N_3S donor set; this complex is achiral with a "side-by-side" disposition of bridging ligands. For comparison purposes we also crystallographically characterised $[Cu_2(L^3)_2]$, where L^3 is $[O_2P(pzpy)_2]^-$, an analogue of L^2 but with a phosphinate rather than thiophosphinate group. This complex is a dinuclear double helicate in which each ligand acts as an *N,N*-bidentate chelate to each metal ion. Comparison of this with the structure of $[Cu_2(L^2)_2]$ shows that it is the involvement of the thiophosphinate S atom of L^2 in coordination that prevents helication from occurring. © 1998 Elsevier Science Ltd. All rights reserved

Keywords: double helicates; copper; crystal structures; dinuclear complexes.

We have been interested in the preparation and coordination chemistry of new multidentate ligands which contain two or three chelating arms linked to a central spacer [1–7]. Some examples are in Scheme 1. The coordination behaviour of these ligands is characterised by a large degree of variability in the structures of their complexes, because the ligands generally have the ability to donate all of their chelating arms to one metal ion if it is large enough, or alternatively to act as a bridge between different metal ions in other cases. The former type of coordination behaviour is exemplified by the mononuclear lanthanide complexes of the podand $[HB(pzpy)_3]^-$ [pzpy denotes the fragment 3-(2-pyridyl)-pyrazol-1-yl] which we have studied in some detail [1,2]; the latter type of behaviour affords a variety of unusual structures such as tetranuclear [3] and trinuclear [4] complexes with $[HB(pzpy)_3]^-$, dinuclear double helicates with $[H_2B(pz\text{-}bpy)_2]^-$ [5], infinite one-dimensional helicates with $[O_2P(pzpy)_2]^-$ [6], and an octanuclear helical molecular ring with $[H_2B(pzpy)_2]^-$ [7].

In seeking to extend this type of chemistry we recently attempted to prepare the podand O=P(pzpy)$_3$, as a neutral analogue of the hexadentate podand $[HB(pzpy)_3]^-$ in which the three bidentate arms were linked by a P=O head-group rather than by a borohydride. However, this compound proved

* Author to whom correspondence should be addressed.

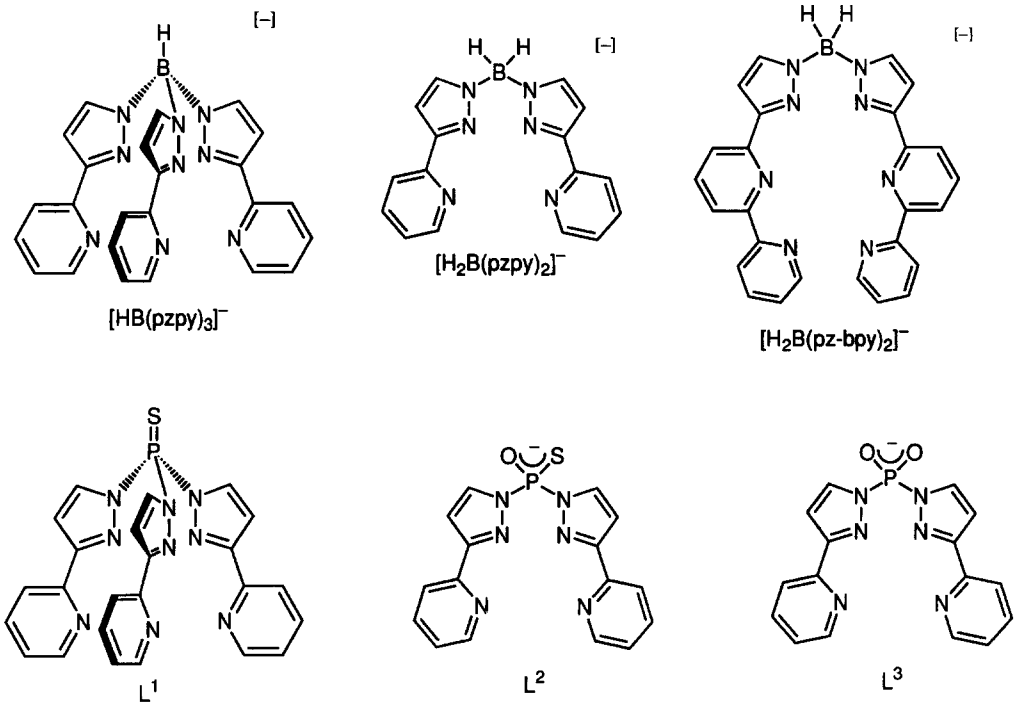

Scheme 1.

too reactive to isolate, giving instead the hydrolysis product $[O_2P(pzpy)_2]^-$ (hereafter L^3) whose coordination behaviour has been examined [6]. We have now prepared the related podand ligand $S{=}P(pzpy)_3$ (L^1), reasoning that replacement of the oxo-substituent by its less electronegative sulfur analogue might render the resulting ligand less susceptible to hydrolysis. In this we were partly correct, as L^1 has been successfully prepared and crystallographically characterised; however, attempts to prepare copper(I) and copper(II) complexes with L^1 have resulted in decomposition of the ligand to give complexes of $[OSP(pzpy)_2]^-$ (L^2), an analogue of L^3 but with one of the oxygen atoms of the phosphinate group replaced by sulfur to give a thiophosphinate. In this paper we describe the synthesis and characterisation of L^1, its reactions with Cu(II) and Cu(I) salts to give complexes of L^2, and a related double-helical Cu(I) complex of L^3.

EXPERIMENTAL

3-(2-Pyridyl)-pyrazole [8] and $[Cu(MeCN)_4][PF_6]$ [9] were prepared according to the published methods; other reagents were obtained commercially and used as received. Instrumentation used for routine spectroscopic analyses has been described previously [1].

Preparation of L^1

A mixture of 3-(2-pyridyl)pyrazole (2.90 g, 20 mmol) was suspended in a mixture of toluene (30 cm^3) and dry Et_3N (2.83 g, 28 mmol). This was cooled to 0°C, and a solution of $PSCl_3$ (0.83 g, 4.9 mmol) in toluene (5 cm^3) was added dropwise; the mixture was then heated to reflux for 18 h to give a clear solution. On cooling to room temperature, $Et_3N \cdot HCl$ separated and was filtered off to leave a clear yellow solution which was evaporated to dryness to give a waxy yellow solid. Trituration with MeCN gave white solid which was filtered off, washed with MeCN and then Et_2O, and dried *in vacuo*. Yield of L^1: 1.98 g (82%). Found: C, 58.0; H, 3.7; N, 25.3. Required for $C_{24}H_{18}N_9PS$: C, 58.2; H, 3.6; N, 25.5%. EI MS: $m/z = 495$ (M^+).

Reaction of L^1 *with copper(II) acetate hydrate*

To a blue-green solution of $[Cu(MeCO_2)_2 \cdot H_2O]$ (0.061 g, 0.31 mmol) in MeOH (10 cm^3) was added L^1 (0.153 g, 0.31 mmol) and the mixture was stirred at room temperature for 1 h. During this time the colour of the solution became dark green, and then a bright turquoise solid precipitated. This was filtered off, washed with MeOH and Et_2O, and dried *in vacuo*. Yield: 75 mg, 42%. Found: C, 48.7; H, 3.6; N, 20.5. Required for $[Cu_2(L^2)_2(\mu\text{-pzpy})_2] \cdot 2H_2O$: C, 48.6; H,

3.4; N, 21.2%. Recrystallisation from MeCN/ether gave X-ray quality crystals of $[Cu_2(L^2)_2(\mu\text{-pzpy})_2]$.

Reaction of L^1 *with* $[Cu(MeCN)_4][PF_6]$

To a solution of $[Cu(MeCN)_4][PF_6]$ (0.174 g, 0.47 mmol) in dry CH_2Cl_2 (10 cm^3) under N_2 was added L^1 (0.232 g, 0.47 mmol), resulting immediately in a bright orange solution which was stirred for 2 h at room temperature, during which time a yellow suspension formed. After addition of hexane (10 cm^3), the suspension was filtered under N_2, washed with a CH_2Cl_2/hexane mixture, and dried *in vacuo* to give $[Cu(L^1)][PF_6]$ in 65% yield. Found: C, 40.2; H, 2.7; N, 17.6. Required for $[Cu(L^1)][PF_6]$: C, 40.9; H, 2.6; N, 17.6%. Recrystallisation under N_2 by cooling a saturated MeCN solution afforded X-ray quality crystals of a decomposition product which proved to be $[Cu_2(L^2)_2]$ (see Results and Discussion section).

Preparation of $[Cu_2(L^3)_2]$

$[Et_3NH][L^3]$ (0.22 g, 0.50 mmol) and $[Cu(MeCN)_4][PF_6]$ (0.19 g, 0.50 mmol) were added to dry MeCN (10 cm^3) under N_2 with stirring. The solution turned orange, and on standing overnight (under N_2) small orange crystals grew. The orange product $[Cu_2(L^3)_2]$ was extremely air-sensitive, reacting rapidly to give a green tetranuclear Cu(II) complex of pzpy (arising from both oxidation of the metal and decomposition of the ligand) which has been previously characterized [10]. Consequently, an elemental analysis of $[Cu_2(L^3)_2]$ could not be obtained.

Crystal structure determinations

Suitable crystals were quickly transferred from the mother liquor to a stream of cold N_2 at $-100°C$ on a Siemens SMART diffractometer fitted with a CCD-type area detector. In all cases data were collected at $-100°C$ using graphite-monochromatised Mo–K_α radiation. A detailed experimental description of the methods used for data collection and integration using the SMART system has been published [1]. For triclinic crystals a full sphere of data was collected to allow a good absorption correction using SADABS; for all other crystal systems a hemisphere is sufficient. Table 1 contains a summary of the crystal parameters, data collection and refinement. In all cases the structures were solved by conventional heavy-atom or direct methods and refined by the full-matrix least-squares method on all F^2 data using the SHELXTL 5.03 package on a Silicon Graphics Indy computer [11]. Non-hydrogen atoms were refined with anisotropic thermal parameters; hydrogen atoms were included in calculated positions and refined with isotropic thermal parameters riding on those of the parent atom.

In all cases data were collected in the first instance to a 2θ limit of 55° (the default setting for our area detector). For the three copper complexes the data were in every case weak and for the final refinement were truncated at a 2θ value above which no significant diffracted intensity was observed. Including of data above this 2θ threshold in the refinement resulted in substantially poorer R indices with no noticeable improvement in the precision of the structures. In every case the data-to-parameter ratio is, however, reasonable.

Crystals of L^1 were stable and diffracted well, and the structural determination presented no problems. There is no imposed symmetry within the molecule.

In $[Cu_2(L^2)_2(\mu\text{-pzpy})_2]$ the crystals were well-formed and stable, but the weak high-angle data and modest level of refinement ($R_1 = 10.8\%$) is ascribable to the high degree of thermal motion of the non-coordinated pendant arm of L^2 which is not constrained by coordination to a metal ion. These atoms consequently have particularly high thermal parameters, but could not be separated into disordered components. The molecule is centrosymmetric, with half of it constituting an asymmetric unit.

Crystals of $[Cu_2(L^2)_2]\cdot 6$ MeCN were rather small and lost solvent rapidly on removal from the mother liquor, resulting in partial decomposition in the few seconds it took to coat the crystals in paraffin oil and transfer them to the cold stream of N_2 on the diffractometer; consequently the data were weak. The complex lies astride an inversion centre, so the asymmetric unit corresponds to $Cu(L^2)\cdot 3$ MeCN. One of the MeCN molecules is well-behaved. The other two are disordered over two positions by swivelling about the methyl carbon atoms, such that the methyl carbon atom is fixed in each case and the other C and N atoms are disordered over two sites with 50:50 site occupancies.

Crystals of $[Cu_2(L^3)_2]\cdot 3$MeCN were likewise small (that used had dimensions $0.20\times 0.10\times 0.05$; the larger ones were not single) and not only lost solvent rapidly but were unstable with respect to aerial oxidation. Again partial decomposition occurred during transfer to the diffractometer and the data were very weak. The complex lies astride a C_2 axis, which runs through the two independent Cu atoms and which therefore have 50% site occupancy. The asymmetric unit therefore corresponds to $Cu(L^1)\cdot 1.5$ MeCN, with one unique acetonitrile molecule and one across an inversion centre. The data was too weak to allow complete resolution of the disorder; the atoms of the solvent molecules were therefore modelled just as carbon atoms and hydrogen atoms were not included in the refinement. The space group $P2_12_12$ is very unusual and is non-centrosymmetric: spontaneous resolution of the helicates has therefore occurred on crystallisation. The absolute structure parameter was zero within experimental error, indicating that the optical configuration was chosen correctly.

Table 1. Crystallographic data for the four new compounds

Complex	L^1	$[Cu_2(L^2)_2(\mu\text{-pzpy})_2]$	$[Cu_2(L^2)_2]\cdot 6MeCN$	$[Cu_2(L^3)_2]\cdot 3MeCN$
Formula	$C_{24}H_{18}N_9PS$	$C_{48}H_{36}N_{18}Cu_2O_2P_2S_2$	$C_{44}H_{42}Cu_2N_{18}O_2P_2S_2$	$C_{38}H_{33}N_{15}Cu_2P_2O_4$
M	495.50	1150.09	1108.1	952.81
System, space group	Triclinic, $P\bar{1}$	Monoclinic, $P2_1/c$	Triclinic, $P\bar{1}$	Orthorhombic, $P2_12_12$
a (Å)	9.863(2)	14.618(6)	10.982(6)	14.498(3)
b (Å)	11.363(4)	10.295(3)	11.238(6)	14.985(3)
c (Å)	11.449(2)	16.951(8)	11.588(9)	8.913(2)
α (°)	74.36(2)	90	84.88(3)	90
β (°)	71.99(2)	102.076(10)	72.63(4)	90
γ (°)	80.00(2)	90	71.62(5)	90
U (Å^3)	1169.3(5)	2494(2)	1295.3(14)	1936.2(7)
Z	2	2	1	2
D_c (g cm^{-3})	1.407	1.531	1.421	1.634
μ (mm^{-1})	0.24	1.061	1.019	1.246
$F(000)$	512	1172	568	972
Crystal size/mm^3	$0.25\times0.20\times0.10$	$0.20\times0.10\times0.10$	$0.25\times0.10\times0.10$	$0.20\times0.10\times0.05$
2θ range for data used (°)	4–55	3–45	4–45	4–40
Unique data, restraints, parameters	5265, 0, 316	3199, 12, 314	3375, 90, 359	1816, 30, 277
Weighting factors (a,b)[a]	0.0822, 0	0.1964, 15.73	0.0861, 0	0.012, 0
Final R_1, wR_2[a,b]	0.0655, 0.1709	0.1076, 0.3637	0.0741, 0.191	0.0601, 0.0988
Largest peak, hole (e Å^{-3})	+0.902, −0.683	+0.876, −0.827	+0.873, −0.577	+0.432, −0.298

[a] $wR_2 = [\Sigma[w(F_o^2-F_c^2)^2]/\Sigma w(F_o^2)^2]^{1/2}$ where $w^{-1} = [\sigma^2(F_o^2)+(aP)^2+bP]$ and $P = [\max(F_o^2,0)+2F_c^2]/3$.

[b] Structure was refined on F_o^2 using all data; the value of R_1 is given for comparison with refinements based on F_o with a threshold of $F \geqslant 4\sigma(F)$.

Table 2. Selected bond lengths (Å) and angles (°) for L^1

P(1)—N(31)	1.694(3)	P(1)—N(11)	1.702(3)
P(1)—N(51)	1.700(3)	P(1)—S(1)	1.9027(13)
N(31)—P(1)—N(51)	102.61(14)	N(31)—P(1)—S(1)	114.04(11)
N(31)—P(1)—N(11)	107.4(2)	N(51)—P(1)—S(1)	117.49(11)
N(51)—P(1)—N(11)	101.53(14)	N(11)—P(1)—S(1)	112.46(11)

Table 3. Selected bond lengths (Å) and angles (°) for $[Cu_2(L^2)_2(\mu\text{-pzpy})_2]$

Cu(1)—N(51)	1.957(6)	Cu(1)—N(52A)	1.977(8)
Cu(1)—N(11)	1.994(11)	Cu(1)—N(61)	2.053(10)
Cu(1)—N(21)	2.358(11)	P(1)—O(1)	1.470(9)
P(1)—S(1)	1.885(9)		
N(51)—Cu(1)—N(52A)	98.1(2)	N(11)—Cu(1)—N(61)	90.7(4)
N(51)—Cu(1)—N(11)	169.7(4)	N(51)—Cu(1)—N(21)	99.1(4)
N(52A)—Cu(1)—N(11)	91.1(4)	N(52A)—Cu(1)—N(21)	96.1(3)
N(51)—Cu(1)—N(61)	80.6(4)	N(11)—Cu(1)—N(21)	75.2(5)
N(52A)—Cu(1)—N(61)	173.8(4)	N(61)—Cu(1)—N(21)	90.1(4)

Table 4. Selected bond lengths (Å) and angles (°) for $[Cu_2(L^2)_2]\cdot 6MeCN$

Cu(1)—N(12)	2.006(7)	Cu(1)—N(31)	2.091(8)
Cu(1)—N(42)	2.063(7)	Cu(1)—S(1)	2.324(3)
P(1)—O(1)	1.471(6)	P(1)—S(1)	1.950(3)
N(12)—Cu(1)—N(42)	138.3(3)	N(12)—Cu(1)—S(1)	94.3(2)
N(12)—Cu(1)—N(31)	113.1(3)	N(42)—Cu(1)—S(1)	118.4(2)
N(42)—Cu(1)—N(31)	78.2(3)	N(31)—Cu(1)—S(1)	114.0(2)

Table 5. Selected bond lengths (Å) and angles (°) for $[Cu_2(L^3)_2]\cdot 3MeCN$

Cu(1)—N(21A)	2.007(9)	Cu(2)—N(32)	2.015(11)
Cu(1)—N(21)	2.007(9)	Cu(2)—N(32A)	2.015(11)
Cu(1)—N(12A)	2.077(9)	Cu(2)—N(41)	2.028(12)
Cu(1)—N(12)	2.077(9)	Cu(2)—N(41A)	2.028(12)
P(1)—O(1)	1.470(9)	P(1)—O(2)	1.478(10)
N(21A)—Cu(1)—N(21)	142.4(5)	N(32)—Cu(2)—N(32A)	123.6(7)
N(21A)—Cu(1)—N(12A)	82.0(4)	N(32)—Cu(2)—N(41)	79.3(5)
N(21)—Cu(1)—N(12A)	117.5(4)	N(32A)—Cu(2)—N(41)	118.7(5)
N(21A)—Cu(1)—N(12)	117.5(4)	N(32)—Cu(2)—N(41A)	118.7(5)
N(21)—Cu(1)—N(12)	82.0(4)	N(32A)—Cu(2)—N(41A)	79.3(6)
N(12A)—Cu(1)—N(12)	119.8(5)	N(41)—Cu(2)—N(41A)	143.8(7)

RESULTS AND DISCUSSION

Synthesis and structure of L^1

Reaction of three equivalents of 3-(2-pyridyl) pyrazole (Hpzpy) with $PSCl_3$ in toluene/Et_3N, according to a published method for reaction of other pyrazoles with $PSCl_3$ [12], afforded L^1 in good yield. The crystal structure is shown in Fig. 1 and confirms the formulation. Each of the three bidentate pzpy arms has a *transoid* conformation to allow the nitrogen lone pairs to avoid each other. Two of the arms are directed away from the capping S atom towards the region of space where metal-ion binding would occur; the third arm is directed away from this area, presumably for steric reasons, by rotation about the P(1)—N(51) bond. The increased length of the P—N bonds (ca 1.70 Å) compared to the B—N bonds of the tris(pyrazolyl)borate analogue $[HB(pzpy)_3]^-$ (ca 1.53 Å) suggest that the cavity of L^1 would be slightly larger than that of $[HB(pzpy)_3]^-$ if it coordinated all of its donor arms to the same metal ion.

Reaction of L^1 *with* Cu(II) *and* Cu(I) *salts to give complexes of* L^2

Reaction of L^1 with copper(II) acetate dihydrate in methanol rapidly resulted in formation of a turquoise precipitate whose elemental analysis did not correspond to any obvious combination of metal, ligand (L^1) and counter-ion.

The crystal structure of the product is in Fig. 2, and showed it to be in fact $[Cu_2(L^2)_2(\mu\text{-pzpy})_2]$ (consistent with the elemental analysis) in which partial solvolysis of L^1 has occurred to give L^2, with two bidentate pzpy arms attached to a thiophosphinate head-group. This results in liberation of one equivalent of the bidentate ligand Hpzpy into the medium *per* molecule of L^2, and both L^2 and (deprotonated) pzpy are coordinated in the dinuclear Cu(II) complex. Each pzpy fragment bridges the two Cu(II) centres, with the bidentate chelating site (pyridyl N and pyrazolyl N^2 atoms) coordinated to one Cu(II) ion, and the pyrazolyl N^3 atom coordinated to the other. The result is a planar $\{Cu_2(\mu\text{-pzpy})_2\}$ fragment of the type we have previously seen in the grid-like tetranuclear Cu(II) complex $[Cu_4(pzpy)_6(dmf)_2]^{2+}$ [10]. Each ligand L^2 is terminally bound to one Cu(II) ion via one of the two chelating arms; the second arm is pendant with a *transoid* conformation of the heterocyclic rings to minimise the lone pair/lone pair repulsion. Each Cu(II) ion is formally five-coordinate in a square-pyramidal geometry, with the axial Cu(1)—N(21) bond [2.358(11) Å] being considerably longer than the four equatorial bonds which all lie in the range 1.96–2.05 Å. The sixth coordination site of each Cu(II) ion is involved in a weak pseudo-axial interaction to the oxygen atom of the thiophosphinate

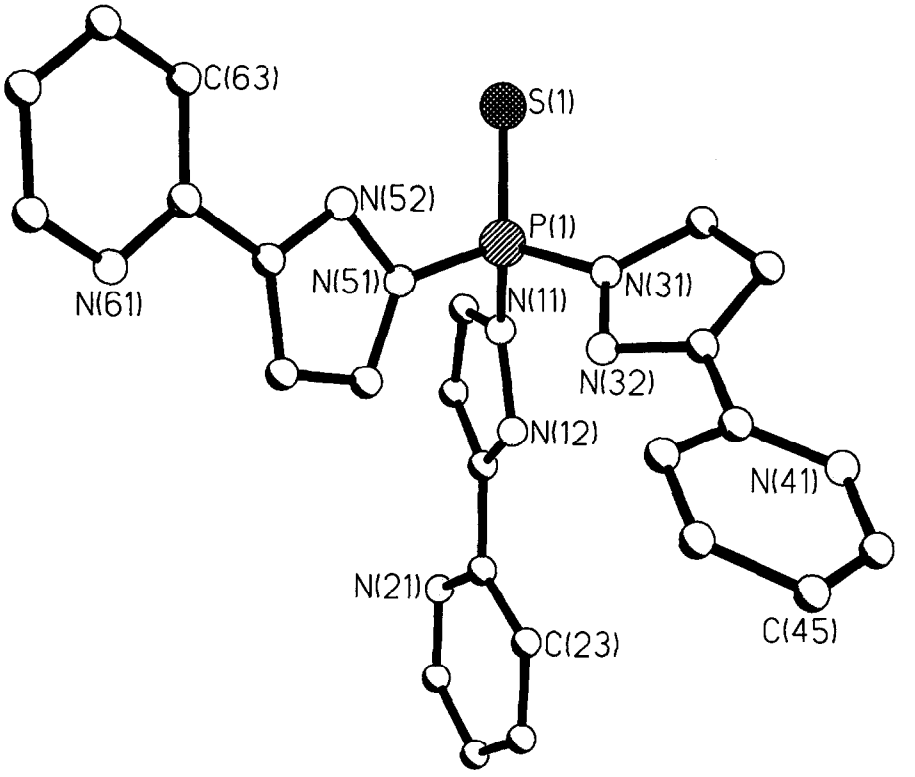

Fig. 1. Crystal structure of L^1.

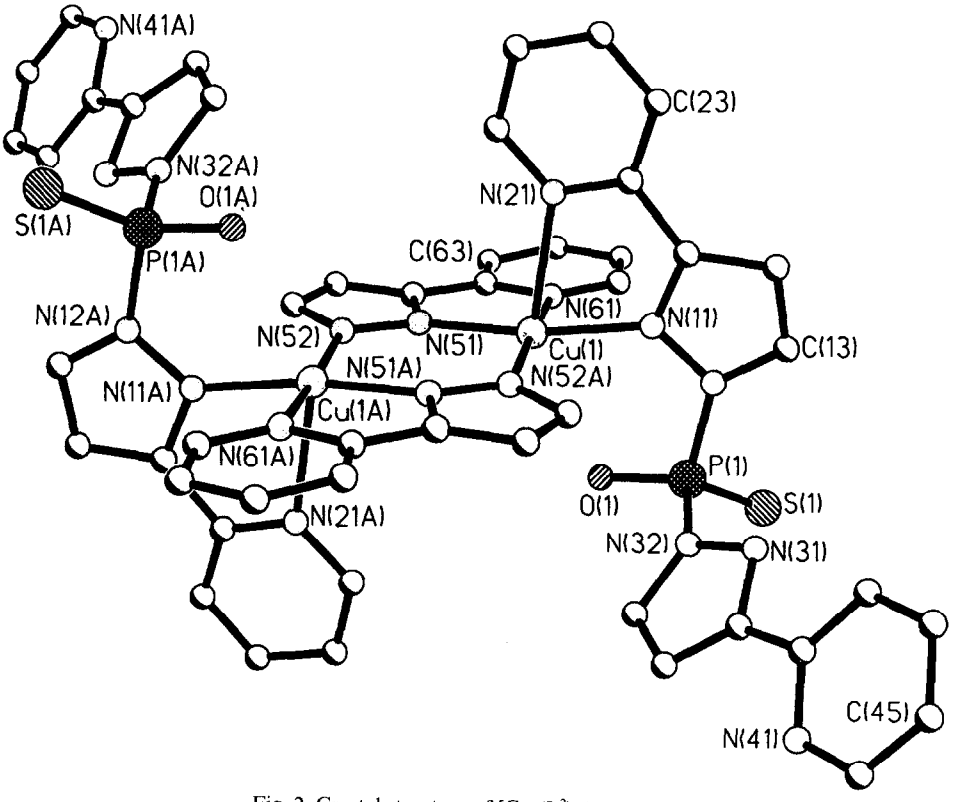

Fig. 2. Crystal structure of $[Cu_2(L^2)_2(\mu\text{-pzpy})_2]$.

group of L^2, with the Cu(1) $\cdots$ O(1) separation being 2.79 Å. Several other planar dinuclear Cu(II) complexes with pyrazolate bridges are known, and they invariably display strong antiferromagnetic exchange [13].

We thought that the hydrolysis of L^1 in the above reaction probably arose from the presence of water of crystallisation in copper(II) acetate. Accordingly we performed the reaction of L^1 with $[Cu(MeCN)_4][PF_6]$ in distilled acetonitrile under N_2. This afforded a yellow solid whose elemental analysis suggested the formulation $[Cu(L^1)][PF_6]$, i.e. a mononuclear complex of the intact ligand L^1. The IR spectrum contained the characteristic hexafluorophosphate bands. X-ray quality crystals were obtained by cooling a saturated MeCN solution of the crude material, still under N_2. In the IR spectrum of the crystals, however, the stretches due to the hexafluorophosphate ion were no longer present, and the structure (Fig. 3) shows again that partial decomposition of the ligand has occurred to give $[Cu_2(L^2)_2]$, despite the use of distilled solvents and an N_2 atmosphere for handling the material at all times.

In $[Cu_2(L^2)_2]$ both ligands are bridging both metal ions, in a centrosymmetric "face to face" (rather than helical) manner. Each ligand coordinates to one Cu ion as a bidentate *N,N*-donor chelate in the usual way via the pyrazolyl and pyridyl groups of one arm, but coordinates to the other Cu ion as an *S,N*-donor chelate via the thiophosphinate S and pyrazolyl groups. The pyridyl group of this ligand arm is therefore pendant, although the N atom is directed towards the Cu ion [non-bonded Cu(1) $\cdots$ N(21) separation, 3.29 Å] indicating a weak residual interaction. Each ligand therefore acts as an N_3S donor with one non-coordinating pyridyl group. The affinity of Cu(I) for thiolate and thioether donors is well known and therefore results in a somewhat unexpected binding mode for L^2 in this structure. The dihedral angle between the CuNN and CuNS planes of each chelating fragment is 83°, consistent with the common preference of Cu(I) for pseudo-tetrahedral geometry.

The double-stranded helicate $[Cu_2(L^3)_2]$

Given coordination of the S atom of L^2 in $[Cu_2(L^2)_2]$, we were interested to see what would happen if the S atom were replaced by an O atom (as in L^3), since the more electronegative O atom would be less likely to coordinate to the "soft" Cu(I) ions. The ligand L^3 is therefore more likely to coordinate solely via its N atoms in its Cu(I) complex, and we found recently that complexes of Ag(I) and Tl(I) with L^3 have unusual infinite one-dimensional helical structures [6].

Reaction of L^3 with $[Cu(MeCN)_4][PF_6]$ in distilled MeCN under N_2 afforded a yellow-orange material which was very air sensitive; exposure to air rapidly gave the green tetranuclear Cu(II) complex of pzpy [10], following hydrolysis of L^3 and oxidation of Cu(I) to Cu(II). This is in strong contrast to the Ag(I) complex with L^3 which is completely stable in air and actually crystallises with water molecules in the lattice [6]. Small crystals of the orange product could be isolated which were just suitable for X-ray diffraction studies, and the crystal structure (Fig. 4) shows the complex to be $[Cu_2(L^3)_2]$.

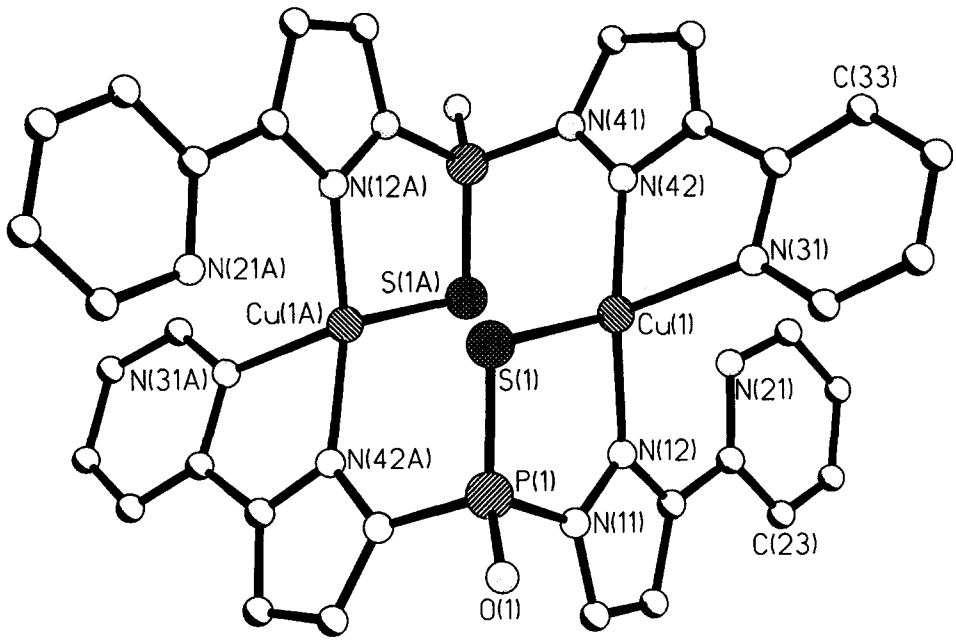

Fig. 3. Crystal structure of $[Cu_2(L^2)_2]$.

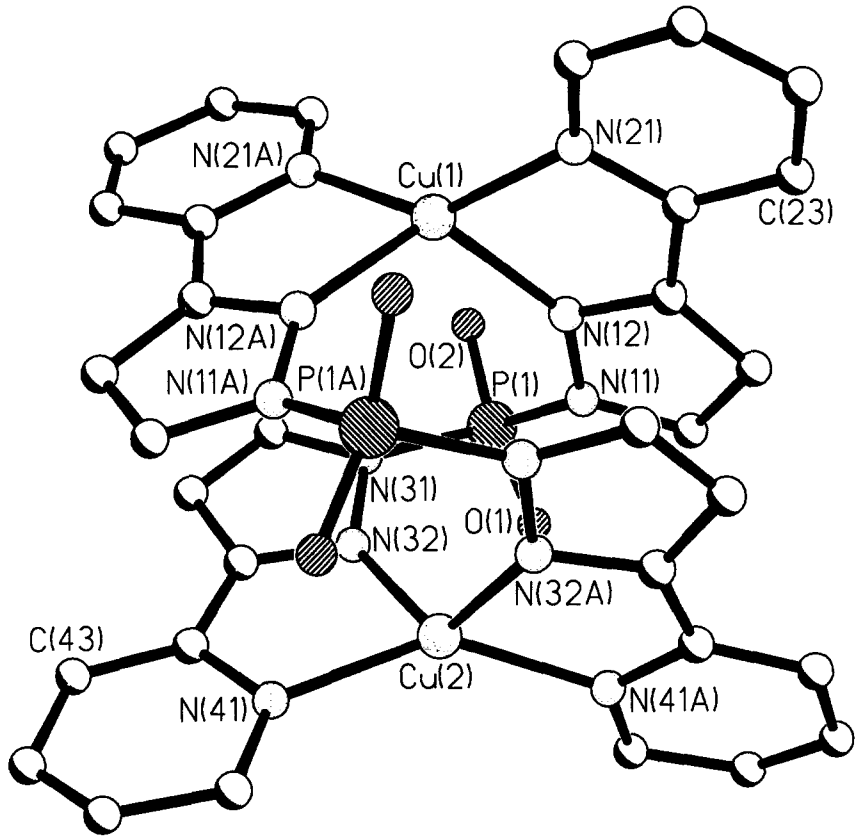

Fig. 4. Crystal structure of $[Cu_2(L^3)_2]$.

The structure is a double-stranded helix, with each Cu(I) ion coordinated by two *N,N*-bidentate chelating fragments, one from each ligand, and the phosphinate group not involved in coordination. As is normal in helicate structures there are π-stacking interactions between overlapping sections of the two ligands, and this is emphasised in Fig. 5; the mean-plane separations of the overlapping areas are in the range 3.2–3.5 Å. The two CuNN planes at each metal ion are approximately mutually perpendicular [79° at Cu(1) and 77° at Cu(2)], and the bond lengths and angles of the metal-ion coordination spheres are entirely typical of Cu(I) complexes with chelating diimine ligands [14]. The Cu(1)···Cu(2) separation is 4.63 Å. Constable and co-workers have prepared a variety of double-helical dinuclear copper(I) complexes with 2,2′:6′,2″:6″,2‴-quaterpyridine and various substituted derivatives in which they showed that the "pitch" of the helix and hence the metal–metal separation depended on the nature of the substituents on the ligand [15]. In the case of $[Cu_2(L^3)_2]$ the $\{PO_2\}^-$ spacer group separating the bidentate fragments results in a greater metal–metal separation than observed in the quaterpyridine complexes.

The structure of $[Cu_2(L^3)_2]$ is of interest not only in comparison to the related quaterpyridine helicates, but in relation to the non-helical, "side-by-side" structure of $[Cu_2(L^2)_2]$, in which the high affinity of the sulfur ligand for Cu(I) precludes a helical conformation. Figure 4 shows clearly that the helical ligand arrangement in $[Cu_2(L^3)_2]$ results in the phosphinate oxygen atoms being directed away from the metal ions and not participating in coordination. If $[Cu_2(L^2)_2]$ were helical it would therefore not be possible for the S atoms to coordinate. We also note that the chemical stability of $[Cu_2(L^2)_2]$ with respect to aerial oxidation, in marked contrast to $[Cu_2(L^3)_2]$, presumably arises from stabilisation of the Cu(I) state by coordination of the sulfur atom.

CONCLUSIONS

The desired podand ligand L^1 could be made easily in high yield and has been crystallographically characterised, but so far we have not been able to isolate complexes of the intact ligand. Reaction with Cu(I) and Cu(II) salts afforded in each case complexes of the thiophosphinate ligand L^2 on recrystallisation, arising from partial hydrolysis of the ligand. The Cu(II) complex $[Cu_2(L^2)_2(\mu\text{-pzpy})_2]$ has a planar dicopper(II) core with two bridging pyrazolate groups, and hypodenate L^2 ligands in which one bidentate arm is pendant. In the Cu(I) complex $[Cu_2(L^2)_2]$ each ligand

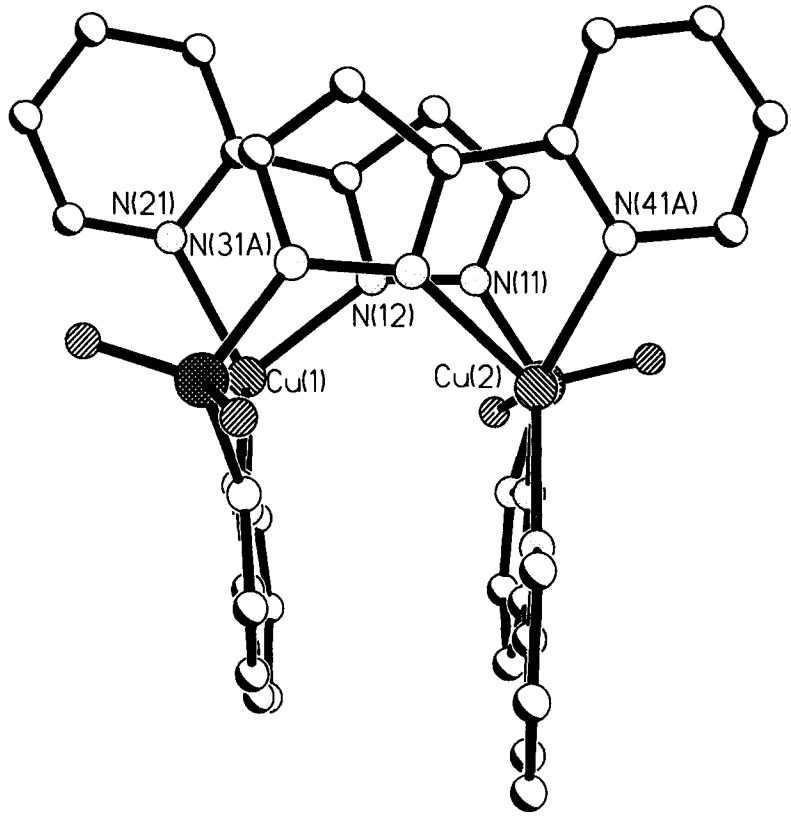

Fig. 5. Alternative view of the crystal structure of $[Cu_2(L^3)_2]$ emphasising the inter-ligand aromatic π-stacking.

L^2 is bridging in an asymmetric manner, acting as an *N,N*-donor to one metal and an *N,S*-donor to the other resulting in an achiral centrosymmetric structure. In contrast $[Cu_2(L^3)_2]$, in which the S atom of the thiophosphinate is replaced by an O atom which no longer coordinates to Cu(I), is a double-stranded helicate in which each ligand bridges symmetrically as an *N,N*-chelate to each metal ion.

Acknowledgement—We thank the EPSRC for financial support.

REFERENCES

1. Jones, P. L., Amoroso, A. J., Jeffery, J. C., McCleverty, J. A., Psillakis, E., Rees, L. H. and Ward, W. D., *Inorg. Chem.*, 1997, **36,** 10.
2. Armaroli, N., Balzani, V., Barigelletti, F., Ward, M. D. and McCleverty, J. A., *Chem. Phys. Lett.*, 1997, **276,** 435.
3. Amoroso, A. J., Jeffery, J. C., Jones, P. L., McCleverty, J. A., Thornton, P. and Ward, M. D., *Angew. Chem., Int. Ed. Engl.*, 1995, **34,** 1443.
4. Amoroso, A. J., Jeffery, J. C., Jones, P. L., McCleverty, J. A., Psillakis, E. and Ward, M. D., *J. Chem. Soc., Chem. Commun.*, 1995, 1175; Jones, P. L., Jeffery, J. C., Maher, J. P., McCleverty, J. A., Rieger, P. H. and Ward, M. D., *Inorg. Chem.*, 1997, **36,** 3088.
5. Psillakis, E., Jeffery, J. C., McCleverty, J. A. and Ward, M. D., *Chem. Commun.*, 1997, 479.
6. Psillakis, E., Jeffery, J. C., McCleverty, J. A. and Ward, M. D., *J. Chem. Soc., Dalton Trans.*, 1997, 1645.
7. Jones, P. L., Byrom, K. J., Jeffery, J. C., McCleverty, J. A. and Ward, M. D., *Chem. Commun.*, 1997, 1361.
8. Amoroso, A. J., Cargill Thompson, A. M. W., Jeffery, J. C., Jones, P. L., McCleverty, J. A. and Ward, M. D., *J. Chem. Soc., Chem. Commun.*, 1994, 2751; Brunner, H. and Scheck, T., *Chem. Ber.*, 1992, **125,** 701.
9. Kubas, G. J., *Inorg. Synth.*, 1979, **19,** 90.
10. Jeffery, J. C., Jones, P. L., Mann, K. L. V., Psillakis, E., McCleverty, J. A., Ward, M. D. and White, C. M., *Chem. Commun.*, 1997, 175.
11. SHELXTL 5.03 program system; Siemens Analytical X-Ray Instruments, Madison, WI, USA, 1995.
12. LeCloux, D. D., Tokar, C. J., Osawa, M., Houser, R. P., Keyes, M. C. and Tolman, W. B., *Organometallics*, 1994, **13,** 2855; Fischer, S., Hoyano,

J. and Peterson, L. K., *Can. J. Chem.*, 1976, **54,** 1995.
13. Otieno, T., Rettig, S. J., Thompson, R. C. and Trotter, J., *Inorg. Chem.*, 1995, **34,** 1718; Hanot, V. P., Robert, T. D., Kolnaar, J., Hassnoot, J. G., Reedijk, J., Koojiman, H. and Spek, A. L., *J. Chem. Soc., Dalton Trans.*, 1996, 4275.
14. Bardwell, D. A., Jeffery, J. C., Otter, C. A. and Ward, M. D., *Polyhedron*, 1996, **15,** 191 and refs. therein.
15. Constable, E. C., Hannon, M. J., Martin, A., Raithby, P. R. and Tocher, D. A., *Polyhedron*, 1992, **22,** 2967; Constable, E. C., Heirtzler, F., Neuburger, M. and Zehnder, M., *J. Am. Chem. Soc.*, 1997, **119,** 5606.

Pergamon

PII: S0277-5387(97)00450-6

Polyhedron Vol. 17, No. 10, pp. 1715–1723, 1998
© 1998 Elsevier Science Ltd
All rights reserved. Printed in Great Britain
0277-5387/98 $19.00+0.00

Host–guest interaction between the dinuclear copper(II) complex of the hexaaza macrocyclic ligand 3,6,9,17,20,23-hexaaza-tricyclo[23.3.1.1^{11,15}]triaconta-1(29),11(30),12,14,25,27-hexaene and malonate, maleate, fumarate, pyrophosphate and orthophosphate anions

Tania F. Pauwels, Werner Lippens, Gerrit G. Herman* and André M. Goeminne

Department of General and Inorganic Chemistry, University of Ghent, Krijgslaan 281, B-9000 Ghent, Belgium

(Received 21 July 1997; accepted 28 October 1997)

Abstract—The hexaaza macrocyclic ligand 3,6,9,17,20,23-hexaazatricyclo[23.3.1.1]triaconta-1(29),11(30),12,14,25,27-hexaene (L), forms strong dinuclear complexes, as well as several protonated and hydroxo chelates, with Cu(II) ions. The host–guest interactions between the dinuclear copper(II) complexes of L and malonate, maleate, fumarate, pyrophosphate and orthophosphate anions were investigated by potentiometric conventional pH-metry as well as by spectrophotometric titrations in 2 : 1 : 1 molar ratio for Cu(II), L and guest. Several ternary complexes are found in aqueous solution as a result of coordinate bonding, hydrogen bond formation and Columbic attraction between the host and guest. The stability constants for all the species found are reported. The dinuclear copper(II) complex of L shows stronger complexation with the maleate anion than with malonate and fumarate anions. It is suggested that the presence of the double bond in maleate offers a more favourable geometry for coordination to the Cu_2L host. Complexation with pyrophosphate and orthophosphate anions show little difference in stability. The big, flexible, pyrophosphate anion probably coordinates outside the macrocycle. © 1998 Elsevier Science Ltd. All rights reserved

Keywords: host–guest; hexaaza macrocyclic ligand; dinuclear complexes.

The chemistry of large polyazamacrocyclic ligands is of considerable interest since the addition to complexing cationic species [1–6], the dinuclear metal complexes are also capable of coordinating anions [7–10]. The study of macrocyclic ligands and their metal complexes can add to a better understanding of certain biological functions as well as to new catalysts of value in chemical synthesis. Recently Martell and coworkers have reported that the macrocyclic hexaamine ligand 3,6,9,16,19,22-hexaaza-27,28-dioxatricyclo[22.2.1.1] - octacosa - 1(26),11,13,24 - tetraene (BFBD, Formula I), is capable of forming mono- through hexaprotonated cationic species as well as both mono- and dinuclear Cu(II) complexes which in turn recognize oxalate, malonate and pyrophosphate anions. Crystal structures confirmed that the binding of anionic substrates to the protonated macrocyclic ligand BFBD is through electrostatic forces and hydrogen bonds [11].

For the ternary Cu(II) complexes it is described that the strength of the coordinate bonds and electrostatic attractive forces all contribute to their stabilities. The binding strength increases with the charge of both hosts and guests, as well as with the basicity of the donor groups of the guests. The ligand L (Formula

* Author to whom correspondence should be addressed.

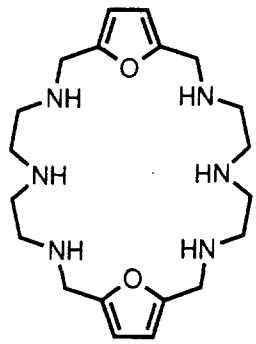

Formula I. BFBD

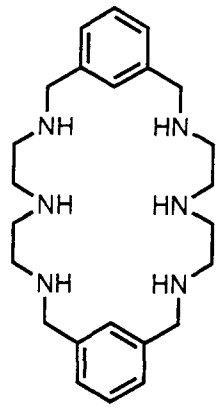

Formula II. L

II), consisting of two diethylenetriamine units separated by m-xylyl bridges, is also capable of forming dinuclear metal complexes, whereby each metal ion is coordinated by three amino nitrogen atoms leaving additional coordination sites available. In aqueous solution these coordination sites could be occupied by H_2O, OH^- or anionic substrates [12].

In this paper we report the formation of dinuclear Cu(II) complexes with L as well as their interaction with malonate, maleate, fumarate, pyrophosphate and orthophosphate anions since only one account of additional substrate binding by these complexes has been described [13].

Potentiometric equilibrium methods and spectrophotometric data are employed to elucidate the nature of the ternary species formed in solution.

EXPERIMENTAL

Reagents

The ligand L was synthesized as described previously [14], but with some minor modifications and was separated as its hexahydrochloride salt ($L \cdot 6HCl.H_2O$). All other reagents were of analytical grade and used as received. Distilled and deionized water (Milli-Q quality, specific conductance < 0.05 $\mu S\ cm^{-1}$) was used throughout for all solutions.

Solutions

Carbonate-free sodium hydroxide solutions (ca 0.500 mol dm^{-3}) were prepared from Titrisol ampoules and were standardized by titration with HCl. The HCl solution was standardized by argentometry. The metal ion stock solution was prepared from metal perchlorate and was standardized by titration with the disodium salt of ethylenediaminetetraacetic acid (EDTA) in the presence of a small amount of the Hg (EDTA) complex using appropriate conditions and electrodes (mercury and calomel electrode) [15]. All final solutions for the potentiometric and spectrophotometric titrations were made up to an ionic strength of 0.1 mol dm^{-3} with sodium perchlorate.

Equipment

The potentiometric measurements were carried out with an automatic titration system, equipped with a Radiometer PHM84 pH meter and a Schott T-100 burette (total volume 5 cm^3). The pH meter was fitted with a Schott H2680 glass electrode and a Schott B3410 calomel electrode with a second salt bridge filled with 0.1 mol dm^{-3} NaCl. A Schott titration assembly was used with a thermostatted vessel (80 cm^3) and a magnetic stirrer. All titrations were performed at 25°C ± 0.1°C under an atmosphere of nitrogen, presaturated with water vapour by bubbling through a 0.1 mol dm^{-3} $NaClO_4$ solution. The program Titrate, slightly modified, was used to monitor the titration [16].

The electrode system was calibrated as a hydrogen ion concentration probe ($pH = -\log[H^+]$) by titrations of hydrochloric acid 40 cm^3 0.0359 mol dm^{-3}) with NaOH(aq). The concentration of HCl was determined by argentometry. The titration data were processed using Gran's method in order to calculate the standard cell potential (E°), the dissociation of water (K_w), together with the correction terms for changes in the liquid junction potential in strong acid medium, a_j ($-\log[H^+] < 2.5$), and for the non-linear electrode response in a strong alkaline medium, b_j ($-\log[H^+] > 11.5$) [17]. The pK_w value was found to be 13.78 in accord with literature values, $a_j = 420$ mV $dm^3\ mol^{-1}$ and $b_j = -90$ mV $dm^3\ mol^{-1}$ [18]. The electromotoric force readings were converted into pH values using eqn (1); pH values were obtained by successive approximations taking $[H^+]$ as zero at the start.

$$pH = (E^\circ - E + a_j[H^+] + b_j K_w[H^+]^{-1})/S \quad (1)$$

The value for the Nernst slope, S, was obtained as the slope of the plot pH_{calc} vs $E_{measured}$ for

$2.4 < pH_{calc} < 3.3$ and was 59.0 ± 0.05 mV. Calibration parameters remained fairly constant with time. Titrations were performed with 0.5302 mol dm^{-3} and with C_M to C_L to C_G ratios of 2 : 1 : 1, G being the guest ligand. Equilibrium times of up to 10 min were required.

The electronic absorption spectra were recorded at 25°C on a Hewlett Packard 8451A diode array spectrophotometer in the wave length region 190 to 820 nm. Spectra were obtained from titrations similar to those in the potentiometric experiments; for each titration point a small amount of the titration solution was injected into a cell of appropriate length and re-injected in the titration vessel after recording the spectrum [19].

Calculations

The calculations of the stability constants of the various species formed in aqueous solution were obtained from numerical analysis of all experimental emf data from the potentiometric titrations using Superquad [20,21]. Titration data were evaluated by testing chemically acceptable complexation models. The best models were selected after successive attempts according to the best agreement between observed and calculated data and by means of an accurate statistic analysis of the global σ-value for the refinement, and goodness of fit (χ^2) and the standard deviation of each formation constant as calculated by Superquad. In addition, the program Equil [22] was used to calculate simulated titration curves for each given set of species and stability constants, and to calculate the species distribution curves relative to total Cu^{2+} present. Due to data entry limitations of this program, no smooth curves were obtained for some complexes at pH ranges corresponding to inflection points.

The protonation as well as the complexation constants of the guest ligands with Cu^{2+} were used as found in the literature at 25°C and ionic strength 0.10 mol dm^{-3} [23].

RESULTS AND DISCUSSION

Protonation constants

The pH titration profile of the ligand has a 4 equivalent buffer region for pH 8–11 ($2 < a < 6$ with a being the number of moles base added to the total number of moles ligand), indicating the presence of four moderately to strong basic amino groups. These amino groups are the ones closest to the benzene ring and their basicities are little influenced by Coulombic effects. The remaining two amino groups have low basicity. It is clear that the central amino groups of the diethylenetriamine moieties in the macrocycle are involved here as their basicities will be strongly influenced by the Coulombic effects of two adjacent (positive) protonated amino groups. These observations are in agreement with the calculated protonation constants given in Table 1.

Copper(II) complexes

The ligand L forms both mononuclear (1 : 1) and binuclear (2 : 1) complexes [24]. The titration conditions were chosen in that way that only the Cu_2L complex was present as final complex.

This complex is formed maximally at pH 6. The calculated stability constants are presented in Table 2 together with values in the literature.

It can be seen that fairly close agreement is obtained for the stability constants of these species that are common to both studies. The small differences may result from the use of different supporting electrolytes.

The species distribution curves are presented in Fig. 1. It is seen that the mononuclear copper complex $CuLH_2$, appears only at low pH. In the region pH 4–7 the Cu_2L complex is dominant, while at higher pH the hydroxo species $Cu_2L(OH)$ and $Cu_2L(OH)_2$ are formed owing to the deprotonation of the water mol-

Table 1. Individual and cumulative protonation constants of the ligand L at 25°C and I = 0.10 mol dm^{-3} $NaClO_4$

Equilibrium[a]	log K
$L + H \Leftrightarrow HL$	9.57
$L + 2H \Leftrightarrow H_2L$	18.41
$L + 3H \Leftrightarrow H_3L$	26.49
$L + 4H \Leftrightarrow H_4L$	33.73
$L + 5H \Leftrightarrow H_5L$	37.32
$L + 6H \Leftrightarrow H_6L$	40.38
$L + H \Leftrightarrow HL$	9.57
$HL + H \Leftrightarrow H_2L$	8.84
$H_2L + H \Leftrightarrow H_3L$	8.08
$H_3L \pm H \Leftrightarrow H_4L$	7.24
$H_4L + H \Leftrightarrow H_5L$	3.59
$H_5L + H \Leftrightarrow H_6L$	3.06

[a] Charges are omitted for clarity.

Table 2. Stability constants of L with Cu(II) ions in 2 : 1 molar Cu : L ratio at T = 25°C, I = 0.10 mol dm^{-3} $NaClO_4$

Equilibrium[a]	log β[b,c]	log β[d]
$Cu + L + 2H \Leftrightarrow CuLH_2$	29.54 (5)	29.23
$2Cu + L \Leftrightarrow Cu_2L$	24.17 (4)	24.49
$2Cu + L + OH \Leftrightarrow Cu_2L(OH)$	16.79 (5)	16.57
$2Cu + L + 2OH \Leftrightarrow Cu_2L(OH)_2$	8.21 (2)	8.74

[a] Charges are omited for clarity.
[b] Relative standard deviations are given in parentheses.
[c] This work.
[d] Ref. [12], 25°C, I = 0.10 mol dm^{-3} KCl.

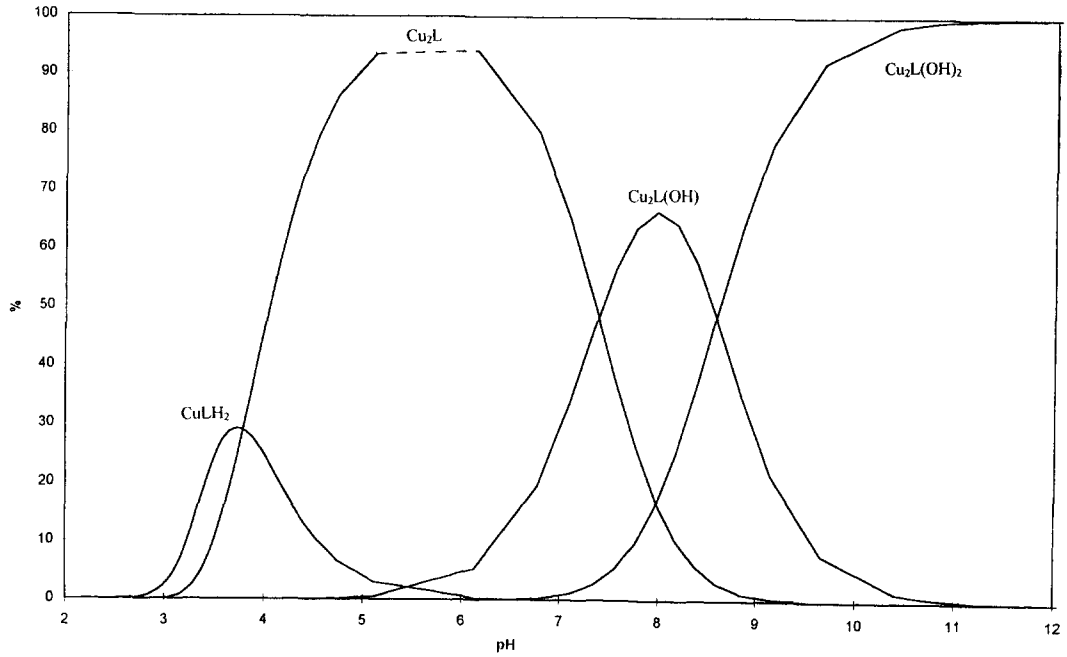

Fig. 1. Species distribution diagram showing the species formed as a function of pH when L and Cu(II) are equilibrated at 25°C and $I = 0.10$ mol dm^{-3} $NaClO_4$ in 1 : 2 molar ratio.

ecules which coordinate the Cu(II) centra in the Cu_2L complex.

The spectrophotometric titration up to $a = 6$ shows the formation of one chromophore with $\lambda_{max} = 645$ nm ($\nu_{d\text{-}d} = 15.530$ cm^{-1}). Beyond $a = 6$ the absorbance decreases while λ_{max} shifts to 630 nm ($\nu_{d\text{-}d} = 15.873$ cm^{-1}) as the $Cu_2L(OH)_2$ complex is formed as final species.

Binding of malonate anion by Cu(II) complexes of L

The titration curve shows two inflection points at $a = 8$ and $a = 10$ corresponding to the formation of Cu_2LMa and $Cu_2L(OH)_2$ complexes. Refinement of the model necessitated the introduction of $CuLMaH_2$ as additional complex. The stability constants obtained for the binding of the malonate anion to the dinuclear Cu(II) complexes are presented in Table 3. Calculated equilibrium constants for the equilibrium of malonate with the host complexes $CuLH_2$ and Cu_2L are also given. The dinuclear ternary complex Cu_2LMa is the most stable among these three species.

In the species distribution diagram (see Fig. 2) it is seen that the Cu_2LMa complex is formed up to 100% and that the mononuclear ternary complex $CuLMaH_2$, which appears only at low pH, only reaches 20% of total metal. Thus the guest complexes $CuLH_2$ and Cu_2L stabilize the malonate anion to the same extent as their individual procentual formation (see Fig. 1).

At the point of the mononuclear ternary complex

Table 3. Stability constants for the ternary complexes formed in the Cu(II)-L-malonate system ($I = 0.10$ mol dm^{-3} $NaClO_4$; 25°C)

Equilibrium[a]	log K
$Cu + L + Ma + 2H \Leftrightarrow CuLMaH_2$	35.13
$2Cu + L + Ma \Leftrightarrow Cu_2LMa$	29.94
$2Cu + L + Ma + OH \Leftrightarrow Cu_2LMa(OH)$	20.26
$CuLH_2 + Ma \Leftrightarrow CuLMaH_2$	5.59
$Cu_2L + Ma \Leftrightarrow Cu_2LMa$	5.77
$Cu_2L(OH) + Ma \Leftrightarrow Cu_2LMa(OH)$	3.47

[a] Charges are omitted for clarity.

$CuLMaH_2$, it is interesting to know where the two protons are located. In the species distribution diagrams (Fig. 1 and 2) it is found that the maximum of the $CuLH_2$ complex is reached at pH 3.6 which is just the same for the $CuLMaH_2$ complex. This indicates that the two protons must be on amino groups of the macrocycle L.

The malonate anion is then coordinated to Cu(II) at one side and hydrogen bonded to the protonated amino groups at the other side of the macrocycle. The suggested binding mode is shown in Chart 1 [25].

At higher pH the hydroxo species $Cu_2LMa(OH)$ is formed. Finally at sufficiently high pH the malonate anion is replaced by hydroxide ions and the $Cu_2L(OH)_2$ becomes the final complex.

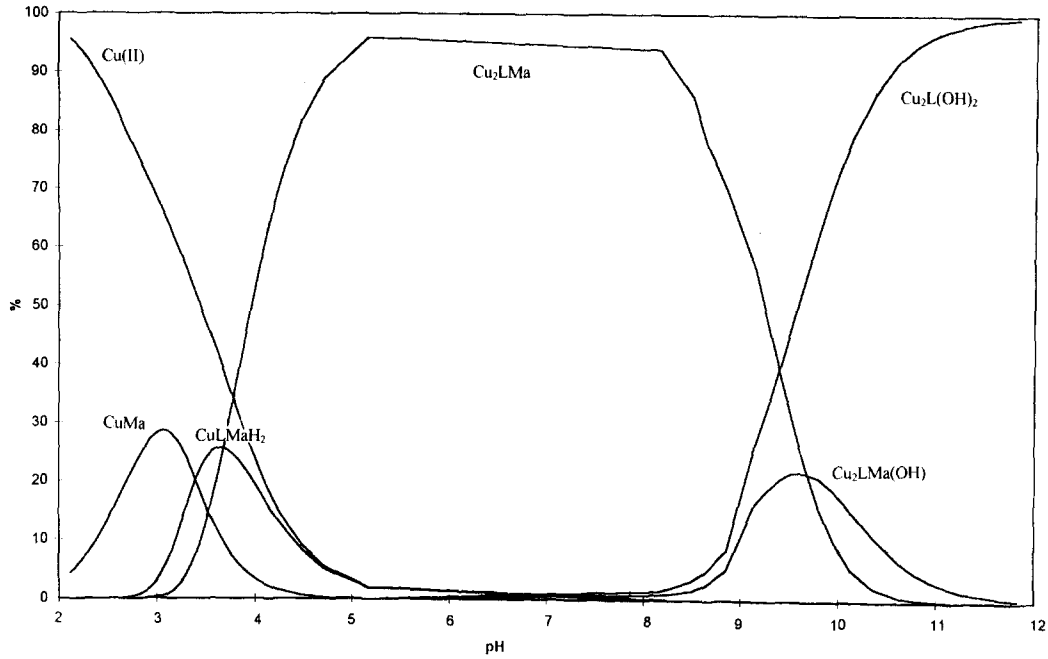

Fig. 2. Species distribution diagram showing the species formed as a function of pH when Cu(II), L and malonate are equilibrated at 25°C and $I = 0.10$ mol dm^{-3} $NaClO_4$ in 2 : 1 : 1 molar ratio.

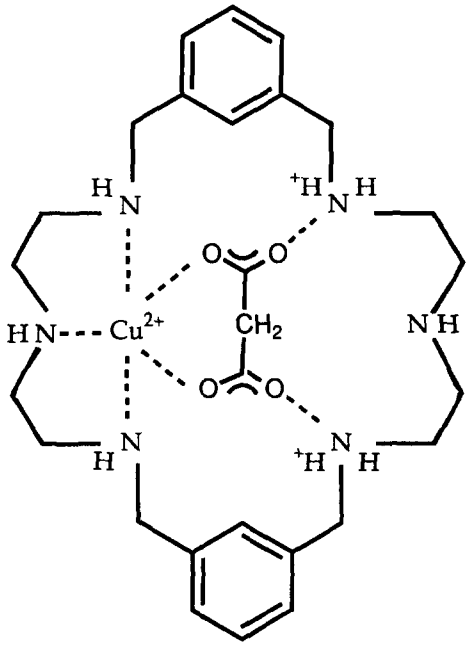

Chart 1. Possible binding mode in $CuLMaH_2$.

It is also noteworthy that at very low pH there is an appreciable interaction between the Cu(II) ion and malonate anion resulting in the CuMa complex. This is not surprising as malonate is a much weaker base than the ligand L.

The spectrophotometric titration shows the build-up of one chromophore to $a = 8$ with $\lambda_{max} = 662$ nm ($\nu_{d\text{-}d} = 15.106$ cm^{-1}) corresponding to the formation of the Cu_2LMa species. After $a = 8$ the absorbance drops and λ moves to lower wavelength. A new maximum is reached by $a = 10$ with $\lambda_{max} = 630$ nm ($\nu_{d\text{-}d} = 15.873$ cm^{-1}) proving that the $Cu_2L(OH)_2$ complex is the final complex.

Binding of maleate anion by Cu(II) complexes of L

The two inflection points in the titration curve correspond to the formation of the following complexes: Cu_2LMale ($a = 8$) and $Cu_2L(OH)_2$ ($a = 10$). Refinement of the model necessitated the introduction of $CuLMaleH_2$ as additional complex. The stability constants obtained for the 2 : 1 : 1 molar ratio of Cu(II) : L : Maleate system are presented in Table 4. These results show the formation of three ternary species in the region pH 2–12, which are the same for the previous system except that the equilibrium constants of this system for the host–guest complexation are higher than for malonate. The distribution diagram for the maleate ternary system (not shown) is similar to that for the malonate system. The following remarks are of interest: (i) the mononuclear ternary complex $CuLMaleH_2$ only appears at low pH and reaches up to 20% of total metal; (ii) the least important species are CuMale and Cu_2L indicating the larger affinity of the maleate anion for Cu(II) ions and its minor affinity for the Cu_2L-complex; (iii) the Cu_2LMale complex is the only important species in solution in the region pH

Table 4. Stability constants for the ternary complexes formed in the Cu(II)-L-maleate system ($I = 0.10$ mol dm^{-3} $NaClO_4$; 25°C)

Equilibrium[a]	log K
$Cu + L + Male + 2H \Leftrightarrow CuLMaleH_2$	38.41
$2Cu + L + Male \Leftrightarrow Cu_2LMale$	30.75
$2Cu + L + Male + OH \Leftrightarrow Cu_2LMale(OH)$	21.98
$CuLH_2 + Male \Leftrightarrow CuLMaleH_2$	8.87
$Cu_2L + Male \Leftrightarrow Cu_2LMale$	6.58
$Cu_2LMale(OH) + Male \Leftrightarrow Cu_2LMale(OH)$	5.19

[a] Charges are omitted for clarity.

5–8.5; (iv) at higher pH the monohydroxo complex $Cu_2LMale(OH)$ is formed, followed by the replacement of the maleate anion by a second hydroxide ion.

It is also interesting to note that this maleate anion forms more stable complexes with Cu_2L than the malonate anion does. This is probably due to the fact that the double bond in the maleate anion causes enhanced rigidity and that the geometry of the rigid anion is more favourable for complexation. In the spectrophotometric titration it is seen that the absorbance steadily rises up to $\lambda_{max} = 630$ nm ($\nu_{d\text{-}d} = 15.873$ cm^{-1}) corresponding to the formation of the Cu_2LMale complex. Then the absorbance drops and also λ_{max} moves up to lower values. A new maximum is reached with $\lambda_{max} = 615$ nm ($\nu_{d\text{-}d} = 1626$ cm^{-1}) probably corresponding to the formation of the $Cu_2L(OH)_2$ species.

Binding of fumarate anion by Cu(II) complexes of L

The pH profile of this system shows two inflection points corresponding to the Cu_2LFum ($a = 8$) and the $Cu_2L(OH)_2$ complex ($a = 10$). Refinement of the model necessitated the introduction of $CuLFumH_2$ as additional complex. The equilibrium constants obtained for the binding of the fumarate anion to the dinuclear Cu(II) complexes are listed in Table 5.

Table 5. Stability constants for the ternary complexes formed in the Cu(II)-L-fumarate system ($I = 0.10$ mol dm^{-3} $NaClO_4$; 25°C)

Equilibrium[a]	log K
$Cu + L + Fum + 2H \Leftrightarrow CuLFumH_2$	35.02
$2Cu + L + Fum \Leftrightarrow Cu_2LFum$	29.14
$2Cu + L + Fum + OH \Leftrightarrow Cu_2LFum(OH)$	18.84
$CuLH_2 + Fum \Leftrightarrow CuLFumH_2$	5.48
$Cu_2L + Fum \Leftrightarrow Cu_2LFum$	4.97
$Cu_2L(OH) + Fum \Leftrightarrow Cu_2LFum(OH)$	2.05

[a] Charges are omitted for clarity.

The species found are the same as the ones found with the malonate and the maleate anion but they are less stable. From Table 5 it is clear that fumarate stabilizes the mononuclear complex more than the dinuclear one. Moreover, comparison with corresponding data in Table 4 shows that the host–guest complexation is stronger with maleate than with fumarate. This observation must be related to the *cis*-position of the carboxylate group on the double bond in maleate, offering a more favourable orientation for interaction with both Cu^{2+} ions in the Cu_2L complex than the trans-orientation in fumarate. The malonate anion which has no double bond is very flexible and can arrange itself in a favourable conformation for coordination.

The distribution diagram for the fumarate ternary system (not shown) is similar to that for the malonate system. The following remarks are of interest: (i) the formation of the mononuclear ternary complex $CuLFumH_2$, reaches a maximum of 30% of total metal only at low pH; (ii) the amount of the Cu_2LFum species rapidly increases to 90% in the pH range 5–9.5; (iii) the monohydroxo complex $Cu_2LFum(OH)$ is formed at high pH while a second hydroxide ion replaces the fumarate anion at pH 10.5.

The spectrophotometric titration indicates the formation of one chromophore to $a = 8$ with $\lambda_{max} = 630$ nm ($\nu_{d\text{-}d} = 15.873$ cm^{-1}). This corresponds to the formation of the Cu_2LFum complex in the titration curve. Further titration causes a decrease in absorbance and λ. A new maximum is reached at $\lambda_{max} = 615$ nm ($\nu_{d\text{-}d} = 1626$ cm^{-1}) at $a = 10$ which corresponds to the $Cu_2L(OH)_2$ species formed at $a = 10$.

Binding of pyrophosphate anion by Cu(II) complexes of L

Table 6 gives the stability constants for the ternary complexes formed for the interactions of two equivalents of Cu(II) with L and the pyrophosphate anion. Six ternary complexes are formed of which two mononuclear and four dinuclear complexes. This greater number of complexes was expected considering the fact that pyrophosphate is a poly-acid. The formation of these ternary complexes can be understood as (i) host–guest interaction between the hosts $CuLH_2$, Cu_2L or $Cu_2L(OH)$ and pyrophosphate (H_2Py or Py) (see Table 6, equilibriums 8, 10 and 15), and (ii) protonation of these ternary complexes (Table 6, equilibriums 9, 11 and 12).

Firstly, the host–guest interactions in the former group of ternary complexes are based on electrostatic attraction since the stability constants of these complexes increase with increasing charges on both positive host and negative guest.

Secondly, if one compares the protonation constants of Cu_2LPy and of Cu_2LPyH (Table 6, equilibriums 11, and 12, respectively) with the first, respectively the second protonation constant of pyro-

Table 6. Stability constants for the ternary complexes formed in the Cu(II)-L-pyrophosphate system ($I = 0.10$ mol dm^{-3} $NaClO_4$; 25°C)

Equilibrium[a]		log K
$Cu + L + Py + 4H \Leftrightarrow CuLPyH_4$	(1)	50.64
$Cu + L + Py + 5H \Leftrightarrow CuLPyH_5$	(2)	53.25
$2Cu + L + Py \Leftrightarrow Cu_2LPy$	(3)	34.85
$2Cu + L + Py + H \Leftrightarrow Cu_2LPyH$	(4)	41.80
$2Cu + L + Py + 2H \Leftrightarrow Cu_2LPyH_2$	(5)	46.36
$2Cu + L + Py + OH \Leftrightarrow Cu_2LPy(OH)$	(6)	25.05
$2Cu + L + Py + 2OH \Leftrightarrow Cu_2LPy(OH)_2$	(7)	10.67
$CuLH_2 + H_2Py \Leftrightarrow CuLPyH_4$	(8)	6.56
$CuLPyH_4 + H \Leftrightarrow CuLPyH_5$	(9)	2.61
$Cu_2L + Py \Leftrightarrow Cu_2LPy$	(10)	10.68
$Cu_2LPy + H \Leftrightarrow Cu_2LPyH$	(11)	6.95
$Cu_2LPyH + H \Leftrightarrow Cu_2LPyH_2$	(12)	4.56
$Cu_2L + HPy \Leftrightarrow Cu_2LPyH$	(13)	9.16
$Cu_2L + H_2Py \Leftrightarrow Cu_2LPyH_2$	(14)	7.65
$Cu_2L(OH) + Py \Leftrightarrow Cu_2LPy(OH)$	(15)	8.26

[a] Charges are omitted for clarity.

phosphate ($\log K_1^H = 8.47$ and $\log K_2^H = 6.07$ for pyrophosphate) [26], a constant difference of -1.50 log K-units is found. It is likely that protonation takes place at the remaining free O^- sites of pyrophosphate since the Cu_2L^{4+}-unit in the ternary complex will lower the basicity of the bound pyrophosphate unit. On the other hand, the protonation constant for the formation of $CuLPyH_5$ (see Table 6, equilibrium 9) is 0.70 log units higher than the $\log K_3^H (= 1.92)$ of pyrophosphate. This indicates that the proton added is shared between an O^- site of pyrophosphate and an amino group of L.

Finally, the higher stability of Cu_2LPy relative to Cu_2LMa, Cu_2LMale and Cu_2LFum prevents the replacement of pyrophosphate by a hydroxide anion in alkaline medium.

The species distribution diagram depicted in Fig. 3 shows the presence of the Cu_2LPyH_2 complex at low pH. By increasing the pH, the Cu_2LPyH complex becomes the only important species in solution till pH 6.5. After that, the Cu_2LPy species becomes more important till pH 10 where the $Cu_2LPy(OH)$ complex becomes the only species in solution. In contrast with the previous observations, the pyrophosphate anion is not replaced by a hydroxide ion at high pH.

Chart 2 shows a possible coordination mode for Cu_2LPy.

The spectrophotometric titration shows a steadily rising absorbance with $\lambda_{max} = 666$ nm ($\nu_{d\text{-}d} = 15.015$ cm^{-1}) corresponding to the formation of the Cu_2LPyH complex in the titration curve. Between pH 6 and 8 the absorbance further increases with a new maximum at $\lambda_{max} = 680$ nm ($\nu_{d\text{-}d} = 14.706$ cm^{-1}). This is in accordance with the formation of the Cu_2LPy species.

Binding of orthophosphate anion by Cu(II) complexes of L

The pH profile of this titration shows an inflection point at $a = 8$ corresponding to the Cu_2LPH complex and a second inflection point at $a = 10$ which corresponds to the $Cu_2LP(OH)$ species. The stability constants for the system Cu(II) : L : Orthophosphate in 2 : 1 : 1 molar ratio are listed in Table 7. Five ternary species are formed of which one mononuclear and four dinuclear complexes. The distribution diagram for the orthophosphate ternary system (not shown) is similar to that for the pyrophosphate system. The following remarks are of interest: (i) the Cu_2LPH_2 complex is the only important species in solution in the low pH region; (ii) the only species found in the pH range 5–8 is Cu_2LPH; (iii) further increase of pH increases the share of the Cu_2LP complex till pH 9 whereafter the $Cu_2LP(OH)$ species becomes important.

The difference in stability values for the dinuclear species can again be explained in terms of electrostatic attractions. If the Cu_2LP, Cu_2LPH and Cu_2LPH_2 complexes are compared (Table 7, equilibriums 7, 10 and 11), it can be seen that the charge on the dinuclear complex remains the same but that the negative charge of the phosphate anion decreases with increasing protonation, thus lowering the electrostatic attraction between the reacting species. It is clear that addition of one proton to the Cu_2LP and Cu_2LPH species (Table 7, equilibriums 8 and 9) must necessarily decrease the strength of coordinate bonding and lead to a decrease in stability. The same explanation can be given for the comparison of Cu_2LP and $Cu_2LP(OH)$ species (Table 7, equilibriums 8 and 12).

A possible binding mode for Cu_2LP is shown in Chart 3.

It can be seen in spectrophotometric titration that the absorbance steadily rises up to $a = 8$ with $\lambda_{max} = 645$ nm ($\nu_{d\text{-}d} = 15.504$ cm^{-1}) corresponding the formation of the Cu_2LPH complex in the titration curve. After $a = 8$ the absorbance and λ_{max} drop to lower values. A new maximum is reached at $a = 10$ with $\lambda_{max} = 615$ nm ($\nu_{d\text{-}d} = 1626$ cm^{-1}) corresponding to the formation of the $Cu_2LP(OH)$ species.

CONCLUSION

Considering the host–guest systems Cu^{2+} : L : G in 2 : 1 : 1 molar ratio, it is noticed that both the $CuLH_2$ and Cu_2L species appear as host while G and protonated forms of G act as guest. The most important species is the dinuclear Cu_2LG complex (90%).

The binding with malonate, maleate and fumarate anions compared well but a preference for the maleate anion was observed. This was caused by the enhanced

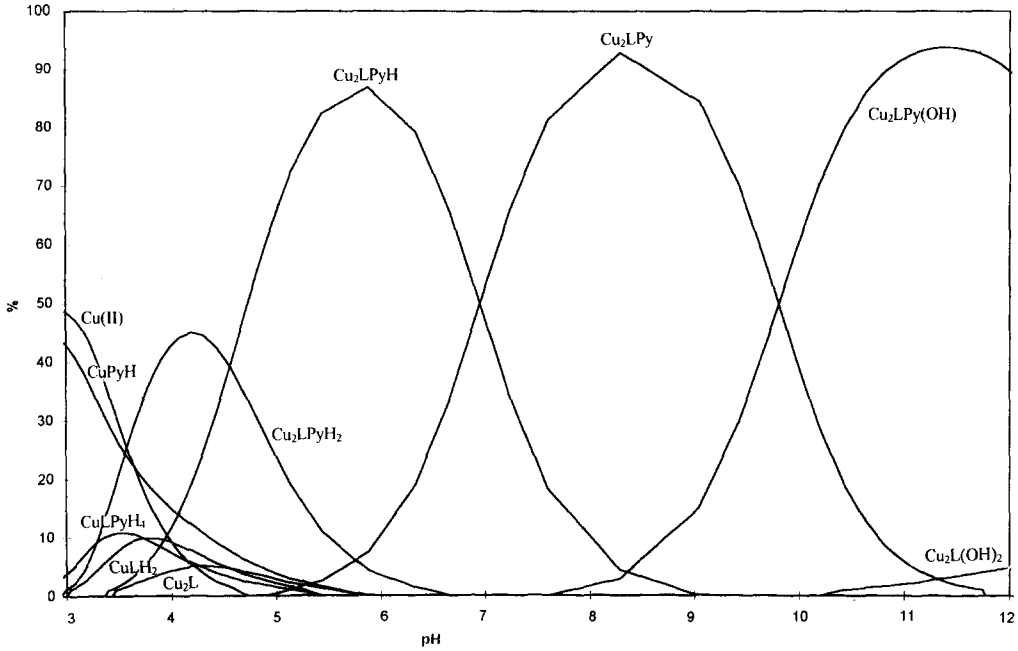

Fig. 3. Species distribution diagram showing the species formed as a function of pH when Cu(II), L and pyrophosphate are equilibrated at 25°C and $I = 0.10$ mol dm^{-3} $NaClO_4$ in 2 : 1 : 1 molar ratio. The $Cu_2LPy(OH)_2$ complex appears only for a little percentage and is not shown.

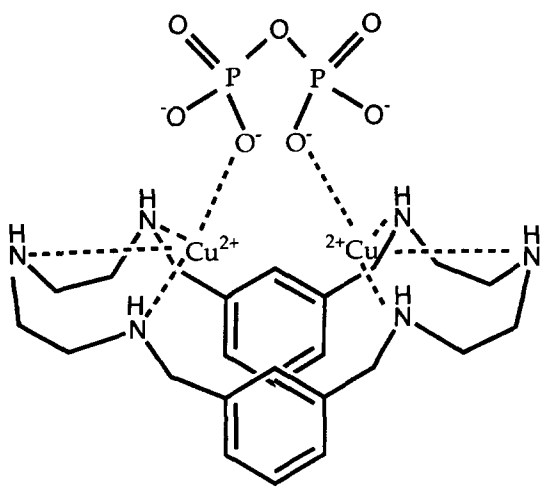

Chart 2. Possible binding mode in Cu_2LPy.

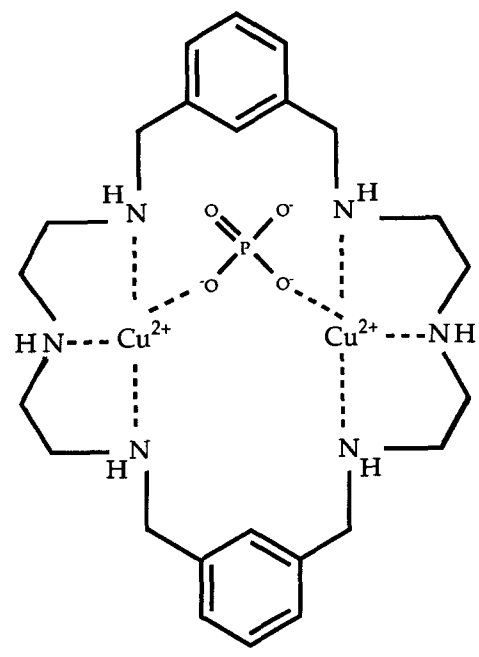

Chart 3. Possible binding mode in Cu_2LP.

rigidity (in comparison with malonate anion) and the favourable *cis*-coordination for complexation (in comparison with fumarate anion).

The complexes obtained with pyrophosphate and orthophosphate anions were also comparable with a slight preference for the former. From log K values a greater stability was expected for pyrophosphate considering the greater number of O^- groups. The loss in stability is caused by the necessarily coordination of the big anion outside the macrocycle.

Table 7. Stability constants for the Cu(II)-L-orthophosphate system (I = 0.10 mol dm^{-3} $NaClO_4$; 25°C)

Equilibrium[a]		log K
$Cu + L + P + 4H \Leftrightarrow CuLPH_4$	(1)	50.74
$2Cu + L + P \Leftrightarrow Cu_2LP$	(2)	34.26
$2Cu + L + P + H \Leftrightarrow Cu_2LPH$	(3)	41.97
$2Cu + L + P + 2H \Leftrightarrow Cu_2LPH_2$	(4)	46.89
$2Cu + L + P + OH \Leftrightarrow Cu_2LP(OH)$	(5)	25.22
$CuLH_2 + H_2P \Leftrightarrow CuLPH_4$	(6)	2.75
$Cu_2L + P \Leftrightarrow Cu_2LP$	(7)	10.09
$Cu_2LP + H \Leftrightarrow Cu_2LPH$	(8)	7.71
$Cu_2LPH + H \Leftrightarrow Cu_2LPH_2$	(9)	4.92
$Cu_2L + HP \Leftrightarrow Cu_2LPH$	(10)	6.06
$Cu_2L + H_2P \Leftrightarrow Cu_2LPH_2$	(11)	4.27
$Cu_2L(OH) + P \Leftrightarrow Cu_2LP(OH)$	(12)	8.43

[a] Charges are omitted for clarity.

Acknowledgement—The authors wish to thank Dr D. Depla and ing T. Haemers for technical assistance.

REFERENCES

1. Lindoy, L. F., *The Chemistry of Macrocyclic Ligand Complexes*, Cambridge Univ. Press, Cambridge, U.K., 1989.
2. Sutherland, I. O., *Pure Appl. Chem.*, 1989, **61,** 1547.
3. Pratt, A., Sutherland, I. O. and Newton, R. F., *J. Chem. Soc., Perkin Trans. I*, 1988, 13.
4. Izatt, R. M., Pawlak, K., Bradshaw, J. S. and Bruening, R. L., *Chem. Rev.*, 1991, **91,** 1721.
5. Bianchi, A., Micheloni, M. and Paoletti, P., *Coord. Chem. Rev.*, 1991, **110,** 17.
6. Dobler, M., *Ionophores and Their Structures*, Wiley Interscience Publication, New York, 1981.
7. Motekaitis, R. J. and Martell, A. E., *Inorg. Chem.*, 1992, **31,** 5534.
8. Llobet, A., Reibenspies, J. J. and Martell, A. E., *Inorg. Chem.*, 1994, **33,** 5946.
9. Fabbrizzi, L., Pallavicini, P., Parodi, L., Perotti, A. and Tagliette, A., *J. Chem. Soc., Chem. Commun.*, 1995, 2439.
10. Jurek, P. E., Martell, A. E., Motekaitis, R. J. and Hancock, R. D., *Inorg. Chem.*, 1995, **34,** 1823.
11. Lu, Q., Reibenspies, J. J., Martell, A. E. and Motekaitis, R. J., *Inorg. Chem.*, 1996, **35,** 2636.
12. Nation, D. A., Martell, A. E., Carroll, R. I. and Clearfield, A., *Inorg. Chem.*, 1996, **35,** 7246.
13. Nation, D. A., Reibenspies, J. J. and Martell, A. E., *Inorg. Chem.*, 1996, **35,** 4597.
14. Martell, A. E. and Menif, R., *J. Chem. Soc., Chem. Commun.*, 1989, 1521.
15. Vogel, A. I., *A Text-book for Quantitative Analysis*, Longraus and Green, New York, 1961, p. 959.
16. Arnold, A. P., Daignault, S. A. and Rabenstein, D. L., *Anal. Chem.*, 1985, **57,** 1112.
17. Gran, G., *Analysts (London)*, 1952, **77,** 661.
18. Martell, A. E. and Smith, R. M., *Critical Stability Constants*, Vol. 6, Plenum Press, New York, 1985.
19. Cattoir, S., Herman, G. G. and Goeminne, A. M., *J. Coord. Chem.*, 1996, **38,** 245. K. I. Dhont, G. G. Herman, A. C. Fabretti, W. Lippens and A. M. Goeminne, *J. Chem. Soc., Dalton Trans.* 1996, 1753.
20. Sabatini, A. Vacca, A. and Gans, P., *Coord. Chem. Rev.*, 1992, **120,** 398.
21. Gans, P., Sabatini, A. and Vacca, A., *J. Chem. Soc., Dalton Trans*, 1985, 1195.
22. Ting-Po, I. and Nancollas, G. M., *Analyt. Chem.*, 1972, **44,** 1940.
23. Martell, A. E. and Smith, R. M., *Critical Stability Constants*, Vol. 3–4, Plenum Press, New York, 1985.
24. Menif, R., Martell, A. E., Squattrito, P. J. and Clearfield, A., *Inorg. Chem.*, 1990, **29,** 4723.
25. Lu, Q., Reibenspies, J. J., Martell, A. E. and Motekaitis, R. J., *Inorg. Chem.*, 1996, **35,** 2630.
26. Motekaitis, R. J., Reibenspies, J. J. and Martell, A. E., *Inorg. Chem.*, 1995, **34,** 4958.

Pergamon

PII: S0277-5387(97)00442-7

Polyhedron Vol. 17, No. 10, pp. 1725–1728, 1998
© 1998 Elsevier Science Ltd
All rights reserved. Printed in Great Britain
0277-5387/98 $19.00+0.00

^{195}Pt NMR spectra of ferrocenylketimine complexes of platinum(II)

Li Ding, Yang Jie Wu* and Da Peng Zhou

Department of Chemistry, Zhengzhou University, Zhengzhou 450052, P.R. China

(Received 25 August 1997; accepted 27 October 1997)

Abstract—The ^{195}Pt NMR spectra of two series of 18 ferrocenylketimine complexes of platinum(II) which include 9 cycloplatinated derivatives [σ-Pt{(η^5-C_5H_3CMe=NAr)Fe(η^5-C_5H_5)}(DMSO)Cl] (**1**) and 9 coordinated compounds [*trans*-$PtCl_2$(DMSO){(η^5-C_5H_4CMe=NAr)}Fe(η^5-C_5H_5)] (**2**) (Ar = substituted phenyl groups) have been recorded. The ^{195}Pt chemical shifts are regularly affected by the substituents in the N-phenyl rings, and satisfactory to excellent linear relationships are found to exist between the ^{195}Pt shifts (δ) and Hammett substituent constants in both series. The directions of the substituent effect on δ(^{195}Pt) are the same in both series, i.e., electron-donating substituents cause shifts to higher frequency, and the coordinated compounds have a better linear relationship. These ^{195}Pt NMR features support the existence of intramolecular coordination between the imino nitrogen atom and the platinum(II) and n-π conjugation between the nitrogen and the N-phenyl ring. © 1998 Elsevier Science Ltd. All rights reserved

Keywords: ^{195}Pt NMR spectra; ferrocenylketimine complexes of platinum(II); substituent effect; intramolecular coordination.

The chemistry of platinum spans a gap which includes heterogeneous catalysts for automobiles [1], homogeneous catalysts for organic synthesis [2], and cancer drugs [3]. Consequently an increasing number of chemists express an interest in ^{195}Pt nuclear magnetic resonance and the number of reports containing ^{195}Pt data on organometallic complexes has steadily increased. To the best of our knowledge, so far none of the ^{195}Pt NMR studies has described the linear correlations between ^{195}Pt shifts (δ) and Hammett substituent constants (σ_p or σ_m). There are only two reports of ^{195}Pt NMR involving ferrocenyl platinum complexes [4]. Herein we report the ^{195}Pt chemical shift in solution and the linear correlations between δ(^{195}Pt) values and Hammett substituent constants σ_p or σ_m for the following ferrocenylketimine derivatives of platinum(II).

RESULTS AND DISCUSSION

^{195}Pt NMR spectra

The ferrocenylketimine complexes of platinum(II) **1** and **2** were synthesized according to the published procedure [5], based on the reaction of the free ligands with stoichiometric amounts of *cis*-Pt(DMSO)$_2$Cl$_2$ in refluxing toluene. The ^{195}Pt chemical shifts for compounds **1** and **2** are listed in Table 1.

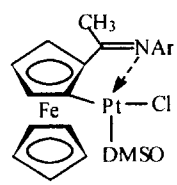

1

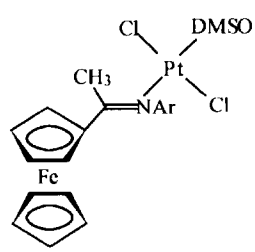

2

* Author to whom correspondence should be addressed.

Table 1. ^{195}Pt NMR chemical shifts δ for compounds **1** and **2**

Compounds	δ_1 (ppm)	Compounds	δ_2 (ppm)
1a	−3790.1	**2a**	−2966.1
1b	−3797.7	**2b**	−2966.9
1c	−3802.7	**2c**	−2968.8
1d	−3804.6	**2d**	−2975.9
1e	−3805.0	**2e**	−2976.1
1f	−3819.7	**2f**	−2988.2
1g	−3800.7	**2g**	−2967.9
1h	−3808.3	**2h**	−2978.0
1i	−3815.0	**2i**	−2985.3

For the *trans* derivatives **2**, the ^{195}Pt chemical shift falls within the range of −2966.1 to −2988.2 ppm, characteristic of a $PtNSX_2$ donor set. An analogue is *trans*-$PtCl_2(NH_3)$(DMSO) for which $\delta(^{195}Pt)$ is −3067 ppm [6]. A $PtNOX_2$ donor set is expected to give values in the range of −1600 to −1800 ppm [4a]. The results obtained confirm that the DMSO is S-bound in solution. Cycloplatination results in a large lower frequency shift to a range of −3790.1 to −3819.7 ppm, making easy identification of this type of product. A closely comparable shift in the literature [4a] was −3899 ppm for compound [σ-Pt{(η^5-$C_5H_3CH(Me)NMe_2$)Fe(η^5-C_5H_5)}(DMSO)Cl].

It is usually convenient to discuss the magnetic shielding of the heavier nuclei principally in terms of local "paramagnetic" and "diamagnetic" contributions σ^p and σ^d. Metal chemical shifts are dominated by changes in the paramagnetic screening contribution, σ^p, to the total shielding [6a]. This term depends upon (a) the asymmetry of the electronic distribution within the valence *5d* and *6p* orbitals of the platinum atom, (b) the mean inverse cube of the distance between these electrons and the platinum nucleus, and (c) the inverse of the energy separations between the ground and excited states for these electrons.

A decrease in halide content normally causes a ^{195}Pt shift to lower frequency on the basis of electronegativity differences and changes in electronic asymmetry [6b], so the lower frequency shift of cycloplatination is a direct consequence of σ-Pt—C bond formation. The higher frequency shift of compounds **2** may be tentatively ascribed to a strong *trans* effect, which makes a difference in σ^p due to the change in electronic excitation energy. This phenomenon is in accordance with that noted elsewhere [6b]: for $[PtCl_2(PR_3)_2]$ and $[PtCl_2(AsR_3)_2]$ types, the shift of the *cis* complex is at lower frequency than that of its *trans* analogue by 400–500 ppm.

Effects of substituents of N-phenyl ring

Electronic withdrawal by a substituent connected to the platinum atom modifies the electronic unbalance among its valence orbitals, and will result in a change in σ^p [7]. As shown in Table 1, the ^{195}Pt shifts show obvious dependence on the nature of the substituents in the N-phenyl ring, with lower frequency shifts resulting from electron-withdrawing groups and with higher frequency shifts resulting from electron-donating groups. Such a trend has also been found in the ^{199}Hg NMR spectra of ferrocenylimine derivatives of mercury [8]. Satisfactory to excellent linear correlations between ^{195}Pt shifts (δ) and Hammett substituent constant σ_p or σ_m [9] were obtained for both series (Eqns (1) and (2) for compounds **1** and **2**, respectively).

$$\delta_1 = -3800.2 - 23.3\sigma \quad n = 9 \quad r = -0.975 \quad (1)$$

$$\delta_2 = -2970.5 - 21.7\sigma \quad n = 9 \quad r = -0.991 \quad (2)$$

However, no obvious correlation with substituent effect has been found for the *meta*- and *para*-substituted arylplatinum cyclooctadiene compounds [7].

It is noteworthy that the ^{195}Pt chemical shifts of compounds **2** are less sensitive to the change of the substituents in the N-phenyl ring in comparison with compounds **1** (see slope in Eqn (1) which is larger than that in Eqn (2)). The X-ray crystal structures [5] (Fig. 1) have shown that Pt—N bond length of compound **2c** is shorter than that of compound **1c**, and the angle between the N-phenyl ring and the plane of C—C=N—C in **2c** is larger than that in **1c** (68.24° and 87.43° for **1c** and **2c**, respectively). If only *n*-π conjugation involving the *n*-electrons of the imino nitrogen and π-electrons of the N-phenyl group is considered, the substituents in the N-phenyl ring should have a much stronger effect on platinum for compounds **2** than that for compounds **1**. A possible explanation is that the substituents affect the platinum of compounds **1** not only by means of the N → Pt interaction, but also via part transmission of electronic effects through the C=N bond and the substituted Cp ring, though the nonplanarity of the N-phenyl ring and the plane C—C=N—C destroys the π-π conjugation between the C=N bond and the N-phenyl group to some extent. As for compounds **2**, there is only N → Pt interaction.

It is believed that there is an interaction between the *n*-electrons and unoccupied *5d* and *6p* orbital of the platinum atom [10]. In this way, the electron-donating groups should enhance the unbalance of electron distribution in the unoccupied orbital of the platinum, thus leading to an increase in the paramagnetic shielding term σ^p with observed higher frequency shift while the electron-withdrawing groups have an opposite effect.

EXPERIMENTAL

The details for the synthesis and characterization of compounds **1** and **2** have been described previously [5].

^{195}Pt NMR spectra were recorded on a Bruker

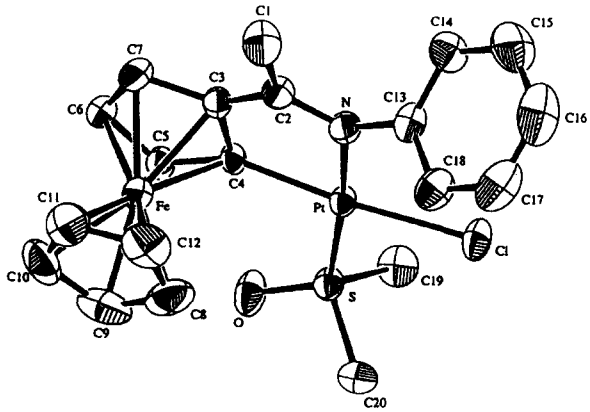

1c: N—Pt 2.095(5) Å
Angles(°) between planes:
A and B 68.24, A and C 62.35.

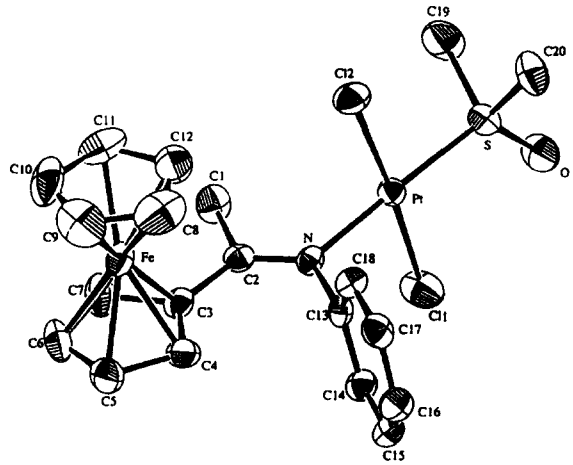

2c: N—Pt 2.049(4) Å
Angles(°) between planes:
A and B 87.43, A and C 90.94.

Fig. 1. The structures and some parameters of the ferrocenylketimine complexes of platinum(II) with A, B and C representing the N—Ar ring, plane of C(Cp ring)—C=N and substituted Cp ring, respectively.

DPX-400 spectrometer in $CDCl_3$ at 20°C with Na_2PtCl_6 in D_2O as an external standard. The operating frequency was 86.0 MHz and the routine acquisition parameters used were as follows: pulse width, 12.00 μs, acquisition time 0.64 s, spectral width 51,546.39 Hz.

Acknowledgements—We are grateful to the National Natural Science Foundation of China (Project 29592066) and the Natural Science Foundation of Henan Province for financial support to this work.

REFERENCES

1. Harrison, B., Cooper, B. J. and Wilkins, A. J. J., *Platinum Metals Reviews*, 1981, **25,** 14.
2. (a) Consiglio, C., Pino, P., Flowers, L. I. and Pittman, C. H., *J. Chem. Soc., Chem. Comm.*, 1983, 612; (b) Bailar, J. C., in *Inorganic Compounds with Unusual Properties*, ed. R. B. King. American Chemical Society, 1979, p. 1.
3. (a) Rosenberg, B. and Van Camp, L., *Cancer Res.*, 1970, **30,** 1799; (b) Lippard, S. J., *Science*, 1982, **218,** 1075; (c) Suzanne, E. and Lippard, S. J., *Chem. Rev.*, 1987, **87,** 1153.
4. (a) Ranatunge-Bandarage, P. R. R., Robinson, B. H. and Simpson, J., *Organometallics*, 1994, **13,** 500; (b) Ranatunge-Bandarage, P. R. R., Duffy, N. W., Johnston, S. M., Robinson, B. H. and Simpson, J., *Organometallics*, 1994, **13,** 511.
5. Wu, Y. J., Ding, L., Wang, H. X., Liu, Y. H., Yuan, H. Z. and Mao, X. A., *J. Organomet. Chem.*, JOM 06948.
6. (a) Pregosin, P. S., in *Annual Reports on NMR Spectroscopy*, Vol. 17, ed. G. A. Webb. Academic Press, p. 285–349 and reference therein; (b) Pregosin, P. S., *Coord. Chem. Rev.*, 1982, **44,** 247 and reference therein.
7. Kennedy, J. D., McFarlane, W., Puddephatt, R. J. and Thompson, P. J., *J. Chem. Soc., Dalton Trans.*, 1976, 874, and reference therein.

8. Wu, Y. J., Huo, S. Q., Yuan, H. Z. and Liu, Y. H., *Main Group Chemistry*, 1996, **1**, 253.
9. Shorter, J., in *Correlation Analysis of Organic Reactivity: With particular reference to multiple regression*, ed. D. Bawden. Research Studies Press, England, 1982, p. 30.
10. Jameson, C. J. and Gutowsky, H. S., *J. Chem. Phys.*, 1964, **40**, 1714.

Pergamon

PII: S0277-5387(97)00464-6

Polyhedron Vol. 17, No. 10, pp. 1729–1733, 1998
© 1998 Elsevier Science Ltd
All rights reserved. Printed in Great Britain
0277-5387/98 $19.00+0.00

Synthesis and characterization of polynuclear complexes of molybdenum carbonyl derivatives with pyridine-2-carbaldehyde azine (pa) and ferrocenylphosphines. Crystal structure of $[Mo_2(CO)_6(\mu\text{-dppf})(\mu\text{-pa})]$ (dppf = 1,1′-*bis*(diphenylphosphino)ferrocene)

Juan Granifo,*[a] Andres Vega[b] and María T. Garland[b]

[a] Departamento de Ciencias Químicas, Facultad de Ingeniería y Administración, Universidad de La Frontera, Casilla 54-D, Temuco, Chile

[b] Facultad de Ciencias Físicas y Matemáticas, Universidad de Chile, Casilla 487-3, Santiago, Chile

(Received 23 August 1997; accepted 27 October 1997)

Abstract—Novel mono- and didentate ferrocenylphosphines containing complexes, $[Mo_2(CO)_6(dfpp)_2(\mu\text{-pa})]$ (dfpp = diferrocenylphenylphosphine) and $[Mo_2(CO)_6(\mu\text{-dppf})(\mu\text{-pa})]$, have been isolated and characterized by infrared and electronic spectroscopy, and cyclic voltammetry. For the $[Mo_2(CO)_6(\mu\text{-dppf})(\mu\text{-pa})]$ complex a single crystal X-ray structure analysis evidences its double bridge nature and the asymmetry of the bridging ligands due to steric constraints. In the visible region, the new compounds show strong solvatochromic bands and this effect has been evaluated by using the E^*_{MLCT} parameter. The redox behaviour of the complexes involves molybdenum and ferrocene-based oxidations and pa-based reductions. The results are compared to the previously characterized analogous complexes based on the related ligands triphenylphosphine and 1,2-*bis*(diphenylphosphino)ethane. © 1998 Elsevier Science Ltd. All rights reserved

Keywords: molybdenum; carbonyl; ferrocenylphosphines; polypyridine complexes.

In a recent article we have reported [1] the reaction chemistry of the novel dinuclear acetonitrile derivated $[Mo_2(CO)_6(NCMe)_2(\mu\text{-pa})]$ (pa = pyridine-2-carbaldehyde azine, Fig. 1) towards the monodentate phosphine PPh_3 and the didentate phosphine 1,2-*bis*(diphenylphosphino)ethane (dppe). The labile MeCN groups of the acetonitrile complex are readily replaced by PPh_3 and dppe to yield the *bis*(PPh_3) compound $[Mo_2(CO)_6(PPh_3)_2(\mu\text{-pa})]$ and the dppe-bridged complex $[Mo_2(CO)_6(\mu\text{-dppe})(\mu\text{-pa})]$, respectively. These homobimetallic species are characterized by strong solvatochromic bands in the visible region (MLCT, pa(π^*) ← Mo(d)) and by molybdenum centered (oxidation) and pa centered (reduction) redox processes. The single crystal X-ray structure of the double bridge complex $[Mo_2(CO)_6(\mu\text{-dppe})(\mu\text{-pa})]$ shows an asymmetric bridging pa ligand because of the shortness of the —CH_2CH_2— chain of the dppe ligand linking the molybdenum atoms.

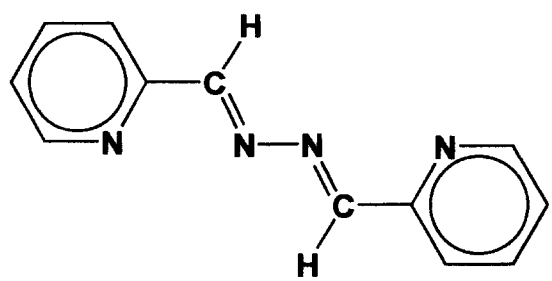

Fig. 1. Structure of the pa ligand.

* Author to whom correspondence should be addressed.

In this work, we further extend the study of the aforementioned synthetic avenue to mono- and didentate ferrocenylphosphines to obtain multinuclear compounds. In this regard, by using the redox-active P-donor metalloligands diferrocenylphenylphosphine (dfpp) and 1,1′-*bis*(diphenylphosphino)ferrocene (dppf) the heterometallic complexes $[Mo_2(CO)_6(dfpp)_2(\mu\text{-pa})]$ and $[Mo_2(CO)_6(\mu\text{-dppf})(\mu\text{-pa})]$ were isolated. The spectroscopic, electrochemical and structural properties of these new ferrocenylphosphine complexes are reported herein.

EXPERIMENTAL

Reagent grade solvents were used for all preparations. Diferrocenylphenylphosphine (dfpp) and 1,1′-*bis*(diphenylphosphino)ferrocene (dppf) were purchased from Aldrich Chemical Co. $[Mo_2(CO)_6(NCMe)_2(\mu\text{-pa})]$ was obtained following similar methods to those described in the literature [1].

Synthesis of $[Mo_2(CO)_6(\mu\text{-dppf})(\mu\text{-pa})]\cdot 1.25(CH_3)_2CO$

Into a solution of 0.125 g (0.192 mmol) of just prepared $[Mo_2(CO)_6(NCMe)_2(\mu\text{-pa})]$ in 40 cm^3 of CH_2Cl_2 were added 0.106 g (0.192 mmol) of dppf and stirred for 3 h under nitrogen. The dark green coloured solution was then filtered. To this filtrate 20 cm^3 of MeOH were added and on standing for 1 h a dark green precipitate was formed, which was filtered off and washed with 3 portions of MeOH (10 cm^3). The resultant crude precipitate was dissolved in Me_2CO (100 cm^3), filtered, and the filtrate was evaporated to ca 10 cm^3 at room temperature. The dark green crystals were separated by filtration and washed with Me_2CO (5 cm^3). Yield: 0.095 g (41%). Anal. Found: C, 55.90; H, 3.80; N, 4.60%. Calc. for $C_{52}H_{38}FeMo_2N_4O_6P_2\cdot 1.25(CH_3)_2CO$: C, 55.84; H, 3.83; N, 4.68%. IR (KBr, disc): $\nu_{C\equiv O}$, 1918 s, 1825 s and 1801 s cm^{-1}.

Synthesis of $[Mo_2(CO)_6(dfpp)_2(\mu\text{-pa})]\cdot 3CH_3OH$

The same procedure for the above dppf complex $[Mo_2(CO)_6(\mu\text{-dppf})(\mu\text{-pa})]$ was followed, but the crude dark green precipitate was dissolved in hot CH_2Cl_2 instead of Me_2CO. After the addition of equal volume of MeOH the solution was concentrated *in vacuo* to half of the volume. The concentrated solution was stored at room temperature (2 h). The needle like dark green crystals were washed with CH_2Cl_2–MeOH (1 : 1). Anal. Found: C, 53.60; H, 4.20; N, 3.40%. Calc. for $C_{73}H_{68}Fe_4Mo_2N_4O_9P_2$: C, 54.04; H, 4.22; N, 3.45%. IR (KBr, disc): $\nu_{C\equiv O}$, 1906 s, 1815 s and 1798 s cm^{-1}.

Instruments

IR spectra were registered as solid KBr samples on a Bruker Model IFS-66V FTIR instrument. The electronic spectra were obtained on a Spectronic 3000 diode array spectrophotometer. Cyclic voltammograms were obtained in CH_2Cl_2 containing 0.10 M $TBAPF_6$ as supporting electrolyte. The three electrode measurements were carried out with a Wenking Potentioscan POS-73 and a X-Y recorder. A platinum-disk working electrode, a platinum wire auxiliary electrode, and a AgCl/Ag reference electrode (with internal reference ferrocenium/ferrocene) were used in the cyclic voltammetry experiments.

X-ray crystal structure of $[Mo_2(CO)_6(\mu\text{-dppf})(\mu\text{-pa})]\cdot 1.25(CH_3)_2CO$

A brownish single crystal suitable for the X-ray diffraction study, measuring $0.50\times 0.16\times 0.08$ mm, was fixed with epoxy resin to a glass fibre and mounted onto a Siemens R3m/V single crystal diffractometer. Intensity data were collected using graphite monochromatized Mo–K_α radiation ($\lambda = 0.71073$ Å). A total of 50 independent reflexions in the range $15 \leqslant 2\theta \leqslant 25^\circ$ were used for crystal system and cell parameters determination. Crystal data: Monoclinic, $P2_1$, $a = 10.925(9)$, $b = 11.070(7)$, $c = 24.15(2)$ Å, $\beta = 102.43(2)^\circ$, $Z = 2$. Data collection and structure determination: 5664 reflections collected in an angle span of $2 \leqslant 2\theta \leqslant 50^\circ$, within index ranges $-13 \leqslant h \leqslant 12, 0 \leqslant k \leqslant 13, 0 \leqslant l \leqslant 28$. Of them, 5332 were independent ($R_{int} = 0.045$), and 4119 considered observed ($I > 2\sigma(I)$). No absorption correction was applied. The structure was partially solved by routine application of direct methods and completed through the iterative use of difference Fourier synthesis. Least squares refinement using F^2 of 679 parameters and 11 soft restraints led to the final indices $R_1 = 0.042$, $wR_2 = 0.099$ [$I = 2\sigma(I)$], $R_1 = 0.069$, $wR_2 = 0.203$ [all data], and the goodness of fit on F^2 is 1.00, max. and min. $\Delta\rho$: 0.50 and -0.38 eÅ^{-3}. Hydrogen atoms were included at their calculated positions and allowed to ride. In the course of the structure resolution, 1.25 acetone molecules per formula unit were found in the form of solvate and split into two different positions with occupancy factors of 0.60 and 0.65, respectively. Programs used: Data reduction, structure solution by direct methods, structure refinement by full matrix least squares on F^2, molecular graphics: SHELXTL-Plus package, version 5.03 (Sheldrick, 1994) [2].

RESULTS AND DISCUSSION

Treatment of $[Mo_2(CO)_6(NCMe)_2(\mu\text{-pa})]$ with dfpp (1 : 2 molar ratio) or dppf (1 : 1 molar ratio) in dichloromethane at room temperature, afforded the new heterometallic complexes $[Mo_2(CO)_6(dfpp)_2(\mu\text{-pa})]$ and $[Mo_2(CO)_6(\mu\text{-dppf})(\mu\text{-pa})]$, respectively. These

dark-green coloured products are air stable. The dppf derivative is soluble in organic solvents such as dichloromethane, chloroform or benzene, but unsoluble in alcohols and light petroleum. The dfpp based complex shows a lower solubility than that of the dppf-based compound in all the solvents.

The molecular structure of the dppf complex $[Mo_2(CO)_6(\mu\text{-dppf})(\mu\text{-pa})]$ is shown in the Fig. 2 with the atomic numbering scheme. The solid state structure is characterized by the two molybdenum atoms, Mo1 and Mo2, bridged by the pa and dppf ligands, and, in addition, each metal centre is coordinated by a set of tricarbonyl groups in a facial arrangement. The ligand geometry around the Mo atoms is distorted octahedral as is inferred from the smaller N1—Mo1—N2 [72.0(3)°] and N3—Mo2—N4 [72.4(3)°] angles, due to the constrain imposed by the five-membered ring of the bonded pa ligand. In spite of this distortion, the lack of planarity around each Mo centre is not strong [the best mean plane defined by N2, N1, C47 and C49 deviate by 0.019(7), −0.024(8), 0.031(9) and −0.038(11) Å, and the homologous one defined by N3, N4, C50 and C52 deviate by 0.014(8), −0.013(8), 0.027(11) and −0.030(11) Å]. All the Mo—N and Mo—CO distances are in accord with the values of other molybdenum carbonyl derivatives [1]. The Mo1—P1 [2.588(3) Å] and Mo2—P2 [2.596(3) Å] lengths are comparable with those observed in the related Mo-dppf compounds $[Mo(CO)_4(dppf)]$ [3] [2.560(16) Å] and $[Mo_2(CO)_{10}(\mu\text{-dppf})]$ [4] [2.532(1) Å]. The pa ligand is forced to be non-planar and to acquire an approximately *trans* configuration by the steric requirements of the dppf ligand [the torsion angle C40—N2—N4—C46 is 140.6(9)°]. The pyridyl rings are rather planar with a maximal deviation of 0.012(12) Å for C42 and of 0.015(13) Å for C37, the dihedral angle between them is 144.3(3)°. The notorious enlargement of the P—Mo—N(hidrazinic) angles in the $[Mo_2(CO)_6(\mu\text{-dppf})(\mu\text{-pa})]$ complex [average P1—Mo1—N2 and P2—Mo2—N4 angles of 97.7(7)°] in comparison with the analogous angles in the dppe complex $[Mo_2(CO)_6(\mu\text{-dppe})(\mu\text{-pa})]$ [89.39(14)°] [1], makes evident the bulkier nature of the ferrocenyl group with respect to the aliphatic $—CH_2CH_2—$ chain. The two cyclopentadienyl rings of the ferrocenyl unit do not deviate significantly from the planarity [maximal deviations on each ring are 0.012(11) Å for C27 and 0.010(9) Å for C31], but they are slightly displaced from a coplanar position as is evidenced by the dihedral angle of 1.1(4)° between both planes. The Fe—cp [cp = centroid of the C_5 ring] distances [P1 ring, 1.647(1) Å; P2 ring, 1.637(1) Å] are in agreement with that found in the literature [5] and the iron atom is slipped from each cyclopentadienyl ring by 0.018(2) and 0.048(3) Å, respectively. The phosphorous atoms of the phosphocyclopentadiene rings, which virtually do not suffer displacement from their respective C_5 ring planes [0.058(3) Å for P1 and 0.013(2)Å for P2], are rotated relative to one another giving a dihedral angle P1—cp1—cp2—P2 of 116.4(4)° and, besides, the two C_5 rings of the ferrocenyl moiety reach a nearly staggered conformation [the angle to get the nearby perfectly staggered situation is approximately 11.0°].

The solid state IR spectra of the $[Mo_2(CO)_6(dfpp)_2(\mu\text{-pa})]$ and $[Mo_2(CO)_6(\mu\text{-dppf})(\mu\text{-pa})]$ complexes have a pattern similar to other molybdenum(0) tricarbonyl species. They present three strong carbonyl stretching bands, the two at lower

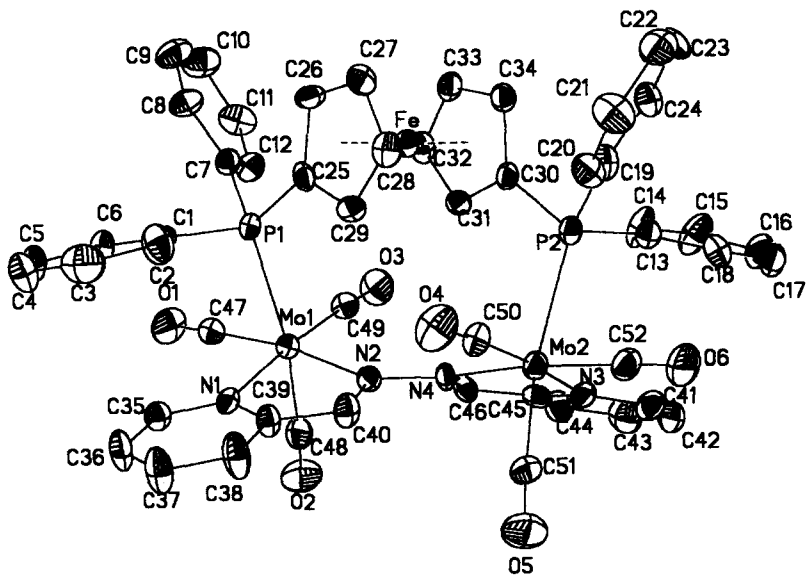

Fig. 2. Schematic view of the complex $[Mo_2(CO)_6(\mu\text{-dppf})(\mu\text{-pa})] \cdot 1.25(CH_3)_2CO$ showing the atomic labelling used and the thermal ellipsoids, drawn at a 50% level (the acetone molecules have been omitted).

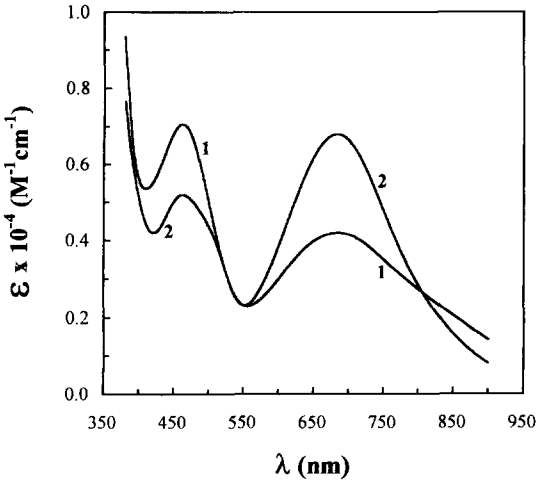

Fig. 3. Electronic spectra recorded in dichloromethane for (**1**) $[Mo_2(CO)_6(dfpp)_2(\mu\text{-pa})]$ and (**2**) $[Mo_2(CO)_6(\mu\text{-dppf})(\mu\text{-pa})]$.

frequency are superimposed. This characteristic pattern has been shown to belong to the *fac* isomers [6].

The electronic absorption spectra in the visible region of the $[Mo_2(CO)_6(dfpp)_2(\mu\text{-pa})]$ and $[Mo_2(CO)_6(\mu\text{-dppf})(\mu\text{-pa})]$ complexes were measured in dichloromethane solution (Fig. 3). Both complexes show two strong solvatochromic absorption bands. Previous work [1] has assigned these bands as MLCT transitions from the Mo t_{2g} orbitals to the first and the second LUMO of the π^* orbitals of the pa ligand, MLCT(1) and MLCT(2) respectively. The longest wavelength MLCT(1) transition of the dfpp complex (690 nm, $\varepsilon = 4200\ M^{-1}\ cm^{-1}$) appears slightly red-shifted with respect to that of the dppf-bridged species (682 nm, $6800\ M^{-1}\ cm^{-1}$). Nevertheless, in the highest energy side the effect works in the opposite way; the MLCT(2) transition of the dfpp compound (462 nm, $7100\ M^{-1}\ cm^{-1}$) is blue-shifted in comparison with the analogue of the dppf-bridged complex (468 nm, $5200\ M^{-1}\ cm^{-1}$). This behaviour is expected considering the existence of different conformations of the pa ligand on each one of these complexes. More specifically, theoretical calculations [1] (extended-Hückel MO calculations with charge iteration) predict a planar conformation (*trans*) for the azine in complexes with monodentate ligands (*viz.*, the dfpp complex) and, besides, if the structure is distorted from the planar situation (*viz.*, the dppf complex) the first and second LUMOs of the pa π^* system become closer in energy (comparatively the changes of energy in the metal orbitals are not significant).

The solvatochromism of the MLCT(1) and MLCT(2) transitions of the dppf complex $[Mo_2(CO)_6(\mu\text{-dppf})(\mu\text{-pa})]$ was evaluated (the low solubility of the dfpp compound precluded this evaluation) by plotting the respective charge-transfer energies MLCT(1) and MLCT(2) vs the E^*_{MLCT} parameter [7] (Table 2). The linear correlations obtained are described by the equation $\bar{\nu}_{MLCT} = A + B \cdot E^*_{MLCT}$ (MLCT(1): $A = 13{,}676$, $B = 1481\ cm^{-1}$, $r = 0.987$; MLCT(2): $A = 20{,}852$, $B = 1128\ cm^{-1}$, $r = 0.993$). The slope B, i.e. the solvent sensitivity, of the MLCT(1) transition is comparable, within the experimental error, to that calculated for the related double bridge complex $[Mo_2(CO)_6(\mu\text{-dppe})(\mu\text{-pa})]$ ($B = 1634\ cm^{-1}$ using the solvents of Table 2) [1], showing that the introduction of the ferrocenyl moiety in place of the aliphatic chain $—CH_2CH_2—$ has no great inci-

Table 1. Selected bond lengths (Å) and angles (°) for $[Mo_2(CO)_6(\mu\text{-dppf})(\mu\text{-pa})] \cdot 1.25(CH_3)_2CO$

Mo1—C49	1.954(11)	Mo2—N4	2.261(7)	Mo2—N4	2.261(7)
Mo1—C47	1.963(10)	Mo2—P2	2.596(3)	Mo2—P2	2.596(3)
Mo1—C48	2.006(11)	P1—C25	1.810(8)	P1—C25	1.810(8)
Mo1—N2	2.271(7)	P1—C7	1.824(9)	P1—C7	1.824(9)
Mo1—N1	2.276(8)	P1—C1	1.841(9)	P1—C1	1.841(9)
Mo1—P1	2.588(3)	P2—C30	1.827(9)	P2—C30	1.827(9)
Mo2—C50	1.925(11)	P2—C13	1.844(9)	P2—C13	1.844(9)
Mo2—C52	1.944(10)	P2—C19	1.864(9)	P2—C19	1.864(9)
Mo2—C51	1.957(11)	N2—C40	1.305(11)	N2—C40	1.305(11)
Mo2—N3	2.259(8)	N4—C46	1.284(11)	N4—C46	1.284(11)
C49—Mo1—C47	88.7(5)	N2—Mo1—P1	98.4(2)		
C49—Mo1—C48	87.3(5)	N1—Mo1—P1	87.0(2)		
C47—Mo1—C48	85.3(4)	C50—Mo2—C51	85.2(5)		
C49—Mo1—N2	100.4(3)	C52—Mo2—C51	84.5(5)		
C47—Mo1—N2	170.5(4)	N2—Mo1—N1	72.0(3)		
C48—Mo1—N2	92.3(3)	C49—Mo1—P1	93.8(3)		
C49—Mo1—N1	172.4(4)	C47—Mo1—P1	83.6(3)		
C47—Mo1—N1	98.9(4)	C48—Mo1—P1	168.8(3)		
C48—Mo1—N1	93.4(4)	C50—Mo2—C52	87.2(4)		

Table 2. Low-energy visible absorption maxima of the complex $[Mo_2(CO)_6(\mu\text{-dppf})(\mu\text{-pa})]$ in several solvents

Solvent (E^*_{MLCT})[a]	$\bar{\nu}_{max}$ (cm^{-1}) MLCT(2)	MLCT(1)
Benzene (0.34)	21,277	14,205
$CHCl_3$ (0.42)	21,277	14,368
THF (0.59)	21,505	14,430
CH_2Cl_2 (0.67)	21,645	14,663
Acetone (0.82)	21,739	14,859
MeCN (0.98)	21,978	15,152
DMSO (1.00)	21,978	15,198

[a] Solvent parameters (E^*_{MLCT}) from Ref. 7.

dence on the interaction with the solvent. The solvent sensitivities of the MLCT(2) transitions seem to be different; the slope B in the dppf complex results lower than that of the dppe ($B = 1692$ cm^{-1}) species. But, this difference is apparent, since it can be attributed to the uncertainty in the measurements of the respective λ_{max}; these bands occur as shoulders of the strong absorptions coming from the UV region.

The cyclic voltammetry studies for the $[Mo_2(CO)_6(dfpp)_2(\mu\text{-pa})]$ and $[Mo_2(CO)_6(\mu\text{-dppf})(\mu\text{-pa})]$ complexes were carried out in CH_2Cl_2 solution. The doubly bridged dppf complex $[Mo_2(CO)_6(\mu\text{-dppf})(\mu\text{-pa})]$ shows an irreversible oxidation wave at $E_p = 0.28$ V followed for a quasi-reversible couple at $E_{1/2} = 0.63$ V. The first wave compares well with that of the molybdenum(0/+1) oxidation of the dppe species $[Mo_2(CO)_6(\mu\text{-dppe})(\mu\text{-pa})]$ [1]. Then, the quasi-reversible remaining couple, absent in the dppe species, is assigned straightforwardly to the one electron ferrocene/ferrocenium oxidation in the dppf ligand [8]. For the *bis*(dfpp) compound was not possible to determine with exactitude the expected anodic processes involving the ferrocenyl groups [9], they appear overlapped with the irreversible Mo(0/+1) wave (the superimposed waves were observed at about 0.3 V). The reduction side for the doubly bridged dppf complex, is characterized by two reversible one electron waves centred on the pa ligand [1] ($E^1_{1/2} = -1.44$ V; $E^2_{1/2} = -1.94$ V). By contrast, in the *bis*(dfpp) system the first one is reversible ($E^1_{1/2} = -1.45$ V) and the more catodic is irreversible ($E_p = -2.04$ V). Probably, this difference is due to the bridge nature of dppf ligand which blocks a following reaction that could occur if two monodentate phosphine dfpp ligands were the coordinating species.

Acknowledgements—Financial support from the Dirección de Investigación y Desarrollo de la Universidad de La Frontera (Project No. 9630) to carry out this work is gratefully acknowledged.

REFERENCES

1. Granifo, J., Vargas, M. E., Dodsworth, E. S., Farrar, D. H., Fielder, S. S. and Lever, A. B. P., *J. Chem. Soc., Dalton Trans.*, 1996, 4369.
2. Sheldrick, G. M., SHELXTL-Plus Release 5.03. Siemens Analytical X-ray Instruments Inc. Madison, WI, U.S.A., 1994.
3. Butler, I. R., Cullen, W. R., Kim, T.-J., Rettig, S. J. and Trotter, J., *Organometallics*, 1985, **4**, 972.
4. Hor, T. S. A., Phang, L.-T., Liu, L.-K. and Wen, Y.-S., *J. Organomet. Chem.*, 1990, **397**, 29.
5. Yam, V. W.-W., Choi, S. W.-K. and Cheung, K.-K., *J. Chem. Soc., Dalton Trans.*, 1996, 3411.
6. Houk, L. W. and Dobson, G. R., *Inorg. Chem.*, 1996, **5**, 2119.
7. Manuta, D. M. and Lees, A. J., *Inorg. Chem.*, 1983, **22**, 3825.
8. Corain, B., Longato, B., Favero, G., Ajò, D., Pilloni, G., Russo, U. and Kreissl, F. R., *Inorganica Chim. Acta*, 1989, **157**, 259.
9. Kotz, J. C., Nivert, C. L., Lieber, J. M. and Reed, R. C., *J. Organomet. Chem.*, 1975, **91**, 87.

Pergamon

PII: S0277-5387(97)00444-0

Polyhedron Vol. 17, No. 10, pp. 1735–1739, 1998
© 1998 Elsevier Science Ltd
All rights reserved. Printed in Great Britain
0277-5387/98 $19.00+0.00

Mononuclear *bis*-chelate and *tris*-chelate complexes of nickel(II) with selenocyanate. Molecular structure of $[Ni(en)_3]$*cis*-$[Ni(en)_2(NCSe)_2]_2X_2$ ($X = PF_6^-$, ClO_4^- and $SeCN^-$) and *trans*-$[Ni(en)_2(NCSe)_2]$

Joan Ribas,[a]* Montserrat Monfort,[a] Inmaculada Resino,[a] Barindra Kumar Ghosh,[a] Xavier Solans[b] and Mercé Font-Bardia[b]

[a] Departament de Química Inorgànica. Universitat de Barcelona. Diagonal, 647. 08028—Barcelona (Spain)

[b] Departament de Cristallografia i Dipòsits Minerals, Universitat de Barcelona, Martí i Franquès s/n, 08028–Barcelona (Spain)

(Received 6 August 1997; accepted 27 October 1997)

Abstract—The reaction of $Ni(ClO_4)_2.aq$, ethylenediamine (en) and KSeCN afford mononuclear $[Ni(en)_3][Ni(en)_2(NCSe)_2]_2(ClO_4)(SeCN)$ (**1**) complexes. The same reaction starting with $Ni(NO_3)_2.aq$ with or without KPF_6 affords two different compounds: $[Ni(en)_3][Ni(en)_2(NCSe)_2]_2(PF_6)_2$ (**2**) and $[Ni(en)_2(NCSe)_2]$ (**3**). The structures of the three compounds were determined by X-ray crystallography. The structures of compounds (**1**) and (**2**) were very similar, consisting of two discrete mononuclear Ni(II) complexes, one *tris*-chelate and the other *cis bis*-chelate with the two selenocyanato ligands linked by the nitrogen atoms. The structure of complex (**3**) is different and consisted of a discrete neutral mononuclear Ni(II) complex *trans bis*-chelate with the two selenocyanato ligands also linked by the nitrogen atoms. Structures, synthetic trends and magnetic behaviour are discussed. © 1998 Elsevier Science Ltd. All rights reserved

Keywords: selenocyanato complexes; mononuclear Ni(II) complexes; magnetism.

Magnetic interactions propagated by pseudohalide bridging ligands between paramagnetic centers have attracted great interest in the past few years. The most comprehensive literature refers to N_3^- bridging ligands: The end-to-end bridging mode creates antiferromagnetic coupling [1] and the end-on mode, ferromagnetic coupling [2]. With cyanato bridging ligands this behaviour is not so clear and the number of reported complexes that have been fully characterized is too low to permit magneto-structural correlations [3]. The literature on thiocyanato ligand is more abundant: the bridge mode usually involves both nitrogen and sulphur, and thus an M—NCS—M linkage occurs [4]. Focusing our attention on Ni(II) polynuclear complexes [5], the Ni—SCN and Ni—NCS angles are almost constant and they all show ferromagnetic behaviour [6]. With the selenocyanato anion only one *bis*(μ-selenocyanato)nickel(II) 1-D complex [7], and one *bis*(μ-selenocyanato)nickel(II) dinuclear complex [8] are reported: both also show ferromagnetic coupling [9]. Owing to the reduced number of selenocyanate derivatives we tried the synthesis of new Ni(II) complexes with $SeCN^-$ as bridging ligand, using the ethylenediamine as terminal ligand. Unfortunately, with nitrate, perchlorate and hexafluorophosphate as counteranion and maintaining an Ni(II): amine: selenocyanato ratio 1:2:1 yield the monomers (**1**), (**2**), (**3**) instead of the desired dimeric product $[Ni_2(en)_4(\mu\text{-}SeCN)_2]X_2$ as the ratio could be expected to furnish.

* Author to whom correspondence should be addressed.

EXPERIMENTAL

Preparation

Caution! Perchlorate salts of metal complexes with organic ligand are potentially explosive. Only a small amount of material should be prepared, and it should be handled with caution.

$[Ni(en)_3][Ni(en)_2(NCSe)_2]_2(ClO_4)(SeCN)$ (**1**). Ethylenediamine (en) (0.12 g, 2 mmol) was added to an aqueous solution (20 cm^3) of $Ni(ClO_4)_2.6H_2O$ (0.36 g, 1 mmol), followed by solid KSeCN (0.15 g, 1 mmol). The mixture was stirred for 15 min afterwards, the blue-violet solution was filtered. Slow evaporation of the clear solution at room temperature afforded, after 1 week, blue-violet crystals suitable for X-ray crystal determination. Yield: 55%. Anal: Calcd for $C_{19}H_{56}ClN_{19}Ni_3O_4Se_5$: C, 18.69; H, 4.62; N, 21.79; Cl, 2.90. Found: C, 18.5; H, 4.6; N, 21.3; Cl, 2.9.

$[Ni(en)_3][Ni(en)_2(NCSe)_2]_2(PF_6)_2$ (**2**). To an aqueous solution (25 cm^3) of $Ni(NO_3)_2.6H_2O$ (0.30 g, 1 mmol), ethylenediamine (en) (0.12 g, 2 mmol) was added, followed by solid KSeCN (0.15 g, 1 mmol). The mixture was stirred for 15 min while solid KPF_6 (0.50 g, 2.7 mmol) was added. The solution was then filtered, and the X-ray quality blue-violet single crystals were obtained by slow evaporation. Yield: 64%. Anal: Calcd for $C_{18}H_{56}F_{12}N_{18}Ni_3P_2Se_4$: C, 16.54; H, 4.29; N, 19.29. Found: C, 16.9; H, 4.3; N, 19.5.

$[Ni(en)_2(NCSe)_2]$ (**3**). This compound was synthesized and crystallized as (**2**) but without adding KPF_6 at the final stage of the synthesis. In this case the yield was poor (20–25%). Anal: Calcd for $C_6H_{16}N_6NiSe_2$: C, 18.53; H, 4.15; N, 21.61. Found: C, 18.7; H, 4.2; N, 21.7.

X-ray data collection and structure determination

Small blue-violet prismatic crystals ($0.1 \times 0.1 \times 0.2$ mm approximately for (**1**), (**2**) and (**3**) respectively) were selected and mounted on an Enraf-Nonius CAD4 four-circle diffractometer, using monochromatic Mo–K_α radiation (0.71069 Å). The crystal system for all three compounds is monoclinic. Unit cell parameters were determined from 25 automatically centered reflections ($12 < \theta < 21°$) and refined by least-squares. Intensity data were collected with the $\omega/2\theta$ scan-technique. Three reflections were measured every 2 h as orientation and intensity control, significant intensity decay was not observed. Lorentz-polarization and empirical absorption corrections (φ-scan method) were performed. The crystallographic data, and some features of the structure, are listed in Table 1. The structure was solved by Patterson synthesis using the SHELXS computer program [10] and refined by full-matrix least-square methods with the SHELX93 computer program [11] using 5153 reflections for (1), 6658 for (2) and 1877 for (3) (the reflections with very negative intensity were not included). The function minimized was $\Sigma w \| F_o|^2 - |F_c|^2|^2$, where $w = [\sigma^2(I) + (kP)^2]^{-1}$, and $P = (|F_o|^2 + 2|F_c|^2)/3$ and $k = 0.1190$ for (**1**); 0.059 for (**2**) and 0.603 for (**3**). f, f′ and f″ were taken from International Tables of Crystallography [12]. For (**1**) the $NCSe^-$ ion was located in a disordered position, an occupancy factor of 0.5 was assigned according to height of the Fourier synthesis. The disorder of perchlorate ions was not located, showing high U_{eq}. Oxygen atoms of perchlorate ions were refined isotropically. 8H atoms were computed and refined with an overall isotropic temperature factor using a riding model.

Physical measurements

Magnetic susceptibility measurements in the range 300–2 K were carried out on an MPMS Quantum Design instrument (with a SQUID detector). Diamagnetic corrections were estimated from Pascal Tables. IR spectra were recorded on a Nicolet 520 FTIR spectrophotometer.

RESULTS

Starting from $Ni(ClO_4)_2$.aq. and working in a ratio Ni/ethylenediamine/KSeCN = 1,2,1, a dinuclear or a 1-D compound with ClO_4^- as counter anion was expected. However, the reaction followed another route, affording the complex $[Ni(en)_3][Ni(en)_2(NCSe)_2]_2(ClO_4)(SeCN)$ (**1**). The same reaction starting from $Ni(NO_3)_2$.aq, and more than two equivalents of KPF_6, a very similar complex was obtained with only a PF_6^- as a counteranion $[Ni(en)_3][Ni(en)_2(NCSe)_2]_2(PF_6)_2$ (**2**). On the other hand, eliminating the KPF_6 in the reaction, a discrete *trans*-$[Ni(en)_2(NCSe)_2]$ (**3**) mononuclear was synthesized.

The IR spectrum of the three compounds shows the characteristic bands attributable to the amine ligands. Compound (**1**) shows very strong and broad bands centred at 1100 cm^{-1} and 600 cm^{-1}, due to the perchlorate anions. A very strong band centred at 830 cm^{-1} corresponding to PF_6^- anion appears in (**2**). Focusing our interest in the stretching mode of the selenocyanate region, all three compounds show two bands in the 2030–2100 cm^{-1} region. For (**2**) and (**3**) the band at lower frequency is very weak while it is stronger in (**1**): this can be interpreted by the presence of only coordinated selenocyanate bridging ligands in *cis* position for (**2**) and (**3**), according to Curtis [13] but in (**1**) there is two kind of selenocyanate: terminal and bridge. The other frequencies due to selenocyanato ligand are masked by the presence of the bands attributable to ethylenediamine.

The crystal structure determination for (**1**) and (**2**) showed that both complexes have two different discrete mononuclear complexes in the crystal lattice: $[Ni(en)_3]^{2+}$ and *cis*-$[Ni(en)_2(NCSe)_2]$, in the 1:2 relation in each unit cell. Crystal lattice were very

Table 1. Crystallographic data for (**1**), (**2**) and (**3**)

	(**1**)	(**2**)	(**3**)
Formula	$C_{19}H_{56}ClN_{19}Ni_3O_4Se$	$C_{18}H_{56}F_{12}N_{18}Ni_3P_2Se_4$	$C_6H_{16}N_6NiSe_2$
Temperature (K)	293	293	293
Space group	*C*2/*c*	*C*2/*c*	$P2_1/n$
a (Å)	24.160(9)	24.736(3)	8.8980(13)
b (Å)	12.824(2)	12.960(4)	8.3851(12)
c (Å)	20.472(4)	20.565(3)	9.626(6)
β (°)	134.47(3)	135.690(10)	112.96(3)
V (Å^3)	4526(2)	4605(2)	661.3(4)
Z	4	4	2
Data collected range θ (°)	1.88–30.00	1.86–29.99	2.65–29.95
Absorption coefficient (mm^{-1})	5.364	4.532	6.952
μ(Mo–K$_\alpha$), cm^{-1}	53.64	45.32	69.52
Max. and min. transmission fact.	0.93, 0.67	0.94, 0.77	0.80, 0.53
Index ranges	$-33 \leqslant h \leqslant 24$	$-34 \leqslant h \leqslant 24$	$-12 \leqslant h \leqslant 11$
	$0 \leqslant k \leqslant 18$	$0 \leqslant k \leqslant 18$	$-2 \leqslant k \leqslant 11$
	$0 \leqslant l \leqslant 28$	$0 \leqslant l \leqslant 28$	$0 \leqslant l \leqslant 13$
Reflections collected	7324	6943	2052
Independent reflections	6596	6709	1927
	[$R_{int} = 0.032$]	[$R_{int} = 0.022$]	[$R_{int} = 0.0091$]
Observed data [$I > 2\sigma(I)$]	5809	3270	1396
No. param. refined	224	299	103
Goodness-of-fit on F^2	0.935	0.884	1.041
Final *R* indices [$I > 2\sigma(I)$]	$R_1 = 0.0648$	$R_1 = 0.0397$	$R_1 = 0.0402$
	$wR_2 = 0.1526$	$wR_2 = 0.0906$	$wR_2 = 0.0910$
R indices (all data)	$R_1 = 0.1533$	$R_1 = 0.1207$	$R_1 = 0.0733$
	$wR_2 = 0.2395$	$wR_2 = 0.1287$	$wR_2 = 0.1161$
Extinction coefficient	0.0000(9)	0.00000(6)	0.042(3)
Largest diff. Peak and hole (e A^{-3})	0.496, −0.917	1.055, −0.845	0.969, −0.471

$R_1 = \Sigma||F_o|-|F_c||/\Sigma|F_o|$; $wR_2 = [\Sigma w(|F_o|-|F_c|)^2/\Sigma w|F_o|^2]^{1/2}$.

similar: same space group and almost similar parameters (see Experimental Part). The only difference between them was the presence of ClO_4^- and $SeCN^-$ in compound (**1**) and PF_6^- in compound (**2**) as counteranion. Molecular structure of the two mononuclear entities for (**1**) and (**2**) are similar and for (**2**) is given in Fig. 1. The main bond distances and angles are gathered in Table 2.

All Ni(II) ions are distorted octahedrally co-ordinated. The two *cis*-$[Ni(en)_2(NCSe)_2]$ entities are more distorted, owing to the smaller Ni—N(CSe) distances (average: 2.06 Å whereas the average for Ni—N-

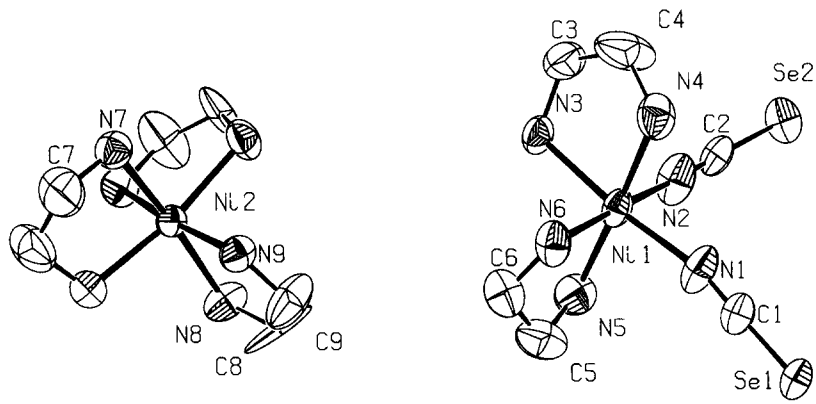

Fig. 1. Plot of the two cationic moieties of $[Ni(en)_3][Ni(en)_2(NCSe)_2]_2$ $(PF6)_2$ (**2**), showing the atom numbering scheme.

Table 2. Main bond lengths (Å) and angles (°) for $[Ni(en)_3][Ni(en)_2(NCSe)_2]_2(ClO_4)$ (SeCN) (**1**) and $[Ni(en)_3][Ni(en)_2(NCSe)_2]_2(PF_6)_2$ (**2**)

cis-$[Ni(en)_2(NCSe)_2]$ moiety		
	(**1**)	(**2**)
Ni(1)—N(1)	2.091(6)	2.066(4)
Ni(1)—N(2)	2.050(6)	2.062(4)
Ni(1)—N(3)	2.129(7)	2.102(4)
Ni(1)—N(4)	2.103(6)	2.126(4)
Ni(1)—N(5)	2.138(5)	2.128(3)
Ni(1)—N(6)	2.154(8)	2.120(4)
N(1)—Ni(1)—N(2)	90.5(2)	91.0(2)
N(1)—Ni(1)—N(3)	90.0(3)	90.1(2)
N(1)—Ni(1)—N(4)	89.2(2)	89.6(2)
N(1)—Ni(1)—N(5)	173.9(3)	174.6(2)
N(1)—Ni(1)—N(6)	92.4(3)	92.0(2)
N(2)—Ni(1)—N(3)	92.7(3)	91.8(2)
N(2)—Ni(1)—N(4)	175.6(3)	175.2(2)
N(2)—Ni(1)—N(5)	88.6(2)	88.8(2)
N(2)—Ni(1)—N(6)	89.1(3)	88.7(2)
N(3)—Ni(1)—N(4)	82.9(3)	83.4(2)
N(3)—Ni(1)—N(5)	96.0(3)	95.4(2)
N(3)—Ni(1)—N(6)	177.0(3)	177.8(2)
N(4)—Ni(1)—N(5)	92.1(2)	91.1(2)
N(4)—Ni(1)—N(6)	95.4(3)	96.0(2)
N(5)—Ni(1)—N(6)	81.6(2)	82.6(2)
$[Ni(en)_3]$ moiety		
	(**1**)	(**2**)
Ni(2)—N(7)	2.128(6)	2.130(3)
Ni(2)—N(8)	2.137(5)	2.135(4)
Ni(2)—N(9)	2.136(6)	2.129(4)
N(7)—Ni(2)—N(7)#1	172.1(3)	170.9(2)
N(7)—Ni(2)—N(9)#1	92.6(2)	93.69(14)
N(7)—Ni(2)—N(9)	93.3(2)	93.22(14)
N(7)—Ni(2)—N(8)	91.4(2)	91.53(14)
N(7)—Ni(2)—N(8)#1	83.2(2)	82.27(13)
N(7)#1—Ni(2)—N(9)#1	93.3(2)	93.22(14)
N(7)#1—Ni(2)—N(9)	92.6(2)	93.69(14)
N(7)#1—Ni(2)—N(8)	83.2(2)	82.27(13)
N(7)#1—Ni(2)—N(8)#1	91.4(2)	91.53(14)
N(8)—Ni(2)—N(8)#1	95.6(4)	93.9(2)
N(8)—Ni(2)—N(9)	91.0(2)	92.9(2)
N(8)—Ni(2)—N(9)#1	172.6(2)	171.9(2)
N(8)#1—Ni(2)—N(9)	172.6(2)	171.9(2)
N(8)#1—Ni(2)—N(9)#1	91.0(2)	92.9(2)
N(9)—Ni(2)—N(9)#1	82.5(3)	80.6(2)

Symmetry transformations used to generate equivalent atoms: #1 $-x, y, -z+1/2$.

(amine) is 2.12 Å). The angles N(amine)—Ni—N(amine) in *cis* arrangement are close to 90°. The N—M—N angles for the chelating *en* ligands are less than 90°, as usual. The N(1)—Ni—N(2), corresponding to the angle between both NCSe ligand is 90.5(2) for (1) and 91.0(2) for (2). The angles corresponding to ligands in *trans* positions are between 174.0 and 177.8°. The tris-chelate moieties are more regular. They have a C_2 axis. The Ni(2)—N(amine) distances moved from 2.140 Å to 2.125 Å. As in the $[Ni(en)_2(NCSe)_2]$ part, the angles N(amine)—Ni—N(amine) in *cis* arrangement are close to 90°. The N—M—N angles for the chelating *en* ligands are less than 90°, as usual. The N(amine)—Ni—N(CSe) angles are 90.09 and 89.91.

The structure of *trans*-$[Ni(en)_2(NCSe)_2]$ (**3**) consists of isolated neutral unities. An ORTEP drawing with the atom-labelling scheme is shown in Fig. 2. The main bond lengths and angles are given in Table 3. The complex has a pseudo-octahedral geometry with an inversion centre in the NiN_6 unit. All Ni—N (amine) distances are 2.104 Å, and both Ni—N(CSe) distances are 2.126 Å. All the N—Ni—N angles in *trans* position are 180°. The angles N(amine)—Ni—N(amine) in *cis* arrangement are close to 90°. As in the structures (**1**) and (**2**), if the two N atoms belong to the same ethylenediamine, this angle, as expected, is lower than for the N atoms not belonging to the same amine. The N(amine)—Ni—N(CSe) angles are 90.09 and 89.91.

The magnetic susceptibility measurements were carried out in the 2–300 K temperature range. The $\chi_M T$ vs T plots for the three complexes are given in Fig. 3. Compounds (**1**) and (**2**) showed the same behaviour. The room temperature $\chi_M T$ values for (**1**) were 3.62 $cm^3\ mol^{-1}\ K$ and 3.48 $cm^3\ mol^{-1}\ K$ for (**2**) (corresponding to a three isolated Ni(II) with $g > 2.00$) and was practically constant in the temperature range analysed.

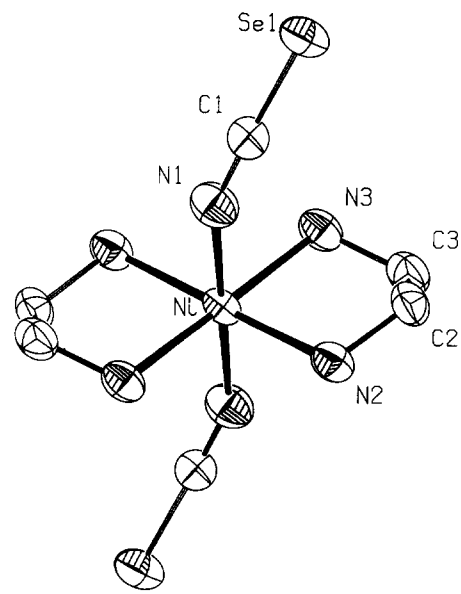

Fig. 2. Plot of *trans*-$[Ni(en)_2(NCSe)_2]$ (**3**) showing the atom numbering scheme.

Table 3. Main bond lengths (Å) and angles (°) for *trans*-[Ni(en)$_2$(NCSe)$_2$] (**3**)

Ni—N(1)	2.126(3)
Ni—N(2)	2.104(3)
Ni—N(3)	2.104(3)
N(1)—Ni—N(1)#1	180.0
N(1)—Ni—N(2)	90.09(13)
N(1)—Ni—N(2)#1	89.91(13)
N(1)—Ni—N(3)	89.3(2)
N(1)—Ni—N(3)#1	90.7(2)
N(1)#1—Ni—N(2)	89.91(13)
N(1)#1—Ni—N(2)#1	90.09(13)
N(1)#1—Ni—N(3)	90.7(2)
N(1)#1—Ni—N(3)#1	89.3(2)
N(2)—Ni—N(2)#1	180.0
N(2)—Ni—N(3)	82.58(13)
N(2)—Ni—N(3)#1	97.42(13)
N(2)#1—Ni—N(3)	97.42(13)
N(2)#1—Ni—N(3)#1	97.42(13)
N(3)—Ni—N(3)#1	180.0

Symmetry transformations used to generate equivalent atoms: #1 $-x+1, -y+1, -z+2$.

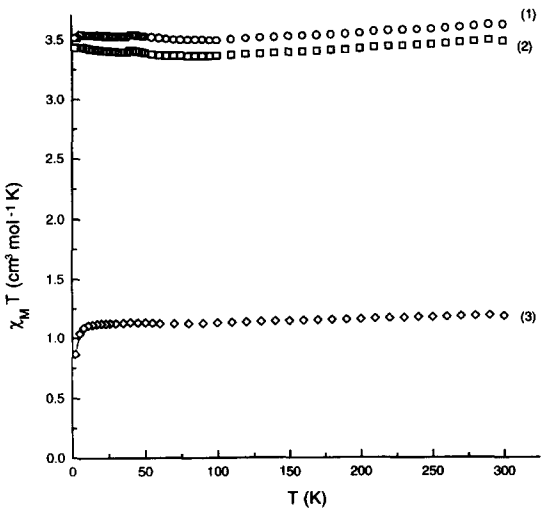

Fig. 3. Plots of the temperature dependence of χ_MT vs T for (**1**), (**2**) and (**3**).

The room temperature χ_MT value for compound (**3**) was 1.18 cm^3 mol^{-1} K which corresponded to an isolated Ni(II), and exhibited a quasi Curie law behaviour with a slight decrease at low temperature as usual in the isolated mononuclears of Ni(II).

As a conclusion, the synthesis of only mononuclear species with selenocyanate anions, could indicate that $NCSe^-$ is a worse bridging ligand than the NCS^- analogue, due to the softer character of the Se atom compared to the S atom, regarding to Ni(II) metallic centre.

Acknowledgements—We are very grateful to DGYCYT (Grant PB93-0772) for financial support and for the grant to B.K.G. and I.R.

REFERENCES

1. (a) Ribas, J., Monfort, M., Diaz, C., Bastos, C. and Solans, X., *Inorg. Chem.*, 1993, **32,** 3557; (b) Escuer, A., Vicente, R., El Fallah, M. S., Ribas, J., Solans, X. and Font-Bardia, M., *J. Chem. Soc., Dalton Trans.*, 1993, 2975; (c) Escuer, A., Vicente, R., Ribas, J., El Fallah, M. S. and Solans, X., *Inorg. Chem.*, 1993, **32,** 1033; (d) Escuer, A., Vicente, R., Ribas, J., El Fallah, M. S., Solans, X. and Font-Bardia, M., *Inorg. Chem.*, 1993, **32,** 3727; (e) Escuer, A., Vicente, R., Ribas, J., El Fallah, M. S., Solans, X. and Font-Bardia, M., *Inorg. Chem.*, 1994, **32,** 695; (f) Ribas, J., Monfort, M., Ghosh, B. K. and Solans, X., *Angew. Chem. Int. Ed. Engl.*, 1994, **33,** 2087.
2. (a) Vicente, R., Escuer, A., Ribas, J., El Fallah, M. S., Solans, X. and Font-Bardia, M., *Inorg. Chem.*, 1993, **32,** 1920; (b) Ribas, J., Monfort, M., Diaz, C., Bastos, C. and Solans, X., *Inorg. Chem.*, 1994, **33,** 484; (c) Ribas, J., Monfort, M., Costa, R. and Solans, X., *Inorg. Chem.*, 1993, **32,** 695. (d) Monfort, M., Ribas, J. and Solans, X., *J. Chem. Soc., Chem. Commun.*, 1993, 350; (e) Ribas, J., Monfort, M., Solans, X. and Drillon, M., *Inorg. Chem.*, 1994, **33,** 742.
3. Escuer, A., Vicente, R., Ribas, J., El Fallah, M. S. and Solans, X., *Inorg. Chim. Acta*, 1994, **216,** 5 and references therein.
4. (a) Haasnoot, J. G., Driessen, W. L., and Reedijk, J., *Inorg. Chem.*, 1984, **23,** 2803; (b) Walz, L. and Haase, W., *J. Chem. Soc., Dalton Trans.*, 1985, 1243.
5. Monfort, M., Ribas, J. and Solans, X., *Inorg. Chem.*, 1994, **33,** 4271 and references therein.
6. (a) Ginsberg, A. P., Martin, R. L., Brookes, R. W. and Sherwood, R. C., *Inorg. Chem.*, 1972, **11,** 2884; (b) Duggan, M. D. and Hendrickson, D. N., *Inorg. Chem.*, 1974, **13,** 2929.
7. Turpeinen, U., *Finn. Chem. Lett.*, 1997, 75.
8. Vicente, R., Escuer, A., Ribas, J., Solans, X. and Font-Bardia, M., *Inorg. Chem.*, 1993, **32,** 6117.
9. Escuer, A. and Vicente, R., have studied the magnetism of the 1-D complex reported by Turpeinen (Ref. 7). It shows small ferromagnetic coupling. (Private communication.)
10. Sheldrick, G. M., *Acta Cryst.*, 1990, **A46,** 467–473.
11. Sheldrick, G. M., SHELXL. *A computer program for crystal structure determination.* University of Göttinger, Germany, 1994.
12. *International Tables of X-ray Crystallography*, Vol. IV. Kynoch Press, Birmingham, England, 1974, p. 99.
13. Curtis, N. F. and Curtis, Y. M., *Aust. J. Chem.*, 1996, **19,** 1423.

Pergamon

PII: S0277-5387(97)00443-9

Polyhedron Vol. 17, No. 10, pp. 1741–1746, 1998
© 1998 Elsevier Science Ltd
All rights reserved. Printed in Great Britain
0277-5387/98 $19.00+0.00

New spectrophotometric evidence for the existence of $HCrO_4^-$

J. J. Cruywagen,* J. B. B. Heyns and E. A. Rohwer

Department of Chemistry, University of Stellenbosch, Stellenbosch 7600, Republic of South Africa

(Received 9 June 1997; accepted 27 October 1997)

Abstract—A spectrophotometric study of the protonation and dimerization of CrO_4^{2-} at different concentrations in the pH range 8–2.5 at 25°C in 0.1 M (Na)Cl medium led to the characterization of $HCrO_4^-$ and $Cr_2O_7^{2-}$ in terms of formation constants and absorption spectra. When the pH is varied at constant Cr(VI) concentration the experimental spectra exhibit one real and three accidental isosbestic points. The results of this investigation do not corroborate recent work in which the non-existence of $HCrO_4^-$ was claimed. The spectrophotometric determined equilibrium constants have been verified by potentiometric titrations. The values are: $\log \beta_{11} = 6.09 \pm 0.04$ and $\log \beta_{22} = 13.94 \pm 0.06$. © 1998 Elsevier Science Ltd. All rights reserved

Keywords: isosbestic point; chromate solution; spectrophotometry.

In a very recent paper in this journal [1] a seemingly quite convincing case was put forward for the non-existence of $HCrO_4^-$. It was claimed that $HCrO_4^-$ is spectrophotometrically undetectable and that $Cr_2O_7^{2-}$ is the only species to be formed upon acidification of CrO_4^{2-}. The authority of textbooks was questioned on the grounds that early results did not prove the existence of $HCrO_4^-$ but were merely consistent with it. An important consideration was four isosbestic points exhibited by the spectra of chromate solutions measured at various concentrations and pH values. The conclusion was further supported by the results of factor analysis and by application of the method of spectral displacement. This work followed after reports by Michel *et al.* [2,3] that the $HCrO_4^-$ ion could not be detected by Raman spectra. These experiments covered conditions for which relatively high percentage concentrations of $HCrO_4^-$ would be expected, that is if the generally accepted equilibrium constants of $HCrO_4^-$ and $Cr_2O_7^{2-}$ are used to calculate the distribution of species.

The implication of these findings is that the many previous investigators of chromate protonation equilibria determined the formation constant of an imaginary ion. Should this be the case it is really astonishing that such consistent values for the equilibrium constants could have been obtained using a variety of experimental techniques [4]. Also, in a recent ^{17}O-oxygen exchange NMR study of CrO_4^{2-} and $Cr_2O_7^{2-}$ an increase in the line width of the ^{17}O signal of CrO_4^{2-} on adding acid was attributed to a much broader signal of $HCrO_4^-$ [5].

From a theoretical point of view there is no reason to doubt the existence of $HCrO_4^-$. For CrO_4^{2-} to dimerize by elimination of a water molecule, protonation should be the first step in the process. If $HCrO_4^-$ would be too strong an acid to occur at say pH = 2.5 then the tendency for dimerization, especially at low concentration, would be very small at this pH and still smaller at pH > 2.5. In other words, if $Cr_2O_7^{2-}$ is the predominating species at a particular pH appropriate dilution at that pH should yield $HCrO_4^-$ ions.

However, to verify that $HCrO_4^-$ really exists under specified conditions, as has been shown by earlier workers and also presented in authoritative textbooks, new experimental evidence is now needed. This basic knowledge is not only of importance in the general context of oxyacids, but also essential, for example, for the interpretation of the mechanisms of redox reactions of Cr(VI) and for an understanding of the toxic and mutagenic effects of Cr(VI) species; at physiological pH (7.4) the $HCrO_4^-$ ion would be an important species [6].

In earlier spectrophotometric work determinations of equilibrium constants have been based on the change in absorbance at one or only a few suitable wavelengths [7]. With modern sophisticated computer

* Author to whom correspondence should be addressed.

programs large volumes of absorbance data can be treated for model testing and to supply equilibrium constants and spectra of the absorbing species.

In this paper we present spectrophotometric results which verify previously determined equilibrium constants for the protonation and dimerization of CrO_4^{2-} and which also confirm the existence of $HCrO_4^-$. In addition complete individual spectra for the species in question are reported, in particular those of the $HCrO_4^-$ and $Cr_2O_7^{2-}$ ions which cannot be measured directly. These curves show at which wavelengths isosbestic points should occur when the pH of a Cr(VI) solution is varied.

EXPERIMENTAL

Analytical grade chemicals (Merck) were used and solutions were prepared with water purified with a Millipore Milli-Q system. A chromium(VI) stock solution of known concentration was prepared by weighing out an appropriate amount of dried potassium dichromate. Hydrochloric acid was standardized against tris(hydroxymethyl)aminomethane.

A GBC 920 UV-VIS double beam spectrophotometer equipped with a Peltier thermocell was used for the absorption measurements. Absorption spectra of chromium(VI) solutions at four different concentrations, viz. 0.10, 0.20, 1.0 and 1.92 mM (M = mol dm^{-3}) were recorded in the range 220–460 nm at intervals of 2 nm. Each experiment was started with 80 cm^3 solution to which carbonate-free sodium hydroxide was added to convert all chromium(VI) to chromate. This solution was kept in a thermostatted water bath at 25°C and titrated with an acidified chromium(VI) solution of the same concentration covering the pH_c range 8.0–2.1. To exclude carbon dioxide from the system a stream of purified nitrogen was passed through 0.10 M NaCl and then bubbled slowly through the titration solution. Silica cuvettes of path length 1.00 and 0.20 cm were used for the low and high concentrations respectively. For recording the spectrum of a chromate solution at much higher concentration, namely 40 mM, a demountable cuvette of path length 0.01 was used. A potentiometric titration of chromate (10 mM) with hydrochloric acid was carried out as described previously [8]. All solutions were made 0.10 M with respect to chloride ions by adding the appropriate amount of NaCl.

The electrode system was standardized in terms of hydrogen ion concentration. The free hydrogen ion concentration, h, was determined by measuring the potential, E, to ± 0.2 mV using a Ross combination electrode (Orion 8102 SC) with a 3.0 M KCl bridge solution. Equation (1) was used to calculate h from the measured potential:

$$E = E^\circ + 59.16 \log h \qquad (1)$$

E° was determined from a titration of 0.1 M NaCl with 0.1000 M HCl as described by Rossotti [9]. For brevity, $-\log h$ is denoted by pH_c.

RESULTS AND DISCUSSION

The change in absorption as a function of pH_c for solutions at two Cr(VI) concentrations, differing by a factor of 19, is shown in Figs 1 and 2. For both concentrations four isosbestic points are seen, one of which occurs at the same wavelength (339.5 nm) in the two plots. Since isosbestic points are by no means confined to two-component systems [10,11], these results should not be regarded as evidence for the existence of only two absorbing species. For this system, comprising three absorbing species, isosbestic points can be expected to occur if the pH is varied at constant Cr(VI) concentration provided the spectra of the individual species intersect [10,11]. Whether the latter condition would be satisfied can only be decided once spectra for the individual species have been determined.

A reliable test for the number of equilibria, especially when minor species are involved, is to compare experimental absorbance values with calculated values using the whole spectrum and in particular those absorbances where the greatest change with pH and concentration occurs. Obviously such model testing will only yield meaningful results if it is based on data of the highest possible accuracy collected under controlled conditions, e.g. constant ionic medium and constant temperature.

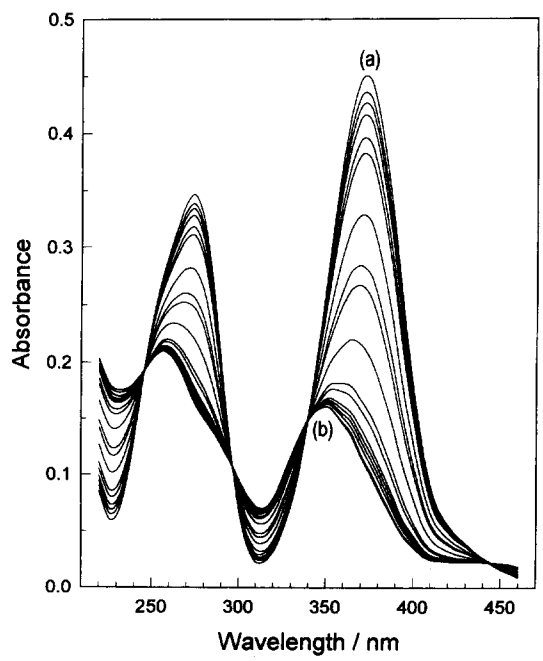

Fig. 1. Change in absorption spectra with change in pH_c from 7 (a) to 2.5 (b) of a 0.1 mM chromium(VI) solution measured in a 1 cm cuvette.

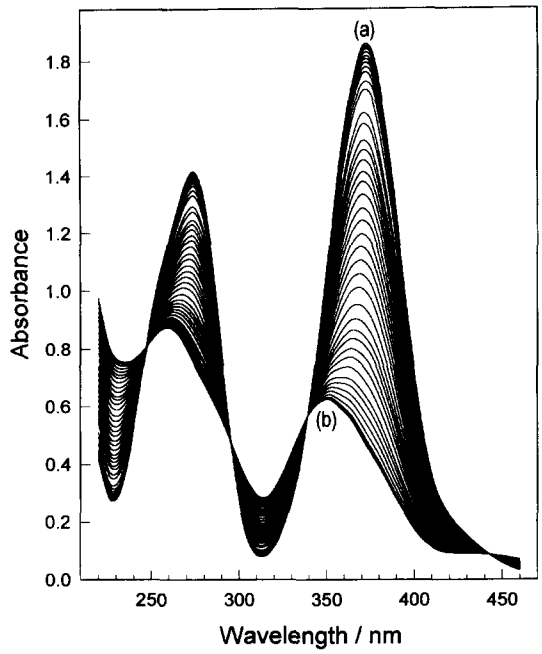

Fig. 2. Change in absorption spectra with change in pH_c from 8 (a) to 2.1 (b) of a 1.92 mM chromium(VI) solution measured in a 0.2 cm cuvette.

The following two reactions were considered in the computer treatment of the data:

$$CrO_4^{2-} + H^+ \rightleftharpoons HCrO_4^- \quad (2)$$

$$2CrO_4^{2-} + 2H^+ \rightleftharpoons Cr_2O_7^{2-} \quad (3)$$

The equilibrium constants are denoted by β_{11} and β_{22} respectively. In this investigation the computer programs PHAB [12] and SPECFIT [13] were employed for model testing. When treating the same data the two programs produced identical values for the equilibrium constants. An advantage of the program PHAB is that it can accommodate more data, accepts known spectra and is faster. The program SPECFIT on the other hand has the facility of factor analysis and also the option of a graphical display of the fit of calculated absorbances on experimental values at any selected wavelength.

After treating the first data set pertaining to Cr(VI) concentration 0.1 mM, it was already clear that $HCrO_4^-$ is the major reaction product at this low concentration. A reaction model assuming the presence of $HCrO_4^-$ resulted in an excellent fit which is significantly better than that for $Cr_2O_7^{2-}$. The results are shown in Table 1. When computations were done with both equilibria then the dichromate ion was rejected. From the constants finally obtained, calculations show that under the conditions of this experiment less than 1% of the Cr(VI) occurs as dichromate. For the data pertaining to a Cr(VI) concentration of 0.2 mM about 2% occurs as dichromate and nearly identical results were obtained. When only the $Cr_2O_7^{2-}$ reaction is considered the absorption/pH plots (at suitable wavelengths) show the expected deviation between calculated and experimental absorbances because in this case the absorption is not dependent on the square of the hydrogen ion concentration.

For the calculations at five-fold higher concentration both equilibria are retained in the model. Although only a relatively small percentage of chromate is converted to dichromate (~8%) a fairly accurate value for β_{22} is acquired and the value of β_{11} is the same as that calculated at the lower concentrations.

For the titration at the highest Cr(VI) concentration (1.92 mM) the best fit again resulted when both $HCrO_4^-$ and $Cr_2O_7^{2-}$ were assumed to be present. For this experiment the maximum percentage of chromate converted to dichromate was about 14%. The equilibrium constants are for practical purposes similar to those obtained from the other sets of data. Results of calculations done with some combinations of data sets are also shown in Table 1. It is reassuring that such consistent results could be obtained despite the relatively low concentration of dichromate in the solutions. At the low ionic strength chosen for the experiments the tendency for hydrogen chromate to dimerize is smaller than at high ionic strength, e.g. 3.0 mol dm^{-3}. The main reason for choosing the low ionic strength was the quest for accuracy. Not only is the background absorption in the UV region much smaller, but the possible introduction of small amounts of protolytic impurities via the high salt concentration is avoided. Ironically, it turned out to be easier to characterize $HCrO_4^-$ than $Cr_2O_7^{2-}$ by spectrophotometry. As an independent check of the accuracy of the spectrophotometric results a potentiometric titration was carried out and the data treated with the program SUPERQUAD [14]. The values of the stability constants thus obtained, log $\beta_{11} = 6.08$ (6.09) and log $\beta_{22} = 13.89$ (13.90) are not only in excellent agreement with the spectrophotometric values but also with literature values (in parentheses) pertaining to the same ionic strength [15].

The individual absorption spectra of the Cr(VI) species obtained from these calculations are shown in Fig. 3; as the experiments were started with chromate the calculated and experimental spectral curves were identical. That the calculated spectra and stability constants give a satisfactory description of the system is also shown by the comparison of a simulated spectrum and an experimental spectrum measured at a much higher concentration namely at 40 mM chromate; at this concentration and $pH_c = 2.3$ about 60% of the chromate is in the form of $Cr_2O_7^{2-}$. The agreement between the two spectral curves (Fig. 4) leaves no doubt about the consistency of the spectrophotometric results. A quite reliable test for the presence of polynuclear species, dinuclear in the present case, and which is based on Beer's Law, is that with a change in total concentration a change in the

Table 1. Results of calculations and values of equilibrium constants at 25°C and 0.10 M NaCl

Data	Number of spectra	$[Cr(VI)]_{Tot}$ (mM)	$\log \beta_{11} \pm 3\sigma$	$\log \beta_{22} \pm 3\sigma$	$\sigma_A \times 10^2$
A	19	0.1	6.103±0.003	—	0.075
			—	(16.05±0.02)	0.29
B	26	0.2	6.098±0.001	—	0.076
			—	(15.88±0.02)	0.87
A+B	45	0.1; 0.2	6.098±0.002	—	0.18
C	25	1.0	6.10±0.05	13.95±0.03	0.23
D	39	1.92	6.07±0.03	13.99±0.02	0.49
C+D	64	1.0; 1.92	6.08±0.01	13.93±0.02	0.67
Potentiometric		10.0	6.08±0.01	13.89±0.08	—
Average		—	6.09±0.05	13.95±0.08	—
Literature [15]	—	6.09±0.04	13.90±0.10	—	

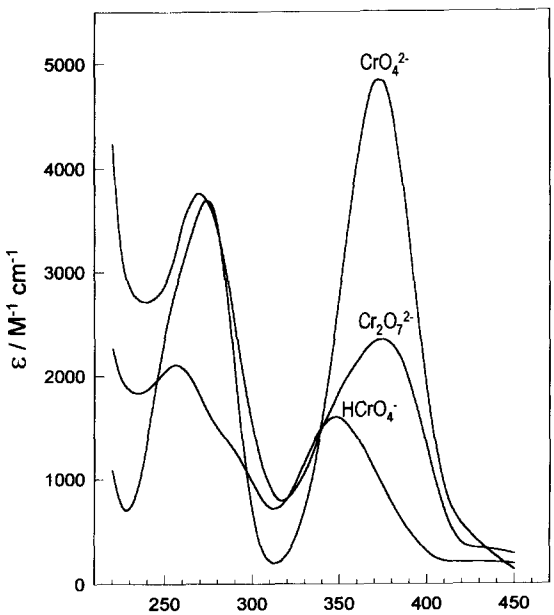

Fig. 3. Calculated absorption spectra of various Cr(VI) species. Molar absorptivities of $Cr_2O_7^{2-}$ have been divided by two in order to present comparable spectra.

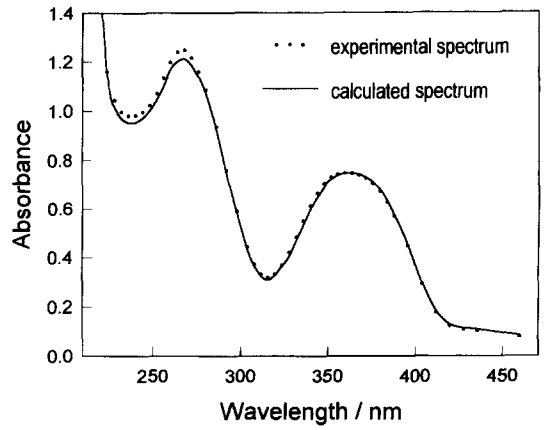

Fig. 4. Experimental and calculated spectra of a solution of 0.04 M Cr(VI) at $pH_c = 2.3$.

molar absorptivity, ε, at a particular wavelength would occur providing nothing else is changed, e.g. constant pH is required. Although Poulopoulou *et al.* [1] compared ε values of solutions over a wide concentration range and at different pH values the focus was mainly on the four observed isosbestic points so that the small changes observed led to the conclusion that $HCrO_4^-$ does not exist. A nice illustration of how the whole spectrum changes due to the presence of both $HCrO_4^-$ and $Cr_2O_7^{2-}$ is shown in Fig. 5 where ε is plotted against wavelength. The spectra of Cr(VI) solutions at low pH_c where all chromate has been converted to $HCrO_4^-$ and $Cr_2O_7^{2-}$ show an increase in ε with increase in concentration at most wavelengths as well as a clear shift of the two absorption peaks to shorter wavelengths. If dichromate were the only species present at low pH_c, as suggested by Poulopoulou *et al.* [1], these curves should have coincided.

Having verified the existence of $HCrO_4^-$ a meaningful discussion of the isosbestic points, whether real or illusory, is now possible because individual spectra of $Cr_2O_7^{2-}$ and $HCrO_4^-$ are available. The experimental spectra shown in Fig. 1 are those of solutions containing only two species in equilibrium, CrO_4^{2-} and $HCrO_4^-$, and the four points of intersection at wavelengths 245.8, 296.5, 339.3 and 443 nm therefore represent the isosbestic points of this two-component system. The same points of intersection are seen in the calculated spectral curves of CrO_4^{2-} and $HCrO_4^-$ (Fig. 3). However, the spectral curve of $Cr_2O_7^{2-}$ intersects at only one of these points namely at 339.3 nm which therefore can be regarded as a real isosbestic point for the three-component system.

For the experimental spectra shown in Fig. 2 about

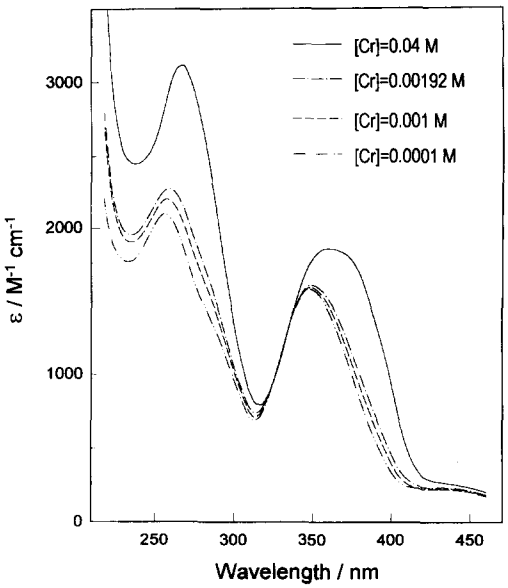

Fig. 5. Change in the molar absorptivity with change in Cr(VI) concentration at $pH_c = 2.3$.

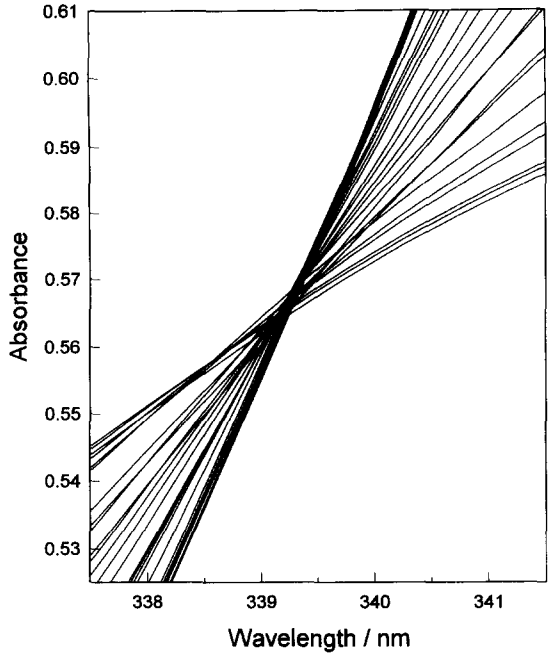

Fig. 7. Small part of Fig. 2 enlarged to show genuine isosbestic point at 339.3 nm.

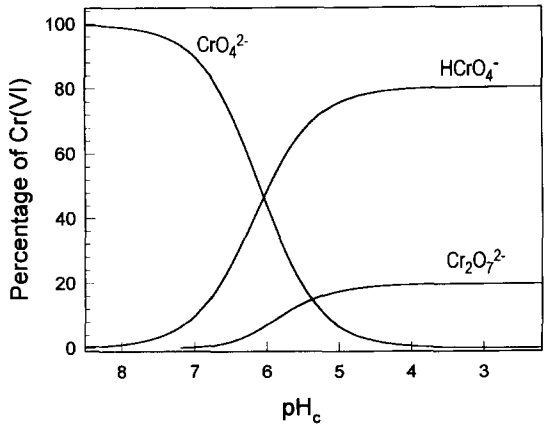

Fig. 6. Distribution of species in a 1.92 mM Cr(VI) solution as a function of pH_c.

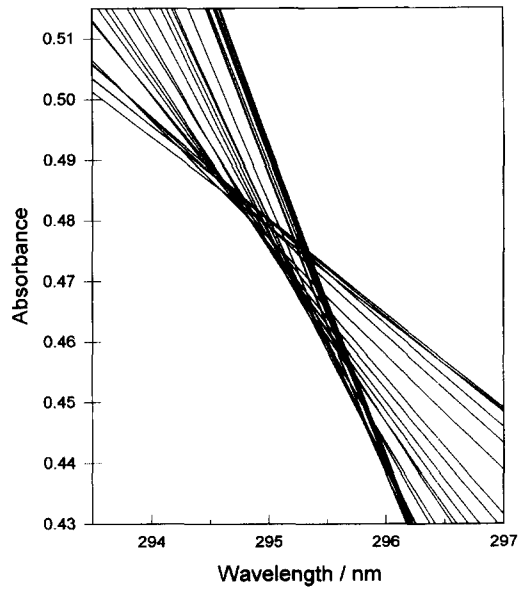

Fig. 8. Small part of Fig. 2 enlarged to show apparent isosbestic point at 295 nm.

14% of the Cr(VI) is converted to dichromate, but four apparently well-defined isosbestic points are still exhibited. However, owing to the very similar shape of the spectra of CrO_4^{2-} and $Cr_2O_7^{2-}$ the changes are hardly discernible as a deviation from the "isosbestic points" of CrO_4^{2-} and $HCrO_4^-$. The isosbestic points at 245.8 and 296.5 nm now occur as points of intersection at approximately 247 and 295 nm while the molar absorbances have increased with about 8% and 15% respectively. The difference between the real isosbestic point at 339.3 nm and an illusory one (e.g. at 295 nm) is illustrated in Figs 7 and 8 where small parts of the experimental spectra of Fig. 2 are "blown up".

These comments also apply to the spectrophotometric results of Poulopoulou *et al.* [1]. For example, using the now-known individual spectra of the three chromate species the five experimental spectra pertaining to 10.0 mM reported by these authors could be simulated to yield four apparently well-defined isosbestic points. However, only the genuine isosbestic point occurred at the same wavelength namely 339.3 nm while the two other points shifted

Table 2. Results of factor analysis of spectrophotometric data showing the decrease in σ_A with increase in the number of factors (1 to 4)

	$\sigma_A \times 10^2$			
$[Cr(VI)]_{Tot}$/mM	1	2	3	4
0.10	3.8	0.056	0.046	0.039
0.20	7.3	0.049	0.043	0.040
1.0	40	0.36	0.14	0.13
1.92	70	1.0	0.3	0.27

from 245.8 to 250 and from 296.5 to 293 nm respectively, owing to the higher percentage concentration of dichromate in the solutions.

Although the interpretation of factor analysis is often ambiguous the result of such analysis of our data using the program SPECFIT [13] gave a clear indication of the number of species at the different concentrations. When the σ_A values for two and three factors are compared (Table 2) the small differences at the lowest Cr(VI) concentration indicate two species, but at the higher concentrations these differences are consistent with three absorbing species.

CONCLUSION

The results of this study have confirmed that $HCrO_4^-$ is an important species in acidified chromate solution and have shown that earlier workers without the benefit of sophisticated instrumentation and high-speed computers gave the correct description of the system. With change in pH the absorption spectra of a solution containing the three absorbing ions, CrO_4^{2-}, $HCrO_4^-$ and $Cr_2O_7^{2-}$ show four apparently well-defined isosbestic points of which only the one occurring at 339.3 nm is real. The small difference in the shape of the spectral curves of CrO_4^{2-} and $Cr_2O_7^{2-}$ as well as the relative changes in absorption with change in pH_c are the main reasons for the occurrence of illusory isosbestic points. For the same reasons it might be difficult to make an unequivocal decision based on the method of spectral displacement [1]. It is also clear now that Raman spectrometry lacks the sensitivity to discriminate between the chromate species in question. The reported spectra [3] do not show any Raman lines other than those corresponding to CrO_4^{2-} and $Cr_2O_7^{2-}$ ions under conditions where more than 60% of the Cr(VI) should exist as $HCrO_4^-$.

With complete spectra for the individual Cr(VI) species now available it is of interest to compare these with the spectra of corresponding vanadium(V) species [16]. The similarities are striking. Protonation of VO_4^{3-}, just like that of CrO_4^{2-}, causes a decrease in absorption and a shift of both bands to shorter wavelengths. Further, dimerization of HVO_4^{2-} to form $V_2O_7^{4-}$ again results in considerably higher absorption together with a shift of the absorption bands to longer wavelengths.

Acknowledgements—Financial support by the Foundation for Research Development and the University of Stellenbosch is gratefully acknowledged.

REFERENCES

1. Poulopoulou, V. G., Vrachnou, E., Koinis, S. and Katakis, D., *Polyhedron*, 1997, **16,** 521.
2. Michel, G. and Machiroux, R., *J. Raman Spect.*, 1983, **14,** 22.
3. Michel, G. and Caha, Y., *J. Raman Spect.*, 1986, **17,** 79.
4. Refs listed by [1–3].
5. Brasch, N. E., Buckingham, D. A., Clark, C. R. and Rowan, A. E., *Aust. J. Chem.*, 1996, **49,** 697.
6. Cieslak-Golonga, M., *Polyhedron*, 1995, **15,** 3667.
7. Sasaki, Y., *Acta Chem. Scand.*, 1962, **16,** 719 and refs therein.
8. Cruywagen, J. J., Rohwer, E. A. and van de Water, R. F., *Polyhedron*, 1996, **16,** 243.
9. Rossotti, H. S., *Talanta*, 1974, **21,** 809.
10. Cohen, M. D. and Fischer, E., *J. Chem. Soc.*, 1962, 3044.
11. Mayer, R. G. and Drago, R. S., *Inorg. Chem.*, 1976, **15,** 2011.
12. Gans, P., Sabatini, A. and Vacca, A., *Talanta*, 1996, **43,** 1739.
13. Maeder, M. and Zuberbühler, A. D., *Anal. Chem.*, 1990, **62,** 2220.
14. Gans, P., Sabatini, A. and Vacca, A., *J. Chem. Soc., Dalton Trans.*, 1985, 1195.
15. Smith, R. M. and Martell, A. E., *Critical Stability Constants*, Vol. 6, second supplement. Plenum Press, New York, 1989.
16. Cruywagen, J. J. and Heyns, J. B. B., *Polyhedron*, 1991, **10,** 249.

Pergamon

PII: S0277-5387(97)00436-1

Polyhedron Vol. 17, No. 10, pp. 1747–1753, 1998
© 1998 Elsevier Science Ltd
All rights reserved. Printed in Great Britain
0277-5387/98 $19.00+0.00

Mixed complexes of 5-nitrosouracil derivatives: Synthesis and structural study of 6-amino-1,3-dimethyl-5-nitrosouracilato (N^5,N^6)-aqua-2,2′-bipyridine (*N*,*N*′)-copper(II) perchlorate hydrate and 2,2′-bipyridine (*N*,*N*′)-chloro-1,3-dimethylviolurato (N^5,O^6)-copper(II) hemihydrate

Francine Bélanger-Gariépy,[a] René Faure,[b] Francisco Hueso-Ureña,[c] Miguel N. Moreno-Carretero,[c,*] Jorge A. Rodríguez-Navarro[d] and Juan M. Salas-Peregrín[d]

[a] Dep. Chimie, Université de Montréal, C. P. 6128, Montréal, Québec H3C 3J7, Canada

[b] Dep. Chimie Analytique 2, Université "Claude Bernard"—Lyon I, 69622 Villeurbanne Cedex, France

[c] Dep. Química Inorgánica y Orgánica, Universidad de Jaén, 23071-Jaén, España

[d] Dep. Química Inorgánica, Universidad de Granada, 18071-Granada, España

(Received 4 August 1997; accepted 24 October 1997)

Abstract—The mixed [Cu(DANU)(bipy)(H_2O)]$ClO_4 \cdot H_2O$ (**1**) and [Cu(DMV)(bipy)Cl]$\cdot 1/2H_2O$ (**2**) complexes have been isolated from the reaction, in water/EtOH medium, of copper(II) perchlorate and chloride with 6-amino-1,3-dimethyl-5-nitrosouracil (HDANU) and 2,2′-bipyridine (bipy). It is noteworthy that, in the second complex, the uracil ligand is the 1,3-dimethyl-violurato monoanion (DMV), appeared from the hydrolysis of HDANU. In addition to X-ray diffraction studies, these compounds have been characterized from IR and EPR spectra and magnetic measurements (77–290 K). The crystal lattice of **1** is made up of discrete square pyramidal [Cu(DANU)(bipy)(H_2O)]$^+$ cations, a disordered perchlorate group and a water molecule. The coordination geometry about the metal centre is square pyramidal (N_4+O). The basal positions are occupied by a bidentate DANU ligand, coordinated through the N15 and N16 donor positions, and a bipyridine ligand. A water molecule (Cu—O1W 2.193(3) Å) occupies the apical site. The compound **2** presents a similar molecular structure to that of **1** with the copper centre lying in a N_3O+Cl environment. In this case, the basal positions are occupied by a bipy ligand and a DMV ligand coordinated through the N15 and O16 donor positions, instead of the DANU ligand found in the previous compound. The apical position is occupied in this case by a chlorine atom (Cu1—Cl1 2.413(2) and Cu2—Cl2 2.389(2) Å). © 1998 Elsevier Science Ltd. All rights reserved

Keywords: crystal structure; complexes; uracil; violuric acid; copper.

There are many bibliographic data relative to structural features [1–3] and coordination modes [4–23] displayed by violuric acids (4-hydroxy-5-nitroso-1,2,3,6-tetrahydro-pyrimidine-2,6-dione) and 6-amino-5-nitrosouracil (4-amino-5-nitroso-1,2,3,6-tetrahydro-pyrimidine-2,6-dione) derivatives (see Fig. 1).

On binding to metal ions, these compounds exhibit well established patterns, which may be described as follows. At first, there are many examples in which the formation of a N5—O4 five-membered chelate ring (O6 if the IUPAC numbering system for pyrimidine heterocycles is followed) is found [12–17]. How-

* Author to whom correspondence should be addressed.

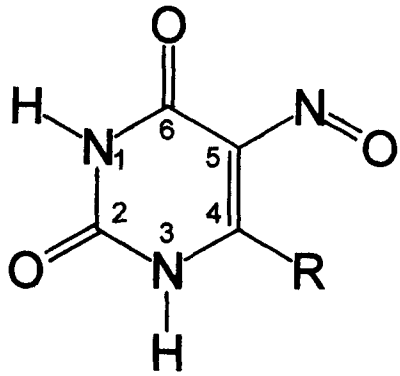

Fig. 1. Molecular structure of 6-amino-5-nitrosouracil (R=NH_2) and violuric acid (R=OH), showing the IUPAC numbering scheme as pyrimidine derivatives.

ever, there are two compounds in which additional coordination schemes are established. In the silver(I)-1,3-dimethylvioluric acid-1,3-dimethyl violurato [18] complex, the metal ion is five-coordinated by two N5,O6 chelates and an O5 atom from a neighbour molecule, resulting in asymmetric chains without metal-metal interactions. The CdL_2 complex with the 6-amino-3-methyl-5-nitrosouracilato anion [19] displays a dodecahedral coordination in which all ligands are equivalents acting as [N5,O4]-[N1,O2] doubly bidentate bridges between two adjacent metal centers.

Moreover, for the 6-amino-5-nitrosouracil derivatives, the bidentate coordination through N5 and N6 atoms has been crystallographically shown [20–23], thus contradicting the authors who pointed out that the primary 6-amino groups are not suitable binding sites due to their low basicity which may be related to the high delocalization of the lone pair of the nitrogen in the heterocyclic ring [24]. These papers describe structures in which there is a N5,N6,N5′,N6′-tetradentate ligand obtained from the condensation of two uracils through the 6-amino group with an alkyl one [21–23] or a roughly planar MN_4 moiety originated by the existence of two N5,N6-bidentate 6-amino-5-nitrosouracil ligands [20].

We have previously reported the structure and properties of 6-amino-1,3-dimethyl-5-nitrosouracilato(N^5,N^6)-2,2′-bipyridine(*N*,*N*′)-ethanol(O)-copper(II) nitrate [25]. Now, as an extension of this work, we report the crystal structure of two new copper(II) mixed bipy complexes with 6-amino-1,3-dimethyl-5-nitrosouracil, $[Cu(DANU)(bipy)(H_2O)]ClO_4 \cdot H_2O$, and 1,3-dimethylvioluric acid, $[Cu(DMV)(bipy)Cl] \cdot \frac{1}{2}H_2O$.

EXPERIMENTAL

Synthesis

All chemicals used in this work were analytical reagent grade. The 6-amino-1,3-dimethyl-5-nitrosouracil (HDANU) was obtained, as monohydrate, by nitrosation of 6-amino-1,3-dimethyluracil (synthesized from condensation of N,N′-dimethylurea and cyanoacetic acid in acetic anhydride) with sodium nitrite and acetic acid.

The synthesis of the complexes was carried out as follows: An aqueous solution (ca 20 ml) containing 0.5 mmol of copper (II) perchlorate (**1**) or copper(II) chloride (**2**) was added, slowly with stirring, to 1 mmol of DANU and 1 mmol of 2,2′-bipyridine, both dissolved in EtOH :water mixture (ca 100 ml). The resulting solutions were stirred for one hour and allowed to stand at room temperature. By evaporation during several days, green crystalline solids were isolated; the yields were ca 85% and 73%, respectively. It must be pointed out that the elemental analysis of the complex **2** clearly indicates the existence of the HDMV (1,3-dimethylvioluric acid) ligand which proceeds from the HDANU hydrolysis; this hydrolysis may be justified by a longer time of crystallisation. However, despite of we have some unpublished results which relate the extent of this reaction with the involvement of the 6-amino group in the hydrogen-bonding in the free ligands, clear conclusions about why and when this process takes place cannot be made. Both solids were filtered off, washed with ethanol and diethylether and air dried. Analytical data were: $[Cu(DANU)(bipy)(H_2O)]ClO_4 \cdot H_2O$. Found: 35.4%C, 3.3%H, 15.1%N, 7.1%H_2O, Calcd 35.7%C, 3.6%H, 15.6%N, 6.7%H_2O; $[Cu(DMV)(bipy)Cl] \cdot \frac{1}{2}H_2O$, Found: 42.5%C, 3.3%H, 15.5%N, 2.2%H_2O, Calcd 42.9%C, 3.4%H, 15.6%N, 2.0%H_2O.

CAUTION! *Perchlorate salts are dangerous and must be handled with care*

Crystallography

Unit cell constants were obtained for crystals of $[Cu(DANU)(bipy)(H_2O)]ClO_4 \cdot H_2O$ (**1**) and $[Cu(DMV)(bipy)Cl] \cdot \frac{1}{2}H_2O$ (**2**) from least squares fits to settings of 25 reflections centred on an Enraf-Nonius CAD-4 diffractometer using graphite-monochromatized Cu-K_α ($\lambda = 1.54056$ Å) and Mo-K_α ($\lambda = 0.71073$ Å) radiations for **1** and **2** respectively. Corrections for absorption were applied: integration (**1**) and Ψ-scans (**2**). The structures were solved by standard Patterson methods and refined by full-matrix least-squares, applying the SHELX-76 [26], SHELXL-93 [27] (**1**) and SDP packages [28] (**2**).

1: $CuClC_{16}H_{19}N_6O_9$, triclinic, space group $P\bar{1}$, $a = 8.049(3)$, $b = 11.946(2)$, $c = 12.024(4)$ Å, $\alpha = 64.71(2)$, $\beta = 86.53(3)$, $\gamma = 88.76(2)^\circ$, $V = 1043.4(5)$ Å^3, $Z = 2$, $F(000) = 550$, $M = 538.36$, $D_c = 1.714$ g cm^{-3}. 3957 independent reflections were collected in the range $2\theta \leqslant 140^\circ$ for a crystal of size $0.53 \times 0.38 \times 0.15$ mm ($\mu = 3.23$ mm^{-1}, max./min. transmission = 0.6252/0.2799). Terminal conventional $R(F_o) = 0.055$ for 3717 reflections with $I > 2\sigma(I)$ and $wR^2(F_o^2, \text{all}) = 0.1647$ ($wR^2 = [\Sigma w(F_o - F_c)^2/\Sigma wF^2]^2$

and $w = [\sigma^2(F_o^2) + (0.1087P)^2 + 0.9972P]^{-1}$ where $P = \frac{1}{3}(F_o^2 + 2F_c^2)$). Max. feature in ΔF map of 0.80 e Å^{-3}. All non-hydrogen atoms were assigned anisotropic temperature factors. The perchlorate group was found to be disordered in three positions with fractional occupation of 0.25, 0.25 and 0.50. Hydrogen atoms of the organic ligands were idealized and those of the water molecules were refined with fixed O—H distances (0.82 Å).

2: $CuClC_{16}H_{15}N_5O_{4.5}$, triclinic, space group $P\bar{1}$, $a = 7.730(9)$, $b = 14.550(6)$, $c = 16.383(8)$ Å, $\alpha = 99.46(4)$, $\beta = 101.55(9)$, $\gamma = 98.43(8)°$, $V = 1750(2)$ Å^3, $Z = 2$, $F(000) = 912$, $M = 448.32$, $D_c = 1.702$ g cm^{-3}. 5889 independent reflections were collected in the range $2\theta \leqslant 50°$ for a crystal of size $0.75 \times 0.35 \times 0.01$ mm ($\mu = 1.49$ mm^{-1}, max./min. transmission 0.993/0.660). Terminal $R(F_o) = 0.067$ for 3825 reflections with $I > 3\sigma(I)$ and $wR(F_o) = 0.084$ ($wR = [\Sigma w(F_o - F_c)^2/\Sigma wF_o^2]^{1/2}$ and $w = 4F_o^2[\sigma^2(I) + (0.1F_o^2)^2]^{-1}$). Max. feature in ΔF map of 0.9 e Å^{-3}. All non-hydrogen atoms were assigned anisotropic temperature factors. Hydrogen atoms of the organic ligands were idealized.

Apparatus

Microanalyses of C, H and N were performed in the Scientific Instrumentation Center of the University of Granada; the water contents of the complexes were determined from the TG plot (Mettler TG-50 thermobalance, air, 10°C min^{-1} heating rate). IR spectra were obtained on a Perkin–Elmer FT-IR 1760x (KBr pellets, 4000–400 cm^{-1}) and Perkin–Elmer 983G spectrophotometer (600–180 cm^{-1}, polyethylene pellets). The EPR spectra were obtained in the X-band at room temperature on a Bruker ESP 300E apparatus, with a microwave frequency of 9.79 GHz and a modulation frequency of 100 kHz. Magnetic measurements were carried out on a Manics DSM-8 system between 77 and 290 K.

RESULTS AND DISCUSSION

Crystal structures

A drawing of molecular units showing the atom numbering is displayed in Fig. 2. Selected bond distances and angles are listed in Table 1.

The crystal lattice of **1** is made up of discrete square pyramidal $[Cu(DANU)(bipy)(H_2O)]^+$ cations, a disordered perchlorate group and a water molecule. The coordination geometry about the metal centre is square pyramidal (N_4+O). The basal positions are occupied by a bidentate DANU ligand, coordinated through the N15 and N16 donor positions and a bipyridine ligand. A water molecule (Cu—O1W 2.193(3) Å) occupies the apical site. The copper centre appears 0.198 Å displaced from the basal plane. The distortion of the polyhedron was calculated by a quantification of the Muetterties and Guggenberger method [29] and the use of trigonal bipyramid (TBP) and square pyramid (SP) as limiting geometries [30], giving an 8% distorted SP (see Table 2).

The structure of **2** is made up of two crystallographically independent square pyramidal [Cu(DMV)(bipy)Cl] entities (I and II) and a crystal lattice water molecule. Compound **2** presents a similar molecular structure to that of **1** with the copper centre laying in a N_3O+Cl environment. In this case, the basal positions are occupied by a bipy ligand and a DMV ligand coordinated through the N15 and O16 donor positions, instead of the DANU ligand found in the previous compound. The apical position is occupied in this case by a chlorine atom (Cu1—Cl1 2.413(2) and Cu2—Cl2 2.389(2) Å). The copper centres are found to be considerably more displaced from the basal plane than in **1**, namely 0.331 and 0.357 Å for Cu1 and Cu2, respectively. This fact may be explained because of considering the covalent radii values of O and Cl, in which it may be deduced a stronger Cu—L axial interaction in compound **2** if it is compared to **1**, which may result in a greater pyramidalization of the coordination polyhedron in **2**. Also, the distortion of the coordination polyhedra in **2** was calculated giving, respectively, 7% and 25% distorted SP for Cu1 and Cu2.

The bond length ratio R(unidentate/bidentate), 1.10 for **1** and 1.20 for **2**, and the normalized bite b (1.29–1.31) of bidentate ligands indicate that these compounds fall into the β class compounds [31]. For those types of molecules nearer the square-pyramid, the structure can be considered to be approaching square-planar four-coordination, with the addition of a fifth more weakly bonded ligand. Both structures are very similar with the related [Cu(DANU)(bipy)(EtOH)]NO_3 [25], in which the ratio R (unidentate/bidentate) is 1.13.

In both cases, the two five-membered chelate rings deviate from planarity, showing an envelope form, and are mutually angled by 11.3° (**1**), and 19.6 (**2**-I) and 23.5° (**2**-II). The uracil moieties are practically planar but are coplanar neither the mean bipy plane (**1**, 5.1°; **2**-I, 12.5°; **2**-II, 18.7°) nor the coordination square-plane [N_4 (**1**) and N_3O (**2**)] (**1**, 4.8°; **2**-I, 4.1°; **2**-II, 11.0°). Also, the mean bipy plane and the coordination plane (**1**, 9.2°; **2**-I, 8.6°; **2**-II, 7.8°) are not coplanar. Finally, both pyridine rings of bipy ligands are slightly angled to each other (**1**, 3.5°; **2**-I, 3.1°; **2**-II, 4.4°).

A very interesting feature is the fact that in **1** the DANU derivative is present whereas in **2** its hydrolysis product DMV appears. However, considered both ligand geometries, it appears difficult to discern which the DANU or the DMV ligand is present in each compound, since there are not statistically significative differences in the C16—N16 (1.242(4) Å) and C16—O16 (1.238(8), 1.263(8) Å) bond distances.

The geometry of pyrimidine moiety in both compounds is very close to those reported for the related

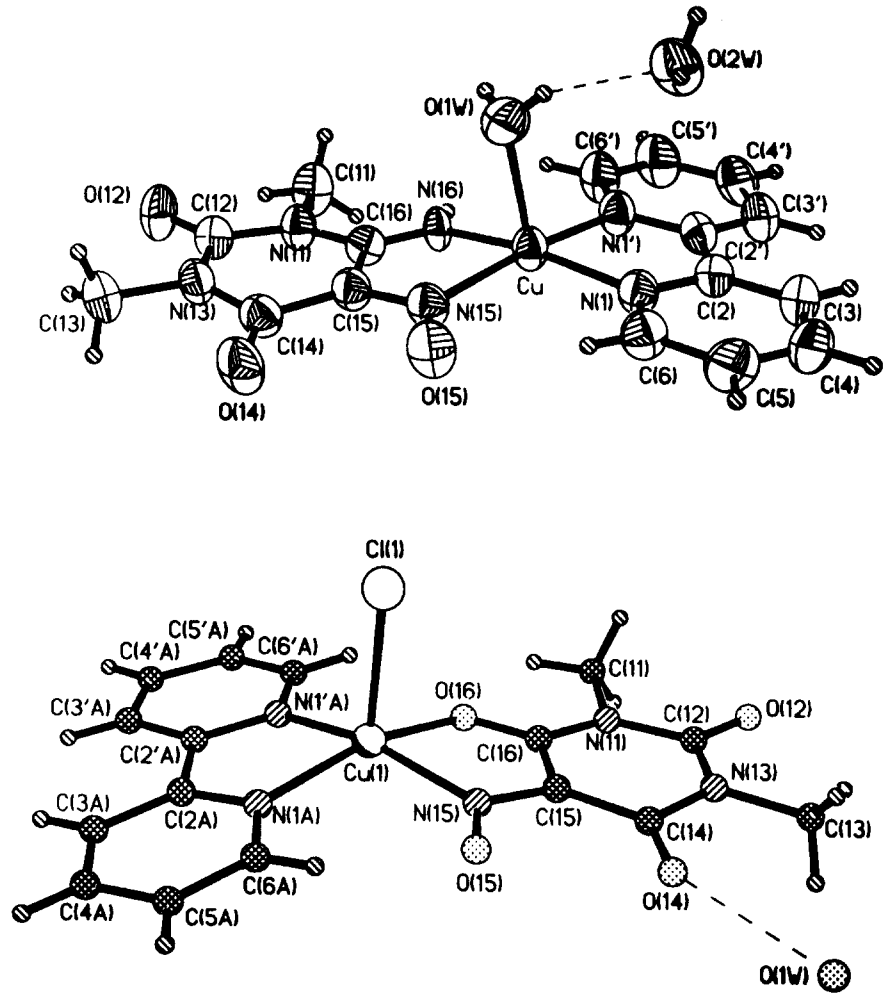

Fig. 2. View of the molecular unit of $[Cu(DANU)(bipy)(H_2O)]ClO_4 \cdot H_2O$ (**1**) (top) and $[Cu(DMV)(bipy)Cl] \cdot \frac{1}{2}H_2O$ (**2**) (bottom). In **1**, disordered perchlorate anions have been omitted for clarity. In **2**, only one unit is displayed; in the other, the DMV atoms are named as X(2*) and the bipy atoms as X(*B).

complexes $[Cu(DANU)_2(H_2O)_2]$ [20], $[Cu(DMV)_2(H_2O)_2]$ [12] and $[Cu(DANU)(bipy)(EtOH)]NO_3$ [25]. The C=O distances correspond to a double bond, the carbonylic character being enhanced on complexation if it is compared with the free ligand [2] although, in the violurato complex, the coordinated C16—O16 and C26—O26 carbonyl groups are significantly longer than the other two ones. In the DANU complex, the C16—N16 distance is shorter (ca 0.06 Å) than the one in the free ligand, showing an increase of the imino character of this group. In all cases, the double N=O bond is also shorter (ca 0.04 Å) in the complex than in the free ligands. On comparing the geometries of all reported data, no significant changes in the bond angles can be detected with the only exception of the angles C14—C15—N15 and N15—C15—C16 which are, on coordinating to the Cu(II) ion, respectively opened and closed (ca 12°) with respect to the free ligand.

The molecules are packed via hydrogen bonding. In **1**, the coordinated water molecule is bonded to the uncoordinated one (O1W···O2W 2.714(4) Å) and to the oxygens of the disordered perchlorate group ($-x$, $-y$, $2-z$) (O1W···O81 2.60(2), O1W···O74 2.86(2) and O1W···O61 2.93(2) Å). Also, the non-coordinated water molecule is involved in hydrogen bonds with the O14 and O15 atoms of uracil moiety ($1-x$, $-y$, $1-z$) (O2W···O14 2.946(4) and O2W···O15 2.935(4) Å) and other perchlorate group ($1+x$, y, z) (O2W···O63 2.87(2), O2W···O71 2.90(2) and O2W···O84 3.07(2) Å). In **2**, there is only a well-established hydrogen bond O1W···O14 (2.952(5) Å) and a weaker contact O1W···Cl1 (3.358(6) Å).

Spectral and magnetic measurements

The IR spectra of these compounds have been compared with those for free HDANU [32] and HDMV [12] and are very similar to those reported for the

Table 1. Bond lengths (Å) and angles (°) around the copper(II)

Compound **1**			
Cu—N1′	1.976(3)	C16—N16	1.242(4)
Cu—N16	1.998(2)	C15—N15	1.335(4)
Cu—N1	2.002(3)	N15—O15	1.246(4)
Cu—N15	2.005(3)	C12—O12	1.206(4)
Cu—O1W	2.193(3)	C14—O14	1.216(4)
N1′—Cu—N16	92.7(1)	N1′—Cu—N1	81.6(1)
N16—Cu—N1	166.8(1)	N1′—Cu—N15	168.2(1)
N16—Cu—N15	80.7(1)	N1—Cu—N15	102.7(1)
N1′—Cu—O1W	98.7(1)	N16—Cu—O1W	93.1(1)
N1—Cu—O1W	99.5(1)	N15—Cu—O1W	91.4(1)
Compound **2**			
Cu1—Cl1	2.413(2)	Cu2—Cl2	2.389(2)
Cu1—N15	2.002(5)	Cu2—N25	2.002(6)
Cu1—O16	1.999(4)	Cu2—O26	2.018(4)
Cu1—N1a	2.024(5)	Cu2—N1b	2.000(5)
Cu1—N1′a	1.991(5)	Cu2—N1′b	2.019(5)
C16—O16	1.238(8)	C26—O26	1.263(8)
C15—N15	1.351(8)	C25—N25	1.348(8)
N15—O15	1.241(6)	N25—O25	1.238(6)
C12—O12	1.196(8)	C22—O22	1.206(8)
C14—O14	1.212(8)	C24—O24	1.202(8)
Cl1—Cu1—N15	96.0(2)	Cl2—Cu2—N25	97.3(2)
Cl1—Cu1—O16	93.7(1)	Cl2—Cu2—O26	103.4(1)
Cl1—Cu1—N1a	106.5(2)	Cl2—Cu2—N1b	101.9(2)
Cl1—Cu1—N1′a	101.2(2)	Cl2—Cu2—N1′b	98.7(2)
N15—Cu1—N1′a	161.2(2)	N25—Cu2—N1b	160.4(2)
O16—Cu1—N1a	159.2(2)	O26—Cu2—N1′b	157.7(2)
O16—Cu1—N1′a	90.9(2)	O26—Cu2—N1b	91.6(2)
N1′a—Cu1—N1a	80.5(2)	N1′b—Cu2—N1b	80.7(2)
N1a—Cu1—N15	102.0(2)	N1′b—Cu2—N25	100.1(2)
N15—Cu1—O16	80.3(2)	N25—Cu2—O26	80.3(2)

related complexes $[Cu(DANU)_2(H_2O)_2]$ [20], $[Cu(DANU)(bipy)(EtOH)]NO_3$ [25] and $[Cu(DMV)_2(H_2O)_2]$ [12]. The main features of the infrared spectra related with the potential donor groups may be described as follows. For DANU complexes, an increase of the imino character of the C6—N6 bond takes place as indicates the shift to upper wavenumber of the band assigned to ν(N—H), which is displaced from 3329 cm^{-1} in the free HDANU [32] to 3466 (**1**), 3473 [25] and 3394 cm^{-1} [20]. This fact may be explained by the behavior of the 6-amino group as a metal binding site. The bands assigned to ν(C=O) carbonyl groups (1729 cm^{-1} in **1** and 1726 in HDANU spectra [32]) remain practically unaffected upon complexation, which is in according with the diffraction results, since the carbonylic oxygen is not involved in the metal-ligand bond. In the other related complexes, this band appears at 1726 [20] and 1729 cm^{-1} [25].

In the IR spectra of DMV complexes, there are no bands around 3300 cm^{-1} assignable to ν(N—H) vibration. This fact was another piece of evidence to the existence of the hydrolysis of DANU to give DMV in the compound **2**. The metal-ligand interaction through the oxygen of one carbonyl group is clearly detected by the changes in the ν(C=O) carbonyl bands, which are all displaced to lower wavenumber with respect to their position in the IR spectrum of the free ligand. In the IR spectrum of **2**, three bands at 1729, 1685 and 1668 cm^{-1} may be assigned to coupled vibrational activity of carbonyl groups. In both title compounds, the band assigned to ν(N=O) of the 5-nitroso group (**1**, 1512 cm^{-1}; **2**, 1510 cm^{-1}) is also shifted to lower wavenumber, as in other related compounds [12,20,25], with respect to its position in the IR spectrum of the free ligands (HDANU, 1518 cm^{-1}; HDMV, 1540 cm^{-1}). Bands corresponding to the main vibrational modes of coordinated 2,2′-bipyridine, clearly distinguished from both HDANU and HDMV bands, appear at 1601, 1585 and 776 cm^{-1} (**1** and **2**) (1579,1558 and 758 cm^{-1} in free bipy), these values being coincident with those found in the spectrum of the related ternary complex $[Cu(DANU)(bipy)(EtOH)]NO_3$ [25]. Also, the infrared spectrum of **1** permits to assign the bands for the

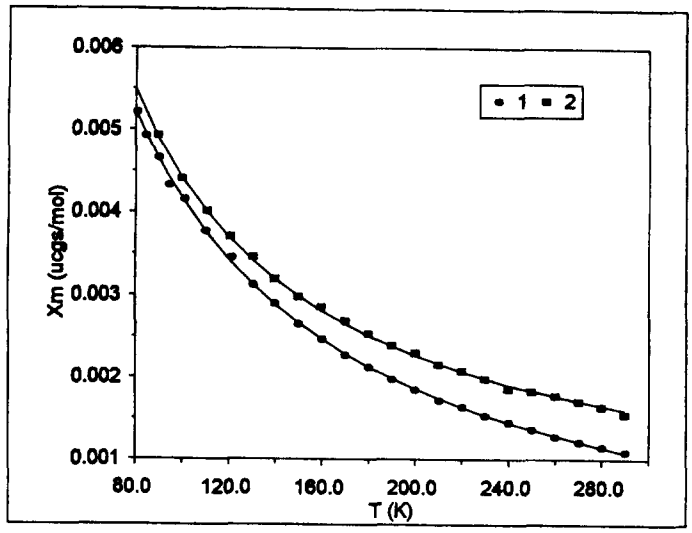

Fig. 3. Magnetic susceptibility values at different temperatures (**1**, circles; **2**, squares).

ν(Cl—O) of perchlorate group [33] (1146, 1117 and 1084 cm^{-1}). The appearance of three bands for this vibration mode in a free tetrahedral anion must be explained by the loss of symmetry that takes place as consequence of the involvement in hydrogen bonds. The analysis of far-IR spectra does not allow us to safely assign any band for metal-ligand vibration modes; only, in the spectrum of **2**, a band at 283 cm^{-1} can be assigned to ν(Cu—Cl) vibration [34].

From the fit of molar susceptibility values at different temperatures (Fig. 3) to the Curie-Weiss' law ($\chi_M = C/[T-\theta]$), the following parameters were obtained: **1**, $C = 0.295(6)$ cgsu K mol^{-1}, $\theta = 33(6)$ K, $r = 0.9950$, $\mu_{eff} = 1.83(4)$ BM and **2**, $C = 0.462(2)$ cgsu K mol^{-1}, $\theta = -3(2)$ K, $r = 0.9998$, $\mu_{eff} = 1.96(6)$ BM. The θ value in the compound **1** indicates that ferromagnetic interactions could be in some extent. However, the confirmation of the apparent trends needs data over a longer temperature range down to 4 K, and that any effects of ferromagnetism must be rather small, particularly in view of the weak intermolecular contacts. In both complexes, the effective magnetic moment for Cu(II) ion, once the diamagnetic corrections were made, is clearly in accord to the existence of magnetically diluted monomeric units [35].

The complexes display axial EPR powder spectra with $g_\perp = 2.03$ and $g_\parallel = 2.25$ (**1**) and $g_\perp = 2.03$ and $g_\parallel = 2.20$ (**2**) and this may be interpreted [36,37] by the existence of a rhombic symmetry with the tetragonal axes parallel, but in which the rhombic component is so small that it is not resolved by the powder technique.

Table 2. Dihedral angles (°) and distortion (Δ) for the coordination polyhedra of **1** and **2**, as proposed by Galy *et al.*, compared to ideal trigonal bipyramid (TBP) and regular tetragonal pyramid (TP) structures[a]

dihedral angles	TBP	1	2 (unit I)	2 (unit II)	TP
δa1	101.5	100.3	97.6	128.8	119.8
δa3	101.5	116.4	113.7	92.2	119.8
δa4	101.5	108.0	104.7	129.7	119.8
δa6	101.5	119.0	113.4	95.7	119.8
δe1	53.1	73.1	97.0	59.3	75.7
δe2	53.1	76.5	78.2	58.6	75.7
δa2	101.5	61.2	64.5	62.6	75.7
δa5	101.5	55.8	58.3	60.1	75.7
δe3	53.1	2.1	2.3	2.5	0
Δ	0	0.92	0.93	0.75	1

[a] Dihedral angles are defined according to Muetterties and Guggenberger. Distortion parameter is defined as

$$\Delta = \frac{|\delta a1+\delta a3+\delta a4+\delta a6-406|}{164.7} + \frac{|\delta e1+\delta e2-106.2|}{203.4} + \frac{|203-\delta a2-\delta a5|}{232.2} + \frac{|53.2-\delta e3|}{477.9}$$

Supplementary material

A list of structure factors and tables with atomic coordinates and isotropic thermal parameters for non-H atoms, bond lengths and angles, anisotropic temperature factors for non-H atoms, hydrogen atom coordinates and equations of planes and dihedral angles are available from author M. N. M.-C. on request.

REFERENCES

1. Craven, B. M. and Mascarenhas Y., *Acta Cryst.*, 1964, **17,** 407.
2. Low, J. N., Howie, R. A., Hueso-Ureña, F. and Moreno-Carretero, M. N., *Acta Cryst.*, 1992, **C48,** 145.
3. Low, J. N., Scrimgeour, S. N., Egglishaw, C., Howie, R. A., Moreno-Carretero M. N. and Hueso-Ureña, F., *Acta Cryst.*, 1994, **C50,** 1329.
4. Riche, C., *C. R. Acad. Sci. Paris*, 1965, **260,** 2516.
5. Gillier, H., *C. R. Acad. Sci. Paris*, 1963, 427.
6. Hamelin, M., *C. R. Acad. Sci. Paris*, 1967, **264,** 2034.
7. Hamelin, M., *C. R. Acad. Sci. Paris*, 1968, **266,** 19.
8. Hamelin, M., *Acta Cryst.*, 1972, **B28.** 228.
9. Raston, C. L. and White, A. H., *J. Chem. Soc., Dalton Trans.*, 1976, 1915.
10. Abraham, F., Nowogrocki, G., Sueur, S. and Bremard, C., *Acta Cryst.*, 1978, **B34,** 1466.
11. Abraham, F., Nowogrocki, G., Sueur, S. and Bremard, C., *Acta Cryst.*, 1980, **B36,** 799.
12. Romero-Molina, M. A., Martin-Ramos, J. D., López-González, J. D. and Valenzuela-Calahorro, C., *An. Quim.*, 1983, **79,** 200.
13. Ruiz-Valero, C., Monge, A., Gutiérrez-Puebla, E. and Gutiérrez-Ríos, E., *Acta Cryst.*, 1984, **C40,** 811.
14. Romero-Molina, M. A., Salas-Peregrín, J. M., Simard, M., Quirós-Olozábal, M. and Beauchamp, A. L., *Polyhedron*, 1990, **9,** 2733.
15. Faus, J., Julve, M., Lloret, F. and Muñoz, M. C., *Inorg. Chem.*, 1993, **32,** 2013.
16. Faus, J., Julve, M., Lloret, F., Real, J. A. and Sletten, J., *Inorg. Chem.*, 1994, **33,** 5535.
17. Moreno-Carretero, M. N., Salas-Peregrín, J. M., Colacio, E., Sánchez-Sánchez, M. P. and Nieto-García, F., *Acta Cryst.*, 1986, **C42,** 407.
18. Ruiz-Valero, C., Monge, A., Gutiérrez-Puebla, E. and Gutiérrez-Ríos, E., *Acta Cryst.*, 1983, **C39,** 1214.
19. Romero-Molina, M. A., Moreno-Carretero, M. N., Sánchez-Sánchez, M. P., Nieto-García, F. and Ruiz, J., *Inorg. Chem.*, 1986, **25,** 1498.
20. Salas-Peregrín, J. M., Romero-Molina, M. A., Sánchez-Sánchez, M. P., Moreno-Carretero, M. N., Quirós-Olozábal, M., Molina-Molina, J. and Faure, R., *Polyhedron*, 1992, **11,** 2217.
21. Colacio, E., Domínguez-Vera, J. M., Escuer, A., Kivëkas, R. and Romerosa, A., *Inorg. Chem.*, 1994, **33,** 3914.
22. Kivëkas, R., Klinga, M., Colacio, E., Domínguez-Vera, J. M. and Romerosa, A., *Acta Cryst.*, 1995, **C51,** 1087.
23. Colacio, E., Domínguez-Vera, J. M., Romerosa, A., Kivëkas, R., Klinga, M. and Escuer, A., *Inorg. Chim. Acta*, 1995, **234,** 61.
24. Martin, R. B. and Mariam, Y. H., *Metal Ions Biol. Syst.*, 1973, **8,** 57.
25. Ferguson, G., Low, J. N., Quirós-Olozábal, M., Salas-Peregrín, J. M., Hueso-Ureña, F. and Moreno-Carretero, M. N., *Polyhedron*, 1996, **15,** 3233.
26. Sheldrick, G. M., *SHELX*-76, *Crystallographic Program System*, University of Cambridge, Cambridge, U.K. 1976.
27. Sheldrick, G. M., *SHELXL*-93, University of Göttingen, Göttingen, Germany, 1993.
28. *SDP Structure Determination Package*, Frenz, B. A. & Associates Inc., College Station, Texas, 1982.
29. Muetterties, E. L. and Guggenberger, L. J., *J. Am. Chem. Soc.*, 1974, **96,** 1748.
30. Galy, J., Bonnet, J. J. and Andersson, S., *Acta Chem. Scand.*, 1979, **A33,** 383.
31. Kepert, D. L., *Inorganic Stereochemistry*, Springer-Verlag, New York, 1982.
32. Salas-Peregrín, J. M., Moreno-Carretero, M. N., Colacio-Rodríguez, E. and Romero Molina, M. A., *Rev. Chim. Minér.* 1984, **21,** 233.
33. Nakamoto, K., *Infrared and Raman Spectra of Inorganic and Coordination Compounds*, 4th edn., Wiley & Sons, New York, 1986.
34. Ferraro, J. R., *Low-Frequency Vibrations of Inorganic and Coordination Compounds*, Plenum Press, New York, 1971.
35. Carlin, R. L., *Magnetochemistry*, Springer-Verlag, Berlin 1986.
36. Pilbrow, J. R., *Transition Ion Electron Paramagnetic Resonance*, Oxford Science Publications, Oxford, 1990.
37. Hathaway, B. J. and Billing, D. E., *Coord. Chem. Rev.*, 1970, **5,** 143.

Pergamon

PII: S0277-5387(97)00430-0

Polyhedron Vol. 17, No. 10, pp. 1755–1758, 1998
© 1998 Elsevier Science Ltd
All rights reserved. Printed in Great Britain
0277-5387/98 $19.00+0.00

The photochemistry of $Ru_3(CO)_{12}$ with HX {X = Cl, Br, I} and the reaction chemistry of $H_2Ru_3(CO)_{10}$ with allyl halides

Nicholas E. Leadbeater,* Jack Lewis, Paul R. Raithby and Moira-Ann Rennie

Department of Chemistry, University of Cambridge, Lensfield Road, Cambridge, CB2 1EW, U.K.

(Received 3 September 1997; accepted 21 October 1997)

Abstract—The potential of photochemistry in cluster synthesis has been demonstrated by the high yield preparation of $(\mu\text{-H})(\mu\text{-X})Ru_3(CO)_{10}$ {X = Cl (**2a**), Br (**2b**), I (**2c**)} from $Ru_3(CO)_{12}$ (**1**) and the molecular structure of $(\mu\text{-H})(\mu Cl)Ru_3(CO)_{10}$ (**2a**) determined by single-crystal X-ray diffraction. As an extension to the work, the halide containing complexes have also been prepared thermally by reaction of the appropriate allyl halide with the novel di-hydrido cluster $H_2Ru_3(CO)_{10}$ (**3**). © 1998 Elsevier Science Ltd. All rights reserved

Keywords: photochemistry; ruthenium; carbonyl clusters.

The photochemistry of organometallic compounds is a developing research area, being of importance both in synthesis and catalysis as well as proving fascinating in its own right [1,2]. Research in our group has focused on harnessing the synthetic potential of photochemistry to generate known and novel compounds efficiently and in high yields [3].

The tri-ruthenium cluster $Ru_3(CO)_{12}$ (**1**) can undergo either photofragmentation or photosubstitution reactions [1]. Our studies have shown that it is possible to control the photoprocesses by simply changing the solvent in which the photolysis is performed [3]. Solvents such as dichloromethane and hexane lead, in the majority of cases, to photofragmentation products. Conversely, photolysis in more polar solvents such as acetonitrile, ethyl acetate or diethyl ether leads to photosubstitution products. In this paper we show that, by irradiating an HX {X = Cl, Br, I} saturated diethyl ether solution of $Ru_3(CO)_{12}$, it is possible to generate the trinuclear clusters $(\mu\text{-H})(\mu\text{-X})Ru_3(CO)_{10}$ in high yield.

As an extension to the work, this class of compound was also formed thermally by reaction of the appropriate allyl halide with the novel di-hydrido cluster $H_2Ru_3(CO)_{10}$ (**3**).

* Author to whom correspondence should be addressed.

EXPERIMENTAL

General

All reactions were performed under an inert atmosphere of dry nitrogen using standard Schlenk techniques and solvents were distilled prior to use. All photochemical reactions were performed in a specially designed glass reaction vessel fitted with a gas bubbler, reflux condenser, solid carbon dioxide cooling finger and a stirrer to ensure that the temperature was even throughout the solution. A 250 W broad-band UV source was used as the light source and reflectors placed around the reaction vessel to maximize efficiency. Solution infrared (IR) spectra were recorded in hexane as solvent using a Perkin–Elmer PE 1710 Fourier-transform infrared spectrometer. ^1H NMR spectra were recorded in $CDCl_3$ as solvent using a Bruker WM250 Fourier-transform NMR spectrometer and data reported using the chemical shift scale in units of ppm relative to the solvent resonance as an internal standard. Ruthenium trichloride was

provided by Johnson Matthey and Co. Ltd and literature methods used to prepare $Ru_3(CO)_{12}$ (**1**) [4] and $H_2Ru_3(CO)_{10}$ (**3**) [5].

Photochemical preparation of $(\mu\text{-H})(\mu\text{-X})Ru_3(CO)_{10}$ {X = Cl (**2a**), Br (**2b**), I (**2c**)}

A diethyl ether solution of **1** (30 mg in 100 ml) was saturated with HX and the reaction mixture then irradiated using the broad-band UV source, the temperature of the solution being maintained around 0°C. The reaction was monitored using IR spectroscopy and deemed complete when there was no further change in the IR spectrum {X = Cl 2 h; Br 3 h; I 5 h}. After evaporating to dryness, the residue was extracted into hexane. After again removing the solvent, the product was recrystallized from pentane yielding pure **2a** (75%) **2b** (60%) or **2c** (50%). Spectroscopic data: **2a** IR(ν_{CO}): 2112 (w), 2077 (s), 2064 (s), 2034 (vs), 2015 (s), 1995 (m) cm^{-1}, ^1H NMR (δ): −13.24 (s, Ru—H); **2b** IR (ν_{CO}): 2116 (w), 2074 (s), 2068 (s), 2027 (vs), 2020 (s), 1994 (m) cm^{-1}, ^1H NMR (δ): −14.42 (s, Ru—H); **2c** IR (ν_{CO}): 2109 (w), 2068 (s), 2062 (s), 2024 (vs), 2007 (s), 1994 (m) cm^{-1}, ^1H NMR (δ): −15.08 (s, Ru—H).

Reaction of $H_2Ru_3(CO)_{10}$ *with allyl halides*

An excess of the appropriate allyl halide was added to a cooled hexane solution of **3** (50 mg in 100 ml). The resultant mixture was stirred for 20 min. After removal of the solvent *in vacuo*, $(\mu\text{-H})(\mu\text{-X})Ru_3(CO)_{10}$ was extracted into cold dichloromethane as the main product (**2a**, 70%; **2b**, 65%; **2c**, 60%), characterised by comparison of IR and ^1H spectral data with that in the literature data [6].

X-ray data collection, structure determination and refinement of $(\mu\text{-H})(\mu\text{-Cl})Ru_3(CO)_{10}$ (**2a**)

Suitable single-crystals of **2a** were grown from a dichloromethane-hexane solution by slow evaporation. Crystal data: $C_{10}HClO_{10}Ru_3$, orange plates, crystal dimensions 0.40 × 0.30 × 0.25 mm, triclinic, $P\bar{1}$ (No. 2), $a = 7.749(5)$ Å, $b = 8.782(6)$ Å, $c = 13.562(8)$ Å, $\alpha = 95.36(3)°$, $\beta = 103.26(3)°$, $\gamma = 110.16(3)°$, $V = 828.1(9)$ Å^3, $D_{calc} = 2.486$ Mg cm^{-3}, $Z = 2$, $F(000) = 580$, Mo–K_α radiation, $\lambda = 0.71073$ Å, μ(Mo–K_α = 2.907 mm^{-1}), $T = 153(2)$ K. Stoe-Siemens AED diffractometer, 2927 reflections collected in the range $3.05 \leqslant \theta \leqslant 25.07$, 2922 unique absorption corrected data ($R_{int} = 0.1159$). The structure was solved by direct methods (Ru atoms) (SHELXTL PLUS [7]) and Fourier difference syntheses and refined with Ru, C and O atoms anisotropic by full-matrix least squares based on F^2 (SHELXL 93 [8]). The bridging hydride was located directly, assigned a fixed thermal displacement parameter and its coordinates refined freely. The refinement converged at $R_1 = 0.0260$ and $wR_2 = 0.0599$ for 2549 observed data [$F > 4\sigma(F)$], and $R_1 = 0.0340$, $wR_2 = 0.0634$ (all data), goodness of fit = 1.059, max, min peak in final difference map = 0.691, −0.604 eÅ^{-3}, max $\Delta/\sigma = 0.001$, weighting scheme $w = 1/[\sigma^2(F_o)^2 + (0.355P)^2 + 0.5868P]$, $P = (F_o^2 + F_c^2)/3$, produced a flat analysis of variance.

RESULTS AND DISCUSSION

Broad-band UV photolysis of a diethyl ether solution of $Ru_3(CO)_{12}$ (**1**) under an atmosphere of HX {X = Cl, Br and I} at 0°C afforded one main product in each case. The reaction products were characterized as the known clusters $(\mu\text{-H})(\mu\text{-X})Ru_3(CO)_{10}$ {X = Cl (**2a**), Br (**2b**), I (**2c**)} (eq. 2) by comparison of spectroscopic data with that in the literature [6].

The photochemical route leads to product yields of approximately 50–75% as compared to about 30% using previous literature methods [6]. This illustrates clearly the advantages of photochemistry as a preparative tool for the synthesis of trinuclear clusters, the reaction here being performed in one stage at room temperature or lower, the yields of the product being high and the reaction time short.

The molecular structure of **2a** was determined by single crystal X-ray analysis (Fig. 1). Selected bond lengths and angles are shown in Table 1. The complex crystallizes in the triclinic space group $P\bar{1}$ (No. 2). The ruthenium and osmium clusters **2a** and $(\mu\text{-H})(\mu\text{-Cl})Os_3(CO)_{10}$ are isomorphous and isostructural, both showing discrete ordered $(\mu\text{-H})(\mu\text{-Cl})M_3(CO)_{10}$ units, separated by normal van der Waals distances [9]. The molecules have approximate C_s symmetry, the doubly-bridged metal–metal bond being slightly longer than the non-bridged bonds. The Ru—Cl—Ru angle in **2a** is relatively acute [71.14(5)°]. By studying the bond lengths in a number of dinuclear ruthenium and osmium complexes containing $(\mu\text{-H})(\mu\text{-Cl})$ bridges it is concluded that there are no clear restraints imposed on the molecule by the [Ru(CO)$_4$] group in **2a** which can, essentially, be considered as a third bridge across the $Ru(\mu\text{-H})(\mu\text{-Cl})Ru$ bond [10].

The molecular structure of $(\mu\text{-H})(\mu\text{-Br})Ru_3(CO)_{10}$ has been reported previously [9]. Unlike **2a, 2b** crystallizes in a monoclinic space group ($P2_1/c$) but both possess the same approximate C_s symmetry in the crystalline state. The di-bridged Ru—Ru bond in **2a** is significantly longer at 2.833(2) Å than that in **2b** {2.819(1) Å} this being interesting since it would be expected that bridging by the larger halogen would lead to a longer metal—metal bond. Also, the Ru—Hal—Ru (Hal = Cl, Br) and Ru—H—Ru angles are larger in the case of **2a** at 70.14(5)° and 96(2)° respectively as compared to **2b** {66.80(5)° and 104.5(1)°}. In both **2a** and **2b** there is a *trans* influence in the Ru—C(O) distances to the carbonyl groups *trans* to the halogen atom {Ru(1)—C(13) = 1.863(5)

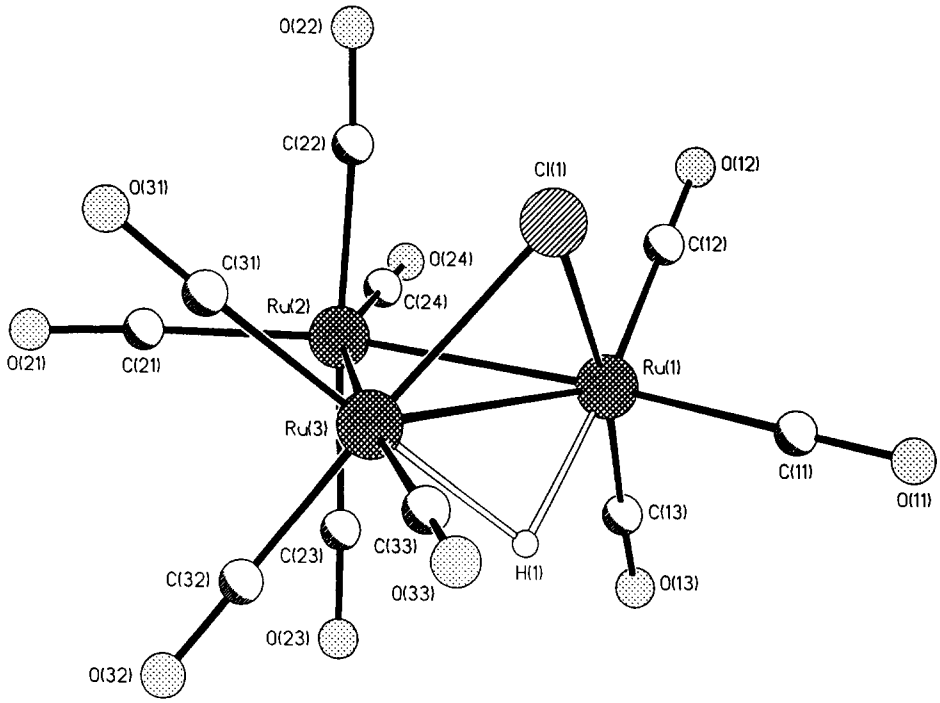

Fig. 1. Molecular structure of **2a**.

Table 1. Selected bond lengths (Å) and angles (°) for **2a**

Ru(1)—Ru(2)	2.810(2)	Ru(3)—Cl(1)	2.433(2)
Ru(1)—Ru(3)	2.833(2)	Ru(1)—H(1)	1.87(5)
Ru(2)—Ru(3)	2.796(2)	Ru(3)—H(1)	1.95(6)
Ru(1)—Cl(1)	2.437(2)		

Ru(1)—Ru(2)—Ru(3)	60.70(5)	Cl(1)—Ru(3)—Ru(1)	54.51(4)
Ru(2)—Ru(3)—Ru(1)	59.88(4)	H(1)—Ru(1)—Ru(3)	43(2)
Ru(3)—Ru(1)—Ru(2)	59.41(3)	H(1)—Ru(3)—Ru(1)	41(2)
Ru(1)—Cl(1)—Ru(3)	71.14(5)	Cl(1)—Ru(1)—H(1)	88(2)
Ru(1)—H(1)—Ru(3)	96(2)	Cl(1)—Ru(3)—H(1)	87(2)
Cl(1)—Ru(1)—Ru(3)	54.35(5)	C(11)—Ru(1)—Ru(3)	113.0(2)

Å, Ru(3)—C(32) = 1.873(5) Å}. This has been observed for similar complexes of general formula $(\mu\text{-H})(\mu\text{-L})Ru_3(CO)_{10}$ {L = COMe [11], $CNMe_2$ [12], NO [13], SCH_2CO_2H [14]}, the *trans* effect in these compounds being even more marked than observed here. Consequently, the differences in these bond lengths are a measure of the donor and π-acceptor properties of L; an increased Ru—X bond strength equating to an increased *trans* Ru—C(O) bond distance. The other Ru—C bond lengths in **2a** range from 1.904(5) to 1.965(5) Å and all the Ru—C—O angles are close to linear, ranging from 175.1(4) to 179.8(4)°.

As well as being synthesised photochemically, **2a**, **2b** and **2c** has been prepared by addition of the appropriate allyl halide to the newly reported di-hydride reagent $H_2Ru_3(CO)_{10}$ (**3**) as in the case of the osmium analogue **4** [15]. This illustrates the potential of **3**, **4** being one of the most versatile tri-osmium clusters known due to its ability to form simple adducts. Of interest is that, even in an excess of allyl halide, the di-halide bridged clusters $(\mu\text{-X})_2Ru_3(CO)_{10}$ are not observed. This is in contrast to **4** where the ratio of $(\mu\text{-H})(\mu\text{-X})Os_3(CO)_{10}$ to $(\mu\text{-X})_2Os_3(CO)_{10}$ is defined by the stoichiometry of reaction [15].

Acknowledgments—We thank Girton College Cambridge for a Research Fellowship (N.E.L.) and the Engineering and Physical Sciences Research Council for support (M.A.R.).

REFERENCES

1. Leadbeater, N. E., *J. Chem. Soc., Dalton Trans.*, 1995, 2923.
2. (a) Perutz, R. N., *Chem. Rev.*, 1993, 361; (b) Geoffroy, G. L. and Wrighton, M. S., *Organometallic Photochemistry*. Academic Press, New York, 1979.
3. Edwards, A. J., Leadbeater, N. E., Lewis, J. and Raithby, P. R., *J. Organomet. Chem.*, 1995, **15,** 512.
4. Eady, C. R., Jackson, P. F., Johnson, B. F. G., Lewis, J., Malatesta, M. C., McPartlin, M. and Nelson, W. J. H., *J. Chem. Soc., Dalton Trans.*, 1980, 383.
5. Leadbeater, N. E., Lewis, J. and Raithby, P. R., *J. Organomet. Chem.*, 1997, **543,** 251.
6. (a) Kampe, C. E., Boag, N. M., Knobler, C. B. and Kaesz, H., *Inorg. Chem.*, 1984, **23,** 1390; (b) Lavigne, G. and Kaesz, H., *J. Am. Chem. Soc.*, 1984, **106,** 4647.
7. Sheldrick, G. M., *SHELXTL-PLUS program for solving, refining and displaying crystal structures from diffraction data*. University of Göttingen, Germany, 1993.
8. Sheldrick, G. M., *SHELXL-93 program for crystal structure refinement*. University of Göttingen, Germany, 1993.
9. Churchill, M. R. and Lashewycz, R. A., *Inorg. Chem.*, 1979, **18,** 1926.
10. For a representative view of molecules containing (μ-H)(μ-Cl) bridges see: (a) Bown, M. and Waters, J. M., *J. Am. Chem. Soc.*, 1990, **112,** 2442; (b) Feng, Q., Ferrer, M., Green, M. L. H., Mountford, P., Mtetura, V. S. B. and Prout, K., *J. Chem. Soc., Dalton Trans*, 1991, 1397; (c) Churchill, M. R. and Ni, S. W. Y., *J. Am. Chem. Soc.*, 1990, **112,** 2442; (d) Churchill, M. R. and Julis, S. A., *Inorg. Chem.*, 1977, **16,** 1488.
11. Johnson, B. F. G., Lewis, J., Orpen, A. G., Raithby, P. R. and Süss-Fink, G., *J. Organomet. Chem.*, 1979, **173,** 187.
12. Churchill, M. R., DeBoer, B. G. and Rotella, F. J., *Inorg. Chem.*, 1976, **15,** 1843.
13. Johnson, B. F. G., Lewis, J. and Zuccaro, C., *J. Chem. Soc., Dalton Trans*, 1980, 99.
14. Jeannin, S., Jeannin, Y. and Lavigne, G., *Inorg. Chem.*, 1978, **17,** 2103.
15. Deeming, A. J. and Hasso, S., *J. Organomet. Chem.*, 1976, **114,** 313.

Pergamon

PII: S0277-5387(97)00429-4

Polyhedron Vol. 17, No. 10, pp. 1759–1765, 1998
© 1998 Elsevier Science Ltd
All rights reserved. Printed in Great Britain
0277-5387/98 $19.00+0.00

Complexes of lanthanide(III) ions with 18-membered Schiff-base macrocycles

Carlos Platas,[a] Rufina Bastida,[b] Andrés de Blas,[a,*] David E. Fenton,[c] Alejandro Macías,[b] Adolfo Rodríguez[b] and Teresa Rodríguez-Blas*[a]

[a] Departamento de Química Fundamental e Industrial, Universidad de La Coruña, Campus de la Zapateira s/n, 15071 La Coruña, Spain

[b] Departamento de Química Inorgánica, Universidad de Santiago de Compostela, Avda. de las Ciencias s/n, 15706 Santiago de Compostela, Spain

[c] Department of Chemistry, The University, Sheffield S3 7HF, U.K.

(Received 4 July 1997; accepted 21 October 1997)

Abstract—18-membered hexadentate N_4O_2 and N_3O_3 Schiff-base polyoxaazamacrocycles derived from 2,6-bis(2-aminophenoxymethyl) pyridine and different organic dicarbonyl compounds are obtained by a template procedure as mononuclear lanthanide(III) complexes. In the absence of the metal salt, macrocycles are not formed. The complexes were characterised by elemental analysis, molar conductivity and mass, UV–V, IR, ^1H NMR and ^{13}C NMR spectroscopy. © 1998 Elsevier Science Ltd. All rights reserved

Keywords: template synthesis; lanthanide(III) complexes; polyoxaazamacrocycle; Schiff-base; ion-selectivity.

The preparation and characterisation of metal complexes with macrocyclic Schiff-base ligands have been the subject of numerous studies in the recent past [1]. This type of ligands have been prepared by cyclo-condensation reaction of appropriate diketo or diformyl and polyamine precursors, often by a template procedure. The presence of a suitable metal ion plays an important role in directing the synthetic pathway of the Schiff base formation and it is now well established that lanthanides can serve as effective templates [2–4].

We are interested in the synthesis and characterisation of new lanthanide coordination compounds with mixed N_xO_y donor set macrocycles. Previously, we have reported the synthesis and spectroscopic properties of lanthanide(III) complexes of N_3O_2, N_3O_3, and N_2O_4 polyoxaaza Schiff-base macrocycles containing aromatic, head and lateral units [5–7]. Herein, we describe the synthesis and characterisation of lanthanide(III) nitrate and perchlorate complexes with the Schiff base polyoxaaza macrocycles L^1 and L^2. Lead(II) complexes with these macrocycles have been previously [8] prepared as intermediates in the preparation of L^3 and L^4, but no further studies were made on them.

* Author to whom correspondence should be addressed. E-mail: mayter@udc.es.

EXPERIMENTAL

Measurements

Elemental analyses, proton and carbon NMR and mass spectra were carried out by Servicios Generales de Apoyo a la Investigación of the Universidad de La Coruña: elemental analyses were carried out on a Carlo Erba 1108 elemental analyser; proton and carbon NMR spectra were run on a Bruker AC 200 F spectrometer and FAB mass spectra were recorded using a FISONS QUATRO mass spectrometer with a Cs ion-gun and using a thioglycerol matrix. The IR spectra were recorded, as KBr discs and/or fluorolube mull, using a Perkin–Elmer 1330 spectrophotometer and the electronic absorption spectra of complexes in acetone solution were recorded at 25°C using a Uvikon 941 Plus spectrophotometer.

Conductivity measurements were carried out in 10^{-3} mol dm^{-3} dimethylformamide or acetonitrile

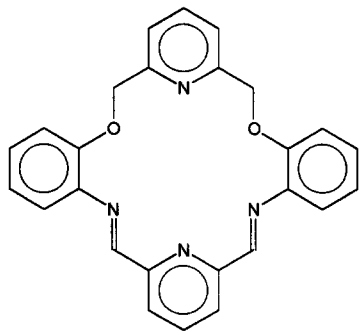

L1

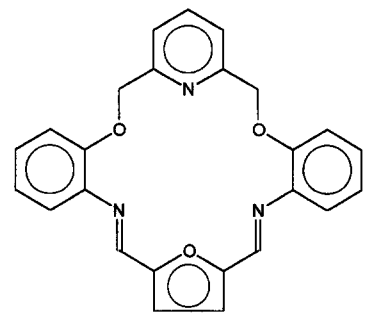

L2

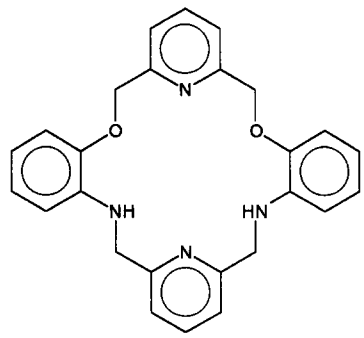

L3

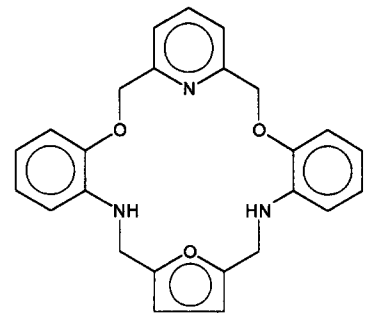

L4

solutions at 25°C using a Crison Micro CM 2201 conductivimeter.

Chemicals and starting materials

2,6-Diformylpyridine and 2,5-diformylfuran were prepared according to literature methods [9–11]. 2,6-bis(2-aminophenoxymethyl)pyridine monohydrate was prepared by reduction of the corresponding dinitro precursor [8]. Lanthanide(III) nitrates and perchlorates were commercial reagents from Aldrich and Alfa laboratories, used without further purification. Solvents were of reagent grade purified by the usual methods. **CAUTION:** perchlorates are potentially explosive!

Condensation between 2,6-diformylpyridine and 2,6-bis(2-aminophenoxymethyl)pyridine monohydrate in the absence of metal ions

Procedure 1. An ethanolic solution of 2,6-diformylpyridine (1 mmol in 25 cm^3) was added dropwise to an ethanolic solution of the diamine (1 mmol in 25 cm^3) with stirring and heating. The solution was refluxed with magnetic stirring for 4 h. The colour changed to yellow and a yellow powder precipitated.

Procedure 2. To a 225 cm^3 of refluxing methanol were simultaneously added, dropwise, two methanolic solutions: 2,6-bis(2-aminomethoxymethyl)pyridine (0.3 mmol in 50 cm^3) and 2,6-diformylpyridine (0.3 mmol in 50 cm^3) over a period of 8 h. The resultant yellow solution was heated for 9 h. No identifiable product could be isolated.

Reaction of 2,6-bis(2-aminophenoxymethyl)pyridine and 2,6-diformylpyridine in the presence of lanthanide(III) ions

General procedure for $[LnL^1][ClO_4]_3$. 2,6-Bis(2-aminophenoxymethyl)pyridine monohydrate (0.3 mmol) and $Ln(ClO_4)_3 \cdot xH_2O$ (Ln = La, Pr, Nd, Sm, Eu, Dy, Ho) were dissolved in hot absolute ethanol (35 cm^3). 2,6-Diformylpyridine (0.3 mmol) dissolved in absolute ethanol (20 cm^3) was slowly added. Stirring and heating of the solution was maintained during the addition and the solution was then refluxed for 2 or 3 h. The yellow powder precipitated was filtered off, washed with diethyl ether and air dried. In some cases, a second portion of the same product was isolated by concentration of the mother liquor.

Ce, Gd, Tb and Er complexes were synthesised by the same procedure using acetonitrile as solvent and the products were isolated from the solution after evaporation until 20 cm^3 and addition of diethyl ether (20 cm^3).

The complexes are air stable in the solid state,

soluble in acetone, acetonitrile, dimethyl sulfoxide and dimethylformamide, moderately soluble in methanol and ethanol and insoluble in chloroform, water and carbon tetrachloride.

General procedure for $[LnL^1][NO_3]_3$. To a solution of 2,6-bis(2-aminophenoxymethyl)pyridine monohydrate (0.3 mmol) in methanol (20 cm^3) was added a solution of the hydrated lanthanide nitrate (0.3 mmol) (Ln = La–Lu, except Pm) in methanol (10 cm^3). The solution was vigorously stirred and heated while a methanolic solution of 2,6-diformylpyridine (0.3 mmol) was dropwise added. Within 5–10 min a yellow precipitate began to appear. Refluxing was maintained for ca 2 h. The product was filtered off, washed with acetone and diethyl ether and dried under vacuum.

The complexes are air stable in the solid state, soluble in dimethyl sulfoxide and insoluble in all other common solvents.

Condensation between 2,5-diformylfurane and 2,6-bis(2-aminophenoxymethyl)pyridine monohydrate in the absence of metal ions

To a 225 cm^3 of refluxing absolute ethanol were simultaneously added, dropwise, two ethanolic solutions of 2,6-bis(2-aminomethoxymethyl)pyridine (0.3 mmol in 50 cm^3) and 2,5-diformylfurane (0.3 mmol in 50 cm^3) over a period of 6 h. The resultant orange solution was heated for 4 h. No identifiable product could be isolated.

Reaction of 2,6-bis(2-aminophenoxymethyl)pyridine and 2,5-diformylfurane in the presence of lanthanide(III) perchlorate ions

General procedure for $[LnL^2][ClO_4]_3$. 2,6-bis(2-aminophenoxymethyl)pyridine monohydrate (0.3 mmol) and $Ln(ClO_4)_3 \cdot xH_2O$ (Ln = La, Pr, Nd, Eu, Gd, Tb, Dy, Ho, Er) were dissolved in hot absolute ethanol (35 cm^3). 2,5-Diformylfurane (0.3 mmol) solved in absolute ethanol (20 cm^3) was slowly added to the former solution. Stirring and heating was maintained during the addition and the solution was then refluxed for 10 min. The powdery precipitate was filtered off, washed and stirred with diethyl ether and dried under vacuum. A second portion of the same product was isolated by concentration of the mother liquor. Cerium and samarium complexes were obtained by the same procedure using acetonitrile as solvent and the product was isolated from the solution after evaporation until 20 cm^3 and addition of diethyl ether (20 cm^3).

The complexes are air stable in solid state, soluble in acetone, acetonitrile, dimethyl sulfoxide and dimethylformamide; moderately soluble in methanol and ethanol and insoluble in chloroform, water and carbon tetrachloride.

RESULTS AND DISCUSSION

Lanthanide(III) complexes of L^1

The template reactions of 2,6-bis(2-aminophenoxymethyl)pyridine and 2,6-diformylpyridine in the presence of hydrated lanthanide perchlorates or nitrates in refluxing absolute ethanol or acetonitrile gave complexes with formula $[LnL^1][ClO_4]_3 \cdot xH_2O$ (Ln = La–Er, except Pm) and $[LnL^1][NO_3]_3$ (Ln = La–Lu, except Pm) in good yields. In general, the yield of the reaction decreases with decreasing ionic radii of the metal ions. The microanalytical data and yields are given in Tables 1 and 2. The conductivity data in dimethylformamide (dmf) for the $[LnL^1][ClO_4]_3 \cdot xH_2O$ are in the range reported for 2 : 1 electrolytes in this solvent (Table 1) [12] and suggest that one perchlorate ion is coordinated, at least in dmf. As we have previously found in other similar compounds [5], the nitrate complexes are less soluble than the corresponding perchlorate ones and their sparing solubility in common solvents has made difficult studies in solution and prevented the measurement of conductivity.

The TG-DTA shows the very high thermal stability of the lanthanide nitrate complexes and supports the proposed formulation. The macrocycle remains intact with the metal ions up to 350°C and no mass loss is observed under this temperature.

All the perchlorate complexes have similar IR spectra indicating that they have similar structures. The absence of carbonyl and amine bands, together with the appearance of an imine band at 1607–1628 cm^{-1}, indicates that condensation and cyclisation has occurred [13]. Medium-to-strong bands at 1580 and 1495 cm^{-1} for the two highest-energy pyridine-ring vibrations are also present. Nitate lanthanide complexes have similar IR spectra exhibiting ν(C=N) as a moderately strong band in the region 1607–1618 cm^{-1}. Information regarding the possible bonding modes of the nitrate and perchlorate anions may also be obtained from the IR spectra. The absorption bands at 1120 cm^{-1} (ν_3) and 627 cm^{-1} (ν_4) present in the perchlorate compounds are assignable to the asymmetric Cl—O stretching and Cl—O bending modes respectively [14–16]. The higher energy band shows considerable splitting, and is actually three maxima at 1144, 1121 and 1088 cm^{-1}, suggesting some interaction of at least one of the ClO_4^- anions with the metal. The greater intensity of the peak at 1121 cm^{-1} compared to those of the side peaks suggests the coexistence of ionic perchlorate [17]. All of the nitrate complexes present bands at 1460, 1280 and 1030 cm^{-1} assignable to the ν(N=O), $\nu_a(NO_2)$ and $\nu_s(NO_2)$ vibrations [18] and clearly identify these species as containing coordinated nitrate groups. The two highest frequency bands are separated 163–185 cm^{-1}, indicating strong interaction between the oxygen atoms from the nitrate with the lanthanide ions and it is typical of bidentate coordination [19,20]. When the

Table 1. Analytical, yield and molar conductance (in dmf) data for the complexes $[LnL^1](ClO_4)_3 \cdot xH_2O$

Ln	x	Analysis (%)[a] C	N	H	Yield (%)	$\Lambda_M/cm^2 \cdot \Omega^{-1} \cdot mol^{-1}$
La	0	36.2(36.4)	6.45(6.5)	2.3(2.35)	81	171
Ce	0	36.0(36.3)	6.5(6.5)	2.2(2.35)	90	168
Pr	1	35.2(35.6)	6.5(6.4)	2.4(2.5)	66	178
Nd	1	35.2(35.4)	6.3(6.7)	2.6(2.5)	71	176
Sm	3	33.6(33.8)	6.0(6.1)	2.7(2.8)	59	178
Eu	1	35.4(35.1)	6.3(6.3)	2.7(2.5)	49	145
Gd	0.5	35.0(35.3)	6.7(6.3)	2.3(2.4)	70	167
Tb	[b]	37.1(37.2)	7.1(6.7)	2.7(2.9)	60	156
Dy	3	33.7(33.4)	6.0(6.0)	2.9(2.8)	55	127
Ho	1	35.0(34.7)	6.2(6.2)	2.7(2.5)	17	132
Er	3	33.2(33.5)	6.0(6.0)	2.8(2.95)	69	160

[a] Required values are given in parentheses.
[b] 0.5 CH_3CN 0.5Et_2O.

Table 2. Analytical and yield data for the complexes $[LnL^1](NO_3)_3$

Ln	Analysis (%)[a] C	N	H	Yield (%)
La	41.9(41.9)	12.9(13.15)	2.5(2.7)	91
Ce	41.95(41.8)	13.1(13.1)	2.7(2.7)	73
Pr	41.75(41.8)	13.1(13.1)	2.6(2.7)	93
Nd	41.3(41.6)	12.6(13.0)	2.6(2.7)	92
Sm	41.5(41.25)	12.9(12.95)	2.5(2.6)	94
Eu	41.0(41.2)	12.8(12.9)	2.5(2.6)	75
Gd	40.7(40.9)	12.7(12.8)	2.5(2.6)	70
Tb	40.7(40.8)	12.6(12.8)	2.8(2.6)	65
Dy	40.2(40.5)	12.4(12.7)	2.5(2.6)	76
Ho	40.3(40.5)	12.5(12.7)	2.7(2.6)	63
Er	40.2(40.4)	12.6(12.7)	2.8(2.6)	73
Tm	40.1(40.3)	12.5(12.65)	2.6(2.6)	64
Yb	40.15(40.1)	12.4(12.6)	2.5(2.6)	50
Lu	41.1(39.95)	12.4(12.55)	2.6(2.6)	61

[a] Required values are given in parentheses.

IR spectra are recorded as KBr discs, a band at 1385 cm^{-1} can be observed; nevertheless, this band, which might be attributed to ionic nitrate, disappears when the spectra is run as fluorolube mulls indicating that there is no ionic nitrate in these compounds [21].

The FAB mass spectra were recorded using thioglycerol as matrix and all of them show the peak at 421 corresponding to $[L^1+1]^+$, confirming the monomeric [1+1] nature of the macrocycle. Likewise, it is possible to observe peaks due to the species $[LnL^1(ClO_4)_2]^+$ (Ln = La, Pr, Nd, Sm, Tb); $[LnL^1(ClO_4)]^+$ (Ln = La, Pr, Nd, Sm, Ho) and $[LnL^1]^+$ (Ln = La, Pr, Nd, Sm, Eu, Ho, Er) in the case of perchlorate complexes and peaks due to the species $[LnL^1(NO_3)_2]^+$ (Ln = Eu, Gd, Tb, Er, Tm, Lu); $[LnL^1(NO_3)]^+$ (Ln = Eu, Gd, Tb, Er, Tm, Lu) and $[LnL^1]^+$ (Ln = Eu, Gd, Tb, Er, Tm, Yb, Lu) for the nitrates.

The electronic absorption spectra of the perchlorate complexes in acetone solutions are virtually identical and present medium to intense bands with maxima at ca 380 nm and a shoulder at ca 350 nm which can be assigned to a transition either on the ligand or to a charge-transfer transition.

The ^1H NMR spectra of lanthanum, cerium, praseodymium, neodymium and samarium perchlorate complexes (Table 3) and the carbon NMR spectrum of lanthanum complex were run in $(CD_3)_2CO$ solution and they are consistent with the proposed formulations. The proton NMR spectrum of the La(III) complex gave the spected simple spectrum, indicating the integrity of the macrocycle in that medium. The spectra obtained after 12 h, 24 h and even some days were similar to the initial one, which indicates the stability of the complex in acetone solution. For the spectrum of the Sm(III) complex with its very small isotropic shifts and sharp signals, assignments could be made by simple comparison with the diamagnetic La(III) complex. For Ce(III), Pr(III) and Nd(III) complexes, resonance assignments were made on the basis of signal integrations and line width analyses. When the spectra of the paramagnetic complexes are compared with that of the lanthanum complex, significant changes in the chemical shifts, in particular for praseodymium and neodymium, are observed: one of the most important occurs for the imine proton signal which is shifted downfield by 6.95 ppm for Pr, 14.92 ppm for Nd and 2.15 ppm for Ce, and upfield by ca 0.5 ppm for Sm. The assignments for the ^{13}C NMR spectrum of the lanthanum complex

Table 3. Proton NMR data of the complexes $[LnL^1](ClO_4)_3$ in d_6-acetone

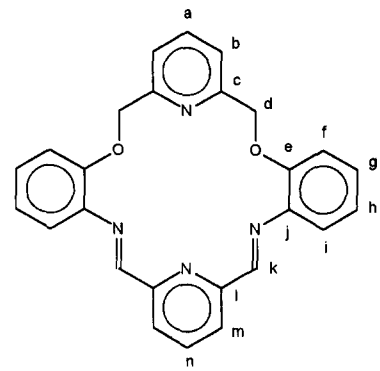

Ln	H_a	H_b	H_d	H_f or H_i	H_g or H_h	H_k	H_m	H_n
La	8.25 (t, 1H)	7.84 (d, 2H)	5.98 (s, 4H)	7.92 (dd, 2H) 7.74 (dd, 2H)	7.64 (td, 2H) 7.39 (td, 2H)	9.48 (s, 2H)	—8.64–8.67 (m, 3H)[a]—	
Ce	—10.20–10.30 (m, 3H)[a]—		2.94 (s, 4H)	4.80 (d, 2H) 4.56 (d, 2H)	5.93 (t, 2H) 5.70 (t, 2H)	11.63 (s, 2H)	7.53 (d, 2H)	8.46 (t, 1H)
Pr	9.95 (t, 1H)	9.09 (d, 2H)	—0.4–1.5 (m, 12H)[a]—			16.43 (s, 2H)	12.73 (d, 2H)	12.43 (t, 1H)
Nd	10.60 (t, 1H)	10.84 (d, 2H)	7.05 (s, 4H)	—6.66–6.02 (m, 8H)[a]—		24.40 (s, 2H)	12.78 (d, 2H)	11.70 (t, 1H)
Sm	8.74 (t, 1H)	8.35 (d, 2H)	6.39 (s, 4H)	7.85 (d, 2H) 7.73 (d, 2H)	7.44 (t, 2H) 7.14 (t, 2H)	8.98 (s, 2H)	—9.35–9.15 (m, 3H)[a]—	

[a] The signals are overlapped.

were achieved with the aid of heteronuclear correlation spectroscopy (^1H-^{13}C COSY), distortionless enhancements by polarisation transfer (DEPT) spectroscopy, and substituent shift calculations: δ_C 164.89 (C_k); 156.24 (C_l); 153.32, 153.01 (C_e, C_j); 143.63 (C_a); 141.54 (C_n); 137.63 (C_c); 132.71 (C_m); 132.35, 125.59 (C_g, C_h), 123.40 (C_b), 121.33 (C_f), 115.74 (C_i); 74.19 (C_d).

It was not possible to run the ^1H NMR spectra of most of the nitrate complexes, because of their poor solubility. The ^1H NMR of lanthanum and samarium complexes were obtained using deuterium dimethyl sulfoxide as solvent. The ^1H NMR spectrum of lanthanum was recorded after different time intervals (3 min, 30 min and 4 h after solution). It becomes more complicated with passage of time and changes in intensity of the signals as well as the appearance of new ones are observed. So, the singlet at 9.24 ppm corresponding to the imine proton is going down in intensity meanwhile other at 9.03 ppm is going up. After four hours, a third signal at 8.67 ppm is also observed. Something similar happens with the signals corresponding to the ethylenic and aromatic protons. The behaviour of perchlorate complexes in this solvent is similar to this one and in either event it is apparent that these compounds are not very stable in this medium. It is possible that this behaviour may be due to the formation of carbinolamines through partial hydrolysis of imine bonds [22], or has been noted previously that there is a loss of metal from the complex on dissolution of polyoxaazamacrocyclic Schiff base complexes in DMSO [23]. In order to understand the real situation, FAB mass spectra of a solution of the $[LaL^1](NO_3)_3$ complex in DMSO were also recorded after different time intervals (immediately after dissolution, and after 1, 3 and 4 h) and all of them show the peak at m/z 421 corresponding to L^1 but no peak corresponding to the complex or to carbinolamines was observed what seems to indicate that the Schiff-base macrocycle L^1 remains intact in the DMSO solution with passage of time and the formation of carbinolamines could be rejected.

The reaction of 2,6-diformylpyridine and 2,6-bis(2-aminophenoxymethyl)pyridine in absolute ethanol or methanol in the absence of metal salt yields a pale yellow solid whose FAB mass spectrum shows a peak at m/z 421, which can be attributable to the Schiff-base diimine macrocycle L^1, nevertheless, the IR spectrum shows a band at 1626 cm^{-1} attributable to $\nu(C{=}N)_{imine}$ together with a carbonyl band at 1721 cm^{-1} indicating formation of acyclic as well as cyclic products. A number of attempts were made to purify the solid but no analytically pure material was obtained. This confirms the importance of the metal ion in directing the steric course of the condensation process; nevertheless, it must be stated that the complexing properties of counterions must be also taking into account in the planning of the template synthesis of macrocyclic

Table 4. Analytical, yield and molar conductance data (in acetonitrile) for the complexes $[LnL^2](ClO_4)_3 \cdot xEt_2O$

Ln	x	Analysis (%)*			Yield (%)	colour	$\Lambda_M/cm^2 \cdot \Omega^{-1} \cdot mol^{-1}$
		%C	%N	%H			
La	0	36.2(35.5)	5.0(5.0)	2.3(2.3)	54	brown	257
Ce	1	34.9(34.7)	5.0(4.85)	2.3(2.2)	60	red	287
Pr	0.5	37.3(36.6)	5.0(4.7)	2.4(2.7)	53	brown	131
Nd	0.5[a]	36.1(35.7)	5.0(4.8)	2.3(2.5)	47	yellow-orange	224
Sm	1	34.1(34.3)	4.8(4.8)	2.1(2.4)	69	red	294
Eu	0.5	36.4(36.2)	5.0(4.7)	2.8(2.7)	61	brown	215
Gd	0.5	36.7(36.0)	5.0(4.7)	2.4(2.7)	45	brown	251
Tb	3[b]	32.4(32.6)	4.7(4.6)	2.6(2.7)	40	red	185
Dy	0.5	36.1(35.7)	5.0(4.6)	2.6(2.7)	58	brown	210
Ho	3[b]	32.6(32.4)	4.3(4.5)	2.9(2.7)	44	brown	152
Er	6[b]	30.1(30.5)	4.0(4.3)	3.1(3.2)	50	red	232

* Required values are given in parentheses.
[a] EtOH.
[b] H_2O.

compounds with particular geometries around the metal ion.

Lanthanide(III) complexes of L^2

The reaction of 2,6-diformylfuran and 2,6-bis(2-aminophenoxymethyl)pyridine in absolute ethanol gave a solid whose IR spectrum shows a band at 1620 cm^{-1} attributable to ν(C=N) together with a carbonyl band at 1735 cm^{-1} indicating formation of acyclic as well as cyclic products. ^1H NMR confirms this situation and shows peaks at δ 9.80 and 8.55 corresponding to the aldehyde and imine protons, respectively. After many attempts to purify the solid, no analytically pure material was obtained.

Condensation between 2,6-bis(2-aminophenoxymethyl)pyridine and 2,5-diformylfuran in the presence of hydrated lanthanide perchlorates in absolute ethanol or acetonitrile gave complexes that agree with formula $[LnL^2][ClO_4]_3 \cdot xEt_2O$ (Ln = La–Er, except Pm) in high yields. The yields of the reactions, analytical and conductivity data are given in Table 4. The molar conductance values of the complexes measured in acetonitrile lie in the range reported for 2:1 electrolytes in this solvent, with the exception of Pr and Ho complexes whose values are in the range reported for 1:1 electrolytes [12].

All the IR spectra show a medium intense band at 1614 cm^{-1} attributable to the azomethine groups. None showed any absorption attributable to ν(C—O) of unchanged carbonyl groups or to ν(NH) of amine groups. The ν_3 and ν_4 bands of the ClO_4^- group occurring at 1121 and 627 cm^{-1} are again split, suggesting some interaction of at least one of the perchlorate anions with the metal [14–16]. Likewise, the greater intensity of the peak at 1121 cm^{-1} compared with the side peaks at 1143 and 1090 cm^{-1} suggests the coexistence of ionic perchlorate [17]. The FAB mass spectra of the complexes in thioglycerol show the peak corresponding to the free macrocycle L^2 at m/z 411, what confirms the monomeric [1+1] nature of the ligand.

The electronic absorption spectra were recorded for freshly prepared solutions in acetone and contain intense and medium bands with maxima at 406–408, 426–430 and 454–458 nm which can be assigned to a transition localised either on the ligand or to a charge-transfer transition.

The ^1H and ^{13}C NMR spectra of the diamagnetic $[LaL^2][ClO_4]_3$ complex was run in $(CD_3)_2SO$ and CD_3CN. The proton spectrum in deuterium dimethyl sulfoxide is complicated, indicating that different types of products are present and it is consistent with the behaviour reported for $[LaL^1]^{3+}$. On dissolution in CD_3CN, however, the expected simple spectra was obtained: δ_H 8.91 (s, 2 H, CH=N), 8.15 (t, 1H pyr H), 7.2–7.8 (m, 12 H, furan H and aryl H) and 5.80 (s, 4 H, CH_2—O) and δ_C 155.35, 153.91, 152.99, 150.42, 141.39, 137.72, 131.99, 126.21, 122.79, 122.64, 120.61, 116.77 and 75.76; this remains unchanged over a period of some days indicating its stability in CD_3CN.

Acknowledgement—We thank Xunta de Galicia (XUGA 20903B94) and the Universidad de La Coruña for financial support.

REFERENCES

1. Guerriero, P., Tamburini, S. and Vigato, P. A., *Coord. Chem. Rev.*, 1995, **139,** 17.
2. Vigato, P. A. and Fenton, D. E., *Inorg. Chim. Acta*, 1987, **139,** 39.

3. Fenton, D. E. and Vigato, P. A., *Chem. Soc. Rev.*, 1988, **17,** 69.
4. Alexander, V., *Chem. Rev.*, 1995, **95,** 73.
5. Bandín, R., Bastida, R., de Blas, A., Castro, P., Fenton, D. E., Macías, A., Rodriguez, A. and Rodriguez, T., *J. Chem. Soc., Dalton Trans.*, 1994, 1185.
6. Bastida, R., de Blas, A., Castro, P., Fenton, D. E., Macías, A., Rial, R., Rodriguez, A. and Rodriguez-Blas, T., *J. Chem. Soc., Dalton Trans.*, 1996, 1493.
7. Adams, H., Bastida, R., de Blas, A., Carnota, M., Fenton, D. E., Macías, A., Rodriguez, A. and Rodriguez-Blas, T., *Polyhedron*, 1997, **16,** 567.
8. Fenton, D. E., Murphy, B. P., Leong, A. J., Lindoy, L. F., Bashall, A. and McPartlin, M., *J. Chem. Soc., Dalton Trans.*, 1987, 2543.
9. Papadoupoulus, E. P., Jarrar, A. and Issidorides, C. H., *J. Org. Chem.*, 1966, **31,** 615.
10. Jerchel, D., Heider, J. and Wagner, H., *Liebigs Ann. Chem.*, 1958, **613,** 153.
11. Oleinik, A. F., and Novitskii, Yu., *J. Org. Chem. USSR*, 1970, **6,** 2643.
12. Geary, W. J., *Coord. Chem. Rev.*, 1971, **7,** 81.
13. Cummings, S. C. and Busch, D. H., *J. Am. Chem. Soc.*, 1970, **92,** 1924.
14. Hathaway, A. J. and Underhill, E., *J. Chem. Soc.*, 1961, 3091.
15. Pavkovik, S. F. and Meek, D. W., *Inorg. Chem.*, 1965, **4,** 1091.
16. Rosenthall, M. R., *J. Chem. Educ.*, 1973, **50,** 331.
17. De Cola, L., Smailes, D. L. and Vallarino, L. M., *Inorg. Chem.*, 1986, **25,** 1739.
18. Nakamoto, K., *Infrared and Raman Spectra of Inorganic and Coordination Compounds*, 3rd edn. Wiley-Interscience, New York, 1977.
19. Guerriero, P., Casellato, U., Tamburini, S., Vigato, P. A. and Graziani, R., *Inorg. Chim. Acta*, 1987, **129,** 127.
20. Forsberg, J. H. and Moeller, T., *Gmelin Handbook. Anorg. Chem.*, Part D1. Springer-Verlag, Berlin, 1980.
21. Avecilla, F., Bastida, R., de Blas, A., Fenton, D. E., Macías, A., Rodríguez, A., Rodríguez-Blas, T., García-Granda, S. and Corzo-Suárez, R., *J. Chem. Soc., Dalton Trans.*, 1997, 409.
22. Abid, K. K. and Fenton, D. E., *Inorg. Chim. Acta*, 1984, **95,** 119.
23. Abid, K. K. and Fenton, D. E., *Inorg. Chim. Acta*, 1984, **82,** 223.

Pergamon

PII: S0277-5387(97)00440-3

Polyhedron Vol. 17, No. 10, pp. 1767–1771, 1998
© 1998 Elsevier Science Ltd
All rights reserved. Printed in Great Britain
0277-5387/98 $19.00+0.00

Structure, spectral and magnetic behaviours of tetrakis(flufenamato)(caffeine)(aqua)di copper(II)—first example of two non-equivalent ligands at the apex

M. Melník,[a] M. Koman,[a]* and T. Glowiak[b]

[a] Department of Inorganic Chemistry, Slovak Technical University, 812 37 Bratislava, Slovak Republic

[b] Institute of Chemistry, University of Wroclaw, F. Joliot-Curie 14, 50-383 Wroclaw, Poland

(Received 6 August 1997; accepted 20 October 1997)

Abstract—The crystal and molecular structure of the tetrakis(flufenamato)(caffeine)(aqua)dicopper(II) $Cu_2(fluf)_4(caf)(H_2O)$, was determined by direct methods and Fourier techniques. The two copper(II) atoms are bridged by four carboxylate group, with the apical ligand of a water molecule around Cu(1), and a caffeine molecule around Cu(2). The spectral and magnetic properties are also discussed. © 1998 Elsevier Science Ltd. All rights reserved

Keywords: copper; structure; flufenamate.

Dimeric copper(II) acetate-type complexes constitute a class of compounds with a long history. The earliest reference to copper acetate is from the year 1597 [1]. In these complexes two copper(II) atoms are bridged by four carboxylate groups in a syn-syn arrangement [2]. The apical positions are usually occupied either by oxygen or nitrogen containing ligands. Each copper displays a distorted square pyramidal geometry. The dimeric complex usually show marked antiferromagnetism [3–5].

Fenamates (mefanamic, niflumic and flufenamic acids) constitute an important group of analgetics which are believed to act through inhibition of prostaglandin biosystems, like other anti-inflammatory analgeties [6]. It is known that some drugs act via chelation [7] or via the inhibition of metalloenzymes [8], but little is known about the modification of activity of most drugs when their ligating potential is utilized. The interaction of the copper(II) atom which plays a vital role in a number of quite different biological processes, with therapeutically administered drugs is a subject of considerable interest.

On the basis of spectral and magnetic properties of copper(II) flufenamate monohydrate a dimeric structure was proposed [9] similar to that of copper(II) acetate monohydrate [10].

In order to better understand some aspects of metal ion-drug interactions, we have studied here the complexation of flufenamic acid [flu, or *N*-(α,α,α-trifluoro-*m*-tolyl)anthranilic acid] in the presence of caffeine (caf). The derivative $Cu_2(fluf)_4(caf)(H_2O)$ was prepared, studied by spectral and magnetic methods and also characterized by X-ray crystallography.

EXPERIMENTAL

Preparation

$Cu(fluf)_2H_2O$ was prepared as described by Melník *et al.* [9]. The green $Cu_2(fluf)_4(caf)(H_2O)$ was prepared by treating caffeine with $Cu(fluf)_2H_2O$ in an equimolar ratio in hot methanol. The resulting solution was fil-

* Author to whom correspondence should be addressed.

tered and the filtrate left to stand at room temperature, allowing fine green crystals to precipitate out. These were filtered off, washed with cold methanol and dried at room temperature. Calc.: for $Cu_2(fluf)_4(caf)(H_2O)$: Cu, 7.59%; C, 51.71%; N, 10.05%; H, 3.62%. Found: Cu, 7.82%; C, 51.4%; N, 8.95%; H, 3.21%.

Spectral studies

Electronic spectrum in the region 10–28 kK was measured with a Perkin–Elmer 450 spectrophotometer. IR spectrum in region 400–3600 cm^{-1} was measured with an IR 10 spectrometer. In both cases, Nujol suspension techniques were used. The EPR spectrum of powdered sample was obtained using a Varian E4 spectrometer at room temperature.

Magnetic susceptibility measurements

Magnetic susceptibility of polycrystaline sample was measured by Faraday method over the temperature range of 77–300 K using a sensitive Cahn RG–HV electrobalance. $Hg[Co(NCS)_4]$ was used as calibrant [11], the value of 16.44 10^{-6} cm^3 g^{-1} was taken as its magnetic susceptibility [12]. Magnetism of sample was found to be field-independent. The effective magnetic moments were calculated from the equation $\mu_{eff} = 2.83\ (X_M \cdot T)^{1/2}$.

Crystallography

Data collection and cell refinement was carried out using Kuma (1991) KM4 diffractometer software [13]. Intensity data were corrected to Lorenz and polarization factors. The structure was solved by the heavy atom method with SHELX86 [14], and subsequent Fourier synthesis using SHELXL93 [15]. Anisotropic thermal parameters were refined for all nonhydrogen atoms. Geometrical analyses was performed using SHELXL93 [15]. The structures were drawn using ORTEP [15]. The final parameters after refinement are summarized in Table 1. Select bond distances and angles are in Table 2.

Supplementary material including non-hydrogen and hydrogen atomic coordinates ($\times 10^4$), anisotropic displacement parameters for nonhydrogen atoms [$Å^2 \times 10^3$] have been deposited at the Cambridge Crystallographic Data Centre. Observed and calculated structural factors are available on request from the correspondence author.

Table 1. Crystal data and structure refinement for $[Cu_2(fluf)_4(caf)(H_2O)]$

Identification code	jon2
Formula	$C_{32.50}H_{23}CuF_6N_4O_6$
FW	743.09
Temperature (K)	293(2)
Wavelength (Å)	0.71069
Crystal system	Monoclinic
Space group	P21/m
a (Å)	11.777(2)
b (Å)	23.156(5)
c (Å)	12.502(3)
α (°)	90
β (°)	95.67(3)
γ (°)	90
V (Å^3)	3392.7(12)
Z	4
D_{calc} (mg m^3)	1.455
Absorption coefficient (mm^{-1})	0.725
$F(000)$	1508
Crystal size (mm)	$0.40 \times 0.31 \times 0.27$
θ range (°)	2.27–25.05
Index ranges	$0/h/14$, $0/k/27$, $-14/l/14$
Reflections collected	6459
Independent reflections	6159 ($R_{int} = 0.0439$)
Absorption correction	No
Refinement method	Full-matrix least-squares on F^2
Data/restraints/parameters	6159/0/472
Goodness-of-fit on F^2	1.001
Final R indices [$I > 2\sigma(I)$]	$R_1 = 0.0489$, $wR_2 = 0.1322$
R indices (all data)	$R_1 = 0.1381$, $wR_2 = 0.1745$
Largest diff. peak and hole (eÅ^{-3})	0.747 and −0.814

RESULTS AND DISCUSSION

The IR spectrum of the complex is very complex. The spectrum of $Cu_2(fluf)_4(caf)(H_2O)$ shows an absorption band at 3250 cm^{-1}. This frequency corresponds to the antisymmetric and symmetric OH stretch and confirms presence of water in the compound. The carboxylate stretching frequencies $\nu_{as}(COO^-)$ at 1625 cm^{-1} and $\nu_s(COO^-)$ at 1390 cm^{-1} are characteristic of copper(II) carboxylate compounds [17]. The stretching vibration of the C=N of heterocyclic ring appears at around 1590 cm^{-1} and on complexation a shift to higher frequencies is observed [18,19]. In the present complex this shift to about 1605 cm^{-1} may suggest bond formation by the metal atom to the nitrogen atom of caffeine, thereby increasing the dipolar contribution of $C{=}N^+$ in the heterocyclic ring.

The electronic spectrum of the complex shows band at 14.2×1000 cm^{-1} (band I) which was identified as *d-d* transition of the copper(II), and a shoulder at 27×1000 cm^{-1} (band II). The shoulder (band II) is characteristic of the bridging system with antiferromagnetic interaction [20].

The EPR spectrum obtained for the powdered sample of $Cu_2(fluf)_4(caf)(H_2O)$ at room temperature contained the typical absorption bands of an axially

Table 2. Selected bond lengths [Å] and angles [°] for $[Cu_2(fluf)_4(caf)(H_2O)]$

Cu(1)—O(11)	1.957(3)	Cu(1)—O(11)#1	1.957(3)
Cu(1)—O(21)	1.956(3)	Cu(1)—O(21)#1	1.958(3)
Cu(1)—O(1)	2.143(5)	Cu(1)—Cu(2)	2.6328(12)
Cu(2)—O(12)	1.958(3)	Cu(2)—O(12)#1	1.958(3)
Cu(2)—O(22)	1.959(3)	Cu(2)—O(22)#1	1.959(5)
Cu(2)—N(31)	2.240(5)	O(11)—C(11)	1.267(5)
O(12)—C(11)	1.242(5)	O(21)—C(21)	1.270(5)
O(22)—C(21)	1.262(5)	N(11)—C(13)	1.381(6)
N(11)—C(18)	1.395(6)	N(21)—C(23)	1.371(7)
N(21)—C(28)	1.397(6)	N(31)—C(38)	1.321(8)
N(31)—C(31)	1.360(7)		

O(11)—Cu(1)—O(11)#1	87.8(2)	O(11)—Cu(1)—O(21)	90.00(13)
O(11)#1—Cu(1)—O(21)	168.92(12)	O(21)—Cu(1)—O(21)#1	90.1(2)
O(11)—Cu(1)—O(1)	97.93(13)	O(21)—Cu(1)—O(1)	93.11(14)
O(21)#1—Cu(1)—O(1)	93.11(14)	O(11)—Cu(1)—Cu(2)	83.94(9)
O(11)#1—Cu(1)—Cu(2)	83.94(9)	O(21)—Cu(1)—Cu(2)	85.03(9)
O(21)#1—Cu(1)—Cu(2)	85.03(9)	O(1)—Cu(1)—Cu(2)	177.39(14)
O(12)—Cu(2)—O(12)#1	88.9(2)	O(12)—Cu(2)—O(22)	90.6(2)
O(12)#1—Cu(2)—O(22)	166.90(13)	O(12)#1—Cu(2)—O(22)#1	90.7(2)
O(22)—Cu(2)—O(22)#1	86.8(2)	O(12)—Cu(2)—N(31)	102.91(13)
O(12)#1—Cu(2)—N(31)	102.91(13)	O(22)—Cu(2)—N(31)	90.1(2)
O(22)#1—Cu(2)—N(31)	89.94(14)	O(12)#1—Cu(2)—Cu(1)	83.89(9)
O(22)—Cu(2)—Cu(1)	82.90(10)	O(22)#1—Cu(2)—Cu(1)	83.04(9)
N(31)—Cu(2)—Cu(1)	170.32(14)	C(11)—O(11)—Cu(1)	123.5(3)
C(11)—O(12)—Cu(2)	124.1(3)	C(21)—O(21)—Cu(1)	123.1(3)
C(21)—O(22)—Cu(2)	125.6(3)	C(38)—N(31)—Cu(2)	110.1(4)
C(31)—N(31)—Cu(2)	146.0(5)		

Symmetry transformations used to generate equivalent atoms: #1 $x, -y+1/2, z$

symmetric binuclear species [21]. The spectral feature of the powder at room temperature shows absorptions at low and high fields (Hz_1 and Hz_2, respectively), with an asymmetrical absorption near 4500 G (H_T2). One absorption is missing because $|D| > h.\nu$ at the X-band frequency used. The spectrum can be interpreted using a spin Hamiltonian for axial symmetry

$$H = g_{II}\beta H_z S_z + g_\perp (H_X S_X + H_Y S_Y) + D(S_Z^2 + 2/3)$$

where $S = 1$ for the thermally accessible triple state and the other symbols have their usual meaning. The value obtained for the spin Hamiltonian parameters are: $g_\perp = 2.065$; $g_{II} = 2.356$; $\langle g \rangle = 2.169$ and $|D| = 0.326\ cm^{-1}$. The $|D|$ value of $0.326\ cm^{-1}$ is large compared to the magnetic quantities (approximately 3.00 G), but is smaller compared to vibrational frequencies. The values are comparable to those found in binuclear copper(II) carboxylates [17].

The molar susceptibilities corrected for diamagnetism and magnetic moments for $Cu_2(fluf)_4(caf)(H_2O)$ are reported at various temperature in Table 3 and graph μ_{eff} (B.M.) against T on Fig. 1.

The temperature susceptibility data can be described by the equation

Table 3. Magnetic data for $Cu_2(fluf)_4(caf)(H_2O)$ (-diamagnetic corr. $\times 10^6 = 347$)

T(K)	$X'_M \times 10^6$	μ_{eff}(B.M.)
93	500	0.60
113	566	0.72
133	642	0.82
153	760	0.95
173	850	1.09
193	895	1.17
213	900	1.24
231	913	1.31
253	945	1.38
273	976	1.46
293	932	1.48

$$X'_M = \frac{g^2 N\beta^2}{3kT} \frac{1}{1+1/3\exp^{-2J/kT}} + N_\alpha$$

where $-2J$ is exchange coupling constant, and other

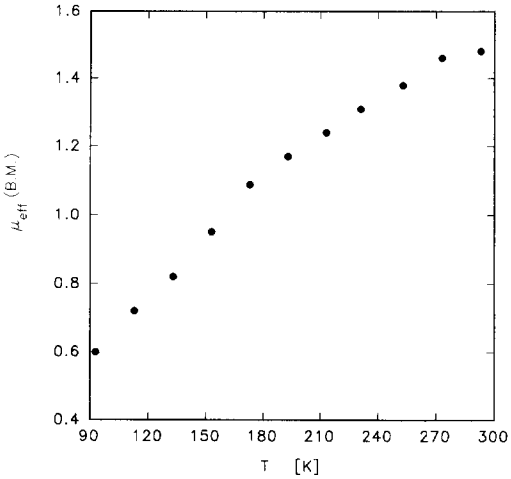

Fig. 1. Temperature dependence of the effective magnetic moment (μ_{eff}) for $Cu_2(fluf)_4(caf)(H_2O)$.

symbols have the usual meaning. The spectroscopic splitting factor g_{av} was obtained from the EPR spectrum and used as constants in the least-square fitting process. The least-squares fitting was performed using a Fortran V program on an Univac 1108 computer. The energy separation ($-2J$) between the triplet and singlet states of 275(10) cm^{-1} which was obtained is similar to those of related copper(II) carboxylates [5,17].

Crystal structure of $Cu_2(fluf)_4(caf)(H_2O)$ with labeling of atoms is shown in Fig. 2. The compound exists as a dimer consisting of two non-equivalent distorted square-based pyramidal copper(II) polyhedra, joined by four carboxilic groups of flufenamato ions formed a square-based around each copper(II) atom. While the apex around Cu(1) is occupied by a water molecule at a distance of 2.141(5) Å, around Cu(2) by a caffeine at a distance of 2.239(5) Å. To our knowledge, this is the first example in this series of dimer copper(II) carboxylates, which the apex position are occupied by two different donor ligands. The Cu—Cu distance is 2.633(1) Å. The displacement of the copper(II) atoms from the basal plane toward the apical ligands also differ, Cu(1) by 0.189 Å and Cu(2) by 0.223 Å.

This molecule follows the trends already noted for this type of dimer. The Cu—Cu separation (2.633(1) Å) as well as Cu—L bond distances are similar to those observed in other Cu(II) carboxylates [2,22].

The bio-test of the compound is in progress and will be published elsewhere.

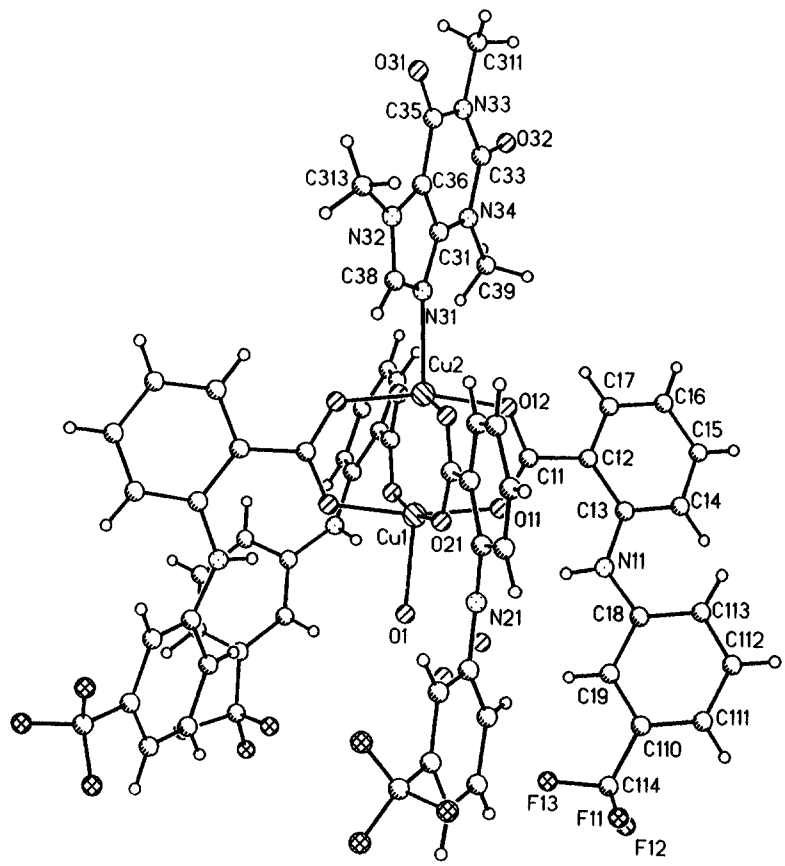

Fig. 2. The molecular structure of $Cu_2(fluf)_4(caf)(H_2O)$.

REFERENCES

1. Libavius, A., *Alchemie reprint "Die Alchemiedes Andreas Libavius. Ein Lehrbuch der Chemie aus dem Jahre* 1957", *Gmelin Institut.* Max-Planck Gesellschaft and Gesellschaft Deutscher Chemister, Verlag Chemie, Weinheim, 1964, p. 381.
2. Melník, M., *Coord. Chem. Rev.*, 1982, **42,** 259.
3. Kato, M., Jannasen, H. B. and Fanning, J. C., *Chem. Rev.*, 1964, **64,** 99.
4. Doedens, R. J., *Progr. Inorg. Chem.*, 1976, **21,** 209.
5. Melník, M., *Kemia-Kemi*, 1982, **12,** 17.
6. Flower, R. J., *Pharm. Rev.*, 1974, **22,** 33.
7. Albert, A., *Selective Toxicity. The Phisicochemical Basic of Therapy*, 6th edn. Chapman and Hall, London, 1979.
8. Hughes, M. N., *The Inorganic Chemistry of Biological Processes*, 2nd edn. Wiley, New York, 1981.
9. Melník, M., Macašková, L. and Mrozinski, J., *Polyhedron*, 1988, **7,** 1745.
10. van Nicker, J. N. and Scholning, F. R. L., *Acta Cryst.*, 1953, **6,** 227.
11. Figgis, B. N. and Nyholm, R. S., *J. Chem. Soc.*, 1958, 4190.
12. König, E., *Magnetic Properties of Coordination and Organometallic Transition Metal Compounds*, Springer Verlag, Berlin, 1966.
13. Kuma, *Kuma KM4 User's Guide.* Version 3.1. Kuma Diffraction, Wroclaw, Poland, 1991.
14. Sheldrick, G. M., *SHELXS*86. *Crystallographic Computing* 3, ed. G. M. Sheldrick, C. Krueger and R. Goddard. Oxford University Press, Oxford, 1985, p. 175.
15. Sheldrick, G. M., *SHELXL*93. Program for Refinement of Crystal Structure. Univ. Göttingen, Germany, 1994.
16. Johnson, C. K., *ORTEP.* Report ORNL-3794. Oak Ridge National Laboratory, Tennessee, 1965.
17. Melník, M., *Coord. Chem. Rev.*, 1981, **36,** 1.
18. Nakamoto, K., Lautil, A., Mantai, C. and Baltanski, M., *J. Chem. Phys.*, 1957, **72,** 1052.
19. Kidani, Y., Noji, M. and Koike, H., *Bull. Chem. Soc. Japan*, 1975, **48,** 249.
20. Dubicki, L. and Martin, R. L., *Inorg. Chem.*, 1966, **5,** 2203.
21. Bleaney, B. and Bowers, K. D., *Proc. Roy. Soc. Lond. A*, 1952, **214,** 451.
22. Sundberg, M. R., Uggla, R. and Melník, M., *Polyhedron*, 1996, **15,** 1157.

Pergamon

PII: S0277-5387(97)00447-6

Polyhedron Vol. 17, No. 10, pp. 1773–1778, 1998
© 1998 Elsevier Science Ltd
All rights reserved. Printed in Great Britain
0277-5387/98 $19.00+0.00

Kinetics of the formation, and optical absorption study of $[IrCl_5(CH_3CN)]^{2-}$ in solution

Jan D'Olieslager, Christiane Görller-Walrand,* Kristel Schoutens and Ben Gilliams

Katholieke Universiteit Leuven, Department of Chemistry, Coordination Chemistry Division, Celestijnenlaan 200F, B-3001 Heverlee (Leuven), Belgium

(Received 1 July 1997; accepted 20 October 1997)

Abstract—In this paper the kinetics of the reaction of $[IrCl_5(H_2O)]^{2-}$ with CH_3CN has been studied. The reaction product was isolated and identified as $K_2[IrCl_5(CH_3CN)]\cdot 2H_2O$. The experimental rate constants show no constant order with respect to the acetonitrile concentration. A preferential solvation of $[IrCl_5(H_2O)]^{2-}$ by acetonitrile in water-acetonitrile mixtures is suggested to explain the data. The obtained optical absorption spectra of $[IrCl_5(CH_3CN)]^{2-}$ are in good agreement with data already published, but another interpretation is given for the observed *d–d* transitions. The low energy transition at about 24,000 cm^{-1} is predicted to be a singlet–singlet transition ($^1A_2 \leftarrow {}^1A_1$), and not a singlet–triplet transition as proposed in other work. © 1998 Elsevier Science Ltd. All rights reserved

Keywords: kinetics; optical absorption spectra; singlet–singlet transition.

Recently transition metal complexes of rhodium and iridium gained renewed interest because of their applications in photographic industry where these compounds are important as doping agents for manufacturing of AgX photographic emulsions [3]. In this context different authors emphasised the importance of mono-substituted transition metal complexes [4–6].

Up to now, little has been reported on substitution reactions of transition metal complexes in mixed solvents, with one or both of these solvents acting as potential ligands. In some cases a preferential solvation of transition metal ions by organic solvents is observed. Some transition metal complexes discriminate in favour of the organic solvent over water with respect to their first shell coordination. Earlier studies on the thermal solvolysis of $[Cr(NCS)_6]^{3-}$ in acetonitrile-water mixtures revealed the strong preference of $[Cr(NCS)_6]^{3-}$ for CH_3CN in CH_3CN–H_2O mixtures [1]. Also *trans*-$[Cr(NH_3)_2(NCS)_4]^-$ in water-acetone mixtures shows a strong preference for acetone in its solvation sphere [2].

In our work on the synthesis and study of the chemical behaviour of complexes with the general formula $[MCl_5X]^{2-}$, M = Rh(III) and Ir(III), X = neutral ligand, we investigated the reaction of $[IrCl_5(H_2O)]^{2-}$ with acetonitrile in mixtures of H_2O—CH_3CN:

$$[IrCl_5(H_2O)]^{2-} + CH_3CN \xrightarrow{k} [IrCl_5(CH_3CN)]^{2-} + H_2O \quad (1)$$

The unusual dependence of the formation rate on the concentration of acetonitrile urged us to examine the kinetics of the reaction in more detail. In order to explain the observed kinetics we suggest a preferential solvation of $[IrCl_5(H_2O)]^{2-}$ by CH_3CN in water-acetonitrile mixtures.

An interpretation of the optical absorption spectrum of $[IrCl_5(CH_3CN)]^{2-}$ is reported, which differs from the one presented earlier [7]. This interpretation is compared with the data for other iridium compounds [8,9].

EXPERIMENTAL

Materials

As a starting product $K_2[IrCl_5(H_2O)]$ is used. This complex was obtained by aquation of $K_3[IrCl_6]$ dissolved in H_2O according to the reaction (eqn (2)) [10].

* Author to whom correspondence should be addressed.

$$[IrCl_6]^{3-} + H_2O \rightarrow [IrCl_5(H_2O)]^{2-} + Cl^- \quad (2)$$

The synthesis of $K_2[IrCl_5(CH_3CN)] \cdot 2H_2O$ was reported earlier by Lebedinskii and Fedorov [11] and by Catsikis and Good [7]. An aqueous solution of $K_3[IrCl_6]$ (5×10^{-2} M) was heated for three hours at 50°C. Under these circumstances, the main complex in the solution is $[IrCl_5(H_2O)]^{2-}$ (>95%) [10]. A 10-fold excess of acetonitrile was added, and the solution was boiled for one min. After cooling, the desired compound precipitated immediately. Addition of absolute ethanol to the filtrate increased the yield. The salt was washed first with absolute ethanol and then with ether. It was dried under vacuum over P_2O_5.

An elemental analysis was performed. The amount of H_2O was determined by a Karl-Fisher titration, K^+, Ir^{3+} were respectively determined by AAS and ICP. Cl^- was determined by Ion Chromatography, after the complex was decomposed by boiling it for 1 h in a solution of Na_2CO_3 (10^{-2} M). The Cl^--ligands are released and the solution turns blue according to the formation of $IrO_2 \cdot 2H_2O$ [12]. Anal: $H_2O = (7.3 \pm 0.3)\%$, $K = (15.0 \pm 0.4)\%$, Cl^- $(36.0 \pm 0.7)\%$, $Ir = (35.5 \pm 0.4)\%$ Calcd for $K_2IrCl_5(CH_3CN) \cdot 2H_2O$: $H_2O = 6.86\%$, $K = 14.8\%$, $Cl^- = 33.6\%$, $Ir = 36.3\%$.

RESULTS

UV-visible absorption spectrum

The UV-visible absorption spectrum of $[IrCl_5(CH_3CN)]^{2-}$ in an aqueous solution is given in Fig. 1. Comparison of our spectrum with the data reported in reference [7] indicate some differences in the position of the absorption peaks as well as in the values of the molar extinction coefficients (see Discussion).

Infrared spectrum

The infrared spectrum in the region 4000–600 cm^{-1} of $K_2[IrCl_5(CH_3CN)] \cdot 2H_2O$, obtained in a KBr pellet, corresponds well with the one reported in literature [7], except for the value of the ν(CN) stretching vibration (Table 1).

Kinetics

When the reaction given in eqn (1) is investigated at a temperature range of 22°C to 42°C, its rate is slowed down sufficiently, to allow a kinetic investigation. Since we observed $[IrCl_5(CH_3CN)]^{2-}$ to be photochemical labile, all experiments were carried out in the absence of light. We checked the stability of $[IrCl_5(CH_3CN)]^{2-}$ spectrophotometrically. The spectral observations indicate that further no secondary reactions occur below 60°C.

The reaction rate was studied spectrophotometrically. The solutions were ca 5 mM respect to the aquapentachloro-iridate(III) complex. The concentration of acetonitrile varied from 0.5 M–7.0 M. $NaClO_4$ was used to keep the ionic strength at a constant value of 0.1 M or 1.0 M. $HClO_4$ was used to adjust the pH of the solution. The solutions were placed in 1 cm quartz cells housed in a thermostated cell holder in the spectrophotometer.

The spectral progress of the reaction of the aquapentachloro-iridate(III) complex with acetonitrile exhibits three isosbestic points at 526 nm, 500 nm and 402 nm. With the reaction order of eqn (1), being first order to the concentration of $[IrCl_5(H_2O)]^{2-}$ in the presence of excess acetonitrile, the system is described by the rate law (eqn (3)):

$$-\frac{d[\{IrCl_5(H_2O)\}^{2-}]}{dt} = k_{exp} \cdot [\{IrCl_5(H_2O)\}^{2-}] \quad (3)$$

The apparent concentration of $[IrCl_5(H_2O)]^{2-}$ is calculated from (eqn (4)):

$$[\{IrCl_5(H_2O)]^{2-}]_t = [\{IrCl_5(H_2O)\}^{2-}]_0 - [\{IrCl_5(CH_3CN)\}^{2-}]_t \quad (4)$$

$[\{IrCl_5(CH_3CN)\}^{2-}]_t$ is measured from the spectral changes at 368 nm, corresponding to the absorption maximum of $[IrCl_5(CH_3CN)]^{2-}$. The experimental rate constants k_{exp} are presented in Table 2. For acetonitrile concentrations below 1.0 M, a deviation of linearity is observed near the end of the reaction. The final spectrum is slightly different from the one in Fig. 1.

Earlier studies by Chang and Garner [13] show that $[IrCl_5(H_2O)]^{2-}$ can undergo a further aquation according to the reaction given in eqn (5). The reaction is first order with respect to the aquapentachloro-iridate(III) ion. The aquation rate constant does not depend on the pH of the solution and it decreases as the ionic strength is increased.

$$[IrCl_5(H_2O)]^{2-} + H_2O \xrightarrow{k_{aq}} [IrCl_4(H_2O)_2]^- + Cl^- \quad (5)$$

Since they measured the values of k_{aq} at an ionic strength of 2.2 M–3.7 M, we repeated their experiments in pure aqueous solutions at 42°C and an ionic strength of 0.1 and 1.0 M corresponding to our reaction conditions. Values of 1.5×10^{-5} s^{-1} and 1.0×10^{-5} s^{-1} are respectively obtained for those reaction conditions.

DISCUSSION

Spectral data (infrared and UV-visible)

Catsikis and Good reported only on the position of the absorption maxima and the corresponding extinc-

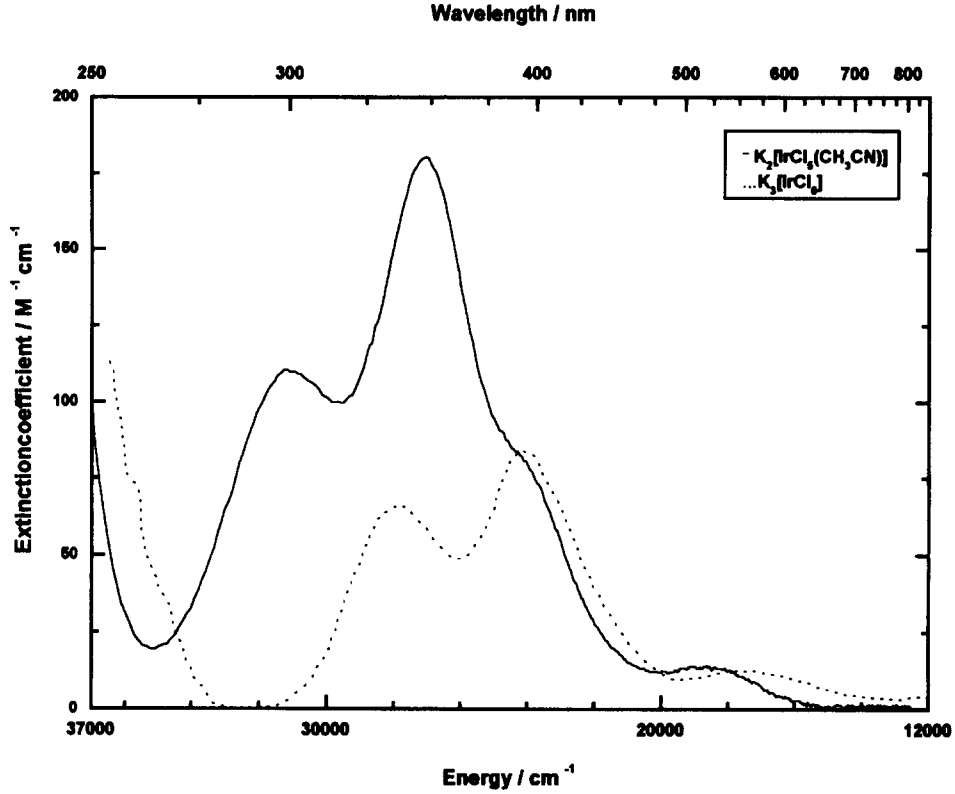

Fig. 1. Optical absorption spectrum of $[IrCl_5(CH_3CN)]^{2-}$ and of $[IrCl_6]^{3-}$ in H_2O at room temperature.

Table 1. IR-peaks of $K_2[IrCl_5(CH_3CN)] \cdot 2H_2O$

IR-peaks (cm^{-1})		
Reference [7]		This work
ν(O—H), $\delta(H_2O)$		3600–3200, 1650–1550
ν(C—H str.)	2941	2940
ν(CN str.)	2381	2320
$\delta(CH_3$ def.)	1408	1408
$\delta(CH_3$ def.)	1361	1360
$\delta(CH_3$ rock.)	1028	1030
ν(C—C str.)	962	962

tion coefficients [7]. A comparison with our data (see Table 3) reveals that although their data for the first absorption band correspond very well, they reported slightly different values for the two other bands. It is difficult to judge over the purity of their product, since only a C, H and N analysis was reported. Taking into consideration their IR-data and more specific the CN-stretching vibration, another significant difference

Table 2. k_{exp} obtained at different reaction conditions

Run No.(°)	T (°C)	$[CH_3CN]$ (mol/l)	μ (M)	pH	$10^3 \cdot k_{exp}$ (s^{-1})[a]
1	42	0.50	0.1	5.6	0.126
2	42	1.00	0.1	5.6	0.29
3	42	1.50	0.1	5.6	0.45
4	42	2.00	0.1	5.6	0.67
5	42	2.50	0.1	5.6	0.91
6	42	3.00	0.1	5.6	1.33
7	42	3.50	0.1	5.6	1.64
8	42	3.95	0.1	5.6	1.98
9	42	4.50	0.1	5.6	2.45
10	42	5.00	0.1	5.6	3.2
11	42	5.50	0.1	5.6	3.8
12	42	6.00	0.1	5.6	4.3
13	42	6.25	0.1	5.6	4.8
14	42	6.50	0.1	5.6	5.1
15	42	7.00	0.1	5.6	6.0
16	42	3.00	1.0	5.6	1.15
17	42	3.00	1.0	1.0	1.19
18	33	4.50	0.1	5.6	0.40
19	23	4.50	0.1	5.6	0.075

[a] Error limits ± 3%.

Table 3. Optical absorption data of $[IrCl_5(CH_3CN)]^{2-}$ in an aqueous solution

Reference [7]				This work				
				Experimental			Calculated	
λ_{max} (nm)	Energy (cm^{-1})	ε ($M^{-1}\,cm^{-1}$)	Assignment	λ_{max} (nm)	Energy (cm^{-1})	ε ($M^{-1}\,cm^{-1}$)	energy (cm^{-1})	Assignment
422	23,700	79	$^3T_{1g} \leftarrow {}^1A_{1g}$	422	23,700	73	24,000	$^1A_2 \leftarrow {}^1A_1$
365	27,400	198	$^1T_{1g} \leftarrow {}^1A_{1g}$	368	27,100	182	26,500	$^1E \leftarrow {}^1A_1$
315	31,700	253	$^1T_{2g} \leftarrow {}^1A_{1g}$	322	31,100	115	31800	$^1E \leftarrow {}^1A_1$
							34,300	$^1B_2 \leftarrow {}^1A_1$

with our spectrum is found (see Table 1). Comparison literature data of other transition metal complexes of the form $[MX_5(CH_3CN)]$ (Table 4) shows that coordinated acetonitrile exhibits a sharp absorption peak in the region of 2320 cm^{-1} to 2330 cm^{-1}. For $Cs_2[RhCl_5(CH_3CN)] \cdot 2H_2O$, a slightly different value is reported by Catsikis and Good [14]. From earlier studies in this laboratory, $Cs_2[RhCl_5(CH_3CN)] \cdot 2H_2O$ is available and we recorded the IR-spectrum. A splitted band with energies of 2304cm^{-1} and 2325 cm^{-1} is observed. The shift of about 60 cm^{-1} for $K_2[IrCl_5(CH_3CN)] \cdot 2H_2O$ is very unlikely, which makes the identity of the product of Catsikis and Good questionable.

Concerning the identification of the optical absorption spectrum we have to point out the difference between the spin-allowed and the spin-forbidden transitions on one hand, and secondly we have to draw the attention to the influence of the introduction of the hetero ligand on the descent in symmetry, causing a split of the degenerate excited states.

The here considered transition metal complex has a t_{2g}^6 ground state configuration ($^1A_{1g}$) and its low lying excited states belong to a $t_{2g}\,{}^5e_g^1$ configuration. For the corresponding hexa-chloro complex, i.e. $[IrCl_6]^{3-}$, the $t_{2g}\,{}^5e_g^1$ configuration gives rise to the $^3T_{1g}$, $^3T_{2g}$, $^1T_{1g}$ and $^1T_{2g}$ representations. From the optical absorption spectrum of $[IrCl_6]^{3-}$ (dotted curve in Fig. 1) the following *d-d* transitions can be identified; $^3T_{1g} \leftarrow {}^1A_{1g}$ at 16,300 cm^{-1}, $^3T_{2g} \leftarrow {}^1A_{1g}$ at 17,900 cm^{-1}, $^1T_{1g} \leftarrow {}^1A_{1g}$ at 24,100 cm^{-1} and $^1T_{2g} \leftarrow {}^1A_{1g}$ at 28,100 cm^{-1} [8]. Although it is hard to interpret and to identify the singlet–triplet transitions (dotted curve in Fig. 1), it is nevertheless obvious that an energy gap of a few 1000 cm^{-1} between the triplet and singlet states is characteristic for such transition metal complexes. As such the singlet–triplet transitions for $[IrCl_5(CH_3CN)]^{2-}$ should be expected at much lower energy than given by Catsikis and Good [7]. Moreover, singlet–triplet *d-d* transitions for octahedrally bound complexes of this kind of compounds are characterised by much smaller intensities than those given by Catsikis and Good (Table 3). It seems then also evident to us to assign the low intensity band at 18,500 cm^{-1} in Fig. 1 as a singlet–triplet transition.

Tetragonal distortion ($O_h \rightarrow C_{4v}$), implied by the substitution of a Cl^- ligand by a CH_3CN ligand causes the T_{1g} and T_{2g} states (in an octahedral parentage scheme) to split in a A_2 and E state for T_{1g}, and in B_2 and E state for T_{2g}. So, for mono-substituted transition metal complexes of this kind, four *d-d* transitions should be observed, but the $^1A_2 \rightarrow {}^1A_1$ and $^1B_2 \rightarrow {}^1A_1$ transitions are allowed only when vibronic coupling is considered. In general the effect of vibronic coupling is not large enough for mono-substituted rhodium and iridium compounds, and rarely a split-

Table 4. Stretching vibration of CN in octahedral transition metal complexes of the form $[MX_5(CH_3CN)]$

Compound	ν(CN) (cm^{-1})	Reference
$K_3[Co(NH_3)_5(CH_3CN)]$	2320	16
$K_2[Rh(CN)_5(CH_3CN)] \cdot 2H_2O$	2325	15
$Cs_2[RhCl_5(CH_3CN)] \cdot 2H_2O$	2304	14
	2304, 2325	This work
$K_2[Ir(CN)_5(CH_3CN)]$	2331	15
$K_2[IrCl_5(CH_3CN)]$	2381	6
	2323	This work

ting of the 2 spin-allowed singlet–singlet transitions is observed [13–15,17–22]. For some complexes the splitting of the first spin-allowed transition is observed, but never a splitting of the second spin-allowed transition [18–20]. This can be explained by looking at the C_4-symmetry representations; here the transitions to the ^1A state are allowed, but those to the ^1B states are forbidden.

We interpret the other transitions observed in Fig. 1 as the $^1A_2 \leftarrow {}^1A_1$ transition at 23,700 cm^{-1}, the $^1E \leftarrow {}^1A_1$ transition at 27,100 cm^{-1} and the $^1E \leftarrow {}^1A_1$ transition at 31,100 cm^{-1}.

A ligand field calculation for $[IrCl_5(CH_3CN)]^{2-}$ was made, using the STATED computer program. Details for the application of this program are given elsewhere [24,25]. We predicted the $^1A_2 \leftarrow {}^1A_1$ transition at approximately 24,000 cm^{-1}; the first $^1E \leftarrow {}^1A_1$ transition at 26,500 cm^{-1}, the second $^1E \leftarrow {}^1A_1$ transition at 31,800 cm^{-1}, and the $^1B_2 \leftarrow {}^1A_1$ transition at 34,300 cm^{-1}. The energies predicted for these transitions correspond pretty well with the experimental results. An even more important conclusion is that the low energy transition at 23,700 cm^{-1} is predicted to be a singlet–singlet transition, and not a triplet–singlet transition as proposed by Catsikis and Good [7]. So $[IrCl_5(CH_3CN)]^{2-}$ can be considered as an example were vibronic coupling is large enough to cause a splitting of the first transition ($^1T_1 \leftarrow {}^1A_1$) and to have two distinguishable transitions to $^1A_2$ respectively to ^1E. The same effect is also observed for some other $[M(NH_3)_5X]^{n+}$ transition metal complexes [18–20] as explained above.

Kinetics

Comparison of our values of k_{aq} with the data presented in Table 2 shows that at high concentrations of CH_3CN (>1 M), the aquation reaction (eqn (5)) is negligible. This is in agreement with the observation that the final spectrum of the reaction progress equals Fig. 1 at high concentrations of CH_3CN. The values of k_{aq} in an aqueous solution indicate that at 0.5 M CH_3CN the aquation reaction starts to contribute to the total reaction, which explains the small deviation of linearity of $\ln([\{IrCl_5(H_2O)\}^{2-}])$ in function of time at 0.5 M CH_3CN.

The data show that k_{exp} does not depend on the pH. This is expected, since $[IrCl_5(H_2O)]^{2-}$ shows only very weak acid properties, the pK_a being 8.8 [10]; 10.1 [26]. A small effect is noted when the ionic strength is raised from 0.1 M to 1.0 M: k_{exp} decreases by about 17%. The Arrhenius activation energy, obtained from a plot of $\ln(k_{exp})$ versus 1/T at a concentration of CH_3CN of 4.5 M and $\mu = 0.1$ M is (30.0±0.5) kcal/mole.

The dependence of k_{exp} on the concentration of acetonitrile is rather unusual. There is no linear relationship between k_{exp} and the concentration of acetonitrile. This implies that the reaction kinetics can not be described by a simple pseudo first order reaction, for which the experimental rate constant is given by $k_{exp} = k \cdot [CH_3CN]^n$, with n expected to be equal to one. A calculation of the order n from a plot of $\ln(k_{exp})$ in function of $\ln([CH_3CN])$ shows that n varies from 1.2 to 1.9 when the acetonitrile concentration varies from 0.5 M to 7.0 M, as shown in Table 5.

Table 5. Formal reaction order n as a function of the bulk acetonitrile concentration

$[CH_3CN]$ (mol/l)	n
0.5–1.5	1.2
1.5–2.5	1.4
2.5–4.5	1.6
4.5–7.0	1.9

To explain this behaviour, one must be aware of the fact that different interactions have to be taken into account in mixed solvents. Evidence exists for short distance ion–solvent interactions, which lead to immediate reagent surrounding, significantly different of the composition of the bulk medium. More specific, it is shown that some transition metal complexes show preferential solvation by an organic solvent in binary mixtures with water. Behrendt *et al.* [1] studied the aquation of $[Cr(NCS)_6]^{3-}$ in CH_3CN–H_2O mixtures. There kinetic results show that the experimental solvolysis rate constant decreases with increasing mole fraction of CH_3CN. The NMR method for determining the composition of the solvation shell of a paramagnetic solute [27] has been applied to reveal a strong preference of $[Cr(NCS)_6]^{3-}$ for CH_3CN in CH_3CN–H_2O mixtures. Similar results are obtained for *trans*-$[Cr(NH_3)_2(NCS)_4]^-$ in acetone-water mixtures [2]. A similar preference of the complex ion for acetone is demonstrated. Our kinetic results point also in the direction of a preferential solvation of $[IrCl_5(H_2O)]^{2-}$ by acetonitrile. If this indeed occurs, the concentration of CH_3CN in the solvation sphere will be higher then the bulk concentration. This would explain why the experimental rate constant shows no constant order with respect to the bulk acetonitrile concentration.

CONCLUSION

In this paper an optical absorption investigation of $[IrCl_5(CH_3CN)]^{2-}$ in an aqueous solution is presented. The obtained spectra are in rather good agreement with data published before, but another interpretation is given for the observed *d-d* transitions. The low energy transition at about 24,000 cm^{-1} is predicted to be a singlet–singlet transition ($^1A_2 \leftarrow {}^1A_1$), and not a singlet–triplet transition as proposed in other work. As such the $[IrCl_5(CH_3CN)]^{2-}$ compound

can be considered as an example were vibronic coupling is large enough to cause a splitting of the (in an octahedral parentage scheme) first $^1T_{1g} \leftarrow {}^1A_{1g}$ transition of the corresponding hexa-compound.

Our kinetic results suggest a preferential solvation of $[IrCl_5(H_2O)]^{2-}$ by acetonitrile in water-acetonitrile mixtures.

Acknowledgements—B.G. (specialisatiebursaal IWT) is indebted to the "Flemish Institute for the Encouragement of Scientific and Technological Research in the Industry (IWT)" for financial aid. Financial support from the Geconcerteerde Onderzoeksacties (Konventie No. 87 93-110) and the IIKW (4.0007.94 and G.0124.95) is also gratefully acknowledged.

REFERENCES

1. Behrendt, S., Langford, C. H. and Frankel, L. S., *J. Am. Chem. Soc.*, 1969, **91,** 2236.
2. Langford, C. H. and White, J. F., *Can. J. Chem.*, 1967, **45,** 3049.
3. Eachus, R. S. and Olm, M. T., *J. Soc. Photogr. Sci. Tech. Japan*, 1991, **54,** 294.
4 . Endo, K. and Saikawa, M., *J. Photogr. Sci.*, 1990, **38,** 210.
5. Marchetti, A. P. and Eachus, R. S., *Adv. Photochem.*, 1992, **17,** 145.
6. Vercammen, H., Ceulemans, T., Schoemaker, D., Moens P. and Vandenbroucke, D., *Phys. Stat. Sol.*, submitted for publication, 1997.
7. Catsikis, B. D. and Good, M. L., *Inorg. Nucl. Chem. Lett.*, 1973, **9,** 1129.
8. Jørgensen, C. K., *Acta Chem. Scand.*, 1956, **10,** 500.
9. Cotton, F. A. and Wilkinson, G., *Advanced Inorganic Chemistry*, 5th edn. John Wiley & Sons, New York, 1988, p. 900.
10. Poulsen, I. A. and Garner, C. S., *J. Am. Chem. Soc.*, 1962, **84,** 2032.
11. Lebedinskii, V. V. and Fedorov, I. A., *Ann. Inst. Platine (U.S.S.R)*, 1935, **12,** 87.
12. Gmelin, *Handbuch der Anorganische Chemie*. Springer-Verlag, Berlin-Heidelberg-New York, 1978.
13. Chang, J. C. and Garner, C. S., *Inorg. Chem.*, 1965, **4,** 209.
14. Catsikis, B. D. and Good, M. L., *Inorg. Chem.*, 1969, **8,** 1095.
15. Geoffroy, G. L., Wrighton, M. S., Hammond, G. S. and Gray, H. B., *Inorg. Chem.*, 1974, **13,** 430.
16. Jordan, R. B., Sargeson, A. M. and Taube, H., *Inorg. Chem.*, 1966, **5,** 1091.
17. Jørgensen, C. K., *Adv. Chem. Phys.*, 1962, **5,** 33.
18. Wentworth, R. A. D. and Piper, T. S., *Inorg. Chem.*, 1965, **4,** 709.
19. Thomas, T. R. and Crosby, G. A., *J. Mol. Spectrosc.*, 1971, **38,** 118.
20. Blanchard, W. D. and Mason, W. R., *Inorg. Chim. Acta*, 1978, **28,** 159.
21. Robb, W. and de Steyn, M. M. V., *Inorg. Chem.*, 1967, **6,** 615.
22. Palmer, D. A. and Harris, G. M., *Inorg. Chem.*, 1975, **14,** 1316.
23. Rosenberg, G. N., Ph.D. thesis, University of British Columbia, 1974.
24. Gilliams, B., Heerman, L. and Görller-Walrand, C., *J. Alloys and Compounds*, 1997, **259,** 153.
25. *STATED—Development of a Computer Program*, A. Ceulemans, Ph.D. thesis (appendix), Katholieke Universiteit Leuven, 1979.
26. Jørgensen, C. K., *Acta Chem. Scand.*, 1957, **11,** 151.
27. Frankel, L. S., Stengle, T. R. and Langford, C. H., *Chem. Comm.*, 1965 373.

Pergamon

PII: S0277-5387(97)00438-5

Polyhedron Vol. 17, No. 10, pp. 1779–1785, 1998
© 1998 Elsevier Science Ltd
All rights reserved. Printed in Great Britain
0277-5387/98 $19.00+0.00

The effect of chelate rings on the structure of copper(II) compounds with triamine derivatives. The crystal structure of [Cu(dptSS)Cl_2]

A. Hatzidimitriou and C. A. Bolos*

Department of General and Inorganic Chemistry, Lab. of Inorganic Chemistry, Aristotle University, Thessaloniki 54006, Greece

(Received May 27 1997; accepted 20 October 1997)

Abstract—The reaction of Schiff bases of dipropylenetriamine (dpt) with 2-thiophenecarboxaldehyde, 2-furaldehyde and pyrrol-2-carboxaldehyde with copper(II) salts in 1 : 2 : 1 molecular ratios, gave compounds of general formula [$CuLX_2$]; [L = Schiff base of dipropylenetriamine with 2-thiophenecarboxaldehyde (dptSS), 2-furaldehyde (dptOO) and pyrrol-2-carboxaldehyde (dptNN) and X = Cl, Br]. The compounds have been characterised by elemental analyses, molar conductance, magnetic, electronic and IR spectral studies. The X-ray crystal structure of the blue-green [Cu(dptSS)Cl_2] has also been solved. Copper(II) is five coordinated with three Cu—N contacts [2.025(3) Å, 2.064(3) Å and 2.004(3) Å] from the tridentate dptSS and two contacts from chlorine atoms at distances 2.545(1) Å and 2.290(1) Å. The five donors form a distorted square pyramid which contains the N(1), N(2), N(3) and Cl(2) on the basal plane and Cl(1) on the apical position. The IR and the electronic spectra are in accordance with the established features of the structure. The molar conductivity indicates that the complexes are 1 :1 electrolytes, while the magnetic moments are consistent with monomeric copper(II) units. © 1998 Elsevier Science Ltd. All rights reserved

Keywords: copper complexes; dipropylentriamine Schiff bases; crystal structure.

The relationship between structure and the chelate ring size of multidentate ligands (i.e. polyamines, Schiff base derivatives etc.) in coordination compounds is a subject of considerable importance, because this relation provides information on physical and chemical properties, biological activities etc. The first takes into account the geometry, the magnetism and spectroscopy coming from the mode of the ligand's coordination and its conformation [1–6]. The second view is related with the variation in biological activity and cytotoxicity depending on the chain length of the ligands and the oxidation state of the metal atom [7,8].

Among the metal atoms, copper(II) readily forms complexes with polyamines and their Schiff bases [9–12]. The geometry of the copper(II) complexes is related to the size of the polyamine ligand and the additional moieties. A recent detailed study [9] has shown that the reaction of Schiff base ligand 1,7-dithenylidine-1,4,7-triazaheptane (dienSS) with $CuCl_2 \cdot 2H_2O$ yields a polymeric compound with extended linear chain structure. The $[Cu_3(dienSS)_2Cl_6]_x$ repeating units occur via a double $CuCl_2Cu$ bridge that connects highly elongated octahedra and a single CuClCu bridge that connects the octahedra with $[CuCl_4]^{2-}$ units. The factors they may rationalise the observed geometry are: (a) vibronic forces; (b) the increased acceptor abilities of the $[Cu(dienSS)]^{2+}$ units, and (c) the inability of Cl^- to afford higher coordination numbers to Cu(II).

Continuing our studies on similar systems, we have prepared and studied a series of Cu(II) complexes with Schiff bases of dipropylenetriamine with heterocyclic aldehydes and we therefore report in this paper the X-ray crystal structure of the [Cu(dptSS)Cl_2] complex. A comparison between the polymeric $[Cu_3(dienSS)_2Cl_6]_x$ and the monomeric [Cu(dptSS)Cl_2] complex is also discussed. The different heterocyclic aldehydes were used to prepare the dipropylenetriamine Schiff bases due to their ability to change the charge on the Cu(II)

* Author to whom correspondence should be addressed.

atom [2], transforming thus the complexes to bioactive reagents.

EXPERIMENTAL SECTION

Materials

$CuCl_2 \cdot 2H_2O$, $CuBr_2$, pyrrol-2-carboxaldehyde, 2-furaldehyde and 4-azaheptamethylenediamine were purchased from Merck and used as received. 2-Thiophenecarboxaldehyde were purchased from Aldrich Chemical Company. The solvents used were reagent grade and were used without any further purification.

Preparation of the complexes

The complexes I–V (Table 1) were prepared from the product of the condensation reaction of dipropylenetriamine with the heterocyclic aldehydes and its further reaction with $CuCl_2 \cdot 2H_2O$ or $CuBr_2$.

[Cu(dptSS)Cl_2]. (I) was prepared as follows: 1.31 g (10 mmol) of dipropylenetriamine was stirred for 20 min with 2.24 g (20 mmol) of 2-thiophenecarboxaldehyde and the oily product was diluted with 20 ml of methanol. A solution of $CuCl_2 \cdot 2H_2O$ (1.71 g, 10 mmol) in 10 ml of methanol was added. The resulting blue-green mixture was then allowed to evaporate slowly kept at 4°C. After 5 days blue-green crystals of the compound (I) were isolated by filtration. Yield: 62%.

[Cu(dptSS)Br_2]. (II) was prepared in a similar manner using $CuBr_2$ and was obtained as bluish-green microcrystalline powder in 80% yield.

[Cu(dptOO)Cl_2]. (III)-Dipropylenetriamine 1.31 g (10 mmol) was mixed with 2.62 g (20 mmol) of 2-furaldehyde and the oily product was diluted with 20 ml of methanol. A solution of $CuCl_2 \cdot 2H_2O$ (1.71 g, 10 mmol) in 10 ml of methanol was added. The resulting green mixture was concentrated to 15 ml volume by rotary evaporation. The solution was allowed further to evaporate in low temperature (4°C). After 48 h green crystals of compound III were isolated in 67% yield.

[Cu(dptOO)Br_2]. (IV) was prepared by an almost similar manner. 1.31 g (10 mmol) of dipropylenetriamine was mixed with 2.62 g (20 mmol) of 2-furaldehyde and the oily product was diluted with 20 ml of methanol. A solution of $CuBr_2$ (2.23 g, 10 mmol) in 20 ml of MeOH was added. The resulting solution was then allowed slowly to evaporate in the air. After 2 weeks bluish-green microcrystalline powder was isolated by filtration, washed with ether, and dried *in vacuo*. Yield: 80%.

[Cu(dptNN)Cl_2]. (V) 1.31 g (10 mmol) of dipropylenetriamine and 1.94 g (20 mmol) pyrrol-2-carboxaldehyde were mixed in methanol (15 ml). To the resulting mixture, a solution of $CuCl_2 \cdot 2H_2O$ (1.71 g, 10 mmol) in methanol was added. The resulting brown solution was concentrated to 10 ml volume by rotary evaporation. Then, the brownish precipitate was filtered off, washed with ether and dried *in vacuo*. Yield: 60%.

The complexes were recrystallised from hot methanol and they are soluble in methanol, water, DMSO and DMF but insoluble in $CHCl_3$, CCl_4 and ether.

Methods

C, H and N were analysed with a Perkin–Elmer elemental analyser and copper was determined by

Table 1. Analytical data, UV-vis bands, magnetic moments and molar conductivity values of the new copper(II) compounds

No	Compound	%C calc. (found)	%H calc. (found)	%H calc. (found)	%Cu calc. (found)	UV-vis (nm) (log ε)	μ_{eff} (BM)	$\Lambda\mu$ ($\mu S \cdot cm^{-1}$)
I	[Cu(dptSS)Cl_2]	42.33 (42.29)	4.63 (4.60)	9.26 (9.24)	14.00 (13.96)	266(4.38) 271(4.26) 633(2.28)	1.73	92
II	[Cu(dptSS)Br_2]	35.40 (35.45)	3.87 (3.91)	7.74 (7.68)	11.72 (11.67)	273(4.18) 290(4.17) 641(2.37)	1.80	107
III	[Cu(dptOO)Cl_2]	45.54 (45.61)	4.98 (4.94)	9.96 (10.01)	15.07 (14.99)	278(4.21) 290(4.18) 646(2.24)	1.76	112
IV	[Cu(dptOO)Br_2]	37.60 (37.61)	4.11 (4.06)	8.23 (8.25)	12.45 (12.47)	269(4.08) 321(4.01) 585 *sh*	1.78	98
V	[Cu(dptNN)Cl_2]	45.76 (45.86)	5.48 (5.48)	16.68 (16.72)	15.14 (15.09)	263(4.11) 339(4.05) 500 *sh*	1.75	85

atomic absorption spectroscopy. IR spectra were recorded with a Perkin–Elmer 1650 FT-IR spectrophotometer in the 400–4000 cm^{-1} region using KBr pellets and in the 200–400 cm^{-1} region using polyethylene disks. Electronic spectra were obtained in methanolic solution on a Shimadzu UV-160A spectrophotometer in the 200–1100 nm region. Molar conductivities were measured with a WTW conductivity bridge and a calibrated dip type cell. Magnetic susceptibilities of powdered samples were recorded by the Faraday method with a home-made balance against Hg[Co(SCN)$_4$] as calibrant. Diamagnetic corrections were estimated from Pascal constants.

Theoretical treatments

Molecular mechanics calculations were carried out using the PCMODEL version 6.0 package [13] implemented on an IBM RISK 6000 computer. The MMX force field parameters used were those standard in the program. The coordinates used were those obtained from the crystal structure analysis.

Collection of X-ray data

A crystal suitable for X-ray diffraction was mounted on an Enraf-Nonius CAD4 diffractometer using graphite-monochromatised Mo–K_α radiation ($\lambda = 0.71069$ Å). Unit cell parameters and orientation matrix were obtained from the setting angles of 25 reflections ($12^\circ < \theta < 15^\circ$) and refined by least-squares. Data were collected at room temperature using an $\omega/2\theta$ motion. No significant decay of the standard intensities, collected 27 times during the data acquisition, was observed. Crystallographic data and other pertinent information are in Table 2. All data were corrected for Lorenz and polarisation as well as for absorption using the DIFABS method. The position of the copper atom and the two chlorine atoms were found by direct methods using SHELXS86 [14] and all subsequent calculations were performed using CRYSTALS [15]. All hydrogen atoms were found but only the positions of those belonging to the methylene and amino groups of dipropylenetriamine were refined. The rest of them were positioned geometrically with recalculation after each refinement cycle. All non-hydrogen atoms were refined anisotropically. In the final stage of the refinement, an overall isotropic extinction parameter was introduced. Final refinement was continued until the sum of the shift/esd (estimated standard deviation) ratio was less than 0.01. Selected bonds and angles are in Tables 4 and 5. Illustrations were drawn using ORTEP II [16]. Further experimental details are deposited with the Editor.

RESULTS AND DISCUSSION

The reaction between Schiff bases, dptSS or dptOO or dptNN and copper salts in methanol yielded solid, air stable, coloured microcrystalline or crystalline compounds of the general formula [Cu(dptYY)X$_2$] (Table 1). Their elemental analyses confirm the proposed stoichiometry. The d^9 electronic configuration of copper(II) is confirmed by room temperature magnetic measurements.

Spectral studies

In IR spectra of the ligands (Table 3), the characteristic bands of N—H and C—H stretching vibrations of polyamines were observed at the regions of 3289–3380 and 2900–3000 cm^{-1} respectively [17,18]. The band at the region 3289–3380 cm^{-1}, which could be assigned to secondary amine group of the Schiff bases, is shifted upon coordination to lower wave numbers. This shift is strong evidence that the nitrogen atom of the secondary amino group is binding to copper atom. The band at 1660 cm^{-1} is assigned to the stretching vibration of C=N and shows the formation of the Schiff bases [19]. This band in the complexes spectra is displaced 20–30 cm^{-1} lower, evidence which supports the binding between copper and the nitrogen atoms of —CH=N— moieties. According to the above observations, we may conclude that the ligands are coordinated in a tridentate mode. The formation of the Cu—N bond is further confirmed [18] from the band at 500–520 cm^{-1}. Lastly, the peaks at 310–325 cm^{-1} and 245–247 regions are due to the stretching vibration [20] of the Cu—Cl and Cu—Br bonds, respectively.

The vis spectra (Table 1) of the complexes I, II and III, in MeOH, show a broad band centered at 633–646 nm, while the IV and V complexes show a shoulder at 585 and 500 nm respectively. These bands are of low intensity and are assigned to a Cu(II) *d-d* transitions [21]. The UV spectra, of all complexes, show very strong bands at 263–290 nm which may be assigned to intraligand transitions, whereas the bands at 321 and 339 nm of IV and V complexes respectively may be tentatively assigned to charge transfer transitions.

The combination of the elemental analysis, the IR and UV-vis spectra shows that the Schiff bases bind with copper in a tridentate fashion through the three nitrogen atoms. X-ray crystallography was used to confirm the molecular geometry (see below).

The values of the magnetic moment for the I–V complexes (Table 1) are in the range of 1.73–1.80 BM, which is consistent with monomeric copper(II) units. Finally the molar conductivity values (Table 1) of the compounds, in methanol, show that they behave as 1 : 1 electrolytes [22].

Description of the crystal and molecular structure of [Cu(dptSS)Cl$_2$]

The unit cell contains two well separated neutral molecules of the complex. A perspective view of the

Table 2. Crystal data and experimental details for the structural study of [Cu(dptSS)Cl_2]

Formula	$C_{16}H_{21}N_3S_2Cl_2Cu$
Molecular mass, M_r	453.84
Crystal parameters	
Crystal shape	blue-green rectangular prisms
Crystal size (mm)	$0.41 \times 0.43 \times 0.39$
Crystal system	Triclinic
Space group	$P\bar{1}$
Reflections for cell measurement	25
Unit cell dimensions	
a (Å)	9. 289(1)
b (Å)	10.454(1)
c (Å)	12.347(1)
α (°)	65.948(5)
β (°)	66.883(6)
γ (°)	64.313(6)
V (Å^3)	952.1(1)
Z	2
D_x (Mg m^{-3})	1.34
Linear absorption coefficient, μ (cm^{-1})	13.59
Measurement of intensity data	
Scan speed (deg min^{-1})	2.0 min ; 20.1 max
ω range	2.6–23.1
Reflections measured	3567
Independent reflections	3343
Reflections observed	2398 reflected [$I \geqslant 3\sigma(I)$]
Indices limits	$-11 \leqslant h \leqslant 0$, $-12 \leqslant k \leqslant 12$, $-14 \leqslant l \leqslant 14$
$F(000)$	466
Refinement	
$R = \Sigma(\|F_o\|-\|F_c\|)/\Sigma\|F_o\|$	0.0321
$w = 1/\sigma(F_o)$	
$R_w = [\Sigma w(\|F_o\|-\|F_c\|)^2/\Sigma w(\|F_o\|^2]^{1/2}$	0.0344

Table 3. The most important IR spectra bands (cm^{-1}) of Cu(II) compounds

Compound	ν(N—H)	ν(C=N)	ν(Cu—O)	(Cu—N)	ν(Cu—X) X=Cl, Br
dptSS	3289	1661			
[Cu(dptSS)Cl_2]	3175	1625	599	530	290 295
[Cu(dptSS)Br_2]	3163	1615	598	528	247
dptOO	3378	1646			
[Cu(dptOO)Cl_2]	3160	1625	590	465	325
[Cu(dptOO)Br_2]	3160	1630	580	475	245
dptNN	3380 *br*	1640			
[Cu(dptNN)Cl_2]	3120	1580	550	425	315

[Cu(dptSS)Cl_2] molecule with the atomic numbering scheme is shown in Fig. 1. The geometry around the metal ion can be described as distorted tetragonal pyramidal with the N(1), N(2), N(3) and Cl(2) atoms forming the square base and Cl(1) on the apical position, at distances from the copper atom 2.025(3) Å, 2.064(3) Å, 2.004(3) Å, 2.290(1) Å, and 2.545(1) Å respectively. All distances are similar to those found in previously reported copper complexes with analogous ligands [9,12]. The equation of the best basal plane is $1.616x-6.573y-8.218z = -5.266$ and the N(1), N(2), N(3), Cl(2) atoms forming it can be considered as lying on it, as their deviations are smaller than the error (0.05 Å). The copper atom was found 0.34(5) Å above this mean plane while the Cl(1) atom was lying in the same direction as copper and at a distance of 2.84(5) Å above the plane.

The carbon atoms C(6), C(7) and C(8) of the dipro-

Table 4. Selected interatomic distances (Å) of [Cu(dptSS)Cl$_2$]

Cu(1)—Cl(1)	2.545(1)
Cu(1)—Cl(2)	2.290(1)
Cu(1)—N(1)	2.025(3)
Cu(1)—N(2)	2.064(3)
Cu(1)—N(3)	2.004(3)
S(1)—C(1)	1.700(5)
S(1)—C(4)	1.720(4)
N(1)—C(5)	1.283(5)
N(1)—C(6)	1.465(5)
N(2)—C(8)	1.479(5)
N(2)—C(9)	1.485(5)
N(3)—C(11)	1.468(5)
N(3)—C(12)	1.292(5)
C(1)—C(2)	1.345(7)
C(2)—C(3)	1.389(6)
C(3)—C(4)	1.386(6)
C(4)—C(5)	1.445(5)
C(6)—C(7)	1.530(6)
C(7)—C(8)	1.516(6)
C(9)—C(10)	1.516(6)
C(10)—C(11)	1.522(6)
C(12)—C(13)	1.458(5)
C(13)—C(14)	1.373(6)
C(13)—S(2)	1.733(4)
C(14)—C(15)	1.415(6)
C(15)—C(16)	1.350(7)
C(16)—S(2)	1.693(5)

Table 5. Selected bond angles (°) of [Cu(dptSS)Cl$_2$]

Cl(2)—Cu(1)—Cl(1)	108.68(4)
N(1)—Cu(1)—Cl(1)	96.16(9)
N(1)—Cu(1)—Cl(2)	89.61(9)
N(2)—Cu(1)—Cl(1)	90.48(9)
N(2)—Cu(1)—Cl(2)	160.1(1)
N(2)—Cu(1)—N(1)	82.7(1)
N(3)—Cu(1)—Cl(1)	100.4(1)
N(3)—Cu(1)—Cl(2)	93.4(1)
N(3)—Cu(1)—N(1)	161.2(1)
N(3)—Cu(1)—N(2)	88.3(1)
C(4)—S(1)—C(1)	91.5(2)
C(5)—N(1)—Cu(1)	119.9(3)
C(6)—N(1)—Cu(1)	118.2(2)
C(6)—N(1)—C(5)	121.8(3)
C(8)—N(2)—Cu(1)	110.5(2)
C(9)—N(2)—Cu(1)	119.8(3)
C(9)—N(2)—C(8)	113.3(3)
C(11)—N(3)—Cu(1)	115.9(2)
C(12)—N(3)—Cu(1)	121.0(3)
C(12)—N(3)—C(11)	120.8(3)
C(2)—C(1)—S(1)	112.6(4)
C(3)—C(2)—C(1)	112.8(4)
C(4)—C(3)—C(2)	112.9(4)
C(3)—C(4)—S(1)	110.2(3)
C(5)—C(4)—S(1)	127.8(3)
C(5)—C(4)—C(3)	122.0(4)
C(4)—C(5)—N(1)	131.7(4)
C(7)—C(6)—N(1)	109.2(3)
C(8)—C(7)—C(6)	113.1(4)
C(7)—C(8)—N(2)	111.4(3)
C(10)—C(9)—N(2)	114.2(3)
C(11)—C(10)—C(9)	112.2(3)
C(10)—C(11)—N(3)	109.6(3)
C(13)—C(12)—N(3)	131.6(4)
C(14)—C(13)—C(12)	121.4(4)
S(2)—C(13)—C(12)	128.2(3)
S(2)—C(13)—C(14)	110.1(3)
C(15)—C(14)—C(13)	112.6(4)
C(16)—C(15)—C(14)	112.9(4)
S(2)—C(16)—C(15)	112.2(4)
C(16)—S(2)—C(13)	92.2(2)

pylenetriamine ligand lie below the previous best basal plane with a maximum deviation of 2.036(6) Å for C(7), while the atoms C(9), C(10) and C(11) lie above the plane with a maximum deviation of 0.78(6) Å for C(11).

The six member coordination rings adopt the first one the *chair* and the second the *boat* conformation. The atoms N(3), C(11), C(9) and N(2) from the *chair* like ring form a plane with equation $0.452x+9.352y+6.013z=6.873$ and a maximum deviation of 0.07 Å (equal with the error) for C(11). The atoms C(10) and Cu lie at the opposite sides of this plane with deviations 0.72(6) Å and 0.93(6) Å, respectively. The mean plane passing through the atoms N(1), C(6), C(8) and N(2) from the *boat* like ring follows the equation $6.478x+4.905y+11.516z=4.280$. The atoms C(7) and Cu lie at the same side of this plane with deviations 0.65(6) Å and 1.19(7) Å, respectively. The deviations of the atoms forming the best plane have a mean value of 0.15(5) Å, evidence that this ring is slightly distorted.

The ability of the two six membered coordination ring to adopt either the *boat* or the *chair* conformation gives rise to three possible conformations for the complex, that is *chair/chair*, *boat/boat* and *chair/boat*. The relative energies of these conformations have been calculated by means of molecular mechanics calculations. The starting geometry was this found from the X-ray structure. In each calculation the X-ray geometry has been distorted and a full optimisation has been performed including both the heavy and the hydrogen atoms.

All the above conformation have been found as minima in the potential energy surface of the complex. The optimised *chair/boat* conformation, which is almost identical with the geometry found from the X-ray structure, is not the global minimum in the potential energy surface. Instead the *chair/chair* conformation is the global with the *chair/boat* and *boat/boat* ones found as local minima located 0.6 and 1.4 kcal mol^{-1} higher in energy, respectively. The preference of the complex to adopt the second most stable conformation must be due to crystal packing effects. This is also supported by the very small energy difference between the *chair/boat* and *chair/chair* structure (0.6 kcal mol^{-1}).

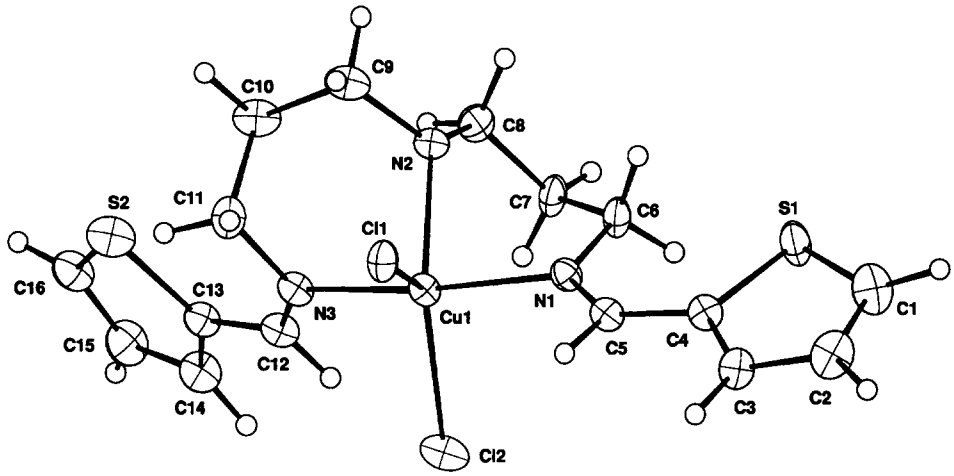

Fig. 1. ORTEP plot showing the molecular structure of the [Cu(dptSS)Cl_2] with the atomic numbering scheme. Atomic thermal ellipsoids are presented at the 50% probability level.

A comparable study of the molecular structures of the complexes [Cu_3(dienSS)$_2Cl_6$]$_x$ [9] and [Cu(dptSS)Cl_2] reveals the reasons leading the first complex being a polymer and forcing the second to remain a monomer.

As far as the polymeric complex [Cu_3(dienSS)$_2Cl_6$]$_x$ is concerned the [Cu(dienSS)] coordination rings are five membered. The size of these two five-membered rings and especially their arrangement (both rings atoms are almost coplanar) gives no protection to the copper ion, allowing chlorine atom from a neighbouring [Cu(dienSS)Cl_2] unit to coordinate the copper atom, forming thus a polymer of coordination octahedra.

In the case of the [Cu(dptSS)Cl_2] complex the existence of one more methylene group in each coordination ring, results in the transformation of the five-member rings of the complex [Cu_3(dienSS)$_2Cl_6$]$_x$ to six-member ones. These formed rings consequently are forced to retain either the *boat* or the *chair* like conformation. The orientation of these *chair* and *boat* like rings above and below the coordination plane, forces the complex [Cu(dptSS)Cl_2] to remain five coordinated, giving no room of approaching to any other bridging atoms to form polymers. As a consequence of the formed chelate rings sizes and their orientation, the complex [Cu(dptSS)Cl_2] is forced to remain a five coordinated monomer, adopting the optimum geometry of the distorted tetragonal pyramid.

Acknowledgement—We thank the Staff of CEMES Laboratory, Toulouse, France, for crystallographic and theoretical facilities. We are also grateful to Prof. M. Sigalas for helpful discussion on theoretical approaches.

REFERENCES

1. Hathaway, B. J. and Billing, D. E., *Coord. Chem. Rev.*, 1970, **5,** 141.
2. Bolos, C. A., Nikolov, G. St., Ecateriniadou, L., Kortsaris, A. and Kyriakidis, D. A., NATO ASI. *Bioinorganic Chemistry*, Book of Abstracts 1994, p. 119.
3. Farrell, N., Almeida, S. G. and Skov, K. A., *J. Am. Chem. Soc.*, 1988, **110,** 5018.
4. Farrell, N. and Qu, Y., *Inorg. Chem.*, 1989, **28,** 3416.
5. Farrell, N., Qu, Y. and Hacker, M. P., *J. Med. Chem.*, 1990, **33,** 2179.
6. Halfpenny, M. T., Levason, W. and McAuliffe, C. A., *Inorg. Chim. Acta*, 1979, **32,** 229.
7. Navarro-Ranninger, C., Amo Ochoa, P., Pérez, J. M., González, V. M., Masaguer, J. R. and Alonso, C., *J. Inorg. Biochem.*, 1994, **53,** 177.
8. Manoussakis, G., Bolos, C., Ecateriniadou, L. and Sarris, C., *Eur. J. Med. Chem.*, 1987, **22,** 421.
9. Christidis, P. C., Bolos, C. A. and Nikolov, G. St., *Inorg. Chim. Acta*, 1995, **237,** 123.
10. Allmann, R., Krestl, M., Bolos, C., Manoussakis, G. and Nikolov, G. St., *Inorg. Chim. Acta*, 1990, **175,** 255.
11. Gliemann, G., Klement, U., Stuckel, C., Bolos, C., Manoussakis, G. and Nikolov, G. St., *Inorg. Chim. Acta*, 1992, **195,** 227.
12. Christidis, P., Triantafyllou, S. T. and Bolos, C. A., *Z. für Kristallographie*, 1994, **209,** 502.
13. MMX program, Version 6.0, Serena Software, Box 3076, Bloomington, IN, 47402-3076, U.S.A.
14. Sheldrick, G. M., SHELX-86, program for crystal structure determination, *Acta Crystallogr.*, 1990, **A 46,** 467.

15. Watkin, D. J., Caruthers, J. R. and Betteridge, P. W., *Crystals*. Chemical Crystallographic Laboratory, Oxford University, 1993.
16. Johnson, C. K., ORTEP II Rep. ORNL-5138, Oak Ridge National Laboratory, TN, U.S.A., 1976.
17. Nakamoto, K., *Infrared and Raman Spectra of Inorganic and Coordination Compounds*. Wiley, New York, 1986.
18. Trendafilova, N., Nikolov, G. St., Bauer, G. and Kellner R., *Inorg. Chim. Acta*, 1993, **210,** 77.
19. Coleman, III W. M., *Inorg. Chim. Acta*, 1981, **49,** 205.
20. Chen, L., Thompson, L. K. and Bridson, J. N., *Inorg. Chem.*, 1993, **32,** 2938.
21. Lever, A. B. P., *Inorganic Electronic Spectroscopy*, 2nd edn. Elsevier, New York, 1984.
22. Geary, W. J., *Coord. Chem. Rev.*, 1971, **7,** 81.

Pergamon

PII: S0277-5387(97)00457-9

Polyhedron Vol. 17, No. 10, pp. 1787–1789, 1998
© 1998 Elsevier Science Ltd
All rights reserved. Printed in Great Britain
0277-5387/98 $19.00+0.00

COMMUNICATION

Synthesis and magnetic properties of a new oxalato-bridged heterotrinuclear complex, $[NiCr_2(bipy)_2(C_2O_4)_4(H_2O)_2]\cdot H_2O$. A rare case of antiferromagnetic coupling between Cr(III) and Ni(II) ions

Nicolae Stanica,[a] Carl V. Stager,[b] Marilena Cimpoesu[a] and Marius Andruh[a]*

[a] University of Bucharest, Faculty of Chemistry, Inorganic Chemistry Laboratory, Str. Dumbrava Rosie nr. 23, 70254 Bucharest, Romania

[b] McMaster University, Department of Physics and Astronomy, Hamilton, Ontario, L8S 4M1, Canada

(Received 28 July 1997; accepted 6 November 1997)

Abstract—A new heterotrinuclear complex, $[NiCr_2(bipy)_2(C_2O_4)_4(H_2O)_2]\cdot H_2O$, has been synthesized by self-assembling $[Cr(bipy)(C_2O_4)_2]^-$ building blocks with Ni(II) ions. The synthesis way consists of the reaction of a barium(II) precursor, $[BaCr_2(bipy)_2(C_2O_4)_4(H_2O)]\cdot H_2O$, with nickel(II) sulfate. Variable-temperature magnetic susceptibility measurements indicate an antiferromagnetic coupling between Ni(II) and Cr(III) ions ($J = -0.6$ cm^{-1}, $\mathbf{D}_{Ni} = 0.4$ cm^{-1}, $\boldsymbol{H} = -J(\mathbf{S}_{Cr1}\mathbf{S}_{Ni} + \mathbf{S}_{Cr2}\mathbf{S}_{Ni}) + \mathbf{S}_{Ni}\mathbf{D}_{Ni}\mathbf{S}_{Ni})$. © 1998 Elsevier Science Ltd. All rights reserved

Keywords: chromium complexes; nickel complexes; oxalato complexes; 2,2′-bipyridine; magnetic properties.

A successful strategy for the design of heteropolymetallic complexes consists in the ingenious use of versatile building blocks, which are usually relatively stable coordination compounds with potential bridging ligands. A particular emphasis has been brought to 2D and 3D multimetallic complexes, with the perspective to design molecular-based magnets [1,2]. On the other hand, oligonuclear systems are useful models for the experimental and theoretical investigation of the factors governing the sign and the magnitude of the exchange interactions between adjacent metal ions [2–4].

Recently, we have reported on the ability of a new molecular brick, $[Cr(bipy)(C_2O_4)_2]^-$, to generate heteropolymetallic complexes with novel topologies of the metallic centers and, consequently, with interesting magnetic properties [5,6]. We have shown that the self-assembly process is strongly influenced by: (i) the coordination algorithm of the assembling cation (Ba^{2+}, Mn^{2+}, Cu^{2+}, Co^{2+}, Zn^{2+}); (ii) the oxidation state of the assembling cation (Ag^+). Divalent cations which prefer a coordination number of six (Co^{2+}, Cu^{2+}, Zn^{2+}) have been found to generate discrete linear {Cr(III)-μ-C_2O_4-M(II)-μ-C_2O_4-Cr(III)} trinuclear species [5–7]. The synthetic route is straightforward and consists in the reaction of a barium-chromium precursor, $[BaCr_2(bipy)_2(C_2O_4)_4(H_2O)]$ H_2O, with the appropriate transition metal sulfate [5]:

$$Ba\{Cr(bipy)(C_2O_4)_2\}_2 + MSO_4 \rightarrow M\{Cr(bipy)(C_2O_4)_2\}_2 + BaSO_4$$

In this note we report on the synthesis and magnetic properties of the nickel derivative, $[NiCr_2(bipy)_2$

* Author to whom correspondence should be addressed.

$(C_2O_4)_4(H_2O)_2]\cdot H_2O$*. The divalent nickel ion has a marked preference for the octahedral stereochemistry. Therefore, the structure of the $\{NiCr_2\}$ complex is quite predictable, namely it should be isostructural with other $\{M^{II}Cr_2\}$ derivatives ($M^{II} = Co^{II}$, Cu^{II}, Zn^{II}). The solid state electronic spectrum exhibits the characteristic features of both octahedral Cr(III) and Ni(II) chromophores, namely *cis*-$[Cr(III)N_2O_4]$ and $[Ni(II)O_6]$ [8]. The first two bands, located at 395 nm and 550 nm, are assigned to the spin-allowed transitions for the Cr(III)-moiety: $^4A_2 \rightarrow {}^4T_1$ and $^4A_2 \rightarrow {}^4T_2$, respectively (assuming the O site symmetry). The shoulder at ~ 700 nm and the band at 1180 nm are assigned to the $^3A_{2g} \rightarrow {}^3T_{1g}$ and $^3A_{2g} \rightarrow {}^3T_{2g}$ transitions for the pseudo-octahedral $[Ni(II)O_6]$ chromophore.

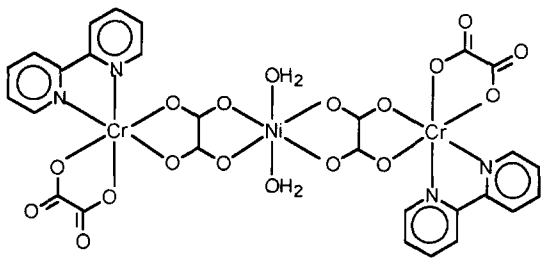

The most intriguing properties of the heteropolymetallic complexes concern the exchange interactions between the paramagnetic centers. The particular pairs Cr(III)—Ni(II) and Cr(III)—Cu(II) mixed-metal ions are among the classical examples illustrating the ferromagnetic coupling due to the strict orthogonality of the magnetic orbitals, $< t_{2g}|e_g > = 0$, $(t_{2g})^3(Cr)$-$(e_g)^{1,2}$ (Cu, Ni) (considering only the unpaired electrons) [2–4]. The crystal structures of the isomorphous compounds, $[MCr_2(bipy)_2(C_2O_4)_4(H_2O)_2]$, M = Co(II), Cu(II) and Zn(II) [5–7], allow for reliable predictions of the magnetic properties for the whole series. The divalent cation, lying on an inversion center, exhibits a tetragonally distorted octahedral stereochemistry. The elongated bonds involve one oxygen atom arising from each oxalato bridging ligands. In the C_i group symmetry of the trinuclear complex, the magnetic orbitals transform as the a_g irreducible representation and are no more orthogonal. Consequently, the Cr(III)—Ni(II) exchange interaction, as the Cr(III)—Cu(II) one [6], should be antiferromagnetic. Indeed, the results of the cryomagnetic investigation of $[NiCr_2(bipy)_2(C_2O_4)_4(H_2O)_2]\cdot H_2O$, shown in the form of $\chi_M T$ versus T plot, clearly indicate the expected antiferromagnetic coupling (Fig. 1). The magnetic susceptibiliy was measured with a SQUID magnetometer (Quantum Design, San Diego, CA) in the temperature range 1.7–300 K. At room temperature, $\chi_M T$ is equal to 4.89 cm^3 mol^{-1} K, which corresponds to the three uncoupled metal ions ($\chi_M T = 4.75$ cm^3 mol^{-1} K if $g_{Ni} = g_{Cr} = 2$). By lowering the temperature, $\chi_M T$ remains constant down to ca 80 K, then decreases more and more, reaching a value of 3.06 cm^3 mol^{-1} K at 1.70 K.

The expression for the magnetic susceptibility has been based on the full-matrix diagonalization of the following phenomenological Hamiltonian:

$$H = -J(\mathbf{S}_{Cr1}\mathbf{S}_{Ni} + \mathbf{S}_{Cr2}\mathbf{S}_{Ni}) + \mathbf{S}_{Ni}\mathbf{D}_{Ni}\mathbf{S}_{Ni}$$

The local anisotropy tensor, $\mathbf{D}_{Ni}$, was taken into account because, in axial symmetry, nickel(II) can have a significant zero-field splitting. The best least-squares fit gives: $g_{av} = 2.03$, $J = -0.6$ cm^{-1}, and $\mathbf{D}_{Ni} = 0.4$ cm^{-1}. The discrepancy factor, defined as $R = \Sigma[(\chi_M T)_{obs} - (\chi_M T)_{calc}]^2/\Sigma[(\chi_M T)_{obs}]^2$, is then equal to 1.5×10^{-5}. For the analogous compound, $\{CuCr_2\}$, the Cu(II)—Cr(III) interaction is also antiferromagnetic ($J = -18.8$ cm^{-1}) [6]. Several other Ni(II)—Cr(III) oligomeric complexes have been synthesized and their magnetic properties investigated. Three of them are oxalato-bridged species and the Cr(III)—Ni(II) coupling was found always ferromagnetic [9,10]. A tetranuclear $\{NiCr_3\}$ dithiooxalato bridged complex has been structurally characterized [11]. The magnitude of the ferromagnetic coupling through the dithiooxalato bridges was found more than twice as large as in the oxalato derivatives. In one Cr(III)—Ni(II) cyanide-bridged heptanuclear

*A suspension of $[BaCr_2(bipy)_2(C_2O_4)_4(H_2O)]H_2O$ (0.5 mmol) in 50 ml of water reacted with the stoichiometric amount of $NiSO_4\cdot 7H_2O$ dissolved in 10 ml of water. The resulting mixture was stirred for 4 h to promote complete precipitation of barium sulfate, which has been removed by filtration. $[NiCr_2(bipy)_2(C_2O_4)_4(H_2O)_2]\cdot H_2O$ was obtained as a red violet microcrystalline powder by slow concentration of the aqueous solution. The heterotrinuclear complex was purified by recrystallization from water. Yield: 84%. FTIR data (KBr, cm^{-1}): 3440 br, 1720 vs, 1690 vs, 1620 m, 1500 w, 1480 w, 1450 m, 1375 s, 1320 w, 1290 w, 1250 w, 1185 w, 1170 w, 1080 w, 1065 w, 1040 w, 900 w, 850 w, 810 m, 780 m, 730 m, 670 w, 560 m, 460 w, 420 w. Correct elemental chemical analyses. The water content was determined by means of thermogravimetric analysis. Any attempt to obtain single crystals failed.

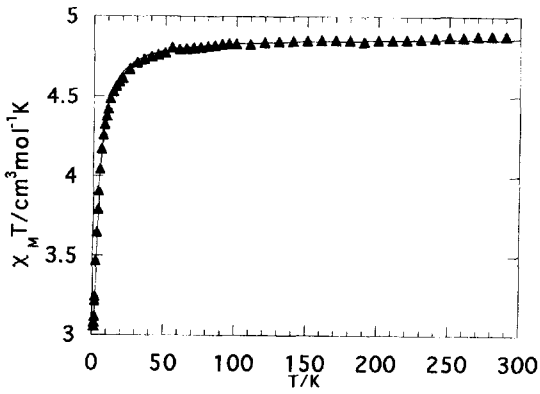

Fig. 1. $\chi_M T$ vs T plot for $[NiCr_2(bipy)_2(C_2O_4)_4(H_2O)_2]\cdot H_2O$.

complex the interaction is ferromagnetic too, as expected from the orthogonality of the magnetic orbitals [12]. An antiferromagnetic coupling was found only in a few Cr(III)—Ni(II) hydroxo-bridged tri- and tetranuclear complexes [13,14].

REFERENCES

1. Kahn, O., Pei, Y. and Journaux, Y., in *Inorganic Materials*, 2nd edn, ed. D. W. Bruce and D. O'Hare. Wiley 1996, p. 66.
2. Kahn, O., *Adv. Inorg. Chem.*, 1995, **43,** 179 and references therein.
3. Kahn, O., *Molecular Magnetism*, VCH Publishers, New York, 1993.
4. Kahn, O., *Struct. Bonding (Berlin)*, 1987, **68,** 89.
5. Rochon, F. D., Melanson, R. and Andruh, M., *Inorg. Chem.*, 1996, **35,** 6086.
6. Andruh, M., Melanson, R., Stager, C. V. and Rochon, F. D., *Inorg. Chim. Acta*, 1996, **251,** 309.
7. Andruh, M. and Rochon, F. D., unpublished.
8. Lever, A. B. P., *Inorganic Electronic Spectroscopy*, 2nd edn. Elsevier, 1984.
9. Pei, Y., Journaux, Y. and Kahn, O., *Inorg. Chem.*, 1989, **28,** 100.
10. Ohba, M., Tamaki, H., Matsumoto, N. and Okawa, H., *Inorg. Chem.*, 1993, **32,** 5385.
11. Mitsumi, M., Okawa, H., Sakiyama, H., Ohba, M., Matsumoto, N., Kurisaki, T. and Wakita, H., *J. Chem. Soc., Dalton Trans.*, 1993, 2991.
12. Mallah, T., Auberger, C., Verdaguer, M. and Veillet, P., *J. Chem. Soc., Chem. Commun.*, 1995, 61.
13. Hodgson, D. J., Michelsen, K., Pedersen, E. and Towle, D. K., *Inorg. Chem.*, 1991, **30,** 815.
14. Corbin, K. M., Glerup, J., Hodgson, D. J., Lynn, M. H., Michelsen, K. and Nielsen, K. M., *Inorg. Chem.*, 1993, **32,** 18.

Pergamon

PII: S0277-5387(97)00461-0

Polyhedron Vol. 17, No. 10, pp. 1791–1793, 1998
© 1998 Elsevier Science Ltd
All rights reserved. Printed in Great Britain
0277-5387/98 $19.00+0.00

COMMUNICATION

X-ray structure and solid state ^{29}Si NMR spectroscopy of the octahalocyclotetrasilanes, Si_4Cl_8 and Si_4Br_8

Julian R. Koe,* Douglas R. Powell, Jarrod J. Buffy and Robert West

Department of Chemistry, University of Wisconsin, Madison, WI 53706 U.S.A.

(Received 16 June 1997: accepted 2 September 1997)

Abstract—The crystallographic and solid state ^{29}Si NMR characterisation of octachlorocyclotetrasilane, **1**, and octabromocyclotetrasilane, **2**, are described. In the solid state, **1** and **2** exist as centrosymmetric square planar molecules. © 1998 Elsevier Science Ltd. All rights reserved

Keywords: octachlorocyclotetrasilane; octabromocyclotetrasilane; cyclotetrasilane; X-ray structure; solid state ^{29}Si NMR spectroscopy.

Small strained silicon rings [1,2] have attracted considerable attention due to their reactivity towards ring-opening, extrusion of silylenes and disilenes, polymerisation, substitution and insertion chemistry. Whereas X-ray structures have been reported for a number of alkyl- and aryl-substituted cyclotetrasilanes [3–5], the structure of the unusually coloured octahalocyclotetrasilanes [6,7], Si_4X_8, has been a matter of debate for the last 20 years and a full structural characterisation is required for a deeper understanding of the nature of these species.

In our work on the chemistry of cyclotetrasilanes and their polymerisation, we synthesised the air- and moisture-sensitive compounds octachlorocyclotetrasilane Si_4Cl_8, **1** and octabromocyclotetrasilane, Si_4Br_8, **2**, according to the reported procedure [6], although our purification method (recrystallisation) differed from that in the literature (sublimation). Crystals suitable for single crystal X-ray diffraction analysis were prepared by recrystallisation from toluene at −20°C, coated with Krytox and mounted on a glass fibre. The structures were obtained using a diffractometer equipped with a CCD area detector, the use of which permitted the rapid collection of data, critical in the analysis due to the extreme moisture-sensitivity of the compounds.

The structures of **1** and **2** with selected bond distances and angles are shown in Figs 1 and 2, respectively. The molecules have similar structures and will therefore be discussed together, except where specified. The compounds possess crystallographic centres of inversion and have very slightly rhomboidally compressed square-planar structures, in qualitative agreement with the planar D_{4h} minimum energy structure obtained for Si_4Cl_8 by semi-empirical (PM3) calculations [8], though in contrast to conclusions based on vibrational spectroscopy [6,7]. Similarly apparently contradictory data were obtained for octamethylcyclotetrasilane, for which X-ray analysis indicated a planar structure [3] while both vibrational [9] and gas electron diffraction [10] data indicated folding (the latter gave a value of 29.4(40)°). The planar structures of Si_4Cl_8 and Si_4Br_8 contrast also with the structures of nearly all other cyclotetrasilanes for which X-ray diffraction analyses have been obtained [2,11,12] (dihedral angles of 12–40° are typical), although octakis(trimethylsilyl)cyclotetrasilane is also planar [13], presumably due to minimisation of interactions between the bulky substituents. It is interesting to compare the structure of Si_4Cl_8 with that of its carbon analogue, C_4Cl_8, for which vibrational spectroscopy [14] indicated a puckered D_{2d} structure. This was borne out in the crystal structure [15] which showed a folded cyclic structure with a dihedral angle of 19°.

* Author to whom correspondence should be addressed.

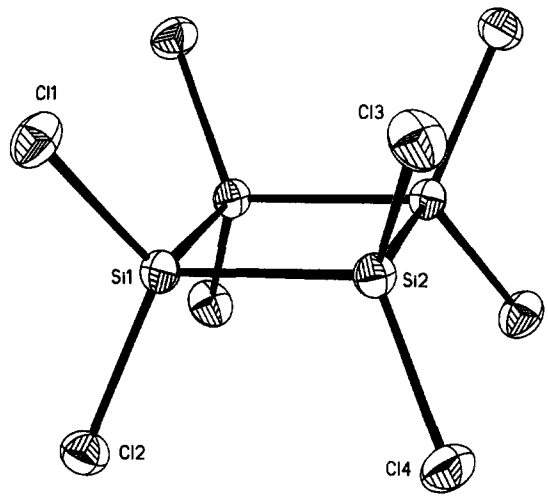

Fig. 1. Molecular structure of Si_4Cl_8 (**1**) with 50% probability thermal ellipsoids. Selected interatomic distances (Å): Si(1)—Cl(1) 2.039(2), Si(1)—Cl(2) 2.049(2), Si(1)—Si(2) 2.372(2), Si(1)—Si(2)$^{\#1}$ 2.372(2). Selected bond angles (°): Si(1)—Si(2)—Si(1)$^{\#1}$ 90.12(5), Si(2)—Si(1)—Si(2)$^{\#1}$ 89.88(5), Cl(1)—Si(1)—Cl(2) 112.17(7), Cl(4)—Si(2)—Cl(3) 111.84(7). $^{\#1}$symmetry transformation used to generate equivalent atoms: $-x+1, -y+1, -z+1$.

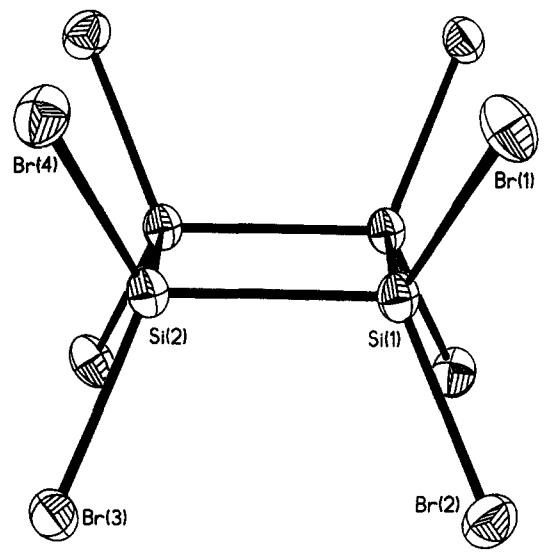

Fig. 2. Molecular structure of Si_4Br_8 (**2**) with 50% probability thermal ellipsoids. Selected interactomic distances (Å): Si(1)—Br(1) 2.203(3), Si(1)—Br(2) 2.202(3), Si(1)—Si(2) 2.370(4), Si(1)—Si(2)$^{\#1}$ 2.372(4). Selected bond angles (°): Si(1)—Si(2)—Si(1)$^{\#1}$ 89.86(12), Si(2)—Si(1)—Si(2)$^{\#1}$ 90.14(12), Br(1)—Si(1)—Br(2) 112.43(11), Br(4)—Si(2)—Br(3) 113.07(11). symmetry transformation used to generate equivalent atoms: $-x+1, -y+1, -z+1$.

The Si—Si bond lengths in **1** (2.372(2)Å) are somewhat longer than in dodecamethylcyclohexasilane [16] (2.338(4)Å) and Si_4Me_8 (mean value: 2.363 Å) [3]. The Si—Si distances in **2** are essentially the same as for **1** within the standard deviational errors. The distances in **1** are also larger than the Si—Si distances in Si_4Me_8 (mean value: 2.363 Å) [3]. The bond lengths are, however, considerably shorter than those reported in the PM3 calculation [8] (2.454 Å) for Si_4Cl_8. Restriction of the Si—Si—Si bond angles to almost 90° permits the opening of the Cl—Si—Cl angles to around 112° and very slightly larger in the case of the bulkier bromo-derivative.

^{29}Si NMR data were also obtained for **1** and **2**. The solid state ^{29}Si MAS-NMR spectrum comprised a single resonance at 7.1 ppm and the solution state ^{29}Si NMR spectrum of **1** gave a signal at 5.44 ppm, which is in reasonable agreement with the published [17] (5.86 ppm) and solid state values. For **2**, a broader peak was observed in the solid state ^{29}Si MAS-NMR spectrum at −8.3 ppm (cf −15.97 for the published [17] solution state spectrum).

We are continuing our endeavours in this area and are currently investigating the cause of the discrepancy between the crystallographic and vibrational data concerning the planarity of the Si_4 ring.

EXPERIMENTAL

Crystallographic data for **1**

Cl_8Si_4: $M = 395.96$; monoclinic, $P2_1/n$; $a = 7.3255(2)$, $b = 7.1815(2)$, $c = 13.2844(4)$Å; $\beta = 104.6800(10)°$; $V = 676.05(3)$Å^3; $Z = 2$; $D_{calc} = 1.945$ g cm^3; Mo-K_α radiation, $\lambda = 0.71073$ Å; absorption coefficient = 1.971 mm^{-1}; $F(000) = 384$; $T = 133(2)$K; yellow transparent prisms. Crystal dimensions: $0.42 \times 0.36 \times 0.25$ mm. 6839 intensity data were collected on a Siemens P4/CCD diffractometer using graphite-monochromated Mo-K_α ($\lambda = 0.71073$ Å) radiation (range $2.91 \leqslant \theta \leqslant 28.01°$; $-9 \leqslant h \leqslant 9$, $0 \leqslant k \leqslant 9$, $0 \leqslant l \leqslant 17$), 1528 independent reflections ($R_{int} = 0.0330$) and 1356 observed [$I > 2\sigma(I)$]. The structure was solved by direct methods and refined by full-matrix least-squares on F^2 using SHELXTL V.5 (1994). Neutral atom scattering factors were taken from ref. 18. $R_1 = 0.0492$ [$I > 2\sigma(I)$], $wR_2 = 0.1337$ (all data); GOF(F^2) = 1.192.

Crystallographic data for **2**: Br_8Si_4: $M = 751.64$; monoclinic, $P2_1/n$; $a = 7.5961(7)$, $b = 7.4198(7)$, $c = 14.0201(13)$Å; $\beta = 103.995(2)°$; $V = 766.74(12)$Å^3; $Z = 2$; $D_{calc} = 3.256$ g cm^3; Mo-K_α radiation, $\lambda = 0.71073$ Å; absorption coefficient = 1.971 mm^{-1}; $F(000) = 672$; $T = 133(2)$K; yellow transparent prisms. Crystal dimensions: $0.44 \times 0.38 \times 0.32$ mm. 3494 intensity data were collected on a Siemens P4/CCD diffractometer using graphite-monochromated Mo-K_α ($\lambda = 0.71073$ Å) radiation (range $2.81 \leqslant \theta \leqslant 28.82°$; $-10 \leqslant h \leqslant 10$, $-7 \leqslant k \leqslant 9$, $-18 \leqslant l \leqslant 10$), 1837 independent reflections ($R_{int} = 0.0325$) and 1462 observed [$I > 2\sigma(I)$]. The

structure was solved by direct methods and refined by full-matrix least-squares on F^2 using SHELXTL V.5 (1994). Neutral atom scattering factors were taken from ref. 18. $R_1 = 0.0643$ [$I > 2\sigma(I)$], $wR_2 = 0.19747$ (all data); GOF(F^2) = 1.051.

Full details of the structure determinations have been deposited at the Cambridge Crystallographic Data Centre.

^{29}*Si NMR data for* **1** *and* **2**

Solution state ^{29}Si NMR experiments were referenced to internal tetramethysilane and recorded in C_6D_6 using a Bruker AM-500 instrument operating at 99.36 MHz. Solid state ^{29}Si MAS-NMR spectra were obtained using zirconia rotors in a Varian Unity-300 spectrometer operating at 59.591 MHz and referenced to external tetrakis(trimethylsilyl)silane.

Acknowledgements—This work was supported by the US Office of Naval Research. We also acknowledge grants from the NSF for the purchase of the X-ray diffractometer and NMR spectrometers.

REFERENCES

1. Weidenbruch, M., *Chem. Rev.*, 1995, **95,** 1479 and references therein.
2. Hengge, E. and Janoschek, R., *Chem. Rev.*, 1995, **95,** 1495 and references therein.
3. Kratky, C., Schuster, H. G. and Hengge, E., *J. Organomet. Chem.*, 1983, **247,** 253.
4. Hurt, C. J., Calabrese, J. C. and West, R., *J. Organomet. Chem.*, 1975, **91,** 273; Parkanyi, L., Sasvari, K. and Barta, I., *Acta Crystallogr.*, 1978, **B34,** 883; Watanabe, H., Kato, M., Okawa, T., Kougo, Y., Nagai, Y. and Goto, M., *Appl. Organomet. Chem.*, 1987, **1,** 157.
5. Weidenbruch, M., Thom, K-L., Pohl, S. and Saak, W., *Monatsh. Chem.*, 1988, **119,** 65; Matsumoto, H., Minemura, M., Takatsuna, K., Nagai, Y. and Goto, M., *Chem. Lett.* 1985, 1005; Matsumoto, H., Takatsuna, K., Minemura, M., Nagai, Y. and Goto, M., *J. Chem. Soc., Chem. Commun.*, 1985, 1366.
6. Hengge, E. and Kovar, D., *Z. anorg. allg. Chem.*, 1979, **458,** 163.
7. Hassler, K., Hengge, E. and Kovar, D., *J. Mol. Struct.*, 1980, **66,** 25.
8. Stüger, H. and Janoschek, R., *Phosphorous, Sulfur and Silicon*, 1992, **68,** 129.
9. Hassler, K., *Spectrochim. Acta*, 1981, **A37,** 541.
10. Mastryukov, V. S., Strelkov, S. A., Vilkov, L. V., Kolonits, M., Rozsondai, B., Schuster, H. G. and Hengge, E., *J. Mol. Struct.*, 1990, **238,** 433.
11. West, R., In *The Chemistry of Organic Silicon Compounds*, ed. S. Patai and Z. Rappoport, Wiley, New York, 1989, Part II, Ch. 19, p. 1207.
12. West, R., In *Comprehensive Organometallic Chemistry II*, Vol. 2, ed. E. W. Abel, F. G. A. Stone and G. Wilkinson, Pergamon, Oxford, 1995, Ch. 3, p. 79.
13. Chen, Y. S. and Gaspar, P. P., *Organometallics*, 1982, **1,** 1410.
14. Miller, F. A. and Capwell, R. J., *Spectochim. Acta*, 1971, **A27,** 1113.
15. Owen, T. B. and Hoard, J. L., *Acta Crystallogr.*, 1951, **4,** 172; Margulis, T. N., *Acta Crystallogr.*, 1965, **19,** 857.
16. Carrell, H. L. and Donohue, J., *Acta Crystallogr.*, 1972, **B28,** 1566.
17. Utvary, K. and Hengge, E., *Monatsh. Chem.*, 1979, **110,** 1295.
18. *International Tables for Crystallography*, Vol. C., Tables 6.1.1.4, 4.2.6.8 and 4.2.4.2, Kluwer, Boston, 1995.

Pergamon

PII: S0277-5387(97)00532-9

Polyhedron Vol. 17, Nos. 11–12, pp. 1795–1801, 1998
© 1998 Elsevier Science Ltd
All rights reserved. Printed in Great Britain
0277-5387/98 $19.00+0.00

Isomerism and redox properties of 1-ferrocenyl-1,3-butanedionate complexes

Piero Zanello,*[a] Fabrizia Fabrizi de Biani,[a] Christopher Glidewell,*[b] Janine Koenig[b] and Steven J. Marsh[b]

[a] Dipartimento di Chimica dell'Università di Siena, Pian dei Mantellini, 44, 53100 Siena, Italy

[b] School of Chemistry, University of St Andrews, St Andrews, Fife KY16 9ST, U.K.

(Received 29 October 1997; accepted 18 December 1997)

Abstract – The ferrocenyl diketone $[(C_5H_5)Fe(C_5H_4)COCH_2COCH_3]$ has been used to form neutral metal complexes of the 1-ferrocenyl-1,3-butanedionate ligand $[(C_5H_5)Fe(C_5H_4)COCHCOCH_3]^-$: the aluminium complex of this ligand, $[Al\{(C_5H_5)Fe(C_5H_4)COCHCOCH_3\}_3]$, has been characterised by ^1H and ^{13}C NMR as a 2:3 mixture of *fac* and *mer* isomers, having C_3 and C_1 molecular symmetry respectively. Electrochemical studies show that each peripheral 1-ferrocenyl-1,3-butanedionate ligand L of both $M^{II}L_2$ (M = Co, Ni, Cu) and $M^{III}L_3$ (M = Al, Cr, Mn, Fe) complexes undergoes reversible one-electron oxidation at potential values essentially overlapping each other. This means that the central metal ions prevent any electronic communication between the two or three ferrocene fragments. In addition to these reversible ferrocene-centred oxidations, there are reversible one-electron reductions centred at M for ML_3 and FeL_3 (but not for CrL_3 or AlL_3), but the metal-centre reductions of $M^{II}L_2$ are irreversible owing to further reactions following reduction. © 1998 Elsevier Science Ltd. All rights reserved

Keywords: ferrocenes; ferrocenyl diketone; metal complexes; electrochemistry.

We have recently reported practical routes to a number of 1,3-diketones containing a ferrocene nucleus, of general types $FcCOCH_2COR$ and $FcCH_2CH(COR)_2$ [Fc = $(C_5H_5)Fe(C_5H_4)$] and to some of the corresponding bis(1,3-diketones) $Fe(C_5H_4COCH_2COR)_2$ and $Fe[C_5H_4CH_2CH(COR)_2]_2$ [1]. The crystal and molecular structures have been reported for two representative examples, $FcCOCH_2COMe$ which exists [2] in the solid state solely in the enol form FcCOCHC(OH)Me, and $FcCH_2CH(COCMe_3)_2$ which exists [3] in the solid state solely in the keto form, although ferrocenyl diketones of both types exist as keto/enol mixtures in solution. Despite the fact that ferrocenyl 1,3-diketones were first described more than thirty years ago [4], there have been remarkably few reports of their application as ligands towards metal ions: Imai and Óta reported the characterisation by electronic spectroscopy of some M(II) complexes derived from the ligand $FcCOCH_2COMe$ **1**, for M = Mn, Co, Ni, Cu and Zn [5], although the preparations were not described. For any asymmetric bidentate ligand of general type L—L′, both square planar $M(L—L')_2$ and octahedral $M(L—L')_3$ complexes have the potential to exhibit geometric isomerism, of *cis/trans* and *mer/fac* types respectively, although this possibility was not addressed by Imai and Óta [5]. We have now synthesised a range of M(II) and M(II) complexes of $(FcCOCHCOMe)^-$ **2** and **3** respectively, including the diamagnetic complex $[(FcCOCHCOMe)_3Al]$, and we report here details of the synthesis, the full structural characterisation of $[(FcCOCHCOMe)_3Al]$ by ^1H and ^{13}C NMR spectroscopy, and an electrochemical study of selected examples.

$[FcCOCHCOCH_3)_3M]$	$[(FcCOCHCOCH_3)_2M]$
2 a M = Al	**3 a** M = VO
b M = Cr(III)	**b** M = Mn(II)
c M = Mn(III)	**c** M = Co(II)
d M = Fe(III)	**d** M = Ni(II)
	e M = Cu(II)

Incorporation of transition metal fragments into redox active ligands may afford materials having unusual properties because of unexpected electronic

* Author to whom correspondence should be addressed.

interactions. In this connection interest is rapidly growing around metalla-ferrocene derivatives and most aspects of their chemistry have been recently reviewed [6]. Our emphasis in the present work is on structural (particularly isomerism) and electrochemical aspects.

EXPERIMENTAL

Synthesis of 1-ferrocenyl-3-hydroxybut-2-en-1-one, **1**

A solution of *n*-butyl lithium (128 cm^3 of a 1.6 mol dm^{-3} solution in hexanes, 205 mmol) was added, under N_2 and at 0°C, to a solution of di-isopropylamine (21–5 g, 223 mmol) in sodium-dried THF (200 cm^3). After stirring for 1 h, acetylferrocene (20.4 g, 89.4 mmol) was added portionwise during 1 h. This mixture was stirred overnight at ambient temperature: after cooling to 0°C, ethyl acetate (18.1 g, 205 mmol) was added during 30 min, and the resulting solution was stirred overnight at ambient temperature. Dry ether (100 cm^3) was then added, and the resulting orange precipitate (the lithium salt of the keto-enolate) was filtered off; this solid was hydrolysed with 10% aqueous HCl (50 cm^3). The filtrate meanwhile, was evaporated to dryness, and the resulting oil was diluted with CH_2Cl_2 (30 cm^3) and chromatographed on alumina, with elution by 10% aqueous HCl. The combined aqueous HCl fractions were extracted with ether: the ether extract was washed with sodium hydrogencarbonate solution and then dried over magnesium sulfate. The ether was evaporated and the resulting solid was recrystallised from hexane to give the product **1** in 51% yield, with spectral data identical to those reported earlier [1,2].

Synthesis of M(III) *complexes*, **2** *of* 1-ferrocenyl-1,3-butanedionate

(*a*) Al(III) *complex*, **2a**. A solution of the diketone **1** (0.40 g, 1.48 mmol) in concentrated aqueous ammonia (19 cm^3) and methanol (66 cm^3) was added in portions to a solution of aluminium sulfate octadecahydrate (0.32 g, 0.48 mmol) in water (3 cm^3). After 30 min, a red solid was filtered off and washed well with water. This solid was then dissolved in the minimum volume of CH_2Cl_2, and the resulting solution was washed with water (3×30 cm^3): the organic layer was dried and evaporated to yield tris(1-ferrocenyl-1,3-butanedionato-*O*,*O*′)aluminium (0.38 g, 0.45 mmol, 94%). Anal.: Found: C, 60.0, H, 4.6%. $C_{45}H_{39}AlFe_3O_6$ requires C, 60.5, H, 4.7%.

(*b*) Cr(III) *complex*, **2b**. Chromium(III) hexahydrate (0.10 g, 0.37 mmol) was dissolved in water (4 cm^3) and urea (0.36 g, 6.0 mmol) was added in small portions: diketone **1** (0.44 g, 1.62 mmol) was then added and the mixture was heated to 80°C for 2 h. After cooling, the mixture was filtered to give a red-brown solid, which was twice recrystallised from cyclohexane to yield **2b** (0.04 g, 0.047 mmol, 13%). Anal.: Found: C, 58.1, H, 4.9%. $C_{42}H_{39}CrFe_3O_6$ requires C, 58.7, H, 4.6%.

(*c*) Mn(III) *complex*, **2c**. Diketone **1** (0.50 g, 1.85 mmol) was added to an aqueous solution (2 cm^3) containing manganese(II) chloride tetrahydrate (0.08 g, 0.40 mmol) and sodium acetate trihydrate (0.13 g, 0.96 mmol). To this solution was then added, dropwise with stirring, a solution of potassium permanganate (0.015 g, 0.095 mmol) in water (10 cm^3), followed by a further solution of acetate trihydrate (0.13 g) in water (10 cm^3). After 10 min, the deep red-brown product was filtered off, and washed with water followed by methanol to give **2c** (0.13 g, 0.15 mmol, 30%). Anal.: Found: C, 58.5, H, 4.5%. $C_{42}H_{39}Fe_3MnO_6$ requires C, 58.5, H, 4.5%.

(*d*) Fe(III) *complex*, **2d**. A solution of diketone **1** (0.40 g, 1.48 mmol) in methanol (40 cm^3) was added in portions to a solution of iron(II) chloride hexahydrate (0.13 g, 0.49 mmol) in water (2 cm^3), followed by a solution of sodium acetate trihydrate (0.21 g, 1.54 mmol) in water (1 cm^3). The entire mixture was stirred at 70 C until all the solvent had evaporated: the residue was slurried with a mixture of water (6 cm^3) and methanol (40 cm^3), and then filtered. The solid product was well washed with water and then dried to provide deep red-purple **2d** (0.32 g, 0.37 mmol, 75%). Anal.: Found: C, 58.4, H, 4.8%. $C_{42}H_{39}Fe_4O_6$ requires C, 58.4, H, 4.6%.

Synthesis of M(II) *complexes*, **3**, *of* 1-ferrocenyl-1,3-butanedionate

(*a*) *Vanadyl complex*, **3a**. A solution of the diketone **1** (0.40 g, 1.48 mmol) in methanol (20 cm^3) was added to a solution of vanadyl sulfate monohydrate (0.12 g, 0.66 mmol) in water (0.5 cm^3): to this mixture was then added an excess of an aqueous solution of sodium carbonate. The resulting solid was filtered off, dried and recrystallised from CH_2Cl_2 to give red-brown **3a** (0.20 g, 0.32 mmol, 48%). Anal.: Found: C, 57.3, H, 4.1%. $C_{28}H_{26}Fe_2O_5V$ requires C, 55.6, H, 4.3%.

(*b*) Mn(II) *complex*, **3b**. A solution of the diketone **1** (0.40 g, 1.48 mmol) in methanol (20 cm^3) was added to a solution of manganese(II) chloride tetrahydrate (0.15 g, 0.76 mmol) in water (0.75 cm^3). To this mixture was added dropwise with stirring an excess of an aqueous solution of sodium acetate trihydrate (0.20 g, 1.40 mmol) in water (0.5 cm^3), followed by three drops of concentrated aqueous ammonia. After stirring for 10 min at ambient temperature the mixture was held at 0°C for 4 h. The resulting precipitate was filtered off and washed with water to yield dark brown **3b** (0.30 g, 0.51 mmol, 69%). Anal.: Found: C, 56.0, H, 4.5%. $C_{28}H_{26}Fe_2MnO_4$ requires C, 56.7, H, 4.4%.

(*c*) Co(II) *complex*, **3c**. A solution of the diketone **1** (0.40 g, 1.48 mmol) in methanol (20 cm^3) was added slowly with stirring to a solution of sodium hydroxide (0.06 g, 1.50 mmol) in water (1 cm^3). This mixture

was added dropwise with stirring to a solution of cobalt(II) chloride hexahydrate (0.18 g, 0.76 mmol) in water (10 cm^3). The resulting solid was filtered off and washed with water; recrystallisation from CH_2Cl_2 gave dark brown **3c** (0.15 g, 0.25 mmol, 34%). Anal.: Found: C, 57.0, H, 4.7%. $C_{28}H_{26}CoFe_2O_4$ requires C, 56.3, H, 4.4%.

(*d*) Ni(II) *complex*, **3d**. A solution of the diketone **1** (0.40 g, 1.48 mmol) in methanol (20 cm^3) was added slowly with stirring to a solution of sodium hydroxide (0.06 g, 1.50 mmol) in water (1 cm^3). To this mixture was added dropwise with stirring a solution of nickel(II) chloride hexahydrate (0.18 g, 0.76 mmol) in water (2 cm^3). The mixture was boiled for 2 min, cooled and exhaustively extracted with CH_2Cl_2: the combined extracts were washed with water, dried, and evaporated to yield purple-brown **3d** (0.24 g, 0.40 mmol, 54%). Anal.: Found: C, 56.7, H, 4.4%. $C_{28}H_{26}Fe_2NiO_4$ requires C, 56.3, H, 4.4%.

(*e*) Cu(II) *complex*, **3e**. A solution of the diketone **1** (0.40 g, 1.48 mmol) in methanol (40 cm^3) was added to a solution of copper(II) acetate monohydrate (0.15 g, 0.75 mmol) in water (3 cm^3): the mixture was shaken vigorously and then heated to 60 °C for 5 min. After cooling to ambient temperature, the resulting solid was filtered off and washed with water, followed by a little cold methanol to give orange-red **3e** (0.27 g, 0.45 mmol, 61%). Anal.: Found: C, 55.8, H, 4.4%. $C_{28}H_{26}CuFe_2O_4$ requires C, 55.9, H, 4.4%.

NMR spectra for Al(FcCOCHCOMe)$_3$, **2a**

Spectra were measured in $CDCl_3$ solution at ambient temperature using Bruker AM-300 spectrometer: the ^{13}C spectrum was assigned by use of appropriate DEPT sequences.

(*a*) fac *isomer*. δ(H) 2.08 (s, 3H, CH_3), 4.21 (s, 5H, C_5H_5), 4.39 (m, 2H) and 4.75 (m, 2H) (C_5H_4), 5.81 (s, 1H, COCHCO); δ(C) 27.2 (q, CH_3), 70.0 (d, C_5H_5), 80.2 (s, ipso of C_5H_4), 96.8$_9$ (d, CH), 188.0 (s) and 188.7 (s) (2 × CO).

(*b*) mer *isomer*. δ(H) 2.10 (s, 3H), 2.11 (s, 3H), and 2.15 (s, 3H) (3 × CH_3); 4.11 (s, 5H), 4.20 (s, 5H) and 4.25 (s, 5H) (3 × C_5H_5); 4.34 (m, 2H), 4.38 (m, 4H), 4.78 (m, 2H), 4.83 (m, 1H), 4.87 (m, 1H) and 4.90 (m, 2H) (3 × C_5H_4); 5.73 (s, 1H), 5.77 (s, 1H) and 5.80 (s, 1H) (3 × COCHCO). δ(C) 27.0 (q), 27.1 (q), and 27.3 (q), (3 × CH_3); 70.2 (d, 3 × C_5H_5); 79.9 (s), 80.1 (s), and 80.3 (s), (3 × ipso of C_5H_4); 96.9$_4$ (d), 97.2 (d), and 97.3 (d) (3 × CH); 188.1$_2$ (s), 188.1$_5$ (s), 188.2 (s), 188.6$_0$ (s), 188.6$_2$ (s), and 188.8 (s) (6 × CO).

(*c*) *Unassigned* CH *resonances in* C_5H_4 *region of* ^{13}C *spectrum*. 68.7, 68.8, 69.0$_3$, 69.0$_5$, 69.1, 69.2, 69.5, 70.4, 70.9, 71.0, 71.1, 71.3.

Electrochemistry

Materials and apparatus for electrochemistry have all been described elsewhere [7]. All potential values are referred to the Standard Calomel Electrode (SCE). Ferrocene can not be used as an internal standard here as its oxidation wave almost overlaps the oxidation waves of the complexes under study: consequently, the formal electrode potential of the couple $[Fe(C_5H_5)_2]/[Fe(C_5H_5)_2]^+$ was determined by cyclic voltammetric experiments performed under precisely the same experimental conditions (solvent, electrode material, supporting electrolyte, scan rate and temperature) as used for the complexes.

RESULTS AND DISCUSSION

The synthesis of the ferrocenyl diketone **1** described in the Experimental section is an improvement of the method described earlier [2], in that the modified work-up procedure provides a rather higher yield.

In the formation of neutral metal complexes from metal ions and neutral 1,3-diketones, protons are liberated [eqn (1)]:

$$M^{x+} + xRCOCH_2COR' \rightarrow [M(RCOCHCCOR')_x] + xH^+ \quad (1)$$

Effective preparative routes therefore require addition of a basic reagent to remove these liberated protons, to ensure efficient complexation of M^{x+}, which do not concurrently effect precipitation of, for example, metal hydroxides; the choice of the bases used in the present work has been guided by experience gained in the synthesis of metal complexes of simple 1,3-diketones. Although the complexes **3b–3e** have been described before [5], the preparative details were not given, and for this reason we report here detailed procedures for their preparations. We have been unable to isolate a zinc complex, although this was described by Imai and Óta. For formation of the Mn(II) and Fe(III) complexes, **3b** and **2d,** the reactions were buffered with sodium acetate, while formation of the Al(III) complex **2a** was promoted by the addition of aqueous ammonia: the formation of the Cr(III) complex **2b** was assisted by addition of urea, which hydrolyses during the course of the reaction to liberate ammonia. Sodium carbonate was employed as the base in the preparation of the vanadyl complex **3a,** while the preparation of both the Co(II) and Ni(II) complexes, **3c** and **3d,** employed preformed ligands generated *in situ* by reaction of the diketone **1** with aqueous sodium hydroxide. The synthesis of the Cu(II) complex **3e** employed the self-buffering copper(II) acetate. The only preparation which did not follow the simple pattern described by eqn (1) is that of the Mn(III) complex **2c**: for this, the Mn(II) complex is synthesised in the presence of an excess of the diketone **1** and, without isolation, converted to the Mn(III) complex in a comproportionation reaction with a stoichiometric quantity of permanganate [eqn (2)]:

$$4[Mn(FcCOCHCOMe)_2]+[MnO_4]^-+ 7FcCOCH_2COMe+H^+ \rightarrow 5[Mn(FcCOCHCOMe)_3]+4H_2O \quad (2)$$

The stoichiometries of all the complexes were established by elemental analysis: although complexes **2** may all be expected to exhibit *fac*/*mer* isomerism (see below), in no case could any chromatography conditions be found which allowed these isomers to be distinguished by means of their R_f values. In consequence no isomer separations were possible and hence, in turn, no structural characterisation by means of single-crystal X-ray diffraction has been possible. For the characterisation of the isomerism in **2**, we have turned instead to the NMR properties of the diamagnetic aluminium complex **2a**.

NMR spectra of complex **2a**

Metal complexes of the pentane-1,3-dionate ligand, of type $[(MeCOCHCOMe)_3M]$ are octahedral with idealised molecular symmetry D_3 [8], except for the Mn(III) complex which shows clear evidence of a Jahn-Teller elongation [9]; hence all can occur in enantiomeric Λ and Δ forms. Despite the enforced absence of structural data from X-ray crystallography, it is a reasonable inference that the complexes **2** will adopt octahedral geometries similar to those of the pentanedionate complexes, and the discussion of the NMR spectra of **2** will proceed on that basis.

In the ^1H NMR spectrum of compound **2a**, those resonances expected to appear as singlets (CH_3, COCHCO, and C_5H_5) all appear as a set of four resonances, three of which have equal intensity. These data indicate the presence of both *fac* and *mer* isomers: the *fac* isomer has idealised C_3 molecular symmetry, with all three ligands equivalent by symmetry, while in the *mer* isomer, of molecular symmetry C_1, the three ligands are all in different environments.

Hence the three equally-intense resonances in each region arise from the three distinct ligands of the *mer* isomer, while the fourth resonance in each group is attributable to the *fac* isomer. Integration of each group of resonances indicates a *fac*:*mer* ratio of 1:1.6, i.e. approximately 2:3. Precisely the same pattern of (3+1) individual resonances is readily identifiable in each of the regions of the ^{13}C NMR spectrum where the number of separate resonances does not cause problems of coincidental overlap, namely the CH_3, CH, C_5H_5 and CO regions; in addition, the *ipso*-carbon resonances of the C_5H_4 groups conform to this pattern. However, the pattern of the CH resonances arising from the C_5H_4 groups is more complex, in both the ^1H and ^{13}C NMR spectrum.

It is generally observed that whenever there is a stereogenic centre adjacent to the *ipso*-carbon in a monosubstituted ferrocene, then the four CH groups of the C_5H_4 fragment are magnetically inequivalent and it is often possible to distinguish four different chemical shifts in both the ^1H and ^{13}C spectra. In both isomers of complex **2a**, the aluminium ion provides a stereogenic centre: although this is three bonds away from the C_5H_4 unit, nonetheless the NMR spectra show clear evidence of magnetically inequivalent CH groups. A similar effect, over three covalent bonds, has been observed for the C_5H_4 unit in the compound $FcCH_2NH(CHMePh)$ [10]. In the ^1H spectrum, two resonances can be assigned to the C_5H_4 unit of the *fac* isomer, each corresponding to two hydrogens per ligand; for the *mer* isomer six chemical shifts can be distinguished, one of which corresponds in intensity to four hydrogens, three others each correspond to two hydrogens, and the final two to one hydrogen each. It is the observation of resonances in the C_5H_4 region whose integrals corresponding to one hydrogen per molecule which provides clear evidence for the

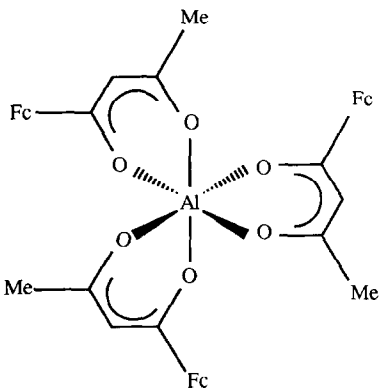

fac isomer

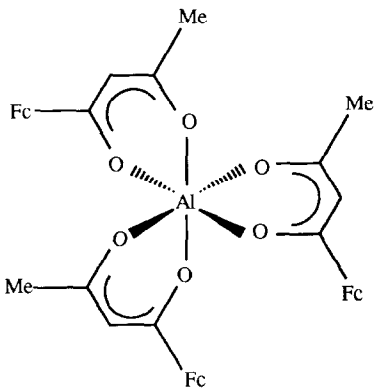

mer isomer

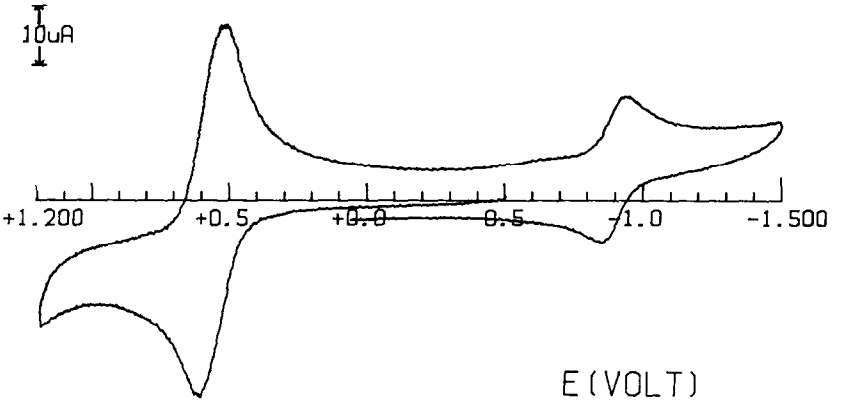

Fig. 1. Cyclic voltammetric response recorded at a platinum electrode on a CH_2Cl_2 solution containing **2d** (0.8×10^{-3} mol dm^{-3}) and $[NBu_4][PF_6]$ (0.2 mol dm^{-3}). Scan rate 0.2 V s^{-1}.

magnetic inequivalence of the CH units in the *mer* isomer C_5H_4 groups. If all such CH units had distinguishable chemical shifts, there would be twelve in all for the *mer* isomer, and four for the *fac* isomer: In the ^{13}C spectrum, a total of twelve resonances assignable to CH units in C_5H_4 groups can be resolved, although assignment of these to individual isomers has not been made: without the stereogenic effect of the metal ion the maximum number expected, for the two isomers together, would be eight. The *fac* and *mer* isomers of a complex $ML_3L'_3$ containing only monodentate ligands L and L′ and having molecular symmetries C_{3v} and C_{2v} respectively, are simple geometric isomers; in the presence of an asymmetric bidentate ligand of type L—L′, as here, giving molecular symmetries C_3 and C_1, the *fac* and *mer* isomers are also diastereoisomers.

Electrochemistry

Cyclic voltammetry and controlled potential coulometry proved that the ligand precursor 1-ferrocenyl-1,3-butanedione (**1**) undergoes in dichloromethane solution a chemically and essentially electrochemically reversible one-electron oxidation. As a matter of fact, controlled potential exhaustive oxidation ($Ew = +0.8$ V) consumes one electron/molecule. Cyclic voltammetry on the resulting solution affords a profile quite complementary to the original one. As a consequence of the electron removal the starting orange solution assumes the green colour ($\lambda_{max} = 640$ nm) typical of the iron-centred ferrocene oxidations. Furthermore, analysis [1] of the cyclic voltammograms exhibited by ligand **1** with scan rate varying from 0.02 V s^{-1} to 1.00 V s^{-1} shows that: (i) the current function $i_{pa}/v^{1/2}$ remains constant; (ii) the peaks-current ratio i_{pc}/i_{pa} is constantly equal to 1; (iii) peak-to-peak separation ΔE_p slightly departs from the theoretical value of 60 mV.

Without exception, members of both the series $M^{III}L_3$ and $M^{II}L_2$ exhibit a single oxidation process having features of chemical reversibility and involving three and two electrons respectively. In some cases reduction processes centred on the central M ions have been also observed, which, but for complexes **2c** and **2d,** are usually complicated by decomposition reactions. As a typical example, Fig. 1 shows the cyclic voltammetric response given by the iron complex **2d**.

As indicated above for all complexes **2,** a single oxidation process is observed for complex **2d,** which consumes three electrons/molecule in controlled potential coulometry ($Ew = +0.8$ V). Upon exhaustive oxidation the original red solution turns green-brown and exhibits a cyclic voltammogram complementary to the starting one. In turn, as far as the chemical reversibility of the Fe(III)/Fe(II) reduction of the central metal ion is concerned it has been also verified by exhaustive cathodic electrolysis ($Ew = -1.1$ V).

Table 1 summarises the formal electrode potentials of the redox changes exhibited by the complexes under study. Without exception, members of the series **2** and **3** exhibit a single oxidation process and consume in controlled potential coulometry three and two electrons respectively.

A comparison of the oxidation potential of **1** with unsubstituted ferrocene points out the electron-withdrawing ability of the diketone group. In addition, it is clearly evident that independent of the nature of the different central metal ions, their complexation to 1-ferrocenyl-1,3-butanedionate somewhat compensates for the inductive effects of the diketonate group.

In none of the complexes studied is there any evidence of electronic communication between the several iron atoms of the ferrocene ligands. Despite the

Table 1. Electrochemical parameters ($E^{\circ\prime}$ in V, ΔE_p in mV) for the redox processes exhibited by complexes ML_3 and ML_2 and related species in dichloromethane solution (supporting electrolyte: $[NBu_4][PF_6]$ (0.2 mol dm^{-3}))

Complex	Ferrocene-centred oxidation			Metal-centred reduction		
	$E^{\circ\prime}$	$\Delta E_p{}^a$	n^b	$E^{\prime}$	$\Delta E_p{}^a$	n^b
1	+0.64	88	1	—	—	—
2a	+0.58	114	3	—	—	—
2b	+0.58	90	3	—	—	—
2c	+0.59	130	3	−0.36	370	1
2d	+0.58	118	3	−0.88	92	1
3c	+0.59	122	2	−0.90[c]	110	1
3d	+0.58	166	2	−0.88[c]	74	1
3e	+0.56	70	2	−1.28[d]	—	[e]
$Fe(C_5H_5)_2$	+0.39	80	1	—	—	—

[a] Measured at 0.1 Vs^{-1}.
[b] coulometrically measured number of electrons involved in the redox change.
[c] complicated by subsequent chemical reactions.
[d] irreversible process.
[e] not measured.

delocalised nature of the π-electrons in each metal diketonate fragment, the individual ferrocene units are effectively insulated from one another. A number of bis-ferrocenyl compounds, in which the two ferrocene fragments are separated by insulating groups, have been found to exhibit two well-separated and reversible one-electron oxidations, indicative of electronic communication between the two fragments. However, in all cases involving such electronic communication the ferrocene fragments are separated by no more than two covalent bonds, as in Fc_2 [12], and in Fc_2CO, Fc_2CH_2, Fc_2CHOH and Fc_2CPhOH [13]. On the other hand, when the insulating spacer is such that the individual ferrocene fragments are separated by more than two covalent bonds, as in $FcCH_2CH_2Fc$ [14], FcCHROCHRFc [13,15], or $(FcCH_2)_2C(COR)_2$ [13], only a single two-electron oxidation is observed. In the complexes **2** and **3** described here, the shortest pathway between ferrocene units requires six bonds. The related Co(II) complex formed by the conjugate base of formylferrocenethiosemicarbazone, in which the two ferrocene groups are also separated by six bonds, similarly shows a single two-electron oxidation consistent with there being no electronic communication between the ferrocenes [16]. This pattern is rather common for metal complexes of simple ferrocenyl ligands [17], and hence it seems unlikely that coordination polymers based upon ferrocene-1,1′-diylbis(1,3-diketone), or similar, ligands will be effective electrical conductors.

Acknowledgements—P.Z. acknowledges the financial support of Italian MURST (quota 60%) and the technical assistance of Mrs G. Montomoli.

REFERENCES

1. Zakaria, C. M., Morrison, C. A., McAndrew, D., Bell, W. and Glidewell, C., *J. Organomet. Chem.*, 1995, **485,** 201.
2. Bell, W., Crayston, J. A., Glidewell, C., Mazid, M. A. and Hursthouse, M. B., *J. Organomet. Chem.*, 1992, **434,** 115.
3. Ferguson, G., Glidewell, C. and Zakaria, C. M., *Acta Cryst.*, 1994, **C50,** 1673.
4. Cain, C. E., Mashburn, Jr, T. A. and Hauser, C. R., *J. Org. Chem.*, 1961, **26,** 1030.
5. Imai, I. and Óta, T., *Bull. Chem. Soc. Jpn.*, 1974, **47,** 2497.
6. Hayashi, T. and Togni, A., eds. *Ferrocenes From Homogeneous Catalysis to Material Science*, VCH Weinheim, 1995.
7. Togni, A., Hobi, M., Rihs, G., Rist, G., Albinati, A., Zanello, P., Zech, D. and Keller, H., *Organometallics*, 1994, **13,** 1224.
8. (a) Kruger, G. J. and Reynhardt, E. C., *Acta Cryst.*, 1974, **B30,** 822; (b) Kuroda, R. and Mason, S. F., *J. Chem. soc., Dalton Trans.*, 1979, 273; (c) Pang, L., Lucken, E. A. C. and Bernadinelli, G., *J. Am. Chem. Soc.*, 1990, **112,** 8754; (d) Pang, L., Whitehead, M. A. and Lucken, E. A. C., *Inorg. Chim. Acta*, 1993, **203,** 239.
9. Stults, B. R., Marianelli, R. S. and Day, V. W., *Inorg. Chem.*, 1979, **18,** 1853.
10. Unpublished work.
11. Brown, E. R. and Sandifer, J. R. In *Physical*

Methods of Chemistry, Electrochemical Methods, Vol. 2, B. W. Rossiter and J. F. Hamilton, Wiley, New York, 1986, Ch. 4.
12. Kotz, J., Neyhart, G., Vining, W. J. and Rausch, M. D., *Organometallics*, 1983, **2,** 79.
13. Ferguson, G., Glidewell, C., Opromolla, G., Zakaria, C. M. and Zanello, P., *J. Organomet. Chem.*, 1996, **517,** 183.
14. Bildstein, B., Denifli, P., Wurst, K., André, M., Baumgarten, M., Friedrich, J. and Ellmerer-Müller, E., *Organometallics*, 1995, **14,** 4334.
15. Silva, N. E. P. R. A., Pombeiro, A. J. L., da Silva, J. J. R. F., Herrmann, R., Deus, N., Castilho, T. J. and Silva, M. F. C. G., *J. Organomet. Chem.*, 1991, **421,** 75.
16. Fleishmann, W.-D. and Fritz, H. P., *Z. Naturforsch.*, 1973, **28b,** 383.
17. Zanello, P. in Ref. 6, pp. 317–430.

Pergamon

PII: S0277-5387(97)00531-7

Polyhedron Vol. 17, Nos. 11–12, pp. 1803–1809, 1998
© 1998 Elsevier Science Ltd
All rights reserved. Printed in Great Britain
0277-5387/98 $19.00+0.00

Synthesis and characterization of some four- and five-coordinate copper(II) complexes of 6-methyl-2-formylpyridinethiosemicarbazone (HNNS) and the X-ray crystal structures of the $[Cu(NNS)(CH_3COO)(H_2O)]$ and $[Cu(HNNS)(H_2O)(SO_4)]\cdot H_2O$ complexes

Mohammad Akbar Ali,*[a] Nor Erawadi Hj Ibrahim,[a] Ray J. Butcher,[b] Jerry P. Jasinski,[c] John M. Jasinski[c] and Jeffrey C. Bryan[d]

[a] Department of Chemistry, University of Brunei Darussalam, BSB 2028, Brunei Darussalam

[b] Department of Chemistry, Howard University, Washington, D.C. 20059, U.S.A.

[c] Department of Chemistry, Keene State College, NH 03431, U.S.A.

[d] Chemical and Analytical Sciences Division, Oak Ridge National Laboratory, Oak Ridge, TN 37831-6119, U.S.A.

(Received 20 October 1997; accepted 18 December 1997)

Abstract—Copper(II) complexes of general formula, $[Cu(NNS)(H_2O)_xX]\cdot nH_2O$ (NNS^- = uninegatively charged tridentate thiosemicarbazone ligand formed from 6-methyl-2-formylpyridine; $X = NCS^-$, CH_3COO^-, N_3^-; $x = 0,1$; $n = 0.5, 1$) and $[Cu(HNNS)(H_2O)(SO_4)]\cdot H_2O$ have been synthesized and characterized by a variety of physico-chemical techniques. Magnetic and spectroscopic evidence support a square-planar structure for the [Cu(NNS)X] ($X = NCS^-$, N_3^-) complexes and a five-coordinate structure for the $[Cu(HNNS)(H_2O)(SO_4)]\cdot H_2O$ complex. The crystal structures of the $[Cu(NNS)(CH_3COO)(H_2O)]$ and $[Cu(HNNS)(H_2O)(SO_4)]\cdot H_2O$ complexes have been determined by X-ray diffraction. The acetato complex has a distorted square-pyramidal geometry with the thiosemicarbazone ligand acting as a uninegatively charged tridentate NNS chelating agent and the fourth and fifth coordination positions of the copper(II) ion are occupied by a unidentate acetate and water ligand, respectively. The sulphato-complex is also five-coordinate with the thiosemicarbazone coordinated as a neutral NNS ligand and the fourth and fifth coordination sites are occupied by a water molecule and a unidentate sulphate ligand, respectively. © 1998 Elsevier Science Ltd. All rights reserved

Keywords: copper(II) complexes; 6-methyl-2-formylpyridinethiosemicarbazone; four- and five-coordinate copper(II) complexes; crystal structures of copper(II) complexes.

Transition metal complexes of thiosemicarbazones have generated considerable interest due to their wide-ranging biological activities [1–3]. Of all the thiosemicarbazones studied so far, the 2-formylpyridinethiosemicarbazone (HPATS) probably got the most attention due to its marked antitumour properties [4]. Its copper(II) complex, Cu(PATS) has been shown to be more active than the free ligand [5]. Structural studies on copper-PATS complexes by X-ray diffraction [6–9] have shown that these complexes are dimeric in the solid state. Since the active antitumour species *in vivo* has been thought to be the monomeric $[Cu(PATS)H_2O]^+$ ion and as HPATS appears to react with copper(II) salts to yield only dimers, we thought it worthwhile to synthesize and

* Author to whom correspondence should be addressed.

characterize some monomeric copper(II) complexes with the same NNS chelate but using a slightly modified HPATS ligand. In a previous paper [10], we reported that the 6-methyl-2-formylpyridinethiosemicarbazone, which is very similar to HPATS, except that it has a methyl group at the sixth position of the pyridine ring, is capable of forming monomeric four-coordinate square-planar copper(II) complexes, in contrast with HPATS which forms dimeric copper(II) chelates. In this paper, we report the preparation and characterization of some new copper(II) complexes of this ligand together with the X-ray crystal structures of the [Cu(NNS)(CHCOO)(H_2O)] and [Cu(HNNS)(H_2O)(SO_4)] · H_2O complexes.

EXPERIMENTAL

The details of physical measurements have been reported previously [10].

Compound preparation

The method of preparation of the ligand is given in our previous paper [10]. The [Cu(NNS)(CH_3COO)(H_2O)] complex was prepared as described previously [10].

Preparation of [Cu(NNS)X](X = NCS^-, N_3^-)

The [Cu(NNS)(CH_3COO)(H_2O)] complex (1 mmol) was dissolved in water (100 ml) to which excess sodium thiocyanate or sodium azide (5 mmol) was added. The product formed was collected by filtration and washed with water followed by methanol and dried in a desiccator over silica gel. Yield: 80–90%.

Preparation of [Cu(HNNS)(H_2O)(SO_4)] · H_2O

Copper(II) sulphate pentahydrate (1 mmol) was dissolved in a minimum amount of water. The solution was mixed with a boiling solution of the ligand (1 mmol) in methanol (100 ml). On heating on a water bath for ca 5 min, the complex crystallized out of the reaction mixture. Recrystallization from water gave beautiful green x-ray diffraction quality crystals. Yield: 85%.

Determination of the crystal structure of the [Cu(HNNS)(H_2O)(SO_4)] · H_2O *complex*

The intensity data were obtained by using an Enraf-Nonius CAD4 diffractometer at 163 K. Intensities were corrected for Lorentz and polarization effects and empirical absorption corrections were applied based on a set of ψ scans. Calculations were carried out using XCAD49 (data reduction), SHELXTL (absorption correction, structure solution/refinement and molecular graphics). All hydrogen atoms were placed in calculated positions, refined using a riding model, and given an isotropic displacement parameter equal to 1.2 (CH, CH2) or 1.5 (CH3, OH) times the equivalent isotropic displacement parameter of the atom to which it is attached. When warranted, methyl hydrogen atomic positions were allowed to rotate about the C—C bond. Full-matrix least-squares refinement of all data against F^2 of the quantity $w(F_o^2 - F_c^2)$ was used to adjust the position and anisotropic thermal parameters of all non-hydrogen atoms. Unit cell dimensions were refined by use of the settings of 25 accurately determined reflections widely separated in reciprocal space. Intensities were measured by ω scans. The structure was solved by direct methods [11] and subsequent Fourier syntheses were used to determine remaining non-hydrogen atomic positions. A summary of the crystallographic data, experimental details and refinement results is given in Table 1.

Determination of the crystal structure of [Cu(NNS)(H_2O)(CH_3COO)]

The intensity data were collected at 296 K by a Rigaku AFC6S diffractometer. Cell constants and orientation matrix for data collection were obtained by least-squares refinement of the diffraction data from reflections in the range 30.03–36.45°. The structure was solved by direct methods. All non-hydrogen atoms were refined anisotropically. Hydrogen atoms were included in structure factor calculations in their calculated positions. The final cycle of full-matrix least-squares refinement was based on 1301 observed reflections. Neutral atom scattering factors were taken from Cromer and Waber [12]. All calculations were performed using the TEXSAN crystallographic software package of molecular structure [13]. A summary of crystal data, experimental details and refinement results are listed in Table 1. The data were corrected for Lorentz and polarization effects. No absorption correction was made.

RESULTS AND DISCUSSION

The 6-methyl-2-pyridinecarboxaldehydethiosemicarbazone (Fig. 1) has a thioamide function, —HN—C(S)NH_2 and consequently, it can exhibit thione-thiol tautomerism.

However, its IR spectrum as Nujol mull does not display any ν(S—H) band at ca 2600 cm^{-1} indicating that, in the solid state, it remains as the thione form (1a). However, in solution and in the presence of copper(II) salts, it can quickly convert to the thiol form (1b) with the concomitant formation of copper(II) complexes of the deprotonated mercaptide form of the ligand. It is only with the copper(II) sulphate salt that the Schiff base yields a copper(II) com-

Table 1. Summary of crystal data, data collection and structure refinement parameters for the $[Cu(NNS)(H_2O)(CH_3COO)]$ and $[Cu(HNNS)(H_2O)(SO4)] \cdot H_2O$ complexes

Compound	$[Cu(HNNS)(H_2O)(SO_4)] \cdot H_2O$	$[Cu(NNS)(H_2O)(CH_3COO)]$
Chemical formula	$C_8H_{14}CuN_4O_6S_2$	$C_{10}H_{14}CuN_4SO_3$
Formula weight	389.89	333.85
Crystal system	monoclinic	monoclinic
Space group	$P2_1/n$	$P2_1/n(14)$
a (Å)	12.147 (2)	7.556 (2)
b (Å)	7.1813 (6)	14.086 (3)
c (Å)	16.2251 (14)	12.447 (2)
β (°)	104.798 (9)	91.54 (2)
V (Å^3)	1368.3 (2)	1324.3 (9)
Z	4	4
Mo–K_α (Å)	0.71073	0.71069
T (K)	153	296
ρ_{calc} (g cm^{-3})	1.893	1.674
μ (mm^{-1})	1.935	1.812
Sample dimension (mm)	$0.45 \times 0.12 \times 0.10$	$0.10 \times 0.10 \times 0.50$
$F(000)$	796	684
$2\Theta_{max}$	50	50
Reflections collected	6392	2623
Independent reflections	2416 ($R_{int} = 0.0862$)	2431 ($R_{int} = 0.050$)
No. of data used for refinement	2416	1301
No. of parameters refined	247	229
Refinement method	Full-matrix least-squares	Full-matrix least squares
R	0.0371	0.043
R_w	0.0500	0.044
Largest peak and smallest peak (e A^{-3})	0.813, −1.280	0.41, −0.37
Goodness of fit on F^2	1.020	1.30

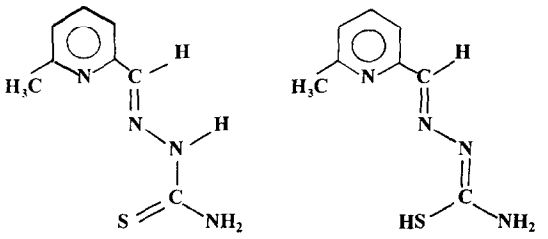

(1a) Thione form (1b) Thiol form

Fig. 1. (a) Thione from (**1a**) and (b) thiol form (**1b**).

plex containing the neutral form of the ligand. The related pyridine-2-carboxaldehydethiosemicarbazone (HPATS) has also been found to coordinate with copper(II) ions in both protonated and deprotonated forms. Recently, a bis-chelated copper(II) complex of 2-acetylpyridinethiosemicarbazone ligand has been reported [14] which is unique in that it has a neutral as well as a deprotonated tridentate NNS ligand coordinated to the copper(II) ion in the same complex.

The complexes isolated in the present study have the empirical formulae, $[Cu(NNS)(X)(H_2O)_x] \cdot nH_2O$ (NNS^- = anionic form of the 6-methylpyridine-2-carboxaldehydethiosemicarbazone ligand; X = NCS^-, N_3^-, CH_3COO^-; $n = 0.5, 1$ $x = 0,1$) and $[Cu(HNNS)(SO_4)(H_2O)] \cdot H_2O$. The characterization data for these complexes are shown in Table 2. The molar conductivities of these complexes in DMSO are well below the range (50–70 ohm^{-1} cm^2 mol^{-1}) found for 1:1 electrolytes, indicating that the anions are coordinated to the copper(II) ion. Coordination of the anions to the copper(II) ion is further supported by the IR spectra of the thiocyanato-, sulphato- and the azido complexes (Table 3).

The IR data (Table 3) also support coordination of the Schiff base via the azomethine nitrogen atom {lowering of the azomethine ν(C=N) band and shift of the hydrazine ν(N—N) band of the free ligand to higher frequencies), the pyridine nitrogen atom (shift of the pyridine ring deformation mode from 562 cm^{-1} to about 595 cm^{-1}) and the sulphur atom (lowering of the ν(C=S) band from 830 cm^{-1} to 720 cm^{-1}).

The room-temperature magnetic moments of the present copper(II) complexes (Table 1) indicate that they are magnetically dilute in nature. Their electronic spectra show bands in the regions 210–345, 380–470 and 660–690 nm, corresponding to the intraligand,

Table 2. Colours, conductivities, magnetic moments and analytical data for the copper(II) complexes

Compound	Colour	Λ[a]	μ[b]	Analytical data[c] C	H	N
[Cu(NNS)(NCS)]	green	29.8	1.85	34.09 (34.33)	2.61 (2.88)	21.85 (22.24)
[Cu(NNS)N_3]·0.5H_2O	green	3.4	1.78	31.22 (31.29)	3.27 (2.96)	31.85 (31.65)
[Cu(HNNS)(SO_4)(H_2O)]·H_2O	bright green	12.1	2.12	24.56 (24.64)	3.42 (3.61)	14.01 (14.36)

[a] Molar conductance (ohm^{-1} cm^{2}mol^{-1}) of ca 10^{-3} M solutions in DMSO.
[b] Effective magnetic moment at 300 K.
[c] Calculated values are given in parentheses.

Table 3. Selected infrared bands (cm^{-1}) and electronic spectral data for the copper(II) complexes

Compound	IR bands (cm^{-1})				Electronic spectra[a]	
	νNH_2	νCN	$\nu N—N$	anion bands	State	λ_{max}(nm)
				ν(C—N):		
[Cu(NNS)(NCS)]	3166 w	1614 s	1034 w	2100 sh	Nujol	655, 419, 360 sh
	3343 w			2118 m	DMSO	668, 412, 330 sh, 295
				2147 m		(2.2) (4.0) (4.2)
				2162 sh		
					Nujol	740, 409, 359
[Cu(NNS)(N_3)]·0.5H_2O	3371 w	1609 m	1039 m	ν(NNN):	DSMO	640, 410, ca330 sh, 294
	3107 w			2064 s		(2.8) (4.1) (4.2)
				2050 s		
[Cu(HNNS)(SO_4)(H_2O)]·H_2O	3231 m	1643 s	1044 s	ν(S—O)	Nujol	800, 400 sh, 344
				1117 s	DMSO	673, 410, 330 sh, 294
				1104 s		(2.4) (4.05) (4.1)
				1044 s		
				1007 s		
				973 m		
				643 s		
				600 s		
HNNS·H_2O[b]	3200 w	1620 s	1000 m			
	3320 w					
	3100 br					

[a] Log ε (litre mol^{-1} cm^{-1}) are given in parentheses.
[b] Ref. 10.

charge transfer and *d-d* transitions, respectively. The sulphur to copper charge transfer band, which is characteristic of copper(II)-thiosemicarbazone complexes [7,8] is observed at ca 410 nm.

The x-ray crystal structures of the [Cu(HNNS)(SO_4)(H_2O)]·H_2O *and* [Cu(NNS)(CH_3COO)(H_2O)] *complexes*

The structures of the sulfato- and the acetato complexes, together with the atom numbering schemes adopted, are shown in Figs 2 and 3, respectively. Tables 4 and 5 list the selected bond lengths and bond angles for the sulfato- and acetato-complexes, respectively. The crystal structures of both complexes contain discrete five-coordinate copper(II) ions. The coordination environment around the copper(II) ion in each complex is five-coordinate with the copper atom lying in an approximate plane of four coordinating atoms, three of which are supplied by the 6-methyl-2-formylpyridinethiosemicarbazone, the fourth coordination position is occupied by an oxygen atom of the sulfate or acetate ligand and the fifth

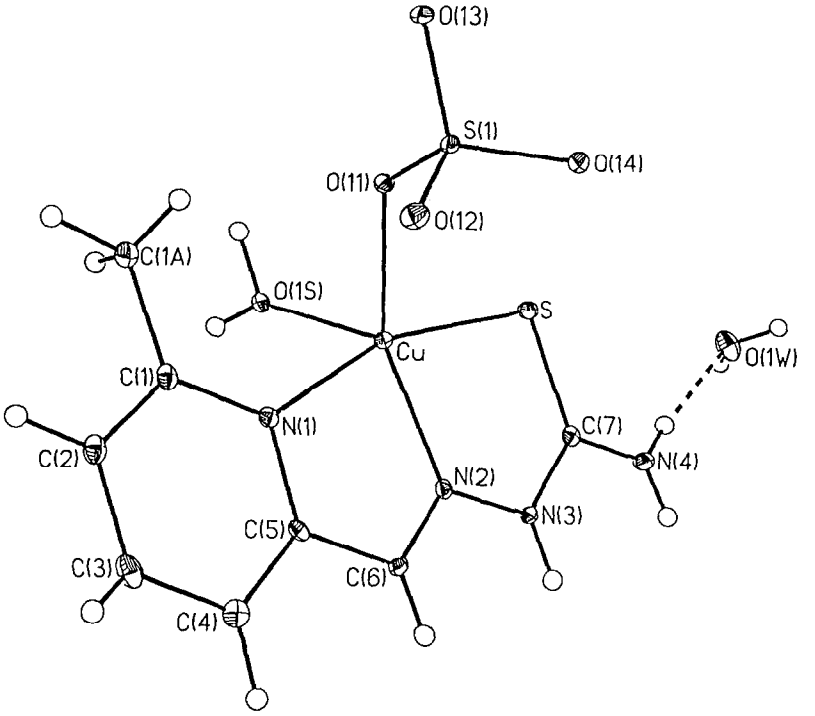

Fig. 2. The structure of [Cu(HNNS)(SO$_4$)(H$_2$O)] · H$_2$O.

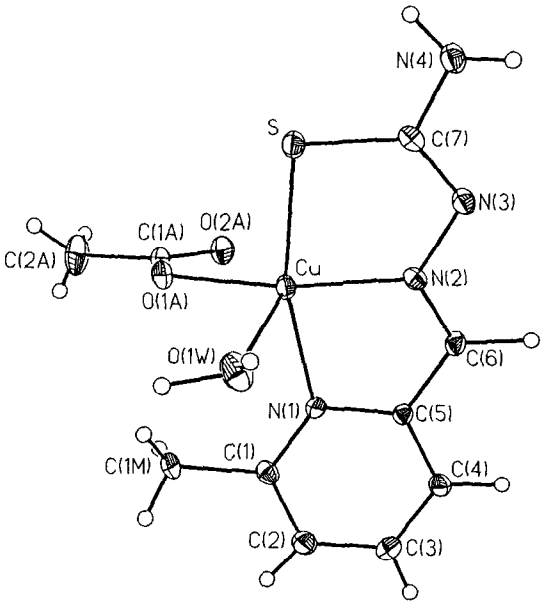

Fig. 3. The molecular structure of [Cu(NNS)(CH$_3$COO)(H$_2$O)] with the atom numbering scheme.

coordination position is completed by an oxygen of the coordinated water molecule. In the [Cu(HNNS)(SO$_4$)(H$_2$O)] · H$_2$O complex, the C(7)—S bond distance (1.710(3) Å) is nearer to that expected of a double bond than a single bond and compares well with that of other thiosemicarbazone-copper(II) complexes containing thione sulfur [7]. Both the sulfato- and acetato-copper(II) complexes of the parent 2-formylpyridinethiosemicarbazone have a dimeric structure with one-atom acetate of sulfate oxygen-bridging [7]. This shows that substitution of a hydrogen atom by a methyl group at the sixth position of the pyridine ring of the ligand prevents formation of a dimer. In spite of the similarity of the coordination sphere around the copper(II) ion in both sulfate and acetate complexes, the crystal structures show that the 6-methyl-2-pyridinecarboxaldehydethiosemicarbazone exists in the deprotonated mercaptide form in the acetate complex, whereas it is present as undeprotonated thione form in the sulfato complex. The deprotonation of the ligand in the [Cu(NNS)(CH$_3$COO)(H$_2$O)] complex is accompanied by tautomerization to the iminothiolate form. While coordinating in the iminothiolate form, the negative charge on the sulfur atom (generated by deprotonation) is delocalized in the C—N—N—C system as indicated by their intermediate bond distances [C(6)—N(2) = 1.273(8) Å, N(2)—N(3) = 1.739(7) Å and N(3)—C(7) = 1.305 Å]. The C(7)—S bond distance (1.728(7) Å) in the acetato-complex, is shorter than that found in the analogous copper(II) complexes containing thiolato sulfur atoms, but the bond orders of the two C—N bonds are closer to two than one. The Cu—S, Cu—N(imine) and Cu—N(py) bond lengths in both complexes (Tables 3 and 4) compare well with those found in other related five-coordinate

Table 4. Selected bond lengths (Å) and bond angles (°) for $[Cu(HNNS)(SO_4)(H_2O)]\cdot H_2O$

Cu—N(2)	1.966(2)	S(1)—O(12)	1.463(2)
Cu—N(1)	2.069(2)	S(1)—O(14)	1.482(2)
Cu—S	2.328(8)	S—C(7)	1.710(3)
Cu—O(11)	1.974(2)	S(1)—O(11)	1.497(2)
Cu—O(1S)	2.163(2)	N(1)—C(5)	1.365(4)
N(2)—N(3)	1.372(3)	N(4)—C(7)	1.310(4)
N(3)—C(7)	1.352(4)		
N(2)—Cu—N(1)	79.93(9)	O(11)—Cu—N(1)	102.02(9)
O(11)—Cu—O(1S)	91.40(8)	N(2)—Cu—O(1S)	117.02(9)
N(2)—Cu—S	82.75(7)	N(1)—Cu—O(1S)	93.91(9)
N(1)—Cu—S	162.47(7)	O(11)—Cu—S	91.94(7)
N(2)—Cu—O(11)	151.45(9)	O(1S)—Cu—S	96.32(7)
C(7)—Cu—S	162.47(7)	C(7)—S—Cu	97.59(10)
O(13)—S(1)—O(14)	110.37(12)	O(12)—S(1)—O(13)	111.78(13)
O(13)—S(1)—O(11)	107.09(11)	S(1)—O(11)—Cu	120.94(11)

Table 5. Selected bond lengths (Å) and bond angles (°) for [Cu(NNS)$(CH_3COO)(H_2O)$]

Cu—S	2.275(2)	N2—C6	1.273(8)
Cu—O(1A)	1.966(5)	N3—C7	1.305(8)
Cu—O1W	2.453(5)	N4—C7	1.365(9)
Cu—N1	2.093(6)	C1A—C2A	1.49(1)
Cu—N2	1.959(6)	O1A—C1A	1.265(9)
S—C7	1.728(7)	O2A—C1A	1.239(8)
N2—N3	1.379(7)	N1—C1	1.344(8)
S—Cu—O1A	93.8(2)	S—Cu—N1	163.6(2)
S—Cu—N2	83.1(2)	O1A—Cu—N1	102.4(2)
O1A—Cu—N2	162.2(2)	N1—Cu—N2	80.7(2)
O1W—Cu—S	99.0(2)	O1A—Cu—O1W	90.5(2)
O1W—Cu—N1	83.5(2)	O1W—Cu—N2	107.3(2)
Cu—S—C7	95.4(3)	Cu—O1A—C1A	111.4(4)
Cu—N2—N3	124.2(4)	Cu—N2—C6	116.9(5)
S—C7—N3	125.8(5)	S—C7—N4	116.8(6)

copper(II) complexes of thiosemicarbazone ligands [7,8]. The stereochemistry around the copper(II) atom in both complexes is intermediate between a square-pyramidal (SPY) and a trigonal-bipyramidal (TBPY) geometry. Illustration of this point can be made by considering the distortion from idealized TBPY geometry. Taking O(11) and N(2) as the axial donors in the $[Cu(HNNS)(SO_4)(H_2O)]\cdot H_2O$ complex, an angle of 151.45(9)° is subtended at the copper(II) ion [*viz.* the O(11)—Cu—N(2) angle] which is much smaller than the theoretical value of 180°. The angles between the two axial donors and the three equatorial donors O(1S), N(1) and S in the sulfato complex range from 102.02(9)° for the O(11)—Cu—N(1) angle to 117.02(9)° for the N(2)—Cu—O(1S) angle. The three equatorial angles range from 162.47(7)° for N(1)—Cu—S, 96.32(7)° for O(1S)—Cu—S and 93.91(9)° for O(1S)—Cu—N(1) showing marked differences from the ideal value of 120°. A similar comparison can be made for an idealized SPY geometry taking O(11) as the apical donor and N(1), N(2) and O(1S) to form the basal plane.

Similarly, taking 01A and N2 as the axial donors for the acetato complex, an angle of 162.2(2)° is subtended at the copper(II) ion, which is smaller than the theoretical value of 180°. The angles between the two axial donors and the three equatorial donors S, N1 and O1W range from 80.7(2) to 102.4(2)°, showing marked differences from the expected value of 120°. In a similar manner, a comparison can be made for an idealized square-pyramidal geometry for the acetato-complex by taking O1W as the apical donor and S, N2, N1 and O1A as the axial donors. The distortion from idealized stereochemistry for both complexes is attributed to the restricted bite angles imposed by the Schiff base.

The molecular packing study for the sulfato-complex confirms the presence of extensive hydrogen

bonding interactions involving the uncoordinated sulfate oxygens, the coordinated and uncoordinated water molecules and the hydrogen atoms attached to N(4). These hydrogen bonding interactions between the hydrogen atom on N(3) and a sulfato ligand are probably responsible for stabilizing the neutral form of the ligand.

The molecular packing study for the [Cu(NNS)(CH_3COO)(H_2O)] complex shows that one of the two NH_2 protons is involved in hydrogen bonding to the coordinated acetate oxygen of an adjoining molecule. The two water protons are both involved in hydrogen bonding interaction to N3 and O2A in other molecules.

CONCLUSION

Although the parent 2-formylpyridine thiosemicarbazone (HPATS) ligand almost invariably forms dimeric copper(II) complexes with copper(II) salts, the present ligand, which is similar to HPATS expect that it has a methyl group attached to the sixth position of the pyridine ring, yields monomeric copper(II) complexes. The sulfato- and acetato-copper(II) complexes of the present ligand, like those of the HPATS ligand, are also five-coordinate but they are not dimeric with oxygen-bridging.

Acknowledgements—Grateful acknowledgement is made to the University of Brunei Darussalam for financial support. One of us (MAA) thanks Mr. Hussain Bin Mohd. Hashim, Laboratory Superintendent and Mr. Mohd. Jamil Abd Hamid, Technical Officer of Chemistry Department, University of Brunei Darussalam, for assistance.

REFERENCES

1. Subsczynski, W. K., Antholine, W. E., Hyde, J. S. and Petering, D. H., *J. Am. Chem. Soc.*, 1987, **109,** 46.
2. Liberta, A. E. and West, D. X., *BioMetals*, 1992, **5,** 125.
3. Scovill, J. P., Klayman, D. L. and Franchino, C. F., *J. Med. Chem.*, 1982, **25,** 1261.
4. (a) Brockman, R. W., Thomson, J. R., Bell, M. J. and Skipper, H. E., *Cancer Res.*, 1956, **16,** 1167; (b) Sartorelli, A. C., Agrawal, K. C., Tsiftsoglou, A. S. and Moore, P. E., In *Advances in Enzyme Regulation*, Vol. 15, ed. G. Weber, Pergamon, New York, 1977, 117.
5. Antholine, W. E., Gunn, P. and Hopwood, L. E., *Intl. Radiat. Oncology, Biol. Phy.*, 1981, **7,** 491.
6. Bell, C. F. and Theocharis, R., *Acta Crystallogr. Section C*, 1987, **43,** 26.
7. Bingham, A. G., Bogge, H., Muller, A., Ainscough, E. W. and Brodie, A. M., *J. Chem. Soc., Dalton Trans.*, 1987, 493.
8. Ainscough, E. W., Brodies, A. M., Ranford, J. D. and Waters, J. M., *J. Chem. Soc., Dalton Trans.*, 1991, 2125.
9. Garcia-Tojal, J., Urtiaga, M. K., Cortes, R., Lezama, L., Rojo, T. and Arriortua, M. I., *J. Chem. Soc., Dalton Trans.*, 1994, 2233.
10. Ali, M. A., Dey, K. K., Nazimuddin, Butcher, R. J., M., Jasinski, J. P. and Jasinski, J. M., *Polyhedron*, 1996, **15,** 3331.
11. Gilmore, C. J., *J. Appl. Cryst.*, 1984, **17,** 42.
12. Cromer, D. T. and Waber, J. T., *International Tables for X-Ray Crystallography*, Table 2.2A, Vol. IV, The Keynoch Press, Birmingham, England, 1994.
13. TEXAN-TEXRAY, Analysis Package. Molecular Structure Corporation, 1985.
14. Souza, P., Matesanz, A. I. and Fernandez, V., *J. Chem. Soc., Dalton Trans.*, 1996, 3011.

Pergamon

PII: S0277-5387(97)00527-5

Polyhedron Vol. 17, Nos. 11–12, pp. 1811–1815, 1998
© 1998 Elsevier Science Ltd
All rights reserved. Printed in Great Britain
0277-5387/98 $19.00+0.00

Synthesis of bis(diphenylphosphino) ethanenickel(II) organodichalcogenide complexes and cyclotrimerisation reaction of dimethylacetylenedicarboxylate: structure of Ni(dppe)(SC_6H_4O)

Mary S. Thomas and J. Darkwa*†

Department of Chemistry, University of the North, Private Bag X1106, Sovenga 0727, South Africa

(Received 21 July 1997; accepted 16 December 1997)

Abstract—Reaction of Ni(dppe)Cl_2 (dppe = bis(diphenylphosphino)ethane) with organodichalcogenide ligands of the type 1,2-HSC_6H_4EH (E = CO_2, O, NH) in the presence of triethylamine to give the products Ni(dppe)($SC_6H_4CO_2$) (**1**), Ni(dppe)(SC_6H_4O) (**2**), and Ni(dppe)(SC_6H_4NH) (**3**). Complex **2** was characterised by single crystal X-ray diffraction, which shows a distorted geometry. Complexes **1–3** and the dithiolato analogues of 1,2-benzenedithiol, Ni(dppe)(SC_6H_4S) (**4**), and 3,4-toluendithiol, Ni(dppe)(SC_6H_3MeS) (**5**), upon reflux with dimethylacetylenedicarboxylate (DMAD) formed the cyclotrimeric product hexamethylbenzene hexacarboxylate (HMBC). © 1998 Elsevier Science Ltd. All rights reserved

Keywords: nickel(II) complexes; crystal structure; cyclotrimerisation; hexamethylbenzene hexacarboxylate.

Since the discovery of the cyclotetramerisation of acetylene by Reppe [1], a number of transition metal complexes have been found to homogeneously catalyse the cyclisation of acetylenes. Much of this work has centred around the group 10 metals, with the cheaper nickel playing quite a prominent role in these studies. Two oxidation states are predominant in the use of nickel as a catalyst for acetylene cyclisation. These are Ni(II) and Ni(0). Early literature reports considered Ni(II) complexes as the active catalysts in the formation of cyclooctatetraenes [2], whereas Ni(0) complexes trimerise acetylenes to benzenoid derivatives [3,4]. In general, studies involving Ni(0) are more abundant than those of Ni(II) mainly because the former readily dissolve in organic solvents whilst Ni(II) salts, that are normally used, are insoluble in such solvents. With the aid of phosphine ancillary ligands the solubility of Ni(II) complexes in organic solvents could be achieved. Such compounds are known to trimerise acetylenes [5]. Recently, Bennet and Wenger [6] have utilised bis(phosphino)nickel(0) complexes to catalytically cyclise a number of alkynes in solution, demonstrating the importance of phosphines in these reactions.

With dithiolato as coligands, phosphinonickel complexes can behave as nucleophilic agents towards acetylenes. Dimethylacetylenedicarboxylate reacts with (triphos)Ni(η^2-S_2CS) (triphos = 1,1,1-tris-(diphenylphosphinomethyl)ethane) to form a heterocyclic five-membered metallo-ring adduct, in which a dimerised DMAD moiety is attached to the C and S ends of the η^2-S_2CS ligand [7]. Adduct formation, through the attachment of dienes to sulfur atoms of bis(1,2-ethylenedithiolato)Ni [8] and of quadricyclane to one sulfur atom of (η^5-C_5H_5)(1,2-BDT)Co(III) (1,2-BDT = 1,2-benzenedithiolato) [9], are known. In an effort to investigate the nucleophilic properties of bis(diphenylphosphino)ethanenickel(II) organodichalcogenide complexes, we reacted the three compounds synthesised in this paper as well as Ni(dppe)(SC_6H_4S) (**4**) and Ni(dppe)(SC_6H_3MeS) (**5**), the synthesis of which has been reported elsewhere

* Author to whom correspondence should be addressed.

† Present address: Department of Chemistry, University of the Western Cape, Private Bag X17, Bellville 7535, South Africa.

[10], with DMAD. Our investigations showed that DMAD readily trimerises to HMBC.

RESULTS AND DISCUSSION

Syntheses of mixed aryldichalcogenide complexes (**1–3**) were performed in good yields, by adding the appropriate chalcogen containing ligand to a solution of $Ni(dppe)Cl_2$ and excess Et_3N (eqn (1)).

$$Ni(dppe)Cl_2 + 1,2\text{-}HSC_6H_4EH \xrightarrow{2Et_3N} Ni(dppe)(SC_6H_4E) + 2Et_3NHCl (E = CO_2\ (\mathbf{1}),\ O\ (\mathbf{2}),\ NH\ (\mathbf{3})) \quad (1)$$

All reactions were complete within 2 h and products could be isolated in analytically pure form. The ^1H NMR of complexes **1–3** displays a pattern which is consistent with the different environment of all four protons of the phenyl group of the chalcogen containing ligands. Compound **3** has an additional broad peak at 4.35 pm, corresponding to the NH group of the aminothiophenolate ligand. The non-equivalence of the two phosphorus atoms of the dppe is clearly indicated by different electronic properties between the S and E of the thiolate ligands. This results in a set of multiplets for the ethane moiety in the dppe. For **1** and **3** there are two sets of multiplets, with each set associated with one P atom; but the multiplets for **2** are not well resolved. The $^{31}P\{^1H\}$ spectra show doublets corresponding to the expected AX (**1, 2**) or AB (**3**) spin system. The latter is similar to the peaks pattern for $[Ni(dippe)(SR)(CNBu^t)]^+$ (dippe = 1,2-bis(diisopropylphosphino)ethane, R = C_6F_5, C_6F_4H, C_6H_4F, Ph) [11].

Compounds **1–5** are stable indefinitely in the solid state in air at room temperature; but on exposure to air, blue solutions of **3** gradually turn purple in 2 days at room temperature. This is accompanied by the disappearance of the NH peak in the ^1H NMR spectrum. Other phenyl peaks of the aminothiophenolate ligand lose their fine structure gradually and broaden over a period of 12 days.

Structure of $Ni(dppe)(SC_6H_4O)$

The co-ordination around the nickel is a distorted square-planar, with a maximum deviation from the least-square of $NiOSP_2$ being 0.19 Å. This deviation from planarity is more pronounced than that found for **4** [10]. The molecular structure of **2** is shown in Fig. 1 and selected bond distances and angles are given in Table 1 and atomic co-ordinates in Table 2. Apart from the Ni—O and the C(1)—O bonds in **2** which do not exist in **4** [10], all other bond distances and angles in the two compounds are comparable. The bond lengths and angles are in the expected ranges for Ni—S [12] and Ni—P [13] distances. In particular the Ni—S and Ni—O distances are similar to those found

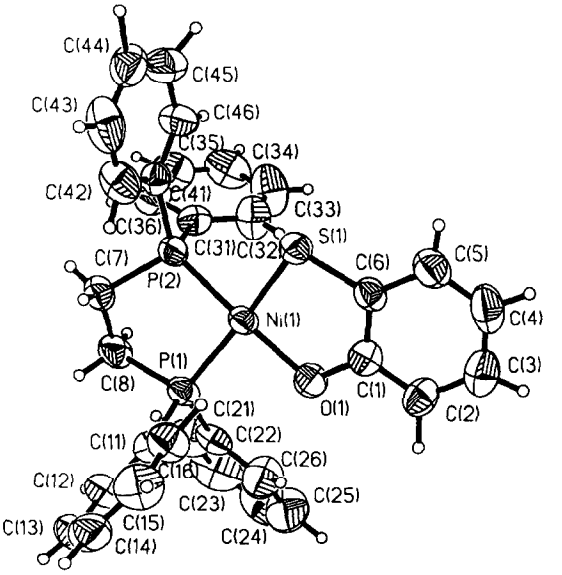

Fig. 1. ORTEP drawing of $Ni(dppe)(SC_6H_4O)$.

in $[^nBuNH]_2[Ni(SC_6H_4O)_2]$, which are 2.153(2) Å and 1.875(3) Å respectively [14].

Reactions with DMAD

When solutions of compounds **2–5** and DMAD in toluene/CH_2Cl_2 (1 : 1) were refluxed, typically for 48 h, HMBC could be isolated (eqn (2)). The reaction is very slow at room temperature and could take up to 1 week to complete, but it is much faster at elevated temperatures.

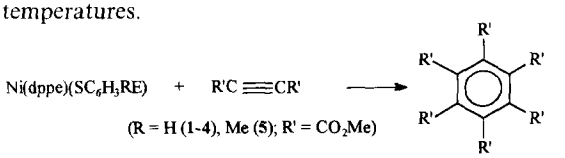

(2)

The product was identified as HMBC by its melting point, IR, ^1H, ^{13}C NMR and mass spectroscopy (see Experimental section). The efficiency of these complexes to effect the cyclotrimerisation ranges from 4% for **3** to 42% for **5**; with the ratio of DMAD to the nickel complexes being about 48 : 1. Nevertheless the yields for all are better than expected from a stoichiometric reaction except for **3**; implying some catalytic activity.

However under similar conditions and work-up procedure, HMBC could not be isolated when **1** reacted with DMAD. A brown precipitate was obtained when solutions, after reflux, were allowed to stand at room temperature for several days. The dominant peak in the ^1H NMR spectrum of this brown solid is 3.88 ppm, with some weak and broad peaks in the phenyl region. ^{13}C NMR spectrum gave

Table 1. Selected bond distances (Å) and angles (°) for **2**

Ni—S(1)	2.158(10)	Ni—O(1)	1.879(3)
Ni—P(1)	2.126(1)	Ni—P(2)	2.174(1)
P(1)—C(8)	1.849(5)	P(2)—C(7)	1.830(4)
P(1)—C(11)	1.815(4)	P(1)—C(21)	1.799(4)
P(2)—C(31)	1.816(4)	P(2)—C(41)	1.808(4)
C(7)—C(8)	1.518(7)	S(1)—C(6)	1.765(4)
O(1)—C(1)	1.320(5)	C(1)—C(6)	1.389(5)

O(1)—Ni—S(1)	90.53(9)	O(1)—Ni—P(1)	91.85(9)
P(2)—Ni—P(1)	86.71(4)	P(2)—Ni—S(1)	92.63(4)
O(1)—Ni—P(1)	169.51(10)	S(1)—Ni—P(1)	170.21(5)
C(6)—S(1)—Ni	95.30(13)	C(1)—O(1)—Ni	115.9(2)
C(7)—P(2)—Ni	108.8(2)	C(8)—C(7)—P(2)	107.0(3)
C(7)—C(8)—P(1)	107.6(3)	C(8)—C(7)—P(2)	107.0(3)
O(1)—C(1)—C(6)	121.2(3)	C(1)—C(6)—S(1)	115.6(3)

peaks assignable to HMBC as the only significant peaks. The parent peak in EIMS of the solid is m/z = 395 and a molecular peak at m/z = 427 (5.7%), which were also observed as the parent and molecular peaks for HMBC. The 395 peak corresponds to a loss of OMe from HMBC. Other peaks in the spectrum were m/z 683, 825, and 967; which we have not been able to assign to any definitive molecular formula. But the difference between peaks show loss of DMAD (m/z = 142). Based on this data it is evident that **1** also cyclotrimerises DMAD, but the HMBC formed could be adsorbed by some reminant nickel complex, thus making it difficult to separate by column chromatography.

NMR tube reaction of **5** and DMAD allowed the progress of the trimerisation to be monitored by ^{1}H NMR spectroscopy. There were not significant changes in the spectrum of **5** during the first 30 min. After 4 h new peaks appeared at 7.08 (d), 7.33 and 7.67, all were weak in intensities, in addition to 7.26 (d), 7.21 (s) and 6.63 (m) for **5**. Peaks of **5** were significantly weaker after 24 h, and the 7.08 peak observed after 24 h had become quite broad. A distinct HMBC peak at 3.88 had begun to emerge at this stage in the reaction. When the spectrum of the mixture was run after 3 days, the peaks found were the same as those of 24 h but better resolved. The ^{31}P NMR after 24 h gave two peaks at 58.62 and 48.22 (intensity ratio 2:1); the 58.62 peak is assignable to **5** but the latter is new. However after 7 days of reaction the peak intensities were equal. Finally, ^{13}C spectrum of this mixture showed the following chemical shifts: 165.2, 152.2, 133.9, 74.5 and 43.4; three of which are the peaks of HMBC (165.8, 133.9 and 53.5). When phenylacetylene and diphenylacetylene were used in place of DMAD, no reaction was observed and the acetylenes could be recovered in near quantitative amounts. This clearly implies that the bulkier and less electrophilic alkynes, could not be activated by the nickel complexes. These observations suggest that the trimerisation process might involve attack of the nickel complex by the alkyne as proposed by Tyler *et al.* [16]. The least efficient of the five complexes in effecting trimerisation was found to be **3** which could be explained by the gradual decomposition of the complex in solution (*vide supra*).

CONCLUSION

With bidentate phosphines as ancillary ligand, homo and mixed aryldichalcogenide nickel(II) complexes could convert the electrophilic acetylene, DMAD, to HMBC catalytically. However bulky acetylenes are unreactive, most likely due to their inability to be activated by the catalysts. The lack of reactivity by the bulkier acetylenes might mean that the initial step in the cyclisation of DMAD is coordination of the acetylene.

EXPERIMENTAL

Materials and instrumentation

All solvents were of analytical grade and were used without further purification. The thiols and 1,2-bis(diphenylphosphino)ethane were purchased from Aldrich and were used as received. Ni(dppe)Cl_2 [16], Ni(dppe)(1,2-BDT) (**4**) and Ni(dppe)(TDT) (**5**) (TDT = 3,4-toluenedithiolato), were prepared by the literature procedure [10].

IR spectra were recorded on a Mattson Polaris or a Nicolet 205 FT-IR. ^{1}H, ^{13}C and ^{31}P NMR were recorded on a Varian Gemini 2000 or a Gemini 300 and referenced to residual $CHCl_3$ for ^{1}H (7.26), ^{13}C (77.0) and externally to 85% H_3PO_4 for ^{31}P. Mass spectra data were collected on a Finnigan MAT SSQ 700 in the electron impact mode and elemental analyses were performed by the microanalytical laboratory

Table 2. Atomic co-ordinates ($\times 10^4$) and equivalent isotropic displacement parameters ($Å^2 \times 10^3$)

	x	y	z	U(eq)[a]
Ni(1)	3400(1)	1189(1)	3633(1)	42(1)
S(1)	4160(1)	2096(1)	3172(1)	50(1)
P(1)	2383(1)	384(1)	4064(1)	46(1)
O(1)	3876(2)	1853(2)	4131(1)	59(1)
C(1)	4583(3)	2473(2)	4040(1)	47(1)
P(2)	3074(1)	267(1)	3109(1)	43(1)
C(2)	5072(4)	2925(3)	4397(2)	61(1)
C(3)	5870(4)	3544(3)	4311(2)	73(1)
C(4)	6130(4)	3746(4)	3864(2)	80(2)
C(5)	5631(4)	3319(3)	3509(2)	67(1)
C(6)	4857(3)	2680(3)	3596(1)	46(1)
C(7)	1842(3)	−321(3)	3246(2)	57(1)
C(8)	1913(4)	−586(3)	3741(2)	60(1)
C(11)	1181(3)	998(3)	4197(1)	47(1)
C(12)	1074(4)	1871(3)	4049(2)	65(1)
C(13)	146(5)	2328(4)	4140(2)	83(2)
C(14)	−692(4)	1925(4)	4364(2)	78(2)
C(15)	−586(4)	1074(4)	4505(2)	74(1)
C(16)	344(4)	610(4)	4425(2)	62(1)
C(21)	2877(3)	−26(3)	4596(1)	55(1)
C(22)	2977(3)	−928(4)	4695(2)	55(1)
C(23)	3387(6)	−1211(5)	5103(3)	104(2)
C(24)	3763(5)	−600(7)	5414(3)	112(3)
C(25)	3664(6)	286(6)	5330(2)	105(2)
C(26)	3232(6)	568(5)	4921(2)	87(2)
C(31)	4112(3)	−567(3)	3236(2)	49(1)
C(32)	5113(4)	−346(3)	3097(1)	70(1)
C(33)	5966(5)	−934(4)	3187(3)	95(2)
C(34)	5778(5)	−1745(4)	3007(2)	88(2)
C(35)	4793(6)	−1987(4)	2878(2)	88(2)
C(36)	3940(5)	−1470(3)	2921(2)	69(1)
C(41)	2956(3)	633(2)	2528(1)	45(1)
C(42)	2076(4)	1096(3)	2389(2)	69(1)
C(43)	1990(5)	1392(4)	1946(2)	87(2)
C(44)	2776(5)	1252(3)	1638(2)	75(1)
C(45)	3665(5)	804(4)	1773(2)	74(1)
C(46)	3769(4)	496(3)	2214(2)	61(1)

[a] U_{eq} is defined as one third of the trace of the orthogonalized U_{ij} tensor.

at the University of Cape Town, South Africa, as a service.

Syntheses of Ni(dppe)organodichalcogenide complexes

All three complexes were prepared and worked-up in a similar manner and typical procedure is described for Ni(dppe)($SC_6H_4CO_2$).

Ni(dppe)($SC_6H_4CO_2$) (**1**). A mixture of Ni(dppe)Cl_2 (1.0 g, 1.89 mmol) and thiosalicylic acid (0.29 g, 1.89 mmol) was degassed and nitrogen saturated CH_2Cl_2 (30 cm^3) added. To the resultant solution was added Et_3N (1.00 cm^3), changing the orange solution to dark red. After stirring the solution for 2 h, hexane (50 cm^3) was added to give an orange brown precipitate. The solid was washed with copious amount of water and recrystallised from CH_2Cl_2/hexane. Yield = 0.88 g, 76%, m.p. = 258–260°C. Anal. Calc. for $C_{33}H_{28}O_2P_2SNi$: C, 65.05; H, 4.63; S, 5.26. Found: C, 63.93; H, 4.70; S, 4.70%. ^1H NMR ($CDCl_3$): 8.11 (q, 1H), 7.30 (q, 1H), 7.01 (m, 2H) ($SC_6H_4CO_2$); 8.03 (m, 8H), 7.51 (m, 12H) (dppe), 2.38 (m, 2H), 2.10 (m, 2H) (dppe). $^{13}C\{^1H\}$ NMR: 168.9 (s) ($SC_6H_4CO_2$), 142.4 (s), 133.5 (d, J_{CP} = 10.20 Hz), 133.1 (d, J_{CP} = 10.30 Hz), 129.2 (d, J_{CP} = 8.30 Hz), 128.7 (s), 123.1 (s) (dppe), 131.9 (s), 131.4 (s), 128.4 (s), 127.4 (s), 126.8 (s) ($SC_6H_4CO_2$), 29.7 (d, J_{CP} = 15.0 Hz), 21.9 (d, J_{CP} = 15.0 Hz) (dppe). $^{31}P\{^1H\}$ NMR: 57.19 (d, J_{PP} = 59.82 Hz), 41.72 (d, J_{PP} = 59.82 Hz). IR (KBr pellet, cm^{-1}): 3043 w, 1592 vs, 1575 vs, 1543 m, 1433 s, 1348 s, 1100 s, 821 s, 752 s, 703 s, 689 s, 528 vs, 488 m.

Ni(dppe)(SC_6H_4O) (**2**). Yield = 0.76 g, 69%; m.p. = 294–296°C. Anal. Calc. for $C_{32}H_{28}OP_2SNi$: C, 66.12; H, 4.86; S, 5.52. Found: C, 65.56; H, 4.83; S, 4.96%. ^1H NMR ($CDCl_3$): 8.08 (t, J_{HH} = 9.0 Hz, 4H), 7.88 (t, J_{HH} = 9.0 Hz, 4H), 7.46 (m, 12H) (dppe), 7.30 (d, J_{HH} = 7.41 Hz, 1H), 6.82 (t, J_{HH} = 8.19 Hz, 1H), 6.72 (d, J_{HH} = 7.98 Hz), 6.50 (t, J_{HH} = 7.41 Hz) (SC_6H_4O), 2.60 (m, 4H) (dppe), $^{13}C\{^1H\}$ NMR: 133.3 (dd, J_{CP} = 9.3 Hz), 131.2 (d, J_{CP} = 22.6 Hz), 128.9 (t, J_{CP} = 10.3 Hz) 115.3 (d, J_{CP} = 33.2 Hz) (dppe), 130.9 (s), 130.3 (s), 129.7 (s), 127.6 (s), 122.5 (s) (SC_6H_4O), 29.5 (d, J_{CP} = 16.0 Hz), 22.7 (d, J_{CP} = 16.0 Hz) (dppe). $^{31}P\{^1H\}$ NMR: 58.88 (d, J_{PP} = 55.46 Hz, 1P), 44.97 (d, J_{PP} = 55.46 Hz, 1P). IR (KBr pellet, cm^{-1}): 3029 m, 1560 m, 1482 w, 1454 vs, 1434 vs, 1274 s, 1231 m, 1100 s, 1021 w, 871 w, 843 w, 818 w, 743 s, 718 m, 689 vs, 529 vs, 488 m.

Ni(dppe)(SC_6H_4NH) (**3**). Yield = 0.82 g, 75%; decompositon = 249.1°C. Anal. Calc. for $C_{32}H_{29}NP_2SNi$: C, 66.23; H, 5.04; N, 2.41; S, 5.53. Found: C, 65.31; H, 5.03; N, 1.94; S, 5.23. ^1H NMR ($CDCl_3$): 7.85 (t, J_{HH} = 7.80 Hz, 8H), 7.46 (m, 12H) (dppe), 6.71 (t, J_{HH} = 6.80 Hz, 1H), 6.43 (dd, J_{HH} = 13.00, 7.20 Hz 2H), 4.38 (s, br, 1H) (SC_6H_4NH), 2.32 (d, 17.60 Hz, 4H) (dppe). $^{13}C\{^1H\}$ NMR: 133.5 (d, J_{CP} = 11.1 Hz), 131.3 (d, J_{CP} = 17.6 Hz), 129.2 (d, J_{CP} = 9.9 Hz), 128.7 (d, J_{CP} = 10.3 Hz) (dppe), 130.0 (s), 127.6 (s), 121.8 (s), 112.9.5 (s) (SC_6H_4NH), 27.9 (t, J_{CP} = 20.1 Hz) (dppe). $^{31}P\{^1H\}$ NMR: 60.44 (d, J_{PP} = 47.56 Hz, 1P), 59.77 (d, J_{PP} = 47.56 Hz, 1P). IR (KBr pellet, cm^{-1}): 3020 m, 1559 s, 1480 w, 1463 s, 1434 vs, 1310 s, 1188 w, 1100 s, 1026 m, 876 m, 851 w, 820 s, 737 s, 689 vs, 528 vs, 480 vs, 432 w, 395 w, 372 m.

Reaction of Ni(dppe) organodichalocogenide *complexes with* DMAD. In a typical reaction excess DMAD (2 cm^3, 16.27 mmol) and Ni(dppe)(SC_6H_4O) (0.20 g, 0.34 mmol) solution in toluene/CH_2Cl_2 (1 : 1) (50 cm^3) was refluxed for 24 h. The dark orange solution obtained was concentrated to about 5 cm^3 and chromatographed (silica gel, CH_2Cl_2/ether 1 : 4) to yield 0.40 g (0.94 mmol) of hexamethylbenzene hexacarboxylate, $C_6(CO_2Me)_6$. ^1H NMR ($CDCl_3$): 3.88

(s, 18H). ^{13}C NMR: 165.2 (s), 133.9 (s), 53.5 (s). IR (KBr pellet cm^{-1}): 3012 m, 2958 s, 1738 vs, 1576 w, 1445 vs, 1413 s, 1363 s, 1332 s, 1235 vs, 1182 vs, 1160 s, 1122 m, 985 vs, 906 w, 872 s, 860 vs, 849 vs, 828 s, 805 w, 787 w, 757 m, 618 s, 603 m, 471 w. MS (EI): *m/z* (relative intensity) 426 (2) (M^+), 395 (100) ($M^+ - OMe$). The other complexes were reacted with DMAD using the same number of moles of nickel complex (0.34 mmol) and DMAD (16.27 mmol). The number of moles of HMBC isolated were **3** (0.23 mmol), **4** (0.52 mmol) and **5** (2.26 mmol).

Crystal structure determination of **2**

Single crystals of **2** suitable for crystal structural determination were obtained by slow diffusion of hexane into a CH_2Cl_2 solution of **2** at room temperature. A dark rectangular plate crystal of size $0.70 \times 0.22 \times 0.11$ mm was mounted in a sealed capillary tube for data collection. All geometric and intensity data were collected on a Siemens SMART diffractometer with a CCD detector. Crystal data for $C_{32}H_{28}OP_2SNi$ ($Mr = 581.25$): orthorhombic, Pbca; $a = 12.5385(6)$ Å, $b = 15.1818(2)$ Å, $c = 29.496(2)$ Å, $V = 5614.7(5)$ Å^3; $Z = 8$; $D_{calc} = 1.375$ Mg m^{-3}; Mo-K_α radiation ($\lambda = 0.71073$ Å); $T = 298$; $\theta = 1.38$–28.29 , 10 s/frame exposure; 0.3 /frame; 6563 independent reflections collected, 4970 unique. Full matrix least-squares refinement [17] of 446 parameters on F^2 gave $R_1 = 0.0698$. $wR_2 = 0.1746$, GoF = 1.253. Max ΔF 0.42 eÅ^{-3}, min -0.25 eÅ^{-3}. An absorption correction based on multiple redundant data analysis was applied [18].

Supplementary material. Further crystallographic details can be obtained on request from the Director of the Cambridge Data Centre, University Chemical Laboratory, Lensfield Road, Cambridge CB2 1EW, U.K.

Acknowledgement—Financial support for this work by the University of the North and the Foundation for Research Development (South Africa) for the purchase of a regional NMR are gratefully acknowledged. We are also grateful to Dr E. Y. Osei-Twum, King Fahd University of Petroleum and Minerals, Saudi Arabia and Dr M. M. Nindi, University of Botswana, for the mass spectral data. We thank Prof. J. C. A. Boeyens and Ms Leanne Cook, University of the Witwatersrand, South Africa, for the X-ray structure determination, which was done as a service.

Note: After we submitted our paper a report on the synthesis of Ni(dppe)($SC_6H_4CO_2$) appeared in the literature [19].

REFERENCES

1. Reppe, W., Schlichting, O., Klager, K. and Toepel, T., *Justus Liebigs Ann. Chem.*, 1948, **561,** 1.
2. Schrauzer, G. N., Glockner, P. and Eichler, S., *Angew. Chem.*, 1964, **76,** 28.
3. (a) Meriwether, L. S., Colthup, E. C., Kennerly, G. W. and Reusch, R. N., *J. Org. Chem.*, 1961, **26,** 5155; (b) Meriwether, L. S., Colthup, E. C. and Kennerly, G. W., *ibid.*, 1961, **26,** 5163; (c) Colthup, E. C. and Meriwether, L. S., *ibid.*, 1961, **26,** 5169; (d) Meriwether, L. S., Leto, C. M. F., Colthup, E. C. and Kennerly, G. W., *ibid.*, 1962, **27,** 3930.
4. (a) Roe, D. M., Calvo, C., Krishnamachari, N., Mosely, K. and Maitlis, P. M., *J. Chem. Soc., Chem. Commun.*, 1973, 436; (b) Roe, D. M., Calvo, C., Krishnamachari, N., Mosely, K. and Maitlis, P. M., *J. Chem. Soc., Dalton Trans.*, 1975, 78.
5. Eisch, J. J. and Galle, J. E., *J. Organomet. Chem.*, 1975, **96,** C23.
6. Bennet, M. A. and Wegner, E., *Organometallics*, 1995, **14,** 1267.
7. Bianchini, C. and Meli, A., *J. Organomet. Chem.*, 1982, **236,** C75.
8. Schrauzer, G. N. and Mayweg, V. P., *J. Am. Chem. Soc.*, 1965, **87,** 1483.
9. Kajitani, M., Hatano, H., Fujita, T., Okumachi, T., Nagao, H., Akiyama, T. and Sugimori, A., *J. Organomet. Chem.*, 1992, **430,** C64.
10. Darkwa, J., *Inorg. Chim. Acta*, 1997, **257,** 137.
11. Tenorio, M. J., Puerta, M. C. and Valerga, P., *J. Chem. Soc., Dalton Trans.*, 1996, 1935.
12. Krüger, H.-J. and Holm, R. H., *Inorg. Chem.*, 1989, **29,** 1148.
13. Mazighi, K., Carrol, P. J. and Sneddon, L. G., *Inorg. Chem.*, 1992, **31,** 3197.
14. Köckerling, M. and Henkel, G., *Chem. Ber.*, 1993, **126,** 951.
15. Mao, F., Schut, D. M. and Tyler, D. R., *Organometallics*, 1996, **15,** 4770.
16. van Hecke, G. R. and deW Horrocks W. Jr., *Inorg. Chem.*, 1996, **5,** 1968.
17. Sheldrick, G. M., *SHELXL*-93, *Program for the Refinement of Crystal Structures*, Universität Göttingen, Germany, 1993.
18. Sheldrick, G. M., *SADABS, An Empirical Absorption Correction*, private communication to subscribers of the Siemens CCD e-mail list.
19. McCaffrey, L. J., Henderson, W., Nicholson, B. K., Mackay, J. E. and Dinger, M. B., *J. Chem. Soc., Dalton Trans.*, 1997, 2577.

Pergamon

PII: S0277-5387(97)00526-3

Polyhedron Vol. 17, Nos. 11–12, pp. 1817–1829, 1998
© 1998 Elsevier Science Ltd
All rights reserved. Printed in Great Britain
0277-5387/98 $19.00+0.00

Synthesis and structural characterization of cobalt(III) complexes of hybrid donor-type didentate or tetradentate ligands bearing dimethylphosphino and thioether groups

Kazuo Kashiwabara,[a]* Norihiko Taguchi,[a] Hideo D. Takagi,[a] Kiyohiko Nakajima[b] and Takayoshi Suzuki[c]*

[a] Department of Chemistry, Graduate School of Science, Nagoya University, Nagoya 464-01, Japan

[b] Department of Chemistry, Aichi University of Education, Kariya 448, Japan

[c] Department of Chemistry, Graduate School of Science, Osaka University, Toyonaka 560, Japan

(Received 14 October 1997; accepted 12 December 1997)

Abstract—The preparation and characterization of new hybrid donor-type phosphine-thioether ligands, a linear tetradentate $Me_2P(CH_2)_2S(CH_2)_3S(CH_2)_2PMe_2$ (dmdtn) and a didentate $Me_2P(CH_2)_2SR$ [R = Me (mtdmp) or Et (etdmp)], and their cobalt(III) complexes are described. The reaction of *trans*-$[CoCl_2(py)_4]Cl$ (py = pyridine) with dmdtn, followed by anion metathesis with $NaPF_6$, afforded green crystals of *trans*(*Cl*,*Cl*)-$[CoCl_2\{meso(S)\text{-dmdtn}\}]PF_6$ (**1**), whose geometrical structure and configuration around S atoms were determined by X-ray analysis. Further reaction of **1** with Li(acac) (acac = pentane-2,4-dionate) and crystallization with $LiBF_4$ gave red crystals of the acac complex **2**. The X-ray analysis of **2** confirmed the structure and configuration of *cis*β-$[Co(acac)\{racemic(S)\text{-dmdtn}\}](BF_4)_2$, indicating the configurational inversion at one sulfur during the derivation of complex **2**. An analogous *N*,*N*-dimethyldithiocarbamate (dtc) complex **3** was also prepared, and the electrochemical properties of complexes **1**–**3** were discussed. For analogous mtdmp and etdmp (P—S) complexes, *trans*(*Cl*,*Cl*)*cis*(*P*,*P*)-$[CoCl_2(P—S)_2]PF_6$ reacted with Li(acac) to give not only *trans*(*P*,*S*)-$[Co(acac)(P—S)_2](PF_6)_2$ but also $[Co(acac)_2(P—S)]PF_6$. Similar reactions with Na(dtc) yielded *cis*-$[Co(dtc)_2(P—S\text{-}\kappa P)_2]$ (**14** for P—S = mtdmp), together with *trans*(*P*,*S*)-$[Co(dtc)(P—S)_2](PF_6)_2$ and $[Co(dtc)_2(P—S)]PF_6$. The structures of these complexes were characterized by NMR and UV-visible spectroscopy and X-ray analysis of **14**. These results suggested that the didentate ligands were hemilabile as similar to previously described SPPS-type tetradentate ligands, but the tetradentate dmdtn ligand was not. © 1998 Elsevier Science Ltd. All rights reserved

Keywords: hybrid donor-type ligand; dimethylphosphino group; thioether; tetradentate ligand; cobalt(III); hemilabile.

Because of the soft base characters of phosphines and thioethers, their complexation behaviours and bonding natures to cobalt(III) of a typical Lewis hard acid are expected to be quite different from those of well-examined hard bases of the analogous amines. In line with this view, we have continued to study cobalt(III) complexes with linear hybrid donor-type tetradentate ligands bearing phosphine and amine groups [1–7] or phosphine and thioether groups [8,9]. In previous reports [8,9], we have prepared a large number of cobalt(III) complexes containing $MeS(CH_2)_2$-$PPh(CH_2)_nPPh(CH_2)_2SMe$ (SPPS; $n = 2$ or 3), in order to compare their properties with those of the complexes containing analogous phosphine-amine (NPPN) ligands. In the SPPS complexes, many complicated stereo and geometrical isomers were possible, because the ligands have two chiral phosphorus atoms in the central part and two prochiral sulfur atoms in the terminal of their skeletons. Further, the thioether moieties often did not coordinate to cobalt(III), the weak donor ability of thioethers toward cobalt(III)

* Authors to whom correspondence should be addressed.

being suggested [10]. In order to examine further the coordination abilities and complexation behaviours of the phosphine-thioether ligands, we have extended the study to the PSSP-type linear tetradentate ligand, which has no chiral phosphorus atoms in its skeleton.

The crystal structures of nickel(II) and palladium(II) complexes containing $Ph_2P(CH_2)_2S(CH_2)_3S(CH_2)_2PPh_2$ (dpdtn) have been reported previously [11–13], and several transition metal(II) complexes containing the related PSSP-type tetradentate ligands, $Ph_2P(CH_2)_nS(CH_2)_nS(CH_2)_nPPh_2$ ($n = 2$ [14] or 3 [15]), have been synthesized. We have tried to synthesize the cobalt(III) complexes of dpdtn, but only *cis*β-[Co(dtc)(dpdtn)]$(BF_4)_2$ could be isolated in very low yield (ca 10%); all the other attempts were unsuccessful [16]. The difficulty in syntheses of such complexes may be caused by the steric bulkiness of the diphenylphosphino groups. Thus, we have prepared a new tetradentate ligand $Me_2P(CH_2)_2S(CH_2)_3S(CH_2)_2PMe_2$ (dmdtn; Scheme 1) and its cobalt(III) complexes, because the dimethylphosphino group has a smaller steric requirement and a stronger donor ability than the diphenylphosphino group. The related didentate phosphine-thioether ligands $Me_2P(CH_2)_2SR$ [R = Me (mtdmp) and Et (etdmp)] and their cobalt(III) complexes were also prepared to examine the effect of sulfur position (central or terminal) in the skeleton.

EXPERIMENTAL

All reactions were handled under a dinitrogen atmosphere using Schlenk techniques until such time that air-stable cobalt(III) complexes were formed. All of the solvents used in the preparation of the phosphines and their complexes were deaerated with dinitrogen for 20 min immediately before use. The $^{13}C\{^1H\}$ NMR spectra were recorded on a Hitachi R-90H spectrometer and referenced to tetramethylsilane. The absorption spectra were measured on a Hitachi U3400 spectrophotometer at room temperature. Cyclic voltammograms were measured on a BAS 100B electrochemical analyzer at a scan rate 100 mV s^{-1} in acetonitrile solutions at 25.0 ± 0.1 ([complex] = 1.0×10^{-3} mol dm^{-3}; 0.1 mol dm^{-3} Bu_4NBF_4). A platinum disk, a platinum wire and a Ag/Ag^+ electrode (Ag/0.01 mol dm^{-3} $AgNO_3$) were used as the working, auxiliary and reference electrodes, respectively, the redox potential of ferrocene/ferrocenium ion being observed at +0.15 V vs Ag/Ag^+.

2,12-*Dimethyl*-2,12-*diphospha*-5,9-*dithiatridecane* (**dmdtn**)

To a liquid ammonia solution (200 cm^3) of sodium metal (2.7 g, 0.12 mol), which was cooled in a dry ice-acetone bath, was added tetramethyldiphosphane [17] (6.3 g, 0.052 mmol) dropwise with stirring. The resulting orange solution was stirred for 1 h, and ethylenesulfide (6.3 g, 0.11 mol) was added dropwise with stirring. After stirring for an additional 1 h, 1,3-dibromopropane (10.5 g, 0.052 mmol) was added and the resulting colourless mixture was stirred further for 1 h. From the mixture liquid ammonia was carefully evaporated by removal of the dry ice-acetone bath, affording pale yellow oily residue with a precipitate of NaBr. The residue was mixed with diethyl ether (100 cm^3) and filtered. The ethereal solution was evaporated under reduced pressure to leave a pale yellow oily product of dmdtn (11.3 g, 74% yield). ^{13}C NMR ($CDCl_3$): δ 13.8 (d, $^1J_{PC}$ = 13.1 Hz, PCH_3), 28.6 (d, $^2J_{PC}$ = 17.6 Hz, SCH_2CH_2P), 29.2 (d, $^4J_{PC}$ = 1.7 Hz, $CH_2CH_2CH_2$), 31.0 (s, $CH_2CH_2CH_2$), 32.2 (d, $^1J_{PC}$ = 12.8 Hz, PCH_2). This is soluble in common organic solvents and was used for the preparation of cobalt(III) complexes without further purification.

2-(*Methylthio*)*dimethylphosphinoethane* (**mtdmp**) *and* 2-(*ethylthio*)*dimethylphosphinoethane* (**etdmp**)

The preparation of mtdmp was described previously [19]. The etdmp was prepared by a method similar to that for mtdmp using (2-chloroethyl)ethylsulfide instead of (2-chloroethyl)methylsulfide (90% yield). ^{13}C NMR ($CDCl_3$): δ 13.8 (d, $^1J_{PC}$ = 12.8 Hz, PCH_3), 14.7 (s, SCH_2CH_3), 25.9 (s, SCH_2CH_3), 28.0 (d, $^2J_{PC}$ = 17.6 Hz, SCH_2CH_2P), 32.1 (d, $^1J_{PC}$ = 12.4 Hz, PCH_2).

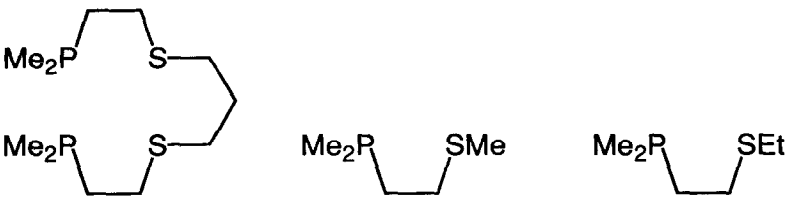

dmdtn **mtdmp** **etdmp**

Scheme 1. The hybrid donor-type phosphine-thioether ligands used in this study.

trans-[$CoCl_2$(dmdtn)]PF_6 (**1**)

To a methanol solution (30 cm^3) of *trans*-[$CoCl_2(py)_4$]Cl·$6H_2O$ [19] (0.59 g, 1.0 mmol) was added dmdtn (0.30 g, 1.1 mmol) with stirring. The mixture was stirred at room temperature for 2 h and then concentrated to ca 5 cm^3 under reduced pressure. The concentrate was applied to a column (ϕ 3.0 × 45 cm) of Sephadex LH-20. The adsorbed products were eluted with methanol, affording faster developing minor green and red bands and then a slowly developing major blue-green band. The major band was collected and concentrated to a small volume. To the concentrate was added a methanol solution of excess $NaPF_6$, giving green precipitate. The crude product obtained was recrystallized by diffusion of diethyl ether vapour into an acetonitrile solution to deposit blue-green crystals of **1** (0.22 g, 40% yield). Found: C, 23.60; H, 4.72. Calc.: for $C_{11}H_{26}Cl_2CoF_6P_3S_2$: C, 23.63; H, 4.69%. ^{13}C NMR (CD_3CN): δ 12.1 (virtual t, J_{PC} = 16.1 Hz, PCH_3), 12.9 (virtual t, J_{PC} = 16.4 Hz, PCH_3), 26.3 (s, $CH_2CH_2CH_2$), 31.5 (s, SCH_2-CH_2P), 33.2 (virtual t, J_{PC} = 16.6 Hz, PCH_2), 34.6 (s, $SCH_2CH_2CH_2S$). This complex is soluble in methanol and acetonitrile, but insoluble in water and diethyl ether.

cisβ-[Co(acac)(dmdtn)]$(BF_4)_2$ (**2**)

A mixture of **1** (0.33 g, 0.59 mmol) and Li(acac) (0.094 g, 0.89 mmol) in methanol (40 cm^3) was stirred for 2 h, and then concentrated to ca 10 cm^3 under reduced pressure. The concentrate was diluted with water (100 cm^3) and applied on a column (ϕ 3.0 × 45 cm) of SP-Sephadex C-25 (Na^+ form). The adsorbed products were eluted with 0.05 mol dm^{-3} aqueous Na_2SO_4 solution, giving a minor yellow band. After the elution of the yellow band, a major red band was eluted with 0.3 mol dm^{-3} aqueous Na_2SO_4 solution. The collected eluate of the red band was evaporated to dryness under reduced pressure, and the residue was extracted with methanol. To the concentrated methanol extract was added a saturated methanol solution of $LiBF_4$ to give a red precipitate. The crude product was recrystallized by diffusion of diethyl ether vapour into an acetonitrile solution to deposit red crystals of **2** (0.23 g, 63% yield). Found: C, 31.07; H, 5.37. Calc: for $C_{16}H_{33}B_2CoF_8O_2P_2S_2$: C, 31.19; H, 5.40%. ^{13}C NMR (CD_3CN): δ 10.4–11.9 (overlapped peaks due to four kinds of PCH_3), 20–35 (overlapped peaks due to SCH_2CH_2P and $SCH_2CH_2CH_2S$), 26.6 (s, CCH_3), 27.8 (d, $^4J_{PC}$ = 4.5 Hz, CCH_3), 102.2 (s, *C*H), 191.5 (s, *C*O), 192.2 (s, *C*O). The complex is soluble in water, methanol and acetonitrile, but not in diethyl ether.

cisβ-[Co(dtc)(dmdtn)]$(PF_6)_2$ (**3**)

To a methanol solution (100 cm^3) of **1** (0.37 g, 0.66 mmol) was added a methanol solution (100 cm^3) of Na(dtc)·$2H_2O$ (0.14 g, 0.78 mmol) dropwise with stirring in an ice bath. The mixture was stirred for 2 h at room temperature, concentrated to ca 10 cm^3, and then diluted with water (100 cm^3). The aqueous solution was applied on a column (ϕ 5.0 × 60 cm) of SP-Sephadex C-25 (Na^+ form), and the adsorbed products were eluted with 0.05 mol dm^{-3} aqueous NaCl solution. After elution of a minor brown band, a major red band was eluted with 0.5 mol dm^{-3} aqueous NaCl solution. The eluate of the red band was evaporated to dryness under reduced pressure, and the residue extracted with a small amount of ethanol. The filtered red extract was concentrated to ca 1 cm^3 under reduced pressure and mixed with a saturated ethanol solution of $NaPF_6$ to afford red precipitate. The crude product obtained was recrystallized by diffusion of diethyl ether vapour into an acetonitrile solution to deposit red crystals of **3** (0.40 g, 80% yield). Found: C, 22.19; H, 4.28; N, 1.98. Calc.: for $C_{14}H_{32}CoF_{12}NP_4S_4$: C, 22.32; H, 4.28; N, 1.86%. ^{13}C NMR (CD_3CN): δ 9.8–12.3 (m, PCH_3), 15.5 (dd, $^1J_{PC}$ = 31.4 Hz, $^3J_{PC}$ = 4.2 Hz, PCH_3), 23.5 (s, $CH_2CH_2CH_2$), 28–37 (overlapped peaks due to SCH_2-CH_2P and $SCH_2CH_2CH_2S$), 30.1 (d, $^1J_{PC}$ = 31.8 Hz, PCH_2), 34.4 (dd, $^1J_{PC}$ = 31.8 Hz, $^3J_{PC}$ = 4.5 Hz, PCH_2), 39.7 (s, NCH_3), 40.3 (s, NCH_3), 199.1 (br, NCS_2). This complex is soluble in water, methanol and acetonitrile, but not in diethyl ether.

trans-[$CoCl_2$(mtdmp)$_2$]PF_6 (**4**)

To a methanol solution (30 cm^3) of *trans*-[$CoCl_2(py)_4$]Cl·$6H_2O$ (3.0 g, 6.0 mmol) was added mtdmp (2.0 g, 15 mmol). The mixture was stirred at room temperature for 2 h and then evaporated to dryness under reduced pressure. The residue was washed with diethyl ether to remove unreacted mtdmp and dissolved in a small amount of water. To the filtered solution was added an aqueous solution of excess $NaPF_6$, affording green precipitate. The crude product obtained was recrystallized by diffusion of diethyl ether vapour into a dichloromethane solution to deposit green crystals of **4** (2.5 g, 70% yield). Found: C, 22.00; 4.44. Calc.: for $C_{10}H_{26}Cl_2CoF_6P_3S_2$: C, 21.95; H, 4.79%. ^{13}C NMR (CD_3CN): δ 11–12 (overlapped peaks due to two kinds of PCH_3), 17.7 (s, SCH_3), 33.8 (s, SCH_2), 35.9 (virtual t, J_{PC} = 18.1 Hz, PCH_2). This complex is soluble in methanol, acetonitrile and dichloromethane, but insoluble in water and diethyl ether.

trans-[$CoCl_2$(etdmp)$_2$]PF_6 (**5**)

This complex was prepared by a method similar to that for **4** using etdmp instead of mtdmp (80% yield). Found: C, 25.22; H, 5.24. Calc.: for $C_{12}H_{30}Cl_2CoF_6P_3S_2$: C, 25.06; H, 5.26%. ^{13}C NMR (CD_3CN): δ 12.0 (virtual t, J_{PC} = 17.4 Hz, PCH_3), 12.2 (virtual t, J_{PC} = 16.8 Hz, PCH_3), 13.0 (s,

SCH_2CH_3), 29.5 (s, SCH_2CH_3), 31.6 (s, SCH_2CH_2P), 36.4 (virtual t, J_{PC} = 18.3 Hz, PCH_2). The solubility of this complex is similar to that of **4**.

trans(*P*,*S*)-[Co(acac)(mtdmp)$_2$](PF$_6$)$_2$ (**6**) *and* [Co(acac)$_2$(mtdmp)]PF$_6$ (**8**)

To a methanol solution (50 cm^3) of **4** (1.0 g, 1.8 mmol) was added a methanol solution (20 cm^3) of Li(acac) (0.40 g, 3.8 mmol) with stirring. The mixture was stirred overnight, then concentrated to ca 5 cm^3 under reduced pressure and diluted with water (2 dm^3). The aqueous solution was applied on a column (ϕ 5.0 × 50 cm) of SP-Sephadex C-25 (Na^+ form), and the adsorbed products were washed thoroughly with water and then eluted with 0.05 mol dm^{-3} aqueous Na_2SO_4 solution to develop violet and orange bands in this order. After the violet band was collected, the eluent was changed to 0.2 mol dm^{-3} aqueous Na_2SO_4 solution. Each eluate was evaporated to dryness under reduced pressure, and the residue was mixed with methanol to extract the violet or orange complex. The methanol extract was concentrated to ca 1 cm^3, and a saturated methanol solution of $NaPF_6$ added until the precipitation of violet or orange complex was completed. The orange crude product was recrystallized from methanol to deposit orange crystals of **6** (0.22 g, 18% yield). Found: C, 25.01; H, 4.62. Calc.: for $C_{15}H_{33}CoF_{12}O_2P_4S_2$: C, 25.10; H, 4.62%. ^{13}C NMR (CD_3CN): δ 7.5–13.3 (overlapped peaks due to four kinds of PCH_3), 16.3 (d, $^3J_{PC}$ = 1.7 Hz, SCH_3), 17.7 (s, SCH_3), 25–40 (overlapped peaks due to CCH_3, PCH_2 and SCH_2), 101.6 (s, *C*H), 191.4 (s, *C*O), 193.0 (d, $^3J_{PC}$ = 2.4 Hz, *C*O). The violet complex was similarly recrystallized to deposit violet crystals of **8** (0.21 g, 21% yield). Found: C, 33.43; H, 4.95. Calc.: for $C_{15}H_{27}CoF_6O_4P_2S$: C, 33.47; H, 5.06%. ^{13}C NMR (CD_3CN): δ 7.5 (d, $^1J_{PC}$ = 30.4 Hz, PCH_3), 8.6 (d, $^1J_{PC}$ = 31.3 Hz, PCH_3), 14.9 (s, SCH_3), 26.1 (s, CCH_3), 26.4 (s, CCH_3), 26.8 (s, CCH_3), 28.0 (d, $^4J_{PC}$ = 7.0 Hz, CCH_3), 30.5 (d, $^1J_{PC}$ = 32.2 Hz, PCH_2), 34.7 (s, SCH_2), 99.1 (s, *C*H), 99.6 (s, *C*H), 188.0 (s, *C*O), 189.7 (s, *C*O), 191.6 (s, *C*O), 192.9 (d, $^3J_{PC}$ = 2.5 Hz, *C*O). The complex **6** is soluble in water, methanol and acetonitrile, while complex **8** is soluble in methanol and acetonitrile but not in water.

trans(*P*,*S*)-[Co(acac)(etdmp)$_2$](PF$_6$)$_2$ (**7**) *and* [Co(acac)$_2$(etdmp)]PF$_6$ (**9**)

These complexes were prepared by methods similar to those for **6** and **8**, using complex **5** as a starting material. The crude orange product was recrystallized by diffusion of diethyl ether vapour into an acetonitrile solution to deposit orange crystals of **7** (16% yield). Found: C, 28.04; H, 4.76. Calc. for $C_{17}H_{27}CoF_{12}O_2P_4S_2$: C, 27.18; H, 4.98%. ^{13}C NMR (CD_3CN): δ 7–20 (overlapped peaks due to PCH_3 and SCH_2CH_3), 25–40 (overlapped peaks due to CCH_3, PCH_2 and CH_2SCH_2), 101.8 (s, *C*H), 192.7 (s, *C*O), 193.3 (d, $^3J_{PC}$ = 2.1 Hz, *C*O). The violet complex was recrystallized from a mixture of methanol and water to deposit violet crystals of **9** (43% yield). Found: C, 35.19; H, 5.45. Calc. for $C_{16}H_{29}CoF_6O_4P_2S$: C, 34.79; H, 5.29%. ^{13}C NMR (CD_3CN): δ 7.5 (d, $^1J_{PC}$ = 30.4 Hz, PCH_3), 8.4 (d, $^1J_{PC}$ = 28.0 Hz, PCH_3), 11.6 (s, SCH_2CH_3), 26.3 (d, $^4J_{PC}$ = 1.0 Hz, CCH_3), 26.8 (s, CCH_3), 27.1 (s, CCH_3), 28.2 (d, $^4J_{PC}$ = 6.9 Hz, CCH_3), 30.6 (d, $^1J_{PC}$ = 32.5 Hz, PCH_2), 31.9 (br, SCH_2CH_3), 32.8 (d, $^2J_{PC}$ = 3.1 Hz, SCH_2CH_2P), 99.0 (s, *C*H), 99.5 (s, *C*H), 187.9 (d, $^3J_{PC}$ = 0.7 Hz, *C*O), 189.6 (s, *C*O), 191.5 (s, *C*O), 192.9 (d, $^3J_{PC}$ = 3.1 Hz, *C*O). The solubilities of these complexes **7** and **9** are similar to those of the corresponding mtdmp complexes **6** and **8**, respectively.

trans(*P*,*S*)-[Co(dtc)(mtdmp)$_2$](PF$_6$)$_2$ (**10**), [Co(dtc)$_2$(mtdmp)]PF$_6$ (**12**) *and cis*-[Co(dtc)$_2$(mtdmp-κP)$_2$]PF$_6$ (**14**)

To a methanol solution (100 cm^3) of **4** (0.55 g, 1.0 mmol) was added a methanol solution (100 cm^3) of Na(dtc)·2H$_2$O (0.18 g, 1.0 mmol) dropwise with stirring in an ice bath. The mixture was stirred for 2 h at room temperature and concentrated to ca 10 cm^3. The concentrate was diluted with water (100 cm^3) and then applied on a column (ϕ 5.0 × 60 cm) of SP-Sephadex C-25 (Na^+ form). The adsorbed products were eluted with 0.01 mol dm^{-3} aqueous NaCl solution, violet (**V1**), violet (**V2**) and red (**R**) bands being eluted in this order. After elution of the violet bands (**V1** and **V2**), a major red band (**R**) was eluted with 0.3 mol dm^{-3} aqueous NaCl solution. The eluate of each band was evaporated to dryness under reduced pressure, and the residue was extracted with a small amount of ethanol. The filtered extract was concentrated to ca 1 cm^3 under reduced pressure and mixed with a saturated ethanol solution of $NaPF_6$ to afford a violet or red precipitate. The crude product obtained from **V1** was recrystallized by diffusion of diethyl ether vapour into a dichloromethane solution to deposit violet crystals of **14** (0.10 g, 14% yield), and those from **V2** and **R** were recrystallized from an aqueous acetone solution to deposit violet crystals of **12** (0.05 g, 9% yield) and red crystals of **10** (0.35 g, 47% yield), respectively. For complex **10**; Found: C, 21.28; H, 4.46; N, 1.86. Calc.: for $C_{13}H_{32}CoF_{12}NP_4S_4$: C, 21.06; H, 4.35; N, 1.89%. ^{13}C NMR (CD_3CN): δ 5.8–16.4 (overlapped peaks due to four kinds of PCH_3), 17.9 (s, SCH_3), 18.7 (d, $^3J_{PC}$ = 4.1 Hz, SCH_3), 25–35 (overlapped peaks due to PCH_2CH_2S), 39.9 (s, NCH_3), 40.9 (s, NCH_3), 196.3 (br, NCS_2). This complex is soluble in methanol, acetone and acetonitrile, but not in water, dichloromethane or diethyl ether. For complex **12**; Found: C, 22.67; H, 4.36; N, 4.79. Calc.: for $C_{11}H_{25}CoF_6N_2P_2S_5$: C, 22.76; H, 4.34; N, 4.83%. ^{13}C NMR (CD_3CN): δ 6.7 (d, $^1J_{PC}$ = 34.9 Hz, PCH_3), 10.6 (d, $^1J_{PC}$ = 30. 4 Hz, PCH_3), 20.2 (s, SCH_3), 30.7

(d, $^2J_{PC}$ = 6.9 Hz, PCH_2CH_2S), 32.9 (d, $^1J_{PC}$ = 30 Hz, PCH_2), 38.8 (br, NCH_3), 39.3 (s, NCH_3), 201.4 (br, NCS_2), 203.4 (s, NCS_2). This complex is soluble in methanol and acetonitrile, but not in water or diethyl ether. For complex **14**; Found: C, 26.92; H, 5.16; N, 3.81. Calc. for $C_{16}H_{38}CoF_6N_2P_3S_6$: C, 26.81; H, 5.34; N, 3.91%. ^{13}C NMR (CD_3CN): δ 2.5 (virtual t, J_{PC} = 14.7 Hz, PCH_3), 13.0 (virtual t, J_{PC} = 16.0 Hz, PCH_3), 20.2 (s, SCH_3), 28.8 (virtual t, J_{PC} = 3.5 Hz, PCH_2CH_2S), 29.2 (virtual t, J_{PC} = 5.7 Hz, PCH_2), 38.5 (s, NCH_3), 38.9 (s, NCH_3), 201.6 (s, NCS_2). This complex is soluble in methanol, dichloromethane and acetonitrile, but not in water or diethyl ether.

trans(*P*,*S*)-[Co(dtc)(etdmp)$_2$](PF$_6$)$_2$ (**11**), [Co(dtc)$_2$-(etdmp)]PF$_6$ (**13**) *and cis*-[Co(dtc)$_2$(etdmp-κP)$_2$]PF$_6$ (**15**)

These complexes were obtained by a method similar to the corresponding mtdmp complexes using complex **5** as a starting material. Complex **11** was obtained as red crystals (67% yield). Found: C, 23.47; H, 4.79; N, 1.96. Calc.: for $C_{15}H_{34}CoF_{12}NP_4S_4$: C, 23.42; H, 4.72; N, 1.82%. ^{13}C NMR (CD_3CN): δ 9.4–11.9 (overlapped peaks due to four kinds of PCH_3), 13.3 (d, $^4J_{PC}$ = 2.1 Hz, SCH_2CH_3), 13.5 (s, SCH_2CH_3), 15–35 (overlapped peaks due to PCH_2CH_2S and SCH_2CH_3), 39.9 (s, NCH_3), 40.5 (s, NCH_3), 199.8 (br, NCS_2). Complex **13** was obtained as violet crystals (9% yield). Found: C, 24.52; H, 4.60; N, 4.70. Calc. for $C_{12}H_{27}CoF_6N_2P_2S_5$: C, 24.24; H, 4.58; N, 4.71%. ^{13}C NMR (CD_3CN): δ 6.7 (d, $^1J_{PC}$ = 34.9 Hz, PCH_3), 10.6 (d, $^1J_{PC}$ = 30.8 Hz, PCH_3), 13.3 (s, SCH_2CH_3), 26.3 (s, SCH_2CH_3), 33.1 (d, $^1J_{PC}$ = 30 Hz, PCH_2), 34.4 (d, $^2J_{PC}$ = 7.1 Hz, PCH_2CH_2S), 38.7 (s, NCH_3), 38.8 (s, NCH_3), 39.2 (s, NCH_3), 201.6 (d, $^3J_{PC}$ = 0.7 Hz, NCS_2), 203.3 (s, NCS_2). Complex **15** was obtained as violet crystalline solid (11% yield). Although the elemental analysis of this product gave no satisfactory result probably due to bad crystallinity of this compound, the ^{13}C NMR and electronic absorption spectra suggested that the product was pure enough for our structural characterization and measurements. ^{13}C NMR (CD_3CN): δ 12.6 (virtual t, J_{PC} = 14.5 Hz, PCH_3), 13.0 (virtual t, J_{PC} = 16.0 Hz, PCH_3), 15.4 (s, SCH_2CH_3), 25–35 (overlapped peaks due to SCH_2-CH_2P and SCH_2CH_3), 29.7 (virtual t, J_{PC} = 11.2 Hz, PCH_2), 38.5 (s, NCH_3), 38.9 (s, NCH_3), 201.6 (s, NCS_2). The solubilities of complexes **11**, **13** and **15** are similar to those of the corresponding mtdmp complexes **10**, **12** and **14**, respectively.

X-ray data collection, structure determination and refinement

A single crystal of each complex **1**, **2** and **14** were glued on top of a glass fibre with epoxy resin. The X-ray intensities were measured at 23°C with graphite-monochromated Mo-K_α radiation (λ = 0.71073 Å) on a Rigaku four-circle diffractometer AFC-5. Final lattice constants were determined by least-squares refinements of the orientation angles of 25 centred reflections in the range $20 \leqslant 2\theta \leqslant 30°$. Three standard reflections were monitored every 150 and showed no serious decomposition. The intensities were collected for $(+h, +k, \pm l)$ octants at $2\theta \leqslant 60°$ using 2θ-ω scan method. The structures were solved by the usual heavy-atom method using the SHELXS-86 program [20] and refined on F by full-matrix least-squares using anisotropic thermal parameters for all non-hydrogen atoms. Hydrogen atoms of **1** and **2** were located in calculated positions and fixed during refinement cycles, and those of **14** were located on the positions given by Fourier-difference syntheses, or by calculation, and refined isotropically. Complex neutral atom scattering factors [21] were used. All calculations were carried out using the XTAL 3.2 software [22].

Crystal data are summarized in Table 1. Atomic coordinates have been deposited with the Cambridge Crystallographic Data Centre.

RESULTS AND DISCUSSION

We have attempted preparing cobalt(III) complexes of dpdtn which is a linear tetradentate phosphine-thioether ligand bearing terminal diphenylphosphino groups. A reaction of a mixture of Co(BF$_4$)$_2$·6H$_2$O and dpdtn in methanol with a dichloromethane solution of tetramethylthiuramdisulfide gave a red complex of *cis*β-[Co(dtc)(dpdtn)](BF$_4$)$_2$ in a poor yield (ca 10%), while all the other attempts were fruitless [16]. The difficulty for preparation of the cobalt(III)-dpdtn complexes would result from the steric bulkiness of diphenylphosphino group. Therefore, we have prepared a new tetradentate ligand dmdtn which is a dimethylphosphino analogue of dpdtn, because the dimethylphosphino group would have a smaller steric requirement and a stronger donor ability to a cobalt(III) centre than diphenylphosphino group. The ligand dmdtn could be prepared in a good yield from sodium dimethylphosphide, ethylenesulfide and 1,3-dibromopropane in liquid ammonia by a one-pot reaction. Owing to its high boiling point, the crude product obtained was used for preparation of cobalt(III) complexes without further purification, and no serious problem was observed in the course of complex preparation.

In order to elucidate the characteristics of dmdtn complexes, analogous didentate phosphine-thioether ligands, mtdmp and etdmp, and their cobalt(III) complexes were also prepared. The preparation of mtdmp and etdmp from sodium dimethylphosphide and (2-chloroethyl)-methylsulfide or -ethylsulfide in liquid ammonia always contained 1,2-bis(dimethylphosphino)ethane (dmpe) as a by-product in ca 5–10%, which was hardly separated because of similar boiling points among mtdmp, etdmp and dmpe. The

Table 1. Crystallographic data for complexes **1**, **2** and **14**

	1	**2**	**14**
Formula	$C_{11}H_{26}Cl_2CoF_6P_3S_2$	$C_{16}H_{33}B_2CoF_8O_2P_2S_2$	$C_{16}H_{38}CoF_6N_2P_3S_6$
Crystal size/mm	0.4 × 0.4 × 0.3	0.6 × 0.4 × 0.3	0.6 × 0.5 × 0.45
Crystal system	Monoclinic	Monoclinic	Monoclinic
Space group	$P2_1/m$ (No. 11)	$P2_1/c$ (No. 14)	$C2/c$ (No. 15)
a (Å)	9.956(1)	9.841(2)	13.169(4)
b (Å)	10.497(1)	20.866(4)	21.046(4)
c (Å)	10.383(2)	12.976(2)	12.785(5)
β (°)	97.19(1)	93.53(1)	118.01(2)
U (Å^3)	1076.5(2)	2659.5(8)	3128(2)
Z	2	4	4
No. of reflns measured	3531	8341	4750
μ(Mo-K_α) (mm^{-1})	1.497	0.980	1.15
Transmission factors	0.689–1.000	—	0.519–0.706
No. of reflns used[a]	2511	3440	1851
No. of parameters	124	298	231
R, R_w[b]	0.044, 0.052	0.056, 0.059	0.078, 0.075

[a] $|F_o| > 3\sigma(|F_o|)$.
[b] $R = \Sigma||F_o| - |F_c||/\Sigma|F_o|$, $R_w = [\Sigma w(|F_o| - |F_c|)^2/\Sigma w|F_o|^2]^{1/2}$ [$w^{-1} = \sigma^2(|F_o|) + (0.015|F_o|)^2$].

contamination of dmpe has no significant influence for preparation of cobalt(III) complexes.

Dichloro complexes

The reaction of *trans*-$[CoCl_2(py)_4]Cl \cdot 6H_2O$ with dmdtn, followed by anion metathesis with $NaPF_6$, afforded a green complex of $[CoCl_2(dmdtn)]PF_6$ (**1**). The yield of complex **1** is relatively low (40%) as compared with the corresponding mtdmp or etdmp complex; a green complex of $[CoCl_2(mtdmp)_2]PF_6$ (**4**) or $[CoCl_2(etdmp)_2]PF_6$ (**5**) was prepared in 70–80% yield by a method similar to that for complex **1**. In contrast to the case of complex **4** or **5**, the preparation of complex **1** was always accompanied by the formation of red and green by-products. The by-products, however, could not be characterized, because they were unseparable from each other by means of fractional recrystallization or column chromatography and unstable in water. Complex **1** is stable in solution even in water, while complexes **4** and **5** are slowly hydrolyzed in aqueous acetone.

The crystal structure of **1** was determined by X-ray diffraction. A perspective view of the complex cation is shown in Fig. 1, and selected bond lengths and angles are listed in Table 2. The Co, Cl(1), Cl(2) and C(6) atoms are located on the crystallographic plane of symmetry, and the geometry around the central Co atom is almost octahedral. Two Cl atoms occupy *trans* positions, and two *cis* sulfur atoms have opposite absolute configurations, i.e., *meso*(S). The five-membered $CoPC_2S$ chelate rings take an envelope conformation and the six-membered $CoSC_3S$ chelate has a chair conformation. Thus, the total geometrical structure of the complex cation is assigned as *trans*(*Cl*,*Cl*)-chair-$[CoCl_2\{meso(S)\text{-dmdtn}\}]^+$ [23].

The Co—P(1) bond length in complex **1** is similar to the Co—P bond lengths in *trans*(*Cl*,*Cl*)-$[CoCl_2\{meso(P)\text{-SPPS}\}]BF_4$ (2.223(3) and 2.230(3) Å; SPPS = $MeS(CH_2)_2PPh(CH_2)_3PPh(CH_2)_2SMe$) [9]. These bond lengths indicate that the *trans* influence of the thioether group is intermediate between those of an amino group and a dimethylphosphino group, because the corresponding Co—P bond lengths in *trans*(*Cl*,*Cl*)*cis*(*P*,*P*)-$[CoCl_2(edmp)_2]^+$ (edmp = $Me_2P(CH_2)_2NH_2$) are 2.190(3) and 2.201(3) Å and those in *trans*-$[CoCl_2(dmpe)_2]^+$ (dmpe = $Me_2P(CH_2)_2PMe_2$) are 2.256(1) and 2.262(1) Å [24]. The Co—Cl bond lengths in complex **1** are also intermediate between those of the edmp complex (2.238(3) and 2.244(3) Å) and the dmpe complex (2.260(1) Å) [24], although the differences among them are rather small. This order is consistent with that of steric congestion due to alkyl groups on P or S atoms which decreases in the order bis(dmpe) > dmdtn > *cis*(*P*,*P*)-bis(edmp). The Co—S bond length in complex **1** is slightly shorter than those in the SPPS complex (2.325(3) and 2.329(3) Å) [9]. The small deviation of the bond lengths probably results from the different relative positions of the S atoms in the ligand skeleton: central positions in dmdtn while terminal in SPPS. The five- and six-membered chelate bite angles are close to a right angle, whereas the P(1)—Co—P(1′) angle is appreciably wider 96.19(3)°. The P—Co—P bond angle is almost equal to that in the edmp complex (96.9(1)°) [24], but relatively larger than the S—Co—S angle in *trans* (*Cl*,*Cl*)-$[CoCl_2\{meso(P)\text{-SPPS}\}]BF_4$ (90.7(1)°) [9]. Therefore, the widening of

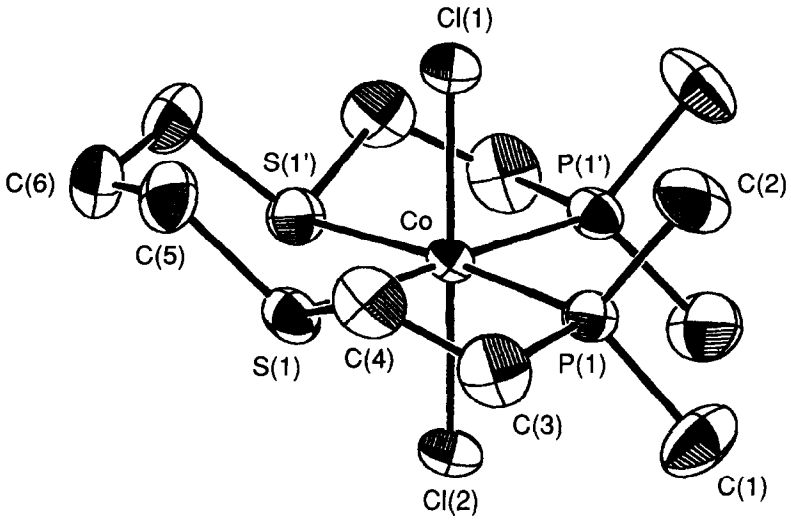

Fig. 1. Perspective drawing of the complex cation in *trans*(*Cl,Cl*)*cis*(*P,P*)-[$CoCl_2${*meso*(S)-dmdtn}]PF_6, **1** (hydrogen atoms are omitted for clarity).

Table 2. Selected bond lengths (Å) and angles (°) for complex **1**

Co—Cl(1)	2.251(1)	Co—Cl(2)	2.244(1)
Co—S(1)	2.2956(9)	Co—P(1)	2.2330(8)
Cl(1)—Co—Cl(2)	179.91(3)		
Cl(1)—Co—S(1)	92.02(3)	Cl(1)—Co—P(1)	90.97(3)
Cl(2)—Co—S(1)	87.92(3)	Cl(2)—Co—P(1)	89.09(3)
S(1)—Co—P(1)	87.73(3)	S(1)—Co—P(1')	175.03(3)
S(1)—Co—S(1')	88.20(3)	P(1)—Co—P(1')	96.19(3)

P—Co—P angle in the dmdtn and edmp complexes can be interpreted by steric repulsion between the mutually *cis*-positioned dimethylphosphino groups.

For the SPPS complexes both green *trans*-[$CoCl_2${*meso*(P)-SPPS}]$^+$ and red *cis*α-[$CoCl_2${*racemic*(P)-SPPS}]$^+$ isomers were obtained [9], but in this study the corresponding *cis*α-isomer could not be isolated. While molecular models indicate that *cis*α-skew-[$CoCl_2${*racemic*(S)-dmdtn}]$^+$ has the least non-bonded steric interaction among the possible isomers (with conformers), the mutual *trans* arrangement of dimethylphosphino groups will be unfavourable because of their strong *trans* influences. The ^{13}C-{^1H} NMR spectrum of a green CD_3CN solution of complex **1**, this green colour suggesting that the *trans* geometrical structure retains in solution as well, shows two kinds of resonances for P—CH_3 and a single resonance for the other carbons. Both conformers of *trans*(*Cl,Cl*)-chair-[$CoCl_2${*meso*(S)-dmdtn}]$^+$ with molecular C_s symmetry (the crystal structure of **1**) and *trans*(*Cl,Cl*)-skew-[$CoCl_2${*racemic*(S)-dmdtn}]$^+$ with molecular C_2 symmetry should give the observed spectral pattern. The former chair conformer is more stable than the latter skew with respect to the $CoSC_3S$ six-membered ring conformation [23], while the steric congestion due to mutually *cis*-positioned PMe_2 groups favour the latter conformer. Although we have no evidence for either conformer, it is more probable for the *trans*(*Cl,Cl*)-chair-[$CoCl_2${*meso*(S)-dmdtn}]$^+$ structure to be maintained in solution as well, since the inversion of absolute configuration at the sulfur in complex **1** will be restricted by chelate rings with stable chair conformation.

For complexes **4** and **5**, there are five possible geometrical isomers (Scheme 2). The absorption spectra of complexes **4** and **5** were quite similar to that of complex **1** (Fig. 2), and the absorption peak positions of the I_a component of the first d-d transition band which appeared at the lowest energy region were almost identical among the three complexes (Table 3). Therefore, the geometrical structures (the donor atoms arrangement) were assigned as *trans*-(*Cl,Cl*)*cis*(*P,P*). Interestingly, the peak positions of the I_a component of the first d-d transition band also coincide with that of *trans*(*Cl,Cl*)*cis*(*P,P*)-[$CoCl_2$(edmp)$_2$]$^+$ (16,600 cm^{-1}, log $\varepsilon = 2.14$) [25].

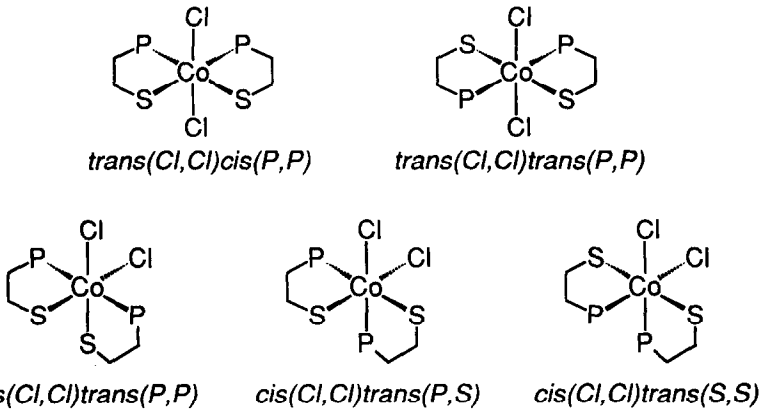

Scheme 2. Five possible geometrical isomers for $[CoCl_2(P—S)_2]^+$ (P—S = mtdmp or etdmp) complexes.

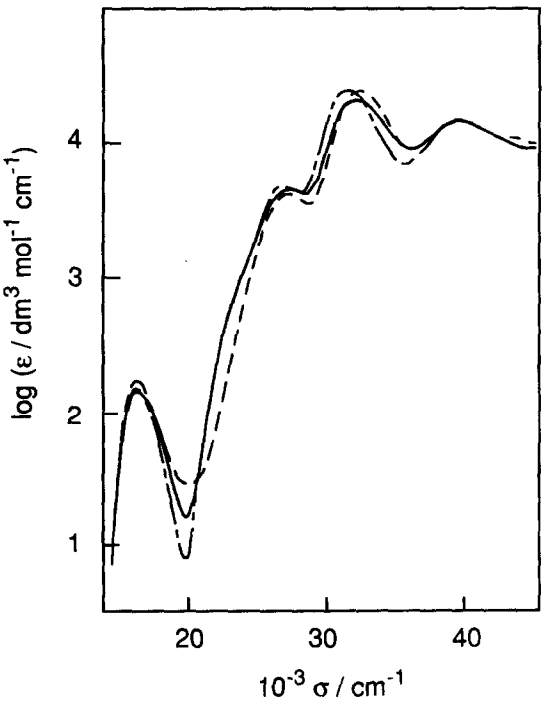

Fig. 2. Absorption spectra of complex **1** in acetonitrile (– –), **4** in methanol (——) and **5** in acetonitrile (– · –) at room temperature.

This indicates that the ligand field strengths of the thioether groups in complexes **1**, **4** and **5** are apparently similar to those of amino group of the corresponding edmp complex, while the ligand field parameters of $\langle—CH_2NH_2\rangle$[5] and $\langle—CH_2SMe\rangle$[5] are previously reported as 21,400 and 17,700 cm^{-1}, respectively [26].

The ^{13}C-$\{^1H\}$ NMR spectra of **4** and **5** in CD_3CN exhibit a spectral pattern similar to that of **1**, i.e., two kinds of resonances for P—CH_3 and a single resonance for the other carbons (except for the overlapped multiplet for P—CH_3 of **4**). This pattern is in contrast to that of the corresponding edmp complex, where only one kind of resonance for P—CH_3 is observed [^{13}C NMR (CD_3CN): δ 11.2 (virtual t, J_{PC} = 16.9 Hz, PCH_3), 34.5 (virtual t, J_{PC} = 15.7 Hz, PCH_2), 41.1 (s, NCH_2)] [16]. The two kinds of P—CH_3 signals observed for complexes **4** and **5** indicate that the configurational inversion at each sulfur is restricted in the complexes. By combination of absolute configuration at two sulfur centres, *meso*(S) and *racemic*(S) diastereomers are possible for the complexes. In these cases, in contrast to complex **1**, the steric factor seems to be dominant. Therefore, the *racemic*(S) isomer is more probable due to steric congestion of mutually *cis*-positioned SR groups, although, again, we have no evidence for this.

As mentioned above, complexes **4** and **5** were prepared in high yields, in contrast to the analogous edmp complex. The reaction of *trans*-$[CoCl_2(py)_4]Cl \cdot 6H_2O$ with edmp in a molar ratio of 1:2 gave *trans*-(*Cl,Cl*)*cis*(*P,P*)-$[CoCl_2(edmp)_2]PF_6$ in only 13% yield together with a large amount of *fac*-$[Co(edmp)_3](PF_6)_3$ (63% yield based on edmp), and the other methods for preparing *trans*(*Cl,Cl*)*cis*(*P,P*)-$[CoCl_2(edmp)_2]^+$ gave similarly low yields (7–10%) due to preferential formation of *fac*-$[Co(edmp)_3]^{3+}$. On the other hand, we could prepare neither [Co(mtdmp or etdmp)$_3$]$^{3+}$ nor [Co(mtdmp or etdmp)(dmdtn)]$^{3+}$ complexes by the reaction of **1**, **4** or **5** with excess mtdmp or etdmp. The steric factor of alkyl substituents on S atoms would result in difficulty in the formation of these $[Co(P)_3(S)_3]^{3+}$-type complexes.

Pentane-2,4-dionate or N,N-dimethyldithiocarbamate complexes

The red complexes of $[Co(acac)(dmdtn)](BF_4)_2$ (**2**) and $[Co(dtc)(dmdtn)](BF_4)_2$ (**3**) were derived from complex **1** in high yields (63–80%), only one isomer

Table 3. Absorption spectral data of complexes[a]

Complex	Solvent	$10^{-3}\ \sigma/cm^{-1}$ [log (ε/dm^3 mol^{-1} cm^{-1})]
1	CH_3CN	16.50 [2.28], 27.59 [3.63], 32.87 [4.28], 39.77 [4.13]
2	CH_3CN	20.88 [3.02], 28.5^{sh} [3.4], 35.8^{sh} [4.4], 42.1^{sh} [4.1]
3	CH_3CN	20.7^{sh} [2.9], 25.31 [2.91], 31.8^{sh} [4.2], 34.69 [4.45], 42.71 [4.17]
4	CH_3OH	16.55 [2.12], 27.78 [3.60], 32.77 [4.23], 40.34 [4.07]
5	CH_3CN	16.41 [2.19], 27.52 [3.60], 32.33 [4.30], 40.14 [4.05]
6	CH_3OH	19.4^{sh} [2.7], 22.39 [2.88], 29.4^{sh} [3.5], 35.24 [4.22]
8	CH_3OH	18.0^{sh} [2.2], 19.77 [2.66], 30.0^{sh} [3.7], 38.22 [4.50]
10	CH_3CN	20.1^{sh} [2.9], 22.8^{sh} [3.0], 35.58 [4.36], 39.77 [4.18]
12	CH_3CN	18.30 [2.76], 23.5^{sh} [3.2], 28.2^{sh} [3.9], 32.2^{sh} [4.4], 34.69 [4.44], 39.72 [4.42]
14	CH_3CN	17.97 [2.56], 25.8^{sh} [3.5], 28.8^{sh} [3.8], 35.32 [4.39], 40.81 [4.28]

[a] *sh* denotes shoulder peak.

for each being isolated in this study. For each reaction a by-product was detected in column chromatography as a yellow (for acac) or brown (for dtc) band, but the relative yield was very low and we could not isolate it as a pure form. Complexes **2** and **3** were assigned as a *cisβ*-isomer by their ^{13}C-{^1H} NMR spectra. While the ^{13}C resonances due to the dmdtn moiety exhibit very complicated patterns with many overlapped peaks, those due to acac or dtc ligand gave their structural information. The methyl groups of acac moiety in complex **2** exhibit two kinds of resonances at δ 26.6 (s) and 27.8 (d, $J = 4.5$ Hz), and those of dtc in complex **3** at δ 39.7 (s) and 40.3 (s); these indicate that the symmetry around the central Co atom is lower than C_2 of *cisα* configuration, that is, C_1 of *cisβ*. The assignment was confirmed by X-ray analysis for complex **2**.

A perspective view of the complex cation in **2** is shown in Fig. 3, and selected bond lengths and angles are listed in Table 4. The complex has a distorted octahedral geometry with *cisβ* configuration of the linear tetradentate dmdtn ligand. The two coordinated sulfur atoms have the same absolute configuration as each other, i.e., *racemic*(S) (*RR*/*SS*). This fact indicates that the configurational inversion at one sulfur atom occurred during the derivation of complex **2** from complex **1**. The central six-membered chelate ring of dmdtn takes a chair conformation, and the total configuration of the dmdtn ligand is *cisβ*-chair-*racemic*(S). A molecular modeling study suggests that this conformer will be more stable than the other possible isomers, *cisβ*-chair-*meso*(S), *cisβ*-skew-*meso*(S) and *cisα*-skew-*racemic*(S), as discussed by Bosnich *et al.* for the analogous linear tetradentate amine-thioether ligand of $NH_2(CH_2)_2S$-$(CH_2)_3S(CH_2)_2NH_2$ (ete) [23].

The Co—P(1) and Co—P(2) bond lengths in complex **2** are similar to each other, although their *trans*-positioned donor atoms are different: O of acac for P(1) and S of dmdtn for P(2). In contrast, the Co—S(1) and Co—S(2) bond lengths are quite different from each other, which results from the stronger *trans* influence of dimethylphosphino group compared to that of acac. The Co—S(1) bond length is nearly equal to that in complex **1**, both of which are *trans* to the dimethylphosphino group of dmdtn. On the other hand, the Co—S(2) bond length is similar to the Co—S bonds in *cisβ*,*trans*(*Cl*,*S*)-[CoCl(NO_2)(ete)]Cl (2.22(1) and 2.24(1) Å) [27]. The small deviation of Co—O bond lengths would also be affected by the *trans* influence of the dimethylphosphino group. Although the five-membered P—Co—S chelate angles and the P(1)—Co—P(2) bond angle in complex **2** are similar to the corresponding angles in complex **1**, the S(1)—Co—S(2) angle in the six-membered chelate ring in **2** is appreciably larger than in **1**. The reason for the widening of S—Co—S angle is not clear.

Although the lack of X-ray analysis for complex **3** prohibits our discussion of the absolute configuration of sulfur atoms and the configuration of chelate rings in detail, the absorption spectrum of complex **3** was similar to that of **2** except for an additional band observed around 25,300 cm^{-1} (Fig. 4), and a *cisβ*-chair-*racemic*(S) form is expected as the most stable isomer.

The reaction of complex **4** or **5** with Li(acac) in methanol afforded an orange complex of [Co(acac)(mtdmp or etdmp)$_2$](PF_6)$_2$ (**6** or **7**) and a violet one of [Co(acac)$_2$(mtdmp or etdmp)]PF_6 (**8** or **9**). For the former there are three possible geometrical isomers with *trans*(*P*,*P*), *trans*(*P*,*S*) and *trans*(*S*,*S*) configurations (Scheme 3). The ^{13}C-{^1H} NMR spectra of the orange complexes exhibit two kinds of signals for carbonyl carbons: δ 191.4 (s) and 193.0 (d, $J = 2.4$ Hz) for complex **6** and 192.7 (s) and 193.3 (d, $J = 2.1$ Hz) for complex **7**. The lower field doublet signal for each complex is assigned to the carbonyl carbon *trans* to the dimethylphosphino group of mtdmp or etdmp [28]. Thus, the orange complexes **6** and **7** are definitely assigned as the *trans*(*P*,*S*)-isomer, which is corresponding to the *cisβ*-isomer of complex **2** in regard to the donor atom arrangements. The absorption spectra of complexes **2** and **6** showed a similar pattern except for the appearance of a shoulder peak at the

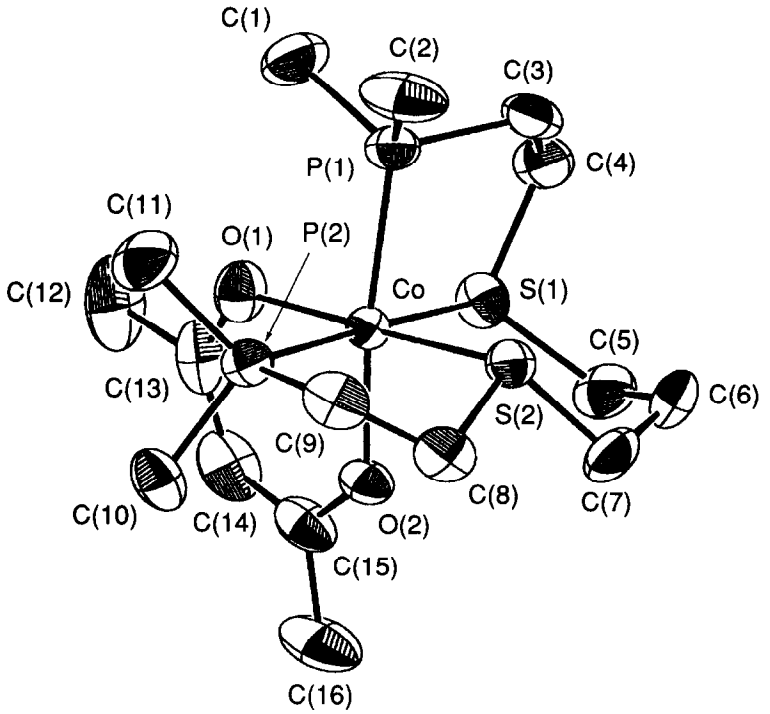

Fig. 3. Perspective drawing of the complex cation in *cisβ*-[Co(acac){*racemic*(S)-dmdtn}]$(BF_4)_2$, **2** (hydrogen atoms are omitted for clarity).

Table 4. Selected bond lengths (Å) and angles (°) for complex **2**

Co—S(1)	2.308(2)	Co—S(2)	2.221(1)
Co—P(1)	2.226(2)	Co—P(2)	2.222(2)
Co—O(1)	1.910(4)	Co—O(2)	1.929(4)
S(1)—Co—S(2)	95.54(6)	P(1)—Co—P(2)	97.33(6)
S(1)—Co—P(1)	86.13(6)	S(1)—Co—P(2)	175.20(7)
S(1)—Co—O(1)	86.9(1)	S(1)—Co—O(2)	87.8(1)
S(2)—Co—P(1)	88.36(6)	S(2)—Co—P(2)	87.91(6)
S(2)—Co—O(1)	176.4(1)	S(2)—Co—O(2)	88.1(1)
P(1)—Co—O(1)	89.2(1)	P(1)—Co—O(2)	172.7(1)
P(2)—Co—O(1)	89.8(1)	P(2)—Co—O(2)	89.0(1)
O(1)—Co—O(2)	94.5(2)		

lower energy side of the first absorption band of complex **6** (Fig. 4(a)).

For $[Co(acac)_2(mtdmp \text{ or } etdmp)]^+$ complexes (**8** or **9**), there are two possible diastereomers, Δ-*R*(S)/Λ-*S*(S) and Δ-*S*(S)/Λ-*R*(S). The $^{13}C\text{-}\{^1H\}$ NMR spectra of these complexes in CD_3CN show a singlet signal for the S—R group, which indicates a rapid configurational inversion at the S atom [*R*(S) ↔ *S*(S)] or a preferential formation of either diastereomer. Since there are no steric factors to prevent the inversion at the sulfur, the observed singlet for the S—R group seems to result from a rapid configurational inversion at the sulfur atom. The inversion of the selenium atom, which seems to be much slower than that of the sulfur in the analogous bis(acac) complexes, is detectable by NMR methods [29].

The reaction of **4** with Na(dtc)·$2H_2O$ afforded two violet complexes **12** and **14** as well as a major orange complex **10**, and a similar reaction of **5** gave the corresponding complexes **11**, **13** and **15**. The three complexes formed in each reaction can be separated by means of column chromatography using SP-Sephadex C-25 resin; the first and the second developing violet complexes are found to have the compositions of $[Co(dtc)_2(mtdmp \text{ or } etdmp)_2]PF_6$ (**14** or **15**) and $[Co(dtc)_2(mtdmp \text{ or } etdmp)]PF_6$ (**12** or **13**), respec-

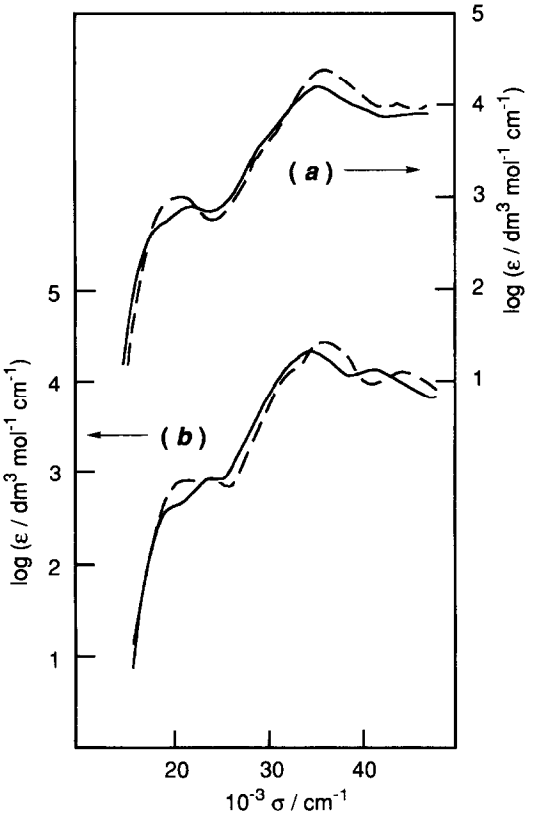

Fig. 4. (a) Absorption spectra of complex **2** in acetonitrile (– –) and **6** in methanol (——), (b) **3** in acetonitrile (– –) and **10** in acetonitrile (——) at room temperature.

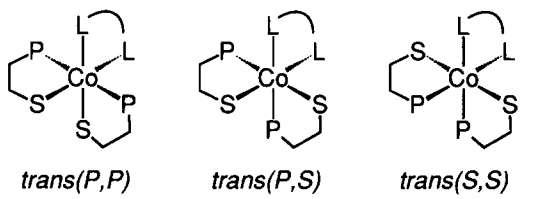

Scheme 3. Three possible geometrical isomers for $[Co(L—L)(P—S)_2]^{2+}$ (L—L = acac or dtc; P—S = mtdmp or etdmp) complexes.

tively, by elemental analyses. The complexes **12** and **13** are assigned as the bis(dtc) analogues of **8** and **9**, respectively, by $^{13}C-\{^1H\}$ NMR spectroscopy.

The structure of complex **14** was determined by X-ray analysis to be *cis*-$[Co(dtc)_2(mtdmp-\kappa P)_2]PF_6$. A perspective view of the complex cation is shown in Fig. 5, and selected bond lengths and angles are listed in Table 5. The Co atom is located on a crystallographic C_2 axis which bisects the P(1)—Co—P(1′) and S(2)—Co—S(2′) angles. The coordination geometry is slightly distorted octahedral with four sulfur and two phosphorus atoms. The two mtdmp ligands function as a monodentate ligand through the coordination of only phosphorus atom and are sited in mutual *cis*-positions. The Co—P bond length in complex **14** was slightly longer than those in complexes **1** and **2**, and the P—Co—P bond angle also wider than a right angle; both of these structural deviations would result from steric repulsion between the mutually *cis*-positioned monodentate phosphines. The corresponding etdmp complex **15** was also characterized as *cis*-$[Co(dtc)_2(etdmp-\kappa P)_2]PF_6$ based on the $^{13}C-\{^1H\}$ NMR spectrum.

The geometrical structures of complexes **10** and **11** are assigned as *trans*(*P*,*S*) isomer based on the $^{13}C-\{^1H\}$ NMR spectra, which are comparable to those of complexes **3**, **7** and **8**. Two kinds of N—CH_3 resonances for dtc moiety and of SR (R = Me for **10** or Et for **11**) for mtdmp or etdmp were exhibited. The absorption spectra of complexes **3** and **10** are also compared in Fig. 4(b). The spectral patterns are similar to each other and to those of the corresponding acac complexes. For each complex two absorption peaks or shoulders appeared in the region 20,000–25,000 cm^{-1}, which are assigned to the first and second d-d transition bands as discussed previously for $[Co(dtc)(dmpe)_2]^{2+}$ (dmpe = $Me_2P(CH_2)_2PMe_2$) [30]. The energy difference between the first and second d-d bands is quite small for mixed donor-type cobalt(III) complexes having both sulfur and phosphorus as donor atoms.

Electrochemistry

The cyclic voltammograms of dmdtn complexes **1**, **2** and **3** are shown in Fig. 6. The latter two *cisβ* complexes exhibited reversible redox waves of Co^{3+}/Co^{2+} at $E_{1/2} = -0.64$ V for the acac complex **2** and -0.82 V for the dtc complex **3**, respectively. On the other hand, the *trans*-dichloro complex **1** gave irreversible reduction waves at -0.52 and -0.82 V, and all of the mtdmp and etdmp complexes also exhibited irreversible reduction waves at -0.5 to -0.8 V; these observations indicated that all complexes other than **2** or **3** are unstable in their Co^{2+} states. The tetradentate ligand with *cisβ* configuration may stabilize their structures even in the Co^{2+} oxidation state. Compared to the reduction potentials of the mono(dtc)-type cobalt(III) complexes, the $E_{1/2}$ value of complex **3** is similar to those of $[Co(dtc)(en)_2]^{2+}$ (-0.75 V) [31] and $[Co(dtc)\{P(OMe)_3\}_4]^{2+}$ (-0.75 V) [32], but fairly shifted to the positive side from those of $[Co(dtc)\{Me_2P(CH_2)_nPMe_2\}_2]^{2+}$ ($n = 1$, 2 or 3; -0.95 to -1.11 V) [31,32]. These redox potentials indicate that the thioether groups are weaker ligands than the dimethylphosphino group in both Co^{3+} and Co^{2+} states.

CONCLUDING REMARKS

In this study three kinds of cobalt(III) complexes containing dmdtn and either dichloro (**1**), acac (**2**) or

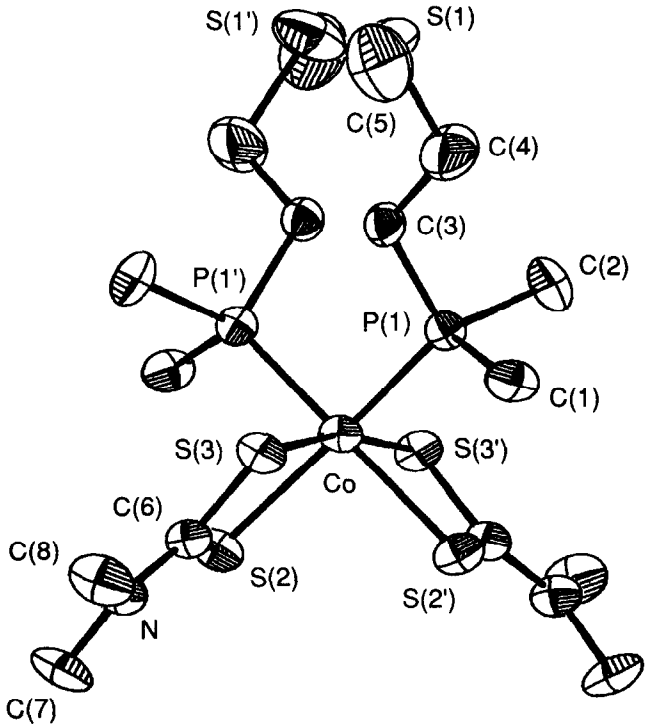

Fig. 5. Perspective drawing of the complex cation in *cis*-[Co(dtc)$_2$(mtdmp-κP)$_2$]PF$_6$, **14** (hydrogen atoms are omitted for clarity).

Table 5. Selected bond lengths (Å) and angles (°) for complex **14**

Co—S(2)	2.312(3)	Co—S(3)	2.275(2)
Co—P(1)	2.241(3)		
S(2)—Co—S(3)	75.6(1)	S(2)—Co—S(3′)	95.1(1)
S(2)—Co—S(2′)	89.0(1)	S(3)—Co—S(3′)	167.1(1)
S(2)—Co—P(1)	162.93(9)	S(2)—Co—P(1′)	89.0(1)
S(3)—Co—P(1)	87.74(9)	S(3)—Co—P(1′)	100.78(9)
P(1)—Co—P(1′)	97.6(1)		

dtc (**3**) ligands are synthesized. For each complex only one isomer can be isolated and the dmdtn acts as a tetradentate ligand. These results are in contrast to the previously described SPPS-type tetradentate ligands, because the SPPS ligands often give more than one isomer due to the relative configurations of the central phosphorus atoms and in some cases act as a didentate diphosphine ligand [8,9]. Several cobalt(III) complexes containing didentate mtdmp or etdmp are also synthesized and compared the properties with those of the analogous dmdtn complexes. The reaction of dichlorobis(mtdmp or etdmp) complex (**4** or **5**) with Li(acac) or Na(dtc) gives not only mono(acac or dtc)-type complexes (**6**, **7**, **10** or **11**) but also bis(acac or dtc)-type complexes (**8**, **9**, **12**, **13**, **14** or **15**). Therefore, it is suggested that the didentate ligands are more labile for substitution than the tetradentate dmdtn and can act as a hemilabile ligand as well as SPPS-type tetradentate ligands.

Acknowledgements—The present work was supported in part

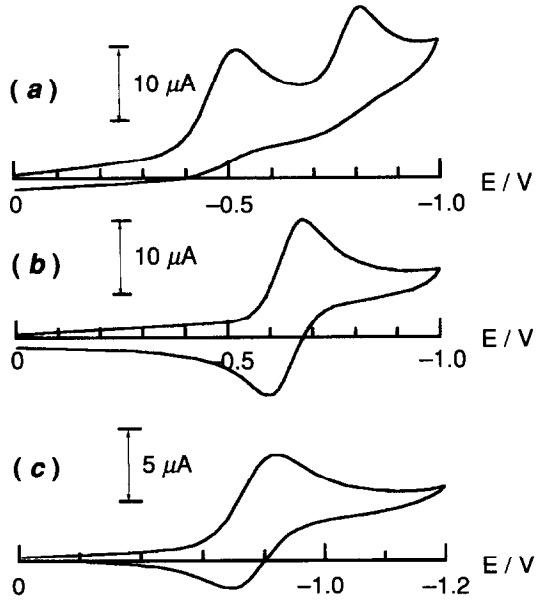

Fig. 6. Cyclic voltammograms of (a) complex **1**, (b) **2** and (c) **3** in acetonitrile at 25.0±0.1°C.

by a Grant-in-Aid for Scientific Research No. 08640709 from Ministry of Education, Science and Culture, Japan.

REFERENCES

1. Kashiwabara, K., Jung, M. and Fujita, J., *Bull. Chem. Soc. Jpn.*, 1991, **64,** 2372.
2. Jung, M., Atoh, M., Kashiwabara, K. and Fujita, J., *Bull. Chem. Soc. Jpn.*, 1990, **63,** 2051.
3. Jung, M., Atoh, M., Kashiwabara, K. and Fujita, J., *Bull. Chem. Soc. Jpn.*, 1988, **61,** 3503.
4. Atoh, M., Sugiura, H., Seki, Y., Kashiwabara, K. and Fujita, J., *Bull. Chem. Soc. Jpn.*, 1987, **60,** 1699.
5. Atoh, M., Kashiwabara, K. and Fujita, J., *Bull. Chem. Soc. Jpn.*, 1986, **59,** 1001.
6. Atoh, M., Kashiwabara, K. and Fujita, J., *Bull. Chem. Soc. Jpn.*, 1985, **58,** 3492.
7. Atoh, M., Kashiwabara, K. and Fujita, J., *Bull. Chem. Soc. Jpn.*, 1985, **58,** 2793.
8. Kitagawa, T., Kita, M., Kashiwabara, K. and Fujita, J., *Bull. Chem. Soc. Jpn.*, 1991, **64,** 2942.
9. Kashiwabara, K., Ito, Y., Kita, M., Fujita, J. and Nakajima, K., *J. Chem. Soc., Dalton Trans.*, 1997, 39.
10. Murray, S. G. and Hartly, F. R., *Chem. Rev.*, 1981, **81,** 365.
11. Aurivillius, K. and Bertinesson, G., *Acta Crystallogr., Sect. B*, 1980, **36,** 790.
12. Aurivillius, K. and Bertinesson, G., *Acta Crystallogr., Sect. B*, 1981, **37,** 2073.
13. Bertinesson, G., *Acta Crystallogr., Sect. C*, 1983, **39,** 698.
14. Degischer, G. and Schwarzenbach, G., *Helv. Chim. Acta*, 1966, **49,** 1927.
15. Dubois, T. D. and Meek, D. W., *Inorg. Chem.*, 1969, **8,** 146.
16. Kashiwabara, K., unpublished results.
17. Butter, S. A. and Chatt, J., *Inorg. Synth.*, 1974, **XV,** 185.
18. Suzuki, T., Morikawa, A. and Kashiwabara, K., *Bull. Chem. Soc. Jpn.*, 1996, **69,** 2539.
19. Glerup, J., Schäffer, C. E. and Springborg, J., *Acta Chem. Scand., A*, 1978, **32,** 673.
20. Sheldrick, G. M., SHELXS-86, Program for Crystal Structure Determination, University of Göttingen, 1986.
21. Cromer, D. T. and Waber, J. T., *International Tables for X-Ray Crystallography*. Vol. 4. Kynoch Press, Birmingham, 1974, vol. 4.
22. Hall, S. R., Flack, H. D. and Stewart, J. M., XTAL 3.2, Program for X-Ray Crystal Structure Analysis, Universities of Western Australia, Geneva and Maryland, 1992.
23. Bosnich, B., Kneen, W. R. and Phillip, A. T., *Inorg. Chem.*, 1969, **8,** 2567.
24. Kita, M., Kashiwabara, K., Fujita, J., Tanaka, H. and Ohba, S., *Bull. Chem. Soc. Jpn.*, 1994, **67,** 2457.
25. Kinoshita, I., Yokota, Y., Matsumoto, K., Ooi, S., Kashiwabara, K. and Fujita, J., *Bull. Chem. Soc. Jpn.*, 1983, **56,** 1067.
26. Shimura, Y., *Bull. Chem. Soc. Jpn.*, 1988, **61,** 693.
27. Murray-Rust, J. and Murray-Rust, P., *Acta Crystallogr., Sect. B*, 1973, **29,** 2606.
28. Kashiwabara, K., Kinoshita, I., Ito, T. and Fujita, J., *Bull. Chem. Soc. Jpn.*, 1981, **54,** 725.
29. Nakajima, K., Kojima, M. and Fujita, J., *Bull. Chem. Soc. Jpn.*, 1986, **59,** 3505.
30. Ohishi, T., Kashiwabara, K. and Fujita, J., *Bull. Chem. Soc. Jpn.*, 1987, **60,** 583.
31. Okuno, M., Kita, M., Kashiwabara, K. and Fujita, J., *Chem. Lett.*, 1989, 1643.
32. Matsui, M., Kita, M., Kashiwabara, K. and Fujita, J., *Bull. Chem. Soc. Jpn.*, 1993, **66,** 1140.
33. Kita, M., Okuno, M., Kashiwabara, K. and Fujita, J., *Bull. Chem. Soc. Jpn.*, 1992, **65,** 3042.

Pergamon

PII: S0277-5387(97)00528-7

Polyhedron Vol. 17, Nos. 11–12, pp. 1831–1841, 1998
© 1998 Elsevier Science Ltd
All rights reserved. Printed in Great Britain
0277-5387/98 $19.00+0.00

Ternary copper(II) complexes with diethylenetriamine and α-(or β-) alaninehydroxamic acids in water solution

Barbara Kurzak,[a]* Danuta Kroczewska[a] and Julia Jezierska[b]

[a] Institute of Chemistry, Pedagogical University, 3-Maja 54, 08-110 Siedlce, Poland

[b] Faculty of Chemistry, University of Wrocław, F. Joliot-Curie 14, 50-383 Wrocław, Poland

(Received 1 October 1997; accepted 12 December 1997)

Abstract—Stabilities of the mixed-ligand complexes of Cu^{2+} ion with diethylenetriamine [bis(2-aminoethyl) amine, dien)] as a primary ligand and α-alaninehydroxamic acid [2-amino-N-hydroxypropanamid, α-Alaha] or β-alaninehydroxamic acid [3-amino-N-hydroxypropanamid, β-Alaha] as a secondary ligand L and their absorption and EPR spectra at various pH values are reported. The visible spectra exhibit a characteristic red shift and a shoulder at lower energies indicating a five-coordinate structure of the formed complexes. The change of the EPR spectral parameters as a function of pH reflects two modes of an equatorial-axial chelation by aminohydroxamic acid ligand L in $[Cu(dien)(HL)]^{2+}$ and $[Cu(dien)(L)]^{+}$ species, while the diethylenetriamine nitrogens are coordinated at three equatorial positions in each case. α-Alaha is a more effective chelating ligand than β-Alaha in the Cu^{2+}-dien-L ternary system. This is reflected in the much higher basicity-adjusted stability constants, $\log K_{Cu(dien)(\alpha\text{-Alaha})(\beta\text{-Alaha})} - \Sigma pK^{H}$. © 1998 Elsevier Science Ltd. All rights reserved

Keywords: copper(II) complexes; mixed-ligands complexes; five-coordinate; aminohydroxamic acids; diethylenetriamine; e.s.r. spectra; vis spectra.

The importance of ternary complexes in biochemical systems has provided a strong impetus to the study of mixed ligand metal(II) complexes [1–5]. The total ligand concentration greatly exceeds the metal content in the mammalian body leading to competition between various complexing species and metal ions present in the living tissues and fluids. Ternary complexes have been implicated in the storage and transport of metal ions and of active substances through membranes [6]. As the mixed-ligand complexes play such a central role it is worthwhile to assemble information on their formation, stability and structure and on the mutual influence of two ligands bound to the same metal ion [2,7–10].

Copper is a bioessential element with truly unique chemical characteristics. It is also toxic with low legal concentration limits, for example, for drinking water or sewage sludge [11]. In view of the increasingly realistic expectations of therapy aimed at the biological cause of genetic disorders, two hereditary diseases concerning copper metabolism, Wilson's disease and Menke's syndrome, have attracted special attention [11,12]. The therapy consists of administration of copper-specific chelating agents, in particular D-penicillamine or—in cases of the not uncommon intolerance to it—of triethylenetetramine [11,13].

Polyamines play an important role in the processes in living organisms. These compounds are found at a significant concentration in young cells and, particularly, in cancer tumor tissues [14,15]. Polyamines are very effective ligands.

The importance of hydroxamic and aminohydroxamic acids in biology, medicine, pharmacology and agriculture is well known [16–19].

The literature on ternary metal complexes involving aminohydroxamic acids is not rich, however some ternary systems involving aminohydroxamic acid and amino acid [20,21], amine [22,23], or other bioligand as the secondary one [24–27], were investigated.

The aim of the present work was to obtain information on the complex formation ability of α-Alaha or β-Alaha towards $[Cu(dien)(H_2O)_3]^{2+}$ complex, and to characterize the structures of the ternary complexes

* Author to whom correspondence should be addressed.

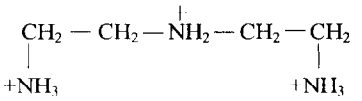

diethylenetriamine (dien)

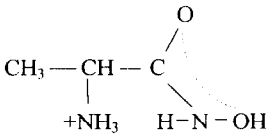

α-alaninehydroxamic acid
(α-Alaha)

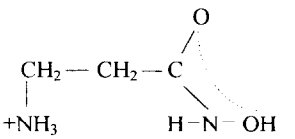

β-alaninehydroxamic acid
(β-Alaha)

Scheme 1.

formed using potentiometric titration and spectroscopic (EPR and visible) techniques.

EXPERIMENTAL

Materials

α-Alaha and β-Alaha were prepared via the methyl ester of the respective amino acid as described in Ref. 28. Dien was from Aldrich (Germany) used without further purification and its purity was greater than 99%. The fully protonated forms of the ligands are shown in Scheme 1.

The purity of the hydroxamic acids and diethylenetriamine and the exact concentrations of the stock solutions were determined by Gran's method [29]. Copper(II) chloride solution was purchased from Merck. For clarity, the charges of the complexes are omitted in the tables. It has to be mentioned, however, that the fully deprotonated forms of aminohydroxamic acids are L^- while the diethylenetriamine is L.

Potentiometric measurements

Protonation constants of the ligands and the stability constants of the binary and ternary complexes were determined by pH-metric titration of 5 cm^3 samples in water solutions in the pH range of 2–11. The stability constants of the complexes formed, together with derived equilibrium constants characteristic of

Table 1. Overall stability constants ($\log\beta$) and characteristic parameters for the stability of Cu^{2+} ternary complexes formed with diethylenetriamine (dien) and α-alaninehydroxamic acid/β-alaninehydroxamic acid (L) at 25°C and $I = 0.2$ mol dm^{-3} (KCl) in water solutions (the ion charges are omitted)

No.	dien + α-Alaha	dien + β-Alaha
1. $\log\beta$[Cu(dien)HL]	28.33(5)	28.77(3)
2. $\log\beta$[Cu(dien)L]	21.11(2)	19.99(2)
3. pK[Cu(dien)(HL)]	7.22	8.78
4. $\log K$[Cu(dien)HL]; [Cu(dien)] + $H_2L^+ \rightleftharpoons$ [Cu(dien)HL] + H^+	−4.22	−5.62
5. $\log K$[Cu(dien)L]; [Cu(dien)] + L ⇌ [Cu(dien)L]	5.10	3.98
6. $\log K$[Cu(dien)L] − ΣpK^H	−11.44	−14.40
7. $\Delta\log K$	−5.75	−8.91
8. $\log\beta^{stat}$	20.74	—
9. $\Delta\log\beta$	0.37	—
10. $\log X$	1.35	—

some stepwise processes of complex formation, are listed in Table 1.

The data for the Cu^{2+}-α-Alaha and Cu^{2+}-β-Alaha binary systems can be found in the our early papers [30–32], but for the sake of comparison these data are included in Table 2. Data for Cu^{2+}-dien binary system can be found in the literature [33], but we had to determine the stability constants under identical conditions to those of ternary systems, i.e. at 298 K and ionic strength of 0.2 mol dm^{-3} (KCl). Refined values (Table 2) are in good agreement with the literature data, after allowing for changes in experimental conditions and calculation methods [33,34]. For the binary system 1 : 1, 1 : 2 and 1 : 4 metal to ligand ratios were used. The concentration of the ligand in the experimental solution was $4 \cdot 10^{-3}$ mol dm^{-3}. For the determination of the stability constants of the mixed ligand complexes the metal(II) concentration in samples were $2 \cdot 10^{-3}$ mol dm^{-3} and $4 \cdot 10^{-3}$ mol dm^{-3} and concentration ratios of metal : dien : α-Alaha/β-Alaha were 1 : 1 : 1, 1 : 1 : 2, 1 : 2 : 1, 1 : 2 : 2 and 1 : 1 : 4. All the pH-metric titrations were carried out with carbonate-free KOH solution of known concentration (ca 0.2 mol dm^{-3}). The pH-metric titrations were performed with a Radelkis OP-208/1 instrument equipped with a micro combination pH electrode (Mettler-Toledo, Type 2) using a ABU-80 titration unit (Radiometer). The electrodes system was calibrated by periodic titrations of an HCl solution ($5 \cdot 10^{-2}$ mol dm^{-3} KCl) against standard KOH solution. Titration EMF data were used to calculate the hydrogen ion concentration, $[H^+]$. Stability constants $\beta_{pqrs} = [M_p(dien)_qL_rH_s]/[M]^p[dien]^q[L]^r[H]^s$ were calculated with the aid of the SUPERQUAD computer program [35]. The reported standard deviations were calculated by assuming random errors.

Spectroscopic studies

The absorption spectra were recorded on a Beckman DU650 spectrophotometer at room temperature. The EPR spectra were performed using a Bruker 300E X-band spectrometer at 77 K in water/ethyleneglycol (80 : 20 v/v) solution. The spectra were analysed by computer simulation program [36] based on resonance fields calculated according to method of Sakaguchi *et al.* [37]. The concentrations were the same as

Table 2. Overall stability constants ($\log\beta$) and stepwise formation constants ($\log K$) for H^+ and Cu^{2+} complexes formed with diethylenetriamine (dien) and α-alaninehydroxamic acid/β-alaninehydroxamic acid (L) in binary systems at 25°C and I = 0.2 mol dm^{-3} (KCl) in water solutions (the ion charges are omitted)

diethylenetriamine		α-alaninehydroxamic acid	
$\log\beta$[Hdien]	9.97(1)	$\log\beta$[HL]	9.20(0)
$\log\beta$[H_2dien]	19.05(1)	$\log\beta$[H_2L]	16.54(1)
$\log\beta$[H_3dien]	23.40(1)	pK_1^{micro}(NH_3^+)	7.48(2)[a]
pK_1(NH_2^+)	4.35	pK_2^{micro}(CONHOH)	7.90(3)[a]
pK_2(NH_3^+)	9.08		
pK_3(NH_3^+)	9.97	$\log\beta$[CuL]	10.85(1)
		$\log\beta$[$Cu_2L_2H_{-1}$]	20.85(2)
$\log\beta$[Cu(dien)]	16.01(1)	$\log\beta$[CuL_2]	19.93(1)
$\log\beta$[Cu(dien)$_2$]	20.94(1)	$\log\beta$[CuL_2H_{-1}]	9.98(2)
$\log\beta$[(Cu(dien)$_2$H]	29.36(3)		
$\log\beta$[Cu(dien)H_{-1}]	6.99(3)	$\log K$[CuL]	10.85
		$\log K$[CuL_2]	9.10
		[CuL] + L ⇌ [CuL_2]	
$\log K$[Cu(dien)]	16.01	pK[CuL_2]	9.95
		$\log(K_{CuL}/K_{CuL_2})$	1.73
$\log K$[Cu(dien)$_2$]	4.93		
[Cu(dien)] + dien ⇌ [Cu(dien)$_2$]			
		β-alaninehydroxamic acid	
$\log K$[Cu(dien)$_2$H]	3.38	$\log\beta$[HL]	9.89(1)
[Cu(dien)] + Hdien ⇌ [Cu(dien)$_2$H]		$\log\beta$[H_2L]	18.38(1)
$\log K$[Cu(dien)H_{-1}]	−9.02	pK_1^{micro}(NH_3^+)	8.85(2)[a]
[Cu(dien)(H_2O)] ⇌ [Cu(dien)(OH)] + H^+		pK_2^{micro}(CONHOH)	8.47(2)[a]
pK[Cu(dien)]	9.02		
pK[Cu(dien)(Hdien)]	8.42	$\log\beta$[CuL]	12.85(3)[b]
$\log(K_{Cu(dien)}/K_{Cu(dien)_2})$	11.08	$\log\beta$[$Cu_5L_4H_{-4}$]	46.66(7)[b]

[a] Ref. 38, (temp. 25°C, I = 0.2).
[b] Ref. 30, (temp. 25°C, I = 0.2).

used in the potentiometric titrations (the metal ion concentration was $4 \cdot 10^{-3}$ mol dm^{-3} and metal to ligands molar ratio were 1 : 1 : 2 for Cu^{2+}-dien-α-Alaha system and 1 : 1 : 4 for Cu^{2+}-dien-β-Alaha system).

RESULTS AND DISCUSSION

The fully protonated form (Scheme 1) of the dien can release three protons in the whole pH range, i.e. one from the NH_2^+ group and two from the NH_3^+ amino groups. The dissociation processes of the two ammonium groups overlap one another, and thus the two higher *pK* values given in Table 2 cannot be ascribed unambiguously. This means that the dissociation constants calculated from the pH-metric data are macroconstants. In this case the dissociation microconstants are not available up to now but this is beyond the scope of the present work.

The dissociation constants found for the fully protonated form of the α-Alaha and β-Alaha in this work are macroconstants. For these ligands both macro- and microconstants are available [38].

Titration

Binary systems. The constants determined by us for the binary Cu^{2+}-dien system agree well with the earlier results [33]. The low stability of $[Cu(dien)_2]^{2+}$ compared with that of $[Cu(dien)]^{2+}$ (Table 2) reflects the fact that only one of the four equatorial coordination positions at Cu^{2+} remains available for the coordination of the second dien and that the expected coordination tendency of the apical positions is low. Formation of $[Cu(dien)_2]^{2+}$ from $[Cu(dien)]^{2+}$ is reflected also by EPR parameters between pH 5.3 and 10 (Table 3). These parameters suggest of 3N,O donor set around Cu^{2+} plane for the latter complex. The apparent decrease in $g_\parallel$ and increase in $A_\parallel$ values confirms that an additional nitrogen atom is involved 4N in-plane coordination in $[Cu(dien)_2]^{2+}$. The change of the parameters is smaller than that expected for the complexes where four nitrogen atoms form strictly planar environment around Cu^{2+} (as in Cu^{2+} complexes with dioxocyclam characterized by $A_\parallel = 215 \cdot 10^{-4}$ cm^{-1} $g_\parallel = 2.171$) [39].

Ternary systems. In spite of the large amount of data which have been collected for mixed chelate systems, it is often not possible to discuss the results

Table 3. EPR parameters of the ternary Cu-dien-β-Alaha and binary Cu-dien and Cu-β-Alaha systems

Systems	pH	g_z	g_x	g_y	A_z	A_x	A_y
Cu-dien-β-Alaha	2.3	2.420[a]	2.085[a]	2.085[a]	130[a]	10[a]	10[a]
		(2.340)	(2.080)	(2.080)	(158)	(10)	(10)
Cu-dien-β-Alaha	3.3	(2.342)	(2.080)	(2.080)	(160)	(10)	(10)
		2.234	2.050	2.050	190	21	21
Cu-dien-β-Alaha	4.9	2.237	2.050	2.050	190	21	21
Cu-dien-β-Alaha	6.0	2.243	2.050	2.050	185	18	18
Cu-dien-β-Alaha	7.1	2.242	2.052	2.052	184	18	18
			$g_{iso} = 2.117$			$A_{iso} = 73$	
Cu-dien-β-Alaha	8.4	2.244	2.050	2.050	183	18	18
		2.212	2.050	2.050	194	14	14
Cu-dien-β-Alaha	9.2	(2.244)	(2.053)	(2.053)	(183)	(18)	(18)
		2.212	2.050	2.050	194	14	14
Cu-dien-β-Alaha	10.3	2.212	2.049	2.049	194	18	18
			$g_{iso} = 2.117$			$A_{iso} = 66$	
Cu-dien	2.9	2.420[a]	2.085[a]	2.085[a]	130[a]	10[a]	10
		(2.234)	(2.055)	(2.055)	(192)	(10)	(10)
Cu-dien	5.3	2.234	2.050	2.050	190	21	21
Cu-dien	7.9	(2.234)	(2.050)	(2.050)	(190)	(21)	(21)
		2.214	2.053	2.053	186	14	14
Cu-dien	9.4	2.215	2.048	2.048	185	10	10
Cu-β-Alaha	3.7	2.420[a]	2.085[a]	2.085[a]	130[a]	10[a]	10[a]
		(2.340)	(2.080)	(2.080)	(159)	(10)	(10)

The anisotropic and isotropic parameters are estimated on the basis of computer simulation of the experimental spectra measured at 77 K and 295 K, respectively.

Parameters *A* are given in [10^{-4} cm^{-1}].

The parameters in the parentheses corresponds to the species existing in an apparently smaller contribution.

[a] The parameters relevant to Cu_{aq}^{2+}.

very deeply, because a number of parameters such as kind and ionic charge of donor atoms, density, configuration of metal ions and ligands etc. are involved. Also, the discussion of mixed species has to be based on experimentally determined values of stability constants and intensive factors, all of which have been calculated with due allowance for the contribution of simple species [1]. The general four-component equilibria can be written as:

$$pM + q(\text{dien}) + r(L) + sH \rightleftharpoons M_p(\text{dien})_q(L)_rH_s$$

where p, q, r and s are the stoichiometric coefficients corresponding to the metal ion, M, dien, L (L = α-Alaha or β-Alaha), and H, respectively; charges are omitted for simplicity. The overall formation constants are defined as:

$$\beta_{pqrs} = [M_p(\text{dien})_q(L)_rH_s]/[M]^p[(\text{dien})]^q[(L)]^r[H]^s$$

The β_{pqrs} constant expresses the stability of the [Cu(dien)L]$^+$ ternary species but does not represent directly the binding strength between the L and copper(II) ions. The equilibrium constant, $K_{Cu(dien)L}$, evaluated from the computed values of the related β_{pqrs} values according to equation: $\log K_{Cu(dien)L} = \log\beta_{Cu(dien)L} - \log\beta_{Cu(dien)}$, shows how tightly L (aminohydroxamic anion) is bound to the binary [Cu(dien)]$^{2+}$ complex. Thus, the binding strength of α-Alaha or β-Alaha in the ternary complexes depends on the stability of the binary complex [Cu(dien)]$^{2+}$; in other words, it depends mainly on the basicity of the coligand (dien).

Different methods are known for the estimation of the formation of mixed ligand complexes [1]. In this respect, Sigel's $\log X_{MAB}$ value (the constant due to the equilibrium $[MA_2] + [MB_2] \rightleftharpoons 2[MAB]$) cannot be calculated for the Cu^{2+}-dien-β-Alaha ternary species, since the complex with 1 : 2 ratio is not formed in the Cu^{2+}-β-Alaha binary system (see Table 2). For the Cu^{2+}-dien-α-Alaha system the $\log X_{Cu(dien)(\alpha\text{-Alaha})}$ value (1.35) is larger than that expected on a statistical basis (0.6), which means that the formation of mixed complexes is favoured in this system (Table 1).

Since statistical effects are important for mixed ligand complex stabilization, we have calculated statistical stability constants:

$$\log\beta_{MAB}^{stat.} = \log 2 + \frac{1}{2}(\log\beta_{MA_2} + \log\beta_{MB_2})$$

$\Delta\log\beta_{MAB}$ value given by the following equation:

$$\Delta\log\beta_{MAB} = \log\beta_{MAB}^{calc.} - \log\beta_{MAB}^{stat.}$$

is a measure of additional influences, other than the statistical one, of ligands on the stability of mixed complexes. Positive $\Delta\log\beta_{Cu(dien)(\alpha\text{-Alaha})}$ value (0.37) exhibits higher stability for the 1 : 1 : 1 : 0 mixed ligand species compared to binary ones. It is interesting to compare the stability of the binary complex $M + B \rightleftharpoons [MB]$ with that of the ternary one $[MA] + B \rightleftharpoons [MAB]$. The difference between the stabilities of those complexes, $\Delta\log K$, given by expression

$$\Delta\log K = \log K_{MAB}^{MA} - \log K_{MB}^{M} = \log K_{MBA}^{MB} - \log K_{MA}^{M}$$

is a way to characterize the tendency to form ternary complex. This relation may be expressed in other terms by

$$\Delta\log K = \log\beta_{MAB} - (\log\beta_{MA} + \log\beta_{MB})$$

The $\Delta\log K$ parameter expresses, as is well known, the effect of the bonded primary ligand (dien) towards an incoming secondary ligand (α-Alaha or β-Alaha anion). Since the aminohydroxamic acid coordinates more easily with the free Cu^{2+} ion than with the complexed metal ion, [Cu(dien)]$^{2+}$, $\Delta\log K$ should be negative. It can be seen, by viewing the $\Delta\log K$ values for different systems, that values of this factor for the Cu^{2+}-dien-α-Alaha and Cu^{2+}-dien-β-Alaha systems are very low (−5.75 and −8.91, respectively). This effect of the ternary complex is due to Cu^{2+} lower (than six) coordination number [40].

Cu^{2+}-dien-α-Alaha system. In the Cu^{2+}-dien-α-Alaha system, the titration data fit satisfactorily to the assumption of the presence of the binary ([Cu(dien)]$^+$, [Cu(α-Alaha)$_2$], [Cu(dien)(H-dien)]$^{3+}$, [Cu(dien)$_2$]$^{2+}$, [Cu(α-Alaha)$_2$H$_{-1}$]$^-$) and the ternary [Cu(dien)(H-α-Alaha)]$^{2+}$ and [Cu(dien)(α-Alaha)]$^+$ complexes. The stability constants obtained for the complexes in the binary and ternary systems are given in Tables 1 and 2. Concentration distribution curves are presented in Fig. 1.

The Cu^{2+}-dien 1 : 1 and 1 : 2 complexes are formed at high concentrations at copper(II) : dien : α-Alaha ratio of 1 : 2 : 2. Under these conditions the ternary complexes are of ca 30% of the total copper content, but at 1 : 1 : 2 ratio the ternary complex reaches of ca 60% (Fig. 1(c)). The latter system was studied in the vis spectroscopy (see below). Additionally, Fig. 1(c) shows that the presence of dien supresses the formation of dimeric [Cu$_2$(α-Alaha)$_2$H$_{-1}$]$^+$ species in the ternary system.

The calculated concentrations of these eight copper(II) complex species, as a function of pH, Cu^{2+}-dien-α-Alaha 1 : 1 : 2 ratio system (shown in Fig. 1(c)) indicate that under these conditions the [Cu(dien)]$^{2+}$ species is present in ca 95%. The next complex, [Cu(α-Alaha)$_2$], observed from 4 to 11 pH range, reaches a maximum concentration (70%) at pH 7.4. The [Cu(dien)(H-dien)]$^{3+}$ complex, from pH 7 to 9, is a minor species (ca 2%), so it can be regarded as negligible. The first ternary species, [Cu(dien)(H-α-Alaha)]$^{2+}$, is seen above pH 4 whereas above pH 6.5 [Cu(dien)(α-Alaha)]$^+$ appears and reaches maximum concentration of ca 60% at pH 9.6. At higher pH the [Cu(α-Alaha)$_2$H$_{-1}$]$^-$ and [Cu(dien)$_2$]$^{2+}$ species become also important. The deprotonation process of [Cu(dien)(H-α-Alaha)]$^{2+}$ leading to the formation of [Cu(dien)(α-Alaha)]$^+$ above pH 7 corresponds to the liberation of the proton from the —NH$_3^+$ group,

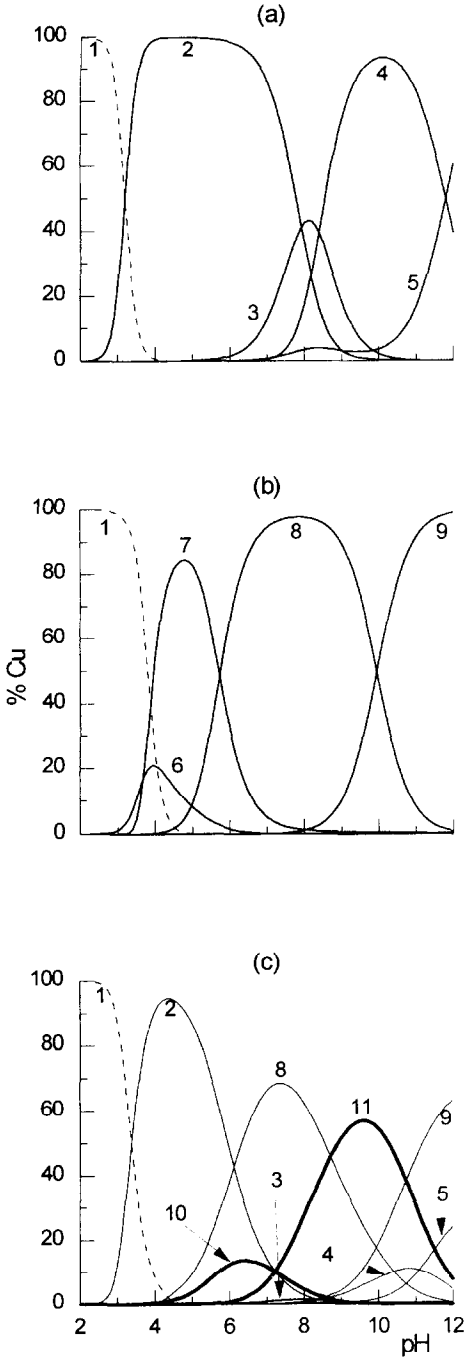

Fig. 1. Species distribution patterns for Cu^{2+} complexes of dien (a) and α-Alaha (b) at 1 : 2 ratio, and dien-α-Alaha (c) at 1 : 1 : 2 ratio; $c_{Cu^{2+}} = 4 \cdot 10^{-3}$ mol dm^{-3}: **1**-Cu^{2+}, **2**-$[Cu(dien)]^{2+}$, **3**-$[Cu(dien)_2H]^{3+}$, **4**-$[Cu(dien)_2]^{2+}$, **5**-$[Cu(dien)H_{-1}]^{+}$, **6**-$[Cu(\alpha\text{-Alaha})]^{+}$, **7**-$[Cu_2(\alpha\text{-Alaha})_2H_{-1}]^{+}$, **8**-$[Cu(\alpha\text{-Alaha})_2]$, **9**-$[Cu(\alpha\text{-Alaha})_2H_{-1}]^{-}$, **10**-$[Cu(dien)(H\text{-}\alpha\text{-Alaha})]^{2+}$, **11**-$[Cu(dien)(\alpha\text{-Alaha})]^{+}$.

which is hardly likely, since the $pK_{Cu(dien)(H\text{-}\alpha\text{-}Alaha)}$ value equal to 7.22 (Table 1 no. 3) is characteristic for the $pK^{micro}_{\alpha\text{-}Alaha}(NH_3^+)$ microconstant. The same effect is observed in the Cu^{2+}-dien-β-Alaha system above pH 8.5; $pK_{Cu(dien)(H\text{-}\beta\text{-}Alaha)} = 8.78$ is characteristic for the $pK^{micro}_{\beta\text{-}Alaha}(NH_3^+)$ microconstant (see Table 2). Taking into account these protonation constants, hydroxamate type (*O*,*O*) coordination of H-α-Alaha and H-β-Alaha ligand can be supposed for the $[Cu(dien)(HL)]^{2+}$ species. The relatively rigid structure of a bound dien molecule enforces deviation of the complex geometry from tetragonal of $[Cu(dien)(H_2O)_3]^{2+}$ to a square pyramidal geometry of $[Cu(dien)(HL)]^{2+}$ as EPR spectra suggest (see below).

The protonated ternary species $[Cu(dien)(H\text{-}\alpha\text{-}Alaha)]^{2+}$ has a maximum concentration at pH 6.5. For the evaluation of the coordinating properties of $H\text{-}\alpha\text{-}Alaha^{+}$ towards $[Cu(dien)]^{2+}$ a comparison of the stabilities of $[Cu(dien)(H\text{-}\alpha\text{-}Alaha)]^{2+}$ and $[Cu(dien)(NH_3)]^{2+}$ is reasonable. This may be done by the corresponding equilibria. For the $Cu(dien)^{2+}$—H—NH_3 system

$$[Cu(dien)]^{2+} + H\text{—}NH_3^+ \rightleftharpoons [Cu(dien)(NH_3)]^{2+} + H^+$$

obtains $\log K_{Cu(dien)(H\text{-}NH3)} = -6.28$ [33]. For the Cu^{2+}-dien-H-α-Alaha system (equilibrium no. 4 in Table 1) $\log K_{Cu(dien)(H\text{-}\alpha\text{-}Alaha)} = -4.22$. It is evident that the coordination tendency of H-α-Alaha towards $[Cu(dien)]^{2+}$ is, by a factor of about 2.06, larger than that of ammonia giving a first hint for an additional apical interaction of H-α-Alaha in $[Cu(dien)(H\text{-}\alpha\text{-}Alaha)]^{2+}$.

Cu^{2+}-dien-β-Alaha system. In the Cu^{2+}-dien-β-Alaha system, the titration data fit satisfactorily to the assumption of the presence of the binary ($[Cu(dien)]^{2+}$, $[Cu(\beta\text{-Alaha})]^{+}$, $[Cu(dien)(H\text{-dien})]^{3+}$, $[Cu(dien)_2]^{2+}$, $[Cu(\beta\text{-Alaha})_2H_{-1}]^{-}$) and the ternary $[Cu(dien)(H\text{-}\beta\text{-Alaha})]^{2+}$ and $[Cu(dien)(\beta\text{-Alaha})]^{+}$ complexes. The stability constants obtained for the complexes in the binary and ternary systems are given in Tables 1 and 2. Concentration distribution curves are presented in Fig. 2.

The Cu^{2+}-dien 1 : 1 and 1 : 2 complexes are formed in high concentrations at copper(II) : dien : β-Alaha ratio of 1 : 2 : 2. Under these conditions the ternary complexes constitute of ca 30% of the total copper content, but at 1 : 1 : 4 ratio they reach of ca 65% (Fig. 2(c)). The latter system was studied in the vis and EPR spectroscopy (see below). Additionally, Figs 2(c) and 7 show that the presence of dien supresses the formation of the polymeric $[Cu_5(\beta\text{-Alaha})_4H_{-4}]^{2+}$ species in the ternary system.

The calculated concentrations of these seven copper(II) complex species, as a function of pH (shown in Fig. 2(c)) indicate that under these conditions the $[Cu(\beta\text{-Alaha})]^{+}$ species constitutes of ca 20%. The next complex, $[Cu(dien)]^{2+}$, observed from 3 to 8 pH range, reaches a maximum concentration (87%) at pH 5. The $[Cu(dien)(H\text{-dien})]^{3+}$ species, from pH 7 to 9, is a minor one (ca 2%), so it can be regarded as negligible. The first ternary species, $[Cu(dien)(H\text{-}\beta\text{-Alaha})]^{2+}$, is seen above pH 6. Above pH 8 $[Cu(dien)(\beta\text{-Alaha})]^{+}$ appears and reaches a

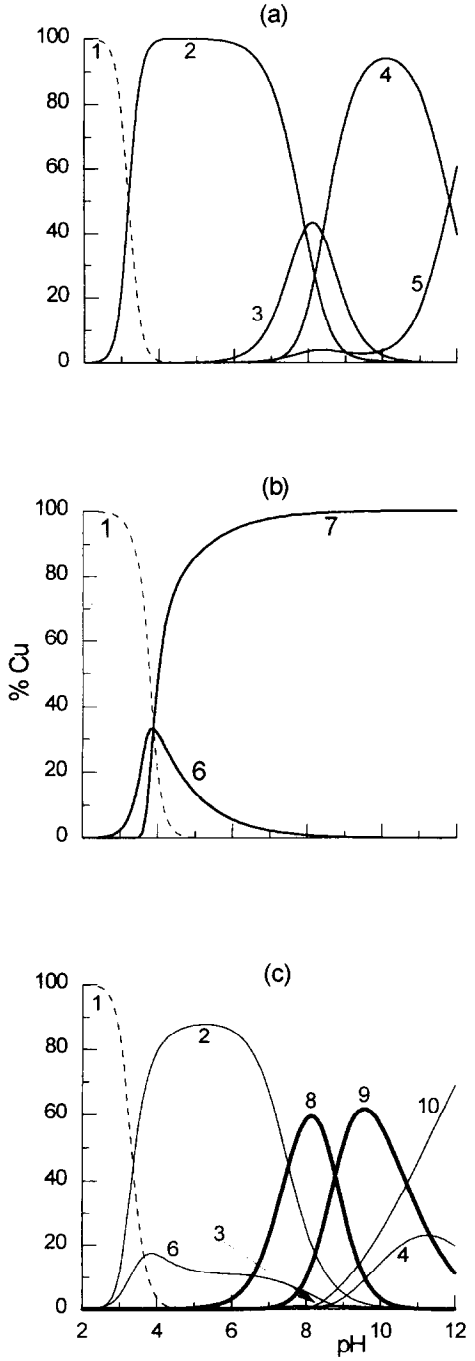

Fig. 2. Species distribution patterns for Cu^{2+} complexes of dien (a) and β-Alaha (b) at 1 : 2 ratio, and dien-β-Alaha (c) at 1 : 1 : 4 ratio; $c_{Cu^{2+}} = 4 \cdot 10^{-3}$ mol dm^{-3}: **1**-Cu^{2+}, **2**-$[Cu(dien)]^{2+}$, **3**-$[Cu(dien)_2H]^{3+}$, **4**-$[Cu(dien)_2]^{2+}$, **5**-$[Cu(dien)H_{-1}]^{+}$, **6**-$[Cu(\beta\text{-Alaha})]^{+}$, **7**-$[Cu_5(\beta\text{-Alaha})_4H_{-4}]^{2+}$, **8**-$[Cu(dien)(H\text{-}\beta\text{-Alaha})]^{2+}$, **9**-$[Cu(dien)(\beta\text{-Alaha})]^{+}$, **10**-$[Cu(\beta\text{-Alaha})_2H_{-1}]^{-}$.

maximum concentration of ca 60% at pH 9.5. Under these conditions at higher pH the $[Cu(\beta\text{-Alaha})_2H_{-1}]^{-}$ and $[Cu(dien)_2]^{2+}$ species become also important (Fig. 2(c)) as a consequence of the "disproportionation" of the ternary species, what can be shown by the following reaction:

$$2[Cu(dien)(\beta\text{-Alaha})]^{+} \rightleftharpoons [Cu(dien)_2]^{2+} + [Cu(\beta\text{-Alaha})_2H_{-1}]^{-} + H^{+}$$

The deprotonation process of the $[Cu(dien)(H\text{-}\beta\text{-Alaha})]^{2+}$ species leading to the formation of the $[Cu(dien)(\beta\text{-Alaha})]^{+}$ complex above pH 8.5 corresponds to the liberation of proton from the $-NH_3^+$ group. This species has a maximum concentration at pH 8. For the evaluation of the coordinating properties of H-β-$Alaha^{+}$ towards $[Cu(dien)]^{2+}$ a comparison of the stabilities of $[Cu(dien)(H\text{-}\beta\text{-Alaha})]^{2+}$ and $[Cu(dien)(NH_3)]^{2+}$ may be done (see above for Cu^{2+}-dien-α-Alaha system). For the Cu^{2+}-dien-β-Alaha system $\log K_{Cu(dien)(H\text{-}\beta\text{-Alaha})} = -5.62$ (Table 1), what means that the coordination tendency of H-β-$Alaha^{+}$ towards $[Cu(dien)]^{2+}$ is, by a factor of about 0.66, larger than that of ammonia.

α-Alaha is more effective chelating ligand than β-Alaha in the Cu^{2+}-dien-L ternary system. This is reflected in the much higher basicity-adjusted stability constants, $\log K_{Cu(dien)(\alpha\text{-Alaha})/(\beta\text{-Alaha})} - \Sigma pK^{H}$. These values are −11.44 and −14.40 for $[Cu(dien)(\alpha\text{-Alaha})]^{+}$ and $[Cu(dien)(\beta\text{-Alaha})]^{+}$, respectively (Table 1). It seems that basicity of the coordinating donor groups is over-compensated by chelating effect which is clearly seen in the case when (N_{amino}, N_{hydrox}) donor set (provided by L ligands) is involved in Cu^{2+} chelation. Thus, due to the preference of Cu^{2+} for five- rather than six-membered chelation [39], the complex with L = α-Alaha is found to be more stable.

Spectroscopy studies

Additional information on the structure of the binary and ternary complexes may be gained from their absorption spectral data. Even at the pH level where the distribution of the ternary $[Cu(dien)(\alpha\text{-Alaha})]^{+}$ species has a maximum, the binary: $[Cu(dien)]^{2+}$, $[Cu(\alpha\text{-Alaha})_2]$, $[Cu(dien)_2H]^{3+}$, $[Cu(dien)_2]^{2+}$, $[Cu(dien)H_{-1}]^{+}$ and $[Cu(\alpha\text{-Alaha})_2H_{-1}]^{-}$ complexes coexist in a greater or smaller extent, as can be seen in Fig. 1(c). Therefore, in the absorption spectra measured even at this pH level would be included the contributions from the binary species. The same problem exists in the Cu^{2+}-dien-β-Alaha system (Fig. 2(c)).

Figure 3 shows the pH-varied absorption spectra of the Cu^{2+}-dien-α-Alaha system (Fig. 3(a)) and Cu^{2+}-dien-β-Alaha one (Fig. 3(b)).

As the pH of the solution increases, the absorbance in the longer wavelength region is greatly enhanced. Such a spectral change, that is the red shift of *d-d* absorption band and the intensity rise, indicates the structural change around the copper(II) ion (from a

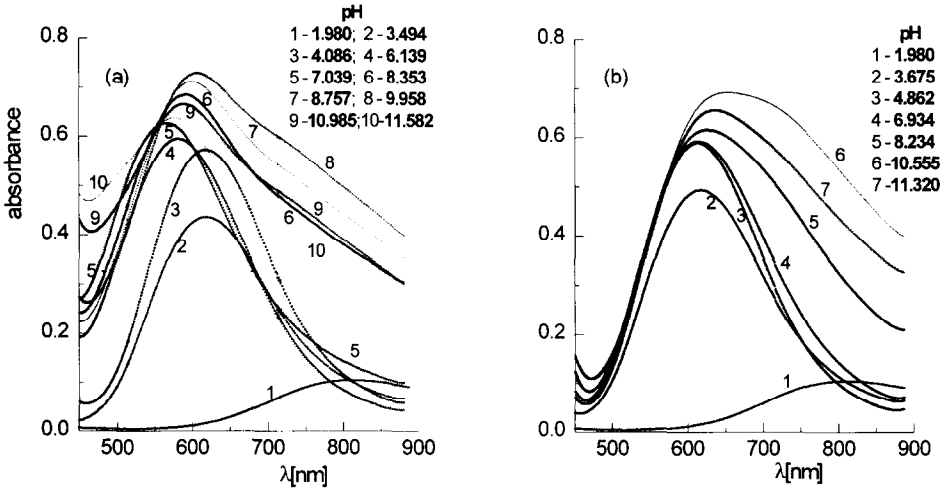

Fig. 3. pH-varied absorption spectra of Cu^{2+}-dien-α-Alaha system at 1 : 1 : 2 ratio (a) and Cu^{2+}-dien-β-Alaha system at 1 : 1 : 4 ratio (b); $c_{Cu^{2+}} = 4 \cdot 10^{-3}$ mol dm^{-3}.

square-planar or tetragonal to a type five-coordination geometry, as is well known) [9,41]. This fact suggests transition from a six to a five-coordination geometry while going from the binary to ternary species.

To extract the net ligand-field absorption band of each ternary species, the spectrum measured at a pH value where each mixed-ligand species exhibits maximal contribution was resolved into the components corresponding to the individual species existing at that pH (as described in Ref. 10). The dotted curves in Fig. 4 show the absorption spectra resolved in this way for the ternary systems.

The molecular absorptivity for the mixed-ligand species was then calculated taking into account their distribution. The distribution-corrected curves are shown in Fig. 5.

The absorption curve for the [Cu(dien)(H-β-Alaha)]$^{2+}$ species (Fig. 5) exhibits a maximum at about 611 nm with ε (molar absorptivity) ~76, a value which almost coincides with that of [Cu(dien)$(H_2O)_3$]$^{2+}$ ($\lambda_{max} = 614$ nm, $\varepsilon = 78$). Titration experiments predict that the amino group of β-Alaha should be protonated in this system. On the other hand, this result is consistent with the expectation of much smaller energy shift upon involvement of oxy-

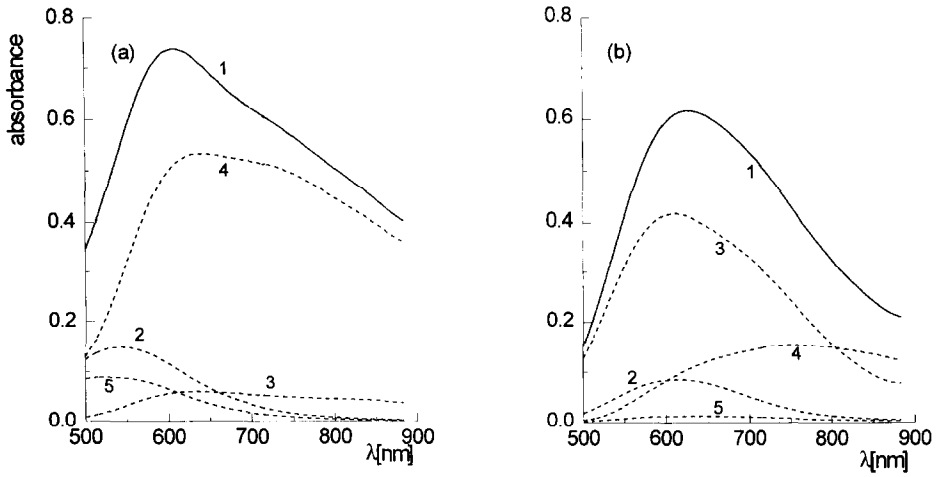

Fig. 4. Species resolutions of the observed spectra of Cu^{2+}-dien-α-Alaha system at pH 9.70 (a) (species and distribution percentages: **2**-[Cu(α-Alaha)$_2$] −22.38%; **3**-[Cu(dien)$_2$]$^{2+}$ −7.00%; **4**-[Cu(dien)(α-Alaha)]$^+$ −56.79%; **5**-[Cu(α-Alaha)$_2$ H_{-1}]$^-$ −12.59%) and Cu^{2+}-dien-β-Alaha at pH 8.23 (b) (**2**-[Cu(dien)]$^{2+}$ −13.79%; **3**-[Cu(dien)(H-β-Alaha)]$^{2+}$ −68.38%; **4**-[Cu(dien)(β-Alaha)]$^+$ −12.73%; **5**-[Cu(β-Alaha)]$^+$ −3.36%).

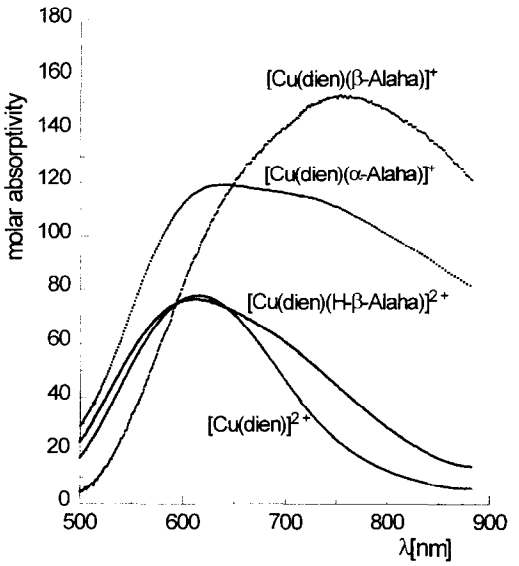

Fig. 5. Distribution-corrected absorption spectra for the $[Cu(dien)]^{2+}$, $[Cu(dien)\text{-}\alpha\text{-}Alaha]^{2+}$, $[Cu(dien)(H\text{-}\beta\text{-}Alaha)]^{2+}$ and $[Cu(dien)\text{-}\beta\text{-}Alaha]^{+}$ species.

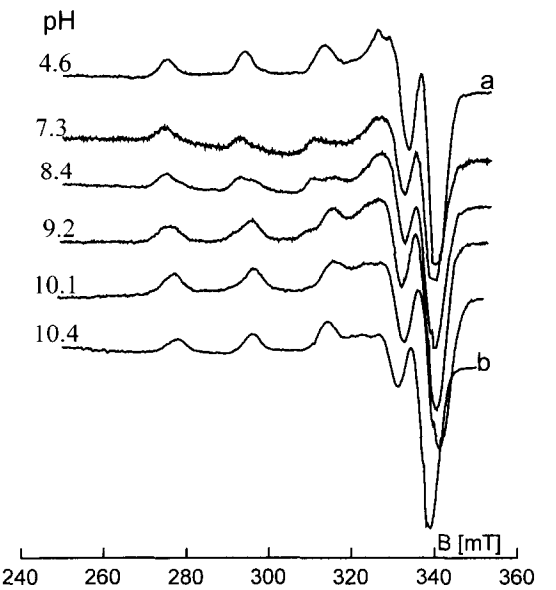

Fig. 7. EPR spectra of Cu^{2+} complexes formed in $Cu(dien)^{2+}$-β-Alaha system as a function of pH at 77 K; **a** and **b** spectra are observed for Cu^{2+}-dien system.

gen than nitrogen donor atom. Therefore, $[Cu(dien)(H\text{-}\beta\text{-}Alaha)]^{2+}$ is expected to have a square-based pyramidal geometry in which dien occupies three equatorial positions and the hydroxamic group forms (*O,O*) type chelate ring involving equatorial and apical positions.

Formation of the $[Cu(dien)(H\text{-}\beta\text{-}Alaha)]^{2+}$ complex is reflected by a distinct change in EPR spectra of mixed ligand Cu^{2+}-dien-β-Alaha system in comparison with those manifested by Cu^{2+}-dien and Cu^{2+}-β-Alaha systems separately, starting from pH 6 (Fig. 7). The variation of the $g_{\parallel}$ and $A_{\parallel}$ parameters is well known and widely used criterion for structural identification of the coordination sphere of Cu^{2+} ion provided by the polyfunctional ligands [31,39,42,43,]. The apparent increase of $g_{\parallel}$ and decrease of $A_{\parallel}$ values in comparison with those relevant to $[Cu(dien)]^{2+}$ should be assigned to the effect of electron donation of hydroxamate oxygen bound at an axial position (Table 3). This effect is pronounced in EPR parameters only when relatively small change occurs in equatorial coordination. It is observed when water at the fourth equatorial position in $[Cu(dien)]^{2+}$ is replaced by the oxygen atom of the hydroxamate group.

The absorption curves for the $[Cu(dien)(\alpha\text{-}Alaha)]^{+}$ and $[Cu(dien)(\beta\text{-}Alaha)]^{+}$ species which exhibit a peaks at 651 nm (119) (and shoulder at ~750 nm) and 755 nm (152), respectively, are drastically different from that for binary $[Cu(dien)]^{2+}$ species. This spectral behaviour reveals the structural transformation around the copper(II) ion strongly suggesting [9,41] the formation of a five-coordinate mixed-ligand complex. A comparison between the species distribution curves (Figs 1(c) and 2(c)) and

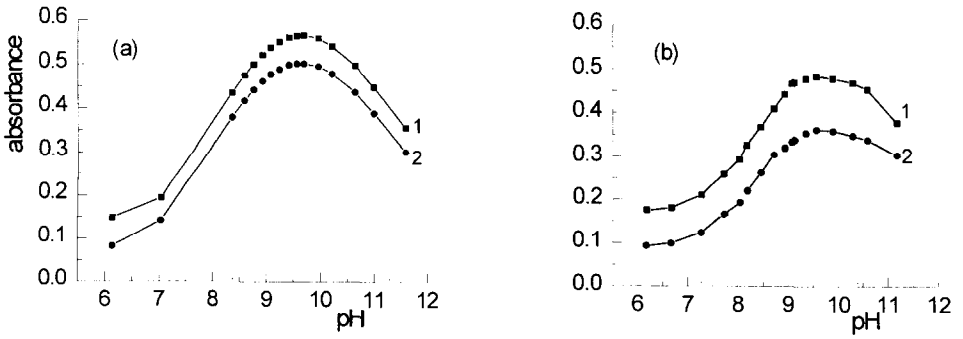

Fig. 6. Plots of absorbance vs pH for the pH-varied spectra of (a) Cu^{2+}-dien-α-Alaha system at 1 : 1 : 2 ratio (**1**—750 nm, **2**—800 nm) and (b) Cu^{2+}-dien-β-Alaha system at 1 : 1 : 4 ratio (**1**—755 nm, **2**—814 nm).

the pH-dependent curves of the absorption (Fig. 3(a) and (b)) clearly indicate that the spectral change shown in Fig. 6(a) and (b) is attributable to the formation and decay of the 1110 species.

EPR spectra allow to detect the formation process of the 1110 species within pH range 8.4–10. An equilibrium between the $[Cu(dien)(H\text{-}\beta\text{-}Alaha)]^{2+}$ and $[Cu(dien)(\beta\text{-}Alaha)]^{+}$ species, of increasing contribution, is demonstrated by Fig. 7.

Replacement oxygen by nitrogen atoms into copper(II) coordination sphere is characterized by substantial increase in $A_{\parallel}$ and decrease of $g_{\parallel}$ in comparison to the $[Cu(dien)(H\text{-}\beta\text{-}Alaha)]^{2+}$ ternary complex (Table 3). Thus, the EPR spectral data unambigously support the coordination of aminohydroxamic acid ligands through (N_{amino}, N_{hydrox}) donor set. The parameters do not reach the values expected for the complex with an exactly planar 4N coordination around copper(II) [39], in agreement with the suspection that electron donating nitrogen atom is coordinated along z axis. This is remarkable that isotropic hyperfine parameter A_{iso}, determined by the analysis of liquid solution EPR spectra is substantially smaller for the complex formed at pH about 10 than for that existing at pH 7. Because the g_{iso} parameters are almost identical, a decrease A_{iso} values is consistent with reduction in the Fermi contact term. This trend is usually treated as an indication of a stronger electron donation imposed by the donor atoms bound at an axial position. It seems to be probable that upon freezing this effect is partly diminished [44].

CONCLUSION

In the copper(II)-dien-α- (or β-) alaninehydroxamic acid system, the potentiometric, vis and EPR results strongly suggest the formation of five-coordination ternary 1111 and 1110 species. A comparison of the absorption spectra with the results of EPR method shows that formation of the (*O*,*O*) hydroxamate chelate occurs at a lower pH (for $[Cu(dien)(HL)]^{2+}$ species) and (N_{amino}, N_{hydrox}) chelate occurs at a higher pH (for $[Cu(dien)L]^{+}$ species).

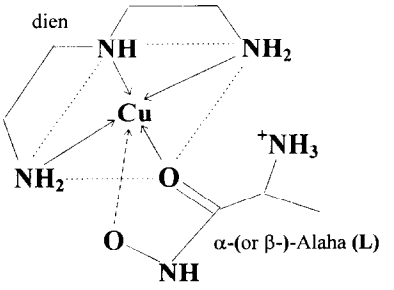

$[Cu(dien)HL]^{2+}$

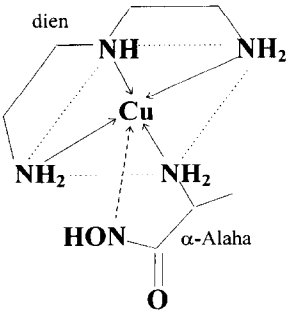

$[Cu(dien)L]^{+}$

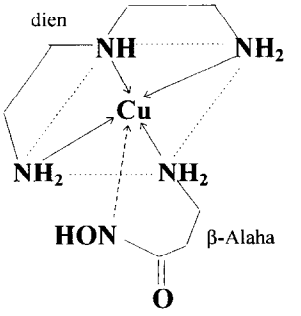

$[Cu(dien)L]^{+}$

Scheme 2.

Acknowledgments—The authors gratefully thank Dr Andre Ozarowski of the University of California (ozarowsk@indigo.ucdavis.edu) for allowing use of his simulation program for EPR spectra. This work was supported by the Polish State Committee for Scientific Research (project KBN, 3/T09A/021/13).

REFERENCES

1. Sigel, H., in *Metal Ions in Biological Systems*, Vol. 2. Marcel Dekker, Inc., New York, 1973.
2. Sigel, H., Fischer, B. E. and Prijs, B., *J. Am. Chem. Soc.*, 1977, **99,** 4489.
3. Bastian, M., Cheng, D., Gregan, F., Liang, G. and Sigel, H., *Z. Naturforsh.*, 1993, **48b,** 1279.
4. Zhang, F. and Liu, Q. T., *J. Coord. Chem.*, 1993, **28,** 197.
5. Sigel, H. and McCormick, D., *Accout. Chem. Res.*, 1970, **3,** 201.
6. Hanaki, A. and Yokoi, H., *Inorg. Chim. Acta*, 1986, **123,** L7.
7. Odani, A., Masuda, H., Inukai, K. and Yamauchi, O., *J. Am. Chem. Soc.*, 1992, **114,** 6294.
8. Bastian, M., Chen, D., Gregan, F., Liang, G. and Sigel, H., *Z. Naturforsch.*, 1993, **48B,** 1279.
9. Sugimori, T., Shibakawa, K., Masuda, H., Odani, A. and Yamauchi, O., *Inorg. Chem.*, 1993, **32,** 4951.
10. Murakami, T., Murata, K. and Ishikawa, Y., *Inorg. Chim. Acta*, 1996, **244,** 51.
11. Kaim, W. and Rall, J., *Angew. Chem., Int. Ed. Engl.*, 1996, **35,** 43.
12. Kaim, W. and Schwederski, B., *Bioinorganic Chemistry: Inorganic Elements in the Chemistry of Life*. Wiley, Chichester, 1994.
13. Laurie, S. H. and Sarkar, B., *J. Chem. Soc., Dalton Trans.*, 1977, 1822.
14. Potkonjak, D. and Pasic, J., *Jugosl. Physiol. Pharmacol. Acta*, 1983, **19,** 170.
15. Tabor, C. W. and Tabor, H., *Ann. Rev. Biochem.*, 1984, **53,** 749.
16. Kehl, H., ed. *Chemistry and Biology of Hydroxamic Acids*. Karger, New York, 1982.
17. Neilands, B., *Struct. Bond., (Berlin)*, 1966, **1,** 59.
18. Maehr, H., *Pure Appl. Chem.*, 1971, **28,** 603.
19. Jackson, W. P., Islip, P. J., Kneem, G., Pugh, A. and Wates, P. J., *J. Med. Chem.*, 1988, **31,** 500 and references therein.
20. Farkas, E. and Buglyó, P., *Magyar Kem. Foly.*, 1990, **96,** 192.
21. Farkas, E. and Kurzak, B., *J. Coord. Chem.*, 1990, **22,** 145.
22. Kurzak, B. and Kroczewska, D., *Transit. Metal Chem.*, 1993, **18,** 295.
23. Kurzak, B. and Kroczewska, D., *J. Coord. Chem.*, 1995, **34,** 67.
24. El-Ezaby, M. S., Marafie, H. M. and Abu-Soud, H. M., *Polyhedron*, 1986, **5,** 973.
25. El-Ezaby, M. S. and Hassan, M. M., *J. Inorg. Biochem.*, 1988, **34,** 241.
26. Shubaid, N. M. and El-Ezaby, M. S., *Polyhedron*, 1995, **14,** 1965.
27. Marafie, H. M., Shubaib, N. M., Ghodsian, R. and El-Ezaby, M. S., *J. Inorg. Biochem.*, 1988, **38,** 27.
28. Blatt, A. H., *Organic Synthesis Collection*, Vol. 2. Wiley, New York, 1943, p. 67.
29. Gran, G., *Acta Chim. Scand.*, 1950, **4,** 599.
30. Kurzak, B., Farkas, E., Głowiak, T. and Kozłowski, H., *J. Chem. Soc., Dalton Trans.*, 1991, 163.
31. Kurzak, B., Kurzak, K. and Jezierska, J., *Inorg. Chim. Acta*, 1986, **125,** 77.
32. Farkas, E., Szöke, J., Kiss, T., Kozłowski, H. and Bal, W., *J. Chem. Soc., Dalton Trans.*, 1989, 2247.
33. Gampp, H., Sigel, H. and Zuberbühler, A. D., *Inorg. Chem.*, 1982, **21,** 1190.
34. Hulanicki, A., Krawczyński, T. and Lewenstam, A., *Anal. Chim. Acta*, 1984, **158,** 343.
35. Gans, P., Sabatini, A. and Vacca, A., *J. Chem. Soc., Dalton Trans.*, 1985, 1195.
36. Ozarowski, A., unpublished program.
37. Sakaguchi, U., Arata, Y. and Fujiwara, S., *J. Magn. Res.*, 1973, **9,** 118.
38. Farkas, E., Kiss, T. and Kurzak, B., *J. Chem. Soc., Perkin Trans.* 2, 1990, 1255.
39. Sovago, I., Sanna, D., Dessi, A., Varnagy K. and Micera, G., *J. Inorg. Biochem.*, 1996, **63,** 99.
40. Ref. 1, pp. 105–107.
41. Duggan, M., Ray, N., Hathaway, B. J., Tomlinson, G., Brint, P. and Pelin, K., *J. Chem. Soc., Dalton Trans.*, 1980, 1342.
42. Kurzak, B., Kozłowski, H. and Farkas, E., *Coord. Chem. Rev.*, 1992, **114,** 169.
43. Boduszek, B., Dyba, M., Jeżowska-Bojczuk, M., Kiss, T. and Kozłowski, H., *J. Chem. Soc., Dalton Trans*, 1997, 973.
44. Antholine, W. E., Riedy, G., Hyde, J. S., Basosi, R. and Petering, D. H., *J. Biomol. Struct. Dynam.*, 1984, **2,** 469.

Pergamon

PII: S0277-5387(97)00521-4

Polyhedron Vol. 17, Nos. 11–12, pp. 1843–1850, 1998
© 1998 Elsevier Science Ltd
All rights reserved. Printed in Great Britain
0277-5387/98 $19.00+0.00

Synthesis and crystal structure of the 1-dimensional dihalide-bridged polymers: dichlorobis(thiazole)iron(II) and dibromobis(thiazole)copper(II)

Michael James,* Hiroyuki Kawaguchi and Kazuyuki Tatsumi

Department of Chemistry, Faculty of Science, Nagoya University, Furo-cho, Chikusa-ku, Nagoya 464-01, Japan

(Received 7 November 1997; accepted 11 December 1997)

Abstract—The new polymeric compound $Fe(thiazole)_2Cl_2$ (**1**) has been synthesised by the addition of thiazole to an ethanolic solution of anhydrous $FeCl_2$. The structure of $Cu(tz)_2Br_2$ (**2**) has also been determined. The structures of both polymers consist of pseudo-octahedral units, doubly linked by halide-bridges to form infinite linear chains. Slight variation in the bonding of the two are observed, relating to the Jahn-Teller nature of Cu^{2+}. Room temperature magnetic susceptibility measurements of **1** give an effective moment of 5.51(2) B.M., indicating high-spin Fe(II). © 1998 Elsevier Science Ltd. All rights reserved

Keywords: dichlorobis(thiazole)iron(II); dibromobis(thiazole)copper(II).

Polymeric systems of Cu and Co containing thiazole (tz) and di-bridging chloro ligands have been known for some time; however, only the structure of dichlorobis(thiazole)copper(II) has previously been reported [1]. Prior studies of the reaction between thiazole and iron(II) chloride have indicated an analogous compound is formed [2], however thus far no structural data have been reported. This paper details the synthesis and structural characterisation of the iron analogue $Fe(tz)_2Cl_2$ (**1**) by single crystal techniques, as well as the structural characterisation of the previously prepared $Cu(tz)_2Br_2$ (**2**). Room temperature magnetic properties of **1** are presented.

EXPERIMENTAL

Anhydrous $CuBr_2$ (99% purity), anhydrous $FeCl_2$ (98% purity) and thiazole (99% purity) were obtained from Aldrich Chemical Co. Inc. and used as obtained. Ethanol and methylene chloride (A.R. grade) were used when freshly distilled. The synthesis of **1** was carried out under dry Ar using Schlenk techniques, while **2** was prepared in air. Elemental analyses were carried out on a LECO CHNS-900 elemental analyser. Infrared spectra were recorded (Nujol mull) in the 350–5200 cm^{-1} range on a Perkin–Elmer FT-IR 2000 spectrophotometer. Magnetic susceptibility measurements were carried out at room temperature using a Sherwood Scientific Gouy balance.

$Fe(tz)_2Cl$ (1)

Thiazole (12 mmol, 2 ml) was added to an ethanolic solution of anhydrous $FeCl_2$ (6 mmol, 16 ml) with constant stirring. A pale yellow precipitate was immediately formed. The sample was stirred for a further 10 min before being centrifuged. The supernatant was reduced to ~10 ml under vacuum and stored in a sealed vessel under dry Ar. Yellow crystals suitable for X-ray diffraction were obtained after 8 weeks. The microcrystalline precipitate was washed with benzene and diethyl ether. Found: C, 24.6; H, 2.0; N, 9.4; S, 21.6%. Calcd for **1**: C, 24.7; H, 2.0; N, 9.1; S, 21.2%. IR (nujol): ν(ligand) 608 (m), 737 (m), 808 (m), 879 (w), 912 (w), 1060 (w), 1112 (w), 1231 (w) cm^{-1}.

*Author to whom correspondence should be addressed: Neutron Scattering Group, ANSTO, Lucas Heights Research Laboratories, PMB 1, Menai NSW 2234, Australia. Fax: 612-9717 3606. E-mail: mja@ansto.gov.au

$Cu(tz)_2Br_2$ (**2**)

Thiazole (12 mmol, 2 ml) was added to an ethanolic solution of anhydrous $CuBr_2$ (6 mmol, 16 ml) with constant stirring. A green precipitate was immediately formed. The sample was stirred for 20 min, collected, washed with ether and benzene and allowed to dry under suction. The product was recrystallised from dimethylformanide by addition of an equal volume of methylene chloride followed by cooling in the freezer compartment of a refrigerator. Dark green needle-like crystals suitable for X-ray diffraction were obtained after 3 weeks. Found: C, 18.5; H, 1.6; N, 6.9; S, 16.6%. Calcd for **2**: C, 18.3; H, 1.5; N, 7.1; S, 16.3%. IR (Nujol): ν(ligand) 612 (s), 635 (w), 738 (s), 810 (s), 882 (m), 920 (m), 1065 (m), 1113 (m), 1237 (m) cm^{-1}.

X-ray crystallography

Measurements were made on a Rigaku AFC7R diffractometer an ambient temperature using monochromated Mo-K_α radiation ($\lambda = 0.71069$ Å). Crystals were mounted on the top of glass fibers. Cell constants were obtained by least-squares analysis of 16 strong reflections in the range $5.53° < 2\theta < 14.33°$ for **1**, and 25 reflections ($29.35° < 2\theta < 29.79°$) for **2**. Details of crystal data, data collection and structure refinement for **1** and **2** are summarised in Table 1. The intensity data were corrected for Lorentz and polarisation effects and an empirical absorption correction based on azimuthal scans of several reflections was also applied.

The structures were solved by direct methods and developed by alternating cycles of difference Fourier syntheses and full matrix least-squares refinements. The positions of the non-hydrogen atoms were determined unequivocally, with the exception of the thiazole ligands in **1**, which displayed static disorder between adjacent carbon and sulfur sites, due to a 180° rotation about its Fe—N bonds. In this case the disorder was modeled by refinement of jointly occupied S/C sites. The minority components of these jointly occupied sites are indicated by a primed label, such that the site S/C′ contains a majority of sulfur, while the adjacent C/S′ site is constrained so as to give an equal proportion of carbon. The occupation factors of sulfur atoms were refined only at the S/C′ sites, while the C′ and S′ occupation factors were constrained so as to give fully occupied sites. The non-hydrogen atoms were refined anisotropically, with the exception of the atoms at the disordered sites which were refined isotropically. Hydrogen atoms were placed at calculated positions. Neutral atom scattering factors were taken from [3], and anomalous dispersion corrections were taken from [4]. Crystallographic calculations were carried ut with a teXsan crystallographic software package of Molecular Structure Corporation (1985 & 1992).

RESULTS AND DISCUSSION

The chemical reactivity of iron(II) chloride with thiazole does not appear to be substantially different

Table 1. Summary of crystallographic data for $Fe(tz)_2Cl_2$ (**1**) and $Cu(tz)_2Br_2$ (**2**)

	1	**2**
Formula	$C_6H_6N_2FeS_2Cl_2$	$C_6H_6N_2CuS_2Br_2$
Formula weight	297.012	393.614
Crystal system	Monoclinic	Monoclinic
Space group	*Cc* (No. 9)	$P2_1/c$ (No. 14)
a (Å)	17.908(9)	7.460(2)
b (Å)	3.717(5)	3.987(3)
c (Å)	14.870(8)	17.757(2)
β (°)	95.30(5)	92.15(1)
V(Å^3)	985(1)	527.8(3)
Z	4	2
Colour, Habit	Yellow, needle	Dark green, needle
D_c (g cm^{-3})	2.001	2.476
μ (Mo-K_α), cm^{-1}	24.42	100.10
$2\theta_{max}$, deg	55.0	55.0
No. of refins used $I > 3\sigma(I)$)	1005	1387
ρ_{max}/ρ_{min}, e Å^{-3}	0.47/−0.59	0.45/−1.09
R^a/R_w^b, %	3.2/4.8	2.9/3.6
GOF[c]	2.33	1.59

[a] $R = \Sigma\|\|F_o| - |F_c\|| / \Sigma|F_o|$.
[b] $R_w = [\Sigma w(|F_o| - |F_c|)^2 / \Sigma w|F_o|^2]^{1/2}$.
[c] $\text{GOF} = [\Sigma(|F_o| - |F_c|)^2 / \Sigma(N_{reflns} - N_{params})]^{1/2}$.

to that observed for copper(II) halides [1]. While compounds of M(II)-thiazole-halides (M = Co, Ni, Cu, Zn and Pd) have been known for some time [5,6], thiazole containing complexes of Fe(II) have only recently been reported [2,7].

Crystal structure of $Fe(tz)_2Cl_2$ (**1**)

The structure of $Fe(tz)_2Cl_2$ (**1**) consists of tetragonally elongated octahedral units, with *N*-donor thiazole ligands in the axial positions. These units are equatorially linked along the *b*-axis by double chloride bridges to form infinite linear chains (Fig. 1). The packing of these chains in the unit cell of **1** is shown in Fig. 2. Selected bond lengths and bond angles for **1** are given in Table 2.

Four distinct Fe—Cl bonds are formed in **1** with roughly equivalent bond lengths ranging between 2.521(2) Å and 2.560(2) Å, which bridge a Fe—Fe distance of 3.717(5) Å. Fe—N bond lengths of 2.196(6) Å (Fe—N1) and 2.150(7) Å (Fe—N2) are typical of those found for the Fe(II)—N bonds (2.21(1) Å) in the complex salt $[Fe(tz)_6][Fe_2OCl_6]$ [7]. The bond angles about Fe in **1** give rise to a pseudo-octahedrally coordinated centre that shows deviations away from regular angles (Table 2). Angles between equivalent chlorine atoms such as Cl1—Fe—Cl1* were found to be ~94°, while those between inequivalent chlorine atoms such as Cl1*—Fe—Cl2 were found to be ~86°. The axial N1—Fe—N2 bond angle (177.4(3)°) also shows a deviation away from regular symmetry.

Constrained refinement of occupation factors for the disordered thiazole ring (N2—C4—C5—S2—C6) revealed that the S2 and C5 sites (as shown in Figs 1 and 2) were approximately 87% occupied with the designated atoms. The C5′ and S2′ atoms that were generated by the 180° rotation about the Fe—N2 bond occupied the remaining 13% of these sites. Orientational static disorder of this type has been previously reported for *trans*-$Mo(tz)_3Br_3$ [23] and $Fe_2O(tz)_4Cl_4$ [2].

The dimensions of the non-disordered thiazole ligand in **1** are typical of those found in other metal thiazole complexes [1,2,7,23]. The axial thiazole ligands of **1** show rotations about their Fe—N bonds with respect to one another (Fig. 1). The thiazole rings N1—C1—C2—S1—C3 (i.e. those labeled A, B, D and F in Fig. 2) are rotated approximately 15° away from the *ac* plane, while the rings N2—C4—C5—S2—C6 (C, E, G and H) are rotated approximately 25° in the opposite direction. The sense of tilting of the thiazole rings in Fig. 2 is indicated such that atoms labeled "+" are positioned above the *ac* plane, while "−" atoms are positioned below.

The crystal structures of a number of polymeric iron(II) compounds have been documented. Of these, the majority are comprised of *O*- [8–15] or *N*-donor

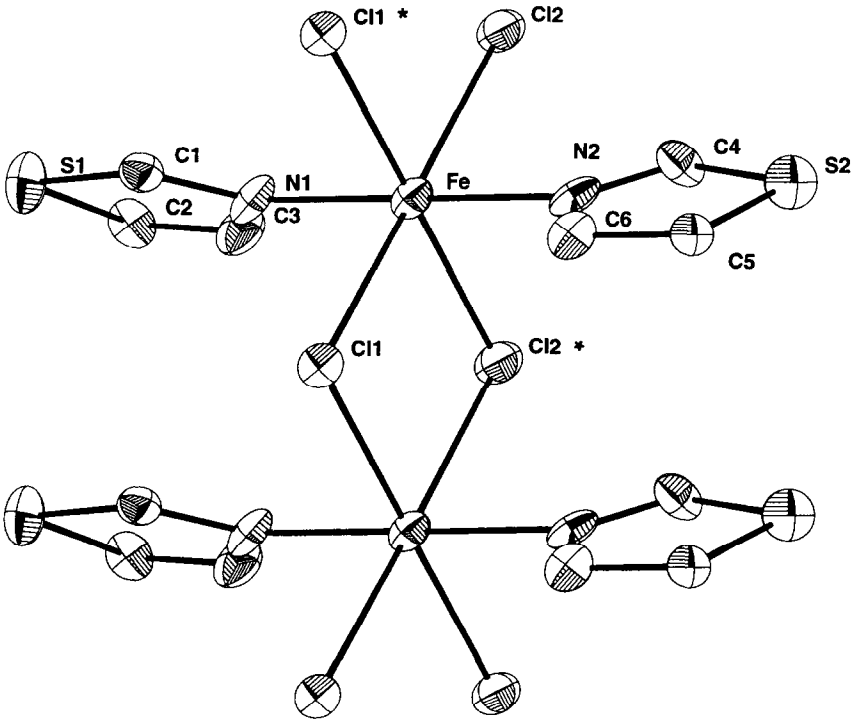

Fig. 1. An ORTEP drawing of linear chains of $Fe(tz)_2Cl_2$ (**1**). H atoms are omitted for clarity. All atoms are represented by the thermal ellipsoids at 50% probability.

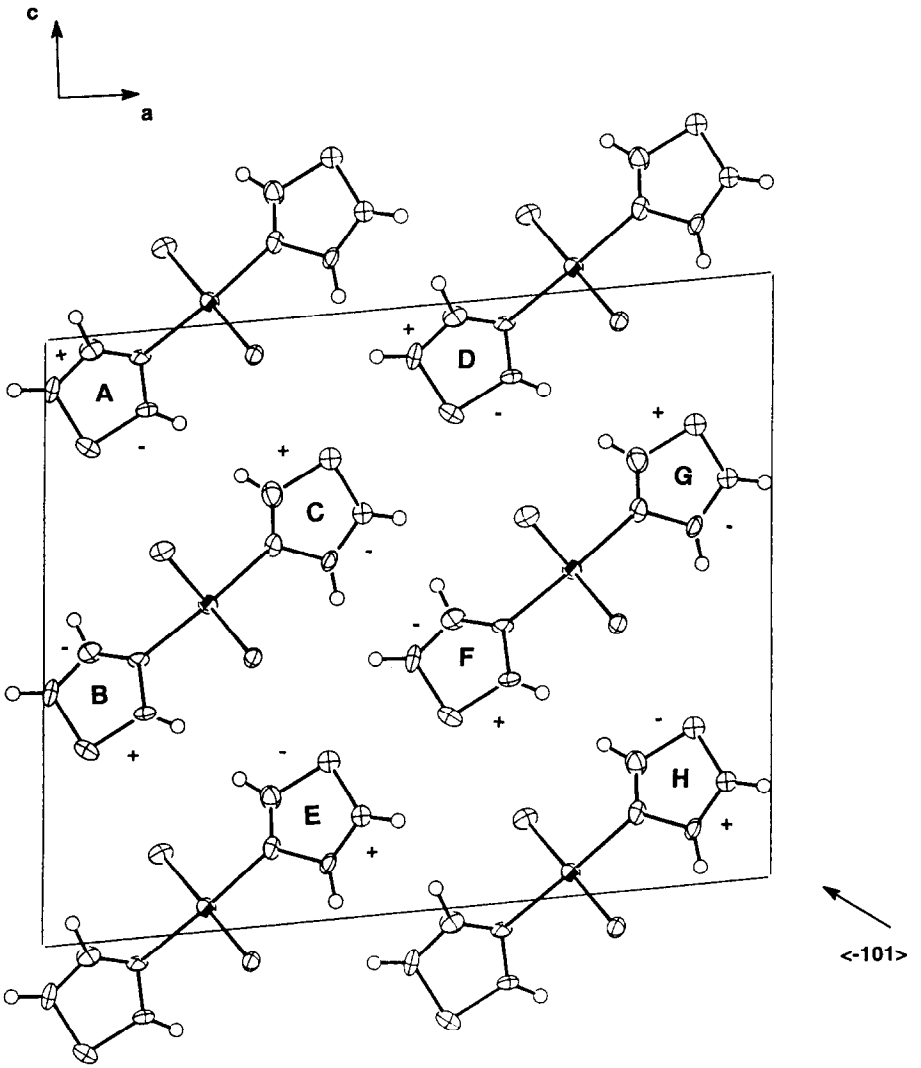

Fig. 2. Packing of infinite linear chains in the unit cell of $Fe(tz)_2Cl_2$ (**1**). The chain direction is into the page (parallel to the *b*-axis).

[16–21] bridging ligands. Polymeric iron(II) complexes based on 1-dimensional di-bridging halide chains are almost unknown. A notable example is that of $[FeCl_2(OPMe_3)]_\infty$ [22], where each iron centre is linked by 2 axial and 2 equatorial bridging chlorine atoms to adjacent iron atoms. The $-OPMe_3$ group adopts a third equatorial position about the Fe atom, leading to a distorted trigonal bipyramidal coordination geometry. Thus, while $[FeCl_2(OPMe_3)]_\infty$ is also a dichloride bridged iron(II) polymer, the bonding relationship between adjacent molecular units is substantially different to that observed in **1**.

A much wider range of Fe—Cl bond lengths (2.350 Å–2.603 Å) are observed in the more highly distorted Fe_2Cl_4 chains of $[FeCl_2(OPMe_3)]_\infty$ [22]. The Fe—Fe bond lengths for this complex (3.688(1) Å and 3.560(1) Å) are also slightly shorter than that found in **1**. The axial Cl—Fe—Cl bond angles of $[FeCl_2(OPMe_3)]_\infty$ are similar (174.14(3)°) to those in **1**, however, by virtue of the trigonal bipyramidal coordination, the equatorial Cl—Fe—Cl bond angle (123.49(3)°) is substantially different.

Crystal structure of $Cu(tz)_2Br_2$ (**2**)

The polymeric compound $Cu(tz)_2Br_2$ (**2**) consists of the same dihalide bridged linear structure as **1** and has been found to be isostructural with $Cu(tz)_2Cl_2$ [1]. The chain structure of **2** is shown in Fig. 3 and the packing of chains in the unit cell is displayed in Fig. 4. Selected bond lengths and bond angles are given in Table 3. The Cu_2Br_2 structural motif based-on di-bridging bromide ligands has been observed in numerous Cu(I) and Cu(II) polymeric complexes [24–32]. In particular the complexes $Cu(3,5\text{-dimethylpyridine})_2Br_2$ [24],

Table 2. Selected bond lengths (Å) and angles (°) for **1**

Fe—Fe*[a]	3.717(5)		
Fe—C11	2.560(2)	Fe—C12	2.539(2)
Fe—C11*	2.521(2)	Fe—C12*	2.527(2)
Fe—N1	2.196(6)	Fe—N2	2.150(7)
N1—C1	1.345(9)	N2—C4	1.29(1)
C1—S1	1.750(7)	C4—S2/C5'[b]	1.630(9)
S2—C2	1.739(7)	S2/C5'—C5/S2'	1.663(3)
C2—C3	1.32(1)	C5/S2'—C6	1.465(9)
C3—N1	1.31(1)	C6—N2	1.451(8)
N1—Fe—N2	177.4(3)		
Fe—C11—Fe*	94.1(1)	Fe—C12—Fe*	94.4(1)
C11—Fe—C11*	94.0(1)	C12—Fe—C12*	94.4(1)
C11*—Fe—C12*	179.1(1)	C11—Fe—C12	179.5(1)
C11*—Fe—C12	86.1(4)	C11—Fe—C12*	85.5(1)
C11—Fe—N1	90.4(2)	C12—Fe—N2	88.6(2)
C11*—Fe—N1	90.9(2)	C12*—Fe—N2	89.6(2)
C11—Fe—N2	91.6(2)	C12—Fe—N1	89.4(2)
C11*—Fe—N2	90.7(2)	C12*—Fe—N1	88.9(2)
Fe—N1—C1	119.2(4)	Fe—N2—C4	131.0(5)
N1—C1—S1	111.5(5)	N2—C4—S2/C5'	119.5(6)
C1—S1—C2	90.0(3)	C4—S2/C5'—C5/S2'	92.3(3)
S1—C2—C3	106.4(6)	S2/C5'—C5/S2'—C6	109.2(3)
C2—C3—N1	121.8(8)	C5/S2'—C6—N2	110.2(5)
Fe—N1—C3	131.0(5)	Fe—N2—C6	120.4(4)

[a] An asterisk denotes a translation of the molecule along the *b* axis.

[b] Sites disordered by 180° rotations about the Fe—N2 bond, with occupancy factors of S2/C5' and C5/S2' = 0.87(1)/0.13.

$Cu(pyridine)_2$-Br_2 [25] and $Cu(N\text{-methylimidazole})_2Br_2$ [26] show essentially isostructural features to **2** with a *trans*-arrangement of Cu—N bonds and di-bridging Br—Cu—Br* bonds. The Cu—N distance in **2** of 1.988(3) Å is essentially identical to that found in the chloro- analogue (1.990(2) Å), while the disparate Cu—Br distances of 2.472(1) Å and 3.120(1) Å are also consistent with those observed for $Cu(tz)_2Cl_2$ (2.322(1) Å and 2.998(1) Å). The essentially regular Br—Cu—Br* angles of 90.2(1)° are in agreement with those observed for other dibromo-bridged copper complexes [24–26].

The structure of **1** is analogous to these $Cu(tz)_2X_2$ (X = Cl and Br) polymers in that it contains a similar di-bridging linear chain structure along the *b*-axis. Closer examination of Figs 1 and 3 however, indicate slightly different structural behaviour, suggesting dissimilar bonding mechanisms in **1** and **2**. In contrast to the opposed rotational behaviour of the thiazole rings in **1**, the rings in **2** show synchronised rotations about their Cu—N bonds of approximately 21° relative to the *ac* plane (Figs 3 and 4). These distinct rotational behaviours are clearly linked to the different transition metal–halide bonding modes in these complexes. Estes and coworkers [1] described the polymer structure of $Cu(tz)_2Cl_2$ as a square-planar array consisting of two thiazole ligands and two short in-plane chloride bonds linked by the two longer out-of-plane Cu—Cl bonds. The bonding arrangement in **2** can also be described in this matter and is reflective of the Jahn-Teller nature of d^9 Cu^{2+}. Given the in-plane nature of the strongest bonds about the Cu centre, it is likely that the single-ion ground state is essentially $d_{x^2-y^2}$ in character.

Examination of the bonding picture about the Fe centre of **1** indicates a much more regular arrangement in terms of the Fe—N and Fe—Cl bond lengths. The square-planar-like arrangement of two halide and two nitrogen bonds, along with the two longer out-of-plane halide bonds that is observed in **2** is inappropriate for describing **1**, where very little variation is shown between each of the four of the Fe—Cl bonds. The pseudo-octahedral arrangement described above provides a more suitable description, given that Jahn-Teller effects do not contribute significantly to the high-spin d^6 ground state configuration of Fe^{2+}.

Comparison of the tilting of the thiazole rings across the iron and copper transition metal centres (Figs 2 and 4) clearly shows the dissimilar nature of these polymer chains within their crystals. This feature leads to the lowering of crystal symmetry and thus the effective doubling of the unit cell volume of **1** as compared to **2**. Despite these different rotation mechanisms however, the packing arrangements in their respective cells are such that nearest-neighbour interactions between thiazole ligands on adjacent

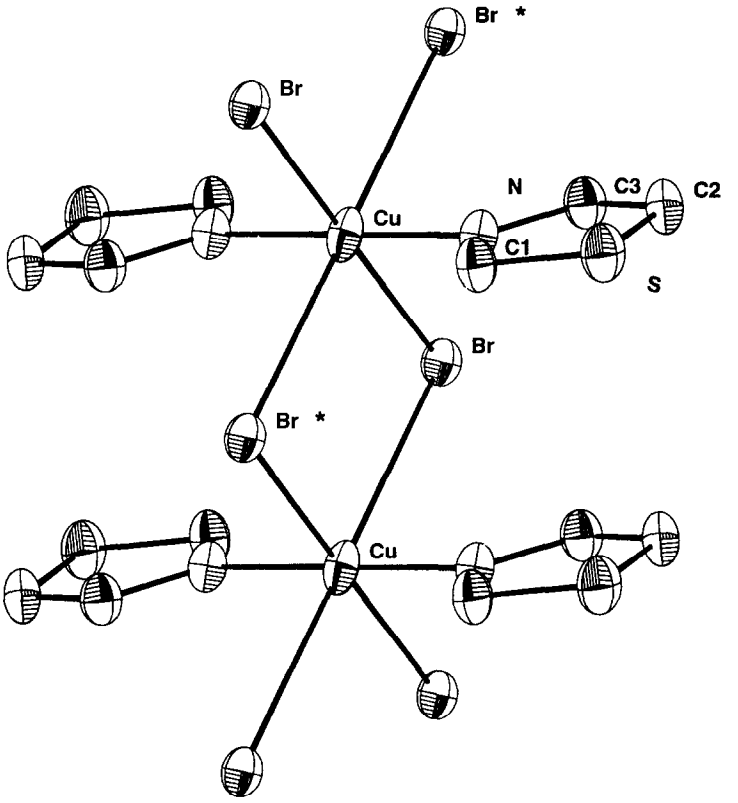

Fig. 3. An ORTEP drawing of linear chains of $Cu(tz)_2Br_2$ (**2**). H atoms are omitted for clarity. All atoms are represented by the thermal ellipsoids at 50% probability.

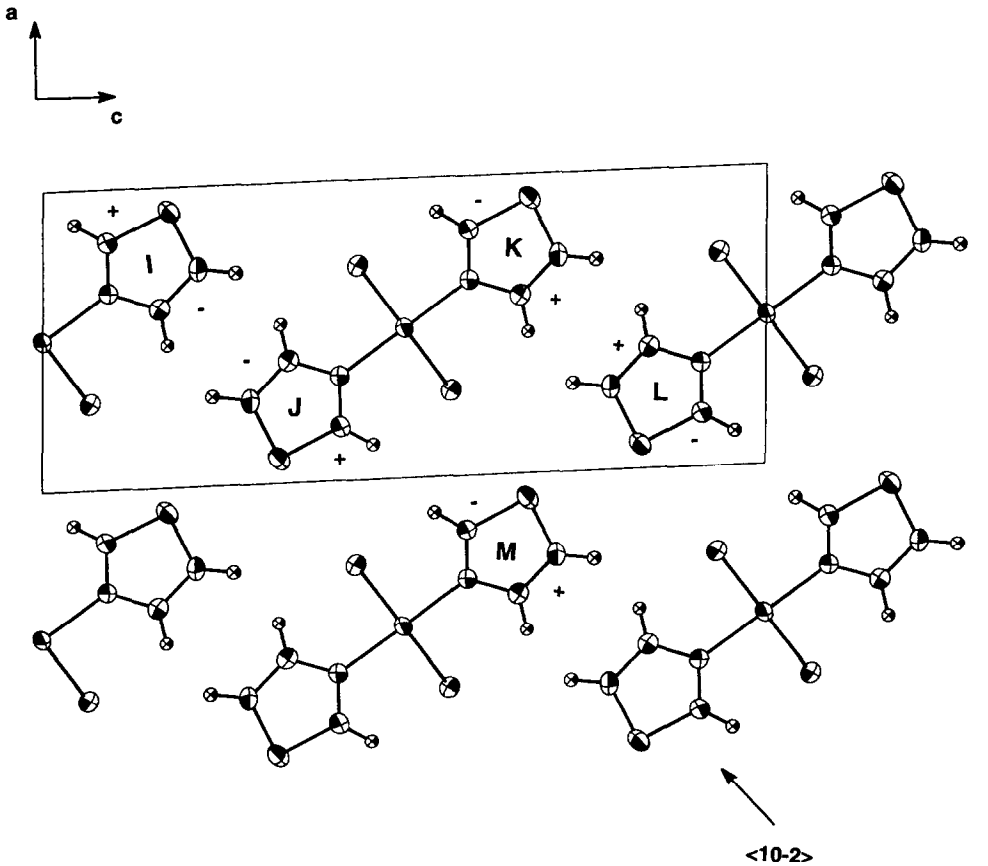

Fig. 4. Packing of infinite linear chains in the unit cell of $Cu(tz)_2Br_2$ (**2**). The chain direction is into the page (parallel to the *b*-axis).

Table 3. Selected bond lengths (Å) and angles (°) for **2**

Cu—Cu*	3.987(3)		
Cu—Br	2.472(1)	Cl—S	1.698(4)
Cu—Br*	3.120(1)	S—C2	1.708(4)
Cu—N	1.988(3)	C2—C3	1.366(6)
N—Cl	1.308(5)	C3—N	1.369(5)
Br—Cu—Br*	90.2(1)	Cu—Br—Cu*	90.2(1)
Cu—N—Cl	124.2(3)	Br—Cu—N	90.0(1)
C2—S—Cl	90.4(2)	Br*—Cu—N	90.1(1)
S—Cl—N	114.1(3)	Cu—N—C3	124.4(3)
Cl—N—C3	111.4(3)	N—C3—C2	114.7(4)
C3—C2—S	109.4(3)		

* An asterisk denotes a translation of the molecule along the *b* axis.

chains are similar. Equivalent interchain relationships are observed along the ⟨−101⟩ direction in **1** (Fig. 2) and the ⟨10–2⟩ direction in **2** (Fig. 4). With respect to the orientation of the thiazole rings, the interchain relationships in **1** between rings C, F and H (Fig. 2) are analogous to those relationships between rings I, J and M in **2** (Fig. 4). The interchain distances between rings in these structures are comparable, although those for **1** tend to be slightly shorter than found in **2** (Table 4).

Although interchain distances are similar for these two complexes, the position of chains along the *b* axis are different in each. Cu centres in **2** occupy high symmetry 2*d* sites (1/2, 1/2, 0 and 1/2, 0, 1/2) in $P2_1/c$, while Fe centres in **1** occupy general 4*a* sites (*x*, *y*, *z*) in *Cc*. The relative positions of adjacent polymer chains along the *c* axis of **1** are therefore shifted in *b* with respect to one another, leading to a modulation throughout the crystal.

Table 4. Selected interchain distances (Å) for **1** and **2**

Ring	Atom	Ring	Atom	Interchain Distance
		1		
C	H6	F	H2	2.46(1)
F	H1	H	H4	2.53(1)
C	H5	F	H3	2.66(1)
F	H2		C11	3.04(1)
F	H1		C12	3.29(1)
C	H5	D	S1	3.25(1)
F	H2		S2	3.33(1)
E	S2	F	S1	3.39(1)
		2		
I	H2	J	H3	2.56(1)
J	H1	M	H1	2.62(1)
I	H3	J	H2	2.67(1)
L	H2		Br	3.01(1)
L	H2	M	S	3.27(1)
L	S	M	S	3.64(1)

Magnetic susceptibility

The molar magnetic susceptibility (χ_{mol}) of $Fe(tz)_2Cl_2$ was measured at room temperature (298 K). Upon correcting for diamagnetism an effective moment (μ_{eff}) was determined as 5.51(2) μ_B; this value being consistent with high-spin Fe^{2+} containing 4 unpaired electrons (S = 2). Cotton *et al.* report a smaller effective moment of 4.90 μ_B for the di-chloro-bridged polymer $[FeCl_2(OPMe_3)]_\infty$ [22], the reduction in magnitude possibly being a reflection of the trigonal bipyramidal coordination geometry. Due to the scarcity of pseudo-octahedral di-halide-bridged Fe(II) 1-dimensional systems, very little has been studied of the magnetic response of these materials to changes in temperature.

The magnetic behaviour of **2,** has previously been characterised [1,5]. Room temperature susceptibility measurements were carried out by Hughes and Rutt [5] who found an effective moment consistent with the 1 unpaired spin of d^9 Cu^{2+} ions (μ_{eff} = 1.77 μ_B). Variable temperature susceptibility data were collected by Estes *et al.* [1] and were able to be fitted by an isotropic Heisenberg model using the relations of Bonner and Fisher [33], giving $J = -10.4$ cm^{-1} and $g = 2.12$. Interestingly, a good fit to the data for $Cu(tz)_2Cl_2$ was found using a model for a two dimensional Heisenberg antiferromagnetic layer, however attempts to fit the $Cu(tz)_2Br_2$ data to this model were unsuccessful. The authors proposed that additional superexchange pathways via sulfur–sulfur contacts played an important role in the dimensionality increase of the chloride system.

The M—M distances observed in **1** and **2** of 3.717 Å and 3.987 Å respectively preclude extensive metal–metal bonding occurring in these complexes, however the possibility of intrachain magnetic superexchange

pathways occurring via the di-halide bridges has been clearly demonstrated in other studies [1,24–26,34–37].

REFERENCES

1. Estes, W. E., Gavel, D. P., Hatfield, W. E. and Hodgson, D. J., *Inorg. Chem.*, 1978, **17,** 1415.
2. James, M., Kawaguchi, H. and Tatsumi, K., *Polyhedron*, 1997, **16,** 1873.
3. Cromer, D. T. and Waber, J. T., *International Tables for X-ray Crystallography*, Vol. VI, ed. T. Hahn. Kynoch, Birmingham, England, 1974, Table 2.2A.
4. Ibers, J. A. and Hamilton, W. C., *Acta Cryst.*, 1964, **17,** 781.
5. Hughes, M. N. and Rutt, K. J., *J. Chem. Soc. A*, 1970, 3015.
6. Eilbeck, W. J., Holmes, F. and Underhill, A. E., *J. Chem. Soc. A*, 1967, 757.
7. James, M., Kawaguchi, H. and Tatsumi, K., *Polyhedron*, in press, 1997.
8. Deyrieux, R. and Peneloux, A., *Bull. Soc. Chim. Fr.*, 1969, 2675.
9. Weber, R. and Bergerhoff, G., *Z. Anorg. Allg. Chem.*, 1991, **598/599,** 371.
10. Weber, G., *Acta Cryst. B*, 1980, **36,** 3197.
11. Strouse, J., Layten, S. W. and Strouse, C. E., *J. Am. Chem. Soc.*, 1977, **99,** 562.
12. Sledzinska, I., Murasik, A. and Piotrowski, M., *Physica B+C*, 1986, **138,** 315.
13. Weiss, A., Riegler, E., Alt, I., Bohme, H. and Robl, C., *Z. Naturforsch. Teil B*, 1986, **41,** 18.
14. Bujoli, B., Courilleau, A., Palvadeau, P. and Rouxel, J., *European J. Solid State Inorg. Chem.*, 1992, **29,** 171.
15. Bujoli, B., Pena, O., Palvadeau, P., Le Bideau, J., Payen, G. and Rouxel, J., *Chem. of Materials*, 1993, **5,** 583.
16. Jooss, R., Kult, A., Lentz, A. and Walz, L., *Z. Kristallogr.*, 1995, **210,** 766.
17. Cingi, M. B., Lanfredi, A. M. M., Tiripicchio, A., Cornelissen, J. P., Haasnoot, J. G. and Reedijk, J., *Inorg. Chim. Acta*, 1987, **127,** 189.
18. Meyer, H. J. and Pickardt, J., *Z. Naturforsch. Teil B*, 1988, **43,** 135.
19. Real, J. A., De Munno, G., Munoz, M. C. and Julve, M., *Inorg. Chem.*, 1991, **30,** 2701.
20. Ozarowski, A., Shunzhong, Yu., McGarvey, B. R., Mislanker, A. and Drake, J. E., *Inorg. Chem.*, 1991, **30,** 3167.
21. Kubel, F. and Strahle, J., *Z. Naturforsch. Teil B*, 1983, **38,** 258.
22. Cotton, F. A., Luck, R. L. and Son, K., *Inorg. Chim. Acta*, 1991, **184,** 177.
23. James, M., Kawaguchi, H. and Tatsumi, K., *Acta Cryst. C*, 1997, **53,** 1391.
24. van Ooijen, J. A. C., Reedijk, J., Sonneveld, E. J. and Visser, J. W., *Tran. Met. Chem.*, 1979, **4,** 305.
25. Morosin, B., *Acta Cryst. B*, 1975, **31,** 632.
26. Jansen, J. C., van Koningsveld, H. and van Ooijen, J. A. C., *Cryst. Struct. Comm.*, 1978, **7,** 637.
27. Julve, M., De Munno, G., Bruno, G. and Verdaguer, M., *J. Chem. Res.*, 1987, 152.
28. Garland, M. T., Grandjean, D., Spondine, E., Atria, A.. M. and Manzur, J., *Acta Cryst. C*, 1988, **44,** 1209.
29. Atria, A. M., Baggio, R., Garland, M. T., Gonzales, O., Manzur, J., Pena, O. and Spondine, E., *J. Cryst. Spectrosc.*, 1993, **23,** 943.
30. Begley, M. J., Eisenstein, O., Hubberstey, P., Jackson, S., Russell, C. E. and Walton, P. H., *J. Chem. Soc., Dalton Trans.*, 1994, 1935.
31. Munakata, M., Kuroda-Sowa, T., Maekawa, M., Honda, A. and Kitagawa, S., *J. Chem. Soc., Dalton Trans.*, 1994, 2771.
32. Fetzer, Th., Lentz, A. and Debaerdemaeker, T., *Z. Naturforsch. Teil B*, 1989, **44,** 553.
33. Bonner, J. C. and Fisher, M. E., *Phys. Rev. A*, 1964, **135,** A640.
34. Duffy, W., Venneman, J., Strandberg, D. and Richards, P. M., *Phys. Rev. B*, 1974, **9,** 2220.
35. Hughes, R., Morosin, B., Richards, P. M. and Duffy, W., *Phys. Rev. B*, 1975, **11,** 1795.
36. Jeter, D. Y. and Hatfield, W. E., *J. Inorg. Nucl. Chem.*, 1972, **34,** 3055.
37. Takeda, K., Matsukawa, S. and Hageda, T., *J. Phys. Soc. Jpn*, 1971, **30,** 1330.

Pergamon

PII: S0277-5387(97)00525-1

Polyhedron Vol. 17, Nos. 11–12, pp. 1851–1861, 1998
© 1998 Elsevier Science Ltd
All rights reserved. Printed in Great Britain
0277-5387/98 $19.00+0.00

Studies on the synthesis of Pb-Ti-oxo-alkoxo-carboxylato complexes

L. Spiccia, B. O. West* and Q. Zhang

Centre for Chemical Synthesis and Department of Chemistry, Monash University, Clayton, Victoria, Australia, 3168

(Received 6 October 1997; accepted 11 December 1997)

Abstract—Reactions between lead carboxylates $Pb(O_2CR)_2$ and $Ti(OPr^i)_4$ produce complexes of empirical formulae $Pb_2Ti_2(O)(O_2CR)_2(OPr^i)_8$ (R = C_3F_7 **1**; $C(CH_3)_3$ **2**) in toluene and $Pb_2Ti_4(O)_2(O_2CR)_2(OPr^i)_{14}$ (R = $CH(CH_3)_2$ **3**) in Pr^iOH solution. ^{207}Pb NMR evidence indicates that both types of complex form in alcoholic solution. The compound **4** having a Pb_3Ti_3 core is produced when $Pb(O_2CCH(CH_3)_2)_2$ reacts with $Ti(OPr^i)_4$ in toluene. Attempts to prepare acetylacetonate derivatives of compounds having 1 : 1 or 1 : 2 Pb : Ti stoichiometries by direct substitution of the compounds gave poorly soluble Pb containing products but direct reaction of $Pb(O_2CCH_3)_2$ or PbO with Ti-acetylacetonate-alkoxide species gave compounds of empirical formulae $Pb_3Ti_3(O)_4(O_2CCH_3)_2(OPr^i)_7(acac)$ **5** and $Pb_2Ti_2(O)(OEt)_8(acac)_2$ **6**. Reaction of $Ti(OR)_4$ (R = OPr^i, Et) with acetic acid yields products which further react with PbO to form the previously characterised Pb—Ti compounds $Pb_2Ti_2(O)(O_2CCH_3)_2(OPr^i)_8$ **7** and $Pb_2Ti_4(O)_2(O_2CCH_3)_2(OEt)_{14}$ **8**. Molecular weight measurements, ^{207}Pb, ^{19}F, ^1H and ^{13}C NMR and IR spectral data have been used to derive empirical formulae for the various complexes isolated. © 1998 Elsevier Science Ltd. All rights reserved

Keywords: lead–titanium; alkoxide; carboxylate; ^{207}Pb; NMR; acetylacetone.

Mixtures of hydrated lead acetate and a titanium alkoxide in alcoholic solution have been used as precursors to the formation of the piezoelectric material $PbTiO_3$ by sol-gel processes. [1–4]. It was recognised that some form of Pb—Ti complex would be formed in such solutions [1] and various empirical formulae were proposed (e.g. $Pb(O_2CCH_3)(O)Ti(OR)_3$, $Pb(O)_2Ti_2(OR)_6$). Subsequent attempts at direct synthesis involving reaction between anhydrous $Pb(O_2CCH_3)_2$ and $Ti(OPr^i)_4$ and $Ti(OEt)_4$ led to the isolation of two compounds each having a different Pb : Ti ratio depending on the alkoxide substituent. The 1 : 1 Pb : Ti ratio complex formed using $Ti(OPr^i)_4$ as reagent [5–7], was shown to be $Pb_2Ti_2(\mu_4\text{-}O)(O_2CCH_3)_2(OPr^i)_8$ **7** by single crystal X-ray analysis [6]. This complex has also been formed by direct reaction of acetic acid on the mixed metal alkoxide $Pb_2Ti_2(\mu\text{-}O)(OPr^i)_{10}$ [8].

The formula of the 1 : 2 complex formed using $Ti(OEt)_4$ has been established as $Pb_2Ti_4(\mu_4\text{-}O)_2(O_2CCH_3)_2(OEt)_{14}$ **8** by two independent X-ray studies [7,9]. The latter complex was the only compound to be isolated whether the Pb : Ti ratio of initial reagents was 1 : 1 or 1 : 2. Each compound has a Pb : acetate ratio of 1 : 1 instead of the 1 : 2 ratio of the starting reagent i.e. acetate has been "lost" in the reaction as had previously been found [10] using various spectroscopic techniques. Moreover an acetate group bridges each of the Pb—Pb and Ti—Ti atom pairs in the 1 : 1 compound while in the 1 : 2 complex, only the pairs of Ti atoms have bridging acetate groups attached i.e. there has been acetate exchange between Pb and Ti as part of the overall reaction. Group exchange between the labile Group 4/14 precursor reagents is not unexpected although the mechanism for the exchange process is unclear. Another extreme case of such an exchange reaction has been observed in the reaction between Zn acetate and a Sn methoxide compound in an attempt to prepare a Sn—Zn heterometallic [11]. Solubility considerations presumably determined that the most readily isolated product was the polymeric homonuclear Zn-acetate-alkoxide $[Zn_2(O_2CCH_3)_3(OCH_3)]_n$.

The isolation of complexes of differing Pb—Ti stoichiometry using the same Pb carboxylate reagent but

* Author to whom correspondence should be addressed.

different Ti alkoxides raises the question as to whether this results from a fortuitous combination of solubility considerations or is due more fundamentally to steric or electronic differences between the alkoxy compounds of Ti, varying bridging capacities of the alkoxide groups or abilities to form oxo groups by ester elimination. Similarly the exchange of acetate groups between Pb and Ti suggests that the alkanoate group could also play a role in determining the final stoichiometry of Pb—Ti compound.

We report here the isolation and empirical formulae of complexes formed by the reactions of $Ti(OPr^i)_4$ with several other lead alkanoates ($Pb(O_2CR)_2$) where R is either strongly electronegative (C_3F_7) or large and capable of exerting steric resistance to bridge formation, ($C(CH_3)_3$, $CH(CH_3)_2$). Also, in view of the addition of acetylacetone to mixtures of a titanium alkoxide and $Pb(O_2CCH_3)_2$ to improve the thickness [12] and electrical properties [13] of $PbTiO_3$ films produced by sol-gel processes we have endeavoured to identify the acetylacetone complexes formed by its reaction with Pb—Ti alkoxide precursors.

A further feature of the two Pb—Ti complexes previously isolated has been the presence of tetrahedrally coordinated oxo groups as key structural features of each complex. In recent years, oxo groups have been found to be common structural units in many other homo- and heteronuclear alkoxides [14] and carboxylato-alkoxides compounds [15,16] even when the compounds have been prepared under scrupulously anhydrous conditions. Although such groups might still result from hydrolytic processes due to the adventitious entry of traces of water, other processes including ether elimination in alkoxides (i)

$$M—OR + RO—M \rightarrow M—O—M + R_2O \qquad (i)$$

and ester elimination in carboxylate-alkoxide reactions (ii)

$$M—OR + R'COO—M \rightarrow M—O—M' + R'COOR \qquad (ii)$$

are more likely to be the routes by which oxo groups are formed. There have been reports of the formation of esters in previous studies of Pb acetate–Ti alkoxide reactions [17–19]. Hubert-Pfalzgraf *et al.* [6] however did not observe ester formation in the room temperature reaction which yielded the 1 : 1 Pb : Ti compound **7** but only when the reactants were initially heated in toluene thus suggesting ether elimination leads to oxo group formation. Extensive ester formation has been reported to occur when mixtures of Zn or other transition metal acetates are heated to high temperatures in decalin with $Al(OR)_3$ [20]. Zn—O—Al and other M—O—Al alkoxy complexes have been proposed to form although their structures are not precisely known. The generality of the formation of oxo groups in reactions leading to alkoxo-carboxylato mixed metal species and indeed polynuclear alkoxides suggests that the fundamental reactions require further study.

The use of PbO as a reagent to produce "basic" lead acetate [21] suggested it be examined as a direct source of oxo groups in the synthesis of Pb—Ti complexes and as part of the present study we have successfully prepared the known 1 : 1 and 1 : 2 Pb : Ti oxo-acetato-alkoxide complexes using the products of reaction of $Ti(OR)_4$ (R = Pr^i, Et) and acetic acid as the titanium reagent. Although strenuous efforts have been made to prepare crystals of suitable quality for X-ray analysis of the new species formed in these studies so far they have been uniformly unsuccessful. Hence the empirical formulae suggested, although supported by spectroscopic and vapour phase osmometric molecular weight measurements, rely greatly on comparisons with other structurally characterised species, where available and on chemically plausible assumptions, particularly with regard to the presence and number of oxo groups in the molecules.

EXPERIMENTAL

All reactions were carried out using dry solvents and manipulations used Schlenk techniques under dry nitrogen. Alcohols were predried over molecular sieves then distilled after the formation of the appropriate Mg alkoxide or in the presence of CaH_2 then stored over molecular sieves. All other solvents were dried by standard procedures.

Molecular weights were measured by vapour phase osmometry (VPO) at 60°K using a Knauer Type II osmometer contained in a dry box facility with benzil as standard. ^{207}Pb NMR spectra were obtained using a Bruker AM-300 spectrometer. Chemical shifts were measured in ppm using $Pb(Me)_4$ as external standard with high field from the standard considered negative. These values were converted to values relative to $Pb(NO_3)_2$ by adding 2961 [22]. ^1H, ^{13}C and ^{19}F spectra were measured at 300 K (unless otherwise stated) on a Varian EM-360A or the Bruker instrument. Tetramethylsilane was used as standard for ^1H and ^{13}C spectra and $CFCl_3$ for ^{19}F spectra. Mass spectra were recorded on VG Micromass 7070F or VG Trio-1 quadrupolar spectrometers. Electron microprobe analyses (EMA) were made with a Cambridge S410 SEM linked through an NEC X-ray detector and pulse processing system to a Packard multichannel analyser. A commercial sample of $PbTiO_3$ (Aldrich) was used as standard. Elemental analyses were by CMAS, Melbourne. $Ti(OPr^i)_4$ (Aldrich) was used as received.

Lead carboxylates

Anhydrous lead acetate. The preparation of 10–20 g quantities, free from evidence for O—H stretching frequencies in the 3000–4000 cm^{-1} region was accomplished by either heating lead acetate trihydrate at 100°C under reduced pressure (10^{-3} Torr) for 5 h or

stirring the hydrate at room temperature with excess acetic anhydride for several hours then removing all volatile materials by pumping at 10^{-3} Torr and 50°C. The product is insoluble in toluene, THF and chloroform, readily soluble in methanol and 2-methoxyethanol and sparingly soluble in ethanol. A typical analysis gave; Found: C, 14.8; H, 1.85. Calc. for $C_4H_6O_4Pb$: C, 14.8; H, 1.85%.

Basic lead acetate $3[Pb(O_2CCH_3)_2]\cdot PbO\cdot H_2O$. The method was based on that of Kwestroo *et al.* [21]. PbO was added to a solution of the trihydrate in water in the mole ratio 1 : 3, oxide to acetate (a slight excess of oxide was used giving a practical mole ratio of 1.05 : 3. The mixture was stirred at room temperature for some hours as the bulk of the oxide slowly dissolved. The solution was finally filtered and evaporated at 40°C under reduced pressure. The powder X-ray pattern of the product was identical with the compound reported [21]. Found: C, 12.0; H, 1.50. Calc. for $C_{12}H_{20}O_{14}Pb_4$: C, 11.8; H, 1.60%.

Lead heptafluorobutyrate trihydrate $Pb(O_2CC_3F_7)_2\cdot 3H_2O$. An aqueous solution of the acid was refluxed with PbO, the solution filtered and allowed to evaporate to crystallisation. Found: C, 13.7; H, 0.2; F, 38.3. Calc. for $C_8H_6F_{14}O_7Pb$: C, 14.0; H, 0.09; F, 38.7%.

Lead pivalate $Pb(O_2CC(CH_3)_3)_2$. PbO was added to a methanol solution containing two equivalents of pivalic acid and the mixture stirred at room temperature until most of the oxide had dissolved. The solution was filtered and on further standing deposited a white solid which was filtered and dried. M.pt. 172–174°C. Found: C, 29.2; H, 4.63. Calc. for $C_{10}H_{18}O_4Pb$: C, 29.3; H, 4.40%.

Lead dimethylacetate $[Pb(O_2CCH(CH_3)_2)_2]_6\cdot 4H_2O$. This compound was prepared by the reported method [23].

1 : 1 *Pb* : *Ti ratio compounds*

$Pb_2Ti_2(O)(O_2CR)_2(OPr^i)_8$. $Ti(OPr^i)_4$ (usually 3.5 mmol) was added dropwise to an equimolar quantity of the carboxylate as a slurry in isopropanol (anhydrous lead acetate [7]) or toluene (lead heptafluorobutyrate) or a solution in toluene (lead pivalate). Volumes of solvent ca 30 cm^3 were found appropriate. The mixtures were refluxed for 2–3 h, filtered, then cooled to 0°C or a lower temperature to induce crystallisation. In the case of the pivalate product the solvent was eventually removed under reduced pressure, the waxy solid remaining redissolved in the minimum of warm toluene and cooled to −20°C until crystals formed. The yields in terms of the amounts of crystalline product recovered were at least 55% in each preparation.

$Pb_2Ti_2(O)(O_2CC_3F_7)_2(OPr^i)_8$ **1**. EMA: Pb : Ti, 1 : 1. Found: C, 26.9; H, 4.10; F, 18.3. Calc. for $C_{32}H_{56}F_{14}O_{13}Pb_2Ti_2$: C, 26.9; H, 3.90; F, 18.6%. Mol. wt. (benzene): 1397 ± 50 (theor. for $C_{32}H_{56}F_{14}O_{13}Pb_2Ti_2$, 1425). NMR: ^1H ($CDCl_3$): δ = 1.22, 1.25, 1.29, 1.35, 1.39, 1.47 (d, $OCH(C\underline{H}_3)_2$, 48H); 4.05, 4.78, 4.97, 5.05, 5.47, 5.70 (sp, $OC\underline{H}(CH_3)_2$, 8H) ppm: ^{19}F ($CDCl_3$): δ = −81.25, −81.72 (t, $O_2CCF_2CF_2C\underline{F}_3$); −118.0, −120.3 (sext, $O_2CCF_2C\underline{F}_2CF_3$); −126.5, −128.1 (t, $O_2CC\underline{F}_2CF_2CF_3$) ppm. IR (Nujol): 2922 (vs), 2854 (vs), 1673 (vs), 1413 (w), 1378 (s), 1337 (vs), 1227 (w), 1220 (vs), 1120 (vs), 1086 (w), 1019 (m), 966 (m), 934 (s), 838 (m), 817 (m), 718 (m), 588 (s) cm^{-1}.

$Pb_2Ti_2(O)((O_2CC(CH_3)_3)_2(OPr^i)_8$ **2**. EMA: Pb : Ti = 1 : 1. Found: C, 34.2; H, 6.31. Calc. for $C_{34}H_{74}O_{13}Pb_2Ti_2$: C, 34.0; H, 6.17%. Mol. wt. (benzene): 1165 ± 50 (theor. for $C_{34}H_{74}O_{13}Pb_2Ti_2$, 1201). NMR: ^1H ($CDCl_3$): δ = 1.16 (s, $O_2CC(C\underline{H}_3)_3$); 1.28 (d, $OCH(C\underline{H}_3)_2$); 1.26 (d, $OCH(C\underline{H}_3)_2$); 1.23 (d, $OCH(C\underline{H}_3)_2$); 4.86 (sp, $OC\underline{H}(CH_3)_2$); 4.82 (sp, $OC\underline{H}(CH_3)_2$); 4.50 (sp, $OC\underline{H}(CH_3)_2$) ppm. IR (Nujol): 2922 (vs), 2854 (vs), 1557 (vs), 1483 (s), 1461 (vs), 1426 (s), 1404 (s), 1375 (vs), 1360 (vs), 1324 (m), 1224 (m), 1162 (vs), 1126 (vs), 1008 (vs), 962 (vs), 834 (m), 727 (m), 587 (vs), 470 (vs) cm^{-1}.

$Pb_2Ti_2(O)(O_2CCH_3)_2(OPr^i)_8$ [8] **7**. EMA: Pb : Ti = 1 : 1. Found: C, 29.9; H, 5.5. Calc. for $C_{28}H_{62}O_{13}Pb_2Ti_2$: C, 30.1; H, 5.6%. Mol. wt. (benzene): 1109 ± 50 (theor. for $C_{28}H_{62}O_{13}Pb_2Ti_2$, 1117). NMR: ^1H ($CDCl_3$) 293 K: δ = 1.23, 1.25, (d, $OCH(C\underline{H}_3)_2$); 1.98, 2.02 (s, $O_2CC\underline{H}_3$); 4.47, 4.99 (sp, $OC\underline{H}(CH_3)_2$) ppm; 217 K: δ = 1.25, 1.28, (d, $OCH(C\underline{H}_3)_2$); 1.98, 2.01 (s, $O_2CC\underline{H}_3$); 4.09, 4.49, 4.86, 4.99 (sp, $OC\underline{H}(CH_3)_2$) ppm: C^{13} ($CDCl_3$): δ = 21.48, 22.43 ($O_2C\underline{C}H_3$); 24.86, 25.47 ($OCH(\underline{C}H_3)_2$; 64.10, 75.41 ($O\underline{C}H(CH_3)_2$); 176.9, 177.0 ($O_2\underline{C}CH_3$) ppm. IR (Nujol): 1556 (vs), 1434 (vs), 1374 (s), 1326 (m), 1126 (vs), 1010 (vs), 839 (m), 786 (m) cm^{-1}.

$Pb_3Ti_3(O)_4(O_2CCH_3)_2(OPr^i)_7(acac)$ **5**. Acetylacetone (0.5 g, 5 mmol) was added dropwise to a solution of $Ti(OPr^i)_4$ (2.84 g, 10 mmol) in Pr^iOH (30 cm^3). The solution was stirred at room temperature for 1 h then evaporated under reduced pressure until an oil remained. This was redissolved in Pr^iOH (30 cm^3) and solid $Pb(O_2CCH_3)_2$ (3.25 g, 10 mmol) added. The mixture was refluxed until all solid had dissolved giving a green-yellow solution. This was filtered and allowed to stand at −20°C and crystalline material (ca 1 g) slowly deposited. Yield: 20%. EMA: Pb : Ti = 1 : 1. Found: C, 24.0; H, 4.09. Calc: for $C_{30}H_{62}O_{17}Pb_3Ti_3$: C, 24.6; H, 4.25% Mol. wt. (Pr^iOH) 1500 ± 50. (theor. for $C_{30}H_{62}O_{17}Pb_3Ti_3$, 1460). NMR: ^1H ($CDCl_3$): δ = 1.19–1.30 (d, $OCH(C\underline{H}_3)_2$, 42H); 1.95–2.24 (s, $O_2CC\underline{H}_3$ and $C\underline{H}_3$ acac total 12H); 4.01–4.83 (sp, $OC\underline{H}(CH_3)_2$ 7H); 5.51 (s, $C\underline{H}$ acac 1H) ppm: ^{13}C ($CDCl_3$): δ = 21.1, 21.8, 22.5 ($O_2C\underline{C}H_3$); 24.7, 25.3 ($OCH(\underline{C}H_3)_2$); 26.6 ($\underline{C}H_3$ acac); 76.6, 78.3 ($O\underline{C}H(CH_3)_2$), 102.6 ($\underline{C}H$ acac); 170.5, 178.8 ($O_2\underline{C}CH_3$); 187.2, 191.2 ($\underline{C}O$ acac) ppm. IR (CCl_4): 1590 (s), 1567 (s), 1526 (s), 1419 (s), 1372 (s), 1127 (m), 1019 (m), 663 (s), 650 (s) cm^{-1}.

$Pb_3Ti_3(O)_4(O_2CCH(CH_3)_2)_2(OPr^i)_8$ **4**. $Pb(O_2C$-

$CH(CH_3)_2)_2$ (1.91 g, 5 mmol) was dissolved in toluene (20 cm^3) then $Ti(OPr^i)_4$ (1.5 ml, 5 mmol) added dropwise. The mixture was warmed at 60°C for several hours then filtered and allowed to stand at room temperature for some days until a small crop (ca 500 mg) of crystals appeared. EMA: Pb: Ti = 1: 1. Found: C, 24.8; H, 4.56. Calc. for $C_{32}H_{70}O_{16}Pb_3Ti_3$: C, 26.0; H, 4.74% M. wt. (benzene): 1445 ± 50 (theor. for $C_{32}H_{70}O_{16}Pb_3Ti_3$, 1476). IR (Nujol): 2926 (vs), 2855 (vs), 1561 (vs), 1532 (vs), 1410 (vs), 1360 (vs), 1274 (vs), 1167 (s), 1117 (vs), 1094 (vs), 972 (s), 928 (m), 850 (s), 811 (s), 765 (m), 727 (vs), 694 (m), 627 (vs) cm^{-1}.

1:2 *Pb*: *Ti ratio compounds*

$Pb_2Ti_4(O)_2(O_2CCH(CH_3)_2)_2(OPr^i)_{14}$ **3**. $Ti(OPr^i)_4$ (2.83 g, 10 mmol) was added dropwise to a suspension of $Pb(O_2CCH(CH_3)_2)_2$ (3.81 g, 10 mmol) in Pr^iOH (30 cm^3) and the mixture refluxed for 20 min. The resulting solution was filtered hot and crystals grew as it cooled to room temperature. Yield: 91%. M.pt. 72–72°C. EMA: Pb: Ti, 1: 2. found: C, 36.7; H, 6.85. Calc. for $C_{50}H_{112}O_{20}Pb_2Ti_4$: C, 36.6; H, 6.84%. Mol. wt. (toluene): 1620 ± 50 (theor. for $C_{50}H_{112}O_{20}Pb_2Ti_4$, 1639). NMR: ^1H (d^8-toluene): $\delta = 1.19$ (d, $O_2CCH(C\underline{H}_3)_2$, 12H, $J = 7.0$ Hz); 1.25, 1.35, 1.52, 1.55 (d $OCH(C\underline{H}_3)_2$, 84H, $J = 6.1$ Hz); 2.46 (sp $O_2CC\underline{H}(CH_3)_2$ 2H, $J = 6.1$ Hz) ppm.

$Pb_2Ti_4(O)_2(O_2CCH_3)_2(OEt)_{14}$ **8** *from "basic" lead acetate*. $Ti(OPr^i)_4$ (2.86 g, 10 mmol) was dissolved in ethanol (30 cm^3) and the solution stirred at room temperature for 30 min before evaporating under reduced pressure until an oily "waxy" solid remained. This was redissolved in ethanol (30 cm^3) and the solution added dropwise to a suspension of "basic" lead acetate (3.04 g, 2.50 mmol) in EtOH (50 cm^3). The resulting mixture was refluxed for 1 h then allowed to cool to room temperature and colourless crystals separated. The complex is readily soluble in hexane, benzene and toluene. Yield: 70%. EMA: Pb: Ti, 1: 2. Found: C, 27.8; H, 5.40. Calc. for $C_{32}H_{76}O_{20}Pb_2Ti_4$: C, 27.7; H, 5.48%. Mol. wt. (benzene): 1350 ± 50 (theor. for $C_{32}H_{76}O_{20}Pb_2Ti_4$, 1387). NMR: ^1H ($CDCl_3$) 300 K: $\delta = 1.22$, 1.24, 1.26 (t, $OCH_2C\underline{H}_3$); 1.98 (s, $O_2CC\underline{H}_3$); 3.72–4.56 (broad band of poorly resolved quartets, $OC\underline{H}_2CH_3$): 217 K: $\delta = 1.20$, 1.23, 1.25 (t, $OCH_2C\underline{H}_3$); 1.98 (s, $O_2CC\underline{H}_3$); 3.70, 4.09, 4.44, 4.51, 5.14 (q, $OC\underline{H}_2CH_3$) ppm; (C_6D_6) 300 K: $\delta = 1.30$, 1.35, 1.54 (t, $OCH_2C\underline{H}_3$); 2.01 s, $O_2CC\underline{H}_3$); 4.53, 4.68, 4.90 (q, $OC\underline{H}_2CH_3$) ppm. ^{13}C ($CDCl_3$): $\delta = 17.8$, 18.4, 19.2 ($OCH_2\underline{C}H_3$); 26.2 ($O_2C\underline{C}H_3$); 68.5, 69.2, 71.0, 72.2 ($O\underline{C}H_2CH_3$); 183.0 ($O_2\underline{C}CH_3$) ppm. IR (Nujol): 1564 (vs), 1434 (vs), 1372 (s), 1131 (s), 1094 (s), 1052 (s), 925 (m), 895 (m), 663 (m) cm^{-1}.

Reaction with $Ti(OPr^n)_4$-"$[Pb_2(O_2CCH_3)_3(OPr^n)]$"

$Ti(OPr^n)_4$ (2.84 g, 10 mmol) was dissolved in Pr^nOH (50 cm^3) and $Pb(O_2CCH_3)_2$ (3.25 g, 10 mmol) added. The mixture was refluxed for 1 h as the acetate dissolved. The resulting clear yellow solution was cooled to room temperature and a white solid precipitated. It recrystallised from Pr^nOH. EMA: Pb only. Found: C, 16.7; H, 2.66. Calc. for $C_9H_{16}O_7Pb_2$: C, 16.6; H, 2.46%. NMR: $^1H(CDCl_3)$: $\delta = 0.94$ (t, $OCH_2CH_2C\underline{H}_3$, 3H); 1.60 (sex, $OCH_2C\underline{H}_2CH_3$, 2H); 2.04 ($O_2CC\underline{H}_3$, 9H); 3.61 (t, $OC\underline{H}_2CH_2CH_3$, 2H). IR (Nujol): 1159 (s), 1423 (s), 1227 (m), 1105 (m), 1070 (s), 1017 (s), 888 (w), 721 (s), 665 (s) cm^{-1}. MS: $m/z = 593$ ($Pb_2(O_2CCH_3)_3^+$, 5%); 489 ($Pb_2O(O_2CCH_3)^+$, 3%); 267 ($Pb(O_2CH_3)^+$ 100%).

Reactions with PbO

$Pb_2Ti_4(\mu\text{-}O)_2(O_2CCH_3)_2(OEt)_{14}$ **8**. $Ti(OEt)_4$ (0.82 g, 3.60 mmol) was dissolved in ethanol (30 cm^3) and glacial acetic acid (0.22 g, 3.60 mmol) added. The mixture was heated under reflux for 30 min, cooled, then PbO (0.8 g, 3.6 mmol) added and the mixture returned to reflux for 3 h. The solution was filtered and left until crystallisation occurred. Found: C, 27.8; H, 5.40. Calc. for $C_{32}H_{76}O_{22}Pb_2Ti_4$: C, 27.7: H, 5.48%. EMA: Pb: Ti, 1: 2. ^{207}Pb NMR (toluene): sharp peak at 2868 ppm.

$Pb_2Ti_2(\mu\text{-}O)(OEt)_8(acac)_2$ **6**. Acetylacetone (1 g, 10 mmol) was added to a solution of $Ti(OEt)_4$ (2.29 g, 10 mmol) in EtOH (50 cm^3), the mixture refluxed for 30 min then cooled to room temperature. PbO (2.23 g, 10 mmol) was then added and the mixture heated at reflux for a further 3 h. The solution was filtered, reduced to half its volume under reduced pressure and allowed to stand whereupon a white solid slowly precipitated. It was recovered by filtration, washed with EtOH and dried under reduced pressure. EMA: Pb: Ti = 1: 1. Found: C, 26.3; H, 4.45. Calc. for $C_{26}H_{54}O_{13}Pb_2Ti_2$: C, 28.7; H, 5.02%. Mol. wt. (benzene): 900 ± 50 (theor. for $C_{26}H_{54}O_{13}Pb_2Ti_2$, 1085). NMR: ^1H ($CDCl_3$): $\delta = 1.19$, 1.22, 1.24 (t, $OCH_2C\underline{H}_3$, 24H); 1.94, 2.05 (s, $C\underline{H}_3$ acac, 12H); 4.42, 4.46 (q, $OC\underline{H}_2CH_3$, 16H); 5.55 (s, $C\underline{H}$ acac, 2H) ppm. ^{13}C ($CDCl_3$): $\delta = 18.3$, 20.2, 20.8, 26.8 ($\underline{C}H_3$ (acac and OEt); 68.7, 72.2 ($O\underline{C}H_2CH_3$); 102.9 (CH acac); 188.0 (CO acac) ppm. IR (Nujol): 1594 (bvs), 1521 (vs), 1442 (vs), 1372 (vs), 1271 (vs), 1146 (vs), 1099 (vs), 1057 (vs), 897 (s) cm^{-1}.

RESULTS AND DISCUSSION

The lead carboxylates

The various lead carboxylates were conveniently prepared by the reactions of PbO, suspended in an organic solvent or water, with the appropriate acid. The heptafluorobutyrate was isolated as a trihydrate similar to the acetate whose structure has been shown to be based on chelated acetate groups bridging Pb atoms [24–26] while the anhydrous trimethylacetate was isolated from methanol solution. The dime-

Table 1. ^{207}Pb NMR spectra of lead carboxylates (concentrations were as close to 0.1 mol dm^{-3} as solubilities allowed)

Compound	Solvent	^{207}Pb chemical shifts (ppm) 300 K	(TK)
$Pb(O_2CCH_3)_2 \cdot 3H_2O$	H_2O	1552	
	MeOH	1973	1776(276) 1679(256)
	DMSO	2327 broad	
	$MeOC_2H_4OH$	1601 broad	
$Pb(O_2CCH_3)_2$	H_2O	1552	
	DMSO	2384	
$3Pb(O_2CCH_3)_2 \cdot PbO \cdot H_2O$	MeOH	no signal	3121, 2818, 2591, 1861(250)
$Pb(O_2CC_3F_7)_2 \cdot 3H_2O$	H_2O	126 broad	
	MeOH	606	116(226)
	DMSO	608	
	$MeOC_2H_4OH$	436	68(226)
	THF	1087	771(226)
$[Pb(O_2CCH(CH_3)_2)_2] \cdot 4H_2O$	$C_6D_5CD_3$		2709, 2661, 2170, 1667
$Pb(O_2CC(CH_3)_3)_2$	H_2O		1426

thylacetate, containing 2/3 of a mole of water per Pb, has been shown [23] to exist in the solid state as the cyclic hexamer $[Pb_6(O_2CCH(CH_3)_2)_{12}] \cdot 4H_2O$ soluble in solvents such as toluene. ^{207}Pb NMR data on the compounds are given in Table 1 together with that for the acetate and "basic" acetate. Single resonances were observed for the C_3F_7, $C(CH_3)_3$ and acetate compounds in water. The 4 resonances found in toluene for the sparingly water insoluble dimethylacetate have been previously discussed in terms of its hexanuclear structure [23]. Harrison *et al.* [27] have previously measured the ^{207}Pb chemical shifts of a number of lead(II) compounds PbX_2 in water, including lead acetate, and concluded that the single resonances observed were due to very rapid equilibration between cation anion complexes as in eqn. (iii). They showed that in consequence the shift values varied quite markedly with concentration unless the salt is completely ionised at all concentrations as is the perchlorate.

$$PbX_2(H_2O)_x \leftrightarrow [PbX(H_2O)_y]^+ + X^- \qquad \text{(iii)}$$

No study of the variation with concentration was made for any of the compounds examined in the present work but as far as permitted by solubility considerations, NMR measurements were made at concentrations close to 0.3 mol dm^{-3}. Allowing for conversion to chemical shifts relative to $Pb(NO_3)_2$ the value of 1552 ppm found in the present work for the acetate at 0.3 M is in good agreement with that of 1557 ppm previously reported [27].

Single ^{207}Pb resonances were also observed for the acetate and heptafluorobutyrate in several ionising coordinating solvents at 300 K and at 226 K in methanol. This implies rapid exchange between the various possible solvated species $[Pb(O_2CR)_2(solv)_x]$ and $[Pb(O_2CR)(solv)_y]^+$, the variation of chemical shift with alkanoate group indicating a difference in equilibrium constants between the complexes of the various alkanoate complexes. The presence of the highly electronegative fluorocarbon group results in a considerable shift to higher field of the observed resonances in each solvent compared to the hydrated acetate.

The "basic" acetate fails to display any resonances in MeOH at 300 K, but multiple resonances were observed at 250 K suggesting either that the compound dissociates in solution giving species that can exchange with each other sufficiently rapidly to prevent NMR detection except at low temperatures or that a single species exists with differently coordinated lead atoms which undergoes such rapid fluxional behaviour at room temperature that single atom resonances are not detected. The crystal structure of the compound has not yet been reported but the tetranuclear empirical formula of the compound, $3Pb(O_2CCH_3)_2 \cdot PbO \cdot H_2O$ [21] may suggest some structural relationship with other tetranuclear, "basic" carboxylates $M_4(\mu_4\text{-}O)(O_2CR)_6$ [28] of Zn, Be and Co which have been structurally characterised and found to have four tetrahedrally arranged metal ions coordinated to a central oxo group with carboxylate ions coordinated in O—O bridging mode to pairs of metal ions. The additional water molecule associated with the empirical formula of the Pb compound could be

coordinated at a single Pb site leading to an overall trigonal pyramidal configuration for the four Pb atoms. Ready displacement of coordinated water from one site and reattachment of MeOH solvent at other Pb sites or the changing of coordination partners of each Pb atom by "opening" and "shutting" of the acetate bridges provides plausible mechanisms of fluxional exchange for such a labile system and even for distinguishing individual Pb atoms when the exchange processes are slowed at low temperatures. The empirical formulation of an oxo group and discrete water molecule however may alternatively represent two OH groups. The only "basic" Pb unit so far structurally defined is the hexanuclear cationic species $[Pb_6O(OH)_6]^{4+}$ found in the "basic" perchlorate salt [29]. It contains one oxo group coordinated to four tetrahedrally arranged Pb atoms with the remaining two Pb atoms linked to two faces of the tetrahedron each by three triply bridging OH groups. This array leads to the presence of three differently coordinated types of Pb atoms in the solid state structure.

Reactions of lead carboxylates with $Ti(OPr^i)_4$

1 : 1 Pb : Ti *ratio complexes.* New complexes having a 1 : 1 Pb : Ti ratio have been obtained from reactions between $Pb(O_2CC_3F_7)_2$ or $Pb(O_2CC(CH_3)_3)_2$ and $Ti(OPr^i)_4$ in hot toluene solution. The solution molecular weights measured for the complexes indicate that they are of comparable stoichiometries to the structurally characterised acetate-isopropoxide complex **7** [6,7] and suggest they have the empirical formulae $Pb_2Ti_2(\mu\text{-}O)(O_2CC_3F_7)_2(OPr^i)_8$ **1** and $Pb_2Ti_2(\mu\text{-}O)(O_2CC(CH_3)_3)_2(OPr^i)_8$ **2**. The ^{207}Pb NMR spectrum of each complex **1**, **2**, **7**, in toluene (and **7** in Pr^iOH) shows two sharp resonances (Table 2), those for the heptafluorobutyrate compound being at notably higher field than for the pivalate or acetate in line with the high field shift shown by the Pb fluoroalkanoate compared to other alkanoates. The structure of complex **7** determined by Hubert-Pfalzgraf *et al.* [5,6] showed a central μ_4-O-(Pb_2-Ti_2) unit with one Pb atom (Pb(1)) 4 coordinate and the other, (Pb(2)), **5** coordinate in the solid state. The pairs of Pb and Ti atoms are each bridged by acetate groups so that there are two differently coordinated carboxylate groups in the crystal structure. The ^{207}Pb NMR spectra are in agreement with the presence of two differently coordinated Pb atoms in each of the Pb—Ti complexes. The 4-coordinate site (Pb(1)) will have a relatively lower electron density than the 5-coordinate (Pb(2)), is therefore less shielded, suggesting that the lower field (2824 ppm) resonance be tentatively assigned to Pb(1) and that at 2447 ppm to Pb(2).

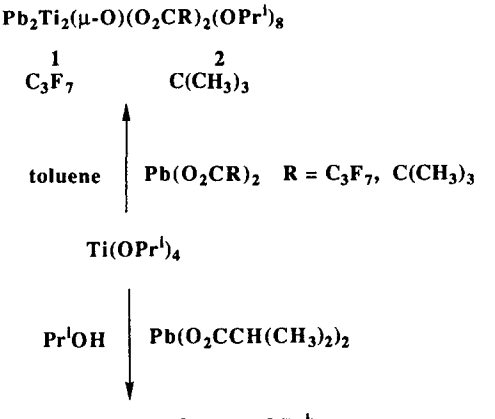

Scheme 1.

Table 2. Empirical formulae of Pb—Ti compounds and ^{207}Pb NMR spectra

Pb : Ti ratio	Complex	^{207}Pb chemical shifts[a] (ppm)
1 : 1	**1** $Pb_2Ti_2(O)(O_2CC_3F_7)_2(OPr^i)_8$	1822, 1717 (1876, 1682, 224 K)
	2 $Pb_2Ti_2(O)(O_2CC(CH_3)_3)_2(OPr^i)_8$	2814, 2336
	4 $Pb_3Ti_3(O)_4(O_2CCH(CH_3)_2)_2(O^iPr)_8$	2397, 2189 (2534, 2397, 2189 Pr^iOH)
	5 $Pb_3Ti_3(O)_4(O_2CCH_3)_7(OPr^i)_7(acac)$	2561, 2161
	6 $Pb_2Ti_2(\mu\text{-}O)(OEt)_8(acac)_2$	2688
	7 $Pb_2Ti_2(O)(O_2CCH_3)_2(OPr^i)_4$	2824, 2447 2750, 2438 (Pr^iOH)
1 : 2	**3** $Pb_2Ti_4(O)_2(O_2CCH(CH_3)_2)_2(OPr^i)_{14}$	2599, 2374, 2176 (2556 Pr^iOH)
	8 $Pb_2Ti_4(O)_2(O_2CCH_3)_2(OEt)_{14}$	2868 (2430, 2110, 1780, EtOH)

[a] Spectra measured at 300 K in toluene solution unless otherwise indicated.

Compounds **1** and **7** show ^{19}F and ^{13}C (**1**) and ^{1}H (**7**) NMR resonances indicative of two separate carboxylate groups at room temperature (see Experimental). However only one ^{1}H resonance was clearly observed for the pivalate in compound **2**. The 7 differing isopropoxide ligands seen in the solid state structure of the acetate (**7**) are not individually distinguishable in the clusters of overlapping doublets ($OCH(C\underline{H}_3)_2$ and septets ($OC\underline{H}(CH_3)_2$) due to these groups in the acetate complex or either of compounds **1** or **2**. While the NMR data reported here were obtained using a spectrometer working at 300 MHz, Hubert-Pfalzgraf *et al.* [6] only detected one ^{207}Pb resonance and one CH_3 acetate ^{1}H resonance for compound **7** at 200 MHz. They have moreover presented evidence for the existence of two fluxional species in solution based on the ^{1}H NMR detection of additional acetate resonances at $-50°C$. In support of this we have observed an increase in the number of resonances ascribable to isopropyl CH groups for compound **7** at 217 K. The molecular weights of the compounds in benzene measured in the present work indicates that little or no dissociation occurs in solution.

The ^{1}H spectrum of the heptafluorobutyrate compound also showed groups of overlapping isopropoxide CH_3 and CH signals but neither showed any marked increase in separation or increase in number at 217 K indicating a lower degree of fluxional behaviour for this complex.

1 : 2 Pb : Ti *ratio complexes*

The structural studies [7,9] of the 1 : 2 Pb—Ti complex containing acetate and ethoxide groups have established its formula to be $Pb_2Ti_4(\mu_4\text{-}O)_2(O_2CCH_3)_2(OEt)_{14}$ **8** with equivalently sited 5 coordinate Pb atoms. The molecular weight measured in toluene is in agreement with such an empirical formula while the observation of a single ^{207}Pb NMR resonance [7,9] (Table 2) indicates that it does not dissociate rapidly in that solvent. The ^{1}H NMR spectrum in $CDCl_3$ at 300 K shows three broad, partially overlapping triplets in the region expected for ethoxide CH_3 resonances. A single broad band of unresolved quartets is observed in the region expected to show methylene protons. At 217 K five peaks can be clearly seen in the methylene region but no resolution of the methyl protons was observed. The spectrum in C_6D_6 shows sets of overlapping resonances in each of the methyl and methylene regions. A single resonance due to the acetate methyl is however clearly recognised in both solvents. At lower temperatures the resonances broaden and the acetate methyl resonance shifts until it merges with the residual toluene methyl resonance at 2.1 ppm. These observations indicate a degree of fluxional behaviour for the molecule in solution probably involving interconversion of bridging and terminal alkoxide groups.

When $Pb(O_2CCH(CH_3)_2)_2$ reacts with $Ti(OPr^i)_4$ in isopropanol even in a 1 : 1 mole ratio a high yield of complex **3** having a 1 : 2 ratio of Pb : Ti is obtained. Its ^{1}H NMR spectrum shows a cluster of resonances that may be assigned to the methyl and methylene groups respectively of the isopropoxide groups together with peaks having chemical shifts representative of the dimethylacetate CH and CH_3 protons. Integration of these regions provides a ratio of OPr^i to $O_2CCH(CH_3)_2$ groups of 7 : 1. The molecular weight for the compound in toluene solution indicated the empirical formula $Pb_2Ti_4(\mu\text{-}O)_2(O_2CCH(CH_3)_2)_2(OPr^i)_{14}$ **3**, similar to that of the 1 : 2 Pb : Ti acetate/ethoxide product **8**. However three ^{207}Pb resonances were observed for the compound in toluene solution and a single resonance in Pr^iOH (Table 2). This contrasts with the single resonance shown by the 1 : 2 acetate-ethoxide compound **8**. The reaction between equimolar quantities of $Pb(O_2CCH(CH_3)_2)_2$ and $Ti(OPr^i)_4$ in toluene allowed isolation of a very small quantity of a complex **4** having a Pb : Ti ratio of 1 : 1. In contrast to the other 1 : 1 ratio compounds isolated which have a Pb_2Ti_2 composition the molecular weight of this product in toluene indicated that it contains a Pb_3Ti_3 core. Insufficient quantity of the product was isolated to allow the full range of NMR measurements to be made but the compound shows two ^{207}Pb NMR resonances in toluene solution and three in Pr^iOH (Table 2) one of the latter (2534 ppm) having close to the same chemical shift as given by the 1 : 2 complex (2556 ppm) prepared and measured in that solvent.

The influence of solvent on the formation of mixtures of Pb—Ti complexes

The reaction of $Pb(O_2CCH(CH_3)_2)_2$ and $Ti(OPr^i)_4$ in both isopropanol and toluene was further examined by removing samples from reaction mixtures containing equimolar amounts of the reagents after some hours of reflux and measuring their ^{207}Pb NMR spectra. In the case of the toluene reaction, three strong peaks at 2599, 2374 and 2176 ppm were observed in the ratio 1 : 2 : 2 together with some far less intense peaks. The sample from the isopropanol reaction similarly showed three strong resonances with almost the same chemical shifts 2529, 2343, and 2195 ppm together with several weaker peaks at lower field. Comparison with the spectra of the isolated compounds measured in each solvent thus indicates that both types of compounds with Pb_2Ti_4 and Pb_3Ti_3 cores are formed whether the reaction solvent is isopropanol or toluene. Each type of complex appears stable in one solvent but undergoes some degree of rearrangement in the other to form the second type of complex, possibly reaching an equilibrium condition. A plausible empirical formula for the 1 : 1 species formed with this combination of reagents in agreement with the

various data is $Pb_3Ti_3(O)_4(O_2CCH(CH_3)_2)_2(OPr^i)_8$ **4**. The ^{207}Pb NMR examination of the reaction mixtures shows the presence of other Pb containing species which were not identified. None of these peaks could be ascribed to the unreacted carboxylate.

X-ray structural data on the two different products is necessary if a detailed understanding of their apparent interconvertability is to be obtained. The structural features so far defined by the acetate/ethoxide 1 : 2 Pb : Ti compound **8** may not be found for the dimethylacetate/isopropoxide complex despite their similar metal ratios and ^{207}Pb NMR features while the Pb_3Ti_3 compound represents a new structural type.

The ^{207}Pb NMR spectral examination of several other reaction mixtures has also disclosed the coincident formation of other Pb : Ti ratio complexes to those which were most readily isolated. Thus a freshly prepared equimolar mixture of anhydrous $Pb(O_2CCH_3)_2$ and $Ti(OPr^i)_4$ in Pr^iOH showed not only two peaks representative of the 1 : 1 Pb : Ti compound **7** isolated but also an additional strong peak at 2987 ppm which may well be due to the parallel formation of a 1 : 2 complex similar to **8** formed by reaction between $Pb(O_2CCH_3)_2$ and $Ti(OEt)_4$. The relatively easy isolation of the 1 : 1 species 7 could be due to its lower solubility and formation in greater amount under the reaction conditions employed. The detection of only two peaks in the ^{207}Pb NMR spectrum of the pure complex dissolved in isopropanol, the solvent used in the reaction, indicates that the 1 : 1 compound retains its stoichiometry and possibly its solid state structure in the alcohol, and does not rearrange to give some 1 : 2 product. However the ^{207}Pb spectrum of the 1 : 2 Pb : Ti acetate/ethoxide complex **8** which displays only one resonance in toluene solution, shows three resonances when measured in ethanol solution indicating some form of decomposition or rearrangement of the 1 : 2 Pb : Ti compound occurs in that solvent. Samples removed at various time intervals from a refluxing equimolar mixture of $Pb(O_2CCH_3)_2$ and $Ti(OEt)_4$ in ethanol, from which can be isolated the 1 : 2 compound **8** show the same three resonances and may well indicate the parallel formation of both 1 : 2 and 1 : 1 ratio acetate-ethoxide species.

Similarly, the reaction between $Ti(OPr^i)_4$ and $Pb(O_2CC(CH_3)_3)_2$, which favoured the isolation of the 1 : 1 ratio Pb : Ti complex **2** in toluene, was also studied in refluxing isopropanol by measuring the ^{207}Pb spectra of samples of the reaction mixture withdrawn at intervals. After 30 min reaction time 5 peaks of equal intensity were observed at 2261, 2336, 2682, 2814 and 3069 ppm. These resonances occur downfield of the resonance shown by the carboxylate alone and indicate that the carboxylate had already reacted to form new species. Further refluxing for up to 3 h, showed an increase in intensity of the peaks at 2336 and 2814 ppm had become the dominant features of the spectrum. These were comparable to the chemical shifts measured in toluene for the 1 : 1 complex **2** subsequently isolated. The other peaks initially observed, although much reduced in intensity, were still detectable.

Such qualitative experiments indicate that a variety of compounds can form from reactions between Pb carboxylates and Ti alkoxides in a given solvent. The complex most readily isolated must depend on its solubility in that solvent and the concentration which it can attain because of the solvent influence on the reaction pathway. The different Pb : Ti ratio complexes may or may not be formed in equilibrium with each other.

Reactions with other Ti alkoxides

Solubility considerations appeared to dominate several other reactions attempted with $Ti(OMe)_4$, $Ti(OBu^n)_4$ or $Ti(OPr^n)_4$. Reaction between $Pb(O_2CCH_3)_2$ and either of the first two alkoxides resulted in solids shown by EMA to be mixtures of Pb and Pb—Ti products which could not be separated. $Ti(OPr^n)_4$ formed a sparingly soluble product containing only Pb whose mass spectrum showed an ion of mass 593 possibly $[Pb_2(O_2CCH_3)_3]^+$ or $[Pb_2(O_2CCH_3))_{3-x}(OPr^n)_x]^+$. Its ^1H NMR spectrum indicated the presence of acetate and alkoxide groups in the ratio 3 : 1. It appears to be $\{Pb_2(O_2CCH_3)_3(OPr^n)\}_n$ a similar type of compound to $\{Zn_2(O_2CCH_3)_3(OMe)\}_n$ [11].

Action of acetylacetone

Only one Pb—Ti complex containing acetylacetone $Pb_2Ti_2(O)(acac)_2(OPr^i)_8$ has previously been reported [8] resulting from the direct reaction of acetylacetone with the "single source" compound $Pb_2Ti_2(O)(OPr^i)_{10}$ in hexane solution. We have attempted the direct substitution of acetylacetone for other coordinated groups by reaction with $Pb_2Ti_2(O)(O_2CCH_3)_2(OPr^i)_8$ **7** in Pr^iOH and $Pb_2Ti_4(O)_2(O_2CCH_3)_2(OEt)_{14}$ **8** in EtOH. In each reaction a precipitate formed which only contained Pb together with acetate, alkoxide and acetylacetonate groups as indicated by IR spectral examination. Hubert-Pfalzgraf *et al.* [6] have reported that $Pb(O_2CCH_3)_2$ is precipitated following reaction of acetylacetone with **7** in toluene. The pretreatment of a slurry of $Pb(O_2CCH_3)_2$ in isopropanol with a solution of the ligand produced a similar insoluble Pb containing product which did not dissolve in the presence of $Ti(OPr^i)_4$ even under reflux.

A successful procedure involved the dissolution of solid $Pb(O_2CCH_3)_2$ in a Pr^iOH solution of $Ti(OPr^i)_4$ containing acac in the ratio acacH : Ti, 0.5 : 1 allowing isolation of a product having a 1 : 1 Pb : Ti ratio. The molecular weight of the complex in Pr^iOH indicated a Pb_3Ti_3 core was present. The ^{13}C NMR spectrum of the product contained peaks that could be assigned

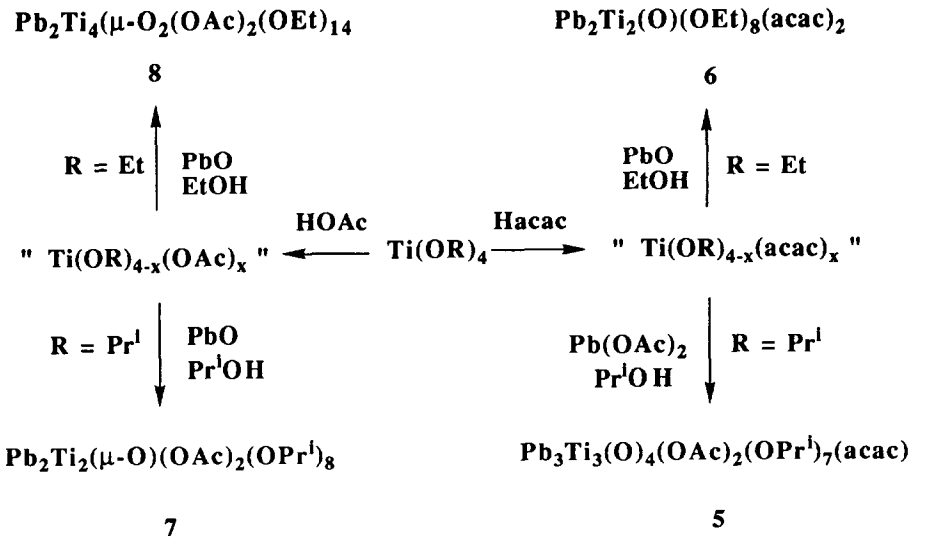

Scheme 2.

to isopropoxide, acetate and acetylacetonate groups. The shifts assigned to the acetylacetonate group were similar to those reported for that ligand in $Ti(OPr^i)_3(acac)$ [30] and $Pb_2Ti_2(O)(acac)_2(OPr^i)_8$ [8] with 2 separate CO resonances being identified suggesting unsymmetrical binding of the acetylacetonate ligand. Non-symmetric bonding of acac has been observed in the dimeric $[Al(OPr^i)_2(acac)]_2$ [31]. Two intense IR spectral bands shown by the Pb—Ti compound at 1567 cm^{-1} and 1419 cm^{-1} are assigned as $\nu_{as}(CO_2)$ and $\nu_{sym}(CO_2)$ respectively, characteristic of an acetate group symmetrically attached to a metal while the difference $\Delta\nu = 148$ cm^{-1} between these frequencies indicates a bridging mode of coordination [32]. Strong metal alkoxide vibrations are observed in the 1000–1200 cm^{-1} region. The ^1H NMR spectrum showed three septets assigned to CH protons of isopropyl groups which integrated to give a ratio of 4 : 2 : 1 from higher to lower field suggesting the presence of non-equivalent isopropyl groups. The splitting of the isopropyl methyl doublets confirms this inequivalence. The methyl resonances of the acac and acetate groups are likely to have similar chemical shifts [33] around 2 ppm. Three peaks are shown by the complex in that region. One sharp (1.95 ppm), the other two broad (2.03 and 2.09 ppm) with integration giving a 2 : 1 : 1 ratio of intensities. Since the IR spectral evidence suggests equivalent acetate coordination, the sharp NMR peak at 1.95 ppm is assigned to an acetate CH_3 resonance with the remaining broader peaks due to dissimilarly placed acac methyl groups. The sharp peak at 5.51 ppm is then assigned to the acac CH proton, the value being similar to that reported for $Ti(OPr^i)_3(acac)$ [30]. The ^{207}Pb NMR spectrum of the complex in toluene showed two broad diffuse peaks at 2561 and 2161 ppm in the ratio 2 : 1 according to the peak width at half height. This would accord with a 2 : 1 ratio of three Pb atoms in the molecule dispersed over two different types of coordination sites but the broad nature of the peaks does not preclude the existence of more separate Pb sites in the molecule with fluxional properties. These data taken in conjunction with its elemental analysis suggest the empirical formula $Pb_3Ti_3(O)_4(O_2CCH_3)_2(OPr^i)_7(acac)$ **5** with acac coordinated to Ti in an unsymmetrical mode.

Reactions involving PbO

Initial experiments showed that no reaction occurred between PbO and $Ti(OPr^i)_4$ or $Ti(OEt)_4$ when the components were refluxed in the parent alcohols but prior reaction of the alkoxide with one equivalent of either acetic acid or acetylacetone gave products which readily dissolved the oxide. Thus a Pr^iOH solution of $Ti(OPr^i)_4$, previously treated with one equivalent of acetic acid, reacted with an equimolar quantity of PbO to give a solution displaying the same ^{207}Pb NMR spectrum as a solution of $Pb(O_2CCH_3)_2$ and $Ti(OPr^i)_4$ refluxed in Pr^iOH. This was considered above to indicate a mixture of the known 1 : 1 Pb : Ti complex $Pb_2Ti_2(\mu\text{-}O)(O_2CCH_3)_2(OPr^i)_8$ **7** together with the as yet uncharacterised 1 : 2 compound $Pb_2Ti_4(\mu\text{-}O)_2(O_2CCH_3)_2(OPr^i)_{14}$. Reaction of PbO with a similarly formed Ti-acetate-ethoxide species in ethanol allowed the isolation of the known compound $Pb_2Ti_4(\mu\text{-}O)_2(O_2CCH_3)_2(OEt)_{14}$, **8** identified by its IR, ^{207}Pb and ^1H NMR spectra and elemental analysis. Similarly, a solution containing the product formed by reaction of equimolar amounts of $Ti(OEt)_4$ and acetylacetone in ethanol was refluxed with sufficient PbO to give a

1 : 1 Pb : Ti mole ratio. A product isolated from the mixture had a Pb : Ti ratio of 1 : 1 and showed only a single ^{207}Pb resonance in toluene solution (Table 2). Its ^{1}H and ^{13}C NMR spectra showed peaks assignable to ethoxide and coordinated acetylacetonate ions. Its integrated ^{1}H NMR spectrum and molecular weight suggest it is the ethoxy analogue of the isopropoxy-acetylacetonate compound previously reported by Hubert-Pfalzgraf *et al.* [8] with empirical formula $Pb_2Ti_2(O)(OEt)_8(acac)_2$ **6**. PbO failed to dissolve in a solution in which $Ti(OPr^i)_4$ had been first reacted with one mole equivalent or acetylacetone.

Although simple stoichiometric formulae $Ti(OR)_{4-n}(O_2CR)_n$ ($n = 1, 2$) have been assigned [34] earlier to the products formed when $Ti(OR)_4$ react with carboxylic acids, recent structural studies have shown that more complex species are formed. Although the specific product formed on reaction of acetic acid with $Ti(OEt)_4$ has not yet been structurally characterised, the compounds formed in other related reactions have been found to be hexanuclear oxo Ti species of the form $Ti_6(\mu\text{-}O)_4(O_2CR)_8(OR')_8$ ($R = CH_3$, $R' = Bu^n$ [35], $R = CH_3$, $R' = Et$ [36], $R = C_6H_5$, $R' = Pr^n$ [37]). The oxo groups have been suggested to derive from hydrolysis by water produced by the esterification reaction between the acid and liberated alcohol [36]. Polynuclear species have also been detected by various spectroscopic techniques in solutions of $Ti(OEt)_4$ which have reacted with acetylacetone [30]. Such considerations make it impossible to conclude from synthetic experiments alone that oxo groups derived from PbO are found in the final Pb—Ti complexes but the experiments at least show that the oxide can be a useful reagent in the synthesis of mixed Pb—Ti derivatives as an alternative to the use of preformed lead carboxylates.

Acknowledgements—This work was supported in part by Australian Research Council and Generic Industrial Research and Development grants (to L.S. and B.O.W.) and Centre for Chemical Synthesis and Overseas Research Scholarships (to Q.Z.).

REFERENCES

1. Gurkovich, S. R. and Blum, J. B., *Ultrastructure Processing of Ceramics, Glasses and Composites*, ed. L. L. Hench and D. R. Ulrich. Wiley, 1984, Chap. 12, 152.
2. Blum, J. B. and Gurkovich, S. R., *J. Mater. Sci.*, 1985, **20,** 4479; *Ferroelectrics*, 1985, **62,** 189.
3. Budd, K. D., Dey, S. K. and Payne, D. A., *Proc. Brit. Ceram. Soc.*, 1985, **36,** 107.
4. Chandler, C. D., Roger, C. and Hampden-Smith, M. J., *Chem. Rev.*, 1993, **93,** 1205.
5. Hubert-Pfalzgraf, L. G., *Polyhedron*, 1994, **13,** 1181.
6. Hubert-Pfalzgraf, L. G., Daniele, S., Papiernik, R., Massiani, M.-C., Septe, B., Vaissermann, J. and Daran, J.-C., *J. Mater. Chem.*, 1997, **7,** 753.
7. Bates, J., Zhang, Q., Spiccia, L. and West, B. O., *J. Sol-Gel Sci. Technol.*, 1994, **2,** 29.
8. Daniele, S., Papiernik, R., Hubert-Pfalzgraf, L. G., Jagner, S. and Håkansson, M., *Inorg. Chem.*, 1995, **34,** 628.
9. Chae, H. K., Payne, D. A., Xu, Z. and Ma, L., *Chem. Mater.*, 1994, **6,** 1589.
10. Ramamurthi, S. D. and Payne, D. A., *Mater. Res. Soc. Symp. Proc.*, 1990, **180,** 79.
11. Chandler, C. D., Fallon, G. D. and West, B. O., *Polyhedron*, 1993, **12,** 2001.
12. Milne, S. J. and Pyke, S. H., *J. Am. Ceram. Soc.*, 1991, **74,** 1407.
13. Ariizumi, A., Kawamura, K., Kikuchi, I. and Kato, I., *Jap. J. Appl. Phys.*, 1985, **24,** Supp. 24-3, 7.
14. Turova, N. Ya., Turevskaya, E. P., Kessler, V. G. and Yanovskaya, M. I., *J. Sol-Gel Sci. Technol.*, 1994, **2,** 17.
15. Caulton, K. G. and Hubert-Pfalzgraf, L. G., *Chem. Rev.*, 1990, **90,** 969.
16. Mehrotra, R. C. and Singh, A., *Chem. Soc. Rev.*, 1996, **25,** 1.
17. Hayashi, Y. and Blum, J. B., *J. Mater. Sci.*, 1987, **22,** 2655.
18. Dekleva, T. W., Hayes, J. M., Cross, L. E. and Geoffroy, G. L., *J. Am. Ceram. Soc.*, 1988, **71,** C-280.
19. Kezuka, K., Hayashi, Y. and Yamaguchi, T., *J. Am. Ceram. Soc.*, 1989, **72,** 1660.
20. Hodes, L., Bioul, J. P., Durbut, P., Hamitou, A., Marbehaut, J. L., Ouhadi, T., Stevens, C. C. and Teyssié, P., *J. Mol. Catal.*, 1977/78, **3,** 135; Ouhadi, T., Bioul, J. P., Stevens, C., Warrin, R., Hochz, L. and P. Teyssié, *Inorg. Chim. Acta*, 1976, **19,** 203.
21. Kwestroo, W. and Langereis, C., *J. Inorg. Nucl. Chem.*, 1965, **27,** 2533.
22. Dechter, J. J., *Prog. Inorg. Chem.*, 1982, **29,** 285; Harris, R. K., Kennedy, J. J. and McFarland, W., *NMR and the Periodic Table*, ed. R. K. Harris and B. E. Mann. Academic Press, New York, 1978.
23. Zhang, Q., Fallon, G. D., West, B. O. and Spiccia, L., *Polyhedron*, 1996, **16,** 19.
24. Harrison, P. G. and Steel, A. T., *J. Organometal. Chem.*, 1982, **239,** 105.
25. Rajaram, R. K. and Mohana Rao, J. K., *Z. Kristallogr.*, 1982, **160,** 225.
26. Bryant, R. G., Chacko, V. P. and Etter, M. C., *Inorg. Chem.*, 1984, **23,** 3580.
27. Harrison, P. G., Healy, M. A. and Steel, A. T., *J. Chem. Soc., Dalton Trans.*, 1983, 1845.
28. *Zn-acetate*: Koyama, H. and Saito, Y., *Bull. Chem. Soc. Jpn*, 1954, **27,** 112; pivalate and benzoate; Clegg, W., Harbron, D. R., Homan, C. D., Hunt, P. A., Little, I. R. and Straughan, B. P., *Inorg. Chim. Acta*, 1991, **186,** 51. *Be-acetate*: Tulinsky, A. and Worthington, C. R., *Acta Crystallogr.*, 1959, **12,** 626. *Co-pivalate*: Blake, A. B., *J. Chem. Soc., Chem. Commun.*, 1966, 569.
29. Spiro, T. G., Templeton, D. H. and Zalkin, A., *Inorg. Chem.*, 1969, **8,** 856; Olin, A. and Soderquist, R., *Acta Chem. Scand.*, 1972, **26,** 3505.
30. Léaustic, A., Babonneau, F. and Livage, J., *Chem. Mater.*, 1989, **1,** 240.

31. Garbauskas, M. F., Wengrovius, J. H., Going, R. C. and Kasper, J. S., *Acta Crystallogr.*, 1984, **C40,** 1536; Wengrovius, J. H., Garbauskas, M. F., Williams, E. A., Going, R. C., Donahue, P. E. and Smith, J., *J. Am. Chem. Soc.*, 1986, **108,** 982.
32. Deacon, G. B. and Philipps, R. J., *Coord. Chem. Rev.*, 1980, **33,** 227.
33. Szymanski, H. A. and Yelin, R. E., *NMR Band Handbook*. IFI/Plenum Data Corporation, New York, 1968.
34. Varma, I. D. and Mehrotra, R. C., *J. prakt, Chem.*, 1959, **8,** 235.
35. Doeuff, S., Dromzee, Y., Taulelle, F. and Sanchez, C., *Inorg. Chem.*, 1989, **28,** 4439.
36. Gautier-Luneau, I., Mosset, A. and Galy, J., *Z. Kristallogr.*, 1987, **180,** 83.
37. Ammala, P., Hockless, D. C. R. and West, B. O., to be published.

Pergamon

PII: S0277-5387(97)00524-X

Polyhedron Vol. 17, Nos. 11–12, pp. 1863–1869, 1998
© 1998 Elsevier Science Ltd
All rights reserved. Printed in Great Britain
0277-5387/98 $19.00+0.00

TCB bridged binuclear and polynuclear copper(II) complexes: a novel three dimension-network structure complex $[(Cudien)_2(Cudien \cdot H_2O)TCB\ (ClO_4)_2 \cdot H_2O]_n$ (TCB = tetracarboxylatobenzene, dien = 3-azapentane-1,5-diamine)

Jian-Zhong Zou,[a]† Qi Liu,[a] Zheng Xu,[a]* Xiao-Zeng You[a] and Xiao-Ying Huang[b]

[a] Coordination Chemistry Institute, State Key Laboratory of Coordination Chemistry, Nanjing University, Nanjing (210093), PR China

[b] State Key Laboratory of Structural Chemistry, Fujian Institute of Research on the Structure of Matter, Chinese Academy of Science, Fuzhou (350002), PR China

(Received 6 August 1997; accepted 11 December 1997)

Abstract—The binuclear copper(II) complexes $[(Cudipn \cdot H_2O)_2\ TCB] \cdot 8H_2O$ and the three-dimensional network complex $[(Cudien)_2(Cudien \cdot H_2O)TCB\ (ClO_4)_2 \cdot H_2O]_n$, where TCB stands for tetracarboxylatobenzene, dipn is *N*-(3-aminopropyl)-1,3-propanediamine, dien is 3-azapentane-1,5-diamine, were synthesized and characterized by IR, ESR and magnetic susceptibility. The compound $[(Cudipn \cdot H_2O)_2TCB] \cdot 8H_2O$ is a TCB bridging binuclear Cu(II) complex. The complex $[(Cudien)_2\ (Cudien \cdot H_2O)TCB\ (ClO_4)_2 \cdot H_2O]_n$ crystallizes in the monoclinic system, space group C2/c, with $a = 26.257(9)$, $b = 8.087(2)$, $c = 19.301(7)$ Å, $\beta = 116.41(3)^\circ$ and $Z = 4$. The copper atoms have two kinds of coordination environment. Cu(2) atom is coordinated in an elongated octahedral arrangement by three nitrogen atoms from dien, two oxygen atoms from two carboxyl groups of two adjacent TCB molecules and one oxygen atom from the water molecule. The other kind of copper atoms Cu(1) and Cu(1c) are coordinated in a square pyramidal environment by three nitrogen atoms from dien and two oxygen atoms from two adjacent TCB molecules, one of which lays above or below the 2-D network plane. These form a three-dimensional network structure. Moreover four carboxyl groups of TCB^{4-} are divided to two types by their different coordination mode: (1) two *para*-carboxyl groups C(14)O(1)O(2) bridge the copper atom Cu(2) with one oxygen atom O(1) in monodentate fashion, (2) other two-carboxyl groups C(15)O(3)O(4) coordinate to Cu(1) and Cu(1d) in a bridging bidentate fashion. The magnetic susceptibility shows the weak antiferromagnetic interaction in two compounds because of the longer distances between two paramagnetic centers. © 1998 Elsevier Science Ltd. All rights reserved

Keywords: crystal structure; polynuclear copper(II) complexes; tetracarboxylatobenzene bridged; magnetic properties.

Owing to its fundamental importance, the study of polynuclear complexes has been an active field of coordination chemistry in recent years [1]. Particular attention is now being paid to synthesis extended transition metal complexes with increasing dimensionally in order to provide efficient exchange pathways between metal ions. Different bridging ligand systems such as cyanide [2], oxalate [3] and oxalate-type ligands [4], end-to-end azide [5], croconate (4,5-dihydroxycyclopent-4-ene-1,2,3-trionate [6], 2,5-dihydroxy-1,4-benzoquinone and its derivatives [7], squa-

* Author to whom correspondence should be addressed.

† Present address: Department of Chemistry & Chemical Engineering, Southeast University, Nanjing (210096), PR China.

rate (3,4-dihydroxycyclobut-3-ene-1,2-dionate) [8], 4,4-bipyridine [9], terephthlate [13–19] have successfully been used to construct polymeric coordination compounds as chains or two or three dimensional infinite networks. Similar to the terephthlate anion, the tetracarboxylatobenzene anion appears to be an ideal ligand with which polynuclear copper(II) compounds are obtained [20], since four carboxyl group, eight O-donor atoms are available for coordination. Furthermore, carboxyl ligand has shown a good capable of bridging and providing exchange pathways when paramagnetic metals are involved. For example [21], they form binuclear or polynuclear complexes with transition metal ions via two oxygen atoms coordinating to two metal atoms, separately, forming a three-atom bridge or even via a single oxygen atom coordinating to two metals forming a one atom bridge.

Continuing our interest in the synthesis of terephthlate anion bridging polynuclear complexes [22], we report a novel three dimension net-work structure of polynuclear copper(II) complex $[(Cudien)_2(Cudien \cdot H_2O)TCB(ClO_4)_2 \cdot H_2O]_n$. To our knowledge, this is the first report about tetracarboxylatobenzene bridging three-dimension polynuclear copper(II) complex.

EXPERIMENTAL

Materials

Dien (3-azapentane-1,5-diamine), dipn (*N*-(3-aminopropyl)-1,3-propane-diamine) and copper(II) perchlorate hexahydrate were used as purchased. Piperidimium tetracarboxylatobenzene was prepared by the literature method [22]. Element analyses (C, H, N) were determined on a Perkin–Elmer 240C microanalysis instrument. IR absorption spectra, as KBr pellets, were recorded on a Nicolet FTIR 170X spectrophotometer. The EPR spectra were recorded on a Bruker ER 200D-SRC. Variable-temperature magnetic susceptibilities were determined on a CF-1 ESM magnetic balance (1.5–300 K) and a CAHN-2000 magnetic balance (75–300 K).

Preparation of $[(Cudien)_2(Cudien \cdot H_2O)TCB(ClO_4)_2 \cdot H_2O]_n$ (**1**)

A methanol solution (50 ml) of copper(II) perchlorate hexahydrate (1.48 g, 4 mmol) was slowly added to the same solution (10 cm^3) of dien (0.43 cm^3, 4 mmol) with stirring. Then the methanol solution (20 cm^3) of piperidimium tetracarboxylatobenzene (594 mg, 1 mmol) was added dropwise. The blue precipitate appeared very soon. The mixture was cooled under refluxing for 1 h, then filtered, washed with methanol and dried. The blue solid was redissolved in hot water (50 cm^3), filtered and the filtrate set aside for one month at room temperature, the blue single crystals were obtained. Calc. (Found) for $C_{22}H_{45}N_9O_{18}Cl_2Cu_3$, C, 26.56 (26.82); H, 4.76 (4.60); N, 12.80 (12.58); Cu, 19.35 (19.00). IR spectrum: 3347 cm^{-1} (s), 3317 (vs), 3248 (s), 3136 (s), 2972 (m), 2933 (s), 2874 (m), 1610 (vs), 1569 (sh), 1564 (vs), 1455 (m), 1409 (s), 1366 (s), 1140 (m), 1100 (vs), 1080 (vs), 1025 (s), 816 (m), 625 (m).

Preparation of $[(Cudipn \cdot H_2O)_2TCB] \cdot 8H_2O$ (**2**)

The same method was followed as for the preparation of the compound (**1**). The blue solid of compound (**2**) was obtained, then redissolved in water. A few days later, the blue crystals were obtained. Calc. (Found) for $C_{22}H_{56}N_6Cu_2O_{18}$: C, 32.03 (32.23), H, 6.62 (6.83), N, 9.62 (10.25). IR spectrum: 3459 cm^{-1} (s), 3378 (s), 3279 (vs), 3136 (s), 2939 (s), 2875 (s), 1690 (sh), 1611 (s), 1572 (vs), 1481 (m), 1412 (m), 1367 (vs), 1322 (s), 1136 (m), 1041 (m), 864 (m), 819 (m).

X-ray structure determination of $[(Cudien)_2(Cudien \cdot H_2O)TCB(ClO_4)_2 \cdot H_2O]_n$

A blue prism crystal with dimensions of $0.65 \times 0.35 \times 0.25$ mm was mounted on an Enraf–Nonius CAD4 diffractometer for data collection using graphite-monochromatic Mo-K_α radiation ($\lambda = 0.71069$ Å) at 296 K. 3445 reflections were collected, of which 3371 were independent and 2399 observed with $I > 3\sigma(I)$. Data were corrected for Lorentz and polarization effects and empirical absorption. The structure was solved by Patterson method, followed by Fourier syntheses and refined by full matrix least squares methods with anisotropic thermal parameters for all non-hydrogen atoms. During the refining, the atoms Cu(2), N(5) and O(5) lie on the C_2 axis, however, in order to reduce the R factor and the remaining peak, let the Cu(2) and N(5) atoms deviate a little from the special site (0, y, 1/4). All hydrogen atoms were found from the difference Fourier map and were refined with isotropic thermal parameters. All calculations were performed on MICRO VAX3100 computer using the MSC TEXSAN V.2.1 programs. The final R value is 0.049 and refinement with the complete data set yielded $\omega R = 0.061$. The crystallographic data are summarized in Table 1.

RESULTS AND DISCUSSION

Crystal structure

Selected bond lengths and angles are shown in Table 2. Figure 1 presents the structure of the cation $[(Cudien)_2(Cudien \cdot H_2O)TCB]^{2+}$ with the atomic-numbering scheme. The unit possesses a center symmetry. Four carboxyl groups of the tetracarboxylatobenzene (TCB^{4-}) anion coordinated to six copper(II) ions with

Table 1. Crystallographic data for $[(Cudien)_2(Cudien\cdot H_2O)TCB(ClO_4)_2\cdot H_2O]_n$

Formula weight	985.19
Temperature	296 K
λ (Mo-K_α)	0.71069 Å
Crystal system	Monoclinic
Space group	$C2/C$
a (Å)	26.257(9)
b (Å)	8.087(2)
c (Å)	19.301(7)
β (°)	116.4(3)
V	3671(2) Å^3
D_c	1.78 Mg/m^3
Absorption coefficient (μ)	1.958 mm^{-1}
Data collection range (θ)	1–25°
Reflections collected	3445
Independent reflections ($I > 2\sigma(I)$)	3371
R (WR)	0.049 (0.061)

two kinds of coordination environment. Two copper(II) ions Cu(2), Cu(2c) have octahedral geometry, of which the equatorial plane consisted of N(4), N(5) and N(4a) from dien and oxygen atom O(5) of the water molecular and the apical positions are occupied by two oxygen atoms O(1) and O(1b) from the carboxyl groups of two TCB^{4-} anions in monodentate fashion, which forms a linear chain. Each of other four copper(II) ions Cu(1), Cu(1c), Cu(1d) and Cu(1e) are located in a square pyramidal environment, as for the Cu(1), the basal plane consists of N(1), N(2) and N(3) of dien and O(3) from carboxyl group of TCB^{4-} anion, the axial is occupied by O(4a) from the carboxyl group of TCB^{4-} anion located on the next layer below the 2-D network plane. All these form a three dimension structure. The coordination environments of these copper atoms are analogous to those in compound (**2**). The molecular structure of the complex $[(Cudipn\cdot H_2O)_2TCB]\cdot 8H_2O$ [22] had been reported (Fig. 2). In the complex (**2**), two copper atoms locate in a square pyramidal environment. The basal plane consists of three nitrogen atoms of dipn and oxygen atom of carboxyl group of TCB^{4-} anion, but the axial

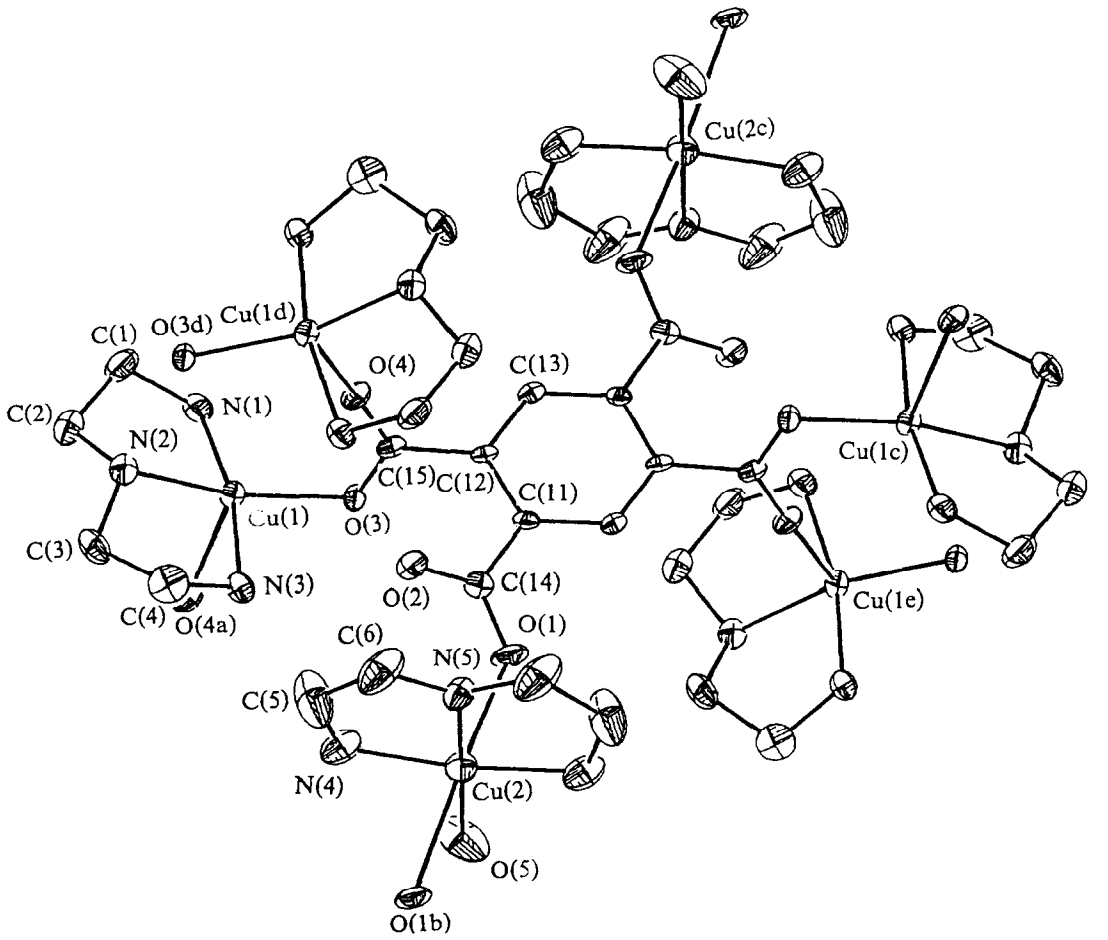

Fig. 1. View of the structure of the title complex (ellipsoids at the 50% probability level).

Table 2. Selected bond lengths (Å) and bond angles (°)

Cu(1)—O(3)	1.975(3)	Cu(1)—N(2)	1.983(4)
Cu(1)—N(1)	1.989(5)	Cu(1)—N(3)	1.989(4)
Cu(1)—O(4a)	2.407(4)	Cu(2)—N(4)	1.912(7)
Cu(2)—N(5)	1.990(9)	Cu(2)—O(5)	1.982(6)
Cu(2)—N(4b)	2.082(7)	O(2)—N(5b)	2.109(9)
Cu(2)—O(1)	2.350(5)	Cu(2)—O(1b)	2.845(5)
O(3)—Cu(1)—N(2)	161.1(2)	O(3)—Cu(1)—N(1)	99.4(2)
O(3)—Cu(1)—N(3)	92.4(2)	O(3)—Cu(1)—O(4a)	98.1(1)
N(2)—Cu(1)—N(1)	85.3(2)	N(2)—Cu(1)—N(3)	85.3(2)
N(2)—Cu(1)—O(4a)	100.4(2)	N(1)—Cu(1)—N(3)	166.9(2)
N(1)—Cu(1)—O(4a)	88.4(2)	N(3)—Cu(1)—O(4a)	84.2(2)
N(4)—Cu(2)—N(5)	83.1(4)	N(4)—Cu(2)—O(5)	97.4(2)
N(4)—Cu(2)—N(4b)	160.7(2)	N(4b)—Cu(2b)—N(5)	87.6(3)
N(4)—Cu(2)—O(1)	110.3(2)	N(5)—Cu(2)—O(5)	176.5(3)
N(5)—Cu(2)—N(4b)	86.4(4)	N(5)—Cu(2)—O(1)	92.7(3)
O(5)—Cu(2b)—N(4)	92.1(2)	O(5)—Cu(2b)—N(5)	152.1(2)
O(5)—Cu(2)—O(1)	90.3(1)	N(5)—Cu(2b)—N(4)	76.3(3)
N(4)—Cu(2)—O(1)	86.3(2)	O(5)—Cu(2b)—O(1)	77.1(3)
N(4b)—Cu(2b)—O(1)	76.5(3)	N(4)—Cu(2b)—O(1)	89.4(2)
N(5b)—Cu(2b)—O(1)	99.7(3)		

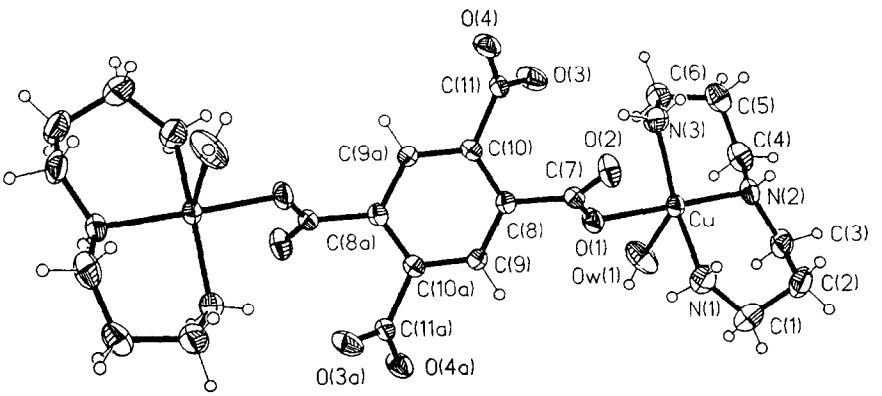

Fig. 2. The molecular structure of the complex $[(Cudipn \cdot H_2O)_2TCB] \cdot 8H_2O$.

position is occupied by the oxygen atom of water molecule. In the complex (**1**), the bond angles of O(4a)—Cu(1)—N(1), O(4a)—Cu(1)—N(2), O(4a)—Cu(1)—N(3) and O(4a)—Cu(1)—O(3) are 88.4 (2)°, 100.4 (2)°, 84.2 (2)° and 98.1 (1)°, respectively. The Cu(1) atom deviates 0.0139 Å from the least square plane consisting of O(3)N(1)N(2)N(3). But in the complex (**2**), the Cu atom lies in the square plane very well, which consists of four atoms: O(1), N(1), N(2) and N(3). It is possible that dipn is more flexible than dien, which produces two quite different results: the complex (**1**) has an infinite structure and the complex (**2**) has a binuclear structure with molecularity.

Four carboxyl groups of TCB^{4-} are divided into two kinds by different coordination modes in complex (**1**). Two *para*-carboxyl groups C(14)O(1)O(2) coordinate to Cu(2) with one oxygen atom O(1) in monodentate fashion. The distance of Cu(2)—O(1) is 2.350(5) Å, which is longer than that of the normal Cu—O (carboxylate) (1.927–2.010 Å) [24]. The distance between the two copper ions Cu(2) and Cu(2c) which were bridged by TCB unit is 10.949(2) Å which is shorter than that in complex (2) (11.194 Å). The other two *para*-carboxyl groups C(15)O(3)O(4) are bound to the Cu(1) and Cu(1d) in a bridging bidentate fashion with a short bond Cu(1)—O(3) (1.957(3) Å) and a long bond Cu(1d)—O(4) (2.407(4) Å). The distance between Cu(1) and Cu(1d) atoms is 4.230(1) Å, this value is the shortest intramolecular distance in complex (**1**).

A carboxylate ion can coordinate to a metal atom in a number of ways [25]. Up to date, five coordination types of carboxyl group have been found, as shown in

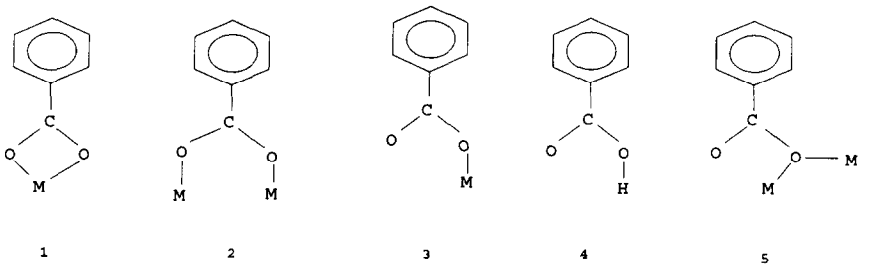

Fig. 3. The coordinating fashion of carboxyl group.

Fig. 3. Their coordination fashions are different: (1) as a bidentate ligand to coordinate with one metal ion; (2) as a bidentate ligand to bridge two metal centers; (3) as a monodentate ligand to bind a metal ion; (4) free COO^- group forming a hydrogen bond with crystal water or coordination water; and (5) as a monoatomic bridge, binding two metal ions. The coordination models of (3) and (4) are present in some carboxyl complexes [13–18]. The mode (5) appears in a few examples [26]. Usually, if the carboxyl group coordinated with mode (2), a layered or three dimensional structure could be formed, such as in a layered structure manganese(II) mellitate $[Mn_2(C_6(COO)_6(H_2O)_6]\,[Mn(H_2O)_6]\cdot 2H_2O]$ [25], the carboxyl groups coordinated to manganese(II) with the model (2). In the complex (**1**), the four carboxyl groups exist in two modes: (2) and (3), a 3-D network structure is obtained. But the other coordinating modes often form molecular complexes. Two *para*-carboxyl groups acted as the model (3) and the other two carboxyl groups are free COO^- (as the model (4)) in the complex (**2**) [22], the complex is a TCB bridging molecular complex.

The crystal packing diagram of the complex $[(Cudien)_2(Cudien\cdot H_2O)\ TCB(ClO_4)_2\cdot H_2O]_n$ is shown in Fig. 4. The noncoordinated perchlorate anions (ClO_4^-) and water molecules fill in the space of an infinite three-dimensional network structure. There are three linear chains in the crystal, one along the diagonal of the cell unit, Cu(2) ions are linked together through the TCB^{4-} unit, in which the carboxyl groups act as in mode (3). The other one along the *c* axis, the carboxyl groups act as the mode (2). Along the *b* axis through the crystal lattice, there is a zigzag chain, in which Cu(1) ions are linked together by carboxyl groups acting as mode (2) from the adjacent layer.

There are six copper atoms around the TCB^{4-} ion and each copper(II) atom is coordinated by the two adjacent TCB^{4-} unit, so, there are three copper(II) ions in each unit.

IR spectrum

The strong broad band at 1569 cm^{-1}, 1564 cm^{-1} and 1366 cm^{-1} for the $\nu_{as}(COO)$ and $\nu_s(COO)$ stretching modes of carboxyl group and ν_s–ν_{as}: 203 cm^{-1} and 198 cm^{-1} respectively in complex (**1**) suggest that there exist two kinds of coordination mode for all carboxyl groups of the TCB^{4-} ligand: an amphimonodentate (end to end) and an anisobidentate (*syn-anti*) coordination models [27] which is proved by the X-ray crystal structure analysis. But for complex (**2**), the shoulder peak at 1690 cm^{-1} belongs to the stretching vibration of the carboxyl free group COO^-. The strong broad bands at 1572, 1367 cm^{-1} are the $\nu_{as}(COO)$ and $\nu_s(COO)$ stretching modes of the monodentate coordinating carboxyl group of TCB [28]. This structure has been proved in our previous work [22].

EPR and magnetic properties

The EPR spectra recorded at room temperature show an isotropic spectrum with $g_{av} = 2.11$ for compound (**1**) and $g_\perp = 2.056$ for compound (**2**). In both the complexes, the half-field peaks are not found which means that the exchange interaction between copper(II) atoms in two compounds are very weak. Variable temperature (1.5–300 K) magnetic susceptibility data were collected for a crystal sample of the complex (**1**). The temperature dependence of the reciprocal magnetic susceptibility $1/\chi_M$ is a linear relationship in the range of 6–300 K with the Weiss constant $\theta = -1.5$, suggesting a very weak antiferromagnetic interaction. In compound (**1**) there are two possible exchange pathways: (i) through the extended terephthalate in two linear chains: along the *c* axis and diagonal of the cell unit with the metal–metal separation 10.949(2) Å. According to the relation proposed by Coffmann and Buetter [30], the separation between the magnetic centers in the range 10–11 Å corresponds to the smallest $|J|$ value of about 0.1 cm^{-1} so the magnetic interactions at these two linear chains could be neglected. (ii) Through the bidentate carboxyl group with the *syn-anti* configuration in the zigzag chain along the *b* axis, the metal–metal separation is 4.230(1) Å which could be responsible for a weak antiferromagentic exchange of the compound (**1**). It is quite similar with the bidentate carboxylate bridged polymeric complex $[Cu(NH_3)_2](CH_3COO)_2]$ ($J/k = -4.3$ K) [27]. This exchange interaction involving overlap between the

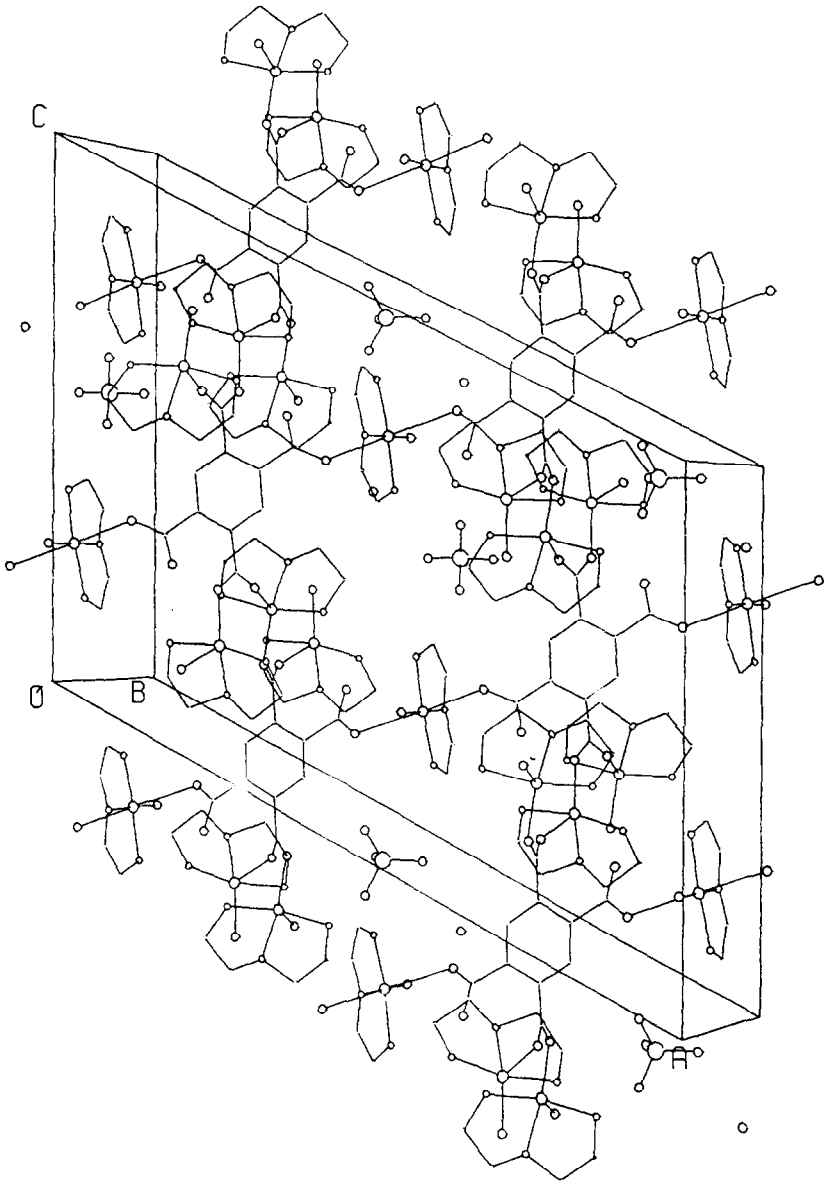

Fig. 4. The crystal packing diagram of the complex $[(Cudien)_2(Cudien \cdot H_2O)TCB(ClO_4)_2 \cdot H_2O]_n$.

two magnetic orbitals of $d_{x^2-y^2}$-type through *syn-anti* carboxyl bridge is very weak.

The thermal dependence of the molar magnetic susceptibility χ_M of complex (**2**) is characterized to an antiferromagnetic interaction between the two copper ions. The susceptibility of the compound was successfully analyzed in the terms of an isotropic exchange interaction for a binuclear species with $H = -JS_1S_2$ and $S_1 = S_2 = 1/2$. The least square analysis for compound (**2**) yields $J = -9.03\ cm^{-1}$ and $g = 2.17$ with $R = 1.81 \times 10^{-4}$ (R is the agreement factor defined as $\Sigma(X_m^{obsd} - X_m^{calc})^2/\Sigma(X_m^{obsd})^2$. The best fit curve is shown in Fig. 5. The J value is much larger than that proposed by Coffmann and Buetter (0.1 cm^{-1}) [30] and shows that the possible magnetic inter-

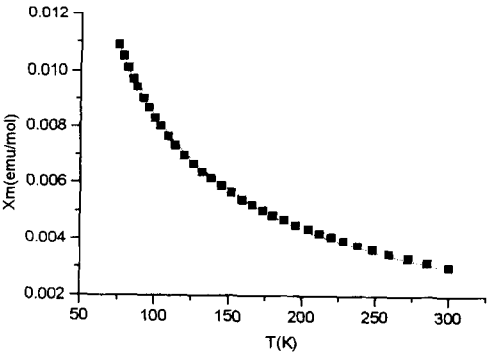

Fig. 5. The best fit curve of the magnetic behavior of the complex (**2**) in the form of χ_M (experiment value: ■ ■ ■; theory value: —) vs T plot.

action pathways of two magnetic centers in complex (**2**) could not go through the TCB^{4-} anion. According to other analogous complexes [19], the intermolecule interaction may be responsible for the magnetic behavior.

The conclusion can be drawn from the two TCB bridged Cu(II) complexes. TCB^{4-} anion has four carboxyl groups which can coordinate with metal atoms in a number of ways, therefore the TCB^{4-} anion is an ideal ligand to synthesize the new structure polynuclear complex. We used two analogous copper complexes Cudien$(ClO_4)_2$ and Cudipn$(ClO_4)_2$ to react with TCB piperidimium salt and two quite different structure complexes were obtained. One is a new three-dimensional infinite structure polynuclear copper complex $[(Cudien)_2(Cudien \cdot H_2O)TCB(ClO_4)_2 \cdot H_2O]_n$ and the other is a binuclear copper complex $[(Cudipn \cdot H_2O)_2\ TCB] \cdot 8H_2O$ with molecularity. The magnetic interaction is very weak, because of the longer distance between two magnetic centers.

Acknowledgment—This work was supported by the National Natural Science Foundation of China and a key research project from the State Science and Technology Commission of China.

REFERENCES

1. *Magneto-Structural Correlations in Exchange Coupled Systems*, ed. R. D. Willett, D. Gattesdhi and O. Kahn. Reidel, Dordrecht, The Netherlands, 1985.
2. Entley, W. R. and Girolami, G. S., *Inorg. Chem.*, 1994, **33,** 5165; Ohba, M., Maruono, N., Okawa, H., Enoki, T. and Latour, J.-M., *J. Am. Chem. Soc.*, 1994, **116,** 11566; Ohba, M., Okawa, H., Ito, T. and Ohto, A., *J. Chem. Soc., Chem. Commun.*, 1995, 1545.
3. De Munno, G., Ruiz, R., Lloret, F., Faus, J., Sessoli, R. and Julve, M., *Inorg. Chem.*, 1995, **34,** 408; De Munno, G., Julve, M., Lloret, F., Faus, J., Verdaguer, M. and Caneschi, A., *Inorg. Chem.*, 1995, **34,** 157.
4. Vicente, R., Ribas, J., Alvarez, S., Segui, A., Solans, X. and Verdaguer, M., *Inorg. Chem.*, 1987, **26,** 4004.
5. Commarmond, J., Plumere, P., Lehn, J. M., Agnus, Y., Louis, R., Weiss, R., Kahn, O. and Morgenstern Badarau, I., *J. Am. Chem. Soc.*, 1982, **104,** 6330; Chaudhuri, P., Oder, K., Wieghardt, K., Nuber, B. and Weiss, J., *Inorg. Chem.*, 1986, **25,** 2818.
6. Castro, I., Sletten, J., Faus, J., Julve, M., Lloret, F. and Alvarez, S., *Inorg. Chem.*, 1992, **31,** 1989; Cornia, A., Fabretti, A. C., Giusti, A., Ferraro, F. and Gatteschi, D., *Inorg. Chim. Acta*, 1993, **121,** 87.
7. Pierpont, C., Franceconi, L. C. and Hendrickson, D. M., *Inorg. Chem.*, 1977, **16,** 2367; Verdaguer, M., Michalowicz, A., Girerd, J. J., Alberding, N. and Kahn, O., *Inorg. Chem.*, 1980, **19,** 327; Folgado, J. V., Ibanez, R., Coronado, E., Beltran, D., Savariault, J. M. and Galy, J., *Inorg. Chem.*, 1988, **27,** 19; Chaudhuri, P. and Ode, K., *J. Chem. Soc., Dalton Trans.*, 1990, 1597.
8. Solans, X., Aguilo, M., Gleizes, A., Faus, J., Julve, M. and Verdaguer, M., *Inorg. Chem.*, 1990, **29,** 175.
9. Julve, M., Verdaguer, M., Faus, J., Tinti, F., Mortal, J., Monge, A. and Guiterrez-Puebla, E., *Inorg. Chem.*, 1987, **26,** 3520.
10. Verdaguer, M., Gouteron, J., Jeannin, S., Jeannin, Y. and Kahn, O., *Inorg. Chem.*, 1984, **23,** 4291.
11. Bakalbassis, E. G., Tsipis, C. A. and Mrozinski, J., *Inorg. Chem.*, 1985, **24,** 4231.
12. Bakalbassis, E. G., Mrozinski, J. and Tsipis, C. A., *Inorg. Chem.*, 1986, **25,** 3684.
13. Bakalbassis, E. G., Bozopoulos, A. P., Mrozinski, J., Rentzeperis, P. J. and Tsipis, C. A., *Inorg. Chem.*, 1988, **27,** 529.
14. Bakalbassis, E. G., Kahn, O., Bergerat, P., Jeannin, S., Jeannin, Y. and Dromzee, Y., *J. Am. Soc., Chem. Commun.*, 1990, 1771.
15. Bakalbassis, E. G., Tsipis, C. A., Bozopoulos, A. P., Dreissig, W., Narl, H. and Mrozinski, J., *Inorg. Chim. Acta*, 1991, **186,** 113.
16. Bakalbassis, E. G., Bergerat, P., Kahn, O., Jeannin, S., Jeannin, Y., Dromzee, Y. and Guillot, M., *Inorg. Chem.*, 1992, **31,** 625.
17. Xanthopoulos, C. E., Siigalas, M. P., Katsoulos, G. A., Tsipis, C. A., Terzis, A., Mentzafos, M. and Hountals, A., *Inorg. Chem.*, 1993, **32,** 5433.
18. Cano, J., De Munno, G., Sanz, J., Ruiz, R., Floret, F., Faus, J. and Julve, M., *J. Chem. Soc., Dalton Trans.*, 1994, 3465.
19. Verdaguer, M., Couteron, J., Jeannin, S., Jeannin, Y. and Kahn, O., *Inorg. Chem.*, 1984, **23,** 4291.
20. Phalguni, C., Karen, O., Karl, W., Stefan, G. and Johannes, W., *J. Am. Chem. Soc.*, 1988, **110,** 3657.
21. Deacon, G. B. and Phillips, R. J., *Coord. Chem. Rev.*, 1980, **33,** 227.
22. Chen, H., Zou, J.-Z., Xu, Z. and You, X.-Z., *Acta Crystal.*, 1996, **C52,** 43.
23. *Org. Synth.*, (Collective Vol. 5), p. 824.
24. van Koningsbruggen, P. J., van Haul, J. W., Muller, E., Graaff, R. A. G., Haasnoot, J. G. and Reedijk, J., *J. Chem. Soc., Dalton Trans.*, 1993, 1371.
25. Wu, L. P., Yamamoto, M., Kuroda-Sowa, Y., Mackawa, M., Fukui, J. and Munakata, M., *Inorg. Chim. Acta*, 1995, **239,** 165.
26. Alyea, E. C., Dias, S. A., Ferguson, G., Khan, M. A. and Roberts, P. J., *Inorg. Chem.*, 1979, **18,** 2433.
27. Carlin, R. L., Kopinga, K., Kahn, O. and Verdaguer, M., *Inorg. Chem.*, 1986, **27,** 1786.
28. Kazuo Nakamoto, *Infrared and Raman Spectra of Inorganic and Coordination Compounds*, 3rd edn. p. 248.
29. Rosenthal, M. R., *J. Chem. Educ.*, 1973, **50,** 331.
30. Coffman, R. E. and Buetter, G. R., *J. Phys. Chem.*, 1979, **83,** 2387.

Pergamon

PII: S0277-5387(97)00522-6

Polyhedron Vol. 17, Nos. 11–12, pp. 1871–1875, 1998
© 1998 Elsevier Science Ltd
All rights reserved. Printed in Great Britain
0277-5387/98 $19.00+0.00

The syntheses and characterisation of some novel difunctional sulfur-nitrogen chains: new dithiadiazenes and trithiadiazenes derived from meta-dimercaptobenzene

John J. Longridge and Jeremy M. Rawson*

Department of Chemistry, The University of Cambridge, Lensfield Road, Cambridge, CB2 1EW, U.K.

(Received 16 October 1997; accepted 10 December 1997)

Abstract—Condensation of *m*-$C_6H_4(SCl)_2$ with $Me_3SiNSNSiMe_3$ in a 1:2 mole ratio produced quantitatively the difunctional chain *m*-$C_6H_4(SNSNSiMe_3)_2$ (**I**) which could be capped with ArSCl [Ar = *p*-$O_2NC_6H_4$, *o*-$O_2NC_6H_4$ and *o,p*-$(O_2N)_2C_6H_3$] to yield the bis(trithiadiazene) chains *m*-$C_6H_4(SNSNSAr)_2$ (**II**–**IV** respectively) or condensed with a further equivalent of *m*-$C_6H_4(SCl)_2$ to give the polymer [*m*-$C_6H_4SNSNS]_n$ (**V**). © 1998 Elsevier Science Ltd. All rights reserved

Keywords: thiazyl; sulfur-nitrogen; polymer.

We have recently become interested [1] in the preparation of novel materials in which redox-active functional groups are linked via a π-delocalised backbone which will facilitate through-bond communication between redox active centres. Our synthetic strategy [1] has been to utilise small fragments of conducting poly(sulfurnitride) [2] to provide the delocalised π-framework. As a first step in this research programme we have examined the possibility of forming oligo-functional thiazyl chains, in which two (or more) sulfur-nitrogen chains are linked together through a phenylene spacer unit [3].

Synthetic strategies for the preparation of simple thiazyl chains with up to nine heteroatoms in the chain, e.g. ArS_5N_4Ar, have been developed by a number of research groups [1]. However, the exploitation of these methodologies to yield oligo-functional materials (Scheme 1) has not been fully investigated. Previously, Rees and co-workers have shown [4] that ring closure is the preferred reaction for the condensation of *ortho*-$C_6H_4(SCl)_2$ with $Me_3SiNSNSiMe_3$ (Scheme 1). However, the analogous reaction of *para*-$C_6H_4(SCl)_2$ with $Me_3SiNSNSiMe_3$ has been shown to yield a mixture of difunctional and polymeric material dependent on the reaction conditions [5,6]. Herein we report the high yielding syntheses of a series of difunctional thiazyl chains derived from *meta*-dimercaptobenzene.

* Author to whom correspondence should be addressed.

RESULTS AND DISCUSSION

Dropwise addition of *m*-$C_6H_4(SCl)_2$ [prepared by chlorination of *m*-$C_6H_4(SH)_2$ with SO_2Cl_2] to $Me_3SiNSNSiMe_3$ in a 1:2 mole ratio at ambient temperature yielded the difunctional thiazyl chain, *m*-$C_6H_4(SNSNSiMe_3)_2$ (**I**). Spectroscopic studies on the reaction mixture indicated that **I** was prepared quantitatively and there was no evidence for either the ring-closure or the potential polymer-forming reactions (*vide infra*) which might have been anticipated. Evaporation of the reaction mixture yielded crude **I** which was typically contaminated with traces of Me_3SiCl. Analytically pure **I** could be recovered in *ca* 70% yield by recrystallisation from hexane and was characterised by ^1H and ^{13}C NMR and microanalytical data. The ^1H NMR (Fig. 1) consists of a multiplet in the aromatic region and a singlet ($\delta = +0.35$) for the $SiMe_3$ functional group in the relative ratio 2:9. The ^{13}C NMR spectrum exhibits a single resonance ($\delta = 1.8$) for the trimethylsilyl C and four magnetically distinct aromatic C nuclei (in the region $\delta = +121$ to $+139$) of which the $\delta = +139$ resonance

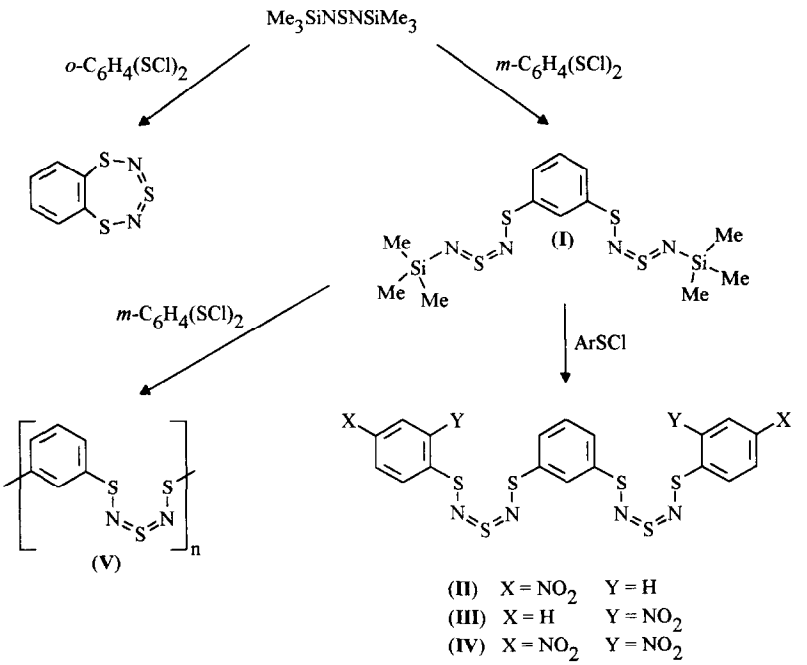

Scheme 1. Condensation pathways between dimercaptobenzenes and bis(trimethylsilyl)sulfurdiimide.

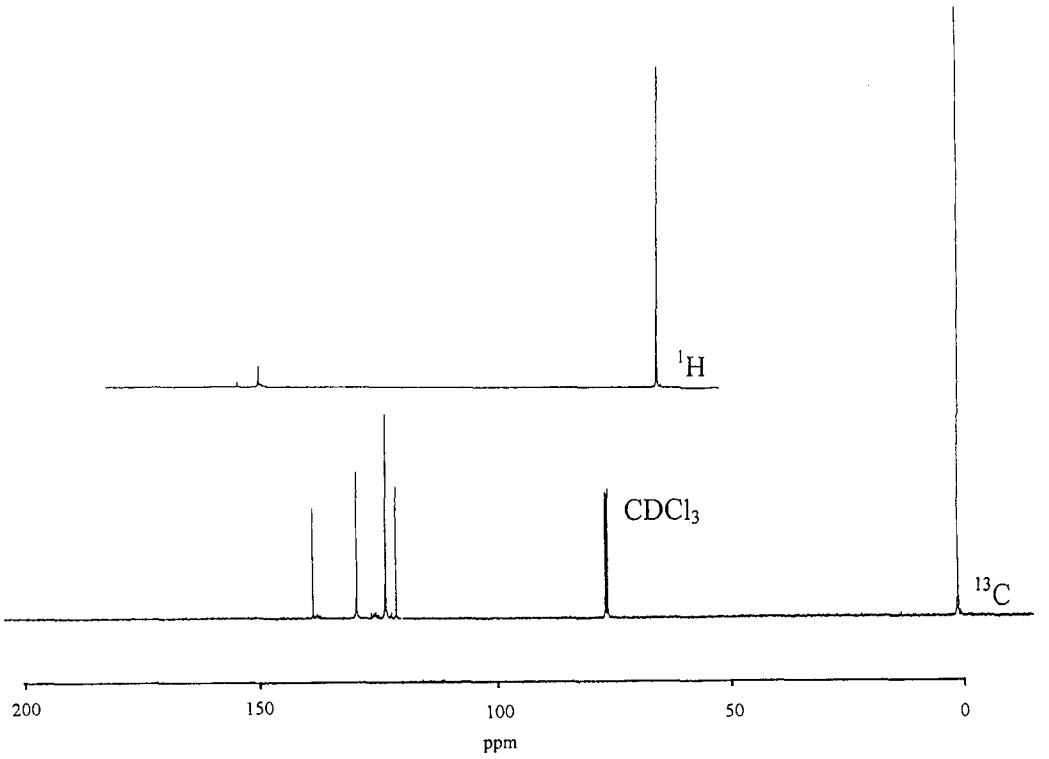

Fig. 1. ^{13}C and ^{1}H (inset) NMR spectra of **I**.

was unambiguously assigned (by APT) as the S-bonded C. The UV–vis spectrum of **I** in $CHCl_3$ exhibited an absorption maxima at 387 nm ($\varepsilon = 2.6 \times 10^4$ mol dm^{-3} cm^{-1}) (Fig. 2) which we attribute to the dithiadiazene chromophore [1]. **I** was found to be soluble in a wide range of solvents including toluene,

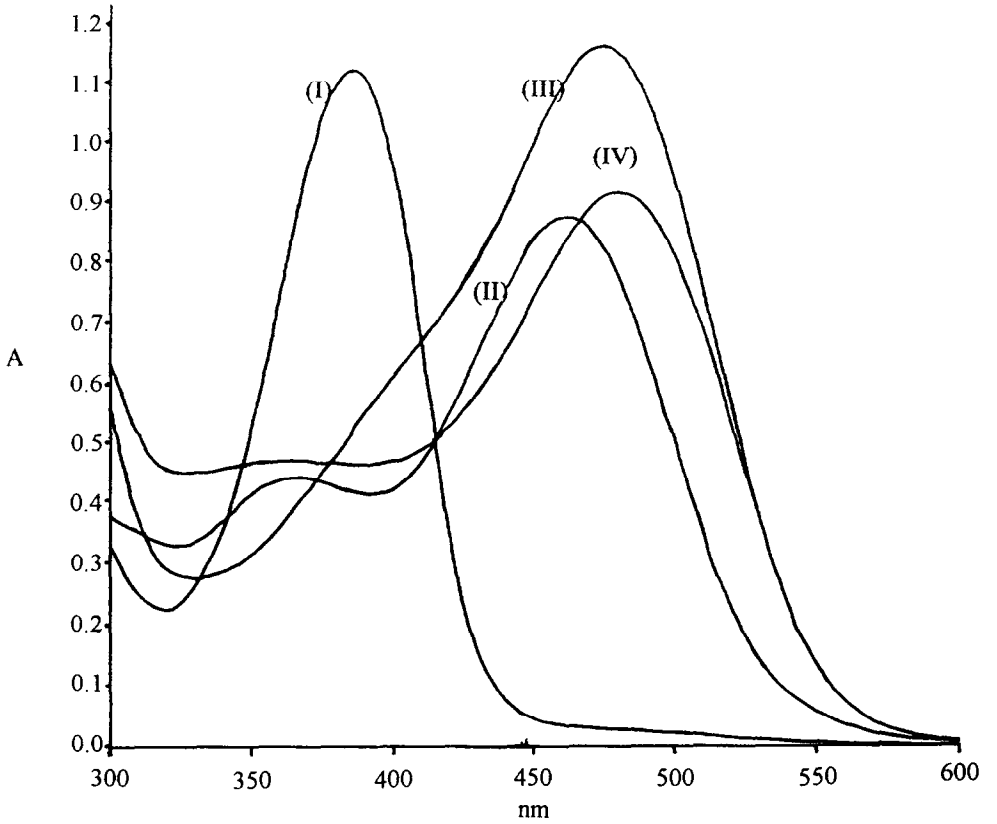

Fig. 2. UV–visible spectra of compounds **I–IV**.

dichloromethane, chloroform and diethyl ether. It is sparingly soluble in hexane.

The quantitative formation of **I**, in preference to polymer-formation, indicated that the trimethylsilyl groups on **I** are significantly less reactive towards *m*-$C_6H_4(SCl)_2$ than those on the sulfurdiimide, Me_3Si NSNSiMe_3. This is in agreement with a report by Kuyper and Street [7] who found that the rate of condensation of the first trimethylsilyl group on Me_3Si-NSNSiMe_3 was significantly greater than the second and this facilitated the isolation of mono-substituted compounds. Nevertheless, the trimethylsilyl groups on **I** are sufficiently reactive to allow **I** to be a useful intermediate for the preparation of longer thiazyl chains. We have found that chain-capping can be achieved via condensation with two equivalents of ArSCl to form the new difunctional chains, *m*-$C_6H_4(SNSNSAr)_2$ [Ar = *p*-$O_2NC_6H_4$ (**II**), *o*-$O_2NC_6H_4$ (**III**) or *o*,*p*-$(O_2N)_2C_6H_3$ (**IV**)] in quantitative yield (by NMR), with recovered yields typically in the range 86–89%. The solubilities of compounds **II–IV** were found to be considerably less than those observed for **I**, although they provided sufficient solubility in chloroform for spectroscopic characterisation. Compounds **II–IV** were characterised by multinuclear NMR and microanalysis. Solution UV–visible studies on compounds **II–IV** exhibited broad absorption maxima (462, 475 and 481 nm respectively, $\varepsilon = 1.3$ to 3.2×10^4 mol dm^{-3} cm^{-1}) "red-shifted" in comparison to **I** (Fig. 2). This "red-shift" is associated with the increased delocalisation, and the absorption maxima for compounds **II–IV** are typical of those observed for simple monofunctional trithiadiazene chains [1]. In addition the relative positions of the three absorption maxima for **II–IV** are entirely consistent with previous observations [1] in which the *ortho*-nitro group produces a shift to higher wavelength of some 15–20 nm, in comparison to the related *para*-nitro substituents.

In Scheme 1, compounds **I–IV** have been represented in the conformations observed for the related crystallographically characterised monofunctional thiazyl chains [1]. However, a variety of geometric isomers are possible for these compounds and the energetic differences between different conformations is small (25–30 kJ mol^{-1}) [8]. This may account for the lack of crystallinity in these difunctional systems. Our attempts to prepare suitable crystals of **I–IV** for X-ray diffraction studies, by slow evaporation, solvent diffusion and cooling saturated solutions, were unsuccessful and produced only microcrystalline precipitates. Attempted vacuum sublimation led only to decomposition at elevated temperatures.

Whereas the longer thiazyl chain compounds exhi-

bit a tendancy to decompose to shorter thiazyl chains via extrusion [1] of S_4N_4, the shorter chains do not undergo similar reactions, although scrambling of thiazyl chains has been reported [9] in the presence of sodium or potassium. In our studies, we have seen no indication of the formation of S_4N_4 by spectroscopic techniques (IR, *m/e*). Furthermore, the effect of the thiazyl-chain on the ^{13}C chemical shift of the aromatic C atoms is sufficiently large that compounds of differing chain-lengths can be clearly identified by ^{13}C NMR and we have seen no indication of chain-scrambling or S_4N_4 extrusion.

Although condensation of *m*-$C_6H_4(SCl)_2$ with $Me_3SiNSNSiMe_3$ in a 1 : 2 mole ratio yielded exclusively **I**, condensation of **I** with a further equivalent of *m*-$C_6H_4(SCl)_2$ at room temperature yielded an insoluble red material of composition $(C_6H_4S_3N_2)_n$ which was characterised as the polymer $(m\text{-}C_6H_4S_3N_2)_n$ (**V**) on the basis of microanalytical data. The analogous polymer $(p\text{-}C_6H_4S_3N_2)_n$, which is also red in colour, has been previously isolated [6] from the reaction of *p*-$C_6H_4(SCl)_2$ with $Me_3SiNSNSiMe_3$.

CONCLUSIONS

This work highlights the use of oligo-functional thiols as suitable precursors for the controlled syntheses of multifunctional thiazyl chains. We are now exploiting similar methodologies to prepare new di- and tri-functional derivatives which possess multiple metal-binding sites and redox-active centres.

EXPERIMENTAL

General procedures

All reactions and manipulations were carried out under an atmosphere of dry nitrogen, using standard double-manifold techniques and a glove box (Saffron Scientific Instruments). Solvents were distilled prior to use. C, H, and N analyses were carried out using an Exeter CE-440 elemental analyser. NMR data was collected on Bruker AM-400 and AC/DPX-250 Fourier transform NMR spectrometers. UV–visible spectra were recorded on a Perkin–Elmer lambda-12 UV–visible spectrophotometer. *m*-dimercaptobenzene (Aldrich) and SO_2Cl_2 (BDH) were used without further purification. $Me_3SiNSNSiMe_3$ was prepared according to the literature method [10].

Synthesis of *m*-$C_6H_4(SNSNSiMe_3)_2$ (**I**). *m*-$C_6H_4(SH)_2$ (1.000 g, 7.03 mmol) in CH_2Cl_2 (20 ml) was added dropwise to a stirred solution of SO_2Cl_2 (3.795 g, 2.3 ml, 28mmol) in CH_2Cl_2 (5 ml) at room temperature. The yellow solution was then refluxed for 1 h, cooled to room temperature and the solvent and excess SO_2Cl_2 removed *in vacuo*, yielding a red oil, *m*-$C_6H_4(SCl)_2$. The oil was redissolved in CH_2Cl_2 (20 ml) and added dropwise to a stirred solution of $Me_3SiNSNSiMe_3$ (2.90 g, 3.4 ml, 14 mmol) in CH_2Cl_2 (5 ml) at room temperature to yield a dark red solution of **I**. After 12 h, the CH_2Cl_2 was removed *in vacuo* yielding crude *m*-$C_6H_4(SNSNSiMe_3)_2$ (**I**) as a pale red solid which was recrystallised (1.9940 g, 70%) from hexane. (Found: C, 35.1; H, 5.2; N, 13.4. Calc.: C, 35.4; H, 5.4; N, 13.8%). ^1H NMR ($CDCl_3$, 250 MHz): δ 0.32, 7.35–7.38, 7.75. ^{13}C NMR ($CDCl_3$, 400 MHz): δ 1.75, 121.3, 123.5, 130.0, 138.9. UV–Visible ($CHCl_3$) λ_{max}/nm 387 ($\varepsilon = 2.6 \times 10^4$ mol dm^{-3} cm^{-1}).

Syntheses of *m*-$C_6H_4(SNSNSAr)_2$ (**II–IV**). A solution of **I** (0.500 g, 1.23 mmol) in CH_2Cl_2 (20 ml) was added dropwise to a stirred solution of ArSCl (2.46 mmol) in CH_2Cl_2 (10 ml) at room temperature, resulting in a dark red solution which was stirred for a further 2 h, prior to removal of solvent *in vacuo*. The crude red solid, *m*-$C_6H_4(SNSNSAr)_2$, was washed with hexane (4 × 5 ml) and dried *in vacuo*. Compound **II**, [Ar = *p*-$O_2NC_6H_4$]: Yield: 0.6140 g, 88%. (Found: C, 38.3; H, 2.3; N, 14.5. Calc.: C, 38.0; H, 2.1; 14.8%). ^1H NMR ($CDCl_3$, 250 MHz): δ 7.31–7.64, 7.81, 7.82, 8.16–8.40. ^{13}C NMR ($CDCl_3$, 400 MHz): δ 122.6, 122.8, 124.5, 124.6, 126.4, 128.7, 137.1, 144.1. UV–Visible ($CHCl_3$) λ_{max}/nm 462 ($\varepsilon = 3.2 \times 10^4$ mol dm^{-3} cm^{-1}). Compound **III**, [Ar = *o*-$O_2NC_6H_4$]: Yield: 0.6220 g, 89%. (Found: C, 38.2; H, 2.1; N, 14.6. Calc.: C, 38.0; H, 2.1; 14.8%). ^1H NMR ($CDCl_3$, 250 MHz): δ 7.31–7.44, 7.67–7.78, 8.03–8.06, 8.14–8.17, 8.33–8.37. ^{13}C NMR ($CDCl_3$, 400 MHz): δ 122.9, 125.1, 125.3, 125.5, 125.8, 126.1, 126.4, 129.9, 134.5, 139.7, 140.8, 141.2. UV–Visible ($CHCl_3$) λ_{max}/nm 475 ($\varepsilon = 2.1 \times 10^4$ mol dm^{-3} cm^{-1}). Compound **IV**, [Ar = *o,p*-$(O_2N)_2C_6H_3$]: Yield: 0.7560g, 86%. (Found: C, 32.8; H, 1.8; N, 17.2. Calc.: C, 32.8; H, 1.5; N, 17.0%). ^1H NMR ($CDCl_3$, 250 MHz): δ 7.31–7.53, 7.68–7.71, 8.20–8.31, 8.48–8.60, 9.15–9.18. UV–Visible ($CHCl_3$) λ_{max}/nm 481 (δ— = 1.8×10^4 mol dm^{-3} cm^{-1}).

Synthesis of $(m\text{-}C_6H_4S_3N_2)_n$ (**V**). A solution of **I** (0.400 g, 0.98 mmol) and *m*-$C_6H_4(SCl)_2$ [prepared as for **I**, from *m*-$C_6H_4(SH)_2$ (0.140 g, 0.98 mmol)] each dissolved in CH_2Cl_2 (25 ml) were simultaneously added dropwise to a stirred reservoir of CH_2Cl_2 (100 ml) over the course of 3 h, yielding a red precipitate. The solution was stirred for a further 1 h and the solid collected by filtration, washing with CH_2Cl_2 (3 × 10 ml) and dried *in vacuo* yielding a red solid of composition $(m\text{-}C_6H_4S_3N_2)_n$ (**V**), (0.1390 g, 35%) which was insoluble in common organic solvents. (Found: C, 35.6; H, 2.3; N, 13.8; Calc.: C, 36.0; H, 2.0; N, 14.0). The filtrate contained a mixture of several uncharacterised soluble products.

Acknowledgements—The authors would like to thank the Royal Society for an equipment grant (J.M.R.), the University of Cambridge, the E.P.S.R.C. and the Newton Trust for a studentship (J.J.L.).

REFERENCES

1. Rawson, J. M. and Longridge, J. J., *Chem. Soc. Rev.*, 1997, **53,** and references therein.

2. Labes, M. M., Love, P. and Nichols, L. F., *Chem. Rev.*, 1979, **79,** 1.
3. Rawson, J. M. and Longridge, J. J., *Phos. Sulf. Silicon*, accepted for publication.
4. Morris, J. L., Rees, C. W. and Rigg, D. J., *J. Chem. Soc., Chem. Commun.*, 1985, 396.
5. Chien, J. C. W. and Zhou, M.-Y., *J. Polymer Sci.*, 1986, **24,** 2947.
6. Scherer, O. J., Wolmershäuser, G. and Jotter, R., *Z. Nautrforsch.*, 1982, **37b,** 432.
7. Kuyper, J. and Street, G. B., *J. Amer. Chem. Soc.*, 1977, **99,** 7848.
8. (a) Gleiter, R. and Bartetzko, R., *Z. Naturforsch.*, 1981, **B36,** 492; (b) Bannister, R. M. and Rzepa, H. S., *J. Chem. Soc., Dalton Trans.*, 1989, 1609.
9. Bestari, K., Oakley, R. T. and Cordes, A. W., *Can. J. Chem.*, 1991, **69,** 94.
10. Warrens, C. P. and Woollins, J. D., *Inorg. Synth.*, 1989, **25,** 43.

Pergamon

PII: S0277-5387(97)00523-8

Polyhedron Vol. 17, Nos. 11–12, pp. 1877–1881, 1998
© 1998 Elsevier Science Ltd
All rights reserved. Printed in Great Britain
0277-5387/98 $19.00+0.00

Synthesis and molecular structure of an *exo*-bicyclic eleven-vertex *closo*-ruthenaborane $[(PPh_3)(C_6H_5COS)_2RuB_{10}H_8] \cdot (CH_2Cl_2)$

Hai-Jun Yao,[a] Chun-Hua Hu,[b] Jian-Min Dou,[b] Jing-De Wei,[a] Ruo-Shui Jin,[a] Wen Li[b] and Pei-Ju Zheng[b]*

[a] Department of Chemistry, Fudan University, Shanghai 200433, P. R. China

[b] Research Center of Analysis and Measurement, Fudan University, Shanghai 200433, P. R. China

(Received 8 August 1997; accepted 10 December 1997)

Abstract—The title compound has been separated in ca 13% yield from the reaction of *closo*-$[B_{10}H_{10}]^{2-}$, $[(PPh_3)_3RuCl_2]$ and C_6H_5COSH in CH_2Cl_2 solution, and characterized by elemental analysis, infrared spectroscopy, ^1H NMR and ^{31}P NMR spectroscopy and single-crystal X-ray diffraction analysis. The molecular structure is based on an eleven-vertex *closo*-type C_{2v} $\{RuB_{10}\}$ cluster-geometry with the ruthenium atom occupying the unique six-connected apical position. The metal center has three exopolyhedral ligands, one triphenylphosphine and two dative thiobenzoate sulfur atoms. The carbonyl oxygen atoms of two thiobenzoxy are additionally bonded to B2 and B3 atoms respectively, resulting in two exocyclic five-membered Ru—S—C—O—B rings. © 1998 Elsevier Science Ltd. All rights reserved

Keywords: synthesis; molecular structure; metallaborane; ruthenaborane; exopolyhedral cyclic; *closo*-type $\{RuB_{10}\}$.

The exopolyhedral heterocyclic metallaborane and metallacarborane compounds with metal-to-cluster linkages have been the interesting subjects recently. Previous work in this area has been confined to four types of linkage. The *ortho*-cycloboronation processes that lead to the formation of the metal-to-boron *ortho*-P-phenyl linkage have been extensively studied in metallaborane chemistry [1–7]. Most of the known *exo*-cyclic metallaborane compounds which exhibited exopolyhedral metal-to-boron acetate linkage were generally obtained by the reactions in the presence of acetic acid [8–9], but the first example of metallacarborane compound with an acetate linkage on a *closo* ten-vertex $\{IrCB_8H_7\}$ system obtained in an obscure reaction process [4]. A series of compounds which exhibit a metal-to-boron dithioformate linkage have been obtained by the reactions between CS_2 and related metallaheteroborane or metallaborane species under reflux conditions [10–15]. The exopolyhedral heterocyclic platinaundecaborane [7-(PMe_2Ph)-2,7-$(\mu$-$S_2CNEt_2)$-*nido*-7-$PtB_{10}H_{11}$] with an exopolyhedral metal-to-boron *N*,*N*-diethyldithio-carbamate linkage is obtained from the reaction of [7,7-(PMe_2Ph)-*nido*-7-$PtB_{10}H_{12}$] with $[AuBr_2(S_2CNEt_2)]$ [16]. All of these facts indicate that the cyclic exopolyhedral metal-to-cluster linkage in polyhedral metallaborane and metallacarborane compounds may be formed in a quite different way. We are interested in the synthesis of exopolyhedral cyclic metallaborane by the reaction of $MCl_2(PPh_3)_x$ (M = Ru, Ni and Pt; $x = 2$ or 3) with $B_{10}H_{10}^{2-}$ in the presence of carboxylic and thiocarboxylic acid in refluxing CH_2Cl_2 solution. We have reported a series of stable metallaboranes containing from one to three five-membered rings [17–20]. Here we report the synthesis and structure of an exopolyhedral cyclic *closo*-$\{RuB_{10}\}$ cluster compound with two five-membered Ru—S—C—O—B rings.

EXPERIMENTAL

The starting compounds $[(PPh_3)_3RuCl_2]$ [21], $[NEt_4]_2[B_{10}H_{10}]$ [22] and C_6H_5COSH [23] were prepared by previously published methods. Dichloromethane, n-pentane and petroleum ether (b.p. 60–

* Author to whom correspondence should be addressed.

90°C) were purified by repeated distillation. Reactions were carried out under dry nitrogen in oxygen-free solvent, but subsequent manipulation and separation were carried out in air. Chromatography was carried out by preparative thin-layer using Kieselgel 60G (Merck) on plates of dimension 20 cm × 20 cm × ca 1mm, made in the laboratory as required.

Synthesis of compound **1**

$[(PPh_3)_3RuCl_2]$ (0.38 g, 0.4 mmol), $[NEt_4]_2[B_{10}H_{10}]$ (0.15 g, 0.4 mmol) and C_6H_5COSH (0.11 g, 0.8 mmol) were stirred together in a refluxing CH_2Cl_2 (70 cm^3) solution under dry nitrogen for 112.5 h. The resulting bright-red solution was reduced (rotary evaporator, 30°C, water pump) to ca 5 cm^3, and chromatographed (t.l.c.) using CH_2Cl_2-light petroleum (b.p. 60–90°C) (5:3) as eluant to give an orange-red compound at $Rf = 0.81$, in ca 13% yield. The product was recrystallized from CH_2Cl_2/*n*-pentane to give air-stable orange-red crystals. Found: C, 48.71; H, 4.30; S, 7.31. $C_{33}H_{35}RuPB_{10}S_2O_2Cl_2$ requires C, 47.25; H, 4.21; S, 7.65%. FTIR(cm^{-1}): 3050 (w), 2516 (vs), 2461 (s), 1786 (w), 1762 (m), 1733 (m), 1685 (vs), 1640 (vs), 1505 (vs), 1453 (s), 1419 (m), 1334 (m), 1303 (s), 1230 (vs), 1164 (m), 1095 (vs), 1025 (w), 974 (s), 763 (m), 731 (s), 680 (s), 554 (w). ^1H NMR ($CDCl_3$): δ ppm 0.87 (q, 2H, BH), δ ppm 1.28 (t, 4H, BH), δ ppm 1.58 (s, 2H, BH), δ ppm 6.81–8.39 (25H, Ph); ^{31}P NMR ($CDCl_3$) δ 21.868 ppm.

Physical measurements

Elemental analyses were performed on a Carlo Erba 1106 elemental analyser.

IR spectra of the complex in the range 400–4000 cm^{-1} as KBr pellets was measured on a NICOLET 5SXC-FTIR spectrometer.

^1H NMR spectra was collected on a BRUCKER spectrometer and using TMS as the internal reference. ^{31}P NMR spectra was collected on a DRX400 spectrometer and using 85% H_3PO_4 as the external reference.

X-ray crystallography

A crystal with dimensions of 0.30 × 0.30 × 0.27 mm was mounted on an Enraf-Nonius CAD4 diffractometer. Unit cell parameters were determined by a least-squares refinement of 25 reflections with $20.8° < 2\theta < 26.4°$ and the data were collected using graphite-monochromatized Mo-K_α radiation ($\lambda = 0.71073$ Å) with $\omega/2\theta$ scan mode ($0 \leqslant 2\theta \leqslant 50$) at 21 ± 1°C. The structure was determined by Direct methods (MULTAN-82). All non-hydrogen atoms were located successfully and all hydrogen atoms were treated as riding on their attached atoms. The refinement of positional and anisotropic thermal parameters was carried out by full-matrix least-squares method. All calculations were carried out on a Micro VAX-II computer with SDP-*Plus* software package. Experimental data are summarized in Table 1.

RESULTS AND DISCUSSION

In addition to the strong B—H stretch bonds [24,25] at 2516 and 2461 cm^{-1}, the infrared spectra of the compound also exhibits a strong absorption at 1095 cm^{-1} due to PPh_3 aromatic vibration involving some P—C stretching, which has a slight shift than the reported data of PPh_3 (1090 cm^{-1}) [26,27]. Three strong absorption bands at 1685, 1230, and 963 cm^{-1} which are assigned to ν(C—O), ν(C—phenyl) and ν(C—S) of thiobenzoxy ligands respectively, are in correspondence with the reported data (1690, 1210, 950 cm^{-1}) [28,29]. We can deduce that compound **1** contains both PPh_3 and thiobenzoxy as ligands.

A drawing of the molecular structure of compound **1** is shown in Fig. 1. The selected bond lengths and bond angles are listed in Table 2 and Table 3 respectively. Both X-ray diffraction analysis and ^1H NMR spectrum have showed that the cluster has an eleven-vertex cluster structure of idealized C_{2v} symmetry. The borane-to-metal bonding mode is boat-hexaphto. The ruthenium center has three exopolyhedral ligands, one triphenylphosphine and two dative S atoms of thiobenzoxy groups. The exopolyhedral ruthenium-bound ligand phosphorus atom is almost in the reflection plane which bisects the two B4—B5 and B6—B7 vectors. The two thiobenzoxy groups behave as bridging ligands between the ruthenium center and two prow boron atoms, in which their two sulfur atoms coordinate to Ru1 and two carbonyl oxygen atoms are bound to B2 and B3 respectively. This results in two nearly symmetric exopolyhedral five-membered Ru—S—C—O—B rings. From Table 2, the interatomic distance of Ru—B and B—B within the $\{RuB_{10}\}$ cage are similar to those observed in reported 11-vertex *closo*-ruthenaundecaborane clusters as shown in literatures 8 and 30–32. The average values of interatomic distances of C7—O1 and C14—O2 is 1.311 Å, which are between those of C—O single-bond (1.43 Å) and C=O double-bond (1.22 Å). This fact indicates that the carbon–oxygen bonds of two thiocarboxyl groups have some double-bond character and is supported by the infrared spectroscopic observation as shown above.

The idealized C_{2v} closed eleven-vertex metallaborane structural type is to be of interest because of its contravention of the simple Wade-Williams cluster-geometry and electron-counting rules. According to the Wade-Williams' electron-counting rules, there are two possible electron structures for this C_{2v} $\{RuB_{10}\}$ cage. The first would be that the [Ru(1-1)PPh_3(SCPh)$_2$] moiety contributes three orbitals and two electrons to cluster bonding, so that the closed structure has two electron less than that required for

Table 1. Crystallographic data

Chemical formula	$RuCl_2S_2PO_2C_{33}B_{10}H_{35}$
Crystal system	Triclinic
Space group	*P*-1
Unit cell dimensions	$a = 12.610(2)$ Å, $\alpha = 110.89(1)°$
	$b = 12.860(2)$ Å, $\beta = 103.52(1)°$
	$c = 14.365(2)$ Å, $\gamma = 106.84(1)°$
Volume	1930(1) Å^3
Z	2
D_{calc}	1.444 g/cm^3
μ	7.1 cm^{-1}
No. of measured reflections	7059
No. of unique reflections	6461
No. of observed [$I > 3\sigma(I)$] reflections	5057
Index ranges	$-15 \leqslant h \leqslant 15$, $-15 \leqslant k \leqslant 15$, $0 \leqslant l \leqslant 17$
Absorption correction	Empirical
Weight scheme	Unit weights
Parameters refined	460
Final R indices [$I > 3\sigma(I)$]	$R = 0.039$, $Rw = 0.054$
Goodness-of-fit (S)	1.91
Largest shift/esd	0.02
Highest peak in the last difference fourier	0.51 e/Å^3

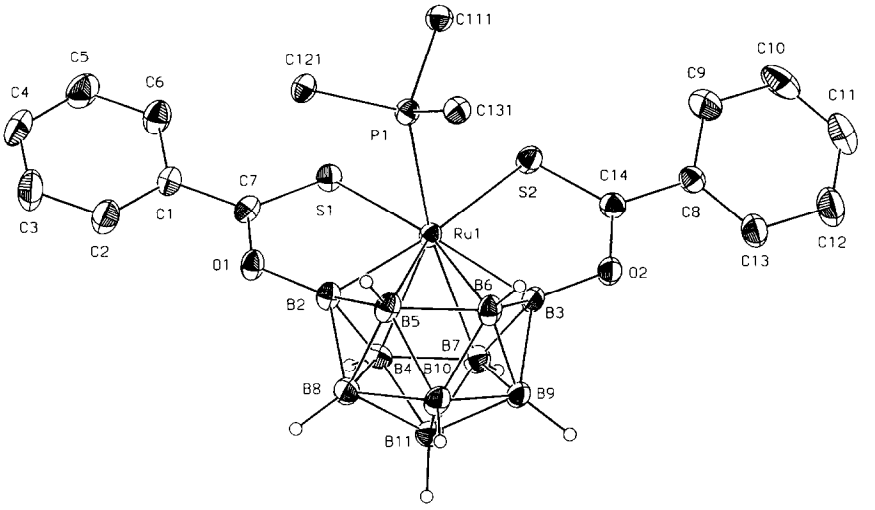

Fig. 1. ORTEP drawing of the title compound (30% probability ellipsoids). Some C and H atoms are omitted for clarity.

Table 2. Selected bond lengths (Å) for compound **1**

Ru1—S1	2.455(1)	Ru1—S2	2.460(1)	Ru1—P1	2.4823(8)
Ru1—B2	2.052(6)	Ru1—B3	2.067(5)	Ru1—B4	2.337(4)
Ru1—B5	2.313(6)	Ru1—B6	2.385(6)	Ru1—B7	2.397(4)
O1—B2	1.430(6)	O2—B3	1.428(6)	B2—B4	1.747(6)
B2—B5	1.717(8)	B2—B8	1.684(6)	B3—B6	1.730(8)
B3—B7	1.762(7)	B3—B9	1.725(7)	B4—B7	1.693(9)
B4—B8	1.843(8)	B4—B11	1.801(8)	B5—B6	1.767(9)
B5—B8	1.822(6)	B5—B10	1.798(6)	B6—B9	1.831(5)
B6—B10	1.780(6)	B7—B9	1.838(9)	B7—B11	1.779(8)
B8—B10	1.775(8)	B8—B11	1.775(7)	B9—B10	1.748(9)
B10—B11	1.754(7)				

Table 3. Selected bond angles (°) for compound **1**

S1—Ru1—S2	88.73(4)	S1—Ru1—P1	82.25(4)	S1—Ru1—B2	74.9(2)
S1—Ru1—B3	148.6(2)	S1—Ru1—B4	83.3(1)	S1—Ru1—B5	117.1(1)
S1—Ru1—B6	161.2(1)	S1—Ru1—B7	111.1(1)	S2—Ru1—P1	85.92(3)
S2—Ru1—B2	161.2(2)	S2—Ru1—B3	74.1(2)	S2—Ru1—B4	123.7(1)
S2—Ru1—B5	152.7(1)	S2—Ru1—B6	110.1(1)	S2—Ru1—B7	92.5(1)
P1—Ru1—B2	100.7(1)	P1—Ru1—B3	121.4(1)	P1—Ru1—B4	146.6(1)
P1—Ru1—B5	89.00(9)	P1—Ru1—B6	97.74(9)	P1—Ru1—B7	166.6(1)
B2—Ru1—B3	115.7(2)	B2—Ru1—B4	46.3(2)	B2—Ru1—B5	45.8(3)
B2—Ru1—B6	86.7(3)	B2—Ru1—B7	85.0(2)		

a formal *closo* electron count, and it would be regarded as "electron hyper-deficient" [33,34]. This situation is based on the assumption that the metal center is electronically saturated. If the metal center is allowed to be electronically unsaturated, the second possible electron structure would be that the [Ru(II) $PPh_3(SCPh)_2$] moiety contributes three obitals and four electrons to cluster bonding, so that the cluster has sufficient electrons for a formal *closo* electron count, in this case the compound would have a formally unsaturated 16-electron Ru(II) center. However, there is also a possible electron structure called *isocloso* structure with the metal center having a four-orbital four-electron contribution [30,35]. All of these views are short of sufficient experimental evidences.

Although the reaction mechanism is complex, overall reaction is stoicheiometric and can easily be expressed by a simple equation [eqn (2)],

$$[(PPh_3)_3RuCl_2] + [B_{10}H_{10}]^{2-} + 2C_6H_5COSH \rightarrow [(PPh_3)(C_6H_5COS)_2RuB_{10}H_8] + 2H_2 + 2Cl^- + 2PPh_3 \quad (2)$$

Two interesting facts show that the reaction mechanism is not simple. The first one is that the ruthenium(II) vertex is coordinated by the sulfur atoms of two thiobenzoxy. This gives an evidence that the elimination of two molecules of hydrogen must involve a series of process, not a simple reaction between the terminal-hydrogen of $[B_{10}H_{10}]^{2-}$ anion and the -SH group of thiobenzoic acid. The second fact is that the carbon-oxygen bond of thiobenzoxy in compound **1** keeps its carbonyl character. It implies that the carbonyl group of thiobenzoic acid plays the role as a Lewis base. As we know that $B_{10}H_{12}L_2$ can react with a strong Lewis base R_3N to give the *closo*-$B_{10}H_{10}^{2-}$:

$$B_{10}H_{12}L_2 + 2R_3N = 2R_3NH^+ + B_{10}H_{10}^{2-} + 2L$$

It is reasonable that the presence of a weak Lewis base species, such as the carbonyl group of carboxy or thiocaboxy ligands, would be favorable for the reverse process which leads to the opening of the $B_{10}H_{10}^{2-}$ cage. Because of the great complexity, the mechanism of this type of reaction needs to be further studied in the future.

Acknowledgements—We thank the support of the Chinese National Natural Science Foundation.

REFERENCES

1. Crook, J. E., Greenwood, N. N., Kennedy. J. D. and McDonald, W. S., *J. Chem. Soc., Chem. Commun.*, 1981, 933.
2. Crook, J. E., Greenwood, N. N., Kennedy, J. D. and McDonald, W. S., *J. Chem. Soc., Chem. Commun.*, 1982, 383.
3. Bould, J., Greenwood, N. N., Kennedy, J. D. and McDonald, W. S., *J. Chem. Soc., Chem. Commun.*, 1982, 465.
4. Crook, J. E., Greenwood, N. N., Kennedy, J. D. and McDonald, W. S., *J. Chem. Soc., Chem. Commun.*, 1983, 83.
5. Bould, J., Crook, J. E., Greenwood, N. N. and Kennedy, J. D., *J. Chem. Soc., Chem. Commun.* 1983, 949.
6. Elrington, M., Greenwood, N. N., Kennedy, J. D. and Thornton-Pett, M., *J. Chem. Soc., Dalton Trans.*, 1986, 2277.
7. Bould, J., Brint, P., Fontaine, X. L. R., Kennedy, J. D., Thornton-Pett, M., *J. Chem. Soc., Chem. Commun.*, 1989, 1763.
8. Fontaine, X. L. R., Greenwood, N. N., Kennedy, J. D., Thornton-Pett, M. and Zheng, P.-J., *J. Chem. Soc., Chem. Commun.*, 1987, 1717.
9. Coldicott, R. S., In *Current Topics in the Chemistry of Boron.* ed. G. W. Kabalka. RSC, Cambridge and London. 1994, 297.
10. Ferguson, G., Faridoon and Spalding, T. R., *Acta Crystallogr. sect. C.*, 1988, **44,** 1368.
11. Faridoon, Spalding, T. R., Ferguson, G., Kennedy, J. D. and Fontaine, X. L. R., *J. Chem. Soc., Chem. Commun.*, 1989, 906.
12. Ferguson, G., Jennings, M. C., Lough, A. J., Coughlan, S., Spalding, T. R., Kennedy, J. D., Fontaine, X. L. R. and stibr., B., *J. Chem. Soc., Chem. Commun.*, 1990, 891.
13. Ferguson, G., Coughlan, S., Spalding, T. R., Fontaine, X. L. R., Kennedy, J. D. and stibr., B., *Acta Crystallogr. sect. C.*, 1990, **46,** 1402.
14. Ferguson, G., Gallagher, J. F., Jennings, M. C.,

Coughlan, S., Spalding, T. R., Kennedy, J. D. and Fontaine, X. L. R., *J. Chem. Soc., Chem. Commun.*, 1994, 1595.
15. Coldicott, R. S., Kennedy, J. D. and Thornton-Pett, M., *J. Chem. Soc., Dalton Trans.*, 1996, 3819.
16. Beckett, M. A., Greenwood, N. N., Kennedy, J. D. and Thornton-Pett, M., *Polyhedron*, 1985, **4**, 505.
17. Yao, H.-J., Fu, J., Jin, R.-S., Wei, J.-D., Chen, J. and Zheng, P.-J., *Chinese J. Struct. Chem.*, 1995, **14**, 364.
18. Dou, J.-M., Hu, C.-H., Yao, H.-J., Li, W., Jin, R.-S. and Zheng, P.-J., *Acta Crystallogr. sect. C.*, 1997, **53**, 693.
19. Hu, C.-H., Dou, J.-M., Yao, H.-J., Li, W., Jin, R.-S. and Zheng, P.-J., *Acta Crystallogr. sect. C.*, 1997, **53**, 695.
20. Dou, J.-M., Hu, C.-H., Sun, J., Wei, J.-D. and Zheng, P.-J., *Polyhedron*, 1997, **16**, 3873.
21. Hallman, P. S., Stephenson, T. A. and Wilkinson, G., *Inorg. Synth.*, 1970, **9**, 16.
22. Guillevic, G., Dazord, J., Mongeot, H. and Cueilleron, J., *J. Chem. Res.*, 1978, 4864.
23. Noble, P. and Terbell, D. S., *Org. Synth. Coll.*, **4**, 924.
24. Brint, P., Sangchakr, B., Fowler, P. W. and Weldon, V. J., *J. Chem. Soc., Dalton Trans.*, 1989, 2253.
25. Leites, L. A., *Chem. Rev.*, 1992, **92**, 279.
26. Daasch, L. W. and Smith, D. C., *Anal. Chem.*, 1951, **23**, 853.
27. Corbridge, D. E. C., *J. Appl. Chem.*, 1956, **6**, 456.
28. Nyquist, R. A. and Potts, W. J., *Spectrochim. Acta*, 1959, **15**, 514.
29. Savant, V. V., Gopalakrishnan, J. and Patel, C. C., *Inorg. Chem.*, 1970, **9**, 748.
30. Crook, J. E., Elrington, M., Greenwood, N. N., Kennedy, J. D., Thornton-Pett, M. and Woolins, J. D., *J. Chem. Soc., Dalton Trans.*, 1985, 2407.
31. Bown, M., Fontaine, X. L. R., Greenwood, N. N., Mackinnon, P., Kennedy, J. D. and Thornton-Pett, M., *J. Chem. Soc., Dalton Trans.*, 1987, 2781.
32. Bown, M., Fontaine, X. L. R., Greenwood, N. N., Kennedy, J. D. and Thornton-Pett, M., *J. Chem. Soc., Dalton Trans.*, 1990, 3039.
33. Johnston, R. L. and Mingos, D. M. P., *Inorg. Chem.*, 1986, **25**, 3321.
34. Baker, R. T., *Inorg. Chem.*, 1986, **25**, 109.
35. Crook, J. E., Elrington, M., Greenwood, N. N., Kennedy, J. D. and Woolins, J. D., *Polyhedron*, 1984, **3**, 901.

Pergamon

PII: S0277-5387(97)00519-6

Polyhedron Vol. 17, Nos. 11–12, pp. 1883–1889, 1998
© 1998 Elsevier Science Ltd
All rights reserved. Printed in Great Britain
0277-5387/98 $19.00+0.00

Synthesis, crystal structure and triboluminescence spectrum of 1,4-dimethylpyridinium tetrakis (2-thenoyltrifluoroacetonato)europate

Xiao-Feng Chen,[a] Shu-Hua Liu,[a] Chun-Yin Duan,[a] Yao-Hua Xu,[a] Xiao-Zeng You,[a]* Jing Ma[b] and Nai-Ben Min[b]

[a] Coordination Chemistry Institute, the State Key Laboratory of Coordination Chemistry, Nanjing University, Nanjing, 210093, PR China

[b] State Key Laboratory of Solid State Microstructures, Nanjing University, Nanjing 210093 PR China

(Received 11 September 1997; accepted 9 December 1997)

Abstract—Triboluminescent phenomenon of 1,4-dimethylpyridinium tetrakis(thenoyltrifluoroacetonato) europate (**1**) was firstly observed. Its crystal structure and the triboluminescent spectrum were successfully determined. The crystal is centrosymmetric and the Eu atom exhibits an eight-coordinate tetragonal antiprismatic geometry. The triboluminescent spectrum of **1** is basically similar to that of photoluminescent spectrum and the observed triboluminescent emission correlates with the disorders of the S atoms and F atoms.
© 1998 Elsevier Science Ltd. All rights reserved

Keywords: europate complex; HTTA; 1,4-dimethylpyridinium; triboluminescence; photoluminescence; disorder.

Triboluminescence is the emission of light produced during mechanical action on solids. Although it is an old phenomenon, its mechanism is not well understood. In recent years, the complexes of the lanthanide elements exhibiting brilliantly triboluminescent properties have been under extensive research [1,2]. In particular, triboluminescent compounds have received more and more attention due in part to a growing need for optical-pressure sensor device [3]. Furthermore, extensive searching for a clear pattern of triboluminescent activity as a function of crystal structure that would permit the construction of a predictive theory of triboluminescence have been under way [4]. Zink [5] estimated that the correlation of triboluminescence activity with noncentrosymmetric space groups was greater than 95%. Sweeting [1] and Rheingold [2] respectively determined the crystal structures of triethylammonium tetrakis (dibenzoylmethanato)europate and piperidinium tetrakis(benzoylacetonato)europate which all display centrosymmetric space groups. They suggested that disorder and ionic compounds play important roles in triboluminescent activity of centrosymmetric materials. In this paper, we report the crystal structure and the triboluminescent spectrum of the firstly observed triboluminescent lanthanide complex **1**. We believe the disorders of the S atoms and F atoms may provide a sufficient condition for the triboluminescence of centrosymmetric crystals of **1**. This result confirms the discovery of Sweeting [1].

EXPERIMENTAL

Preparations

All the chemicals were analytical grade and used without further purification. Iodine 1,4-dimethyl-

* Author to whom correspondence should be addressed.

pyridinium was prepared according to the literature method.

Synthesis of **1**. 1.04 g (4.68 mmol) HTTA (2-thenoyltrifluoroacetone) and 0.275 g (1.17 mmol) Iodine 1,4-dimethylpyridinium was dissolved in 20 ml of ethanol, by heated to boiling, then 0.187 g (4.68 mmol) NaOH in 10 ml water was added. Under vigorous stirring, $Eu(NO_3)_3$ (1.17 mmol) solution was added dropwise and the resultant mixture was refluxed for 3 h with stirring. After hot filtration, the filtrate was allowed to cool slowly at room temperature for several days. Orange single crystals suitable for X-ray analysis were obtained. Found: C, 40.69; H, 2.43; N, 1.24. Calc.: for $EuC_{39}H_{26}F_{12}NO_8S_4$: C, 40.77; H, 2.61; N, 1.22%. The medium-IR of **1** showed peaks at 3089 (w), 3055 (w), 1607 (s), 1537 (s), 1503 (s), 1467 (m), 1411 (s), 1355 (s), 1300 (s), 1246 (m), 1299 (m), 1185 (s), 1137 (s), 1082 (m), 1059 (m), 1032 (w), 1012 (w), 931 (w), 858 (w), 828 (w), 784 (m), 766 (w), 750 (w), 717 (m), 694 (w), 680 (w), 642 (m), 605 (w), 579 (m), 493 (w), 460 (w). Mp: 190–192°C.

Physical measurements

Elemental analysis were performed on a Perkin–Elmer 240C analysical instrument. The IR spectrum was recorded on a Nicolet FT-IR 170sx spectrophotometer with KBr pellet in the range of 4000–400 cm^{-1}. Triboluminescence spectrum was obtained using an Acton Research Corporation (ARC) SpectraPro-750, Santa Barbara Instruments Group (SBIG) CCD Detection System. The grating chosen was blazed for 500 nm with 1200 grooves per mm. The 10 μm slit used gave a resolution of 0.023 nm. Wavelength accuracy is ± 0.1 nm with the 1200 g mm grating. A curve was acquired with no crushing sample, no triboluminescence. It was set as background. The curve that has been set as the background will be subtracted from each new curve input from the camera. The sample was placed as close as possible to the slit in the quartz colorimetric tube and was ground by hand, drawing up a small portion with a glass rod, crushing it against the side of the tube. Photoluminescence spectrum was obtained on ARC SpectraPro-750, (SBIG) CCD and Nd: YAG laser. 355 nm laser line of Nd: YAG with 20 ns pulse width was used to pump the sample.

X-ray crystal structure determination

A crystal having dimensions of $0.48 \times 0.42 \times 0.36$ mm was mounted on a glass fibre. The intensities were collected on a Siemens P4 four-circle diffractometer with monochromated Mo-Kα ($\lambda = 0.71073$ Å) radiation at room temperature. All computation were carried out on a Pc-586 computer using the SHELXTL-Pc Program Package [7]. Compound **1** crystallizes in the monoclinic space group $P2_1/n$ with $a = 14.333(2)$, $b = 17.640(3)$, $c = 18.169(3)$ Å; $\beta = 103.503(14)°$; $V = 4466.6(11)$ Å^3; $Z = 4$; $D_{calc} = 1.702$ g cm^{-3}. A total of 8463 reflections, of which 4229 reflections were unique ($R_{int} = 0.096$), were collected in the range $3.5 \leqslant 2\theta \leqslant 50°$ using $\omega/2\theta$ scan mode with a variable scan speed 5.0–50.0° min^{-1} in ω. The data were corrected for Lorentz and polarization effects during data reduction using XSCANS [6] and the linear absorption coefficient was 1.692 mm^{-1}. The structure was solved by direct methods and refined on F^2 by full-matrix least-squares methods using SHELXTL version 5.0 [7]. The S(1), S(3) and S(4) atoms (site occupancy factor (sof) for S(1) and S(1′), S(3) and S(3′), S(4) and S(4′) fixed at 0.5 respectively) and F(1), F(2), F(3), F(4), F(5), F(6), F(10), F(11) and F(12) (sof = 0.5) were found disordered. All the non-hydrogen atoms were refined anisotropically. Hydrogen atoms were placed in calculated positions (C—H, 0.96 Å) assigned fixed isotropic thermal parameters at 1.2 times the equivalent isotropic U of the atoms to which they are attached (1.5 times for methyl groups) and allowed to ride on their respective parent atoms. The contributions of these hydrogen atoms were included in the structure-factors calculations. The final cycle of refinement included 578 parameters and converged with unweighted and weighted agreement factors of $R = 0.0593$ and $R_w = 0.1560$; GOF = 1.046 (on F^2) (The weighting scheme was $w^{-1} = \sigma^2 (F_o^2) + (0.06P)^2$, $P = (F_o^2 + 2F_c^2)/3$). The maximum and minimum peaks on the final difference Fourier map corresponded to 0.419 and -0.526 eÅ^{-3}.

RESULTS AND DISCUSSION

The structure and labeling schemes of **1** is shown in Fig. 1. Selected bond distances and angles are listed in Table 1. It is tetra-bidentate, eight-coordinate Eu(III) complex containing four HTTA anionic ligands. Many aspects of the eight-coordinated geometry structural europium complexes have been previously discussed. The Eu atom in **1** also has an eight-coordinate tetragonal antiprismatic geometry. The tetragonal planes are defined as [O(1)O(2)O(5)O(7)] and [O(3)O(4)O(6)O(8)] (Fig. 2). The complex **1** possesses an approximate 2-fold rotational axis C (2) (Fig. 3). The average Eu—O distance of **1** (2.385(3) Å) is somewhat shorter than those of 4-methylpyridium tetrakis (thenoyltrifluoroacetonato)europate (**2**) (2.391(7) Å) [8] and N-ethylpyridinium tetrakis(thenoyltrifluoroacetonato)europate (**3**) (2.391 Å) [9] and is longer than that of 3,6-di(dimethylamine)-diphenyliodonium tetrakis(thenoyltrifluoroacetonato)europate (**4**) (2.381 Å) [10]. The average of C—O bond in **1** (1.241 Å) is shorter than those of in **2** (1.261 Å), in **3** (1.259 Å) and in **4** (1.258 Å). It reflects the lower π atom delocalization of C—O double bond in **1**. The O—Eu—O angles within a chelate ring have the following similar averages: **1**, 72.60°; **2**, 71.25°; **4**, 71.0°. 1,4-dimethylpyridinium is a cation and does not coordinate with Eu(III). The C—N bond distance

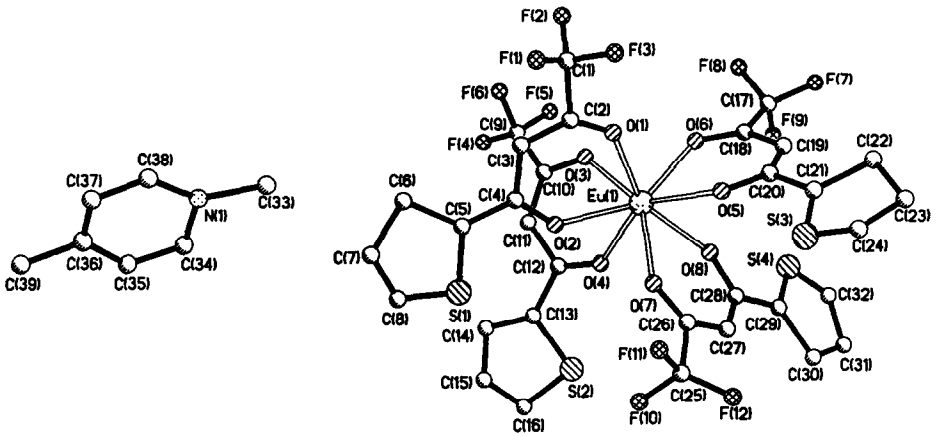

Fig. 1. Molecular structure and labeling scheme for **1**.

Table 1. Selected bond distances (Å) and angles (°) for **1**

Eu—O(1)	2.397(2)	Eu—O(2)	2.369(3)
Eu—O(3)	2.389(3)	Eu—O(4)	2.379(2)
Eu—O(5)	2.415(3)	Eu—O(6)	2.370(2)
Eu—O(7)	2.368(3)	Eu—O(8)	2.393(3)
O(1)—C(2)	1.189(5)	O(2)—C(4)	1.245(6)
O(3)—C(10)	1.299(6)	O(4)—C(12)	1.201(5)
O(5)—C(20)	1.247(5)	O(6)—C(18)	1.235(5)
O(7)—C(26)	1.249(6)	O(8)—C(28)	1.262(6)
F(1)—C(1)	1.306(4)	F(2)—C(1)	1.308(5)
F(3)—C(1)	1.322(5)	F(1′)—C(1)	1.291(5)
F(2′)—C(1)	1.432(6)	F(3′)—C(1)	1.275(7)
F(4)—C(9)	1.322(5)	F(5)—C(9)	1.330(5)
F(6)—C(9)	1.303(4)	F(4′)—C(9)	1.441(8)
F(5′)—C(9)	1.320(7)	F(6′)—C(9)	1.580(6)
F(7)—C(17)	1.310(4)	F(8)—C(17)	1.307(4)
F(9)—C(17)	1.304(3)	F(10)—C(25)	1.323(5)
F(11)—C(25)	1.313(4)	F(12)—C(25)	1.314(5)
F(10′)—C(25)	1.340(6)	F(11′)—C(25)	1.214(8)
F(12′)—C(25)	1.363(7)	C(33)—N(1)	1.529(9)
C(34)—N(1)	1.447(6)	C(38)—N(1)	1.377(8)

O(7)—Eu—O(2)	73.07(10)	O(7)—Eu—O(6)	137.69(10)
O(2)—Eu—O(6)	148.05(10)	O(7)—Eu—O(4)	81.19(9)
O(2)—Eu—O(4)	71.62(9)	O(6)—Eu—O(4)	114.63(8)
O(7)—Eu—O(3)	145.70(9)	O(2)—Eu—O(3)	79.04(10)
O(6)—Eu—O(3)	74.25(10)	O(4)—Eu—O(3)	71.21(10)
O(7)—Eu—O(8)	73.82(9)	O(2)—Eu—O(8)	133.88(9)
O(6)—Eu—O(8)	74.57(9)	O(4)—Eu—O(8)	72.36(10)
O(3)—Eu—O(8)	114.78(9)	O(7)—Eu—O(1)	106.27(9)
O(2)—Eu—O(1)	70.83(9)	O(6)—Eu—O(1)	88.33(9)
O(4)—Eu—O(1)	137.30(10)	O(3)—Eu—O(1)	82.36(10)
O(8)—Eu—O(1)	150.34(9)	O(7)—Eu—O(5)	71.08(9)
O(2)—Eu—O(5)	120.87(9)	O(6)—Eu—O(5)	74.54(9)
O(4)—Eu—O(5)	142.56(11)	O(3)—Eu—O(5)	142.32(9)
O(8)—Eu—O(5)	76.01(10)	O(1)—Eu—O(5)	76.15(10)

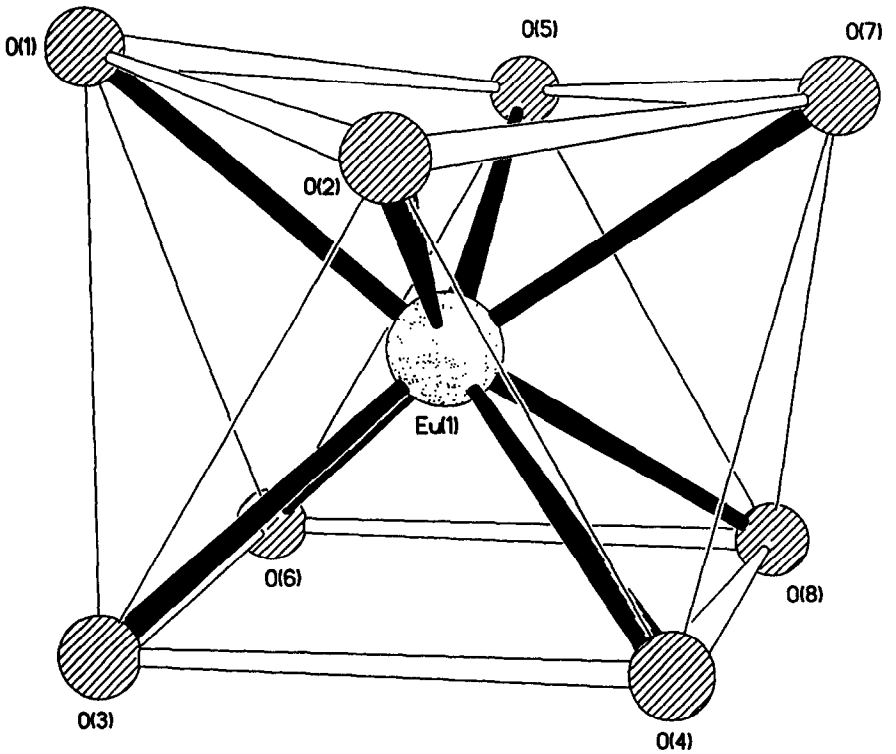

Fig. 2. The antiprismatic coordination geometry for **1**.

(1.529 Å) between the methyl C and N atom is longer than σ typical C—N single bond (1.479 Å). It was the result that *N*-methyl was absorbed by F(4), F(5) and F(6) atoms. So the F(4)—C(9), F(5)—C(9) and F(6)—C(9) bond distances were longer than other F—C bond distances. Two C—N bond distances in the pyridine ring were 1.377(8) Å and 1.447(6) Å respectively. It was the result of π atom delocalization. It is noted that three S atoms of the four crystallographically thienyl rings and three of the four CF_3 in **1** display equally occupied alternative positions.

Complex **1** is highly luminescent in the solid state. Its photoluminescence spectrum at room temperature is shown in Fig. 4. This luminescence is typical of the europium centered transitions from $^5D_0$ levels to the lower $^7F_{0\text{-}4}$ levels of the ground multiplet and has been assigned in Table 2. The transition from $^5D_0$ to $^7F_0$ hasn't been observed. The complex **1** belongs to monoclinic system, the partial symmetry of Eu^{3+} may be C_{2h} after it was excited [11]. Complex **1** which was obtained from the saturated solution was strongly triboluminescent in darkness. When **1** was recrystallized from CH_3CN or CH_3CN-C_2H_5OH, it was triboluminescent with red light emission in daylight. The triboluminescence of **1** is independent of time, but smaller crystals appear to emit less light. The triboluminescence spectrum of **1** is given in Fig. 5. There is no detectable dinitrogen emission. The triboluminescence emission is weaker than that of photoluminescence. So we only observed a part of the emission in the range 550–720 nm which corresponded the most intense emission of the photoluminescence. Other Eu^{3+} ion characteristic emission is much weaker than that of the most intense emission, they haven't been observed in the triboluminescence spectrum. Rheigold [2] stated that the most visible component of their triboluminescent emission of lanthanide complexes is the characteristic photoluminescence of the metallic element. It is apparent that the triboluminescence maximum of complex **1** is similar to that of photoluminescence. Therefore we think that the part of the triboluminescence spectrum does prove that this is europium emission. The emissions observed in triboluminescence is centered transition of the europium from $^5D_0$ level to $^7F_2$ level. The signal to noise ratios which were not very well didn't affect the assignment of the emission [1b,12].

Several mechanism have been proposed for triboluminescence. There is substantial evidence that charge separation created during fracture is the immediate precursor of the triboluminescence emission [13]. It is generally accepted that the primary event in the triboluminescence is the recombination of charges separated during fracture. It has been asserted that only piezoelectric (noncentrosymmetric) crystals may be triboluminescent because only such crystals can develop opposite charges on the opposing faces of a developing crack. The crystal structures of tri-

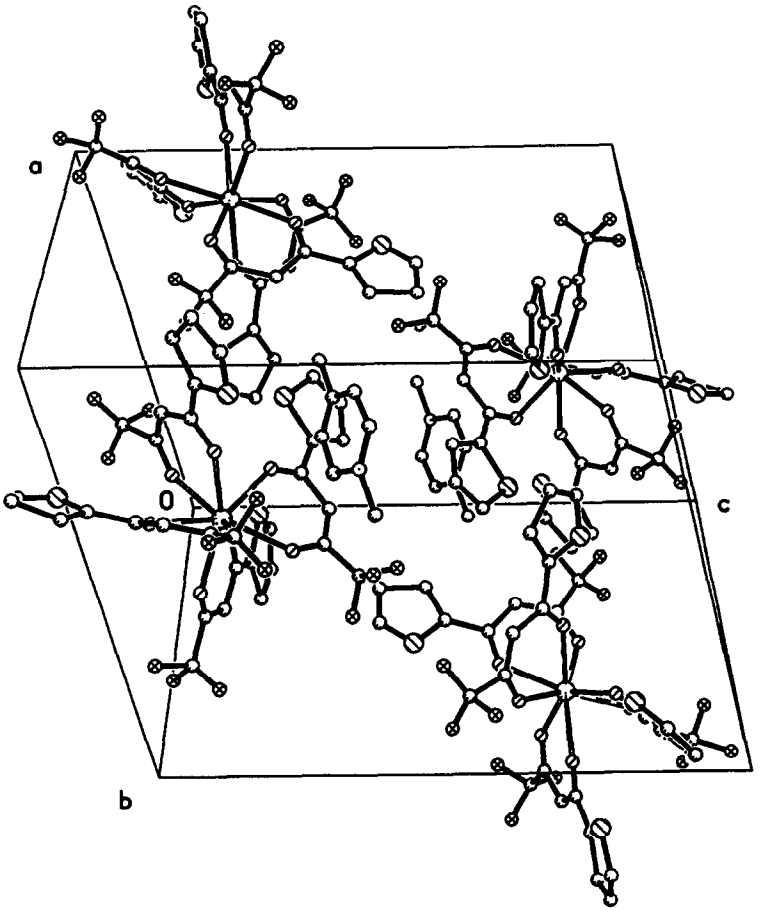

Fig. 3. Unit cell packing diagram for **1**.

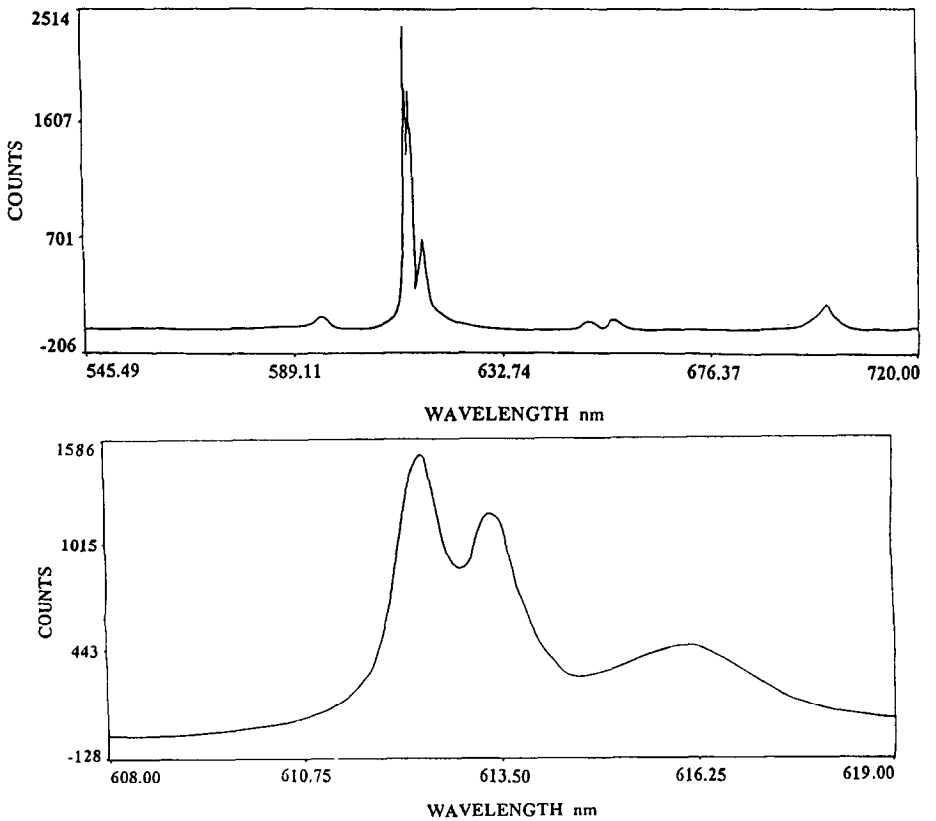

Fig. 4. (a) Emission spectrum (λex = 355 nm) of solid **1** in the range 550–720 nm at room temperature; (b) The most intense emission of solid **1** at room temperature.

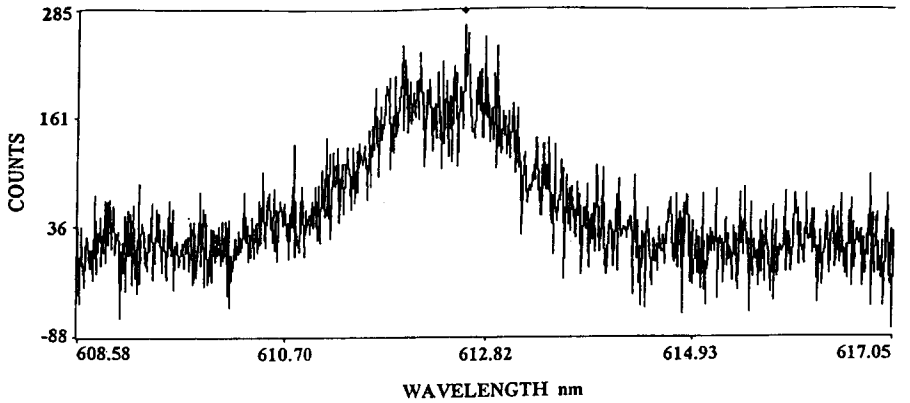

Fig. 5. Triboluminescent spectrum of 1 at room temperature.

boluminescent materials show that a noncentrosymmetric space group is neither necessary nor sufficient for triboluminescence. There are many centrosymmetric crystals which are triboluminescent and many noncentrosymmetric crystals which are not. The present study again demonstrates that materials which are centrosymmetric can be triboluminescent: **1** crystallizes in $P2_1/n$. In the discussion of relation of structure and triboluminescence activity, Sweeting [1] suggested that the phenyl-ring and cation disorder in triethylammonium tetrakis(dibenzoylmethanato) europate which is one of the most brilliantly triboluminescent compounds known provided a sufficient source of localized polarity to produce the observed activity. We are now faced with the similar example. A similar effect is also evident in **1**. The disorders of S atoms and F atoms in **1** may provide a structural basis for charge separation by creating randomly distributed sites of slightly different ionization potentials and electron affinities at the faces of developing cracks. It is not clear which disorder is more important to the triboluminescence between S atoms and F atoms. It is interesting to note that **2** and **3** crystallize in the centric space group $P\bar{1}$ and **4** crystallizes in the centric space group $P2_1/n$. They all appear to exhibit no disorder of S atoms and F atoms and exhibit no triboluminescent activity from the parameters. Therefore, we think the disorder of **1** may play an important role in centrosymmetric **1** for triboluminescence. The disorder in the fluorescent europate ion provides the local dissymmetry needed to support charge separation. In conclusion the Sweeting theory, i.e. the disorder provides sufficient condition for the triboluminescent activity of the centrosymmetric crystals, and appears to be correct for the complexes. We are currently searching for other materials to confirm the discovery of Sweeting.

Table 2. Luminescence spectra data of the complex **1**

Photoluminescence		Triboluminescence	
λ (nm)	assignment	λ (nm)	assignment
595.67	$^5D_0 \rightarrow {}^7F_1$		
612.46	$^5D_0 \rightarrow {}^7F_2$	612.15	$^5D_0 \rightarrow {}^7F_2$
613.39	$^5D_0 \rightarrow {}^7F_2$	612.59	$^5D_0 \rightarrow {}^7F_2$
615.97	$^5D_0 \rightarrow {}^7F_2$		
650.78	$^5D_0 \rightarrow {}^7F_3$		
655.68	$^5D_0 \rightarrow {}^7F_3$		
701.08	$^5D_0 \rightarrow {}^7F_4$		

Acknowledgements—This work was supported by grants from the State Science and Technology Commission and the National Natural Science Foundation of China.

REFERENCES

1. (a) Sweeting, L. M. and Rheingold, A. L., *J. Am. Chem. Soc.*, 1987, **109,** 2652; (b) Sweeting, L. M., Casel, M. L. and Rosenblatt, M. M., *J. Lumin.*, 1992, **52,** 281.
2. (a) Rheingold, A. L. and King, W., *Inorg. Chem.*, 1989, **28,** 1715; (b) Zink, J. I., *J. Am. Chem. Soc.*, 1981, **103,** 1074.
3. Zhu, W. and Huang, W., *J. Rare Earth* (*Chinese*), 1990, **8,** 102.
4. Sweeting, L. M. and Rheingold, A. L., *J. Phys. Chem.*, 1988, **92,** 5648.
5. Zink, J. I., *Private Communication*, 1989.
6. Siemens, *XSCANS* (*Version* 2.1), Siemens Analytical X-ray Instruments Inc. Madison, U.S.A., 1994.
7. Siemens, *SHELXTL* (*Version* 5.0), Siemens Industrial Automation, Inc, Analytical Instrumentation, U.S.A., 1995.
8. Huang, C. H., Zhu, X. Y., Guo, F. W., Song, J. Q., Xu, Z. H. and Liao, C. S., *Acta Sientiarum Naturalium Universitatis Pekinensis*, 1992, **28,** 428.
9. Wei, A. Z., Teng, M. K., Dai, J. B. and Liang, T. C., *J. Struct. Chem.* (*Chinese*), 1983, **2,** 237.

10. Chen, B. T., Zhang, Y. G., Gao, L. and Wang, M. Z., *Acta Chimica Sinica*, 1997, **55,** 553.
11. Zhang, Y., Lin, L. P. and Lu, S. Z., *J. Inorg. Chem.* (*Chinese*), 1997, **13,** 280.
12. Hocking, M. B., VandervoortMaarschalk, F. W., McKiernan, J. and Zink, J. I., *J. Lumin*, 1992, **51,** 323.
13. (a) Dickinson, J. T., Brix, L. B. and Jensen, L. C., *J. Phys. Chem.*, 1984, **88,** 1698 ; (b) Das, J. N., *J. Phys.*, 1973, **B23,** 962.

Pergamon

PII: S0277-5387(97)00516-0

Polyhedron Vol. 17, Nos. 11–12, pp. 1891–1895, 1998
© 1998 Elsevier Science Ltd
All rights reserved. Printed in Great Britain
0277-5387/98 $19.00+0.00

Effects of the benzosubstitution of cryptands for the complex formation between protons, alkali and alkaline earth cations in water

D. A. Dantz, H.-J. Buschmann* and E. Schollmeyer

Deutsches Textilforschungszentrum Nord-West e.V., Frankenring 2, D-47798 Krefeld, Germany

(Received 10 October 1997; accepted 5 December 1997)

Abstract—The protonation reactions of the cryptand (222), benzocryptand (222B) and dibenzocryptand (222BB) and the complexation of alkali and alkaline earth cations in aqueous solution have been studied using pH-metric and calorimetric titrations. The results show that the first proton of all protonated ligands is located inside, and the second proton outside, the cavity. The benzo substituents have no influence upon the enthalpy of the protonation. The entropy of the protonation decreases slightly with the number of benzo substituents due to the lower flexibility of the cryptands. The increasing number of benzo groups leads to lower stability constants for the alkali and alkaline earth cations. These cryptands shield the complexed cations more efficiently from the solvent. Comparing the complexation entropies of the cryptands of barium ion with those of potassium ion it is shown that in the case of the barium ion one more water molecule is released compared with the potassium ion during the complex formation with all three cryptands examined. © 1998 Elsevier Science Ltd. All rights reserved

Keywords: cryptand; benzocryptand; dibenzocryptand; alkali cations; alkaline earth cations; complexes; stability constants; thermodynamic properties.

INTRODUCTION

The first stability constants for the complexation of alkali and alkaline earth cations with cryptands were reported more than 25 years ago [1]. The authors of that article show the dependence of the complex stability on the ionic radius of the complexed ion, the cavity size and the nature of the donor atoms in the cryptand. In the meantime, a large number of articles has been published reporting the complexation of cryptands with a variety of cations in different solvents [2–7]. However, concerning the complexation reaction of benzo or dibenzo substituted cryptands in aqueous solution only few thermodynamic data have been published because of the low solubility of the benzo and the dibenzo cryptands in water [12]. More data are available for the complexation reaction in other solvents as methanol or propylene carbonate [9–12]. The hydrophobic benzo groups of the cryptands (222B) and (222BB) influence the complexation behaviour of these ligands. The flexibility and the basicity of the oxygen atoms next to the benzene rings are reduced. Thus, the benzo groups can directly influence the complex formation and indirectly the interactions between the complexed cation and solvent molecules.

EXPERIMENTAL

The cryptands 4,7,13,16,21,24-hexaoxa-1,10-diazabicyclo[8.8.8]hexacosan (Kryptofix 222, Merck) and 5,6–14,15-dibenzo-4,7,13,16,21,24-hexaoxa-1,10-diazabicyclo[8.8.8]hexacosan (Kryptofix 222BB, Merck) were used without further purification. The cryptand 5,6-benzo-4,7,13,16,21,24-hexaoxa-1,10-diazabicyclo[8.8.8]hexacosan (Kryptofix 222B, Merck) is available as solution in toluene. After evaporation of the solvent the cryptand is dissolved in water. The concentration of the ligand in aqueous solution was determined by potentiometric titration. The chemical structures of the ligands used are given in Fig. 1.

The salts $LiNO_3$, NaCl, KCl, RbCl, CsCl, $Ca(NO_3)_2$, $Sr(NO_3)_2$, $BaCl_2$, $Cu(NO_3)_2$, $Pb(NO_3)_2$,

* Author to whom correspondence should be addressed.

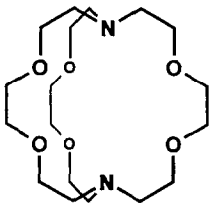

Cryptand (222)

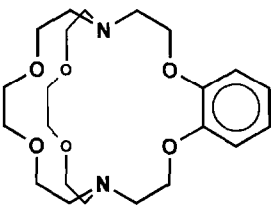

Benzocryptand (222B)

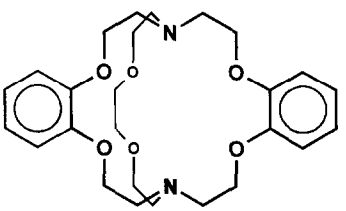

Dibenzocryptand (222BB)

Fig. 1. Chemical structure of the cryptands used.

$Cd(NO_3)_2$, $(CH_3)_4NClO_4$ and $(CH_3)_4NOH$ were of the highest commercially available purity. All solutions were prepared with bidistilled water.

The protonation constants of the cryptand (222B) and the stability constants of the cation cryptand (222B) complex with a log K value higher than 3 were determined by potentiometric titrations [13]. A solution of tetramethyl ammonium hydroxide (0.06 mol/l) was titrated into 20 ml aqueous solution containing the cryptand (0.01 mol/l) and hydrochloric acid (0.04 mol/l). During the titrations the ionic strength was kept constant using tetraethyl ammonium perchlorate (0.05 mol/l) as supporting electrolyte. The titration was performed automatically using a Metrohm Dosimat 665 and a pH-electrode (Metrohm 6.0203.100).

The determinations of the thermodynamic values of the complexation reactions with the cryptands (222B) and (222BB) were performed by calorimetric titrations. The reaction enthalpies were determined using a Tronac Model 450 calorimeter. The measured heat Q produced during the titration is related to the reaction enthalpy ΔH after correction of all non-chemical heat effects by the following equation:

$$Q = \Delta H \cdot \Delta n \qquad (1)$$

where Δn is the number of moles of the complex formed during the titration. The evalution of the data has been described in detail [14–16].

The reaction enthalpy of the monoprotonation reaction K_1 was measured by titrating continuously a solution (0.15 ml) of hydrochloric acid (0.02–0.05 mol/l) into 40 ml solution of the ligands (0.0008–0.003 mol/l) during 30 s. Under these experimental conditions the actual proton concentration in the reaction vessel is much lower than the ligand concentration so only monoprotonation of the ligand takes place. The reaction enthalpy of the second protonation step K_2 is determined by titrating a solution of the ligand (0.00082–0.003 mol/l) into 40 ml hydrochloric acid (0.05 mol/l). Thus, the proton concentration is much higher compared with the ligand concentration. As a result, both nitrogen atoms are protonated. According to the prior measured value of the reaction enthalpy for the monoprotonation, the reaction enthalpy for the second protonation step can be calculated.

The reaction enthalpy of the complexation reaction with the alkali and alkaline earth cations were measured by titrating a solution of the salt (0.03 mol/l) into a solution of the cryptand. The concentration of the cryptand (222B) and (222BB) was 0.003 mol/l and 0.00082 mol/l, respectively. In the case of the cryptand (222BB) a saturated aqueous solution was used. The concentration of the cryptand (222BB) in this solution is known from the literature [8].

RESULTS AND DISCUSSION

The results of the protonation and the complexation of alkali and alkaline earth cations with the different cryptands in aqueous solution are summarized in Table 1. The enthalpies for the complex formation of the cryptands (222B) and (222BB) with alkaline earth cations reported in the literature [17] have been calculated from kinetic measurements at different temperatures. Thus, the accuracy of these values is expected not to be as high as from calorimetric measurements.

The protonated cryptands can exist in three different conformations as shown in Fig. 2. The first protonation K_1 of the cryptand (222) has to be compared with the protonation reaction of trimethylamine due to the decreasing basicity of the nitrogen atoms from primary to secondary and tertiary amines. The first protonation enthalpy of the cryptand (222) ($\Delta H_1 = -47.9$ kJ/mol) is higher than that for the protonation of trimethylamine ($\Delta H = -36.9$ kJ/mol). This indicates that the proton of the protonated cryptand (222) is located inside the cavity where additional interactions with the hetero atoms especially with the second nitrogen atom are possible [13]. The value of the enthalpy for the second protonation K_2 is $\Delta H_2 = -24.5$ kJ/mol. This value is about 12 kJ/mol lower than that for the protonation of trimethylamine. The free electron pair of the second nitrogen atom has to turn from inside the cavity to outside. The addition of the first and the second protonation enthalpy of the cryptand (222) is -72.4 kJ/mol which is twice as much as the enthalpy for the

Table 1. Stability constants log K, (K in dm^3/mol) and thermodynamic values ΔH, $T\Delta S$ (kJ/mol) for the reaction of cryptands with several cations and the protonation reaction in aqueous solutions at 25°C

Cation	(222) log K	(222) $-\Delta H$	(222) $T\Delta S$	(222B) log K	(222B) $-\Delta H$	(222B) $T\Delta S$	(222BB) log K	(222BB) $-\Delta H$	(222BB) $T\Delta S$
H^+ (K_1)	10.00	47.9	9.1	9.27	46.6	6.3	9.5[c]	46.1	8.1
	10.21[a]	51.9[a]	6.4[a]	9.08[a]	59.0[a]	−4.7[a]			
	9.71[b]	45.2[b]	10.2[b]						
H^+ (K_2)	7.45	24.5	18.0	6.21	18.6	16.8	6.2[c]	21.4	14.0
	7.55[a]	29.9[a]	13.0[a]	6.10[a]	22.2[a]	13.1[a]			
	7.31[b]	18.8[b]	22.8[b]						
Li^+	1.5[f]	6.4	4.4	1.7	5.7	3.8		[i]	
Na^+	4.11[b]	31.0[b]	−7.5[b]	3.9	26.2	−3.9	4.13[c]	10.8	12.8
	4.1[f]	36.1[f]	−10.0[f]	4.0[b]			3.44[g]		
K^+	5.58[b]	46.1[b]	−14.3[b]	5.1	38.3	−9.2	5.01[c]	36.7	−8.1
	6.0[f]	52.3[f]	−18.2[f]	4.9[b]			4.35[g]		
							4.62[g]		
Rb^+	4.06[b]	49.4[b]	−26.2[b]	3.9	26.9	−4.6	2.60[e]	[i]	
	5.7[f]	51.0[f]	−18.6[f]	3.4[b]					
Cs^+	3.3[f]	2.4[f]	−16.4[f]	2.4	1.8	−11.9	1.08[c]	[i]	
Ca^{2+}	4.57[b]	0.8[b]	25.3[b]	3.9	2.8	19.5[c]	3.23[c]	0.6	17.8
	5.9[f]	−2.3[f]	31.2[f]	3.8[c]	12.1[c]	9.6[c]	2.66[c]	−3.8[c]	19.0[c]
				3.8[b]			3.45[d]		
				4.0[d]					
Sr^{2+}	8.26[b]	44.4[b]	−2.7[b]	7.1	38.1	2.4	4.76[c]	29.6	−2.4
	7.3[f]	43.4[f]	−1.9[f]	7.4[c]	41.9[c]	0.3[c]	5.7[c]	43.5[c]	−11.0[c]
				6.9[b]			6.38[d]		
				7.5[d]					
Ba^{2+}	9.7[b]	59.9[b]	−4.6[b]	7.6	50.5	−0.9	5.65[d]	30.6	1.6
	9.5[f]	62.8[f]	−8.8[f]	8.0[c]	60.7[c]	−15.1[c]	5.4[c]	15.5[c]	15.3[c]
				7.4[b]			>5[c]		
				7.9[d]			5.65[g]		

[a] Ref. 13; [b] Ref. 19; [c] Ref. 17; [d] Ref. 9; [e] Ref. 8; [f] Ref. 27; [g] Ref. 28; [h] Ref. 29; [i] not enough heat produced during titration.

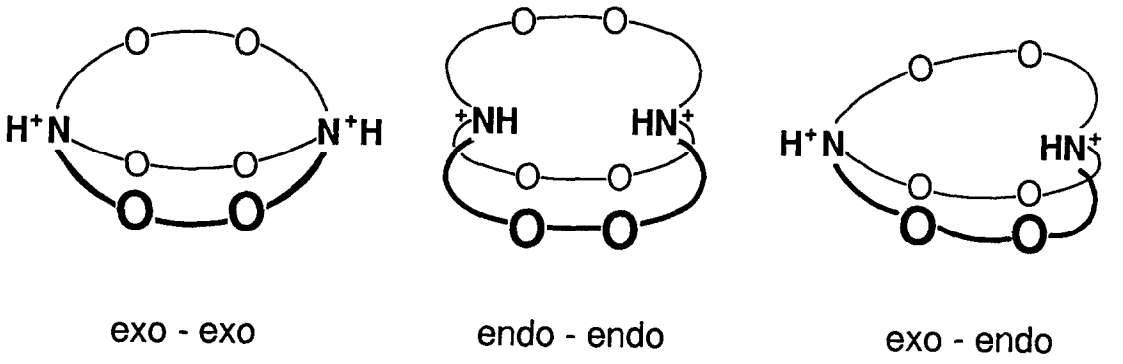

Fig. 2. Possible conformations of the diprotonated cryptands.

protonation of trimethylamine ($2\Delta H = -73.8$ kJ/mol). This shows that both protons mainly interact with the nitrogen atoms in aqueous solution. In the case of the noncyclic analogues of the cryptand (222) no intramolecular interactions of the protonated amine with the oxygen atoms have been observed [18].

The enthalpies of the first protonation step K_1 of the cryptands (222), (222B) and (222BB) are nearly constant. Thus, the decreasing basicity of the oxygen atoms due to the benzo substitution has no effect on the enthalpy of the first protonation. This indicates that generally both nitrogen atoms participate in the first protonation reaction in aqueous solution.

The enthalpy of the second protonation K_2 is almost

constant for all three cryptands used. This is not surprising, because if the second proton is located outside the cavity, the number of benzo substituents should have no influence on the second enthalpy. The entropy of the second protonation decreases slightly which can be explained by the more rigid structure of the benzo-substituted cryptands. In turning the free electron pair of one nitrogen atom from inside to outside, the side chains of the cryptands also have to change their conformation.

Recently crystal structures of the diprotonated cryptand (222) have been published where both protons are located inside the cavity (endo-endo conformation) of the cryptand [20,21]. This structure is in accordance with the molecular dynamic simulation of the protonated cryptand (222) [22]. In this case, both protonated amines are stabilized by the nearest three oxygen atoms. The crystal structure of the diprotonated cryptand (211) is also known from the literature [23]. In contrast to the endo-endo conformation of the crystal structure of the diprotonated cryptand exists in solution the endo-exo conformation. Our results clearly demonstrate that the solvent plays an important role during the formation of the diprotonated cryptand (222).

In the case of the complex formation with alkali and alkaline earth cations the benzo substitution of the cryptand may lead to the following effects:

(a) the cavity size decreases due to the shorter bond of the benzene ring compared with a carbon-carbon single bond;
(b) the rigidity of the cryptand increases;
(c) the benzo ring lowers the basicity of the oxygen donor atoms next to the benzene rings;
(d) the cryptand thickness increases with the number of the benzo substituents. Thicker ligands like the benzosubstituted cryptands shield the cations from the solvent which decreases the stability of the complex. This effect increases with an increasing dielectric constant of the solvent [24].

The potassium (r = 1.38 Å) [25] and barium ion (r = 1.36 Å) [25] fit best into the cavity of the cryptand (222) (r = 1.4 Å) [24] which is shown by the highest stability constant compared with the other alkali and alkaline earth cations, respectively. These stability constants decrease drastically with an increasing number of benzo substituents.

On the other hand, the complex stabilities of the smaller sodium ion (r = 1.02 Å) [25] remains nearly constant with an increasing number of benzo substituents. The decreasing cavity size from the cryptand (222) to (222BB) allows the interaction of the sodium ion with more donor atoms. Thus, the effect of the lower basicity of the oxygen atoms is compensated by the additional interactions with the oxygen atoms. The calcium ion has the same size as the sodium ion (r = 1.00 Å) [25]. In contrast to the stability constants of the sodium ion cryptand complexes the stability constants of the calcium ion cryptand complexes decrease with an increasing number of benzo substituents. The explanation for this result is the increasing ligand thickness which has an effect four times higher for alkaline earth than for alkali ions caused by the charge of the cation [24].

The lithium ion (r = 0.73 Å) [25] is much smaller than the cavity size of the cryptand (222) and therefore the lithium ion interacts only with some donor atoms of the ligand. The decreasing cavity size from the cryptand (222) to (222B) also allows no additional interactions of the lithium ion with other donor atoms in the cryptands. Thus, no changes of the stabilities or enthalpies of the complexation reaction comparing the cryptands (222) and (222B) could be observed. The rubidium (r = 1.49 Å) [25] and caesium ion (r = 1.70 Å) [25] are too big to fit into the cavity of the cryptand (222). These ions are located at one side of the cavity and do not interact with all of the donor atoms of the cryptands. Therefore, the enthalpy of the complexation reaction decreases for these cations. Also the lower basicity of the oxygen atoms next to the benzo groups of the cryptand has an influence upon the enthalpy.

The benzo substitution has also an effect on the solvation sphere of the cryptand cation complex. The ionic radii of the potassium and the barium ion are nearly identical. During complex formation with both cations all contributions e.g., cryptand deformation, cryptand solvation and changes in the structual freedom of the cryptand, are nearly the same. Thus, the observed differences in the entropies which are 9.7, 8.3 and 9.7 kJ/mol for the cryptands (222), (222B) and (222BB), respectively, can only be caused by changes in the number of solvent molecules liberated during the reaction. Dividing these differences of molar entropy for barium as against potassium by the molar entropy for the melting of ice (7.6 kJ/mol) [26] shows that in the case of the reaction of the barium ion with the cryptands are additional water molecule set free compared with the potassium ion. Due to the constant differences between the reaction entropies for barium and potassium ion complexation, it is obvious that the benzo groups of the cryptands have no influence upon the solvation of the complexes. These results are different from those in the solvent methanol, where the substitution of the side chains of the cryptand with benzo groups influences significantly the solvation sphere [12].

Acknowledgements—Financial support by the Ministry of Science and Technology of Nordrhein-Westfalen, Germany is gratefully acknowledged.

REFERENCES

1. Lehn, J.-M. and Sauvage, J. P., *Chem. Commun.*, 1971, 440.
2. Christensen, J. J., Eatough, D. J. and Izatt, R. M., *Chem. Rev.*, 1974, **74**, 351.

3. Izatt, R. M., Lamb, J. D., Eatough, D. J., Christensen, J. J. and Rytting, J. H., *Design of Selective Ion Binding Macrocyclic Compounds and Their Biological Applications*, Medicinal Chemistry Vol. 11, Drug Design 8, ed. E. J. Ariens, Academic Press, New York, 1979.
4. Izatt, R. M., Bradshaw, J. S., Nielsen, S. A., Lamb, J. D. and Christensen, J. J. *Chem. Rev.*, 1985, **85,** 271.
5. Izatt, R. M., Pawlak, K., Bradshaw, J. S. and Bruening, R. L., *Chem. Rev.*, 1991, **91,** 1721.
6. An, H., Bradshaw, J. S. and Izatt, R. M., *Chem. Rev.*, 1992, **92,** 543.
7. Izatt, R. M., Pawlak, K., Bradshaw, J. S. and Bruening, R. L., *Chem. Rev.*, 1995, **95,** 2529.
8. Buschmann, H.-J., Cleve, E., Denter, U. and Schollmeyer, E., *J. Phys. Org. Chem.*, 1994, **7,** 479.
9. Cox, B. G., van Truong, N., and Schneider, H., *J. Am. Chem. Soc.*, 1984, **106,** 1273.
10. Cox, B. G., Knop, D. and Schneider, H., *J. Phys. Chem.*, 1980, **84,** 320.
11. Cox, B. G., Garcia-Rosas, J. and Schneider, H., *Ber. Bunsenges. Phys. Chem.* 1982, **86,** 293.
12. Buschmann, H.-J., *Inorg. Chim. Acta*, 1987, **134,** 225.
13. Buschmann, H.-J., Carvalho, C., Cleve, E., Wenz, G. and Schollmeyer, E., *J. Coord. Chem.*, 1994, **31,** 347.
14. Christensen, J. J., Ruckman, J., Eatough, D. J. and Izatt, R. M., *Thermochim. Acta*, 1972, **3,** 203.
15. Eatough, D. J., Christensen, J. J. and Izatt, R. M., *Thermochim. Acta*, 1972, **3,** 219.
16. Eatough, D. J., Izatt, R. M. and Christensen, J. J., *Thermochim. Acta*, 1972, **3,** 233.
17. Bemtgen, J. M., Springer, M. E., Loyola, V. M., Wilkins R. G. and Taylor, R. W., *Inorg. Chem.*, 1984, **23,** 3348.
18. Dantz, D. A., Buschmann, H.-J. and Schollmeyer, E., *Thermochim. Acta*, 1997, **294,** 133.
19. Anderegg, G., *Helv. Chim. Acta*, 1975, **58,** 1218.
20. MacGillivray, L. R., Atwood, J. L., *Angew. Chem. Int. Ed. Engl.*, 1996, **35,** 1828.
21. MacGillivray, L. R., Atwood, J. L., *J. Org. Chem.*, 1995, **60,** 4972.
22. Auffinger, P. and Wipff, G., *J. Incl. Phenom. Mol. Recognit. Chem.*, 1991, **11,** 71.
23. Luger, P., Buschmann, J., Knöchel, A., Tiemann, D. and Patz, M., *Acta Cryst.*, 1991, **C47,** 1860.
24. Lehn, J.-M., *Struct. Bonding (Berlin)*, 1973, **16,** 1.
25. Shannon, R. D. and Prewitt, C. T., *Acta Crystallogr.*, 1969, **B25,** 925.
26. Marcus, Y., *J. Solution Chem.*, 1985, **15,** 291.
27. Buschmann, H.-J., Cleve, E. and Schollmeyer, E., *J. Coord. Chem.*, 1996, **39,** 293.
28. Chantooni, M. K. and Kolthoff, J. K., *Proc. Natl. Acad. Sci. U.S.A.*, 1981, **78,** 7245.
29. Dietrich, B., Lehn, J.-M. and Sauvage, J.-P., *J. Chem. Soc., Chem. Comm.*, 1973, 15.

Pergamon

PII: S0277-5387(97)00520-2

Polyhedron Vol. 17, Nos. 11–12, pp. 1897–1906, 1998
© 1998 Elsevier Science Ltd
All rights reserved. Printed in Great Britain
0277-5387/98 $19.00+0.00

Synthesis, characterization and reactivity of *cis*-Ru(L)(PPh_3)Cl_2; L = 2-pyridyl-N-(2′-methylthiophenylmethyleneimine): crystal structure of *cis*-Ru(L)(PPh_3)Cl_2 and [Ru(L)(PPh_3)(bpy)]$(ClO_4)_2$

Mosarraf Hossain,[a] Milan Maji,[a] Shyamal Kumar Chattopadhyay,[b] Saktiprosad Ghosh*[a] and Alexander J. Blake[c]

[a] Department of Inorganic Chemistry, Indian Association for the Cultivation of Science, Calcutta 700 032, India

[b] Department of Chemistry, Bengal Engineering College (Deemed University), Howrah 711 103, West Bengal, India

[c] Department of Chemistry, The University of Nottingham, University Park, Nottingham, NG7 2RD, England, U.K.

(Received 15 July 1997; accepted 4 December 1997)

Abstract—A number of ruthenium(II) complexes containing an NNS chelating thioether ligand (L) have been synthesized and characterized by elemental analysis, UV-visible, IR and ^1H NMR spectroscopy and cyclic voltammetry. Ru(L)(PPh_3)Cl_2 (**1**) has been characterized by X-ray diffraction. Structural features of (**1**) indicate a distorted octahedral coordination environment around the ruthenium(II) centre. The two chlorides are *cis* to each other with the Ru—Cl(1) bond *trans* to PPh_3 longer than the Ru—Cl(2) bond. Several mixed-ligand complexes containing bipyridine, phenanthroline, 2-picolinate and oxalate were also isolated and the structure of one of the heterochelates has been solved. [Ru(L)(PPh_3)(bpy)]$(ClO_4)_2$ (**2**) has also been structurally characterized. The structure and properties of (**2**) correspond to the predictions based on the structure of (**1**).
© 1998 Elsevier Science Ltd. All rights reserved

Keywords: ruthenium(II) complexes; NNS donor ligand; mixed ligand complexes; crystal structures; electrochemical study.

Ruthenium(II) complexes of nitrogen and thioether-sulfur chelating ligands received little attention [1–4] over the last few decades even though one such complex was reported way back in 1960 [5]. The N—S chelated ruthenium complexes reported so far, the sulfur donor centres are confined mainly to thiolato sulfur. The lower reactivity [6] of the thioether complexes of the first row transition metals, probably arising out of the steric hindrance at the sulfur atom offered by the alkyl group attached to it and consequent lowering of the nucleophilicity, may have been the discouraging factor. In contrast, thioether complexes of the second row transition metals are quite reactive towards oxidation [7]. Despite some reports [3,7–8] of the synthesis of some ruthenium(II) thioether complexes as a part of the exploration of the reactivity of thiolato complexes towards CH_3I, interest in structural characterization of the resultant thioether complexes was singularly lacking. It has been observed that use of ruthenium substituted metalloproteins where ruthenium is linked to methionine-sulfur of proteins sometimes provide valuable information for the purpose of exploring the local protein structure and their influence on electron transfer reactions [21]. To date, only three structure determinations of thioether complexes of ruthenium(II) are reported by Sheldrick *et al.* [10,11]. These are

* Author to whom correspondence should be addressed.

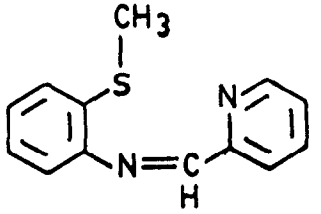

L

ruthenium(II) complexes of an amino acidate ligand, one of which is an organometalic complex [(nbd)Ru(D,L-metme)Cl_2] [10]. [nbd = norbornadiene; metme = methionine methyl ester] and the other two complexes are [RuCl(L-metme)$_2$(PPh_3)]Cl and [RuCl(L-metme)$_2$(PPh_3)] [11]. In this paper we report the synthesis and structure determination of a ruthenium(II) complex of the NNS-chelating thioether ligand 2-pyridyl-N-(2′-methylthiophenyl)methyleneimine(L). The structure of the complex Ru(L)(PPh_3)Cl_2 (**1**) has been determined and the *cis* disposition of the two chloro ligands suggests that substitution by a bidentate chelating ligand is quite feasible and may lead to facile synthesis of mixed chelates. The structure of [Ru(L)(PPh_3)(bpy)](ClO_4)$_2$ one of the derivatives of (**1**), is also determined and discussed.

EXPERIMENTAL

$RuCl_3$ was obtained from Arora-Matthey Limited. Ru(PPh_3)$_3Cl_2$ was prepared by a published procedure [12]. The ligand 2-pyridyl-*N*-(2′-methylthiophenyl)methyleneimine (L) was prepared according to the literature [13]. All other common chemicals were of reagent grade and were used as received. Reagent grade solvents were dried and distilled by usual methods and the solvents were stored over molecular sieves (4 Å). Tetraethylammonium perchlorate (TEAP) was prepared from tetraethylammonium bromide (Fluka AG) by a standard procedure [7] and was recrystallized twice from water and then dried at 110°C for 24 h. Dinitrogen gas was purified by bubbling it successively through alkaline dithionite solution and concentrated sulfuric acid.

Physical measurements

Electronic spectra were recorded with a Shimadzu Model UV-2100 spectrophotometer. Electrochemical data were collected with a Bioanalytical system CV-27 Electrochemicalanalyser and a BAS model X-Y recorder at 298 K. Cyclic voltammetric experiments were carried out with platinum working and counter electrode and a Ag/AgCl reference electrode which was separated from the working compartment by a medium glass frit. Potentials were referenced internally to the ferricenium/ferrocene couple (Fc^+/Fc, 0.46 V vs Ag/AgCl). ^{1}H NMR data were obtained with a Varian XL 100 FT-NMR spectrometer using TMS as the internal reference. Magnetic data were obtained with help of a Princeton Applied Research Model 155 vibrating sample magnetometer using Hg[Co(SCN)$_4$] as the calibrant. Infrared spectra were recorded with a Perkin–Elmer 783 Spectrophotometer as KBr or CsBr pellets. Microanalysis were carried out using a Perkin–Elmer 240 C,H,N analyser. Solution electrical conductivity was measured with a Philips PR-9500 conductivity bridge fitted with a dip-type cell calibrated with 0.02 M KCl solution.

Preparation of the complexes

cis-Ru(L)(PPh_3)Cl_2 (**1**). 960 mg (1 mmol) of Ru(PPh_3)$_3Cl_2$ was dissolved in 40 ml benzene and the solid ligand (470 mg, 2 mmol) was added to it followed by 30 ml of benzene. The colour changed to red-violet immediately. The mixture was refluxed for ca 5 h. The compound separated out within 30 min. The reaction mixture was cooled and filtered. The dark violet residue was washed thoroughly with benzene and dried *in vacuo* over fused $CaCl_2$. Yield: 570 mg, 86% (Found: C, 56.3; H, 4.2; N, 4.3. Calcd for $RuC_{31}H_{27}N_2SPCl_2$: C, 56.2; H, 4.1; N, 4.2%). Conductance in CH_3CN (Λ_M): 52 (ohm^{-1} cm^2 mol^{-1}).

[Ru(L)(PPh_3)(bpy)](ClO_4)$_2$ (**2**) *and* [Ru(L)(P-Ph_3)(bpy)](PF_6)$_2$ (**3**). **Warning**: Perchlorate salts of metal complexes are potentially explosive [14].

About 330 mg (~0.5 mmol) of compound **1** was dissolved in 50 ml of MeOH. 80 mg (~0.5 mmol) of 2,2′-bipyridine was added to it followed by 10 ml MeOH and the mixture was refluxed in a nitrogen atmosphere for about 24 h. After cooling, it was filtered and the volume of the filtrate was reduced to one third of its original volume in a rotary evaporator. It was then divided into two parts. In one part excess aqueous $LiClO_4$ solution was added and the precipitate was allowed to stand in a refrigerator for 1/2 h. It was filtered and washed thoroughly with water. The compound was dried over fused $CaCl_2$ and recrystallized from MeOH/Et_2O. Yield: 187 mg, 79% (Found for **2**: C, 52.2; H, 3.8; N, 5.8. Calcd for $RuC_{41}H_{35}N_4SPCl_2O_8$: C, 52.0; H, 3.7; N, 5.9%). Conductance for **2** in CH_3CN (Λ_M): 219 (ohm^{-1} cm^2 mol^{-1}).

To the other part excess aqueous NH_4PF_6 was added and the compound was isolated and purified similarly as above. Yield: 215 mg 83% (Found for **3**: C, 47.5; H, 3.5; N, 5.2. Calcd for $RuC_{41}H_{35}N_4SP_3F_{12}$: C, 47.4; H, 3.4; N, 5.4%). Conductance for **3** in CH_3CN (Λ_M): 248 (ohm^{-1} cm^2 mol^{-1}).

[Ru(L)(PPh_3)(phen)](ClO_4)$_2$ (**4**), [Ru(L)(PPh_3)(phen)](PF_6)$_2$ (**5**) *and* [Ru(L)(PPh_3)(2-Picolinate)](PF_6) (**6**). These compounds were prepared and purified by a method similar to that used for

preparing the compounds **2** and **3** except the fact that *o*-phenanthroline for **4** and **5** and 2-picolinic acid for **6** was used in place of 2,2′-bipyridine. Yields: 725 mg (75%) for **4**, 775 mg (73%) for **5** and 600 mg (70%) for **6**. [(Found for **4**: C, 53.0; H, 3.6; N, 5.6. Calcd for $RuC_{43}H_{35}N_4SPCl_2O_8$: C, 53.2; H, 3.6; N, 5.8%). Conductance for **4** in CH_3CN (Λ_M): 281 (ohm^{-1} cm^2 mol^{-1})]. [(Found for **5**: C, 48.8, H, 3.1; N, 5.1. Calcd for $RuC_{43}H_{35}N_4SP_3F_{12}$: C, 48.6; H, 3.3; N, 5.3%). Conductance for **5** in CH_3CN (Λ_M): 285 (ohm^{-1} cm^2 mol^{-1})]. [(Found for **6**: C, 51.6; H, 3.8; N, 4.8. Calcd for $RuC_{37}H_{31}N_3SO_2P_2F_6$: C, 51.7; H, 3.6; N, 4.9%). Conductance for **6** in CH_3CN (Λ_M): 136 (ohm^{-1} cm^2 mol^{-1})].

[Ru(L)(PPh$_3$)(C$_2$O$_4$)]·2H$_2$O (**7**). About 330 mg (~0.5 mmol) of **1** was dissolved in 50 ml of MeOH followed by 208 mg (~1 mmol) of $AgClO_4$. The mixture was refluxed for 1 h under nitrogen atmosphere. It was cooled and filtered to remove the precipitated AgCl. Excess aqueous solution of sodium oxalate was added to it, when a red precipitate separated out. It was filtered and washed thoroughly with water. The dried compound was recrystallized from MeOH/Et$_2$O. Yield: 235 mg, 66% (Found: C, 55.3; H, 3.8; N, 4.2. Calcd for $RuC_{33}N_2H_{31}SO_6P$: C, 55.4; H, 3.9; N, 4.3%). Conductance in CH_3CN (Λ_M): 33 (ohm^{-1} cm^2 mol^{-1}).

Crystallographic structure determinations

Single crystals of *cis*-Ru(L)(PPh$_3$)Cl$_2$] (**1**) and [Ru(L)(PPh$_3$)(bpy)](ClO$_4$)$_2$] (**2**) were grown by slow diffusion of *n*-Hexane into CH_2Cl_2 solutions of the complexes at room temperature. Dark red crystal of dimension $0.58 \times 0.19 \times 0.08$ mm for **1** and $0.60 \times 0.31 \times 0.14$ mm for **2** were selected for diffraction studies. The crystals were flash-cooled in a mineral oil film by placing it in the cold nitrogen stream of an Oxford Cryosystems low-temperature device [15] mounted on a Stöe Städi-4 four circle diffractometer. The reflection widths were derived from on-line profile fitting whose parameters were updated continuously [16]. The intensities of three standard reflections monitored every 60 min showed no significant variation. The lattice parameters were refined from 2θ values (30°–38°) for complex **1** of 35 reflections and (24°–26°) for complex **2** of 19 reflections measured at $\pm\omega$. The structure was solved by using the PATTY routine of DIRDIF [7] and refined on F^2 using SHELXL-93 [18]. All non-hydrogen atoms were allowed anisotropic thermal motion and phenyl rings were constrained to be rigid groups. Hydrogen atoms were included in calculated positions and thereafter allowed to ride on their parent atoms with $U_{iso}(H) = 1.2\ U_{aq}$ (C). Table 1 summarizes the data and information relating to data collection and structure refinement; the fractional atomic coordinates of the compound **1** are given in Table 2 and those of **2** are included in Table 3. The relevant bond distance and bond angle data of compound **1** and **2** are presented in Tables 4 and 5 respectively. The angle between the planes were calculated using a standard program [19].

Table 1. Crystallographic Data for *cis*-Ru(L)(PPh$_3$)Cl$_2$ (**1**) and [Ru(L)(PPh$_3$)(bpy)](ClO$_4$)$_2$ (**2**)

	(1)	(2)
Formula	$C_{31}H_{27}Cl_2N_2PRuS$	$C_{41}H_{35}Cl_2N_4O_8PRuS$
FW	662.55	946.73
Space group	*P*2(1)/C	*P*-1
Crystal system	Monoclinic	Triclinic
a (Å)	10.077(3)	9.911(13)
b (Å)	11.068(3)	10.86(2)
c (Å)	25.021(8)	20.25(3)
α (°)	90	78.33(12)
β (°)	94.62(3)	79.05(6)
γ (°)	90	67.95(6)
V (Å^3)	2781.6(14)	1963(5)
Z	4	2
T(K)	150.0(2)	150.0(2)
λ (Å)	0.71073	0.71073
ρ_{calc} (g cm^{-1})	1.582	1.602
μ (mm^{-1})	0.913	0.69
$R(F)^a$	0.0409	0.0522
$R_w(F)^b$	0.0645	0.0829
GOF (F^2)	1.106	1.079

$^a R(F) = \Sigma\|F_o\| - |F_c\|/\Sigma|F_o|$.
$^b R_w(F) = [\Sigma w(|F_o| - |F_c|)^2/\Sigma w|F_o|^2]^{1/2}$.

RESULTS AND DISCUSSION

The ruthenium compounds reported in this study are sufficiently pure and gave satisfactory analytical results. The formula of the neutral, monocationic and dicationic compounds are supported by their respected conductance values. All the complexes are dimagnetic and hence the formal oxidation state of ruthenium in them is +2. ^{1}H NMR spectra of the ligand and metal complexes were recorded in $CDCl_3$. The methyl signal of the ligand (L) at 2.37 ppm is shifted to 3.09 ppm on complexation indicating M—S bond formation. The ill-resolved ^{1}H NMR spectra at 7.00 ppm region is due to the overlapping bands of the phenyl ring protons and the pyridine ring protons. Theoretically two isomers are possible for 6, but only one could be detected by the TLC technique.

Description of the crystal structures

Figure 1 and Fig. 2 (complex cation only) show the ORTEP diagrams of the complexes **1** and **2** respectively along with their atom numbering scheme. The coordination geometry around ruthenium is distorted octahedral and the NNS ligand occupies a meridional plane. The other meridional plane is occupied by the

Table 2. Atomic coordinates ($\times 10^4$) and equivalent isotropic displacement parameters ($Å^2 \times 10^3$) for *cis*-Ru(L)(PPh_3)Cl_2 (**1**). U(eq) is defined as one third of the trace of the orthogonalized Uij tensor

atom	*x*	*y*	*z*	*U*(eq)
Ru	5603(1)	7528(1)	3432(1)	15(1)
Cl(1)	3413(1)	7747(1)	2925(1)	24(1)
Cl(2)	4922(1)	5493(1)	3638(1)	24(1)
C(1)	3129(6)	8445(5)	4231(2)	37(1)
S(2)	4910(1)	8461(1)	4186(1)	22(1)
C(3)	5218(5)	9992(4)	3996(2)	20(1)
C(4)	5014(5)	10947(4)	4340(2)	28(1)
C(5)	5381(6)	12102(5)	4208(2)	31(1)
C(6)	5946(5)	12313(4)	3731(2)	29(1)
C(7)	6160(5)	11381(4)	3382(2)	26(1)
C(8)	5780(5)	10205(4)	3511(2)	19(1)
N(9)	5955(4)	9187(3)	3174(2)	18(1)
C(10)	6236(4)	9286(4)	2677(2)	18(1)
C(11)	6493(4)	8180(4)	2404(2)	18(1)
N(12)	6321(4)	7149(3)	2696(1)	17(1)
C(13)	6621(5)	6085(4)	2484(2)	21(1)
C(14)	7130(5)	5991(5)	1989(2)	25(1)
C(15)	7298(5)	7017(5)	1693(2)	25(1)
C(16)	6952(5)	8134(4)	1897(2)	20(1)
P	7681(1)	7297(1)	3864(1)	17(1)
C(11P)	7913(3)	6701(3)	4549(1)	23(1)
C(12P)	9189(3)	6689(3)	4805(1)	30(1)
C(13P)	9414(3)	6175(3)	5311(1)	39(1)
C(14P)	8362(4)	5671(3)	5561(1)	46(2)
C(15P)	7086(3)	5682(3)	5305(1)	42(2)
C(16P)	6861(3)	6197(3)	4799(1)	29(1)
C(21P)	8769(3)	6217(2)	3539(1)	21(1)
C(22P)	9938(3)	6501(2)	3308(1)	27(1)
C(23P)	10595(3)	5620(3)	3034(1)	33(1)
C(24P)	10084(3)	4455(3)	2992(1)	33(1)
C(25P)	8915(3)	4170(2)	3223(1)	29(1)
C(26P)	8257(3)	5051(3)	3497(1)	25(1)
C(31P)	8555(3)	8754(2)	3913(1)	23(1)
C(32P)	8594(3)	9415(3)	4386(1)	27(1)
C(33P)	9115(4)	10578(3)	4404(1)	30(1)
C(34P)	9598(3)	11080(2)	3949(1)	34(1)
C(35P)	9560(3)	10419(3)	3476(1)	29(1)
C(36P)	9038(3)	9256(3)	3457(1)	25(1)

Table 3. Atomic coordinates ($\times 10^4$) and equivalent isotropic displacement parameters ($Å^2 \times 10^3$) for [Ru(L)(PPh_3)(bpy)]$(ClO_4)_2$ (**2**). U(eq) is defined as one third of the trace of the orthogonalized Uij tensor

atom	*x*	*y*	*z*	*U*(eq)
Ru	609(1)	3296(1)	2581(1)	13(1)
C1	981(9)	−98(7)	2825(4)	29(2)
S2	−363(2)	1579(2)	2763(1)	18(1)
C3	−1064(7)	1657(6)	3635(3)	19(1)
C4	−1780(9)	796(7)	3998(4)	30(2)
C5	−2431(9)	951(8)	4658(4)	36(2)
C6	−2363(9)	1955(8)	4961(4)	33(2)
C7	−1660(8)	2809(7)	4613(3)	24(2)
C8	−975(7)	2655(6)	3959(3)	19(1)
N9	−202(5)	3473(5)	3567(3)	16(1)
C10	150(7)	4292(6)	3823(3)	19(1)
C11	997(7)	5031(6)	3382(3)	17(1)
N12	1324(6)	4785(5)	2717(3)	18(1)
C13	2085(7)	5455(7)	2286(4)	22(2)
C14	2580(8)	6350(7)	2473(4)	29(2)
C15	2283(8)	6586(7)	3132(4)	24(2)
C16	1445(7)	5928(7)	3596(4)	22(2)
N1B	2668(6)	1881(5)	2805(3)	15(1)
C2B	3071(7)	1380(7)	3434(3)	23(2)
C3B	4364(8)	360(8)	3554(4)	31(2)
C4B	5283(9)	−218(8)	3000(4)	38(2)
C5B	4866(8)	278(8)	2355(4)	29(2)
C6B	3582(7)	1356(7)	2263(3)	21(1)
C7B	3123(7)	2055(6)	1597(3)	19(1)
C8B	3993(8)	1772(7)	985(4)	24(2)
C9B	3584(8)	2596(7)	385(3)	26(2)
C10B	2308(8)	3710(7)	420(3)	24(2)
C11B	1453(8)	3907(7)	1035(3)	21(2)
N12B	1813(6)	3092(5)	1618(3)	18(1)
P	−1637(2)	4752(2)	2224(1)	14(1)
C11P	−2294(7)	4249(6)	1572(3)	19(1)
C12P	−1435(8)	3163(6)	1234(3)	22(2)
C13P	−1977(8)	2816(7)	740(3)	26(2)
C14P	−3394(8)	3528(7)	597(4)	30(2)
C15P	−4266(8)	4603(8)	929(4)	31(2)
C16P	−3724(8)	4960(7)	1415(3)	26(2)
C21P	−3153(7)	4906(6)	2914(3)	17(1)
C22P	−3832(7)	3947(6)	3055(3)	20(1)
C23P	−4809(7)	3896(7)	3640(4)	28(2)
C24P	−5111(8)	4796(7)	4090(4)	31(2)
C25P	−4469(8)	5769(8)	3946(3)	30(2)
C26P	−3498(7)	5822(7)	3362(3)	22(2)
C31P	−1701(7)	6462(6)	1873(3)	21(2)
C32P	−1955(8)	6998(7)	1202(3)	28(2)
C33P	−1848(9)	8235(8)	912(4)	38(2)
C34P	−1510(10)	8977(8)	1286(4)	43(2)
C35P	−1250(8)	8470(7)	1955(4)	32(2)
C36P	−1334(7)	7234(6)	2234(3)	21(1)
C11	2347(2)	2586(2)	−4691(1)	21(1)
O11	2097(6)	4003(5)	−4909(3)	31(1)
O12	2115(7)	2326(6)	−3960(3)	41(1)
O13	1317(7)	2237(5)	−4954(3)	38(1)
O14	3791(7)	1805(6)	−4939(4)	51(2)
C12	7259(2)	1031(2)	9091(1)	35(1)
O21	8543(7)	−56(7)	8901(3)	54(2)
O22	6247(8)	1322(7)	8606(4)	61(2)
O23	7616(9)	2203(7)	9074(4)	61(2)
O24	6609(8)	654(7)	9753(3)	72(3)

PPh_3 and two chlorides in **1** and two nitrogen atoms of bipyridyl moiety in **2**. Both the Ru—Cl distances in **1** are somewhat long, but the Ru—Cl(1) bond *trans* to PPh_3 is slightly longer than Ru—Cl(2), due to the greater *trans* effect of phosphorus donor centre over nitrogen. It has been reported [21] that the highest occupied molecular orbital in a thioether is essentially a sulphur 3p orbital which is perpendicular to the SC_2 plane defined by S(2), C(1) and C(3). Thus the Ru—S sigma bond is derived from overlap of a vacant ruthenium $d\sigma$ orbital with the S(3p) HOMO. Hence the strength of Ru—S bond is expected to be maximum when SC_2 plane is perpendicular to the Ru—S bond. One may define [21] X as the mid-point

Table 4. Selected bond lengths [Å] and angles [deg] for Ru(L)(PPh$_3$)Cl$_2$ (**1**)

Bond lengths			
Ru—Cl(1)	2.467(2)	C(8)—N(9)	1.427(6)
Ru—Cl(2)	2.4221(13)	N(9)—C(10)	1.301(6)
Ru—S(2)	2.3086(13)	C(10)—C(11)	1.436(6)
Ru—N(9)	1.988(4)	C(11)—N(12)	1.374(6)
Ru—N(12)	2.075(4)	C(11)—C(16)	1.385(6)
Ru—P	2.292(2)	N(12)—C(13)	1.336(6)
C(1)—S(2)	1.807(6)	P—C(31P)	1.837(2)
S(2)—C(3)	1.794(5)	P—C(11P)	1.835(2)
C(3)—C(8)	1.400(6)	P—C(21P)	1.853(2)

Bond angles			
N(9)—Ru—N(12)	79.3(2)	C(3)—C(8)—N(9)	117.2(4)
N(9)—Ru—P	94.36(11)	C(7)—C(8)—N(9)	123.3(4)
N(12)—Ru—P	91.45(11)	C(10)—N(9)—C(8)	123.0(4)
N(9)—Ru—S(2)	85.74(11)	C(10)—N(9)—Ru	116.5(3)
N(12)—Ru—S(2)	165.07(11)	C(8)—N(9)—Ru	120.3(3)
P—Ru—S(2)	89.39(5)	N(9)—C(10)—C(11)	116.4(4)
N(9)—Ru—Cl(2)	171.59(11)	N(12)—C(11)—C(10)	114.8(4)
N(12)—Ru—Cl(2)	97.22(11)	C(16)—C(11)—C(10)	123.6(4)
P—Ru—Cl(2)	93.40(4)	C(13)—N(12)—Ru	129.5(3)
S(2)—Ru—Cl(2)	97.61(5)	C(11)—N(12)—Ru	111.8(3)
N(9)—Ru—Cl(1)	85.32(11)	N(12)—C(13)—C(14)	122.3(4)
N(12)—Ru—Cl(1)	85.73(11)	C(31P)—P—C(11P)	103.2(2)
P—Ru—Cl(1)	177.17(4)	C(31P)—P—C(21P)	107.3(2)
S(2)—Ru—Cl(1)	93.39(5)	C(11P)—P—C(21P)	98.2(2)
Cl(2)—Ru—Cl(1)	86.78(4)	C(31P)—P—Ru	110.40(12)
C(3)—S(2)—C(1)	102.7(2)	C(11P)—P—Ru	121.58(12)
C(3)—S(2)—Ru	97.8(2)	C(21P)—P—Ru	114.59(12)
C(1)—S(2)—Ru	114.5(2)		

between C(1)···C(3) vector and the Ru—S—X angle is expected to be 90° for maximum strength of the Ru—S bond. In compound **1** this angle is found to be 87.26° and in compound **2** the corresponding angle is 87.15°. Thus the Ruthenium-thioether bond is expected to be very strong. This is amply reflected in the Ru—S bond length (2.309 in **1** and 2.340 in **2**), which are among the shortest reported for ruthenium-thioether complexes. Compared to that of compound **1** the slight lengthening of the Ru—S bond in **2** may be due to steric repulsion of the bypyridyl ring with the alkyl groups of the thioether ligand. The Ru—P bond lengths are also quite short, indicating pronounced "soft" character of the Ru(II) core, which results in strong back bonding between the metal centre and the phosphine moiety. Again, the slightly longer Ru—P bond in **2** probably arises due to steric effect as well as competition for back bonding between triphenyl phosphine and bipyridyl moiety. For the same reason the Ru—N9 (imine) bond length in **1** (1.988) is shorter than that in **2** (2.025).

IR spectra

Selected IR bands and their assignments are listed in Table 6. A fairly strong band at 1620 cm^{-1}, assigned to ν(CN) vibration of the ligand underwent blue shift due to M—N bond formation in complexes [22]. The ν(CS) bands present at 790 and 760 cm^{-1} in the ligand are lowered by 10–15 cm^{-1} on complexation and point to the formation of M—S bond [23]. The shift of the pyridine ring vibration at 630 and 430 cm^{-1} in all the complexes also indicates that coordination takes place from the pyridine ring nitrogen. In addition, the presence of the broad and strong bands at 1100 cm^{-1} and 850 cm^{-1} in the complexes containing perchlorate and hexafluorophosphate respectively is symptomatic of the ionic nature of these two anions. The strong bands of the free oxalate ion at 1690 cm^{-1} and 1710 cm^{-1} are considerably modified in the corresponding complex **6** pointing to the coordination of the oxalate moiety to the ruthenium(II) centre. The medium intensity ν(Ru—Cl) bands at 315 and 360 cm^{-1} in complex **1** are indicative of the *cis*-disposition of the two coordinated chloride ligands [24].

Electrochemistry

The results of the cyclic voltametric experiments for various Ru(II) complexes are listed in Table 7. Cyclic voltammograms of complex **1** and **2** in acetonitrile and **1** in dichloromethane is shown in Fig. 3. Potential

Table 5. Selected bond distances [Å] and angles [deg] for $[Ru(L)(PPh_3)(bpy)](ClO_4)_2$ (**2**)

Bond lengths			
Ru—S2	2.340(3)	N1B—C6B	1.355(9)
Ru—N9	2.025(6)	C2B—C3B	1.368(10)
Ru—N12	2.077(6)	C3B—C4B	1.397(11)
Ru—N1B	2.109(6)	C4B—C5B	1.385(11)
Ru—N12B	2.089(6)	C5B—C6B	1.382(10)
Ru—P	2.342(3)	C6B—C7B	1.470(10)
C1—S2	1.804(7)	C7B—N12B	1.362(8)
S2—C3	1.776(7)	C7B—C8B	1.387(10)
C3—C8	1.412(10)	C8B—C9B	1.385(10)
C8—N9	1.414(9)	C9B—C10B	1.385(10)
N9—C10	1.292(9)	C10B—C11B	1.373(10)
C10—C11	1.441(9)	C11B—N12B	1.344(9)
C11—N12	1.378(9)	P—C11P	1.829(7)
C11—C16	1.379(10)	P—C21P	1.829(7)
N12—C13	1.330(9)	P—C31P	1.831(7)
N1B—C2B	1.352(9)		
Bond angles			
N9—Ru—N12	79.7(2)	C10—N9—C8	122.9(6)
N9—Ru—N12B	169.2(2)	C10—N9—Ru	115.3(4)
N12—Ru—N12B	93.2(2)	C8—N9—Ru	121.6(4)
N9—Ru—N1B	94.2(2)	N9—C10—C11	118.1(6)
N12—Ru—N1B	88.0(2)	N12—C11—C10	114.8(6)
N12B—Ru—N1B	77.3(2)	C16—C11—C10	123.5(6)
N9—Ru—S2	84.2(2)	C13—N12—Ru	130.6(5)
N12—Ru—S2	163.6(2)	C11—N12—Ru	112.0(4)
N12B—Ru—S2	102.4(2)	N12—C13—C14	123.4(7)
N1B—Ru—S2	90.4(2)	C2B—N1B—C6B	118.9(6)
N9—Ru—P	91.4(2)	C2B—N1B—Ru	125.7(4)
N12—Ru—P	96.1(2)	C6B—N1B—Ru	115.0(4)
N12B—Ru—P	97.4(2)	C11B—N12B—Ru	126.6(5)
N1B—Ru—P	173.6(2)	C7B—N12B—Ru	115.5(4)
S2—Ru—P	87.07(13)	C11P—P—C21P	101.8(3)
C3—S2—C1	100.1(3)	C11P—P—C31P	103.6(3)
C3—S2—Ru	98.1(3)	C21P—P—C31P	106.5(3)
C1—S2—Ru	114.8(3)	C11P—P—Ru	116.5(2)
C7—C8—N9	124.0(6)	C21P—P—Ru	112.0(2)
C3—C8—N9	116.1(6)	C31P—P—Ru	115.0(2)

separations between anodic and cathodic waves, ΔE_p vary between 60 and 90 mV. The peak separations are generally larger than the ideal Nernstian value of 59 mV, but are commonly observed for complexes of this type [2,25], apparently due to uncompensated solution resistance [25]. Plot of peak currents vs the square root of the scan rates are linear, indicating that diffusion-controlled redox processes are occurring at the electrode. The reversible nature of Ru(III)/Ru(II) electron transfer processes is evident from their i_{pc}/i_{pa} ratio of ~1.0. The oxidative response is dominated by a single reversible redox wave corresponding to a Ru(III)/Ru(II) couple. The effect of various parameters on the Ru(III)/Ru(II) couple can be summarized as follows:

(a) $E_{1/2}$(Ru(III)/Ru(II)) values of the neutral complexes $Ru(L)(PPh_3)Cl_2$ (**1**) (0.81 V) and $Ru(L)(PPh_3)(C_2O_4)$(**7**)(E_{pa} = 1.0 V) are lower than that of the monocationic complex **6** (1.19 V) and the dicationic complexes **2, 3, 4** and **5** (~1.50 V) presumably because of their lower formal charge. Similar results were previously observed for other thioether, thiolato [2] and phosphine complexes [26]. It may be noted that redox potential differences between $M^{+1/0}$, $M^{+2/+1}$ and $M^{+3/+2}$ couples are expected simply because the different charge-types lead to different changes in solvation energy for the redox process. The same effect of formal charge is evident if we compare $E_{1/2}$ values of the dicationic thioether complexes $[Ru(L)(PPh_3)(bpy)]^{+2}$ (1.51 V) and $[Ru(L)(PPh_3)(phen)]^{+2}$ (~1.51 V) which are about 0.5 to 0.6 V higher than the corresponding monocationic complexes $[Ru(pabt)(PPh_3)(bpy)]^{+}$ (1.01 V) and $[Ru(pabt)(PPh_3)(Phen)]^{+}$ (1.03 V) (Pabt = demethylated form of L) [27].

(b) On replacing the two chlorides of [Ru(L)(P-

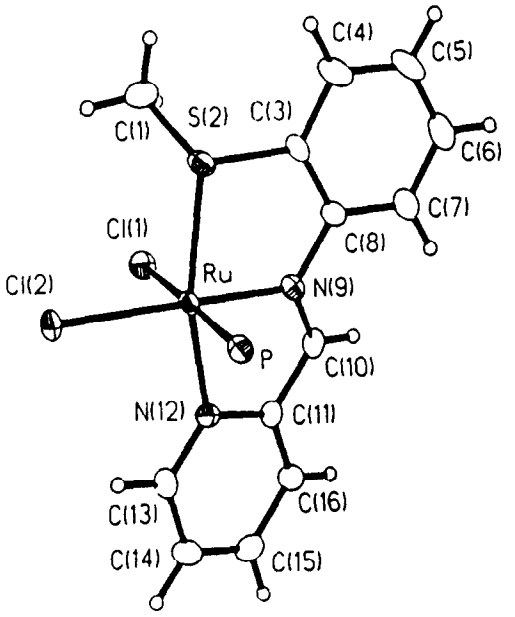

Fig. 1. ORTEP diagram and atom numbering scheme of *cis*-Ru(L)(PPh$_3$)Cl$_2$ (**1**) (the phenyls of the triphenylphosphine ligand have been omitted).

compared to the chloride donors and this is responsible for increase in the $E_{1/2}$ value.

(c) It is interesting to note that the dicationic monothioether complex *cis*-[(bpy)$_2$Ru(PPh$_3$)(S-(CH$_2$CH$_3$)$_2$)]$^{2+}$ exhibits Ru(III)/(II) oxidation [2] at 1.55 V (vs Ag/AgCl) which is almost identical to those of compounds **3** and **5**. This is quite expected, if one assumes that the pyridine-2-aldimino part of the tridentate Schiff base used in this work behaves like a bpy ligand and thus the coordination environment of ruthenium(II) in **3** and **5** is identical to that of [(bpy)$_2$Ru(PPh$_3$)(S(CH$_2$CH$_3$)$_2$)]$^{2+}$ consisting of two bipyridine, one triphenylphosphine and one thioether moiety.

(d) A peak of appreciable current height at 1.11 V present in MeCN solution of **1** disappears in CH$_2$Cl$_2$. This peak is assigned to a solvolysed product of **1** whereby one of the two chlorides is replaced by a MeCN moiety and the resultant species undergoes oxidation at a higher positive potential than the parent complex [28]. It is quite possible that Cl(1) is preferentially replaced by a MeCN molecule due to the greater *trans* effect of PPh$_3$ lying opposite to it. (Λ_M in MeCN of **1** after 12 h standing (R.T.) = 122 ohm^{-1} cm^2 mol^{-1}).

Ph$_3$)Cl$_2$] (**1**) by more electronegative O—O donor to form [Ru(L)(PPh$_3$)(C$_2$O$_4$)] (**7**) the $E_{1/2}$ increases from 0.79 to 1.0 V. The more electronegative oxygen atom increases the effective nuclear charge on the metal

Electronic spectra

Table 8 contains the electronic spectral data of the ligand (L) and the complexes. The visible-near UV

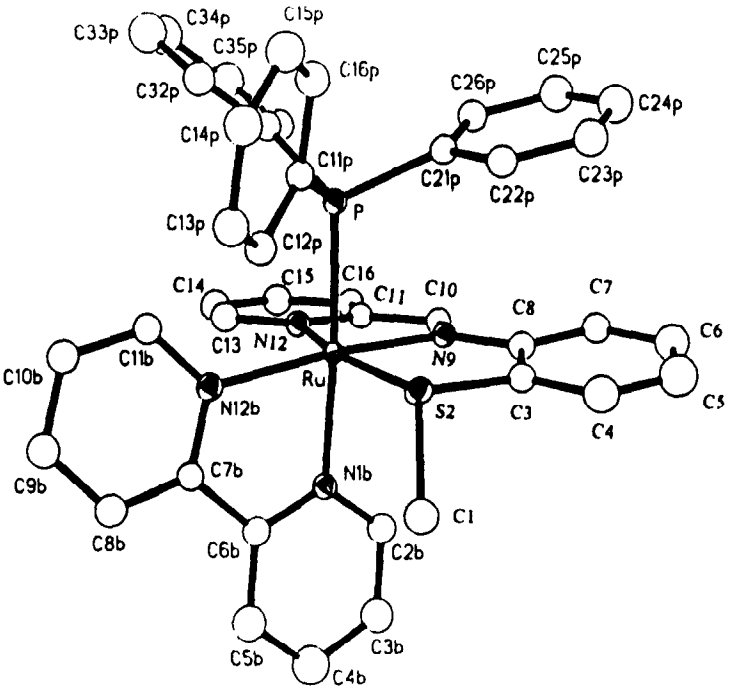

Fig. 2. ORTEP diagram and atom numbering scheme of [Ru(L)(PPh$_3$)(bpy)](ClO$_4$)$_2$] (**2**) (Complex cation only).

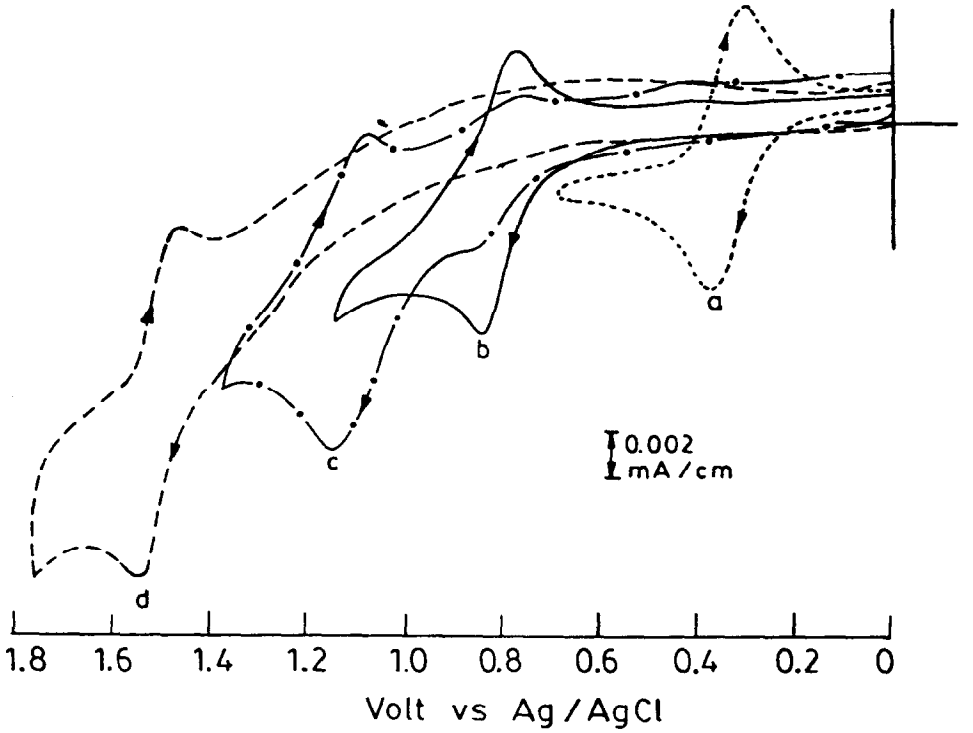

Fig. 3. Cyclic voltammograms (scan rate 200 mVs $^{-1}$) of 10^{-3} M solutions of (a) *cis*-$Ru(bpy)_2Cl_2 \cdot 2H_2O$ in acetonitrile (– – –), (b) *cis*-$Ru(L)(PPh_3)Cl_2$ (**1**) in dichloromethane (——), (c) *cis*-$Ru(L)(PPh_3)Cl_2$ (**1**) in acetonitrile (– · – · –) and (d) $[Ru(L)(PPh_3)(bpy)](ClO_4)_2$ (**2**) (— — —) in acetonitrile (0.1 M TEAP) at a platinum electrode (298 K).

Table 6. Important IR bands (cm^{-1}) of the compounds

Compound	ν(C=N) + ν(C=C)	ν(CS)	Other characteristics vibration
L	1620, 1580, 1570, 1560	790, 760	630, 560, 490, 420
cis-$Ru(L)(PPh_3)Cl_2$ (**1**)	1630(sh), 1590, 1520	775, 750	620, 570, 480, 440, 360, 315
$[Ru(L)(PPh_3)(bpy)](ClO_4)_2$ (**2**)	1620(sh), 1600	775, 750	1090(s, br)[a], 630, 565, 460, 430
$[Ru(L)(PPh_3)(bpy)](PF_6)_2$ (**3**)	1620(sh), 1600, 1580, 1570	775, 755	850(s, br)[b], 630, 560(s)[b], 470, 430
$[Ru(L)(PPh_3)(phen)](ClO_4)_2$ (**4**)	1625, 1600, 1580, 1535, 1515	780, 750	1090(s, br)[a], 635, 580, 460, 430
$[Ru(L)(PPh_3)(phen)](PF_6)_2$ (**5**)	1625, 1600, 1580, 1535, 1515	780, 750	850(s, br)[b], 660, 620, 560(s)[b], 460, 430
$[Ru(L)(PPh_3)(2\text{-picolinate})](PF_6)$ (**6**)	1650, 1630, 1595	780, 750	850(s, br)[b], 560(s)[b], 530, 460, 430
$Ru(L)(PPh_3)(C_2O_4) \cdot 2H_2O$ (**7**)	1650(s), 1585, 1530	790, 750	1710(sh)[c], 620, 435, 370

sh = shoulder, s = strong, br = broad, [a] νClO_4, [b] νPF_6, [c] νCO.

region of the spectra is dominated by strong charge transfer bands responsible for the intense colour of the complexes in the solid state as well as in solution. In the ligand L there are several low lying acceptor orbitals e.g. pyridine π^*, aldimine π^* and low lying vacant *d* orbitals of thioether sulfur. So there may be up to three expected MLCT transitions in the ruthenium complexes of the ligand. Moreover, since all the complexes contain some additional π accepting ligands like triphenylphosphine, bpy or *o*-phen, which themselves contain vacant π^* acceptor orbitals, the actual number of MLCT transitions observed may be much more. Extensive overlapping between these transitions as well as those of the intraligand transitions which, for the free ligand was observed at 363, 251 and 210 nm, make the actual assignment extremely difficult, particularly for the transitions in the UV region. However, the first high intensity band in complex **1** may be reasonably assigned to a $Ru(d\pi) \rightarrow \pi^*(L)$ transition. On substituting the two

Table 7. Cyclic voltammetric results[a,b] at 298 K

Complex	Oxidation $E_{1/2}$, V (ΔE_p, mV)
cis-Ru(L)(PPh$_3$)Cl$_2$ (**1**)	0.79(65), 1.11(60), 0.81(90)[c]
[Ru(L)(PPh$_3$)(bpy)](ClO$_4$)$_2$ (**2**)	1.51(65)
[Ru(L)(PPh$_3$)(bpy)](PF$_6$)$_2$ (**3**)	1.51(75)
[Ru(L)(PPh$_3$)(phen)](ClO$_4$)$_2$ (**4**)	1.51(75)
[Ru(L)(PPh$_3$)(phen)](PF$_6$)$_2$ (**5**)	1.51(75)
[Ru(L)(PPh$_3$)(2-picolinate)](PF$_6$) (**6**)	1.19(75)
Ru(L)(PPh$_3$)(C$_2$O$_4$)·2H$_2$O (**7**)	E_{pa} = 1.00[d]

[a] Conditions: 0.1 M TEAP in CH_3CN vs Ag/AgCl; Solution concentration 10^{-3} M; Working electrode, Platinum; Scan rate 200 mVs^{-1}.

[b] $E_{1/2} = 0.5\ (E_{pa} + E_{pc})$, $\Delta E_p = E_{pc} - E_{pa}$, where E_{pc} and E_{pa} are cathodic and anodic peak potentials, respectively.

[c] Data in CH_2Cl_2. Corresponding E_{pc} = 0.73 V.

CONCLUSION

Apart from the synthesis, characterization and structure determination of two ruthenium(II) complexes of a new NNS chelating thioether ligand, this work clearly demonstrates how determination of structure of a new compound can help to predict its reactivity and to frame synthetic strategies for the preparation of a host of interesting mixed ligand complexes. The *cis* disposition of the two coordinated chloride ion in Ru(L)(PPh$_3$)Cl$_2$ (**1**) pointed to the possible synthesis of heterochelates with different types of bidentate chelating ligands which is realized in this work. It is also demonstrated here that Ru(II) complexes of the thioether ligand 2-pyridyl-N-(2′-methylthiophenyl)-methyleneimine are quite reactive chemically as well as electrochemically.

Acknowledgements—Financial assistance from the Department of Science and Technology (DST), Government of India, New Delhi is gratefully acknowledged.

Table 8. Electronic spectral data for the ruthenium complexes in acetonitrile

Complex	$\lambda_{max,nm}(\varepsilon_{max} \times 10^{-3}, M^{-1}\ cm^{-1})$
L	363(3.16), 251(14.41), 210(16.91)
cis-Ru(L)(PPh$_3$)Cl$_2$ (**1**)	592(0.61), 520(1.34), 360(3.30), 345(5.01), 305(7.12), 280(4.50)
[Ru(L)(PPh$_3$)(bpy)](ClO$_4$)$_2$ (**2**)	486(2.67), 367(7.04), 350(9.46), 290(19.29), 225(39.11)
[Ru(L)(PPh$_3$(bpy)](PF$_6$)$_2$ (**3**)	485(3.19), 465(2.95), 365(8.42), 307(13.10)
[Ru(L)(PPh$_3$)(phen)](ClO$_4$)$_2$ (**4**)	480(3.67), 455(sh)(3.58), 360(sh)(12.39), 347(14.55), 300(18.52)
[Ru(L)(PPh$_3$)(phen)](PF$_6$)$_2$ (**5**)	477(3.72), 367(12.22), 347(14.26), 292(23.22), 265(37.03), 228(62.20)
[Ru(L)(PPh$_3$)(2-picolinate)](PF$_6$) (**6**)	515(2.97), 365(sh)(6.52), 343(sh)(90.4), 308 (15.24), 239(sh)(26.70), 212(49.80)
Ru(L)(PPh$_3$)(C$_2$O$_4$)·2H$_2$O (**7**)	550(2.41), 365(3.81), 312(11.18), 278(6.58)

sh = shoulder.

chlorides by bipyridyl or *o*-phen the first charge transfer band in the visible region exhibits appreciable blue shift, as anticipated. The bands at 280–300 nm are probably due to π–π^* transitions of the ligand and of bipyridyl or *o*-phen moieties [29]. Other bands in the higher energy region may also be assigned to π–π^* and n–π^* transitions of the phenyl, pyridine or bpy/*o*-phen moieties [3].

REFERENCES

1. Mahapatra, A. K., Datta, S., Goswami, S., Mukherjee, M., Mukherjee, A. K. and Chakravorty, A., *Inorg. Chem.*, 1986, **25**, 1715.
2. Root, M. J., Sullivan, B. P., Meyer, T. J. and Deutsch, E., *Inorg. Chem.*, 1985, **24**, 2731.
3. Root, M. J. and Deutsch, E., *Inorg. Chem.*, 1984, **23**, 622.

4. Saleem, A. M., Samha, H. A., Hodali, H. A. and Seyam, A. M., *Synth. React. Inorg. Met.-Org. Chem.*, 1992, **22,** 805.
5. Goodwin, H. A. and Lions, F., *J. Am. Chem. Soc.*, 1960, **82,** 5013.
6. Gainsford, G. J., Jackson, W. G. and Sargeson, A. M., *J. Am. Chem. Soc.*, 1982, **104,** 137.
7. Root, M. J. and Deutsch, E., *Inorg. Chem.*, 1985, **24,** 1464.
8. Sellmann, D. and Kappler, O., *Angew. Chem. Ed. Int. Engl.*, 1988, **27,** 689.
9. Sellmann, D., Barth, I. and Moll, M., *Inorg. Chem.*, 1990, **29,** 176.
10. Sheldrick, W. S. and Exner, R., *J. Organomet. Chem.*, 1990, **386,** 375.
11. Sheldrick, W. S. and Exner, R., *Inorg. Chim. Acta*, 1992, **195,** 1.
12. Stephenson, T. A. and Wilkinson, G., *J. Inorg. Nucl. Chem.*, 1966, **28,** 945.
13. Chia, P. S. K. and Livingstone, S. E., *Aust. J. Chem.*, 1969, **22,** 1825.
14. Wolsey, W. C., *J. Chem. Educ.*, 1973, **50,** A335.
15. Cosier, J. and Glazer, A. M., *J. Appl. Cryst.*, 1986, **19,** 105.
16. Clegg, W., *Acta Cryst.*, 1981, **A37,** 22.
17. Beurskens, P. T., Admiraal, G., Beurskens, G., Bosman, W. P., Garcia Granda, S., Gould, R. O., Smits, J. M. M. and Smykalla, C., *The DIRDIF program system, Technical Report of the Crystallography Laboratory*, University of Nijmegen, The Netherlands, 1992.
18. Sheldrick, G. M., SHELXL-93, *Program for crystal structure refinement*, University of Gottingen, Germany, 1993.
19. World List of Crystallographic Computer Programs, *J. Appl. Cryst.*, 1973, **6,** 309.
20. Sheldrick, G. M., *SHELXTL/PC version* 4.3. *Siemens Analytical X-ray Instrumentation Inc.*, Madison, WI, U.S.A., 1992.
21. Krogh-Jespersen, K., Zhang, X., Westbrook, J. D., Fikar, R., Nayak, K., Kwik, W. L., Potenza, J. A. and Schugar, H. J., *J. Am. Chem. Soc.*, 1989, **111,** 4082.
22. Campbell, M. J., Grzeskowiak, R. and Thomas, R., *Spectrochim. Acta*, 1976, **32A,** 556.
23. Sutton, G. J., *Aust. J. Chem.*, 1963, **16,** 1137.
24. Gilbert, J. D., Rose, D. and Wilkinson, G., *J. Chem. Soc.*, (*A*), 1970, 2765.
25. Callahan, R. W., Keene, F. R., Meyer, T. J. and Salmon, D. J., *J. Am. Chem. Soc.*, 1977, **99,** 1064.
26. Sullivan, B. P., Salmon, D. J. and Meyer, T. J., *Inorg. Chem.*, 1978, **17,** 3334.
27. Hossain, M., Chattopadhyay, S. K. and Ghosh, S., *Polyhedron*, 1997, **16,** 1793.
28. Wheeler, S. H., Mattson, B. M., Miessler, G. L. and Pignolet, L. H., *Inorg. Chem.*, 1978, **17,** 340.
29. Masui, H., Lever, A. B. P. and Auburn, P. R., *Inorg. Chem.*, 1991, **30,** 1240.

Pergamon

PII: S0277-5387(97)00514-7

Polyhedron Vol. 17, Nos. 11–12, pp. 1907–1912, 1998
© 1998 Elsevier Science Ltd
All rights reserved. Printed in Great Britain
0277-5387/98 $19.00+0.00

Additional reactions of inorganic condensed phosphate oligomers during their degradation reactions in the presence of aluminum(III) ions

Genichiro Kura,* Yoshinobu Miyazaki and Jun Sakamoto

Department of Chemistry, Fukuoka University of Education, Akama, Munakata, Fukuoka 811-4192, Japan

(Received 13 October 1997; accepted 2 December 1997)

Abstract—When linear di-, tri-, or tetraphosphate was degraded in the presence of Al^{3+}, in addition to the usual degradation products, phosphates formed which possessed one more PO_4 group than the parent phosphates. This was confirmed by using HPLC. Tetraphosphate produced from the hydrolysis of triphosphate in the presence of Al^{3+} was isolated with the use of an anion-exchange column, and its structure was ascertained by ^{31}P-NMR measurement. Moreover, linear tetra-, penta- and hexaphosphates resulted from the six-membered *cyclo*-triphosphate in the presence of Al^{3+} ions. The yield of the unusual hydrolysis products of the phosphates became maximum when an equimolar amount of Al^{3+} ion was used. © 1998 Elsevier Science Ltd. All rights reserved

Keywords: condensed phosphates; hydrolysis; aluminum(III) ion; HPLC; ^{31}P NMR.

Condensed phosphate oligomers are very interesting polyvalent electrolytes which carry a high charge within their relatively compact molecules [1]. In this group, *cyclo*-polyphosphate anions are relatively weak Brønsted bases in aqueous solutions, and they can exist as high-valent anions [2]. However, they form complexes or ion-pairs with many cations other than tetra-alkylammonium ions [3], and these complexes or ion-pair formations must be considered when their reactions in aqueous solutions are investigated. Linear polyphosphate anions have terminal PO^- groups which are very strong as Brønsted bases [4], and it is necessary to have accurate knowledge of their acid dissociation constants to predict their effect in aqueous solutions. Generally, linear polyphosphate oligomers have a stronger complexibility than cyclic oligomers [5] with the same polymerization degree, though, unlike their cyclic counterpart are highly dependent upon the pH of the aqueous solutions. Moreover, the degradation reactions of P—O—P bonds in the condensed phosphate oligomers must be kept in mind when these entities are used in aqueous solutions. If degradation reactions occur, the chemical properties, especially the complexibilities, of these oligomers vary considerably. It then becomes important to fully understand the nature of the degradation process and the products that result from it.

Both *cyclo*- and linear-polyphosphate oligomers finally decompose to monophosphate [6]. For the last decade the hydrolysis reactions of *cyclo*- and linear-polyphosphate oligomers have been investigated using liquid chromatography. It has been found that in acidic solutions linear oligomers are hydrolyzed faster than cyclic oliogomers, except for *cyclo*-triphosphate [7], and in basic solutions cyclic ones degrade faster [8]; however, the differences in the rate constants of both oligomers in states of the polymerization higher than 6 become smaller, and the degradation rates are also highly dependent upon the cations present [9–12]. When the effect of aluminum(III) ions on the rate of degradation of the oligomers was investigated, it was found that unusual reactions occurred during the degradation reactions [13]. When linear diphosphate was hydrolyzed in the presence of Al^{3+} ions, triphosphate, which has a higher polymerization degree than

* Author to whom correspondence should be addressed.

the parent diphosphate, was found in addition to monophosphate, which is the usual hydrolysis product. Similarly, when tri- and tetraphosphate were degraded in the presence of Al^{3+} ion, tetra- and pentaphosphate, respectively, were found among the hydrolysis products.

In this study, these "unusual reactions" were investigated using HPLC, and the degradation products of triphosphate were separated by the use of an anion-exchange column; tetraphosphate was then isolated from the other degradation products, and its structure was ascertained not only by HPLC but also by ^{31}P NMR spectra measurements. Furthermore, linear tetra-, penta-, and hexaphosphate were found in the degradation products of pure *cyclo*-triphosphate in the presence of Al^{3+} ion. In order to elucidate the mechanism of the new reactions, the ratio of the initial concentration of the condensed phosphate oligomers to that of the Al^{3+} ions was changed, and the relative yields of "degradation products" having an increased degree of polymerization were determined. The yields were consequently highest when the ratio of the concentration of phosphate oligomers to that of Al^{3+} ion was nearly 1 : 1.

These reactions were not observed in the presence of Cu^{2+}, Ni^{2+}, Mg^{2+}, or La^{3+} ions. The reaction mechanism seemed related to the slow exchange of coordinated molecules of the Al^{3+} ion. Since phosphate moieties formed by the cleavage of the P—O—P bond and the parent phosphate are coordinated around the same Al^{3+} ion having relatively long residence times, they can recombine with each other, resulting in the formation of phosphates possessing one more PO_4 group than the parent entity. When *cyclo*-triphosphate is degraded, linear triphosphate as a first degradation product may recombine with linear mono-, di-, and triphosphate, which are the usual degradation products of *cyclo*-triphosphate, thereby producing linear tetra-, penta- and hexaphosphate.

In this paper, *cyclo*- and linear polyphosphates are abbreviated as P_{nm} and P_n, respectively, where n is the number of phosphorus atoms per molecule.

EXPERIMENTAL

Chemicals

Linear di- and triphosphate were of commercial origin and they were recrystallized repeatedly until their purity became satisfactory. Linear tetraphosphate was prepared by the alkaline hydrolysis of sodium *cyclo*-tetraphosphate with NaOH and crystallized as a guanidium salt [14]. Sodium salt of *cyclo*-tri- and *cyclo*-tetraphosphate were prepared following the method described in the literature [15]. The purity of these phosphates was checked by HPLC [16].

Hydrolysis

The initial concentration of diphosphate to be degraded was 2.5×10^{-4} mol/l and the concentration of Al^{3+} ion added was adjusted to 2.5×10^{-4} mol/l. When the concentration of both phosphate and Al^{3+} ion were increased to greater than 2.5×10^{-4} mol/l, a precipitate formed. The initial concentrations of triphosphate samples were 5×10^{-4} mol/l and 2.5×10^{-3} mol/l. The concentration of Al^{3+} ion was varied to achieve a molar ratio ($[Al^{3+}] : [P_3]$) of 1 : 1 or 2 : 1, under which conditions the yield of tetraphosphate formed was measured. The initial concentrations of *cyclo*-triphosphate were 2.5×10^{-4} mol/l or 2.5×10^{-3} mol/l, and the concentration of Al^{3+} to be added were also varied to achieve molar ratios ($[Al^{3+}]$: of 1 : 2, 1 : 1, 2 : 1, 3 : 1, and 5 : 1. The hydrolysis temperature was maintained at 70°C using a thermostat. The hydrolysis samples were then analyzed with an HPLC system devised earlier [16].

Isolation of tetraphosphate in the hydrolysis sample of triphosphate

Tetraphosphate formed from hydrolysis of an equimolar mixture of triphosphate and Al^{3+} ion was isolated with an anion-exchange resin colum. The initial solution contained 3.0×10^{-3} mol/l of triphosphate and Al^{3+} ion, and was hydrolyzed for 5 h at 70°C, after which 10 ml of the sample was passed through the anion-exchange column (ϕ 10 mm × 400 mm) containing Dowex 1-X4 resin (100–200 mesh).

The tetraphosphate was separated with a gradient elution system. The volume of the mixing chamber was 1000 ml, the concentration of KCl solution originally in the mixing chamber was 0.22 mol/l, and the concentration of KCl in the upper reservoir was 0.5 mol/l. The pH of the eluent solution was adjusted to 10.5. The effluent was fractionated with a fraction collector. The fractions which contained tetraphosphate were combined and the tetraphosphate was concentrated to about one-fifth volume with the use of a small amount (0.5 g) of anion-exchange resin. The sample thus isolated was used for HPLC analysis and for NMR measurement, after which the sample was hydrolyzed again at pH 3, 60°C, for 3 h and analyzed with HPLC.

NMR measurement

The ^{31}P NMR spectra were recorded on a JEOL JNM-GSX 500 with a 10 mm multinuclear probe tuned to 202.5 MHz. The NMR parameters were chosen as follows: the flip angle was ca 45° (10 μs), the pulse repetition time was 3 s, and the spectral width was 36 kHz. The chemical shifts were reported with respect to 85% H_3PO_4 as an external reference. A field/frequency lock was achieved with the ^2H resonance of D_2O contained in a 2 mm tube.

RESULTS AND DISCUSSION

In this study triphosphate in the presence of equimolar Al^{3+} ion, 2.5×10^{-3} mol/l, was hydrolyzed at 70°C and pH 3. The chromatograms of its hydrolysis samples are shown in Fig. 1(a). At time 0, trace amounts of mono- and diphosphate were found, though a large portion of the sample remained as triphosphate. After 5 h a significant amount of linear tetraphosphate, never before observed as a hydrolysis product of triphosphate, was found (Fig. 1(b)). This was confirmed by HPLC. Upon isolating this tetraphosphate from the hydrolysis products of triphosphate, it was further examined to reconfirm its identity. A preliminary experiment revealed that linear mono-, di-, tri-, and tetraphosphate can be successively separated from each other by the gradient elution described in the Experimental section. Under these elution conditions, the hydrolysis products of triphosphate which contained tetraphosphate were analyzed, and the chromatograms obtained are shown in Fig. 2. The fractions from 350 to 400 ml were collected, and tetraphosphate as a "hydrolysis product" was isolated. The tetraphosphate thus isolated was chromatographed again, as represented in Fig. 3, and its peak volume agreed with that of standard tetraphosphate synthesized separately. Moreover the tetraphosphate sample was hydrolyzed at pH 3 and at 60°C for 5 h in the absence of Al^{3+} ion. The chromatogram of the hydrolysis products is shown in Fig. 4. The presence of tri-, di-, and monophosphate, the expected hydrolysis products of tetraphosphate, confirmed the identity of the sample.

These facts demonstrate the tetraphosphate was undoubtedly contained in the hydrolysis sample of triphosphate in the presence of Al^{3+} ion. The isolated

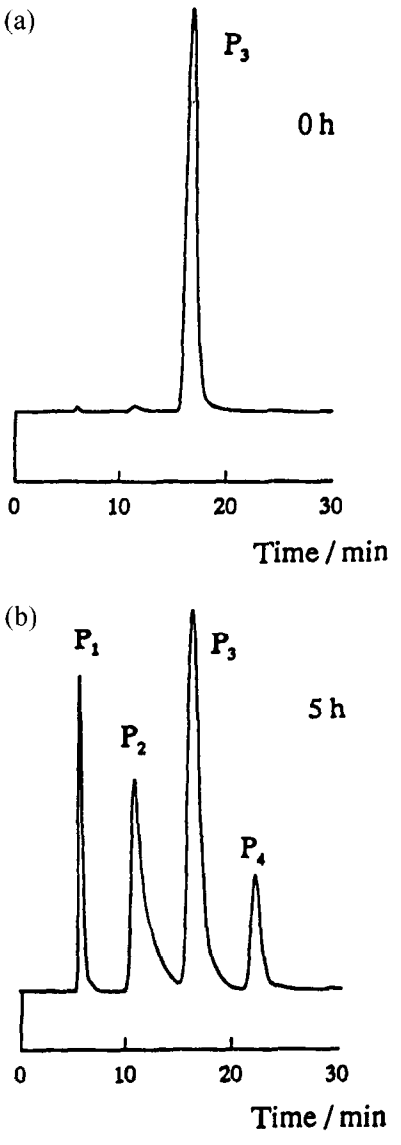

Fig. 1. Chromatogram of the hydrolysis samples of triphosphate in the presence of equimolar Al^{3+}: (a) at time 0 (b) after 5 h.

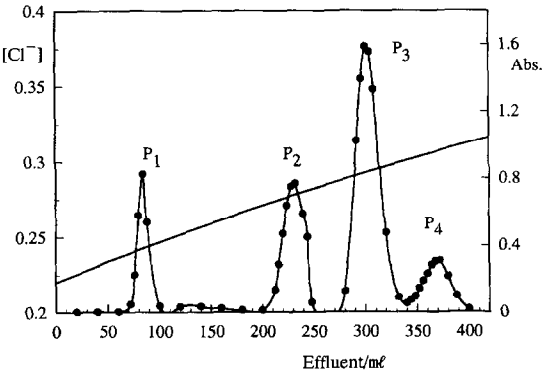

Fig. 2. Isolation of tetraphosphate from the hydrolysis product of triphosphate.

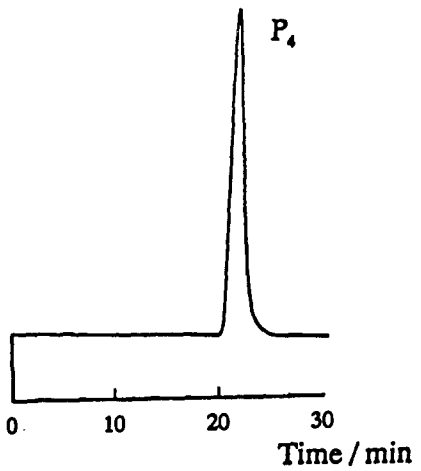

Fig. 3. HPLC analysis of the tetraphosphate isolated.

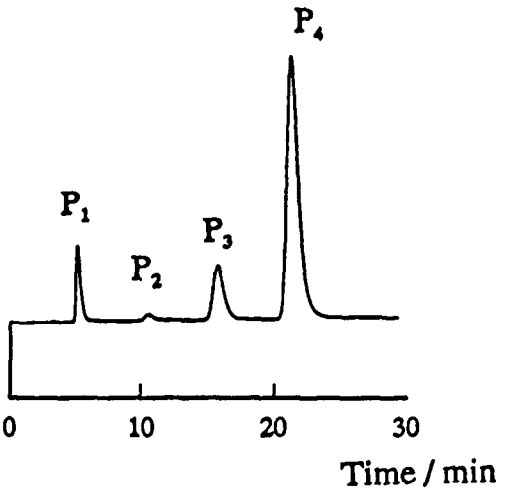

Fig. 4. HPLC analysis of the hydrolysis product of the tetraphosphate isolated.

tetraphosphate initially contained a large amount of KCl. It was therefore diluted greatly with water and wholly adsorbed with 0.5 g of anion-exchange resin, and eluted with 5 ml of 2 M $(CH_3)_4NCl$. The ^{31}P NMR spectra of the sample solution of tetraphosphate thus concentrated and desalted was measured, as shown in Fig. 5. At -6.53 ppm, a peak due to the end PO^- groups of typical linear polyphosphate, and a peak attributed to the middle PO^- groups at -22.42 ppm were observed. The areas under the two peaks above are almost same, indicating the tetraphosphate structure, which has two end PO^- and two middle PO^- groups.

The experimental results cited above therefore show that when linear triphosphate is degraded under the presence of equimolar Al^{3+} ion, it produces tetraphosphate, even though this product has one more PO_4 unit than its parent.

Next, the chromatograms of the products of *cyclo*-triphosphate hydrolyzed in the presence of equimolar Al^{3+} ion are shown in Fig. 6. Other than the usual hydrolysis products of *cyclo*-triphosphate, appreciable amount of linear tetra-, penta- and hexaphosphate were observed. This may be explained by the degradation of *cyclo*-triphosphate into "active" triphosphate, which would attack mono-, di-, or triphosphate, the usual hydrolysis products of *cyclo*-triphosphate, to form linear tetra-, penta-, or hexaphosphate, respectively.

To consider the mechanism of these unusual reactions, the molar ratio of Al^{3+} ion to be added to the linear phosphates or *cyclo*-triphosphate was varied, and the yield of the polyphosphates which were of polymerization degrees higher than that of parent phosphates was determined. As shown in Table 1, when the molar ratio of Al^{3+} ion to triphosphate or *cyclo*-triphosphate was 1 : 1, the yield became maximum. Moreover, as shown in Tables 1 and 2, the yield increased with the increase in the initial concentration of parent phosphates. If the concentration of Al^{3+} is high compared to that of condensed phosphate oligomers (parent phosphates), the phosphate moieties formed by the degradation are coordinated with the different Al^{3+} ions and thus the probabilities of the recombination reactions between parent phosphates and degradation products may decrease. On the other hand, when the concentration of Al^{3+} ion is lower than that of the parent phosphate, the rate of degradation of the parent phosphates becomes slower, and the probability of the addition reactions might likewise become lower.

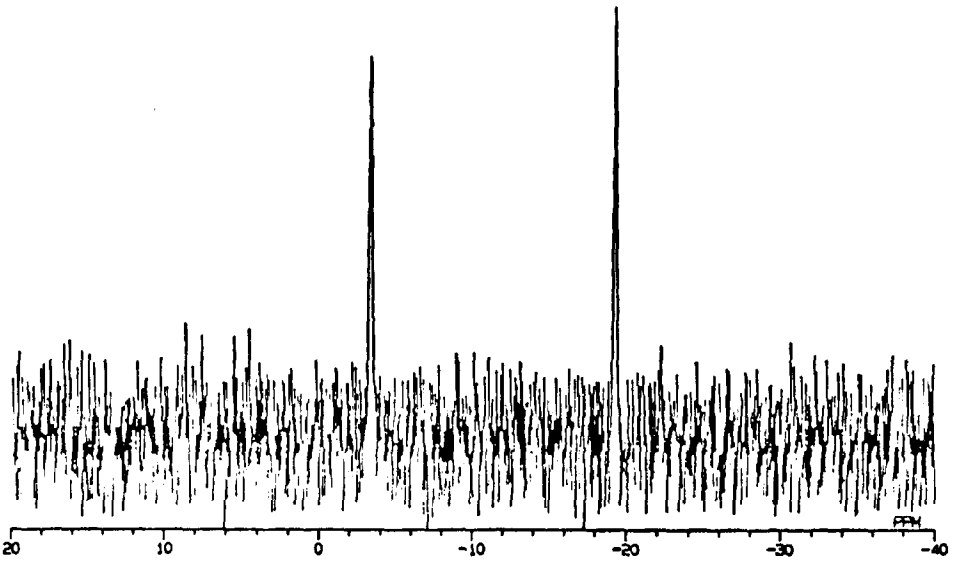

Fig. 5. ^{31}P-NMR spectra of the tetraphosphate isolated.

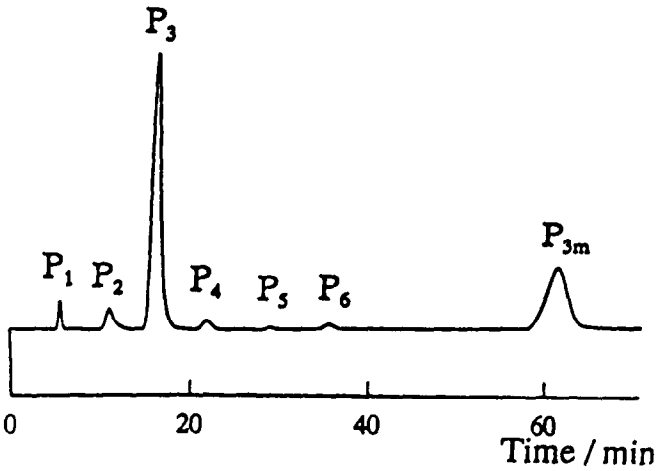

Fig. 6. The chromatogram of the hydrolysis samples of *cyclo*-triphosphate in the presence of equimolar Al^{3+}.

Table 1. Yield of the tetraphosphate when both initial concentration of the triphosphate and the ratio of the phosphates to Al^{3+} were changed

	Yield of P_4/%		
$[P_3$ or $P_{3m}]/[Al^{3+}]$	$[P_3]$; 5×10^{-4} M	$[P_3]$; 2.5×10^{-3} M	$[P_{3m}]$; 2.5×10^{-4} M
2	2.5 (6 h)[a]	6.5 (6 h)[a]	0.8 (1.5 h)[b]
1	5.6 (6 h)[a]	11.1 (5 h)[a]	2.21 (1.5 h)[b]
0.5	0.25 (6 h)[a]	1.9 (5 h)[a]	1.71 (1.5 h)[b]

[a] at 70 C.
[b] at 80 C.

Table 2. Yield of the higher linear polyphosphate oligomers when the initial concentration of *cyclo*-triphosphate was changed under the presence of equimolar Al^{3+} at 80 C

	Yield after 0.25 h/%		
	P_4	P_5	P_6
2.5×10^{-4} M	0.9	0.1	0.2
2.5×10^{-3} M	2.3	0.6	1.5

Acknowledgments—We wish to thank Dr Hirofumi Sakashita and Dr Hirohisa Tsuzuki for their help in obtaining NMR data using a JEOL JNM-GSX 500 spectrometer at the Center of Advanced Instrumental Analysis, Kyushu University, Japan.

REFERENCES

1. Van Wazer, J. R., *Phosphorus and Its Compounds*, Vol. I. Interscience, New York, 1958.
2. Kura, G. and Ohashi, S., *J. Inorg. Nucl. Chem.*, 1972, **34**, 3899.
3. Kura, G. and Ohashi, S., *J. Inorg. Nucl. Chem.*, 1976, **38**, 1151.
4. Watters, J. I., Sturrock, P. E. and Simonaitis, R. E., *Inorg. Chem.*, 1963, **2**, 765.
5. Van Wazer, J. R. and Callis, C. F., *Chem. Rev.*, 1958, **58**, 1011.
6. Kura, G., *Recent Res. Devel in Pure & Applied Chem.*, 1997, **1**, 17.
7. Kura, G., *Bull. Chem. Soc. Jpn.*, 1983, **56**, 3769.
8. Kura, G., *Bull. Chem. Soc. Jpn.*, 1987, **60**, 2857.
9. Kura, G., *Polyhedron*, 1987, **6**, 1863.
10. Kura, G., *Polyhedron*, 1990, **9**, 2177.
11. Kura, G., *Polyhedron*, 1991, **10**, 697.

12. Kura, G. and Tsukuda, T., *Polyhedron*, 1993, **12,** 865.
13. Kura, G. and Ninomiya, J., *Chem. Lett.*, 1995, 819.
14. Quimby, O. T., *J. Phys. Chem.*, 1954, **58,** 603.
15. Brauer, G., *Handbuch der Präprativen Anorganischen Chemie.* Ferdinand Enke Verlag. Stuttgart, 1962, p. 494.
16. Kura, G., *J. Chromatogr.*, 1988, **447,** 91.

Pergamon

PII: S0277-5387(97)00512-3

Polyhedron Vol. 17, Nos. 11–12, pp. 1913–1922, 1998
© 1998 Elsevier Science Ltd
All rights reserved. Printed in Great Britain
0277-5387/98 $19.00+0.00

A facile and preferential synthesis of the complexes, *cis-trans-cis*-$Ru^{II}[NC_5H_4$-N=N-$C_6H_4(R)]_2$ (R = H, *o*-Me/Cl, *m*-Me/Cl, *p*-Me/Cl). Synthesis, spectroscopic characterization and electron-transfer properties

Pradip Munshi, Ramapati Samanta and Goutam Kumar Lahiri*

Department of Chemistry, Indian Institute of Technology, Bombay, Powai, Mumbai-400076, India

(Received 25 August 1997; accepted 2 December 1997)

Abstract—A group of seven complexes of the type *ctc*-$Ru^{II}L_2Cl_2$ (**2a** **2g**) (L = NC_5H_4-N=N-$C_6H_5(R)$, R = H, *o*-Me/Cl, *m*-Me/Cl, *p*-Me/Cl and *ctc* = *cic-trans-cis* with respect to chlorides, pyridine and azo nitrogens, respectively) have been synthesized and characterized. The complexes are diamagnetic (Ru^{II}, t_{2g}^6, S = 0) and electrically neutral. The molecular geometry of the complexes (**2**) in solution has been established by ^1H NMR spectroscopy. They exhibit a strong metal to ligand charge-transfer band in the range 582–603 nm and intra ligand π–π^* transition near 320 nm. In acetonitrile solution the complexes display reversible ruthenium(II) $\rightleftharpoons$ ruthenium(III) oxidation couples in the range 1.02 → 1.36 V vs SCE. Two successive quasi-reversible ligand reductions are observed for each complex in the ranges −0.42 → −0.60 V and −0.68 → −0.85 V vs SCE, respectively. The complexes **2a** and **2e** have been oxidized to the corresponding trivalent species (**3a** and **3e**) by using HNO_3 as oxidizing agent and isolated in solid state as perchlorate salts. Complexes are one-electron paramagnets (Ru^{III}, t_{2g}^5, S = 1/2) and show 1 : 1 conductivity in acetonitrile solution. The presence of perchlorate counter ion in the complexes has been evidenced by the strong infrared bands near 1100 and 600 cm^{-1}. Complexes exhibit a strong ligand to metal charge-transfer band near 530 nm and intra ligand π–π^* transition near 370 nm. In glassy condition (77 K) complexes display rhombic EPR spectra corresponding to the distorted octahedral geometry. © 1998 Elsevier Science Ltd. All rights reserved

Keywords: ruthenium; synthesis; spectra; redox.

Selectivity in chemical reactions is one of the primary objectives particularly where the reactions prefer to form multiple products. One example of such kind of reactions is the interaction of ruthenium trichloride salt with the unsymmetrical 2-(arylzao)pyridine (NC_5H_4-N=N-$C_6H_5(R)$, L) ligand. The unsymmetrical nature of L leads to the formation of isomeric dichloro complexes, $[Ru(L)_2Cl_2]$. Out of the expected five isomers of $[Ru(L)_2Cl_2]$ (*ctc*, *ccc*, *ttt*, *cct* and *tcc* with respect to chlorides pyridine and azo nitrogens, respectively) a mixture of three isomeric complexes, *ctc*, *ccc* and *ttt*-$Ru(L)_2Cl_2$ have been obtained from the reaction of ruthenium trichloride with the ligand, L [1]. Extensive chromatographic purifications and further chemical processes are required to get the individual isomeric species from the reaction mixture. In fact almost a week is needed to prepare the thermodynamically end product pure *ctc* isomer [1]. Although *ctc* isomer is found to be an attractive precursor to synthesize various interesting other complexes [2] and itself has shown important reactivities such as oxo-transfer [3], catalysis [4], electrocatalysis [4], electropolymerization [4], aromatic thiolation [5], cleavage of C—S bond of organic molecules [5], there is no direct and convenient method to synthesize this particular *ctc*-isomer. Therefore, there is an obvious need to develop a direct and convenient procedure for the synthesis of the important *ctc*-$Ru(L)_2Cl_2$ isomer.

In this article we would like to report a facile one-pot synthesis of a group of selective *ctc*-$[Ru^{II}(L)_2Cl_2]$ complexes. The complexes have been prepared by

* Author to whom correspondence should be addressed.

reacting the azopyridine ligand, L with the μ-dichloro diruthenium starting complex, $[Cl(CS)(PPh_3)_2Ru^{II}\mu\text{-}(Cl)]_2$, **1**. Their spectroscopic characterization, electron-transfer properties and spectroelectrochemical correlation have been described.

EXPERIMENTAL

Materials

Commercial ruthenium trichloride (S.D. Fine Chemicals, Bombay, India) was converted to $RuCl_3 \cdot 3H_2O$ by repeated evaporation to dryness with concentrated hydrochloric acid. The starting complex **1** was prepared according to the reported procedure [6]. Other chemicals and solvents were reagent grade and used as received. Silica gel (60–120 mesh) used for chromatography was purchased from S.D. Fine Chemicals, Bombay, India. For spectroscopic and electrochemical studies HPLC grade solvents were used. Tetrabutyl ammonium perchlorate (TBAP) used for electrochemical works was purchased from Aldrich, USA.

Physical measurements

Solution electrical conductivity was checked using Systronic conductivity bridge-305. Electronic spectra (1100–200 nm) were recorded using a Shimadzu UV 160 spectrophotometer. Infrared (4000–300 cm^{-1}) spectra were taken on a Perkin-Elmer 783 spectrophotometer. Magnetic moments were measured with the help of a PAR vibrating—sample magnetometer. ^1H NMR spectra were obtained with the use of a 300 MHz Varian FT-NMR spectrometer. Cyclic voltammetric measurements were carried out using a PAR model 362 scanning potentiostat electrochemistry system. A platinum wire working electrode, a platinum wire auxiliary electrode, and an aqueous saturated calomel reference electrode (SCE) were used in a three electrode configuration. TBAP was the supporting electrolyte and the solute concentration was $\sim 10^{-3}$ M. The half wave potential E^0_{298} was set equal to 0.5 $(E_{pa}+E_{pc})$, where E_{pa} and E_{pc} are anodic and cathodic cyclic voltammetric peak potentials, respectively [7]. The scan rate used was 50 mV s^{-1}. The coulometric experiments were done with a PAR model 370-4 electrochemistry apparatus incorporating 179, digital coulometer. A platinum wire gauze working electrode was used in coulometric experiments. All experiments were carried out under dinitrogen atmosphere and are uncorrected for junction potentials. EPR measurements were made with a Varian model 109 E-line X-band spectrometer fitted with a quartz dewar for measurements at 77 K (liquid nitrogen). The spectra were calibrated by using tetracyanoethylene (TCNE) ($g = 2.0037$). The elemental analyses were carried out with a Carlo Eraba (Italy) elemental analyzer.

Caution! Perchlorate salts of metal complexes are generally explosive. Care should be taken while handling such complexes.

Synthesis of ligands and complexes. The ligands L^1–L^7 were prepared by condensing 2-aminopyridine with the appropriate nitrosobenzene by following the available procedure [8].

The complexes (**2a**–**2g**) were prepared by using a general procedure. Yield varies in the range 65–70%. Specific details are given for one representative complex.

ctc - Bis[2 - (*p-chlorophenylazo*)*pyridine*]*dichloro ruthenium*(*II*), $[Ru(L^7)_2Cl_2]$ (**2g**). The precursor diruthenium complex $[Ru^{II}(CS)(PPh_3)_2Cl_2]_2$, **1** (200 mg, 0.135 mmol) and the ligand 2-(*p*-chlorophenylazo) pyridine, L^7 (118 mg, 0.54 mmol) were dissolved in 15 ml of methanol. The resulting mixture was heated to reflux for a period of 2 h. The initial red brown solution was gradually turned to blue-violet color. The progress of the reaction was monitored periodically by TLC. The solvent was removed under reduced pressure. The crude product was then purified by column chromatography on a silica gel (60–120 mesh) column. Unreacted excess ligand was eluted first with benzene and was rejected. The pure blue colored complex was eluted with 50 : 1 ratio of chloroform and acetonitrile solvents leaving behind a dark band at the top of the column. On removal of the solvent mixture under reduced pressure fine dark crystalline complex $[Ru(L^7)_2Cl_2]$ was obtained. Yield: 102 mg, 70%.

ctc-Bis[2 - (*m-chlorophenylazo*)*pyridine*]*dichloro-ruthenium*(*III*) *perchlorate, monohydrate*, *ctc*-$[Ru(L^5)_2Cl_2]ClO_4 . H_2O$, (**3e**). Finely powdered *ctc*-$[Ru(L^5)_2Cl_2]$ (100 mg) was dissolved in nitric acid. A deep red solution was immediately developed with the evolution of nitrous fumes. The solution was cooled to 273 K and a saturated aqueous solution of sodium perchlorate was added. The deposited dark red solid was filtered off and washed with dilute nitric acid and a small amount of ice-cold water. The oxidized product was then dried in vacuo over P_4O_{10} (yield: 81 mg, 70%).

RESULTS AND DISCUSSION

Seven substituted 2-(arylazo) pyridine ligands used are abbreviated as L^1–L^7. The azopyridine ligand binds to the metal ions in a bidentate N_p, N_a manner forming a five membered chelate ring, ML.

During our recent reactivity studies of the dichloro bridged diruthenium complex, $[Ru^{II}Cl_2(CS)(PPh_3)_2]_2$, **1** we had the occasion to conduct the reaction of azopyridine ligands (L) with the **1**. The reaction of L with the metal complex **1** unexpectedly leads to the formation of selective *ctc*-$Ru(L)_2Cl_2$, **2** isomer as a sole product eqn (1). Although the isolation of pure *ctc* isomer **2** by the conventional method takes nearly one week, the pure complex **2** is achieved here within 2 h.

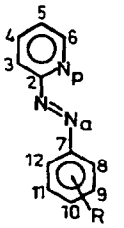

L

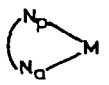

ML

$L^1 \rightarrow R = H$

$L^2 \rightarrow R = 8Me$

$L^3 \rightarrow R = 8Cl$

$L^4 \rightarrow R = 9Me$

$L^5 \rightarrow R = 9Cl$

$L^6 \rightarrow R = 10Me$

$L^7 \rightarrow R = 10Cl$

The conversion of the complex **1** to **2** involves the cleavage of μ-chloro bonds and the replacement of two phosphines and one thiocarbonyl (CS) group from each of the ruthenium centers by the two azopyridine ligands, L. Under identical reaction conditions the reaction of **1** with the similar strong π-acidic but symmetric N,N donor ligands such as 2,2′-bipyridine and 1,10-phenanthroline result in the dimeric and monomeric complexes, **3** and **4**, respectively [6]. In both the complexes (**3** and **4**) phosphine ligands remain unaffected. Thus the replacement of terminal thiocarbonyl (CS) and chloride groups from each of the ruthenium centers of **1** by the bipyridine molecule facilitates the formation of **3**. In case of incoming phenanthroline ligand dimeric structure of **1** has been lost via the cleavage of μ-Cl bonds. In the present case the situation is more complex, here the complete removal of phosphine from the metal center is an additional step. The removal of bulkier *trans* triphenylphosphines from the $Ru(PPh_3)_2$ core is not a common situation [9]. The driving force of the facile conversion of **1** to **2** is not clear.

To generalize the reaction we have used a group of seven azopyridine ligands, L^1–L^7 which are varying depending on the nature and the position of the substituents present in the phenyl ring. The complexes **2a** and **2d** were prepared earlier by following the conventional routes and the stereochemistry of the com-

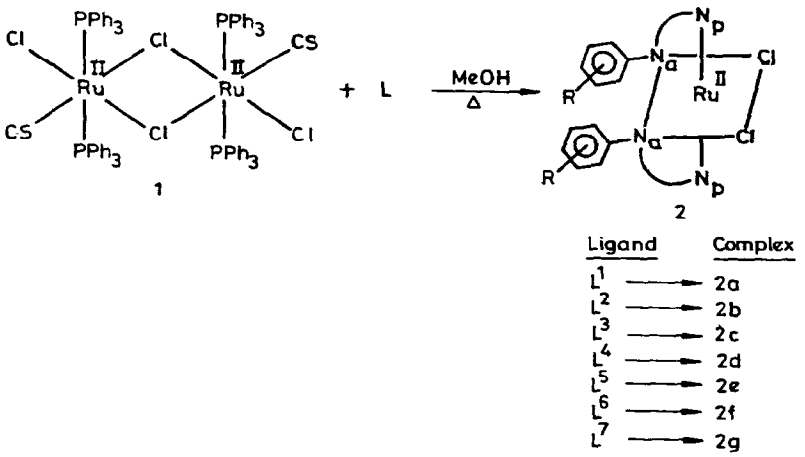

(1)

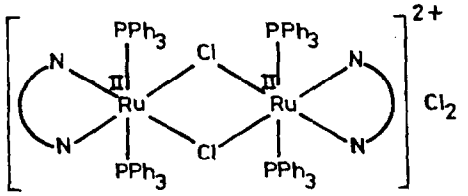

3

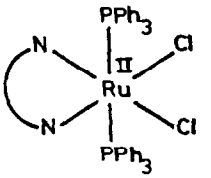

4

plex **2a** was established by single crystal X-ray structure. The ligands L^2, L^3, L^5, L^6, L^7 and their corresponding complexes **2b, 2c, 2e, 2f, 2g** have been prepared first time.

The microanalytical data of the complexes **2** (Table 1) are in good agreement with the calculated values and thus confirming the composition of the complexes, $Ru(L)_2Cl_2$ (**2**). Solid state magnetic moment measurements at 298 K indicate that the complexes are uniformly diamagnetic (t_{2g}^6, S = 0). In acetonitrile, dimethyl formamide and methanol solvents the complexes are non-conducting. Since the spectral properties of the complexes (**2a–2g**) are akin to those of the earlier reported two complexes **2a** and **2d**, it is therefore inferred that all the complexes (**2a–2g**) have very similar isomeric configuration.

Spectral study

I.R. spectra. I.R. spectra of the complexes **2** display several intense bands in the region 4000–300 cm^{-1}. No attempt was made to assign all the bands, however, there are two notable figures: (i) A strong band near 1300 cm^{-1} due to ν(N=N) stretching frequency of the coordinated azopyridine ligand has been observed for all the complexes (Table 1). The N=N stretching frequency of the free L appears near 1425 cm^{-1} [1].

Table 1. Microanalytical, infrared and electronic spectral data

Comp.	Elemental analysis (%)[a] C	H	N	Infrared spectral data (cm^{-1})[b] $\nu_{N=N}$	ν_{Ru-Cl}	Ligand	Electronic spectral data[c] λ_{max} (nm) (ε[d], M^{-1} cm^{-1})
2a	49.22	3.31	15.42	1310	335, 310	L^1	445(760, 321(19,500)
	(49.06)	(3.34)	(15.61)				583(11417), 462[e](1870), 319(24,427)
2b	50.71	3.41	14.70	1326	332, 310	L^2	451(905), 319(21,990)
	(50.87)	(3.38)	(14.84)				589(12,955), 465[e](2256), 316(22,785)
2c	43.33	2.60	13.96	1321	330, 312	L^3	452(808), 319(21,770)
	(43.48)	(2.63)	(13.83)				603(12,820), 462[e](1417), 305(23,107)
2d	50.99	3.45	14.97	1305	330, 305	L^4	450(860), 320(22,100)
	(50.87)	(3.38)	(14.84)				582(10,701), 470[e](2022), 322(23,533)
2e	43.62	2.60	13.72	13.08	328, 302	L^5	451(527, 317(21,970)
	(43.48)	(2.63)	(13.83)				603(15,015), 478[e](2345), 311(26,755)
2f	50.74	3.31	14.69	1328	327, 303	L^6	450(650), 319(21,820)
	(50.87)	(3.38)	(14.84)				589(9332), 473[e](2214), 328(22,555)
2g	43.42	2.75	13.95	1319	335, 315	L^7	447(532), 321(21,450)
	(43.48)	(2.63)	(13.83)				602(12,893), 462[e](2007), 304(22,794)
3a	40.41	3.15	12.95	1340	345, 320		570[e](4000), 532(5100), 374(21,200)
	(40.27)	(3.05)	(12.81)				
3e	36.61	2.30	11.65	1343	347, 327		572[e](3600), 535(6090), 370(20,400)
	(36.43)	(2.48)	(11.59)				

[a] Calculated values are in parentheses.
[b] In KBr discs.
[c] In dichloromethane solution.
[d] Extinction coefficient.
[e] Shoulder.

This appreciable lowering of the N=N frequency while moving from the free ligand (L) to the complexes (**2**) is attributed to the presence of strong $d\pi(Ru^{II}) \rightarrow \pi^*(L)$ back bonding in the ground state of ruthenium (II), where $\pi^*(L)$ is the LUMO of the azoimine chromophore [2]. (ii) All the complexes exhibit systematically two bands near 300 cm^{-1} (Table 1) in accordance with the *cis* configuration of the coordinated two chlorides.

^1H NMR spectra. All the complexes display well resolved ^1H NMR spectra in $CDCl_3$ solvent. Chemical shift and spin–spin splitting (among nearest neighbor protons) values are depicted in Table 2. Two representative spectra and schematic representation of inter spectral correlations are shown in Fig. 1. The presence of C_2 symmetry in the *ctc* isomer makes each half of the molecule equivalent. Thus one methyl signal has been observed for the complexes **2b, 2d** and **2f**. Similarly aromatic region of the spectra exhibit calculated number of protons correspond to one particular ligand in accord with the C_2 symmetry of the *ctc* isomer. The individual aromatic proton resonances were assigned (Table 2) on the basis of their relative intensities, spin-spin structure and substituent-induced change in splitting patterns [10]. Chemical shifts are also considered as additional indicators such as 8-H and 12-H are coincident doublets in complex **2a** whereas 8-H signal appears as a separate singlet for the *meta* substituted complexes, **2d** and **2e**. Further, the 8-H singlet is significantly shifted to higher and lower fields in the complexes **2d** and **2e**, respectively, compared to **2a** (Table 2) based on the electron releasing and withdrawing properties of the methyl and chloride substituents, respectively. *Ortho* substituted (**2b, 2c**) and *para* substituted (**2f, 2g**) complexes also show the expected changes in the distributions of the phenyl ring proton signals with respect to the unsubstituted complex (**2a**).

The effect of the specific position of methyl group in the phenyl ring of the complexes **2b, 2d, 2f** has been clearly reflected in the corresponding chemical shifts of the methyl groups (Table 2). The chemical shift of the methyl group follows the order: *o*-Me (**2b**), 2.40 ppm > *p*-Me (**2f**), 2.24 ppm > *m*-Me (**2d**), 2.13 ppm, indicating the effect of nearby electron withdrawing azo group on the *ortho* and *para* methyl groups is more compared to the *meta* methyl group as expected.

Electronic spectra. Solution electronic spectra of the ligands (L^1–L^7) and the complexes (**2a–2g**) were studied in dichloromethane solvent in the range 200–1100 nm. The spectral data are listed in Table 1 and representative spectra are shown in Fig. 2. The azopyridine ligands (L) are exhibiting two bands near 450 nm ($\varepsilon \rightarrow$ in the range of 500–1000) and near 320 nm

Table 2. ^1H NMR spectral data in $CDCl_3$

Comp.	δ (J/Hz)[a] 6H	3H	4H	5H	8H	9H	10H	11H	12H
2a	9.36 (6.0)[b]	8.57 (5.52)[b]	7.99 (7.71)[c] (7.71)	7.52 (6.85)[c] (6.85)	6.82 (8.57)[b]	7.11 (7.8)[c] (7.8)	7.28 (6.85)[c] (6.85)	7.11 (7.8)[c] (7.8)	6.82 (8.57)[b]
2b	9.16 (5.17)[b]	8.53 (7.9)[b]	7.97 (6.9)[c] (6.9)	7.4 (6.9)[c] (6.9)	(Me) 2.4	5.85 (6.9)[b]	7.07 (7.9)[c] (7.9)	6.61 (6.9)[c] (6.9)	7.2 (8.6)[b]
2c	8.95 (6.75)[b]	8.56 (9.0)[b]	8.01 (8.25)[c] (8.25)	7.4 (6.6)[c] (6.6)	(Cl)	7.23 (5.3)[b]	7.09 (6.0)[c] (6.0)	7.2[d]	7.2[d]
2d	9.38 (6.2)[b]	8.52 (8.0)[b]	7.98 (8.0)[c] (8.0)	7.54 (6.5)[c] (6.5)	6.60[e]	(Me) 2.13	7.08 (8.1)[b]	6.98 (7.8)[c] (7.8)	6.58 (9.1)[b]
2e	9.4 (5.9)[b]	8.57 (8.0)[b]	8.02 (8.0)[c] (8.0)	7.6 (6.3)[c] (6.3)	7.26[e]	(Cl)	6.77 (7.4)[b]	7.09 (7.15)[c] (7.15)	6.74 (4.2)[b]
2f	9.42 (5.47)[b]	8.48 (8.42)[b]	7.98 (7.56)[c] (7.56)	7.55 (8.42)[c] (8.42)	6.87 (8.42)[b]	6.72 (8.42)[b]	(Me) 2.24	6.72 (8.42)[b]	6.87 (8.42)[b]
2g	9.4 (5.45)[b]	8.53 (7.8)[b]	8.04 (7.8)[c] (7.8)	7.56 (8.3)[c] (8.3)	6.76 (9.0)[b]	7.11 (9.01)[b]	(Cl)	7.11 (9.01)[b]	6.76 (9.01)[b]

[a] Tetramethyl silane is the internal standard.
[b] Doublet.
[c] Triplet.
[d] Multiplate pattern, centered at 7.2 ppm.
[e] Singlet.

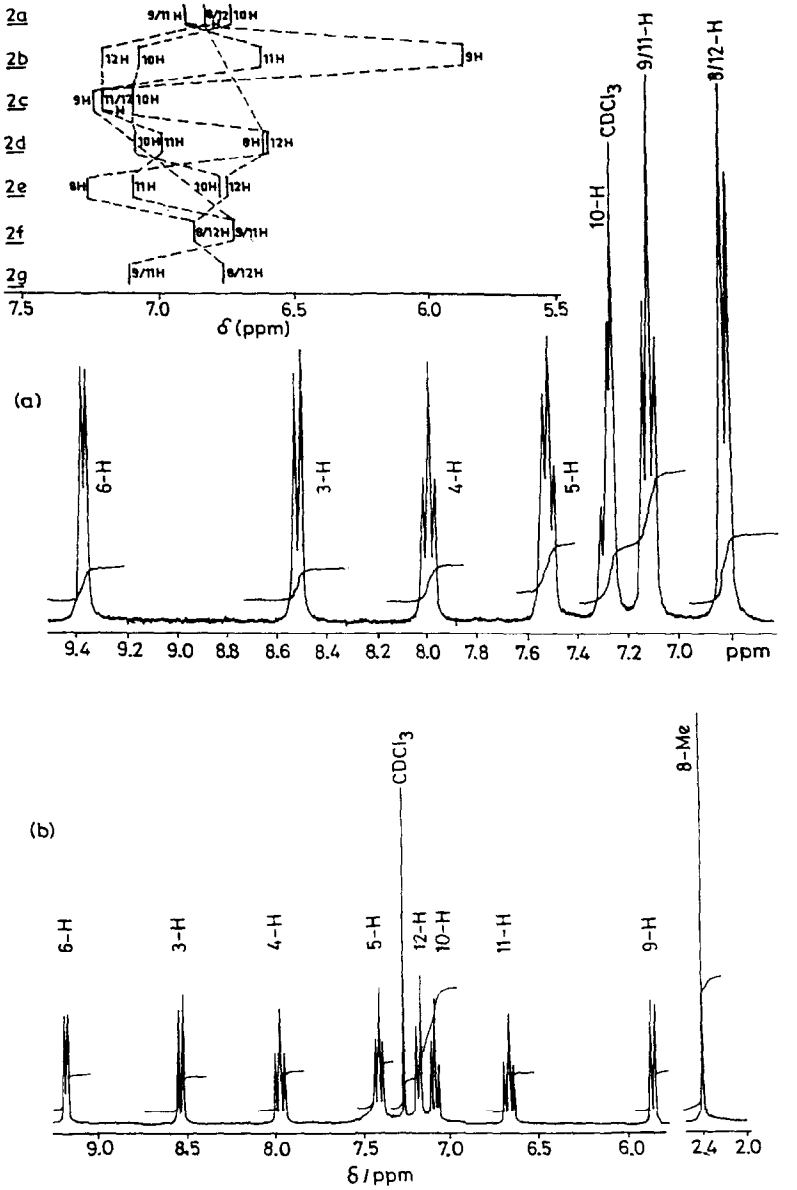

Fig. 1. ^{1}H NMR spectra of (a) *cis*-$Ru^{II}(L^1)_2Cl_2$, **2a** and (b) *cis*-$Ru^{II}(L^2)_2Cl_2$, **2b** in $CDCl_3$. The inset shows a schematic representation of chemical shifts for the phenyl ring protons [-C_6H_4(R)] of **2a**–**g**.

($\varepsilon \sim 20{,}000$) (Table 1), these are possibly due to $n \rightarrow \pi^*$ and $\pi \rightarrow \pi^*$ transitions, respectively, centered primarily on the azo group [11]. All the complexes display two major intense bands near 600 nm and 320 nm (Table 1). The lower energy band near 600 nm is associated with a shoulder at the higher energy part near 470 nm. The band near 600 nm is assigned to $d\pi(Ru^{II}) \rightarrow L(\pi^*)$ [where $L(\pi^*)$ is dominated by the LUMO of the azoimine chromophore] MLCT (metal-to-ligand-charge-transfer) transition. Transition of this type are well documented in ruthenium(II) complexes of unsaturated ligands [12]. The band near 320 nm may be due to intra ligand $\pi \rightarrow \pi^*$ transition.

Electron-transfer properties

Metal redox and ligand reductions. All the complexes are electroactive with respect to metal as well as ligand centers. Redox properties of the complexes have been studied in dichloromethane solution by cyclic voltammetry (CV) using a platinum working electrode. All the complexes display the same three redox processes in the potential range ± 1.5 V vs saturated calomel electrode (SCE) (tetrabutyl ammonium perchlorate used as electrolyte, 298 K). Representative voltammograms are shown in Fig. 3. The peak-to-peak separations of the couples lie in the range 80–

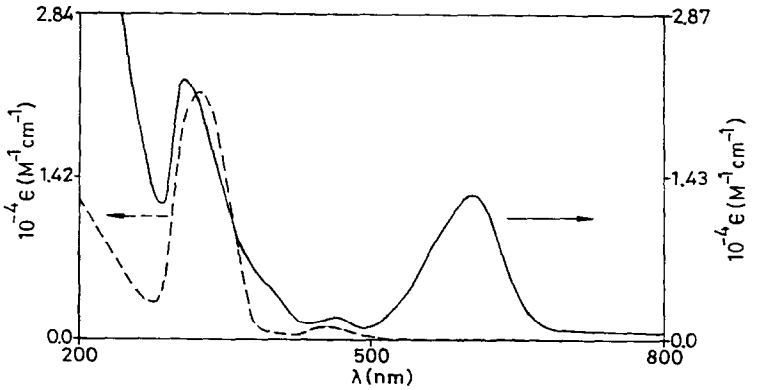

Fig. 2. Electronic spectra of *cis*-$Ru^{II}(L^3)_2Cl_2$, **2c** (—) and the free ligand, L^3 (- - -) in dichloromethane.

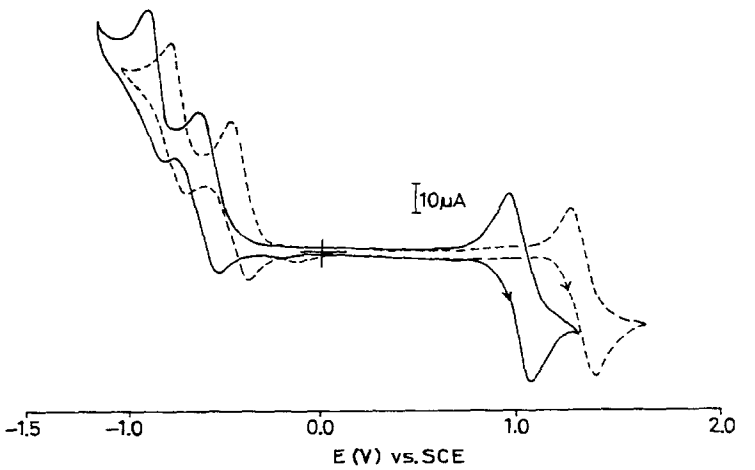

Fig. 3. Cyclic voltammograms of $\sim 10^{-3}$ M solution of the complexes *cis*-$Ru^{II}(L^2)_2Cl_2$, **2b** (—) and *cis*-$Ru^{II}(L^3)_2Cl_2$, **2c** (- - -) in dichloromethane.

110 mV. Reduction potentials data are listed in Table 3.

All the complexes display one reversible oxidative response near 1 V which is assigned to ruthenium(II) to ruthenium(III) oxidation eqn (2). The one-electron nature of the couple eqn (2) was confirmed by constant potential

$$[Ru^{III}(L)_2Cl_2]^+ + e^- \rightleftharpoons Ru^{II}(L)_2Cl_2 \qquad (2)$$

coulometry (Table 3). Here metal oxidation potential varies depending on the nature and the specific location of the substituents present in the phenyl ring of the ligands. The presence of electron donating methyl group in the complexes **2b, 2d, 2f** decreases the metal oxidation potential as compared to the complex **2a** (Table 3). Furthermore, the effect of the position of the methyl group in the ligands has been reflected directly on the metal redox and it follows the order: 1.09 V, *m*-Me (**2d**) > 1.04 V, *p*-Me (**2f**) > 1.02 V, *o*-Me (**2b**). Similarly electron withdrawing chloride group in the complexes **2c, 2e, 2g** increases the metal oxidation potential and depending on the specific position of chloride group in the ligands the metal oxidation potential follows the order: 1.36 V, *o*-Cl (**2c**) > 1.30 V, *p*-Cl (**2g**) > 1.25 V, *m*-Cl (**2e**). Hence, metal oxidation potential can be tuned in the desired direction by introducing specific group in the selective position of the ligand.

All the complexes exhibit two successive quasi-reversible one-electron reductions in the ranges $-0.48 \rightarrow -0.59$ V and $-0.69 \rightarrow -0.85$ V vs SEC, respectively (Fig. 3, Table 3). Azopyridine ligand is a well known potential electron-transfer center and can accept two electrons in one electrochemically accessible LUMO (lowest unoccupied molecular orbital) which is primarily azo in character [13]. Since two electroactive azo groups are present in the complexes **2**, four successive one-electron reductions are therefore expected for each complex. However, in practice we have observed two one-electron reductions cor-

Table 3. Electrochemical data at 298 K[a]

Comp.	Ru^{III}/Ru^{II} couple E^0_{298}/V (ΔE_p/mV)	n^b	Ligand reductions E^0_{298}/V (ΔE_p/mV)	ΔE^0/V[c]	ν_{MLCT}/cm^{-1} Cal.[d]	Obs.[e]
2a	1.13 (90)	1.03	−0.52 (80) −0.75 (90)	1.65	16,307	17,153
2b	1.02 (100)	1.07	−0.60 (90) −0.85 (100)	1.62	16,065	16,978
2c	1.36 (100)	0.94	−0.42 (90) −0.73 (100)	1.78	17,355	16,583
2d	1.09 (90)	1.09	−0.55 (80) −0.78 (90)	1.64	16,227	17,182
2e	1.25 (100)	1.05	−0.48 (80) −0.68 (100)	1.73	16,952	16,583
2f	1.04 (100)	1.09	−0.57 (90) −0.82 (100)	1.61	15,984	16,978
2g	1.30 (100)	0.97	−0.45 (80) −0.69 (90)	1.75	17,114	16,611

[a] Condition: solvent, dichloromethane; supporting electrolyte, TBAP; reference electrode, SCE; solute concentration, $\sim 10^{-3}$ M; working electrode, platinum wire.

[b] $n = Q/Q'$, where Q' is the calculated coulomb count for 1 e^- transfer and Q is the coulomb count found after exhaustive electrolysis of $\sim 10^{-2}$ M solution of the complex.

[c] Calculated by using eqn (6) of the text.

[d] Using eqn (5) of the text.

[e] In dichloromethane solution.

responding to eqns (3) and (4) within the ±1.5 V potential range. The other expected two reductions could not be seen presumably due to solvent cut-off.

$$[Ru^{II}(L)_2Cl_2] + e^- \rightleftharpoons [Ru^{II}(L)(L^{\cdot-})Cl_2]^- \quad (3)$$

$$[Ru^{II}(L)(L^{\cdot-})Cl_2]^- + e^- \rightleftharpoons [Ru^{II}(L^{\cdot-})(L^{\cdot-})Cl_2]^{2-} \quad (4)$$

The reduction potentials of the coordinated ligands systematically vary based on the nature and the position of the substituents present in the ligands (Table 3).

Spectroelectrochemical correlation. The lowest energy metal to ligand charge-transfer (MLCT) bands of the complexes (**2a–2g**) are observed in the range 582–603 nm (Table 1). The reduction potentials of the reversible ruthenium(III)–ruthenium(II) couple and the first ligand reduction (reduction of the azo function) of the complexes have been observed in the ranges 1.02 → 1.36 V and −0.42 → −0.60 V vs SCE, respectively. The lowest energy MLCT transition involves excitation of the electron from the field t_{2g} orbital of ruthenium(II) to the lowest π^* orbital of the azopyridine ligand (dominated by the azoimune, -N=N-C=N- fragment). The energy of the MLCT band for each complex (**2a–2g**) can be predicted from the experimentally observed electrochemical data by considering the following eqns (5)–(6) [14]. Here E^0_{298} (Ru^{II}/Ru^{II}) and E^0_{298} (L) are the formal potentials (in V) of the ruthenium(III)–ruthenium(II) couple and the first

$$\nu_{MLCT} = 8065(\Delta E^0) + 3000 \quad (5)$$

$$\Delta E^0 = E^0_{298}(Ru^{III}/Ru^{II}) - E^0_{298}(L) \quad (6)$$

ligand reduction, respectively. The ν_{MLCT} is the frequency of the lowest energy MLCT transition (in cm^{-1}). The factor 8065 in eqn (5) is used to convert potential difference ΔE from volt to cm^{-1} and the term 3000 cm^{-1} is of empirical origin. The calculated and experimentally observed ν_{MLCT} transition frequencies for all the complexes are listed in Table 3 and there is a linear relationship between the ν_{MLCT} and ΔE (Fig. 4). Here, the calculated values for all the complexes lie within the 900 cm^{-1} of the experimentally observed MLCT energies which are in very good agreement with the previously observed correlations in the other ruthenium complexes [15].

Trivalent ruthenium congener, ctc-$[Ru^{III}(L)_2Cl_2]^+$, **3** *and distortion parameters.* Common oxidizing agents such as ceric ammonium sulfate in $HClO_4$, chlorine gas and hydrogen peroxide cannot oxidize the $[Ru^{II}(L)_2Cl_2]$ (**2**) complexes. However, the strong oxidizing agent, HNO_3 can easily generate the red colored oxidized complexes $[Ru^{III}(L)_2Cl_2]^+$ (**3**) eqn (7).

$$ctc\text{-}[Ru^{II}(L)_2Cl_2] + HNO_3 \rightarrow ctc\text{-}[Ru^{III}(L)_2Cl_2]^+ \quad (7)$$
2 **3**

Oxidized complexes are not stable enough, slowly undergo reductions to the corresponding parent bivalent complexes, $[Ru^{II}(L)_2Cl_2]$ (**2**) both in the solid

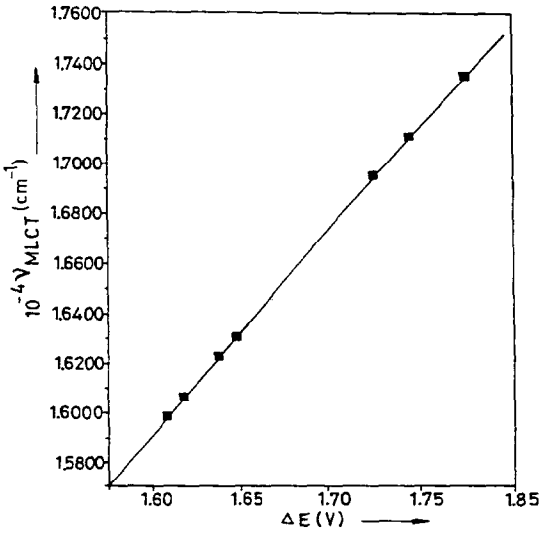

Fig. 4. Least squares plot of the lowest energy metal-to-ligand charge-transfer band (γ_{MLCT}, cm^{-1}) vs the difference in potential (ΔE, V) between the $Ru^{II/III}$ couple and the first ligand reduction.

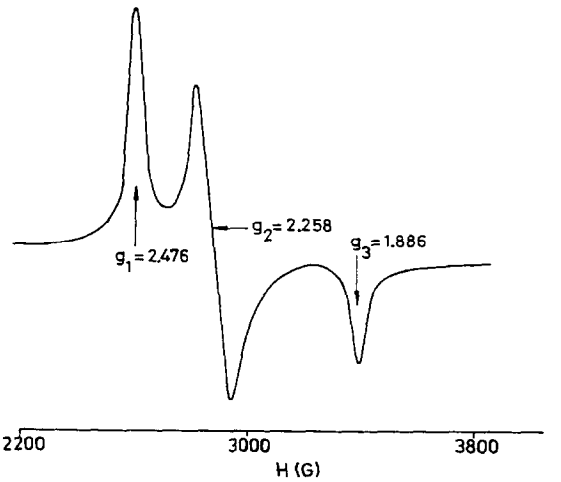

Fig. 5. X-band EPR spectrum of the oxidized complex, *ctc*-$[Ru^{III}(L^5)_2Cl_2](ClO_4)$. H_2O, **3e** in chloroform at 77 K.

and solution states. Coulometric oxidations of the complexes (**2**) at a potential 100 mV positive to the corresponding E_{pa} of Ru^{II}/Ru^{III} couple in acetonitrile solution at 273 K produced red-colored oxidized species (**3**). Oxidized complexes (**3**) can be quantitatively reduced to the corresponding bivalent species (**2**) electrochemically or chemically by using ascorbic acid as reducing agent. The presence of trivalent ruthenium in the oxidized solutions has been established by the characteristic rhombic EPR spectra of the oxidized complexes in chloroform solvent at 77 K (liquid nitrogen) [16]. Although all the complexes (**2**) behave equally on oxidation, two particular oxidized complexes **3a** and **3e** have been isolated in pure solid state as monohydrated perchlorate salts and characterized. Microanalytical data of the complexes (**3**) are in good agreement with the calculated values (Table 1). Both the complexes show 1 : 1 conductivity in acetonitrile solvent (Table 4). Solid state magnetic moment measurements indicate that the complexes are one-electron paramagnates (low-spin Ru^{III}, t_{2g}^5, $S = 1/2$) (Table 4). There is 1 : 1 correspondence in the IR bands of the oxidized complexes, $[Ru^{III}(L)_2Cl_2]ClO_4 \cdot H_2O$ and their corresponding bivalent analogues, $[Ru^{II}(L)_2Cl_2]$ except the former show additional bands due to the lattice water (3400 cm^{-1}) and ionic perchlorate (1100 and 630 cm^{-1}). The azo stretching frequency and the Ru–Cl stretching frequencies are found to be shifted to higher energy in the trivalent complexes (Table 1) [17]. Electronic spectra of the complexes were recorded in dichloromethane solvent and the values are shown in Table 1. In the visible region the complexes exhibit one intense band near 530 nm with a shoulder at the lower energy part. The intense visible band near 530 nm is assigned to ligand to metal charge-transfer (LMCT) transition [18]. In the UV region the complexes show ligand based transition near 370 nm. One-electron paramagnetic trivalent ruthenium complexes (**3**) exhibit rhombic EPR spectra in glassy condition (77 K) (Fig. 5) due to the molecular distortion (EPR g values are listed in Table 4).

Table 4. Magnetic moments,[a] molar conductivities[b] and EPR g values[c]

Comp.	μ_{eff}/B M	π_M/Ω^{-1} cm^2 mol^{-1}	g_1	g_2	g_3
3a	1.94	144	2.513	2.249	1.871
3e	1.98	152	2.476	2.258	1.886

[a] In the solid state at 298 K.
[b] In acetonitrile solvent at 298 K.
[c] In chloroform solvent at 77 K.

CONCLUSIONS

We have thus observed an unusual but facile synthetic method for the preferential formation of *ctc*-$Ru(L)_2Cl_2$ isomer, which is conveniently a multistep and cumbersome procedure. Systematic variation of the substituents in the ligand has been directly reflected in the spectral and redox properties of the complexes. It shows that both the nature and the respective location of the substituents in the ligand frame play the crucial role to tune the redox stability of the metal ion in the complexes.

Acknowledgements—Financial support received from the

Department of Science and Technology, New Delhi, India is gratefully acknowledged. We are grateful to Professor A. Q. Contractor and Ms Sukeerthi, I.I.T. Bombay for assistance with electrochemical measurements and Mr P. K. Kolay, Civil Engineering Department, I.I.T. Bombay for some computer programming. Special acknowledgement is made to Regional Sophisticated Instrumental Center, RSIC, IIT Bombay for providing NMR and EPR facilities.

REFERENCES

1. (a) Goswami, S., Chakravarty, A. R. and Chakravorty, A., *Inorg. Chem.*, 1981, **20,** 2246; (b) Krause, R. A. and Krause, K., *Inorg. Chem.*, 1980, **19,** 2600.
2. (a) Bag, N., Pramanik, A., Lahiri, G. K. and Chakravorty, A., *Inorg. Chem.*, 1992, **31,** 40; (b) Rao, P. S., Thakur, G. A. and Lahiri, G. K., *Indian J. Chem.*, 1996, **35A,** 946; (c) Bhattacharya, S., *Polyhedron*, 1993, **12,** 235; (d) Goswami, S., Chakravarty, A. R. and Chakravorty, A., *Inorg. Chem.*, 1982, **21,** 2737; (e) Goswami, S., Chakravarty A. R. and Chakravorty, A., *Inorg. Chem.*, 1983, **22,** 602; (f) Goswami, S., Mukherjee, R. N. and Chakravorty, A., *Inorg. Chem.*, 1983, **22,** 2825; (g) Ghosh, P and Chakravorty, A., *J. Chem. Soc., Dalton Trans.*, 1985, 361; (h) Deb, A. K., Paul, P. C. and Goswami, S., *J. Chem. Soc., Dalton Trans.*, 1988, 2051.
3. Goswami, S., Chakravorty, A. R. and Chakravorty, A., *J. Chem. Soc. Chem. Commun.*, 1982, 1288.
4. Lahiri, G. K., Bhattacharya, S., Goswami, S. and Chakravorty, A., *J. Chem. Soc., Dalton Trans.*, 1990, 561.
5. (a) Santra, B. K., Thakur, G. A., Ghosh, P., Pramanik, A. and Lahiri, G. K., *Inorg. Chem.*, 1996, **35,** 3050; (b) Santra, B. K. and Lahiri, G. K., *J. Chem. Soc., Dalton Trans.*, 1997, 129.
6. Gilbert, J. D., Baird, M. C. and Wilkinson, G., *J. Chem. Soc.*, (A) 1968, 2198.
7. Sawyer, D. T., Sobkowiak, A. and Roberts, J. L. Jr., *Electrochemistry for Chemists*, 2nd edn. Wiley, New York, 1995.
8. Campbell, Henderson, A. W. and Taylor, D., *J. Chem. Soc.*, 1953, 1281.
9. Bag, N., Lahiri, G. K., Basu, P. and Chakravorty, A., *J. Chem. Soc., Dalton Trans.*, 1992, 113.
10. Pesce, B., *Nuclear Magnetic Resonance in Chemistry*, p. 174. Academic Press, New York, 1965.
11. Kalia, K. C. and Charavorty, A., *J. Org. Chem.*, 1970, **35,** 2231.
12. (a) Bryant, G. M., Fergusson, J. E. and Powell, H. K. J., *Aust. J. Chem.*, 1971, **24,** 257; (b) Ceulemans, A. and Vanquickborne, L. G., *J. Am. Chem. Soc.*, 1981, **103,** 2238; (c) Felix, F., Ferguson, J., Gudel, H. U. and Ludi, A., *J. Am. Chem. Soc.*, 1980, **102,** 4096; (d) Decurtins, S., Felix, F., Ferguson, J., Gudel, H. U. and Ludi, A., *J. Am. Chem. Soc.*, 1980, **102,** 4102; (e) Bardwell, D. A., Jeffery, J. C., Schatz, E., Tilley, E. E. M. and Ward, M. D., *J. Chem. Soc., Dalton Trans.*, 1995, 826; (f) Bag, N., Lahiri, G. K., Bhattacharya, S., Falvello, F. R. and Chakravorty, A., *Inorg. Chem.*, 1988, **27,** 4396.
13. Santra, B. K. and Lahiri, G. K., *J. Chem. Soc., Dalton Trans.*, 1997, 1883.
14. Ghosh, B. K. and Chakravorty, A., *Coord. Chem. Rev.*, 1989, **95,** 239.
15. (a) Santra, B. K., Menon, M., Pal, C. K. and Lahiri, G. K., *J. Chem. Soc., Dalton Trans.*, 1997, 1387; (b) Keerthi, K. D., Santra, B. K. and Lahiri, G. K., *Polyhedron*, 1997, 000.
16. (a) Holligan, B. M., Jeffery, J. C., Norgett, M. K., Schatz, E. and Ward, M. D., *J. Chem. Soc., Dalton Trans.*, 1992, 3345; (b) Lahiri, G. K., Bhattacharya, S., Mukherjee, M., Mukherjee, A. K. and Chakravorty, A., *Inorg. Chem.*, 1987, **26,** 3359.
17. Nakamoto, K., *Infrared Spectra of Inorganic and Coordination Compounds*. Wiley, New York, 1963.
18. Pramanik, A., Bag, N., Lahiri, G. K. and Chakravorty, A., *J. Chem. Soc., Dalton Trans.*, 1990, 3823.

Pergamon

PII: S0277-5387(97)00513-5

Polyhedron Vol. 17, Nos. 11–12, pp. 1923–1930, 1998
© 1998 Elsevier Science Ltd
All rights reserved. Printed in Great Britain
0277-5387/98 $19.00+0.00

Synthesis and solid-state structures of three magnesium diamide complexes derived from $RN(H)CH_2CH_2N(H)R$ diamine precursors (R = Ph or $PHCH_2$)

William Clegg,[a] Lynne Horsburgh,[a] Robert E. Mulvey,[b]* Michael J. Ross,[b] René B. Rowlings[b] and Victoria Wilson[b]

[a] Department of Chemistry, University of Newcastle, Newcastle upon Tyne NE1 7RU, U.K.

[b] Department of Pure and Applied Chemistry, University of Strathclyde, Glasgow G1 1XL, U.K.

(Received 10 October 1997; accepted 28 November 1997)

Abstract—Three new magnesium diamide complexes have been prepared by treating the diamine precursors *N,N'*-diphenylethylenediamine or *N,N'*-dibenzylethylenediamine with the commercial reagent dibutylmagnesium in the presence of a donor solvent (THF or HMPA). Their crystal structures have been determined. Both $[\{MgN(Ph)CH_2CH_2N(Ph)\cdot 2THF(1.5\ THF)\}_2]$ and $[\{MgN(CH_2Ph)CH_2CH_2N(CH_2Ph)\cdot HMPA\}_2]$ adopt dimeric arrangements based on *trans*-5.4.5-fused ring systems. The former structure is distinctive and noteworthy for exhibiting a five-coordinate, distorted trigonal bipyramidal Mg centre, instead of the more usual four-coordinate, distorted tetrahedral geometry found in the latter structure. Replacing the two THF ligands of the former structure by two HMPA molecules leads to deaggregation, in the form of the monomeric complex $[MgN(Ph)CH_2CH_2N(Ph)\cdot 2HMPA]$, which also displays an unremarkable distorted tetrahedral Mg coordination. Comparisons are made with other dimeric and monomeric, magnesium amide and related complexes. © 1998 Elsevier Science Ltd. All rights reserved

Keywords: chelates; crystal structure; diamides; magnesium.

Recently we have shown that it is possible to construct unusual three-dimensional magnesium–nitrogen bonded cage architectures by doubly deprotonating the primary diamine precursors **1** and **2**. Thus, THF solvate **3** is hexameric with an interpenetrated Mg_6/N_{12} octahedral/cuboctahedral arrangement [1], and HMPA solvate **4** is trimeric with a Mg_3 equilateral triangle encapsulated within a N_6 trigonal prism [2]. A key condition for such cage construction is that the steric bulk of the metal binding sites of these bifunctional dianions must be small; hence, the presence of the hydrogen atom in the "$[RN(H)^-]$" moieties is thought to be critical. Even methyl substituents appear to be too sterically demanding to permit cage formation. Methyl analogues of **3** and **4** are not available for direct comparison, but a close analogy exists in the alkylamide $[\{MeMgN(Me)CH_2CH_2NMe_2\}_2]$, one of the earliest reported magnesium amide crystal structures [3], which adopts a (non-cage) dimeric structure based on a planar $(MgN)_2$ ring with additional Mg—N and Mg—C terminal bonds that complete the distorted tetrahedral metal geometry. We therefore expected to form structures of this more conventional type, either dimeric or monomeric depending on the degree of solvation, when extending our magnesiation studies to *N,N'*-diphenylethylenediamine, **5** and *N,N'*-dibenzylethylenediamine, **6**, i.e. secondary diamine precursors with greater steric requirements than the aforementioned primary systems. As reported herein, whilst our expectations have been realised through the synthesis and crystallographic characterisations of the dimers **7** and **8**, and monomer **9**, surprising features have nevertheless emerged. Most significantly, the Mg centres in dimeric **7**, depart from the normal four-coordination [4]: unusually, the four-membered $(MgN)_2$ ring is tetrasolvated by tetrahydrofuran (THF) ligands, thus lead-

* Author to whom correspondence should be addressed.

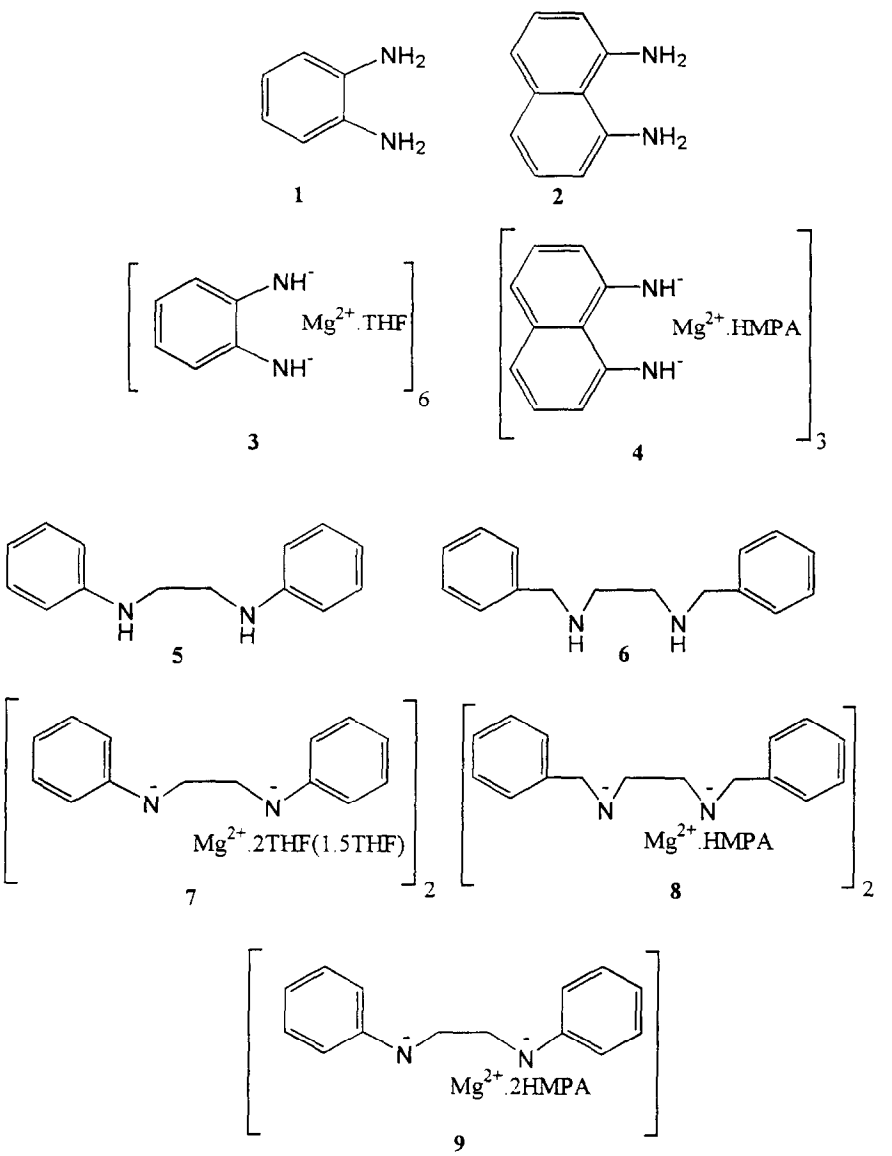

ing to a higher five-coordinate Mg geometry. Also, although structures **7** and **9** involve the same dianion and have equal numbers of solvent molecules attached to their Mg centres, they differ in terms of aggregation number *n* (i.e. 2 and 1 respectively). This provides an interesting contrast with the recently reported THF and hexamethylphosphoramide (HMPA) 1 : 1 solvates of magnesium bis(dibenzylamide), $[\{Mg[N(CH_2Ph)_2]_2 \cdot THF\}_2]$ and $[\{Mg[N(CH_2Ph)_2]_2 \cdot HMPA\}_2]$, both of which are dimeric [5].

RESULTS AND DISCUSSION

Synthesis and characterisation

Double deprotonation of the precursor diamines was achieved using the commercial reagent dibutylmagnesium (which contains a statistical mixture of Bu^n and Bu^s groups), by the general reaction shown in eqn (1). The reactions were facile, and complete by the time the chilled solutions reached room temperature.

$$Bu_2Mg + RN(H)CH_2CH_2N(H)R \rightarrow \text{“}[Mg(RNCH_2CH_2NR)]\text{”} + 2BuH \quad (1)$$

In each case an excess of donor solvent was needed to completely dissolve the precipitate initially formed by this magnesium-hydrogen exchange process. Approximately three and five-molar equivalents of HMPA proved sufficient in the preparation of **8** and **9**, respectively. However, it required nearly seventy molar equivalents of the weaker donor THF to accomplish the same task in the case of **7**. This there-

fore denied the opportunity for any stoichiometric control of the degree of solvation [cf, the aforementioned magnesium bis(dibenzylamide) system [5], where, in contrast, mono- and bis-solvates are isolable]. The crystalline solids isolated from solution are each solvated to a different extent. Benzyl-substituted **8** contains one HMPA ligand per metal centre, while phenyl analogue **9** contains two. In the THF solvate **7**, two solvent molecules directly bind to the Mg centre, but there are also additional THF molecules of crystallisation (three for every dimeric molecule) throughout the lattice. The empirical formula of each new compound was confirmed by running ^{1}H NMR spectra in DMSO solution (see Experimental section). A full spectroscopic investigation is planned for a future study. Note that the compounds possess extremely limited solubility in arene solvents.

Attempts to make a THF analogue of **8** to complete the series of solvates proved unsuccessful. As in the preparation of **7**, the precipitate formed initially upon magnesiation of the diamine could only be dissolved (with difficulty) in a large volume of THF. No solid product could then be coaxed from the resulting solution despite prolonged cooling at low temperature. Repeating the attempted preparation in an alternative THF/HMPA solvent mixture afforded, as expected, only the THF-free crystalline HMPA solvate **8**.

X-ray crystallographic studies

The molecular structures of dimers **7** and **8** (Figs 1 and 2, respectively) share similar characteristics. Both

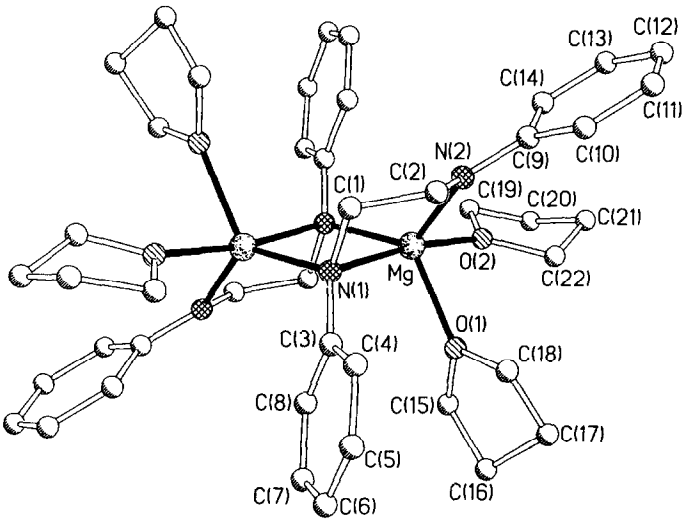

Fig. 1. Molecular structure of **7** showing atom-labelling scheme. Hydrogen atoms, minor disorder components, and THF molecules of crystallisation are omitted.

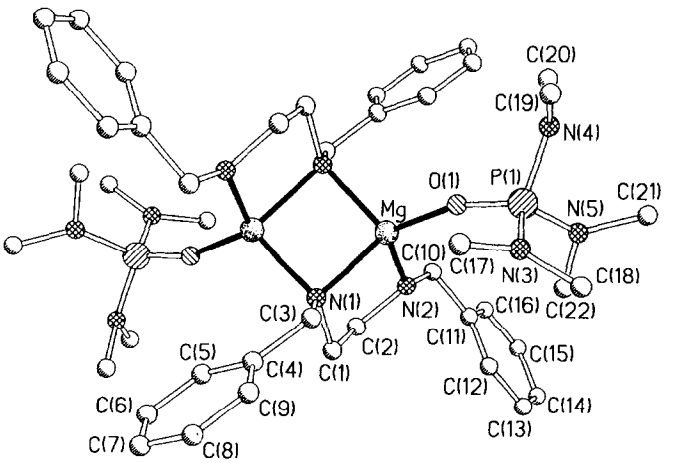

Fig. 2. Molecular structure of **8** showing atom-labelling scheme. Hydrogen atoms are omitted.

are centrosymmetric, with a planar rhomboidal $(MgN)_2$ cyclic ring. Two five-membered MgNCCN chelate rings, arising from the ligation of the second N anion of the diamide [N(2)], lie on opposite sides of this central ring to complete a *trans*-5.4.5-fused ring system. The ladder-like frameworks fashioned by the fusing of the three rings are subtly different: the non-planar MgNCCN chelate rings have an envelope-type appearance with the flap at the C(2) apex; with respect to the central ring, this flap is positioned *exo* in **7** (Fig. 3), but *endo* in **8** (Fig. 4). Steric interferences of the additional atoms (i.e. of a methylene group) within the amido substituent of **8** are minimised by the switch to an *endo* conformation. A more conspicious distinction exists between the two structures: each Mg centre is bis-solvated (by THF) in **7**, and mono-solvated (by HMPA) in **8**. Concomitantly, the metal coordination geometry is distorted trigonal bipyramidal [axial atoms, N(1) and O(2)] in **7**, and distorted tetrahedral in **8**. Five-coordination is rare for Mg in amide crystal structures. At the time of writing, there is no other magnesium amide dimer in the Cambridge Crystallographic Database [6] which exhibits this high coordination number. Commonly, such structures have a steric preference for four-coordinate Mg geometries as illustrated by the alkyl (amide) $[\{Bu^nMgN(CH_2CH_2NMe_2)CH_2Ph\}_2]$ [7], which also features a *trans*-5.4.5-fused ring system with *endo* C flaps (note the presence of the benzyl substituent) like that in **8**. The architectures of the cage structures of **3** and **4**, discussed in the Introduction, do allow for the higher coordination state; however, in contrast to that in **7**, the five ligating atoms are arranged in a distorted square-based pyramidal geometry.

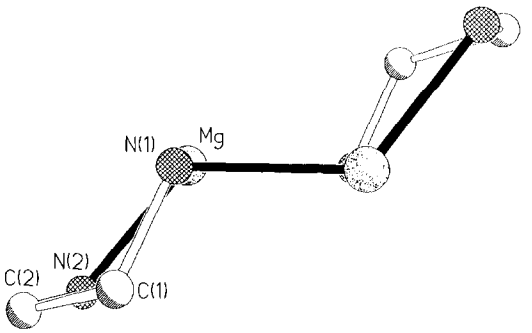

Fig. 3. *trans*-5.4.5-fused ring system of **7** showing *exo* orientation of C(2) atom.

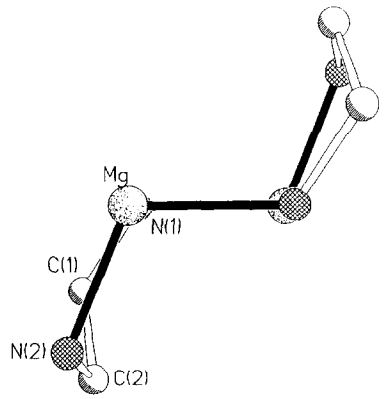

Fig. 4. *trans*-5.4.5-fused ring system of **8** showing *endo* orientation of C(2) atom.

Tables 1 and 2 give individual bond lengths and bond angles for **7** and **8** respectively, while Table 3 compares a selection of them with those in related 5.4.5-fused ring systems. It is immediately obvious from this comparative data that the steric constraints placed on the structures by the fusing of the three rings causes dimensions, in general, to be similar. Illustrating this point, the two sets of Mg—N bonds in the central $(MgN)_2$ rings tend to be non-equivalent, and their lengths show little variation throughout the series (range, 2.077–2.290 Å). Also, the bite angles of the diamine ligands [N(1)MgN(2)] cover a narrow range (84.22–87.83°). In four of the structures the endocyclic bond angles within the central $(MgN)_2$ rings follow the same pattern: acute at N and obtuse at Mg, but close to 90° (mean values, 87.06 and 92.94°). Out of line is structure **7** which displays sharper Mg corners [value, 87.64(8)° cf 92.36(8)° at N]. This anomaly is an effect of the unique five-coor-

Table 1. Selected bond lengths (Å) and angles (°) for **7**

Mg—N(1)	2.290(2)	Mg—N(1A)	2.099(2)
Mg—N(2)	2.040(2)	Mg—O(1)	2.083(2)
Mg—O(2)	2.167(2)		

N(2)—Mg—O(1)	109.26(9)	N(2)—Mg—N(1A)	127.58(9)
O(1)—Mg—N(1A)	122.64(9)	N(2)—Mg—O(2)	100.35(9)
O(1)—Mg—O(2)	81.59(8)	N(1A)—Mg—O(2)	94.13(8)
N(2)—Mg—N(1)	84.22(8)	O(1)—Mg—N(1)	91.34(8)
N(1A)—Mg—N(1)	87.64(8)	O(2)—Mg—N(1)	172.52(8)
Mg—N(1)—Mg(A)	92.36(8)		

Symmetry transformations used to generate equivalent atoms:
A: $-x+1, -y+1, -z+1$.

Table 2. Selected bond lengths (Å) and angles (°) for **8**

Mg—N(1)	2.113(2)	Mg—N(1A)	2.077(2)
Mg—N(2)	1.982(3)	Mg—O(1)	1.938(2)
O(1)—Mg—N(2)	117.86(10)	O(1)—Mg—N(1A)	116.35(10)
N(2)—Mg—N(1A)	112.75(10)	O(1)—Mg—N(1)	123.18(9)
N(2)—Mg—N(1)	87.83(10)	N(1A)—Mg—N(1)	93.76(9)
Mg—N(1)—Mg(A)	86.24(9)		

Symmetry transformations used to generate equivalent atoms:
A: $-x+1, -y+2, -z$.

Table 3. Comparison of selected bond lengths (Å) and angles (°) in corresponding sections of various 5.4.5-fused ring systems

Bond	Magnesium amide 7	8	10	11	12
Mg—N central ring	2.290	2.113	2.082	2.107/2.118	2.113
Mg—N′ central ring	2.099	2.077	2.085	2.102/2.097	2.116
Mg—N terminal	2.040	1.982	1.997	2.190/2.182	2.200
Mg—O donor	2.167 2.083	1.938	2.041	—	—
N—Mg—N′ central ring	87.64	93.76	93.9	91.70/91.38	92.4
Mg—N—Mg central ring	92.36	86.24	86.1	88.30/88.62	87.6
N—Mg—N bite angle	84.22	87.83	87.8	83.36/83.97	84.6

10 = $[\{MeMgN(Me)CH_2CH_2NMe_2\}_2]$; **11** = $[\{Mg[N(SiMe_3)C_6H_4N(SiMe_3)\text{-}o](OEt_2)\}_2]$; **12** = $[\{Bu^nMgN(CH_2CH_2NMe_2)CH_2Ph\}_2]$.

dination at this atom, with these corners representing axial-equatorial bond angles. Turning to the chelate outer-rings, where the N centres of the rings are anionic (in **7**, **8**, and $[\{Mg[N(SiMe_3)C_6H_4N(SiMe_3)\text{-}o](OEt_2)\}_2]$ [8]), their bonds to Mg are significantly shorter than those in the central rings, reflecting their terminal, sp^2 nature (cf sp^3 nature of the bridging N centres). The reverse is true in the other two structures (i.e. the terminal Mg—N bonds are longer), as these are dative bonds involving neutral, sp^3 N centres. A further point of interest, pertaining to **7** only, is that the two Mg—O (THF) bonds have different lengths in keeping with the asymmetrical character of the $(MgN)_2$ cyclic core: the equatorial one involving O(1) is 0.084 Å shorter than the axial one involving O(2). The stronger oxygen-donor HMPA found in **8** forms the shortest Mg—O bond (by 0.145 Å) of the dimer series.

Two crystallographically independent monomers of nearly identical molecular structure were found in the unit cell of **9**. For brevity, only one monomer is shown in Fig. 5; but dimensions for both are listed in Table 4. Comparing this data with that of **7** which involves the same dianion reveals that the metal-diamide attachment is shorter (mean Mg—N bond length, 2.023 Å) and more symmetrical in the monomer. The bite angle of the chelating ligand is also slightly wider in **9** (mean value, 87.02°). To prevent eclipsing of the methylene units in **9** there is a twist in the NC $(H)_2C(H)_2N$ bridge (e.g. N—C—C—N torsion angles 46.1° and 44.5° in the two molecules), which forces the attached Ph rings out of co-planarity (dihedral angles 36.9° and 35.8°). The distorted tetrahedral coordination of the Mg centre is completed by two HMPA ligands, which engage in Mg—O bonds of nearly equivalent length, the mean value of which (1.943 Å) is within the error limits of the corresponding bond in the mono-solvated dimer **8**. In **9** the two HMPA molecules are separated by a mean OMgO angle of 100.12°; the mean NMgO angle is considerably larger at 117.75°. Similar dimensions (mean Mg—O bond length, 1.973 Å; O—Mg—O bond angle, 102.9°) to those in **9** are found in the previously reported bis-HMPA-solvated magnesium amide monomer $[Mg\{N(H)Mes\}_2\cdot(HMPA)_2]$ (Mes = 2,4,6-$Me_3C_6H_2$-), as the steric influence of the bulky aryl group is moderated by the fact that the second substituent is a hydrogen atom [9].

A number of other monomeric, magnesium amide and related complexes have been reported. Most exhibit distorted tetrahedral Mg coordination [10–15]. The structure of $[Mg\{N(SiMe_3)_2\}_2\cdot 2THF]$ [16], which has a mean Mg—N bond length of 2.021 Å, is representative of this four-coordinate type. There are, however, particularly interesting examples where the metal centre has a lower or higher coordination

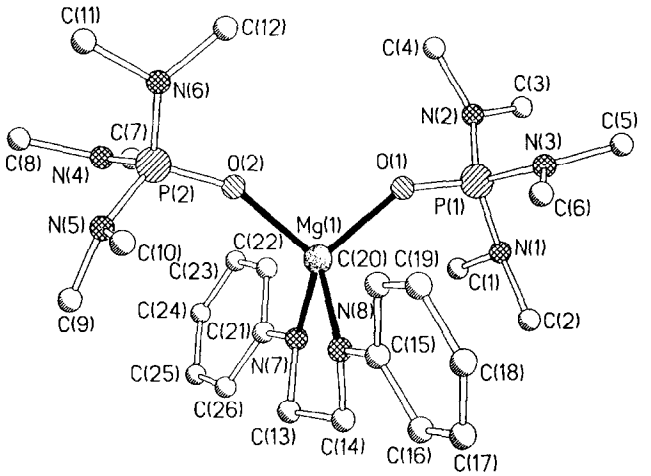

Fig. 5. One of the crystallographically independent monomeric structures of **9** showing atom-labelling scheme. Hydrogen atoms are omitted.

Table 4. Selected bond lengths (Å) and angles (°) for **9**

Mg(1)—N(7)	2.031(3)	Mg(1)—N(8)	2.024(3)
Mg(1)—O(1)	1.960(2)	Mg(1)—O(2)	1.944(2)
Mg(2)—N(15)	2.021(3)	Mg(2)—N(16)	2.014(3)
Mg(2)—O(3)	1.921(2)	Mg(2)—O(4)	1.946(2)
O(2)—Mg(1)—O(1)	101.74(10)	O(2)—Mg(1)—N(8)	118.75(11)
O(1)—Mg(1)—N(8)	116.22(11)	O(2)—Mg(1)—N(7)	115.92(11)
O(1)—Mg(1)—N(7)	118.08(10)	N(8)—Mg(1)—N(7)	87.03(11)
O(3)—Mg(2)—O(4)	98.50(11)	O(3)—Mg(2)—N(16)	118.00(11)
O(4)—Mg(2)—N(16)	118.97(11)	O(3)—Mg(2)—N(15)	121.88(11)
O(4)—Mg(2)—N(15)	114.18(11)	N(16)—Mg(2)—N(15)	87.00(11)

number. In the former category is the two-coordinate silylamide $[Mg\{N(SiMePh_2)_2\}_2]$ [17], notable for its lack of donor ligands, which has a near-linear N—Mg—N geometry (angle, 162.8°) with short bonds (mean length, 1.966 Å). At the opposite extreme is the hypercoordinated iminoaminosulfinate $[Mg\{(Me_3SiN)_2SPh\}_2 \cdot (THF)]$ which possesses four long Mg—N bonds (mean length, 2.142 Å) and one Mg—O(THF) bond [18]: note that five-coordination is made possible here, as in the aforementioned cage complexes **3** and **4**, by the bidentate (*N,N'*) nature of the ligand, though in this case the ligand is monoanionic, not dianionic.

Finally, for completeness, it should be pointed out that the lithium analogue of **9** is available for comparison [19]. An earlier X-ray crystallographic study revealed it to be the monomeric, dinuclear sesqui-HMPA solvate ($PhLiNCH_2CH_2NLiPh \cdot 3HMPA$). Its salient feature is an N_2Li_2 double bridge, reminiscent of the C_2Li_2 "ion-triplet" structures encountered in many dilithiated hydrocarbons [20,21]. The double bridging of two Li^+ cations and one $(N \cdots N)^{2-}$ dianion is electrostatically favoured as it sets up four attractive contacts at the expense of only two repulsive ones. In this diamide system, there can be no equivalent Mg structure on account of the formal 2+ charge on the alkaline-earth metal cation; hence, **9** adopts the simpler single ion-pair arrangement.

EXPERIMENTAL

Syntheses

All reactions were performed in conventional Schlenk apparatus under a protective atmosphere of dry, oxygen-free argon gas.

Compound **7**. A commercial solution of dibutylmagnesium (10 mmol in heptane: purchased from Aldrich) was added via syringe to a chilled solution of *N,N'*-diphenylethylenediamine (10 mmol) in THF (20 ml). Warming the mixture to room temperature gave a cream-coloured precipitate, which was dissolved by the introduction of further THF (40 ml) and on heating to 50°C. Only microcrystalline solid was deposited on cooling this solution, so more THF

(20 ml) was added and the mixture was rewarmed. Allowing the solution to cool to room temperature over twenty-four hours produced colourless needle crystals of **7**. These crystals quickly turn green on the surface when isolated. Yield: 2.01g (20.7%). M.p. 102–104°C. Elemental analyses; Found: C, 69.0; H, 8.2; N, 6.1; Mg, 4.3. Calc. for $C_{56}H_{84}N_4Mg_2O_7$; C, 69.2; H, 8.7; N, 5.8; Mg, 4.9; O, 11.5%. ^{1}H NMR (400 MHz, DMSO-d_6, 25°C) δ 1.77 (t, CH_2 of THF), 3.20 (s, CH_2), 3.61 (t, OCH_2 of THF), 6.53 (m, *p*Ph), 6.58 (m, *o*Ph), 7.07 (m, *m*Ph).

Compound **8**. Dibutylmagnesium (10 mmol in heptane) was added dropwise to neat *N,N'*-dibenzylethylenediamine (10 mmol) which had been cooled beforehand. An off-white precipitate formed on stirring. The heptane solvent was removed *in vacuo* and replaced by toluene (10 ml). Despite vigorous heating complete dissolution could not be achieved, so HMPA was added in small aliquots until this occurred (total amount added, 30 mmol). Hexane (2 ml) was also added since it was found to aid the crystallisation process. Cooling of the solution to −5°C afforded a large crop of colourless crystals of **8**. These crystals turn brown and become sticky on isolation, and thus their melting point could not be obtained. Yield: 0.57g (36.5%). Elemental analyses; Found C, 58.7; H, 8.5; N, 15.3; Mg, 5.1. Calc. for $C_{22}H_{36}N_5Mg_1O_1P_1$; C, 59.8; H, 8.2; N, 15.9; Mg, 5.5; O, 3.6; P, 7.0%. ^{1}H NMR (400 MHz, DMSO-d_6, 25°C) δ 2.52 (d, HMPA), 2.57 (s, CH_2CH_2), 3.65 (s, CH_2), 7.21 (m, *p*Ph), 7.28 (m, *o*/*m*Ph).

Compound **9**. Dibutylmagnesium (10 mmol in heptane) was added dropwise to a chilled hexane suspension of *N,N'*-diphenylethylenediamine (10 mmol). A mildly exothermic reaction ensued producing an amorphous solid. Neither the addition of THF (10 ml) or of pyridine (10 ml) could dissolve this solid. To the pyridine mixture was added HMPA (8 ml). This gave a brown solution initially, before rapidly precipitating a solid. Pale brown/colourless needle crystals of **9** were obtained on recrystallising this solid by adding a toluene/HMPA (5 ml/1 ml) mixture. Yield: 2.55g (43.0%). M.p. 195°C (decomp.) Elemental analyses; Found C, 52.2; H, 7.5; N, 19.3; Mg, 3.4. Calc. for $C_{26}H_{50}N_8Mg_1O_2P_2$; C, 52.7; H, 8.4; N, 18.9; Mg, 4.1; O, 5.4; P, 10.5%. ^{1}H NMR (400 MHz, DMSO-d_6, 25°C) δ 2.49 (d, HMPA), 3.17 (s, CH_2CH_2), 6.50 (t, *p*Ph), 6.55 (d, *o*Ph), 7.04 (t, *m*Ph).

Elemental analysis was carried out using a Perkin-Elmer 2400 elemental analyser and magnesium analysis was performed by atomic absorption using a PU9100 Philips spectrometer.

Table 5. Crystallographic data

Compound	**7**	**8**	**9**
Formula	$C_{56}H_{84}Mg_2N_4O_7$	$C_{44}H_{72}Mg_2N_{10}O_2P_2$	$C_{26}H_{50}MgN_8O_2P_2$
M	973.9	883.7	593.0
Crystal system	monoclinic	triclinic	triclinic
Space group	C_2/c	$P\bar{1}$	$P\bar{1}$
a (Å)	21.035(2)	10.764(2)	11.116(4)
b (Å)	13.6823(11)	11.130(2)	15.945(4)
c (Å)	19.4391(15)	11.463(2)	19.872(7)
α (°)	90	89.025(7)	73.71(2)
β (°)	104.368(2)	70.839(4)	83.81(2)
γ (°)	90	72.483(6)	81.62(3)
V (Å^3)	5419.7(7)	1232.0(4)	3336.4(19)
Z	4	1	4
D_{calc} (g cm^{-3})	1.194	1.191	1.181
μ (mm^{-1})	0.098	0.159	0.184
F (000)	2112	476	1280
Crystal size (mm)	0.65 × 0.42 × 0.41	0.78 × 0.44 × 0.20	0.83 × 0.58 × 0.31
θ_{max} (°)	28.52	28.43	22.56
Maximum indices *hkl*	28, 18, 26	14, 14, 15	11, 17, 21
Reflections measured	16,525	7756	15,195
Unique reflections	6213	5383	8724
R_{int}	0.0353	0.0884	0.0416
Weighting parameters a, b	0.1259, 6.6952	0.1315, 1.1177	0.0479, 3.1800
Extinction coeff. x	0.0017(5)	0	0.0005(2)
No. of refined parameters	336	277	728
wR_2 (all data)	0.2433	0.2258	0.1240
R ("observed" data)	0.0742 (4709)	0.0752 (4391)	0.0439 (6496)
Goodness of fit	1.104	1.076	1.057
Max., min. el. density (e Å^3)	0.98, −0.19	0.79, −0.86	0.42, −0.36

X-ray crystallography

Crystal data for **7, 8** and **9,** are shown in Table 5, together with information on data collection and structure determination procedures. Measurements for 7 and **8** were at 160 K on a Siemens SMART CCD diffractometer. Cell parameters were refined from the observed ω angles of all strong reflections in each complete data set, which was recorded with frames of 0.3° in ω. Measurements for **9** were made at 160 K on a Stoe-Siemens four-circle diffractometer. Cell parameters were refined from 2θ values of 31 reflections (20–23°) measured at $\pm\omega$ to minimise systematic errors. Intensities were measured with profile-fitted ω/θ scans [22]. No absorption corrections were applied.

The structures were solved by direct methods, and refined by full-matrix least squares on F^2, with weighting $W^{-1} = \sigma^2(F_o^2) + (aP)^2 + (bP)$, where $P = (F_o^2 + 2F_c^2)/3$ [23]. An isotropic extinction coefficient x was refined, whereby $F_c' = F_c/(1 + 0.001xFc^2\lambda^3/\sin 2\theta)^{1/4}$.

Anisotropic displacement parameters were refined for all non-hydrogen atoms while hydrogen atoms were included with riding model constraints. For **7** two-fold disorder was resolved for one coordinated THF and for an uncoordinated THF molecule across a two-fold rotation axis, and was refined with the assistance of geometrical restraints. For the uncoordinated THF molecules, oxygen and carbon atoms could not be distinguished, and hydrogen atoms were not included. The residuals are defined as $wR_2 = \{\Sigma[w(F_o^2 - F_c^2)]/\Sigma[w(F_o^2)^2]\}^{1/2}$ for all data, conventional $R = \Sigma||F_o| - |F_c||/\Sigma|F_o|$ for reflections having $F_o^2 > 2\sigma(F_o^2)$; the goodness of fit is calculated on F^2 for all data. Programs: standard Siemens SMART and Stoe DIF4 control software. Siemens SAINT area-detector frame integration, SHELXTL [23], and local programs.

Complete bond lengths and angles, coordinates and displacement parameters have been deposited at the Cambridge Crystallographic Data Centre. (See Information for Authors, Issue No. 1).

Acknowledgement—The EPSRC are thanked for sponsoring this research.

REFERENCES

1. Clegg, W., Frank, M., Mulvey, R. E. and O'Neil, P. A., *J. Chem. Soc., Chem. Commun.*, 1994, 97.
2. Clegg, W., Horsburgh, L., Mulvey, R. E. and Rowlings, R., *J. Chem. Soc., Chem. Commun.*, 1996, 1739.
3. Magnuson, V. R. and Stucky, G. D., *Inorg. Chem.*, 1969, **8,** 1427.
4. For a review of the structures of magnesium organic derivatives see: Markies, P. R., Akkerman, O. S., Bickelhaupt, F., Smeets, W. J. J. and Spek, A. L., *Adv. Organomet. Chem.*, 1991, **32,** 147.
5. Clegg, W., Craig, F. J., Henderson, K. W., Kennedy, A. R., Mulvey, R. E., O'Neil, P. A. and Reed, D., *Inorg. Chem.*, 1997, **36,** 6238.
6. Allen, F. H. and Kennard, O., *Chem. Des. Autom. News*, 1993, **8,** 31.
7. Henderson, K. W., Mulvey, R. E., Clegg, W. and O'Neil, P. A., *J. Organomet. Chem.*, 1992, **439,** 237.
8. Duff, A. W., Hitchcock, P. B., Lappert, M. F., Taylor, R. G. and Segal, J. A., *J. Organomet. Chem.*, 1985, **293,** 271.
9. Olmstead, M. M., Grigsby, W. J., Chacon, D. R., Hascall, T. and Power, P. P., *Inorg. Chim. Acta*, 1996, **251,** 273.
10. Kuhn, N., Schulten, M., Boese, R. and Bläser, D., *J. Organomet. Chem.*, 1991, **421,** 1.
11. Englehardt, L. M., Junk, P. C., Patalinghug, W. C., Sue, R. E., Raston, C. L., Skelton, B. W. and White, A. H., *J. Chem. Soc., Chem. Commun.*, 1991, 930.
12. Westerhausen, M. and Hausen, H.-D., *Z. Anorg. Allg. Chem.*, 1992, **615,** 27.
13. Veith, M., Gaffing, F. and Huch, V., *Z. Naturforsch*, 1988, **43b,** 846.
14. Lorenz, V., Thiele, K. H. and Neumüller, B., *Z. Anorg. Allg. Chem.*, 1994, **620,** 691.
15. Gardiner, M. G., Hanson, G. R., Henderson, M. J., Lee, F. C. and Raston, C. L., *Inorg. Chem.*, 1994, **33,** 2456.
16. Bradley, D. C., Hursthouse, M. B., Ibrahim, A. A., Malik, K. M. A., Motevalli, M., Möseler, R., Powell, H., Runnacles, J. D. and Sullivan, A. C., *Polyhedron*, 1990, **9,** 2959.
17. Bartlett, R. A., Olmstead, M. M. and Power, P. P., *Inorg. Chem.*, 1994, **33,** 4800.
18. Freitag, S., Kolodziejski, W., Pauer, F. and Stalke, D., *J. Chem. Soc., Dalton Trans.*, 1993, 3479.
19. (a) Armstrong, D. R., Barr, D., Brooker, A. T., Clegg, W., Gregory, K., Hodgson, S. M., Snaith, R. and Wright, D. S., *Angew. Chem.*, 1990, **102,** 443; (b) *Angew. Chem. Int. Ed. Engl.*, 1990, **29,** 410.
20. (a) Schleyer, P. v. R., *Pure Appl. Chem.*, 1983, **55,** 355; (b) 1984, **56,** 151.
21. Streitwieser, A., *Acc. Chem. Res.*, 1984, **17,** 353.
22. Clegg, W., *Acta Cryst., Sect. A*, 1981, **37,** 22.
23. Sheldrick, G. M., SHELXTL User Manual, Siemens Analytical X-ray Instruments Inc., Madison, WI, U.S.A.; version 5, 1994.

Pergamon

PII: S0277-5387(97)00488-9

Polyhedron Vol. 17, Nos. 11–12, pp. 1931–1936, 1998
© 1998 Elsevier Science Ltd
All rights reserved. Printed in Great Britain
0277-5387/98 $19.00+0.00

The preparation and kinetics of aquation of diastereoisomeric complexes of *trans*-$[Cr(Me_8[14]aneN_4)Cl_2]^+$ ($Me_8[14]aneN_4$ = 3,5,7,7,10,12,14,14-octamethyl-1,4,8,11-tetra-azacyclotetradecane)

Robert W. Hay[a]* and Iain Fraser[b]

[a] School of Chemistry, University of St Andrews, St Andrews, KY16 9ST, U.K.

[b] Chemistry Department, University of Stirling, Stirling FK7 9AG, U.K.

(Received 4 August 1997; accepted 26 November 1997)

Abstract—1,2-Propanediamine monohydroperchlorate reacts with acetone to give the dihydroperchlorate salt of 3,5,7,7,10,12,14,14-octamethyl-1,4,8,11-tetra-azacyclotetradeca-4,11-diene, $Me_8[14]dieneN_4$. The reaction is stereospecific giving only the 3,10-C-*meso* diastereoisomer (L_I). Reduction of L_I with $NaBH_4$ in methanol–water solution gives three isomeric $Me_8[14]aneN_4$ ligands (L_A, L_B and L_C). These saturated macrocycles give green *trans*-$[CrLCl_2]^+$ complexes which have been characterised by infrared and visible spectra. The red chloroaqua complexes *trans*-$[CrL(OH_2)Cl]Cl_2 \cdot H_2O \cdot H_2SO_4$ have also been prepared and characterised. The aquation of the dichloro-complexes to the chloro–aqua derivatives has been studied kinetically over a temperature range and rate constants (k_{aq}) and activation parameters are reported. The substantial negative values of $\Delta S^{\ddagger}$ observed are consistent with an associative I_a mechanism. © 1998 Elsevier Science Ltd. All rights reserved

Keywords: tetraaza macrocycle; alkyl substitution; chromium(III); aquation kinetics.

Reduction of $Me_8[14]dieneN_4$ (L_I) with sodium borohydride in methanol–water gives three diastereoisomeric $Me_8[14]aneN_4$ macrocycles (L_A, L_B and L_C) [1], Scheme. The 3,10-C-*meso* configuration of the parent diene has been established on the basis of ^1H NMR spectra [2,3] and confirmed by X-ray crystallography on the nickel(II) complex [2]. The three diastereoisomeric $Me_8[14]aneN_4$ macrocycles can be separated by fractional crystallisation from xylene [1]. Structures have been assigned on the basis of ^1H and ^{13}C NMR spectra and the configuration of L_B confirmed by X-ray crystallography [1]. The preparation of the *trans*-$[Co(Me_8[14]aneN_4)Cl_2]ClO_4$ complexes and the crystal structure of *trans*-$[CoL_ACl_2]ClO_4$ have been described [4]. The present paper deals with the preparation of the $[CrLCl_2]^+$ complexes and the determination of their aquation rates.

* Author to whom correspondence should be addressed.

EXPERIMENTAL

Synthesis

3,10-C-*meso*-3,5,7,7,10,12,14,14-Octamethyl-1,4,8,11-tetra-azacyclotetradeca-4,11-diene dihydroperchlorate ($Me_8[14]dieneN_4 \cdot 2HClO_4$) was prepared as follows. 1,2-Diaminopropane (74 cm^3, 1 mol) was dissolved in acetone (500 cm^3) and cooled in an ice-salt bath. Perchloric acid (99 cm^3, 70%, 1 mol) was added dropwise with continuous stirring. An orange colour developed in the solution. After the addition of the perchloric acid was completed the mixture was stirred at room temperature for ca 4 h until precipitation began. After standing overnight at room temperature, the fine white crystalline product was removed by filtration, washed with ethanol, then ether and dried *in vacuo*.

CAUTION! perchlorate salts of amines are hazardous materials and should not be heated. They can detonate with great violence.

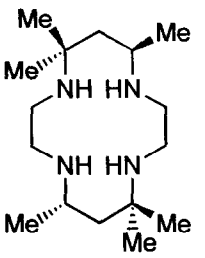

tet a
C-meso
(1)

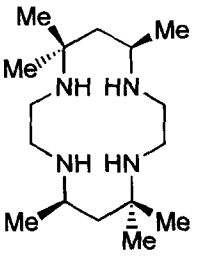

tet b
C-racemic
(2)

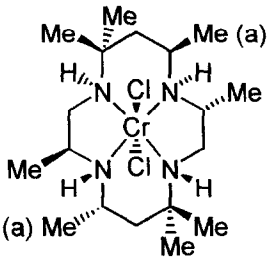

(3) L_A complex

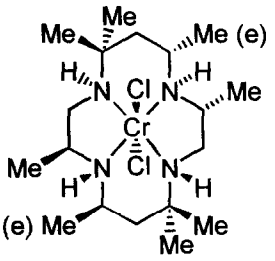

(4) L_B complex

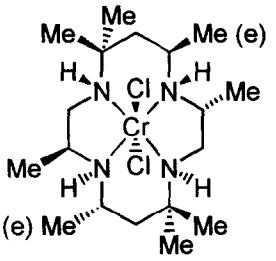

(5) L_C complex

Reduction of 3,10-C-*meso*-Me_8[14]dieneN$_4$·$2HClO_4$ with $NaBH_4$ in 1 : 1 water–methanol was carried out essentially as previously described and the diastereoisomers L_A, L_B and L_C separated by crystallisation from xylene [1]. The ligand L_A is insoluble in hot xylene and has m.p. 350°C (decomp.). L_B the first fraction from xylene was recrystallised from ether, m.p. 122°C. L_C was obtained as cubic crystals as the last fraction from xylene and was also recrystallised from ether, m.p. 85°C.

The complex *trans*-$[CrL_ACl_2]Cl \cdot 2H_2O \cdot HCl$ was prepared as follows. A suspension of L_A (0.20 g, 0.64 mmol) in DMF (3 cm^3) was added to a solution of $CrCl_3 \cdot 6H_2O$ (0.17 g, 0.64 mmol) in DMF (3 cm^3) which had been previously boiled for 10 min. for dehydration. The reaction mixture was refluxed for 30 min. before being filtered warm. The DMF was then removed by gentle boiling to give a green solid, which was dissolved in hot dilute HCl (5 cm^3). The solution was filtered and conc. HCl (3 cm^3) added. On standing at 4°C for several days green crystals formed, which were filtered off, washed with a 1 : 1 ethanol/diethyl ether mixture and dried *in vacuo*. Yield 0.11 g (39%). (Found: C, 40.3; H, 8.6; N, 10.4. Calc. for $C_{18}H_{45}Cl_4CrN_4O_2$: C, 39.8; N, 8.4; N, 10.3%). IR ν H_2O 3369; ν NH 3202 cm^{-1}.

The ligands L_B and L_C are much more soluble in DMF than L_A. As a result, on mixing DMF solutions of the ligands (0.20 g, 0.64 mmol) and $CrCl_3 \cdot 6H_2O$ (0.17 g, 0.64 mmol) the reaction was complete after 15 min. at a reaction temperature of 100°C. The macrocyclic chromium(III) complexes were isolated and recrystallised as described above for *trans*-$[CrL_ACl_2]^+$. Yields 0.21 g (75%) for *trans*-

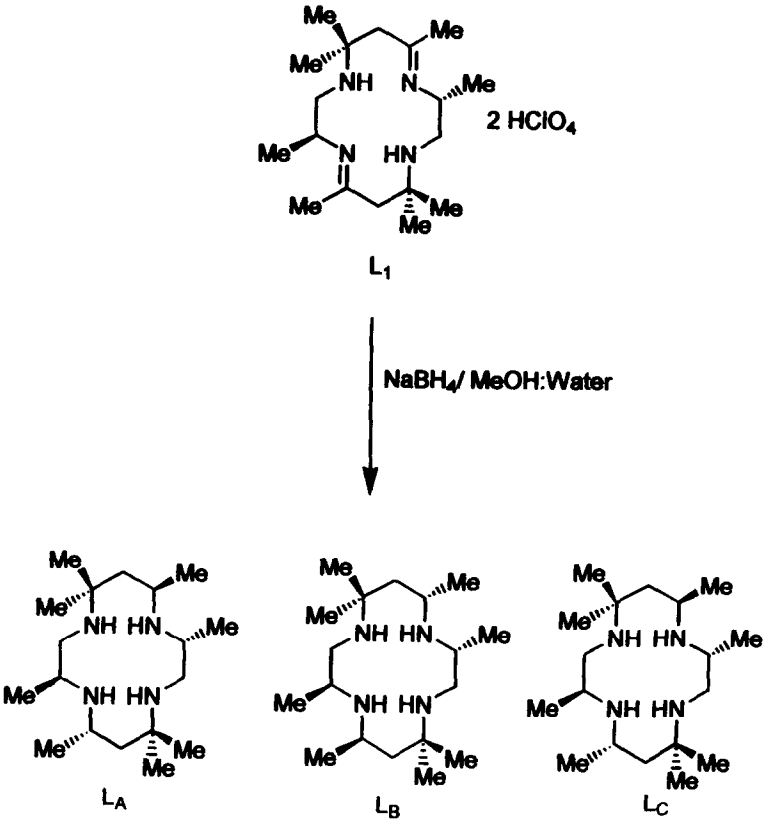

Scheme 1.

$[CrL_BCl_2]Cl \cdot 2H_2O \cdot HCl$ and 0.19 g (68%) for the L_C derivative. (Found (L_B): C, 39.7; H, 8.2; N, 9.9. Found (L_C): C, 40.2; H, 8.5; N, 10.1. Calc. for $C_{18}H_{45}Cl_4CrN_4O_2$: C, 39.8; H, 8.35; N, 10.3%). IR (L_B) H_2O 3375, ν NH 3203. For L_C ν H_2O 3372, ν NH 3208 cm^{-1}.

The red *trans*-$[CrLCl(OH_2)]Cl_2 \cdot H_2O \cdot H_2SO_4$ complexes (L = L_A, L_B or L_C) were prepared by dissolving the dichloro-complexes in 0.05 mol dm^{-3} H_2SO_4. On standing at room temperature for several weeks, red crystalline solids deposited. These solids were filtered off, washed with ethanol then diethyl ether and dried *in vacuo*. (Found (L_A): C, 35.3; H, 7.2; N, 10.2. Found (L_B): C, 35.2; N, 7.4; N, 8.8. Found (L_C): C, 35.1; N, 7.25; N, 8.85. Calc. for $C_{18}H_{46}Cl_3CrN_4O_6S$: C, 35.7; H, 7.7; N, 9.26. IR for L_A ν H_2O 3455; ν NH 3202; ν SO_4^{2-} 1162, 1132, 600 cm^{-1}. For L_B ν H_2O 3400; ν NH 3205, 3125; ν SO_4^{2-} 1170, 1140. For L_C ν H_2O 3479; ν NH 3208, 3104; ν SO_4^{2-} 1158, 1134, 603 cm^{-1}.

The dihydroxo complexes were prepared by dissolving the dichloro complexes in 0.1 mol dm^{-3} sodium hydroxide solution. The diaqua complexes were prepared by acidification of the dihydroxo complexes with 1 mol dm^{-3} nitric acid (one drop was normally sufficient). The UV-visible spectra of the complexes are summarised in Table 1.

Measurements

Infrared spectra were recorded as KBr discs on a Shimadzu IR-435 instrument. Electronic absorption spectra were obtained using a Perkin–Elmer Lambda 5 spectrophotometer.

Kinetics

Loss of the first chloro ligand was monitored spectrophotometrically. Measurements were made using 0.05 mol dm^{-3} solutions of sulphuric acid ($I = 0.05$ mol dm^{-3} as $pK_1 = -3$ and $pK_2 = 2$ for sulphuric acid). The dichloro complexes have very limited solubility in HNO_3 and $HClO_4$. The kinetics were monitored at 510 nm (absorption increase) using a Gilford SP 500 spectrophotometer interfaced with a PC. Rate constants were obtained from the slope of the linear plots of $\ln(A_\infty - A_t)$ vs time t, where A_∞ is the final absorbance at 510 nm and A_t is the absorbance at time t. Absorbance changes were monitored over 4–9 half lives.

RESULTS AND DISCUSSION

The reaction of $[CrCl_3(DMF)_3]$ prepared *in situ* by dehydration of $CrCl_3 \cdot 6H_2O$ in DMF solution with

Table 1. Electronic spectra of the complexes

Complex	λ_{max} (ε) (nm) ($dm^3\ mol^{-1}\ cm^{-1}$)
trans-$[CrL_ACl_2]^+$	577 (26), 430 (sh), 384 (58), 255 (sh), 214 (15400)
trans-$[CrL_BCl_2]^+$	580 (31), 430 (sh), 384 (54), 255 (sh), 214 (14820)
trans-$[CrL_CCl_2]^+$	580 (24), 430 (sh), 385 (46), 255 (sh), 214 (19400)
trans-$[CrL_A(OH_2)Cl]^{2+}$	577 (sh), 505 (42), 398 (78), 296 (55), 207 (11500)
trans-$[CrL_B(OH_2)Cl]^{2+}$	580 (sh), 510 (28), 400 (82), 208 (10100)
trans-$[CrL_C(OH_2)Cl]^{2+}$	580 (sh), 510 (29), 400 (71), 208 (12680)
trans-$[CrL_A(OH)_2]^+$	500 (33), 396 (43)
trans-$[CrL_B(OH)_2]^+$	480 (34), 396 (46), 320 (55)
trans-$[CrL_C(OH)_2]^+$	500 (35), 398 (41), 310 (23)
trans-$[CrL_A(OH_2)_2]^{3+}$	540 (21), 420 (sh), 364 (61)
trans-$[CrL_B(OH_2)_2]^{3+}$	520 (23), 420 (sh), 360 (74)
trans-$[CrL_C(OH_2)_2]^{3+}$	525 (16), 420 (sh), 368 (61)

sh = shoulder.

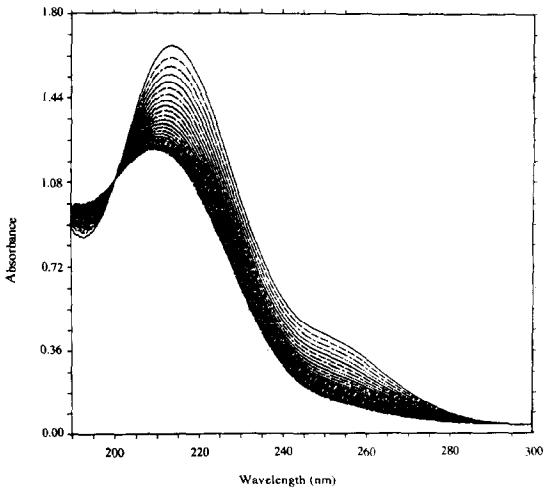

Fig. 1. Interval scan spectrum for the aquation of $[CrL_ACl_2]^+$ in acidic solution at 30 °C. The time interval between scans is 10 min.

L_A, L_B and L_C gives the green *trans*-$[CrLCl_2]^+$ complexes. The reaction of cyclam (1,4,8,11-tetra-azacyclotetradecane) [5] and 5,12-dimethyl-cyclam [6] with $[CrCl_3(DMF)_3]$ gives predominantly the violet-purple *cis*-isomer with only ca 10% of the green *trans*-isomer. The ligand tet *a* (1) gives *trans* complexes with Cr(III), while tet *b* (2) gives *cis* complexes [7]. The ligand tet *b* is known to readily fold to give *cis*-octahedral complexes with the (RRRR, SSSS) *sec*-NH chiral nitrogen configuration and two equatorial methyls and one axial methyl substituent on each six-membered chelate ring. The ligand tet *a* only folds with difficulty because of the unfavourable interaction of axial methyl substituents in the six-membered chelate rings with ligands in the axial positions of the octahedral coordination sphere of the metal. The additional steric interactions in the octamethyl ligands would obviously be expected to favour the formation of the *trans* isomer and this was found to be the case.

The reaction of L_A with $[CrCl_3(DMF)_3]$ in DMF solution requires some 30 min. for completion in refluxing DMF. However, due to the greater solubility of L_B and L_C in DMF solution these reactions are complete in 15 min. The green *trans* complexes analyse as $[CrLCl_2]Cl \cdot 2H_2O \cdot HCl$ and presumably contain the species $[H_5O_2]^+Cl^-$ as previously observed [7] in *trans*-$[Cr(tet\ a)Cl_2 \cdot 2H_2O \cdot HCl$.

Electronic spectra

The electronic spectra of the various complexes prepared are summarised in Table 1. In O_h symmetry three ligand field bands are expected for a d^3 ion $^4A_{2g} \rightarrow {}^4T_{2g}$ and $^4A_{2g} \rightarrow {}^4T_{1g}(F)$ and the two electron transition $^4A_{2g} \rightarrow {}^4T_{1g}(P)$. The electronic spectra are very similar to those previously reported for chromium(III) complexes of macrocyclic tetra-aza ligands [6]. The more symmetrical *trans*-isomers (D_{4h}) normally have absorption coefficients < 30 and the lowest energy *d–d* band occurs in the region 510–570 nm. The less symmetrical *cis*-isomers (C_{2v}) have much higher absorption coefficients ($> 100\ dm^3\ mol^{-1}\ cm^{-1}$) for the lowest energy *d–d* band which occurs in the region 500–560 nm. The spectra of all of the complexes prepared are fully consistent with the *trans* stereochemistry. Bembi and coworkers [4] have recently characterised the diastereoisomeric *trans*-$[Co(Me_8[14]aneN_4)Cl_2]^+$ complexes. Significantly only green *trans*-complexes were characterised and no evidence for *cis*-complexes was obtained. Cobalt(III) gives both *cis*- and *trans*-$[Co(cyclam)Cl_2]^+$ with 1,4,8,11-tetra-azacyclotetradecane [8] and folded *cis*-complexes can

Table 2. Rate constants for the aquation of the *trans*-$[CrLCl_2]^+$ complexes in 0.05 mol dm^{-3} sulphuric acid (L = L_A, L_B or L_C)

Complex	Temp. (°C)	$10^4 k_{aq}$ (s^{-1})	$10^4 k_{aq}$ (calc.)[a] (s^{-1})
$[CrL_ACl_2]^+$	33	2.24	2.25
	40	2.84	2.83
	46	3.43	3.42
	52	4.07	4.10
$[CrL_BCl_2]^+$	36	1.71	1.73
	41	2.96	3.01
	44	4.33	4.16
	51	8.44	8.67
	53	10.71	10.64
$[CrL_CCl_2]^+$	34	1.76	1.73
	37	2.43	2.43
	42	4.21	4.23
	46	6.21	6.50
	50	9.67	9.90

[a] Calculated from the activation parameters in Table 3.

Table 3. Rate constants at 25 °C and activation parameters for the aquation of the *trans*-$[CrLCl_2]^+$ complexes (L = L_A, L_B or L_C)

Complex	$10^5 k_{aq}^{25}$ (s^{-1})	$\Delta H^\ddagger$ (kJ mol^{-1})	$\Delta S^\ddagger$ (JK^{-1} mol^{-1})
$[CrL_ACl_2]^+$	18.3	23.4	−238
$[CrL_BCl_2]^+$	4.7	87	−36
$[CrL_CCl_2]^+$	6.5	85	−40

readily be obtained with chelating bidentate ligands such as oxalate, 1,2-diaminoethane and acetylacetonate [9]. The presence of the eight methyl substituents in the 14-membered ring favours the formation of *trans*-isomers.

Aquation studies

All three dichloro-complexes aquate in 0.05 mol dm^{-3} sulphuric acid to give pink solutions of *trans*-$[CrL(OH_2)Cl]^{2+}$. Tight isosbestic points are observed on spectrophotometric monitoring of the reactions. Interval scan spectra for the hydrolysis of *trans*-$[CrL_ACl_2]^+$ at 30 °C are shown in Fig. 1. The products of aquation *trans*-$[CrL(OH_2)Cl]^{2+}$ are stable in aqueous sulphuric acid for several weeks at room temperature. On slow evaporation, red crystalline solids *trans*-$[CrL(OH_2)Cl]Cl_2 \cdot H_2O \cdot H_2SO_4$ were obtained. The presence of sulphate is indicated by the infrared spectra which exhibit ν (SO_4^{2-}) at ca 1600, 1130 and 600 cm^{-1}.

The kinetics of aquation to the chloro–aqua complexes was monitored spectrophotometrically over a temperature range. Values of k_{aq} are listed in Table 2. Activation parameters and values of k_{aq} at 25 °C are summarised in Table 3. The quite substantial negative values of $\Delta S^\ddagger$ observed for the aquation of chromium(III) complexes has been attributed to an associative mechanism and typical values for some *trans*-$[Cr(N_4)Cl_2]^+$ complexes (N_4 = a series of four nitrogen donors) are summarised in Table 4. Most of these reactions exhibit quite negative entropies of activation consistent with an I_a mechanism. The low enthalpy of activation for the complex *trans*-$[CrL_ACl_2]^+$ is compensated by a large negative value of $\Delta S^\ddagger$ and aquation at 25 °C is only some 3–4 times faster than that of the corresponding L_B and L_C complexes which have very similar activation parameters to those obtained for the aquation of *trans*-$[Cr(tet\ a)Cl_2]^+$ [10]. Somewhat similar results have been obtained by Bembi *et al.* [11] for the analogous cobalt(III) derivatives where all of the complexes have aquation rates in the range 4.7×10^{-4}–8.7×10^{-4} s^{-1} at 25 °C.

Stereochemistry

The crystal structure of *trans*-$[CoL_ACl_2]ClO_4$ (α-isomer) has recently been determined [4]. In these complexes a variety of diastereoisomers are possible

Table 4. Rate constants and activation parameters for the aquation of *trans*-$[Cr(N_4)Cl_2]^+$ complexes at 25 °C

Complex	k_{aq} (s^{-1})	$\Delta H^\ddagger$ (kJ mol^{-1})	$\Delta S^\ddagger$ (JK^{-1} mol^{-1})	Ref.
trans-$[Cr(2,3,2\text{-tet})Cl_2]^+$	3.23×10^{-6}	107	0	[13]
trans-$[Cr(3,2,3\text{-tet})Cl_2]^+$	1.06×10^{-6}	95	−50	[14]
trans-$[Cr(cyclam)Cl_2]^+$	2×10^{-8}	116	−8	[15]
trans-$[Cr(tet\ a)Cl_2]^+$	1.26×10^{-5}	93	−37	[10]
trans-$[CrL_ACl_2]^+$	1.8×10^{-4}	23	−238	This work
trans-$[CrL_BCl_2]^+$	4.7×10^{-5}	87	−36	This work
trans-$[CrL_CCl_2]^+$	6.5×10^{-5}	85	−40	This work

due to the presence of the four chiral *sec*-NH centres although normally it is only possible to isolate the most stable of these. The α-isomer of *trans*-$[CoL_A Cl_2]ClO_4$ has the stereochemistry shown in (3). The complex has the trans III arrangement of the *sec*-NH centres. The two single methyl groups in the six-membered rings are axial so that steric crowding around both chloride ligands is identical.

If the ligands L_B and L_C also adopt the most thermodynamically stable trans III configuration in the chromium(III) complexes the configurations of $[CrL_BCl_2]^+$ and $[CrL_CCl_2]^+$ will be as shown in (4) and (5) respectively. In both the L_B and L_C complexes the two single methyl groups in the six-membered rings are diequatorial. These configurations are those defined by the ^1H NMR results in the diamagnetic cobalt(III) complexes. Confirmatory evidence is provided by the crystal structure of the α-isomer of $[NiL_C](ClO_4)_2$ which is found to have the ligand conformation shown in (5) [12].

REFERENCES

1. Bembi, R., Sondhi, S. M., Singh, A. K., Jhanji, A. K., Roy, T. G., Lown, J. W. and Ball, R. G., *Bull. Chem. Soc. Jpn.*, 1989, **62,** 3701.
2. Curtis, N. F., Swan, D. A., Water, T. N. and Maxwell, I. E., *J. Am. Chem. Soc.*, 1969, **91**(4), 4588.
3. Ito, T. and Busch, D. H., *Inorg. Chem.*, 1974, **13,** 1770.
4. Bembi, R., Drew, M. G. B., Singh, R. and Roy, T. P., *Inorg. Chem.*, 1991, **30,** 1403.
5. Ferguson, J. and Tobe, M. L., *Inorg. Chim. Acta*, 1970, **4,** 109.
6. Hay, R. W., Pujari, M. P., Bembi, R., Jeragh, B. and Norman, P. R., *Transition Met. Chem.*, 1989, **14,** 393.
7. House, D. A., Hay, R. W. and Akbar Ali, M., *Inorg. Chim. Acta*, 1983, **72,** 239.
8. For *cis*-complexes see Poon, C. K. and Tobe, M. L., *J. Chem. Soc.* (A), 1968, 1549. For *trans*-complexes see Bosnich, B., Poon, C. K. and Tobe, M. L., *Inorg. Chem.*, 1965, **4,** 1102.
9. See for example, Ali, M. A., Hay, R. W. and Lawrance, G. A., *Inorg. Chim. Acta*, 1983, **70,** 65.
10. Yang, D. and House, D. A., *Inorg. Chim. Acta*, 1982, **64,** L167.
11. Bembi, R., Roy, T. G., Jhanji, A. K. and Maheswari, A., *J. Chem. Soc., Dalton Trans.*, 1990, 3531.
12. Ferguson, G., Lough, A. L. and Bembi, R., *Acta Crystallogr.*, 1990, **C46,** 213.
13. Kutal, C. and Adamson, A. W., *Inorg. Chem.*, 1973, **12,** 1990.
14. Yang, D. and House, D. A., *Inorg. Chem.*, 1982, **21,** 2999.
15. Campi, E., Ferguson, J. and Tobe, M. L., *Inorg. Chem.*, 1970, **9,** 1781.

Pergamon

PII: S0277-5387(97)00530-5

Polyhedron Vol. 17, Nos. 11–12, pp. 1937–1942, 1998
© 1998 Published by Elsevier Science Ltd
All rights reserved. Printed in Great Britain
0277-5387/98 $19.00+0.00

Synthesis, NMR (^{13}C, ^{111}Cd, ^{199}Hg) spectra and structures of $(Ph_4As)_2[Hg_2Cl_4(SC(O)Ph)_2]$ and $(Ph_4As)_2[CdCl_4Hg(SC(O)Ph)_2]$

Jagadese J. Vittal‡ and Philip A. W. Dean*

Department of Chemistry, University of Western Ontario, London, Ontario N6A 5B7, Canada

(Received 15 September 1997; accepted 25 November 1997)

Abstract—Combination of $Ph_4AsCl \cdot H_2O$, $Hg(SC(O)Ph)_2$ and $HgCl_2$ or $CdCl_2 \cdot 2.5H_2O$ in the required stoichiometric ratio gives $(Ph_4As)_2[MCl_4Hg(SC(O)Ph)_2]$, M = Hg (**1**) or Cd (**2**). Crystals of **1** were also isolated in an unsuccessful attempt to prepare the complex $(Ph_4As)[Na\{Hg(SC(O)Ph)_3\}_2]$. X-ray crystallographic analyses of **1** and **2** show both to contain a Hg(II) bonded to two thiobenzoate ligands with a near-linear S—Hg—S skeleton. The S—Hg—S angle is 174.9(2)° in **1** and 175.4(1)° in **2**. In each, the $Hg(SC(O)Ph)_2$ moiety is involved in weak interactions with two chlorine atoms from $[MCl_4]^{2-}$. Mercury-199 and ^{111}Cd NMR spectral studies indicate that the $Hg(SC(O)Ph)_2$ remains intact in solution, and that scrambling or transfer of ligands between the linear and tetrahedral metal centres does not occur. Carbon-13 and ^{199}Hg NMR data are reported for $Hg(SC(O)Ph)_2$. © 1998 Published by Elsevier Science Ltd. All rights reserved

Keywords: cadmium; chloride; mercury; NMR; thiobenzoate; X-ray analysis.

We have been interested in metal complexes of the thiobenzoate anion, thb^- [1–5]. Recently, we reported the synthesis and the structures of $[M(thb)_3]^-$ (M = Zn, Cd and Hg) [4]. Earlier, we had shown [1] that in the presence of the sodium cation Cd(II) forms the $[Na\{Cd(thb)_3\}_2]^-$ anion in which each Cd(II) is bound strongly to three sulfur atoms and Na^+ to six oxygen atoms, three from each $Cd(thb)_3$ moiety. Thus $[Cd(thb)_3]^-$ exhibits monoanionic tridentate ligand behaviour towards Na^+. In an attempt to demonstrate analogous ligand behaviour by $[Hg(thb)_3]^-$, we tried to isolate the $[Na\{Hg(thb)_3\}_2]^-$ anion. From this synthesis we isolated, in crystalline form, an unexpected product that still contained chloride. Thereafter, starting with $Hg(thb)_2$, we were able to prepare this product, $(Ph_4As)_2[Hg_2(thb)_2Cl_4]$, **1**, more directly, as well as to extend the synthesis to the related compound $(Ph_4As)_2[Hg(thb)_2CdCl_4]$, **2**. Both **1** and **2** have been characterized in the solid state by single-crystal X-ray diffraction techniques. In solution they, and $Hg(thb)_2$, have been characterized by multi-NMR (^{13}C, $^{111/113}Cd$, ^{199}Hg).

EXPERIMENTAL

General procedures

All starting materials were obtained commercially and used as received. All solvents were dried by allowing them to stand over 3A molecular sieves. All syntheses and preparations of NMR samples were carried out under an atmosphere of Ar(g). However, neither

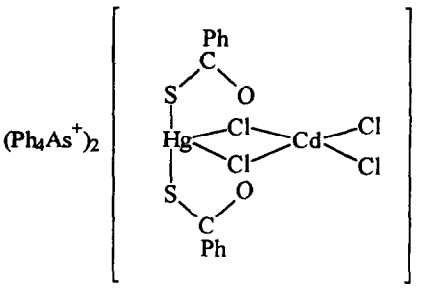

* Author to whom correspondence should be addressed.
‡ Present address: Department of Chemistry, National University of Singapore, Lower Kent Ridge Road, Singapore 119 260.

solid $Hg(thb)_2$ nor solid **1** or **2** appear to be very air-sensitive. NMR spectra were recorded at ambient probe tempearture using either a Varian Gemini 200 (for ^{13}C or ^{199}Hg) or a Varian XL-300 spectrometer system (for ^{13}C, ^{23}Na, ^{111}Cd or ^{199}Hg), in unlocked mode. Field drift was negligible. (Cadmium-111, rather than the slightly more sensitive ^{113}Cd, was observed because there was interference for ^{113}Cd in the region of interest; no measurable primary isotope effect is expected between ^{111}Cd and ^{113}Cd.) Samples were prepared in CH_2Cl_2 in 10 mm o.d. standard NMR tubes on the basis of mass/volume of solvent. Carbon-13 NMR spectra were referenced to internal TMS using the solvent signal as secondary, internal reference, while ^{23}Na, ^{111}Cd and ^{199}Hg NMR spectra were referenced to external 0.1 M $NaBPh_4$ in Me_2CO, 0.1 M $Cd(ClO_4)_2$(aq) and pure $HgMe_2$ (**Caution!** Highly toxic! [6]) by sample interchange.

$Hg(SC(O)Ph)_2$

This was prepared by Dr Yang Wu, of these laboratories, following Ref. 7 [8]. PhC(O)SH (2.76 g, 20.0 mmol) was added dropwise to a solution of $Hg(CN)_2$ (2.53 g, 10.0 mmol) in EtOH (50 ml). White crystals formed immediately. The mixture was cooled in ice for 1 h, then the product was separated by filtration, washed with ice-cold EtOH, and dried *in vacuo*. Yield: 4.6 g, 86%. Anal. Calc. for $C_{14}H_{10}HgO_2S_2$: C, 35.41, H, 2.12; Found: C, 35.64, 35.48, H, 2.00, 2.03. Carbon-13 NMR (CH_2Cl_2, 293 K): 197.3 (Ph*C*(O)S), 138.4 (C_1), 134.1 (C_4), 129.2 ($C_{2/6 \text{ or } 3/5}$), 128.9 ($C_{3/5 \text{ or } 2/6}$).

$(Ph_4As)_2[Hg_2Cl_4(SC(O)Ph)_2]$ (**1**)

The solids $Hg(SC(O)Ph)_2$ (0.475 g, 1.0 mmol), $HgCl_2$ (0.271 g, 1.0 mmol) and $Ph_4AsCl \cdot H_2O$ (0.844 g, 2 mmol) were added to 15 ml MeOH with stirring. After 5 min Me_2CO (15 ml) was added to get a clear solution, which was was filtered and left at room temperature for crystallization. Long flat crystals were separated by decantation, washed with Et_2O and dried in air. Yield: 1.1 g (69.5%). Anal. Calc. for $C_{62}H_{50}As_2Cl_4Hg_2O_2S_2$: C, 45.20; H, 3.06; Found: C, 46.76, 46.93; H, 3.16, 3.08. Carbon-13 NMR (CH_2Cl_2, 293 K, concentration 0.05 mol/l): 196.9 (Ph*C*(O)S), 139.8 (C_1, PhC(O)S), 135.3 (C_4, Ph_4As^+), 133.4 ($C_{2,6}$, Ph_4As^+), 132.7 (C_4, PhC(O)S), 131.7 ($C_{3,5}$, Ph_4As^+), 128.9 ($C_{2/6 \text{ or } 3/5}$, PhC(O)S), 128.4 ($C_{3/5 \text{ or } 2/6}$, PhC(O)S), 120.9 (C_1, Ph_4As^+); with full relaxation, integration of the $C_{2/6}$ and $C_{3/5}$ signals gives Ph(of Ph_4As^+)/Ph(of PhC(O)S) = 4.0. The product isolated from an attempted preparation of $(Ph_4As)[\{Hg(SC(O)Ph)_2\}_2HgCl_4]$ gave the same ratio of intensities and was, therefore, **1**.

Single crystals that proved, by X-ray diffraction, to be **1** were isolated during an attempted synthesis of $(Ph_4As)[Na\{Hg(SC(O)Ph)_3\}_2]$. In this attempted synthesis, a methanolic solution of NaSC(O)Ph was prepared by the addition of PhC(O)SH (2.02 g, 14.6 mmol) in MeOH (10 ml) to a solution of NaOMe prepared *in situ* by dissolution of Na metal (0.30 g, 13.2 mmol) in MeOH (10 ml). To the resultant yellow solution, $HgCl_2$ (1.19 g, 4.4 mmol) in MeOH (20 ml) was added with stirring to get a white precipitate. Stirring was continued for 5 min, then a solution containing $Ph_4AsCl \cdot H_2O$ (1.92 g, 4.4 mmol) in MeOH (20 ml) was added. This mixture was stirred for a further 30 min, when CH_2Cl_2 (10 ml) and Me_2CO (20 ml) were added to give a clear supernatant liquid over a precipitate that was presumed to be NaCl. The precipitate was removed by filtration. Volatiles were removed from the filtrate *in vacuo* to get a white solid. This was dissolved in CH_2Cl_2 (25 ml), layered with Et_2O and left at room temperature for crystallization. The crystals were washed with Et_2O and dried in air. Yield: 4.57 g. The data crystals used for X-ray analysis were picked from this batch. No resonance was observed in the ^{23}Na NMR spectrum of the bulk material, and the signals observed in the ^{13}C NMR spectrum were those of neither **1** (see above) nor $(Ph_4As)[Hg(SC(O)Ph)_3]$ [4].

$(Ph_4As)_2[CdCl_4Hg(SC(O)Ph)_2]$ (**2**)

The synthesis was carried out following the method used for the direct synthesis of **1** (see above), except that $CdCl_2 \cdot 2.5H_2O$ replaced $HgCl_2$ as starting material. The crude product was crystallized from a mixture of CH_2Cl_2 and Et_2O. Yield: 1.06 g (73.5%). Anal. Calc. for $C_{62}H_{50}As_2CdCl_4HgO_2S_2$: C, 49.78, H, 3.37; Found C, 48.60, 48.43, H, 3.12, 3.17 Carbon-13 NMR (CH_2Cl_2, 296 K, concentration 0.025 mol/l): 197.1 (Ph*C*(O)S), 139.4 (C_1, PhC(O)S), 135.2 (C_4, Ph_4As^+), 133.4 ($C_{2,6}$, Ph_4As^+), 133.1 (C_4, PhC(O)S), 131.7 ($C_{3,5}$, Ph_4As^+,), 129.0 ($C_{2/6 \text{ or } 3/5}$, PhC(O)S), 128.5 ($C_{3/5 \text{ or } 2/6}$, PhC(O)S,), 120.8 (C_1, Ph_4As^+); with full relaxation, integration of the $C_{2/6}$ and $C_{3/5}$ signals gives Ph(of Ph_4As^+)/Ph(of PhC(O)S) = 3.9.

Crystallographic studies

Crystals of **1**, $(Ph_4As)_2[Hg_2Cl_4(SC(O)Ph)_2]$, that were suitable for X-ray analysis were obtained during the attempted synthesis of $(Ph_4As)[Na\{Hg(thb)_3\}_2]$ (see above) while those of **2**, $(Ph_4As)_2$ $[CdCl_4Hg(SC(O)Ph)_2]$, were obtained during the direct synthesis and recrystallization of this compound. For diffraction experiments, the data crystals were mounted at the end of a glass fibre using expoxy glue.

For both **1** and **2** the diffraction experiments were carried out on a Siemens P4 diffractometer with the XSCANS software package [9], using graphite monochromated Mo-K_α radiation at 25°C. *SHELXTL* [10] programs were used for data processing, solution and the least-squares refinements on F^2. The cell constants were obtained by centering 26 high angle reflections

($24.8 \leqslant 2\theta \leqslant 25.1°$) for **1** and 38 high angle reflections ($10.2 \leqslant 2\theta \leqslant 25.1°$) for **2**. During the data collection four standard reflections were monitored at the end of every 296 reflections. At the end of the data collection, face-indexed absorption correction was applied to the data.

The non-hydrogen atoms of the $[Hg(SC(O)Ph)_2MCl_4]^{2-}$ anions, and the arsenic atoms, were refined anisotropically. In the cations, isotropic thermal parameters were refined for the carbon atoms of the phenyl rings and two-fold symmetry constraints were applied to the phenyl rings. Riding models were used to place all the hydrogen atoms in the calculated ideal positions for the purpose of structure factor calculations only. There were no shifts in the final least-squares cycles. The crystal data and the experimental details are given in Table 1.

RESULTS AND DISCUSSION

The compounds **1** and **2** are isolated readily from mixtures of $Ph_4AsCl \cdot H_2O$, $Hg(SC(O)Ph)_2$ and $HgCl_2$ or $CdCl_2 \cdot 2.5H_2O$ in the correct stoichiometric ratio in $MeOH : Me_2CO$. An attempt to prepare $(Ph_4As)[Na\{Hg(SC(O)Ph)_3\}_2]$ from the correct stoichiometric ratio of $Ph_4AsCl \cdot H_2O$, $HgCl_2$ and $Na^+PhC(O)S^-$ in $MeOH : Me_2CO : CH_2Cl_2$ gave, as a minor product, crystalline **1**.

Structures of **1** *and* **2**

The structures of **1** and **2** were determined by single crystal X-ray diffraction analysis. The compounds were found to be isotypical in the solid state. Within the structures, the cations are unexceptional and will not be discussed further. Perspective views of the anions in **1** and **2** are shown in Figs 1 and 2, which also show the numbering scheme. Selected bond distances and angles for the anions in **1** and **2** are in Table 2.

In both the anions, there are recognizable $Hg(thb)_2$ molecules. The Hg—S distances and S—Hg—S bond

Table 1. Crystal Data for$(Ph_4As)_2$ $[Hg_2Cl_4(SC(O)Ph)_2]$ (**1**) and $(Ph_4As)_2$ $[CdCl_4Hg(SC(O)Ph)_2]$ (**2**)

	1	**2**
Empirical formula	$C_{62}H_{50}As_2Cl_4Hg_2O_2S_2$	$C_{62}H_{50}As_2CdCl_4HgO_2S_2$
Temperature (K)	298	
Wavelength (Å)	0.71073	
Crystal system	Monoclinic	
Space group	$P2_1/c$	
a (Å)	10.848(2)	10.855(1)
b (Å)	21.554(3)	21.514(2)
c (Å)	25.831(3)	25.799(2)
β (°)	97.82(1)	97.83(1)
V (Å^3)	5984(2)	5968.8(9)
Z	4	
D_{calc} (g cm^{-3})	1.758(5)	1.665
Crystal color and habit	colorless and platy	
Crystal size (mm)	$0.38 \times 0.32 \times 0.12$	$0.30 \times 0.20 \times 0.15$
θ range (°)	1.85–23.00	
Index range	$-1 \leqslant h \leqslant 11$, $-1 \leqslant k \leqslant 23$, $-28 \leqslant l \leqslant 28$	
Scan mode	θ-2θ scans	ω-scans
Total reflections	9963	10,042
Independent reflections	8204 ($R = 0.0327$)	8270 ($R = 0.0405$)
Absorption correction	Gaussian method involving face indexing	
Max. and min. transmission	0.530 and 0.225	0.724 and 0.586
Refinement method	Full-matrix least-squares on F^2	
Data/restraints/param.	8204/680/427	4563/64/421
GOF on F^2	1.017	1.011
Final $R[I > 2\sigma(I)]$	$R_1 = 0.0569$	$R_1 = 0.0583$
	$wR_2 = 0.0984$	$wR_2 = 0.1022$
R indices (all data)	$R_1 = 0.1398$	$R_1 = 0.1347$
	$wR_2 = 0.1234$	$wR_2 = 0.1294$
Largest diff. peak, Hole (e Å^{-3})	0.751, −0.693	0.690, −0.489

$R_1 = \Sigma(||F_o| - |F_c||)/\Sigma|F_o|$; $wR_2 = [\Sigma w(F_o^2 - F_c^2)^2/\Sigma wF_o^4]^{1/2}$.

GOF $= [\Sigma w(F_o^2 - F_c^2)^2/(n-p)]^{1/2}$, where n is the number of reflections and p is the number of parameters refined.

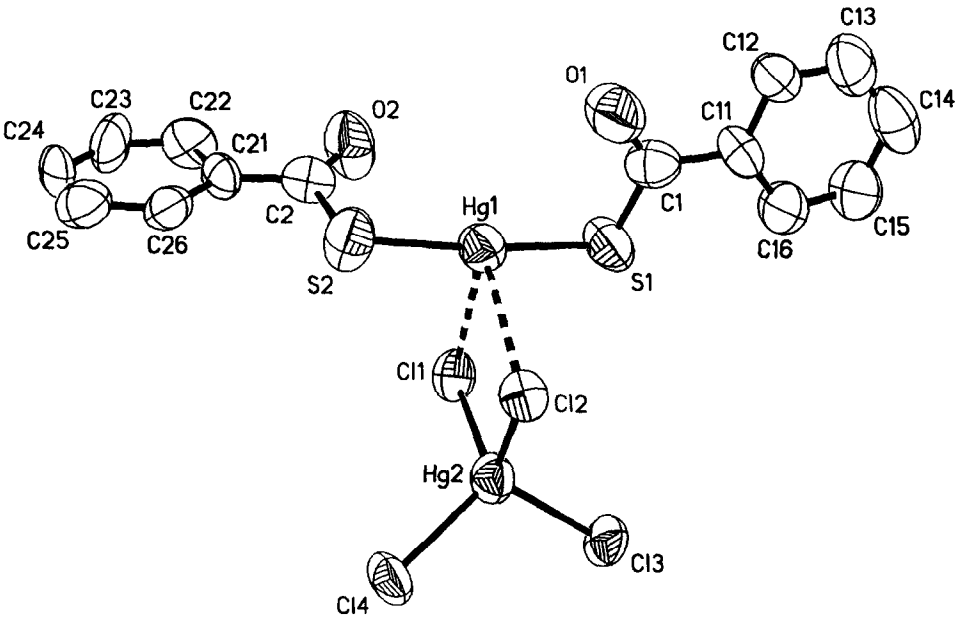

Fig. 1. A view of the $[HgCl_4Hg(SC(O)Ph)_2]^{2-}$ anion in **1**. The hydrogen atoms are omitted for clarity.

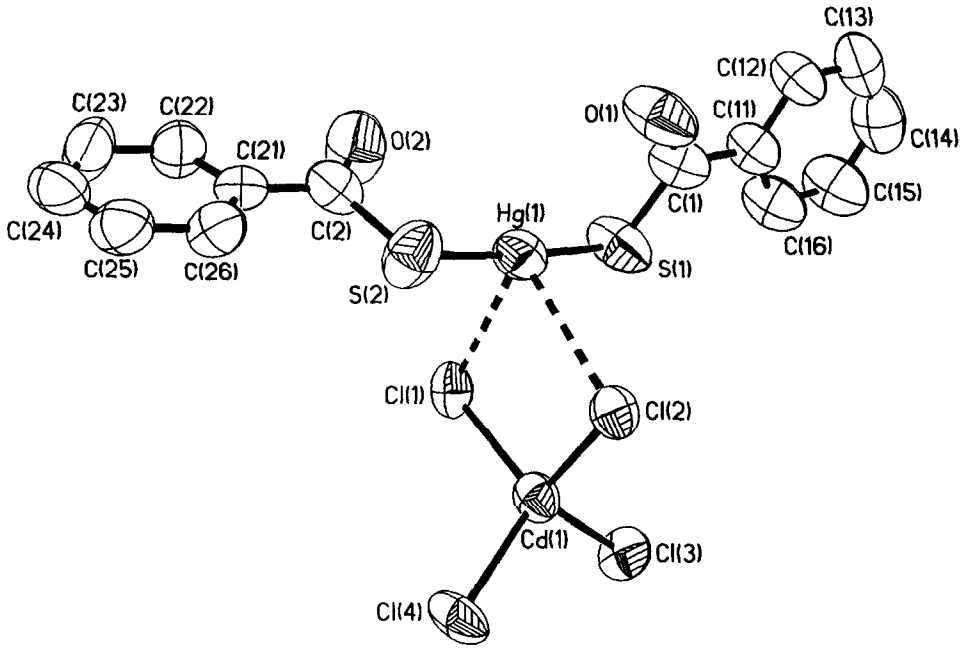

Fig. 2. A view of the $[CdCl_4Hg(SC(O)Ph)_2]^{2-}$ anion in **2**. The hydrogen atoms are omitted for clarity.

angle are 2.345(5) and 2.360(5) Å and 174.9(2)° in **1**, and 2.345(4) and 2.348(4) Å and 175.4(1)° in **2**. The near linearity of the HgS_2 skeleton in the anions of **1** and **2** suggests that these anions may be thought of as weak MCl_4^{2-} : $Hg(thb)_2$ donor : acceptor complexes. Consistent with the presence of a very weak donor : acceptor interaction are the Hg(1)—Cl(1) and Hg(1)—Cl(2) distances, 2.985(4) and 3.065(4) Å in **1**, and 2.990(3) and 3.103(3) Å in **2**, which approach the sum of the van der Waals radii, 3.2–3.4 Å [11,12]. Such long interactions are a common feature of mercury chemistry [13]. A CSD search [14] reveals that in discrete $HgCl_4^{2-}$ anions Hg—Cl distances range from 2.386–2.643 Å and Cl—Hg—Cl angles from 92.018–141.061°. It is difficult therefore to conclude that the $HgCl_4^{2-}$ in **1**, with Hg(2)—Cl distances 2.444(4)–

Table 2. Selected bond distances (Å) and angles (°) for the anions in **1** and **2** (M = Hg(2) in **1**, M = Cd(1) in **2**)

	1	**2**
Hg(1)—S(1)	2.345(5)	2.345(4)
Hg(1)—S(2)	2.360(5)	2.348(4)
Hg(1)—Cl(1)	2.985(4)	2.990(3)
Hg(1)—Cl(2)	3.065(4)	3.103(3)
S(1)—C(1)	1.712(15)	1.733(13)
S(2)—C(2)	1.734(14)	1.742(13)
M—Cl(1)	2.482(4)	2.471(3)
M—Cl(2)	2.548(3)	2.502(3)
M—Cl(3)	2.444(4)	2.438(3)
M—Cl(4)	2.461(4)	2.469(3)
S(1)—Hg(1)—S(2)	174.9(2)	175.40(14)
S(1)—Hg(1)—Cl(1)	87.62(13)	87.34(11)
S(1)—Hg(1)—Cl(2)	91.7(2)	91.13(12)
S(2)—Hg(1)—Cl(1)	97.0(2)	96.95(12)
S(2)—Hg(1)—Cl(2)	91.29(13)	91.35(10)
Cl(1)—Hg(1)—Cl(2)	78.66(10)	78.28(8)
C(1)—S(1)—Hg(1)	103.2(6)	103.1(5)
C(2)—S(2)—Hg(1)	100.8(6)	101.5(5)
Cl(1)—M—Cl(2)	99.34(12)	101.34(10)
Cl(3)—M—Cl(1)	108.88(14)	108.99(11)
Cl(3)—M—Cl(2)	112.93(13)	112.93(13)
Cl(3)—M—Cl(4)	111.43(13)	109.62(11)
Cl(4)—M—Cl(1)	118.18(14)	116.42(11)
Cl(4)—M—Cl(2)	105.53(13)	106.75(10)
M—Cl(1)—Hg(1)	92.54(11)	91.76(9)
M—Cl(2)—Hg(1)	89.40(11)	88.57(9)

2.548(3) Å and Cl—Hg(2)—Cl angles 99.34(12)–118.18(14)°, has been significantly distorted by its interaction with the $Hg(thb)_2$ moiety. However, the bonds Hg(2)—Cl(1) and Hg(2)—Cl(2) in **1**, which involve bridging Cl, are longer than the terminal Hg—Cl distances, as is commonly found for mercury [13].

Similarly, a CSD search [14] shows that bond distances and angles for discrete $CdCl_4^{2-}$ fall in the ranges 2.412–2.565 Å and 94.980–135.794°. Hence, the $CdCl_4^{2-}$ in **2**, with Cd(1)—Cl in the range 2.438(3)–2.502(3) Å and Cl—Cd(1)—Cl angles in the range 101.34(10)–116.42(11)°, is not unusually distorted by its interaction with $Hg(thb)_2$. The mean Hg(1)—Cl_{br} distance for **2** is marginally larger than that for **1** (3.05 Å vs 3.03 Å), and consistent with this the M—Cl_{br} and M—Cl_t distances in **2** are less well differentiated for **2** than for **1**, although we note that the longest and shortest Cd(1)—Cl distances in **2** are associated with bridging and terminal Cd(1)—Cl bonds.

The compound **2** appears to be only the second structurally-characterized compound containing Cd and Hg bridged by halogen atoms. In $I_2Cd(\mu\text{-}I)_2Hg(PPr_3)_2$, as in **2**, there is a tendency of the Hg(II) towards linear co-ordination as evidenced by the P—Hg—P angle of 152.8(1)° [15].

NMR spectra

Mercury thiobenzoate, $Hg(thb)_2$, has a concentration-independent ^{199}Hg chemical shift: $\delta_{Hg}(\Delta\nu_{1/2}) = -1265(\sim 20$ Hz) in CH_2Cl_2. The resonance is shielded relative to that of $Hg(SPh)_2$, e.g. $\delta_{Hg}(Hg(SPh)_2) = -1065$ for a saturated solution in $CHCl_3$ [16]. Shielding of the metal resonances of complexes of $PhC(O)S^-$ relative to those of the corresponding PhS^- complexes appears to be a general phenomenon [1–4].

At ambient probe temperature, $\delta_{Hg}(\Delta\nu_{1/2}) = -1143(\sim 85$ Hz) for a solution containing 0.025 mol of **2**/L of CH_2Cl_2. In the general context of ^{199}Hg NMR chemical shifts [17], the change in δ_{Hg} relative to that of $Hg(thb)_2$ is a minor one, showing that the $Hg(thb)_2$ in **2** has remained intact. The ^{111}Cd NMR chemical shift is ≈ 425 ppm for the very broad ^{111}Cd resonance ($\Delta\nu_{1/2} \approx 2500$ Hz) of the same solution. This signal is in the region expected for $CdCl_4^{2-}$ [18,19]. Apparently no interchange or transfer of ligands has occurred between Cd and Hg in the solution of **2**. On reduction of the concentration, δ_{Hg} moves towards that of free $Hg(thb)_2$, e.g. $\delta_{Hg}(\Delta\nu_{1/2}) = -1157(95$ Hz) for a solution with 0.0125 mol of **2**/L of CH_2Cl_2. Evidently **2** dissociates to $Hg(thb)_2$ and $CdCl_4^{2-}$ in solution, but not completely. In this case, the broadness of the ^{111}Cd resonance for **2** can be attributed to an intermediate rate of exchange (on the timescale of $\Delta\delta_{Cd}$) between free and bound $CdCl_4^{2-}$.

A single ^{199}Hg NMR signal is observed for a solution containing 0.05 mol of **1** l of CH_2Cl_2, with $\delta_{Hg}(\Delta\nu_{1/2}) = \sim -1040(\sim 400$ Hz). This signal does not shift significantly on modest dilution. The resonance is assigned to a $Hg(thb)_2$ moiety. The increase of ~ 225 ppm in δ_{Hg} that accompanies the change from $Hg(thb)_2$ to **1**, and the lack of a change in δ_{Hg} for **1** upon dilution, suggests that the anion of **1** is not extensively dissociated in CH_2Cl_2. However, no ^{199}Hg NMR signal was observed for $HgCl_4^{2-}$. This resonance must be exceedingly broad. By analogy with the results for **2**, we attribute this result to exchange of $HgCl_4^{2-}$ between free and bound sites, indicating the presence of *some* (apparently slight) dissociation of **1**.

CONCLUSIONS

The compounds $(Ph_4As)_2[Hg(SC(O)Ph)_2MCl_4]$ (M = Hg or Cd) can be synthesized readily from $Ph_4AsCl \cdot H_2O$, $Hg(SC(O)Ph)_2$ and $HgCl_2$ or $CdCl_2 \cdot H_2O$. X-ray analysis shows that in the new anions $Hg(SC(O)Ph)_2$, acting as a weak acceptor, is linked to MCl_4^{2-} through two chlorines. Metal NMR suggests that no ligand exchange or transfer occurs between $Hg(SC(O)Ph)_2$ and MCl_4^{2-}, and that when M = Hg, the complex dissociation dissociates only slightly in CH_2Cl_2, while the complex with M = Cd is

more extensively dissociated to $Hg(SC(O)Ph)_2$ and $CdCl_4^{2-}$.

Supplementary material

Tables of bond distances and angles, close nonbonded contacts, positional and thermal parameters, anisotropic thermal parameters, calculated hydrogen atom coordinates, selected torsion angles and selected weighted least-squares planes for **1** and **2** have been deposited with the Cambridge Crystallographic Data Centre.

Acknowledgment—This work was made possible by funding from the Natural Sciences and Engineering Research Council of Canada in the form of an Individual Research Grant to P.A.W.D.

REFERENCES

1. Vittal, J. J. and Dean, P. A. W., *Inorg. Chem.*, 1993, **32,** 791.
2. Burnett, T. R., Dean, P. A. W. and Vittal, J. J., *Can. J. Chem.*, 1993, **72,** 1127.
3. Vittal, J. J. and Dean, P. A. W., *Acta Crystallogr., Section C*, 1996, **C52,** 1180.
4. Vittal, J. J. and Dean, P. A. W., *Inorg. Chem.*, 1996, **35,** 3089.
5. Vittal, J. J. and Dean, P. A. W., *Acta. Crystallogr., Section C*, 1997, **C53,** 409.
6. Blayney, M. B., Winn, J. S. and Nierenberg, D. W., *Chem. Eng. News*, 1997, **75**(19), 7.
7. Wertheim, E., *J. Am. Chem. Soc.*, 1929, **51,** 3661.
8. An alternative synthesis is available: Savant, V. V., Gopalakrishnan, J. and Patel, C. C., *Inorg. Chem.*, 1970, **9,** 748.
9. XSCANS version 2.1, Siemens Analytical X-Ray Instruments Inc., Madison, WI, U.S.A., 1994.
10. SHELXTL Software version 5.0, Siemens Analytical X-Ray Instruments Inc., Madison, WI, U.S.A., 1994.
11. Bondi, A. J., *Phys. Chem.*, 1964, **68,** 441.
12. There is disagreement over the van der Waals radius of Hg: Canty, A. J. and Deacon, G. B., *Inorg. Chim. Acta*, 1980, **45,** L225.
13. (a) Grdenić, D., *Quart. Rev. Chem. Soc., London*, 1969, **19,** 303; (b) Dean, P. A. W., *Prog. Inorg. Chem.*, 1978, **24,** 109; (c) House, D. A., Robinson, W. T. and McKee, V., *Coord. Chem. Rev.*, 1994, **135/136,** 533.
14. Allen, F. H. and Kennard, O., *Design Automation News*, 1993, **8,** 31.
15. Bell, N. A., Goldstein, M., March, L. A. and Nowell, I. W., *Inorg. Chim. Acta*, 1984, **83,** 75.
16. Dean, P. A. W., Vittal, J. J. and Trattner, M. H., *Inorg. Chem.*, 1987, **26,** 4245.
17. (a) Kidd, R. G. and Goodfellow, R. J., in *NMR and the Periodic Table*, ed. R. K. Harris and B. E. Mann. Academic, New York, 1978, p. 266ff.; (b) Goodfellow, R. J., in *Multinuclear NMR*, ed. J. Mason. Plenum, New York, 1987, p. 577ff.
18. Colton, R. and Dakternieks, D., *Austral. J. Chem.*, 1980, **33,** 2405.
19. Kostelnik, R. J. and Bothner-By, A. A., *J. Mag. Reson.*, 1974, **14,** 141.

Pergamon

PII: S0277-5387(97)00482-8

Polyhedron Vol. 17, Nos. 11–12, pp. 1943–1952, 1998
© 1998 Elsevier Science Ltd
All rights reserved. Printed in Great Britain
0277-5387/98 $19.00+0.00

Synthesis, crystal structures and electrochemical properties of Cu^{II} and Ni^{II} complexes with hexadentate ligands containing thioether-amido-pyridyl donor set

Yukinari Sunatsuki,* Takehisa Matsumoto, Yuuji Fukushima, Masaaki Mimura, Masaaki Hirohata, Naohide Matsumoto and Fumiaki Kai*

Department of Chemistry, Faculty of Science, Kumamoto University, Kurokami 2-39-1, Kumamoto 860-8555, Japan

(Received 24 September 1997; accepted 19 November 1997)

Abstract—Novel two acyclic hexadentate ligands, 1,4-bis[*o*-(pyridine-2-carboxamidophenyl)]-1,4-dithiobutane (H_2bpctb) and 1,4-bis[*o*-(pyridine-2-carboxamidophenyl)]-1,5-dithiopentane (H_2bpctp), containing thioether functions were synthesized and their copper(II) and nickel(II) complexes [(Cu(bpctb)], **1**; [Cu(bpctp)], **2**; [Ni(bpctb)], **3** and [Ni(bpctp)], **4**) were prepared. The structures of **1**–**4** were determined by X-ray crystallography. The coordination geometries of **3** and **4** are octahedral with two amido and two pyridyl nitrogen atoms and two thioether sulfur atoms of hexadentate ligand. However, the coordination geometry of **2** is a flattened tetrahedron combining two amido nitrogen atoms and two pyridyl nitrogen atoms of hexadentate ligand without thioether coordination. X-ray crystallography and ESR spectroscopic studies revealed that the coordination geometry of **1** is an uncommon equatorially elongated octahedron in solid state. However, this coordination geometry changes to an axially elongated one in solution. The copper(II/I) redox processes for **1** and **2** are around −1.2 V and the nickel(II/III) processes for **3** and **4** at around 0.3 V vs ferrocene/ferrocenium couple were observed in DMSO. © 1998 Elsevier Science Ltd. All rights reserved

Keywords: hexadentate thioether ligand; crystal structure; ESR spectra; redox potential; equatorially elongated octahedral copper(II) complex.

The coordination chemistry of thioether sulfur is of great interest in bioinorganic chemistry [1]. Usually, a sulfur atom in a free thioether has a poor coordinating ability to metal ions. However, the thioether sulfur in macrocyclic ligands can coordinate to transition metals, and a number of these type of complexes have been synthesized and characterized [2]. The thioether sulfur can also coordinate to metal ions by using acyclic multidentate ligands containing the thioether function on the internal position [3,4].

In this connection, we designed new acyclic hexadentate ligands containing thioether-amido-pyridyl donor set; 1,4-bis[*o*-(pyridine-2-carboxamidophenyl)]-1,4-dithiobutane (H_2bpctb) and 1,4-bis[*o*-(pyridine-2-carboxamidophenyl)]-1,5-dithiopentane (H_2bpctp). Herein, we describe the synthesis, structure and electrochemical property of the copper(II) and nickel(II) complexes derived from these ligands.

* Author to whom all correspondence should be addressed.

EXPERIMENTAL

Materials

All chemicals used for synthetic work were of reagent grade and used without further purification. All solvents used for physical measurements were purified according to the literature methods [5] and stored under nitrogen atmosphere.

The diamines as precursors of thioether-system ligands, 1,2-bis(2-aminophenylthio)ethane (bape) and 1,3-bis(2-aminophenylthio)propane (bapp), were prepared according to the literature [6].

Two ligands, H_2bpctb and H_2hpctp, were prepared by the procedure in the literature [7]. As an example,

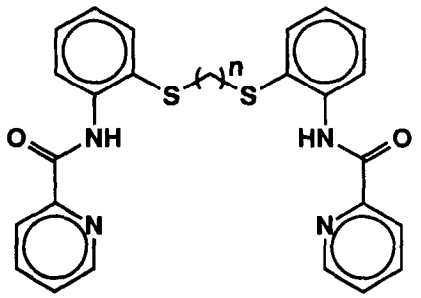

n = 2; H_2bpctb
n = 3; H_2bpctp

Abbreviation for complexes

[Cu(bpctb)] ; 1
[Cu(bpctp)] ; 2
[Ni(bpctb)] ; 3
[Ni(bpctp)] ; 4

Scheme 1. Structural formula and abbreviations for ligands and complexes.

the synthesis of 1,4-bis[*o*-(pyridine-2-carboxamidephenyl)]-1,4-dithiobutane (H_2bpctb, Scheme 1) is described here. To a solution of 2-pyridinecarboxylic acid (0.6 mol) in pyridine (240 ml) was added bape (0.3 mol) in pyridine (60 ml). After an addition of triphenylphosphite (0.6 mol) in this mixture, the reaction solution was heated on a steam bath for 4 h and allowed to stand at room temperature overnight. Colorless needles were collected and washed with methanol. Anal. Calcd for $C_{26}H_{22}N_4O_2S_2$: C, 64.17; H, 4.56; N, 11.52%. Found: C, 64.26; H, 4.58; N, 11.39%. IR 3284 cm^{-1}, ν_{NH}(amido); 1689 cm^{-1}, ν_{CO} (amido). ^1H NMR (90 MHz, $CDCl_3$, δ_{TMS} ppm): 11.2 (sb, 2H), NH; 8.69–6.92 (m, 16H), aromatic; 3.0 (s, 4H), SCH_2. m.p. 184°C. H_2bpctp; Colorless needles. Anal. Calcd for $C_{27}H_{24}N_4O_2S_2$: C, 58.18; H, 3.97; N, 10.06%. Found: C, 57.96; H, 3.99; N, 9.90%. IR 3328 cm^{-1}, ν_{NH}(amido); 1686 cm^{-1}, ν_{CO}(amido). ^1H NMR (90 MHz, $CDCl_3$, δ_{TMS} ppm): 11.2 (sb, 2H), NH; 8.69–6.91 (m, 16H), aromatic; 3.0 (t, 4H), SCH_2; 1.8 (quint., 2H), CH_2. m.p. 113°C.

Preparation of complexes

The general procedure was followed for all complexes. Details are given for **1** as an example. Methanol solution of copper(II) acetate monohydrate (1.0 mmol) was added to a hot methanol solution of H_2bpctb (1.0 mmol). The mixture was then heated on a water bath for 0.5 h, then deep green microcrystals were separated, and were washed with methanol. Crude product was recrystallized from DMSO/CH_2Cl_2 mixed solution. Deep green prisms were obtained. Anal. Calcd for $C_{26}H_{20}N_4O_2S_2Cu$: C, 56.97; H, 3.68; N, 10.22%. Found: C, 56.68; H, 3.70; N, 10.10%. IR 1617 cm^{-1}, ν_{CO}(amido). UV(log ε) 317 (4.30), 424 sh (2.54), 708 (2.13) nm in CH_2Cl_2; 432 sh, 622 sh, 726 nm in solid state. μ_{eff} (R.T.) = 1.82 BM.

Other complexes were obtained by the method similar to that for **1**. **2**·DMSO; Dark green prisms. Anal. Calcd for $C_{27}H_{22}N_4O_2S_2Cu \cdot C_2H_6OS$: C, 54.40; H, 4.41; N, 8.75%. Found: C, 54.47; H, 4.41; N. 8.08%. IR 1624 cm^{-1}, ν_{CO}(amido); 1028 cm^{-1} ν_{SO}(DMSO). UV(log ε) 330 (4.13), 426 sh (2.92), 652 (2.26), 826 (2.49) nm in CH_2Cl_2; 442 sh, 678 sh, 822 nm in solid state. μ_{eff} (R.T.) = 2.08 BM. **3**; Red prisms. Anal. Calcd for $C_{26}H_{20}N_4O_2S_2Ni$: C, 57.48; H, 3.71; N, 10.31%. Found: C, 57.33; H, 3.80; N, 10.35%. IR 1614 cm^{-1}, ν_{CO}(amido). UV(log ε) 345 (4.21), 526 sh (1.41), 842 (1.82) nm in CH_2Cl_2; 538 sh, 834 nm in solid state. μ_{eff} (R.T.) = 2.96 BM. **4**; Red prisms. Anal. Calcd for $C_{27}H_{22}N_4O_2S_2Ni$: C, 58.18; H, 3.97; N, 10.06%. Found: C, 57.96; H, 3.99; N, 9.90%. IR 1612 cm^{-1}, ν_{CO}(amido). UV(log ε) 343 (4.25), 544 sh (1.31), 856 (1.83) nm in CH_2Cl_2; 536 sh, 842 nm in solid state. μ_{eff} (R.T.) = 3.05 BM.

Physical measurements

Elemental analyses for C, H, and N were performed at the Elemental Analysis Service Center of Kyushu University. Electrical conductivity measurements were carried out on a Horiba DS-14 conductivity meter in 10^{-3} mol dm^{-3} solution at room temperature. Infrared spectra were measured on KBr disks with JASCO A-102 spectrophotometer. ^1H NMR spectra were recorded in $CDCl_3$ on a JEOL EX 90 spectrometer. Electronic spectra were measured on a Hitachi U-4000 spectrophotometer by the use of the 10^{-3} mol dm^{-3} solutions. Electrochemical measurements were carried out on a Yanagimoto P-1100 polarographic analyzer equipped with three electrodes of a glassy carbon working electrode, a platinum wire auxiliary electrode, and a saturated calomel electrode (SCE) as the reference, in which tetra-*n*-butylammonium perchlorate was employed as the supporting electrolyte. The concentration of the supporting electrolyte in sample solution was adjusted to 0.1 mol dm^{-3}. The sample solutions were deoxidized by nitrogen bubbling for 15 min before measurements. All the observed potentials were corrected by the Fc^+/Fc couple of ferrocene as an internal standard. ESR spectra were recorded on a JEOL TE200 spectrometer at liquid nitrogen temperature. Magnetic susceptibilities at room temperature were measured on a Faraday balance, where the calibration was made with $[Ni(en)_3]S_2O_3$ (en = ethylenediamine) [8]. Corrections were applied for diamagnetism calculated from Pascal's constants [9]. Effective magnetic moments were calculated by the equation $\mu_{eff} = 2.828(\chi_A T)^{1/2}$, where χ_A is the magnetic susceptibility per metal ion.

X-ray data collection, reduction, and structure determination

All measurements were made on a Rigaku AFC7R diffractometer with graphite monochromated Mo–K_α radiation ($\lambda = 0.71069$ Å) and a 12 kW rotating anode generator. The data were collected at a temperature of 20 ± 1°C using ω-2θ scan technique at a scan speed of 16.0° min^{-1} (in omega). The weak reflections ($I < 10.0\sigma(I)$) were rescanned (maximum of 3 scans) and the counts were accumulated to ensure good counting statistics. Stationary background counts were recorded on each side of the reflection. The ratio of peak counting time to background counting time was 2 : 1. The intensities of three representative reflections were measured after every 150 reflections, showing a good stability of the intensities. An empirical absorption correction based on azimuthal scans of several reflections was applied. The data were corrected for Lorentz and polarization effects.

The structures were solved by direct methods [10] and expanded using Fourier techniques [11]. The non-hydrogen atoms were refined anisotropically. Hydrogen atoms were included in the structure factor calculation. Full-matrix least-squares refinements based on the observed reflections ($I > 3.00\sigma(I)$) were employed, where the unweighted and weighted agreement factors of $R = \Sigma||F_o| - |F_c||/\Sigma|F_o|$ and $Rw = [\Sigma w(|F_o| - |F_c|)^2/\Sigma w|F_o|^2]^{1/2}$ are used. The weighting scheme was based on counting statistics. Neutral atomic scattering factors were taken from Cromer and Waber [12b]. Anomalous dispersion effects were included in F_{calc}; the values $\Delta f'$ and $\Delta f''$ where those of Creagh and McAuley [12a]. All calculations were performed using the teXsan crystallographic software package of Molecular Structure Corporation [13].

Crystal data and details of the structure determination for **1–4** are summarized in Table 1.

RESULTS AND DISCUSSIONS

Synthesis and characterization

Two ligands, H_2bpctb and H_2bpctp, were prepared by the same procedure for 1,2-bis(2-pyridinecarboxamido)benzene [7] with high yield (ca 80%). For all complexes, ν_{NH} band was not observed and ν_{CO} bands were shifted to a lower wavenumber in the IR spectra compared with those of ligands. These results indicate that deprotonated amido nitrogen atoms are coordinating to a metal ion in all complexes [14]. The electronic absorption band observed at 317–345 nm in CH_2Cl_2 was assigned to $\pi \rightarrow \pi^*$ transition and the others were assigned to *d-d* transition of the metal ion. Electronic spectra show that the coordination geometry of **1**, **3** and **4** is the octahedron. For compound **1**, however, *d-d* band at 708 nm is splitting in two at 622 nm (shoulder) and 726 nm. It is expected that the transformation occurs between structure of **1** in solid state and in solution. It was obvious that compound **2** had a flattened tetrahedral coordination geometry as described below.

Structural description of compound **1**, [Cu(bpctb)]

An ORTEP view of **1** with the atom numbering scheme is shown in Fig. 1. Selected bond distances and angles are reported in Table 2(a). This complex has a 2-fold axis passing through Cu(1) and the midpoint of C(13) and C(13)*. A copper(II) ion assumes an octahedral coordination geometry with two amido

Table 1. Crystallographic data for compounds **1–4**

	1	**2**·DMSO	**3**	**4**
Formula	$C_{26}H_{20}N_4O_2S_2Cu$	$C_{29}H_{28}N_4O_3S_3Cu$	$C_{26}H_{20}N_4O_2S_2Ni$	$C_{27}H_{22}N_4O_2S_2Ni$
Formula weight	548.14	640.29	543.29	557.32
Crystal color	Deep green	Dark green	Red	Red
Crystal system	monoclinic	monoclinic	monoclinic	monoclinic
Space group	C_2/c	C_2/c	$P2_1/c$	C_2/c
a (Å)	20.739(2)	15.579(3)	10.700(2)	12.902(2)
b (Å)	9.785(2)	17.311(3)	14.207(3)	18.341(2)
c (Å)	14.862(1)	12.172(3)	16.182(2)	10.342(1)
β (°)	128.162(4)	120.49(1)	107.80(1)	95.695(9)
V (Å^3)	2371.4(5)	2828(1)	2342.4(6)	2435.3(4)
Z	4	4	4	4
D_{calc} (g cm^{-3})	1.535	1.503	1.540	1.520
μ (cm^{-1})	11.30	10.27	10.40	10.02
No. of reflections	1722	2649	4561	3015
R	0.035	0.040	0.027	0.058
Rw	0.047	0.049	0.031	0.053

$R = \Sigma||F_o| - |F_c||/\Sigma|F_o|$, $Rw = [\Sigma w(|F_o| - |F_c|)^2/\Sigma w|F_o|^2]^{1/2}$, $w = 1/[\sigma(F_o)^2]$.

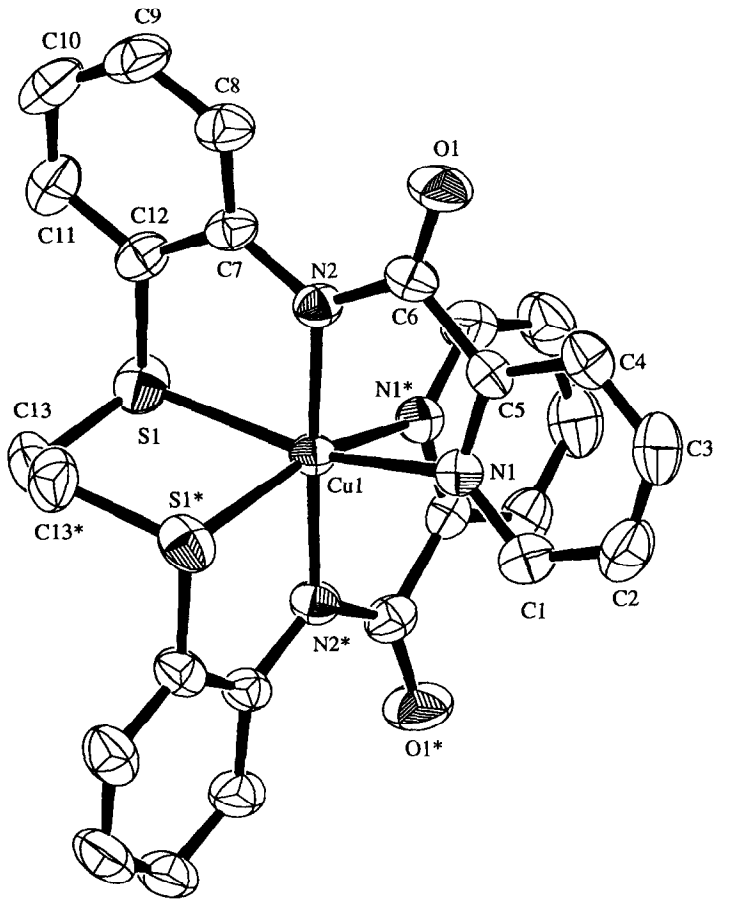

Fig. 1. An ORTEP drawing of compound **1** with atom numbering scheme, showing 50% probability ellipsoids

Table 2. Selected bond distances (Å) and angles ( ) with the estimated standard deviation in parentheses for copper(II) complexes

	(a) Compound **1**		
Cu(1)—S(1)	2.503(1)		
Cu(1)—N(1)	2.155(4)	Cu(1)—N(2)	1.977(3)
S(1)—C(12)	1.781(4)	S(1)—C(13)	1.817(5)
N(1)—C(1)	1.337(5)	N(1)—C(5)	1.339(5)
N(2)—C(6)	1.348(5)	N(2)—C(7)	1.412(5)
S(1)—Cu(1)—S(1)*	86.85(6)		
S(1)—Cu(1)—N(1)	164.97(9)	S(1)—Cu(1)—N(1)*	94.60(9)
S(1)—Cu(1)—N(2)	84.1(1)	S(1)—Cu(1)—N(2)*	97.8(1)
N(1)—Cu(1)—N(1)*	87.9(2)	N(2)—Cu(1)—N(2)*	177.3(2)
N(1)—Cu(1)—N(2)	80.9(1)	N(1)—Cu(1)—N(2)*	97.2(1)
	(b) Compound **2**		
Cu(1)—N(1)	2.056(3)	Cu(1)—N(2)	1.952(3)
S(1)—C(12)	1.775(4)	S(1)—C(13)	1.808(4)
N(1)—C(1)	1.344(4)	N(1)—C(5)	1.338(4)
N(2)—C(6)	1.340(4)	N(2)—C(7)	1.422(4)
N(1)—Cu(1)—N(1)*	134.9(2)	N(2)—Cu(1)—N(2)*	172.3(2)
N(1)—Cu(1)—N(2)	81.9(1)	N(1)—Cu(1)—N(2)*	101.2(1)
C(12)—S(1)—C(13)	102.0(2)		
C(1)—N(1)—C(5)	118.7(3)	C(6)—N(2)—C(7)	118.5(3)

and two pyridyl nitrogen atoms and two thioether sulfur atoms of hexadentate ligand. The bond distance of Cu(1)—S(1) is 2.503(1) Å. This bond distance lies in the middle of the axial Cu(1)—S distances (2.59–2.64 Å) and the equatorial one (2.32–2.48 Å) for the copper(II) complex with thioether ligands [4,15]. The copper(II) to pyridyl nitrogen bond distance of Cu(1)—N(1) and the copper(II) to amido nitrogen bond distance of Cu(1)—N(2) are 2.155(4) Å and 1.977(3) Å, respectively. This Cu(1)—N(1) bond distance is longer than the normal value of 1.96–2.08 Å for the copper(II) to pyridyl nitrogen equatorial bond distances [16]. On the other hand, Cu(1)—N(2) bond distance lies in the range of normal values for copper(II) to deprotonated amido nitrogen bond distances [16(f),17]. Thus, coordination geometry of this complex is described as an equatorially elongated octahedron which is occupied by N(1), S(1), N(1)*, and S(1)* on the equatorial site and N(2) and N(2)* on the axial site (see ESR spectroscopic study).

Structural description of compound **2**·DMSO, [Cu(bpctp)]·DMSO

An ORTEP view of **2**·DMSO with the atom numbering scheme is shown in Fig. 2. Selected bond distances and angles are listed in Table 2(b). This complex has a 2-fold axis passing through Cu(1) and C(14). Figure 2 shows that the structure of **2** is essentially different from that of **1**. A copper(II) ion assumes a flattened tetrahedral coordination geometry with two amido nitrogen atoms and two pyridyl nitrogen atoms of hexafunctionalized ligand with the bond angles of N(1)—Cu(1)—N(1)* and N(2)—Cu(1)—N(2)* are 134.9° and 172.3°, respectively. The bond distances of Cu(1)—N(1) and Cu(1)—N(2) are 2.056(3) Å and 1.952(3) Å, respectively. These distances are shorter than the corresponding distances of **1**. Neither of the thioether sulfur atoms coordinate to the copper center. A six membered chelate ring containing two thioether sulfur atoms as coordination atom may be unsuitable for the ligation between the thioether sulfur and the copper(II) ion. However, two sulfur atoms, S(1) and S(1)*, sit on two *cis* sites for Cu(1) with the distance of 3.006(1) Å. This value of the distance suggests that the weak interaction exists between Cu and S. On account of this fact, the coordination geometry of Cu(1) can also be described as a distorted octahedral with *cis*-open sites and two S atoms interact weakly on the open sites.

Structural description of compound **3**, [Ni(bpctb)]

An ORTEP view of **3** with the atom numbering scheme is shown in Fig. 3. Selected bond distances and angles are listed in Table 3(a). A nickel(II) ion assumes an octahedral coordination geometry with two amido and two pyridine nitrogen atoms and two thioether sulfur atoms of hexadentate ligand. The average bond distances of Ni(1)—S, Ni(1)—N_{amido}, and Ni(1)—$N_{pyridyl}$ are 2.4058 Å, 2.026 Å, and 2.067 Å,

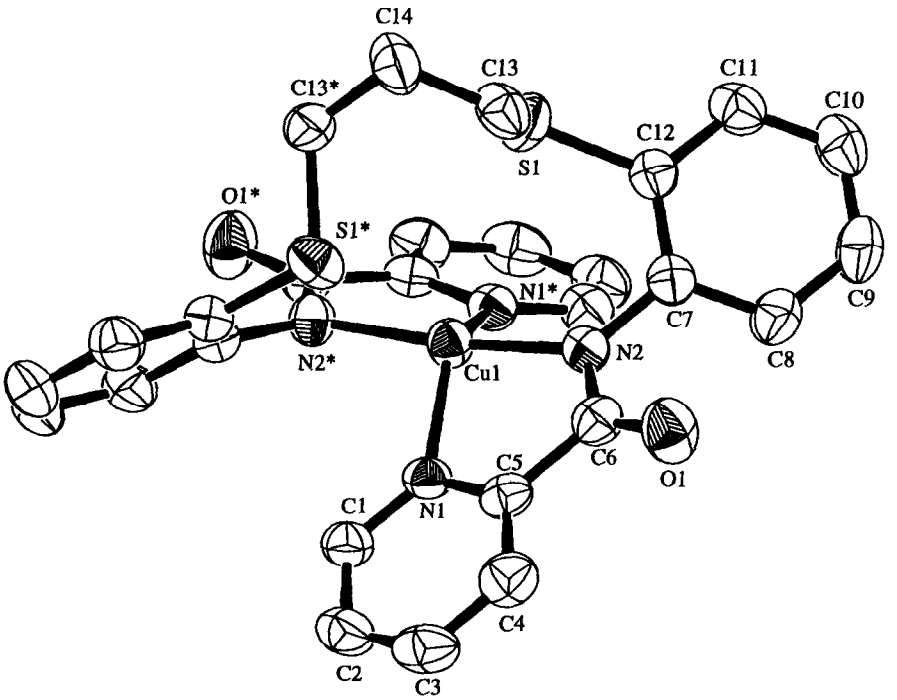

Fig. 2. An ORTEP drawing of compound **2**·DMSO with atom numbering scheme, showing 50% probability ellipsoids.

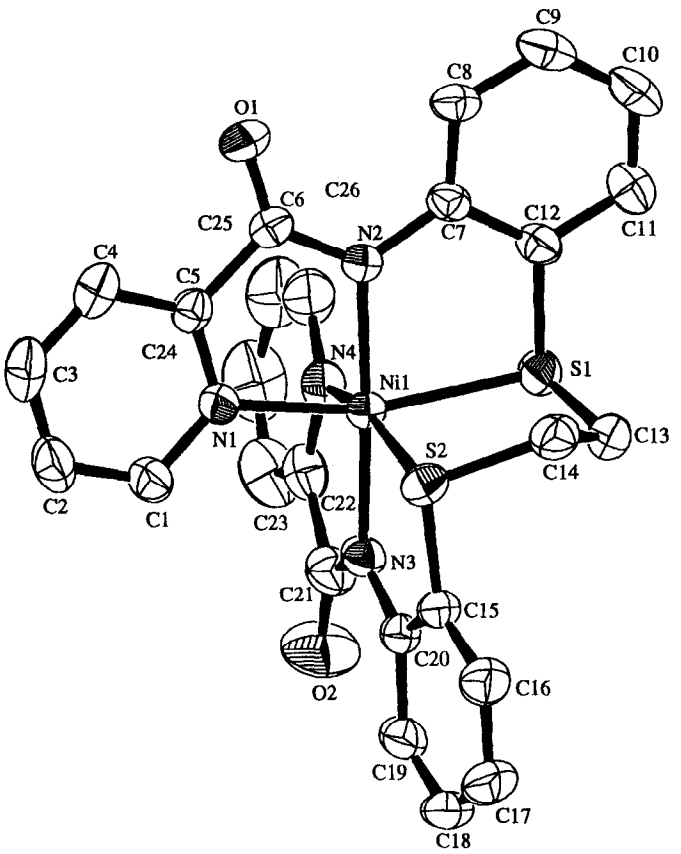

Fig. 3. An ORTEP drawing of compound **3** with atom numbering scheme, showing 50% probability ellipsoids.

respectively. This nickel(II) to thioether sulfur bond distance is within the range of the normal values of 2.39–2.55 Å for octahedral Ni^{II} complexes [1a,3]. These Ni—N bond distances lie in the general value of Ni—N bond distances for octahedral complexes [1a]. Especially, the Ni—N_{amido} bond distance is close to the normal values of ca 2.01 Å for octahedral complexes[18]. Bond angles around the Ni^{II} are close to the corresponding angles of **1**.

Structural description of compound **4**, [Ni(bpctp)]

An ORTEP view of **4** with the atom numbering scheme is shown in Fig. 4. Selected bond distances and angles are listed in Table 3(b). This complex has a 2-fold axis passing through Cu(1) and the midpoint of C(14) and C(14)*, and shows disorder in the propylene bridge (C(14), C(14)*). A nickel(II) ion assumes an octahedral coordination geometry with two amido and two pyridyl nitrogen atoms and two thioether sulfur atoms of hexadentate ligand. The bond distances of Ni(1)—S(1), Ni(1)—N(1), and Ni(1)—N(2) are 2.418(1) Å, 2.063(3) Å, and 2.020(3) Å, respectively. This complex resembles **3** in the structure. However, Ni(1)—S(1) bond distance is longer and S(1)—Ni(1)—S(1)* bond angle is larger than those of **3** with increase the number of carbon atom of alkyl bridge between two sulfur atoms.

ESR spectroscopic study for Cu^{II} *complexes*

The ESR spectra for powder samples of compounds **1** and **2** at the liquid nitrogen temperature are shown in Fig. 5. The powder spectrum of **1** (Fig. 5(a)) is typical of an axial pattern with $g_\perp > g_\parallel$. This spectrum shows that the unpaired electron lies on the d_{z^2} orbital and the coordination geometry of **1** is the uncommon equatorially elongated octahedron in solid state. The result is consistent with the X-ray crystallographic structure of **1**. However, the $CHCl_3$ glass spectrum of **1** (Fig. 5(b)) is of an axial pattern with $g_\parallel > g_\perp$ ($g_\parallel = 2.20$, $g_\perp = 2.07$, $A_\parallel = 12.5$ mT), contrary to the powder spectrum. This fact indicates that the structure of **1** in solid state changes in the $CHCl_3$ solution from an equatorially elongated octahedron to an axially elongated one. In other words, bond distances of Cu^{II} to amido nitrogen atoms are longer and the distances of Cu^{II} to sulfur atoms and Cu^{II} to pyridyl nitrogen atoms are shorter in solution, compared with those in solid state. The same change in a spectrum was also observed in frozen DMF solution.

The powder spectrum of **2** (Fig. 5(c)) shows a rhom-

Table 3. Selected bond distances (Å) and angles (°) with the estimated standard deviation in parentheses for nickel(II) complexes

	(a) Compound **3**		
Ni(1)—S(1)	2.4036(7)	Ni(1)—S(2)	2.4080(7)
Ni(1)—N(1)	2.060(2)	Ni(1)—N(2)	2.026(2)
Ni(1)—N(3)	2.025(2)	Ni(1)—N(4)	2.073(2)
S(1)—C(12)	1.781(2)	S(1)—C(13)	1.817(3)
S(2)—C(14)	1.816(3)	S(2)—C(15)	1.787(2)
N(1)—C(1)	1.344(3)	N(1)—C(5)	1.345(3)
N(2)—C(6)	1.340(3)	N(2)—C(7)	1.405(3)
N(3)—C(20)	1.405(3)	N(3)—C(21)	1.335(3)
N(4)—C(22)	1.341(3)	N(4)—C(26)	1.340(3)
S(1)—Ni(1)—S(2)	88.01(2)		
S(1)—Ni(1)—N(1)	164.96(5)	S(1)—Ni(1)—N(2)	84.34(5)
S(1)—Ni(1)—N(3)	97.56(6)	S(1)—Ni(1)—N(4)	90.83(6)
S(2)—Ni(1)—N(1)	92.77(5)	S(2)—Ni(1)—N(2)	98.06(5)
S(2)—Ni(1)—N(3)	84.14(6)	S(2)—Ni(1)—N(4)	164.44(6)
N(1)—Ni(1)—N(2)	80.67(7)	N(1)—Ni(1)—N(3)	97.46(7)
N(1)—Ni(1)—N(4)	92.35(7)	N(2)—Ni(1)—N(3)	177.16(7)
N(2)—Ni(1)—N(4)	97.26(8)	N(3)—Ni(1)—N(4)	80.64(8)
	(b) Compound **4**		
Ni(1)—S(1)	2.418(1)		
Ni(1)—N(1)	2.063(3)	Ni(1)—N(2)	2.020(3)
S(1)—C(12)	1.776(4)	S(1)—C(13)	1.817(5)
N(1)—C(1)	1.335(5)	N(1)—C(5)	1.343(4)
N(2)—C(6)	1.355(5)	N(2)—C(7)	1.392(5)
S(1)—Ni(1)—S(1)*	96.21(6)		
S(1)—Ni(1)—N(1)	164.87(9)	S(1)—Ni(1)—N(1)*	87.06(9)
S(1)—Ni(1)—N(2)	83.90(9)	S(1)—Ni(1)—N(2)*	98.58(9)
N(1)—Ni(1)—N(1)*	93.6(2)	N(2)—Ni(1)—N(2)*	176.3(2)
N(1)—Ni(1)—N(2)	81.0(1)	N(1)—Ni(1)—N(2)*	96.5(1)

bic pattern with $g_1 = 2.22$, $g_2 = 2.10$ and $g_3 = 2.03$, and reflects the crystal structure of this compound. The glass spectrum of **2** is essentially the same pattern with the hyperfine structure due to the Cu nucleus, regardless of the solvent. No structural change like compound **1** was observed.

Electrochemical property

Electrochemical measurements for the complexes were carried out in the DMSO solutions; the potentials are summarized in Table 4. The quasi-reversible process of the copper(II) complexes observed at

Table 4. Electrochemical data for compounds **1–4**

Compound	E_{pc}/V	E_{pa}/V	ΔE_p/mV	$E'_{1/2}$/V[a]	$E_{1/2}$/V
1	−1.303	−1.183	120	−1.243	−1.224
2	−1.139	−1.073	66	−1.106	−1.108
3	0.205	0.271	66	0.238	0.246
4	0.365	0.429	64	0.397	0.391

[a] $E'_{1/2} = (E_{pc} + E_{pa})/2$.

All the observed potentials were corrected by the Fc^+/Fc couple of ferrocene which was employed as the internal standard. Tetra-*n*-butylammonium perchlorate was employed as supporting electrolyte. All measurements were carried out in DMSO.

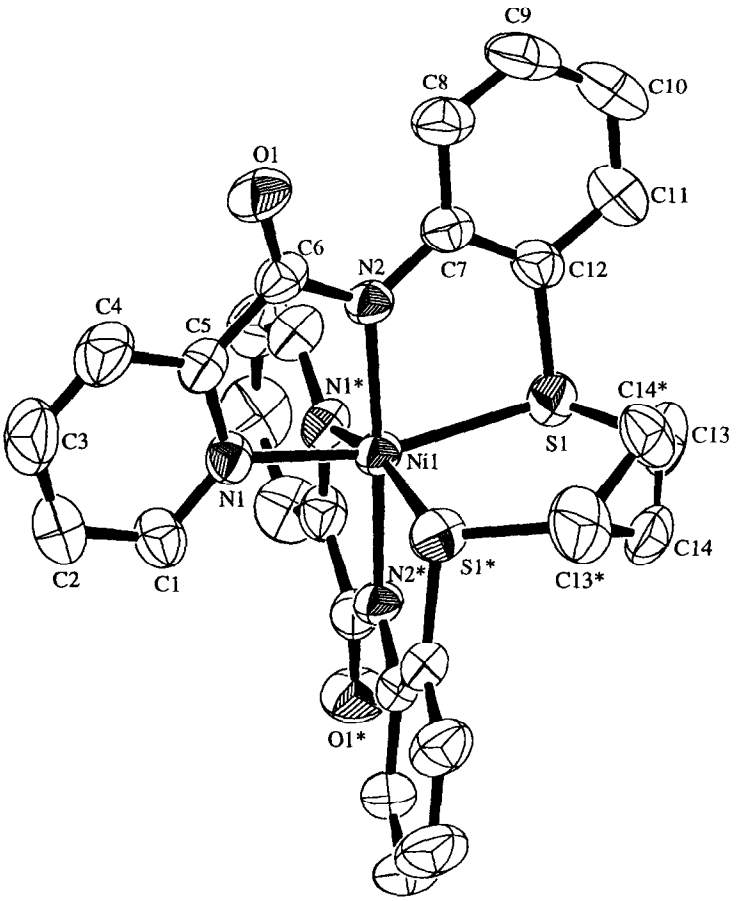

Fig. 4. An ORTEP drawing of compound **4** with atom numbering scheme, showing 50% probability ellipsoids.

-1.224 V for **1** and at -1.108 V for **2** vs the ferrocene/ferrocenium couple is assigned to Cu^{II} to Cu^{I} process. The deprotonated amido nitrogen is known as a strong donor atom and can stabilize the high oxidation state of metal ions [19]. However, Cu^{II} to Cu^{III} process of those complexes was not observed in DMSO. Shukla *et al.* had reported that the copper(II/III) redox process was observed at near $+0.53$ V vs SCE (ca $+0.08$ V vs Fc/Fc^{+}) for Cu^{II} complexes using N_2S_4 ligands which have the thiophenolate groups instead of pyridyl one of our ligands [20]. Thiophenolate sulfur is known as a coordinating atom which has an ability to stabilize the high oxidation state of metal ion [21]. Thus, our ligands have a weaker ability to stabilize the high oxidation state of metal ions, compared with Shukla's ligand system. In addition, the ESR study revealed that the Cu^{II}—N_{amido} bond of **1** is elongated by the solvation and **2** has the tetrahedral coordination geometry. Both of them are disadvantageous to stabilize the high oxidation state of metal ions. Therefore, Cu(II/III) redox process was not observed in the present copper(II) complexes.

The quasi-reversible process of the nickel(II) complexes observed at 0.246 V for **3** and at 0.391 V for **4** vs the ferrocene/ferrocenium couple is assigned to Ni^{II} to Ni^{III} process of them. Contrary to the Cu^{II} complexes, this process is not observed for Shukla's ligand system [20]. As described in crystallographic section, Ni—S bond distance of **4** is longer than that of **3** with increase of the number of carbon atom of alkyl bridge between two sulfur atoms. Owing to this difference, the redox potential of **4** is ca 0.15 V higher than that of **3**.

REFERENCES

1. (a) Halcrow, M. A. and Christou, G., *Chem. Rev.*, 1994, **94**, 2421; (b) Kaim, W. and Rall, J., *Angew. Chem., Int. Ed. Engl.*, 1996, **35**, 43.
2. Cooper, S. R. and Raule, S. C., *Structr. Bonding*, 1990, **72**, 1; Blake, A. J. and Schroder, M., *Adv. Inorg. Chem.*, 1990, **35**, 1.
3. (a) Mohanty, J. G., Singh, R. P. and Chakravorty, A., *Inorg. Chem.*, 1975, **14**, 2178; (b) Lappin, A. G., Laranjeira, M. C. M. and Peacock, R. F., *Inorg. Chem.*, 1983, **22**, 786; (c) Choudhury, S. B., Ray, D. and Chakravorty, A., *Inorg. Chem.*, 1991, **30**, 4354; (d) Choudhury, S. B., Ray, D. and Chakravorty, A., *J. Chem. Soc., Dalton*

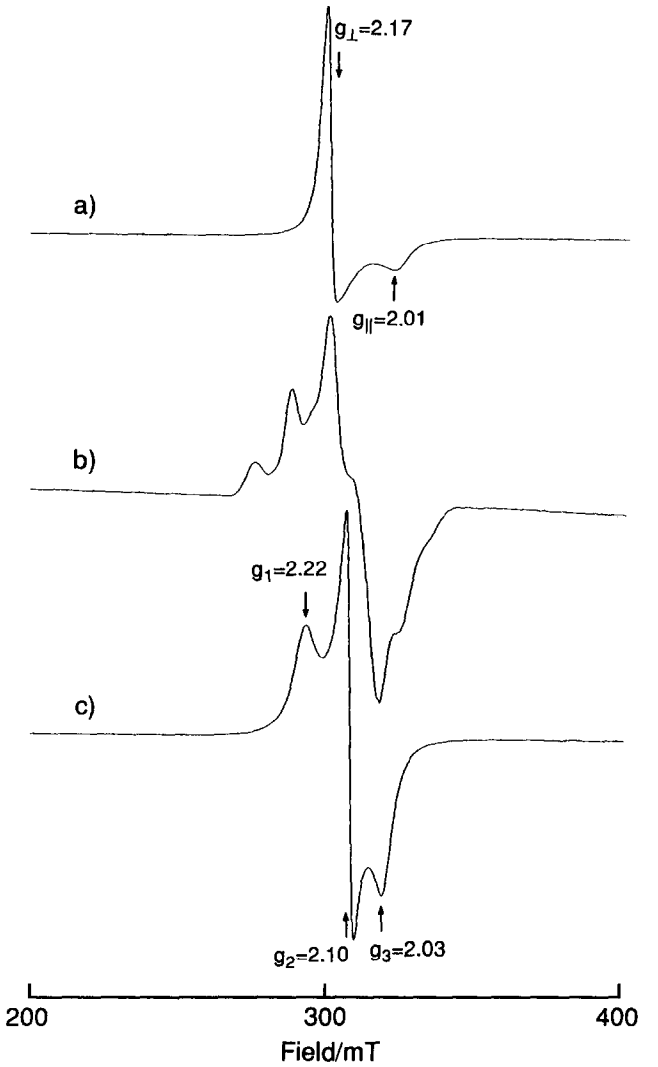

Fig. 5. ESR spectra of copper(II) complexes at liquid nitrogen temperature; (a) the powder spectrum of **1**; (b) the $CHCl_3$ glass spectrum of **1**; (c) the powder spectrum of **2**.

Trans., 1992, 107; (e) Karmakar, S., Choudhury, S. B., Ray, D. and Chakravorty, A., *Polhyedron*, 1993, **12**, 291; (f) Karmakar, S., Choudhury, S. B., Ray, D. and Chakravorty, A., *Polyhedron*, 1993, **12**, 2325.

4. (a) Dagdigian, J. V., Mckee, V. and Reed, C. A., *Inorg. Chem.*, 1982, **21**, 1332; (b) Latour, J. M., Limosin, D. and Ray, P., *J. Chem. Soc., Chem. Commun.*, 1985, 464; (c) Benzekri, A., Dubourdeaux, P., Latour, J. M., Laugier, J. and Ray, P., *J. Chem. Soc., Chem. Commun.*, 1987, 1564; (d) Benzekri, A., Dubourdeaux, P., Latour, J. M., Laugier, J. and Ray, P., *Inorg. Chem.*, 1988, **27**, 1564; (e) Benzekri, A., Dubourdeaux, P., Latour, J. M., Laugier, J. and Ray, P., *J. Chem. Soc., Dalton Trans.*, 1991, 3359.
5. Perrin, D. and Armarego, W. F. L., *Purification of Laboratory Chemicals*, 3rd edn. Pergamon, 1988.
6. (a) Jaunin, R. and Holl, R., *Helv. Chim. Acta*, 1958, **41**, 1783; (b) Unger, O., *Chem. Ber.*, 1987, **30**, 607; (c) Dwyer, F. P., Gills, N. S., Gyartas, S. C. and Lions, F., *J. Am. Chem. Soc.*, 1954, **76**, 383.
7. Barnes, D. J., Chapman, R. L., Vagg, R. S. and Watton, E. C., *J. Chem. Eng. Data*, 1978, **4**, 349.
8. Lindoy, L. F., Katovic, V. and Busch, D. H., *J. Chem. Educ.*, 1972, **49**,.
9. Earnshaw, A., *Introduction to Magnetochemistry*. Academic Press, New York, 1968.
10. (a) Fan Hai-Fu. SAPI91: Structure Analysis Programs with Intelligent Control, Rigaku Corporation, Tokyo, Japan, 1991; (b) Debaerdemaeker, T., Germain, G., Main, P., Refaat, L. S., Tate, C. and Woolfson, M. M., MULTAN88: Computer program for the automatic solution of crystal structures from X-ray diffraction data, University of York, U.K., 1988; (c) Sheldrick, G. M., SHELXS86: A program for X-ray crystal structure determination, University of Cambridge, 1986.

11. Beurskens, P. T., Admiraal, G., Beurskens, G., Bosman, W. P., Garcia-Granda, S., Gould, R. O., Smits, J. M. M. and Smykalla, C., DIRDIF91: The DIRDIF program system, Technical Report of the Crystallography Laboratory, University of Nijimegen, The Netherlands, 1992.
12. (a) Creagh, D. C. and McAuley, W. J., *International Tables for Crystallography*, Vol. C, ed. A. J. C. Wilson. Kluwer Academic Publishers, Boston, 1992; (b) Cromer, D. T. and Waber, J. T., *International Tables for X-ray Crystallography*, Vol. IV. The Kynoch Press, Birmingham, U.K., 1974.
13. teXsan: Crystal Structure Analysis Package, Molecular Structure Corporation, 1985 and 1992.
14. Bellamy, L. J., *The Infra-red Spectra of Complex Molecules*, 3rd edn. Chapman and Hall, London 1975.
15. (a) Pattanayak, S., Chakraborty, P., Chandra, S. K. and Chakravorty, A., *Polyhedron*, 1995, **15,** 1121; (b) Nanda, K. K., Addison, A. W., Sinn, E. and Thompson, L. K., *Inorg. Chem.*, 1996, **35,** 5966.
16. (a) Chapman, R. L., Stephens, F. S. and Vagg, R., *Inorg. Chim. Acta*, 1980, **43,** 29; (b) Jacobson, R. R., Tyeklar, Z., Farooq, A., Karlin, K. D., Liu, S. and Zubieta, J., *J. Am. Chem. Soc.*, 1988, **110,** 3690; (c) Lubben, M., Hage, R., Meetsma, A., Bÿma, K. and Feringa, B. L., *Inorg. Chem.*, 1995, **34,** 2217; (d) Ghosh, D., Lal, T. K., Ghosh, S. and Mukherjee, R., *J. Chem. Soc., Chem. Commun.*, 1996, 13; (e) Kayatani, T., Hayashi, Y., Inomata, K. and Uehara, A., *Bull. Chem. Soc. Jpn*, 1996, **69,** 389; (f) Akagi, F., Nakao, Y., Matsumoto, K., Takamizawa, S., Mori, W. and Suzuki, S., *Chem. Lett.*, 1997, 181.
17. (a) Diaddario, L. L., Robinson, W. R. and Margerum, D. W., *Inorg. Chem.*, 1983, **22,** 1021; (b) Tokii, T., Mikuriya, M., Okawa, H., Murase, I. and Kida, S., *Bull. Chem. Soc. Jpn*, 1984, **57,** 2098; (c) Koikawa, M., Okawa, H., Matsumoto, N., Gotoh, M., Kida, S. and Kohzuma, T., *J. Chem. Soc., Dalton Trans.*, 1989, 2089; (d) Stumpf, H. O., Pei, Y., Kahn, O., Sletten, J. and Renard, J. P., *J. Am. Chem. Soc.*, 1993, **115,** 6738; (e) Sanz, J. L., Cervera, B., Ruiz, R., Bois, C., Faus, J., Lloret, F. and Julve, M., *J. Chem. Soc., Dalton Trans.*, 1996, 1359; (f) Sunatuki, Y., Hirata, R., Motoda, Y., Nakamura, M., Matsumoto, N. and Kai, F., *Polyhedron*, 1997, **16,** 4105.
18. Lewis, R. M., Nancollas, G. H. and Coppens, P., *Inorg. Chem.*, 1972, **6,** 1371.
19. Collins, T. J., *Acc. Chem. Res.*, 1994, **27,** 279 and references therein.
20. Shukla, R., Mandel, S. and Bharadwaj, P. K., *Polyhedron*, 1993, **12,** 83.
21. Krüger, H.-J. and Holm, R. H., *Inorg. Chem.*, 1987, **26,** 3647.

Pergamon

PII: S0277-5387(97)00481-6

Polyhedron Vol. 17, Nos. 11–12, pp. 1953–1957, 1998
© 1998 Elsevier Science Ltd
All rights reserved. Printed in Great Britain
0277-5387/98 $19.00+0.00

A new one-dimensional 4,4′-bipy-bridged compound $[Mn(hfac)_2(4,4'\text{-bipy})]_n$ (hfac = hexafluoroacetetylacetonato; 4,4′-bipy = 4,4′-bipyridine). Synthesis, crystal structure and magnetic properties

Hao-Yu Shen,[a] Dai-Zheng Liao,*[a] Zong-Hui Jiang,[a] Shi-Ping Yan,[a] Bai-Wan Sun,[a] Geng-Lin Wang,[a] Xin-Kan Yao[b] and Hong-Gen Wang[b]

[a] Department of Chemistry, Nankai University, Tianjin, 300071, P.R. China

[b] Central Laboratory, Nankai University, Tianjin, 300071, P.R. China

(Received 18 September 1997; accepted 19 November 1997)

Abstract—A one-dimensional 4,4′-bipy-bridged compound $[Mn(hfac)_2(4,4'\text{-bipy})]_n$ (hfac = hexafluoroacetetylacetonato; 4,4′-bipy = 4,4′-bipyridine) has been prepared and its structure has been determined. The structure consists of a zigzag-one-dimensional chain in which Mn(II) ion is bridged by 4,4′-bipy. The coordination environment is distorted octahedral for Mn(II), and $Mn(hfac)_2(4,4'\text{-bipy})$ has a *cis* coordination. Magnetic investigation shows that this compound presents a very weak antiferromagnetic interaction ($J = -0.196\ cm^{-1}$, $g_{Mn} = 2.02$, $F = 2.24 \times 10^{-3}$). © 1998 Elsevier Science Ltd. All rights reserved

Keywords: one-dimensional compound; 4,4′-bipy-bridged compound; crystal structure; magnetic properties.

High-dimensional compounds are of interest in the field of molecular based magnets because on one side they should help researchers gain a better understanding of the correlation between the magnetism and structure, and on the other side high-dimensional antiferro- or ferromagnets are attractive for possible technical applications. Our interest is to obtain high-dimensional compounds to study magneto-structure correlation. 4,4′-bipyridine and $NaNO_2$ are both good bridging ligand to mediate magnetic interaction between metal ions [1–7]. $Mn(hfac)_2$ is a widely used precursor compound which has two vacant or two substitutable coordination sites to form high dimensional compounds with suitable bridging ligand.

In order to prepare high dimensional compound, we used 4,4′-bipyridine and $NaNO_2$ and $Mn(hfac)_2$ as reaction masses. Unexpectedly $NaNO_2$ did not react in this system; we only got a one-dimensional chain compound $Mn(hfac)_2(4,4'\text{-bipy})$. Although the present compound has a same mononuclear fragment $[Mn(hfac)_2]$ as that of $[Mn(hfac)_2L]$ (L = *trans*-1,2-bis(4-pyridyl)ethylene) which is previously reported by Okawa *et al.* [5], the bridging ligands of the two compounds are different.

In this paper, we report a new one-dimensional 4,4′-bipy bridged compound $Mn(hfac)_2(4,4'\text{-bipy})$ and its magnetic properties.

EXPERIMENTAL

Synthesis

To 10 ml ethanol solution of $Mn(hfac)_2$ (103.5 mg, 0.5 mmol) was added 4,4′-bipy (96.11 mg, 0.5 mmol) dissolved in 10 ml methane alcohol. This mixture solution was added to aqueous $NaNO_2$ (34.5 mg, 0.5 mmol). The clear yellow solution was left to stand undisturbed at room temperature. Several days later, X-ray quality brown-red single crystals were obtained by slow evaporation, which were filtered, washed with water, methane alcohol, ether, and air dried. Yield: 72%. Elemental analysis: Found: C, 44.78; H, 3.28;

* Author to whom correspondence should be addressed.

N, 34.55. Calc. for $[MnC_{20}H_{10}F_{12}N_2O_4]$: C, 44.59; H, 3.74; N, 34.67%. m.p. 260°C (decomp.).

Physical measurements

Elemental analyses of carbon, hydrogen and nitrogen were carried out with a Perkin–Elmer analyzer model 240. The electronic spectrum was measured with a Perkin–Elmer Hitachi-240 spectrophotometer. The infrared spectroscopy on KBr pellets was performed on a Nicolet 5DX FT-IR spectrophotometer in the 4000–400 cm^{-1} region. Magnetic susceptibility measurement of a crystalline sample was carried out in the temperature range 1.3–300 K on a vibrating sample magnetometer, model CF-1.

Crystallographic data collection and structure determination

A brown-red monoclinic crystal with dimensions $0.2 \times 0.3 \times 0.3$ mm^3 was mounted on a computer-controlled Enraf-Nonius CAD4 diffractometer equipped with a graphite-monochromatized Mo-K_α radiation ($\lambda = 0.71073$ Å). Crystal data for [Mn(hfac)(4,4′-bipy)], $MnC_{20}H_{10}F_{12}N_2O_4$: Space group C_2/c, $a = 9.852(2)$ Å, $b = 17.026(3)$ Å, $c = 14.208(3)$ Å, $\alpha = \gamma = 90.00(0)°$, $\beta = 94.68(3)°$, $V = 2375(1)$ $Å^3$, $\rho_{calcd} = 1.748$ g cm^{-3}, $Z = 4$, $\mu = 0.6541$ mm^{-1}, $F(000) = 1236$.

The cell parameters were determined by a least-squares calculations based on the setting angles and 25 reflections with 2θ angles ranging from 8.35 to 12.14° at 299(1) K. The intensities of the $\pm hkl$ reflections were measured up to $\theta_{max} = 23°$, the ω-2θ scan technique was employed, the ω-scan width equal to $(0.6 \pm 0.35 \tan\theta)°$, and the scan speed 0.92–5.49° min^{-1}. A total of 1616 independent reflections was measured giving 1309 observed reflections ($I > 3\sigma(I)$) used in the refinement. Three standard reflections monitored every 60 min showed no intensity variation during the data collection. No absorption correction was made during processing.

The structure was solved by direct method (SHELXS-86) using SDP-PLUS program [8,9] and refined by the full-matrix least-squares method with use of the SHELXL-93 package of program. Atomic scattering factors were taken from Ref. 10. The final R and wR values were 0.047 and 0.053 respectively ($R = \Sigma\|F_o| - |F_c\|/\Sigma|F_o|$. $wR = [\Sigma(w|F_o| - |F_c|)^2/\Sigma w|F_o|^2]^{1/2}$; $w = 1/(\sigma^2(F) + 99.0000\ F^2$; $[\Sigma w(|F_o| - F_c|)^2/(N_{obs} - N_{para})]^{1/2}$), and goodness of fit 2.14 for all observed reflections.

RESULTS AND DISCUSSION

Description of the crystal structure

Selected interatomic bond distances and bond angles are given in Table 1. The molecular structure is shown in Fig. 1.

The structure consists of chains in which *cis*-$Mn(hfac)_2$ are bridged by 4,4′-bipy. the chains are generated in the unit cell with *cis*-$Mn(hfac)_2$(4,4′-bipy), as shown in Fig. 1.

The Mn(II) ion assumes a distorted octahedral coordination geometry. The deviation from octahedral coordination geometry is probably due to the large steric hindrance between hfac molecules and 4,4′-bipy. Mn(II) is coordinated with four oxygen atoms from two hfac ligands [Mn(1)—O(1) = Mn(1)—O(1a) = 2.134(4) Å, Mn(1)—O(2) = Mn(1)—O(2) = 2.186(4) Å], and two nitrogen atoms from two 4,4′-bipy ligands [Mn(1)—N(11) = Mn(1)—N(11a) = 2.257(5) Å]. The other nitrogen atoms of the two 4,4′-bipy ligands are coordinated to two adjacent manganese ions. In the crystal lattice, the Mn ion lies on a two-fold rotation axis. From Fig. 2, we can see complex $Mn(hfac)_2$(4,4′-bipy) had a zigzag-chain structure. The two pyridine rings of a 4,4′-bipyridine is in a plane. The dihedral angle is 0.03°. The metal–metal separation across the bridging 4,4′-bipy is 11.674 Å for Mn(1)···Mn(1c).

IR spectrum

The IR spectrum of the compound exhibits two characteristic strong bonds at 1650–1660 and 1490 cm^{-1} attributed to the $\nu_{C=O}$ and $\nu_{C=C}$ stretching vibrations of the hfac respectively, suggesting an enol coordination mode for hfac ligands [11]. Because of the strong absorption of hfac in IR, most absorption bands of 4,4′-bipy were screened by the absorption of hfac, but some characteristic absorption can also be observed: a sharp band at 1610 cm^{-1} attributed to the ν_{ring} and another sharp one at 1410 cm^{-1} attributed to the $\nu_{C=C}$ stretching vibrations, also two sharp unsymmetric bands at 800 cm^{-1} attributed to the ν_{C-H} stretching vibrations [12].

Magnetic properties

The magnetic behavior of the compound is represented in Fig. 3, in the forms of $\chi_m T$ vs T. The observed $\chi_m T$ value is 4.65 cm^3 K mol^{-1} at 295 K, which is slightly higher than the spin-only value of 4.34 cm^3 K mol^{-1} for Mn(II) ($S = 5/2$) and $g_{Mn} = 2$. When the temperature is lowered, $\chi_m T$ remains almost constantly until 6.5 K and then decreases sharply to 0.8 cm^3 K mol^{-1} at 1.5 K, indicating the presence of a weak antiferromagnetic exchange interaction within the chain.

On the base of magneto-structural data on the complex, an antiferromagnetic exchange coupling within 1-D 4,4′-bipy-bridged chain is expected. In principle, the magnetic data for complex can be analyzed with the Hamiltonian $\hat{H} = -2J\Sigma\hat{S}_{2i} \cdot \hat{S}_{2i+1}$, where J is the exchange coupling parameter associated with a particular manganese(II) ion [13]. Since such a Hamiltonian cannot presently be used for an exact

Table 1. Selected interatomic bond distances (Å) and angles (°)

Mn(1)—O(1)	2.134(4)	Mn(1)—O(2)	2.186(4)
Mn(1)—N(11)	2.257(5)	Mn(1)—O(1a)	2.134(4)
Mn(1)—O(2a)	2.186(4)	Mn(1)—N(11a)	2.257(5)

O(1)—Mn(1)—O(2)	86.6(1)	O(1)—Mn(1)—N(11)	93.4(2)
O(2)—Mn(1)—N(11)	92.4(2)	O(1)—Mn(10—O(1a)	176.9(2)
N(11)—Mn(1)—O(1a)	88.6(2)	O(1)—Mn(1)—O(2a)	83.3(2)
N(11)—Mn(1)—O(2a)	169.8(2)	O(1a)—Mn(1)—O(2a)	82.6(1)
O(10—Mn(1)—O(11a)	88.6(2)	O(2)—Mn(1)—N(11a)	169.8(2)
N(11)—Mn(1)—N(11a)	93.3(2)	O(1a)—Mn(1)—N(11a)	93.5(2)
O(2a)—Mn(1)—N(11)	92.4(2)		

Symmetry code a = $-x$, y, $0.5-z$; b = $0.5-x$, $0.5-y$, $1-z$; c = $0.5+x$, $0.5-y$, $0.5+z$; d = $-0.5-x$, $0.5-y$, $-z$; e = $-0.5+x$, $0.5-y$, $-0.5+z$.

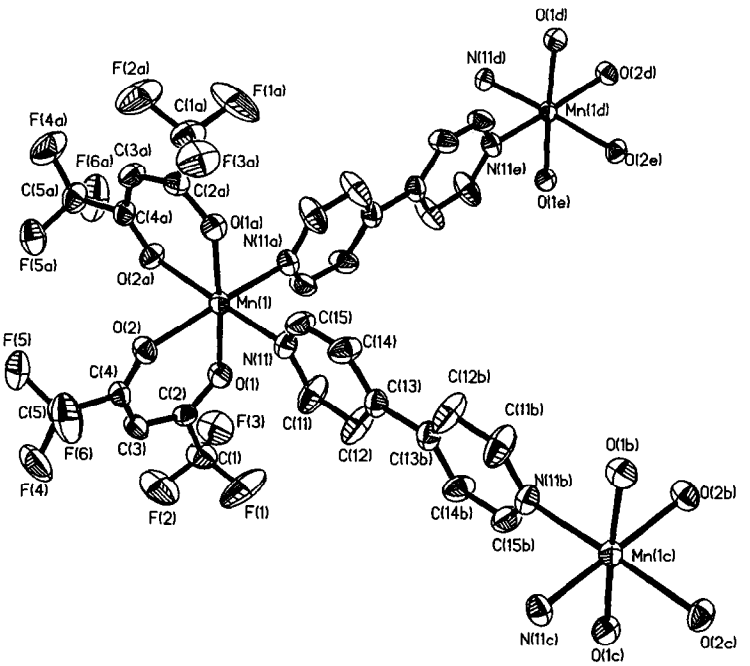

Fig. 1. The ORTEP drawing of $Mn(hfac)_2(4,4'\text{-bipy})$.

solution in the $S = 5/2$ case, we can only treat the present complex by using approximate model. It was found that the polynomial expression (eqn (1)) of Hatfield and co-workers [14] gives a fairly good fit to the data of complex.

$$\chi = \frac{Ng_{Mn}^2\beta^2}{KT}[A + Bx^2]/[1 + Cx + Dx^3] \qquad (1)$$

where $A = 2.9167$, $B = 208.04$, $C = 15.543$, $D = 2707.2$, and $x = |J|/KT$.

The least-squares fit from eqn (1) to the data was found with $J = -0.196(1)$ cm^{-1}, $g_{Mn} = 2.02$, where a very weak antiferromagnetic intrachain interaction between the nearest Mn(II) ions is present. The agreement factor, defined as $F = \Sigma_i(\chi_i^{obs} - \chi_i^{calcd})^2/\Sigma_i(\chi_i^{obs})^2$, was 2.24×10^{-3} for all of the 96 observations.

If we compare this J value with those previously reported for other complexes with 4,4′-bipy bridging ligands, we see that the coupling constant is similar to all the others [1–4,6]. The low value of J might be due to the following reasons: (1) the existence of Mn^{II}-(4,4′-bipy)-Mn^{II} pathway is not a sufficient condition for superexchange; (2) the Mn^{II}—Mn^{II} separation of 11.674 Å is clearly too large to permit larger overlap between magnetic orbitals.

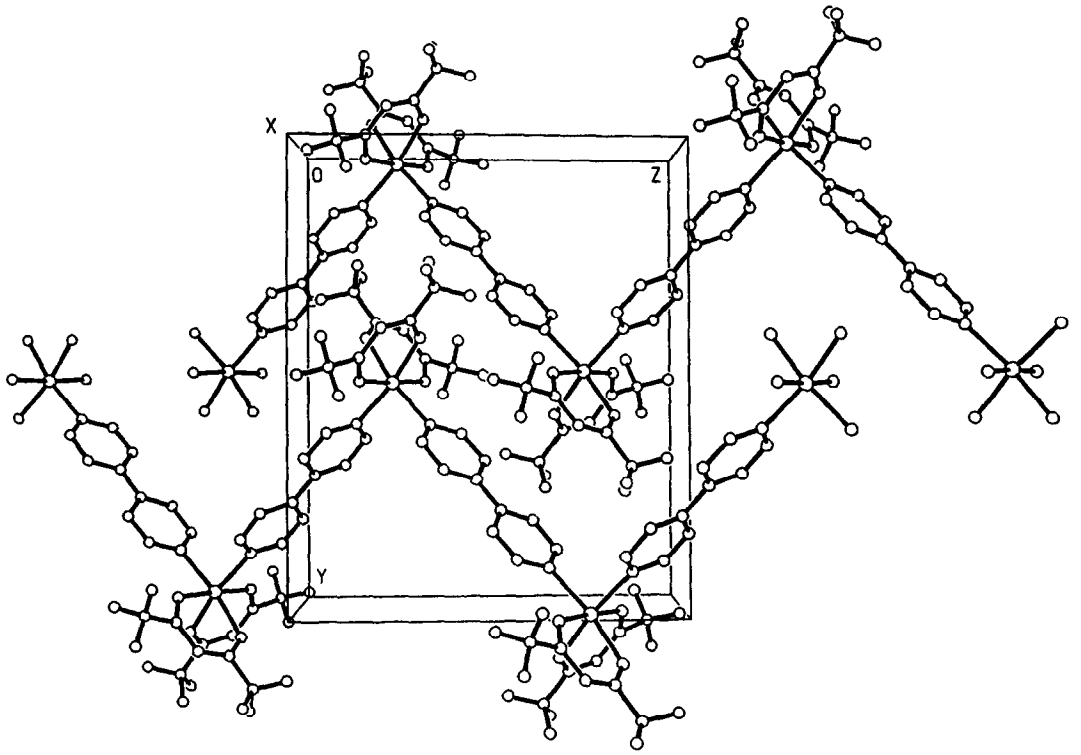

Fig. 2. View of the crystal cell of the compound.

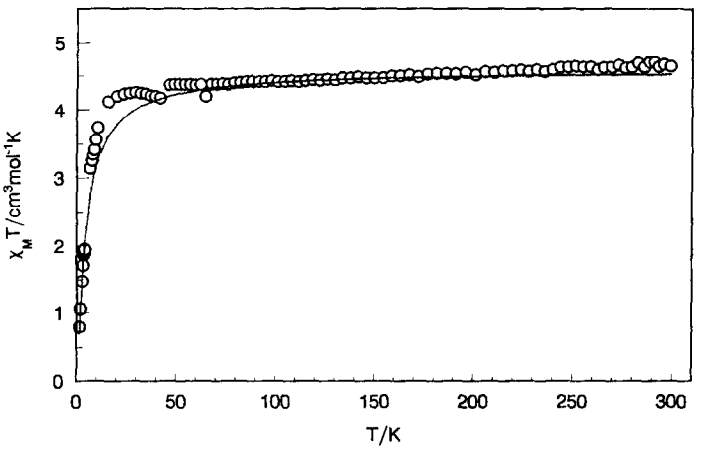

Fig. 3. Plots of the products $\chi_m T$ vs temperature for $Mn(hfac)_2(4,4'\text{-bipy})$. The solid line represents the best fitting (see text for the fitted parameters).

Acknowledgement—This work was supported by the National Natural Science Foundation of China.

REFERENCES

1. Tosik, A., Bukowska-Strzyzewska, M. and Mroziński, J., *J. Coord. Chem.*, 1990, **21,** 253.
2. Slangen, P. M., van Koningsbruggen, P. J., Haasnooot, J. G., Jansen, J., Gorter, S., Reedijk, J., Kooijman, H., Smeets, W. J. J. and Spek, A. L., *Inorg. Chim. Acta*, 1993, **212,** 289.
3. Julve, M., Verdaguer, M., Faus, J., Tinti, F., Moratal, J., Monge, A. and Gutiérrez-Puebla, E., *Inorg. Chem.*, 1987, **26,** 3520.
4. Haddad, M. S., Hendrickson, D. N., Cannady, J. P., Drago, R. S. and Bieksza, D. S., *J. Am. Chem. Soc.*, 1979, **101,** 898.

5. Mago, G., Hinago, M., Miyssaka, H., Matsumoto, N. and Okawa, H., *Inorg. Chim. Acta*, 1997, **245,** 145.
6. Li, M.-X., Xu, Z., You, X.-Z. and Chen, C.-G., *Acta Chimica Sinica*, 1994, **58,** 274.
7. Escuer, A., Vicente, R. and Solans, X., *J. Chem. Soc., Dalton Trans.*, 1997, 531.
8. SPD-PLUS, Enraf-Nonius, Delft, The Netherlands, 1985.
9. Sheldrick, G. M., *Acta Crystallogr.*, 1990, **A46,** 467.
10. *International Tables for X-Ray Crystallography*, Vol. 4. Kynoch Press, Birmingham, England, 1974.
11. Deacon, G. B. and Phillips, R. J., *Coord. Chem. Rev.*, 1980, **22,** 33.
12. Czakis-Sulikowska, D. M., Radwańska-Doczkalska, J. and Sójka, G., *Monatch. Chem.*, 1984, **115,** 961.
13. Kahn, O., *Molecular Magnetism*. VCH, New York, 1993.
14. Hiller, W., Strähle, J., Datz, A., Hanack, M., Hatfield, W. E., der Haar, L. W. and Gütlich, P., *J. Am. Chem. Soc.*, 1984, **106,** 329.

Pergamon

PII: S0277-5387(97)00485-3

Polyhedron Vol. 17, Nos. 11–12, pp. 1959–1974, 1998
© 1998 Elsevier Science Ltd
All rights reserved. Printed in Great Britain
0277-5387/98 $19.00+0.00

Bismuth(III) coordination compounds. Synthesis, characterization, and X-ray structures of $[Bi(Cl)(\mu\text{-}Cl)_2(THF)_2]_\infty$, $Bi(O_2CMe)_3(Solv)_x$ (Solv = py, $x = 2$ or MeIm, $x = 4$) [1], and $[Bi(\mu\text{-}OCH_2CMe_3)(OCH_2CMe_3)_2(Solv)]_2$ (Solv = $HOCH_2CMe_3$ or py)

Timothy J. Boyle,*[a] Dawn M. Pedrotty,[a] Brian Scott[b] and Joseph W. Ziller[c]

[a] Sandia National Laboratories, Advanced Materials Laboratory, 1001 University Boulevard SE, Albuquerque, New Mexico, 87106, U.S.A.

[b] Los Alamos National Laboratories, CST-18, Chemical Science and Technology Division—X-ray Diffraction Laboratory, Los Alamos, New Mexico 87545, U.S.A.

[c] Department of Chemistry—X-ray Facilities, University of California-Irvine, Irvine, CA 92717, U.S.A.

(Received 12 August 1997; accepted 19 November 1997)

Abstract—We have isolated and structurally characterized several novel bismuth coordination compounds. Dissolution of $Bi(NO_3)_3 \cdot 5H_2O$ in concentrated HCl, followed by crystallization from THF lead to the isolation of $[Bi(Cl)(\mu\text{-}Cl)_2(THF)_2]_\infty$, **1**. Each bismuth metal center of **1** adopts a 7-coordinated pentagonal bipyramidal geometry. One THF solvent molecule and one terminal chloride ligand are located in each of the axial positions. A terminal THF solvent molecule and four bridging chlorides reside in the equatorial positions. Dissolution of $Bi(O_2CMe)_3$ in pyridine (py) or N-methylimidazole (MeIm) results in the isolation of the appropriate amine adduct, either $Bi(O_2CMe)_3(py)_2$, **2** or $Bi(O_2CMe)_3(MeIm)_3 \cdot (MeIm)$, **3**. Compound **2** uses two py molecules to adopt an unusual (for bismuth acetate species) 8-coordinated triangular dodecahedral geometry. In contrast, **3** incorporates three MeIm molecules to adopt the 9-coordinated tricapped trigonal prismatic geometry typically observed for bismuth acetate compounds (a "free" MeIm molecule is located in the lattice). The reaction of $Bi[N(SiMe_3)_2]_3$ with $HOCH_2CMe_3$ (HONp) yields $[Bi(\mu\text{-}ONp)(ONp)_2(HONp)]_2$, **4**. An alternative synthetic route to **4** is the metathical exchange between $BiCl_3$ and 3 equivalents of NaONp in the presence of HONp. The bismuth atoms of **4** are 5-coordinated and adopt an apical-shared, square base pyramidal (SP) arrangement. Recrystallization of **4** from py yields the dinuclear complex $[Bi(\mu\text{-}ONp)(ONp)_2(py)]_2$, **5**. The Bi atoms of **5** also adopt a 5-coordinated SP geometry; however, the two metal centers are linked through a basal-shared arrangement. The apical ONp ligands are in an up-down relationship to each other. © 1998 Elsevier Science Ltd. All rights reserved

Keywords: bismuth; halide; acetate; alkoxide; neopentoxide.

Coordination compounds of bismuth are of interest for such varied applications as oxidation catalysts [2–5], medicinal and biomedical practices [6–11], superconductors [7,12,13], and other oxide based materials [1,2,7,14]. Thus, much attention has focused on identification of new bismuth compounds that are suitable for these applications. We are interested in highly soluble Bi compounds for use in precursor solutions to produce ferroelectric thin films. Ferroelectric materials are those ceramics that possess a spontaneous polarization that can be reoriented with an

* Author to whom correspondence should be addressed.

applied electric field [15]. This leads to a hysteresis in the polarization-voltage response and is the basis of computer memory applications. A wide range of ferroelectric materials that contain bismuth and may potentially be used as memory, piezoelectric, or electro-optic devices would include: $Bi_4Ti_3O_{12}$, $SrBi_2Nb_2O_9$, $BiCaNb_2O_9$, $BiCaTa_2O_9$, $Bi_4Ba_2Ti_5O_{18}$, $Bi_4BaTi_4O_{15}$, $BiNaTi_2O_6$, and $BiKTi_2O_6$ [15]. Currently, the most research activity surrounding bismuth ceramics involves the layered-perovskite ferroelectric material $SrBi_2Ta_2O_9$ (SBT) [1,16–19]. SBT materials are of great interest for non-volatile memory applications due to their promise of non-fatigue with extended electrical cycling.

Since the preparation of these bismuth oxide materials requires extremely pure and well-characterized compounds, it is important to know the solid and solution state characteristics of these precursors in order to exploit their properties to the fullest extent. Even though a wide number of bismuth compounds have been crystallographically characterized. [1–3,6,8,10,12–14,20–52], few of these compounds are suitable for the solution processes used to generate films [53]. Recently, we reported the use of pyridine (py) to dissolve $[Bi(O_2CMe)_3]_\infty$ as a key component in the production of low temperature SBT thin films [1,15]. From this investigation, two amine solvated $Bi(O_2CMe)_3$ complexes were isolated [1]. In looking for further alternative precursors, we have investigated ONp derivatives of bismuth. We become interested in the *neo*-pentoxide (OCH_2CMe_3 = ONp) ligand for materials applications due to the combination of favorable characteristics of the hydrocarbon chain [54]. The β-hydrogens of the ONp ligand are easily eliminated upon hydrolysis, allowing for rapid organic decomposition which is vital for production of uniform materials at low temperature. The OBu^t moiety of the ONp ligand greatly increases the solubility of the resulting metal alkoxide by introducing steric bulk around the metal center, inhibiting oligomerization. The combination of these two attributes makes the ONp ligand an ideal candidate to produce well-characterized highly soluble bismuth alkoxides.

This report details the synthesis, characterization, and X-ray structural information of a number of bismuth coordination compounds: (i) the halide precursor, $[Bi(Cl)(\mu\text{-}Cl)_2(THF)_2]_\infty$ **1**, (ii) two solvated acetates, $Bi(O_2CMe)_3(py)_2$, **2** [1,19], and $Bi(O_2CMe)_3(MeIm)_3 \cdot (MeIm)$, **3** [1,19], and (iii) two new solvated bismuth alkoxides, $[Bi(\mu\text{-}ONp)(ONp)_2(HONp)]_2$, **4** and $[Bi(\mu\text{-}ONp)(ONp)_2(py)]_2$, **5**. The solution behaviors of these compounds, based on NMR and molecular weight studies are also discussed.

EXPERIMENTAL

All compounds were handled under an inert atmosphere using standard Schlenk and glove box techniques, unless otherwise noted, as previously described [55]. FT-IR data were obtained on a Nicolet, Magna System Spectrometer-550. Thermal gravimetric analysis/differential thermal analysis (TGA/DTA) experiments were performed on a Polymer Laboratories STA 1500 Instrument. Elemental Analysis was performed on a Perkin–Elmer 2400 CHN-S/O Elemental Analyzer. NMR spectral data were collected on an AC-250 or Brucker 400 MHz spectrometer. All spectra were referenced against the residual proton impurity in the appropriate pre-dried deuterated solvent. The following compounds were used as received (Aldrich): concentrated HCl, $Bi(NO_3)_3 \cdot 5H_2O$, $HOCH_2CMe_3$ (HONp), N-methylimidazole (MeIm), $LiN(SiMe_3)_2$, $BiCl_3$ and $Bi(O_2CMe)_3$ (Alpha). Immediately prior to use, toluene and tetrahydrofuran (THF) were dried over and distilled from Na/benzophenone, whereas pyridine (py, Fisher) was dried over and distilled from CaO. $Bi[N(SiMe_3)_2]_3$ was synthesized according to literature reports [$BiCl_3$ (Aldrich) and 3 $LiN(SiMe_3)_2$ (Aldrich) in THF] [26]. NaONp, synthesized by either the reaction between Na° or NaH with HONp, was purified by sublimation.

$[Bi(Cl)(\mu\text{-}Cl)_2(THF)_2]_\infty$, 1

To a Schlenk flask charged with $Bi(NO_3)_3 \cdot 5H_2O$ (10.0 g, 20.6 mmol), concentrated HCl (20 ml) was slowly added by addition funnel. The reaction mixture, evolves as gas (bubbles) and turns yellow. The reaction mixture was allowed to stir at 60°C under an argon atmosphere. Periodically, excess pressure was removed by introduction of a slight vacuum. After 12 h, the reaction mixture was cooled to room temperature and all of the volatile materials were removed *in vacuo*. The resulting pale yellow powder was dissolved in THF and allowed to sit at glovebox temperatures for several days. The resulting X-ray quality crystals proved to be $[Bi(Cl)(\mu\text{-}Cl)_2(THF)_2]_\infty$, **1**. Yield first crop 4.3 g (47.5%). Repetition of concentration and sitting of the mother liquor leads to a quantitative yield of **1**. TGA/DTA (oxygen) [weight loss up to T°C (total weight loss (%))/thermal event, T°C]: 160°C (30.0)/endo (sm), 70.0°C; 103°C (73.6)/exo (m), 278°C; 395°C (74.0)/exo (m), 360°C. Elem. Anal. Calcd for $C_8H_{16}BiO_2Cl_3$ (two THF): 20.90, C; 3.51, H; for $C_4H_8BiOCl_3$ (one THF): 12.40, C; 2.08, H. Found: 12.46, C; 2.13, H.

$Bi(O_2CMe)_3(py)_2$, 2

$Bi(O_2CMe)_3$ (1.00 g, 2.59 mmol) was dissolved in a minimum amount of py (~1.53 ml), stirred for 12 h, centrifuged to remove any undissolved powder, and then concentrated by rotary evaporation. After sitting at circumjacent glovebox temperatures for 2–3 days, X-ray quality crystals were isolated and proved to be $Bi(O_2CMe)_3(py)_2$, **2**. Repetition of the concentration

and sitting of the mother liquor leads to a quantitative yield of **2**. ^{1}H NMR (400.1 MHz, $CDCl_3$) δ 8.60 (4.5H, bs, NC(*H*)C(H)C(H)C(H)C(H)), 7.71 (2H, mult., NC(H)C(H)C(*H*)C(H)C(H), 7.33 (4.3H, mult., NC(H)C(*H*)C(H)C(H)C(H)), 2.05 (9H, mult., O_2CMe). IR (KBr, partial 1800–1200 cm^{-1}) 1555 (bs, mult. sh.: 1560, 1580, 1545), 1493 (m), 1419 (bs, mult. sh.: 1453, 1448, 1403, 1392) 1336 (m), 1263 (w). TGA/DTA (oxygen) [weight loss up to T°C (total weight loss (%))/thermal event, T°C]: 70°C (25.5)/endo (sm), 70°C; 200°C (27.8)/none; 263°C (41.3)/exo (sm), 263°C; 321°C (52.1)/exo (1 g), 304°C and exo(1 g), 321°C. Elem. Anal. Calcd for $C_{16}H_{19}BiN_2O_6$ (two py): 35.31, C; 3.52, H; 2.57, N; $C_{11}H_{14}BiNO_6$ (one py): 28.39, C; 3.03, H; 3.01, N. Found: 28.93, C; 3.23, H; 3.48, N.

$Bi(O_2CMe)_3(MeIm)_3 \cdot MeIm$, 3

$Bi(O_2CMe)_3$ (1.00 g, 2.59 mmol) was dissolved in a minimum amount of MeIm (~1.00 ml), stirred for 12 h, centrifuged to remove an undissolved powder, and then concentrated by rotary evaporation. After sitting at circumjacent glovebox temperatures for 2–3 days, X-ray quality crystals were isolated and proved to be $Bi(O_2CMe)_3(MeIm)_3 \cdot MeIm$, **3**. Repetition of concentration and sitting of the mother liquor leads to a quantitative yield of **3**. ^{1}H NMr (250 MHz, $CDCl_3$) δ 7.53 (4.3H, s, N=C*H*N(CH$_3$)C*H*=C*H*), 7.05 (4.6H, s, N=C*H*N(CH$_3$)C*H*=C*H*), 6.82 (4.6H, s, N=C*H*N(CH$_3$)C*H*=C*H*), 3.63 (14.5H, s, N=CHN(C*H*$_3$)CH=CH), 1.89 (9H, s, O_2CCH_3). IR (KBr, partial 1800–1200 cm^{-1}) 1563 (strong broad with multiple shoulders), 1553 (bs, mult. sh.), 1415 (s), 1348 (s), 1282 (w), 1262 (w), 1231 (m). TGA/DTA (oxygen) [weight loss up to T°C (total weight loss (%))/thermal event, T°C]: 82°C (2.8)/endo (sm), 77°C; 198°C (21.0/endo (m), 198°C; 278°C (58.8)/exo (m), 270°C; 339°C (64/)exo (1 g), 314; 357°C (65.5)/exo (1g), 330°C. Elem. Anal. Calcd for $C_{22}H_{38}BiN_8O_6$: 36.72, C; 5.32, H; 15.57, N. Found: 37.66, C; 5.23, H, 17.59, N.

$Bi(\mu\text{-}OCH_2CMe_3)(OCH_2CMe_3)_2(HOCH_2CMe_3)]_2$, 4

Method A. To a solution of $Bi[N(SiMe_3)_2]_3$ (15.0 g, 218 mmol) in toluene (100 ml), $HOCH_2CMe_3$ (8.62 g, 9.80 mmol) was added via an additional funnel. The bright yellow solution was heated to 65°C until the reaction mixture turns pale yellow (~2.5 h). The volatile components were removed *in vacuo*, the resulting powder was washed with hexanes and extracted with toluene (*note*: extraction of the dried material with THF leads to a higher yield of a white powder with identical analytical data as noted for the crystalline material of **4**). The toluene soluble fraction was cooled to −35°C yields crystals which proved to be $[Bi(\mu\text{-}OCH_2CMe_3)(OCH_2CMe_3)_2(HOCH_2CMe_3)]_2$, **4**. Yield 6.14 g (50.5%). ^{1}H NMR (250.1 MHz, toluene-d_8) 4.22 (2H, s, OCH_2CMe_3), 1.04 (12H, s, OCH_2CMe). ^{13}C NMR (100.6 MHz, toluene-d_8) 74.9 (OCH_2CMe), 34.8(OCH_2CMe), 27.3 (OCH_2CMe). FT-IR (KBr, cm^{-1}) 3477 (w), 2953 (s), 2903 (w), 2863 (m), 2813 (w), 2743 (w), 2696 (m), 1477 (m), 1462 (w), 1391 (m), 1357 (m), 1302 (w), 1260 (m), 1215 (w), 1048 (s), 1006 (s), 930 (w), 897 (m), 622 (m), 584 (m), 564 (m), 534 (m).

Method B. To a solution of NaONp (0.67 g, 6.12 mmol) and HONp (0.27 g, 0.31 mmol) in toluene (30 ml), $BiCl_3$ (0.50 g, 2.04 mmol) was slowly added. The reaction mixture immediately turned cloudy. After stirring for 24 h, the reaction mixture was separated by centrifugation and the volatile materials of the soluble fraction were removed by rotary evaporation. The analytical data of the bulk powder proved consistent with **4** generated by method A. Crystalline yield 0.601 g (52.7%)

$[Bi(\mu\text{-}OCH_2CMe_3)(OCH_2CMe_3)_2(py)]_2$, 5

In a vial, **4** (0.50 g, 0.45 mmol) was dissolved in py (7.5 ml), stirred for 12 h, the solution concentrated, and cooled to −35°C. The resulting crystals proved to be $[Bi(\mu\text{-}OCH_2CMe_3)(OCH_2CMe_3)_2(py)]_2$, **5**. Yield 44.6% (0.22 g). ^{1}H NMR (400.1 MHz, pyridine-d_5, partial coordinated py not differentiated from solvent) δ 4.43 (OCH_2CMe_3), 1.08 (OCH_2CMe_3). ^{13}C NMR (100.6 MHz, pyridine-d_5) δ 73.7 (OCH_2CMe_3), 26.7 (OCH_2CMe_3), 25.9 (OCH_2CMe_3). FT-IR (KBr, cm^{-1}) 2953 (s), 2853 (m), 2793 (w), 2694 (w), 1574 (m), 1474 (m), 1461 (sh), 1401 (m), 1348 (m), 1262 (m), 1063 (s), 1010 (m), 798 (m), 751 (sh), 639 (bw), 553 (w).

X-ray collection, structure determination and refinement

Table 1 lists the data collection parameters for **1**–**5**. All compounds were handled using standard inert atmosphere oil coating techniques. For all of the crystals, the determination of the Laue symmetry, crystal class, unit cell parameters and the orientation matrix were carried out according to standard procedures [56]. Intensity data were collected using a $2\theta/\omega$ scan technique with Mo-K_α radiation and monitored after 97 reflections. The raw data were processed with either: (a) a local version of CARESS [57] which employs a modified version of the Lehman-Larsen algorithm to obtain intensities and standard deviations from the measured 96-step profiles or (b) the SHELXTL PC Version 4.2/360 software using SHELX 93 software for structure refinement corrected for absorption using the ellipsoidal option in the XEMP facility of SHLXTL PC. All data were corrected for Lorentz and polarization effects and were placed on approximately absolute scale. Structures were solved in the proper space group using

Table 1. Collection data for $[Bi(Cl)(\mu\text{-}Cl)_2(THF)_2]_n$, **1**, $Bi(O_2CMe)_3(py)_2$, **2**, $Bi(O_2CMe)_3(MeIm)_3 \cdot MeIm$, **3**, $[Bi(\mu\text{-}ONp)(ONp)_2(HONp)]_2$, **4**, and $[Bi(\mu\text{-}ONp)(ONp)_2(py)]_2$, **5**

Compound	**1**	**2**	**3** [58]	**4**	**5**
Formula	$C_8H_{16}BiO_2Cl_3$	$C_{16}H_{16}BiN_2O_6$	$C_{22}H_{38}BiN_8O_6$	$C_{40}H_{88}Bi_2O_8$	$C_{40}H_{76}Bi_2N_2O_6$
Formula weight	459.54	544.31	719.58	1115.06	1098.99
Temperature (K)	158	163	173	103	158
Space group	$P2_1/n$	$P2_1/n$	$P\bar{1}$	$P\bar{1}$	$P2_1/c$
Crystal system	monoclinic	monoclinic	triclinic	triclinic	monoclinic
a (Å)	7.982(1)	13.316(1)	9.371(1)	10.383(2)	9.733(1)
b (Å)	9.006(1)	9.533(1)	11.1830(10)	11.923(1)	23.328(2)
c (Å)	18.642(2)	16.626(1)	14.354(2)	11.931(1)	10.504(1)
α (°)			67.79(1)	107.94(1)	
β (°)	98.74(1)	123.05(1)	89.67(1)	113.58(1)	93.76(1)
γ (°)			83.16(1)	92.82(1)	
V (Å^3)	1324.6(3)	1769.0(3)	1381.5(3)	1262.4(3)	2379.7(3)
Z	4	4	2	1	2
λ (Mo–K_α radiation) (Å)	0.71073	0.71073	0.71069	0.71069	0.71073
D_{calcd} (Mg m^{-3})	2.304	2.044	1.730	1.467	1.534
μ (mm^{-1})	13.892	10.001	6.432	7.000	7.425
$R_1{}^a$ (%)	3.97[c]	2.71[d]	4.88[e]	5.90[f]	3.18[g]
$wR_2{}^b$ (%)	9.30	5.38	12.72	11.22	7.13
$[I > 2\sigma(I)]$					
$R_1{}^a$ (%)	7.51[c]	4.72[d]	6.51[e]	9.59[f]	5.29[g]
$wR_2{}^b$	10.65	5.93	15.12	12.83	8.34
[all data]					

[a] $R_1 = \Sigma||F_o| - |F_c||/\Sigma|F_o| \times 100$.
[b] $wR_2 = [\Sigma w(F_o^2 - F_c^2)^2/\Sigma (w|F_o|^2)^2]^{1/2} \times 100$.
Final weighting scheme calc:
[c] $w = 1/[\sigma^2(F_o^2) + (0.0577P)^2 + 2.0058P]$.
[d] $w = 1/[\sigma^2(F_o^2) + (0.0237P)^2 + 4.1816P]$.
[e] $w = 1/[\sigma^2(F_o^2) + (0.1143P)^2 + 3.7910P]$.
[f] $w = 1/[\sigma^2(F_o^2) + (0.0257P)^2 + 8.5167P]$.
[g] $w = 1/[\sigma^2(F_o^2) + (0.0397P)^2 + 6.3928P]$.
where $P = (F_o^2 + 2F_c^2)/3$.

Patterson and difference Fourier techniques. Compounds **1, 2,** and **5** were solved by direct methods and refined on F^2 by full-matrix least-squares technique. The analytical factors for neutral atoms were used throughout the analysis.

For **1,** all 3265 data were corrected for decay (20%), absorption, Lorentz, and polarization effects, and placed on an approximately absolute scale. The diffraction symmetry was $2/m$ with systematic absences $0k0$ for $k = 2n+1$ and $h0l$ for $h+l = 2n+1$. The centrosymmetric monoclinic space group $P2_1/n$ space group was therefore uniquely defined. Compound **1** is polymeric with repeating $BiCl_3(THF)_2$ unit and is disordered. To account for this disorder, two components were included for atoms Bi(1), Cl(3), O(2), C(5), and C(8) (see Fig. 1). Hydrogen atoms were not included in the refinement due to the disorder. At convergence, $wR_2 = 0.1065$ and GOF = 1.057 for 175 variables refined against all 3051 unique data (for comparison, refinement on F, $R_1 = 0.0397$ for those 2065 data with $F > 4.0\sigma(F)$).

For compound **2** all 3267 data were corrected for absorption and for Lorentz and polarization effects and were placed on an approximately absolute scale. The diffraction symmetry was $2/m$ with systematic absences $0k0$ for $k = 2n+1$ and $h0l$ for $l = 2n+1$. The centrosymmetric monoclinic space group $P2_1/c$[C_{2h}^5; No. 14] is therefore uniquely defined. Hydrogen atoms were included using a riding model in the solution of the structure of **2**. At convergence, $wR_2 = 0.0593$ and GOF = 1.082 for 227 variables refined against all 3124 unique data (for comparison, refinement on F, $R_1 = 0.0271$ for those 2454 data with $F > 4.0\sigma(F)$).

Compound **3** was successfully solved in the $P\bar{1}$ space group. This solution yielded the Bi atom position and the majority of the carbon, nitrogen and oxygen atom positions. Subsequent Fourier synthesis gave the remaining atomic positions of **3**. At this time a methyl imidazole was found in the lattice. The hydrogen atoms were fixed in positions of ideal geometry, with a C—H distance of 0.93 Å for phenyl hydrogens and 0.96 Å for methyl hydrogens and refined using the riding model in the SFIX facility in SHELXL 93. These idealized hydrogen atoms had their isotropic temperature factors fixed at 1.2 times (phenyl) or 1.5 times (methyl) the equivalent isotropic U of the C

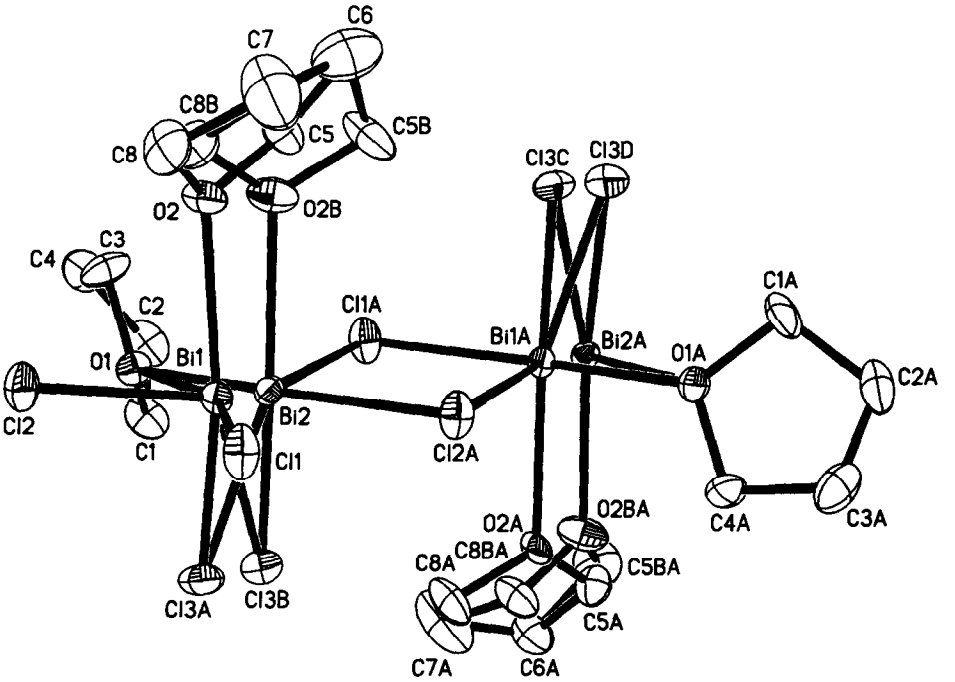

Fig. 1. Thermal ellipsoid plot of $[Bi(Cl)(\mu\text{-}Cl)_2(THF)_2]_\infty$, **1**. Thermal ellipsoids are drawn at the 50% level.

atoms they were bonded to. The final refinement included anisotropic thermal parameters on all non-hydrogen atoms and converged to $R_1 = 0.0488$ and $R2_w = 0.1272$. Another unit cell and space group were also solved for a similar $Bi(O_2CMe)_3(MeIm)_3$ complex but only $\frac{1}{2}$MeIm was located in the unit cell lattice. This compound is referred to as $Bi(O_2CMe)_3(MeIm)_3 \cdot \frac{1}{2}MeIm$, **3a** [58]. A full listing, detailing the collection parameters for this molecule can be found in the supplementary information.

Compound **4** was successfully solved in the $P\bar{1}$ space group. This solution yielded the bismuth atom and the majority of all other atoms. Subsequent Fourier synthesis gave all remaining carbon and oxygen atom positions. All hydrogen atoms were fixed in positions of ideal geometry, with a C—H distance of 0.97 Å for ethyl hydrogens and 0.96 Å for methyl hydrogens and refined using the riding model in the SFIX facility in SHELXL 93. These idealized hydrogen atoms had their isotropic temperature factors fixed at 1.2 times (ethyl) or 1.5 times (methyl) the equivalent isotropic U of the carbon atom they were bonded to. The final refinement included anisotropic thermal parameters on all non-hydrogen atoms and converged to $R_1 = 0.0590$ and $R2_w = 0.1122$ for $I < 2\sigma < (I)$.

For **5**, all 576 data were corrected for decay (15%), absorption, Lorentz and polarization effects, and were placed on an approximately absolute scale. The diffraction symmetry was $2/m$ with systematic absences $0k0$ for $k = 2n+1$ and $h0l$ for $l = 2n+1$. The centrosymmetric monoclinic space group $P2_1/c$ [C_{2h}^5; No. 14] is therefore uniquely defined. Hydrogen atoms were included using a riding model for solving of the structure. The molecule is dinuclear and located about an inversion center. At convergence, $wR_2 = 0.0834$ and GOF = 1.033 for 226 variables refined against all 5468 unique data (for comparison, refinement on F, $R_1 = 0.0318$ for those 4205 data with $F > 4.0\sigma(F)$).

RESULTS AND DISCUSSION

Due to the interest in bismuth containing species, we isolated and characterized a series of bismuth coordination compounds: (a) a THF adduct of $BiCl_3$, (b) two amine adducts of $Bi(O_2CMe)_3$, and (c) two, solvent modified bismuth alkoxide compounds. The solid state structures and solution state behavior were determined.

Synthesis

$BiCl_3$ was generated by the dissolution of $Bi(NO_3)_3 \cdot 5H_2O$ in THF, followed by addition of (concentrated) HCl, and stirring for over 12 h at room temperature (eqn (1)).

$$Bi(NO_3)\cdot 5H_2O + (xs)HCl \xrightarrow[THF]{-5H_2O,\ -3HNO_3} [Bi(\mu\text{-}Cl)_2(Cl)(THF)_2]_\infty \quad (1)$$

After this time, all of the volatile materials were removed *in vacuo*. The resulting powder was re-dissolved in a minimum amount of THF and allowed to

sit at glove box temperature for several days. Large crystals formed which proved to be $[BiCl_3(THF)_2]_\infty$, **1** (see Fig. 1). TGA/DTA analyses indicated that 2 molecules of THF for every Bi atom were present which is consistent with the NMR data (*vide infra*); however, the elemental analysis revealed only one molecule of THF per molecule. As was noted for $BiCl_3(THF)_3$ [35], the THF ligands are volatile and the degree of coordination of THF for **1** is influenced by the time/temperature of drying. $BiCl_3(THF)_3$ was formed at low temperature (−20°C), whereas, **1** was grown at glovebox temperature and this may explain the structure difference (losing one of the labile THF ligands from $BiCl_3(THF)_3$ to form **1** is easily envisioned).

$[Bi(O_2CMe)_3]_\infty$ compounds are reportedly soluble in amine solutions resulting in coordination of the solvent; however, no structural studies on the solvated compounds have been reported [44]. Pyridine (py) and N-methylimidazole (MeIm) were chosen to solubilize $[Bi(O_2CMe)_3]_\infty$ since these amines are highly coordinating Lewis bases and would disrupt the polymer. Using a minimum of amount of the appropriate amine, $[Bi(O_2CMe)_3]_\infty$ was dissolved and allowed to sit at glovebox temperature for 2–3 days. A quantitative yield of crystalline material was isolated from the synthetic route shown in eqn (2).

$$Bi(O_2CMe)_3 + Solv \rightarrow Bi(O_2CMe)_3(Solv)_x \cdot (Solv)_y \quad (2)$$

Solv = pyridine, $x = 2, y = 0$, **2**.
= 1-methyl imidazole, $x = 3, y = 1$, **3**,
$x = 3, y = 1/2$, **3a**.

These solvents have resulted in unusual transition metal and the lanthanide [59–66] complexes necessitating structural determination of the resulting amine coordinated products. The use of py results in the formation of the clear crystalline material of $Bi(O_2CMe)_3(py)_2$, **2**; whereas, using MeIm as a solvent results in the isolation of a slightly yellow colored crystalline material $Bi(O_2CMe)_3(MeIm)_3 \cdot (MeIm)$, **3**. Thermal ellipsoid plots of **2** and **3** are shown in Figs 2 and 3, respectively. NMR data reveal two molecules of py are coordinated to the metal center (*vide infra*) but elemental analyses indicate only one molecule of py is associated with **2**. As was noted for the coordinated THF molecules of **1**, the coordinated py molecules of **2** are labile and the temperature and/or time of drying can influence the number of associated solvent molecules. For the elemental analysis of **3**, the data is consistent with a slight excess of MeIm (a reflection of the low volatility of MeIm upon drying). Due to the additional coordination of the amines, the solubility of **2** and **3** is slightly enhanced in toluene. This simple recrystallization step also turns out to be an excellent method for further purification of these compounds [the starting material (sold as 99.999% pure) had several impurities present by ICP-MS].

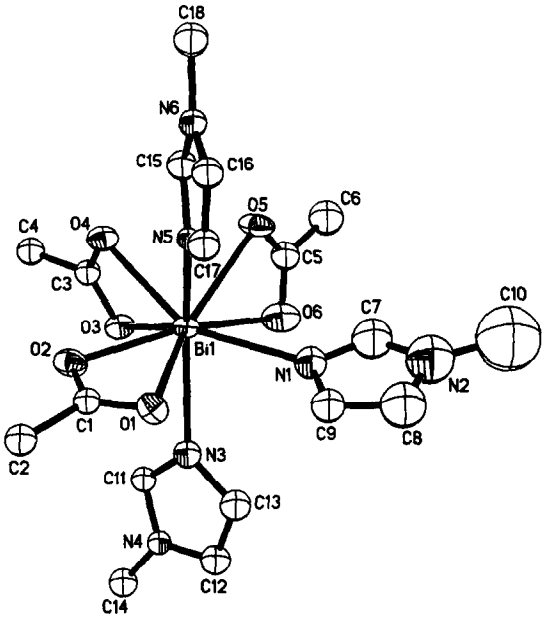

Fig. 2. Thermal ellipsoid plot of $Bi(O_2CMe)_3(py)_2$, **2** Thermal ellipsoids are drawn at the 50% level.

Alcoholysis exchange of $Bi(N(SiMe_3)_2)_3$ with HONp produces $[Bi(ONp)_3(HONp)]_2$, **4**, eqn (3a) (see Fig. 4).

$$2Bi[N(SiMe_3)_2]_3 + 9HONp \xrightarrow[-6HN(SiMe_3)_2]{\text{toluene}} [Bi(\mu\text{-}ONp)(ONp)_2(HONp)]_2 \quad (3a)$$

$$3BiCl_3 + 6NaONp + (xs)HONp \xrightarrow[-6NaCl]{\text{toluene}} [Bi(\mu\text{-}ONp)(ONp)_2(HONp)]_2 \quad (3b)$$

The loss of yellow color of the initial solution was used as an indication that the reaction was finished. At room temperature, this reaction can take one week to reach completion; however, careful heating reduces the reaction time to 2–3 h (*note*: uncontrolled and unmonitored heating, results in decomposition of **4** producing a black precipitate proven by XRF to be Bi/BiO). Removal of the solvent, followed by redissolution in toluene and cooling to −35°C yields X-ray quality crystals of **4**. Extraction of **4** with THF yields a powder with identical analytical data as noted for the crystalline material. As was observed for other amide alcohol exchange reactions, the parent amine is often noted as a minor impurity [67]. Historically, these impurities are removed by heating a toluene solution of the product at reflux temperatures; however, in solution, **4** decomposes at relatively low temperatures (<60°C). An alternative synthesis that produces **4** is the metathical exchange of $BiCl_3$ with NaONp/HONp in toluene (eqn (3b)). Elemental analysis of **4** has proven inconsistent due to its extreme sensitivity to relative humidity and the volatility of

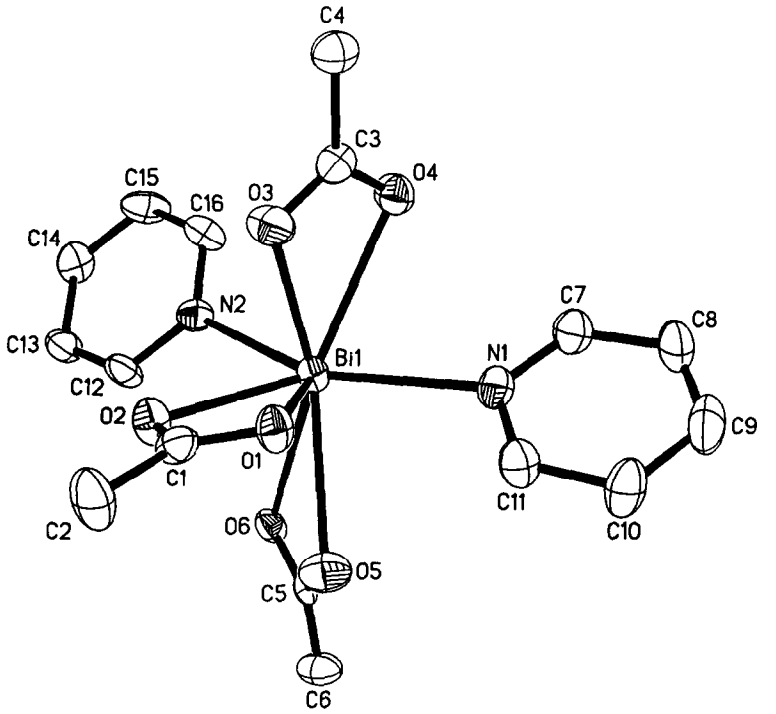

Fig. 3. Thermal ellipsoid plot of $Bi(O_2CMe)_3(MeIm)_3 \cdot MeIm$, **3**. Thermal ellipsoids are drawn at the 50% level. The lattice MeIm is not shown.

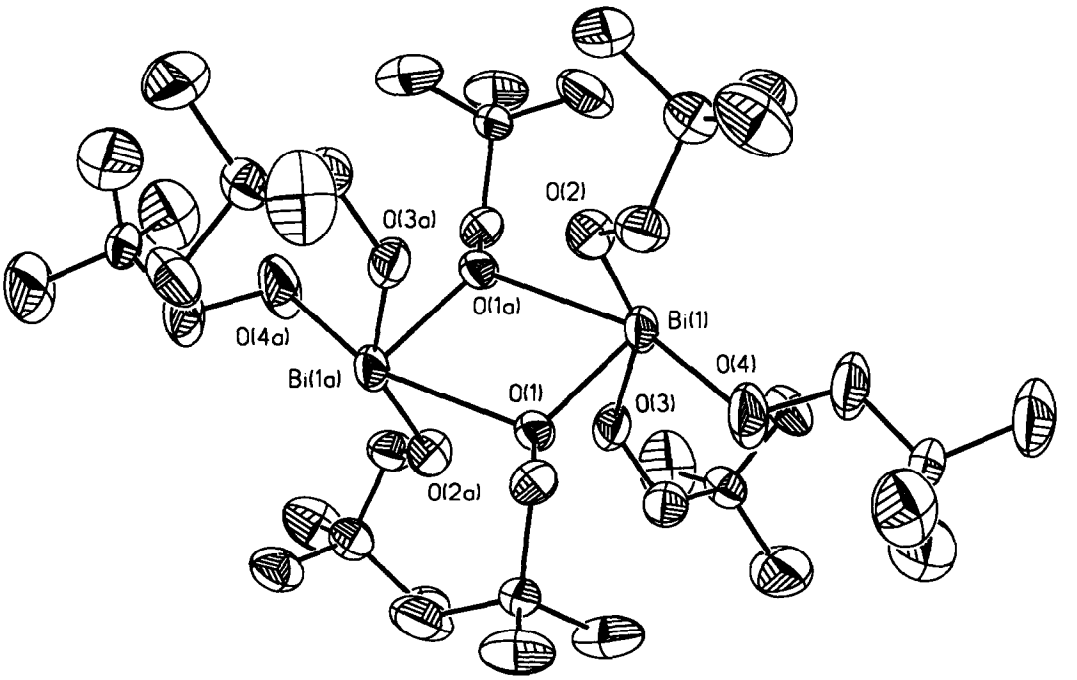

Fig. 4. Thermal ellipsoid plot of $[Bi(\mu\text{-}ONp)(ONp)_2(HONp)]_2$, **4**. Thermal ellipsoids are drawn at the 50% level.

this compound. This bismuth alkoxide is stable in a sealed solution (toluene or THF) for extended period of times at room temperature. Attempts to sublime this material have been successful at temperatures < 100 °C ($@ 10^{-3}$ Torr); however, there is a significant amount of decomposition accompanied by this process.

In an attempt to replace the coordinated HONp alcohol of **4**, several Lewis basic solvents were investigated. As observed for the acetate system, amine solvents readily bind to the bismuth metal center. Redissolution of **4** in py resulted in replacement of the coordinated HONp, eqn (4).

$$[Bi(\mu\text{-ONp})(ONp)_2(HONp)]_2 + py \xrightarrow[-2HONp]{py} [Bi(\mu\text{-ONp})(ONp)_2(py)]_2 \quad (4)$$

Crystals were grown by cooling (−35 C) a concentrated solution of **4** in py and crystallographically characterized as $[Bi(\mu\text{-ONp})(ONp)_2(py)]_2$, **5**, verifying that the dinuclear structure is retained in the presence of py. The thermal ellipsoid plot of **5** is shown in Fig. 5. Elemental analysis of **5** has also proven to be inconsistent due to its sensitivity to the atmospheric water as well as its volatility.

SOLID STATE

Crystallographic studies [21–23]

Table 1 is a tabulation of the X-ray collection data for compounds **1**–**5**. Tables 2–6 are the atomic coor-

Table 2. Atomic coordinates ($\times 10^5$) for **1**

Atoms	*x*	*y*	*z*	U(eq)[a]
Bi(1)	2071(1)	1023(1)	2149(1)	18(1)
Bi(2)	2068(1)	1963(1)	2139(1)	16(1)
O(1)	249(6)	1452(5)	927(2)	22(1)
O(2)	−652(16)	904(13)	2770(7)	28(3)
Cl(1)	3897(2)	−403(2)	3228(1)	29(1)
Cl(2)	1112(2)	−1585(2)	1791(1)	27(1)
Cl(3A)	4416(4)	928(4)	1405(2)	30(1)
Cl(3B)	4403(5)	2031(5)	1388(2)	31(2)

[a] U(eq) is defined as one third of the trace of the orthogonalized U_{ij} tensor.

Table 3. Atomic coordinates ($\times 10^5$) for **2**

Atoms	*x*	*y*	*z*	U(eq)[a]
Bi(1)	−2679(1)	−590(1)	5542(1)	21(1)
O(1)	−2250(4)	−2829(4)	5122(3)	28(1)
O(2)	−2062(4)	−2587(5)	6502(3)	31(1)
O(3)	−706(4)	−488(5)	6128(3)	35(1)
O(4)	−1410(4)	1611(5)	5567(3)	33(1)
O(5)	−4608(4)	−2278(5)	4687(3)	40(1)
O(6)	−4611(4)	−992(5)	5750(3)	23(1)
N(1)	−3336(5)	−317(6)	3748(4)	27(1)
N(2)	−1990(4)	265(5)	7209(4)	25(1)

[a] U(eq) is defined as one third of the trace of the orthogonalized U_{ij} tensor.

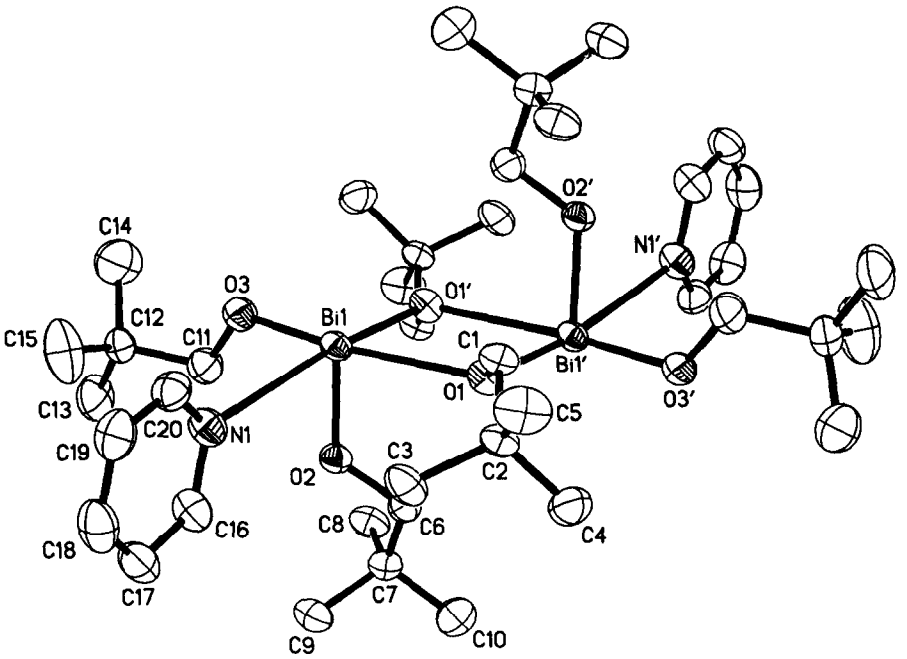

Fig. 5. Thermal ellipsoid plot of $[Bi(\mu\text{-ONp})(ONp)_2(py)]_2$, **5**. Thermal ellipsoids are drawn at the 50% level.

Table 4. Atomic coordinates ($\times 10^5$) for **3**

Atoms	x	y	z	U(eq)[a]
Bi(1)	1527(1)	3668(1)	2700(1)	14(1)
O(1)	−554(7)	5348(7)	2105(5)	28(2)
O(2)	1467(7)	6105(7)	2240(5)	27(2)
O(3)	1678(7)	3791(8)	4454(5)	32(2)
O(4)	−168(7)	2944(7)	4116(5)	28(2)
O(5)	3097(7)	2718(7)	1526(5)	26(2)
O(6)	1761(7)	4635(6)	869(5)	25(1)
N(1)	2557(9)	1245(7)	3826(6)	23(2)
N(2)	3943(10)	−623(9)	4298(6)	32(2)
N(3)	−204(8)	2522(7)	2112(5)	19(2)
N(4)	−1723(8)	2109(8)	1151(6)	21(2)
N(5)	4191(8)	4012(8)	2885(6)	21(2)
N(6)	6028(8)	4607(8)	3475(6)	21(2)
N(7)	3589(10)	−684(9)	1656(7)	37(2)
N(8)	5499(14)	−2061(11)	1805(9)	59(2)

[a] U(eq) is defined as one third of the trace of the orthogonalized U_{ij} tensor.

Table 5. Atomic coordinates ($\times 10^5$) for **4**

Atoms	x	y	z	U(eq)[a]
Bi(1)	1617(1)	856(1)	86(1)	50(1)
O(1)	462(7)	942(6)	1170(6)	34(2)
O(2)	−90(8)	1639(6)	−1126(7)	44(2)
O(3)	2485(8)	−656(7)	1238(7)	49(2)
O(4)	2901(11)	2512(9)	1492(9)	100(4)

[a] U(eq) is defined as one third of the trace of the orthogonalized U_{ij} tensor.

Table 6. Atomic coordinates ($\times 10^5$) for **5**

Atoms	x	y	z	U(eq)[a]
Bi(1)	1822(1)	4670(1)	4912(1)	26(1)
O(1)	−115(4)	5318(1)	3860(3)	29(1)
O(2)	1005(4)	3993(2)	3856(3)	30(1)
O(3)	2957(4)	4087(2)	6101(4)	33(1)
N(1)	3805(5)	4475(2)	3162(4)	35(1)

[a] U(eq) is defined as one third of the trace of the orthogonalized U_{ij} tensor.

Table 7. Selected bond distances (Å) and angles ( ) for **1**

Distance		1
Bi···Bi	Bi(1)···Bi(2)	0.847
	Bi(1)···Bi(1A)	4.710
	Bi(2)···Bi(1A)	3.915
	Bi(2)···Bi(2A)	4.720
Bi—Cl	Bi(1)—Cl(3A)	2.495(3)
	Bi(2)—Cl(3B)	2.495(4)
	Bi(2)—Cl(3A)	2.652(3)
	Bi(1)—Cl(3B)	2.665(4)
Bi—(μ-Cl)	Bi(1)—Cl(1)	2.632(2)
	Bi(2)—Cl(1)	2.555(2)
	Bi(1)—Cl(2)	2.529(2)
	Bi(2)—Cl(2)	2.631(2)
Bi—O_{THF}	Bi(1)—O(1)	2.539(4)
	Bi(1)—O(2)	2.615(13)
	Bi(1)—O(2B)	2.738(14)
	Bi(2)—O(1)	2.535(4)
	Bi(2)—O(2B)	2.598(13)
Angles		1
(μ-Cl)—Bi—Cl	Cl(1)—Bi(1)—Cl(3A)	91.9(1)
	Cl(1)—Bi(1)—Cl(3B)	102.9(1)
	Cl(2)—Bi(1)—Cl(3A)	92.5(1)
	Cl(2)—Bi(1)—Cl(3B)	112.6(1)
	Cl(1′)—Bi(2)—Cl(3A)	113.3(1)
	Cl(1′)—Bi(2)—Cl(3B)	92.7(1)
	Cl(2)—Bi(2)—Cl(3A)	102.4(1)
	Cl(2)—Bi(2)—Cl(3B)	92.3(1)
(μ-Cl)—Bi—(μ-Cl)	Cl(2)—Bi(1)—Cl(1)	81.9(1)
	Cl(1′)—Bi(2)—Cl(2)	81.4(1)
Cl—Bi—O_{THF}	Cl(3A)—Bi(1)—O(1)	83.2(1)
	Cl(3B)—Bi(1)—O(1)	79.7(1)
	Cl(3A)—Bi(1)—O(2)	171.4(3)
	Cl(3A)—Bi(1)—O(2B)	162.0(3)
	Cl(3B)—Bi(1)—O(2)	160.8(3)
	Cl(3B)—Bi(1)—O(2B)	140.5(3)
	Cl(3A)—Bi(2)—O(1)	80.2(1)
	Cl(3B)—Bi(2)—O(1)	83.1(1)
	Cl(3A)—Bi(2)—O(2B)	159.9(3)
	Cl(3B)—Bi(2)—O(2B)	173.9(3)
(μ-Cl)—Bi—O_{THF}	Cl(1)—Bi(1)—O(1)	159.2(1)
	Cl(1)—Bi(1)—O(2)	92.5(3)
	Cl(1)—Bi(1)—O(2B)	101.2(3)
	Cl(1′)—Bi(2)—O(1)	79.7(1)
	Cl(2)—Bi(1)—O(1)	78.2(1)
	Cl(2)—Bi(2)—O(1)	160.3(1)
	Cl(2)—Bi(2)—O(2B)	91.4(3)

dinates for **1**–**5**, respectively. The metrical data for **1** is shown in Table 6, for $Bi(O_2CMe)_3$, **2**, and **3** in Table 7, and for **4** and **5** in Table 8.

Bismuth halides. Typically bismuth(III) halides are mononuclear species of general formula $BiX_3(cmplx)_n$ (X = Cl, Br, or I; cmplx = macrocylces [27,33,43,50], solvent [35,38,41,45,48], and other complexing agents [10,20,49,68] with coordination numbers ranging from 6 to 9). Whitmire and co-workers have shown by crystallographic investigations that $BiCl_3$ is easily complexed using oxygen donor ligands to produce $[BiCl_3(Solv)_3]_n$ (Solv = THF, $n = 1$; diglyme, $n = 2$; and diethylcarbitol, $n = 2$) complexes [35]. The THF

Table 8. Selected bond distances (Å) and angles (°) for $Bi(O_2CMe)_3$, **2** and **3**

Distances	$Bi(O_2CMe)_3$		**2**		**3**	
Bi—O	Bi(1)—O(1)	2.341	Bi(1)—O(1)	2.409(4)	Bi(1)—O(1)	2.448(7)
	Bi(1)—O(2)	2.516	Bi(1)—O(2)	2.327(4)	Bi(1)—O(2)	2.543(7)
	Bi(1)—O(3)	2.376	Bi(1)—O(3)	2.251(4)	Bi(1)—O(3)	2.578(6)
	Bi(1)—O(4)	2.622	Bi(1)—O(4)	2.680(5)	Bi(1)—O(4)	2.517(7)
	Bi(1)—O(5)	2.546	Bi(1)—O(5)	2.688(5)	Bi(1)—O(5)	2.663(6)
	Bi(1)—O(6)	2.244	Bi(1)—O(6)	2.803(5)	Bi(1)—O(6)	2.454(6)
	av.	2.44(14)	av.	2.53(23)	av.	2.53(8)
Bi—N			Bi(1)—N(1)	2.623(5)	Bi(1)—N(1)	2.641(7)
			Bi(1)—N(2)	2.533(5)	Bi(1)—N(3)	2.514(7)
					Bi(1)—N(5)	2.601(7)
Angles	$Bi(O_2CMe)_3$		**2**		**3**	
O—Bi—O	O(1)—Bi(1)—O(2)	53.2	O(1)—Bi(1)—O(2)	54.7(1)	O(1)—Bi(1)—O(2)	52.3(2)
	O(1)—Bi(1)—O(3)	69.4	O(1)—Bi(1)—O(3)	76.1(2)	O(1)—Bi(1)—O(3)	94.1(2)
	O(1)—Bi(1)—O(4)	120.0	O(1)—Bi(1)—O(4)	116.8(1)	O(1)—Bi(1)—O(4)	77.2(2)
	O(1)—Bi(1)—O(5)	124.7	O(1)—Bi(1)—O(5)	68.0(2)	O(1)—Bi(1)—O(5)	124.5(2)
	O(1)—Bi(1)—O(6)	87.5	O(1)—Bi(1)—O(6)	107.1(1)	O(1)—Bi(1)—O(6)	76.0(2)
	O(2)—Bi(1)—O(3)	117.9	O(2)—Bi(1)—O(3)	81.2(2)	O(2)—Bi(1)—O(3)	78.5(2)
	O(2)—Bi(1)—O(4)	152.4	O(2)—Bi(1)—O(4)	130.3(2)	O(2)—Bi(1)—O(4)	105.1(2)
	O(2)—Bi(1)—O(5)	77.9	O(2)—Bi(1)—O(5)	75.6(2)	O(2)—Bi(1)—O(5)	115.0(2)
	O(2)—Bi(1)—O(6)	75.8	O(2)—Bi(1)—O(6)	78.9(2)	O(2)—Bi(1)—O(6)	73.7(2)
	O(3)—Bi(1)—O(4)	51.1	O(3)—Bi(1)—O(4)	51.9(2)	O(3)—Bi(1)—O(4)	51.3(2)
	O(3)—Bi(1)—O(5)	127.3	O(3)—Bi(1)—O(5)	143.9(2)	O(3)—Bi(1)—O(5)	139.9(2)
	O(3)—Bi(1)—O(6)	80.6	O(3)—Bi(1)—O(6)	152.3(2)	O(3)—Bi(1)—O(6)	150.8(2)
	O(4)—Bi(1)—O(5)	90.6	O(4)—Bi(1)—O(5)	152.8(1)	O(4)—Bi(1)—O(5)	139.7(2)
	O(4)—Bi(1)—O(6)	77.2	O(4)—Bi(1)—O(6)	135.9(1)	O(4)—Bi(1)—O(6)	146.1(2)
	O(5)—Bi(1)—O(6)	53.4	O(5)—Bi(1)—O(6)	46.1(1)	O(5)—Bi(1)—O(6)	51.1(2)
O—Bi—N			O(1)—Bi(1)—N(1)	75.1(2)	O(1)—Bi(1)—N(1)	148.4(2)
			O(2)—Bi(1)—N(1)	129.4(2)	O(2)—Bi(1)—N(1)	150.4(2)
			O(3)—Bi(1)—N(1)	94.3(2)	O(3)—Bi(1)—N(1)	78.8(2)
			O(4)—Bi(1)—N(1)	75.9(2)	O(4)—Bi(1)—N(1)	74.4(2)
			O(5)—Bi(1)—N(1)	80.1(2)	O(5)—Bi(1)—N(1)	72.9(2)
			O(6)—Bi(1)—N(1)	113.2(2)	O(6)—Bi(1)—N(1)	123.5(2)
			O(1)—Bi(1)—N(2)	155.4(2)	O(1)—Bi(1)—N(3)	78.4(2)
			O(2)—Bi(1)—N(2)	74.4(2)	O(2)—BI(1)—N(3)	127.7(2)
			O(3)—Bi(1)—N(2)	82.6(2)	O(3)—Bi(1)—N(3)	126.6(2)
			O(4)—Bi(1)—N(2)	83.2(2)	O(4)—Bi(1)—N(3)	75.7(2)
			O(5)—Bi(1)—N(2)	116.3(2)	O(5)—Bi(1)—N(3)	76.7(2)
			O(6)—Bi(1)—N(2)	73.6(1)	O(6)—Bi(1)—N(3)	78.9(2)
					O(1)—Bi(1)—N(5)	127.2(2)
					O(2)—Bi(1)—N(5)	75.0(2)
					O(3)—Bi(1)—N(5)	76.7(2)
					O(4)—Bi(1)—N(5)	125.6(2)
					O(5)—Bi(1)—N(5)	71.5(2)
					O(6)—Bi(1)—N(5)	87.4(2)
N—Bi—N			N(1)—Bi(1)—N(2)	155.4(2)	N(1)—Bi(1)—N(3)	81.5(2)
					N(1)—Bi(1)—N(5)	81.4(2)
					N(3)—Bi(1)—N(5)	147.1(2)

Table 9. Selected bond distances (Å) and angles (°) for **4** and **5**

Distances		**4**		**5**
Bi···Bi		3.74		3.88
Bi—OR[a]	Bi(1)—O(2)	2.247(7)	Bi(1)—O(2)	2.058(3)
	Bi(1)—O(4)	2.098(8)	Bi(1)—O(3)	2.109(4)
Bi—(μ-OR)	Bi(1)—O(1)	2.072(6)	Bi(1)—O(1)	2.606(4)
	Bi(1)—O(1′)	2.546(6)	Bi(1)—O(1′)	2.170(3)
Bi—Solv	Solv = HOR		Solv = py	
	Bi(1)—O(3)	2.579(8)	Bi(1)—N(1)	2.789(5)
Angles		**4**		**5**
O—Bi—O	O(2)—Bi(1)—O(3)	153.1(3)	O(2)—Bi(1)—O(3)	89.7(2)
	O(2)—Bi(1)—O(4)	95.8(4)		
	O(3)—Bi(1)—O(4)	103.5(4)		
O—Bi—(μ-O)	O(1)—Bi(1)—O(2)	86.1(3)	O(1)—Bi(1)—O(2)	88.5(1)
	O(1)—Bi(1)—O(3)	76.2(3)	O(1)—Bi(1)—O(3)	164.1(1)
	O(1)—Bi(1)—O(4)	87.9(3)	O(2)—Bi(1)—O(1′)	92.7(1)
	O(2)—Bi(1)—O(1′)	79.2(2)	O(3)—Bi(1)—O(1′)	92.8(1)
	O(3)—Bi(1)—O(1′)	76.2(2)		
	O(4)—Bi(1)—O(1′)	159.6(3)		
(μ-O)—Bi—(μ-O)	O(1)—Bi(1)—O(1′)	72.1(3)	O(1)—Bi(1)—O(1′)	71.5(1)
O—Bi—N			O(2)—Bi(1)—N(1)	77.2(1)
			O(3)—Bi(1)—N(1)	85.8(1)
(μ-O)—Bi—N			O(1)—Bi(1)—N(1)	109.1(1)
			O(1′)—Bi(1)—N(1)	169.8(1)

[a] OR = OCH_2CMe_3.

complex in this investigation was found to be a mononuclear species.

In contrast, the product from eqn (1) proved to be the polynuclear complex, $[Bi(\mu\text{-}Cl)_2Cl(THF)_2]_\infty$, **1** (see Fig. 1). The Bi metal centers of **1** are 7-coordinated in a slightly distorted pentagonal bipyramidal arrangement. The equatorial positions are filled by one THF molecule and two bridging chloride atoms. The remaining equatorial positions consist of the two bridging chlorides associated with the next metal center. The axial positions are filled by a terminal chloride ligand and a solvent molecule of THF. Several crystals were investigated and all proved to be the polymeric structure of **1**. This structure is consistent with the hypervalencey normally associated with Bi compounds [35]. Several of the atoms of compound **1** are disordered and due to the proximity of these atoms, several anomalous short distances and angles are noted in Table 7. If these are not included in the discussion of the metrical data for **1**, the Bi—Cl and Bi—O distances and angles of **1** are in agreement with those previously reported [35]. As expected, the μ-Cl distances are slightly longer than those noted for the terminal ligands.

Bismuth acetates. An excellent review of bismuth carboxylates, alkoxides and β-diketonates has been published by Pisarevskii and Martynenko [42]. The polymeric structure of $[Bi(O_2CH)_3]_\infty$ was solved in 1969 [46]. Since then only two other structures containing the tri-acetate arrangement have been reported: the polymeric $[Bi(O_2CMe)_3]_\infty$ [47] and the tetranuclear pivalate adduct, $[Bi(O_2CC(CH_3)_3)_3]_4$ [12]. Each of these compounds has a bismuth center that is 9-coordinated due to oligomerization through bridging oxygen atoms. The increased steric repulsion of the pivalate results in a tetranuclear species, not infinite chains. There is a report on the crystal structure of bismuth(III) trifluoroacetate trifluoroacetic acid $[Bi(O_2CCF_3)_3 \cdot HO_2CCF_3]_\infty$ which maintains a polymeric structure even with the coordination of HO_2CCF_3 [52]. Interestingly, there are two mondentate acetate ligands noted for this compound [52]. Other solvated $Bi(O_2CMe)_3$ compounds have been reported. These include the thiourea solvated species which were characterized as the molecular 9-coordinated species $[Bi_2(O_2CMe)_6 \cdot 3SC(NH_2)_2$ and $Bi(O_2CMe)_3(SC(NH_2)_2)_3]$ [29]. The latter complex has the oxygen atoms on one side of the Bi atom and the S atoms on the other.

While it is known that $[Bi(O_2CMe)_3]_\infty$ will dissolve in amine solvents [44], no amine solvated structures of this compound have been reported to date. Due to

the dearth of structurally characterized amine adducts and the unique characteristics imparted by coordination of imidazole molecules [59–66], the crystal structures of the $Bi(O_2CMe)_3$ amine compounds were solved. Figure 2 is the thermal ellipsoid plot of $Bi(O_2CMe)_3py_2$, **2**. Compound **2** is an unusual 8-coordinated bismuth acetate wherein 6 of the sites are filled by the acetate ligands. The remaining two sites are filled by two molecules of py. Eight-coordinated molecules are found to adopt either a cube, a square antiprism or a triangulated dodecahedron (TD) arrangement [69]. On the basis of the observed angles, **2** adopts a distorted TD geometry with N(1) as the lone capping atom and O(2) and N(2) as the shared capping atoms of the dodecahedron (see Fig. 2). Due to the lability of the py molecules associated with **2**, it is not unreasonable to suggest that several different structures of $Bi(O_2CMe)py_x$ ($x = 1$ or 3) are isolable as well.

In contrast to the 8-coordinated structure of **2**, $Bi(O_2CMe)_3(MeIm)_3 \cdot MeIm$, **3**, (see Fig. 3) is a typical 9-coordinated tricapped trigonal prism complex with 3 molecules of MeIm coordinated on the same side of the bismuth atom. Another MeIm is observed co-crystallizing within the defined unit cell, well away from the bismuth metal center (the three closest contacts to the Bi atom are 4.98, 5.67, and 5.75 Å from the C(22), C(21), and N(7) atoms, respectively). A crystal that has an identical structural arrangement of the $Bi(O_2CMe)_3(MeIm)_3$ core was solved in an alternative space group [58]; however, only $\frac{1}{2}$ of a MeIm was located in the unit cell lattice to form $Bi(O_2CMe)_3(MeIm)_3 \cdot \frac{1}{2}MeIm$, **3a**. Structural information concerning both crystal structure solutions has been deposited in the supplementary information section. The metrical data listed in Table 7 and discussed in this paper were chosen due to the slightly improved R values for **3** versus **3a**.

An average Bi—O distance of 2.53 Å was observed for both **2** and **3** (standard values range from 2.18–2.94 Å; $[Bi(O_2CMe)_3]_\infty = 2.44$ Å). The average Bi—N distance recorded for both **2** and **3** is ~2.58 Å. Typical values for the O—Bi—O angles of a single carboxylate ligand range from 40 to 57 and the angles for **2** and **3** fall within this range as well.

Bismuth alkoxides. Typically bismuth alkoxides are polymeric unless sterically demanding ligands are utilized [24–26,34,39,42]. For example, the first structurally characterized bismuth alkoxide by Evans *et al.* used aryl oxide ligands to form the mononuclear complex $Bi(OC_6H_3Me_2\text{-}2,6)_3$ [34]. The Buhro group [26], and independently Hubert-Pfalzgraf and co-workers [24,25], found that using the less sterically demanding methoxyethanol (OC_2H_4OMe or OEtOMe) yielded the polymeric $[Bi(\mu\text{-}OEtOMe)(OEtOMe)_2]_\infty$. Herrmann *et al.* have isolated a mononuclear β-methoxy alcohol [i.e., $Bi(OCHMe_2CH_2OMe)_3$] derivative but no structure was reported [70]. The majority of other monodentate alkoxide compounds of bismuth (i.e., $Bi(OR)_3$ where R = Me, Et, and Pr^i) are poorly characterized, display low solubility and sublime in low yield [24,25]. The Hubert-Pfalzgraf group also reports the synthesis of the monomeric $Bi(OBu^t)_3$ (nuclearity based on partial X-ray crystallographic results) [24,25]. Whitmire and co-workers have reported a series of fluorinated alkoxides, $Bi(\mu\text{-}OCH(CF_3)_2)(OCH(CF_3)_2)_2(THF)]_2$, $[Bi(\mu\text{-}OC_6F_5)(OC_6F_5)_2 \cdot Solv]_2 \cdot Solv$ (Solv = toluene, THF, cyclohexane) with intermediate ligands that produce dinuclear species [39]. The reported long F···Bi interactions along with increased size of F versus H atoms help reduce oligomerization, creating soluble and volatile precursors.

The structure of $[Bi(\mu\text{-}ONp)(ONp)_2(HONp)]_2$, **4**, (see Fig. 4) proved to be a dinuclear species with each 5-coordinated bismuth adopting a distorted square pyramidal (SP) arrangement of ONp ligands. Table 8 lists the bond distances and angles for **4**. One of the alkoxides of **4** must be considered a coordinated alcohol to maintain charge balance. The O(3) atom was assigned as the oxygen of the coordinated HONp based on the Bi—O(3) bond length being ~0.5 Å longer than the rest of the terminal alkoxides. The C—O—Bi bond angle is not significantly varied from the other ligands but this may be due to steric constraints. Unfortunately, no peaks corresponding to hydrogen atoms could be located on any of the oxygens. Further evidence of this coordinated alcohol was found in the FT-IR spectral data, bond distances (*vide infra*) and the replacement of this ligand by recrystallization from py (see compound **5**). The HONp solvent ligand is located *trans* to the longest Bi—O distance in **4**. It is assumed the 6th coordination site is filled by the lone pair of electrons. Compound **4** has both apical ONp ligands bridge to the basal site of the other metal center (apical shared). The geometry around the metal centers of **4** is distorted from an ideal SP geometry to accommodate the apical bridging ligand [O(1)—Bi(1)—O(basal), 80.5° (av.) for **4**] and the lone pair of electrons [O(basal)—Bi—O(basal), 156° (av.) for **4**] of the Bi metal center. The internal core has acute angles of 72.1(3)° which are slightly greater than those observed for the fluorinated $OCH(CF_3)_2$ complex [70.9(3)] but smaller than that of the OEtOMe [73.0(3) and 72.7(3)] complex [24,25]. The central Bi_2O_2 core of **4** consists of one long and one short Bi—(μ-O) bond distance as was noted for the other compounds [24,25]. The asymmetric core leads to a Bi···Bi bond distance of 3.74 Å for **4**. This distance is consistent with the other bismuth alkoxides (3.64 Å for OEtOMe derivatives within the dinuclear unit (3.96 Å between each moiety) and 3.98 Å for the $OCH(CF_3)_2$ derivative). *Trans* to the shortest ligand (the apical ligand) is the lone pair of electrons of the bismuth metal center. The Bi—OR [2.17 Å (av.) for **4**] and Bi—-(μ-OR) [2.31 Å (av.) for **4**] distances are in agreement with other bismuth alkoxide compounds in the literature [24,25,34,39].

Compound **5** was characterized as [Bi(μ-

ONp)(ONp)$_2$py]$_2$ (see Fig. 5) with bond distances and angles tabulated in Table 8. Compound **5** is derived from the replacement of the coordinated HONp ligands in **4** with py molecules. **5** consists of two SP Bi metal centers linked through basal ONp ligands with the apical ONp ligands pointed in opposite directions. The arrangement observed for **5** is similar to that observed for the [Bi(OCH(CF$_3$)$_2$)$_3$(THF)]$_2$ [39] and the central moiety of [(Bi(OEtOMe)$_3$)$_2$]$_x$ [24,25]. The O(2)—Bi(1)—O(basal) and O(2)—Bi(1)—N(1) angles are 87.0° (av.). The average O(basal)—Bi—O(basal) angle is 167.0°. The asymmetric internal O—Bi—O core (71.55°) leads to a Bi···Bi bond distance of 3.88 Å for **5**. This value and the Bi—OR and Bi—(μ—OR) distances (2.08 Å (av.) and 2.39 Å (av.), respectively) are consistent with literature values [24–26,34,39,42]. Once again the apical ligand has the shortest recorded Bi—O distance in the molecule and is located *trans* to the lone pair of electrons. The more idealized SP geometry of **5** can be accounted for by reduction of steric bulk around the metal center through the replacement of the HONp ligands for the relatively flat py molecules. The coordinated py is 2.79 Å from the Bi metal center and is *trans* to the longest Bi—O distance recorded for **5**.

The reduced oligomerization of **4** and **5** in comparison to the [Bi(OEtOMe)$_3$)$_2$]$_x$ or the fluorinated alkoxides must be due to the steric bulk of the ONp ligand since there is no obvious H bonding to aid in reducing the hypervalencey. Extended F···Bi interactions were noted for the fluorinated compounds [39].

FT-IR *spectroscopy*

The FT-IR carbonyl stretches of Bi carboxylate compounds fall within the range of 1565 to 1525 cm^{-1} and 1410 to 1400 cm^{-1} for the asymmetric and symmetric stretches of the carboxylate ligands, respectively [42]. Furthermore it has been noted that the carboxylate stretches that are split or broadened into several lines may be due to inequivalent carboxylic ligands [42]. This would explain the number of bands observed for the asymmetric structures of compounds **2** (1555, 1493, 1419 cm^{-1}) and **3** (1563, 1553, 1415 cm^{-1}).

The IR spectrum of **4** shows a broad stretch around 3200 cm^{-1} consistent with the coordinated alcohol. For **5**, this stretch is no longer present due to the coordination of the amine solvent. The three standard ONp bands [54] for **4** and **5** appear around 2900 cm^{-1}; however, the amine solvent stretches of **5** make this region more complicated. For **4** and **5** the methyl stretches of the ONp ligands are consistent with other ONp [54,71] and Bi(OR)$_3$ complexes [24,25,34,39,42]. For **5**, three other broad peaks associated with the py are present at 1580, 1262, and 797 cm^{-1}. Consistent with literature reports, the Bi—O stretching peaks of **4** and **5** appear around 550 cm^{-1}.

TGA/DTA

Since **2**–**5** are potentially precursors for bismuth oxide materials, determination of their thermal decomposition characteristics was necessary; therefore, TGA/DTA spectra (under oxygen) were obtained for these compounds. The TGA weight losses associated with volatilization of solvent molecules for **2** and **3** are accompanied by endotherms in the DTA. The remaining thermal events in the DTA are exothermic, consistent with the loss of acetate ligands recorded in the TGA/DTA spectra for [Bi(O$_2$CMe)$_3$]$_x$. Hence, the coordinated solvents of **2** and **3** do not appear to effect the decomposition route of the Bi(O$_2$CMe)$_3$ moiety. The theoretical conversion of **2** to Bi$_2$O$_3$ would involve a weight loss of ~57%. The recorded weight loss of 52.1% for **2** is more consistent with one pyridine coordinated (~50%). This again shows the lability of the pyridine molecules as was evidenced by the elemental analysis. The theoretical weight loss for **3** (67.6%) is consistent with the experimentally recorded weight loss (65.5%). True TGA/DTA spectra were not obtainable for compounds **4** and **5** due to the sensitivity of these compounds to ambient atmospheric conditions and their volatility upon heating.

TGA/DTA spectra were also obtained on BiCl$_3$ and **1** to further investigate solvent effects on decomposition pathways. The resulting TGA spectrum of **1** is not fully understood due to the large weight loss recorded (75.3% versus 51.0% for theoretical conversion to Bi$_2$O$_3$). However, the unsolvated BiCl$_3$ DTA spectrum revealed two medium sized endotherms in the DTA; whereas, **1** had a combination of small endotherms and medium sized exotherms. Unlike what was observed for **2** and **3**, the coordinated solvent of **1** appears to alter the thermal decomposition pathway in comparison to the unsolvated parent halide.

SOLUTION STATE

Typically coordination compounds of bismuth display poor solubility due to increased oligomerization induced by the high coordination numbers achieved with the large Bi cation (calculated radii of 1.10, 1.17, and 1.31 Å for C.N. = V, VI and VIII, respectively) [72]. Due to the coordinating solvents and increased steric bulk of the ONp ligands, we have substantially reduced the oligomerization and increased the solubility of these Bi compounds. Molecular weight and NMR data were obtained to elucidate their solution behavior. All samples were investigated by redissolving the dried crystalline material in the appropriate solvent.

Molecular weight determinations

All molecular weight determinations were performed by the Singer method [73]. The molecular

weight of **1** in THF was found to be 840 ± 84. This is consistent with an average nuclearity of 3.6 or a complex larger than a trinuclear species. The molecular weight of **2** in py was found to be 589 ± 59, consistent with the crystallographically isolated mononuclear complex (MW = 544.31). Compound **3** is assumed to be mononuclear as well due to the structural similarities of **2** and **3** and the greater Lewis basicity of MeIm vs py. Molecular weight determinations of **4** in toluene were found on average to be 1080 ± 108. This appears to be in agreement with the solid state molecular weight (1115.06), indicating a dinuclear species exists in solution. This is consistent with previous reports of sterically hindered bismuth alkoxides [24,25]. Once again, due to the structural similarities of **4** and **5**, the py adduct is also thought to retain its dinuclear complexation in solution.

NMR spectroscopy

Crystalline materials of **2** and **3** were redissolved in $CDCl_3$. Based upon the integration of the appropriate peaks, for a free flowing powder there are two molecules of py per bismuth center for **2** and four MeIm molecules per Bi atom for **3**. Both of these observations are in agreement with the solid state structure (the lattice solvent molecule of **3** does not appear to be more labile than the bound solvent molecules). The acetate resonance of **3** appears ~ 0.1 ppm upfield from that of **2**. Samples of **2** and **3**, redissolved in pyridine-d_5, display methyl acetate resonances at ~ 2.00 ppm. The downfield shift of the acetate resonance for **3** in py is a reflection of the MeIm being replaced by the excess py ultimately forming **2**.

The ^{1}H NMR spectrum of **4** reveals two resonances at δ 4.22 (2H) for the methylene and δ 1.04 (9H) for the methyl groups. This indicates either rapid exchange of the bridging and terminal ligands or adoption of a mononuclear structure in solution. The ^{13}C NMR displays three resonances consistent with the carbons of ONp ligands and does not aid in distinguishing between the two possible interactions. Low temperature variable temperature NMR spectroscopy reveals significant broadening of the ONp peaks and the ingrowth of more than 6 methylene resonances (213 K). The large number of resonances must be due to either the formation of an asymmetric dinuclear complex or the freezing out of dinuclear rotomers. While we cannot distinguish between these two species, both proposed explanations invoke dinuclear compounds. Therefore, the NMR experiments coupled with the results from the molecular weight studies indicate that for **4** a dinuclear species must be present in solution.

The ^{1}H and ^{13}C NMR spectra of **5** in py also reveal only one set of resonances associated with the ONp alkoxide ligands. As was noted for **4**, the terminal and bridging ligands of compound **5** are in rapid exchange. The py resonances of **5** cannot be distinguished from the py solvent; however, in $CDCl_3$, py resonances can be observed with an integration of one py per bismuth metal center. If a sample of **4** is redissolved in pyridine-d_5 the previously coordinated alcohol can be observed in the ^{1}H NMR spectrum as free alcohol.

CONCLUSIONS

We have synthesized and crystallographically characterized a wide variety of bismuth containing complexes: $[BiCl_3(THF)_2]_\infty$ **1**, $Bi(O_2CMe)_3(py)_2$, **2**, $Bi(O_2CMe)_3(MeIm)_3 \cdot MeIm$, **3**, $[Bi(ONp)_3(HONp)]_2$, **4**, and $[Bi(ONp)_3(py)]_2$, **5**. Compound **1** proved to be polynuclear in solution and solid state. The structures of **2** and **3** add to the family of solvated $Bi(O_2CMe)_3$ compounds as the first structurally characterized amine solvated bismuth acetates. There appears to be little change observed in the metrical data for these complexes species vs that of the unsolvated $[Bi(O_2CMe)_3]_\infty$; however, a change in solubility of these compounds in other organic solvents when crystallized from an amine solution has been noted. The first crystallographically characterized monodentate bismuth alkoxide, **4**, is easily modified by addition of Lewis bases, as evidenced in the characterization of **5**. Due to the hypervalencey and increased acidity of the bismuth metal center, these compounds adopt dinuclear structures and possess coordinated Lewis basic solvents.

Acknowledgments—This work was supported by the United States Department of Energy under contract number DE-ACO4-94AL85000. Sandia is a multiprogram laboratory operated by Sandia Corporation, a Lockeed Martin Company, for the United States Department of Energy.

The authors would also like to thank C. D. Buchheit, C. J. Tafoya and B. A. Hernandez for their technical assistance and Dr Todd M. Alam for NMR investigations.

Supporting information—A complete listing of crystal data collection, positional and thermal parameters, and bond distances and angles for **1–5** (64 pages) are available.

REFERENCES

1. Boyle, T. J., Buchheit, C. D., Rodriguez, M. A., Al-Shareef, H. N., Hernandez, B. A., Scott, B. and Ziller, J. W., *J. Mater. Res.*, 1996, **11**, 2274.
2. Devillers, M., Tirions, O., Cadus, L., Ruiz, P. and Delmon, B., *J. Solid State Chem.*, 1996, **126**, 152.
3. Postel, M. and Dunach, E., *Coord. Chem. Rev.*, 1996, **155**, 127.
4. Kallal, K., Coin, C. and Postel, M., *New J. of Chem.*, 1997, **21**, 495.
5. Williams, S., Puri, M. and Mims, C. A., *Catalysis Today*, 1997, **37**, 43.
6. Agocs, L., Briand, G. G., Burford, N., Cameron, T. S., Kwiatkowski, W. and Robertson, K. N., *Inorg. Chem.*, 1997, **36**, 2855.
7. Wullens, H., Deviller, M., Tinant, B. and Declercq, J. P., *J. Chem. Soc., Dalton Trans.*, 1996, 2023.

8. Ferrari, M. B., Capacchi, L. C., Cavalca, L. and Gasparri, G. F., *Acta Cryst.*, 1972, **B28,** 1169.
9. Asato, E., Driessen, W. L., de Graaff, R. A. G., Hulsbergern, F. B. and Reedijk, J., *Inorg. Chem.*, 1991, **30,** 4210.
10. Belicchi, R., Capacchi, C. L., Cavalca, L. and Gasparri, G. F., *Acta Cryst.*, 1972, **B28,** 1169.
11. Meyer, J. M., Ryu, A. and Danziger, L. H., *Antimicrobial Agents and Chemotherapy*, 1997, **41,** 1607.
12. Troyanov, S. I. and Pisarevsky, A. P., *J. Chem. Soc., Chem. Commun.*, 1993, 335.
13. Rogers, R. D., Bond, A. H. and Aguinaga, S., *J. Am. Chem. Soc.*, 1992, **114,** 2960.
14. Devillers, M., Desmet, F. and Tirions, O., *Thermochimica Acta*, 1995, **260,** 165.
15. Jaffe, B., Cook, W. R. J. and Jaffe, H., *Piezoelectric Ceramics*. 1971, Academic Press Inc., New York.
16. Amanuma, K., Hase, T. and Miyasaka, Y., *Appl. Phys. Lett.*, 1995, **66,** 221.
17. Amanuma, K., Hase, T. and Miyasaka, Y., *Mater. Res. Soc. Symp. Proc.*, 1995, **361,** 21.
18. Chen, S.-Y., Du, X.-F. and Chen, I.-W., *Mater. Res. Soc. Symp. Proc.*, 1995, **361,** 15.
19. Rodriguez, M. A., Boyle, T. J., Hernandez, B. A., Buchheit, C. D. and Eatough, M. O., *J. Mater. Res.*, 1996, **11,** 2282.
20. Carmalt, C. J., Cowley, A. H., Culp, R. D., Jones, R. A., Kamepalli, S. and Norman, N. C., *Inorg. Chem.*, 1997, **36,** 2770.
21. The Cambridge Structural Database was used for determination of structure types, literature references, bond distances, and bond angles.
22. Allen, F. H., Bellard, S., Brice, M. D., Cartwright, B. A., Doubleday, A., Higgs, H., Hummelink, T., Hummelink-Peters, B. G., Kennard, O., Motherwell, W. D. D., Rodgers, J. R. and Watson, D. G., *Acta Cryst.*, 1979, **B35,** 146.
23. Allen, F. H., Kennard, O. and Taylor, R., *Acc. Chem. Res.*, 1983, **16,** 146.
24. Massiani, M.-C., Papiernik, R., Hubert-Pfalzgraf, L. G. and Daran, J.-C., *J. Chem. Soc., Dalton Trans.*, 1990, 301.
25. Massiani, M.-C., Papiernik, R. and Hubert-Pfalzgraf, L. G., *Polyhedron*, 1991, **10,** 437.
26. Matchett, M. A., Chiang, M. T. and Buhro, W. E., *Inorg. Chem.*, 1990, **29,** 358.
27. Alcock, N. W., Ravindran, M. and Willey, G. R., *J. Chem. Soc., Chem. Commun.*, 1989, 1063.
28. Beck, J., Brendel, C. J., Bengtssonkloo, L., Grebs, G., Mummert, M., Stankowski, A. and Ulvenlun, S, *Chem. Berichte*, 1996, **129,** 1219.
29. Bensch, W., Blazso, E., Dubler, E. and Oswald, H. R., *Acta Cryst.*, 1987, **C43,** 1699.
30. Bochmann, M., Song, X. J., Hursthouse, M. B. and Karaulov, A., *J. Chem. Soc., Dalton Trans.*, 1995, 1649.
31. Carmalt, C. J., Cowley, A. H., Decken, A., Lawson, Y. G. and Norman, N. C., *Organometallics*, 1996, **15,** 887.
32. Carmalt, C. J., Cowley, A. H., Decken, A. and Norman, N. C., *J. Organomet. Chem.*, 1995, **496,** 59.
33. Drew, M. G., Nicholson, D. G., Sylte, I. and Vasudevan, A., *Inorg. Chim. Acta*, 1990, **171,** 11.
34. Evans, W. J., Hain, J. H. J. and Ziller, J. W., *J. Chem. Soc., Chem. Commun.*, 1989, 1628.
35. Eveland, J. R. and Whitmire, K. H., *Inorg. Chim. Acta*, 1996, **249,** 41.
36. Eveland, J. R., Whitmire, K. H. and Saillard, J. Y., *Inorg. Chem.*, 1996, **35,** 4400.
37. Forster, G. E., Begley, M. J. and Sowerby, D. B., *J. Chem. Soc., Dalton Trans.*, 1995, 383.
38. Frank, W., Schneider, J. and Muller-Becker, S., *J. Chem. Soc., Chem. Commun.*, 1993, 799.
39. Jones, C. M., Burkart, M. D., Bachman, R. E., Serra, D. L., Hwu, S.-J. and Whitmire, K. H., *Inorg. Chem.*, 1993, **32,** 5136.
40. Li, X. W., Lorberth, J., Masa, W. and Wocadlo, S., *J. Organomet. Chem.*, 1995, **485,** 141.
41. Mitzi, D. B., *Inorg. Chem.*, 1996, **35,** 7615.
42. Pisarevskii, A. P. and Martynenko, L. I., *Russian J. Coord. Chem.*, 1994, **20,** 303.
43. Rogers, R. D., Bond, A. H., Aguinaga, S. and Reyes, A., *J. Am. Chem. Soc.*, 1992, **114,** 2967.
44. Reese, A. L., McMartin, K., Miller, D. and Wickham, P. P., *J. Org. Chem.*, 1973, **38,** 764.
45. Schier, A., Wallis, J. M., Muller, G. and Schmidbaur, H., *Angew. Chem., Int. Ed. Eng.*, 1986, **25,** 757.
46. Stalhandske, C. I., *Acta Chim. Scand.*, 1969, **23,** 1525.
47. Tryoanov, S. I. and Pisarevskii, A. P., *Koord. Khim.*, 1991, **17,** 909.
48. Vezzosi, M., Zanoli, A. F., Pietro, L. and Corradi, A. B., *J. Chem. Soc., Dalton Trans.*, 1988, 191.
49. Willey, G. R., Rudd, M. D., Samuel, C. J. and Drew, M. G. B., *J. Chem. Soc., Dalton. Trans.*, 1995, 759.
50. Willey, G. R., Daly, L. T. and Rudd, M. D., *Polyhedron*, 1995, **14,** 315.
51. Jolas, J. L., Hoppe, S. and Whitmire, K. H., *Inorg. Chem.*, 1997, **36,** 3335.
52. Reiss, G. J., Frank, W. and Schneider, J., *Main Group Metal Chem.*, 1995, **18,** 287.
53. Tuttle, B. A. and Schwartz, R. W., *Mater. Res. Soc. Bull.*, 1996, **21,** 49.
54. Boyle, T. J., Alam, T. M., Mechenbeir, E. R., Scott, B. and Ziller, J. W., *Inorg. Chem.*, 1997, **36,** 3293.
55. Boyle, T. J., Schwartz, R. W., Doedens, R. J. and Ziller, J. W., *Inorg. Chem.*, 1995, **34,** 1110.
56. XSCANS Software Users Guide, Version 2.1, Siemens Industrial Automation, Inc., Madison, WI, 1994. XSCANS and SHELXTL PC are products of Siemens Analytical X-ray Instruments, Inc., 6300 Enterprise Lane, Madison, WI 53719.
57. Braoch, R. W., *Argonne National Laboratory, Illinois*, 1978.
58. The crystal of $Bi(O_2CMe)_3(MeIm)_3 \cdot MeIm$, **4,** was also identified in the monoclinic space group C_2/c with unit cell parameters $a = 17.614(3)$ Å, $b = 9.205(2)$ Å, $c = 30.946(5)$ Å, $\beta = 91.74(8)^\circ$, $V = 5015.0(1)$ Å^3, for $Z = 8$. $R_1 = 5.53$ and $wR_2 = 12.63$ for $I < 2\sigma(I)$. $R_1 = 8.44$ and wR_2 15.20 for all data. $R_1 = \Sigma||F_o| - |F_c||/\Sigma|F_o| \times 100$; $wR_2 = [\Sigma w(F_o^2 - F_c^2)^2/\Sigma(w|F_o|^2)^2]^{1/2} \times 100$. Final weighting scheme calc: $w = 1/[\alpha^2(F_o^2) + (0.0431P)^2 + 312.0559P]$ where $P = (F_o^2 + 2F_c^2)/3$.

59. Dev, S., Ramli, E., Rauchfuss, T. B. and Stern, C. L., *J. Am. Chem. Soc.*, 1990, **112,** 6385.
60. Dev, S., Ramli, E., Rauchfuss, T. B. and Wilson, S. R., *Inorg. Chem.*, 1991, **30,** 2514.
61. Ramli, E., Rauchfuss, T. B. and Stern, C. L., *J. Am. Chem. Soc.*, 1990, **112,** 4043.
62. Rauchfuss, T. B., Dev, S. and Wilson, S. R., *Inorg. Chem.*, 1992, **31,** 154.
63. Sundberg, R. J. and Martin, R. B., *Chem. Rev.*, 1974, **74,** 471.
64. Evans, W. J., Shreeve, J. S., Boyle, T. J. and Ziller, J. W., *J. Coord. Chem.*, 1995, **34,** 229.
65. Evans, W. J., Rabe, G. W. and Ziller, J. W., *Inorg. Chem.*, 1994, **33,** 3072.
66. Evans, W. J., Rabe, G. W. and Ziller, J. W., *J. Organomet. Chem.*, 1994, **483,** 39.
67. Vaartstra, B. A., Huffman, J. C., Gradeff, P. S., Hubert-Pfalzgraf, L. G., Daran, J.-C., Parraud, S., Yunlu, K. and Caulton, K. G., *Inorg. Chem.*, 1990, **29,** 3126.
68. Williams, D. J., Carter, T., Fahn, K. L. and V. D., *Inorg. Chim. Acta*, 1995, **228,** 1995.
69. Cotton, F. A. and Wilkinson, G., *Advanced Inorganic Chemistry Fifth Edition*, John Wiley & Sons, New York, 1988.
70. Herrmann, W. A., Huber, N. W., Anwander, R. and Priermeier, T., *Chem. Berichte*, 1993, **126,** 1127.
71. Boyle, T. J., Alam, T. A., Dimos, D., Moore, G. J., Buchheit, C. D., Al-Shareef, H. N., Mechenbier, E. R. and Bear, B. R., *Chem. Mater.*, 1997, in press.
72. Shannon, R. D., *Acta Cryst.*, 1976, **A32,** 751.
73. Clark, E. P., *Analytical Ed.*, 1941, 820.

Pergamon

PII: S0277-5387(97)00478-6

Polyhedron Vol. 17, Nos. 11-12, pp. 1975-1982, 1998
© 1998 Elsevier Science Ltd
All rights reserved. Printed in Great Britain
0277-5387/98 $19.00+0.00

Synthesis and structural characterization of zinc(II) complexes of 2,5,9,12-tetramethyl-1,4,8,11-tetraazacyclotetradecane

Ki-Young Choi

Department of Chemistry, Mokwon University, Taejon 301-729, Korea

(Received 21 October 1997; accepted 19 November 1997)

Abstract—The synthesis and structural characterization of $ZnLX_2$ (X = H_2O(**1**), N_3^-(**2**), and NCS^-(**3**); L = 2,5,9,12-tetramethyl-1,4,8,11-tetraazacyclotetradecane) complexes are reported. The crystal structure analysis was employed to determine solid state structures. The crystal structures of these complexes have an axially elongated octahedral geometry with two axial ligands and adopt the *trans*-III conformation. The long Zn—O bond distance of 2.343(5) Å in complex **1** has a high pK_a value of 11.2. © 1998 Elsevier Science Ltd. All rights reserved

Keywords: characterization of zinc(II) complexes with tetramethyl tetraaza macrocycle.

Recently, there has been great interest for the role of metal ions in the active centers of hydrolytic metalloenzymes such as carbonic anhydrases, carboxypepdidase, and phosphatase [1]. As one of the approaches, various types of zinc(II) complexes have been designed to account for or mimic the functions played by the central Zn(II) ions [2–4]. In carbonic anhydrases the active site of the enzyme consists of a zinc center coordinated to three histidine imidazole groups and a water molecule in which the pK_a value (H_2O) lies ca 7.5 [5,6]. Furthermore, Zn(II) complexes of macrocyclic triamines [7–10] and tetraamines [11–13] have been the most widely studied models due to their similar structural, thermodynamic and kinetic properties with carbonic anhydrases. In these complexes the Zn(II) ion is coordinated to three or four secondary amine groups and a water molecule, which can dissociate giving a Zn—OH species with pK_a values of 7.3–9.8 [7–12]. The nuclephilicity of the zinc hydroxide unit is related to the pK_a of the coordinated water, and among the macrocyclic triamine systems, the less stable complexes yield lower pK_a values. On the other hand, the well-recognized inhibition of carbonic anhydrases by a variety of simple anions has been repeatedly exploited as a probe of its catalytic activity [14]. Recently, X-ray crystal analysis of the SCN^- binding to carbonic anhydrases [15], 1,5,9-triazacyclododecane (L^1) [16] and 3,14-dimethyl-2, 6, 13, 17-tetraazatricyclo(14.4.$0^{1,18}$,$0^{7,12}$)docosane (DTAD) [17] complexes of Zn(II) showed a five-coordinate complexes with SCN^- and water bound.

In this study, we report the synthesis and characterization of $ZnLX_2$ (X = H_2O(**1**), N_3^-(**2**) and NCS^-(**3**); L = 2,5,9,12-tetramethyl-1,4,8,11-tetraazacyclotetradecane) complexes. To understand the nature of the axial ligands, the solid state X-ray crystal structures of $ZnLX_2$ are determined. We have also investigated the acidity of the bound water of complex **1**.

EXPERIMENTAL

Materials and analytical methods

All solvents were reagent grade and purified according to the literature [18]. Reagents such as $ZnCl_2$, methyl vinyl ketone, 1,2-diaminopropane, perchloric acid and $NaBH_4$ were purchased from Aldrich and were used without further purification. All other reagents were reagent grade. Distilled water was used for all reactions. The ligand 2,5,9,12-tetramethyl-1,4,8,11-tetraazacyclotetradecane was prepared according to literature methods [19]. Infrared spectra of solid complexes were recorded on a Perkin–Elmer Paragon 1000 FT-IR spectrophotometer. High-resolution fast atom bombardment spectrometry (FAB mass) were performed by using a Jeol JMS-HA 100A/100A instrument. Elemental analyses were car-

ried out by the Korea Research Institute of Chemical Technology Taejon, Korea.

Preparation of $[ZnL(H_2O)_2]Cl_2$ (**1**)

A methanol solution (20 cm^3) of L (513 mg, 2 mmol) and $ZnCl_2$ (273 mg, 2 mmol) was heated at reflux for 2 h. The solution was allowed to cool at room temperature and was then filtered. The filtrate was evaporated to dryness. The product was redissolved in a minimum amount of water. After the solution was allowed to stand at room temperature over a several day period, colorless crystals formed. Recrystallization from water/acetonitrile (1 : 1, 10 cm^3), filtration, washing with diethyl ether, and drying *in vacuo* produced a white solid (583 mg, 68% yield). Found : C, 39.4 : H, 8.5 : N, 13.2. Calc. For $ZnC_{14}H_{36}N_4O_2Cl_2$: C, 39.2 : H, 8.5 : N, 13.1%. IR (KBr, cm^{-1}) : 3336 (ν_{OH}), 3246 (ν_{OH}), 3172 (ν_{NH}), 3101 (ν_{NH}), 1647 (ν_{HOH}). FAB mass (CH_2Cl_2, *m/z*) : 428.7$(M)^+$.

Preparation of $[ZnL(N_3)_2]$ (**2**)

To a methanol solution (20 cm^3) of **1** (214 mg, 0.5 mmol) was added NaN_3 (65 mg, 1 mmol) and the mixture refluxed for 1 h. The solution was filtered and the filtrate was evaporated to dryness. The product was dissolved in water/acetonitrile (1 : 1, 10 cm^3). When this mixture was allowed to stand for a few days, colorless crystals were obtained. These were filtered off, washed with diethyl ether and dried *in vacuo* (154 mg, 76% yield). Found : C, 41.4 : H, 8.0 : N, 34.7. Calc. For $ZnC_{14}H_{32}N_{10}$: C, 41.4 : H, 8.0 : N, 34.5%. IR (KBr, cm^{-1}) : 3164 (ν_{NH}), 2036 ($\nu_{N=N}$). FAB mass (CH_2Cl_2, *m/z*) : 405.8$(M)^+$.

Preparation of $[ZnL(NCS)_2]$ (**3**)

This compound was synthesized from **1** (214 mg, 0.5 mmol) and KSCN (97 mg, 1 mmol) following the procedure reported for **2**, obtaining **3**, as colorless crystals (171 mg, 78% yield). Found : C, 44.0 : H, 7.4 : N, 19.1. Calc. For $ZnC_{16}H_{32}N_6S_2$: C, 43.9 : H, 7.4 : N, 19.2%. IR (KBr, cm^{-1}) : 3218 (ν_{NH}), 2049 ($\nu_{C=N}$). FAB mass (CH_2Cl_2, *m/z*) : 437.9$(M)^+$.

Potentiometric titrations

Potentiometric titrations were carried out on a Radiometer TIM 900 Titration Manager fitted with

Table 1. Crystallographic data

	1	**2**	**3**
Formula	$ZnC_{14}H_{36}N_4O_2Cl_2$	$ZnC_{14}H_{32}N_{10}$	$ZnC_{16}H_{32}N_6S_2$
Formula weight	428.75	405.85	437.96
Crystal system	triclinic	triclinic	monoclinic
Space group	$P\bar{1}$	$P\bar{1}$	$P2_1/c$
a (Å)	7.934(2)	7.852(1)	8.253(1)
b (Å)	9.612(2)	9.095(1)	17.940(2)
c (Å)	7.476(1)	7.279(2)	7.734(2)
α (°)	109.79(2)	95.95(2)	90.0
β (°)	104.29(2)	97.20(2)	111.21(2)
γ (°)	84.65(2)	111.15(1)	90.0
V (Å^3)	519.9(2)	474.7(2)	1067.5(4)
Z	1	1	2
F(000)	228.6	216.3	465.1
D_{calc} (g cm^{-3})	1.370	1.420	1.363
λ (Mo–K_α) (Å)	0.71069	0.71069	0.71069
μ (mm^{-1})	1.48	1.34	1.38
T (K)	288	288	288
Scan width	$0.8 \pm 0.34 \tan\theta$	$0.8 + 0.34 \tan\theta$	$0.8 + 0.34 \tan\theta$
h, *k*, *l* range	−9 9, 0 11, −8 8	−9 8, 0 11, −8 8	−10 9, 0 22, 0 9
2θ range (°)	49.84	51.82	51.82
No. of unique reflections	1838	1861	2088
No. of observed reflections $[F_o > 3\sigma(F_o)]$	1308	1492	1074
R^a	0.047	0.036	0.040
$R_w{}^b$	0.051	0.039	0.043
GoF^c	0.55	0.47	0.53

$^a R = \Sigma(|F_o| - |F_c|)/\Sigma|F_o|$.
$^b R_w = [\Sigma w(|F_o| - |F_c|)^2/\Sigma w(|F_o|)^2]^{1/2}$.
^{c} GoF $= [\Sigma(w|F_o| - |F_c|)^2/(\text{No. of reflns} - \text{No. of params})]^{1/2}$.

a Radiometer combination electrode. The electrode response was standardized with buffer solution at pH 4.00 and 7.00 (25.0 ± 0.1°C). An aqueous solution (10 cm^3) of 1 : 1 ($C_L = 1.0 \times 10^{-2}$ M, $C_M = 1.0 \times 10^{-2}$ M) ratio for the mixture was titrated with a carbonate-free 0.0982 M KOH at 25.0 ± 0.1°C and $I = 0.2$ ($NaClO_4$). Humidified nitrogen gas free carbon dioxide (through 1N NaOH solution) was passed over the solution during the potentiometric measurements. The hydrogen ion concentrations were obtained from the measured pH values by the method of Martell *et al.* ($pK_w = 13.78$) [20]. Since Zn(II) complexation equilibrium was very slow, the pH values were read after sufficient time (1 h) at each titration point. The complexation constants were obtained by fitting the potentiometric data and the protonation constants [21] to the BEST program [20].

X-ray crystallographic analysis

A summary of crystal data, data collection and refinement for all crystallographically characterized compounds are given in Table 1. Colorless crystals of dimensions $0.2 \times 0.2 \times 0.2$ for **1**, $0.2 \times 0.1 \times 0.2$ for **2** and $0.3 \times 0.2 \times 0.2$ for **3** were mounted on an Enraf-Nonius CAD4 diffractometer with graphite monochromated Mo-K_α radiation ($\lambda = 0.71069$). Accurate cell parameters and an orientation matrix were determined from the least-squares fit of 25 reflections. Intensity data were collected in the $\omega - 2\theta$ scan mode. For all crystals three standard reflections were measured every 240 min. Data were corrected for Lorentz and polarization effects. No absorption correction was applied. The structures were solved by use of heavy-atom methods. All remaining non-hydrogen atoms were found by iterative cycles of full-matrix least squares refinement and difference-Fourier synthesis using NRCVAX [22]. All non-hydrogen atoms were refined anisotropically. All hydrogen atoms were included at calculated positions ($d_{C-H} = 1.08$ Å) and refined isotropically at the final cycle. Full crystallographic details, atomic coordinates, interatomic distances and angles, hydrogen atom coordinates, anisotropic displacement parameters and structure factor tables for **1**, **2** and **3** have been deposited with the editor as supplementary material.

RESULTS AND DISCUSSION

Description of structures

In the present compounds, two alternating five- and six-membered chelate rings are in the gauche and chair form with most stable *trans*-III conformations. An inversion center of these complexes exits on the central Zn(II) ion. The N—Zn—N angles of the six-membered chelate rings are larger than those of the five-membered chelate rings.

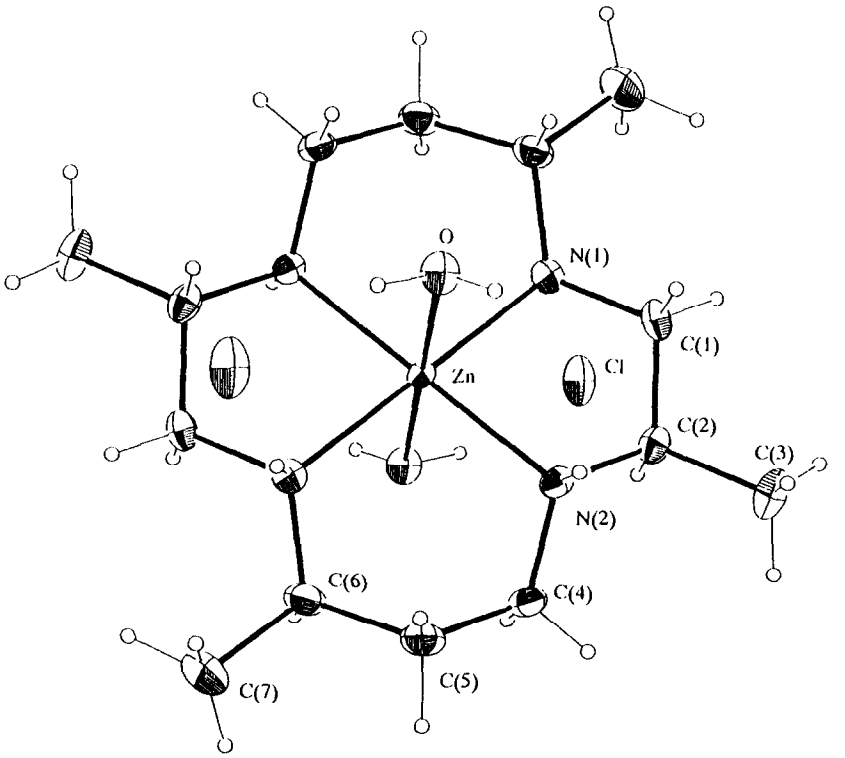

Fig. 1. ORTEP drawing of **1** with the atom-numbering scheme.

Figure 1 shows an ORTEP drawing of **1** with the atomic numbering scheme. Selected interatomic bond distances and angles are listed in Table 2. The crystal structure of **1** consists of $[ZnL(H_2O)_2]^{2+}$ cation and two Cl^- anions. The coordination environment around Zn(II) ion shows an axially elongated octahedron with two oxygen atoms of water molecules and four nitrogen atoms of the macrocyclic ligand. The average Zn—N bond distance of 2.094(5) Å is similar to those found in $[Zn(DTAD)(H_2O)_2]Cl_2$ (2.099(2) Å) [13] and $Zn(O_2COCH_3)$ ([14]aneN_4) (2.099(2) Å) [11] which have the tetragonal six-coordinate complexes. Zn—OH_2 bond distance in five-coordinate complexes with square-pyramidal geometry, [Zn(N,N′)-*bis*(salicylidene)(ethylenediamine)(H_2O)] [23] is reported to be ca 2.0 Å, whereas those in a tetragonal six-coordinate complexes, [Zn(8)-hydroxyquinoline$(H_2O)_2$] [24] and [Zn(DTAD)$(OH_2)_2$] Cl_2 [13], lengthens to 2.263(5) Å and 2.338(3) Å. The Zn—O bond distance of **1** was found to be 2.343(5) Å. The elongation of Zn—O distance in complex **1** may be attributed to the detrimental

Table 2. Selected interatomic bond distances (Å) and angles ( )

		1	
Zn—O	2.343(5)	Zn—N(2)	2.092(4)
Zn—N(1)	2.096(5)		
O—Zn—N(1)	90.2(2)	Zn—N(1)—C(1)	105.7(4)
O—Zn—N(2)	90.1(2)	Zn—N(1)—C(6)^a	115.8(4)
N(1)—Zn—N(2)	84.5(2)	Zn—N(2)—C(2)	106.5(3)
N(1)—Zn—N(2)^a	95.5(2)	Zn—N(2)—C(4)	113.5(4)
		2	
Zn—N(1)	2.111(3)	N(3)—N(4)	1.180(4)
Zn—N(2)	2.099(3)	N(4)—N(5)	1.164(4)
Zn—N(3)	2.308(3)		
N(1)—Zn—N(3)	84.6(1)	Zn—N(1)—C(1)	105.5(2)
N(2)—Zn—N(3)	89.3(1)	Zn—N(1)—C(6)^a	116.0(2)
N(1)—Zn—N(2)	85.0(1)	Zn—N(2)—C(2)	105.6(2)
N(1)—Zn—N(2)^a	95.0(1)	Zn—N(2)—C(4)	113.5(2)
Zn—N(3)—N(4)	124.4(2)	N(3)—N(4)—N(5)	179.0(3)
		3	
Zn—N(1)	2.088(5)	N—C	1.115(10)
Zn—N(2)	2.098(4)	S—C	1.625(8)
Zn—N	2.461(7)		
N(1)—Zn—N	87.9(2)	Zn—N(1)—C(1)	104.9(4)
N(2)—Zn—N	90.2(2)	Zn—N(1)—C(6)^a	117.8(4)
N(2)—Zn—N(2)	95.1(2)	Zn—N(2)—C(2)	106.5(3)
N(1)—Zn—N(2)^a	84.9(2)	Zn—N(2)—C(4)	113.5(4)
Zn—N—C	115.1(5)	N—C—S	108.9(7)

^{a} $-x, -y, -z$.

Table 3. Hydrogen-bond parameters (Å,) for **1**

D—H···A	D—H (Å)	H···A (Å)	D—A (Å)	D—H···A ( )
N(1)^a—NH(1)^a···Cl	0.72(6)	2.65(6)	3.352(6)	165(6)
O—H(O1)···Cl	0.94(7)	2.19(7)	3.102(6)	164(5)
O—H(O2)···Cl^b	0.72(7)	2.43(7)	3.140(6)	167(7)
N(2)—NH(2)···Cl^b	0.81(6)	2.57(5)	3.369(5)	168(5)

^{a} $-x, -y, -z$.
^{b} $-x, -y, 1-z$.

effect by the steric hinderance of the four methyl groups on the ligand. Figure 2 shows that the water molecule coordinates to the central Zn(II) ion, accompanied by chlorides and secondary amines of macrocycle which are located close to the coordinated water through the four hydrogen-bonding chelate rings (Table 3).

Figure 3 shows an ORTEP drawing of **2** with the atomic numbering scheme. Selected interatomic bond distances and angles are listed in Table 2. The structure of **2** reveals a six-coordinated octahedral geometry with bonds to the four secondary amines of the macrocycle and to the two axial azide ligands. The average Zn—N (secondary amines) distance of 2.105(3) Å is longer than those observed in the four-coordinated complex $[Zn(L^5)]^{2+}$ (L^5 = 1,4,8,11-tetraazacyclotetradecane) (2.088(2) Å) [25], but are similar to those reported for the six-coordinated complex $[Zn(DTTD)](ClO_4)_2 \cdot H_2O$ (DTTD = 6,13-dimethyl-1,4,8,11-tetraazacyclotetradecane-6,13-diamine) (2.100(5) Å) [26]. The axial Zn—N(3) bond distances of 2.308(3) Å are equivalent, but both are ca 0.2 Å longer than equatorial Zn—N (secondary amines) bonds which indicate an axially elongated octahedral geometry. The axial Zn—N(3) linkage is bent slightly off the perpendicular to the ZnN_4 plane by 0.71–5.44°. The azido group is slightly asymmetric [N(3)—N(4) = 1.180(4) and N(4)—N(5) = 1.164(4) Å] and linear within the experimental error [N(3)—N(4)—N(5) angle = 179.0(3)°].

Figure 4 shows an ORTEP drawing of **3** with the atomic numbering scheme. Selected interatomic bond distances and angles are listed in Table 2. The structure of **3** shows that the Zn(II) is coordinated by the secondary amines of the macrocycle and that the axial positions are weakly bonded by two nitrogen atoms of the thiocyanate ligands. The average Zn—N (secondary amines) distance of 2.093(5) Å is shorter than those reported for the complex $[Zn(L^5)(NCS)_2]$ (2.104(11) Å) [27], while the axial Zn—N (thiocyanate) distance of 2.461(4) Å is longer than that to the thiocyanate ligands in $[Zn(L^5)(NCS)_2]$ (2.371(13) Å) [27], giving an axially elongated octahedral geometry. Also, the axial Zn—N bond is not perpendicular to ZnN_4 plane with N(1)—Zn—N and N(2)—Zn—N angles of 87.9(2) and 90.2(2)°. The Zn—N—C and N—C—S angles related to the thiocyanate ligand are 115.1(5) and 178.9(7)°, respectively.

Complexation constants

The titration data as shown in Fig. 5 were treated for the 1 : 1 H_4L and $ZnCl_2$ in aqueous solution of 0.20 ($NaClO_4$) at 25.0±0.1 C. The Zn(II) complexation constants K_{ZnL} and K_a are defined as follows:

$$Zn(II) + L \rightleftarrows ZnL \quad K_{ZnL} \tag{1}$$

$$ZnL \rightleftarrows ZnH_{-1}L + H^+ \quad K_a \tag{2}$$

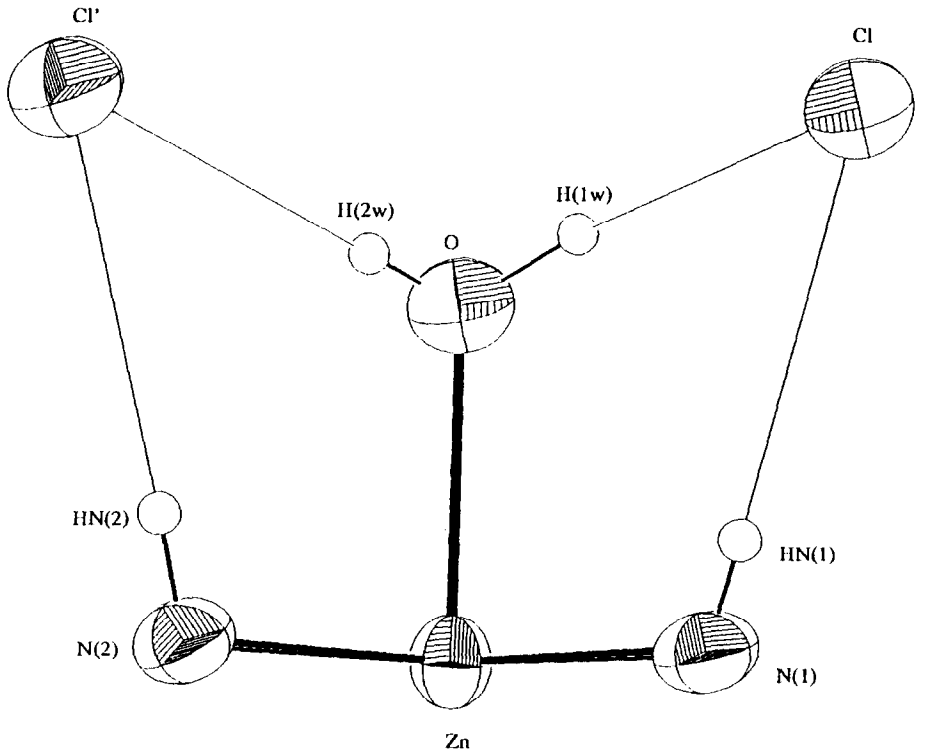

Fig. 2. Hydrogen-bond system of **1**.

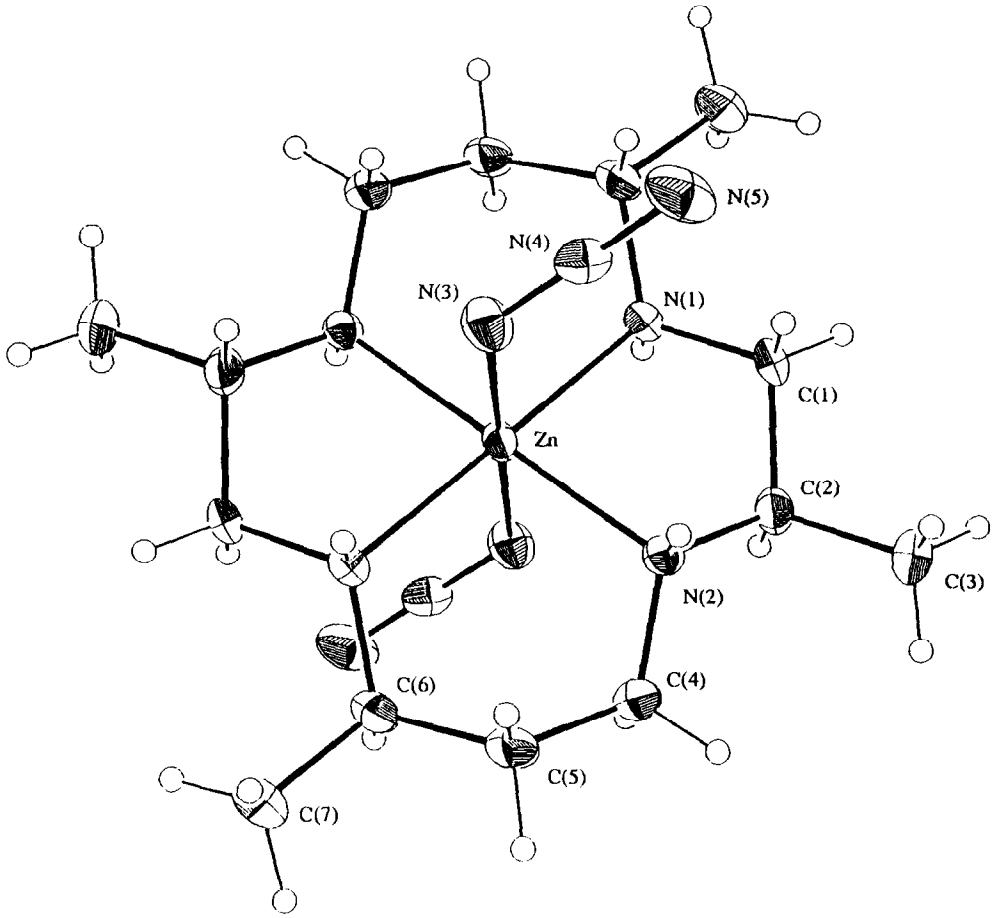

Fig. 3. ORTEP drawing of **2** with the atom-numbering scheme.

Table 4. Zn(II) complex formation constants ($\log K_{ZnL}$) and deprotonation constants (pK_a) of Zn(II)-bound H_2O at 25.0±0.1°C and $I = 0.20$ ($NaClO_4$)

Ligands	$\log K_{ZnL}$	pK_a	Ref.
L^1	8.41±0.02[a]	7.30±0.02[a]	7
L^2	7.01±0.02[a]	7.34±0.02[a]	7
L^3	10.41[b]	8.20[b]	8
L^4	16.2[c]	8.02±0.03[a]	7, 28
L^5	15.5[c]	9.77±0.05[a]	7, 28
L^6	10.4[d]	8.36[d]	10
L^7	—	10.7[e]	9
L	18.7	11.2	this work

[a] $I = 0.10$ ($NaClO_4$), [b] $I = 0.1$ (KNO_3), [c] $I = 0.2$ ($NaClO_4$), [d] $I = 0.1$ ($NaNO_3$), [e] $I = 0.1$ ($NaClO_4$). Abbreviations: L^1 = 1,5,9-triazacyclododecane, L^2 = 1,4,10-triazacyclododecane, L^3 = 1,4,8-triazacycloundecane, L^4 = 1,4,7,10-tetrazacyclododecane, L^5 = 1,4,8,11-tetraazacyclotetradecane, L^6 = 1,4,8,11-tetramethyl-1,4,8,11-tetraazacyclotetradecane, L^7 = 2-(2-hydroxyphenyl)-1,5,9-triazacyclododecane.

Table 4 summarizes the obtained $\log K_{ZnL}$ and pK_a values in comparison with the reported values of macrocyclic polyamines. The pK_a value of 11.2 with **1** is considerably high compared with those of other Zn(II)—OH_2 macrocyclic tetraamines. It is generally understood that the acidity of Zn(II)—OH_2 moiety is greatly influenced by the nature of macrocyclic polyamines and coordination environments at Zn(II). For instance, the Zn(II) complexes of macrocyclic triamines having larger cavities such as L^1 and L^2 show the most acidic in nature with pK_a values of 7.3 [7], while the Zn(II) complexes of macrocyclic tetraamines show less acidic with pK_a values of 9.77 and 8.36, respectively [7,10]. The high pK_a of H_2O bound to Zn(II) in the hexacoordinate environment is expected with the longer Zn—O bond distances seen in the octahedral geometries. With a longer bond distance the water ligand should be less polarized and result in a decreased acidity. It is also anticipated that an increasing coordination number at Zn(II) decreases the acidity of bound water. Kimura *et al.* reported, on the Zn(II) complex with a [2-(2-hydroxyphenyl)-1,5,9-triazacyclododecane] (L^7), that the H_2O bound

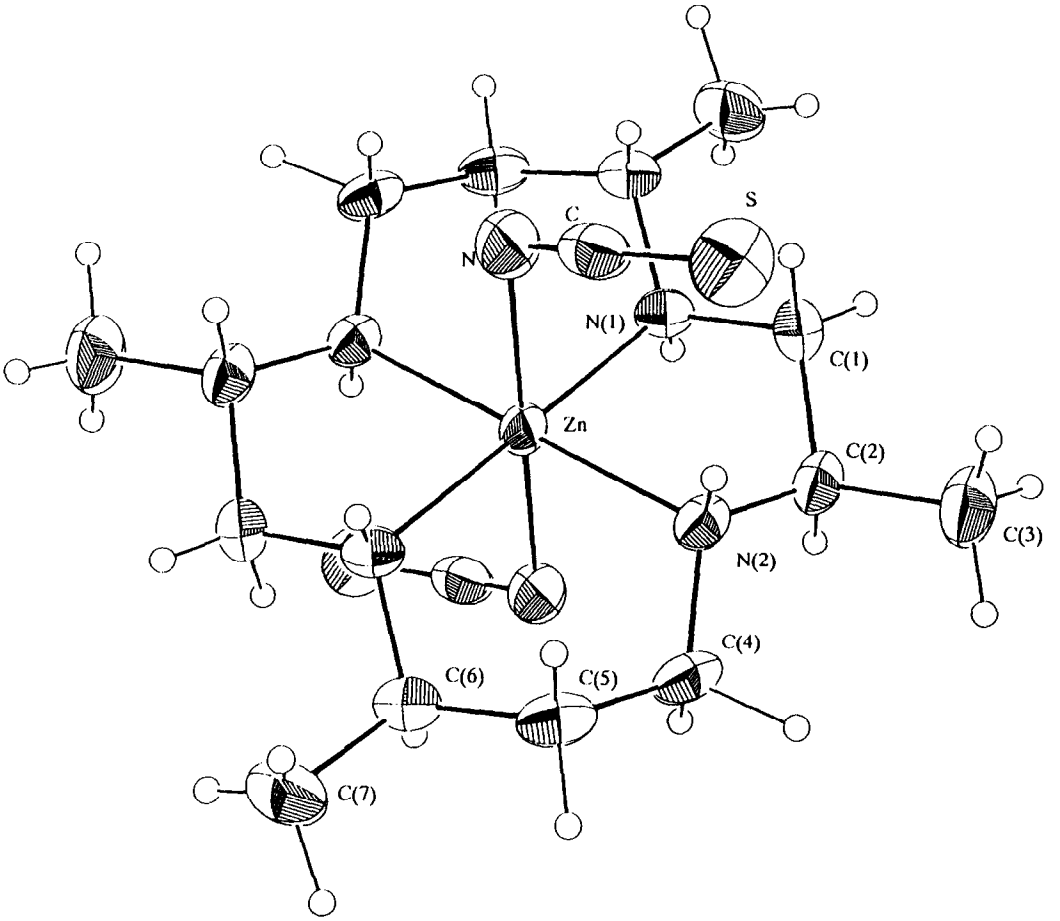

Fig. 4. ORTEP drawing of **3** with the atom-numbering scheme.

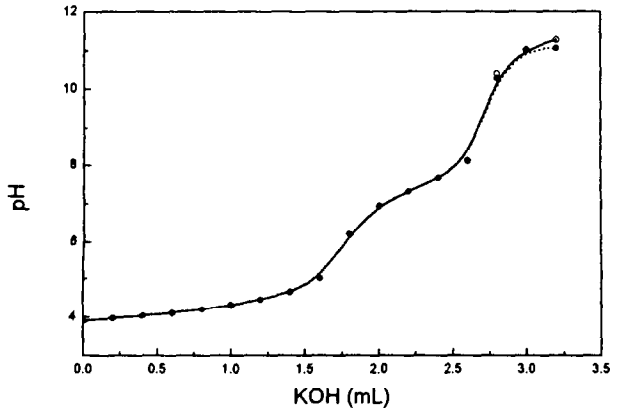

Fig. 5. Titration curve for 10 mL of 1 : 1 ($C_L = 1.0 \times 10^{-2}$ M, $C_M = 1.0 \times 10^{-2}$ M) mixture with 0.0982 M KOH at 25.0 ± 0.1°C and $I = 0.20$ ($NaClO_4$).

to Zn(II) (distance 2.22 Å) has a pK_a value of 10.7 [9], indicating a greatly reduced (from 7.3 of L^1) acidity of Zn(II) due to the phenolate ($pK_a = 6.8$) coordination. The much low acidity of **1** may be due to the long Zn—O bond distance of 2.388(3) Å in the octahedral geometry.

Acknowledgements—This work was supported by the Basic Science Research Institute Program of Education of Korea, Project No. BSRI-97-3435 and the Research Fund of Mokwon University, 1977.

REFERENCES

1. Bertini, I., Luchinat, C., Maret, W. and Zeppezauer, M., *Zinc Enzymes*. Birkhauser, Boston, MA, 1986.
2. Looney, A., Runyu, H., McNeill, K. and Parkin, G., *J. Am. Chem. Soc.*, 1993, **115,** 4690.
3. Kitajima, N., Hikichi, S., Tanaka, M. and Morooka, Y., *J. Am. Chem. Soc.*, 1993, **115,** 5496.
4. Kimura, E., *Prog. Inorg. Chem.*, 1994, **41,** 443.
5. Pocker, Y. and Sarkanen, S., *Adv. Enzymol.*, 1987, **47,** 149.
6. Kimura, E., Koike, T. and Toriuni, K., *Inorg. Chem.*, 1988, **27,** 3687.
7. Kimura, E., Shiota, T., Koike, T., Shiro, M. and Kodama, M., *J. Am. Chem. Soc.*, 1990, **112,** 5805.
8. Zompa, L. J., *Inorg. Chem.*, 1978, **17,** 2531.
9. Nakani, B. S., Welch, J. J. B. and Hancock, R. D., *Inorg. Chem.*, 1983, **22,** 2956.
10. Kimura, E., Yamaoka, M., Morioka, M. and Koike, T., *Inorg. Chem.*, 1986, **25,** 3883.
11. Kata, M. and Ito, T., *Inorg. Chem.*, 1985, **24,** 509.
12. Norman, P. R., *Inorg. Chim. Acta*, 1987, **130,** 1.
13. Choi, K. Y., Suh, I. H. and Kim, J. C., *Polyhedron*, 1997, **16,** 1783.
14. Pocker, Y. and Thomas, L. D., *J. Am. Chem. Soc.*, 1982, **104,** 2424.
15. Eriksson, A. E., Kylsten, P. M., Jones, T. A. and Liljas, A., *Proteins*, 1988, 283.
16. Kimura, E., Koike, T., Shionoya, M. and Shiro, M., *Chem. Lett.*, 1992, 787.
17. Cho, K. Y. and Suh, I. H., *Polyhedron*, 1997, **16,** 2393.
18. Perrin, D. D., Armarego, W. L. F. and Perrin, D. R., *Purification of Laboratory Chemicals*, 2nd edn. Pergamon Press, New York, 1985.
19. Kolinski, R. A., Korybut-Daszkiewicz, B. and Kubaj, Z., *Inorg. Chem. Acta*, 1982, **57,** 269.
20. Martell, A. E. and Motekaitis, R. J., *Determination and Use of Stability Constants*, 2nd edn. VCH, New York, 1992.
21. Protonation constants (log K_i) in 0.20 M $NaClO_4$ and at 25.0 ± 0.1°C are 11.16, 10.96, 2.74 and 0.91, which are calculated by fitting the potentiometric data to the PKAS program [20].
22. Gabe, E. J., Page, Y. L., Charland, J. P., Lee, F. L. and White, P. S., *J. Appl. Cryst.*, 1989, **22,** 384.
23. Hall, D. and Moore, F. H., *J. Chem. Soc. A*, 1966, 1822.
24. Palenik, G. J., *Acta Cryst.*, 1964, **17,** 696.
25. Tyson, T. A., Hodgson, K. O., Hedman, B. and Clark, G. R., *Acta Cryst.*, 1990, **C46,** 1638.
26. Bernhardt, P. V., Lawrance, G. A., Maeder, M. and Hambley, T. W., *J. Chem. Soc., Dalton Trans.*, 1991, 1167.
27. Ito, T., Kato, M. and Ito, H., *Bull. Chem. Soc. Jpn*, 1984, **57,** 2636.
28. Kodama, M. and Kimura, E., *J. Chem. Soc., Dalton Trans.*, 1977, 2269.

Pergamon

Polyhedron Vol. 17, Nos. 11–12, pp. 1983–1989, 1998
© 1998 Elsevier Science Ltd
All rights reserved. Printed in Great Britain
0277-5387/98 $19.00+0.00

PII: S0277-5387(97)00480-4

The reaction of P_4 with $[Cp'Mo(CO)_3]_2$ ($Cp' = \eta^5$-C_5H_4tBu)—the structure of $[Cp'Mo(CO)_2\langle(\eta^3\text{-}P_4)\{Cr(CO)_5\}_4(H)\rangle]$

Manfred Scheer,* Uta Becker and Jörg Magull†

Institut für Anorganische Chemie der Universität Karlsruhe, Engesserstraße, Geb. 30.45, D-76128 Karlsruhe, Germany

(Received 1 October 1997; accepted 17 November 1997)

Abstract—The photochemical reaction of $[Cp'Mo(CO)_3]_2$ ($Cp' = \eta^5$-C_5H_4tBu) with white phosphorus in the presence of $[Cr(CO)_5thf]$ leads to the P_n ligand complexes $[Cr(CO)_4\langle(\eta^4\text{-}P_4)\{Cr(CO)_5\}_4\rangle]$ (**1**), $[Cp'Mo(CO)_2\langle(\eta^3\text{-}P_4)\{Cr(CO)_5\}_4(H)\rangle]$ (**2**) and $[\{Cp'Mo(CO)_2\}_2\langle(\mu,\eta^2\text{-}P_2)\{Cr(CO)_5\}_2\rangle]$ (**3**). The products were characterized by NMR, IR and partially by X-ray structure analysis. The reaction proceeds via a P—P bond cleavage leading to the bent *cyclo*-P_4 complex $[Cp'Mo(CO)_2\langle(\eta^3\text{-}P_4)\{Cr(CO)_5\}_4\{Cp'Mo(CO)_3\}\rangle]$ (**2a**), which hydrolysis during the chromatographic work-up to give the more stable compound **2**. Furthermore, a P_3/P_1 fragmentation of **2a** occurs to form the phosphido complex intermediate $[Cp'(CO)_2Mo{\equiv}P \rightarrow Cr(CO)_5]$. The latter dimerises resulting in the formation of the tetrahedral compound **3**, containing a Mo_2P_2 moiety.
© 1998 Elsevier Science Ltd. All rights reserved

Keywords: P_n-ligands; molybdenum complexes; bent *cyclo*-P_4-ligand; Mo_2P_2-tetrahedral complex; phosphido complex intermediate.

Reactions of white phosphorus with transition metal complexes afford co-ordination compounds containing P_n-ligands without organic substituents [1]. While numerous publications exist discussing the structural variety of such compounds, only a few investigations of the reaction pathway have been done so far [2]. In order to study the transformation pathway of the P_4 tetrahedron in the co-ordination sphere of transition metals we developed the concept of the three-component-reaction [3,4]. These reactions are carried out starting from white phosphorus and the corresponding metal carbonyl complex ML_n, e.g. $[Cp''Rh(CO)_2]$ ($Cp'' = \eta^5$-$C_5H_3tBu_2$) as shown in Scheme 1, in the presence of a Lewis-acidic compound like $[Cr(CO)_5thf]$. The lone pairs of the initially formed P_n-ligands are thus able to co-ordinate to the chromium pentacarbonyl units. Therefore, it becomes possible to stabilise intermediates along the reaction pathway. A second function of the $[Cr(CO)_5]$ moieties is the activation of the metal carbonyl complex ML_n by promoting the loss of CO based on the formation of the very stable $[Cr(CO)_6]$ [3]. Due to the steric influence of the $[Cr(CO)_5]$ groups, the reaction pathway of a three-component-reaction may differ from the corresponding two-component-reaction without $[Cr(CO)_5thf]$ [3b,5a].

The reaction pathway of three-component-reactions depends on the nature of the metal complexes used, i.e. they have to be subdivided into those forming fragments with an even or an odd number of valence electrons. In the case of complex fragments with an even number of valence electrons, such as $[Cp^xM(CO)]$ ($Cp^x = \eta^5$-C_5H_4tBu (Cp'), η^5-$C_5H_3tBu_2$ (Cp''), η^5-C_5Me_5 (Cp*); M = Co [5], Rh [3] (Scheme 1), Ir [6]), a stepwise P—P bond cleavage under formation of a bicyclotetraphosphine intermediate is observed. These reactions yield products containing *cyclo*-P_4 moieties. The use of co-ordination compounds forming fragments with an odd number of valence electrons, e.g. $[Cp^*Ni(\mu\text{-}CO)]_2$, however lead to a bent *cyclo*-P_4 ligand complex and a Ni_2P_4 pris-

* Author to whom correspondence should be addressed. Telefax: +49(0)(721)661921; e-mail: mascheer@achibm6.chemie.uni-karlsruhe.de

† Present address: Institut für Anorganische Chemie der Universität Göttingen, Tammannstr. 4, D-37077 Göttingen, Germany.

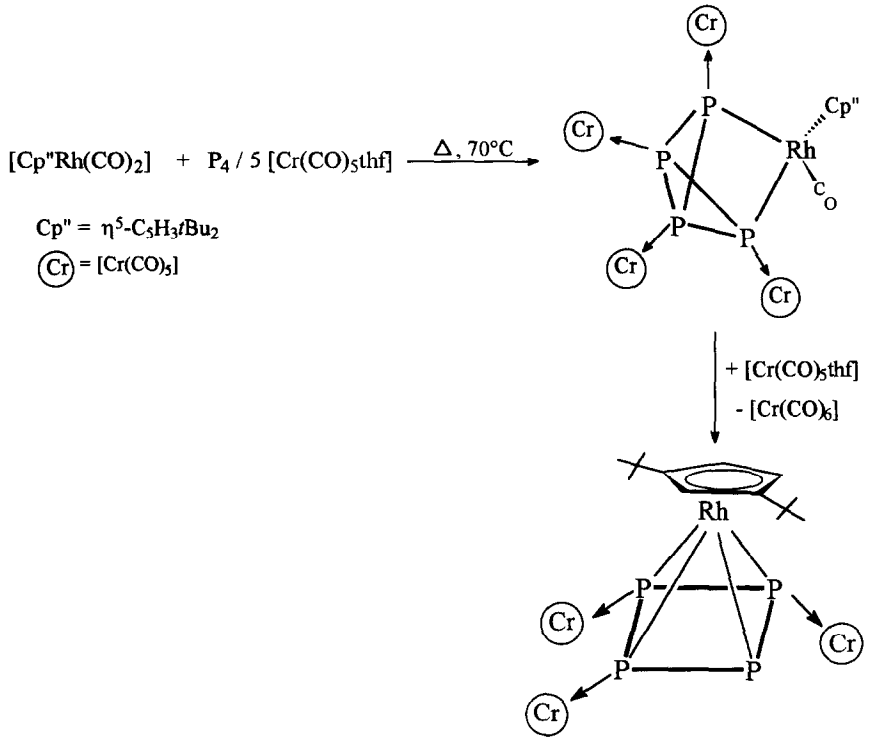

Scheme 1. Three-component-reaction starting from $[Cp''Rh(CO)_2]$ and P_4 in the presence of $[Cr(CO)_5thf]$.

mane, respectively [7]. A P_1/P_3 fragmentation is only observed in a small extent (5%). $[Cp'Mo(CO)_n]_2$ ($n = 2, 3$) also forms fragments with an odd number of valence electrons. Scherer *et al.* showed that the two-component-reaction of $[Cp^*Mo(CO)_2]_2$ with P_4 affords the tetrahedral complexes $[Cp^*Mo(CO)_2(\eta^3\text{-}P_3)]$ and $[\{Cp^*Mo(CO)_2\}_2(\mu,\eta^2\text{-}P_2)]$, as well as $[(Cp^*Mo)_2(\mu,\eta^6\text{-}P_6)]$, containing a hexaphosphabenzene-ligand, and $[\{Cp^*Mo(CO)\}_2(\mu,\eta^2\text{-}P_2)_2]$ bearing two separated P_2 units [8].

Herein we report our results of the corresponding three-component-reaction starting from $[Cp'Mo(CO)_3]_2$ ($Cp' = \eta^5\text{-}C_5H_4tBu$) and the proposed transformation pathway of the tetrahedral P_4 phosphorus.

RESULTS AND DISCUSSION

Synthesis, properties and spectroscopic data of the complexes 1–3

The thermal reaction of $[Cp'Mo(CO)_3]_2$ with P_4 in the presence of $[Cr(CO)_5thf]$ exclusively affords the complex $[Cr(CO)_4\langle(\eta^4\text{-}P_4)\{Cr(CO)_5\}_4\rangle]$ (**1**). The molybdenum starting compound is not involved in the reaction [eqn (1)].

Under UV conditions, however, $[Cp'Mo(CO)_3]_2$ participates in the three-component-reaction (2).

The $^{31}P\{^1H\}$ NMR spectrum of the crude reaction mixture (2) reveals signals for the compounds **1–3** as the main products. Chromatographic work-up of the reaction mixture results in the isolation of the orange crystalline compound **2** and the reddish brown product **3**, besides some unreacted starting material. The products are slightly soluble in hexane and readily soluble in toluene, CH_2Cl_2 or THF.

Table 1 shows the spectroscopic data for **1–3**. The spectroscopic data of **1** and **3** correspond to those of the compounds we obtained by the cothermolysis of P_4 with $[Cr(CO)_5thf]$ [9] and by the reaction of $[\{Cr(CO)_5\}_2PCl]$ with $[Cp'Mo(CO)_3]K$ [10], respectively.

The IR spectrum of **2** shows five bands in the region of the CO stretching frequencies (Table 1) corresponding to the $2A_1 + E$ bands of the distorted C_{4v} symmetry of the $[Cr(CO)_5]$ units and the coupled CO vibrations of the $[Cp'Mo(CO)_2]$ group.

For $[Cp'Mo(CO)_2\langle(\eta^3\text{-}P_4)\{Cr(CO)_5\}_4(H)\rangle]$ (**2**) a proton decoupled and a coupled ^{31}P NMR spectrum was recorded. In the decoupled spectrum an AMX_2 spin system is observed [$\delta(P_A) = 184.8$ ppm, $\delta(P_M) = 63.7$ ppm, $\delta(P_X) = 25.4$ ppm; $P_A = P(3)$, $P_M = P(1)$, $P_X = P(2)$, P(4), Fig. 2]. The P_A nucleus reveals a triplet at 185.0 ppm. Each of the three lines of the triplet additionally shows a fine splitting [$^2J(P_AP_M)$: 24 Hz; Fig. 1a]. In the proton coupled ^{31}P spectrum (AM_2XH spin system) a pseudo quintet for the P_A phosphorus atom is observed due to the additional coupling with the proton attached to it

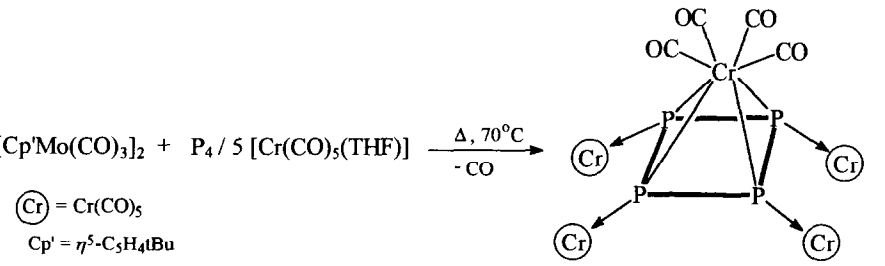

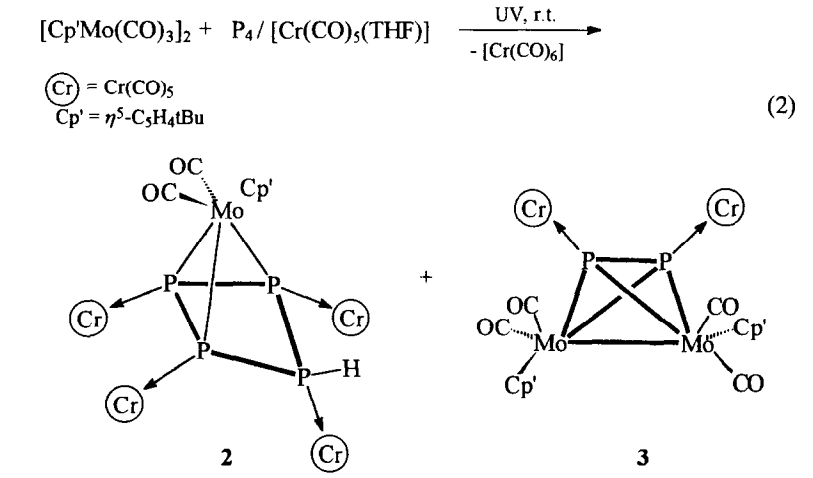

Scheme 2.

Table 1. NMR and IR spectroscopic data for **1–3**

	1	**2**	**3**
$^1H^a$		2.17 (s, 9H)	1.3 (s, 9H)
(ppm)		4.93 (s, 2H)	5.3 (s, 4H)
		5.03 (s, 2H)	
$^{31}P^b$	158.6 (s)	P_A: 184.8 (td)	−22 (s)
(ppm)		P_M: 63.7 (*t*)	
		P_X: 25.4 (dd)	
J(Hz)		P_AP_X: 147	
		P_MP_X: 310	
		P_AP_M: 24	
		P_AH: 277	
$\tilde{\nu}$(CO)	2062 (m)^c	2063 (w)^d	2061 (m)^d
(cm^{-1})	1936 (vs)	2042 (s)	2049 (m)
		2014 (m)	1991 (s)
		1998 (sh)	1979 (s)
		1955 (vs)	1956 (sh)
			1936 (vs)

^{a} In $CDCl_3$; ^{b} in CD_2Cl_2; ^{c} in KBr; ^{d} in CH_2Cl_2.

(Fig. 1b). Since the $J(P_AH)$ coupling at 277 Hz is almost double that of the $J(P_AP_X)$ coupling of 147 Hz, the outermost lines of the both triplets appear only as one line which results in the pattern shown in Fig. 1b ($w_{1/2} \approx 40$ Hz). The P_X nuclei P(2) and P(4) appear as a doublet of doublets at $\delta(P_X) = 25.4$ ppm with the two coupling constants $J(P_AP_X) = 147$ Hz and $J(P_MP_X) = 310$ Hz. The smaller coupling $J(P_AP_X)$ is in accordance with the longer P(2)—P(3) and P(3)—P(4) bonds [2.247(2) and 2.234(3) Å]. The considerably larger $J(P_MP_X)$ corresponds to the shorter P—P distances of the P(1)—P(4) and P(1)—P(2) bonds [2.173(2) and 2.180(2) Å] (Table 2).

Molecular structure of **2**

An ORTEP drawing of the molecular structure of **2** is given in Fig. 2. Selected bond distances and angles are given in Table 2.

The X-ray structure analysis of **2** reveals a $[Cp'Mo(CO)_2]$ moiety capping an allylic P_3 subunit of

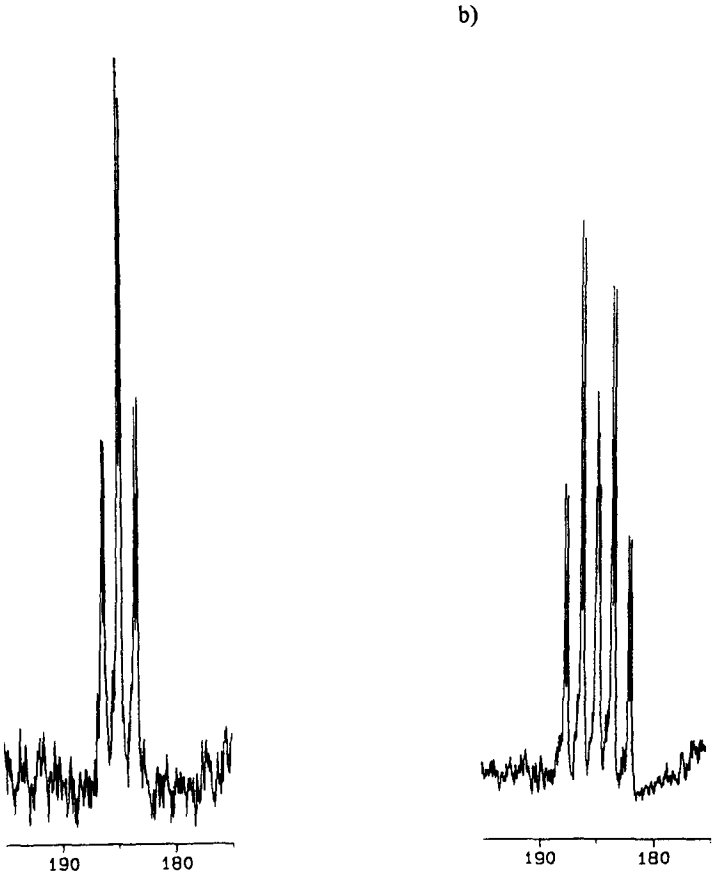

Fig. 1. Details of the ^1H decoupled (a) and coupled (b) ^{31}P NMR spectra for the P_A nucleus of **2**.

Table 2. Selected bond lengths (Å) and selected bond angles (°) for **2**

Mo—P(1)	2.592(2)	P(4)—Mo—P(2)	69.44(7)
Mo—P(2)	2.549(2)	P(4)—Mo—P(1)	50.07(5)
Mo—P(4)	2.542(2)	P(2)—Mo—P(1)	50.17(5)
P(1)—P(2)	2.180(2)	P(4)—P(1)—P(2)	83.54(8)
P(1)—P(4)	2.173(2)	P(1)—P(2)—P(3)	88.94(9)
P(2)—P(3)	2.247(2)	P(4)—P(3)—P(2)	80.64(9)
P(3)—P(4)	2.234(3)	P(1)—P(4)—P(3)	89.45(9)
Cr(1)—P(1)	2.372(2)		
Cr(2)—P(2)	2.355(2)		
Cr(3)—P(3)	2.349(2)		
Cr(4)—P(4)	2.361(2)		

a *cyclo*-P_4 ligand. Additionally all P atoms co-ordinate to $[Cr(CO)_5]$ moieties. The Mo atom is located at a distance of 2.139 Å above the P_3 plane. The P—P bond distances to the P(3) atom, which does not co-ordinate to the Mo atom, are found to be 2.247(2) and 2.234(3) Å, respectively. They are in the range of P—P single bonds [11], whereas the other P—P bond lengths [$\bar{d}$(P(1)—P(2)/(4)) = 2.1765(2) Å] are shorter. Such a P_3/P_1 distortion is also observed in the complexes $[Cp^*Ni(\eta^3\text{-}P_4)\{Cr(CO)_5\}_3\{Cp^*Ni(CO)\}]$ (**4**) [7] and $[\{(CH_3CN)_2(CO)_2WCl\}(\eta^3\text{-}P_4)\{W(CO)_5\}_3(OH)]$ **5** [12]. The P—P bond lengths in **4** and **5** are slightly shorter than in **2** (**4**: $\bar{d}$(P(2)—P(1)/(3)) = 2.166(2) Å, $\bar{d}$(P(4)—P(1)/(3)) 2.217(2) Å; **5**: $\bar{d}$(P(1)—P(2)/(3)) = 2.165(5) Å, $\bar{d}$(P(4)—P(2)/(3)) = 2.207(5) Å). The P(3) atom in **2** lies 42.8° out of the plane defined by the other P atoms. In **5** this angle is almost identical (42°), but the Ni complex **4** shows a considerably smaller angle (28.2°).

We already described the X-ray structure of the Mo_2P_2 tetrahedral complex **3** in [10]. A discussion of the structure of the analogous tungsten complex of **1** can be found in [9].

Discussion of the reaction pathway

The structures of the isolated products give some evidence concerning the transformation pathway of the P_4 tetrahedron in reaction (2). It appears probably that in the first step a P—P bond cleavage in the P_4 tetrahedron occurs and the Mo—Mo bond in $[Cp'Mo(CO)_3]_2$ is split. The formed bicy-

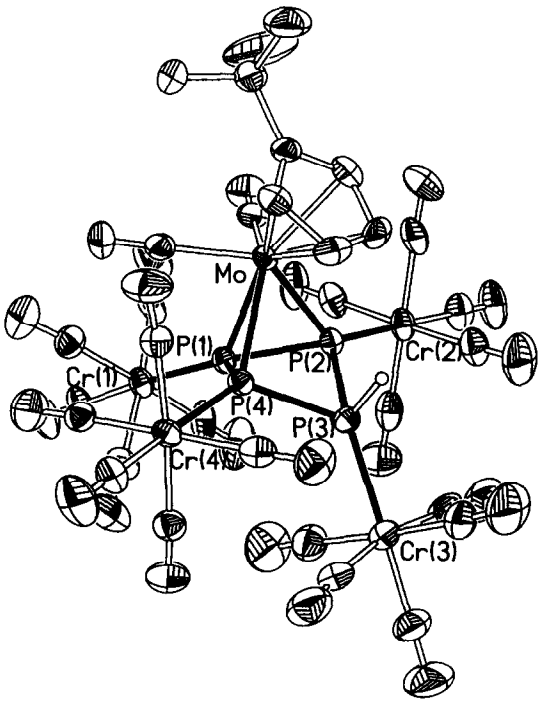

Fig. 2. ORTEP view of the $[Cp'Mo(CO)_2\langle(\eta^3\text{-}P_4)\{Cr(CO)_5\}_4(H)\rangle]$ (**2**) molecule giving the atom number scheme used in Table 2. Thermal ellipsoids are of 50% probability.

clotetraphosphine complex with two σ bound $[Cp'Mo(CO)_3]$ units reacts under CO elimination. Afterwards the formed $[Cp'Mo(CO)_2]$ complex fragment shifts into a capping position in order to yield a η^3-co-ordinating bent *cyclo*-P_4-ligand complex $[Cp'Mo(CO)_2\langle(\eta^3\text{-}P_4)\{Cr(CO)_5\}_4\{Cp'Mo(CO)_3\}\rangle]$ (**2a**). This compound cannot be isolated after chromatographic work-up. The formation of **2** could be caused by a hydrolysis of the σ bound $[Cp'Mo(CO)_3]$ moiety. The further P_3/P_1 fragmentation of **2a** seems to be the main reaction pathway of reaction (2). It should lead to a P_3 ligand complex with all lone pairs of the P atoms co-ordinating to $[Cr(CO)_5]$ groups. It was not possible, to assign signals in the $^{31}P\{^1H\}$ NMR spectrum unambiguously to such a compound due to the possible existence of several products of $[Cp'Mo(CO)_2(\eta^3\text{-}P_3)\{Cr(CO)_5\}_n]$ with a different number of $[Cr(CO)_5]$ units. The P_1 species, formed at the same time, could be a phosphido complex [13] with the formula $[Cp'(CO)_2Mo{\equiv}P \rightarrow Cr(CO)_5]$. Such species with metals in a low oxidation state are not stable as monomers and a dimerisation to the tetrahedral Mo_2P_2 complex **3** readily occurs [14].

The comparison of the discussed pathway of reaction (2) with the three-component-reaction starting from $[Cp^*Ni(\mu\text{-}CO)]_2$ shows an analogy in the two reactions [7]. In both cases the first step seems to be the appearance of an unstable bicyclotetraphosphine complex followed by the formation of a complex with a η^3-co-ordinating, bent P_4 ligand. $[Cp^*Ni(\eta^3\text{-}P_4)\{Cr(CO)_5\}_3\{Cp^*Ni(CO)\}]$ (**4**) is the starting point of two different reaction pathways [7]; (i) the formation of the prismane $[Cp^*_2Ni_2P_4\{Cr(CO)_5\}_2]$ as the main reaction mode and (ii) a P_3/P_1 fragmentation to form the tetrahedral complexes $[Cp^*Ni(\eta^3\text{-}P_3)\{Cr(CO)_5\}_3]$ and $[(Cp^*Ni)_2\{(\mu,\eta^2\text{-}P_4)\{Cr(CO)_5\}_2\}]$, respectively. However, **2a** seems to react exclusively under P_3/P_1 fragmentation to the tetrahedron **3** and a P_3-ligand complex.

EXPERIMENTAL

General

All experiments were performed under a purified N_2 atmosphere using Schlenk techniques. The solvents were dried, degassed and stored under N_2. The molybdenum starting complex $[Cp'Mo(CO)_3]_2$ was pre-

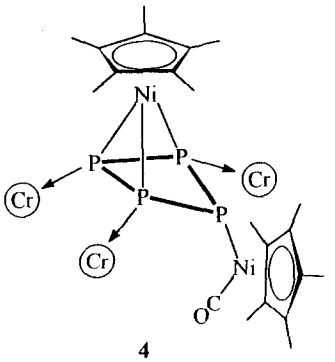

4

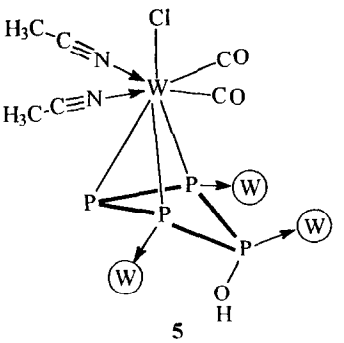

5

(M) = $M(CO)_5$

M = Cr, W

Scheme 3.

pared as previously described [15]. Infrared (IR) spectra were recorded on a Perkin-Elmer PE 883 IR spectrometer, the ^1H and ^{31}P NMR spectra on a Bruker AC 250 [^1H: 250.13 MHz; ^{31}P: 101.256 MHz, Standard: Me_4Si (^1H); 85% H_3PO_4 (^{31}P)].

Reaction of $[Cp'Mo(CO)_3]_2$ *with* P_4 *in the presence of* $[Cr(CO)_5thf]$, *the preparation of* $[Cp'Mo(CO)_2\langle(\eta^3\text{-}P_4)\{Cr(CO)_5\}_4(H)\rangle]$ **(2)** *and* $[\{Cp'Mo(CO)_2\}_2\langle(\mu,\eta^2\text{-}P_2)\{Cr(CO)_5\}_2\rangle]$ **(3)**

(*a*) *Under thermal conditions.* 602 mg (1 mmol) $[Cp'Mo(CO)_3]_2$, 124 mg P_4 (1 mmol) and a solution of 6 mmol $[Cr(CO)_5thf]$ in 20 ml THF, prepared by irradiation of 1.4 g $[Cr(CO)_6]$ in THF, were refluxed for 2 h. The ^{31}P NMR spectrum of the crude reaction mixture shows the exclusive formation of $[Cr(CO)_4\langle(\eta^4\text{-}P_4)\{Cr(CO)_5\}_4\rangle]$ **(1)** [9], which decomposes during chromatographic work-up and unreacted P_4.

(*b*) *Under photochemical conditions.* 602 mg (1 mmol) $[Cp'Mo(CO)_3]_2$, 124 mg P_4 (1 mmol) and a solution of 6 mmol $[Cr(CO)_5thf]$ in 20 ml of THF, prepared by irradiation of 1.4 g $[Cr(CO)_6]$ in THF, were irradiated for 2 h in 250 ml of THF in a UV apparatus (low pressure mercury lamp, TQ 150, Hanau) under internal water cooling to 15°C. All the solvent was removed in vacuum. Unreacted P_4 and $[Cr(CO)_6]$ were removed by sublimation (10^{-3} Torr) at 50–60°C. The brown residue was dissolved in 5 ml CH_2Cl_2, 5 g silicagel was added and subsequently the solvent was removed to dryness. The chromatographic separation on a silicagel column (30 × 1.5 cm; Merck 230–400 mesh) packed with hexane yielded red starting compound $[Cp'Mo(CO)_3]_2$ (240 mg, 40% yield), eluted with hexane, followed by the orange product **2** (90 mg, 8% yield after recrystallization from CH_2Cl_2) eluted with 5:1 hexane/toluene. The reddish brown compound **3** was eluted with 1:2 hexane/toluene (70 mg, 7% yield after recrystallization from CH_2Cl_2).

Crystal structure analysis of **2**

The crystal structure analysis was performed on a STOE STADI IV (ω-scan mode) diffractometer with Mo-K_α radiation ($\lambda = 0.71073$ Å) with empirical absorption corrections (5 Psi-scans). $F(000) = 2296$, $D_{calc} = 1.763$ mg/m^{-3}, 566 parameters, crystal size $0.25 \times 0.20 \times 0.08$ mm, $T = 203(1)$ K, $3 < 2\theta < 50°$. Number of reflections measured 7238, 6635 independent reflections [R(int) = 0.0508] of which 4075 were assigned observed [$I > 2\sigma(I)$], absorption coefficient 1.460 mm^{-1}. The refinement converged at residuals $wR_2 = 0.0966$ for all reflections, corresponding to a conventional $R = 0.0457$ for the observed F_o data. The proton H(3) attached to the P(3) atom was freely refined. Further crystal data and data collection parameters are summarized in Table 3. The structures were solved by direct methods using SHELXS-86 [16a], full-matrix-least-squares refinement on F^2 in SHELXL-93 [16b] with anisotropic displacement for non-H atoms, hydrogen atoms, except H(3), located in idealized positions and refined isotropically according to the riding model. Atomic co-ordinates have been deposited with the Cambridge Crystallographic Data Centre.

Table 3. Crystallographic data for **2**

Formula	$C_{31}H_{14}Cr_4MoO_{22}P_4$
Formula weight (g mol^{-1})	1166.24
Crystal color	Orange
Space group	$P2_1/n$
a(Å)	11.494(7)
b(Å)	16.565(7)
c(Å)	23.497(9)
β(°)	100.88(6)
V(Å^3)	4393(4)
Z	4
D_{calc} (g cm^{-3})	1.763
μ(Mo-K_α) (cm^{-1})	14.60
Temp. (K)	203(1)
R_1[a] ($I > 2\sigma(I)$)	0.0457
wR_2[b] ($I > 2\sigma(I)$)	0.0852

[a] $R_1 = \Sigma||F_o| - |F_c||/\Sigma|F_o|$.
[b] $R_2 = [\Sigma\omega(F_o^2 - F_c^2)^2]/[\Sigma(F_o^2)^2]^{1/2}$.

Acknowledgements—We are grateful to the Deutsche Forschungsgemeinschaft and the Fonds der Chemischen Industrie for financial support.

REFERENCES

1. Reviews: Scheer, M. and Herrmann, E., *Z. Chem.*, 1990, **29,** 41–55; Scherer, O. J., *Angew. Chem.*, 1990, **102,** 1137–1155; *Angew. Chem. Int. ed. Engl.*, 1990, **29,** 1104–1122.
2. Scherer, O. J., Schwarz, G. and Wolmershäuser, G., *Z. anorg. allg. Chem.*, 1996, **622,** 951–957; For possibilities of the transformation of As_4, see: Scherer, O. J., Pfeifer, K. and Wolmershäuser, G., *Chem. Ber.*, 1993, **125,** 2367–2372.
3. (a) Scheer, M., Troitzsch, C. and Jones, P. G., *Angew. Chem.*, 1992, **104,** 1395–1397; *Angew. Chem. Int. ed. Engl.*, 1992, **31,** 1377–1379; (b) Scheer, M., Troitzsch, C., Hilfert, L., Dargatz, M., Kleinpeter, E., Jones, P. G. and Sieler, J., *Chem. Ber.*, 1995, **128,** 251–257.
4. Scheer, M. and Becker, U., *Phosphorus, Sulfur, Silicon*, 1994, **93–94,** 391–392.
5. (a) Scheer, M., Becker, U., Huffman, J. C. and Chisholm, M. H., *J. Organomet. Chem.*, 1993, **461,** C1–C3; (b) Scheer, M. and Becker, U., *J. Organomet. Chem.*, 1997, in press.
6. Scheer, M., Becker, U. and Matern, E., *Chem. Ber.*, 1996, **129,** 721–724.
7. Scheer, M. and Becker, U., *Chem. Ber.*, 1996, **129,** 1307–1310.

8. Scherer, O. J., Sitzmann, H. and Wolmershäuser, G., *Angew. Chem.*, 1985, **97,** 358; *Angew. Chem. Int. Ed. Engl.*, 1985, **24,** 351.
9. Scheer, M., Herrmann, E., Sieler, J. and Oehme, M., *Angew. Chem.*, 1991, **103,** 1023; *Angew. Chem. Int. Ed. Engl.*, 1991, **30,** 969.
10. Scheer, M., Schuster, K., Krug, A. and Hartung, H., *Chem. Ber.*, 1996, **129,** 973–979.
11. Maxwell, L. R., Hendrichs, S. B. and Mosley, Y. M., *J. Chem. Physics*, 1935, **3,** 699; Simon, A., Borrmann, H. and Craubner, H., *Phosphorus and Sulfur*, 1987, **30,** 507; Simon, A., Bormann, H. and Horakh, J., *Chem. Ber.*, 1997, **130,** 1235–1240.
12. Scheer, M. and Dargatz, M., *J. Organomet. Chem.*, 1992, **435,** 259.
13. (a) Scheer, M., Schuster, K., Budzichowski, T. A., Chisholm, M. H. and Streib, W. E., *J. Chem. Soc., Chem. Commun.*, 1995, 1671; (b) Laplaza, C. E., Davis, W. M. and Cummins, C. C., *Angew. Chem.*, 1995, **107,** 2181; *Angew. Chem. Int. Ed. Engl.*, 1995, **34,** 2042; (c) Schrock, R. R., Zanetti, N. C. and Davis, W. N., *Angew. Chem.*, 1995, **107,** 2184; *Angew. Chem. Int. Ed. Engl.*, 1995, **34,** 2044; (d) Scheer, M., Müller, J. and Häser, M., *Angew. Chem.*, 1996, **108,** 2637–2641; *Angew. Chem. Int. Ed. Engl.*, 1996, **35,** 2492–2496.
14. Reviews: Scheer, M., *Coord. Chem. Rev.*, 1997, **163,** 271–286; Scheer, M., *Angew. Chem.*, 1995, **107,** 2151–2153; *Angew. Chem. Int. Ed. Engl.*, 1995, **34,** 1997–1999.
15. Scheer, M., Schuster, K., Schenzel, K., Herrmann, E. and Jones, P. G., *Z. anorg. allg. Chem.*, 1991, **600,** 109.
16. (a) Sheldrick, G. M., *SHELXS*-86, University of Göttingen, 1986; (b) Sheldrick, G. M., *SHELXL*-93, University of Göttingen, 1993.

Pergamon

PII: S0277-5387(97)00479-8

Polyhedron Vol. 17, Nos. 11-12, pp. 1991-1995, 1998
© 1998 Elsevier Science Ltd
All rights reserved. Printed in Great Britain
0277-5387/98 $19.00+0.00

About the existence of Th(III) in aqueous solution

G. Ionova,[a] C. Madic[a] and R. Guillaumont*[b]

[a] DCC/DRDD, Service d'Etude et de Modélisation des Procédés, CEA, ValRhô-Marcoule, BP 171, 30207 Bagnols sur Ceze, Cedex, France

[b] Institut de Physique Nucléaire, IN2P3-CNRS, 91406 Orsay, Cedex, France

(Received 18 September 1997; accepted 17 November 1997)

Abstract—Recently [1] it was claimed that (i) the reaction of $ThCl_4$ with HN_3 in slightly acidic aqueous solution produces the aqueous ion of Th(III) according to the thermodynamically allowed reaction: $Th^{4+} + HN_3 \rightarrow Th^{3+} + 1.5N_2 + H^+$; (ii) Th(III) was identified by its absorption (UV–vis. 200–1300 nm) and ESR spectra. This paper is aimed to prove that the aqueous ion Th^{3+}(aq) is thermodynamically unstable and that the identification of Th(III) in the considered solutions ask for new experiments. © 1998 Elsevier Science Ltd. All rights reserved

Keywords: actinides; thorium; electronic configuration; crystal field effect.

Among the chemical properties of the lanthanides, Ln, and actinides, An, the stabilities of aqueous ions in "unusual" oxidation states involving a *d*-electron in the electronic configuration of the ground state of Ln and An is of particular interest [2,3]. The ground electronic configuration of an ion is not always the same in the gaseous state, for instance for Ln and An it could be f^q or $f^{q-1}d$, $f^{q-1}s$ or $f^{q-1}p$ [4,6]. For a gaseous ion, these two configurations are separated by the promotion energy, ΔE. For Th^{3+} gaseous ion, it is known from 50 years ago [4a] that the energies of the configurations $6d^1$ ($^2D_{3/2}$), $7s^1$ ($^2S_{1/2}$) and $7p^1$ ($^2P_{1/2}$) relative to $5f^1$ ($^2F_{5/2}$) are respectively: 1.13856 eV, 2.869 eV and 7.482 eV. Thus for Th^{3+} gaseous ion ΔE, between $5f^1$ and $6d^1$ configurations, is equal to 1.14 eV. This ion belongs to the same category as Np^{2+} ($\Delta E = 0.51$ eV), Pu^{2+} ($\Delta E = 1.61$ eV), Cm^{2+} ($\Delta E = 0.88$ eV) and Pa^{3+} ($\Delta E = 2.07$ eV) [4].

The crystal field effect of ligands, i.e. water molecules, measured by $\Delta(d)$, stabilizes the electronic configurations $6d^1$ by an energy D ($D > 0$, $D > \Delta E$). That is the reason why the old, -3.7 V, [6] recommended redox potential for the pair Th^{4+} (aq)/Th^{3+} (aq) was increased to -3.0 V [5]. It was recently claimed that such potential, -3 V, allows the reduction of Th^{4+} aqueous ion to a Th^{3+} ion, using hydrazoic acid HN_3 [1].

* Author to whom correspondence should be addressed.

The first part of this paper is devoted to a short analysis of the potentials $E^0(3/2)$ with $f^{q-1}d$ electronic configuration for the reduced specie, to the comparison between $E^0(4/3)$ for Th and Pa and a discussion of the recommended potentials $E^0(4/3)$ for Th given in [5] and [6] in the frame of the crystal field stabilization, D, of a $6d$ electron. In the second part the possibility of the reduction of Th^{4+} ion by HN_3 is considered. Finally, in the last part absorption and ESR spectra, assigned in [1] to a trivalent thorium species, are discussed.

CONSIDERATION ABOUT THORIUM IV/III REDOX POTENTIAL

The stabilization of *d* electrons by crystal field effect was taken into account for the first time in [6] and then in [5], to estimate the redox potentials $E^0(3/2)$ and $E^0(4/3)$ of Ln and An. Unfortunately in [5] the crystal field stabilization was taken twice resulting in an increase of the redox potentials $E^0(3/2)$ (more positive than -3 V) for some dipositive Ln (La^{2+}, Ce^{2+}, Gd^{2+}) and An (Pa^{2+}, U^{2+}, Np^{2+}) ions. Therefore it was emphasized that the ions Ac^{2+}, Th^{2+}, Pa^{2+}, U^{2+}, Np^{2+}, La^{2+}, Ce^{2+} and Gd^{2+} could be stable in aqueous solution.

On the other hand, it was proposed that for the two cations Pa^{3+} (aq) and Th^{3+} (aq) the electronic

configurations are respectively, fd and f [5]. Regarding the crystal field stabilization effect, D, two limiting cases have to be considered, the weak, $D < \Delta E$, and the strong one, $D > \Delta E$ (Fig. 1). In the former case the electronic configurations f^1 and f^2 should be realized in Th^{3+}(aq) and Pa^{3+}(aq) respectively. The value for the $E^0(4/3)$ (in short for $M^{4+}(aq)/M^{3+}(aq)$) of An with the f^q electron configuration for An^{3+} is given according to [6] by:

$$E^0(4/3)(V) = -4.00 + 1.37\,(q-1) + F_{q-1} \quad (1)$$

From the eqn (1) and with F_{q-1} values from [6] one has: $q = 1$, $F_{q-1} = 0.18$ V and $E^0_{Th}(4/3) = -3.82$ V for Th; $q = 2$, $F_{q-1} = 0.53$ V and $E^0_{Pa}(4/3) = -2.1$ V for Pa if $D(Th^{3+}(aq)) < 1.14$ eV and $D(Pa^{3+}(aq)) < 2.07$ eV, which correspond to the case of a weak crystal field effect.

In order to realize respectively the fd and d electronic configurations in Pa^{3+}(aq) and Th^{3+}(aq) ΔE should be higher than 1.4 eV in the case of Th^{3+}(aq) and higher than 2.07 eV for Pa^{3+}(aq). In this case the eqn (1) is rewritten:

$$E^0(4/3) = -4.00 + 1.37\,(q-1) + F_{q+1} - D - \Delta E \quad (2)$$

or

$$E^0_{Th}(4/3) = -4.96 + D \quad (3)$$

$$E^0_{Pa}(4/3) = -4.17 + D \quad (4)$$

For the Ln and An complexes there are no experimental data concerning the crystal field effects $\Delta(d)$ and the stabilization energy D. From calculations for U(IV) complexes with ligands L = F, O, Cl, Br and I in octahedral ($CN = 6$) and cubic ($CN = 8$) crystal fields by relativistic Xα SW method, the values of $\Delta(d)$ have been calculated [7]. In the case of cluster complexes $U(IV)O_6^{8-}$, which are the closer to the Th(IV) aqueous ion, the calculated values $\Delta(d)$ are 3.15 and 2.80 eV respectively. The $6d$ electron stabilizations D are 1.26 eV ($CN = 6$) and 1.68 eV ($CN = 8$). For a given element the value of D decreases with the decrease of the oxidation state. Thus, in the case U^{3+} (and Th^{3+}) the stabilization energy, D, should be less than 1.3 eV ($CN = 6$) and 1.70 eV ($CN = 8$). From spectral data (d-d transitions) for fluoride complexes of $5d$ metals, even in the oxidation states IV–VI, the values of D do not exceed 1.7 eV. Consequently the electronic configuration of Pa^{3+}(aq) is rather f^2 with a small energy gap f^2–fd and $E^0_{Pa}(4/3) = -2.1$ V according to eqn (1). The small excitation energy f^2–fd is one of the reasons of the instability of Pa^{3+}(aq).

The same situation (but with d-f electronic transition or $E(fd) < 0$) occurs for the Th^{3+} species with $D < 1.7$ eV for Th^{3+}(aq) ($CN = 8$–9). The value of $E^0_{Th}(4/3)$ may follow both the eqn (1) or (2) since

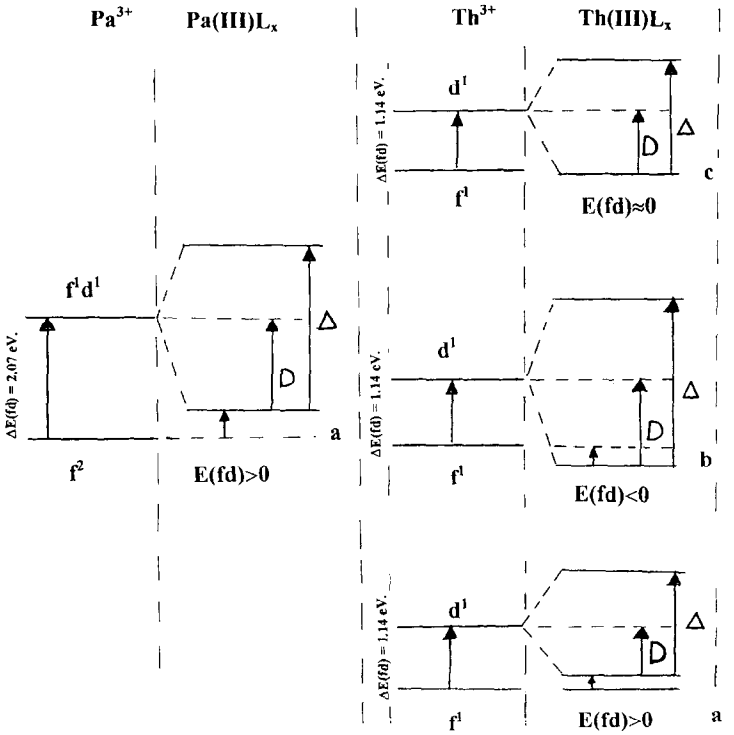

Fig. 1. Stabilization of a $6d$ electron of Th^{3+} and Pa^{3+} by crystal field effect; a: $D < \Delta E(fd)$; b: $D > \Delta E(fd)$; c: D around $\Delta E(fd)$.

$\Delta E(\mathrm{Th}) = 1.14$ eV $< \Delta E(\mathrm{Pa}) = 2.07$ eV. The probability that d^1 configuration is the lowest in energy is larger for $Th^{3+}(aq)$ than for $Pa^{3+}(aq)$. In [5] and [6] the values of D are 1.96 and 1.26 eV respectively. The first one seems too large and the second one rather small. Thus, with an average value of 1.16 eV (Fig. 1b) and accordingly to the eqn (2) corresponding to a $6d$ lowest configuration, the redox potential $E^0_{\mathrm{Th}}(4/3) = -3.35$ V.

For these reasons the instability of $Th^{3+}(aq)$ like $Pa^{3+}(aq)$ ion seems clear. Thus, with a good probability we may accept that $E^0_{\mathrm{Th}}(4/3) = -3.35$ V (d electronic configuration) (Fig. 1b) $> E^0_{\mathrm{Th}}(4/3) > -3.82$ V (f electronic configuration) (Fig. 1a), considering that for $Th^{3+}(aq)$ a pseudo-degenerated f and d configuration can not be completely ruled out (Fig. 1c).

The reducing ability of HN_3

The dissolution of HN_3 in water gives a weakly acidic solution [9] and its redox behaviour in acidic solutions is quite complex, as the following reactions show:

$$HN_3 = H^+(aq) + N^{3-}(aq) \quad pK_a = 4.77 \qquad (5)$$

$$3NH_4^+ = HN_3 + 11H^+ + 8e^- \quad E^0_{298} = +0.66\ V \qquad (6)$$

$$NH_4^+ + N_2 = HN_3 + 3H^+ + 2e^- \quad E^0_{298} = +1.82\ V \qquad (7)$$

$$HN_3 = 3/2\,N_2 + H^+ + e^- \quad E^0_{298} = -2.80\ V \qquad (8)$$

In [1] the value of the redox potential for the reaction (8), $E^0(8)$, used for the discussion was fixed at -3.54 V but not at -2.80 V and for the reaction:

$$Th^{4+} + HN_3 = Th^{3+} + 1.5\,N_2 + H^+ \qquad (9)$$

the potential ΔE^0 was estimated as

$$\Delta E^0 = E^0_{\mathrm{Th}}(4/3) - E^0(8) = -3.0 + 3.54 = +0.54\ V \qquad (10)$$

which was the basis to conclude that the reaction (9) is thermodynamically allowed. With the potential $E^0_{\mathrm{Th}}(4/3) = -3.35$ V or -3.82 (and even with -3.0 V) and $E^0(8) = -2.8$ V, ΔE^0 has a negative value, which indicates that, in fact, the reaction (9) is not thermodynamically allowed.

But there are other reasons. The potential $E^0(UO_2^{2+}/U^{4+})$ in acid solution is $+0.27$ V [10]. Using the eqns (9) and (10) to forecast the reduction of U(VI) by HN_3, led to the conclusion that this reduction is thermodynamically allowed, but it was established that HN_3 does not reduce U(VI) or U(IV) [21]. The matter is that in acid solution the scheme of potentials for HN_3 follows the step reactions (6) to (8). In analytical chemistry, the reaction of formation of ferric azide, FeN_3^{2+}, when hydrazoic acid reacts with ferric chloride is used for the qualitative test of the presence of Fe(III) [11]. However the hydrazoic acid does not reduce Fe(III) to Fe(II) although the potential $E^0(3/2)$ for Fe is $+0.77$ V [12]. Finally in neutral solution of thorium salt, the azide anion promotes thorium hydroxide formation and does not form thorium azide:

$$Th(NO_3)_4 + 4KN_3 + 4H_2O = Th(OH)_4 + 4KNO_3 + 4HN_3 \qquad (11)$$

The reaction (11) is used both in qualitative and quantitative determination of Th in the presence of lanthanides. Under the same circumstances, U and Zr are also precipitated as hydroxides [13].

In conclusion there is no firm basis to consider the reaction (9) as thermodynamically allowed.

About the identification of Th^{3+} *in* HN_3 *solutions*

In the resultant solutions of the reduction of $ThCl_4$ with HN_3 the complexes of Th(III), $[Th(H_2O)_x(N_3)_yCl_z]^{3-y-z}$, are supposed to involve N_3, Cl and H_2O ligands. In the tetravalent azido-chloro-complexes of tetravalent Ti, Zr and Hf both terminal, $[(MCl_4(N_3)_2]^{2-}$, and 1, 1μ-N, $[(M_2Cl_8(N_3)_2]^{2-}$, bonding was found for N_3 [14]. If Th(III) or Th(IV) azides exist within the conditions of the considered experiments, the absorption spectra must be explained.

In [1] room temperature optical spectra of proposed Th(III) solution were measured and discussed for a Th concentration of 0.3 mol l^{-1} at pH around 3.5. The quoted concentration is not the result of measurements but is based on the assumption of a 100% yield for the reaction (9) starting with HN_3 2 mol l^{-1} and Th 0.3 mol l^{-1}. The broad band with a maximum at 460 nm = 21.7 kK (which could correspond also to the absorption of ferric azide FeN_3^{2+} [11]), and the peaks at 332 nm = 30.1 kK, 190 mm = 52.6 kK and 185 nm = 54.1 kK were assigned to the $f \Rightarrow d$ and metal $\Rightarrow$ ligand allowed transitions.

Since reaction (9) is not thermodynamically allowed, let us accept for the discussion that the measured spectrum corresponds to an azide complex of Th(IV) involving also chlorine ligands. The linear azide anion belongs to $D_{\infty h}$ point group. In the $^1\Sigma_g^+$ ground state the 16 valent electrons occupy the 6 MO: $1\sigma_g^2\ 1\sigma_u^2\ 2\sigma_g^2\ 2\sigma_u^2\ 1\pi_u^4\ D_{\infty h} 1\pi_g^4$. The highest occupied molecular orbital is the non bonding π_g. Complexes of Th(IV) with ligands having mobile π electron system (most often azo-group) like the azide anion with the non-bonding π electrons have absorption bands within 320–680 nm [15]. For example the dissolution of $Th(C_9H_6ON)_4$, which is the precipitate of Th by 8-hydroxyquinoline, in 0.1 mol l^{-1} HCl shows absorption at 320–330 nm [15]. In contrast with that on the spectrum reported in [1] at below 650 nm the broad

band until 420 nm (centred at 460 nm) was interpreted as the $f \Rightarrow d$ transition for a trivalent Th complex.

Two kinds of charge transfer bands in the considered complex can be proposed: $N_3^- \Rightarrow Th^{4+}$ and $Cl^- \Rightarrow Th^{4+}$. The intensive absorption at 332, 190 and below 185 nm were interpreted as charge transfer transitions. In fact, the first one (at 332 and 460 nm) could be assigned to $N_3^- \Rightarrow Th^{4+}$ transition and the second and third (at 190 and below 185 nm) could be assigned to the charge transfer $Cl^- \Rightarrow Th^{4+}$.

The equation connecting the charge transfer bands $E(Cl^- \Rightarrow An^{3+})$ and $E(Cl^- \Rightarrow An^{4+})$ for the tetravalent and trivalent actinide chlorine complexes is:

$$E(Cl^- \Rightarrow An^{4+}) = E(Cl^- \Rightarrow An^{3+}) + V_q + \Delta F_q \quad (12)$$

with $V_q = -33.28$ kK and ΔF_q being evaluated using the approach given in [6]. The correlation between $E(Cl^- \Rightarrow An^{4+})$ and $E(Cl^- \Rightarrow An^{3+})$ can be established (Table 1). For simplicity octahedral complexes MCl_6^{3-} and MCl_6^{2-} are only considered, although the charge transfer energies can be easily recalculated for any symmetry and any CN.

The agreement between the experimental and calculated values $E(Cl^- \Rightarrow An^{4+})$ for An = Pa, U, Np and Pu shows the good validity of eqn (12). It means that values of the charge transfer energies for the considered thorium complexes are satisfactory. The charge transfer energies $E(Cl^- \Rightarrow An^{3+})$ and $E(Cl^- \Rightarrow An^{4+})$ differ approximately on 30 kK. Thus, the intensive absorption "below 185 nm = 54 kK" [1] corresponds to the chlorine-Th(IV) charge transfer (in $ThCl_6^{2-}$ one is at 156 nm ≈ 64.2 kK). In the case of non-octahedral symmetry and higher CN the charge transfer energy would be a little changed. In the part of spectra at about 100 nm (eqn (12) and Table 1) where the charge transfer $Cl^- \Rightarrow Th^{3+}$ is expected, any absorption is measured in [1]. With other hand, the $f \Rightarrow d$ transition in Th(III) complex is waited to be about 1200–1300 nm. These transitions are not observed in [1].

Optical spectra do not confirm firmly the existence of trivalent thorium but rather those of Th(IV) complexes.

Finally, the ESR spectrum of a frozen solution was given in [1]. The very broad signal is seen very similar in shape to that of UCl_5SOCl_2. The average value of g tensor was measured as $g = 2.19$.

For $[Th(III)\{\eta^5\text{-}C_5H_3(SiMe_3)_2\}]$ the average experimental value of g, $g = 1.91 \pm 0.001$, is interpreted with the assumption of a $6d$ electron configuration [18]. One can see that g values in [1] and [18] differ significantly for a $6d$ electron configuration, which exist in the former case and is assumed in the later. To go further in the discussion let us propose a $5f^1$ configuration for Th, it is to say let assume the existence of Th(III). The g values for the $5f^1$ electron configuration, for example, in UCl_5SOCl_2, UCl_5, $PaCl_5$, $RbUCl_6$ and other compounds is about 1.1 with the sign undetermined (+ or −) [19]. In [20] the value of g for UCl_5SOCl_2 is negative, $g = -1.18$. Thus, it is difficult to understand why the authors of [1] consider an ESR spectrum with $g = 2.19$ as "very similar" to the spectra of UCl_5SOCl_2 with $g = -1.18$.

It seems that the measured ESR spectrum is not connected with Th(III). Without the measurement of the concentration of spins, it is impossible to discuss ESR spectra. Besides, it is known that the decomposition of HN_3 can go through a variety of ways involving the formation of various radicals like nitrogen and imine radical [9,16].

CONCLUSION

In conclusion thermodynamic considerations, room temperature absorption spectra as well as ESR investigations do not support the first observation of Th(III) species in aqueous solution.

REFERENCES

1. Klapotke, T. M. and Schulz, A., *Polyhedron*, 1997, **16**(6), 989.

Table 1. Relation between the charge-transfer energy for the tri- and tetravalent actinide chlorine complexes. All data are in kK

An (ΔF_q) [6]	$E(Cl^- \Rightarrow An^{3+})$ [2]	$E(Cl^- \Rightarrow An^{4+})$ calc. [2]	$E(Cl^- \Rightarrow An^{4+})$, exp. [17]
Th (2.825)	94.6	64.2	—
Pa (0.805)	82.9	82.9	50.4
U (−5.08)	77.02	38.7	39.0
Np (−5.566)	71.65	32.8	31.0
Pu (−0.161)	60.86	27.4	27.0
Am (0.483)	49.0	16.2	—
Cm (−26.46)	64.95	5.21	—
Bk (2.03)	51.98	20.7	21.0

2. Ionova, G., Krupa, J. C., Gerard, I. and Guillaumont, R., *New J. Chem.*, 1995, **19**(19), 677.
3. David, F., Ionova, G. and Guillaumont, R., *J. Radioanal. Nucl. Lett.*, 1995, **199**(1), 35.
4. (a) Klinkerberg, P. F. and Lang, R. G., *Physica*, 1949, **15,** 774; (b) Nugent, L. J. and Vander Sluis, K. L., *J. Opt. Soc. Am.*, 1971, **61,** 1112.
5. Bratsch, S. G. and Lagowski, J. J., *J. Phys. Chem.*, 1986, **90,** 307.
6. Nugent, L. J., Baybarz, R. D., Burnett, J. L. and Ryan, J. L., *J. Phys. Chem.*, 1973, **77,** 1528.
7. Suraeva, N. I., Ph. Dissertation, Institute of Physical Chemistry of Russian Academy of Sciences, Moscow, 1989.
8. Lever, A. B., *Inorganic Electronic Spectroscopy*. Elsevier, 1968, p. 118.
9. Jones, K., In *Comprehensive Inorganic Chemistry*, Vol. 1, ed. J. C. Baylar. Pergamon Press, 1973, 294.
10. Morss, L. R., *Chemistry of Actinide Elements*, 2nd edn, Vol. 2, ed. J.. J. Katz and L. Morss. Chapman and Hall, New York, 1986, p. 1278.
11. Roberson, C. E. and Austin, C. M., *Anal. Chemistry*, 1957, **29**(5), 854.
12. Latimer, W. M., *The Oxidation States of the Elements and their Potentials in Aqueous Solutions*, 2nd edn. Prentice Hall, 1952.
13. Muller, M., *Inorganic and Theoretical Chemistry*, Vol. 2. Longmans, Green and Co, London, 1957, p. 334–354.
14. Wilkinson, G., *Comprehensive Coordination Chemistry*, Vol. 2. Pergamon Press, 1987, p. 228.
15. Ryabchikov, D. I. and Gol'braikh, E. K., *The Analytical Chemistry of Thorium*. Pergamon Press, 1963, p. 35.
16. Kelly, P. and Smith, M., *J. Chem. Soc.*, 1961, 1479.
17. Jörgensen, C. K. and Ryan, J. L., *Mol. Phys.*, 1963, **7,** 17.
18. Kot, W., Salimoff, G. and Edelstein, N. M., *J. Am. Chem. Soc.*, 1988, **110,** 986.
19. Selbin, J. and Ortego, J. D., *Chem. Rev.*, 1969, **7,** 657.
20. Karraker, D. G., *Inorg. Chem.*, 1964, **3,** 1618.
21. Maslenikov, A. and Nikitenko, S., Private communication.

Pergamon

PII: S0277-5387(97)00486-5

Polyhedron Vol. 17, Nos. 11–12, pp. 1997–2007, 1998
© 1998 Elsevier Science Ltd
All rights reserved. Printed in Great Britain
0277-5387/98 $19.00+0.00

Synthesis and structures of ruthenium(II) mono[1,2-phenylenebis(dimethylarsine)] complexes: precursors to *trans* metal-to-ligand charge-transfer chromophoric assemblies

Benjamin J. Coe,* Christopher I. McDonald and Roy L. Beddoes

Department of Chemistry, University of Manchester, Oxford Road, Manchester M13 9PL, U.K.

(Received 30 September 1997; accepted 14 November 1997)

Abstract—The complex *fac*-[$RuCl_3$(pdma)(NO)] [pdma = 1,2-phenylenebis(dimethylarsine)] reacts with silver(I) salts, AgX, at room temperature in acetonitrile to afford disubstituted derivatives *cis*-[$RuClX_2$(pdma)(NO)] (X^- = trifluoroacetate **1**, *p*-toluenesulphonate **2** or nitrate **3**). Reflux of *fac*-[$RuCl_3$(pdma)(NO)] in 1 : 4 pyridine/methanol containing an excess of AgO_2CCF_3 causes conversion into *cis*-[Ru(OMe)(pdma)$(py)_2$(NO)][PF_6]$_2$ **4** (py = pyridine). Reaction of *fac*-[$RuCl_3$(pdma)(NO)] in refluxing 1 : 7 pyridine/acetonitrile containing 2 equivalents of AgO_2CCF_3 affords *cis*-[RuCl(pdma)$(py)_2$(NO)][PF_6]$_2$ (**5**). **5** is also prepared by reaction of **1** in refluxing pyridine/acetonitrile. The mixed-chelate salts *trans*-[RuCl(pdma)(L—L)(NO)][PF_6]$_n$ [n = 2, L—L = 2,2′-bipyridine **6**, 1,10-phenanthroline **7**, 4,4′-dimethyl-2,2′-bipyridine **8** or 1,2-bis(diphenylphosphino)ethane **9**; n = 1, L—L = picolinate **10**] are produced by reaction of *fac*-[$RuCl_3$(pdma)(NO)] with an excess of L—L in refluxing methanol. The yields of the reactions to produce **5–10** vary according to the ligating ability of the incoming ligand(s). Single-crystal structures of *fac*-[$RuCl_3$(pdma)(NO)], **2**·Me_2CO, **3** and **6** have been determined. **3** is the first ruthenium complex containing monodentate nitrato ligand(s) to be structurally characterized. © 1998 Elsevier Science Ltd. All rights reserved

Keywords: ruthenium complexes; ligands; synthesis.

Photoactive ruthenium(II) complexes containing α-diimmine ligands such as 2,2′-bipyridine (bipy) or 1,10-phenanthroline (phen) are of particular current interest for potential applications in "photochemical molecular devices" (PMDs) [1]. A metal-based PMD exploits metal-to-ligand charge-transfer (MLCT) excitations to trigger electron or energy-transfers which result in potentially useful phenomena, e.g. long-lived photoinduced charge-separations. A combination of electronic and stereochemical factors determine the utility of an MLCT chromophore in a PMD, and recent studies in this field have featured an increasing emphasis on stereochemical aspects [2–4]. We are developing strategies for controlled ligand substitutions at octahedral metal centres as a means to create functionalized chromophoric *trans* complexes. Work with complexes based on *trans*-$\{Ru(bipy)_2\}^{2+}$ centres was synthetically successful [5], but the products suffer from poor photostability and tend to isomerize to their more stable *cis* forms. Related complexes containing only a single bipy or other α-diimmine ligand are expected to feature potentially useful photoexcitation properties, combined with greatly improved stability.

We have recently begun to explore the derivative chemistry of the complex *trans*-[$RuCl(pdma)_2(NO)]^{2+}$ [pdma = 1,2-phenylenebis(dimethylarsine)] [6]. The *trans*-$\{Ru(pdma)_2\}^{2+}$ core provides a highly stable platform for stepwise axial substitutions of the chloride and nitrosyl ligands, without any isomerization. We have incorporated this non-chromophoric centre into ligand-bridged dinuclear complexes which are of interest for the study of intervalence transfer properties [7]. The complex *fac*-[$RuCl_3$(pdma)(NO)] was first reported in 1966 [8], together with a series of related complexes *fac*-[$RuCl_3L_2$(NO)] (L = triphenylphosphine, etc.). The only one of these to be subjected to attempts at chloride substitutions, *fac*-

* Author to whom correspondence should be addressed. E-mail: b.coe@man.ac.uk

$[RuCl_3py_2(NO)]$ (py = pyridine) was reportedly inert, even drastic reaction conditions leading only to decomposition. However, *fac*-$[RuCl_3(pdma)(NO)]$ is known to be an intermediate in the synthesis of *trans*-$[RuCl(pdma)_2(NO)]Cl_2$ [9], demonstrating that the former is amenable to chloride substitutions. We hence sought to investigate the derivative chemistry of *fac*-$[RuCl_3(pdma)(NO)]$, with the primary objective of preparing mixed-chelate *trans*-NO/Cl complexes of α-diimmine ligands which will serve as precursors to stable MLCT chromophoric assemblies.

EXPERIMENTAL

Materials and procedures

The compound $RuCl_3 \cdot 2H_2O$ was supplied by Johnson Matthey plc and pdma was obtained from Dr P. G. Edwards, University of Wales College of Cardiff. The complex *fac*-$[RuCl_3(pdma)(NO)]$ was prepared according to a published procedure [8]. All other reagents were obtained commercially and used as supplied. All reactions were conducted under an argon atmosphere. Products were dried overnight at room temperature in a vacuum desiccator ($CaSO_4$) prior to characterization.

Instrumentation

^{1}H NMR spectra were recorded on a Varian Gemini 200 spectrometer and all shifts are referenced to $SiMe_4$. The complex fine splitting of the pyridine or 2,2′-bipyridine proton resonances is ignored and the signals are reported as simple doublets or triplets. The ^{19}F NMR spectrum of **1** was recorded on a Varian Unity 500 spectrometer with $CFCl_3$ as reference. Elemental analyses were performed by the Microanalytical Laboratory, University of Manchester. Infrared spectra were obtained as KBr discs with an ATI Mattson Genesis Series FTIR instrument. FAB mass spectra were recorded using a Kratos Concept spectrometer with a 6–8 keV Xe atom beam and 3-nitrobenzyl alcohol as matrix.

Cyclic voltammetric measurements were carried out using an EG&G PAR model 173 potentiostat/galvanostat with a model 175 universal programmer. A single-compartment cell was used with the saturated calomel reference electrode (SCE) separated by a salt bridge from the platinum-bead working electrode and platinum-wire auxiliary electrode. Acetonitrile (HPLC grade) was used as received and tetra-*n*-butylammonium hexafluorophosphate, twice recrystallized from ethanol and dried *in vacuo*, was used as supporting electrolyte. Solutions containing ca 10^{-3} mol dm^{-3} analyte (0.1 mol dm^{-3} electrolyte) were deaerated by purging with N_2. All $E_{1/2}$ values were calculated from $(E_{pa}+E_{pc})/2$ at a scan rate of 200 mV s^{-1}.

Preparations

cis-$[RuCl(CF_3CO_2)_2(pdma)(NO)]$ (**1**). To a solution of *fac*-$[RuCl_3(pdma)(NO)]$ (100 mg, 0.191 mmol) in acetonitrile (30 cm^3) was added AgO_2CCF_3 (136 mg, 0.616 mmol) in acetonitrile (5 cm^3). Immediate precipitation of AgCl was observed, and the reaction was stirred at room temperature for 24 h. The solvent was reduced to a small volume *in vacuo*, and the AgCl was removed by filtration through celite. Addition of water to the golden filtrate solution caused precipitation of the product which was filtered off and washed with water. The product was precipitated once more from acetone-water and dried to yield a pale golden solid. Yield: 85 mg, 66%. Found: C, 25.2; H, 2.35; N, 2.55. Calc. for $C_{14}H_{16}As_2ClF_6NO_5Ru$: C, 24.8; H, 2.40; N, 2.05%. ^{1}H NMR data (200 MHz, CD_3COCD_3): δ 8.22 (2 H, m, C_6H_2), 7.83 (2 H, m, C_6H_2), 2.18 (6 H, s, 2AsMe), 2.15 (6 H, s, 2AsMe). ^{19}F NMR data (500 MHz, CD_3COCD_3): δ −75.38 (s). ν(N≡O) 1882 vs, ν(C=O) 1688 vs, ν(C—O) 1195 vs and 1141 s cm^{-1}. *m/z*: 566 ($[M-CF_3CO_2^-]^+$) and 453 ($[M-2CF_3CO_2^-]^+$).

cis-$[RuCl(C_7H_7SO_3)_2(pdma)(NO)]$ (**2**). This complex was prepared in similar manner to **1** by using $AgO_3SC_7H_7$ (174 mg, 0.624 mmol) in place of AgO_2CCF_3. After evaporation to a small volume, dichloromethane was added and the AgCl and excess $AgO_3SC_7H_7$ were removed by filtration through celite. The solution was evaporated to dryness and dichloromethane was added. Further $AgO_3SC_7H_7$ was removed by filtration through celite and acetone was added to the filtrate. Slow evaporation of the dichloromethane *in vacuo* caused precipitation of the product. This was filtered off, washed with acetone then water, and dried to yield a golden microcrystalline solid. Yield: 106 mg, 65%. Found: C, 37.95; H, 4.05; N, 1.55; S, 7.35. Calc. for $C_{24}H_{30}As_2ClNO_7RuS_2 \cdot C_3H_6O$: C, 38.0; H, 4.25; N, 1.65; S, 7.50%. ^{1}H NMR data (200 MHz, $CDCl_3$): δ 7.86 (4 H, d, J = 8.1 Hz, Me-C_6H_4-SO_3), 7.77 (4 H, m, C_6H_4), 7.17 (4 H, d, J = 8.1 Hz, Me-C_6H_4-SO_3), 2.49 (6 H, s, 2AsMe), 2.38 (6 H, s, 2Me), 2.06 (6 H, s, 2AsMe). ν(N≡O) 1881 vs, ν(S=O) 1256 s, 1153 s and 1102 s cm^{-1}. *m/z*: 625 ($[M-C_7H_7SO_3^-]^+$) and 453 ($[M-2C_7H_7SO_3^-]^+$).

cis-$[RuCl(NO_3)_2(pdma)(NO)]$ (**3**). This complex was prepared in similar manner to **1** by using $AgNO_3$ (83 mg, 0.489 mmol) in place of AgO_2CCF_3. The AgCl was removed by filtration through celite and the yellow filtrate was evaporated almost to dryness. This caused precipitation of the orange product which was filtered off and washed with acetonitrile. The product was washed with aqueous $Na_2S_2O_3$ to remove residual AgCl, then washed with water and dried. Yield: 70 mg, 64%. Found: C, 20.5; H, 3.10; N, 7.25. Calc. for $C_{10}H_{16}As_2ClN_3O_7Ru$: C, 20.85; H, 2.80; N, 7.30%. ν(N≡O) 1865 vs, $\nu_{as}(NO_2)$ 1477 vs, $\nu_s(NO_2)$ 1262 vs, ν (N—O) 1000 m cm^{-1}.

cis-$[Ru(OMe)(pdma)(py)_2(NO)]PF_6]_2$ (**4**). A solu-

tion of *fac*-[$RuCl_3$(pdma)(NO)] (100 mg, 0.191 mmol) and AgO_2CCF_3 (215 mg, 0.973 mmol) in methanol (40 cm^3) and pyridine (10 cm^3) was heated at reflux for 14 h. The solvent was reduced to a small volume *in vacuo*, acetone was added and the AgCl was removed by filtration through celite. Aqueous NH_4PF_6 was added to the filtrate and the acetone was evaporated slowly *in vacuo*, causing formation of a yellow precipitate which was filtered off and washed with water. The crude product was reprecipitated from acetone-aqueous NH_4PF_6 and dried (130 mg). Purification was effected by three precipitations from acetone-diethyl ether to afford a gold solid. Yield: 73 mg, 43%. Found: C, 28.3; H, 3.70; N, 4.80. Calc. for $C_{21}H_{29}As_2F_{12}N_3O_2P_2Ru$: C, 28.15; H, 3.25; N, 4.70%. ^1H NMR data (200 MHz, CD_3COCD_3): δ 9.03 (4 H, d, $2H^{2,6}$), 8.38 (2 H, m, C_6H_2), 8.31 (2 H, t, H^4), 8.00 (2 H, m, C_6H_2), 7.85 (4 H, t, $2H^{3,5}$), 3.77 (3 H, s, OMe), 2.34 (6 H, s, 2AsMe), 2.22 (6 H, s, 2AsMe). ν(C—H) 2934 m and 2807 m, ν(N≡O) 1848 vs cm^{-1}. *m/z*: 752 ($[M-PF_6^-]^+$).

cis-[RuCl(pdma)$(py)_2$(NO)][PF_6]$_2$ (**5**). A solution of *fac*-[$RuCl_3$(pdma)(NO)] (100 mg, 0.191 mmol) and AgO_2CCF_3 (85 mg, 0.385 mmol) in acetonitrile (35 cm^3) and pyridine (5 cm^3) was heated at reflux for 30 min. The solvent was reduced to a small volume *in vacuo*, aqueous NH_4PF_6 was added and the precipitate was filtered off and washed with water. The crude product was dissolved through the frit in acetone to leave most of the AgCl, the remainder of which was removed by filtration through celite. The product was then precipitated by addition of aqueous NH_4PF_6, filtered off, washed with water and dried. Purification was effected by two precipitations from acetone-diethyl ether to afford a pale yellow solid. Yield: 67 mg, 39%. Found: C, 27.05; H, 2.85; N, 4.50. Calc. for $C_{20}H_{26}As_2ClF_{12}N_3OP_2Ru$: C, 26.65; H, 2.90; N, 4.65%. ^1H NMR data (200 MHz, CD_3COCD_3): δ 9.02 (4 H, d, $2H^{2,6}$), 8.41–8.32 (4 H, m, $2H^4$ and C_6H_2), 7.97 (2 H, m, C_6H_2), 7.89 (4 H, t, $2H^{3,5}$), 2.41 (6 H, s, AsMe), 2.30 (6 H, s, AsMe). ν(N≡O) 1893 vs cm^{-1}. *m/z*: 755 ($[M-PF_6^-]^+$), 612 ($[M-2PF_6^-]^+$), 531 ($[M-2PF_6^- - py]^+$) and 452 ($[M-2PF_6^- - 2py]^+$).

trans-[RuCl(pdma)(bipy)(NO)][PF_6]$_2$ (**6**). A solution of *fac*-[$RuCl_3$(pdma)(NO)] (100 mg, 0.191 mmol) and 2,2′-bipyridine (305 mg, 1.95 mmol) in methanol (40 cm^3) was heated at reflux for 3 h. The solvent was reduced to a small volume *in vacuo*, diethyl ether was added and the precipitate was filtered off and washed with diethyl ether. The crude product was dissolved through the frit in water to leave a small amount of insoluble material. The product was precipitated by addition of aqueous NH_4PF_6, filtered off, washed with water and dried to yield a pink solid (128 mg). Purification was effected by three precipitations from acetonitrile-diethyl ether to afford a pale yellow solid. Yield: 87 mg, 51%. Found: C, 26.9; H, 2.50; N, 4.35. Calc. for $C_{20}H_{24}As_2ClF_{12}N_3OP_2Ru$: C, 26.75; H, 2.70; N, 4.70%. ^1H NMR data (200 MHz, CD_3CN): δ 8.93 (2 H, d, $H^{6,6'}$), 8.72 (2 H, d, $H^{3,3'}$), 8.53 (2 H, t, $H^{4,4'}$), 8.15 (2 H, m, C_6H_2), 8.01 (2 H, t, $H^{5,5'}$), 7.93 (2 H, m, C_6H_2), 2.36 (6 H, s, AsMe), 2.27 (6 H, s, 2AsMe). ν(N≡O) 1878 vs cm^{-1}. *m/z*: 754 ($[M-PF_6^-]^+$), 609 ($[M-2PF_6^-]^+$) and 579 ($[M-2PF_6^- - NO]^+$).

trans-[RuCl(pdma)(phen)(NO)][PF_6]$_2$ (**7**). This was prepared and purified in identical fashion to **6** by using 1,10-phenanthroline (346 mg, 1.92 mmol) in place of bipy. From 160 mg of crude pale orange product, a pale yellow solid was obtained. Yield: 101 mg, 57%. Found: C, 28.6; H, 2.65; N, 4.50. Calc. for $C_{22}H_{24}As_2ClF_{12}N_3OP_2Ru$: C, 28.65; H, 2.60; N, 4.55%. ^1H NMR data (200 MHz, CD_3CN): δ 9.33 (2 H, dd, J = 1.2, 5.3 Hz, $H^{2,9}$), 9.11 (2 H, dd, J = 1.2, 8.3 Hz, $H^{4,7}$), 8.41 (2 H, s, $H^{5,6}$), 8.31 (2 H, dd, J = 5.3, 8.3 Hz, $H^{3,8}$), 8.20 (2 H, m, C_6H_2), 7.96 (2 H, m, C_6H_2), 2.44 (6 H, s, 2AsMe), 2.37 (6 H, s, 2AsMe). ν(N≡O) 1874 vs cm^{-1}. *m/z*: 733 ($[M-2PF_6^-]^+$) and 603 ($[M-2PF_6^- - NO]^+$).

trans-[RuCl(pdma)(4,4′-Me_2bipy)(NO)][PF_6]$_2$ (**8**). This was prepared and purified in identical fashion to **6** by using 4,4′-dimethyl-2,2′-bipyridine (354 mg, 1.92 mmol) in place of bipy. A pale yellow solid was obtained. Yield: 91 mg, 51%. Found: C, 28.45; H, 3.05; N, 4.80. Calc. for $C_{22}H_{28}As_2ClF_{12}N_3OP_2Ru$: C, 28.5; H, 3.05; N, 4.55%. ^1H NMR data (200 MHz, CD_3CN): δ 8.73 (2 H, d, J = 5.8 Hz, $H^{6,6'}$), 8.56 (2 H, d, J = 1.5 Hz, $H^{3,3'}$), 8.14 (2 H, m, C_6H_2), 7.92 (2 H, m, C_6H_2), 7.80 (2 H, dd, J = 5.9, 1.5 Hz, $H^{5,5'}$), 2.71 (6 H, s, 2Me), 2.33 (6 H, s, 2AsMe), 2.24 (6 H, s, 2AsMe). ν(N≡O) 1875 vs cm^{-1}. *m/z*: 637 ($[M-2PF_6^-]^+$) and 607 ($[M-2PF_6^- - NO]^+$).

trans-[RuCl(pdma)(dppe)(NO)][PF_6]$_2$ (**9**). This was prepared in similar fashion to **6** by using 1,2-bis(diphenylphosphino)ethane (764 mg, 1.92 mmol) in place of bipy. Some of the dppe remained undissolved throughout the reaction. After refrigeration this was filtered off and washed with methanol. The pale golden filtrate was reduced to a small volume *in vacuo* and water was added to precipitate the remaining dppe. This was removed by extraction with dichloromethane (4 × 5 cm^3) and then aqueous NH_4PF_6 was added to the aqueous layer. The crude product was filtered off, washed with water and dried (67 mg). This material was shown by proton NMR to contain ca 5% *trans*-[RuCl(pdma)$_2$(NO)][PF_6]$_2$. The latter was removed by reprecipitation from acetone/NBu^n_4Cl followed by precipitation from water/aqueous NH_4PF_6; *trans*-[RuCl(pdma)$_2$(NO)]Cl_2 is less soluble in acetone than is *trans*-[RuCl(pdma)(dppe)(NO)]Cl_2 and so precipitates first upon addition of NBu^n_4Cl, despite being the minor component. This process was repeated to afford the pure product as a pale yellow solid. Yield: 28 mg, 13%. Found: C, 38.0; H, 3.60; N, 1.55; P, 10.60. Calc. for $C_{36}H_{40}As_2ClF_{12}NOP_4Ru$: C, 37.9; H, 3.55; N, 1.25; P, 10.85%. ^1H NMR data (200 MHz, CD_3COCD_3): δ 8.19 (2 H, m, C_6H_2), 7.98–7.67 (22 H, c m, C_6H_2 and $4C_6H_5$), 4.18 (2 H, c m, CH_2), 3.77 (2 H, c m, CH_2), 2.51 and 2.50 (6 H, s, s, 2AsMe), 1.03 and 1.02 (6 H, s, s, 2AsMe). ν(N≡O) 1873 s cm^{-1}. *m/z*: 996 ($[M-PF_6^-]^+$), 851 ([M–

$2PF_6^-]^+$), 821 ($[M-2PF_6^- -NO]^+$) and 785 ($[M-2PF_6^- -NO-Cl]^+$).

trans-[RuCl(pica)(pdma)(NO)]PF_6 (**10**). A solution of *fac*-[$RuCl_3$(pdma)(NO)] (100 mg, 0.191 mmol) and picolinic acid (236 mg, 1.92 mmol) in methanol (40 cm^3) was heated at reflux for 30 min. The solvent was reduced to a small volume *in vacuo*, water was added and the precipitate was filtered off and washed with water to leave a small amount of insoluble material. The addition of aqueous NH_4PF_6 to the filtrate precipitated the product which was filtered off, washed with water and dried to yield a pale golden solid (83 mg). This material was shown by proton NMR to contain ca 15% *trans*-[RuCl(pdma)$_2$(NO)][PF_6]$_2$. The latter was precipitated by the slow addition of NBu^n_4Cl to an acetone solution of the product mixture. After filtration, the slow addition of aqueous NH_4PF_6 caused precipitation of $NBu^n_4PF_6$ which was filtered off and washed with water. The addition of further aqueous NH_4PF_6 to the filtrate caused precipitation of the product which was filtered off, washed with water and dried. Remaining traces of $NBu^n_4PF_6$ were removed by precipitation from acetonitrile-diethyl ether to afford **10** as a pale yellow solid. Yield: 40 mg, 29%. Found: C, 26.8; H, 2.60; N, 4.00. Calc. for $C_{16}H_{20}As_2ClF_6N_2O_3PRu$: C, 26.7; H, 2.80; N, 3.90%. ^1H NMR data (200 MHz, CD_3COCD_3): δ 9.20 (1 H, d, H^6), 8.52 (1 H, td, J = 1.4, 7.6 Hz, H^4), 8.39–8.32 (3 H, m, H^3 and C_6H_2), 8.05 (1 H, m, H^5), 7.92 (2 H, m, C_6H_2), 2.47 (3 H, s, AsMe), 2.39 (3 H, s, AsMe), 2.37 (6 H, s, 2AsMe). ν(N≡O) 1872 s cm^{-1}, ν(C=O) 1671 s cm^{-1}. m/z: 574 ($[M-PF_6^-]^+$).

X-ray crystallography

Crystals of *fac*-[$RuCl_3$(pdma)(NO)] were obtained by slow cooling of a boiling methanolic solution to room temperature. Those of the other compounds were grown by slow evaporation at room temperature; **2**·Me_2CO from acetone/dichloromethane, **3** from an acetonitrile reaction solution and **6** from acetonitrile/toluene.

A prismatic crystal of each compound was selected for diffraction study, having the following colours and dimensions: *fac*-[$RuCl_3$(pdma)(NO)] (red; 0.15 × 0.25 × 0.45 mm), **2**·Me_2CO (orange; 0.10 × 0.10 × 0.17 mm), **3** (yellow; 0.05 × 0.15 × 0.30 mm) and **6** (yellow; 0.05 × 0.15 × 0.35 mm). The crystals were mounted on glass fibres and data were collected on a Rigaku AFC5R diffractometer at ambient temperature. The structures of *fac*-[$RuCl_3$(pdma)(NO)], **2**·Me_2CO and **3** were solved by standard direct methods using SHELXS86 [10] for *fac*-[$RuCl_3$(pdma)(NO)] and SIR92 [11] for **2**·Me_2CO and **3**. In the case of **6**, heavy-atom Patterson methods [12] were employed. For **2**·Me_2CO, **3** and **6** the structures were expanded using Fourier techniques with DIRDIF94 [13]. In all cases refinement was by full-matrix least-squares on F_o for all unique reflections.

Data were corrected for Lorentz-polarization effects and for absorption with maximum and minimum transmission factors of 1.00 and 0.74 for *fac*-[$RuCl_3$(pdma)(NO)], 1.00 and 0.94 for **2**·Me_2CO, 1.00 and 0.72 for **3** and 1.00 and 0.78 for **6**. All non-hydrogen atoms, including those of the acetone of crystallization in **2**·Me_2CO, were refined anisotropically and hydrogen atoms were included in idealized positions. All calculations were performed using the TEXSAN crystallographic software package [14]. The complexes *fac*-[$RuCl_3$(pdma)(NO)] and **2**·Me_2CO lie on crystallographic mirror planes. Complex **3** has approximate mirror symmetry, but no ambiguity exists with respect to an alternative centrosymmetric space group. Salt **6** is prone to form laminates, which caused some problems with structure solution due to reflection twinning. There is still some distortion present in the final model, mainly in the bipy ligand, which is presumably due to the superposition of a small proportion of the twin in the lattice.

ORTEP [15] diagrams showing views of the complexes are given in Figs 1–4. Crystallographic data and refinement details are presented in Table 2, and selected bond lengths and angles in Tables 3–6. Fractional atomic coordinates, anisotropic thermal parameters, and full listings of bond lengths and angles have been deposited at the Cambridge Crystallographic Data Centre.

RESULTS AND DISCUSSION

Synthesis and characterization

The complex *fac*-[$RuCl_3$(pdma)(NO)] reacts with silver(I) salts, AgX, at room temperature in acetonitrile to afford disubstituted derivatives *cis*-[$RuClX_2$(pdma)(NO)] [X^- = trifluoroacetate, CF_3CO_2 (**1**), *p*-toluenesulphonate, $C_7H_7SO_3$ (**2**) or nitrate (**3**)] in reasonable yield. Yields are independent of the nature of X^- and are unaffected by using an excess of AgX. Selective substitution of the equatorial chlorides in *fac*-]$RuCl_3$(pdma)(NO)] is possible because the linearly bonded nitrosyl ligand delabilizes the axial chloride, as manifested in the Ru—Cl bond lengths (see later). The insoluble product **3** was identified by infrared spectroscopy and by X-ray crystallography (see later) as the neutral complex containing two monodentate nitrato ligands, rather than the isomeric chelate salt, *trans*-[RuCl(*O*,*O*-NO_3)(pdma)(NO)]NO_3.

Fac-[$RuCl_3$(pdma)(NO)] reacts very slowly in refluxing pyridine to afford *cis*-[RuCl(pdma)$(py)_2$(NO)]$^{2+}$ in low yield, accompanied by decomposition to give an insoluble black material. This reaction is predictably much faster in a protic medium, the initial chloride substitution being complete after 30 min at reflux in 1:4 pyridine-methanol,

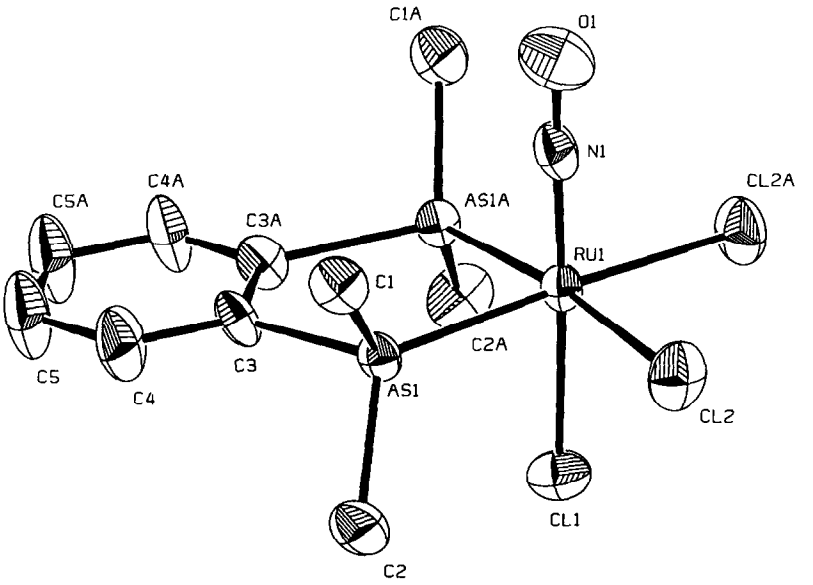

Fig. 1. Structural representation of the complex *fac*-[$RuCl_3$(pdma)(NO)], with hydrogen atoms omitted (50% probability ellipsoids).

as evidenced by an absence of water-insoluble starting material. However, it is not possible to obtain a good yield of *cis*-[RuCl(pdma)$(py)_2$(NO)]$^{2+}$ via this method, and extended reflux times produce an intractable product mixture. Proton NMR spectra indicate that this is due to the participation of methoxide ion as a ligand. In the presence of 3 equivalents of AgO_2CCF_3 the major product of this reaction is the trisubstituted derivative *cis*-[Ru(OMe)(pdma)$(py)_2$(NO)]$^{2+}$, isolated as its PF_6^- salt **4** in reasonable yield.

Reaction of *fac*-[$RuCl_3$(pdma)(NO)] with 2 equivalents of AgO_2CCF_3 in refluxing acetonitrile produces the known [9] complex *trans*-[RuCl(pdma)$_2$(NO)]$^{2+}$ in low yield via scrambling of the pdma ligands.* The most efficient method for the synthesis of *cis*-[RuCl(pdma)$(py)_2$(NO)]$(PF_6)_2$ (**5**) is via the reaction of *fac*-[$RuCl_3$(pdma)(NO)] in 1:7 pyridine-acetonitrile in the presence of 2 equivalents of AgO_2CCF_3. Yields are modest and decrease with extended reflux times, as the production of *trans*-[RuCl(pdma)$_2$(NO)]$^{2+}$ and also of another complex, believed to be *cis*-[Ru(OH)(pdma)$(py)_2$(NO)]$^{2+}$, increases.† **5** can also be prepared by reaction of the trifluoroacetate complex **1** with pyridine in acetonitrile, but this gives slightly poorer yields than the direct reaction.

The mixed-chelate salt *trans*-[RuCl(pdma)(bipy)(NO)]$[PF_6]_2$ (**6**, bipy = 2,2′-bipyridine) is produced in reasonable yield by reaction of *fac*-[$RuCl_3$(pdma)(NO)] with an excess of bipy in refluxing methanol. This reaction is considerably more efficient than that with pyridine due to the superior ligating ability of the chelating bipy. The salts **7**, **8** and **9** are produced in analogous fashion to **6** by using 1,10-phenanthroline, 4,4′-dimethyl-2,2′-bipyridine or 1,2-bis(diphenylphosphino)ethane in place of bipy. The poor yield of **9** is ascribed to diminished ligating ability due to the steric bulk of the dppe ligand. Several attempts at preparing **9** via **1** gave similarly low yields. In the case of **10** a shorter reaction time is necessary in order to minimize the production of *trans*-[RuCl(pdma)$_2$(NO)]$^{2+}$, demonstrating the inferior ligating ability of the picolinate ligand with respect to bipy or phen. We have found that the reaction of

* A partial solution of *fac*-[$RuCl_3$(pdma)(NO)] (100 mg, 0.191 mmol) and AgO_2CCF_3 (96 mg, 0.435 mmol) in acetonitrile (40 cm^3) was heated at reflux for 3 h. After cooling, the solvent was evaporated *in vacuo* to ca 3 cm^3, and the AgCl was removed by filtration through celite. Addition of aqueous NH_4PF_6 gave a sticky golden precipitate which was collected by filtration and washed with water. This was purified by precipitation, first from acetone-aqueous NH_4PF_6 and then from acetone-diethyl ether to afford a yellow solid. Yield: 16 mg, 16%. Found: C, 23.1; H, 3.20; N, 1.40. Calc. for $C_{20}H_{32}As_4ClF_{12}NOP_2Ru$: C, 23.35; H, 3.15; N, 1.35. ^1H NMR data (200 MHz, CD_3COCD_3): δ 8.46 (4 H, m, $2C_6H_2$), 7.99 (4 H, m, $2C_6H_2$), 2.56 (6 H, s, 2AsMe), 2.38 (6 H, s, 2AsMe). ν(N≡O) 1881 vs cm^{-1}.

† The complex *cis*-[Ru(OH)(pdma)$(py)_2$(NO)]$^{2+}$ is identified by the presence of a clearly resolved, minor set of signals attributable to a *cis*-{Ru(X)(pdma)$(py)_2$}$^+$ moiety in the proton NMR spectrum; in particular, a singlet at 6.30 ppm integrating for 1 proton is assigned to the OH resonance. Small amounts of *trans*-[RuCl(pdma)$_2$(NO)]$[PF_6]_2$ or *cis*-[Ru(OH)(pdma)$(py)_2$(NO)]$[PF_6]_2$ can be separated from **5** by precipitation from acetone-diethyl ether or from acetone-aqueous NH_4PF_6, respectively.

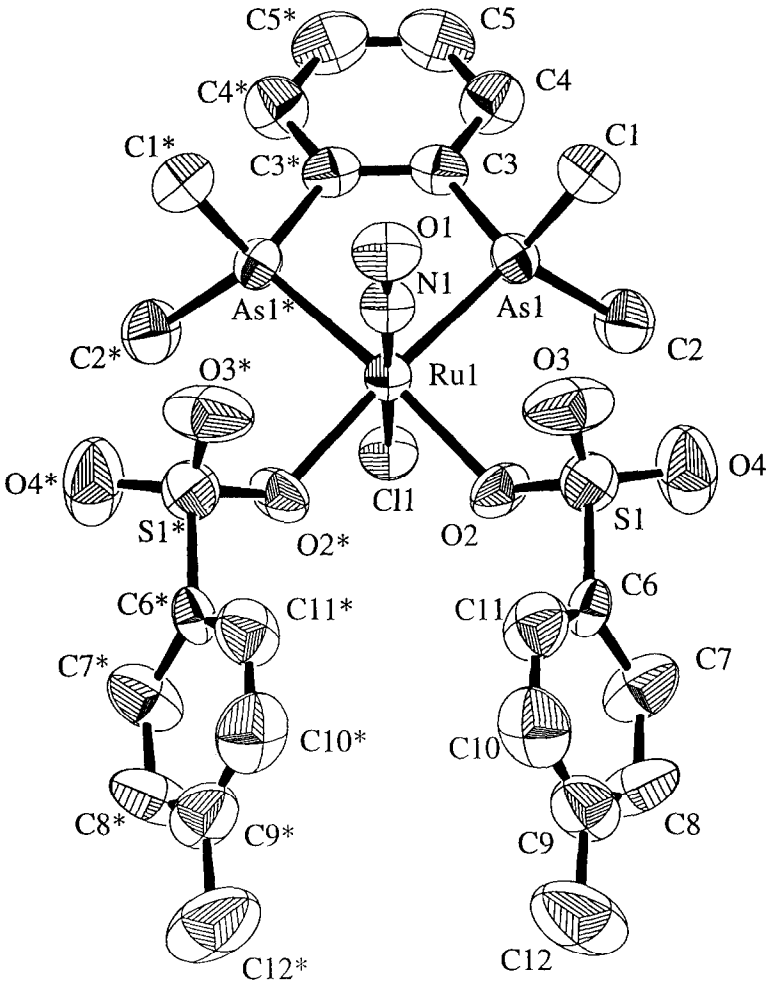

Fig. 2. Structural representation of the complex in *cis*-[RuCl($C_7H_7SO_3$)$_2$(pdma)(NO)]·Me_2CO (**2**·Me_2CO), details as in Fig. 1.

fac-[$RuCl_3$(pdma)(NO)] with α-diimines in refluxing methanol is surprisingly sensitive to the nature of the ligand. Following the synthetic procedure for **6–8**, but using 2,2′-bipyrimidine, 4,5-diazafluoren-9-one, 2,2′-biquinoline or 2,9-dimethyl-1,10-phenanthroline, the only isolable product is *trans*-[RuCl(pdma)$_2$(NO)]$^{2+}$. Investigations are ongoing in order to explain these seemingly anomalous results. The syntheses of **1–10** are shown in Scheme 1.

All of the new complexes display ν(N≡O) bands in the region 1900–1840 cm^{-1}, consistent with the presence of linearly bonded nitrosyl ligands, and confirmed by crystallographic studies (see later). The ν(N≡O) frequencies of **1–3** and **5–10** vary predictably with the nature of the equatorial ligand(s). Replacement of the *trans* chloride in **5** by the more basic methoxide in **4** produces a low-energy shift of 45 cm^{-1} in the ν(N≡O) band. The nitrato ligands in **3** give rise to bands at 1477, 1262 and 1000 cm^{-1} ($\Delta\nu$ = 215 cm^{-1}) consistent with monodentate coordination [16]. Absorptions at similar energies have been assigned to monodentate nitrato ligands in complexes of Ru(IV) [17]. Intense bands characteristic of the other ligands, particularly the CF_3CO_2 and $C_7H_7SO_3$ anions, are also observed.

For **1**, **2** and **4–8** the *trans*-NO/Cl geometry and resulting C_s symmetry is confirmed by the presence of a single 1,2-disubstituted benzene AA′BB′ pattern and two methyl singlets due to the pdma ligands in the ^1H NMR spectrum, accompanied by signals characteristic of the other ligands. Loss of the symmetry plane in **9** and **10** causes splitting of the $AsMe_2$ signals, but only a single AA′BB′ pattern is observed in each case.

Electrochemical studies

The electrochemical properties of the complexes in **4–10** were studied by cyclic voltammetry in acetonitrile, and results are presented in Table 1, together with data for *trans*-[RuCl(pdma)$_2$(NO)][PF_6]$_2$, *trans*-

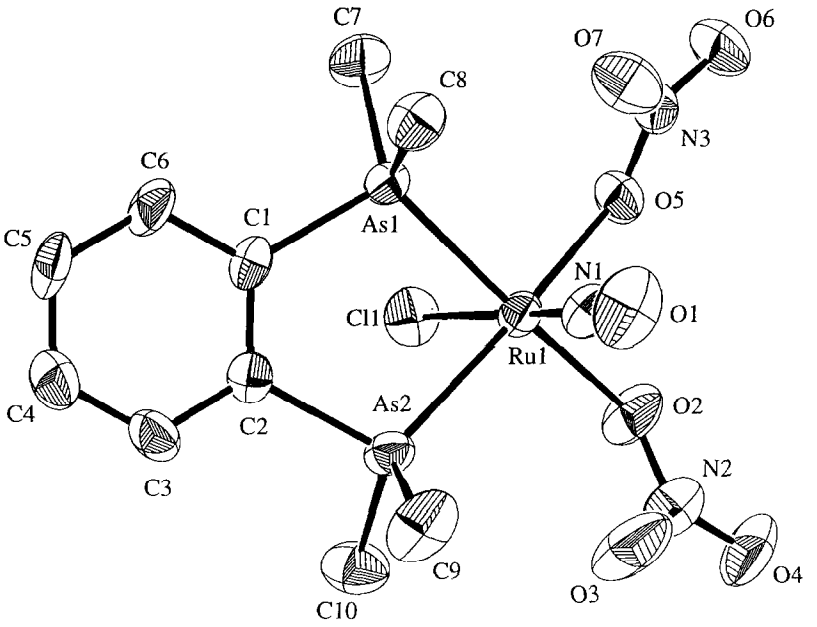

Fig. 3. Structural representation of the complex *cis*-[RuCl(NO_3)$_2$(pdma)(NO)] (**3**), details as in Fig. 1.

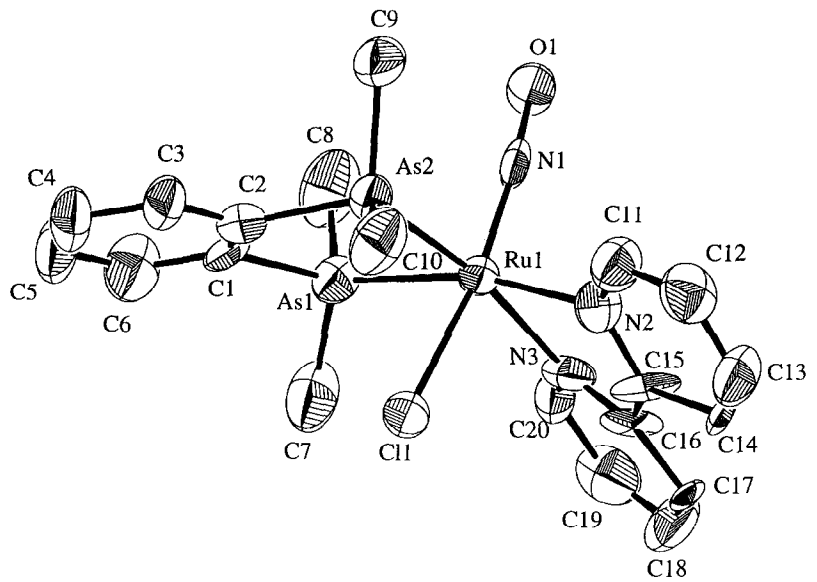

Fig. 4. Structural representation of the cation in salt **6**, *trans*-[RuCl(pdma)(bipy)(NO)]$^{2+}$, details as in Fig. 1.

[RuCl(py)$_4$(NO)][PF_6]$_2$ and *trans*-[RuCl(bipy)$_2$(NO)][PF_6]$_2$ for purposes of comparison [6,18, 19].

With the exception of **4**, all of the new complexes show reversible waves between 0.14 and −0.16 V vs SCE, assigned to one-electron reductions of the {Ru(NO)}$_6$ moieties [20]. Although the potentials of these processes are influenced by the nature of the co-ligands, they cannot generally be correlated with ligand basicity. The only clear trend is that the most negative potentials are observed for the complexes containing the strongly basic anions methoxide or picolinate (in **4** and **10**). Either one or two further reduction waves are observed on cathodic scanning which are irreversible in all cases except for the third reduction of **9**. The redox behaviour of **6–8** and *trans*-[RuCl(bipy)$_2$(NO)][PF_6]$_2$ contrasts with that of *trans*-[RuCl(pdma)$_2$(NO)][PF_6]$_2$, for which quasi-reversible second and third reductions indicate increased stability of the two and three-electron reduced forms [6].

Table 1. Electrochemical data in acetonitrile

Complex salt	$E_{1/2}$/V vs SCE (ΔE_p/mV)[a] or E_{pc}	
	$\{Ru(NO)\}^{3+/2+}$	other waves
trans-$[RuCl(pdma)_2(NO)][PF_6]_2$ [6]	0.06 (65)	−0.47 (115)
		−1.59 (100)
trans-$[RuCl(py)_4(NO)][PF_6]_2$ [18]	0.30 (80)	−0.60
trans-$[RuCl(bipy)_2(NO)][PF_6]_2$ [19]	0.22 (70)	−0.40
4 *cis*-$[Ru(OMe)(pdma)(py)_2(NO)][PF_6]_2$	−0.29 (70)[b]	
5 *cis*-$[RuCl(pdma)(py)_2(NO)][PF_6]_2$	0.12 (60)	−0.54
		−1.47
6 *trans*-$[RuCl(pdma)(bipy)(NO)][PF_6]_2$	0.05 (80)	−0.57
7 *trans*-$[RuCl(pdma)(phen)(NO)][PF_6]_2$	0.05 (85)	−0.57
8 *trans*-$[RuCl(pdma)(4,4'\text{-}Me_2bipy)(NO)][PF_6]_2$	0.02 (70)	−0.57
9 *trans*-$[RuCl(pdma)(dppe)(NO)][PF_6]_2$	0.12 (60)	−0.38
		−1.47 (85)
10 *trans*-$[RuCl(pica)(pdma)(NO)]PF_6$	−0.16 (70)	−0.75

[a] Using solutions ca 10^{-3} mol dm^{-3} in complex salt and 0.1 mol dm^{-3} in $NBu^n_4PF_6$ at a platinum-bead working electrode with a scan rate of 200 mV s^{-1}. Ferrocene internal reference $E_{1/2} = 0.40$ V, $\Delta E_p = 60$ mV.

[b] Irreversible reduction process as evidenced by $i_{pc} > i_{pa}$.

Table 2. Crystallographic data and refinement details

	fac-$[RuCl_3(pdma)(NO)]$	**2**·Me_2CO	**3**	**6**
Formula	$C_{10}H_{16}As_2Cl_3NORu$	$C_{27}H_{36}As_2ClNO_8RuS_2$	$C_{10}H_{16}As_2ClN_3O_7Ru$	$C_{20}H_{24}As_2ClF_{12}N_3OP_2Ru$
FW	523.51	853.07	576.62	898.72
Crystal system	monoclinic	orthorhombic	orthorhombic	monoclinic
Space group	*Cm*	*Pnma*	$Pna2_1$	$P2_1/n$
a (Å)	11.260(8)	20.172(3)	22.983(4)	13.221(3)
b (Å)	14.201(3)	16.476(4)	8.110(2)	11.474(3)
c (Å)	6.347(4)	10.254(3)	9.688(1)	20.471(5)
β (°)	119.63(5)			100.40(2)
U (Å^3)	882(1)	3407(2)	1805(1)	3054(1)
Z	2	4	4	4
D_c (Mg m^{-3})	1.970	1.663	2.121	1.954
Temperature (K)	294	296	295	291
λ (Å)	0.710 69 (Mo-K_α)	0.710 69 (Mo-K_α)	0.710 69 (Mo-K_α)	0.710 69 (Mo-K_α)
F(000)	504	1712	1120	1752
μ (mm^{-1})	5.036	2.634	4.690	2.933
Scan type	$\omega/2\theta$	$\omega/2\theta$	$\omega/2\theta$	ω
2θ limit (°)	50.0	50.1	50.1	50.1
h, *k*, *l* Ranges	0–13, 0–16, −7–6	0–24, 0–19, −12–0	0–27, 0–9, 0–11	0–15, 0–13, −24–23
Reflections collected	859	3428	1880	5975
Unique reflections (R_{int})	816 (0.058)	3428	1880	5713 (0.046)
Observed reflections [$I > 3\sigma(I)$]	748	1812	1429	3140
R[a]	0.034	0.043	0.030	0.068
R_w[a]	0.041	0.030	0.024	0.061
Goodness of fit, (*S*)	1.76	1.53	1.70	3.02
No. parameters	86	199	216	379
Peak and hole (e Å^{-3})	1.05, −0.93	0.53, −0.61	0.54, −0.45	1.70, −0.85

[a] $R = \Sigma(|F_o| - |F_c|)/\Sigma|F_o|$; $R_w = [\Sigma w(F_o - F_c)^2/\Sigma wF_o^2]^{1/2}$; $S = [\Sigma w(F_o - F_c)^2/(\text{no. of reflns} - \text{no. of params})]^{1/2}$.

Table 3. Selected bond distances (Å) and angles (°) for *fac*-[$RuCl_3$(pdma)(NO)]

Ru(1)—As(1)	2.382(2)	Ru(1)—N(1)	1.72(2)
Ru(1)—Cl(1)	2.350(5)	N(1)—O(1)	1.15(2)
Ru(1)—Cl(2)	2.420(3)		
As(1)—Ru(1)—As(1)a	87.68(9)	Cl(1)—Ru(1)—Cl(2)	89.4(1)
As(1)—Ru(1)—Cl(1)	84.9(1)	Cl(1)—Ru(1)—N(1)	177.2(5)
As(1)—Ru(1)—Cl(2)	88.16(9)	Cl(2)—Ru(1)—Cl(2)a	95.5(2)
As(1)—Ru(1)—Cl(2)a	173.2(1)	Cl(2)—Ru(1)—N(1)	92.5(3)
As(1)—Ru(1)—N(1)	93.1(3)	Ru(1)—N(1)—O(1)	178(1)

Table 4. Selected bond distances (Å) and angles (°) for complex **2**·Me_2CO

Ru(1)—As(1)	2.402(1)	Ru(1)—O(2)	2.101(5)
Ru(1)—Cl(1)	2.334(3)	N(1)—O(1)	1.164(9)
Ru(1)—N(1)	1.700(8)		
As(1)—Ru(1)—As(1)*	86.26(5)	Cl(1)—Ru(1)—N(1)	173.5(3)
As(1)—Ru(1)—Cl(1)	83.53(6)	O(2)—Ru(1)—O(2)*	83.8(3)
As(1)—Ru(1)—O(2)	94.1(1)	O(2)—Ru(1)—N(1)	98.5(2)
As(1)—Ru(1)—O(2)*	169.8(1)	Ru(1)—O(2)—S(1)	129.4(3)
As(1)—Ru(1)—N(1)	91.7(2)	Ru(1)—N(1)—O(1)	174.4(8)
Cl(1)—Ru(1)—O(2)	86.4(1)		

Table 5. Selected bond distances (Å) and angles (°) for complex **3**

Ru(1)—As(1)	2.410(1)	N(2)—O(2)	1.31(1)
Ru(1)—As(2)	2.422(1)	N(2)—O(3)	1.22(1)
Ru(1)—Cl(1)	2.313(3)	N(2)—O(4)	1.22(1)
Ru(1)—O(2)	2.112(7)	N(3)—O(5)	1.29(1)
Ru(1)—O(5)	2.112(7)	N(3)—O(6)	1.22(1)
Ru(1)—N(1)	1.723(9)	N(3)—O(7)	1.24(1)
N(1)—O(1)	1.14(1)		
As(1)—Ru(1)—As(2)	84.73(5)	Cl(1)—Ru(1)—O(2)	85.8(2)
As(1)—Ru(1)—Cl(1)	84.95(8)	Cl(1)—Ru(1)—O(5)	85.2(2)
As(1)—Ru(1)—O(2)	168.8(2)	Cl(1)—Ru(1)—N(1)	174.1(3)
As(1)—Ru(1)—O(5)	96.2(2)	O(2)—Ru(1)—O(5)	76.7(3)
As(1)—Ru(1)—N(1)	90.3(3)	O(2)—Ru(1)—N(1)	99.3(4)
As(2)—Ru(1)—Cl(1)	83.02(8)	O(5)—Ru(1)—N(1)	98.8(4)
As(2)—Ru(1)—O(2)	100.4(2)	Ru(1)—N(1)—O(1)	175.4(9)
As(2)—Ru(1)—O(5)	168.0(2)	Ru(1)—O(2)—N(2)	122.7(7)
As(2)—Ru(1)—N(1)	93.1(3)	Ru(1)—O(5)—N(3)	122.7(7)

Structural studies

Single-crystal structures were determined for *fac*-[$RuCl_3$(pdma)(NO)], **2**·Me_2CO, **3** and **6**. Representations of the complexes are shown in Figs 1, 2, 3 and 4, respectively.

All of the complexes show the expected *trans*-NO/Cl arrangement, with typical values for Ru—As bond lengths and As—Ru—As chelate angles [6,7]. In each case the Ru—NO unit is essentially linear, consistent with the infrared data (see earlier). The cation in **6** shows a small deviation from ideal octahedral geometry with a N(1)—Ru—Cl(1) angle of 170.5(4)°, the bipy bending away from the nitrosyl ligand.

In *fac*-[$RuCl_3$(pdma)(NO)] the equatorial Ru—Cl

Table 6. Selected bond distances (Å) and angles (°) for salt **6**

Ru(1)—As(1)	2.447(2)	Ru(1)—N(2)	2.14(1)
Ru(1)—As(2)	2.448(2)	Ru(1)—N(3)	2.15(1)
Ru(1)—Cl(1)	2.337(4)	N(1)—O(1)	1.14(1)
Ru(1)—N(1)	1.73(1)		

As(1)—Ru(1)—As(2)	83.83(6)	As(2)—Ru(1)—N(3)	167.3(3)
As(1)—Ru(1)—Cl(1)	82.1(1)	Cl(1)—Ru(1)—N(1)	170.5(4)
As(1)—Ru(1)—N(1)	92.4(4)	Cl(1)—Ru(1)—N(2)	86.3(3)
As(1)—Ru(1)—N(2)	167.4(3)	Cl(1)—Ru(1)—N(3)	86.5(3)
As(1)—Ru(1)—N(3)	98.2(3)	N(1)—Ru(1)—N(2)	99.8(5)
As(2)—Ru(1)—Cl(1)	81.3(1)	N(1)—Ru(1)—N(3)	101.9(5)
As(2)—Ru(1)—N(1)	90.5(4)	N(2)—Ru(1)—N(3)	76.1(4)
As(2)—Ru(1)—N(2)	99.3(3)	Ru(1)—N(1)—O(1)	174(1)

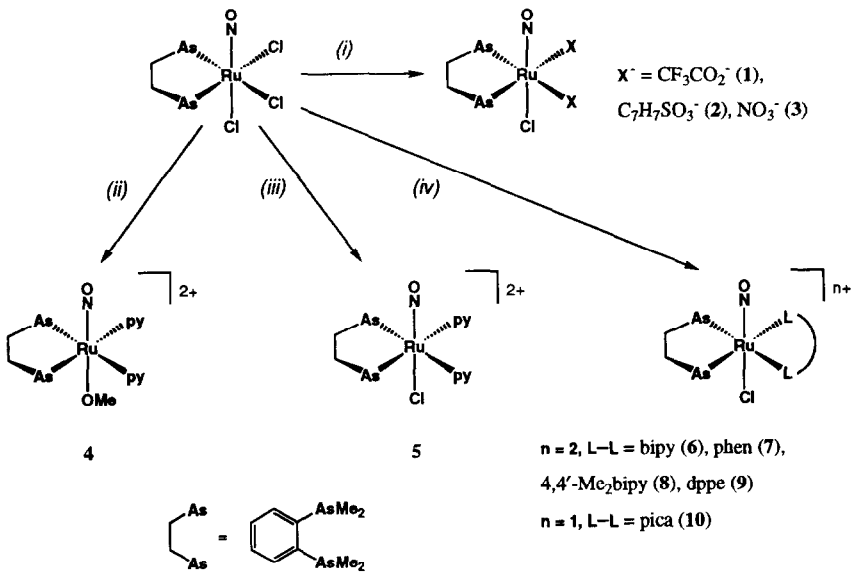

Scheme 1. Synthesis of the complexes **1**–**3** and the cations in the salts **4**–**10**: (*i*) excess AgX, MeCN, r.t.; (*ii*) AgO_2CCF_3 (3 equivalents), MeOH/pyridine, reflux; (*iii*) AgO_2CCF_3 (2 equivalents), MeCN/pyridine, reflux; (*iv*) excess L—L, MeOH, reflux.

bond lengths are longer than the axial one by 0.07 Å, consistent with the observed preferential labilization of the equatorial chlorides. In the related complex *fac*-[$RuCl_3$(bipy)(NO)], the extension of the equatorial vs the axial Ru—Cl bond lengths is only ca 0.03 Å [Ru—Cl_{eq} = 2.383(2)/2.390(1) Å; Ru—Cl_{ax} = 2.354(2) Å] [21]. The pdma ligand hence exerts a greater *trans* labilizing influence on chloride than does bipy in *fac*-[$RuCl_3$(L—L)(NO)] complexes.

To our knowledge, **3** is the first ruthenium complex containing monodentate nitrato ligands to be crystallographically characterized. The Ru(IV) 2,7-dimethylocta-2,6-diene-1,8-diyl complex [Ru(η^3:η^3-$C_{10}H_{16}$)(NO_3)$_2$] features two "semi-chelating" nitrato ligands with Ru—O bond lengths of 2.091(5) and 2.548(8) Å [17], the former being similar to that found in **3**. The free nitrate N—O bonds in **3** are shorter than the coordinated bonds, the average bond lengths of 1.23(1) Å and 1.30(1) Å, respectively, being consistent with partial double bond character in the uncoordinated bonds. **2**·Me_2CO and **3** adopt similar conformations, with the uncoordinated O atoms of the oxoanion ligands directed away from the chlorides. The geometric parameters of the *p*-toluenesulphonate ligands in **2**·Me_2CO are similar to those found in *cis,cis*-[Ru($C_7H_7SO_3$)$_2$(PPh_3)$_2$(CO)(H_2O) [22].

CONCLUSION

Due to the *trans* influence of the pdma ligand, the complex *fac*-[$RuCl_3$(pdma)(NO)] serves as a con-

venient precursor to a variety of derivatives. The mixed-chelates *trans*-[RuCl(pdma)(L—L)(NO)]$^{2+}$ (L—L = bipy or phen) will act as precursors to stable, functionalized *trans* derivatives containing visible MLCT chromophores.* The results of these studies will form the basis of a forthcoming report.

Acknowledgements—Thanks are due to The Nuffield Foundation and the EPSRC for financial support and to Johnson Matthey plc for a generous loan of ruthenium trichloride.

REFERENCES

1. Balzani, V. and Scandola, F., *Supramolecular Photochemistry*. Ellis Horwood, Chichester, 1991.
2. Sauvage, J.-P., Collin, J.-P., Chambron, J.-C., Guillerez, S., Coudret, C., Balzani, V., Barigelletti, F., De Cola, L. and Flamigni, L., *Chem. Rev.*, 1994, **94,** 993.
3. Grosshenny, V., Harriman, A., Hissler, M. and Ziessel, R., *Platinum Metals Rev.*, 1996, **40,** 26 and 72.
4. Barigelletti, F., Flamigni, L., Collin, J.-P. and Sauvage, J.-P., *Chem. Commun.*, 1997, 333.
5. Coe, B. J., Friesen, D. A., Thompson, D. W. and Meyer, T. J., *Inorg. Chem.*, 1996, **35,** 4575.
6. Coe, B. J., Chery, M., Beddoes, R. L., Hope, H. and White, P. S., *J. Chem. Soc., Dalton Trans.*, 1996, 3917.
7. Coe, B. J., Hayat, S., Beddoes, R. L., Helliwell, M., Jeffery, J. C., Batten, S. R. and White, P. S., *J. Chem. Soc., Dalton Trans.*, 1997, 591.
8. Fairy, M. B. and Irving, R. J., *J. Chem. Soc. A*, 1966, 475.
9. Douglas, P. G., Feltham, R. G. and Metzger, H. G., *J. Am. Chem. Soc.*, 1971, **93,** 84.
10. Sheldrick, G. M., In *Crystallographic Computing* 3, ed. G. M. Sheldrick, C. Krueger and R. Goddard. Oxford University Press, 1985.
11. Altomare, A., Cascarano, M., Giacovazzo, C. and Guagliardi, A., *J. Appl. Crystallogr.*, 1993, **26,** 343.
12. Beurskens, P. T., Admiraal, G., Buerskens, G., Bosman, W. P., Garcia-Granda, S., Gould, R. O., Smits, J. M. M. and Smykalla, C., The DIRDIF program system, Technical Report of the Crystallography Laboratory, University of Nijmegen, The Netherlands, 1992.
13. Beurskens, P. T., Admiraal, G., Buerskens, G., Bosman, W. P., de Gelder, R., Israel, R. and Smits, J. M. M., The DIRDIF-94 program system, Technical Report of the Crystallography Laboratory, University of Nijmegen, The Netherlands, 1994.
14. TEXSAN-TEXRAY Structure Analysis Package, Molecular Structure Corporation, 1985 and 1992.
15. Johnson, C. K., ORTEP, a Fortran thermal ellipsoid plot program, Technical report ORNL-5138, Oak Ridge National Laboratory, Oak Ridge, TN, 1976.
16. Nakamoto, K., *Infrared and Raman Spectra of Inorganic and Coordination Complexes*, 4th edn. Wiley, New York, 1986.
17. Steed, J. W. and Tocher, D. A., *Polyhedron*, 1994, **13,** 167.
18. Coe, B. J., Meyer, T. J. and White, P. S., *Inorg. Chem.*, 1995, **34,** 593.
19. Nagao, H., Nishimura, H., Funato, H., Ichikawa, Y., Howell, F. S., Mukaida, M. and Kakihana, H., *Inorg. Chem.*, 1989, **28,** 3955.
20. Callahan, R. W. and Meyer, T. J., *Inorg. Chem.*, 1977, **16,** 574.
21. Haukka, M., Venäläinen, T., Ahlgrén, M. and Pakkanen, T. A., *Inorg. Chem.*, 1995, **34,** 2931.
22. Harding, P. A., Robinson, S. D. and Henrick, K., *J. Chem. Soc., Dalton Trans.*, 1988, 415.
23. Coe, B. J. and McDonald, C. I., work in progress.

*Although salts **6**–**8** are almost colourless, exhibiting MLCT bands in the UV region, these absorptions are markedly red-shifted in axial derivatives containing N-heterocyclic ligands, e.g. *trans*-[RuCl(pdma)(bipy)(py)]PF_6 is orange and shows an MLCT maximum at 430 nm in acetonitrile [23].

Pergamon

PII: S0277-5387(97)00487-7

Polyhedron Vol. 17, Nos. 11–12, pp. 2009–2012, 1998
© 1998 Elsevier Science Ltd
All rights reserved. Printed in Great Britain
0277-5387/98 $19.00+0.00

Reductive dimerization of phenyl isocyanate by divalent samarium complex: Synthesis and crystal structure of $[(ArO)_2(DME)Sm]_2[\mu\text{-}\eta^4\text{-}(PhN)OCCO(NPh)]\cdot 4THF$ (ArO = 2,6-di-tertbutyl-4-methylphenoxo)

Fugen Yuan,[a] Qi Shen[a]* and Jie Sun[b]

[a] School of Chemistry and Chemical Engineering, Suzhou University, Suzhou 215006, China

[b] Laboratory of Organometallic Chemistry, Shanghai Institute of Organic Chemistry, Chinese Academy of Sciences, Shanghai 200032, China

(Received 15 September 1997; accepted 14 November 1997)

Abstract—The reaction of divalent $(ArO)_2Sm(THF)_3\cdot THF$ with phenyl isocyanate directly gives a bimetallic complex $[(ArO)_2(DME)Sm]_2[\mu\text{-}\eta^4\text{-}(PhN)OCCO(NPh)]\cdot 4THF$ (ArO = 2,6-di-tertbutyl-4-methylphenoxo) via one-electron reduction and coupling reactions. In this complex, the deprotonated *N,N'*-diphenyloxamide ligand bridges two units of $(ArO)_2(DME)Sm$ with C(5)—C(5*), Sm—N and Sm—O(1) bonds of 1.43(2), 2.549(8) and 2.318(7) Å, respectively. © 1998 Elsevier Science Ltd. All rights reserved

Keywords: coupling reaction; samarium; oxamide; crystal structure.

The reactivity of divalent lanthanide complexes as strong reducing agents has been widely studied [1]. They are reported to react with a variety of unsaturated substrates such as $C_6H_{11}NC$ [2], PhC≡CPh [3], PhC≡CC≡CPh [4], PhN=NPh [5], PyCH=CHPy [6], CO [7], ^{t}BuC≡P [8], PhC≡CH [9], etc., and to show plentiful reaction patterns. For example, $(C_5Me_5)_2Sm(THF)]_2$ reacts with CO at 90 psi to give the ketenecarboxylate of lanthanocene $[(C_5Me_5)_4Sm_2(O_2CCCO)(THF)_2$ [7]. The CO molecules undergo one-electron reduction reactions plus the appropriate coupling. The reaction of $(C_5Me_5)_2Sm$ with PhC≡CH leads to coupling of two phenylethynyl ligands into $(C_5Me_5)_4Sm_2(Ph_2C_4)$ [9].

Isocyanates, as their own structural features, have been widely used in both polymer synthesis [10] and organic synthesis [11]. Study on the reaction of lanthanide complexes with isocyanates should be interesting. Although SmI_2 together with HMPA has been reported to make aromatic isocyanates couple into aromatic oxamides [11a,b], no details about the reaction itself were reported. We are interested in exploring the reactivity of divalent $(ArO)_2Sm(THF)_3\cdot THF$ (ArO = 2,6-di-tertbutyl-4-methylphenoxo) and have studied its reaction with phenyl isocyanate. Here we report the results.

EXPERIMENTAL

Materials and measurements

All operations were performed under pure argon by Schlenk techniques. Pre-dried THF, toluene and DME were distilled from sodium benzophenone ketyl. $(ArO)_2Sm(THF)_3\cdot THF$ was prepared from $SmI_2(THF)_x$ and ArONa in THF and crystallized in toluene [12]. PhNCO was stirred over P_2O_5 for 24 h and then distilled under vacuum. Melting point was determined in a sealed argon-filled capillary and uncorrected. Infrared spectra were recorded on a Magna

* Author to whom correspondence should be addressed.

550 spectrometer (KBr pellet). Proton NMR spectra were recorded on a DRX-400 spectrometer with positive fields being downfield from the external standard $SiMe_4$.

Preparation

To a solution of $(ArO)_2Sm(THF)_3 \cdot THF$ (1.77 g, 2.02 mmol) in 30 ml of toluene was added 0.22 ml of PhNCO (0.24 g, 2.02 mmol) with a syringe. The color of the solution changed from dark brown to yellow-green immediately. The reaction was kept for 24 h with stirring. After the toluene was removed by vacuum and a yellow-green viscose solid was obtained. The residue was dissolved in DME with small amount of hexane. Yellow-green crystals of $[(ArO)_2(DME)Sm]_2[\mu\text{-}\eta^4(PhN)OCCO(NPh)] \cdot 4THF$ (1.14 g, 58.8%) was obtained at -20°C. Crystals suitable for X-ray analysis were grown in THF-DME at 5 C. m.p. 105–110°C. Found: C, 62.3; H, 7.9; N, 1.6; Sm, 15.7. Calc. for $C_{98}H_{154}N_2O_{14}Sm_2$: C, 62.4; H, 8.2; N, 1.5; Sm, 15.9%. IR (cm^{-1}): 2956 s, 1667 s, 1605 m, 1528 m, 1435 s, 1397 m, 1312 w, 1234 m, 1158 m, 1119 w, 1026 w, 864 w, 756 w. ^1H NMR (C_6D_6, 300 K), δ (ppm): 0.96 and 3.34 (THF), 1.42 (aromatic tert-butyl), 2.29 (aromatic methyl), 2.93 and 3.00 (DME), 7.09 (aromatic CH), 7.20 (phenyl ring).

X-ray crystallography

A yellow-green prismatic crystal of approximate dimensions $0.20 \times 0.20 \times 0.30$ mm was sealed in a thin-walled glass capillary under pure argon. Measurements were made on a Rigaku AFC7R diffractometer with graphite monochromated Mo–K_α radiation. Cell constants and an orientation matrix for data collection were obtained from a least-squares refinement using the setting angles of 20 carefully centered reflections in the range $18.37 \leqslant 2\theta \leqslant 21.65$°. The data were collected at a temperature of 20 ± 1°C using the ω-2θ scan technique to a maximum 2θ value of 45.0°. The data were corrected for Lorentz and polarization effects. The structure was solved by heavy-atom Patterson method and expanded using Fourier techniques. Some non-hydrogen atoms were refined anisotropically, while the rest were refined isotropically. all calculations were performed using the TEXSAN crystallographic software package [13].

Crystal data and experimental conditions: $C_{98}H_{154}N_2O_{14}Sm_2$, triclinic, $P\bar{1}$(#2), $a = 14.32(1)$, $b = 14.603(7)$, $c = 13.577(8)$ Å, $\alpha = 97.94(4)$, $\beta = 114.00(5)$, $\gamma = 74.28(5)$°, $V = 2495(2)$ Å^3, $Z = 1$, total reflections 6532, unique 6037 ($R_{int} = 0.136$), observed 4532 ($I > 3\sigma(I)$), $R = 0.063$, $Rw = 0.075$, transmission factors 0.90–1.03. Selected bond distances and bond angles are given in Table 1.

RESULTS AND DISCUSSION

Reductive coupling reactions of some substances mediated by divalent bis(pentamethyl cyclopentadienyl) samarium complex have been reported including the reactions of $^tBuC{\equiv}P$ [8], $PhC{\equiv}CH$ [9], pyridazine [14], benzaldehyde azine [14] and 1,2-di-2-pyridylethene [15]. These reactions all afford the corresponding bimetallic products, characterized by X-ray crystallography. When PhNCO was added into a dark brown solution of $(ArO)_2Sm(THF)_3 \cdot THF$ in toluene at room temperature, the solution color changed immediately to yellow-green indicating the oxidation of Sm^{2+} into Sm^{3+}. After work up, yellow-green air-sensitive crystals of $[(ArO)_2(DME)Sm]_2[\mu\text{-}\eta^4\text{-}(PhN)OCCO(NPh)] \cdot 4THF$ (**1**) were isolated from the THF-DME solution in good yield.

$$(ArO)_2Sm(THF)_3 \cdot THF + PhNCO \xrightarrow{(1)\text{toluene (2)THF-DME}} [(ArO)_2(DME)Sm]_2[\mu\text{-}\eta^4\text{-}(PhN)OCCO(NPh)] \cdot 4THF$$

In the reaction, two phenyl isocyanate molecules undergo reductive dimerization and the resulting new ligand keeps coordinating to samarium atoms to form a bimetallic complex. Figure 1 shows the molecular

Table 1. Selected bond distances (Å) and bond angles (°)

Sm—O(1)	2.318(7)	Sm—O(2)	2.571(8)
Sm—O(3)	2.576(8)	Sm—O(4)	2.183(10)
Sm—O(5)	2.207(9)	Sm—N	2.549(8)
N—C(5)	1.32(1)	N—C(6)	1.45(1)
C(5)—C(5*)	1.43(2)	C(5)—O(1*)	1.29(1)
O(1)—Sm—N	66.1(2)	O(1)—Sm—O(4)	99.1(3)
O(1)—Sm—O(5)	119.1(3)	N—Sm—O(4)	99.9(3)
N—Sm—O(5)	87.1(3)	O(4)—Sm—O(5)	140.4(2)
Sm—N—C(5)	114.5(6)	Sm—N—C(6)	129.3(6)
Sm—O(1)—C(5*)	123.1(5)	N—C(5)—C(5*)	117(1)
N—C(5)—O(1*)	123.8(8)	O(1)—C(5*)—C(5)	119(1)

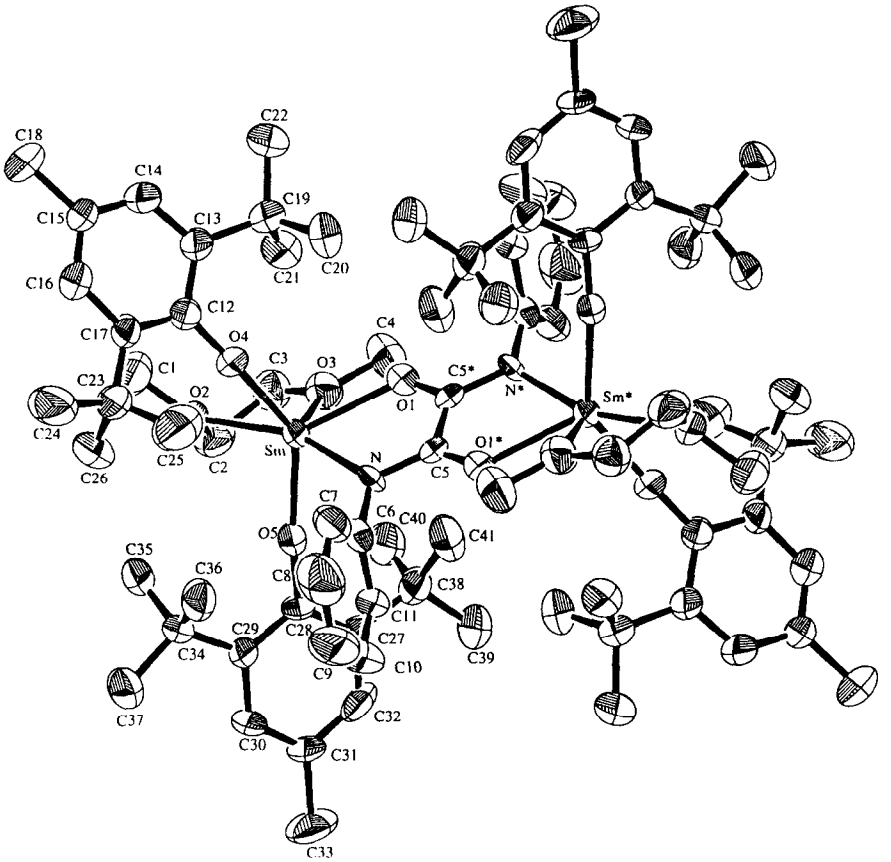

Fig. 1. Molecular structure of **1**.

structure of **1**. Two phenoxo ligands are asymmetrically located on the plane consisting of Sm, N, C(5), C(5*) and O(1) atoms. Sm atom is surrounded by five oxygen atoms and a nitrogen atom to form six-coordinate. The dianionic oxamide ligand [(PhN)OCCO(NPh)]$^{2-}$ connects two samarium atoms. The geometry of **1** is similar to that of $[(C_5Me_5)_2Sm]_2[\mu$-η^4-(PhN)OCCO(NPh)]$\cdot 2C_7H_8$ (**2**) which was formed by the reaction of $(C_5Me_5)_2Sm(\mu$-$\eta^1:\eta^1$-$PhN_2Ph)$ with CO [5]. The Sm—O(Ar) distances are normal. The Sm—O(1) bond is a little longer than Sm—O(Ar) bond, but much shorter than Sm—O(DME) bond. So it is a single bond. The Sm—N distance of 2.549(8) Å in **1** is in agreement with a donor bond, for the donor bond distance for a six-coordinated Sm^{3+} is expected to be 2.41–2.65 Å [5,16]. The distances of N—C bond (1.32(1) Å) and C—O bond (1.29(1) Å) are intermediate between a double bond distance (N=C, 1.29 Å; C=O, 1.20–1.22 Å) and a single bond distance (N—C, 1.47 Å; C—O, 1.43 Å), which are comparable with 1.31(1) and 1.26(1) Å, respectively, in **2**. These distances are consistent with one multiple bond delocalized over the —N—C—O— unit. The C(5)—C(5*) distance of 1.43(2) Å in **1** is shorter than 1.57(2) Å in **2**. The latter is more typically close to a single bond than the former. These bond parameters indicate that [(PhN)OCCO(NPh)]$^{2-}$ dianion in complex **1** highly delocalizes its electrons as well as that in **2**. Figure 2 shows the bond fashion. Although the difference in bond distances between **1** and **2** is small, the bond angles in the two complexes are not fully comparable. For example, the Sm—N—C(5) angle and N—C(5)—O(1*) angle, 114.5(6)° and 123.8(8)° respectively, in **1** are smaller than the corresponding angles, 118.7(6)° and 130.4(10)° respectively, in **2**. It is not clear now whether these differences come from the different metal ionic radii due to their different coordinate numbers.

These results confirm that both C_5Me_5 ligands and ArO ligands here can lead to the same type of complex, which contains a tetradentate oxamide ligand.

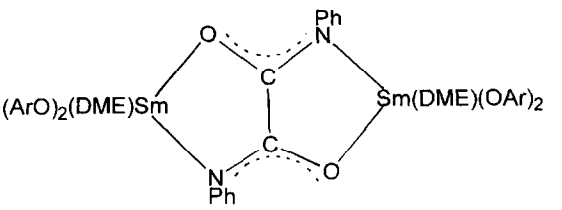

Fig. 2. Bond fashion of dianionic ligand in **1**.

Acknowledgements—The authors thank the Chinese National Science Foundation, Natural Science Foundation of Jiangsu Province and the Laboratory of Organometallic Chemistry, Shanghai Institute of Organic Chemistry, Academia Sinica, for financial support.

REFERENCES

1. Evans, W. J., *Polyhedron*, 1987, **6,** 803; Molander, G. A., *Chem. Rev.*, 1992, **92,** 29; Molander, G. A. and Harris, C. R., *Chem. Rev.*, 1996, **96,** 307.
2. Evans, W. J. and Drummond, D. K., *Organometallics*, 1988, **7,** 797.
3. Evans, W. J., Hughes, L. A., Drummond, D. K., Zhang, H. and Atwood, J. L., *J. Am. Chem. Soc.*, 1986, **108,** 1722.
4. Evans, W. J., Keyer, R. A., Zhang, H. and Atwood, J. L., *J. Chem. Soc., Chem. Commun.*, 1987, 837.
5. Evans, W. J., Drummond, D. K., Chamberlain, L. R., Doedens, R. J., Bott, S. G., Zhang, H. and Atwood, J. L., *J. Am. Chem. Soc.*, 1988, **110,** 4983.
6. Evans, W. J. and Drummond, D. K., *J. Am. Chem. Soc.*, 1988, **110,** 2772.
7. Evans, W. J., Grate, J. W., Hughes,, L. A., Zhang, H. and Atwood, J. L., *J. Am. Chem. Soc.*, 1985, **107,** 3728.
8. Recknagel, A., Stalke, D., Roesky, H. W. and Edelmann, F. T., *Angew. Chem.*, 1989, **101,** 496.
9. Evans, W. J., Keyer, R. A. and Ziller, J. W., *Organometallics*, 1990, **9,** 2628.
10. Shashoua, V. E., *J. Am. Chem. Soc.*, 1959, **81,** 3156; Patten, T. E. and Novak, B. M., *Macromolecules*, 1993, **26,** 436; Patten, T. E. and Novak, B. M., *J. Am. Chem. Soc.*, 1993, **113,** 5065; Hoff, S. M. and Novak, B. M., *Macromolecules*, 1993, **26,** 4067; Okamoto, Y., Matsuda, M., Nakano, T. and Yashima, E., *J. Polym. Sci., Polym. Chem.*, 1994, **32,** 309.
11. (a) Liu, Y., Bei, M., Zhou, Z. and Fujiwara, Y., *Chem. Lett.*, 1992, 1143; (b) Liu, Y. and Bei, M., *Youji Huaxue (China)*, 1994, **14,** 34; (c) Arnold, R. G. , Nelson, J. A. and Verbanc, J. J., *Chem. Rev.*, 1957, **57,** 47.
12. Qi, G., Shen, Q. and Lin, Y., *Acta Cryst.*, 1994, **C50,** 1456.
13. TEXSAN. Crystal structure analysis package, Molecule structure Corporation, Woodlands, TX, 1992.
14. Evans, W. J. and Drummond, D. K., *J. Am. Chem. Soc.*, 1989, **111,** 3329.
15. Evans, W. J., Keyer, R. A., Rabe, G. W., Drummond, D. K. and Ziller, J. W., *Organometallics*, 1993, **12,** 4664.
16. Shannon, R. D., *Acta Cryst.*, 1976, **A32,** 751.

Pergamon

PII: S0277-5387(97)00510-X

Polyhedron Vol. 17, Nos. 11–12, pp. 2013–2020, 1998
© 1998 Elsevier Science Ltd
All rights reserved. Printed in Great Britain
0277-5387/98 $19.00+0.00

Physico-chemical parameter correlations in the $[RuCl_2(CO)(L)(PPh_3)_2]$ complexes (L = *N*-heterocycles)

Karen Wohnrath,[a] Alzir A. Batista,[a]* Antonio Gilberto Ferreira,[a] Julio Zukerman-Schpector,[a] Luiz Antonio A. de Oliveira[b] and Eduardo E. Castellano[c]

[a] Departamento de Química, Universidade Federal de São Carlos, CP 676, 13565-905 São Carlos, SP, Brazil

[b] Instituto de Química, Universidade Estadual Paulista Júlio de Mesquita Filho, UNESP-CP 355, Campus de Araraquara, 14800-900 Araraquara, SP, Brazil

[c] Instituto de Física de São Carlos, Universidade de São Paulo, C.P. 369, 13560-970, São Carlos(SP), Brazil

(Received 5 July 1997; accepted 13 November 1997)

Abstract—Fourteen complexes in the series $[RuCl_2(CO)(L)(PPh_3)_2]$ (where L = N-heterocycles) have been prepared and characterized by IR and NMR spectroscopies, and cyclic voltammetry. A good correlation is found between observed and calculated electrochemical potentials; $E_{1/2}$ vs pK_a or (G_p, σ_m for a series of similar ligands. It is now reported that the carbonyl stretching frequency, ν_{CO}, and the ^{13}C and ^{31}P NMR signals do not correlate well with any of the physico-chemical parameters used ($E_{1/2}$, Taft's and Hammett's parameters). This behaviour is probably due to the characteristics of the Ru(II) species, which does not transmit the steric and electron donor/acceptor properties of the ligands to the carbonyl group, or because the measurements are not able to detect the effect induced by the changes in the ligand L. Indeed, good correlations are obtained when the measurements directly involve the metal centre, as is the case in the $E_{1/2}$ measurements. Crystals of $[RuCl_2(CO)(4\text{-pic})(PPh_3)_2]$ are monoclinic, space group $P2_1/n$, a = 12.019(2), b = 13.825(3) and c = 22.253(3) Å. The structure was solved by the Patterson method and was refined by full-matrix least-squares procedure to R = 0.054 and R_w = 0.055, for 2114 reflections with $I > 3\sigma(I)$.

For L = 2-acetylpyridine and 2-methylimidazole, complexes with formulae $[RuCl_2(CO)(L)(PPh_3)] \cdot L$ and $[RuCl_2(CO)(L)_2(PPh_3)]$, respectively, were obtained. © 1998 Elsevier Science Ltd. All rights reserved

Keywords: ruthenium; Lever's parameters; X-ray structure.

Different physico-chemical measurements, such as carbonyl stretching or its force constants [1–9] and chemical shifts [2,4,7,10–12] have been used to study the structural and electronic properties of transition metal carbonyl complexes through correlations with empirical substituent parameters, such as Taft's σ_I [13,14], Hammett's σ parameters [15], Kabachnik's parameters σ^{PH} [16] and pK_a of ligands [17]. Although for certain types of carbonyl complexes it is possible to relate the σ-donor and π-acceptor ability of ligands with ν(CO) frequencies, for other types of ligands there is little correlation [5]. In the complexes *cis*-$[Pt(\eta^1\text{-}C_6H_4X\text{-}p)_2(PPh_3)_2]$ and *cis*-$[Pt(\eta^1\text{-}C_6H_4X\text{-}p)_2(Ph_2PC_2H_4PPh_2)]$ the coupling constant ^1J(Pt—P) increases as X becomes more electron withdrawing and they show a good correlation with σ_I but not σ_p or σ_p^o [18]. Such a correlation is in accord with the *trans*-influence theory and with the notion that the magnitude of s-electron density in the Pt—P bonds increases with decreasing s-electron density on the bonded carbon of the *trans*-ligand [18]. It is interesting to note, however, that the ^{31}P chemical shifts are insensitive to the nature of X. Similar observations were reported [19] for *trans*-$[Pt(CH_3)(XC_5H_4N)(Ph_2PC_2H_4PPh_2)]$ (X = 4-$N(CH_3)_2$, 4-CH_3, H, 4-

* Author to whom correspondence should be addressed: Tel.: 55-16-274-8285. Fax: 55-16-274-8350. E-mail: daab@.power.ufscar.br

CO_2CH_3, 4-$COCH_3$, or 4-CN) for which ^1J(Pt—P) shows a correlation with σ but the ^{31}P chemical shift for the P atom *trans* to the substituted pyridine does not. The nature of the metal may play a role in determining whether a successful correlation is observed, since a linear correlation exists between the ^{31}P chemical shifts and σ or the analogous palladium complexes, *trans*-[$Pd(CH_3)(XC_5H_4N)(Ph_2PC_2H_4PPh_2)$] [19].

The lack of good correlation of the electron density around the molybdenum atom, as indicated by $\delta(^{95}Mo)$ in a series of [$Mo(CO)_3$(bipy){$P(p\text{-}C_6H_4X)_3$}] [X = Cl,F,H,CH_3,OCH_3,$N(CH_3)_2$] complexes with the pK_a of the ligands supported the argument that pK_a values are not an appropriate measure of the interaction between phosphines and soft acid species such as low-valent transition metal centres. This can be attributed to the fact that pK_a values are dependent on the interaction between the phosphine and the hard acid, H^{+2}.

Cyclic voltammetry in acetonitrile has been used to study the reversible one electron reduction in the complex [$RuCl(bipy)_2(4\text{-}XC_6H_4NO)]^{2+}$. Hammett plots of $E_{1/2}$ versus σ_R, σ_R^o and $\sigma_p - \sigma_m$ were linear, a reaction constant, $\rho = 1.05$ was noted in the correlation with σ_R indicating that the redox potential is very sensitive to the nature of X [20]. Since these correlations involve parameters which measure pure resonance effects, the effect of X is presumably transmitted to the metal centre via the π-electron system of the nitrosoarene. Recently, a ligand electrochemical parameter, $E_L(L)$, based upon the Ru^{III}/Ru^{II} reduction potential as an electrochemical standard was introduced [21] and developed [22,23]. This allows one to predict the metal-centered redox potential of a variety of complexes on the basis of the additivity of the $E_L(L)$ parameters. The prediction is made using the linear relationship

$$E_{calc} = S_M[\Sigma E_L(L_i)] + I_M \quad (1)$$

where the slope, S_M, and the intercept, I_M, are constant for all derivatives of a given coordination number, stereochemistry, and spin state undergoing a defined redox process.

This report deals with physico-chemical data for [$RuCl_2(CO)(L)(PPh_3)_2$] complexes. By systematically changing L, we hoped to probe the nature of the bonding between a d^6 metal centre in a low valence oxidation state, and carbon monoxide, triphenylphosphine and various nitrogen donor ligands, especially *N*-heterocycles ones. Our aim in this work is to test the validity of the above equation for the series of complexes with the general formula [$RuCl_2(CO)(L)(PPh_3)_2$] and to evaluate the role of the Ru(II) ion nature in correlations between some physico-chemical parameters.

EXPERIMENTAL

All reactions and manipulations were carried out under a dry, oxygen-free argon or dinitrogen atmosphere. The chemicals employed in this work were of reagent grade quality (Aldrich). Tetrabutylammonium perchlorate (Fluka purum) was recrystallized from ethanol/water and dried overnight, under vacuum, at 100°C. Reagent grade solvents (Merck) were appropriately distilled, dried and stored over Linde 4 Å molecular sieves. Infrared spectra were recorded as CsI pellets on a Bomem–Michelson 102 instrument, and UV-Vis spectra in CH_2Cl_2 on a HP 8452A spectrophotometer and are given as λ_{max} (nm) (ε in $M^{-1}\,cm^{-1}$). ^{1}H, ^{13}C and $^{31}P\{^1H\}$ NMR spectra were obtained in $CDCl_3$ (Aldrich) or CH_2Cl_2 solutions at room temperature with a Bruker 200 MHz spectrometer. All ^{31}P spectra were proton decoupled and an internal 85% phosphoric acid reference was used. Cyclic and differential pulse voltammetries were carried out at room temperature in freshly distilled dichloromethane containing 0.1 M $Bu_4N^+ClO_4^-$ (TBAP), using an EG&G/PARC electrochemical system consisting of a 273A potentiostat. A three electrode system with resistance compensation was used throughout. The working and auxiliary electrodes were a stationary platinum foil and a platinum wire, respectively. The reference electrode was Ag/AgCl in a Luggin capillary, 0.1 mol/L TBAP in CH_2Cl_2, a medium in which ferrocene is oxidized at 0.42 V (Fc^+/Fc). The measured potentials were converted to the standard hydrogen scale by adding 0.222 V. The scans were recorded at different scanning speeds in the range 50–500 mV s^{-1}. Conductivity was measured using 10^{-3} M solutions of the complexes at 25°C under N_2, using a Micronal conductivity bridge, and are quoted in units of $\Omega^{-1}\,cm^2\,mol^{-1}$. Elemental analyses were performed at the Institute of Chemistry of the University of São Paulo, São Paulo.

ttt-[$RuCl_2(CO)_2(PPh_3)_2$] and [$RuCl_2(CO)$(DMF)$(PPh_3)_2$] (DMF = *N*,*N*-dimethylformamide) were prepared according to literature methods [24,25]. In the present work, a series of complexes of composition [$RuCl_2(CO)(L)(PPh_3)_2$] was obtained in the solid state for L = pyridine (py), pyrazine (pz), 2-cyanopyridine (2-pyCN), 3-cyanopyridine (3-pyCN), 4-cyanopyridine (4-pyCN), 2-picoline (2-pic), 3-picoline (3-pic), 4-picoline (4-pic), isonicotinamide (iso), 4-aminopyridine (4-pyam), 4-dimethylaminopyridine (4-pydiam), 2-aminoethylpyridine (2-pyame), imidazole (im) and 1-methylimidazole (1-Meim), where all ligands are coordinated by the nitrogen atom of the pyridine ring. For L = 2-acetylpyridine (2-pyac) and 2-methylimidazole (2-Meim), compounds of composition [$RuCl_2(CO)$(2-pyac)(PPh_3)·2-pyac and [$RuCl_2(CO)$(2-Meim)$_2(PPh_3)$], were obtained. In a typical synthesis the ligand in excess was added to 4 ml of dichloromethane contained in a 15 ml two neck flask and the mixture was deoxygenated with argon, subsequently 0.1 g of *ttt*-[$RuCl_2(CO)_2(PPh_3)_2$] or [$RuCl_2(CO)$(DMF)$(PPh_3)_2$] was added. After 25 min of stirring at room temperature, the solution volume was reduced to approximately 2 ml and ether was added to precipitate a yellow solid, which was filtered

off, washed well with ether and vacuum dried. Yield: ca 80%. For the synthesis of complexes with sterically hindered ligands, such as 2-cyanopyridine or 2-methylpyridine, the procedure was conducted with neat ligand as solvent. The microanalyses data are reported in Table 1.

Crystals of $[RuCl_2(CO)(4\text{-pic})(PPh_3)_2]$ suitable for X-ray crystallography were grown by slow evaporation of a chloroform/ether solution. A single crystal was used for data collection and cell parameter determination on an Enraf–Nonius CAD-4 diffractometer, using graphite monochromatized Mo–K_α radiation at room temperature ($T = 292$ K). Unit cell parameters were obtained by least-squares from the setting angle of 25 reflections. Intensity data were collected in the $\omega/2\theta$ scan mode up to $\theta_{max} = 25$°, with scan rates between 1.4–6.7° min^{-1}. The intensities of 2 standard reflections were essentially constant during the measurement. Data were corrected for Lorentz polarization (correction factors 0.66, 1.00) and absorption effects, following the procedure of Walker and Stuart [26]. The structure determination and refinement were performed with the SHELX76 system of programs [27], Fig. 1 was drawn with ORTEP [28]. In the final cycles of least-squares refinement, all non-hydrogen atoms were treated anisotropically. All hydrogen atoms were assumed in their calculated position by the geometry of the ligand atom and included in the least-squares calculation with fixed isotropic temperature factor (6.0 $Å^2$). The function minimized was $\Sigma w(|F_o| - |F_c|)^2$, where $w^{-1} = \sigma^2(F_o) + 0.0003 F_o^2$, and the refinement converged to final $R = 0.054$, $R_w = 0.056$, $R_{all} = 0.099$ and $S = 1.38$. In the final refinement cycle, the maximum shift/e.s.d. ratio was 0.001 and the maximum and minimum electron densities in the difference map were 0.65 and −0.50 e $Å^{-3}$, respectively. Scattering factors for non-hydrogen atoms were taken from Cromer and Mann [29] with corrections for anomalous dispersion from Cromer and Liberman [30], and for hydrogen atoms from Stewart *et al.* [31].

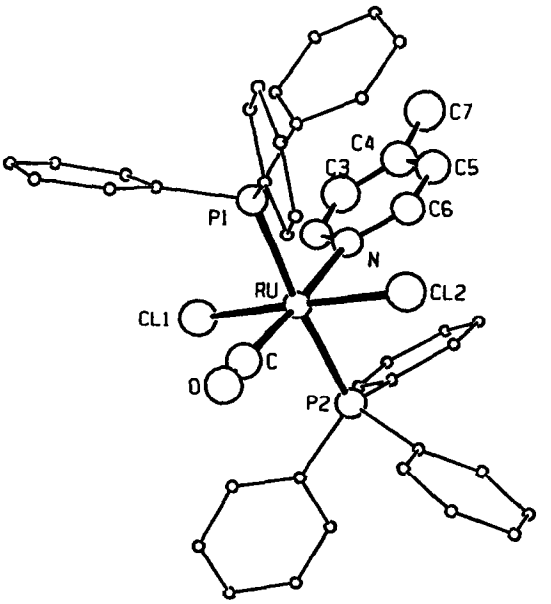

Fig. 1. ORTEP drawing of $[RuCl_2(CO)(4\text{-pic})(PPh_3)_2]$ with the atom numbering scheme.

Table 1. Elemental analysis of the complexes of general formula $[RuCl_2(CO)(L)(PPh_3)_2]$

	Results					
	Calculated			experimental		
	%C	%H	%N	%C	%H	%N
py	62.8	4.4	1.7	61.9	4.3	1.9
2-pyCN	62.3	4.1	3.4	61.4	4.1	3.3
3-pyCN	62.3	4.1	3.4	61.4	4.1	3.4
4-pyCN	62.3	4.1	3.4	61.5	4.1	3.3
2-pic	63.2	4.6	1.7	62.4	4.5	1.7
3-pic	63.2	4.6	1.7	63.5	4.6	2.0
4-pic	63.2	4.6	1.7	62.4	4.6	1.9
iso	61.0	4.3	3.3	60.7	4.3	3.3
4-pyam	61.6	4.4	3.4	57.8	4.3	3.1
4-pydiam	62.4	4.8	3.3	61.7	4.7	3.3
2-pyame	62.5	4.4	1.7	59.1	4.1	3.1
2-pyac[a]	61.0	4.5	3.5	62.9	4.5	2.3
pz	61.2	4.3	3.5	61.2	4.4	3.6
im	60.6	4.3	3.5	60.1	4.3	3.7
1-Meim	61.0	4.5	3.4	60.9	4.5	3.8
2-Meim[b]	51.7	4.3	8.9	50.2	4.4	9.3

[a] Values calculated for the formula $[RuCl_2(CO)(2\text{-pyac})(PPh_3)]$.2-pyac.

[b] Values calculated for the formula $[RuCl_2(CO)(2\text{-Meim})_2(PPh_3)]$.

The data collection and experimental details are summarized in Table 2. The relevant interatomic bond lengths and angles are listed in Table 3. Figure 1 shows the ORTEP drawing of the molecule with the atom numbering scheme.

RESULTS AND DISCUSSION

It is a well known fact that in a complex such as *ttt*-$[RuCl_2(CO)_2(PPh_3)_2]$ with two *trans* carbon monoxide ligands, one of these CO ligands is labile [32]. This property has been used in our laboratory [33] for the synthesis of mononuclear and binuclear complexes, where the labilized CO ligand is substituted by *N*-heterocycle ligands.

The crystal structure of $[RuCl_2(CO)(4\text{-pic})(PPh_3)_2]$ in Fig. 1 shows that the 4-pic ligand is *trans* to CO, the two chlorides are *trans* and the two phosphine groups are *trans*. A similar structure was found previously for the complex *ttt*-$[RuCl_2(CO)_2(PPh_3)_2]$ [34]. Three coordination planes are well defined and their angles

Table 2. Crystal data and summary of intensity data collection and structure refinement

Compound	$C_{43}Cl_2H_{37}NOP_2Ru$
Color/Shape	Yellow/irregular
Form. wt.	817.70
Space group	$P2_1/n$
Temp., °C	19
Cell constants[a]	
a (Å)	12.019(2)
b (Å)	13.825(3)
c (Å)	22.253(3)
β, (°)	99.06(1)
Cell Vol., (Å^3)	3651(1)
Formula units/unit cell	4
Calculated density, g cm^{-3}	1.487
μ calc., cm^{-1}	6.89
Diffractometer/scan	Enraf Nonius CAD-4/ω-2θ
Radiation, graphite monochromator	λ Mo-K_α (=0.71073 Å)
Max. crystal dimensions, mm	0.25 × 0.15 × 0.05
Scan width	0.80 + 0.35 tan θ
Standard reflections	−4 5 6; 0 10 0
Decay of standards	±0.9%
Reflections measured	4864
2θ range, deg.	0–25°
Range of h, k, l	±14, +16, +26
Reflections observed [$I > 3\sigma(I)$]	2113
No of parameters varied	234
Weights	$[\sigma(F_o) + 0.0003\ F_o^2]^{-1}$
GOF	1.38
R	0.054
R_w	0.054
Largest features final diff. map, e Å^{-3}	0.64; −0.50

[a] Least squares refinement of $((\sin\theta)/\lambda)^2$ values for 25 reflections $7 > \theta > 17°$.

are of a slightly distorted octahedron, attributed to the absence of significant steric effects between the ligands. The Ru—P, Ru—Cl and Ru—C bond distances are similar to those found in analogous system [34–36], as can be seen in Table 4.

All the complexes show single, strong IR absorptions in the range 1930–1960 cm^{-1} (attributed to the symmetric stretching frequency of the carbonyl ligand) and also single weak absorptions in the range 320–335 cm^{-1} ($\nu_{Ru\ Cl}$). The absorption frequencies involving the carbonyl groups and the Ru—Cl bonding are summarized in Table 5.

The $^{31}P\{^1H\}$ NMR data for the series of complexes $[RuCl_2(CO)(L)(PPh_3)_2]$, shown in Table 5, present only singlets around $\delta = 30$, indicating that in all complexes the two phosphorus atoms of the two triphenylphosphine ligands are equivalents. This fact is consistent with the two phosphines being *trans* to each other, which allows us to assume a structure similar to the one found in the solid state for the 4-pic ligand complex. When L = 2-Meim the microanalysis data for the complex with this ligand (Table 1) suggest the formulation $[RuCl_2(CO)(2\text{-Meim})_2(PPh_3)]$. The fact that the ^{31}P NMR signal for this complex is found at a lower frequency compared with the other members in the series, suggests that the phosphine is *trans* to a good acceptor ligand. Thus the IR and ^{31}P NMR data for this complex allow us to propose a structure where the CO is *trans* to the phosphine and the imidazoles are *trans* to each other, which is in agreement with chlorides being mutually *trans*. The ^{31}P NMR of the 2-acetylpyridine complex is essentially identical to the other complexes where the phosphine is *trans* to a substituted pyridine. Considering the ^{31}P NMR data, the microanalysis data, which is consistent with the presence of two molecules of the ligand, and the fact that the IR spectrum of this compound shows only a single ν_{Ru-Cl} at 331cm^{-1}, we suggest that this complex incorporates two monocoordinated 2-acetylpyridines, one of which is *trans* to the phosphine and the other of which *trans* to the carbon monoxide.

The ^{13}C NMR data for the series of complexes $[RuCl_2(CO)(L)(PPh_3)_2]$, show three triplets and one singlet in the region between $\delta = 140$ and $\delta = 120$, attributed to the carbon atoms of PPh_3 ligands, peaks between $\delta = 155$ and $\delta = 110$, attributed to the aromatic carbon atoms of the coordinated *N*-heterocyclic ligands, and triplets around $\delta = 205$. The data for the

Table 3. Selected bond lengths (Å) and angles (°) for $[RuCl_2(CO)(4\text{-pic})(PPh_3)_2]$, with e.s.d.s in parentheses

Ru—Cl(1)	2.413(4)	P(1)—C(111)	1.83(1)
Ru—Cl(2)	2.421(4)	P(1)—C(121)	1.82(1)
Ru—C	2.02(1)	P(1)—C(131)	1.83(1)
Ru—N	2.202(1)	P(2)—C(211)	1.84(1)
Ru—P(1)	2.406(4)	P(2)—C(221)	1.83(1)
Ru—P(2)	2.404(4)	P(2)—C(231)	1.83(1)
C—O	1.10		
Cl(1)—Ru—Cl(2)	178.8(2)	Ru—C—O	176(1)
Cl(1)—Ru—C	87.3(4)	Ru—NC—(2)	121.2(9)
Cl(1)—Ru—N	89.6(3)	Ru—N—C(6)	121.1(9)
Cl(1)—Ru—P(1)	93.1(1)	C(2)—N—C(6)	118(1)
Cl(1)—Ru—P(2)	90.6(1)	N—C(2)—C(3)	123(1)
Cl(2)—Ru—C	93.5(4)	C(2)—C(3)—C(4)	120(1)
Cl(2)—Ru—N	89.5(3)	Ru—P(1)—C(111)	119.0(4)
Cl(2)—Ru—P(1)	87.8(1)	Ru—P(1)—C(121)	116.5(4)
Cl(2)—Ru—P(2)	88.5(1)	Ru—P(1)—C(131)	111.8(4)
C—Ru—N	175.5(5)	C(111)—P(1)—C(121)	100.4(6)
C—Ru—P(1)	88.4(4)	C(111)—P(1)—C(131)	100.5(6)
C—Ru—P(2)	94.3(4)	C(121)—P(1)—C(131)	106.7(6)
N—Ru—P(1)	88.5(3)	P(1)—C(111)—C(112)	116.0(9)
N—Ru—P(2)	89.0(3)	P(1)—C(111)—C(116)	124(1)
P(1)—Ru—P(2)	175.5	C(112)—C(111)—C(116)	120(1)

Table 4. Representative structural data for some ruthenium(II) complexes

	Distances (Å)				
Complex	Ru—P	Ru—Cl	Ru—C	C—O	Ref
$[RuCl_2(CO)(4\text{-pic})(PPh_3)_2]$	2.405	2.417	2.01	1.10	This work
ttt-$[RuCl_2(CO)_2(PPh_3)_2]$	2.39	2.43	1.96	1.10	34
ttt-$[RuCl_2(CO)_2(PBz_3)_2]$	2.398	2.418	1.948	1.122	35
cct-$[RuCl_2(CO)_2(PPh_3)_2]$	2.424	2.439	1.859	1.130	36

latter region, shown in Table 5, are of special interest, since they correspond to the signal of the carbon atom of the CO group, being consistent with the carbon atom interacting with two equivalent phosphorus atoms which are mutually *trans*. For L = py, besides the expected triplet in $\delta = 205.08$, two additional singlets around $\delta = 204$ were also observed. These singlets are tentatively attributed to the presence of two nonequivalent CO groups in the binuclear species $[Ru_2Cl_4(CO)_2(py)_2(PPh_3)_2]$ formed in solution and having two bridging Cl groups. Additional evidence for the existence of the equilibrium between mono- and binuclear complexes proposed comes from the ^{31}P NMR spectra where, besides the expected intense signal of the mononuclear complex at $\delta = 30.53$, signals are found at $\delta = -5.0$, 22.26 and 49.17. The negative chemical shift signal is characteristic of the presence of free phosphine in solution, possibly liberated during the process of binuclear complex formation. The signals at $\delta = 22.26$ and 49.17 can be attributed to the coordinated phosphines *trans* to pyridine and CO, respectively, in agreement with the previous discussion about the 2-methylimidazole complex.

When L = 2-pyac, the ^{13}C NMR spectrum is more complicated in the region close to $\delta = 205$, indicating the presence of more than one type of CO. When L = 2-Meim, no ^{13}C signal was observed in this region, probably due to the low solubility of this complex in the chloroform solvent.

The electronic spectra of the complexes $[RuCl_2(CO)(L)(PPh_3)_2]$ show two intense absorptions in the UV-region ($\varepsilon_{max} \cong 10^4\ M^{-1}\ cm^{-1}$) below 350 nm due to internal transitions of the ligands. These bands can be attributed to internal $\pi \rightarrow \pi^*$ transitions in the coordinated aromatic ligands [37]. In the visible

Table 5. Spectroscopic data of the complexes of general formula [Ru(Cl)2(CO)(L)(PPh3)2][a]

L	$\nu_{(CO)}$ (cm^{-1})	$\nu_{(Ru-CO)}$ (cm^{-1})	λ_1 (nm), (ε_{max} (M^{-1} cm^{-1}))[b]	λ_2 (nm), (ε_{max} (M^{-1} cm^{-1}))[b]	ν_2 (kK)	$\delta^{13}C(CO)$	$\delta^{31}P$
2-pyCN	1959	580		460 (45)	21.74	198.08	21.42
pz	1950	589	362 (200)	411(382)	24.33	206.03	32.38
2-pyac	1941	588	369 (700)			205.89	32.41
3-pyCN	1947	591	365 (154)	417 (275)	23.98	205.83	32.89
4-pyCN	1947	563	372 (240)	435 (103)	22.99	205.90	32.14
iso	1954	588	368 (175)	433 (129)	23.09	205.44	32.13
py	1946	596	375 (151)	430 (377)	23.25	205.08	30.51
3-pic	1946	595	372 (120)	445 (128)	22.47	205.43	31.71
2-pic	1942	592	364 (164)	448 (96)	22.32	205.73	31.41
4-pic	1944	593	375 (113)	450 (133)	22.22	205.74	31.34
im	1941	594	362 (225)	444 (153)	22.52	205.92	33.35
1-Meim	1934	594	363 (110)	450 (151)	22.22	205.96	33.51
2-Meim	1954	601	378 (143)	450 (196)	22.22		41.62
2-pyame	1928	588	360 (148)	453 (100)	22.07	205.11	33.05
4-pyam	1946	594	375 (160)	445 (118)	22.47	205.64	30.62
4-pydiam	1947	593	370 (142)	447 (275)	22.37	205.46	30.79

[a] Except for L = 2-pyac and 2-Meim, where compositions $[RuCl_2(CO)(2\text{-pyac})(PPh_3)]$ and $[RuCl_2(CO)(2\text{-Meim})_2(PPh_3)]$ were found.

[b] Absorption maxima and intensity determined by Gaussian deconvolution of the spectra.

region all the complexes, except when L = 2-pyCN and 2-pyac, show two absorption bands (λ_1 and λ_2) of low intensity ($\varepsilon_{max} \cong 10^2\ M^{-1}\ cm^{-1}$), attributed to *d–d* transitions. The position and intensity of the *d–d* bands of all the complexes studied, after deconvolution to correct the strong effect of the intense UV bands, are shown in Table 5.

Experimental data of ν_{CO}, ν_2, δ ^{13}C and δ ^{31}P (Table 5), when correlated with Taft's and Hammett's substituent parameters listed in Table 6, showed very poor agreements. Apparently the effect of the substituent in the *N*-heterocycle ligands is not transmitted to the other ligands through the Ru(II) central atom, or the effect is too small to be detected by the techniques employed in these measurements.

If this is so, better correlations are expected when the measurements are related to properties involving the central metal atom, as in $E_{1/2}$ measurements. The cyclic voltammograms of all the complexes prepared consist of a pair of reversible peaks ($i_a/i_c \cong 1$), attributed to the one electron Ru^{III}/Ru^{II} couple, and the $E_{1/2}$ values are shown in Table 7.

Indeed, for the series of substituted pyridine ligands lacking significant steric effects (L = 3-pyCN, 4-pyCN, iso, py, 3-pic, 4-pic, 4-pyam, 4-pydiam), a reasonable linear plot of $E_{1/2}$ vs pK_a (Fig. 2), correlation coefficient $R = -0.99$ and slope -0.02 was observed. Similar results were obtained when the Hammett parameters ($E_{1/2}$ vs σ_M, σ_P; $R = 0.98$) or Taft parameters ($E_{1/2}$ vs σ^o_M, σ^o_P; $R = 0.97$) were used. As suggested by the decrease of the $E_{1/2}$ values with increasing values of pK_a of L ligands, more effective back-bonding ligands increase $E_{1/2}$ by stabilizing Ru(II) mainly due to this effect.

The experimental and calculated electrochemical data for the series of complexes of general formula $[RuCl_2(CO)(L)(PPh_3)_2]$ by using Lever's equation [1] and the $E_L(L)$ values taken from the literature [21] (for $Ru^{(III/II)}$ couples in organic solvent, $E_{calc} = 0.97[\Sigma_i E_L(L_i)] + 0.04$]) are shown in Table 7. For the same set of substituted pyridinic ligands used before in Fig. 2, a correlation coefficient $R = 0.99$ and a slope equal to 1.02 were obtained for the plot E_{calc} vs $E_{1/2}$ (Fig. 3). Ideally, the best straight line that correlates the observed and calculated values should have a slope of unity, but in view of the small set of data available for our correlation the result obtained can be considered good enough. Similar results were obtained recently in substituted-polypyridyl complexes of ruthenium containing II-acceptor ligands [44], where a slope of 1.2 was observed. If we had included the ligands im, 1-Meim, 2-pyame and pz, the *R* value would decrease to 0.78 and the slope to 0.88. These data together show the utility of the electrochemical parameters proposed by Lever [21], considering the variety of ligands and substrates used in this work.

CONCLUSION

The results obtained in this work suggest that to consider correlations of ligand substituent parameters with physico-chemical properties of coordination

Table 6. Taft's and Hammett's substituent parameters of the ligands L of the complexes of general formula $[Ru(Cl)_2(CO)(L)(PPh_3)_2]$

L	σ_p, σ_m[a]	σ_p^-, σ_m^+[b]	σ_p^-[b]	σ_p^o, σ_m^o[c]	σ_I^o[d]	σ_R^o[d]
3-pyCN	0.56	0.56		0.62	0.57	0.08
4-pyCN	0.66	0.66	1.00	0.69	0.52	0.14
iso	0.36		0.61		0.30	0.20
py	0.0	0.0	0.0	0.0	0.0	0.0
3-pic	−0.07	−0.07			−0.01	−0.16
4-pic	−0.17	−0.31	−0.17	−0.12	−0.05	−0.10
4-pyam	−0.66	−1.30	−0.15	−0.38	0.10	−0.48
4-pydiam	−0.83	−1.70	−0.12	−0.44	0.05	−0.52

[a] Ref. 15; [b] Refs 13 and 15; [c] Ref. 38; [d] Ref. 39.

The parameter σ is defined through the famous Hammett equation ($\sigma = \log k_X - \log k_H$) where k_H is the ionization constant for benzoic acid in water at 25°C and k_X is the ionization constant for a *meta* (σ_m) or *para* (σ_p) derivative under the same experimental conditions. Positive values of (represent electron withdrawal by the substituent from the aromatic ring; negative σ values indicate electron release to the ring. The parameters σ_p^+ and σ_m^+ were defined for systems where a positive charge is delocalized between substituent and reaction centre via "through resonance"; the σ_p^- served for groups with loosely held lone pair electrons conjugated with a substituent capable of accepting a pair of electrons via resonance. The normalized (σ_p^o, σ_m^o) constants were formulated the ionization of phenylacetic acids from other systems which all through resonance would be eliminated, preventing resonance interaction. σ_I^o, σ_R^o constants have been developed by Taft to separete the inductive and resonance contributions of substituents [13–15].

Table 7. Electrochemical parameters of the complexes $[Ru(Cl)_2(CO)(L)(PPh_3)_2]$[a]

L	pK_a	$E_{1/2}$ (V) vs NHE	E_{calc} (V) vs NHE[e]
2-pyCN	−0.26[a]	1.40	
pz	0.65[b]	1.55	1.61
2-pyac	0.78[c]	1.43	
3-pyCN	1.36[a]	1.39	1.59
4-pyCN	1.86[a]	1.40	1.60
iso	3.65[b]	1.37	1.54
py	5.25[b]	1.33	1.53
3-pic	5.68[b]	1.31	1.51
2-pic	5.97[b]	1.31	1.50
4-pic	6.02[b]	1.30	1.51
im	6.95[b]	1.24	1.40
1-Meim	6.95[b]	1.28	1.37
2-Meim	7.85[c]	1.04	
2-pyame	8.78[d]	1.36	1.42
4-pyam	9.11[b]	1.23	1.44
4-pydiam	9.71[c]	1.22	1.42

[a] Ref. 40.
[b] Ref. 41.
[c] Value calculated using the equation $pK_a = 5.03 - 11.88\Sigma\sigma_M$, Ref. 17.
[d] Ref. 42.
[e] Ref. 43.
[f] Refs 21, 23; [g] Except for L = 2-pyac and 2-Meim.

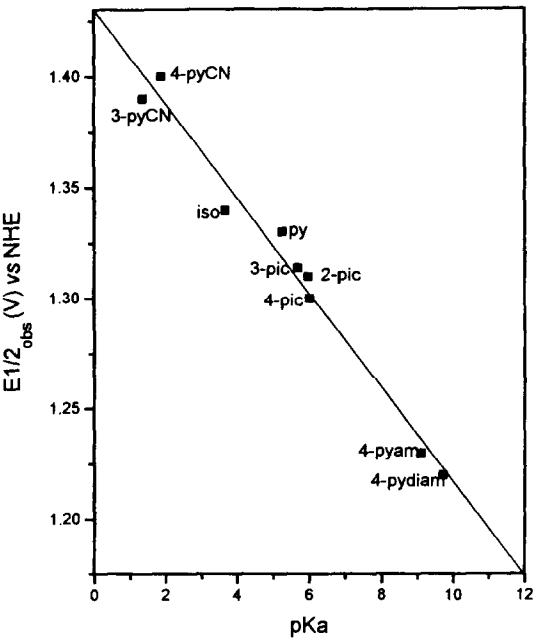

Fig. 2. Correlation of measured values of $E_{1/2}$ for the $[RuCl_2(CO)(L)(PPh_3)_2]$ complexes with pK_a of free ligands (L) (L = N-heterocycles). See text for correlation coefficient and slope value.

compounds, the nature of the central metal atom and the technique to be used for measurements are fundamental. In our study, the effect of the ligand substituents reflects in the properties directly related to the "soft" central metal atom, which does not strongly transmit the steric and donor/acceptor properties of the substituents in the *N*-heterocycle species to the remaining ligands.

Acknowledgements—We thank FAPESP, CAPES, CNPq and FINEP for financial support of this work. We wish to

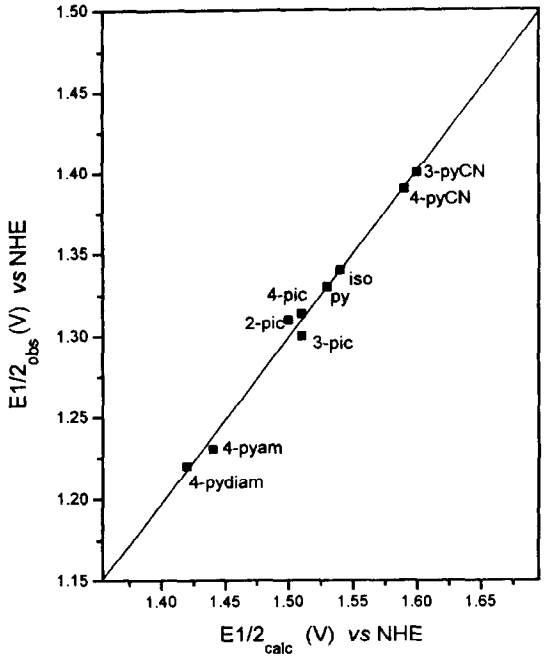

Fig. 3. Correlation of measured values of $E_{1/2}$ vs E_{calc} for the $[RuCl_2(CO)(L)(PPh_3)_2]$ complexes. See text for correlation coefficient and slope value.

thank Prof. Chris Orvig and Prof. A.B.P. Lever for a helpful discussion.

REFERENCES

1. Bitterwolf, T. E., *Polyhedron*, 1988, **7,** 1382.
2. Alyea, E. C., Gossage, R. A., Malito, J. and Munir, Z. A., *Polyhedron*, 1990, **9,** 1059.
3. Gray, G. M. and Gray, R. J., *J. Magn. Reson.*, 1984, **57,** 347.
4. Box, J. W. and Gray, G. M., *Magn. Reson. Chem.*, 1986, **24,** 527.
5. Alyea, E. C., Fisher, K. J. and Gossage, R. A., *Spectrochimica Acta*, 1989, **45A,** 203.
6. Fisher, R. D., *Chem. Ber.*, 1991, **103,** 162.
7. Romeo, R., Arena, G. and Scolaro, L. M., *Inorg. Chem.*, 1992, **31,** 4879.
8. Box, J. W. and Gray, G. M., *Inorg. Chem.*, 1987, **26,** 2774
9. Bursten, B. E. and Green, M. R., *Prog. Inorg. Chem.*, 1988, **36,** 393.
10. Alyea, E. C. and Song, S., *Inorg. Chem.*, 1992, **31,** 4909.
11. Bitterwolf, T. E., *Polyhedron*, 1988, **7,** 409.
12. Malito, J., Alyea, E. C. and Gossage, R. A., *Spectrochimica Acta*, 1992, **48A,** 873.
13. Hansch, C., Leo, A. and Taft, R. W., *Chem. Rev.*, 1991, **91,** 165.
14. Hansch, C. and Leo, A., *Substituent Constants for Correlation Analysis in Chemistry and Biology*, 1st edn. John Wiley & Sons, New York, 1979.
15. Johnson, C. D., *The Hammett Equation*. Cambridge University Press, New York, 1973.
16. Allman, T. and Goel, R. G., *Can. J. Chem.*, 1982, **60,** 716.
17. Perrin, D. D., Dempsey, B. and Serjeant, E. P., *pK_a Prediction for Organic Acids and Bases*. Chapman and Hall, New York, 1981.
18. Eaborn, C., Odell, K. J. and Pidcock, A., *J. Chem. Soc., Dalton Trans.*, 1978, 357.
19. Clark, H. C. and Milne, C. R., *Can. J. Chem.*, 1979, **57,** 958.
20. Bowden, W. L., Little, W. F., Meyer, T. J. and Salmon, D., *J. Am. Chem. Soc.*, 1975, **97,** 6897
21. Lever, A. B. P., *Inorg. Chem.*, 1990, **29,** 1271.
22. Lever, A. B. P., *Inorg. Chem.*, 1991, **30,** 1980.
23. Masui, H. and Lever, A. B. P., *Inorg. Chem.*, 1993, **32,** 2199.
24. Stephenson, T. A. and Wilkinson, G., *J. Inorg. Nucl. Chem.*, 1966, **28,** 945.
25. James, B. R., Markham, L. D., Hui, B. C. and Rempel, G. L., *J. Chem. Soc. Dalton Trans.*, 1973, 2247.
26. Walker, N. and Stuart, D., *Acta Cryst.*, 1983, **A39,** 158.
27. Sheldrick, G. M., SHELX-76. Program for Crystal Structure Determination (University of Cambridge, U.K., 1976.
28. Johnson, C. K., ORTEP, Report ORNL-3794, Oak Ridge National Laboratory, Tennessee, U.S.A., 1965.
29. Cromer, D. T. and Mann, J. B., *Acta Cryst.*, 1968, **A24,** 321.
30. Cromer, D. T. and Liberman, D., *J. Chem. Phys.*, 1970, **53,** 1891.
31. Stewart R. F., Davidson, E. R. and Simpson, W. T., *J. Chem. Phys.*, 1965, **42,** 3175.
32. Krassowski, D. W., Nelson, J. H., Brower, K. R., Hauenstein, D. and Jacobson, R. A., *Inorg. Chem.*, 1988, **27,** 4294.
33. Batista, A. A., Porcu, O. M., Nascimento, O. R. and Barbosa, V. M., *J. Coord. Chem.*, 1993, **32,** 345.
34. Oliva, G. and Batista, A. A., unpublished data.
35. Wilkes, L. M., Nelson, J. H., Mitchener, J. P., Babich, M. W., Riley, W. C., Helland, B. J., Jacobson, R. A., Cheng, M. Y., Seff, K. and McCusker, L. B., *Inorg. Chem.*, 1982, **21,** 1376.
36. Batista, A. A., Zukerman-Schpector, J., Porcu, O. M., Queiroz, S. L., Araujo, M. P., Oliva, G. and Souza, D. H. F., *Polyhedron*, 1994, **13,** 689.
37. Coel, B. J., Meyer, T. J. and White, P. S., *Inorg. Chem.*, 1995, **34,** 593.
38. Fujita, T. and Nishioka, T., *Prog. Phys. Org. Chem.*, 1976, **12,** 49.
39. Taft, R. W., *J. Phys. Chem.*, 1960, **64,** 1805.
40. Zanella, A. W. and Ford, P. C., *Inorg. Chem.*, 1975, **14,** 42.
41. CRC: *Handbook of Chemistry and Physics*, 1st ed. CRC press, U.S.A., 1991.
42. Martell, A. L., *Stability Constants of Metal-Ion Complexes*: Section II: Organic Ligands. The Chemical Society, London, 1964.
43. Scriven, E. F. V., *Pyridines and Their Benzo Derivatives*. In: *Comprehensive Heterocyclic Chemistry*, Vol. 2, eds A. R. Katriztky and C. W. Rees. Pergamon Press, Oxford, 1984.
44. Dovletoglou, A., Adeyemi, S. A. and Meyer, T. J., *Inorg. Chem.*, 1996, **35,** 4120.

Pergamon

PII: S0277-5387(97)00476-2

Polyhedron Vol. 17, Nos. 11–12, pp. 2021–2028, 1998
© 1998 Elsevier Science Ltd
All rights reserved. Printed in Great Britain
0277-5387/98 $19.00+0.00

Synthesis, thermodynamics and relaxivity studies for the complexation of Gd^{3+}, Ca^{2+}, Cu^{2+} and Zn^{2+} by *N,N″*-bis(amide) derivatives of diethylenetriaminepentaacetic acid

Yun-Ming Wang,*[a] Su-Tin Lin,[a] Yueh-Ju Wang[a] and Reu-Sheng Sheu[b]

[a]School of Chemistry, Kaohsiung Medical College, No. 100 Shih-Chuan 1st Road, Kaohsiung, Taiwan 807, Republic of China

[b]Department of Radiology, Kaohsiung Medical College, No. 100 Shih-Chuan 1st Road, Kaohsiung, Taiwan 807, Republic of China

(Received 19 September 1997; accepted 12 November 1997)

Abstract—Three bis(amide) derivatives of H_5dtpa [(carboxymethyl)iminobis(ethylenenitrilo)tetraacetic acid], H_3L^1 = bis(adamantanamide), H_3L^2 = bis(2-methoxybenzylamide), and H_3L^3 = bis(2-methoxyphenethylamide) were synthesized. Their protonation constants were determined by potentiometric titration in 0.10 mol dm^{-3} KCl and by NMR pH titration at 25.0±0.1 °C. Stability and selectivity constants are measured to evaluate the possibility of using the corresponding gadolinium(III) complexes for magnetic resonance imaging contrast agents. Low stability or selectivity constants indicate higher possibility for releasing free Gd^{3+} ion and free ligand as well from gadolinium(III) complexes. The formations of gadolinium(III), copper(II), zinc(II), and calcium(II) complexes were investigated quantitatively by the potentiometry. The stability constant for gadolinium(III) complex is larger than those for Ca(II), Zn(II), and Cu(II) complexes for these three octadentate ligands. The selectivity constants and modified selectivity constants of the amides for Gd^{3+} over endogenously available metal ions were calculated. Effectiveness of all three ligands in binding divalent and trivalent metal ions in biological media is assessed by comparing pM values at physiological pH 7.4. Spin-lattice relaxivity R_1 for Gd(III) complexes was also determined. The observed relaxivity were found to decrease with increasing pH in the acid range below pH 3 and relaxivity values were become invariant with respect to pH changes over the range of 3–10. © 1998 Elsevier Science Ltd. All rights reserved

Keywords: gadolinium complexes; contrast agents; relaxivity; MRI; thermodynamics; paramagnetic complexes.

This report describes the synthesis of three *N,N″*-bis(amide) derivatives of H_5dtpa ((carboxymethyl) iminobis(ethylenenitrilo)tetraacetic acid) i.e. H_3L^1 = bis(adamantanamide), H_3L^2 = bis(2-methoxybenzylamide), and H_3L^3 = bis(2-methoxyphenethylamide). Their protonation constants, thermodynamic, and conditional stability constants of complexes with Gd^{3+}, Cu^{2+}, Zn^{2+}, and Ca^{2+} and their selectivity for Gd^{3+} over endogenously available metal ions are discussed. The spin-lattice relaxivity R_1 of the [GdL^1], [GdL^2], and [GdL^3] are also described.

* Author to whom correspondence should be addressed. Tel.: 00 886 7 3121101 ext 2218. Fax: 00 886 7 3125339. E-mail: m825010@cc.kmc.edu.tw.

EXPERIMENTAL

Materials

Gadolinium chloride (>99.9%) was obtained from Aldrich Chemical Co. and oven dried at 110 °C for at least 24 h before use. All other reagents used for the synthesis of the amides were purchased from commercial sources unless otherwise noted. Proton NMR spectra and elemental analyses were used to confirm the composition of the products.

Chart I

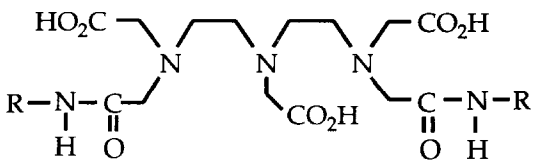

	R
H_3L^1	
H_3L^2	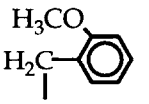
H_3L^3	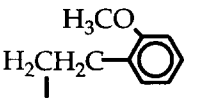

Preparations

Diethylenetriamine-N,N′,N″-*triacetic*-N,N″-*dianhydride*. The anhydride was prepared according to the method of Eckelman *et al.* [1]. White solid (33.23 g, 93%); m.p. 183–185 °C; δ_H [200 MHz, solvent $(CD_3)_2SO$; standard $SiMe_4$] 3.71 (8 H, s, terminal NCH_2CO_2), 3.31 (2 H, s, central NCH_2CO_2), 2.75 (4 H, t, NCH_2), and 2.60 (4 H, t, NCH_2).

N,N″-*Bis*(*amides*) *of* H_5dtpa: H_3L^1, H_3L^2, *and* H_3L^3. The compounds H_3L^1, H_3L^2, and H_3L^3 were synthesized by a modification of the procedure of Konings *et al.* [2]. The dianhydride (5.0 g, 13.99 mmol) was added in portions over 1 h to ice-cold stirred 99% alkylamine (140 mmol). After 30 min, the ice bath was removed and the reaction mixture was stirred at room temperature for 20 h. It was concentrated under reduced pressure to an oil, diluted with water (30 cm^3), and adjusted to pH 1.5 with concentrated HCl. The colourless solid formed was collected and recrystallized from water–acetone to give colourless crystals.

N,N″-*Bis*(*adamantanamide*) H_3L^1. White crystals (3.9 g, 57%), m.p. 192–193 °C (Found: C, 48.8; H, 7.8; N, 14.05. $C_{20}H_{37}N_5O_8 \cdot H_2O$ requires C, 48.65; H, 7.95; N, 14.2%); δ_H (200 MHz; solvent D_2O/NaOD standard $SiMe_4$) 1.65 (6 H, s, $NCCH_2CHCH_2$), 1.94 (6 H, s, $NCCH_2CH_2$), 2.03 (3 H, s, $NCCH_2CHCH_2$), 3.15 (4 H, s, NCH_2CON), 3.16 (4H, s, terminal NCH_2CO_2), 3.52 (2 H, s, central NCH_2CO_2), and 3.1, 2.89 (8 H, s, NCH_2CH_2N).

N,N″-*Bis*(2-*methoxybenzylamide*) H_3L^2. White crystals (6.35 g, 72%), m.p. 152–154 °C (Found: C, 57.1; H, 6.65; N, 11.1. $C_{30}H_{41}N_5O_{10} \cdot H_2O$ requires C, 57.1; H, 6.55; N, 11.1%); δ_H 7.18, 6.93 (8 H, m, C_6H_4) 4.32 (4 H, s, $ArCH_2N$), 3.79 (6 H, s, OCH_3), 3.15 (4 H, s, NCH_2CON), 3.07 (4 H, s, terminal NCH_2CO_2), 3.01 (2 H, s, central NCH_2CO_2), and 2.53 (8 H, m, NCH_2CH_2N).

N,N″-*Bis*(2-*methoxylphenethylamide*) H_3L^3. White crystals (6.19 g, 67%), m.p. 105–107 °C (Found: C, 55.1; H, 7.1; N, 10.1. $C_{32}H_{45}N_5O_{10} \cdot 2H_2O$ requires C, 55.25; H, 7.1; N, 10.1%); δ_H 7.09, 6.92 (8 H, m, C_6H_4), 3.77 (6H, s, OCH_3), 3.41 (4 H, t, $NHCH_2CH_2Ar$), 2.99 (4 H, s, terminal NCH_2CO_2), 3.30 (2 H, s, central NCH_2CO_2), 3.01 (4 H, s, NCH_2CON), and 2.73 (8 H, s, NCH_2CH_2N).

General techniques

Solutions of amides (0.1 mol dm^{-3}) for NMR pH titration were made up in D_2O, and pD was adjusted with DCl or CO_2-free NaOD. Proton NMR spectra were measured in D_2O solution on a Varian XL-200E spectrometer. The final pD of the amide solutions were determined with a microelectrode. The final pD was obtained from the equation pD = pH + 0.40 [3]. The hydrogen electrode used in the present study allows a reliable and accurate determination of the proton activity over an extended pH range.

Solution preparations

Stock solutions of Ca^{2+}, Zn^{2+}, Cu^{2+}, and Gd^{3+} were prepared between 0.015 and 0.02 mol dm^{-3} from the nitrate salts with demineralized water (obtained by a Millipore/Milli-Q system) and standardized by titration with Na_2H_2edta (disodium salt of ethylenedinitrilotetraacetic acid) [4] or atomic absorption spectrophotometry.

Potentiometric measurements

Potentiometric titrations were performed with an automatic titrator system to determine the protonation constants of the amides and the stability constants of the metal complexes. The autotitrating system consists of a 702 SM Titroprocessor, a 728 stirrer, and a PT-100 combination pH electrode (Metrohm). Each titration was performed at least three times. Since the Gd^{3+} chelate is completely or almost completely formed at low pH, their stability constant could not be determined from the normal potentiometric titration method. Therefore, these stability constants were evaluated by a ligand–ligand competition potentiometric titration in this study [5–7]. A 1:1:1 molar ratio of Gd^{3+}, amide, and a reference ligand with a known metal chelate stability was titrated. A good reference ligand for the Gd^{3+} systems was found to be H_4edta. H_4edta forms a complex with Gd^{3+} whose stability constant is accurately known.

Computational method

The protonation constants of the amides were calculated using a FORTRAN computer program PKAS [8] written for polyprotonic weak acid equilibria. The stability constants of normal chelates and the protonated metal chelates were determined from the titration data with the FORTRAN computer program BEST [8]. The average difference between observed and calculated $-\log[H^+]$ was <0.04 throughout all titration. A value of 13.78 was employed for the pK_w at 25 C. The species distribution diagrams were calculated with the FORTRAN program SPE and SPEPLOT [8].

Relaxation time measurement

The Gd^{III} chelate solution was prepared by combining equal molar amounts of the stock $GdCl_3$ and the amides solution. A slight excess (3%) of the amide was used and the solution was allowed to react for at least 2 h at room temperature to ensure completion of the complexation. The Gd^{III} chelate solutions under various pH values were prepared by combining the buffer solution with an appropriately diluted Gd^{III} complex solution in a 1:1 (*v/v*) ratio. The following buffer systems (all 0.10 mol dm^{-3}, except those at pH 7–8) were used: chloroacetic acid/NaOH (pH 2 and 3), acetic acid/NaOH (pH 4 and 5), Tris (=tris(hydroxymethyl)aminomethane)/HCl (pH 7 and 8), and ammonia/HCl (pH 9 and 10) [9]. These buffer solutions were used to maintain constant ionic strength (i.e. 0.10 mol dm^{-3}). The 0.10 mol dm^{-3} buffers were sufficient to keep the solution pH within the desired range in most cases. However, the 0.10 mol dm^{-3} Tris buffer was too weak to maintain Gd^{III} complex solution at pH 7, and a 1.0 mol dm^{-3} Tris buffer solution was used instead. The buffered Gd^{III} chelate solutions were all allowed to equilibrate for at least 2 h. The pH of these solutions was determined immediately before relaxation time T_1 measurements.

Relaxation times T_1 of aqueous solutions of gadolinium(III) complexes of linear bis(amide) derivatives of H_5dtpa were measured to determine relaxivity R_1. All measurements were made using an NMR spectrometer operating at 20 MHz and 37.0 ± 0.1 C (NMS 120 Minispec, Bruker). Before each measurement the spectrometer was tuned and calibrated. The value of T_1 was measured from eight data points generated by an inversion-recovery pulse sequence. The slopes of plots of $1/T_1$ vs concentration give R_1 in dm^3 $mmol^{-1}$ s^{-1}.

RESULTS AND DISCUSSION

Protonation constants

The amide protonation constants are expressed as in eqn (1).

$$K_n = [H_nL]/([H_{n-1}L][H^+]) \quad (1)$$

Table 1 summarizes the protonation constants of the bis(amides) measured in the range pH 3–10. The titration curves of H_3L^1, H_3L^2, and H_3L^3 all show a very sharp increase between pH 9.0 and 4.0 (moles of base per mol amide present = 2). This is due to the large difference between the first ($\log K_1$) and second protonation constant ($\log K_2$), i.e. 9.35 and 4.85, 9.33 and 4.64, and 9.12 and 4.61, respectively. The $\log K_3$ (third protonation constant) values are 3.73, 3.78, and 3.46, respectively. The carboxylates have $\log K_4$ and $\log K_5$ values below 2 (not observed in this study). The protonation constants are very similar to those of the H_3dmdtta ($\log K_1 = 9.37$, $\log K_2 = 4.38$, $\log K_3 = 3.31$ in 0.1 mol dm^{-3} $NaClO_4$) [10].

The replacement of the two carboxylate groups in H_5dtpa by the two *N*-adamantane-, *N*-2-methoxybenzyl-, and *N*-2-methoxyphenethyl-amide groups results in a decrease in $\log K_1$ (i.e. 1.14, 1.16, 1.37 units), $\log K_2$ (i.e. 3.75, 3.96, 3.99 units), $\log K_3$ (i.e. 0.55, 0.50, 0.82 units), and ΣpK_a values (i.e. 8.08, 8.26, 8.82 units). These significant differences in basicity of the amine groups (ΣpK_a) are presumably due to hydrogen bonding from the terminal nitrogen atom and carboxylate to amide protons in the bis(amides) [11–13].

Table 1. Protonation constants log K_n with uncertainty (σ) in parentheses

	log K_n [25.0 ± 0.1 C, I = 0.10 mol dm^{-3} (KCl)]				
Equilibrium	H_3L^1	H_3L^2	H_3L^3	H_3dmdtta[a]	H_5dtpa[b]
[HL]/[L][H]	9.35(0.03)	9.33(0.07)	9.12(0.07)	9.37(0.01)	10.49
[H_2L]/[HL][H]	4.85(0.02)	4.64(0.01)	4.61(0.01)	4.38(0.01)	8.60
[H_3L]/[H_2L][H]	3.73(0.01)	3.78(0.01)	3.46(0.01)	3.31(0.04)	4.28
[H_4L]/[H_3L][H]					2.64
ΣpK_a	17.93	17.75	17.19	17.06	26.01

[a] Data were obtained from Ref. 10.
[b] Ref. 18.

NMR pH titration

The macroscopic protonation constants of the amides in Table 1 are determined by the potentiometric titration technique. However, the microscopic protonation scheme is obtained by NMR spectroscopy coupled with pH titration [14]. The proton NMR spectra of H_3L^1 as a function of pH are shown in Fig. 1. These show that the central nitrogen atom is the most basic. Coalescence of the triplets corresponding to the ethylenic group occurs about pH > 9.5 for the H_3L^1, H_3L^2, and H_3L^3. Plots of the chemical shift values (δ) of the methylenic resonance of H_3L^1 as a function of pH was given in Fig. 2. There are three inflections centred at pH about 9.5, 4.5, and 3.5 for the H_3L^1, H_3L^2, and H_3L^3. Only one inflection centred at pH about 9.5 was determined for H_3L^3 because the ligand precipitated below pH 5. The downfield shift of δ in the region pH 4.5–9.5 indicate that the first observed protonation occurred on the central nitrogen atom, which is common to all these *N*-substituted carboxylic systems. At about pH 4.5 a downfield δ shift was also observed for one of the terminal nitrogen atoms which is the second protonation site. These values correlate quite well with the protonation constants of the amides in Table 1 and reflect stepwise protonation of the amino groups of the bis(amides) of H_5dtpa with the formation of the species HL^{2-}, H_2L^-, and H_3L. The species distribution curves for H_3L^1, H_3L^2, and H_3L^3 are shown that the dominant species is the monoprotonated ligand between pH 6.0 and 8.5.

Thermodynamic stability constants

The normal chelate thermodynamic stability constants [$K_{ML(therm)}$] are expressed as in eqn (2) where M represents

$$K_{ML(therm)} = [ML]/([M][L]) \quad (2)$$

the free, unhydrolysed aquametal ion, L the uncomplexed, total deprotonated form of the ligand and ML is the normal unprotonated and unhydrolysed complex. The potentiometric titration curves for the complexes of Gd^{3+}, Cu^{2+}, Ca^{2+}, and Zn^{2+} with H_3L^1 have an inflection point at 3 mol base added per mol amide. Titration curves corresponding to other mixtures, like 2:1 or 1:2, were not significantly different from those of ratio 1:1. Thus, no 2:1 and 1:2 metal:ligand species were observed in these complexes. The $[CaL^1]^-$, $[CaL^2]^-$, and $[CaL^3]^-$ curves increase rapidly from pH 6 to 10. The titration curves for the complexes of Cu^{2+}, and Zn^{2+} with H_3L^1, H_3L^2, and H_3L^3 increase from pH 3.5 to 10. The Gd^{3+} reacts strongly with the amides and at considerably lower pH than do the divalent metals. The stability constants of the complexes of Gd^{3+} with H_3L^1, H_3L^2, and H_3L^3 were derived from the competition reaction H_4edta. In Table 2, the thermodynamic stability constants are presented for the linear poly(aminocarboxylates) H_3L^1, H_3L^2, H_3L^3, H_3dmdtta, and H_5dtpa [10,13]. The similar stability constants of the complexes of Gd^{3+}, Cu^{2+}, Ca^{2+}, and Zn^{2+} with the bis(amides) throughout the series (i.e. H_3L^1, H_3L^2, H_3L^3, H_3dmdtta, H_3dipdtta (dipdtta = di(iso-propylcarbamoyl methyl)diethylenetrinitrilo triacetic acid), H_3dtbdtta (dtbdtta = di(tert-butylcarbamoylmethyl)diethylenetrinitrilo triacetic acid), and H_3dbdtta (dbdtta = di(benzylcarbamoylmethyl)diethylenetrinitrilo triacetic acid)) may indicate similar ligand basicities [10,15,16]. Since the basicity of H_3L^1 (ΣpK_a = 17.93), H_3L^2 (17.75), and H_3L^3 (17.19) is very similar to those of H_3dmdtta (17.06), H_3dipdtta (17.59), H_3dtbdtta (18.01), and H_3dbdtta (17.50) the contribution of the enthalpy term to the thermodynamic stability should be similar in the complexes of Gd^{3+}, Ca^{2+}, Cu^{2+}, and Zn^{2+}. Thus, the lower stability of the bis(amide) of H_5dtpa chelates when compared to the H_5dtpa chelates is assigned to the weaker donor ability of the amide group and the lower basicity of the terminal nitrogen atoms.

Conditional stability constants and selectivity constants

For biological studies the conditional stability constants ($K_{ML(cond)}$) of a metal chelate under physiological conditions (pH 7.4) is more important than the thermodynamic stability constant [14,17]. In Table

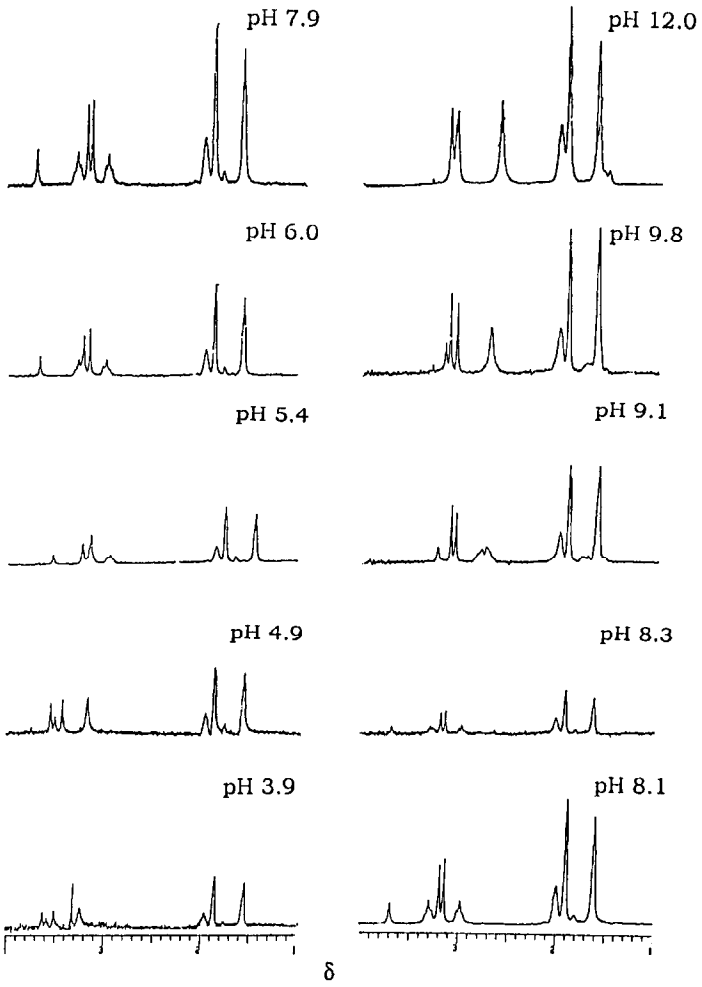

Fig. 1. Proton NMR spectra of H_3L^1 as a function of pH.

2, the conditional stability constants at pH 7.4 are presented for the five poly(aminocarboxylates) H_3L^1, H_3L^2, H_3L^3, H_5dmdtta, and H_5dtpa. Their order is $[Gd(dtpa)]^{2-} > [GdL^1] \approx [GdL^2] \approx [GdL^3] \approx [Gd(dmdtta)]$. This suggests the conditional stability constants of the gadolinium(III) complexes are dependent on the ligand basicity. The thermodynamic stability constants at pH > 11 for $[Gd(dtpa)]^{2-}$ and the gadolinium(III) complexes of the bis(amide) derivatives differ by a factor of the $10^{5.5}$–$10^{6.0}$ that is higher than that at pH 7.4 ($10^{3.0}$–$10^{3.5}$). This indicates that the stability of $[Gd(dtpa)]^{2-}$ is only slightly higher than those of $[GdI^1]$, $[GdL^2]$, and $[GdL^3]$ at pH 7.4.

Stability constants do not provide directly comparable basis for the measuring total ion sequestering abilities of the ligands at physiological conditions (pH 7.4), and therefore they were used to calculate pM values [20]. The advantage of comparing pM values rather than stability constants of the complexes is that the pM values reflect the influence of ligand basicity and metal chelate protonation. The larger the pM value, the higher is the affinity of that ligand for the metal ion under the specified conditions. The relative order of the stability constants may change if a different set of conditions (concentration and pH) is used to calculate the pM values. The results given in Table 3 indicate that the H_5dtpa is much stronger gadolinium(III) chelating agents than are those of the H_3L^1, H_3L^2, and H_3L^3. The pM values of $[GdL^1]$, $[GdL^2]$, and $[GdL^3]$ are larger than those of $[CaL^1]^-$, $[CaL^2]^-$, and $[CaL^3]^-$, $[CuL^1]^-$, $[CuL^2]^-$, and $[CuL^3]^-$ and $[ZnL^1]^-$, $[ZnL^2]^-$, and $[ZnL^3]^-$, respectively. Therefore, the competition among Gd^{3+}, Ca^{2+}, Cu^{2+}, and Zn^{2+} with H_3L^1, H_3L^2 and H_3L^3 is seem to favour Gd^{3+} at pH 7.4, indicating that the complexes should be stable enough to avoid interference by Ca^{2+}, Cu^{2+}, and Zn^{2+}. Even though the stability constants for H_5dtpa chelates are larger than those of the corresponding amides chelates, the pGd values for GdL^1, GdL^2 and GdL^3 are about 3 log unit less than those of $[Gd(dtpa)]^{2-}$, because H_5dtpa has high protonation constants, and therefore formations of its complexes are subject to stronger hydrogen ion competition. Species distribution curves of $[GdL^1]$, $[GdL^2]$, and

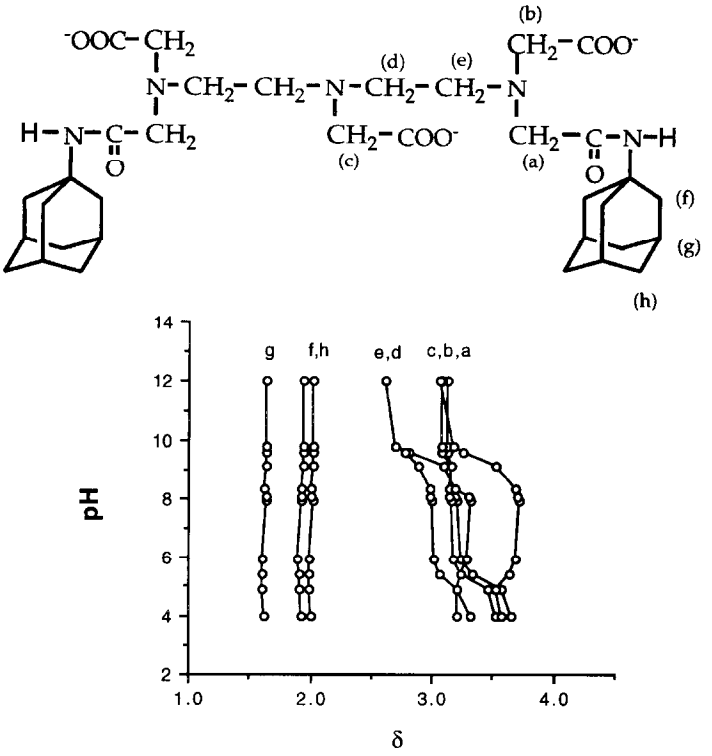

Fig. 2. Proton NMR titration curves for H_3L^1.

Table 2. Stability constants and selectivity constants of the complexes of Gd^{3+}, Zn^{2+}, Ca^{2+} and Cu^{2+}. Uncertainty (σ) in log K values are given in parentheses

	log K [25.0 ± 0.1 C, I = 0.10 mol dm^{-3} (KCl)]				
	H_3L^1	H_3L^2	H_3L^3	H_3dmdtta[a]	H_5dtpa[b]
$K_{GdL(therm)}$	16.85(0.03)	16.82(0.04)	16.91(0.03)	16.85(0.05)	22.46
$K_{GdL(cond)}$	14.89	14.88	15.18	14.84	18.14
$K_{CaL(therm)}$	7.49(0.04)	7.74(0.04)	7.54(0.07)	7.17(0.04)	10.75
$K_{CaHL(therm)}$	5.27(0.04)	5.22(0.04)	5.37(0.06)	4.45(0.02)	—
$K_{CaL(cond)}$	5.53	5.80	5.81	5.11	6.43
$K_{CuL(therm)}$	12.86(0.05)	13.42(0.04)	13.28(0.08)	13.03(0.03)	21.38
$K_{CuHL(therm)}$	3.47(0.05)	3.19(0.06)	3.71(0.06)	3.36(0.02)	—
$K_{CuL(cond)}$	10.90	11.48	11.55	11.06	17.06
$K_{ZnL(therm)}$	11.90(0.09)	12.48(0.03)	12.79(0.08)	12.04(0.03)	18.70
$K_{ZnHL(therm)}$	4.47	3.00(0.03)	3.96(0.04)	4.04(0.04)	—
$K_{ZnL(cond)}$	9.94	10.54	11.06	10.02	14.38
[log K_{sel}(Gd/Zn)]	4.95	4.34	4.12	4.81	3.76
[log K_{sel}(Gd/Ca)]	9.36	9.08	9.37	9.68	11.71
[log K_{sel}(Gd/Cu)]	3.99	3.40	3.63	3.82	1.08
log K_{sel}	9.18	8.57	8.40	9.03	7.04

[a] Data were obtained from Ref. 14.
[b] Refs 18 and 19.

[GdL^3] have been generated from the potentiometric data given in Table 2 indicate that there is still some free Gd^{3+} at pH 1 but by pH 3 the complex is fully formed. However, the octachelated structure is dominant species at physiological pH 7.4.

The logarithmic selectivity constant [14,17] of H_3L^1, H_3L^2, H_3L^3, H_3dmdtta, and H_5dtpa for Gd^{3+} over Zn^{2+}, Ca^{2+}, and Cu^{2+} is the difference between log K_{GdL} and log K_{ML} (M = Zn^{2+}, Ca^{2+} or Cu^{2+}) i.e. log K_{sel}(Gd/Zn), log K_{sel}(Gd/Ca), and

Table 3. The pM[a] values of the complexes of Gd^{3+}, Zn^{2+}, Ca^{2+} and Cu^{2+} at pH 7.4

	H_3L^1	H_3L^2	H_3L^3	H_3dmdtta	H_5dtpa
pGd	13.72	13.84	14.15	13.88	17.14
pCu	9.90	10.48	10.55	10.05	16.06
pCa	4.53	4.81	4.82	4.19	5.45
pZn	8.94	9.54	10.06	9.06	13.39

[a] $pM = -\log[M]_{free}$ at pH 7.4, $[\text{metal ion}]_{total} = 1$ μmol dm^{-3}, and $[\text{ligand}]_{total} = 1.1$ μmol dm^{-3}.

$\log K_{sel}$(Gd/Cu). The selectivity constants are also given in Table 2. Since the basicity of H_3L^1, H_3L^2, and H_3L^3 is very similar to those of H_3dmdtta, H_3dipdtta, H_3dtbdtta, and H_3dbdtta [15], the contribution of the stability constant to the selectivity constant should be similar for the complexes of Gd^{3+}, Cu^{2+}, Ca^{2+}, and Zn^{2+}. From the selectivity constants, H_3L^1, H_3L^2, and H_3L^3 show a slightly more favourable selectivity toward Gd^{3+} over Zn^{2+} than does H_5dtpa.

The consequences of the modified selectivity constants (K_{sel}) for Gd^{3+} over other endogenous metal ions (Cu^{2+}, Ca^{2+}, and Zn^{2+}) and H^+ for a ligand can be calculated [14]. Table 2 shows the modified selectivity constants of H_3L^1, H_3L^2, H_3L^3, H_3dmdtta, and H_5dtpa at pH 7.4. The concentrations of Ca^{2+}, Cu^{2+}, and Zn^{2+} used were 2.5, 1.0×10^{-3} and 5.0×10^{-2} mmol dm^{-3}, respectively [15]. The $\log K_{sel}$ of H_3L^1 (9.18), H_3L^2 (8.57), and H_3L^3 (8.40) are very similar to that of H_3dmdtta (9.03), but slightly higher than that of H_5dtpa (7.04). Thus, H_3L^1, H_3L^2, and H_3L^3 form the gadolinium(III) complexes that are more stable than $[Gd(dtpa)]^{2-}$ toward transmetallation with endogenous metal ions at pH 7.4.

Relaxometry studies

The spin-lattice relaxivities R_1 of $[GdL^1]$, $[GdL^2]$, and $[GdL^3]$ are given in Table 4. The R_1 values are similar to the 3.90 and 4.08 dm^3 mmol^{-1} s^{-1} determined for the gadolinium(III) complex of H_3dmdtta and H_3dbdtta [15,16,21] under the same experimental conditions, respectively. Since the complexes of gadolinium(III) with H_3L^2 and H_3L^3 studied consist of gadolinium(III) bound to similar amides for the current study. The relaxivity R_1 of a paramagnetic metal chelate is governed by an exchange between coordinated water molecule and surrounding water molecules in solution [22,23]. With everything else being equal the exchange process is only dependent on the hydration number of the metal complex. However, hydration number of the complexes of gadolinium(III) with H_3L^1, H_3L^2, and H_3L^3 may be the same with [Gd(dmdtta)] and [Gd(dbdtta)] [10,15,21,24] leading to almost identical R_1 values. The relaxivity of $[GdL^1]$ is 4.99 dm^3 mmol^{-1} s^{-1} higher than those of $[GdL^2]$ and $[GdL^3]$, and this is undoubtedly due in part to the larger molecular size, which lead to a longer rotational correlation time.

The relaxivities R_1 for the complexes $[GdL^1]$, $[GdL^2]$, and $[GdL^3]$ at various pH values are given in Fig. 3. The relaxivity R_1 curve exhibits no pH dependence over the pH range 3–10. Therefore, no ligand dissociation for gadolinium(III) complexes occurred with varying pH of the solution. It is concluded that

Table 4. Relaxivities R_1 gadolinium(III) complexes

Complex	pH	R_1 relaxivity[a] /dm^3 mmol^{-1} s^{-1}
$[GdL^1]$	7.5±0.1	4.99±0.05
	limiting[a]	5.75±0.03
$[GdL^2]$	7.6±0.1	4.01±0.05
	limiting[a]	4.75±0.07
$[GdL^3]$	7.6±0.1	3.89±0.03
	limiting[a]	4.65±0.05

[a] Average of relaxivity values over the pH range 3–10.

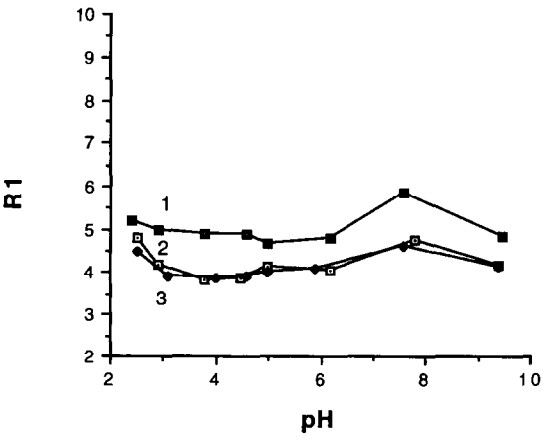

Fig. 3. pH dependence of the relaxivity for the complexes GdL^1, GdL^2, and GdL^3, all in 0.10 mol dm^{-3} buffers (pH 7 data excluded) at 20 MHz and T = 37.0±0.1 C.

the hydration number remains constant in this pH range.

The water solubility of [GdL^2] and [GdL^3] (6.79 g and 7.19 g in 100 g of water at 25°C, respectively) are considerably higher than that of [Gd(dbdtta)] (1.15 g in 100 g of water) [15]. Introducing hydrophilic methoxyl moiety covalently linked to ligand H_3dbdtta exhibits lower lipophicity than that of [Gd(dbdtta)]. High stability and high relaxivity R_1 of the gadolinium(III) chelates are important prerequisites for potential use as magnetopharmaceuticals. The amides, H_3L^1, H_3L^2, and H_3L^3 produce nonionic complexes when they chelate with gadolinium(III). Such nonionic complexes may have good membrane permeability. The fact that the complexes of gadolinium(III) with H_3L^1, H_3L^2, and H_3L^3 are quite stable in the aqueous solution, does not dissociate under physiological conditions (pH 7.4) and do not exchange with Ca^{2+}, Cu^{2+}, and Zn^{2+} to an appreciable extent show that they may be effective MRI contrast agents.

Acknowledgements—We are grateful to the National Science Council of the Republic of China for financial support under Contract No. NSC 86-2113-M037-009. This research was also supported in part by grants from Department of Health under contrast No. DOH86-HR-501.

REFERENCES

1. Eckelman, W. C., Karesh, S. M. and Reba, R. C., *J. Pharm. Sci.*, 1975, **64,** 704.
2. Konings, M. S., Dow, W. C., Love, D. B., Raymond, K. N., Quay, S. C. and Rocklage, S. M., *Inorg. Chem.*, 1990, **29,** 1488.
3. Mikkelsen, K. and Nielsen, S. O., *J. Phys. Chem.*, 1960, **64,** 632.
4. Chang, C. A., Brittain, H. G., Telser, J. and Tweedle, M. F., *Inorg. Chem.*, 1990, **29,** 4468.
5. Harris, W. R. and Martell, A. E., *Inorg. Chem.*, 1976, **15,** 713.
6. Li, Y., Martell, A. E., Hancock, R. D., Reibenspies, J. H., Anderson, C. J. and Welch, M. J., *Inorg. Chem.*, 1996, **35,** 404.
7. Taliaferro, C. H., Motekaitis, R. J. and Martell, A. E., *Inorg. Chem.*, 1984, **23,** 1188.
8. Martell, A. E. and Motekaitis, R. J., *Determination and Use of Stability Constants*, 2nd edn. VCH, New York, 1992.
9. Chang, C. A., Brittain, H. G., Telser, J. and Tweedle, M. F., *Inorg. Chem.*, 1990, **29,** 4468.
10. Cacheris, W. P., Quay, S. C. and Rocklage, S. M., *Magn. Reson. Imaging*, 1990, **8,** 467.
11. Sudmeier, J. L. and Reilley, C. N., *Anal. Chem.*, 1964, **36,** 1698.
12. Fujiwara, Y. and Reilley, C. N., *Anal. Chem.*, 1968, **40,** 890.
13. Geraldes, C. F. G. C., Urbano, A. M., Alpoim, M. C., Sherry, A. D., Kuan, K.-T., Rajagopalan, R., Maton, F. and Muller, R. N., *Magn. Reson. Imaging*, 1995, **13,** 401.
14. Sherry, A. D., Cacheris, W. P. and Kuan, K.-T., *Magn. Reson. Med.*, 1988, **8,** 180.
15. Wang, Y. M., Cheng, T. H., Liu, G. C. and Sheu, R. S., *J. Chem. Soc., Dalton Trans.*, 1997, 883.
16. Wang, Y. M., Cheng, T. H., Sheu, R. S., Chen, I. T. and Chiang, M. Y., *J. Chin. Chem. Soc.*, 1997, **44,** 123.
17. Kumar, K., Tweedle, M. F., Malley, M. F. and Gougoutas, J. Z., *Inorg. Chem.*, 1995, **34,** 6472.
18. Wright, D. L., Holloway, J. H. and Reilley, C. N., *Anal. Chem.*, 1965, **37,** 884.
19. Smith, R. M. and Martell, A. E., *Critical Stability Constants*, Vols 1–4. Plenum, New York, 1975–1977.
20. Bannochie, C. J. and Martell, A. E., *Inorg. Chem.*, 1991, **30,** 1385.
21. Chang, C. A., *Invest. Radiol.*, 1993, **28,** S21.
22. Lauffer, R. B., *Chem. Rev.*, 1987, **87,** 901.
23. Zhang, X., Chang, C. A., Brittain, H. G., Garrison, J. M., Telser, J. and Tweedle, M. F., *Inorg. Chem.*, 1992, **31,** 5597.
24. Bligh, S. W. A., Chowdhury, A. H. M. S., McPartlin, M., Scowen, I. J. and Bulman, R. A., *Polyhedron*, 1995, **14,** 567.

Pergamon

PII: S0277-5387(97)00473-7

Polyhedron Vol. 17, Nos. 11–12, pp. 2029–2035, 1998
© 1998 Elsevier Science Ltd
All rights reserved. Printed in Great Britain
0277-5387/98 $19.00+0.00

Gold complexes with mono- or di-chalcogenides of bis(diphenylphosphino)methanide ligands. X-ray crystal structure of $[Au(C_6F_5)_2\{(SPPh_2)_2C(AuAsPh_3)_2\}]ClO_4$

Beatriz Alvarez,[a] Eduardo J. Fernández,[a] M. Concepción Gimeno,[b] Peter G. Jones,[c] Antonio Laguna[b]* and José M. López-de-Luzuriaga[a]

[a] Departamento de Química, Universidad de La Rioja, Obispo Bustamante 3, E-26001 Logroño, Spain

[b] Departamento de Química Inorgánica, ICMA, Universidad de Zaragoza-CSIC, E-50009 Zaragoza, Spain

[c] Institüt für Anorganische und Analytische Chemie der Technischen Universität, Postfach 3329, D-38023 Braunschweig, Germany

(Received 18 September 1997; accepted 12 November 1997)

Abstract—The reaction between the chalcogenide derivatives $[Au(C_6F_5)_3(PPh_2CH_2PPh_2E)]$ (E = S, O) and [Au(acac)PPh_3] or [Au(TfO)PPh_3] leads to the dinuclear compounds $[Au(C_6F_5)_3\{PPh_2CH(AuPPh_3)PPh_2E\}]$ (E = S, O) or $[Au(C_6F_5)_3\{PPh_2CH_2PPh_2(SAuPPh_3)\}]$, respectively. When the phosphine disulphide complex $[Au(C_6F_5)_3(SPPh_2CH_2PPh_2S)]$ is employed, the reaction with [Au(acac)PPh_3] promotes the double substitution of the methylenic protons. The reaction of [Au(acac)L] (L = PPh_3, $AsPh_3$) with the six-membered auracycle $[Au(C_6F_5)_2\{(SPPh_2)_2CH_2\}]ClO_4$ leads to the double substitution of both methylenic protons by $[AuL]^+$ fragments, keeping the auracycle intact. The crystal structure of one such product, $[Au(C_6F_5)_2\{(SPPh_2)_2C(AuAsPh_3)_2\}]ClO_4$ has been established by X-ray diffraction studies. Starting from the methanide derivative $[Au(C_6F_5)_2(SPPh_2CHPPh_2S)]$, the reaction with [Au(acac)PPh_3] leads to the synthesis of the four-membered ring methanide $[Au(C_6F_5)_2\{SPPh_2C(AuPPh_3)PPh_2S\}]$ © 1998 Elsevier Science Ltd. All rights reserved

Keywords: gold; diphosphinedichalcogenide; diphosphinemonochalcogenide; methanide; crystal structure.

In the last few years there has been a renewed interest in the chemistry of diphosphine chalcogenide ligands and their methanide derivatives [1–5], which can be attributed to the tendency of the diphosphine chalcogenides to charge delocalization, thus enhancing the acidity of the methylenic protons as well as the lability of the chalcogen–metal bonds [6]. This lability can give rise to dynamic processes and thus renders these ligands appropiate for catalytic applications [7–10].

The introduction of oxygen or sulfur atoms at one or both phosphorus centres in bis(diphenylphosphino)methane after or prior to metal complexation can change the character of the donor atom or lead to metallacycle ring expansion, depending on the starting complex employed. This may have a significant influence on the coordination properties or on the reactivity of these products.

The present paper reports the synthesis of some gold(III) derivatives containing mono- or di-chalcogenides of bis(diphenylphosphino)methane and their reactivity towards reagents of the type [Au(acac)L] (acac = acetylacetonate) forming methanide complexes. We employed tris(pentafluorophenyl)gold(III) derivatives, which afford non-cyclic methanides in a different way from that recently described [11] or $[Au(C_6F_5)_2(SPPh_2CH_2PPh_2S)]ClO_4$ [12], from which we have synthesized methanediide species containing a six-membered metallacycle. These last products are not accessible through other

* Author to whom correspondence should be addressed.

classical methods, which lead instead to the formation of four-membered rings.

RESULTS AND DISCUSSION

The reaction of $[Au(C_6F_5)_3(PPh_2CH_2PPh_2)]$ and equimolecular amounts of sulfur leads to the sulfuration of the free phosphorus to give $[Au(C_6F_5)_3(PPh_2CH_2PPh_2S)]$ (**1**) (see Scheme 1).

Compound **1** is stable to air and moisture, soluble in most common organic solvents and insoluble in hexane. The IR spectrum of this compound shows the characteristic pattern of tris(pentafluorophenyl) gold(III) groups [13]. Besides, a weak band at 611 cm^{-1} corresponding to the ν(P—S) vibration appears [14]. The $^{31}P\{^1H\}$ and ^{19}F NMR spectra of this compound are also in accordance with the proposed structure (see Experimental section).

The presence of the chalcogenide atom near the phosphorus increases the acidity of the methylenic protons of the phosphine and this increase is greater for the sulfur than for the oxygen derivative. Thus, the resonance of the methylene group in complex **1** appears at $\delta = 3.66$ (t), shifted downfield compared to the starting material ($\delta = 3.2$) and making it appropriate for further deprotonations.

When complex **1** or the corresponding oxygen derivative $[Au(C_6F_5)_3(PPh_2CH_2PPh_2O)]$ [15] are treated with equimolecular amounts of [Au(acac)PPh_3] in dichloromethane, a methylenic proton is substituted by an $[AuPPh_3]^+$ group, affording the dinuclear species $[Au(C_6F_5)_3\{PPh_2CH(AuPPh_3)PPh_2E\}]$ (E = S (**2**), O (**3**)) (Scheme 1). As we already observed in previous studies [16], the substitution of a methylenic proton by an $[AuL]^+$ fragment (L = tertiary phosphine) also increases the acidity of the second methylenic H atom. However, in this case an excess of [Au(acac)PPh_3] does not produce the double substitution.

Complexes **2** and **3** are air and moisture-stable solids, soluble in chlorinated solvents, acetone and diethyl ether and insoluble in hexane. Their analytical and spectroscopic data are in accordance with the proposed formulation; e.g. they display three resonances with relative intensities 1:1:1 in their $^{31}P\{^1H\}$ spectra.

The reaction of complex **1** with the aurating agent [Au(TfO)PPh_3] (TfO = trifluoromethanesulfonate), prepared *in situ* by reaction of [AuClPPh_3] and AgTfO in dichloromethane, leads to the dinuclear complex $[Au(C_6F_5)_3\{PPh_2CH_2PPh_2(SAuPPh_3)\}]TfO$ (**4**), in which the coordination of the new $[AuPPh_3]^+$ fragment takes place at the sulfur atom.

When the phosphine disulphide derivative $[Au(C_6F_5)_3(SPPh_2CH_2PPh_2S)]$ [12] is employed instead of the monosulphide, its reaction with [Au(acac)PPh_3] leads to the synthesis of the di-substituted product $[Au(C_6F_5)_3\{SPPh_2C(AuPPh_3)_2PPh_2S\}]$ (**5**), whatever the molar ratio of the gold(I) derivative and without formation of the monosubstituted species $[Au(C_6F_5)_3\{SPPh_2CH(AuPPh_3)PPh_2S\}]$ (Scheme 1). This result is probably attributable to two factors: (i) the increase of the acidity that the second sulfur atom produces in the methylenic protons and (ii) the increase of the length of the phosphine ligand, reducing the steric restrictions that prevented the synthesis of disubstituted non-cyclic methanides as reported in a previous paper [11].

Complex **5** is obtained as a pale yellow stable solid soluble in acetone, ether and chlorinated solvents and insoluble in hexane. Its $^{31}P\{^1H\}$ NMR spectrum dis-

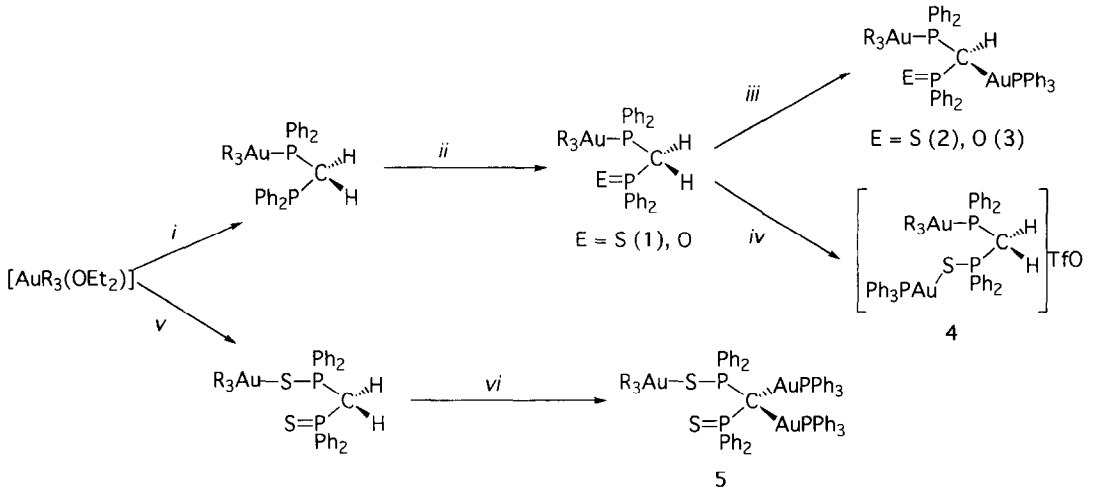

Scheme 1. $R = C_6F_5$; (i) $PPh_2CH_2PPh_2$; (ii) 1/8 S_8 or H_2O_2; (iii) [Au(acac)PPh_3]; (iv) [Au(PPh_3)]TfO; (v) $SPPh_2CH_2PPh_2S$; (vi) **1** or **2** equiv. [Au(acac)PPh_3].

plays two different resonances for the diphosphine phosphorus and a pseudo-triplet at $\delta = 35.2$ from both phosphorus atoms of the PPh_3 groups.

In the case of the diaryl complex $[Au(C_6F_5)_2(SPPh_2CH_2PPh_2S)]ClO_4$ [12], which contains the phosphine disulphide as a chelate, the increase of acidity produced by the sulfur centres is also demonstrated by its reaction with [Au(acac)L] (L = PPh_3, $AsPh_3$). Treatment of one equivalent of the starting complex with two equivalents of [Au(acac)L] results in the substitution of both methylenic protons by two $[AuL]^+$ groups with formation of $[Au(C_6F_5)_2\{(SPPh_2)_2C(AuL)_2\}]ClO_4$ (L = PPh_3 (**6**), $AsPh_3$ (**7**)) (Scheme 2). This is a surprising result in view of our previous studies with the same starting complex, because the employment of stronger deprotonating agents, such as NaH, led to the formation of four membered rings [12].

Complexes **6** and **7** are pale yellow solids, moisture and air stable. They are soluble in chlorinated solvents and acetone and they behave as 1 : 1 electrolytes in this solvent. Their analytical and spectroscopic data are in accordance with their formulation. The resonance from the phosphorus of the diphosphine sulphide appears as a triplet at $\delta = 43.9$ (**6**) or as a singlet at $\delta = 42.6$ (**7**) in their $^{31}P\{^1H\}$ NMR spectra. In the spectrum of the triphenylphosphine derivative **6** the signal corresponding to the PPh_3 groups is located at $\delta = 36.3$ and appears as a triplet because of the coupling with both phosphorus of the chelating ligand.

The crystal structure of complex **7** has been determined. The cation is shown in Fig. 1, with selected bond lengths and angles in Table 1. The complex crystallizes with two independent formula units; the overall distances and angles are very similar and consequently we will comment on only one of them. The precision is not very good for reasons discussed below. The coordination around the gold(III) center is slightly distorted from square planar, whereby the wide bite of the diphosphine disulphide ligand represents the major deviation from ideal geometry, S(2)—Au(1)—S(1) 102.0(2)°. This bite angle is unusually high for a chelating ligand in gold(III) complexes, compared with other examples such as $[Au(C_6F_5)_2(SPPh_2CHPPh_2)]$ (S—Au—P 89.6(1)°) [17] or $[Au(C_6F_5)_2\{(PPh_2)_2C(AuPPh_3)_2\}]ClO_4$ (P—Au—P 70.5(3)°) [16]. The gold(III) atom is coplanar with the C(11), C(21), S(1) and S(2) atoms. The Au—S distances, 2.390(7) and 2.357(8) Å, are longer than those found in $[Au(C_6F_5)_2(SPPh_2CHPPh_2)]$ (2.345(2) Å). The P—S bond lengths are 2.029(11) and 2.050(10) Å corresponding to a slightly shortened single bond. The gold(I) atoms exhibit essentially linear geometry and lie only 2.873(2) Å from each other. These short gold–gold contacts are very frequent in this type of polynuclear methanide complexes e.g., $[Au(C_6F_5)_2\{(PPh_2)_2C(AuPPh_3)_2\}]ClO_4$ (Au···Au 2.826(2) Å) or $[Au_2\{(PPh_2)_2C(AuPPh_3)_2\}_2](ClO_4)_2$ [18] (Au···Au 2.920(2)–2.987(2) Å). The Au—As bond lengths 2.365(3) and 2.370(3) Å are similar to those in the complexes $[Au(CH_3)(AsPh_3)]$ (2.3800(11) Å) [19] or $[Au(CH_2CH_3\text{-}closo\text{-}C_2B_{10}H_{10})(AsPh_3)]$ [19] (2.3740(8) Å) which also have a carbon donor ligand *trans* to the Au—As bond.

Using the same starting complex we have synthesized another methanide featuring a four-membered ring instead a six-membered one. This is made possible by treating it first with NaH, which causes a change in the coordination of the chelating ligand: one sulfur atom is replaced by the new methanide carbon atom at the gold(III) centre. If this product is now treated with one equivalent of $[Au(acac)PPh_3]$, the second methylenic proton is then removed and the $[AuPPh_3]^+$ takes its place (see Scheme 2).

Complex **8** is a yellow solid stable to air and moisture. It is soluble in chlorinated solvents and insoluble in diethyl ether or hexane. The IR spectrum shows two bands at 575 (w) and 625 (m) cm^{-1} due to the ν(P—S) vibration, in accordance with the presence of a free and a coordinated sulfur atom [20]. In the $^{31}P\{^1H\}$ NMR spectrum the signals corresponding to the three non equivalent phosphorus appear at $\delta = 46.9$, 37.5 and 34.8 with 1 : 1 : 1 relative intensity and no coupling between the different phosphorus is observed.

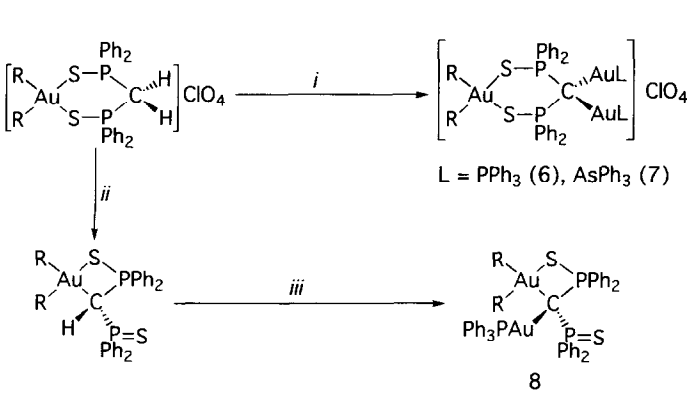

Scheme 2. $R = C_6F_5$; (i) **2** [Au(acac)L]; (ii) NaH; (iii) $[Au(acac)PPh_3]$.

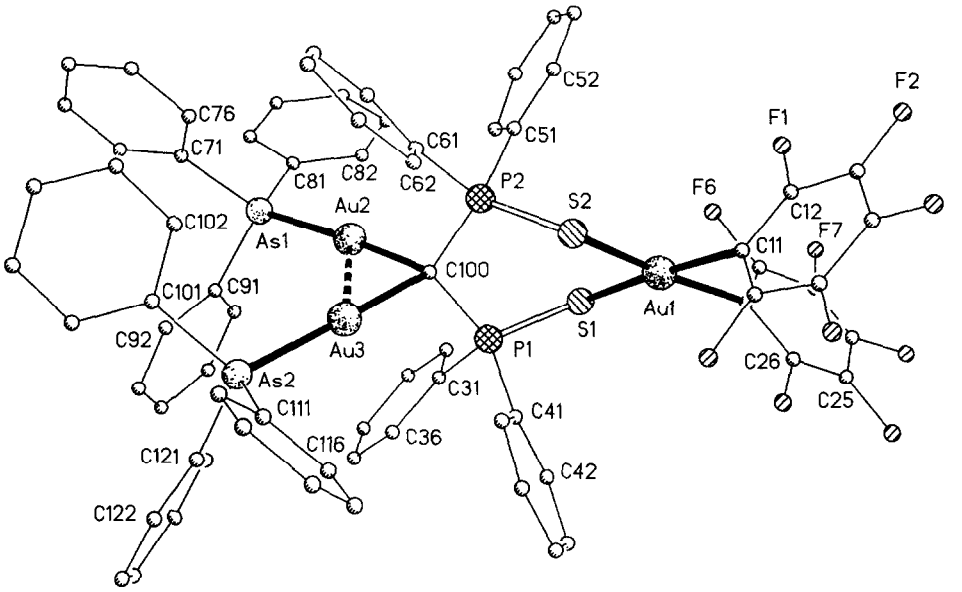

Fig. 1. The cation of complex **7** in the crystal with the atom labelling scheme. H atoms are omitted for clarity, radii are arbitrary.

EXPERIMENTAL

General

NMR spectra were recorded on a Bruker ARX 300 spectrometer in $CDCl_3$ solutions. Chemical shifts are quoted relative to $SiMe_4$ (^1H, external), $CFCl_3$ (^{19}F, external) and H_3PO_4 (85%) (^{31}P, external). All experiments were carried out at room temperature and under nitrogen except for **1**.

$[Au(C_6F_5)_3(PPh_2CH_2PPh_2S)]$ (**1**)

To a toluene solution of $(Au(C_6F_5)_3(PPh_2CH_2PPh_2)]$ [13] (0.27 g, 0.25 mmol) was added S (0.009 g, 0.3 mmol). The mixture was refluxed for 24 h and the solvent was evaporated to dryness. The dry solid was then treated with diethyl ether and insoluble material was filtered off over celite. The solution was concentrated to ca 5 cm^3 and hexane was added to give complex **1** as a white solid. Yield: 77%. m.p. 123°C. $C_{43}H_{22}AuF_{10}P_2S$ (1114.583). Calc: C, 46.3; H, 2.0; S, 2.9. Found: C, 46.9; H, 2.15; S, 2.4. $^{31}P\{^1H\}$ NMR: $\delta = 8.5$ (m, 1P, Au(III)-PPh_2) and 33.2 (d, 1P, SPPh_2, [^2J(P—P) = 17.2 Hz]); ^1H NMR: $\delta = 3.6$ ("t", 2H, CH_2, $N = 11.3$ Hz); ^{19}F NMR: $\delta = -118.9$ (m, 4F, *o*-F), −119 (m, 2F, *o*-F), −156.4 (t, 2F, *p*-F, [^3J(FF) = 20.1 Hz]), −157.2 (t, 1F, *p*-F, [^3J(FF) = 19.9 Hz]), −160.5 (m, 4F, *m*-F) and −160.6 (m, 2F, *m*-F).

$[Au(C_6F_5)_3\{PPh_2CH(AuPPh_3)PPh_2E\}]$ (E = S (**2**), O (**3**))

To a dichloromethane solution of $[Au(C_6F_5)_3(PPh_2CH_2PPh_2E]$ (0.278 g, 0.25 mmol, $E = S$ (**1**)) or (0.274 g, 0.25 mmol, $E = O$ [11]) was added [Au(acac)PPh_3] (0.139 g, 0.25 mmol). After stirring for 2 h the mixture was filtered through a layer of celite and the solvent was evaporated to ca 5 cm^3. Addition of 20 ml of hexane led to the precipitation of **2** or **3** as a pale yellow solids. Yield: 60% **2**, 66% **3**. m.p. 113°C, **2**, 78°C, **3**. $C_{61}H_{36}Au_2F_{10}SP_3$ (1572.833) **2**. Calc: C, 46.6; H, 2.3; S, 2.03. Found: C, 46.8; H, 2.6; S, 2.15. $C_{61}H_{36}Au_2F_{10}OP_3$ (1556.768) **3**. Calc: C, 47.1; H, 2.3. Found: C, 47.2; H, 2.9. NMR **2**: $^{31}P\{^1H\}$: $\delta = 21.8$ (m, 1P, Au(III)-PPh_2) 41.3 (dd, 1P, SPPh_2, [^2J(P-P) = 37.8 Hz], [^3J(P-P) = 12.8 Hz]) and 38.6 ("t", 1P, PPh_3, $N = 11$ Hz). ^1H: $\delta = 3.75$ ("c", 1H, CH, $N = 7.33$ Hz). ^{19}F: $\delta = -118.4$ (m, 4F, *o*-F), −121.2 (m, 2F, *o*-F), −157.8 (t, 1F, *p*-F, [^3J(FF) = 19.9 Hz]), −158.1 (t, 2F, *p*-F, [^3J(FF) = 19.9 Hz]), −160.9 (m, 4F, *m*-F) and −161 (m, 2F, *m*-F). NMR **3**: $^{31}P\{^1H\}$: $\delta = 21.6$ (m, 1P, Au(III)-PPh_2), 29.4 (dd, 1P, SPPh_2, [^2J(P−P) = 33.9 Hz], [^3J(P-P) = 11.3 Hz]) and 38.6 ("t", 1P, PPh_3, $N = 11.3$ Hz). ^1H: $\delta = 3.79$ ("q", 1H, CH, [N(HP) = 8.57 Hz]). ^{19}F: $\delta = -119.4$ (m, 4F, *o*-F), −121.1 (m, 2F, *o*-F), −157.8 (t, 1F, *p*-F, [^3J(FF) = 20.1 Hz]), −158.1 (t, 2F, *p*-F, [^3J(FF) = 19.9 Hz]), −161.5 (m, 4F, *m*-F) and −161.6 (m, 2F, *m*-F).

$[Au(C_6F_5)_3\{PPh_2CH_2PPh_2(SAuPPh_3)\}]$ TfO (**4**)

To a freshly prepared dichloromethane solution of [Au(TfO)PPh_3] (0.25 mmol) was added $[Au(C_6F_5)_3(PPh_2CH_2PPh_2S)]$ (0.278 g, 0.25 mmol) and the mixture was stirred for 2 h. Evaporation of the solvent to

Table 1. Selected bond lengths (Å) and angles ° for complex **7**

Au(1)—C(11)	2.02(3)	Au(1)—C(21)	2.08(4)
Au(1)—S(2)	2.357(8)	Au(1)—S(1)	2.390(7)
Au(2)—C(100)	2.10(3)	Au(2)—As(1)	2.370(3)
Au(2)—Au(3)	2.873(2)	Au(3)—C(100)	2.04(3)
Au(3)—As(2)	2.365(3)	As(1)—C(81)	1.91(2)
P(1)—S(1)	2.029(11)	P(2)—S(2)	2.050(10)
Au(4)—C(141)	2.02(2)	Au(4)—C(131)	2.05(3)
Au(4)—S(3)	2.375(7)	Au(4)—S(4)	2.385(7)
Au(5)—C(200)	2.13(3)	Au(5)—As(3)	2.371(3)
Au(5)—Au(6)	2.840(2)	Au(6)—C(200)	2.07(3)
Au(6)—As(4)	2.368(3)	P(3)—S(3)	2.007(10)
P(4)—S(4)	2.047(11)		

C(11)—Au(1)—C(21)	84.9(10)	C(11)—Au(1)—S(2)	84.8(7)
C(21)—Au(1)—S(2)	169.6(8)	C(11)—Au(1)—S(1)	173.2(7)
C(21)—Au(1)—S(1)	88.3(8)	S(2)—Au(1)—S(1)	102.0(2)
C(100)—Au(2)—As(1)	175.3(7)	C(100)—Au(2)—Au(3)	45.2(7)
As(1)—Au(2)—Au(3)	130.31(9)	C(100)—Au(3)—As(2)	177.6(7)
C(100)—Au(3)—Au(2)	47.0(7)	As(2)—Au(3)—Au(2)	130.63(9)
C(81)—As(1)—Au(2)	113.4(7)	C(71)—As(1)—Au(2)	114.8(6)
C(91)—As(1)—Au(2)	113.0(7)	C(121)—As(2)—Au(3)	112.4(6)
C(101)—As(2)—Au(3)	113.2(6)	C(111)—As(2)—Au(3)	112.5(7)
C(100)—P(1)—S(1)	115.8(10)	C(31)—P(1)—S(1)	105.3(8)
C(41)—P(1)—S(1)	107.6(8)	C(100)—P(2)—S(2)	113.9(10)
C(61)—P(2)—S(2)	105.9(8)	C(51)—P(2)—S(2)	107.1(8)
P(1)—S(1)—Au(1)	102.9(4)	P(2)—S(2)—Au(1)	104.8(4)
P(2)—C(100)—P(1)	112.4(14)	P(2)—C(100)—Au(3)	116(2)
P(1)—C(100)—Au(3)	111.9(14)	P(2)—C(100)—Au(2)	115.1(14)
P(1)—C(100)—Au(2)	111.0(14)	Au(3)—C(100)—Au(2)	87.8(10)
C(141)—Au(4)—C(131)	89.4(8)	C(141)—Au(4)—S(3)	172.2(6)
C(131)—Au(4)—S(3)	82.8(6)	C(141)—Au(4)—S(4)	86.1(6)
C(131)—Au(4)—S(4)	175.0(6)	S(3)—Au(4)—S(4)	101.7(2)
C(200)—Au(5)—As(3)	174.2(7)	C(200)—Au(5)—Au(6)	46.7(7)
As(3)—Au(5)—Au(6)	128.02(9)	C(200)—Au(6)—As(4)	173.8(7)
C(200)—Au(6)—Au(5)	48.4(7)	As(4)—Au(6)—Au(5)	125.66(9)
C(191)—As(3)—Au(5)	110.2(8)	C(201)—As(3)—Au(5)	113.0(7)
C(211)—As(3)—Au(5)	118.2(7)	C(241)—As(4)—Au(6)	115.6(8)
C(231)—As(4)—Au(6)	115.3(7)	C(221)—As(4)—Au(6)	108.0(6)
C(200)—P(3)—S(3)	112.0(10)	C(151)—P(3)—S(3)	105.4(7)
C(161)—P(3)—S(3)	107.9(8)	C(200)—P(4)—S(4)	114.7(10)
C(181)—P(4)—S(4)	107.6(8)	C(171)—P(4)—S(4)	106.3(8)
P(3)—S(3)—Au(4)	102.0(4)	P(4)—S(4)—Au(4)	102.8(4)
P(4)—C(200)—P(3)	112.6(14)	P(4)—C(200)—Au(6)	112.8(14)
P(3)—C(200)—Au(6)	116.9(14)	P(4)—C(200)—Au(5)	115.4(14)
P(3)—C(200)—Au(5)	111.5(14)	Au(6)—C(200)—Au(5)	85.0(10)

ca 5 cm^3 and addition of 20 cm^3 of hexane led to the precipitation of **4** as a microcrystalline white solid. Yield: 55%. m.p. 114°C. $C_{62}H_{37}Au_2F_{13}O_3P_3S_2$ (1722.909). Calc: C, 43.2; H, 2.15; S, 3.7. Found: C, 43.6; H, 2.2; S, 3.6. Λ_m (5×10^{-4} M) = 133 ($ohm^{-1}\cdot cm^2\cdot mol^{-1}$). $^{31}P\{^1H\}$ NMR: δ = 5.1 (m, 1P, Au(III)-*P*Ph_2), 36.4 (m, 1P, S*P*Ph_2) and 43.6 (m, 1P, *P*Ph_3). ^1H NMR: δ = 4.55 ("t", 2H, CH_2, N = 10.4 Hz). ^{19}F NMR: δ = −117.6 (m, 4F, *o*-F), −120.5 (m, 2F, *o*-F), −155.5 (t, 2F, *p*-F, [^3J(FF) = 19.9 Hz]), −156.5 (t, 1F, *p*-F, [^3J(FF) = 19.9 Hz]), −160.0 (m, 4F, *m*-F), −161.0 (m, 2F, *m*-F) and −120.4 (CF_3SO_3).

$[Au(C_6F_5)_3\{SPPh_2C(AuPPh_3)_2PPh_2S\}]$ (**5**)

To a dichloromethane solution of $[Au(C_6F_5)_3(SPPh_2CH_2PPh_2S)]$ (0.286 g, 0.25 mmol) was added [Au(acac)PPh_3] (0.279 g, 0.50 mmol). After stirring for 1 h the mixture was filtered through a layer of celite and the solvent was evaporated to ca 5 cm^3.

Addition of 20 cm^3 of hexane led to the precipitation of **5** as a pale yellow solid. Yield: 71%. m.p. 110°C. $C_{79}H_{50}Au_3F_{10}S_2P_4$ (2063.147). Calc: C, 46.0; H, 2.4; S, 3.1. Found: C, 46.4; H, 2.1; S, 2.9. $^{31}P\{^1H\}$ NMR: δ = 47.0 (m, 1P, Au(III)-PPh_2), 50.6 (m, 1P, $SPPh_2$) and 35.2 ("t", 1P, PPh_3, N = 7.3 Hz). ^{19}F NMR: δ = −121.2 (m, 4F, *o*-F), −122.2 (m, 2F, *o*-F), −158.6 (t, 1F, *p*-F, [^3J(FF) = 19.9 Hz]), −158.8 (t, 2F, *p*-F, [^3J(FF) = 19.9 Hz]), −162 (m, 4F, *m*-F) and −163.4 (m, 2F, *m*-F).

$[Au(C_6F_5)_2\{(SPPh_2)_2C(AuL)_2\}]ClO_4$ (L = PPh_3 (**6**), $AsPh_3$ (**7**))

A solution of $[Au(C_6F_5)_2(SPPh_2CH_2PPh_2S)]ClO_4$ (0.27 g, 0.25 mmol) in 25 cm^3 of dichloromethane was treated with [Au(acac)PPh_3] (0.279 g, 0.50 mmol (**6**)) or [Au(acac)$AsPh_3$] (0.30 g, 0.50 mmol (**7**)). After stirring for 2 h the mixture was filtered through a layer of celite and the solvent was evaporated to ca 5 cm^3. Addition of 20 cm^3 of diethyl ether led to the precipitation of **6** or **7** as a pale yellow solids. Yield: 80% **6**, 74% **7**. $C_{73}H_{50}Au_3ClF_{10}O_4P_4S_2$ (1995.56) **6**. Calc: C, 43.95; H, 2.5. Found: C, 43.65; H, 2.35. $C_{73}H_{50}Au_3As_2ClF_{10}O_4P_2S_2$ (2083.457) **7**. Calc. C, 42.1; H, 2.4; S, 3.1. Found: C, 42.5; H, 2.1; S, 3.4. Λ_m ($5 \cdot 10^{-4}$ M): 143 (**6**), 140 (**7**) (ohm $^{-1} \cdot cm^2 \cdot mol^{-1}$). NMR **6**: $^{31}P\{^1H\}$: δ = 43.9 (t, 2P, Au(III)-$SPPh_2$, [^{3}J(P-P) = 5.6 Hz]) and 36.3 (t, 2P, PPh_3, [^3J(P-P) = 5.6 Hz]). NMR **7**: $^{31}P\{^1H\}$: δ = 42.6 (s, 2P, Au(III)-PPh_2); ^{19}F: δ = −121.8 (m, 4F, *o*-F), −155.7 (t, 2F, *p*-F, [^3J(FF) = 19.9 Hz]) and −160.5 (m, 4F, *m*-F).

$[Au(C_6F_5)_2\{SPPh_2C(AuPPh_3)PPh_2S\}]$ (**8**)

To a dichloromethane solution of $[Au(C_6F_5)_2(SPPh_2CHPPh_2S)]$ (0.195 g, 0.20 mmol) was added [Au(acac)PPh_3] (0.112 g, 0.20 mmol). After stirring for 1 h the mixture was filtered through a layer of celite and the solvent was evaporated to ca 5 cm^3. Addition of 20 cm^3 of hexane led to the precipitation of **8** as a yellow solid. Yield: 53%. $C_{55}H_{35}Au_2F_{10}P_3S_2$ (1436.85). Calc: C, 45.95; H, 2.45. Found: C, 45.65; H, 2.8. $^{31}P\{^1H\}$ NMR: δ = 46.9 (m, 1P, Au(III)-PPh_2), 34.8 (m, 1P, $SPPh_2$) and 37.5 (s, 1P, PPh_3).

Crystal structure determination of $7 \cdot 2CH_2Cl_2$

Crystal data. $C_{74}H_{52}As_2Au_3Cl_3F_{10}O_4P_2S_2$, M_r = 2168.31, monoclinic, space group $P2_1/n$, a = 18.134(4), b = 15.805(3), c = 51.489(9) Å, β = 95.52(2)°, V = 14689(9) $Å^3$, Z = 8, D_c = 1.961 Mg m^{-3}, μ = 7.156 mm^{-1}, $F(000)$ = 8272, T = −100°C. Colourless prism 0.40 × 0.30 × 0.20 mm.

Data collection and reduction. The crystal was mounted in inert oil on a glass fibre. Data were collected using monochromated Mo-K_α radiation (λ = 0.71073 Å) on a Siemens P4 diffractometer with an LT-2 low temperature attachment to $2\theta_{max}$ = 45°. 19,516 intensities were collected of which 18,818 (R_{int} = 0.070) were independent. An absorption correction based on Ψ-scans gave transmissions factors 0.693–0.904. Cell constants were refined from setting angles of 55 reflection in the 2θ range 6–23°.

The structure was solved by direct methods and subjected to full-matrix least-squares refinement on F^2 (program SHELXL-93) [21]. Au, P, As, S and F atoms were refined anisotropically, others isotropically. Hydrogen atoms were included using a riding model. The final $\omega R(F^2)$ was 0.211 for 18,789 reflections, 751 parameters and 358 restraints, conventional $R(F)$ 0.0812. S = 1.028, maximum $\Delta\rho$ 1.94 e $Å^{-3}$. The poor R value is caused by two factors: (i) the disorder of an perchlorate with very badly defined O atoms (the dichloromethane molecules also display high U values) and, more seriously, (ii) the reflection overlap caused by the long axis (despite narrow reflections and the use of ω scans). A systems of restraints to P, S and F atom displacement-factor components and local ring symmetry was used. CCDC reference number 100612.

Acknowledgements—We thank the Dirección General de Investigación Científica y Técnica (No. PB94-0079) and the Fonds der Chemischen Industrie for financial support.

REFERENCES

1. Browning, J., Dixon, K. R. and Hilts, R. W., *Organometallics*, 1989, **8,** 552.
2. Berry, D. E., Browning, J., Dixon, K. R., Hilts, R. W. and Pidcock, A., *Inorg. Chem.*, 1992, **31,** 1479.
3. Slawin, A. M. Z., Smith, M. B. and Woollins, J. D., *J. Chem. Soc., Dalton Trans.*, 1996, 1283.
4. Slawin, A. M. Z., Smith, M. B. and Woollins, J. D., *J. Chem. Soc., Dalton Trans.*, 1996, 3659.
5. Paul, M. and Schmidbaur, H., *Chem. Ber.*, 1996, **129,** 77.
6. Laguna, A. and Laguna, M., *J. Organomet. Chem.*, 1990, **394,** 743.
7. Tanke, R. S. and Crabtree, R. M., *J. Chem. Soc., Chem. Commun.*, 1990, 1056.
8. Mazany, A. M. and Fackler, J. P., *Organometallics*, 1982, **1,** 752.
9. Browning, J., Bushnell, G. M., Dixon, K. R. and Pidcok, A., *Inorg. Chem.*, 1983, **22,** 2226.
10. Browning, J., Beveridge, K. A., Bushnell, G. M. and Dixon, K. R., *Inorg. Chem.*, 1986, **25,** 1987.
11. Fernández, E. J., Gimeno, M. C., Laguna, A., López de Luzuriaga, J. M. and Olmos, E., unpublished results.
12. Laguna, A., Laguna, M., Rojo, A. and Fraile, M. N., *J. Organomet. Chem.*, 1986, **315,** 269.
13. Usón, R., Laguna, A., Laguna, M., Fernández, E. J., Jones, P. G. and Sheldrick, G. M., *J. Chem. Soc., Dalton Trans.*, 1982, 1971.
14. Teichmann, H. and Hilgetag, G., *Angew. Chem., Int. Ed. Engl.*, 1967, **6,** 1013.

15. Alvarez, B., Fernández, E. J., Gimeno, M. C., Jones, P. G., Laguna, A., Laguna, M. and López de Luzuriaga, J. M., *J. Organomet. Chem.*, 1996, **525,** 109.
16. Fernández, E. J., Gimeno, M. C., Jones, P. G., Laguna, A., Laguna, M. and López de Luzuriaga, J. M., *J. Chem. Soc., Dalton Trans.*, 1992, 3365.
17. Usón, R., Laguna, A., Laguna, M., Fraile, M. N., Jones, P. G. and Erdbrügger, C. F., *J. Chem. Soc., Dalton Trans.*, 1989, 73.
18. Fernández, E. J., Gimeno, M. C., Jones, P. G., Laguna, A. Laguna, J. and López de Luzuriaga, J. M., *Angew. Chem. Int. Ed. Engl.*, 1994, **33,** 87.
19. Reid, B. D. and Welch, A. J., *J. Organomet. Chem.*, 1992, **438,** 371.
20. Wheatland, D. A., Clapp, C. H. and Waldron, R. W., *Inorg. Chem.*, 1972, **11,** 2340.
21. Sheldrick, G. M., SHELXL-93, *Program for Crystal Structure Refinement*. University of Göttingen, 1993.

Pergamon

PII: S0277-5387(97)00474-9

Polyhedron Vol. 17, Nos. 11–12, pp. 2037–2042, 1998
© 1998 Elsevier Science Ltd
All rights reserved. Printed in Great Britain
0277-5387/98 $19.00+0.00

Synthesis and structural characterization of chalcogenido-bridged trinuclear palladium(II) dialkyldithiophosphates, $[Pd_3(\mu_3\text{-}E)_2\{S_2P(OR)_2\}_2(PR'_3)_2]$ (E = S or Se, R = Et, Pr^n, Pr^i, Bu^s and R′ = Ph, Et)

Sanjay Narayan,[a] Vimal K. Jain[a]* and R. J. Butcher[b]

[a] Chemistry Division, Bhabha Atomic Research Centre, Trombay, Mumbai-400 085, India

[b] Department of Chemistry, Howard University, Washington, DC-20059, U.S.A.

(Received 15 September 1997; accepted 12 November 1997)

Abstract—Reaction of $[PdCl\{S_2P(OR)_2\}(PR'_3)]$ with sodium sulfide or selenide in acetone afforded neutral trinuclear palladium(II) complexes of the type $[Pd_3(\mu_3\text{-}E)_2\{S_2P(OR)_2\}_2(PR'_3)_2]$ (E = S or Se; R = Et, Pr^n, Pr^i, Bu^s, R′ = Et or Ph) in 24–42% yield. These complexes were characterized by elemental analysis, NMR (^1H, ^{31}P, ^{77}Se) and FAB mass spectral data. The molecular structure of $[Pd_3(\mu_3\text{-}S)_2\{S_2P(OEt)_2\}_2(PPh_3)_2]$ (**1**) was determined by X-ray diffraction. The molecule consists of three distorted square-planar palladium atoms sharing two μ_3-S ligands. One of the palladium atoms is linked with two triphenylphosphine ligands while each of the remaining two palladium atoms is coordinated with chelating dithiophosphate group. © 1998 Elsevier Science Ltd. All rights reserved

Keywords: palladium; chalcogen; dithiophosphate; ^{77}Se NMR; X-ray.

Interest in the chemistry of metal chalcogenide complexes continues to grow [1–4] due to their applications in metal catalyzed hydrodesulfurization [5,6] and in materials science [4,7]. Substitution reactions in palladium(II) dithiolate complexes are quite facile and give a variety of products [8]. The reactions of $[PdCl(S_2CNMe_2)(PEt_3)]$ with thiols in the presence of base have been reported recently to give monomeric palladium thiolate, $[Pd(SR)(S_2CNMe_2)(PEt_3)]$ [9]. We carried out a reaction of $[PdCl\{S_2P(OR)_2\}(PR'_3)]$ with Na_2S/Na_2Se with the hope of isolating binuclear chalcogenido-bridged complexes, similar to Cp*M-Te-MCp* (M = Ti, Zr and Hf) [10]. However, neutral chalcogenido-bridged trinuclear palladium complexes were isolated.

EXPERIMENTAL SECTION

All reactions were carried out in anhydrous solvents under N_2 atmosphere. $[PdCl\{S_2P(OR)_2\}(PR'_3)]$ (R = Et, Pr^n, Pr^i, Bu^s; and R′ = Ph, Et) [11] and Na_2S [12], Na_2Se [12] were prepared by the literature methods. Analysis were performed by the Analytical Chemistry Division of this research centre. The ^1H, $^{31}P\{^1H\}$ and $^{77}Se\{^1H\}$ NMR were recorded in 5 mm NMR tubes as $CDCl_3$ solution on a Varian VXR-300 instrument. Chemical shifts are referenced with internal chloroform peak (δ 7.26 ppm) for ^1H, external 85% H_3PO_4 for $^{31}P\{^1H\}$, Me_2Se for $^{77}Se\{^1H\}$. FAB Mass spectra were recorded on a JEOL SX 102/DA-6000 Mass spectrometer using Argon/Xenon (6 KV, 10 mA) as the FAB gas. m-Nitrobenzyl alcohol was used as the matrix.

Synthesis

$[Pd_3(\mu_3\text{-}S)_2\{S_2P(OEt)_2\}_2(PPh_3)_2]$ (**1**). To an acetone solution (25 ml) of $[PdCl\{S_2P(OEt)_2\}(PPh_3)]$ (150 mg, 0.255 mmol), solid Na_2S (15 mg, 0.192 mmol) was added and the reaction mixture was stirred at room temperature under N_2 for 48 h. The solvent was

* Author to whom correspondence should be addressed.

removed *in vacuo*. The residue was extracted with diethylether and filtered. The filtrate was concentrated to 5 ml and hexane (5 ml) was added. This solution on cooling in a freezer for a week gave orange crystals, which were separated by decanting the solvent and recrystallized again from acetone-hexane (Yield: 31 mg, 29%), m.p. 171–173°C (dec.). Anal. Calcd for $C_{44}H_{50}O_4S_6P_4Pd_3$: C, 41.4; H, 4.0. Found: C, 41.0; H, 3.8. ^{1}H NMR in $CDCl_3$: 1.38, 1.47 (each t, 7.1 Hz, 6H each, OCH_2Me); 4.26, 4.34 (each dq, J_{PH} 9.6 Hz (d), J_{HH} 7.1 Hz (q), 4H each, OCH_2-); 7.18–7.54 (m, 30H, *Ph*). $^{31}P\{^1H\}$ in $CDCl_3$: 22.8 (s, *P*Ph$_3$); 103.7 [s, $S_2P(OEt)_2$]. The supernatant on drying *in vacuo* gave a brown paste. The ^{1}H and $^{31}P\{^1H\}$ NMR spectra showed the existence of a mixture of products together with **1**.

$[Pd_3(\mu_3\text{-}S)_2\{S_2P(OPr^n)_2\}_2(PPh_3)_2]$ (**2**). This complex was prepared in an analogous manner to **1** and was recrystallized from acetone-hexane in 41% yield, m.p. 195–197°C (dec.). Anal. Calcd for $C_{48}H_{58}O_4S_6P_4Pd_3$: C, 43.2; H, 4.4. Found: C, 43.1; H, 4.1. ^{1}H in $CDCl_3$: 0.98, 1.04 (each t, 7.1 Hz, 6H, OCH_2CH_2Me); 1.76, 1.84 (each sextet, 7.1 Hz, 4H each, OCH_2CH_2-); 4.15, 4.23 (each dt, J_{PH} 9.0 Hz (d), J_{HH} 7.1 Hz (t), 4H each, OCH_2-); 7.18–7.55 (m, 30H, P*Ph*$_3$). $^{31}P\{^1H\}$ in $CDCl_3$: 21.6 (s, *P*Ph$_3$); 103.2 [s, $S_2P(OPr^n)_2$].

$[Pd_3(\mu_3\text{-}Se)_2\{S_2P(OPr^n)_2\}_2(PPh_3)_2]$ (**3**). To an acetone solution of $[PdCl\{S_2P(OPr^n)_2\}(PPh_3)]$ (2.147 g, 3.48 mmol) solid Na_2Se (449 mg, 3.59 mmol) was added. The reaction mixture was stirred at room temperature under a nitrogen atmosphere for 36 h. The solvent was evaporated *in vacuo*. The residue was washed thoroughly with hexane (5 × 10 ml), dried *in vacuo*, dissolved in acetone (20 ml) and passed through a Florisil column. To the solution, hexane (15 ml) was added to give brown crystals which were separated and again recrystallized from a cold acetone-hexane mixture. The yield of maroon crystals thus obtained was 35% (580 mg, based on Pd contents); m.p. 198–202°C (dec.). Anal. Calcd for $C_{48}H_{58}O_4S_4Se_2P_4Pd_3$: C, 40.4; H, 4.4. Found: C, 40.5; H, 3.9. ^{1}H NMR in $CDCl_3$: 0.97, 1.04 (each t, 7.4 Hz, 6H each, $POCH_2CH_2Me$); 1.75, 1.84 (each q, 7.1 Hz, 4H each, $POCH_2CH_2$-); 4.13, 4.21 (each m, 4H each, $POCH_2$–); 7.16–7.54 (m, 30H, P*Ph*$_3$). $^{31}P\{^1H\}$ in $CDCl_3$: 13.7 (s, *P*Ph$_3$) 103.2 [s, $S_2P(OPr^n)_2$]. $^{77}Se\{^1H\}$ NMR in $CDCl_3$: −98.7 (d, $^2J(^{77}Se\text{-}^{31}P) = 48$ Hz). FAB mass: *m/e* 1428 (molecular ion); 1215 $[Pd_3(\mu_3\text{-}Se)_2\{S_2P(OPr^n)_2\}(PPh_3)_2]$; 1166 $[Pd_3(\mu_3\text{-}Se)_2\{S_2P(OPr^n)_2\}_2(PPh_3)]$; 1089 $[Pd_3(\mu_3\text{-}Se)_2\{S_2P(OPr^n)_2\}_2(PPh_2)]$; 953 $[Pd_3(\mu_3\text{-}Se)_2\{S_2P(OPr^n)_2\}(PPh_3)]$.

$[Pd_3(\mu_3\text{-}Se)_2\{S_2P(OEt)_2\}_2(PPh_3)_2]$ (**4**). This complex was prepared in an anologous manner to compound **3** and was recrystallized from acetone-hexane mixture in 24% yield, m.p.: 197–198°C (dec.). Anal. Calcd For $C_{44}H_{50}O_4S_4Se_2P_4Pd_3$: C, 38.5; H, 3.7. Found: C, 38.7; H, 3.2. ^{1}H NMR in $CDCl_3$: 1.37, 1.46 (each t, 7.0 Hz, 6H each, $POCH_2Me$); 4.24, 4.33 (each dq, J_{HH} 7 Hz (q), J_{PH} 9.5 Hz (d), 4H each, $POCH_2$-); 7.15–7.54 (m, 30 H, P*Ph*$_3$). $^{31}P\{^1H\}$ in $CDCl_3$: 12.1 (s, *P*Ph$_3$), 101.0 [s, $S_2P(OEt)_2$].

$[Pd_3(\mu_3\text{-}Se)_2\{S_2P(OPr^i)_2\}_2(PPh_3)_2]$ (**5**). This complex was prepared in an analogous manner to **3** and was recrystallized from acetone-hexane in 25% yield, m.p. 224–225°C (dec.). Anal. Calcd for $C_{48}H_{58}O_4S_4Se_2P_4Pd_3$: C, 40.4; H, 4.4. Found: C, 39.5; H, 3.9. ^{1}H NMR in $CDCl_3$: 1.37, 1.47 (each d, 6.2 Hz, 12H each, $POCHMe_2$); 4.98 (m, 4H, $POCH$-); 7.18–7.52 (m, 30H, P*Ph*$_3$). $^{31}P\{^1H\}$ in $CDCl_3$: 15.0 (s, *P*Ph$_3$), 101.1 [s, $S_2P(OPr^i)_2$].

$[Pd_3(\mu_3\text{-}Se)_2\{S_2P(OBu^s)_2\}_2(PPh_3)_2]$ (**6**). This was prepared in an analogous manner to **3**. The complex was recrystallized from diethylether-hexane in 36% yield, m.p. 173–175°C (dec.). Anal. Calcd for $C_{52}H_{66}O_4S_4Se_2P_4Pd_3$: C, 42.1; H, 4.5. Found: C, 42.0; H, 3.7. ^{1}H NMR in $CDCl_3$: 0.95, 1.01 (each t, 7.5 Hz, 6H each, $POCHCH_2Me$); 1.36, 1.47 (each d, 6.2 Hz, 6H each, $POCHMe$); 1.74 (m, 8H, $POCHCH_2$-); 4.76 (m, 4H, $POCH$-); 7.17–7.57 (m, 30H, P*Ph*$_3$). $^{31}P\{^1H\}$ in $CDCl_3$: 12.0 (s, *P*Ph$_3$), 99.0 [s, $S_2P(OBu^s)_2$].

$[Pd_3(\mu_3\text{-}Se)_2\{S_2P(OPr^n)_2\}_2(PEt_3)_2]$ (**7**). This complex was prepared in an analogous manner to **3**, and was recrystallized by cooling a diethylether-hexane mixture in a freezer for a week (yield 42%) m.p. 163–165 C. Anal. Calcd for $C_{24}H_{58}O_4S_4Se_2P_4Pd_3$: C, 25.3; H, 5.1. Found: C, 24.5; H, 4.9. ^{1}H NMR in $CDCl_3$: 0.94 (dt, J_{HH} 7.5 Hz (t), J_{PH} 22 Hz (d), 18H, PCH_2Me); 1.22, 1.28 (each t, 7.5 Hz, 6H each, $POCH_2CH_2Me$); 1.71 (m, 12H, PCH_2-); 1.92 (m, 8H, $POCH_2CH_2$-); 3.97, 4.13 (each dt, J_{HH} 7 Hz (t), J_{PH} 9 Hz (d), 4H each, $POCH_2$-); $^{31}P\{^1H\}$ in $CDCl_3$: 11.4 (s, *P*Et$_3$), 101.7 [s, $S_2P(OPr^n)_2$]. FAB mass: *m/e* 1140 (molecular ion).

X-ray crystallography

All measurements were made at 20 ± 2°C on a Rigaku AFC 6S diffractomer using graphite monochromated Mo–K_α radiations ($\lambda = 0.71073$ Å). Crystal data and data collection details are given in Table 1. The data were corrected for Lorentz and polarization effects. Semi-empirical absorptions correction was based on Ψ scan of several reflections (maximum and minimum transmission factors: 0.57 and 0.26, respectively). The structure was solved by a combination of the Patterson and direct methods and refined by full-matrix least-squares on F^2. Neutral atom factors were taken from Cromer and Waber [14]. Anamolous dispersion effects were included in F_{calc} [15]. All calculations were performed using the TEXSAN [16] crystallographic software package of the Molecular Structure Corporation. The ORTEP [17] plot of the molecule is shown in Fig. 1.

RESULTS AND DISCUSSION

Treatment of $[PdCl\{S_2P(OR)_2\}(PR'_3)]$ with sodium sulfide or selenide in acetone gave neutral chal-

Table 1. Crystal data and structure refinement for $[Pd_3(\mu\text{-}S)_2\{S_2P(OEt)_2\}_2(PPh_3)_2]$

Empirical formula	$C_{44}H_{50}O_4P_4Pd_3S_6$
Formula weight	1278.28
Temperature (K)	293(2)
Wavelength (Å)	0.71073
Crystal system	Triclinic
Space group	$P\bar{1}$
a (Å)	11.988(4)
b (Å)	13.523(5)
c (Å)	18.953(8)
α ( )	77.18
β ( )	82.18
γ ( )	69.370(10)
V (Å)^3	2798(2)
Z	2
D_{calc} (Mg m^3)	1.517
Absorption coefficient (mm $^{-1}$)	1.328
F(000)	1280
Crystal size	$0.39 \times 0.25 \times 0.12$ mm
θ range for data collection ( )	2.65 to 25.00
Index ranges	$0 \leqslant h \leqslant 14$, $-15 \leqslant k \leqslant 16$, $-22 \leqslant l \leqslant 22$
Reflection collected	10343
Independent reflections	9832($R_{int} = 0.0591$)
Absorption correction	SHELXA
Refinement method	Full-matrix least-squares on F^2
Data/restraints/parameters	9823/0/556
Goodness-of-fit on F^2	1.014
Final R indices [$I > 2(I)$]	$R_1 = 0.0644$, $wR_2 = 0.0994$
R indices (all data)	$R_1 = 0.1608$, $wR_2 = 0.1354$
Extinction coefficient	0.0000(2)
Largest diff. peak and hole (e Å $^{-3}$)	0.583 and -0.585

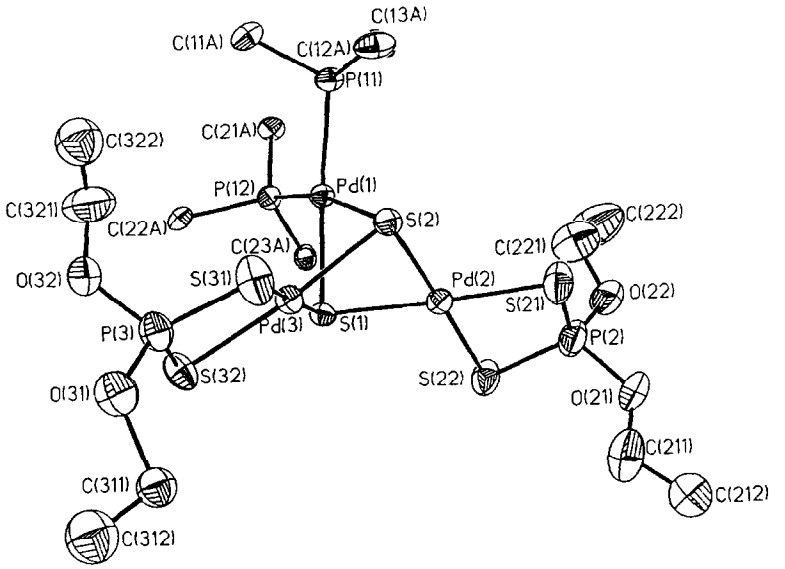

Fig. 1. Molecular structure of $[Pd_3(\mu_3\text{-}S)_2\{S_2P(OEt)_2\}_2(PPh_3)_2]$. Phenyl groups of PPh_3 are omitted for the sake of clarity.

ogenido-bridged trinuclear palladium(II) complexes of the type $[Pd_3(\mu_3\text{-}E)_2\{S_2P(OR)_2\}_2(PR'_3)_2]$ (E = S, Se; R = Et, Pr^n, Pr^i, Bu^s and R′ = Et, Ph) (Scheme 1) in 24–42% yield. The ^{1}H NMR showed two sets of OR proton resonances in 1 : 1 ratio indicating non-equivalence of the alkoxy groups on the dithi-

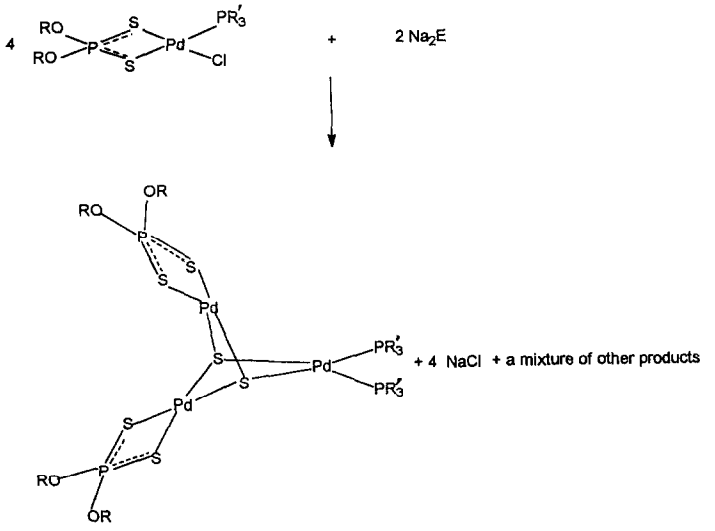

	R	R′	E
1	Et	Ph	S
2	Pr^n	Ph	S
3	Pr^n	Ph	Se
4	Et	Ph	Se
5	Pr^i	Ph	Se
6	Bu^s	Ph	Se
7	Pr^n	Et	Se

Scheme 1.

ophosphate ligand. The $^{31}P\{^1H\}$ NMR spectra showed singlets for the triphenylphosphine and dialkyldithiophosphate moiety. The ^{31}P resonance for triphenylphosphine is more shielded for the selenido-bridged complexes than the corresponding sulfido-bridged derivatives. The $^{77}Se\{^1H\}$ NMR spectrum (^{77}Se $I = 1/2$, natural abundance 7.58%) of **3** showed a doublet at -98.7 ppm with $^2J(^{77}Se\text{-}^{31}P)_{trans}$ of 48 Hz. FAB mass spectra of $[Pd_3(\mu_3\text{-}Se)_2\{S_2P(OPr^n)_2\}_2(PR'_3)_2]$ (R′ = Et, Ph) showed molecular ion peaks. Other prominent ions observed in the spectra are due to the species formed either by loss of a dithiophosphate ligand or triphenylphosphine ligand. The isotopic patterns for these species are in accord with the pattern calculated for $Pd_3Se_2S_4$ fragment.

The structure of **1**, established by X-ray study, shows that this is a sulfido-bridged trinuclear palladium(II) complex (Fig. 1). Molecule consists of three distorted square-planar palladium atoms sharing two μ_3-S ligands. The molecular geometry may alternatively be viewed of a trigonal bipyramidal Pd_3S_2 core with one palladium atom linked with two triphenylphosphine and each of the remaining two palladium atoms is coordinated with chelating dithiophosphate group. The central palladium atoms in the triangle are not equilateral, the two Pd—Pd distances (av. 3.0446(14) Å) are shorter than the third one (3.217(2) Å). Although **1** is the first neutral trinuclear sulfido-bridged complex, the Pd—Pd distances are in accord with the Pd—Pd bond lengths reported in $[Pd_3(\mu\text{-}S)_2(PMe_3)_6][BPh_4]_2$ [18]. However, the metal–metal distances in other ionic chalcogenido-bridged trinuclear complexes, $[Pt_3(\mu_3\text{-}Te)_2(PEt_3)_6][PF_6]_2$ [19], $[Pt_3(\mu_3\text{-}Te)_2(dppe)_3][BPh_4]_2$ [20], $[Ni_3(\mu_3\text{-}E)_3(PR_3)_6]^{2+}$ (E = S, Se) [21], are equidistant.

The dithiophosphate ligands are symmetrically chelated to the palladium atoms, the Pd—$S_{(dithio)}$ distances are essentially the same (i.e. av. 2.383 Å) and are in good agreement with the values reported for chelated dithio palladium complexes [22,23]. The P—S bond lengths (av. 1.982(5) Å) are intermediate between the double bond (1.94 Å) and single bond (2.09 Å) values confirming the partial double bond character, as expected from symmetrically chelated dithiophosphate ligand. The angles S(21)—Pd(2)—S(22) (84.16(11)°), S(31)—Pd(3)—S(32) (83.64(11)°), S(1)—Pd(2)—S(2) (78.96(9)°), S(1)—Pd(3)—S(2) (78.50(9)°) and S(1)—Pd(1)—S(2) (76.87(9)°) are

Table 2. Selected bond distances (Å) and angles (deg) for $[Pd_3(\mu_3\text{-}S)_2\{S_2P(OEt)_2\}_2(PPh_3)_2]$

		Distances	
Pd(1)—S(1)	2.348(3)	Pd(3)—S(32)	2.370(3)
Pd(1)—S(2)	2.337(3)	S(31)—P(3)	1.980(5)
Pd(1)—P(11)	2.292(3)	S(32)—P(3)	1.973(4)
Pd(1)—P(12)	2.328(3)	P(3)—O(31)	1.572(8)
Pd(2)—S(1)	2.301(3)	P(3)—O(32)	1.575(9)
Pd(2)—S(2)	2.280(3)	Pd(1)—Pd(2)	3.0930(14)
Pd(2)—S(21)	2.384(3)	Pd(1)—Pd(3)	2.9962(14)
Pd(2)—S(22)	2.386(3)	Pd(2)—Pd(3)	3.217(2)
S(21)—P(2)	1.985(5)	P(11)—C(11A)	1.794(10)
S(22)—P(2)	1.989(5)	P(11)—C(12A)	1.833(10)
P(2)—O(21)	1.573(9)	P(11)—C(13A)	1.815(11)
P(2)—O(22)	1.584(10)	P(12)—C(21A)	1.826(10)
Pd(3)—S(1)	2.304(3)	P(12)—C(22A)	1.834(10)
Pd(3)—S(2)	2.300(3)	P(12)—C(23A)	1.815(10)
Pd(3)—S(31)	2.392(2)		
		Angles	
S(1)—Pd(1)—P(11)	168.68(10)	Pd(3)—Pd(1)—P(11)	121.19(8)
S(2)—Pd(1)—P(11)	92.04(10)	Pd(3)—Pd(1)—P(12)	123.38(7)
S(1)—Pd(1)—S(2)	76.87(9)	Pd(2)—Pd(1)—S(1)	47.65(7)
S(1)—Pd(1)—P(12)	90.21(9)	Pd(2)—Pd(1)—S(2)	47.16(7)
P(11)—Pd(1)—P(12)	100.98(10)	Pd(3)—Pd(1)—S(1)	49.26(7)
S(2)—Pd(1)—P(12)	166.72(9)	Pd(3)—Pd(1)—S(2)	49.21(7)
Pd(2)—Pd(1)—P(11)	125.24(8)	Pd(2)—Pd(1)—Pd(3)	63.75(4)
Pd(2)—Pd(1)—P(12)	121.02(7)		
Pd(1)—S(1)—Pd(2)	83.40(9)	Pd(1)—S(2)—Pd(2)	84.10(9)
Pd(1)—S(1)—Pd(3)	80.19(8)	Pd(1)—S(2)—Pd(3)	80.49(9)
Pd(2)—S(1)—Pd(3)	88.61(9)	Pd(2)—S(2)—Pd(3)	89.22(9)
Pd(1)—Pd(2)—Pd(3)	56.66(3)	Pd(1)—Pd(3)—Pd(2)	59.59(3)
Pd(1)—Pd(2)—S(1)	48.95(6)	Pd(1)—Pd(3)—S(1)	50.55(6)
Pd(1)—Pd(2)—S(2)	48.74(7)	Pd(1)—Pd(3)—S(2)	50.30(7)
Pd(3)—Pd(2)—S(1)	45.73(6)	Pd(2)—Pd(3)—S(1)	45.66(7)
Pd(3)—Pd(2)—S(2)	45.64(7)	Pd(2)—Pd(3)—S(2)	45.13(6)
S(1)—Pd(2)—S(2)	78.96(9)	S(1)—Pd(3)—S(2)	78.50(9)
S(1)—Pd(2)—S(21)	176.47(11)	S(1)—Pd(3)—S(31)	178.02(11)
S(1)—Pd(2)—S(22)	99.29(10)	S(1)—Pd(3)—S(32)	98.26(10)
S(2)—Pd(2)—S(21)	97.61(11)	S(2)—Pd(3)—S(31)	99.68(11)
S(2)—Pd(2)—S(22)	177.92(11)	S(2)—Pd(3)—S(32)	172.62(11)
S(21)—Pd(2)—S(22)	84.16(11)	S(31)—Pd(3)—S(32)	83.64(11)
Pd(2)—S(21)—P(2)	83.5(2)	Pd(3)—S(31)—P(3)	83.39(14)
Pd(2)—S(22)—P(2)	83.37(14)	Pd(3)—S(32)—P(3)	84.08(14)
S(21)—P(2)—S(22)	107.1(2)	S(31)—P(3)—S(32)	106.9(2)
S(21)—P(2)—O(21)	114.4(4)	S(31)—P(3)—O(31)	115.6(4)
S(22)—P(2)—O(21)	114.0(4)	S(32)—P(3)—O(31)	113.0(4)
S(21)—P(2)—O(22)	113.4(4)	S(31)—P(3)—O(32)	112.5(4)
S(22)—P(2)—O(22)	113.6(4)	S(32)—P(3)—O(32)	114.2(4)

compressed owing to the formation of four-membered chelate rings. Consequently other angles have opened. The Pd—P [9,23,24], Pd—$S_{(sulfido)}$ [18] are in good agreement with the reported values. It may be noted that the two of the palladium-sulfido bonds for the palladium linked to triphenylphosphines are longer (0.04 Å) than the other Pd—S bonds where palladium atoms are bound to the dialkyldithiophosphate groups. Selected bond lengths and angles are given in Table 2.

Acknowledgments—One of the authors (S.N.) is grateful to DAE for the award of a Junior Research Fellowship to him. Authors thank Drs J. P. Mittal and C. Gopinathan for encouragements of this work. The Facilities provided by RSIC, IIT Mumbai for recording NMR (^1H, ^{31}P, ^{77}Se) spec-

tra; Analytical Chemistry Division, BARC for microanalyses and Dr. Ramachandra Bhat for calculation of isotopic pattern for $Pd_3Se_2S_4$ fragment are gratefully acknowledged.

REFERENCES

1. Brennan, J. G., Siegrist, T., Stuezynshi, S. M. and Steigerwald, M. L., *J. Am. Chem. Soc.*, 1990, **112,** 9233–9236.
2. Dobbs, D. A. and Bergman, R. G., *J. Am. Chem. Soc.*, 1992, **114,** 6908–6909.
3. Liu, C. W., Stubbs, T., Staples, R. J. and Fackler, J. P. Jr, *J. Am. Chem. Soc.*, 1995, **117,** 9778–9779.
4. Steigerwald, M. L., Siegerist, T., Stuczynski, S. M. and Kwon, Y. U., *J. Am. Chem. Soc.*, 1992, **114,** 3155–3156.
5. Chen, J., Daniels, L. M. and Angelici, R. J., *J. Am. Chem. Soc.*, 1990, **112,** 199–204.
6. Spies, G. and Angelici, R. J., *Organometallics*, 1987, **6,** 1897–1903.
7. (a) Boussean, M., Valade, L., Legros, J. P., Cassoux, P., Garbauskas, M. and Interrante, L. V., *J. Am. Chem. Soc.*, 1986, **108,** 1908; (b) Heuer, W. B. and Hoffman, B. M., *J. Chem. Soc., Chem. Commun.*, 1986, 174.
8. Hutton, A. T., *Comprehensive Coordination Chemistry*. Vol. 4, ed. G. Wilkinson, R. D. Gillard and J. A. McCleverty. Pergamon Press, 1987, Chap. 51.8, p. 1131.
9. Reger, D. L. and Collins, J. E., *Inorg. Chem.*, 1995, **34,** 2473–2475.
10. (a) Howard, W. A. and Parkin, G., *J. Am. Chem. Soc.*, 1994, **116,** 606; (b) Howard, W. A. and Parkin, G., *J. Organomet. Chem.*, 1994, **472,** C1; (c) Fischer, J. M., Piers, W. E., MacGillivry, L. R. and Zaworotko, M. J., *Inorg. Chem.*, 1995, **34,** 2499.
11. Cornock, M. C. and Stephenson, T. A., *J. Chem. Soc., Dalton Trans.*, 1977, 501.
12. Lio, L. H., Varatsis, C. and Kanatzidis, M. G., *Inorg. Chem.*, 1993, **32,** 2453.
13. Calabrese, J. C. Ph.D. thesis, University of Wisconsin, Madison (1972): Beurskens, P. T. Technical Report 1984/1 Crystallography Laboratory, Toernoolveld 6225 Ed. Nijmegin, The Netherlands.
14. Cromer, D. T. and Waber, J. T., *International Tables for X-ray Crystallography*, Vol. 4. Kynoch Press, Birmingham, 1974, Table 2.2A.
15. Ibers, J. A. and Hamilton, W. C., *Acta Cryst.*, 1964, **17,** 781.
16. TEXSAN, Structure Analysis Package, Molecular Structure Corporation, 1985.
17. Johnson, C. K., ORTEP II, Report ORNEL-5138. Oak Ridge National Laboratory, Oak Ridge, TN, 1976.
18. Werner, H., Bortleff, W. and Schubest, U., *Inorg. Chim. Acta*, 1980, **43,** 199–204.
19. Ma, A. L., Thoden, J. B. and Dahl, L. F., *J. Chem. Soc., Chem. Commun.*, 1992, 1516–1518.
20. Mastumoto, K., Ikuzawa, M. K., Kamikubo, M. and Ooi, S., *Inorg. Chim. Acta*, 1994, **217,** 129–134.
21. (a) Cecconi, F., Ghilardi, C. A. and Midollini, S., *Inorg. Chem.*, 1983, **22,** 3802–3808; (b) Mastumoto, K., Saiga, N., Tanaka, S. and Ooi, S., *J. Chem. Soc., Dalton Trans.*, 1991, 1265–1271.
22. (a) Reger, D. L., Garza, D. G. and Lebioda, L., *Organometallics*, 1991, **10,** 902–906; (b) Reger, D. L., Garza, D. G. and Lebioda, L., *Organometallics*, 1992, **11,** 4285–4292.
23. Fackler, J. P. Jr, Thomson, L. D., Lin, I. J. B., Stephenson, T. A., Gould, R. O., Alison, J. M. C. and Fraser, A. J. F., *Inorg. Chem.*, 1982, **21,** 2397–2403.
24. Ghilardi, C. A., Midollini, S., Nuzzi, F. and Orlandini, A., *Trans. Met. Chem.*, 1983, **8,** 73–75.

Pergamon

PII: S0277-5387(97)00517-2

Polyhedron Vol. 17, Nos. 11–12, pp. 2043–2047, 1998
© 1998 Elsevier Science Ltd
All rights reserved. Printed in Great Britain
0277-5387/98 $19.00+0.00

Supramolecular self-assembly in triphenyllead(IV) dimethylphosphinodithioate, $^{1}_{x}[Ph_3PbS_2PMe_2]$, a chain polymer built through intermolecular Pb···S secondary bonds

Frank T. Edelmann,[a]* Ionel Haiduc,[b] Cristian Silvestru,[b] Hans-Georg Schmidt[c] and Mathias Noltemeyer[c]

[a] Chemisches Institut, Otto-von-Guericke-Universität Magdeburg, D-39106 Magdeburg, Germany

[b] Facultatea de Chimie, Universitatea "Babes-Bolyai", RO-3400 Cluj-Napoca, Roumania

[c] Institut für Anorganische Chemie der Universität Göttingen, Tammannstr. 4, D-37077 Göttingen, Germany

(Received 10 September 1997; accepted 3 November 1997)

Abstract—The first structural characterization of an organolead phosphinodithioate is reported. According to an X-ray diffraction study, the title compound triphenyllead(IV) dimethylphosphinodithioate, $^{1}_{x}[Ph_3PbS_2PMe_2]$, forms a linear polymer in the solid state. Supramolecular association through secondary bonds of the type P=S···Pb leads to a polymeric chain formed by –Pb–S–P=S···Pb– units. The inorganic backbone is wrapped in a lipophilic "hose" made up of methyl and phenyl groups. © 1998 Elsevier Science Ltd. All rights reserved

Keywords: lead; organolead compounds; phosphinodithioates; supramolecular association; secondary bonds.

Supramolecular chemistry is defined as "the chemistry of molecular assemblies and of intermolecular bonds" and deals with "organised entities that result from the association of two or more chemical species held together by intermolecular forces" [1]. The formation of supramolecular structures is the result of a spontaneous association of a large number of components (self-assembly) and can involve various types of interactions, such as metal ion coordination, secondary bonding, hydrogen bonding, electrostatic forces and others.

Metal and organometal derivatives of phosphorodithioato [2a] and phosphinodithioato [2b] ligands display a remarkable diversity of coordination patterns. The ability of these ligands to function as bridging groups in Main Group metal compounds via secondary bonds, M—S—P=S···M, often leads to supramolecular self-assembly [3].

Crystal structure investigations of a number of lead(II) phosphorodithioates, $Pb[S_2P(OR)_2]_2$, with R = Et [4], Pr^i [5], Bu^i [4b], and Ph [4b] and phosphinodithioates, $Pb(S_2PR_2)_2$, with R = Me [6], Et [7] and Ph [8], revealed in all cases supramolecular self-assembly involving P=S···Pb secondary bonds. Moreover, each compound displayed a different structure and there were no two identical modes of association of the $Pb(S_2PR_2)_2$ building blocks.

In spite of the often fascinating structures produced by the two types of phosphoro- and phosphinodithioato ligands, they have been little used in organolead chemistry, and only two organolead(IV) com-

* Author to whom correspondence should be addressed.

pounds have been structurally characterised. Triphenyllead(IV) diethylphosphorodithioate, $Ph_3PbS_2P(OEt)_2$, contains discrete tetrahedral molecules and the ligand is monodentate, (a) with the second sulfur atom pointing away from the metal [9]. Diphenyllead(IV) dibenzylphosphorodithioate, $Ph_2Pb[S_2P(O\text{-}CH_2Ph)_2]_2$, is a dimer, in which the molecules are connected in pair by weak Pb···S secondary bonds, as shown in (b) [9a].

The only organolead phosphinodithioate investigated by X-ray diffraction is the diphenyllead derivative $Ph_2Pb(S_2PPh_2)_2$ [9b].

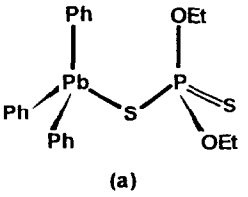

(a)

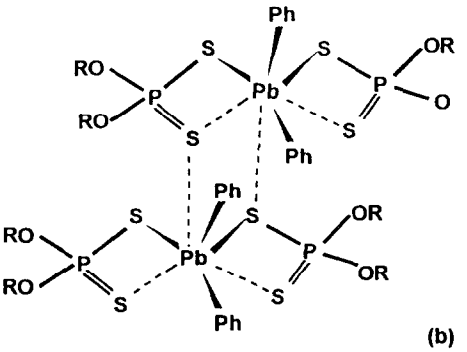

(b)

Reported here is the crystal structure of triphenyllead(IV) dimethylphosphinodithioate, $Ph_3PbS_2PMe_2$, the preparation of which has been previously reported [10]. Unlike the diethylphosphorodithioate (a), our compound is a linear polymer, containing a 1–Pb—S—P=S···Pb– chain, wrapped in a lipophilic "hose" made up of methyl groups (on phosphorus) and phenyl groups (on lead).

EXPERIMENTAL

The compound investigated has been obtained in a previously reported work [10].

Crystallographic data for $^1_\infty[Ph_3PbS_2PMe_2]$

$C_{20}H_{21}PPbS_2$. M = 563.65, orthorhombic, space group *Pbca*; a = 1149.6(2) pm, b = 1197.8(2) pm, c = 2.997.3(6) pm, $\alpha = \beta = \gamma = 90°$, V = 4.1273(13) nm^3; $Z = 8$; D_{calc} = 1.814 Mg/m^3, absorption coefficient 8.454 mm^{-1}, $F(000)$ 2160. Data were collected on a Siemens-Stoe AED2 diffractometer, at 153(2) K for 7572 reflections of which 1907 independent reflections (R_{int} = 0.1372) were used in the full-matrix least-squares refinement on F^2 with the SHELXS-90 Program System [11]. The final R indices [$I > 2\sigma(I)$] are R_1 = 0.0519, wR_2 = 0.1343, with R indices (all data) R_1 = 0.0719, wR_2 = 0.1662. Goodness-of-fit on F^2 1.081. The largest difference peak and hole 1786 and −1680 e nm^{-3}.

RESULTS AND DISCUSSION

The structure of triphenyllead(IV) dimethylphosphinodithioate, $^1_\infty[Ph_3PbS_2PMe_2]$, consists of molecules connected into infinite chains. An ORTEP drawing of the unit with the atom numbering scheme is shown in Fig. 1 and the packing of polymeric chains is shown in Fig. 2. Selected interatomic distances and bond angles are given in Table 1.

In the monomeric building block the lead atom is five-coordinate in a trigonal bipyramidal geometry, with the phenyl groups in equatorial positions and two sulfur atoms in axial positions. The two lead-sulfur bonds are not identical, with the shortest Pb(1)—S(1) bond [270.8(4) pm] connected to the sulfur atom single-bonded to phosphorus [P(1a)—S(1) 204.3(5) pm] as primary bond, and the longest Pb(1)—S(2) bond [302.8(4) pm] to the sulfur atom doubly bonded to phosphorus [P(1)=S(2) 197.9(6) pm]. This longer lead–sulfur distance corresponds to a Pb···S secondary bond, and is larger than the sum of covalent radii for lead and sulfur (estimated 250 pm) but significantly shorter than the sum of van der Waals radii (estimated 380 pm).

The phosphinodithioato ligand is bridging, as evident from Fig. 2, and this explains the lengthening of the P=S double bond involved, compared with pure P=S double bonds. The resulting polymeric chain consists of nearly linear S—Pb···S segments [bond angle 165.4(1)°]; bending of the chains occurs at the sulfur sites, with P(1)—S(2)—Pb(1) 126.1(2)° and P(1a)—S(1)—Pb(1) 101.4(2)°. The bending is more pronounced at the primary bonded sulfur atom than at the sulfur atom involved in the secondary bond.

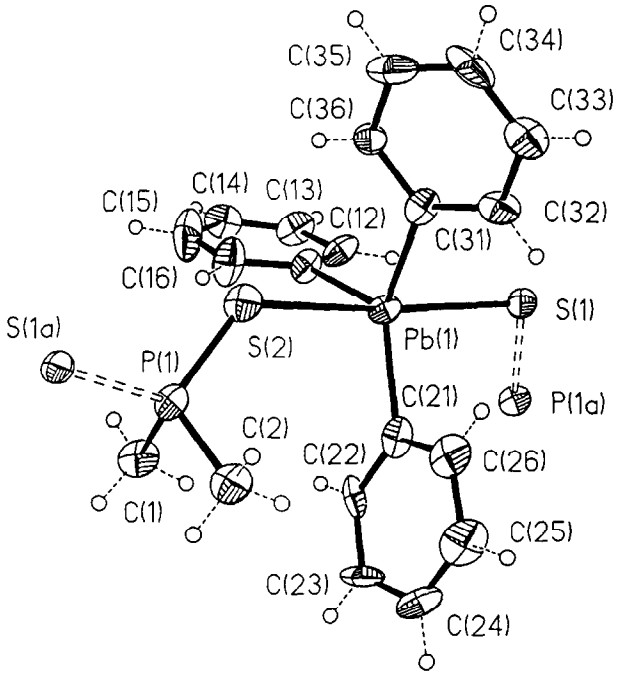

Fig. 1. ORTEP drawing of a monomeric unit in $^{1}_{\infty}[Ph_3PbS_2PMe_2]$.

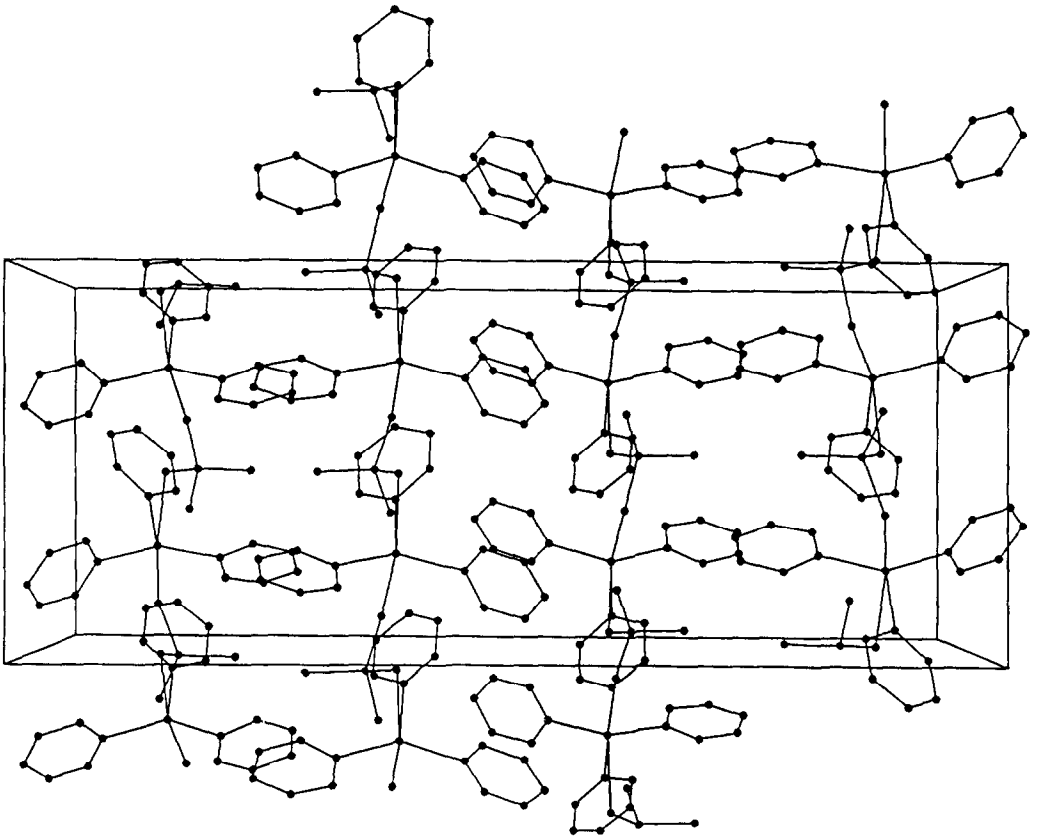

Fig. 2. Packing diagram of the polymeric chains in $^{1}_{\infty}[Ph_3PbS_2PMe_2]$.

Table 1. Selected bond lengths (pm) and angles (°) for $^1_\infty$[$Ph_3PbS_2PMe_2$]

Pb(1)—C(11)	224(2)	Pb(1)—C(21)	222(2)
Pb(1)—C(31)	220(2)	Pb(1)—S(1)	270.8(4)
Pb(1)—S(2)	302.8(4)	S(1)—P(1)[a]	204.3(5)
S(2)—P(1)	197.9(6)	P(1)—C(1)	180(2)
P(1)—C(2)	1.83(2)	P(1)—S(1)[b]	2.043(5)
C(31)—Pb(1)—C(21)	117.4(6)	C(31)—Pb(1)—C(11)	111.2(5)
C(21)—Pb(1)—C(11)	128.0(6)	C(31)—Pb(1)—S(1)	90.4(4)
C(21)—Pb(1)—S(1)	96.5(4)	C(11)—Pb(1)—S(1)	100.6(4)
C(31)—Pb(1)—S(2)	77.2(4)	C(21)—Pb(1)—S(2)	82.7(4)
C(11)—Pb(1)—S(2)	91.1(4)	S(1)—Pb(1)—S(2)	165.4(1)
P(1)[a]1—S(1)—Pb(1)	101.4(2)	P(1)—S(2)—Pb(1)	126.1(2)
C(1)—P(1)—C(2)	105.7(8)	C(1)—P(1)—S(2)	112.9(6)
C(2)—P(1)—S(2)	110.9(6)	C(1)—P(1)—S(1)[b]	105.8(6)
C(2)—P(1)—S(1)[b]	108.4(5)	S(2)—P(1)—S(1)[b]	112.7(2)

Symmetry transformations used to generate equivalent atoms: [a] $-x+1/2, y+1/2, z$; [b] $-x+1/2, y-1/2, z$.

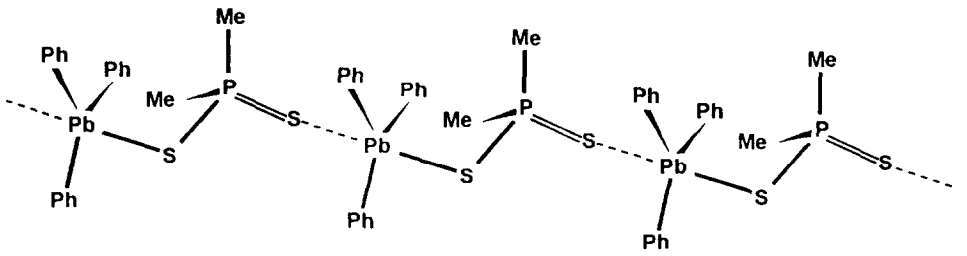

The Pb—S primary bond lengths (270.8 pm) are comparable with the Pb—S interatomic distances measured in lead(II) phosphinodithioates [2b] and lead(II) phosphorodithioates [2a] (range 275–298 pm). The Pb···S secondary bonds in $^1_\infty$[$Ph_3PbS_2PMe_2$] (302.8 pm) are comparable, even somewhat shorter than other intermolecular lead–sulfur secondary bonds observed in lead(II) phosphoro- and phosphinodithioates [2].

The peripheral organic groups at phosphorus and lead wrap the inorganic chain in a lipophilic "hose" and the intermolecular contacts between chains are determined by the mutual orientation and packing of these groups, interacting through van der Waals forces only. This is obvious from the space filling illustration of the polymeric chains, shown in Fig. 3. It can be seen that alternating phenyl groups at lead and methyl groups at phosphorus are intercalated in the space around the inorganic inner core in such a way as to minimise the exposure of the Pb—S—P chain backbone.

Triphenyllead(IV) dimethylphosphinodithioate is the first self-assembled organo–lead compound displaying a chain structure similar to those found in other Main Group organometal phosphinodithioates, e.g. $^1_\infty$[$PhHgS(S)PEt_2$], [12], $^1_\infty$[$Me_2SbS(S)PMe_2$] [13], or $^1_\infty$[$PhTeS(S)PPh_2$] [14]. There are, however, differences in the coordination mode of the phosphinodithioato ligand, which forms chelate rings in the building blocks of the PhHg and Me_2Sb compounds but participates with only one sulfur atom in the PhTe compound. In the lead derivative, the bridging ligand participates with both sulfur atoms, but no intra-unit chelate rings are formed.

Acknowledgements—This work was financially supported by the Otto-von-Guericke-Universität Magdeburg. A research fellowship (to I.H.) from the Alexander von Humboldt-Stiftung is gratefully acknowledged.

REFERENCES

1. (a) Lehn, J. M., *Angew. Chem.*, 1988, **100**, 91; *Angew. Chem. Int. Ed. Engl.*, 1988, **27**, 89; (b) Lehn, J. M., in *Perspectives in Coordination Chemistry*. ed. A. F. Williams, C. Floriani and A. E. Mehrbach. Verlag Helvetica Chimica Acta Basel and VCH Weinheim, 1992, p. 447; (c) Lehn, J.

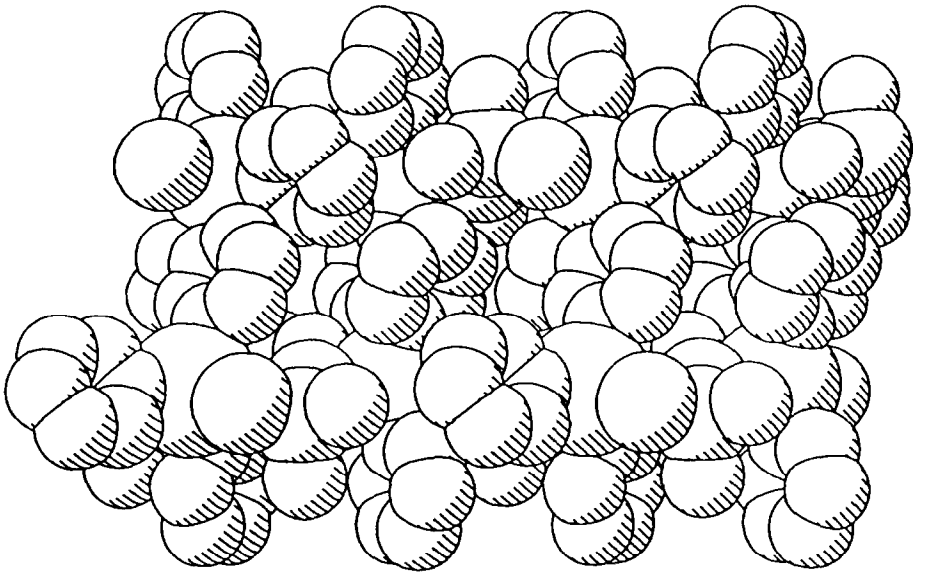

Fig. 3. Space filling diagram of the polymeric chains in $^{1}_{\infty}[Ph_3PbS_2PMe_2]$.

M., *Supramolecular Chemistry. Concepts and Perspectives*. VCH Weinheim, 1995, p. 1.
2. (a) Haiduc, I., Sowerby, D. B. and Lu, S., *Polyhedron*, 1995, **14,** 3389; (b) Haiduc, I. and Sowerby, D. B., *Polyhedron*, 1996, **15,** 2469.
3. Haiduc, I., *Coord. Chem. Rev.*, 1997, **158,** 325.
4. (a) Ito, T., *Acta Cryst.*, 1972, **B28,** 1034; (b) Harrison, P. G., Steel, A., Pelizzi, G. and Pelizzi, C., *Main Group Metal Chem.*, 1988, **11,** 181.
5. Lawton, S. L. and Kokotailo, G. T., *Inorg. Chem.*, 1972, **11,** 363.
6. Silvestru, C., Haiduc, I., Cea-Olivares, R. and Hernandez-Ortega, S., *Inorg. Chim. Acta*, 1995, **233,** 51.
7. Svensson, G. and Albertsson, J., *Acta Chem. Scand.*, 1991, **45,** 820.
8. Ebert, K. H., Breunig, H. J., Silvestru, C., Stefan, I. and Haiduc, I., *Inorg. Chem.*, 1994, **33,** 1695.
9. (a) Begley, M. G., Gafney, C., Harrison, P. G. and Steel, A., *J. Organomet. Chem.*, 1985, **289,** 281; (b) Olafsson, S. N., Petersen, T. N. and Andersen, P., *Acta Chem. Scand.*, 1966, **50,** 745.
10. Silvestru, C., Silvestru, A., Haiduc, I., Gavino-Ramirez, R. and Cea-Olivares, R., *Heteroatom Chem.* 1994, **5,** 327.
11. Sheldrick, G. M., *Acta Crystallogr. Sect. A*, 1990, **46,** 467.
12. Casas, J. S., Castineiras, A., Sanchez, A., Sordo, J. and Vazquez-Lopez, E. M., *J. Organomet. Chem.*, 1994, **468,** 1.
13. Ebert, K. H., Breunig, H. J., Silvestru, C. and Haiduc, I., *Polyhedron*, 1994, **13,** 2531.
14. (a) Silvestru, A., Haiduc, I., Ebert, K. H. and Breunig, H. J., *Inorg. Chem.*, 1994, **33,** 1253; (b) Silvestru, A., Haiduc, I., Ebert, K. H., Breunig, H. J. and Sowerby, D. B., *J. Organomet. Chem.*, 1994, **482,** 253.

Pergamon

Polyhedron Vol. 17, Nos. 11–12, pp. 2049–2063, 1998
© 1998 Elsevier Science Ltd
All rights reserved. Printed in Great Britain
PII: S0277-5387(97)00483-X
0277-5387/98 $19.00+0.00

Pd(II) and Pt(II) complexes with mixed phosphorus–oxygen donor ligands

Jui-Sui Sun, Calvin E. Uzelmeier, Donald L. Ward and Kim R. Dunbar*

Department of Chemistry, Michigan State University, East Lansing, MI 48824–1322, U.S.A.

(Received 29 September 1997; accepted 31 October 1997)

Abstract A series of new complexes have been synthesized from reactions of $[M(NCCH_3)_4][BF_4]_2$ (M = Pd, Pt) with the mixed donor ligand tris(2,4,6-trimethoxyphenyl) phosphine (TMPP). Reaction of $[Pd(NCCH_3)_4][BF_4]_2$ with two equivalents of TMPP in acetone produces the ether-phosphine complex $[Pd(TMPP)_2][BF_4]_2$, **1**. In this molecule the Pd atom is situated at the center of a pseudo-octahedron, with the phosphorus atoms in a *cis* orientation. The complex was also characterized by infrared, electronic, and NMR spectroscopies as well as by cyclic voltammetry. Reaction of $[Pd(NCCH_3)_4][BF_4]_2$ with four equivalents of TMPP in acetone yields the neutral phosphino-phenoxide compound Pd(TMPP-*O*)$_2$, **2**, where TMPP-*O* is the demethylated form of TMPP. ^1H and $^{31}P\{^1H\}$ NMR studies of **2** support the assignment of a solution structure that involves free rotation of the uncoordinated phenyl rings of the TMPP ligands. Reaction of $[Pt(NCCH_3)_4][BF_4]_2$ with two equivalents of TMPP in acetonitrile yields $[PT(NCCH_3)_2(TMPP)_2][BF_4]_2$, **3**. Structural and spectroscopic data for **3** indicate that free rotation of the arene rings in solution is restricted due to steric influences of the two CH_3CN co-ligands. Reaction of $PtCl_2(NCCH_3)_2$ with two equivalents of TMPP in acetone or reaction of $[Pt(NCCH_3)_4][BF_4]_2$ with four equivalents of TMPP in acetone gives Pt(TMPP-*O*)$_2$, **4**. Reaction of $PtCl_2(NCCH_3)_2$ with two equivalents of TMPP in tetrahydrofuran yields the neutral compound PtCl(TMPP)(TMPP-*O*), **5**. Although suitable single crystals were not obtained, the structure of compound **5** was deduced from infrared and NMR spectroscopies to be a square planar molecule with one neutral TMPP ligand coordinated in an η^1 fashion and a demethylated TMPP group bound as an η^2-P,O ligand where the phosphorus atoms are *trans* and the other two coordination sites are occupied by a phenoxide oxygen and a Cl atom. © 1998 Elsevier Science Ltd. All rights reserved

Keywords: Pd(II) complex; Pt(II) complex; donor ligands.

Transition metal complexes with ether-functionalized phosphine ligands have been found to exhibit enhanced reactivity due to the presence of weak metal-ether interactions that are often labile in the solid-state as well as in solution [1–4]. As a result of this behavior, ether-phosphine ligands have been referred to as "hemi-labile", a term coined specifically for such ligands with the complexes themselves being referred to as "incipiently coordinatively unsaturated" [1d,5,6].

In view of the interest in such molecules, our group has been investigating the unusual ether phosphine tris(2,4,6-trimethoxyphenyl)phosphine (TMPP). Special characteristics of this ligand are high basicity, a large cone angle of 184°, and the presence of *ortho*-methoxy substituents that can act as "built-in" solvent molecules in the chemistry. Among the unusual complexes that have been isolated with this ligand are mononuclear Rh(II) d^7 radicals, molecules that are ordinarily very unstable but which are indefinitely stable towards air and moisture in the presence of TMPP [3a].

One of our goals in this project has been to design homologous series of d^6, d^7 and d^8 TMPP complexes that differ only in the coordination mode adopted by the TMPP [3]. These related compounds are of general interest for probing the structural and reactivity differences exhibited by compounds that possess the same ligand set but a different metal electron count. Earlier work from our laboratories had shown that homoleptic TMPP compounds of Rh^I, Rh^{II} and Rh^{III} exhibit interesting redox chemistry and that they undergo reversible small molecule reactions based on the ability of the ether groups to dissociate [3a–c,e,n]. Given these promising results, it was logical to extend

* Author to whom correspondence should be addressed.

these studies to Pd(II) and Pt(II) which are known to be useful in catalytic applications when weakly bonded ligands are involved [5j,k,7 9]. In addition, polydentate ligands such as TMPP with steric requirements that favor octahedral coordination may enforce this geometry on metals for which six coordination is rarely observed [10,11]. In spite of the considerable interest, a fairly limited number of such compounds have been studied [5]. During the course of preparing this manuscript, a paper by Lindner and coworkers appeared which describes the reactivity of $[Pd(P \cap O)_2]^{2+}$ complexes as CO/ethene copolymerization catalysts, where P ∩ O is an η^2-coordinated polysiloxane-bound ether-phosphine [5k]. Herein we report the syntheses, X-ray structures, and spectroscopic data for a series of Pd(II) and Pt(II) complexes supported by TMPP or phenoxide derivatives of TMPP. In the new compounds, the ligands are shown to adopt η^1, η^2 and η^3 binding modes in square planar or six-coordinate environments. Some of these results have appeared in communication form [3j].

EXPERIMENTAL

Physical measurements

Infrared spectra were recorded on a Nicolet 740 FT-IR spectrophotometer. ^{1}H NMR spectra were measured on Varian 300 or 500 MHz spectrometers; chemical shifts were referenced relative to the residual proton impurities of acetone-d_6 (2.04 ppm with respect to TMS), acetonitrile-d_3 (1.93 ppm with respect to TMS) or chloroform-d_1 (7.24 ppm with respect to TMS). ^{31}P $\{^1$H$\}$ NMR spectra were obtained on Varian 300 or 500 MHz spectrometers operating at 121.4 MHz and 203.6 MHz respectively, and were referenced relative to an external standard of 85% phosphoric acid. Spin-simulation experiments were carried out by using the LAME program which is included in the VNMR software package. Elemental analyses were performed at Galbraith Laboratories, Inc., Knoxville, TN, or Desert Analytics, Tucson, AZ. Electrochemical measurements were carried out by using an EG&G Applied Research Model 362 scanning potentiostat in conjunction with a BAS Model RXY recorder. Cyclic voltammetric experiments were carried out at 22 ± 2°C using 0.1 M tetra-*n*-butylammonium hexafluorophosphate ($TBAPF_6$) as the supporting electrolyte. $E_{p,a}$ and $E_{p,c}$ were referenced to a Ag/AgCl electrode and are uncorrected for junction potentials.

Starting materials

The starting materials $PtCl_2(NCC_6H_5)_2$ and Pd sponge were purchased from Strem Chemicals, Inc. and were used as received. Tris(2,4,6-trimethoxyphenyl)phosphine (TMPP) was prepared according to published methods [3m] or purchased from Aldrich and used without further purification [12]. $[M(NCCH_3)_4][BF_4]_2$ (M = Pd [13a], Pt [13b]), and $[Cp_2Fe][BF_4]$ [13c] salts were prepared as described in the literature. Acetone was distilled over 3 Å molecular sieves, methanol was distilled over $Mg(OMe)_2$ under a nitrogen atmosphere, and methylene chloride was distilled over P_2O_5 under a nitrogen atmosphere. Benzene, diethyl ether, THF, and toluene were distilled over sodium-potassium/benzophenone. Unless otherwise specified, all reactions were carried out under an argon atmosphere by using standard Schlenk-line techniques.

$[Pd(TMPP)_2][BF_4]_2$ (**1**). An acetone solution (10 ml) containing two equivalents of TMPP (0.476 g, 0.900 mmol) was added dropwise to an acetone solution (10 ml) of $[Pd(NCCH_3)_4][BF_4]_2$ (0.200 g, 0.450 mmol) at −44°C which effected an immediate color change from pale yellow to red. The resulting solution was stirred for 40 min at −44°C and evaporated to dryness *in vacuo*. The compound was recrystallized from acetone and diethyl ether to give a brick-red solid in 82% yield (0.993 g). ^{1}H NMR in acetone-d_6 at −80°C (δ ppm): -OMe 3.32 (s, 6H); 3.34 (s, 6H); 3.47 (s, 6H); 3.52 (s, 6H); 3.83 (br, 18H); 4.03 (s, 6H); 4.25 (s, 6H); *meta*-H: 5.70 (br, 2H), 5.92 (br, 2H), 6.19 (br, 2H), 6.30 (br, 2H), 6.43 (br, 2H), 6.78 (br, 2H). ^{31}P$\{^1$H$\}$ NMR in acetone-d_6 (300 MHz, δ ppm): +1.67. Anal. Calcd for **1**, $PdP_2C_{54}O_{18}H_{66}B_2F_8$: C, 48.22; H, 4.95. Found: C, 48.29; H, 5.05. UV–Vis (CH_2Cl_2): λ_{max} (nm) (ε in M^{-1}, cm^{-1}) 485 (2.3×10^4), 373 (3.7×10^4), 260 (1.7×10^5).

Pd(TMPP-*O*)$_2$ (**2**). An acetone solution (15 ml) containing four equivalents of TMPP (0.719 g, 1.352 mmol) was added dropwise to an acetone solution (10 ml) of $[Pd(NCCH_3)_4][BF_4]_2$ (0.150 g, 0.338 mmol) at 0°C which effected an immediate color change from pale yellow to orange. The resulting solution was stirred for 2 h at 0°C, then warmed to room temperature and stirred for an additional 12 h. The solvent was removed by evaporation to yield an orange solid. This solid was recrystallized from THF and diethyl ether, then washed with a mixture of hexanes and acetone (v/v 2/3) to remove trace amounts of [CH_3-TMPP][BF_4]. The orange product is obtained in 78% yield (0.301 g). ^{1}H NMR (δ ppm in $CDCl_3$): -OMe: 3.10 (s, 6H), 3.12 (s, 24H), 3.66 (s, 6H), 3.75 (s, 12H); *meta*-H: 5.34 (br, 2H), 5.80 (br, 8H), 6.13 (br, 2H). ^{31}P$\{^1$H$\}$ NMR (300 MHz, δ ppm in $CDCl_3$), −3.07.

$[Pt(NCCH_3)_2(TMPP)_2][BF_4]_2$ (**3**). A solution of CH_3CN (10 ml) and two equivalents of TMPP (0.240 g, 0.450 mmol) was added dropwise to 5 ml of a CH_3CN solution of $[Pt(NCCH_3)_4][BF_4]_2$ (0.120 g, 0.225 mmol) at 0°C. The resulting solution was stirred for 40 min at 0°C and the solvent was removed *in vacuo* to give a pale yellow solid. The solid was recrystallized from CH_2Cl_2 and Et_2O; 73% yield (0.250 g). ^{1}H NMR (δ ppm in CD_3CN): 3.33 (s, 6H, CH_3CN); -OMe: 3.42 (br, 12H), 3.61 (br, 24H), 3.78 (s, 6H), 4.82 (s, 12H); *meta*-H: 6.11 (t, 4H), 6.15 (d, 8H). ^{31}P$\{^1$H$\}$

NMR (300 MHz, δ ppm in CD_3CN), −44.5 (d, $^1J_{PtP}$ = 2422 Hz).

Pt(TMPP-*O*)$_2$ (**4**). An acetone solution (20 ml) containing four equivalents of TMPP (0.600 g, 1.13 mmol) was added dropwise to an acetone solution (10 ml) of $[Pt(NCCH_3)_4][BF_4]_2$ (0.150 g, 0.281 mmol) at 0°C. The resulting solution was stirred for 12 h after which time the solvent was removed by evaporation to give a pale yellow residue. The solid was recrystallized from THF and Et_2O to give a pale yellow solid, which was dissolved in a mixture of THF and Et_2O and filtered through Celite to remove the insoluble methylphosphonium salt, $[CH_3\text{-TMPP}][BF_4]$. The volume of the filtrate was reduced under vacuum and the resulting yellow product was washed with Et_2O and dried *in vacuo*, 58% yield (0.201 g). X-ray quality single crystals of Pt(TMPP-*O*)$_2$ were obtained from a solution of the compound in EtCN and Et_2O at 0°C. ^{1}H NMR (δ ppm in CD_3CN), -OMe: 3.40 (s, 6H), 3.58 (s, 24H), 3.69 (s, 6H), 3.82 (s, 12H); *meta*-H: 5.58 (d-d, 2H), 5.81 (d-d, 2H), 6.15 (d, 8H). $^{31}P\{^1H\}$ NMR (300 MHz, δ ppm in CD_3CN), 24.9 (d, $^1J_{PtP}$ = 1950 Hz). Anal. Calcd for $PtP_2C_{54}O_{18}H_{66}B_2F_8$: C, 50.61; H, 4.90. Found: C, 49.57; H, 5.05.

PtCl(TMPP)(TMPP-*O*) (**5**). A mixture of $PtCl_2(NCC_6H_5)_2$ (0.150 g, 0.318 mmol) and TMPP (0.33 g, 0.636 mmol) were loaded in a Schlenk flask, dissolved in 30 ml of THF and stirred for 2 days under reduced pressure to remove the CH_3Cl(g) by-product. A pale yellow precipitate and a yellow solution were obtained. The precipitate was discarded, the yellow solution was filtered into a second flask, and the volume of the filtrate was reduced under vacuum. Et_2O was then added to precipitate a pale yellow solid, which was washed with a mixture of acetone and Et_2O to remove trace quantities of $[CH_3\text{-TMPP}]^+$, washed with Et_2O and finally dried under vacuum to yield a pale yellow compound in 40% yield (0.163 g). IR (Nujol, cm^{-1}) ν(Pt-Cl) 326. ^{1}H NMR (δ ppm in CD_3CN), -OMe: 3.28 (s, 3H), 3.38 (s, 30H), 3.58 (s, 3H), 3.75 (s, 9H), 3.77 (br, 6H); *meta*-H: 5.29 (m, 1H), 5.38 (m, 1H), 5.99 (d, 6H), 6.04 (d, 4H). $^{31}P\{^1H\}$ NMR (500 MHz, δ ppm in CD_3CN), −20.47 (dd, $^1J_{PtP}$ = 3212 Hz, $^2J_{PP}$ = 561 Hz), −26.85 (dd, $^1J_{PtP}$ = 2993 Hz, $^2J_{PP}$ = 561 Hz).

X-ray crystallographic studies

Crystallographic data for compounds **1**–**4** were collected on a Rigaku AFC6S diffractometer equipped with monochromated Mo–K_α radiation produced by a 2 kW sealed tube generator. Crystallographic computing for **1**, **3**, and **4** was performed on a VAXSTATION 4000 by using the Texsan crystallographic software package [14]. Computing for **2** was performed on a Silicon Graphics Indigo II workstation using the Texsan and SHELXTL [15] software system. Crystal parameters and basic information pertaining to data collection and structure refinement are summarized in Table 1.

$[Pd(TMPP)_2][BF_4]_2$ (**1**). Single crystals of **1** were grown by slow diffusion of diethyl ether into a CH_2Cl_2 solution of compound **1**. A red crystal of dimensions 0.50 × 0.40 × 0.36 mm was secured on the tip of a glass fiber with Dow Corning silicone grease and placed in a cold N_2(g) stream. Least-squares refinement using 21 well-centered reflections in the range $25 \leqslant 2\theta \leqslant 35°$ indicated an orthorhombic crystal system. The data were collected at −110 ± 1°C using the ω-2θ scan technique to a maximum 2θ value of 47°. A total of 4837 reflections was collected, of which 4181 data with $I > 0.01\sigma(I)$ were used for F^2 refinement, and 3298 data with $I > 3.00\sigma(I)$ were used for F refinement. An empirical absorption correction based on azimuthal scans of three reflections near $\chi = 90°$ was applied which resulted in transmission factors ranging from 0.92 to 1.00. The data were corrected for Lorentz and polarization effects. The space group was determined to be $Pna2_1$ based on the observed systematic absences. The structure was solved by the MITHRIL [16] program, and subsequent cycles of DIRDIF [17] were used to locate the atom positions for full-matrix least-squares refinement. The phenyl rings of the TMPP ligands were refined isotropically for the F^2 refinement and treated as rigid groups for the F refinement to reduce the number of parameters. F^2 refinement of 585 parameters resulted in residuals of $R = 0.075$ and $R_w = 0.101$, while refinement on F of 433 parameters resulted in residuals of $R = 0.057$ and $R_w = 0.074$. Attempts to solve the structure in the higher symmetry space group *Pnma* (#62) were unsuccessful. Both enantiomorphs of the noncentrosymmetric space group $Pna2_1$ (#33) were refined, but no statistically significant difference in the residuals R and R_w (0.0751, 0.1009 for #62 and 0.0750, 0.1009 for #33) were observed.

Pd(TMPP-*O*)$_2$·3.73CH_2Cl_2·H_2O (**2**)·3.73CH_2Cl_2·H_2O. Single crystals of **2** were grown by a slow diffusion of diethyl ether into a CH_2Cl_2 solution of compound **2**. An orange crystal of dimensions 0.98 × 0.40 × 0.22 mm was secured on the tip of a glass fiber with Dow Corning silicone grease and placed in a cold N_2(g) stream. Least-squares refinement using 25 well-centered reflections in the range $15.0 \leqslant 2\theta \leqslant 22.3°$ indicated that the crystal is consistent with an orthorhomic crystal system. The data were collected at −85 ± 1°C using the ω-2θ scan technique to a maximum 2θ value of 47°. Of the 10,169 reflections that were collected, 815 were systematically absent. An empirical absorption correction based on azimuthal scans of three reflections with χ near 90° was applied which resulted in transmission factors ranging from 0.55–1.00. The data were corrected for Lorentz and polarization effects. The structure was solved in the space group *Pbcn* using the MITHRIL [16] and DIRDIF [17] structure solution programs and refined by full-matrix least-squares refinement on F [15]. Methoxy methyl groups centered about atoms

Table 1. Summary of crystallographic data for $[Pd(TMPP)_2][BF_4]_2$ (**1**), Pd(TMPP-*O*)$_2$ (**2**)·3.73CH_2Cl_2 H_2O, $[Pt(NCCH_3)_2(TMPP)_2][BF_4]_2$ (**3**), Pt(TMPP-*O*)$_2$ (**4**)·3EtCN

	1	**2**·3.73CH_2Cl_2·H_2O	**3**	**4**·3EtCN
Formula	$PdP_2F_8O_{18}C_{54}B_2H_{66}$	$PdCl_{7.5}P_2O_{19}C_{55.7}H_{67.5}$	$PtP_2F_8O_{18}N_2C_{58}BH_{72}$	$PtP_2O_{18}N_3C_{61}H_{75}$
Formula weight	1345.07	1376.27	1515.85	1395.31
Color	Red	Orange	Yellow	Yellow
Crystal size (mm^3)	$0.36\times0.40\times0.50$	$0.22\times0.40\times0.98$	$0.30\times0.30\times0.44$	$0.27\times0.36\times0.36$
Space group	$Pna2_1$	$Pbcn$	$P\bar{1}$	$P2_1/c$
a (Å)	20.71(1)	20.162(9)	14.578(3)	12.958(5)
b (Å)	17.838(3)	24.62(2)	18.291(3)	33.262(7)
c (Å)	15.908(2)	24.326(11)	13.229(2)	14.697(5)
α (°)	90	90	104.40(1)	90
β (°)	90	90	109.24(1)	100.68(3)
γ (°)	90	90	88.41(2)	90
V ($Å^3$)	5876(5)	12,566(11)	3220(1)	6225(3)
Z	4	8	2	4
d_{calc} (g cm^{-3})	1.520	1.455	1.563	1.489
m (cm^{-1})	4.56	6.47	23.38	23.96
Temperature (°C)	-110 ± 1	-85 ± 1	-100 ± 1	-100 ± 1
R^a	0.075	0.1065	0.036	0.042
$R_w{}^b$, $wR2^c$	0.101[b]	0.2598[c]	0.045[b]	0.047[b]
Goodness of Fit[d]	2.28	1.030	1.64	1.39

[a] $R = \Sigma\|F_o| - |F_c\|/\Sigma|F_o|$.
[b] $R_w = [\Sigma w(|F_o| - |F_c|)^2/\Sigma w|F_o|^2]^{1/2}$; $w = 1/s^2(|F_o|)$.
[c] $wR2 = [S[w(F_o^2 - F_c^2)^2]/S[w(F_o^2)^2]]^{1/2}$.
[d] Goodness-of-fit = $[Sw(|F_o| - |F_c|)^2/(N_{obs} - N_{parameter})]^{1/2}$.

C39, C47, and C48 were found to be disordered, and each was refined isotropically as twin methyl groups, A and B, with a combined occupancy of 1.0 and with restraints on C—O and C···C. All other non-hydrogen atoms were refined anisotropically, except for solvent molecules. Treatment of the dichloromethane molecules is described in the following section. The final full-matrix least-squares refinement was based on 9199 reflections that were used to fit 774 parameters with 540 restraints to give $R_1 = 0.1065$ and $wR_2 = 0.2598$. The goodness-of-fit index was 1.030, and the maximum shift in the final difference map was 0.002 $Å^3$ associated with C173. After convergence, the mean shift/ESD was 0.006 and the highest peak in the difference Fourier map was 1.16 e $Å^{-3}$ which is associated with the solvent molecule containing C172.

Dichloromethane molecules were located using electron density difference maps generated using the SHELXTL software package [15]. The disordered CH_2Cl_2 molecules were modeled with restraints on the C—Cl and C···Cl distances. All C—Cl bond distances were constrained to 1.79 Å. Occupancies were also refined, resulting in a total of 3.73 dichloromethane molecules per Pd atom. An additional isolated atom was added as the oxygen of a water molecule and refined isotropically.

$[Pt(NCCH_3)_2(TMPP)_2][BF_4]_2$ (**3**). Single crystals of **3** were grown by slow diffusion of diethyl ether into a solution of **3** in acetone and CH_2Cl_2. A pale yellow crystal of dimensions $0.30\times0.44\times0.30$ mm^3 was secured on the tip of a glass fiber with Dow Corning silicone grease and placed in a cold N_2(g) stream. Least-squares refinement using 21 well-centered reflections in the range $20 \leqslant 2\theta \leqslant 26°$ indicated a triclinic crystal system. The data were collected at -100 ± 1°C using the ω-2θ scan technique to a maximum 2θ value of 47°. Of the 9951 reflections that were collected, 9519 were unique. An empirical absorption correction based on azimuthal scans of three reflections with χ near 90° was applied which resulted in transmission factors ranging from 0.84 to 1.00. The data were corrected for Lorentz and polarization effects. The structure was solved in the space group $P\bar{1}$ with the program PHASE [18] followed by DIRDIF [17] structure solution programs and refined by full-matrix least-squares refinement. All non-hydrogen atoms were refined anisotropically. The final full-matrix least-squares refinement was based on 7081 observed reflections with $F_o^2 > 3\sigma(F_o^2)$ that were used to fit 820 parameters to give $R = 0.036$ and $R_w = 0.045$. The goodness-of-fit index was 1.64, and the highest peak in the final difference map was 1.59 e $Å^{-3}$ which is associated with the $[BF_4]^-$ counterion.

Pt(TMPP-*O*)$_2$·3EtCN (**4**)·3EtCN. A pale yellow crystal of dimensions $0.36\times0.36\times0.27$ mm^3 was secured on the tip of a glass fiber with Dow Corning silicone grease and placed in a cold N_2(g) stream. Least-squares refinement using 21 well-centered reflections in the range $20 \leqslant 2\theta \leqslant 24°$ indicated that the crystal belonged to a monoclinic crystal system.

The data were collected at -100 ± 1°C using the ω-scan technique to a maximum 2θ value of 47°. Of the 9900 reflections that were collected, 9420 were unique and were corrected for Lorentz and polarization effects. The space group was determined to be $P2_1/c$ based on the observed systematic absences. An empirical absorption correction based on azimuthal scans of three reflections with χ near 90° was applied which resulted in transmission factors ranging from 0.95 to 1.00. The structure was solved and developed with the use of the MITHRIL [16] and DIRDIF [17] structure solution programs and refined by full-matrix least-squares refinement. All non-hydrogen atoms were refined anisotropically, with the final cycle being based on 6082 observed reflections with $F_o^2 > 3\sigma(F_o^2)$ that were used to fit 766 parameters to give $R = 0.042$ and $R_w = 0.047$. The goodness-of-fit index was 1.39 and the highest peak in the final difference map was 0.85 e Å^{-3}.

RESULTS AND DISCUSSION

Preparation of Pd^{II} TMPP complexes

The unusual brick-red compound $[Pd(TMPP)_2][BF_4]_2$ (**1**) is readily prepared from $[Pd(NCCH_3)_4][BF_4]_2$ and two equivalents of TMPP in acetone. This compound is thermally unstable in solution, however, and readily converts to the phenoxide derivative Pd(TMPP-*O*)$_2$ (**2**) where TMPP-*O* refers to the mono-demethylated derivative of TMPP. The demethylation reaction is accelerated in the presence of excess TMPP which acts as a nucleophile to react with the electrophilic methoxy groups associated with the metal. This type of decomposition reaction has been previously documented in the analogous Rh, Co and Ni compounds [3b,g,i,l], as well as in the chemistry of TMPP with Rh and Ir olefins [3k]. In an effort to avoid sacrificing TMPP in a rational synthesis of Pd(TMPP-*O*)$_2$, $[Pd(TMPP)_2][BF_4]_2$ was combined with other nucleophiles such as KI, $LiNMe_2$, and NaOMe. Unfortunately, these reactions led to complex mixtures of $[CH_3\text{-TMPP}][BF_4]$, **1** and **2**, as evidenced by ^1H and $^{31}P\{^1H\}$ NMR spectroscopies. Ultimately, compound **2** was obtained in the best yield and in the purest form from the reaction of $[Pd(NCCH_3)_4][BF_4]_2$ with four equivalents of TMPP (75% yield). The reaction of Pd(II) with TMPP are summarized in Scheme 1.

Preparation of Pt^{II} TMPP complexes

The compound $[Pt(TMPP)_2][BF_4]_2$ is obtained from acetone solutions of $[Pt(NCCH_3)_4][BF_4]_2$ that have been treated with two equivalents of TMPP. The product of the same reaction performed in CH_3CN is $[Pt(NCCH_3)_2(TMPP)_2][BF_4]_2$ (**3**) as verified by X-ray crystallography. In $[Pt(NCCH_3)_2(TMPP)_2][BF_4]_2$ only two of the original CH_3CN ligands have been replaced with monodentate TMPP molecules; obviously the ether interactions are prevented due to the presence of the more basic CH_3CN ligands.

$PtCl_2(NCC_6H_5)_2$ was found to react with TMPP in the presence of two equivalents of $NaBPh_4$ to yield Pt(TMPP-*O*)$_2$ (**4**), PtCl(TMPP)(TMPP-*O*) (**5**), NaCl, and $[CH_3\text{-TMPP}][BPh_4]$. These reactions are designed to make use of the chloride ligands for dealkylation of the *ortho*-substituted methoxy-phosphines with the liberation of MeX [1a,b,d,f]. Single crystals of Pt(TMPP-*O*)$_2$ (**4**) were obtained by chilling a CH_3CH_2CN/Et_2O solution of the products to 0°C. The presence of **5** suggests that the second *O*-metalation at the remaining chloride ligand is slow and that more forcing conditions are required to drive the reaction to completion. A similar observation was reported by Shaw and co-workers [1a,b,f]. A much higher yield route to Pt(TMPP-*O*)$_2$ is the slow addition of an acetone solution of four equivalents of TMPP to an acetone solution of $[Pt(NCCH_3)_4][BF_4]_2$. The reactions of Pt(II) with TMPP are summarized in Scheme 2.

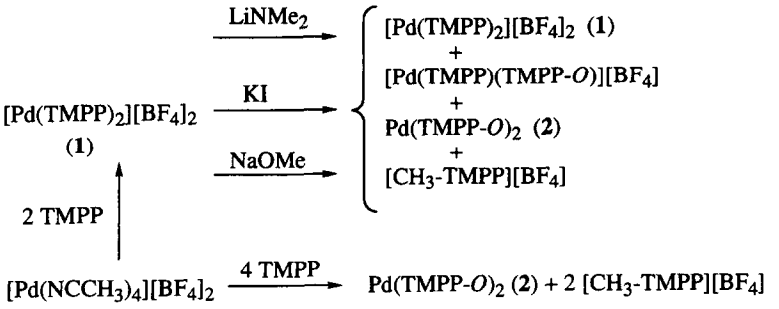

TMPP = P{$C_6H_2(OCH_3)_3$}$_3$ tris(2,4,6-trimethoxy)phenylphosphine

TMPP-*O* = [P{$OC_6H_2(OCH_3)_2$}{$C_6H_2(OCH_3)_3$}$_2$]$^-$

bis(2,4,6-trimethoxy)phenyl 4,6-trimethoxy-2-phenoxide phosphine

Scheme 1. Reactions of Pd(II) with various nucleophiles.

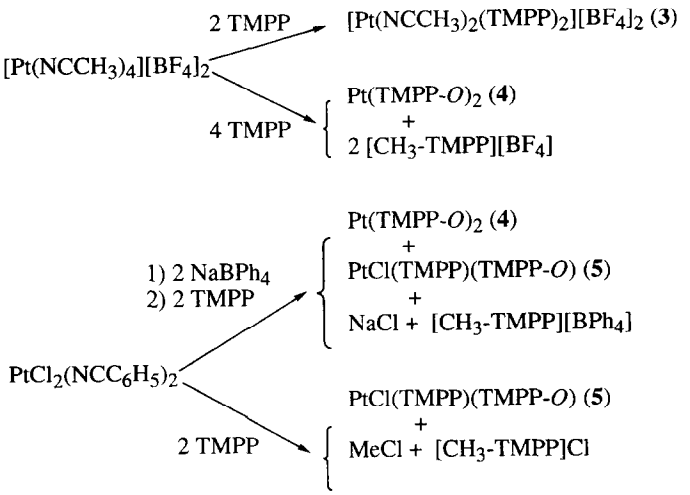

Scheme 2. Reactions of Pt(II) starting materials with TMPP.

Molecular structures of **1** *and* **2**.

ORTEP drawings of the molecular cation of **1** and **2** are displayed in Figs 1 and 2, with selected bond distances and angles provided in Tables 2 and 3. The Pd atom of **1** resides at the center of a pseudo-octahedron defined by P1, P2 and the two ether-oxygen atoms O1 and O10 in an equatorial arrangement; two ether oxygen atoms O4 and O13 occupy axial positions. The deviation of the geometry around the Pd atom from square-planar is evident from the acute angles defined by the five-membered metallacycles Pd1—P1—C1—C2—O1 for which P1—Pd1—O1 = 78.3(2)° and Pd1—P2—C19—C20—O10 for which P2—Pd1—P10 = 78.1(2)°. The average Pd—O_{axial} distance of 2.651 Å is the shortest axial contact reported to data for a Pd(II) compound [19–22]. In comparison, the corresponding distances in $Pd^{II}L_6$

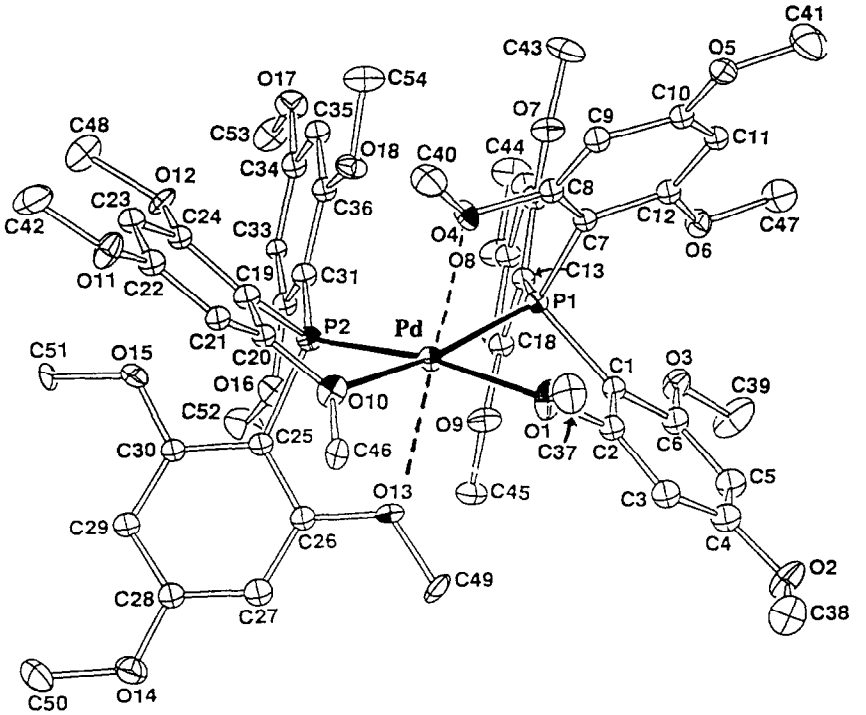

Fig. 1. ORTEP drawing of $[Pd(TMPP)_2][BF_4]_2$ (**1**). Thermal ellipsoids are drawn at the 25% probability level. Hydrogen atoms have been removed for clarity. Selected distances (Å) and angles (°) for **1** can be found in Table 3.

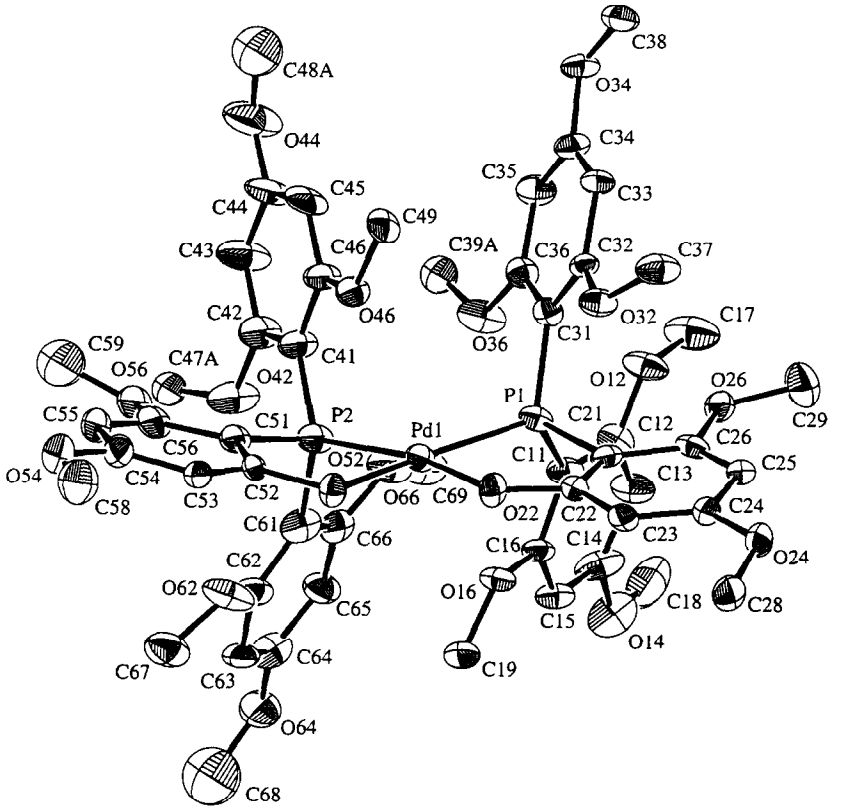

Fig. 2. ORTEP drawing of Pd(TMPP-*O*)$_2$ (**2**). Thermal ellipsoids are drawn at the 25% probability level. Hydrogen atoms have been removed for clarity. Selected distances (Å) and angles (°) for **2** can be found in Table 2.

Table 2. Selected bond distances (Å) and bond angles (°) for [Pd(TMPP)$_2$][BF$_4$]$_2$ (**1**)

Bond distances			
Pd1—P1	2.216(4)	P1—C1	1.85(1)
Pd1—P2	2.215(4)	P1—C7	1.82(1)
Pd1—O1	2.195(7)	P1—C13	1.82(1)
Pd1—O10	2.177(8)	P2—C19	1.83(1)
Pd1—O4	2.671(7)	P2—C25	1.82(1)
Pd1—O13	2.632(7)	P2—C31	1.80(1)
Bond angles			
P1—Pd1—P2	105.92(8)		
P1—Pd1—O1	78.3(2)		
P1—Pd1—O10	168.6(2)		
P2—Pd1—O1	170.1(2)		
P2—Pd1—O10	78.1(2)		
Pd1—P1—C1	96.6(4)		
Pd1—P1—C7	106.1(4)		
Pd1—P1—C13	123.0(4)		
Pd1—P2—C19	96.5(4)		
Pd1—P2—C25	105.7(4)		
Pd1—P2—C31	123.0(4)		

Table 3. Selected bond distances (Å) and bond angles (°) for Pd(TMPP-*O*)$_2$·3.73CH$_2$Cl$_2$O (**2**·3.73CH$_2$Cl$_2$·H$_2$O)

Bond distances			
Pd1—P1	2.270(4)	P1—C11	1.822(13)
Pd1—P2	2.251(4)	P1—C21	1.832(12)
Pd1—O22	2.047(7)	P1—C31	1.824(13)
Pd1—O52	2.047(8)	P2—C41	1.81(2)
O22—C22	1.363(4)	P2—C51	1.78(2)
O52—C52	1.363(4)	P2—C61	1.87(2)
Bond angles			
P2—Pd1—P1	109.4(2)		
O22—Pd1—P1	84.9(2)		
O52—Pd1—P1	165.2(2)		
O22—Pd1—O52	81.2(3)		
C11—P1—Pd1	118.1(5)		
C21—P1—Pd1	97.6(4)		
C11—P1—C31	111.5(6)		
C11—P1—C21	104.2(6)		
C22—O22—Pd1	121.1(7)		
C52—O52—Pd1	117.5(8)		

complexes supported by trigonal (*S,S,S*) or (*S,S,N*) ligands fall in the range 2.95–3.27 Å [21–23]. The geometry about the Pd atom of **2** is square planar, consisting of a *cis* arrangement defined by P1, P2 and the phenoxide oxygen atoms O22 and O52. Ring strain in **2** is evidenced by angles of O22—Pd1—O52 = 81.4(3)°, O52—Pd1—P2 = 84.6(2)°, and P2—Pd1—P1 = 109.4(2)°. Axial ether-oxygen atoms O16 and O46 are at distances of 2.887 and 3.025 Å which are much longer than the analogous interactions in **1**.

Molecular structures of **3** *and* **4**

ORTEP drawings of the compounds $[Pt(NCCH_3)_2(TMPP_2)][BF_4]_2$ (**3**) and Pt(TMPP-*O*)$_2$ (**4**) are presented in Figs 3 and 4, while selected bond distances and angles are provided in Tables 4 and 5, respectively. The coordination number of $[Pt(NCCH_3)_2(TMPP)_2][BF_4]_2$ is four with mutually *trans* monodentate TMPP and CH_3CN ligands. The ⟨P1—Pt1—N1 and ⟨P2—Pt1—N2 angles are 87.0(2)° and 90.3(2)°, respectively, leading to a nearly perfect square planar geometry around the metal center. The *trans* atoms define angles of ⟨P1—Pt1—P2 = 175.67(7)° and ⟨N1—Pt1—N2 = 177.0(3)°. The molecular geometry of Pt(TMPP-*O*)$_2$ consists of a *cis* arrangement of phosphorus and methoxy-oxygen atoms about the metal center and long axial interactions to ether-oxygen atoms. The distortion observed in Pt(TMPP-*O*)$_2$ involves ring strain of the five-membered metallacycles (Pt1—P1—C1—C2—O1 and Pt1—P2—C19—C20—O10) for which the angles are ⟨C2—Pt1—P1 = 84.1(2)° and ⟨O10—Pt1—P2 = 84.2(2)° compared to the η^1-TMPP ligands observed in compound $[Pt(NCCH_3)_2(TMPP)_2][BF_4]_2$ (**3**). Free rotation of arene rings on the η^1-TMPP ligands in **3** is effectively blocked by the CH_3CN ligands, which are in the rotational pathway of pendant methoxy groups of TMPP. This is evident in the space filing diagram of the compound depicted in Fig. 5. The solid-state structure is evidently retained in solution as judged by the results of NMR spectroscopy (*vide infra*).

The average Pt—P bond distances in $[Pt(NCCH_3)_2(TMPP)_2][BF_4]_2$ and Pt(TMPP-*O*)$_2$ of 2.356(2) and 2.255(2) Å respectively are similar to those observed in phosphine and phosphite complexes of Pt(II) (2.2 to 2.4 Å) [23]. The η^1-Pt—P bond distances in $[Pt(NCCH_3)_2(TMPP)_2][BF_4]_2$ are longer than those found in Pt(TMPP-*O*)$_2$ which may be due to the chelate effect of the η^2-TMPP ligands in the latter compound and also to the *trans* effect of the TMPP vs the phenoxide ligand. The average Pt—O bond distance of 2.047(5) Å in Pt(TMPP-*O*)$_2$ is longer than the corresponding bond distance reported in the platinum-alkoxide complex, *cis*-$[Pt(PPh_2CH_2CMe_2O)_2]$

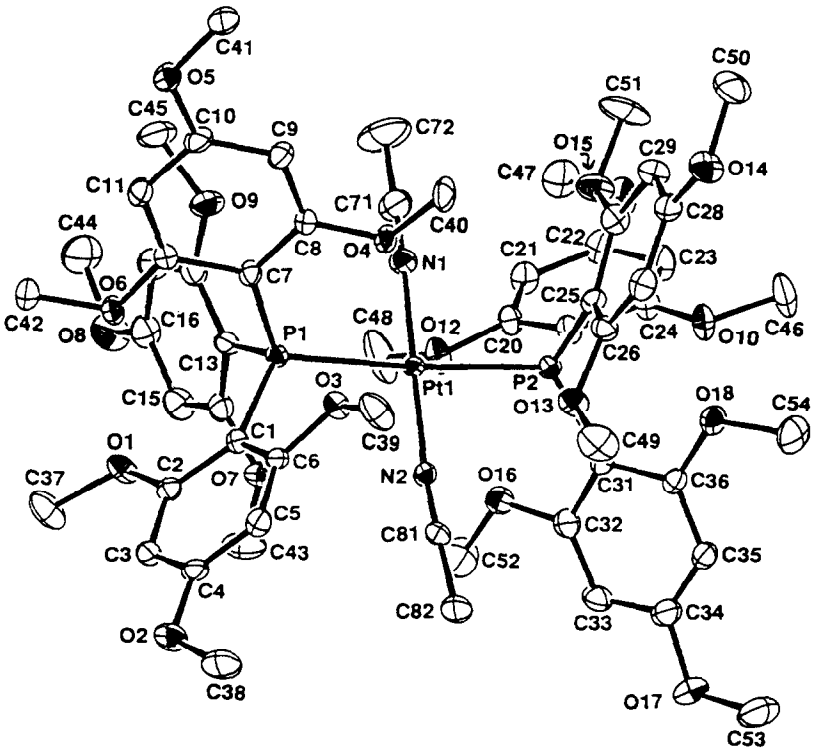

Fig. 3. ORTEP drawing of $[Pt(NCCH_3)_2(TMPP)_2][BF_4]_2$ (**3**). Hydrogen atoms have been removed for clarity. Thermal ellipsoids are drawn at the 25% probability level. Selected distances (Å) and angles (°) for **3** can be found in Table 4.

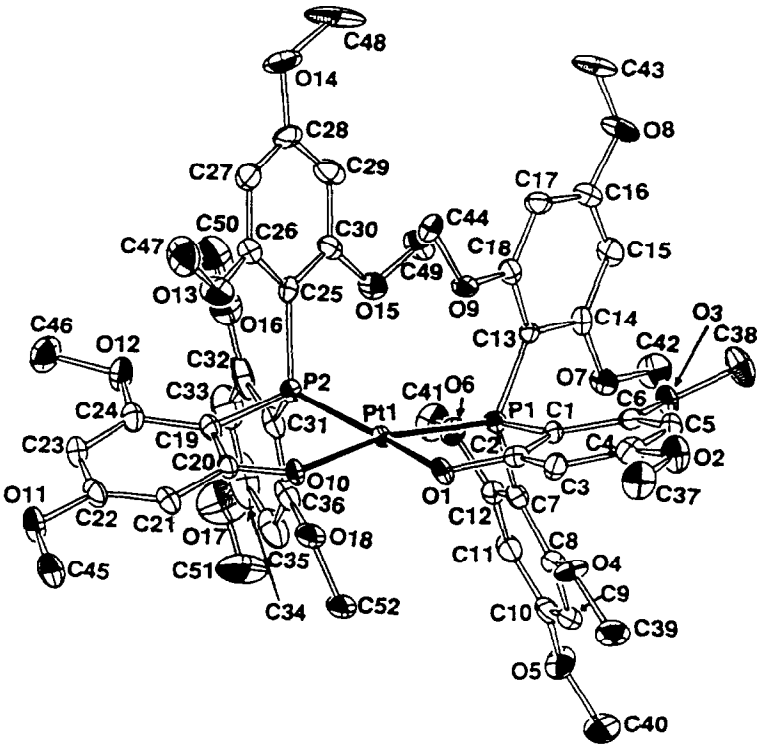

Fig. 4. ORTEP drawing of Pt(TMPP-*O*)$_2$ (**4**). Hydrogen atoms have been removed for clarity. Thermal ellipsoids are drawn at the 25% probability level. Selected distances (Å) and angles (°) for **4** can be found in Table 5.

(2.013(4) Å) [25a] and *cis*-[Pt($Ph_2PCH_2CH_2O$)$_2$]·H_2O (2.039(5) Å) [25b], but shorter than those found in two platinum-ether complexes (2.144(9) Å and 2.192(7) Å) [5f,g]. Axial interactions in the molecule Pt(TMPP-*O*)$_2$ that involve the Pt center and pendant methoxy groups are longer than the sum of the covalent radii of the two atoms (Pt1—O9 = 3.110(5) Å and Pt1—O18 = 3.130(7) Å).

Table 4. Selected bond distances (Å) and bond angles (°) for [Pt($NCCH_3$)$_2$(TMPP)$_2$][BF_4]$_2$ (**3**)

Bond distances			
Pt1—P1	2.357(2)	P1—C1	1.822(7)
Pt1—P2	2.356(2)	P1—C7	1.814(7)
Pt1—N1	1.972(7)	P1—C13	1.806(7)
Pt1—N2	1.961(6)	P2—C19	1.810(7)
N1—C71	1.12(1)	P2—C25	1.808(7)
N2—C81	1.141(9)	P2—C31	1.820(7)
Bond angles			
P1—Pt1—P2	175.67(7)		
P1—Pt1—N1	87.0(2)		
P1—Pt1—N2	93.9(2)		
P2—Pt1—N1	88.9(2)		
P2—Pt1—N2	90.3(2)		
N1—Pt1—N2	176.9(3)		
Pt1—N1—C71	171.9(8)		
Pt1—N2—C81	174.0(6)		
N1—C71—C72	176(1)		
N2—C81—C82	178.7(8)		

^1H *and* $^{31}P\{^1H\}$ NMR *studies*

Compounds (**1**) *and* (**2**). Variable-temperature ^1H NMR studies of [Pd(TMPP)$_2$][BF_4]$_2$ (**1**) in acetone-d_6 from +20 to −80°C indicate that the TMPP ligands are involved in a fluxional process which is not unusual for these types of complexes [9]. The ^1H NMR spectrum at 20°C contains a broad resonance at 6.3 ppm due to the *m*-protons of the phenyl rings, a sharp resonance at 3.8 ppm assigned to the equivalent *para*-methoxy substituents and a broad signal at 3.6 ppm due to the *ortho*-methoxy substituents. The ^1H NMR spectrum at −80°C contains three resonances between δ = 3.5–6.5 ppm, six distinct resonances in the range δ = 5.60–6.80 ppm assigned to inequivalent *meta* protons, six resonances between δ = 3.30–4.25 ppm due to inequivalent *ortho*-methoxy groups, and one broad resonance at δ = 3.83 ppm due to three *para*-methoxy substituents. This spectrum is consistent with free rotation of the unmetalated aryl groups. A room temperature $^{31}P\{^1H\}$ NMR spectrum of **1** in acetone-d_6 exhibits a single resonance at δ = +1.67 ppm. These data are in accord with the presence of only one type of coordinated phosphine

Table 5. Selected bond distances (Å) and bond angles ( ) for Pt(TMPP-*O*)$_2$·3EtCN (**4**·3EtCN)

Bond distances			
Pt1—P1	2.255(2)	P1—C1	1.810(8)
Pt1—P2	2.255(2)	P1—C7	1.821(9)
Pt1—O1	2.044(5)	P1—C13	1.830(8)
Pt1—O10	2.049(5)	P2—C19	1.817(8)
Pt1—O9	3.119(5)	P2—C25	1.836(9)
Pt1—O18	3.130(7)	P2—C31	1.845(9)
Bond Angles			
P1—Pt1—P2	110.85(8)		
P1—Pt1—O1	84.1(2)		
P1—Pt1—O10	164.0(2)		
P2—Pt1—O1	163.2(2)		
P2—Pt1—O10	84.2(2)		
Pt1—P1—C1	98.7(3)		
Pt1—P1—C7	111.9(3)		
Pt1—P1—C13	123.5(3)		
Pt1—P2—C19	99.1(3)		
Pt1—P2—C25	111.0(3)		
Pt1—P2—C31	124.0(3)		

ligand and support a close relationship between the solution and solid-state structures of the cation. A fluxional process such as this indicates that, for a given phosphine ligand, there are six *ortho*-methoxy oxygen atoms competing for a total of two coordination sites. Such exchange within the coordination sphere is a potentially valuable characteristic for the design of catalytically active complexes.

The ^{1}H NMR spectrum of Pd(TMPP-*O*)$_2$ (**2**) reveals only four distinct features in the methoxy region of the TMPP-*O* ligands between 3.0 and 3.8 ppm, which indicates that the unbound rings on the TMPP ligands are involved in free rotation on the NMR time scale. The Ni(II) analog also behaves in this manner [3i,26]. Two of these four resonances are due to the inequivalent *para* (a) and *ortho* (b) methyl groups of the bonded ring while the other two are due to four equivalent *ortho* (c) and two equivalent *para* (d) methyl groups of the free rings, as depicted in Fig. 6. Three distinct resonances appear in the *meta* proton region of TMPP-*O* ligands between 5.3 and 6.2 ppm. Two of these three resonances are assigned to two inequivalent *meta* protons (1 and 2) of the bonded ring and the third one is attributed to four equivalent *meta* protons (3) of the free rings as indicated on the spectrum. A ^{31}P$\{^1$H$\}$ NMR spectrum of Pd(TMPP-*O*)$_2$ (**2**) in chloroform-d$_1$ at room temperature exhibits a single resonance at $\delta = -3.07$ ppm.

Compounds **3**–**5**. The room temperature ^{1}H NMR spectrum of [Pt(NCCH$_3$)$_2$(TMPP)$_2$][BF$_4$]$_2$ (**3**) (Fig. 7) reveals six distinct resonances in the methoxy region between 3.3 and 3.9 ppm and two resonances in the *meta* proton region between 6.1 and 6.2 ppm due to the TMPP ligands. This pattern indicates that the solution structure of **3** possesses two magnetically inequivalent methoxyphenyl rings which is consistent with the solid-state structure as mentioned earlier. An assignment of the resonances in [Pt(NCCH$_3$)$_2$(TMPP)$_2$][BF$_4$]$_2$ is provided in the inset on the NMR spectrum in Fig. 7. Two rings above and below the plane defined by the three atom sequence P—Pt—P are symmetry related by a mirror plane bisecting the third ring and containing the two phosphorus atoms and the metal center. One singlet at 3.33 ppm is assigned to two CH$_3$CN ligands (a), while the res-

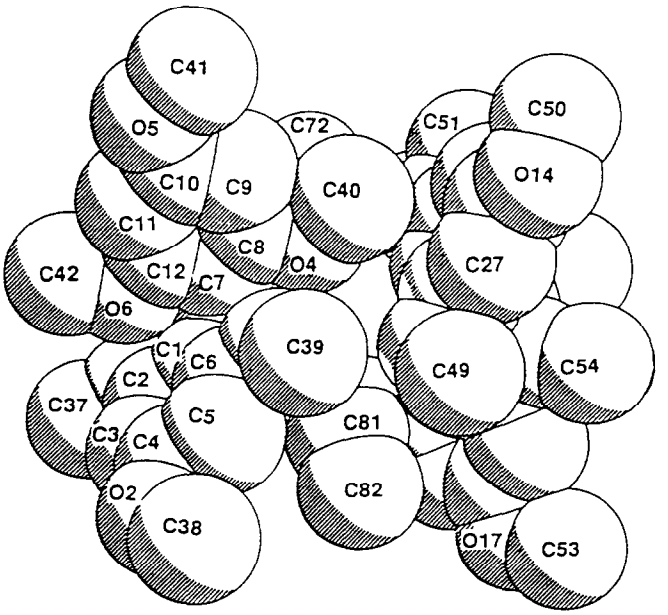

Fig. 5. Space filling diagram of [Pt(NCCH$_3$)$_2$(TMPP)$_2$][BF$_4$]$_2$ (**3**). Hydrogen atoms have been removed for clarity.

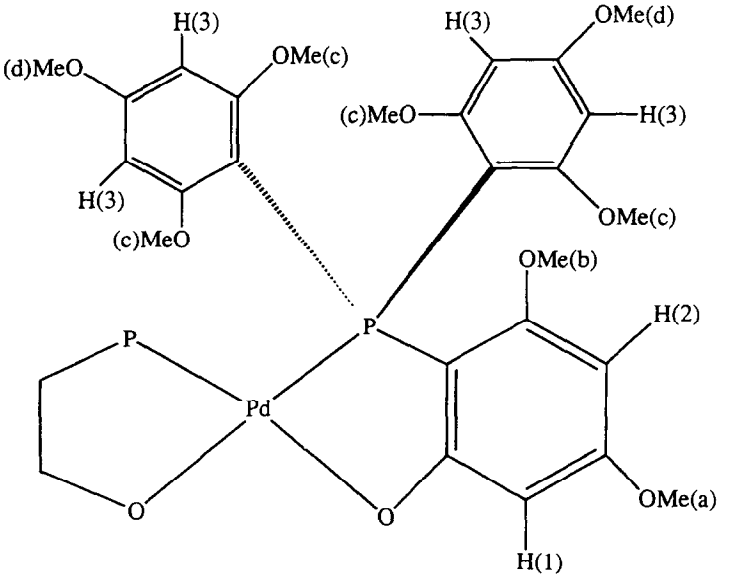

Fig. 6. Illustration of Pd(TMPP-*O*)$_2$ (**2**) with hydrogen atoms labeled. The other half of the molecule is omitted for clarity.

onances at 3.41 and 3.78 ppm are assigned to be the *ortho* (b) and *para* (c) methyl groups on the rings of the TMPP ligands distal from the CH_3CN groups. The two resonances at 3.61 and 3.82 ppm are assigned to the *ortho* (d) and *para* (e) methyl groups on the rings of TMPP ligands proximal to CH_3CN. The triplet and the doublet are attributable to four equivalent *meta* (1) protons on the two distal rings and eight protons (2) on the four proximal phenyl groups rings. The virtual triplet observed in the *meta* proton region of the TMPP ligand is indicative of a *trans* geometry for the two phosphorus atoms, which is supported by the X-ray structure.

The room temperature ^{1}H NMR spectrum of Pt(TMPP-*O*)$_2$ (**4**), shown in Fig. 8, resembles that of Pd(TMPP-*O*)$_2$ and contains four distinct resonances in the methoxy region of the TMPP-phenoxide ligands between 3.3 and 3.9 ppm. This indicates that the unbound rings of the TMPP ligand are free to rotate which has also been observed in the Ni(II) [3i,26] and

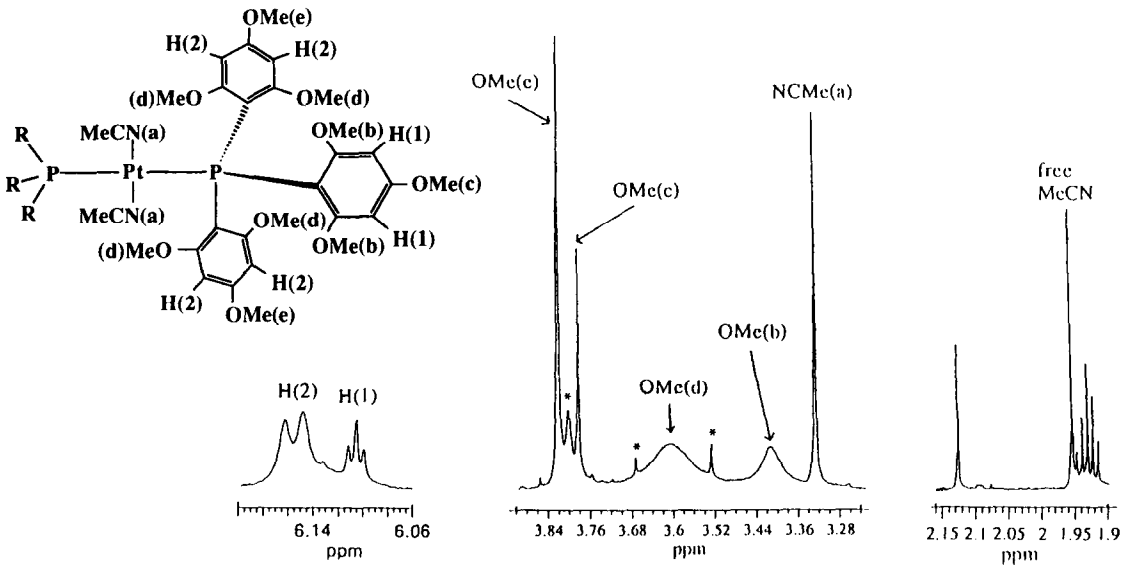

Fig. 7. Room temperature ^{1}H NMR spectrum of [Pt(NCCH$_3$)$_2$(TMPP)$_2$][BF$_4$]$_2$ (**3**). (*) Signals due to demethylation products that are always present in small quantities.

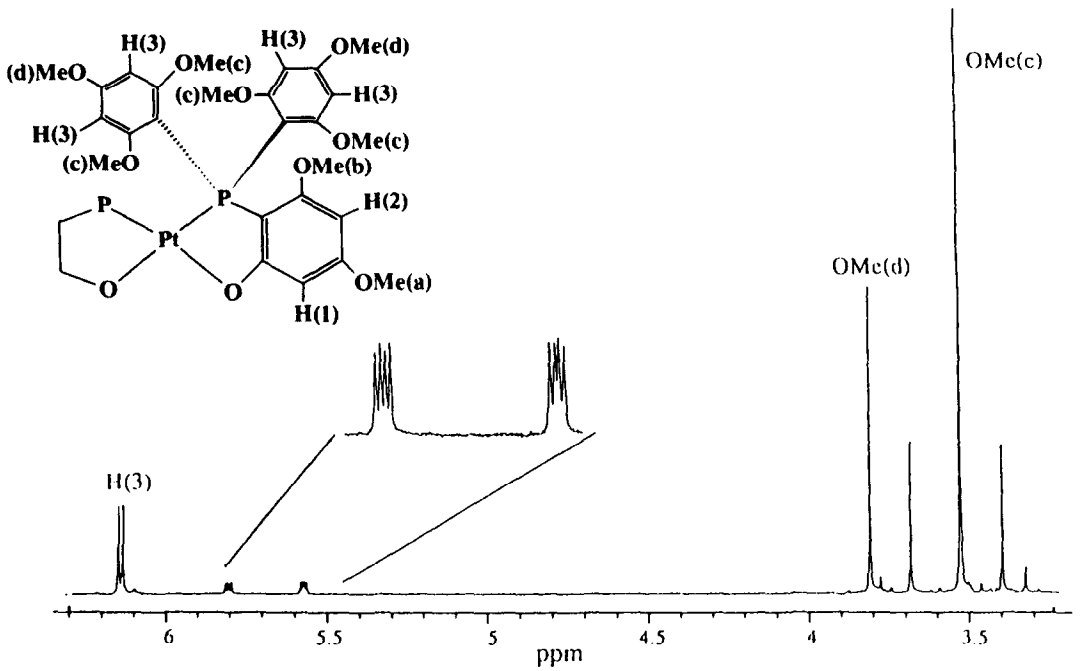

Fig. 8. Room temperature ^{1}H NMR spectrum of Pt(TMPP-*O*)$_2$ (**4**) in acetonitrile-d$_3$.

Pd(II) analogues [3j]. Two of these four resonances are due to the inequivalent *ortho* and *para* methyl groups of the bonded ring and the other two are due to four equivalent *ortho* and two equivalent *para* methyl groups of the free rings. Three distinct resonances occur in the *meta* proton region between 5.5 and 6.2 ppm. Two of these three resonances are due to two inequivalent *meta* protons of the bonded ring and the last one is due to four equivalent *meta* protons of the free rings. A ^{31}P{^{1}H} NMR spectrum of Pt(TMPP-*O*)$_2$ in acetonitrile-d$_3$ at room temperature exhibits a single resonance at $\delta = -24.97$ ppm with a coupling constant $^1J_{Pt\text{-}P}$ of 1950 Hz, which is in the range of values reported in the literature for *cis* phosphine ligands [23]. Despite the increased electron density at the metal center in the neutral compound **4**, the ^{31}P spectrum exhibits a downfield shift as compared to $\delta = -44.5$ ppm for the dicationic complex **3**. Such a shift can be explained by ring contributions from the formation of five-membered rings [24]. These NMR data are in accord with the presence of two types of unsymmetrically coordinated rings of the TMPP ligand.

The room temperature ^{1}H NMR spectrum of PtCl(TMPP)(TMPP-*O*) (**5**) (Fig. 9) reveals five resonances in the methoxy region of the TMPP and TMPP-*O* ligands between 3.2 and 3.9 ppm. These data indicate that the unbound rings of the bidentate TMPP ligand are involved in free rotation. Two of these five resonances are due to the inequivalent *ortho* (a) and *para* (b) methoxy groups of the bonded ring of the TMPP-*O* moiety, while a second set are due to the *para* (c and d) methoxy groups on the free rings of the TMPP and TMPP-*O* ligands. Integration requires the fifth resonance to be an overlap of *ortho* (e) methoxy groups on the free rings of both the TMPP and TMPP-*O* ligands. Four distinct features in the *meta* proton region of TMPP and TMPP-*O* ligands appear between 5.3 and 6.1 ppm. Two multiplets at 5.29 and 5.38 pm are due to the two *meta* (H1 and H2) protons of the bonded ring of the TMPP-*O* moiety, while a doublet at 6.04 ppm is attributed to four *meta* (H3) protons of the free rings. The final doublet at 5.99 ppm is assigned to six equivalent *meta* (H4) protons of the η^1-TMPP ligand. A ^{31}P{^{1}H} NMR spectrum of **5** in acetonitrile-d$_3$ at room temperature exhibits an ABX second-order pattern with satellites, indicating the presence of two inequivalent phosphorus atoms coupled to ^{195}Pt ($I = 1/2$, 33% abundance) [1a–c,23]. Successful simulation of this spectrum was obtained by first simulating the ABX splitting pattern which gave the satellite positions, followed by simulation of the AB P_A—P_B coupling. These two simulations were then combined with appropriate weighting of the satellite intensities. The best fit was achieved with chemical shift values of P_A, $\delta = -20.48$ ppm, P_B, $\delta = -26.39$ ppm and coupling constants of ^1J(Pt—P_A) = 3212 Hz, ^1J(Pt—P_B) = 2993 Hz and ^2J(P_A—P_B) = 561 Hz (Fig. 9). These NMR data are in accord with the molecular geometry depicted in Fig. 10 wherein one neutral TMPP ligand is coordinated in an η^1 fashion and a demethylated TMPP group is bound as an η^2-P,O ligand with *trans* P atoms (deduced from the large magnitude of ^2J(P_A—P_B)), a phenoxide O and a Cl$^-$ ion in a square plane.

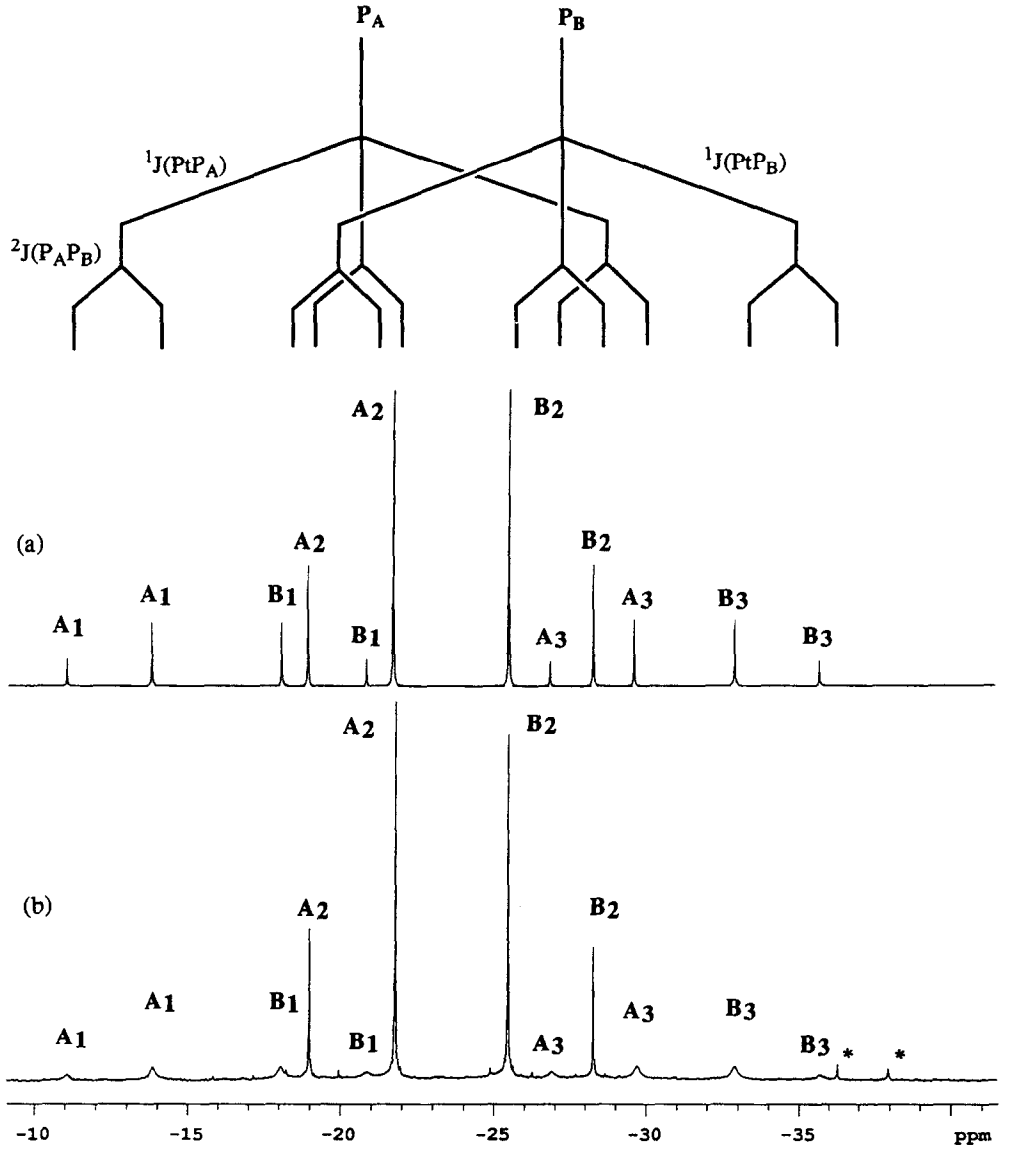

Fig. 9. The splitting diagram for (a), calculated and (b) experimental $^{31}P\{^1H\}$ NMR spectrum of PtCl(TMPP)(TMPP-*O*) (**5**) in acetonitrile-d_3 at room temperature. (*) Signals due to demethylation products that are always present in small quantities.

CONCLUSIONS

Reactions of divalent palladium and platinum complexes with 2,4,6-tris(trimethoxyphenyl)phosphine lead to the formation of new phosphinoether and phosphinophenoxide compounds including a six-coordinate Pd(II) complex possessing the shortest axial contacts reported in the literature to date. Unlike most other P,O chelates reported in the literature, the TMPP ligand appears to be sufficiently flexible to adopt a myriad of bonding modes. This point is well-demonstrated by the observed hapticity changes of TMPP from monodentate in $[Pt(NCCH_3)_2(TMPP)_2][BF_4]_2$ (**3**) to bidentate in Pd(TMPP-*O*)$_2$ (**2**) and Pt(TMPP-*O*)$_2$ (**4**) to tridentate in $[Pd(TMPP)_2][BF_4]_2$ (**1**). The results of this study, taken together with the data obtained in earlier investigations, support the conclusion that homoleptic TMPP complexes of the platinum group metals are fairly unstable due to electrophilic reactions of the coordinated methoxy groups that lead to phenoxide formation. It appears that the TMPP phosphine molecule itself is the most useful demethylation reagent for the high-yield preparation of the demethylated compounds M(TMPP-*O*)$_2$ (M = Pd, Pt), with other nucleophiles being much less specific in their reactions with $[M(TMPP)_2]^{2+}$ species. The fluxional nature of $[Pd(TMPP)_2][BF_4]_2$ allows for the *in situ* formation of open coordination sites which

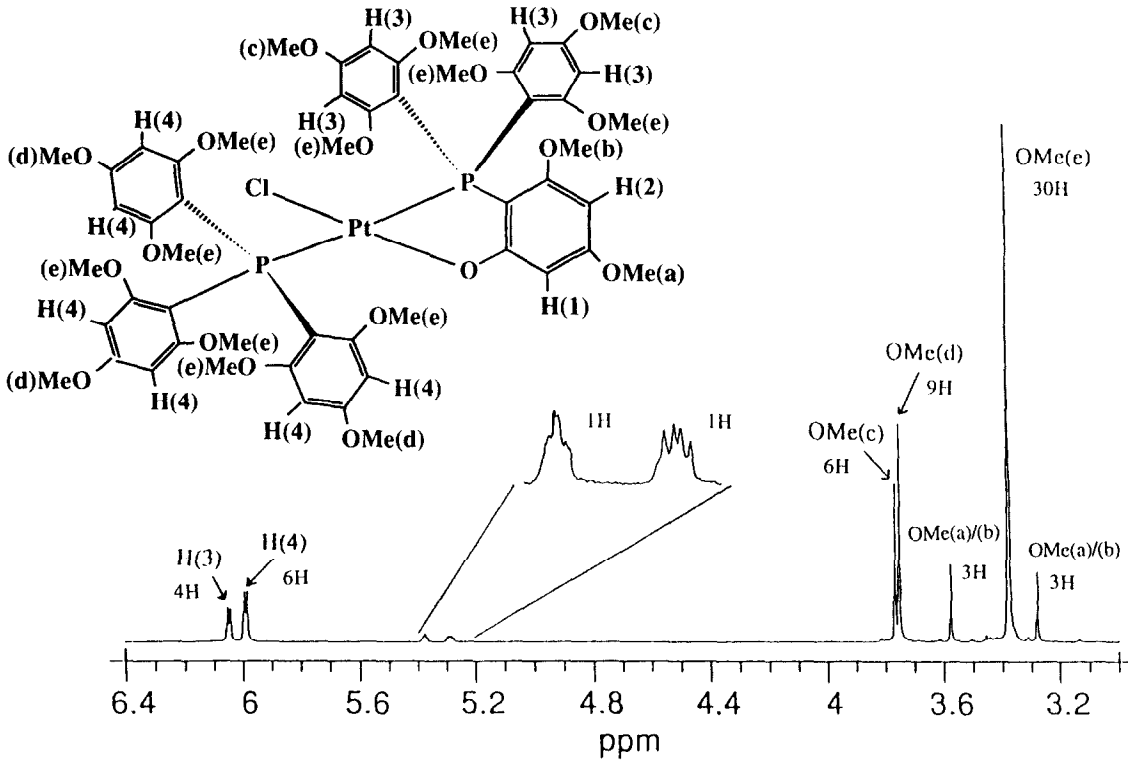

Fig. 10. Room temperature ^{1}H NMR spectrum of PtCl(TMPP)(TMPP-*O*) (**5**) in acetonitrile-d_3.

opens up the potential for small molecule activation or catalytic activity, possibilities that are currently being explored.

Acknowledgements—We gratefully acknowledge the National Science Foundation (Grant CHE-8914915 to K.R.D.) and the Camille and Henry Dreyfus Foundation for financial support. We also thank Michigan State University for providing The Herbert T. Graham fellowship for C.E.U. The X-ray equipment was purchased by grants from the National Science Foundation (Grants CHE-8403823 and CHE-8908088). The NMR equipment was supported by a grant from the National Institutes of Health (Grant No. 1-510-RR04750-01).

Supporting information available—

Tables of crystal data, atomic coordinates, bond lengths and angles, anisotropic displacement parameters, and positional and thermal parameters for **1, 2, 3,** and **4** (51, 70, 75 and 67 pages, respectively). Ordering information is given on any current masthead page.

REFERENCES

1. (a) Jones, C. E., Shaw, B. L. and Turtle, B. L., *J. Chem. Soc., Dalton Trans.*, 1974, 992; (b) Empsall, H. D., Shaw, B. L. and Turtle, B. L., *J. Chem. Soc., Dalton Trans.*, 1976, 1500; (c) Empsall, H. D., Heys, P. N. and Shaw, B. L., *J. Chem. Soc., Dalton Trans.*, 1978, 257; (d) Jeffrey, J. C. and Rauchfuss, T. B., *Inorg. Chem.*, 1979, **18,** 2658; (e) Moulton, C. J. and Shaw, B. L., *J. Chem. Soc., Dalton Trans.*, 1980, 299; (f) Miller, E. M. and Shaw, B. L., *J. Chem. Soc., Dalton Trans.*, 1974, 480.
2. See for example: Lindner, E. and Dettinger, J. Z., *Naturforsch.*, 1991, **46b,** 432 and references therein.
3. (a) Dunbar, K. R., Haefner, S. C. and Pence, L. E., *J. Am. Chem. Soc.*, 1989, **111,** 5504; (b) Dunbar, K. R., Haefner, S. C. and Bender, C., *J. Am. Chem. Soc.*, 1991, **113,** 9540; (c) Dunbar, K. R., Haefner, S. C. and Swepston, P. N., *J. Chem. Soc., Chem. Commun.*, 1991, 460; (d) Chen, S.-J. and Dunbar, K. R., *Inorg. Chem.*, 1991, **30,** 2918; (e) Dunbar, K. R. and Haefner, S. C., *Organometallics*, 1992, **11,** 1431; (f) Dulebohn, J. I., Haefner, S. C., Bergland, K. R. and Dunbar, K. R., *Chem. of Mat.*, 1992, **4,** 506; (g) Dunbar, K. R. and Quillevéré, A., *Organometallics*, 1993, **12,** 618; (h) Dunbar, K. R., Matonic, J. H. and Saharan, V., *Inorg. Chem.*, 1994, **33,** 25; (i) Dubar, K. R., Quillevéré, A. and Sun, J.-S., *Inorg. Chem.*, 1994, **33,** 3598; (j) Dunbar, K. R. and Sun, J.-S., *J. Chem. Soc., Chem. Comm.*, 1994, 2387; (k) Dunbar, K. R., Haefner, S. C., Uzelmeier, C. E. and Howard, A., *Inorg. Chim. Acta*, 1995, **240,** 527; (l) Quillevéré, A., Sun, J.-S., Uzelmeier, C. E. and Dunbar, K. R., manuscript in preparation; (m) Dunbar, K. R. and Haefner, S. C., *Polyhedron*, 1994, **13,** 727; (n) Haefner, S. C.,

Uzelmeier, C. E. and Dunbar, K. R., manuscript in preparation.
4. Werner, H., Stakr, A., Schultz, M. and Wolf, J., *Organometallics*, 1992, **11,** 1126.
5. (a) Anderson, G. K. and Kumar, R., *Inorg. Chem.*, 1984, **23,** 4064; (b) Braunstein, P., Matt, D. and Dusausay, Y., *Inorg. Chem.*, 1983, **22,** 2043; (c) Podlahová, J., Kratochvil, B. and Langer, V., *Inorg. Chem.*, 1981, **20,** 2160; (d) Empsall, H. D., Johnson, S. and Shaw, B. L., *J. Chem. Soc., Dalton Trans.*, 1980, 302; (e) O'Flynn, K. H. P. and McDonald, W. S., *Acta Cryst.*, 1977, **B33,** 194; (f) Anderson, G. K., Corey, E. R. and Kumar, R., *Inorg. Chem.*, 1987, **26,** 97; (g) Alcock, N. W., Platt, A. W. G. and Pringle, P. G., *J. Chem. Soc., Dalton Trans.*, 1989, 2069; (h) Reddy, V. V. S., Whitten, J. E., Redmill, K. A., Varshney, A. and Gray, G. M., *J. Organomet. Chem.*, 1989, **372,** 207; (i) Braunstein, P., Matt, D., Dusausoy, Y., Fischer, J., Mitschler, A. and Ricard, L., *J. Am. Chem. Soc.*, 1981, **103,** 5115; (j) Lindner, E., Schrieber, R., Kemmler, M., Schneller, T. and Mayer, H. A., *Chem. Matter.*, 1995, **7,** 1951; (k) Lindner, E., Schrieber, R., Schneller, T., Wegner, P. and Mayer, H. A., *Inorg. Chem.*, 1996, **35,** 514.
6. Bader, A. and Lindner, E., *Coord. Chem. Rev.*, 1991, **108,** 27.
7. (a) Peuckert, M. and Keim, W., *Organometalics*, 1983, **2,** 594; (b) Huang, Q., Xu, M., Qian, Y., Xu, W., Shao, M. and Tang, Y., *J. Organomet. Chem.*, 1985, **287,** 419; (c) Keim, W., Behr, A., Hoffmann, B., Kowaldt, F. H., Kürschner, U., Limbäcker, B. and Sistig, F., *Organometalics*, 1986, **5,** 2356; (d) Klabunde, U. and Ittel, S. D., *J. Molec. Catal.*, 1987, **41,** 123.
8. (a) Schrock, R. R. and Osborn, J. A., *J. Am. Chem. Soc.*, 1976, **98,** 2134; (b) Davies, J. A., Hartley, F. R. and Murray, S. G., *Inorg. Chem.*, 1980, **19,** 2299; (c) Sen, A. and Lai, T. W., *Organometalics*, 1982, **1,** 415.
9. Boeré, R. T., Montgomery, C. D., Payne, N. C. and Willis, C. J., *Inorg. Chem.*, 1985, **24,** 3680.
10. (a) Blake, A. J., Gould, R. O., Lavery, A. J. and Schröder, M., *Angew. Chem. Int. Ed. Engl.*, 1986, **25,** 274; (b) Wieghardt, K., Küppers, H.-J., Raabe, E. and Krüger, C., *Angew. Chem. Int. Ed. Engl.*, 1986, **25,** 1101; (c) Blake, A. J., Holder, A. J., Hyde, T. I., Roberts, Y. V., Lavery, A. J. and Schröder, M., *J. Organomet. Chem.*, 1987, **323,** 261; (d) Grant, G. T., Sanders, K. A., Setzer, W. N. and VanDerveer, D. G., *Inorg. Chem.*, 1991, **30,** 4053; (e) de Groot, B., Hanan, G. S. and Loeb, S. J., *Inorg. Chem.*, 1991, **30,** 4644.
11. Blake, A. J., Crofts, R. D., de Groot, B. and Schröder, M., *J. Chem. Soc., Dalton Trans.*, 1993, 485.
12. (a) Protopopov, I. S. and Kraft, M. Ya., *Zh. Obshch. Khim.*, 1963, **33,** 3050; (b) Protopopov, I. S. and Kraft, M. Ya., *Med. Prom. USSR*, 1959, **13,** 5.
13. (a) Thomas, R. R. and Sen, A., *Inorg. Synth.*, 1989, **26,** 128; (b) de Renzi, A., Panunzi, A. and Vitagliano, A., *J. Chem. Soc., Chem. Commun.*, 1976, 47; (c) Hendrickson, D. N., Sohn, Y. S. and Gray, H. B., *Inorg. Chem.*, 1971, **10,** 1559.
14. TEXSAN-TEXRAY Structure Analysis Package, Molecular Structure Corporation, 1985, 1996.
15. SHELXTL v. 5.04, G. M. Sheldrick and Siemens Analytical X-ray Systems, Inc., 1997, 6300 Enterprise Lane, Madison WI. 53719.
16. MITHRIL: Integrated Direct Methods Computer Program, Gilmore, C. J., *J. Appl. Cryst.*, 1984, **17,** 42.
17. DIRDIF: Direct Methods for Difference Structure, An Automatic Procedure for Phase Extension; Refinement of Difference Structure Factors: Beurskens, R. T. Technical Report, 1984.
18. PHASE: Calbrese, J. C., *PHASE—Patterson Heavy Atom Solution Extractor*. University of Wisconsin, Madison, PhD. Thesis, 1972.
19 (a) Wieghardt, K., Walz, W., Nuber, B., Weiss, J., Ozarowski, A., Stratemeier, H. and Reinen, D., *Inorg. Chem.*, 1986, **25,** 1650; (b) Zompa, L. J. and Margulis, T. N., *Inorg. Chem. Acta*, 1978, **28,** L157.
20. (a) Bosnich, B., Mason, R., Pauling, P. J., Robertson, G. B. and Tobe, M. L., *J. Chem. Soc., Chem. Commun.*, 1968, 97; (b) Ito, T., Sugimoto, M., Toriumi, K. and Ito, H., *Chem. Lett.*, 1981, 1477; (c) van der Merwe, M. J., Boeyens, J. C. A. and Hancock,. R. D., *Inorg. Chem.*, 1983, **22,** 3489; (d) Wada, A., Sakabe, N. and Tanaka, J., *Acta Crystallogr.*, 1976, **B32,** 1121; (e) Szalda, D. J., Macartney, D. H. and Sutin, N., *Inorg. Chem.*, 1984, **23,** 3473; (f) Krüger, H.-J. and Holm, R., H., *J. Am. Chem. Soc.*, 1990, **112,** 2955.
21. (a) Holm, R. H. and Krüger, H.-J., *Inorg. Chem.*, 1987, **26,** 3647; (b) Castro, B. and Freire, C., *Inorg. Chem.*, 1990, **29,** 5113; (c) Choudhury, S. B., Ray, D. and Chakravorky, A., *Inorg. Chem.*, 1990, **29,** 4603; (d) Krüger, H.-J., Peng, G. and Holm, R. H., *Inorg. Chem.*, 1991, **30,** 734; (e) Franolic, J. D., Wang, W. Y. and Millar, M., *J. Am. Chem. Soc.*, 1992, **114,** 6587 and references therein; (f) Blake, A. J., Gould, R. O., Halcrow, M. A., Holder, A. J., Hyde, T. I. and Schröder *J. Chem. Soc., Chem. Commun.*, 1992, 3427; (g) Cha, M., Gatlin, C. L., Critchlow, S. C. and Kovacs, J. A., *Inorg. Chem.*, 1993, **32,** 5868.
22. (a) Armstrong, J. McD., Meyer, D. V., Verpoorte, J. A. and Edsall, J. T., *J. Biol. Chem.*, 1966, **241,** 5137; (b) Chlebowski, F. and Coleman, J. E., *Metal Ions in Biological Chemistry*, ed. H. Sigel, 1976, **6,** 1.
23. (a) *Comprehensive Coordination Chemistry*, Vol. 5, ed. G. Wilkinson, R. D. Gillard, and J. A. McCleverty. Pergamon Press, Oxford, U.K., 1987, chap. 52 and references therein.
24. (a) Garrou, P. E., *Chem. Rev.*, 1981, **81,** 229; (b) Lindner, E., Haustein, M., Mayer, H. A., Schneller, T., Fawzi, R. and Steinmann, E., *Inorg. Chim. Acta*, 1995, **231,** 201.
25. (a) Alcock, N. W., Platt, A. W. and Pringle, P., *J. Chem. Soc., Dalton Trans.*, 1987, 2273; (b) Alcock, N. W., Platt, A. W. G. and Pringle, P. G., *J. Chem. Soc., Dalton Trans.*, 1989, 139.

Pergamon

PII: S0277-5387(97)00432-4

Polyhedron Vol. 17, Nos. 11–12, pp. 2065–2072, 1998
© 1998 Elsevier Science Ltd
All rights reserved. Printed in Great Britain
0277-5387/98 $19.00+0.00

Palladium(II) and platinum(II), (IV) complexes of acetamidrazones

M. Teresa Cocco,[b] Valentina Onnis,[b] Gustavo Ponticelli*[a] and Antonio Spanu[a]

[a] Dipartimento di Chimica e Tecnologie Inorganiche e Metallorganiche, Via Ospedale 72, 09124 Cagliari, Italy

[b] Dipartimento Farmaco Chimico Tecnologico, Via Ospedale 72, 09124 Cagliari, Italy

(Received 28 July 1997; accepted 21 October 1997)

Abstract—Palladium(II) and platinum(II),(IV) complexes with N^1-acylacetamidrazones (**L1–L5**) and N^1-acyl-2-phenylacetamidrazones (**L6–L9**) are described. The complexes have been prepared by reaction of the corresponding metal chloride with the ligand in the required stoichiometrical ratio and were characterized by chemical analyses and physical measurements. The stereochemistry has been assigned on the basis of IR, far IR spectroscopy, electronic reflectance spectra and molar conductivity values. © 1998 Elsevier Science Ltd. All rights reserved

Keywords: palladium(II) chloride; platinum(II),(IV) chloride; N^1-acylacetamidrazone ligands; complexes; synthesis.

The amidrazones RC(=NH)NHNHR′ (R, R′ = H, alkyl, aryl) have been studied very little as ligands of transition metals [1]. Some published results are available on the structure and catalytic activity of nickel(II) and copper(II) complexes with amidrazones [2], and the structure of cobalt(II) complexes with N^1-aryl-substituted arylamidrazones [3]. Furthermore in the literature were found only the X-ray structure for two novel oxopersulphidoamidrazone tungstate complexes $WO(S_2)_2$[RC(=NH)NHNH] where R = CH_3, C_2H_5 [4]; in the molecular structures the tungsten atom is coordinated by a terminal oxoligand, to two persulphido S_2^{2-} ligands and one bidentate amidrazone ligand. The coordination polyhedron of the tungsten atom is pentagonal bipyramidal, whose two axial ligands are formed by terminal oxoatom and the *N*(H) coordinating atom of the NHNH in amidrazone [4].

The antibacterial activity of first transition metals complexes with picolinamidrazones derivatives [5] and the antibacterial and antitumoral activities of platinum(II) complexes with N^1-phenylsubstituted amidrazones [6] have been also reported.

While, as far as the acetamidrazone complexes are concerned, at the best of our knowledge no references are available. The amidrazones were previously utilized by us in the synthesis of potential biologically active heterocyclic compounds. For example N^1-acetylacetamidrazone **L1**, N^1-ethoxycarbonylacetamidrazone **L2** and N^1-ethoxycarbonyl-2-phenylacetamidrazone **L6** were used as starting materials for the synthesis of imidazole derivatives that have shown a moderate antimicrobial activity [7,8].

EXPERIMENTAL

Solvents and reagents were purified according to standard laboratory techniques.

Microanalysis were carried out with a Fisons EA 1108 elemental analyser.

The IR spectra were recorded in the 4000–180 cm^{-1} range with a Perkin–Elmer mod. 983; the near IR spectra were recorded in KBr pellets, while the far IR spectra were recorded in Nujol mulls (CsI). The electronic reflectance spectra were recorded with a Varian Cary 5 in the 50,000–15,000 cm^{-1} range.

The conductivity measurements were carried out with a WTW, LBR model, conductance bridge at 25°C for 10^{-3} M solution in DMF.

The ^{1}H NMR spectra of ligands and complexes were taken in DMSO-d_6 solution with a Varian Unity

* Author to whom correspondence should be addressed.

300 spectrometer. The chemical shifts are given in ppm relative to TMS as internal standard. The ^{1}H NMR spectra of the complexes, taken in DMSO-d_6 solution showed no signals due to the complexes, probably because the DMSO substituted the ligand in the complexes. It was not possible to register the ^{1}H NMR spectra of the complexes in $CDCl_3$ since they are insoluble in this solvent.

The mass spectra of the complexes were taken via the solid inlet from solid samples in glass capillary sealed on the other end with excitations energies 16–70 eV with a Fisons QMD 1000 spectrometer in EI mode. Unfortunately the molecular peak of all the complexes was not obtained even though the conditions for the mass spectral measurements were varied. Typical by the mass spectra of all complexes were mainly those of the corresponding N^1-acylacetamidrazone ligand.

The N^1-acetyl-,N^1-ethoxycarbonyl- and N^1-benzoylacetamidrazones (**L1, L2, L6**) were prepared according to established procedures [9].

Synthesis of N^1-benzoylacetamidrazones (**L3–L5, L7–L9**)

A mixture of ethyl acetimidate derivative (0.01 mol) and the appropriate acylhydrazine (0.01 mol) in 50 ml of anhydrous ethanol was heated at 70–75 °C for 1–2 min and then kept at room temperature for one night. The precipitate was collected by filtration, throughly washed with ethyl ether and recrystallized from the solvent indicated below.

N^1-benzoylacetamidrazone (**L3**) was obtained from ethylacetimidate and benzoyl hydrazine in 87% yield; M.p. 163–165°C (ethanol); Found: C, 61.0; H, 6.3; N, 23.6%. Calc. for $C_9H_{11}N_3O$: C, 61.0; H, 6.2; N, 23.6%.

^{1}H NMR (DMSO-d_6): δ 1.91 (s, 3H, CH_3), 6.22 (br s, 2H, NH_2), 7.37, 7.88 (m, 5H, Ar), 9.66 (br s, 1H, NH).

N^1-(4-methylbenzoyl)acetamidrazone (**L4**) was obtained from ethylacetimidate and 4-methylbenzoyl hydrazine in 78% yield; M.p. 185 °C (ethanol); Found: C, 62.7; H, 6.9; N, 21.5%. Calc. for $C_{10}H_{13}N_3O$: C, 62.8; H, 6.8; N, 21.5%.

^{1}H NMR (DMSO-d_6): δ 1.92 (s, 3H, CH_3), 2.30 (s, 3H, CH_3), 6.27 (br s, 2H, NH_2), 7.15, 7.77 (m, 4H, Ar), 9.65 (br s, 1H, NH).

N^1-(4-chlorobenzoyl)acetamidrazone (**L5**) was obtained from ethylacetimidate and 4-chlorobenzoyl hydrazine in 86% yield; M.p. 180 °C (ethanol); Found: C, 51.0; H, 4.7; N, 20.0%. Calc. for $C_9H_{10}ClN_3O$: C, 51.1; H, 4.8; N, 20.0%.

^{1}H NMR (DMSO-d_6): δ 1. (s, 3H, CH_3), 6.31 (br s, 2H, NH_2), 7.36, 7.96 (m, 4H, Ar), 9.84 (br s, 1H, NH).

N^1-benzoyl-2-phenylacetamidrazone (**L7**) was obtained from ethyl phenylacetimidate and benzoyl hydrazine in 82% yield; M.p. 175–6 °C (ethanol); Found: C, 71.2; H, 6.0; N, 16.9%. Calc. for $C_{15}H_{15}N_3O$: C, 71.1; H, 6.0; N, 16.6%.

^{1}H NMR (DMSO-d_6): δ 3.49 (s, 2H, CH_2), 6.33 (br s, 2H, NH_2), 7.30, 7.86 (m, 10H, Ar), 9.74 (br s, 1H, NH).

N^1-(4-methylbenzoyl)-2-phenylacetamidrazone (**L8**) was obtained from ethyl phenylacetimidate and 4-methylbenzoyl hydrazine in 70% yield; M.p. 170–72 °C (acetonitrile); Found: C, 71.7; H, 6.4; N, 15.7%. Calc. for $C_{16}H_{17}N_3O$: C, 71.9; H, 6.4; N 15.7%.

^{1}H NMR (DMSO-d_6): δ 2.30 (s, 3H, CH_3), 3.47 (s, 2H, CH_2), 6.38 (br s, 2H, NH_2), 7.30, 7.75 (m, 9H, Ar), 9.68 (br s, 1H, NH).

N^1-(4-chlorobenzoyl)-2-phenylacetamidrazone (**L9**) was obtained from ethyl phenylacetimidate and 4-chlorobenzoyl hydrazine in 70% yield; M.p. 180 °C (ethanol); Found: C, 62.8; H, 5.0; N, 14.7%. Calc. for $C_{15}H_{14}ClN_3O$: C, 62.6; H, 4.9; N, 14.6%.

^{1}H NMR (DMSO-d_6): δ 3.66 (s, 3H, CH_2), 6.40 (br s, 2H, NH_2), 7.30, 7.93 (m, 9H, Ar), 9.93 (br s, 1H, NH).

Synthesis of the palladium(II) complexes

A mixture of the $PdCl_2$ (0.18 g, 1 mmol) and the ligand in the appropriate stoichiometrical ratio was heated for 48 h at reflux in the solvent indicated below. The **A1, A6** complexes were prepared in ethanol using ligand and salt in 3 : 1 ratio. The palladium complexes with amidrazones **L3–L5** and **L7–L9** were prepared in acetone, using ligand and salt in 2 : 1 ratio.

$Pd(L1)_2Cl_2$ (**A1**). To an ethanolic solution (10 ml) of $PdCl_2$ (0.18 g, 1 mmol) N^1-acetylacetamidrazone (**L1**) (0.24 g, ~2 mmol) was added and the resulting mixture was heated at reflux with stirring for 6 h. The formed precipitate was collected by filtration, washed with hot ethanol (5 ml) and dried *in vacuo* over P_4O_{10}. Yield: 0.20 g, 50%.

Synthesis of the platinum(II) complexes

A mixture of the $PtCl_2$ (0.27 g, 1 mmol) and the ligand (3 mmol) was heated for 6 h at reflux in the acetone. The complex **B1** was prepared in ethanol utilizing ligand and salt in 2 : 1 ratio.

$[Pt(L3)_2 \cdot L3 \cdot 2H_2O$ (**B3**). To a Me_2CO solution (20 ml) of $PtCl_2$ (0.27 g, 1 mmol) N^1-benzoylacetamidrazone (**L1**) (0.24 g, ~2 mmol) was added and the resulting mixture was refluxed for 6 h. The formed precipitate was filtered off, washed with hot Me_2CO (10 ml) and dried *in vacuo* over P_4O_{10}. Yield: 0.3 g, 65%.

Synthesis of the platinum(IV) complexes

$Pt(L2)_2Cl_4$ (**B2**). To a Me_2CO solution (20 ml) of $PtCl_4$ (0.34 g, 1 mmol) N^1-ethoxycarbonyl-

acetamidrazone (**L2**) (0.3 g, ~2 mmol) was added and the resulting mixture was refluxed for two days. The formed precipitate was filtered off, washed with hot Me_2CO (10 ml) and dried *in vacuo* over P_4O_{10}. Yield: 0.19 g, 30%.

RESULTS AND DISCUSSION

In this work we describe the preparation of N^1-acylacetamidrazones (**L1–L5**) and N^1-acyl-2-phenylacetamidrazones (**L6–L9**) and their complexes with Pd(II), Pt(II) and Pt(IV) (Scheme and Figure 1).

The synthesis of acetamidrazones was carried out in mild conditions. Short heating of a mixture of acetimidates and acylhydrazines in ethanol gave high yield of **L1–L9** at almost pure state. The ^1H NMR data, recorded in DMSO-d_6 solution, provide evidence for only an amide hydrazone tautomeric species. The complexes were prepared by heating at reflux the salts and an excess of acetamidrazones. A variety of experimental conditions were tested changing the solvent and the ligand/salt ratio. Depending on reaction conditions and on starting compounds, ionic or neutral complexes were obtained.

For **L1, L2** and **L6** we isolated complexes of formula $M(L)_2Cl_2$ where M = Pd(II), Pt(II) and $Pt(L)_nCl_4$; $n = 2, 4$. For **L3–L5, L7–L9** we have obtained complexes of the type $Pt(L)_2 \cdot L \cdot mH_2O$; while for **L3–L5** and **L7** we have isolated $Pd(L)_2 \cdot mH_2O$ complexes and for **L8** and **L9,** also $Pd(L)_2Cl_2 \cdot mH_2O$ type complexes, where $m = 0–2$, were isolated.

For the formation of complexes $Pt(L)_3 \cdot mH_2O$ and $Pd(L)_2 \cdot mH_2O$ without halogens, we can hypothesize that in these reactions HCl is free and that metal ions are coordinated with two anionic ligands.

To establish the coordination behaviour of the ligands and the stereochemistry of the complexes, all the isolated complexes have been studied by infrared, electronic reflectance spectra and by conductivity molar measurements in DMF.

Analytical and physical data of the complexes are reported in Table 1. These compounds are microcrystalline and/or powderlike, coloured from yellow to deep brown, generally soluble in DMF or DMSO and insoluble in other organic solvents. All the attempts made for recrystallize our palladium(II) and platinum(II), (IV) complexes for a X-ray structural investigation were unsuccessful.

The conductivity molar values are typical of non-conductors, except for complexes **B2** and **B6,** that are characteristic respectively of uni-univalent and uni-bivalent electrolites.

The ν(NH) and ν(CO) of the near infrared spectra for the complexes and ligands are reported in Table 2. Generally in the near infrared spectra of the complexes the ν(NH) are shifted to lower energy in the 36–200 cm^{-1} range when compared with the parent ligands. This shift is characteristic for a coordination of a NH_2 or NH group to the metallic ion [10–12]. In some cases **A1,** and **B6** the ν(NH) is either not shifted or moved to higher wavenumbers shifted with respect to the free ligand [13]. Generally the complexes with **L1** show the ν(CO) shifted to lower wavenumbers with respect to that of the free ligand, this fact has confirmed that the oxygen of the CO is involved in the coordination of the metal (Table 2).

In the far infrared spectra of **L1** complexes ν(M—N) [14] and ν(M—O) are present at 380–372 cm^{-1} and 450–429 cm^{-1}respectively, so that the complexes can be described as $[M(L1)_2]Cl_2$, (M = Pd, Pt) (Table 3). The low conductivity values typical for non electrolytes, can be explained by postulating that the complexes are rearranged in solution.

These infrared assignement for $M(L1)_2Cl_2$ complexes could be confirmed by an X-ray investigation [15] on a cobalt(II) complex $Co(L1)_2Cl_2 \cdot H_2O$, which has shown that this complex is ionic and that the

L 1 -L9

L	R	R'	L	R	R'
L1	CH_3	CH_3	L6	$C_6H_5CH_2$	OC_2H_5
L2	CH_3	OC_2H_5	L7	$C_6H_5CH_2$	C_6H_5
L3	CH_3	C_6H_5	L8	$C_6H_5CH_2$	4-$CH_3C_6H_4$
L4	CH_3	4-$CH_3C_6H_4$	L9	$C_6H_5CH_2$	4-ClC_6H_4
L5	CH_3	4-ClC_6H_4			

Scheme 1.

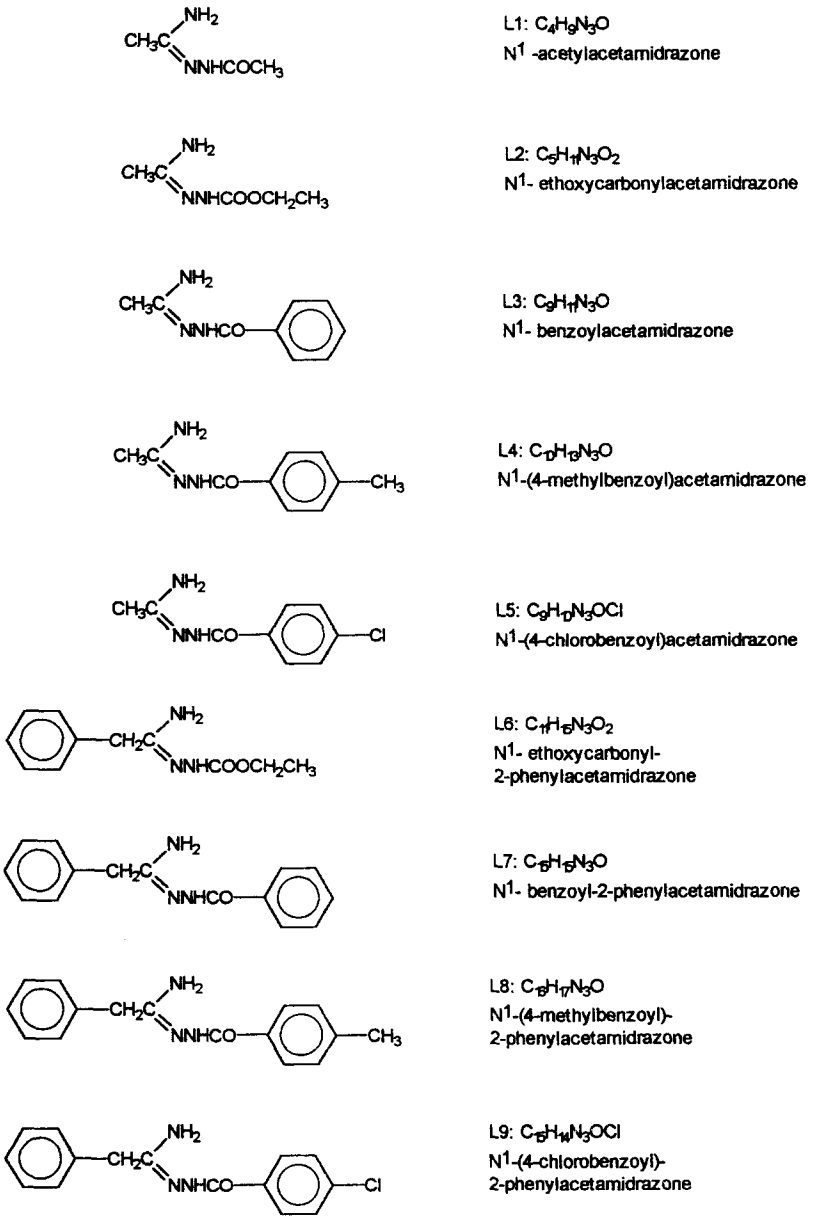

Fig. 1. **L1–L9** ligands.

complex is octahedral with two **L1** chelate coordinated molecules via N^3 and O of CO, two water molecules coordinated to the cobalt ion and two chloride ions out of the coordination sphere.

The reflectance electronic spectra of $[M(L)_2]Cl_2$ complexes where M = Pd(II) and Pt(II) (Table 4) are indicative of a square planar geometry [16,17]. The bands in the 26,180–23,000 cm^{-1} range could be assigned to the ν_1 transition $^1A_{1g} \rightarrow {}^1B_{1g}$. In the UV spectra there are strong absorptions in the 44,400–30,490 cm^{-1} range that may be due to the charge transfer band $L \rightarrow M$. By assuming a value of $F_2 = 10F_4 = 600$ cm^{-1} for the Slater Condon interelectronic repulsion parameters [18] it is possible to derive from the first spin-allowed transition d-d the value $\Delta = \nu_1 + 3.5F_2$. These values lie in the 28,280–25,630 cm^{-1} range.

The complexes of **L2** and **L6** do not show the negative shift of the ν(CO) and there is a negative shift of ν(NH) when compared with the free ligand.

For **A6, B2** and **B6** complexes, the presence of a not shifted or a shifted ν(NH) band to higher wavenumbers respect to the free ligand has been attributed to the presence of the free ligand, so that these compounds can be respectively described as $[Pd(L6)_2Cl_2] \cdot L6$, $[Pt(L2)Cl_4] \cdot L2$ and $[Pt(L6)_2Cl_4] \cdot$

Table 1. Analytical and physical data

Mark	Complex	M.p. (°C)	Colour	Found (calc.) %			Λ_M (DMF)
A1	$Pd(L1)_2Cl_2$	[a]	tan	23.0(23.6)	3.9(4.4)	19.9(20.6)	—
A3	$Pd(L3)_2 \cdot H_2O$	254	tan	45.0(45.3)	4.7(4.2)	17.3(17.6)	—
A4	$Pd(L4)_2 \cdot 2H_2O$	229	tan	45.6(45.9)	5.1(5.4)	15.8(16.1)	—
A5	$Pd(L5)_2 \cdot 2H_2O$	216	light yellow	38.1(38.3)	4.4(3.9)	15.5(14.9)	6
A6	$Pd(L6)_2Cl_2$	302	light yellow	30.7(31.2)	3.4(3.4)	17.6(18.2)	6
A7	$Pd(L7)_2 \cdot 2H_2O$	227	tan	55.8(55.7)	5.0(4.4)	11.9(12.3)	—
A8	$Pd(L8)_2Cl_2$	216	tan	54.8(54.1)	4.7(4.5)	11.9(11.8)	7
A9	$Pd(L9)_2Cl_2 \cdot H_2O$	273	light tan	46.4(46.6)	4.1(3.7)	11.6(10.9)	—
B1	$Pt(L1)_2Cl_2$	[a]	medium grey	19.6(19.4)	3.2(3.7)	39.9(39.9)	—
B2	$Pt(L2)_2Cl_4$	185	ivory	19.4(19.1)	3.9(3.8)	13.3(13.4)	90
B3	$Pt(L3)_3 \cdot 2H_2O$	210	lilac	42.5(42.6)	5.0(4.6)	16.5(16.6)	5
B4	$Pt(L4)_3$	219	yellow	47.7(47.0)	6.0(4.9)	16.9(16.4)	10
B5	$Pt(L5)_3 \cdot H_2O$	237	yellow	41.0(40.9)	4.5(3.6)	15.9(15.9)	3
B6	$Pt(L6)_4Cl_4$	185	pearl grey	19.7(19.3)	3.5(3.6)	16.9(16.9)	149
B7	$Pt(L7)_3$	207	ivory	56.8(56.7)	4.3(4.5)	13.8(13.2)	6
B8	$Pt(L8)_3 \cdot H_2O$	212	light yellow	56.6(56.9)	5.4(5.1)	12.4(12.4)	8
B9	$Pt(L9)_3$	214	ivory	51.9(51.2)	4.4(3.8)	12.2(11.9)	4

[a] Compounds that decompose without melting.
— Insoluble or little soluble.

Table 2. Absorption bands in the near IR spectra (4000–500 cm^{-1} range)

Mark	Compound	ν(N—H)	$\Delta\nu$	ν(C=O)
L1	$C_4H_9N_3O$	3393 msbr, 3197 sbr		1658 s, 1686 s
A1	$Pd(L1)_2Cl_2$	3341 s, 3357 sbr	36	1642 s, 1632 s
B1	$Pt(L1)_2Cl_2$	3335 vsbr	48	1642 vs, 1632 vs
L2	$C_5H_{11}N_3O_2$	3378 ms, 3268 sh, 3218 ms, 3188 sh		1685 s
B2	$Pt(L2)_2Cl_4$	3442 mw, 3250 vs, 3115 vsbr	143	1718 vs, 1700 vs
L3	$C_9H_{11}N_3O$	3480 ms, 3460 ms, 3400 s, 3200 vs		1633 vs
A3	$Pd(L3)_2 \cdot H_2O$	3420 ms, 3180 s	60	1650 s
B3	$Pt(L3)_3 \cdot 2H_2O$	3498 m, 3356 ms, 3180 s	124	1647 vs
L4	$C_{10}H_{13}N_3O$	3456 s, 3198 sbr		1643 s
A4	$Pd(L4)_2 \cdot 2H_2O$	3418 ms, 3180 s	38	1646 vs
B4	$Pt(L4)_3$	3398 sh, 3270 sh	58	1645 vs
L5	$C_9H_{10}ClN_3O$	3414 vs, 3399 m, 3300 m		1628 s
A5	$Pd(L5)_2 \cdot H_2O$	3420 msbr, 3185 vsbr	115	1620 s
B5	$Pt(L5)_3 \cdot H_2O$	3337 s	77	1661 vs
L6	$C_{11}H_{15}N_3O_2$	3419 m, 3346 vw, 3240 ms, 3198 ms		1712 m, 1701 m
A6	$Pd(L6)_3Cl_2$	3240 s, 3215 vsbr, 3120 s	204	1756 mw, 1737 mw
B6	$Pt(L6)_4Cl_4$	3421 w, 3277 vs, 3185 s, 3124 sh	142	1725 vs, 1704 s
L7	$C_{15}H_{15}N_3O$	3432 ms, 3297 mbr, 3152 sbr		1621 s
A7	$Pd(L7)_2 \cdot 2H_2O$	3402 ms, 3330 ms	30	1650 s
B7	$Pt(L7)_3$	3430 s, 3202 sh	200	1650 vs
L8	$C_{16}H_{17}N_3O$	3460 s, 3195 s		1631 s
A8	$Pd(L8)_2Cl_2$	3480 m, 3405 m, 3322 m	55	1650 s
B8	$Pt(L8)_3 \cdot H_2O$	3330 vs	130	1650 vs
L9	$C_{15}H_{14}ClN_3O$	3420 ms, 3307 ms, 3150 s		1614 s
A9	$Pd(L9)_2Cl_2 \cdot H_2O$	3402 m, 3250 ms, 3140 s	170	1650 s
B9	$Pt(L9)_3$	3378 ms, 3270 s, 3170 vsbr	42	1658 vs

Table 3. Absorption bands in the far IR spectra (500–180 cm^{-1} range)

Mark	Compound	ν(M—O)	ν(M—N)	ν(M—X)	Other bands
L1	$C_4H_9N_3O$				472w, 394 vwbr, 345 m, 322 sh, 313 sh, 300 w, 273 w, 248 mw, 218 m
A1	$Pd(L1)_2Cl_2$	450 mw	380 m		439 mw
B1	$Pt(L1)_2Cl_2$	429 wbr	372 m		323 w
L2	$C_5H_{11}N_3O_2$				410 m, 320 m, 301 w, 273 wbr, 242 mw, 220 m
B2	$Pt(L2)_2Cl_4$		381 m	340 sh, 330 vsbr, 318 sh	396 mbr
L3	$C_9H_{11}N_3O$				445 m, 433 m, 409 w, 395 w, 365 vw, 344 ms, 320 w, 311 w, 300 mw, 275 mw, 242 ms, 220 m
A3	$Pd(L3)_2 \cdot H_2O$		340 mw		
B3	$Pt(L3)_2 \cdot 2H_2O$		337 mw		456 w, 420 vw, 355 wbr
L4	$C_{10}H_{13}N_3O$				470 m, 460 sh, 422 mw, 381 sh, 366 m, 339 ms, 321 m, 312 sh, 299 mw, 272 mw, 243 m, 221 ms
A4	$Pd(L4)_2 \cdot 2H_2O$		347 mw		
B4	$Pt(L4)_2$		312 w		
L5	$C_9H_{10}ClN_3O$				465 m, 380 vs, 372 sh, 351 sh, 321 w, 310 s, 229 sh, 272 m, 242 m, 219 m
A5	$Pd(L5)_2 \cdot 2H_2O$		348 m, 340 m		363 sh
B5	$Pt(L5)_4 \cdot H_2O$		335 m		351 mw, 262 mw, 440 w, 394w
L6	$C_{11}H_{15}N_3O_2$				474 ms, 405 vwbr, 353 w, 320 w, 310 w, 300 w, 273 mw, 242 mw, 220 m, 202 m
A6	$Pd(L6)_3Cl_2$		383 s		
B6	$Pt(L6)_4Cl_4$		365 vw	333 s	344 ms
L7	$C_{15}H_{15}N_3O$				495 m, 460 m, 412 wbr, 392 w, 381 vw, 349 ms, 333 vw, 323 ms, 313 sh, 300 mw, 272 m, 266 sh, 242 ms, 220 ms
A7	$Pd(L7)_2 \cdot H_2O$		344 m		
B7	$Pt(L7)_3$		320 m		280 mw
L8	$C_{16}H_{17}N_3O$				470 s, 456 sh, 424 m, 407 vw, 381 sh, 366 ms, 339 s, 322 ms, 300 w, 277 w, 243 m, 218 s, 206 w
A8	$Pd(L8)_2Cl_2$		345 sh		336 ms
B8	$Pt(L8)_2 \cdot H_2O$		322 m		491 w, 390 vw br, 257 m
L9	$C_{15}H_{14}ClN_3O$				479 m, 457 m, 416 vw, 391 w, 367 m, 348 m, 332 w, 318 sh, 312 ms, 300 m, 296 sh, 273 m, 243 ms, 219 ms
A9	$Pd(L9)_2Cl_2 \cdot H_2O$		[a]	353 vs	
B9	$Pt(L9)_3$		320 m		443 w

[a] ν(Pd—N) is covered by ν(Pd—Cl).

Table 4. Reflectance spectra (50,000–15,000 cm^{-1} range)

Mark	Compound	Bands[a]
A1	$[Pd(L1)_2Cl_2]$	30,675, 23,800(25,900)
B1	$[Pt(L1)_2Cl_2]$	26,180(28,280)
B2	$[Pt(L2)Cl_4]\cdot L2$	32,895, 32,050, 29,850
A3	$[Pd(L3)_2]\cdot H_2O$	44,440, 36,360, 29,410, 24,690(26,790)
B3	$[Pt(L3)_2]\cdot L3\cdot 2H_2O$	41,670, 35,710, 27,030
A4	$[Pd(L4)_2]\cdot 2H_2O$	33,900, 32,260, 28,570, 25,000(27,100)
B4	$[Pt(L4)_2]\cdot L4$	35,710, 28,170
A5	$[Pd(L5)_2]\cdot 2H_2O$	42,550, 34,480, 32,260, 25,000(27,100)
B5	$[Pt(L5)_2]\cdot L5\cdot H_2O$	40,820, 28,570
A6	$[Pd(L6)_2Cl_2]\cdot L6$	30,490, 23,310(25,410)
B6	$[Pt(L6)_2Cl_2]Cl_2\cdot 2L6$	30,860, 29,500
A7	$[Pd(L7)_2]\cdot 2H_2O$	41,670, 26,670, 23,810(25,910)
B7	$[Pt(L7)_2]\cdot L7$	44,440, 36,360, 32,790, 26,320(28,420)
A8	$[Pd(L8)_2]Cl_2$	44,440, 31,250, 23,810(25,910)
B8	$[Pt(L8)_2]\cdot L8\cdot H_2O$	41,670, 36,360, 30,300, 25,640(27,740)
A9	$[Pd(L9)_2]Cl_2\cdot H_2O$	44,440, 40,000, 32,260, 23,530(25,630)
B9	$[Pt(L9)_2]\cdot L9$	42,550, 37,730, 30,300, 25,000

[a] The values of Δ are shown in brackets.

2L6. For the absence of the ν(M—Cl) bands in the expected range, we can conclude that the complexes can be described as $[M(L)_2]Cl_2\cdot mL$.

Some platinum(IV) complexes as **B2** and **B6** show IR absorption bands at 340, 330, 318 and at 333 cm^{-1} respectively, assigned to ν(Pt—Cl) [19,20]. All the complexes with **L2** and **L6** show a band in the 381–359 cm^{-1} range assigned to ν(M—N) [14] (Table 3).

From the infrared spectra and conductivity molar values equal to 149 cm^2 Ω^{-1} mol^{-1}, characteristic for an unibivalent electrolyte, we can describe **B6** as $[Pt(L6)_2Cl_2]Cl_2\cdot 2L6$, while **B2** has a $\Lambda_M = 90$ cm^2 Ω^{-1} mol^{-1} which can be explained by postulating that in DMF is present a partial dissociation of the complex $Pt(L2)_2Cl_4$ described as $[Pt(L2)Cl_4]\cdot L2$.

The shape of the reflectance electronic spectra of the Pt(IV) complexes [21,22] (Table 4) and the far infrared spectra confirm that these compounds are hexacoordinate.

In conclusion the bidentate chelate N^1-acylacetamidrazone derivatives **L** have shown some different patterns of coordination: **L1** coordinates with nitrogen of the N^2 and oxygen of carbonylic group, **L2** and **L6** with the nitrogens of N^3 and N^1. **L3–L5** and **L7–L9** coordinate only two molecules of the anionic species with the nitrogens of N^3 and N^1. Furthermore all the studied compounds are generally non-electrolytes because the complexes are rearranged in solution: we can suggest a square planar stereochemistry for $M(L)_2Cl_2$ (M = Pd(II), Pt(II)) and a distorted octahedral structure for $Pt(L)_nCl_4$ (n = 2, 4) where L = **L1**, **L2** and **L6**. For $M(L)_n\cdot mH_2O$ complexes, where L = **L3–L8**, M = Pd(II), n = 2; M = Pt(II), n = 3, m = 0–2, we can suggest a square planar geometry. For the **L9** $Pd(L9)_2Cl_2\cdot H_2O$ and $Pt(L9)_3$ complexes also square planar structure can be suggested.

REFERENCES

1. Jerchel, D. and Kuhn, R., *Annales*, 1950, **56,** 185.
2. Gerbeleu, N. V., Palanciuc, S. S., Simonov, Yu. A., Dvorkin, A. A., Bourosh, P. N., Reetz, M. T., Arion, V. B. and Tollner, K., *Polyhedron*, 1995, **14,** 521.
3. Bezuglaya, Z. V., Zaitsen, B. E., Ivlieva, K. M., Avramenko, B. I. and Stepanov, B. I., *Koord. Khim.*, 1987, **13,** 191.
4. Du, S., Zhu, N. and Wu, X., *Polyhedron*, 1994, **13,** 301.
5. Samus, N. M., Toleva, A. D., Tsapkov, V. I., Burdenko, T. A. and Videlingam, A. H., *Khim. Farm. Zh.*, 1992, **26,** 75.
6. Pelova, R., Spassowska, N., Manieva, L. and Taxirov, S., *Pharmazie*, 1987, **42,** 251.
7. Cocco, M. T., Congiu, C., Plumitallo, A., Schivo, M. L. and Palmieri, G., *Farmaco*, 1987, **42,** 347.
8. Cocco, M. T., Olla, C., Onnis, V., Schivo, M. L. and De Logu, A., *Farmaco*, 1992, **47,** 229.
9. Glover, E. E., Rowbottom, K. T. and Bishop, D. C., *J. C. S. Perkin I*, 1972, **23,** 2927.
10. Ponticelli, G., *Inorganica Chimica Acta*, 1971, **5,** 461.
11. Schlessinger, G. G., *Bull. New Jersey Acad. Sci.*, 1967, **12,** 42.
12. Curtis, N. F., Raimond, R. W. and Curtis, Y. M., *J. Chem. Soc.* (A), 1968, 182.
13. Sing, P. P. and Rivest, R., *Can. J. Chem.*, 1968, **46,** 2361.

14. Sacconi, L. and Sabatini, A., *J. Inorg. Chem.*, 1963, **25,** 1389 and references therein.
15. Cocco, M. T., Ianelli, S., Ponticelli, G., *Cryst. Struct. Comm.*, submitted.
16. Efimenko, I. A., Kurbakova, A. P. and Matovic, Z. D., *Transition Metal Chem.*, 1994, **19,** 539.
17. Pinna, R., Ponticelli, G. and Preti, C., *J. Inorg. Nucl. Chem.*, 1975, **37,** 1681.
18. Latham, A. R., Hascall, V. and Gray, G., *Inorg. Chem.*, 1965, **4,** 788.
19. Massacesi, M., Pinna, R. and Puggioni, G., *J. Inorg. Biochem.*, 1987, **28,** 95.
20. Floris, G., Padiglia, A., Ponticelli, G. and Puggioni, G., *Transition Metal Chem.*, 1992, **17,** 145.
21. Ponticelli, G., Matovic, Z. D., Miletic, V. D., Efimenko, I. A., Kurbakova, A. P. and Radanovic, D. J., *Bull. Chem. Techn. Mac.*, 1996, **15,** 9.
22. Azarita, T. N. and Bora, T., *Polyhedron*, 1984, **3,** 121.

Pergamon

PII: S0277-5387(97)00422-1

Polyhedron Vol. 17, Nos. 11–12, pp. 2073–2077, 1998
© 1998 Elsevier Science Ltd
All rights reserved. Printed in Great Britain
0277-5387/98 $19.00+0.00

Dinuclear iridium alkoxy complexes of C_{60} fullerene

Merja Soimasuo, Tuula T. Pakkanen, Markku Ahlgrén and Tapani A. Pakkanen*

Department of Chemistry, University of Joensuu, P.O. Box 111, FIN-80101 Joensuu, Finland

(Received 31 October 1996; accepted 17 October 1997)

Abstract—Reactions of C_{60} with iridium cyclo-octadiene dimers containing bridging alkoxide groups, $Ir_2(OR)_2(1,5\text{-}COD)_2$ (R = Me, Et, *n*-Pr, Ph), in a 1 : 1 mole ratio at ambient temperature produced brown solid materials. On the basis of chemical and single crystal X-ray analysis and IR spectra, formulations $Ir_2(OR)_2(1,5\text{-}COD)_2(C_{60})$ are proposed for these compounds. © 1998 Elsevier Science Ltd. All rights reserved

Keywords: fullerene; iridium; alkoxy bridged; cyclo-octadiene; X-ray structure; infrared.

Fullerenes were discovered experimentally in 1985 [1], but they were studied only theoretically until a method of preparation for quantitative amounts of fullerenes was invented in 1990 [2]. Since then fullerenes have been investigated intensively.

Because of their spherical form, fullerenes are unique ligands for organometallic compounds. Several organometallic derivatives of fullerenes have already been synthesized. The first structurally characterized organometallic fullerene derivative was synthesized by Fagan *et al.* [3] in 1991. In this monoadduct $(\eta^2\text{-}C_{60})Pt(PPh_3)_2$ the metal is bound to the fullerene surface in η^2-fashion at the 6-6 ring fusion. In every structurally characterized organometallic fullerene compound the metal is bound to the fullerene surface similarly. In addition to several monoadducts [4], some di- [5] and hexa [6]-adducts have been synthesized.

We have previously synthesized the first ruthenium carbonyl fullerene derivative, $Ru(CO)_4C_{60}$ [7]. This compound was soluble in common organic solvents; and when characterized spectroscopically (IR and ^{13}C NMR spectroscopy), it was found to be similar to the other fullerene compounds.

We have also been able to synthesize and crystallize the compound $C_{60}\{Ir_2Cl_2(1,5\text{-}COD)_2\}_2$ [8], in which the two iridiums bind to two adjacent 6 :6 ring fusions, being the first example of this kind of bonding in fullerenes. It is remarkable because it shows that the neighboring π-bonds of a six-membered ring of C_{60} can also be activated in the formation of a metal complex [8].

Recently the synthesis and crystallographic characterization of two dinuclear derivatives $Cp^*_2Ru_2(\mu\text{-}H)(\mu\text{-}Cl)(C_{60})$ and $Cp^*_2Ru_2(\mu\text{-}Cl)_2(C_{60})$ was reported [9]. These compounds have also two metal centers coordinated to two adjacent 6-6 junctions of C_{60}.

In the present study we have extended the synthesis and characterization of dimeric transition metal derivatives of C_{60} to alkoxy bridged iridium compounds. As starting materials, we have used coordinately unsaturated alkoxy-bridged iridium compounds $Ir_2(OR)_2(1,5\text{-}COD)_2$, where R = CH_3 [10], C_2H_5, *n*-C_3H_7 or C_6H_5 [11]. The influence of the length of the carbon chain (R) attached to the oxygen bridge in $Ir_2(OR)_2(1,5\text{-}COD)_2$ on the reactivity with fullerenes has been also investigated.

EXPERIMENTAL

Materials

All reactions were carried out under either nitrogen or argon, and the solvents used were purged with nitrogen gas and dried over molecular sieves. Commercial fullerenes (purchased from Texas Fullerenes Corporation) were used without further purification. Alkoxy-bridged iridium dimers $Ir_2(OR)_2(1,5\text{-}COD)_2$, where 1,5-COD = 1,5-cyclo-octadiene and R = CH_3 =

* Author to whom correspondence should be addressed.

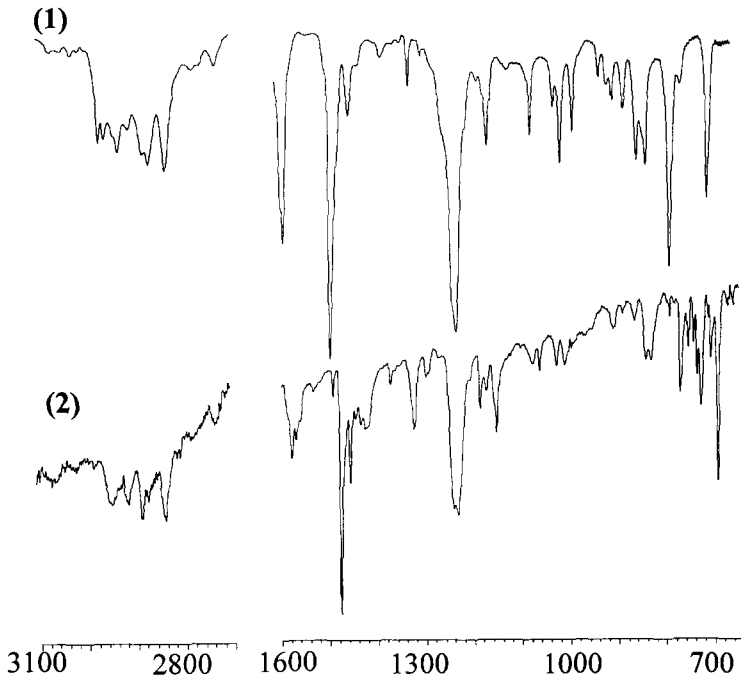

Fig. 1. IR-spectra of the compounds (1) $Ir_2(OMe)(OPh)(1,5\text{-}COD)_2$ and (2) $Ir_2(OMe)(OPh)(1,5\text{-}COD)_2C_{60}$ in KBr.

Me, C_2H_5 = Et, $n\text{-}C_3H_7$ = *n*-Pr or C_6H_5 = Ph (Fig. 2), were synthesized according to procedures described in the literature [10,11] starting from $IrCl_3nH_2O$ or $Ir_2Cl_2(1,5\text{-}COD)_2$ (both purchased from Strem Chemicals).

IR spectra and chemical analyses

The IR spectra were measured with a Nicolet Magna-IR 750 spectrometer. Solid samples were mixed with KBr and pressed into pellets. The pellets were then scanned 100 times in the range 4000–650 cm^{-1} with a resolution of 2 cm^{-1}. The chemical analyses were determined with a Carlo Erba CHN+O/S 1106 analysator. Every observed value is the average of three measurements.

Synthesis of $Ir_2(OR)_2(1,5\text{-}COD)_2C_{60}$. Buckminsterfullerene and iridium compounds, except for $Ir_2(OMe)(OPh)(1,5\text{-}COD)_2$, were dissolved in toluene. Compound $Ir_2(OMe)(OPh)(1,5\text{-}COD)_2$ was insoluble in toluene and was therefore dissolved in dichloromethane. Solutions of fullerene and each iridium dimer were combined in a 1 : 1 mole ratio and stirred at room temperature for 18–24 h except in the case of $Ir_2(OMe)_2(1,5\text{-}COD)_2$ for 2 h. The color of the solutions changed immediately to dark red. During the reaction, a brown precipitate was formed in each reaction. According to TLC, the solutions contained

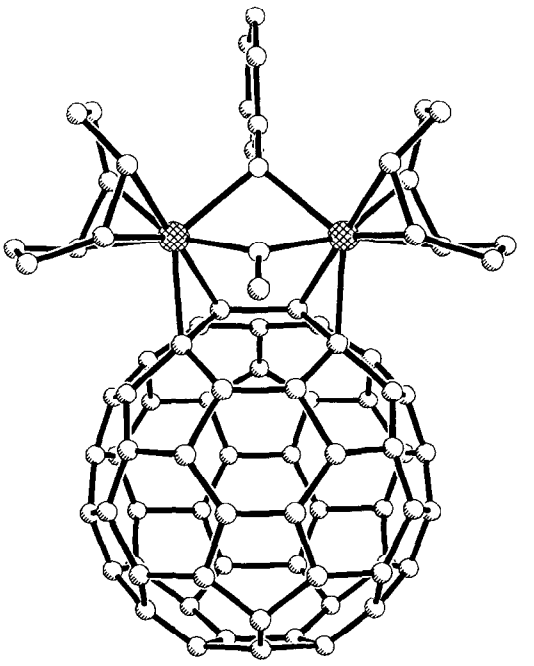

Fig. 2. Perspective view of $Ir_2(OMe)(OPh)(1,5\text{-}COD)_2C_{60}$. The disordered solvent molecule (CH_2Cl_2) has been omitted for clarity.

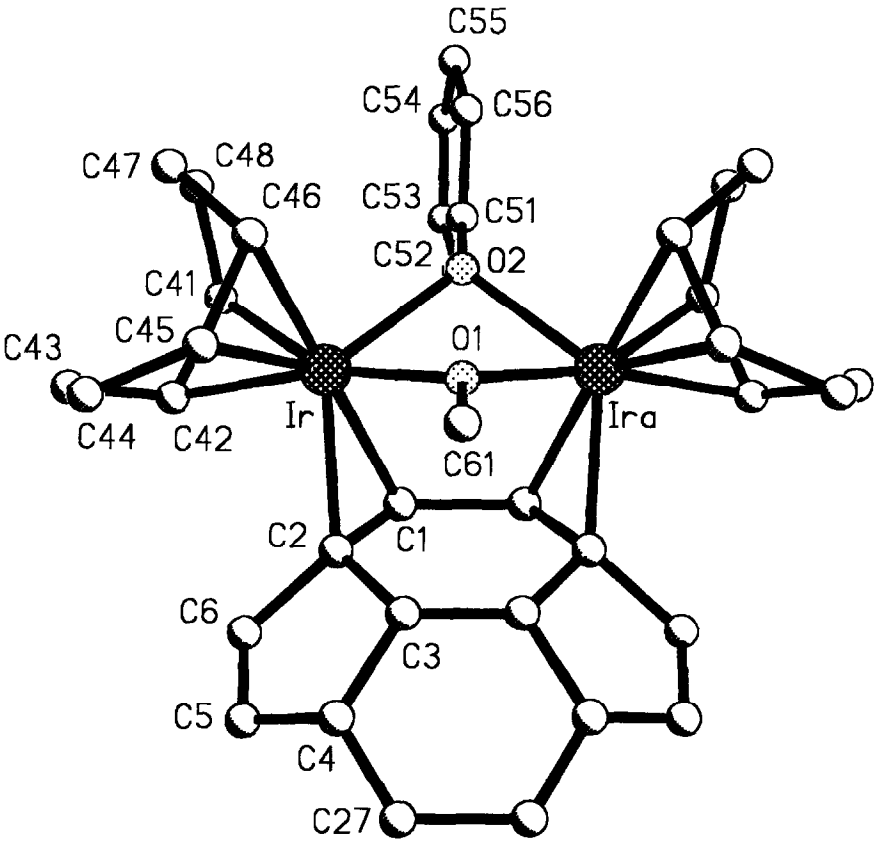

Fig. 3. Detailed view of the coordination of $Ir_2(OMe)(OPh)(1,5\text{-}COD)_2$ onto the surface of the fullerene molecule.

only unreacted starting materials. The resulting precipitate was separated by decantation, washed several times with small amounts of toluene and dried *in vacuo* at room temperature.

Elemental analysis and IR-spectroscopic data

$Ir_2(OMe)_2(1,5\text{-}COD)_2C_{60}$. C(Calc.: 67.7, Found: 68.4), H(Calc.: 2.2, Found: 2.3); IR absorptions in KBr: 2920, 2884, 2832, 1459, 1425, 1328, 1189, 1079, 1041, 739, 734, 710, 695 cm^{-1}.

$Ir_2(OEt)_2(1,5\text{-}COD)_2C_{60}$. C(Calc.: 68.1, Found: 67.2), H(Calc.: 2.4, Found: 2.1); IR absorptions in KBr: 2915, 2879, 2829, 1458, 1414, 1341, 1325, 1259, 1078, 1010, 796, 729 cm^{-1}.

$Ir_2(O\textit{n}\text{-}Pr)_2(1,5\text{-}COD)_2C_{60}$. C(Calc.: 68.4, Found: 68.6), H(Calc.: 2.7, Found: 2.1); IR absorptions in KBr: 2913, 2879, 2830, 1460, 1414, 1341, 1327, 1241, 1081, 1008, 919, 730, 694 cm^{-1}.

$Ir_2(OMe)(OPh)(1,5\text{-}COD)_2C_{60}\cdot CH_2Cl_2$. C(Calc.: 69.1, Found: 70.7), H(Calc.: 2.3, Found: 2.3); IR absorptions in KBr: 2944, 2883, 2834, 1579, 1478, 1460, 1328, 1233, 1155, 846, 835, 774, 730, 694 cm^{-1}.

X-ray structure determination of $Ir_2(OMe)(OPh)(1,5\text{-}COD)_2C_{60}\,CH_2Cl_2$

A crystal with approximate dimensions of $0.05\times0.25\times0.45$ mm was measured with a Nicolet R3m diffractometer using an ω-scan data-collection mode and graphite-monochromatized Mo–K_α radiation ($\lambda = 0.71073$ Å). Accurate cell parameters were obtained from 25 automatically centered reflections. Intensities were corrected for background, Lorentz-polarization factors, as well as for absorption from ψ-scan data, the maximum and minimum transmission factors being 0.489 and 0.300, respectively.

The crystal structure was determined by direct methods with SHELX86 [12] and subsequent Fourier synthesis with SHELXL93 [13]. The Ir, Cl and O atoms were refined anisotropically and the C atoms isotropically. The phenyl rings of the phenoxy group was refined as a rigid group (disordered over the mirror plane) with a common isotropic temperature factor. H atoms were placed in calculated positions and not refined, except those attached to the C atom of the methoxy group and those attached to CH_2Cl_2 which were omitted. Details of the crystal data and the structure refinement are given in Table 1.

Table 1. Crystallographic data of $C_{60}\{Ir_2(OMe)(OPh)(1,5\text{-}COD)_2\}\cdot CH_2Cl_2$

Formula	$C_{84}H_{26}Cl_2Ir_2O_2$
FW	1522.35
Crystal system	Monoclinic
Space group	$P2_1/m$
a (Å)	14.198(3)
b (Å)	13.661(3)
c (Å)	14.496(4)
β (°)	118.53(2)
V (Å^3)	2470.2(10)
Z	2
D_{calcd} (g cm^{-3})	2.047
μ (cm^{-1}) (Mo–K$_\alpha$)	55.54
$F(000)$	1468
$2\theta_{max}$ (°)	50
Unique refl. collected	4405
Observed refl. [$F > 4\sigma(F_o)$]	2495
Parameters	210
$R[F^2 > 4\sigma(F^2)]$	0.110
$wR(F^2)$	0.241
S	1.707

RESULTS AND DISCUSSION

The dimeric alkoxy-bridged iridium compounds all reacted with C_{60} in a 1 : 1 mole ratio. The reaction was fast for $Ir_2(OMe)_2(1,5\text{-}COD)_2$. The precipitate began to form gradually after the solutions had been combined. The other iridium complexes required a longer time to react with fullerene. In each reaction the color of the solution turned dark red immediately, but with $Ir_2(OR)_2(1,5\text{-}COD)_2$ (R = Et, *n*-Pr, Ph), the precipitate took longer time to form. The longer the alkyl group attached to oxygen was, the longer was the needed reaction time.

The products were insoluble in common organic solvents. Due to the lack of solubility, the products could be characterized primarily by chemical analysis and IR spectroscopy. Based on the results of chemical analysis, all of the new compounds synthesized are 1 : 1 compounds, i.e., in each compound one fullerene molecule is attached to one dimeric iridium molecule. All experimentally observed carbon and hydrogen contents agree with the theoretical values.

The IR spectra of the starting materials and the products were compared and the wavenumbers of the strongest vibrations are given in the experimental section for the products. The observed IR spectra of the starting materials are similar to the IR spectra given in the literature [11] for these compounds. The IR spectra of $Ir_2(OMe)(OPh)(1,5\text{-}COD)_2$ and $C_{60}\{Ir_2(OMe)(OPh)(1,5\text{-}COD)_2\}$ are presented in Fig. 1.

The coordinated cyclo-octadiene ligand in compound $Ir_2Cl_2(1,5\text{-}COD)_2$ has CH-vibrations at wavenumbers 2958, 2914, 2874 and 2830 cm^{-1} [14]. These vibrations can be found in the spectrum of every starting material and product either at exactly the same or slightly different wavenumbers. CH-vibrations due to methyl, ethyl, *n*-propyl or phenyl groups can also be found in the appropriate wavenumber area. Based on the observed CH-vibrations in the IR spectra of the products, some conclusions can be made. Every new compound synthesized in this study contains cyclo-octadiene ligands coordinated to iridium. These complexes have also similar alkyl or aryl groups as the starting materials. Therefore the dimeric structure of the iridium compounds is very likely retained in the new fullerene complexes.

Buckminsterfullerene has only four IR active vibrations at wavenumbers 1429, 1182.5, 576.5 and 527 cm^{-1} [15]. When fullerene reacts with the metal compound, the effect of coordination on the fullerene core is only local. Since the fullerene core remains largely unaffected, IR active vibrations usually remain at the same or nearly the same wavenumbers. This situation can also be seen in the present study. In every spectrum of the product, vibrations due to the fullerene core can be seen at wavenumbers 1439–1407 cm^{-1} and 1189–1183 cm^{-1}.

Attempted crystallizations by the slow diffusion method were accomplished only in the case of $Ir_2(OPh)(OMe)(1,5\text{-}COD)_2C_{60}$ producing thin aggregated plates. The crystal structure determination was successful giving the crystal structure of the compound. The structure refinement was not completed to the standard accuracy due to the data quality (all crystals containing small satellite crystals) and disordered solvent molecules. The coordination geometry (Figs 2 and 3) of the two iridium atoms is similar to that of $C_{60}\{Ir_2Cl_2(1,5\text{-}COD)_2\}_2$, where the metals bind to two adjacent 6 : 6 ring fusions [8]. Selected bond lengths and angles for $Ir_2(OPh)(OMe)(1,5\text{-}COD)_2C_{60}$ are given in Table 2. The bond distances (av. 2.2 Å) between iridium and fullerene carbon atoms in $Ir_2(OPh)(OMe)(1,5\text{-}COD)_2C_{60}$ are similar to those (av. 2.221 Å) found in $C_{60}\{Ir_2Cl_2(1,5\text{-}COD)_2\}_2$. The iridium–oxygen distances in the methoxy and phenoxy bridges are 2.07 and 2.26 Å, respectively.

Table 2. Selected bond lengths (Å) and bond angles (°) of $C_{60}\{Ir_2(OMe)(OPh)(1,5\text{-}COD)_2\}$

Ir—O_1	2.07(2)	Ir—C_{45}	2.10(4)
Ir—O_2	2.26(2)	Ir—C_{46}	2.15(3)
Ir—C_1	2.22(2)	C_1—C_2	1.55(3)
Ir—C_2	2.18(2)	C_2—C_3	1.46(3)
Ir—C_{41}	2.13(3)	C_1—C_1^i	1.50(5)
Ir—C_{42}	2.19(3)	C_3—C_3^i	1.34(5)

O_1—Ir—O_2	71.6(8)	C_{42}—Ir—C_{45}	82.5(12)
C_1—Ir—C_2	41.2(8)	C_1—Ir—C_{41}	104.4(10)
C_{41}—Ir—C_{42}	39.8(10)	C_1—Ir—C_{46}	175.3(10)
C_{45}—Ir—C_{46}	40.2(11)	C_2—Ir—C_{42}	86.0(9)
C_{41}—Ir—C_{46}	80.3(11)	C_2—Ir—C_{45}	96.1(11)

equivalent positions: $i = x, \frac{1}{2}-y, z$.

Coordinatively unsaturated iridium molecules undergo oxidative-addition reactions rather easily. The formation of these new fullerene complexes with alkoxy-bridged iridium dimers is a new example of this type of reaction. The only change in the dimeric starting materials is the attachment of the new ligand, fullerene. In these reactions the iridium center becomes coordinatively saturated.

CONCLUSIONS

Our results proved that it is possible to prepare fullerene derivatives starting from iridium dimers with different bridging groups. Careful selection of the bridging and terminal group of the starting material is essential.

These investigations open up a new area of fullerene chemistry. The next goal is to investigate different iridium dimers. Because it is possible to activate adjacent 6 : 6 ring bonds, it might be possible to synthesize compounds with more than two metal atoms attached to the fullerene core. The reactivity of other metal compounds with similar structures should be tested.

Acknowledgement—Financial support from the Academy of Finland is gratefully acknowledged.

REFERENCES

1. Kroto, H. W., Heath, J. R., O'Brien, S. C., Curl, R. F. and Smalley, R. E., *Nature*, 1985, **318,** 162.
2. Krätschmer, W., Lamb, L. D., Fostiropoulos, K. and Huffman, D. R., *Nature*, 1990, **347,** 354.
3. Fagan, P. J., Calabrese, J. C. and Malone, B., *Science*, 1991, **252,** 1160.
4. (a) Balch, A. L., Catalano, V. J. and Lee, J. W., *Inorg. Chem.*, 1991, **30,** 3980; (b) Balch, A. L., Lee, J. W., Noll, B. C. and Olmstead, M. M., *Inorg. Chem.* 1993, **32,** 3577; (c) Bashilov, V. V., Petrovskii, P. V., Sokolov, V. I., Lindeman, S. V., Guzey, I. A. and Struchkov, Y. T., *Organometallics*, 1993, **12,** 991; (d) Douthwaite, R. E., Green, M. L. H., Stephens, A. H. H. and Turner, J. F. C., *J. Chem. Soc., Chem. Commun.*, 1993, 1522; (e) Park, J. T., Cho, J.-J. and Song, H., *J. Chem. Soc., Chem. Commun.*, 1995, 15; (f) Balch, A. L., Catalano, V. J., Lee, J. W., Olmstead, M. M. and Parkin, S. R., *J. Am. Chem. Soc.*, 1991, **113,** 8953. (g) Balch, A. L., Ginwalla, A. S., Lee, J. W., Noll, B. C. and Olmstead, M. M., *J. Am. Chem. Soc.*, 1994, **116,** 2227.
5. (a) Balch, A. L., Lee, J. W., Noll, B. C. and Olmstead, M. M., *J. Am. Chem. Soc.*, 1992, **114,** 10984; (b) Balch, A. L., Lee, J. W., Noll, B. C. and Olmstead, M. M., *Inorg. Chem.* 1994, **33,** 5238; (c) Balch, A. L., Lee, J. W. and Olmstead, M. M., *Angew. Chem. Int. Ed. Engl.* 1992, **31,** 1356.
6. (a) Fagan, P. J., Calabrese, J. C. and Malone, B., *J. Am. Chem. Soc.*, 1991, **113,** 9408; (b) Fagan, P. J., Calabrese, J. C. and Malone, B., *Acc. Chem. Res.*, 1992, **25,** 134.
7. Rasinkangas, M., Pakkanen, T. T. and Pakkanen, T. A., *J. Organomet. Chem.*, 1994, **476,** C6.
8. Rasinkangas, M., Pakkanen, T. T., Pakkanen, T. A., Ahlgrén, M. and Rouvinen, J., *J. Am. Chem. Soc.*, 1993, **115,** 4901.
9. Maremkal, I. J., Chi, Y., Peng, S.-M. and Lee, G.-H., *Organometallics*, 1995, **14,** 4454.
10. Uson, R., Oro, L. A. and Cabeza, J. A., *Inorganic Syntheses*, 1985, **23,** 126.
11. Pannetier, G., Fougeroux, P., Bonnaire, R. and Platzer, N., *Journal of the Less-Common Metals*, 1971, **24,** 83.
12. Sheldrick, G. M., *Acta Crystallogr. A*, 1990, **46,** 467.
13. Sheldrick, G. M., SHELX93: Program for the Refinement of Crystal Structures; University of Göttingen, Germany, 1993.
14. Winkhaus, G. and Singer, H., *Chemische Berichte*, 1966, **99,** 3610.
15. Hare, J. P., Dennis, T. J., Kroto, H. W., Taylor, R., Allaf, A. W., Balm, S. and Walton, D. R. M., *J. Chem. Soc., Chem. Commun.*, 1991 412.

Pergamon

PII: S0277-5387(97)00433-6

Polyhedron Vol. 17, Nos. 11–12, pp. 2079–2085, 1998
© 1998 Elsevier Science Ltd
All rights reserved. Printed in Great Britain
0277-5387/98 $19.00+0.00

The $[Cu(tmen)(OH)(OH_2)]^+$ promoted hydrolysis of 2,4-dinitrophenyl diethyl phosphate and *O*-isopropyl methylphosphonofluoridate (Sarin) (tmen = *N*,*N*,*N*′,*N*′-tetramethyl-1,2-diaminoethane)

Robert W. Hay* and Norman Govan†

School of Chemistry, University of St Andrews, St Andrews, KY16 9ST, U.K.

(Received 15 September 1997; accepted 16 October 1997)

Abstract– The hydrolysis of the phosphate triester 2,4-dinitrophenyl diethyl phosphate to diethyl phosphate is catalysed by $[Cu(tmen)(OH)(OH_2)]^+$ in the pH range 6.5 to 8.0. At pH 7 with a catalyst concentration of 2.5×10^{-3} mol dm^{-3} the rate enhancement is ca 10^4 fold. The pH dependence of the catalysis is consistent with the hydroxoaqua complex being the active species in the hydrolysis. The greater kinetic effectiveness of this weak base, compared with hydroxide ion on a molar basis, indicates a bifunctional mechanism in which bound hydroxide acts as a nucleophile in conjunction with electrophilic catalysis by copper at the phosphoryl oxygen. The copper complex is an excellent catalyst for the hydrolysis of *O*-isopropyl methylphosphonofluoridate (Sarin). At pH 7 and 25°C using a Sarin concentration of 4.5×10^{-2} mol dm^{-3} and a $[Cu(tmen)(OH_2)_2]^{2+}$ concentration of 5×10^{-3} mol dm^{-3}, complete hydrolysis (9 turnovers) occurs in 13 min. © 1998 Elsevier Science Ltd. All rights reserved

Keywords: copper(II); tmen; catalysis; phosphotriester; sarin; hydrolysis.

In recent years there has been considerable interest in the metal complex promoted hydrolysis of phosphate esters [1]. Studies have involved kinetically inert cobalt(III) [2] and labile copper(II) [3] and zinc(II) [4] complexes with monoesters, diesters and triesters of phosphoric acid as substrates. A number of phosphate esters and related phosphorus(V) compounds are potent nerve agents and are used in chemical weaponry [5,6]. As a result the development of catalyst systems for the hydrolysis of such compounds is of considerable importance. The present paper discusses the $[Cu(tmen)(OH)(OH_2)]^+$ promoted hydrolysis of 2,4-dinitrophenyl diethyl phosphate. Due to steric effects, *N*-methylation of ethylenediamine leads to the formation of *mono* rather than *bis* complexes with copper(II). A variety of hydroxoaquo complexes of copper(II) and zinc(II) have been found to be active catalysts in the hydrolysis of phosphate esters, and for this reason the present catalyst system was developed. The triester 2,4-dinitrophenyl diethyl phosphate (**1**) is a suitable substrate as it is water soluble and its hydrolysis can readily be monitored by standard spectrophotomeric procedures.

EXPERIMENTAL

Synthesis

2,4-Dinitrophenyl diethyl phosphate was prepared as follows. Diethyl chlorophosphate (63 g, 0.366 mol) was added dropwise to a stirred suspension of dry sodium 2,4-dinitrophenoxide (75.4 g, 0.366 mol) in toluene (450 cm^3). On completion of the addition, the mixture was refluxed for five hours, cooled, washed with ice water (150 cm^3) followed by cold 5% sodium carbonate solution (150 cm^3) then ice water (150 cm^3). The toluene layer was dried over $MgSO_4$ and concentrated *in vacuo* to give the crude 2,4-dinitrophenyl

* Author to whom correspondence should be addressed.
† Present address, CBD, Porton Down, Salisbury, Wilts, SP4 0JQ, U.K.

diethyl phosphate in 60% yield. The crude ester was kept in a deep freeze and aliquots purified immediately before use as described below.

CAUTION: phosphate esters of this type exhibit anticholinersterase activity. Great care should be exercised in their handling and use.

Glassware should be decontaminated with solutions of hypochlorite (bleach).

Immediately prior to use, the ester (1.0 g) was dissolved in ice-cold chloroform, and the solution shaken with ice-cold 5% $NaHCO_3$ (25 cm^3), then ice-water (25 cm^3), followed by ice cold 0.1 mol dm^{-3} HCl (25 cm^3) then finally two aliquots (2×25 cm^3) of ice-cold water. The organic layer was dried over Na_2SO_4 for several hours and finally the solvent was removed at 40°C under vacuum. The phosphate ester residue was used for the kinetic experiments. (Found: C, 37.4; H, 4.1; N, 8.2. $C_{10}H_{13}N_2O_8P$ Calcd C, 37.5; H, 4.1; N, 8.75%.) ^{13}C NMR (reference TMS), 16.3 (doublet, $J = 7.34$ Hz; CH_3); 65.8 (doublet, $J = 7.34$ Hz; $—CH_2—$); 121.6; 129.1 (—C—H); 140.7; 143.8; 148.4 (—C—X). IR 1542 (NO_2), 1350 (P=O), 1032 (P—O—alkyl), 1270 (P—O—aryl).

[Cu(tmen)Cl_2]. A solution of *N,N,N′,N′*-tetramethylethylenediamine (1.45 g, 12.5 mmol) in ethanol (40 cm^3) was added dropwise with stirring to a filtered solution of $CuCl_2 \cdot 2H_2O$ (2.55 g, 15 mmol) in methanol (100 cm^3). The mixture was rotary evaporated to half volume. On standing overnight at room temperature, the dark blue complex crystallised and was filtered off and recrystallised from methanol-ether and dried *in vacuo*. (Found: C, 28.4; H, 6.4; N, 10.9. $C_6H_{16}N_2Cl_2Cu$ Calcd C, 28.75; H, 6.4; N, 11.2%.) The complex has λ_{max} 655 nm in water ($\varepsilon = 55$ dm^3 mol^{-1} cm^{-1}) and is a 2:1 electrolyte in water with $\Lambda_M = 202$ S cm^2 mol^{-1} at 25°C.

Kinetics

The kinetics of base hydrolysis of 2,4-dinitrophenyl diethyl phosphate was followed spectrophotometrically using a stopped-flow system, by monitoring the release of the 2,4-dinitrophenoxide ion at 360 nm.

The copper(II) promoted hydrolysis was studied at 35°C using a Gilford 2400 spectrophotometer interfaced with a PC. In order to avoid possible complications due to buffer catalysis the metal complex ($pK_1 = 7.40$ at 35°C) was used as the buffer system. Reactions were initiated by the addition of 50 μl of a ca 5×10^{-3} mol dm^{-3} solution of the ester in acetonitrile to the spectrophotometer cell containing the metal complex previously adjusted to the desired pH. Release of the 2,4-dinitrophenoxide ion was monitored at 400 nm. The reactions were first order in the phosphate ester (ca 8×10^{-5} mol dm^{-3} initial concentration) and excellent first order kinetics were observed. Plots of $\ln(A_\infty - A_t)$ versus time were linear for several half lives.

Measurements with Sarin

Measurements with Sarin (O-isopropyl methylphosphonofluoridate = GB; $LD_{50} = 0.025$ mg/kg) were made at CBD, Porton Down. Hydrolysis in the presence of $[Cu(tmen)(OH_2)_2]^{2+}$ was carried out by monitoring the release of fluoride using a fluoride specific electrode. The measurements were made at 25°C and pH 7 using HEPES buffer (1 mol dm^{-3}). The concentration of copper complex employed was 5×10^{-3} mol dm^{-3} and the concentration of Sarin 4.5×10^{-2} mol dm^{-3}.

Potentiometric titrations

Potentiometric titrations were carried out with a Radiometer Titralab system using G202B glass and K401 calomel electrodes. The electrode system was standardised before and after each titration using Radiometer standard buffer solutions (pH 7.00 and 9.18). The temperature was controlled by circulating water from a Haake FE thermostat. Aqueous solutions of [Cu(tmen)Cl_2] prepared from the solid complex were titrated using standard NaOH (ca 0.1 mol dm^{-3}) under nitrogen. Sufficient KNO_3 was added to maintain the ionic strength at 0.1 mol dm^{-3}. The pK_1 values for $[Cu(tmen)(OH_2)_2]^{2+}$ at 25°C and 35°C were obtained from the relationship, $pH = pK + \log([A^-]/[HA])$ and are thus practical constants involving the hydrogen ion activity and the concentration of the other species.

RESULTS AND DISCUSSION

The complex [Cu(tmen)Cl_2] is readily characterised as dark blue crystals. In the solid state the complex is a chloride bridged dimer. On dissolution in water, the chloride ligands are displaced to give $[Cu(tmen)(OH_2)_2]^{2+}$ according to the reaction,

$$[Cu(tmen)Cl_2] + 2H_2O \rightarrow [Cu(tmen)(OH_2)_2]^{2+} + 2Cl^-$$

In water the complex behaves as a 2:1 electrolyte and has λ_{max} 655 nm consistent with a CuN_2O_4 chromophore. Potentiometric titration of $[Cu(tmen)(OH_2)_2]^{2+}$ with standard sodium hydroxide gives a well defined end point after addition of one equivalent of base, Fig. 1. This end point can be attributed to the ionisation,

$$[Cu(tmen)(OH_2)_2]^{2+} \rightleftharpoons [Cu(tmen)(OH)(OH_2)]^+ + H^+; \quad K_1 \quad (1)$$

to give the hydroxoaqua complex. Analysis of the potentiometric data, Table 1, gives $pK_1 = 7.58 \pm 0.02$ at 25°C and $pK_1 = 7.40$ at 35°C. The *N*-permethylated ethylenediamine sterically hinders the formation of

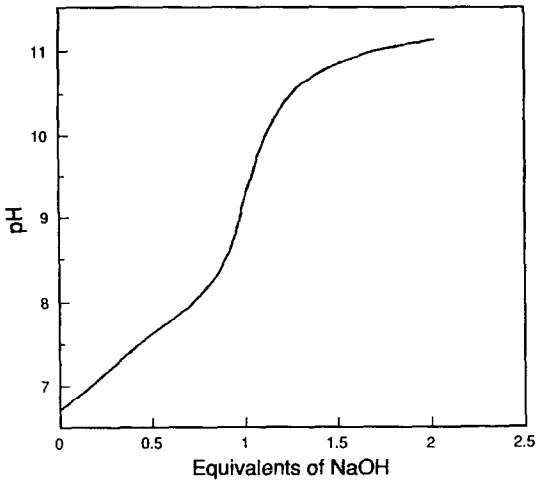

Fig. 1. Potentiometric titration of $[Cu(tmen)(OH_2)_2]^{2+}$ (2.48×10^{-3} mol dm^{-3}) with standard sodium hydroxide (0.10 mol dm^{-3}) at 35 °C and $I = 0.1$ mol dm^{-3} (KNO_3).

Table 1. Determination of pK_1 for $[Cu(tmen)(OH_2)_2]^{2+}$ at 25 °C and $I = 0.1$ mol dm^{-3} (KNO_3)

Vol NaOH (cm^3)	pH	pK_1
0.04	6.85	7.58
0.06	7.06	7.57
0.08	7.23	7.57
0.10	7.39	7.58
0.12	7.53	7.58
0.14	7.67	7.58
0.16	7.82	7.58
0.18	7.96	7.59

The titrating base was 0.985 mol dm^{-3} sodium hydroxide. The end point of the titration was 0.255 cm^3 of base.

bis-complexes in solution, and only the 1 : 1 complex is formed at 1 : 1 ligand to metal ratios. Additional potentiometric work established that dimerisation of the hydroxoaqua complex to the hydroxy-bridged dimer was not significant at concentrations below 10^{-3} mol dm^{-3}.

Kinetic studies

The base hydrolysis of 2,4-dinitrophenyl diethyl phosphate, was studied over the temperature range 9.3 to 42.5 °C giving $\Delta H^{\ddagger} = 50.6$ kJ mol^{-1} and $\Delta S^{\ddagger}_{298} = -79$ J K^{-1} mol^{-1}. At 35 °C and $I = 0.1$ mol dm^{-3}, the value of $k_{OH} = 1.55$ dm^3 mol^{-1} s^{-1}, Table 2.

In the pH range 6.5 to 7.7 the hydrolysis of the ester is markedly catalysed by $[Cu(tmen)(OH)(OH_2)]^+$. The reactions were studied using the copper(II) complex in greater than ten fold excess over the phosphate ester. Values of the observed first order rate constant (k_{obs}) for the disappearance of the ester are listed in Table 3 as a function of the copper complex concentration and the pH. At constant pH the reaction displays a linear dependence on the concentration of the copper(II) complex, Fig. 2. At pH 6.53 no evidence was obtained for the onset of saturation kinetics even when the copper(II) complex was in ca 40 fold excess. Values of the second order rate constant $k_{cat} = k_{obs}/(\text{Complex})_{Total}$ were obtained from the least squares slope of the plots of k_{obs} versus the total concentration of the copper complex, Table 4. Values of k_{cat} increase with the pH in a sigmoidal manner over the pH range 6.5 to 7.9, Fig. 3, consistent with the hydroxoaqua complex being the active species in the reaction. If this is the case values of k_{cat}/α, where α is the fraction of the total complex ionised to the hydroxoaqua complex should be effectively constant. Values of α were calculated from the pH and the experimentally determined ionisation constant at 35 °C. Values of k_{cat}/α are reasonably constant, Table

Table 2. Rate constants for the hydrolysis of 2,4-dinitrophenyl diethyl phosphate at $I = 0.1$ mol dm^{-3} over the temperature range 10–45 °C

Temp. (°C)	$10^6 k_{H_2O}$ (s^{-1})	$10^2 k_{OH}$ (dm^3 mol^{-1} s^{-1})	$10^2 k_{OH}$ (dm^3 mol^{-1} s^{-1})
10.0			11.75
15.0			16.95
20.0			22.2
25.0	1.2	30.5	29.2
30.0	1.7	41.7	39.6
35.0	2.26	56.5	57.8
40.0	3.03	75.8	80.2
45.0	4.10	100.0	101.0

The rate constants k_{OH} listed in the final column were determined by stopped-flow measurements. All other rate constants were obtained using pH-stat methods. For base hydrolysis $\Delta H^{\ddagger} = 50.7 \pm 1.0$ kJ mol^{-1} and $\Delta S^{\ddagger}_{298} = -79 \pm 2$ J K^{-1} mol^{-1}.

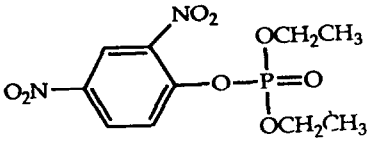

(1)

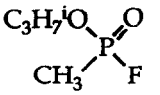

GB (Sarin)

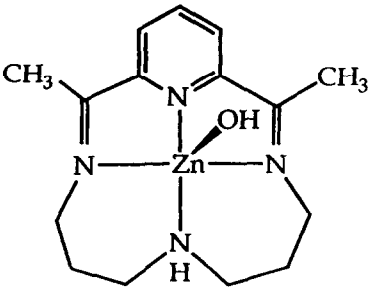

(2)

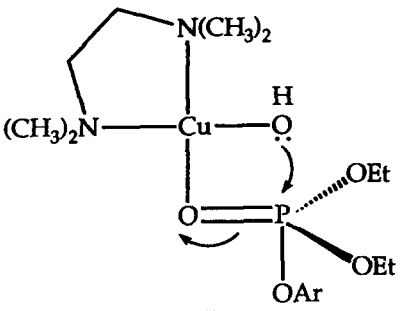

(3)

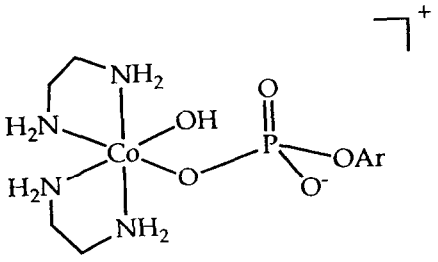

(4)

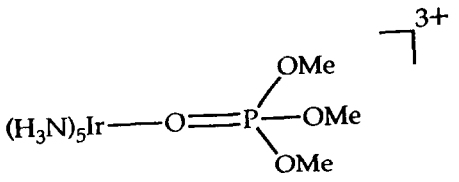

(5)

Table 3. Values of k_{obs} for the [Cu(tmen)(OH$_2$)$_2$]$^{2+}$ catalysed hydrolysis of 2,4-dinitrophenyl diethyl phosphate at 35°C and I = 0.1 mol dm^{-3} over a range of pH

pH	10^3[Cu(tmen)[$^{2+}$ (mol dm^{-3})	$10^3 k_{obs}$ (s^{-1})
6.53	0.50	0.44
	1.00	0.84
	1.50	1.15
	2.00	1.52
	2.50	1.95
	3.00	2.32
6.73	0.50	0.60
	1.00	1.18
	1.50	1.73
	2.00	2.27
	2.50	2.83
6.93	0.50	0.80
	1.00	1.59
	1.50	2.56
	2.00	3.17
	2.50	4.11
7.13	0.50	1.10
	1.00	2.10
	1.50	3.27
	2.00	4.25
	2.50	5.38
7.33	0.50	1.15
	1.00	2.50
	1.50	4.25
	2.00	4.95
	2.50	6.05
7.53	0.50	1.31
	1.00	2.94
	1.50	4.40
	2.00	5.55
	2.50	6.93
7.73	0.05	1.14
	1.00	3.45
	1.50	4.99
	2.00	6.60
	2.50	7.93

[a] The total catalyst concentration, i.e. ([Cu(tmen)(OH$_2$)$_2$]$^{2+}$ + ([Cu(tmen)(OH)(OH$_2$)]$^+$). The initial 2,4-dinitrophenyl diethyl phosphate concentration was 8×10^{-5} mol dm^{-3}.

The quoted rate constants are the average values obtained in three kinetic runs.

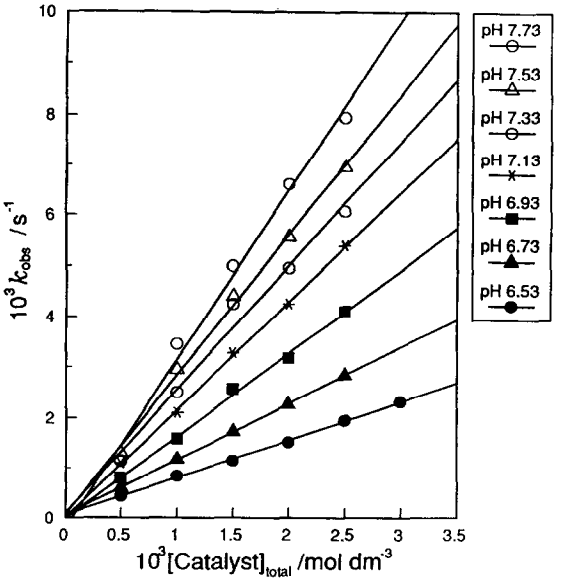

Fig. 2. Plot of k_{obs} versus the total concentration of [Cu(tmen)(OH$_2$)$_2$]$^{2+}$ for the catalysed hydrolysis of 2,4-dinitrophenyl diethyl phosphate at 35°C at various pH values and I = 0.1 mol dm^{-3} (KNO$_3$).

4 giving an average value for $k = k_{cat}/\alpha = 5.7$ dm^3 mol^{-1} s^{-1} at 35°C and I = 0.1 mol dm^{-3}. Some drift in the rate constant is expected as formation of the hydroxoaqua complex is expected to lead to some production of the inactive dihydroxo bridged dimer by the reaction

$$2[Cu(tmen)(OH)(OH_2)]^+ \rightleftharpoons [Cu(tmen)(OH)_2Cu(tmen)]^{2+} + 2H_2O \quad (2)$$

An interesting feature of the reaction is that k is some four fold greater than k_{OH} (1.55 dm^3 mol^{-1} s^{-1} at 35°C) for the base hydrolysis of the ester. Since free hydroxide is at least 10^6 stronger as a base than [Cu(tmen)(OH)(OH$_2$)]$^+$ this observation effectively excludes the copper complex acting as a general base catalyst in the reaction. The present results are consistent with the observations of Gellman, Petter and Breslow [4a] on the [Zn(CR)OH]$^+$ (**2**) catalysed hydrolysis of 2,4-dinitrophenyl diphenyl phosphate. Kinetic studies established that the catalytically active complex is the zinc hydroxo species (pK = 8.7). The second order rate constant for attack of the fully ionised [Zn(CR)OH]$^+$ on the triester is ca 2.8×10^{-1} dm^3 mol^{-1} s^{-1} at 25°C, compared with $k_{OH} = 2.8 \times 10^{-2}$ dm^3 mol^{-1} s^{-1}, which is an order of magnitude *smaller*

Table 4. The pH dependence of the second order rate constants k_{cat} as a function of the fraction of the complex [Cu(tmen)(OH$_2$)$_2$]$^{2+}$ ionised to the hydroxoaqua complex at 35°C and I = 0.1 mol dm^{-3}

pH	k_{cat} (dm^3 mol^{-1} s^{-1})	α	k_{cat}/α (dm^3 mol^{-1} s^{-1})
6.53	0.75	0.12	6.3
6.73	1.10	0.18	6.1
6.93	1.64	0.25	6.6
7.13	2.14	0.35	6.1
7.33	2.45	0.46	5.3
7.53	2.77	0.57	4.9
7.73	3.24	0.68	4.8

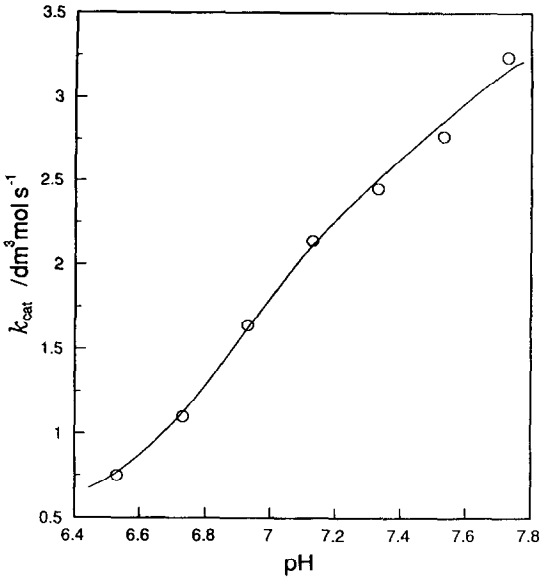

Fig. 3. Plot of k_{cat} versus pH for the $[Cu(tmen)(OH_2)_2]^{2+}$ catalysed hydrolysis of 2,4-dinitrophenyl diethyl phosphate at 35°C and $I = 0.1$ mol dm^{-3} (KNO_3).

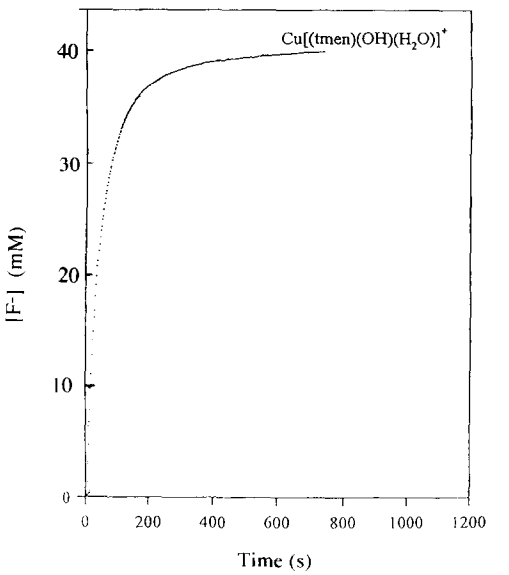

Fig. 4. Hydrolysis of Sarin (O-isopropyl methylfluorophosphonate) at pH 7.0 in 1 mol dm^{-3} HEPES buffer in the presence of the copper(II)-tmen complex. The reaction was monitored using a fluoride specific electrode. The concentration of Sarin was 4×10^{-2} mol dm^{-3} and the total copper(II) complex concentration was 5×10^{-3} mol dm^{-3}.

for the base hydrolysis reaction. To account for such experimental observations it is necessary to invoke a bifunctional "push-pull" mechanism. The metal centre delivers a coordinated hydroxide ion to the triester while simultaneously withdrawing electron density from the phosphorus atom by interacting with the phosphoryl oxygen. This mechanism is illustrated in (**3**). All four atoms of the transient four membered ring have almost normal bond angles and there is little or no strain in the formation of the trigonal-pyramidal phosphorane intermediate. Similar bifunctional mechanisms have been observed in catalytically active cobalt(III) complexes. For example, the hydrolysis of 4-nitrophenyl phosphate in (**4**) has been shown to occur by intramolecular attack by coordinated hydroxide at phosphorus to give initially a five-coordinate phosphorane which decays to $[Co(en)_2PO_4]$ containing bidentate phosphate and 4-nitrophenol [2c]. The effectiveness of Lewis acid catalysis alone in polarising the phosphoryl group can be gauged from the observation that k_{OH} for trimethyl phosphate hydrolysis is increased 400 fold when the phosphoryl group is coordinated to iridium(III) in the complex (**5**) [7].

A true catalytic system should exhibit turnover. Turnover experiments were carried out by pH-stat methods. In a typical run a solution of 7.25×10^{-4} mol dm^{-3} 2,4-dinitrophenyl diethyl phosphate and 5×10^{-5} mol dm^{-3} of the copper(II) complex (ratio 1 : 15) was adjusted to pH 7.6 and the release of H^+ due to ester hydrolysis monitored by the automatic addition of 0.10 mol dm^{-3} sodium hydroxide solution. Measurements were made at 25 and 35°C. At pH 7.6 and 35°C the half life of the ester is 71 hours in the absence of any catalyst. At 25°C there were some 20.6 turnovers per hour using the $[Cu(tmen)(OH)(OH_2)]^+$ catalyst. A few experiments were also carried out by ^{31}P NMR methods. The reaction was run for a period of time and the copper(II) removed by treating with H_2S. The solution was normally analysed before one equivalent of 2,4-dinitrophenolate was produced. The NMR measurements confirmed that only unreacted ester and diethyl phosphate were present in solution.

Measurements were also carried out with *O*-isopropyl methylfluorophosphonate (Sarin) to assess the effectiveness of $[Cu(tmen)(OH)(OH_2)]^+$ as a catalyst for its hydrolysis. The reaction was monitored using a fluoride specific electrode at pH 7.0 controlled by HEPES buffer. The measurements were made at 25°C using a total sarin concentration of 4×10^{-2} mol dm^{-3}. A typical plot for fluoride release versus time is shown in Fig. 4. Complete hydrolysis of the fluorophosphonate occurs in some 700 seconds under these conditions. The copper(II) complex is a very effective catalyst for the hydrolysis of the nerve agent. There was no evidence for product inhibition of the reaction even at quite high Sarin concentrations. However, pH control presents a problem due to the release of HF which lowers the pH so that little of the active hydroxoaqua complex is present in solution.

REFERENCES

1. For a review see Chin, J., *Acc. Chem. Res.*, 1991, **24**, 145.

2. (a) Connolly, J. A., Kim, J. H., Banaszczyk, M., Drouin, M. and Chin, J., *Inorg. Chem.*, 1995, **34,** 1094; (b) Norman, P. R. and Cornelius, R. D., *J. Am. Chem. Soc.*, 1982, **104,** 2356; (c) Jones, D. R., Lindoy, L. F. and Sargeson, A. M., *J. Am. Chem. Soc.*, 105, 7327; (d) Milburn, R. M., Gautem-Basak, M., Tribolet, T. and Sigel, H., *J. Am. Chem. Soc.*, 1985, **107,** 3315; (e) Kim, J. H. and Chin, J., *J. Am. Chem. Soc.*, 1992, **114,** 9792.
3. (a) Young, M. J. and Chin, J., *J. Am. CHem. Soc.*, 1995, **117,** 10577; (b) Wall, M., Hynes, R. C. and Chin, J., *Angew. Chem.*, 1993, **105,** 1695; (c) Wahnon, D., Hynes, R. C. and Chin, J., *J. Chem. Soc., Chem. Commun.*, 1994, 1441; (d) Burstyn, J. N. and Deal, K. A., *Inorg. Chem.*, 1993, **32,** 3585; (e) Clewley, R. G., Slebocka-Tilk, H. and Brown, R. S., *Inorg. Chem. Acta*, 1989, **157,** 233; (f) Morrow, J. and Trogler, W. C., *Inorg. Chem.*, 1989, **27,** 2330; (g) Menger, F. M., Gan, L. H., Johnson, E. and Durst, D. H., *J. Am. Chem. Soc.*, 1987, **109,** 2800.
4. (a) Gellman, S. N., Petter, R. and Breslow, R., *J. Am. Chem. Soc.*, 1986, **108,** 2388; (b) Gultneh, Y., Allwar, Ahvazi, B., Blaise, D., Butcher, R. J., Jasinski, J. and Jasinski, J., *Inorg. Chim. Acta*, 1996, **241,** 31.
5. Yang, Y.-C., *Chem. and Ind.*, 1995, 334.
6. Yang, Y.-C., Baker, J. A. and Ward, J. R., *Chem Rev.*, 1992, **92,** 1729.
7. Hendry, P. and Sargeson, A. M., *J. Chem. Soc., Chem. Commun.*, 1982, 164.

Pergamon

PII: S0277-5387(97)00426-9

Polyhedron Vol. 17, Nos. 11–12, pp. 2087–2093, 1998
© 1998 Elsevier Science Ltd
All rights reserved. Printed in Great Britain
0277-5387/98 $19.00+0.00

Synthesis, molecular structure and reactivity of the first secondary carbaboranylbisphosphine 1,2-bis(phenylphosphino)-1,2-dicarba-*closo*-dodecaborane(12)

Viktor P. Balema,[a] Maren Pink,[a] Joachim Sieler,[a] Evamarie Hey-Hawkins*[a] and Lothar Hennig[b]

[a] Institut für Anorganische Chemie der Universität Leipzig, Talstrasse 35, D-04103 Leipzig, Germany

[b] Institut für Organische Chemie der Universität Leipzig, Talstrasse 35, D-04103 Leipzig, Germany

(Received 1 September 1997; accepted 16 October 1997)

Abstract—The reaction of a diastereomeric mixture of 1,2-bis(phenylchlorophosphino)-1,2-dicarba-*closo*-dodecaborane(12) (**1**) with $LiAlH_4$, followed by hydrolysis with H_2O, gives a 4:1 mixture of *rac*- and *meso*-1,2-bis(phenylphosphino)-1,2-dicarba-*closo*-dodecaborane(12) (**2a, b**) or 1-phenylphosphino-1,2-dicarba-*closo*-dodecaborane(12) (**3**), depending on the stoichiometry employed. A mixture of **2a, b** reacts with sulfur in undecane at 190°C or without solvent at 105–110°C to give exclusively the cyclic anhydride of 1,2-bis(phenylthiophosphoryl)-1,2-dicarba-*closo*-dodecaboranyl(12)-dithiodiphosphinic acid (**6**). **2, 3** and **6** were characterised spectroscopically (^1H, ^{31}P, ^{11}B, ^{13}C NMR, IR, MS) and X-ray structure determinations were carried out on the racemic isomers **2a** and **6**. © 1998 Elsevier Science Ltd. All rights reserved

Keywords: secondary carbaboranylbisphosphine; cyclic anhydride of 1,2-bis(phenylthiophosphoryl)-1,2-dicarba-*closo*-dodecaboranyl(12)-dithiodiphosphinic acid.

Organic or organo-element derivatives of dicarba-*closo*-dodecaboranes(12) have received increasing attention during the past decade as they exhibit interesting chemical and physical properties. Thus, these compounds have been employed as catalysts [1,2], as doping reagents in semiconductor materials [3], as precursors for ceramic materials [4], and in neutron-capture therapy of tumors (boron neutron capture therapy) [5] and other medical areas [6,7]. Hence applications in medicine can be envisioned for related carbaboranylphosphines and transition metal complexes thereof [8].

While tertiary phosphino derivatives of dicarba-*closo*-dodecaboranes(12), which were first reported in 1963 [9], have been employed as ligands in transition metal chemistry and as starting materials for the preparation of other *closo*-carbaborane(12)-containing organophosphorus compounds [10], their secondary analogues have remained largely unexplored. The only report on the attempted synthesis of secondary phosphinocarbaboranes, by A.V.Kasantsev *et al.* in 1971, claims that the reaction of 2-substituted 1-phenylchlorophosphino-1,2-dicarba-*closo*-dodecaboranes(12) with $LiAlH_4$ yields the corresponding 1-phenylphosphino-1,2-dicarba-*closo*-dodecaboranes (12), which, however, decompose under the reaction conditions with formation of C-substituted 1,2-dicarba-*closo*-dodecaboranes(12) and primary phosphines [11].

We now report the synthesis and spectroscopic properties of the first secondary bisphosphinocarbaboranes, *rac*- and *meso*-1,2-bis(phenylphosphino)-1,2-dicarba-*closo*-dodecaborane(12) (**2a, 2b**) and 1-phenylphosphino-1,2-dicarba-*closo*-dodecaborane(12) (**3**), as well as the separation of the diastereoisomers of **2** and the molecular structure of the *racemic* isomer **2a**. **2a, b** react with sulfur in boiling

* Author to whom correspondence should be addressed

undecane or at elevated temperature without solvent to give the cyclic anhydride of 1,2-bis(phenylthiophosphoryl)-1,2-dicarba-*closo*-dodecaboranyl (12)-dithiodiphosphinic acid (**6**), which was also structurally characterised.

RESULTS AND DISCUSSION

Synthesis and properties of 2, 3 *and* 6

A mixture (4:1) of *rac*- and *meso*-1,2-bis(phenylphosphino)-1,2-dicarba-*closo*-dodecaborane(12) (**2a, 2b**) was obtained in 91% yield by reacting a diastereomeric mixture of *rac*- and *meso*-1,2-bis(phenylchlorophosphino)-1,2-dicarba-*closo*-dodecaborane(12) (**1**) [9] (^{31}P: 80.54 and 80.62 ppm) with 1.1 eqv. $LiAlH_4$ in ether and subsequent hydrolysis with 10 eqv. H_2O (Scheme 1). It was observed previously [11] that the P—C bond is cleaved by an excess of $LiAlH_4$ and H_2O. Thus, when a 50% excess of $LiAlH_4$ and 50 eqv. of H_2O are employed, only 1-phenylphosphino-1,2-dicarba-*closo*-dodecaborane (12) (**3**) is obtained, in 42% yield, as well as insoluble boron- and phosphorus-containing products (Scheme 1).

The carbaboranylphosphines **2** and **3** are obtained as air- and water-stable colourless solids, soluble in organic solvents, and purifiable by column chromatography. The better solubility of **2b** in hexane allows the diastereoisomers of **2** to be separated.

In the $^{31}P\{H\}$ NMR spectrum, the two diastereoisomers of **2** exhibit singlets at −15.15 for **2a** and −14.98 ppm for **2b**; for **3**, the resonance is shifted to low field (−2.67 ppm, $^1J_{PH}$ 229 Hz). On proton coupling, the HPC—CPH fragments in **2a** and **2b** show the signals of an AA′XX′ spin system. The coupling constants ($^1J_{PH}$ 244 Hz **2a**, 239 Hz **2b**; $^3J_{PP}$ 84 Hz **2a**, 87 Hz **2b**) were obtained from simulated ^{1}H NMR spectra [12]. However, the two signals of the diastereoisomers of *o*-phenylenebisphosphine, 1,2-$(PhPH)_2C_6H_4$ (−41.8, −42.4 ppm) [13], and 1,2-bis(phenylphosphino)ethane, $PhP(H)CH_2CH_2(H)$-PPh (−45.6, −45.9 ppm) [14], are observed in the same range as those of their corresponding monophosphines, Ph_2PH (−41 ppm) [15] and Ph(Et)PH (−46 ppm) [15]. The observation of no notable chemical shift difference in the ^{31}P NMR spectra indicates only minor magnetic interaction of the P atoms in these bisphosphines. Thus, the low-field shift of the resonance of **3** relative to **2** cannot be attributed to steric or electronic effects of the second PHPh group. Therefore, the observed difference in the chemical shifts of **2** and **3** must be due to the influence of the 1,2-dicarba-*closo*-dodecaborane(12) cluster. This assumption is supported by the observed difference in the ^{31}P chemical shifts of 1-diphenylphosphino-1,2-dicarba-*closo*-dodecaborane(12) (25.6 ppm) [16] and 1,2-bis(diphenylphosphino)-1,2-dicarba-*closo*-dodecaborane(12) (8.2 ppm) [17].

To investigate the chemical reactivity of **2a, b**, its reaction with sulfur was studied (Scheme 2). No reaction was observed on heating a *racemic* mixture of **2a, b** (4:1) and sulfur in THF or toluene under refluxing conditions. However, when the reaction was carried out in undecane at 190°C or without solvent at 105–110°C, the cyclic anhydride of 1,2-bis(phenylthiophosphoryl)-1,2-dicarba-*closo*-dodecaboranyl-(12)-dithiodiphosphinic acid (**6**) was obtained in 67 (undecane) or 44% (without solvent) yield.

The course of the reaction, followed by ^{31}P NMR spectroscopy, indicated that the reactivity of **2a, b** is rather different to that of other secondary 1,2-diphosphines [18–20]. **2a, b** were heated with sulfur without solvent and samples were taken after 10 min, 1 h, 2 h, 5 h and 6 h, dissolved in C_6D_6 and studied by ^{31}P NMR spectroscopy.

After 10 *min*. A very intense signal for the starting material **2a, b** is observed at ca −15 ppm and several very weak singlets in the range of +64 to +90 ppm, which could not be assigned. In addition, signals for the two diastereoisomers of **4** [doublets at −13.4 ppm (J_{PP} 59 Hz) and −12.3 ppm (J_{PP} 45 Hz) and doublets at +32.2 ppm (J_{PP} 58 Hz) and +33.4 ppm (J_{PP} 45 Hz)] were observed. On proton coupling, the signals

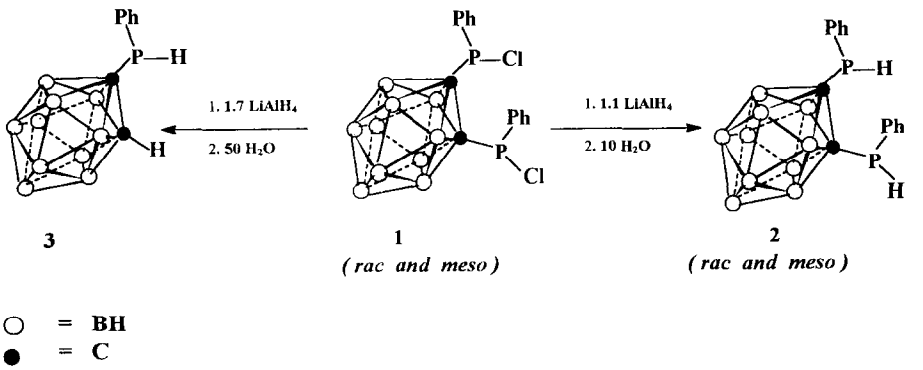

Scheme 1.

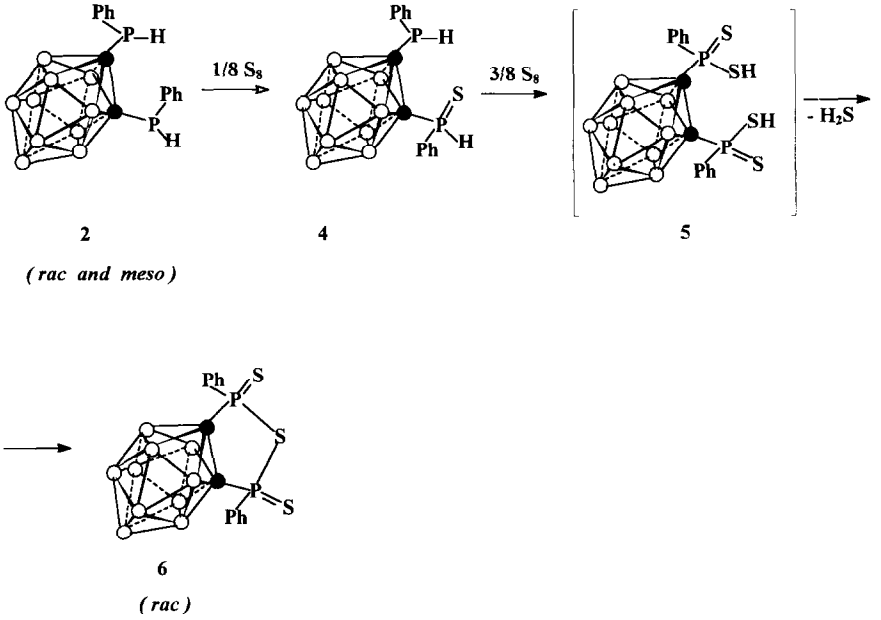

Scheme 2.

at low field show additional P—H coupling [J_{PH} 572 Hz (δ 32.2 ppm) and J_{PH} 513 Hz (δ 33.4 ppm)], indicating the presence of a P(=S)H group [15], while those at high field exhibit coupling constants of 240 and 210 Hz, characteristic of secondary phosphines. The ^{31}P NMR data indicate that this compound is the intermediate 1-phenylphosphino-2-phenylthiophosphoryl-1,2-dicarba-*closo*-dodecaborane(12) (**4**) shown in Scheme 2.

After 1 *h*, 2 *h*, 5 *h and* 6 *h*. Samples taken after 1–6 h show decreased intensity of the signals of **2a, b** and **4**, while a singlet at +75 ppm increases in intensity, indicating the formation of **6**. A crystal structure determination (*vide infra*) showed that **6** consists of the *racemic* isomer only. Surprisingly, no signals for the proposed intermediate, the bis(phosphinesulfide) derivative, are observed. In contrast, the reaction of related 1,2-diphosphines, $H(Ph)P(CH_2)_nP(Ph)H$ (n = 2–6), with sulfur gave the corresponding disulfides, $H(S)(Ph)P(CH_2)_nP(Ph)(S)H$, as the only reaction products [19].

Molecular structure of **2a** *and* **6**

Crystal structure determinations were carried out on the *racemic* isomer **2a** (Fig. 1) and on **6**. The latter proved to be the *racemic* isomer (Fig. 2). To our knowledge, **2a** is the first structurally characterised secondary 1,2-dicarba-*closo*-dodecaboranyl(12)-bisphosphine, and **6** the first structurally characterised cyclic 1,2-bis(thiophosphoryl)-1,2-dicarba-*closo*-dodecaboranyl(12)-dithiodiphosphinic acid anhydride.

2a crystallises in the centrosymmetric monoclinic space group $C2/c$, and the molecule is located on a crystallographic C_2 axis which bisects the C(1)—C(1)′ and B(2)—B(2)′ bonds. The cyclic anhydride of 1,2-bis(phenylthiophosphoryl)-1,2-dicarba-*closo*-dodecaboranyl(12)-dithiodiphosphinic acid (**6**) crystallises in the centrosymmetric monoclinic space group $P2_1/n$. Of the two possible diastereomers, the *racemic* form is present. Due to the presence of an inversion centre in both space groups, both enantiomeric forms of **2a** and **6** (*R,R*) and (*S,S*), are present in the unit cell. Selected bond lengths and bond angles are given in Tables 1 and 2.

The $B_{10}H_{10}C_2P_2Ph_2$ fragments of **6** and **2a** are similar. A comparison of the P—C and C—C bond lengths of **2a** and **6** with the related phosphino-1,2-dicarba-*closo*-dodecaboranes(12), 1-diphenylphosphino-2-thioisopropyl-1,2-dicarba-*closo*-dodecaborane(12) **7** [21], 1-diphenylphosphino-2-methyl-1,2-dicarba-*closo*-dodecaborane(12) **8** [22], and 1,2 bis(diisopropylphosphino)-1,2-dicarba-*closo*-dodecaborane (12) **9** [23], shows only a small shortening of the $C_{carbaborane}$—$C_{carbaborane}$ bond length in **2a** [1.683(2) Å] and **6** [1.658(3)] compared with **7** [1.747(5) Å], **8** [1.702(6) Å] and **9** [1.719(3) Å]. The P—$C_{carbaborane}$ [1.8727(13) for **2a**, 1.870(2), 1.862(2) for **6**, 1.884(4) for **7**, 1.884(4) for **8** and 1.891(3), 1.894(3) Å for **9**] and P—C_{Ph} bond lengths [1.8244(14) for **2a**, 1.807(3), 1.805(2) for **6**, 1.832(5) Å, 1.822(5) Å for **7**, and 1.829(4) Å, 1.832(4) Å for **8**] remain largely unchanged.

Dithiodiphosphinic acid anhydrides structurally related to **6** are rare. A similar (S)P—S—P(S) frame-

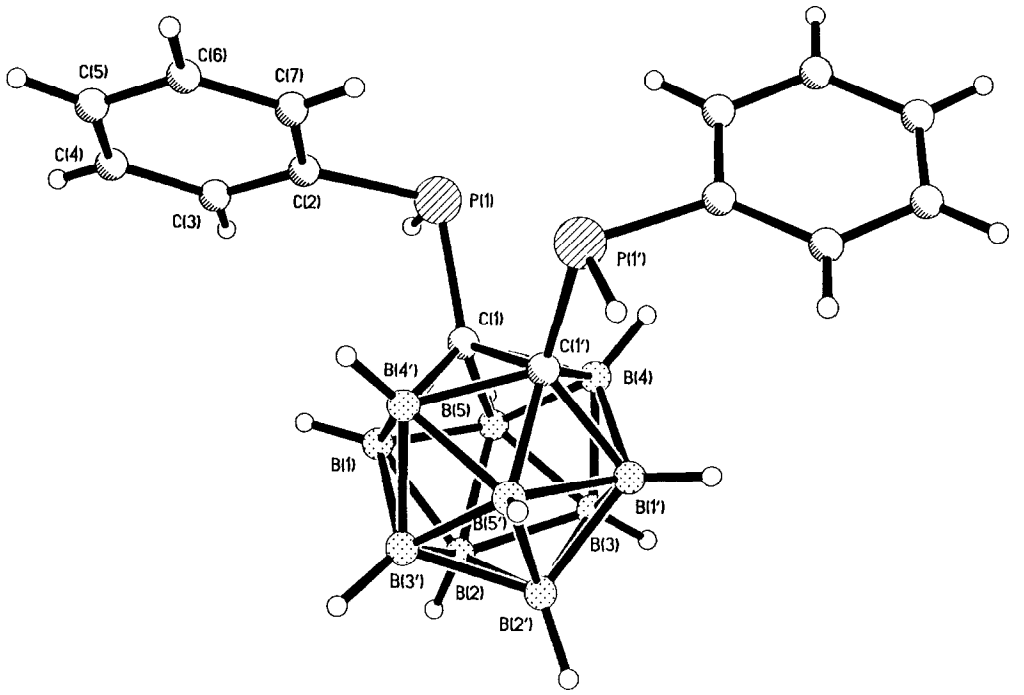

Fig. 1. Molecular structure of **2a** showing the atom numbering scheme employed (SHELXTL PLUS; XP) [26].

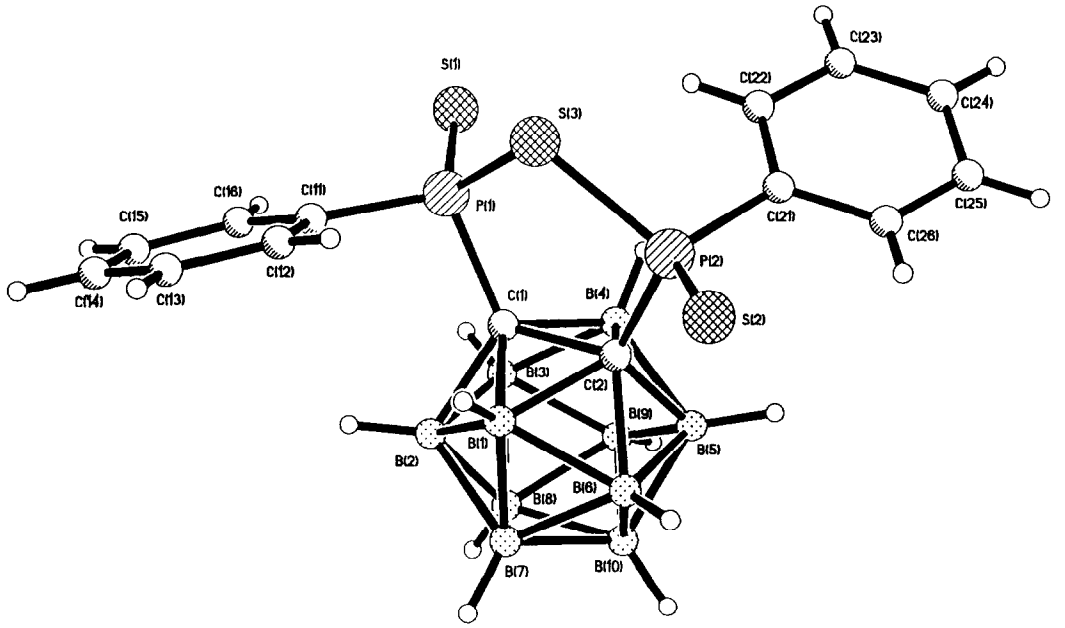

Fig. 2. Molecular structure of **6** showing the atom numbering scheme employed (SHELXTL PLUS; XP) [26].

work is observed in **6** [P=S 1.9154(9), 1.9218(9), P—S 2.1106(9), 2.1211(9) Å], *rac*-[Me(Bu^t)P(S)]$_2$S (**10**) [24] [P=S 1.939(1), 1.941(1), P—S 2.126(1), 2.123(1) Å], and 3,5-di-*tert*-butyl-1,8-epithio-1λ^5,8λ^5-naphthol-[1,8-*cd*][1,7,2,6]benzodioxadiphosphonine-1,8-dithione (**11**) [25] [P=S 1.917(2), 1.905(2), P—S 2.074(2), 2.087(2) Å]. The latter is, however, obtained as the *meso* form only, due to the presence of two fused rings [$C_3P(=S)_2S$ and $C_2O_2P(=S)_2S$]. The P—S—P [**6**: 103.44(4), **10**: 104.78(5)°] and S—P—S

Table 1. Selected bond lengths (Å) and angles (°) for **2a**

P(1)—C(1)	1.8727(13)	P(1)—C(2)	1.8244(14)
P(1)—H(1P)	1.32(2)	C(1)—C(1)′	1.683(2)
B(1)—C(1)	1.712(2)	B(4)—C(1)′	1.714(2)
B(4)—C(1)	1.737(2)	B(5)—C(1)	1.712(2)
B—B from 1.769(2) to 1.792(2)		B—H from 1.05(2) to 1.09(2)	
C(2)—P(1)—C(1)	104.58(6)	C(2)—P(1)—H(1P)	98.6(8)
C(1)—P(1)—H(1P)	92.4(8)	C(1)—B(1)—B(3)′	105.2(1)
C(1)—B(1)—B(4)′	58.78(8)	C(1)—B(1)—B(2)	105.1(1)

Table 2. Selected bond lengths (Å) and angles (°) for **6**

S(1)—P(1)	1.9154(9)	S(2)—P(2)	1.9218(9)
S(3)—P(2)	2.1106(9)	S(3)—P(1)	2.1211(9)
P(1)—C(11)	1.807(3)	P(1)—C(1)	1.870(2)
P(2)—C(21)	1.805(2)	P(2)—C(2)	1.862(2)
C(1)—C(2)	1.658(3)	C(1)—B(3)	1.709(4)
C(1)—B(2)	1.713(3)	C(1)—B(1)	1.731(4)
C(1)—B(4)	1.731(4)	C(2)—B(5)	1.709(4)
C(2)—B(6)	1.724(4)	C(2)—B(1)	1.727(4)
C(2)—B(4)	1.736(4)		
B—B from 1.764(4) to 1.791(5)			
P(2)—S(3)—P(1)	103.44(4)	C(11)—P(1)—C(1)	104.05(11)
C(11)—P(1)—S(1)	115.38(9)	C(1)—P(1)—S(1)	113.61(8)
C(11)—P(1)—S(3)	105.62(9)	C(1)—P(1)—S(3)	99.95(8)
S(1)—P(1)—S(3)	116.42(4)	C(21)—P(2)—C(2)	106.71(11)
C(21)—P(2)—S(2)	115.40(9)	C(2)—P(2)—S(2)	113.13(8)
C(21)—P(2)—S(3)	107.02(9)	C(2)—P(2)—S(3)	101.01(8)
S(2)—P(2)—S(3)	112.39(4)	C(2)—C(1)—P(1)	116.6(2)
C(1)—C(2)—P(2)	116.2(2)		

[**6**: 116.42(4), 112.39(4), **10**: 115.68(5), 117.36(5)°] bond angles of **6** and **10** are in the same range, while those of **11** are much smaller [P—S—P 97.21(6), S—P—S 109.90(8), 110.51(8)°] as the P—S—P group is part of two strained fused cyclic systems.

CONCLUSION

The results presented here show that the secondary carbaboranylphosphines **2** and **3** are readily accessible, air- and water-stable solids. The diastereoisomers **2a** and **2b** can be separated by fractional crystallisation. The reaction of **2a, b** with sulfur indicates that the reactivity of secondary carbaboranylphosphines differs significantly from that of secondary alkyl- or arylbisphosphines. Further studies of the reactivity of **2** are under way.

EXPERIMENTAL

All experiments were carried out under purified dry argon. Solvents were dried and freshly distilled under argon. NMR spectra: Avance DRX 400 (Bruker), standards: ^{1}H NMR (400 MHz): trace amounts of protonated solvent, C_6D_6, ^{13}C NMR (100.6 MHz): internal solvent, ^{31}P NMR (162 MHz): external 85% H_3PO_4, ^{11}B NMR: external $BF_3 \cdot Et_2O$. The IR spectra were recorded as KBr mulls on a Perkin–Elmer FT-IR spectrometer System 2000 in the range 350–4000 cm^{-1}. The melting points were determined in sealed

capillaries under argon and are uncorrected. *Rac*- and *meso*-1,2-bis(phenylchlorophosphino)-1,2-dicarba-*closo*-dodecaborane(12) (**1**) were prepared by literature procedures [9] and obtained in 80% yield.

Synthesis of rac- and meso-1,2-bis(phenylphosphino)-1,2-dicarba-*closo*-dodecaborane(12) (**2a**), (**2b**)

A suspension of $LiAlH_4$ (0.5 g, 13 mmol) in 25 cm^3 ether was added to a solution of **1** (5.1 g, 11.8 mmol) in 125 cm^3 ether at 0 °C over 1.5 h. The reaction was kept at 0 °C for 1 h, then for 1 h at 16 °C; finally, the mixture was refluxed for 1 h. After cooling to r.t., 2.1 cm^3 H_2O was added, the mixture filtered and the solution dried over $NaHSO_4$. The ether was removed *in vacuo* to give 3.9 g (91%) **2**. The diastereoisomers were separated by fractional crystallisation from hexane. After 6 crystallisations, 0.8 g of pure **2a** or, after 10 crystallisations, 0.06 g of **2b** were obtained. M.p. 148–149 °C, **2a**; 120–124 °C, **2b**. Found: C, 46.93; H, 6.01; P, 16.49. Calc.: for $C_{14}H_{22}B_{10}P_2$: C, 46.68; H, 6.10; P, 17.16%. IR for **2a, 2b** (KBr) cm^{-1}: 3072 (C—H); 2626, 2606, 2583, 2561 (B—H); 2323 (P—H); 1957, 1814 (Ph); 1584; 1483; 1436; 1310; 1276; 1113; 1079; 1026; 1000; 941; 919; 876; 813; 741; 728; 689; 483; 407.

Spectroscopic data for **2a** (C_6D_6, 25 °C). ^1H NMR (400 MHz): δ 7.30 (m, 4H, Ph), 7.00 (m, 6H, Ph), 4.78 (dt, 2H, P—H, $^1J_{PH}$ 244 Hz, $^3J_{PP}$ 82 Hz), 3.5–1.6 ppm (br, m, B—H); ^{31}P (161.9 MHz): $\delta -15.15$ ppm (dt, $^1J_{PH}$ 246 Hz, $^3J_{PP}$ 84 Hz); ^{13}C (100.6 MHz): δ 136.8 (m, *ipso*-C, Ph), 131.0, 130.9, 129.0 (Ph), 76.3 ppm (m, $C_2B_{10}H_{10}$); ^{11}B (128.4 MHz): $\delta -0.9$ (2B, $^1J_{BH}$ 142 Hz), -7.2 (4B, $^1J_{BH}$ 144 Hz), -9.4 (2B, $^1J_{BH}$ 225 Hz), -11.3 ppm (2B).

Spectroscopic data for **2b** (C_6D_6, 25 °C). ^1H NMR (400 MHz): δ 7.30 (m, 4H, Ph), 7.00 (m, 6H, Ph), 4.78 (dt, 2H, P—H, $^1J_{PH}$ 239 Hz, $^3J_{PP}$ 87 Hz), 3.5–1.6 ppm (br, m, B—H); ^{31}P (161.9 MHz): $\delta -14.98$ ppm (dt, $^1J_{PH}$ 239 Hz, $^3J_{PP}$ 87 Hz); ^{13}C (100.6 MHz): δ 136.8 (m, *ipso*-C, Ph), 131.0, 130.9, 129.0 (Ph), 77.6 ppm (m, $C_2B_{10}H_{10}$); ^{11}B (128.4 MHz): $\delta -0.9$ (2B, $^1J_{BH}$ 142 Hz), -7.2 (4B, $^1J_{BH}$ 144 Hz), -9.4 (2B, $^1J_{BH}$ 225 Hz), -11.3 ppm (2B).

Synthesis of 1-phenylphosphino-1,2-dicarba-*closo*-dodecaborane(12) (**3**)

3 was prepared analogously to **2** from **1** (5.7 g, 13.3 mmol) in 125 cm^3 ether, 0.8 g (21 mmol) $LiAlH_4$ in 30 cm^3 ether and 10.5 cm^3 H_2O. **3** was purified by column chromatography (hexane/acetone 4:1), yield 1.4 g (42%). M.p. 33–36 °C. ^1H NMR (400 MHz, C_6D_6, 25 °C): δ 7.05, 7.00, 6.92 (m, 5H, Ph), 4.57 (d, 1H, $^1J_{PH}$ 229 Hz, P—H), 3.5–1.6 ppm (br, m, B—H); ^{31}P (161.9 MHz, C_6D_6, 25 °C): $\delta -2.67$ ppm (d, $^1J_{PH}$ 229 Hz); ^{11}B (128.4 MHz, C_6D_6, 25 °C): $\delta -1.2$ (1B, $^1J_{BH}$ 160 Hz), -2.7 (1B, $^1J_{BH}$ 170 Hz), -7.6 (2B, $^1J_{BH}$ 152 Hz), -9.5 (1B, $^1J_{BH}$ 182 Hz), -11.0 (1B, $^1J_{BH}$ 200 Hz), -12.8 ppm (4B); ^{13}C (100.6 MHz, C_6D_6, 25 °C): δ 136.7 (d, $^1J_{CP}$ 18 Hz, *ipso*-C, Ph), 131.8, 130.6, 129.8 (Ph), 69.0 (d, $^1J_{CP}$ 60 Hz, $C_2B_{10}H_{11}$), 63.8 ppm (d, $^1J_{CH}$ 196 Hz, $C_2B_{10}H_{11}$); IR (KBr) cm^{-1}: 3058, 2957, 2927 (C—H); 2586 (B—H); 2320 (P—H); 1957, 1884 (Ph); 1585; 1483; 1437; 1308; 1275; 1172; 1115; 1091; 1072; 1025; 1001; 944; 918; 900; 827; 795; 739; 720; 692; 628; 481; 408. Found: C, 39.07; H, 6.77; P, 11.50. Calc.: for $C_8H_{17}B_{10}P$: C, 38.14; H, 6.75; P, 12.28%.

Synthesis of the cyclic anhydride of 1,2-bis(phenylthiophosphoryl)-1,2-dicarba-*closo*-dodecaboranyl-(12)-dithiodiphosphinic acid (**6**)

In undecane. A racemic mixture of **2a, b** (0.72 g, 2.0 mmol) and sulfur (0.07 g, 9.0 mmol) were heated in undecane (20 cm^3) at 190–200 °C for 5 h. The solvent was distilled off *in vacuo*, the greyish residue was then dissolved in hot hexane and filtered. **6** was obtained on cooling the hexane solution to −5 °C, yield 0.6 g (67%). M.p. 229–232 °C. ^1H NMR (400 MHz, C_6D_6, 25 °C): δ 8.15 (m, Ph), 6.93 (m, Ph), 3.5–1.9 ppm (br, m, B—H); ^{31}P (161.9 MHz, C_6D_6, 25 °C): δ 75.1 ppm; ^{11}B (128.4 MHz, C_6D_6, 25 °C): $\delta -2.7$ (J_{BH} 167 Hz), -4.2 (J_{BH} 166 Hz), -10.3 ppm; ^{13}C (100.6 MHz, C_6D_6, 25 °C): δ 134.3, 133.8, 130.1, 128.9 (Ph), 85.4 (m, $C_2B_{10}H_{10}$). IR (KBr) cm^{-1}: 3059 (C—H); 2664, 2651, 2615, 2583, 2571, 2554 (B—H); 1815 (Ph); 1580; 1480; 1437; 1311; 1187; 1161; 1092; 1078; 1027; 997; 903; 848; 799; 735; 722; 687; 671 ($\nu_s P_2S_2$); 625; 614; 560; 535; 475; 430; 417. Vibrations for P—S—P and $\nu_{as}P_2S_2$ are expected in the range 450–600 cm^{-1} [28]; however, they cannot be unambiguously assigned. Found: C, 37.04; H, 4.89; S, 20.92; P, 13.23. Calc.: for $C_{14}H_{20}B_{10}P_2S_3$: C, 37.00; H, 4.40; S, 21.04; P, 13.59%.

Without solvent. A racemic mixture of **2a, b** (1.0 g, 2.7 mmol) and sulfur (0.35 g, 10.9 mmol) were heated at 105–110 °C for 6 h. After 10 min, 1, 2, 5 and 6 h the reaction mixture was cooled to room temperature and samples were taken for ^{31}P NMR spectroscopic studies. After completion of the reaction, the white mixture was dissolved in hot hexane and worked up as described above giving 0.53 g (44%) of **6**.

Data collection and structural refinement of **2a** *and* **6**

Crystal data for **2a**. $C_{14}H_{22}B_{10}P_2$, $M = 360.36$, white crystals, $0.4 \times 0.3 \times 0.2$ mm, monoclinic, space group $C2/c$ (no. 15), $T = 293(2)$ K, $a = 20.2581(13)$, $b = 8.8653(6)$, $c = 11.8046(9)$ Å, $\beta = 112.374(1)°$, $V = 1960.4(2)$ Å^3, $Z = 4$, $D_c = 1.221$ g cm^{-3}, $F(000) = 744$, μ(Mo-K_α) = 0.216 mm^{-1}, 7114 reflections collected with $2 < \Theta < 26°$; of these 1826 were independent; 162 parameters, refinements converge to $R_1 = 0.0317$, $wR_2 = 0.0816$ (for reflections with $I > 2\sigma(I)$), $R_1 = 0.0359$, $wR_2 = 0.0837$ (all data).

Crystal data for **6**. $C_{14}H_{20}B_{10}P_2S_3$, $M = 454.52$,

white crystals, $0.3 \times 0.2 \times 0.2$ mm, monoclinic, space group $P2_1/n$ (no. 14), $T = 223(2)$ K, $a = 13.5378(9)$, $b = 11.0197(7)$, $c = 15.6155(10)$ Å, $\beta = 104.996(1)^\circ$, $V = 2250.2(3)$ Å^3, $Z = 4$, $D_c = 1.342$ g cm^{-3}, $F(000) = 928$, $\mu(\text{Mo-}K_\alpha) = 0.472$ mm^{-1}, 9685 reflections collected with $1.8 < \theta < 26^\circ$; of these 4015 were independent; 342 parameters, refinements converge to $R_1 = 0.0413$, $wR_2 = 0.0893$ (for reflections with $I > 2\sigma(I)$), $R_1 = 0.0564$, $wR_2 = 0.0975$ (all data).

Data (Mo-K_α, $\lambda = 0.71073$ Å) were collected with a Siemens CCD (SMART). All observed reflections (2θ range: 4–52°) were used for determination of the unit cell parameters. The structures were solved by direct methods (SHELXTL PLUS [26]) and subsequent difference Fourier syntheses and refined by full-matrix least-squares on F^2 (SHELXTL PLUS [26]). Restrictions for **2a**: P, B, and C atoms anisotropic, H atoms located and refined isotropically. Restrictions for **6**: S, P, B, and C atoms anisotropic, H atoms located and refined isotropically. Atomic coordinates, bond lengths and angles, and thermal parameters have been deposited at the Fachinformationszentrum [27].

Acknowledgements—We gratefully acknowledge support from the Fonds der Chemischen Industrie. Chemetall has provided a generous donation of lithium alkyls.

REFERENCES

1. Hart, F. A. and Owen, D. W., *Inorg. Chim. Acta*, 1985, **103,** L1.
2. Longato, B. and Bresadola, S., *Inorg. Chem.*, 1982, **21,** 168.
3. Bakun, A. V., Dokuchaev, Yu. P., Lapidis, I. I., Moskovskii, Yu. V., Skvortsov, I. M. and Antokin, B. G., *USSR Pat.*, 402241.
4. Hsu, M. T. S., Chen, T. S. and Riccitiello, S. R., *J. Appl. Polym. Sci.*, 1991, **42,** 851.
5. Hawthorne, M. F., *Angew. Chem.*, 1993, **105,** 997.
6. Gelen, M., Bouhdid, A., Willem, R., Bregadze, V. I., Ermanson, L. V. and Tiekink, E. R. T., *J. Organomet. Chem.*, 1995, **501,** 277.
7. Godovikov, N. N., Balema, V. P., Rys, E. G., Zhukovskiy, Yu. G., Sotchilina, E. E. and Moralev, S. N., *Bioorganicheskja khimija* (*Bioorganic Chemistry Russ.*), 1993, **19,** 1077.
8. *Metal Complexes in Cancer Chemotherapy*, ed. B. K. Keppler, VCH, Weinheim, New York, 1993.
9. Alexander, R. P. and Schroeder, H., *Inorg. Chem.*, 1963, **2,** 1107.
10. Bregadze, V. J., *Chem. Rev.*, 1992, **92,** 209.
11. Kasantsev, A. V., Zhubekova, M. N. and Zakharkin, L. I., *Zh. Obshch. Khim.*, 1971, **41,** 2027.
12. VARIAN VNMR SOFTWARE, Version 4.1 Revision C, SunOS™ 4.1.2.
13. Hitchcock, P. B., Lappert, M. F., Leung, W.-P. and Yin, P., *J. Chem. Soc., Dalton Trans.*, 1995, 3925.
14. Kimpton, B. R., McFarlane, W., Muir, A. S., Patel, P. G. and Bookham, J. L., *Polyhedron*, 1993, **12,** 2525.
15. Nifant'ev, E. E., *Spektroskopie* ^{31}P; MGPI, Moskau 1986, p. 149.
16. Kivekäs, R., Teixidor, F., Viñas, C. and Nuñez, R., *Acta Cryst.*, 1995, **C51,** 1868.
17. Hill, W. E., Rackley, B. G. and Silva-Trivino, L. M., *Inorg. Chim. Acta*, 1983, **75,** 51.
18. Issleib, K. and Döll, G., *Z. anorg. allg. Chem.*, 1963, **324,** 259.
19. Grossmann, G., Walther, B. and Gastrock-May, U., *Phosphorus and Sulfur*, 1981, **11,** 259.
20. Corbridge, D. E. C., *Phosphorus. An Outline of its Chemistry, Biochemistry and Technology*, Elsevier, Amsterdam–New York, 1980.
21. Teixidor, F., Viñas, C., Benakki, R., Kivekäs, R. and Sillanpää, R., *Inorg. Chem.*, 1997, **36,** 1719.
22. Kivekäs, R., Sillanpää, R., Teixidor, F., Viñas, C. and Nuñez, R., *Acta Cryst.*, 1994, **C50,** 2027.
23. Kivekäs, R., Sillanpää, R., Teixidor, F., Viñas, C., Nuñez, R. and Abad, M., *Acta Cryst.*, 1995, **C51,** 1864.
24. Wunderlich, H. and Wussow, H.-G., *Z. Naturforsch.*, 1984, **39b,** 1581.
25. Foreman, M. R. St. J., Slawin, A. M. Z. and Woollins, J. D., *J. Chem. Soc., Chem. Commun.*, 1995, 2217.
26. SHELXTL PLUS, Siemens Analyt. X-ray Inst. Inc., 1990, XS: *Program for Crystal Structure Solution*, XL: *Program for Crystal Structure Determination*, XP: *Interactiv Molecular Graphics*.
27. Further details of the structure determination may be obtained upon request from the Fachinformationszentrum Karlsruhe, D-76344 Eggenstein-Leopoldshafen, Germany, giving reference to the depository number CSD 407662 (for **2a**) and CSD 408309 (for **6**), and citing the authors and this paper.
28. Weidlein, J., Müller, U. and Dehnicke, K., *Schwingungsfrequenzen I*, G. Thieme Verlag, Stuttgart–New York, 1981.

Pergamon

PII: S0277-5387(97)00427-0

Polyhedron Vol. 17, Nos. 11–12, pp. 2095–2100, 1998
© 1998 Elsevier Science Ltd
All rights reserved. Printed in Great Britain
0277-5387/98 $19.00+0.00

Synthesis, crystal structure and properties of $[Fe_2O(bipy)_4Cl_2](ClO_4)_2 \cdot 0.25CH_3CN \cdot 0.25CH_3OH \cdot 0.25H_2O$, a μ-Oxo diiron(III) complex

Dao Feng Xiang,[a] Xiang Shi Tan,[a] Si Wei Zhang,[a] Yu Han,[b] Kai Bei Yu[c] and Wen Xia Tang[a]*

[a] Coordination Chemistry State Key Laboratory, Coordination Chemistry Institute, Nanjing University, Nanjing 210093, PR China

[b] Chemistry Department of Nanjing University, Nanjing 210093, PR China

[c] Analysis Center, Chengdu Branch of Chinese Academy of Science, Chengdu 610041, PR China

(Received 15 July 1997; accepted 16 October 1997)

Abstract—A μ-Oxo binuclear iron(III) complex $[Fe_2O(bipy)_4Cl_2](ClO_4)_2 \cdot 0.25CH_3CN \cdot 0.25CH_3OH \cdot 0.25H_2O$ with 2,2′-bipyridine and chlorine anion as terminal ligands has been prepared and characterized by X-ray crystallography, Mössbauer and magnetic spectroscopic measurements. The dimeric cation exhibits typical Fe—μ—O bond lengths of 1.786 Å and a bridge angle of 167.0°. The Fe···Fe separations are 3.549 Å. Magnetic susceptibility data have been measured in the temperature range 75–300 K. The μ-Oxo bridge could mediate a strong antiferromagnetic exchange interaction ($J = 115.3\ cm^{-1}$) between the two Fe(III) centers in high spin states. The data of isomer shift and quadrupole splitting obtained from Mössbauer spectrum are in agreement with the distorted octahedral coordination sphere of Fe(III) sites in high spin states. © 1998 Elsevier Science Ltd. All rights reserved

Keywords: μ-Oxo iron(III) complexes; dinuclear iron complexes; magnetism; Mössbauer; electronic spectra; infrared spectra.

The (μ-Oxo) diiron(III) complexes bridged by an oxide (or hydroxide, alkoxo, etc) and carboxylates have long been of considerable interest as a result of their distinctive magnetic properties, spectroscopic properties and their relevance to diiron nonheme proteins, such as the invertebrate dioxygen carriers hemerythrin and myohemerythrin, the R2 protein of the ribonucleotide reductase (RNR) from *Escherichia coli*, rubrerythrin and the purple acid phosphatases [1–3]. In the past decade a number of (μ-Oxo) complexes have been reported, of which the (μ-Oxo) diiron(III) complexes bridged by a single oxide is an important category [4,5] and even at present much attention is still paid to this field [6–9]. The crystal structure of μ-Oxo binuclear iron(III) complex using bidentate ligand phenanthroline as terminal ligands ($[Fe_2O(phen)_4(H_2O)]_2(NO_3)_2 \cdot 3.5H_2O$) has been reported [10]. The μ-Oxo binuclear iron(III) complex using bidentate ligand bipyridine as terminal ligands ($[Fe_2O(bipy)_4](SO_4)_2 \cdot 3.5H_2O$) was also synthesized early [11], but the relevant crystal structures have not been obtained until now and the magnetic properties was poorly characterized. In our efforts to synthesize terephthalate-bridged polynuclear iron(III) complex, we obtained the single crystals of the title compound unexpectedly in organic solvent (CH_3OH and CH_3CN). Herein we reported the synthesis, crystal structure, Mössbauer and magnetic spectroscopic properties of the title compound.

* Author to whom correspondence should be addressed.

EXPERIMENTAL

Preparations

All the chemicals used were of reagent grade and used as received. The piperidinium salt of terephthalic acid was prepared as previously described [12]. The complex $[Fe(bpy)_3](ClO_4)_3 \cdot 3H_2O$ was prepared by the method of Burstall and Nyholm [13]. All operations were carried out under aerobic conditions at ambient temperature.

$[Fe_2O(bipy)_4Cl_2](ClO_4)_2 \cdot 0.25CH_3CN \cdot 0.25CH_3OH \cdot 0.25H_2O$ was prepared as follows: A methanolic solution (15 ml) of bipyridine (2 mmol) and piperidinium isophthalate (0.5 mmol) was added to a solution (15 ml) of iron(III) chloride hexahydrate (1 mmol) in the same solvent with continuously stirring. Then a methanolic solution (10 ml) of sodium perchlorate (2 mmol) was added, whereupon a yellow precipitate formed. The solid was filtered out, washed with methanol and air-dried. Good shaped black single crystals of X-ray quality were obtained in a 54% yield by dispersing ether into CH_3CN solution of the title complex for about two weeks. Anal. Calc.: for $C_{40.75}H_{34.25}Cl_4Fe_2N_{8.25}O_{9.50}$: C, 46.83; H, 3.30; N, 11.06; Fe, 10.69. Found: C, 46.56; H, 3.35; N, 10.92, Fe, 10.98%.

X-ray structure determination

Details of the X-ray diffraction studies of the title compound may be found in Table 1. Diffraction data were collected at 295 ± 2 K on a P4 four-circle diffractometer with graphite-monochromated Mo-K_α radiation ($\lambda = 0.71073$ Å) by using the ω-$/2\theta$ scan technique. Intensity data were collected in the 2θ range of 3–46°. A total of 6233 reflections were collected and 3124 of them considered as observed [$I > 2\sigma(I)$] and used for the refinement of the structure. The intensities were corrected for Lorentz-polarisation and absorption. Two iron atoms were located by direct method. The positions of all non-hydrogen atoms were created by Fourier syntheses. The C43 in the solvent CH_3OH was found to exhibit locally positional disorder and it has two possible positions (symmetry operation: #1: $-x+1$, y, $-z+5/2$). The hydrogen atoms in C2, C13, C14, C17, C18, C22, C27, C29, C38 were placed in calculated idealized positions (the C—H bond length is 0.930). The hydrogen atoms of crystallization H_2O molecules and solvent H_2O molecules were not disposed. All the other hydrogen atoms were created using difference Fourier syntheses. The final cycle of full-matrix least-squares refinement on F^2 was based on 3124 observed reflections [$I > 2\sigma(I)$] and variable parameters and converged with unweighted and weighted agreement factors of $R = \Sigma||F_o| - |F_c||/\Sigma|F_o| = 0.059$, $wR_2 = [\Sigma[W(F_o^2 - F_c^2)^2]/\Sigma[W(F_o^2)^2]]^{1/2} = 0.1387$. ($W = 1/[\sigma^2(F_o^2) + (0.0920 \times p)^2$, where $p = [\max(F_o^2, 0) + 2F_c^2]/3$). The maximum and minimum peaks on the final difference Fourier map corresponded to 0.645 and 0.356 eÅ^{-3}, respectively. The selected bond lengths and angles are listed in Table 2. Complete listing of atomic coordinates, bond lengths and angles, and thermal parameters are included in the supplementary material.

Table 1. Crystal data for the title compound

Formula	$C_{40.75}H_{34.25}Cl_4Fe_2N_{8.25}O_{9.5}$
Mr	1045.01
Temperature (K)	295(2)
Crystal dimensions (mm)	$0.48 \times 0.48 \times 0.24$
Crystal system	Monoclinic
Space group	C2/c
a/Å	32.195(6)
b/Å	17.997(3)
c/Å	22.379(4)
β/°	131.250(10)
V/Å^3	9749(3)
z	8
ρ_{calc} (Mg/m^3)	1.432
λ (Mo-K_α)/Å	0.71073
Scan type	ω-2θ
2θ range/°	3–46
No. of total reflections	6223
No. of independent reflections	5803
Data/restraints/parameters	5798/12/694
R, *wR* [$I > 2\sigma(I)$]	0.0571, 0.1387
GOF	0.872 (on F^2)

Physical measurements

UV-Vis spectra were recorded on an Shimadzu UV-visible recording spectra photometer (UV-240) in 1-cm quartz cuvette using H_2O as a solvent. IR spectra were recorded on a Fourier Transform Infrared Spectrometer (170SX) and samples were dispersed in 13-mm diameter KBr pellets. Magnetic susceptibility data on powder-samples were measured over a temperature range of 75–300 K at a measuring 6000 G by using a CAHN-2000 Faraday-type magnetometer. The apparatus was calibrated with $[Ni(en)_3]S_2O_3$ (en = ethylenediamine). Diamagnetic corrections were made using Pascal's constants. Mössbauer spectra were measured with a symmetrical constant acceleration mode at room temperature. Data were collected with an LSI based 256 channel multichannel analyzer using 15 mCi^{57}Co(Pd) as a radiation source. Spectra were fitted with a Lorentzian line shape.

RESULT AND DISCUSSION

Structure description

The labeled molecular structure of the title compound is depicted in Fig. 1. The two ferric atoms are

Table 2. Selected bond lengths (Å) and bond angles (°) for the title compound

		bond lengths	
Fe(1)—O(1)	1.788(4)	Fe(1)—N(1)	2.131(5)
Fe(1)—N(4)	2.161(6)	Fe(1)—N(3)	2.195(6)
Fe(1)—N(2)	2.286(6)	Fe(1)—Cl(1)	2.325(2)
Fe(2)—O(1)	1.785(4)	Fe(2)—N(8)	2.124(6)
Fe(2)—N(5)	2.154(6)	Fe(2)—N(6)	2.191(6)
Fe(2)—N(7)	2.242(5)	Fe(2)—Cl(2)	2.315(2)
		bond angles	
O(1)—Fe(1)—N(1)	95.6(2)	O(1)—Fe(1)—N(4)	101.6(2)
N(1)—Fe(1)—N(4)	159.0(2)	O(1)—Fe(1)—N(3)	95.9(2)
N(1)—Fe(1)—N(4)	92.4(2)	N(4)—Fe(1)—N(3)	74.1(3)
O(1)—Fe(1)—N(2)	168.3(2)	N(1)—Fe(1)—N(2)	73.4(2)
N(4)—Fe(1)—N(2)	88.3(2)	N(3)—Fe(1)—N(2)	80.5(2)
O(1)—Fe(1)—Cl(1)	98.4(2)	N(1)—Fe(1)—Cl(1)	96.22(2)
N(4)—Fe(1)—Cl(1)	93.1(2)	N(3)—Fe(1)—Cl(1)	162.5(2)
N(2)—Fe(1)—Cl(1)	87.3(2)	O(1)—Fe(2)—N(8)	97.7(2)
O(1)—Fe(2)—N(5)	97.2(2)	N(8)—Fe(2)—N(5)	159.3(2)
O(1)—Fe(2)—N(6)	91.4(2)	N(8)—Fe(2)—N(6)	90.8(2)
N(5)—Fe(2)—N(6)	74.5(3)	O(1)—Fe(2)—N(7)	169.6(2)
N(8)—Fe(2)—N(7)	73.7(2)	N(5)—Fe(2)—N(7)	89.9(2)
N(6)—Fe(2)—N(7)	83.0(2)	O(1)—Fe(2)—Cl(2)	01.1(2)
N(8)—Fe(2)—Cl(2)	94.8(2)	N(5)—Fe(2)—Cl(2)	96.4(2)
N(6)—Fe(2)—Cl(2)	165.5(2)	N(7)—Fe(2)—Cl(2)	85.7(2)

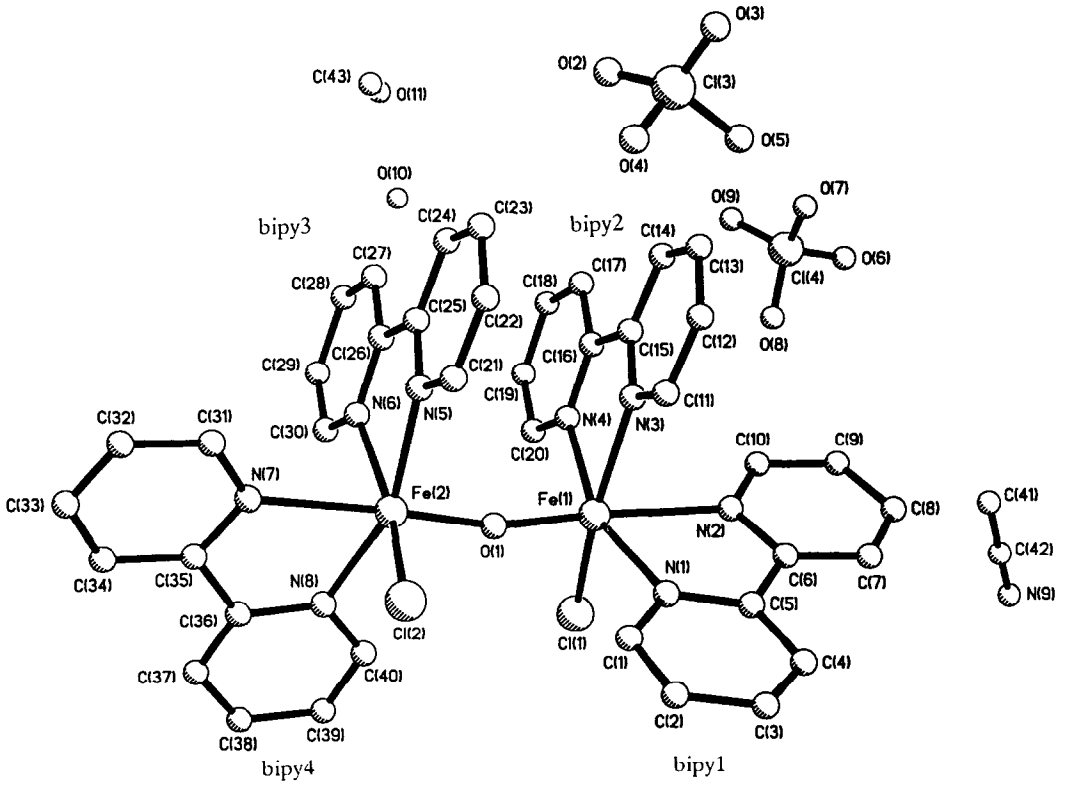

Fig. 1. Plot of the structure of the title compound, together with the numbering scheme used in the structural discussion. Hydrogen atoms are omitted for clarity.

bridged by a single oxo ligand. Each of the two Fe atoms is hexacoordinate and possesses an N_4ClO environment by virtue of four nitrogen atoms [N(1), N(2), N(3), N(4) for Fe(1) and N(5), N(6), N(7), N(8) for Fe(2)] from two chelating bipy groups, a terminal chlorine atom [Cl(1) for Fe(1) and Cl(2) for Fe(2)] and a bridging oxygen atom [O(1)]. The chloride ligand is *cis* to the bridging oxo atom in each case. The Fe(1)—N (bipy) average bond length is 2.193 Å and Fe(1)—Cl(1) bond length is 2.353 Å, while Fe(2)—N (bipy) average bond length is 2.178 Å and Fe(2)—Cl(2) bond length is 2.315 Å. For Fe(1) and Fe(2) the large deviations of bond angle from 90° of the idealized octahedral geometry are found for angles N(1)—Fe(1)—N(2) [73.4(2)°], N(4)—Fe(1)—N(3) [74.1(3)°] and N(8)—Fe(2)—N(7) [73.7(2)°], N(5)—Fe(2)—N(6) [74.5(3)], respectively. So the Fe atoms both have distorted-octahedral coordination sphere. Fe(1) is 0.299(5) Å out of the best equatorial plane which is defined by N(1), N(3), N(4) and Cl(1) (the largest deviation from the mean plane is 0.0325 Å for N(3)), while Fe(2) is 0.271(7) Å out of the best equatorial plane which is defined by N(5), N(6), N(8) and Cl(2) (the largest deviation from the mean plane is 0.0325 Å for N(6)). The Fe—O—Fe linkage is nonlinear, exhibiting an angle (Fe(1)—O—Fe(2)) of 167.0°C. This value is in the range of Fe—O—Fe angles (139–180°) known from previous studies [4,5]. The Fe—μ—O distances (Fe(1)—μ—O = 1.788(4) Å, Fe(2)—μ—O = 1.785(4) Å) are entirely characteristic of such linkages with a known range of 1.755–1.82 Å [4,5]. The combination of the nonlinear bridge and the strong Fe—μ—O bonding produces an intermetallic spacing of 3.54 Å. Because N(2) and N(7) trans to the μ-Oxo ligand are subject to a significant *trans* influence from that strongly bond bridging group, the bond lengths of Fe(1)—N(2) and Fe(2)—N(7) (2.286(6) and 2.242(5)) are apparently longer than those for other Fe—N bond lengths. Two of the chelate rings, bipy2 and bipy3 (Fig. 1) are nearly parallel to one another (dihedral angle 2.114°).

Magnetic properties

The temperature dependence of the molar magnetic susceptibility of the title compound in the form of χ_M versus T is shown in Fig. 2. The effective magnetic moment at 300 K is 2.34μ_B and 0.68μ_B at 75 K. This gradual decrease of μ_{eff} as the temperature is lowered indicated an antiferromagnetic exchange between the two iron(III) centers. The magnetic behavior of the title compound was interpreted by use of the Heisenberg Dirac. Van Vleck $S_1 = S_2 = 5/2$ spin-coupled dimer model ($H = -2JS_1S_2$), where S_1 and S_2 are the spin operators for the two iron(III) centers [14]. The expression of magnetic susceptibility of the title compound is

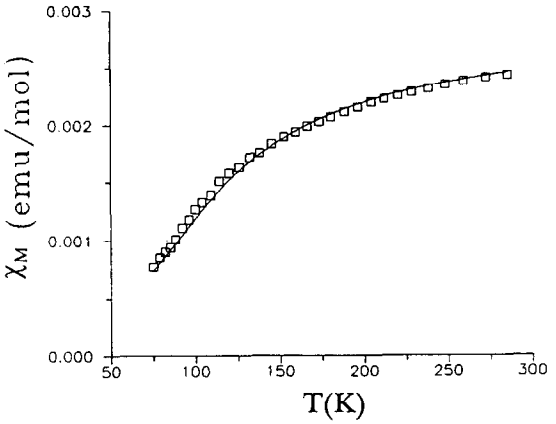

Fig. 2. Experimental (□) and calculated (—) temperature dependent molar magnetic susceptibility.

$$\chi_M = (1-\rho)Ng^2\beta^2/kT\cdot[(2e^{2x}+10e^{6x}+28e^{12x}+60e^{20x}+110e^{30x})/(1+3e^{2x}+5e^{6x}+7e^{12x}+9e^{20x}+11e^{30x})]+35\rho/8T$$

where $x = -J/kT$, ρ = mole fraction of paramagnetic impurities with ($S = 5/2$) spin-only behavior. N, g, β, k and T have their usual meanings.

Using the equation, the least-squares fit to the magnetic susceptibility data gives the parameters: $J = -115.3$ cm^{-1}, $\rho = 4.8\times10^{-3}$ and $R = 2.51\times10^{-3}$ [$R = \Sigma(\chi_{calc}-\chi_{obs})^2/\Sigma(\chi_{obs})$], assuming $g = 2$. The J value indicates a strong antiferromagnetic exchange coupling between the two Fe(III) centers. For complex $[Fe_2O(bipy)_4](SO_4)_2\cdot3.5H_2O$ [11], since the possible small amount of paramagnetic monomer was not considered in the fitting of the magnetic susceptibility data, its magnetic properties was poorly characterized.

The exchange interaction parameters in most of μ-Oxo binuclear iron complexes are from 80 to 130 cm^{-1} [4–9]. The value found here is therefore consistent with the range. Superexchange pathways within a Fe_2O^{4+} unit consist of various orbital overlaps which serve to couple $S = 5/2$ Fe(III) ions via the diamagnetic oxide bridge. For (μ-o) and μ-carboxylates bridged iron(III) complexes Gorun and Lippard have proposed a correlation between J and the shortest superexchanges pathway, but the correlation does not apply to the single μ-Oxo bridged diiron(III) centers [15]. The exchange interaction parameters J values and some structural parameters of a series of single μ-Oxo bridged diiron(III) complexes are listed in Table 3 [16–28]. Although no quantitative correlation between any geometric parameters and the magnitude of the exchange coupling is established from the table, it can be found that J increase with an increased Fe—O—Fe angle and with a decrease in the average. Fe—(μ—O) bond length, approximately.

Table 3. Structural and magnetic parameters for some known μ-Oxo bridge binuclear iron(III) complexes

Formula	$-J/cm^{-1}$	Fe—O/Å	Fe···Fe/Å	Fe—O—Fe/°	Ref
$enH_2[FeHEDTA)_2O]\cdot 6H_2O$	95	1.795(1)	3.56(1)	165(1)	9
$[(FeB(H_2O))_2O](ClO_4)_4$	100	1.8	3.6	178	10
$[Fe(3\text{-}tBusaltmen)]_2O$	100	1.779(5)	3.551	173.42	11
$\{[(TACN)Fe(acac))]_2O\}ClO_4$	89	1.787(5)	3.512	158.6(3)	12
$\{Fe[TABB(OMe)_2]\}_2O$	118	1.777(6)	3.552(1)	176.3(3)	13
$[Fe(TPC)]_2O$	129	1.755(5)	3.510(8)	180	14
$[Fe(FF)]_2O\cdot H_2O\cdot 2C_6H_5CH_3$	108	1.787(17)	3.525_{calc}	161.1(4)	15
$[Fe_2O(N_5)Cl_3]Cl\cdot 2C_2H_5OH$	125	1.751(4)	3.412(1)	149.8(3)	16
$[Fe(Cl\text{-}dipic)]_2O\cdot 4H_2O$	107	1.772(3)	3.545(1)	180	17
$[Fe_2O(tetren)_2]I_4$	98	1.77(1)	3.531_{calc}	172	18
$[Fe(mhq)_2]_2O\cdot CHCl_3$	80	1.780(11)	$3.45(1)_{calc}$	151.6(1)	19
$[Fe_2O(bbimae)_2Cl_2](NO_3)_2$	103	1.7816(7)	3.563(1)	180	20
$[Fe(cpbN)]_2O\cdot C_8H_{10}$	80	1.806(3)	3.440_{calc}	144.5(2)	21
$[tpa(OH)FeOFe(H_2O)tpa](ClO_4)_3$	97	1.810	3.389(2)	138.9(4)	3c
$[tpa(Cl)FeOFe(Cl)tpa](ClO_4)_2$	116	1.785(1)	3.565	174.7(5)	3c
$[Fe_2O(bpy)_4Cl_2](ClO_4)_2\cdot 0.25C$ $H_3CN0.25CH_3OH\cdot 0.25H_2O$	115.3	1.787(5)	3.549	167.0	this work

Mössbauer spectra

The Mössbauer spectrum of the compound at room temperature was measured and the nonlinear least fit gives an isomer shift of 0.3620 mm/s and a quadrupole splitting of 1.364 mm/s. The isomer shift is in the range 0.35–0.60 mm/s which are characteristic of 5- or 6-coordinate high-spin diferric μ-Oxo and μ-hydroxo complexes [4]. The isomer shift reported here supported the high-spin state of iron(III) ($S = 5/2$) determined by magnetism susceptibility fit. The magnitude of the quadrupole splitting is a reflection of the unsymmetrical electric field gradient about each high-spin iron(III) site. The majority of the oxo-bridged diferric complexes gave quadrupole splittings >1 mm/s [4]. The relatively large quadrupole splitting observed here indicate an unsymmetric ligand field about the iron(III) atoms and this result is consistent with the distorted octahedral coordination sphere of Fe(III) centers in the title compound.

Electronic spectra and infrared spectra

The electronic spectrum of an aqueous solution of the title compound show that the well-resolved optical maxima occur at ~230 and ~275 nm with extinction coefficients 31,500 M^{-1} cm^{-1} and 39,500 M^{-1} cm^{-1}. Two shoulders are apparent at ~470 and ~510 nm with $\varepsilon = 550$ M^{-1} cm^{-1} and 450 M^{-1} cm^{-1}, which are assigned to $^6A_1 \rightarrow (^1E, ^4A_1)$ ligand field transition, enhanced by nearby oxo LMCT bands [29]. In addition, a well-resolved optical maxima with an apparent $\lambda_{max} \sim 350$ nm ($\varepsilon \sim 7000$ M^{-1} cm^{-1}) may be noted, which lie in the so-called oxo dimer region and has been assigned to $O^{2-} \rightarrow$ Fe(III) charge-transfer transitions [30].

Infrared spectra of 2,2′-bipyridine, the $[Fe(bipy)_3]^{3+}$ monomer, and the title complex were examined and compared. As observed, the dimer has a strong new absorption at 824 cm^{-1}, which is characteristic of the asymmetric stretch of an Fe—O—Fe moiety [9].

REFERENCES

1. Blake, A. J., Grant, C. M., Parsons, S., Solan, G. A. and Winpenny, R. E. P., *J. Chem. Soc., Dalton Trans.*, 1996, 321.
2. Que, Jr., L. and True, A. E., *Prog. Inorg. Chem.*, 1990, **38,** 97.
3. Feig, A. L., and Lippard, S. J., *Chem. Rev.*, 1994, **94,** 759.
4. Kurtz, Jr., D. M., *Chem. Rev.*, 1990, **90,** 585.
5. Murray, K. S., *Coord. Chem. Review*, 1974, **12,** 1.
6. Jones, P. L., Jeffery, J. C., McCleverty, J. A. and Ward, M. D., *Polyhedron*, 1997, **16,** 1567.
7. Vernik, I. and Stynes, D. V., *Inorg. Chem.*, 1996, **35,** 2006.
8. Martens, C. F., Murthy, N. N., Obias, H. V. and Karlin, K. D., *J. Chem. Soc., Chem. Commun.*, 1996, 629.
9. Hazell, A., Jensen, K. B., McKenzie, C. J. and Toftlund, H., *Inorg. Chem.*, 1994, **33,** 3127.
10. Plowman, J. E., Loehr, T. M., Schauer, C. K. and Anderson, O. P., *Inorg. Chem.*, 1984, **23,** 3553.
11. Reiff, W. M., Baker, Jr., W. A. and Erickson, N. E., *J. Am. Chem. Soc.*, 1968, **90,** 4794.
12. Verdaguer, M., Gouteron, J., Jeannin, S., Jeannin, Y. and Kahn, O., *Inorg. Chem.*, 1984, **23,** 4291.
13. Burstall, F. H. and Nyholm, R. S., *J. Chem. Soc.*, 1952, 3570.

14. O'Connor, C. J., *Prog. Inorg. Chem.*, 1982, **29,** 203.
15. Gorun, S. M. and Lippard, S. J., *Inorg. Chem.*, 1991, **30,** 1625.
16. Lippard, S. J., Schugar, H. and Walling, C., *Inorg. Chem.*, 1967, **6,** 1825.
17. Fleischer, E. and Hawkinson, S., *J. Am. Chem. Soc.*, 1967, **89,** 720.
18. Mukherjee, R. N., Stack, T. D. P. and Holm, R. H., *J. Am. Chem. Soc.*, 1988, **110,** 1850.
19. Wieghardt, K., Pohl, K., Bossek, U., Nuber, B. and Weiss, J. Z., *Naturforsch.*, B43 198, 1184.
20. Katovic, V., Vergez, S. C. and Busch, D. H., *Inorg. Chem.*, 1977, **16,** 1716.
21. Strauss, S. H., Pawlik, M. J., Skowyra, J., Kennedy, J. R., Anderson, O. P., Spatalian, K. and Dye, J. L., *Inorg. Chem.*, 1987, **26,** 724.
22. Landrum, J. T., Grimmet, D., Haller, K. J., Scheidt, W. R. and Reed, C. A., *J. Am. Chem. Soc.*, 1981, **103,** 2640.
23. Gomez-Romero, P., Whitten, E. H., Reiff, W. M., Backes, G., Sanders-Loehr, J. and Jameson, G. B., *J. Am. Chem. Soc.*, 1989, **111,** 9039.
24. Ou, C. C., Wollman, R. G., Hendrickson, D. N., Potenza, J. A. and Schugar, H. J., *J. Am. Chem. Soc.*, 1978, **100,** 4717.
25. Hanson, M. V., Marsh, W. E. and Carlisle, G. O., *Nucl. Chem. Lett.*, 1977, **13,** 277.
26. Mabbs, F. E., McLachlan, V. N., McFadden, D. and McPhall, A. F., *J. Chem. Soc., Dalton Trans.*, 1973, 2016.
27. Takahashi, K., Nishida, Y., Maeda, Y. and Kida, S., *J. Chem. Soc., Dalton Trans.*, 1985, 2375.
28. Mockler, G. M., DeJersey, J., Zerner, B., O'Connor, C. J. and Sinn, E., *J. Am. Chem. Soc.*, 1983, **105,** 1891.
29. Norman, R. E., Holz, R. C., Ménage, S., O'Connor, C. J., Zhang, J. H. and Que, Jr., L., *Inorg. Chem.*, 1990, **29,** 4629.
30. Reem, R. C., McCormick, J. M., Devlin, D. E., Stephens, P. J., Musselman, R. L. and Solomon, E. I., *J. Am. Chem. Soc.*, 1989, **111,** 4688.

Pergamon

PII: S0277-5387(97)00462-2

Polyhedron Vol. 17, Nos. 11–12, pp. 2101–2104, 1998
© 1998 Elsevier Science Ltd
All rights reserved. Printed in Great Britain
0277-5387/98 $19.00+0.00

The crystal structure of *trans*-$CrBr_2(pyridine)_4 \cdot 2pyridine$

David G. Holah,*[a] Alan N. Hughes,[a] Craig Lundeen[b] and Vincent R. Magnuson[b]

[a] Department of Chemistry, Lakehead University, Thunder Bay, Ontario, Canada, P7B 5E1

[b] Department of Chemistry, University of Minnesota-Duluth, Duluth, MN 55812, U.S.A.

(Received 4 August 1997; accepted 9 October 1997)

Abstract—The structure of $CrBr_2 \cdot 6(py)$ (py = pyridine) consists of a Cr atom at the intersection of three 2-fold axes in the space group *Ccca*. The Cr is coordinated to 4 N atoms of py ligands [CrÅN distances of 2.135(4) and 2.164(5) Å] and interacts weakly with 2 Br ions [Cr—Br distance 2.998(1) Å] giving the CrN_4Br_2 unit D_{2h} symmetry. There are two py molecules per Cr centre trapped in the lattice. © 1998 Elsevier Science Ltd. All rights reserved

Keywords: $[CrBr_2(pyridine)_4] \cdot 2pyridine$; X-ray structure.

Interest in Jahn-Teller distortions, particularly in d^9 and d^4 systems, has remained high over many years. For example, many crystallographic studies have been completed on copper^{II} complexes. Much less has been done with the high-spin d^4 systems Cr^{II} and Mn^{III}. To isolate structural distortions caused by electronic effects from those due to the presence of non-equivalent ligands on a metal centre, monomeric complexes with six equivalent monodentate ligands are of particular importance. Amongst the very few structurally characterized compounds in this category are $[Mn(urea)_6][ClO_4]_3$ [1], $[Cr(CNPh)_6][PF_6]_2$ [2], $[Cr(H_2O)_6][SiF_6]$ [3], CrF_6 units in $CrNbF_6$ [4] and $Cr(H_2O)_6^{2+}$ octahedra in the lattices of Tutton salts [5]. Such compounds are therefore rare relative to those of the type ML_4X_2 and it has recently been shown [6] that even the complex with the empirical formula $Cr(py)_6(PF_6)_2$ (py = pyridine) is an example of the latter type. In this complex, only four of the py molecules are coordinated to the Cr atom and there are weak axial interactions with F atoms of PF_6^- species. It was considered likely at the time of its synthesis that the related complex $CrBr_2 \cdot 6py$, **1**, contains the $[Cr(py)_6]^{2+}$ cation [7]. Thermogravimetric analysis of **1** showed [7] the rapid loss of between 3 and 4 py molecules, with no evidence for even the transitory existence of $CrBr_2 \cdot 4py$, as might perhaps be expected if **1** is analogous to the PF_6 compound. It was therefore of interest to determine the structure of **1**.

EXPERIMENTAL

Crystals of **1** were prepared as previously described [7]. A suitable crystal was sealed in a nitrogen-filled Lindemann capillary and stored in liquid nitrogen to prevent slow decomposition and loss of py.

X-ray crystallographic data collection was carried out on an Enraf-Nonius CAD-4 diffractometer using graphite monochromated Mo–K_α radiation at 173 K. Crystal structure refinement calculations were carried out (at UMD) on a PC Express computer with the SHELX program system [8]. NRCVAX programs were used for scaling and data reduction [9]. Unit cell parameters were obtained by least squares analysis of 25 low angle reflections. The stability of the crystal was measured by monitoring periodically three standard reflections; no systematic intensity variations were observed. Intensity data were corrected for Lorentz and polarization factors. Atomic scattering factors were taken from tabulated values.

The Cr atom was found using direct methods and cycles of Fourier and difference Fourier calculations were used to find the remaining atoms. All atoms were refined with anisotropic thermal displacement

* Author to whom correspondence should be addressed.

Table 1. Crystal data and structure refinement for **1**

Empirical formula	$C_{30}H_{30}N_6CrBr_2$
Formula weight	686.4
Temperature (K)	173(2)
Wavelength (Å)	0.71073
Crystal system	Orthorhombic
Space group	*Ccaa*
a (Å)	14.856(2)
b (Å)	11.681(3)
c (Å)	16.807(3)
V (Å^3)	2916.6
Z	4
D_{calc} (g cm^{-3})	1.563
Absorption coefficient (mm^{-1})	3.163
F(000)	1384.0
Crystal size (mm)	$0.78 \times 0.73 \times 0.36$
Crystal description	dark green needle
Range (°)	2.42–24.16
Index ranges	$-16 <= h <= 17$, $-12 <= k <= 13$, $-19 <= l <= 13$
Reflections collected	5508
Independent reflections	1163 [$R_{int} = 0.0435$]
Refinement method	Full-matrix least-squares on F^2
Data/restraints/parameters	1163/0/93
Goodness-of-fit on F^2	1.129
Final *R* indices[a]	$R_1 = 0.0382$, $wR_2 = 0.0850$ [$911 F_o > 4\sigma(F_o)$]
R indices (all data)	$R_1 = 0.0526$, $wR_2 = 0.0914$
Largest diff. peak and hole (e Å^{-3})	0.819 and −0.265

[a] $R_1 = \Sigma||F_o| - |F_c||/\Sigma|F_o|$; $wR_2 = [\Sigma[w(F_o^2 - F_c^2)^2]/\Sigma[w(F_o^2)^2]]^{0.5}$.

parameters except H atoms whose calculated ideal positions were included but not refined. Relevant data concerning the crystal, data collection and structure solution are recorded in Table 1. (Tables of crystallographic data, including a listing of anisotropic displacement parameters, bond lengths and angles and observed and calculated structure factors for **1** have been deposited with the Cambridge Crystallographic Data Center.)

RESULTS AND DISCUSSION

The problem of py loss, resulting in rapid decomposition of crystals sealed in capillaries at room temperature, was overcome by freezing the sample and collecting the data at low temperatures.

Figure 1 is an ORTEP view of **1** and shows that each Cr atom is surrounded by four py molecules and the two Br atoms. Two py molecules are trapped in the lattice. Compound **1** crystallizes in the space group *Ccca* with 4 molecules in the unit cell and with each Cr atom at the intersection of the three 2-fold axes passing through N1—Cr, N3—Cr and Br—Cr. The relevant bond lengths are Cr—N(1) 2.135(4), Cr—N(3) 2.164(5) and Cr—Br 2.998(1) Å, giving the CrN_4Br_2 unit D_{2h} symmetry. The Cr—N bond lengths are comparable with those found in similar complexes containing $Crpy_4X_2$ units (X = Cl [10], X = FPF_5 [6]) and in other related complexes [11]. The Cr—Br distance of ~3 Å is significantly longer than those found (2.36–2.839 Å) in other Cr(II) complexes [12]. It is also approximately 0.24 Å longer than the sum of the ionic radii of the two ions [13]. At best, therefore, the Br interacts only very weakly with the Cr centre. A similar situation has been found for the Cr—Cl interaction in $Crpy_4Cl_2$ [10]. The C—N, C—C and C—H distances in the py rings are normal.

For clarity, only the unique atoms are labelled in Fig. 1 which also shows the positions of the py molecules trapped in the lattice. Although the molecule contains only two lattice py units per Cr atom, Fig. 1 shows the positions of all the symmetry-related lattice py molecules in the environment of each Cr atom. The view down the N3—Cr axis (Fig. 2) shows this more clearly. Notice that the plane of the py ring of N3 on *one* side of the Cr—N1 py plane is parallel (within 2.8°) with the planes of the two lattice py rings on the *opposite* side of the Cr—N1 py plane. Figure 2 also illustrates that the lattice py molecules are somewhat closer to the N1 py (2.4–2.9 Å) than to the N3 py (2.9–3.3 Å). This crowding of the N1 py may be responsible for the slightly shorter Cr—N1 distance compared to

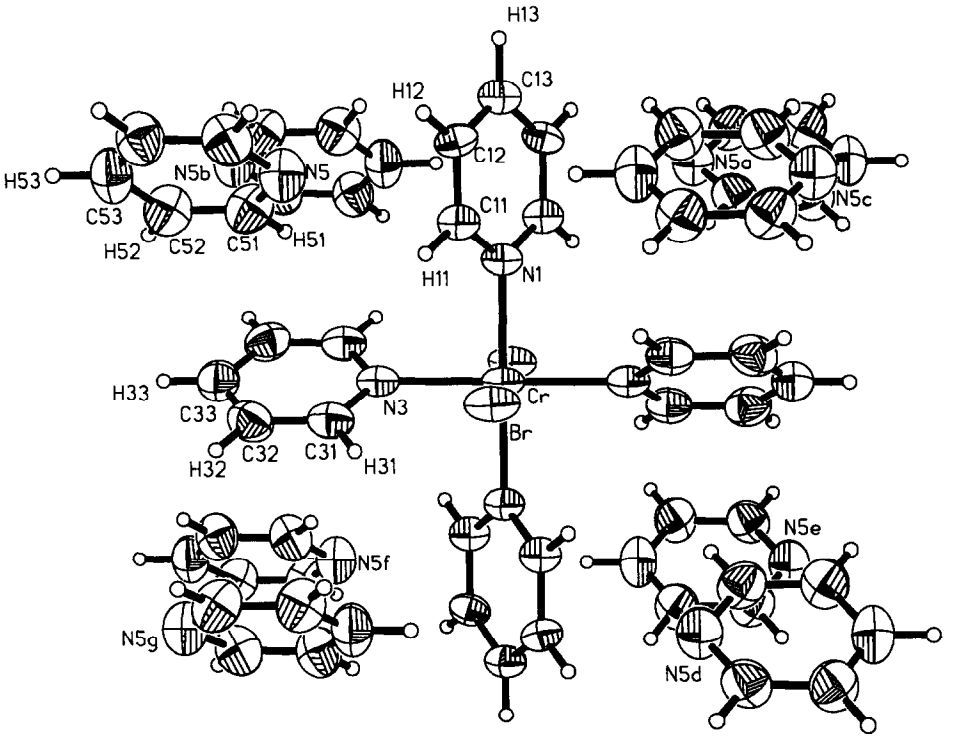

Fig. 1. Diagram of **1** looking down the Cr—N3 axis showing the relationship between coordinated and lattice pyridine molecules.

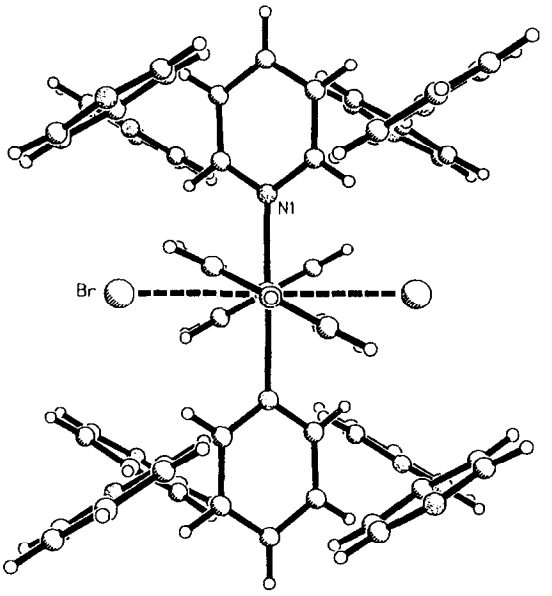

Fig. 2. ORTEP diagram of complex **1** looking down the Cr—Br axis.

the Cr—N3 distance since there is no electronic reason associated with the d^4 configuration of the Cr atom that requires this.

Thus, despite its thermochemical behaviour, **1** does not contain 6 equivalent ligands. It is simply another example of the common ML_4X_2 arrangement about which much has been written in terms of the Jahn-Teller effect.

Acknowledgements—We thank the Lakehead University Senate Research Committee and the Natural Sciences and Engineering Research Council of Canada for financial support. We also thank E. Prokopchuk for technical assistance.

REFERENCES

1. Aghabozorg, H., Palenik, G. J., Stoufer, R. C. and Summers, J., *Inorg. Chem.*, 1982, **21**, 3903.
2. Bohling, D. A. and Mann, K. R., *Inorg. Chem.*, 1984, **23**, 1426.
3. Cotton, F. A. Falvello, L. R.. Murillo C. A and Quesada, J. F., *J. Solid State Chem.*, 1992, **96**, 192.
4. Goubard, F., Chassaing, J., Bizot, D. and Quarton, M., *Eur. J. Solid State Inorg. Chem.*, 1994, **31**, 223.
5. Cotton, F. A., Daniels, L. M., Falvello, L. R., Murillo, C. A. and Schultz, A. J., *Inorg. Chem.*, 1994, **33**, 5396 and references therein.
6. Fochi, G., Stähle, J. and Ging, F., *Inorg. Chem.*, 1991, **30**, 4669.
7. Holah, D. G. and Fackler, Jr., J. P., *Inorg. Chem.*, 1965, **4**, 1112.

8. Sheldrick, G. M., SHELXL-93, Program System for X-ray Structure Determination, University of Cambridge, 1963.
9. Gabe, E. J., Le Page, Y., Charland, J. P., Lee, F. L. and White, P. S., *J. Appl. Cryst.*, 1989. **22,** 384, PC version of the system.
10 Cotton, F. A., Daniels, L. M., Feng, X., Maloney, D. J., Murillo, C. A. and Zuniga, L. A., *Inorg. Chim. Acta*, 1995, **235,** 21.
11. Cotton, F. A., Daniels, L. M., and Murillo, C. A., *Polyhedron*, 1992, **11,** 2475.
12. Larkworthy, L. F., Nolan, K. B. and O'Brien, P., in *Comprehensive Coordination Chemistry*, Vol. 3, ed. G. Wilkinson, R. D. Gillard and J. A. McCleverty. Pergamon Press, Oxford, 1987, Ch. 35.
13. Huheey, J. E., Keiter, E. A. and Keiter, R. A., *Inorganic Chemistry*, 4th edn. Harper Collins, 1993, p. 114.

Pergamon

PII: S0277-5387(97)00439-7

Polyhedron Vol. 17, Nos. 11–12, pp. 2105–2108, 1998
© 1998 Published by Elsevier Science Ltd
All rights reserved. Printed in Great Britain
0277-5387/98 $19.00+0.00

The syntheses and crystal structures of $[PPh_4][In(SePh)_4]$ and $[PPh_4][In(SePh)_3(SeH)]$

Donna M. Smith and James A. Ibers*

Department of Chemistry, Northwestern University, 2145 Sheridan Road, Evanston, Illinois 60208-3113, U.S.A.

(Received 15 September 1997; accepted 30 September 1997)

Abstract—The reaction of $InCl_3$ with NaSePh in ethanol followed by addition of PPh_4Cl affords tetraphenylphosphonium tetra(benzeneselenolato)indium(III), $[PPh_4][In(SePh)_4]$ (**1**). Reaction of the $[In(SePh_4)]^-$ reaction mixture with $NaBH_4$ and elemental sulfur followed by the addition of PPh_4Cl yields tetraphenylphosphonium tri(benzeneselenolato)(hydroselenido)indium(III), $[PPh_4][In(SePh)_3(SeH)]$ (**2**). The structures of **1** and **2**, as determined from single-crystal X-ray data, feature well-separated cations and anions with the In(III) centers of the anions tetrahedrally coordinated to four $[SePh]^-$ ligands or three $[SePh]^-$ ligands and one $[SeH]^-$ ligand, respectively. © 1998 Published by Elsevier Science Ltd. All rights reserved

Keywords: indium-selenolate complexes; synthesis; X-ray structures.

Many indium thiolates and selenolates have been synthesized [1–3], owing to the potential of such materials as single-source precursors [3,4]. Here we report the syntheses and characterization of the anionic indium selenolates $[In(SePh)_4]^-$ and $[In(SePh)_3(SeH)]^-$ as their PPh_4^+ salts. Apparently, only one other anionic indium selenolate has been reported, namely $[InBr(SePh)_3]^-$ as its $[PPh_4]^+$ salt, although it has not been structurally characterized [2]. Little reaction chemistry of main-group benzeneselenolate compounds has been reported.

EXPERIMENTAL

All manipulations were carried out under N_2 with the use of standard Schlenk techniques. Solvents were purchased from Baxter Scientific Products Inc., McGaw Park, IL and were distilled, dried, and degassed before use. EtOH was dried over MgI_2; CH_3CN was dried over CaH_2. The remaining reagents were purchased from Aldrich Chemical Co., Milwaukee, WI and used as received. The ^{77}Se NMR spectra were obtained with the use of a Varian 400 MHz Unity Plus spectrometer equipped with a 10 mm tunable broad-band probe, a variable temperature apparatus, and a deuterium lock. All ^{77}Se NMR chemical shifts are referenced to the external Ph_2Se_2 standard at 460 ppm, which in turn is referenced to $(CH_3)_2Se$ at 0 ppm.

Preparation of $[PPh_4][In(SePh)_4]$ (1)

NaSePh was prepared *in situ* by the reaction of $NaBH_4$ (0.113 g; 3.0 mmol) in 10 ml EtOH with Ph_2Se_2 (0.468 g; 1.5 mmol) in 10 ml EtOH. A suspension of $InCl_3$ (0.221 g; 1.0 mmol) in 10 ml EtOH was added with stirring to the pale yellow NaSePh solution. After the solution was stirred for several hours, PPh_4Cl (0.430 g; 1.15 mmol) in 10 ml EtOH was added to give a white precipitate. The precipitate was collected by filtration and redissolved in acetonitrile. The solvent was removed under vacuum to afford light yellow crystals of **1**. Yield: 0.50 g; 46% based on In. Found: In, 10.94; C, 51.15; H, 4.39. Calc. for $C_{48}H_{40}InPSe_4$: In, 10.65; C, 53.46; H, 3.74. ^{77}Se NMR (d-DMF, 25°C): $\delta = 69.9$ ppm.

Preparation of $[PPh_4][In(SePh)_3(SeH)]$ (2)

$InCl_3$ (0.110 g; 0.5 mmol) in 15 ml EtOH was reacted with NaSePh (2.0 mmol prepared as described

* Author to whom correspondence should be addressed.

above). The resultant yellow solution was filtered into a flask containing the dry reagents $NaBH_4$ (0.067 g; 1.5 mmol) and elemental sulfur (0.019 g; 0.5 mmol). The solution fizzed and a milky white precipitate formed immediately. The solution was filtered again and PPh_4Cl (0.21 g; 0.5 mmol) in 5.0 ml EtOH was added. Slow evaporation of the solvent afforded white needles (**2**) and a light yellow precipitate. Crystals of **2** were manually separated from the yellow powder. Yield: 0.20 g; 40% based on In. IR: ν(Se—H) 2241 cm^{-1}.

Crystallographic studies

Intensity data were collected at 113(2) K with Mo-K_α radiation on a Picker diffractometer for **1** and with Cu-K_α radiation on an Enraf-Nonius CAD4 diffractometer for **2**. The number of reflections used to obtain unit cell parameters and the 2θ ranges involved were **1**: 25, 30–35°; **2**: 25, 30.1–36.1°. In each study, six standard reflections were monitored and were found to be constant within counting statistics. Continuous scan data were collected for **1** and processed [5] whereas profile data were collected for **2** and processed accordingly. Both data sets were corrected for absorption by means of the analytical method [6]. Additional experimental details are given in Table 1.

The structures were solved by direct methods [7] and were refined by full-matrix least squares methods [8]. Phenyl H atoms were placed in calculated positions and were refined with the use of a riding model. Anisotropic displacement parameters were refined for the heavy atoms and the majority of the C atoms in **1**; the ellipsoids for atoms C(34), C(35), C(52), C(65), C(76), and C(81) were non-positive definite and thus isotropic displacement parameters were refined for these atoms. Anisotropic displacement parameters were refined for all of the non-hydrogen atoms in **2**. No unusual features were observed in the final difference electron-density maps. Lists of final coordinates, displacement parameters, bond distances and angles, hydrogen coordinates, and structure factors have been deposited as supplementary data with the Editor.

Table 1. Crystal data and structure refinement for $[PPh_4][In(SePh)_4]$ and $[PPh_4][In(SePh)_3(SeH)]$

Compound	$[PPh_4][In(SePh)_4]$	$[PPh_4][In(SePh)_3(SeH)]$
Chemical formula	$C_{48}H_{40}InPSe_4$	$C_{42}H_{35}InPSe_4$
Formula weight	1078.43	1001.33
a (Å)	9.459(2)	9.873(2)
b (Å)	20.769(4)	13.430(5)
c (Å)	21.786(4)	30.096(7)
β (°)	92.13(3)	97.83(2)
V (Å^3)	4277(2)	3953(2)
Space group	C_{2h}^5-$P2_1/n$	C_{2h}^5-$P2_1/c$
Z	4	4
D calc (g cm^{-3})	1.675	1.682
Temperature (K)[a]	113(2)	113(2)
μ (cm^{-1})	40	96
Transmission factors[b]	0.658–0.780	0.243–0.638
$R(F)$	0.080	0.061
$R_w(F^2)$[c]	0.174	0.138

[a] The low-temperature system is based on a design by Huffman [16]. The diffractometer was operated with the use of the Indiana University PCPS system [17].

[b] The analytical method as employed in the Northwestern absorption program AGNOST was used for the absorption correction [6].

[c] $R(F_o) = \Sigma||F_o|-|F_c||/|F_o|$; $F_o^2 > 2\sigma(F_o^2)$. $R_w(F_o^2) = \{\Sigma[w(F_o^2-F_c^2)^2]/\Sigma wF_o^4\}^{1/2}$; $w^{-1} = \sigma^2(F_o^2)+(0.04\times F_o^2)^2$ for $F_o^2 \geq 0$ and $w^{-1} = \sigma^2(F_o^2)$ for $F_o^2 < 0$.

RESULTS AND DISCUSSION

The structure of $[PPh_4][In(SePh)_4]$ (**1**) comprises well-separated cations and anions. The In(III) center is tetrahedrally coordinated to four $[SePh]^-$ ligands (Fig. 1). The In—Se bond distances range from 2.570(2) to 2.584(2) Å (Table 2), comparable to the In—$Se_{terminal}$ bond distances in $K_8In_4Se_{10}\cdot 16H_2O$ (average 2.543(2) Å) [9] and in $[MeIn(\mu\text{-}SePh)(SePh)]_\infty$ (2.541(4) and 2.542(3) Å) [3]. The Se—In—Se bond angles in $[PPh_4][In(SePh)_4]$ range from 102.00(7) to 112.58(7)°, slightly distorted from tetrahedral, probably as a result of the steric crowding of the bulky phenyl rings. The structure of $[PPh_4][In(S^tBu)_4]$ also features an In(III) atom in a slightly distorted tetrahedral environment [10].

As expected, the ^{77}Se NMR spectrum of $[PPh_4][In(SePh)_4]$ shows a single resonance (δ = 69.9 ppm). This value falls in the broad range observed for organometallic selenolates [11] and is close to that observed for $In(SePh)_3$ (δ = 38.8 ppm) [12].

The structure of $[PPh_4][In(SePh)_3(SeH)]$ (**2**) also comprises well-separated cations and anions. The In(III) center is tetrahedrally coordinated to three

Table 2. Selected bond distances (Å) and angles (°) for $[PPh_4][In(SePh)_4]$ (**1**) and $[PPh_4][In(SePh)_3(SeH)]$ (**2**)

Distance or Angle	1	2
In(1)—Se(1)	2.584(2)	2.553(1)
In(1)—Se(2)	2.571(2)	2.533(1)
In(1)—Se(3)	2.575(2)	2.555(1)
In(1)—Se(4)	2.570(2)	2.521(2)[a]
Se(2)—In(1)—Se(1)	102.00(7)	117.83(5)
Se(3)—In(1)—Se(1)	110.33(8)	100.20(4)
Se(4)—In(1)—Se(1)	112.47(8)	109.67(5)
Se(3)—In(1)—Se(2)	112.34(8)	122.08(5)
Se(4)—In(1)—Se(2)	106.61(8)	99.40(5)
Se(4)—In(1)—Se(3)	112.58(7)	107.18(5)

[a] Se(4) is the Se atom of the SeH group.

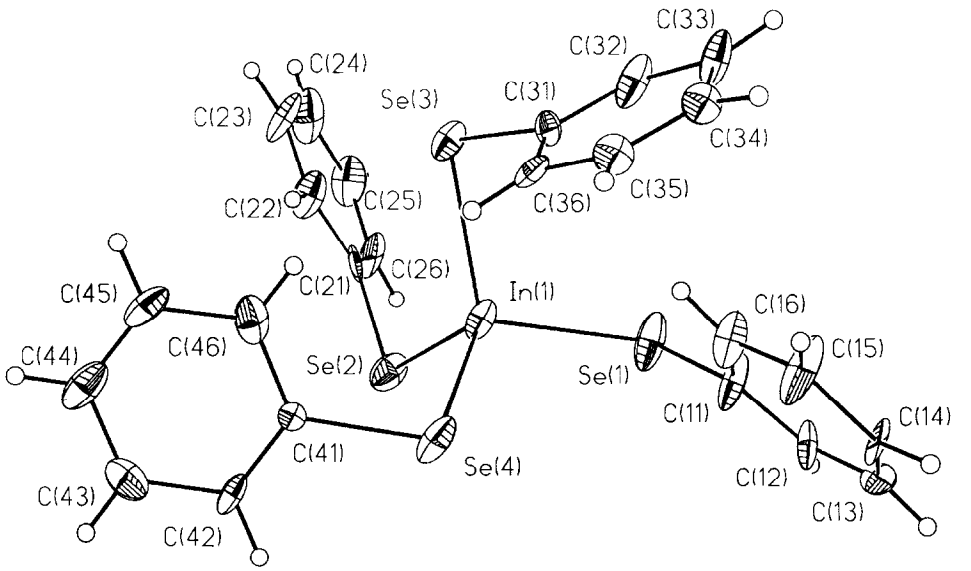

Fig. 1. View of the $[In(SePh)_4]^-$ anion. Here and in the succeeding figure the 50% probability displacement ellipsoids are shown.

$[SePh]^-$ ligands and one $[SeH]^-$ ligand (Fig. 2). The H atom of the $[SeH]^-$ ligand, though not located directly from crystallographic data, was detected spectroscopically (ν(Se—H) = 2241 cm^{-1}). This value may be compared with those of 2260 cm^{-1} in $[(pp_3)RhSeH]$ (pp_3 = tris(2-(diphenylphosphino) ethyl)phosphine) [13] and 2250 cm^{-1} in $[Pd_7Se_6(SeH)Cl(PPh_3)_7]$ [14].

In **2** the In—Se(Ph) bond distances (2.533(1) to 2.555(1) Å) are shorter than those in **1** (2.570(2) to 2.584(2) Å) (Table 2). The In—Se(H) bond distance (2.521(2) Å) is probably shorter than the In—Se(Ph)

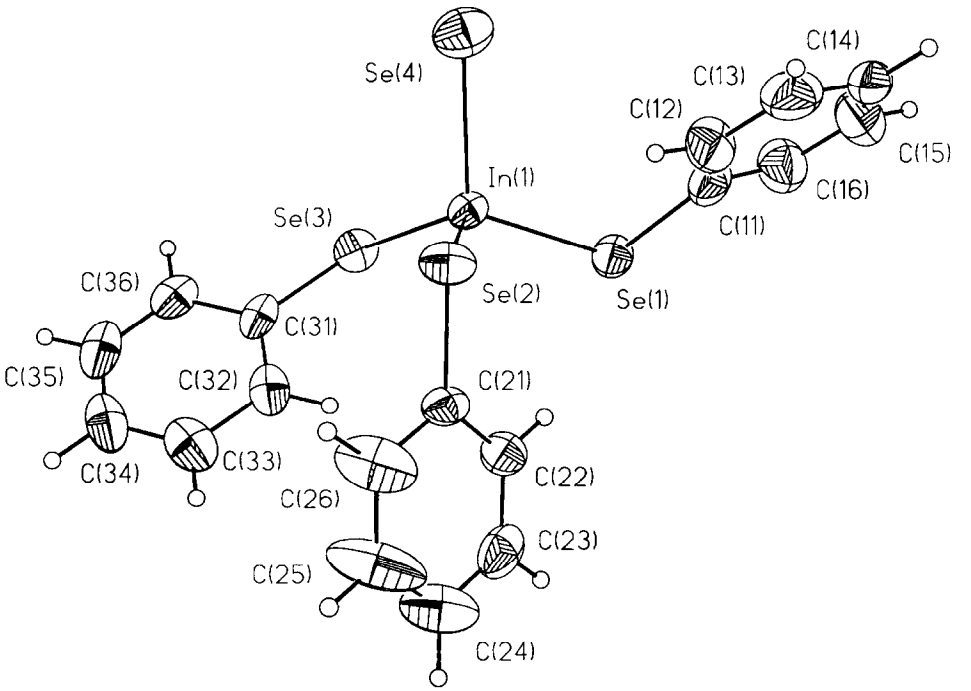

Fig. 2. View of the $[In(SePh)_3(SeH)]^-$ anion.

distances. The In center is again in a distorted tetrahedral environment with the Se—In—Se bond angles ranging from 99.41(5) to 122.10(5)°.

Indium selenolates have been isolated from reactions involving a variety of starting materials. Most often the In source is either In metal [2], $InCl_x$ (x = 1, 3) [4], or InR_3 (R = Me, Mes) [3]. For the synthesis of $[PPh_4][In(SePh)_4]$, $InCl_3$ is reacted with 4 equiv. of NaSePh. Interestingly, if In metal is reacted with 1.5 equiv. of Ph_2Se_2 then $In(SePh)_3$ is isolated [1,2]. $In(SePh)_3$ in turn reacts with PPh_4Br to afford $[PPh_4][InBr(SePh)_3]$ [1,2]. For the synthesis of $[PPh_4][In(SePh)_3(SeH)]$, $InCl_3$ is again reacted with 4 equiv. of NaSePh. The reaction mixture is then added to a flask containing $NaBH_4$ and elemental sulfur to afford **2**. When the reaction is carried out without sulfur or with elemental selenium in place of sulfur crystals of **1** are obtained. In the synthesis of **2** $NaBH_4$ provides a source of hydride and sulfur may act as a phenyl scavenger to afford Ph_2S_2.

Of the few compounds containing $[SeH]^-$ ligands reported, only one was prepared from the reaction of a phenylselenide. Treatment of $Os_6(CO)_{18}$ with $NaBH_4$ followed by the addition of PhSeCl affords the neutral cluster $[Os_6(\mu\text{-H})(CO)_{18}(\mu\text{-SeH})]$ [15]. Here the $[SeH]^-$ unit acts as a bridging ligand.

Acknowledgment—This research was funded by the National Science Foundation, Grant No. CHE95-31232.

REFERENCES

1. Annan, T. A., Kumar, R., Mabrouk, H. E., Tuck, D. G. and Chadha, R. K., *Polyhedron*, 1989, **8,** 865–871.
2. Kumar, R., Mabrouk, H. E. and Tuck, D. G., *J. Chem. Soc., Dalton Trans.*, 1988, 1045–1047.
3. Rahbarnoohi, H., Kumar, R., Heeg, M. J. and Oliver, J. P., *Organometallics*, 1995, **14,** 3869–3875.
4. Hirpo, W., Dhingra, S., Sutorik, A. C. and Kanatzidis, M. G., *J. Am. Chem. Soc.*, 1993, **115,** 1597–1599.
5. Waters, J. M. and Ibers, J. A., *Inorg. Chem.*, 1977, **16,** 3273–3277.
6. de Meulenaer, J. and Tompa, H., *Acta Crystallogr.*, 1965, **19,** 1014–1018.
7. Sheldrick, G. M., SHELXTL PC Version 4.1 An integrated system for solving, refining, and displaying crystal structures from diffraction data. Siemens Analytical X-Ray Instruments Inc., Madison, WI, U.S.A.
8. Sheldrick, G. M., SHELXL-96 Unix Beta-test Version.
9. Krebs, B., Voelker, D. and Stiller, K.-O., *Inorg. Chim. Acta*, 1982, **65,** L101–L102.
10. Hirpo, W., Sutorik, A. C., Dhingra, S. and Kanatzidis, M. G., *Polyhedron*, 1994, **13,** 2797–2800.
11. Duddeck, H., *Prog. NMR Spec.*, 1995, **27,** 1–323.
12. Kumar, R. and Tuck, D. G., *Can. J. Chem.*, 1989, **67,** 127–129.
13. Fenske, D., Fleischer, H., Krautscheid, H., Magull, J., Oliver, C. and Weisgerber, S., *Z. Naturforsch., B: Chem. Sci.*, 1991, **46,** 1384–1394.
14. Di Vaira, M., Peruzzini, M. and Stoppioni, P., *Inorg. Chem.*, 1991, **30,** 1001–1007.
15. Layer, T. M., Lewis, J., Martín, A., Raithby, P. R. and Wong, W.-T., *J. Organomet. Chem.*, 1993, **444,** C57–C59.
16. Huffman, J. C., Ph.D. thesis (Indiana University, 1974).
17. Huffman, J. C. and Streib, W. E., unpublished work.

Pergamon

PII: S0277-5387(97)00419-1

Polyhedron Vol. 17, Nos. 11–12, pp. 2109–2114, 1998
© 1998 Elsevier Science Ltd
All rights reserved. Printed in Great Britain
0277 5387/98 $19.00+0.00

Voltammetric study of the redox chemistry of 2,3-dihydroxy-quinoxaline and its zinc complexes in non-aqueous medium

Mario E. Bodini,* M. Angélica del Valle, Georgina E. Copia and Cecilia Soto

Departamento de Química Inorgánica, Facultad de Química, Pontificia Universidad Católica de Chile, Casilla 306, Santiago de Chile, Chile

(Received 7 February 1997; accepted 26 September 1997)

Abstract—The electrochemical behaviours of 2,3-dihydroxy-quinoxaline (2,3-DH_2Qx) and the complex species formed with zinc(II) have been studied in non-aqueous media. Using dimethylsulphoxide or *N*,*N*-dimethylformamide as solvents the monoanion of the ligand is obtained quantitatively after reduction of one of the hydroxylic protons. The reduction potential for the hydroxylic proton is −1.93 V *vs* S.C.E. in DMSO and −1.68 V *vs* S.C.E. in DMF, reflecting the different donor number of the solvents. If acetonitrile is used, the simultaneous reduction of both hydroxylic protons is observed. The oxidation to the semiquinone is observed at −0.12 V *vs* S.C.E. in DMSO and DMF whereas it appears at −0.02 V *vs* S.C.E. in acetonitrile.

Neither the protonated ligand nor its quinonic form exhibit the formation of stable complexes with zinc(II) whereas the dianionic species produces two coordination compounds having M : L stoichiometric ratios of 1 : 1 and 1 : 2.

The semiquinone form of the ligand by itself shows the tendency to polymerize on the surface of the electrode and it is not stabilized in the presence of this metal ion. A neutral insoluble compound that passivates the electrode is formed when the semiquinone and this metal ion interact. It was not possible to study this complex in detail but the electrochemical evidence indicates that it has formed on the surface of the electrode. © 1998 Elsevier Science Ltd. All rights reserved

Keywords: zinc; 2,3-dihydroxy-quinoxaline; complexes; aprotic medium; voltammetry.

A great deal of information is known concerning biological systems whose functions are facilitated by zinc metal ions. For instance, many enzymes involved in the replication process through DNA and RNA contain zinc in their structure [1] like the RNA-polymerase and the DNA-polymerase enzymes isolated from *Escherichia coli* and the inverse transcriptase isolated from some viruses [2,3]. A totally synthetic model for the photosynthetic process in chlorophyl has been developed in which a tetraphenylporphyrin complex of zinc has been used to capture the visible photons. In this case the electron carriers are ferro- and ferricyanide ions [4,5].

Catechols are bidentate ligands that form a great number of stable metal complexes and that are used by biological systems for the transport and storage of these metal ions [6]. The oxidized form of catechols, quinones, can be reduced reversibly to the semiquinone radical form through one electron transfer. For example, flavins can be reduced through one or two-electron transfer processes to yield the semiquinone or the hydroquinone species [7]. Many other examples of coordination compounds with dioxolenes ligands that are important in biological processes are known [8] as is the case of the stabilization of semiquinone radicals formed by oxidation of dopa by Zn(II) [9]. On the other hand, the extreme reactivity of the Zn(II) dianionic catechol species has been reported [10]. It is clear that these compounds will be the basis for the development of effective catalysts for redox processes.

Trying to develop complexes that can be oxidized at a more positive potential, yielding species with a better reducing power, we have thought of studying the redox chemistry of complexes with a ligand having nitrogen atoms as part of the aromatic ring and two adjacent hydroxyl groups in order to be similar to a catechol and to have a good coordinating capacity.

* Author to whom correspondence should be addressed.

The electron-withdrawing nitrogen atoms caused a deactivation of the ring and the donating ability of the hydroxy groups will be facilitated, making more difficult the release of an electron with the subsequent oxidation of the catecholic residue. Therefore, the oxidation of the dihydroxy species to the corresponding semiquinone will occur at more positive potentials and the coordination compounds will also show this behaviour. We have chosen the compound 2,3-dihydroxy-quinoxaline in which two nitrogen atoms are present in the quinoxaline ring:

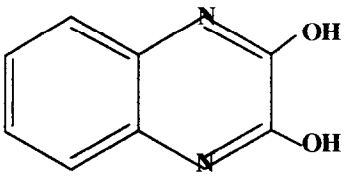

2,3 - Dihydroxyquinoxaline (2,3-DH2Qx)

The study of the redox chemistry of this ligand will be done in non-aqueous solvents in order to stabilize any possible radical species that might be formed as the consequence of the electron-transfer processes. The interaction of the different forms of this ligand with the Zn(II) ion will be studied to obtain knowledge of the redox chemistry of the complexes formed with this metal ion.

EXPERIMENTAL

Equipment

A three-electrode potentiostat (Bioanalytical Systems) Model CV-1A 230 and a Linear Model 8036 X-Y recorder were used for the cyclic voltammetric experiments. Controlled-potential electrolysis was accomplished with a Bioanalytical Systems Model SP-2 and a PUC coulometer.

The electrochemical cell was equipped with a Beckman platinum-inlay working electrode (area 0.23 cm^2), a platinum coil auxiliary electrode and an Ag/AgCl reference electrode filled with an aqueous tetramethylammonium chloride solution and adjusted to 0.00 V vs S.C.E. The latter was contained in a Pyrex tube with a soft-glass cracked tip; this electrode was placed inside a Luggin capillary. For controlled-potential electrolysis a platinum mesh working electrode was employed.

A Milton Roy Model Spectronic 3000 diode array spectrophotometer was used for UV–vis spectrophotometric measurements.

Reagents

The reagents for the investigation and synthesis included $Zn(ClO_4)_2 \cdot 6H_2O$ (G. Frederick Smith), tetrabutylammonium hydroxide (TBAOH, 1.0 M in methanol, Aldrich) and tetramethyl-ammonium chloride (Aldrich). Tetraethylammonium perchlorate (TEAP) was obtained from reaction of a 25% aqueous solution of tetraethylammonium hydroxide (Aldrich) and concentrated perchloric acid (Merck) and recrystallized from anhydrous ethyl alcohol. The ligand 2,3-dihydroxyquinoxaline was obtained from Aldrich Chemical Co.

Aldrich "Gold Label" solvents were used without further purification for all the experiments. High purity argon was used to deaerate solutions.

Since the solvation water of $Zn(ClO_4)_2 \cdot 6H_2O$ interfered with the stoichiometric formation of the complexes under study, $[Zn^{II}(DMU)_6][ClO_4]_2$ (DMU = dimethylurea) [11] was used in all the experiments in which the zinc complexes were formed *in situ*.

RESULTS AND DISCUSSION

In order to study the redox chemistry of this ligand the cyclic voltammetric experiments with its solutions in different solvents yielded the voltammograms illustrated in Fig. 1. In dimethylsulphoxide a reduction process is observed at -1.93 V vs S.C.E. if the potential is scanned initially in the negative direction. Upon reversal of the scan direction two anodic peaks show

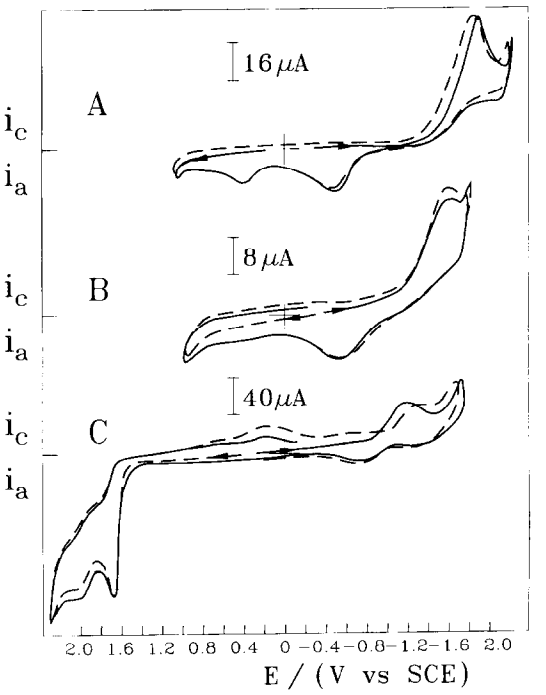

Fig. 1. Cyclic voltammograms of solutions of 2,3-DH_2QX (a) 3 mM in DMSO; (b) 1 mM in DMF and (c) 1 mM in acetonitrile. The scan rate is 100 mV s^{-1}. The supporting electrolyte is 0.1 M TEAP.

up at −0.52 V vs S.C.E. and at +0.42 V vs S.C.E. The anodic peaks are associated with the former reduction process because an initial potential scan toward positive potentials does not show the presence of these processes. Controlled-potential electrolysis at −2.0 V vs S.C.E. indicated that the residual current was attained after the transfer of one equivalent of charge. The dependence of the peak current with the square root of the scan rate for these voltammetric peaks when DMSO is used as the solvent is illustrated in Fig. 2. We can conclude from these results that we are in the presence of a diffusion-controlled process. However, the dependence of the peak current of the anodic peak at −0.52 V vs S.C.E. with the scan rate is not linear. This is characteristic of the oxidation of hydrogen gas on the surface of the electrode which was generated in the previous reduction process. This phenomenon is observed every time a ligand with acidic protons is studied voltammetrically in non-aqueous solvents [12,13,14] and the activation of molecular hydrogen has been described and analyzed very carefully [15]. An analysis of the dependence of the peak current with the square root of the scan rate for the other anodic peak at +0.42 V vs S.C.E. shows that again a linear dependence is obtained indicating that it corresponds to the oxidation of a species in the solution that remains nearby the surface of the electrode.

The molecular structure of this compound makes possible the existence of two forms in equilibrium in which the protons are located either on the oxygen atoms of the hydroxy groups or on the heterocyclic nitrogen atoms of the quinoxaline residue.

Therefore, the reduction process observed can be represented by:

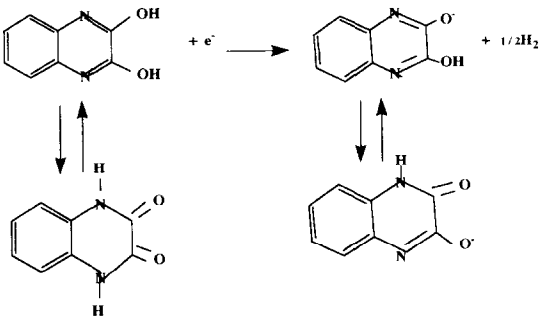

Consequently, the process observed at −0.42 V vs S.C.E. corresponds to the irreversible oxidation of the monoanionic form of the ligand to the protonated semiquinone.

$$[2,3\text{-DHQx}]^- \xrightarrow{-0.42\,V} [2,3\text{-DHSQx}]\cdot + e^-$$

The cyclic voltammogram of a solution of 2,3-DH_2Qx in dimethylformamide is shown in Fig. 1(b). In this case the reduction of one of the acidic protons is observed at −1.68 V vs S.C.E., the oxidation of hydrogen shows up at −0.58 V vs S.C.E. and the oxidation of the monoanion becomes apparent only at +0.50 V vs S.C.E. If the potential is scanned initially in the positive direction the peak at +0.50 V vs S.C.E. can be observed as a very small signal indicating that the monoanionic species is initially present in the solution. The reason for this behaviour is that dimethylformamide has a more basic character than dimethylsulphoxide. The ligand in this solution partially dissociates forming the corresponding monoanion. If we compare the electrochemical behaviour of this ligand in DMF and in DMSO, namely the results of controlled-potential electrolysis and the dependence of the peak current with the square root of the scan rate, we can see that they are very similar. Therefore, we must conclude that the electrode process is the same in both cases.

If acetonitrile is used as the solvent, the voltammetric behaviour is illustrated in Fig. 1(c). In this case the proton reduction shows up at −1.26 V vs S.C.E. with the corresponding oxidation at −0.56 V vs S.C.E. The most important difference in this case with respect to the other two solvents is that a controlled-potential experiment indicates that two equivalents of charge are being transferred in this process. This is indicative that the two protons are reduced simultaneously in this solvent or, at least, as one proton is being reduced the reduction potential of the

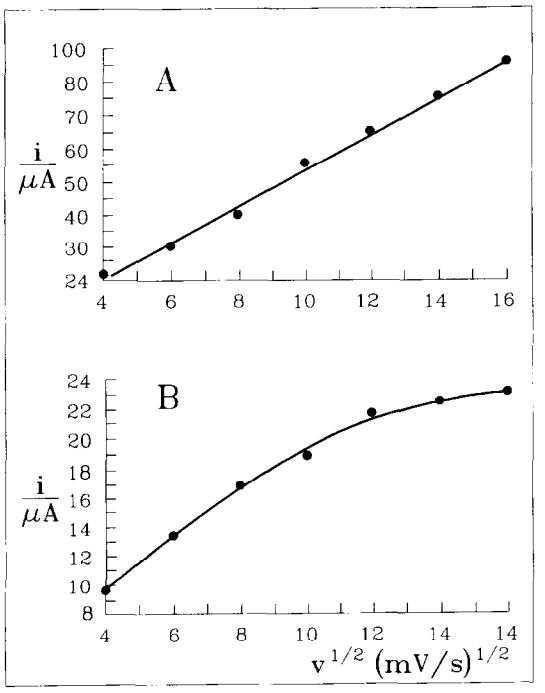

Fig. 2. Dependence of the peak current (a) for the cathodic process at −1.94 V vs S.C.E. and (b) for the anodic process at −0.52 V vs S.C.E. of 2,3-DH_2Qx in DMSO with the square root of the scan rate.

Table 1. Reduction potential for the hydroxylic proton of the ligand and donor numbers of the utilized solvents

Solvent	Ep 2,3-DH_2Qx	Donor effect [16]
DMSO	−1.90 V vs S.C.E.	29.8
DMF	−1.68 V vs S.C.E.	26.6
ACN	−1.26 V vs S.C.E.	14.1

other is shifted so that it is not possible to differentiate them.

$$[2,3\text{-}DH_2Qx]+2e^- \rightarrow [2,3\text{-}DQx]^{2-}+H_2(ads)$$

In this solvent the largest electrochemical window is obtained in the positive side of potentials and two peaks are now observed corresponding to the oxidation of the ligand to yield a radical species which decomposes. Therefore, its reduction is observed only if a very fast scan rate is used. Table 1 illustrates the reduction potentials for the hydroxylic proton of the ligand along with the donor numbers of the solvents used in this work.

If two equivalents of base are added to a solution of 2,3-DH_2Qx to form the dianion no reduction peaks are observed in the solvents studied which is indicative

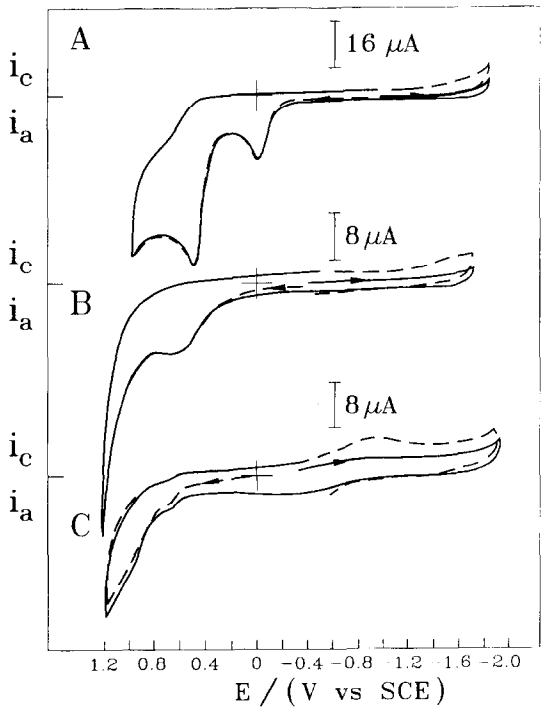

Fig. 3. Cyclic voltammograms of a solution 1 mM in 2,3-DH_2Qx and 2 mM in TBAOH using as solvents (a) DMSO; (b) DMF and (c) acetonitrile. The scan rate is 100 mV s^{-1} and the supporting electrolyte is 0.1 M TEAP.

Table 2. Peak potentials for the oxidation of the dianion in the solvents considered

Solvent	Peak	Peak potential (volts vs S.C.E.)
DMSO	a	−0.12
DMF	a	−0.12
ACN	a	−0.02
DMSO	b	+0.46
DMF	b	+0.46
ACN	b	+0.46
DMSO	c	+0.92
DMF	c	+0.84
ACN	c	+1.86

that no reducible protons are present under these conditions. The cyclic voltammograms for this solution are illustrated in Fig. 3. Notice that three anodic peaks are observed (peaks (a), (b) and (c) in the figure) whose peak potentials in the three solvents are summarized in Table 2.

It is interesting to notice that the peak potentials for peaks (a) and (b) are very similar in the three solvents with the only exception of peak (a) in acetonitrile which shows up at a potential slightly more positive. Peak (c) is found very close to peak (b) in DMSO and DMF precluding a good resolution of the voltammogram. In acetonitrile peak (c) appears at a very positive potential so that the three anodic processes are better resolved. Controlled-potential electrolysis at a potential 100 mV more positive than the peak potential for this process in the three solvents studied indicated that one equivalent of charge was transferred in all chases. The dependence of the peak current with the square root of the scan rate corresponded to a diffusion controlled process. At high scan rates the current does not increase accordingly because a high current density causes a very high local concentration of the radical species produced in the charge-transfer process and its polymerization will block the surface of the electrode.

Accordingly, the oxidation process corresponding to peak (a) must correspond to the generation of the semiquinone species and it can be represented by:

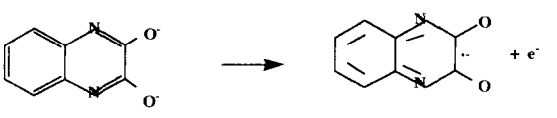

The assignment of peak (b) was not possible because the attempt to do controlled-potential electrolysis at a potential 100 mV more positive than its peak potential resulted in the passivation of the

electrode in the three solvents studied. Considering that the area of this voltammetric peak is similar to that of peak (a) we can suggest that this process also involves the transfer of one equivalent of charge leading to the production of the quinone species. Finally, peak (c) would correspond to a further oxidation of the quinone producing some radical species which would originate some polymeric product considering its molecular structure and the positive potential this process takes place at.

The interaction with Zinc(II) was studied using the dianion of the ligand because no change was observed in the UV–vis spectrum of the quinone in the presence of this metal ion leading us to conclude that no complex is formed between these two species. Figure 4 illustrates the UV–vis spectra of a solution of the quinone generated by controlled-potential electrolysis at 0.6 V vs S.C.E. and a solution of the quinone in the presence of an equimolar amount of Zn(II) ion.

The voltammetric behaviour of solutions of the dianion of the ligand in dimethylsulphoxide in the presence of different amounts of Zn(II) are shown in Fig. 5. If the metal-to-dianion of the ligand mole ratio is 1 : 3 no free metal ion is detected as the voltammetric peak corresponding to the reduction of free Zn(II) to Zn(0), which appears at −1.05 V vs S.C.E., is not observed. On the other hand, the anodic peak corresponding to the oxidation of the free dianion to the corresponding semiquinone shows up at −0.12 V vs S.C.E. Therefore, in this case an excess of the dianion of the ligand is detected. If the metal-to-dianion of the ligand mole ratio is made 1 : 2 no excess either of the metal ion or the dianion of the ligand is detected (Fig. 5(b)) indicating that this is the exact stoichiometry of a complex formed. Only one anodic peak is observed in this case, which must correspond to the oxidation of bound ligand.

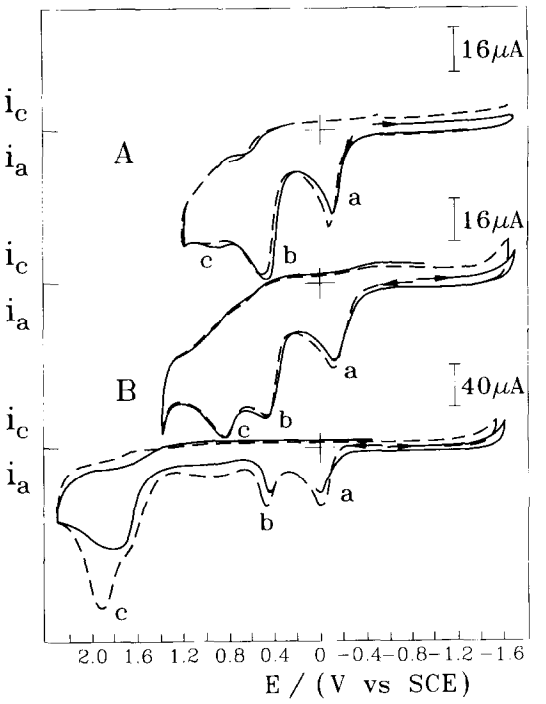

Fig. 5. Cyclic voltammograms of solutions that are 1 mM in 2,3-DQx^{-2} and 2 mM in TBAOH in the presence of (a) 0.33 mM Zn(II). The scan rate is 100 mV s^{-1} and the supporting electrolyte is 0.1 M TEAP.

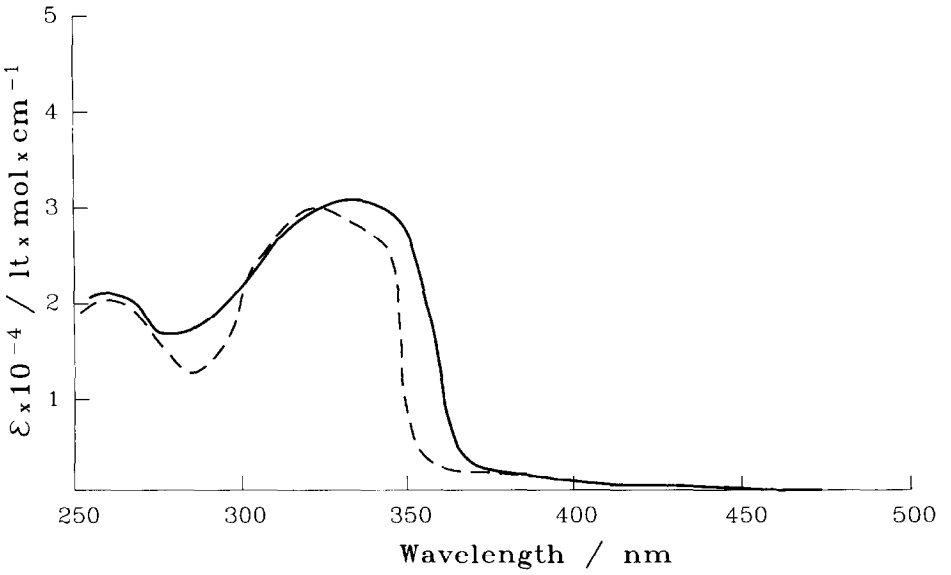

Fig. 4. UV–vis spectra of solutions: (a) 3 mM of the quinone in DMSO generated by controlled-potential electrolysis of the dianion at −0.6 V vs S.C.E. and (b) 3 mM of the quinone and 3 mM of Zn(II) ion.

An attempt to do controlled-potential electrolysis to study this process in detail was not possible because the current dropped to zero very quickly, indicating that in this case the product formed is neutral, it precipitates and blocks the surface of the electrode.

Therefore, we can conclude that a complex with a 1:2 metal-to-dianion of the ligand stoichiometry is formed in solution and that its oxidation can be explained according to the following electrode reaction:

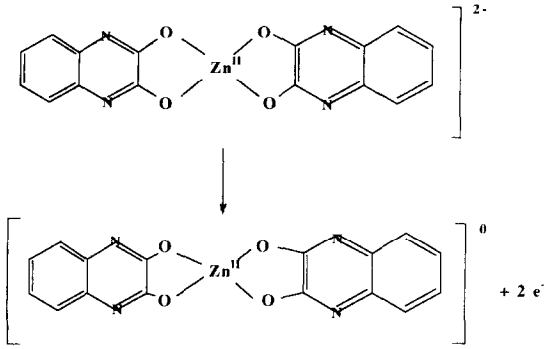

Figure 5(c) shows that in the case of 1:1 metal-to-ligand mole ratio no reduction of the free metal ion is observed if the potential is scanned initially in the negative direction indicating that the metal ion is forming a complex. An anodic peak appears at a potential very close to the solvent discharge. After this oxidation process the presence of free zinc ion becomes evident. In this case, the oxidation of the ligand produces the decomposition of the complex leading to the formation of free quinone and free zinc(II) ion.

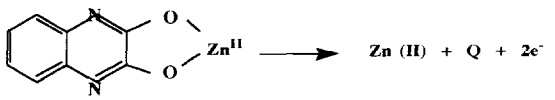

The presence of free quinone after the charge transfer process is inferred by the appearance of free metal ion after the oxidation process and that the UV–vis spectra of a solution of the quinone both in the presence and in the absence of zinc(II) ion look exactly the same. Furthermore, no formation of complexes is observed in the case of 3,5-ditertbutyl-1,2-benzoquinone and Zn(II) ion in dimethylsulphoxide [10].

Therefore, we can finally conclude that the dianion of the ligand 2,3-dihydroxyquinoxaline forms two complexes with Zn(II) having 1:2 and 1:1 metal-to-ligand stoichiometries and that the 1:1 species forms on the surface of the electrode. These complexes probably have a tetrahedral symmetry with two solvent molecules to complete the coordination sphere in the case of the 1:1 complex. The following is a summary of the charge transfer reactions of the different forms of this ligand and the corresponding zinc complexes:

$$[2,3\text{-DHQx}^{=}] \overset{-0.42\,V}{\rightarrow} [2,3\text{-DHSQx}]^{\cdot -} + e^{-}$$

$$[2,3\text{-DHQx}^{=}] \overset{-0.12\,V}{\rightarrow} [2,3\text{-DSQx}^{=}]^{\cdot -} + e^{-}$$

$$Zn[2,3\text{-DQx}]_2 \overset{-0.63\,V}{\rightarrow} Zn[2,3\text{-DSQx}]_2 + 2e^{-}$$

$$Zn[2,3\text{-DQx}] \overset{0.93\,V}{\rightarrow} Zn(II) + Qx + 2e^{-}$$

with the corresponding peak potentials observed. Notice that in this case the oxidation potential for the oxidation of the dianion to the corresponding semiquinone is more positive than in the case of 3,4-ditertbutyl-catechol [10] and in the case of 2,3-dihydroxynaphthalene [17] due to the deactivating effect of the two nitrogen atoms in the quinoxaline residue. In the presence of zinc the oxidation potential of the bound ligands shifts to an even more positive value probably as a consequence of the high stability of the complexes being formed.

These results indicate that this ligand will be very appropriate to stabilize complexes with high oxidation state metal ions considering its high resistance to oxidation.

REFERENCES

1. Ochiai, E., *Bioinorganic Chemistry*, Reverte S.A., 1985, pp. 355–359.
2. Mildvan, A. S., *Ann. Rev. Biochem.*, 1974, **43**, 357.
3. Slater, J. P., Mildvan, A. S. and Loeb, L. A., *Biochim. Biophys., Res. Commun.*, 1971, **44**, 37.
4. Wang, J. H., *Proc. Nat. Acad. Sci. U.S.A.*, 1969, **62**, 653.
5. Huheey, J. E., *Inorganic Chemistry, Principles of Structure and Reactivity*. Harper & Row, 2nd edn, 1981, p. 788.
6. Pierpont, C. G. and Buchanan, R. M., *Coord. Chem. Rev.*, 1981, **38**, 45.
7. Hartland, F. and Vicek Jr., A., *Inorg. Chem.*, 1994, **35**, 1957.
8. Pierpont, C. G. and Lange, C. W., *Prog. Inorg. Chem.*, 1994, **41**, 331–442.
9. Kalyanaraman, B. and Sealy, R. C., *Biochem. Biophys. Res. Commun.*, 1982, **106**, 1119.
10. Bodini, M. E., Copia, G., Robinson, E. and Sawyer, D. T., *Inorg. Chem.*, 1983, **22**, 126.
11. van Loenwen, P. W. and Groenweld, W. L., *J. Inorg. Nucl. Chem. Lett.*, 1967, **3**, 145.
12. Bodini, M. E. and del Valle, M. A., *Polyhedron*, 1990, **9**, 1181.
13. Bodini, M. E., del Valle, M. A. and Arancibia, V., *Polyhedron*, 1993, **12**, 1733.
14. Bodini, M. E., Osorio, C., del Valle, M. A., Arancibia, V. and Muñoz, G., *Polyhedron*, 1993, **14**(20-21), 2933.
15. Barrette, W. C. and Sawyer, D. T., *Anal. Chem.*, 1984, **56**, 563.
16. Sawyer, D. T., Sobkowiak, A. and Roberts Jr., J. L., *Electrochemistry for Chemist*. 2nd edn, Wiley-Interscience, New York, 1995, p. 327.
17. Bodini, M. E. and Arancibia, V., *Trans. Met. Chem.*, 1997, **22**, 150.

Pergamon

PII: S0277-5387(97)00385-9

Polyhedron Vol. 17, Nos. 11–12, pp. 2115–2125, 1998
© 1998 Elsevier Science Ltd
All rights reserved. Printed in Great Britain
0277-5387/98 $19.00+0.00

The reactivity of $[Rh(S_2CNEt_2)(CO)_2]$ towards Hpz^{An}

Mercedes Cano,* Paloma Ovejero, Jose V. Heras, Elena Pinilla, Francisco A. Ruiz and A. Monge

Departamento de Química Inorgánica I and Laboratorio de Difracción de Rayos-X, Facultad de Ciencias Químicas, Universidad Complutense, 28040-Madrid

Instituto de Ciencias de los Materiales, sede D, C.S.I.C., Cantoblanco, Madrid, Spain

(Received 4 June 1997; accepted 18 September 1997)

Abstract—The reaction of $[Rh(S_2CNEt_2)(CO)_2]$ and Hpz^{An} (3(5)-*p*-methoxyphenylpyrazole) in acetone at room temperature yields to a mixture of $[Rh(\mu\text{-}pz^{An})(S_2CNEt_2)(CO)]_2$ (**2**) and $[Rh(S_2CNEt_2)_3]$ (**3**). The same results were obtained from the reaction of $[RhCl(CO)_2(H\text{-}pz^{An})]$ with NaS_2CNEt_2. The first reaction in boiling solvents (acetone, dichloromethane) didn't yield to the binuclear complex (**2**) but an unexpected complex $[Rh(S_2CNEt_2)(CO)]_2$ (**1**) was obtained. Complex (**1**) was proved to be the evolution result of the starting $[Rh(S_2CNEt_2)(CO)_2]$ in boiled solvents. The molecular structure of complex (**3**) has been determined. Crystals of (**3**) are monoclinic, space group C2/c, and is a different form than that previously reported for $[Rh(S_2CNEt_2)_3]$. Subtle differences between the molecular structures are also found. © 1998 Elsevier Science Ltd. All rights reserved

Keywords: dithiocarbamate; rhodium; pyrazole.

We have recently described the chemical behaviour of $[Rh(S_2CNEt_2)(CO)_2]$ towards P-donor ligands [1]. In those reactions the substitution of one or both carbonyl groups was induced by the $R_2NCS_2^-$ ligands giving rise to $[Rh(S_2CNR_2)(CO)(P(4\text{-}XC_6H_4)_3)]$ or $[Rh(S_2CNR_2)(P(4\text{-}XC_6H_4)_3)_2]$ (R = Et, Me; X = Cl, F, CH_3, CH_3O) depending on the stoichiometry and reaction conditions [1].

On the other hand, *N*-donor ligands containing the pyrazol functionality have proved to be versatile ligands towards rhodium being attached to the metal either an unidentate neutral (Hpz) or bridging anionic mode (pz) [2,3].

Although the proton loss of the Hpz groups was common by the presence of alkali in the reaction, several other examples indicate that factors like the nature of the other ligands on the metal or the nucleophilicity of the pyrazole group could give rise to the formation of binuclear pyrazolate species [4].

Following our precedents in Rh(I) chemistry we decide to investigate the coordinative ability of the Hpz^{An} (An = 3(5)-*p*-methoxyphenyl) towards $[Rh(S_2CNEt_2)(CO)_2]$. That pyrazol was chosen because in previous works the chemistry of Rh(I) compounds containing this ligand [2,3] had been well established and crystalline structures of $[RhCl(CO)_2(H\text{-}pz^{An})]$ [2] and $[Rh(\mu\text{-}pz^{An})(CO)_2]_2$ [5] solved.

In this work the reactivity of $[RhCl(CO)_2(H\text{-}pz^{An})]$ towards $Et_2NCS_2^-$ ligand has also been analyzed. From that reaction the same $[Rh(\mu\text{-}pz^{An})(S_2CNEt_2)(CO)]_2$ (**2**) and $[Rh(S_2CNEt_2)_3]$ (**3**) compounds were identified as final products.

The crystalline structure of (**3**) is also described and compared with that previously reported [6]. We also comment on the ligands redistribution process from the starting compound $[Rh(S_2CNEt_2)(CO)_2]$ towards the dimer $[Rh(S_2CNEt_2)(CO)]_2$ (**1**).

RESULTS AND DISCUSSION

The reaction of $[Rh(S_2CNEt_2)(CO)_2]$ and Hpz^{An} (3(5)-*p*-methoxyphenylpyrazole) has been carried out. Different solvents, temperature and reaction times

* Author to whom correspondence should be addressed.

were tried in order to achieve carbonyl derivatives containing $Et_2NCS_2^-$ and pyrazol ligands.

It is interesting to note that in acetone or dichloromethane at reflux temperature, after ca 2 or 6 h of reaction respectively an unexpected product was formed. The new compound was characterized as $[Rh(S_2CNEt_2)(CO)]_2$ (**1**) as will be described below.

The same complex (**1**) was also performed from $[Rh(S_2CNEt_2)(CO)_2]$ both in solid state and in solution.

On the other hand, the complex $[Rh(\mu\text{-}pz^{An})(S_2CNEt_2)(CO)]_2$ (**2**) was achieved from the above reaction at room temperature after ca 10 days independently of the solvent used.

It was remarkable that in all cases the complex $[Rh(S_2CNEt_2)_3]$ (**3**) was also obtained as by-side product.

In the following points the complexes (**1**), (**2**) and (**3**) will be discussed.

$[Rh(S_2CNEt_2)(CO)]_2$ (1)

$[Rh(S_2CNEt_2)(CO)_2]$ in acetone at room temperature evolves after 9 days to a shine black solid product from which the dinuclear complex $[Rh(S_2CNEt_2)(CO)]_2$ (**1**) was separated after several recrystallizations. $[Rh(S_2CNEt_2)_3]$ (**3**) was also obtained as by-side product and identified by X-ray diffraction. Its crystalline structure which was also solved will be described below. Despite repeated attempts to eliminate (**3**) from the mixture it was not possible as we deduced by ^1H NMR.

If in the above treatment the temperature is increased until reflux of acetone or dichloromethane, the same evolution products were raised after ca 2 or 6 h respectively.

Therefore the observed evolution of $[Rh(S_2CNEt_2)(CO)_2]$ towards $[Rh(S_2CNEt_2)(CO)]_2$ (**1**) appears to be responsible that the reaction of $[Rh(S_2CNEt_2)(CO)_2]$ with Hpz^{An} ligand at reflux temperature doesn't give rise to the desired pyrazolil derivative. The mixture of (**1**), (**3**) and an unidentified product was also obtained after a slow evolution of $[Rh(S_2CNEt_2)(CO)_2]$ in the solid state.

Reaction of $[Rh(S_2CNEt_2)(CO)]_2$ (**1**) with Hpz^{An} was tried, however it didn't work under any conditions.

The complex (**1**) was characterized by elemental analyses, IR and ^1H-NMR spectroscopies, mass spectrometry and magnetic measurements.

IR spectroscopy was used to monitor the course of the evolution (Fig. 1). The complete transformation of the starting complex in solution towards complex (**1**) was observed after 9 days at room temperature.

The IR spectrum (in KBr disc) of the new compound (**1**) (Table 1) shows two ν(CO) bands at 2020 and 1967 cm^{-1} which are shifted to lower frequencies to respect to dicarbonylic precursor. Those values are consistent with an oxidation state + I on the rhodium atom and with a *cis*-$Rh(CO)_2$ distribution [7]. The remaining bands from the dithiocarbamate ligands are similar to those of the related compounds, $[Rh(S_2CNEt_2)_3]$ (**3**) and $[Rh(S_2CNEt_2)(CO)_2]$ [8]. The unique band showing a significant shift is the ν(CN) band which moves 10 cm^{-1} to lower frequencies to respect to the starting monomer. Such a shift has been attributed to the presence of bridging dithiocarbamate ligands [9].

The ^1H NMR spectrum in $CDCl_3$ (Table 1) shows three resonances at δ 3.81, 3.72 and 3.60 ppm as multiplets. The signals at δ 3.72 and 3.60 ppm are assigned to the *N*-methylene protons of two unequivalent ethyl groups of the diethyldithiocarbamate ligands of complex (**1**) and the multiplets at δ 3.81 and 3.60 ppm (as superimposed signal) evidence the presence of $[Rh(S_2CNEt_2)_3]$ (**3**). The multiplet at δ 1.26 ppm includes the signal corresponding to CH_3 groups of both compounds.

The mass spectrum of complex (**1**) does not contain a parent-ion peak being the highest value *m/e* peak at 945.9 corresponding to $[Rh_2(S_2CNEt_2)_3]^+$ ion. Related ion peaks at 797.9 and 649.9 from $[Rh_2(S_2CNEt_2)_4]^+$ and $[Rh_2(S_2CNEt_2)_3]^+$ respectively are also observed. An explanation for that behaviour emerges by considering the interaction of the $[Rh(S_2CNEt_2)_2]^+$ and $[Rh(S_2CNEt_2)_3]^+$ fragments from the mixture of (**1**) and (**3**) derivatives.

The magnetic susceptibility of sample (mixture of (**1**) and (**3**) (as impurity)) was measured showing the diamagnetic character of described complex (**1**).

From the above findings we suggested a structure for (**1**) as depicted in Fig. 2. In that the $[Rh(CO)_2]$ fragment is bonded to the $[Rh(S_2CNEt_2)_2]$ group with the dithiocarbamate ligands acting as chelating to a metal centre and bridging by a S atom to the other rhodium atom. Related structures has also been observed in some dinuclear complexes [9–11].

$[Rh(\mu\text{-}pz^{An})(S_2CNEt_2)(CO)]_2$ (2)

Reaction of the compound $[Rh(S_2CNEt_2)(CO)_2]$ with a stoichiometric amount of Hpz^{An} in acetone solution at room temperature leads to the dinuclear $[Rh(\mu\text{-}pz^{An})(S_2CNEt_2)(CO)]_2$ (**2**) which was isolated after 10 days of reaction as air-stable orange solid, mixed with orange crystal of $[Rh(S_2CNEt_2)_3]$ (**3**). Due to the similar solubility of both products all attempts to obtain pure complex (**2**) were unrewarding as deduced by the analytical data. However the product could be characterized by mass spectrometry, IR and ^1H NMR spectroscopy.

The diamagnetic character of sample was determined suggesting the diamagnetism of complex (**2**).

The dimeric nature of complex (**2**) was evidenced by mass spectrometry. The mass spectrum of (**2**) contains a parent-ion peak at 905 corresponding to the dimer $[Rh(\mu\text{-}pz^{An})(S_2CNEt_2)(CO)]_2$ and other peaks at 876.1, 848.1 and 675.0 corresponding to the $[Rh_2(\mu$-

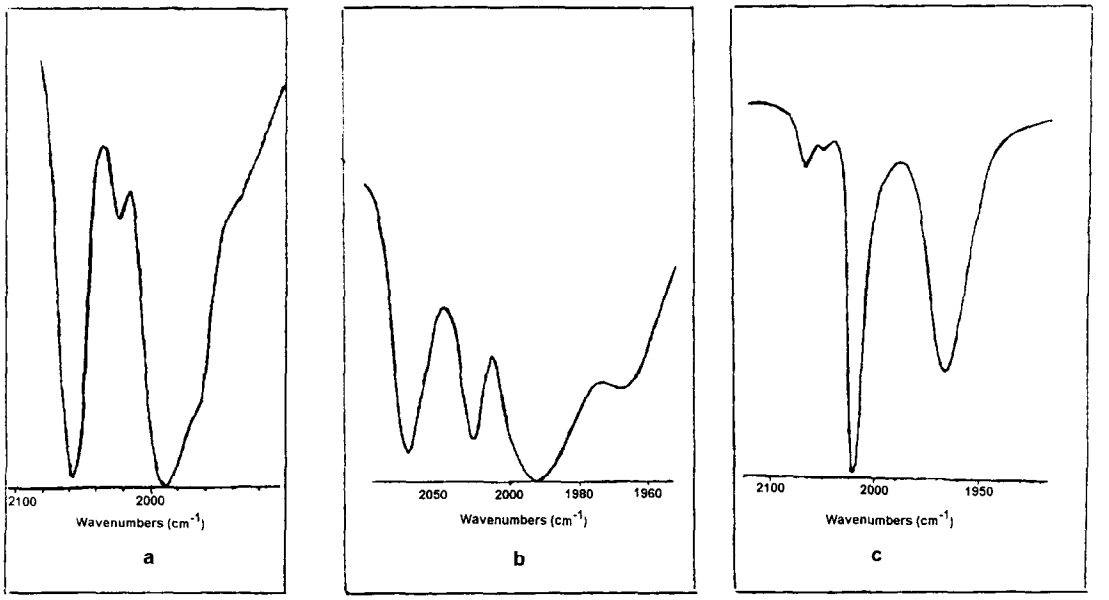

Fig. 1. Observed evolution of $[Rh(S_2CNEt_2)(CO)_2]$ compound in solid state in the IR carbonyl region. (a) 5 h, (b) 6 days and (c) 9 days.

Table 1. IR (cm^{-1}), ^1H NMR (δ, (ppm) J(Hz)) spectroscopic data for the complexes (**1**), (**2**), (**3**) and the parent compound $[Rh(S_2CNEt_2)(CO)_2]$

	IR[a]		^1H NMR[b]					
	CO	$Et_2NCS_2^-$	$Et_2NCS_2^-$		Pyrazole protons			
Complex	ν(CO)	ν(CN)	$\delta(CH_2)$	$\delta(CH_3)$	$\delta(H_3)$	$\delta(H_4)$	$\delta(p\text{-}OMeC_6H_4)$	
(**1**)	2020 vs	1508 vs	3.60 m	1.26 m				
	1967 vs		3.72 m					
			3.81 m					
(**2**)	2070 vs	1506 vs	3.82 m	1.25 m	7.72 (d, 2.4)	6.50 (br s)	7.97 (d, 8.4)H_o	7.96 (d, 8.1)H_o
	2005 vs		3.60 m		7.56 (d, 2.1)	6.36 (d, 2.7)	7.87 (d, 8.4)H_o	7.84 (d, 8.4)H_o
					7.47 (br s)	6.344 (d, 2.1)	7.00 (d, 8.4)H_m	6.93 (d, 8.1)H_m
					7.44 (br s)	6.342 (d, 2.4)	3.89 (s, —OMe)	3.83 (s, —OMe)
(**3**)		1497 vs	3.60 m	1.26 m				
			3.82 m					
$[Rh(S_2CNEt_2)(CO)_2]$	2.54 vs	1518 vs	3.77 q	1.28 t				
	1998 vs							
	1980 vs							

[a] In KBr discs.

[b] In $CDCl_3$ solution. vs = very strong; m = multiplet; t = triplet; q = quartet; d = doublet; br s = broad signal; s = singlet.

$pz^{An})_2(S_2CNEt_2)_2(CO)]^+$ $[Rh_2(\mu\text{-}pz^{An})_2(S_2CNEt_2)_2]^+$ and $[Rh_2(\mu\text{-}pz^{An})(S_2CNEt_2)_2]^+$ fragments respectively. An ion peak at 547 from $[Rh(S_2CNEt_2)_3]^+$ is also present.

On the other hand, some characteristic features were observed in the IR spectrum of the complex (**2**) (Table 1).

1. The two carbonyl bands characteristic of a *cis*-$Rh(CO)_2$ group [7] are moved ca 15 cm^{-1} towards higher energy and the ν(CN) band is also shifted 12 cm^{-1} towards lower energy to respect to the parent dicarbonyl complex. Although those displacements agree with an increase in the oxidation state on the rhodium atom the latter one has also been considered as the result of a decrease in the number of ligands sharing the same positive charge [9].

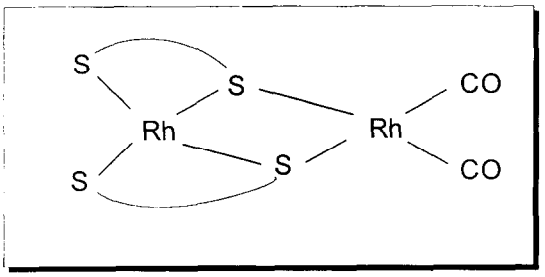

Fig. 2.

2. The compound (**2**) shows the unexpected absence of ν(N—H) of the pyrazole group, which agree with the presence of pyrazolate groups. The derivative (**2**) has been obtained in the absence of alkali, thus providing another example of the formation of a pyrazolate derivative rather than the neutral pyrazole product expected under such conditions. Several other examples of such proton loss exist [4].

From the above results we suggest two types of environment for each Rh in the dinuclear complex (**2**). In that, the $[Rh(S_2CNEt_2)_2]$ fragment should be bonded to a *cis*-$Rh(CO)_2$ group through two pyrazolate bridging ligands.

The ^{1}H NMR data in $CDCl_3$ solution were recorded and listed in Table 1. No signals of H—N protons are observed in agreement with the IR ν(NH) absence confirming the pyrazolate nature of these groups and supporting the suggested formula.

On the other hand, the pattern of signals was more complicated than that expected for one complex containing only one type of $Et_2NCS_2^-$ and pyrazolate groups. So four signals at δ 7.72, 7.56, 7.47 and 7.44 ppm as well as other four signals at 6.50, 6.36, 6.35, and 6.34 ppm are attributed to the H_5 and H_4 protons respectively of four unequivalence pyrazolate rings. In addition four signals at δ 7.97, 7.96, 7.87 and 7.84 ppm corresponding to H(orto) and two signals at δ 7.00 and 6.93 ppm from the related H(meta) of the phenyl substituent are also observed. All of those data imply the presence of a mixture of pyrazolate complexes.

Due to unsymmetrical substitution of the bridging pyrazolate ligands the dinuclear complexes of the type $[Rh(\mu\text{-}pz^R)(L_2)]_2$ [2] may exist as two geometrical isomers, H—H and H—T and indeed both isomers were detected by ^{1}H NMR in the related compound $[Rh(\mu\text{-}pz^{An})(CO)_2]_2$ [2]. Although these types of isomers could also be proposed in complex (**2**), for that the presence of two different metal environments $[Rh(CO)_2]$ and $[Rh(S_2CNEt_2)_2]$ suggests a third new form H—H(B) as depicted in Fig. 3. Therefore the above ^{1}H NMR results could be considered as due to the mixture of the three isomeric forms: H—H(A), H—H(B) and H—T (Fig. 3).

On the other hand, the *N*-methylene proton signals of the $Et_2NCS_2^-$ ligands appear as two multiplets at δ 3.82 and 3.60 ppm of marked different shape and intensity. Both of them are consistent with the presence of $[Rh(S_2CNEt_2)_3]$ (as will be discussed below) but the CH_2 *N*-methylene protons of complex (**2**) should be also included in the broad signal at δ 3.82 ppm. In addition the chemical shifts of the OMe protons of anysol substituent are also observed at δ 3.89 and 3.83 ppm (as superimposed signals to the multiplet at δ 3.82 ppm).

The methyl proton resonance of the $Et_2NCS_2^-$ ligands appears as a broad signal at δ 1.25 ppm in which the characteristic triplet of $[Rh(S_2CNEt_2)_3]$ is also superimposed.

An alternative route to product the complex (**2**) was also found by reaction of the square planar complex $[RhCl(CO)_2(H\text{-}pz^{An})]$ with NaS_2CNEt_2 ligand. The reaction solution colour changed from orange-yellow to dark orange immediately. The course of reaction was monitored by IR spectroscopy. After 9 days a mixture of (**1**) and (**2**) was detected and both complexes mixed with the complex (**3**) were isolated from the solution. It was noteworthy to indicate that the reaction occurs through $[Rh(S_2CNEt_2)(CO)_2]$ as intermediate which was detected after 3 h.

A schematic representation of the reactions is depicted in Scheme 1.

$[Rh(S_2CNEt_2)_3]$ (3)

As we have described above during the study of the reactivity of $[Rh(S_2CNEt_2)(CO)_2]$ with Hpz^{An} we proved the formation of $[Rh(S_2CNEt_2)_3]$ (**3**) as a by-side product in all of the realized treatments.

Complex (**3**) was isolated as orange crystals which were separated from the mixture of products and its crystalline structure solved. The identity of (**3**) as $[Rh(S_2CNEt_2)_3]$ was also evidenced by comparation of its ^{1}H NMR spectrum with that obtained from the product synthetized by reaction of $RhCl_3$ and NaS_2CNEt_2 [12].

Particular results from ^{1}H NMR and X-ray diffraction crystalline structure studies of (**3**) were obtained and reported here.

^{1}H NMR

The ^{1}H NMR studies of diamagnetic *N,N*-dialkildithiocarbamate derivatives of trivalent transition metals have been described in terms of the cobalt(III) behaviour [12]. Therefore for our propose ^{1}H NMR data of $[Co(S_2CNEt_2)_3]$ were used as reference [12].

A ^{1}H NMR study for (**3**) in a range of solvents

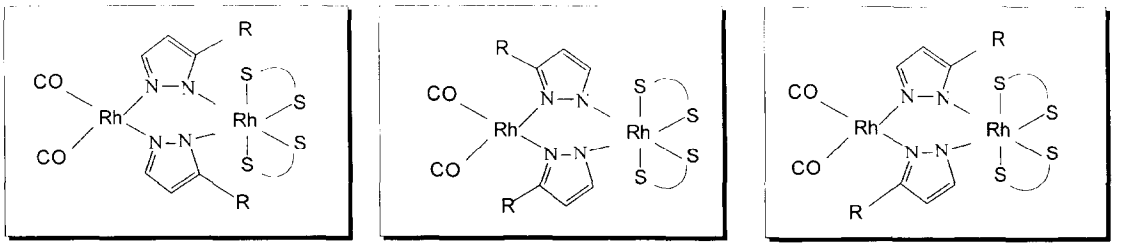

H - H (A) H - H (B) H - T

R = p-$CH_3OC_6H_4$

$\widehat{SS}$ = $Et_2NCS_2^-$

Fig. 3.

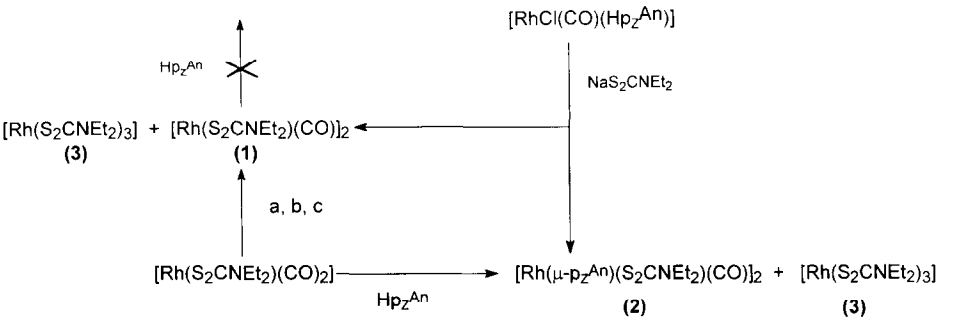

a room temperature for 9 days

b reflux temperature of acetone or dichlorometane

c evolution of solid state

Fig. 3.

and temperatures was achieved. $CDCl_3$, $(CD_3)_2CO$, CD_3OD, $(CD_3)_2SO$ and C_6D_6 were used as solvents.

In $CDCl_3$ at room temperature the protons of the *N*-methylene groups appear as a pair of well defined multiplets at δ 3.82 and 3.60 ppm (Fig. 4) in contrast with the multiplet observed for $[Co(S_2CNEt_2)_3]$ in the same solvent and temperature conditions [12]. However, while the former one was performed with a 300 MHz spectrometer the latter one had been registered with a 60 MHz one. Both multiplets characteristic of an ABX_3 system were the result of the magnetic unequivalence of the *N*-methylene protons in agreement with the noncentrosymmetric structure of $[Rh(S_2CNEt_2)_3]$. In all of the other solvents the ^1H NMR spectra of (**3**) show one multiplet for the *N*-methylene protons being the separation of its components increased in the order $C_6D_6 < (CD_3)_2SO < CD_3OD < (CD_3)_2CO$ (Fig. 4).

A strong interaction of the chloroform solvent with $[Rh(S_2CNEt_2)_3]$ (**3**) is proposed as responsible of its ^1H NMR behaviour. The interpretation of this chloroform-dithiocarbamate interaction has been suggested elsewhere that occurs at the nitrogen atom [13], although structural results for dithiocarbamate derivatives indicate that the S···H interactions are the dominant intermolecular forces within the crystal lattices [13].

From our results, chloroform-dithiocarbamate interaction was clearly established but weak similar interactions with *O*-donor solvents should not be excluded. Related with this consideration it was interesting to note that only in C_6D_6 solution in which there was not solvent interaction the ^1H NMR spectrum of (**3**) gave the typical quartet-triplet of symmetric dithiocarbamate complexes.

X-ray crystal structure

The crystal structure of the title compound $[Rh(S_2CNEt_2)_3]$ (**3**) has been determined by X-ray diffraction. In previous studies the crystal structure of $[Rh(S_2CNEt_2)_3]$ has already been reported, the crystal system being monoclinic space group $P2_1/a$ [6]. How-

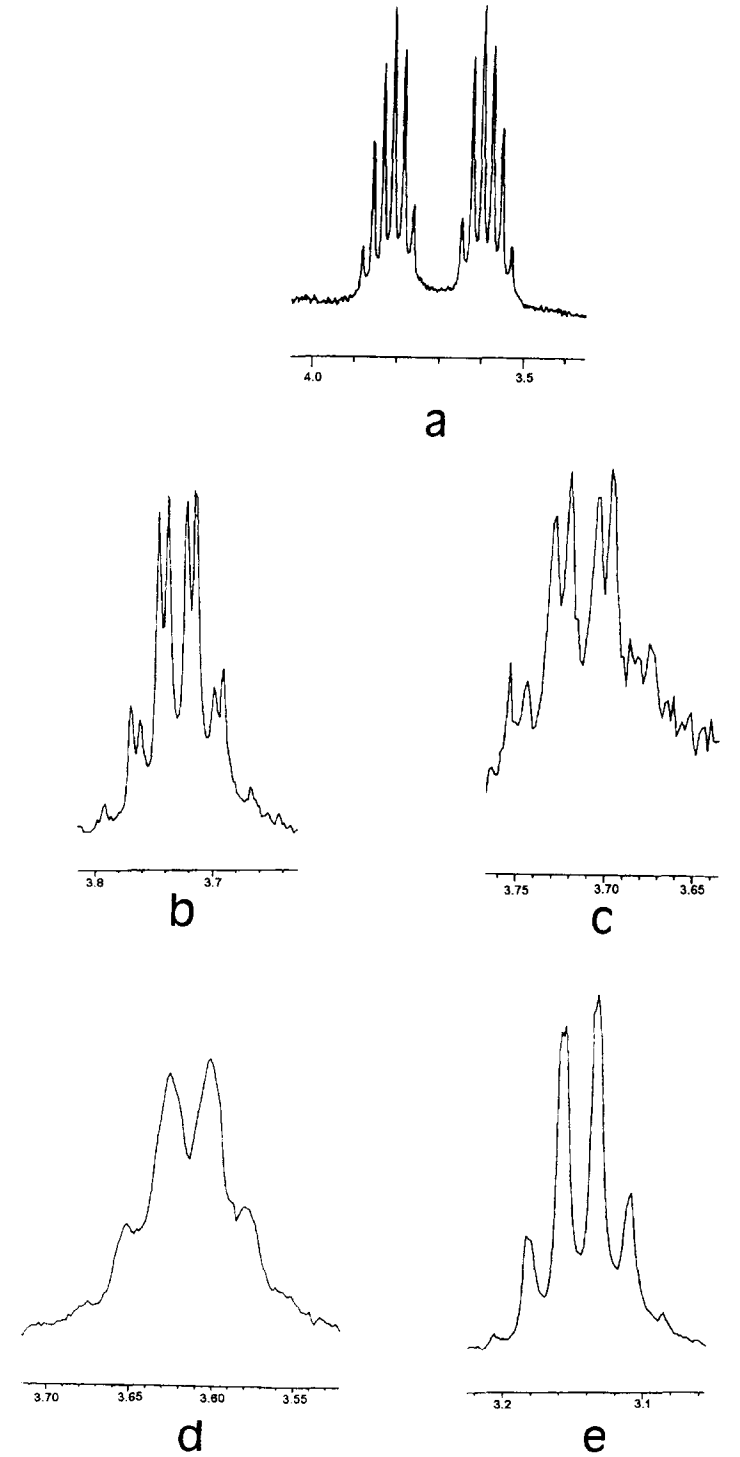

Fig. 4. *N*-methylene proton signals from ^{1}H NMR of (**3**) in different solvents: (a) $CDCl_3$, (b) $(CD_3)_2CO$, (c) CD_3OD, (d) $(CD_3)_2SO$, (e) C_6D_6.

ever, from the structural data of the well formed prismatic crystals of (**3**) we deduced that a new crystalline form had been isolated, cell symmetry *C*2/c. It was elsewhere reported that for complexes of type $[M(S_2CNEt_2)_3]$ subtle differences in the crystalline packing occur as the metal-sulphur distances *r* change. So, the molecular array commons shown a symmetry *C*2/c when $r <$ ca 2.36 Å, a symmetry *A*2/a when

$r >$ ca 2.43 Å and a $P2_1/c$ in the intermediate range [6]. A metal-sulphur distance of 2.352(2) Å (Table 2) was observed in (**3**) in agreement with the space group $C2/c$.

For (**3**), the lattice consists of discrete molecules of $[Rh(S_2CNEt_2)_3]$, which bear a two-fold symmetry axis passing through the rhodium atom and the axis if ligand 1, lying the plane of this ligand approximately parallel to the xy face (Fig. 5). As in the isostructural Co(III) [14] and Ir(III) [15] derivatives each molecule consists of a metal atom coordinated by three bidentate ligands being the MS_6 core geometry a good approximation to D_3.

As usual, the S_2CNC_2 section of the ligands are substantially planar. The best least-squares plane for S_2CNC_2 shows a maximum deviation of 0.0187(7) Å for C2 atom and of 0.046(6) for C7 atom (Fig. 6), of ligand 1 and 2 respectively [16].

The terminal methyl groups on the ligand adopt the usual conformation lying on alternate sides of the ligand plane at the same way that it was observed for $[Rh(S_2CNEt_2)_3]$ $P2_1/a$ [6]. However while the latter one shows almost equivalent distances of the groups to the ligand planes, the former one exhibits marked differences of those distances in two of the ligands (2 and 2′). In addition the methyl-methyl distance in ligands 2 and 2′ was shorter than in ligand 1, in other words the methyl groups of two ligands (2 and 2′) are approached but distanced in other one (1) (Table 3). In Fig. 7 the schematic representation of the two types of molecules founded for $[Rh(S_2CNEt_2)_3]$ were depicted.

Other difference emerges [15] by considering the values of $\theta = 22.03$ and $h = 1.20$ (θ = angle twist about the three-fold axis, h = S—S′ distance divided by M—S distance) following Kepert's ligand repulsion model [17]. From those values a lower distortion from the octahedral geometry than that observed in described crystal $P2_1/c$ was deduced.

EXPERIMENTAL

All reactions were performed under dioxygen-free dry dinitrogen, using freshly distilled, dried and degassed solvents. Syntheses of starting Rh-complex and the ligand have been described previously: $[Rh(S_2CNEt_2)(CO)_2]$ [8], $[RhCl(CO)_2(H\text{-}pz^{An})]$ [2] and Hpz^{An} [18].

Elemental analyses for carbon, hydrogen and nitrogen were carried out by the Microanalytical Service of the Complutense University. IR spectra were recorded on a FT-IR Nicolet magna 550 spectrometer in KBr discs. ^1H NMR spectra were performed on a Varian VXR XL-300 (299.95 MHz). Chemical shifts δ are listed in parts per million relative to tetramethylsilane; coupling constants J are in hertz. The ^1H chemical shifts and coupling constants are accurate to 0.01 ppm and 0.2 Hz respectively. FAB mass spectra were recorded on a VG AutoSpec spectrometer. Magnetic measurements were made using a Faraday type susceptometer equipped with a nitrogen continuous-flow cryostat.

Preparation of $[Rh(S_2CNEt_2)(CO)]_2$ (**1**)

An orange solution of $[Rh(S_2CNEt_2)(CO)_2]$ (0.4 mmol) in acetone (15 ml) was stirred at room tem-

Table 2. Selected bond distances (Å) and angles (°) for $[Rh(S_2CNEt_2)_3]$ with e.s.d.'s in parentheses

Rh—S1	2.351(2)	S3—C4	1.709(5)
Rh—S2	2.353(2)	N2—C4	1.330(6)
Rh—S3	2.351(1)	N2—C5	1.468(8)
S1—C1	1.712(4)	N2—C7	1.461(7)
C1—N1	1.33(1)	C5—C6	1.437(8)
N1—C2	1.460(8)	C7—C8	1.474(11)
C2—C3	1.474(12)	S1—S1′	2.834(2)
S2—C4	1.704(5)	S2—S3	2.821(2)
S3—Rh—S1′	96.69(5)	N1—C2—C3	113.4(6)
S2—Rh—S1′	166.3(6)	Rh—S2—C4	87.4(2)
S2—Rh—S3	73.69(5)	Rh—S3—C4	87.4(1)
S1—Rh—S1′	74.1(6)	C5—N2—C7	118.1(4)
S1—Rh—S3	94.48(5)	C4—N2—C7	120.7(4)
S1—Rh—S2	96.75(7)	C4—N2—C5	120.6(4)
Rh—S1—C1	87.09(7)	S3—C4—N2	123.9(4)
S1—C1—S1′	111.7(1)	S2—C4—N2	124.7(4)
S1—C1—N1	124.14(9)	S2—C4—S3	111.5(2)
C1—N1—C2	120.7(3)	N2—C5—C6	115.0(6)
C2—N1—C2′	118.7(4)	N2—C7—C8	112.5(5)

′ $1-x, y, 1/2-z$.

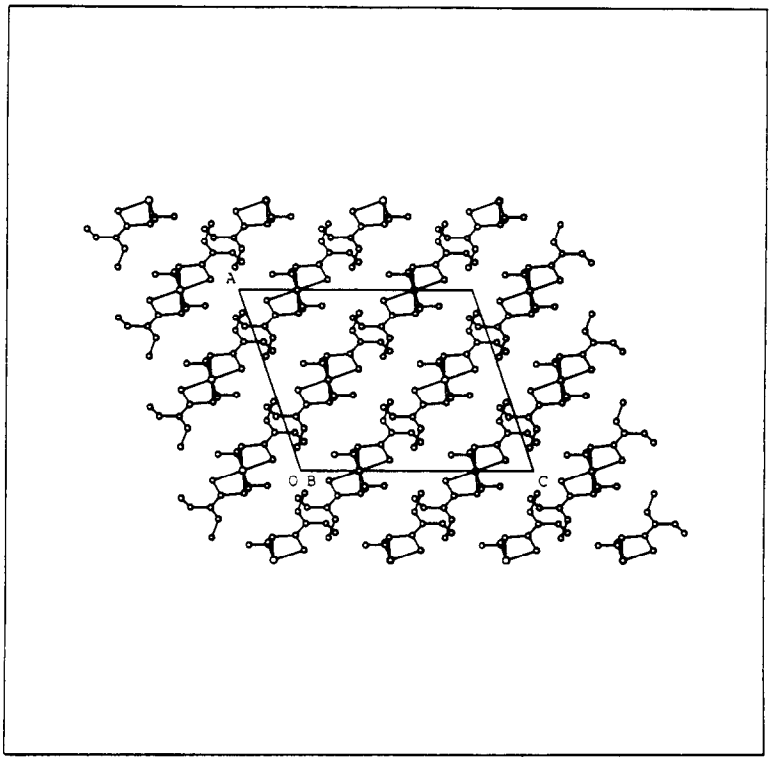

Fig. 5. Packing arrangement in (**3**) viewed down the *b* axis.

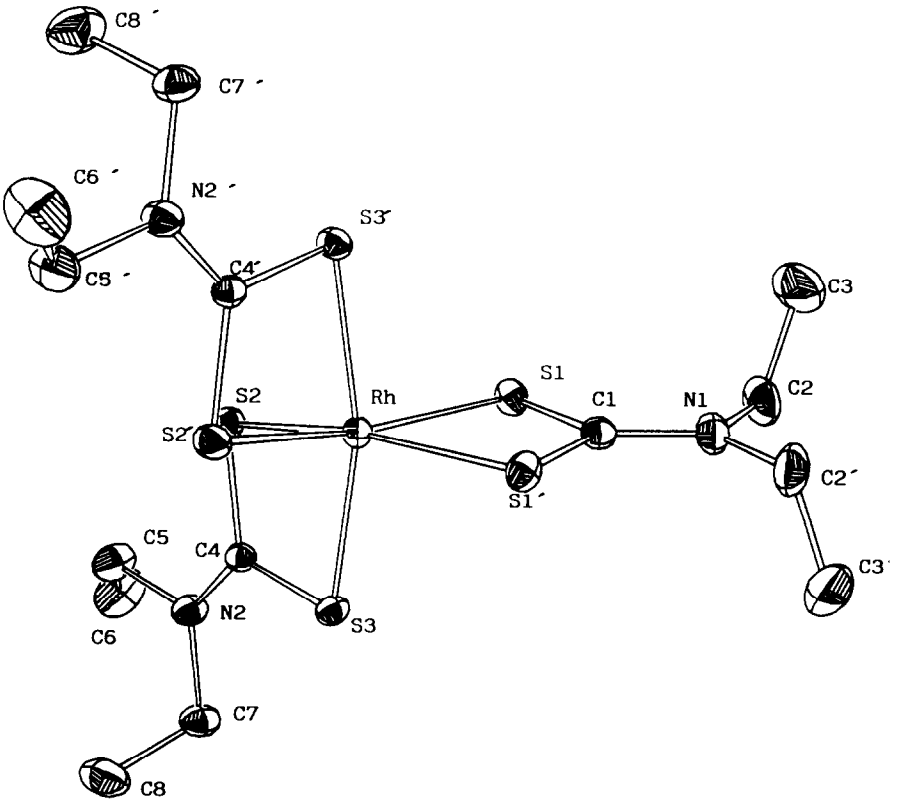

Fig. 6. Perspective ORTEP drawing of (**3**), with atomic numbering scheme.

Table 3. Deviation (Å) of the least-squares planes defined by the S_2CNC_2 fragments by the carbon atoms of the ethyl groups

	$[Rh(S_2CNEt_2)_3]^a$			$[Rh(S_2CNEt_2)_3]^b$			
ligand atom	1	2	3	atom	1	atom	2,2′
C2	−0.08	0.01	0.03	C2	−0.018(7)	C5,C5′	−0.035(7)
C3	1.22	−1.41	−1.30	C3	1.368(8)	C6,C6′	0.813(9)
C4	0.07	0.01	−0.02	C2′	0.018(7)	C7,C7′	−0.046(6)
C5	−1.29	1.46	1.39	C3′	−1.368(8)	C8,C8′	−1.396(9)

Angle ( ) between the planes (1)–(2) 84.76(7).

[a] From Colin L. Raston and Allan H. White, *J. Chem. Soc., Dalton Trans.*, 1975, 2426.
[b] our work.
[c] $1-x, y, 1/2-z$.

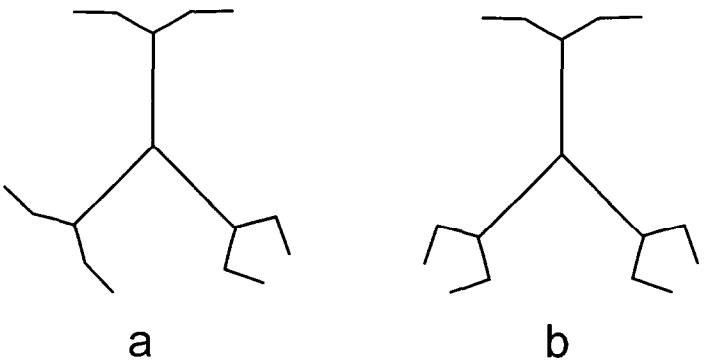

Fig. 7. (a) From Raston, C. L. and White, A. H., *J. Chem. Soc., Dalton Trans.*, 1975, 2425. (b) Our work.

perature for 9 days. The initial orange solution changed to brown with the time. Then, the volume was reduced *in vacuo* to approx. 3 ml. Addition of hexane caused the precipitation of a brown solid, which was filtered off, washed several times with methanol and dried *in vacuo*. The solid was recrystallized from acetone/hexane and identified as complex (**1**). Anal. Found: C, 24.93; H, 3.51; N, 4.68. Calc.: C, 25.80; H, 3.58; N, 5.01. The red-orange crystals obtained from filtrate solution corresponding to the complex $[Rh(S_2CNEt_2)_3]$ (**3**).

This same compound was obtained in a shorter time when the reaction was carried out at reflux temperature in dichloromethane (2 h) or acetone (6 h) as solvents. Also was obtained by evolution of the starting dicarbonyl complex in solid state.

Preparation of $[Rh(\mu\text{-}pz^{An})(S_2CNEt_2)(CO)]_2$ (**2**)

To a solution of $[Rh(S_2CNEt_2)(CO)_2]$ (0.4 mmol) in acetone (15 ml) was added the Hpz^{An} (0.4 mmol) ligand. The orange solution formed was stirred at room temperature for 10 days. The initial orange colour of the solution changed to dark orange. Then, the volume was reduced *in vacuo* to approx. 3 ml; hexane was added to precipitate an orange solid identified as (**2**), which was filtered off, washed several times with diethylether and dried *in vacuo*. Anal. Found: C, 42.38; H, 4.19; N, 9.27. Calc.: C, 41.55; H, 4.08; N, 9.10. Red-orange crystals of $[Rh(S_2CNEt_2)_3]$ (**3**) were obtained from filtrate solution.

On the other hand, complexes (**1**) and (**2**) were also obtained by a different route. To a solution of $[RhCl(CO)_2(H\text{-}pz^{An})]$ (0.163 mmol) in acetone (15 ml) was added the diethyldithiocarbamate ligand as a sodium salt (0.163 mmol). The initial orange-yellow colour of the solution changed to dark orange. The mixture was stirred for 9 days, and then the volume was reduced to approx. 3 ml; hexane was added and a brown-yellow solid precipitated which was filtered off, washed with methanol and dried *in vacuo*. This complex was identified as compound (**1**). The filtrate solution was evaporated to dryness; the orange solid obtained identified as a mixture of (**2**) and (**3**) was washed with diethyl ether and dried *in vacuo*.

Table 4. Crystal and refinement data for $[Rh(S_2CNEt_2)_3]$

Formula	$RhS_6N_3C_{15}H_{30}$
Mr	547.69
Crystal system	monoclinic
Space group	$C2/c$
a (Å)	14.044(4)
b (Å)	10.407(2)
c (Å)	16.952(3)
β (°)	109.03(2)
V (Å^3)	2342(1)
Z	4
$F(000)$	1128
ρ_{calcd} (g cm^{-3})	1.55
Temperature (K)	295
μ (cm^{-1})	12.4
Crystal size (mm)	$0.15 \times 0.12 \times 0.12$
Diffractometer	Enraf-Nonius CAD4
Radiation	Graphite-monochromated Mo–K_α ($\lambda = 0.71069$ Å)
Scan technique	ω-2θ
Data collected	(-16, 0, 0) to (16, 12, 20)
θ	$1 < \theta < 25$
Unique data	2067
Unique data (I) $\geq 2\sigma(I)$	1585
R_{int} (%)	0.05
Standard reflections	3/96
R_F (%)	3.2
RW_F (%)	3.4
Average shift/error	0.004

Table 5. Atomic coordinates and thermal parameters for non-hydrogen atoms of $[Rh(S_2CNEt_2)_3]$

Atom	x	y	z	U_{eq}
RH	0.5000(0)	0.2476(1)	0.2500(0)	314(2)*
S1	0.3984(1)	0.4279(1)	0.2481(1)	432(5)*
C1	0.5000(0)	0.5202(7)	0.2500(0)	40(3)
N1	0.5000(0)	0.6482(6)	0.2500(0)	55(3)
C2	0.4103(6)	0.7198(6)	0.2495(5)	75(3)
C3	0.4126(8)	0.7617(9)	0.3332(5)	111(4)
S2	0.3707(1)	0.0933(1)	0.2215(1)	436(5)*
S3	0.4413(1)	0.2204(1)	0.1044(1)	380(4)*
N2	0.2930(3)	0.0451(5)	0.0568(3)	46(2)
C4	0.3582(4)	0.1101(5)	0.1186(3)	35(2)
C5	0.2292(5)	−0.0550(7)	0.0746(4)	66(3)
C6	0.1274(5)	−0.0584(9)	0.0184(5)	96(4)
C7	0.2935(4)	0.0581(6)	−0.0289(3)	51(2)
C8	0.3435(6)	−0.0508(8)	−0.0549(5)	84(3)

$U_{eq} = 1/3\Sigma_i\Sigma_j U_{ij} a_i^* a_j^* \mathbf{a}_i \cdot \mathbf{a}_j \times 10^3$.
* $U_{eq} \times 10^4$ for Rh and S atoms.

X-ray structure determination of $[Rh(S_2CNEt_2)_3]$ (**3**)

Yellow, prismatic single crystal of $[Rh(S_2CNEt_2)_3]$ (**3**) was obtained from acetone-hexane. The data were collected on an Enraf-Nonius CAD4 diffractometer and unit cell constants were refined from least-squares fitting of the θ values of 25 reflections with 2θ range 30–14. A summary of the fundamental crystal data is given in Table 4. The intensities were corrected for Lorentz and polarization effects. Scattering factors for neutral atoms and anomalous dispersion corrections for Rh and S were taken from the International Tables for X-ray Crystallography [19].

The structure was solved by Patterson and Fourier methods. Empirical absorption corrections [20] were applied at the end of the isotropic refinement with unit weights and fixed coordinates and isotropic factors for the hydrogen atoms led to $R = 0.032$ and $Rw = 0.034$. Final difference synthesis showed no significantly electron density. No trend in F versus F_o or $(\sin\theta)/\lambda$ was observed. Most of the calculations were carried out with the X-ray 80 program [21]. Table 5 shows the final atomic parameters.

Acknowledgements—We thank the DGES of Spain for financial support (Projects PB92-0213 and PB95-0370).

Supplementary material—Tables giving fractional coordinates, thermal parameters, and bond distances and angles for $[Rh(S_2CNEt_2)_3]$ (6 pages). Tables of observed and calculated structure factors (14 pages) can be obtained from the authors.

REFERENCES

1. Cano, M., Heras, J. V., Lobo, M. A., Ovejero, P., Campo, J. A. and Pinilla, E., *Rhodium Express*, 1995, **9**, 8.
2. Cano, M., Campo, J. A., Heras, J. V., Lafuente, J., Rivas, C. and Pinilla, E., *Polyhedron*, 1994, **14**, 1139.
3. López, C., Jiménez, J. A., Claramunt, R. M., Cano, M., Heras, J. V., Campo, J. A., Pinilla, E. and Monge, A., *J. Organomet. Chem.*, 1996, **511**, 115.
4. Banditelli, G., Bandini, A. L., Bonati, F. and Minghetti, G., *J. Organomet. Chem.*, 1981, **218**, 229.
5. Cano, M., Heras, J. V., Lobo, M. A., Guzmán, E. and Pinilla, E., to be published.
6. Raston, C. L. and White, A. H., *J. Chem. Soc., Dalton Trans.*, 1975, 2425.
7. Brauns, T. B., Carriedo, C., Cockayne, J. S., Connelly, N. G., García Herbosa, G. and Guy Orpen, A., *J. Chem. Soc., Dalton Trans.*, 1989, 2049.
8. Heras, J. V., Pinilla, E. and Ovejero, P., *J. Organomet. Chem.*, 1984, **269**, 277.
9. Hendrickson, A. R., Martin, R. L. and Taylor, D., *J. Chem. Soc., Dalton Trans.*, 1975, 2182.
10. Hendrickson, A. R., Martin, R. L. and Taylor, D., *Aust. J. Chem.*, 1976, **29**, 269.
11. Raston, C. L. and White, A. H., *J. Chem. Soc., Dalton Trans.*, 1975, 2410.
12. Golding, R. M., Healy, P. C., Newman, P. W. G., Sinn, E. and White, A. H., *Inorg. Chem.*, 1972, **11**, 2435.

13. Raston, C. L. and White, A. H., *J. Chem. Soc., Dalton Trans.*, 1975, 2405.
14. Raston, C. L., White, A. H. and Willis, A. C., *J. Chem. Soc., Dalton Trans.*, 1975, 2429.
15. Raston, C. L. and White, A. H., *J. Chem. Soc., Dalton Trans.*, 1975, 32.
16. Nardelli, M., Musatti, A., Domiano, P. and Andreetti, G. D., *Ric. Sci., Parte* 2: *Sez. A*, 1965, **8,** 807.
17. Kepert, D. L., *Inorg. Chem.*, 1972, **11,** 1561.
18. Trofimenko, S., Calabrese, J. C., Kochi, J. K., Wolowiec, F. B., Hulsbergen, F. B. and Reedjik, J., *Inorg. Chem.*, 1992, **31,** 3943.
19. *International Tables for X-ray Crystallography*, Vol. 4, Kynoch Press, Birmingham, 1974, pp. 72–98.
20. Walker, N. and Stuart, D., *Acta Crystallogr., Sect. A*, 1983, **39,** 158.
21. Steward, J. M., *The X-ray* 80 *System*. Computer Science Centre, University of Maryland, College Park, Maryland, 1985.

Pergamon

PII: S0277-5387(97)00358-6

Polyhedron Vol. 17, Nos. 11–12, pp. 2127–2136, 1998
© 1998 Elsevier Science Ltd
All rights reserved. Printed in Great Britain
0277-5387/98 $19.00+0.00

Ternary complex formation kinetics involving (1,4,7,10-tetraazacyclododecane)nickel(II) and bidentate ligands

Chung-Yu Lai, Wei-Jen Lan, Chi Wang and Chung-Sun Chung*

Department of Chemistry, National Tsing-Hua University, Hsinchu, Taiwan 30043, Republic of China

(Received 5 May 1997; accepted 15 August 1997)

Abstract—The kinetics of reactions of (1,4,7,10-tetraazacyclododecane)nickel(II), NiT^{2+}, with 1,10-phenanthroline, ethylenediamine, and glycine were studied at 25.0°C and $\mu = 0.10$ mol dm^{-3} (NaCl). T is a tetradentate ligand. All reactions were first order in NiT^{2+} and reversible. The reaction with 1,10-phenanthroline was first order in 1,10-phenanthroline with the formation rate constant $k_{NiL}^{phen} = 1.31 \times 10^4$ dm^3 mol^{-1} s^{-1} and the dissociation rate constant $k_d = 19.6$ s^{-1}, followed the Eigen-Tamm mechanism. Ring closure was rate determining. The reaction involving ethylenediamine was resolved into the terms with formation rate constants $k_{NiL}^{en} = 1.61 \times 10^5$ dm^3 mol^{-1} s^{-1}, $k_{NiL}^{Hen} = 4.64 \times 10^3$ dm^3 mol^{-1} s^{-1}, and dissociation rate constants $k^{NiT(en)} = 4.55$ s^{-1} and $k_H^{NiT(en)} = 9.62 \times 10^7$ dm^3 mol^{-1} s^{-1}. Ring closure was rate determining in the en pathway but not in the Hen^+ pathway. The reaction involving glycine varies in order as a function of the glycine concentration, being first order in glycine at low glycine concentration and shifting toward a zero-order dependence a high glycine concentration. The mechanism involves a singly O-bonded LNi—O—N^+ intermediate in rapid equilibrium with reactants, $K_1 = 1.10 \times 10^3$ dm^3 mol^{-1}, followed by a slow ring closure, $k_2 = 5.29 \times 10^2$ s^{-1}. The dissociation rate constant is $k_d = 6.00$ s^{-1}. The important factors affecting the rates and the mechanisms of these reactions are the steric and inductive effects of the coordinated tetradentate ligand, the conformation angle distortion involving the "bite angle" of the two open coordination sites on NiL^{2+}, and the internal conjugate base effect of the attacking bidentate ligand. © 1998 Elsevier Science Ltd. All rights reserved

Keywords: kinetics; ternary complex formation; nickel(II) complexes.

The kinetics of reactions of (triethylenetetramine) nickel(II), N(trien)$^{2+}$, with 1,10-phenanthroline (phen), ethylenediamine (en), and glycine (gly) have been reported by Steinhaus *et al.* [1,2]. In the current investigation, we have attempted to gain a more detailed understanding of the effects that a coordinated tetradentate ligand has upon ternary complex formation. To accomplish this, we have studied the kinetics of complexation reactions of (1,4,7,10-tetraazacyclododecane)nickel(II), $[Ni([12]aneN_4)(H_2O)_2]^{2+}$, with phen, en, and glycine as shown in eqn 1, with L representing any bidentate ligand and T representing $[12]aneN_4$.

$$NiT(H_2O)_2^{2+} + L^{n-} \rightleftharpoons NiTL^{(2-n)+} + 2H_2O \quad (1)$$

The X-ray structure of $[Ni([12]aneN_4)(H_2O)_2]^{2+}$ has been reported [3] and shown in Fig. 1. The tetradentate $[12]aneN_4$ is folded so that the water molecules can be accommodated in *cis* positions. Thus, $[Ni([12]aneN_4)(H_2O)_2]^{2+}$ is a suitable distorted octahedral nickel(II) substrate, with the $[12]aneN_4$ acting as a non-removable tetradentate ligand and the two *cis*-coordinated aqua groups replaceable by a variety of bidentate ligands as shown in eqn 1.

EXPERIMENTAL

Reagents

$[12]aneN_4$ was prepared by the method of Richman and Atkins [4]. $Ni([12]aneN_4)(NO_3)_2$ was prepared by mixing anhydrous ethanolic solutions of the ligand (0.5 g, 0.0029 mol/50 cm^3) and $NiNO_3 \cdot 6H_2O$ (1 g,

* Author to whom correspondence should be addressed.

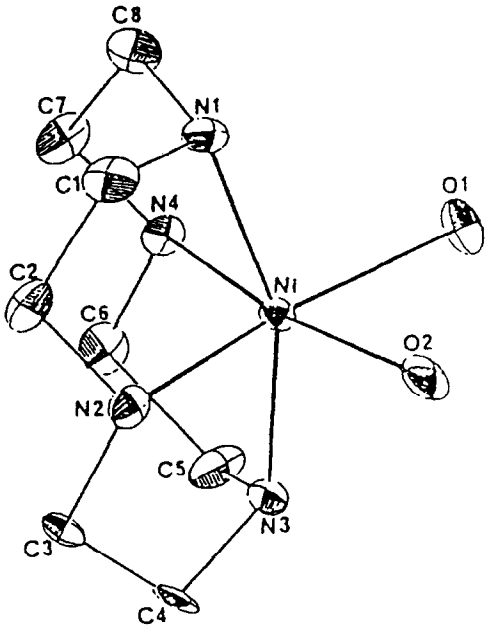

Fig. 1. Crystal structure of $[Ni([12]aneN_4)(H_2O)_2]^{2+}$.

0.0034 mol/100 cm^3) in a water bath with stirring. The mixture turned from green to violet. Reducing the volume to 20 cm^3 by further heating in a water bath, the solution was cooled in a refrigerator for several hours. The violet product was filtered off and recrystallized from methanol (Found: C, 27.1; H, 5.65; N, 23.7. Calc. for $NiC_8H_{20}N_6O_6$: C, 27.0; H, 5.7; N, 23.7%).

All chemicals used were of GR grade (Merck of Fluka). Glycine and 1,10-phenanthroline were recrystallized before use. Ethylenediamine was distilled and standardized by a potentiometric titration against standard HCl solution (Merck). The buffers used were N-(2-hydroxyethyl)piperazine-N′-2-ethanesulfonic acid (HEPES, $pK_a = 7.75$) and {[tris(hydroxymethyl) methyl]amino}-propane (TAPS, $pK_a = 8.4$). NaCl and $NaClO_4$ were used to control the ionic strength.

Kinetic measurements

The kinetics of ternary complex formation between $[Ni([12]aneN_4)(H_2O)_2]^{2+}$ and bidentate ligands were followed at 25.0±0.1°C and $\mu = 0.10$ mol dm^{-3} with the use of a Union Giken RA-401 stopped-flow spectrophotometer equipped with a Union RA-415 rapid-scan attachment. The reactions should be carried out with $NaClO_4$ to maintain the ionic strength. Unfortunately, the solubilities of these complexes in 0.1 mol dm^{-3} [$NaClO_4$] is extremely low. Precipitation prevents us from using $NaClO_4$ to maintain the ionic strength. This is the reason why R. K. Steinhaus, B. L. Lee and L. H. Kolopajlo studied the reactions of (triethylenetetraamine)nickel(II) with glycine, 1,10-phenanthroline, ethylenediamine, bipyridine and sarcosine with NaCl being used to maintain the ionic strength [1,2]. In order to compare our results with the reactions of (triethylenetetraamine)nickel(II) with these bidentate ligands, NaCl was used to maintain the ionic strength. Absorbance vs time data were collected at 347, 250, and 248 nm for the reactions of $[Ni([12]aneN_4)(H_2O)_2]^{2+}$ with phen, ethylenediamine and glycine, respectively. Pseudo-first-order conditions were maintained by using at least a 10-fold excess of the bidentate ligand to $[Ni([12]aneN_4)]^{2+}$ in each run. Good first-order kinetics were observed in all cases. The rate constants were obtained by linear least-squares fit for the data by using a computer.

RESULTS AND DISCUSSION

$[Ni([12]aneN_4)(H_2O)_2]^{2+}$-1,10-phenanthroline

The kinetics of ternary complex formation between $[Ni(12]aneN_4)(H_2O)_2]^{2+}$ and phen were studied over a pH range from 7.05 to 7.58, covering a phen concentration range of $(1.21–4.39)\times10^{-3}$ mol dm^{-3} at 25.0°C and $\mu = 0.1$ mol dm^{-3} (NaCl). All reactions were carried out with at least a 12-fold excess of phen to $[Ni(12)aneN_4)]^{2+}$ both with and without buffer. The pseudo-first-order constants are listed in Table 1. Under these conditions, $[Ni([12]aneN_4)phen]^{2+}$ is incompletely formed; the reaction is therefore a reversible reaction and follows the rate expression

Table 1. Experimental values of the rate constants for the reaction of $[Ni([12]aneN_4)]^{2+}$ with 1,10-phenanthroline at 25.0±0.1°C and $\mu = 0.1$ mol dm^{-3} (NaCl)

pH	10^3 [phen], mol dm^{-3}	k_{obsd}, s^{-1}	pH	10^3 [phen], mol dm^{-3}	k_{obsd}, s^{-1}
7.16	1.21	35.0	7.57	1.21	35.0
7.22	1.67	41.9	7.56	1.67	41.3
7.23	2.12	47.7	7.55	2.12	47.5
7.23	2.58	53.6	7.58	2.58	53.4
7.24	3.03	59.3	7.55	3.03	59.1
7.22	3.48	65.4	7.60	3.48	64.5
7.21	3.94	71.1	7.57	3.94	69.0
7.24	4.39	77.5	7.55	4.39	77.5
7.42	1.21	35.3	7.14[b]	1.21	35.1
7.41	1.67	41.6	7.10[b]	1.67	41.3
7.42	2.12	47.5	7.05[b]	2.12	47.6
7.41	2.58	53.5	7.13[b]	2.58	53.5
7.41	3.03	59.6	7.11[b]	3.03	59.4
7.41	3.48	64.8	7.07[b]	3.48	65.0
7.41	3.94	71.8	7.13[b]	3.94	69.9
7.39	4.39	77.3	7.06[b]	4.39	76.9

[a] All runs at 1.02×10^{-4} mol dm^{-3} $Ni([12]aneN_4)^{2+}$ and [buffer] = 0.01 mol dm^{-3} HEPES.

[b] [buffer] = 0.00 mol dm^{-3}.

$$-\frac{d[\mathrm{NiT}]}{dt} = k^{\mathrm{L}}_{\mathrm{NiT}}[\mathrm{NiT}][\mathrm{L}] - k_{\mathrm{d}}[\mathrm{NiTL}] \qquad (2)$$

with L = phen and T = [12]aneN$_4$. The observed pseudo-first-order rate constants are plotted vs the concentration of phen and followed eqn (3). This plot is shown in Fig. 2.

$$k_{\mathrm{obsd}} = k^{\mathrm{L}}_{\mathrm{NiT}}[\mathrm{L}] + k_{\mathrm{d}} \qquad (3)$$

Values of $k^{\mathrm{L}}_{\mathrm{NiT}}$ and k_{d} obtained from this plot are given in Table 2 along with corresponding values for the reaction of $[\mathrm{Ni(trien)(H_2O)_2}]^{2+}$ with phen reported by Steinhaus and Lee [1].

In all formation reactions involving nickel(II), the Eigen-Tamm mechanism has been found to hold [5]. As shown in eqns (4), (5) and (6), $\mathrm{NiT(H_2O)_2^{2+}}$ is $[\mathrm{Ni([12]aneN_4)(H_2O)_2}]^{2+}$, L-L is phen, species II is an outer-sphere complex, species III is mono-coordinated, and species IV is chelated.

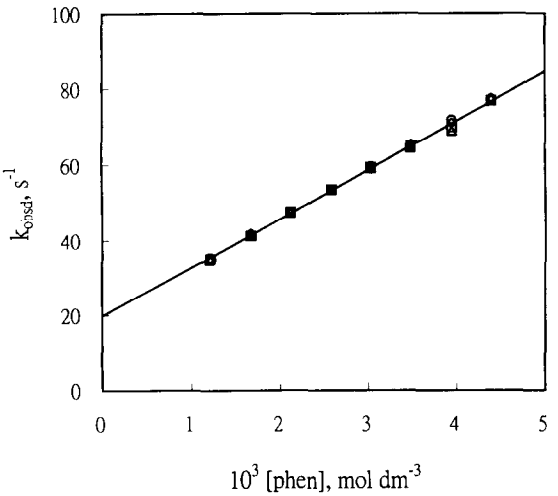

◇ pH 7.2 ○ pH 7.4 △ pH 7.6 □ pH 7.1

Fig. 2. Dependence of k_{obs} upon [phen] for reaction of $[\mathrm{Ni([12]aneN_4)(H_2O)_2}]^{2+}$ and phen (μ = 0.1 mol dm^{-3}, 25.0 C): runs with buffer (◇, ○, △); runs without buffer (□). Solid line is least-squares best fit of the points.

$$\underset{\mathrm{I}}{\mathrm{NiT(H_2O)_2^{2+}}} + \mathrm{L\text{-}L} \underset{k_{-1}}{\overset{k_1}{\rightleftharpoons}} \underset{\mathrm{II}}{\mathrm{NiT(H_2O)_2 \cdot L\text{-}L^{2+}}} \qquad (4)$$

$$\underset{\mathrm{II}}{\mathrm{NiT(H_2O)_2 \cdot L\text{-}L^{2+}}} \underset{k_{-2}}{\overset{k_2}{\rightleftharpoons}} \underset{\mathrm{III}}{\mathrm{NiT(H_2O)\text{-}L\text{-}L^{2+}}} + \mathrm{H_2O} \qquad (5)$$

$$\underset{\mathrm{III}}{\mathrm{NiT(H_2O)\text{-}L\text{-}L^{2+}}} \underset{k_{-3}}{\overset{k_3}{\rightleftharpoons}} \underset{\mathrm{IV}}{\mathrm{TNi}\begin{array}{l}\diagup\ L^{2+}\\ \\ \diagdown\ L\end{array}} + \mathrm{H_2O} \qquad (6)$$

If the usual assumption are made that (1) the outer-sphere reaction is rapid ($K_{\mathrm{os}} = k_1/k_{-1}$), and that (2) the singly bonded species (III) is a steady-state intermediate, then formation rate constant can be written as shown in eqn (7).

$$k^{\mathrm{phen}}_{\mathrm{NiT}} = \frac{K_{\mathrm{os}}k_2k_3}{k_{-2}+k_3} \qquad (7)$$

If ring closure (k_3) were much faster than bond rupture of species III (k_{-2}), then initial complex formation (k_2) were rate limiting and the formation rate constant could be predicted as eqn (8).

$$k^{\mathrm{phen}}_{\mathrm{NiT}} = K_{\mathrm{os}}k^{-\mathrm{H_2O}}\ (2/6) \qquad (8)$$

The value of K_{os} at 25°C was estimated theoretically to be 0.16 dm^3 mol^{-1} (Ref. 6), and the water exchange rate constant for $[\mathrm{Ni([12]aneN_4)(H_2O)_2}]^{2+}$, $k^{-\mathrm{H_2O}}$, is 2.00×10^7 s^{-1} (Ref. 7); the intimate mechanism of this process is probably dissociative (Ref. 8). The statistical factor of 2/6 accounts for the number of available coordination sites of $[\mathrm{Ni([12]aneN_4)(H_2O)_2}]^{2+}$ relative to $[\mathrm{Ni(H_2O)_6}]^{2+}$. The value of $k^{\mathrm{phen}}_{\mathrm{NiT}}$ calculated from eqn (8) is 1.1×10^6 dm^3 mol^{-1} s^{-1}. As listed in Table 2, this value is 84 times larger than the observed value of $k^{\mathrm{phen}}_{\mathrm{NiT}}$. This difference indicates that the coordinated [12]aneN$_4$ exerts a significant decelerating effect on the complexation of the attacking phen and suggests that ring closure contributes to the rate of formation. Thus, the rate-determining step is the formation of the second Ni—N bond. The coordinated [12]aneN$_4$ increases the lability at the remaining coordination sites and increases the monodentate phen dissociation rate constant (k_{-2}). In addition, the steric

Table 2. Rate constant values for $[\mathrm{Ni(trien)(H_2O)_2}]^{2+}$-phen[a] and $[\mathrm{Ni([12]aneN_4(H_2O)_2}]^{2+}$-phen systems at 25.0 C and μ = 0.10 mol dm^{-3} (NaCl)

	$[\mathrm{Ni([12]aneN_4(H_2O)_2}]^{2+}$-phen	$[\mathrm{Ni(trien)(H_2O)_2}]^{2+}$-phen[a]
$k^{\mathrm{phen}}_{\mathrm{NiT}}$	$(1.31 \pm 0.01) \times 10^4$ dm^3 mol^{-1} s^{-1}	$(7.9 \pm 0.6) \times 10^3$ dm^3 mol^{-1} s^{-1}
	1.1×10^6 dm^3 mol^{-1} s^{-1}[b]	2.7×10^5 dm^3 mol^{-1} s^{-1}[b]
k_{h}	19.6 ± 0.5 s^{-1}	6.2 ± 2.0 s^{-1}

[a] Values taken from Ref. 1.
[b] Calculated value from eqn 8.

effect of the coordinated [12]aneN$_4$ strongly blocks the formation of the second Ni—N bond so that ring closure contributes to the rate.

The formation rate constant for the reaction of phen with $Ni(H_2O)_6^{2+}$ and the water exchange rate constant of $[Ni(H_2O)_6]^{2+}$ are 1.6×10^{3} dm^3 mol^{-1} s^{-1} and 3.2×10^{4} s^{-1}, respectively [7,9]. [12]aneN$_4$ increases the rate of water loss of nickel(II) by a factor of about 630, but phen reacts only 8 times faster with $[Ni([12]aneN_4)(H_2O)_2]^{2+}$ than with $[Ni(H_2O)_6]^{2+}$. The relatively low rate of reaction between $[Ni([12]aneN_4)(H_2O)_2]^{2+}$ and phen is further evidence of steric effect coordinated [12]aneN$_4$ has upon the formation reaction.

As shown in Table 2, the rate constants of phen reacting with $[Ni([12]aneN_4)(H_2O)_2]^{2+}$ and [Ni(trien)$(H_2O)_2]^{2+}$ are similar. These results indicate that the steric effect of coordinated [12]aneN$_4$ upon the formation reaction of its nickel(II) complex with phen is very similar to that of coordinated trien.

$[Ni([12]aneN_4)(H_2O)_2]^{2+}$-*ethylenediamine*

The kinetics of ternary complex formation between $[Ni([12]aneN_4)(H_2O)_2]^{2+}$ and ethylenediamine were studied at 25.0°C and $\mu = 0.1$ mol dm^{-3} ($NaClO_4$) over a pH range of 7.35–8.12, covering an ethylenediamine concentration range of $(2.97\text{–}6.93)\times10^{-3}$ mol dm^{-3}. All reactions were carried out with at least a 12-fold excess of en to $[Ni([12]aneN_4)(H_2O)_2]^{2+}$. Under these conditions, the reaction is first order in $[Ni([12]aneN_4)(H_2O)_2]^{2+}$ and is reversible. The observed rate constants are listed in Table 3 and followed the expression shown in eqn (9) with L = en and T = [12]aneN$_4$, where $[en]_T$ refers to the total concentration of protonated and unprotonated en.

$$-\frac{d[NiT]}{dt} = k_f[NiT][en]_T - k_d[NiTL] \qquad (9)$$

With the assumption that $[en]_T$ remains constant, eqn (9) can be expressed to eqn (10).

$$k_{obsd} = k_f[en]_T + k_d \qquad (10)$$

Plots of k_{obs} vs $[en]_T$ give straight lines according to eqn (10) (Fig. 3). The values of k_f and k_d as a function of pH are given in Table 4.

In the pH range of this study, the reactive species are the unprotonated and monoprotonated ethylenediamine, en and Hen$^+$. Reactions of these species with $[Ni([12]aneN_4)(H_2O)_2]^{2+}$ to produce the ternary complex is then considered to occur as in eqns (11 and 12).

$$NiT(H_2O)_2^{2+} + en \underset{k^{NiT(en)}}{\overset{k^{en}_{NiT}}{\rightleftharpoons}} NiT(en)^{2+} + 2H_2O \qquad (11)$$

$$NiT(H_2O)_2^{2+} + Hen^+ \underset{k^{NiT(en)}_H}{\overset{k^{Hen}_{NiT}}{\rightleftharpoons}} NiT(en)^{2+} + H^+ + 2H_2O \qquad (12)$$

Table 3. Experimental values of the rate constants for the reaction of $Ni([12]aneN_4)^{2+}$ with ethylenediamine at 25.0 ± 0.1°C and $\mu = 0.1$ mol dm^{-3} ($NaClO_4$)

pH	10^4 [Ni([12]aneN$_4$)$^{2+}$], mol dm^{-3}	10^3 [en], mol dm^{-3}	k_{obsd}, s^{-1}
7.35	2.50	2.97	18.73
		3.96	21.92
		4.95	24.60
		5.94	27.76
		6.93	30.45
7.53	2.50	2.97	18.64
		3.96	23.16
		4.95	25.82
		5.94	29.59
		6.93	33.11
7.73	2.50	2.97	19.62
		3.96	23.68
		4.95	27.24
		5.94	32.16
		6.93	37.65
7.92	2.50	2.97	20.68
		3.96	26.27
		4.95	31.42
		5.94	35.33
		6.93	39.49
8.12	2.50	2.97	23.65
		3.96	28.58
		4.95	34.62
		5.94	41.50
		6.93	47.12

Table 4. Rate constants for formation (k_f) and dissociation (k_d) reactions of $[Ni([12]aneN_4(en)]^{2+}$ at 25.0 ± 0.1°C and 0.1 mol dm^{-3} ($NaClO_4$)

pH	k_f, dm^3 mol^{-1} s^{-1}	k_d, s^{-1}
7.35	2.93×10^3	10.16
7.53	3.57×10^3	8.38
7.73	4.50×10^3	5.79
7.92	4.72×10^3	7.28
8.12	6.05×10^3	5.09

Thus the rate law can be written as two formation terms and two dissociation terms as shown in eqn 13.

$$-\frac{d[NiT(H_2O)_2^{2+}]}{dt} = k^{en}_{NiT}[en][NiT(H_2O)_2^{2+}] + k^{Hen}_{NiT}[Hen^+][NiT(H_2O)_2^{2+}] - k^{NiT(en)}[NiT(en)^{2+}] - k^{NiT(en)}_H[NiT(en)^{2+}][H^+] \qquad (13)$$

Comparing this with eqn 9 yields

$$k_f[en]_T = k^{en}_{NiT}[en] + k^{Hen}_{NiT}[Hen^+] \qquad (14)$$

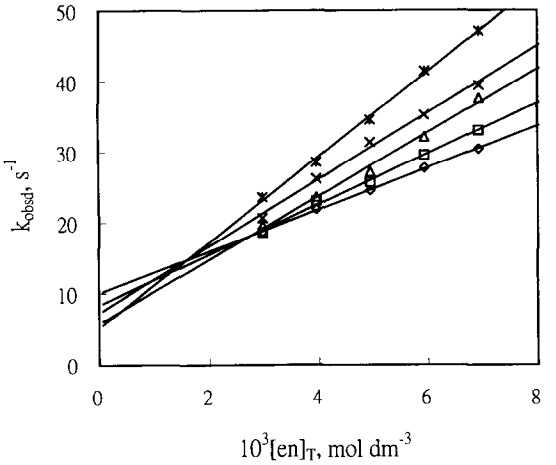

◇ pH 7.35 □ pH 7.53 △ pH 7.73 × pH 7.92 ✱ pH 8.12

Fig. 3. Plots of k_{obsd} vs $[en]_T$ for the reaction of $[Ni([12]aneN_4)(H_2O)_2]^{2+}$ and ethylenediamine (25.0°C, $\mu = 0.1$ mol dm^{-3}).

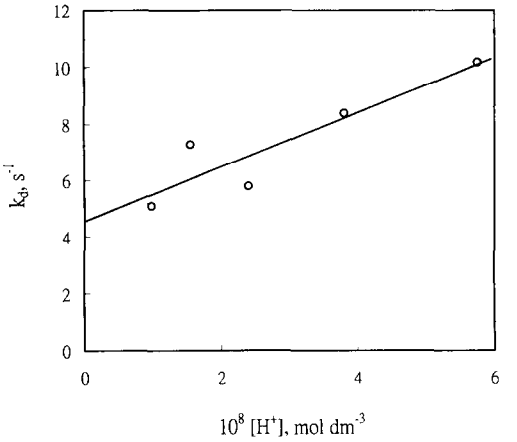

Fig. 5. Dependence of k_d upon $[H^+]$ for the reaction of $[Ni([12]aneN_4)(H_2O)_2]^{2+}$ and ethylenediamine (25.0°C, $\mu = 0.1$ mol dm^{-3}).

and

$$k_d = k^{NiT(en)} + k_H^{NiT(en)}[H^+] \quad (15)$$

Equation (14) can be rearranged to eqn (16) and plotted as shown in Fig. 4. A plot of k_d

$$k_f \frac{[\Sigma L]}{[en]} = k_{NiT}^{en} + k_{NiT}^{Hen} K_1^H [H^+] \quad (16)$$

vs $[H^+]$ is shown in Fig. 5. The values of k_{NiT}^{en}, k_{NiT}^{Hen}, k^{NiTen} and $k_H^{NiT(en)}$ obtained from these plots are listed in Table 5 along with corresponding values for the reaction of $[Ni(trien)(H_2O)_2]^{2+}$ with en and Hen^+ reported by Steinhaus and Kolopajlo [2].

The results in this table indicate both reactive unprotonated and monoprotonated terms are found. These results can be explained by modifying the mechanism proposed by Steinhaus and Kolopajlo [2] shown in Fig. 6. Assuming that the outer-sphere reaction is rapid, that the singly bonded species is a steady-state intermediate, and that the protonation equilibrium is rapid leads to the rate expressions in eqns (17 and 18).

$$k_{NiT}^{en} = \frac{2}{6} \frac{K_{os} k_1 k_2}{k_{-1} + k_2} \quad (17)$$

$$k_{NiT}^{Hen} = \frac{2}{6} \frac{K_{os} k'_1 k_2}{k'_{-1} K'_H [H^+] + k_2} \quad (18)$$

For the reaction of Hen^+ with $[Ni([12]aneN_4)(H_2O_2)]^{2+}$, Fig. 4, a plot of eqn (16), shows k_f to be a linear function of $[H^+]$ throughout the pH range studied and thus gives a value of k_{NiT}^{Hen} from the slope that is independent of $[H^+]$. This result indicate that $k'_{-1}K'_H[H^+]$ should be smaller than k_2. Thus eqn (18) simplifies to eqn (19) and the formation of the singly bonded species (II′) may be the rate-determining step.

$$k_{NiT}^{Hen} = \frac{2}{6} K'_{os} k_1 \quad (19)$$

If the steric effect of the coordinated $[12]aneN_4$ upon the reaction of $[Ni([12]aneN_4)(H_2O)_2]^{2+}$ with Hen^+ were negligibly small, the value of $(k_{NiT}^{HL})'$ can be estimated by eqn (20).

$$(k_{NiT}^{Hen})' = \frac{2}{6} K'_{os} k^{-H_2O} \quad (20)$$

The value of K'_{os} calculated from a modification of the Fuoss equation [6] is 0.044 dm^3 mol^{-1}; the value of k^{-H_2O} is 2.00×10^7 s^{-1} [7]. The predict value of $(k_{NiT}^{Hen})'$, given in Table 5, is 63 times larger than that observed. It has been estimated that an intramolecularly hydrogen bonded form of Hen^+ slows down the reaction of Hen^+ with nickel(II) by a factor of 3 [11]. Thus, the

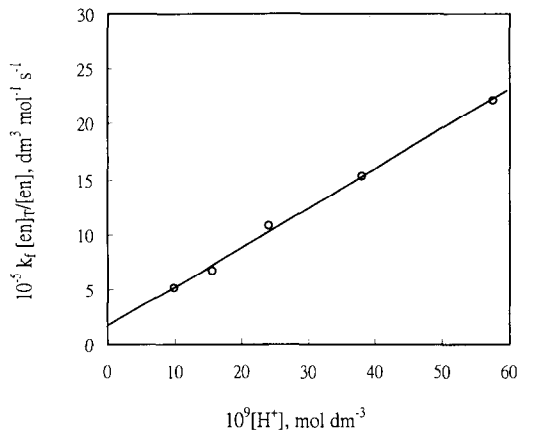

Fig. 4. Dependence of $k_f[en]_T/[en]$ upon $[H^+]$ for the reaction of $[Ni([12]aneN_4)(H_2O)_2]^{2+}$ and ethylenediamine (25.0 C, $\mu = 0.1$ mol dm^{-3}).

Table 5. Rate constant values for $[Ni([12]aneN_4)(H_2O)_2]^{2+}$-en and $[Ni(trien)(H_2O)_2]^{2+}$-en[a] systems at 25.0 C and $\mu = 0.10$ mol dm^{-3}

	$[Ni([12]aneN_4)(H_2O)_2]^{2+}$-en	$[Ni(trien)(H_2O)_2]^{2+}$-en[a]
k_{NiT}^{en}, dm^3 mol^{-1} s^{-1}	$(1.69 \pm 0.43) \times 10^5$	$(2.67 \pm 1.23) \times 10^4$
$(k_{NiT}^{en})'$, dm^3 mol^{-1} s^{-1}[b]	9.7×10^6	4×10^6
k_{NiT}^{Hen}, dm^3 mol^{-1} s^{-1}	$(4.61 \pm 0.14) \times 10^3$	$(1.77 \pm 0.13) \times 10^3$
$(k_{NiT}^{Hen})'$, dm^3 mol^{-1} s^{-1}[c]	2.9×10^5	7×10^4
$k_H^{NiT(en)}$, dm^3 mol^{-1} s^{-1}	$(9.62 \pm 2.55) \times 10^7$	
$k^{NiT(en)}$, s^{-1}	4.55 ± 0.98	8.62 ± 1.43

[a] Values taken from Ref. 2.
[b] Rate constant values for the reactions of unprotonated en with Ni(II) complexes.
[c] Predicted from eqn 21.
[d] Rate constant values for the reactions of monoprotonated Hen with Ni(II) complexes.
[e] Predicted from eqn 20.

actual steric factor of $[Ni([12]aneN_4)(H_2O)_2]^{2+}$ reacting with Hen^+ is about 21, which is slightly larger than that of $[Ni(trien)(H_2O)_2]^{2+}$ reacting with Hen^+[2].

If the first Ni—N bond formation is the rate-determining step for the reaction of $[Ni([12]aneN_4)(H_2O)_2]^{2+}$ with en, the value of formation rate constant $(k_{NiT}^{en})'$ can be predicted from eqn (21).

$$(k_{NiT}^{en})' = \frac{2}{6} K_{os} k_1 \qquad (21)$$

The steric factor of the reaction of en with $[Ni([12]aneN_4)(H_2O)_2]^{2+}$ is similar to that of the reaction of Hen^+ with $[Ni([12]aneN_4)(H_2O)_2]^{2+}$ since the uprotonated end of Hen^+ is the initial reaction site. Equation (21) incorporating an accelerating internal-conjugate-base factor [2] of 190 and a retarding steric factor of 21, predicts a value of $(k_{NiT}^{en})' = 9.7 \times 10^6$ dm^3 mol^{-1} s^{-1}, which is about 50 times larger than the experimentally observed value of $k_{NiT}^{en} = 1.61 \times 10^5$ dm^3 mol^{-1} s^{-1}. The large difference between $(k_{NiT}^{en})'$ and k_{NiT}^{en} indicates the first Ni—N bond formation of en to $[Ni([12]aneN_4)(H_2O)_2]^{2+}$ is not rate determining. The coordinated $[12]aneN_4$ molecule increases the lability at the remaining coordination sites and strongly hinders the formation of the second Ni—N bond. Therefore, the ring closure rate is slower than the

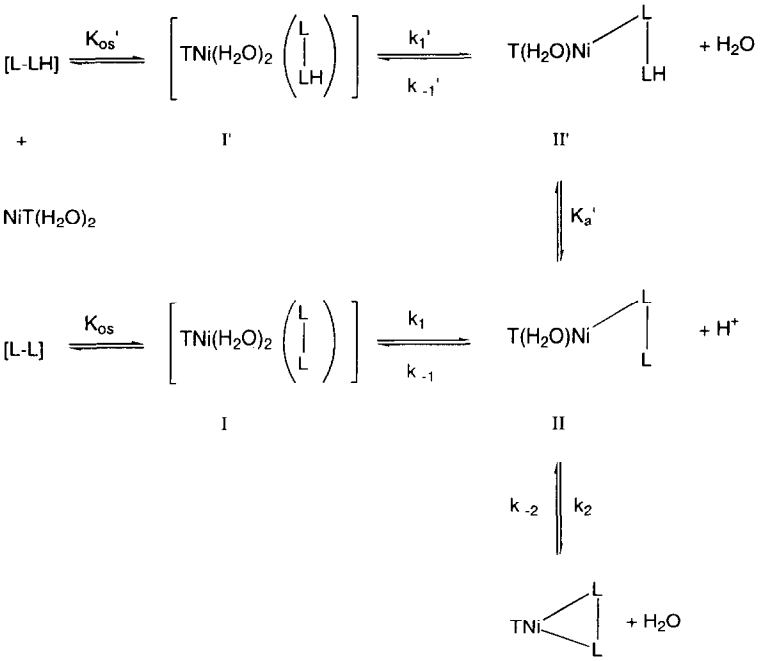

Fig. 6. Proposed mechanism for the reaction of en and Hen^+ with $[Ni([12]aneN_4)(H_2O)_2]^{2+}$.

monodentate en dissociation rate with the result that the second Ni—N bond formation is the rate-determining step.

As pointed out by Steinhaus [2], en requires a bond angle of about 82° when coordinated to nickel(II). The crystal structure of $[Ni([12]aneN_4)(H_2O)_2]^{2+}$ (Fig. 1) reveals that the bond angle formed between the two H_2O ligands and nickel(II) is 82.5°. Therefore, the conformation-angle-distortion (CAD) effect should be very small in the reaction of $[Ni([12]aneN_4)(H_2O)_2]^{2+}$ with en. By contrast, the CAD effect in the reaction of $[Ni(trien)(H_2O)_2]^{2+}$ with en is very large. As shown in Table 5, the formation rate constants k_{NiT}^{en} and k_{NiT}^{Hen} for the reactions of $[Ni([12]aneN_4)(H_2O)_2]^{2+}$ are larger than those of $[Ni(trien)(H_2O)_2]^{2+}$; on the other hand, the dissociation rate constant $k^{NiT(en)}$ for the reaction of $[Ni([12]aneN_4)(H_2O)_2]^{2+}$ is smaller than that of $[Ni(trien)(H_2O)_2]^{2+}$. The relatively large formation rate constants for the reaction of $[Ni([12]aneN_4)(H_2O)_2]^{2+}$ is mainly due to the fact that the labilizing effect of the four [12]aneN$_4$ nitrogens is slightly larger than that of the four trien nitrogens. The relatively large k_d value for the reaction of $[Ni(trien)(en)]^{2+}$ may be due to the relatively large CAD effect of $[Ni(trien)(en)]^{2+}$ compared to that of $[Ni([12]aneN_4)(en)]^{2+}$. As pointed out by Steinhaus and Kolopajlo [2], coordination of trien to nickel(II) forces a bite angle of 92.7° on $Ni(trien)^{2+}$ involving the two open coordination sites. On the other hand, coordination of [12]aneN$_4$ to nickel(II) give a bite angle of 82.5° on $[Ni([12]aneN_4)]^{2+}$ involving the two open coordination sites [3]. Therefore, the CAD accelerating effect for the reaction of $[Ni(trien)(en)]^{2+}$ is much larger than that for the reaction of $[Ni([12]aneN_4)(en)]^{2+}$.

$[Ni([12]aneN_4)(H_2O)_2]^{2+}$-*glycine*

The kinetics of ternary complex formation between $[Ni([12]aneN_4)(H_2O)_2]^{2+}$ and gly were studied at 25.0°C and $\mu = 0.10$ mol dm^{-3} (NaCl), over a pH range from 6.82 to 7.83, covering a gly concentration of 5.00×10^{-3} mol dm^{-3}–1.50×10^{-2} mol dm^{-3}. Kinetic studies were carried out under pseudo-first-order conditions by using at least a 10-fold excess of gly to $[Ni([12]aneN_4)(H_2O)_2]^{2+}$. The observed pseudo-first-order rate constants are given in Table 6. Under these conditions, $[Ni([12]aneN_4)gly]^{+}$ is incompletely formed; the reaction is therefore a reversible reaction. Plots of the observed pseudo-first-order rate constant, k_{obsd}, against total glycine concentration at a constant pH are shown in Fig. 7. The plots were linear up to pH 7.4. Higher pHs showed a curvature indicative of a shift from first-order to zero-order behaviour in glycine as shown by the pH 7.6 and pH 7.8 curves of Fig. 7. The intercepts of the plots at pHs less than 7.4, listed in Table 7, were constant and gave an average value of 6.00 s^{-1}, which is independent of glycine, hydrogen, or hydroxide ion and buffer anion and protonated buffer. Plots above pH 7.4 appear to intercept at the same point. This value must represent a reaction involving only $[Ni([12]aneN_4)(H_2O)_2]^{2+}$ and cannot involve $[Ni([12]aneN_4)(H_2O)(OH)]^{+}$ or $[Ni([12]aneN_4H)(H_2O)_2]^{3+}$ species since these would show a pH dependence. Again, as with the $[Ni([12]aneN_4)(H_2O)_2]^{2+}$-phen system, no biphasic behavior was seen so that the intercepts indicate a reversible reaction with k_{obsd} described by eqn 22.

$$k_{obsd} = k_{NiT}^{gly}[gly] + k_b \quad (22)$$

The average value of 6.00 s^{-1} was subtracted from

Table 6. Experimental values of the rate constants for the reaction of $[Ni([12]aneN_4)(H_2O)_2]^{2+}$ with glycine at 25.0 ± 0.1°C and $\mu = 0.1$ mol dm^{-3} (NaCl)

pH	10^3 [gly]$_T$, mol dm^{-3}	k_{obsd}, s^{-1}	pH	10^3 [gly]$_T$, mol dm^{-3}	k_{obsd}, s^{-1}
6.82	5.00	10.1	7.44	5.00	21.7
	7.50	11.7		7.50	30.5
	10.0	13.7		10.0	39.8
	12.5	16.0		12.5	47.2
	15.0	17.8		15.0	54.6
7.05	5.00	12.7	7.64	5.00	32.9
	7.50	16.0		7.50	47.1
	10.0	19.3		10.0	55.8
	12.5	23.2		12.5	63.6
	15.0	25.7		15.0	74.1
7.27	5.00	17.3	7.83	5.00	46.7
	7.50	21.0		7.50	61.6
	10.0	27.8		10.0	78.8
	12.5	33.2		12.5	84.5
	15.0	38.0		15.0	95.6

All runs at 5.00×10^{-4} mol dm^{-3} $Ni([12]aneN_4)^{2+}$ and [buffer] = 0.10 mol dm^{-3}.

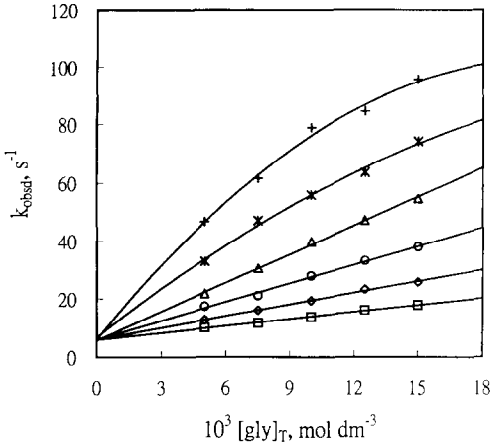

□ pH 6.8 ◇ pH 7.1 ○ pH 7.3 △ pH 7.4 ✱ pH 7.6 + pH 7.8

Fig. 7. Dependence of k_{obsd} upon total glycine concentration at various pH values for reaction of $[Ni([12]aneN_4)(H_2O)_2]^{2+}$ and glycine (μ = 0.1 mol dm^{-3}, 25 C). Solid lines at pH 6.8, 7.1, 7.3 and 7.4 are least-squares best fit of the points.

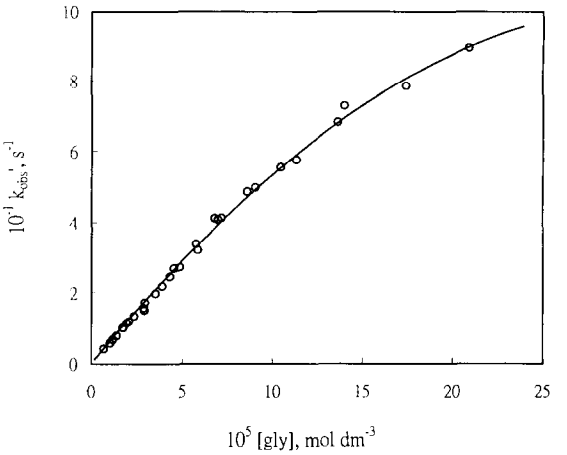

Fig. 8. Dependence of k'_{obsd} upon glycinate ion concentration over pH range of 7.0–8.2 for reactions of $[Ni([12]aneN_4)(H_2O)_2]^{2+}$ and glycine (μ = 0.1 mol dm^{-3}, 25 C).

$$k'_{obsd} = \frac{ab[gly]}{1 + a[gly]} \tag{24}$$

Table 7. Rate constant and equilibrium constant values for $[Ni([12]aneN_4)(H_2O)_2]^{2+}$-gly and $[Ni(trien)(H_2O)_2]^{2+}$-gly[a] systems at 25.0 C and μ = 0.10 mol dm^{-3}

	$[Ni([12]aneN_4)(H_2O)_2]^{2+}$-gly	$[Ni(trien)(H_2O)_2]^{2+}$-gly[a]
k_d	6.0 ± 0.2 s^{-1}[b]	8.7 ± 2.0 s^{-1}[f]
	6.1 ± 0.3 s^{-1}[c]	7.6 ± 1.0 s^{-1}[g]
	6.0 ± 0.8 s^{-1}[d]	8.1 ± 0.9 s^{-1}[h]
	5.8 ± 0.8 s^{-1}[e]	
K_1	$(1.10 \pm 1.58) \times 10^3$ dm^3 mol^{-1}	$(6.9 \pm 2.6) \times 10^2$ dm^3 mol^{-1}
k_2	$(5.29 \pm 7.56) \times 10^2$ s^{-1}	$(1.3 \pm 0.5) \times 10^2$ s^{-1}

[a] Values taken from Ref. 1.
[b] pH 6.8.
[c] pH 7.1.
[d] pH 7.3.
[e] pH 7.4.
[f] pH 7.0.
[g] pH 7.0.
[h] pH 7.5.

k_{obsd} for the glycine reactions. When this corrected value, k'_{obsd}, was plotted against the glycinate ion concentration with $K_a = 2.69 \times 10^{-10}$ for glycine, according to eqn 23, all points covering all pHs and glycine

$$k'_{obsd} = k^{gly}_{NiT}[gly] = k^{gly}_{NiT}\left(\frac{K_a[gly]_T}{K_a + [H^+]}\right) \tag{23}$$

concentrations studied fell on the same line. The plot, shown in Fig. 8 has a definite curvature to it. Behavior such as this is represented by the rate expression shown in eqn (24). Equation 24 can be rearranged to eqn

(25) and plotted as shown in Fig. 9. Values of a and b obtained from this plot

$$\frac{1}{k'_{obsd}} = \frac{1}{ab[gly]} + \frac{1}{b} \tag{25}$$

are $a = 1.10 \times 10^3$ dm^3 mol^{-1} and $b = 5.29 \times 10^2$ s^{-1}. Although all points appear to fit the line (Fig. 9), the standard deviations of K_1 and k_2 of $[Ni\{1,4,7,10\text{-tetraazacyclododecane}\}(H_2O)_2]^{2+}$-gly system shown in Table 7 are very large. We have repeated this experiment, similar results were found. The large deviations are mainly due to the very small intercept of this

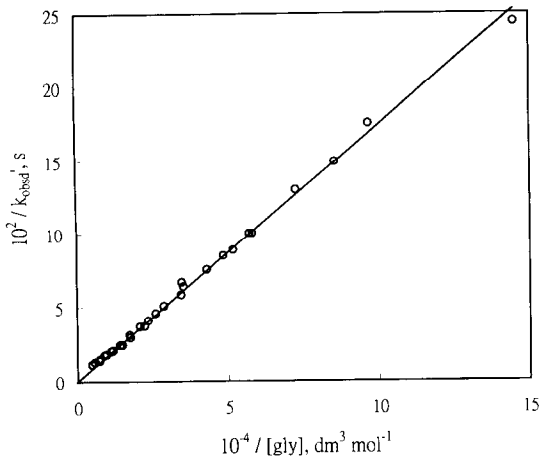

Fig. 9. Resolution of k'_{obsd} for reaction of $[Ni([12]aneN_4)(H_2O)_2]^{2+}$ with glycine into terms a and b of eqn 25. Plot covers glycinate ion concentration range of 1.0×10^{-4} to 2.1×10^{-3} mol dm^{-3}. Solid line is least-squares best fit of the data.

plot (Fig. 9). The standard deviations of other rate constants and equilibrium constants are small. Attempts were made to fit the data to other rate laws containing monoprotonated glycine without success. No reactive protonated terms were found.

The mechanism for the reaction of $[Ni(trien)(H_2O)_2]^{2+}$ and gly has been thoroughly studied by Steinhaus and Lee [1]. This mechanism shown in eqn (26) is consistent with the kinetic results of the reaction between $[Ni([12]aneN_4)(H_2O)_2]^{2+}$ and gly.

$$[(H_2O)_2Ni(T)] + \begin{matrix} O \\ | \\ N \end{matrix} \overset{K_1}{\rightleftharpoons} \left[H_2O(T)Ni \begin{matrix} O \\ | \\ N \end{matrix} \right] + H_2O$$

$$\downarrow k_2$$

$$\left[(T)Ni \begin{matrix} O \\ | \\ N \end{matrix} \right] + H_2O \quad (26)$$

Assuming that the mono-coordinated intermediate is in equilibrium with $[Ni([12]aneN_4)(H_2O)_2]^{2+}$ and gly leads to the kinetic expression given in eqn (27) which is identical with eqn (24) [1]. Thus $a = K_1$ and $b = k_2$. These values are given in Table 7 along with corresponding values for the reaction of $[Ni(trien)(H_2O)_2]^{2+}$ with gly reported by Steinhaus and Lee [1].

$$k'obsd = \frac{K_1 k_2 [gly]}{1 + K_1 [gly]} \quad (27)$$

The equilibrium type of mechanism followed by a slow ring closure of glycine indicates the carboxylate groups bonds first in $[Ni([12]aneN_4)(H_2O)_2]^{2+}$-gly reaction. If the amino group coordinates before the carboxylate group, k_{-1} could not be much larger than k_2 and the equilibrium type of mechanism would not be seen.

Although the basicity of the carboxylato group of gly is weaker than that of acetate, the value of K_1 shown in Table 7 is 220 times larger than the stability constant of Ni(acetate)$^+$ (K = 5.0 dm^3 mol^{-1}) [12]. These results indicate the internal conjugate base (ICB) effect is very important in the reaction of $[Ni([12]aneN_4)(H_2O)_2]^{2+}$ and gly.

The labilizing effect of the four [12]aneN$_4$ nitrogens is 4 times larger than that of the four trien nitrogens. Similarly, the k_2 value for the reaction of $[Ni([12]aneN_4)(H_2O)_2]^{2+}$ and gly is 4 times larger than that of $[Ni(trien)(H_2O)_2]^{2+}$ and gly.

Although the labilizing effect of the four [12]aneN$_4$ nitrogens is larger than that of the four trien nitrogens, it is interesting that the k_d value for the reaction of $[Ni(trien)(gly)]^+$ is larger than that of $[Ni([12]aneN_4)(gly)]^+$. The relatively large k_d value for the reaction of $[Ni(trien)(gly)]^+$ may be due to the relatively large CAD effect of $[Ni(trien)(gly)]^+$ compared to that of $[Ni([12]aneN_4)(gly)]^+$. As pointed out by Steinhaus and Kolopajlo [2], coordination of trien to nickel(II) forces a bite angle of 92.7° on Ni(trien)$^{2+}$ involving the two open coordination sites. On the other hand, coordination of [12]aneN$_4$ to nickel(II) give a bite angle of 82.5° on $[Ni([12]aneN_4)]^{2+}$ involving the two open coordination sites [3]. Therefore, the CAD accelerating effect for the reaction of $[Ni(trien)(gly)]^+$ is much larger than that for the reaction of $[Ni([12]aneN_4)(gly)]^+$.

Acknowledgement— The support of the Chemistry Research Center, National Science Council of the Republic of China, under Grants NSC 86-2113-M-007-023, is gratefully acknowledged.

REFERENCES

1. Steinhaus, R. K. and Lee, B. I., *Inorg. Chem.*, 1982, **21**, 1829.
2. Steinhaus, R. K. and Kolopajlo, L. H., *Inorg. Chem.*, 1985, **24**, 1839.
3. Bencini, A., Bianchi, A., Garcia-España, E., Jeannin, Y., Julve, M., Marcelino, V. and Philoche-Levisalles, M., *Inorg. Chem.*, 1990, **29**, 963.
4. Richman, I. E. and Atkins, T. I., *J. Am. Chem. Soc.*, 1974, **96**, 2268.
5. Margerum, D. W., Caley, C. W., Weatherburn, D. C. and Pagenkopf, G. K., *Coordination Chemistry*, ed. A. E. Martell. American Chemical Society, Washington, DC, 1978, ACS Monogr. No. 174, pp. 7–8.
6. Wilkins, R. G., *Kinetics and Mechanism of Reactions of Transition Metal Complexes*. VCH, New York, 1991, pp. 206–207.
7. Wilkins, R. G., *Kinetics and Mechanism of Reactions of Transition Metal Complexes*. VCH, New York, 1991, p. 214.
8. Nichols, P. J., Frésard, Y., Ducommun, Y. and Merbach, A. E., *Inorg. Chem.*, 1984, **23**, 4341.
9. Holyer, R. H., Hubbard, C. D., Kettle, S. F. A. and Wilkins, R. G., *Inorg. Chem.*, 1965, **4**, 929.
10. Margerum, D. W., Caley, C. W., Weatherburn, D. C. and Pagenkopf, G. K., *Coordination Chem-*

istry, ed. A. E., Martell. American Chemical Society, Washington, DC, 1978, ACS Monogr. No. 174, p. 133.
11. Taylor, R. W., Stepien, H. K. and Rorabacher, D. B., *Inorg. Chem.*, 1974, **13,** 1282.
12. Silken, L. and Martell, A., *Stability Constants of Metal-Ion Complexes*. The Chemical Society, London, 1964.

Pergamon

PII: S0277-5387(97)00472-5

Polyhedron Vol. 17, Nos. 11–12, pp. 2137–2140, 1998
© 1998 Elsevier Science Ltd
All rights reserved. Printed in Great Britain
0277-5387/98 $19.00+0.00

COMMUNICATION

Ligand control of molecular helicity in the coordination of toxic heavy metal ions: crystal structure of a monohelical cadmium(II) complex

Nesrin Beynek,[a] Mary McPartlin,[b] Brian P. Murphy[c]* and Ian J. Scowen[b]

[a] Department of Chemistry, UMIST, PO Box 88, Manchester, M60 1QD, U.K.

[b] School of Chemistry, University of North London, Holloway Road, London N7 8DB, U.K.

[c] Department of Chemistry, John Dalton Building, Manchester Metropolitan University, Chester Street, Manchester, M1 5GD, U.K.

(Received 25 August 1997; accepted 10 November 1997)

Abstract—The new semi-rigid diimine ligand, $OpyNpy_2$, coordinates the toxic heavy metals ions Cd(II) and Hg(II) in a monohelical fashion, as established, in the former, by X-ray crystallography and, in both, by ^1H NMR spectroscopy; ligand control is attributed to the helical topology of these complexes of stereochemically non-demanding ions. © 1998 Elsevier Science Ltd. All rights reserved

Keywords: ligand; monohelical; cadmium(II) complex.

Metal-ion coordination chemistry plays a fundamental role in the controlled assembly of novel molecular and supramolecular structures, with particular interest surrounding the topology and intrinsic chirality of helicates [1]. While much attention has focused on double [2,3] and triple [4] helical systems, controlled assembly of single helicates remains limited to only a few examples [5,6]. The relationship between the single/double helices and mononuclear acyclic/macrocyclic ligand complexes can readily be conceptualized as illustrated (Scheme 1). While examples of the former have recently appeared [2], cases of the latter are much less common [5,6]. In this communication, we describe the syntheses and characterization of Cd(II) and Hg(II) complexes that correspond to examples of the monohelical topology.

To produce systems with a propensity for monohelical coordination, we have synthesized the linear diimine ligand, $OpyNpy_2$, attempting to limit free rotation of its multidentate backbone by incorporating unsaturated imine functions and sterically demanding aromatic substituents, together with "hinge" methylene groups in order to generate a conformationally restricted acyclic system for binding in a mononuclear fashion. The complex $[Cd(OpyNpy_2)](NO_3)_2 \cdot 2H_2O$, reported herein is, to the best of our knowledge, the first structurally characterized monohelical Cd(II) complex of an acyclic ligand. The Cd(II) complex similar to the helical Zn(II) complex of $SpyNpy_2$ [5], the sulphur analogue of $OpyNpy_2$.

The complexes $[M(OpyNpy_2)](X)_2$ [where

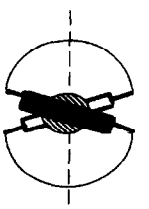

Figure-of-eight

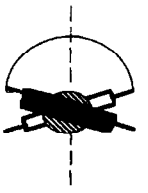

Monohelical

Scheme 1.

* Author to whom correspondence should be addressed.

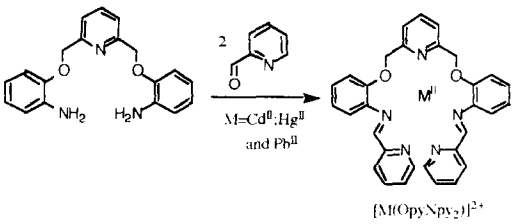

Scheme 2.

M = Cd(II) or Hg(II); X = $(NO_3)^-$ or $(ClO_4)^-$] were obtained from [1 + 2] Schiff-base condensation 2,6-*bis*(2-aminophenoxymethyl) pyridine [7] and 2-pyridinecarboxaldehyde in methanol in the presence of the appropriate metal salt (Scheme 2) and were fully characterized by IR, ^{1}H NMR, fast atom bombartment (FAB) mass spectrometry and elemental analyses.†

Crystals of $[Cd(OpyNpy_2)](NO_3)_2 \cdot 2H_2O$ were obtained by slow diffusion of diethyl ether into acetonitrile : methanol (1 : 2 v/v) solution of the complex. Crystals of one enantiomer only were obtained. The crystal selected for structure determination‡ was found to occur in the chiral space group $P6_122$, giving monohelical *P*(plus) configuration only (Fig. 1). The metal coordinates to all the potential donors of the ligand. However, significantly longer Cd—O than Cd—N bonds are observed which, as indicated in analogous structures [8], presumably result from relatively weak electrostatic metal-ether oxygen interactions common with these d^{10} ions. The 7-coordinate metal sphere is somewhat irregular although is best envisaged as a capped octahedron with N(1A), N(2A), O(1A) and N(2B) describing the equatorial plane and N(3) capping the O(1A), O(1B), N(2B) face. The "crossed" meridional orientation of planar N_2O units within the octahedron [dihedral angle 66.4(4)] underpins the helicity of the complex with the principal twists in the ligand strand occurring across the CH_2O linkages.

^{1}H NMR spectra of $[Cd(OpyNpy_2)](X)_2$ and $[Hg(OpyNpy_2)](X)_2$ in acetonitrile-d_3 (Fig. 2) are broadly similar. The spectra show two key features. Signals arising from the 2-pyridylimine protons in the complexes are flanked by satellites arising from spin-spin coupling to $I = 1/2$ metal nuclei (^{111,113}Cd and ^{199}Hg)§ indicating that the complexes are kinetically inert on the NMR timescale. Observations of this kind are relatively unusual in nitrogen–oxygen donor ligands and have hitherto been limited to macrocyclic [7–9] and cryptate [10] ligands. Notably, this is the second report of mercury(199)–proton coupling through an imine donor; the first corresponding to the thioether analogue of this complex[5]. Furthermore, spectra of both complexes show AB subspectra arising from diastereotopic environments of the methylene protons of the ligand. Such observations are consistent with the assignment of chiral complexes in solution. Consideration of the retention of metal-to-imine (proton) coupling together with the geminal coupling observed in the methylene region suggests that any mechanism of rapid interconversion of helical enantiomers in solution does not involve extensive ligand dissociation. Indeed, the weakly bonding oxygen donors, as evidenced by the X-ray structural data, might facilitate localized dissociation in any such racemization.

These studies show that restricting the degrees of freedom in semi-rigid open-chain ligands can produce monohelical complexes, even with metals that have little geometrical preference. We are currently examining the variation of ligand parameters such as denticity, flexibility and donor type as well as detailed NMR studies.

Acknowledgement—We are grateful to the University of

† FAB(MS), IR and C, H, N analysis were expected.

$[Cd(OpyNpy_2)](ClO_4)_2$: ^{1}H NMR (300 MHz, CD_3CN, 298 K): δ 5.38 (2H, d, J 15.2 Hz, CH_aH_b), 5.86 (2H, d, J 15.2 Hz, CH_aH_b), 7.47 (2H, t, J 7.2 Hz), 7.61 (2H, d, J 7.8 Hz), 7.66–7.78 (4H, m), 7.84 (2H, t, J 5.0 Hz), 8.00–8.10 (3H, m), 8.27 (2H, d, J 7.7 Hz), 8.39 (2H, t, J 7.7 Hz), 8.57 (2H, d, J 5.0 Hz), 9.51 (2H, s, HC=N).

$[Cd(OpyNpy_2)](NO_3)_2 \cdot 2H_2O$: ^{1}H NMR (300 MHz, CD_3CN, 298 K): δ 5.61 (4H, s, CH_2), 7.46 (2H, t, J 7.2 Hz), 7.60–7.77 (6H, m), 7.82 (2H, t, J 6.3 Hz), 8.00–8.09 (3H, m), 8.27 (2H, d, J 7.5 Hz), 8.38 (2H, t, J 7.7 Hz), 8.56 (2H, d, J 4.2 Hz), 9.51 (2H, s, HC=N).

$[Hg(OpyNpy_2)](NO_3)_2 \cdot 2H_2O$; ^{1}H NMR (300 MHz, CD_3CN, 298 K): δ 5.56 (4H, s (br), CH_2), 7.44 (2H, t, J 7.3 Hz), 7.64–7.70 (4H, m), 7.76 (2H, d, J 8.4 Hz), 7.89–8.09 (6H, m), 8.33–8.44 (5H, m), 8.60 (2H, d, J 4.3 Hz), 9.68 (2H, s, HC=N).

‡ Crystal data for $[Cd(OpyNpy_2)](NO_3)_2 \cdot 2H_2O$, $C_{31}H_{29}N_7O_{10}Cd$, $M = 734.51$, hexagonal, space group $P6_122$, $a = b = 15.68762(4)$, $c = 45.378(4)$ Å, $U = 9670.8(10)$ Å^3, $Z = 12$, $F(000) = 4704$, $D_c = 1.591$ g cm^{-3}, μ(Cu–K_α) = 6.03 mm^{-1}, λ(Cu–K_α) = 1.54178 Å. A yellow-brown crystal ($0.4 \times 0.4 \times 0.5$ mm^3) was mounted on a quartz fibre and data were collected on a Siemens P4 four-circle diffractometer in the θ range 3.25–55.0°. Of 9568 data collected, 4055 were unique ($R_{int} = 0.0521$). The structure was solved by direct methods and refined on F_o^2 with all non-hydrogen atoms of the complex assigned aniostropic thermal parameters. Residual electron density was assigned to two disordered water molecules. All hydrogens of the complex cation were included in idealized positions and assigned a fixed thermal parameter of 0.08 Å^2. Final wR_2 and R_1 values were 0.1601 and 0.0674 for all data, and 0.1335 and 0.0541 for data with $I > 2\sigma(I)$. Calculated Flack x parameter was 0.013(17). The weighting scheme used was $w^{-1} = \sigma^2 F_o^2 + (0.0823P)^2$ where P = [max. $(F_o^2, 0) + 2F_c^2$]/3. Programs: SHELXTL PC version 5.03, Siemens Analytical X-Ray Instruments, Madison, WI, 1994.

§ The intensities of the NMR satellites relative to the central imine singlet are: 1 : 6 for $[Cd(OpyNpy_2)](X)_2$ {X = $[ClO_4]^-$ and $[NO_3]^-$} and 1 : 10 for $[Hg(OpyNpy_2)](NO_3)_2$, corresponding closly to the natural abundances of the respective $I = 1/2$ nuclei (^{113}Cd + ^{111}Cd = 25%; ^{199}Hg = 16.84%).

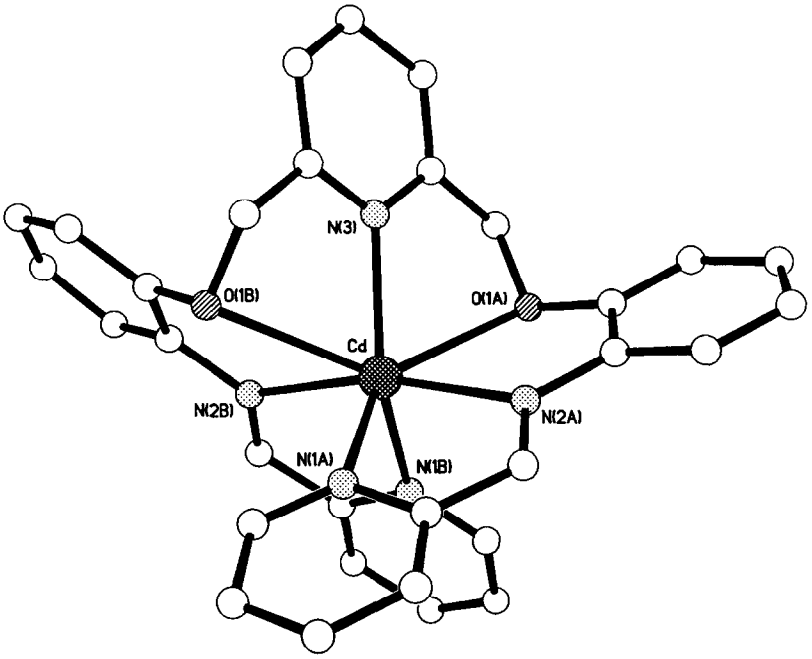

Fig. 1. The crystal structure of $[Cd(OpyNpy_2)](NO_3)_2 \cdot 2H_2O$, the principal bond lengths Å and angles ( ) are Cd—N(3) 2.299(8), Cd—N(1A) 2.308(8), Cd—N(1B) 2.326(8), Cd—N(2A) 2.348(8), Cd—N(2B) 2.366(7), Cd—O(1A) 2.598(8), Cd—O(1B) 2.708(8), N(3)—Cd—N(1A) 127.4(3), N(3)—Cd—N(1B) 135.6(3), N(1A)—Cd—N(1B) 96.9(2), N(3)—Cd—N(2A) 98.8(3), N(1A)—Cd—N(2A) 71.7(3), N(1B)—Cd—N(2A) 97.2(2), N(3)—Cd—N(2B) 94.7(3), N(1A)—Cd—N(2B) 102.2(3), N(1B)—Cd—N(2B) 70.9(3), N(2A)—Cd—N(2B) 166.3(3), N(3)—Cd—O(1A) 68.1(3), N(1A)—Cd—O(1A) 136.8(3), N(1B)—Cd—O(1A) 81.6(2), N(2A)—Cd—O(1A) 65.7(3), N(2B)—Cd—O(1A) 117.5(2), N(3)—Cd—O(1B) 67.8(3), N(1A)—Cd—O(1B) 76.2(3), N(1B)—Cd—O(1B) 130.6(2), N(2A)—Cd—O(1B) 124.8(2), N(2B)—Cd—O(1B) 63.4(3), O(1A)—Cd—O(1B) 135.7(3).

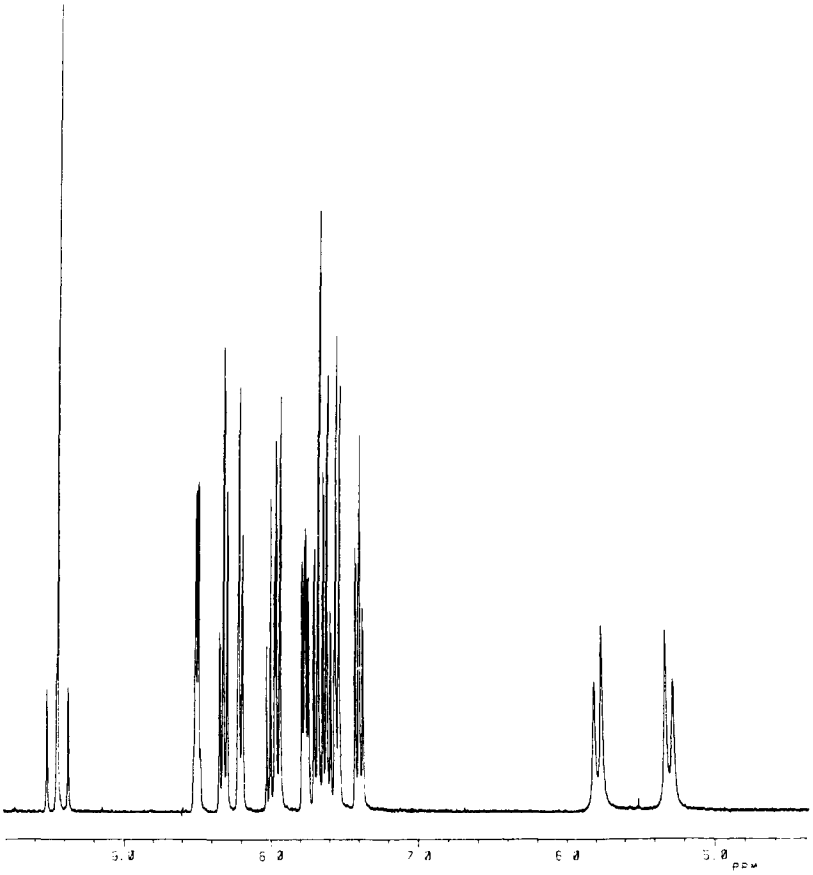

Fig. 2. ^1H NMR spectrum (300 MHz; 5.38–9.51 ppm range) of CD_3CN solution of $[Cd(OpyNpy_2)](ClO_4)_2$.

Trakya (Turkey) (N.B.) and the EPSRC (I.J.S.) for financial support and to Siemens plc (Karlsruhe) for X-ray data collection.

REFERENCES

1. (a) For example *Comprehensive Coordination Chemistry*, Vol. 9, ed. J.-M. Lehn, volume ed. J.-P. Sauvage and M. W. Hosseini. Pergamon, Oxford, 1996; (b) Constable, E. C., in *Comprehensive Supramolecular Chemistry*, Vol. 9, ed. J.-M. Lehn. Elsevier, 1996; (c) Constable, E. C., Kulke, T. Neuburger, M. and Zehnder, M., *J. Chem. Soc., Chem. Commun.*, 489 (1997); (d) Baum, G., Constable, E. C., Fenske, D. and Kulke, T., *J. Chem. Soc., Chem. Commun.*, 1997, 2043.
2. (a) For example Fenton, D. E., Matthews, R. W., McPartlin, M., Murphy, B. P., Scowen, I. J. and Tasker, P. A., *J. Chem. Soc., Dalton Trans.*, 1996, 3421; (b) Comba, P., Fath, A., Huttner, G. and Zsolnai, L., *J. Chem. Soc., Chem. Commun.*, 1996, 1885; (c) Bryant, Jr. L. H., Lachgar, A. and Jackels, S. C., *Inorg. Chem.*, 1995, **34,** 4230; (d) Comba, P., Fath, A., Hambley, T. W. and D. T. Richens, *Angew. Chem. Int. Ed. Eng.*, 1995, **34,** 1883; (e) Fenton, D. E., Matthews, R. W., McPartlin, M., Murphy, B. P., Scowen, I. J. and Tasker, P. A., *J. Chem. Soc., Chem. Commun.*, 1994, 1391.
3. (a) Hasenknopf, B., and Lehn, J.-M., *Helv. Chim. Acta*, 1996, **79,** 1643; (b) Chotalia, R., Constable, E. C., Neuburger, N., Smith, D. R. and Zehnder, M., *J. Chem. Soc., Dalton Trans.*, 1996, 4207; (c) Constable, E. C., Heirtzler, F. R., Neuburger, M. and Zehnder, M., *J. Chem. Soc., Chem. Commun.*, 1996, 933; (d) Piguet, C., Bernardinelli, G., Williams, A. F. and Bocquet, B., *Angew. Chem. Int. Ed. Eng.*, 1995, **34,** 582; (e) Bligh, S. W. A., Choi, N., Evagorou, E. G., Li, W.-S. and McPartlin, M., *J. Chem. Soc., Chem. Commun.*, 1994, 2399; (f) Potts, K. T., Keshavarz-K, M., Tham, F. S., Abruna, H. D. and Arana, C. R., *Inorg. Chem.*, 1993, **32,** 4422, 4436; (g) Judice, J. K., Keipert, S. J. and Cram, D. J., *J. Chem. Soc., Chem Comm.*, 1993, 1323; (h) Constable, E. C., *Tetrahedron*, 1992, 10013 and refs therein; (i) Constable, E. C., Hannon, M. J., Martin, A., Raithby, P. R. and Tocher, D. A., *Polyhedron*, 1992, **11,** 2967.
4. (a) For example Piguet, C. Hopfgartner, G., Williams, A. F. and Bunzli, J.-C. G., *J. Chem. Soc., Chem. Commun.*, 1995, 491; (b) Charbonniere, L. J., Bernardinelli, G., Piguet, C., Sargeson, A. M. and Williams, A. F., *J. Chem. Soc., Chem. Commun.*, 1994, 1419; (c) Kramer, R., Lehn, J.-M., de Cian, A. and Fischer, J., *Angew. Chem., Int. Ed. Eng.*, 1993, **32,** 703; (d) Bernardinelli, G., Piguet and C., Williams, A. F., *Angew. Chem. Int. Ed. Eng.*, 1992, **31,** 1622.
5. Adatia, T., Beynek, N. and Murphy, B. P., *Polyhedron*, 1995, **14,** 335.
6. (a) Tulchinsky, M. L., Demina, L. I., Lindeman, S. V. and Struchkov, Yu. T., *Inorg. Chem.*, 1994, **33,** 5836; (b) Constable, E. C., Chotalia, R. and Tocher, D. A., *J. Chem. Soc., Chem. Commun.*, 1992, 771; (c) Constable, E. C., Walker, J. V., Tocher, D. A. and Daniels, M. A. M., *J. Chem. Soc., Chem. Commun.*, 1992, 768; (d) Constable, E. C., Drew, M. G. B., Forsyth, G. and Ward, M. D., *J. Chem. Soc., Chem. Commun.*, 1988, 1450; (e) Lindoy, L. F., Bush, D. H. and Goedken, V., *J. Chem. Soc., Chem. Commun.*, 1972, 683.
7. Fenton, D. E., Murphy, B. P., Leong, A. J., Lindoy, L., Bashall, A. and McPartlin, M., *J. Chem. Soc., Dalton Trans.*, 1987, 2543.
8. (a) Adam, K. R., Donelly, S., Leong, A. J., Lindoy, L. F., McCool, B. J., Bashall, A., Dent, M. R., Murphy, B. P., McPartlin, M., Fenton, D. E. and Tasker, P. A., *J. Chem. Soc., Dalton Trans.*, 1990, 1635; (b) Bashall, A., McPartlin, M., Murphy, B. P., Fenton, D. E., Kitchen, S. J. and Tasker, P. A., *J. Chem. Soc., Dalton Trans.*, 1990, 505.
9. Biyk, A., Harding, M. M., Turner, P. and Hambley, T. W., *J. Chem. Soc., Dalton Trans.*, 1994, 2783; (b) Adams, H., Bailey, N. A., Fenton, D. E., Ford, I. G., Kitchen, S. J., Williams, M. G., Tasker, P. A., Leong, A. J. and Lindoy, L. F., *J. Chem. Soc., Dalton Trans.*, 1991, 1665; (c) Bailey, N. A., Fenton, D. E., Kitchen, S. J., Lilley, T. H., Williams, M. G., Tasker, P. A., Leong, A. J. and Lindoy, L. F., *J. Chem. Soc., Dalton Trans.*, 1991, 627.
10. (a) Janssen, R. J. A., Lindoy, L. F., Matthews, O. A., Meehan, G. V., Sobolev, A. N. and White, A. H., *J. Chem. Soc., Chem. Commun.*, 1995, 735; (b) Drew, M. G. B., Howarth, O. W., Morgan, G. G. and Nelson, J., *J. Chem. Soc., Dalton Trans.*, 1994, 3149.

Pergamon

PII: S0277-5387(98)00082-5

Polyhedron Vol. 17, Nos 13–14, pp. 2141–2151, 1998
© 1998 Elsevier Science Ltd
All rights reserved. Printed in Great Britain
0277-5387/98 $19.00+0.00

Synthesis and dynamic NMR studies of Rhenium(I) tricarbonyl bromide complexes of benzimidazolylpyridine ligands. Crystal structure of [ReBr(CO)$_3${2,6-bis(1′, 5′, 6′-trimethylbenzimidazol-2′-yl)pyridine}]

Andrew Gelling[a], Keith G. Orrell[a], Anthony G. Osborne[a]*, Vladimir Šik[a], Michael B. Hursthouse[b], David E. Hibbs[b] and K. M. Abdul Malik[b]

[a]Department of Chemistry, The University, Exeter EX4 4QD, U.K.

[b]Department of Chemistry, University of Wales Cardiff, P.O. Box 912, Park Place, Cardiff CF1 3TB, U.K.

(Received 8 December 1997; accepted 19 February 1998)

Abstract—Pentacarbonylbromorhenium(I) reacted with 2,6-bis(benzimidazol-2′-yl)pyridine (bbip), 2,6-bis(1′-methylbenzimidazol-2′-yl)pyridine (bmbip), 2,6-bis(5′,6′-dimethylbenzimidazol-2′-yl)pyridine (bdmbip), and 2,6-bis(1′,5′,6′-trimethylbenzimidazol-2′-yl)pyridine (btmbip) to form stable octahedral complexes of type *fac*-[ReBr(CO)$_3$L] (L = bbip, bmbip, bdmbip or btmbip) in which L is acting as a bidentate chelate ligand. At above-ambient temperatures in solution the complexes are fluxional with the nitrogen ligand oscillating between equivalent bidentate bonding modes. Rates and activation energies for these fluxions have been investigated by NMR methods. At low temperatures rotation of the uncoordinated benzimidazolyl unit is restricted and for *fac*-[ReBr(CO)$_3$(btmbip)] in CD_2Cl_2 solution, two preferred rotamers exist in 89:11% relative abundances. A rotational energy barrier has been estimated. The X-ray crystal structure of *fac*-[ReBr(CO)$_3$)(btmbip)] confirms the bidentate chelate bonding of btmbip with a N–Re–N angle of 74.2°. The pendant benzimidazole unit is inclined at an angle of 60.7° to the pyridine ring. © 1998 Elsevier Science Ltd. All rights reserved

Keywords: rhenium; benzimidazolylpyridine; fluxionality; dynamic NMR.

Following the discovery of a 1,4-metallotropic shift in metal complexes of 2,2′:6′,2″-terpyridine (terpy) in which the terpy was bonded as a bidentate chelate ligand to a kinetically inert metal centre [1–5], we have been interested in investigating the generality of this phenomenon. We extended our studies to a series of nitrogen ligands analogous to terpy in which one or both of the outer pyridine rings were replaced by pyrazoles [6, 7, 8, 9].

We now report the results of a study on some rhenium(I) complexes of terpy analogues in which both outer pyridine rings have been replaced by benzimidazole derivatives, namely 2,6-bis(benzimidazol-2′-yl)pyridine (bbip), 2,6-bis(1′-methylbenzimidazol-2′-yl)pyridine (bmbip), 2,6-bis(5′,6′-dimethylbenzimidazol-2′-yl)pyridine (bdmbip), and 2,6-bis-(1′,5′,6′-trimethylbenzimidazol-2′-yl)pyridine (btmbip).

Variable temperature NMR studies of the solution fluxionality of the complexes *fac*-[ReBr(CO)$_3$L] (L = bbip, bmbip, bdmbip and btmbip) and a crystal structure of *fac*-[ReBr(CO)$_3$(btmbip)] are presented.

*Author to whom correspondence should be addressed.

EXPERIMENTAL

Materials

Previously described methods were used to prepare the complex [ReBr(CO)$_5$] [10] and the ligands bbip, bdmbip, bmbip, and btmbip [11, 12].

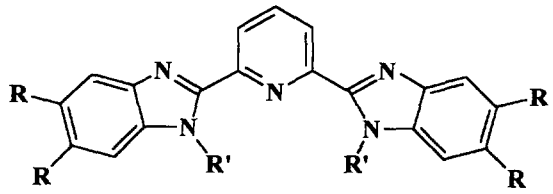

R	R'	
H	H	bbip
H	Me	bmbip
Me	H	bdmbip
Me	Me	btmbip

Synthesis of complexes

All preparations were performed by standard Schlenk techniques [13] under purified nitrogen using freshly distilled, dried and degassed solvents. The complexes $[ReBr(CO)_3L]$ (L = bbip, bdmbip, bmbip and btmbip) were all prepared in an analogous manner, synthetic data being given in Table 1. The preparation of $[ReBr(CO)_3(bmbip)]$ is given as a representative example.

2,6-Bis(1'-methylbenzimidazol-2'-yl)pyridinebromotricarbonylrhenium(I)

The compounds $[ReBr(CO)_5]$ (0.1 g, 0.25 mmol) and bmbip (0.1 g, 0.29 mmol) were stirred and heated under reflux in methanol (20 cm^3) for 4 h. The solution was cooled to ambient temperature and the supernatant liquid was decanted off. The orange solid was washed *in situ* with methanol (2 × 10 cm^3), diethylether (10 cm^3) and then dried under vacuum to give orange crystals. Yield 0.16 g (95%). A sample for analysis was dried under vacuum at 50°C for 8 h.

Physical methods

Infrared spectra of dichloromethane solutions of the complexes were recorded on a Perkin–Elmer 881 spectrometer calibrated from the line of polystyrene at 1602 cm^{-1}. Elemental analyses (C, H, N) were carried out by Butterworth Laboratories, Teddington, Middlesex, UK.

^1H NMR spectra were recorded on either a Bruker AC300 FT spectrometer operating at 300.13 MHz or on a Bruker DRX–400 FT spectrometer operating at 400.13 MHz. Chemical shifts are quoted relative to Me_4Si ($\delta = 0$) as an internal standard. Variable temperature NMR spectra were obtained using the Bruker variable temperature units B-VT100 (AC300) and B-VT2000 (DRX-400). Rate data were derived from bandshape analysis of ^1H NMR spectra using a version of the DNMR3 program [14]. Activation parameters based on experimental rate data were calculated using the THERMO program [15].

X-ray crystallography

The crystal used for X-ray work was obtained as described above. All measurements were made on a Delft Instruments FAST area detector diffractometer positioned at the window of a rotating anode generator with Mo-Kα radiation by following procedures described earlier [16]. The crystal data, details of data collection and structure refinement are summarised in Table 2. The cell parameters were determined by least-squares refinement of diffractometer angles for 250 reflections. The data were corrected for Lorentz and polarisation factors and also for absorption effects (DIFABS) [17].

Table 1. Synthetic and analytical data for the complexes *fac*-$[ReBr(CO)_3L]$ (L = bbip, bdmbip, bmbip, or btmbip)

Complex	Yield[a] (%)	ν(CO)[b] /cm^{-1}	Analysis[c] (%) C	H	N
$[ReBr(CO)_3(bbip)]$	68	2040s 1930m 1900m	39.5 (39.9)	2.0 (2.0)	10.3 (10.6)
$[ReBr(CO)_3(bdmbip)]$	40	2025s 1920m 1885m	42.7 (43.5)	3.2 (2.9)	9.4 (9.8)
$[ReBr(CO)_3(bmbip)]$	95	2025s 1915m 1900m	43.1 (43.0)	2.4 (2.6)	10.5 (10.5)
$[ReBr(CO)_3(btmbip)]$	38	2020s 1915m 1895m	45.3 (45.1)	3.5 (3.4)	9.1 (9.4)

(a) Yield quoted relative to metal containing reactant.
(b) Recorded in CH_2Cl_2 solution; s = strong, m = medium.
(c) Calculated values in parentheses.

Table 2. Crystal data and details of data collection and structure refinement for $[ReBr(CO)_3(C_{25}H_{25}N_5)]$. CH_3OH.

Empirical formula	$[C_{28}H_{25}BrN_5O_3Re]$. CH_3OH
Formula weight	777.68
Temperature	150(2) K
Wavelength	0.71069 Å
Crystal system	Triclinic
Space group	P-1 (No. 2)
Unit cell dimensions	$a = 10.712(2)$ Å
	$b = 11.507(2)$ Å
	$c = 13.886(3)$ Å
	$\alpha = 104.26(2)$
	$\beta = 95.24(2)$
	$\gamma = 116.743(9)$
Volume	1440.5(5) Å^3
Z	2
Density (calculated)	1.793 Mg/m^3
Absorption coefficient	5.648 mm^{-1}
$F(000)$	760
Crystal size	0.28 × 0.24 × 0.18 mm
Theta range for data collection	2.09 to 25.05
Index ranges	$-12 \le h \le 10$, $-13 \le k \le 8$, $-14 \le l \le 15$
Reflections collected	4926
Independent reflections	3788 [R(int) = 0.0637]
Absorption correction factors	0.865–1.109
Refinement method	Full-matrix least-squares on F^2
Data / restraints / parameters	3788 / 36 / 369
Goodness-of-fit on F^2	0.577
Final R indices (all 3788 data)	$R_1 = 0.0522$, $wR_2 = 0.0762$
R indices [2698 data with $I > 2\sigma(I)$]	$R_1 = 0.0348$, $wR_2 = 0.0716$
Largest diff. peak and hole	0.956 and −0.730 e. Å^{-3}

$R_1 = \Sigma(F_o - F_c)/\Sigma(F_o)$; $wR_2 = [\Sigma\{w(F_o^2 - F_c^2)^2\}/\Sigma\{(wF_o^2)^2\}]^{1/2}$; $w = 1/[\sigma^2(F_o^2)]$

The structure was solved by Patterson methods (SHELXS86) [18] and refined by full-matrix least-squares on F^2 using all unique data with intensities greater than 0 (SHELXL93) [19]. The non-hydrogen atoms were all anisotropic, but it was necessary to use an ISOR = 0.005 restraint for N(2), C(13), C(19), C(22), C(01) and O(01) to prevent these atoms becoming 'non-positive-definite'. The hydrogen atoms were included in calculated positions (riding model) with $U_{iso} = n \times U_{eq}$ ($n = 1.2$ for CH, and 1.5 for OH and CH_3 groups) of the parent atoms. Final R-values are given in Table 2. The diagram was drawn using SNOOPI [20]. Sources of scattering factor data are given in ref. [19]. The calculations were done on a 200 MHz personal computer.

Full details of crystallographic study including the atomic coordinates and displacement coefficients, hydrogen atom parameters, full list of bond lengths and angles have been deposited as supplementary material.

RESULTS

The complexes $[ReBr(CO)_3)L]$ (L = bbip, bmbip, bdmbip and btmbip) were obtained as orange crystalline air-stable solids solvated with methanol from reactions of $[ReBr(CO)_5]$ with the ligand in refluxing methanol. The complexes were not very soluble in the common organic solvents but, as would be expected, the presence of methyl groups in the nitrogen ligand, markedly increased the solubility of the ligand and the complex. In solution all the complexes displayed three strong carbonyl stretching bands in the infrared (Table 1) indicative of a *fac* stereochemistry for the complex and implying that the nitrogen ligands were acting as bidentate chelates. This was confirmed by solution NMR studies.

NMR studies

The ^1H chemical shift data for the four ligand molecules bbip, bmbip, bdmbip and btmbip, are given in Table 3. The structures are shown with a *trans*, *trans* configuration for the pyridine nitrogen and the imidazole nitrogen atoms not bearing an exocyclic group, as this is the structure most likely to be preferred in view of the solid state structure of the protonated form of bmbip [21]. An analogous *trans*, *trans* configuration of nitrogen atoms is also found in the solid

Table 3. ^{1}H NMR chemical shift data[a] for the bis(benzimidazolyl)pyridine ligands at 303 K.

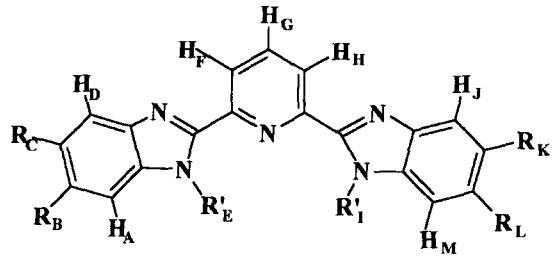

Ligand	Solvent	A	B	C	D	E	F	G	H	I	J	K	L	M
bbip[b]	$(CD_3)_2CO$	7.80	7.32	7.32	7.67	9.70	8.50	8.20	8.50	9.70	7.67	7.32	7.32	7.80
bdmbip[c]	$(CDCl_2)_2$	7.40	2.40	2.40	7.40	f	8.32	7.84	8.32	f	7.40	2.40	2.40	7.40
bmbip[d]	$(CDCl_2)_2$	7.85	7.37	7.37	7.47	4.20	8.40	8.06	8.40	4.20	7.47	7.37	7.37	7.85
btmbip[e]	$CDCl_3$	7.61	2.43	2.45	7.22	4.20	8.36	7.99	8.36	4.20	7.22	2.45	2.43	7.61

(a) Relative to TMS, $\delta = 0$. (b) $R_{B,C,K,L} = R'_{E,I} = H$. (c) $R_{B,C,K,L} = Me$, $R'_{E,I} = H$.
(d) $R_{B,C,K,L} = H$, $R'_{E,I} = Me$. (e) $R_{B,C,K,L} = R'_{E,I} = Me$. (f) Not detected.

state structures of terpy and 2,6-bis(pyrazol-1-yl) pyridine [22]. The spectra show the expected seven chemical shifts.

At ambient temperatures the four metal complexes show spectra consistent with the N_3 ligand bonding to the rhenium in a bidentate chelate manner. The assignments of the ^{1}H signals due to all thirteen different chemical environments are given in Table 4.

On raising the temperature of the solutions of all four rhenium complexes changes occurred which were consistent with the metal moiety undergoing a metallotropic shift as indicated at the head of Table 4. Such a Re–N bond fluxion will cause exchanges (i) between the aromatic hydrogen or methyl environments, namely A⇌M, B⇌L, C⇌K and D⇌J, (ii) between the pyridyl hydrogens F⇌H and (iii) between the -N-H (or -N-R) environments E⇌I. It is notable that the pyridyl environment H_G will be totally unaffected by this fluxion.

The ^{1}H NMR spectra of the individual complexes will now be described.

[ReBr(CO)$_3$(btmbip)]

This was the most soluble of the four complexes studied, presumably as a result of the heavy methylation of the ligand, and its ^{1}H NMR spectra were easily analysed. Its ambient temperature spectrum, in $(CDCl_2)_2$ solvent, consisted of 13 signals consistent

Table 4. ^{1}H NMR chemical shift data[a] for the complexes [ReBr(CO)$_3$L] at 303 K.

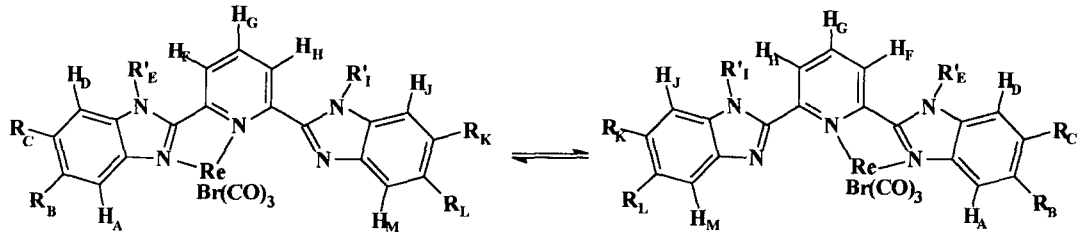

L	Solvent	A	B	C	D	E	F	G	H	I	J	K	L	M
bbip[b]	$(CD_3)_2SO$	7.87	7.57	7.57	7.87	13.25	8.67	8.54	8.06	13.25	7.75	7.31	7.31	7.64
bdmbip[c,d]	$(CDCl_2)_2$	7.81	2.49	2.18	6.95	10.29	8.02	7.53	7.79	10.29	7.76	2.54	2.52	7.65
bmbip[e]	$(CDCl_2)_2$	8.16	7.67	7.67	7.95	4.38	8.45	8.33	7.80	3.93	7.58	7.48	7.48	7.53
btmbip[f]	$(CDCl_2)_2$	7.88	2.51	2.53	7.40	4.30	8.35	8.24	7.70	3.86	7.32	2.51	2.47	7.69

(a) Relative to TMS, $\delta = 0$. (b) $R_{B,C,K,L} = R'_{E,I} = H$. (c) $R_{B,C,K,L} = Me$, $R'_{E,I} = H$. (d) At 333 K.
(e) $R_{B,C,K,L} = H$, $R'_{E,I} = Me$. (f) $R_{B,C,K,L} = R'_{E,I} = Me$.

with a static bidentate chelate complex. Unambiguous assignments of all signals (with the exception of the four closely separated C-methyl signals) were made with the aid of NOE difference experiments. The aromatic region of the spectrum is depicted in Fig. 1. On warming, pairs of signals show mutual exchange broadening consistent with the 1,4-metallotropic shift, with the exception of the triplet signal of H_G ($^3J_{GH} = {}^3J_{GF} = 7.9$ Hz) which remains sharp. At the highest temperature reached (413 K), a broad coalescence of the signals due to H_F, H_H, H_A and H_M can be noted, whereas at this temperature the signals due to H_D and H_J have already coalesced and sharpened to a fairly sharp averaged signal. Changes in the N-methyl region (δ 3.8–4.3) were simpler to follow and total bandshape analysis was performed on the pair of exchanging signals. Experimental and computer simulated spectra are shown in Fig. 2, with the 'best-fit' rate constants for each temperature given. Activation energies were computed in the usual way (Table 5). In

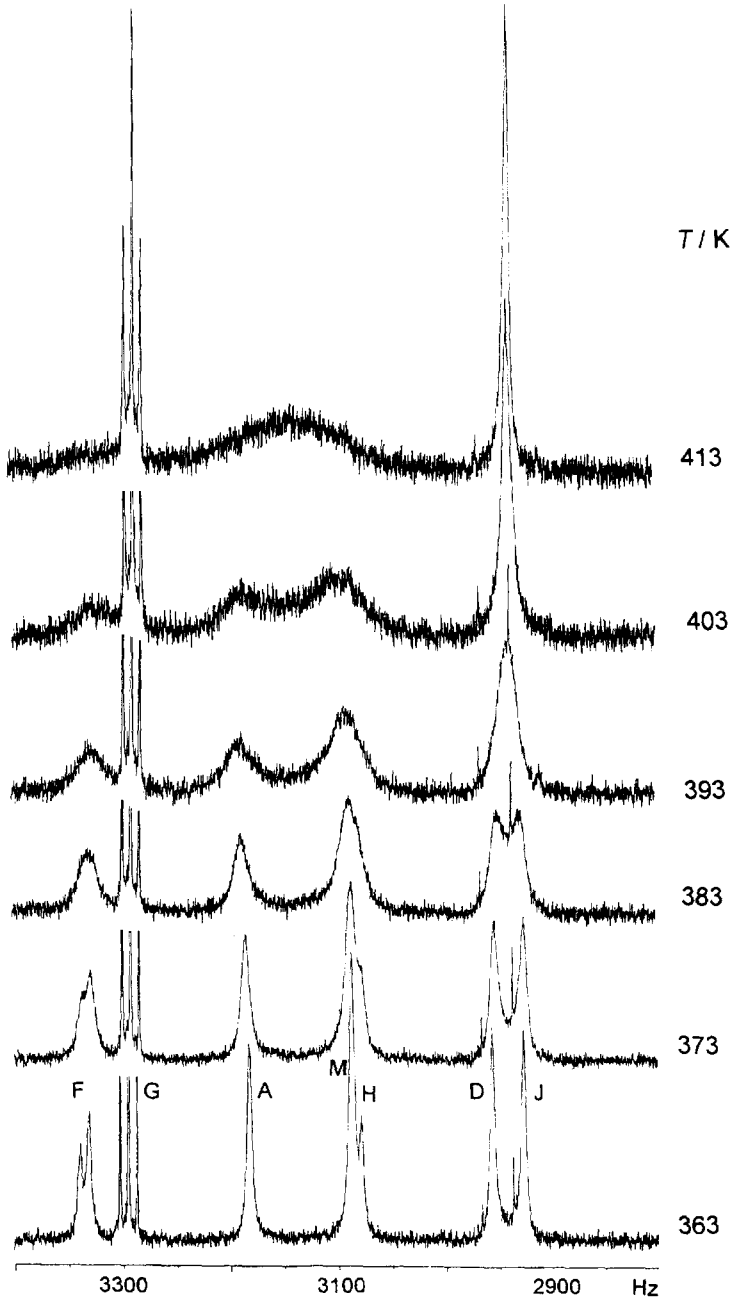

Fig. 1. Variable temperature ^{1}H NMR spectra (400 MHz) of the complex [ReBr(CO)$_3$(btmbip)] in $(CDCl_2)_2$ showing the effects of the Re-N fluxion on the aromatic hydrogens. Labelling refers to Table 4.

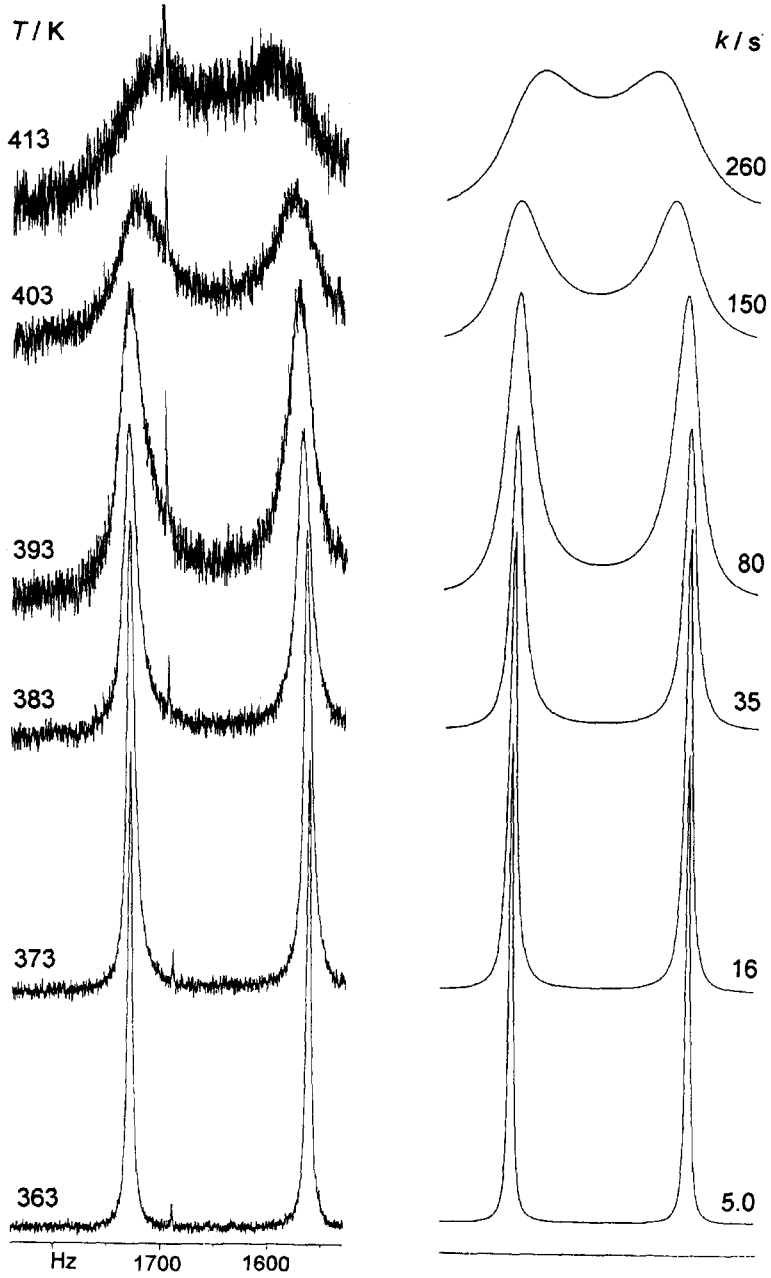

Fig. 2. Variable temperature ^{1}H NMR spectra (400 MHz) of the complex [ReBr(CO)$_3$(btmbip)] showing the effect of the Re-N fluxion on the N-methyl signals. Computer simulated spectra are shown alongside.

Table 5. Activation energy data for the 1,4 Re-N fluxions in the [ReBr(CO)$_3$L] complexes.

L	$\Delta H^{\ddagger}$/ kJ mol^{-1}	$\Delta S^{\ddagger}$/ J K^{-1} mol^{-1}	$\Delta G^{\ddagger a}$/ kJ mol^{-1}
bbip	72.5±2.5	−5.4±7.1	74.1±0.3
bdmbip	87.7±4.0	−2.0±10.3	88.3±1.0
bmbip	76.5±3.2	−13.3±8.3	80.4±0.7
btmbip	94.4±4.5	28.4±11.5	85.9±1.0

(a) Measured at 298.15 K.

the room temperature spectrum of this complex, the two N-methyl signals Me_E and Me_I were of different widths, with the broader signal due to Me_I having a half-height width of ~5 Hz. This suggested that it might be displaying effects of restricted rotation of the pendant benzimidazolyl portion of the ligand. A low temperature NMR study of this complex in CD_2Cl_2 solvent was therefore performed. On cooling to 213 K (Fig. 3) this signal continued to broaden and eventually split into an unequal intensity pair of signals denoted by I and I′ in Fig. 3 and Table 6. This indi-

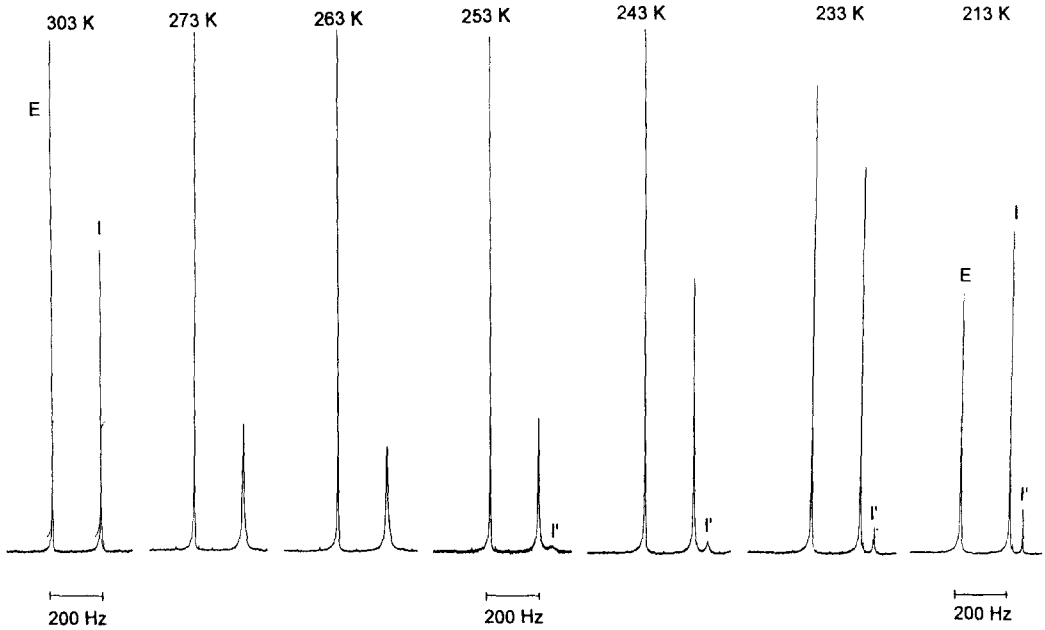

Fig. 3. Low temperature ^{1}H NMR spectra (400 MHz) of the complex [ReBr(CO)$_3$(btmbip)] in CD_2Cl_2 showing the effects of restricted rotation on the N-methyl signal of the pendant benzimidazolyl function.

cated a pair of rotameric species (rel. populations 0.89/0.11) as depicted in Table 6. Cooling of the sample also led to broadening and splitting of some of the ring hydrogen signals, notably H_F, H_H and H_M. The shifts of their minor counterparts $H_{F'}$, $H_{H'}$ and $H_{M'}$ are given in Table 6. An estimate was made of the energy barrier to rotation by fitting the bandshapes for the Me_I and $Me_{I'}$ signals (Fig. 3) at temperatures on either side of the coalescence temperature of 263 K. The activation energy, $\Delta G^{\ddagger}$ (298 K), for the process was calculated (Table 7).

The preferred solution rotamer is presumed to have a geometry similar to that exhibited in the solid state, where, according to the X-ray crystal structure (see

Table 6. ^{1}H-NMR chemical shift data[a] for hydrogens affected by the restricted ring rotation in the complex [ReBr(CO)$_3$(btmbip)] in CD_2Cl_2 at 203 K

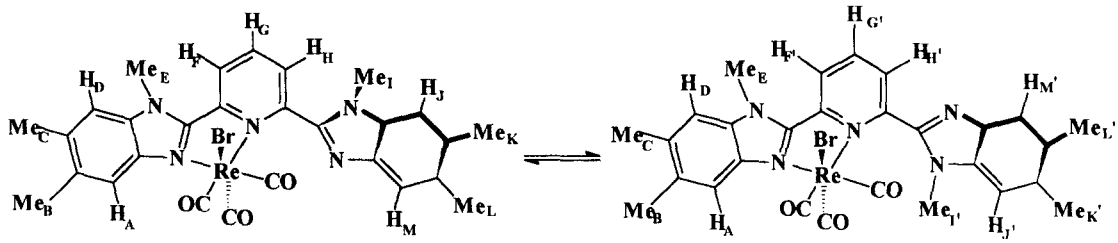

F	G	H	I	J	K	L	M
8.43	8.32	7.73	3.80	7.30	2.41	2.38	7.56

F'	G'	H'	I'	J'	K'	L'	M'
8.40	8.32	7.85	3.67	7.30	2.41	2.38	7.64

(a) Relative to TMS, $\delta = 0$. Shifts $\delta_A - \delta_E$ were not affected by the restricted rotation and are not quoted.

Table 7. Energy barriers for restricted rotation[a] of the ligand pendant heterocyclic ring in [ReBr(CO)$_3$L] (L = terpy, pbipy, dmpbipy, mpbipy, or btmbip) complexes.

Complex	Pendant ring	Rotamer populations	$\Delta G^{\ddagger b}$/kJ mol^{-1}	Ref.
[ReBr(CO)$_3$(terpy)]	pyridine	~0.5/0.5	not measureable	[3]
[ReBr(CO)$_3$(pbipy)]	pyrazole	0.5/0.5	43.0	[9]
[ReBr(CO)$_3$(dmpbipy)]	3,5-dimethylpyrazole	0.975/0.025	58.4	[9]
[ReBr(CO)$_3$(mpbipy)]	4-methylpyrazole	0.5/0.5	38.5[c]	[9]
[ReBr(CO)$_3$(btmbip)]	1,5,6-trimethylbenzimidazole	0.89/0.11	56.9	This work

a. Major → minor species

b. At 298.15 K

c. Estimated from measurements at the coalescence temperature (≅ 193 K)

terpy = 2,2′:6′,2″-terpyridine, pbipy = 6-(pyrazol-1-yl)-2,2′-bipyridine, dmpbipy = 6-(3,5-dimethylpyrazol-1-yl)-2,2′-bipyridine, mpbipy = 6-(4-methylpyrazol-1-yl)-2,2′-bipyridine.

later), the pendant benzimidazolyl unit is rotated from the plane of the pyridine ring by an amount given by the torsion angle N(2)–C(12)–C(13)–N(4) of 60° and the N-methyl group is in a near *cis*- relationship to Br. The structure of the other solution rotamer is likely to differ from the favoured rotamer by a near 180° rotation of the pendant benzimidazole function, thus causing the N-methyl to be approximately *trans* to Br.

[ReBr(CO)$_3$(bmbip)]

The ^{1}H NMR spectra of this complex showed analogous changes to the btmbip complex (above). The 1,4-metallotropic shift was clearly monitored by the exchanges of the ring pyridyl signals H_F and H_H and the N-methyl signals R_E and R_I. The energy barrier of the fluxion was determined by bandshape analysis of the N-methyl signals in the temperature range 353–413 K. Good agreement between experimental and computer fitted line shapes was achieved for seven temperatures in the above range and reliable activation energy data obtained (Table 5).

[ReBr(CO)$_3$(bdmbip)]

The existence of the 1,4-Re-N fluxion was also displayed in the variable temperature spectra of this complex. At temperatures up to 333 K, the spectra were indicative of a bidentate, chelate complex which was static on the NMR chemical shift timescale. Table 4 lists the chemical shifts of the four aromatic singlets, the three pyridyl signals (H_F, H_H doublets, H_G triplet) and the four C-methyl signals and the 2 N–H signals. On warming, the expected pairs of signals exchanged. The clearest exchanges were between the pyridyl signals H_F and H_H and these were used for bandshape analysis. Five fittings were achieved in the temperature range 373–413 K and an activation energy was calculated (Table 5).

[ReBr(CO)$_3$(bbip)]

This was the least soluble of the complexes and $(CD_3)_2SO$ had to be chosen as solvent.

At room temperature the ^{1}H spectrum was rather complex and the signal assignments (Table 4) are somewhat tentative. However, signals due to the pyridyl hydrogens H_F, H_G and H_H were clearly identified. On warming the solution, the signals H_F and H_H broadened, coalescing around 383 K and then sharpening. Bandshape fittings were made at six temperatures in the range 323–373 K, and activation energy data calculated (Table 5).

Activation energies

The energy data for the Re–N bond fluxions (Table 5) show that magnitudes of $\Delta H^{\ddagger}$ are in the range 72–94 kJ mol^{-1} and magnitudes of $\Delta G^{\ddagger}$ (298.15 K) in the range 74–88 kJ mol^{-1}. $\Delta S^{\ddagger}$ values are small in most cases as expected for purely intramolecular rearrangements, with the exception of the value for the btmbip complex. The positive $\Delta S^{\ddagger}$ value implies a much more weakly bound transition state structure than for the other complexes. This may be a reasonable assumption in view of the high degree of methylation of the benzimidazolyl moiety. This $\Delta S^{\ddagger}$ value causes the trend in $\Delta G^{\ddagger}$ values for the fluxion to differ slightly from that of the $\Delta H^{\ddagger}$ values. It was therefore felt more meaningful to discuss relative activation energies in terms of $\Delta H^{\ddagger}$ data, where the ligand order is btmbip > bdmbip > bmbip > bbip. This implies that methyl substitution on the aromatic ring of the benzimidazole unit causes an increase in the activation energy for the fluxion as does substitution of -N-H

by -N-Me groups. The former effect is quite large ($\Delta\Delta H^{\ddagger} = 15-18$ kJ mol^{-1}) whereas the latter effect is rather smaller ($4-7$ kJ mol^{-1}).

The magnitudes of these 1,4-Re-N fluxion energies are similar to that of the 2,2′:6′,2″-terpyridine complex [ReBr(CO)$_3$(terpy)] ($\Delta H^{\ddagger} = 79.8$ kJ mol^{-1}) [3], but significantly greater than that of the bispyrazolylpyridyl complexes [ReBr(CO)$_3$(bppy)] (bppy = 2,6-bis(pyrazol-1-yl) pyridine, $\Delta H^{\ddagger} = 50.8$ kJ mol^{-1}) and [ReBr(CO)$_3$(tmbppy)] (tmbppy = 2,6-bis(3,5-dimethylpyrazol-1-yl)pyridine, $\Delta H^{\ddagger} = 68.5$ kJ mol^{-1}) [6]. It should be noted that in this pair of complexes introduction of methyl groups to the ligand again causes a significant increase in the energy barrier for the fluxion.

The activation energy ($\Delta G^{\ddagger}$) for the restricted rotation of the unbound 1′,5′,6′-trimethylbenzimidazole function is 56.9 kJ mol^{-1} which is similar in magnitude to that of the pendant 3,5-dimethylpyrazole ring in the complex [ReBr(CO)$_3$(dmpbipy)] [9], (Table 7). When there are no methyl groups on the 3- and 5-positions of the pyrazole ring, as in the corresponding pbipy and mpbipy complexes (Table 7), the rotation barrier falls considerably. Clearly the steric bulk of the rotating unit is the crucial factor in determining the rotation barrier. Also, it would appear that the greater the steric hindrance the greater the population imbalance of the solution rotamers (Table 7).

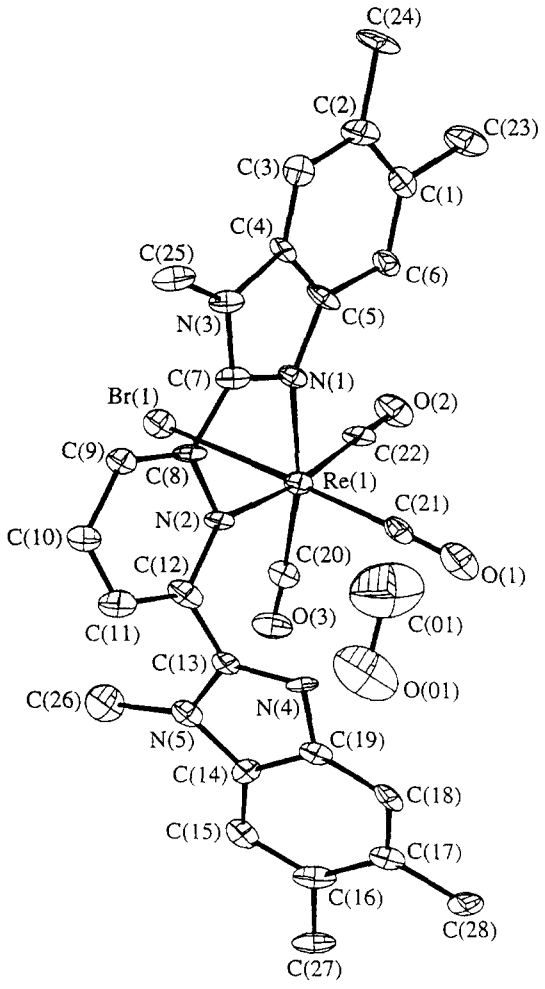

Fig. 4. Structure of [ReBr(CO)$_3$(btmbip)].CH$_3$OH showing the atom numbering scheme. Thermal ellipsoids are drawn at 50% probability level. The hydrogen atoms are omitted for clarity.

Crystal structure of [ReBr(CO)$_3$(btmbip)].CH$_3$OH

In order to confirm the bidentate chelate nature of the N_3 ligand in the complexes in the solid state, to compare the structure with an analogous terpy complex, [ReBr(CO)$_3$(terpy)] [3] and with the structure of the monoprotonated form of bmbip [21] the X-ray crystal structure of [ReBr(CO)$_3$(btmbip)] was determined and found to be a methanol solvate.

A view of the molecule indicating the numbering scheme adopted is shown in Fig. 4. This displays the expected *fac* octahedral coordination for Re and confirms the bidentate chelate nature of the btmbip ligand. As far as we are aware the only other example of a N_3 ligand with the 2,6-bis(benzimidazol-2-yl) pyridine structure acting as a bidentate chelate is in a complex of bmbip with copper [23]. Selected bond lengths and bond angles are given in Table 8.

The Re–N bond distances are unequal with Re–N(1) 2.152(7) and Re–N(2) 2.236(7) Å but they compare with corresponding distances of 2.143 and 2.209 Å in the analogous compound [ReBr(CO)$_3$(terpy)] [3]. Another similarity to the terpy complex is also evident in that the Re–N bond distance to the central N of the N_3 ligand is longer than the bond distance to the terminal N atom.

Inspection of the bond angles at Re shows there to be some distortion from a regular octahedral geometry. The main distortions arise from the small bite angle, N(1)–Re–N(2) 74.2(3)° of the nitrogen ligand, and also the angle C(20)–Re–N(2) of 100.9(4)°. These values are virtually identical to the corresponding values (74.3 and 100.6°) for *fac*-[ReBr(CO)$_3$(terpy)] [3].

The dihedral angles between the ring planes of the N_3 ligand are of interest. The pyridine ring and the coordinated benzimidazolyl unit are inclined to each other at an angle of 7.1(5)°. This compares with values of 30.5 and 45.3° for dihedral angles between adjacent rings in the monoprotonated free ligand bmbip [21], and 12° for the coordinated pyridines in [ReBr(CO)$_3$(terpy)] [3]. The pendant benzimidazolyl unit is rotated from the plane of the pyridine ring, as defined by the torsion angle N(2)-C(12)-C(13)-N(4) of 60.7(12)°. This group is also involved in short hydrogen bonding with the methanol solvate, as exemplified

Table 8. Selected bond lengths (Å) and angles (°) for $[ReBr(CO)_3(C_{25}H_{25}N_5)].CH_3OH$.

Re(1)–C(20)	1.905(10)	Re(1)–C(22)	1.912(10)
Re(1)–C(21)	1.919(11)	Re(1)–N(1)	2.152(7)
Re(1)–N(2)	2.236(7)	Re(1)–Br(1)	2.6244(12)
O(1)–C(21)	1.157(11)	O(2)–C(22)	1.142(10)
O(3)–C(20)	1.157(10)	N(1)–C(7)	1.346(11)
N(1)–C(5)	1.395(11)	N(2)–C(12)	1.342(11)
N(2)–C(8)	1.400(10)	N(3)–C(7)	1.390(11)
N(3)–C(4)	1.399(11)	N(3)–C(25)	1.445(11)
N(4)–C(13)	1.305(10)	N(4)–C(19)	1.397(10)
N(5)–C(13)	1.364(11)	N(5)–C(14)	1.402(10)
N(5)–C(26)	1.466(11)	C(1)–C(6)	1.369(13)
C(1)–C(2)	1.413(13)	C(2)–C(3)	1.428(13)
C(3)–C(4)	1.342(12)	C(4)–C(5)	1.386(12)
C(5)–C(6)	1.401(12)	C(7)–C(8)	1.425(12)
C(8)–C(9)	1.382(12)	C(9)–C(10)	1.400(12)
C(10)–C(11)	1.370(11)	C(11)–C(12)	1.375(13)
C(12)–C(13)	1.475(12)	C(14)–C(19)	1.373(12)
C(14)–C(15)	1.393(12)	C(15)–C(16)	1.398(12)
C(16)–C(17)	1.408(13)	C(17)–C(18)	1.387(12)
C(18)–C(19)	1.404(11)		

C(20)–Re(1)–C(22)	84.8(4)	C(20)–Re(1)–C(21)	91.2(4)
C(22)–Re(1)–C(21)	89.1(4)	C(20)–Re(1)–N(1)	170.0(3)
C(22)–Re(1)–N(1)	99.3(3)	C(21)–Re(1)–N(1)	98.0(4)
C(20)–Re(1)–N(2)	100.9(4)	C(22)–Re(1)–N(2)	171.8(3)
C(21)–Re(1)–N(2)	96.6(3)	N(1)–Re(1)–N(2)	74.2(3)
C(20)–Re(1)–Br(1)	87.5(3)	C(22)–Re(1)–Br(1)	92.0(3)
C(21)–Re(1)–Br(1)	178.2(3)	N(1)–Re(1)–Br(1)	83.3(2)
N(2)–Re(1)–Br(1)	82.4(2)	C(7)–N(1)–C(5)	107.0(7)
C(7)–N(1)–Re(1)	115.6(6)	C(5)–N(1)–Re(1)	135.8(6)
C(12)–N(2)–C(8)	117.5(8)	C(12)–N(2)–Re(1)	127.4(6)
C(8)–N(2)–Re(1)	113.5(5)	C(7)–N(3)–C(4)	107.4(7)
C(7)–N(3)–C(25)	127.9(8)	C(4)–N(3)–C(25)	124.7(8)
C(13)–N(4)–C(19)	104.6(8)	C(13)–N(5)–C(14)	105.3(7)
C(13)–N(5)–C(26)	129.0(8)	C(14)–N(5)–C(26)	125.1(8)
C(3)–C(4)–N(3)	129.9(9)	C(5)–C(4)–N(3)	106.3(8)
C(4)–C(5)–N(1)	109.4(8)	N(1)–C(5)–C(6)	130.3(9)
N(1)–C(7)–N(3)	109.9(8)	N(1)–C(7)–C(8)	119.4(8)
N(3)–C(7)–C(8)	130.6(8)	C(9)–C(8)–N(2)	121.3(8)
C(9)–C(8)–C(7)	125.2(8)	N(2)–C(8)–C(7)	113.4(8)
C(8)–C(9)–C(10)	119.2(8)	C(11)–C(10)–C(9)	118.6(9)
C(10)–C(11)–C(12)	120.7(10)	N(2)–C(12)–C(11)	122.4(9)
N(2)–C(12)–C(13)	115.2(8)	C(11)–C(12)–C(13)	122.4(9)
N(4)–C(13)–N(5)	114.1(8)	N(4)–C(13)–C(12)	123.1(9)
N(5)–C(13)–C(12)	122.9(8)	C(19)–C(14)–C(15)	123.5(8)
C(19)–C(14)–N(5)	105.9(8)	C(15)–C(14)–N(5)	130.6(9)
C(14)–C(19)–N(4)	110.2(7)	C(14)–C(19)–C(18)	119.7(9)
N(4)–C(19)–C(18)	129.8(9)	O(3)–C(20)–Re(1)	175.0(9)
O(1)–C(21)–Re(1)	177.7(9)	O(2)–C(22)–Re(1)	177.3(9)

by the values O(01)–N(4) 2.830, H(01)–N(4) 1.994 Å, angle O(01)–H(01)–N(4) 173°. The N-methyl group of the pendant imidazolyl moiety is *cis* to Br. The bond lengths and angles associated with the organic ligand are as expected. The C–O (carbonyl) distances are 1.142(10) to 1.157(11) Å and the Re–C–O units are close to linearity with angles of 175.0(9) to 177.7(9)°.

Acknowledgements—We thank the EPSRC for postdoctoral support to one of us (A.G.), and also for support to the X-ray facilities at Cardiff.

REFERENCES

1. Abel, E. W., Long, N. J., Orrell, K. G., Osborne, A. G., Pain, H. M. and Šik, V., *J. Chem. Soc., Chem. Commun.*, 1992, 303.

2. Abel, E. W., Dimitrov, V. S., Long, N. J., Orrell, K. G., Osborne, A. G., Šik, V., Hursthouse, M. B. and Mazid, M. A., *J. Chem. Soc., Dalton Trans.*, 1993, 291.
3. Abel, E. W., Dimitrov, V. S., Long, N. J., Orrell, K. G., Osborne, A. G., Pain, H. M., Šik, V., Hursthouse, M. B. and Mazid, M. A., *J. Chem. Soc., Dalton Trans.*, 1993, 597.
4. Abel, E. W., Orrell, K. G., Osborne, A. G., Pain, H. M. and Šik, V., *J. Chem. Soc., Dalton Trans.*, 1994, 111.
5. Abel, E. W., Gelling, A., Orrell, K. G., Osborne, A. G. and Šik, V., *J. Chem. Soc., Chem. Commun.*, 1996, 2329.
6. Abel, E. W., Hylands, K. A., Olsen, M. D., Orrell, K. G., Osborne, A. G., Šik, V. and Ward, G. N., *J. Chem. Soc., Dalton Trans.*, 1994, 1079.
7. Gelling, A., Orrell, K. G., Osborne, A. G. and Šik, V., *J. Chem. Soc., Dalton Trans.*, 1994, 3545.
8. Garcia, M. A. M., Gelling, A., Noble, D. R., Orrell, K. G., Osborne, A. G. and Šik, V., *Polyhedron*, 1996, **15,** 371.
9. Gelling, A., Orrell, K. G., Osborne, A. G., Šik, V., Hursthouse, M. B. and Coles, S. J., *J. Chem. Soc., Dalton Trans.*, 1996, 203.
10. Kaesz, H. D., Bau, R., Hendrickson, D. and Smith, J. M., *J. Am. Chem. Soc.*, 1967, **89,** 2844.
11. Addison, A. W. and Burke, P. J., *J. Heterocycl. Chem.*, 1981, **18,** 803.
12. Kikugawa, Y., *Synthesis*, 1981, 124.
13. Shriver, D. F., *Manipulations of Air-Sensitive Compounds*, McGraw-Hill, New York, 1969.
14. Kleier, D. A. and Binsch, G., DNMR3 Program 165. Quantum Chemistry Program Exchange, Indiana University, IN, 1970.
15. Šik, V., Ph.D. thesis. University of Exeter, 1979.
16. Darr, J. A., Drake, S. R., Hursthouse, M. B. and Malik, K. M. A., *Inorg. Chem.*, 1993, **32,** 5704.
17. Walker, N. P. C. and Stuart, D., DIFABS Program for Absorption Correction, *Acta Crystallogr. Sect. A.*, 1983, **39,** 158. Adapted for FAST geometry by A. I. Karaulov, University of Wales Cardiff, 1991.
18. Sheldrick, G. M., SHELXS86 Program for Crystal Structure Solution, *Acta Crystallogr. Sect. A*, 1990, **46,** 467.
19. Sheldrick, G.M., SHELXL93 Program for Crystal Structure Refinement. University of Gottingen, Germany, 1993.
20. Davies, K., SNOOPI Program for Crystal Structure Drawing. University of Oxford, U.K., 1983.
21. Petoud, S., Bunzli, J-C. G., Schlenk, K. J. and Piguet, C., *Inorg. Chem.*, 1997, **36,** 1345.
22. Bessel, C. A., See, R. F., Jameson, D. L., Churchill, M. R. and Takeuchi, K. J., *J. Chem. Soc. Dalton Trans.*, 1992, 3223.
23. Sanni, S. B., Behm, H. J., Beurskens, P. T., van Albada, G. A., Reedijk, J., Lenstra, A. T. H., Addison, A. W. and Palaniandavar, M., *J. Chem. Soc., Dalton Trans.*, 1988, 1429.

Pergamon

PII: S0277-5387(98)00080-1

Polyhedron Vol. 17, Nos 13-14, pp. 2153-2159, 1998
© 1998 Elsevier Science Ltd
All rights reserved. Printed in Great Britain
0277-5387/98 $19.00+0.00

Stereospecific synthesis and crystal structure of the racemate of 1-thia-2-tellura-1(1-allyl-4-chloro)cyclopentane 2,2,2-trichloride

Jan Bergman[a], Tarja Laitalainen[b], Markku R. Sundberg[c], Rolf Uggla[c] and Raikko Kivekäs[c]

[a]Department of Organic Chemistry, CNT, NOVUM, S-14157 Huddinge, Sweden

[b]Department of Chemistry, Laboratory of Organic Chemistry, PO Box 55, FIN-00014 University of Helsinki, Helsinki, Finland

[c]Department of Chemistry, Laboratory of Inorganic Chemistry, PO Box 55, FIN-00014 University of Helsinki, Helsinki, Finland

(Received 11 November 1997; accepted 17 February 1998)

Abstract—Tellurium tetrachloride and diallyl sulfide react to stereospecifically formed crystals of 1-thia-2-tellura-1(1-allyl-4-chloro)cyclopentane 2,2,2-trichloride. According to single-crystal X-ray determination the structure consists of the (R,R)-(S,S) racemate unit with a centre of symmetry. In the asymmetric units the Te^{IV}-atoms display distorted ψ octahedral coordination. Although the equatorial Te-S bond length is 2.763(1) Å, the Natural Bond Order (NBO) analysis reveals significant electronic interaction. © 1998 Elsevier Science Ltd. All rights reserved

Keywords: tellurium heterocycle; stereoselectivity; NBO; crystal structure.

INTRODUCTION

According to Migalina [1–3] compounds of the general structure **1** (Fig. 1) are formed by interaction of (TeO_2 + HCl) in diethyl ether with diallyl derivatives of the general structure [$(CH_2{=}CHCH_2)_2Z$, Z = NH,NCH_3,O,S]. Such compounds would be obvious candidates for couplings to e.g. functionalized pyrrole derivatives, such as **2** and maybe also piperidones **3**, if similar carbonyl insertions observed [4, 5] in the aromatic series could be extended to the aliphatic series. In this connection the reported conversion [6], induced by degassed Raney nickel of e.g. 2,6-diethoxy-3,5-dimethyl-1,4-oxaselenane **4** dichlorides [6, 7] to 3,4-dimethylfurane is of interest.

Attempts to reproduce the synthesis of (**1**, Z = NH,X = Cl) failed and experiments [8] with $(CH_2{=}CHCH_2)_2NAc$ and $TeCl_4$ gave the zwitterionic oxazoline **5** rather than a compound of type **1**.

1,5-Hexadiene and TeX_4 has been claimed to yield the symmetrical tellurophene derivative **6**. This reaction has been reinvestigated [8] and its formation has been confirmed [9]. In addition the C-C coupled products **7** and **8** are produced. Such formation of carbocycles are in line with the previous cyclizations [10–12] of 1,5-hexadiene induced by $Pb(OAc)_4$ and $Hg(OAc)_2$.

Migalina *et al* [1–3], also claimed the preparation of **1** (Z = S,X = Cl). However, attempts to reproduce these experiments gave compounds of type **9**. A related oxygen system, **10** has previously been studied by Detty [13, 14], whereas its sulfur isologue does not seem to have appeared in the literature. Ring systems with S-Te bonds are however rare although *e.g.* compound **11** has been prepared by Irgolic *et al* [15]. Other more or less related compounds [16] have been discussed in four recent reviews [17–20].

Compound **9** can be synthesised in a number of solvents (*e.g.*, benzene and chloroform), but the best yields were obtained in acetonitrile. The nature of the reagent depends on the solvent and evidently $TeCl_4$ exists in acetonitrile as a mononuclear species.

Attempts to synthesise a Se-analogue of **9** with $SeCl_4$ failed and elemental selenium fell out.

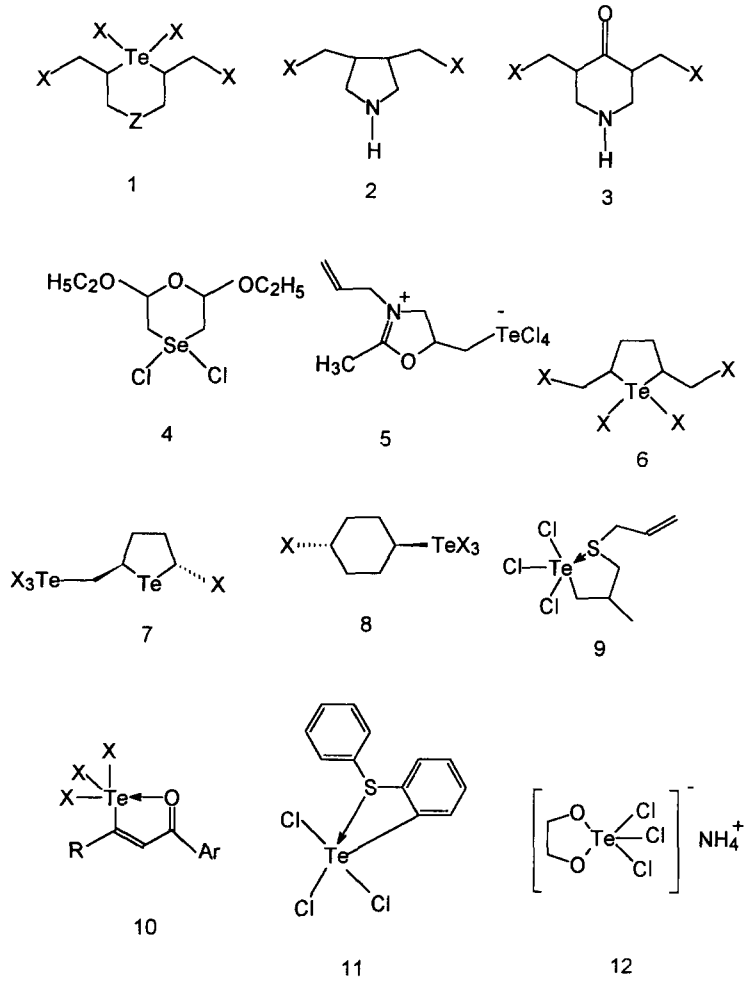

Fig. 1. The tellurium and some related compounds discussed in the present paper.

RESULTS AND DISCUSSION

The synthetic pathway

Unlike the reaction of $TeCl_4$ with diallyl ether, which gives the 1,4-oxatellurane derivative **1** (Z = O,X = Cl) stereoselectively with *cis*-configuration [20], the reaction with diallyl sulfide affords **9** as a racemic mixture of the (R,R) and (S,S) stereoisomers in the solid state (The Scheme). Neither the (R,S)-(S,R) racemate nor any mixed versions were formed. Accordingly, the reaction of $TeCl_4$ with C=C and S-centres takes place by a mechanism, which confers stereochemical control. A relevant question is, whether the crystal (R,R)-(S,S) racemate arises from a stereospecific reaction, or is a result of the crystallisation. Diallyl sulfide has two types of nucleophilic centres, the double bonds and the S-atom. Both paths, (a) and (b), are conceivable. Considering the fact, that the reaction of diallyl ether gives **1**, it is difficult to see, why the regiochemistry would be reversed, if path (a) were followed. It is therefore more likely that Te-S-interaction dominates the initiation of the reaction and the path (b) will dictate the regiochemical result. Then the new chiral centre at the S-atom would react stereospecifically in such a way that (S) would create (S)-configuration at C2 (Fig. 2) and (R) would create (R). Further coordination to give the solid state structure involves the racemate crystallisation and simultaneous expansion of the coordination sphere of the Te-atom. The stability of the chiral centre at the S-atom in solution is not obvious, since the Te-S bond can best be described as a coordinate bond (see *ab initio* calculations) and a decoordination-recoordination sequence is conceivable.

The molecular structure of the racemate of **9** is given in Fig. 2. with selected intermolecular distances. The crystal structure is shown in Fig. 3. The bond lengths and angles are given in Table 1 and contact distances in Table 2.

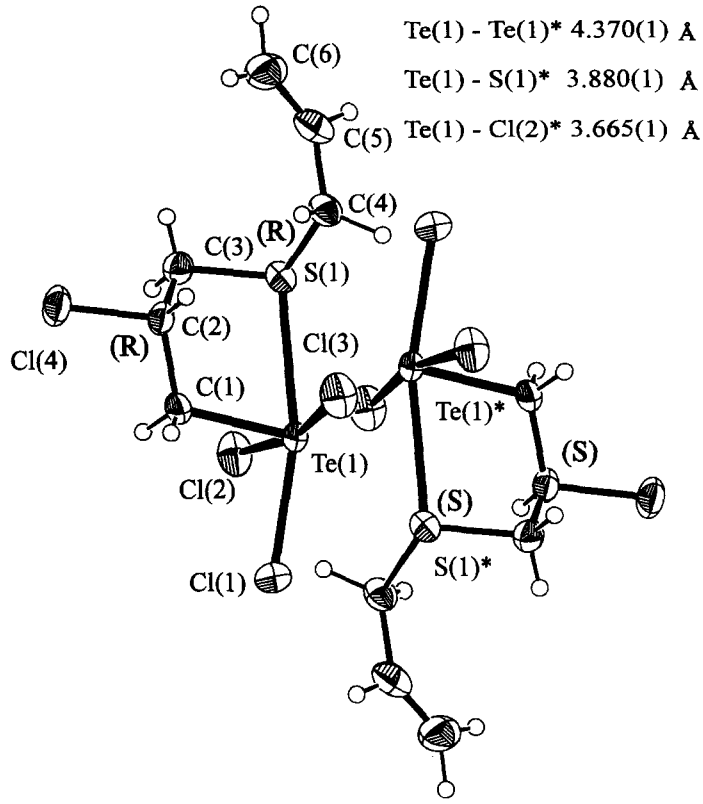

Fig. 2. ORTEP drawing of the racemate of 1-thia-2-tellura-1(1-allyl-4-chloro)cyclopentane 2,2,2-trichloride **9**. The thermal ellipsoids for the non-hydrogen atoms are drawn at 50% level of probability. (S) and (R) denote absolute configuration.

In the solid state the enantiomers of the racemate of **9** are related through a centre of symmetry. The racemic unit forms parallel sheets, which interact through Cl · · · Cl contacts. All Cl-atoms participate in two contacts.

Description of the structure **9**.

The title compound is a new example of tellurium(IV) forming a heterocycle with a C-Te-S bond system (Fig. 2). A previous structure determination of

Table 1. Bond Lengths (Å) and Angles (°) with their Standard Deviations for 1-Thia-2-tellura-(1-allyl-4-chloro)cyclopentane 2,2,2-trichloride **9**.

Te(1) - Cl(1)	2.424(1)	Cl(1) - Te(1) - Cl(2)	93.19(4)
Te(1) - Cl(2)	2.5549(9)	Cl(2) - Te(1) - Cl(3)	168.91(4)
Te(1) - Cl(3)	2.4527(8)	Cl(2) - Te(1) - C(1)	85.87(8)
Te(1) - C(1)	2.139(4)	Cl(1) - Te(1) - Cl(3)	95.18(4)
Te(1) - S(1)	2.763(1)	Cl(1) - Te(1) - C(1)	87.9(1)
S(1) - C(3)	1.810(5)	Cl(3) - Te(1) - C(1)	87.17(8)
S(1) - C(4)	1.828(2)	C(3) - S(1) - C(4)	102.2(2)
C(1) - C(2)	1.508(5)	Te(1) - C(1) - C(2)	113.5(2)
C(2) - C(3)	1.506(5)	Cl(4) - C(2) - C(1)	106.5(2)
Cl(4) - C(2)	1.808(4)	Cl(4) - C(2) - C(3)	107.9(3)
C(4) - C(5)	1.480(6)	C(1) - C(2) - C(3)	114.3(3)
C(5) - C(6)	1.304(7)	S(1) - C(3) - C(2)	110.8(3)
		S(1) - C(4) - C(5)	108.9(2)
		C(4) - C(5) - C(6)	125.2(5)

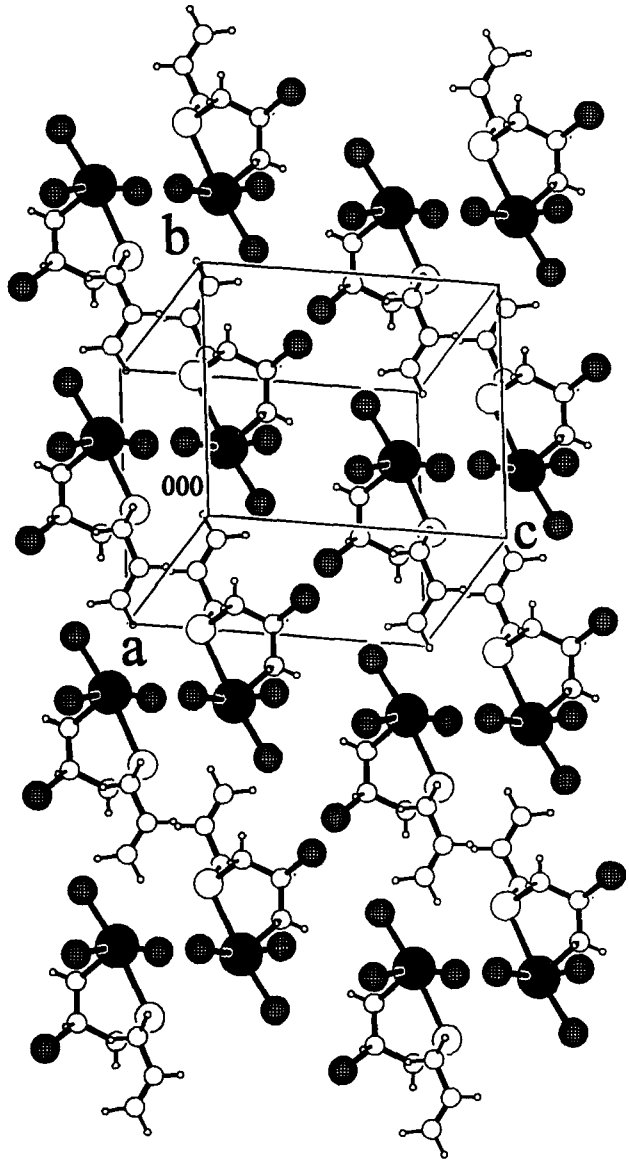

Fig. 3. A view of the packing of 1-thia-2-tellura-1(1-allyl-4-chloro)cyclopentane 2,2,2-trichloride **9**.

Table 2. The Shortest Intermolecular Distances in the Crystal Structure of 1-Thia-2-tellura-1(1-allyl-4-chloro)cyclopentane 2,2,2-Trichloride **9**. The Roman Superscripts Refer to the Given Symmetry Operations.

	distance /Å	symmetry operation	description
Te(1)•••S(1)^{i}	3.880(1)	$-x+1,-y+1,-z$	intradimer
Te(1)•••Cl(2)^{i}	3.665(1)	$-x+1,-y+1,-z$	intradimer
Cl(1)•••Cl(4)^{ii}	3.758(1)	$x,y-1,z$	intralayer
Cl(1)•••Cl(3)^{iii}	3.783(2)	$-x+1,-y+1,-z+1$	interlayer
Cl(2)•••S(1)^{i}	3.479(2)	$-x+1,-y+1,-z$	intradimer
Cl(3)•••Cl(4)^{iv}	3.559(1)	$x+1,y,z$	interlayer
Cl(4)•••Cl(4)^{v}	3.778(1)	$-x+1,-y+2,-z+1$	intralayer

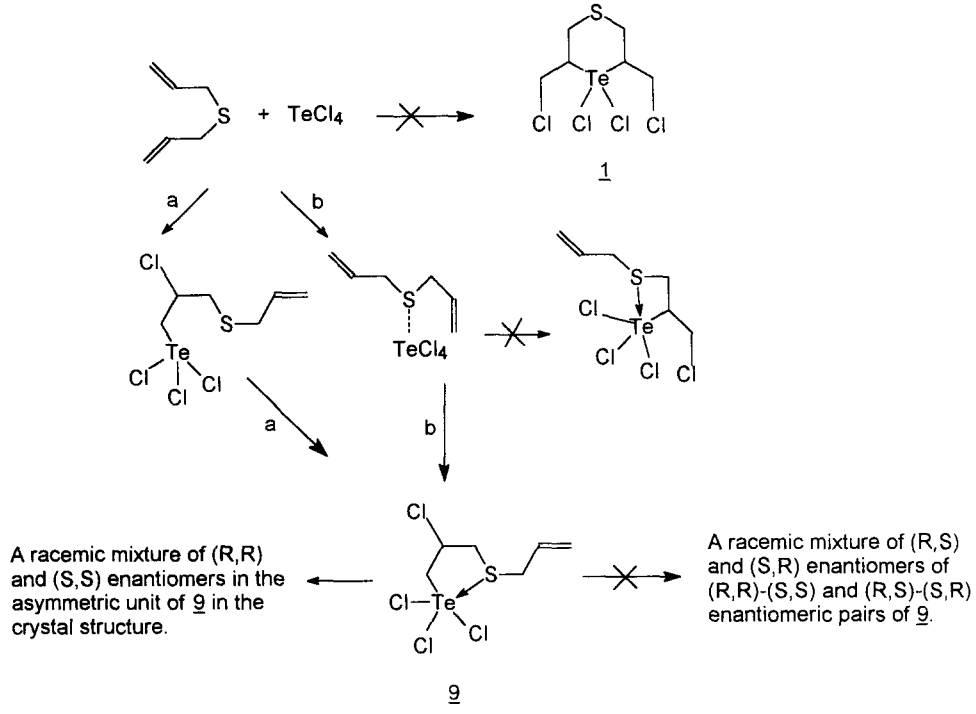

a related Te-compound **11** (Fig. 1) was reported by Irgolic *et al* [15]. The coordination sphere around Te(IV) is distorted ψ octahedron consisting of the above mentioned bonding system and three additional Te-Cl bonds in the equatorial position. The axial positions are occupied by the C(1)-atom and a lone pair of electrons. The average value of the three Te-Cl bonds, 2.477 Å, is shorter than the average value of 2.530 Å found in $[TeCl_6]^{2-}$ anion [22]. The Te-Cl bond lengths appear in the range of 2.34–2.60 with average value of 2.52(3) Å reported for 22 compounds [23]. The Te(1)-Cl(1) bond is shorter than the Te-Cl(2) or Te-Cl(3) bond. It is even shorter than the equivalent Te-Cl(1) bond in trichloro(ethane-1,2-diolato-O,O')tellurate(IV) **12** [2.722(2) Å] [24]. The Te(1)-S(1) bond length [2.763(1) Å] is significantly longer than the average value of 2.541 Å found in bromobis(dimethyldithiocarbamato-*S*,*S*')tellurium(IV) tetrabromo(dimethyldithiocarbamato-*S*,*S*') tellurate(IV)-dioxane(1/1) [25]. The Te(1)-S(1) distance is longer than the sum of the respective covalent radii [2.37 Å] [26]. However, it is shorter than the sum of the van der Waals radii [3.90 Å]. The length of the Te-C(1) bond 2.139(4) Å matches with the average value of 2.139 Å calculated from six Te-C bond containing molecules found from CSD [27].

The racemate of **9** forms layers running along *h*00 planes (Fig. 3). The Te···Cl(2)^{i} distance is significantly shorter than the sum of van der Waals radii [4.00 Å]. These interactions may explain the relatively long Te(1)-Cl(2) bond length of 2.555(1) Å.

Ab initio *calculations for* 9

To elucidate the bonding in **9**, NBO analyses were carried out. Separate calculations were carried out by STO-3G* and LANL1DZ basis sets to evaluate the contribution of the relativistic effect. The atomic coordinates for the racemic unit of **9** (Fig. 2) obtained from X-ray analysis were used as input data.

The results form the population analysis are given in Table 3. The central Te(1)-atom carries a positive charge. The value of 1.121 is less than found in trichloro(ethane-1,2-diolato-O,O')tellurate(IV) **12**, where the value of 1.368 was obtained when calculated at the RHF/STO-3G* level of theory [24]. All the atoms bonded to the Te(1)-atom have negative charges, except the S(1)-atom. The mutually opposite Cl(2)- and Cl(3)-atoms are more negative than the Cl(1)-atom. There seems to be a correlation between the Te-Cl bond lengths and the charge resting on a Cl-atom: the longer the Te-Cl bond is, the more negative charge there will be on a Cl-atom. As expected, the relativistic effect is affecting the Te(1)-atom and its coordination sphere. Especially the positive charge of the Te(1)-atom increases, while the atoms bonded to the Te(1)-atom have received electrons.

Table 3. Summary of Natural Population Analysis (NPA) for the Non-Hydrogen Atoms of 1-Thia-2-tellura-1(1-allyl-4-chloro)cyclopentane 2,2,2-Trichloride **9**.

Atom	Natural Charge	
	STO-3G*	LANL1DZ
Te(1)	1.12111	1.58874
S(1)	0.38445	0.16713
Cl(1)	−0.36436	−0.46503
Cl(2)	−0.51978	−0.62685
Cl(3)	−0.44994	−0.54467
Cl(4)	−0.16568	−0.12205
C(1)	−0.30081	−0.61826
C(2)	0.13503	−0.05490
C(3)	−0.24093	−0.37592
C(4)	−0.19567	−0.41255
C(5)	−0.01665	−0.15607
C(6)	−0.08053	−0.34298

The covalent bonds can be evaluated with the help of NBO analyses (Table S1, Supplementary Material). Although the usual way to interpret the hypervalency is to use the 3c-4e concept, no such bonds were found for the Te(1)-atom. Each Cl-atom has three lone pairs of electrons, the S(1)-atom has two and the central Te(1)-atom one. Although the NBO subprogram does not recognise a covalent Te(1)-S(1) bond, it appears that the lone pair LP2 of the S(1)-atom has 10.7% contribution from Te(1)-atom.

When the relativistic effect is taken into account, the bonding system undergoes a change. The lone pair LP2 of the S(1)-atom gains now 8.7% contribution from Te(1)-atom, and the contribution from C(1)-atom has diminished into 0.6%. Interestingly, there are also interactions across the enantiomeric units. While the lone pair LP2 of the S(1)-atom gains contribution from the Te(1)-atom, the LP1 gets 0.126% of the electron pair from the Te(1)-atom from the neighbouring unit.

The Te(1)-S(1) and Te(1)-Cl(2) bonding can be evaluated with the help of second order perturbation theory analysis of Fock matrix in NBO basis (Table S2, Supplementary Material). When the relativistic effect is not taken into account, the S(1)-atom donates an electron pair partly to the Te(1)-atom and partly to Te(1)-Cl(1) and Te(1)-C(1) bonds. Moreover, the electrons are pushed into the antibonding orbitals of the Te(1)-Cl(1) and Te-C(1) bond. It is relevant to notice that the Te-Cl(2) bond is the longest one among the Te(1)-Cl bonds. This fact may be connected to the participation of the Cl(2)-atom in the shortest intermolecular contacts.

On the basis of the NBO analysis, the Te(1)-S(1) bond can be characterised as a coordinative bond, although it has also features from covalent and charge transfer bonding. When the relativistic effect is included in the calculations, both Te(1)-S(1) and Te(1)-Cl(2) interactions are mostly of charge-transfer type.

EXPERIMENTAL

Spectra

IR spectra were recorded on a Perkin Elmer 1600 FTIR Spectrometer. The NMR spectra were recorded by Bruker AM 400 Instrument.

Synthesis

Tellurium tetrachloride (5.38 g, 2 mmol) was added to a stirred solution of diallyl sulfide (2.58 ml, 2 mmol) in acetonitrile (30 ml) at 35°C. A clear solution was quickly obtained from which soon a white solid was formed. After 2 h at 35°C the mixture was cooled and the solid collected and recrystallised from acetonitrile, yield 6.02 g (75%), mp. 140°C (dec.). IR (KBr): 3018, 2979, 2955, 2941, 1635, 1422, 1404, 1394, 1267, 1235, 1200, 1193, 1168, 1004, 1092, 990, 967, 948, 842, 801, 767, 734, 708 cm^{-1}. ^1H NMR (δ) (CD_3CN): 3.30 (t, 1 H), 3.72(m, 3 H), 3.85 (t, 1 H), 4.45 (m, 1 H), 4.87 (m, 1 H), 5.39 (d, 1 H), 5.50 (d, 1 H) and 5.88 (m, 1 H); ^{13}C NMR (δ) (CD_3CN): 38.54 (CH_2), 40.27 (CH_2), 55.03 (CH), 67.33 (CH_2), 123.14 (CH_2) and 130.3 (CH).

X-ray study

Crystal Data for **9**. $C_6H_{10}Cl_4STe$, $M=383.61$, triclinic, $a=8.2594(11)$, $b=8.8432(11)$, $c=10.469(2)$ Å, $\alpha=96.126(12)$, $\beta=107.610(12)$, $\gamma=117.788(11)°$, $V=616.3(2)$ $Å^3$ (by least-squares refinement of diffractometer angles for 25 independent well-centred reflections, $\lambda=0.71069$ Å), space group $P\bar{1}$ no. 2, $Z=2$, $D_c=2.07$ g cm^{-3}, Crystal dimensions $0.14\times0.21\times0.44$ mm, $\mu=3.47$ mm^{-1}.

Data Collection and Processing. Nicolet P3 diffractometer, ω scan mode, variable scan speed 2.0-20.0°min^{-1}, graphite monochromated Mo-$K\alpha$ radiation, 3604 unique reflections measured ($5°\leq2\Theta\leq60°$), empirical absorption correction based on ι-scans, giving 3241 independent reflections with $F>6\sigma(F_o)$. No decay, but Lorentz and polarization corrections were made.

Structure Analysis and Refinement. Direct methods [28] followed by difference Fourier techniques. The structure was refined by full-matrix least squares techniques with all non-hydrogen atoms having anisotropic and the hydrogen atoms isotropic temperature factors. The function minimised was $\Sigma w(|F_o|-|F_c|)^2$ with $w=1/\sigma^2_F$. The highest peaks in the final difference Fourier maps were near to the Te- and Cl-atoms. Final R and R' ($1/\sigma^2$ weights) values are 0.027 and

0.030, respectively. The neutral atom scattering factors and correction factors for anomalous scattering were those included in the program package. The calculations were carried out with XTAL software [29]. The neutral atom scattering factors were those included in the program. Anisotropic thermal parameters and listings for the observed and calculated structure factors are available as Supplementary Material from the authors on request.

Ab initio *calculations*

The calculations were carried out at the HF/STO-3G* and HF/LANL1DZ levels of theory by the GAUSSIAN92 program package [30] installed on a CRAY-XMP supercomputer. The electronic charges and the bonding properties were analyzed with the NBO program [31], which is a subprogram in GAUSSIAN92. The atomic coordinates for the racemic unit shown in Fig. 2 were used as input data.

Acknowledgement—Financial support of the Academy of Finland, the Technology Development Centre and the University of Helsinki is gratefully acknowledged. The Centre for Scientific Computing, Espoo Finland, provided the necessary computing resources.

REFERENCES

1. Migalina, Yu. V., Balog, I. M., Lendel, V. G., Koz'min. A. S. and Zefirov, N. S., *Khim. Geterotsikl. Soedin*, 1978, 1212.
2. Migalina, Yu. V., Staninets, V. I., Lendel, V. G., Balog, I. M., Palyulin, V. A., Koz'min, A. S. and Zefirov, N. S., *Khim. Geterotsikl. Soedin.*, 1977, 58.
3. Lendel, V. G., Sani, A. Yu., Migalina, Yu. V., Pak, B. I., Balog, I. M., *Khim. Geterotsikl. Soedin.*, 1989, 564.
4. Bergman, J. and Engman, L., *J. Organomet. Chem.*, 1979, **175,** 233.
5. Takahashi, H., Ohe, K., Uemura, S. and Sugita, N., *J. Organomet. Chem.*, 1987, **C43,** 334.
6. Bergman, J. and Laitalainen, T., *Heterocycles*, 1985, **23,** 37.
7. Bergman, J., Laitalainen, T., Kaltia, S., Klinga, M. and Kivekäs, R., *Acta Chem. Scand., Sect. B.*, 1986, **40,** 715.
8. Bergman, J., Siden, J. and Haartmann-Moe, K., *Tetrahedron*, 1984, **40,** 1607.
9. Bergman, J. and Siden, J., Unpublished results.
10. Tabushi, I. and Oda, R., *Tetrahedron Lett.*, 1966, 2487.
11. Julia, M. and Gasquez, E. C., *Bull. Soc. Chim. France*, 1973, 17.
12. Gasquez, E.C., Ph.D, Thesis, Paris, 1970.
13. Detty, M. R. and Luss, H. R., *J. Org. Chem.*, 1983, **48,** 5149.
14. Detty, M. R., Luss, H. R., McKelvey, J. M. and Geer, S. M., *J. Org. Chem.*, 1983, **48,** 149.
15. Chakravorty, R., Irgolic, K. J. and Meyers, E. A., *Acta Crystallogr., Sect. C*, 1985, **41,** 1545.
16. Ogawa, S., Yamashita, M. and Sato, R., *Tetrahedron Lett.*, 1993, **36,** 587.
17. Sadekov, I. D., Abakarov, G. M., Sadekova, Y. I. and Minkin, V. I., *Sulfur Reports*, 1986, **6,** 15.
18. Renson, M., The Chemistry of Organic Selenium and Tellurium Compounds; S. Patai, Z. Rappoport, Eds, Wiley-Interscience, Chichester, (1986), Chap. 13.
19. Detty, M., Tellurium Containing Heterocycles, Wiley, New York, 1994.
20. Haiduc, I., King, R. B. and Newton, M. G., *Chem. Rev.*, 1994, **94,** 301.
21. Laitalainen, T., Sundberg, M. R., Uggla, R. and Bergman, J., *Polyhedron*, 1997, **16,** 2441.
22. Ault, H. K. and Husebye, S., *Acta Chem. Scand., Sect. A*, 1978, **32,** 157.
23. Allen, F. H., Kennard, O., Watson, D. G., Brammer, L., Orpen, A. G. and Taylor, R., *J. Chem. Soc., Perkin Trans. II*, 1987 S(1).
24. Sundberg, M. R., Uggla, R., Laitalainen, T. and Bergman, J., *J. Chem. Soc., Dalton Trans.*, 1994, 3279.
25. Schnabel, W., von Deuten, K. and Klar, G., *Phosphorus Sulfur*, 1982, **13,** 345.
26. Huheey, J. E., Inorganic Chemistry, Harper Collins College Publishers, New York, 4th ed., 1993, p.292.
27. Cambridge Crystallographic Data Centre. User Manual, 3rd ed., Cambridge University, 1988.
28. Sheldrick, G. M., *Acta Crystallogr., Sect. A*, 1990, **46,** 467.
29. Hall, S. R. and Stewart, J. M., (ed). XTAL 3.0 User's Manual, Universities of Western Australia and Maryland, 1988.
30. Gaussian 92, Revision. Frisch, C. M. J., Trucks, G. W., Head-Gordon, M., Gill, P. M. W., Wong, M. W., Foresman, J. B., Johnson, B. G., Schlegel, H. B., Robb, M. A., Replogle, E. S., Gomperts, R., Andres, J. L., Raghavachari, K., Binkley, J. S., Gonzalez, C., Martin, R. L., Fox, D. J., Defrees, D. J., Baker, J., Stewart, J. J. P., Pople, J. A., Gaussian, Inc., Pittsburgh PA, 1992.
31. NBO, Version 3.1, Glendening, E. D., Reed, A. E., Carpenter, J. E. and Weinhold, F. link 607 in Gaussian 92.

Pergamon

PII: S0277-5387(98)00081-3

Polyhedron Vol. 17, Nos 13–14, pp. 2161–2166, 1998
© 1998 Elsevier Science Ltd
All rights reserved. Printed in Great Britain
0277-5387/98 $19.00+0.00

A new coordination mode for the tartrato ligand. Synthesis of vanadium(V) oxo peroxo tartrato complexes and the X-ray crystal structure of $K_2[\{VO(O_2)(L\text{-}tartH_2)\}_2(\mu\text{-}H_2O)].5H_2O$

P. Schwendt[a]*, P. Švančárek[a], L. Kuchta[a] and J. Marek[b]

[a]Department of Inorganic Chemistry, Faculty of Natural Sciences, Comenius University, 842 15 Bratislava, Slovak Republic

[b]Department of Inorganic Chemistry, Faculty of Natural Sciences, Masaryk University, 611 37 Brno, Czech Republic

(Received 24 October 1997; accepted 17 February 1998)

Abstract—Vanadium(V) oxo peroxo tartrato complexes $M_2[\{VO(O_2)(L\text{-}tartH_2)\}_2(\mu\text{-}H_2O)].5H_2O$ ($M=K^+$, NH_4^+; $tart^{4-}=C_4O_6H_2^{4-}$) have been prepared from aqueous-ethanolic medium and characterized by elemental analysis and IR spectroscopy. The X-ray crystal structure of $K_2[\{VO(O_2)(L\text{-}tartH_2)\}_2(\mu\text{-}H_2O)].5H_2O$, as the first crystal structure of a vanadium(V) tartrato complex has been determined. The dinuclear anion exhibits two pentagonal bipyramidal polyhedra about vanadium atoms which are joined to each other by sharing two oxygen atoms of hydroxyl groups and oxygen atom from water molecule. The tartrate group is bonded to the vanadium atom in a bidentate way via oxygen atoms of neighbouring carboxylic and hydroxyl groups. The coordinated hydroxyl oxygen atom is bonded also to the second vanadium atom, but in a monodentate way. This type of bonding of tartrate group was not observed so far. © 1998 Elsevier Science Ltd. All rights reserved

Keywords: peroxo tartrato complexes of vanadium; crystal structure.

Since discovery of the insulin mimetic effect of vanadium(V) compounds [1], the structure and reactivity of vanadium(V) complexes with biologically important ligands have been intensively studied [2]. Peroxo complexes constitute a new group of powerful insulin mimics [3–5]. On the other hand vanadium(V) peroxo complexes are probably formed as intermediates in oxidation reactions catalyzed by vanadium bromoperoxidase, an enzyme from marine algae [6]. Anions of α-hydroxycarboxylic acids, which are involved in many biochemical processes, represent an interesting class of biogenic ligands. Vanadium (V) monoperoxo complexes with citrate [7] and malate [8] have been prepared and structurally characterized. Both compounds contain dinuclear complex anion with a double bridge formed by oxygen atoms of hydroxyl groups (Fig. 1).

The tartrato ligand, as another example of this class

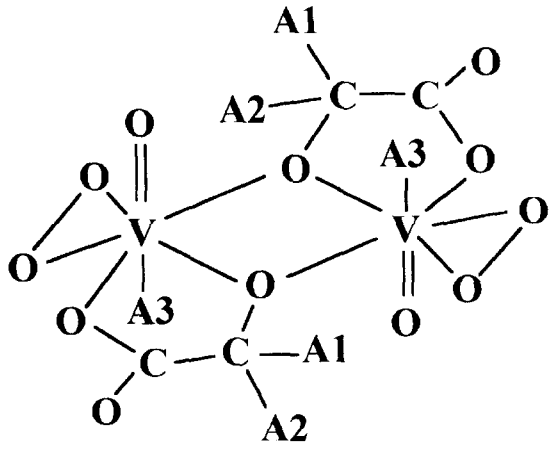

Fig. 1. Schematic structure of α-hydroxycarboxylato monoperoxo complexes of vanadium(V).Malato: A1=H, A2=CH_2–COOH, A3=O (carboxylato, from A_2)Citrato: A1=CH_2–COO(H), A2=CH_2–COO(H), A3=O (carboxylato, from A_2)

*Author to whom correspondence should be addressed.

of ligands, has several alternatives, considering its coordination to central atom. The tartrate anion can act as mono-, bi-, or tridentate ligand with different combinations of donor atoms. Moreover, both hydroxyl and carboxylic groups or the ligand as the whole, can make various bridges between metal atoms, thus forming dimeric or polymeric structures. A number of dimeric tartrato complexes of vanadium(IV) has been structurally characterized e.g. [9, 10], and the synthesis of vanadium(V) complexes e.g. $K_3[HV_2O_5(tart)].H_2O$ and $Na_4[V_4O_8(tart)_2].6H_2O$ [11–14] has been described. The structure reported here represents the first crystal structure of a vanadium(V) tartrato complex. In the dinuclear anion a novel type of tartrato group ligation has been observed.

EXPERIMENTAL

Preparation of complexes

Chemicals. KVO_3 was prepared by thermal decomposition of crystallohydrate obtained by reaction of V_2O_5 with KOH at pH 8. All other chemicals were of analytical grade and used as supplied (Loba Chemie, Lachema).

$$K_2[\{VO(O_2)(L-H_2tart)\}_2\mu-H_2O].5H_2O$$

A solution of KVO_3 (0.69 g, 5 mmol) in 20 cm^3 water was mixed with a solution of L-tartaric acid (0.75 g, 5 mmol) in 5 cm^3 water. After cooling (0°C) of the resulting solution H_2O_2 (30%, 1 cm^3) and ethanol (5 cm^3, dropwise) were added under constant stirring. Light red crystals were isolated after 6 hours standing at 5°C. Found: C 14.67, H 2.71, O_2^{2-} 9.71, V 15.10. Calc. for $C_8H_{20}K_2O_{24}V_2$: C 14.12, H 2.96, O_2^{2-} 9.41, V 14.98%.

The deuterated complex was obtained using D_2O, D_2O_2, and C_2H_5OD instead of H_2O, H_2O_2, and C_2H_5OH.

$$(NH_4)_2[\{VO(O_2)(L-H_2tart)\}_2\mu-H_2O].5H_2O$$

NH_4VO_3 (0.575 g, 5 mmol) and L-tartaric acid (0.75 g, 5 mmol) were dissolved in 10 cm^3 water. After cooling of the solution (0°C) H_2O_2 (30%, 2.5 cm^3) and ethanol (10 cm^3) were added under continuous stirring. The red complex was isolated after 6 hours standing at 5°C. Found: C 15.00, H 4.18, N 4.19, O_2^{2-} 10.09, V 16.04. Calc. for $C_8H_{28}N_2O_{24}V_2$: C 15.06, H 4.42, N 4.39, O_2^{2-} 10.03, V 15.96%.

Both compounds are soluble in water. Solid complexes are stable at −15°C for at least 20 days. The

Table 1. Crystal data and structure refinement for $K_2[\{VO(O_2)(L\text{-}H_2tart)\}_2\mu\text{-}H_2O].5H_2O$

Formula	$C_8H_{16}K_2O_{24}V_2$
Formula weight	676.29
Crystal system	Orthorhombic
Space group	$C222_1$
T (°C)	153 K
a (Å)	11.489(2)
b (Å)	11.836(2)
c (Å)	32.900(4)
V (Å^3)	4473.9(11)
Z	8
D_c (g·cm^{-3})	2.008
μ (mm^{-1})	1.320
λ (Å)	0.71073
$F(000)$	2720
Crystal size (mm)	0.70 × 0.70 × 0.15
Θ range (°)	1.24 to 25.10
Index ranges	$-13 \le h \le 1$, $0 \le k \le 14$, $0 \le l \le 39$
Reflections collected	2322
Independent reflections	2319 (R_{int} = 0.0473)
Goodness-of-fit on F^2	1.026
Final R indices ($I>2\sigma I$)[a]	R_1 = 0.0433, R_{w2} = 0.1240
R indices (all data)[a]	R_1 = 0.0566, R_{w2} = 0.1882
Absolute structure parameter	0.04(6)
Largest diff. peak and hole	1.023 and −0.814 e Å^{-3}
Refinement method	Full-matrix least-squares on F^2
Data / restraints / parameters	2310/6/384

[a] $R_1 = \Sigma \| Fo| - |Fc| / |Fo|$

$R_{w2} = \{\Sigma[w(F^2_o - F^2_c)^2] / \Sigma[w(F^2_o)^2]\}^{1/2}$

decomposition at room temperature is accompanied by succesive colour changes from red through brown to black.

Caution: In some cases an explosive decomposition of the ammonium complex occured at room temperature. It is recommended to handle only small amounts of it (up to 20 mg).

Physical measurements and analyses

Infrared spectra were measured on a Nicolet 750 Magna FTIR Spectrometer with the samples as KBr pellets or nujol mulls.

Vanadium(V) was reduced to vanadium(IV) using ascorbic acid. An access of standard EDTA solution was added to the obtained solution and the vanadium content was determined by a back titration with $ZnCl_2$.

Peroxidic oxygen was determined by titration with $KMnO_4$.

Carbon, hydrogen and nitrogen were estimated on a Carlo Erba 1106 C H N analyzer.

X-ray structure determination

Low-temperature X-ray measurements were made on a KUMA KM4 diffractometer with graphite monochromated Mo-Kα radiation using the ω-2θ scan technique. Cell parameters and an orientation matrix for data collection were obtained from least-squares refinement, using the setting angles of 64 reflections in the range $5.82^\circ < \theta < 12.05^\circ$. No significant decay of the intensity of the three standard reflections recorded after every 90 reflections was observed. Data were not corrected for absorption effects. 2319 unique reflections were obtained, of which 2075 with $I > 2\sigma_I$ were classified as observed. The additional crystal data and refinement results are given in Table 1. The structure was solved by a combination of Patterson and difference Fourier methods, and refined by a full-matrix least-squares procedure (SHELLXL-93) [15] on $|F^2|$. Non-hydrogen atoms were refined anisotropically. Hydrogen atoms were obtained from a difference Fourier map and were refined isotropically. Not all crystal water hydrogen atoms were found. The final refinement was carried out with a weighting scheme of $w = 1/[\sigma^2(F^2_o) + (0.0975P)^2 + 30000P]$, where $p = (F^2_o + 2F^2_c)/3$ *and* 2310 *reflections. Refinement converged at* $R_1(F) = 0.0433$ and $R_{w2}(F^2) = 0.1240$ for observed reflections and 384 refined parameters. The largest positive and negative peaks in the difference map were 1.023 and $-0.814\,e \cdot Å^{-3}$, respectively. Additional material which comprises the final coordinates of atoms, anisotropic displacement parameters and a list of observed and calculated structure factors is available from the Cambridge Crystallographic Data Centre.

RESULTS AND DISCUSSION

The red complexes, $M_2[\{VO(O_2)\ (L\text{-}H_2tart)\}_2\ \mu\text{-}H_2O].\ 5\ H_2O$ (M = K, NH_4), were obtained by crystallization from MVO_3 — L-tartaric acid — H_2O_2 — H_2O — ethanol systems. At room temperature, the complexes decompose both in solid state and aqueous solution. The release of peroxidic oxygen is followed by reduction of vanadium (V), which manifests itself by colour change from red, through brown and green to black.

In the infrared spectra (Table 2), the bands corresponding to the OH stretching vibrations of protonated carboxylic and alcoholic groups can be easily assigned, but not mutually distinguished. The bands at 1736 and 1716 cm^{-1} unambiguously prove the presence of protonated and evidently uncoordinated carboxylic group. The bands at 1662, 1636, 1375, and 1359 cm^{-1} can be assigned to stretching vibrations of deprotonated and coordinated carboxylic group. The COO^- group is coordinated in a monodentate way. This is substantiated by the Δ value ($\Delta = \nu_{as}(COO^-) - \nu_s(COO^-) = 248\ cm^{-1}$), which is typical for this mode of bonding [16]. Deprotonation of alcoholic groups is not easily ascertainable from the IR spectra. Nevertheless the stoichiometry of the complex requires the charge of the ligand to be 2−, therefore the simultaneous presence of a protonated and a deprotonated alcoholic groups in the ligand can be assumed. The bands of the $VO(O_2)$ group are in the range characteristic for monoperoxo complexes of vanadium [17, 18].

The conclusions based on the IR studies were confirmed by X-ray structure analysis. The crystals of

Table 2. Characteristic IR bands for $M_2[\{VO(O_2)\ (L\text{-}H_2tart)\}_2\ \mu\text{-}H_2O].\ 5\ H_2O$ (M = K, NH_4)

K^+	K^+ (D)[a]	NH^+_4	Assignment
3648 m	2672 m (1.36)	3635 m	ν(OH)[c]
3575 m	2630 m (1.36)	3584 m	
3422 s	2533 s (1.35)	3429 s	ν(OH)[d]
3351 m-s	2509 m (1.34)	3269 s	
1736 s	1736 s	1735 m	ν(C=O)[e]
1716 m	1716 m		
1662 vs	1662 vs	1635 s	$\nu_{as}(COO^-)$
1636 m	1636 m		
1375 m	1375 m	1374 sh	$\nu_s(COO^-)$
1359 s	1358 m		
[b]	1281 w		$\delta(H_2O)$
986 vs	984 vs	987 s	ν(V=O)
935 vs	933 vs	935 s	ν(O−O)

[a] Partially deuterated complex; the ratio $\tilde{\nu}$(deuterated)/$\tilde{\nu}$(nondeuterated) is given in parenthesis.
[b] Obscured by other bands.
[c] Carboxylic and alcoholic groups
[d] H_2O
[e] Protonated, uncoordinated carboxylic group

$K_2[\{VO(O_2)(L\text{-}H_2tart)\}_2\ \mu\text{-}H_2O].\ 5\ H_2O$ contain eight formula units in the orthorhombic cell. The K^+ cations, $[\{VO(O_2)(L\text{-}H_2tart)\}_2\ \mu\text{-}H_2O]^{2-}$ anions and molecules of crystal water are held together by electrostatic forces and hydrogen bounds. The bond lengths and angles which are in the expected ranges are in Tables 3 and 4.

In the dinuclear anion (Fig. 2), vanadium atoms are bridged by O7 and O7* hydroxyl oxygens from both L-tartrato ligands and by O4 oxygen atom of a water molecule. The coordination about each vanadium atom is that of distorted pentagonal bipyramid which was found, with exception of $[VO(O_2)(glygly)]^-$ [19] in all thirty one structures of monoperoxo complexes of vanadium [20]. The equatorial positions are occupied by peroxo groups (O1, O2 and O1*, O2*), both bridging hydroxyl oxygens (O7, O7*) and oxygen atoms from the monodentate carboxylic groups (O5, O5*). The axial positions are taken by double bonded oxygen atoms O3 and O3*, and the bridging oxygen atom from the water molecule.

The significant differencies between the structure of peroxo- L-tartrato complex presented here and the related structures of malato and citrato complexes (Fig. 1) are summarized in Table 5.

There are fifty structures of tartrato complexes (except complexes with substituted tartrato group, e.g. esters) registered in the Cambridge Structural Database (1996). A monodentate tartrato ligand was found in three structures, bidentate in fourty one, and tridentate only in one structure. In the remaining five structures, tartrato groups with more than one type of bonding (e.g. mono- and bidentate) were found. The coordination mode of the tartrato ligand in complexes with a bidentate tartrato group can be classified, according to the type and number of donor atoms, into five groups (Table 6). As can be seen from this table, the type of tartrate group ligation in $K_2[\{VO(O_2)\ (L\text{-}H_2tart)\}_2\ \mu\text{-}H_2O].\ 5\ H_2O$ differs from the other ones, especially from that found in the related structure of $(N(CH_3)_4)_2\ [MoO_2(L\text{-}H_2tart)_2].\ C_2H_5OH.\ 1.5H_2O$ [21] (type C), thus representing a new type of ligation of the tartrato ligand (type E).

Table 3. Selected bond lengths (Å) for $K_2[\{VO(O_2)\ (L\text{-}H_2tart)\}_2\ \mu\text{-}H_2O].\ 5\ H_2O$

V1–O3	1.588(5)	V1′–O3′	1.584(6)
V1–O2	1.861(5)	V1′–O2′	1.878(5)
V1–O1	1.895(5)	V1′–O1′	1.895(5)
V1–O5	2.007(6)	V1′–O5′	1.997(5)
V1–O7	2.010(5)	V1′–O7′	2.026(5)
V1–O7[1]	2.015(5)	V1′–O7′[2]	2.003(5)
V1–$O4_w$	2.398(6)	V1′–$O4_w$′	2.390(6)
O1–O2	1.423(7)	O1′–O2′	1.444(7)
O5–C1	1.282(9)	O5′–C1′	1.271(9)
O6–C1	1.223(10)	O6′–C1′	1.220(10)
O7–C2	1.410(9)	O7′–C2′	1.415(9)
O8–C3	1.398(10)	O8′–C3′	1.407(10)
O9–C4	1.208(9)	O9′–C4′	1.210(10)
O10–C4	1.317(9)	O10′–C4′	1.317(10)
C1–C2	1.525(11)	C1′–C2′	1.538(10)
C2–C3	1.545(10)	C2′–C3′	1.507(11)
C3–C4	1.500(11)	C3′–C4′	1.518(11)

Symmetry transformations used to generate equivalent atoms:

[1] -x, y, 1.5-z

[2] x, 1-y, 1-z

Table 4. Bond angles (°) and torsion angles (°) for $K_2[\{VO(O_2)\ (L\text{-}H_2tart)\}_2\ \mu\text{-}H_2O].\ 5\ H_2O$

O3–V1–O2	102.5(3)	O3′–V1′–O2′	102.0(3)
O3–V1–O1	102.5(3)	O3′–V1′–O1′	102.4(3)
O2–V1–O1	44.5(2)	O2′–V1′–O1′	45.0(2)
O3–V1–O5	97.9(3)	O3′–V1′–O5′	98.1(3)
O2–V1–O5	122.2(2)	O2′–V1′–O5′	122.4(2)
O1–V1–O5	78.5(2)	O1′–V1′–O5′	78.2(2)
O3–V1–O7	99.5(3)	O3′–V1′–O7′	98.8(3)
O2–V1–O7	147.6(2)	O2′–V1′–-O7′	148.5(2)
O1–V1–O7	149.2(2)	O1′–V1′–O7′	149.3(2)
O5–V1–O7	77.3(2)	O5′–V1′–O7′	77.0(2)
O3–V1–O7[1]	96.3(2)	O3′–V1′–O7′[2]	96.8(2)
O2–V1–O7[1]	83.8(2)	O2′–V1′–O7′[2]	84.3(2)
O1–V1–O7[1]	127.5(2)	O1′–V1′–O7′[2]	128.3(2)
O5–V1–O7[1]	146.3(2)	O5′–V1′–O7′[2]	145.4(2)
O7–V1–O7[1]	70.3(2)	O7′–V1′–O7′[2]	69.9(2)
O3–V1–$O4_w$	168.2(2)	O3′–V1′–$O4_w$′	167.6(2)
O2–V1–$O4_w$	81.2(2)	O2′–V1′–$O4_w$′	83.4(2)
O1–V1–$O4_w$	88.1(2)	O1′–V1′–$O4_w$′	89.3(2)
O5–V1–$O4_w$	89.3(2)	O5′–V1′–$O4_w$′	88.2(2)
O7–V1–$O4_w$	72.9(2)	O7′–V1′–$O4_w$′	72.0(2)
O7[1]–V1–$O4_w$	72.8(2)	O7′[5]–V1′–$O4_w$′	72.4(2)
O2–O1–V1	66.4(3)	O2′–O1′–V1′	66.9(3)
O1–O2–V1	69.0(3)	O1′–O2′–V1′	68.1(3)
V1–$O4_w$–V1[1]	80.8(2)	V1′–$O4_w$′–V1′[2]	81.6(3)
C1–O5–V1	120.2(5)	C1′–O5′–V1′	121.7(5)
C2–O7–-V1	118.8(4)	C2′–O7′–V1′	118.4(4)
C2–O7–V1[1]	128.4(4)	C2′–O7′–V1′[2]	127.7(4)
V1–O7–V1[1]	101.0(2)	V1′–O7′–V1′[2]	101.6(2)
O6–C1–O5	123.3(7)	O6′–C1′–O5′	124.7(7)
O6–C1–C2	122.0(7)	O6′–C1′–C2′	121.0(7)
O5–C1–C2	114.7(7)	O5′–C1′–C2′	114.3(6)
O7–C2–C1	108.2(6)	O7′–C2′–C1′	108.0(6)
O7–C2–C3	109.3(6)	O7′–C2′–C3′	109.9(6)
C1–C2–C3	110.1(7)	C1′–C2′–C3′	110.4(6)
O8–C3–C4	111.0(7)	O8′–C3′–C4′	110.9(7)
O8–C3–C2	106.4(6)	O8′–C3′–C2′	106.0(6)
C4–C3–C2	112.5(7)	C4′–C3′–C2′	111.8(7)
O9–C4–O10	123.9(7)	O9′–C4′–O10′	124.3(8)
O9–C4–C3	122.6(7)	O9′–C4′–C3′	123.1(8)
O10–C4–C3	113.5(7)	O10′–C4′–C3′	112.6(7)
O7–V1–O5–C1	-9.6(6)	O7′–V1′–O5′–C1′	-6.8(6)
V1–O5–C1–C2	10.3(10)	V1′–O5′–C1′–C2′	6.2(10)
O5–C1–C2–O7	-3.9(11)	O5′–C1′–C2′–O7′	-0.8(10)
C1–C2–O7–V1	-4.0(9)	C1′–C2′–O7′–V1′	-4.6(9)
C2–O7–V1–O5	7.1(6)	C2′–O7′–V1′–O5′	6.0(6)

Symmetry transformations used to generate equivalent atoms:

[1] -x, y, 1.5-z

[2] x, 1-y, 1-z

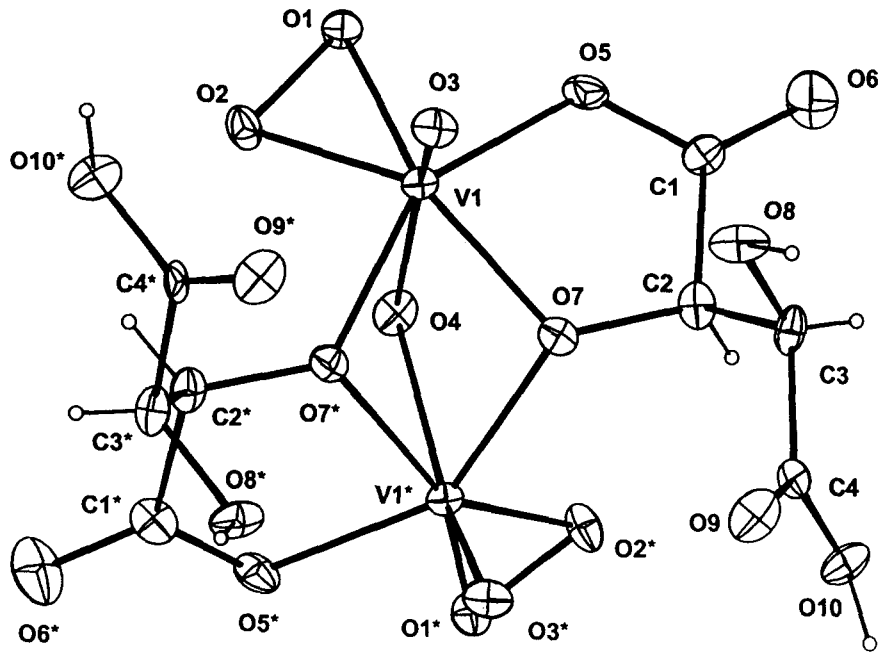

Fig. 2. ORTEP presentation at the 50% probability of the $[\{VO(O_2)\ (L\text{-}H_2tart)\}_2\ \mu\text{-}H_2O]^{2-}$ anion. The position of atoms designated by astericks are generated by twofold axis going through O4 atom.

Table 5. Some differences between structures of α-hydroxycarboxylato peroxo complexes of vanadium(V).

	Malato, Citrato	L-tartrato
Axial positions in pentagonal bipyramide	O (V=O) O (COO^-)	O (V=O) O_b (H_2O)
Type of bridging	Double bridge	Triple bridge
Geometry of the V $(O_b)_2$ V group	~ Planar	Nonplanar
Angle between the two pentagonal planes	~ Coplanar	~ 61
Mutual position of the V=O bonds in the anion	Antiparallel	~ 58 Oriented to the same side from pentagonal planes

Acknowledgements—This work was supported by the Ministry of Education of the Slovak Republic (Grant 1/2169/1995), Comenius University (Grant UK/1576/97), Ministry of Education of the Czech Republic (Grant VS 96095) and by the Grant Agency of the Czech Republic (Grants 203/95/1190 and 203/96/0111).

REFERENCES

1. Shechter, J. and Karlish, S. J. D., *Nature*, 1980, **284,** 556.
2. Crans, D. C., in *Metal ions in biological systems*, **31**; *Vanadium and Its Role in Life*, H. Sigel, A. Sigel, (Eds.), p.147, Marcel Dekker, New York, Basel, Hong Kong, 1995.
3. Shaver, A., Ng, J. B., Hall, D. A., Lum, B. S., Posner, B. I. *Inorg. Chem.*, 1993, **32**, 3109; Posner, B. I., Faure, R., Burges, J. W., Bevan, A. P., Lachance, D., Zhang-Sun, G., Fantus, I. G., Ng, J. B., Hall D. A., Lum, B. S. and Shaver, A., *J. Biol. Chem.*, 1994, **269**, 4596.
4. Shaver, A., Ng, J. B., Hynes, R. C. and Posner, B. I., *Acta Crystallogr.*, 1994, **C50,** 1044.
5. Shaver, A., Hall, D. A., Ng, J. B., Lebuis, A. M., Hynes, R. C. and Posner, B. I., *Inorg. Chim. Acta*, 1995, **229,** 253.
6. Vilter, H., in *Metal ions in biological systems*, Vol. 31, *Vanadium and Its Role in Life*, H. Sigel, and A. Sigel, (Eds.), p. 325, Marcel Dekker, New York, Basel, Hong Kong, 1995.
7. Djordjevic, C. and Lee, M., Sinn, E., *Inorg. Chem.*, 1988, **28,** 719.
8. Djordjevic, C., Lee-Renslo, M. and Sinn, E., *Inorg. Chim. Acta*, 1985, **233,** 97.
9. Tapscott, R. E., Belford, R. L. and Paul, I. C., *Inorg. Chem.*, 1968, **7,** 356.
10. Forrest J. G. and Prout C. K., *J. Chem. Soc.*, (A) 1967, 1312.
11. Jahr, K. F., Preuss, F. and Rosenhahn, L., *J. Inorg. Nucl. Chem.*, 1969, **31,** 297.

Table 6. Bonding in tartrato complexes with bidentate tartrato ligand.

Type	N[a]	Way of bonding	n[b]
A	4 (bis bidentate)	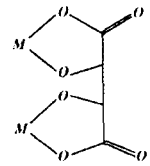	38
B	2	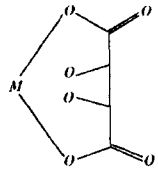	1
C	2	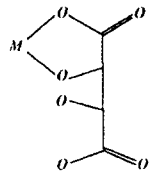	1
D	3 (mono + bidentate)	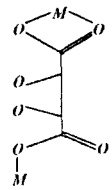	1
E	2 (mono + bidentate)	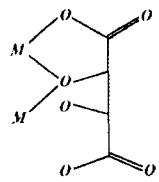	This work

a) N- number of oxygen atoms bonded to central atom(s)
b) n- number of structures in Cambridge Structural Database

12. Sivák, M., *Acta F. R. N. Univ. Comen.-Chimia*, 1980, **28,** 69.
13. Sivák, M., *Acta F. R. N. Univ. Comen.-Chimia*, 1981, **29,** 37.
14. Sivák, M., *Acta F. R. N. Univ. Comen.-Chimia*, 1981, **29,** 47.
15. Sheldrich G. M., SHELXL93. Program for Refinement of Crystal Structures. University of Göttingen, Germany, 1993.
16. Nakamoto K., *Infrared and Raman Spectra of Inorganic and Coordination Compounds*, 4th edn., p. 253, J. Wiley and Sons, New York, Chichester, Brisbane, Toronto, Singapore, 1996.
17. Mimoun, H., Saussine, L., Daire, E., Postel, M., Fischer, J. and Weiss, R., *J. Am. Chem. Soc.*, 1983, **105,** 3101.
18. Kuchta L., Sivák M. and Pavelčík F., *J. Chem. Research*, (S) 1993, 393.
19. Einstein, F. W. D., Batchelor, R. J., Angus-Dunne, S. J. and Tracey, A. S., *Inorg. Chem.*, 1996, **35,** 1680.
20. Schwendt, P. and Sivák, M., ACS Volume Based on the Symposium, Chemistry, Biochemistry, and Insulin Mimetic Influences of Vanadium. in *The 5th Chemical Congress of North America*, Cancun, Mexico 1997 (In Press).
21. Robinson, W. T. and Wilkins, C. J., *Transition Met. Chem.*, 1986, **11,** 86.

Pergamon

PII: S0277-5387(98)00075-8

Polyhedron Vol. 17, Nos 13–14, pp. 2167–2171, 1998
© 1998 Elsevier Science Ltd
All rights reserved. Printed in Great Britain
0277-5387/98 $19.00+0.00

Copper(II) complexes of 10-methyl-10-amino-1,4,8,12-tetra-azacyclopentadecane. Synthesis, protonation and formation constants and kinetics of the acid-catalysed dissociation

Robert W. Hay,* Erzsebet Kiss, Claudia Loechel and Thomas Clifford

School of Chemistry, University of St Andrews, St Andrews, KY16 9ST U.K.

(Received 23 June 1997; accepted 12 February 1998)

Abstract—The ligand 10-methyl-10-amino-1,4,8,12-tetra-azacyclopentadecane has been prepared by the reduction of (10-methyl-10-nitro-1,4,8,12-tetra-azacyclopentadecane)copper(II) nitrate with Zn/HCl. The protonation constants of the ligand at 25°C and $I = 0.1$ mol dm^{-3} are $\log K_{11} = 10.79$, $\log K_{12} = 9.37$, $\log K_{13} = 5.21$, $\log K_{14} = 2.78$ and $\log K_{15} = < 2.0$. The formation constants for the equilibria

$$Cu^{2+} + L + H^{+} \rightleftarrows CuLH^{3+}; \quad \log \beta_{CuLH}$$

$$Cu^{2+} + L \rightleftarrows CuL^{2+}; \quad \log \beta_{CuL}$$

are $\log \beta_{CuLH} = 25.57 \pm 0.03$ and $\log \beta_{CuL} = 21.63 \pm 0.04$. The pK for the ionisation of the protonated 10-amino group in the copper(II) complex, $CuLH^{3+} \rightleftarrows CuL^{2+} + H^{+}$ is 3.94 ± 0.05. The protonated complex is four-coordinate and becomes five-coordinate as the protonated amino group ionises. A new band appears in the visible spectrum of the copper complex at *ca.* 800 nm as the five-coordinate complex is formed. Spectrophotometric titrations using the 800 nm band give a $pK = 3.94 \pm 0.05$. The kinetics of the acid-catalysed dissociation of the copper complex have been studied. © 1998 Elsevier Science Ltd. All rights reserved

Keywords: copper complex; macrocycle; formation constants; dissociation kinetics.

In a recent paper [1], one of us discussed some aspects of the chemistry of the copper(II) complex of 10-methyl-10-nitro-1,4,8,12-tetra-azacyclopentadecane (1). Reduction of this complex with Zn/HCl to give the amino-substituted macrocycle (2 = L) has recently been reported by Bayada and coworkers [2]. This paper also describes the crystal structure of $H_5L.3Cl^{-}.2ClO^{-}_4.2H_2O$. It has recently been found [3] that a variety of bis-cyclam macrocycles, of the type shown in (3) and (4) are very active against HIV-1 and HIV-2 and have considerable chemotherapeutic potential. Some of these compounds are currently undergoing clinical trials in the United States. The macrocycle (2) can form interesting bis-macrocycles by a [2+1] Schiff base condensation with a suitable dialdehyde 'spacer'. The imine linkages can then be readily reduced with sodium borohydride to give derivatives such as (5) which may have pharmaceutical applications.

The present paper discusses the synthesis of (2) and its coordination chemistry with copper(II).

EXPERIMENTAL

Synthesis

(10-*methyl*-10-*nitro*-1,4,8,12-*tetra-azacyclopentadecane*) *copper(II) nitrate*. The tetra-amine 1,10-diamino-4,7-diazadodecane (3,2,3-tet) (35 g, 0.20 mol) was added to copper(II) nitrate dihydrate (48 g, 0.20 mol) in methanol (1500 cm^3). The resulting dark blue solution was warmed with stirring and triethylamine (22 g, 0.22 mol), nitroethane (37 g, 0.49 mol) and formaldehyde (100 cm^3, 40% aqueous solution, 1.44 mol)

*Author to whom correspondence should be addressed.

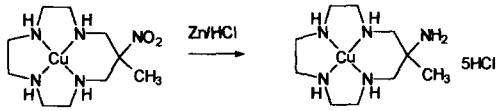

(1) (2)

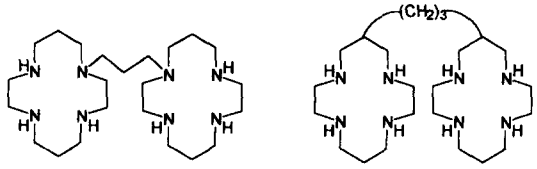

(3) (4)

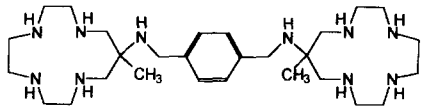

(5)

added. After heating at 55°C for 30 min. the solution was allowed to cool at room temperature overnight. The beautiful blue-purple crystals obtained were filtered off, washed with methanol then diethyl ether and dried in *vacuo*. Yield 64 g (70%). Found: C, 31.2; H, 6.4; N, 21.3. Calc. for $C_{12}H_{27}CuN_7O_8$: C, 31.3; H, 5.9; N, 21.3%.

10-*methyl*-10-*amino*-1,4,8,12-*tetra-azacyclopentadecane*.5*HCl*. The copper(II) complex prepared above (30 g, 0.065 mol) in distilled water (600 cm^3), were simultaneously added, dropwise, to Zn dust (75 g, 1.15 mol) over a period of 2.5 hr. The solution was heated and stirred during the addition, then filtered and the colourless filtrate diluted to 5 litres. The solution was then added to a cation exchange column in the acid form. The column employed had the dimensions 25 × 7 cm. The zinc(II) was removed from the column by the addition of 1 M HCl (about 1.5 litres), then the macrocycle was eluted by the addition of 5 M HCl (about 2.5 litres are required). Evaporation of the HCl solution gave the pentahydrochloride which was washed with ethanol then diethyl ether. The hydrochloride was recrystallised by dissolving in water, adding HCl and precipitating by the addition of ethanol. The hydrochloride was obtained as a very fine white solid which is quite difficult to filter. The hydrochloride was thoroughly dried in *vacuo* over silica gel. Yield 23 g (84%).

Potentiometric measurements

The titrant was added by a microprocessor controlled (VIT90 video titrator) piston burette (ABU91 Radiometer autoburette). Measurements of pH were made with an Orion Ross combination electrode (Model 8102). The titration data were passed from the VIT90 video titrator to a 386 PC using the program TITRAFILE. Conversion of the data to SUPERQUAD format was made using the Fortran program VITOQUAD. The data was processed using the SUPERQUAD program [4] to give the equilibrium constants.

Solutions of copper(II) nitrate were standardised against standard 0.1 mol dm^{-3} EDTA (Aldrich) in a complexometric titration monitored by a copper(II) selective electrode (Orion 9429). The voltage output from the selective electrode was measured relative to SCE (Orion 900200 reference electrode). Standard sodium hydroxide was prepared by dilution of concentrated sodium hydroxide ampoules (Rhone–Poulenc). The sodium hydroxide solution was standardised by titration against accurately weighed samples of potassium hydrogen phthalate. The standard solution was protected against atmospheric CO_2 by calcium oxide (carbosorb, BDH). Stock solutions of hydrochloric and nitric acid were standardised against standard sodium hydroxide. All aqueous solutions were prepared with boiled out distilled water (kept under a stream of argon during cooling). During the titration, the titration vessel was partially sealed and protected against ingress of atmospheric CO_2 by blowing nitrogen gas over the solution surface. The temperature of the solution was maintained at 25°C using a water jacketed cell and Heto circulator. All measurements were carried out at $I = 0.1$ mol dm^{-3} adjusted with KNO_3 (Aldrich 99.99%). Experimental parameters for the potentiometric measurements are summarised in Table 1.

Spectrophotometric titrations

Approximately the same conditions were used as for the potentiometric titrations. An acidic mixture of

Table 1. Summary of experimental parameters for the potentiometric study of the system Cu(II)-L

Solution composition	
$[T_L]$ range (mol dm^{-3})	2.0×10^{-3}–8.5×10^{-4}
$[T_{Cu(II)}]$ range (mol dm^{-3})	1.3×10^{-3}–7.5×10^{-4}
I (mol dm^{-3}) electrolyte	0.1, KNO_3
pH Range	2.0–11.0
Experimental method	pH titration, calibrated by standard buffers
T (°C)	25 ± 0.1
Total number of data points	
Protonation	291 (3 curves)
Copper complexation	177 (3 curves)
Method of calculation	SUPERQUAD

the metal ion (1.9×10^{-3} mol dm^{-3}) and the ligand (2.0×10^{-3} mol dm^{-3}) was titrated with base and at suitable intervals during the titration the UVis spectrum was determined over the wavelength range 1100–350 nm. The measurements were made over the pH range 2.0 to 11.0 at $I = 0.1$ mol dm^{-3} (KNO_3). Absorption spectra were obtained using a Perkin Elmer Lambda 14P instrument controlled by an IBM compatible PC. The cell compartment was thermostated at 25 C.

Kinetics

The kinetics of dissociation of the copper(II) complex were monitored spectrophotometrically at 570 nm which is λ_{max} for the complex. Plots of $\ln(A_t - A_\infty)$ versus time were linear for several half lives and values of k_{obs} (the observed first order rate constant at constant hydrogen ion concentration) were determined from the slope of these plots. The measurements were made at 25 C using nitric acid solutions

RESULTS AND DISCUSSION

Reduction of the nitro group of (1) with Zn/HCl takes place readily and, under the conditions employed, demetalation of the complex occurs to give the ligand pentahydrochloride (2), which was isolated by ion exchange methods.

Potentiometry

The titration curve, Fig. 1, for the protonated ligand shows a buffer region corresponding to the loss of two protons, then a fairly sharp inflexion point after the addition of two equivalents of base. The pK of only one of these acidic protons could be determined, the pK of the other proton being less than 2. A second buffer region corresponds to the titration of a single proton and a third buffer region indicates the removal of two strongly basic protons. The log β values are listed in Table 2. The β values for the protonation of 10-methyl-10-amino-1,4,8,12-tetra-azacyclopentadecane correspond to the following stepwise protonation constants

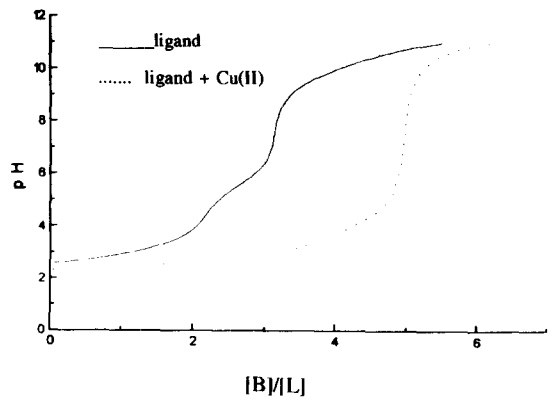

Fig. 1. Titration curves for the ligand pentahydrochloride and for the ligand pentahydrochloride in the presence of one equivalent of copper(II).

Table 2. Protonation constants for L and stability constants for copper(II) complexes.

Protonation constants (ligand = H_4L, errors as σ)		
$\log\beta_{HL}$	$H^+ + L = HL^+$	10.79 ± 0.01
$\log\beta_{H2L}$	$2H^+ + L = H_2L^{2+}$	20.16 ± 0.02
$\log\beta_{H3L}$	$3H^+ + L = H_3L^{3+}$	25.37 ± 0.02
$\log\beta_{H4L}$	$4H^+ + L = H_4L^{4+}$	28.15 ± 0.02
Copper(II) stability constants		
$\log\beta_{CuLH}$	$Cu^{2+} + L + H^+ = CuLH^{3+}$	25.57 ± 0.03
$\log\beta_{CuL}$	$Cu^{2+} + L = CuL^{2+}$	21.63 ± 0.04

$$H^+ + L \rightleftarrows HL^+; \quad \log K_{11} = 10.79 \pm 0.01$$
$$H^+ + HL^+ \rightleftarrows H_2L^{2+}; \quad \log K_{12} = 9.37 \pm 0.02$$
$$H^+ + H_2L^{2+} \rightleftarrows H_3L^{3+}; \quad \log K_{13} = 5.21 \pm 0.03$$
$$H^+ + H_3L^{3+} \rightleftarrows H_4L^{4+}; \quad \log K_{14} = 2.78 \pm 0.03$$
$$H^+ + H_4L^{4+} \rightleftarrows H_5L^{5+}; \quad \log K_{15} < 2$$

Electrostatic repulsion between the protonated amino groups can account for the low values of $\log K_{14}$ and $\log K_{15}$. The high values of $\log K_{11}$ and $\log K_{12}$ may be indicative of intramolecular hydrogen bonding between the protonated and deprotonated amino groups.

Copper complexation

Potentiometric titrations made at a 1:1 metal to ligand ratio were used to calculate the stability constants of the copper(II) complexes using the SUPERQUAD program [4]. A plot of pH *versus* [B]/[L] is shown in Fig. 1, and Fig. 2 shows the speciation curve for the copper(II) complexes formed in the system Cu-L. Hydroxy complexes are not formed as there is a sharp inflexion point after addition of five equivalents of base. This result indicates that the deprotonation and the coordination of the pendant primary amino group occurs. At approximately pH 3–5, the titration curve indicates the formation of a protonated complex $CuLH^{3+}$ which is expected to be four-coordinate with a protonated 10-amino group. For the equilibrium

$$CuLH^{3+} \rightleftarrows CuL^{2+} + H^+; \log K_1$$

$$\log K_1 = (\log \beta_{CuLH} - \log \beta_{CuL}) = 3.94 \pm 0.05$$

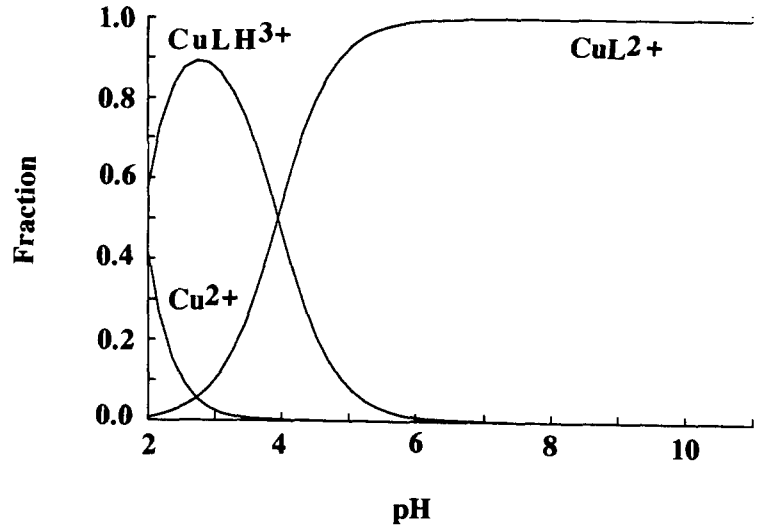

Fig. 2. Speciation curve for the copper(II) complexes. The ligand and copper(II) concentrations are both 1.5×10^{-3} mol dm^{-3}.

Spectrophotometric titrations

Five-coordinate copper(II) complexes normally display two bands in their *d-d* spectrum. Copper(II) complexes of penta-aza macrocycles have the main band near 600 nm and there is an additional band of lower intensity around 800 nm. Exactly analogous behaviour is observed with the copper(II) complex of 10-methyl-10-amino-1,4,8,12-tetra-azacyclopentadecane. At low pH the complex displays a single *d-d* band at 590 nm, Fig. 3. On raising the pH, a new band appears in the spectrum at *ca.* 800 nm. Detailed analysis of the pH-dependence of the intensity of the 800 nm band indicates a $pK = 3.95 \pm 0.05$, fully consistent with the potentiometric measurements.

Kinetics of acid dissociation

A brief investigation of the acid dissociation kinetics of the copper(II) complex was carried out using nitric acid solutions in the concentration range 1.0 to

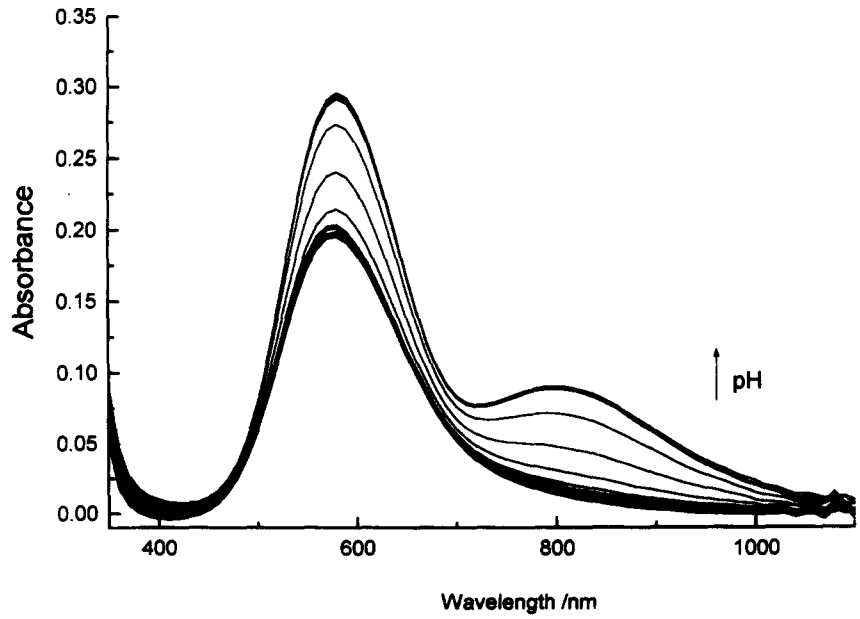

Fig. 3. pH-dependence of the spectrum of $[CuLH]^{3+}$ showing the formation of the five coordinate 'arm on' complex. The measurements cover the pH range 2.0 to 11.0.

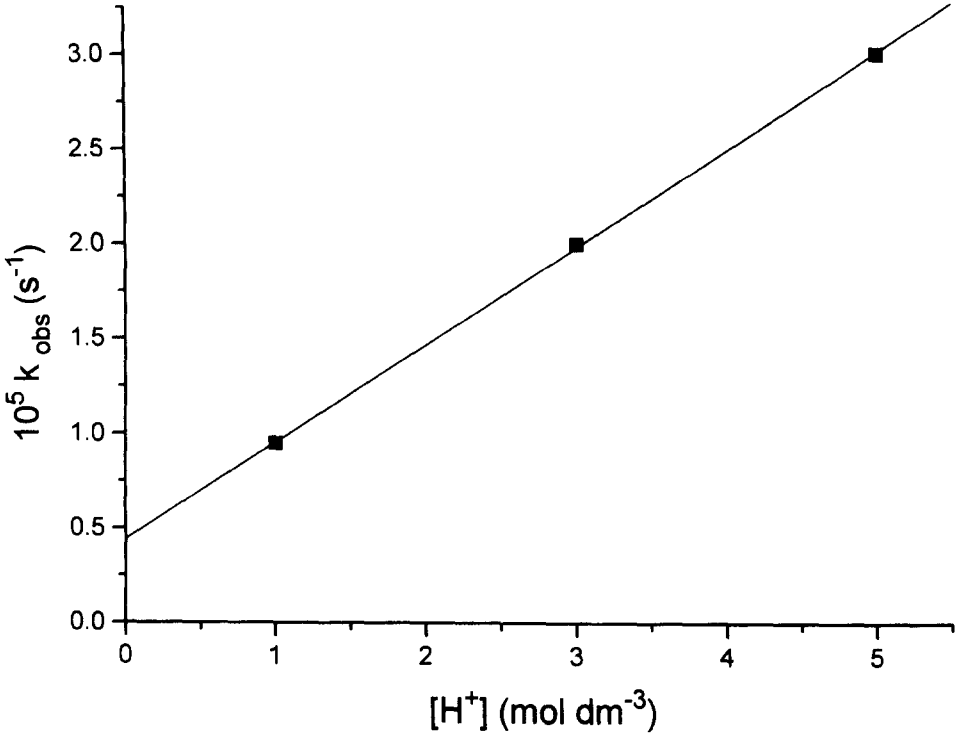

Fig. 4. Plot of k_{obs} *versus* the hydrogen ion concentration for the acid-catalysed dissociation of $[CuLH]^{3+}$ in nitric acid solution at 25°C.

5.0 mol dm^{-3} at 25°C. The plot of k_{obs} (the observed first order rate constant at constant hydrogen ion concentration) *versus* the hydrogen ion concentration is linear, with a small positive intercept, so that $k_{obs} = k_o + k_H[H^+]$, Fig. 4. The rate constant, k_o, relates to the spontaneous dissociation of the complex in water and $k_o = 4.5 \times 10^{-6}\ s^{-1}$ at 25°C. The slope of the plot gives $k_H = 5.1 \times 10^{-6}\ dm^3\ mol^{-1}\ s^{-1}$ at 25°C. The reaction displays kinetic behaviour similar to that observed in the dissociation of the copper(II) complex of [13]aneN$_4$ [5] in a nitric acid solution, where $k_H = 8.0 \times 10^{-4}\ dm^3\ mol^{-1}\ s^{-1}$ at 25°C and I = 5.0 mol dm^{-3}. The dissociation kinetics of the copper(II) complex of [15]aneN$_4$ have previously been studied in some detail [5, 6]. The reaction displays saturation kinetics at high acidities (> 2 mol dm^{-3} H^+) and the hydrolysis can be represented by the equation [5]

$$\text{rate} = k_1[H^+][\text{Complex}]/(1 + k_2[H^+])$$

where $k_1 = 1.4 \times 10^{-2}\ dm^3\ mol^{-1}\ s^{-1}$, $k_2 = 9.91 \times 10^{-1}\ dm^3\ mol^{-1}$ at 25°C and I = 5.0 mol dm^{-3} (HNO_3 + $NaNO_3$). The limiting rate is given by the ratio $k_1/k_2 = 1.4 \times 10^{-3}\ s^{-1}$. The reaction is considerably faster than observed with the present complex and this is probably associated with the difficulty of protonating the species $[CuLH]^{3+}$, which is formed below pH 4.

REFERENCES

1. Hay, R. W. and Fraser, I., *Transition Met. Chem.*, 1991, **16**, 9.
2. Bayada, A., Lawrence, G. A., Maeder, M., Martinez, M., Skelton, B. W. and White, A. H., *Inorg. Chim. Acta*, 1994, **227**, 71.
3. See for example De Clercq, E., Yamamoto, N., Pauwels, R., Baba, B., Schols, D., Nakashima, H., Balzarini, J., Debster, Z., Murrer, B. A., Schwarz, D., Thornton, D., Bridger, G. J., Fricker, S., Henson, G., Abrams, M. and Picker, D., *Proc. Nat. Acad. Sci. U.S.A*, 1992, **89**, 5286; Inouye, Y., Kanamori, T., Yoshida, T., Bu, X., Shionoya, M., Koike, T. and Kimura, E., *Antiviral Chem. Chemother.*, 1995, **6**, 337; Bridger, G. J., Skerlji, R. T., De Clercq, S. and De Clercq, E., *J. Med. Chem.*, 1996, **39**, 109; Bridger, G. J. and Skerlji, R. D., *J. Med. Chem.*, 1995, **38**, 366.
4. Gans, P., Sabatini, A. and Vacca, J., *J. Chem. Soc. Dalton Trans.*, 1985, **00**, 1195.
5. Lan, W. J. and Chung, C. S., *J. Chem. Soc. Dalton Trans.*, 1994, **00**, 191.
6. Hassan, M. M., Ph.D. thesis. University of St Andrews, 1992.

Pergamon

PII: S0277-5387(98)00060-6

Polyhedron Vol. 17, Nos 13–14, pp. 2173–2178, 1998
© 1998 Elsevier Science Ltd
All rights reserved. Printed in Great Britain
0277-5387/98 $19.00+0.00

The crystal stucture of the nitric acid adducts of triphenylarsine oxide and triphenylphosphine oxide

Ruth V. Batt, David P. Bullivant, Kathryn E. Elkington, Sally E. Hill, Jack Hilton, Timothy J. Houghton, Maurice Hovell and Stephen C. Wallwork*

Department of Chemistry, University of Nottingham, University Park, Nottingham NG7 2RD, U.K.

(Received 21 November 1997; revised 4 February 1998)

Abstract—Molecular dimensions suggest that three crystal forms of the nitric acid adduct of triphenylarsine oxide have the bridging proton more closely associated with the As=O group than with the nitrate moiety, whereas the corresponding phosphorus compound has the proton more closely associated with the nitrate moiety. In all cases, strong hydrogen bonds are formed between the two moieties resulting in X–O bonds (where X=As or P) intermediate in character between single and double bonds. © 1998 Elsevier Science Ltd. All rights reserved

Keywords: X-ray structure; triphenylarsine oxide; triphenylphosphine oxide; nitric acid adduct; hydrogen bond.

A series of compounds containing group 15 elements was reported by Tranter [1] as having the constitution $[(C_6H_5)_3XNO_3]_2O$, where X=P, As, Sb. It was suggested that X might have a trigonal bipyramidal coordination with equatorial phenyl groups, apical nitrate groups and the oxygen atom bridging the two halves of the molecule. However, a preliminary crystal structure determination [2], by one of us, of the arsenic compound (hereafter ASNIT) showed it to be the nitric acid adduct of triphenylarsine oxide, (Fig. 1, X=As). Accurate molecular dimensions were not obtained in that determination, so it was decided to seek more accurate nitrate dimensions by replacing As by the lighter P atom. Although X-ray data were obtained for the phosphorus compound (PNIT), judged to be isomorphous from the similarity of cell dimensions, the structure would not refine if coordinates from the As compound were used as a starting point. It was decided, therefore, to collect more accurate X-ray data for the As compound. However, the next few attempts to prepare a new sample resulted in two further crystalline forms of the nitric acid adduct of triphenylarsine oxide (PASNIT1 and PASNIT2) and a material later identified as diphenyl-dihydroxyarsine nitrate. Eventually, a preparation yielded a good sample of ASNIT and an accurate redetermination of the structure was carried out. This paper reports the crystal structures of the three forms of the triphenylarsineoxide adduct and also that of PNIT. The X-ray data for diphenyl-dihydroxyarsine nitrate were too poor to warrant publication of its structural data, though the the structure was reliable enough to establish the molecular formula.

EXPERIMENTAL

The materials were prepared according to the method described by Tranter [1, 3]. All the X-ray data were obtained using a Hilger and Watts computer-controlled, four-circle diffractometer, MoKα radiation ($\lambda=0.71069$ Å) and a $\omega/2\theta$ scan, up to $\theta=25°$. Further data collection and crystal data are in Table 1. The structures of all the materials except PNIT were solved by the heavy-atom Patterson method and all were refined using the CRYSTALS suite of programs

*Author to whom correspondence should be addressed.

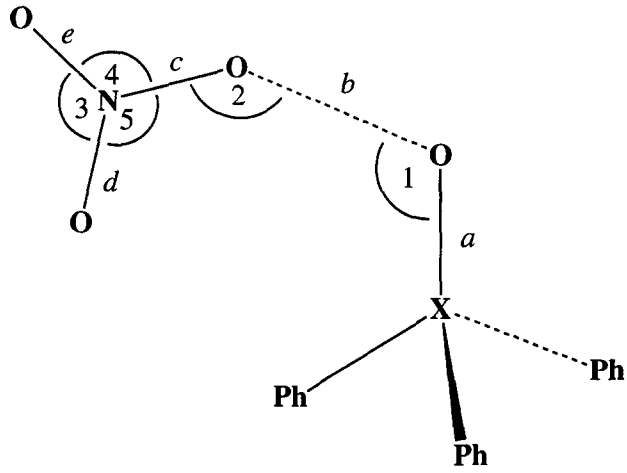

X = P or As

Fig. 1. Schematic molecular structure showing bonds a to e (b being a hydrogen bond) and angles 1 to 5, the dimensions of which are given in Table 2.

Table 1. Data collection and crystal data.

	PNIT	ASNIT	PASNIT1	PASNIT2
Formula	ϕ_3PO.HNO$_3$	ϕ_3AsO.HNO$_3$	ϕ_3AsO.HNO$_3$	ϕ_3AsO.HNO$_3$
M	341.30	385.25	385.25	385.25
Crystal system	monoclinic	monoclinic	monoclinic	monoclinic
Space group	$P2_1/c$	$P2_1/c$	$P2_1/c$	$C2/c$
a (Å)	9.632(1)	10.448(3)	16.74(1)	21.706(2)
b (Å)	17.076(1)	16.302(1)	12.59(1)	12.358(3)
c (Å)	12.139(9)	11.612(1)	20.62(1)	17.410(5)
β (°)	122.33(1)	121.15(1)	125.64(1)	132.53(2)
U (Å^3)	1687(2)	1693(1)	3532(1)	3442(1)
Z	4	4	8	8
D_m (g cm^{-3})	1.34(1)	1.51(1)	1.45(1)	1.48(1)
D_c (g cm^{-3})	1.344	1.512	1.449	1.487
μ(cm^{-1})	1.90	21.4	20.5	21.1
F(000)	712	784	1568	1568
Data collected	3432	3100	6540	3200
Unique observations [$I > 3\sigma(I)$]	2310	2234	3723	2333
No. of parameters refined	281	217	434	217
R[a]	0.050	0.039	0.051	0.051
R_w[b]	0.060	0.041	0.071	0.068

[a] $R = \Sigma||F_o|-|F_c||/\Sigma|F_o|$

[b] $R_w = \{\Sigma w(|F_o|-|F_c|)^2/\Sigma w|F_o|^2\}^{1/2}$

[4]. In view of the refinement problem mentioned above, PNIT was solved by direct methods using SHELX76 [5]. In the later stages of refinement, H atoms were included in calculated positions with fixed isotropic thermal parameters and were not refined, except in the case of PNIT. In that material, H atoms were located in difference maps and their positions and isotropic thermal parameters were refined. Generally, refinement was of the full-matrix type but block diagonal refinement was used for PASNIT1. Weigh-

ting schemes were introduced in the final few cycles of each refinement.

The atomic coordinates, thermal parameters and details of the molecular geometries have been deposited at the Cambridge Crystallographic Data Centre.

RESULTS AND DISCUSSION

A summary of the most significant molecular dimensions in all four compounds is shown in Table 2, a line drawing representation is given in Fig. 1, the molecular structures of PNIT and ASNIT are shown in Fig. 2(a) and Fig. 2(b), respectively, and the crystal structure of ASNIT is shown in Fig. 3. In the case of PASNIT1, there are two crystallographically independent molecules (PASNIT1a and PASNIT1b) in the asymmetric unit, providing two sets of dimensions. Since all four dimensions for the three As compounds are so similar, they must represent the same molecule in slightly different environments. They are therefore averaged in the last column of Table 2. Even allowing for an expected increase of about 0.15 Å between equivalent P–O and As–O bonds [6], it is clear that PNIT has significantly different dimensions. These are consistent with the proton in the X–O..H..ONO_2 hydrogen bond being more closely associated with As–O in the As compounds and with N–O in PNIT. In both situations, however, a strong hydrogen bond is formed, so the X–O bonds are all intermediate in character between single and double bonds, and the $(H)ONO_2$ aduct is intermediate between HNO_3 and NO_3^-. Thus, the N–O bond adjacent to the hydrogen bond in PNIT is 1.302(4) Å in length (about 0.10 Å longer than the other two N–O bonds. This compares with lengths 1.24 to 1.26 Å in the arsenic adducts, which are only 0.03 to 0.04 Å longer than the other N–O bonds. (In nitric acid vapour [7], the N–O(H) bond length is 1.406(10) Å and the other two bonds have lengths 1.211(10) and 1.199(10) Å.)

Confirmation of the hydrogen-bonding proton's position from difference Fourier maps was unreliable but a position approximately equidistant between the two moieties was indicated in PNIT, compared with a position about 0.03 Å nearer As–O than N–O in ASNIT. Support from the As–O and P–O lengths for the two different degrees of proton association was also rather weak in view of the intermediate nature of these bonds in the compounds studied. However, an examination of lengths of hydrogen-bonded X–O and X–OH bonds in the Cambridge Crystallographic Database [8, 9] suggests that the cross-over point from X–O..HO to X–OH..O occurs approximately at the X–O distances 1.52-1.53 Å for P and 1.67-1.68 Å for As. The P–O distance in PNIT is 1.499(2) Å, on the P=O side of the cross-over point, and the As–O distances in ASNIT, PASNIT1, and PASNIT2 range from 1.690(5) Å to 1.710(3) Å, all on the As–OH side.

The relationship between the $(C_6H_5)_3XO$ and NO_3 moieties in PNIT and ASNIT is illustrated in Fig. 2; the arrangements in the other structures involving As–O are not appreciably different from ASNIT. In each structure, one nitrate O atom [O(2) in Fig. 2(a) and Fig. 2(b)] approaches a phenyl ring in the same hydrogen-bonded pair more closely than do the other oxygens. However, whereas in PNIT the hydrogen

Table 2. Comparison of molecular dimensions (as indicated in Fig. 1)

	PNIT	ASNIT	PASNIT1a[a]	PASNIT1b[a]	PASNIT2	Mean As[b]
a	1.499(2)	1.691(3)	1.709(5)	1.690(5)	1.710(3)	1.700(10)
b	2.517(3)	2.498(5)	2.418(8)	2.443(8)	2.491(6)	2.462(36)
c	1.302(4)	1.239(5)	1.241(9)	1.259(9)	1.241(6)	1.245(14)
d	1.206(4)	1.216(5)	1.217(8)	1.200(9)	1.239(9)	1.218(21)
e	1.193(4)	1.209(5)	1.212(8)	1.224(10)	1.221(6)	1.216(8)
Mean X-C	1.793(3)	1.903(6)	1.906(10)	1.901(10)	1.897(6)	1.902(5)
Angle						
1	121.0(1)	128.2(2)	128.5(4)	122.4(4)	125.0(2)	126.0(36)
2	110.7(2)	110.9(3)	117.8(6)	116.8(6)	117.4(3)	115.7(48)
3	124.8(4)	121.7(5)	123.0(8)	122.7(9)	121.1(5)	122.1(10)
4	117.3(3)	118.5(5)	118.7(8)	119.0(9)	118.6(5)	118.7(3)
5	117.8(3)	119.8(5)	118.3(8)	118.3(8)	120.3(5)	119.2(11)
Mean C(CX)C	119.1(6)	121.0(4)	121.8(10)	121.2(5)	120.8(2)	121.2(6)

[a] PASNIT1a and 1b indicate the two crystallographically independent molecules in the the asymmetric unit of PASNIT1.

[b] Mean of all dimensions of this type except for PNIT; The number following each mean dimension is the spread of values, not the standard deviation.

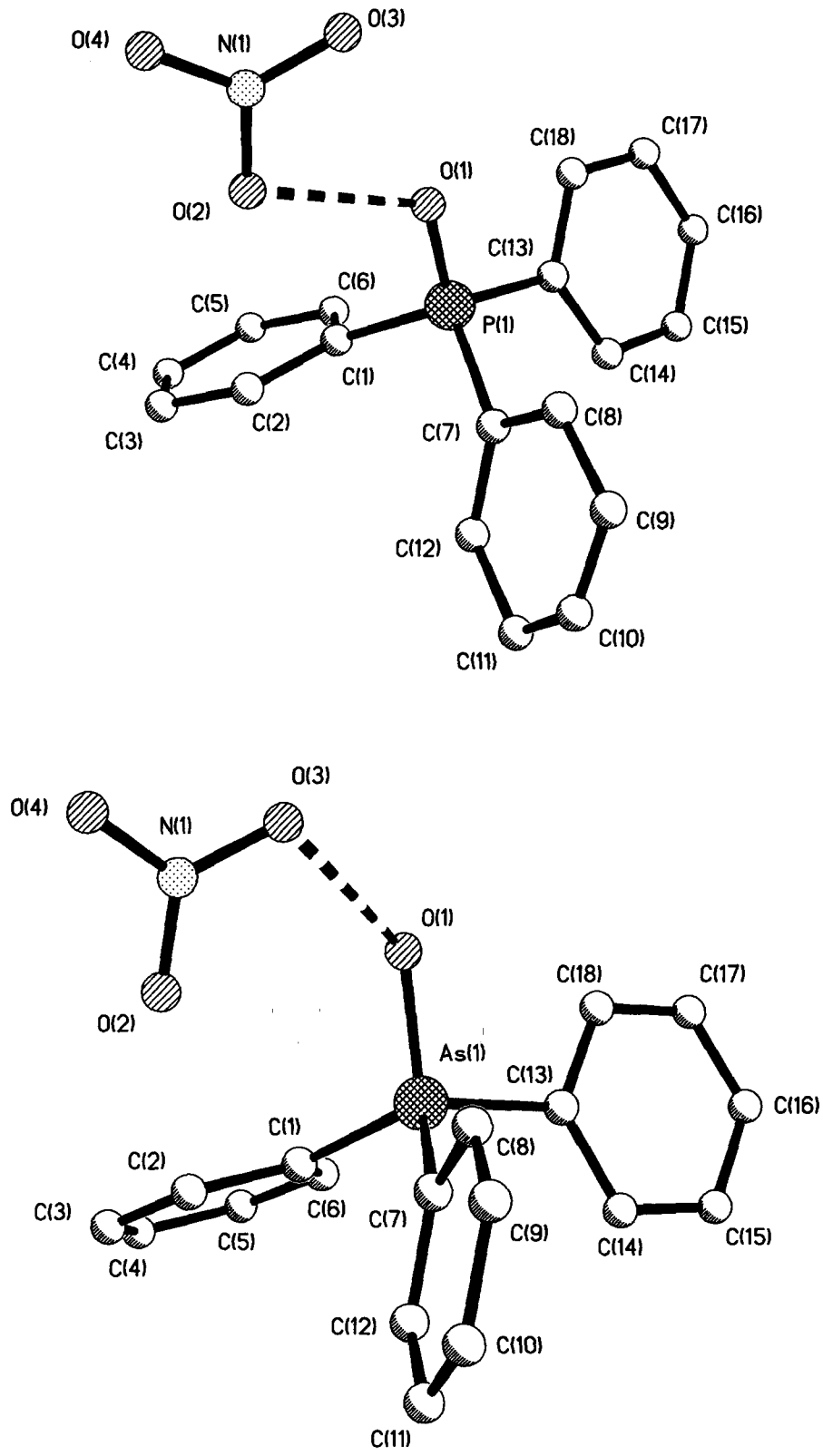

Fig. 2. Molecular structures of (a) PNIT and (b) ASNIT. The broken lines represent hydrogen bonds

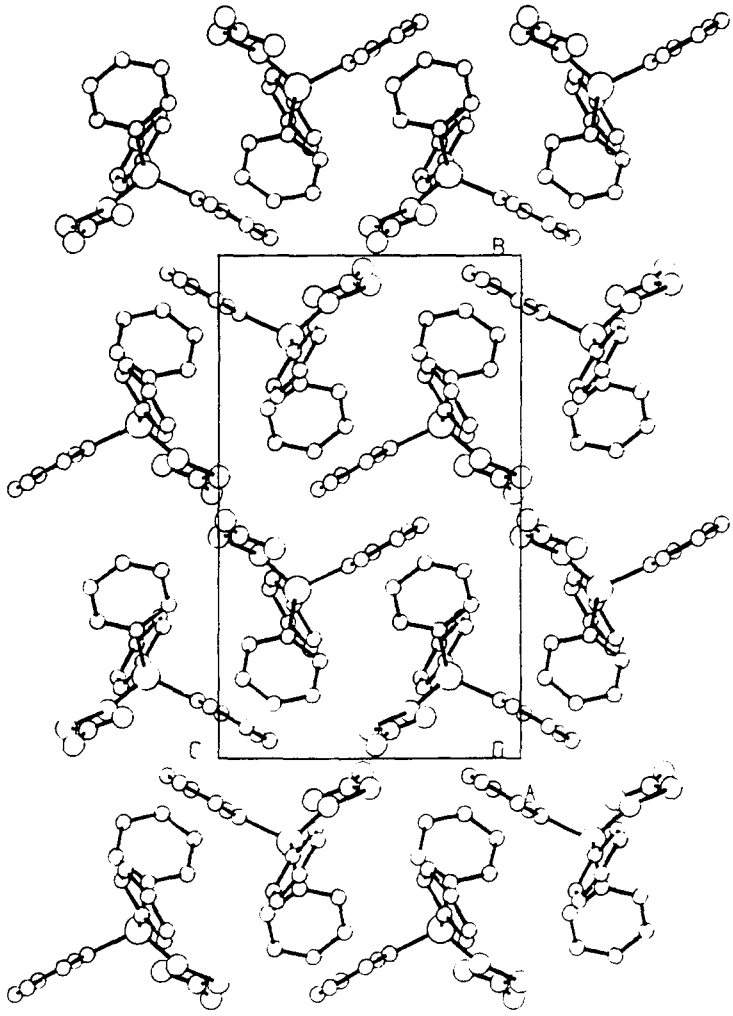

Fig. 3. The crystal structure of ASNIT (a) projected along the a-axis, (b) projected along the c-axis.

bond is formed to this same O atom, in the other structures a hydrogen bond of similar length is formed to a more distant O [O(3) in Fig. 2(b)]. This difference between the P and As structures, and the much greater divergence from planarity of As and the two nearest O atoms of the nitrate group, round the O of the As–O group in all three As structures, compared with the corresponding arrangement round P in PNIT, again indicates a difference in proton location. This difference indicates a greater basicity of As=O compared with P=O in these compounds, consistent with the increasing basicity of Group 15 oxides on descending the group in the periodic table.

The crystal structures may all be thought of in terms of approximately close packed columns of molecules, of van der Waals diameter between 8 and 9 Å. The repeating unit of each column consists of a pair of molecules and varies in length from 11.6 Å in ASNIT to 12.6 Å in PASNIT1. In PNIT and ASNIT, the two molecules comprising each pair are related by a **c**-glide plane, whereas in PASNIT1 and PASNIT2 the two are related by the screw axis parallel to **b**. Figure 3(b), which is a projection of the ASNIT structure along the **c**-axis, shows the view along the columns for this structure and indicates how the columns are arranged in approximately close-packed layers parallel to (010). Figure 3(a), the projection of ASNIT along the **a**-axis, shows how the molecules are arranged within the columns. PNIT is almost identical and PASNIT1 has similar columns extended along the **b**-axis in layers parallel to (001). In PASNIT2, similar columns are again extended along the **b**-axis but the layers are parallel to $(\bar{1}01)$.

Acknowledgements– The late Professor T. J. King assisted with the data collection and the computing and we thank Dr. P. Mountford, Dr. A. J. Blake and Dr. D. J. Watkin for assistance in the preparation of the paper. We acknowledge

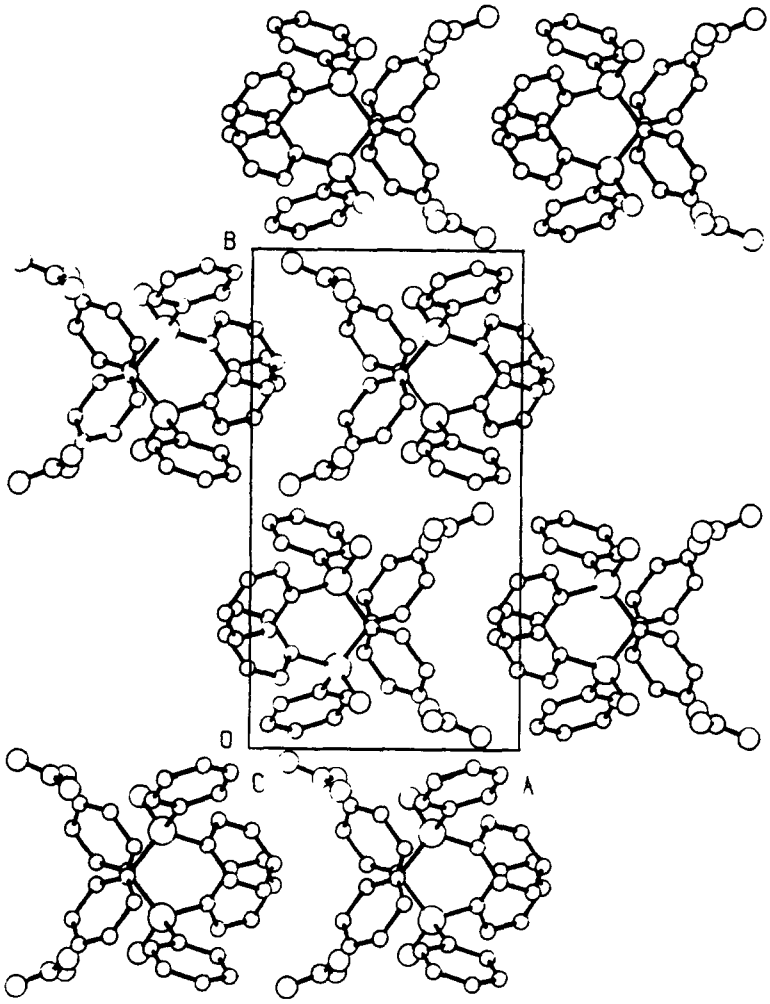

Fig. 3.—continued.

the use of the EPSRC's Chemical Database Service at Daresbury.

REFERENCES

1. Tranter, G. C., Aspects of the nitrate chemistry of group V elements, Ph.D. thesis, University of Nottingham, 1967.
2. Hilton, J., The crystal structures of some anhydrous metal nitrates and their complexes, Ph.D. thesis, University of Nottingham, 1968.
3. Tranter, G. C., Addison, C. C. and Sowerby, D. B., *J. Organometallic Chem.*, 1968, **12,** 369–376.
4. Rollett, J. S. and Carruthers, R. J., CRYSTALS Manual. Oxford University Computing Laboratory, 19 Parks Road, Oxford, UK, 1975.
5. Sheldrick, G. M., SHELX76. Program for crystal structure determination, University of Cambridge, UK, 1976.
6. Ferraris, G. and Ivaldi, G., *Acta Cryst.*, 1984, **B40,** 1–6.
7. Cox, A. P. and Riveros, J. M., *J. Chem. Phys.*, 1965, **42,** 3106–3112.
8. Allen, F. H. and Kennard, O., *Chemical Design Automation News*, 1993, **8,** 1 and 31.
9. Fletcher, D. A., McMeeking, R. F. and Parkin, D., *J. Chem. Inf. Comput. Sci.*, 1996, **36,** 746.

Pergamon

PII: S0277-5387(98)00059-X

Polyhedron Vol. 17, Nos 13-14, pp. 2179-2186, 1998
© 1998 Elsevier Science Ltd
All rights reserved. Printed in Great Britain
0277-5387/98 $19.00+0.00

Cis-facial coordination of bis(pyrid-2-ylmethyl)amine (bpma). Synthesis, structure and spectral behaviour of $[Ni(bpma)_2]^{2+}$

Marappan Velusamy[a], Mallayan Palaniandavar[a]* and K. R. Justin Thomas[b]

[a]Department of Chemistry, Bharathidasan University, Tiruchirappalli, 620 024 India

[b]Regional Sophisticated Instrumentation Centre, Indian Institute of Technology, Chennai, 600 036 India

(Received 8 December 1997; accepted 29 January 1998)

Abstract—Nickel(II) bis-complexes of bis(pyrid-2-ylmethyl)amine (bpma) and bis(benzimidazol-2-ylmethyl)amine (bbma) have been isolated. The complexes have been characterised using IR, UV-VIS and ^{1}H NMR spectral techniques. The pink complex $[Ni(bpma)_2](ClO_4)_2$ crystallises in the orthorhombic space group *Fdd*2, with $a=22.12(2)$, $b=28.087(2)$, $c=8.857(3)$ Å, $\alpha=\beta=\gamma=90^\circ$ and $Z=8$. The nickel(II) atom has a slightly distorted octahedral structure in which the ligands are *cis-facially* coordinated. The $M\text{-}N_{py}$ bond length in $[M(bpma)_2]^{2+}$ [M = Mn(II), Fe(II), Ni(II), Cu(II), Zn(II)] complexes decrease and then increase with increase in d-orbital population. The ligand field parameters of the new complexes are compared with those of other complexes with NiN_6 chromophore. © 1998 Elsevier Science Ltd. All rights reserved

Keywords: nickel(II); synthesis; spectra; crystal structure; NiN_6 chromophore; cis-facial coordination.

Linear tridentate triaza ligands have attracted considerable interest [1] because of their ability to coordinate facially. The factors favouring facial or meridional coordination of these ligands have been discussed [1b]. When the terminal coordination sites of these ligands are primary amines with strong σ-donor ability, meridional coordination (a) is preferred in bis complexes. Thus the complexes $[Cu(dien)_2]^{2+}$ [dien = diethylenetriamine] [2], $[Ni(dien)_2]^{2+}$ and $[Ni(dptn)_2]^{2+}$ [dptn = dipropylenetriamine] [3] have been isolated as *mer* isomers. On the other hand, when the two terminal arms are pyridyl groups as in bis(pyrid-2-ylmethyl)amine [1c] (bpma) or bulky benzimidazolyl groups as in bis(benzimidazol-2-ylmethyl)amine [1b] (bbma), facial coordination is facilitated. Thus, the bpma ligand complexes $[M(bpma)_2]^{2+}$ exhibit *trans*-facial coordination [*meso* isomer (b)] when M = Cu(II) [1c], Zn(II)) [1a] and *cis*-facial coordination [*rac* isomer (c)] when M = Mn(II) [1a], Fe(II) [1e] Cd(II) [1a], Zn(II) [1a]. Further, the branched chain tridentate ligand di-2-pyridylmethanamine (dipa) designed to impose facial coordination in $[M(dipa)_2]^{2+}$ complexes display *rac* isomerism when M = Fe(II), Co(II) but *meso* isomerism when M = Cu(II), Ni(II) [4]. In continuing our work with facially coordinating ligands [1b], [1c], [1d]], we report in this paper the isolation and successful X-ray crystal structure determination of $[Ni(bpma)_2]^{2+}$ complex which crystallizes in *rac* rather than *meso* isomeric form. Though this is expected on the basis of the known *rac* structures of $[M(bpma)_2]^{2+}$ [M = Mn(II), Fe(II), Zn(II)], it is unexpected in view of the *meso* structures of $[M(dipa)_2]^{2+}$ [M = Cu(II), Ni(II)] and $[Cu(bpma)_2]^{2+}$ complexes.

EXPERIMENTAL

Materials

Bis(pyrid-2-ylmethyl)amine was a gift from Reilly Industries, USA. Bis(benzimidazol-2-ylmethyl)amine was prepared as described elsewhere [5]. $Ni(ClO_4)_2.6H_2O$ and organic reagents were used as received. Solvents were purified by using established procedures [6].

*Author to whom correspondence is to be addressed.

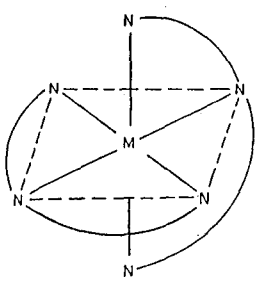

(a)

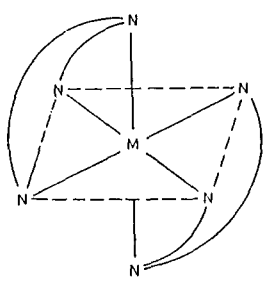

(b)

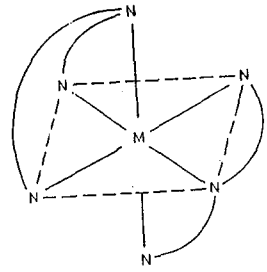

(c)

Physical measurements

Elemental analyses were performed at CDRI, Lucknow, India. Electronic spectra were measured on a Hitachi U-3410 double beam UV/Vis-NIR spectrophotometer. Infrared spectra were obtained using a Bruker IFS 66 FT-IR instrument. The ^{1}H NMR spectra were obtained on a JEOL GSX-400 spectrometer. Conductivity measurements were done with an Elico Type CM-82 T conductivity bridge (Hyderabad, India) with solute concentrations of *ca* 1.0×10^{-3} mol dm^{-3} at 25°C. The nickel content of the complexes were analysed gravimetrically as its dimethylglyoximate.

Preparation of complexes

$[Ni(bpma)_2](ClO_4)_2$ (**1**). A methanolic solution (20 mL) of $Ni(ClO_4)_2.6H_2O$ (0.36 g, 1.0 mmol) was added to a solution of bis(pyrid-2-ylmethyl)amine (0.4 g, 2.0 mmol) in methanol (10 mL) with constant stirring (5 min). The pink coloured precipitate obtained was filtered off, washed with small amounts of cold methanol and then dried under vacuum (yield 0.60 g, 90%). An acetonitrile solution of the complex on slow evaporation yielded pink needle shaped crystals suitable for X-ray diffraction studies. Anal. Calcd for $C_{24}H_{26}N_6Cl_2O_8Ni$: Ni, 8.95; C, 43.94; H, 3.99; N, 12.81. Found: Ni, 8.90; C, 44.00; H, 4.10; N, 13.00.

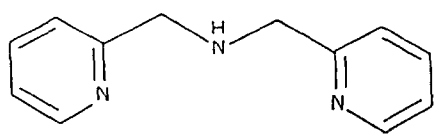

bpma

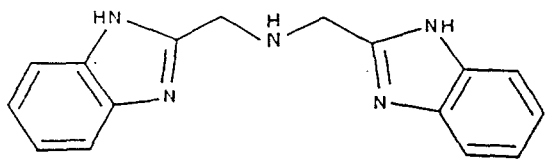

bbma

$[Ni(bbma)_2](ClO_4)_2$ (**2**). This complex was synthesized employing the procedure described above for **1** but by using bis(benzimidazol-2-ylmethyl)amine instead of bpma (yield: 0.7 g, 85%). The crude product was dissolved in acetonitrile and kept for slow evaporation. The pink coloured crystals obtained were not suitable for X-ray diffraction. Anal. Calcd for $C_{32}H_{30}N_{10}Cl_2O_8Ni$: Ni, 7.23; C, 47.32; H, 3.72; N, 17.24. Found: Ni, 7.30; C, 46.98; H, 3.50; N, 17.45.

Structure analysis

A summary of crystal data and experimental parameters for $[Ni(bpma)_2]^{2+}$ are given in Table 1. Diffraction intensities were collected at 293 K on an Enraf-Nonius CAD4 diffractometer employing graphite monochromated Cu-Kα radiation. Unit cell parameters were determined from 25 reflections ($5 < 2\theta < 65$) and refined by least-squares method. The intensities of representative reflections were measured after every 100 reflections. No significant intensity decay was observed. Intensity data were corrected for Lorentz and polarization effects and analytical absorption corrections were applied. The structure was solved by the heavy atom method and refined on F^2 by full-matrix least-squares procedures. The SHELXL-93 of programs was used for structure analysis and refinement.

RESULTS AND DISCUSSION

On the basis of the results of elemental analysis both the complexes **1** and **2** may be formulated as $[ML_2](ClO_4)_2$ where L = bpma or bbma. This is supported by the IR spectra of the complexes, which show an unsplit band around 1150 cm^{-1} characteristic [7] of uncoordinated ClO_4^-. Electrical conductivity data show that both the complexes behave as 1:2 elec-

Table 1. Crystal data and structure refinement for 1.

Empirical formula	$C_{24}H_{26}Cl_2N_6NiO_8$
Formula weight	656.12
Temperature	293(2) K
Wavelength	1.54184 Å
Crystal system	Orthorhombic
Space group	*Fdd*2 [No. 43]
Unit cell dimensions	$a = 22.12(2)$ Å $\alpha = 90$
	$b = 28.087(2)$ Å $\beta = 90$
	$c = 8.857(3)$ Å $\gamma = 90$
Volume	5502(6) Å^3
Z	8
Density (calculated)	1.584 Mg/m^3
Absorption coefficient	3.328 mm^{-1}
$F(000)$	2704
Crystal size	0.43 × 0.14 × 0.25 mm
Theta range for data collection	5.09 to 64.92
Index ranges	$0 \le h \le 25$, $0 \le k \le 32$, $0 \le l \le 9$
Reflections collected	1227
Independent reflections	1227 [R(int) = 0.0000]
Absorption correction	PSI Scans
Max. and min. transmission	99.93 and 52.82
Refinement method	Full-matrix least-squares on F^2
Data/restraints/parameters	1227/1/203
Goodness-of-fit on F^2	1.072
Final R indices [$I > 2\sigma(I)$)]	$R1 = 0.0400$, $wR2 = 0.1042$
R indices (all data)	$R1 = 0.0402$, $wR2 = 0.1044$
Absolute structure parameter	0.00(3)
Extinction coefficient	0.00123(9)
Largest diff. peak and hole	0.557 and −0.375 e.Å^{-3}

trolytes in acetonitrile solution ($\Lambda_M = 240$ for **1** and 260 Ω^{-1} cm^2 mol^{-1} for **2**).

Crystal structure of $[Ni(bpma)_2](ClO_4)_2$

The ORTEP view of the complex cation $[Ni(bpma)_2]^{2+}$, also showing the atomic numbering scheme is depicted in Fig. 1. The principal bond lengths and angles are given in Table 3. The nickel(II) is surrounded by two ligands, each coordinating in a tridentate manner. The nitrogen atom of the secondary amino group and two pyridyl nitrogens are involved in coordination. Both the ligands are facially coordinated with the two coordinating amino groups being *cis* to each other. Hence the nickel ion is on a site of C_2 symmetry, the two-fold axis relating one ligand to the other. So the isomer isolated is the *cis-facial* isomer represented in (c). This is interesting because the nonlinear ligand dipa coordinates but *trans*-facially in $[Ni(dipa)_2]^{2+}$ eventhough such a coordination is less stable than the *cis*-facial coordination, as predicted by molecular mechanics calculations [4].

The Ni–N_{py} bond lengths, Ni–N(1) [2.093(4) Å] and Ni–N(3) [2.073(4) Å] are shorter than the Ni–N_{amine} bond length Ni–N(2) of 2.106(4) Å, obviously due to

Table 2. Atomic coordinates ($\times 10^4$) and equivalent isotropic displacement parameters (Å$^2 \times 10^3$) for 1. U(eq) is defined as one third of the trace of the orthogonalized U_{ij} tensor.

	x	y	z	U(eq)
Ni	0	0	14(1)	40(1)
N(1)	−52(2)	−577(1)	−1474(5)	46(1)
N(2)	144(2)	554(1)	1574(5)	53(1)
N(3)	892(2)	−211(1)	263(5)	47(1)
Cl	1296(1)	364(1)	4860(1)	54(1)
O(1)	1571(2)	−74(2)	5265(8)	98(2)
O(2)	670(2)	286(2)	4560(6)	86(1)
O(3)	1359(2)	688(2)	6097(6)	87(1)
O(4)	1579(2)	558(2)	3574(6)	98(2)
C(1)	−216(2)	−983(2)	−800(7)	61(1)
C(2)	−134(4)	−1423(2)	−1455(9)	90(2)
C(3)	142(4)	−1447(2)	−2852(10)	112(3)
C(4)	334(4)	−1032(2)	−3525(8)	85(2)
C(5)	215(2)	−604(2)	−2817(6)	62(1)
C(6)	−440(2)	705(2)	2216(6)	61(1)
C(7)	479(3)	925(2)	751(8)	72(2)
C(8)	1370(2)	−66(2)	−558(7)	55(1)
C(9)	1948(2)	−221(2)	−284(8)	64(2)
C(10)	2039(2)	−543(2)	886(8)	67(1)
C(11)	1549(2)	−714(2)	1688(7)	61(1)
C(12)	985(2)	−540(1)	1340(6)	50(1)

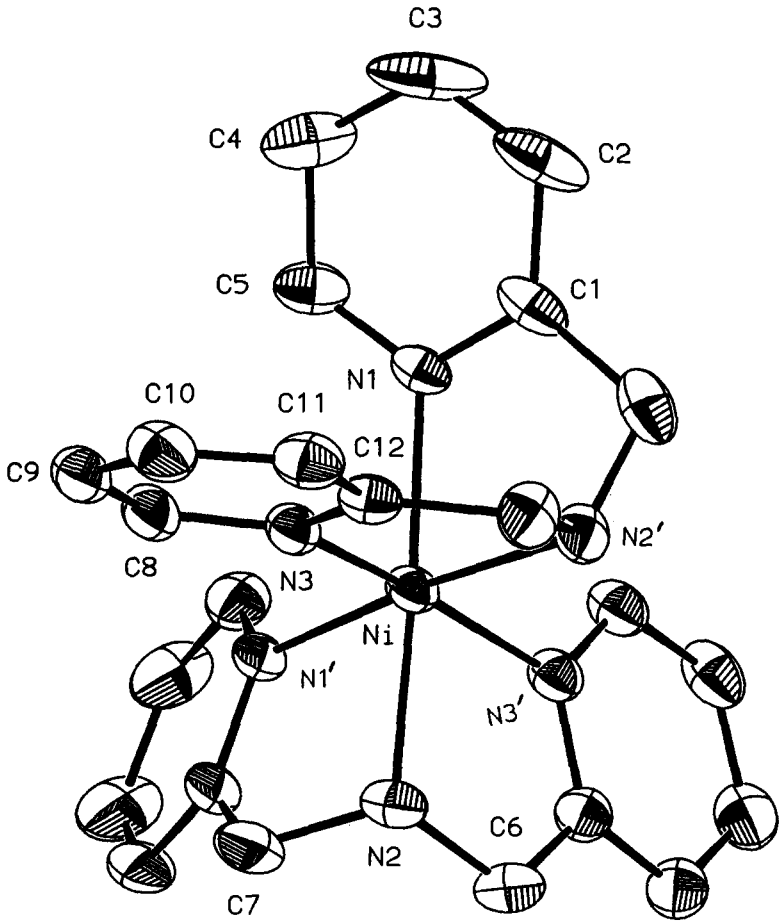

Fig. 1. ORTEP drawing of the $[Ni(bpma)_2]^{2+}$ ion (H atoms have been omitted for clarity).

Table 3. Selected bond lengths (Å) and angles (°) for 1.

Ni–N(3)	2.073(4)
Ni–N(1)	2.093(4)
Ni–N(2)	2.106(4)
N(3)–Ni–N(3)#1	167.8(2)
N(3)–Ni–N(1)	84.11(14)
N(3)#1–Ni–N(1)	103.69(14)
N(3)–Ni–N(1)#1	103.69(14)
N(3)#1–Ni–N(1)#1	84.11(14)
N(1)–Ni–N(1)#1	101.9(2)
N(3)–Ni–N(2)	89.9(2)
N(3)#1–Ni–N(2)	82.08(14)
N(1)–Ni–N(2)	173.9(2)
N(1)#1–Ni–N(2)	80.33(14)
N(3)–Ni–N(2)#1	82.08(14)
N(1)–Ni–N(2)#1	80.33(14)
N(2)–Ni–N(2)#1	98.00(3)

Symmetry transformations used to generate equivalent atoms: #1 $-x, -y, z$

the difference in the state of hybridisation of the amine and pyridine nitrogens. Each of the ligands form two five-membered chelate rings and thus pinches together the three Ni–N bonds leading to intrachelate N–Ni–N bond angles $\sim 10°$ less than the 90° ideal. Thus the octahedral environment around Ni(II) is distorted significantly. When the $M-N_{py}$ bond lengths in $[M(bpma)_2]^{2+}$ [M = Mn(II), Fe(II), Ni(II), Cu(II), Zn(II) (rac)] complexes are plotted as a function of the d-orbital population (Fig. 2) they decrease with the addition of electrons into the t_{2g} orbitals and then increase, as anticipated [8]. On the other hand, the $Cu-N_{amine}$ distance in *meso* $[Cu(bpma)_2]^{2+}$ is higher than the $Zn-N_{amine}$ distance in *meso*-$[Zn(bpma)_2]^{2+}$, which may be due to Jahn-Teller effect and/or hydrogen bonding interaction of coordinated N–H group [1c] in the former. However, it is interesting that the $Zn-N_{amine}$ distance in *meso* isomer is less than that in *rac* isomer.

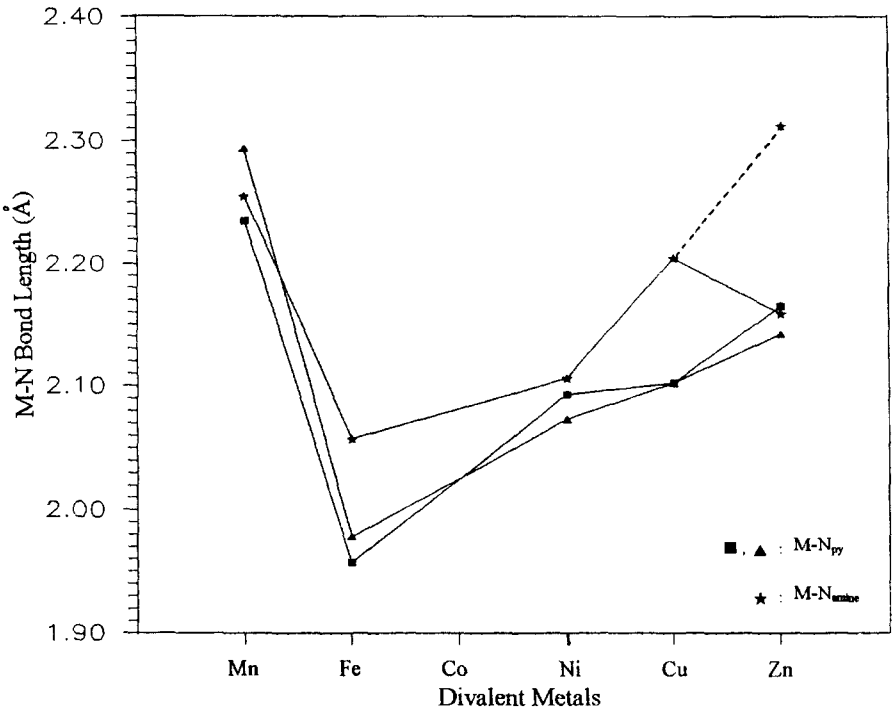

Fig. 2. Plot of M–N bond length versus divalent metals.

The perchlorate anions are apparently ordered, the Cl–O bonds of 1.42(5) Å and associated O–Cl–O angles being normal [109.9(3)°]. This confirms the IR spectral observations that the anion is not involved in coordination.

Electronic absorption spectra

The electronic spectra of both **1** and **2** consist of two principal bands (Fig. 3). In **1** a shoulder occurs on the low-energy side of the lower energy band, whereas in **2** it occurs on the high energy side. Consistency in their assignment [9] and fitment into the equations for the electronic energy levels is achieved by assigning the less intense shoulders to the first spin-forbidden transition $^3A_{2g} \rightarrow {}^1E_g(D)$, and the main bands to the first two spin-allowed transitions $^3A_{2g} \rightarrow {}^3T_{2g}$ (ν_1) and $^3A_{2g} \rightarrow {}^3T_{1g}(F)$ (ν_2) [9]. The third spin-allowed band $^3A_{2g} \rightarrow {}^3T_{1g}(P)$ is predicted to be in the range 29,300–30,540 cm^{-1} (Table 4), but is obviously obscured by the intense ligand bands. The value of the ligand field parameter *Dq* is slightly higher for **1** than for **2**; this illustrates the importance of the strongly π-back bonding pyridine donors in **1** over the strongly σ-donating [10] but sterically demanding bzim nitrogens in **2**. This is consistent with the higher value of the covalency parameter β (Table 5) for the py complex **1**, indicating that the nickel t_{2g} electrons are significantly delocalized over the molecular orbitals of the complex more in **1** than in **2** [11]. It is interesting to note that the $[Ni(dipa)_2]^{2+}$ complex with the same number of pyridine nitrogen donors as for **1** exhibits the same amount of covalency and that the $[Ni(bbp)_2]^{2+}$ [bbp = 2,6-bis(benzimidazol-2-yl)pyridine] [16] complex shows a higher covalency than the bbma complex. The complexes with no pyridine nitrogen as in $[Ni(NH_3)_6]^{2+}$ and $[Ni(dien)_2]^{2+}$ show decreased metal-ligand covalency as expected.

^1H NMR spectra

The ^1H NMR spectroscopy was performed in order to show that the solid state structure of **1** is preserved in solution and to assess the solution structure of its analogue **2**, the crystal structure of which could not be determined for lack of availability of good crystals. Figure 4 shows the ^1H NMR spectrum of **1**, and the chemical shifts for the two complexes are collected in Table 6 along with our proposed assignments. These assignments are based on comparisons with the spectra of Ni(II) complexes [12] of analogous thioether-benzimidazole ligands and Fe(III)-tris(2-pyridylmethyl)amine [13] complex and their relative intensities. The spectral features of **1** and **2** lie in the range 13–50 ppm down field with reference to tetramethylsilane (TMS). The peaks between 40–50 ppm in **1** may be assigned to the pyridine ring protons [H(3) + H(5) and H(6)], with the broad and maximum contact-shifted 50 ppm peak being due to H(6) protons located closest to the nickel(II) center. The broadest peak at 24.9 ppm is assigned to the N–H proton of coordinated secondary amino group. The sharp split

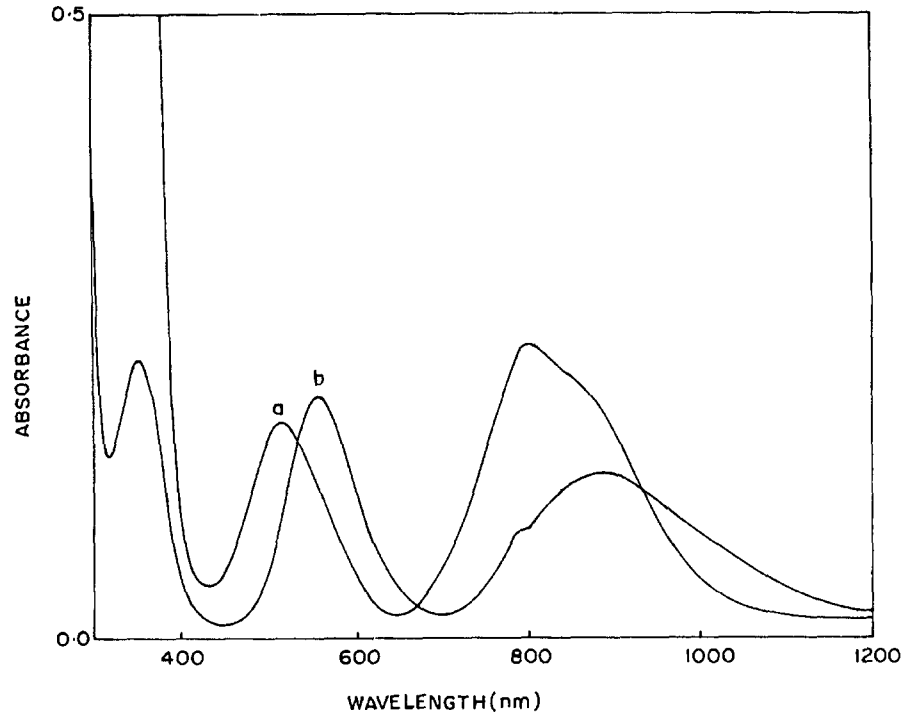

Fig. 3. Electronic absorption spectra of $[Ni(bpma)_2](ClO_4)_2$ (a) and $[Ni(bbma)_2](ClO_4)_2$ (b) in CH_3CN.

Table 4. Electronic Spectral Data for Nickel(II) Complexes in Acetonitrile Solution

Complex	$\bar{\nu}_{max}$, cm^{-1} (ϵ, $M^{-1}cm^{-1}$)						
	$^3A_{2g}\rightarrow{}^3T_{2g}$	$^3A_{2g}\rightarrow{}^1E_g(D)$	$^3A_{2g}\rightarrow{}^3T_{1g}(F)$	$^3A_{2g}\rightarrow{}^3T_{1g}(P)$ observed	calculated	Dq, cm^{-1}	B', cm^{-1}
$[Ni(bpma)_2]^{2+}$	12,450 (8.6)	11,760(sh)	19,420 (5.9)	32,260 (388)*	30,540	1245	831
$[Ni(bbma)_2]^{2+}$	11,310 (6.7)	12,740(sh)	17,920 (8.6)	28,240 (10.1)	29,330	1131	921

* Overlap with ligand based transitions.

Table 5. Comparison of the Ligand Field and Covalency Parameters of Nickel(II) Complexes of Amine Ligands

Complex	Donor Atom Set	Dq, cm^{-1}	B', cm^{-1}	β	ref
$[Ni(NH_3)_6]^{2+}$	N_6	1075	972	0.08	[23]
$[Ni(dien)_2]^{2+}$	N_6	1150	1032	0.02	[23]
$[Ni(dipa)_2]^{2+}$	$N_2N_4^a$	1270	838	0.21	[9]
$[Ni(bpma)_2]^{2+}$	$N_2N_4^a$	1248	831	0.22	this work
$[Ni(bbma)_2]^{2+}$	$N_2N_4^b$	1114	921	0.15	this work
$[Ni(bbp)_2]^{2+}$	$N_2^aN_4^b$	1162	874	0.17	[24]

N = amine, N^a = pyridine nitrogen, N^b = benzimidazole nitrogen

resonance at 13.6 ppm is assigned to the CH_2 proton of the ligand backbone. Further, the splitting (doubling) of the CH_2 proton signal is characteristic of complexes having a C_2 axis of symmetry [14] evident in the X-ray structure. However, no doubling is experienced by the py ring proton resonances probably because all of them experience an equivalent ligand field environment in solution.

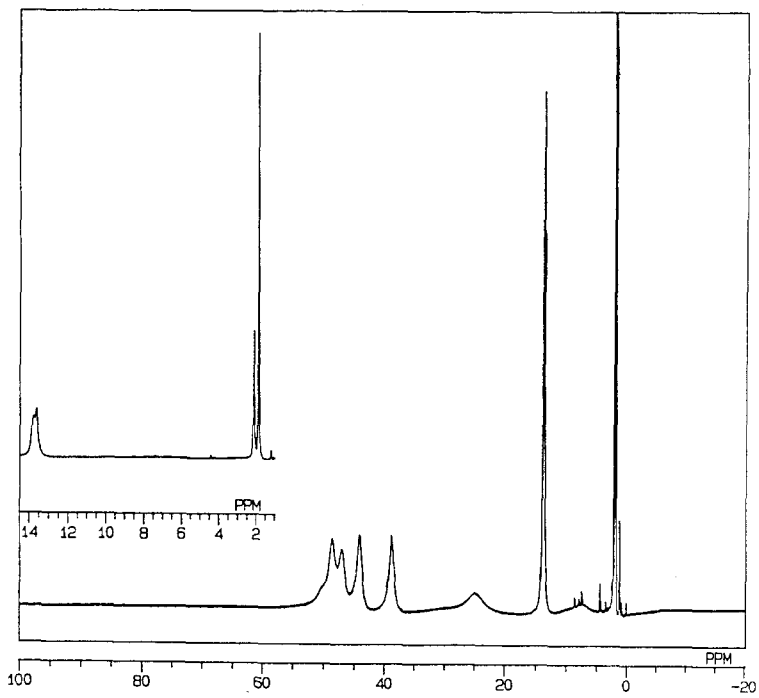

Fig. 4. ^{1}H NMR spectrum of **1** in CD_3CN.

Table 6. ^{1}H NMR Parameters of Ni(II) Complexes

$Ni(bpma)_2]^{2+}$	Int*	Assignment	$Ni(bbma)_2]^{2+}$	Int*	Assignment
13.6	4	CH_2	17.3	2	N–H(bzim)
24.9	1	N–H	29.1	4	CH_2
38.6	2	C(4)–H	34.1	1	N–H
43.9	6	C(3)–H	45.9	2	C(4)–H
		C(5)–H	51.8		
47.5		C(6)–H	6.5–7.4	6	C(5)–H
					C(6)–H
					C(7)–H

* Relative intensity

The complex **2** displays the most contact-shifted doublet signal (49.5, 51.8 ppm, Fig. 5) which is assigned to C(4)-H proton of bzim ring, lying closest to Ni(II). The sharpest peaks in the range 6.5–7.4 ppm correspond to other bzim ring protons lying furthest away from Ni(II). The broadest signal located around 34.1 ppm may be assigned to the N-H proton of the coordinated secondary amino group, as in **1**. The similarly broadened resonance around 17.3 ppm is assigned to bzim N-H protons. As for **1** the CH_2 proton (29.1 ppm) signal is split suggesting that the bbma complex also exists as a *rac* isomer in solution.* This is in contrast to the *meso* isomerism shown by $[Cu(bbma)_2](BF_4)_2$ complex [3]. The dipolar broadened isotropically contact-shifted resonances observed for both **1** and **2** in the range 6.5–51.8 ppm are typical [12, 14] of high spin nickel(II). Further, the sign of the shifts is indicative of dominant σ-spin delocalisation mechanism.

CONCLUSION

The ligand bis(pyrid-2-ylmethyl)amine is *cis*-facially coordinated in the Ni(II) bis-complex both in

* The X-ray crystal structure of this complex has been reported [25] after the submission of this manuscript and is consistent with the structure predicted here in solution.

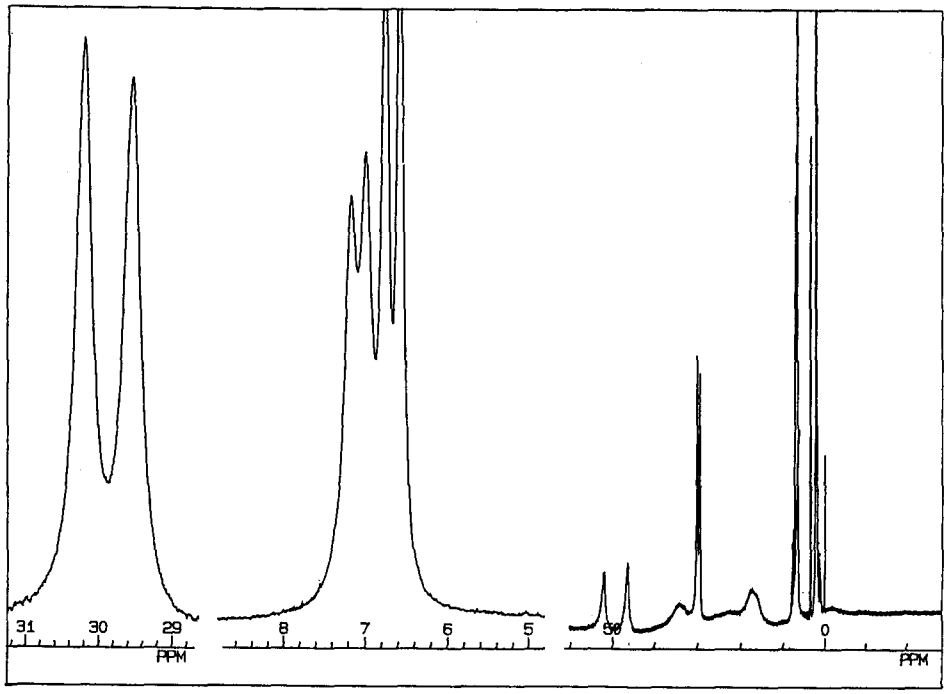

Fig. 5. ^{1}H NMR spectrum of **2** in CD_3CN.

the solid state and in solution. The benzimidazole analogue of this ligand also possesses a similar coordination behaviour in solution.

REFERENCES

1. Glerup, J., Goodson, P. A., Hodgson, D. J., Michelsen, K., Nielsen, K. M. and Weihe, H., *Inorg. Chem.*, 1992, **31,** 4611.
2. Palaniandavar, M., Pandiyan, T., Lakshminarayanan, M. and Manohar, H., *J. Chem. Soc., Dalton Trans.*, 1995, 455.
3. Palaniandavar, M., Butcher, R. J. and Addison, A. W., *Inorg. Chem.*, 1996, **35,** 467.
4. Viswanathan, R., Palaniandavar, M., Balasubramanian, T. and Muthiah, P. T., *J. Chem. Soc., Dalton Trans*, 1996, 2519.
5. Butcher, R. J. and Addison, A. W., *Inorg. Chim. Acta*, 1989, **158,** 211.
6. Stephens, F. S., *J. Chem. Soc.*, 1969, **A,** 883.
7. Hodgson, P. G. and Penfold, B. R., *J. Chem. Soc., Dalton Trans.*, 1974, 1870.
8. Biagini, S. and Cannas, M., *J. Chem. Soc., A*, 1970, 2398.
9. Bernhardt, P. V., Comba, P., Rickenbach, A. M., Stebler, S., Steiner, S., Varnagy, K. and Zehnder, M., *Inorg. Chem.*, 1992, **31,** 4194.
10. Nishida, Y. and Takahashi, K., *J. Chem. Soc., Dalton Trans.*, 1988, 691.
11. Perrins, D. D., Armarego, W. L. F. and Perrins, D. R., *Purification of Laboratory Chemicals*, Pergamon Press, London, 1980.
12. Huheey, J. E., Inorganic Chemistry, *Principles of Structure and Reactivity*, 3rd Edn., p. 388, Harber International SI Edition, 1990.
13. Hathaway, B. J., in *Comprehensive Coordination Chemistry*, G. Wilkinson, R. G. Gillard and J. A. McCleverty (Eds.), Vol. 2, p. 413, Pergamon, Oxford, 1987.
14. Lever, A. B. P., *Inorganic Electronic Spectroscopy*, (Second Edition) Elsevier, Amsterdam, 1986.
15. Uma, R., Viswanathan, R., Palaniandavar, M. and Lakshminarayanan, M., *J. Chem. Soc., Dalton Trans.*, 1994, 1219.
16. Pandiyan, T., Palaniandavar, M., Lakshminarayanan, M. and Manohar, H., *J. Chem. Soc., Dalton Trans.*, 1992, 3377.
17. Blake, A. J., Holder, A. J., Hyde, T. I. and Schroder, M., *J. Chem. Soc., Chem. Commun.*, 1989, 1433.
18. Lucas, C. R., *Can. J. Chem.*, 1983, **61,** 1096.
19. Lucas, C. R., *Can. J. Chem.*, 1986, **64,** 1758.
20. Batra, G. and Mathur, P., *Polyhedron*, 1994, **13,** 3219.
21. Norman, R. E., Yan, S., Que, L., Backes, G., Ling, J., Loehr, J. S., Zhang, J. H. and O'Connor, C. J., *J. Am. Chem. Soc.*, 1990, **112,** 1554.
22. Beritini, I., Sacconi, L. and Speroni, G. P., *Inorg. Chem.*, 1972, **109,** 5227.
23. Jorgensen, C. K., *Acta. Chem. Scand.*, 1955, **9,** 1362.
24. Linert, W., Konecny, M. and Renz, F., *J. Chem. Soc., Dalton Trans.*, 1994, 1523.
25. Pandiyan, T., Bernes, S. and Duran de Bazua, C., *Polyhedron*, 1997, **16,** 2819.

Pergamon

PII: S0277-5387(98)00051-5

Polyhedron Vol. 17, Nos 13-14, pp. 2187-2190, 1998
© 1998 Elsevier Science Ltd
All rights reserved. Printed in Great Britain
0277-5387/98 $19.00+0.00

Syntheses and characterization of organoimido complexes of tantalum; potential single-source precursors to tantalum nitride

Hsin-Tien Chiu,[a]* Shiow-Huey Chuang,[a] Chung-En Tsai,[a] Gene-Hsiang Lee,[b] and Shie-Ming Peng[b]*

[a]Department of Applied Chemistry, National Chiao Tung University, Hsinchu, Taiwan 30050, Republic of China

[b]Department of Chemistry, National Taiwan University, Taipei, Taiwan 10764, Republic of China

(Received 2 December 1996; accepted 26 January 1998)

Abstract—New single-source precursor to tantalum nitride thin films, $(Bu^tN)Ta(NEt_2)_3$, and related complexes, $(RN)Ta(NEt_2)_3$ (R = Pr^i and Pr^n), were prepared by reacting corresponding $(RN)TaCl_3py_2$ complexes (R = Bu^t, Pr^i and Pr^n) with $LiNEt_2$ in hydrocarbon solvents. The structure of $(Bu^tN)TaCl_3py_2$ was determined by X-ray crystallography. © 1998 Elsevier Science Ltd. All rights reserved

Keywords: organoimide complexes; tantalum complexes; CVD precursors.

Imido ligands, =NR, can stabilize early transition metals in high-oxidation states by metal-nitrogen π-bonding [1]. There are many interesting reactions involving these complexes. For example, use of these complexes in homogeneous catalysis, such as olefin metathesis, has been explored [2]. Recently, imido complexes have been employed as precursors to metal nitride and carbonitride thin films by chemical vapor deposition (CVD) [3–6]. For example, cubic phase tantalum nitride thin films can be grown from an ethylimido complex of tantalum, $(EtN)Ta(NEt_2)_3$ [3]. The metal-nitrogen multiple bond of this molecule is speculated to play a major role for the preservation of nitrogen atoms into the solids. However, $(\eta^2\text{-}EtN{=}CHMe)Ta(NEt_2)_3$, a precursor of $(EtN)Ta(NEt_2)_3$, is always in presence with $(EtN)Ta(NEt_2)_3$ [7]. Due to their similar physical properties, complete separation of one from the other is difficult. This makes reaction pathway elucidation complex. The use of other similar organoimido tantalum complexes, such as $(Bu^tN)Ta(NMe_2)_3$, has been considered [8]. The yield of $(Bu^tN)Ta(NMe_2)_3$, however, is low in our hands. Here in we report the systematic syntheses and characterization of $(RN)TaCl_3py_2$ (**1a**, R = Bu^t; **1b**, R = Pr^i; **1c**, R = Pr^n; py = pyridine). These complexes can be converted into $(RN)Ta(NEt_2)_3$ (**2a**, R = Bu^t; **2b**, R = Pr^i; **2c**, R = Pr^n), all of which are volatile liquids at room temperature. These properties make them good candidates for CVD applications; for example, **2a** has been employed successfully as a single-source precursor to grow tantalum nitride thin films by CVD for electronic device applications [9–11].

RESULTS AND DISCUSSION

The air- and moisture-sensitive organoimido complexes $(RN)TaCl_3py_2$ were conveniently prepared in good yields by reacting $TaCl_5$ with the corresponding amines $R(Me_3Si)NH$ and py in hydrocarbon solvents (Scheme 1). The synthetic procedure employed here parallels the methods used to prepare some other organoimido complexes of Ta, for example $(Me_3SiN)TaCl_3L_2$ and $[TaCl(\mu\text{-}Cl)(NBu^t)(NHBu^t)(NH_2Bu^t)]_2$ [12, 13].

Single crystals of **1a** were grown from a toluene solution at −15°C. An ORTEP of **1a**, from an X-ray diffraction study, is shown in Fig. 1. Bond distances and bond angles are listed in Table 1. **1a** has a distorted octahedral geometry. The distance between Ta

*Authors to whom correspondence should be addressed.

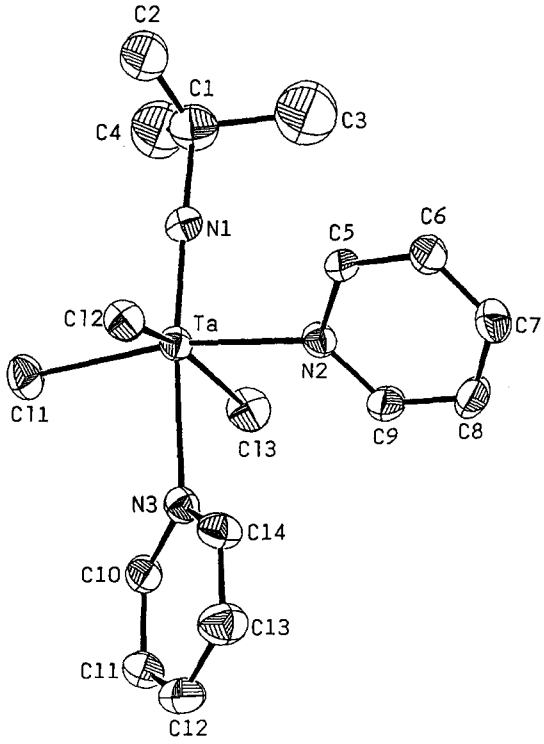

Fig. 1. ORTEP drawing of (Bu^{t}N)TaCl$_3$py$_2$ (**1a**) showing the atom numbering scheme. Only one orientation of the disordered Bu^t group is shown.

Table 1. Selected bond distances and bond angles of **1a**

Bond Distance (Å)		Bond Angle (°)	
Ta-Cl(1)	2.368(2)	Cl(1)-Ta-Cl(2)	92.96(7)
Ta-Cl(2)	2.406(2)	Cl(1)-Ta-Cl(3)	93.77(7)
Ta-Cl(3)	2.382(2)	Cl(1)-Ta-N(1)	99.3(2)
Ta-N(l)	1.745(5)	Cl(l)-Ta-N(2)	168.8(1)
Ta-N(2)	2.273(5)	Cl(1)-Ta-N(3)	86.4(1)
Ta-N(3)	2.452(5)	Cl(2)-Ta-N(3)	160.84(7)
N(1)-C(1)	1.475(1)	Cl(2)-Ta-N(1)	99.6(2)
		Cl(2)-Ta-N(2)	84.6(1)
		Cl(2)-Ta-N(3)	81.5(1)
		Cl(3)-Ta-N(1)	97.0(2)
		Cl(3)-Ta-N(2)	85.4(1)
		Cl(3)-Ta-N(3)	81.1(1)
		N(1)-Ta-N(2)	91.9(2)
		N(1)-Ta-N(3)	174.1(2)
		N(2)-Ta-N(3)	82.4(2)
		Ta-N(1)-C(1)	175.0(5)

and N(1) is short, 1.745(5) Å while the Ta-N(1)-C(1) angle is almost linear, 175.0(5)°. This closely resembles (PhN)TaCl$_3$THF(PEt$_3$), which has a Ta-N distance of 1.765(5) Å and a Ta-N-C angle of 173.3(4)° [14]. The Ta-N(3) distance, 2.452(5) Å, is significantly longer than the Ta-N(2) distance, 2.273(5) Å, reflecting the strong trans influence of the imido ligand. The structure of **1a** derived from solution NMR spectra, which show two sets of non-equivalent py signals, is consistent with the diffraction results. Since **1b** and **1c** showed very similar NMR spectra in the py region, they are thought to be isostructural with **1a**.

The complexes (RN)TaCl$_3$py$_2$ react with LiNEt$_2$ to generate (RN)Ta(NEt$_2$) in good yield (Scheme 1). The three complexes are air- and moisture-sensitive liquids. In a mass spectrometer, they all showed M^+ signals corresponding to the m/z values for the $(RN)Ta(NEt_2)_3^+$ ions. NMR data show resonance signals which can be assigned to the alkyl groups on the imdo and the amido ligands. Based on the data, **2** are proposed to have structures resembling those of tris(dimethylamido)(tertbutylimido)tantalum(V) and tris(dimethylamido)(2,6-diisopropylphenylimido) niobium(V) [8, 15]. Being volatile liquids at 60°C under vacuum is a significant advantage for **2** to be considered as CVD precursors. **2a** has been employed successfully as a single-source precursor to deposit good quality tantalum nitride thin films for electronic device applications [9–11]. Investigations are underway to study the potential applications of **2b** and **2c** as the CVD precursors to TaN thin films.

EXPERIMENTAL

All chemicals and solvents were manipulated under dry and oxygen-free environments. TaCl$_5$ was purchased from Strem and used without further purification. RNH$_2$ and pyridine were supplied by Merck and degassed before use. Me$_3$SiCl was obtained from Janssen and used as received. LiNEt$_2$ was prepared from HNEt$_2$ and Bu^{n}Li (Janssen) in hexane. All ^{1}H and ^{13}C{^{1}H} NMR spectra were recorded at 300 and 75-MHz, respectively, on a Varian Unity-300 spectrometer at +25°C. Mass spectra were measured (Vacuum Generator Trio-2000) by the direct insertion method. Elements were analyzed with a Heraeus CHN-O-Rapid Analyzer.

Preparation of (Bu^{t}N)TaCl$_3$py$_2$ **1a**

To Bu^t(Me$_3$Si)NH (2.3 cm^3, 12 mmol), prepared *in situ* by reacting Me$_3$SiCl (1.5 cm^3, 12 mmol) with Bu^{t}NH$_2$ (2.6 cm^3, 25 mmol) in toluene (100 cm^3), TaCl$_5$ (2.0 g, 5.5 mmol) was added. After the mixture was stirred for 1 h at room temperature, pyridine (1.6 cm^3, 21 mmol) was added. The mixture was stirred overnight then filtered. A yellow solid was separated after the filtrate was concentrated (2.4 g, 85% based on Ta). Recrystallization from toluene at −15°C gave large crystals suitable for X-ray structural analysis. ^{1}H NMR (benzene-d_6): 1.53 (s, 9H, Me_3CN), 6.27 (t, 2H, m-C$_6H_5$N), 6.52 (br, 2H, m-C$_6H_5$N), 6.67 (t, 1H, p-C$_6H_5$N), 6.84 (br, 1H, p-C$_6H_5$N), 8.89 (d, 2H, o-C$_6H_5$N). 9.18 (br, 2H, o-C$_6H_5$N). ^{13}C NMR (chloroform-d): 31.6 (Me_3CN), 66.2 (Me$_3$$C$N), 124.2 (m-

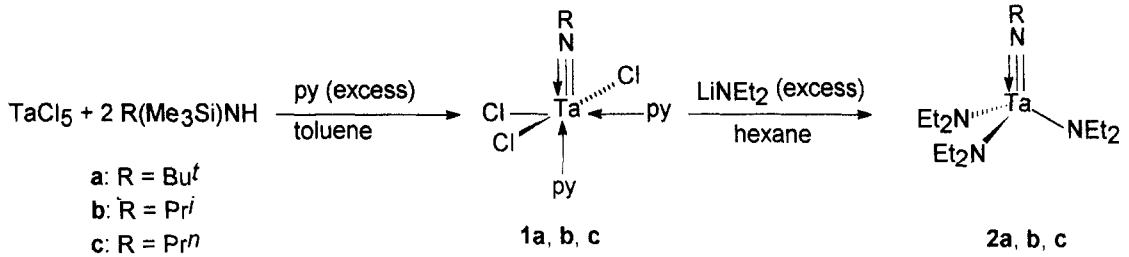

Scheme 1. Syntheses of **1** and **2**.

C_6H_5N), 124.5 (m-C_6H_5N), 139.2 (p-C_6H_5N), 140.6 (p-C_6H_5N), 151.6 (o-C_6H_5N), 152.9 (o-C_6H_5N). Mass (EI, m/z, ^{35}Cl, ^{181}Ta): 342 [M-2 py-Me]$^+$. Anal. Calcd. for $TaC_{14}H_{19}N_3Cl_3$: C, 32.54; H, 3.68; N, 8.13. Found: C, 32.50; H, 3.84; N, 8.02.

Preparation of (Pr^iN)$TaCl_3py_2$ **1b** and (Pr^nN)$TaCl_3py_2$ **1c**

By using $Pr^i(Me_3Si)NH$ and $Pr^n(Me_3Si)NH$, **1b** and **1c** were synthesized by a procedure similar to the one used to prepare **1a**.

1b ^1H NMR (benzene-d_6): 1.38 (d, 6H, Me_2CHN), 5.22 (m, 1H, Me_2CHN), 6.28 (t, 2H, m-C_6H_5N), 6.59 (br, 2H, m-C_6H_5N), 6.82 (t, 1H, p-C_6H_5N), 6.92 (br, 1H, p-C_6H_5N), 8.81 (d, 2H, o-C_6H_5N). 9.15 (br, 2H, o-C_6H_5N). ^{13}C NMR (chloroform-*d*): 25.1 (Me_2CHN), 61.9 (Me_2CHN), 124.3 (m-C_6H_5N), 124.7 (m-C_6H_5N), 139.0 (p-C_6H_5N), 140.2 (p-C_6H_5N), 151.6 (o-C_6H_5N), 152.8 (o-C_6H_5N). Mass (EI, m/z, ^{35}Cl, ^{181}Ta): 343 [M-2 py]$^+$. Anal. Calcd. for $TaC_{13}H_{17}N_3Cl_3$: C, 31.06; H, 3.38; N, 8.36. Found: C, 30.95; H, 3.72; N, 8.21.

1c ^1H NMR (benzene-d_6): 1.02 (t, 3H, $MeCH_2CH_2N$), 1.62 (m, 2H, $MeCH_2CH_2N$), 5.02 (t, 2H, $MeCH_2CH_2N$), 7.34 (m, 4H, m-C_6H_5N), 7.81 (t, 1H, p-C_6H_5N), 7.90 (t, 1H, p-C_6H_5N), 8.77 (d, 2H, o-C_6H_5N). 8.88 (br, 2H, o-C_6H_5N). ^{13}C NMR (chloroform-*d*): 12.0 ($MeCH_2CH_2N$), 26.2 ($MeCH_2CH_2N$), 63.1 ($MeCH_2CH_2N$), 124.4 (m-C_6H_5N), 124.8 (m-C_6H_5N), 138.6 (p-C_6H_5N), 140.1 (p-C_6H_5N), 151.5 (o-C_6H_5N), 152.5 (o-C_6H_5N). Mass (EI, m/z, ^{35}Cl, ^{181}Ta): 343 [M-2 py]$^+$. Anal. Calcd. for $TaC_{13}H_{17}N_3Cl_3$: C, 31.06; H, 3.38; N, 8.36. Found: C, 30.71; H, 3.43; N, 8.23.

Preparation of (Bu^tN)$Ta(NEt_2)_3$ **2a**

To **1a** (2.4 g, 4.6 mmol) suspended in hexane (100 cm^3), $LiNEt_2$ (1.8 g, 23 mmol) suspended in hexane (50 cm^3) was added slowly. The mixture turned brown gradually as it was stirred overnight. After filtration, the filtrate was concentrated to a brown liquid. Purification by vacuum distillation (60°C, 10^{-1} mm Hg) gave a yellow liquid (1.4 g, 65% based on Ta). ^1H NMR (benzene-d_6): 1.15 (t, 18H, $MeCH_2N$), 1.43 (s, 9H, Me_3CN), 3.47 (q, 12H, $MeCH_2N$). ^{13}C NMR (benzene-d_6): 17.2 ($MeCH_2N$), 34.5 (Me_3CN), 47.6 ($MeCH_2N$), 66.2 (Me_3CN). Mass (EI, m/z, ^{181}Ta): 468 [M]$^+$. A satisfactory carbon analysis was not obtained. Anal. Calcd. for $TaC_{16}H_{39}N_4$: C, 41.02; H, 8.39; N, 11.96. Found: C, 40.35; H, 8.30; N, 11.93.

Preparation of $Ta(NPr^i)(NEt_2)_3$ **2b** and $Ta(NPr^n)(NEt_2)_3$ **2c**

2b and **2c** were synthesized by a procedure similar to the one used to prepare **2a**.

2b ^1H NMR (benzene-d_6): 1.17 (t, 18H, $MeCH_2N$), 1.32 (d, 6H, Me_2CHN), 3.45 (q, 12H, $MeCH_2N$), 4.38 (m, 1H, Me_2CHN). ^{13}C NMR (benzene-d_6): 17.3 ($MeCH_2N$), 28.1 (Me_2CHN), 47.8 ($MeCH_2N$), 62.2 (Me_2CHN). Mass (EI, m/z, ^{181}Ta): 454 [M]$^+$. Satisfactory C and H analyses were not obtained. Anal. Calcd. for $TaC_{15}H_{37}N_4$: C, 39.65; H, 8.21; N, 12.33. Found: C, 40.35; H, 6.84; N, 12.53.

2c ^1H NMR (benzene-d_6): 1.04 (t, 3H, $MeCH_2CH_2N$), 1.19 (t, 18H, $MeCH_2N$), 1.70 (m, 2H, $MeCH_2CH_2N$), 3.44 (q, 12H, $MeCH_2N$), 4.16 (t, 2H, $MeCH_2CH_2N$). ^{13}C NMR (benzene-d_6): 11.9 ($MeCH_2CH_2N$), 17.3 ($MeCH_2N$), 28.2 ($MeCH_2CH_2N$), 47.8 ($MeCH_2N$), 64.0 ($MeCH_2CH_2N$). Mass (EI, m/z, ^{181}Ta): 454 [M]$^+$. A satisfactory carbon analysis was not obtained. Anal. Calcd. for $TaC_{15}H_{37}N_4$: C, 39.65; H, 8.21; N, 12.33. Found: C, 38.29; H, 7.96; N, 12.64.

Structure determination of **1a**

A single crystal of **1a** was sealed in a glass capillary under an inert atmosphere. Data were collected on a Nonius CAD-4 using graphite-monochromated Mo Kα radiation, and the structure was solved by the heavy-atom method; all data reduction and structural refinements were performed with the NRCC SDP package. Crystal data, details of data collection, and structural analysis are summarized in Table 2. The methyl groups of Bu^t are disorder with half occupancies. They are designated as C(2), C(3), C(4) and C(2)′, C(3)′, C(4)′, and refined isotropically. The other non-hydrogen atoms were refined with anisotropic parameters. Only hydrogen atoms of pyridine were placed in idealized positions and included in the cal-

Table 2. Crystal data and conditions for crystallographic data collection and structure refinement

Formula	$C_{14}H_{19}N_3Cl_3Ta$
Formula weight	516.72
Space group	$P2_1/c$
a (Å)	9.664(5)
b (Å)	13.535(2)
c (Å)	14.569(3)
β (°)	90.25(3)
V (Å)3	1905.5(11)
Z	4
ρ_{calc}, g cm^{-3}	1.769
λ (Å)	0.7107
F(000)	992
Unit cell determination: number; (2θ range)	25; (17.00–34.00 deg.)
Scan type	$\theta/2\,\theta$
Scan width (°)	$2(0.65+0.35\tan(\theta))$
$2\,\theta$ (max)	50.0
μ, cm^{-1}	61.228
crystal size, mm	$0.50\times0.50\times0.50$
T, °C	25
Number of observed reflections (I > 2.0 sig(I))	2733
Number of unique reflections	3347
R_F[a], R_w[b],	0.031, 0.032
GoF[c]	2.62
Refinement program	NRCVAX
Number of refined parameters	188 (2733 out of 3347 reflections.)
Minimize function	$\Sigma(w(F_o\text{-}F_c)^2)$
Weights scheme	$(1/\sigma(F_o)^2)$
g (2nd. extinction coefficient) $\times 10^4$	1.56(4)
(δ/σ)max	0.0480
(D-map)max.min e/Å^3	−1.260; 1.000

a, $R_F=\Sigma(F_o\text{-}F_c)/\Sigma\ F_o$; *b*, $R_w=[\Sigma(w(F_o\text{-}F_c)^2/\Sigma wF_o^2]^{1/2}$; *c*, $GoF=[\Sigma(w(F_o\text{-}F_c)^2)/(\text{No. of reflections-No. of parameters})]^{1/2}$ Standard reflections: No. 3; Decay 5%; every 3600 seconds; [t]Bu disorder.

culations. Atomic coordinates, bond lengths and angles, and thermal parameters have been deposited at the Cambridge Crystallographic Data Centre.

Acknowledgements—We thank the National Science Council of the Republic of China (NSC-84-2113-M-009-012) for support.

REFERENCES

1. For review, see: (a) Nugent, W. A. and Mayer, J. M., *Metal-Ligand Multiple Bonds*; Wiley, New York (1987). (b) Wigley, D. E., in *Progress in Inorganic Chemistry*; K. D. Karlin, ed., Wiley, New York (1994), Vol. 42.
2. Schaverien, C. J., Dewan, J. C. and Schrock, R. R., *J. Am. Chem. Soc.*, 1986, **108,** 2771.
3. Chiu, H.-T. and Chang, W.-P., *J. Mater. Sci. Lett.*, 1992, **11,** 96.
4. Chiu, H.-T. and Chuang, S.-H., *J. Mater. Res.*, 1993, **8,** 1353.
5. Chiu, H.-T., Ho, W.-Y. and Chuang, S.-H., *J. Mater. Res.*, 1994, **9,** 1622.
6. Winter, C. H., Sheridan, P. H., Lewkebandara, T. S., Heeg, M. J. and Proscia, J. W., *J. Am. Chem. Soc.*, 1992, **114,** 1095.
7. Takahashi, Y., Onoyama, N., Ishikawa, Y., Motojima, S. and Sugiyama, K., *Chem. Lett.* 1978, 525.
8. Nugent, W. A. and Harlow, R. L., *J. Chem. Soc., Chem. Commun.*, 1978, 579.
9. Tsai, M.-H., Sun, S.-C., Chiu, H.-T., Tsai, C.-E. and Chuang, S.-H., *Appl. Phys. Lett.*, 1995, **67,** 1128.
10. Tsai, M.-H., Sun, S.-C., Lee, C.-P., Chiu, H.-T., Tsai, C.-E., Chuang, S.-H. and Wu, S.-C., *Thin Solid Films*, 1995, **270,** 531.
11. Tsai, M.-H., Sun, S.-C., Tsai, C.-E., Chuang, S.-H. and Chiu, H.-T., *J. Appl. Phys.*, 1996, **79,** 6932.
12. Jones, C. M., Lerchen, M. E., Church, C. J., Schomber, B. M. and Doherty, N. M., *Inorg. Chem.*, 1990, **29,** 1679.
13. Jones, T. C., Nielson, A. J. and Rickard, C. E., *J. Chem. Soc., Chem. Commun.*, 1984, 205.
14. Churchill, M. R. and Wasserman, H. J., *Inorg. Chem.*, 1982, **21,** 223.
15. Herrmann, W. A., Baratta, W. and Herdtweck, E., *Angew. Chem. Int. Ed. Engl.*, 1996, **35,** 1951.

Pergamon

PII: S0277-5387(98)00052-7

Polyhedron Vol. 17, Nos 13–14, pp. 2191–2197, 1998
© 1998 Elsevier Science Ltd
All rights reserved. Printed in Great Britain
0277-5387/98 $19.00+0.00

Chemistry of osmium phenolates. Synthesis, structure and redox properties

Falguni Basuli,[a] Shie-Ming Peng[b] and Samaresh Bhattacharya[a]

[a]Department of Chemistry, Inorganic Chemistry Section, Jadavpur University, 700 032 Calcutta, India

[b]Department of Chemistry, National Taiwan University, Taipei, Taiwan, R.O.C.

(Received 25 September 1997; accepted 23 January 1998)

Abstract—The reaction of three phenolic ligands (*viz.* salicylaldehyde, Hsal; 2-hydroxyacetophenone, Hacp and 2-hydroxynaphthaldehyde, Hnap; generally abbreviated as HL, where H stands for the phenolic proton) with $[Os(bpy)_2Br_2]$ has afforded complexes of type $[Os(bpy)_2(L)]^+$, which have been isolated as the perchlorate salts. The complexes are diamagnetic (low-spin d^6, $S=0$) and in acetonitrile solution shows several MLCT transitions in the visible region. Structure of the $[Os^{II}(bpy)_2(sal)]ClO_4$ complex has been determined by X-ray crystallography. The salicylaldehydate anion is coordinated to osmium as a bidentate O,O-donor and the OsN_4O_2 coordination sphere is distorted octahedral. Cyclic voltammetry shows a reversible osmium(II)-osmium(III) oxidation in the range of 0.17–0.25 V *vs* SCE follwed by an irreversible osmium(III)-osmium(IV) oxidation in the range of 1.38–1.48 V *vs* SCE. Three one-electron reductions of the coordinated bpy ligands are also observed on the negative side of SCE (−1.49– −2.08 V). Chemical or electrochemical oxidation of the $[Os^{II}(bpy)_2(L)]ClO_4$ complex affords green $[Os^{III}(bpy)_2(L)]^{2+}$ species, which have been isolated as the perchlorate salts. These complexes are one-electron paramagnetic (low-spin d^5, $S=1/2$) and in acetonitrile solution show LMCT transitions in the visible region. Reduction of the green $[Os^{III}(bpy)_2(L)](ClO_4)_2$ complexes gives back the respective brown $[Os^{II}(bpy)_2(L)]ClO_4$ complexes. © 1998 Elsevier Science Ltd. All rights reserved

Keywords: osmium; phenolates; synthesis; structure; redox properties.

The chemistry of osmium has been receiving continuous attention [1] largely due to the interesting redox properties exhibited by its complexes. Osmium offers a wide range of chemically accessible oxidation states. The stability and the interconvertibility of these different oxidation states are directed by the coordination environment around the metal ion. Coordination of osmium by ligands of different types is of particular importance in this respect. In the present study, phenolic ligands of type **1** have been used as the principal ligand. The ligands are abbreviated in general as HL, where H stands for the dissociable phenolic proton. The phenolate anions (L^-) bind metal ions as bidentate O,O-coordinator forming six membered chelate ring(**2**). Coordination by phenolate oxygen is known to be very effective in stabilizing the higher oxidation states of osmium [2]. For example, in the tris-catecholato osmium complex, osmium is in +6 oxidation state, which is stabilized by the six coordinated phenolate oxygens [2a, 2b, 2e]. The three phenolic ligands that have been used in the present work are salicylaldehyde (Hsal, **3**), 2-hydroxyacetophenone (Hacp, **4**) and 2-hydroxynaphthaldehyde (Hnap, **5**). It may be noted here that while ruthenium chemistry of these ligands has received considerable attention [3], the analogous osmium chemistry appears to remain unexplored. Herein we have restricted our studies on a group of osmium complexes having only one coordinated L. To satisfy the remaining four coordination sites of osmium in this OsL moiety, 2,2′-bipyridine (bpy) has been used as the

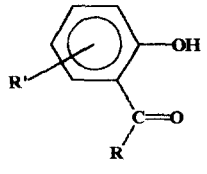

1

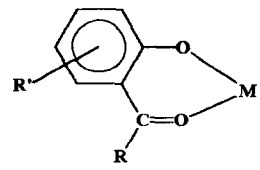

2

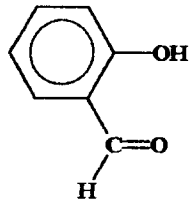

Hsal

3

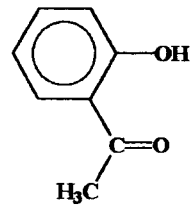

Hacp

4

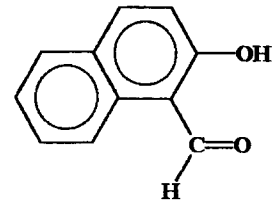

Hnap

5

coligand. The synthesis and characterization of three $[Os(bpy)_2(L)]ClO_4$ complexes and their spectroscopic and electron-transfer properties are reported in this paper.

EXPERIMENTAL

Materials

Osmium tetroxide was purchased from Arora Matthey, Calcutta, India and was converted into $[NH_4]_2[OsBr_6]$ by reduction with HBr [4]. $[Os(bpy)_2Br_2]$ was synthesized from $[NH_4]_2[OsBr_6]$ using a literature method [5]. 2,2′-Bipyridine was purchased from Loba Chemie, Mumbai, India. Salicylaldehyde, 2-hydroxyacetophenone and 2-hydroxynaphthaldehyde were obtained respectively from S.D. (Mumbai), Spectrochem(Mumbai) and Aldrich. All other chemicals and solvents were reagent grade commercial materials and were used as received. Purification of acetonitrile and preparation of tetraethylammonium perchlorate (TEAP) for electrochemical work were performed as reported in the literature [6, 7].

Preparation of complexes

The $[Os^{II}(bpy)_2(L)]ClO_4$ and $[Os^{III}(bpy)_2(L)](ClO_4)_2$ complexes, reported in this work, were prepared by following two general methods. Specific details are given below for two representative cases.

$[Os^{II}(bpy)_2(sal)]Clo_4$ $[Os(bpy)_2Br_2]$ (100 mg, 0.15 mmol) was taken in 3:1 EtOH-water (40 cm^3) and to the solution was added Hsal (20 mg, 0.16 mmol) followed by NEt_3 (16 mg, 0.16 mmol). The solution was then heated at reflux for 6 h. After being cooled to room temperature, a saturated solution of $NaClO_4$ (1 cm^3) was added to it and the volume of the solution was reduced to about 15 cm^3 under reduced pressure. The solution was then kept in the refrigerator for ~24 h. $[Os(bpy)_2(sal)]ClO_4$ precipitated as a dark brown microcrystalline solid, which was collected by filtration, washed with little ice-cold water and dried *in vacuo* over P_4O_{10}. Purification of the product was done by recrystallization from dichloromethane-benzene solution. The yield was 85 mg (78%).

$[Os^{III}(bpy)_2(sal)](Clo_4)_2$ $[Os^{II}(bpy)_2(sal)]ClO_4$ (100 mg, 0.14 mmol) was dissolved in acetone (20 cm^3) and one drop of bromine was added to it. An instantaneous colour change, from brown to green, took place. The solution was then stirred for 10 min and a saturated aqueous solution of $NaClO_4$ (0.5 cm^3) was added to it. Upon partial evaporation of the solution $[Os(bpy)_2(sal)](ClO_4)_2$ precipitated as a green microcrystalline solid, which was collected by filtration, washed with little ice-cold water and dried *in vacuo* over P_4O_{10}. The yield was 90 mg (79%).

Physical measurements

Microanalyses (C,H,N) were performed using a Perkin-Elmer 240C elemental analyser. Infrared spectra were obtained on a Perkin-Elmer 783 spectrometer with samples prepared as KBr pellets. Electronic spectra were recorded on a Simadzu UV 1601 spectrophotometer. Magnetic susceptibilities were measured using a PAR 155 vibrating sample magnetometer fitted with a Walker Scientific L75FBAL magnet. ^1H NMR spectra were obtained on a Brucker AC-200 NMR spectrometer using TMS as the internal standard. ESR spectra studies were done using a Varian E-109C spectrometer fitted with a quartz Dewar for measurement at 77 K (liquid nitrogen). Solution electrical conductivities were measured using a Philips PR 9500 bridge with a solute concentration of 10^{-3} M. Electrochemical measurements were made using a PAR model 273 potentiostat. A platinum disc or graphite working electrode, a platinum wire auxiliary electrode and an aqueous saturated calomel reference electrode (SCE) were used in a three electrode configuration. A platinum wire gauze working electrode was used in the coulometric experiments. A RE 0074 X–Y recorder was used to trace the voltammograms. Electrochemical measurements were per-

Table 1. Crystallographic data for $[Os(bpy)_2(sal)]ClO_4 \cdot CH_2Cl_2$

formula	$C_{28}H_{23}N_4O_6Cl_3Os$
f_w	807.5
space group	Monoclinic, $P2_1/n$
a, Å	9.084(2)
b, Å	20.020(4)
c, Å	15.998(4)
β, (°)	92.95(2)
V, Å^3	2905.3(11)
Z	4
crystal size, mm	$0.20 \times 0.25 \times 0.25$
T, K	298
μ, cm^{-1}	46.301
R_f	0.043
R_w	0.039
GOF	1.50

$R_f = \Sigma \| F_o| - |F_c| / \Sigma |F_o|$.
$R_w = [\Sigma w(|F_o| - |F_c|)^2 / \Sigma w(F_o)^2]^{1/2}$.

formed under a dinitrogen atmosphere. All electrochemical data were collected at 298 K and are uncorrected for junction potentials.

Crystallography

Single crystals of $[Os(bpy)_2(sal)]ClO_4$ were grown by slow diffusion of benzene into a dichloromethane solution of the complex. Selected crystal data and data collection parameters are given in Table 1. The unit cell dimensions were determined by a least-squares fit of 25 machine-centered reflections ($15.00 < 2\theta < 21.84$°). Data were collected on a Enraf–Nonius CAD-4 diffractometer using graphite monochromated Mo–Kα radiation ($\lambda = 0.7107$ Å) by θ-2θ scans within the angular range 3.0–45.0°. Three standard reflections, measured every 3600 seconds of X-ray exposure, showed no significant intensity variation over the course of data collection. X-ray data reduction, and structure solution and refinement were done using the NRCVAX package. The structure was solved by the Patterson method. Final cycles of refinement converged with discrepancy indices of $R_f = 0.043$ and $R_w = 0.039$.

RESULTS AND DISCUSSION

The three phenolic ligands (HL, **3**–**5**) react smoothly with $[Os(bpy)_2Br_2]$ in 3:1 ethanol-water in the presence of triethylamine to afford complexes of type $[Os(bpy)_2(L)]^+$, which have been isolated subsequently as the perchlorate salts in the solid state. Some characterization data of the complexes are given in Table 2. Elemental (C,H,N) analytical data are in excellent agreement with the compositions of the complexes. ^{1}H NMR spectra of the $[Os(bpy)_2(L)]^+$ complexes have been recorded in $CDCl_3$ solution. The aromatic region of the spectra is rather complex in nature due to overlap of signals and hence assignment of signals in this region to specific protons has not

Table 2. Characterization data of the $[Os(bpy)_2(L)]ClO_4$ complexes

Compound	Analytical data[a]			Λ_M[b]	Electronic spectral data[b]	Cyclic voltammetric data[b,c]
	%C	%H	%N	Ω^{-1} cm^2 M^{-1}	λ_{max}, nm (ϵ, M^{-1} cm^{-1})	E, V *vs* SCE
$[Os(bpy)_2(sal)]ClO_4$	44.66 (44.84)	2.98 (2.90)	7.73 (7.75)	140	746(3800), 585[d](5500) 500(10600), 431(12000) 355[d](9200), 297(46800), 245(35000), 221[d](30700).	0.25[e](60[f]), 1.48[g], −1.49[h], −1.80[h], −2.04[h]
$[Os(bpy)_2(acp)]ClO_4$	45.57 (45.62)	3.15 (3.12)	7.62 (7.60)	155	739(3800), 589[d](5900), 506(10500), 429(12700), 354(9700), 296(45700), 246(33600), 215[d](29500).	0.17[e](60[f]), 1.02[g], −1.54[h], −1.77[h], −2.05[h].
$[Os(bpy)_2(nap)]ClO_4$	48.14 (48.15)	3.01 (2.98)	7.29 (7.25)	148	677(4800), 584[d](6200), 489(13100), 435(14800), 362(12300), 296(53400), 236[d](37800), 220(57000).	0.24[e](60[f]), 1.48[g], −1.52[h], −1.78[h], −2.08[h].

[a]Calculated values are in parantheses.
[b]In acetonitrile solution.
[c]Supporting electrolyte, TEAP; scan rate, 50 mVs^{-1}.
[d]Shoulder.
[e]$E_{1/2} = 0.5(E_{pa} + E_{pc})$, where E_{pa} and E_{pc} are anodic and cathodic peak potentials respectively.
[f]$\Delta E_p = E_{pa} - E_{pc}$, in mV.
[g]E_{pa} value.
[h]E_{pc} value.

been attempted. However, intensity measurement of these signals corresponds to the total number of aromatic protons present in the respective complexes. In both $[Os(bpy)_2(sal)]^+$ and $[Os(bpy)_2(nap)]^+$ complexes, the aldehyde proton of the sal and nap ligands shows a distinct resonance at 9.29 ppm. In the $[Os(bpy)_2(acp)]^+$ complex, the methyl signal of the acp ligand appears at 2.31 ppm.

Molecular structure of $[Os(bpy)_2(sal)]ClO_4$ has been determined by X-ray crystallography. A view of the molecule is shown in Fig. 1 and selected bond distances and angles are listed in Table 3. The OsN_4O_2 coordination sphere is distorted octahedral, which is reflected in the three non-linear trans-angles and the twelve cis-angles (non 90°) as well. The salicylaldehyde anion is coordinated to osmium as bidentate O,O-donor with a bite angle of 91.8(3)°.

Infrared spectra of the $[Os(bpy)_2(L)]ClO_4$ complexes shows many vibrations of different intensities below 1700 cm^{-1}. Comparison of these spectra with the spectrum of $[Os(bpy)_2Br_2]$ shows that besides the presence of some similar vibrations, which are prob-

Table 3. Selected bond distances and bond angles for $[Os(bpy)_2(sal)]ClO_4.CH_2Cl_2$

	Bond Distances (Å)		
Os-O1	2.033(7)	C1-O1	1.263(15)
Os-O2	2.052(7)	C1-C2	1.426(18)
Os-N1	2.035(9)	C2-C3	1.438(18)
Os-N2	1.979(9)	C3-C4	1.336(20)
Os-N3	2.021(9)	C4-C5	1.405(21)
Os-N4	2.042(9)	C5-C6	1.343(19)
C6-C7	1.416(17)		
C7-C2	1.412(17)		
C7-O2	1.290(13)		
	Bond Angles (°)		
O1-Os-N2	172.9(3)		
O2-Os-N3	172.6(3)		
N1-Os-N4	177.1(4)		
O1-Os-O2	91.8(3)	O1-Os-N1	94.7(4)
O1-Os-N3	87.5(3)	O1-Os-N4	86.7(3)
O2-Os-N1	89.2(3)	O2-Os-N2	85.6(3)
O2-Os-N4	93.3(3)	N1-Os-N2	78.6(4)
N1-Os-N3	98.2(4)	N2-Os-N3	95.9(3)
N2-Os-N4	100.1(4)	N3-Os-N4	79.3(4)

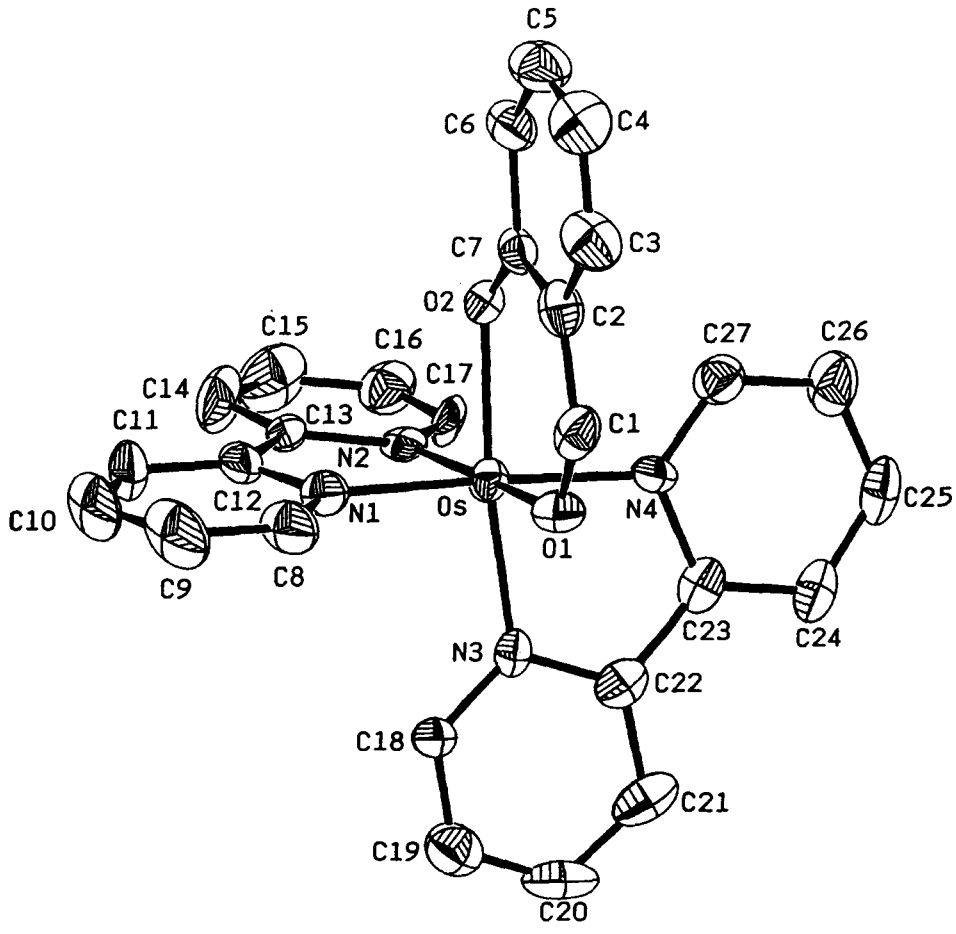

Fig. 1. Structure of $[Os(bpy)_2(sal)]^+$ cation.

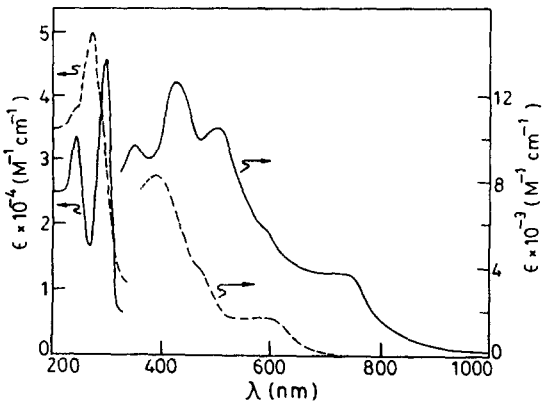

Fig. 2. Electronic spectra of $[Os^{II}(bpy)_2(acp)]ClO_4$. (——) and $[Os^{III}(bpy)_2(acp)](ClO_4)_2$ (– – –) in acetonitrile solution.

ably due to the common $Os(bpy)_2$ moiety, some additional vibrations are observed in the spectra of the $[Os(bpy)_2(L)]ClO_4$ complexes. Of these additional vibrations, the two intense ones observed near 1100 cm^{-1} and 620 cm^{-1} in all these complexes, are attributed to the perchlorate ion. The other new vibrations are obviously due to the coordinated phenolate ligand L. The $[Os(bpy)_2(L)]ClO_4$ complexes are soluble in common polar organic solvents like ethanol, acetone, dichloromethane, acetonitrile etc., producing solutions in different shades of brown. Conductance measurement in acetonitrile solution shows that these complexes behave as 1:1 electrolytes (Table 2), as expected. Electronic spectra of the $[Os(bpy)_2(L)]ClO_4$ complexes have been recorded in acetonitrile solution. Spectral data are presented in Table 2 and a selected spectrum is displayed in Fig. 2. Each complex shows several intense absorptions in the visible region and a few absorptions of very high intensity in the ultraviolet region. The absorptions in the ultraviolet region are attributed to transitions within the ligand orbitals. The intense absorptions in the visible region are probably due to allowed metal-to-ligand charge-transfer transitions. Multiple charge-transfer transitions in these mixed-ligand complexes may result from lower symmetry splitting of the metal level, the presence of different acceptor orbitals and from the mixing of singlet and triplet configurations in the excited state through spin-orbit coupling [8].

CYCLIC VOLTAMMETRIC STUDIES

Electron-transfer properties of the $[Os(bpy)_2(L)]ClO_4$ complexes have been studied in acetonitrile solution (0.1 M TEAP) by cyclic voltammetry. All the complexes show two oxidative responses on the positive side of SCE and three reductive responses on the negative side. Voltammetric data are presented in Table 2 and a selected voltammogram is displayed in Fig. 3.

The first oxidative response exhibited by each complex in the range of 0.17–0.25 V (all potentials are referenced to SCE) is assigned to the osmium(II)-osmium(III) oxidation [eqn. (1)]. This oxidation

$$[Os(bpy)_2(L)]^+ \rightleftharpoons [Os(bpy)_2(L)]^{2+} + e \qquad (1)$$

is reversible, characterized by a peak-to-peak separation (ΔE_p) of 60 mV which remains unaltered upon changing the scan rate. The anodic peak current (i_{pa}) is almost equal to the cathodic peak current (i_{pc}), as expected for a reversible couple. The one-electron nature of this oxidation has been confirmed by constant potential coulometric experiments (*vide infra*). The osmium(II)-osmium(III) oxidation potential in $[Os(bpy)_3]^{2+}$ is 0.84 V [9]. In the $[Os(bpy)_2(L)]^+$ complexes the same oxidation is taking place near 0.2 V. The negative shift of oxidation potential observed upon replacing one bpy by one L reflects the ability of these phenolate ligands to stabilize the +3 state of osmium. Similar systematic variation in redox potentials by stepwise substitution of pyridine ligands by phenolates in ruthenium complexes is well documented in literature [10]. This further points to the fact that inspite of coordination by the soft carbonyl oxygen, coordination by phenolate oxygen has been very effective in lowering the osmium(II)-osmium(III) oxidation potential. Comparison of the osmium(II)-osmium(III) oxidation potential in $[Os(bpy)_2(sal)]^+$ (0.25 V) with the ruthenium(II)-ruthenium(III) oxidation potential in $[Ru(bpy)_2(sal)]^+$ (0.64 V)[3d] shows that the oxidation is much easier in the osmium complexes, as expected.

A second oxidative response, irreversible in nature, is shown by $[Os(bpy)_2(L)]ClO_4$ complexes in the range of 1.38–1.48 V but its assignment is unclear. The one-electron nature of this oxidation is established by com-

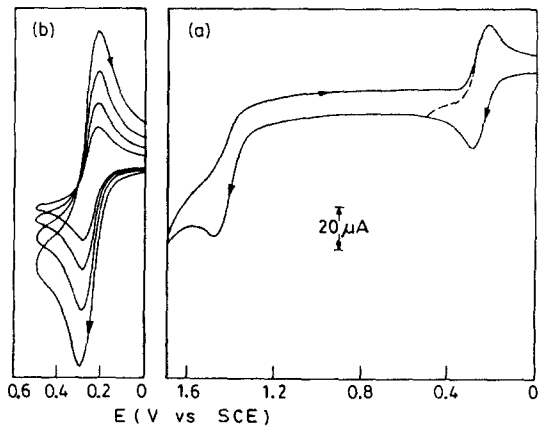

Fig. 3. Cyclic voltammograms of $[Os(bpy)_2(sal)]ClO_4$ in acetonitrile solution (0.1 M TEAP) (a) at a scan rate of 50 mVs^{-1} and (b) at scan rates of 50, 100, 200 and 400 mVs^{-1}.

paring its current height (i_{pa}) with that of osmium(II)-osmium(III) couple.

The three reductive responses, exhibited by the $[Os(bpy)_2(L)]^+$ complexes on the negative side of SCE, are assigned to the reductions of the coordinated bpy ligands as shown in eqs (2)–(4).

$$[Os^{II}(bpy)_2(L)]^+ + e^- \leftrightharpoons [Os^{II}(bpy)(b\dot{p}y)(L)] \quad (2)$$

$$[Os^{II}(bpy)(b\dot{p}y)(L)] + e^- \leftrightharpoons [Os^{II}(b\dot{p}y)_2(L)]^- \quad (3)$$

$$[Os^{II}(b\dot{p}y)_2(L)]^- + e^- \leftrightharpoons [Os^{II}(b\dot{p}y)(b\ddot{p}y)(L)]^{2-} \quad (4)$$

It is well documented in the literature that each bpy ligand can successively accept two electrons in its lowest unoccupied molecular orbital [11]. Hence in these $[Os(bpy)_2(L)]^+$ complexes four successive reductions may be expected, of which three have been experimentally observed. The fourth reduction could not be observed due to solvent cut-off.

$[Os^{III}(bpy)_2(L)]^{2+}$ *complexes*

The reversible nature of the osmium(II)-osmium(III) oxidation in the $[Os(bpy)_2(L)]^+$ complexes shows that the $[Os^{III}(bpy)_2(L)]^{2+}$ species are stable, at least on the cyclic voltammetric time scale. The oxidation potentials are relatively low, which further suggest that the oxidized complexes would be stable much longer time scale. To investigate the stability of the $[Os^{III}(bpy)_2(L)]^{2+}$ complexes, they were electrochemically generated by coulometric oxidation of the $[Os^{II}(bpy)_2(L)]^+$ species at 0.5 V. The oxidations were smooth and quantitative, resulting in a colour change of brown to green. The green solution of the $[Os^{III}(bpy)_2(L)]^{2+}$ complexes shows identical cyclic voltammograms as their respective precursors, except that the osmium(II)-osmium(III) couple now appears as a reductive response. This indicates that no change in the coordination environment around osmium took place during oxidation. Coulometric reduction of the green solutions at 0.0 V gave back brown solutions of the respective $[Os^{II}(bpy)_2(L)]^+$ complexes, which were identified by their characteristic electronic spectra. Chemical oxidation of the $[Os^{II}(bpy)_2(L)]^+$ complexes by bromine in acetone solution also afforded the $[Os^{III}(bpy)_2(L)]^{2+}$ species, which were isolated as the perchlorate salt in the solid state. Characterization data of the $[Os^{III}(bpy)_2(L)](ClO_4)_2$ complexes are given in Table 4. Composition of these complexes have been confirmed by their microanalitical data. Except small shift in band positions, the IR spectra of these oxidized complexes are almost identical to their respective $[Os^{II}(bpy)_2(L)]ClO_4$ precursors. The $[Os^{III}(bpy)_2(L)](ClO_4)_2$ complexes are one-electron paramagnetic, which is in accordance with +3 state of osmium (low-spin d^5, $S = 1/2$) in these complexes. However, ESR studies shows that these $[Os^{III}(bpy)_2(L)](ClO_4)_2$ complexes are ESR-silent. The ESR-inactivity in low-spin d^5 complexes is known to result from extensive mixing of the Kramers doublets by strong spin-orbit coupling which gives rise to short electronic relaxation time [12]. In acetonitrile solution these $[Os^{III}(bpy)_2(L)](ClO_4)_2$ complexes behave as 1:2 electrolytes, as expected. Electronic spectra of the $[Os^{III}(bpy)_2(L)](ClO_4)_2$ complexes have been recorded in acetonitrile solution. Each complex shows five absorptions, three intense ones in the visible region and two very intense ones in the UV region (Table 4, Fig. 2). The absorptions in the visible region are attributed to ligand-to-metal charge-transfer transitions and those in the UV region are assigned to transitions within the ligands orbitals. Chemical reduction of the green $[Os^{III}(bpy)_2(L)](ClO_4)_2$ complexes in acetonitrile solution by hydrazine quantitatively affords the respective brown $[Os^{II}(bpy)_2(L)]ClO_4$ complexes. This shows that the osmium(II)-osmium(III) oxidation [eqn (1)] is chemically reversible as well.

Table 4. Characterization data of the $[Os^{III}(bpy)_2(L)](ClO_4)_2$ Complexes.

Compound	Analytical data[a]			μ_{eff}[b]	Electronic spectral data[c]
	%C	%H	%N	μ_B	λ_{max}, nm (ϵ, $M^{-1}cm^{-1}$)
$[Os(bpy)_2(sal)](ClO_4)_2$	39.48 (39.42)	2.60 (2.55)	6.80 (6.81)	1.93	614(2100), 452[d](5700), 382(11200), 284(53000), 244(50400).
$[Os(bpy)_2(acp)](ClO_4)_2$	40.20 (40.19)	2.77 (2.75)	6.68 (6.70)	1.85	594(1800), 470[d](4000), 388(8300), 274(50200), 240[d](37900).
$[Os(bpy)_2(nap)](ClO_4)_2$	42.71 (42.66)	2.63 (2.64)	6.44 (6.42)	1.88	648(1100), 442[d](5300), 387(10700), 291(37600), 237[d](43300).

[a]Calculated values are in parantheses.
[b]In the solid state at 298 K; $\mu_B \sim 9.27402 \times 10^{-24}$ JT^{-1}.
[c]In dichloromethane solution.
[d]Shoulder.

CONCLUSION

The present study on the $[Os(bpy)_2(L)]ClO_4$ complexes reveals that coordination by phenolate oxygen is very effective in stabilizing the higher oxidation states of osmium. The observed shift in osmium(II)-osmium(III) oxidation potential in going from $[Os(bpy)_3]^{2+}$ (0.84 V) to $[Os(bpy)_2(sal)]^+$ (0.25 V) indicates that in the osmium complexes having more of these phenolate ligands, this oxidation will be much easier. For example, in the $[Os(bpy)(sal)_2]^{n+}$ and $[Os(sal)_3]^{m+}$ complexes, the same osmium(II)-osmium(III) oxidation may be expected to appear near -0.3 V and -0.9 V respectively. Therefore the air-stable oxidation state of osmium in these two complexes will be $+3$ or higher. Studies on these two and other osmium-phenolate complexes are currently in progress.

Acknowledgements—Financial assistance received from the Council of Scientific and Industrial Research, New Delhi [Grant No. 01(1408)/96/EMR-II] is gratefully acknowledged. Thanks are also due to the Third World Academy of Sciences for financial support for the purchase of an electrochemical cell system. The authors thank Dr. Sreebrata Goswami of Indian Association for the Cultivation of Science, Calcutta, and Dr. Rupendranath Banerjee of Jadavpur University, Calcutta, for their help. FB thanks the University Grants Commission, New Delhi, for her fellowship.

REFERENCES

1. (a) Seddon, K. R., *Coord. Chem. Rev.*, 1982, **41,** 159; (b) Moore, D. S., *Coord. Chem. Rev.*, 1982, **44,** 127; (c) Gulliver, D. J. and Levason, W., *Coord. Chem. Rev.*, 1982, **46,** 1; (d) Seddon, E. A., *Coord. Chem. Rev.*, 1985, **67,** 243. (e) Albers, M. O., Robinson, D. J. and Singleton, E., *Coord. Chem. Rev.*, 1987, **79,** 1; (f) Thomas, N. C., *Coord. Chem. Rev.*, 1989, **93,** 225; (g) Rong, D., Hong, H. G., Kim, Y. I., Krueger, J. S., Mayer, J. E. and Mallouk, T. E., *Coord. Chem. Rev.*, 1990, **97,** 237; (h) Yam, V. W. W. and Che, C. M., *Coord. Chem. Rev.*, 1990, **97,** 93; (i) Hage, R., *Coord. Chem. Rev.*, 1991, **111,** 161; (j) Collin, J. P., Guillerez, S., Sauvage, J. P., Barigelletti, F., Flamigni, L., Cola, L. D. and Balzani, V., *Coord. Chem. Rev.*, 1991, **111,** 291; (k) Cola, L. D., Barigelletti, F., Balzani, V., Belser, P., Zelewsky, A. V., Seel, C., Frank, M. and Vogtle, F., *Coord. Chem. Rev.*, 1991, **111,** 255; (l) Constable, E. C. and Housecroft, C. E., *Coord. Chem. Rev.*, 1993, **124,** 183; (m) Ward, M.D., *Coord. Chem. Rev.*, 1993, **127,** 1; (n) Furue, M., Maruyama, K., Kanematsu, Y., Kushida, T. and Kamachi, M., *Coord. Chem. Rev.*, 1994, **132,** 201; (o) Collin, J. P., Sauvage, J. P., Sour, A., Constable, E. C. and Thompson, A. M. W. C., *Coord. Chem. Rev.*, 1994, **132,** 209; (p) Kalyansundaram, K., Zakeeruddin, S. M. and Nazeeruddin, M. K., *Coord. Chem. Rev.*, 1994, **132,** 259; (q) Richmond, M. G., *Coord. Chem. Rev.*, 1995, **141,** 63; (r) Ward, M. D., *Coord. Chem. Rev.*, 1995, **146,** 99.
2. (a) Hursthouse, M. B., Fram, T., New, L., Griffith, W. P. and Nielson, A., *Transition Met. Chem.*, 1973, **3,** 255; (b) Nielson, A. and Griffith, W. P., *J. Chem. Soc., Dalton Trans.*, 1978, 1501; (c) Lahiri, G. K., Bhattacharya, S., Ghosh, B. K. and Chakravorty, A., *Inorg. Chem.*, 1987, **26,** 4324; (d) Haga, M., Isobe, K., Boone, S. R. and Pierpont, C .G., *Inorg. Chem.*, 1990, **29,** 3795; (e) Bhattacharya, S., Boone, S. R., Fox, G. A. and Pierpont, C. G., *J. Am. Chem. Soc.*, 1990, **112,** 1088; (f) Bhattacharya, S. and Pierpont, C. G., *Inorg. Chem.*, 1991, **30,** 2906; (g) Bhattacharya, S. and Pierpont, C. G., *Inorg. Chem.*, 1992, **31,** 35.
3. (a) Gopinathan, S., Joseph, K. and Gopinathan, C., *Indian J. Chem.*, 1987, **26A,** 128; (b) Joseph, K., Despande, S. S., Pardhy, S. A., Unny, I. R., Pandit, S. K., Gopinathan, S. and Gopinathan, C., *Inorg. Chim. Acta*1984, **82**(1), 59; (c) Gopinathan, S., Pardhy, S. A. and Gopinathan, C., *Synth. React. Inorg. Met.-Org. Chem.*, 1986, **16,** 475; (d) Bag, N., Lahiri, G. K., Bhattacharya, S., Falvello, L. R. and Chakravorty, A., *Inorg. Chem.*, 1988, **27,** 4396; (e) Chakravarty, J. and Bhattacharya, S., *Polyhedron*, 1996, **15,** 257.
4. Dwyer, F. P. and Hogarth, J. W., *Inorg. Synth.*, 1957, **5,** 204.
5. Kober, E. M., Casper, J. V., Sullivan, B. P. and Meyer, T. J., *Inorg. Chem.*, 1988, **27,** 4587.
6. Sawyer, D. T. and Roberts Jr., J. L. *Experimental Electrochemistry for Chemists*., John Wiley, New York, 1974, pp. 167–215.
7. Walter, M. and Ramaley, L., *Anal. Chem.*, 1973, **45,** 165
8. (a) Pankuch, B. J., Lacky, D. E. and Crosby, G. A., *J. Phys. Chem.*, 1980, **84,** 2061; (b) Ceulemans, A., Vanquickenborne, L. G., *J. Am. Chem. Soc.*, 1981, **103,** 2238; (c) Decurtis, S., Felix, F., Ferguson, J., Gudel, H. U. and Ludi, A., *J. Am. Chem. Soc.*, 1980, **102,** 4102; (d) Kober, E. M. and Meyer, T. J., *Inorg. Chem.*, 1982, **21,** 3967.
9. This oxidation potential has been determined by us.
10. Bardwell, D. A., Black, D., Jeffery, J. C., Schatz, E. and Ward, M. D., *J. Chem. Soc., Dalton Trans.*, 1993, 2321.
11. (a) Vlcek, A. A., *Coord. Chem. Rev.*, 1982, **43,** 39; (b) Kahl, J. L., Hanck, K. W. and DeArmond, K., *J. Phys. Chem.*, 1978, **82,** 540.
12. Shirin, Z. and Mukherjee, R. N., *Polyhedron*, 1992, **11,** 2625.

Pergamon

PII: S0277-5387(98)00047-3

Polyhedron Vol. 17, Nos 13–14, pp. 2199–2206, 1998
© 1998 Elsevier Science Ltd
All rights reserved. Printed in Great Britain
0277-5387/98 $19.00+0.00

Self assembly in transition metal complexes: structural characterisation of the zinc carboxylate{bis(2-pyrrolecarboxylato)bis(1-methylimidazole)}zinc(II)

Thomas A. Zevaco,[a]* Helmar Görls[b] and Eckhard Dinjus[c]

[a]Projektgruppe "CO2-Chemie" an der Friedrich-Schiller-Universität Jena, Lessingstraße 12, 07743 Jena, Germany

[b]Institut für Anorganische und Analytische Chemie der Universität, August-Bebel-Straße 2, D-07743 Jena, Germany

[c]Forschungszentrum Karlsruhe GmbH, Institut für Technische Chemie-Chemisch-Physikalische Verfahren, Postfach 3640, 76021 Karlsruhe, Germany

(Received 24 September 1997; accepted 23 January 1998)

Abstract—The synthesis, spectral characterisation of the zinc(II) pyrrolecarboxylates, $[Zn(2\text{-Hpyrrc})_2(H_2O)]$ (**1**) and $[Zn(2\text{-Hpyrrc})_2(1\text{-methylimidazole})_2]$ (**2**) ($2\text{-}H_2$pyrrc = 2-pyrrolecarboxylic acid) is reported as well as the X-ray structure determination of the latter compound. The molecular structure of **2** exhibits a distorted tetrahedral geometry around the zinc atom. The pyrrole-2-carboxylic acid acts as a monodentate ligand, *syn*-bound via one carboxylate oxygen atom. In the crystal structure, the discrete molecules of **2** are organised in dimers linked by a complex network of hydrogen bonds. A comparative IR study confirms the existence of different types of hydrogen bonding. © 1998 Elsevier Science Ltd. All rights reserved.

Keywords: crystal structure; zinc carboxylate; imidazole; pyrrole; IR-spectroscopy; self-assembly.

INTRODUCTION

During the course of our studies on new potential carbon dioxide activators, we became interested in systems involving zinc(II) carboxylates since these compounds are known to be effective catalysts for the copolymerisation of CO_2 and epoxides [1, 2]. The most efficient carboxylates are obtained from dicarboxylic acids and display most of the time polymeric frameworks [3–5]. The structural characterisation of such catalysts is poorly documented and the exact nature of the active site remains controversial. Our interest was attracted by carboxylic acids including a pyrrole moiety which might engineer, through hydrogen bonding, new low-molar-weight oligomeric carboxylates. Molecules having self complementary arrays of hydrogen bond donors and acceptors are a topic of main interest in organic chemistry for their ability to build supramolecular assemblies [6–9]. The preparation of hydrogen-bonded aggregates incorporating metal ions is less documented and attracts an ever-growing interest by associating versatile nanoarchitectures and transition metal characteristics [10]. The control of the molecular aggregation should allow, in our case, an easier investigation of the zinc-catalyzed reaction of carbon dioxide with epoxides. Surprisingly, despite a number of extensive studies on the co-ordination of pyrrolecarboxylic acids to metal centres performed with spectroscopic [11, 12] and calorimetric methods [13], no crystallographic data are available, to our knowledge, for the corresponding

* Author to whom correspondence should be addressed.

transition metal carboxylates. We decided to undertake as first part of our study the structural characterisation of such carboxylates. We report here the first X-ray structure of a zinc(II) pyrrolecarboxylate, $[Zn(2\text{-}PyrrcH)_2(1\text{-methylimidazole})_2]$ (**2**).

RESULTS AND DISCUSSION

The reaction of zinc oxide with two equivalents of the 2-pyrrolecarboxylic acid, noted 2-H_2pyrrc, under reflux in aqueous media affords the carboxylato compound, $[Zn(2\text{-}Hpyrrc)_2.H_2O]$, (**1**). This zinc carboxylate reacts with 1-methylimidazole to afford, after recrystallisation from acetonitrile, red parallelepipedic crystals. The analytical and spectral results are consistent with a monomeric compound, $[Zn(2\text{-}Hpyrrc)_2(1\text{-methylimidazole})_2]$ (**2**), presenting a monodentate co-ordination of the carboxylate ligand.

Crystallographic study of 2

The molecular structure of **2** with atomic labelling is given in Fig. 1. Selected distances and angles are given in Table 1. $[Zn(2\text{-}Hpyrrc)_2(1\text{-methylimidazole})_2]$ crystallises in the monoclinic space group $P2_1/c$ with four discrete molecules per unit cell. Each molecule is linked *via* two hydrogen bonds with a centrosymmetrically related counterpart to form a dimer as depicted in Fig. 2. The structural characterisation of such hydrogen-bonded dimeric compounds linked by self complementary donor/acceptor groups is well documented in organic chemistry [14–18] but remains scarce for inorganic compounds. We are aware of only a few transition metal carboxylates of, e.g. zinc [19] and platin [20] displaying such pairs of symmetric C=O . . . H–N bridges.

The zinc atom is tetracoordinated occupying the center of a tetrahedron characterised by a dihedral

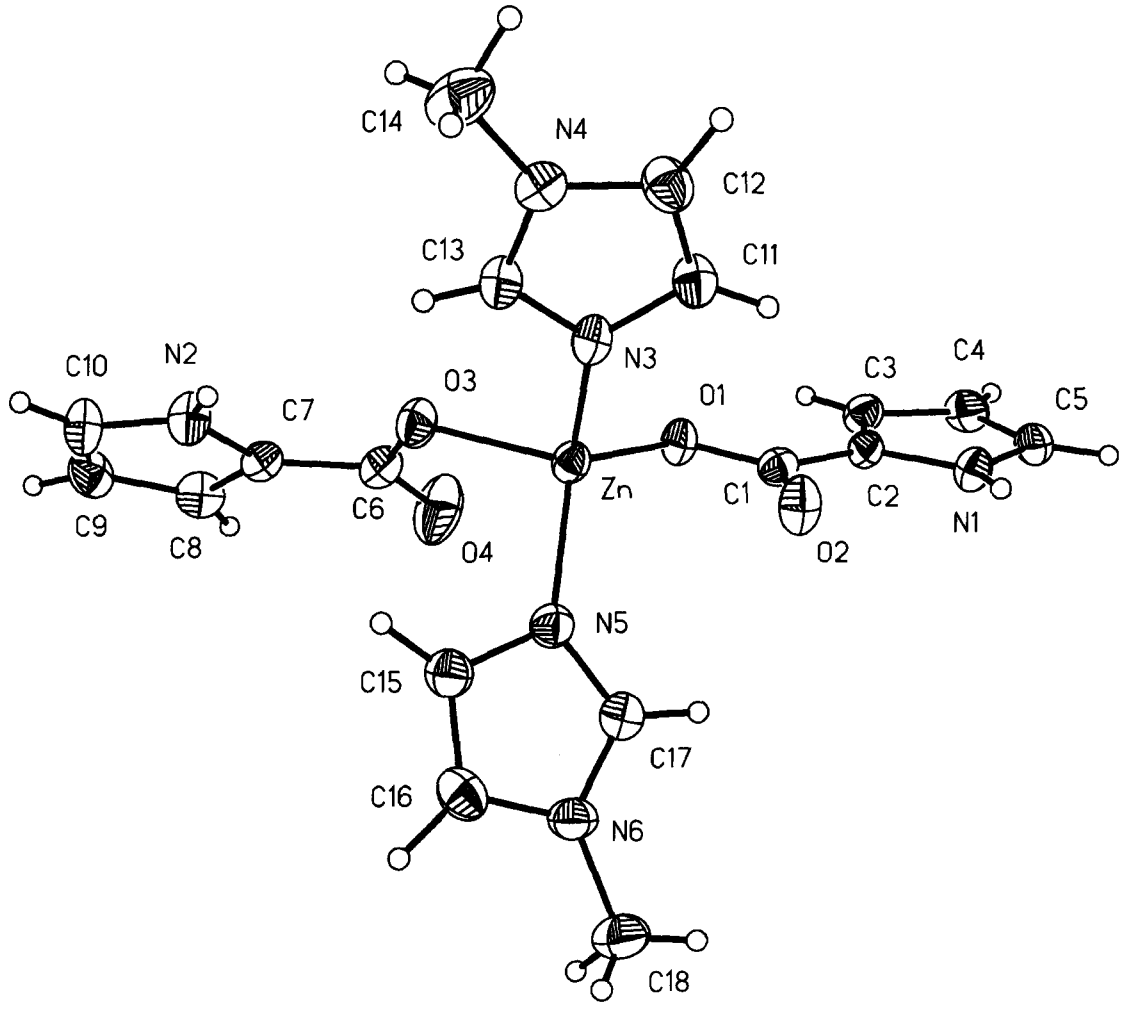

Fig. 1. Molecular structure of $[Zn(2\text{-pyrrolecarboxylato})_2(1\text{-methylimidazole})_2]$ (**2**), with 50% probability thermal ellipsoids for non-hydrogen atoms.

Table 1. Selected bond lengths[Å] and angles [ ] for [Zn(2-pyrrolecarboxylato)$_2$(1-methylimidazole)$_2$]

Bond lengths	Angles and intermolecular distances		
Zn-O(1)	1.969(2)	N(5)-Zn-N(3)	112.25(9)
Zn-O(2)	2.717(2)	O(1)-Zn-O(3)	113.71(8)
Zn-O(3)	1.950(2)	O(1)-Zn-N(3)	112.07(8)
Zn-O(4)	3.037(2)	N(5)-Zn-O(3)	101.95(9)
Zn-N(3)	2.012(2)	O(2)-C(1)-O(1)	122.4(2)
Zn-N(5)	2.002(2)	O(3)-C(6)-O(4)	124.8(3)
C1-O(1)	1.288(3)		
C1-O(2)	1.243(3)	O(2)· · N(1a)	2.801(3)
C6-O(3)	1.285(3)	O(4a)· · N(2b)	2.994(3)
C6-O(4)	1.226(3)	O(1a)· · N(2b)	3.114(3)

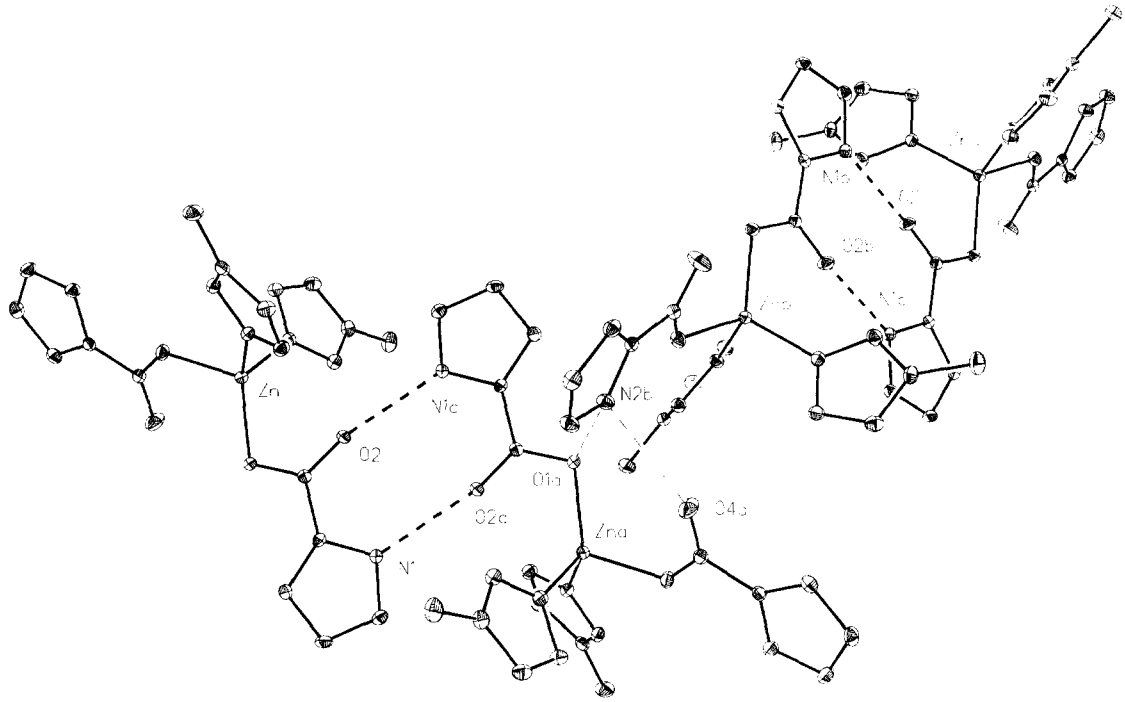

Fig. 2. Representation illustrating the hydrogen bondings within and between the adjacent pairs of **2**. Hydrogen atoms are omitted for clarity. Symmetry transformations used: #a): $-x,1-y,2-z$; #b): $-x,-0.5+y,1.5-z$; #c): $x,0.5-y,-0.5+z$. Intermolecular bond lengths (Å): O(2) . . . N(1a) = 2.801(3), O(4a) . . . N(2b) = 2.994(3), O(1a) . . . N(2b) = 3.114(2) Å.

angle of 90.70(8)° between the planes defined by N(3)-Zn-N(5) and O(3)-Zn-O(1). The angles within the tetrahedron are shifted from the theoretical value and range from 98.62(8)° to 116.44(8)°. The carboxylate groups are bound in a *syn*-monodentate way. This geometry is commonly found in zinc aminocarboxylates and was already described for, e.g. the dichlorobis(L-proline)zinc(II) [21] and bis(L-pyroglutamat)zinc(II) dihydrate. [22]

The ligand-metal distances are 1.969(2) Å and 1.950(2) Å for the Zn-O bonds and 2.002(2) Å and 2.012(2) Å for the Zn-N bonds. The Zn-O bond lengths are within the range reported for tetrahedral environments [21, 22, 23]. The Zn-N bond lengths are similar to those found in other tetrahedral zinc complexes of imidazole (Zn-N: 1.995–2.020 Å) [21, 24] and are shorter than those found in octahedral imidazole complexes [25, 26] (distances ranging from 2.144 to 2.199(4) Å).

The C-O_{sp2} distances measured in the carboxylates groups suggest unequivalent values with 1.226(3) Å and 1.243(3) Å. The latter distance may indicate a weakening of the double bond character and can be compared to those usually found in monodentate zinc

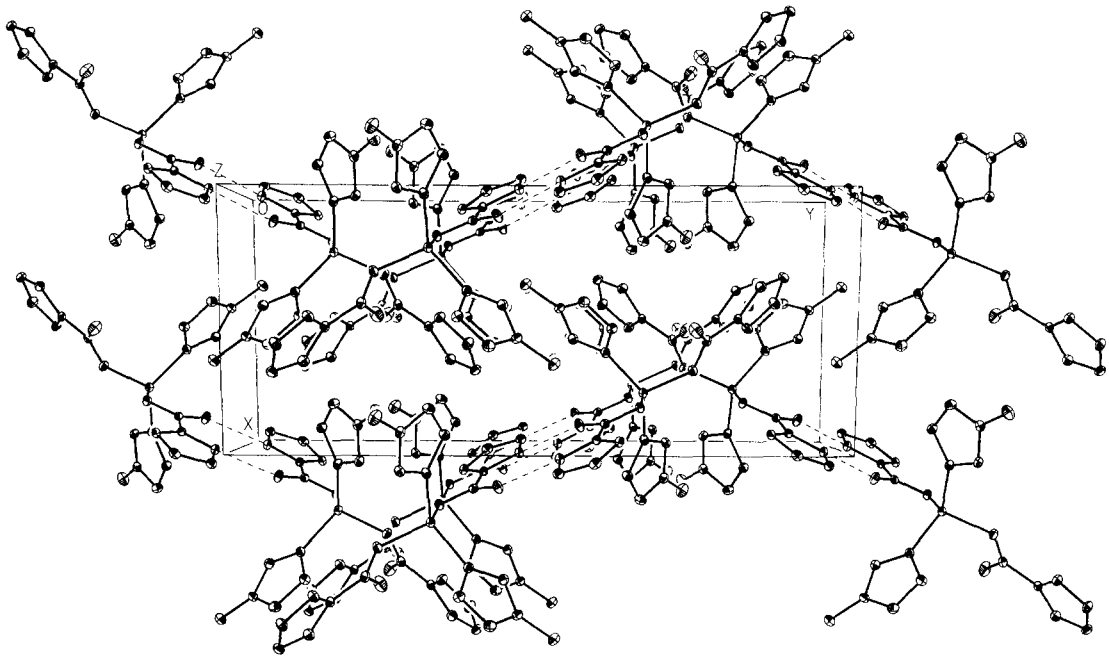

Fig. 3. Unit cell of [Zn(2-pyrrolecarboxylato)$_2$(1-methylimidazole)$_2$] **2**, viewed along the *c* axis.

carboxylates stabilised by hydrogen-bonded networks [19, 22, 27]. As expected, hydrogen bonding plays a significant role in the crystal structure and takes place on two levels, giving rise to interesting structural patterns. Firstly, a "strong"† hydrogen bond is found implicating the pendant oxygens O(2) and the nitrogen atoms N(1a) of pyrrolecarboxylate fragments in two adjacent molecules [O(2)$\cdots$N(1a) = 2.801(2) Å], this interaction accounts for the formation of the above-mentioned dimer. These distant contacts are comparable to hydrogen bond distances found in the crystal structures of many secondary amides involving dimeric arrangements [14]. A second interaction is detected between the oxygen O(4a), the metal-bonded oxygen O(3a) and a pyrazolic nitrogen atom N(2b) belonging to an other adjacent hydrogen-bonded dimer as illustrated in Fig. 2 [O(4a)$\cdots$N(2b) = 2.994(2) Å; O(1a)$\cdots$N(2b) = 3.114(2) Å]. These contacts can be considered as "weak" hydrogen bonds owing to the fact that the carboxylic group O(4a),C(6a),O(3a) is located in the same plane as the pyrazolic nitrogen (deviation ca. 0.025 Å) and directed towards the orbital lobes of the sp^2-hybridised oxygen O(4a) [28]. Likewise, the interaction between O(1a) and N(2b) can be regarded as a weak hydrogen bonding assuming an sp^3 hybridisation for the metal-bonded O(1a) atom [angles within the O(1a)-centred tetrahedron ranging from 105.3(8) to 109.8(8)°] [29]. This kind of secondary "weak" hydrogen bonds may explain some of the features found in the molecular structure such as: i) the different conformations of the pyrrolecarboxylate ligands, whose amino groups display *cis* and *trans* geometries in respect to the pendant carbonyl oxygens and, ii) the distortions observed in the co-ordination geometry of the carboxylato groups to the zinc atom [Zn-O(2): 3.037(2) Å and Zn-O(4): 2.717(2) Å].

The complex hydrogen-bonded network resulting from the combination of these "strong" and "weak" hydrogen bondings links the pseudo-dimers of **2** into staggered sheets which propagate parallel to the [011] plane as depicted in Fig. 3. The methylation at N(4) and N(6) precludes the formation of further hydrogen-bonded networks between the distinct layers.

IR spectroscopic studies

Evidence of hydrogen bonding can also be found in the IR spectra of both zinc carboxylates. Infrared spectra of compounds **1**, **2** and of the ionic sodium pyrrolecarboxylate were run and comparisons were made between the frequencies of the N-H stretching bands in the solid state and the frequency found for the free pyrrolecarboxylic acid in solution ($CHCl_3/CH_3CN$, ν(N-H): 3432 cm^{-1}). Selected IR frequencies are summarised in Table 2.

The spectrum of **1** shows one strong band assigned to the N-H stretching mode at 3350 cm^{-1} comparable

† The terms "strong" and "weak" are used to distinguish the two-centred hydrogen bond (2.801(2)Å) from the three-centred hydrogen bond (2.994(2) and 3.114(2) Å).

Table 2. Selected vibrational frequencies (KBr, $\pm 2\,cm^{-1}$) of compounds **1**, and **2** and of the sodium pyrrole-2-carboxylate. (s = strong, m = medium, w = weak, br = broad, sh = shoulder)

Compound	$\nu(OH_2)$	ν(N-H)	$\delta(OH_2)$	ν_{as}(COO)	ν(C=C), ν(C-N)+ δ(CN-H)	ν(C-C)+ ν_s(COO)
[Zn(2-Hpyrrc)$_2$(H_2O)] **1**	3418m,br	3348s $\Delta_a = -82$	1636sh,br	**1562s**	1510vs	1462m,sh **1442s** 1390w,sh $\Delta\nu_c = 120$
[Zn(2-Hpyrrc)$_2$1-methylimidazole)$_2$] **2**	—	3338m 3234s $\Delta_a = -94, -198$	—	**1608vs** **1574vs**	1546s,	1436s, 1414s **1350vs** $\Delta\nu_c = 258, 224$
Na(2-Hpyrrc) **3**	—	3262s $\Delta_a = -170$	—	**1556s**	1528vs	1426m **1468s** 1388m,sh $\Delta\nu_c = 88$

Δ_a shift defined as: ν(N-H) of the free acid in solution $-\nu$(N-H) of the carboxylate in the solid state.
$\Delta\nu_c$ difference defined as: $\nu_{sym}(COO) - \nu_{sym}(COO)$ of the carboxylate in the solid state.

to the vibration found in the solid-state spectrum of the free 2-pyrrolecarboxylic acid. The absence of band shift indicates that the amine of the 2-pyrrolecarboxylic acid is not co-ordinated to the zinc atom [30]. The comparison with the solution spectrum of the free acid reveals a bathochromic shift of $82\,cm^{-1}$ indicating the presence in compound **1**, as in the free carboxylic acid, of a "weak" hydrogen bonding implicating aminogroups and carboxylic oxygens (entry 1, Tab. 2). This bonding might also implicate the water molecule as suggested by the presence of a broad ν(O-H) band at $3418\,cm^{-1}$ [32]. Compound **2** exhibits in the region characteristic of the N-H stretching vibrations two strong well resolved bands at 3338 and $3234\,cm^{-1}$ (bathochromic shift of 94 and $198\,cm^{-1}$, respectively) consistent with the presence of two amino groups engaged in hydrogen bonding of different intensities (entry 2, Tab. 2). In comparison, the spectrum of the ionic sodium pyrrolecarboxylate, **3**, displays only one strong ν(N-H) band at $3262\,cm^{-1}$ (shift of $170\,cm^{-1}$) which would be concordant with a dimeric structure involving strong hydrogen bonds between *cis*-aminogroups and carbonyl oxygens (entry 3, Tab. 2).

Differences in the spectra of **1** and **2** are also observed in the $1700–1350\,cm^{-1}$ range in which the stretching frequencies of the carboxylate group must appear. An unequivocally attribution is arduous owing to the extensive hydrogen bonding and the presence in the same spectral region of stretching vibrations of the pyrrole ring and deformation modes of the amine. However it is possible, according to comprehensive literature studies [30–39], to propose some band attributions. Thus, in compound **1**, the asymmetric ν(COO) vibration can be found at $1562\,cm^{-1}$ whereas the symmetric ones appear, combined with stretching vibrations of the pyrrole rings, at 1442 and $1390\,cm^{-1}$ [34, 35]. The medium bands at 1510 and $1462\,cm^{-1}$ can be attributed, most probably, to the ν(C=C) band and a combination of the ν(C-N) and δ(CN-H) bands [33]. The carboxylate **2** displays a similar pattern with a larger splitting of the different absorption bands due to the presence of both terminal monodentate carboxylate and terminal carboxylate engaged in strong directive hydrogen bonding. The asymmetric ν(COO) bands are located at 1608 and $1574\,cm^{-1}$, confirming the presence of two distinct carboxylate groups [32]. The symmetric ν(COO) bands, associated with stretching modes of both pyrrole and imidazole rings, can be localised, at 1414, 1436 and $1350\,cm^{-1}$. The strong absorption band noticed at $1546\,cm^{-1}$ can be attributed to the stretching mode of the double bonds [33].

The separation $\Delta\nu$, defined as $\nu_{as}(COO)$-$\nu_s(COO)$, provides some useful information on the bonding mode of the carboxylate group [37, 38, 39]. Deacon and Phillips have established, in the case of acetato compounds, some correlations between the $\Delta\nu$ values and the different modes of bonding of the carboxylato moiety found in the molecular structure: i) monodentate complexes display a greater $\Delta\nu$ than the corresponding ionic complexes, ii) chelating complexes exhibit lower $\Delta\nu$ values than the ionic compounds, and iii) bridging carboxylates give raise to $\Delta\nu$ values greater than those of chelating carboxylates and close to those found in ionic compounds. An unambiguous calculation of $\Delta\nu$ is more difficult than usually reported in the literature due to the mixing of the C-C and COO stretching modes which affords more than one symmetric ν(COO) band.[34–39] However, this

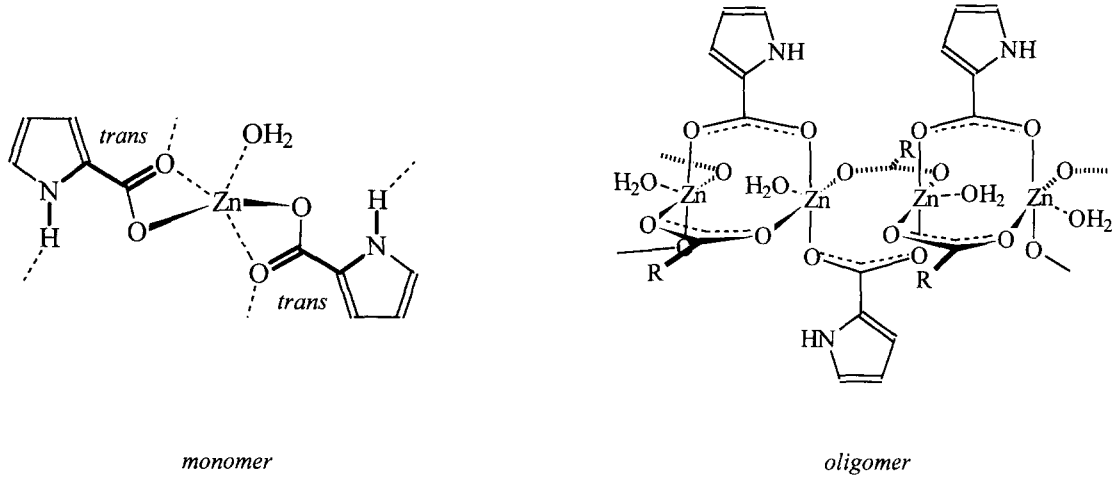

Fig. 4. Potential structures of [Zn(2-pyrrolecarboxylato)$_2$(OH_2)], **1**.

relationship can supply, at least in general terms, some information on the structure of compound **1**. The Δ value found for the compound **1** (120 cm^{-1}) is bigger than that found for the ionic sodium pyrrolecarboxylate **3** (90 cm^{-1}) and is significantly lower than the values found for the monodentate carboxylate **2** (ca. 225 and 260 cm^{-1}). This suggests for compound **1** a near-to-symmetrical bonding of the carboxylate groups to the zinc atom. Two types of solid state structure are therefore conceivable for compound **1** (Fig. 4): on one hand, a mononuclear complexe with carboxylato groups nearly bound in a chelate way such as in [$Zn(O_2CCH_3)(H_2O)_2$] [40] or, on the other hand, an oligomer presenting an O,O′-bridging mode for the carboxylato groups comparable to the bonding described for the anhydrous zinc 2-chlorobenzoate [41] and zinc crotonate [42]. The latter compound was reported to react with an N-donor base to afford low-molar-weighted oligomeric structures such as, e.g.[$Zn_2(CH_3CH=CHCO_2)_4$(quinoline)$_2$] [43]. Such a mechanism might be also conceivable in the case of the pyrrolecarboxylates **1** and **2**, the monomer **2** being the result of the fragmentation of the oligomer **1**. Without an X-ray crystal structure for compound **1** it is not possible to rule out one of these geometries. Such a structural characterisation would also define the nature of the hydrogen bonding in compound **1**, a participation of a further hydrogen bonding occurring between pendant carbonyl oxygens and water molecules cannot be excluded. This interaction can also compensate the asymmetry produced by a monodentate co-ordination of the carboxylate and can consequently decrease the Δν value [40]. More work is planned to elucidate precisely the solid state structure of compound **1** and to rationalise the dependence of the hydrogen-bonded network found in compound **2** on the nature of the present ligands.

EXPERIMENTAL

Reagents and physical measurements

2-pyrrolecarboxylic acid was purchased from Aldrich and used as received. Solvents and reagents were purified by literature methods [44]. 1-methylimidazole was distilled *in vacuo* from calcium hydride (50°C at 0.1 bar). ^1H and ^{13}C NMR data were recorded on a Bruker AC-200 NMR spectrometer. Infrared spectra were measured from KBr pellets in the range of 4000–400 cm^{-1} on a Perkin Elmer PE-16 FT-IR spectrometer. Microanalysis for carbon, hydrogen and nitrogen was carried out by the Institut für Organische und Makromolekulare Chemie of Jena.

Synthesis

Preparation of [Zn(2-Hpyrrc)$_2$.H_2O] (**1**): zinc oxide (0.5 g, 5.1 mmol) was added to a solution of 2-pyrrolecarboxylic acid (1.37 g, 12.3 mmol) in 20 ml of deionized water. The white suspension was refluxed for ca. 12 hours. The reaction mixture was cooled down to room temperature, concentrated (ca. 5 ml), filtered off and washed with acetone. The white precipitate is soluble in MeOH, Acetonitrile, THF and fairly soluble in water.

The solid was recrystallised from hot water (white needles) (1.8 g, 92%) [Zn(2-Hpyrrc)$_2$(H_2O)] Anal. Calc. for $C_{10}H_{10}N_2O_5Zn$: C, 39.55;H, 3.29; N, 9.23. Found: C, 39.37; H, 3.38; N, 9.26. Attempts to isolate singlecrystals of this hydrated carboxylate were not successful.

Spectral characterisation of 1

IR: Table 2; ^1H-NMR in THF d8, δ [ppm] (multiplicity, assignment): 11.01 (s, sharp, N-H); 6.85(s,

pyrrole H3); 6.79 (s, pyrrole H5); 6.10 (s, pyrrole H4); 4.62(s, very broad, H_2O) (The singulets at 11.01 and 4.62 ppm disappear after D_2O addition); ^{13}C-NMR, δ [ppm]: 166.30 (C=O); 126.76, 122.46, 115.30, 109.66, (respectively C2, C5, C3 and C4 of the pyrrole ring).

Preparation of [*zn*(2-*hpyrrc*)$_2$(1-methylimidazole)$_2$] (**2**):

1-methylimidazole (4 ml, 50 mmole) was added to an acetonitrile solution of compound **1** (0.5 g, 1,65 mmole). The colourless solution was refluxed for 10 minutes, filtered and allowed to stand at room temperature. Over a period of ca. 2 weeks, the solution turned slowly to red and deep red crystals suitable for an X-ray structure determination formed (0.2 g, 27%). The crystals are fairly soluble in dmso.[Zn(2-Hpyrrc)$_2$(1-methylimidazole)$_2$] Anal. Calc. for $C_{18}H_{20}N_6O_4Zn$: C, 48.07; H, 4.48; N, 18.68. Found: C, 48.03; H, 4.55; N, 18.79.

Spectral characterisation of 2

IR: Table 2; 1*H-NMR* in dmso d6, δ [ppm] (multiplicity, assignment): 11.12 (s, N-H); 8.16(s, imidazole H2); 7.29 (s, 1-Me-im. H4); 7.23 (s, 1-Me-im. H5); 6.76(s, pyrrole H3); 6.56 (s, pyrrole H5); 6.03 (s, pyrrole H4); 3.72(s, CH3); 13*C-NMR*, δ [ppm]: 166.57(-COO); 121.36, 120.11, 111.97, 108.25, (C2, C5, C3 and C4 of the pyrrole ring);139.43, 127.93, 127.45 (1-Me-im. C2, C4 and C5 sp^2), 30.74 (1-Me-im. C sp^3).

Crystallography of compound 2

X-ray diffraction data: CAD4 diffractometer using graphite-monochromated Mo-Kα radiation. The crystals were mounted in a cold nitrogen stream. Data were corrected for Lorentz and polarisation effects, but not for absorption [45]. The structure was solved by direct methods (SHELXS)[46] and refined by full-matrix least squares techniques against F_0^2 (SHELXL-93)[47]. The hydrogen atoms were located by difference Fourier synthesis and refined isotropically. Finally all non-hydrogen atoms were refined anisotropically. XP (SIEMENS Analytical X-ray Instruments, Inc.) was used for structure representations.

$C_{18}H_{20}N_6O_4Zn$, Mr = 449.77 g.mol^{-1}, monoclinic, space group $P2_1/c$, a = 9.106(1), b = 21.127(3), c = 10.468(2) Å, β = 102.70(1)°, V = 1964.6(4) Å3, Z = 4, $D_{calcd.}$ = 1.521 g.cm^{-3}, T = 183°K, λ = 0.71069 Å, μ (Mo-Kα) = 10.39 cm^{-1}, red parallelepipeds, size 0.40 × 0.38 × 0.36 mm^3, F(000) = 928, 4730 reflections in ±h, −k, +l, measured in the range 2.39° ≤ Θ ≤ 27.44°, 4488 independent reflections, R_{int} = 0.024, 2527 reflections with $F_o > 4\sigma(F_o)$, 342 parameters, R = 0.0347, wR^2 = 0.079, GOF = 1.004, largest difference peak: 0.417 e Å^{-3}.

Acknowledgements—We gratefully acknowledge the Max-Planck-Gesellschaft for financial support and for a post-doctoral fellowship (T.A.Z.).

REFERENCES

1. Inoue, S., *Makromol. Chem., Rapid Commun.* 1980, **1,** 775.
2. Soga, K., Uenishi, K. and Ikeda, S., *J. Polym. Sci.: Polym. Chem. Ed.*, 1979, **17,** 415.
3. Motika, S. A., Pickering, T. L., Rokicki, A., Stein, B. K., *US.Pat.* 5,026,676.
4. Sun, H.-N., *US.Pat.* 4,783,445.
5. Rokicki, A., *US.Pat.* 4,943,677.
6. Rebek Jr., J., *Chem. Soc. Rev.*, 1996, 255.
7. Subramanian, S. and Zaworotko, M. J., *Coord. Chem. Rev.*, 1994, **137,** 357.
8. McDonald, J. C. and Whitesides, G.M., *Chem. Rev.*, 1994, **94,** 2383.
9. Aakeröy, C. B. and Seddon K. R., *Chem. Soc. Rev.*, 1993, 397.
10. Burrows, A. D., Chan, C. W., Chowdhry, M. M., Mc Grady, J. E. and Mingos, D. M. P., *Chem. Soc. Rev.*, 1995, 329.
11. Hammershøi, A., Hartshorn, R. M. and Sargeson, A. M. M. *J. Chem. Soc., Dalton Trans.*, 1991, 621.
12. Erlenmeyer, H., Griesser, R., Prijs, B. and Sigel, H., *Helv. Chim. Acta*, 1968, **51**(2), 339.
13. Aruga, R., *Aust. J. Chem.*, 1981, **34,** 501.
14. Liserowitz, L. and Tuval, M., *Acta Cryst.*, 1978, **B34,** 1230.
15. Berkovitch-Yellin, Z. and Leiserowitz, L., *J. Am. Chem. Soc.*, 1980, **102,** 7677.
16. Hagler, A. T., Huler, E. and Lifson, S., *J. Am. Chem. Soc.*, 1974, **96,** 5319.
17. Kvick, A. and Booles, S. S., *Acta Cryst.*, 1972, **B28,** 3405.
18. Simard, M., Su, D. and Wuest, J. D., *J. Am. Chem. Soc.*, 1991, **113,** 4696.
19. Rodier, N., Ceolin, R., Plat, M. and Zumbihl, H., *Acta Cryst.*, 1990, **C46,** 324.
20. Burrows, A. D., Mingos, D. M. P., White, A. J. P. and Williams. D. J. *J. Chem. Soc., Dalton Trans.*, 1996, 3805.
21. Yukawa, Y., Yasukawa, N., Inomata, Y. and Takeuchi, T., *Bull. Chem. Soc. Jpn.*, 1985, **58,** 1591.
22. Schmidbaur, H., Bach, I., Wilkinson, D. L. and Müller, G., *Chem. Ber.*, 1988, **121,** 1441.
23. Kennard, C. H. L., Smith, G., O'Reilly, E. J., Stadnicka, K. M. and Oleksyn, B.J., *Inorg. Chim. Acta*, 1982, **59,** 241.
24. Lundberg, B. K. S., *Acta Cryst.*, 1966, **21,** 901.
25. Garret, T. P. J., Guss, J. M. and Freeman, H. C., *Acta Cryst.*, 1983, **C39,** 1027.
26. [*Zn*(2-*quinolinecarboxylato*)$_2$(1-methylimidazole)$_2$], T.A. Zevaco, H. Görls, E. Dinjus, *Inorg. Chim. Acta, in press.*.
27. Ferrari, A., Braibanti, A., Bigliardi, G. and Lanfredi, A. M., *Acta Cryst.*, 1965, **19,** 548.
28. Taylor, R., Kennard, O. and Versichel, W., *J. Am. Chem. Soc.*, 1984, **106,** 244.
29. Murray-Rust, P. and Glusker, J.P., *J. Am. Chem. Soc.*, 1984, **106,** 1018.
30. Battaglia, L. P., Bonamartini-Corradi, A., Mar-

cotrigiano, G., Menabue, L. and Pellacani, G. C., *J. Am. Chem. Soc.*, 1980, **102,** 2663.
31. Battaglia, L. P., Bonamartini-Corradi, A., Marcotrigiano, G., Menabue, L. and Pellacani, G. C., *Inorg. Chem.*, 1981, **20,** 1075.
32. Miernik, D. and Lis, T., *J. Chem. Cryst.*, 1994, **24,** 731.
33. Günzler, H. and Böck, H., *IR-Spektroskopie*, 2nd edn., p.226., VCH, Weinheim (1990).
34. Percy, G. C. and Stenton, H. S. *J. Chem. Soc., Dalton Trans.*, 1976, 2429.
35. Vansant, C., Desseyn, H. O., Tangoulis, V., Raptopoulou, C. P., Terzis, A. and Perlepes, S. P., *Polyhedron*, 1995, **14,** 2115.
36. Hodgson, J. B., Percy, G. C. and Thornton, D. A., *J. Mol. Struct.*, 1980, **66,** 81.
37. Deacon, G. B. and Phillips, R. J., *Coord. Chem. Rev.*, 1980, **33,** 227.
38. K. Nakamoto, *Infrared and Raman Spectra of Inorganic and Coordination Compounds*, 4th edn., p.231., Wiley Interscience, New York, 1986.
39. Catterick, J. and Thornton, P., *Adv. Inorg. Chem. Radiochem*, 1977, **20,** 291.
40. Van Niekerk, J. N., Schoening, F. R. L. and Talbot, J.H., *Acta Cryst.*, 1953, **6,** 720.
41. Nakacho, Y., Misawa, T., Fujiwara, T., Wakahara, A. and Tomita, K., *Bull. Chem. Soc. Jpn.*, 1976, **49,** 58.
42. Clegg, W., Little, I. R. and Straughan, B.P., *Acta. Cryst.*, 1986, **C42,** 919.
43. Clegg, W., Little, I. R. and Straughan, B. P., *J. Chem. Soc., Dalton Trans.*, 1986, 1283.
44. Perrin, D. D. and Armarego, W. L., *Purification of Laboratory Chemicals*, 3rd edn., Pergamon, New York, 1988.
45. MOLEN, An Interactive Structure Solution Procedure, Enraf-Nonius, Delft, The Netherlands, 1990.
46. Sheldrick, G. M., *Acta Cryst.*, 1990, **A46,** 467.
47. Sheldrick, G. M., University of Göttingen, Germany, 1993.

Pergamon

PII: S0277-5387(98)00043-6

Polyhedron Vol. 17, Nos 13–14, pp. 2207–2211, 1998
© 1998 Elsevier Science Ltd
All rights reserved. Printed in Great Britain
0277-5387/98 $19.00+0.00

Synthesis and structure of a two-dimensional copper(II) coordination polymer with 3,4,9,10-perylenetetracarboxylic acid and ethylenediamine

Yusaku Suenaga,[a]* Takayoshi Kuroda-Sowa,[a] Megumu Munakata[a] and Masahiko Maekawa[b]

[a] Department of Chemistry, Kinki University, Kowakae, Higashi-Osaka, Osaka 577, Japan

[b] Research Institute for Science and Technology, Kinki University, Kowakae, Higashi-Osaka, Osaka 577, Japan

(Received 24 October 1997; accepted 21 January 1998)

Abstract—The crystal and molecular structure of a dinuclear copper(II) complex with 3,4,9,10-perylenetetracarboxylic acid (H_4ptca) and ethylenediamine (en) $[Cu_2(en)_4(\mu\text{-ptca})](EtOH)_2(H_2O)_6$ has been determined by X-ray structural analysis. Each copper atom is coordinated by four nitrogen atoms of two en molecules , one oxygen atom of bridging $ptca^{4-}$ and one water molecule in an octahedral arrangement. The resulting dinuclear copper(II) complex forms two-dimensional network through intermolecular hydrogen bonds between carboxylate of $ptca^{4-}$ and the water. © 1998 Elsevier Science Ltd. All rights reserved

Keywords: copper(II) complex; 3,4,9,10-perylenetetracarboxylic acid; ethylenediamine; hydrogen-bonding network.

A unique network structure of metal complex polymer is designed by covalent bonds, some weaker intermolecular interactions such as hydrogen bonds, π–π stacking and S···S contacts. The hydrogen bonding of the interaction plays an important role in designing and creating a variety of molecular architectures for molecular self-assembly and molecular recognition in chemical, physical, and biological sciences [1]. Etter's work provides useful structural generalizations and predictive guidelines for patterns of solid-state hydrogen-bonded networks [2]. The types of hydrogen bonding in the metal complex polymer with carboxylate group can be classified as Fig. 1 and Table 1 according to their coordination environment: (A) acting as a bidentate ligand to coordinate one metal atom in the formation of four-membered chelate rings; (B) acting as a bidentate ligand to coordinate one metal atom through hydrogen bond (L = H_2O,

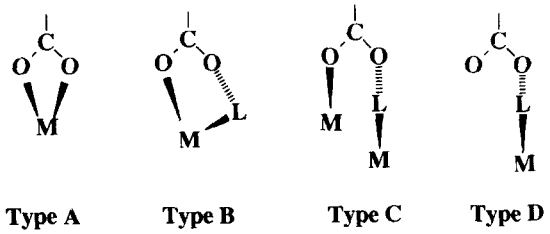

Fig. 1. Types of the hydrogen bond. Type A: bidentate ligand to coordinate one metal atom in the formation of four-membered chelate rings, Type B: bidentate ligand to coordinate one metal atom through hydrogen bond, Type C: bidentate ligand to coordinate two metal atoms through hydrogen bond, Type D: monodentate fashion through hydrogen bond.

* Author to whom correspondence should be addressed.

Table 1. Types of the hydrogen bond

Type	Metal complexes	Hydrogen bond distance (Å)		Reference
B, C	$[Ag_2\{C_6H_4(CO_2)_2\}(NH_3)_2]$	N—H···O	3.089, 3.108, 2.994	[3]
A, C	$[NH_4][Ag\{C_4H_2N_2(CO_2)_2\}]$	N···O	2.82–3.20	[3]
A, B	$M_3(BTC)_2 \cdot 12H_2O$ (M = Co, Ni, Zn)	O—H···O	2.554–3.120	[4]
C	$[\{Cu(tzq)_2(HCO_2)\}_2(\mu\text{-}HCO_2)_2] \cdot 4H_2O$	O—H···O	2.81	[5]
C	$[M(H_3TETP)](OH)_2(H_2O)_2 \cdot 3H_2O$ (M = Gd, Eu)	N···O	2.78, 2.75	[6]
A, C, D	$\{La[C_6(CO_2)_6](H_2O)_9\} \cdot 2H_2O$	O···O	2.690–2.995	[7]

BTC; 1,3,5-benzenetricarboxylic acid.
tzq; [1,2,3]triazolo[1,5-a]quinoline.
TETP; 1,4,8,11-tetrakis-(2-carboxyethyl)-1,4,8,11-tetraazacyclotetradecane.

NH_4, organic ligands); (C) acting as a bidentate ligand to coordinate two metal atoms through hydrogen bond (L = H_2O, NH_4, organic ligands); (D) acting in a monodentate fashion through hydrogen bond. (L = H_2O, NH_4, organic ligands).

In this paper, we report the crystal structure and physical properties of the copper(II) perylenetetracarboxylic acid ($ptca^{4-}$) complex with hydrogen bonding of type C and D. Our interests in two and three-dimensional polymers of metal ions interconnected by aromatic ligands with novel stereochemistry and unique physical properties led to the study of the preparation and structure determination of this complex reported herein.

EXPERIMENTAL

Preparations were performed using the usual Schlenk techniques. All solvents were dried and distilled by standard methods before use. The standard chemicals were obtained from Wako Chemical Co., Japan, and used without further purification. IR spectra were measured as KBr disks on a JASCO FT/IR-8000 spectrometer. ESR spectrum was recorded on a JES-TE200 spectrometer. UV-Vis spectrum was recorded on an Hitachi 150-20 spectrophotometer. ^1H NMR were obtained with a JEOL GSX-270 FT-NMR spectrometer at 23°C. Tetramethylsilane was used as an internal reference.

Synthesis of H_4ptca [8]

A solution of 0.85 g (15.1 mmol) of 85% potassium hydroxide in 150 ml water in a 500 ml beaker is heated to 70–80°C, and 1 g (2.6 mmol) of commercial 3,4,9,10-perylenetetracarboxylic acid dianhydride is stirred in. The pH of the resultant deep-green solution is adjusted to a value of 7 and 6N hydrochloric acid and 3N potassium hydroxide. It is treated with 5 g of decolorizing carbon and filtered. This operation is repeated. The filtrate is heated to 80–90°C and acidified with concentrated hydrochloric acid to pH 1. 3,4,9,10-perylenetetracarboxylic acid precipitates. It is separated from the hot mixture by filtration or centrifugation. It is then suspended in 500 ml of water at 90–95°C, separated by filtration, and washed successively with 300 ml of water, 300 ml of 50% ethanol, and 300 ml of 90% ethanol. After being dried at 80°C/2 mm Hg in a vacuum oven, the 3,4,9,10-perylenetetracarboxylic acid weighs 0.7 g (64%). It does not melt by 300°C.

IR data (KBr, 4000–400 cm^{-1}): 3445 (m broad), 3001 (m, broad), 2658 (m, broad), 1695 (s), 1435 (m), 1396 (w), 1371 (w), 1284 (s).

Anal. Calcd for $C_{24}H_{12}O_8$: C, 67.3; H, 2.8%, Found: C, 67.6; H, 2.5%.

Preparation of metal complex

Crystals of $[Cu_2(en)_4(\mu\text{-}ptca)](EtOH)_2(H_2O)_6$ suitable for single crystal X-ray analysis were obtained by reaction of $Cu(CH_3COO)_2$ (5 mM) and H_4ptca (10 mM) in an en/water (1/5) aqueous solution (8 ml); the pH of the solution was unadjusted. The mixture was stirred and then filtered. The filtrate and the diffusion solvent, EtOH, were sealed in a glass tube and after standing for one week at room temperature, brown plate crystals were obtained.

IR data (KBr, 4000–400 cm^{-1}): 3304 (s), 3215 (s), 3138 (s), 2964 (m), 1591 (s), 1560 (s), 1412 (m), 1385 (m), 1352 (s), 1043 (m).

X-ray structure determination

Crystal data. $C_{18}H_{32}N_4CuO_8$, M = 496.02, monoclinic, space group $P2_1/c$, $a = 8.538(2)$, $b = 11.361(2)$, $c = 23.019(3)$ Å, $\beta = 97.60(2)°$, $V = 2213.1(6)$ Å^3, $Z = 4$, $D_c = 1.488$ g/cm^3, $\lambda(Mo\text{-}K_\alpha) = 0.71069$ Å, $\mu = 10.34$ cm^{-1}, $F(000) = 1044.00$.

A single crystal of dimensions $0.20 \times 0.20 \times 0.30$ mm was mounted with paraffin on a thin glass fibre. Intensity data were measured on a Rigaku AFC-5R four-circle diffractometer by an ω-2θ scan at 23°C and

Table 2. Crystallographic data for $[Cu_2(en)_4(\mu\text{-ptca})](EtOH)_2(H_2O)_6$

Empirical formula	$C_{18}H_{32}N_4CuO_8$
Formula weight	496.02
Color; habit	Brown, plate
Crystal size (mm)	$0.20 \times 0.20 \times 0.30$
Crystal system	Monoclinic
Space group	$P2_1/c$
Unit cell dimensions	
a (Å)	8.538(2)
b (Å)	11.361(2)
c (Å)	23.019(3)
β (°)	97.60(2)
V (Å^3)	2213.1(6)
Z	4
Density (calc.) (g cm^{-3})	1.488
$F(000)$	1044.00
λ (Å)	0.71069 (Mo–K_α)
μ (cm^{-1})	10.34 (Mo–K_α)
Scan method	ω–2θ
Scan speed (° min^{-1})	8
2θ range (°)	$0.89 + 0.30 \tan\theta$
No. reflections measured	5697 (total), 5349 (unique)
No. observed reflections	2785 ($I = 3\sigma(I)$)
R	0.063
R_w	0.076

were corrected for Lorentz and polarization effects. Empirical absorption corrections were applied. A total of 5697 reflections for which $2\theta_{max} = 55.0°$ were collected. Of these data 5349 were unique.

The structure was solved by the direct method (MITHRIL) [9] and refined anisotropically for non-hydrogen atoms by block diagonal least-squares calculations. Reliability factors are defined as $R = \Sigma(F_o - F_c)\Sigma F_o$ and $R_w = \{\Sigma w(F_o - F_c)^2 \Sigma w F_o^2\}^{1/2}$, where $w = 4F_o^2\sigma(F_o^2)$. Atomic scattering factors and anomalous dispersion terms were taken from the *International Tables for X-ray Crystallography*, Vol. IV [10]. All calculations were performed on a micro VAX computer using the TEXSAN crystallographic software package [11]. The final R and R_w values are 0.063 and 0.076, respectively. The details of the X-ray data collection, structure solution and refinement, a full set of bond lengths and angles, thermal parameters, and complete F_c and F_o tables are available from authors.

RESULTS AND DISCUSSION

The final atomic coordinates for non-hydrogen atoms and equivalent thermal parameters are given in Table 3; selected bond lengths and bond angles in Table 4, respectively. Figure 2 shows the perspective view and atom labeling scheme of a segment of the structure.

The molecule has a distorted octahedral geometry about the central copper atom. The carboxylic oxygen

Table 3. Atomic coordinates and isotropic thermal parameters for non-hydrogen atoms in $[Cu_2(en)_4(\mu\text{-ptca})](EtOH)_2(H_2O)_6$

Atom	x	y	z	B(eq)
Cu(1)	0.76087(9)	0.54267(7)	0.70639(4)	3.35(2)
O(1)	1.0866(5)	0.3490(4)	0.7045(2)	4.1(1)
O(2)	0.8608(5)	0.3873(4)	0.6465(2)	3.7(1)
O(3)	0.8121(5)	0.1653(4)	0.7145(2)	3.9(1)
O(4)	0.5750(5)	0.2142(4)	0.6670(2)	4.4(1)
O(5)	0.3535(5)	0.2211(4)	0.7452(2)	4.3(1)
O(6)	0.7208(6)	0.0512(5)	0.8072(2)	5.4(1)
O(7)	0.519(1)	0.1348(9)	0.0673(5)	13.3(3)
O(8)	0.775(2)	0.191(2)	−0.0484(9)	27.7(8)
N(1)	0.9079(6)	0.4957(5)	0.7789(2)	3.3(1)
N(2)	0.6015(6)	0.4399(5)	0.7377(3)	3.8(1)
N(3)	0.9147(7)	0.6628(5)	0.6803(3)	4.3(1)
N(4)	0.6134(7)	0.5911(6)	0.6350(3)	5.0(2)
C(1)	0.819(1)	0.4222(9)	0.8147(4)	6.9(3)
C(2)	0.652(1)	0.4225(10)	0.7985(4)	7.7(3)
C(3)	0.832(1)	0.725(1)	0.6314(6)	11.1(4)
C(4)	0.694(2)	0.679(1)	0.6038(5)	11.0(4)
C(5)	1.0221(7)	0.2328(5)	0.6187(3)	2.8(1)
C(6)	1.1666(7)	0.2415(6)	0.5992(3)	3.4(2)
C(7)	1.2117(7)	0.1681(6)	0.5552(3)	3.4(2)
C(8)	1.1090(7)	0.0860(5)	0.5285(3)	2.6(1)
C(9)	0.9558(6)	0.0724(5)	0.5474(2)	2.3(1)
C(10)	0.8475(7)	−0.0107(5)	0.5191(2)	2.4(1)
C(11)	0.6979(7)	−0.0199(6)	0.5363(3)	3.1(1)
C(12)	0.6574(7)	0.0483(6)	0.5832(3)	3.2(1)
C(13)	0.7612(7)	0.1263(5)	0.6128(3)	2.7(1)
C(14)	0.9124(7)	0.1456(5)	0.5939(2)	2.5(1)
C(15)	0.9843(8)	0.3297(5)	0.6604(3)	3.1(1)
C(16)	0.7128(7)	0.1752(6)	0.6690(3)	3.1(2)
C(17)	0.831(3)	0.077(2)	−0.028(1)	21.8(9)
C(18)	0.692(3)	0.055(2)	0.001(1)	21.2(9)

atom and aqua-oxygen atom occupy the axial positions while the equatorial plane is formed by four nitrogen atoms of two en molecules. The greatest deviations from ideal octahedral geometry are found for the O(2)—Cu—O(5*) angle of 171.7(2)° and Cu—O(2) and Cu—O(5*) distances of 2.461(4), 2.568(4) Å, respectively. The coordination mode of $ptca^{4-}$ is of special interest. Among the four carboxylate groups of $ptca^{4-}$, two form coordination bonds to different copper atoms as a bidentate, respectively (type C, O—H···O 2.760 Å), and the remaining groups form hydrogen bonds to water molecules coordinated with copper atoms, (type D, O—H···O 2.779 Å). All the hydrogen bond distances of O—H···O, Table 5, are as expected [7]. The total result of this hydrogen-bonding gives rise to two-dimensional infinite arrangement. However, the close distances between perylenes is 10.75 Å, indicative of negligible interactions of π–π stacking due to the long separations. The molecular packing of this complex is shown in Fig. 3. Interatomic distances and angles of $ptca^{4-}$ are within the range of values previously

Table 4. Selected bond lengths (Å) and bond angles (°) for $[Cu_2(en)_4(\mu\text{-ptca})](EtOH)_2(H_2O)_6$

Cu(1)—O(2)	2.461(4)	Cu(1)—O(5*)	2.568(4)
Cu(1)—N(1)	2.024(5)	Cu(1)—N(2)	1.998(5)
Cu(1)—N(3)	2.039(5)	Cu(1)—N(4)	2.011(6)
O(1)—C(15)	1.267(8)	O(2)—C(15)	1.246(7)
O(3)—C(16)	1.263(8)	O(4)—C(16)	1.253(7)
O(8)—C(17)	1.43(3)		
O(2)—Cu—O(5*)	171.7(2)	O(2)—Cu—N(1)	92.8(2)
O(2)—Cu—N(2)	94.9(2)	O(2)—Cu—N(3)	91.7(2)
O(2)—Cu—N(4)	88.0(2)	O(5*)—Cu—N(1)	94.6(2)
O(5*)—Cu—N(2)	89.3(2)	O(5*)—Cu—N(3)	84.1(2)
O(5*)—Cu—N(4)	84.6(2)		

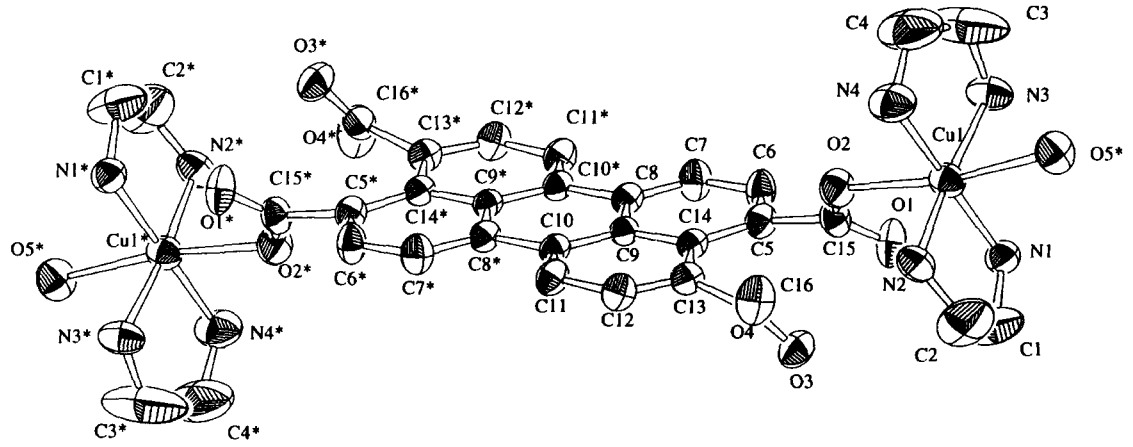

Fig. 2. ORTEP view of the Cu-ptca complex.

Table 5. Hydrogen bond distances Å

O(1)···O(5*)	2.760(7)	O(4)···O(5*)	2.779(6)

reported for perylene [12]. The benzene ring is planar with the maximum deviation of 0.0207 Å. Each plane of the carboxylate group is twisted out of the plane of the benzene ring ca 50°.

These twists and deviations might be due to the repulsion of the oxygen atoms of the adjacent carboxylate groups, and also to the formation of the hydrogen-bonding network, as was discussed. The C—O distances in the present compound, ranging from 1.246 Å–1.267 Å, are not significantly different compared with those in M_3 (1,3,5-benzenetricarboxylic acid)$_2 \cdot 12H_2O$ (M = Co, Ni, Zn) complex [4].

The IR spectrum of the free H_4ptca molecule shows the C=O stretching band at 1695 cm^{-1}. Upon coordination with copper(II), this frequency shifts to 1591 and 1560 cm^{-1}. This indicates ionic coordination between copper(II) cation and $ptca^{4-}$ anion. Also, the N—H stretching band of en is shown at 3304, 3215, and 3138 cm^{-1}. The O—H broad stretching band is shown in range from 3360–3100 cm^{-1}. These data clearly show the formation of the complex and hydrogen-bonding. The solid state electronic spectrum of the complex has three bands at ca 422 nm, 443 nm, and 485 nm, and in comparison, free H_4ptca molecule shows a maximum at ca 500 nm with a broad slope in visible region. This shift of UV-Vis spectrum of the complex may be attributable to the ionic coordination and the hydrogen bond formation between $ptca^{4-}$ and water molecules. ESR spectrum for the crystal sample was measured at room temperature which shows a typical signal pattern for a monomeric copper(II) complex, indicative of negligible interactions of copper(II)-copper(II) due to the long separations of the metal ions (Cu—Cu distance 7.65 Å).

Electrical resistivity of compacted pellets was measured by the conventional two-probe technique. Although the complex behave as a semiconductor with conductivity of 4.6×10^{-5} S cm^{-1}, electrical resistivity of the complex increased with time and finally changed an insulator. This may mean that conductivity mechanism is ionic mechanism.

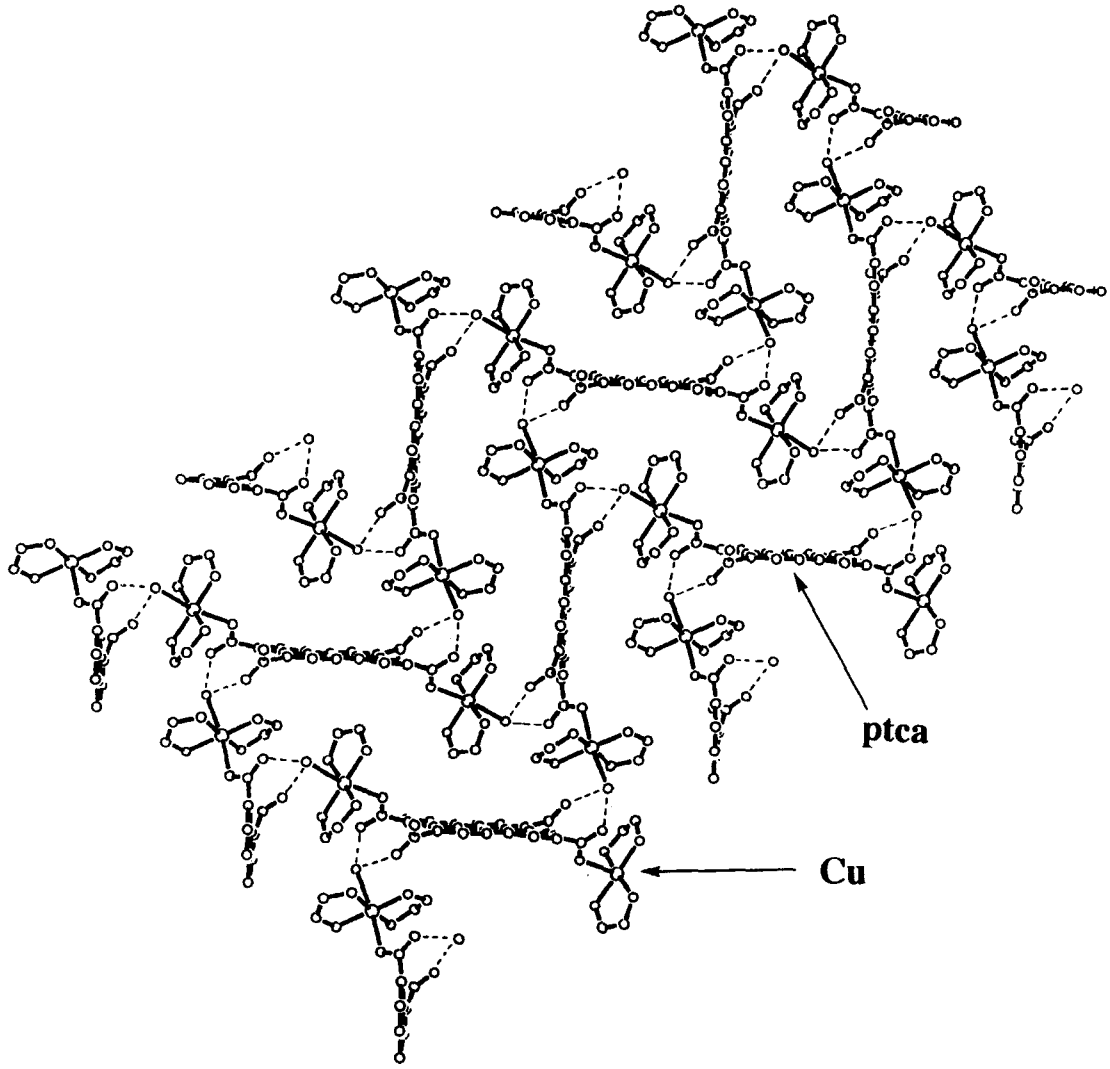

Fig. 3. Molecular structure of $[Cu_2(en)_4(\mu\text{-ptca})](EtOH)_2(H_2O)_6$ assembled by O—H···O hydrogen-bonds.

Acknowledgements—The authors thank Ms M. Sunagawa, Ms A. Shimada and Mr T. Ohno for their assistance with the X-ray measurements.

REFERENCES

1. (a) Nakasuji, K., Sugiura, K., Kitagawa, T., Toyoda, J., Okamoto, H., Okaniwa, K., Mitani, T., Yamamoto, H., Murata, I., Kawamoto, A. and Tanaka, J., *J. Am. Chem. Soc*, 1991, **113,** 1862; (b) Oshio, H., Watanabe, T., Ohta, A., Ito, T. and Masuda, H., *Inorg. Chem.*, 1996, **35,** 472.
2. Etter, M. C., *Acc. Chem. Res.*, 1990, **23,** 120.
3. Smith, G., Reddy, A. N., Byriel, K. A. and Kennard, H. L., *J. Chem. Soc., Dalton Trans.*, 1995, 3565.
4. Yaghi, O. M., Li, H. and Groy, T. L., *J. Am. Chem. Soc.*, 1996, **118**(38), 9096.
5. Escriva, E., Server-Carrio, J., Lezama, L., Folgado, J. V., Piazarro, J. R., Ballesteros, R. and Abarca, B., *J. Chem. Soc., Dalton Trans.*, 1997, 2033.
6. Lecomte, C., Dahaoui-Gindrey, V., Chollet, H., Gros, C., Mishra, A. K., Barbette, F., Pullumbi, P. and Guilard, R., *Inorg. Chem.*, 1997, **36,** 3827.
7. Wu, L. P., Munakata, M., Yamamoto, M., Kuroda-Sowa, T. and Maekawa, M., *J. Coord. Chem.*, 1996, **37,** 361.
8. Org. Synth. V, 813.
9. *MITHRIL*, an integrated direct method computer program, University of Glasgow, Gilmore, C. J., *J. Appl. Crystallogr.*, 1984, **17,** 42.
10. *International Tables for X-Ray Crystallography*, Kynoch Press, Birmingham, 1974, Vol. 4.
11. *TEXSAN-TEXRAY*, Structure Analysis Package, Molecular Structure Corporation, The Woodlands, TX, 1985.
12. Schmitt, R. D., Wing, R. M. and Maki, A. H., *J. Am. Chem. Soc.*, 1969, **91**(16), 4394.

Pergamon

PII: S0277-5387(98)00053-9

Polyhedron Vol. 17, Nos 13–14, pp. 2213–2224, 1998
© 1998 Elsevier Science Ltd
All rights reserved. Printed in Great Britain
0277-5387/98 $19.00+0.00

Conformational studies of 5′-deoxyadenosyl-13-epicobalamin, a coenzymatically active structural analog of coenzyme B_{12}

Kenneth L. Brown,[a]* Shifa Cheng[a] and Helder M. Marques[b]*

[a]Department of Chemistry, Ohio University, Athens, Ohio 45701, U.S.A.

[b]Centre for Molecular Design, Department of Chemistry, University of the Witwatersrand, P.O. Wits, 2050 Johannesburg, South Africa

(Received 15 January 1998; accepted 19 January 1998)

Abstract—5′-Deoxyadenosyl-13-epicobalamin(Ado-13-epiCbl) is a coenzymatically active structural analog of coenzyme B_{12} (5′-deoxyadenosylcobalamin, AdoCbl) in which epimerization at the corrin ring C13 places the *e* propionamide side chain in an "upwardly" axial position. This would seem to bring the *e* side chain into direct steric contact with the adenosyl (Ado) moiety in its normal "southern" conformation (with the purine above the C ring) seen in the solid state for AdoCbl. Molecular mechanics calculations show that this conformation is the global minimum for AdoCbl, but that three other conformations represent local minima, including a "western", a "northern", and an "eastern" conformation, the last of which is known to be populated at room temperature from NMR studies. A structure for Ado-13-epiCbl has been generated by molecular dynamics/simulated annealing calculations starting from the neutron diffraction coordinates for AdoCbl after epimerization at C13. Molecular mechanics calculations on the resulting structure show that a "western" conformation is the global minimum, but that three other conformations, a "northern", an "eastern", and a "northeastern", are of relatively low energy and separated by relatively low energy barriers. The traditional "southern" conformation does not appear as a local energy minimum and is some 6 kcal mol^{-1} destabilized relative to the global minimum due to geometric distortions to relieve steric strain. Two-dimensional homonuclear NMR experiments show extraordinary conformational flexibility in Ado-13-epiCbl with 21 NOE crosspeaks between Ado protons and non-Ado protons, 50% more than in AdoCbl itself. Together with the calculated geometries for the four Ado-13-epiCbl conformers, these data suggest that at least three, and possibly all four of the conformers are populated at room temperature, in contrast to AdoCbl, in which only the "southern" and "eastern" conformers are populated under these conditions. Considering the enzymology of Ado-13-epiCbl, the inaccessibility of its "southern" conformation, and the activity of other AdoCbl analogs structurally modified in the Ado moiety, it is suggested that it may well be the "eastern" conformation, accessible to both AdoCbl and Ado-13-epiCbl, which is enzymatically active. © 1998 Elsevier Science Ltd. All rights reserved

Keywords: Vitamin B_{12}; cobalamin; coenzyme B_{12}; conformation; NMR; molecular modeling.

The means by which 5′-deoxyadenosylcobalamin (AdoCbl)[1]-requiring enzymes "activate" this coenzyme (Fig. 1) by catalyzing the homolytic dissociation of its carbon-cobalt bond by as much as 10^{12}-fold (or higher) [2–6] remains an outstanding problem in vitamin B_{12} biochemistry of keen interest to chemists and biochemists alike. One of the most interesting, and potentially informative, aspects of coenzyme B_{12} enzymology is the fact that at least some AdoCbl-requiring enzymes† are quite promiscuous in terms of using structurally modified analogs of AdoCbl as active coenzymes. Thus, a number of AdoCbl analogs modified at the corrin ring side chains [8–12], on the

* Authors to whom correspondence should be addressed.

† It now appears [7] that AdoCbl-requiring enzymes will fall into two classes, one of which (apparently including the enzymes that catalyze carbon-skeleton rearrangements) shows much more stringent structural requirements for the coenzyme than the other.

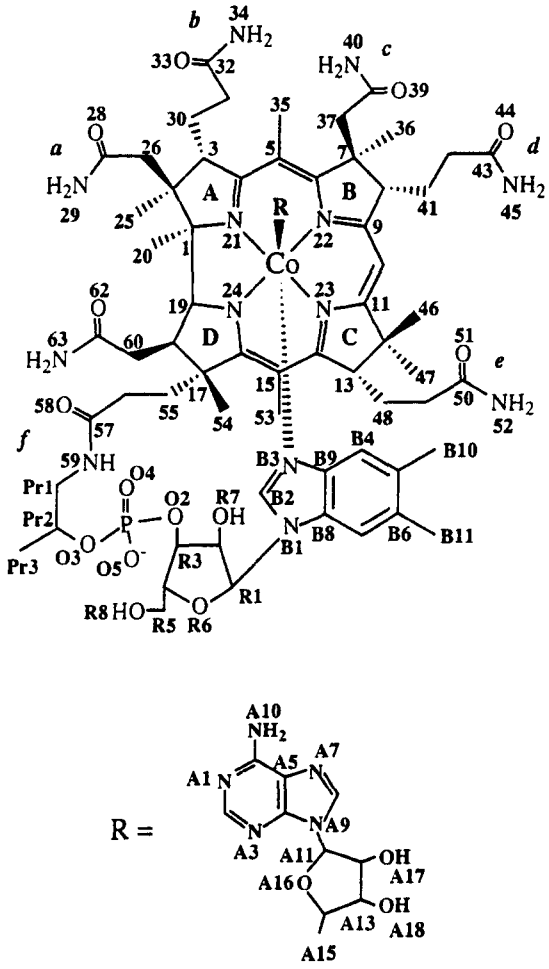

Fig. 1. Structure and numbering scheme of AdoCbl. In Ado-13-epiCbl, epimerization at C13 places the *e* propionamide side chain in an "upwardly" axial position.

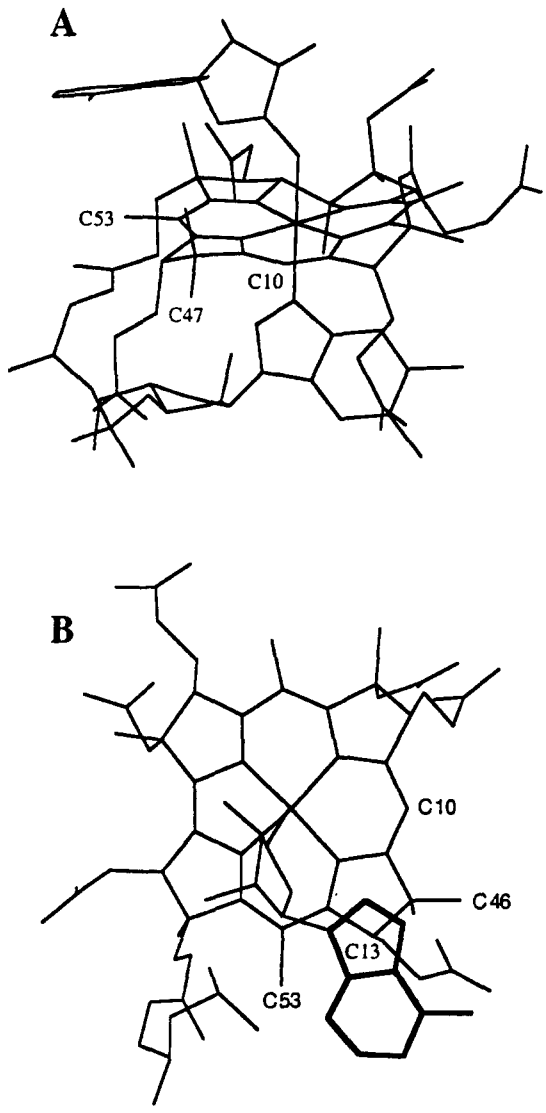

Fig. 2. A. Line drawing of the neutron diffraction structure of AdoCbl (reference 13a) showing the disposition of the adenosine moiety from the "eastern" perspective. B. Top-down view of the same structure of AdoCbl showing the adenine moiety in the "southern" conformation. The axial Bzm ligand has been removed for clarity.

corrin ring itself [13, 14], in the nucleotide loop [8, 15, 16], and in the adenine moiety itself [8, 17–19], are active coenzymes (although others are not), albeit with reduced coenzymic activity. These active analogs potentially have much to tell us about the mechanism(s) by which the B_{12}-requiring enzymes "activate" AdoCbl.

One of the most intriguing of the active AdoCbl analogs is the C13 epimer, Ado-13-epiCbl (Fig. 1), in which the *e* propionamide side chain adopts an "upwardly" axial configuration. This is the case because of certain peculiarities of the structure of AdoCbl. In all of the available crystal structures of AdoCbl [20–25], the conformation of the adenosyl moiety with respect to the remainder of the complex is as shown in Fig. 2. In this universal conformation, the five-membered ribose ring is roughly perpendicular to the corrin macrocycle, pointing towards C15, while the adenine purine is nearly parallel to the corrin ring and deployed over its "southern" quadrant. Molecular mechanics calculations [26–28] have shown, however, that while this "southern" conformation is indeed the global minimum, rotation about the Co–C bond leads to three other reasonably stable local minimum conformations in which the adenine is in the "eastern," "northern," or "western" quadrants. While earlier NMR data [29] had led to the proposal that an "eastern" conformations was, in fact, populated at room temperature, subsequent NMR work [28] showed that the "northern" and "western" conformations could only be populated at elevated temperatures as predicted by the molecular mechanics calculations.

In the 13-epicorrinoids [30, 31], epimerization at

C13 leads to twisting of the C pyrrol ring and an "upwardly" axial disposition of the *e* propionamide side chain, as seen in the X-ray crystal structures of CN-13-epiCbl [32, 33] and in the molecular mechanics calculations of this structure [26]. Since in the global minimum "southern" conformation of AdoCbl, the five-membered ring of the adenine moiety lies directly above the corrin ring C13 (Fig. 2B), it seems highly unlikely that Ado-13-epiCbl can adopt a "southern" conformation. If this is correct, the fact that Ado-13-epiCbl is a partially active coenzyme [14] would seem to suggest that a specific conformation of the Ado moiety relative to the remainder of the cobalamin is not required for catalytic activity. However, studies with AdoCbl analogs modified in the Ado moiety [17–19] suggest that this cannot be correct. This important work shows that the A7 ring nitrogen and the exocyclic primary amino group (A10) of the Ado moiety are essential for catalytic activity in diol dehydrase [18, 19], implying that these groups are specific association points with the enzyme active site, presumably via hydrogen bonding.

The coenzymic activity of Ado-13-epiCbl thus presents a potential dilemma, if it is indeed unable to adopt a normal "southern" conformation. Unfortunately, despite over a year of effort, Ado-13-epiCbl has stubbornly refused to crystallize, preventing an X-ray diffraction study. We have consequently performed the NMR and molecular mechanics study of Ado-13-epiCbl reported below, to address the issue of the conformation of this intriguing AdoCbl analog and confront the question of the importance of Ado conformation and coenzymic activity thus raised.

EXPERIMENTAL

CN-13-epiCbl[30, 31] was prepared from CNCbl and dry trifluoroacetic acid in the presence of 5% (v/v) trifluoroacetic anhydride as previously described [34]. 5′-Deoxy-5′-chloroadenosine was prepared from adenosine by the method of Kikugawa and Ichino [35]. Ado-13-epiCbl was prepared as follows. CN-13-epiCbl (100 mg, 0.074 mmol) was dissolved in 20 mL of 10% NH_4Cl solution. After purging with argon for 60 min, excess Zn wool, freshened by briefly stirring in 1.0 N HCl, was added and the reduction to 13-epicob(II)alamin was allowed to proceed for 60 min. In the dark, an excess of 5′-deoxy-5′-chloroadenosine in deaerated methanol was added, and the alkylation reaction was allowed to proceed overnight. After desalting on Amberlite XAD-2 and purification by HPLC [36–38], Ado-13-epiCbl was obtained in 85% yield (99.1 mg, 0.063 mmol).

NMR spectra were obtained using a Varian Unity Inova 500 MHz NMR spectrometer equipped with pulsed field gradients and operating at 499.899 MHz (^{1}H) and 125.709 MHz (^{13}C). The sample contained 20 mM Ado-13-epiCbl and TSP as an internal reference in 90% H_2O/10% D_2O. All NMR data was collected in the hypercomplex phase-sensitive mode except the HMBC data which were presented in absolute value mode. Data for the TOCSY experiments with watergate solvent suppression were collected into $2K \times 512$ data matrices using 32 scans per t_1 increment, preceded initially by 8 dummy scans. The sweep width was 5400 Hz and the spin-lock field strength was 8.8 kHz. The total spin lock period was 10, 20, or 70 ms. The data matrices were zero filled to $4K \times 4K$ and apodized with a shifted Gaussian function. The data for the watergate ROESY spectra were collected into a $3K \times 512$ data matrix with 64 scans per t_1 increment preceded initially by 64 dummy scans. The sweep width was 5400 Hz, the mixing time was 200 ms, and the spin-lock field strength was 2.5 kHz. The data matrix was zero filled to $4K \times 4K$ and apodized with a shifted Gaussian function. Data for the phase sensitive gradient enhanced HMQC spectrum were collected into a $4K \times 512$ data matrix using 32 scans, preceded initially by 64 dummy scans, over sweep widths of 9115 Hz (^{1}H) and 25,000 Hz (^{13}C). The matrix was zero filled to $4K \times 4K$ and apodized with a shifted Gaussian function. Data for the HMBC experiment were collected into a $2K \times 256$ data matrix using 128 scans, preceded initially by 8 dummy scans, using sweep widths of 5400 Hz (^{1}H) and 37,709 Hz (^{13}C) and a 1.0 s presaturation pulse. A 55 ms transfer delay and an 80 ms homospoil pulse were employed. The matrix was zero filled to $4K \times 4K$ and processed with a shifted Gaussian function.

We have previously described [26] a set of parameters for use with a modified version of the molecular mechanics (MM^1) program MM2(87) [39, 40] for modeling the cobalt corrinoids. We have recently begun to make increasing use of the version of MM2 available in the HYPERCHEM suite of programs and referred to as MM+ [41] because of the visualization graphics capabilities missing from Allinger's original program. The potential energy functions used in MM+ are virtually identical to those used in MM2, but metal ions are handled with a "points on a sphere" model [42]. We have modified [43] our original parameter set [26] to take this into account.

All calculations were performed using MM+ and the force field parameters for the cobalt corrinoids [43] on a 200 MHz PC. Geometry optimizations were carried out using a conjugate-gradient algorithm with a convergence criterion of 0.01 kcal mol^{-1} Å^{-1} r.m.s.d. in the gradient. The steric barriers to rotation of the alkyl ligand in AdoCbl were examined by driving the Co-bound alkyl ligand through 360° in steps of 5° with the starting coordinates those of the neutron diffraction structure of the coenzyme [21]. The dihedral angle, ω_1, chosen for this purpose was the N24-Co-A15-A14 angle, and rotation was performed both in a clockwise and counter-clockwise direction. At each value of ω_1, a full energy minimization was performed, and the structure with the lowest strain energy found at each value of ω_1 was chosen.

To study the possible conformations of Ado-13-

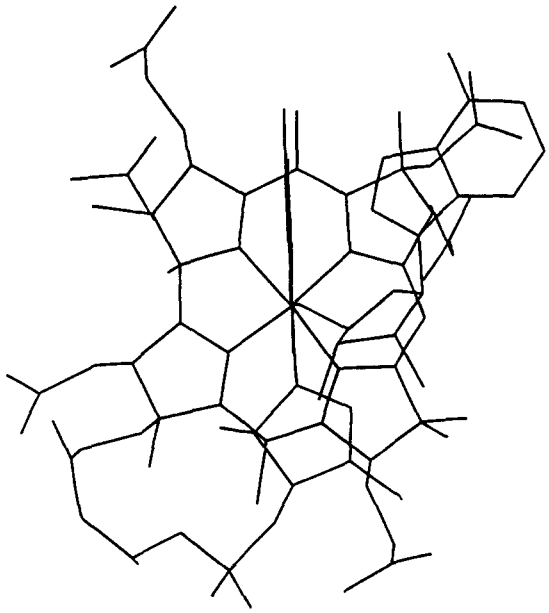

Fig. 3. Line drawing ("top" down perspective) of the structure of Ado-13-epiCbl calculated by the MD/SA procedure described in the text.

epiCbl, in which the *e* side chain at C13 has been epimerized from the lower (α) face to the upper (β) face of the corrin ring, the entire *e* side chain of the neutron diffraction structure of AdoCbl was moved from the lower to the upper face and the C13 proton was moved from the upper to the lower face using the molecular structure editing facilities of HYPERCHEM. The C ring was energy minimized, and the entire structure was then subjected to the following MD/SA procedure: heat from 300 K to 1000 K in 2 ps; run for 20 ps; cool from 1000 K to 300 K over 10 ps; full energy minimization. The annealed structure (Fig. 3) has the Ado ligand over the northeast corner of the corrin ring. This structure was then used as the starting structure for the rotational strain energy profile investigation of the Ado ligand, performed as described above for AdoCbl.

RESULTS

NMR assignments of Ado-13-epiCbl

The ^{1}H and ^{13}C NMR spectra of Ado-13-epiCbl were assigned (Table 1) using the now standard battery of homonuclear and heteronuclear 2D NMR experiments and assignment strategies detailed elsewhere [44, 45], except that the order of resonances in a given spin system was determined using a TOCSY experiment with a decreased spin-lock period (10 or 20 ms instead of 70 ms) rather than a COSY experiment.

The use of pulsed-field gradient solvent suppression in the homonuclear NMR experiments on an aqueous (10% D_2O) sample permits the observation and assignment of the resonances of the exchangeable amide hydrogens. These resonances were assigned from their proximity to ring and side chain hydrogens revealed in the ROESY spectrum using the assignment strategies previously employed for cobalt corrinoids in DMSO-d_6 [46–48]. Absolute assignment of the primary amide *syn* and *anti* protons could be made on the basis of stronger NOE cross peaks from the adjacent methylene protons to the *anti* proton than to the *syn* proton [49, 50]. For each amide except the *d* side chain amide, the *anti* proton was found to be the more downfield member of each pair of coupled amide protons. For the *d* amide, this order was reversed, and the chemical shifts of the *syn* and *anti* protons were much closer together than for the other amides, as is also the case for other Cbls in water [50]. No NOE crosspeaks were found for the *e* amide *syn* proton so it was assigned to the resonance at 6.81 ppm based on a correlation between this signal and that of the *e* amide *anti* proton in the TOCSY spectrum (and an anti-phase Hartmann-Hahn effect cross peak in the ROESY spectrum).

The ^{13}C NMR spectrum of Ado-13-epiCbl is similar to that of AdoCbl [33, 51] but with significant differences around the C pyrrol ring and elsewhere, as shown in **1**, below. By far the largest difference occurs for the C46 and C47 *gem* methyls attached to C12. In AdoCbl, these two resonances occur at 23.9 and 34.2 ppm based on HMQC correlations to ^{1}H signals showing NOE connectivities to C13H [51]. The more downfield ^{13}C resonance has been assigned [51] to the upwardly axial [21–24] C46 methyl group based on its HMBC correlation to C13H which is more strongly coupled to C46 due to their *cis* relationship. The equatorial [21–24] C47 is gauche to C13H and lacks an HMBC correlation to this proton. In addition, the ^{1}H resonance of the group assigned to the equatorial C47 has NOE cross peaks to one of the C48 protons and to the C49 protons, while the ^{1}H resonance of the group assigned to the axially upward C46 methyl lacks these, but has NOE correlations with the Ado protons on A11 and A14. In Ado-13-epiCbl, an HMBC correlation to C13H is seen only for the more downfield methyl at 33.4 ppm. In addition, the protons having an HMQC correlation to this carbon have no NOE correlations to the now upwardly pseudoaxial *e* side chain C48 and C49 methylene protons. However, the protons of an upfield methyl carbon at 23.2 ppm have NOE crosspeaks to both of the C48 methylene protons and to the A2 and A8 Ado protons. Hence, the ^{13}C chemical shifts of the C46 and C47 methyls are interchanged in Ado-13-epiCbl relative to AdoCbl, and the C46 resonance is now shifted upfield due to steric crowding by the C48 methylene.

Surprisingly, there is little difference between the ^{13}C chemical shifts of C13 in AdoCbl and Ado-13-epiCbl; the latter is very close to the chemical shift of C13 in CN-13-epiCbl [33]. Other differences seen in **1**

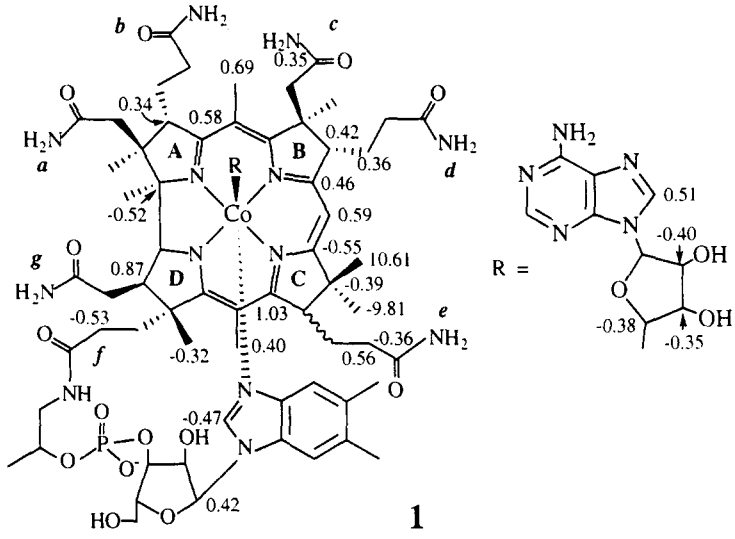

1

$\delta_{AdoCbl} - \delta_{Ado\text{-}13\text{-}epiCbl}$

include some quite remote from the site of epimerization and extending into the "northern" hemisphere, as was also the case with CN-13-epiCbl [33]. These differences might be associated with a larger corrin ring fold angle in the C13 epimer as seen in the X-ray structures of CN-13-epiCbl [33] and CNCbl [52]. In addition, there are several significant chemical shift differences between Ado-13-epiCbl and AdoCbl in the Ado moiety.

Molecular modeling of ado-13-epicbl

The variation in strain energy with rotation of the Ado ligand in AdoCbl was re-examined using the modified force field parameter set [43]. The results are given in Fig. 4 and are very similar to those obtained previously [26–28] except (i) the eastern (E) conformation is better defined; (ii) the position of the Ado ligand in the northern (N) conformation has been shifted in a clockwise direction by about 30°; and (iii) the western (W) conformation is somewhat higher in energy than before ($\triangle$E, the difference in energy between the western conformation and the global minimum found, the southern (S) conformation, is 3.8 kcal mol^{-1}, previously 1.8 kcal mol^{-1}).

The strain energy profile for rotation of the Ado ligand in Ado-13-epiCbl is shown in Fig. 5. The lowest energy structure has the Ado ligand over the western quadrant of the molecule, nestled above and between the *g* and *a* side chains. A large energy barrier separates this from the eastern conformation, where the Ado ligand's five membered ring is over C10. A small energy barrier separates the eastern from a northeastern conformation (NE) with Ado over C7, and another small barrier leads to the northern conformation in which the Ado is somewhat to the left of C5 when viewed from above.

We have previously shown [27] that there are 32 structures, each with a particular set of orientations of the side chains, which account for $\gtrsim$99.9% of the population of an alkylcobalamin at 300 K. The alkyl ligand in Ado-13-epiCbl was set to, but not constrained to, each of the four lowest energy conformations identified in the strain energy profile (Fig. 5), and the complex was energy-minimized in each of the 32 lowest energy side chain conformations. A Boltzmann distribution was then performed over all such energy-minimized conformations at 300 K. Those conformations with $\gtrsim$0.1% of the population were taken to be significant, and the Co–C bond length and Co–C–C bond angle determined as a population-weighted average; the values found were Co–C = 2.040(17) Å and Co–C–C = 126.8(2.7)°. For comparison, the same technique applied to AdoCbl gave Co–C = 2.039(18) Å and Co–C–C = 123.3(1.0)° (while the solid state values [21] are 2.039 Å and 120.7°, respectively).

The nucleotide loop in the structure of Ado-13-epiCbl obtained from the MD/SA procedure (Fig. 3) is in a different conformation to that in AdoCbl (Fig. 2) [20–24]. We have recently shown in our NOE-restrained MD/SA calculations on the solution structure of CNCbl [53] that a range of conformations is accessible to the nucleotide loop. These range from an "outward" conformation where the *f* side chain orientation is such that the O58 carbonyl oxygen lies beneath C60 and points outward, towards the southwest, the phosphate is beneath and somewhat

Table 1. ^{1}H and ^{13}C NMR Assignments for Ado-13-epiCbl [a]

Group	$\delta 13_C$, ppm	$\delta 1_H$, ppm	Group	$\delta 13_C$, ppm	$\delta 1_H$, ppm
C53	17.59	2.51	A11	90.67	5.66
C35	17.77	2.44	C10	96.80	5.82
C25	19.43	1.38	C15	106.94	
C54	19.60	1.24	C5	108.22	
C36	21.19	1.68	B7	113.00	7.20
Pr3	21.45	1.26	B4	120.90	6.24
B11	21.86	2.22	A5	121.47	
B10	22.09	2.22	B8	132.97	
C20	23.03	0.48	B5	133.89	
C46	23.23	1.42	B6	136.26	
A15	27.20	0.93, 1.82	B9	140.63	
C41	28.07	0.83, 1.77	A8	142.92	7.98
C30	28.92	2.01, 2.13	B2	144.75	7.07
C48	30.10	1.72, 1.79	A4	151.19	
C47	33.40	1.27	A2	155.46	8.20
C55	34.09	2.20, 2.52	A6	158.22	
C60	34.38	2.64	C14	165.79	
C42	34.42	0.83, 1.75	C6	166.02	
C56	34.70	1.83, 2.44	C9	172.32	
C49	37.20	2.46, 2.53	C38	177.24	
C31	37.84	2.50, 2.57	C57	177.66	
C18	41.40	2.65	C11	177.83	
C37	45.05	1.62, 2.07	C4	177.86	
C26	45.61	2.48, 2.66	C61	178.60	
Pr1	47.67	3.09, 3.59	C16	178.66	
C2	49.07		C27	179.01	
C12	49.49		C43	179.79	
C7	52.74		C32	180.67	
C13	55.22	3.32	C50	181.13	
C8	56.64	3.25	R7		5.54
C3	57.79	4.17	$d\mathrm{H_A}$		6.29
C17	60.78		$d\mathrm{H_S}$		6.44
R5	63.01	3.81, 3.97	$c\mathrm{H_S}$		6.76
R2	71.60	4.42	$e\mathrm{H_S}$		6.81
Pr2	75.33	4.41	$b\mathrm{H_S}$		6.88
A12	75.54	4.52	$g\mathrm{H_S}$		7.03
R3	75.65	4.66	$a\mathrm{H_S}$		7.12
C19	76.34	4.38	$c\mathrm{H_A}$		7.44
A13	76.46	3.98	$b\mathrm{H_A}$		7.61
R4	83.87	4.13	$e\mathrm{H_A}$		7.65
R1	88.57	6.28	$g\mathrm{H_A}$		7.84
A14	88.57	2.42	$a\mathrm{H_A}$		7.85
C1	88.57		*f*H		8.19

[a] In 90% H_2O/10%D_2O, 25°C. Chemical shifts are relative to internal TSP. The *syn* and *anti* amide H's are designated $a\mathrm{H_S}$, $a\mathrm{H_A}$, $b\mathrm{H_S}$, $b\mathrm{H_A}$, etc., respectively, where *a*, *b*, etc., refer to the standard side chain lettering.

between C17 and C53, and the ribose R4 is beneath C14, close to the C ring, to an "inward" conformation in which the O58 carbonyl oxygen points to the southeast, towards C53 and the *e* side chain, the phosphate is tucked in below C57, and the ribose R4 is beneath C53. Although the "outward" nucleotide loop conformation, calculated here for Ado-13-epiCbl, is somewhat unusual as far as the solid state structures of Cbls are concerned, it is not without precedent. Fig. 6 shows two views of the superposition (at the D ring) of 15 Cbl crystal structures. Fourteen of these have the nucleotide loop in the "inward" conformation, but one, the recently reported 10-chloro-aquacobalamin structure [54] (bold line), has the "outward" conformation, demonstrating that Cbls can crystallize in this nucleotide loop conformation. Our calculations [54] show that there is little energy difference between these conformations.

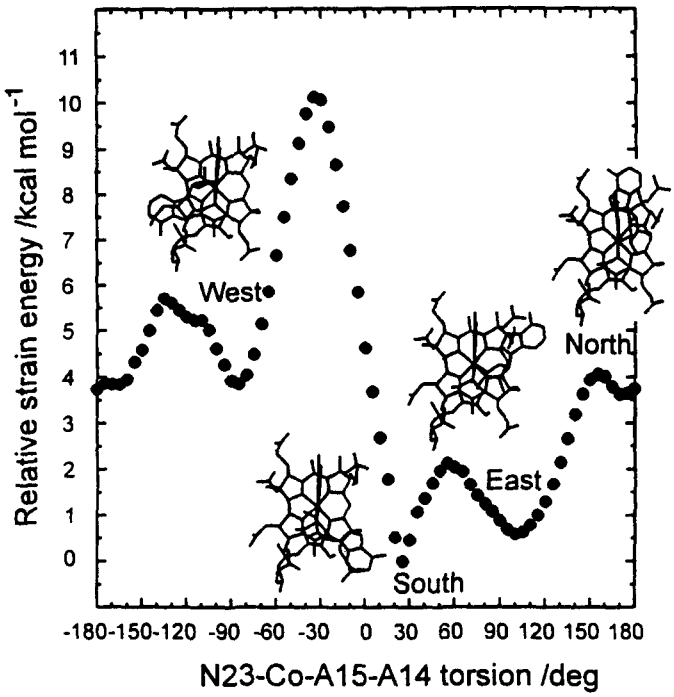

Fig. 4. Strain-energy profile for rotation of the Ado ligand of AdoCbl about the Co–C bond by driving the N24-Co-A15-A14 torsion angle. Line drawings of energy-minimized structures of each of the local minima are also shown.

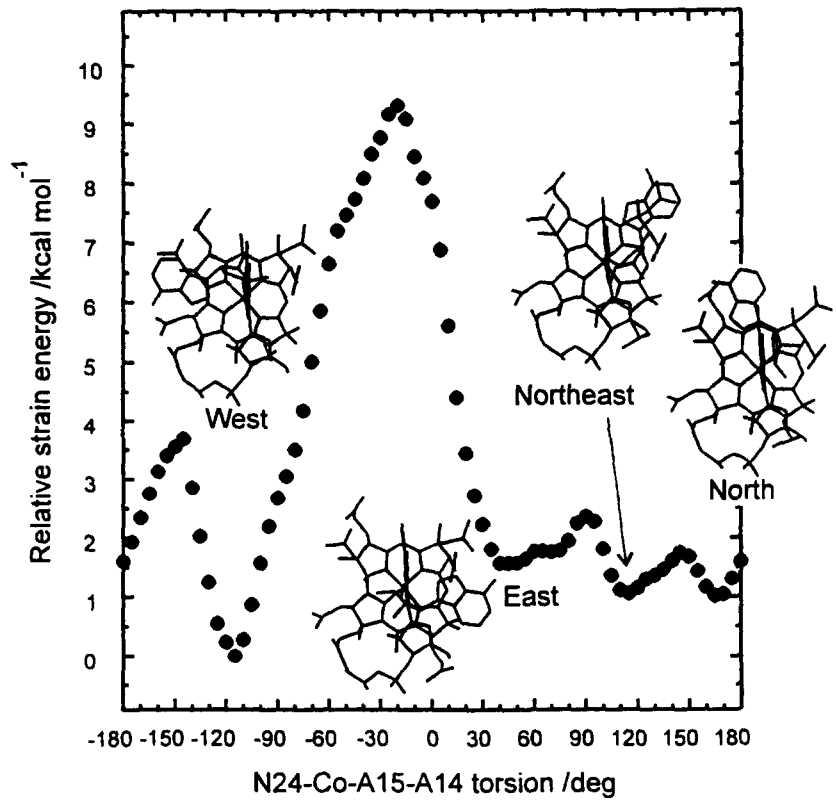

Fig. 5. Strain-energy profile for rotation of the Ado ligand of Ado-13-epiCbl about the Co–C bond by driving the N24-Co-A15-A14 torsion angle. Line drawings of energy-minimized structures of each of the local minima are also shown.

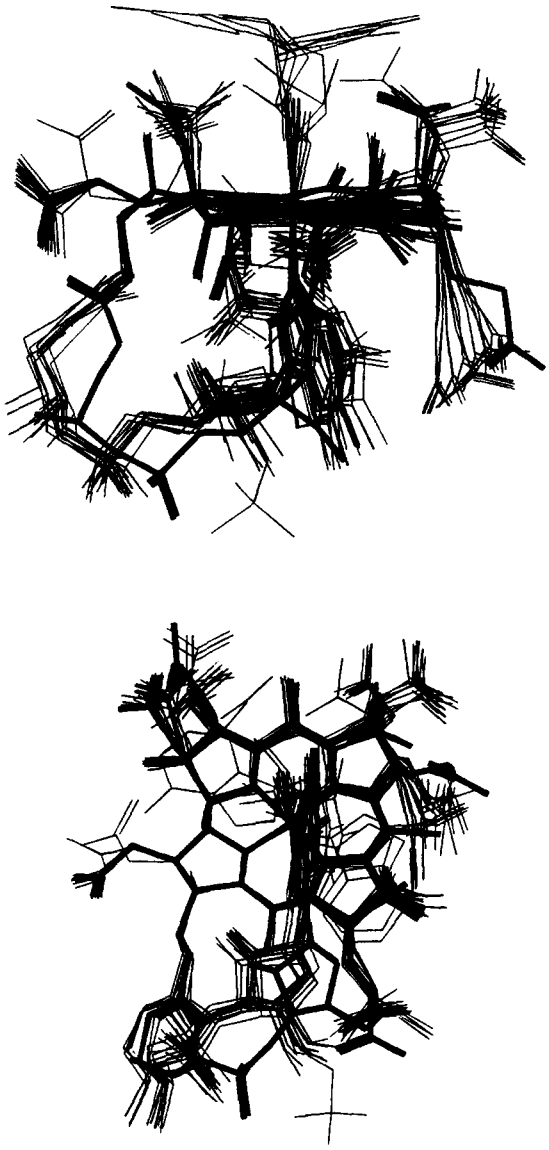

Fig. 6. Superposition (at the D ring) of 15 solid state structures of cobalamins showing that most adopt the "inward" nucleotide loop conformation, but one, 10-chloro-aquacobalamin(bold line) adopts the "outward" nucleotide loop conformation (see text).

Table 2. NOEs Between Ado Protons and Non-Ado Protons in Ado-13-epiCbl and Calculated Interproton Distances for the Four Ado-13-epiCbl Conformers

	Distance, Å[a]			
NOE	West	East	Northeast	North
A15″-C37″	5.47	**3.59**	**3.60**	4.84
A15″-C37′	**4.68**	**2.36**	**3.39**	4.97
A15′-C19	**3.62**	**2.43**	**1.95**	**2.68**
A14-C10	5.37	6.26	**4.06**	**3.60**
A13-C46	**4.31**	5.20	4.90	**4.48**
A13-C26′	4.98	**3.52**	**3.95**	**4.07**
A11-C54	7.41	5.13	8.31	8.96
A11-C37″	5.58	5.97	**3.13**	**2.84**
A11-C37′	4.87	7.42	**4.26**	**2.32**
A11-C48″	7.04	**2.44**	**4.45**	6.70
A11-C46	7.71	**3.39**	**3.01**	5.68
A11-C49′	9.54	**4.77**	6.30	6.59
A11-C26′	**3.01**	6.98	6.91	5.08
A8-C54	**4.42**	7.12	7.48	6.34
A8-C46	6.06	**4.25**	5.96	6.53
A8-C37″	6.75	**3.92**	**3.80**	5.49
A8-C37′	6.33	**3.08**	**4.39**	5.98
A8-C26″	5.30	6.38	5.48	**3.85**
A8-C26′	**4.40**	5.16	**4.09**	**3.03**
A2-C26″	**4.58**	11.73	11.47	8.23
A2-C46	11.84	**3.63**	7.14	10.25

[a]Distance between the indicated hydrogen in the energy-minimized molecular mechanics structures. For methyl and methylene protons, the closest distance is given. Distances $\lesssim$4.8 Å are shown in boldface.

NMR analysis of Ado-13-epiCbl conformation

Table 2 shows the NOEs observed at 500 MHz between Ado and non-Ado protons for Ado-13-epiCbl at 25°C, along with the calculated inter-proton distances for each NOE in each of the four stable conformations. These data are extraordinary in that many more such NOEs (21) are observed for Ado-13-epiCbl than could be observed (9 at 500 MHz [29], 12 at 600 MHz [26], for 14 total [28]) for AdoCbl itself. Assuming that at the current field strength, observation of an NOE requires an inter-proton distance of less than about 4.8 Å, only a single NOE, A11-C54, is not accounted for by the current calculations. This NOE is most likely due to the eastern conformation if the inter proton distance for this conformation is slightly shorter than the current calculations suggest. Many of the observed NOEs are compatible with two or more of the calculated conformations. However, importantly, three NOEs (A11-C49′, A8-C46, and A2-C46) are compatible only with the eastern conformation, three (A11-C26′, A8-C54, and A2-C26″) are compatible only with the western conformation, and one (A8-C26″) is compatible only with the northern conformation.

DISCUSSION

The largest differences in ^{13}C chemical shift between Ado-13-epiCbl and AdoCbl occur at the C46 and C47 methyls, which generally appear near 34 and 22 ppm, respectively, in the normal cobalamins. The upfield displacement of the ^{13}C resonance of the equatorial C47 methyl in the normal Cbl's has been attributed [33] to steric crowding [55–58] by the pseudoaxially downward *e* side chain. In the 13-epicorrinoids, these *gem* dimethyl substituents are displaced by the epimerization at C13, so that C46 becomes equatorial

and *gauche* to C13H and C47 becomes downwardly axial and *cis* to C13H [32, 33]. Consequently, it is the equatorial C46 which is sterically crowded by the now pseudoaxially upward *e* side chain, so that its ^{13}C resonance is shifted to high field.

The strain energy profile for rotation of the Ado ligand about the Co–C bond in Ado-13-epiCbl (Fig. 5) predicts four conformations of relatively similar energy, with a western conformation as the global minimum. There is a local minimum at $\omega_1 = 40°$, quite close to the value ($\omega_1 = 25°$) for the global minimum southern conformation for AdoCbl (Fig. 4). However, care must be exercised in comparing Figs 4 and 5. Although the southern conformation of AdoCbl and the eastern conformation of Ado-13-epiCbl appear to be close on the ω_1 axis, the orientations of the Ado ligands are quite different. In AdoCbl, the southern conformation has the Ado ligand over the C ring (as it is in the crystal structures [20–25] while in the eastern conformation of Ado-13-epiCbl, the imidazole ring of the Ado ligand lies over C10 (Fig. 5). Hence, the ω_1 dihedral angle is not necessarily a definitive indicator of the position of the Ado ligand when *different* structures are compared. This is due to flexibility in the Ado ligand itself. Thus, the N24-Co-A15-A14, Co-A15-A14-A16, and A15-A14-A16-A11 torsion angles in the southern conformer of AdoCbl and the eastern conformer of Ado-13-epiCbl are 25° and 40°, 72° and 84°, and 156° and 132°, respectively. This type of internal flexibility in the Ado ligand is responsible for the different disposition of the adenine moiety in the southern conformation of AdoCbl and the eastern conformation of Ado-13-epiCbl, despite the similarity of the ω_1 values for these two conformations. The conformation of Ado-13-epiCbl in which the adenine moiety is in the same position over the C ring as in the southern conformation of AdoCbl occurs at $\omega_1 \approx 10°$, and is consequently some 6 kcal mol^{-1} higher in energy than the global minimum conformation (Fig. 5). In this truly southern conformation of Ado-13-epiCbl, there is considerable distortion to relieve steric contacts with the upwardly-projecting *e* side chain. The Co–C–C bond angle increases to 131.4°, the Co–C bond angle lengthens to 2.084 Å, the C ring becomes planar, and both C46 and the *e* side chain are forced downward into pseudo-equatorial positions. Thus, the conformation of Ado-13-epiCbl in which the adenine has the same spatial orientation as that in AdoCbl is a highly distorted structure due to steric repulsions between the *e* side chain and the adenine.

NOE crosspeaks between Ado protons and protons elsewhere in the molecule in homonuclear 2D NOE spectra have been used to infer conformation in AdoCbl [28, 29]. The original analysis of these NOE's by Bax, *et al* [29], led to the discovery of an eastern conformation for AdoCbl, populated at room temperature, since several NOEs between Ado and non-Ado protons were incompatible with the southern conformation of the neutron diffraction structure [21]. Subsequent NMR studies at elevated temperatures [28] revealed additional NOE's which were incompatible with both the southern and eastern conformations of AdoCbl, and suggested that the northern, and possibly the western conformations could be populated as well at elevated temperatures.

For Ado-13-epiCbl, there are far more NOE's between Ado and non-Ado protons observed at room temperature, and many of these are compatible only with comformations other than the global minimum western conformation (Table 2). We conclude that Ado-13-epiCbl is substantially more conformationally flexible than AdoCbl with respect to the disposition of the Ado ligand. Evidently at least three of the conformations (eastern, western, and northern) are populated at room temperature, and, judging from the rotational strain energy profile (Fig. 5), most likely all four of the conformers contribute significantly at ordinary temperature. These results strongly suggest that while Ado-13-epiCbl is a highly conformationally mobile molecule, it cannot adopt the well-known southern conformation associated with AdoCbl in the solid state [20–25] and in solution [26–28]. Thus, the known catalytic activity of this AdoCbl analog [14] raises important questions regarding the conformation of the catalytically active species at the enzyme active site, and, indeed, even the importance of AdoCbl conformation to activity.

One possible explanation for the coenzymic activity of Ado-13-epiCbl is that the enzyme enforces a catalytically active southern conformation on this analog, using binding energy to overcome the substantial steric strain inherent in this conformation for Ado-13-epiCbl. Studies of vitamin B_{12} binding proteins show that proteins are capable of binding cobalamins extraordinarily tightly, with the release of as much as 23 kcal mol^{-1} of binding free energy [59–63]. However, AdoCbl-requiring enzymes bind AdoCbl many orders of magnitude less tightly.* Consequently, substantial binding energy may well be available for ground state distortion of the coenzyme.

The loss of AdoCbl-enzyme binding energy upon epimerization at C13 can be estimated using Fersht's work on the thermodynamics of the association of substrate analogs with enzymes and of substrates with mutant enzymes [67–69] and Toraya's data [14] for the activity of Ado-13-epiCbl with diol dehydrase. The value of $\triangle\triangle G_b = -RT \ln [(k_{cat}/K_m)_{Ado\text{-}13\text{-}epiCbl}/(k_{cat}/K_m)_{AdoCbl}]$ for diol dehydrase is then 2.7 kcal mol^{-1}. The MM calculations described above suggest

* For instance, the K_m for AdoCbl with the diol dehydrase of *Aerobacter aerogenes* [9] is 0.99 μmM, so that $K_b < 1.0 \times 10^6$ M^{-1} and $-\triangle G^\circ_b < 8.2$ kcal mol^{-1}, and the K_m for AdoCbl with the methylmalonylCoA mutase of *Propionibacterium shermanii* is 3.5×10^{-8} M [64, 65] so that $K_b < 2.9 \times 10^7$ M^{-1} and $-\triangle G^\circ_b < 10.2$ kcal mol^{-1}. For the ribonucleotide reductase of *Lactobacillus leichmanii*, the maximum binding constant for AdoCbl in the presence of the allosteric effector dGTP, is 5×10^3 M^{-1} ($\triangle G^\circ_b = -3.1$ kcal mol^{-1}) [66].

that this binding energy difference is insufficient to overcome the steric energy strain and enforce a traditional southern conformation on Ado13-epiCbl, for which this conformation is about 6 kcal mol^{-1} higher in energy than the global minimum conformation.

It is anticipated that Cbl side chain amide functionalities represent important hydrogen bonding contacts for the association of Cbls with proteins, since it is hard to imagine that the binding of CNCbl to haptocorrin could release nearly 23 kcal of free energy [63] without extensive hydrogen bonding contacts utilizing the side chain amides. The two existing X-ray structure determinations of the binding pockets of Cbl-requiring enzymes [70, 71], both show evidence of extensive hydrogen bonding to side chain amides, including, in one case, multiple H-bonded contacts to the *e* side chain. Unfortunately, in the X-ray structure of the methylmalonylCoA-AdoCbl complex [71], the Ado ligand is missing, so that important questions regarding AdoCbl conformation at an enzyme active site cannot be answered directly from this structure. Nonetheless, displacement of the *e* side chain amide from its normal position in the epimerized Ado-13-epiCbl must be expected to result in the loss of hydrogen bonding contacts. Thus, the 2.7 kcal mol^{-1} loss in binding energy to diol dehydrase upon *e* side chain epimerization, roughly the amount expected for two hydrogen bonds [72], is most likely attributable to the placement of the *e* side chain in an unnatural position in which hydrogen bonding amino acid residues are not available. Consequently, diol dehydrase is unlikely to force Ado-13-epiCbl into a southern conformation and such an enzyme-induced conformational change is unlikely to explain the catalytic activity of this coenzyme analog.

A second possibility to account for the coenzymic activity of Ado-13-epiCbl is that the disposition of the Ado moiety in AdoCbl is not important in enzyme catalysis. However, this would seem to contradict work with coenzyme analogs altered in the Ado moiety [8, 17–19], which suggest that specific interactions of the enzymes with specific structural features of the Ado ligand are essential for activity. Thus, Toraya and coworkers report that A1-deaza-AdoCbl and A3-deaza-AdoCbl (Fig. 1) are partially active coenzymes for diol dehydrase (56% and 46% as active as AdoCbl, respectively), but A7-deaza-AdoCbl and A10-*N*,*N*-dimethyl-AdoCbl are completely inactive competitive inhibitors [18, 19]. Yakusheva and coworkers have reported that A10-*N*-monomethyl-AdoCbl is a partially active coenzyme for the glycerol dehydrase of *Aerobacter aerogenes* with 12% of the activity of AdoCbl [8]. The most straightforward interpretation of these results is that the A7 endocyclic nitrogen and the A10 exocyclic amino group represent essential points of hydrogen bonding contacts with the enzyme and that the latter acts as a donor in two hydrogen bonds. Presumably, the atom substitutions at A1 and A3 in A1-deaza- and A3-deaza-AdoCbl alter the pK_a's at the A7 and A10 sites, lowering the strength of the essential hydrogen bonds, but not abolishing activity. If this interpretation is correct, then a specific conformation of the coenzyme is required at the active site to bring the essential A7 and A10 hydrogen bonding functionalities into juxtaposition with the putative active site amino acid residues which are their hydrogen bonding partners. This line of reasoning argues strongly against the possibility of conformational promiscuity accounting for the coenzymic activity of Ado-13-epiCbl.

It thus may be necessary to conclude that the traditional southern conformation of AdoCbl, always found in the solid state and calculated to be the global minimum, cannot be the coenzymatically active conformation at the enzyme active site. Since both molecular modeling and NMR studies show that an eastern conformation is of reasonably low energy and populated at ordinary temperatures for both AdoCbl and Ado-13-epiCbl, it is possible that it is the eastern conformation of AdoCbl which is the enzymatically active one. It is consequently most unfortunate that the recent X-ray crystal structure determination of methylmalonylCoA mutase [71] failed to reveal the Ado moiety of the bound coenzyme,* as it seems likely that only through such structural studies can this question be definitively answered.

Acknowledgements—This research was supported by the National Institute of General Medical Sciences, Grant GM 48858 (KLB), the Foundation for Research Development, Pretoria, South Africa, and the University of the Witwatersrand (HMM).

REFERENCES

1. Abbreviations: AdoCbl, 5'-deoxyadenosylcobalamin (coenzyme B_{12}); Ado-13-epiCbl, 5'-deoxyadenosyl-13-epicobalamin; CNCbl, cyanocobalamin (vitamin B_{12}); CN-13-epiCbl, cyano-13-epicobalamin (neovitamin B_{12}); Bzm, 5,6-dimethylbenzimidazole; MM, molecular mechanics; MD, molecular dynamics; SA, simulated annealing.
2. Finke, R. G. and Hay, B. P., *Inorg. Chem.*, 1984, **23,** 3041.
3. Finke, R. G. and Hay, B. P., *Inorg. Chem.*, 1985, **24,** 1278.
4. Hay, B. P. and Finke, R. G., *J. Am. Chem. Soc.*, 1986, **108,** 4820.
5. Hay, B. P. and Finke, R. G., *J. Am. Chem. Soc.*, 1987, **109,** 8012.

* However, it should be pointed out that methylmalonylCoA mutase belongs to the class of AdoCbl-requiring enzymes that have stringent structural requirements for the coenzyme [7]. The possibility that this enzyme, and the other mutases, has different conformational requirements for AdoCbl conformation and different mechanisms of coenzyme activation than the dehydrases and the AdoCbl-dependent ribonucleotide reductases is quite real.

6. Brown, K. L., Cheng, S., Zubkowski, J. D. and Valente, E.J., *Inorg. Chem.*, 1997, **36,** 1772.
7. Buckel, W. Paper presented at the 4th European Symposium on Vitamin B_{12} and B_{12}-Proteins, Sept. 2–6, 1996, Innsbruck, Austria.
8. Yakusheva, M. I., Poznanskaya, A. A., Pospelova, T. A., Rudakove, I. P., Yurkevich, A. M. and Yakovlev, V. A., *Biochim. Biophys. Acta.*, 1977, **484,** 216.
9. Toraya, T., Krodel , E., Mildvan, A. S. and Abeles, R. H., *Biochemistry.*, 1979, **189,** 417.
10. Morley, C. G. D., Blakley, R. L. and Hogenkamp, H. P. C., *Biochemistry.*, 1968, **7,** 1231.
11. Anton, D. L., Tsai, P. K. and Hogenkamp, H. P. C., *J. Biol. Chem.*, 1980, **255,** 4507.
12. Toraya, T. and Fukui, S., *Adv. Chem. Ser.*, 1980, **191,** 139.
13. Tamao, T., Morikawa, Y., Shimizu, S. and Fukui, S., *Biochim. Biophys. Acta.*, 1968, **151,** 260.
14. Toraya, T., Shirakashi, T., Fukui, S. and Hogenkamp, H. P. C., *Biochemistry* , 1975, **14,** 3949.
15. Toraya, T. and Ishida, A., *J. Biol. Chem.*, 1991, **266,** 5430.
16. Toraya, T., Miyoshi, S., Mori, M. and Wada, K., *Biochim. Biophys. Acta.*, 1994, **1204,** 169.
17. Sando, G. N., Blakley, R. L., Hogenkamp, H. P. C. and Hoffman, P. J., *J. Biol. Chem.*, 1975, **250,** 8774.
18. Ushio, K., Fukui, S. and Toraya, T., *Biochim. Biophys. Acta*, 1984, **788,** 318.
19. Toraya, T., Matsumoto, T., Ichikawa, M., Itoh, T., Sugawara, T. and Mizuno, Y., *J. Biol. Chem.*, 1986, **261,** 9289.
20. Lenhert, P. G., *Proc. R. Soc. London.*, 1968, **A303,** 45.
21. Savage, H. F. J., Lindley, P. F., Finney, J. L. and Timmins, P. A., *Acta Cryst.*, 1987, **B43,** 280.
22. Savage, H., *Biophys. J.*, 1989, **50,** 947.
23. Bouquiere, J. P., Finney, J. L., Lehman, M. S., Lindley, P. F. and Savage, H. F. J., *Acta Cryst.*, 1993, **B49,** 79.
24. Bouguiere, J. P., Finney, J. L. and Savage, H. F. J., *Acta Cryst.*, 1994, **B50,** 566.
25. Bouquiere, J. P., *Physica B.*, 1992, **180 & 181,** 745.
26. Marques, H. M. and Brown, K. L., *J. Mol. Struct. (Theochem).*, 1995, **340,** 97.
27. Marques, H. M. and Brown, K. L., *Inorg. Chem.*, 1995, **34,** 3733.
28. Brown, K. L. and Marques, H. M., *Polyhedron*, 1996, **13,** 2187.
29. Bax, A., Marzilli, L. G. and Summers, M. F., *J. Am. Chem. Soc.*, 1987, **109,** 566.
30. Bonnett, R., Godfrey, J. M., Math, V. B., Edmond, E., Evans, H. and Hodder, O. J. R., *Nature*, 1971, **229,** 473.
31. Bonnett, R., Godfrey , J. M. and Math, V. B., *J. Chem. Soc. C.* 3736., 1971, **0,** 3736.
32. Stoeckli-Evans, H., Edmond, E. and Hodgkin, D. C., *J. Chem. Soc., Perkin Trans* 2., 1972, **0,** 605.
33. Brown, K. L., Evans , D. R., Zubkowski, J. D. and Valente, E. J., *Inorg. Chem.*, 1996, **35,** 415.
34. Brown, K. L., Zou, X. and Evans, D. R., *Inorg. Chem.*, 1994, **33,** 5713.
35. Kikugawa K. and Ichino, M. *Tetrahedron Lett.*, 1971, 87.
36. Jacobsen, D. W., Green, R. and Brown, K. L., *Methods Enzymol.*, 1986, **123,** 4.
37. Brown, K. L. and Zou, X., Salmon, L., *Inorg. Chem.*, 1991, **30,** 1949.
38. Brown, K. L., Salmon, L. and Kirby, J. A., *Organometallics.*, 1992, **11,** 422.
39. Allinger, N. L., *J. Am. Chem. Soc.*, 1979, **99,** 8127.
40. Allinger, N. L., Yuh, Y., MM2(87), distributed to academic users by QCPE, under special agreement with Molecular Design Ltd., San Leandro, CA.
41. HYPERCHEM, Version 4.5, Hypercube Ltd., 419 Phillip Street, Waterloo, ON, N2L 3X2, Canada.
42. Hay, B. P., *Coord. Chem. Rev.*, 1993, **126,** 177.
43. Marques, H. M., Warden, C., Monye. M., Shongwe M. S. and Brown, K. L., *Inorg. Chem.*, in press.
44. Brown, K. L., Zou, X., Savon, S. R. and Jacobsen, D. W., *Biochemistry*, 1993, **32,** 8421.
45. Brown, K. L., Zou, X., Wu, G.-Z., Zubkowski, J. D. and Valente, E. J., *Polyhedron.*, 1995, **14,** 1621.
46. Brown, K. L., Brooks, H. B., Gupta, B. D., Victor, M., Marques, H. M., Scooby, D. C., Goux, W. J. and Timkovich, R., *Inorg. Chem.*, 1991, **30,** 3430.
47. Brown, K. L. and Zou, X., *J. Am. Chem. Soc.*, 1993, **115,** 1478.
48. Brown, K. L. and Evans, D. R., *Inorg. Chem.*, 1993, **32,** 2544.
49. Kratky, C., Fäber, G., Gruber, K., Wilson, K., Dauter, Z., Nolting, H.-F., Konrat, R. and Kräutler, B., *J. Am. Chem. Soc.*, 1995, **117,** 4654.
50. Brown , K. L. and Zou, X., *Magn. Reson. Chem.*, 1997, **35** , 889.
51. Summers, M. F., Marzilli, L. G. and Bax, A., *J. Am. Chem. Soc.*, 1986, **108** , 4285.
52. Kräutler, B., Konrat, R., Stupperich, E., Fäber, G., Gruber, K. and Kratkey, C., *Inorg. Chem.*, 1994, **33** , 4128.
53. Marques, H. M., Hicks, R. P. and Brown, K. L., *Chem. Commun.*, 1996, **0,** 1427.
54. Brown, K. L., Cheng, S., Zubkowski, J. D., Valente, E. J., Knapton, L. and Marques, H. M., *Inorg. Chem.*, 1977, **36,** 3666.
55. Grant, D. M. and Cheney, B. V., *J. Am. Chem. Soc.*, 1967, **89,** 5315.
56. Cheney, B. V. and Grant, D. M., *J. Am. Chem. Soc.*, 1967, **89,** 5319.
57. Schneider, H.-J., Price, R. and Keller, T., *Angew. Chem., Int. Ed. Engl.*, 1971, **10,** 730.
58. Breitmaier E. and Voelter, W., Carbon-13 NMR Spectroscopy; VCH, Weinheim, Germany (1989).
59. Nexø, E., Hansen M. R. and Olesen, H., in Vitamin B_{12}; Edited by B. Zagalak and W. Friedrich) deGruyter, Berlin (1979); pp 851-854. .
60. Nexø, E. and Olesen, H., *Biochim. Biophys. Acta.*, 1981, **667,** 370.
61. Nexø E. and Olesen, H. in B_{12}; (Edited by D. Dolphin), Vol. 2. Wiley, New York, (1982); pp 57–85 and 87–104.
62. Newmark, P. A., Green , R., Musso, A. M. and Mollin, D. L., *Br. J. Haematol.*, 1973, **25,** 359.
63. Marchaj, A., Jacobsen, D. W., Savon, S. R. and Brown, K. L., *J. Am. Chem. Soc.*, 1995, **117,** 11640.

64. Overath, P., Stadtman, E. R., Kellerman, G. M. and Lynen, F., *Biochem. Z.*, 1962, **336,** 77.
65. Kellermeyer, R. W., Allen, S. H. G., Stjernholm, R. and Wood, H. G., *J. Biol. Chem.*, 1964, **239,** 2562.
66. Singh, D., Tamao, Y. and Blakley, R. L., *Adv. Enzyme Reg.*, 1977, **15,** 81.
67. Fersht, A. R., *Proc. R. Soc. London, Ser. B.*, 1974, **187,** 397.
68. Fersht, A. R., *Enzyme Structure and Mechanism*; Freeman, W. H., San Francisco; chapters 9 and 11.
69. Wilkinson, A. J., Fersht, A. R., Blow, D. M. and Winter, G., *Biochemistry*, 1983, **22,** 3581.
70. Drennan, C. L., Huang, S., Drummond, J. T., Matthews, R. G. and Ludwig, M. L., *Science*, 1994, **266,** 1669.
71. Mancia, F., Keep , N. H., Nakagawa, A., Leadley, P. F., McSweeney, S., Rasmussen, B., Bösecke, P., Diat, O. and Evans, P. R., *Structure*, 1996, **4,** 339.
72. Fersht, A. R., Shi, J.-P., Knill-Jones, J., Cowe, D. M., Wilkinson, A. J., Blow, D. M., Brick, P., Carter, P., Waye, M. M. Y. and Winter, G., *Nature*, 1985, **314,** 235.

Pergamon

PII: S0277-5387(98)00054-0

Polyhedron Vol. 17, Nos 13–14, pp. 2225–2230, 1998
© 1998 Elsevier Science Ltd
All rights reserved. Printed in Great Britain
0277-5387/98 $19.00+0.00

Redox properties of 17-electron thiolate complexes of cyclopentadienyl iron (III)

C. Díaz,* E. Araya and M. A. Santa Ana

Departamento de Química, Facultad de Ciencias, Universidad de Chile, Casilla 653 Santiago, Chile

(Received 12 January 1998; accepted 15 January 1998)

Abstract—The redox electrochemistry of iron (III) thiolate complexes of the type [CpFe(dppe)-SR]PF_6 R = CH_3, C_3H_7, C_6H_5, p-C_6H_4Br and thiobenzothiazole has been examined by cyclic voltammetry, coulometry and spectroelectrochemistry methods. Four redox waves were observed in the range −1.5 to +1.5 V (S.C.E) in CH_2Cl_2. Around 0.0 V the metal centered reduction Fe (III)→Fe (II) process was observed, while that around +0.5 V the wave observed was attributed to a ligand centered oxidation. Strongly irreversible waves of oxidation near 1.3 V were assigned to the oxidation of RSSR while a reduction wave also strongly irreversible at very high negative potential was attributed to the reduction of the RSSR free ligand, RSSR + 2e→2RS^-. The redox wave observed for the disulphides compounds are discussed in terms of a reductive elimination of RSSR. Chemical and electrochemical reduction of the complexes [CpFe(dppe)-SR]PF_6 was accomplished by the color changes blue → red-brown characteristic of the redox change 17e→18e. © 1998 Elsevier Science Ltd. All rights reserved

Keywords: thiolate; iron complexes; redox properties; phosphine-iron complexes.

INTRODUCTION

The chemistry of transition metal thiolates is currently attracting considerable attention, largely as a result of the possible significance of such complexes in metalloenzyme systems [1–3].

Electron transfer processes on metal complexes containing sulfur ligands are very important for the understanding of redox processes occurring at the thiolate-coordinated metal ions in the active sites of several redox-active enzymes [1–3]. Specifically iron-sulfur thiolate bonds are involved in important metalloproteins [3].

Among the known metal-thiolate compounds, those of iron [3] are relatively more abundant than those of other metals [1, 2]. Although there are now several well-demonstrated methods for synthesizing iron (II)-thiolate compounds [2], few iron (III)-thiolate complexes have been reported [4–6]. We have recently reported a general method of obtaining cyclopentadienyl-iron (III) thiolate complexes in a simple step, starting from the organometallic precursor CpFe(dppe)I and the disulfide RSSR [4, 5].

$$2\text{CpFe(dppe)I} + \text{RSSR} \xrightarrow[\text{CH}_3\text{OH}]{\text{NH}_4\text{PF}_6} 2[\text{CpFe(dppe)SR}]\text{PF}_6 \quad (1)$$

As previously suggested[6], the formation of the iron (III)-thiolate complexes from the iron (II) precursor involves an intramolecular electron-transfer reaction in the intermediate disulfide complex

$$2\text{CpFe(dppe)I} + 2\text{RSSR} \xrightarrow[\text{CH}_3\text{OH}]{\text{NH}_4\text{PF}_6} 2[\text{CpFe(dppe)RSSR}]\text{PF}_6 \quad (2)$$

$$2\text{CpFe}^{\text{II}}\text{(dppe)RSSR} \rightarrow 2\text{CpFe}^{\text{III}}\text{(dppe)} - \text{SR}^+ + \text{RSSR} \quad (3)$$

Fe (III)-thiolate complexes have also recently been obtained by oxidative-addition of thiols to CpFe $(dppe)^+$ -fragment.

$$\text{CpFe(dppe)I} + \text{HSR} \xrightarrow[\text{CH}_3\text{OH}]{\text{NH}_4\text{PF}_6} [\text{CpFe(dppe)} - \text{SR}]\text{PF}_6 + [\text{H}] \quad (4)$$

(In this reaction the unidentified product containing the hydrogen thiol is denoted [H] see ref.[6]). It was

*Author to whom correspondence should be addressed.

suggested [4, 6] that this reaction occurs through the intermediate [CpFe(dppe)HSR]PF_6 which after an intramolecular electron transfer leads to the Fe (III)-thiolate product. The oxidative-addition described above for RSSR and RSH has been reported for other organometallic compounds [7].

Because of much of the chemical transformations involved in biological processes involve an electron-transfer process through a bond Fe-S, the redox behaviour of metal-thiolate complexes is essential, for the understanding of the mechanism of such processes.

Although the redox behaviour of molybdenum thiolates and other metal-thiolates have been examined [8, 9], few electrochemical studies on iron (II) and iron (III)-thiolate compounds have been reported [10, 11]. In this paper we describe the electrochemical behaviour of a series of iron (III)-thiolate complexes [CpFe(dppe)SR]PF_6, where R=CH_3, 1; C_3H_7, 2; C_6H_5, 3, C_6H_4Br, 4; thiobenzothiazole, 5.

RESULTS AND DISCUSSION

The electrochemical behaviour of the series of thiolates [CpFe(dppe)-SR]PF_6 was studied by cyclic voltammetry in CH_2Cl_2 solution. Almost all the complexes undergo a reversible (irreversible for 1 and 5) reduction in the range 0.1 V to −0.4 V. (see Fig. 1 and Table 1). The electron transfer associated with this redox process can be assigned to the reduction of the Fe (III)-thiolate complex CpFe(dppe)-$SR^+ + e \rightarrow$ CpFe(dppe)-SR. Thus, the cyclic voltammogram of [CpFe(dppe)-SC_6H_5] exhibits a one electron oxidation wave at −0.25 V corresponding to the Fe (II)→Fe (III) oxidation process [10]. On the other hand, the

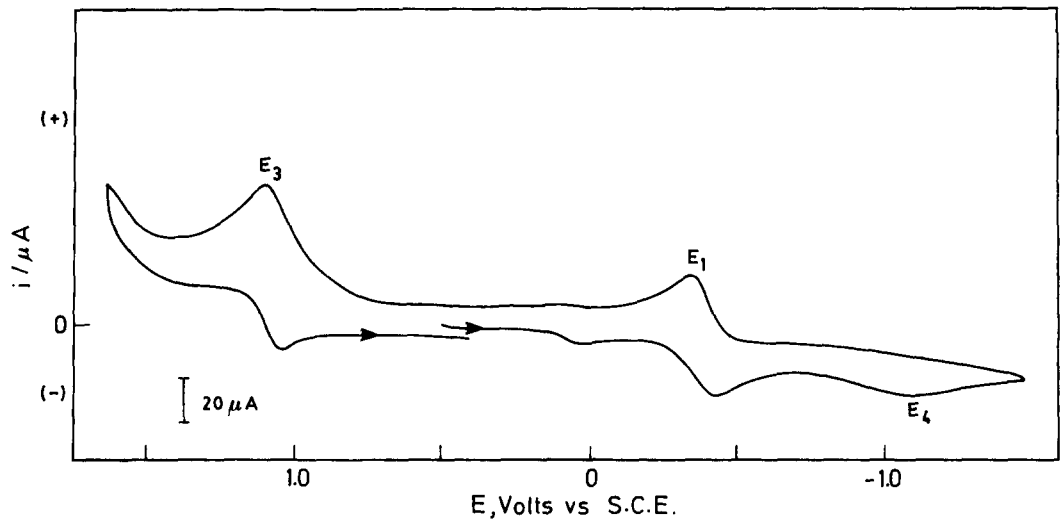

Fig. 1. Cyclic voltammogram for [CpFe(dppe)-S-C_3H_7]PF_6 in CH_2Cl_2 at 25°C and scan rate of 100 mv/s.

Table 1. Electrochemical data for [CpFe(dppe)-SR]PF_6 compounds

Compound	Peak potential, [a] V				
	E1 (ΔEp)(ipa/ipc)	E2 (ΔEp)(ipa/ipc)	E3 (ΔEp)(ipa/ipc)	E4 (ΔEp)(ipa/ipc)	Farad/mol[d]
[CpFe(dppe)-SCH_3]PF_6	−0.35(0.1)(i)[b]	54(0.04)(0,83)	1.3(i)(i)	< −2.0(i)(i)	—
[CpFe(dppe)-S-C_3H_7]PF_6	−0.37(0.1)(0.95)	[c]	1.1(i)(0.98)	−1.07(i)(i)	0.90
[CpFe(dppe)-S-C_6H_5]PF_6	−0.293(0.056)(0.82)	—	1.2(0.06)(0.86)	< −2.0(i)(i)	0.89
[CpFe(dppe)-S-C_6H_4-Br]PF_6	−0.22(.12)(0.90)	—	12(i)(i)	< −1.4(i)(i)	0.91
[CpFe(dppe)-S-benzotiazole]PF_6	−0.3(i)(i)	0.54(0.09)(0.81)	1.11(i)(i)	−1,1(i)(i)	—

[a] From cyclic voltammograms in CH_2Cl_2 solution at 100 m V/seg. Values referenced to S.C.E

[b] (i) Indicate a chemical or electrochemical irreversible process electrode.

[c] Wave not observed.

[d] Coulometry data for E1 process at the volt of the bulk electrolysis value indicated in column 1. Data for irreversible processes could be not, measured.

complex $CpFe(PMe_3)_2SC_6H_5$ undergoes an oxidation process at -0.20 V [11]. Furthermore, metal thiolates of the type $Ln\ M(SR)^{+z}$ with the metal in an accessible higher oxidation state $Ln\ M\ (SR)^{+(Z+1)}$ in general, exhibit an initial oxidation metal based with $E_{1/2}$ values near 0 V [9]. Its appears to be that the high polarisable and soft thiolate ligand [1] induces a high electron density on the metal atom, which provokes a low facile oxidation of the thiolate complexes. This can be also due to the electron rich nature of the fragment $CpFe(dppe)^+$ [10, 12].

As expected the controlled potential coulometry confirm that the reduction of the complexes [CpFe(dppe)-SR] PF_6 is a one electron process. Data are shown in Table 1. This was also corroborated by UV-visible spectroscopy. The initial blue solution of the thiolate iron (III) complex turned yellow-brown after total electrochemical reduction. The UV-visible changes for $[CpFe(dppe)\text{-}S\text{-}C_3H_7]PF_6$ are shown in Fig. 2. Similar UV-visible spectral changes are observed in the chemical reduction using Red-Al as reducing agent as is shown in Fig. 3.

The second one electron oxidation wave observed in the cyclic voltammogram of the complexes (which is absent in complexes 2–4), can be assigned to a ligand based oxidation (reaction Eq. (6)) according to previous electrochemistry studies on metal-thiolate compounds [8, 9]. Cyclic voltammogram for complex 5 is shown in Fig. 4.

$$2CpFe(dppe)-SR \xrightarrow{solv} 2CpFe(dppe)Solv^+ + RSSR + e \quad (5)$$

In agreement with this suggestion we have detected in the cyclic voltammograms of the complexes 1–5, the typical oxidation of RSSR [9, 13] (peak E_3) in the range 1.1–1.3 V as well as their reduction at very negative potentials (termed peak E_4). Furthermore we have observed similar oxidation and reduction waves in the cyclic voltammetry of the free RSSR ligands as is shown in Table 2.

All these results are consistent with the scheme shown in Fig. 5, for the redox behaviour of the complexes [CpFe(dppe)-SR]PF_6. The absence of the oxidation peak E_2 for the complexes 2–4 can be due to the high stability of the Fe (II) species CpFe(dppe)-SR, which preclude the oxidation of the thiolate ligand. In fact the ip_a/ip_c ratio parameter value near 1 for these complexes, indicates a high chemical reversibility. In complexes 2–4 however in spite of that the peak 2 is not obseved, the peak corresponding to the

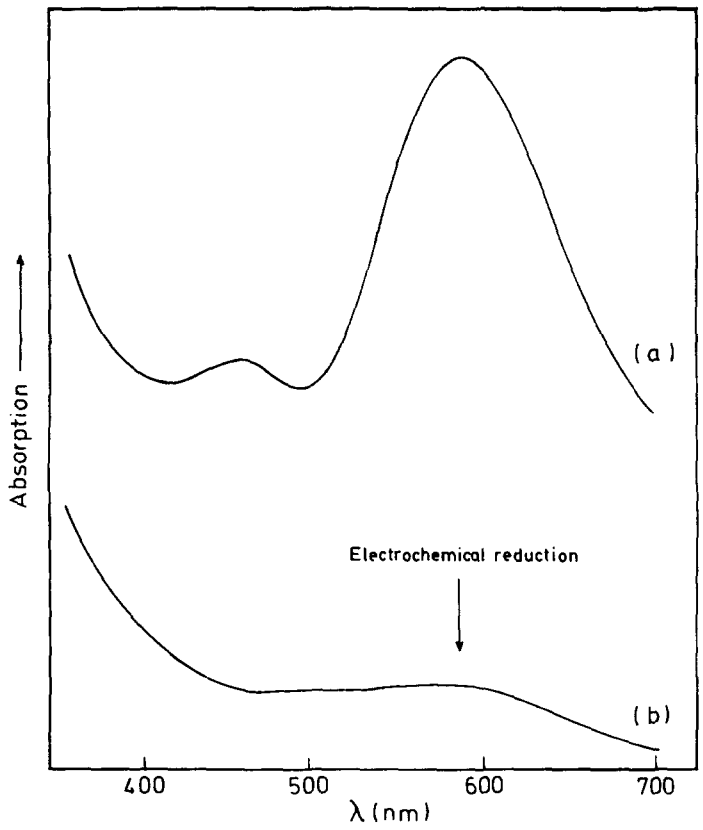

Fig. 2. UV-vis spectra of $[CpFe(dppe)\text{-}S\text{-}C_3H_7]PF_6$ in CH_2Cl_2 solution (a) before the reduction (b) after electrochemical reduction.

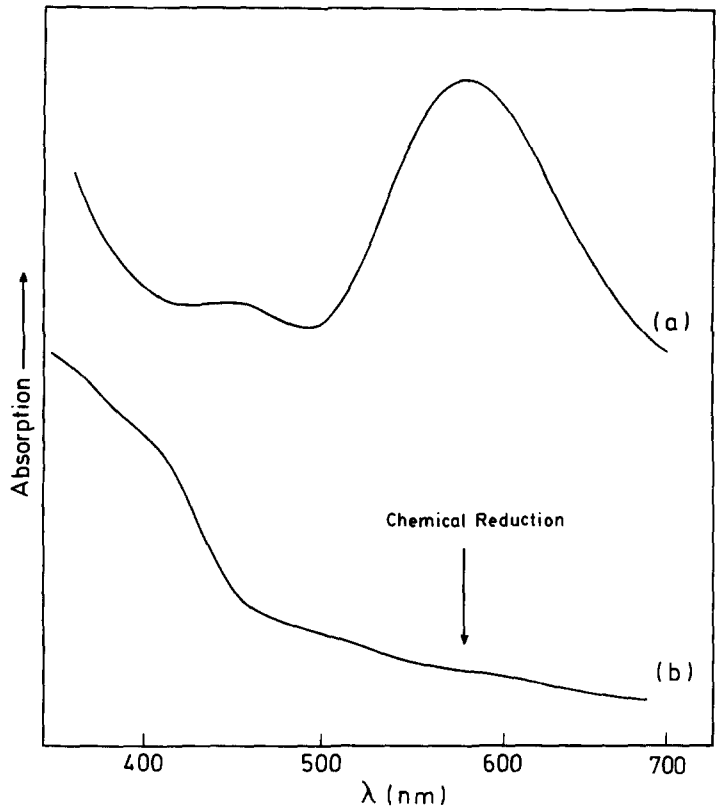

Fig. 3. UV-vis spectra of [CpFe(dppe)-S-C_3H_7]PF_6 in CH_2Cl_2 solution (a) before the reduction (b) after the chemical reduction with Red-Al.

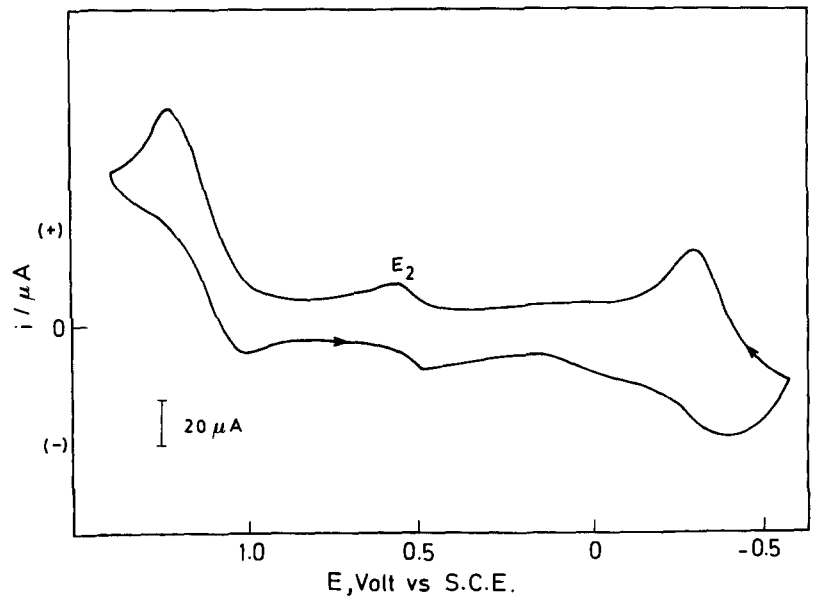

Fig. 4. Cyclic voltammogram for [CpFe(dppe) benzotiazole]PF_6 in CH_2Cl_2 solution at 25°C and scan rate of 100 mv/s.

Table 2. Cyclic Voltammetry Data for Disulfides RSSR[a]

Compound	Epa (V)	Epc (V)	Ref.
Me-S-S-Me	1.62	< -1.8	This work
C_3H_7-S-S-C_3H_7	> 1.8	-0.89	This work
C_6H_5-S-S-C_6H_5	1.4	~ 0	13a
$C_6H_5CH_2$-S-S CH_2-C_6H_5	—	-2.0	9a
CH_3-C_6H_4-S-S-C_6H_4-CH_3	1.3	-2.3	9a
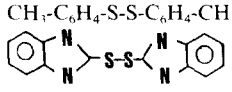	1.1	-1.05	This work
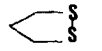	$+1.17$	-1.77	

[a] Main peaks. For dithiobenzotiazole an oxidation peak was observed at 0.2 V. For C_3H_7-S-S-C_3H_7 a reduction peak at -0.5 V was also observed See ref [9]. and [13].

oxidation of the dithioether appears at ~ 0.5 V which suggest that the chemical equilibrium Eq. (6) could exist.

$$2CpFe(dppe)-SR^{+} \rightleftarrows 2CpFe(dppe)^{+} + RSSR \quad (6)$$

Reductive eliminations of RSSR as the shown in eq. (6) have been previously proposed in the formation of thiolate-bridged dimers of group 6B metals [14, 15]. Thus the 16e specie CpFe(dppe)(solvent)$^{+}$ has been detected by UV-visible spectroscopy [16].

EXPERIMENTAL

All solution manipulations were carried out under purified argon or dinitrogen. Compounds [CpFe(dppe)-SR]PF_6 where R = CH_3, C_3H_7, C_6H_5 and p-C_6H_4Br were synthesized as described previously [1, 6]. The new complex CpFe(dppe)-S-benzo-thiazol was prepared as follow:**[CpFe(dppe)-S-benzothiazol]PF_6**, CpFe(dppe).I 0.15 g (0.23 mmol) and 2,2′-Dithiobis (benzothiazole) 0.076 g (0.23 mmol) in the presence of NH_4 PF_6 1 g (0.69 mmol) where stirred in CH_3 OH (30 ml) for 24 h. After this time, the solvent was removed under reduced pressure until dryness and the solid extracted with dichloromethane, filtered through celite and the solution concentrated to c.a. 10 ml. Upon addition of a 1:1 n-hexane-diethyl ether mixture the precipitate, a dark-blue solid, was washed twice with the same mixture and the solid residue dried under vacuo. Yield. 0.11 g, 57%. Anal.: Found C 53.5 H 3.8 Calcd. For C_{32} $H_{33}N$ F_6 S_2 P Fe; C 53. 48 H 3.98 Ir (K Br). 1090 δ (C-H) bend in plane vibration of C_5H_5 group (see ref.[4]); 840 ν (PF_6); 700 δ (C-H) bending-out-plane vibration of group C_6H_5 of dppe (see refs.[4–6]).

Electrochemistry

The cyclic voltrammetry experiments were done with a PARC model 370 electrochemistry system in a specially designed three-electrode glass cell [17, 18]. The working electrode was a carbon glassy disk, the counter was a platinum wire, and the reference electrode an aqueous saturated calomel electrode (S.C.E.) connected to the working cell through a Luggin capillary placed ca. 1 mm from the working electrode. A 0.1 M $[Bu_4N]PF_6$ solution in CH_2Cl_2 was used as supporting electrolyte. Solutions were degassed with nitrogen and a nitrogen atmosphere was maintained

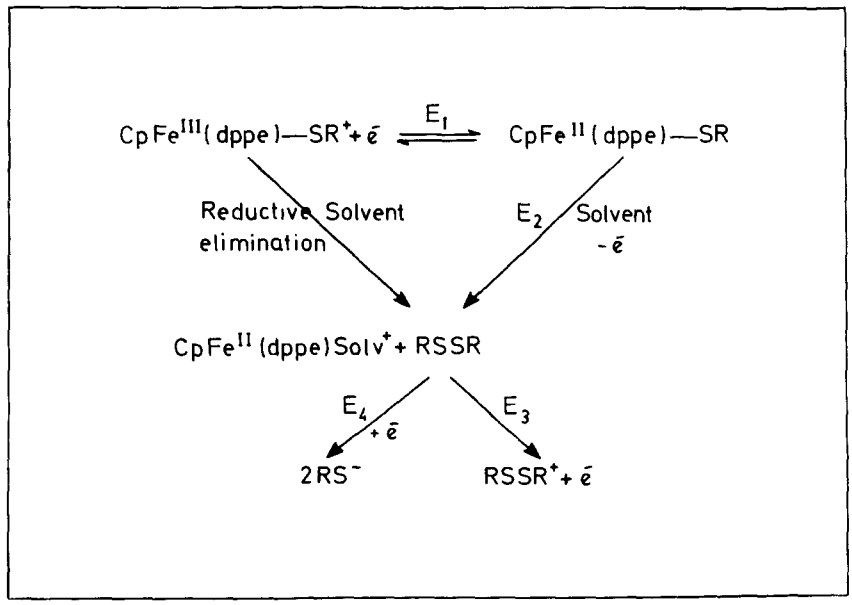

Fig. 5. Redox behavior of [CpFe(dppe)-SR]PF_6 complexes.

over the solution during the experiment. The peak potentials values reported were determined at the first cyclic voltammogram and referenced to the S.C.E.

Controlled potential electrolyses were carried out in the same supporting electrolyte solution using a three electrolysis cell (adapted from Figs 3.14 and 3.16 in ref.[17]) with a platinum gauze as cathode, a platinum wire counter electrode isolated from the working solution by a medium porosity glass frit. The saturated calomel electrode was introduced to the cell through a luggin capillary and placed near the cathode. The charge transfered in the electrolysis was determined with a PARC 179 digital coulometer.

Acknowledgements—We are grateful to the FONDECYT, Project 1950305, and D.I.D. Universidad de Chile for financial support.

REFERENCES

1. Kuehn, Ch.T. and Isied, S., *Prog. Inorg Chem.*, 1990, **27,** 153.
2. Dance, I. G. *Polyhedron*, 1986, **5**, 1037; Blower, P. J. and Dilworth, J. R., *Coord. Chem. Rev.*, 1989, **76**, 121.
3. Beinert, H., Hohn, R. H. and Münck, E., *Science*, 1977, **277**, 653 and reference therein. Evans, D. J., Hughes, D. L. and Silver, J., *Inorg. Chem.*, 1977, **36**, 747. Butt, J. N., Armstrong, F. A., Breton, J., George, S. J., Thomson, A. J. and Hatchikion, E., *J. Am. Chem. Soc.*, 1991, **113**, 6663. Butt, J. N., Sucheta, A., Armstrong, F. A., Breton, J., Thomson, A. J. and Hatchikion, E. C., *J. Am. Chem. Soc.*, 1993, **115**, 1413. Dawson, J. H. and Sono, M., *Chem. Rev.*, 1987, **87**, 1255.
4. Díaz, C., Leal, C. and Yutronic, N., *J. Organomet. Chem.*, 1996, **516,** 59 and references cited therein.
5. Díaz, C., Leal, C. and Yutronic, N., *Bol. Soc. Chil. Quím.*, 1996, **41,** 99.
6. Díaz, C., *Polyhedron*, 1997, **16,** 999.
7. Ju, T. D., Capps, K. B., Lang, R. F. and Hoff, C.D., *Inorg. Chem.*, 1997, **36,** 614.
8. Katz, J. C., Vining, W., Coco, W., Rosen, R., Romao Dias, A. and García, M.H., *Organometallics*, 1983, **2,** 68.

9a. Bradbury, J. R., Masters, A. F., McDonell, A. C., Brunette, A. A., Bond, A. M. and Wedd, A. G., *J. Amer. Chem. Soc.*, 1981, **103**, 1959. Sawyer, D. T., Susan Srivatsa, G., Bodini, M. E., Schaefer, W. P. and Wing, R. M., *J. Am. Chem. Soc.*, 1986, **108**, 93. Barnard, K. R., Bruck, M., Huber, S., Grittini, C., Enemark, J. H., Gable, R. W. and Wedd, A. G., *Inorg. Chem.*, 1997, **36**, 637. .

10. Treichel, P. M., Molzahn, D. C., and Wagner, K. P., *J. Organomet. Chem.*, 1979, **179**, 191. Treichel, P. M. and Komar, D. A., *J. Organomet. Chem.*, 1981, **206**, 77.
11. Roth, E. K. and Jordanov, J., *Inorg. Chem.*, 1992, **31,** 240.
12. Legzdins, P., McNeil, W. S., Rettig, S. J. and Smith, K.M., *J. Am. Chem. Soc.*, 1997, **119,** 3513.

13a. Magno, F., Bontempelli, G. and Pilloni, G., *Electroanal. Chem. and Interf. Electrochem.*, 1971, **30,** 375.

13b. Wowie, J. K., Houts, J. and Sawyer, D. T., *J. Am. Chem. Soc.*, 1977, **99,** 6323.

14. Boorman, P. R., Chivers, T., Mahadev, K. N. and O'Dell, B. D., *Inorg. Chin. Acta*, 1976, **19,** L35.
15. Boorman, P. M., Patel, V. D., Kerr, K. A., Codding, P. W. and Van Rocy, P., *Inorg. Chem.*, 1980, **19,** 3508.
16. Díaz, C. and Yutronic, N., *Polyhedron*, 1996, **15,** 1001.
17. Sawyer, D. T. and Roberts, J. L. Experimental Electrochemistry for Chemists, John Wiley; New York, 1974, p. 147 and 151.
18. González, G., Santa Ana, M. A. and Chadwick, I. *J. Chem. Soc. Perkin Trans. II*, 1983, 1803.

Pergamon

PII: S0277-5387(98)00048-5

Polyhedron Vol. 17, Nos 13–14, pp. 2231–2235, 1998
© 1998 Elsevier Science Ltd
All rights reserved. Printed in Great Britain
0277-5387/98 $19.00+0.00

Mononuclear palladium(II) complexes with the phenylselenolato ligand. The crystal and molecular structure of *trans*-[Pd(SePh)$_2$(P(*n*-Bu)$_3$)$_2$].

Elmer C. Alyea,* George Ferguson* and Shanmugaperumal Kannan

Department of Chemistry and Biochemistry, University of Guelph, Guelph, Ontario, Canada, N1G 2W1.

(Received 5 January 1998; accepted 15 January 1998)

Abstract—Mononuclear palladium(II) complexes of the type [Pd(SePh)$_2$L$_2$] [where L = PMe$_3$, PEt$_3$, P(n-Bu)$_3$, PMePh$_2$ or TPA (1,3,5-triaza-7-phosphaadamantane)] have been prepared and characterized by elemental analysis, ^{1}H, ^{13}C{^{1}H} and ^{31}P{^{1}H} NMR data and in the case of [Pd(SePh)$_2$(P(n-Bu)$_3$)$_2$] by single-crystal X-ray diffraction methods. Crystals of [Pd(SePh)$_2$(P(n-Bu)$_3$)$_2$] are triclinic, space group $P\bar{1}$, a = 8.4798(7), b = 10.3002(15), c = 12.254(2)Å, α = 77.957(15), β = 85.806(11), γ = 83.550(9)°, Z = 1. The structure was refined by full-matrix least-squares calculations on F^2 to final R values R_{obs} = 0.0267 (for 3187 reflections with $I \geq 2\sigma(I)$) and wR(F^2) = 0.0657 (for all 4549 measured reflections). The structure determination shows that the Pd atom lies on an inversion centre so that the coordination geometry is necessarily *trans* and planar. Main bond lengths are Pd-P 2.3334(7) and Pd-Se 2.4609(4)Å. © 1998 Elsevier Science Ltd. All rights reserved

Keywords: palladium-selenium bonding; phosphine ligands; crystal structure.

Transition metal organochalcogenide complexes are of significant current interest owing to their structural and chemical reactivity [1]. These complexes have attractive potential in material science [2] and in constructing model complexes for catalysis [3]. Pertinent to this work, a large number of mononuclear thiolato complexes of palladium(II), [PdX(SR)L$_2$] and [Pd(SR)$_2$L$_2$] have been prepared and characterized [4]. However the mononuclear complexes of palladium(II) with heavier organochalcogenides (SeR or TeR; R = alkyl or aryl group) have rarely been studied except for a few poorly characterized complexes [5], even though the corresponding platinum complexes are well established [6]. As a part of our work on the complexes of transition metal ions with heavier organochalcogenide ligands, we report here the complexes of palladium(II) with the phenylselenolato ligand and the first structurally characterized mononuclear palladium(II) complex containing an organoselenolato group, viz. *trans*-[Pd(SePh)$_2$(P(*n*-Bu)$_3$)$_2$].

*Authors to whom correspondence should be addressed: E-mail addresses: alyea@chembio.uoguelph.ca; and ferguson @chembio.uoguelph.ca

RESULTS AND DISCUSSION

Preparation and characterization

The reaction of *cis*-[PdCl$_2$(L)$_2$] with NaSePh in dichloromethane /methanol yielded orange coloured mononuclear complexes [Pd(SePh)$_2$(L)$_2$] (equation 1).

$$[PdCl_2(L)_2] + 2NaSePh \rightarrow [Pd(SePh)_2(L)_2] + 2NaCl$$

(L = PMe$_3$, PEt$_3$, P(n-Bu)$_3$, PMePh$_2$ or TPA;

TPA = 1,3,5-triaza-7-phosphaadamantane)

The ^{31}P{^{1}H} MR of all the complexes showed a single resonance (Table 1), indicating that the complexes exist exclusively in one isomeric form (*cis* or *trans*). The ^{1}H NMR spectra of all the complexes have the expected peak multiplicities and integrations (Table 1). The phosphines containing a methyl group (PMe$_3$ and PMePh$_2$) show a virtual triplet in these spectra indicating that most likely the complexes exist exclusively in the *trans* isomeric form [6b, 7]. Similarly, the ^{13}C{^{1}H} NMR spectra of all the complexes show a characteristic triplet for the carbon attached to the phosphorus atom. Since the generality of this latter

Table 1. The ^{1}H, $^{13}C\{^{1}H\}$ and ^{31}P NMR data for $[Pd(SePh)_2(L)_2]$.

Complex	^{31}P NMR (δ in ppm)	^{1}H NMR(δ in ppm)	$^{13}C\{^{1}H\}$ NMR(δ in ppm)
$[Pd(SePh)_2(PMe_3)_2]$	−14.37	1.41(t,18H,3.5 Hz,PMe); 7.02(m,6H,C_6H_5); 7.65(m, 4H,C_6H_5).	15.6(t,^{1}J(P-C)=16.5 Hz; 124.04 (C-4); 128.6(C-3,5); 134.4(C-2,6); 139.2(Se-C).
$[Pd(SePh)_2(PEt_3)_2]$	10.0	0.96(q,18H,$PCCH_3$); 1.92 m,12H,PCH_2); 6.99(m,6H, C_6H_5); 7.64(m,4H,C_6H_5).	8.77(CH_3); 15.8(t,^{1}J(P-C)=14.5 Hz); 123.8(C-4); 128.4(C-3,5); 134.77(C-2,6); 139.1(Se-C).
$[Pd(SePh)_2(P(n\text{-}Bu)_3)_2]$	2.50	0.74(t,18H,7Hz,CH_3); 1.19(m,24H,CH_2); 1.82(m, 12H,PCH_2); 6.92(m,6H, C_6H_5); 7.58(m,4H, C_6H_5).	13.86(CH_3); 23.31(t,^{1}J(P-C)= 14 Hz,PC); 24.5(t,^{2}J(P-C)=7 Hz, PCC); 27.01(PCCC); 123.75(C-4) 128.3(C-3,5); 134.83(C-2,6); 139.18(Se-C).
$[Pd(SePh)_2(PMePh_2)_2]$	5.78	1.96(t,6H,3.3Hz,PCH_3); 6.59-7.51(m,30H,C_6H_5).	15.43(t,^{1}J(P-C)=17 Hz,PMe); 123.8(C-4, SePh); 128.05(C-3,5, SePh); 128.34(C-4,PPh); 128.44(C-2,6,SePh); 128.54(C-3,5,PPh); 130.21(C-2,6,PPh); 133.05(t,^{1}J(P-C)=6Hz,PC,PPh); 139.2(SePh).
$[Pd(SePh)_2(TPA)_2]$	−66.1	4.06(s,br,12H,PCH_2); 4.25(q,NCH_2,12H); 7.04 (m,6H,C_6H_5); 7.52(m,4H, C_6H_5).	—

observation relating the spectral pattern to the identification of *trans* vs. *cis* isomers is currently being explored [8], the $^{13}C\{^{1}H\}$ NMR spectral data will be discussed later together with that for a wide range of palladium-phosphine complexes. The chemical shift of the carbon attached to the 'Se' atom agrees well with the earlier reported values for related platinum complexes [6].

Crystal structure of $[Pd(SePh)_2(P(n\text{-}Bu)_3)_2]$

The molecular structure of the complex *trans*-$[Pd(SePh)_2(P(n\text{-}Bu)_3)_2]$ is shown in Fig. 1 and selected dimensions are given in Table 2. The Pd atom lies at an inversion centre and the coordination geometry is thus required to be *trans* and strictly planar. The planar coordination is not exactly square as the crystalographically unique P-Pd-Se angle is 93.58(2)°. The Pd-P and Pd-Se distances (2.3334(7) and 2.4609(4)Å respectively) agree well with the relevant values (2.323(2) and 2.456(1)Å respectively) reported [9] for *trans*-$[Pd(4\text{-}MeC_6H_4COSe)_2(PEt_3)_2]$. A search of the October 1996 release of the Cambridge Crystallographic Database [10] for further PdP_2Se_2 fragments only revealed two compounds [11], $\{Pd[Ph_2P(CH_2)_nPPh_2](SeCN)_2\}$, n=2 or 3, both with *cis*-stereochemistry and with Pd-P 2.275(2)-2.286(2)Å and Pd-Se 2.458(1)-2.488(1)Å. The Pd1-Se1-C11 angle (104.82(8)°) falls between the Pt-Se-C values (104.2(5), 107.1(5)°) reported [6b] for *trans*-$[Pt(SePh)_2(PPh_3)_2]$.

Reaction of NaSePh with $PdCl_2L_2$ (L = PPh_3 *or 0.5 Diphenylphosphinomethane (DPPM)*)

The reaction of NaSePh with $[PdCl_2L_2]$ (where L = PPh_3 or 0.5 DPPM) yielded brown coloured products, which showed many peaks in their ^{31}P NMR spectra. Either decomposition or polymerization of the mononuclear complexes apparently occurred. However the corresponding platinum complexes are very stable under similar reaction conditions [6a].

Reaction of $[Pd(SePh)_2(L)_2]$ (L = PMe_3, PEt_3, $P(n\text{-}Bu)_3$, $PMePh_2$ *or TPA) with Chloroform*

It was noticed that all the alkylphosphine complexes slowly decompose to give some insoluble brown solids, when solutions in $CDCl_3$ were kept for three to four days after recording the NMR spectrum. This shows clearly that the complexes are unstable in chloroform although they are stable in dichloromethane for several more days.

EXPERIMENTAL

Materials

Diphenyldiselenide and $[PdCl_2(PhCN)_2]$ were obtained from commercial sources (Aldrich). The complexes $[PdCl_2(L)_2]$ [12] and $[PdCl_2(TPA)_2]$ [13] were prepared according to literature methods.

Physical measurements

The ^{1}H and $^{13}C\{^{1}H\}$ NMR spectra were recorded in $CDCl_3$ on a Varian Gemini-200 MHz instrument and the chemical shifts are relative to the internal chloroform resonance (at δ 7.26 ppm for ^{1}H and δ 77.0 ppm for ^{13}C). The $^{31}P\{^{1}H\}$ NMR spectra were

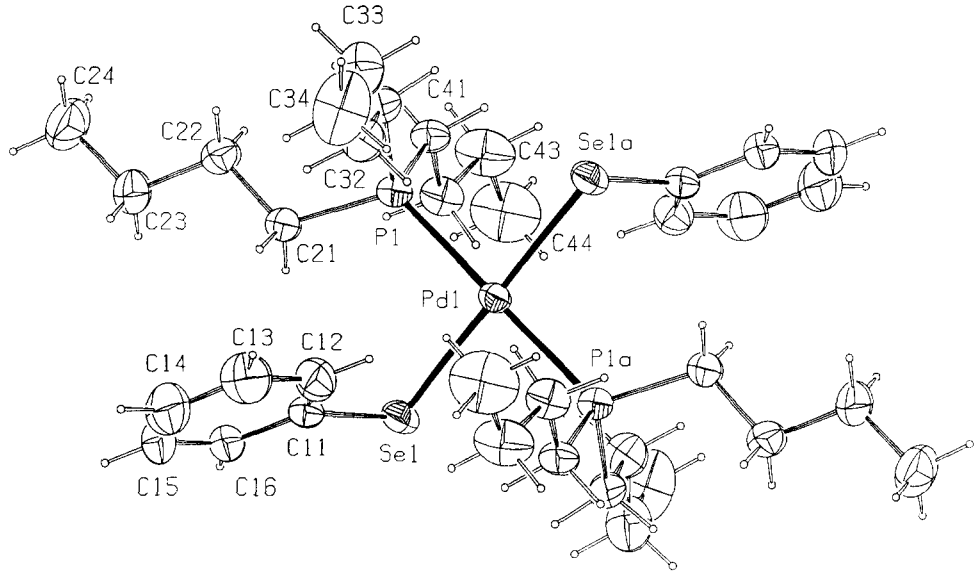

Fig. 1. A view of $[Pd(SePh)_2(P(n\text{-}Bu)_3)_2]$ with our numbering scheme. Anisotropic displacement ellipsoids are shown at the 30% probability level.

Table 2. Selected bond distances (A) and angles( ) for $[Pd(SePh)_2(P(n\text{-}Bu)_3)_2]$ with e.s.d.s in parentheses.

Pd1 Se1	2.4609(4)
Pd1 P1	2.3334(7)
Se1 C11	1.903(3)
P1 C21	1.833(3)
P1 C31	1.829(2)
P1 C41	1.816(3)
P1 Pd1 Se1	93.58(2)
Pd1 Se1 C11	104.82(8)
Pd1 P1 C21	118.78(8)
Pd1 P1 C31	115.05(9)
Pd1 P1 C41	108.68(9)
C21 P1 C31	104.20(13)
C21 P1 C41	104.69(13)
C31 P1 C41	104.03(12)

recorded in $CDCl_3$ on a Varian Unity-400 MHz instrument and the chemical shifts are relative to the external 85% H_3PO_4 resonance. C, H and N analyses were performed by M-H-W Laboratories, Arizona, U.S.A. Melting points were recorded in open capillaries and are uncorrected.

X-ray crystallography

Crystallographic data together with data collection and structure solution refinement details are given in Table 3. All non-H atoms were allowed anisotropic displacement parameters. The ORTEP [16] plot of the molecule is shown in Fig. 1.

Atomic coordinates, anisotropic displacement parameters and full details of molecular dimensions have been deposited with the Cambridge Crystallographic Data Centre (CCDC). See Information for Authors, Issue No. 1. Any requests to the CCDC for this material should quote the full literature citation and the reference number. These data are also available electronically in CIF format from the authors.

Preparation of $[Pd(SePh)_2(P(n\text{-}Bu)_3)_2]$

To a methanolic solution of PhSeSePh (0.538 g, 1.72 mmol), $NaBH_4$ in methanol was added slowly with constant stirring. Addition of $NaBH_4$ was stopped when a colourless solution of PhSeNa formed. To this a solution of $[PdCl_2(P(n\text{-}Bu)_3)_2]$ in dichloromethane (1.08 g, 1.72 mmol) was added and stirred for 5 h. The solvent was evaporated in vacuum, the residue was extracted with dichloromethane (20 mL) and the solution filtered. To the filtrate, 5 mL of methanol was added and the solution was kept for crystallization (yield 1.2 g, 85%). All the other complexes were prepared in an analogous manner and the pertinent data are given in the Supplementary Data as Table 4.

CONCLUSION

The reaction of $PdCl_2(L)_2$ (L = alkylphosphine) with NaSePh yielded the desired mononuclear palladium(II) complexes of the type $[Pd(SePh)_2L_2]$, which are stable in the solid state but decompose in chloroform, whereas the reaction involving L = PPh_3 or 0.5 DPPM gave no products which could be isolated.

Table 3. Summary of Crystal Data, Data Collection, Structure Solution and Refinement Details **1**

(a) **Crystal Data**	
empirical formula	$C_{36}H_{64}P_2PdSe_2$
molar mass	823.13
color, habit	orange, block
crystal size, mm	$0.42 \times 0.35 \times 0.30$
crystal system	triclinic
a, Å	8.4798(7)
b, Å	10.3002(15)
c, Å	12.254(2)
α, °	77.957(15)
β, °	85.806(11)
γ, °	83.550(9)
V, Å^3	1038.8(2)
space group	$P\bar{1}$
Z	1
molecular symmetry	molecule lies on an inversion centre
$F(000)$	424
d_{calc}, g cm^{-3}	1.316
μ, mm^{-1}	2.296
(b) **Data acquisition**[a]	
temp, K	294(1)
unit-cell reflcns (θ-range°)	25 (9.4 17.2)
max. θ (°) for reflcns	27.0
hkl range of reflcns	−10 10; 0 13; −15 15
decay in 3 standard reflcns	2.0%
reflcns measured	4549
unique reflcns	4549
reflcns with $I > 2\sigma(I)$,	3187
absorption correction type	Ψ-scans
min. max. abs. corr.	0.4573, 0.5456
(c) **Structure Solution and Refinement**[b]	
refinement on	F^2
solution method	Patterson heavy-atom
H-atom treatment	riding (C-H 0.93-0.97Å)
no. of variables in L.S.	188
weights:k in $w = 1/(\sigma^2Fo^2 + k)$ [$P = (Fo^2 + 2Fc^2)/3$]	$(0.0340P)^2 + 0.0607P$
R, R_w, gof	0.0267, 0.0657, 1.038
density range in final Δ-map, e Å^{-3}	−0.430, 0.448
final shift/error ratio	0.001
sec. extnct. type	SHELXL
sec. extnct. correction	0.0089(7)

[a] Data collection on an Enraf Nonius CAD4 diffractometer with graphite monochromatised Mo-Kα radiation (λ 0.7107 Å).

[b] All calculations were done on a Silicon Graphics 4D-35TG computer system with the NRCVAX system of programs (E.J. Gabe, Y. Le Page, J-P. Charland, F.L. Lee and P.S. White, *J. Appl. Cryst.* (1989), **22**, 384–389) for refinement with observed data on F, or with SHELXL-93 (G.M. Sheldrick, 1993) for refinement with all data on F^2.

A *trans* geometry was established by X-ray crystallography for the $P(n\text{-}Bu)_3$ complex.

Acknowledgements—ECA and GF thank NSERC (Canada) for Research Grants. SK thanks the Bhabha Atomic Research Centre, Bombay, India for a leave of absence.

REFERENCES

1. Blower, P. J. and Dilworth, J. R. *Coord. Chem. Rev.*, 1987, **76**, 121; Kanatzidis, M. G. and Huang, S., *Coord. Chem. Rev.*, 1994, **130**, 509; Brennan, J. G., Siegrist, T., Carroll, P. J., Stuczynski, S. M., Brus, L. E. and Steigerwald, M. L., *J. Am. Chem. Soc.*, 1989, **111**, 4141; Liaw, W. F., Chuang, C. Y., Lee, W. Z., Lee, C. K., Lee, G. H. and Peng, S. M., *Inorg. Chem.*, 1996, **35**, 2530.
2. Bousseau, M., Valade, L., Legros, J. P., Casssoux, P., Garbauskas, M. and Interrante, L. V., *J. Am. Chem. Soc.*, 1986, **108**, 1908; Brennan, J. G., Siegrist, T., Stuczynski, S. M. and Steigerwald, M. L.,

J. Am. Chem. Soc., 1989, **111**, 9240; Osakada, K. and Yamamoto, T., *Inorg. Chem.*, 1991, **30**, 2328; Hirpo, W., Dhingra, S. and Kanatzidis, M. G., *J. Chem. Soc. Chem. Commun.*, 1992, 557.

3. Weisser, O. and Landa, S., Sulfide Catalysis: Their Properties and Applications, Pergamon Press, Oxford, 1973; Rakowski DuBois, M., Vanderveer, M. C., DuBois, D. L., Haltiwanger, R. C. and Miller, W. K., *J. Am. Chem. Soc.*, 1980, **102**, 7456.
4. Braterman, P. S., Wilson, V. A. and Joshi, K. K., *J. Organomet. Chem.*, 1971, **31**, 123; Aresta, M. and Nyholm, R. S., *J. Organomet. Chem.*, 1973, **56** 395; Dixon, K. R., Moss, K. C. and Smith, M. A. R., *J. Chem. Soc. Dalton Trans.*, 1973, 1528; Rauchfuss, T. B., Shu, J. S. and Roundhill, D. M., *Inorg. Chem.*, 1976, **15**, 2096; Roundhill, D. M., *Inorg. Chem.*, 1980, **19**, 557; Davidson, J. L., Preston, P. N. and Russo, M. V., *J. Chem. Soc. Dalton Trans.*, 1983, 783.
5. Khandelwal, B. L. and Gupta, S. K., *Inorg. Chim. Acta*, 1989, **166**, 199; Gupta, S. K. and Khandelwal, B. L., *Indian. J. Chem. Sec.* A, 1990, **29**, 977.
6. (a) Jain, V. K., Kannan, S., Butcher, R. J. and Jasinski, J. P., *J. Chem. Soc. Dalton Trans.*, 1993, 1509; (b). Jain, V. K., Kannan, S. and Tiekink, E. R. T., *J. Chem. Res* (M)., 1994, 509.
7. Redfield, D. A., Cary, L. W. and Nelson, J. H., *Inorg. Chem.*, 1976, **15,** 1128.
8. Alyea, E. C. and Kannan, S., unpublished work.
9. Kawahara, Y., Kato, S., Kada, T., Murai, T. and Miki, K., *J. Chem. Soc. Dalton Trans.*, 1996, 79.
10. Allen, F. H., Kannard, O. and Taylor, R., *Acc. Chem. Res.*, 1993, **16,** 146.
11. Grygon, C. A., Fultz, W. C., Rheingold, A. L. and Burmeister, J. L., *Inorg. Chim. Acta*, 1988, **144,** 31.
12. Hartley, F. R., The Chemistry of Platinum and Palladium, Applied Science Publishers Ltd., London, 1973.
13. Alyea, E. C., Ferguson, G. and Kannan, S. *Polyhedron*, 1998, **17**, in press.
14. Sheldrick, G. M., SHELXL-93. A program for the refinement of crystal structures. University of Göttingen, Germany, 1993.
15. Gabe, E. J., LePage, Y., Charland, J. P., Lee, F. L. and White, P. S., *J. Appl. Cryst.*, 1989, **22,** 384.
16. Johnson, C. K., ORTEP II, ORNL, Report 5136, Oak Ridge National Laboratory, TN, U.S.A. 1976.

Pergamon

PII: S0277-5387(98)00057-6

Polyhedron Vol. 17, Nos 13–14, pp. 2237–2242, 1998
© 1998 Elsevier Science Ltd
All rights reserved. Printed in Great Britain
0277-5387/98 $19.00+0.00

Syntheses and reactions of tetrazole-group 13 complexes

Miguel-Angel Muñoz-Hernández, Michael S. Hill and D. A. Atwood*

Center for Main Group Chemistry, Department of Chemistry, North Dakota State University, Fargo, North Dakota, 58105-5516, U.S.A.

(Received 31 October 1997; accepted 15 January 1998)

Abstract—The combination of 5-phenyl-1-H-tetrazole (tet) with AlR_3 in stoichiometries of 1–3 leads to the compounds $[(tet)AlR_2]_n$ R = Me (**1**), Et (**2**), ^{t}Bu (**3**), $[(tet)_2AlMe]_n$ (**4**), and $[(tet)_3Al]_n$ (**5**). The addition of pyridine to **1** leads to a soluble compound with the formulation, $[(tet)AlMe_2\text{-pyridine}]_n$ (**6**). Likewise the addition of $AlMe_3$ to **1** and **4** leads to the products $[(tet)AlMe_2\text{-}AlMe_3]_2$ (**7**) and $[(tet)_2AlMe\text{-}AlMe_3]_n$ (**8**). The compounds were characterized by standard techniques and, in the case of **7** by X-ray crystallography. Compounds **1, 4** and **5** were examined (unsuccessfully) as potential unimolecular precursors to aluminum nitride.
© 1998 Elsevier Science Ltd. All rights reserved

Keywords: aluminum; tetrazole; precursor.

Interesting supramolecular assemblies have been obtained in combinations between tetrazole ligands and tin [1]. Otherwise the tetrazole ligands have had a limited usage with the main group elements. Past work has generally involved the formation, and subsequent reactions of the tetrazoles in the absence of metals [2]. The present work has two goals. The first is an exploration into the various compounds that are possible between this ligand system and alkylaluminum reagents. The second goal involves the use of selected tetrazole-aluminum compounds as unimolecular precursors to aluminum nitride. Recent work into group 13 nitride formation has focused on the use of nitrogen rich ligands to overcome a nitrogen deficiency in the resulting solid state materials [3]. The azide group, for instance, has been used with great efficacy in molecular combinations with alkyl- or amido-group 13 compounds [4]. The tetrazole ligand also contains an excess of nitrogen and should warrant similar consideration. It may be envisioned to decompose to aluminum nitride with the release of dinitrogen and benzonitrile. Unfortunately, the results presented herein will demonstrate that the tetrazole does not undergo this favorable decomposition, although some unique chemistry may yet be accessible.

* Author to whom correspondence should be addressed. E-mail: Datwood@plains.nodak.edu

RESULTS AND DISCUSSION

Synthesis and characterization

The tetrazole (5-phenyl-1-H-tetrazole) is combined with AlR_3 in a 1:1 stoichiometry to form the oligomeric (or polymeric) derivatives **1–3** in high yield. The polymer is formed due to the ability of the tetrazole ligands to form both covalent and (at least one) bridging coordinate covalent bond. This situation is demonstrated in the crystal structures of several supramolecular tin derivatives [1]. The solubilities of **1–3** increase in the order Me < Et < ^{t}Bu such that the ^{1}H NMR of the latter derivative can be taken in C_6D_6. Otherwise they must be dissolved in d_6-DMSO. The DMSO presumably acts to depolymerize the parent compound. The fact that **1, 4** and **5** have the same solubility in DMSO lends support to this supposition. The addition of two and three equivalents of tetrazole to $AlMe_3$ leads to compounds **4** and **5**, respectively. In the NMR the Al-Me resonances of **1** and **4** are similar (δ −1.06 and −1.02 ppm, respectively).

The intermolecular bridge-bonding in **1** can be disrupted by adding either a Lewis base, to coordinate to the aluminum atom, or a Lewis acid, to one of the remaining pairs of electrons on the tetrazole nitrogens. More specifically, the addition of pyridine to **1** leads to a compound having the general formula, $Me_2Al(tet)$-pyridine (**6**). Its Al-Me chemical shift is a singlet at δ -0.31 ppm. When $AlMe_3$ is added to **1** a dimeric compound results (**7**). Three of the tetrazole nitrogens are involved in bonding to an aluminum atom. The ^1H NMR spectrum contains two singlets at high field (δ -1.05 and -0.54 ppm) which can be attributed to the $AlMe_3$ and $AlMe_2$ groups, respectively.

Structural characterization

The molecular structure of **7** is shown in Fig. 1. It is dimeric with bridging tetrazole groups. This creates an Al_2N_4 six-membered ring that adopts a boat conformation. The two aluminum atoms are 0.63 Å (A11) and 0.52 Å (A12) above the plane formed by the four nitrogen atoms. This arrangement is very reminiscent of aluminum [5] and gallium [6] complexes of the pyrazolyl ligands. Indeed the structural parameters of the $[Me_2Al(tet)]_2$ core is isomorphous to that of $[Me_2Al(pyrazolyl)]_2$ [5]. The difference, of course, is that the tetrazole derivative features an additional two equivalent $AlMe_3$ units which are peripherally coordinated to a third tetrazole nitrogen. This interaction is presumably why a molecular species can be isolated from the polymeric parent.

Decomposition studies of compounds **1**, **4** *and* **5**. Thermogravimetric analyses of **1**, **4** and **5** indicated that the compounds decompose to eliminate N_2 in the range of 200–340°C with a weight loss in the range of 48–62%. In order to explore the possibility that these compounds might be suitable precursors for the low temperature deposition of aluminum nitride several experiments were conducted. First, the compounds (150 mg) were (individually) heated at 250°C for 12 h under static vacuum in a closed side arm flask. The IR of the remaining solids showed that organic material was present but not a stretching frequency corresponding to AlN (~ 700 cm^{-1}). Similar experiments to that described above were performed but heating the precursors under a flow of N_2 and H_2 and subsequently washing the remaining material with CH_2Cl_2 and toluene. The IR of the remaining solids using both gases also showed the remnants of organic material and the filtrates contained aryl resonances in the ^1H NMR but which could not be ascribed to benzonitrile. In an effort to completely remove the organic material from any aluminum nitride which might be forming the compounds were heated in a hot-walled pyrolysis unit at 500°C for 12 h under a flow of N_2 and in the same type of experiments, under a flow of H_2. Again, the IR spectra showed organic material remaining in the solid residues. Finally, **1** was heated at 200°C for 4 h in a sublimation apparatus. The solid which remained in the bottom of the flask showed a ^1H NMR spectrum identical to **1**. Conversely the sublimed material showed a completely different ^1H NMR. Full characterization of the sublimed material led to the conclusion that the molecules were indeed decomposing to eliminate N_2 but that the by-product of this decomposition was a stable

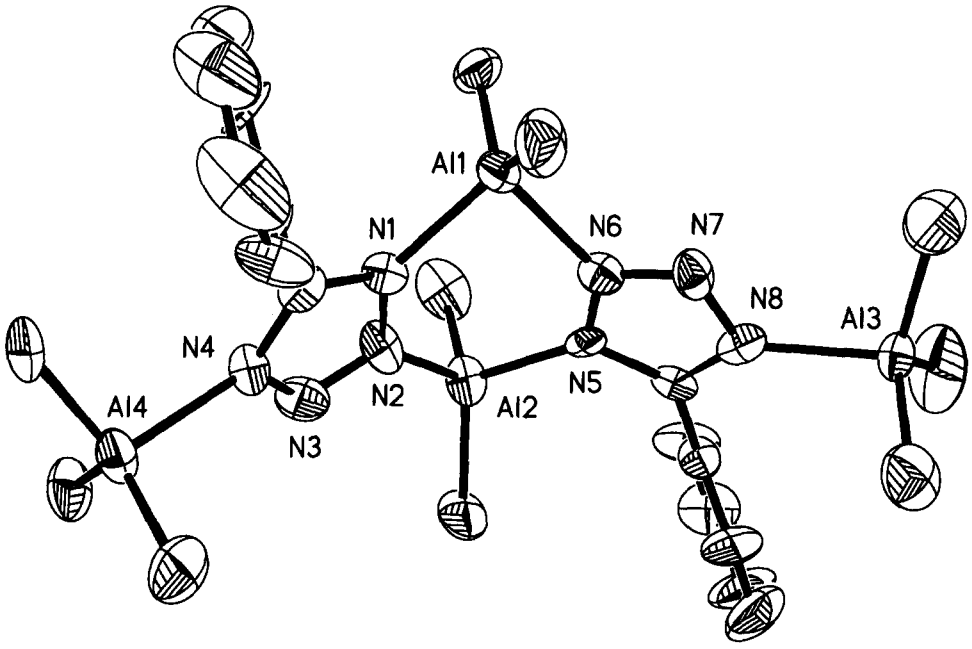

Fig. 1. Molecular structure and atom numbering scheme for compound 7.

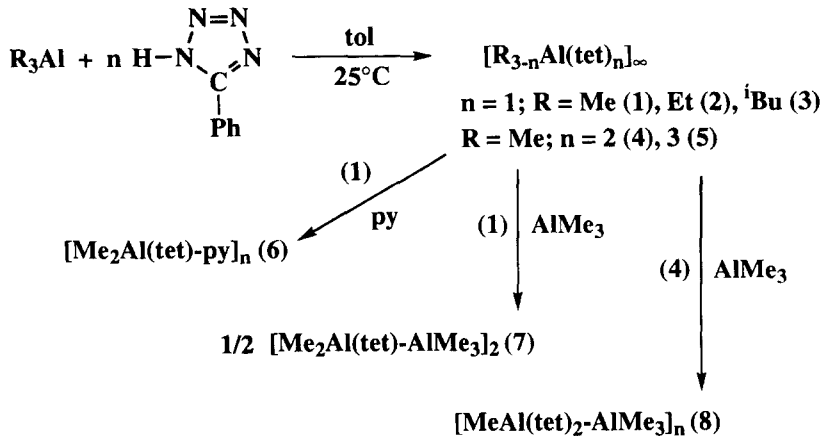

Scheme 1. General syntheses of compounds **1**–**8**.

aluminum containing compound (Scheme 2). Related compounds have been obtained (although not specifically for aluminum) from the decomposition of other tetrazole compounds [2].

CONCLUSIONS

It would thus appear that the tetrazole ligand is a poor choice as a source of nitrogen for aluminum nitride. Stable aluminum containing compounds are produced when either **1**, **4** or **5** are heated to 500 °C. Once a means has been found to prevent polymerization (either with the addition of Lewis bases or acids) tetrazole-aluminum combinations should follow what is known for the related pyrazolyl systems.

EXPERIMENTAL

General considerations

All manipulations were conducted using Schlenk techniques in conjunction to an inert atmosphere glove box. All solvents were rigorously dried prior to use. NMR data were obtained on JEOL-GSX-400 and -270 instruments at 270.17 (^{1}H) MHz in C_6D_6 unless otherwise indicated. Chemical shifts are reported relative to $SiMe_4$ and are in ppm. Elemental analyses were obtained on a Perkin–Elmer 2400 Analyzer. Infrared data were recorded as KBr pellets on a Matheson Instruments 2020 Galaxy Series spectrometer and are reported in cm^{-1}. X-ray data were collected on a Siemens CCD diffractomer using graphite monochromated Mo–K_α (0.71073 Å) radiation. All calculations were performed on a PC using the Siemens software package, SHELXTL-Plus. Selected bond lengths and angles are given in Table 1 while details of the crystal data and a summary of data collection parameters for the complexes are given in Table 2. The data ($\theta = 45°$) for this structure was somewhat weak and there were two molecules of toluene in the lattice. The lowest R value was obtained by narrowing the range to 19.00°. At this point all of the non-hydrogen atoms of the compound were able to be refined with anisotropic parameters but the carbons of the two toluene molecules could only be refined with isotropic parameters.

[$Me_2Al(tet)$]$_n$ (**1**). A solution of trimethyl aluminum (0.25 g, 3.43 mmol) in toluene (10 ml) was added to a stirred suspension of 5-phenyl-1-H-tetrazole (0.5 g, 3.43 mmol) in toluene (20 ml) causing a vigorous gas evolution and the formation of a colorless clear solution, this was stirred for 12 h. Removal of volatiles under reduced pressure produced a white solid which was washed with 10 ml of hexanes, filtration and vacuum dried of the remaining solid afforded **1** in 93% yield as a white toluene insoluble material (mp > 260 °C). ^{1}H NMR (DMSO-d_6): δ −1.06 (s, 6H, $AlCH_3$), 7.52 (m, 3H, C_6H_5), 8.01 (d, 2H, C_6H_5). IR (cm^{-1}): 2962 (m), 1541 (w), 1458 (s), 1400 (m),

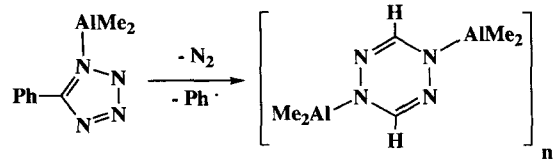

Scheme 2. Postulated product from the thermal decomposition of compound **1**.

Table 1. Selected bond lengths (Å) and angles (°) for **7**

Al(1)—C(15)	1.90(2)	C(15)—Al(1)—C(16)	125.1(9)
Al(1)—C(16)	1.95(2)	C(15)—Al(1)—N(1)	108.6(8)
Al(1)—N(1)	1.99(2)	C(16)—Al(1)—N(1)	111.3(9)
Al(1)—N(6)	2.01(2)	C(15)—Al(1)—N(6)	109.5(7)
Al(2)—C(17)	1.93(2)	C(16)—Al(1)—N(6)	104.5(9)
Al(2)—C(18)	1.91(2)	N(1)—Al(1)—N(6)	93.1(8)
Al(2)—N(2)	1.97(2)	C(17)—Al(2)—C(18)	126(1)
Al(2)—N(5)	1.98(2)	C(18)—Al(2)—N(2)	107.2(9)
Al(3)—C(19)	1.96(2)	C(17)—Al(2)—N(2)	107.8(8)
Al(3)—C(20)	1.94(2)	C(18)—Al(2)—N(5)	110.1(8)
Al(3)—C(21)	1.95(2)	C(17)—Al(2)—N(5)	108.1(8)
Al(3)—N(8)	2.06(2)	N(2)—Al(2)—N(5)	91.6(8)
Al(4)—C(22)	1.98(2)	N(5)—N(6)—Al(1)	128(2)
Al(4)—C(23)	1.96(2)	N(7)—N(6)—Al(1)	119(2)
Al(4)—C(24)	1.97(1)	N(2)—N(1)—Al(1)	125(2)
Al(4)—N(4)	2.07(2)	C(1)—N(1)—Al(1)	127(2)
		N(3)—N(2)—Al(2)	122(2)
		N(1)—N(2)—Al(2)	133(2)
		N(6)—N(5)—Al(2)	130(2)
		C(8)—N(5)—Al(2)	129(2)

Table 2. Summary of data collection and structure solution parameters for **7**

Formula	$C_{43}H_{62}Al_2N_8$
Formula weight	744.97
Crystal system	monoclinic
Space group	$P2_1/c$
a (Å)	12.576(2)
b (Å)	18.358(3)
c (Å)	20.262(3)
β (°)	93.272(4)
V (Å^3)	4670.6(11)
Z	4
F (000)	1304
D_{calc} (Mg m^3)	1.059
Crystal size (mm^3)	$(0.4)^3$
Color, habit	pale yellow block
Temperature (K)	298
Absorbtion coefficient (mm^{-1})	0.098
θ range for data collection (°)	1.50 to 19.00
Reflections collected	10,828
Independent reflections	3714
Data/restraints/parameters	3660/0/342
R_1	0.1237
R_{all}	0.2863
Goodness of fit on F^2	0.778
Largest diff. peak and hole	0.425 and −0.288

1261 (m), 1203 (m), 1076 (s), 1018 (s), 802 (m), 756 (m), 696 (s), 592 (w). Anal. Calcd for $C_9H_{11}AlN_4$: C, 53.74; H, 5.48; N, 27.71. Found: C, 49.84; H, 4.95; N, 26.58.

$[Et_2Al(tet)]_n$ (**2**). To a stirred suspension of 5-phenyl-1-H-tetrazole (0.5 g, 3.43 mmol) in 30 ml of toluene was added with a syringe triethyl aluminum (0.47 ml, 3.43 mmol) causing a vigorous gas evolution and the formation of a colorless clear solution. The reaction mixture was stirred for an additional 12 h, thereafter removal of the solvent under reduced pressure until 10 ml and storage of the solution at −35°C for 1 week afforded **2** as a white solid in 48%; mp 262–264°C which is partially soluble in toluene. ^{1}H NMR (DMSO-d_6): δ −0.35 (q, 1H, $AlCH_2CH_3$), −0.34 (q, 1H, $AlCH_2CH_3$), −0.23 (q, 2H, $AlCH_2CH_3C_6H_5$), 0.94 (t, 6H, $AlCH_2CH_3$), 7.41 (m, 3H, C_6H_5), 7.99 (d, 2H, C_6H_5). IR (cm^{-1}): 2941 (s), 2903 (s), 2862 (s), 1453 (s), 1399 (m), 1281 (w), 1074 (s), 802 (m), 758 (m), 698 (s), 682 (m). Anal. Calcd for $C_{11}H_{15}AlN_4$: C, 57.38; H, 6.57; N, 24.33. Found: C, 54.32; H, 6.68; N, 24.02.

$[^iBu_2Al(tet)]_n$ (**3**). To a stirred suspension of 5-phenyl-1-H-tetrazole (0.5 g, 3.43 mmol) in 30 ml of toluene was added with a syringe triisobutyl aluminum (0.87 ml, 3.43 mmol) causing a vigorous gas evolution and the formation of a colorless clear solution. Removal of volatiles produced a liquid which was redissolved in 20 ml of hexanes. The solution was canula filtered and the solvent removed *in vacuo* affording **3** as a white sticky solid in 83% yield; mp 33°C. ^{1}H NMR (C_6D_6): δ 0.74 [d, 2H, $AlCH_2CH(CH_3)_2$], 1.09 [d, 6H, $AlCH_2CH(CH_3)_2$], 2.10 [dh, 1H, $AlCH_2CH(CH_3)_2$], 7.06 (m, 3H, C_6H_5), 8.27 (m, 2H, C_6H_5). IR (cm^{-1}): 3053 (w), 3024 (w), 2949 (s), 2863 (s) 1460 (s), 1395 (m), 1362 (m), 1262 (w), 818 (w), 679 (s). Anal. Calcd for $C_{15}H_{23}AlN_4$: C, 62.92; H, 8.10; N, 19.37. Found: C, 62.51; H, 8.66; N, 17.30.

$[MeAl(tet)_2]$ (**4**). Prepared as described for **1** from

trimethyl aluminum (0.25 g, 3.43 mmol) and 5-phenyl-1-H-tetrazole (1 g, 6.86 mmol). Yield: 94%; mp > 260 C. ^{1}H NMR (DMSO-d_6): δ −1.02 (s, 3H, AlCH_3), 7.32 (m, 6H, C_6H_5), 8.03 (m, 4H, C_6H_5). IR (cm^{-1}): 3099 (m), 1610 (w), 1525 (w), 1450 (s), 1402 (m), 1282 (w), 1074 (m), 1016 (m), 731 (m), 694 (s), 513 (m). Anal. Calcd for $C_{15}H_{13}AlN_8$: C, 54.22; H, 3.94; N, 33.72. Found: C, 50.31; H, 4.49; N, 28.88.

Synthesis of [Al(tet)$_3$] (**5**). Prepared as described above for **1** from trimethyl aluminum (0.16 g, 2.28 mmol) and 5-phenyl-1-H-tetrazole (1 g, 6.86 mmol). Yield: 96%; mp > 260 C. ^{1}H NMR (DMSO-d_6): δ 7.52 (m, 9H, C_6H_5), 8.03 (d, 6H, C_6H_5). IR (cm^{-1}): 3134 (m), 1450 (s), 1400 (m), 1261 (m), 1097 (s), 1020 (s), 798 (m), 731 (m), 696 (s), 532 (m). Anal. Calcd for $C_{21}H_{15}AlN_{12}$: C, 54.55; H, 3.27; N, 36.35. Found: C, 52.49; H, 3.97; N, 32.23.

[Me$_2$Al(tet)·Py] (**6**). Compound **1** (1.0 g, 4.95 mmol) was suspended in toluene (20 ml). Pyridine (2 ml) was added causing the formation of a colorless solution which was stirred for 2 h. Removal of solvent under reduced pressure produced **6** as a viscous oil which crystallized in stoichiometric yield on standing for 24 h. mp 95 C. ^{1}H NMR ($CDCl_3$): δ −0.31 (s, 6H, AlCH_3), 7.4 (m, 3H, C_6H_5), 7.57 (m, 2H, C_6H_5), 7.06 (m, 3H, C_6H_5), 8.27 (m, 2H, C_6H_5). IR (cm^{-1}): 2357 (w), 1458 (m), 1400 (m), 1261 (s), 1099 (s), 1026 (s), 692 (w).

[Me$_2$Al(tet)-AlMe$_3$]$_2$ (**7**). A solution of trimethyl aluminum (0.25 g, 3.43 mmol) in toluene (10 ml) was added to a stirred suspension of 5-phenyl-1-H-tetrazole (0.5 g, 3.43 mmol) in toluene (20 ml) causing a vigorous gas evolution and the formation of a colorless clear solution. The solution was stirred for 1 h, and then trimethyl aluminum (0.25 g, 3.43 mmol) in toluene (10 ml) was added causing the formation of a colorless crystalline suspension. This was stirred for a further 12 h before **7** was isolated by filtration in 95% yield. Single crystals suitable for X-ray analysis were isolated from the filtrate after several weeks at −30 C. mp 235 C. ^{1}H NMR (DMSO-d_6): δ −1.05 [s, 9H, Al(CH_3)$_3$], −0.54 [s, 6H, Al(CH_3)$_2$], 7.67 (m, 5H, C_6H_5). IR (cm^{-1}): 2933 (m), 2887 (m), 1608 (w), 1527 (w), 1458 (s), 1383 (m), 1288 (w), 1203 (m), 1608 (w), 691 (s). Anal. Calcd for $C_{29}H_{40}Al_4N_8$: C, 52.55; H, 7.35; N, 20.43. Found: C, 47.37; H, 5.97; N, 20.29.

[MeAl(tet)$_2$-AlMe$_3$]$_n$ (**8**). A solution of trimethyl aluminum (0.25 g, 3.43 mmol) in toluene (10 ml) was added to a stirred suspension of 5-phenyl-1-H-tetrazole (1.0 g, 6.86 mmol) in toluene (20 ml) causing a vigorous gas evolution and the formation of a white precipitate. The solution was stirred for 1 h, and then trimethyl aluminum (0.25 g, 3.43 mmol) in toluene (10 ml) was added causing the formation of a colorless crystalline suspension. This was stirred for a further 12 h before **8** was isolated by filtration in 93% yield. mp > 220 C. ^{1}H NMR (DMSO-d_6): δ −0.92 [s, 9H, Al(CH_3)$_3$], −0.54 (s, 3H, AlCH_3), 7.64 (m, 10H, C_6H_5). IR (cm^{-1}): 2936 (m), 2884 (m), 1609 (w), 1528 (m), 1458 (s), 1383 (m), 1289 (w), 1204 (m), 1020 (m), 693 (s). Anal. Calcd for $C_{18}H_{22}N_8Al_2$: C, 53.46; H, 5.48; N, 27.71. Found: C, 52.34; H, 5.01; N, 27.43.

Characterization data for the sublimate from heating **1** *to* 200 *C.* [C_6D_6: δ −0.57 (s, 6H), 7.16 (s, 5H)] and IR [cm^{-1} 3129 (m), 2951 (m), 2847 (m), 2145 (w), 1451 (m), 1400 (w), 1204 (m), 1053 (m), 1015 (m), 693 (s)]. EI-MS [*m*/*z* (intensity %): 57 (100, Me_2Al^+), 71 (70, Me_2AlN^+), 97 (50, $Me_2AlN_2^+$), 111 (39, $Me_2AlN_3^+$), 125 (14, $Me_2AlN_4^+$)]; Elemental analysis (C, 49.65, H, 3.92, N, 29.09).

Acknowledgements—This work was funded principally by the Office of Naval Research EPSCoR program (N00014-96-1-1271). Partial funding was supplied by the National Science Foundation (Grant 9452892) and the donors of the Petroleum Research Fund (Grant 31901-AC3), administered by the American Chemical Society. The receipt of an NSF-CAREER award (CHE-9625376) is also gratefully acknowledged.

REFERENCES

1. (a) Goodger, A., Hill, M., Mahon, M. F., McGinley, J. and Molloy, K., *J. Chem. Soc., Dalton Trans.*, 1996, 847; (b) Hill, M., Mahon, M. F. and Molloy, K., *J. Chem. Soc., Dalton Trans.*, 1996, 1857.
2. Butler, R. N., in *Comprehensive Heterocyclic Chemistry*, ed. R. A. Katritzky and C. W. Rees, Pergamon Press, Oxford, 1984, **5,** 791.
3. Neumayer, D. A. and Ekerdt, J. G., *Chem. Mater.*, 1996, **8,** 9.
4. For some recent examples: (a) Neumayer, D. A., Cowley, A. H., Decken, A., Jones, R. A., Lakhotia, V. and Ekerdt, J. G., *J. Am. Chem. Soc.*, 1995, **117,** 5893; (b) Miehr, A., Ambacher, O., Rieger, W., Metzger, T., Born, E. and Fischer, R. A., *Chem. Vap. Deposition*, 1996, **2,** 51; (c) Kouvetakis, J., McMurran, J., Matsunaga, P., O'Keeffe, M. and Hubbard, J. L., *Inorg. Chem.*, 1997, **36,** 1792.
5. Arduini, A., *J. Chem. Soc., Dalton Trans.*, 1974, 503.
6. See for examples: (a) Louie, B. M., Rettig, S. J., Storr, A. and Trotter, J., *Can. J. Chem.*, 1985, **63,** 703; (b) Nussbaum, S. and Storr, A., *Can. J. Chem.*, 1985, **63,** 2550.

CHEMICAL ABSTRACTS

The combination of 5-phenyl-1-H-tetrazole (tet) with AlR_3 in stoichiometries of 1–3 leads to the compounds [(tet)AlR_2]$_n$ R = Me (**1**), Et (**2**), ^{t}Bu (**3**), [(tet-)$_2$AlMe]$_n$ (**4**), and [(tet)$_3$Al]$_n$ (**5**). The addition of pyridine to **1** leads to a compound with the formulation, [(tet)$AlMe_2$-pyridine]$_n$ (**6**). Likewise the addition of $AlMe_3$ to **1** and **4** leads to the products, [(tet)$AlMe_2$-$AlMe_3$]$_2$ (**7**) and [(tet)$_2$AlMe-$AlMe_3$]$_n$ (**8**). The compounds were characterized by standard techniques and, in the case of **7** by X-ray crystallography (monoclinic, $P2_1/c$, a = 12.576(2) Å, b = 18.358(3) Å, c = 20.262(3) Å, β = 93.272(4)°, V = 4670.6(11) Å^3, Z = 4, with 3714 indp. reflections R_1 = 12.37%).

Compounds **1** and **4** and **5** were examined (unsuccessfully) as potential unimolecular precursors to aluminum nitride.

GRAPHICAL ABSTRACT

The combination of 5-phenyl-1-H-tetrazole (tet) with AlR_3 in stoichiometries of 1–3 leads to a series of poorly soluble compounds having the general formula, $[(tet)_nAlR_{3-m}]_n$ where $m = 1$–3. More soluble compounds can be obtained by the addition of either a strong Lewis base (such as pyridine) or an additional equivalent of $AlMe_3$. This latter reaction results in the formation of a dimeric compound for R = Me (shown). Several of the compounds were examined (unsuccessfully) as potential unimolecular precursors to aluminum nitride.

Pergamon

PII: S0277-5387(98)00045-X

Polyhedron Vol. 17, Nos 13–14, pp. 2243–2248, 1998
© 1998 Elsevier Science Ltd
All rights reserved. Printed in Great Britain
0277-5387/98 $19.00+0.00

Edta-linked 4f-3d heterometallic two dimensional sheet in $Ln_2M_3(edta)_3(H_2O)_{11}\cdot 12H_2O$ (Ln=Nd, Gd; M=Mn,Co)

Tao Yi, Song Gao* and Biaoguo Li

State Key Laboratory of Rare Earth Materials Chemistry & Applications, College of Chemistry and Molecular Engineering, Peking University, Beijing 100871, China

(Received 4 June 1997; accepted 14 January 1998)

Abstract—Two novel edta-linked 4f-3d heterometallic two-dimensional coordination polymers $Nd_2Mn_3(edta)_3(H_2O)_{11}\cdot 12H_2O$ (**A**) and $Gd_2Co_3(edta)_3(H_2O)_{11}\cdot 12H_2O$ (**B**) were synthesized by reaction of $Ln(OH)_3$ (Ln = Nd, Gd), $MnCO_3$ or $Co(OH)_2$ with H_4edta (edta = ethylenediamine-NNN′N′-tetra-acetate) in water. **A** and **B** crystallize in the monoclinic space group C2 with cell parameters a = 16.003(3), 15.799(5), b = 14.733(3), 14.603(5), c = 14.819(3), 14.690 Å, β = 116.21(2), 116.64(3)°, V = 3135(1), 3029(2) Å^3, and Z = 2. **A** or **B** consists of a two-dimensional heterometallic sheet in which the Ln(III) ion is ten coordinated by six carboxyl oxygen atoms from edta and four oxygen atoms from H_2O molecules, the M(II) ion is seven coordinated by two nitrogen, four oxygen from edta and one oxygen from H_2O molecule. Each Ln(III) ion has three M(II) neighbours, while each M(II) is connected to two Ln(III) ions. The Ln(III) and M(II) ions are linked by tridendate bridging carboxylate oxygen atoms with considerable short Ln-M separations in the range of 4.82 to 4.90 Å, which are shorter than the distances between metal ions in heterometallic 3d complexes of edta. The heterometallic sheets are connected by H_2O molecules through hydrogen bonds. © 1998 Elsevier Science Ltd. All rights reserved

Keywords: edta; 4f-3d heterometallic; crystal structure; two dimensional sheet.

The magnetic properties of heteropolymetallic compounds have attracted considerable interest in the last two decades [1, 2]. Great attention has been paid to extended coordination polymer systems, since they often show long range ferro- or ferri- magnetic ordering in the liquid-helium temperature range. To our knowledge, all of them involve only transition-metal ions except for one series, 'oxamato' bridged compounds $[Ln_2Cu_3]$, which contain both lanthanide and transition metal ions with 1-D or 2-D structures [3–5]. As to edta linked, extended heterometallic 3d compounds, two families are known to date [6–10]. One concerns $MM'(edta)\cdot 6H_2O$ with ferrimagnetic chains ([MM′] = [MnCo], [MnNi], [MnCu], [CoNi], [CoCu], [NiNi]). The other series is a 3-D coordination polymer with general formula $M''M(M'edta)_2\cdot 4H_2O$ ([M″MM′] = [CoCoCo], [CoCoNi], [CoNiNi], [ZnNiNi]). Both series exhibit ferrimagnetic ordering below 1.06 K. In this paper, structures of two novel edta linked 4f-3d heterometallic 2-dimensional coordination polymers were reported, tridentate bridging mode of carboxylate group and seven coordinated Co(II) were observed in the complexes.

EXPERIMENTAL

All starting chemical reagents were commercially available and were of reagent grade. Elemental analysis (C, H, N) was performed by the Carlo Erba 1106. IR spectra were recorded on a Nicolet 750 FTIR spectrometer. The thermogravimetric analysis was made by an LT-1 model thermobalance under atmosphere.

*Author to whom correspondence should be addressed.

The proportions of Ln(III) and M(II) were determined by Inductively Coupled Plasma (ICP).

Preparation of $Nd_2Mn_3(edta)_3(H_2O)_{11} \cdot 12H_2O$ (**A**)

Nd_2O_3 (99.9%) was dissolved in aqueous HNO_3, from which $Nd(OH)_3$ was precipitated by 6N NaOH. 1 mmol $MnCO_3$ (99.9%), 2 mmol $Nd(OH)_3$ and 2 mmol H_4edta (>99%) were added to 10 ml water. After stirring and heating, the solids were dissolved, yielding an almost transparent solution, which then was filtered. Pink crystals were obtained after a few months. Found: C, 20.80; H, 4.75; N, 4.73%. Anal. Calc. for $C_{30}H_{82}Mn_3N_6Nd_2O_{47}$: C, 20.80; H, 4.73; N, 4.85%.

Preparation of $Gd_2CO_3(edta)_3(H_2O)_{11} \cdot 12H_2O$ (**B**)

$Gd(OH)_3$ and $Co(OH)_2$ were made in a manner similar to $Nd(OH)_3$. 3 mmol $Co(OH)_2$, 2 mmol $Gd(OH)_3$ and 2 mmol H_4edta were mixed in water. After stirring and heating, the mixture became an almost clear solution which was then filtered. Rose-red single crystals were formed after a few weeks. Found: C, 20.30; H, 4.29; N, 4.70%. Anal. Calc. for $C_{30}H_{82}Co_3Gd_2N_6O_{47}$: C, 20.35; H, 4.63; N, 4.75%.

Crystallography of $[Nd_2Mn_3]$ (**A**) and $[Gd_2CO_3]$ (**B**)

The diffraction data of $[Nd_2Mn_3]$ (**A**) and $[Gd_2Co_3]$ (**B**) were collected on an Enraf-Nonius CAD-4 diffractometer using graphite-monochromated Mo Kα radiation in the θ-scan mode ($2\theta_{max} = 50$ and 46°) at room temperature. Cell Parameters of **A** and **B** were determined from 25 reflections in the θ range of 9.32–12.25° (for **A**) and 9.22–12.35° (for **B**) respectively. An empirical absorption correction was applied to the original data set [11]. The crystallographic data of **A** and **B** was summarized in Table 1. The structures were solved using direct methods and refined by a full-matrix, least-squares technique (SDP-PLUS and SHELXL97) [12, 13]. The quantity minimized was $\Sigma w(|F_o|^2 - |F_C|^2)$ with $w = 1/[\sigma^2(F^2_O) + (0.1157*P)^2 + 19.4077*P]$ for **A** and $1/[\sigma^2(F^2_O) + (0.0945*P)^2 +$

Table 1. Crystallographic Data for $[Nd_2Mn_3]$ and $[Gd_2Co_3]$

	$[Nd_2Mn_3]$	$[Gd_2Co_3]$
Empirical formula	$C_{30}H_{82}Mn_3N_6Nd_2O_{47}$	$C_{30}H_{82}Co_2Gd_2N_6O_{47}$
crystal system	monoclinic	monoclinic
space group	C2	C2
a, Å	16.003(3)	15.799(5)
b, Å	14.733(3)	14.603(5)
c, Å	14.819(3)	14.690(3)
β, deg	116.21(2)	116.64(3)
V, Å^3	3135(1)	3029(2)
Formula weight	1732.3	1770.3
λ, Å	0.71069	0.71069
Z	2	2
D_x, g cm^{-3}	1.835	1.941
$F(000)$	1750	1778
Crystal size	0.30 × 0.30 × 0.20 mm	0.30 × 0.20 × 0.20 mm
T, K	299 ± 1	299 ± 1
Theta	2.09 to 24.97°	2.01 to 22.99°
Index ranges	$-19 \le h \le 17$, $0 \le k \le 17$, $0 \le l \le 17$	$0 \le h \le 17$, $0 \le k \le 16$, $-16 \le l \le 14$
μ, mm^{-1}	2.329	3.081
Refl. collected/unique	2982/2865 [R(int) = 0.0411]	2199/2199 [R(int) = 0.0000]
Max. and min. transm.	0.6531 and 0.5417	0.5777 and 0.4583
Refinement method	Full-matrix least-squares on F^2	
Parameters	368	368
Goodness-of-fit on F^2	1.059	1.099
Final R indices [$I > 2\sigma(I)$]	$R_1 = 0.0527$, $wR_2 = 0.1388$	$R_1 = 0.0368$, $wR_2 = 0.1034$
R indices (all data)	$R_1 = 0.0539$, $wR_2 = 0.1399$	$R_1 = 0.0394$, $wR_2 = 0.1048$
Abs. struc. parameter	0.23(3)	0.00(2)
Largest diff. peak and hole	1.444 and −2.958 e.Å^{-3}	0.909 and −1.097 e.Å^{-3}

$R_1 = \Sigma||F_O| - |F_C||/\Sigma|F_O|$

$wR_2 = [\Sigma w(F^2_O - F^2_C)^2/\Sigma w(F^2_O)^2]^{1/2}$

0.0000*P] for **B**, where $P=[Max(F^2_O,0)+2*F^2_C]/3$. The final refinement for **A** converged to $R_1=0.0527$ and $wR_2=0.1388$ for 2787 observed reflections ($I>2\sigma(I)$). The maximum residual hole in the last difference fourier map was $-2.958\,e\text{Å}^{-3}$ (0.97 Å from Nd). The final refinement for **B** was reached with $R_1=0.0368$ and $wR_2=0.1034$ for 2082 observed reflections ($I>2\sigma(I)$). The maximum residual hole in the last different fourier map is $-1.097\,e\text{Å}^{-3}$.

RESULTS AND DISCUSSIONS

Thermal stability of **A**

Thermogravimetric analysis of **A** showed that twenty-three waters were lost during two steps below 162°C, and the cumulative loss was 23.85% (calc. 23.90%). The complex was decomposed and oxidized between 313–412°C and the remaining weight was 27.99%, according to Nd_2O_3 and MnO_2 (calc. 34.47%). The thermal data was confirmed by the crystal structure data.

IR spectra

The IR spectra of H_4edta, complex **A** and **B**, were measured. Compared to the IR spectra of H_4edta, the stretching vibration absorption peak of the carboxylic group of **A** and **B** shifted from a broad band 1674–1704 cm^{-1} to a sharp peak at 1587 cm^{-1} for **A** and 1593 cm^{-1} for **B**. This indicated that the carboxylic group coordinated to the metal ions and the bond length of C–O tends to be unified. This result was also supported by the crystal structure discussed in the next part. Furthermore, the strong ν(O–H) at 3436 cm^{-1} became wider, which anticipated the existence of more hydrogen bonds in the complexes.

Crystal structure of **A** *and* **B**

X-ray crystallography has established that complexes **A** and **B** are isostructural as shown in Fig. 1. The Ln(III) (Ln = Nd, Gd) ion is ten coordinated by six carboxylate oxygen atoms from edta and four oxygen atoms from H_2O molecules, forming a distorted, bicapped tetragonal anti-prismatic coordination polyhedron with the bond lengths of Ln–O in the range of 2.466–2.791 Å (for **A**) and 2.392–2.766 Å (for **B**). In **A**, O5, O10, O21 and O24 form a plane (distance to the plane: O5, 0.21(1); O10, 0.20(1); O21, −0.19(1); O24, −0.22(1)), while O2, O6, O22 and O23 form another plane (distances to the plane: O2,0.13(1); O6, −0.14(1); O22, 0.20(1); O23, −0.19(1)) and the dihedral angle between the two planes is 15.5(2)°. The distances from Nd(III) to the bridged oxygen atoms, O2, O6 and O9 in **A** are a bit longer than those of the other seven non-bridged oxygen atoms. A similar situation was observed in **B**. M(II) ion is seven coordinated by two nitrogen, four oxygen atoms from the carboxylate group of edta and one oxygen atom from the H_2O molecule. **B** is the second seven coordinate cobalt-aqua-edta complex, average bond lengths of Co–O (2.18 Å) and Co–N (2.24 Å) are a little longer than those in the other Co-edta compounds. A similar coordination number and geometry for Co(II) was also found in $[Co(edtaH_2)(H_2O)]\cdot 2H_2O$ [14]. Meanwhile, seven coordinated Mn(II) complexes are not

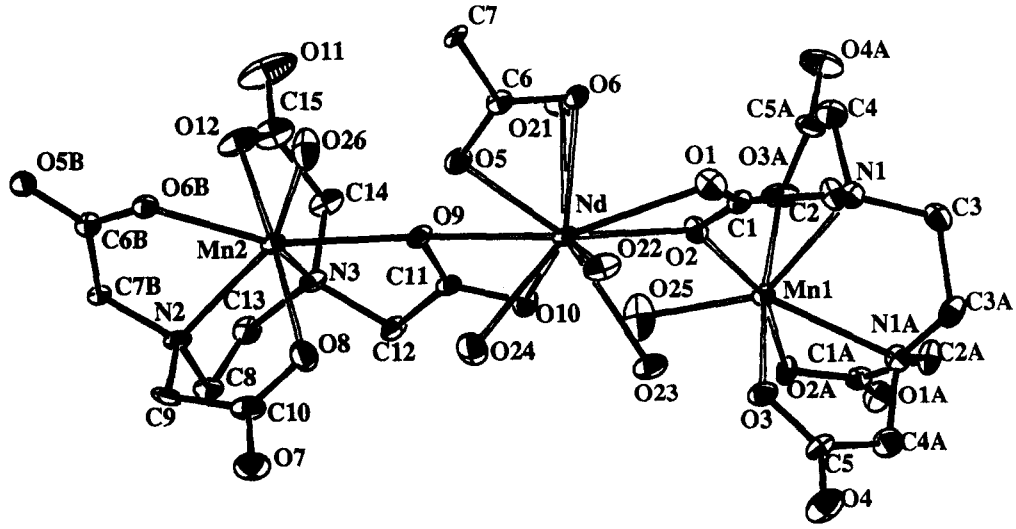

Fig. 1. The ORTEP view of $Nd_2Mn_3(edta)_3(H_2O)_{11}\cdot 12H_2O$ (30% probability displacement ellipsoids). H atoms have been omitted for clarity.

Table 2. Selected Bond Distances and Angles in [Nd_2Mn_3] and [Gd_2Co_3]

Bonds	Nd_2Mn_3	Gd_2Co_3	Bonds	Nd_2Mn_3	Gd_2Co_3
		Bond Lengths (Å)			
Ln-O(5)	2.466(9)	2.411(8)	M(1)-O(2)	2.332(8)	2.311(8)
Ln-O(24)	2.478(10)	2.424(9)	M(1)-N(1)	2.392(10)	2.252(9)
Ln-O(10)	2.493(9)	2.465(8)	M(2)-O(12)	2.149(10)	2.095(8)
Ln-O(22)	2.502(9)	2.418(8)	M(2)-O(26)	2.161(12)	2.057(11)
Ln-O(23)	2.502(8)	2.411(9)	M(2)-O(8)	2.187(9)	2.131(9)
Ln-O(21)	2.508(7)	2.442(7)	M(2)-N(2)	2.281(10)	2.213(10)
Ln-O(1)	2.510(11)	2.392(9)	M(2)-O(6)#3	2.318(8)	2.322(8)
Ln-O(9)	2.659(9)	2.707(9)	M(2)-N(3)	2.380(9)	2.252(8)
Ln-O(6)	2.732(8)	2.688(8)	M(2)-O(9)	2.380(10)	2.327(9)
Ln-O(2)	2.791(8)	2.766(8)	Ln... M1	4.904(2)	4.897(2)
M(1)-O(25)	2.128(16)	2.119(15)	Ln... M2	4.821(2)	4.838(2)
M(1)-O(3)	2.188(9)	2.091(8)			
		Selected Angles (deg)			
Angles	Nd_2Mn_3	Gd_2Co_3	Angles	Nd_2Mn_3	Gd_2Co_3
O(5)-Ln-O(24)	77.2(4)	75.0(3)	O(1)-Ln-O(2)	48.1(3)	48.6(3)
O(5)-Ln-O(10)	118.8(3)	117.2(3)	O(9)-Ln-O(2)	111.3(3)	109.9(2)
O(24)-Ln-O(10)	77.6(3)	77.5(3)	O(6)-Ln-O(2)	106.9(2)	107.5(2)
O(5)-Ln-O(22)	76.4(3)	77.8(3)	O(25)-M(1)-O(3)	93.5(3)	88.3(3)
O(24)-Ln-O(22)	73.4(4)	73.4(3)	O(3)-M(1)-O(3)#2	173.0(6)	176.6(5)
O(10)-Ln-O(22)	143.0(3)	142.2(3)	O(3)-M(1)-O(2)#2	102.7(3)	102.0(3)
O(5)-Ln-O(23)	144.1(3)	144.9(3)	O(25)-M(1)-O(2)	80.5(2)	77.2(2)
O(24)-Ln-O(23)	74.3(3)	75.7(3)	O(3)-M(1)-O(2)	78.5(3)	77.3(3)
O(10)-Ln-O(23)	75.5(3)	74.3(3)	O(2)#2-M(1)-O(2)	161.0(4)	154.4(4)
O(22)-Ln-O(23)	74.9(3)	75.6(3)	O(25)-M(1)-N(1)	142.7(2)	140.5(2)
O(5)-Ln-O(21)	82.3(3)	81.4(3)	O(3)-M(1)-N(1)	101.5(4)	106.3(4)
O(24)-Ln-O(21)	140.3(4)	137.5(3)	O(3)#2-M(1)-N(1)	72.8(3)	76.4(3)
O(10)-Ln-O(21)	83.4(3)	82.7(3)	O(2)#2-M(1)-N(1)	127.7(3)	132.0(3)
O(22)-Ln-O(21)	133.5(3)	135.0(3)	O(2)-M(1)-N(1)	69.5(3)	70.9(3)
O(23)-Ln-O(21)	133.5(3)	133.7(3)	O(25)-M(1)-N(1)#2	142.7(2)	140.5(2)
O(5)-Ln-O(1)	116.6(3)	118.2(3)	O(3)#2-M(1)-N(1)#2	101.5(4)	106.3(4)
O(24)-Ln-O(1)	142.2(3)	144.4(3)	N(1)-M(1)-N(1)#2	74.6(5)	79.0(5)
O(10)-Ln-O(1)	117.5(3)	117.0(3)	O(12)-M(2)-O(26)	86.4(5)	85.9(5)
O(22)-Ln-O(1)	76.1(3)	77.4(3)	O(12)-M(2)-O(8)	173.5(4)	178.9(4)
O(23)-Ln-O(1)	76.6(3)	77.6(4)	O(26)-M(2)-O(8)	100.1(5)	93.8(5)
O(21)-Ln-O(1)	77.4(4)	78.1(4)	O(12)-M(2)-N(2)	100.5(4)	103.3(4)
O(5)-Ln-O(9)	68.4(3)	66.8(3)	O(26)-M(2)-N(2)	145.2(4)	143.4(5)
O(24)-Ln-O(9)	66.4(3)	65.4(3)	O(8)-M(2)-N(2)	73.9(4)	76.4(4)
O(10)-Ln-O(9)	50.4(3)	50.4(2)	O(12)-M(2)-O(6)#3	78.5(4)	76.4(3)
O(22)-Ln-O(9)	131.0(3)	130.8(3)	O(26)-M(2)-O(6)#3	78.0(4)	76.2(4)
O(23)-Ln-O(9)	117.4(3)	116.6(3)	O(8)-M(2)-O(6)#3	102.4(4)	102.5(3)
O(21)-Ln-O(9)	74.6(4)	72.9(3)	N(2)-M(2)-O(6)#3	70.3(3)	71.9(3)
O(1)-Ln-O(9)	150.6(2)	149.5(3)	O(12)-M(2)-N(3)	72.9(3)	76.2(3)
O(5)-Ln-O(6)	49.4(3)	50.3(3)	O(26)-M(2)-N(3)	137.2(5)	137.7(5)
O(24)-Ln-O(6)	118.1(3)	117.3(3)	O(8)-M(2)-N(3)	102.2(4)	104.7(4)
O(10)-Ln-O(6)	149.8(3)	149.0(3)	N(2)-M(2)-N(3)	76.6(3)	78.7(4)
O(22)-Ln-O(6)	66.5(3)	67.9(3)	O(6)#3-M(2)-N(3)	130.8(3)	133.4(3)
O(23)-Ln-O(6)	131.9(3)	133.9(3)	O(12)-M(2)-O(9)	99.2(4)	99.5(4)
O(21)-Ln-O(6)	68.2(3)	68.1(3)	O(26)-M(2)-O(9)	77.8(4)	75.1(4)
O(1)-Ln-O(6)	67.3(3)	67.9(3)	O(8)-M(2)-O(9)	82.7(3)	81.4(3)
O(9)-Ln-O(6)	109.5(3)	108.5(2)	N(2)-M(2)-O(9)	133.3(3)	135.7(3)
O(5)-Ln-O(2)	148.5(3)	148.4(3)	O(6)#3-M(2)-O(9)	155.7(3)	151.3(3)
O(24)-Ln-O(2)	133.1(3)	134.1(3)	N(3)-M(2)-O(9)	69.5(3)	70.6(3)
O(10)-Ln-O(2)	69.5(3)	68.5(2)	M(1)-O(2)-Ln	146.2(4)	149.2(4)
O(22)-Ln-O(2)	116.5(3)	118.0(3)	M(2)#1-O(6)-Ln	149.3(4)	150.4(4)
O(23)-Ln-O(2)	65.9(3)	66.1(3)	M(2)-O(9)-Ln	146.2(4)	147.8(4)
O(21)-Ln-O(2)	68.0(3)	68.1(3)			

Symmetry transformations used to generate equivalent atoms:
#1 $-x+1/2, y+1/2, -z+2$
#2 $-x, y, -z+1$
#3 $-x+1/2, y-1/2, -z+2$

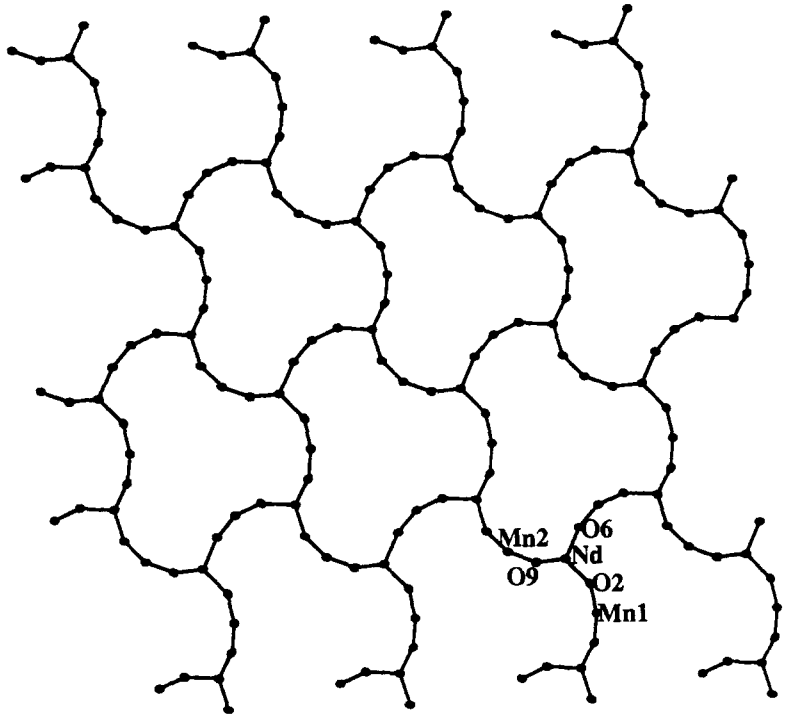

Fig. 2. The connection of metal ions through O atoms in two-dimensional sheet.

rare, such as $Mn_2edta \cdot 9H_2O$ and $Mn_3(edta)_2 \cdot 10H_2O$ [15].

In the title complex, each Ln(III) ion is connected to three M(II) ions by three tridentate carboxylate-O,O′ bridges, while each M(II) ion has two Ln(III) neighbours. Comparing the structures of the title compounds and other edta linked 3d complexes, the most important and significant structural character is based on the bridging modes of the carboxylate group. In carboxylato-linked 4f-3d heteronuclear complexes, such as $\{[GdMn(dtpa)(H_2O)_5]_2 \cdot H_2O\}_n$ [18] and $[Cu_3Gd_2(O_2CCH_2Cl)_{12}(H_2O)] \cdot 2H_2O$ [19]. It is the special bridging mode of the carboxylate group of edta that makes the distances (4.8-4.9 Å) between bridged metal atoms Ln and M significantly shorter than those in 3d heterometallic edta complexes (> 6 Å) [6–10] and other 4f-3d low-dimensional compounds (5.6–5.8 Å) [3–5].

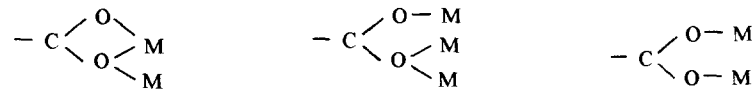

$[Ln_2M_3]$, the bridging carboxylate-O,O′ group is in a less common situation (a). One of its oxygen atoms is used to link Ln(III) and M(II), the other one is bound to Ln(III). This means that the two atoms of a tridentate carboxylate-O,O′ group are used to coordinate only two metal atoms, which is different from the common tridentate bridging mode (b) in which the two O atoms of a carboxylate group are dentate to three metal centers [16]. Meanwhile, the most conventional bridging mode of carboxylate group is bidentate, type (c) [17], which was also found in edta linked 3d heterometallic compounds [6–10], and some

The complex molecule of $[Ln_2M_3]$ consists of 12-membered metal (6Ln, 6M) circle motifs, which were linked together by twelve oxygen atoms to form a two dimensional sheet, as shown in Fig. 2. In the sheet, the nearest M(II)–M(II) and Ln(III)–Ln(III) distances are larger than 8.1 and 8.4 Å respectively. The sheets are connected by H_2O molecules through hydrogen bonds, as shown in Fig. 3. The structure of title compounds is different from the structure of $MM(edta) \cdot 6H_2O$, which consists of 1-D zigzag chains built up from two alternating octahedral sites, referred to as 'chelated' or 'hydrate' according to their local environ-

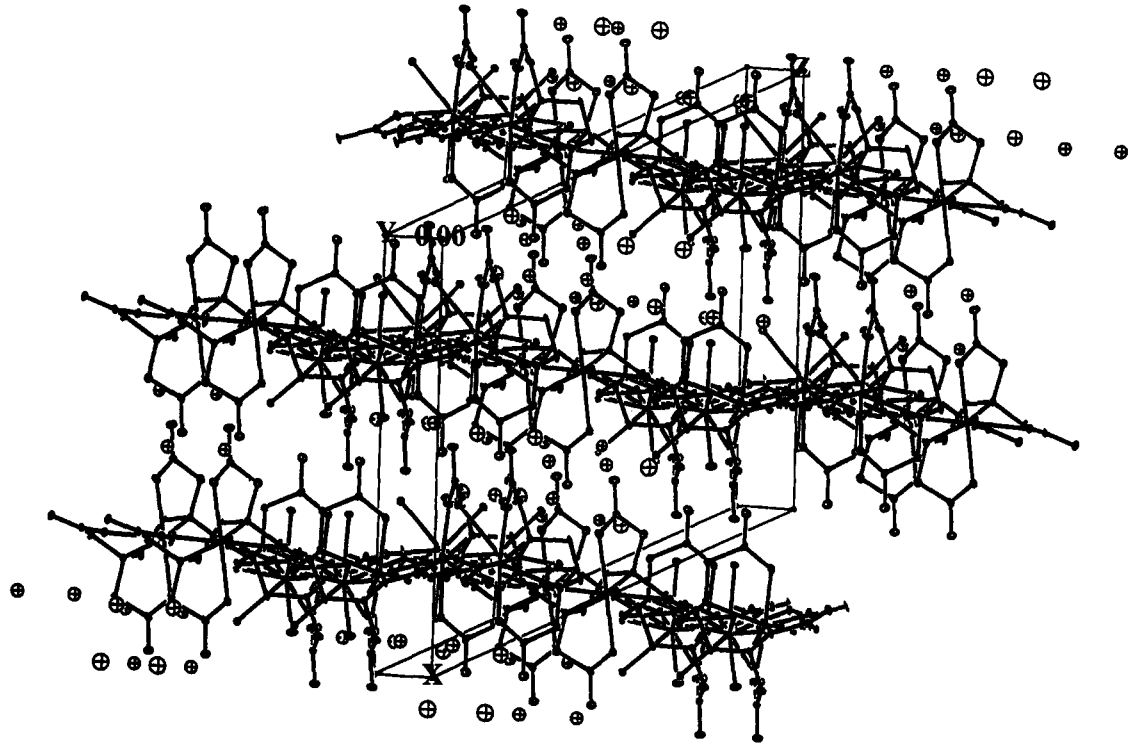

Fig. 3. The packing of 2-D sheets in a unit cell of $[Ln_2M_3]$. H_2O molecules are filled between the layers.

ment and is also different from the layered 3-D $M''M(M'edta)_2 \cdot 4H_2O$. Thus the title complexes may be served as the first 2-D edta coordination polymers, containing both lanthanide and transition metal ions. The investigation of magnetic properties for these complexes is in progress.

Acknowledgments—This work was supported by The State Key Project for Fundamental Research. S.G. thanks Prof. Dr. H. Lueken for helpful discussion and the Alexander von Humboldt Stiftung for a fellowship and NSFC (29771001).

REFERENCES

1. Kahn, O., *Structure and Bonding*, 68, Berlin, 1987, p. 89.
2. Kahn, O., *Advances in Inorganic Chemistry*, 1995, **43,** 179.
3. Guillou, O., Kahn, O. and Oushoorn, R. L., *Inorg. Chem. Acta.*, 1992, **198-120,** 119–131.
4. Kahn, O., Guillou, O., Oushoorn, R. L., Drillon, M., Rabu, P., Boubekeur, K. and Batail, P., *New J. Chem.*, 1995, **19,** 655–660.
5. Guillou, O., Bergerat, P., Kahn, O., Bakalbasis, E., Boubekeur, K., Batail, P. and Guillot, M., *Inorg. Chem.*, 1992, **31,** 110–114.
6. Coronado, E., Drillon M. and Georges, R., in *Research Frontiers in Magnetochemistry*, C. J. O'Connor (Ed.), World Scientific, 1993, pp. 27–66.
7. Coronado, E., in *Magnetic Molecular Materials*, D. Gatteschi, O. Kahn, J. S. Miller and F. Palacio (Eds.), Kluwer, 1991, NATO ASI Series, Vol. E-198, pp. 267–279.
8. Borras-Almenar, J. J. and Coronado, E., *Inorg. Chem. Acta*, 1993, **207,** 105–109.
9. Coronado, E., Drillon, M., Nugteren, P. R., Jongh, L. J., Beltran, D. and Georges, R., *J. Am. Chem. Soc.*, 1989, **111,** 3874.
10. Sapina, F., Coronado, E., Beltran, D. and Burriel, R., *J. Am. Chem. Soc.*, 1991, **113,** 7940.
11. Walker, N. and Stuart, D., *Acta Crystallogr.*, 1983, **A39,** 158–166.
12. Frenz B. A. and Associates, Inc., College Station, Texas 77840 and Enraf–Nonius, Delft, The Netherlands.
13. Sheldrick, G. M., *SHELXL97, PC Version*, University of Goettinggen, Germany, 1997.
14. Zubkowski J. D., Perry D. L., Valente E. J. and Lott S., *Inorg. Chem.* 1995, **34**, 6409–6411; *Inorg.Chem.*, 1996, **35**, 6352.
15. Richards, S., Pedersen, B., Silverton, J. V. and Hoard, J. L., *Inorg. Chem.*, 1964, **3,** 27.
16. Mounts, R. D., Ogura, T. and Fernando, Q., *Inorg.Chem.*, 1974, **13,** 802.
17. Oldham, C., in *Comprehensive Coordination Chemistry*, G. Wilkinson, R. D. Gillard, and J. A. McCleverty (Eds.), Pergamon Press: Oxford, U.K., 1987; **Vol.2**, Chapter 15.6, pp. 437–440.
18. Jin, T.-Z., Zhao, S.-F., Xu, G.-X., Zhen, H.-Y., Shi, N.-C. and Ma, Z.-S., *Acta Chimica Sinica*, 1991, **19,** 569 (Chinese).
19. Chen, X.-M., Tong, M.-L., Wu, Y.-L. and Luo, Y.-J., *J. Chem. Soc., Dalton Trans.*, 1996, **0,** 2181–2182.

Pergamon

PII: S0277-5387(98)00035-7

Polyhedron Vol. 17, Nos 13–14, pp. 2249–2256, 1998
© 1998 Elsevier Science Ltd
All rights reserved. Printed in Great Britain
0277-5387/98 $19.00+0.00

Synthesis, crystal structure and spectroscopic properties of diorganothallium(III) derivatives of 2,6-diacetyl-pyridine-monothiosemicarbazone

J. S. Casas,[a]* E. E. Castellano,[b] M. S. García-Tasende,[a] A. Sánchez,[a] J. Sordo[a] and M. J. Vidarte[a]

[a]Departamento de Química Inorgánica, Universidade de Santiago de Compostela, 15706 Santiago de Compostela, Galicia, Spain

[b]Instituto de Física e Química de Sao Carlos, USP, CEP 13560, Sao Carlos, Brazil

(Received 13 November 1997; accepted 12 January 1998)

Abstract—Dimethyl(2,6-diacetyl-pyridine-monothiosemicarbazonato)thallium(III), $[TlMe_2(L)]$, and Diphenyl-(2,6-diacetyl-pyridine-monothiosemicarbazonato)thallium(III) chloroform solvate, $[TlPh_2(L)],CHCl_3$ were prepared by reacting the corresponding diorganothallium(III) hydroxide with 2,6-diacetyl-pyridinemonothiosemicarbazone (HL). $[TlMe_2(L)]$ crystallizes in the triclinic space group $P\bar{1}$ (no. 2) with $a = 7.064(3)$, $b = 9.149(2)$, $c = 12.377(2)$Å, $\alpha = 79.378(11)$, $\beta = 74.92(2)$, $\gamma = 82.75(2)$, $Z = 2$, $R_1 = 0.0305$, $Rw_2 = 0.0673$. $[TlPh_2(L)].CHCl_3$ crystallizes in the monoclinic space group $C2/c$ with $a = 23.559(3)$, $b = 13.582(2)$, $c = 16.808(3)$Å, $\beta = 106.04(1)°$, $Z = 8$, $R_1 = 0.0620$, $Rw_2 = 0.1155$. Both complexes consist of molecules in which the deprotonated ligand is S,N(3),N(4),O-bonded to the thallium atom $[TlMe_2(L)]$, Tl—S = 2.872(2), Tl—N(3) = 2.590(6), Tl—N(4) = 2.686(2), Tl—O = 2.883(6)Å; $[TlPh_2(L)].CHCl_3$, Tl—S = 2.791(6), Tl—N(3) = 2.56(2), Tl—N(4) = 2.579(14), Tl—O = 2.86(1)Å]. A weak bond Tl...O′ $[TlMe_2(L)]$, 3.050(2) Å; $[TlPh_2(L)].CHCl_3$, 3.42(1) Å] between neighbouring molecules give rise to weakly bonded dimers. The ^1H, ^{13}C and ^{205}Tl NMR spectra of both compounds in DMSO indicate that the bonding scheme observed in solid state is only partially retained in solution, where at least two isomers are observed. © 1998 Elsevier Science Ltd. All rights reserved

Keywords: crystal structure; thallium complexes; diorganothallium complexes; thiosemicarbazone complexes.

The usefulness of $TlMe_2^+$ cation for isolating, in the solid state, different conformational and tautomeric forms of thiosemicarbazones was pointed out in a preceeding paper [1]. The thiosemicarbazone backbone has several possibilities of coordination to metals, *N*, *S*-coordination **(A)** using the azomethine nitrogen [N(3)] being the most common [2].

This mode of coordination was observed in dimethylthallium(III) cyclopentanone thiosemicarbazonate [3] and in dimethylthallium pyridine-2-carbaldehyde thiosemicarbazonate [4] (although in this last case also the N atom of the pyridine ring contributes to the metal-ligand bond). Nevertheless, other coordinative options exist: (*p*-Anisaldehyde thiosemicarbazonato)-dimethylthallium(III) [5] contains the metal N(2), *S*-coordinated, while the ligand retains the typical structure of free thiosemicarbazones **(B)** and $[TlMe_2(HA)(H_2O)]$ (HA = monoanion of pyridoxal thiosemicarbazone) [1] has the ligand *S*-coordinated (if the very weak interaction of the thallium with the phenolic hydroxyl group of the 3-hydroxy-5-hydroxymethyl-2-methyl-pyridine ring is ignored) **(C)**.

The present study was carried out to explore the coordinative behaviour of the new ligand 2,6-diacetyl-pyridine monothiosemicarbazone (HL), serendipitously isolated in a preceeding work [6]. Its reaction with aqueous TlR_2OH (R = Me, Ph) afforded the complexes $[TlMe_2(L)]$ and $[TlPh_2(L)].CHCl_3$. Although in solid state the thiosemicarbazone chain adopts in both compounds the

* Author to whom correspondence should be addressed.

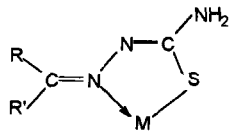

(A)

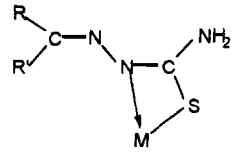

(B)

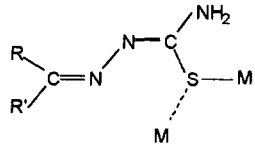

(C)

more usual conformation and is N(3), *S*-bonded to the metal, in DMSO solution there are at least two isomers. The structure of these isomers is discussed.

EXPERIMENTAL

Thiosemicarbazide (Merck), 2,6-diacetylpyridine (Aldrich), thallium(I) iodide (Merck), thallium(I) bromide, methyl lithium (Ega-chemie), methyl iodide (Probus), Bromine (Merck) and phenylboronic acid (Aldrich) were used as received. HL, $TlMe_2OH$ and $TlPh_2OH$ were prepared as described elsewhere [6,7].

Elemental analyses were performed with a FISONS Instrument EA 1108 analyser. Melting points were determined with a Gallenkamp Melting Point Apparatus. Mass spectra were obtained using a KRATOS MS50 spectrometer connected to a DS90 data system and operating under FAB conditions (*m*-nitrobenzyl alcohol, Xe, 8 eV). ^1H (300.14 MHz), ^{13}C (62.83 MHz) and ^{205}Tl (173.1287 MHz) NMR spectra in DMSO were recorded at room temperature in a Bruker WM 250 (^{13}C spectra) and AMX 300 (^1H and ^{205}Tl) apparatuses. Chemical shifts in ppm (δ) were referred to TMS using the solvent signal for ^1H and ^{13}C spectra and aqueous $TlClO_4$ after extrapolation to infinite dilution in ^{205}Tl spectra.

Synthesis of $[TlMe_2(L)]$

1.75 ml of an aqueous solution of $TlMe_2OH$ (0.054 g, 0.21 mmol) was added to a suspension containing 0.05 g of HL (0.21 mmol) in 10 ml of hot methanol. The orange solution obtained was refluxed and stirred for 3 h and then left to stand overnight at room temperature. After cooling for one day at 4°C, a crystalline orange solid formed, adequate for X-ray study; it was isolated and dried *in vacuo*. M.p. 175°C (decomposition). Anal. Found: C, 30.7; H, 3.7; N, 11.9; S, 6.5, Calc. for $C_{12}H_{17}N_4OSTl$, C, 30.7; H, 3.6; N, 11.7; S, 6.8%. The main metallated ions in the FAB spectrum were at m/z(%): 470 (M+H, 29), 454 (M−Me, 33), 388 ($C_{11}H_9N_3Tl$, 11), 235 ($TlMe_2$, 25), 205 (^{205}Tl, 100).

Synthesis of $[TlPh_2(L)] \cdot CHCl_3$

0.17 g of HL (0.72 mmol) were suspended in 20 ml of hot methanol and to this suspension was added an aqueous solution (10 ml) of $TlPh_2OH$ (0.27 g, 0.72 mmol). The orange solution obtained was refluxed and stirred affording an orange solid, which was isolated after cooling to room temperature. Single crystals suitable for the X-ray study were obtained by recrystallisation in chloroform. M.p. 170°C. Anal. Found: C, 38.8; H, 2.9; N, 8.1; S, 5.35, Calc. for $C_{23}H_{22}Cl_3N_4OSTl$: C, 38.7; H, 3.1; N, 7.9; S, 4.5%. The main metallated ions in the FAB spectrum were at m/z(%): 595 (M+H, 20), 517 (M−Ph, 63), 440 (M−2Ph, 3), 359 ($TlPh_2$, 100), 205 (^{205}Tl, 49).

Crystal structure determinations

X-ray crystallography was performed using an Enraf–Nonius CAD-4 difractometer with graphite monochromated Mo–Kα radiation ($\lambda = 0.71073$). Crystal data and experimental conditions are listed in Table 1. Numerical absorption corrections were carried out [8].

Structures were solved using the standard heavy atom Patterson method and difference Fourier Techniques. In the final cycles of full-matrix least-squares refinement all non-H atoms were treated anisotropically. In $[TlPh_2(L)].CHCl_3$ the thermal parameter U33 of atom C(5) would refine to a non physical low value, giving rise to a non-definite-positive thermal tensor; it was for that reason, fixed to the value of 0.035, close to the equivalent ones of neighboring atoms. H atoms in $[TlMe_2(L)]$ were included, as fixed contributors, all with a common isotropic displacement parameter that refined to 0.113(11)Å^2. For $[TlPh_2(L)] \cdot CHCl_3$, all H atoms, except those of the two methyl and one amino groups that were not included in the model, were located on stereochemical grounds [U(eq) = 0.065(18) Å^2]. Atomic scattering factors were taken from Ref. [9]. The programs used were SHELX76[10], SHELXL93 [11] and ORTEP [12].

RESULTS AND DISCUSSION

Crystal structures of the complexes

$[TlMe_2(L)]$. Figure 1 shows the molecular structure of this compound with the numbering scheme used. Selected bond distances and bond angles are listed in Table 2. The thallium atom is coordinated to two

Table 1. Crystallographic data

	$[TlMe_2(L)]$	$[TlPh_2(L)]\cdot CHCl_3$
Formula	$C_{12}H_{17}N_4OSTl$	$C_{23}H_{22}Cl_3N_4OSTl$
Molecular weight	469.73	713.23
Crystal class	Triclinic	Monoclinic
Space group	*P*1(bar)(no. 2)	*C*2/*c*
a (Å)	7.064(3)	23.559(3)
b (Å)	9.149(2)	13.582(2)
c (Å)	12.377(11)	16.808(3)
α (°)	79.378(11)	90.000
β (°)	74.94(2)	106.04(1)
γ (°)	82.75(2)	90.000
V (Å^3)	756.7(3)	5169(2)
Z	2	8
D_c(g.cm^{-3})	2.062	1.833
Crystal size (mm)	0.125 × 0.086 × 0.225	0.225 × 0.125 × 0.050
Colour	orange	orange
μ(mm^{-1})	10.808	6.664
F(000)	444	2752
Transmission factors	0.4397, 0.2635	0.733, 0.477
θ(°) range	1.73–24.97	1.75–24.96
h, *k*, *l*, range	−7, 8; −10, 10; 0, 14	−27, 26; 0, 16; 0, 19
Total no. of reflections measured	2663	3648
No. of unique reflections, Rint	2540, 0.016	3581, 0.050
R_1^a, Rw_2^b	0.0305, 0.0673	0.0620, 0.1155
S on F^2	1.050	1.072
Peaks/holes(eÅ^{-3})	0.614/−0.821	1.166/−1.685

[a] $R_1 = F_o - F_c/F_o$, [b] $Rw_2 = [w(F_o^2 - F_c^2)^2/w(F_o^2)^2]^{1/2}$

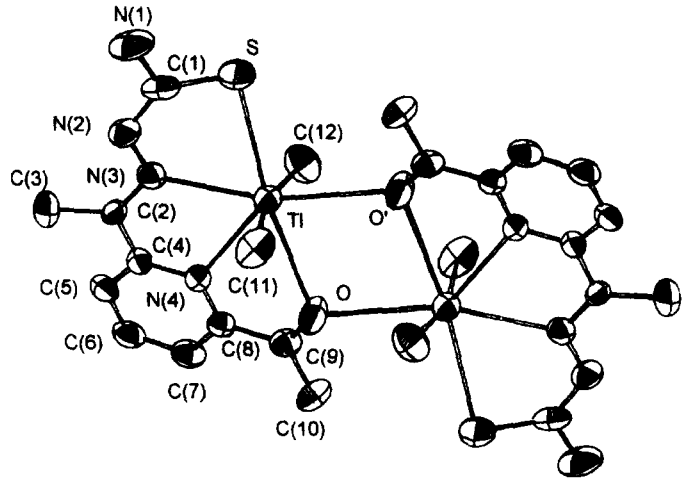

Fig. 1. Crystal structure of $[TlMe_2(L)]$ showing the atom number scheme used.

carbon atoms from the methyl groups [Tl—C(11) = 2.133(9), Tl—C(12) = 2.128(9)Å], one sulphur and one nitrogen atoms from the thiosemicarbazone chain [Tl—S = 2.872(2), Tl—N(3) = 2.590(6) Å], one nitrogen atom from the pyridinic ring [Tl—N(4) = 2.686(2) Å], and one oxygen atom from the CH_3CO group [Tl—O = 2.883(6) Å]. These six interactions together with a weak contact with the O′ atom from a neighbouring molecule ($^I = -x+2, -y+1, -z+1$) give rise to a distorted pentagonal bipyramidal coordination sphere, with the C atoms in apical positions, for the thallium atom, where the main distortions are at the C(11)—Tl—C(12), N(4)—Tl—O and S—Tl—O′ angles (164.3(4), 57.7(2) and 95.62(13) instead of 180, 72 and 72°, respectively, in regular pentagonal bipyr-

Table 2. Selected bond distances (Å) and bond angles (°) for [$TlMe_2(L)$]

Tl—C(11)	2.133(9)	O—C(9)	1.210(9)
Tl—C(12)	2.128(9)	N(1)—C(1)	1.376(10)
Tl—N(3)	2.590(6)	N(2)—C(1)	1.300(11)
Tl—N(4)	2.686(2)	N(3)—C(2)	1.289(10)
Tl—S	2.872(2)	N(3)—N(2)	1.364(8)
Tl—O	2.883(6)	N(4)—C(4)	1.337(9)
Tl—O′	3.050(6)	N(4)—C(8)	1.343(9)
S—C(1)	1.696(10)	C(4)—C(2)	1.475(11)
C(11)—Tl—C(12)	164.3(4)	C(11)—Tl—O′	81.4(3)
C(11)—Tl—N(3)	104.3(3)	C(12)—Tl—O′	86.0(3)
C(11)—Tl—N(4)	88.9(3)	O—Tl—O′	78.8(2)
C(11)—Tl—S	90.4(3)	C(2)—N(3)—Tl	121.1(5)
C(11)—Tl—O	82.8(3)	N(2)—N(3)—Tl	121.5(5)
C(12)—Tl—N(3)	90.7(3)	C(1)—N(2)—N(3)	115.6(7)
C(12)—Tl—N(4)	93.9(3)	C(2)—N(3)—N(2)	115.6(6)
C(12)—Tl—O	85.6(3)	N(1)—C(1)—S	115.6(7)
C(12)—Tl—S	100.2(3)	N(2)—C(1)—S	130.7(6)
N(3)—Tl—N(4)	62.8(2)	N(2)—C(1)—N(1)	113.7(6)
N(3)—Tl—S	66.3(2)	N(3)—C(2)—C(4)	119.1(6)
N(3)—Tl—O	119.9(2)	N(4)—C(4)—C(2)	117.3(7)
N(4)—Tl—S	127.07(13)	N(4)—C(8)—C(9)	116.2(6)
N(4)—Tl—O	57.7(2)	N(4)—C(8)—C(7)	123.3(7)
S—Tl—O	171.73(14)	O—C(9)—C(8)	119.3(7)
S—Tl—O′	95.62(13)		

′ $-x+2, -y+1, -z+1$.

amidal geometry). The Tl—N and Tl—S distances are within the range observed in other thiosemicarbazone-dimethylthallium(III) complexes [1, 3–5]. The Tl—O distance is clearly shorter than the sum of van der Waals radii (3.48 Å [13]) suggesting a significant bonding interaction. The intermolecular Tl···O′ secondary bond which connects dimers, although shorter than that sum, is weaker than the intramolecular thallium-oxygen bond.

When this coordination sphere is compared with that found in the complex dimethylthallium pyridine-2-carbaldehyde thiosemicarbazonate [4] where the ligand is analogous to L except for the CH_3CO group, it is evident that the incorporation of the Tl—O bond and the replacement of a weak interaction Tl···S for a weak interaction Tl···O in the coordination sphere of the thallium atom lengthens the Tl—S bond (2.825 Å (*av.* value) in the pyridine-2-carbaldehyde-thiosemicarbazone complex [4]) whereas the Tl—N(4) bond is not affected.

The thiosemicarbazone chain C(2)—N(3)—N(2)—C(1)(S)—N(1) adopts an E conformation about the aldimine C(2)—N(3) bond and the thioamide S atom is *cis* respect to the hydrazinic NH–N group, as in the $CdCl_2$ adduct $[CdCl_2(HL)(H_2O)].H_2O$ [6]. The C(1)—S distance is similar in both $CdCl_2$ and $TlMe_2^+$ compounds suggesting that, although in the thallium compound the ligand is deprotonated, the C(1)—S bond retains a close to double bond multiplicity. Nevertheless, although the thione-to-thiol evolution is limited, deprotonation of HL lengthens C(1)—N(1) and shortens C(1)—N(2) as usually occurs in other thiosemicarbazonates.

For the CH_3CO group, the C—O bond distance is that corresponding to a double bond and is also very close to that found in the $CdCl_2$ adduct [6], however in the $TlMe_2^+$ compound this oxygen atom also bridges two thallium atoms which gives rise to a centrosymmetric dimer.

$[TlPh_2(L)] \cdot CHCl_3$. The molecular structure of this complex together with the numbering scheme used is in Fig. 2. Selected bond distances and bond angles are listed in Table 3.

The coordination sphere of the thallium atom is very similar to that described for the dimethylthallium derivative. As in that case, two carbon atoms from the phenyl groups, one S atom, two nitrogens [N(3) and N(4)] and two oxygen atoms give rise to a distorted pentagonal bipyramid coordination sphere, with the carbon atoms occupying the apical positions. Possibly the lower steric hindrance of the phenyl groups relative to the methyl groups (although electronic effects cannot be excluded) allows all the intramolecular metal-ligand bond distances (mainly Tl—S and Tl—N) to be shorter in the diphenyl derivative. Also the angle C—Tl—C is slightly wider.

As a consequence of this stronger intramolecular coordination, the intermolecular interaction Tl···O′ which associates the molecules forming dimers is weaker in the phenyl derivative (Tl···O′ = 3.418 Å).

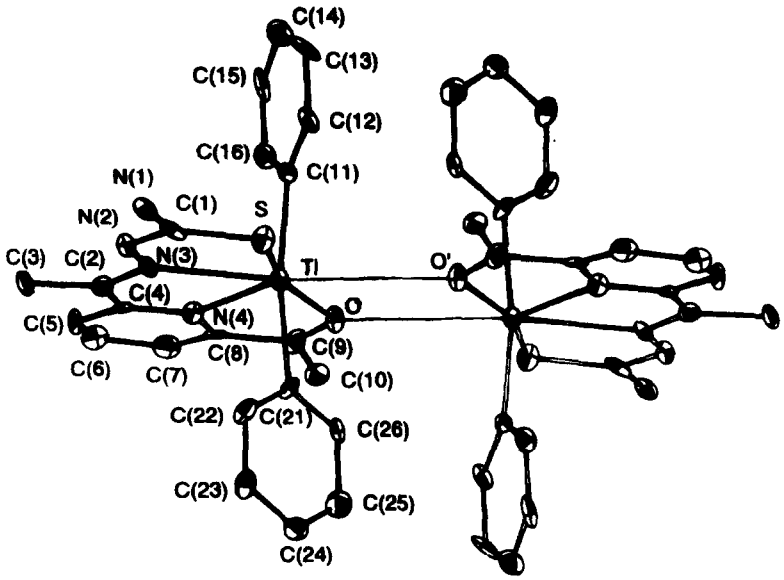

Fig. 2. Crystal structure of $[TlPh_2(L)] \cdot CHCl_3$ showing the atom number scheme used ($CHCl_3$ not shown).

Table 3. Selected bond distances [Å and bond angles (°)] for $[TlPh_2(L)] \cdot CHCl_3$

Tl—C(11)	2.16(2)	N(2)—C(1)	1.29(2)
Tl—C(21)	2.13(2)	N(2)—N(3)	1.35(2)
Tl—N(3)	2.56(2)	N(3)—C(2)	1.27(2)
Tl—N(4)	2.579(14)	N(4)—C(4)	1.35(2)
Tl—S	2.791(6)	N(4)—C(8)	1.41(2)
Tl—O	2.86(1)	C(2)—C(4)	1.45(3)
Tl—O′	3.42(1)	S—C(1)	1.71(2)
N(1)—C(1)	1.34(2)		

C(11)—Tl—C(21)	169.2(6)	C(8)—N(4)—Tl	122.6(12)
C(11)—Tl—N(3)	94.4(6)	Tl—O—Tl′	109.9(5)
C(11)—Tl—N(4)	92.0(6)	C(1)—N(2)—N(3)	120.0(2)
C(11)—Tl—S	94.5(6)	C(2)—N(3)—N(2)	120.0(2)
C(21)—Tl—N(3)	95.7(6)	N(1)—C(1)—S	116(2)
C(21)—Tl—N(4)	88.8(6)	N(2)—C(1)—N(1)	115(2)
C(21)—Tl—S	92.6(4)	N(2)—C(1)—S	129(2)
N(3)—Tl—N(4)	64.9(5)	N(3)—C(2)—C(4)	122(2)
N(3)—Tl—S	69.1(3)	N(4)—C(4)—C(2)	118(2)
N(4)—Tl—S	133.8(4)	N(4)—C(8)—C(9)	117(2)
C(2)—N(3)—Tl	118.0(12)	O—C(9)—C(8)	120(2)
N(2)—N(3)—Tl	122.2(11)	O—C(9)—C(10)	125(2)
C(4)—N(4)—Tl	117.1(11)		

′$1/2-x, 3/2-y, 1-z$.

The ligand, as in the dimethyl derivative, is tetradentate and practically plane. Nevertheless, differences in the Tl-ligand bond distances are accompanied by small differences in the thiosemicarbazone backbone bond distances. Thus, the shorter Tl—S bond corresponds with a larger C(1)—S bond in the diphenylthallium(III) complex.

NMR studies

^1H, ^{13}C and ^{205}Tl NMR data in DMSO-d_6 for HL and its diorganothallium complexes are listed in Table 4. ^1H and ^{13}C NMR spectra of both compounds in DMSO solutions show two different groups of signals for all the protons and carbons of the ligand, sug-

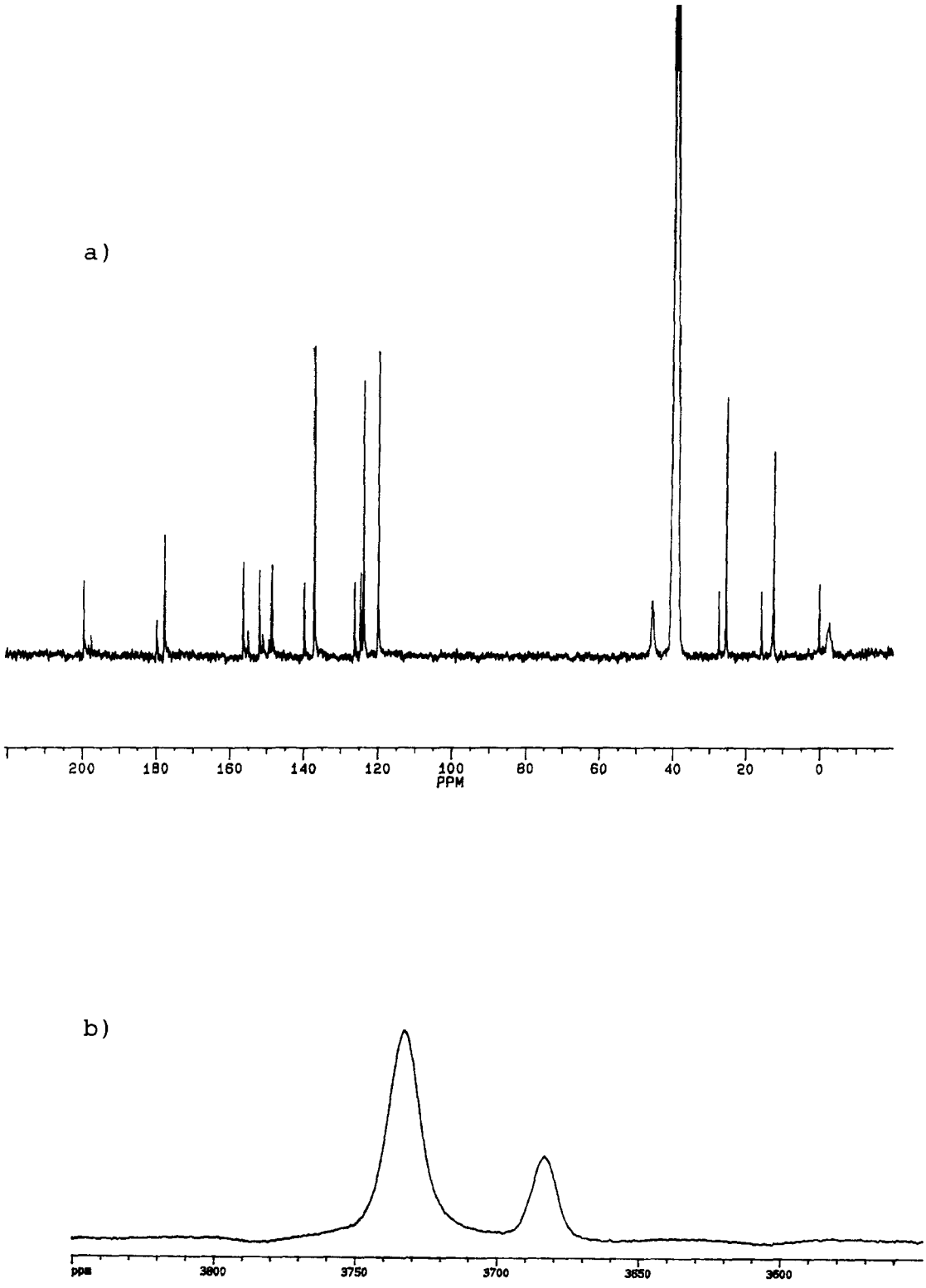

Fig. 3. (a) ^{13}C and (b) ^{205}Tl NMR spectra of $[TlMe_2(L)]$ in DMSO.

gesting an equilibrium between two different isomers.

Figure 3 shows the ^{13}C and ^{205}Tl NMR spectra of $[TlMe_2(L)]$. This last spectrum also shows two different signals, separated ca 50 ppm, confirming two different environments for the thallium atom. Integration of ^{1}H NMR spectrum of this derivative indi-

Table 4. NMR data for HL its diorganothallium derivatives in DMSO-d_6

Compound	N(2)H	$N(1)H_2$	C(5)H	C(7)H	C(6)H	$C(3)H_3$	$C(10)H_3$	R—Tl
HL	10.36s[a]	8.45sb 8.23sb	8.72d	8.72d	7.96t	2.45s	2.66s	
$[TlMe_2(L)]$[c]		7.19sb[b] 7.03sb[b]	8.59d[b]	7.85m[b]	7.85m[b]	2.30s[b]	2.68s[b]	0.85[c]
$[TlPh_2(L)]\cdot CHCl_3$[d]		6.50sb [e]	7.99d 8.63d[b] 7.96d	8.18m 7.80m[b] 8.07m	8.18m 7.85m[b] 8.13m	2.47s 2.14	2.72s 2.57	6.4 8.5

	C(9)	C(1)	C(4)	C(8)	C(2)	C(6)	C(5)	C(7)	C(10)	C(3)	R—Tl
HL	199.3	179.2	154.3	151.9	147.0	137.6	124.7	121.1	25.5	12.0	
$[TlMe_2(L)]$[c]	199.7[b]	177.8[b]	156.5[b]	152.0[b]	148.6[b]	137.1[b]	124.0[b]	119.9[b]	25.5[b]	12.6[b]	21.5[c]
	197.7	179.9	155.1	151.0	149.4	139.8	126.3	124.7	27.5	15.8	
$[TlPh_2(L)]\cdot CHCl_3$	199.5[b]	177.5[b]	155.8[b]	151.8[b]	149.1[b]	137.1[b]	124.11[b]	120.11[b]	25.4[b]	12.7[b]	125.2 140.2
	197.8	179.6	154.3	150.7	150.0	140.0	126.4	122.4	27.6	15.9	

[a] s = singlet, b = broad, d = doublet, m = multiplet.
[b] Major isomer.
[c] $^2J(^1H\text{-}^{205}Tl) = 425.6$ Hz; $^1J(^{13}C-^{205}Tl) = 3032.2$Hz; $\delta(^{205}Tl) = 3734, 3684$ ppm.
[d] $\delta(^{205}Tl) = 3403, 3343$ ppm.
[e] Not observed.

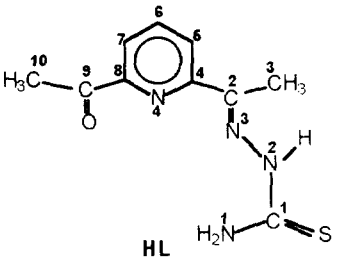

cates that the ratio between both isomers is about 4 : 1. The main changes of the ligand signals in the ^1H NMR spectrum of the major isomer with respect to the free ligand are: (a) the disappearance of the N(2)H signal (at 10.36 ppm in HL) due to deprotonation, (b) the shielding of the NH_2 signal which remains split in two broad bands, (c) the slight shielding of C(5)H, C(6)H and C(7)H (by 0.05–0.1 ppm), (d) the shielding of $C(3)H_3$ (by 0.15 ppm) while $C(10)H_3$ is practically at the same position as that in the free ligand.

In the ^{13}C NMR spectrum the main changes are: (a) C(2), C(3) and C(4) are deshielded by complexation, (b) C(1) and C(7) are shielded while C(5), C(6), C(8), C(9) and C(10) are not affected by deprotonation and metallation. All these changes suggest that, in this tautomeric form, the CH_3CO group and the pyridinic nitrogen probably do not coordinate the metallic center. The shielding of C(1) (about 1 ppm) indicates some evolution of the ligand to the thiol form and the fact that the NH_2 groups still gives two different broad signals may be indicative of either that L retains the typical configuration of the free thiosemicarbazones allowing N(1)H···N(3) hydrogen bonding or that the C(1)—N(1) bond still has enough multiplicity to avoid the free rotation about the $N(1)H_2$ group. These data, together with the chemical shift in the ^{205}Tl NMR spectrum (3734) ppm) suggest that the major tautomeric form may have the structure **(B)** similar to that already described, in solid state, for a dimethylthallium complex with p-anisaldehyde thiosemicarbazone [5].

With regard to the minor isomer, its ^1H and ^{13}C NMR spectra significantly differs from those obtained for the major isomer. The $N(1)H^2$ group gives now just one signal at 6.50 ppm, C(5)H is shielded about 0.6 ppm with respect to the major isomer, while C(6)H and C(7)H are slightly deshielded. In the ^{13}C NMR spectrum significant changes with respect to the major isomer are: (a) a slight shielding of C(9), (b) a slight deshielding of C(1) and (c) a strong deshielding of C(3) and C(4). These results, together with the signal in the ^{205}Tl NMR spectrum (3684 ppm), suggest that the oxygen atom from the CH_3CO group coordinates the thallium atom, together with N(3), N(4) and probably the sulphur, as in solid state. It may therefore be concluded that this isomer has low solubility in the $MeOH/H_2O$ solution used in synthesis, and for that reason this is the one isolated in solid state. $[TlPh_2(L)]\cdot CHCl_3$ behaves similarly to the dimethylthallium derivative in DMSO solution, so the conclusions obtained above can be applied to it.

REFERENCES

1. Casas, J. S., Castellano, E. E., Rodriguez-Argüe-

lles, M. C., Sánchez. A., Sordo, J. and Zukerman-Schpector, J., *Inorg. Chim. Acta*, 1997, **260,** 183.
2. West, D. X., Padhye, S. B. and Sonawane, P. B., *Structure and Bonding*, 1991, **76,** 1.
3. Macías, A., Rodriguez-Argüelles, M. C., Suárez, M. I., Sánchez, A., Casas, J. S. and Sordo, J., *J. Chem. Soc., Dalton Trans.*, 1989, 1787.
4. Casas, J. S., Castaño, M. V., Rodriguez-Argüelles, M. C., Sánchez, A. and Sordo, J., *J. Chem. Soc., Dalton Trans.*, 1993, 1253.
5. Casas, J. S., Castellano, E. E., Macías, A., Rodriguez-Argüelles, M. C., Sánchez, A. and Sordo, J., *J. Chem. Soc., Dalton Trans.*, 1993, 353.
6. Casas, J. S., Castellano, E. E., García-Tasende, M. S., Sánchez, A., Sordo, J. and Zukerman-Schpector, J., *Z. anorg. allg. Chem.*, 1997, **623,** 825.
7. García-Tasende, M. S., Sánchez, A., Casas, J. S. and Sordo, J., *Inorg. Chim. Acta.*, 1992, **210,** 35.
8. Busing, W. R., Levy, H. A., *Acta Crystallogr.*, 1957, **10,** 180.
9. *International Tables for X-ray Crystallography*, Vol. IV, Kynoch, Birmingham, U.K., 1974.
10. Sheldrick, G. M., SHELX76, *Program for Crystal Structure Determination*, University of Cambridge, 1976.
11. Sheldrick, G. M., SHELX93, *Program for Crystal Structure Refinement*, University of Göttingen, 1993.
12. Johnson, C. K., ORTEP, Report ORNL-3794, Oak Ridge National Laboratory, TN, U.S.A., 1965.
13. Bondi, A., *J. Phys. Chem.*, 1964, **68,** 441.

Pergamon

PII: S0277-5387(98)00029-1

Polyhedron Vol. 17, Nos 13–14, pp. 2257–2265, 1998
© 1998 Elsevier Science Ltd
All rights reserved. Printed in Great Britain
0277-5387/98 $19.00+0.00

Chain and rhomboidal "box"-like polymeric metal complexes of *N,N'*-1,2-ethylenebis(pyridin-2-thione)

Zeno Atherton, David M. L. Goodgame,* Dean A. Katahira, Stephan Menzer, Andrew J. P. White and David J. Williams

Chemistry Department, Imperial College of Science, Technology and Medicine, London SW7 2AY, U.K.

(Received 27 October 1997; accepted 12 January 1998)

Abstract—The preparations are reported of a range of complexes of Fe^{II}, Co^{II}, Ni^{II}, Cu^{I}, Ag^{I}, Zn and Cd with *N,N'*-1,2-ethylenebis(pyridin-2-thione) (EBPYT) together with relevant spectroscopic data. The compounds $Co(EBPYT)Br_2$ (**1**) and $[Ni(EBPYT)_3](ClO_4)_2 \cdot 2MeOH \cdot MeNO_2$ (**2**) have been studied by X-ray crystallography. Compound **1** has a chain structure in which tetrahedrally coordinated cobalt centres are linked by bridging EBPYT ligands. In compound **2** octahedrally coordinated "NiS_6" centres are connected by EBPYT bridges so as to form a polymeric three-dimensional array of rhomboidal "boxes". © 1998 Elsevier Science Ltd. All rights reserved

Keywords: X-ray structures; polymeric complexes; bis(pyridine-2-thione) ligand.

A major component of the very rapidly developing field of supramolecular chemistry is the synthesis of new metal complexes with polymeric sheet or 3D-network structures and in particular those forming cavities or channels capable of taking up guest molecules. The great majority of organic ligands that have been used for this purpose hitherto have involved nitrogen donor groups [1] or, to a somewhat lesser extent, oxygen donors such as carboxylate anions [2] or neutral ligands with O-donor groups [3]. The use of extended reach sulphur donor ligands to form such networks has, surprisingly, received far less attention [4], although a number of dithia-alkanes have been shown to form individual, large metallacyclic rings [5]. In view of the observation [4b] that *N,N'*-ethylenebis(pyridin-2-thione) (**I**, EBPYT) forms chains of 4-, 18- and 36-membered rings in the Cu^{I} compound $\{[Cu_2(EBPYT)_3](PF_6)_2\}_n$ we have extended our studies with EBPYT to a wider range of metal ions and we describe here the results of this work.

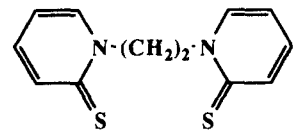

I

EXPERIMENTAL

Preparation of compounds

N,N'-ethylenebis(pyridin-2-thione). This was prepared as described previously [4b].

Metal complexes of EBPYT

Analytical data (Microanalytical Laboratory Imperial College), colours and yields of the complexes

* Author to whom correspondence should be addressed.

of EBPYT are given in Table 1. Preparative details are summarised below.

Caution! Although we did not observe any explosive behaviour with the perchlorate compounds described below, all metal perchlorates must be regarded as potentially explosive and appropriate safety measures taken.

$FeCl_2$(EBPYT). Addition of a solution of hydrated iron(II) chloride (0.31 mmol) in ethanol (5 cm^3), which had been "deoxygenated" by passage of nitrogen, to a solution of EBPYT (0.31 mmol) in deoxygenated nitromethane (6 cm^3) gave an orange precipitate.

$CoCl_2$(EBPYT). A solution of hydrated cobalt(II) chloride (0.11 mmol) in the minimum amount of hot ethanol was added to a hot solution of EBPYT (0.24 mmol) in a mixture of nitromethane (3 cm^3) and ethyl acetate (3 cm^3). The clear green solution quickly deposited a green solid which was filtered off, washed with nitromethane and dried.

$CoBr_2$(EBPYT). This bright green compound separated on mixing hot solutions of hydrated cobalt(II) bromide (0.17 mmol) in ethanol (2 cm^3) and EBPYT (0.24 mmol) in nitromethane (6 cm^3).

CoI_2(EBPYT). This was obtained as for the cobalt(II) bromide complex but using methanol as the solvent for the cobalt iodide.

$Co(NO_3)_2$(EBPYT). A solution of hydrated cobalt(II) nitrate (0.18 mmol) in 0.3 cm^3 of a 1 : 1 mixture of methanol and nitromethane was added to one of EBPYT (0.24 mmol) in nitromethane (6 cm^3). On heating the resulting deep blue-green solution a deep blue-purple solid separated.

$Co(EBPYT)_2(ClO_4)_2 \cdot 2H_2O$. A solution of cobalt(II) perchlorate hexahydrate (0.06 mmol) in ethanol (2 cm^3) was added to a hot solution of EBPYT (0.20 mmol) in nitromethane (3 cm^3). The dark green solution gave a green precipitate on cooling.

$NiBr_2$(EBPYT). This bright green complex precipitated immediately on addition of a solution of hydrated nickel bromide (0.18 mmol) in 0.6 cm^3 of a 1 : 1 mixture of methanol and nitromethane to a hot solution of EBPYT (0.24 mmol) in nitromethane (6 cm^3).

$Ni(EBPYT)_2(BF_4)_2$. Hydrated nickel(II) tetrafluoroborate (0.07 mmol) dissolved in the minimum amount of methanol (0.2 cm^3) was boiled with 2,2-dimethoxypropane (2 cm^3) until the volume was approximately halved. The resulting solution was added to one of EBPYT (0.24 mmol) in nitromethane (8 cm^3) at ca 25°C to give a very finely divided deep blue-green solid. This was collected by centrifugation and washed with nitromethane and then diethylether.

$Ni(EBPYT)_2(ClO_4)_2$ *and* $Ni(EBPYT)_3(ClO_4)_2$. Hydrated nickel perchlorate (0.06 mmol) in warm methanol (2 cm^3) was added to a solution of EBPYT (0.20 mmol) in nitromethane (5 cm^3). The clear brown solution quickly became yellow but, after heating, the

Table 1. Analytical data, colours and yields of the complexes formed by **I** (= L)

Complex	Colour	Analysis (%)[a] C	H	N	Yield (%)
$FeCl_2L$	Orange	38.1 (38.4)	3.0 (3.2)	7.4 (7.5)	76
$CoCl_2L$	Green	38.0 (38.1)	3.2 (3.2)	7.3 (7.4)	74
$CoBr_2L$	Green	31.0 (30.9)	2.5 (2.6)	5.9 (6.0)	95
CoI_2L	Green	26.0 (25.7)	2.1 (2.2)	5.3 (5.0)	60
$Co(NO_3)_2L$	Indigo	33.1 (33.4)	2.6 (2.8)	12.7 (13.0)	76
$Co(ClO_4)_2L_2 \cdot 2H_2O$	Green	36.2 (36.5)	3.4 (3.6)	7.0 (7.1)	57
$NiBr_2L$	Green	30.7 (30.9)	2.5 (2.6)	6.0 (6.0)	93
$Ni(ClO_4)_2L_2$	Deep blue-green	38.6 (38.2)	2.9 (3.2)	7.4 (7.4)	66
$Ni(BF_4)_2L_2$	Deep blue-green	39.9 (39.5)	3.1 (3.3)	7.4 (7.7)	40
Cu_2Cl_2L	Orange	32.1 (32.3)	2.7 (2.7)	6.4 (6.3)	100
Cu_2Br_2L	Orange	27.4 (26.9)	2.1 (2.3)	5.7 (5.2)	100
$Cu_2(ClO_4)_2L_3$	Orange	39.8 (40.4)	3.3 (3.5)	7.6 (7.7)	96
$Cu_2(BF_4)_2L_3$	Orange	41.2 (41.4)	3.1 (3.5)	8.0 (8.0)	100
$Ag_2(ClO_4)_2L_3$	Yellow	37.3 (37.3)	3.1 (3.1)	7.4 (7.3)	81
$Ag_2(BF_4)_2L_3$	Yellow	38.0 (38.1)	3.0 (3.2)	7.2 (7.4)	85
$ZnCl_2L$	Pale yellow	37.2 (37.5)	3.2 (3.1)	7.3 (7.3)	70
$Zn(NCS)_2L$	Pale yellow	39.5 (39.1)	2.7 (2.8)	13.5 (13.0)	83
$Zn(ClO_4)_2L_2$	Cream	37.7 (37.9)	3.1 (3.2)	7.3 (7.4)	53
$CdCl_2L$	Pale yellow	33.4 (33.4)	2.9 (2.8)	6.7 (6.5)	80
$CdBr_2L$	Pale yellow	27.8 (27.7)	2.4 (2.3)	5.6 (5.4)	98
CdI_2L	Pale yellow	24.0 (23.5)	2.0 (2.0)	4.6 (4.6)	82
$Cd(NO_3)_2L$	Yellow	29.9 (29.7)	2.4 (2.5)	11.5 (11.6)	63
$Cd(ClO_4)_2L_2$	Pale yellow	35.4 (35.7)	3.0 (3.0)	7.4 (6.9)	100

[a] Calculated values are given in parentheses.

brown colour returned and the compound Ni(EBPYT)$_2$(ClO$_4$)$_2$ separated as a dark blue-green solid. This was filtered off, washed with nitromethane, then diethyl ether, and dried. Another reaction mixture, initially prepared as above, was not heated but simply allowed to evaporate slowly in air. The precipitate of Ni(EBPYT)$_2$(ClO$_4$)$_2$ which separated was filtered off and the mother liquor again allowed to evaporate slowly. Small red blocks crystallised, together with some free ligand and a further amount of Ni(EBPYT)$_2$(ClO$_4$)$_2$. The red crystals were separated by hand, carefully washed with a little nitromethane and characterised by X-ray diffraction methods.

Cu$_2$Cl$_2$(EBPYT) *and* Cu$_2$(EBPYT)$_3$(BF$_4$)$_2$. The respective, hydrated copper(II) salt (0.10 mmol) in a 1 : 1 mixture of methanol and nitromethane (total volume 0.3 cm^3) was added to one of EBPYT (0.24 mmol) in nitromethane (6 cm^3). A brown solid which formed initially redissolved on stirring and was replaced by an orange precipitate.

Cu$_2$Br$_2$(EBPYT), Cu$_2$(EBPYT)$_3$(ClO$_4$)$_2$ *and* Ag$_2$(EBPYT)$_3$X$_2$ (X = ClO$_4$, BF$_4$). These compounds precipitated immediately on mixing solutions of the appropriate Cu(II) or Ag(I) salt (0.016 mmol; but 0.011 mmol in the case of copper(II) perchlorate) in a 1 : 1 mixture of methanol and nitromethane with one of EBPYT (0.32 mol) in a 1 : 1 mixture of dichloromethane and nitromethane.

ZnCl$_2$(EBPYT). A solution of anhydrous zinc chloride (0.31 mmol) in warm ethanol (0.3 cm^3) was mixed with a warm solution of EBPYT (0.32 mmol) in a mixture of ethanol (2 cm^3) and nitromethane (4 cm^3). The pale yellow complex which precipitated on heating the solution was collected and then washed with diethyl ether.

Zn(NCS)$_2$(EBPYT). Addition of a solution of zinc thiocyanate (0.32 mmol) in methanol (2.5 cm^3) to a warm solution of EBPYT (0.32 mmol) in nitromethane (6 cm^3) gave an immediate yellow precipitate.

Zn(EBPYT)$_2$(ClO$_4$)$_2$. This was obtained as for the previous complex, but using a 2 : 1 EBPYT : Zn mole ratio, and the product separated more slowly.

Cadmium complexes. These compounds precipitated immediately on adding a solution of the appropriate cadmium salt (0.10 mmol for the halides, 0.16 mmol for the perchlorate, and 0.32 mmol for the nitrate) in the minimum amount (ca 0.4 cm^3) of hot dimethylformamide to a solution of EBPYT (0.32 mmol) in nitromethane (6 cm^3).

Spectroscopy

The electronic spectra of the solid compounds were obtained by the reflectance method using powdered samples and a Beckman DK2 spectrometer. IR spectra were recorded on a Perkin–Elmer 1720 FT spectrometer as Nujol mulls using CsI plates. The Mössbauer spectra of Fe(EBPYT)Cl$_2$ were obtained by Dr Q. A. Pankhurst of the Department of Physics and Astronomy, University College London under the ULIRS service.

Crystallography

Crystal data. For CoBr$_2$(EBPYT), **1**: C$_{12}$H$_{12}$N$_2$S$_2$Br$_2$Co, M = 467.1, monoclinic, space group $P2_1/n$ (no. 14), a = 6.88(2), b = 14.35(2), c = 15.34(2) Å, β = 91.2(1)°, U = 1514(4) Å^3, Z = 4, D_c = 2.05 g cm^{-3}, μ(Mo–K$_\alpha$) = 66.8 cm^{-1}, F(000) = 908. A green needle of dimensions 0.42 × 0.15 × 0.06 mm was used.

For [Ni(EBPYT)$_3$](ClO$_4$)$_2$, **2**: [C$_{36}$H$_{36}$N$_6$S$_6$Ni][ClO$_4$]$_2$ · 2MeOH · MeNO$_2$, M = 1127.8, rhombohedral, space group $R\bar{3}/c$ (no. 167), $a = b$ = 15.914(1), c = 35.966(5) Å, U = 7888(1) Å^3, Z = 6 (the molecule has crystallographic D_3 symmetry), D_c = 1.42 g cm^{-3}, μ(Mo–K$_\alpha$) = 7.7 cm^{-1}, F(000) = 3504. A red block of dimensions 0.30 × 0.21 × 0.18 mm was used.

Data collection and processing

Data for both structures were collected on a Siemens P4/PC diffractometer with graphite monochromated Mo–K$_\alpha$ radiation using ω-scans, 1921 (1546) Independent reflections were measured for **1** (**2**) respectively [$2\theta \leqslant 45$ (50)°] of which 902 (1146) had $|F_o| > 4\sigma(|F_o|)$ and were considered to be observed. The data were corrected for Lorentz and polarisation factors, and in the case of **1** an empirical absorption correction was applied; the maximum and minimum transmission factors were 0.67 and 0.20 respectively.

Structure analysis and refinement

Both structures were solved by direct methods. In **1** all of the non-hydrogen atoms were refined anisotropically. In **2**, though the atoms of the complex were ordered and refined anisotropically, both the perchlorate counter ion and the methanol and nitromethane included solvent molecules were found to be disordered. The anion was disordered over a crystallographic mirror plane, and this was modelled by a single one-third occupancy molecule that was refined anisotropically. The methanol molecules were distributed over two reduced occupancy sites, with one of them overlapping one of the partial occupancy nitromethane positions—all of these atoms were refined isotropically. The hydrogen atoms of the ligands in both structures were placed in calculated positions, assigned isotropic thermal parameters, [U(H) = 1.2U_{eq}(C)], and allowed to ride on their parent carbon atoms. The hydrogen atoms of the included solvent molecules in **2** could not be located. Refinements were by full-matrix least-squares based on F^2 to give R_1 = 0.094 (0.066), wR_2 = 0.206 (0.220) for 902 (1146) independent observed reflections and 172 (146) parameters respectively. The maximum and

minimum residual electron densities in the final ΔF maps were 0.66 (0.62) and −0.67 (−0.57) eÅ^{-3} for **1** and **2** respectively. The mean and maximum shift/error ratios in the final refinement cycle were 0.001 (0.000) and −0.005 (0.001) respectively. Computations were performed using the SHELXTL-PC system version 5.03 [6]. Important bond lengths and angles for compounds **1** and **2** are listed in Table 2.

RESULTS AND DISCUSSION

The ligand EBPYT readily forms solid complexes with a range of transition metal ions (Table 1) but only in two cases, Co(EBPYT)Br_2 (**1**) and [Ni(EBPYT)$_3$]$(ClO_4)_2$ (**2**), were we able to obtain crystals of appropriate quality for the single crystal X-ray studies required for elucidation of their extended polymeric structures. These structures are discussed below. Some further, albeit more limited, information about the coordination geometry of the metal ions in the other compounds was obtained by spectroscopic methods.

Metal halide complexes

The metal halide complexes of Fe^{II}, Co^{II}, Ni^{II}, Zn and Cd have stoichiometry M(EBPYT)X_2. The reactions between EBPYT and copper(II) chloride and bromide caused reduction of the copper and the formation of essentially quantitative yields of copper(I) complexes of stoichiometry Cu_2X_2(EBPYT), where X = Cl or Br.

The electronic spectra of the cobalt(II) complexes Co(EBPYT)X_2 (X = Cl, Br, I) in the solid state (Table 3) are typical of an essentially tetrahedral coordination geometry about the Co centre [7], showing strong overlapping bands in the range 5000–8000 cm^{-1} [transitions to components of $^4T_1$(F)] and a strong multicomponent band in the visible region [transitions to components of $^4T_1$(P)]. The electronic spectra of Fe(EBPYT)Cl_2 and Ni(EBPYT)Br_2 (Table 3) are also consistent with a tetrahedral geometry [7–9]. For the compounds M(EBPYT)Cl_2 (M = Fe, Co and Zn) further evidence [10] for tetrahedral coordination geometry is provided by their low frequency IR spectra, which have ν(M—Cl) bands at 296 and 333 cm^{-1} for M = Fe, 300 and 322 cm^{-1} for M = Co, and 291 and 309 cm^{-1} for M = Zn.

The Mössbauer spectrum of Fe(EBPYT)Cl_2 comprises a quadrupole split doublet with Q.S. values of 3.00 mm s^{-1} at 295 K and 3.09 mm s^{-1} at 80 K and with chemical shift (δ) values, relative to α-Fe metal, of 0.74 mm s^{-1} at 295 K and 0.86 mm s^{-1} at 80 K (Fig. 1). Further cooling to 20 K results in little change in these parameters (Q.S. 3.08 mm s^{-1}, δ 0.86 mm s^{-1} at 20 K) but at that temperature the line width increases slightly and with some indication of incipient ordering. The observed parameters, and particularly the δ values, correspond well with other essentially tetrahedral FeL_2Cl_2 complexes where L is a monodentate sulphur donor ligand [11].

Because of the difficulty in growing suitable crystals, X-ray confirmation of these conclusions could be obtained only for Co(EBPYT)Br_2 and even then the crystals were of rather poor quality. They were, however, sufficient to define both the coordination geometry about the metal ion and the long-range structure.

Structure of Co(EBPYT)Br_2 (**1**)

The X-ray study of **1** confirms the essentially tetrahedral coordination at each cobalt centre (Fig. 2) though the S—Co—S angle [92.4(3)°] is significantly distorted from ideal. There are two crystallographically independent EBPYT ligands, each of which has an inversion centre in the middle of the ethylene bridge producing an extended *anti* geometry, the N—CH_2—CH_2—N backbone being inclined by

Table 2. Selected bond lengths (Å) and angles (°) for **1** and **2**

Compound **1**			
Co—S(1)	2.314(7)	Co—S(2)	2.336(8)
Co—Br(1)	2.369(6)	Co—Br(2)	2.379(5)
S(1)—Co—S(2)	92.4(3)	S(1)—Co—Br(1)	111.1(2)
S(2)—Co—Br(1)	112.8(2)	S(1)—Co—Br(2)	114.9(2)
S(2)—Co—Br(2)	113.9(3)	Br(1)—Co—Br(2)	110.6(2)
C(11)—S(1)—Co	109.0(9)	C(21)—S(2)—Co	111.4(8)
Compound **2**			
Ni—S	2.459(1)		
S—Ni—S_a	82.84(5)	S—Ni—S_c	94.20(6)
S—Ni—S_d	100.31(6)	S—Ni—S_e	175.41(5)
C(1)—S—Ni	117.0(2)		

Table 3. Electronic spectra[a] (cm^{-1}) of some complexes formed by EBPYT

$FeCl_2$(EBPYT)	5600
$CoCl_2$(EBPYT)	5800, 7400, 13,600, 15,500, 17,100
$CoBr_2$(EBPYT)	5600, 7100, 13,500, 15,200, 16,100
CoI_2(EBPYT)	5400, 7000, 12,800, 14,200, 14,800
$Co(EBPYT)_2(ClO_4)_2 \cdot 2H_2O$	4900, 6500, 7300sh, 12,500, 14,600, 17,200
$Co(NO_3)_2$(EBPYT)	6900, 8500, 12,500, 17,700
$NiBr_2$(EBPYT)	5400, 9100, 13,600, 15,200
$Ni(EBPYT)_2(BF_4)_2$	23,200, 17,200
$Ni(EBPYT)_2(ClO_4)_2$	23,400, 17,400

[a] By reflectance method.

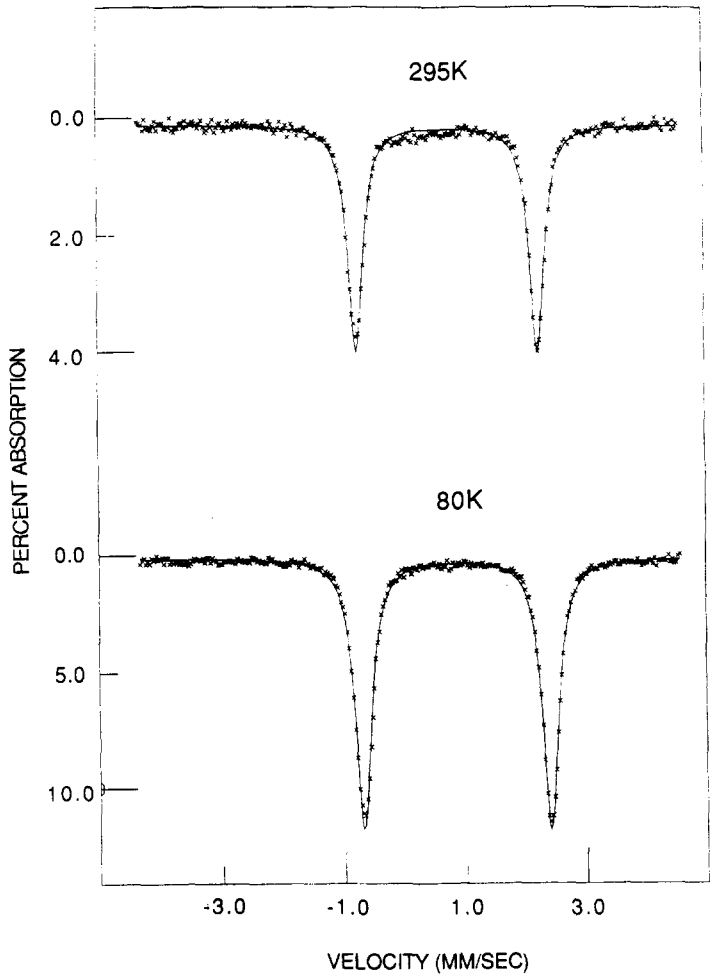

Fig. 1. Mössbauer spectra of $Fe(EBPYT)Cl_2$ at 295 K and 80 K.

ca 85° to the plane of the aryl ring. The EBPYT ligands link adjacent cobalt centres to form polymer chains (Fig. 3). Despite the presence of two independent EBPYT ligands, the chains have C_s symmetry with respect to the $CoBr_2$ plane. Each ligand exhibits a 15° torsional twist about the S-aryl bond, thus producing a "winged" geometry for the $CoBr_2$(-S-aryl)$_2$ unit.

Although there is a superficial stacking of the aryl rings along the crystallographic *a* direction, there is only very minimal ring overlap (ring centroid/ring centroid 4.33 Å) and the rings lie more over the coor-

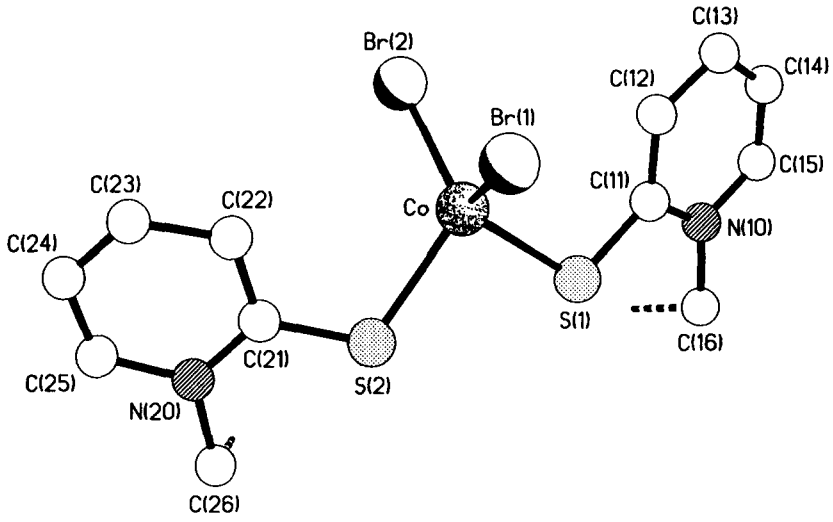

Fig. 2. The coordination geometry about Co in the structure of **1**.

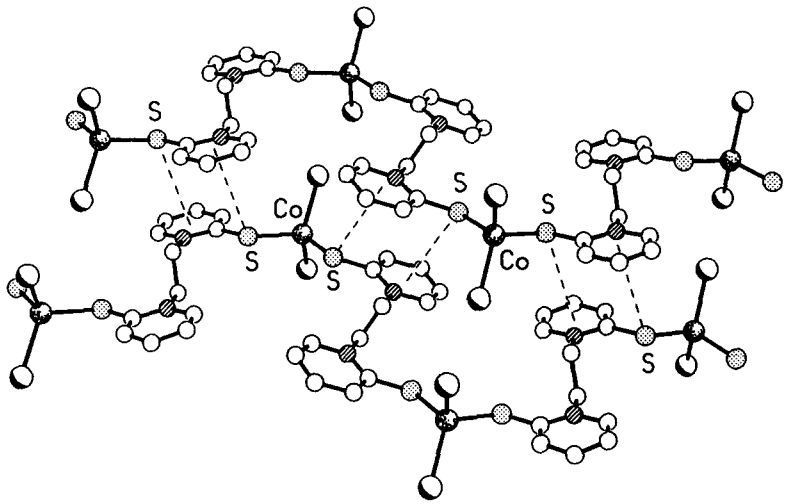

Fig. 3. Part of two adjacent stacked polymeric chains in the structure of **1**. The dashed lines indicate the 3.62 Å sulphur-ring centroid separation referred to in the text.

dinated sulphur atoms, which are at 3.62 Å from the ring centroid. Non-stacked chains pack in a "parquet" pattern with their glide-related neighbours.

Complexes with metal perchlorates and tetrafluoroborates

Addition of a hot solution of nickel tetrafluoroborate hexahydrate in 2,2-dimethoxy-propane, containing a small amount of methanol, to a nitromethane solution of EBPYT gave a very dark blue-green complex of stoichiometry $Ni(EBPYT)_2(BF_4)_2$. This compound was found to be diamagnetic, pointing to a planar NiS_4 coordination geometry, and its electronic spectrum in the solid state (Table 3) is also consistent [12] with that geometry.

Reaction of nickel perchlorate hexahydrate with EBPYT in a mixture of methanol and nitromethane gave, on heating, a precipitate of the analogous very dark blue-green, diamagnetic compound $Ni(EBPYT)_2(ClO_4)_2$. However, slow concentration of the reaction mixture at room temperature resulted in the formation of small red block-like crystals of a new compound (**2**) along with $Ni(EBPYT)_2(ClO_4)_2$. Attempts to isolate **2** free from $Ni(EBPYT)_2(ClO_4)_2$ by recrystallisation resulted in crystal decomposition, so the red crystals were hand-selected and characterised by X-ray diffraction methods.

Structure of $[Ni(EBPYT)_3](ClO_4)_2$ (**2**)

The X-ray analysis of **2** established the compound to have the stoichiometry $Ni(EBPYT)_3(ClO_4)_2$. The nickel atoms are six-coordinate being bonded to a sulphur atom from each of six EBPYT ligands in a D_3 symmetric arrangement (Fig. 4). The distortion from O_h symmetry takes the form of a 6° twist of the opposite faces of the octahedron from a perfectly staggered geometry. The *cis* angles at nickel range between 82.84(5) and 100.31(6) ; the *trans* angles are all 175.42(5) . The Ni—S bond lengths are all 2.459(1) Å and are typical for monodentate sulphur donor ligands octahedrally coordinated to nickel(II).

The torsional twist about each S-aryl bond is 31 which results in a significant flattening of the Ni(-S-aryl)$_6$ unit and overlap of pairs of aryl groups from the upper and lower triangular faces. The ring centroid/ring centroid separations are 3.59 Å and overlapping rings are inclined by 18 , thus indicating a degree of π–π stabilisation of the complex conformation.

As in **1**, the EBPYT ligands have a crystallographic inversion centre at the mid-point of the ethylene bridge, with the plane of the N—CH_2—CH_2—N backbone being inclined by 82° to the aryl ring plane. This *anti* geometry for the ligand results in formation of EBPYT bridges to adjacent, symmetry equivalent nickel centres, thus producing a polymeric network structure. The basic component of the network is a rhombohedron with nickel atoms at each vertex and edges formed by the EBPYT ligands; this is depicted schematically in Fig. 5. The Ni···Ni separation is 10.97 Å and the angles subtended by the Ni—Ni vectors are either 87 or 93 .

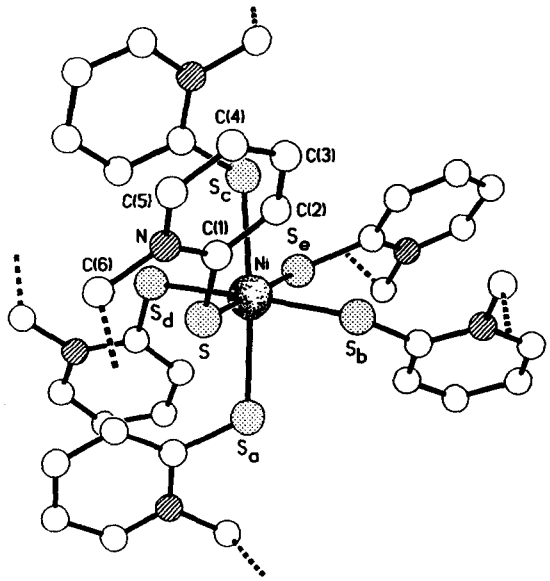

Fig. 4. The coordination geometry about Ni in the structure of **2**: S, S_{a-e} are equivalent by symmetry.

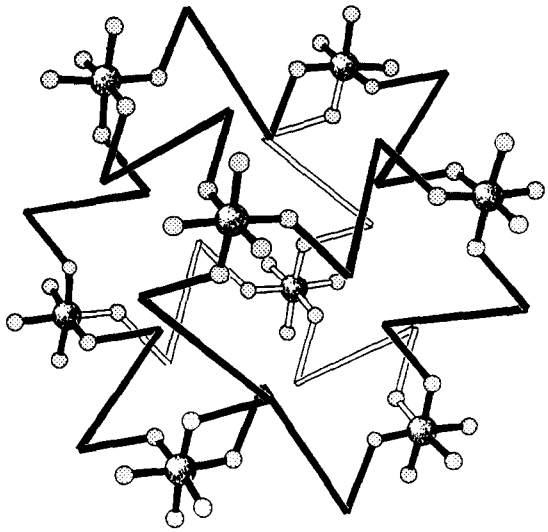

Fig. 5. Schematic representation of one of the contiguous rhomboidal "boxes" forming the polymeric structure of **2**; the long spacer lines link ligand aryl ring centroids.

The network structure we observe here for **2** is similar to those formed by $[Mn\{N,N'$-*p*-phenylenedimethylenebis(4-methylpyridin-2-one)$\}_3](ClO_4)_2$, **3** [3b], and $[Mn(N,N'$-butylenebisimidazole$)_3](ClO_4)_2$, **4** [13]. However in **2** the rhomboid volume (1315 Å^3) is marginally less than that in **3** (1450 Å^3) but is significantly smaller than that in **4** (1950 Å^3). In **4** the free volume is such that rhomboid interpenetration occurs to fill the cavities, whereas in **3** voids are localised along the body diagonals. In **2**, however, the free volume of the central core has a diameter of only ca 5 Å (being restricted by edge-on, inwardly directed aryl rings) and the perchlorate ions are located in the "windows" between adjacent rhomboids (Fig. 6). The smaller central core is populated by disordered molecules of solvation.

Other complexes

The reaction between cobalt(II) perchlorate hexahydrate and EBPYT in a mixture of hot ethanol and nitromethane resulted in the precipitation of a bright green complex of stoichiometry $Co(EBPYT)_2(ClO_4)_2 \cdot 2H_2O$, the solid state electronic spectrum of which (Table 3) is characteristic of an essentially tetrahedral coordination geometry about cobalt(II). The bands arising from the transitions to the components of both $^4T_1(F)$ (in the near IR region) and $^4T_1(P)$ (in the visible region) show pronounced splitting, suggesting that the CoS_4 coordination geometry is somewhat distorted, probably because of steric constraints arising from the form of the bridging action required for the EBPYT ligand to link the tetrahedral metal centres into a polymeric array.

As in the case of the copper(II) halides, reaction

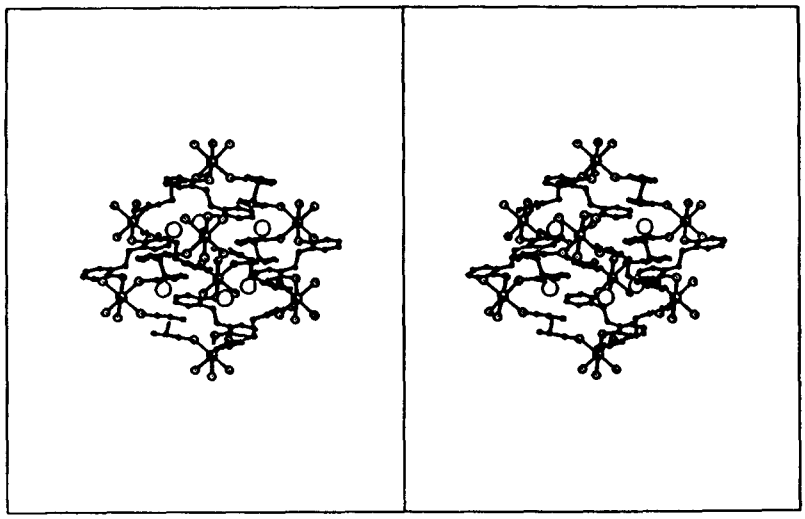

Fig. 6. Stereoscopic view of one of the rhomboidal "boxes" in **2**, with the positions of the perchlorate ions in the "windows" indicated by open circles.

of EBPYT with hydrated copper(II) perchlorate or tetrafluoroborate in mixtures of methanol and nitromethane (and dichloromethane in the case of the perchlorate) resulted in rapid reduction ofthe copper salt and the formation of orange copper(I) complexes of stoichiometry $Cu_2(EBPYT)_3X_2$ ($X = ClO_4$ or BF_4). Analogous complexes $Ag_2(EBPYT)_3X_2$ ($X = ClO_4$ or BF_4) were also formed by silver(I). As the stoichiometry of these complexes is the same as that reported previously [4b] for the complex $\{[Cu_2(EBPYT)_3](PF_6)_2\}_n$, obtained by reaction of $Cu(MeCN)_4(PF_6)$ with EBPYT in acetonitrile, it is quite likely that these new compounds also form sheet polymers in which 4-membered $M_2(\mu\text{-}S)_2$ units are further linked by the EBPYT ligands into arrays of contiguous 18- and 36-membered rings, but single crystals of these compounds were not obtained.

In summary, even though with EBPYT it proved difficult to obtain crystalline samples suitable for full X-ray characterisation, the results of this work, and particularly the structure of **2**, demonstrate that "extended reach" bis-pyridine-2-thione ligands of this type are a potentially fruitful source of new polymeric network complexes. Appropriate ligand modifications, involving substitution on the pyridinthione rings and/or changes in the nature and length of the "spacer" group between the rings, should permit both enhanced crystallinity and a further diversity in the types of arrays that can be formed.

Acknowledgements—We thank the EPSRC for a Research Studentship (to Z.A.), for a post-doctoral fellowship (to S.M.) and for equipment and Dr Pankhurst of the ULIRS Mössbauer service for Mössbauer spectra. D.A.K. thanks Ripon College for granting sabbatical leave to visit Imperial College during the fall of 1993 when part of this work was carried out.

REFERENCES

1. For lead-in reference see: (a) Bertelli, M., Carlucci, L., Ciani, G., Proserpio, D. M. and Sironi, A., *J. Mater. Chem.*, 1997, **7**, 1271; (b) Hoskins, B. F., Robson, R. and Slizys, D. A., *J. Am. Chem. Soc.*, 1997, **119**, 2952; (c) Whiteford, J. A., Lu, C. V. and Stang. P. J., *J. Am. Chem. Soc.*, 1997, **119**, 2524; (d) Liu, J., Paliwala, T., Lim, S. C., Yu, C., Niu, T. and Jacobson, A. J., *Inorg. Chem.*, 1997, **36**, 923; (e) Blake, A. J., Hill, S. J., Hubbersty, P. and Li, W. S., *J. Chem. Soc., Dalton Trans.*, 1997, 913; (f) Hartshorn, C. M. and Steel, P. J., *Chem. Commun.*, 1997, 541; (g) Keller, S. W., *Angew. Chem., Int. Ed. Eng.*, 1997, **36**, 247; (h) Chen, J., Goodgame, D. M. L., Menzer, S. and Williams, D. J., *Polyhedron*, 1997, **16**, 1679; (i) Losier, P. and Zaworotko, M. J., *Angew. Chem., Int. Ed. Eng.*, 1996, **35**, 2779; (j) Fujita, M. and Ogura, K., *Bull. Chem. Soc. Japan*, 1996, **69**, 1471.
2. See, for example: (a) Yaghi, O. M., Jernigan, R., Li, H., Davis, C. E. and Groy, T. L., *J. Chem. Soc., Dalton Trans.*, 1997, 2383; (b) Chung, K. H., Hong, E., Do, Y. and Moon, C. H., *J. Chem. Soc., Dalton Trans.*, 1996, 3363; (c) Wei, P. R., Wu, B. M., Leung, W. P. and Mak, T. C. W., *Polyhedron*, 1996, **15**, 4041; (d) Gutschke, S. O. H., Molinier, M., Powell, A. K., Winpenny, R. E. P. and Wood, P. T., *Chem. Commun.*, 1996, 823.
3. (a) Zhang, R. H., Ma, B. Q., Bu, X.H., Wang, H. G. and Yao, X. K., *Polyhedron*, 1997, **16**, 1123; (b) Goodgame, D. M. L., Menzer, S., Smith, A. M. and Williams, D. J., *J. Chem. Soc., Dalton Trans.*, 1997, 3213, and references therein.
4. (a) Atherton, Z., Goodgame, D. M. L., Katahira, D. A., Menzer, S. and Williams, D. J., *J. Chem. Soc., Chem. Commun.*, 1994, 1423; (b) Goodgame, D. M. L., Katahira, D. A., Menzer, S. and Williams, D. J., *Inorg. Chim. Acta*, 1995,

229, 77; (c) Munakata, M., Wu, L. P., Kuroda-Sowa, T., Maekawa, M., Suenaga, S. and Nakagawa, S., *J. Chem. Soc., Dalton Trans.*, 1996, 1525.
5. e.g. (a) Errington, J., McDonald, W. S. and Shaw, B. L., *J. Chem. Soc., Dalton Trans.*, 1980, 2309; (b) Stephan, D. W., *Organometallics*, 1991, **10,** 2037; (c) Huang, Y., Drake, R. J. and Stephan, D. W., *Inorg. Chem.*, 1993, **32,** 3022.
6. Sheldrick, G. M., SHELXTL Version 5.03, University of Göttingen, Germany, 1995.
7. Goodgame, D. M. L. and Goodgame, M., *Inorg. Chem.*, 1965, **4,** 139.
8. Forster, D. and Goodgame, D. M. L., *J. Chem. Soc.*, 1965, 454.
9. Burbridge, C. D. and Goodgame, D. M. L., *J. Chem. Soc.(A)*, 1968, 1074.
10. (a) Nakamoto, K., *Infrared and Raman Spectra of Inorganic and Coordination Compounds*, 3rd edn, Wiley, New York, 1977, Part III, pp. 317 324; (b) Adams, D. M., *Metal-Ligand and Related Vibrations*, Edward Arnold, London, 1967, p. 277 and references therein.
11. e.g (a) Birchall, T. and Morris, M. F., *Canad. J. Chem.*, 1971, **50,** 211; (b) Petillon, F., Guerchais, J. E. and Goodgame, D. M. L., *J. Chem. Soc., Dalton Trans.*, 1973, 1209.
12. Holt, S. L. and Carlin, R. L., *J. Am. Chem. Soc.*, 1964, **86,** 3017.
13. Duncan, P. C. M., Goodgame, D. M. L., Menzer, S. and Williams, D. J., *Chem. Commun.*, 1996, 2127.

Pergamon

PII: S0277-5387(98)00015-1

Polyhedron Vol. 17, Nos. 13–14, pp. 2267–2770, 1998
© 1998 Elsevier Science Ltd
All rights reserved. Printed in Great Britain
0277-5387/98 $19.00+0.00

Mercury(II) complexes of 4,5-ethylenedithio-1,3-dithiole-2-thione, having S···S and S···Cl contact assembled ribbon structure

Jie Dai,*[a] Megumu Munakata,[b] Guo-qing Bian,[a] Qing-feng Xu,[a] Takayoshi Kuroda-Sowa[b] and Masahiko Maekawa[b]

[a] Department of Chemistry, Suzhou University, Suzhou 215006, P.R. China

[b] Department of Chemistry, Kinki University, Kowakae 3-4-1, Higashi-Osaka 577, Japan

(Received 20 October 1997, accepted 6 January 1998)

Abstract—Two mercury(II) complexes of 4,5-ethylenedithio-1,3-dithiole-2-thione ($C_5H_4S_5$), $[Hg_2(C_5H_4S_5)_2Cl_4]$ (**1**) and $[Hg_2(C_5H_4S_5)_2Br_4]$ (**2**), were synthesized and the structure of complex **1** was characterized crystallographically. Complex **1** has a dimeric structure, in which each mercury atom takes a tetrahedral geometry and is coordinated by two bridging chloride, one terminal chloride and one thiocarbonyl sulfur atom (C=S) of the ligand. These dimers are further packed to form a one dimensional ribbon structure via intermolecular S···S and S···Cl contacts. All of the ligands in the ribbon are co-planar and weakly conjugated. © 1998 Elsevier Science Ltd. All rights reserved

Keywords: mercury(II) complexes; sulfur-rich compounds; crystal structure; intermolecular contacts.

In most conductive sulfur-rich donor-acceptor compounds or radical salts, intermolecular interactions such as S···S contacts have been found to play an important role in the conductivity of these compounds. The molecular packing that influences the S···S interaction is mainly controlled by the identity of the molecule itself, the size of counter ions and co-crystallized solvent molecules [1]. On the other hand, metal ions have properties of special interest as components of supramolecular systems and linkers for self-assembly [2]. Our recent interest was focused on the assembling of sulfur-rich donor compounds via both coordination bonds and S···S interactions [3–5], since the packing and interactions of organic molecules in the coordination compounds have more variety than is observed in pure organic compounds.

To introduce metal ions to these donor-acceptor systems, a sulfur-rich compound of 4,5-ethylenedithio-1,3-dithiole-2-thione ($C_5H_4S_5$), which is known as an electron donor and has available site to coordinate to metal ions [6], was selected as a ligand in this work. The ligand is also a derivative of dmit

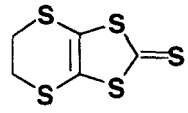

$C_5H_4S_5$

(4,5-disulfanyl-1,3-dithio-2-thionate) and has a similar structure to half of BEDT-TTF [bis(ethylenedithio)tetrathiafulvalene]. Recently we have reported four complexes of $C_5H_4S_5$, $[Ag(C_5H_4S_5)_2NO_3]_x$ [3], $[Cu_4I_4(C_5H_4S_5)_4]_x$ [4], $\{[Ag(C_5H_4S_5)_3]ClO_4 \cdot CH_3CN\}_2$ [5] and $[Ag(C_5H_4S_5)CF_3SO_3]_x$ [5]. Each of them has a unique molecular structure and a S···S contact assembled network. In this paper we report two new mercury(II) complexes of $C_5H_4S_5$. One of which was characterized crystallographically, showing a dimer structure with two kind of intermolecular interactions.

EXPERIMENTAL

The reagent $C_5H_4S_5$ was obtained from Tokyo Kasei Co. and used without further purification. Ace-

* Author to whom correspondence should be addressed.

tonitrile was dried and distilled by a standard method before use. Infrared spectra were measured as KBr and CsI discs on a JASCO FT/IR 8000 spectrometer and electronic spectra were recorded with a Hitachi 150-20 spectrophotometer. Electrical resistivity was measured by a conventional two-probe method at room temperature with a compressed pellet.

Preparation of $[Hg_2(C_5H_4S_5)_2Cl_4]$ (**1**)

To an acetone solution (4 cm^3) of $C_5H_4S_5$ (11.5 mg, 0.05 mmol) was added $HgCl_2$ (27.0 mg, 0.1 mmol) in acetone (2 cm^3). The mixture was stirred for 20 min at room temperature under an argon atmosphere. A red precipitate formed and it was filtered and dried in argon. Suitable crystals for X-ray measurement were grown at $-5°C$ from the filtrate which was sealed in a glass tube. Anal: Calc. for $C_5H_4Cl_2HgS_5$: C, 12.11; H, 0.81. Found: C, 12.26; H, 0.76%.

Preparation of $[Hg_2(C_5H_4S_5)_2Br_4]$ (**2**)

The complex **2** was prepared via a similar method as that of **1**. Instead of $HgCl_2$, $Hg(ClO_4)_2 \cdot H_2O$ and $(C_4H_9)_4NBr$ (in 1 : 2 ratio) were used as the starting materials. Anal: Calc. for $C_5H_4Br_2HgS_5$: C, 10.27; H, 0.69. Found: C, 10.65; H, 0.73%.

The iodine-doped compounds of **1** and **2** were prepared by gaseous diffusion. A small amount of powder of the complex and solid I_2 were separately placed in an H-shaped tube which was then sealed under argon and was allowed to stand for one month at ambient temperature. Red-black I_2-doped compounds were obtained.

X-ray structure determination

A red crystal of **1** was mounted on a Rigaku AFC7R four-circle diffractometer equipped with a graphite monochromator utilizing Mo–K_α radiation. The data were collected by using the ω-2θ scan technique to a maximum 2θ value of 54.9°. Of the 2801 reflections collected, 2622 were unique. An empirical correction based on azimuthal scans of several reflections was applied and the data were corrected for Lorentz and polarization effects. The structure was solved by direct methods (SAPI91) [7], and expanded using Fourier techniques [8]. The non-hydrogen atoms were refined anisotropically. Hydrogen atoms were included but not refined. The final cycle of full-matrix least-squares refinement was based on 2435 observed independent reflections [$I > 3\sigma(I)$] and 118 variable parameters. The final R and R_w values were 0.034 and 0.057, respectively. All calculations were performed using the TEXSAN program system [9]. Details of crystal data are summarized in Table 1.

Table 1. Crystallographic data for the complex **1**

	1
Formula	$C_5H_4Cl_2HgS_5$
Formula weight	495.88
Crystal color, habit	red, prismatic
Crystal dimensions (mm)	$0.20 \times 0.30 \times 0.30$
Crystal system	triclinic
Space group	$P\bar{1}$
a (Å)	8.550(2)
b (Å)	9.8476(8)
c (Å)	8.298(2)
α (°)	100.69(1)
β (°)	118.07(2)
γ (°)	102.79(1)
V (Å^3)	572.9(2)
Z	2
D_{calc} (g cm^{-3})	2.874
F_{000}	456.00
μ (Mo-K_α) (cm^{-1})	147.92
T (K)	23.0
$2\theta_{max}$ (°)	54.9
Total reflections	2801
Unique reflections	2622
Observations ($I > 3\sigma(I)$)	2435
R^a	0.034
Rw^b	0.057
Goodness of fit indicator	2.75
Max shift/error	0.00
$\Delta\rho_{min}$, $\Delta\rho_{max}$ (eÅ^{-3})	−2.43, 0.97

$^a R = \Sigma(||F_o| - |F_c||)/\Sigma|F_o|$.
$^b Rw = \{\Sigma w(|F_o| - |F_c|)^2/\Sigma w|F_o|^2\}^{1/2}$.
$w = 4F_o^2/\Sigma\sigma^2(F_o^2)$.

RESULTS AND DISCUSSION

Structural description and discussion

The complex $[Hg_2(C_5H_4S_5)_2Cl_4]$ (**1**) is found to be a halogen-bridged dimer related by an inversion centre. An ORTEP view of the complex together with the atomic labeling scheme is given in Fig. 1. Each mercury atom is four-coordinated with significant distortion from tetrahedral. Two of these bonds are formed by two asymmetric chloride bridges, while the remaining two bonds are formed by a terminal chloride ion and thiocarbonyl sulfur atom of the ligand. The selected bond lengths and angles for the complex are listed in Table 2, in which the data of the dimeric unit are comparable to those reported in the literature for related chloride bridged dimeric Hg(II) complexes [10,11].

Coordination modes of the $C_5H_4S_5$ ligand have been classified into four types by our previous report [5]. They are monodentate coordination by the thiocarbonyl group (type I), bridge formation by the

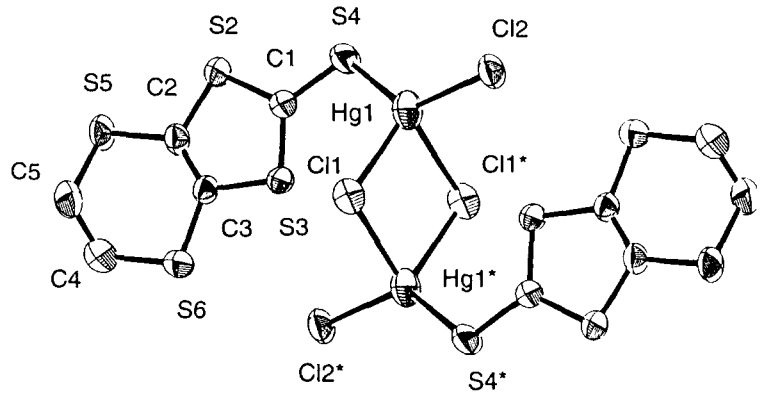

Fig. 1. An ORTEP view of the dimeric structure of $[Hg_2(C_5H_4S_5)_2Cl_4]$.

Table 2. Selected bond lengths (Å) and angles (°) for $[Hg_2(C_5H_4S_5)_2Cl_4]$ (**1**)

Hg(1)—Cl(1)	2.569(2)	Hg(1)—Cl(1′)	2.808(2)
Hg(1)—Cl(2)	2.395(2)	Hg(1)—S(1)	2.467(2)
S(1)—C(1)	1.702(7)		
Cl(1)—Hg(1)—Cl(1′)	85.24(6)	Cl(1)—Hg(1)—Cl(2)	112.1(7)
Cl(1′)—Hg(1)—Cl(2)	102.22(6)	Cl(1)—Hg(1)—S(1)	113.71(6)
Cl(1′)—Hg(1)—S(1)	101.63(7)	Cl(2)—Hg(1)—S(1)	129.42(6)
Hg(1)—Cl(1)—Hg(1′)	94.76(6)		

sulfur of the thiocarbonyl group (type II), bidentate coordination by both thiocarbonyl group and thioether group (type III) and tridentate coordination by the thiocarbonyl sulfur (acting as a bridge) and the thioether sulfur (type IV). Although the coordination of the ligand in type I has been found in complex $[Cu_4I_4(C_5H_4S_5)_4]_\infty$ and $\{[Ag(C_5H_4S_5)_3]ClO_4 \cdot CH_3CN\}_2$ [4,5], other coordination types are co-exist in these complexes. $[Hg_2(C_5H_4S_5)_2Cl_4]$ is the complex found in the coordination of the ligands only in type I. The S(1)—C(1) distance of 1.702 Å in **1** is longer than that for the free ligand 1.633 Å [12] and is the longest found in the complexes of $C_5H_4S_5$. This longer S(1)—C(1) distance attributes to the strong coordination of the thiocarbonyl sulfur to soft mercury(II) ion that weakens the S(1)—C(1) bond.

We are paying significant attention to the S···S contacts in complexes with sulfur-rich ligands, since S···S contact is one of the most important factors by which the compounds exhibit high conductivity [13–16]. We also found that the coordination linkage in metal complexes can be expected to control or change the intra- or inter-molecular interactions in supermolecules [3–5,17]. In the present complex, the S···S contact of 3.583(3) Å between nearby dimeric units is less than the sum 3.70 Å of van der Waals radii of two S atoms. There is another type interaction within the chain, that is strong Cl···S contact. The contact distance of 3.288(3) Å significantly shorter than the sum 3.60 Å of van der Waals radii. Thus, this complex has a one-dimensional supramolecular structure assembled by both S···S and Cl···S contacts. A view of the S···S and Cl···S contacts assembled ribbon structure is given in Fig. 2.

For the head-to-tail S···S contacts (thiocarbonyl to thioether) and the Cl···S contacts, all of the ligands in the ribbon are co-planar and weakly conjugated that indicates an efficient intermolecular π-π orbital interactions and forms a broadened energy band over the whole lattice. Most of the TTF and dmit based superconductors have this character.

Spectroscopic studies and the iodine doped compounds

The IR spectra of **1** and **2** show one broad $\nu_{(C=S)}$ stretching frequency of the heterocyclic ring at 1010 and 1008 cm^{-1} respectively. The C=S stretching frequency of 1477 cm^{-1} for the free ligand [12] is shifted to 1441 cm^{-1} for both of the complexes. These shifts are larger than those of the silver(I) and copper(I) complexes [3–5], attributing to the strong coordination of the mercury(II) with thiocarbonyl sulfur. This result is in accordance with that found in the C=S distances. The infrared frequencies of Hg—X (X = Cl, Br) for complexes **1** and **2** were measured using CsI discs. Comparing with the spectrum of the ligand, the ν(Hg—Cl)$_t$ and ν(Hg—Br)$_t$ (t = terminal)

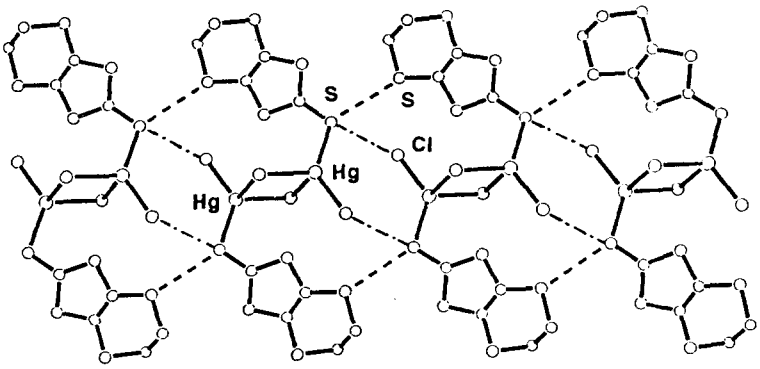

Fig. 2. The one-dimensional ribbon structure assembled by intermolecular S···S and S···Cl contacts.

are 280 and 201 cm^{-1} respectively, and the $\nu(Hg—Cl)_b$ and $\nu(Hg—Br)_b$ (b = bridge) are 226 and 154 cm^{-1} respectively. The dimeric halogen-bridged complexes have been reviewed by P. A. W. Dean in detail [11]. Although only the observation of a bridging Hg—X frequency is probably insufficient to discriminate between halogen-bridged dimers and halogen-bridged polymers with tetrahedral coordination of mercury, considering the other habits of the complex **2**, it should have a dimeric structure as in complex **1**. Both the complexes formed red prismatic crystals and showed high solubility in acetone and acetonitrile. The solid-state electronic spectra of the complexes showed a strong broad peak at about 500 nm assigned to a metal–ligand charge transfer for the red complexes. On the other hand, a weak broad peak at 900 nm can be explained by the intermolecular interactions.

Halogen doping of conjugated electron donors has been shown to be an effective strategy for the synthesis of electrically conductive compounds. Although the iodine doped free $C_5H_4S_5$ ligand is an insulator ($\sigma < 10^{-12}$ S cm^{-1}) the iodine doped complex **1** and **2** exhibit electrical conductivity (σ) of 3.0×10^{-5} S cm^{-1} and 1.5×10^{-5} s cm^{-1} at room temperature. The increase of electronic conductivity is due to the partial oxidation of the ligands and the short S···S contacts within the 1D structure.

Acknowledgments—The financial support from the Ministry of Education, Science, Sports and Culture in Japan and the government of Jiangsu province in China are greatly appreciated.

REFERENCES

1. Schlueter, J. A., Willimas, J. M., Geiser, U., Wang, H. H., Kini, A. M., Kelly, M. and Dudek, J. D., *Mol. Cryst. Liq. Cryst.*, 1996, **285**, 43.
2. Lehn, J.-M., *Supramolecular Chemistry*. VHC, Weinheim, 1995.
3. Dai, J., Munakata, M., Kuroda-Sowa, T., Suenaga, Y., Wu, L. P. and Yamamoto, M., *Inorg. Chim. Acta*, 1997, **225**, 163.
4. Dai, J., Munakata, M., Wu, L. P., Kuroda-Sowa, T. and Suenaga, Y., *Inorg. Chim. Acta*, 1997, **258**, 65.
5. Dai, J., Kuroda-Sowa, T., Munakata, M., Maekawa, M., Suenaga, Y. and Ohno, Y., *J. Chem. Soc., Dalton Trans.*, 1997, 2363.
6. Svenstrup, N. and Becher, J., *Synthesis*, 1995, 215.
7. SAPI91 : Fan, H. F., Structure Analysis Programs with Intelligent Control, Rigaku Cirporation, Tokyo, Japan, 1991.
8. Beurskens, P. T., Admiraal, G., Beurskens, G., Bosman, W. P., Gelder, R. de, Israel, R. and Smits, J. M. M., DIRDIF94, University of Nijmegen, 1994.
9. TEXSAN: Crystal Structure Analysis Package, Molecular Structure Corpration, 1992.
10. Brodersen, K. and Hummel, H.-U. In *Comprehensive coordination Chemistry*, Vol. 5, ed. G. Wilkinson, R. D. Gillard and J. A. McCleverty, Pergamon, New York, 1987, pp. 1047–1170.
11. Dean, P. A. W., *Progress in Inorganic Chemistry*, 1978, **24**, 109.
12. Drew, M. G. B., KIsenyi, J. M. and Parish, R. V., *J. Chem. Soc., Dalton Trans.*, 1987, 1605.
13. Williams, J. M., Wang, H. H., Emge, T. J., Geiser, U., Beno, M. A., Leung, P. C. W., Carlson, K. D., Thorn, R. J., Schultz, A. J. and Whangbo, M., *Prog. Inorg. Chem.*, 1987, **35**, 1.
14. Bryce, M. R., *Chem. Soc. Rev.*, 1991, **20**, 355.
15. Olk, R. M., Olk,, B., Dietzsch, W., Kirmse, R. and Hoyer, E., *Coord. Chem. Rev.*, 1992, **117**, 99.
16. Cassoux, P., Valade, L., Kobayashi, H., Kobayashi, A., Clark, R. A. and Underhill, A. E., *Coord. Chem. Rev.*, 1991, **110**, 115.
17. Munakata, M., Dai, J., Maekawa, M., Kuroda-Sowa, T. and Fukui, J., *J. Chem. Soc., Chem. Commun.*, 1994, 2331.

Pergamon

PII: S00277-5387(98)00010-2

Polyhedron Vol. 17, Nos 13-14, pp. 2271-2278, 1998
© 1998 Elsevier Science Ltd
All rights reserved. Printed in Great Britain
0277-5387/98 $19.00+0.00

Hydrolysis of methionine-containing peptides in binuclear and mononuclear palladium(II) complexes

Xiaohua Chen, Xuemei Luo, Yongcheng Song, Shaozhen Zhou and Longgen Zhu*

Coordination Chemistry Institute, State Key Laboratory of Coordination Chemistry, Nanjing University, Nanjing, Jiangsu, 210093, P.R. China

(Received 14 October 1997; accepted 5 January 1998)

Abstract—The diaqua complexes of *trans*-$[Pd(py)_2Cl_2]$ (Py-pyridine), *cis*-$[Pd(edta)Cl_2]$ (edta-ethylene diamine tetraacetic acid) (complex A), *cis*-$[Pd(temed)Cl_2]$ (temed-N,N,N′,N′-tetramethylethylene diamine) and *cis*-1,2-bis(2-formylglycinebenzenesulfenyl)ethane Pd(II) dichloride (complex C) react with methionine-containing dipeptides (AcMet-aa) (aa-amino acid) via the thioether group in the methionyl side chain. The *trans*-$Pd(py)_2(H_2O)_2]^{2+}$ and *cis*-$[Pd(temed)(H_2O)_2]^{2+}$ yield binuclear complex $[Pd_2(\mu\text{-AcMet-aa})_2(H_2O)_4]^{4+}$, the diaqua complexes of complex A and complex C yield mononuclear complexes, $[PdL(AcMet\text{-aa})(H_2O)]^{2+}$ (L-edta, 1,2-bis(2-formylglycinebenzenesulfenyl)ethane). These reactions and hydrolytic cleavage of the Met-aa amide bond in the coordinated AcMet-aa are conveniently monitored by ^1H NMR spectroscopy. The *trans*-$Pd(py)_2(H_2O)_2]^{2+}$ is a very efficient promoter. The hydrolytic rate promoted by it is almost equal to that promoted by $[Pd(H_2O)_3(OH)]^+$, the fastest one up to now. Although reaction of *trans*-$[Pd(py)_2(H_2O)_2]^{2+}$ and *cis*-$[Pd(temed)(H_2O)_2]^{2+}$ with AcMet-aa yield the same binuclear complex, $[Pd_2(\mu\text{-AcMet-aa})_2(H_2O)_4]^{4+}$, the kinetic data showed that the hydrolytic rate promoted by *cis*-$[Pd(temed)(H_2O)_2]^{2+}$ was actually controlled by temed release. The new mononuclear complexes, $[PdL(AcMet\text{-aa})(H_2O]^{2+}$, observed for the first time, are also hydrolytically active. It is of interest because they are closely associated with protein cleavage promoted by simple mononuclear Pd(II) complexes. © 1998 Elsevier Science Ltd. All rights reserved

Keywords: palladium; hydrolysis; peptide cleavage; artificial metallopeptidase.

Selective cleavage of peptides and proteins is one of the most common tasks and the most important procedure in analytic biochemistry. Although several proteolytic enzymes are available for this purpose, its number is very limited and only trypsin is highly regioselective [1]. Furthermore, since the requirements for the traditional applications are changing today, new methods for cleavage are needed for many tasks in biochemistry and molecular biology: semisynthesis of proteins; sequencing of large or blocked proteins; structural and functional analysis of protein domain; development of new drugs, and so on. Chemical (non-enzymatic) reagents are well suited for many of these tasks. Although the need for them is growing, only one, cyanogen bromide, is available for routine use [1]. But it has several shortcomings. It is volatile and toxic, requires harsh conditions, and often produces incomplete cleavage.

Transition metal complexes are also suited for cleavage of inactivated amide bonds in peptides [2–22] and proteins [23–31]. In the early studies, complexes of cobalt(III) and copper(II) were studied more than any other. Kinetic and mechanistic studies have been done almost exclusively with amides that variously activated by substituents, by ring strain, by forced non-planarity, or by proximate functional group [2–13]. These complexes are not suitable to a practical use for analytic biochemistry, because only the N-terminal amide bond is cleaved. Practical applications, however, usually require cleavage of internal amide bonds.

In recent studies, a variety of metal complexes have been developed for direct hydrolytic or oxidative cleavage of amide bonds in peptides [14–22] and proteins [23–31]. One of them is simple palladium(II)

* Author to whom correspondence should be addressed

aqua complexes that bind to the side chains of methionine [15–19,22] and histidine [20,21] residues in short peptides followed by selectively hydrolytic cleavage of the adjacent amide group, even with turnover [21,22]. In order to further develop this new method for practical application, it is necessary to synthesize new palladium(II) complexes and investigate the action of cleavage reaction as well as understand the stereochemical requirements for cleavage. In this article, we report some palladium(II) complexes that hydrolyze Met-aa(amino acid) amide bond with different behavior. A monodentate palladium(II) complex, *trans*-$[Pd(py)_2(H_2O)_2]^{2+}$, fast hydrolyzes Met-aa amide bond with a hydrolytic rate comparable with that promoted by $[Pd(H_2O)_3(OH)]^+$. Unlike $[Pd(H_2O)_3OH)]^+$, *trans*-$[Pd(py)_2(H_2O)_2]^{2+}$ is more stable and easy to prepare. An N,N-chelated palladium(II) complex, *cis*-$[Pd(temed)(H_2O)_2]^{2+}$ (temed-N,N,N′,N′-tetramethyl ethylene diamine) hydrolyzes Met-aa amide bond with hydrolytic rate controlled by temedH_2^{2+} release. The action of the other two complexes, *cis*-$[Pd(edta)Cl_2]$ (edta-ethylenediaminetetraacetic acid) designated complex A and *cis*-1,2-bis(2-formylglycinebenzenesulfenyl) ethane Pd(II) dichloride designated complex C differs from their similar complexes of *cis*-$[Pd(en)Cl_2]$ (en-ethylenediamine) and *cis*-$[Pd(dtco\text{-}3\text{-}OH)Cl_2]$ (dtco-3-OH-1,5-dithiacyclooctan-3-ol). Although palladium(II) is added to the methionine-containing peptides in the form of mononuclear complexes, the complexes studied so far that actually undergo hydrolysis are binuclear complexes shown as $[Pd_2(\mu\text{-AcMet-aa})_2(H_2O)_4]^{4+}$. Both NMR spectra and kinetic experiments support this conclusion. However, when the diaqua complexes of complex A and complex C were used as promoters, a new hydrolytically active mononuclear Pd(II) complex was observed for the first time. This active monomer may closely be relative to hydrolysis reaction proceeded in proteins because its steric bulk prevents formation of active binuclear complexes. This study contributes to our further understanding of the mechanism of hydrolytic cleavage of peptides and brings us a step closer to our ultimate goal, design of palladium(II) complexes as artificial metallopeptidases.

EXPERIMENTAL

Chemicals

Distilled water was demineralized. The deuterium-containing compounds D_2O, DMSO-d_6 and K_2PdCl_4 were obtained from Aldrich Chemical Co. Dipeptides Met-Gly, Met-Ala, and Met-Val were obtained from Sigma Chemical Co. The terminal amino group in each dipeptide was acetylated by a published procedure [15]. All other common chemicals were of reagent grade.

The following dichloro complexes were prepared by published procedures: *cis*-$[Pd(en)Cl_2]$ [32], $[Pd(H_2O)_3(OH)]^+$ [15], *cis*-$[Pd(temed)Cl_2]$ [32], [Pd(dien)I]I (dien-diethylenetriamine) [33].

Trans-$[Pd(py)_2Cl_2]$. 0.5 g of $PdCl_2$ was suspended in 5 ml of pyridine. The mixture was stirred and heated to 80°C. After the solid was almost dissolved, the hot solution was filtered. 50 ml of benzene was poured into the filtrate. The yellow precipitate was collected, washed with benzene and dried *in vacuo*. Yield 90%. Diffusion of methanol into the N,N-dimethyl formamide (DMF) solution of *trans*-$[Pd(py)_2Cl_2]$ in six days produced the yellow single crystals. Its crystal data were reported in literature [34].

Cis-$[Pd(edta)Cl_2]\cdot 5H_2O$. It was prepared by mixing dihydrogen disodium ethylenediaminetetraacetate (Na_2H_2EDTA) with K_2PdCl_4 in water and crystallized from concentrated hydrochloric acid. The bright yellow crystals of *cis*-$[Pd(edta)Cl_2]\cdot 5H_2O$ was obtained. Its crystal data were determined [35].

1,2-bis(2-formylglycinebenzenesulfenyl)ethane Pd(II)dichloride complex designated complex C. It was synthesized according to standard method as described in our previous paper [36]. PhCOOH → 2-HSPh COOH → (2-SPhCOOH)CH_2CH_2(2-SPhCOOH) → (2-SPhCONHCH_2COOH)CH_2CH_2(2-SPhCONH CH_2COOH) → complex C. Molecular structure of the complex C was determined [36].

The corresponding diaqua complexes were obtained by stirring the precursors with 2.0 equivalents of $AgNO_3$ in a solution of pH* 2 for 4 h at 35°C and removal of AgCl by centrifugation, all in the dark. Since the solvent was D_2O the ligand were actually D_2O, but the formulas will be written simply with H_2O. The aqua complexes were always prepared fresh and used as solutions. For complex C, because of low solubility of corresponding diaqua complex, it was treated with DMSO-d_6 instead and designated complex D.

The ^1H NMR spectra of the acetylated dipeptides in D_2O showed the following principal δ values: AcMet-Gly, 2.04, s, CH_3CO; 2.11, s, CH_3S; 3.99, q, GlyCH_2; AcMet-Ala, 2.03, s, CH_3CO; 2.11, s, CH_3S; 1.44, d, AlaCH_3; 4.39, q, AlaCH; AcMet-Val, 2.03, s, CH_3CO; 2.11, s, CH_3S; 4.27, d, ValCH; 0.96, dd, ValCH_3. Stringent control experiments showed that these peptides are stable for long time in solution of pH $\leqslant$ 1.0 and ruled out simple acid catalysis of the peptides hydrolysis [15,16]. Acidic solutions are needed to suppress formation of oligomeric palladium(II) complexes with hydroxo bridges [15,16].

Measurements

Proton NMR spectra at 500 MHz of D_2O solutions, containing sodium 4,4-dimethyl-4-silapentane-1-sulfonate (DSS) as an internal reference, were recorded with an AM500 spectrometer. The sample temperature was kept at 40 ± 0.5°C. The pH was measured with an Orion 901 instrument and a phoenix Ag-AgCl

reference electrode. The uncorrected values in D_2O solutions are designated pH*.

Kinetics of hydrolysis

Stock solutions of all palladium(II) complexes were prepared fresh in D_2O or DMSO-d_6. The concentration of these Pd(II) complexes was 100 mM. Equimolar amounts of AcMet-aa(aa-Gly, Ala, Val) and of the Pd(II) complexes were mixed rapidly in an NMR tube, so that the final concentration of each was 10.0–20.0 mM. The total volume was 600 μl. pH* was adjusted with 1.0 M $HClO_4$ in D_2O solution, and was measured at beginning and the end of the reaction. The difference between two measurements is always less than 0.1 pH*. Acquisition of the ^1H NMR spectra began as soon as possible, and 16 or 32 scans were taken for each time. The hydrolysis products were monitored by enhancements of the ^1H NMR resonance of free amino acids. The concentrations of the hydrolysis products (Ct and C∞) were determined on the basis of resonance area; the estimated error is ±5%. First-order plots of -ln[(C∞-Ct)/C∞] versus time contained 13–20 points and were linear over at least three half-lives, with correlation coefficients of 0.994–0.999. The observed rate constants, k_{obsd}, are the slopes of these plots. The reactions were run for six half-lives.

RESULTS AND DISCUSSION

Hydrolysis of peptides promoted by trans-$[Pd(py)_2(H_2O)_2]^{2+}$

We reasonably assume that the replacement of the two chloride anions in *trans*-$[Pd(py)_2Cl_2]$ by two aqua ligands would not alter the structure. As scheme 1 shows, after mixing the *trans*-$[Pd(py)_2(H_2O)_2]^{2+}$ with AcMet-Gly, free pyH^+ can be quickly detected by ^1H NMR. This release is favored by the labilizing *trans* effect of the py (compared to H_2O) and thioether and by the acid in solution. The resonance of SCH_3 of AcMet-Gly at 2.46 ppm shows that the active form is a binuclear complex [15,16,18,22]. Hydrolysis of AcMet-Gly and s-methylglutathione (GSMe) promoted by $[Pd(H_2O)_3(OH)]^+$, *trans*-$[Pd(py)_2(H_2O)_2]^{2+}$ and *cis*-$[Pd(en)(H_2O)_2]^{2+}$ is listed in Table 1. for hydrolysis of AcMet-Gly, these three complexes have the same active from, μ_2-s-bridged binuclear complex, that effectively promotes the hydrolysis of peptides in it. However, compared with en, pyridine is a unidentate, weak ligand and more rapidly detached after mixing with the substrate. Therefore, *trans*-$[Pd(py)_2(H_2O)_2]^{2+}$ is a more efficient promoter. The hydrolytic rate promoted by it is almost equal to that promoted by $[Pd(H_2O)_3(OH)]^+$, the fastest one up to now. The great advantage of the *trans*-$[Pd(py)_2(H_2O)_2]^{2+}$ is that it is easy to prepare and stable for stocking. As shown from Table 1, the hydrolysis of s-

Table 1. Hydrolysis of AcMet-Gly and GSMe promoted by palladium(II) complexes at 40 C

Promoter	Substrate	pH*	k_{obsd} 10^4, min^{-1}
$[Pd(H_2O)_3(OH)]^+$	AcMet-Gly	1.07	360
trans-$[Pd(py)_2(H_2O)_2]^{2+}$	AcMet-Gly	1.05	330
cis-$[Pd(en)(H_2O)_2]^{2+}$	AcMet-Gly	1.05	199
$[Pd(H_2O)_3(OH)]^+$	GSMe	0.95	8.9
trans-$[Pd(py)_2(H_2O)_2]^{2+}$	GSMe	0.94	7.8
cis-$[Pd(en)(H_2O)_2]^{2+}$	GSMe	1.00	3.0

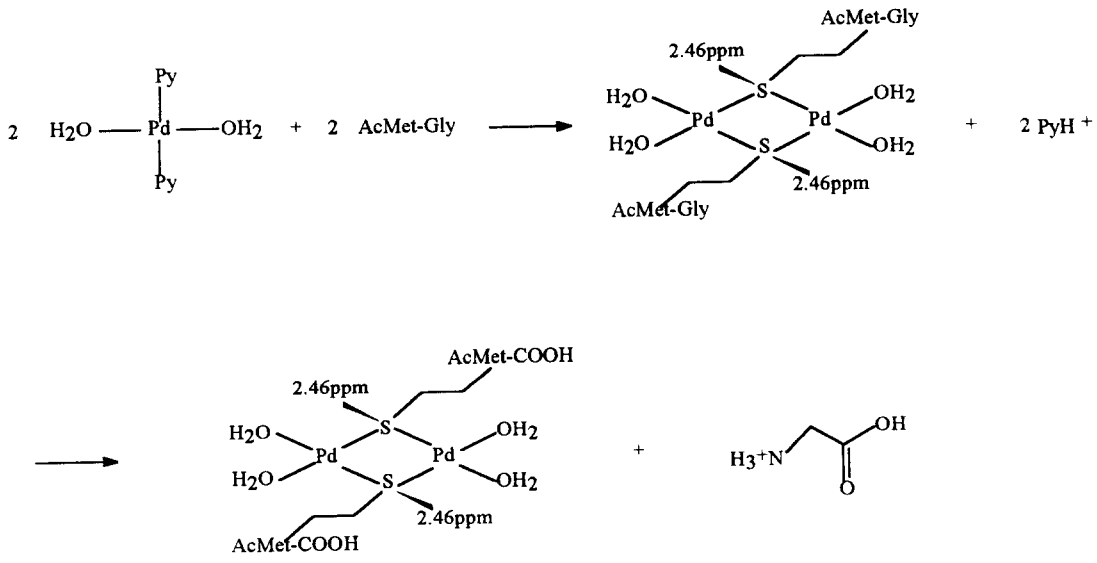

Scheme 1.

methylglutathione is much slower (40–60 times slower) than that of AcMet-Gly. Previous studies showed that s-methylglutathione reacts with Pd(II) complexes to form a binuclear complex as shown below [17].

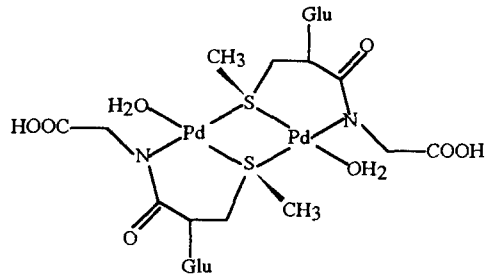

Palladium(II) can effectively induce deprotonation of the amide nitrogen by binding to it [33]. When palladium(II) is already anchored to the side chain, this process is especially favorable due to six-membered chelating ring formation. The estimated pK_a for this reaction is ca 2, and displacement was observed even in solution with pH < 2.0 [37–42]. The coordination of the amide nitrogen to Pd(II) will stabilize the amide bond [15], and suppress the coordination of the carbonyl oxygen to Pd(II). This type of coordination enables to polarize the carbonyl group and activate it toward external attack by solvent water. Because, in this case, coordination of the amide nitrogen is predominant, the hydrolysis of GSMe is very slow. While, as far as AcMet-Gly is concerned, the longer side chain makes the above two types of coordination less likely because they form a seven-membered chelate ring. The aqua ligands attached to palladium(II) and *cis* to the substrates can be delivered to the carbonyl group internally. Therefore, the hydrolysis of AcMet-Gly is fast.

Dependence of hydrolysis rate constant on ligand substitution reaction

The structures of *cis*-$[Pd(temed)(H_2O)_2]^{2+}$ and *cis*-$[Pd(en)(H_2O)_2]^{2+}$ are similar. They are both N,N-chelated Palladium(II) complexes. Their difference lies in that four hydrogen atoms in en are replaced by four methyl groups in temed. As the two complexes mixed with substrate AcMet-aa (aa-Gly, Ala, Val), the sulfur atom in the side chain of substrate substitutes the coordinated water, and at the same time the chemical shift of CH_3S is downfield from 2.11 ppm to 2.50 ppm. The reaction is very fast, it has completed at the beginning of monitoring. A dimer $[Pd_2(\mu\text{-AcMet-aa})_2L_2]^{4+}$ (aa-Gly, Ala, Val; L-en, temed) is formed. After formation of the dimer, $[Pd_2(\mu\text{-AcMet-Gly-})_2(temed)_2]^{4+}$, the signal of free glycine at 3.90 ppm increased. ^1H NMR also showed another two single peaks appeared at 2.62 ppm and 2.99 ppm that are assigned CH_3 and CH_2 in temed. It is clear that the release of free glycine is accompanied by the detachment of temed ligand. Therefore, we can simultaneously determine the observed rate constant of peptide hydrolysis, designated k^h_{obsd} and observed rate constant of substitution reaction of termed by water, designated k^s_{obsd}. The results are listed in Table 2. The k^s_{obsd} of en release is not given in the Table because enH_2^{2+} release in $[Pd_2(\mu_2\text{-AcMet-aa})_2(en)_2]^{4+}$ was too fast to monitor and completed only in 20 min. To compare the rates of ligand release more carefully, we have done some kinetic study on the reaction of the promoters with AcCysMe(acetyl-s-methylcysteine) at 25°C and pH* 1.52. The k^s_{obsd} values are as follows: $10^3K^s_{obsd}$ of $temedH_2^{2+}$ release is 3.56 min^{-1} and $10^3k^s_{obsd}$ of enH_2^{2+} release is 77.1 min^{-1}, 20-fold faster. Comparing the k^h_{obsd} with the k^s_{obsd} in $[Pd_2(\mu\text{-AcMet-aa})_2(temed)_2]^{4+}$, it revealed for the first time that the hydrolysis rate of dipeptides in the binuclear Pd(II) complex is governed by the temed-substitution reaction. The relationship between k^s_{obsd} and k^h_{obsd} can be explained by a consecutive kinetic equation as follows:

$$[Pd_2(\mu\text{-AcMet-aa})_2L_2]^{4+} + 4H_3^+O \xrightarrow{k^s} [Pd_2(\mu\text{-AcMet-aa})_2(H_2O)_4]^{4+} + 2H_2L^{2+} \quad (1)$$

$$[Pd_2(\mu\text{-AcMet-aa})_2(H_2O)_4]^{4+} + 2H_3^+O \xrightarrow{k^h} [Pd_2(\mu\text{-AcMetH})_2(H_2O)_4]^{4+} + 2Haa^+ \quad (2)$$

$$[H^+aa]_t = 2Co[1-(k^h/(k^h-k^s))\exp(-k^st) + (k^s/(k^h-k^s))\exp(-k^ht)]$$

Where Co is the initial concentration of the $[Pd_2(\mu\text{-AcMet-aa})_2L_2]^{4+}$. Because pH* values measured at the beginning and at the end of reaction were always less than 0.1 pH*, we assumed that the concentration of H^+ was unchanged during the reaction. As seen from the equations, the hydrolysis reaction of peptides promoted by palladium(II) complexes proceeds stepwise. First step is detachment of ligand from Pd(II) caused by *trans* effect of thioether and by the acid in solution. Second step is the aqua ligands that *cis*-positioned to the substrate can be delivered to the carbonyl group internally, resulting in scissile of the amide bond. When $k^h \gg k^s$, that means eqn (1) is rate determining step, the hydrolysis rate is governed by detachment of the ligand. If $k^s \gg k^h$, that means eqn (2) is rate determining step, the hydrolysis rate is determined by k^h. When the ligand is temed, as shown in Table 2, the k^s_{obsd} and k^h_{obsd} are well comparable each other. In other words, in this case, the hydrolysis of peptides is governed by detachment of temed ligand and obeys the first order kinetic equation, its k_{obsd} is equal to that of ligand release. When ligand is en or py, because the detachment of en or py is fast, the hydrolysis rate of peptides is mostly governed by eqn (2).

Table 2. The k^{h}_{obsd} of dipeptides hydrolysis and the k^{s}_{obsd} of ligand release in $[Pd_2(\mu_2\text{-Ac-Met-aa})_2L_2]^{4+}$ (L-temed, en) complexes at 40 C and pH* 0.93–1.04

Promoter	Substrate	$10^3\ k^{s}_{obsd}$, min^{-1}	$10^3\ k^{h}_{obsd}$, min^{-1}
cis-$[Pd(temed)(H_2O)_2]^{2+}$	AcMet-Gly	7.20	6.30
	AcMet-Ala	5.90	5.10
	AcMet-Val	4.30	3.86
cis-$[Pd(en)(H_2O)_2]^{2+}$	AcMet-Gly		19.9
	AcMet-Ala		10.4
	AcMet-Val		4.6

Hydrolysis of peptides in mononuclear palladium(II) *complexes*

The chloride ions in complex A and complex C were removed by $AgNO_3$ in D_2O and DMSO-d_6, respectively. As schemes 2 and 3 show, complex B and complex D were formed as promoters used in hydrolysis reaction. The CH_3S resonance of the free AcMet-aa (aa-amino acid) appears at δ 2.11. The CH_3S resonances of terminal and double-bridging thioether ligands fall in two nonoverlapping intervals, 2.26–2.41 and 2.44–2.65 ppm, respectively [15–18,22]. Initial attachment of the promoter to the substrate amounts to displacement of a solvent ligand by the thioether group in the side chain. The displacement is accompanied by migration of chemical shift of the CH_3S toward downfield. Results of mixing the complex B or complex D with the dipeptides AcMet-aa (aa-Ala, Val) are shown in Table 3. Previous studies, such as *cis*-$[Pd(en)(H_2O)_2]^{2+}$ and *cis*-$[Pd(dtco\text{-}3\text{-}OH)(H_2O)_2]^{2+}$ etc as promoters, contained various kinetic evidences that the hydrolytically active form of substrate-containing complex is binuclear complex in spite of starting promoter is monomer or dimer [15–18,22]. However, when mixing of complex B or complex D with AcMet-aa, as Table 3 shows, only one ^1H NMR resonance of SCH_3 appeared at 2.34 or 2.35 ppm that is characteristic of the mononuclear complexes (2.41 ppm in mononuclear complex $[Pd(dien)(AcMet\text{-}aa)]^{2+}$). Although complex B is a N,N-chelated palladium(II) complex, it differs from *cis*-$[Pd(en)(H_2O)_2]^{2+}$. When *cis*-$[Pd(en)(H_2O)_2]^{2+}$ attached to substrate, the thioether group coordinates to palladium(II) and a μ_2-thioether bridged dimer is formed accompanied by the detachment of the en ligand. However, when complex B reacts with substrate, because of steric bulk and weak protonation of

Table 3. Effect of coordination of AcMet-aa to palladium(II) on chemical shift (δ, ppm) of CH_3S group at pH* = 1

Promoter	AcMet-Ala	AcMet-Val
none	2.11	2.11
complex B	2.34	2.34
complex D	2.35	2.35
$[Pd(dien)(H_2O)]^{2+}$	2.41	2.41

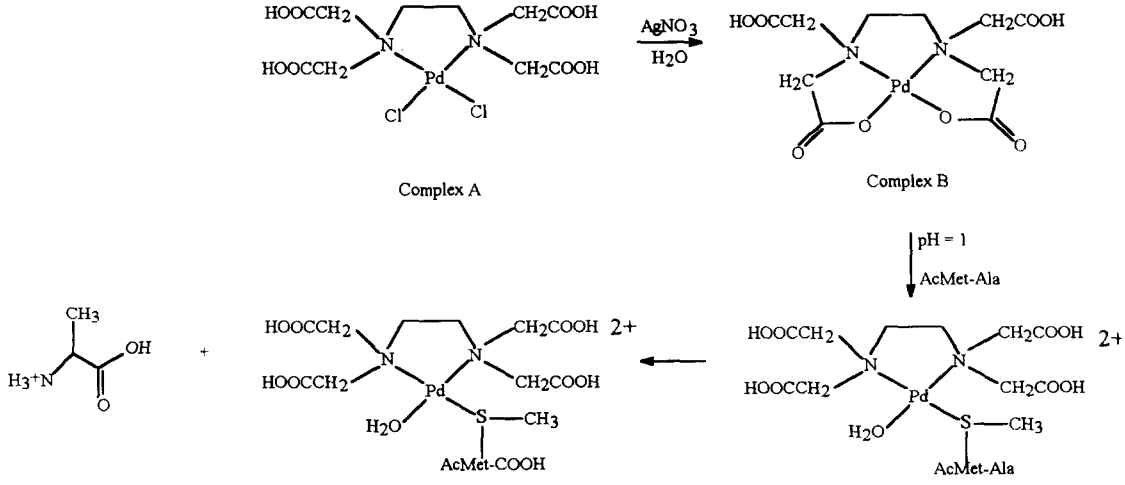

Scheme 2.

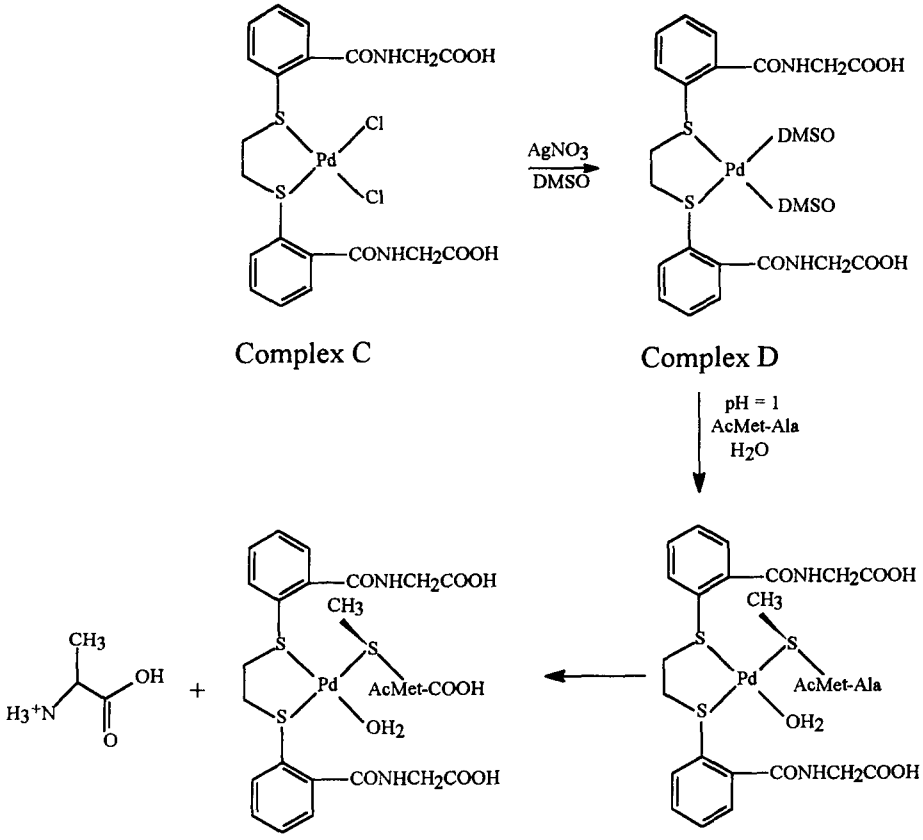

Scheme 3.

nitrogen atom of edta, a mononuclear complex that contained edta ligand and one substrate as terminal ligand was formed. The *trans* effect of thioether group in this monomer is not enough to detach two nitrogen atoms in edta without their protonation. Complex D is similar with *cis*-$[Pd(dtco\text{-}3\text{-}OH)(H_2O)_2]^{2+}$ in that they are both s,s-chelated complexes, but complex D is more bulky and prevents the formation of binuclear complex with substrate, and a mononuclear complex is formed instead, with no free glycine detected. The hydrolysis of substrates in the monomers was monitored by ^1H NMR. The observed rate constants, k_{obsd}, are listed in Table 4. As seen from the Table, although complex B and complex D have different coordinated atoms from ligands, their rate of peptide hydrolysis are quite similar. The k_{obsd} values also depend on the leaving group in the mononuclear complexes as they do in the binuclear complexes [16]. The rate of hydrolysis decreased with increase of the volume from analine to valine. In $[Pd(dien)(AcMet\text{-}aa)]^{2+}$ complex, we did not observe the hydrolysis reaction of AcMet-aa. These results confirm our conclusion that at least one aqua ligand is required for palladium(II) to promote peptide hydrolysis no matter in monomer or in

Table 4. Hydrolysis of the Met-aa bond in mononuclear Pd(II) complexes $[PdL(AcMet\text{-}aa)(H_2O)]^{2+}$ (L-edta, 1,2-bis(2-formylglycinebenzene sulfenyl)ethane; aa-Ala, Val) at pH* ≈ 1 and 50°

Promoter	Solvent	Substrate	$10^3 k_{obsd}$, min^{-1}
complex B	H_2O	AcMet-Ala	4.8
		AcMet-Val	2.3
complex D	100% DMSO	AcMet-aa	no reaction
	20% DMSO + 80% H_2O	AcMet-Ala	5.9
		AcMet-Val	3.4
$[Pd(dien)(H_2O)]^{2+}$	H_2O	AcMet-aa	no reaction

dimer [18]. Comparing the data in Table 1 with that in Table 4, although peptide hydrolysis in mononuclear complexes is much slower than that in binuclear complexes, it is important and of interest. Because this hydrolysis reaction in mononuclear complexes may closely relate to hydrolysis reaction proceeded in horst heart cytochrome *c* [28] and horse heart myoglobin [31] because of the steric bulk of proteins.

CONCLUSION

This study provides new evidences for understanding mechanism of the hydrolytic cleavage of peptides promoted by palladium(II) complexes. The Pd(II) complex with more labile ligand, such as pyridine, is a better promoter. The active species, $[Pd_2(\mu\text{-AcMet-aa})_2(H_2O)_4]^{4+}$, was formed by substitution of py with thioether group of AcMet-aa prior to hydrolysis of AcMet-aa. Although reaction of *trans*-$Pd(py)_2(H_2O)_2]^{2+}$, *cis*-$[Pd(en)(H_2O)_2]^{2+}$ and *cis*-$[Pd(temed)(H_2O)_2]^{2+}$ with AcMet-aa yields the same binuclear complex, $[Pd_2(\mu\text{-AcMet-aa})_2(H_2O)_4]^{4+}$, the hydrolysis of peptides in $[Pd_2(AcMet\text{-aa})_2(L)_2]^{4+}$ (L-en or temed) proceeds via a consecutive reaction: firstly detachment of the ligand en or temed, followed by cleavage of peptide in $[Pd_2(\mu\text{-AcMet-aa})_2(H_2O)_4]^{4+}$. The new mononuclear complexes reported here, $PdL(AcMet\text{-aa})(H_2O)]^{2+}$ (L-edta etc), are also hydrolytically active. It further confirmed that at least one aqua ligand *cis* to the substrate is required for observation of hydrolysis reaction of peptides promoted by Pd(II) complexes.

Acknowledgements—This work was supported by the National Natural Science Foundation of China and the Natural Science Foundation of Jiangsu Province.

REFERENCES

1. Croft, L. R., Handbook of protein sequence analysis, 2nd edn., Wiley, Chichester, 1980.
2. Sutton, P. A. and Buckingham, D. A., *Acc. Chem. Res.*, 1987, **20,** 357.
3. Chin, J., *Acc. Chem. Res.*, 1991, **24,** 145.
4. Chin, J., Banaszczyk, M., Jubian, V., Kim, J. H. and Mrejen, K., In *Bioorganic Chemistry Frontiers*, Vol. 2, ed. H. Dugas, Springer-Verlag, Berlin, 1991.
5. Dixon, N. E. and Sargeson, A. M., In *Zinc Enzymes*, ed. T. G. Spiro, Wiley, New York., 1983, Chap. 7, 254.
6. Suh, J., *Acc. Chem. Res.*, 1992, **25,** 273.
7. Fife, T. H., *Acc. Chem. Res.*, 1993, **25,** 325.
8. Fife, T. H., In *Perspective on Bioinorg. Chem.*, Vol. 1, ed. Hay, R. W., Dilworth, J. R., Nolan, K. B., JAI, Press, Greenwich, 1991, 43.
9. Kluger, R. and Hunt, J. C., *J. Am. Chem. Soc.*, 1989, **111,** 5921.
10. Kluger, R., Chin, J. and Chog, W.-W., *J. Am. Chem. Soc.*, 1979, **101,** 6976.
11. Menger, F. M. and Ladika, M., *J. Am. Chem. Soc.*, 1988, **110,** 6794.
12. Blageva, I. B. and Kirby, A. J., *J. Chem. Soc., Perkin Trans.*, 1985, **2,** 1017.
13. Suh, J., Kim, J. J. and Seong, N. J., *J. Org. Chem.*, 1981, **46,** 4354.
14. Burgeson, I. E. and Kostić, N. M., *Inorg. Chem.*, 1991, **30,** 4299.
15. Zhu, L. and Kostić, N. M., *Inorg. Chem.*, 1992, **31,** 3994.
16. Zhu, L. and Kostić, N. M., *J. Am. Chem. Soc.*, 1993, **115,** 4566.
17. Zhu, L. and Kostić, N. M., *Inorg. Chim. Acta*, 1994, **217,** 21.
18. Chen, X., Zhu, L., Yan, H., You, X. and Kostić, N. M., *J. Chem. Soc., Dalton Trans.*, 1996, 2653.
19. Korneeva, E. N., Ovchinnikov, M. V. and Kostić, N. M., *Inorg. Chim. Acta*, 1996, **243,** 9.
20. Parac, T. N. and Kostić, N. M., *J. Am. Chem. Soc.*, 1996, **118,** 51.
21. Parac, T. N. and Kostić, N. M., *J. Am. Chem. Soc.*, 1996, **118,** 5946.
22. Chen, X., Zhu, L., You, X. and Kostić, N. M., *J. Bioinorg. Chem.*, 1998, in press.
23. Rana, T. M. and Meares, C. F., *Proc. Natl. Acad. Sci. USA*, 1991, **88,** 10578.
24. Rana, T. M. and Meares, C. F., *J. Am. Chem. Soc.*, 1990, **113,** 1859.
25. Rana, T. M. and Measures, C. F., *J. Am. Chem. Soc.*, 1990, **112,** 2457.
26. Platis, I. E., Ermacora, M. R. and Fox, R. O., *Biochemistry*, 1993, **32,** 12761.
27. Ettner, N., Hillen, W. and Ellestad, G. A., *J. Am. Chem. Soc.*, 1993, **115,** 2546.
28. Zhu, L., Qin, L., Parac, T. N. and Kostić, N. M., *J. Am. Chem. Soc.*, 1994, **116,** 5218.
29. Hegg, E. L. and Burstyn, J. N., *J. Am. Chem. Soc.*, 1995, **117,** 7015.
30. Allen, G. and Campbell, R. O., *Int. J. Peptide Protein Res.*, 1996, **48,** 265.
31. Zhu, L., Bakhtiar, R. and Kostić, N. M., Submitted for publication.
32. Hohmann, H. and van Eldik, R., *Inorg. Chim. Acta*, 1990, **174,** 87.
33. Burgess, C., Hartley, F. R. and Searle, G. W., *J. Organomet. Chem.*, 1974, **76,** 247.
34. Viossat, B., Dung, N.-H. and Robert, E., *Acta Crystallogr.*, 1993, **C49,** 84.
35. Preliminary structural data for *cis*-$[Pd(edta)Cl_2]$ were obtained: orthorhombic, space group P2(1)2(1)2(1), $a = 10.212(4)$ Å, $b = 10.236(4)$ Å, $c = 20.983(5)$ Å, $\alpha = \beta = \gamma = 90°$. Pd—N distances are 2.063(5) and 2.102(3) Å. Pd—Cl distances are 2.299(2) and 2.301(1) Å.
36. Yu, Z., Hu, M., Chen, X., Song, Y. and Zhu, L., *J. Inorg. Chem. (Chinese)*, 1996, **4,** 403. The complex C belongs to monoclinic, space group C_2/c, $a = 16.34(2)$ Å, $b = 8.07(1)$ Å, $c = 22.23(2)$ Å, $\alpha = \gamma = 90°$, $\beta = 120.38°$, $R = 0.0257$, $Rw = 0.0671$. Pd—S distance is 2.264(2) Å. Pd—Cl distance is 2.322(2) Å.
37. Sigel, H. and Martin, R. B., *Chem. Rev.*, 1982, **82,** 385.
38. Sovago, I. and Martin, R. B., *J. Inorg. Nucl. Chem.*, 1981, **43,** 425.

39. Menabue, L., Saladini, M. and Sola, M., *Inorg. Chem.*, 1990, **29,** 1293.
40. Kasselauri, S., Garoufis, A., Hadjiliadis, M. and Hadjiliadis, N., *Coord. Chem. Rev.*, 1990, **104,** 1
41. Wilson, E. W. and Martin, R. B., *Inorg. Chem.* 1970, **9,** 528.
42. Laussac, J. P., Haran, R. and Hadjiliadis, N. C R., *Acad. Sci. Paris, Ser.* 2, 1985, **300,** 137.

Pergamon

PII: S0277-5387(98)00008-4

Polyhedron Vol. 17, Nos 13–14, pp. 2279–2288, 1998
© 1998 Elsevier Science Ltd
All rights reserved. Printed in Great Britain
0277-5387/98 $19.00+0.00

On the bonding in π-complexes of borazine

Adam J. Bridgeman

University Chemical Laboratories, Lensfield Road, Cambridge CB2 1EW, UK

(Received 6 October 1997; accepted 5 January 1998)

Abstract—The electronic structure of $[Cr(\eta^6\text{-}B_3N_3H_6))(CO)_3]$ has been investigated in detail using high quality density functional calculations. The bonding is found to be similar to the well established scheme in the arene analogue with the usual ring → metal donation and metal → ring backdonation utilizing the π bonding and anti-bonding orbitals respectively of the ring. The interactions are not localized Cr—N bonds and the ring does not bind as a triamine ligand. The polarization of the π bonding and anti-bonding functions of the free and complexed ligand is however key in determining the adoption of a structure with the CO ligands located *trans* to the nitrogen atoms of the ring in contrast to the structure found for the arene analogue. Puckering of the borazine ring is due to the repulsive interactions between high lying, boron dominated, ring σ-bonding orbitals and the metal's 'lone pairs'. The electronic structure of the unknown diborazine chromium complex is also investigated. Its likely conformation and possible reasons for its instability are suggested. © 1998 Elsevier Science Ltd. All rights reserved

Keywords: borazine; tricarbonyl; arene; chromium; sandwich; DF.

The bonding in the borazine molecule and its derivatives continues to stimulate interest and study. The isoelectronic relationship between benzene and borazine and their similar structural and physical properties has led to borazine being referred to as 'inorganic benzene' These similarities suggest that the bonding in borazine should be represented in an analogous way to that used for benzene. This is illustrated in Scheme 1(a). Chemically though the molecules are known to act rather differently. Lewis acids attack borazine by adding to N whilst Lewis basis add to B. The chemical properties of borazine strongly suggest that the N atom retains some basic character so that the bonding shown in Scheme 1(b) might be a more appropriate formulation. Numerous studies of the bonding and the degree of aromaticity in the borazine molecule and its derivatives have been reported [1].

One of the chemical properties of borazines and arenes that is often used as an illustration in undergraduate courses [2] of the similar behaviour of the two systems is the formation of half-sandwich, η^6 complexes with tricarbonyl chromium. The similarity in the formulation and structures of the complexes of general formula $[Cr(\eta^6\text{-}R_3B_3N_3R'_3)(CO)_3]$ and $[Cr(\eta^6\text{-}R_6C_6)(CO)_3]$ has been taken to infer similar bonding interactions [3,4]. No detailed bonding study of the borazine complex has previously been reported.

The crystal structure [5] of $[Cr(\eta^6\text{-}Et_3B_3N_3Et_3)(CO)_3]$ however reveals a number of differences between the structure of the borazine and arene complexes. The B_3N_3 ring in the free ligand is planar but upon complexation the ring puckers slightly. This leads to unequal Cr—N and Cr—B distances with the former somewhat shorter.

Lagowski [6] argues that the average Cr—N bond length of 2.2 Å is close to that expected for a tetrahedrally coordinated nitrogen atom. In addition, Lagowski points out the ∠B—N—B angle and the non-planarity of the R—NB_2 group and suggests tetrahedrally bonded nitrogen. The essentially planar geometry around the B atoms and the ∠N—B—N angles are consistent with an sp^2 B and Lagowski suggests that the Cr—B bond length is too long for a bonding interaction between these two elements in the complex. Lagowski proposes that the bonding in $[Cr(\eta^6\text{-}R_3B_3N_3R'_3)(CO)_3]$ species should be compared to that in complexes of a tridentate triamine ligand, such as that shown in Scheme 2, so that the borazine is acting as in formulation (b) in Scheme 1.

Scotti *et al.* [3] and Herberich [4] have reported rather different conclusions about the bonding in η^6-bonded borazine complexes. The CO stretching frequencies in $[Cr(\eta^6\text{-}R_3B_3N_3R'_3)(CO)_3]$ species are approximately the same as those in the arene analogues implying overall similar donor/acceptor properties for the η^6-ligand. In addition, the B—N

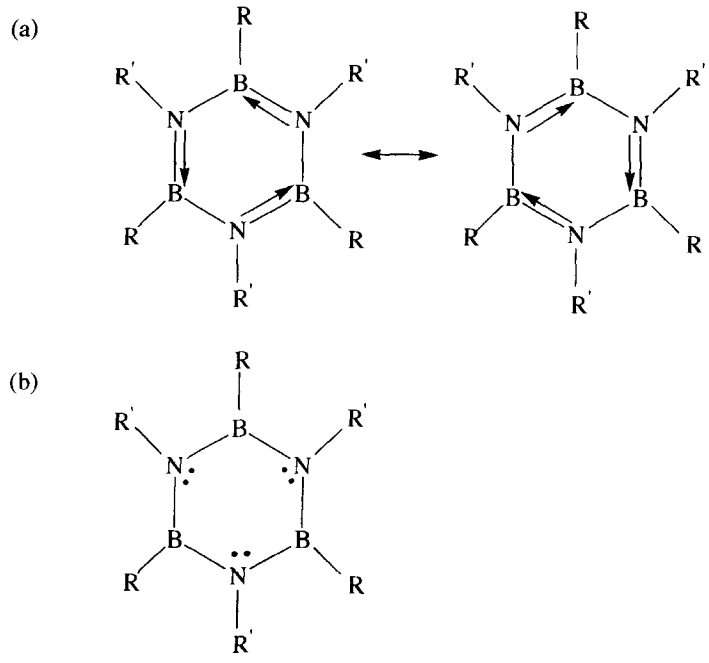

Scheme 1.

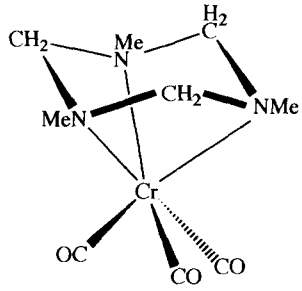

Scheme 2.

bond lengths in the borazine molecule do not increase greatly upon complexation suggesting rather weak Cr-ring interactions and incomplete localization of the nitrogen lone pairs between the chromium and nitrogen atoms. Herberich points out that the difference between the Cr—B and Cr—N bond lengths is similar to the difference in the covalent radii of the main group elements. It is thus argued that the distortion of the ring occurs to accommodate the differing size of the ligand atoms and that the Cr—B bond length is not too long for a bonding interaction.

Herberich also notes that localized Cr—N bonds as argued by Lagowski [6] are inconsistent with the structure of the complex and with the ^{11}B NMR [7]. The puckering of the borazine ring upon complexation is actually rather small. The average torsional angle [5] about the B—N bonds is ca 9°. The torsional angle in truly chair shaped cyclotriborazanes is ca 54.7° whilst the C—N torsional angle [8] in the complex of the triamine shown in Scheme 2 ca 67.2°. Localized Cr—N bonds would result in a low-field shift of the ^{11}B chemical shift upon complexation. A high-field shift is actually observed.

Scotti *et al.* [3] conclude that the ring → Cr σ-donation is more localized between the Cr and N atoms whilst the π-acceptor rôle of the ring is more localized between the Cr and B atoms. This was represented by these workers as in Scheme 3. In a later paper, Scotti *et al.* [9] estimated that the Cr-borazine bond strength is around half that of the Cr-arene bond.

A further structural feature of the borazine complexes is of interest. The CO groups are found [5] to be eclipsed with the B atoms whereas the structure

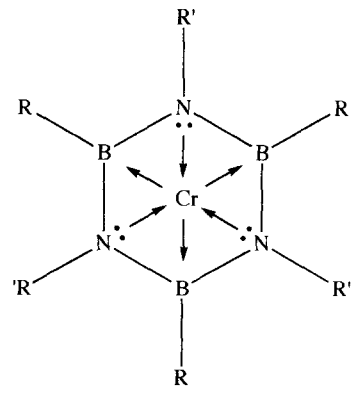

Scheme 3.

[10] of $(\eta^6\text{-}C_6H_6)Cr(CO)_3$ shows the CO groups to be staggered relative to the carbon atoms of the ring.

The purpose of the present work is to study the nature of the bonding in the η^6-borazine complexes and to compare this with that in the arene analogues. The structural features outlined above, namely the puckering of the ring and the positions of the CO groups in the complex, are addressed.

COMPUTATIONAL DETAILS

All density functional (DF) calculations [11–14] were performed here using the 'DeFT' code written by St-Amant [15] in the linear combination of Gaussian-type orbitals (LCGTO) framework. The calculations set used the Vosko–Wilk–Nusair [16] local spin density approximation of the correlation part of the exchange-correlation potential with non-local corrections using the Becke [17] functional for exchange and the Perdew [18] functional for correlation.

The Gaussian basis sets (GTOs) and the auxiliary basis sets needed for the Coulomb and exchange potential were optimized specifically for LSD calculations by Godbout *et al.* [19] GTO sets of double-ζ quality with the contraction patterns (63321/531*/41+) for chromium, (721/51*/1+) for boron, carbon and nitrogen and (41) for hydrogen were used. All calculations were performed in an all electron treatment.

Bond orders were calculated according to the prescription suggested by Mayer [20]. Calculations were performed using the simplest borazine $B_3N_3H_6$ rather than the alkyl substituted molecules to assist computational efficiency. Calculations were performed using the coordinates determined from crystallographic studies as well as using idealized structures to investigate the structural issues identified above.

RESULTS

(*a*) *Borazine and benzene*

Although many comparative studies of borazine and benzene have been performed [1], it is instructive to report the results at the same level of theory used for the complexed systems. Figure 1 shows a Kohn-Sham eigenvalue diagram for the π-functions of the two molecules and an illustration of the corresponding orbitals. The labels correspond to D_{6h} for benzene, D_{3h} for borazine and to C_{3v} in parentheses. The latter are appropriate to the complex ligands. The occupied borazine orbitals are polarized towards the more electronegative nitrogen whilst the virtual orbitals are more boron in character. Nevertheless, the orbitals show that delocalization is important in both systems.

Table 1 lists Mulliken populations and σ and π bond orders. The π bond order in borazine is approximately a third smaller than in benzene. The B—N bond order in borazine is considerably larger than in the NH_3BH_3 adduct but the breakdown into σ and π contributions shows that this is only partially due to the introduction of a π component. The π-bonding acts to shorten the B—N bond and, as revealed by the Mulliken charges, also acts to make the bond less polar. Both of these act to increase the σ contribution to the bond order.

Distortion to the puckered conformation adopted by the complexed borazine ring requires around 15 kJ mol^{-1} and does not significantly alter the B—N bond order. Similar puckering of benzene requires around 26 kJ mol^{-1}.

(*b*) *$Cr(CO)_3$ fragment*

The valence orbitals of a transition metal $M(CO)_3$ fragment have been discussed [21,22] in detail and only the key aspects are reviewed here. The σ lone pairs (5σ) of the three CO ligands transform as a_1+e. The π* orbitals transform as a_2+e and a_1+e for the sets tangentially and radially orientated respectively relative to the base of the $M(CO)_3$ pyramid. The metal orbitals transform as a_1 (4s, 3_{z^2} and $4p_z$) and $3\times e$ ($\{3d_{x^2-y^2}, 3d_{xy}\}$, $\{3d_{xz}, 3d_{yz}\}$ and $\{4p_x, 4p_y\}$). Calculations were performed using an idealized fragment with dimensions based upon those in $[Cr(\eta^6\text{-}Et_3B_3N_3Et_3)(CO)_3]$. The resulting eigenvalue diagram is shown in Fig. 2.

As shown on Fig. 2, there are three occupied levels, $1a_1+1e$, at low energy corresponding to the Cr—CO σ-bonds. The metal $\{d_{xz}, d_{yz}\}$ e orbitals are orientated to overlap well with the matched σ functions of the ligands. This results in a low lying e level corresponding to Cr—CO σ-bonding and an antibonding level primarily metal d in character. Hybridization of the metal d_{z^2} orbital with the 4s lessens the antibonding interaction with the CO σ-functions. More importantly, it is stabilized by the interaction with the a_1 combination of the CO π* orbitals. The metal $\{d_{x^2-y^2}, d_{xy}\}$ e orbitals are correctly orientated to donate into the matching CO π* functions. The $2a_1+2e$ functions are thus mostly metal d-orbital in character and correspond to metal → CO π-donation.

Mixing of the three pairs of metal orbitals of e symmetry can further increase the bonding in the fragment. Mixing of the $\{d_{xz}, d_{yz}\}$ pair into the $\{d_{x^2-y^2}, d_{xy}\}$ pair tilts [22] the latter so as to maximize the bonding with the CO π* functions. Similarly mixing of the $\{d_{x^2-y^2}, d_{xy}\}$ pair into the $\{d_{xz}, d_{yz}\}$ pair tilts the latter so as to maximize overlap with the CO σ functions. The 2e functions are the M—CO π bonding functions. Figure 3(a) illustrates the π bonding orbital for a single M—CO unit and Fig. 3(b) shows the appropriate combination of these to give the 2e functions for the $M(CO)_3$ unit. The 3e functions are the M—CO σ* orbitals and so maximize diametrically opposite the M—CO vectors. Figure 4(a) illustrates σ* for a single M—CO unit and Fig. 4(b) shows the

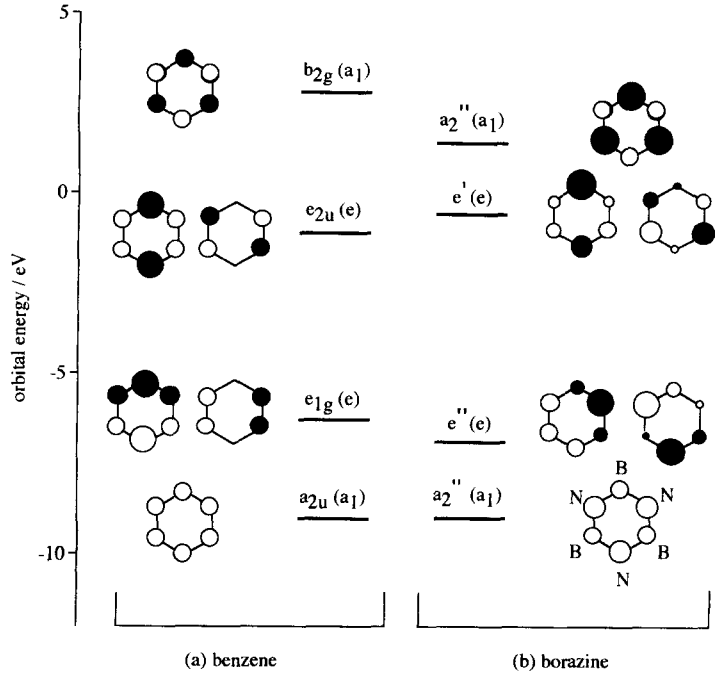

Fig. 1. Kohn-Sham eigenvalue diagram and qualitative representation of the corresponding functions for the π levels of benzene and borazine. The labels correspond to the molecular point groups whilst those in parentheses are appropriate to the functions in the η^6 complexes of $Cr(CO)_3$.

Table 1. Mulliken charges and bond orders for benzene, ethane, borazine and the NH_3-BH_3 adduct

Molecule	Mulliken charge		C—C/B—N bond order σ	π	Total
C_6H_6	C −0.26	H +0.26	0.91	0.46	1.45
CH_3CH_3	C −0.46	H +0.46	0.98	—	0.98
$B_3N_3H_6$	B −0.21	N −0.23	0.97	0.34	1.31
	H_B +0.13	H_N +0.31			
BH_3NH_3	B −0.40	N −0.59	0.68	—	0.68
	H_B +0.1	H_N +0.23			

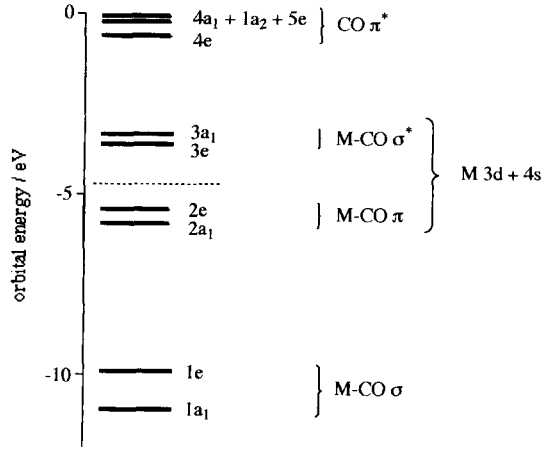

Fig. 2. Kohn–Sham eigenvalue diagram for the $Cr(CO)_3$ fragment. An approximate description of the orbitals is given.

appropriate combination of these for the 2e functions for the $M(CO)_3$ unit. Albright and Hoffmann identify [22] the 2e electrons as 'lone pairs' which orientate themselves in $LM(CO)_3$ complexes to regions of low electron density on the ligand L. Similarly, the empty 3e levels form an acceptor set which seek out regions of high electron density on L.

(*c*) (*Borazine*)*Cr*(*CO*)$_3$

The ring-metal distances were optimized leading to bond lengths of 2.35, 2.39 and 1.52 Å for the Cr—N, Cr—B and B—N bonds respectively. These compare favourably with the observed [5] bond lengths of 2.21, 2.31 and 1.44 Å in $[Cr(\eta^6\text{-}Et_3B_3N_3Et_3)(CO)_3]$. More importantly in the context of the discussion below, the ring is predicted to have the same conformation relative to the carbonyl groups as observed experimentally and to be slightly puckered with a torsional angle about the B—N bonds of ca 6°.

Table 2 lists the Kohn–Sham eigenvalues, their form and an approximate description of their character. The symmetry of the borazine complex is rather

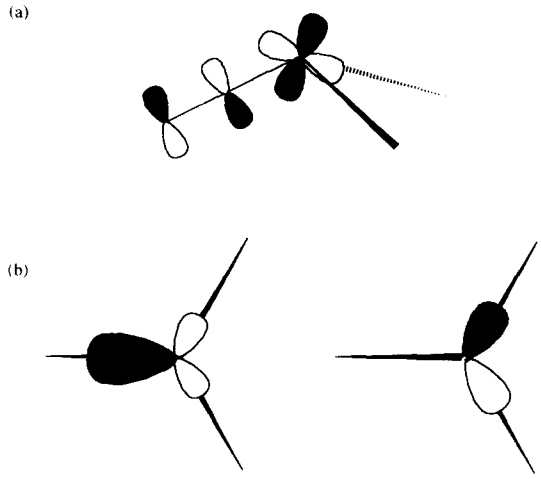

Fig. 3. Representation of (a) a local M—CO π bonding function and (b) the 2e functions of the $M(CO)_3$ fragment.

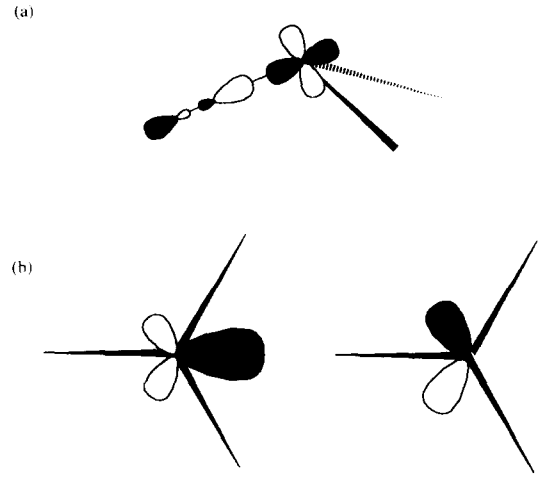

Fig. 4. Representation of (a) a local M—CO σ* function and (b) the 3e functions of the $M(CO)_3$ fragment.

less than the ideal C_{3v} due to unequal bond lengths and angles and this is evident in the splitting of the degenerate functions listed in the table. Table 3 lists Mulliken populations for the complex and for the analogous arene system. The Cr—B, Cr—N, Cr—C, B—N and C—O bond orders in (borazine)$Cr(CO)_3$ are calculated to be 0.30, 0.31, 1.25, 1.24 and 2.32 respectively. The Cr—C_{ring}, Cr—$C_{carbonyl}$, C—C and C—O bond orders in (benzene)$Cr(CO)_3$ are calculated to be 0.40, 1.20, 1.26 and 2.31 respectively. The B—N, C—C and C—O bond orders in the free ligands are 1.31, 1.45 and 2.64 respectively.

The B—N bond order of borazine is slightly reduced upon complexation due to donation from its π system to the metal and acceptance of electron density into the π* functions. This reduction is consistent with the slight increase in the B—N bond length and the small shift in the B—N stretching frequency [3,23]. The size of the reduction however does not suggest complete localization of the π electrons at the nitrogen sites. The Cr—N bond orders are also quite small indicating that the individual interactions are quite weak and are not of the metal-amine type indicated by a formulation such as that shown in Scheme 2. Lagowski proposed [6] that the Cr—B bond length was too long for a bonding interaction. The Cr—B bond order is however of a similar magnitude to that of the Cr—N bond despite the longer bond length. The contributions to the orbitals shown in Table 2 also show that ring → metal donation and metal → ring back donation involve contributions from boron *and* nitrogen. The borazine ring is certainly not bonding as a triamine.

The ring → metal donation is more nitrogen centered due to the polarization of the occupied π orbitals of the ring towards the more electronegative atom. The higher electronegativity of nitrogen, however, also dictates that borazine is a less good donor to the metal than the carbon ring. Similarly, the lower electronegativity of boron ensures that the acceptor functions of the borazine ring are more boron centred and that it is a less good acceptor to the metal than the carbon ring.

The C—C bond order of benzene suffers a rather larger reduction upon complexation indicating that the ring-metal interaction is larger in the arene complex. The C—C bond order quoted above is in fact an average of the values 1.31 and 1.21 for the bonds located *trans* and between the Cr—CO groups respectively. This indicates a small degree of localization of the π bonding in the benzene ring to maximize the donation into the acceptor functions of the $Cr(CO)_3$ unit which are directed at the *trans* C—C bonds, pictured in Fig. 4(b). The carbonyl Cr—C and C—O bond orders and the CO orbital populations are quite similar in the two systems. This is consistent with the similarity in the observed C—O stretching frequencies [3,23]. The Cr—B and Cr—N bond orders are both smaller than that of the ring Cr—C bond in the arene system. The dissociation energies for the processes,

$$\text{(borazine)Cr(CO)}_3 \rightarrow \text{borazine} + \text{Cr(CO)}_3,$$

and

$$\text{(benzene)Cr(CO)}_3 \rightarrow \text{benzene} + \text{Cr(CO)}_3$$

were calculated to be 125 and 241 kJ mol^{-1} respectively. These compare well with the experimental estimates [9] of 105 and 206 kJ mol^{-1}.

(*i*) *Twisting the borazine ring.* The adopted geometry of the complex has the nitrogen atoms *trans* to the three CO ligands. These positions maximize the overlap between the highest lying, nitrogen dominated π function of borazine (the e″ orbital shown in Fig. 1) and the 3e acceptor functions of the $Cr(CO)_3$ fragment, shown in Fig. 4(b). This geometry also max-

Table 2. Kohn–Sham eigenvalues and approximate characters for $[Cr(\eta^6\text{-}H_3B_3N_3H_3))(CO)_3]$

Orbital	Energy/eV	Character	% contributions Cr 3d	Cr 4s	Cr 4p	B 2s	B 2p	N 2s	N 2p	H_B 1s	H_N 1s	C 2s	C 2p	O 2s	O 2p
$9a_1$	−5.67	M—CO π	67	1	2	3	1		1			2	7		15
11e	−5.59, −5.61	M—CO π	60		1	4	8		3				7		15
10e	−8.65, −8.80	B—N, B—H	2	2	2		42		33	15			1		3
9e	−9.30, −9.39	B—N π (/M—CO σ)	10		5	4	18		40	1			8		15
8e	−9.67, −9.87	(B—N π/) M—CO σ	12	3	1	5	11		11	5		7	19		34
$8a_1$	−9.95	(B—N π/) M—CO σ	17		1	3	5		19	1		8	20		23
$2a_2$	−10.20	CO 1π				1	2		3			2	27		60
$7a_1$	−10.23	CO 1π/B—N, B—H	6		4	3	4		2	2		4	29		45
$6a_1$	−10.48	CO 1π/B—N, B—H	3	2	1	10	14	2	6	9	1	3	2		29
7e	−10.77, −10.80	Co 1π	5		2	1	4		9			3	27	1	47
6e	−11.23, −11.36	CO 1π	3	9	1								32		63
$5a_1$	−11.60	B—N π/M—CO σ	2	1	8		11		26			3	15	9	28
5e	−12.27, −12.29	B—N	1			2	19	3	54	2	10		1	3	5
$1a_2$	−12.50	B—N				34		57							
4e	−12.97, −12.16	CO 4σ	4		2				3			34	3	26	26
$4a_1$	−13.95	CO 4σ	1	5	10				2			36	10	24	16
3e	−14.63, −14.90	B—N, N—H	1			35	6		50	1	4				
$3a_1$	−15.58	B—N, N—H	2	2	1	3	11	7	58		16				
2e	−22.27, −22.52	B—N, N—H	1		1	5	12	74	2		5				
$2a_1$	−24.12	CO 3σ	1	2	2	15	7	68	2		3				
1e	−26.82, −27.23	CO 3σ	1	1	1							13	11	64	9
$1a_1$	−28.20	CO 3σ	1	1	1							14	13	59	10

Table 3. Mulliken populations and charges for (borazine)$Cr(CO)_3$ and (benzene)$Cr(CO)_3$

(Borazine)$Cr(CO)_3$						(Benzene)$Cr(CO)_3$					
Cr	charge = +0.12					charge = −0.06					
d_{z^2}	$d_{x^2-y^2,xy}$	$d_{xz,yz}$	s	p_z	p_x, p_y	d_{z^2}	$d_{x^2-y^2,xy}$	$d_{xz,yz}$	s	p_z	p_x, p_y
0.93	2.53	1.28	0.45	0.31	0.37	0.95	2.59	1.35	0.43	0.25	0.37
B	charge = −0.17		N	charge = −0.17		C (ring)	charge = −0.19				
2s	$2p_\sigma$	$2p_\pi$	2s	$2p_\sigma$	$2p_\pi$	2s	$2p_\sigma$	$2p_\pi$			
0.87	1.79	0.51	1.35	2.37	1.45	1.17	2.08	0.94			
H_B	charge = +0.14		H_N	charge = +0.40		H	charge = +0.32				
1s			1s			1s					
0.86			0.60			0.68					
C	charge = +0.03		O	charge = −0.27		C	charge = +0.02		O	charge = −0.26	
2s	2p		2s	2p		2s	2p		2s	2p	
1.30	2.67		1.73	4.54		1.29	2.69		1.72	4.53	

imizes the interaction between the high lying donor 2e orbital of the $Cr(CO)_3$ fragment and the boron dominated π acceptor function of borazine (the e′ orbital shown in Fig. 1). The barrier to rotation is calculated to be 22 kJ mol^{-1}; a substantial barrier compared to kT and to the size of the Cr-borazine dissociation energy which has been estimated [9] to be around 105 kJ mol^{-1}.

Figure 5 shows the reduction in the Cr—N and Cr—B bond orders as the ring is twisted from its preferred geometry ($\theta = 0°$) to one with the CO units *trans* to the B atoms ($\theta = 60°$). The high lying 11e orbitals are, as shown in Table 2, M—CO π bonding in character with small, but important, contributions from the acceptor functions on borazine. As the ring is twisted, the overlap between the $Cr(CO)_3$ donor

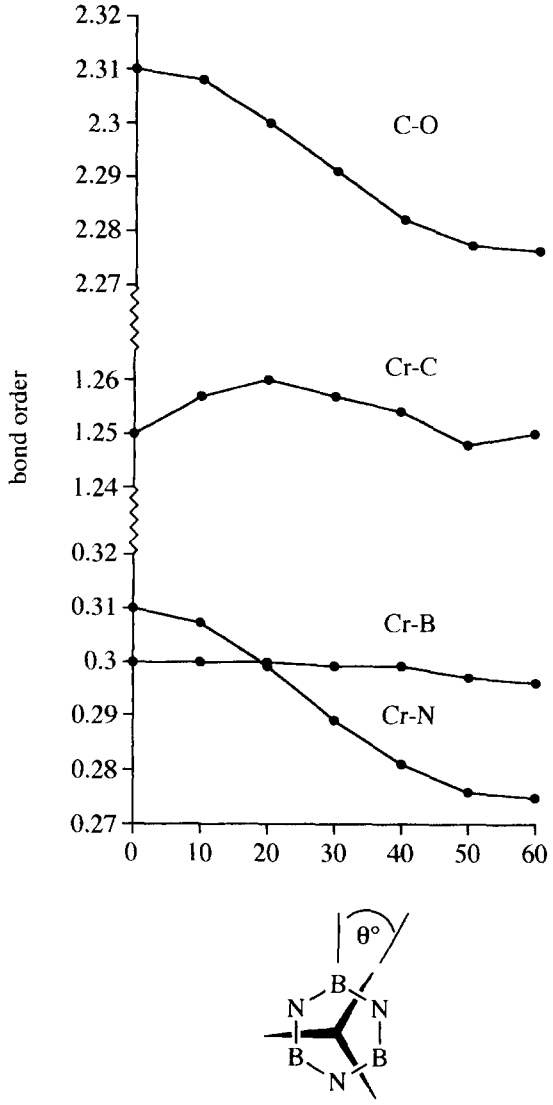

Fig. 5. Bond orders as a function of the twist angle (θ) between borazine and the $Cr(CO)_3$ fragment.

and the borazine acceptor functions decreases. Additionally the $Cr(CO)_3$ donor functions are brought spatially closer to the donor functions of the ring with resulting repulsion. The energy of the orbital increases by 0.12 eV between $\theta = 0$ and 60°.

The 9e orbitals of the complex are, as shown in Table 2, B—N π bonding and ring-Cr bonding in character. They are dominated by the interaction between the ring donor and the $Cr(CO)_3$ acceptor functions. As the ring is twisted, the overlap between the $Cr(CO)_3$ acceptor and the borazine donor functions decreases. As noted directly above, twisting also brings the ring donor functions closer to the donor functions of the $Cr(CO)_3$ fragment. The result is an increase in the energy of the 9e orbital of 0.4 eV between $\theta = 0$ and 60°.

It is interesting to note the character of the B—N π bonding orbital involved in the 9e function of the complex. The ratio of the boron : nitrogen contributions to the e″ orbital of the free ligand is roughly 1 : 2.5. This ratio is approximately maintained in the complex with $\theta = 0°$. When the ring is twisted, however, the boron contribution to this orbital increases whilst that of nitrogen of decreases. The ratio is roughly 1 : 1 when $\theta = 60°$. Thus as the ring is twisted, the B—N π orbital becomes less polarized towards the nitrogen so that donation to the metal is maintained. The increase in the N $p_\pi \rightarrow$ B p_π donation also reduces the repulsion between the donor functions of the ring and those of the $Cr(CO)_3$ fragment. The result is an *increase* in the B—N bond order from 1.24 to 1.30.

The 10e orbital of the complex is predicted to be stabilized by 0.2 eV when the borazine ring is twisted. These orbitals, as shown in Table 2, involve contributions from σ-orbitals of the ring. They are involved in the B—N and B—H σ-bonds and are highly boron in character. The stabilization upon twisting reflects the decease in the repulsive interactions between these high lying orbitals and the spatially and energetically close M—CO σ and π-bonding functions, 8e and 11e respectively. This repulsion acts to destabilize the borazine complex and is also, as discussed below, key in the preference for a puckered ring. Twisting also enables donation from these boron based σ-orbitals into the appropriately aligned acceptor functions on the $Cr(CO)_3$ fragment.

The 10e orbitals in (benzene)$Cr(CO)_3$ are predicted by DF and self consistent field [24] calculations to lie at somewhat lower energy and below that of the ring π function corresponding to the 9e orbital in the borazine system reflecting the intermediate electronegativity of carbon.

As shown in Fig. 5, the C—O bond order also decreases as the ring is twisted from $\theta = 0$ to 60°. This is related for the most part to the increase in the π-back donation from the metal. As outlined above, twisting the ring leads to a decrease in both the ability of the borazine ring to donate and accept electron density. The decrease in the donation by the ring into the M—CO σ* functions (corresponding to the 3e orbitals of the $Cr(CO)_3$ fragment as shown in Fig. 2) leads to an increase in the σ-donation by the CO ligands. Similarly, the decrease in the acceptance by the ring from the M—CO π-bonding orbitals (corresponding to the 2e orbitals of the $Cr(CO)_3$ fragment) leads to an increase in the π-acceptance by the CO ligands. The Cr—C bond order increases as shown in Fig. 5, to a maximum before decreasing as θ approaches 60°. This decrease is related to the repulsive interaction between the ring donor functions and the M—CO π-bonding orbitals.

Whilst borazine is bonding as a π ligand, the polarization of its donor and acceptor functions is key both to the conformation of the ring and the lower stability compared to the arene system.

(*ii*) *Puckering of the borazine ring.* As discussed in

Section (a), puckering of the planar borazine ring to that observed in the η^6 complex requires approximately 15 kJ mol^{-1}. The centre of the coordinated ring was maintained in all of the model calculations and this was chosen to be at the same distance as that of the ring in the observed structure of [Cr(η^6-$Et_3B_3N_3Et_3$)$(CO)_3$]. The ring was then puckered by altering the torsional angles of the B—N bonds. In these calculations, the system was found to be approximately 10 kJ mol^{-1} more stable in the puckered form. The main changes in the orbital energies involve the 9e, 10e and 11e orbitals of the complex. The 9e orbital decreases in energy upon puckering by approximately 0.1 eV because of the increase in the overlap of the acceptor functions of the $Cr(CO)_3$ fragment with the donor functions of the ring as the nitrogen approaches more closely. the Cr—N bond order increases from 0.26 to 0.30. More sizeable stabilizations of 0.25 and 0.21 eV are found for the 10e and 11e levels respectively. Puckering of ring decreases metal → ring donation leading to a reduction in the Cr—B bond order from 0.32 to 0.30. The observed stabilization of the 11e and the 10e functions upon puckering appears to be a result of the decrease in the repulsive interaction between the high lying, boron dominated B—N and B—H σ-orbitals of the ring and the chromium 3d dominated M—CO π bonding functions.

(d) Diborazine chromium

There appear to have been no reports of the preparation of the full sandwich complexes [Cr(η^6-$R_3B_3N_3R'_3)_2$]. Model calculations were performed using averaged structural parameters from the (borazine)$Cr(CO)_3$ system and idealized symmetry. The eigenvalues of the Cr(borazine) fragment are shown in Fig. 6.

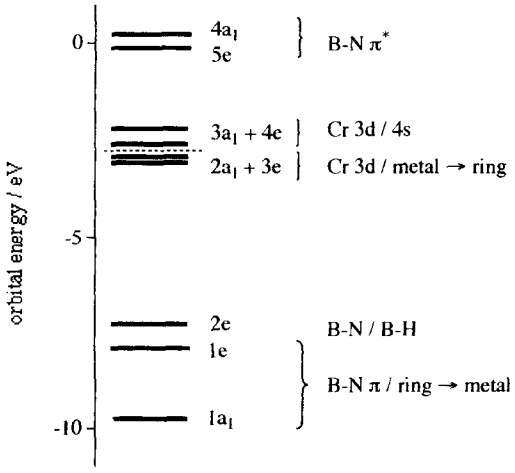

Fig. 6. Kohn–Sham eigenvalue diagram for the Cr(borazine) fragment. An approximate description of the orbitals is given.

The orbitals presented to the incoming ligand by the Cr(borazine) unit are very similar to those of the $Cr(CO)_3$ fragment. The unit presents three 'lone pairs' of $a_1 + e$ symmetry. These are essentially metal → ring donor functions. To maximize interaction with the acceptor functions on the ring, the metal orbitals are tilted towards the boron atoms of the ring to maximize overlap. The resulting 'lone pairs' are thus directed towards the sites diametrically opposite the boron positions of the fragment. There are also three low lying acceptor functions which are essentially the ring → metal antibonding orbitals. As the donor functions of the borazine ring are centred on the nitrogen atoms, the ring → metal bonding functions are tilted to ensure maximum overlap. The resulting antibonding orbitals are thus directed towards the sites diametrically opposite the nitrogen positions of the fragment.

The model calculations predict that the fully staggered geometry is the most stable. This geometry has D_{3d} symmetry and the boron atoms of one ring directly above the nitrogen atoms of the second ring, and *vice versa*. The barrier to rotation of a borazine ring is predicted to require 18 kJ mol^{-1}. In the staggered conformation, the B—N π bonding orbitals then transform as $a_{1g} + a_{2u} + e_g + e_u$ as do the corresponding anti-bonding functions.

Table 4 lists the calculated eigenvalues and a description of the eigenfunctions of the staggered system. Comparison with the results for the tricarbonyl complex listed in Table 2 shows the smaller stabilization of the highest energy, chromium 3d dominated orbitals reflecting the greater acceptor properties of the oxygen dominated carbonyl functions.

Table 5 lists the Mulliken populations and bond orders for the diborazine complex together with those calculated for the dibenzene complex. The increased Cr—C and Cr—B and the decreased C—C and B—N bond orders show increased backdonation to the ring in both cases compared to the tricarbonyl systems. The absence of backdonation to the carbonyl ligands also results in appreciably smaller ring → metal donation. In the diborazine system, this results in a substantial reduction in the Cr—N bond order. Nitrogen is unable to donate effectively to the electron rich metal.

As a borazine ligand is rotated from the fully staggered conformation, the Cr—B and Cr—N bond orders drop and the energies of the $6e_g$ and $4e_g$ orbitals, which correspond to the metal → ring and ring → metal donation respectively, rise. This can be directly related to the discussion above of the donor and acceptor orbitals of the Cr(borazine) fragment which favour the staggered conformation. Just as in the tricarbonyl system, the diborazine complex has high energy, boron dominated, ring σ-bonding orbitals ($5e_g$ and $5e_u$). As the ring is rotated the repulsive interaction between these orbitals and the metal based

Table 4. Kohn–Sham eigenvalues and approximate characters for $[Cr(\eta^6\text{-}H_3B_3N_3H_3)_2]$

			% contributions								
			Cr			B		N		H_B	H_N
Orbital	Energy/eV	Character	3d	4s	4p	2s	2p	2s	2p	1s	1s
$5a_{1g}$	−3.08	M—(BN) π	83	3		5	2	2	1	1	2
$6e_g$	−3.62	M—(BN) π	66			6	22		3		
$5e_g$	−7.58	B—N, B—H	4				39		40		17
$5e_u$	−7.66	B—N, B—H			1		42		37		18
$4e_u$	−8.10	B—N π			3		18		71		3
$4e_g$	−8.30	B—N π	10		10	19		58		5	
$4a_{2u}$	−8.93	B—N, B—H			2	17	38	2	17	23	1
$4a_{1g}$	−9.08	B—N, B—H	1	3		22	37	5	2	28	2
$3a_{2u}$	−9.54	B—N π			5	8	24	1	59	3	
$3a_{1g}$	−10.43	B—N π	2	13		1	23		60		
$1a_{2g}$	−11.17	B—N					42		58		
$1a_{1u}$	−11.22	B—N					42		58		
$3e_u$	−11.25	B—N, N—H				2	11	3	59	2	12
$3e_g$	−11.31	B—N, N—H	3			2	20	2	59	2	12
$2e_u$	−13.38	B—N, N—H			1	35	6		53	2	4
$2e_g$	−13.56	B—N, N—H	2			40	5		49	1	4
$2a_{2u}$	−14.32	B—N, N—H			4	3	11	7	58		17
$2a_{1g}$	−14.53	B—N, N—H	3	3		5	11	6	56		15
$1e_u$	−21.21	B—N, N—H			1	5	11	75	2		5
$1e_g$	−21.24	B—N,N—H	2			4	11	75	2		5
$1a_{2u}$	−22.69	B—N, N—H			7	15	6	66	2		4
$1a_{1g}$	−22.93	B—N, N—H	2	1		16	6	67	2		3

Table 5. Mulliken populations and charges and bond orders for diborazine and dibenzene chromium

$Cr(\eta^6\text{-}H_3B_3N_3H_3)_2$						$Cr(\eta^6\text{-}C_6H_6)_2$					
Cr	charge = +0.58					charge = +0.67					
d_{z^2}	$d_{x^2-y^2,xy}$	$d_{xz,yz}$	s	p_z	p_x, p_y	d_{z^2}	$d_{x^2-y^2,xy}$	$d_{xz,yz}$	s	p_z	p_x, p_y
1.67	2.47	0.67	0.24	0.27	0.10	1.67	2.39	0.85	0.33	0.09	0.12
B	charge = −0.03		N	charge = −0.17		C (ring)	charge = −0.41				
2s	$2p_\sigma$	$2p_\pi$	2s	$2p_\sigma$	$2p_\pi$	2s	$2p_\sigma$	$2p_\pi$			
0.85	1.55	0.57	1.35	2.36	1.46	1.18	2.10	1.13			
H_B	charge = +0.12		H_N	charge = +0.38		H	charge = +0.28				
1s			1s			1s					
0.88			0.62			0.72					
Bond orders						Bond orders					
Cr—B	0.36	Cr—N	0.18	B—N	1.25	Cr—C	0.40	C—C	1.24		

"lone pairs" increases—strongly favouring the fully staggered conformation.

The inability of nitrogen to donate to the low valent metal and the poorer acceptor role of boron ensure that the bonding of the borazine ligand is weaker than that of a benzene ring. In the tricarbonyl complexes, the electronically flexible CO ligands are able to tune the metal somewhat to the requirements of the ring. In the diborazine system, however, the electron rich character of the metal is more evident resulting in weaker interaction with the ligands. The repulsive interactions between high lying σ-orbitals on the rings is also important in destabilizing the complex.

Acknowledgements—The author would like to thank Dr

Alain St-Amant of the University of Ottawa for making the DeFT code publicly available.

REFERENCES

1. Graffeuil, M. and Labarre, J. F., *J. Chim. Phys. Physicochim. Biol.*, 1971, **68,** 1379; Serafini, A., Labarre, J. F. and Gallais, F., *Proc. Int. Conf. Coord. Chem. 16th*, 1974, **2.4a,** 3; Serafini, A. F. and Labarre, J. F., *J. Mol. Struct.*, 1975, **26,** 129; Guest, M. F., Hillier, I. H. and Shenton, I. C., *Tetrahedron*, 1975, **31,** 1943; Vasudevan, K. and Grein, F., *Theor. Chim. Acta*, 1979, **52,** 219; Jug, K., *J. Org. Chem.*, 1983, **48,** 1344; Boyd, R. J., Choi, S. C. and Hale, C. C., *Chem. Phys. Lett.*, 1984, **112,** 136; Doering, J. P., Gedanken, A., Hitchcock, A. P., Fischer, P., Moore, J., Olthoff, J. K., Tossel, J., Raghavachari, K. and Robin, M. B., *J. Am. Chem. Soc.*, 1986, **108,** 3602; Dewar, M. J. S., Jie, C. and Zoebisch, E. G., *Organomet.*, 1988, **7,** 513; Nelson, J. T., Pietro, W. J., *Inorg. Chem.*, 1989, **28,** 544; Cooper, D. L., Wright, S. C., Gerratt, J. and Hyams, P. A., *J. Chem. Soc., Perkin Trans.*, 1989, 719; Jayasuriya, K., *Theochem.-J. Mol. Struct.*, 1991, **82,** 381; Fink, W. H. and Richards, J. C., *J. Am. Chem. Soc.*, 1991, **113,** 3393; Tossel, J. A., Moore, J. H., McMillan, K., Subramaniam, C. K. and Coplan, M. A., *J. Am. Chem. Soc.*, 1992, **114,** 1114; Satsunaga, N., Cundari, T. R., Schmidt, M. W. and Gordan, M. S., *Theor. Chim. Acta*, 1992, **83,** 57.
2. Greenwood, N. N. and Earnshaw, A., *Chemistry of the Elements*, Pergamon Press, Oxford, 1986; Cotton, F. A. and Wilkinson, G., *Advanced Inorganic Chemistry*, 5th edn, Wiley-Interscience, New York, 1988.
3. Scotti, M. and Werner, H., *Helv. Chim. Acta*, 1974, **57,** 1234.
4. Herberich, H., p 381 in 'Comprehensive Organometallic Chemistry', ed. G. Wilkinson, Pergamon Press, New York, 1982.
5. Huttner, G. and Krieg, B., *Angew. Chem. Int. Ed. Engl.*, 1971, **10,** 512; Huttner, G. and Krieg, B., *Chem. Ber.*, 1972, **105,** 3437.
6. Lagowski, J. J., *Coord. Chem. Rev.*, 1977, **22,** 185.
7. Werner, H., Prinz, R. and Deckelmann, E., *Chem. Ber.*, 1969, **102,** 105.
8. Armanasco, N. L., Baker, M. V., North, M. R., Skelton, B. W. and White, A. H., *J. Chem. Soc., Dalton Trans.*, 1997, 1363.
9. Scotti, M., Werner, H., Brown, D. L. S., Cavell, S., Connor, J. A. and Skinner, H. A., *Inorg. Chim. Acta*, 1977, **25,** 261.
10. Rees, B. and Coppens, P., *Acta Cryst.*, 1973, **B29,** 2516.
11. *Local Density Approximations in Quantum Chemistry and Solid-State Physics*, eds. Dahl, J. P. and Avery, J., Plenum, New York, 1989.
12. Parr, R. G. and Yang, W., *Density-Functional Theory of Atoms and Molecules*, Oxford University Press, Oxford, 1989.
13. Labanowski, J. K. and Andzelm, J. W., *Density Functional Methods in Chemistry*, Springer, New York, 1991.
14. Ziegler, T., *Chem. Rev.*, 1991, **91,** 65.
15. St-Amant, A., DeFT, a FORTRAN program (University of Ottawa, 1994).
16. Vosko, S. H., Wilk, L. and Nusair, M., *Can. J. Phys.*, 1980, **58,** 1200.
17. Becke, A. D., *Phys. Rev. A*, 1988, **38,** 3098.
18. Perdew, J. P., *Phys. Rev. B*, 1986, **33,** 8822.
19. Godbout, N., Salahub, D. R., Andzelm, J. and Wimmer, E., *Can. J. Chem.*, 1992, **70,** 1992.
20. Mayer, I., *Chem. Phys. Lett.*, 1983, **97,** 270; Mayer, I., *Int. J. Quantum Chem.*, 1984, **26,** 151.
21. Elian, M. and Hoffmann, R., *Inorg. Chem.*, 1975, **14,** 1058; Whitesides, T. H., Lichtenberger, D. L. and Budnik, R. A., *Inorg. Chem.*, 1975, **14,** 68; Elian, M., Chen, M. M. L., Mingos, D. M. P. and Hoffmann, R., *Inorg. Chem.*, 1976, **15,** 1148; Lichtenberger, D. L. and Fenske, R. F., *J. Am. Chem. Soc.*, 1976, **98,** 50; Burdett, J. K., *J. Chem. Soc., Faraday Trans. II*, 1977, 1599.
22. Albright, A. and Hoffmann, R., *Chem. Ber.*, 1978, **111,** 1578.
23. Lagowski, J. J., *Proc. 13th Int. Conf. Coord. Chem.*, 1970, **2,** 380; Adcock, J. L. and Lagowski, J. J., *Inorg. Chem.*, 1973, **12,** 2533.
24. Guest, M. F., Hillier, I. H., Higginson, B. R. and Lloyd, D. R., *Mol. Phys.*, 1975, **29,** 113.

Pergamon

PII: S0277-5387(98)00004-7

Polyhedron Vol. 17, Nos 13–14, pp. 2289–2293, 1998
© 1998 Elsevier Science Ltd
All rights reserved. Printed in Great Britain
0277-5387/98 $19.00+0.00

[Re(CO)$_3$(3,3′-trimethylene-2,2′-biquinoline)(p-substituted-py)]$^+$ complexes. Preparation and characterization

S. A. Moya,[a]* J. Guerrero,[a] R. Pastene,[a] A. J. Pardey[b] and P. Baricelli[c]

[a] Departamento de Química Aplicada, Facultad de Química y Biología, Universidad de Santiago de Chile, Santiago, Chile

[b] Escuela de Química, Facultad de Ciencias, Universidad Central de Venezuela, Caracas, Venezuela

[c] Centro de Investigaciones Químicas, Facultad de Ingeniería, Universidad de Carabobo, Valencia, Venezuela

(Received 21 July 1997; accepted 30 December 1997)

Abstract—A series of new rhenium(I) complexes of the type [Re(CO)$_3$(3,3′-trimethylene-2,2′-biquinoline)(L)](CF$_3$SO$_3$)$_n$, (L = CF$_3$SO$_3^-$, pyridine (py) or para-substituted pyridine like HO-py, ph-py or NC-py; n = 0 or 1) were prepared and characterized by FTIR, ^{1}H NMR, and UV–vis spectroscopies and by cyclic voltammetry. The pseudo-octahedral facial configuration of these compounds was established by FTIR. The differences found in the spectroscopical and electrochemical results were associated to the effect of the para-position substituent of the L pyridine ligand. © 1998 Elsevier Science Ltd. All rights reserved

Keywords: metallic carbonyl complexes; rhenium complexes; heterocyclic nitrogen ligand.

The chemical, photochemical, and photocatalytic properties of rhenium(I) complexes with polypyridine ligands make them potential agents to promote thermal, photochemical and electrochemical catalysis [1]. Examples of this include the electroreduction and photoreduction of CO_2, the latter being a process of interest in the conversion and storage of solar energy [2].

The MLCT and LLCT transitions in this type of compounds have been proposed as key states in some photochemical processes [1c,3]. Thus, the control or modulation of the absorption and/or emission energy can provide a very important tool to modify the catalytic behaviour of these complexes.

In order to evaluate the effect of structural modifications in the polypyridine ligand on the properties of the ground and excited states in these complexes, we have studied complexes of the general structure ReBr(CO)$_3$(L) with L = bidentate polypyridine ligand [4]. In previous works with ReBr(CO)$_3$(3,3′-R,R′-2,2′-biquinoline), (with R = R′ = H, CH$_3$ or R-R′ = dimethylene and trimethylene bridge) we found that the extended conjugation in the biquinoline, as compared to 2,2′-bipyridine, causes a shift towards lower energy both in the MLCT band and in the reduction potential of the polypyridine ligand [4b,d]. Moreover, the distortion degree from the planarity in the polypyridine ligand induces a slight variation of these energies [4d]. We have associated the emissions in these complexes with parallel relaxation processes from an IL and a MLCT state [4e].

The substitution of the bromide atom in these compounds by para-substituted pyridines (L) with electron donating or electron attracting groups can be a good alternative to obtain an electronic state, *[Re(CO)$_3$(3,3′-R,R′-2,2′-biquinoline)(L)]$^+$, closer to the MLCT state [3,4e]. In order to have new rhenium complexes that can help prove the existence of this electronic state, we report here the synthesis and spectroscopical characterization of a new series of complexes of the type [Re(CO)$_3$(3,2N)(L)]$^{+n}$ (3,2N = 3,3′-trimethylene-2,2′-biquinoline, L = CF$_3$SO$_3^-$, pyridine (py), para-substituted pyridine like HO-py, bz-py (bz = benzyl) or NC-py; n = 0 or 1) (Fig. 1).

* Author to whom correspondence should be addressed.

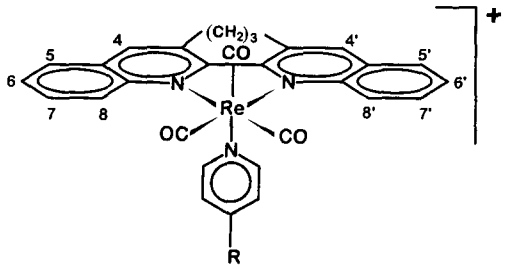

Fig. 1. $[Re(CO)_3(3,3'$-trimethylene-2,2'-biquinoline)(p-R-pyridine)$]^+$ complexes with R = H, CN, benzyl, or OH showing hydrogen positions for NMR discussions.

EXPERIMENTAL

Physical measurements

IR spectra were obtained from solid KBr disk and in $CHCl_3$ solution using a Bruker IFS-66 V FT-IR spectrophotometer. A 0.2 mm KBr cell was used scanning at least 100 times. ^1H NMR spectra were recorded in a 250 MHz Bruker spectrometer. Absorption spectra were recorded on a Shimadzu UV-160 spectrophotometer, using different and previously purified solvents, in quartz cells at ambient temperature. Molar conductivities were determined from 10^{-3} mol dm^{-3} solutions of complex in CH_3CN at 25°C using a Cole-Parmer 01481 conductivity meter. Electrochemical data were acquired in anhydrous acetonitrile solutions of the complexes containing 10^{-1} mol dm^{-3} tetrabutylammonium perchlorate (TBAP) via cyclic voltammetry using a Bank-Wenking POS 73 potentiostat with a Gould OS 4100 oscilloscope, and a Graphtec XY WX 4301 recorder. A three-electrode configuration, a working electrode was a platinum disk, the reference and counter electrodes were an aqueous calomel and a platinum wire, respectively. The test solution was separated from a reference electrode by Vycor bridge filled with corresponding solvent/supporting electrolyte system. A sweep rate of 200 mV s^{-1} was used for all the scans. Potentials were reported as $E_{\frac{1}{2}}^{l} = \frac{1}{2}(Ep_a + Ep_c)$, where Ep_a and Ep_c were the anodic and cathodic peak potentials, respectively. Ferrocene was used as an internal standard to compensate for the junction potential variability among experiments.

Materials

All the operations were carried out under purified nitrogen by standard Schlenk and vacuum-line techniques using freshly distilled, dried and degassed solvents. The solvents used in preparations, recrystallizations, and spectroscopic analysis (Mallinckrodt, grade HPLC) were treated and distilled prior to use. In electrochemical studies, anhydrous acetonitrile was dried using CaH_2 under nitrogen atmosphere at reflux for 2 h, and freshly distilled prior to use. Tetrabutylammonium perchlorate (TBAP) from Fluka was recrystallized twice from HPLC grade ethyl acetate (Mallinckrodt) prior to use. TBAP was stored in a vacuum desiccator over indicating Drierite ($CaSO_4$ anhydrous, Aldrich Chemical Co.) until needed for electrochemical studies. The pyridine ligand, $AgCF_3SO_3$, and $ReBr(CO)_5$, commercially available (Aldrich Chemical Co) were used without further purification. The synthesis of the biquinoline ligand (3,2N) and precursor complex $ReBr(CO)_3$(3,2N) have been previously described [4b,d].

Synthesis of rhenium complexes

The new complexes were obtained at 50°C under an inert atmosphere through stoichiometric precipitation of the corresponding bromide with silver triflate in methylene chloride solutions. Silver bromide was filtered under nitrogen pressure through celite. The filtrate was stirred at 50°C with a stoichiometric amount of the specific pyridine. The resulting orange solution was concentrated and the product purified using a chromatographic column of alumina. The starting material was eluted with methylene chloride and the complexes were eluted with a 5% *v/v* methylene chloride/methanol mixture. The solution was concentrated and the microcrystalline orange product was obtained after dropwise addition of cool hexane.

The $[Re(CO)_3(3,2N)(CF_3SO_3)]$ complex was obtained by concentration of the solution obtained after that the silver bromide was filtered. The product was purified using a chromatographic column of alumina with methylene chloride as eluent and isolated as pure crystals.

$[Re(CO)_3(3,2N)(CF_3SO_3)]$. Yield: 81%. ν_{CO} (in KBr disk) 2014, 1900 (broad) cm^{-1}, (in $CHCl_3$ solution at 25°C) 2013, 1923, 1894 cm^{-1}. Molar conductivity (in acetonitrile) 30 S cm^2 mol^{-1}. Melting point 182°C (d).

$[Re(CO)_3(3,2N)(HO\text{-}py)]^+$. Yield: 58%. ν_{CO} (in KBr disk) 2016, 1895 (broad) cm^{-1}, (in $CHCl_3$ solution at 25°C) 2225, 1917 (broad) cm^{-1}. Molar conductivity (in acetonitrile) 113 S cm^2 mol^{-1}. Melting point 156°C (d).

$[Re(CO)_3(3,2N)(bz\text{-}py)]^+$. Yield: 21%. ν_{CO} (in KBr disk) 2015, 1900 (broad) cm^{-1}, (in $CHCl_3$ solution at 25°C) 2033, 1934 (broad) cm^{-1}. Molar conductivity (in acetonitrile) 140 S cm^2 mol^{-1}. Melting point 130°C (d).

$[Re(CO)_3(3,2N)(py)]^+$. Yield: 55%. ν_{CO} (in KBr disk) 2015, 1900 (broad) cm^{-1}, (in $CHCl_3$ solution at 25°C) 2019, 1830 (broad) cm^{-1}. Molar conductivity (in acetonitrile) 113 S cm^2 mol^{-1}. Melting point 135°C (d).

$[Re(CO)_3(3,2N)(NC\text{-}py)]^+$. Yield: 52%. ν_{CO} (in KBr disk) 2032, 1911 (broad) cm^{-1}, (in $CHCl_3$ solution at 25°C) 2034, 1930 (broad) cm^{-1}. Molar con-

ductivity (in acetonitrile) 140 S cm^2 mol^{-1}. Melting point 113°C (d).

RESULTS AND DISCUSSION

The prepared complexes are stable in air, either as solid or in solution. They are soluble in several solvents of medium polarity. The formulas proposed of the general type [Re(CO)$_3$(3,3′-trimethylene-2,2′-biquinoline)(L)]$^{+n}$ for the products, are supported by melting points, conductivity measurements and spectroscopical results including FTIR, ^{1}H NMR and UV vis.

The conductivity values indicate a non-electrolyte compound for the [Re(CO)$_3$(3,2N)(CF$_3$SO$_3$)] complex and the existence of a species constituted by two ions for the other complexes.

The IR spectra show no important differences when compared with the characteristic spectra of the co-ordinated and the free pyridine ligands. The spectrum in solution for the [Re(CO)$_3$(3,2N)(CF$_3$SO$_3$)] complex show three strong bands in the carbonyl region which arise from a facial conformation with a local C_s symmetry around a hexacoordinated rhenium. For the other compounds with L = substituted pyridines, the spectra exhibit two intense bands in the typical carbonyl stretching region. This behaviour is consequent with a C_{3v} local symmetry for a facial stereochemistry in these complexes. The lowest energy signal for CO groups appears as a very broad band, which can be attributed to the decreasing of symmetry [5].

The proton NMR spectra of the complexes are summarized in Table 1. The assignments for the complexes were made considering the data and conclusions that we have reported previously for the free ligand and for the precursor complex [4d,6]. For those complexes we found that co-ordination shifts the signal of all the protons of the biquinoline ligand to lower fields. In the new complexes this deshielding increase. The effect is larger for the $H_{4'}$ and $H_{4''}$ protons localized in the para-position to the co-ordinated heterocyclic nitrogens. This behaviour is a good indication that the pyridine ligand induces a lower electronic density over the rhenium atom as compared to bromide ligand in the precursor complex. In the same way, the differences in the $\delta_{complex}-\delta_{precursor}$ values for the series indicate that the substitution in para position of the co-ordinated pyridine also provides an effect that should be considered. Although the pyridine aromatic protons show signals at high field with a characteristic AB pattern in the complexes, in the benzylpyridine complex a multiplet signal is observed due to this proton appears overlapped with the five protons of the phenyl ring. The three-signal pattern (q, m, q) of the aliphatic methylene protons is a consequence of the impossibility of the biquinoline molecule to rotate around of the C_2—$C_{2'}$ bond, but it becomes a two-signal pattern (t, m) in the [Re(CO)$_3$(3,2N)(bz-py)]$^+$ complex. This change suggests, that rotation is allowed in this complex under the working temperature.

The UV–vis spectroscopical data for the complexes are shown in Table 2. Over 400 nm, one or two shoulders of low intensity can be clearly observed. Upon increasing the polarity of the solvent, these shoulders are shifted to the high energy region. This type of band can be assigned as a rhenium-to-biquinoline-charge-transfer (MLCT) transition. Because it is

Table 1. ^{1}H NMR spectral data for the [Re(CO)$_3$(3,2N)(L)]$^{+n}$ (n = 0 or 1) complexes and the free ligand (3,2N)[a]

	aromatic protons (3,2N)					aliphatic protons(3,2N)			L protons		
Compound	$H_{4,4'}$	$H_{6,6'}$	$H_{8,8'}$	$H_{5,5'}$	$H_{7,7'}$	H_a	H_b	H_c	H_γ	H_β	
3,2N	8.00 s	7.54 t	8.35 d	7.81 d	7.69 t	2.70 t	2.20 q				
ReBr(CO)$_3$(3,2N)	8.25 s	7.69 t	8.82 d	7.90 m	7.90 m	2.83 q	2.74 m	2.43 q			
[Re(CO)$_3$(3,2N)(CF$_3$SO$_3$)]	8.33 s	7.77 t	8.89 d	7.97 m	7.97 m	3.01 q	2.81 m	2.50 q			
$\delta_{complex}-\delta_{precursor}$	+0.08	+0.08	+0.07	+0.07	+0.07						
[Re(CO)$_3$(3,2N)(HO-py)]$^+$[b]	8.37 s	7.78 t	8.86 d	8.01 m	8.01 m	2.92 q	2.81 m	2.51 q	5.91 d	7.59 d	2.74 s[c]
$\delta_{complex}-\delta_{precursor}$	+0.12	+0.09	+0.04	+0.11	+0.11						
[Re(CO)$_3$(3,2N)(bz-py)]$^+$	8.67 s	7.89 t	8.79 d	8.20 d	8.09 t	2.58 t	2.43 m		6.70 to 7.30[e]		3.85 s[d]
$\delta_{complex}-\delta_{precursor}$	+0.42	+0.20	−0.03	+0.30	+0.19						
[Re(CO)$_3$(3,2N)(NC-py)]$^+$	8.61 s	7.93 m	8.83 d	8.15 m	8.15 m	2.98 q	2.80 m	2.56 q	7.93 m	7.65 d	
$\delta_{complex}-\delta_{precursor}$	+0.36	+0.24	+0.01	+0.25	+0.25						
Re(CO)$_3$(3,2N)(py)]$^+$	8.66 s	7.90 m	8.82 d	8.29 d	8.13 m	2.79 q	2.58 m	2.42 q	7.29 dd	7.14 dd	8.13 m[e]
$\delta_{complex}-\delta_{precursor}$	+0.41	0.21	0.00	+0.39	+0.23						

[a] δ in ppm relative to internal SiMe$_4$ at 25 C in CDCl$_3$.
[b] four pyridine protons and five phenyl protons signals.
[c] OH of p-hydroxypyridine.
[d] CH_2 of p-benzylpyridine.
[e] p-protons pyridine signal.

Table 2. UV–vis spectral data for rhenium complexes and ligand (3,2N) at 25°C

Compound	solvent[a]	λ_{abs},nm (10^{-3} ε, dm^3 mol^{-1} cm^{-1}) ($t_{2g} \rightarrow \pi^*_L$)		($\pi \rightarrow \pi^*$))
3,2N	DCM			319 (98.84)
$ReBr(CO)_3(3,2N)$[b]	TOL	491 (sh)	450 (3.15)	369 (h)
	DCM	480 (sh)	435 (2.85)	371 (151.55)
	ACET	467 (sh)	418 (2.85)	369 (153.89)
$[Re(CO)_3(3,2N)(CF_3SO_3)]$	DCM		425 (sh)	369 (49.50)
	ACET		424 (sh)	368 (18.60)
	AN	463 (sh)	414 (sh)	368 (114.0)
$[Re(CO)_3(3,2N)(HO\text{-}py)]+$	DCM		431 (sh)	384 (11.00)
	ACET		430 (sh)	367 (151.40)
	AN	441 (sh)	411 (sh)	367 (18.64)
$[Re(CO)_3(3,2N)(bz\text{-}py)]+$	DCM		430 (sh)	371 (32.50)
	ACET	434 (sh)	373 (21.80)	
	AN	462 (sh)	420 (sh)	370 (20.20)
$[Re(CO)_3(3,2N)(NC\text{-}py)]+$	DCM	471 (sh)	437 (sh)	421 (7.20)
	ACET		440 (sh)	372 (186.20)
	AN	431 (sh)	429 (sh)	386 (20.12)
$[Re(CO)_3(3,2N)(py)]+$	DCM		430 (sh)	471 (7.20)
	ACET		435 (sh)	372 (186.20)
	AN	450 (sh)	425 (sh)	371 (20.12)

[a] DCM : methylene chloride, TOL : toluene, ACET : acetone, AN : acetonitrile.
[b] Ref. 4d.

difficult to unequivocally assign the absorption maximum for this band, we cannot tell if the presence of the pyridine ligand has some influence over the energy of this transition. This difficulty is also related with the position, just under 400 nm, expected for the rhenium-to-p-substituted-pyridine charge transfer band according with the less extensive conjugation of the pyridine compared with the biquinoline [4d]. The latest band appears overlapped by more intense bands corresponding to intraligand transitions ($\pi \rightarrow \pi^*$ biquinoline).

The redox potentials obtained by cyclic voltammetry at 200 mV s^{-1} in acetonitrile solution of the rhenium complexes are collected in Table 3. The complexes showed two successive reversible or quasi-reversible reduction waves between 0.00 to −2.00 volts range (vs SCE). In every case, the first reduction wave could be attributed to the ligand-centered process which involves the addition of an electron to the π^* orbital on the biquinoline ligand. Each of the complexes displayed a reversible or irreversible oxidation in the 0.80 to 1.44 volts range (vs SCE) assigned to a metal-centered process Re(II/I). This processes involves removal of an electron from the $d\pi$ orbital on rhenium(I) [4d,7].

The differences in the redox potential values for the rhenium compounds do not show a relationship with the basicity of the pyridine ligand. Similar behaviour has been reported for analogous complexes [8].

Table 3. Electrochemical data of the new rhenium complexes[a]

Complex	redox potential redn		oxidn
$ReBr(CO)_3(3,2N)$[b]	−0.99	−1.58	+1.18
$[Re(CO)_3(3,2N)(CF_3SO_3)]$	−1.08	−1.41[d]	+1.24
$[Re(CO)_3(3,2N)(HO\text{-}py)]^+$	−1.03[c]	−1.51	+1.35[c]
$[Re(CO)_3(3,2N)(bz\text{-}py)]^+$	−0.88	−1.36	+0.95[c]
$[Re(CO)_3(3,2N)(NC\text{-}py)]^+$	−1.08[d]	−1.46	+1.44[c]
$[Re(CO)_3(3,2N)(py)]^+$	−1.00[d]	−1.42	+1.40[c]

[a] Potentials are in volts vs SCE in 10^{-1} mol dm^{-3} TBPA/acetonitrile solution at ambient temperature, scan rate was 200 mV s^{-1}.
[b] Ref. 4d.
[c] Values represent anodic peak potentials.
[d] ΔE_p = 170 mV.
[e] ΔE_p = 180 mV.

Acknowledgements—We thanks DICYT-USACH, FONDECYT-CHILE, for the financial support and MOLY-MET-CHILE S.A. for a generous gift of rhenium. Useful comments provided by J. Cornejo are also acknowledged. P.B. thanks CODECHYT/UC, A.J.P. CONICIT/Venezuela and CDCH/UCU.

REFERENCES

1. (a) Juris, A., Balzani, V., Barigelletti, F., Campagna, S., Belser, P. and von Zelewsky, A., *Coord. Chem. Rev.*, 1988, **84,** 85; (b) Barigelletti, F., Campagna, S., Belser, P. and von Zelewsky,

A., *Coord. Chem. Rev.*, 1988, **84,** 5; (c) Kalyanasundaram, K., *Photochemistry of Polypyridine and Porphyrin Complexes*, Academic Press, London, 1992; (d) Shoonover, J. R., Strouse, G. F., Dyer, R. B., Bates, W. D., Chen, P. and Meyer, T. J., *Inorg. Chem.*, 1996, **35,** 273; (e) Treadway, J. A., Loeb, B., Lopez, R., Anderson, P., Keene, F. R. and Meyer, T. J., *Inorg. Chem.*, 1996, **35,** 2242; (f) Rossenaar, B. D., Hartl, F. and Stufkens, D. J., *Inorg. Chem.*, 1996, **35,** 6194.

2. (a) Grätzel, M., *Energy Resources Through Photochemistry and Catalysis*, Academic Press, New York, 1983; (b) Ruiz, E., Wolcan, E., Capparelli, A. L. and Feliz, M. R., *J. Photochem. Photobiol. A. Chem.*, 1995, **89,** 61; (c) Hawecker, J., Lehn, J. M. and Ziessel, R., *J. Chem. Soc., Chem. Commun.*, 1983, 536; (d) Pac, C., Ishii, K. and Yanagida, S., *Chem. Lett.*, 1989, 765.
3. (a) Feliz, M., Ferraudi, G. and Altmiller, H., *J. Phys. Chem.*, 1992, **96,** 257; (b) Kutal, C., Corbin, A. J. and Ferraudi, G., *Organometallics*, 1987, **6,** 553.
4. (a) Moya, S. A., Pastene, R., Schmidt, R., Guerrero, J., Sariego, R. and Sartori, R., *Bol. Soc. Chil. Quim.*, 1992, **37,** 43; (b) Sartori, R., Guerrero, J., Pastene, R., Schmidt, R., Sariego, R. and Moya, S. A., *Bol. Soc. Chil. Quim.*, 1992, **37,** 311; (c) Moya, S. A., Pastene, R., Schmidt, R., Guerrero, J. and Sartori, R., *Polyhedron*, 1992, **11,** 1665; (d) Moya, S. A., Guerrero, J., Pastene, R., Schmidt, R., Sariego, R., Sartori, R., Sans-Aparicio, J., Fonseca, I. and Martinez-Ripoll, M., *Inorg. Chem.*, 1994, **33,** 2341; (e) Ferraudi, G., Feliz, M., Wolcan, E., Hsu, Y., Moya, S. A. and Guerrero, J., *J. Chem. Phys.*, 1995, **99,** 4929; (f) Moya, S. A., Pastene, R., Pardey, A. J. and Baricelli, P., *Bol. Soc. Chil. Quim.*, 1996, **41,** 251.
5. Bermejo, M. J., Ruiz, J. Y., Solans, X. and Vinaixa, J., *Inorg. Chem.*, 1988, **27,** 4385.
6. Thummel, R. P. and Lefoulon, F., *J. Org. Chem.*, 1985, **50,** 666.
7. (a) World, L. A., Duesing, R., Cheng, P., Dellaciana, L. and Meyer, T. J., *J. Chem. Soc., Dalton Trans*, 1991, 849; (b) Yang, W. and Schanze, K. S., *Inorg. Chem.*, 1994, **33,** 1354; (c) Moya, S. A., Pastene, R., Sartori, R., Dixneuf, P. and Le Bozec, H., *J. Braz. Chem. Soc.*, 1995, **6,** 29.
8. Sacksteder, L. A., Zipp, A. P., Brown, E. A., Streich, J., Demas, J. N. and De Graff, B. A., *Inorg. Chem.*, 1990, **29,** 4335.

Pergamon

PII: S0277-5387(98)00003-5

Polyhedron Vol. 17, Nos 13–14, pp. 2295–2299, 1998
© 1998 Elsevier Science Ltd
All rights reserved. Printed in Great Britain
0277-5387/98 $19.00+0.00

Competition study for the base hydrolysis of trans- $[Co(NH_3)_4(NH_2CH_3)X]^{n+}$ complexes

Fabian Benzo, Carolina Mendoza, Marcelo Queirolo and Beatriz Sienra*

Química Inorgánica, Facultad de Química, C. C.1157, Montevideo, Uruguay

(Received 16 October 1997; accepted 28 December 1997)

Abstract—Nitrite ion competition has been measured for the base hydrolysis reaction of *trans*-$Co(NH_3)_4(NH_2CH_3)X^{n+}$ ions (X = Cl^-, Br^-, NO_3^- and SO_4^{2-}) in 1.0 M $NaNO_2$ at 25°C. Both O- and N- bonded $Co(NH_3)_4(NH_2CH_3)NO_2^{2+}$ are formed. Subsequently the $Co(NH_3)_4(NH_2CH_3)ONO^{2+}$ isomer rearranges in OH^- to give the thermodynamically more stable $Co(NH_3)_4(NH_2CH_3)NO_2^{2+}$ ion. The total NO_2^- captured shows a slight dependence on the overall charge of the complex and on the nature of X (R = 2.2, 2.1, 3.6 and 1.2±0.5% for X = Cl^-, Br^-, NO_3^- and SO_4^{2-}, respectively). These results differ from those observed with complexes of the type $Co(NH_3)_5X^{n+}$ and $Co(NH_2CH_3)_5X^{n+}$ where X includes a variety of anions. © 1998 Elsevier Science Ltd. All rights reserved

Keywords: base hydrolysis; trans-$[Co(NH_3)_4(NH_2CH_3)X]^{n+}$ complexes.

Competition experiments have provided information on the detailed mechanism of base hydrolysis of pentaamminecobalt(III) ions, $Co(NH_3)_5X^{n+}$. The thrust of these studies has been the close examination of the leaving group (X) dependence of the product distribution for the reaction of $Co(NH_3)_5X^{n+}$ in aqueous OH^- containing competing Y^- [1–9]. There is ample evidence to show that neutral leaving groups (i.e. X = Me_2SO, $(NH_2)_2CO$, $(MeO)_3PO$) result in enhanced Y^- entry, usually reported as $\%Co(NH_3)_5Y^{2+} = 10^2\,[Co(NH_3)_5Y^{2+}]/[Co(NH_3)_5Y^{2+}]+[Co(NH_3)_5(H_2O)^{3+}]$, when compared to uninegative leaving groups, X^-, and SO_4^{2-}. For example, if Y^- = N_3^- ion, $\%Co(NH_3)_5N_3^{2+}$ are 12 for 3+complexes [4], 8.5–10 for 2+complexes [1,3] and 5.8 [4], 7.2 [7] for X = SO_4^{2-}. Among the 2+complexes, there is an increase in the percentage of $Co(NH_3)_5N_3^{2+}$ as the $Co(NH_3)_5X^{2+}$ complex becomes easier to hydrolyze; this trend appears to approach a limiting value of ~10.5% for the most labile complexes [9].

The products of the base hydrolysis of the more strained $Co(NH_2CH_3)_5X^{n+}$ complexes, have also been studied, with azide ion as competitor (X = $OSO_2CF_3^-$, Me_2NCHO, Cl^-). It was found that these complexes, whose enhanced sensitivity to base hydrolysis is well known [10,11] give rise to much higher azide competition than the $Co(NH_3)_5X^{n+}$ complexes ($\%Co(NH_2CH_3)_5N_3^{2+}$ = 36 [8], 52 [12] and 49 [12] respectively).

The present paper explores the competition properties of *trans*-$Co(NH_3)_4(NH_2CH_3)X^{n+}$ complexes (X = Cl^-, Br^-, NO_3^- and SO_4^{2-}), using nitrite ion as competitor. The kinetics of the base hydrolysis reaction of these complexes has been recently reported [13], and it was found that methylation of the NH_3 ligand, *trans* to the leaving group, produces a modest increase on the reaction rate. Nitrite ion competition has been measured for the base hydrolysis reaction of a series of $Co(NH_3)_5X^{n+}$ ions in 1.0 M $NaNO_2$ [5]. It was found that both O- and N- bonded $Co(NH_3)_5(NO_2)^{2+}$ ions are formed, along with $Co(NH_3)_5(OH)^{2+}$ complex. It is also known that in aqueous base the $Co(NH_3)_5(ONO)^{2+}$ ion isomerizes completely to the $Co(NH_3)_5NO_2^{2+}$ ion, through a base-catalyzed path [14]. It seemed reasonable that the *trans*-$Co(NH_3)_4(NH_2CH_3)X^{n+}$ complexes will show the same behaviour.

We have chosen NO_2^- ion to compete with H_2O for the following reasons: (i) the rate of base hydrolysis for the $Co(NH_3)_4(NH_2CH_3)(NO_2)^{2+}$ complex is con-

* Author to whom correspondence should be addressed.

siderably slower than that for *trans*-$Co(NH_3)_4(NH_2CH_3)X^{n+}$ ions [13]; (ii) the synthesis and spectral properties of $Co(NH_3)_4(NH_2CH_3)(NO_2)^{2+}$ and $Co(NH_3)_4(NH_2CH_3)(ONO)^{2+}$ complexes are known [15].

EXPERIMENTAL

C, H, N elemental analysis were carried out with a Carlo Erba EA1108 elemental analyzer. Visible spectra (ε, $M^{-1}cm^{-1}$; λ, nm) were obtained with a Spectronic 3000 diode array spectrophotometer. ^1H NMR spectra were recorded on a Varian Unity spectrometer operating at 100 MHz and 35°C; signals are described in terms of chemical shifts (δ) with tetramethylsilane (tms) as internal reference. Ion-exchange chromatographies were performed with the use of a Dowex (50W × 8, 50–100 mesh; Na^+ form) cation-exchange resin. HPLC experiments were carried out with a Merck Hitachi D2500 apparatus using a cationic-exchange column (PRP-X200-10μ, 4 × 250 mm).

Materials

trans-$[Co(NH_3)_4(NH_2CH_3)(OSO_3)]HSO_4 \cdot H_20$ was prepared as follows. The complex *trans*-$[Co(NH_3)_4(NH_2CH_3)(SO_3)]Cl$ [16] (7.0 mmol) was dissolved in H_2SO_4 (98%; 15 ml) saturated with Li_2SO_4 at ambient temperature. The resultant pink solution was poured carefully into cold methanol (0.4 l) to precipitate the desired compound. This was collected and washed with methanol and ether. Yield: 68%. Anal: Calcd for $CoH_{20}N_5S_2O_9C$: C, 3.25; H, 5.42; N, 18.97. Found: C, 3.37; H, 5.24; N, 18.79. Visible spectrum: ε_{357} 55.1, ε_{520} 65.4 in water. The ^1H NMR spectra confirmed the isomeric purity of the compound (methyl signal δ 1.74, in D_2O). Ion-exchange chromatography was the major tool used to establish the absence of trace impurities, in particular *trans*-$Co(NH_3)_4(NH_2CH_3)(OH_2)^{3+}$. The complex was absorbed onto a cation-exchange resin and was eluted as a single band with 0.4 M $NaClO_4$.

trans-$[Co(NH_3)_4(NH_2CH_3)Cl](ClO_4)_2$ and *trans*-$[Co(NH_3)_4(NH_2CH_3)Br](ClO_4)_2$ were prepared from the chloride [16] and bromide [17] salts, respectively, by routine treatment with silver perchlorate. *trans*-$[Co(NH_3)_4(NH_2CH_3)(ONO_2)](NO_3)_2$, *trans*-$[Co(NH_3)_4(NH_2CH_3)(OH_2)](ClO_4)_3$, *trans*-$[Co(NH_3)_4(NH_2CH_3)(ONO)]Cl_2$ and *trans*-$[Co(NH_3)_4(NH_2CH_3)(NO_2)]Cl_2$ complexes were prepared as described previously [15,17].

All the complexes salts analyzed satisfactorily for at least three elements, and their absorption and ^1H NMR spectra agreed with the literature data. None of the ^1H NMR spectra of the complexes in concentrated Me_2SO-d_6 solution (except the aqua complex) showed the characteristic Co—OH_2 signal (δ 5.62) [3]. All other reagents and solvents used were of analytical grade.

Competition experiments

The competition experiments were performed at 25°C by dissolving the complexes (0.5 mmol) in 5 ml of water; immediately, these solutions and solutions 2.0M $NaNO_2$ (5 ml, 0.25 M in NaOH) were mixed. In some experiments, weighed samples of the complexes (0.5 mmol) were dissolved directly in 1.0 M $NaNO_2$ (10 ml, 0.125M NaOH); the results did not differ significantly. After 5 min if $X = Cl^-$, Br^- or SO_4^{2-}, or 2 min for $X = NO_3^-$ (>10 $t_{1/2}$) the reaction mixtures were diluted with cold water to quench the reaction and avoid further decomposition of the products.

The product mixtures were sorbed on a column of Dowex resin and then thoroughly washed with water. The sorbed complexes were eluted with 1 M NaCl (pH 4) to separate first the 2+complexes and then with 3M NaCl to recover the $Co(NH_3)_4(NH_2CH_3)(OH_2)^{3+}$ ion (further called aqua complex). Each band was observed spectrophotometrically and compared with the spectra of the pure complexes. The first one (2+complexes) was a mixture of $Co(NH_3)_4(NH_2CH_3)(ONO)^{2+}$ (further called nitrito complex) and $Co(NH_3)_4(NH_2CH_3)(NO_2)^{2+}$ (further called nitro complex) complexes and the rearrangement of the former into the latter complex could be observed. However, complete separation of the two bands was not achieved, although different experimental conditions were tested (column length, concentration and rate of the eluant). Accordingly, in order to determine the amount of each product, a more efficient and less time consuming analytical method was chosen: HPLC. The complexes (0.2 mmol) were dissolved in water (2 ml) and these solutions were immediately mixed with solutions 2.0 M $NaNO_2$ (2 ml, 0.25 M in NaOH). All the competition experiments were performed at 25°C. After 5 min if $X = Cl^-$, Br^- or SO_4^{2-}, or 2 min for $X = NO_3^-$ (>10 $t_{1/2}$) the reaction mixtures were diluted with cold water and 20 μl of these mixtures were analyzed by HPLC. Nitro and nitrito complexes were separated from the aqua complex by eluting with 0.16 M Na_2SO_4, using a flow (1 ml/min) which provided convenient retention times. Complexes concentrations in the eluate fractions were determined spectrophotometrically at 367 nm (see Results); at this wavelength the molar absorption coefficients are 543 M^{-1} cm^{-1} for nitro and nitrito complexes and 33.5 M^{-1} cm^{-1} for aqua complex. Complete elution was confirmed in all the experiments by washing the column with concentrated solutions of Na_2SO_4. The retention times were compared with those of pure and mixed solutions of nitro, nitrito and aqua complexes separately.

RESULTS AND DISCUSSION

The products of the base hydrolysis reaction of the *trans*-$Co(NH_3)_4(NH_2CH_3)X^{n+}$ ions ($X = Cl^-$, Br^-,

NO_3^- and SO_4^{2-}) in the presence of 1.0 M $NaNO_2$ at 25 C, after neutralization, were both O- and N-bonded $Co(NH_3)_4(NH_2CH_3)(NO_2)^{2+}$, and $Co(NH_3)_4(NH_2CH_3)(OH_2)^{3+}$. The presence of both, nitro and nitrito complexes, as reaction products was confirmed by HPLC and cation-exchange experiments.

Attempts at measuring the amounts of nitrito and nitro complexes separately failed because it was not possible to find appropriate experimental conditions to obtain reproducible results. On the other hand, the nitrito complex isomerizes slowly ($t_{1/2}$ = 114 min, 25 C) but completely to the nitro complexes in solution [20]. Therefore, both isomers were measured together at the isosbestic point, ε_{367} 543 $M^{-1}cm^{-1}$.

A representative chromatogram is given in Fig. 1. The chromatogram shows three peaks at 2.2, 4.9 and 6.9 min, corresponding to the excess of NO_2^- present in the solution, the mixture of nitro and nitrito complexes and aqua complex respectively.

The competition was defined as: P (product distribution) = [nitro + nitrito]/[aqua] and %(nitro + nitrito) = 10^2 [nitro + nitrito]/[nitro + nitrito] + [aqua] = $10^2P/1+P$. The conventional [21] competition ratio R was given by $P/[NO_2^-]$.

The product distributions were calculated from the peak areas (A) and the values of the molar absorption coefficients at 367 nm, as follows:

$$P = (\varepsilon_{aqua}/\varepsilon_{nitro\text{-}nitrito})(A_{nitro\text{-}nitrito}/A_{aqua}).$$

There is substantial evidence for a conjugate-base mechanism for hydrolysis of Co (III) amine complexes in basic solutions (Scheme I).

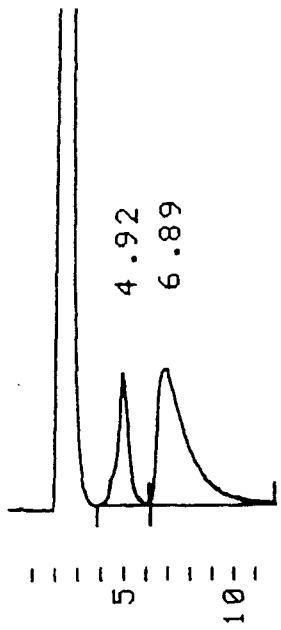

Fig. 1. HPLC chromatogram of the products of base hydrolysis at 25 C of the *trans*-$Co(NH_3)_4(NH_2CH_3)Cl^{2+}$ in the presence of 1.0 M $NaNO_2$.

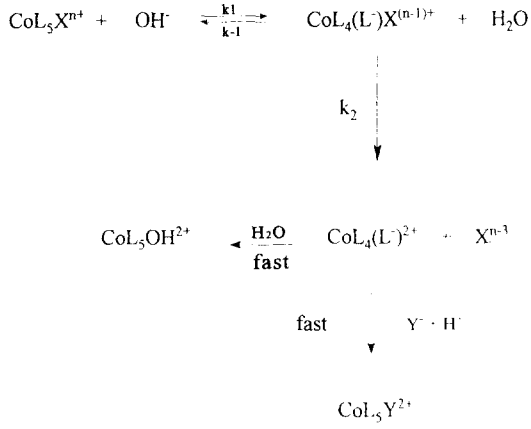

L = amine and L⁻ = deprotonated amine

Scheme I.

It is apparent that if a common intermediate is produced (S_N1CB or D_{CB} mechanism) a constant competition ratio should be found for each species of Y. The results of the competition experiments at 25 C are listed in Table 1. The reported values are averages over at least five independent measurements.

Kinetic and competition data for the base hydrolysis of $Co(NH_3)_5X^{n+}$ and $Co(NH_2CH_3)_5X^{2+}$ ions in the presence of various anions at 25 C, are included in Table 2 and Table 3 for comparison.

These results show, within the experimental error, the following: (i) The *trans*-$Co(NH_3)_4(NH_2CH_3)X^{2+}$ complexes give more nitro complex than the *trans*-$Co(NH_3)_4(NH_2CH3)(OSO_3)^+$ ion. A similar trend has been found for the $Co(NH_3)_5X^{n+}$ complexes; (ii) Among the *trans*-$Co(NH_3)_4(NH_2CH_3)X^{2+}$ complexes there is an increase in the amount of nitro complex found as the complex becomes easier to hydrolyze. The $Co(NH_3)_5X^{2+}$ complexes show a similar behaviour but for the $Co(NH_2CH_3)_5X^{2+}$ this trend is inverted at least for the two complexes already studied ($X = OSO_2CF_3^-$ and Cl^-); (iii) The competition

Table 1. Kinetic and competition data for the base hydrolysis of *trans*-$Co(NH_3)_4(NH_2CH_3)X^{n+}$ in the presence of $NaNO_2$ at 25 C

X	$k_{OH}(s^{-1}M^{-1})$	%CoY[a]	R
SO_4^{2-}	0.56[b]	1.2[d]	0.012[d]
Cl^-	4.8[c]	2.2[d]	0.023[d]
Br^-	14[c]	2.1[d]	0.021[d]
NO_3^-	59[c]	3.6[d]	0.037[d]

[a] % CoY is the %(nitro + nitrito); estimated error in %CoY: ±0.5.
[b] Data from Ref. 18.
[c] Data from Ref. 13.
[d] This work.

Table 2. Kinetic and competition data for the base hydrolysis of $Co(NH_3)_5X^{n+}$ in the presence of various anions at 25°C

X	$k_{OH}(s^{-1}M^{-1})$	$\%CoN_3^{2+}$ [a]	$\%CoNO_2^{2+}$ [b]	$\%CoSCN^{2+}$ [c]
SO_4^{2-}	0.07[d]	5.4[e],5.8[f]	—	4.1[g]
Cl^-	0.60[h]	8.5[i],8.7[e]	4.2[i]	5.5[f]
Br^-	3.3[h]	8.7[i],9.5[e]	5.0[i]	6.1[f]
NO_3^-	9.2[h]	10.4[f],10.3[e]	5.1[f],7.5[j]	7.1[f],7.4[g]
Me_2SO	5.4[f]	12.3[f],12.6[e]	7.8[k],8.8[j]	9.2[f],9.0[g]

[a] $CoN_3^{2+} = Co(NH_3)_5(N_3)^{2+}$.
[b] $CoNO_2^{2+} = Co(NH_3)_5(NO_2)^{2+}$ or $Co(NH_3)_5(ONO)^{2+} + Co(NH_3)_5(NO_2)^{2+}$.
[c] $CoSCN^{2+}$ is the calculated amount of $Co(NH_3)_5(NCS)^{2+}$ after complete reaction of first-formed $Co(NH_3)_5(SCN)^{2+}$.
[d] Data from Ref. 18.
[e] Data from Ref. 9.
[f] Data from Ref. 4.
[g] Data from Ref. 6.
[h] Data from Ref. 13.
[i] Data from Ref. 1.
[j] Data from Ref. 5.
[k] Data from Ref. 19.

Table 3. Kinetic and competition data for the base hydrolysis of $Co(NH_2CH_3)_5X^{n+}$ in the presence of NaN_3 at 25°C

X	k_{OH} ($s^{-1}M^{-1}$)	$\%CoN_3^{2+}$ [a]	R
Cl^-	1.8×10^{3}[b]	49[c]	0.96[c]
$OSO_2CF_3^-$	$> 10^{7}$[d]	36[d]	0.56[d]
Me_2NCHO		52[c]	1.07[c]

[a] $CoN_3^{2+} = Co(NH_3)_5(N_3)^{2+}$.
[b] Data from Ref. 11.
[c] Data from Ref. 12.
[d] Data from Ref. 8.

ratios for the *trans*-$Co(NH_3)_4(NH_2CH_3)X^{n+}$ complexes are smaller than those of the $Co(NH_3)_5X^{n+}$ ions and those of the $Co(NH_2CH_3)_5X^{n+}$ are the biggest ones.

Two generalizations can be drawn from these observations:

(i) The three types of reactants, $Co(NH_3)_5X^{n+}$, *trans*-$Co(NH_3)_4(NH_2CH_3)X^{n+}$ and $Co(NH_2CH_3)_5X^{n+}$ do not exhibit the same behaviour. The competition ratios are different for each substrate and there is not a correlation between those and the reactions rates;

(ii) For each of the three types of reactants the competition ratios differ on the charge of the leaving group X and for a given charge type of X there is a significant variation of R with the nature of the leaving group.

The dependence of anion competition on the formal charge of the $Co(NH_3)_5X^{n+}$ complexes has been interpreted by Jackson and Sargeson in terms of the conjugate base dissociative (S_N1CB) mechanism "where the short lived intermediate five-coordinated species captures the atmosphere of its immediate precursor" [4–7]. On the other hand, Rotzinger [12,22] has asserted that the base hydrolysis of the $Co(NH_3)_5X^{n+}$ complexes proceeds via hexacoordinated intermediates $Co(NH_3)_4(NH_2)\ldots X^{(n-1)+}$: "these intermediates are hexacoordinated, because the ionic strength dependence of the competition ratios showed unambiguously that the leaving group is present in the first coordination sphere during the product formation step".

The competition properties of the $Co(NH_2CH_3)_5X^{n+}$ complexes have also been studied and compared with the competition ratios of the $Co(NH_3)_5X^{n+}$ ions. Sargenson *et al.* [8] have argued that the competition ratios imply a common intermediate arising from the different leaving groups for each set of the $Co(NH_3)_5X^{n+}$ and $Co(NH_2CH_3)_5X^{n+}$ ions and an increased lifetime for $Co(NH_2CH_3)_4(NHCH_3)^{2+}$ relative to $Co(NH_3)_4(NH_2)^{2+}$. On the contrary, Rotzinger [12] has asserted that the pentacoordinated intermediate $Co(NH_2CH_3)_4(NHCH_3)^{2+}$ exhibits a shorter lifetime than the hexacoordinated intermediates $Co(NH_3)_4(NH_2)\ldots X^{(n-1)+}$. The present (limited) data for the *trans*-$Co(NH_3)_4(NH_2CH_3)X^{n+}$ complexes indicate that no two complexes behave the same. The results do not prohibit the formation of the same five-coordinated species for all substrates in a purely dissociative process, but its lifetime has to be so short that it captures ligating groups from the solvent cage before it has had time to adjust to its changed situation. In summary, we think that the base hydrolysis competition results to date are inconclusive, and that the questions of the competition and lifetime of intermediates have not been finally settled.

Acknowledgements—We are grateful for the financial assistance from CONICYT, Uruguay.

REFERENCES

1. Buckingham, D. A., Olsen, I. I. and Sargeson, A. M., *J. Am. Chem. Soc.*, 1966, **88,** 5443.
2. Buckingham, D. A., Creaser, I. I. and Sargeson, A. M., *Inorg. Chem.*, 1970, **9,** 655.
3. Buckingham, D. A., Cresswell, P. J., Sargeson, A. M. and Jackson, W. G., *Inorg. Chem.*, 1981, **20,** 1647.
4. Dixon, N. E., Jackson, W. G., Marty, W. and Sargeson, A. M., *Inorg. Chem.*, 1982, **21,** 688.
5. Jackson, W. G., Randall, M. L., Sargeson, A. M. and Marty, W., *Inorg. Chem.*, 1983, **22,** 1013.
6. Jackson, W. G. and Hookey, C. N., *Inorg. Chem.*, 1984, **23,** 668.
7. Jackson, W. G., Hookey, C. N., Randall, M. L., Comba, P. and Sargeson, A. M., *Inorg. Chem.*, 1984, **23,** 2473.
8. Curtis, N. J., Lawrance, G. A., Lay, P. A. and Sargeson, A. M., *Inorg. Chem.*, 1986, **25,** 484.
9. Brasch, N. E., Buckingham, D. A., Clark, C. R. and Finnie, K. S., *Inorg. Chem.*, 1989, **28,** 4567.
10. Tobe, M. L., *Advances in Inorganic and Bioinorganic Mechanisms*, Vol. 2, ed. A. G. Sykes. Academic Press, London, 1983, p. 1.
11. Buckingham, D. A., Foxman, B. M. and Sargeson, A. M., *Inorg. Chem.*, 1970, **9,** 1790.
12. Rotzinger, F. P., *Inorg. Chem.*, 1991, **30,** 2763.
13. Benzo, F., Massaferro, A., Capparelli, A. L., Mártire, D. O., Queirolo, M. and Sienra, B., *Polyhedron*, 1996, **15,** 1915.
14. Jackson, G. W., Lawrance, G. A., Lay, P. A. and Sargeson, A. M., *Inorg. Chem.*, 1980, **19,** 904.
15. Massaferro, A., Queirolo, M. and Sienra, B., *An. Quím.*, 1992, **88,** 230.
16. Balt, S., Gamelkoorn, H. J., Píriz Mac-Coll, C. R. and Renkema, W. E., *Trans. Met. Chem.*, 1984, **9,** 224.
17. Sienra, B., Massaferro, A. and Píriz Mac-Coll, C. R., *Z. anorg. allg. Chem.*, 1990, **590,** 222.
18. Benzo, F., Capparelli, A. L., Mártire, D. O. and Sienra, B., unpublished work.
19. Birus, M., Reynolds, W. L., Pribanic, M. and Asperger, S., *Proc. Int. Conf. Coord. Chem.*, 1974, **16,** 3.6.
20. Bozoglián, F., Queirolo, M. and Sienra, B., unpublished work.
21. Haim, A. and Taube, H. *Inorg. Chem.*, 1963, **2,** 1199.
22. Rotzinger, F. P., *Inorg. Chem.*, 1988, **27,** 772.

Pergamon

PII: S0277-5387(98)00001-1

Polyhedron Vol. 17, Nos 13–14, pp. 2301–2307, 1998
© 1998 Elsevier Science Ltd
All rights reserved. Printed in Great Britain
0277-5387/98 $19.00+0.00

The anions $[(ZrOH(CO_3)_3)_2]^{6-}$ and $[(ZrOH(C_2O_4)_3)_2]^{6-}$: single crystal X-ray diffraction studies of the complexes guanidinium zirconium carbonate $[(C(NH_2)_3)_3ZrOH(CO_3)_3 \cdot H_2O]_2$ and sodium zirconium oxalate $Na_6(ZrOH(C_2O_4)_3)_2 \cdot 7H_2O$

Susan Morris, Matthew J. Almond,* Christine J. Cardin, Michael G. B. Drew, David A. Rice and Yan Zubavichus

Department of Chemistry, The University of Reading, P.O. Box 224, Whiteknights, Reading RG6 6AD, U.K.

(Received 20 October 1997; accepted 18 December 1997)

Abstract—The complex $[(C(NH_2)_3)_3ZrOH(CO_3)_3 \cdot H_2O]_2$ (**A**) has been shown by means of a single crystal X-ray diffraction study to contain $[C(NH_2)_3]^+$ cations and dimeric anions of formulation $[(ZrOH(CO_3)_3)_2]^{6-}$. The anion is centrosymmetric with each metal being bonded to two bridging OH groups and three chelating CO_3^{2-} ions. The Zr atoms are thus eight coordinate with a dodecahedral environment. The Zr—O distances formed by the bridging OH groups are shorter than those formed through zirconium carbonate interactions. The non-bonded Zr···Zr distance is 3.47(2) Å. An infrared spectroscopic investigation of **A** provides data which support the findings of the crystallographic study. Likewise the complex $Na_6(ZrOH(C_2O_4)_3)_2 \cdot 7H_2O$ (**B**) contains the anion $[(ZrOH(C_2O_4)_3)_2]^{6-}$. This anion is structurally related to the anion in **A** as each Zr atom has an eight-coordinate dodecahedral environment being bonded to two bridging OH groups and three chelating oxalate ligands, but has no imposed crystallographic symmetry. The Zr···Zr non-bonded distance is 3.50(1) Å. The O—Zr—O bridge angles are 69.7(4)° in **A** and 67.4(3)° in **B**. © 1998 Elsevier Science Ltd. All rights reserved

Keywords: anions; single crystal X-ray diffraction.

Zirconia (ZrO_2) is a material which finds a wide range of industrial applications. These range from use as a light scatterer in ophthalmic glasses [1,2], as a toughener in composite ceramics [3], in X-ray photography [2], as heat shields, in the high temperature filtration of corrosive liquids [4] and in the production of crucibles and furnace cores [4]. Some of these industrial uses require zirconia in a particular phase. For example the cubic phase is often required for optical applications since it has a refractive index of 2.4 and is thus efficient at scattering light [1]. By contrast the tetragonal phase is normally required when zirconia is used to toughen composite ceramics. These phases are only stable at high temperatures (cubic above 2370°C; tetragonal between 1170 and 2370°C) and unfortunately cannot normally be retained by rapid quenching. According these phases are typically stabilised by adding a dopant to the ZrO_2 e.g. the addition of small amounts of yttria (Y_2O_3) to the ZrO_2 may stabilise the cubic or tetragonal forms [3,5]. Adding yttria (or other dopants e.g. CaO) to ZrO_2 also has the effect of increasing the electrical conductivity of the material (pure ZrO_2 is an insulator with a resistivity of about 10^{12} Ωm at room temperature) allowing its use as an electrolyte [6].

In our current investigations one aim is to search for coordination compounds of zirconium, typically containing oxo ligands, which readily yield zirconia upon calcination. Thus we hope to find routes, not

* Author to whom correspondence should be addressed.

only to ZrO_2 itself, but also—by forming complexes which contain alongside Zr other metal ions e.g. Y^{3+} or Ca^{2+}—to doped zirconia. Various complexes have been suggested and used as precursors to zirconia by calcination. Two such classes of compounds are the carbonates and oxalates. Thermal decomposition experiments [7–11] have shown that oxalate complexes of zirconium decompose via carbonates to yield ultimately oxide products.

We have synthesised three closely related zirconium carbonate complexes—$[(C(NH_2)_3)_3ZrOH(CO_3)_3 \cdot H_2O]_2$ (**A**), $[(NH_4)_3ZrOH(CO_3)_3 \cdot 2H_2O]_2$ (**C**) and $[K_3ZrOH(CO_3)_3 \cdot 3H_2O]_2$ (**D**)—during the course of our investigations. **C** [12] and **D** [13] have previously been the subject of single crystal X-ray diffraction studies. Both crystallise in the monoclinic space group $P2_1$. However, it is quite likely that subtle differences in structure may arise between **A** and the other two compounds when it is borne in mind that hydrogen bonding involving the guanidinium cation and water molecules will doubtless play an important role in **A**. We also noted from a preliminary X-ray powder diffraction study that, unlike **C** and **D**, **A** crystallises in the triclinic space group P-1. Previous comments regarding the possible structure **A** [14] have not been based upon any structural data. Indeed in proposing structures for **A**, Dervin *et al.* [14] appeared to be unaware of the earlier X-ray work performed on single crystals of **C** [12] and **D** [13] since no reference is made to these structures. Accordingly we have carried out a single crystal X-ray diffraction study of **A**. We have supported these data by an infrared spectroscopic investigation of the three compounds **A**, **C** and **D**.

Our interest in oxalato complexes of zirconium is driven partly by the scarcity of published work detailing such compounds since the pioneering work of Venables and Baskerville in 1897 [15]. There have been two single crystal X-ray diffraction studies of monomeric zirconium oxalate complexes: $K_4Zr(C_2O_4)_4 \cdot 5H_2O$ [16] and $Na_4Zr(C_2O_4)_4 \cdot 3H_2O$ [17]. Our synthesis of **B** was, however, quite fortuitous. We were attempting to follow the method of Blumental [2] for the preparation of a mixed carbonate/oxalate of zirconium. A small number of crystals were isolated which were shown to be **B** by means of a single crystal X-ray diffraction study.

EXPERIMENTAL

Compound **A** was prepared following the method described by Pospelova and Zaitsev [18]. Saturated aqueous ammonium carbonate solution (9 cm^3) and guanidinium carbonate (4 g, 0.02 mol in 10 cm^3 water) were mixed and solid zicronyl chloride (2 g, 0.01 mol) was added. The mixture was filtered to remove any solid residue and the filtrate was left in a desiccator over H_2SO_4 (conc). After a few days tiny, rod-shaped crystals formed. These were isolated by filtration. The zirconium content of **A** was found by direct calcination. C, H and N analysis was performed using a Perkin–Elmer 240B microanalyser by Medac Ltd at Brunel University. Found: Zr, 19.7%, C, 15.0%, H, 4.2%, N, 26.3%; Calc.: Zr, 19.1%, C, 15.1%, H, 4.4%, N, 26.4%.

A small number of crystals of **B** were prepared during the attempted preparation of a mixed carbonate/oxalate of zirconium following the method of Blumental [2]. "Hydrous carbonated zirconia" [18] was first prepared by adding zirconyl chloride (10 g, 0.04 mol) to sodium carbonate (5 g, 0.05 mol) in aqueous solution. The product (1 g, 0.002 mol) was dissolved in the minium of water and crystals of oxalic acid were added until the solution was saturated. The solution effervesced upon addition of the acid. The residue was filtered and the filtrate set aside. After a few days a micro-crystalline precipitate had formed together which a small quantity of needle-shaped crystals of **B**. The precipitate was found to be multicrystalline and analysis suggested that it consisted of a mixture of compounds which proved impossible to separate. This finding endorses a point made previously by Solovkin and Tsvetkova that "a characteristic feature of (the chemistry of) zirconium is the formation of precipitates of indefinite composition" [19]. The needle-shaped crystals of **B** were studied by single crystal X-ray diffraction. Unfortunately the small quantity of crystals produced did not allow any other form of analysis to be performed.

Crystal data for **A** and **B** are given in Table 1 together with refinement details. For both compounds data were collected with Mo–K_α radiation using the MAR research image plate system. The crystals were positioned at 75 mm from the image plate. Ninety-five frames were measured at 2° intervals, each with a counting time of 2 min. Data analyses were carried out with the XDS program [20]. The structures were solved by the Patterson method using the program Shelx 86 program [21]. In both cases the non-hydrogen atoms were refined anisotropically. Hydrogen atoms on the cations in **A** were included in geometric positions, but those on oxygen could not be located. Hydrogen atoms on the bridging hydroxide in **B** were located in a different Fourier map and refined independently. However, hydrogen atoms in the water molecules could not be located. The structures were then refined on F^2 using SHELXL [22]. Bond lengths and angles in the metal coordination spheres for **A** and **B** are given in Tables 2 and 3. Crystallographic data for **A** and **B** have been deposited at the Cambridge Crystallographic Database. Infrared spectra were recorded on samples of **A** in pressed KBr discs using a Perkin–Elmer model 1720-X Fourier transform spectrometer.

RESULTS AND DISCUSSION

Single crystal X-ray diffraction study of **A**

A is an ionic compound and contains $[C(NH_2)_3]^+$ cations and dimeric anions of formulation

Table 1. Crystal data and structure refinement for **A** and **B**

Empirical formula	$C_{12}H_{36}N_{18}O_{20}Zr_2$	$C_{12}H_{16}Na_6O_{33}Zr_2$
Formula weight	935.04	1008.63
Temperature (K)	293(2)	293(2)
Wavelength (Å)	0.71070	0.71073
Crystal system	triclinic	triclinic
Space group	*P*-1	*P*-1
Unit cell dimensions		
a (Å)	6.842(5)	8.094(6)
b (Å)	10.706(8)	10.984(6)
c (Å)	11.801(8)	18.409(6)
α (°)	109.08(5)	91.91(6)
β (°)	94.50(5)	96.78(6)
γ (°)	104.86(5)	109.92(6)
V (Å^3)	777.0	1523.2
Z	1	2
D_{calc} (Mg m^{-3})	1.998	2.199
Absorption coefficient (mm^{-1})	0.785	0.900
F(000)	474	996
Crystal size	0.1 × 0.1 × 0.15 mm	0.1 × 0.1 × 0.3 mm
θ range for data collection (°)	1.86 to 24.97	2.19 to 24.60
Index range	$0 < h < 7, -12 < k < 12, -12 < l < 13$	$0 < h < 9, -12 < k < 12, -21 < l < 21$
Reflections collected	2079	4241
Data/parameters	2079/247	4219/545
Goodness-of-fit on F^2	1.023	1.320
Final *R* indices [$I > 4\sigma(I)$]	$R_1 = 0.0605, wR_2 = 0.1889$	$R_1 = 0.0814, wR_2 = 0.1922$
R indices (all data)	$R_1 = 0.1184, wR_2 = 0.3098$	$R_1 = 0.1180, wR_2 = 0.2480$
Largest diff. peak and hole (e Å^{-3})	1.743 and −2.454	1.280 and −1.173

$[(ZrOH(CO_3)_3)_2]^{6-}$. The anion is the most interesting moiety in the structure and it is depicted in Fig. 1 together with the atom numbering scheme. The anion is centrosymmetric with each metal atom being bonded to two bridging OH groups and three chelating CO_3^{2-} ions. Thus the zirconium atoms are eight coordinate. The Zr—O distances formed by the bridging OH groups [2.112(8) Å (Zr—O(1)); 2.119(9) Å (Zr—O(1)*)] are shorter than those formed through zirconium-carbonate interactions. Of these latter the Zr—O bond formed with O(12) [2.162(11) Å] appears shorter than the others that span the range 2.204(9) Å [Zr—O(22)] to 2.252(10) Å [Zr—O(31)]. The structure of the anion found in **A** has been previously reported as part of a study of $(NH_4)_6[Zr(OH)(CO_3)_3]_2$ (**C**) [12]. The data reported in this earlier study are of poorer quality than are those given here. However, the Zr—O bridging distances in **C** were found to be 2.11(1) Å with the Zr—O (carbonate) distances ranging from 2.18(2) Å to 2.25(2) Å. Thus the distances from the two structure determinations are in accord. The angles in **A** subtended by the chelating carbonate groups range from 57.6(3)° [O(32)—Zr—O(31)] to 59.7(4)° [O(12)—Zr—O(11)] and these are the smallest angles subtended at the metal centre. The next smallest angle is that formed by the two bridging OH groups; an angle of 69.7(4)° is found at the metal centre and the dependent Zr—O(1)—Zr* angle is thus 110.3(4)°. The geometry of the metal coordination sphere can best be considered to be a slightly distorted dodecahedron. The Zr···Zr* distance is 3.471(2) Å which is shorter than that previously reported for **C** [3.498(2) Å] [12]. Each of the 18 hydrogen atoms from the amine groups in the three guanidinium cations form a hydrogen bond to a carbonate oxygen atom with distances ranging from 2.67(1) to 3.15(1) Å.

Single crystal X-ray diffraction study of **B**

In the unit cell of **B** there are two $Na_6[Zr(OH)(C_2O_4)_3]_2 \cdot 7H_2O$ moieties which contain the anion $[(Zr(OH)(C_2O_4)_3)_2]^{6-}$ which has no crystallographically imposed symmetry. This anion is depicted in Fig. 2 where the atom numbering scheme is also given. One of the sodium ions (Na(5)) is disordered over two sites (5A and 5B), as is the oxygen atom of one water molecule (2W). The anion, $[(ZrOH(C_2O_4)_3)_2]^{6-}$ is non-centrosymmetric. The two metal centres in the anion have similar but not identical coordination geometries. Each metal atom is eight coordinate being bonded to three chelating oxalate groups and two bridging OH anions. Thus the coordination geometries found here are similar to those seen in **A**. The Zr—O distances formed with the chelate oxalate anions range from 2.178(9) Å to 2.239(9) Å for Zr(1) and 2.185(9) Å to 2.224(8) Å for Zr(2) and cover a similar range to those formed by the

Table 2. Bond lengths (Å) and angles (°) for **A**

Zr—O(1)*	2.112(8)
Zr—O(1)	2.119(9)
Zr—O(12)	2.162(11)
Zr—O(22)	2.204(9)
Zr—O(11)	2.213(7)
Zr—O(32)	2.231(8)
Zr—O(21)	2.240(8)
Zr—O(31)	2.252(10)
O(1)*—Zr—O(1)	69.7(4)
O(1)*—Zr—O(12)	82.8(4)
O(1)—Zr—O(12)	132.5(3)
O(1)*—Zr—O(22)	95.5(4)
O(1)—Zr—O(22)	87.3(3)
O(12)—Zr—O(22)	134.6(3)
O(1)*—Zr—O(11)	98.4(4)
O(1)—Zr—O(11)	86.2(4)
O(12)—Zr—O(11)	59.7(4)
O(22)—Zr—O(11)	161.6(4)
O(1)*—Zr—O(32)	156.4(4)
O(1)—Zr—O(32)	133.9(3)
O(12)—Zr—O(32)	79.3(3)
O(22)—Zr—O(32)	86.3(4)
O(11)—Zr—O(32)	85.9(3)
O(1)*—Zr—O(21)	83.0(3)
O(1)—Zr—O(21)	134.4(4)
O(12)—Zr—O(21)	75.8(4)
O(22)—Zr—O(21)	59.0(4)
O(11)—Zr—O(21)	134.8(4)
O(32)—Zr—O(21)	77.8(3)
O(1)*—Zr—O(31)	146.0(3)
O(1)—Zr—O(31)	76.3(3)
O(12)—Zr—O(31)	123.1(4)
O(22)—Zr—O(31)	81.4(4)
O(11)—Zr—O(31)	80.3(4)
O(32)—Zr—O(31)	57.6(3)
O(21)—Zr—O(31)	122.0(4)
Zr*—O(1)—Zr	110.3(4)

*Symmetry transformations used to generate equivalent atoms:
$x, -y, -z$.

Table 3. Bond lengths (Å) and angles (°) for **B**

Zr(1)—O(2)	2.098(8)
Zr(1)—O(1)	2.122(8)
Zr(1)—O(14)	2.178(9)
Zr(1)—O(21)	2.191(9)
Zr(1)—O(34)	2.193(8)
Zr(1)—O(31)	2.202(8)
Zr(1)—O(11)	2.236(8)
Zr(1)—O(24)	2.239(9)
O(2)—Zr(1)—O(1)	67.4(3)
O(2)—Zr(1)—O(14)	99.1(3)
O(1)—Zr(1)—O(14)	80.7(3)
O(2)—Zr(1)—O(21)	95.3(3)
O(1)—Zr(1)—O(21)	80.1(3)
O(14)—Zr(1)—O(21)	149.3(3)
O(2)—Zr(1)—O(34)	148.3(3)
O(1)—Zr(1)—O(34)	144.2(3)
O(14)—Zr(1)—O(34)	88.5(3)
O(21)—Zr(1)—O(34)	93.3(4)
O(2)—Zr(1)—O(31)	139.9(3)
O(1)—Zr(1)—O(31)	72.6(3)
O(14)—Zr(1)—O(31)	76.9(3)
O(21)—Zr(1)—O(31)	74.6(3)
O(34)—Zr(1)—O(31)	71.8(3)
O(2)—Zr(1)—O(11)	78.1(3)
O(1)—Zr(1)—O(11)	130.5(3)
O(14)—Zr(1)—O(11)	70.6(3)
O(21)—Zr(1)—O(11)	139.4(3)
O(34)—Zr(1)—O(11)	75.5(3)
O(31)—Zr(1)—O(11)	134.0(3)
O(2)—Zr(1)—O(24)	79.1(3)
O(1)—Zr(1)—O(24)	132.0(3)
O(14)—Zr(1)—O(24)	139.8(3)
O(21)—Zr(1)—O(24)	69.5(3)
O(34)—Zr(1)—O(24)	75.5(3)
O(31)—Zr(1)—O(24)	129.1(3)
O(11)—Zr(1)—O(24)	69.8(3)
Zr(2)—O(2)	2.110(9)
Zr(2)—O(1)	2.111(8)
Zr(2)—O(41)	2.185(9)
Zr(2)—O(61)	2.190(8)
Zr(2)—O(54)	2.204(8)
Zr(2)—O(51)	2.211(9)
Zr(2)—O(44)	2.212(9)
Zr(2)—O(64)	2.224(8)
O(2)—Zr(2)—O(1)	67.4(3)
O(2)—Zr(2)—O(41)	118.0(4)
O(1)—Zr(2)—O(41)	76.1(3)
O(2)—Zr(2)—O(61)	77.8(3)
O(1)—Zr(2)—O(61)	140.8(3)
O(41)—Zr(2)—O(61)	139.1(3)
O(2)—Zr(2)—O(54)	82.9(3)
O(1)—Zr(2)—O(54)	84.0(3)
O(41)—Zr(2)—O(54)	141.1(3)
O(61)—Zr(2)—O(54)	74.0(3)
O(2)—Zr(2)—O(51)	138.6(3)
O(1)—Zr(2)—O(51)	78.7(3)
O(41)—Zn(2)—O(51)	73.2(3)
O(61)—Zr(2)—O(51)	121.4(3)
O(54)—Zr(2)—O(51)	70.3(3)
O(2)—Zr(2)—O(44)	77.8(3)

chelating carbonate groups [2.162(11) Å to 2.252(10) Å]. The two metal centres are linked by two OH bridges. The uncertainties in the OH distances are, as expected, large [1.0(2) Å O(1)—H(1); 0.9(2) Å O(2)—H(2)] but the hydrogen atoms were detectable. The Zr(1)—O(1) and Zr(1)—O(2) distances are 2.122(8) Å and 2.098(8) Å respectively while the related distances for Zr(2) are 2.111(8) Å [to O(1)] and 2.110(9) Å [to O(2)]. Thus all the zirconium–oxygen bridging bonds are equal and of equivalent length to the bridging bonds found in **A** [2.112(8) and 2.119(9) Å]. The zirconium–zirconium distance [3.501(1) Å] is longer than the metal–metal distance in **A** [3.471(2) Å].

The angles subtended at the metal centres by the chelating oxalate fragments range from 69.5(3)° to

Table 3.—*Continued*

O(1)—Zr(2)—O(44)	110.3(4)
O(41)—Zr(2)—O(41)	70.1(3)
O(61)—Zr(2)—O(44)	78.0(4)
O(54)—Zr(2)—O(44)	148.7(3)
O(51)—Zr(2)—O(44)	138.4(3)
O(2)—Zr(2)—O(64)	144.2(3)
O(1)—Zr(2)—O(64)	147.2(3)
O(41)—Zr(2)—O(64)	78.0(3)
O(61)—Zr(2)—O(64)	71.1(3)
O(54)—Zr(2)—O(64)	104.6(3)
O(51)—Zr(2)—O(64)	74.9(3)
O(44)—Zr(2)—O(64)	78.7(4)
Zr(2)—O(1)—Zr(1)	111.6(4)
Zr(1)—O(2)—Zr(2)	112.6(4)

71.8(3) for Zr(1) and 70.1(3)° to 71.1(3)° for Zr(2). These angles being part of five-membered rings are, as expected, larger than the angles subtended at the zirconium centres by the chelating carbonate ions in **A** which range from 57.6(3)° to 59.7(4)° and are part of four-membered rings. The geometry of the metal coordination spheres are slightly distorted dodecahedral. The five-membered oxalato chelate ligands are, within experimental error, planar while the uncertainties associated with the C—O distances are such that no significant difference was detected in the bond distances between the bonded and non-bonded C—O groups. The sodium ions are coordinated to oxygen atoms from both the oxalate groups and water molecules. The two bridging OH anions form hydrogen bonds to adjacent dimers $O(1)\cdots O(65)$ $(x-1, y, z)$ 2.75(1) Å and $O(2)\cdots O(35)$ $(x+1, y, z)$ 2.69(1) Å. In addition each water molecule forms at least two hydrogen bonds to oxygen atoms in the oxalate anions or to other water molecules.

Infrared spectroscopic study of **A**

A shows infrared absorptions at the following wavenumbers (ν/cm^{-1}): 1684 (br), 1559 (br), 1361 (s), 1318 (m), 1303 (m), 1051 (w), 1036 (w), 1008 (w), 945 (w), 858 (w), 847 (m), 783 (m), 758 (s), 690 (w), 622 (vw), 554 (br) and 355 (m). Features are also seen in the regions 1680–1720 cm^{-1} [attributable to ν(C—N) vibrations] and 2900–3600 cm^{-1} [attributable to ν(C—H), ν(O—H) and ν(N—H) vibrations]. However, bands in these last two regions were

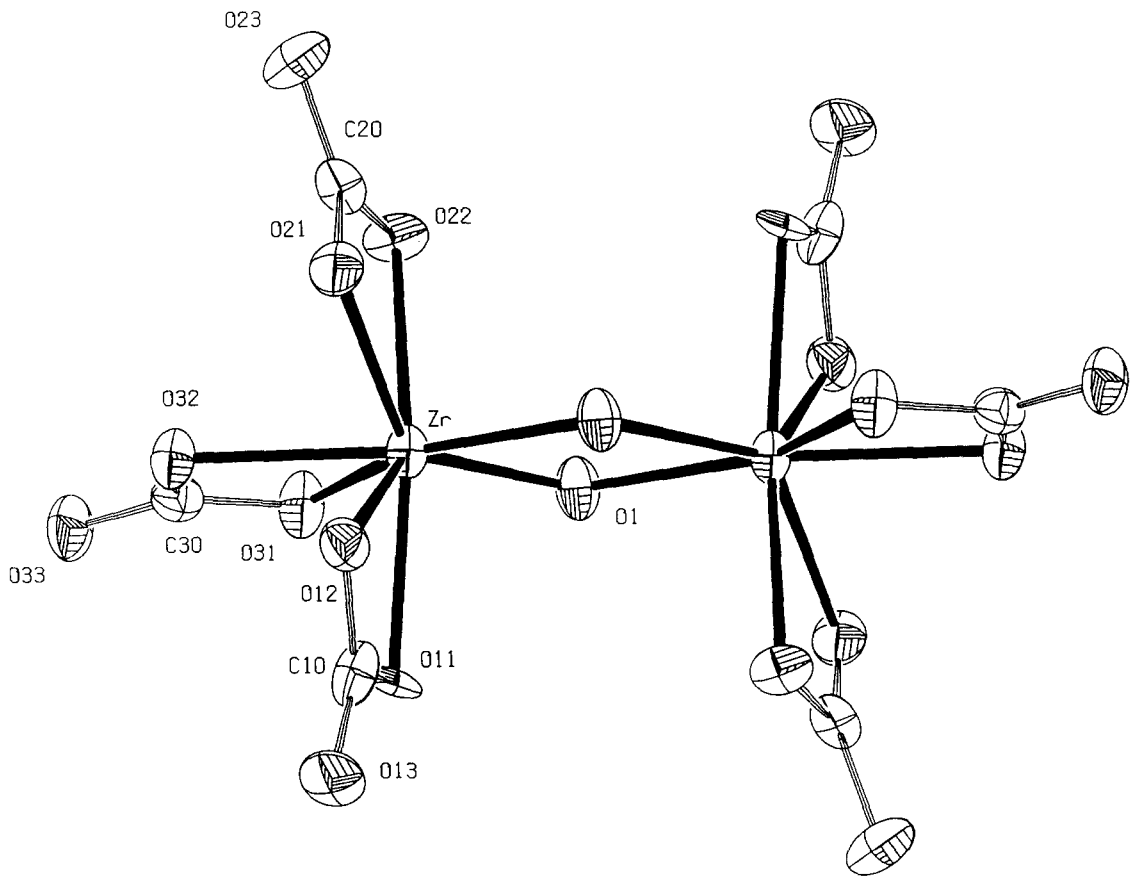

Fig. 1. The $[(ZrOH(CO_3)_3)_2]^{6-}$ anion showing the atomic numbering scheme. Ellipsoids are shown at 50% probability.

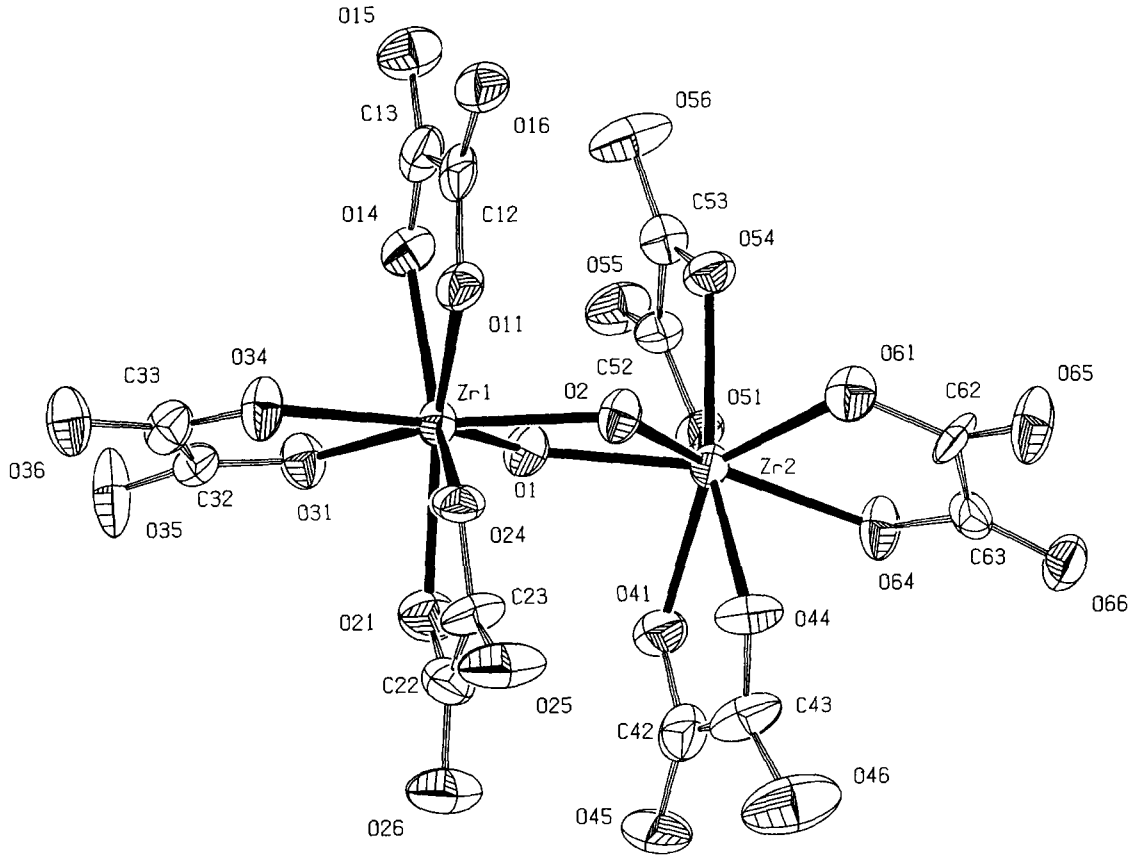

Fig. 2. The $[(ZrOH(C_2O_4)_3)_2]^{6-}$ anion showing the atom numbering scheme. Ellipsoids are shown at 50% probability.

extremely broad and its is difficult to make a detailed analysis or to draw definite conclusions from them. Some points of interest emerge, however, from the infrared data which is listed above, although the situation is necessarily complicated by overlapping of bands and by coupling of vibrations within the molecule. It is possible to distinguish between bands arising from the guanidinium cation or from the anion by a comparison of the spectrum of **A** with spectra of the related compounds **C** and **D** which contain the same anion [12,13]. In order to allow a direct comparison between the infrared spectra of **A, C** and **D** spectra of **C** and **D** were recorded as part of our study under identical conditions used for obtaining the spectrum of **A**. Vibrations which arise from the anion give rise to bands in very similar positions in the spectra of each of the three compounds. The bands of **A** at 1559, 1318 and 1051 cm^{-1} may thus be assigned to stretching vibrations of the coordinated carbonato groups (**C** shows corresponding bands at 1559, 1330 and 1050; **D** at 1560, 1324 and 1048 cm^{-1}). The position of these bands is typical of *chelating* CO_3^{2-} [23,24]. In particular the presence of one higher frequency mode (in **A** at 1559 cm^{-1}) allows an assignment to be made to chelating bidentate as opposed to monodentate CO_3^{2-} [23,24]. The feature at 1008 cm^{-1} most probably arises from the Zr—O(H)—Zr bending mode. **C** and **D** show corresponding features at 997 and 1004 cm^{-1} respectively. This vibration has been found to occur typically in the range ca 950–1000 cm^{-1} for a wide range of complexes [23,25], although Tarte has reported values from 677 to 1000 cm^{-1} for a number of copper compounds [26]. The combination of infrared spectroscopic and single crystal X-ray diffraction data allow us to confirm that compounds **A, C** and **D** have similar structures, although in **A** and **C** (but not **D**) the structure is somewhat complicated by the presence of hydrogen bonding involving the guanidinium (**A**) or ammonium (**C**) cations and water molecules.

Acknowledgements—We are grateful to Cookson's Ltd., Yarnton, Oxon., U.K. and SERC for the provision of a CASE award for S.M. We thank the Rotary Club of Caversham, Berks., U.K. and Sun Microsystems for financial help in supporting a visit of Y.Z. from the Russian Academy of Sciences, Moscow, Russia during which this work was completed.

REFERENCES

1. Singer, F. and German, W. L., *Ceramic Glasses*. Borax Consolidated, London, 1960.

2. Blumenthal, W. B., *The Chemical Behavior of Zirconium*. Van Nostrand, New Jersey, 1958.
3. Heuer, A. H. and Hobbs, L. W., eds, *Advances in Ceramics*, 1984, **3**, 1
4. Greenwood, N. N. and Earnshaw, A., *Chemistry of the Elements*. Pergamon, Oxford, 1984.
5. McDougall, A., *Fuel Cells*. Macmillan, London, 1976.
6. Liebhasky, H. A. and Cairns, E. J., *Fuel Cells and Fuel Batteries*. J. Wiley, New York, 1968.
7. Gangadevi, T., Subba Row, M. and Kutty, T. R. N., *Ind. J. Chem.*, 1980, **19A,** 303, 309.
8. Gangadevi, T., Muraleedharan, K. and Kannan, M. P., *Thermochim. Acta*, 1989, **144,** 109.
9. Sheinkman, A. P., Yunusova, N. V., Osachev, V. P. and Kondrashenkov, A. A., *Russ. J. Inorg. Chem.*, 1974, **19,** 206.
10. Gangadevi, T., Muraleedharan, K. and Kannan, M. P., *Thermochim. Acta*, 1989, **146,** 225.
11. Gangadevi, T., Muraleedharan, K. and Kannan, M. P., *Thermochim. Acta*, 1991, **191,** 105.
12. Clearfield, A., *Inorg. Chim. Acta*, 1970, **3,** 166.
13. Gorbunova, Y. E., *Zh. Stukt. Khim.*, 1968, **9,** 918.
14. Dervin, J., Faucherre, J. and Prusek, H., *Rev. Chim. Min.*, 1974, **11,** 372.
15. Venables, F. P. and Baskerville, C., *J. Am. Chem. Soc.*, 1897, **19,** 13.
16. Kojic-Prodic, B., Ruzic-Toros, Z. and Sljukic, M., *Acta Cryst.*, 1978, **B34,** 2001.
17. Glen, G. L., Silverton, J. V. and Hoard, J. L., *Inorg. Chem.*, 1963, **2,** 250.
18. Pospelova, L. A. and Zaitsev, L. M., *Russ. J. Inorg. Chem.*, 1966, **11,** 996.
19. Solovkin, A. S. and Tsvetkova, S. V., *Russ. Chem. Rev.*, 1962, **31,** 655.
20. Kabsch, W., *J. Appl. Cryst.*, 1988, **21,** 916.
21. Sheldrick, G. M., SHELX86, *Acta Cryst.*, 1990, **A46,** 467.
22. Sheldrick, G. M., SHELXL93, program for crystal structure refinement, University of Gottingen.
23. Nakamoto, K., *Infrared and Raman Spectra of Inorganic and Coordination Compounds*, 4th edn, J. Wiley, New York, 1986.
24. Fujita, J., Martell, A. E. and Nakamoto, K., *J. Chem. Phys.*, 1962, **36,** 339.
25. Scargill, D., *J. Chem. Soc.*, 1961, 4444.
26. Tarte, P., *Spectrochim. Acta*, 1958, **13,** 107.

Pergamon

PII: S00277-5387(98)0005-9

Polyhedron Vol. 17, Nos 13-14, pp. 2309-2311, 1998
© 1998 Elsevier Science Ltd
All rights reserved. Printed in Great Britain
0277-5387/98 $19.00 + 0.00

A new argument in favor of the ether elimination mechanism: formation of acetals on action of molybdenum alkoxides on carbonyl compounds

Vadim G. Kessler,*[a] Kirill V. Nikitin[b] and Alexandr I. Belokon'[c]

[a] Department of Chemistry, Swedish University of Agricultural Sciences, Box 7015, S-75007, Uppsala, Sweden

[b] Department of Chemistry, Lomonosov Moscow State University, 119899, Moscow, Russia

[c] A. N. Nesmeyanov Institute of Organoelement compounds, 117813, Moscow, Russia

(Received 15 August 1997; accepted 18 December 1997)

Abstract—Molybdenum oxomethoxide and ethoxide are found to react very rapidly with aldehydes and ketones in both alcohol and hydrocarbon media transforming the latter into acetals and ketals respectively. The colloid solution of the molybdenum blue usually formulated as "$MoO_{2.88} \cdot H_2O$" appears to be the major inorganic product of this reaction. The reaction mechanism includes presumably formation of a semiacetal molybdate and its subsequent decomposition with elimination of acetal. Different reaction pathways of metal alkoxides interaction with aldehydes and ketones are discussed. © 1998 Elsevier Science Ltd. All rights reserved

Keywords: acetals; molybdenum alkoxides; carbonyl compounds.

The interest in the mechanistic aspects of metal alkoxides transformation into oxoalkoxides and finally into oxides has risen during the last decade, on one hand, by the prospect of their practical application as precursors of oxide materials in sol-gel and MO CVD processes, and, on the other, by the tremendous increase in both crystallographic and synthetic data available, showing the occurrence of a large variety of transformation pathways beyond hydrolysis or radical pyrolysis, considered traditionally to be the main routes of this conversion [1,2]. The trend to achieve better control over the structure and stoichiometry of the products prepared urged the development of already a series of approaches to non-hydrolytic sol-gel processes, such as cocondensation with metal halides or carboxylic acid salts, accompanied by alkyl halide [3] or ester [4] elimination respectively. In the case of pure metal alkoxides there are two different non-redox transformation pathways evidenced so far, the first of them being the ether elimination reaction that was found to be characteristic of niobium [5,6], and molybdenum and tungsten alkoxides [7,8] and simultaneous elimination of alkene and alcohol observed for the derivatives of zirconium and hafnium [9,10] and also tin and lead alkoxides [10]. The mechanism of the first of these processes was proposed by D. C. Bradley [5]:

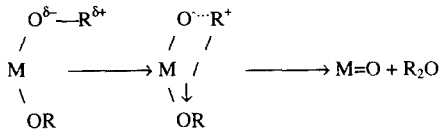

and included at the first step the charge redistribution and formation of a carbocation. The analogous mechanism was recently proved experimentally by J. A. Osborn [11] to be true for molybdenum allyloxides structural rearrangements.

In the course of our recent studies of anodic oxidation of molybdenum and tungsten in alcohols [12], we observed formation of mainly oxo-derivatives and found the oxidation of alcohol with formation of aldehyde or ketone to be an important side reaction. However, when the molybdenum dissolution was carried out in ethanol it was not acetaldehyde but its diacetal

* Author to whom correspondence should be addressed.

Table 1. Interaction of alkoxides (5 mmol) with carbonyl compounds (10 mmol) in 10 ml of solvent at 20°C

Alkoxide	Carbonyl compound	Solvent	Reaction time	Yields of reaction products, %
$MoO(OEt)_4$	CH_3CHO	EtOH	2 min	$CH_3CH(OEt)_2$,96
$MoO(OMe)_4$	$(CH_3CHO)_3$	PhMe	1 min	$CH_3CH(OMe)_2$,73; $CH_3CHOMeOH$,24
$MoO(OMe)_4$	CH_3COCH_3	EtOH	2 h	$(CH_3)_2C(OEt)_2$,62; $(CH_3)_2COEtOH$,36
$Ti(OEt)_4$	CH_3CHO	EtOH	8 h	$CH_3CH(OEt)_2$,12; $CH_3CH{=}CHCHO$,20
$MoO(OMe)_4$	PhCHO	EtOH	10 min	$PhCH(OEt)_2$, 28 $CH_3CH(OEt)_2$,25 PhCHOEtOH,8 $PhCH_2OEt$, 8

that was isolated. We decided, therefore to study the interaction of molybdenum alkoxides with different aldehydes and ketones to prove if the action of the former is catalytical or it undergoes a quantitative transformation and to determine the nature of the latter.

The choice of the possible molybdenum reagents was limited due to the practical reasons, e.g. the isopropoxides in both homological series—$MoO(OR)_4$ and $MoO_2(OR)_2$ decompose on storage due to redox transformations [13–14], while stable $MoO_2(OR)_2$ (R = Me, Et) have poor solubility; and therefore the prospects of practical application of any kind are open only for methoxide and ethoxide of monooxo series, $MoO(OR)_4$.

The synthesis of molybdenum alkoxides—$MoO(OMe)_4$ and $MoO(OEt)_4$ was carried out in inert atmosphere according to techniques described in literature [3,8]. All the operations connected with investigation of reactivity were carried out in ambient atmosphere but as quickly as possible. Anhydrous solvents (ethanol, toluene, acetone) for reactivity investigations were purchased from Merck (dried, for analysis grade) and used without further purification. For each experiment a measured quantity of molybdenum alkoxide (about 5 mmol in each case) was dissolved in 10 ml of solvent, and then to the solution obtained was added a double quantity of carbonyl compound and the mixture was subjected to vigorous stirring. The reaction speed was monitored following the color changes from yellow, via colorless to dark blue corresponding to transformation of $MoO(OR)_4$ into $MoO_2(OR)_2$ and finally $MoO_{2.88}\cdot H_2O$, which is usually observed in the course of ether elimination reaction [15]. On storage for several weeks the dark blue sediment precipitated, revealing the powder pattern of $MoO_{2.88}\cdot H_2O$ (registered using DRON-3M powder diffractometer). GLC-MS studies of the organic products, separated by vacuum distillation at 50–60°C into a vessel refrigerated by liquid nitrogen, were carried out using a Kratos MS-890 device (source temperature 200°C, SE-30 column).

We have found that the action of molybdenum alkoxides, namely $MoO(OMe)_4$ and $MoO(OEt)_4$ transforms the carbonyl compounds into acetals and ketals respectively (Table 1).

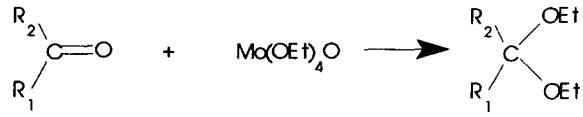

Thus acetaldehyde in solution in ethanol gives ethylal in quantitative yields already after 10 min. Reaction of $MoO(OMe)_4$ with trimers of acetaldehyde in hydrocarbons gives mainly dimethylacetal. Titanium ethoxide, which activity was also tested under analogous conditions gives in its turn only 12% of acetal, promoting aldol condensation as a parallel reaction. Acetone reacts much slower with $MoO(OMe)_4$ in EtOH giving semiketal $(CH_3)_2COH(OEt)$ in considerable amounts. Transformation of benzaldehyde is complicated by its reduction into benzyl alcohol with subsequent formation of benzyl acetal.

The reaction mechanism includes, presumably, quick formation of semiacetal and its rapid exchange with the inner co-ordination sphere of the alkoxide molecule. The other possibility of formation of a mixed-ligand derivative is provided by coordination of the molecule of carbonyl compound by the alkoxide, being a Lewis acid, with subsequent transfer of one OR-group to the carbon atom of the carbonyl group (the latter pathway appears to be more probable in the hydrocarbon media). The mixed alkoxide thus formed undergoes acetal elimination analogous to the ether elimination described in literature.

The reaction needs therefore neither basic nor acidic catalysis (which is usually required for the formation of acetals [16]) and proceeds under rather mild conditions. In an alcohol-free media the reaction occurs, presumably, via formation of a semiacetal derivative via addition of aldehyde to the molecule of initial alkoxide; the second step in this case is the same as that in the alcohol. Molybdenum alkoxides are thus undergoing a quantitative transformation into a colloid oxide product.

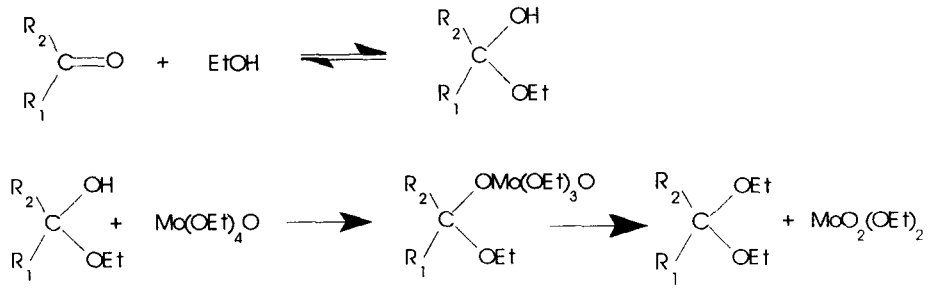

The condensation of metal alkoxides on action of carbonyl compounds, namely, aceton, has been earlier described in literature for zinc [17] and titanium [18] alkoxides. It was supposed then that the non-hydrolytic condensation proceeded solely due to formation of intermediate enolate compounds and an intermediate oxo-enolate of $Ti_3(\mu_3\text{-}O)_2(O^iPr)_5(OCMe{=}CH_2)_3(^iPrOH)$ really was isolated in the latter case, but the results of the present work permit to suppose that it might not be the only reaction pathway for this kind of transformation.

REFERENCES

1. Hubert-Pfalzgraf, L. G., *New J. Chem.*, 1987, **11,** 663.
2. Caulton, K. G. and Hubert-Pfalzgraf, L. G., *Chem. Rev.*, 1990, **90,** 969.
3. Andrianainarivelo, M., Corriu, R. J. P., Leclercq, D., Mutin, P. H. and Vioux, A., *J. Sol-Gel Sci. Tech.*, 1997, **8,** 89.
4. Caruso, J. and Hampden-Smith, M., *J. Sol-Gel Sci. Tech.*, 1997, **8,** 35.
5. Bradley, D. C., Chakravarti, B. N. and Wardlaw W. J., *Chem. Soc.*, 1956. **11,** 4439.
6. Kessler, V. G., Turova, N. Ya., Yanovskii, A. I., Belokon', A. I. and Struchkov, Yu. T., *Russ. J. Inorg. Chem. (Engl)*, 1991, **36,** 938.
7. Turova, N. Ya., Kessler, V. G. and Kucheiko, S. I. *Polyhedron*, 1991, **10,** 2617.
8. Turova, N. Ya. and Kessler, V. G., *Russ. J. General Chem. (Engl)* 1990, **60,** 99.
9. Turevskaya, E. P. Kozlova, N. I. Turova, N. Ya. Belokon', A. I. Berdyjev, D. V. Kessler, V. G. and Grishin, Yu. K., *Bull. Russ. Acad. Sci. (Russ), Chem. Ser.*, **1995,** 752.
10. Teff, D. J., Huffman, J. C. and Caulton, K. G., *J. Am. Chem. Soc.*, 1996, **118,** 4030.
11. Belgacem, J., Kress, J. and Osborn, J. A., *J. Am. Chem. Soc.*, 1996, **114,** 1501.
12. Kessler, V. G., Panov, A. N., Turova, N. Ya., Pisarevsky, A. P., Starikova, Z. A., Yanovsky, A. I. and Struchkov, Yu. T., *J. Chem. Soc., Dalton Trans.*, 1998, (submitted).
13. Chisholm, M. H., Huffman, J. C., Folting, K. and Kirkpatric, C. C., *Inorg. Chem.* 1984, **23,** 1021.
14. Kessler, V. G., Shevelkov, A. V. and Bengtsson-Kloo, L. A., *Polyhedron*, 1997, **16,** (in press).
15. Yanovskaya, M. I., Obvintseva, I. E., Kessler, V. G., Galyamov, Sh., Kucheiko, S. I., Shifrina, R. R. and Turova, N. Ya., *J. Non-Cryst. Solids*, 1990, **124**(1), 155.
16. Buehler, C. A. and Pearson, D. E., *Survey of Organic Synthesis*, J. Wiley and Sons, New York, 1970.
17. Goel, S. C., Chang, M. Y., Gibbons, P. C. and Buhro, W. E., *Mater. Res. Soc. Proc.* 1992, **271,** 3.
18. Hubert-Pfalzgraf, L. G., Daniele, S., Decams, J. M. and Vaisserman, J., *J. Sol-Gel Sci. Tech.*, 1997, **8,** 49.

Pergamon

PII: S0277-5387(97)00534-2

Polyhedron Vol. 17, Nos 13–14, pp. 2313–2319, 1998
© 1998 Elsevier Science Ltd
All rights reserved. Printed in Great Britain
0277-5387/98 $19.00+0.00

Electron transfer between nickel(IV) oxime-imine complexes and nitrite: kinetics and mechanism

Amitava Dutta, Santanu Bhattacharya and Pradyot Banerjee*

Department of Inorganic Chemistry, Indian Association for the Cultivation of Science, Calcutta 700 032, India

(Received 1 October 1997; accepted 17 December 1997)

Abstract—The oxidation of nitrite ion by two nickel(IV) oxime-imine complexes, $[Ni^{IV}(L^1)]^{2+}$ and $[Ni^{IV}(L^2)_2]^{2+}$ (where H_2L^1 = 3,14-dimethyl-4,7,10,13-tetraazahexadeca-3,13-diene-2,15-dione dioxime and HL^2 = 6-amino-3-methyl-4-azahex-3-en-2-one oxime) has been investigated in aqueous perchlorate medium in the range pH 4.50–7.00 by UV–vis spectrophotometry. The reduction of $[Ni^{IV}(L^2)_2]^{2+}$ involves 2 e^- transfer (one-step) path at pH $\leqslant$ 6.0 and above this, it shows biphasic steps involving Ni^{III} as intermediate. The reduction of $[Ni^{IV}(L^1)]^{2+}$ is, however, biphasic in nature throughout the whole range of pH studied. The reaction rate exhibits a notable dependence on the product Ni^{II} complex added externally. The experimental findings and the low value of the calculated ion-pair constant suggest that the mode of electron transfer is likely to be of outer-sphere type.
© 1998 Elsevier Science Ltd. All rights reserved

Keywords: electron transfer; UV–vis spectrophotometry; nickel(IV) oxime-imine complexes; nitrite.

The interaction of small nitrogen containing species, e.g., nitrite with metal complexes is not only of importance for developing reductase models, but also of interest in a number of other areas. The effective use of nitrite for the contribution of certain types of microbes [1] as well as the prevention of corrosion in iron and steel by nitrite is well documented in literature [2–5]. The electron transfer chemistry of nitrite is thereby worth pursuing. In recent times a number of papers have appeared from our laboratory using nickel(IV) and nickel(III) oxime-imine complexes as oxidants [6–9]. This has been substantiated by a review which encompasses the electron transfer reactions of various types of nickel(III) and nickel(IV) complexes published during the period 1981–1997 [10]. The study of the reaction of nitrite ion with these types of nickel(IV) complexes, $[Ni^{IV}(L^1)]^{2+}$ and $[Ni^{IV}(L^2)_2]^{2+}$ (where H_2L^1 = 3,14-dimethyl-4,7,10,13-tetraazahexadeca-3,13-diene-2,15-dione dioxime (**1**) and HL^2 = 6-amino-3-methyl-4-azahex-3-en-2-one oxime (**2**) appears to be a fertile endeavor with regard to mechanistic chemistry. The system may turn out as a possible model for the oxidation of nitrite to nitrate in biological system.

* Author to whom correspondence should be addressed.

EXPERIMENTAL

Materials

The complexes $[Ni^{IV}(L^1)]^{2+}$ and $[Ni^{IV}(L^2)_2]^{2+}$ (also designated as $[Ni^{IV}(L_y)]^{2+}$) were prepared, characterised and standardised by the method reported earlier [11,12]. Sodium nitrite was purchased from Aldrich and its purity was initially checked by the OCl^- oxidation method as reported earlier [13]. The solutions were prepared by dissolving exact amount of the reagents in doubly distilled water. The solutions were deaerated by bubbling dinitrogen through them. The pH of the solutions was measured in a Systronics digital pH meter (μ-pH system 361, India). High purity perchloric acid, reagent-grade (recrystallised) sodium acetate and sodium dihydrogen phosphate were used as buffers to adjust the pH of the reaction solutions.

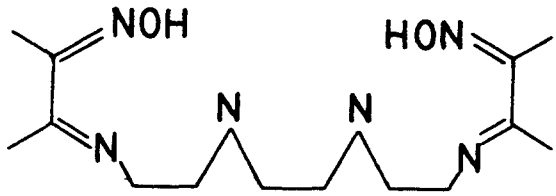

H_2L

(1)

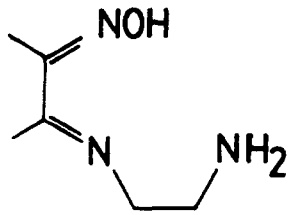

HL^2

(2)

Methods

All the kinetic runs were followed spectrophotometrically at 500 nm and 505 nm, λ_{max} for $[Ni^{IV}(L^1)]^{2+}$ and $[Ni^{IV}(L^2)_2]^{2+}$ respectively ($\varepsilon^{500}_{max} = 6300$ dm^3 mol^{-1} cm^{-1} and $\varepsilon^{505}_{max} = 6100$ dm^3 mol^{-1} cm^{-1}) maintaining pseudo-first-order conditions with large excess of nitrite ion concentration over the oxidants. The measured pH was calculated in terms of the activity of the hydrogen ion. The hydrogen ion concentration was calculated by using the following relationship [14]

$$[H^+] = 10^-[(pH-0.131)/0.982]$$

where 0.131 is the factor due to ligand junction potential between the glass electrode and the solution, and 0.982 denotes the activity coefficient in the reaction medium. Kinetic measurements were monitored using a Shimadzu (Japan) UV–vis 2100 spectrophotometer. The temperature of the reaction medium was maintained within the limit ± 0.1°C by a Haake F-3 thermostat.

RESULTS

The stoichiometries of the reactions for both the oxidants with nitrite were determined by reacting varied concentrations of nitrite with a measured excess of the oxidants at a constant ionic strength, $I = 0.2$ mol dm^{-3} ($NaClO_4$) and pH 4.75. After the completion of the reaction, the excess unreacted $[Ni^{IV}(L_x)^{2+}]$ were measured spectrophotometrically. The ratio of the moles of Ni^{IV} consumed to moles of nitrite consumed was found to be 1.02 ± 0.02. These results agree with the overall reaction

$$[Ni^{IV}(L_x)]^{2+} + NO_2^- + H_2O \rightarrow [Ni^{II}(L_x)] + NO_3^- + 2H^+ \quad (1)$$

A single step 2 e$^-$ transfer path occurs in the range $4.5 \leqslant pH \leqslant 6.0$ for the reduction of $[Ni^{IV}(L^2)_2]^{2+}$ and then the reduction up to pH 7.0 becomes biphasic in nature. In the case of $[Ni^{IV}(L^1)]^{2+}$ a distinct biphasic 1 e$^-$ transfer reduction occurs throughout the experimental pH range (pH 4.5–7.0). In the biphasic reactions for both the oxidants,the initial faster step corresponds to the conversion of $Ni^{IV} \rightarrow Ni^{III}$ followed by a relatively slower decay of $Ni^{III} \rightarrow Ni^{II}$. In the case of the monophasic reduction for $[Ni(L^2)_2]^{2+}$ in the range $4.5 \leqslant pH \leqslant 6.0$, $Ni^{IV} \rightarrow Ni^{III}$ conversion is rate determining followed by a very fast reduction of $Ni^{III} \rightarrow Ni^{II}$ showing an overall single step 2 e$^-$ transfer process. For $[Ni^{IV}(L^2)_2]^{2+}$, the plots of–log A_t vs t (where A_t is the absorbance at time t) for the single step 2 e$^-$ transfer process were linear up to ca 80% of the total reaction indicating first-order dependence of the reaction rate on $[Ni^{IV}(L^2)_2{}^{2+}]$. In the case of biphasic reaction traces, the first phase accounted for 30–40% of the observed absorbance change and the reactions proceeded to 95–100% yield of the product. For the two consecutive steps, the absorbance vs time curves were successfully treated in terms of two first-order reactions and values of k^I_{obs} ($Ni^{IV} \rightarrow Ni^{III}$) and k^{II}_{obs} ($Ni^{III} \rightarrow Ni^{II}$) were obtained from the initial and the final slopes (clearly distinct) of the plots of $-\log A_t$ vs t.

Dependence on nitrite ion concentration

The dependence of observed rates (k_{obs}) on reductant concentrations were investigated at pH 6.0 for $[Ni^{IV}(L^1)]^{2+}$ and at pH 4.5 and 6.5 for $[Ni^{IV}(L^2)_2]^{2+}$ under the following conditions, $[Ni^{IV}(L_x)^{2+}] = 5.0 \times 10^{-5}$ mol dm^{-3}, $I = 0.20$ mol dm^{-3} ($NaClO_4$), temperature 30°C, [Buffer] = 0.02 mol dm^{-3} (acetate or phosphate as required), [ ] = 0.01–0.09 mol dm^{-3} for $[Ni^{IV}(L^1)]^{2+}$ and 0.001–0.01 mol dm^{-3} and 0.01–0.10 mol dm^{-3} for $[Ni^{IV}(L^2)_2]^{2+}$, pH 4.5 and 6.0 respectively. The plots of k_{obs} vs $[NO_2^-]^2$ were straight lines with positive intercepts indicating a second-order dependence of reaction rate on $[NO_2^-]$. The rate law can thereby be expressed as

$$-d/dt[Ni^{IV}(L_x)^{2+}] = k[Ni^{IV}(L_x)^{2+}][NO_2^-]^2 + k_d[Ni^{IV}(L_x)^{2+}]$$
$$= (k[NO_2^-]^2 + k_d)[Ni^{IV}(L_x)^{2+}] \quad (2)$$

where k_d is the auto redox-decomposition rate constant of the respective oxidant at 30°C and $I = 0.20$ mol dm^{-3} ($NaClO_4$). This auto-decomposition to Ni^{II} complex may occur by the withdrawal of imino-hydrogen atom by OH^- of the medium, thereby causing transference of the electron from $N^- \rightarrow Ni^{IV}$. This auto-decomposition rate constants for both the oxidants are found to be pH dependent [15]. At 30°C and $I = 0.20$ mol dm^{-3} ($NaClO_4$) with $[Ni^{IV}] = 5.0 \times 10^{-5}$ mol dm^{-3} k_d varies from 5.40×10^{-6} s^{-1} to 7.20×10^{-4} s^{-1} in our experimental pH range. While calculating the actual k_{obs} values, the auto-decomposition of the complexes at each pH were taken into account. Subtracting the k_d value from the calculated k_{obs} value, we get the actual k_{obs} value and then the k_{obs} vs $[NO_2^-]^2$ plots for both the oxidants give straight lines passing through the origin (Table 1) leading to Eqn (2a)

$$-d/dt[Ni^{IV}(L_x)^{2+}] = k[Ni^{IV}(L_x)^{2+}][NO_2^-]^2 = k_{obs}[Ni^{IV}(L_x)^{2+}] \quad (2a)$$

Dependence on pH

The effect of acidity on the reaction rate was verified in the range pH 4.5–7.0 at $[NO_2^-] = 0.09$ mol dm^{-3} and 0.08 mol dm^{-3} for $[Ni^{IV}(L^1)]^{2+}$ and $[Ni^{IV}(L^2)_2]^{2+}$ respectively. The buffer used up to pH 6.0 was NaOAc–HOAc. Buffering at pH > 6.0 was maintained by Na_2HPO_4–NaH_2PO_4. The pH was adjusted by addition of small amounts of a 0.1 mol dm^{-3} perchloric acid solution. Throughout the experimental pH region, the rate of reaction was found to be independent (within ±4% error) of pH for both the oxidants.

Table 1. Pseudo-first-order rate constants for the oxidation of nitrite by $[Ni^{IV}(L^1)]^{2+}$ and $[Ni^{IV}(L^2)_2]^{2+}$ at two different pHs at 30°C, $I = 0.20$ mol dm^{-3} ($NaClO_4$), $[Ni^{IV}] = 5.0 \times 10^{-5}$ mol dm^{-3}, [buffer] = 0.02 mol dm^{-3} (acetate or phosphate)

Oxidants	$[NO_2^-]$/ mol dm^{-3}	$10^4 k_{obs}$/s^{-1} pH 4.5[c]	pH 6.0[d]	
$[Ni^{IV}(L^1)]^{2+}$	0.01		0.30[a]	0.02[b]
	0.03		0.94[a]	0.06[b]
	0.05		2.89[a]	0.17[b]
	0.07		4.76[a]	0.25[b]
	0.08		6.81[a]	0.35[b]
	0.09		8.31[a]	0.42[b]
$[Ni^{IV}(L^2)_2]^{2+}$	0.001	0.10		
	0.003	0.62		
	0.005	1.50		
	0.007	2.97		
	0.01	5.80	4.0[a]	0.10[b]
	0.03		6.21[a]	0.57[b]
	0.05		15.2[a]	1.52[b]
	0.07		26.3[a]	2.45[b]
	0.08		35.0[a]	3.35[b]
	0.09		56.5[a]	5.23[b]

[a] For $Ni^{IV} \rightarrow Ni^{III}$.
[b] For $Ni^{III} \rightarrow Ni^{II}$.
[c] Acetate buffer.
[d] Phosphate buffer.

Effect of buffer

To see the effect of the buffer components on the reaction rate, the kinetics were monitored at pH 5.0 and 6.5 with the varied concentrations of respective buffers (0.005–0.05 mol dm^{-3}) for both the complexes leaving other conditions same as those for pH variation studies. The reaction rates remain unaltered (within ±3% error) indicating that the buffer species do not have any significant interaction with the redox active nickel complexes.

Effect of metal ions

To test for the effect of trace metal ions (Cu^{2+} or Fe^{2+} etc.) on the reaction rate, experiments were conducted by adding phenanthroline (1.0×10^{-4} mol dm^{-3}) externally to the reaction mixture at pH 4.5 leaving other reaction conditions intact. Since no effect was observed, it is concluded that these metal ions are not present in sufficient amounts to effect the reaction rate.

Effect of Ni^{II} (product complex) added externally

A complicated reaction occurs in the presence of $[Ni^{II}(H_2L^1)]^{2+}$ or $[Ni^{II}(HL^2)_2]^{2+}$ (designated as Ni^{II}) added externally. A rapid increase of absorbance takes place initially (Fig. 1) followed by a steady decrease in absorbance with time. With the increase of added $[Ni^{II}]_0$ at a fixed $[NO_2^-]$, the rate of reduction ($Ni^{IV} \rightarrow Ni^{II}$) becomes slower (Fig. 3). Under pseudo-first-order conditions as stated before, in the presence of a large excess Ni^{II} over the Ni^{IV} complexes, a plot of $(A_t)^{-1}$ vs t shows linearity up to ca 80% of the total reactions indicating a second-order dependence of rate on $[Ni^{IV}]$ (Fig. 2). The reaction is also second-order with respect to $[NO_2^-]$. Variation of $[H^+]$ was found to have no effect on the reaction rate. The variation of $[Ni^{II}]_0$ (3.0×10^{-3}–3.0×10^{-4} mol dm^{-3}) added externally shows an inverse first-order dependence in initial $[Ni^{II}]_0$ (Fig. 3). These results point to a different mechanism operative under these conditions.

DISCUSSION

The monophasic ($Ni^{IV} \rightarrow Ni^{II}$) and biphasic ($Ni^{IV} \rightarrow Ni^{III}$, $Ni^{III} \rightarrow Ni^{II}$) nature of reactions in the reduction of the Ni^{IV} complexes concerned at lower and higher pH respectively can be understood on the

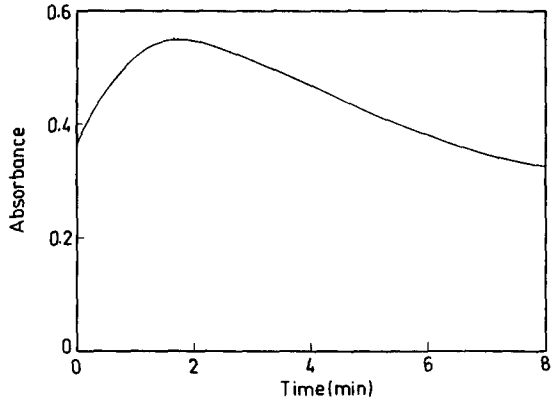

Fig. 1. Change of absorbance with time for the reaction between $[Ni^{IV}(L^1)]^{2+}$ and nitrite in presence of $[Ni^{II}]_0$ at 500 nm. The conditions adopted are: $[Ni^{IV}] = 5.0 \times 10^{-5}$ mol dm^{-3}, $[NO_2^-] = 0.01$ mol dm^{-3}, $[Ni^{II}]_0 = 5.0 \times 10^{-4}$ mol dm^{-3}, $I = 0.20$ mol dm^{-3} ($NaClO_4$), pH = 4.5, [acetate] = 0.02 mol dm^{-3} and temp. = 30°C.

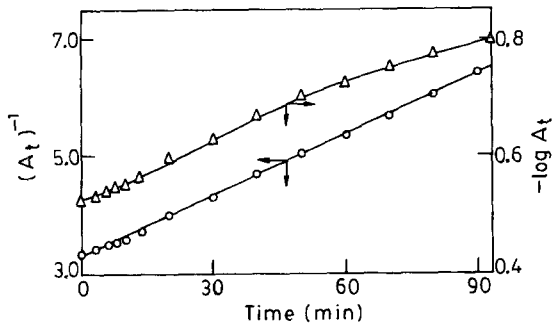

Fig. 2. Plots of (a) $(A_t)^{-1}$ vs time and (b) $-\log A_t$ vs time for the reaction between $[Ni^{IV}(L^2)_2]^{2+}$ and nitrite in presence of $[Ni^{II}]_0$ at 505 nm. Other conditions remain the same as in Fig. 1.

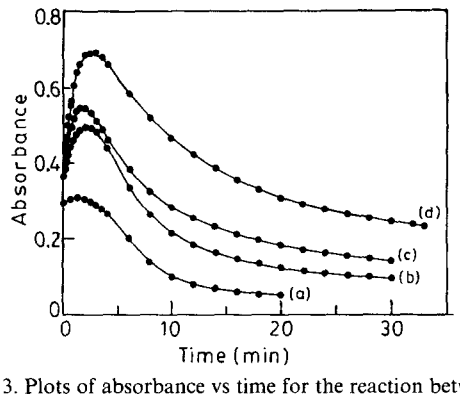

Fig. 3. Plots of absorbance vs time for the reaction between $[Ni^{IV}(L^2)_2]^{2+}$ and nitrite in presence of varying $[Ni^{II}]_0$ at 505 nm (a) $[Ni^{II}]_0 = 1.0 \times 10^{-4}$ mol dm^{-3}; (b) $[Ni^{II}]_0 = 3.0 \times 10^{-4}$ mol dm^{-3}; (c) $[Ni^{II}]_0 = 5.0 \times 10^{-4}$ mol dm^{-3}; (d) $[Ni^{II}]_0 = 7.0 \times 10^{-4}$ mol dm^{-3}. Other conditions are the same as in Fig. 1.

basis of the expected greater proton affinity of Ni^{II} complexes compared to that of Ni^{III} and Ni^{IV} species and also from the E^0 values of the couples present as discussed in our earlier papers [7,8]. Since at low pH E^0_{298} $[Ni^{IV}$–$Ni^{III}] \ll E^0_{298}$ $[Ni^{III}$–$Ni^{II}]$, the reduction of $Ni^{IV} \rightarrow Ni^{III}$ is the rate determining step followed by a very rapid reduction of $Ni^{III} \rightarrow Ni^{II}$. Thus as soon as Ni^{III} is generated from Ni^{IV}, it is reduced to Ni^{II} and hence the single step $2e^-$ transfer process without the involvement of any Ni^{III} intermediate is observed at low pH. However, at higher pH E^0_{298} $[Ni^{IV}$–$Ni^{III}] >$ E^0_{298} $[Ni^{III}$–$Ni^{II}]$ for the proton independent $Ni^{III} \rightarrow Ni^{II}$ transformation but for proton dependent $Ni^{III} \rightarrow Ni^{II}$ transformations have got comparable E^0 values with that of Ni^{III}–Ni^{II} couples. These result in the phase separation at the higher pH.

There are some reports [16–18] where the reactions of nitrite ion have been performed in acidic medium (pH $\leqslant$ 4.25). While preparing nitrite solutions at pH 2.0–4.25, we observed the evolution of small gas bubbles from the solution. Attempted kinetic study shows a strong dependence on $[H^+]$ in this region, and the results are erroneous. This may be due to the presence of kinetically active oxynitrogen species in acidic solutions [19]. Hence the reactions of nitrite would lead to greater complications owing to the rapidly established equilibria:

$$HNO_2 \overset{K_a}{\Leftrightarrow} H^+ + NO_2^- \quad (3)$$

$$H^+ + HNO_2 \Leftrightarrow H_2NO_2^- \quad (\text{or } H_2O + NO^+) \quad (4)$$

$$2HNO_2 \Leftrightarrow N_2O_3 + H_2O \quad (5)$$

$$N_2O_3 \Leftrightarrow NO + NO_2 \quad (6)$$

$$2NO_2 \Leftrightarrow N_2O_4 \quad (7)$$

$$N_2O_4 + H_2O \Leftrightarrow HNO_2 + NO_3^- + H^+ \quad (8)$$

Great care must, therefore, be taken in carrying out such studies in order to determine the proper reactant species. To avoid these, kinetic study has been performed in the range pH $\geqslant$ 4.5. From cyclic voltammetric and spectroscopic studies, it has been reported that the pK_{HS} for $[Ni^{IV}(L_x)]^{2+}$ (involving oxime protons) are less than 1.0 [11,12]. The pK_a of nitrous acid is reported to be 2.95 [eqn (3)] [20]. Hence in the experimental range of pH, only the deprotonated species of both the oxidants and reductant would be expected to exist which could justify the observed lack of $[H^+]$ dependence on the reaction rates (within ±4% deviation). The most characteristic feature of the present reactions is the second-order dependence of rate on $[NO_2^-]$. At first sight this seems rather surprising but it may be relatively simply understood if one considers the involvement of N_2O_4 as an intermediate which may eventually decompose by hydrophylic dismutation. Such an intermediate will also explain the lack of hydrogen ion dependence in the rate-law. The possibility of hydrogen bond formation as encountered in some of the earlier reactions

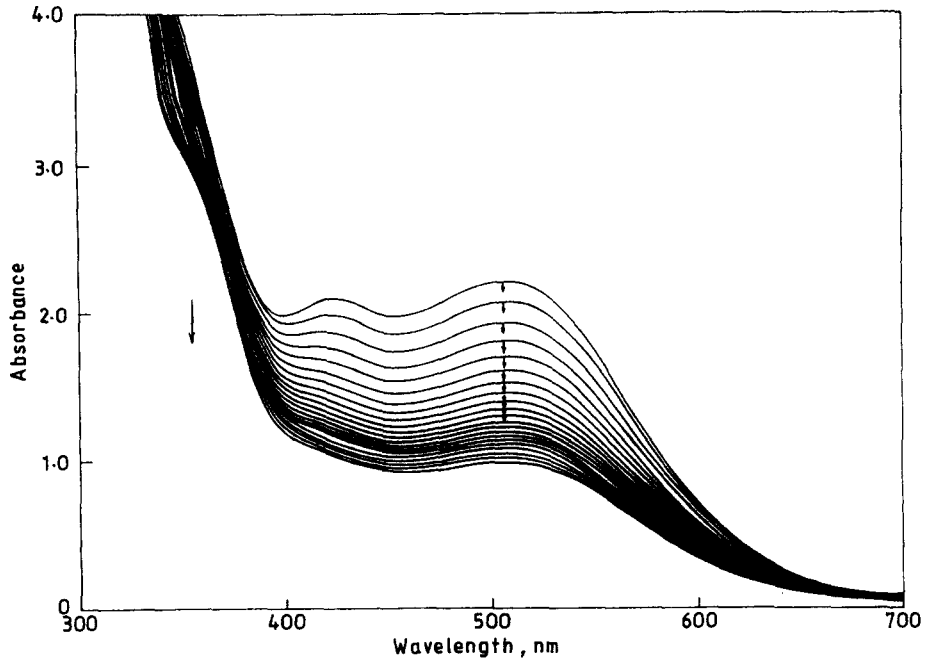

Fig. 4. Spectral scanning for the reaction between $[Ni^{IV}(L^2)_2]^{2+}$ and nitrite at 30°C with $[Ni^{IV}] = 5.0 \times 10^{-5}$ mol dm^{-3}.

[8] is eliminated since the oximato ligand does not find any proton bound on the nitrite reductant. A likely mechanism of the reaction can, thereby, be framed by considering the formation of an outer-sphere associated species between the two oppositely charged reactants [eqn (9)]. A second molecule of nitrite ion then reacts in the rate determining step with the ion-paired species (IP) giving the Ni^{II} product(s) and N_2O_4 [eqn (10)]. The hydrolysis of N_2O_4 takes place rapidly through the k_2 path [eqn (11)].

$$[Ni^{IV}(L_x)]^{2+} + NO_2^- \overset{K_1}{\Leftrightarrow} IP \qquad (9)$$

$$IP + NO_2^- \underset{\text{r.d.s}}{\overset{k_1}{\rightarrow}} [Ni^{II}(L_x)] + N_2O_4 \qquad (10)$$

$$N_2O_4 + H_2O \underset{\text{rapid}}{\overset{k_2}{\rightarrow}} NO_2^- + NO_3^- + 2H^+ \qquad (11)$$

The above scheme leads to a rate-law

$$-d/dt[Ni^{IV}(L_x)^{2+}] = k_1K_1[Ni^{IV}(L_x)^{2+}][NO_2^-]^2 \qquad (12)$$

This is identical to eqn (2a) with $k_1K_1[NO_2^-]^2 = k[NO_2^-]^2 = k_{obs}$, i.e., $k = k_1K_1$. The values of k_1K_1 were evaluated by a least-squares fitting of kinetic data. For monophasic reduction of $[Ni^{IV}(L^2)_2]^{2+}$ at pH 4.5, the value is (5.75 ± 0.07) dm^6 mol^{-2} s^{-1}. For biphasic reduction of both the oxidants at pH 6.0 the values evaluated are: (0.10 ± 0.003) dm^6 mol^{-2} s^{-1} and $(5.04 \pm 0.23) \times 10^{-3}$ dm^6 mol^{-2} s^{-1} for $[Ni^{IV}(L^1)]^{2+}$; (0.532 ± 0.02) dm^6 mol^{-2} s^{-1} and $(7.75 \pm 0.50) \times 10^{-3}$ dm^6 mol^{-2} s^{-1} for $[Ni^{IV}(L^2)_2]^{2+}$ owing to $Ni^{IV} \rightarrow Ni^{III}$ and $Ni^{III} \rightarrow Ni^{II}$ reduction steps respectively. The true comparison between k_1 and k_2 would be possible when one gets an insight into the magnitude of the ion-pair formation constant (K_1) in eqn (9). The value of the ion-pair constant (K_1) can be calculated theoretically using eqns (13)–(15) [21].

$$K_1 = Q_{IP} = \{(4\pi Na^3)/3000\} \exp(-U(a)/KT) \qquad (13)$$

$$U(a) = (Z_1Z_2e^2)/\{Da(1+\kappa a)\} \qquad (14)$$

$$\kappa = \{(8\pi Ne^2\mu)/(1000DKT)\}^{1/2} \qquad (15)$$

where N = Avogadro number, a = distance of closest approach, A = Boltzman constant, T = absolute temperature, Z_1 and Z_2 are the charges on respective ion, e = electronic charge, D = bulk dielectric constant of the medium (water) and μ is the ionic strength. $a = r_1 + r_2$, where r_1 and r_2 are the radii of Ni^{IV} and NO_2^- ions respectively. Values of r_1 and r_2 are considered as 5.1 Å [7] and 1.9 Å [17] respectively. The value of K_1 was calculated to be 2.31 dm^3 mol^{-1}. Dividing k_1K_1 by this value, the rate constant (k_1) was evaluted as: for monophasic reduction of $[Ni^{IV}(L^2)_2]^{2+}$ at pH 4.5 the value is (2.49 ± 0.03) dm^3 mol^{-1} s^{-1}. For biphasic reduction of both the oxidants at pH 6.0, the values evaluated are: (0.04 ± 0.001) dm^3 mol^{-1} s^{-1} and $(2.18 \pm 0.10) \times 10^{-3}$ dm^3 mol^{-1} s^{-1} for $[Ni^{IV}(L^1)]^{2+}$; (0.23 ± 0.01) dm^3 mol^{-1} s^{-1} and $(7.75 \pm 0.50) \times 10^{-3}$ dm^3 mol^{-1} s^{-1} for $[Ni^{IV}(L^2)_2]^{2+}$

for $Ni^{IV} \rightarrow Ni^{III}$ and $Ni^{III} \rightarrow Ni^{II}$ steps respectively. The value of k_2 has been reported to be $1.0 \times 10^3\ s^{-1}$ [22]. Converting it to a second-order parameter with $[H_2O] = 55.5\ mol\ dm^{-3}$, it turns out to $18.0\ dm^3\ mol^{-1}\ s^{-1}$. This shows that the hydrolysis path (k_2) of N_2O_4 is a faster step and not involved in the rate-law.

Nitrite ion can function as both oxidant and reductant [19]. Let us now look into the reactivity features critically when the product Ni^{II} complex is added externally at the onset of the reaction. The nitrite ion may oxidise this Ni^{II} into Ni^{III} or Ni^{IV} due to which there is an initial rise in absorbance and thus loses its initial concentration in the medium. The effective concentration of NO_2^- will go on decreasing as we increase the $[Ni^{II}]_0$ and this clearly justifies the inverse dependence of rate on $[Ni^{II}]_0$ added externally. To explain the second-order dependence on both $[Ni^{IV}]$ and $[NO_2^-]$ and the inverse dependence on $[Ni^{II}]_0$, a possible mechanistic path could be framed as

$$2[Ni^{IV}(L_x)]^{2+} + 2NO_2^- \overset{K_2}{\Leftrightarrow} 2[Ni^{IV}(L_x)\cdots NO_2^-]^+ \quad (16)$$

$$2[Ni^{IV}(L_x)\cdots NO_2^-]^+ \overset{K_3}{\Leftrightarrow} [Ni^{III}(L_x)]^+ + [Ni^{IV}(L_x)\cdots N_2O_4]^+ \quad (17)$$

$$[Ni^{IV}(L_x)\cdots N_2O_4]^+ \underset{k_4}{\overset{k_3}{\Leftrightarrow}} [Ni^{III}(L_x)]^+ + N_2O_4 \quad (18)$$

$$2[Ni^{III}(L_x)]^+ \overset{k_5}{\rightarrow} [Ni^{II}(L_x)] + [Ni^{IV}(L_x)]^{2+} \quad (19)$$

$$N_2O_4 + H_2O \overset{k_6}{\rightarrow} NO_2^- + NO_3^- + 2H^+ \quad (20)$$

The overall stoichiometric reaction can, therefore, be written as

$$[Ni^{IV}(L_x)]^{2+} + NO_2^- + H_2O \rightarrow [Ni^{II}(L_x)] + NO_3^- + 2H^+$$

and this is identical to eqn (1).

Comparison of reactivity of the two Ni^{IV} *complexes*

The reactivity of $[Ni^{IV}(L^2)_2]^{2+}$ towards nitrite ion is found to be greater than that of $[Ni^{IV}(L^1)]^{2+}$. This reflects the ease of rearrangement of tridentate bis-(oxime) ligand (HL^2) having no continuity of the backbone compared to the single-chain hexadentate (continuous) system (H_2L^1) where all sites may be affected equally, although in both the cases there is a change in electronic structure from a low spin t_{2g}^6 to a $t_{2g}^6\ e_g$ configuration.

Conclusion

Preliminary spectral scanning (Fig. 4) shows no indication for the formation of an appreciable amount of thermodynamically stable intermediate species during the reaction. Moreover both the Ni^{IV} and Ni^{III} components of the redox couples have pseudo-octahedral geometry and moderate reduction potential values. These are expected to show low substitution labilities ($< 10^2\ s^{-1}$) [7]. Unfortunately, we could not apply here the Marcus cross-relation equations to test the validity for outer-sphere reactions as the reactions are second-order on $[NO_2^-]$ for both the oxidants. The experimental findings and the low value of the calculated ion-pair constant can best be explained by considering an outer-sphere electron transfer process as above. The present work reveals some interesting aspects: (i) the overall reaction order is three; (ii) the reaction order turns to four in the presence of externally added Ni^{II}-product complex (2–15 times); (iii) presence of kinetically active oxynitrogen species at low pH (< 4.25) renders complicacy and erroneous pH dependency on rate is noted and (iv) low calculated values of ion-pair formation constant are suggestive for the operation of outer-sphere electron transfer route.

Acknowledgement—S.B. acknowledges the Council of Scientific and Industrial Research (New Delhi) for a Research Fellowship. P.B. acknowledges the said Council for a Research Project.

REFERENCES

1. Reddy, D., Lancaster, J. R. and Cornforth, D. P., *Science*, 1983, **221,** 769.
2. Kralic, J., in *Kirk-othmer Encyclopedia of Chemical Technology*. Wiley, New York, 1983, **21,** 244.
3. Cohen, M., *Corrosion* (*Houston*), 1976, **32,** 461.
4. Gouda, V. K. and Sayed, S. M., *Corros. Sci.*, 1973, **13,** 841.
5. Pyke, R. and Cohen, M., *Trans. Electrochem. Soc.*, 1948, **93,** 63.
6. Bhattacharya, S., Dutta, A. and Banerjee, P., *Acta Chem. Scand.*, 1997, **51,** 676.
7. Bhattacharya, S., Ali, M., Gangopadhyay, S. and Banerjee, P., *J. Chem. Soc., Dalton Trans.*, 1994, 3733.
8. Bhattacharya, S., Ali, M., Gangopadhyay, S. and Banerjee, P., *J. Chem. Soc., Dalton Trans.*, 1996, 2645.
9. Saha, B., Dutta, A., Gangopadhyay, S. and Banerjee, P., *Int. J. Chem. Kinet.*, 1997, **29,** 225.
10. Bhattacharya, S., Saha, B., Dutta, A. and Banerjee, P., *Coord. Chem. Rev.*, in press.
11. Mohanty, J. G., Singh, R. P. and Chakravorty, A., *Inorg. Chem.*, 1975, **14,** 2178.
12. Singh, A. N., Singh, R. P. and Chakravorty, A., *Inorg. Chem.*, 1977, **16,** 259.
13. Kolthoff, I. M., Sandell, E. B., Mechan, E. J. and Bruckenstein, S., in *Quantitative Chemical*

Analysis, 4th edn. Mcmillan, New York, 1969, 821.
14. Linert, W., Hertinger, E. and Jameson, R. F., *J. Chem. Soc., Perkin Trans.*, 1993, **2,** 2435.
15. Bhattacharya, S. and Banerjee, P., *Bull. Chem. Soc. Jpn*, 1996, 3475.
16. Dozsa, L. and Beck, M. T., *Inorg. Chim. Acta*, 1970, 219.
17. deMaine, M. M. and Stanbury, D. M., *Inorg. Chem.*, 1991, **30,** 2104.
18. Kundu, S., Bhattacharya, A. K. and Banerjee, R., *J. Chem. Soc., Dalton Trans.*, 1996, 3951.
19. Fanning, J. C., *Coord. Chem. Rev.*, 1991, **110,** 235.
20. Ram, M. S. and Stanbury, D. M., *J. Am. Chem. Soc.*, 1984, **106,** 8136.
21. Furholz, U. and Haim, A., *Inorg. Chem.*, 1987, **26,** 3243.
22. Jones, T. E. and Hamm, R. E., *Inorg. Chem.*, 1975, **14,** 1027.

Pergamon

PII: S0277-5387(97)00533-0

Polyhedron Vol. 17, Nos 13–14, pp. 2321–2326, 1998
© 1998 Elsevier Science Ltd
All rights reserved. Printed in Great Britain
0277-5387/98 $19.00+0.00

Some aspects of the coordination chemistry of 2-pyridinecarbaldehyde azine, (2-paa). The crystal structure of a complex with manganese(II), *cis*-$[MnCl_2(2\text{-paa})_2]$

Dennis A. Edwards,* Grace M. Hoskins, Mary F. Mahon, Kieran C. Molloy and Guy R. G. Rudolph

School of Chemistry, University of Bath, Bath BA2 7AY, U.K.

(Received 11 September 1997; accepted 17 December 1997)

Abstract—In the complex *cis*-$[MnCl_2(2\text{-paa})_2]$, (2-paa = 2-pyridinecarbaldehyde azine) each 2-paa behaves as a bidentate chelating ligand using adjacent pyridyl and azine nitrogen donor atoms. Twisting about the N—N bonds removes the remaining two nitrogen donor atoms of each 2-paa away from the vicinity of the metal centre. This complex is the first to be reported containing two bidentate 2-paa ligands. Only one previous example of a metal complex involving a single bidentate 6-methyl-2-paa ligand has been examined structurally. The complexes $[Mn_2Cl_4(2\text{-paa})]$, $[Zn_2(NO_3)_4(2\text{-paa})]\cdot 2H_2O$ and $[Ag_2(NO_3)_2(2\text{-paa})]$ have also been isolated, NMR evidence indicating that in the zinc and silver complexes the 2-paa ligands act in a double bidentate coordination mode. © 1998 Elsevier Science Ltd. All rights reserved

Keywords: 2-pyridinecarbaldehyde azine; 2-pyridinaldazine; manganese(II); structure; zinc; silver.

Potentially tetrafunctional azines have long found use as ligands and as analytical reagents [1]. One such ligand, 2-pyridinecarbaldehyde azine (**I**, R = R¹ = H), also known as 2-pyridinaldazine, was the subject of an extensive study [2] in the late 1950s and 1960s when cationic complexes with stoichiometries $[M(2\text{-paa})_2]^{2+}$ (M = Fe or Ni) and $[M_2(2\text{-paa})_3]^{4+}$ (M = Fe, Ni or Co), as well as the copper(I) and -(II) complexes $[CuCl(2\text{-paa})]Cl$, $[Cu_2Cl_4(2\text{-paa})]$ and $[Cu_2Cl_2(2\text{-paa})]$, were isolated.

Although the locations of the four donor nitrogen atoms of 2-paa are such as to make their coordination to a single metal centre extremely unlikely, 2-paa is a versatile ligand because of three possible geometric isomers arising from the orientation of the pyridyl groups about each azine C=N unit. Thus, in order to act as a double bidentate chelating ligand and so provide a bridge between two metal centres, it will likely be in a *trans*, *trans*-configuration as proposed for $[M_2(2\text{-paa})_3]^{4+}$ (M = Fe or Ni) [2] and $[Mo_2(CO)_8(2\text{-paa})]$ [3]. Alternatively, it will take up

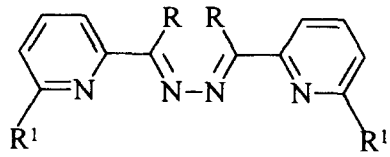

(I)

the *cis*, *trans*-configuration in order to act as a tridentate chelating ligand where both pyridyl and one azine nitrogen atoms are donors, as proposed for $[M(2\text{-paa})_2]^{2+}$ [2]. Coordination to metals in a *cis*, *cis*-configuration has not been confirmed or, indeed, even proposed and is the least likely arrangement for a metal complex involving 2-paa. Some iridium [4] and molybdenum [5] complexes containing 2-paa have been reported. The 2-paa ligands in $[Ir(NO)(PPh_3)_2(2\text{-paa})]^{2+}$ and $[Mo(CO)_3L(2\text{-paa})]$, (L = CO, MeCN or PPh_3) will be bidentate. However, in $[Ir_2(CO)_2(PPh_3)_4(2\text{-paa})]^{2+}$, $[Ir_2H_4(PPh_3)_4(2\text{-paa})]^{2+}$ and in $[Mo_2(CO)_6L_2(2\text{-paa})]$ (L = MeCN, PPh_3 or 1/2

* Author to whom correspondence should be addressed.

μ-dppe) and $[Mo_2(CO)_7(PPh_3)(2\text{-paa})]$ 2-paa is acting as a double bidentate ligand. A variety of lanthanide and actinide complexes of unusual stoichiometries and unknown structures containing this ligand have also been reported recently [6].

Remarkably few crystal structure determinations of complexes containing 2-paa or related ligands have been published. The first [7] showed that five-coordinate $[ZnCl_2(2\text{-paa})]$ contained *cis*, *trans*-tridentate 2-paa. Conversely, the 6-methyl derivative (**I**, R = H, R^1 = Me) is bidentate and in a *trans*, *trans*-configuration in $[IrH_2(PPh_3)_2(6\text{-Me-2-paa})]^+$ [4]. Double bidentate coordination of 2-paa has been confirmed [5] for $[Mo_2(CO)_6(\mu\text{-dppe})(2\text{-paa})]$, the 2-paa not being planar as a result of the short span of the bridging dppe ligand. The 2-paa ligand is, however, closer to being in a *trans*- rather than a *cis*-arrangement. Finally, the structures of two copper(II) complexes containing bis(2-pyridylmethyl)ketazine ligands, (**I**, R = Me, R^1 = H), have been elucidated, the ligand being *trans*, *trans*-double bidentate in $[Cu_2Cl_4(\text{ligand})]$ but *cis*, *trans*-tridentate in $[Cu(NO_3)_2(\text{ligand})]$ [8].

Although, as mentioned, the structure of $[ZnCl_2(2\text{-paa})]$ has been determined, the preparation of this and any other zinc-2-paa complexes have not been reported. Similarly, there are no reports of manganese-2-paa complexes. Therefore, we report here the preparations of zinc nitrate, silver nitrate and two manganese(II) chloride-2-paa complexes, together with the crystal structure of one of the manganese complexes.

EXPERIMENTAL

Infrared spectra (4000–200 cm^{-1}) were recorded as Nujol or hexachlorobutadiene mulls on CsI plates using a Perkin–Elmer 597 spectrophotometer. Proton NMR spectra were recorded on a Jeol GX 270 spectrometer. Room temperature magnetic susceptibilities were measured using a Johnson Matthey magnetic balance. Microanalyses were carried out using a Carlo Erba microanalyser. All solvents were dried over 4A molecular sieves but metal salts were used as received.

Preparation of 2-pyridinecarbaldehyde azine (2-paa)

A solution of hydrazine hydrate (62%; 5.1 cm^3) in ethanol (20 cm^3) was added slowly to a solution of 2-pyridinecarbaldehyde (16 g, 0.15 mol) in a similar volume of ethanol. An exothermic reaction ensued and fine yellow needles of the product appeared. After cooling in ice, the crystals were collected and recrystallised from ethanol. Yield: 8.1 g, 51%. m.p. 148°C (lit. 149°C). (Found: C, 68.4; H, 4.9; N, 26.5. $C_{12}H_{10}N_4$ requires C, 68.5; H, 4.8; N, 26.6%.) ^{1}H NMR ($CDCl_3$), δ 7.35 (m, H^4; $J_{3,4}$ 7.6, $J_{4,5}$ 4.9, $J_{2,4}$ 1.0 Hz), 7.79 (dt, H^3; $J_{2,3}$ 7.6, $J_{3,5}$ 1.8 Hz), 8.13 (ddd, H^2; $J_{2,5}$ 0.9 Hz), 8.70 (s, N=C*H*), 8.73 (ddd, H^5)—assignments relate to protons attached to carbons as numbered in Fig. 1.

Preparation of dinitrato(2-pyridinecarbaldehyde azine)disilver(I)

A solution of 2-paa (0.50 g, 2.4 mmol) in acetone (20 cm^3) was added dropwise with stirring to an aqueous solution of silver nitrate (1.19 g, 7.0 mmol). A yellow precipitate formed immediately and was filtered, washed with water, ethanol and diethyl ether and dried *in vacuo*. Yield: 1.06 g, 81%. (Found: C, 25.9; H, 1.8; N, 15.1. $C_{12}H_{10}Ag_2N_6O_6$ requires C, 26.2; H, 1.8; N, 15.3%.) ^{1}H NMR (CD_3CN) δ 7.77 (m, H^4; $J_{3,4}$ 6.3, $J_{4,5}$ 4.4, $J_{2,4}$ 1.0 Hz), 7.90 (dd, H^2; $J_{2,3}$ 6.3, $J_{2,5}$ 0.9 Hz), 8.15 (dt, H^3; $J_{3,5}$ 1.0 Hz), 8.73 (dd, H^5), 8.88 (s, N=C*H*).

Preparation of tetranitrato(2-pyridinecarbaldehyde azine)dizinc(II) dihydrate

Mixing warm solutions of zinc nitrate hexahydrate (1.20 g, 4.0 mmol) and 2-paa (0.42 g, 2.0 mmol) in acetonitrile followed by cooling gave a yellow precipitate which was filtered, washed with ethanol and diethyl ether and dried *in vacuo*. Yield: 0.97 g, 78%. (Found: C, 22.8; H, 2.4; N, 17.9. $C_{12}H_{14}N_8O_{14}Zn_2$ requires C, 23.0; H, 2.3; N, 17.9%.) ^{1}H NMR (CD_3CN) δ 7.76 (m, H^4), 8.18 (d, H^2 and H^3), 8.82 (d, H^5), 8.88 (s, N=C*H*).

Preparation of tetrachloro(2-pyridinecarbaldehyde azine)dimanganese(II)

A mixture of manganese dichloride tetrahydrate (0.25 g, 1.26 mmol) and 2-paa (0.20 g, 0.95 mmol) were reacted in refluxing ethanol or acetonitrile (30 cm^3) for 1 h. After cooling in ice, the yellow product was filtered, washed with ethanol and diethyl ether and dried *in vacuo*. Yield: 0.24 g, 41%. (Found: C, 31.6; H, 2.3; N, 11.9. $C_{12}H_{10}Cl_4Mn_2N_4$ requires C, 31.2; H, 2.2; N, 12.1%.)

Preparation of cis-dichlorobis(2-pyridinecarbaldehyde azine)manganese(II)

A solution of 2-paa (0.21 g, 1.00 mmol) in ethanol (25 cm^3) was slowly added to a stirred aqueous solution of manganese dichloride tetrahydrate (0.20 g, 1.00 mmol). An aqueous solution of potassium iodide (1.00 g, 6.3 mmol) was then added. No obvious reaction was evident so the solution was allowed to slowly evaporate at room temperature. After two weeks a small crop of wine red crystals began to appear and after a further week these were collected, washed with water and ethanol and dried *in vacuo*. (Found: C, 52.2; H, 3.7; N, 20.9. $C_{24}H_{20}Cl_2MnN_8$ requires C,

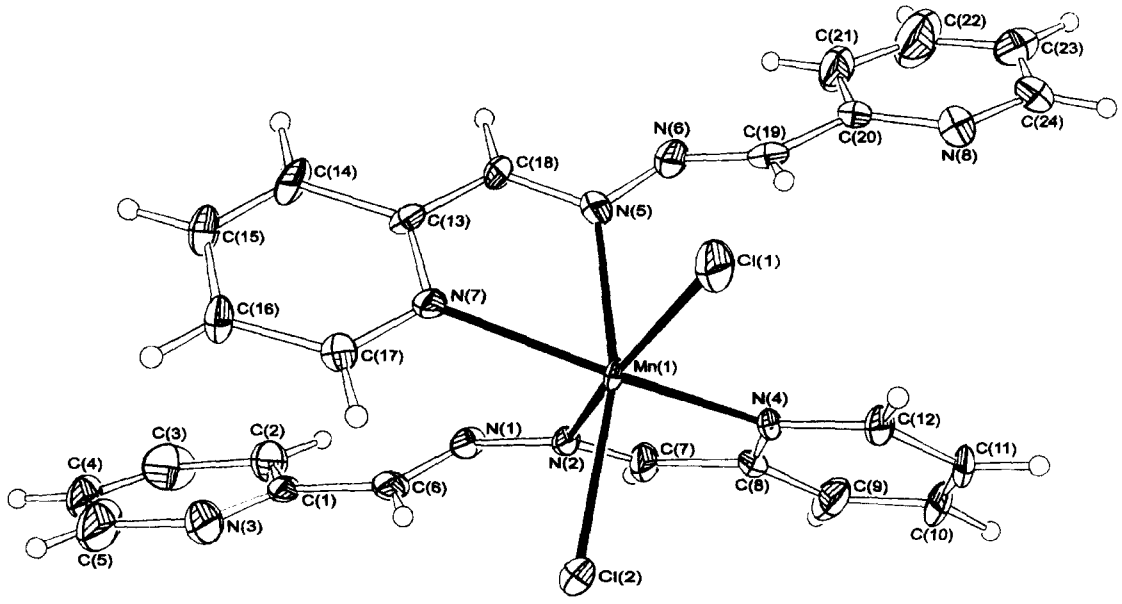

Fig. 1. The asymmetric unit of *cis*-$[MnCl_2(2\text{-paa})_2]$ with atom labelling. Thermal ellipsoids are represented at the 30% probability level.

52.8; H, 3.7; N, 20.5%.) Several preparations carried out as above gave clusters of large crystals but by varying the quantities of solvent smaller crystals were obtained, one of which was selected for a crystal structure determination.

X-ray crystallography

Crystal data: $C_{24}H_{20}Cl_2MnN_8$, M 546.32, triclinic, space group $P\bar{1}$ (No. 2), $a = 8.633(2)$, $b = 9.253(2)$, $c = 16.300(3)$ Å, $\alpha = 100.22(2)$, $\beta = 91.32(2)$, $\gamma = 93.00(3)^\circ$, $V = 1279.0(5)$ Å^3, $Z = 2$, $D_{calc} = 1.419$ g cm^{-3}, $\mu = 0.754$ mm^{-1}, $F(000) = 558$. Data were collected at room temperature, 293(2) K, on a Hilger and Watts Y290 four-circle diffractometer in the range $2.24 < \theta < 22.00^\circ$ using Mo–K_α (0.71069 Å) radiation. A crystal of dimensions $0.4 \times 0.4 \times 0.5$ mm was selected for the structure determination. The index ranges were $0 \leq h \leq 9$; $-9 \leq k \leq 9$; $-16 \leq l \leq 16$. The diffraction intensities were corrected for Lorentz and polarisation effects and for absorption [9]. 3325 Reflections were measured of which 3119 were independent [$R_{int} = 0.0227$]. The structure was solved by Patterson methods. Solution and refinement was achieved using the SHELX suite of programs [10]. Hydrogen atoms were included at calculated positions where relevant throughout. In the final least squares cycles all atoms were allowed to vibrate anisotropically. The large residuals (maximum and minimum 2.904 and -3.133 e Å^{-3} respectively) are a consequence of a very limited batch of crystals, poor crystal quality and several "shadow" peaks close to the heavy atom in the final difference Fourier map despite application of an absorption correction. The goodness-of-fit on F was 1.150 with final R indices [$I > 2\sigma(I)$] of $R_1 = 0.2175$ and $wR_2 = 0.5550$ and R indices (all data) of $R_1 = 0.2415$ and $wR_2 = 0.5864$. The weighting scheme employed was $1/[\sigma^2(F_o^2) + (0.5499P)^2 + 3.8735P]$ where $P = (F_o^2 + 2F_c^2)/3$. Selected bond lengths and angles are given in Table 1. Additional material is available from the Cambridge Crystallographic Data Centre and comprises final fractional atomic coordinates, thermal parameters, hydrogen atom coordinates and a complete listing of bond lengths and angles. The molecular structure, produced using ORTEX [11], is shown, together with the labelling scheme in Fig. 1.

RESULTS AND DISCUSSION

Four previously unreported complexes containing the potentially tetradentate ligand 2-pyridinecarbaldehyde azine (2-paa) have been isolated. The azine itself has prominent IR bands at 1630, ν(C=N), and at 1582, 1570, 1484 and 1437 (pyridine bands) cm^{-1} and its ^{1}H NMR spectrum can be fully assigned (see Experimental section). Two metal nitrate complexes, $\{[Ag(NO_3)]_2(2\text{-paa})\}$ and $\{[Zn(NO_3)_2]_2(2\text{-paa})\} \cdot 2H_2O$ have been prepared and their ^{1}H NMR spectra can be assigned on the basis that a symmetrical ligand arrangement is retained on coordination to the metals. (Proton assignments refer to the related carbon positions shown in Fig. 1.) For the silver complex, only five individual resonances with appropriate multiplicities and couplings are observed for the eight pyridine ring protons and the

Table 1. Selected bond lengths (Å) and angles (°) for *cis*-$[MnCl_2(2\text{-paa})_2]$

Mn(1)—N(7)	2.262(11)	N(1)—N(2)	1.43(2)
Mn(1)—N(4)	2.268(12)	N(2)—C(7)	1.33(2)
Mn(1)—N(2)	2.373(13)	N(5)—C(18)	1.27(2)
Mn(1)—Cl(1)	2.391(5)	N(5)—N(6)	1.43(2)
Mn(1)—N(5)	2.398(13)	N(6)—C(19)	1.28(2)
Mn(1)—Cl(2)	2.421(4)	C(1)—C(6)	1.46(2)
N(1)—C(6)	1.28(2)	C(19)—C(20)	1.45(2)
N(7)—Mn(1)—N(4)	153.6(5)	Cl(1)—Mn(1)—Cl(2)	103.6(2)
N(7)—Mn(1)—N(2)	87.3(4)	N(5)—Mn(1)—Cl(2)	161.5(3)
N(4)—Mn(1)—N(2)	70.2(4)	C(6)—N(1)—N(2)	112(2)
N(7)—Mn(1)—Cl(1)	101.0(3)	C(7)—N(2)—N(1)	111.0(14)
N(4)—Mn(1)—Cl(1)	97.9(3)	C(7)—N(2)—Mn(1)	117.9(9)
N(2)—Mn(1)—Cl(1)	163.8(4)	N(1)—N(2)—Mn(1)	130.4(10)
N(7)—Mn(1)—N(5)	70.2(5)	C(18)—N(5)—N(6)	113.8(14)
N(4)—Mn(1)—N(5)	90.8(4)	C(18)—N(5)—Mn(1)	114.1(11)
N(2)—Mn(1)—N(5)	76.9(4)	N(6)—N(5)—Mn(1)	131.4(8)
Cl(1)—Mn(1)—N(5)	92.7(3)	C(19)—N(6)—N(5)	111(2)
N(7)—Mn(1)—Cl(2)	97.8(3)	N(2)—C(7)—C(8)	113(2)
N(4)—Mn(1)—Cl(2)	95.5(3)	N(5)—C(18)—C(13)	119(2)
N(2)—Mn(1)—Cl(2)	88.9(3)	N(6)—C(19)—C(20)	122(2)

two N=CH protons. A comparison with the chemical shifts of 2-paa itself shows that the resonances assigned to H^4, H^3 and the N=CH protons move downfield, that of H^2 moves upfield and that of H^5 is unchanged on coordination to silver. For the zinc complex only four resonances appear in the δ 7.5–9.0 region of relative intensities 1 : 2 : 1 : 1. Although fewer couplings are observed than for the silver complex, the chemical shifts are similar but those of H^2 and H^3 are accidentally identical. The overall simplicity of both spectra shows that the azine is acting as a double bidentate ligand in both complexes, each of the metal centres being bonded to a pyridyl and an azine nitrogen to generate five-membered rings.

Two manganese(II)-2-paa complexes, $[Mn_2Cl_4(2\text{-paa})]$ and *cis*-$[MnCl_2(2\text{-paa})_2]$, have also been isolated. The former was obtained as a yellow precipitate from a reaction between manganese dichloride tetrahydrate and a slight molar deficiency of 2-paa in either refluxing ethanol or acetonitrile. One compound of the type $[M_2Cl_4(2\text{-paa})]$, where M = Cu, has been reported previously [2] and it was suggested that it contains square planar copper(II) with doubly bidentate 2-paa and terminal chloride ligands. A crystal structure of the closely related complex $[Cu_2Cl_4(\text{ligand})]$ where ligand = bis(2-pyridylmethyl)ketazine (**I**, R = Me, R^1 = H) confirmed this arrangement [8]. Although an analogous structure is conceivable for the manganese complex, we cannot advance any evidence in support. A magnetic moment of 5.90 B.M. at 294 K is merely indicative of high spin manganese(II) irrespective of geometry and the IR spectrum shows ν(C=N) at 1635 cm^{-1} and pyridine ring vibrations at 1580 and 1569 sh cm^{-1}. It would seem likely that the two metal ions are in identical environments and this would be achieved by the presence of doubly bidentate 2-paa.

The second manganese complex was obtained from a reaction designed to produce $[MnI_2(2\text{-paa})]$. Thus, aqueous $MnCl_2 \cdot 4H_2O$ was reacted with an equimolar amount of 2-paa in ethanol and a large excess of aqueous potassium iodide added subsequently. No precipitate appeared but slow evaporation at room temperature over a two-week period led to a low yield of wine-red crystals which contained no iodide and were then characterised as *cis*-$[MnCl_2(2\text{-paa})_2]$ with a magnetic moment of 5.92 B.M. at 295 K and IR bands at 1630, 1580 and 1567 cm^{-1}.

The structure of this complex has been elucidated by a single crystal X-ray crystallographic study. Only one other metal halide-2-paa complex, $[ZnCl_2(2\text{-paa})]$, appears to have had its structure confirmed crystallographically [7] and in that complex 2-paa is *cis*, *trans*-tridentate. However, in *cis*-$[MnCl_2(2\text{-paa})_2]$, (Fig. 1), both 2-paa ligands are, rather surprisingly, merely bidentate and as such this is the first metal-azine complex to show this structural feature. The only other compound with a crystallographically confirmed structure involving a bidentate chelating pyridine-azine ligand is $[IrH_2(PPh_3)_2(6\text{-Me-2-paa})]SbF_6$ [4]. The manganese compound consists of distorted octahedral monomeric molecules with two *cis*-chlorides [Mn—Cl 2.391(5) and 2.421(4) Å; Cl—Mn—Cl, 103.6(2)°] and four donor nitrogen atoms comprising a pyridine and an azine nitrogen from each bidentate ligand. The greatest distortion of the octahedral array arises from constraints imposed by the pyridyl and azine moieties which prohibit an N—Mn—N bite of

Table 2. Comparison of bond parameters for *cis*-$[MnCl_2(LL)_2]$ where LL = 2-paa (this work), bipy (Ref. 13) or phen (Ref. 14)

LL =	2-paa	bipy	phen
Mn—Cl	2.391(5), 2.421(4)	2.436(2), 2.449(1)	2.438(1), 2.451(1)
Mn—N trans to N	2.262(11), 2.268(12)	2.276(3), 2.264(3)	2.295(3), 2.294(3)
Mn—N trans to Cl	2.398(13), 2.373(13)	2.353(3), 2.331(3)	2.344(3), 2.369(3)
N—Mn—N	70.2(4), 70.2(5)	70.2(—), 70.3(—)	71.25(11), 70.93(10)
Cl—Mn—Cl	103.6(2)	not quoted	104.09(4)

90°, the actual angles being 70.2(4) and 70.2(5)° in forming MnN_2C_2 five-membered rings.

A recent [5] semi-empirical AM1 electronic structure calculation carried out for 2-paa predicts that the lowest energy conformation of the free ligand is neither *cis*- nor *trans*. An arrangement with an azine CNNC torsion angle of 102° is predicted with the pyridine rings being twisted out of the plane of the central part of the molecule by approximately 50°. This is not supported by the results from a single crystal structure determination* that we have carried out on the free ligand [12]. This shows that 2-paa crystallises in a centrosymmetric space group and is *trans*-planar with the two pyridyl nitrogens on opposite sides of the azine N—N bond and a consequent CNNC torsion angle of 180.0°. In the manganese complex, the uncoordinated nitrogen atoms of each 2-paa ligand are well removed from the metal centre by twisting about the N—N bond so that the strictly *trans*-configuration of the free ligand is destroyed but still leaving the non-coordinated ends of the 2-paa ligands positioned well away from each other. This is illustrated by the C(18)—N(5)—N(6)—C(19) and C(6)—N(1)—N(2)—C(7) torsion angles of 150.8 and 141.3°, respectively. The 2-paa ligands are arranged in such a way that the two coordinated pyridyl nitrogens are *trans* to each other [N(4)—Mn(1)—N(7), 153.6(5)°], whereas the two coordinated azine nitrogens are *cis* to each other [N(2)—Mn(1)—N(5), 76.9(4)°] and *trans* to chlorides [Cl(1)—Mn(1)—N(2), 163.8(4)° and Cl(2)—Mn(1)—N(5), 161.5(3)°]. The octahedral arrangement can therefore be viewed as a plane containing two chlorides and two azine nitrogens with the two pyridine nitrogens positioned axially. The Mn—N(pyridine) bond lengths of 2.262(11) and 2.268(12) Å are significantly shorter than the Mn—N(azine) bond lengths of 2.373(13) and 2.398(13) Å. No significant differences are evident between the lengths of the C=N bonds which are adjacent to or distant from the coordinated pyridine rings. Average C—C and C—N bond lengths within the pyridine rings and C—C bond lengths external to the pyridine rings are in the expected ranges [1.38(3), 1.34(2) and 1.46(2), respectively].

This structure can be compared to those of *cis*-$[MnCl_2(bipy)_2]$ [13] and *cis*-$[MnCl_2(phen)_2]$ [14] (bipy = 2,2′-bipyridyl; phen = 1,10-phenanthroline), significant bond lengths and angles being displayed in Table 2. All three structures involve constrained chelate ring systems with N—Mn—N angles much reduced to around 70°, Cl—Mn—Cl angles around 14° greater than 90° and Mn—N bonds significantly shorter where *trans* to another nitrogen rather than where *trans* to a chloride ligand.

* 2-paa is monoclinic, space group $P2_1/c$, with $a = 10.054(2)$, $b = 4.648(4)$, $c = 11.691(2)$ Å and $\beta = 91.03(2)°$. The poor quality of the crystals grown resulted in large residuals on attempts to solve the structure. Consequently, bond parameters are not discussed here but use is made of the overall structural arrangement in this Discussion section.

REFERENCES

1. (a) de Torres, A. G., Valcarcel, M. and Pino, F., *Talanta*, 1973, **20**, 919; (b) de Castro, M. D. L. and Valcarcel, M., *Analyt. Lett.*, 1978, **A11**, 1.
2. (a) Stratton, W. J. and Busch, D. H., *J. Am. Chem. Soc.*, 1958, **80**, 1286 and 3191; (b) *ibid.*, 1960, **82**, 4834; (c) Stratton, W. J., Rettig, M. F. and Drury, R. F., *Inorg. Chim. Acta*, 1969, **3**, 97.
3. Haga, M. A. and Koizumi, K., *Inorg. Chim. Acta*, 1985, **104**, 47.
4. (a) Ghedini, M., Longeri, M. and Neve, F., *J. Chem. Soc., Dalton Trans.*, 1986, 2669; (b) Lahoz, F. J., Tiripicchio, A., Neve, F. and Ghedini, M., *ibid.*, 1989, 1075.
5. Granifo, J., Vargas, M. E., Dodsworth, E. S., Farrar, D. H., Fielder, S. S. and Lever, A. B. P., *J. Chem. Soc., Dalton Trans.*, 1996, 4369.
6. (a) Dawod, M. M., Khalili, F. I. and Seyam, A. M., *Polyhedron*, 1989, **8**, 21; (b) *ibid.*, 1990, **9**, 2987.
7. Smith, H. W., *Acta Cryst., Sect. B*, 1975, **31**, 2701.
8. O'Connor, C. J., Romananch, R. J., Robertson, D. M., Eduok, E. E. and Fronczek, F. R., *Inorg. Chem.*, 1983, **22**, 449.

9. Walker, N. and Stuart, D., *Acta Cryst., Sect. A*, 1983, **39,** 158.
10. Sheldrick, G. M., SHELXL93, A computer program for crystal structure refinement, University of Gottingen (1993); SHELX86, A computer program for crystal structure solution, *Acta Cryst., Sect. A*, 1990, **46,** 467.
11. McArdle, P., *J. Appl. Cryst.*, 1994, **27,** 438.
12. Hoskins, G. M. and Mahon, M. F., unpublished results.
13. Lumme, P. O. and Lindell, E., *Acta Cryst., Sect. C*, 1988, **44,** 463.
14. Malinowski, T. J., Kravtsov, V. C., Simonov, Y. A., Lipkowski, J. and Bologa, O. A., *J. Coord. Chem.*, 1996, **37,** 187.

Pergamon

PII: S0277-5387(97)00511-1

Polyhedron Vol. 17, Nos 13–14, pp. 2327–2330, 1998
© 1998 Elsevier Science Ltd
All rights reserved. Printed in Great Britain
0277-5387/98 $19.00+0.00

Synthesis and crystal structure of chiral bis(cyclopentadienyl) samarium Schiff base complexes bearing intramolecular C—C bond formation and hydrogen transfer

Qiancai Liu*†, Mengxian Ding, Yonghua Lin and Yan Xing‡

Polymer Chemistry Laboratory, Changchun Institute of Applied Chemistry, Chinese Academy of Sciences, 159 Renmin Street, Changchun 130022, People's Republic of China

(Received 11 September 1997; accepted 2 December 1997)

Abstract—$SmCl_3$ reacted with CpNa (Cp = Cyclopentadienyl) in the ratio of 1:3 in THF, which then was reacted with (*S*)-(+)-*N*-1-(phenylethyl)salicylideneamine/toluene to yield the title complex,

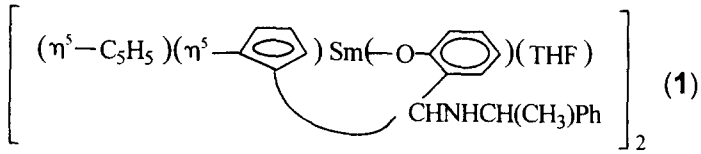

(1)

The X-ray crystal structure determination of the title complex reveals that **1** is a dimer with intramolecular C—C bond formation and hydrogen transfer, which leads to the configuration turnover of the carbon atom at the benzyl position of the ligand, while those of the newly formed asymmetric centers may have either *R* or *S* type configurations. © 1998 Elsevier Science Ltd. All rights reserved

Keywords: samarocene complex; chirality; Schiff base; crystal structure; hydrogen transfer; C—C bond formation.

One of the most attractive fields of organolanthanide chemistry is the synthesis and application of optically active lanthanide complexes due to their excellent catalytic properties for polymerization and asymmetric synthesis [1–5]. Moreover, only a few of lanthanide Schiff base complexes synthesized in non-aqueous condition have been determined [6]. Until now, no information of organolanthanocene Schiff base complexes has been available for comparison with these organolanthanocene alkoxides and/or phenoxides [7–8]. In previous communication, we reported on the synthesis and crystal structure of a dimeric organoneodymocene complex with a chiral Schiff base ligand whose structure provided an information of internal C—C bond formation and hydrogen transfer [9]. In order to provide further information about the properties of this type of complex, we report the synthesis and the crystal structure of the title complex.

EXPERIMENTAL

All the procedures were performed using Schlenk techniques. The solvents were dried over NaOH and distilled under argon from sodium benzophenone ketyl. Anhydrous $SmCl_3$ was prepared by Taylor's method [10]. IR spectra was recorded on a Bio-Rad FTS-7 spectrometer as KBr pellets. The Sm analysis was carried out by complexomeric titration.

* Author to whom correspondence should be addressed.

† Present address: Institute of Applied Chemistry, East China University of Science and Technology (ECUST), Box 421, 130 Meilong Road, Shanghai 200237, China.

‡ Y.L. and Y.X. are responsible for crystal structure determination.

Preparation of **1**

A stirred suspension of $SmCl_3$ (2.424 g, 9.442 mmol) in THF (40 cm^3) was added dropwise to a solution of C_5H_5Na (28.0 ml, M = 1.075 mol/l, 30.10 mmol) in THF under argon atmosphere at room temperature. The resulting mixture was stirred for 24 h, then 15 ml toluene solution of (S)-(+)-*N*-1-phenylethylsalicylideneamine (**2**) (2.12 g, 9.430 mmol) [11] was added and the reaction continued for 3 days. After centrifugation and subsequent extraction of the residue with THF (3 × 20 ml), the combined solution was concentrated under reduced pressure. Yellow crystals were obtained several weeks later in 32% yield (1.75 g). M.p. 214–216°C (dec.), $[\alpha]_D^{20} = -2257°$ (c 0.0542, THF). $C_{58}H_{64}N_2O_4Sm_2$ requires: Sm, 26.06. Anal. Found: Sm, 25.74. IR (KBr, cm^{-1}): 3059 (w), 3019 (w), 2961 (w), 2877 (w), 1588 (w), 1568 (w), 1470 (w), 1444 (w), 1366 (w), 1285 (w), 1232 (m), 1092 (w), 1056 (w), 1020 (w), 912 (w), 877 (w), 851 (w), 815 (w), 780 (w), 761 (s), 755 (s), 700 (m), 681 (w), 573 (m), 544 (w), 488 (w).

X-ray crystallography of **1**

A yellow crystal with dimensions of 0.40 × 0.26 × 0.20 mm was sealed under argon in a glass capillary and mounted on a Siemens P4 four-circle diffractometer. Lattice parameters were determined at 293 K from the angular settings of 30 fine reflections measured from $9.88° \leqslant 2\theta \leqslant 25.21°$. Relevant crystal and data parameters are given in Table 1. Corrections for Lorentz polarization and absorption were applied to the reflection data. During the data collection, the intensities of three standard check reflections measured every 100 reflections varied about ±2%. A combination of Patterson and difference Fourier techniques provided the locating positions of all non-hydrogen atoms, which were refined anisotropically using full-matrix least-squares methods. The final difference map contained no recognizable features and its maximum and minimum peaks were of heights 0.913 and −1.904 $eÅ^{-3}$. All calculations were carried out by means of a Siemens Nixdorf PCD 4 computer with the SHELXTL-Plus (Sheldrick, 1993) program. Table 2 lists the selected bond distances and angles.

Table 1. Crystal data for **1**

Formula	$Sm_2C_{58}H_{64}N_2O_4$
FW	1153.81
Crystal system	Monoclinic
Space group	$P2_1$
Cell constants	
a (Å)	11.165(2)
b (Å)	20.326(3)
c (Å)	12.005(4)
β (°)	110.640(10)
V (Å^3)	2549.5(10)
D_c (g·cm$_{-3}$)	1.503
μ (mm^{-1})	2.328
Z	2
F(000)	1164
Radiation	Mo Kα
λ (Å)	0.71073
Crystal size (mm)	0.40 × 0.26 × 0.26
Data collection, 2θ range (°)	3–50
h, k, l	−1 to 13, −1 to 24, −14 to 13
Reflections collected	5885
Unique reflections	4904

Tables of atomic and coordinate anisotropic thermal parameters, bond lengths and angles and observed and calculated structure factors have been deposited.

RESULTS AND DISCUSSION

The reaction of $LnCl_3$ with CpNa in THF led to the formation of $Cp_3Ln(THF)$, which was subsequently treated with the toluene solution of (*S*)-(+)-*N*-1-phenylethyl salicylideneamine resulting in the formation of orange-red suspension. After workup, the concentrated orange solution was set aside for several weeks, deep yellow crystals were isolated in the yield of 32%. IR spectra did not show the feature characteristic peak of C=N double bond. The X-ray determination shows that the C=N double bond was changed to C—N single bond during the reaction process. Furthermore, the configurations of the benzyl carbon centers (C26 and C45) of ligands were both changed from *S* to *R*, while the newly-formed asymmetric carbon centers (C19 and C44) may have either *R* or *S* configurations. Although reactions of organolanthanide metallocenes with phenols have been reported to generate phenoxide complexes, no C—C bond formation or hydrogen transfer occurred in these cases [7–8].

Structure of **1**

The molecule crystallizes in dimeric units. Complex **1** is isostructural to its Nd analogue (**3**) [9]. A line draw view of **1** is shown in Fig. 1. The two samarium centers are each bonded to two Cp rings and three oxygens: one from a THF molecule and the other two from Schiff bases in μ_2-fashion, to form a distorted trigonal bipyrimidal geometry with two oxygen atoms occupying the apical sites, while the centers of cyclopentadienyl rings and a μ_2-oxygen atom are at the triangular plane. The average Sm—C bond lengths for Sm1 are 2.82 and 2.70 Å, while those for Sm2 and 2.66 and 2.76 Å, the average Sm—C distance is 2.74 Å, which is comparable to that in **3** (2.77 Å). The Sm—O distances for Sm1 are 2.399(13) Å, 2.278(12) Å and 2.650(14) Å, and for Sm2 are 2.377(14) Å,

Table 2. Selected bond lengths (Å) and angles ( ) for **1**

Sm(1)—O(2)	2.278(12)	Sm(1)—O(1)	2.399(13)
Sm(1)—O(3)	2.650(14)	Sm(1)—C(39)	2.67(2)
Sm(1)—C(42)	2.68(3)	Sm(1)—C(40)	2.71(2)
Sm(1)—C(41)	2.73(2)	Sm(1)—C(43)	2.72(2)
Sm(1)—C(37)	2.75(2)	Sm(1)—C(36)	2.80(3)
Sm(1)—C(38)	2.80(3)	Sm(1)—C(34)	2.87(3)
Sm(1)—C(35)	2.89(5)	Sm(2)—C(17)	2.75(4)
Sm(2)—O(1)	2.377(14)	Sm(2)—O(2)	2.484(13)
Sm(2)—O(4)	2.55(2)	Sm(2)—c(13)	2.61(3)
Sm(2)—C(9)	2.64(3)	Sm(2)—C(10)	2.66(3)
Sm(2)—C(11)	2.70(3)	Sm(2)—C(12)	2.71(3)
Sm(2)—C(15)	2.74(3)	Sm(2)—C(14)	2.75(2)
Sm(2)—C(18)	2.78(2)	Sm(2)—C(16)	2.82(2)
C(19(— N(1)	1.51(2)	C(44)—N(2)	1.44(3)
C(26)—N(1)	1.46(3)	C(34)—N(2)	1.41(3)

Sm(2)—O(1)—Sm(1)	110.8(6)	Sm(1)—O(2)—Sm(2)	111.3(5)
O(2)—Sm(1)—O(1)	70.3(4)	O(2)—Sm(2)—Sm(2)—O(1)	67.3(4)
O91)—Sm(2)—O(4)	80.4(5)	O(2)—Sm(1)—O(3)	81.1(4)
O(2)—Sm(2)—O(4)	147.7(5)	O(1)—Sm(1)—O(3)	151.3(5)

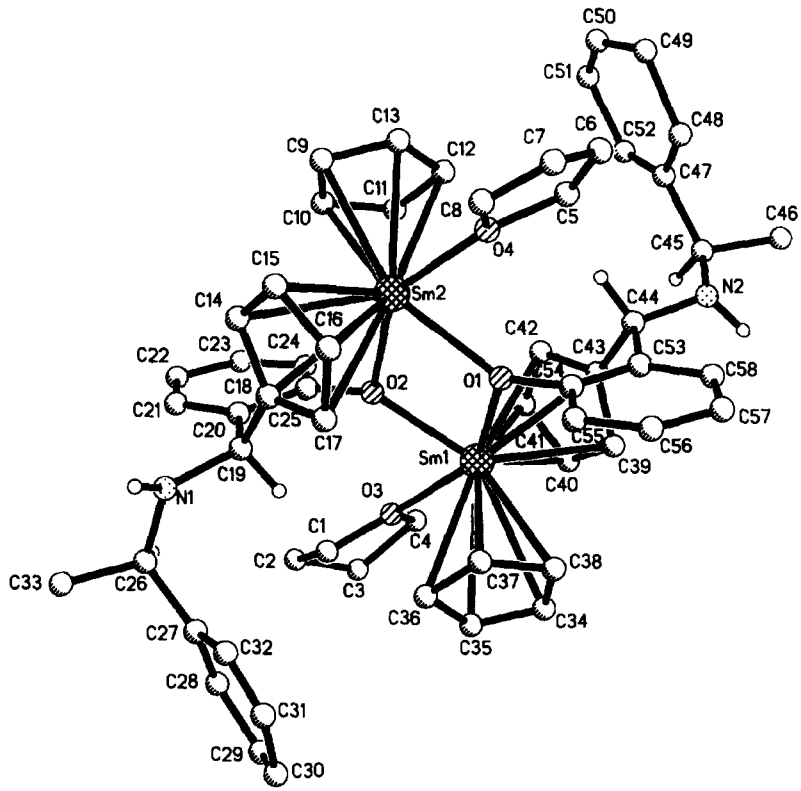

Fig. 1. Molecular structure of **1**. Most hydrogen atoms have been omitted for clarity.

2.484(13) Å and 2.55(2) Å, and the average Sm—O in **1** is 2.60 Å, which is nearly the same as that in **3** (2.602 Å).

Of the greatest interest is the geometry involving the two samarium centers and the Schiff base ligand themselves. The crystal structure of **1** shows that the newly-formed asymmetric carbon centers may bear *R*- or *S*- configuration (e.g. C19 is *S* configuration while

C44 is *R*). The oxygen atoms lie only 0.046 Å from the plane (P1) defined by Sm1, Sm2, O1 and O2 [the sum of the angles in this tetragonal plane = 359.7°]. The dihedral angle between Cp1(C34–C38) and Cp2(C39–C43) is 55.66°, while that of Cp3(C9–C13) and Cp4(C14–C17) is 59.83°, and those of P1 with Cp1, Cp2, Cp3 and Cp4 are 28.34°, 27.34°, 32.67° and 27.30°, respectively. The C19—N1, C26—N1, C44—N2 and C45—N2 bond lengths are 1.51(4), 1.46(3), 1.44(3), 1.41(3) Å, respectively, and are assigned as single bonds by comparison with those in transitional metal complexes and the ligand [9,12]. We think that the formation of **1** can be explained as follows: (1) the reaction of $SmCl_3$ with C_5H_5Na to form tris(cyclopentadienyl)samarium; (2) the protonation of the hydroxy group of Schiff base with one cyclopentadienyl ring omitting CpH; (3) a C—H bond on the cyclopentadienyl ring is activated by the C=N bond of Schiff base which leads to the C—C bond formation; and (4) the hydrogen atom on the Cp ring is transferred onto the nitrogen atom in 1,3-shift fashion and the Cp ring is re-aromatized.

REFERENCES

1. Giardello, M. A., Yamamoto, Y., Brard, L. and Marks, T. J., *J. Am. Chem. Soc.*, 1995, **117,** 3276 and references therein.
2. Mitchell, J. P., Hajela, S., Brookhart, S. K., Hardcastle, K. I., Henling, L. M. and Bercaw, J. E., *J. Am. Chem. Soc.*, 1996, **118,** 1045.
3. Stendel, A., Stehr, J., Siebel, E. and Fisher, R. D., *J. Organomet. Chem.*, 1996, **510,** 197 and references therein.
4. Shibasaki, M. and Sasai, H., *Pure & Appl. Chem.*, 1996, **68,** 113 and references cited.
5. Marko, I. E., Evans, G. R., Seres, S., Chelle, I. and Janousek, Z., *Pure & Appl. Chem.*, 1996, **68,** 923 and references cited.
6. Blech, P. and Floriani, C., *J. Chem. Soc., Dalton Trans.*, 1990, 3557 and references therein.
7. Evans, W. J., Hanusa, T. P. and Levan, K. R., *Inorg. Chim. Acta.*, 1985, **110,** 191 and references cited therein.
8. Zhou, X. G., Wu, Z. Z. and Jin, Z. S., *J. Organomet. Chem.*, 1992, **431,** 289 and references therein.
9. Liu, Q. and Ding, M., *J. Organomet. Chem.*, 1997, in press.
10. Taylor, M. P. and Carter, C. P., *J. Inorg. & Nucl. Chem.*, 1964, **24,** 387.
11. Synthesis of **2** was accomplished by the reaction of salicylaldehyde with *S*-phenylethylamine in the boiling toluene by azeotropic distillation, see: H. E. Smith, S. C. Cook and M. E. Warren, *J. Org. Chem.*, 1964, **29,** 2265.
12. Brunner, H., Qeschey, R. and Nuber, B., *J. Chem. Soc., Dalton Trans.*, 1996, 1499.

Pergamon

PII: S0277-5387(97)00508-1

Polyhedron Vol. 17, Nos 13–14, pp. 2331–2336, 1998
© 1998 Elsevier Science Ltd
All rights reserved. Printed in Great Britain
0277-5387/98 $19.00+0.00

Pd(II) and Pt(II) complexes with chalcogenide derivatized phosphathia ligands

Julie Connolly, Anthony R. J. Genge, Simon J. A. Pope and Gillian Reid*

Department of Chemistry, University of Southampton, Highfield, Southampton SO17 1BJ, U.K.

(Received 24 October 1997; Accepted 24 November 1997)

Abstract—The mixed phosphine sulfide/thioether and phosphine selenide/thioether ligands L^1–L^4 react with $PdCl_2$ or $PtCl_2$ in the presence of $TlPF_6$ in $MeNO_2$ solution to give the distorted square planar complexes $[Pd(L)](PF_6)_2$ or $[Pt(L)](PF_6)_2$ as powdered solids. IR spectroscopy shows ν(P=S) or ν(P=Se) for the complexes are to low frequency of free L^1–L^4, indicating coordination via the sulfide or selenide. $^{31}P\{^1H\}$, $^{77}Se\{^1H\}$ and ^{195}Pt NMR studies confirm η^4-ligation in solution, and the spectra do not alter significantly upon cooling. Also, the ^{195}Pt NMR chemical shifts indicate that the mixed phosphine sulfide/thioether donor set results in a very similar electronic environment at Pt(II) to a homoleptic tetrathioether donor set. $\delta(^{195}Pt)$ for the mixed phosphine selenide/thioether complexes of Pt(II) occur at slightly lower frequency. The crystal structure of L^3 is also reported. © 1998 Elsevier Science Ltd. All rights reserved

Keywords: Pd(II); Pt(II); chalcogenide.

We have recently been interested in establishing the coordinating abilities of polydentate and macrocyclic phosphathia ligands to transition metal centres. These ligands are of interest since they combine relatively poor σ-donor thioethers with strong σ-donor phosphines in a single ligand. This combination allows a direct comparison of these donor types and can also lead to structural diversity [1–6] In addition, Rh(I) carbonyl complexes containing phosphino–thiolate and phosphino–thioether ligands have been shown to be very active in catalysing the carbonylation of methanol to ethanoic acid [7].

In our recent work we have shown that the macrocycle Ph_2[14]aneP_2S_2 (8,12-diphenyl-1,5-dithia-8,12-diphosphacyclotetradecane) [1] and the acyclic ligands 1–3, in which the phosphine functions (good σ-donors) are specifically located at the termini, coordinate to a range of metal ions yielding various structural motifs including, for example, $[Au_2(1)_2]Cl_2$ which shows a helical binuclear arrangement with linear P_2 coordination at Au(I) from two bridging phosphathia ligands, and a trapped Cl^- anion within the metallocyclic cavity [2], distorted tetrahedral $[M(L)]^+$ (M = Cu or Ag; L = 1–3) [3] and octahedral *cis*-$[M'Cl_2(L)]^+$ (M' = Co; L = 1, 2; M' = Rh; L = 1–3 or Ph_2[14]aneP_2S_2; M' = Ir; L = 1) [1,4]. With Pd(II) and Pt(II), these ligands also coordinate via both the phosphine and thioether functions, yielding distorted square planar species, $[M(L)]^{2+}$ (M = Pd or Pt; L = 1–3 or Ph_2[14]aneP_2S_2). The resulting Pt(II) species undergo oxidation with halogen (Cl_2 or Br_2) to yield relatively stable octahedral Pt(IV) species $[PtX_2(L)]^{2+}$, demonstrating that the P_2S_2-donor ligands can also support the relatively hard Pt(IV) centre [5]. We have also shown that the sulfide and

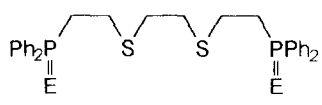

E = S: L^1

E = Se: L^2

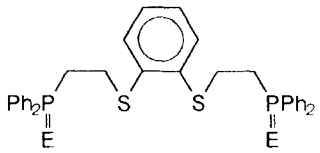

E = S: L^3

E = Se: L^4

* Author to whom correspondence should be addressed.

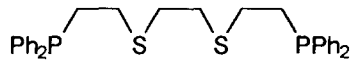

1

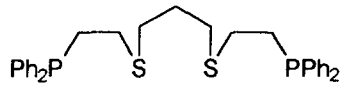

2

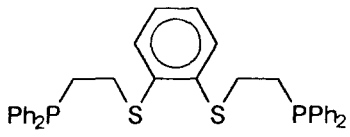

3

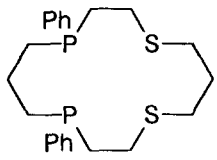

$Ph_2[14]aneP_2S_2$

selenide derivatives of 1–3 react readily with the group 11 metals yielding species such as the distorted tetrahedral cations $[M(L)]^+$ (M = Cu or Ag), in which the ligands are bound in an η^4-mode via both the P-bound chalcogen donors and the thioether donors [6]. Introduction of the chalcogen donors results in these species being considerably more labile in solution than the analogous complexes with 1–3. The catalytic potential of phosphine chalcogenide ligands has also been noted [8,9].

In this paper we report the results of our investigations into the synthesis and characterisation of the Pd(II) and Pt(II) complexes incorporating the sulfide and selenide derivatives of 1 and 3, $[M(L)](PF_6)_2$ (M = Pd, Pt; L = L^1, L^2, L^3, L^4). A single crystal X-ray structure determination on L^3 is also reported.

RESULTS AND DISCUSSION

Reaction of MCl_2 (M = Pd or Pt) with one molar equivalents of L^1–L^4 and two molar equivalents of $TlPF_6$ in degassed MeCN or $MeNO_2$ solution affords a white precipitate (TlCl) and a yellow or orange solution. After removing the TlCl, the complexes $[M(L)](PF_6)_2$ were isolated as powdered solids. Using MeCN typically led to rather low yields and more difficulty in purifying the products. This is probably due to the increased coordinating ability of the MeCN over $MeNO_2$, and contrasts with our observations for the preparation of Pd(II) and Pt(II) complexes of the parent diphosphadithia ligands 1–3 which form readily and in high yield in refluxing MeCN [5] IR spectroscopy confirms the presence of the phosphine ligands, ν(P=S) or ν(P=Se) occurring at ca 610 or 520 cm^{-1} respectively, i.e. to low frequency of free L^1–L^4, indicating coordination of the sulfide or selenide donors to Pd(II) or Pt(II). In addition, strong peaks around 840 and 555 cm^{-1} are attributed to $\nu(PF_6^-)$ and $\delta(PF_6^-)$, respectively. The electrospray mass spectra (MeCN) reveal peaks with the correct isotopic distributions for $[M(L)]PF_6^+$ and/or $[M(L)]^+$. These data, together with ^1H NMR spectroscopy and microanalyses, confirm the formulations $[M(L)](PF_6)_2$ (L = L^1–L^4) for the products.

The $^{31}P\{^1H\}$, $^{77}Se\{^1H\}$ and ^{195}Pt NMR data for these complexes are listed in Table 1. The $^{31}P\{^1H\}$ spectra show a singlet (with satellites in the case of the Pt compounds) shifted a few ppm either to higher or lower frequency compared to free L^1–L^4, as well as a septet at ca −145 ppm (PF_6^-). These signal integrate as 1 : 1, indicating one L per metal ion, and cooling to 200 K does not significantly alter the spectra. For the Pt(II) species $^2J_{PtP}$ is ca 100 Hz, considerably smaller than $^1J_{PtP}$ in $[Pt(L)]^{2+}$ (L = 1–3, or $Ph_2[14]aneP_2S_2$) which are typically ca 3000 Hz [1,5]. For the phosphine selenide derivatives (L^2 and L^4), $^{77}Se\{^1H\}$ NMR spectra were also recorded. For the Pd(II) complexes the $^{77}Se\{^1H\}$ NMR spectra each show a doublet ca 100 ppm to high frequency and with $^1J_{PSe}$ reduced substantially compared to the free ligands (ca 540 Hz vs 732 Hz for free L^2 and L^4). For the Pt(II) complexes $\delta(^{77}Se)$ is to higher frequency than for the Pd(II) analogues, with $^1J_{PSe}$ even smaller (ca 515 Hz). These data confirm coordination of L^2 and L^4 to Pd(II) or Pt(II) via the Se donors. The ^{195}Pt NMR spectra for the Pt(II) complexes of the sulfide derivatives each show a triplet at −4238 and −4182 ppm respectively for L^1 and L^2. This is the same region as $\delta(^{195}Pt)$ for Pt(II) complexes of tetrathioether macrocycles which we have previously reported, e.g. $[Pt([16]aneS_4)](PF_6)_2$ ([16]$aneS_4$ = 1,5,9,13-tetrathiacyclohexadecane) −4177 ppm, $[Pt([14]aneS_4)]$

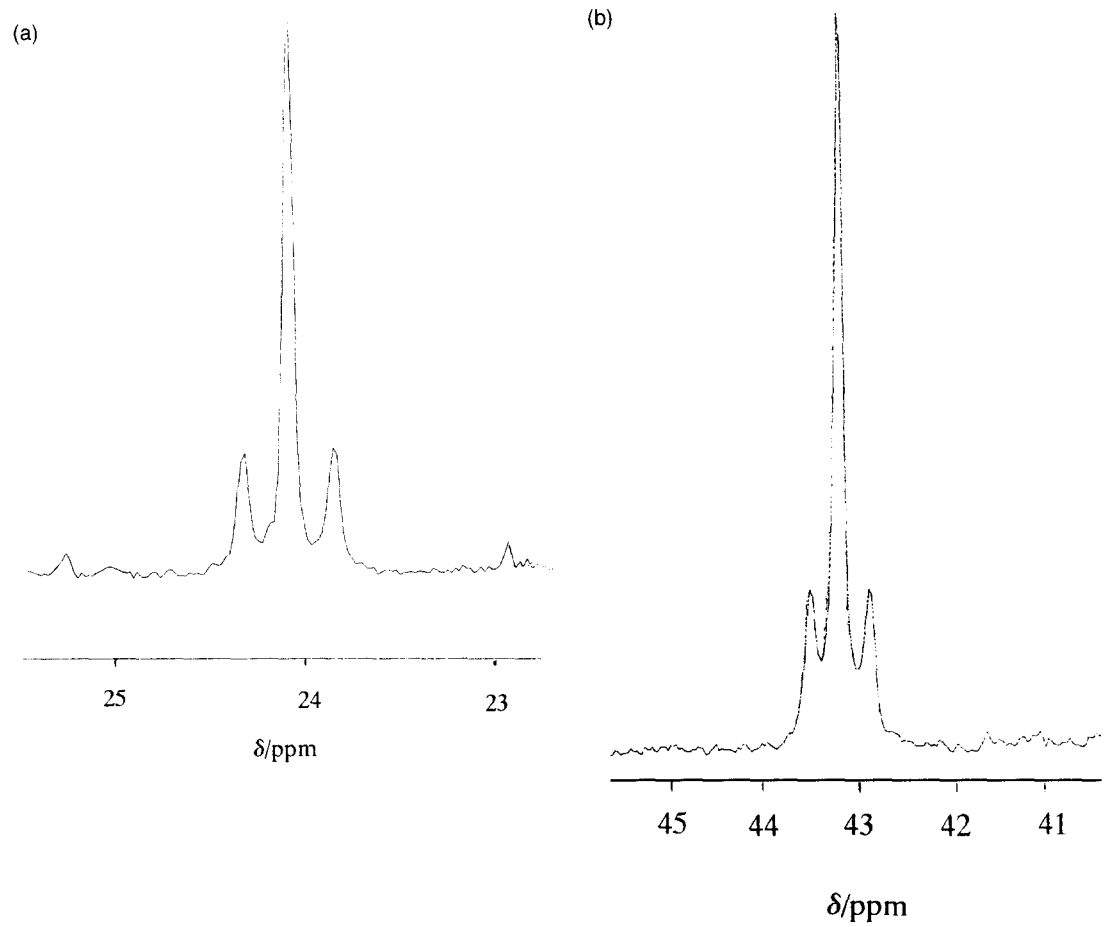

Fig. 1. $^{31}P\{^1H\}$ NMR spectrum of $[Pt(L^2)](PF_6)_2$ (a) and $[Pt(L^3)](PF_6)_2$ (b).

$(PF_6)_2$ ([14]aneS$_4$ = 1,4,8,11-tetrathiacyclotetra-decane) −4645 ppm [10], indicating that the homoleptic S(thioether)-donor set in the macrocyclic complexes generates a similar electronic environment to the mixed thioether/sulfide donor set in the new compounds. In the ^{195}Pt NMR spectra of the selenide species the triplets are centred at approximately −4500 ppm. This compares with −4750 ppm for $[Pt([16]aneSe_4)](PF_6)_2$ ([16]aneSe$_4$ = 1,5,9,13-tetra-selenacyclohexadecane) [11].

Table 1. NMR spectroscopic data

Complex	$\delta^{31}P\{^1H\}$/ppm	$\delta^{77}Se\{^1H\}$/ppm	$\delta^{195}Pt$/ppm	$^2J_{PtP}$/Hz	$^1J_{PSe}$/Hz	$^1J_{PtSe}$/Hz
$[Pd(L^1)](PF_6)_2$	44.5	—	—	—	—	—
$[Pd(L^2)](PF_6)_2$	43.0	—	—	—	—	—
$[Pd(L^3)](PF_6)_2$	27.2	−249	—	—	543	—
$[Pd(L^4)](PF_6)_2$	28.4	−266	—	—	540	—
$[Pt(L^1)](PF_6)_2$	39.0	—	−4238 t	103	—	—
$[Pt(L^2)](PF_6)_2$	43.5	—	−4182 t	96	—	—
$[Pt(L^3)](PF_6)_2$	24.1	−277	−4502 t	105	519	55
$[Pt(L^4)](PF_6)_2$	28.3	−212	−4452 t	100	514	Not resolved

$\delta^{31}P$: L^1, 41.2; L^2, 41.2; L^3, 32.8; L^4, 32.6.
$\delta^{77}Se\{^1H\}$: L^3, −352; L^4, −353.
$^1J_{PSe}$: L^3, 732; L^4, 732 Hz.
t = triplet.

Extensive studies have previously been conducted on chalcogenide derivatives of iminobis(diphenylphosphine), $PPh_2P(E)NHP(E)Ph_2$ (E = O, S or Se) [12]. These studies include complexes of Pd(II) and Pt(II), and the NMR properties of the deprotonated neutral species $[M\{Ph_2P(Se)NP(Se)Ph_2\}_2]$ are very similar to those in Table 1. Thus, for M = Pt $\delta(^{195}Pt)$ is −4242 ppm, $^2J_{PPt}$ = 105 Hz and $^1J_{PSe}$ = 543 Hz [13].

Crystals of L^3 suitable for an X-ray crystallographic study were obtained from a solution of L^3 in CH_2Cl_2/hexane. The crystal structure of L^3 shows the expected structure (Fig. 2, Table 2) with P(1)=S(3) = 1.939(1) and P(2)=S(4) = 1.956(1) Å, significantly shorter than *d*(P=Se) in L^4, 2.099(2), 2.111(2) Å [6]. The angles subtended at P lie in the range 103.4(2)–114.5(1)°, indicating approximately tetrahedral phosphorus atoms.

EXPERIMENTAL

Infrared spectra were measured as KBr or CsI discs or as nujol mulls using a Perkin–Elmer 983G spectrometer over the range 200–4000 cm^{-1}. Mass spectra were run by positive electrospray (ES) using a VG Biotech Platform. ^1H NMR spectra were recorded using a Bruker AM300 spectrometer operating at 300 MHz. $^{31}P\{^1H\}$, $^{77}Se\{^1H\}$ and ^{195}Pt NMR spectra were recorded in 10 mm o.d. tubes containing ca 10% deuterated solvent, using a Bruker AM360 spectrometer operating at 145.8, 68.68 and 77.7 MHz respectively and are referenced to external 85% H_3PO_4 [$\delta(^{31}P) = 0$], neat Me_2Se [$\delta(^{77}Se) = 0$] or aqueous $Na_2[PtCl_6]$ [$\delta(^{195}Pt) = 0$]. Microanalyses were performed by the Imperial College microanalytical service. L^1–L^4 were prepared as described previously [6].

Preparations

$[Pd(L^1)](PF_6)_2$. $PdCl_2$ (0.015 g, 0.09 mmol), L^1 (0.050 g, 0.09 mmol) and 2 molar equivalents of $TlPF_6$ (0.063 g, 0.18 mmol) were added to MeCN (20 cm^3). This mixture was then refluxed for 24 h under a N_2 atmosphere during which time a white solid (TlCl) was deposited and a yellow/orange solution formed. After filtering through celite to remove the TlCl, the solution was concentrated and Et_2O added to yield an orange solid. This was collected by filtration, washed with Et_2O and dried *in vacuo* (Yield 0.034 g, 41%). Calc. for $C_{30}H_{32}F_{12}P_4PdS_4 \cdot CH_2Cl_2$: C = 35.0, H = 3.2%. Found: C = 35.0, H = 3.3%. Electrospray mass spectrum (MeCN): found *m/z* = 344; calc. for $0.5[^{106}Pd(L^1)]^{2+}$ *m/z* = 344. ^1H NMR spectrum (300 MHz, $CDCl_3$, 300 K): δ 7.3–8.0 (*m*, Ph), 2.9–3.9 (*m*, CH_2). IR spectrum (CsI disk): 3050 w, 2920 w, 1480 m, 1435 s, 1360 w, 1248 s, 1230 m, 1180 m, 1104 s, 1061 w, 1031 m, 997 w, 840 vs, 748 m, 729 m, 716 m, 690 m, 573 m, 559 s, 522 w, 508 w, 488 w cm^{-1}.

$[Pd(L^2)](PF_6)_2$. Method as for $[Pd(L^1)](PF_6)_2$ above, but using $PdCl_2$ (0.010 g, 0.06 mmol), L^2 (0.038 g, 0.06 mmol) and $TlPF_6$ (0.041 g, 0.12 mmol) giving an orange solid. (Yield 0.032 g, 50%). Calculated for $C_{30}H_{32}F_{12}P_4PdS_2Se_2 \cdot CH_2Cl_2$: C = 30.9, H = 2.9%. Found: C = 30.7, H = 2.6%. Electrospray mass spectrum (MeCN): found *m/z* = 392; calc. for

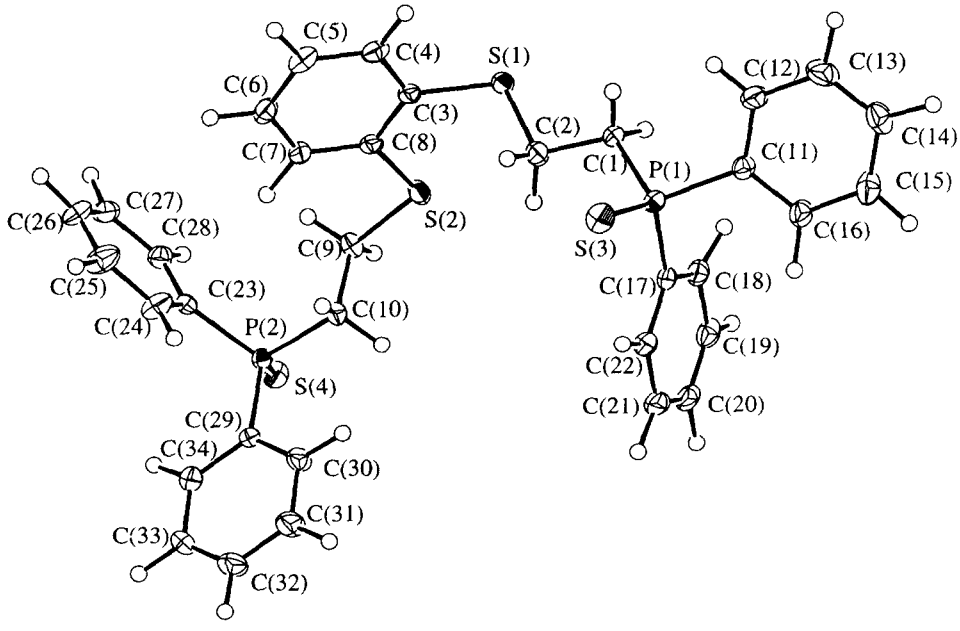

Fig. 2. View of the structure of L^3 with the numbering scheme adopted. Ellipsoids are drawn at the 40% probability level.

Table 2. Selected bond lengths and angles for L^3

S(1)—C(2)	1.830(4)	S(1)—C(3)	1.782(3)
S(2)—C(8)	1.770(3)	S(2)—C(9)	1.813(3)
S(3)—P(1)	1.939(1)	S(4)—P(2)	1.956(1)
P(1)—C(1)	1.824(4)	P(1)—C(11)	1.820(4)
P(1)—C(17)	1.811(4)	P(2)—C(10)	1.817(3)
P(2)—C(23)	1.815(3)	P(2)—C(29)	1.798(4)
C(1)—C(2)	1.513(5)	C(3)—C(4)	1.385(5)
C(3)—C(8)	1.408(4)	C(4)—C(5)	1.396(5)
C(5)—C(6)	1.381(5)	C(6)—C(7)	1.393(5)
C(7)—C(8)	1.390(5)	C(9)—C(10)	1.529(5)

C(2)—S(1)—C(3)	100.7(2)	C(8)—S(2)—C(9)	103.5(2)
S(3)—P(1)—C(1)	112.8(1)	S(3)—P(1)—C(11)	113.6(1)
S(3)—P(1)—C(17)	114.5(1)	C(1)—P(1)—C(11)	104.8(2)
C(1)—P(1)—C(17)	105.2(2)	C(11)—P(1)—C(17)	104.9(2)
S(4)—P(2)—C(10)	112.4(1)	S(4)—P(2)—C(23)	114.6(1)
S(4)—P(2)—C(29)	113.2(1)	C(10)—P(2)—C(23)	103.4(2)
C(10)—P(2)—C(29)	106.8(2)	C(23)—P(2)—C(29)	105.6(2)
P(1)—C(1)—C(2)	112.9(2)	S(1)—C(2)—C(1)	107.8(2)
S(1)—C(3)—C(4)	119.3(3)	S(1)—C(3)—C(8)	120.9(3)
C(4)—C(3)—C(8)	119.8(3)	C(3)—C(4)—C(5)	120.4(3)
C(4)—C(5)—C(6)	119.9(3)	C(5)—C(6)—C(7)	120.2(3)
C(6)—C(7)—C(8)	120.4(3)	S(2)—C(8)—C(3)	116.4(3)
S(2)—C(8)—C(7)	124.4(3)	C(3)—C(8)—C(7)	119.3(3)
S(2)—C(9)—C(10)	112.9(2)	P(2)—C(10)—C(9)	110.7(2)

$0.5[^{106}Pd(L^2)]^{2+}$ $m/z = 392$. ^1H NMR spectrum (300 MHz, $CDCl_3$, 300 K): δ 7.1–7.9 (*m*, aromatic C*H*), 2.5–3.1 (*m*, CH_2). IR spectrum (CsI disk): 3062 w, 2920 w, 2860 w, 1433 m, 1408 m, 1358 m, 1259 s, 1095 m, 845 vs, 802 s, 743 m, 729 m, 691 m, 586 m, 558 s, 531 s, 495 m, 394 w cm^{-1}.

$[Pd(L^3)](PF_6)_2$. $PdCl_2$ (0.014 g, 0.08 mmol), L^3 (0.050 g, 0.08 mmol) and $TlPF_6$ (0.058 g, 0.017 mmol) were stirred for 24 h in degassed $MeNO_2$ (20 cm^3) at room temperature, giving a white precipitate (TlCl) and a yellow solution. Removal of the TlCl by filtration, followed by addition of Et_2O to the filtrate gave a yellow solid. (Yield 0.019 g, 23%). Calc. for $C_{34}H_{32}F_{12}P_4PdS_4$: C = 39.7, H = 3.1%. Found: C = 39.5, H = 3.3%. Electrospray mass spectrum (MeCN): found m/z = 883, 737, 368; calc. for $[^{106}Pd(L^3)]PF_6^+$ $m/z = 881$; $[^{106}Pd(L^3)]^+$ $m/z = 736$; $0.5[^{106}Pd(L^3)]^{2+}$ $m/z = 368$. ^1H NMR spectrum (300MHz, $CDCl_3$, 300 K): δ 7.1–7.8 (*m*, aromatic C*H*), 2.6–3.2 (*m*, CH_2). IR spectrum (CsI disk): 3050 w, 2960 w, 2916 w, 1480 m, 1435 m, 1357 m, 1262 w, 1098 s, 1061 w, 1031 m, 997 w, 838 vs, 759 m, 748 m, 718 m, 682 m, 613 m, 557 s, 529 m cm^{-1}.

$[Pd(L^4)](PF_6)_2$. Method as for $[Pd(L^3)](PF_6)_2$ above, but using $PdCl_2$ (0.015 g, 0.08 mmol), L^4 (0.060 g, 0.08 mmol) and $TlPF_6$ (0.061 g, 0.17 mmol) giving an orange solid. (Yield 0.038 g, 41%). Calc. for $C_{34}H_{32}F_{12}P_4PdS_2Se_2 \cdot CH_2Cl_2$: C = 34.8, H = 2.8%. Found: C = 34.7, H = 2.7%. Electrospray mass spectrum (MeCN): found m/z = 831; calc. for $[^{106}Pd(L^4)]^+$ $m/z = 832$. ^1H NMR spectrum (300 MHz, $CDCl_3$, 300 K): δ 7.3–7.8 (*m*, aromatic C*H*), 2.7–3.1 (*m*, CH_2). IR spectrum (CsI disk): 3062 w, 2960 w, 2921 w, 2852 w, 1435 m, 1357 m, 1260 w, 1099 s, 841 vs, 747 m, 722 m, 693 m, 613 m, 558 s, 523 w, 507 w cm^{-1}.

$[Pt(L^1)](PF_6)_2$. Method as for $[Pd(L^1)](PF_6)_2$ above, but using $PtCl_2$ (0.023 g, 0.09 mmol), L^1 (0.050 g, 0.09 mmol) and $TlPF_6$ (0.063 g, 0.18 mmol) giving a pale yellow solid. (Yield 0.067 g, 73%). Calc. for $C_{30}H_{32}F_{12}P_4PtS_4$: C = 33.7, H = 3.0%. Found: C = 33.4, H = 2.7%. Electrospray mass spectrum (MeCN): found m/z = 777; calc. for $[^{195}Pt(L^1)]^+$ $m/z = 777$. ^1H NMR spectrum (300 MHz, $(CD_3)_2SO$, 300 K): δ 7.5–8.1 (*m*, aromatic C*H*), 2.9–3.8 (*m*, CH_2). IR spectrum (CsI disk): 3055 w, 297 w, 2958 w, 2912 w, 1582 w, 1481 m, 1437 s, 1360 w, 1232 m, 1189 m, 1106 s, 1061 w, 997 w, 840 vs, 768 w, 752 m, 716 m, 689 m, 610 sh, 558 s, 523 w, 488 m cm^{-1}.

$[Pt(L^2)](PF_6)_2$. Method as for $[Pd(L^1)](PF_6)_2$ above, but using $PtCl_2$ (0.020 g, 0.08 mmol), L^2 (0.051 g, 0.08 mmol) and $TlPF_6$ (0.055 g, 0.16 mmol) giving a pale yellow solid. (Yield 0.040 g, 46%). Calc. for $C_{30}H_{32}F_{12}P_4PtS_2Se_2 \cdot CHCl_3$: C = 29.1, H = 2.6%. Found: C = 28.7, H = 3.1%. Electrospray mass spectrum (MeCN): found m/z = 871, 791; calc. for $[^{195}Pt(L^2)]^+$ $m/z = 873$, $[^{195}Pt(L^2\text{-}Se)]^+$ $m/z = 793$. ^1H NMR spectrum (300 MHz, $CDCl_3$, 300 K): δ 7.3–7.8 (*m*, aromatic C*H*), 2.4–3.1 (*m*, CH_2). IR spectrum (CsI disk): 3050 w, 2962 w, 2920 w, 1584 w, 1481 m,

1435 s, 1179 s br, 1101 s, 1049 m, 997 w, 838 vs, 748 m, 722 m, 715 m, 688 m, 579 m, 557 s, 522 m, 505 w cm^{-1}.

$[Pt(L^3)](PF_6)_2$. Method as for $[Pd(L^3)](PF_6)_2$ above, but using $PtCl_2$ (0.020 g, 0.07 mmol), L^3 (0.047 g, 0.07 mmol) and $TlPF_6$ (0.055 g, 0.016 mmol) giving a cream coloured solid. (Yield 0.048 g, 57%). Calc. for $C_{34}H_{32}F_{12}P_4PtS_4 \cdot CH_2Cl_2$: C = 36.0, H = 2.8%. Found: C = 35.7, H = 2.1%. Electrospray mass spectrum (MeCN): found $m/z = 825$, 412; calc. for $[^{195}Pt(L^3)]^+$ $m/z = 825$; $0.5[^{195}Pt(L^3)]^{2+}$ $m/z = 412$. ^1H NMR spectrum (300 MHz, $CDCl_3$, 300 K): δ 7.6–8.1 (*m*, aromatic C*H*), 3.6–4.1 (*m*, CH_2). IR spectrum (CsI disk): 3058 w, 2960 w, 2923 w, 2851 w, 1437 m, 1356 m, 1260 m, 1103 s, 1026 m, 841 vs, 758 m, 725 m, 716 m, 687 m, 612 m, 558 s, 524 m, 486 w cm^{-1}.

$[Pt(L^4)](PF_6)_2$. Method as for $[Pd(L^3)](PF_6)_2$ above, but using $PtCl_2$ (0.024 g, 0.09 mmol), L^4 (0.061 g, 0.09 mmol) and $TlPF_6$ (0.067 g, 0.19 mmol) giving a pale yellow solid. (Yield 0.079 g, 72%). Calc. for $C_{34}H_{32}F_{12}P_4PtS_2Se_2$: C = 33.8, H = 2.7%. Found: C = 34.2, H = 2.8%. Electrospray mass spectrum (MeCN): found $m/z = 1065$, 919, 460; calc. for $[^{195}Pt(L^4)]PF_6^+$ $m/z = 1066$, $[^{195}Pt(L^4)]^+$ $m/z = 919$, $0.5[^{195}Pt(L^4)]^{2+}$ $m/z = 460$. ^1H NMR spectrum (300 MHz, CD_3NO_2, 300 K): δ 7.4–8.1 (*m*, aromatic C*H*), 3.4–3.8 (*m*, CH_2). IR spectrum (CsI disk): 3058 w, 2958 w, 2921 w, 2854 w, 1435 m, 1356 m, 1258 w, 1101 s, 995 w, 842 vs, 762 w, 723 w, 684 w, 612 w, 558 s, 522 m, 510 w cm^{-1}.

X-Ray structure determination on L^3

Colourless blocks L^3 in were obtained from a solution of CH_2Cl_2 and hexane. The selected crystal ($0.55 \times 0.50 \times 0.15$ mm) was coated with mineral oil and mounted on a glass fibre under a stream of cold N_2 gas.

Crystal data. $C_{34}H_{32}P_2S_4$, $M = 630.81$, triclinic, space group $P\bar{1}$ (No. 2), $a = 10.291(7)$, $b = 18.819(9)$, $c = 9.012(3)$ Å, $\alpha = 90.30(4)$, $\beta = 114.06(3)$, $\gamma = 95.51(5)^\circ$, $V = 1584(1)$ Å^3 [from 2θ values of 16 reflections measured at $\pm\omega$ ($2\theta = 20.0$–28.2°, $\lambda = 0.71073$ Å)], $Z = 2$, $D_c = 1.322$ g·cm^{-3}, $\mu = 4.09$ cm^{-1}, $F(000) = 660$.

Data collection and processing. Data collection used a Rigaku AFC7S diffractometer equipped with an Oxford Systems cryostream operating at 150 K, using graphite monochromated Mo-K_α radiation, (ω-2θ scan technique), 5927 data collected ($2\theta_{max}$ 50.0°), 5590 unique data ($R_{int} = 0.026$ based on F^2). Preliminary psi-scans showed no significant absorption, and no crystal decay or movement were observed.

Structure solution and refinement. The structure was solved by direct methods [14] and expanded using Fourier techniques to locate all non-H atoms for the one complete molecule in the asymmetric unit [15]. All non-H atoms were refined anisotropically and hydrogen atoms were included in fixed calculated positions [with d(C—H) = 0.96 Å] but not refined. The final cycle of full-matrix least-squares refinement (on F) was based on 3799 observed reflections with ($I > 2.5\sigma(I)$) and 361 variable parameters and converged with $R = 0.039$, R_w 0.040, using the weighting scheme $w^{-1} = \sigma^2(F)$. The maximum residual peak and minimum residual trough corresponded to +0.38 and −0.27 eÅ^{-3}. Selected bond lengths and angles are given in Table 2.

Atomic coordinates, anisotropic thermal parameters and bond lengths and angles have been deposited at the Cambridge Crystallographic Data Centre (CCDC).

Acknowledgements—We thank the EPSRC for support and for provision of the X-ray diffractometer. We also thank Johnson Matthey plc for loans of $PdCl_2$ and $PtCl_2$.

REFERENCES

1. Champness, N. R., Frampton, C. S., Reid, G. and Tocher, D. A., *J. Chem. Soc., Dalton Trans.*, 1994, 3031.
2. Gibson, A. M. and Reid, G., *J. Chem. Soc., Dalton Trans.*, 1996, 1267.
3. Doel, C. L., Gibson, A. M., Reid, G. and Frampton, C. S., *Polyhedron*, 1995, **14,** 3139.
4. Champness, N. R., Forder, R. J., Frampton, C. S. and Reid, G., *J. Chem. Soc., Dalton Trans.*, 1996, 1261; Forder, R. J. and Reid, G., unpublished results.
5. Connolly, J., Forder, R. J. and Reid, G., *Inorg. Chim. Acta*, 1997, **264,** 137.
6. Genge, A. R. J., Gibson, A. M., Guymer, N. K. and Reid, G., *J. Chem. Soc., Dalton Trans.*, 1996, 4099.
7. Dilworth, J. R., Miller, J. R., Wheatley, N., Baker, M. J. and Sunley, J. G., *J. Chem. Soc., Chem. Commun.*, 1995, 1579.
8. Baker, M. J., Giles, M. F., Orpen, A. G., Taylor, M. J. and Watt, R. J., *J. Chem. Soc., Chem. Commun.*, 1995, 197.
9. Wong, T. Y. H., Barnabas, A. F., Sallin, D. and James, B. R., *Inorg. Chem.*, 1995, **34,** 2278.
10. Blake, A. J., Bywater, M. J., Crofts, R. D., Gibson, A. M., Reid, G. and Schroder, M., *J. Chem. Soc., Dalton Trans.*, 1996, 2979.
11. Champness, N. R., Kelly, P. F., Levason, W., Reid, G., Slawin, A. M. Z. and Williams, D. J., *Inorg. Chem.*, 1995, **34,** 651.
12. Woollins, J. D., *J. Chem. Soc., Dalton Trans.*, 1996, 2893 and references therein.
13. Bhattacharyya, P., Novosad, J., Philips, J., Slawin, A. M. Z., Williams, D. J. and Woolins, J. D., *J. Chem. Soc., Dalton Trans.*, 1995, 1607.
14. SHELXS-86, program for crystal structure solution, Sheldrick, G. M., *Acta Crystallogr., Sect. A*, 1990, **46,** 467.
15. TeXsan: Crystal Structure Analysis Package, Molecular Structure Corporation, The Woodlands, Texas, 1995.

Pergamon

PII: S0277-5387(97)00477-4

Polyhedron Vol. 17, Nos 13-14, pp. 2337-2343, 1998
© 1998 Elsevier Science Ltd
All rights reserved. Printed in Great Britain
0277-5387/98 $19.00+0.00

Reactions of platinum(II) anticancer drugs. Kinetics of acid hydrolysis of *cis*-diammine(cyclobutane-1,1-dicarboxylato)platinum(II) "Carboplatin"

Robert W. Hay* and Sian Miller

School of Chemistry, University of St Andrews, St Andrews, KY16 9ST, U.K.

(Received 6 November 1996; accepted 21 November 1997)

Abstract—The kinetics of acid hydrolysis of "carboplatin" [*cis*-diammine(cyclobutane-1,1-dicarboxylato)platinum(II)] has been studied over a range of acidities at constant ionic strength (I = 1.0 mol dm^{-3}) and various temperatures. Loss of the substituted malonato ligand occurs in a biphasic reaction involving a ring opening step and a slower step in which loss of the monodentate malonato ligand occurs. At low acidities the first step k_{obs} (**1**) is approximately ten times faster than the second step (k_{obs} (**2**)). At higher acidities this ratio falls to *ca* four fold. Plots of k_{obs} (**1**) vs [H$^+$] are linear with a positive intercept and the plots can be adequately described by the relationship k_{obs} (**1**) = $k_0 + k_1$[H$^+$] with $k_0 = 6 \times 10^{-5}$ s^{-1} and $k_1 = 3.3 \times 10^{-4}$ s^{-1} at 25°C and I = 1.0 mol dm^{-3}. The rate constant k_{obs} (**2**) = k_2[H$^+$] with $k_2 = 1.1 \times 10^{-4}$ s^{-1} at 25°C and I = 1.0 mol dm^{-3}. The antitumour activity of carboplatin is discussed in terms of the kinetic results obtained. © 1998 Elsevier Science Ltd. All rights reserved

Keywords: carboplatin; kinetics; acid hydrolysis; ring opening; malonato ring.

"Cisplatin" (*cis*-diamminedichloroplatinum(II)) (**1**) is a well established and effective antitumour agent which is most active against testicular and ovarian cancers [1]. However, the dose-limiting side effect of nephrotoxicity has led to the development of second and third generations of platinum based complexes showing antitumour activity [2]. Of the second generation compounds the complex *cis*-diammine(cyclobutane-1,1-dicarboxylato)platinum(II), [Pt(NH$_3$)$_2$(cbda)] or "carboplatin" (**2**) was found to be an effective antitumour agent [3] with approximately the same spectrum of activity as cisplatin but with reduced toxicity [4].

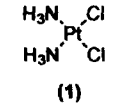

(1)

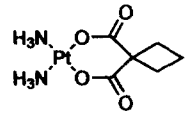

(2) = carboplatin

The mechanism of action of cisplatin involving its hydrolysis *in vivo* to the active species *cis*-[PtCl(NH$_3$)$_2$(OH$_2$)]$^+$ [5,6] and its subsequent binding to DNA is relatively well established. However, the mode of action of carboplatin remains uncertain and a number of reaction pathways are possible. For both carboplatin and cisplatin it is known that the *cis*-diammineplatinum(II) species binds to DNA *in vivo* [7]. However, it has not been confirmed that the aqua species derived from carboplatin is the active complex. Aquated platinum(II) species are produced more slowly from carboplatin as opening of the malonato ring is a very slow process compared with the ready hydrolysis of cisplatin. The half life of carboplatin in chloride-free phosphate buffer at pH 7 and 37°C is 268 h compared with 24 h for cisplatin under these conditions [8]. In view of the relative chemical inertness of carboplatin, a variety of suggestions have been

* Author to whom correspondence should be addressed.

made to account for its activity such as enzymatic activation [9,10], reaction with sulphur nucleophiles or direct interaction with DNA itself [11]. The topic has been recently reviewed [12] and an NMR study of the reactions of carboplatin in solution has been published [13].

The kinetics of displacement of cyclobutane-1,1-dicarboxylate from $[Pt(NH_3)_2(cbda)]$ is of considerable interest as it may lead to an understanding of the mode of action of the drug. In addition, the information is also of importance in defining the mechanism of displacement of oxygen donor ligands from four-coordinate Pt(II) complexes [14–18]. Canovese and coworkers [17] have studied the kinetics of ring opening and displacement of the malonato ligand in carboplatin in acidic solution. In the presence of acid it was found that the process was biphasic, resembling the successive displacement of two monodentate carboxylate ligands. The first (ring opening) step followed the rate law $k_{obs} = (k_0 + k_1 K[H^+])/(1 + K[H^+])$ where $k_0 = 8 \times 10^{-5}$ s^{-1}, K = 0.6 dm^3 mol^{-1} s^{-1} and $k_1 = 8.0 \times 10^{-4}$ s^{-1} at 25°C. The second step was found to follow the simple relationship $k_{obs} = k[H^+]$ with $k = 1.61 \times 10^{-4}$ dm^3 mol^{-1} s^{-1} at 25°C. Canovese *et al.* [17] also found that in the absence of acid and other nucleophiles carboplatin was inert. However, in the presence of Cl^- the displacement of the ligand follows a first order dependence on the chloride ion concentration with $k_{obs} = k_{Cl}[Cl^-]$. At 80°C $k_{Cl} = 1.32 \times 10^{-4}$ dm^3 mol^{-1} s^{-1}. In hydrochloric acid solution it was also observed that carboplatin gave yellow crystals of cisplatin as hydrolysis took place.

The present paper describes kinetic studies on the hydrolysis of carboplatin in perchloric acid solution under conditions of constant ionic strength as part of a program to define the mechanism of action of the drug.

EXPERIMENTAL

Diammine(cyclobutane-1,1-dicarboxylato) platinum(II) was purchased from both Strem and Sigma and used without further purification. All other reagents were of AnalaR quality or the best reagent grade available.

Kinetic studies were carried out as follows. Solutions (3.5 cm^3) of perchloric acid (1.0, 0.8, 0.6, 0.4 and 0.2 mol dm^{-3}) and the required amount of $NaClO_4 \cdot H_2O$ to give an ionic strength of 1.0 mol dm^{-3} were allowed to reach thermal equilibrium in a 1 cm quartz spectrophotometer cell placed in the temperature-controlled cell compartment of a Perkin-Elmer Lambda 5 UV-vis spectrophotometer. The reaction was initiated by the addition of solid $[Pt(NH_3)_2(cbda)]$ to the reaction medium. The solid dissolved rapidly on stirring and interval scan or fixed wavelength (245 nm) data collection modes were begun. The reaction was monitored until no further change in absorbance occurred (ca six to eight half lives). The observed first order rate constants k_{obs} (**1**) and k_{obs} (**2**) for the two consecutive reactions were calculated from the absorbance vs time data using standard equations [18].

RESULTS AND DISCUSSION

Canovese *et al.* [17] have found that the UV spectrum of carboplatin in water remains constant for many weeks at 25°C. However, acidification of the solution with dilute perchloric acid leads to an immediate change in the absorbance followed by a slow decrease in the absorbance over the whole range of wavelengths scanned. The final product spectrum closely resembled that of a freshly prepared solution of *cis*-$[Pt(NH_3)_2(OH_2)_2]^{2+}$. Similar observations were made in the present work. At 245 nm the absorbance increased rapidly then slowly decreased with time consistent with a biphasic reaction involving an initial ring opening step followed by a slower loss of the monodentate malonato ligand. No isosbestic points were observed and the final spectrum was consistent with that reported [19,20] for *cis*-$[Pt(NH_3)(OH_2)_2]^{2+}$, Fig. 1. In hydrochloric acid solution, yellow crystals of *cis*-$[Pt(NH_3)_2Cl_2]$ were obtained as the reaction progressed. It is thus quite clear that loss of the malonato ligand occurs under acidic conditions.

The observed first order rate constants k_{obs} (**1**) and k_{obs} (**2**) relating to the first and second steps of the biphasic reaction were calculated from the absorbance-time data for each stage. The infinity absorbance for the first reaction could be estimated from the absorbance-time data and directly measured for the second. As ring opening is faster than the loss of the monodentate malonato ligand, it was necessary to use two different temperature ranges to study the two

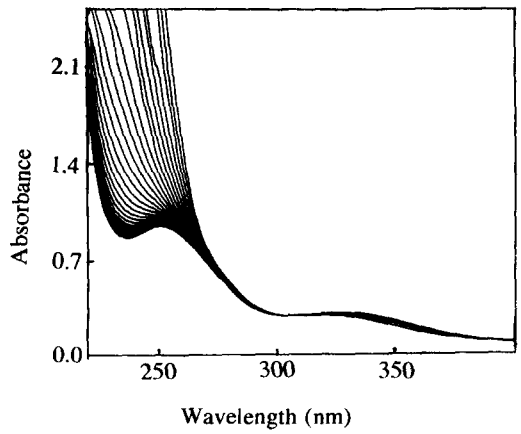

Fig. 1. Spectrophotometric scans for the acid hydrolysis of carboplatin in 0.8 mol dm^{-3} $HClO_4$ (I = 1.0 mol dm^{-3}) at 34.8°C. The scan interval is 10 min. The absorption maximum at 245 nm decreases with time to give a final spectrum with $\lambda_{max} = 252 \pm 1$ nm identical with that of *cis*-$[Pt(NH_3)_2(OH_2)_2]^{2+}$ (see Ref. [20]).

Table 1. Spectrophotometric rate constants for the first (k_{obs} (**1**)) and the second (k_{obs} (**2**)) stages of the displacement of cyclobutane-1,1-dicarboxylate from $[Pt(NH_3)_2(cbda)]$ in $HClO_4$ at $I = 1.0$ mol dm^{-3} ($NaClO_4$)[a]

Temp. (°C)	$[HClO_4]$ (mol dm^{-3})	$10^4 k_{obs}$ (**1**) (s^{-1})	$10^5 k_{obs}$ (**2**) (s^{-1})
19.8	0.2	0.91±0.27	
	0.4	1.31±0.04	
	0.6	1.70±0.31	
	0.8	1.97±0.63	
	1.0	2.25±0.53	
25.0	0.2	1.22±0.32	0.64±0.05
	0.4	2.04±0.18	2.37±0.14
	0.6	2.52±0.66	4.77±0.26
	0.8	3.13±0.26	7.59±0.65
	1.0	3.96±0.46	9.05±0.56
30.0	0.2	1.60±0.54	2.67±0.25
	0.4	2.73±0.71	6.26±0.37
	0.6	3.94±0.70	9.37±0.45
	0.8		12.6±0.7
	1.0		20.3±2.6
34.8	0.2		4.31±0.36
	0.4		9.60±0.67
	0.6		10.37±0.7
	0.8		23.2±2.7
	1.0		33.9±1.7

[a] Absorbance vs time data were collected at 245 nm.

reactions. The rate constant k_{obs} (**1**) was determined at 20, 25 and 30°C and k_{obs} (**2**) at 25, 30 and 35°C. The rate constants obtained are summarised in Table 1. A plot of k_{obs} (**1**) vs the perchloric acid concentration at 25°C is shown in Fig. 2. The plot is linear with a positive intercept and k_{obs} (**1**) $= k_0 + k_1[H^+]$

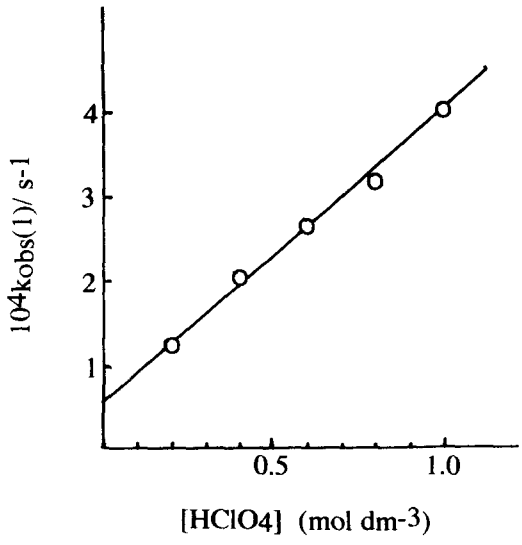

Fig. 2. Plot of k_{obs} (**1**) vs the hydrogen ion concentration at 25°C.

Table 2. Rate constants for the first step (k_0 and k_1) and for the second step (k_2) for the hydrolysis of carboplatin in $HClO_4$ at $I = 1.0$ mol dm^{-3} ($NaClO_4$)

Temp. (°C)	$10^5 k_0$ (s^{-1})	$10^4 k_1$ (dm^3 mol^{-1} s^{-1})	$10^4 k_2$ (dm^3 mol^{-1} s^{-1})
19.8	6.27	1.67	
25.0	6.03	3.29	1.11
30.0		5.85	2.08
34.8			3.64

The temperature dependence of k_1 gives $\Delta H^{\ddagger} = 88.4$ kJ mol^{-1} and $\Delta S^{\ddagger}_{298} = -15$ JK^{-1} mol^{-1}. The temperature dependence of k_2 gives $\Delta H^{\ddagger} = 90.0$ kJ mol^{-1} and $\Delta S^{\ddagger}_{298} = -19$ JK^{-1} mol^{-1}.

here k_0 relates to the spontaneous ring opening reaction and k_1 to the acid-catalysed process. Values of k_0 and k_1 at various temperatures are listed in Table 2. The rate constants k_0 are somewhat approximate as they were obtained from the extrapolated intercepts of the plots.

Plots of k_{obs} (**2**) vs the perchloric acid concentration are also linear and have a negligible intercept with k_{obs} (**2**) $= k_2[H^+]$. Values of k_2 are also listed in Table 2. At low acid concentrations the rate constant k_{obs} (**1**) is some ten times greater than k_{obs} (**2**) for the second step. At higher acidities the ratio falls to approximately four.

Cyclobutane-1,1-dicarboxylate is a relatively weak acid and its displacement from Pt(II) would be expected to be subject to acid catalysis. Attempts were made to detect a pre-equilibrium protonation by studying the initial absorbance of solutions of carboplatin in perchloric acid (0.2 to 1.0 mol dm^{-3} at $I = 1.0$ mol dm^{-3} ($NaClO_4$)). No evidence for such an equilibrium could be obtained with the absorbance being essentially constant within experimental error over this acidity range.

The hydrolysis of carboplatin at constant hydrogen ion concentration corresponds to two consecutive reactions

$$A \xrightarrow{k_1} B \xrightarrow{k_2} C$$

the concentrations of A, B and C as a function of time are given by the eqns (1–3)

$$A = A_0 e^{-k_1 t} \quad (1)$$

$$B = A_0 k_1 (e^{-k_1 t} - e^{-k_2 t})/(k_2 - k_1) \quad (2)$$

$$C = A_0[1 + (k_1 - k_2)^{-1}(k_2 e^{-k_1 t} - k_1 e^{-k_2 t})] \quad (3)$$

where A_0 is the initial concentration of A. The functions A/A_0, B/A_0 and C/A_0 can readily be computed from these equations [26]. At 25°C in 1 mol dm^{-3} perchloric acid $k_1 = 2.17 \times 10^{-2}$ min^{-1} and $k_2 = 9.66 \times 10^{-3}$ min^{-1}. The relative concentrations

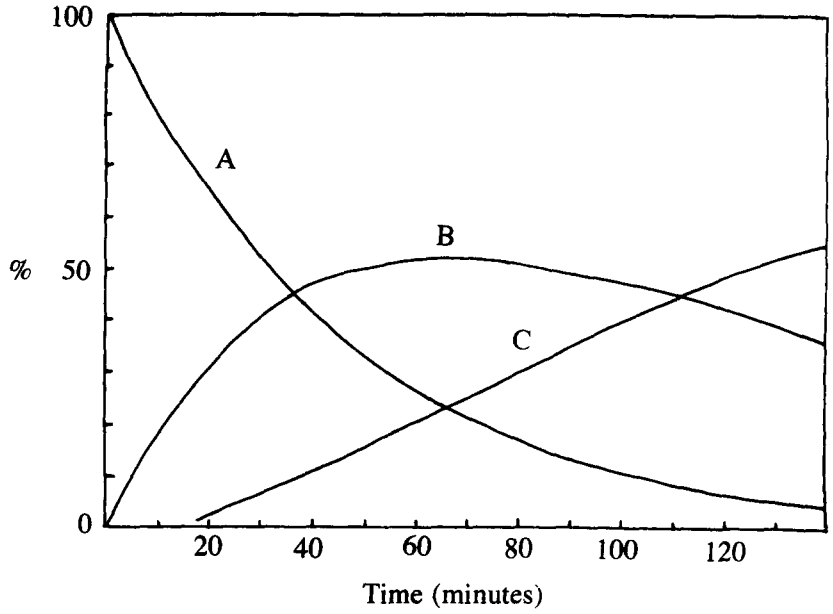

Fig. 3. Concentration vs time curves for the hydrolysis of carboplatin in 1 mol dm^{-3} $HClO_4$ at 25°C and I = 1.0 mol dm^{-3}; A = carboplatin; B = the monodentate carboxylato complex and C = $[Pt(NH_3)_2(OH_2)_2]^{2+}$. The curves are calculated using the equations discussed in the text with $k_1 = 2.17 \times 10^{-2}$ min^{-1} and $k_2 = 9.66 \times 10^{-3}$ min^{-1}. The maximum concentration of B is 50% and is reached at 67.2 min.

of A, B and C are shown in Fig. 3. The maximum concentration of B is 50% and is reached at 67.2 min calculated using the expressions

$$\tau_{max} = \ln Z/(Z-1)$$

$$\beta_{max} = Z^{Z/(1-Z)}$$

where $Z = k_2/k_1$. Because of the rather similar rates of ring opening and hydrolysis of the monodentate carboxylato complex it is not easy to determine the spectrum of the intermediate.

Mechanistic conclusions

The acid hydrolysis of carboplatin can be represented as shown in the Scheme. Ring opening involves a rapid pre-equilibrium protonation of the carboxylato ligand followed by a slow ring opening step. The kinetic behaviour observed will depend on the degree of protonation of the complex. If A represents carboplatin, the ring opening scheme can be summarised

$$A + H^+ \rightleftharpoons AH^+ ; K$$

$$AH^+ \xrightarrow{k} \text{Products}$$

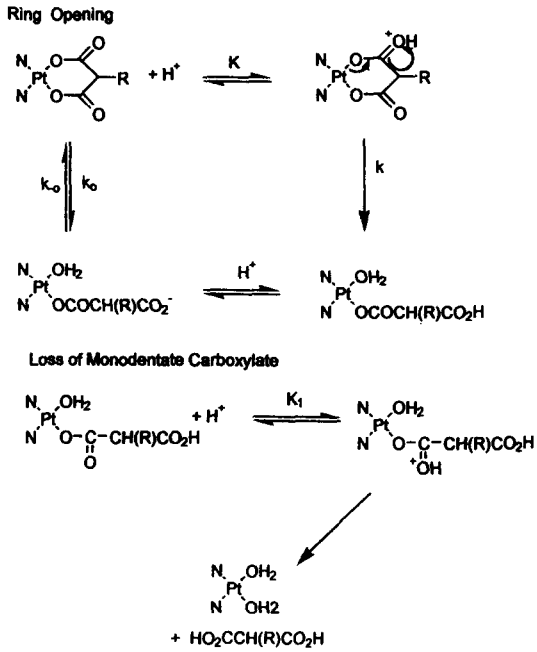

Scheme 1.

and k_{obs} ($[A]+[AH^+]$) = $k[AH^+] = kK[A][H^+]$, so that $k_{obs} = kK[H^+]/(1+K[H^+])$. In the present work we found that plots of k_{obs} (**1**) vs $[H^+]$ are linear and display no curvature. Canovese *et al.* [17] obtained somewhat similar results but with a considerable degree of scatter in the experimental data. The kinetic results previously obtained [17] are plotted in Fig. 4. Least squares analysis gives $k_0 = 8 \times 10^{-5}$ s^{-1} and $k_1 = 3 \times 10^{-4}$ dm^3 mol^{-1} s^{-1} from the slope which is in good agreement with our values of $k_0 = 6 \times 10^{-5}$

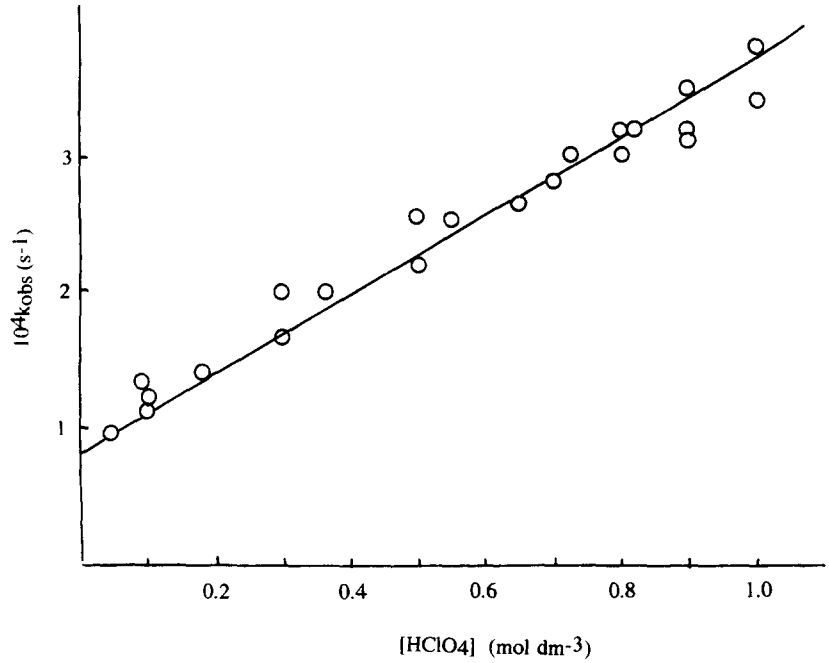

Fig. 4. Plot of k_{obs} vs the concentration of $HClO_4$ for the ring-opening reaction using the data of Canovese *et al.* (Ref. [17]).

s^{-1} and $k_1 = 3.3 \times 10^{-4}$ dm^3 mol^{-1} s^{-1} at 25°C and $I = 1.0$ mol dm^{-3}.

Canovese *et al.* [17] considered that there was curvature in the plot and fitted the data to the eqn $k_{obs} = k_0 + k_1[H^+]/(1 + K[H^+])$ with $K = 0.6$ dm^3 mol^{-1}. This is a remarkably high value for the equilibrium constant and would suggest that the complex is some 35% protonated in 1 mol dm^{-3} $HClO_4$. A carboxylato ligand would be expected to be a very weak base and its protonation behaviour would be predicted to be rather similar to that of a carboxylic acid, $RCO_2H + H^+ \rightleftharpoons RCO_2H_2^+$. The pK_{BH^+} for the protonation of acetic acid is -6 [21], i.e. the acid is 50% protonated at $H_0 = -6$ which occurs in >10 mol dm^{-3} perchloric acid [22]. The previous workers noted very minor absorbance changes (0.02 absorbance units) in the absorbance of carboplatin in the acidity range 0–1.0 mol dm^{-3} $HClO_4$ and attributed these changes to protonation of the complex. We were unable to detect any *systematic* change in the absorbance of the platinum complex as a function of the perchloric acid concentration although random minor variations were observed which we attributed to experimental error in the measurements and/or medium effects.

We conclude that for the ring opening step the kinetics can be adequately described by the eqn k_{obs} (**1**) $= k_0 + k_1[H^+]$. A similar rate expression is observed in the acid-catalysed decarboxylation of cobalt(III) carbonato complexes *cis*-$[CoL(CO_3)]^+ + H^+ \rightarrow [CoL(OH_2)_2]^{3+}$. These reactions have been studied in considerable mechanistic detail [23] and display deuterium solvent isotope effects k_{D_2O}/k_{H_2O} of ca 2.3 consistent with a rapid pre-equilibrium protonation of the complex followed by a slow ring opening step. Deuterium oxide is a weaker base than water and therefore more of the protonated complex occurs in deuterium oxide than in water. These reactions also display a k_0 term attributed to the spontaneous ring-opening step in aqueous solution. These "spontaneous" reactions are observed in acidic solution as the carboxylate group is immediately protonated and this greatly decreases the rate of the reverse ring closure step. Ring closure requires the removal of the carboxylate proton by a base (water) and since water is a much weaker base than the carboxylate group, the reaction is slow

$$RCO_2H + H_2O \rightleftharpoons RCO_2^- + H_3O^+ ; k_f, k_r$$

The equilibrium constant $K = k_f/k_r$ and since K is small $k_f \ll k_r$. Many examples of this effect are seen in the literature [24].

Our results for the second step of the reaction with k_{obs} (**2**) $= k_2[H^+]$ with $k_2 = 1.1 \times 10^{-4}$ s^{-1} at 25°C are in good agreement with the results obtained by Canovese who determined a similar rate law with $k_2 = 1.6 \times 10^{-4}$ s^{-1} at 25°C. It should also be stressed that the reactions described in the present paper were carried out under conditions of constant ionic strength so that medium effects were minimised.

Biological aspects

In the absence of acid and nucleophiles, carboplatin is stable in water for a period of many weeks at 25°C

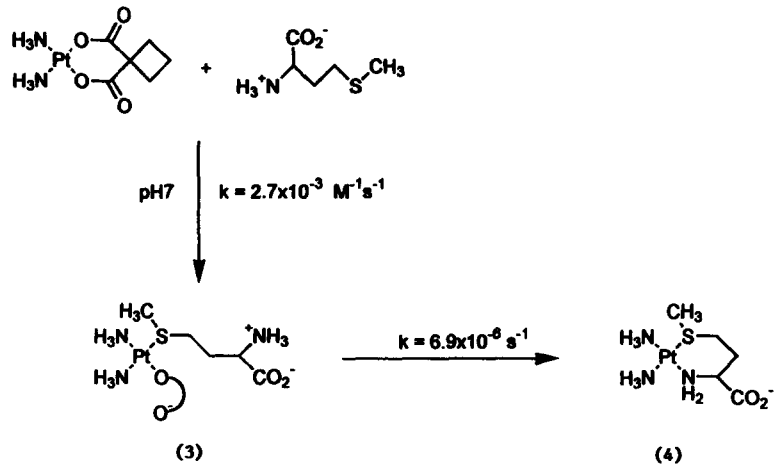

and it has been suggested [17] that for ring opening in water $k < 10^{-8}$ s^{-1}. A recent NMR study suggests that $k < 5 \times 10^{-9}$ s^{-1} at 37°C [13]. In the presence of chloride there is a first order dependence [17] of ring opening on the chloride concentration with $k_{obs} = k_{Cl}[Cl^-]$ where $k_{Cl} = 1.3 \times 10^{-4}$ dm^3 mol^{-1} s^{-1} at 80°C. The plasma chloride concentration is 104 mM (compared with 4 mM within cells) so that at plasma chloride concentrations $k_{obs} = 1.3 \times 10^{-5}$ s^{-1} at 80°C ($t_{1/2}$ = 14.7 h). At 37°C the half life of the Cl^- reaction is likely to be of the order of 250 h. Such a slow reaction is unlikely to be of biological importance and effectively excludes the idea that carboplatin is simply a prodrug for cisplatin.

We have observed that carboplatin reacts readily with thiol ligands such as glutathione and cysteine, thioethers such as methionine and directly with guanosine in a monophasic reaction. These observations are consistent with recent results reported by Sadler *et al.* [13,25]. Thiols react slowly and sulphur-bridged species containing four-membered Pt_2S_2 rings are the predominant products. Reactions with thioether ligands are much more rapid and a rate constant $k = 2.7 \times 10^{-3}$ dm^3 mol^{-1} s^{-1} at pH 7.0 and 37°C has been reported for the reaction of methionine with carboplatin to give the ring opened complex (**4**) with $k = 6.9 \times 10^{-6}$ s^{-1} at 37°C, Scheme 2.

Carboplatin also reacts with 5′-guanosine monophosphate (5′-GMP) in aqueous solution [13] and the complex *cis*-[Pt(NH$_3$)$_2$(cbda-O)(5′-GMP)] has been detected during the course of the reaction (H$_2$cbda = cyclobutane-1,1-dicarboxylic acid). These results suggest that the direct attack of nucleotides on carboplatin may be of importance in the mechanism of action of the drug.

Acknowledgement—We would like to thank the International Association for Cancer Research for financial support for this work.

REFERENCES

1. Prestayko, A. W., Crooke, S. T. and Carter, S. K. ed. *Cisplatin: Current Status and New Developments* Academic Press, New York, 1980.
2. Drobnik, J., *Cancer Chemother. Pharmacol.*, 1983, **10,** 145.
3. Dabrowiak, J. C. and Bradner, W. T., *Progr. Med. Chem.*, 1987, **24,** 129.
4. Harrap, K. R., Jones, M., Wilkinson, C. R., Clink, H. McD., Sparrow, S., Mitchley, B. C. V., Clarke, S. and Veasey, A. in *Cisplatin: Current Status and New Developments*, ed. A. W. Prestayko, S. T. Crooke and S. K. Carter, Academic Press, New York, 1980, p 193.
5. Miller, S. and House, D. A., *Inorg. Chim. Acta*, 1990, **173,** 53.
6. Bancroft, D. P., Lepre, C. A. and Lippard, S. J., *J. Am. Chem. Soc.*, 1990, **112,** 6860.
7. Abrams, M. J. in *Chemistry of Antitumour Agents*, ed. D. E. Wilman, Blackie, London, 1990.
8. Roberts, J. J., Knox, R. J., Friedlos, F. and Lydall, D. A. in *Biochemical Mechanisms of Platinum Anticancer Drugs*, ed. D. C. H. McBrien and T. F. Slater, IRL Press, Oxford, 1986, p 29.
9. Cleare, M. J., Hydes, P. C., Malerbi, B. W. and Watkins, D. M., *Biochimie*, 1978, **60,** 835.
10. Cleare, M. J., *Coord. Chem. Rev.*, 1974, **12,** 349.
11. Knox, R. J., Friedlos, F., Lydall, D. A. and Roberts, J. J., *Cancer Res.*, 1986, **46,** 1972.
12. Reedijk, J., *Inorg. Chim. Acta*, 1992, **198,** 200, 873; Reedijk, J., *J. Chem. Soc. Chem. Commun.*, 1996, 801.
13. Frey, U., Ranford, J. D. and Sadler, P. J., *Inorg. Chem.*, 1993, **32,** 1333.
14. Annibale, G., Canovese, L., Cattalini, L., Maragoni, G., Michelon, G. and Tobe, M. L., *J. Chem. Soc. Dalton Trans.*, 1984, 1641.
15. Canovese, L., Catalini, L., Maragoni, G. and Tobe, M. L., *J. Chem. Soc., Dalton Trans.*, 1985, 731.
16. Canovese, L., Tobe, M. L., Annibali, G. and Cattalini, L., *J. Chem. Soc., Dalton Trans.*, 1986, 1107.

17. Canovese, L., Cattalini, L., Chesa, G. and Tobe, M. L., *J. Chem. Soc., Dalton Trans.*, 1988, 2135.
18. Canovese, L., Catalini, L., Gemelli, L. and Tobe, M. L., *J. Chem. Soc., Dalton Trans.*, 1988, 1049.
19. Miller, S. E. and House, D. A., *Inorg. Chim. Acta*, 1989, **161,** 131.
20. Millar, S. E. and House, D. A., *Inorg. Chim. Acta*, 1989, **166,** 189.
21. Arnett, E. M., *Progr. Phys. Org. Chem.*, 1963, **1,** 223.
22. Paul, M. A. and Long, F. A., *Chem. Rev.*, 1957, **57,** 1. For a discussion see K. B. Wiberg *Physical Organic Chemistry*, John Wiley, New York, 1964.
23. See for example, Hay, R. W. and Jeragh, B., *J. Chem. Soc., Dalton Trans.*, 1979, 1343; Hay, R. W. and Jeragh, B., *Transition Met. Chem.*, 1979, **4,** 288; Dasgupta, T. P., *Inorg. Chim. Acta*, 1976, **20,** 33; Sastri, V. S. and Harris, G. M., *J. Am. Chem. Soc.*, 1970, **92,** 2943.
24. Typical examples are $Cu^{2+} + en \rightleftharpoons Cu(en)^{2+}$ and $Cu^{2+} + Hen^{+} \rightleftharpoons Cu(en)^{2+} + H^{+}$ where $k_f = 3.8 \times 10^9$ dm^3 mol^{-1} s^{-1} and 1.4×10^5 dm^3 mol^{-1} s^{-1} respectively. For compilations of rate constants see Sharma, V. S. and Leussing, D. L. in *Metal Ions in Biological Systems* ed. H. Sigel, Vol **2,** p. 127, Dekker, New York, 1973 and Kustin, K. and Swinehart, J., *Prog. Inorg. Chem.*, 1970, **13,** 107.
25. Barnham, K. J., Djuran, M. I., Murdoch, P. S., Ranford, J. D. and Sadler, P. J., *Inorg. Chem.*, 1996, **35,** 1065.
26. Frost, A. A. and Pearson, R. G., *Kinetics and Mechanism*, 2nd edn., John Wiley, London, 1961.

Pergamon

PII: S0277-5387(97)00460-9

Polyhedron Vol. 17, Nos 13–14, pp. 2345–2351, 1998
© 1998 Elsevier Science Ltd
All rights reserved. Printed in Great Britain
0277-5387/98 $19.00+0.00

Rhodium complexes with secondary phosphine and phosphinite ligands and the crystal structures of $[(PPh_2OH)_2(PPh_2O)Rh(\mu\text{-}Cl)_3Rh(PPh_2OH)(PPh_2O)_2]$ and $[(PPh_2OH)(PPh_2O)Cl(NCMe)Rh(\mu\text{-}Cl)_2Rh(PPh_2OH)(PPh_2O)Cl(NCMe)]\cdot 2thf$

Bhavesh Patel, Simon J. A. Pope and Gillian Reid*

Department of Chemistry, University of Southampton, Highfield, Southampton SO17 1BJ, U.K.

(Received 30 September 1997; accepted 11 November 1997)

Abstract—$RhCl_3\cdot 3H_2O$ reacts with ca six molar equivalents of PPh_2H or PCy_2H in EtOH solution under a N_2 atmosphere and in the presence of excess NH_4PF_6 to yield $[RhCl_2(PPh_2H)_4]PF_6$ or $[RhCl_2(PCy_2H)_4]PF_6$ respectively as yellow solids. $^{31}P\{^1H\}$ NMR spectroscopy shows the presence of the *trans* isomer only in chlorocarbon solutions, with J_{RhP} ca 80 Hz. Upon standing a solution of *trans*-$[RhCl_2(PPh_2H)_4]PF_6$ in a MeCN/thf mixture results in the production of yellow crystals of $[(PPh_2OH)(PPh_2O)Cl(NCMe)Rh(\mu\text{-}Cl)_2Rh(PPh_2OH)(PPh_2O)Cl(NCMe)]\cdot 2thf$, the structure of which shows an edge-bridged bioctahedral arrangement with d(Rh···Rh) = 3.74 Å. The NCMe ligands lie *trans* to the terminal Cl ligands, while the PPh_2OH and PPh_2O ligands are *trans* to the bridging Cl ligands. The crystal structure of the triply-bridged dimer $[(PPh_2OH)_2(PPh_2O)Rh(\mu\text{-}Cl)_3Rh(PPh_2OH)(PPh_2O)_2]$ has also been determined, showing a face-sharing bioctahedral arrangement, with d(Rh···Rh) = 3.39 Å. Both dinuclear species show significant P—O—H···O—P hydrogen-bonding interactions. © 1998 Elsevier Science Ltd. All rights reserved

Keywords: rhodium; phosphine; X-ray structure; phosphinite.

In contrast to tertiary phosphines, the coordination chemistry of primary and secondary phosphines has been largely neglected. This is in part due to the fact that coordination to a metal ion leads to the P-bound proton becoming very acidic and hence these species are liable to deprotonate yielding phosphido derivatives [1]. We have been investigating the chemistry of primary and secondary phosphines with the platinum group metals with a view to using these as neutral formally two-electron donors [2–5]. In our recent work we have isolated the stable cationic species $[MCl(PCy_2H)_3]^+$ (M = Pd, Pt) [2], and the neutral complexes $[M'X_2(L)_4]$ (X = Cl or Br, M' = Ru: L = PPh_2H, $PPhH_2$; M' = Os: L = PPh_2H, $PPhH_2$, PCy_2H). $^{31}P\{^1H\}$ NMR spectroscopic studies, together with X-ray crystallographic studies on several of these, confirm the *trans*-dihalo arrangement, with the four neutral phosphine ligands occupying the equatorial plane. The Ru and Os compounds exhibit reversible M(II)/(III) redox couples [3,4]. We now report the preparation and spectroscopic characterisation of the Rh(III) species *trans*-$[RhCl_2(PR_2H)_4]PF_6$ (R = Ph, Cy), together with single crystal X-ray structure determinations on two unusual chloro-bridged bioctahedral dimers $[(PPh_2OH)_2(PPh_2O)Rh(\mu\text{-}Cl)_3Rh(PPh_2OH)(PPh_2O)_2]$ and $[(PPh_2OH)(PPh_2O)Cl(NCMe)Rh(\mu\text{-}Cl)_2Rh(PPh_2OH)(PPh_2O)Cl(NCMe)]\cdot 2thf$, isolated as decomposition products.

Several Rh(I) and Ir(I) complexes with secondary phosphines have been reported previously, including $[M(PR_2H)_4]^+$ (M = Rh, Ir; R = Cy, Ph, Et) and $[Rh(PBu^t_2H)_3Cl]$ [6]. Also, in an early paper Hayter reported the preparation of the neutral Rh(III) complexes $[RhCl_3(PPh_2H)_3]$ and $[RhCl_3(PEt_2H)_3]$ by reaction of $RhCl_3\cdot 3H_2O$ with three molar equivalents of

* Author to whom correspondence should be addressed.

the phosphine in EtOH, although the characterisation of these species was very limited [7].

RESULTS AND DISCUSSION

Reaction of $RhCl_3 \cdot 3H_2O$ with six molar equivalents of PPh_2H or PCy_2H in degassed EtOH solution affords a colour change to yellow. In the presence of NH_4PF_6 concentration of the solution *in vacuo* gives the complexes $[RhCl_2(PPh_2H)_4]PF_6$ or $[RhCl_2(PCy_2H)_4]PF_6$ respectively as yellow solids. IR spectroscopy confirms the presence of the phosphine ligands and ν(P—H) occurs as a weak absorption at ca 2370 cm^{-1}. In addition, strong peaks around 840 and 555 cm^{-1} are assigned to $\nu(PF_6^-)$ and $\delta(PF_6^-)$ respectively, confirming the presence of the non-coordinating anion. The electrospray mass spectra reveal peaks with the correct isotopic distributions at $m/z = 883$ and 847 for the former, corresponding to $[RhCl(PPh_2H)_4]^+$ and $[Rh(PPh_2H)_4]^+$, and 965 and 767 for the latter, corresponding to $[RhCl_2(PCy_2H)_4]^+$ and $[RhCl_2(PCy_2H)_3]^+$. There was no evidence for other Rh-containing species such as dimers at higher m/z.

The $^{31}P\{^1H\}$ NMR spectrum of $[RhCl_2(PPh_2H)_4]PF_6$ reveals a doublet at +1.2 ppm indicative of a *trans*-dichloro geometry with four equivalent PPh_2H ligands coordinated in the equatorial plane, $J_{RhP} = 83$ Hz; typical of Rh(III) phosphine couplings. A septet at −146.3 ppm is also observed due to the PF_6^- and these signals integrate as 4 : 1. Similarly, for $[RhCl_2(PCy_2H)_4]PF_6$ a doublet at −5.0 ppm and septet at −146.3 ppm are observed, $J_{RhP} = 74$ Hz. In both cases the proton coupled ^{31}P NMR spectrum shows a distinctive second order pattern due to the coordinated secondary phosphines (Fig. 1), as expected given the direct one-bond P—H coupling, coupling to the P—H protons from *cis* and *trans* phosphine ligands and coupling to the phenyl or cyclohexyl ring protons. These data, together with ^1H NMR spectroscopy and microanalyses, confirm the products to be the Rh(III) tetrakis-phosphine complexes *trans*-$[RhCl_2(PPh_2H)_4]PF_6$ and *trans*-$[RhCl_2(PCy_2H)_4]PF_6$.

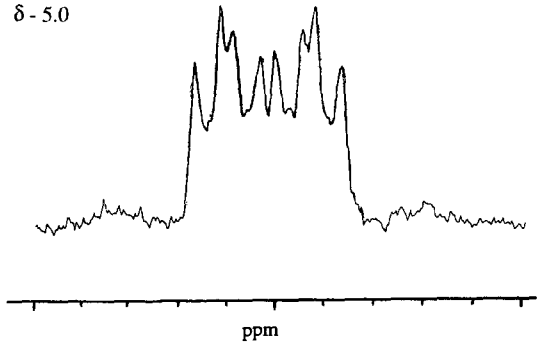

Fig. 1. ^{31}P NMR spectrum of *trans*-$[RhCl_2(PCy_2H)_4]PF_6$ showing the coordinated phosphine region.

In an attempt to grow crystals suitable for a single crystal X-ray structure analysis, a solution of *trans*-$[RhCl_2(PPh_2H)_4]PF_6$ in MeCN/thf was allowed to stand for several days at ca −15°C. This resulted in the formation of a few yellow columnar crystals, along with phosphine oxide. A structure analysis performed on one of these crystals showed them in fact to be the unusual $(\mu\text{-Cl})_2$ edge-bridged bioctahedral species $[(PPh_2OH)(PPh_2O)Cl(NCMe)Rh(\mu\text{-}Cl)_2Rh(PPh_2OH)(PPh_2O)Cl(NCMe)] \cdot 2thf$, formed by oxidation of the secondary phosphine complex. The structure shows (Fig. 2, Table 1) a centrosymmetric dinuclear species in which each Rh(III) centre is coordinated to two bridging Cl ligands, one terminal Cl ligand, one PPh_2OH, one PPh_2O^- and one NCMe ligand, giving a distorted octahedral arrangement, Rh—P(1) = 2.267(3), Rh—P(2) = 2.268(3), Rh—Cl(1) = 2.321(3), Rh—Cl(2) = 2.493(2), Rh—N(1) = 2.015(8) Å. The bridging Cls are *trans* to the diphenylphosphinous acid and diphenylphosphinite ligands, leaving the terminal Cl and NCMe ligands mutually *trans*. The phosphinous acid proton was located in the difference map, and the position of this between the two O atoms, together with the O(1)···O(2) distance of 2.38 Å, suggests a significant H-bonding interaction involving the P—O—H···O—P fragments. This type of H-bonding arrangement has been observed previously in several species including for example $[(PPh_2OMe)_2(PPh_2OH)Ru(\mu\text{-}Cl)_3Ru(PPh_2OH)_2(PPh_2O)]$ [8], $[PtH(PPh_2O^nBu)(PPh_2OH)(PPh_2O)]$ [9], $[Pd(S_2PMe_2)(PPh_2O)(PPh_2OH)]$ [10] and $[(PPh_2OH)(PPh_2O)ClRh(\mu\text{-}Cl)_3RhCl(PPh_2O)(PPh_2OH)]^-$ [11]. The Rh···Rh distance is 3.74 Å in our product, indicating non-interacting metal centres. This compares with an Rh···Rh distance of 3.745(15) Å for $[(Rh_2(PBu^n_3)_4Cl_6]$ [12].

Since only a few crystals of this material were produced, a full spectroscopic study was not possible. Importantly however, an electrospray mass spectrum of these did not reveal the same peaks as observed for $[RhCl_2(PPh_2H)_4]PF_6$ (above), showing instead peaks with the correct isotopic distributions at $m/z = 1122$ and 582, assigned to $[Rh_2Cl_3(PPh_2OH)_2(PPh_2O)_2]^+$ and $[RhCl(PPh_2OH)(PPh_2O)(MeCN)]^+$ respectively.

In a separate experiment, upon standing an ethanol solution containing $RhCl_3 \cdot 3H_2O$ and three molar equivalents of PPh_2H, a few orange prism crystals of a second dinuclear species, $[(PPh_2OH)_2(PPh_2O)Rh(\mu\text{-}Cl_3)Rh(PPh_2OH)(PPh_2O)_2]$, were produced (together with phosphine oxide and other decomposition products). The crystal structure of this material shows (Fig. 3, Table 2) a $(\mu\text{-Cl})_3$ confacial bioctahedral geometry, in which one Rh(III) centre is formally ligated to two PPh_2OH and one PPh_2O^- ligands and three bridging Cl's, while the other formally has one PPh_2OH, two PPh_2O^- and three bridging Cls. The phosphinous acid protons were not identified in the difference map in this case, however they are again implicated by the

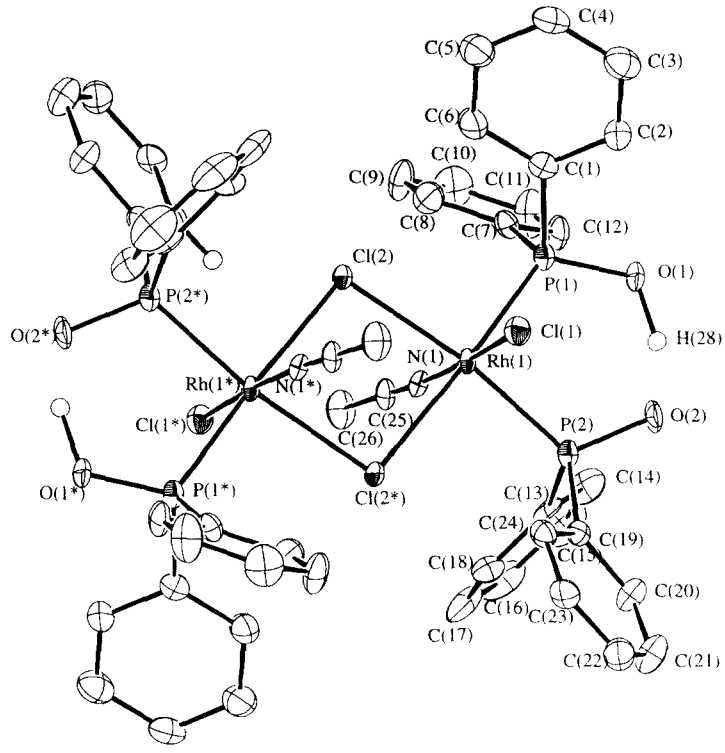

Fig. 2. View of the structure of $[(PPh_2OH)(PPh_2O)Cl(NCMe)Rh(\mu\text{-}Cl)_2Rh(PPh_2OH)(PPh_2O)Cl(NCMe)]$ with the numbering scheme adopted. Atoms marked * are related by a crystallographic inversion centre.

Table 1. Selected bond lengths and angles for $[(PPh_2OH)(PPh_2O)Cl(NCMe)Rh(\mu\text{-}Cl)_2Rh(PPh_2OH)(PPh_2O)Cl(NCMe)]$

Bond lengths (Å)

Atom	Atom	Distance	Atom	Atom	Distance
Rh(1)	Cl(1)	2.321(3)	Rh(1)	Cl(2)*	2.493(2)
Rh(1)	Cl(2)	2.500(3)	Rh(1)	P(1)	2.267(3)
Rh(1)	P(2)	2.268(3)	Rh(1)	N(1)	2.015(8)
P(1)	O(1)	1.552(6)	P(1)	C(1)	1.823(10)
P(1)	C(7)	1.808(9)	P(2)	O(2)	1.549(6)
P(2)	C(13)	1.801(10)	P(2)	C(19)	1.803(9)
N(1)	C(25)	1.14(1)	C(25)	C(26)	1.46(1)

Bond angles (°)

Atom	Atom	Atom	Angle	Atom	Atom	Atom	Angle
Cl(1)	Rh(1)	Cl(2)	93.23(9)	Cl(1)	Rh(1)	Cl(2)	96.35(9)
Cl(1)	Rh(1)	P(1)	86.37(10)	Cl(1)	Rh(1)	P(2)	89.40(9)
Cl(1)	Rh(1)	N(1)	176.9(2)	Cl(2)	Rh(1)	Cl(2)*	83.04(8)
Cl(2)	Rh(1)	P(1)	94.35(9)	Cl(2)	Rh(1)	P(2)	171.90(10)
Cl(2)	Rh(1)	N(1)	83.7(2)	Cl(2)*	Rh(1)	P(1)	176.3(1)
Cl(2)*	Rh(1)	P(2)	89.06(9)	Cl(2)*	Rh(1)	N(1)	83.7(2)
P(1)	Rh(1)	P(2)	93.5(1)	P(1)	Rh(1)	N(1)	93.5(2)
P(2)	Rh(1)	N(1)	93.7(2)	Rh(1)	Cl(2)	Rh(1)*	96.96(8)
Rh(1)	P(1)	O(1)	114.4(3)	Rh(1)	P(1)	C(1)	116.0(3)
Rh(1)	P(1)	C(7)	109.1(3)	O(1)	P(1)	C(1)	104.5(4)
O(1)	P(1)	C(7)	107.7(4)	C(1)	P(1)	C(7)	104.5(4)
Rh(1)	P(2)	O(2)	115.3(3)	Rh(1)	P(2)	C(13)	107.7(3)
Rh(1)	P(2)	C(19)	118.3(3)	O(2)	P(2)	C(13)	107.5(4)
O(2)	P(2)	C(19)	103.4(4)	C(13)	P(2)	C(19)	103.6(4)

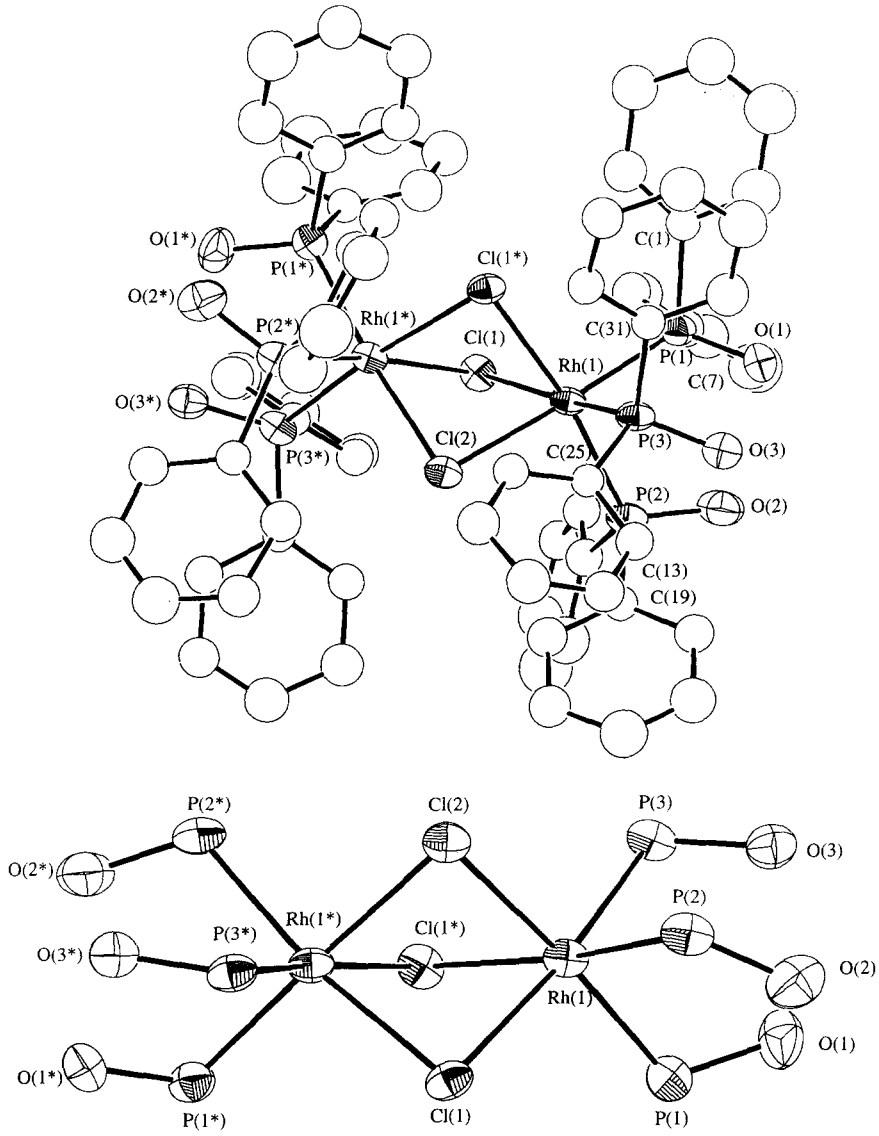

Fig. 3. View of the structure of $[(PPh_2OH)_2(PPh_2O)Rh(\mu\text{-}Cl)_3Rh(PPh_2OH)(PPh_2O)_2]$ (a) with the numbering scheme adopted and (b) showing the chloro-bridged core. Atoms marked * are related by a crystallographic 2-fold axis.

O···O distances, O(1)···O(2) = 2.55, O(1)···O(3) = 2.54, O(2)···O(3) = 3.01 Å. Hence these interatomic distances suggest that the most plausible arrangement is for O(1) to be deprotonated, since this allows a significant H-bonding interaction of O(1) with both the proton on O(2) and O(3). The third phosphinous acid proton is disordered across a crystallographic two-fold axis and must be associated with either O(2) or O(3) and only on one half of the molecule. However, there is little doubt over its presence since otherwise, counting charges would imply a Rh(II)/Rh(III) dimer which is highly unlikely, and further, there was no evidence for any other species in the difference map. Stephenson and co-workers reported a similar disorder problem in the structure of the Ru(II)/Ru(II) dimer $[(PPh_2OEt)_2(PPh_2OH)Ru(\mu\text{-}Cl)_3Ru(PPh_2OH)_2(PPh_2O)]$, which also crystallises in the space group F_{ddd} with a half-molecule in the asymmetric unit. In this case there was substantial disorder of the PPh_2O^- and PPh_2OEt ligands about a two-fold axis or centre of symmetry [8]. They also reported a full structure determination on the related confacial bioctahedral Ru(II)/Ru(II) dimer $[(PPh_2OMe)_2(PPh_2OH)Ru(\mu\text{-}Cl)_3Ru(PPh_2OH)_2(PPh_2O)]$, formed by pyrolysis of $[PPh_2OMe)_3Ru(\mu\text{-}Cl)_3Ru(PPh_2OMe)_3]Cl$ for 12 h at 120°C [8]. The Rh···Rh distance in $[(PPh_2OH)_2(PPh_2O)Rh(\mu\text{-}Cl)_3Rh(PPh_2OH)(PPh_2O)_2]$ is 3.39 Å. The only previously reported dinuclear Rh(III) complex which involves similar phosphinito ligation is the anionic dimer $[(PPh_2OH)(PPh_2O)ClRh(\mu\text{-}Cl)_3RhCl(PPh_2O)(PPh_2OH)]^-$ for which d(Rh···Rh) is 3.2262(16) [11].

Table 2. Selected bond lengths and angles for $[(PPh_2OH)_2(PPh_2O)Rh(\mu\text{-}Cl)_3Rh(PPh_2OH)(PPh_2O)_2]$

Bond lengths (Å)

Atom	Atom	Distance	Atom	Atom	Distance
Rh(1)	Cl(1)	2.517(5)	Rh(1)	Cl(1)*	2.458(5)
Rh(1)	Cl(2)	2.459(5)	Rh(1)	P(1)	2.293(6)
Rh(1)	P(2)	2.312(6)	Rh(1)	P(3)	2.282(5)
P(1)	O(1)	1.55(1)	P(1)	C(1)	1.81(2)
P(1)	C(7)	1.85(2)	P(2)	O(2)	1.59(2)
P(2)	C(13)	1.82(2)	P(2)	C(19)	1.83(2)
P(3)	O(3)	1.56(1)	P(3)	C(25)	1.79(2)
P(3)	C(31)	1.84(2)			

Bond angles (°)

Atom	Atom	Atom	Angle	Atom	Atom	Atom	Angle
Cl(1)	Rh(1)	Cl(1)*	78.4(2)	Cl(1)	Rh(1)	Cl(2)	77.8(1)
Cl(1)	Rh(1)	P(1)	96.8(2)	Cl(1)	Rh(1)	P(2)	99.2(2)
Cl(1)	Rh(1)	P(3)	171.5(2)	Cl(1)	Rh(1)	Cl(2)	78.9(1)
Cl(1)*	Rh(1)	P(1)	99.9(2)	Cl(1)*	Rh(1)	P(2)	170.9(2)
Cl(1)*	Rh(1)	P(3)	93.5(2)	Cl(2)	Rh(1)	P(1)	174.6(2)
Cl(2)	Rh(1)	P(2)	92.0(2)	Cl(2)	Rh(1)	P(3)	98.1(2)
P(1)	Rh(1)	P(2)	89.1(2)	P(1)	Rh(1)	P(3)	87.2(2)
P(2)	Rh(1)	P(3)	88.4(2)	Rh(1)	Cl(1)	Rh(1)*	85.9(2)
Rh(1)	Cl(2)	Rh(1)*	87.1(2)	Rh(1)	P(1)	O(1)	113.5(6)
Rh(1)	P(1)	C(1)	116.9(7)	Rh(1)	P(1)	C(7)	112.9(7)
O(1)	P(1)	C(1)	103.4(9)	O(1)	P(1)	C(7)	106.9(9)
C(1)	P(1)	C(7)	102.1(9)	Rh(1)	P(2)	O(2)	113.7(6)
Rh(1)	P(2)	C(13)	114.0(7)	Rh(1)	P(2)	C(19)	114.8(7)
O(2)	P(2)	C(13)	102.8(9)	O(2)	P(2)	C(19)	105.8(9)
C(13)	P(2)	C(19)	104.5(9)	Rh(1)	P(3)	O(3)	112.3(5)
Rh(1)	P(3)	C(25)	115.0(7)	Rh(1)	P(3)	C(31)	114.1(6)
O(3)	P(3)	C(25)	105.6(8)	O(3)	P(3)	C(31)	106.7(8)
C(25)	P(3)	C(31)	102.1(9)				

A mass spectrum of the remaining crystals showed peaks around $m/z = 1487$ corresponding to loss of one Cl from the neutral dimer, and once again there was no evidence for any rhodium species involving PPh_2H ligands. Furthermore, an IR spectrum showed peaks due to the PPh_2OH and PPh_2O^- ligands as well as a weak absorption at 253 cm^{-1} assigned to $\nu(Rh—Cl_{bridging})$.

These results show that while PPh_2H and PCy_2H react readily with Rh(III) to give the tetrakis phosphine cations $[RhCl_2(L)_4]^+$, the diphenylphosphine complex is not very stable in solution, readily undergoing oxidation and dimerisation. This is in contrast to the behaviour of the Ru(II) and Os(II) species *trans*-$[MX_2(L)_4]$ (X = Cl or Br; L = PPh_2H, PCy_2H, $PPhH_2$) which are apparently much more stable [3,4]. The dinuclear species reported here presumably precipitate out of solution due to their poor solubilities. Prior to this work there was only one reported Rh(III) chloro-bridged dimer involving phosphinite ligands [11]. Current work is aimed at finding alternative, more direct, synthetic routes to these and other rhodium phosphinite derivatives.

EXPERIMENTAL

Infrared spectra were measured as KBr or CsI discs or as Nujol mulls using a Perkin–Elmer 983G spectrometer over the range 180–4000 cm^{-1}. Mass spectra were run by positive electrospray (ES) using a VG Biotech Platform. ^1H NMR spectra were recorded using a Bruker AM300 spectrometer operating at 300 MHz. $^{31}P\{^1H\}$ NMR spectra were recorded in 10 mm o.d. tubes containing ca 10% deuterated solvent, using a Bruker AM360 spectrometer operating at 145.8 MHz and are referenced to external 85% H_3PO_4 [$\delta(^{31}P) = 0$]. Microanalyses were performed by the Imperial College microanalytical service. PCy_2H was purchased from Strem and PPh_2H was prepared by the literature procedure [13].

PREPARATIONS

trans-$[RhCl_2(PPh_2H)_4]PF_6$

$RhCl_3 \cdot 3H_2O$ (0.106 g, 0.40 mmol), PPh_2H (0.45 ml, 2.4 mmol) and a small excess of NH_4PF_6 (0.08 g,

0.5 mmol) were added to stirring, degassed EtOH (30 cm^3) under a N_2 atmosphere. This solution was stirred at room temperature for 1 day during which time a light yellow precipitate was deposited. This was collected by filtration, washed with Et_2O and dried *in vacuo* (Yield: 0.41 g, 95%). Calc. for $C_{48}H_{44}Cl_2F_6P_5Rh$: C = 54.2, H = 4.1%; Found: C = 53.8, H = 3.8%. Electrospray mass spectrum (MeCN): found $m/z = 883$, 847; Calc. for $[^{103}Rh^{35}Cl(PPh_2H)_4]^+$ $m/z = 882$, $[^{103}Rh(PPh_2H)_4]^+$ $m/z = 847$. $^{31}P\{^1H\}$ NMR spectrum ($CH_2Cl_2/CDCl_3$, 300 K): $\delta + 1.2$ (*d*, PPh_2H, 4P, $J_{RhP} = 83$ Hz), -146.3 (*spt*, PF_6^-, 1P). ^1H NMR spectrum (300 MHz, $CDCl_3$, 300 K): δ 7.1–7.4 (*m*, Ph), 5.7 (*m*, P*H*). IR spectrum (CsI disk): 3051 w, 2372 w, 1460 m, 1375 m, 1308 m, 1182 m, 1161 m, 1071 m, 923 m, 840 vs, 735 m, 557 s, 504 m, 477 w, 448 m, 420 w, 365 w cm^{-1}.

trans-$[RhCl_2(PCy_2H)_4]PF_6$

$RhCl_3 \cdot 3H_2O$ (100 mg, 0.38 mmol) dissolved in a minimum volume of H_2O was added to deoxygenated EtOH (20 cm^3). Excess PCy_2H (0.45 cm^3, 2.3 mmol) was added to the solution and the mixture was refluxed under N_2 for 3 h, yielding a yellow solution. Addition of excess NH_4PF_6 gave a yellow solid which was collected by filtration, washed with Et_2O and dried *in vacuo* (Yield: 0.22 g, 52%). Calc. for $C_{48}H_{88}Cl_2F_6P_5Rh$: C = 51.9, H = 8.3%; Found: C = 51.6, H = 8.1%. Electrospray mass spectrum (MeCN): found $m/z = 965$, 767; calculated for $[^{103}Rh^{35}Cl_2(PCy_2H)_4]^+$ $m/z = 965$, $[^{103}Rh^{35}Cl_2(PCy_2H)_3]^+$ $m/z = 767$. $^{31}P\{^1H\}$ NMR spectrum ($CH_2Cl_2/CDCl_3$, 300 K): δ -5.0 (*d*, PCy_2H, 4P, $J_{RhP} = 74$ Hz), -146.3 (*spt*, PF_6^-, 1P). IR spectrum (CsI disk): 2921 s, 2851 sm, 2362 w, 2321 w, 1460 m, 1375 m, 1290 w, 1263 w, 1226 w, 1199 w, 1175 w, 1075 m, 1048 w, 1002 m, 936 w, 920 w, 836 vs, 722 m, 559 s 513 wm 478 m, 449 w, 432 w, 389 w, 343 m, 281 w cm^{-1}.

X-RAY CRYSTALLOGRAPHY

$[(PPh_2OH)(PPh_2O)Cl(NCMe)Rh(\mu\text{-}Cl)_2Rh(PPh_2OH)(PPh_2O)Cl(NCMe)] \cdot 2thf$

Yellow, columnar crystals of $[(PPh_2OH)(PPh_2O)Cl(NCMe)Rh(\mu\text{-}Cl)_2Rh(PPh_2OH)(PPh_2O)Cl(NCMe)] \cdot 2thf$ were obtained from a solution of *trans*-$[RhCl_2(PPh_2H)_4]PF_6$ in MeCN/thf. The selected crystal ($0.30 \times 0.20 \times 0.15$ mm) was coated with mineral oil and mounted on a glass fibre under a cold stream of N_2 gas.

Crystal data. $C_{60}H_{56}Cl_4N_2O_6P_4Rh_2$, $M = 1372.6$, triclinic, space group P_1 (#2), $a = 13.056(2)$, $b = 13.920(3)$, $c = 9.276(4)$ Å, $\alpha = 107.50(2)$, $\beta = 100.50(2)$, $\gamma = 103.32(2)^\circ$, $V = 1504.4(8)$ Å^3 [from 2θ values of 20 reflections measured at $\pm\omega$], $\lambda = 0.71073$ Å, $Z = 1$, $D_{calc} = 1.515$ g cm^{-3}, $\mu = 8.82$ cm^{-1}, $F(000) = 696$.

Data collection and processing. Data collection used a Rigaku AFC7S diffractometer equipped with an Oxford Systems cryostream operating at 150 K, using graphite monochromated Mo-K_α radiation, (ω-2θ scan technique), 5542 data collected ($2\theta_{max}$ 50.0°), 5290 unique data ($R_{int} = 0.063$ based on F^2). As there were no identifiable faces an empirical absorption correction was applied using ψ-scans (min. and max. transmission factors were 0.738 and 1.000 respectively).

Structure solution and refinement. The structure was solved by direct methods [14] and expanded using Fourier techniques to locate all non-H atoms in the half-molecule in the asymmetric unit (related to the other half by a centre of symmetry) [15]. During refinement one fully occupied THF solvent molecule was also identified in the asymmetric unit. All non-H atoms were refined anisotropically and hydrogen atoms were included in fixed calculated positions [with d(C—H) = 0.96 Å] but not refined. The H atom associated with the PPh_2OH ligands was located in the difference map and included but not refined. The final cycle of full-matrix least-squares refinement (on *F*) was based on 2859 observed reflections with ($I > 2.5\sigma(I)$) and 352 variable parameters and converged with $R = 0.053$, R_w 0.059, using the weighting scheme $w^{-1} = \sigma^2(F)$. The maximum residual peak and minimum residual trough corresponded to $+1.33$ and -1.45 eÅ^{-3}. Selected bond lengths and angles are given in Table 1.

$[(PPh_2OH)_2(PPh_2O)Rh(\mu\text{-}Cl)_3Rh(PPh_2OH)(PPh_2O)_2]$

Orange prisms of $[(PPh_2OH)_2(PPh_2O)Rh(\mu\text{-}Cl)_3Rh(PPh_2OH)(PPh_2O)_2]$ were obtained from a solution of $RhCl_3 \cdot 3H_2O$ (0.094 g, 0.36 mmol) and three molar equivalents of PPh_2H (1.08 mmol) in EtOH (20 cm^3), which was refluxed for one hour to give an organge solution, and then maintained at ca -15°C over several days. The selected crystal ($0.55 \times 0.40 \times 0.30$ mm) was coated with mineral oil and mounted on a glass fibre under a cold stream of N_2 gas.

Crystal data. $C_{72}H_{63}Cl_3O_6P_6Rh_2$, $M = 1522.30$, orthorhombic, space group F_{ddd}, $a = 25.861(6)$, $b = 43.002(5)$, $c = 23.924(5)$ Å, $V = 26605(7)$ Å^3 [from 2θ values of 20 reflections measured at $\pm\omega$], $\lambda = 0.71073$ Å, $Z = 16$, $D_{calc} = 1.520$ g cm^{-3}, $\mu = 8.13$ cm^{-1}, $F(000) = 12384$.

Data collection and processing. Data collection used a Rigaku AFC7S diffractometer equipped with an Oxford Systems cryostream operating at 150 K, using graphite monochromated Mo-K_α radiation. Using the ω scan technique 6235 data were collected ($2\theta_{max}$ 50.0°). As there were no identifiable faces an empirical absorption correction was applied using ψ-scans (min.

and max. transmission factors were 0.910 and 1.000 respectively).

Structure solution and refinement. The structure was solved by direct methods [14] and expanded using Fourier techniques to locate all non-H atoms in the half-molecule in the asymmetric unit (related to the other half by a crystallographic two-fold axis) [15]. The Rh, Cl, P and O atoms were refined anisotropically and hydrogen atoms were included in fixed calculated positions [with d(C—H) = 0.96 Å] but not refined. The H atoms associated with the PPh_2OH ligands were not located in the difference map, and were therefore omitted from the final structure factor calculation. The final cycle of full-matrix least-squares refinement (on F) was based on 2461 observed reflections with ($I > 2.5\sigma(I)$) and 222 variable parameters and converged with $R = 0.076$, R_w 0.104, using the weighting scheme $w^{-1} = \sigma^2(F)$. The maximum residual peak and minimum residual trough corresponded to +2.19 (attempts were made to refine this as a partially occupied O atom e.g. from a H_2O solvent molecule, but without success) and −0.78 e $Å^{-3}$. Selected bond lengths and angles are given in Table 2.

Atomic coordinates, anisotropic thermal parameters and bond lengths and angles for the two structures have been deposited at the Cambridge Crystallographic Data Centre (CCDC).

Acknowledgements—We thank the EPSRC for a studentship (S.J.A.P.) and for provision of the X-ray diffractometer. We also thank Johnson Matthey plc for loans of $RhCl_3 \cdot 3H_2O$.

REFERENCES

1. (a) For examples see *The Chemistry of Organophosphorus Compounds*, Vol. 1, ed. F. R. Hartley. Wiley, 1990; (b) Brauer, D. J., Knuppel, P. C. and Stelzer, O., *Chem. Ber.*, 1987, **120,** 81; (c) Bartsch, R., Hietkamp, S., Morton, S., Peters, H. and Stelzer, O., *Inorg. Chem.*, 1983, **22,** 3624; (d) Brauer, D. J., Gol, F., Hietkamp, S., Peters, H., Sommer, H., Stelzer, O. and Sheldrick, W. S., *Chem. Ber.*, 1986, **119,** 349; (e) Sanders, J. R., *J. Chem. Soc. A*, 1971, 2991; (f) *J. Chem. Soc., Dalton Trans.*, 1973, 743; (g) Cotton, F. A., Frenz, B. A. and Hunter, D. L., *Inorg. Chim. Acta*, 1976, **16,** 203; (h) McAslan, E. B., Blake, A. J. and Stephenson, T. A., *Acta Cryst., Sect. C*, 1989, **45,** 1811; (i) Levason, W., McAuliffe, C. A. and Riley, B., *Inorg. Nucl. Chem. Lett.*, 1973, **9,** 1201; Brandon, J. B. and Dixon, K. R., *Can. J. Chem.*, 1981, **59,** 1188.
2. Forder, R. J., Mitchell, I. S., Reid, G. and Simpson, R. H., *Polyhedron*, 1994, **13,** 2129.
3. Blake, A. J., Champness, N. R., Forder, R. J., Frampton, C. S., Frost, C. A., Reid, G. and Simpson, R. H., *J. Chem. Soc., Dalton Trans.*, 1994, 3377.
4. Forder, R. J. and Reid, G., *Polyhedron*, 1996, **15,** 3249.
5. Doel, C. L., Frampton, C. S., Gibson, A. M. and Reid, G., *Polyhedron*, 1995, **14,** 3139.
6. (a) Rigo, P. and Bressan, M., *Inorg. Chem.*, 1976, **15,** 220; (b) Holah, D. G., Hughes, A. N. and Hui, B. C., *Can. J. Chem.*, 1972, **50,** 3714.
7. Hayter, R. G., *Inorg. Chem.*, 1964, **3,** 301.
8. Gould, R. O., Jones, L., Sims, W. J. and Stephenson, T. A., *J. Chem. Soc., Dalton Trans.*, 1977, 669.
9. Cornock, M. C., Gould, R. O., Jones, C. L. and Stephenson, T. A., *J. Chem. Soc., Dalton Trans.*, 1997, 1307.
10. Kong, P.-C. and Roundhill, D. M., *J. Chem. Soc., Dalton Trans.*, 1974, 187.
11. (a) Duncan, J. A. S., Hedden, D., Roundhill, D. M., Stephenson, T. A. and Walkinshaw, M., *Angew. Chem., Int. Ed., Engl.*, 1982, **21,** 452; (b) Duncan, J. A. S., Hedden, D., Roundhill, D. M., Stephenson, T. A. and Walkinshaw, M., *J. Chem. Soc., Dalton Trans.*, 1984, 801.
12. Muir, J. A., Muir, M. M. and Rivera, A. J., *Acta Crystallogr., Sect. B*, 1974, **30,** 2062.
13. Biancho, V. D. and Doronzo, S., *Inorg. Synth.*, 1976, **16,** 161.
14. Sheldrick, G. M., SHELXS-86, program for crystal structure solution, *Acta Crystallogr., Sect. A*, 1990, **46,** 467.
15. TeXsan: Crystal Structure Analysis Package, Molecular Structure Corporation, The Woodlands, Texas, 1995.

Pergamon

PII: S0277-5387(97)00518-4

Polyhedron Vol. 17, Nos 13–14, pp. 2353–2361, 1998
© 1998 Elsevier Science Ltd
All rights reserved. Printed in Great Britain
0277-5387/98 $19.00 + 0.00

Transformation of cadmium ferricyanide by heating, milling and sonication

E. Reguera,[a]* J. Balmaseda,[b] G. Quintana,[a] A. Gomez[b] and J. Fernandez-Bertran[c]

[a] Institute of Materials and Reagents, University of Havana, San Lazaro and L, 10400 Havana, Cuba;

[b] National Center for Scientific Research, P.O. Box 6990, Havana, Cuba;

[c] Center for Pharmaceutical Chemistry, P.O. Box 16042, Havana, Cuba

(Received 12 May 1997; accepted 10 November 1997)

Abstract—On heating, milling and sonication, cadmium ferricyanide decomposes and reduces to cadmium ferrocyanide. Two compositions were studied, pure cadmium ferricyanide and mixed potassium–cadmium ferricyanide. The role of reducing agent is played by the CN^- anions liberated during the decomposition process. The solid decomposition product is composed by several phases of cadmium ferrocyanide, an Fe^{3+} phase and also potassium ferrocyanide in the case of the mixed complex salt. The decomposition process was monitored using DTA, XRD, IR and Mössbauer techniques. No occurrence of linkage isomerization in cadmium ferricyanide was detected. © 1998 Elsevier Science Ltd. All rights reserved

Keywords: cadmium ferricyanide; reducing agent; decomposition.

Transformation of hexacyanometallates through linkage isomerization was predicted and observed approximately 30 years ago [1–3]. The phenomena have been well established for ferrous chromicyanide and manganicyanide which transform spontaneously into the corresponding ferrocyanides [2–5]. The change in the structural chain M—NC—M′ can be envisaged as a flipping of the CN ligands through an unstable intermediate ferric salt produced by an electron transfer which reduces the inner cation to Cr^{II} and Mn^{II} [5]. Other results such as the isomerization of cobaltous chromicyanide [2] and silver cobalticyanide [6] have been contested [5,7]. House *et al.* have reported the isomerization of $KCd[Fe(CN)_6]\cdot 5H_2O$ on heating at above 110°C [8] and on sonication [9]. In this report we present evidence that $Cd_3[Fe(CN)_6]_2\cdot 12H_2O$ and $KCd[Fe(CN)_6]\cdot 5H_2O$ undergo reduction to ferrocyanides when heated, milled or sonicated, without linkage isomerization. The processes were followed by DTA, XRD, IR and Mössbauer techniques.

* Author to whom correspondence should be addressed.

EXPERIMENTAL

Cadmium ferricyanide was prepared in two different compositions: $Cd_3[Fe(CN)_6]_2\cdot 12H_2O$ and $KCd[Fe(CN)_6]\cdot 5H_2O$; in the following, $Cd_3Fe_2^{III}$ and $KCdFe^{III}$, respectively. The former composition was obtained mixing five-fold excess of cadmium chloride with potassium ferricyanide as aqueous solutions. The precipitate was filtered, washed several times with distilled water and dried in a desiccator over silica gel. $KCdFe^{III}$ was prepared in the same manner but using a large excess of potassium ferricyanide. By the same procedure cadmium ferrocyanide ($Cd_2[Fe(CN)_6]\cdot xH_2O$) and mixed potassium–cadmium ferrocyanide ($CdK_2[Fe(CN)_6]\cdot xH_2O$), which we will label Cd_2Fe^{II} and CdK_2Fe^{II}, were also prepared. In the preparation of Cd_2Fe^{II} and CdK_2Fe^{II}, ferrocyanic acid and potassium ferrocyanide, respectively, were used. Mixed potassium–cadmium ferrocyanide was also obtained by mechanochemical reduction of $Cd_3Fe_2^{III}$ and $KCdFe^{III}$ by milling with KBr [10,11]. These last two complexes together with manganous ferrocyanide ($Mn_2[Fe(CN)_6]\cdot 8H_2O$), in the following Mn_2Fe^{II}, were used as reference compounds. The preparation of Mn_2Fe^{II} is reported elsewhere [12]. The compositions

suggested by the above abbreviations were confirmed by chemical analysis. Hydration degree was determined using thermogravimetry.

The nature and transformations of $Cd_3Fe_2^{III}$, $KCdFe^{III}$, Cd_2Fe^{II}, CdK_2Fe^{II} and Mn_2Fe^{II} were followed by IR spectroscopy in Nujol mulls between CaF_2 plates and in KBr disks, using an ATI Mattson (Genesis Series) FT-IR spectrometer, in the frequency range of 4000–400 cm^{-1}. The structural characterization was performed through XRD with monochromated CuK_α and CoK_α radiations in a HZG-4 diffractometer (Carl Zeiss). Thermal analysis was carried out in a MOM Q-1500 equipment.

The Mössbauer spectra were recorded at room temperature with a Co^{57} in Rh source, using a constant acceleration spectrometer (from Mosstec). All spectra were fitted using an iterative least-squares minimisation algorithm and pseudo-Lorentzian line shapes to obtain the values of isomer shift (δ), quadrupole splitting (Δ), linewidth (Γ) and relative area (A). The isomer shift values are reported relative to sodium nitroprusside.

Isothermal heating of samples was carried out in air in the temperature range of 100–150°C using a sand-bath regulated at ± 3°C and heating times from some minutes to 100 h. Samples were also heated in vacuum at a pressure of 10^{-6} Torr. Irradiation with microwaves was performed using a domestic oven (from Sanyo) operated at 500 watts. For sonication experiments 0.1 g of sample was mixed with 20 ml of dioxane in a glass container and then irradiated up to 2 h using a laboratory ultrasound apparatus (homemade). The effect of milling on the compounds was studied grinding the samples at room temperature and at 80°C in an agate mortar. Samples were also milled in a micronizer (ZM-1 Retsch) at 20,000 rpm.

Table 1. Crystal data of $Cd_2[Fe(CN)_6]\cdot 3H_2O$

hkl	d_{obs}	$d_{calc.}$	I/I_o	*hkl*	d_{obs}	$d_{calc.}$	I/I_o
100	6.338	6.336	33	220	2.240	2.241	44
001	5.481	5.492	4	202	2.073	2.073	3
101	4.146	4.145	100	212	1.970	1.970	15
200	3.169	3.168	32	003	1.826	1.827	9
210	2.835	2.832	32	103	1.756	1.755	9
201, 002	2.744	2.746	5	321	1.675	1.675	5
102, 211	2.515	2.516	14	203	1.582	1.583	8

Crystal Cell: Tetragonal; Cell parameters (Å): $a = 6.346(1)$; $b = 6.346(1)$; $c = 10.959(1)$.

Table 2. Crystal data of $CdK_2[Fe(CN)_6]\cdot 2H_2O$

hkl	d_{obs}	$d_{calc.}$	I/I_o	*hkl*	d_{obs}	$d_{calc.}$	I/I_o
110	5.977	5.986	8	320	2.501	2.500	5
101	5.737	5.753	8	122	2.465	2.464	5
011	5.074	5.078	73	130	2.399	2.399	4
111	4.539	5.543	6	321	2.354	2.353	6
020	3.700	3.703	30	312	2.310	2.310	7
211	3.590	3.593	100	420	2.095	2.095	12
002	3.489	3.489	22	402	2.055	2.054	12
012	3.156	3.156	5	330	1.996	1.995	3
121	3.113	3.114	9	132	1.976	1.977	4
301	3.046	3.048	9	501	1.952	1.952	3
112	3.016	3.014	12	040	1.852	1.852	4
311	2.819	2.819	7	422	1.797	1.796	11
221	2.751	2.751	5	141	1.762	1.763	3
212	2.683	2.681	3	042	1.636	1.636	4

Crystal cell: Orthorhombic; $Z = 2$; $\rho_m = 2.75$ g cm^{-3}; $\rho_c = 2.77$ g cm^{-3}.

Cell parameters (Å): $a = 10.166(2)$; $b = 7.406(1)$; $c = 6.978(2)$.

RESULTS AND DISCUSSION

Characterization of the initial compounds and standards

As far as we know, the crystalline structure of Cd_2Fe^{II} and CdK_2Fe^{II} have not been previously reported. We have found these compounds tetragonal and orthorhombic, respectively, their crystal data are given in Tables 1 and 2. Some of the reported XRD powder patterns for cadmium ferrocyanide [13–15] can be indexed using these two unit cells. The structural refinement of these compounds will be reported elsewhere. According to their XRD powder patterns, both $Cd_3Fe_2^{III}$ and $KCdFe^{III}$ crystallise in the fcc crystal cell (Fm3m) of Prussian Blue analogs [16–18] with slightly different cell edges (a_0); see Fig. 1a. As the structural model for $Cd_3Fe_2^{III}$ can be used, the reported structure for divalent transition metal hexacyanometallates(III) [19–26], where 33% of the complex anions positions are left vacant. The vacant sites are occupied by water molecules which replace some CN ligands of the outer Cd^{2+} cations. The structure of $KCdFe^{III}$ has a cubic framework of Fe^{III}—CN—Cd^{2+} chains with potassium cations occupying half of the small cubic voids of the network, similar to that of soluble Prussian Blue $KFe[Fe(CN)_6]\cdot xH_2O$ [17].

The IR spectra of Cd_2Fe^{II} and CdK_2Fe^{II}, both in anhydrous and hydrated forms, are similar, with a strong ν(CN) band at 2063 cm^{-1} and a weak band at 2030 cm^{-1}; see Fig. 2a and Table 3. The origin of that weak band at 2030 cm^{-1} will be discussed below. Their δ(Fe—C≡N) and ν(Fe—C) vibrations fall at 595 cm^{-1} and 450 cm^{-1}, respectively. The IR spectra of $Cd_3Fe_2^{III}$ and CdK_2Fe^{III} are also similar with ν(CN), δ(Fe—C≡N) and ν(Fe—C) at 2152 cm^{-1}, 528 cm^{-1} and 415 cm^{-1}, respectively; see Fig. 2b and Table 3.

Mössbauer spectra of Cd_2Fe^{II} and CdK_2Fe^{II} are single lines, while for $Cd_3Fe_2^{III}$ and $KCdFe^{III}$ they are quadrupole doublets, see Fig. 3 and Table 4. No sig-

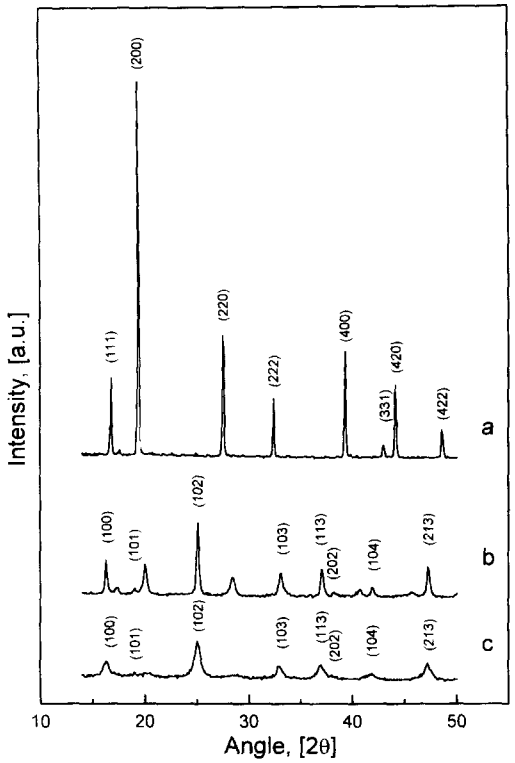

Fig. 1. XRD powder patterns of (a) cadmium ferricyanide; (b) cadmium ferricyanide heated for 50 h in air at 120°C; (c) cadmium ferricyanide milled for 2 h in agate mortar at 80°C. The decomposition products (b) and (c) are of low crystallinity, however their main reflections correspond to $Cd_2[Fe(CN)_6]\cdot xH_2O$.

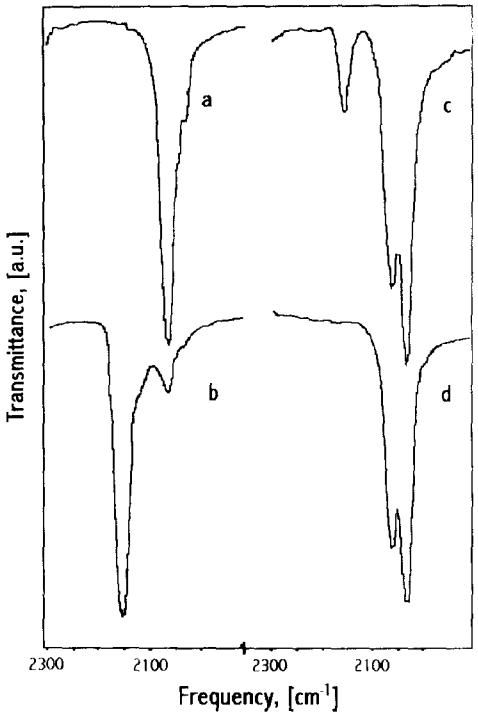

Fig. 2. IR spectra (CN stretching region) of (a) cadmium ferrocyanide; (b) cadmium ferricyanide with impurities of cadmium ferrocyanide; (c) cadmium ferricyanide heated for 20 h in air at 120°C; (d) cadmium ferricyanide heated for 50 h in air at 120°C.

nificant differences in Mössbauer parameters between pure and mixed salts are observed.

Transformations of $Cd_3[Fe(CN)_6]_2\cdot 12H_2O$

We have carried out a parallel study of the two compositions of cadmium ferricyanide. With minor differences, which will be discussed below, their behaviour on the different treatments is similar. In the following we will discuss in detail the results concerning $Cd_3Fe_2^{III}$ which is a simple salt.

Isothermal and microwave heating

When $Cd_3Fe_2^{III}$ samples are isothermally heated above 100°C, chemical processes take place. Thermal analysis shows an endothermic effect with loss of weight due to a dehydration process, which begins at about 70°C, followed at a higher temperature by a strong exothermic peak with its maximum at 150°C. Most ferricyanides decompose on heating with initial reduction as the first step, with loss of CN ligands. The free CN^- reduces the ferricyanide to ferrocyanide and at the end an oxidised phase of Fe^{3+} remains [27–32]. The heated product shows a decrease in the intensity of the 2152 cm^{-1} band until its total disappearance. New bands appear at 2063 cm^{-1} and 2030 cm^{-1}; see Fig. 2c,d and Table 3. The 2063 cm^{-1} band corresponds to Cd_2Fe^{II}. When the heating is performed in vacuum, the 2030 cm^{-1} is the main band in the decomposition product. Equal result is obtained by microwave heating; see Fig. 4a,b. Four bands at 611 cm^{-1}, 595 cm^{-1}, 456 cm^{-1} and 450 cm^{-1} appear in the low frequency region ; see Fig. 5b. The bands at 595 cm^{-1} and 450 cm^{-1} correspond to δ(Fe—C≡N) and ν(Fe—C) vibrations of Cd_2Fe^{II}. Since the pair at 611cm^{-1} and 456 cm^{-1} is dominant when the band at 2030 cm^{-1} is the most intense CN vibration (samples heated in vacuum), obviously these three bands can be assigned to a reduction product, which we interpreted as an anomalous cadmium ferrocyanide phase; in the following labelled as $Cd_2Fe^{II}(A)$. The well defined set of ν(CN), δ(Fe—C≡N) and ν(Fe—C) vibration modes supports the interpretation of that anomalous species as a metal hexacyanometallate.

XRD powder patterns confirm the decomposition of $Cd_3Fe_2^{III}$ on heating and the formation of products of low crystallinity; see Fig. 1. Samples with strong IR absorption bands at 2063 cm^{-1} and 2030 cm^{-1} have XRD powder patterns which can be interpreted

Table 3. ν(CN) frequencies of some selected samples of cadmium hexacyanoferrates and manganous ferrocyanide

Starting compound	Sample history	ν(CN) in [cm^{-1}]	Line intensity[a]	Assignment
Cd_2Fe^{II}	Without treatment	2063	S	Cd_2Fe^{II}
		2030	W	Anomalous Cd_2Fe^{II}
Cd_2Fe^{II}	Heated for 100 h in air at 150°C	2063	S	Cd_2Fe^{II}
		2030	W	Anomalous Cd_2Fe^{II}
Cd_2Fe^{II}	Very prolonged milling	2063	S(VB)	Amorphous Cd_2Fe^{II}
		2030	VW	Anomalous Cd_2Fe^{II}
Cd_2Fe^{II}	Heated for 1 h in vacuum at 400°C	2063	S	Cd_2Fe^{II}
		2030	M	Anomalous Cd_2Fe^{II}
$Cd_3Fe_2^{III}$	Without treatment	2152	S	$Cd_3Fe_2^{III}$
		2063	W	Cd_2Fe^{II}
		2030	VW	Anomalous Cd_2Fe^{II}
$Cd_3Fe_2^{III}$	Heated for 20 h in air at 120°C	2152	M	$Cd_3Fe_2^{III}$
		2063	S	Cd_2Fe^{II}
		2030	S	Anomalous Cd_2Fe^{II}
$Cd_3Fe_2^{III}$	Heated for 50 h in air at 120°C	2063	S	Cd_2Fe^{II}
		2030	S	Anomalous Cd_2Fe^{II}
$Cd_3Fe_2^{III}$	Heated for 20 h in vacuum at 140°C	2152	M	Cd_2Fe^{II}
		2063	M	Cd_2Fe^{II}
		2030	S	Anomalous Cd_2Fe^{II}
$Cd_3Fe_2^{III}$	Microwave heated for 1 h at 500 watts	2152	S	$Cd_3Fe_2^{III}$
		2063	W	Cd_2Fe^{II}
		2030	M	Anomalous Cd_2Fe^{II}
$Cd_3Fe_2^{III}$	Milled in agate mortar for 2 h at 80°C	2063	W	Cd_2Fe^{II}
		2030	S	Anomalous Cd_2Fe^{II}
$Cd_3Fe_2^{III}$	Sonicated for 1 h at room temperature	2152	S	$Cd_3Fe_2^{III}$
		2063	M	Cd_2Fe^{II}
		2030	VW	Anomalous Cd_2Fe^{II}
Mn_2Fe^{II}	Without treatment	2066	S	Hydrated Mn_2Fe^{II}
Mn_2Fe^{II}	Dehydrated at 140°C	2032	S	Anhydrous Mn_2Fe^{II}

[a] S, strong; M, medium; W, weak; VW, very weak; VB, very broad.

as normal Cd_2Fe^{II} (see Fig. 1b and Table 1) and minor diffraction peaks of non-identified decomposition products, probably phases of Fe^{3+} and Cd^{2+}. According to these results, Cd_2Fe^{II}(A) is amorphous since in spite of being the majority phase it does not produce an XRD powder pattern.

Mössbauer spectra of totally reduced $Cd_3Fe_2^{III}$ samples can be fitted as a superposition of two quadrupole doublets plus a singlet; see Fig. 3c and Table 4. According to its isomer shift value ($\delta = 0.16$ mm/s) the singlet was assigned to normal Cd_2Fe^{II}. The doublet with larger Δ value has an isomer shift ($\delta = 0.61$ mm/s) typical of high spin Fe^{3+} [33,34]. This ferric phase results from the decomposition process of $Cd_3Fe_2^{III}$ on heating. The other doublet with $\delta = 0.08$ mm/s and $\Delta = 0.20$ mm/s was assigned to Cd_2Fe^{II}(A). The high spin Fe^{3+} phase was not identified because it does not produce a reliable XRD pattern. However, it is probably a ferric oxide phase with very low particle size, which is in accordance with its Mössbauer spectra. Fe^{3+} oxide and oxihydroxide of low particle size have Mössbauer spectra at room temperature consisting in broad doublets due to their superparamagnetic behaviour [35–38].

Effect of mechanical milling and irradiation with ultrasound

Mechanical milling in an agate mortar or in a micronizer has the same effect on $Cd_3Fe_2^{III}$ that heating. In this process the rupture of metal–ligand bonds takes place induced by the mechanical deformation originated in the milling process and/or by the local heating generated in the colliding points of the crystals [39–41]. When the grinding is carried out at room temperature, to reach a 100% decomposition one must mill several hours in the agate mortar and always the resulting product shows the two CN absorption bands at 2063 cm^{-1} and 2030 cm^{-1} with approximately the same intensity. However, if the grinding process is performed at above 70°C the decomposition is fast with formation of mainly the Cd_2Fe^{II}(A) species with CN band at 2030 cm^{-1}; see Fig. 4c.

By hot-milling it is possible to obtain a decomposition product of $Cd_3Fe_2^{III}$ practically free of normal Cd_2Fe^{II}. A typical XRD powder pattern of totally reduced $Cd_3Fe_2^{III}$ sample by milling is shown in Fig. 1c. In that pattern the diffraction peaks corresponding to normal Cd_2Fe^{II} are weak and broaded. The

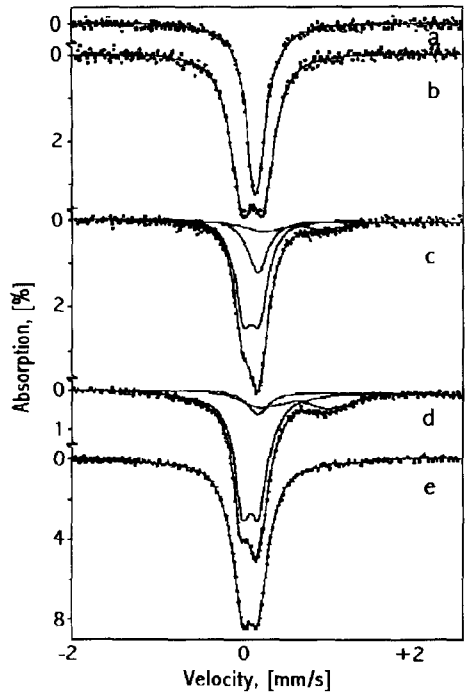

Fig. 3. Mössbauer spectra at room temperature of (a) cadmium ferrocyanide; (b) cadmium ferricyanide; (c) cadmium ferricyanide heated for 50 h in air at 120°C; (d) cadmium ferricyanide milled for 2 h in an agate mortar at 80°C; (e) anhydrous manganous ferrocyanide obtained by vacuum dehydration at 140°C.

observed broadening of the diffraction peaks can be explained as due to the preparation method. The milling process produces a material with very low particle size and deformed micro-crystals. In the Mössbauer spectra of hot-milled $Cd_3Fe_2^{III}$ samples it is also dominant the doublet corresponding to $Cd_2Fe^{II}(A)$ with about a 70% of the relative area and only a contribution of about a 9% from normal Cd_2Fe^{II}; see Fig. 3d and Table 4. The low frequency region of IR spectra is simple with the absorption bands corresponding to δ(Fe—C≡N) and ν(Fe—C) at 612 cm^{-1} and 455 cm^{-1}, respectively.

Irradiation with ultrasound in essense is similar to mechanical milling [42]. When a slurry of crystalline material is sonicated the collapse of acoustic bubbles originates the collision of particles at high speed causing their fracture [43–45] and probably also an increase of the local temperature. Our results of sonication of $Cd_3Fe_2^{III}$ samples reproduce those previously reported for $KCdFe^{III}$ submitted to similar treatment [9]. On sonication $Cd_3Fe_2^{III}$ decomposes but the decomposition product is practically free of $Cd_2Fe^{II}(A)$; see Fig. 5d and Table 3. However, we interpreted the absorption at 2063 cm^{-1} as due to normal ferrocyanide and not as occurrence of linkage isomerization in $Cd_3Fe_2^{III}$, as reported by House *et al.* [9]. With ultrasound the decomposition rate is low and even after several hours of treatment in the IR spectra of sonicated $Cd_3Fe_2^{III}$ samples the most intense band falls at 2152 cm^{-1}, corresponding to the starting compound. The absence of $Cd_2Fe^{II}(A)$ in this process could be related with that low decomposition rate. In contrast, heating and milling are more drastic processes which favour the formation of amorphous phases, like $Cd_2Fe^{II}(A)$.

Decomposition products of $CdK[Fe(CN)_6]\cdot 5H_2O$

Mixed potassium–cadmium ferrocyanide decomposes by reduction as does the pure cadmium complex ($Cd_3Fe_2^{III}$) when it is submitted to the above discussed processes. However, in the case of $CdKFe^{III}$ the IR spectra of the decomposition product are very complex with new absorption bands in the range of 2020–2100 cm^{-1}. When this product is washed with water the solid precipitate shows the CN absorption bands characteristic of the two species of Cd_2Fe^{II} while from the filtrate potassium ferrocyanide, $K_4[Fe(CN)_6]$ which we will label KFe^{II}, can be crystallised by evaporation. Potassium ferrocyanide in its anhydrous form has six CN absorption bands at 2027, 2042, 2047, 2064, 2071 and 2093 cm^{-1} [46,47]. This explains why in the IR spectra of decomposed $CdKFe^{III}$ several additional CN absorption bands are observed. During the decomposition of $CdKFe^{III}$ the formation of anhydrous KFe^{II} also takes place. The formation of single complex salts from mixed hexacyanoferrates is also observed in oxidation processes of hexacyanometallates in solid state [12].

XRD corroborates the IR results. In XRD powder patterns of decomposed $CdKFe^{III}$ samples diffraction peaks of KFe^{II} and normal Cd_2Fe^{II} can be detected. Similar information is derived from the Mössbauer spectra where also the doublet corresponding to $Cd_2Fe^{II}(A)$ is observed.

Another important peculiarity of the decomposition process of $CdKFe^{III}$ compared with $Cd_3Fe_2^{III}$ is related with their decomposition rate. Parallel heating of $Cd_3Fe_2^{III}$ and $CdKFe^{III}$ samples shows that the mixed complex presents higher stability. This could be explained by the role of crystallisation water. In alkali ferricyanides hydration water catalyses the decomposition process [31]. This fact could also explain the higher stability observed for $Cd_3Fe_2^{III}$ when it is heated in vacuum or by microwave irradiation compared with its conventional heating in air.

On the nature of anomalous cadmium ferrocyanide

In a first attempt to understand the nature of $Cd_2Fe^{II}(A)$, normal Cd_2Fe^{II} was submitted to the above discussed processes (heating, milling and sonication), however, no significant changes were observed in its IR and Mössbauer spectra; see Tables 3 and 4.. Since $Cd_2Fe^{II}(A)$ is amorphous, Cd_2Fe^{II} was

Table 4. Mössbauer parameters at room temperature of some selected samples of cadmium hexacyanoferrates and manganous ferrocyanide

Starting compound	Sample history	δ^a	Δ	Γ	A	Assignment
		(%)	(mm/s)			
Cd_2Fe^{II}	Without treatment	0.163	—	0.273	100	Cd_2Fe^{II}
Cd_2Fe^{II}	Heated for 100 h in air at 150°C	0.165	—	0.284	100	$100Cd_2Fe^{II}$
Cd_2Fe^{II}	Very prolonged milling	0.160	—	0.417	100	Amorphous Cd_2Fe^{II}
$Cd_3Fe_2^{III}$	Without treatment	0.107	0.256	0.305	100	$Cd_3Fe_2^{III}$
$Cd_3Fe_2^{III}$	Heated for 50 h in air at 120°C	0.163	—	0.273	14	Cd_2Fe^{II} Anomalous Cd_2Fe^{II}
		0.083	0.188	0.248	63	Fe^{3+} phase
		0.619	0.791	0.544	23	
$Cd_3Fe_2^{III}$	Milled in agate mortar for 2 h at 80°C	0.163	—	0.273	8	Cd_2Fe^{II} Anomalous Cd_2Fe^{II}
		0.085	0.201	0.257	70	Fe^{3+} phase
		0.615	0.803	0.558	22	
Mn_2Fe^{II}	Without treatment	0.184	—	0.260	100	Hydrated Mn_2Fe^{II}
Mn_2Fe^{II}	Dehydrated at 140°C	0.072	0.207	0.262	100	Anhydrous Mn_2Fe^{II}

[a] Isomer shift values relative to sodium nitroprusside; errors in isomer shift (δ), quadrupole splitting (Δ) and linewidth (Γ) are smaller than 0.01 mm/s.

amorphized by very prolonged milling but the resulting amorphous Cd_2Fe^{II} has IR and Mössbauer spectra very different to those observed for Cd_2Fe^{II}(A). The CN absorption of amorphous Cd_2Fe^{II} is a broad band at 2063 cm^{-1}; see Fig. 6a. The milling process partially removes the degeneration of the allowed F_{1u} triplet [17,48,49] which is observed as a broadening in the CN

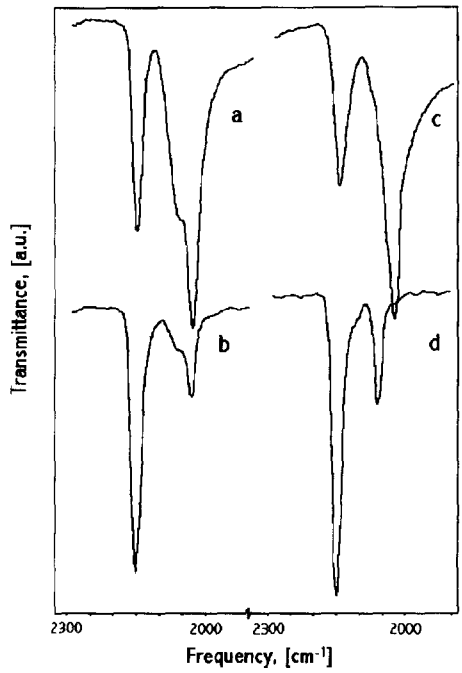

Fig. 4. IR spectra (CN stretching region) of cadmium ferricyanide (a) heated for 20 h in vacuum at 140°C; (b) irradiated with microwaves for 1 h at 500 watts; (c) milled for 30 min in agate mortar at 80°C; (d) sonicated for 1 h at room temperature.

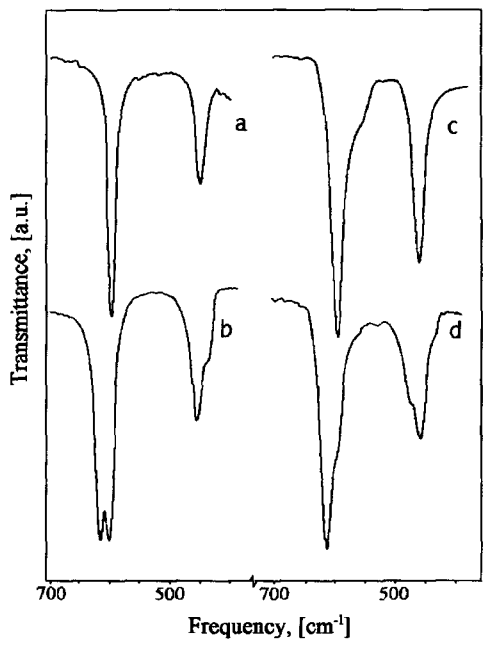

Fig. 5. IR spectra (low frequency region) of (a) cadmium ferrocyanide; (b) cadmium ferricyanide heated for 50 h in air at 120°C; (c) manganous ferrocyanide hydrate; (d) partially dehydrated manganous ferrocyanide (mixture of anhydrous and hydrated phases).

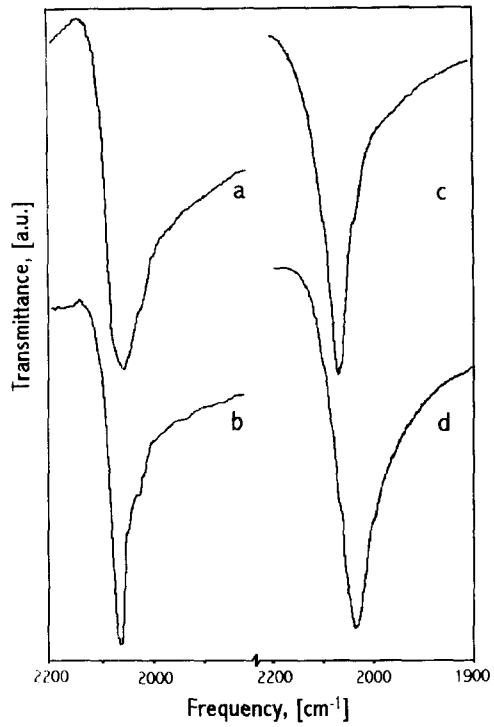

Fig. 6. IR spectra (CN stretching region) of (a) amorphous cadmium ferrocyanide (obtained by prolonged milling of ordered cadmium ferrocyanide); (b) cadmium ferrocyanide pyrolized for 1 h in vacuum at 400°C; (c) manganous ferrocyanide hydrate; (d) anhydrous manganous ferrocyanide.

absorption. The Mössbauer spectra of this amorphous Cd_2Fe^{II} can be fitted as a broad singlet or an unresolved doublet (see Table 4) which is also different to the resolved doublet observed for $Cd_2Fe^{II}(A)$.

An insight to the nature of $Cd_2Fe^{II}(A)$ can be obtained by comparing to the behaviour of manganous ferrocyanide. When Mn_2Fe^{II} is dehydrated the ν(CN) band changes from 2066 cm^{-1} to 2032 cm^{-1}; see Fig. 6c,d. This frequency shift of 34 cm^{-1} is analogous to that observed in Cd_2Fe^{II} species, of 32 cm^{-1}. The analogy is also valid for the low frequency region where the frequency shift of δ(Fe—C≡N) and ν(Fe—C) vibrations of Mn_2Fe^{II} on dehydration is 16 cm^{-1} and 5 cm^{-1}, respectively, similar to the corresponding shift observed in Cd_2Fe^{II} species; see Fig. 5c,d. In the structure of Mn_2Fe^{II} the structural $Mn_2[Fe(CN)_6]$ units are linked by three water molecules and three CN ligands [50]. On dehydration the water bridges are eliminated and these structural units remain linked by only three CN ligands, resulting in a complex where a 50% of the Fe^{II}—CN—Mn^{2+} chains are unlinked. From this point of view, $Cd_2Fe^{II}(A)$ can be imaged as a complex with many Fe^{II}—CN—Cd^{2+} chains unlinked. This picture is in accordance with the observed release of CN^- ligands during the decomposition process of $Cd_3Fe_2^{III}$ and with the amorphous character of the resulting $Cd_2Fe^{II}(A)$. A random loss of CN^- ligands must destroy the skeletal structure of the complex giving an amorphous material. The Mössbauer results also support this hypothesis. The Mössbauer spectrum of hydrated manganous ferrocyanide is a single absorption line typical of metal ferrocyanide [51–53] while in its anhydrous state the Mössbauer absorption is a doublet with δ and Δ values close to those found for $Cd_2Fe^{II}(A)$ [35]; see Fig. 2e and Table 4. The value of $\Delta \neq 0$ in this case is sensing an asymmetrical environment for Fe^{II} (lattice contribution) since low spin ferrous cation does not have electronic contribution to Δ [34,35].

Metal ferrocyanides decompose at higher temperature than the corresponding ferricyanides but also lossing CN ligands. From this fact $Cd_2Fe^{II}(A)$ could be obtained pyrolizing $CdFe^{II}$ in vacuum. When Cd_2Fe^{II} was pyrolized in vacuum above 400°C, in the resulting product appears the CN absorption at 2030 cm^{-1}, characteristics of $Cd_2Fe^{II}(A)$; see Fig. 6b.

Anomalous metal ferrocyanides are also observed in decomposition products of other metal hexacyanoferrates (II and III). A detailed study of these anomalous complexes is now in progress.

Expected Mossbauer and IR spectra for isomerized cadmium ferricyanide

Cd^{2+} forms di- and tetracyano complexes with CN ligands [17,54,55]. In consequence, a maximum of two thirds of the Fe^{3+}—CN—Cd^{2+} chains could be converted to Fe^{3+}—NC—Cd^{2+}. In an isomerized cadmium ferricyanide Fe^{3+} cations must have a mixed coordination sphere formed by four N and two C of CN ligands. Since Fe^{3+} forms low spin complexes when coordinated with CN ligands at the C end and adopts the high spin electronic configuration when the coordination takes place at the N end [34,56–60], there are two possibilities for Fe^{3+} cation in an isomerized cadmium ferricyanide: it remains in low spin state or it passes to the high spin configuration. In both possibilities the Mössbauer spectra of the isomerized species and of the initial compounds must be very different. In the former possibility a larger quadrupole splitting must be expected since in addition to the electronic contribution to the value of Δ now a lattice contribution is also present (due to the mixed coordination sphere). In the second possibility the most significant variation must be observed in the value of δ, changing from about 0.10 mm/s for the low spin configuration to about 0.64 mm/s in the high spin one [59–61].

The changes in IR spectra on isomerization of cadmium ferricyanide must also be significant and very different from those reported for thermal-treated and sonicated $KCdFe^{III}$ samples [8,9]. In $KCdFe^{III}$ or $Cd_3Fe_2^{II}$ the symmetry around the central cation (Fe^{3+}) is O_h type and only a CN absorption band is observed (degenerated F_{1u} vibrational state) but in

partially isomerized samples the point symmetry around the new central cation (Cd^{2+}) will be C_{4v} or less; in consequence the degeneration must be removed and several CN absorption bands will be observed [48,62]. Furthermore, the CN absorption corresponding to the chains Fe^{3+}—NC—Cd^{2+} must fall above 2140 cm^{-1} since this is the frequency of the anion $[Cd(CN)_4]^{2-}$ [48]. Isomerized cadmium ferricyanide should present a CN triplet near 2160 cm^{-1} [63,64].

The processes which take place in heated and sonicated cadmium ferricyanides are the normal decomposition and reduction observed in metal ferricyanides and not linkage isomerization as reported [8,9].

CONCLUSIONS

When cadmium ferricyanide or mixed potassium–cadmium ferricyanide are heated in air or in vacuum above 100°C, or irradiated with microwaves or ultrasound, or milled in a mortar or in a micronizer, the decomposition of these compounds take place with formation of several phases of cadmium ferrocyanide. In this transformation the role of reducing agent is played by the CN^- anions liberated in the decomposition process. The CN absorption bands at 2030 cm^{-1} and at 2063 cm^{-1} in the decomposition products are assigned to anomalous and normal cadmium ferrocyanides, respectively. The appearance of these two CN absorptions cannot be interpreted as occurrence of a linkage isomerization process in cadmium ferricyanide when this compound is heated or sonicated as have been reported [8,9].

Acknowledgements—The authors thank J. C. Llopiz for IR and DTA facilities, and E. Gonzalez and A. Penton for their assistance in DTA and XRD measurements, respectively. We also appreciate the help of L. Nunez in the preparation of the manuscript.

REFERENCES

1. Shriver, D. F., Shriver, S. A. and Anderson, S. E., *Inorg. Chem.*, 1965, **4,** 725.
2. Brown, D. B., Shriver, D. F. and Schwartz, L. H., *Inorg. Chem.*, 1968, **7,** 77.
3. Brown, D. B. and Shriver, D. F., *Inorg. Chem.*, 1969, **8,** 37.
4. House, J. E. Jr. and Bailar, J. C. Jr., *Inorg. Chem.*, 1969, **8,** 672.
5. Reguera, E., Fernandez-Bertran, J. and Nunez, L., *Polyhedron*, 1994, **13,** 1619.
6. Kob, N. E. and House, J. E. Jr., *Trans. Metal Chem.*, 1994, **19,** 31.
7. Reguera, E., Quintana, G. and Fernandez-Bertran, J., *Trans. Metal. Chem.*, 1997, Accepted for publication (TMC-3946).
8. Cosmano, R. J. and House, J. E. Jr., *Thermochim. Acta*, 1975, **13,** 127.
9. House, J. E. Jr. and Kob, N. E., *Inorg. Chem.*, 1993, **32,** 1053.
10. Fernandez-Bertran, J., Blanco, J. and Hernandez, M., *Spectrochim. Acta*, 1987, **43A,** 981.
11. Fernandez-Bertran, J., Blanco, J., Hernandez, M. and Rodriguez, R., *React. of Solids*, 1988, **5,** 95.
12. Reguera, E., Fernandez-Bertran, J. and Duque, J., *Polyhedron*, 1994, **13,** 479.
13. PDF 24-163, PDF-24-164; JCPDS (International Centre for Diffraction Data, 1992).
14. Kuznetsov, V. G., Popova, Z. V. and Seifer, G. B., *Russ. J. Inorg. Chem.* (Engl. Transl.), 1970, **15,** 1084.
15. Cola, M., Ganzerlini Valentini, M. T. and Borroni, P., *J. Inorg. Nucl. Chem.*, 1978, **40,** 1041.
16. Shriver, D. F., *Struct. Bonding*, 1966, **1,** 32.
17. Sharpe, A. G., in *The Chemistry of Cyano Complexes of the Transition Metals.* Academic Press, London, New York, San Francisco, 1976.
18. Reguera, E., Fernandez-Bertran, J. and Nunez, L., *Z. Naturforsch.*, 1995, **50B,** 1067.
19. Ludi, A. and Gudel, H. U., *Struct. Bonding*, 1973, **14,** 1.
20. Ludi, A., Gudel, H. U. and Ruegg, M., *Inorg. Chem.*, 1970, **9,** 2224.
21. Ron, R. G., Ludi, A. and Engel, P., *Chimica*, 1973, **27,** 77.
22. Beall, G. W., Milligan, W. O., Korp, J. and Bernal, I., *Inorg. Chem.*, 1977, **16,** 2715.
23. Mullica, D. F., Milligan, W. O., Beall, G. W. and Reeves, W. L., *Acta Cryst.*, 1978, **B34,** 3558.
24. Mullica. D. F., Milligan. W. O. and Hill, F. W., *J. Inorg. Nucl. Chem.*, 1979, **15,** 361.
25. Milligan, W. O., Mullica, D. F. and Hill, F. W., *J. Inorg. Nucl. Chem.*, 1981, **43,** 3119.
26. Mullica, D. F., Gage, J. L. and Sappenfield, E. L., *J. Solid State Chem.*, 1994, **112,** 312.
27. Chamberlain, M. M. and Greene, A. F. Jr., *J. Inorg. Nucl. Chem.*, 1963, **25,** 1471.
28. Seifer, G. B. and Makarova, Z. A., *Dokl. Akad. Nauk SSR*, 1966, **169,** 358.
29. Gallagher, P. K. and Prescott, B., *Inorg. Chem.*, 1970, **9,** 2510.
30. Fanning, J. C., Elrod, C. L., Franke, B. S. and Melnik, J. L., *J. Inorg. Nucl. Chem.*, 1972, **34,** 139.
31. Raj, D. and Danon, J., *J. Inorg. Nucl. Chem.*, 1975, **37,** 2039.
32. Bonnet, M. G. and Paris, R. A., *Bull. Soc. Chim. France*, 1975, **5–6,** 1063.
33. Long, G. J. and Grandjean, F. eds. *Mössbauer Spectroscopy Applied to Magnetism and Materials Science.* Plenum Press, New York and London, 1993.
34. Gutlich, P., in *Mössbauer Spectroscopy*, ed. U. Gonser. Springer-Verlag, Berlin, Heidelberg, New York, 1975, p. 68.
35. Reguera, E. and Fernandez-Bertran, J., *Hyp. Interact.*, 1994, **88,** 49.
36. Goldanskii, V. I. and Herber, R. H., eds. *Chemical Applications of Mössbauer Spectroscopy.* Academic Press, New York, 1968.
37. Bancroft, G. M., *Mössbauer Spectroscopy. An Introduction for Inorganic Chemists and Geochemists.* McGraw-Hill, London, New York, 1973.

38. Greenwood, N. N. and Gibb, T. C., *Mössbauer Spectroscopy*. Adam Hilger, London, 1971.
39. Boldyrev, V. V., *Solid State Ionics*, 1995, **63–65,** 537.
40. Heinicke, G., *Tribochemistry*. Akademic Verlag, Berlin, 1984.
41. Fernandez-Bertran, J., Gonzalez, E. E., de Onate, J., Lopez, R. and Navarro, E., *J. Solid State Chem.*, 1993, **107,** 314.
42. Boldyrev, V. V., *Ultrasonic Sonochem.*, 1995, **2,** 143.
43. Suslick, K. S. and Casadonte, D. J., *J. Amer. Chem. Soc.*, 1987, **109,** 3459.
44. Suslick, K. S. and Doktycz, S. J., *J. Amer. Chem. Soc.*, 1989, **111,** 2342.
45. Suslick, K. S., Casadonte, D. J. and Doktycz, S. J., *J. Chem. Mater.*, 1989, **1,** 6.
46. Reguera, E. and Fernandez-Bertran, J., *Spectrosc. Lett.*, 1996, **30,** 89.
47. Fernandez-Bertran, J. and Reguera, E., *Solid State Ionics*, 1996, **93,** 139
48. Nakamoto, K., in *Infrared Spectra of Inorganic and Coordination Compounds*. Wiley, New York, London, Sidney, Toronto, 1970.
49. Fernandez-Bertran, J., Reguera, E., Dago, A., Lopez, C. and Infante, G., *Polyhedron*, 1996, **15,** 315.
50. Ruegg, M., Ludi, A. and Rieder, K., *Inorg. Chem.*, 1971, **10,** 1773
51. Fluck, E., Kerler, W. and Neuwirth, W., *Angew. Chem.*, 1963, **75,** 461.
52. Rasmussen, P. G. and Meyers, E. A., *Polyhedron*, 1984, **3,** 183.
53. Reguera, E. and Fernandez-Bertran, J., *Eur. J. Solid State Inorg. Chem.*, 1994, **31,** 1021.
54. Nishikiori, S., Ratcliffe, C. I. and Ripmeester, J. A., *J. Amer. Chem. Soc.*, 1992, **114,** 8590.
55. Chadwick, B. M. and Sharpe, A. G., *Adv. Inorg. Chem. Radiochem.*, 1966, **8,** 83.
56. Danon, J., in *Applications of the Mössbauer Effect in Chemistry and Solid State Physics*. Technical Report Series No. 50. IAEA, Vienna, 1966, p. 89.
57. Ito, A., Suenagua, M. and Ono, K., *J. Chem. Phys.*, 1968, **4,** 3597.
58. Fluck, E., Inoue, H. and Yanagisawa, S., *Z. anorg. allg. Chem.*, 1977, **430,** 241.
59. Reguera, E., Fernandez-Bertran, J., Diaz, C. and Molerio, J., *Hyperf. Interact.*, 1992, **73,** 285.
60. Reguera, E., Fernandez-Bertran, J., Dago, A. and Diaz, C., *Hyperf. Interact.*, 1992, **73,** 295
61. Reguera, E., Fernandez-Bertran, J., Diaz, C., Blanco, J. and Rondon, S., *Hyperf. Interact.*, 1990, **55,** 391.
62. Jones, L. H., in *Inorganic Vibrational Spectroscopy*. Vol. 1. Marcel-Dekker, New York, 1971.
63. Fernandez-Bertran, J., Blanco, J. and Reguera, E., *Spectrochim. Acta*, 1990, **46A,** 685.
64. Fernandez-Bertran, J., Reguera, E. and Blanco, J., *Spectrochim. Acta*, 1990, **46A,** 1679.

Pergamon

PII: S0277-5387(97)00445-2

Polyhedron Vol. 17, Nos 13–14, pp. 2363–2371, 1998
© 1998 Elsevier Science Ltd
All rights reserved. Printed in Great Britain
0277-5387/98 $19.00 + 0.00

Calorimetric determination of the enthalpies of coordination of competitive ternary mixed-ligand complex compounds. Copper(II)-12-(2′-hydroxy-5′-bromo-benzyl)-1,4,7,10-tetraazacyclo-tridecane-11,13-dione-α-aminoacids and 5-substituted 1,10-phenanthrolines systems†

Hua-Kuan Lin,* Shou-Rong Zhu, Zhi-Fen Zhou, Xun-Cheng Su, Zong-Xin Gu and Yun-Ti Chen

Department of Chemistry, Nankai University, Tianjin, 300071, P.R. China

(Received 6 August 1997; accepted 27 October 1997)

Abstract—The enthalpies of protonation of 12-(2′-hydroxy-5′-bormo-benzyl)-1,4,7,10-tetraazacyclotridecane-11,13-dione(HBTADO) have been determined in aqueous solution at 25.0 ± 0.1°C and ionic strength 0.1 mol dm^{-3} KNO_3 by means of model RD-1 automatic conduction calorimeter. The enthalpies of coordination of the binary complex compounds of this ligand with copper(II) and the ternary complex compounds of this ligand copper(II)-5-substituted 1,10-phenanthrolines have also been determined under identical conditions of the ternary complex compounds of the type Cu(II)-α-aminoacids-HBTADO have been evaluated through "overall calculation". Linear enthalpy relationships, linear enthalpy-entropy relationships have been found to exist between the enthalpies of formation of ternary complex compounds Cu(II)-R′Phen-HRTADO and the enthalpies, entropies of protonation of ligands HRTADO. In addition, linear enthalpy relationships have been found to exist between the enthalpies of formation of ternary complex compounds Cu(II)-α-aminoacids-HRTADO and the enthalpies of formation of binary complex compounds $Cu(II)H_{-1}A$ and linear entropy relationships have been found to exist between the entropies of formation of ternary complex compounds Cu(II)-α-aminoacids-HRTADO and the entropies of formation of binary complex compounds $Cu(II)H_{-1}A$.
© 1998 Elsevier Science Ltd. All rights reserved

Keywords: enthalpy of protonation; enthalpy of coordination; HBTADO.

Macrocyclic oxopolyamines are unique metal chelators, their structure bearing the dual features of macrocyclic polyamines and oligopeptides [1–4]. Because of their important biological functions and some unusual properties, oxopolyamines have been extensively studied, and structural features for their biological significance are well recognized [1–11]. A calorimetric study of the coordination reaction in aqueous solution for these macrocyclic dioxotetraamines with metal ions can provide useful information, in particular, in understanding the high stability of these complex compounds formed from these macrocyclic polyamines with metal ions arises from enthalpy effect or entropy effect and if Linear Enthalpy Relationships (LERs) exist in these systems. In previous papers [12–15], we reported the calorimetric measurements of the enthalpies of protonation of 12-(2′-hydroxy-3′,5′-dibromobenzyl)-1,4,7,10-tetraazacyclo-tridecane-11,13-dione (HDBTADO), 12-(2′-hydroxy-benzyl)-1,4,7,10-tetraazacyclotridecane-11,13-dione(HTADO), 12-(2′-hydroxy-3′-methoxy-benzyl)1,4,7,10-tetraazacyclotridecane-11,13-dione(HMTADO), 1,4,7,10-tetraazacyclo-

* Author to whom correspondence should be addressed.

† This work 2967102 was supported by the National Natural Science Foundation of China.

tridecane-11,13-dione(TADO) and of the enthalpies of coordination of the bianary complex compounds of Cu(II)-HDBTADO, -HTADO, -HMTADO and -TADO and of the ternary complex compounds of Cu(II)-5-substituted phenanthrolines(R′Phen)-HDBTADO, -HTADO, -HMTADO and -TADO and of Cu(II)-α-aminoacids-HDBTADO, -HTADO, -HMTADO and -TADO. In order to understand how the substituents of benzyl of these macrocyclic dioxotetraamines with pendant group influence their enthalpies of coordination and entropies of coordination, in this paper, we report the study on the thermodynamical properties of protonation of 12-(2′-hydroxy-5′-bromo-benzyl)-1,4,7,10-tetraazacyclotridecane-11,13-dione(HBTADO) and of coordination of its binary complex compounds with Cu(II) as well as its ternary complex compounds with Cu(II)-R′Phen and Cu(II)-α-aminoacids.

THEORETICAL

The two amido groups in macrocyclic dioxotetraamines are equivalent upon coordination to a 3d metal ion and both are deprotonated simultaneosly [11]. The following two eqns (1) and (2) must be considered in addition to those eqns for the calculation reported earlier [16].

$$Cu + A = CuH_{-2}A + 2H$$

$$\beta_{CuH_{-2}A} = [CuH_{-2}A][H]^2/[Cu][A] \quad (1)$$

$$Cu + A = CuH_{-1}A + H$$

$$\beta_{CuH_{-1}A} = [CuH_{-1}A]/[Cu][A] \quad (2)$$

where A denotes HBTADO; H denotes hydrogen ion. Charges omitted for clarity.

EXPERIMENTAL

HBTADO was prepared and its structure determined by means of elemental analysis, IR, NMR and MS as reported earlier [17]. The rest of all chemical reagents, the experimental conditions were reported previously [12]. The methods for the measurement of all heat effects were the same as reported previously [16]. A model RD-1 automatic conduction calorimeter with a precision of ±0.5% has been used to measure the heat effect [18].

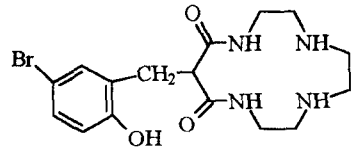

Fig. a.

RESULTS AND DISCUSSION

The experimental results of the protonation study of ligand HBTADO are presented in Table 1. The values of the enthalpies of coordination of the binary systems Cu(II)-HBTADO and of the ternary systems Cu(II)-R′Phen-HBTADO and Cu(II)-α-aminoacids-HBTADO are collected in Tables 2, 3, and 4, respectively. Thermodynamic functions of coordination of binary systems Cu(II)-HRTADO(12-(2′-hydroxy-3′,5′-substituted benzyl)-1,4,7,10-tetraazacyclotridecane-11,13-dione) (and of protonation of ligands HRTADO) and ternary systems Cu(II)—R′Phen-HRTADO and Cu(II)-α-aminoacids-HRTADO are summarized in Tables 5, 6 and 7, respectively.

As can be seen from Table 1, the enthalpy of first protonation ligand HBTADO, i.e., the enthalpy of coordination of proton to oxygen atom of pendant group, is -29.3 ± 0.2 kJ mol^{-1}. This value is slightly larger than that of phenol, -25.5 kJ mol^{-1} [19]. As can be seen from Table 2, the enthalpies of coordination of binary complex compounds $CuH_{-2}A$ and $Cu(II)H_{-1}A$ are -12.7 ± 0.2 and -13.8 ± 0.5 kJ mol^{-1}, respectively.

These values are negative, indicating that the overall enthalpy effects of coordination of Cu(II) to ligand HBTADO are exothermic. Because the coordination of Cu(II) with the four nitrogen atoms of the HBT-

Table 1. Determination of the enthalpies of protonation of ligand HBTADO (temperature 25±0.1°C; $I = 0.1$ mol dm^{-3} KNO_3; $\Delta H_N = -59.78$ kJ mol^{-1}; $\gamma = 0.8318$)

n	$10^3 T_H$ mol dm^{-3}	$10^3 T_A$ mol dm^{-3}	pH_i	pH_f	Q_c J	pK_{D1}	pK_{D2}	pK_{D3}	ΔH_{HA} kJ mol^{-1}	ΔH_{H_2A} kJ mol^{-1}	ΔH_{H_3A} kJ mol^{-1}
4	3.047	1.016	9.72	3.44	−1.20±0.01	3.67[27]			−29.3±0.2		
4	3.047	1.523	9.96	4.65	−1.54±0.01		8.81			−24.4±0.3	
4	3.047	3.047	10.18	9.12	−1.82±0.01			9.78			−24.4±0.3

n is the number of the measurement; T_H is the total concentration of the acid; T_a is the total concentration of the HBTADO ligand; pH_i is the pH value of initial solution of HBTADO ligand; pH_f is the pH value of mixed solution of the HBTADO with acid; Q_c is the corrected heat effect of the measurement; pK_{D1}, pK_{D2}, pK_{D3} are the first, second, third dissociation constants of HBTDO ligand, respectively.

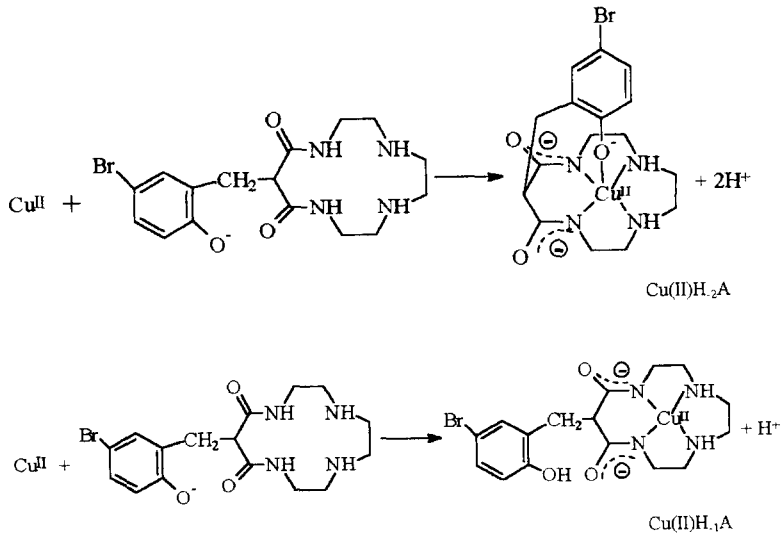

Fig. b.

Table 2. Determination of the enthalpies of formation of binary complex compound Cu(II)-HBTADO (temperature 25 ± 0.1°C; $I = 0.1$ mol dm^{-3} KNO_3)

n	10^3T_A mol dm^{-3}	10^3T_{Cu} mol dm^{-3}	pH_i	pH_f	Q_c J	$\log\beta_{CuH_{-2}A}$	$\log\beta_{CuH_{-1}A}$	$\Delta H_{CuH_{-2}A}$ kJ mol^{-1}	$\Delta H_{CuH_{-1}A}$ kJ mol^{-1}
4	3.974	1.987	10.63	8.76	-1.26 ± 0.01	1.07[28]	6.63	-12.7 ± 0.2	
4	1.987	1.987	10.03	5.27	-0.61 ± 0.01				-13.8 ± 0.5

Table 3. Determination of the enthalpies of formation of ternary complex compounds Cu(II)-R'Phen-HBTADO (temperature 25.0 ± 0.1°C; $I = 0.1$ mol dm^{-3} KNO_3)

R	n	10^3T_A mol dm^{-3}	10^3T_{Cu}RPhen mol dm^{-3}	pH_i	pH_f	Q_c J	$\log\beta_{CuRPhenA}$	$\Delta H_{CuRPhenA}$ kJ mol^{-1}
CH_3	2	1.755	1.807	10.57	8.74	-0.59 ± 0.01	9.93[27]	-6.51 ± 0.26
H	2	1.755	1.800	10.57	8.41	-0.68 ± 0.01	9.97	-8.72 ± 0.26
Cl	3	1.755	1.807	10.48	8.23	-0.64 ± 0.01	10.05	-11.2 ± 0.3
NO_2	2	1.755	1.807	10.41	7.71	-0.66 ± 0.01	10.12	-14.2 ± 0.3

Table 4. Determination of the enthalpies of formation of ternary complex compounds Cu(II)-AA-HBTADO (temperature 25.0 ± 0.1°C; $I = 0.1$mol dm^{-3} KNO_3)

α-amino acid	n	10^3T_A mol dm^{-3}	10^3T_B mol dm^{-3}	10^3T_{Cu} mol dm^{-3}	pH_i	pH_f	Q_c J	$\log\beta_{CuAE}$	ΔH_{CuAB} kJ mol^{-1}
proline	5	1.801	1.808	1.807	9.87	5.52	-0.67 ± 0.01	20.00[28]	-60.7 ± 1.0
α-aminoisobutyric acid	4	4.513	4.498	4.517	9.42	4.94	-0.90 ± 0.01	19.67	-69.7 ± 0.4
isolecuine	2	1.804	1.797	1.807	9.45	5.28	-0.72 ± 0.01	19.44	-65.9 ± 1.0
glycine	2	1.805	1.803	1.807	9.89	5.79	-1.43 ± 0.01	19.31	-65.3 ± 0.9
valine	2	1.801	1.805	1.807	9.54	5.40	-0.82 ± 0.01	19.43	-65.3 ± 0.8
serine	3	1.801	1.813	1.807	9.45	5.65	-1.01 ± 0.01	19.22	-63.0 ± 0.6

Table 5. The thermodynamic functions of protonation and coordination with Cu(II) for 1,4,7,10-tetraazacyclotridecane-11,13-dione(TADO) and its derivations(HRTADO), 25±0.1°C; I = 0.1 mol dm^{-3} KNO_3

HRADO	ΔG_{HA}	ΔG_{H_2A}	ΔG_{H_3A} kJ mol^{-1}	$\Delta G_{CuH_{-2}A}$	$\Delta G_{CuH_{-1}A}$
TADO [29]	−50.2	−20.6		13.5	
HMTADO [28]	−58.6	−51.6	−20.4	−8.96	−41.2
HTADO [28]	−57.2	−51.7	−20.9	−9.02	−40.0
HBTADO [28]	−55.8	−50.3	−21.0	−6.11	−37.9
HDBTADO	−53.6	−41.8	−31.4	3.83	−27.6
	ΔH_{HA}	ΔH_{H_2A}	ΔH_{H_3A} kJ mol^{-1}	$\Delta H_{CuH_{-2}A}$	$\Delta H_{CuH_{-1}A}$
TADO [15]	−36.8±0.2	−30.2±0.2		13.9±0.4	
HMTADO [14]	−35.6±0.3	−19.1±0.1	−18.4±0.4	−17.6±0.2	−18.8±0.4
HTADO [13]	−32.7±0.3	−22.8±1.1	−19.6±1.4	−15.1±0.2	−16.1±0.5
HBTADO	−29.3±0.2	−24.4±0.3	−24.4±0.3	−12.7±0.2	−13.8±0.5
HDBTADO [12]	−25.1±0.3	−17.0±0.7	−13.8±1.0	5.40±0.26	4.81±0.13
	ΔS_{HA}	ΔS_{H_2A}	ΔS_{H_3A} J K^{-1} mol^{-1}	$\Delta S_{CuH_{-2}A}$	$\Delta SH_{CuH_{-1}A}$
TADO	44.9	−32.2		−1.34	
HMTADO	77.1	109	6.7	−29.0	75.1
HTADO	82.2	96.9	4.4	−20.4	80.1
HBTADO	88.9	86.9	−11.4	−22.1	80.8
HDBTADO	95.6	83.2	59.0	5.3	109

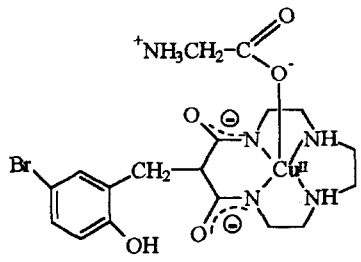

Fig. c.

ADO ligand would simultaneously release two hydrogen ions from the amido groups, a certain amount of energy was consumed, but an oxygen atom on the phenol group of HBTADO ligand binding with Cu(II)(for $CuH_{-2}A$) or hydrogen ion (for $CuH_{-1}A$) will give out a certain amount of energy which is larger than the consumed energy ($\Delta H_{CuH_{-2}TADO}$ = 13.85±0.43 kJ mol^{-1} [15]).

As can be seen from Table 3, the values of the enthalpies of coordination of ternary complex compounds CuR′PhenA are −6.51±0.26(CH_3Phen), −8.71±0.26(Phen), −11.2±0.3(ClPhen) and −14.2±0.3(NO_2Phen) kJ mol^{-1}, respectively. As the tendency of Cu(II) to coordinate R′Phen is very strong, the CuR′Phen complex does not dissociate in the pH range 2–7 and it may be regarded as a stable series. Therefore, CuR′Phen can coordinate with only two nitrogen atoms of the amindo groups of HBTADO and it cannot form a planar structure with four nitrogen atoms of the ligand HBTADO. Thus, the bond of CuR′Phen with HBTADO may bend, with energy expenditure, but the oxygen atom of phenol group takes part in the coordination with Cu(II) of Cu(II)-R′Phen by releasing of certain amount of energy to exceed the energy consumed. Therefore, enthalpies of coordination of ternary systems Cu(II)-R′Phen-HBTADO are negative values. Furthermore, a d-p back π bonding takes place between the 3d electron cloud of Cu(II) and p-orbital of R′Phen; this decreases the electron density at Cu(II), strengthens the bonding between Cu(II)-R′Phen and HBTADO, and increases the enthalpies of coordination of Cu(II)-R′Phen to HBTADO. When the substituents R′on Phen vary from CH_3 to NO_2 the coordination tendency increases, while the enthalpies of protonation of ligands R′Phen decrease with substituents varying from CH_3 to NO_2. By plotting of the enthalpies of coordination of CuR′Phen with ligand HBTADO against the enthalpies of protonation of the ligands R′Phen ($\Delta H_{HR'Phen}$ CH_3: −16.7; H: −15.1; Cl: −11.6; NO_2: −8.4 kJ mol^{-1}) [20], a straight line is obtained with a negative slope.

Table 6. The thermodynamic functions of the formation of ternary complex compounds Cu(II)-R′Phen-TADO(or its derivations HRTADO) at 25±0.1°C; $I = 0.1$ mol dm^{-3} KNO_3 in aqueous solution

HRTADO	$\Delta G_{CuR'PhenA}$ kJ mol^{-1}	$\Delta H_{CuR'PhenA}$ kJ mol^{-1}	$\Delta S_{CuR'PhenA}$ J K^{-1} mol^{-1}
		5-CH_3Phen	
TADO	−35.4 [29]	4.90±0.31 [15]	135
HMTADO	−59.8 [27]	−20.6±0.3 [14]	132
HTADO	−58.4 [27]	−12.0±0.3 [13]	156
HBTADO	−56.7 [27]	−6.51±0.26	168
HDBTADO	−46.1 [27]	1.69±0.25 [12]	160
		Phen	
TADO	−35.5 [29]	3.46±0.31 [15]	131
HMTADO	−60.3 [27]	−22.0±0.3 [14]	129
HTADO	−58.8 [27]	−13.8±0.3 [13]	151
HBTADO	−56.9 [27]	−8.72±0.26	161
HDBTADO	−46.5 [27]	0.30±0.25 [12]	157
		5-ClPhen	
TADO	−35.7 [29]	−0.15±0.32 [15]	119
HMTADO	−60.8 [27]	−24.6±0.3 [14]	122
HTADO	−59.5 [27]	−16.8±0.3 [13]	143
HBTADO	−57.4 [27]	−11.2±0.3	155
HDBTADO	−47.0 [27]	−2.85±0.25 [12]	148
		5-NO_2Phen	
TADO	−35.8 [29]	−3.14±0.32 [15]	110
HMTADO	−61.4 [27]	−28.0±0.3 [14]	112
HTADO	−60.0 [27]	−19.3±0.3 [13]	137
HBTADO	−57.8 [27]	−14.2±0.3	146
HDBTADO	−47.6 [27]	−5.44±0.30 [12]	142

The regression equation is as follows:

$$\Delta H_{CuR'Phen} = -21.65-0.8874\Delta H_{HR'Phen}$$

$$\gamma = -0.9947$$

The linear enthalpy relationship indicates that the enthalpies of coordination of ligand HBTADO to CuR′Phen strongly depend on the enthalpies of protonation of ligands R′Phen.

It is apparent from Table 4 that the enthalpies of coordination ternary complex compounds Cu(II)-α-aminoacids-HBTADO(CuAB) have values ranging from −(60–69) kJ mol^{-1}. These values were larger than the enthalpies of coordination of binary complex compound $CuH_{-2}A$(−12.7±0.2 mol^{-1}) and $CuH_{-1}A$(−13.8±0.5 kJ mol^{-1}).

In forming these ternary complex compounds, the ligand HBTADO will simultaneously release two protons from the amido groups. When the α-aminoacid coordinated to Cu(II) with its carboxyl oxygen, one of the protons released from amido groups of ligand HBTADO would combine with the amino group nitrogen of α-aminoacid. When the stability constants of the ternary complex compounds Cu(II)-HBTADO-α-aminoacids were calculated with TITFIT [21], only the model $\log\beta_{CuAB}$ was simulated and the result of calculation was convergent. Judging from the released heats and the colour of final solutions, both the binary system Cu(II)-HBTADO and the ternary systems Cu(II)-HBTADO-α-aminoacids appear to have been formed.

The absorption maximum is at 510 nm for Cu(II)-HBTADO binary system and at 600–620 nm for Cu(II)-α-aminoacids-HBTADO ternary systems. This indicates that the α-aminoacids take part in the coordination with Cu(II)-HBTADO in the ternary complex systems Cu(II)-HBTADO-α-aminoacids.

In Table 4 also reported the pH values of the solutions before the reaction are in the range of 9.4–9.9 (the α-aminoacids thus exist in deprotonation form) while after reaction the pH values of the solutions are in the range 4.9–5.8; the α-aminoacidic carboxyl group cannot accept a proton under these conditions. One of the two protons released from the amido groups of HBTADO must therefore bind to the nitrogen atom of the amino group of the α-aminoacids and the oxygen atom of the carboxyl group of the the α-aminoacids would coordinate to the Cu(II) of Cu(II)-HBTADO. The crystal structures of the five coordination compounds of Cu(II) with the 4-(quinolin-8-ylmethyl)-1.4.7.10-tetraazacyclotridecane-11.13-dione and with 4,7-bis(quinolin-8-ylmethyl)-1,4,7.10-

Table 7. The thermodynamic function of the formation ternary complex compounds Cu(II)-TADO(or its derivations HRTADO)(A)-α-aminoacids(B) at 25±0.1°C; $I = 0.1$ mol dm^{-3} KNO_3 in aqueous solution

HRTADO	ΔG_{CuAB} kJ mol^{-1}	ΔH_{CuAB} kJ mol^{-1}	ΔS_{CuAB} J K^{-1} mol^{-1}
		proline	
TADO	−65.3 [29]	−37.7±0.5 [15]	86.6
HMTADO	−116.8 [28]	−66.8±1.3 [14]	168
HTADO	−115.3 [28]	−64.6±2.3 [13]	170
HBTADO	−114.1 [28]	−60.7±1.0	179
HDBTADO	−109.2 [28]	−42.6±0.4 [12]	223
		α-aminoisobutyric acid	
TADO	−60.9 [28]	−46.2±0.6 [15]	49.3
HMTADO	−115.2 [28]	−74.7±1.2 [14]	136
HTADO	−113.5 [28]	−72.2±1.5 [16]	139
HBTADO	−112.2 [28]	−69.7±0.4	143
HDBTADO	−107.1 [28]	−51.3±0.4 [12]	187
		isoleucine	
TADO	58.6 [29]	−43.1±0.7 [15]	52.0
HMTADO	−114.1 [28]	−71.5±1.1 [14]	143
HTADO	−112.4 [28]	−68.3±1.3 [13]	148
HBTADO	−110.9 [28]	−65.9±1.0	151
HDBTADO	−105.0 [28]	−47.8±0.5 [12]	192
		glycine	
TADO	−57.4 [29]	−42.3±0.8 [15]	50.7
HMTADO	−113.4 [28]	−70.4±1.7 [14]	144
HTADO	−110.9 [28]	−67.5±1.8 [13]	146
HBTADO	−110.2 [28]	−65.3±0.9	151
HDBTADO	−104.4 [28]	−47.2±0.4 [12]	192
		serine	
TADO	−57.0 [29]	−39.9±0.6 [15]	57.4
HMTADO	−112.5 [28]	−68.2±0.9 [14]	149
HTADO	−110.3 [28]	−66.0±1.2 [13]	149
HBTADO	−110.0 [28]	−63.0±0.6	158
HDBTADO	−102.8 [28]	−45.1±0.4 [12]	194
		valine	
TADO	−57.9 [29]	−42.4±0.7 [15]	52.0
HMTADO	−113.7 [28]	−69.8±0.4 [14]	147
HTADO	−112.1 [28]	−67.5±0.4 [13]	150
HBTADO	−110.9 [28]	−65.3±0.8	153
HDBTADO	−104.9 [28]	−46.7±0.5 [12]	195

tetraazacyclotridecane-11,13-dione have been obtained [22]. Furthermore, five coordination compounds, in which the water molecule coordinates with the Cu(II) of Cu(II)-TADO, have been crystallographically established [23]. These crystal structure determinations indicated that the five coordination structures proposed for the mixed complex compounds Cu(II)-HBTADO-α-aminoacids (CuAB) are reasonable. According to the above assumption, for the Cu(II)-HBTADO-α-aminoisobutyric acid ternary complex compound, the enthalpy of coordination of HBTADO to Cu(II) with concomitant double deprotonation of amido groups is −13.8 kJ mol^{-1}, the enthalpy of protonation of the nitrogen atom of amino group of α-aminoisobutyric acid −51.9±0.1 kJ mol^{-1} [16], the enthalpy of coordination of oxygen atom of carboxyl group of α-aminoisobutyric acid to copper(II) (i.e. the difference between the enthalpy of first coordination of α-aminoisobutyric acid to copper(II), −25.8±0.3 kJ mol^{-1} [16], and the enthalpy of first coordination of ammonia with copper(II), −23 kJ mol^{-1} [19]) is about −2.8 kJ mol^{-1}. Thus, the total amount of these enthalpies is −68.5 kJ mol^{-1}, which approximately equals the enthalpy of coordination of the ternary complex compound Cu(II)-HBTADO-α-aminoisobutyric acid, −69.7 kJ mol^{-1}. For Cu(II)-HBTADO-proline the calculated value is −59.9 kJ mol^{-1},

the experimental one is -60.7 kJ mol^{-1}. For Cu(II)-HBTADO-isoleucine the calculated value is -65.1 kJ mol^{-1}, the experimental one is -65.9 kJ mol^{-1}. For Cu(II)-HBTADO-glycine the calculated value is -64.3 kJ mol^{-1}, the experimental one is -65.3 kJ mol^{-1}. For Cu(II)-HBTADO-valine the calculated value is -63.9 kJ mol^{-1}, the experimental one is -65.3 kJ mol^{-1}. For Cu(II)-HBTADO-serine the calculated value is -62.1 kJ mol^{-1}, the experimental one 63.0 kJ mol^{-1}.

These findings again show that the enthalpy of coordination of ternary complex compounds are approximately the sum of the enthalpy of coordination of the corresponding parent binary complex compounds provided no d-p back π bonding exists in the ternary system [16]. However, a linear enthalpy relationship was found to exist between the enthalpies of coordination of ternary complex compounds CuAB and the enthalpies of protonation of ligand α-aminoacids (ΔH_{HB}: Pro, -43.3 ± 0.1; Aib, -51.9 ± 0.1; iLe, -48.5 ± 0.1; Gly, -47.7 ± 0.2; Val, -47.3 ± 0.1; Ser, -45.5 ± 0.1 kJ mol^{-1}) [16] with the following correlation equation:

$$\Delta H_{CuAB} = -15.28 + 1.049\Delta H_{AB}$$
$$r = 0.9974$$

The linear enthalpy relationship indicates that the enthalpies of coordination of ternary complex compounds Cu(II)-α-aminoacids-HBTADO strongly depend on the enthalpies of protonation of ligands α-aminoacids. The slope of the line is approximately unity.

It is found from Table 5 that the protonation of these macrocyclic ligands, HRTADO(12-(2′-hydroxy-3′,5′-substituted benzyl)-1,4,7,10-tetraazacyclotridecane-11,13-dione) has three steps. Enthalpies of first protonation (i.e. the enthalpies of protonation of oxygen atom of phenol group, ΔH_{HA} values decrease with the change of substituents from methoxyl to dibromo. Because the values of enthalpies of first protonation depended on the densities of electron cloud on the oxygen atom of phenol group. Furthermore, due to the stacking effect [24,25], the oxygen atom of the phenol group is drawn near to nitrogen atom of amino group of macrocyclic ring. When first proton coordinated to the oxygen atom of the phenol group, it may be bridged to two nitrogen atoms of two amino group of HRTADO ligands. This effect will increase the enthalpies of first protonation of the macrocyclic ligands HRTADO. Therefore, the enthalpies of the first protonation of HMTADO, HTADO ligands (-35.6 ± 0.3, -32.7 ± 0.3 kJ mol^{-1}) much exceed -25.5 kJ mol^{-1}, the enthalpy of protonation of phenol. Although Br atom, two Br atoms on phenyl ring decrease the electron density on oxygen atom of phenol group for HBTADO, HDBTADO ligands, respectively, but the enthalpies of first protonation of HBTADO, HDBTADO still are -29.7 ± 0.2, -25.1 ± 0.3 kJ mol^{-1}. When the second and the third protons coordinate to two nitrogen atoms of two amino groups of HRTADO ligands, first must break the bridged bond of first proton with two nitrogen atoms of two amino groups. This need consumes certain energy and this consumed energy decreased with varying of substituents from CH_3 to 2Br. Therefore, ΔH_{H_2A} and ΔH_{H_3A} are -19.1 ± 0.1, -22.8 ± 1.1, -24.4 ± 0.3, -17.0 ± 0.7 and -18.4 ± 0.4, -19.6 ± 1.4, -24.4 ± 0.3, -13.8 ± 1.0 kJ mol^{-1}, respectively. These values all are smaller than -36.8 ± 0.2 and -30.2 ± 0.2 kJ mol^{-1} (see ΔH_{HA} and ΔH_{H_2A} of TADO in Table 5). But ΔH_{H_2A} and ΔH_{H_3A} of HDBTADO appear out of the ordinary. Again see ΔS_{H_2A} and ΔS_{H_3A} of HDBTADO in Table 5, we find that ΔS_{H_2A} is ordinary and ΔS_{H_3A} appear special large. (A substance of this phenomenon is not understood and further investigation needs to be done.) Above factors cause that ΔG_{H_2A} and ΔG_{H_3A} of HDBTADO are out of the ordinary. This phenomenon also is found to exist in the binary and ternary complexes.

It is also seen from Tables 5 and 6 that the linear enthalpy relationships have been found to exist between the enthalpies of coordination of ternary complex compounds Cu(II)—R′Phen-HRTADO(A) and the enthalpies of protonation of the first step of ligands A, ΔH_{HA}, with correlation equations as following:

Cu(II)-CH_3Phen-A ternary system:
$\Delta H_{CuCH_3Phen} = 53.78 + 2.058\Delta H_{HA}$ $\quad r = 0.9929$
Cu(II)-Phen-A ternary system:
$\Delta H_{CuPhenA} = 51.96 + 2.054\Delta H_{HA}$ $\quad r = 0.9944$
Cu(II)-ClPhen-A ternary system:
$\Delta H_{CuClPhen} = 48.10 + 2.020\Delta H_{HA}$ $\quad r = 0.9960$
Cu(II)-NO_2Phen-A ternary system:
$\Delta H_{CuNO_2PhenA} = 46.85 + 2.073\Delta H_{HA}$ $\quad r = 0.9926$

It is seen from Tables 5 and 6 that some linear enthalpy-entropy relationships have been found to exist between the enthalpy of coordination of ternary complex compounds Cu(II)—R′Phen-A and the entropy of protonation of ligands A with correlation equations as follows:

Cu(II)-CH_3Phen-A ternary system:
$\Delta H_{CuCH_3Phen} = -108.7 + 1.156\Delta S_{HA}$ $\quad r = 0.9920$
Cu(II)-Phen-A ternary system:
$\Delta H_{CuPhenA} = -110.0 + 1.151\Delta S_{HA}$ $\quad r = 0.9919$
Cu(II)-ClPhen-A ternary system:
$\Delta H_{CuClPhen} = -111.3 + 1.134\Delta S_{HA}$ $\quad r = 0.9946$
Cu(II)-NO_2Phen-A ternary system:
$\Delta H_{CuNO_2PhenA} = -116.7 + 1.163\Delta S_{HA}$ $\quad r = 0.9906$

This existence of these two linear relationships has its internal correlation. Since the benzyl hydroxy group of macrocyclic ligands can take part not only in combing with hydrogen ion but also can take part in coordination with Cu(II)-R′Phen. When the substituents on the benzyl group are different the enthalpies of coordination of ternary complex compounds Cu(II)-R′Phen-A and the enthalpy and entropy of

protonation of macrocyclic ligands A vary accordingly. As can be seen from Tables 5 and 7, some linear enthalpy relationships also exist between the enthalpies of coordination of ternary complex compounds Cu(II)-HRTADO(A)-α-aminoacids(B) and the enthalpies of coordination of the binary complex compounds Cu(II)H-1A with correlation equations as the following (except the Cu(II)-α-aminoacids-TADO ternary systems):

Cu(II)-Pro-A ternary system:
$\Delta H_{CuProA} = -47.42 + 1.025\Delta H_{CuH_{-1}A}$ $\gamma = 0.998$
Cu(II)-Aib-A ternary system:
$\Delta H_{CuAibA} = -56.08 + 0.993\Delta H_{CuH_{-1}A}$ $\gamma = 1.000$
Cu(II)-iLe-A ternary system:
$\Delta H_{CuiLeA} = -52.49 + 0.992\Delta H_{CuH_{-1}A}$ $\gamma = 1.000$
Cu(II)-Gly-A ternary system:
$\Delta H_{CuGlyA} = -51.88 + 0.997\Delta H_{CuH_{-1}A}$ $\gamma = 1.000$
Cu(II)-Val-A ternary system:
$\Delta_{HCuValA} = -51.50 + 0.987\Delta H_{CuH_{-1}A}$ $\gamma = 1.000$
Cu(II)-Ser-A ternary system:
$\Delta_{HCuSerA} = -49.80 + 0.987\Delta H_{CuH_{-1}A}$ $\gamma = 1.000$

As can be seen also from Tables 5 and 7 that some linear entropy relationships have been found to exist between the entropies of coordination of the ternary complex compounds Cu(II)-HRTADO(A)-α-aminoacids (B) and the entropies of coordination of the binary complex compounds Cu(II)H-1A with correlation equations as follows(except the Cu(II)-TADO-α-aminoacids ternary system):

Cu(II)-Pro-A ternary system:
$\Delta S_{CuProA} = 41.66 + 1.662\Delta S_{CuH_{-1}A}$ $\gamma = 0.991$
Cu(II)-Aib-A ternary system:
$\Delta S_{CuAibA} = 17.07 + 1.556\Delta S_{CuH_{-1}A}$ $\gamma = 0.997$
Cu(II)-iLe-A ternary system:
$\Delta S_{CuiLeA} = 32.01 + 1.467\Delta S_{CuH_{-1}A}$ $\gamma = 0.999$
Cu(II)-Gly-A ternary system:
$\Delta S_{CuGlyA} = 31.62 + 1.468\Delta S_{CuH_{-1}A}$ $\gamma = 0.995$
Cu(II)-Val-A ternary system:
$\Delta S_{CuValA} = 34.70 + 1.467\Delta S_{CuH_{-1}A}$ $\gamma = 0.997$
Cu(II)-Ser-A ternary system:
$\Delta S_{CuSerA} = 44.00 + 1.374\Delta S_{CuH_{-1}A}$ $\gamma = 0.986$

The existence of these linear relationships indicates that the values of enthalpies and entropies of coordination of the ternary complex compounds Cu(II)AB strongly depend on the values of enthalpies and entropies of coordination of the binary complex compounds Cu(II)H$_{-1}$A. As reported above the enthalpies of coordination of ternary complex compounds, Cu(II)AB can be related to additivity effect to the parent binary complex compounds, i.e. the enthalpies of ΔH_{CuAB} are equivalent to the sum of the enthalpies of protonation of nitrogen atom on the amino group of α-ammoniac's, the enthalpies of coordination of oxygen atom on carboxyl group of α-aminocids with Cu(II) of binary complex compounds Cu(II)H$_{-1}$A and the enthalpies of coordination of the binary complex compounds Cu(II)H$_{-1}$A.

It is seen from Table 6 that the values of enthalpies of coordination of ternary complex compounds Cu(II)-R′Phen-A are rather small, the range of 2 to -2.8 kJ mol^{-1}, but the values of entropies of coordination of ternary complex compounds Cu(II)-R′Phen-A are larger, about 120 to 170 kJ^{-1} mol^{-1}, i.e. the values of $-T\Delta S_{CuR'PhenA}$ of ternary complex compounds Cu(II)-R′Phen-A are -32 to -50 kJ mol^{-1}. It means that the high stability of ternary complex compounds Cu(II)-R′Phen-A mainly arises from their entropy effects, which might be resulted from the stacking effect of aromatic ring of 5-substituted phenanthrolines with the macrocyclic ring and phenyl ring of HRTADO ligands [24–26].

REFERENCES

1. (a) Luo, Q. H., Zhu, S. R., Shen, M. C., Yu, S. Y., Zhang, Z., Huang, X. Y. and Wu, Q. J., *J. Chem. Soc., Dalton Trans.*, 1994, 1873; (b) Zhu, S. R., Lin, H. K., Lin, C. C., Kou, F. P. and Chen, Y. T., *Inorg. Chim. Acta*, 1995, **228,** 225.
2. (a) Kodama, M. and Kimura, E., *J. Chem. Soc., Dalton Trans.*, 1979, **325,** 1783; (b) *ibid*, 1981, 694; (c) Kimura, E., Sakonaka, A., Machida, R. and Kodama, M., *J. Am. Chem. Soc.*, 1982, **104,** 4225; (d) Machida, R., Kimura, E. and Kuski, Y., *Inorg. Chem.*, 1986, **25,** 3461.
3. Lampeka, Y. D. and Gavrish, S. P., *J. Coord. Chem.*, 1990, **21,** 351.
4. Fabrizzi, L., Montagna, L. and Poggi, A., *J. Chem. Soc., Dalton Trans.*, 1987, 2631.
5. (a) Luo, Q. H., Zhu, S. H., Shen, M. C., Tu, Q. Y., Dai, A. B., Liu, A. D., Gu, H. C., Li, F. M. and Di, S. J., *Kexue Tongbao(Chin.)*, 1992, 1288; (b) Shen, M. C., Luo, Q. H., Zhu, S. R., Tu, Q. Y., Dai, A. B., Liu, A. D., Gu, H. C., Li, F. M. and Di, S. J., *Chem. J. Chinese Univ., Ser. B*, 1990, **6,** 354; (c) Luo, Q. H., Zhu, S. R., Shen, M. C. and Zhang, Z., *Acta Chim. Sinica*, 1994, **52,** 699.
6. Kimura, E., Yatsunami, T., Watanabe, A., Michida, R., Koike, T., Fujioka, H., Kuramota, Y., Sumomogi, M., Kunimitsu, K. and Yamashita, A., *Biochim. Biophys. Acta*, 1983, **745,** 37.
7. Kirksey, Jr. S. T., Neubecker, T. A. and Margerum, D. W., *J. Am. Chem. Soc.*, 1979, **101,** 1631.
8. Diaddario, L. L., Robinson, W. R. and Margerum, D. W., *Inorg. Chem.*, 1983, **22,** 1021.
9. Rybka, J. S., Kurtz, J. I., Neubecker, T. A. and Margerum, D. W., *Inorg. Chem.*, 1980, **19,** 2791.
10. Bossu, F. P., Chellappa, K. L. and Margerum, D. W., *J. Am. Chem. Soc.*, 1977, **99,** 2195.
11. Kimura, E., *J. Coord. Chem.*, 1986, **15,** 1; (b) *ibid, Tetrahedron*, 1992, **48,** 6175; (c) Kimura, E., Koike, T., Michida, R., Nagi, R. and Komada, M., *Inorg. Chem.*, 1980, **23,** 4181.
12. Lin, H. K., Zhu, S. R., Gu, Z. X. and Chen, Y. T., *J. Chem. Soc., Dalton Trans.*, 1995, 1879.
13. Lin, H. K., Zhu, S. R., Gu, Z. X. and Chen, Y. T., *Thermo. Acata*, 1995, **259,** 215.
14. Lin, H. K., Zhu, S. R., Gu, Z. X. and Chen, Y. T., *Polyhedron*, 1996, **15,** 3241.
15. Lin, H. K., Zhu, S. R., Gu, Z. X. and Chen,

Y. T., *Gazzetta Chim. Italiana*, 1996, **126,** 835.
16. Lin, H. K., Gu, Z. X., Chen, X. M. and Chen, Y. T., *Thermo. Acta*, 1988, **123,** 201.
17. Zhu, S. R., Lin, H. K., Lin, C. C., Kou, F. P. and Chen, Y. T., *Inorg. Chim. Acta*, 1995, **228,** 225.
18. Den, Y., Tian, A., Qin, Z., Zeng, X. and Zhan, S., *Chem. J. Chinese Univ.*, 1981, **2,** 244.
19. (a) Martell, A. E. and Smith, R. M., *Critical Stability Constants*, Vol 3. Plenum, New York, London, 1977, p. 181; (b) Vol. 4, p. 40.
20. Chen, Y. T., Lin, H. K. and Zhu, J. Y., *J. Chem. Soc., Dalton Trans.*, 1990, 3445.
21. Zuberbuhler, A. D. and Kaden, J. A., *Talanta*, 1982, **29,** 201.
22. Bu, X. H., An, D. L., Chen, Y. T., Shionoya, M. and Kimura, E., *J. Chem. Soc., Dalton Trans.*, 1995, 2289.
23. Zhu, S. R., Luo, Q. H., Shen, M. C., Dai, A. B. and Huang, L. R., *Polyhedron*, 1992, **11,** 941.
24. Sigel, H., *Pure & Appl. Chem.*, 1989, **61,** 923.
25. Scheraga, H. A., *Acc. Chem. Res.*, 1979, **12,** 7.
26. Lin, H. K., Gu, Z. X., and Chen, Y. T., *Thermo. Acta*, 1993, **219,** 115.
27. Xian, J. C., Zhu, S. R., Lin, H. K. and Chen, Y. T., *Acta Physico-Chimica Sinica*, 1994, 10, 841.
28. Xian, J. C., Zhu, S. R., Lin, H. K. and Chen, Y. T., *Chem. J. of Chinese Univer.*, 1994, **15,** 163.
29. Xian, J. C., Zhu, S. R., Lin, H. K. and Chen, Y. T., *J. of Inorganic Chemistry(Chin.)*, 1994, **10,** 189.

Pergamon

PII: S0277-5387(97)00420-8

Polyhedron Vol. 17, Nos 13–14, pp. 2373–2378, 1998
© 1998 Elsevier Science Ltd
All rights reserved. Printed in Great Britain
0277-5387/98 $19.00+0.00

Coordination compounds of 4,2′-6′,4″-terpyridine, [MCl_2(4,2′-6′,4″-terpyridine)], M = Mn(II), Co(II), Ni(II), Cu(II) or Zn(II). Crystal structure of *catena*-poly [(dichlorozinc)-μ-(4,2′-6′,4″-terpyridine)]

Montserrat Barquín,[a] Juan Cancela,[a] María J. González Garmendia,*[a] Javier Quintanilla[a] and Ulises Amador[b]†

[a] Grupo de Química Inorgánica, Facultad de Ciencias Químicas, Universidad del País Vasco UPV/EHU, Apartado 1072, 20080 San Sebastián, Spain

[b] C.A.I. de Difracción de Rayos X, Facultad de Ciencias Químicas, Universidad Complutense, 28040 Madrid, Spain

(Received 1 July 1997; accepted 9 October 1997)

Abstract—MCl_2 (4,2′-6′,4″-terpyridine) compounds, where M = Mn(II), Co(II), Ni(II), Cu(II) or Zn(II), have been synthesized and characterized by IR and electronic spectroscopy and susceptibility magnetic measurements. Crystalline structure of the Zn(II) complex has been determined by X-ray diffraction. The Zn(II) atom shows to be in a highly distorted tetrahedral environment, defined by two Cl atoms and two N atoms of two ligand molecules, that act as bridges bound through the N atoms of the external pyridine rings. The structure is made of chains that do not interact among them. © 1998 Elsevier Science Ltd. All rights reserved

Keywords: coordination compounds; MCl_2(4,2′-6′,4″-terpyridine) compounds; *catena*-poly [(dichlorozinc)-μ-(4,2′-6′,4″-terpyridine)].

INTRODUCTION

The different relative position of the N atoms in the terpyridine isomers leads to different coordination behaviour.

4,2′-6′-4″-terpyridine(I) possesses three pyridinic N-atoms with donor character. However, due to its relative position, they cannot coordinate to the same metallic cation as it happens with the 2,2′-6′-2″-terpyridine(II) isomer.

2,2′-6′,4″-perpyridine(III) is a bidentate ligand through the two nearest N atoms or a cyclometalling ligand, with N_2C donor set, with Ru [1], possessing a non-chelating pyridine ring which is protonated.

No reference related to the isomer (I) complex formation has been found. However it seems likely that it can behave as a bridge ligand coordinated through the N-atoms of the external rings.

In the present work we describe the synthesis and characterization of the complexes [MCl_2 (4,2′-6′,4″-terpyridine)], M = Mn(II), Co(II), Ni(II), Cu(II) and Zn(II). For the Zn(II) complex we were able to determine its crystalline structure. The ligand behaves as a bridge through the N-atoms of the external rings.

EXPERIMENTAL

Preparation of complexes

All complexes were synthesized by adding, with stir and at room temperature, an ethanolic solution of the ligand (0.5 mmol in 5 ml) to an aqueous solution of the metal chloride (0.5 mmol in 3 ml), in stoichiometric

* Author to whom correspondence should be addressed.

† Present address: Departamento de Química Inorgánica y Materiales, Facultad de Ciencias Experimentales y Técnicas, Universidad San Pablo-CEU, Urb. Montepríncipe, 28688-Boadilla del Monte, Madrid, Spain

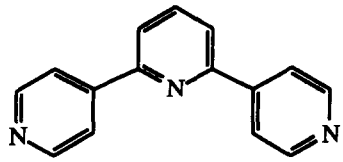

(I)

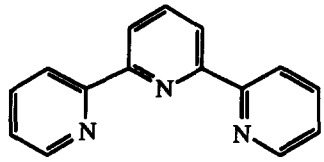

(II)

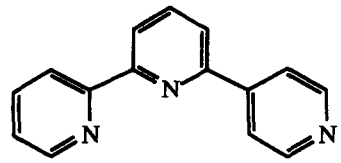

(III)

quantities. The resulting precipitate was washed with ethanol and air dried.

Table 1 collects analytical results and yields of complexes preparation.

By evaporation of a solution of Zn(II) complex in DMS some translucent and colourless crystals were obtained.

Physical measurements

C, H and N were analysed using a Perkin–Elmer 240C Elemental Analyzer. Conductivity measurements were made using a Metrhom E518 conductimeter with a Metrhom 6.0901.110 cell (constant = 0.74 cm^{-1}). IR spectra were recorded in the 4.000–65 cm^{-1} region, on a Nicolett 740 FT-IR spectrometer, with KBr pellets in the middle range and with Nujol on a polyethylene film under 650 cm^{-1}. Electronic spectra, as diffuse reflectance, were registered on a Schimadzu UV-265 FW instrument, in the 900–190 nm range. Magnetic susceptibilities were determined with a DSM8 susceptometer, with a Drusch M 1119 power source and an Oxford ITC4 temperature controller. Diamagnetic corrections were applied [2].

X-ray crystal structure determination

A colourless crystal of needle-like shape and dimensions $0.10 \times 0.10 \times 0.25$ mm^3 was mounted on a Nonius CAD-4 diffractometer and used for the structure determination. Table 2 collects the main crystal data and the refinement parameters for $ZnC_{15}N_3H_{11}Cl_2$. Graphite monochromated Mo-K_α ($\lambda = 0.71069$ Å) was used in the data collection carried out at 295 K. The unit cell parameters were determined by least-square refinement of the 2θ values of 25 strong well

Table 2. Crystallographic parameters for $ZnC_{15}N_3H_{11}Cl_2$

Chemical Formula	$ZnC_{15}N_3H_{11}Cl_2$
Formula weight	369.6
Crystal system	Monoclinic
Space group	$P2_1/n$ (N.14)
a (Å)	6.649(3)
b (Å)	14.078(2)
c (Å)	16.345(3)
β (°)	83.93(3)
Z	4
V (Å^3)	1521.4(8)
ρ_{calcd} (g cm^{-3})	1.61
Crystal dimensions, (mm^3)	$0.1 \times 0.1 \times 0.25$
Data Collection	
Unique data	4594
Observed reflections $I > 3\sigma(I)$	2044
R_{int}, %	1.5
$F(000)$	744
μ(Mo-K_α), cm^{-1}	20.2
Structure solution and refinement	
$R(F)^a$	$R = 0.043$
$R_w(F)^b$	$R_w = 0.048$

$^a R = \Sigma|F_o - F_c|/\Sigma|F_o|$

$^b R_w = (\Sigma w (F_o - F_c)^2/\Sigma w|F_o|^2)^{1/2}$

Table 1. Analytical results and yields of complexes preparation

Compound	Colour	% Found (Calc.) C	H	N	Yield (%)
$MnCl_2L$	white	50.33 (50.17)	2.95 (3.09)	11.59 (11.70)	43.6
$CoCl_2L$	violet	49.90 (49.65)	3.00 (3.06)	11.70 (11.58)	66.6
$NiCl_2L$	yellow	49.64 (49.65)	3.02 (3.05)	11.25 (11.57)	55.6
$CuCl_2L$	blue	48.77 (48.99)	2.98 (3.02)	11.05 (11.43)	70.7
$ZnCl_2L$	white	49.42 (48.75)	3.04 (3.00)	11.47 (11.37)	85.7

centered reflections in the angular range $13° < 2\theta < 35°$. The intensities were measured in the angular range $1° < 2\theta < 60°$ (hkl range, 9,0,0 to 9,19,23) using the $\omega/2\theta$ scan technique. There was no appreciable change in the intensities of three standard reflections periodically monitored. The raw data were corrected for Lorentz and polarization effects. Scattering factors for neutral atoms were taken from the "*International Tables for X-Ray Crystallography*" [3].

The heavy atoms (Zn and Cl) were located using the Patterson function while the other non-hydrogen atoms (N and C) positions were determined by subsequent Fourier syntheses. Since no trends in ΔF vs F_o or $\sin\theta/\lambda$ were observed, unit weights were assigned. Due to the crystal size and to the low absorption coefficient, no absorption correction was applied. A final refinement was undertaken with anisotropic thermal motion for the non-hydrogen atoms with the hydrogen atoms at the positions determined by the molecular geometry and keeping the isotropic thermal parameters constant and equal for all of them. Full-matrix least-square refinement minimized $\Sigma w(|F_o|-|F_c|)^2$. The maximum and average shift-to-error ratios were 0.001 and 0.0004 respectively, while the maximum residual electron density, located near the Zn atom, was 0.6 $e\text{Å}^{-3}$. Most of the calculations were carried out with the XRAY80 program [4].

RESULTS AND DISCUSSION

Due to the insolubility of most complexes in the habitual solvents, it was not possible to carry out conductivity measurements. However zinc complex, which was soluble in DMSO, showed to be no-conductor.

Crystalline structure of $ZnCl_2$(4,2′-6′,4″-terpy)

Table 3 collects the main interatomic distances (Å) and angles (degrees). The compound consist of infinite zigzag chains of composition $ZnCl_2$(4,2′-6′,4″-terpy) running parallel to the *b*-axis. Figure 1 shows an ORTEP view of the molecule and Fig. 2 depicts the molecular packing in the crystal.

The zinc atoms are coordinated to two chlorine atoms and to two nitrogen atoms, N(1) and N(3′), of two different terpy ligands. These atoms are arranged in a very distorted tetrahedron with two long Zn—Cl distances, 2.214 Å and 2.192 Å, and to two Zn—N shorter bonds, 2.051 Å and 2.071 Å. These distances

Table 3. Selected bond lengths (Å) and angles (°) for Zn(4,2′-6′,4″-terpy)Cl_2

Zn—Cl(1)	2.214(2)		
Zn—Cl(2)	2.192(2)	C(3)—C(4)	1.397(8)
Zn—N(1)	2.051(5)	C(3)—C(6)	1.500(8)
Zn—N(3′)	2.071(5)	C(4)—C(5)	1.386(9)
N(2)—C(6)	1.326(7)	C(6)—C(7)	1.382(8)
N(2)—C(10)	1.349(7)	C(7)—C(8)	1.388(9)
N(1)—C(1)	1.342(8)	C(8)—C(9)	1.374(9)
N(1)—C(5)	1.321(8)	C(9)—C(10)	1.381(9)
N(3)—C(13)	1.345(8)	C(11)—C(12)	1.370(9)
N(3)—C(14)	1.326(8)	C(11)—C(15)	1.396(9)
C(1)—C(2)	1.378(9)	C(12)—C(13)	1.372(0)
C(2)—C(3)	1.376(8)	C(14)—C(15)	1.362(8)
Cl(1)—Zn—Cl(2)	121.9(1)	C(3)—C(4)—C(5)	118.6(6)
Cl(1)—Zn—N(1)	106.0(1)	N(1)—C(5)—C(4)	123.0(6)
Cl(1)—Zn—N(3′)	109.5(2)	N(2)—C(6)—C(3)	114.7(5)
Cl(2)—Zn—N(1)	113.1(2)	C(3)—C(6)—C(7)	122.3(5)
Cl(2)—Zn—N(3′)	105.3(2)	N(2)—C(6)—C(7)	123.0(5)
N(1)—Zn—N(3′)	98.6(2)	C(6)—C(7)—C(8)	117.9(6)
C(6)—N(2)—C(10)	118.8(5)	C(7)—C(8)—C(9)	119.6(6)
C(1)—N(1)—C(5)	118.2(5)	C(8)—C(9)—C(10)	119.0(6)
C(13)—N(3)—C(14)	116.6(5)	N(2)—C(10)—C(9)	121.7(5)
N(1)—C(1)—C(2)	122.8(6)	C(12)—C(11)—C(15)	116.3(6)
C(1)—C(2)—C(3)	119.2(6)	C(11)—C(12)—C(13)	120.5(6)
C(2)—C(3)—C(6)	119.7(5)	N(3)—C(13)—C(12)	122.9(6)
C(2)—C(3)—C(4)	118.2(5)	N(3)—C(14)—C(15)	123.8(6)
C(4)—C(3)—C(6)	122.1(5)	C(11)—C(15)—C(14)	120.0(6)

Atoms labelled by prime are obtained by applying the symmetry operation $(x-1/2, -y+1/2, z-1/2)$

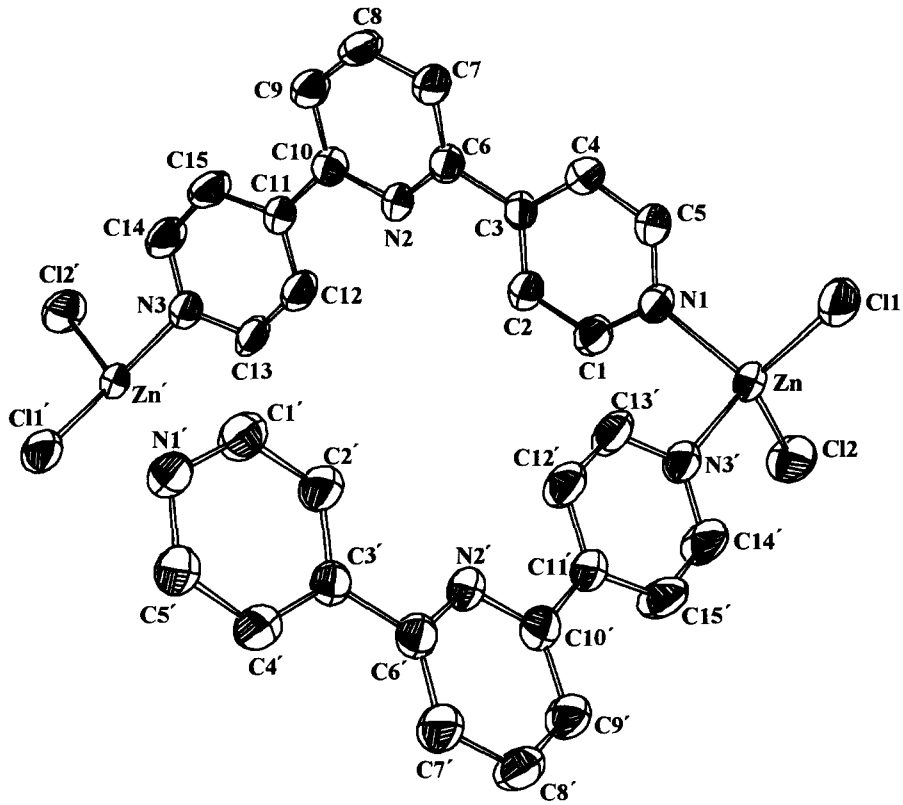

Fig. 1. The ORTEP view of $Zn(4,2'\text{-}6',4''\text{-terpy})Cl_2$

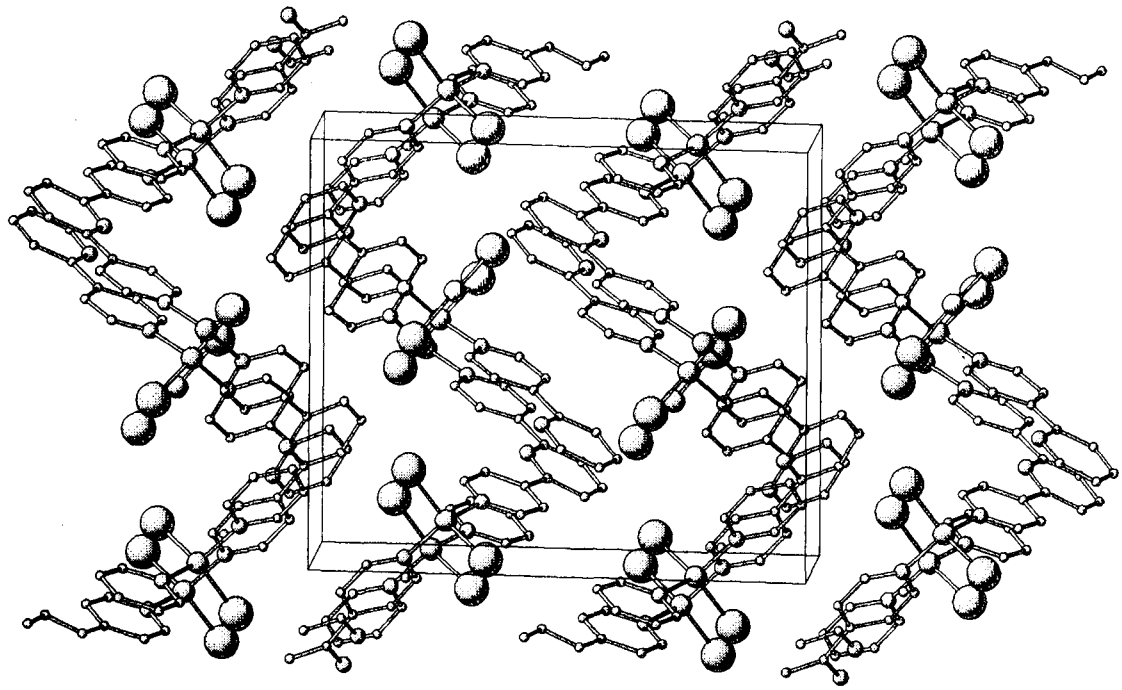

Fig. 2. Molecular packing in the crystal of $Zn(4,2'\text{-}6',4''\text{-terpy})Cl_2$

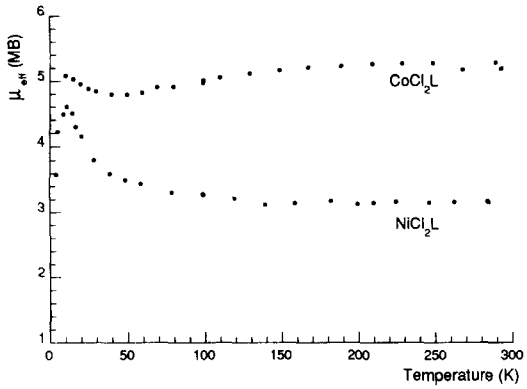

Fig. 3. Magnetic moment vs temperature for Co(II), and Ni(II) complexes.

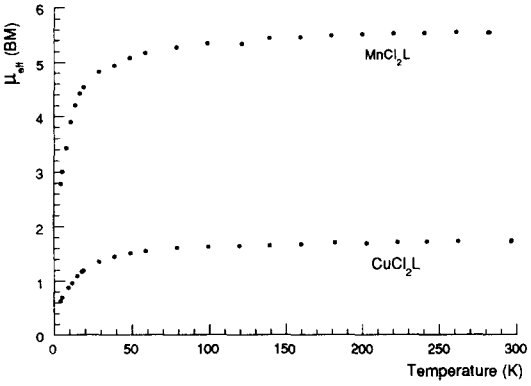

Fig. 4. Magnetic moment vs temperature for Mn(II) and Cu(II) complexes.

are similar to that observed in other monomeric complexes: d(Zn—Cl) = 2.22 Å and 2.23 Å, d(Zn—N) = 2.05 Å in $ZnCl_2(py)_2$ [5], and d(Zn—Cl) = 2.26 Å, d(Zn—N) = 2.09 Å, 2.18 Å and 2.14 Å in $ZnCl_2$(2,2′-6′,2″-terpy) [6]. The angles Cl(1)—Zn—Cl(2) (121.9°) and N(1)—Zn—N(3′) (98.6°) are very different from the value of a regular tetrahedron (109.5°); this is probably a steric requirement of the large chlorine atoms bonded to the zinc. The rest of the tetrahedral angles are much closer to their ideal value. The zinc atoms of neighbouring chains are at a distance of 6.649 Å, the length of the *a*-axis. The shortest distance between a zinc and a chlorine atom of neighbouring chains is at least of 5.8 Å. These long distances exclude any type of interchain interactions.

The molecules of the ligand are coordinated to two different metallic atoms by the nitrogen atoms of both the terminal rings, N(1) and N(3), acting as bridges, while the central ring is not coordinated. Every pyridine ring of the ligand keeps its planarity. However, the terpy molecule as a whole is not planar: the angle is defined by rings containing the N(1) and N(2) atoms is only 9.0° while the angle between the central ring and that containing the N(3) atom is 106.8°. This is necessary to allow the tetrahedral coordination of the metallic atoms.

X-ray diffraction of the other complexes

Powder diffractograms of Mn(II), Co(II), Ni(II) and Cu(II) complexes showed them to be analogues. However they are different to the Zn(II) complex diffractogram, denoting that they have structural differences.

We suppose for those cations, an octahedral environment in the solid state, in accordance with the other experimental results.

Infrared spectra

Complexes infrared spectra reproduce basically that of the ligand with some modifications due to its coordination. The ligand shows a band at 1593 cm^{-1}, related to pyridine ring vibrations that shifts to higher frequencies in the metal complexes with an increase of 15 to 22 cm^{-1}, depending on the metal.

The assignation of the far infrared bands is not feasible due to the many peaks that the ligand itself shows in this area. Around 340 cm^{-1} there is a clear band that is not present in the ligand, and it is assigned to the stretching frequency of M—Cl.

Electronic spectra

Only diffuse reflectance spectra were recorded due to the insolubility of most of the complexes. The ligand shows a band in the ultraviolet region centered at 290 nm with a shoulder that starts under 450 nm, assigned to a π-π^* transition. All the five complexes clearly show this shoulder.

In Table 4 are summarized the bands and their assignation on the bases of an octahedral environment for the metallic cation.

The $CuCl_2L$ complex shows a very broad band at 700 nm (14,200 cm^{-1}) that is assigned to the $^2E_g \rightarrow {}^2T_{2g}$ transition, from which a 10 Dq value of 14,200 cm^{-1} is estimated. The complex of Ni(II) presents two bands, one at 700 nm assigned to the $^3A_{2g} \rightarrow {}^3T_{1g}(F)$ transition and other around 23,800 cm^{-1} assigned to the $^3Ag_{2g} \rightarrow {}^3T_{1g}(P)$ transition. From these two bands a 10 Dq value of 9,000 cm^{-1} and a *B* value of 740 cm^{-1} are obtained. The band corresponding to the $^3Ag_{2g} \rightarrow {}^3T_{2g}$ transition is not observed, as it should appear at lower frequencies.

The Co(II) complex also shows two bands centered at 620 and 530 nm (16,100–18,900 cm^{-1}), assigned to $^4T_{1g}(F) \rightarrow {}^4T_{1g}(P)$ and $^4T_{1g}(F) \rightarrow {}^4A_{2g}$ transitions, respectively. The values of 10 Dq = 10,500 and B = 712 cm^{-1} are deduced from these bands.

The complexes of Zn(II) and Mn(II) showed only

Table 4. Assignation of the found bands and calculated values of 10 Dq and *B*

Compound	ν (cm^{-1})	Assignation	10 Dq (cm^{-1})	B (cm^{-1})
$CoCl_2L$	16,100 cm^{-1}	$^4T_{1g}(F) \rightarrow {}^4T_{1g}(P)$		
	18,900 cm^{-1}	$^4T_{1g}(F) \rightarrow {}^4A_{2g}(F)$	10,500	712
$NiCl_2L$	14,200 cm^{-1}	$^3A_{2g} \rightarrow {}^3T_{1g}(F)$		
	23,800 cm^{-1}	$^3A_{2g} \rightarrow {}^3T_{1g}(P)$	9,000	740
$CuCl_2L$	14,200 cm^{-1}	$^2E_g \rightarrow {}^2T_{2g}$	14,200	

the ligand bands, as it was expected, due to their d^{10}–d^5 configurations.

Using Jørgensen's expression 10 Dq = f(ligand)·g(cation)·10^3 cm^{-1} it is possible to calculate a 10 Dq value for the complexes, estimating, from the Co(II) complex results, a value of $f = 1.13$ for both ligands and accepting the parameter g for the cations Cu^{2+} (12) and Mn^{2+} (8.5) [7]. The resulting values for 10 Dq are 13,560 cm^{-1} for $CuCl_2L$, and 9,600 cm^{-1} for $MnCl_2L$.

Magnetic measurements

Table 5 shows the magnetic values for the temperature range in which the Curie-Weiss law is obeyed.

$ZnCl_2L$ complex is diamagnetic as it was expected for a d^{10} configuration.

Table 5. Magnetic results

Compound	T (°K)	θ (°K)	μ (BM)[a]	
$MnCl_2L$	100–295	−14.0	5.69	(d^5, high spin)
$CoCl_2L$	100–295	−9.1	5.31	(d^7, high spin)
$NiCl_2L$	100–295	3.4	3.13	(d^8)
$CuCl_2L$	100–295	−22.8	1.79	(d^9)

[a] Calc. from the Curie constant value.

For Mn^{2+} and Co^{2+} complexes the μ_{eff} value is in agreement with a high spin value for d^5 and d^7 configurations, respectively.

The representation of μ vs T at low temperatures shows an antiferromagnetism interaction in the cases of Mn and Cu complexes, and a ferromagnetic interaction for the Ni complex. This result agrees with the sign of θ. As the solid structures are unknown it is not possible to make an adjustment of the found data.

Acknowledgements—This work has been supported by the Diputación Foral de Guipuzcoa, San Sebastian, Spain.

REFERENCES

1. Constable, E. C., Carllig Thompson, A. M. W., Cherryman, J. and Liddiment, T., *Inorg. Chim. Acta*, 1995, **235**, 165.
2. O'Connor, Ch., *Prog. Inorg. Chem.*, 1982, **29**, 203.
3. *International Tables for X-Ray Crystallography*, Vol. IV, Kynoch Press, Birmingham, U.K., 1974, p. 72.
4. Stewart, J. M., *The X-RAY80 System*, Computer Science Center, University of Maryland, College Park, MD, U.S.A. 1980.
5. Stefen, W. L. and Palenik, G. J., *Acta Crystallogr. Sect. B*, 1976, **32**, 298.
6. Einstein, F. W. B. and Pendolf, B. R., *Acta Cryst.*, 1966, **20**, 924.
7. Wilkinson, G., Gillard, R. D. and McCleverty, J. A. (eds), *Comprehensive Coordination Chemistry*, *Vol.* 1, Pergamon Press, 1987, p. 251.

Pergamon

PII: S0277-5387(97)00463-4

Polyhedron Vol. 17, Nos 13–14, pp. 2379–2410, 1998
© 1998 Elsevier Science Ltd
All rights reserved. Printed in Great Britain
0277-5387/98 $19.00+0.00

Synthesis, crystal structure and a spectroscopic study of *bis*(triphenylphosphine)gold(I)$^+$ TCNQ$^-$

N. C. Baenziger, W. E. Bennett, D. M. Soboroff, P. S. O'Donnell and J. R. Doyle*

Department of Chemistry, University of Iowa, Iowa City, IA 52242, U.S.A.

(Received 30 June 1997; accepted 6 October 1997)

Abstract—The complex of the *bis*(triphenylphosphine)gold(I) cation and the radical anion of 2,2′-(2,5-cyclohexadiene-1,4-diylidene)bispropanedinitrile, (TCNQ), has been prepared and characterized by spectroscopic and X-ray crystallographic methods. The solid state structure consists of the linear (P—Au—P) cation *bis*(triphenylphosphine)gold(I) and the approximately planar radical anion of TCNQ. The bond lengths are: Au—P 2.300(2); P—C 1.800(11), 1.789(11), 1.800(11); C≡N 1.175(16), 1.128(16). The infrared spectrum of the complex exhibits bands at 2176 and 2150 cm^{-1} in the nitrile region. The electron spin resonance spectrum of this compound, in benzene, is consistent with a structure in which the TCNQ radical anion is symmetrically oriented about the *bis*(triphenylphosphine)gold(I) cation. The hyperfine coupling constants are: $a^N = 0.981$, $a^H = 1.379$, $a^P = 0.095$ gauss. © 1998 Elsevier Science Ltd. All rights reserved

Keywords: TCNQ; spectroscopy; X-ray crystallography.

Recent interest [1–4] in the radical anion salts of *bis*(triphenylphosphine)gold(I)$^+$ prompted a reexamination of research previously conducted in our laboratory [5]. The initial interest in this class of compounds was aroused by the potentially unique electrical and magnetic properties of the radical anion salts of TCNQ and TCNE. Since certain aspects of our initial study differ from those recently reported [2,4] we have redetermined the crystal structure and reinvestigated the ESR spectrum of the *bis*(triphenylphosphine)gold(I)$^+$ TCNQ$^-$ salt and report the results here.

EXPERIMENTAL

Preparation of chloro(triphenylphosphine)gold(I)

To a solution of hydrated chloroauric acid (0.97 g, 2.58 mmol) in ethanol (20 cm^3) was added triphenylphosphine (1.27 g, 4.84 mmol). The solution was stirred for 15 min during which time the yellow color of the gold(III) dissipated and a white crystalline product separated. The product was recovered by filtration, washed with ethanol (5 cm^3) and finally with diethyl ether (5 cm^3). The product was recrystallized from ethanol: m.p. 239–241°. Calc. for $C_{18}H_{15}PAuCl$: C, 43.70; H, 3.06. Found: C, 43.54; H, 2.70.

Preparation of bis(triphenylphosphine)gold(I)$^+$ TCNQ$^-$

A mixture of triphenylphosphine (1.80 g, 6.86 mmol) and chloro(triphenylphosphine)gold(I) (3.26 g, 6.59 mmol) was suspended in ethanol (75 cm^3) and the mixture heated until the solution cleared (about 10 min). Potassium hydroxide (0.40 g, 7.13 mmol) was added and the solution refluxed an additional fifteen minutes. The resulting hot red solution was filtered into a suspension of TCNQ (1.56 g, 7.64 mmol) in ethanol (30 cm^3). The solution turned green and dark green crystals separated from the mixture. The product may be purified by dissolution in benzene and reprecipitation by the addition of pentane. Calc.: C, 62.30; H, 3.67; N, 6.05. Found: C, 62.24; H, 3.52; N, 5.96.

* Author to whom correspondence should be addressed.

Infrared spectra

The infrared spectrum of TCNQ was recorded in a KBr pellet, Nujol and chloroform. Where the medium does not absorb, the features of these spectra are identical. A medium intensity, sharp single band at 2220 cm^{-1} is assigned to the nitrile stretching frequency and a medium intensity band at 1540 cm^{-1} is assigned to the C=C stretching frequency. The frequencies correspond to the assignments reported by Acker and Hertler [6].

The infrared spectrum of *bis*(triphenylphosphine)gold(I)$^+$ TCNQ$^-$ was recorded in Nujol, benzene and a KBr pellet. Where the solvent does not absorb, the features of the spectrum are identical in Nujol and benzene. The nitrile frequencies are assigned to the bands at 2176 and 2150 cm^{-1}. The spectrum observed in the KBr pellet appears to be a composite of the spectrum of bromo (triphenylphosphine)gold(I) and potassium TCNQ.

Electron spin resonance spectrum

The electron spin resonance spectrum of *bis*(triphenylphosphine)gold(I)$^+$ TCNQ$^-$ was recorded at a concentration of 1×10^{-4} in benzene. The solvent was deoxygenated by introducing it into a vacuum line (which had been pumped down to a pressure of 10^{-5} torr), and freezing it to liquid nitrogen temperature. The cycle of freezing and thawing was repeated several times. After the solvent was deoxygenated it was transferred on the vacuum line to the sample holder. The sample holder consisted of a compartment for the solvent, a compartment for the sample and an ESR tube. These compartments were connected by a common junction which was fitted with a vacuum stopcock and an O-ring joint. The device could be attached to the vacuum system via the O-ring connector and in this manner the sample and solvent could be handled in a vacuum and mixed just prior to recording the spectrum. The hyperfine components resulting from four equivalent nitrogen, hydrogen and carbon atoms and two equivalent phosphorus atoms have been resolved. The hyperfine coupling constants are: $a^N = 0.981$, $a^H = 1.379$, $a^P = 0.095$ and $a^{C\text{-}13}$ for four equivalent, nitrile carbon atoms was estimated to be 0.19.

A g-value of 2.0113(2) was calculated by comparing the spectrum of the gold complex with that of Fremeys salt by use of a dual cavity and dual channel recorder. The center of the spectrum of Fremeys salt was estimated to be 3390 gauss.

A spin concentration experiment was performed in order to show that the observed spectrum was that of the gold compound and not that of an impurity. A solution of the gold complex of known concentration was placed in one section of the cavity and a sample of DPPH in the other section. Suitable signal levels and modulation amplitudes were chosen such that only the envelopes of the two curves were apparent. The spectra of both samples were recorded; then a sample of pitch in KCl was substituted for the sample containing the gold compound. The number of spins in the sample of DPPH was then calculated by comparison of the curves. The DPPH was used as a secondary standard because of experimental difficulties in observing the spectrum of pitch in KCl at an intensity sufficient to compare it directly to the gold complex. A value of 9.75×10^{16} spins was calculated from this experiment compared to the calculated value of 7.9×10^{16} from the solution concentration.

X-ray crystallography

Bis(triphenylphosphine)gold(I)$^+$ TCNQ$^-$ forms dark green parallelepipeds elongated along the a axis. Crystals suitable for structural analysis were obtained from an ethanol solution.

The lattice constants were determined on a Picker four circle automated diffractometer using Ni-filtered $CuK_{\alpha 1}$ radiation ($\lambda_{\alpha 1} = 1.54051$ Å). The constants are: $a = 10.937(2)$, $b = 13.267(2)$, $c = 9.2299(7)$, $\alpha = 107.48(1)$, $\beta = 100.34(1)$, $\gamma = 119.73(2)$ at 295°K. The intensity data were determined on a Picker four circle diffractometer using Zr-filtered Mo–K_α radiation ($\lambda = 0.7107$). The intensity measurements utilized the step scan method detailed elsewhere [7] and were corrected for absorption [9]. Further experimental details are given in Table 1.

The calculated X-ray density is 1.52 g cm^{-3} ($Z = 1$, $M.W. = 925.76$). A measured density of 1.49 g cm^{-3} was determined psychometrically using iosoctane.

Precession photographs revealed that the crystal either belonged to the space group $P\bar{1}$ or $P1$. Examination of the Patterson map and subsequent refinement revealed that the compound belonged to the triclinic space group $P\bar{1}$.

The crystal used for structural analysis was mounted along the a axis and data collected to $\theta = 25°$.

Structure determination and refinement

The structure of *bis*(triphenylphosphine)gold(I)$^+$ TCNQ$^-$ was solved using heavy atom techniques, employing a program previously developed at the University of Iowa. The atom scattering factors were taken from "International Tables for X-ray Crystallography" [13]. All atoms were assumed to be neutrally charged. Both real and imaginary dispersion corrections were applied for gold and phosphorus during all stages of the refinement.

The progress of the refinement was followed using the relation:

$$R_2 = [\Sigma w(\Delta F)^2 / \Sigma w(F_o)^2]^{1/2}$$

where $\Delta F = F_o - F_c$. The function minimized was $\Sigma w(\Delta F)^2$. In the final refinement step, anisotropic ther-

Table 1. Crystallographic data and processing parameters

Molecular formula	$C_{48}H_{34}AuN_4P_2$
Molecular weight	925.76
$F(000)$	459
Crystal system	Triclinic
Space group	$P\bar{1}$
a (Å)	10.937(2)
b (Å)	13.267(2)
c (Å)	9.2299(7)
α (°)	107.48(1)
β (°)	100.34(1)
γ (°)	119.73(2)
Cell dimension	12 refl., 90 to 120° 2θ ($\lambda_{K\alpha1}$ = 1.54051 Å)
Z	1
V (Å^3)	1018.3
D_{calc} (Mg m^{-3})	1.52
D_{obs} (Mg m^{-3})	1.49
Crystal size (mm)	0.06 × 0.12 × 0.22
μ(Mo–K$_\alpha$) (mm^{-1})	2.54
Abs. Corr. (Max/min)	0.862/0.633
Data collection limits to θ	25°
Scan mode [7] θ-2θ step size	0.08°
Octants sampled	full sphere
Decay	~1%
Total refl.	8168
$F_o > 3\sigma(F_o)$	2896
Least squares parameters	214
Data/parameters	2896/214
R	0.0417
R_w	0.0627
Weighting scheme [8]	$P = 0.04$, $Q = 0$ $wt = 1/(\sigma_F^2 + (PF)^2 + Q)$
Residual extrema in final difference map (e Å^{-3})	+1.6 to −1.2

mal displacement factors were used for all non-hydrogen atoms. Hydrogen atoms were included at fixed positions, 0.95 Å, with isotropic thermal displacement factors. The phenyl groups were constrained to be idealized planar groups with exact distances of 1.40 Å.

RESULTS AND DISCUSSION

The synthesis of *bis*(triphenylphosphine)gold(I)$^+$ TCNQ$^-$ differs from the previously reported procedure, involving the reaction of lithium salt of TCNQ$^-$ and *bis*(triphenylphosphine)gold(I) perchlorate, and consists of the formation of an intermediate gold cluster compound and the oxidation of this compound by TCNQ to yield the green crystalline unsolvated product. The intermediate solution of the polygold compound was not isolated but is similar to that reported by Malatesta [10] from which polygold compounds have been previously isolated.

The infrared spectrum in the nitrile region (2176 and 2150 cm^{-1}) corresponds to the values reported for the solvated species [2,4].

The electron spin resonance spectrum of the titled compound is shown in Fig. 1a along with the simulated spectrum of the compound, 1b, and the spectrum of the TCNQ radical anion, 1c, reported by Fischer and McDowell [12]. In contrast to the spectra of the solvated species the unsolvated form displays extensive hyperfine interactions.

The spectrum was recorded in benzene at a concentration of 10^{-4} M. The hyperfine components resulting from four equivalent nitrogen, hydrogen,

Table 2. Selected bond distances (Å) and bond angles (°)

Au—P	2.309(1)	C(21)—C(20)	1.38(1)
P—C(1)	1.801(6)	C(21)—C(19)	1.40(2)
P—C(7)	1.790(7)	C(22)—C(21)	1.45(2)
P—C(13)	1.801(6)	C(22)—C(23)	1.41(2)
C(19)—N(1)	1.17(2)	C(22)—C(24)	1.40(1)
C(20)—N(2)	1.13(2)	C(23)—C(24′)	1.37(2)
P—Au—P	180.0	C(20)—C(21)—C(19)	118(1)
Au—P—C(1)	116.9	C(20)—C(21)—C(22)	122(1)
Au—P—Cl(7)	110.0	C(19)—C(21)—C(22)	120(1)
Au—P—C(13)	111.3	C(21)—C(22)—C(23)	120(2)
C(1)—P—C(7)	106.1(3)	C(21)—C(22)—C(24)	121(1)
C(1)—P—C(13)	104.7(5)	C(23)—C(22)—C(24)	119(1)
C(7)—P—C(13)	107.2(4)	C(22)—C(23)—C(24′)	122(1)
N(1)—C(19)—C(21)	176.2(2)	C(22)—C(24)—C(23′)	119(1)
N(2)—C(20)—C(21)	176.5(1)		

Distances assigned to the phenyl groups: C—C 1.40; C—H 0.95 Å; bond angles 120°.

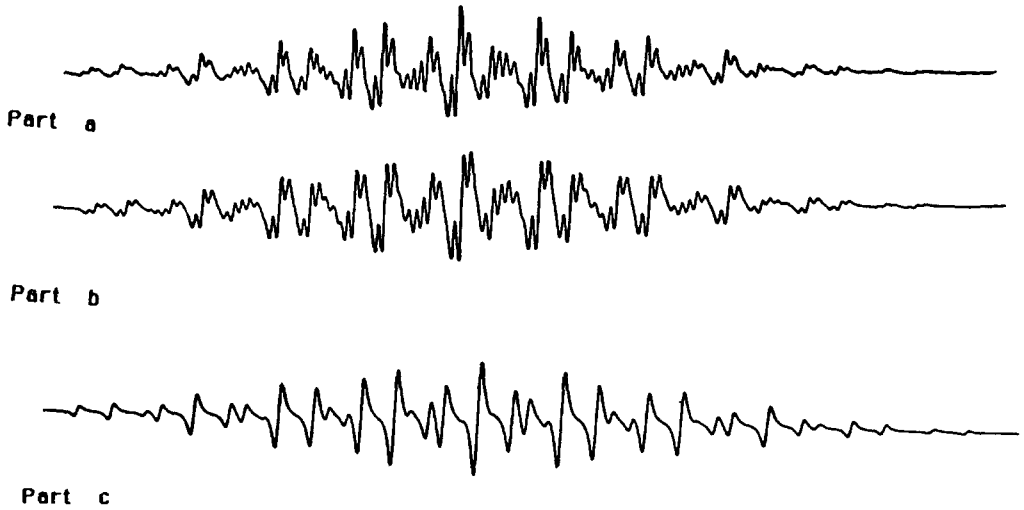

Fig. 1. (a) The ESR spectrum of *bis*(triphenylphosphine)gold(I)$^+$ TCNQ$^-$; (b) the simulated spectrum of *bis*(triphenylphosphine)gold(I)$^+$ TCNQ$^-$; (c) the spectrum [12] of the TCNQ radical anion.

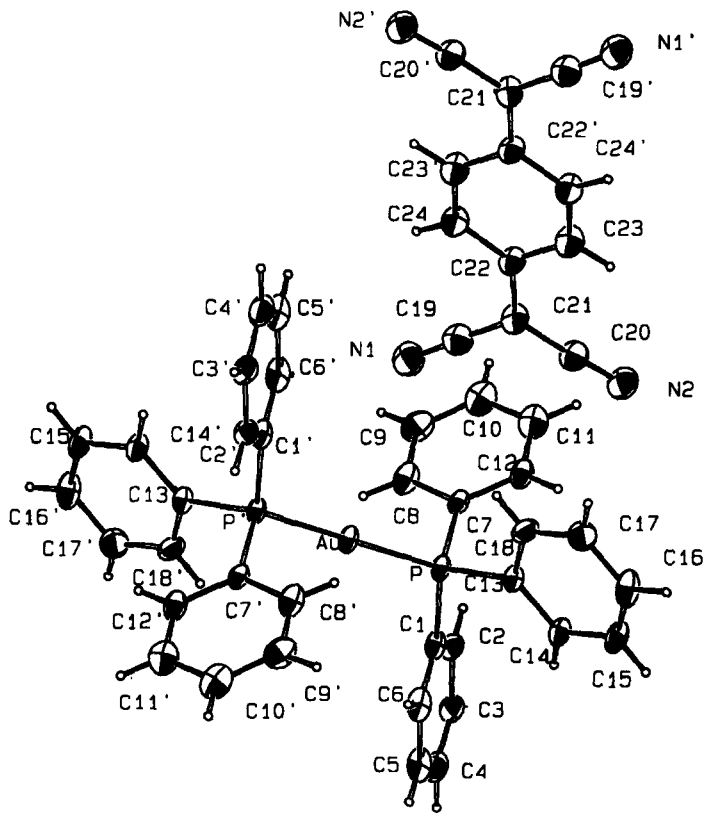

Fig. 2. The molecular geometry and numbering scheme of *bis*(triphenylphosphine)gold(I)$^+$ TCNQ$^-$.

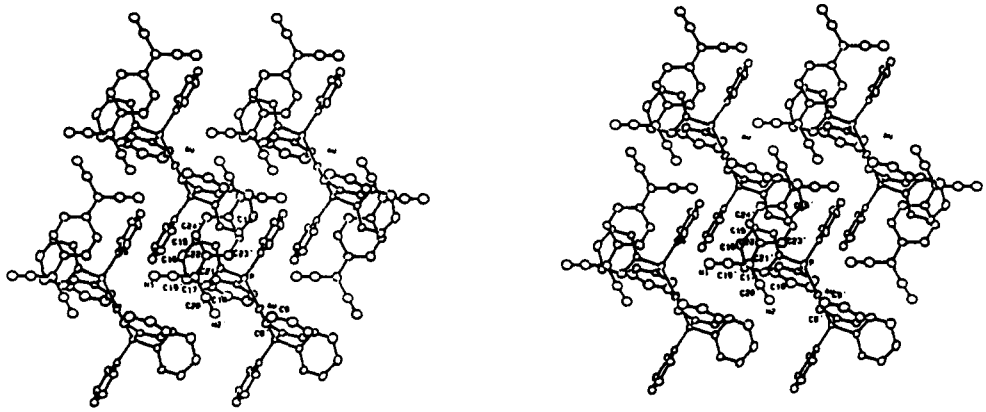

Fig. 3. Stereoplot of the structure of *bis*(triphenylphosphine)gold(I)$^+$ TCNQ$^-$, viewed approximately perpendicular to the *a*, *c* face.

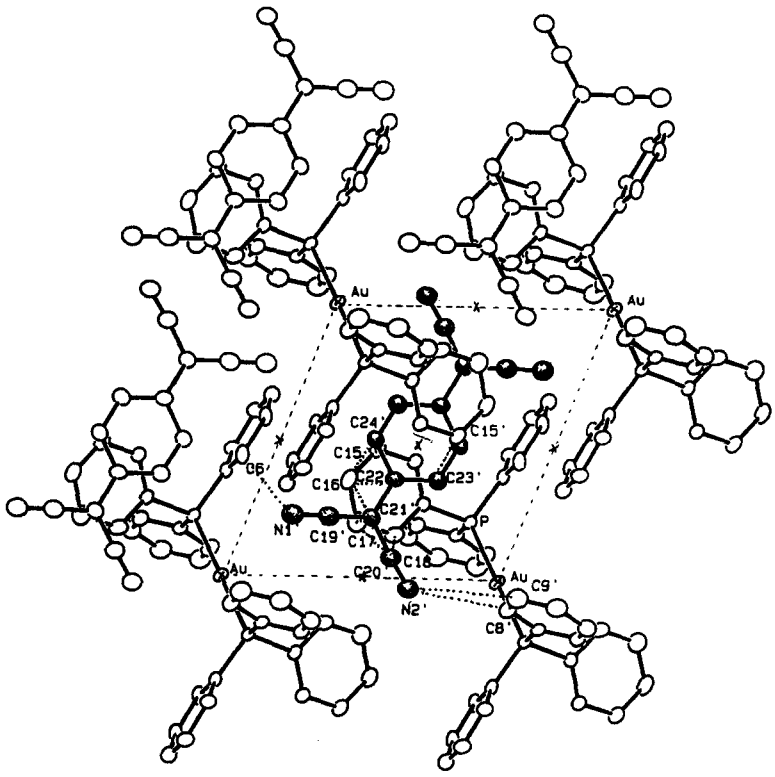

Fig. 4. A packing diagram of *bis*(triphenylphosphine)gold(I)$^+$ TCNQ$^-$. View of *a*, *c* face showing interspecies contacts. TCNQ anion is highlighted to distinguish it from the cation. Centers of symmetry are denoted by x. Intermolecular contacts are indicated by dotted lines. A few of the close contact lines have been omitted for clarity. See interspecies distances Table A4.

and carbon-13 atoms and two equivalent phosphorus atoms were resolved. The hyperfine coupling constants are: $a^N = 0.981$, $a^H = 1.379$, $a^P = 0.095$, and $a^{C\text{-}13}$ for one set of four equivalent, nitrile, carbon atoms was estimated to be 0.19, with an average line width of 0.0716 gauss. The g-value was found to be 2.0113(2). It should be noted that no splitting due to the gold atom was observed which may be due to the fact that the hyperfine coupling constant for gold is probably very small and thus this component was not resolved.

The fact that there are four equivalent nitrogen atoms, four equivalent hydrogen atoms, and two equivalent phosphorus atoms indicates that the cation is symmetrically arranged with respect to the anion, $TCNQ^-$, in a solvent cage of benzene. One cannot exclude the possibility of two equivalent hydrogen atoms on the triphenylphosphine accounting for the additional splitting instead of the phosphorus atoms. It would, however, be a very fortuitous situation if only two triphenylphosphine hydrogens were involved in the splitting and if this were the case then one would anticipate a^H to be much larger.

Table 1 lists the crystallographic data and processing parameters and intermolecular distances and bond angles are listed in Table 2. Figure 2 illustrates the molecular configuration and atom numbering scheme. Figure 3 is a stereoplot viewed perpendicular to the a, c face, and Fig. 4 is a packing diagram featuring the a, c face.

The crystals belong to the triclinic, centrosymmetric space group $P\bar{1}$ in contrast to the arrangement of the solvated form which has been assigned to the noncentrosymmetric, monoclinic space group $C2$. The geometry about the gold atom is linear with a P—Au—P bond angle of 180°. The TCNQ anion is slightly distorted from planarity with a center of symmetry located at the center of the anion. The planes containing the TCNQ anions are separated by the cations at a distance of 12.78 Å. The bond distances and bond angles of the phenyl groups were fixed and refined as a group. With the exception of the nitrile groups the distances within the anion were close to normal values as reported in Table 2.

REFERENCES

1. Baykova, T. V., Ellert, O. G., Kuz'mina, L. G., Dvortsova, N. V., Lemenovskil, D. A. and Rubezhov, A. Z., *Mendeleev Commun.*, 1991, **1,** 22.
2. Alonso, P. J., Cerrada, E., Garin, J., Gimeno, M. C., Luguna, A. and Jones, P. G., *Synthetic Metals*, 1993, **55–57,** 1772.
3. Cerrada, E., Gimeno, M. C., Jimenez, J., Laguna, A., Laguna, M. and Jones, P. G., *Organometallics*, 1994, **13,** 1470.
4. Cerrada, E., Garin, J., Gimeno, M. C., Laguna, A., Laguna, M. and Jones, P. G., *Spec.-R. Soc. Chem.*, 1993, **131** (Chemistry of the Copper and Zinc Triads), 164.
5. Soboroff, M., PhD. Thesis, The University of Iowa, Iowa City, Iowa, 1973, (C. Abs. **80,** 66297k).
6. Acker, D. S. and Hertler, W. R., *J. Am. Chem. Soc.*, 1962, **84,** 3370.
7. Baenziger, N. C., Foster, B. A., Howells, M., Howells, R., Vander Valk, P. and Burton, D. J., *Acta Cryst.*, 1977, **B33,** 2327.
8. Killean, R. C. G. and Lawrence, J. L., *Acta Cryst.*, 1969, **B25,** 1750.
9. Templeton, L. and Templeton, D., *ABSORB, Am. Crystallogr. Assoc. Meet. Storrs*, Connecticut, 1973, Abstract E10, p. 143; modified for local use by F. J. Hollander.
10. Malastesta, I., Naldini, I., Simonetta, G. and Curiata, F., *Coor. Chem. Revs.*, 1966, **1,** 255.
11. Johnson, C. K., ORTEPII, Report ONRL-5138, Oak Ridge National Laboratory, Tennessee, U.S.A., 1976.
12. Fischer, P. H. H. and McDowell, C. A., *J. Am. Chem. Soc.*, 1963, **85,** 2694.
13. *International Tables for X-ray Crystallography.* Kynoch Press, Birmingham, 1974.

APPENDIX

Table A1. Atomic coordinates for atoms refined in *bis*(triphenylphosphine)gold(I)$^+$ TCNQ$^-$

	x	*y*	*z*	U_{eq}
Au	0.00000	0.00000	0.00000	0.0360(2)
P	0.21153(22)	0.20503(19)	0.19712(25)	0.0335(6)
N(1)	0.7726(13)	0.1126(12)	0.1674(17)	0.079(5)
N(2)	1.0296(12)	0.2872(11)	0.7034(16)	0.075(4)
C(19)	0.7755(14)	0.1287(12)	0.3000(22)	0.070(5)
C(20)	0.9184(13)	0.2208(11)	0.5897(17)	0.062(4)
C(21)	0.7778(12)	0.1403(9)	0.4570(14)	0.054(4)
C(22)	0.6356(10)	0.0677(9)	0.4763(14)	0.051(3)
C(23)	0.6384(13)	0.0746(12)	0.6324(16)	0.064(4)
C(24)	0.4933(12)	−0.0062(11)	0.3435(14)	0.060(4)
	(Atom positions calculated from ideal phenyl model + orientation matrix)			
C(1)	0.3808	0.2740	0.1530	0.042(3)
C(2)	0.4599	0.4007	0.1687	0.046(3)
C(3)	0.5981	0.4547	0.1468	0.057(4)
C(4)	0.6570	0.3821	0.1092	0.068(5)
C(5)	0.5779	0.2555	0.0935	0.074(5)
C(6)	0.4397	0.2015	0.1155	0.056(4)
C(7)	0.1645	0.3192	0.2315	0.037(3)
C(8)	0.0942	0.3236	0.0934	0.057(4)
C(9)	0.0527	0.4097	0.1138	0.076(5)
C(10)	0.0816	0.4914	0.2725	0.071(5)
C(11)	0.1520	0.4870	0.4106	0.065(4)
C(12)	0.1934	0.4009	0.3902	0.048(3)
C(13)	0.2738	0.2064	0.3926	0.037(2)
C(14)	0.4288	0.2726	0.4907	0.046(3)
C(15)	0.4709	0.2729	0.6433	0.057(4)
C(16)	0.3580	0.2069	0.6978	0.059(4)
C(17)	0.2030	0.1407	0.5997	0.074(5)
C(18)	0.1609	0.1404	0.4470	0.058(4)
	(calculated hydrogen atom positions)			
	x	*y*	*z*	U_{iso}
H(2)	0.420	0.450	0.194	0.050
H(3)	0.652	0.541	0.157	0.063
H(4)	0.751	0.419	0.094	0.080
H(5)	0.618	0.206	0.068	0.096
H(6)	0.386	0.115	0.105	0.070
H(8)	0.074	0.268	−0.014	0.065
H(9)	0.005	0.412	0.020	0.096
H(10)	0.053	0.550	0.286	0.088
H(11)	0.172	0.542	0.518	0.077
H(12)	0.241	0.398	0.484	0.055
H(14)	0.505	0.317	0.454	0.054
H(15)	0.576	0.318	0.710	0.068
H(16)	0.387	0.207	0.801	0.073
H(17)	0.126	0.096	0.637	0.091
H(18)	0.056	0.095	0.380	0.069
H(23)	0.733	0.129	0.725	0.075
H(24)	0.487	−0.009	0.239	0.072

Table A2. Group parameters and errors for *bis*(triphenylphosphine)gold(I)$^+$ TCNQ$^-$

		Phenyl Group I			
Rotation Angles			Center of Gravity		
About *i*	About *j*	About *k*	*x*	*y*	*z*
−174.74(3)	−11.46(3)	150.27(3)	0.5189(5)	0.3281(5)	0.1311(5)
Calculated errors in C(1)			0.3808(5)	0.2740(5)	0.1530(5)
Orthonormal equation of plane: $-0.1988i+0.0898j-0.9759k = -1.3996$					
		Phenyl Group II			
−83.75(5)	41.10(3)	2.69(4)	0.1231(5)	0.4053(4)	0.2520(6)
Calculated errors in C(7)			0.1645(5)	0.3192(4)	0.2315(6)
Orthonormal equation of plane: $-0.6574i-0.7490j-0.0820k = -1.7406$					
		Phenyl Group III			
122.70(4)	33.62(4)	−100.19(3)	0.3159(5)	0.2066(4)	0.5452(5)
Calculated errors in C(13)			0.2738(5)	0.2064(5)	0.3926(5)
Orthonormal equation of plane: $0.5537i-0.7008j-0.4499k = -1.4090$					
		TCNQ Group			
Orthonormal equation of plane:		$0.6056(31)i-0.7560(24)j-0.2484(21)k = -3.218(13)$			
Deviation of atoms from plane:		N(1) 0.30(2), N(2) −0.15(1), C(19) 0.13(2), C(20) −0.06(2), C(21) 0.02(1), C(22) 0.00(1), C(23) −0.17(2), C(24) −0.08(1)			
		Angles between plane normals			
Phenyl 1	Phenyl 2	81.8	Phenyl 2	Phenyl 3	78.6
Phenyl 1	Phenyl 3	74.6	Phenyl 2	TCNQ	79.1(2)
Phenyl 1	TCNQ	86.9(1)	Phenyl 3	TCNQ	12.4(7)

Table A3. U-values for *bis*(triphenylphosphine)gold(I)$^+$ TCNQ$^-$

	U11	U12	U13	U22	U23	U33
Au	0.0443(3)	0.0134(2)	0.0010(2)	0.0344(3)	0.0093(2)	0.0390(3)
P	0.0406(10)	0.0163(8)	0.0056(8)	0.0354(10)	0.0105(8)	0.0366(11)
N1	0.082(7)	0.032(6)	0.033(7)	0.086(8)	0.030(7)	0.101(9)
N2	0.070(6)	0.036(6)	0.032(6)	0.089(7)	0.027(7)	0.098(8)
C1	0.056(5)	0.032(4)	0.014(4)	0.058(5)	0.019(4)	0.035(4)
C2	0.046(4)	0.016(4)	0.014(4)	0.047(5)	0.017(4)	0.059(6)
C3	0.049(5)	0.016(5)	0.014(5)	0.074(7)	0.018(6)	0.064(7)
C4	0.064(7)	0.038(7)	0.017(5)	0.117(10)	0.031(7)	0.054(7)
C5	0.095(8)	0.087(9)	0.038(6)	0.135(11)	0.044(7)	0.054(6)
C6	0.083(7)	0.057(5)	0.029(5)	0.082(7)	0.027(5)	0.044(5)
C7	0.036(4)	0.017(3)	0.008(3)	0.042(4)	0.014(4)	0.046(5)
C8	0.068(6)	0.038(5)	0.014(50	0.062(5)	0.032(5)	0.072(7)
C9	0.085(8)	0.060(7)	0.028(7)	0.089(8)	0.052(8)	0.104(10)
C10	0.073(7)	0.049(6)	0.024(7)	0.072(7)	0.022(7)	0.043(10)
C11	0.070(6)	0.042(6)	0.032(6)	0.066(6)	0.018(6)	0.091(8)
C12	0.052(5)	0.026(4)	0.013(4)	0.056(5)	0.014(5)	0.056(6)
C13	0.051(4)	0.022(4)	0.013(4)	0.039(4)	0.018(3)	0.040(4)
C14	0.053(4)	0.029(4)	0.010(4)	0.062(5)	0.019(4)	0.045(5)
C15	0.069(6)	0.042(6)	0.010(5)	0.083(7)	0.029(5)	0.049(6)
C16	0.093(8)	0.040(6)	0.015(6)	0.064(6)	0.028(5)	0.052(6)
C17	0.094(8)	0.038(7)	0.029(7)	0.090(7)	0.060(7)	0.080(8)
C18	0.056(5)	0.027(5)	0.012(5)	0.071(6)	0.046(6)	0.076(7)
C19	0.073(7)	0.036(6)	0.034(7)	0.068(7)	0.032(7)	0.101(11)
C20	0.064(7)	0.026(5)	0.025(6)	0.058(6)	0.024(6)	0.089(8)
C21	0.064(6)	0.032(5)	0.029(5)	0.053(5)	0.015(5)	0.072(7)
C22	0.050(5)	0.026(4)	0.021(5)	0.051(5)	0.016(5)	0.074(7)
C23	0.071(6)	0.045(6)	0.033(6)	0.075(7)	0.024(6)	0.082(8)
C24	0.066(6)	0.044(5)	0.032(5)	0.074(6)	0.026(6)	0.074(7)

Table A4. Interspecies distances (Å) and errors for *bis*(triphenylphosphine)gold(I)$^+$ TCNQ$^-$

N(1′)—C(6)	3.36(1)	C(21′)—C(16)	3.74(1)
N(2′)—C(8)	3.38(2)	C(21′)—C(17)	3.72(1)
N(2′)—C(9)	3.55(1)	C(22′)—C(15)	3.78(1)
N(2′)—C(3)	3.40(1)[a]	C(22′)—C(16)	3.55(1)
N(2′)—C(4)	3.52(1)[a]	C(23′)—C(15)	3.87(2)
N(2′)—C(10)	3.66(2)[a]	C(24′)—C(15)	3.78(2)
C(20′)—C(17)	3.75(2)	C(24′)—C(16)	3.71(2)
C(20′)—C(18)	3.62(2)		
C(20′)—C(10)	3.64(2)[a]		

[a] Not shown in Fig. 4. These atoms are from cations displaced along *b*. Closest C—H and N—H distances are: N(1′)—H(6), 2.67; N(2′)—H(3), 2.78; N(2′)—H(10)), 2.72; C(20′)—H(10), 2.74 Å.

Table A5. Structure factor values for *bis*(triphenylphosphine)gold(I)$^+$ TCNQ$^-$

h	k	l	$10F_c$	$10F_c$	$10S_g$	h	k	l	$10F_o$	$10F_c$	$10S_g$	h	k	l	$10F_o$	$10F_c$	$10S_g$	h	k	l	$10F_o$	$10F_c$	$10S_g$
0	0	1	373	351	11	0	5	−10	228	208	−45	0	9	−1	266	279	8	1	−11	6	246	252	5
0	0	2	475	449	9	0	5	−9	195	187	21	0	9	0	318	318	6	1	−11	7	139	147	12
0	0	3	283	268	8	0	5	−8	219	217	4	0	9	1	357	366	21	1	−11	8	75	69	−13
0	0	4	207	213	8	0	5	−7	220	229	18	0	9	2	238	236	12	1	−11	9	77	89	−33
0	0	5	465	456	9	0	5	−6	382	376	11	0	9	3	155	175	9	1	−10	−3	155	172	9
0	0	6	402	381	48	0	5	−5	520	513	5	0	9	4	118	127	13	1	−10	−2	174	167	19
0	0	9	177	157	7	0	5	−4	218	230	2	0	10	−10	157	154	17	1	−10	−1	322	320	−16
0	1	−9	153	152	9	0	5	−3	456	459	5	0	10	−9	93	115	10	1	−10	0	306	311	15
0	1	−8	114	126	9	0	5	−2	640	642	6	0	10	−8	97	88	−16	1	−10	1	211	211	6
0	1	−7	249	257	5	0	5	−1	596	633	6	0	10	−7	146	149	12	1	−10	2	292	312	6
0	1	−6	414	423	4	0	5	0	606	583	6	0	10	−6	271	271	11	1	−10	3	221	222	7
0	1	−5	521	505	5	0	5	1	628	642	13	0	10	−5	306	313	12	1	−10	4	386	395	19
0	1	−4	255	254	5	0	5	2	253	263	15	0	10	−4	217	227	17	1	−10	5	298	311	9
0	1	−3	1061	993	11	0	5	3	293	316	9	0	10	−3	211	208	8	1	−10	6	69	56	−16
0	1	−2	1747	1633	17	0	5	4	293	291	6	0	10	−2	167	168	18	1	−10	7	160	169	8
0	1	−1	943	906	9	0	5	5	392	386	8	0	10	−1	320	333	10	1	−10	8	152	158	12
0	1	0	765	732	15	0	5	6	231	226	7	0	10	0	369	369	11	1	−10	9	179	184	5
0	1	1	328	323	16	0	5	7	129	137	10	0	10	1	209	204	8	1	−10	10	127	152	13
0	1	2	90	83	7	0	6	−10	127	128	−59	0	10	2	135	116	−22	1	−9	−4	186	154	7
0	1	3	464	452	23	0	6	−9	167	157	17	0	11	−9	67	76	−18	1	−9	−3	170	191	8
0	1	4	884	826	62	0	6	−8	148	149	−36	0	11	−7	140	140	14	1	−9	−2	378	383	19
0	1	5	429	428	21	0	6	−7	235	238	7	0	11	−6	331	339	13	1	−9	−1	295	286	24
0	1	6	368	350	26	0	6	−6	381	403	15	0	11	−5	148	135	7	1	−9	0	241	228	12
0	1	7	214	201	6	0	6	−5	344	345	7	0	11	−4	120	124	8	1	−9	1	238	244	10
0	1	8	198	214	8	0	6	−4	488	489	5	0	11	−3	207	215	6	1	−9	2	387	402	4
0	1	9	195	192	−40	0	6	−3	531	533	5	0	11	−2	264	257	8	1	−9	3	306	321	3
0	2	−10	228	71	−40	0	6	−2	449	461	4	0	11	−1	305	311	33	1	−9	4	320	322	10
0	2	−7	479	485	14	0	6	−1	476	512	5	0	11	0	158	152	17	1	−9	5	238	249	5
0	2	−6	352	356	4	0	6	0	406	412	12	0	11	1	137	131	8	1	−9	6	157	173	22
0	2	−5	534	510	21	0	6	1	355	351	4	0	12	−8	182	184	15	1	−9	7	243	257	7
0	2	−4	421	425	4	0	6	2	274	277	5	0	12	−7	136	133	7	1	−9	8	273	284	5
0	2	−3	544	521	5	0	6	3	376	389	15	0	12	−6	156	152	6	1	−9	9	182	177	26
0	2	−2	674	654	7	0	6	4	374	375	4	0	12	−5	73	91	−17	1	−9	10	91	69	13
0	2	−1	485	480	15	0	6	5	249	261	7	0	12	−4	162	165	13	1	−8	−5	136	143	12
0	2	0	161	171	6	0	6	6	71	81	13	0	12	−3	227	213	20	1	−8	−4	235	218	7
0	2	1	695	687	69	0	7	−10	192	71	−33	0	12	−1	161	159	−30	1	−8	−3	231	272	7
0	2	2	764	763	53	0	7	−9	159	152	3	0	12	0	128	107	−22	1	−8	−2	391	375	8
0	2	3	785	769	40	0	7	−8	213	217	4	0	13	−7	95	84	12	1	−8	−1	206	204	6

Table A5 *Continued.*

h	*k*	*l*	$10F_c$	$10F_c$	$10S_g$	*h*	*k*	*l*	$10F_o$	$10F_c$	$10S_g$	*h*	*k*	*l*	$10F_o$	$10F_c$	$10S_g$	*h*	*k*	*l*	$10F_o$	$10F_c$	$10S_g$
0	2	4	509	516	20	0	7	−7	284	290	14	0	13	−6	77	90	−26	1	−8	0	303	311	3
0	2	5	269	276	5	0	7	−6	404	416	28	0	13	−5	130	132	8	1	−8	1	334	358	3
0	2	6	279	288	6	0	7	−5	287	284	3	0	13	−4	197	190	6	1	−8	2	513	531	10
0	2	8	204	236	8	0	7	−4	324	323	10	0	13	−3	186	178	11	1	−8	3	464	481	5
0	3	−10	123	94	19	0	7	−3	385	409	4	0	13	−2	160	158	6	1	−8	4	262	277	10
0	3	−9	264	230	5	0	7	−2	466	483	5	1	−14	3	151	153	8	1	−8	5	260	275	3
0	3	−8	364	354	7	0	7	−1	380	400	8	1	−14	4	173	176	7	1	−8	6	342	366	7
0	3	−7	364	259	3	0	7	0	352	351	11	1	−14	5	118	119	15	1	−8	7	272	282	3
0	3	−6	249	249	10	0	7	1	328	319	10	1	−14	6	90	83	13	1	−8	8	194	199	14
0	3	−5	226	251	14	0	7	2	378	383	11	1	−13	−5	171	50	−28	1	−8	9	110	108	−19
0	3	−4	599	588	6	0	7	3	321	340	6	1	−13	1	150	159	7	1	−8	10	92	91	−32
0	3	−3	837	841	8	0	7	4	240	256	7	1	−13	2	210	212	6	1	−7	−6	82	86	−15
0	3	−2	549	547	5	0	7	5	115	116	10	1	−13	3	217	209	71	1	−7	−5	198	191	8
0	3	−1	1128	1117	11	0	8	−10	92	87	9	1	−13	4	139	143	24	1	−7	−4	369	367	4
0	3	0	279	273	6	0	8	−9	184	181	26	1	−13	5	96	100	15	1	−7	−3	318	320	3
0	3	1	598	596	30	0	8	−8	231	236	9	1	−13	6	122	122	−22	1	−7	−2	292	289	3
0	3	2	703	715	28	0	8	−7	296	305	3	1	−13	7	106	116	15	1	−7	−1	225	240	4
0	3	3	485	510	24	0	8	−6	162	151	5	1	−13	8	146	146	13	1	−7	0	530	515	11
0	3	4	358	363	11	0	8	−5	274	277	16	1	−12	−1	158	146	9	1	−7	1	737	766	7
0	3	5	228	227	5	0	8	−4	327	332	3	1	−12	0	194	185	31	1	−7	2	369	390	7
0	3	6	369	357	26	0	8	−3	491	500	10	1	−12	1	220	219	7	1	−7	3	414	429	12
0	4	−9	205	207	21	0	8	−2	377	392	4	1	−12	2	233	227	16	1	−7	4	295	301	3
0	4	−8	256	245	8	0	8	−1	207	219	4	1	−12	3	173	162	−34	1	−7	5	299	306	9
0	4	−7	218	220	17	0	8	0	307	310	3	1	−12	4	125	116	14	1	−7	6	360	365	4
0	4	−6	318	319	3	0	8	1	328	325	13	1	−12	5	114	119	8	1	−7	7	270	264	3
0	4	−5	572	569	6	0	8	2	341	358	3	1	−12	6	270	269	13	1	−7	8	158	173	6
0	4	−4	649	647	13	0	8	3	223	239	7	1	−12	7	187	191	22	1	−7	9	126	134	8
0	4	−3	610	589	6	0	8	4	168	166	8	1	−12	8	127	130	22	1	−7	10	172	161	9
0	4	−8	427	419	4	0	9	−10	157	148	9	1	−12	9	86	79	10	1	−6	−7	74	104	−18
0	4	−1	256	269	3	0	9	−9	201	200	8	1	−11	−2	143	145	20	1	−6	−5	356	355	18
0	4	0	703	691	14	0	9	−8	153	142	−31	1	−11	−1	182	175	13	1	−6	−4	287	302	6
0	4	1	766	780	31	0	9	−7	222	222	4	1	−11	0	248	245	12	1	−6	−3	244	259	5
0	4	1	398	780	28	0	9	−6	106	98	8	1	−11	1	272	265	5	1	−6	−2	309	311	9
0	4	3	493	490	25	0	9	−5	363	371	25	1	−11	2	183	183	6	1	−6	−1	485	498	19
0	4	4	275	281	5	0	9	−4	383	385	34	1	−11	3	179	187	5	1	−6	0	866	833	17
0	4	5	257	243	5	0	9	−3	295	303	21	1	11	4	235	245	5	1	−6	1	500	529	15
0	4	6	345	342	17	0	9	−2	147	151	4	1	−11	5	314	328	9	1	−6	2	218	236	2

Table A5—*Continued.*

h	k	l	$10F_c$	$10F_c$	$10S_g$	h	k	l	$10F_o$	$10F_c$	$10S_g$	h	k	l	$10F_o$	$10F_c$	$10S_g$	h	k	l	$10F_o$	$10F_c$	$10S_g$
1	−6	3	218	226	4	1	−1	−4	503	481	25	1	3	6	365	360	37	1	8	−2	225	199	4
1	−6	4	481	497	5	1	−1	−3	410	387	25	1	4	−10	225	224	7	1	8	−1	180	174	13
1	−6	5	342	366	3	1	−1	−2	926	837	37	1	4	−9	160	150	−41	1	8	0	341	344	14
1	−6	6	437	428	17	1	−1	−1	709	679	14	1	4	−8	157	154	11	1	8	1	386	383	8
1	−6	7	265	263	11	1	−1	0	1041	1025	21	1	4	−7	224	231	7	1	8	2	279	283	11
1	−6	8	206	229	4	1	−1	1	914	967	9	1	4	−6	425	416	13	1	9	−10	142	149	11
1	−6	9	162	146	11	1	−1	2	147	140	7	1	4	−5	556	560	22	1	9	−9	111	125	10
1	−6	10	194	176	17	1	−1	3	169	167	14	1	4	−4	380	388	8	1	9	−8	108	101	−28
1	−5	−6	302	309	6	1	−1	4	495	478	5	1	4	−3	652	633	7	1	9	−7	127	130	−31
1	−5	−5	314	312	6	1	−1	5	726	723	7	1	4	−2	478	460	5	1	9	−6	289	288	9
1	−5	−3	364	360	7	1	−1	6	485	468	24	1	4	−1	738	721	22	1	9	−5	368	347	18
1	−5	−2	636	629	19	1	−1	8	166	156	8	1	4	0	630	657	6	1	9	−4	246	234	17
1	−5	−1	684	700	27	1	−1	9	135	141	11	1	4	1	247	274	12	1	9	−3	177	162	11
1	−5	0	443	426	13	1	0	−7	285	286	3	1	4	2	295	283	12	1	9	−2	202	208	10
1	−5	1	280	292	8	1	0	−6	393	403	16	1	4	3	304	301	9	1	9	−1	313	313	13
1	−5	2	463	480	5	1	0	−5	569	555	6	1	4	4	400	413	4	1	9	0	392	392	20
1	−5	3	315	328	3	1	0	−4	437	439	9	1	4	5	429	426	4	1	9	1	250	250	5
1	−5	4	790	789	8	1	0	−3	811	780	32	1	4	6	217	211	6	1	9	2	181	169	18
1	−5	5	477	482	10	1	0	−2	552	540	17	1	5	−10	114	110	−34	1	9	3	114	124	13
1	−5	6	409	401	12	1	0	−1	971	924	10	1	5	−9	117	111	−24	1	10	−10	67	70	−20
1	−5	7	201	198	12	1	0	0	530	516	16	1	5	−8	258	254	13	1	10	−9	211	71	−40
1	−5	8	244	231	5	1	0	1	331	325	3	1	5	−7	254	246	5	1	10	−8	129	129	−34
1	−5	9	222	208	7	1	0	2	646	645	6	1	5	−6	491	502	5	1	10	−7	197	194	14
1	−5	10	191	164	13	1	0	3	709	706	28	1	5	−5	382	380	11	1	10	−6	258	247	13
1	−4	−8	175	174	10	1	0	4	894	855	9	1	5	−4	253	247	5	1	10	−5	200	199	12
1	−4	−6	211	192	6	1	0	5	513	502	5	1	5	−3	384	380	8	1	10	−4	154	152	−44
1	−4	−5	290	290	38	1	0	6	56	63	−15	1	5	−2	670	649	7	1	10	−2	289	291	6
1	−4	−4	359	362	7	1	0	8	181	174	7	1	5	−1	519	516	5	1	10	−1	326	332	10
1	−4	−3	425	438	21	1	1	−10	81	85	−31	1	5	0	379	380	4	1	10	0	201	205	24
1	−4	−2	483	486	24	1	1	−7	406	402	4	1	5	1	283	300	11	1	10	1	114	104	−18
1	−4	−1	884	872	44	1	1	−6	512	519	5	1	5	2	532	526	11	1	10	2	150	148	12
1	−4	0	113	120	3	1	1	−5	268	270	3	1	5	3	332	343	7	1	11	−9	100	94	−21
1	−4	1	588	610	6	1	1	−4	600	580	6	1	5	4	359	373	7	1	11	−8	147	140	7
1	−4	2	628	648	6	1	1	−3	326	319	7	1	5	5	295	313	6	1	11	−7	227	221	25
1	−4	3	731	727	15	1	1	−2	930	916	9	1	5	6	109	111	13	1	11	−6	156	159	6
1	−4	4	871	846	17	1	1	−1	725	695	22	1	6	−10	70	74	−16	1	11	−5	133	127	−31
1	−4	5	304	303	9	1	1	0	112	100	6	1	6	−9	133	135	−23	1	11	−4	210	213	6
1	−4	6	299	311	15	1	1	1	1095	1037	11	1	6	−8	269	274	5	1	11	−3	215	218	6

Table A5—*Continued.*

h	*k*	*l*	$10F_c$	$10F_c$	$10S_g$	*h*	*k*	*l*	$10F_o$	$10F_c$	$10S_g$	*h*	*k*	*l*	$10F_o$	$10F_c$	$10S_g$	*h*	*k*	*l*	$10F_o$	$10F_c$	$10S_g$
1	−4	7	295	293	9	1	1	2	825	798	8	1	6	−7	321	321	10	1	11	−2	204	210	18
1	−4	8	247	229	5	1	1	3	606	587	6	1	6	−6	214	224	17	1	11	−1	186	204	7
1	−4	9	271	230	5	1	1	4	426	410	4	1	6	−5	276	286	3	1	11	0	190	62	−33
1	−3	−5	255	262	5	1	1	5	296	295	6	1	6	−4	435	426	4	1	12	−8	139	147	15
1	−3	−4	450	437	27	1	1	6	234	226	7	1	6	−3	256	268	10	1	12	−7	123	137	−29
1	−3	−3	517	521	16	1	1	7	311	292	6	1	6	−2	724	713	22	1	12	−6	180	67	−33
1	−3	−2	771	748	39	1	2	−9	174	168	19	1	6	−1	430	443	4	1	12	−5	121	131	19
1	−3	−1	829	825	25	1	2	−8	349	354	3	1	6	0	400	388	4	1	12	−4	198	189	10
1	−3	0	123	113	6	1	2	−7	338	345	7	1	6	1	288	288	3	1	12	−3	188	186	6
1	−3	1	1001	1057	10	1	2	−6	291	282	3	1	6	2	378	393	4	1	12	−2	129	135	22
1	−3	2	789	794	8	1	2	−5	225	240	2	1	6	3	342	373	10	1	12	−1	149	143	−35
1	−3	3	1023	1000	10	1	2	−4	756	742	8	1	6	4	261	270	5	1	13	−6	98	106	10
1	−3	4	401	402	4	1	2	−3	473	444	9	1	6	5	141	138	10	1	13	−4	163	161	16
1	−3	5	400	406	4	1	2	−2	437	439	4	1	7	−10	125	110	8	2	−14	2	173	151	17
1	−3	6	215	226	9	1	2	−1	557	521	6	1	7	−9	195	186	8	2	−14	3	192	180	8
1	−3	7	308	310	3	1	2	0	927	882	19	1	7	−8	205	217	12	2	−14	4	121	128	12
1	−3	9	170	153	8	1	2	1	624	626	12	1	7	−7	318	327	16	2	−14	5	100	74	11
1	−2	−9	162	170	11	1	2	2	856	846	17	1	7	−6	146	148	4	2	−14	6	180	178	−31
1	−2	−8	202	195	6	1	2	3	537	537	5	1	7	−5	270	276	5	2	−14	7	109	109	−26
1	−2	−7	152	154	8	1	2	4	285	292	14	1	7	−4	439	447	4	2	−13	0	191	187	17
1	−2	−5	407	409	4	1	2	5	272	256	5	1	7	−3	420	422	4	2	−13	1	227	223	18
1	−2	−4	667	654	7	1	2	6	354	347	7	1	7	−2	565	567	6	2	−13	2	149	160	7
1	−2	−3	660	637	13	1	2	7	244	226	7	1	7	−1	235	244	7	2	−13	3	155	171	19
1	−2	−2	465	447	9	1	3	−9	258	238	21	1	7	0	232	238	5	2	−13	4	121	116	−28
1	−2	−1	598	565	18	1	3	−8	263	259	5	1	7	1	386	377	19	2	−13	5	158	158	−34
1	−2	0	593	581	6	1	3	−7	207	213	10	1	7	2	328	344	7	2	−13	6	165	174	13
1	−2	1	1097	1201	22	1	3	−6	302	304	3	1	7	3	297	298	15	2	−13	7	180	167	9
1	−2	2	1146	1123	23	1	3	−5	347	357	7	1	7	4	149	162	9	2	−13	8	97	94	−25
1	−2	3	407	409	4	1	3	−4	727	714	15	1	7	5	100	131	14	2	−12	−2	137	123	12
1	−2	4	106	120	6	1	3	−3	532	526	5	1	8	−10	180	173	11	2	−12	−1	203	198	20
1	−2	5	332	320	10	1	3	−2	317	307	9	1	8	−9	213	220	28	2	−12	0	223	217	4
1	−2	6	393	386	16	1	3	−1	1068	1045	11	1	8	−8	145	145	7	2	−12	1	229	225	7
1	−2	7	401	397	4	1	3	0	802	847	8	1	8	−7	196	198	18	2	−12	2	139	132	6
1	−1	−9	115	135	−23	1	3	1	748	777	22	1	8	−6	168	163	18	2	−12	3	171	175	5
1	−1	−7	217	214	4	1	3	2	409	418	4	1	8	−5	341	340	20	2	−12	4	189	178	25
1	−1	−6	336	329	3	1	3	3	252	249	5	1	8	−4	435	423	4	2	−12	5	274	279	16
1	−1	−5	587	574	18	1	3	4	284	287	14	1	8	−3	416	400	17	2	12	6	201	194	32

Table A5—*Continued.*

h	k	l	$10F_c$	$10F_c$	$10S_g$	h	k	l	$10F_o$	$10F_c$	$10S_g$	h	k	l	$10F_o$	$10F_c$	$10S_g$	h	k	l	$10F_o$	$10F_c$	$10S_g$
2	−12	7	180	169	5	2	−7	9	130	135	13	2	−2	2	227	231	2	2	2	4	273	266	19
2	−12	8	92	74	8	2	−7	10	179	140	−31	2	−2	3	387	392	4	2	2	5	382	379	4
2	−12	9	105	101	−17	2	−6	−7	132	136	12	2	−2	4	872	820	44	2	2	6	269	294	5
2	−11	−3	133	138	11	2	−6	−4	216	201	6	2	−2	5	733	707	29	2	3	−10	186	181	−38
2	−11	−2	169	177	13	2	−6	−3	286	294	3	2	−2	6	542	526	5	2	3	−9	170	178	22
2	−11	−1	219	220	22	2	−6	−2	434	440	9	2	−2	7	153	153	8	2	3	−8	75	58	−12
2	−11	0	282	271	17	2	−6	−1	640	623	58	2	−2	8	92	91	11	2	3	−7	133	126	8
2	−11	1	165	169	7	2	−6	0	382	384	11	2	−1	−9	133	159	12	2	3	−6	500	522	10
2	−11	2	211	215	4	2	−6	1	407	428	4	2	−1	−7	309	306	9	2	3	−5	499	493	20
2	−11	3	276	290	6	2	−6	2	442	458	13	2	−1	−6	309	319	15	2	3	−4	615	605	18
2	−11	4	310	317	12	2	−6	3	469	485	5	2	−1	−5	516	498	26	2	3	−3	549	534	5
2	−11	5	310	330	6	2	−6	4	638	684	13	2	−1	−4	236	244	9	2	3	−2	422	405	4
2	−11	6	121	123	6	2	−6	5	352	372	11	2	−1	−3	450	430	41	2	3	−1	704	683	7
2	−11	7	103	120	8	2	−6	6	242	253	10	2	−1	−2	475	473	9	2	3	0	651	645	26
2	−11	8	119	137	8	2	−6	7	180	192	18	2	−1	−1	899	854	18	2	3	1	534	519	5
2	−11	9	169	173	7	2	−6	8	236	213	7	2	−1	0	522	508	5	2	3	2	267	254	13
2	−10	−4	147	131	13	2	−6	9	238	215	10	2	−1	1	677	693	7	2	3	3	372	374	4
2	−10	−3	173	163	5	2	−6	10	162	148	13	2	−1	2	945	952	9	2	3	4	407	402	8
2	−10	−2	247	233	10	2	−5	−8	137	167	10	2	−1	3	965	904	68	2	3	5	410	385	41
2	−10	−1	377	365	26	2	−5	−5	130	141	9	2	−1	4	675	641	40	2	3	6	185	199	7
2	−10	0	228	234	11	2	−5	−4	290	291	6	2	−1	5	399	383	20	2	3	7	144	156	12
2	−10	1	219	223	9	2	−5	−3	426	414	4	2	−1	6	119	116	8	2	4	−10	187	83	−33
2	−10	2	348	359	10	2	−5	−2	430	456	4	2	−1	7	92	79	−19	2	4	−9	63	68	−16
2	−10	3	340	353	7	2	−5	−1	749	698	75	2	−1	8	261	235	5	2	4	−8	224	226	4
2	−10	4	334	345	13	2	−5	0	467	458	5	2	−1	9	247	239	7	2	4	−7	323	332	13
2	−10	5	140	134	6	2	−5	1	578	589	12	2	0	−10	77	85	13	2	4	−6	543	548	5
2	−10	6	155	170	19	2	−5	2	728	762	22	2	0	−9	92	125	15	2	4	−5	416	424	12
2	−10	7	197	204	22	2	−5	3	489	525	10	2	0	−7	266	271	5	2	4	−4	225	206	2
2	−10	8	198	199	6	2	−5	4	388	407	8	2	0	−6	370	370	4	2	4	−3	459	460	5
2	−10	9	189	195	15	2	−5	5	417	408	13	2	0	−5	265	270	3	2	4	−2	398	388	4
2	−10	10	70	65	−16	2	−5	6	242	247	5	2	0	−4	368	380	4	2	4	−1	516	529	5
2	−9	−4	168	173	8	2	−5	7	294	317	6	2	0	−3	937	910	19	2	4	0	656	646	26
2	−9	−3	314	314	3	2	−5	8	228	219	7	2	0	−2	803	776	16	2	4	1	278	284	11
2	−9	−2	378	378	8	2	−5	9	272	241	5	2	0	−1	1436	1341	14	2	4	2	478	461	29
2	−9	−1	275	276	3	2	−5	10	80	100	−22	2	0	0	576	573	6	2	4	3	366	364	18
2	−9	0	182	193	5	2	−4	−6	171	162	7	2	0	1	478	499	10	2	4	4	376	368	30
2	−9	1	299	309	27	2	−4	−4	504	500	5	2	0	2	605	573	30	2	4	5	233	232	7
2	−9	2	397	417	4	2	−4	−3	584	578	6	2	0	3	620	592	37	2	5	−10	80	61	−13

Table A5—*Continued.*

h	k	l	$10F_c$	$10F_c$	$10S_g$	h	k	l	$10F_o$	$10F_c$	$10S_g$	h	k	l	$10F_o$	$10F_c$	$10S_g$	h	k	l	$10F_o$	$10F_c$	$10S_g$
2	−9	3	410	416	12	2	−4	−2	633	517	6	2	0	4	443	426	18	2	5	−9	167	167	17
2	−9	4	197	206	4	2	−4	−2	503	517	10	2	0	5	123	105	7	2	5	−8	243	247	5
2	−9	5	247	252	5	2	−4	−1	399	400	8	2	0	6	332	319	47	2	5	−7	406	416	12
2	−9	6	262	282	8	2	−4	0	1326	1297	13	2	0	7	328	285	7	2	5	−6	212	222	6
2	−9	7	260	272	8	2	−4	1	87	91	8	2	1	−10	96	96	−26	2	5	−5	251	264	13
2	−9	8	208	201	4	2	−4	3	905	924	9	2	1	−9	187	176	7	2	5	−4	331	321	10
2	−9	9	135	131	7	2	−4	4	287	301	3	2	1	−8	277	280	3	2	5	−3	378	387	4
2	−9	10	96	90	13	2	−4	5	268	266	3	2	1	−7	351	361	4	2	5	−2	608	586	6
2	−8	−6	103	94	−23	2	−4	6	321	338	6	2	1	−6	289	289	12	2	5	−1	555	545	6
2	−8	−5	215	215	6	2	−4	7	304	310	6	2	1	−5	434	431	9	2	5	0	377	372	8
2	−8	−4	326	335	10	2	−4	9	177	180	7	2	1	−4	576	563	6	2	5	1	338	347	14
2	−8	−3	392	392	12	2	−3	−9	131	147	8	2	1	−3	783	739	8	2	5	2	353	374	7
2	−8	−2	151	153	6	2	−3	−8	141	139	10	2	1	−2	1056	1002	11	2	5	3	320	335	10
2	−8	−1	226	232	11	2	−3	−7	130	139	6	2	1	−1	321	308	6	2	5	4	267	272	5
2	−8	0	373	363	15	2	−3	−6	255	259	5	2	1	0	165	168	7	2	6	−10	113	126	12
2	−8	1	483	492	14	2	−3	−5	457	449	5	2	1	1	933	1027	19	2	6	−9	237	229	5
2	−8	2	546	558	27	2	−3	−4	423	436	13	2	1	2	506	502	10	2	6	−8	207	215	12
2	−8	3	386	399	4	2	−3	−3	628	635	6	2	1	3	677	632	41	2	6	−7	343	346	3
2	−8	4	150	166	4	2	−3	−2	268	271	3	2	1	4	302	298	6	2	6	−6	85	91	9
2	−8	5	345	363	10	2	−3	−1	827	271	8	2	1	5	268	255	5	2	6	−5	286	295	3
2	−8	6	332	348	3	2	−3	0	1866	1792	37	2	1	6	439	398	35	2	6	−4	419	420	4
2	−8	7	267	275	5	2	−3	1	388	417	4	2	1	7	279	244	6	2	6	−3	468	463	5
2	−8	8	191	196	6	2	−3	2	516	552	10	2	1	8	222	203	7	2	6	−2	378	383	4
2	−8	9	116	116	8	2	−3	3	328	347	3	2	2	−10	205	186	8	2	6	−1	387	394	8
2	−8	10	146	144	−25	2	−3	5	388	386	8	2	2	−9	311	283	6	2	6	0	302	315	3
2	−7	−3	232	226	5	2	−3	6	530	534	5	2	2	−8	282	273	28	2	6	1	322	324	16
2	−7	−2	262	255	5	2	−3	7	393	391	4	2	2	−7	160	166	5	2	6	2	316	316	16
2	−7	−1	353	349	14	2	−3	8	286	265	6	2	2	−6	193	195	10	2	6	3	346	360	31
2	−7	0	712	698	14	2	−2	−9	142	148	10	2	2	−5	459	457	5	2	6	4	153	152	8
2	−7	1	608	630	18	2	−2	−6	344	323	41	2	2	−4	590	580	18	2	6	5	135	156	−35
2	−7	2	183	207	4	2	−2	−5	569	592	34	2	2	−3	615	599	6	2	7	−10	168	175	7
2	−7	3	284	299	6	2	−2	−4	376	382	30	2	2	−2	100	96	7	2	7	−9	192	205	33
2	−7	4	410	429	8	2	−2	−3	467	468	23	2	2	−1	707	694	14	2	7	−8	161	159	5
2	−7	5	463	487	23	2	−2	−2	772	695	54	2	2	0	803	780	16	2	7	−7	107	90	9
2	−7	6	370	387	11	2	−2	−1	660	635	7	2	2	1	920	958	9	2	7	−6	264	267	11
2	−7	7	203	195	6	2	−2	0	580	580	6	2	2	2	433	423	9	2	7	−5	302	290	6
2	−7	8	217	211	4	2	−2	1	240	265	5	2	2	3	356	345	14	2	7	−4	389	376	4

Table A5—*Continued.*

h	k	l	$10F_c$	$10F_c$	$10S_g$	h	k	l	$10F_o$	$10F_c$	$10S_g$	h	k	l	$10F_o$	$10F_c$	$10S_g$	h	k	l	$10F_o$	$10F_c$	$10S_g$
2	7	−3	476	444	19	3	−13	5	227	229	5	3	−7	−2	463	438	46	3	−2	−5	310	312	12
2	7	−2	272	258	3	3	−13	6	96	103	−16	3	−7	−1	740	729	7	3	−2	−4	631	580	44
2	7	−1	247	240	5	3	−13	7	146	131	7	3	−7	0	256	248	15	3	−2	−3	228	228	2
2	7	0	319	337	6	3	−13	8	93	90	−21	3	−7	1	494	498	20	3	−2	−2	675	669	7
2	7	1	384	388	15	3	−12	−2	219	199	13	3	−7	2	269	289	8	3	−2	−1	1117	1060	22
2	7	2	253	265	8	3	−12	−1	216	202	15	3	−7	3	426	438	9	3	−2	0	587	583	6
2	7	3	195	194	8	3	−12	0	223	213	4	3	−7	4	538	557	5	3	−2	1	354	352	7
2	7	4	144	126	9	3	−12	1	164	168	25	3	−7	5	294	313	12	3	−2	2	477	501	5
2	8	−10	80	98	12	3	−12	2	181	179	29	3	−7	6	156	163	20	3	−2	3	479	495	5
2	8	−9	108	90	−27	3	−12	3	207	207	10	3	−7	7	179	187	25	3	−2	4	505	491	30
2	8	−8	163	167	7	3	−12	4	239	233	5	3	−7	8	217	220	13	3	−2	5	387	379	39
2	8	−7	82	75	8	3	−12	5	247	244	5	3	−7	9	243	231	27	3	−2	6	261	260	5
2	8	−6	385	376	15	3	−12	6	189	172	6	3	−7	10	185	153	9	3	−2	8	262	250	8
2	8	−5	332	317	3	3	−12	7	103	126	16	3	−6	−5	149	160	7	3	−1	−10	228	80	−40
2	8	−4	261	246	5	3	−12	8	139	143	7	3	−6	−4	271	275	5	3	−1	−9	73	95	−16
2	8	−3	218	222	4	3	−12	9	147	152	12	3	−6	−3	420	421	4	3	−1	−7	354	354	4
2	8	−2	218	221	17	3	−11	−3	153	139	9	3	−6	−2	478	469	10	3	−1	−6	381	370	4
2	8	−1	336	336	10	3	−11	−2	235	229	12	3	−6	−1	782	765	23	3	−1	−5	233	238	12
2	8	0	335	344	17	3	−11	−1	228	230	5	3	−6	0	172	144	12	3	−1	−4	423	417	13
2	8	1	265	265	13	3	−11	0	280	271	8	3	−6	1	635	645	6	3	−1	−3	420	416	4
2	8	2	158	155	−31	3	−11	1	211	212	8	3	−6	2	487	517	15	3	−1	−2	574	572	17
2	8	3	135	130	7	3	−11	2	241	240	5	3	−6	3	555	583	11	3	−1	−1	925	869	9
2	9	−10	70	71	−13	3	−11	3	321	326	6	3	−6	4	310	336	6	3	−1	0	753	721	8
2	9	−9	60	93	14	3	−11	4	309	311	3	3	−6	5	291	310	3	3	−1	1	236	240	5
2	9	−8	193	184	19	3	−11	5	190	187	13	3	−6	6	221	226	18	3	−1	2	655	688	13
2	9	−7	146	155	9	3	−11	6	141	143	14	3	−6	7	305	325	3	3	−1	3	593	584	42
2	9	−6	284	280	11	3	−11	7	159	183	10	3	−6	8	282	256	3	3	−1	4	541	545	27
2	9	−5	198	191	4	3	−11	8	168	160	−33	3	−6	9	233	205	16	3	−1	6	317	313	10
2	9	−4	145	154	−28	3	−11	9	133	144	8	3	−5	−8	181	183	9	3	−1	7	272	234	5
2	9	−3	211	210	8	3	−10	−4	186	191	7	3	−5	−5	205	207	6	3	−1	8	246	248	7
2	9	−2	350	332	14	3	−10	−2	350	348	14	3	−5	−4	494	508	5	3	0	−10	109	115	13
2	9	−1	304	314	6	3	−10	−1	268	268	16	3	−5	−3	561	554	6	3	0	−8	278	280	6
2	9	0	176	197	21	3	−10	0	211	198	4	3	−5	−2	533	553	5	3	0	−7	299	319	3
2	9	1	125	129	8	3	−10	1	285	288	11	3	−5	−1	218	221	2	3	0	−6	199	194	10
2	9	2	156	166	12	3	−10	2	266	274	5	3	−5	0	325	328	3	3	0	−5	147	165	13
2	10	−9	97	94	10	3	−10	3	357	367	4	3	−5	1	788	777	16	3	0	−4	456	464	9
2	10	−8	149	148	7	3	−10	4	228	237	7	3	−5	2	568	600	6	3	0	−3	841	811	84
2	10	−7	182	189	31	3	−10	5	119	119	10	3	−5	3	514	540	15	3	0	−2	719	681	7

Table A5 *Continued.*

h	*k*	*l*	$10F_c$	$10F_c$	$10S_g$	*h*	*k*	*l*	$10F_o$	$10F_c$	$10S_g$	*h*	*k*	*l*	$10F_o$	$10F_c$	$10S_g$	*h*	*k*	*l*	$10F_o$	$10F_c$	$10S_g$
2	10	−6	197	182	8	3	−10	6	253	259	8	3	−5	4	313	331	3	3	0	−1	1019	976	10
2	10	−5	109	114	8	3	−10	7	259	263	26	3	−5	5	340	355	3	3	0	0	286	282	3
2	10	−4	201	209	8	3	−10	8	202	203	22	3	−5	6	319	327	3	3	0	1	644	654	6
2	10	−3	273	260	19	3	−10	9	125	116	−41	3	−5	7	367	370	4	3	0	2	551	565	44
2	10	−2	247	251	5	3	−9	−5	239	245	7	3	−5	8	257	259	5	3	0	3	440	449	4
2	10	−1	155	162	11	3	−9	−3	328	329	10	3	−5	9	170	149	9	3	0	4	351	354	11
2	10	0	153	149	6	3	−9	−2	224	221	7	3	−4	−5	477	474	5	3	0	5	176	173	7
2	10	1	153	142	20	3	−9	−1	82	70	−16	3	−4	−4	486	511	19	3	0	6	372	365	7
2	11	−8	140	144	−34	3	−9	0	362	343	4	3	−4	−3	296	306	15	3	0	7	352	298	7
2	11	−7	134	137	9	3	−9	1	339	358	3	3	−4	−2	317	296	28	3	1	−10	196	175	8
2	11	−6	103	96	7	3	−9	2	421	455	4	3	−4	−1	200	197	2	3	1	−8	250	230	5
2	11	−5	138	126	8	3	−9	3	243	253	5	3	−4	0	902	883	9	3	1	−7	109	109	5
2	11	−4	217	215	17	3	−9	4	269	278	3	3	−4	1	819	815	8	3	1	−6	192	189	8
2	11	−3	193	196	8	3	−9	5	308	331	3	3	−4	2	585	626	6	3	1	−5	571	564	6
2	11	−2	195	195	6	3	−9	6	366	385	15	3	−4	3	461	473	5	3	1	−4	530	523	11
2	11	−1	83	58	9	3	−9	7	237	243	14	3	−4	4	332	340	3	3	1	−3	944	882	9
2	12	−7	222	60	−40	3	−9	8	173	179	5	3	−4	5	456	476	5	3	1	−2	574	546	6
2	12	−6	81	97	−15	3	−9	9	72	72	12	3	−4	6	370	370	7	3	1	−1	114	106	5
2	12	−5	208	192	25	3	−9	10	107	111	10	3	−4	7	379	388	11	3	1	0	436	432	9
2	12	−4	143	156	7	3	−8	−6	173	164	10	3	−4	8	147	142	9	3	1	1	598	605	6
2	12	−3	126	131	20	3	−8	−3	123	126	7	3	−4	9	178	57	−33	3	1	2	574	565	52
3	−15	3	146	126	12	3	−8	−2	174	168	5	3	−3	−9	138	147	11	3	1	3	295	295	12
3	−15	4	112	111	−24	3	−8	−1	459	480	18	3	−3	−6	334	345	3	3	1	4	294	294	12
3	−15	5	83	63	−14	3	−8	0	468	467	9	3	−3	−5	348	360	10	3	1	5	559	537	17
3	−14	1	197	185	6	3	−8	1	501	512	30	3	−3	−4	279	284	8	3	1	6	256	251	5
3	−14	2	168	167	7	3	−8	2	400	424	12	3	−3	−3	338	324	3	3	1	7	239	206	7
3	−14	3	145	132	7	3	−8	3	214	231	9	3	−3	−2	597	568	18	3	2	−10	150	140	20
3	−14	4	140	127	21	3	−8	4	506	523	10	3	−3	−1	697	674	14	3	2	−9	148	127	9
3	−14	5	175	164	28	3	−8	5	344	360	3	3	−3	0	937	929	9	3	2	−8	226	211	−60
3	−14	6	172	154	19	3	−8	6	328	348	3	3	−3	1	766	768	8	3	2	−7	99	88	10
3	−14	7	128	129	13	3	−8	7	131	120	5	3	−3	2	536	556	5	3	2	−6	484	490	15
3	−13	−1	160	156	18	3	−8	8	116	118	−37	3	−3	3	221	238	13	3	2	−5	577	574	12
3	−13	0	226	219	7	3	−8	9	178	151	12	3	−3	4	505	510	5	3	2	−4	515	497	10
3	−13	1	204	196	20	3	−8	10	154	159	25	3	−3	5	632	630	44	3	2	−3	112	117	11
3	−13	2	185	190	24	3	−7	−7	170	182	10	3	−3	8	98	91	−39	3	2	−2	398	392	8
3	−13	3	115	104	13	3	−7	−6	173	162	7	3	−3	9	212	168	6	3	2	−1	755	735	30
3	−13	4	193	179	21	3	−7	−3	260	265	10	3	−2	−6	365	367	11	3	2	0	662	649	7

Table A5—*Continued.*

h	k	l	$10F_c$	$10F_c$	$10S_g$	h	k	l	$10F_o$	$10F_c$	$10S_g$	h	k	l	$10F_o$	$10F_c$	$10S_g$	h	k	l	$10F_o$	$10F_c$	$10S_g$
3	2	1	440	469	4	3	7	−4	223	215	18	4	−12	3	273	273	5	4	−7	2	336	351	7
3	2	2	526	523	5	3	7	−2	186	193	19	4	−12	4	176	184	25	4	−7	3	585	610	6
3	2	3	355	351	4	3	7	−1	436	420	44	4	−12	5	244	238	5	4	−7	4	348	366	3
3	2	4	385	370	27	3	7	0	317	304	19	4	−12	6	173	169	23	4	−7	5	237	241	5
3	2	5	367	345	51	3	7	1	336	297	7	4	−12	7	184	179	17	4	−7	6	258	274	5
3	2	6	185	165	7	3	7	2	137	154	11	4	−12	8	150	160	7	4	−7	7	268	254	40
3	2	7	126	120	10	3	7	3	134	122	11	4	−12	9	112	119	9	4	−7	8	258	258	10
3	3	−10	108	121	9	3	8	−10	105	96	9	4	−11	−3	265	250	5	4	−7	9	170	156	24
3	3	−9	94	84	15	3	8	−9	119	124	17	4	−11	−2	177	184	9	4	−6	−8	144	155	12
3	3	−8	172	178	5	3	8	−8	156	164	22	4	−11	−1	151	122	12	4	−6	−6	147	151	9
3	3	−7	342	351	7	3	8	−7	198	206	4	4	−11	0	169	171	15	4	−6	−4	380	368	4
3	3	−6	383	398	11	3	8	−6	192	195	10	4	−11	1	230	246	5	4	−6	−3	438	443	13
3	3	−5	297	312	30	3	8	−5	180	170	7	4	−11	2	295	312	9	4	−6	−2	528	531	5
3	3	−4	434	429	4	3	8	−4	199	190	4	4	−11	3	381	398	4	4	−6	−1	80	71	−15
3	3	−3	254	266	3	3	8	−3	224	218	11	4	−11	4	252	249	13	4	−6	0	269	270	3
3	3	−2	964	935	10	3	8	−2	264	248	24	4	−11	5	186	184	20	4	−6	1	523	520	5
3	3	−1	424	425	4	3	8	−1	443	428	13	4	−11	6	150	153	11	4	−6	2	627	662	6
3	3	0	525	509	26	3	8	0	132	130	7	4	−11	7	185	190	6	4	−6	3	556	602	11
3	3	1	299	310	9	3	8	1	208	186	8	4	−11	8	167	170	8	4	−6	4	309	333	3
3	3	2	314	311	3	3	8	2	150	145	22	4	−11	9	73	79	−16	4	−6	5	235	250	9
3	3	3	405	384	28	3	9	−9	179	77	−33	4	−10	−5	141	158	10	4	−6	6	348	365	3
3	3	4	354	340	11	3	9	−8	146	146	−33	4	−10	−4	173	212	9	4	−6	8	238	224	12
3	3	5	206	208	14	3	9	−7	171	176	15	4	−10	−3	160	165	8	4	−6	9	117	102	−33
3	4	−10	80	79	−14	3	9	−6	172	175	9	4	−10	−2	195	207	8	4	−5	−8	131	164	9
3	4	−9	135	158	13	3	9	−5	132	130	7	4	−10	−1	111	113	−23	4	−5	−5	400	409	4
3	4	−8	190	216	6	3	9	−4	188	173	8	4	−10	0	372	374	15	4	−5	−4	296	295	6
3	4	−7	416	426	12	3	9	−3	249	246	20	4	−10	1	467	474	5	4	−5	−3	339	348	7
3	4	−6	259	261	18	3	9	−2	258	258	18	4	−10	2	349	371	7	4	−5	−2	283	279	3
3	4	−5	243	248	5	3	9	−1	242	241	5	4	−10	3	228	221	18	4	−5	−1	419	402	8
3	4	−4	413	384	17	3	9	0	84	121	15	4	−10	4	114	120	6	4	−5	0	795	770	8
3	4	−3	440	431	4	3	9	1	169	164	−33	4	−10	5	187	188	6	4	−5	1	789	793	8
3	4	−2	476	452	5	3	10	−9	80	100	−19	4	−10	6	305	310	9	4	−5	2	559	598	6
3	4	−1	338	324	3	3	10	−8	147	150	−34	4	−10	7	191	200	10	4	−5	3	303	321	12
3	4	0	305	303	24	3	10	−7	119	129	12	4	−10	8	181	175	16	4	−5	4	291	286	3
3	4	1	350	382	3	3	10	−6	83	89	−30	4	−10	9	93	83	14	4	−5	5	390	413	4
3	4	2	421	419	17	3	10	−5	136	131	8	4	−9	−6	174	171	17	4	−5	6	335	336	10
3	4	3	362	352	7	3	10	−4	236	226	7	4	−9	−5	179	176	9	4	−5	7	235	227	7
3	4	4	328	314	3	3	10	−3	243	236	5	4	−9	−3	209	220	6	4	−5	8	167	160	7

Table A5—*Continued.*

h	*k*	*l*	$10F_o$	$10F_c$	$10S_g$	*h*	*k*	*l*	$10F_o$	$10F_c$	$10S_g$	*h*	*k*	*l*	$10F_o$	$10F_c$	$10S_g$	*h*	*k*	*l*	$10F_o$	$10F_c$	$10S_g$
3	4	5	191	164	−43	3	10	−2	200	200	6	4	−9	−2	159	161	6	4	−5	9	106	93	12
3	5	−10	115	140	8	3	10	−1	100	93	−44	4	−9	−1	394	388	4	4	−4	−8	137	107	8
3	5	−9	266	261	21	3	11	−7	107	81	12	4	−9	0	504	499	15	4	−4	−7	87	106	−22
3	5	−8	168	175	5	3	11	−6	95	106	12	4	−9	1	276	283	14	4	−4	−6	248	257	5
3	5	−7	271	274	11	3	11	−5	202	198	14	4	−9	2	283	296	6	4	−4	−5	405	405	12
3	5	−6	59	61	8	3	11	−4	162	172	13	4	−9	3	77	78	7	4	−4	−4	273	286	3
3	5	−5	282	262	11	3	11	−3	129	119	16	4	−9	4	392	403	8	4	−4	−3	511	491	5
3	5	−4	393	387	4	4	−15	2	136	130	8	4	−9	5	413	417	4	4	−4	−2	421	410	8
3	5	−3	453	446	5	4	−15	3	116	115	10							4	−4	−1	835	803	8
3	5	−2	470	465	5	4	−15	4	101	83	−33	4	−9	6	282	301	8	4	−4	0	560	577	17
3	5	−1	271	260	5	4	−15	5	149	143	7	4	−9	7	164	169	7	4	−4	1	374	380	11
3	5	0	379	386	4	4	−15	6	138	129	8	4	−9	8	121	100	13	4	−4	2	387	414	4
3	5	1	365	412	7	4	−14	0	182	180	13	4	−9	9	151	157	26	4	−4	3	433	455	4
3	5	2	379	369	4	4	−14	1	147	143	24	4	−8	−5	148	161	9	4	−4	4	342	356	10
3	5	3	269	264	5	4	−14	2	149	151	7	4	−8	−3	175	182	7	4	−4	5	424	442	4
3	5	4	200	192	6	4	−14	3	125	122	−30	4	−8	−2	287	288	6	4	−4	6	259	263	23
3	5	5	138	153	11	4	−14	4	157	151	16	4	−8	−1	579	575	6	4	−4	7	167	179	7
3	6	−10	155	155	6	4	−14	5	198	196	6	4	−8	0	470	465	19	4	−4	8	189	154	−33
3	6	−9	118	121	−24	4	−14	6	138	120	−24	4	−8	1	171	168	3	4	−4	9	192	193	19
3	6	−8	111	99	10	4	−14	7	90	89	−15	4	−8	2	318	321	3	4	−3	−9	98	77	11
3	6	−7	104	117	7	4	−13	−2	137	130	7	4	−8	3	453	484	9	4	−3	−8	85	113	14
3	6	−6	204	200	4	4	−13	−1	250	225	25	4	−8	4	416	432	4	4	−3	−6	372	383	15
3	6	−5	515	492	10	4	−13	0	184	168	6	4	−8	5	298	308	3	4	−3	−5	350	341	3
3	6	−4	441	435	18	4	−13	1	149	153	21							4	−3	−4	334	318	3
3	6	−3	355	353	7	4	−13	2	177	174	19	4	−8	6	206	203	6	4	−3	−3	505	486	5
3	6	−2	203	208	14	4	−13	3	165	156	26	4	−8	7	168	161	5	4	−3	−2	592	584	12
3	6	0	423	399	4	4	−13	4	219	207	18	4	−8	8	167	175	22	4	−3	−1	295	280	15
3	6	1	294	317	18	4	−13	5	144	148	7	4	−8	9	232	229	21	4	−3	0	582	587	6
3	6	2	312	302	9	4	−13	6	136	119	8	4	−7	−7	161	180	10	4	−3	1	616	620	6
3	6	3	183	172	7	4	−13	7	123	123	14	4	−7	−6	164	190	8	4	−3	2	303	327	3
3	6	4	153	152	9	4	−13	8	99	110	10	4	−7	−5	129	133	19	4	−3	3	415	441	4
3	7	−10	76	78	−23	4	−12	−3	151	151	12	4	−7	−4	175	181	7	4	−3	4	510	540	15
3	7	−9	100	91	8	4	−12	−2	225	219	4	4	−7	−3	444	456	4	4	−3	5	282	283	8
3	7	−8	151	145	14	4	−12	−1	216	218	4	4	−7	−2	551	545	6	4	−3	6	311	319	3
3	7	−7	267	266	21	4	−12	0	143	148	13	4	−7	−1	308	300	3	4	−3	7	183	189	7
3	7	−6	341	334	14	4	−12	1	150	149	6	4	−7	0	602	585	12	4	−3	8	250	219	35
3	7	−5	312	305	3	4	−12	2	180	172	5	4	−7	1	51	67	−13	4	−2	−8	192	192	6

Table A5—*Continued.*

h	k	l	$10F_c$	$10F_c$	$10S_g$	h	k	l	$10F_o$	$10F_c$	$10S_g$	h	k	l	$10F_o$	$10F_c$	$10S_g$	h	k	l	$10F_o$	$10F_c$	$10S_g$
4	−2	−7	329	318	3	4	2	−3	177	191	5	4	7	−6	216	218	4	5	−10	8	98	105	−32
4	−2	−6	266	271	8	4	2	−2	723	683	7	4	7	−5	162	149	10	5	−10	9	137	130	−25
4	−2	−5	313	312	6	4	2	−1	938	902	38	4	7	−4	234	231	9	5	−9	−6	161	187	10
4	−2	−4	396	380	4	4	2	0	399	379	16	4	7	−3	279	269	3	5	−9	−4	194	213	8
4	−2	−3	268	278	3	4	2	1	248	251	5	4	7	−2	298	282	18	5	−9	−3	201	208	6
4	−2	−2	674	659	7	4	2	2	250	274	10	4	7	−1	244	236	12	5	−9	−2	117	137	16
4	−2	−1	524	518	5	4	2	3	432	442	9	4	7	0	223	238	4	5	−9	−1	440	444	4
4	−2	0	437	423	4	4	2	4	350	338	14	4	7	1	156	165	8	5	−9	0	141	148	4
4	−2	1	730	714	15	4	2	5	215	215	6	4	7	2	140	152	8	5	−9	1	335	339	10
4	−2	2	332	371	3	4	2	6	198	175	−70	4	8	−9	84	69	11	5	−9	2	206	213	6
4	−2	3	659	680	7	4	3	−10	86	77	14	4	8	−8	160	145	16	5	−9	3	352	367	4
4	−2	4	444	457	13	4	3	−9	112	129	8	4	8	−7	166	167	7	5	−9	4	471	485	5
4	−2	5	206	204	6	4	3	−8	170	163	10	4	8	−6	188	185	13	5	−9	5	312	326	3
4	−2	6	308	289	22	4	3	−7	349	345	24	4	8	−5	166	164	13	5	−9	6	140	154	6
4	−2	7	206	207	8	4	3	−6	243	247	10	4	8	−4	171	173	9	5	−9	7	153	160	8
4	−2	8	231	219	7	4	3	−5	169	171	5	4	8	−3	198	198	14	5	−9	8	117	131	8
4	−1	−10	86	87	−14	4	3	−4	345	332	3	4	8	−2	279	277	6	5	−9	9	183	178	16
4	−1	−9	188	189	8	4	3	−3	664	645	20	4	8	−1	168	174	13	5	−8	−5	99	125	16
4	−1	−7	236	254	7	4	3	−2	585	583	6	4	8	0	191	195	6	5	−8	−2	457	464	9
4	−1	−6	207	209	6	4	3	−1	307	319	3	4	8	1	127	150	13	5	−8	−1	301	305	6
4	−1	−5	182	189	4	4	3	0	288	289	3	4	9	−9	107	99	14	5	−8	0	314	325	3
4	−1	−4	398	402	12	4	3	1	310	309	3	4	9	−8	153	144	20	5	−8	1	373	367	11
4	−1	−3	814	798	8	4	3	2	309	329	3	4	9	−7	116	134	19	5	−8	2	338	367	3
4	−1	−2	363	352	7	4	3	3	442	431	13	4	9	−6	91	83	15	5	−8	3	525	545	5
4	−1	−1	785	744	8	4	3	4	205	212	8	4	9	−5	176	163	7	5	−8	4	302	311	3
4	−1	0	496	475	5	4	3	5	227	200	36	4	9	−4	170	184	7	5	−8	5	181	173	4
4	−1	1	706	709	7	4	4	−10	78	82	−16	4	9	−3	233	235	14	5	−8	6	142	142	11
4	−1	2	435	481	4	4	4	−9	211	211	34	4	9	−2	194	196	16	5	−8	7	235	225	16
4	−1	3	433	452	4	4	4	−8	260	265	5	4	9	−1	104	106	7	5	−8	8	202	207	6
4	−1	4	272	277	8	4	4	−7	81	86	8	4	10	−8	70	91	−17	5	−8	9	136	136	8
4	−1	7	322	309	6	4	4	−6	223	236	18	4	10	−7	89	98	11	5	−7	−5	98	140	11
4	0	−9	184	172	7	4	4	−5	205	210	4	4	10	−6	92	93	9	5	−7	−3	396	397	4
4	0	−8	150	169	9	4	4	−4	432	433	4	4	10	−5	200	204	16	5	−7	−2	377	384	8
4	0	−7	129	123	6	4	4	−3	554	545	6	4	10	−4	170	163	7	5	−7	−1	184	177	7
4	0	−6	308	315	6	4	4	−2	371	382	4	4	10	−3	116	133	19	5	−7	0	406	400	8
4	0	−5	476	465	5	4	4	−1	174	179	3	5	−15	1	124	117	9	5	−7	1	463	467	9
4	0	−4	625	604	6	4	4	0	252	247	13	5	−15	2	92	82	10	5	−7	2	503	525	5
4	0	−3	781	743	8	4	4	1	402	399	8	5	−15	3	101	86	12	5	−7	3	307	319	9

Table A5– *Continued.*

h	k	l	$10F_c$	$10F_c$	$10S_g$	h	k	l	$10F_o$	$10F_c$	$10S_g$	h	k	l	$10F_o$	$10F_c$	$10S_g$	h	k	l	$10F_o$	$10F_c$	$10S_g$
4	0	−2	221	221	2	4	4	2	348	365	3	5	−15	4	144	137	14	5	−7	4	198	203	8
4	0	−1	381	386	4	4	4	3	280	280	8	5	−15	5	153	154	8	5	−7	5	242	253	5
4	0	0	520	517	5	4	4	4	203	195	20	5	−15	6	129	123	19	5	−7	6	178	190	11
4	0	1	546	569	5	4	4	5	195	168	18	5	−14	−1	187	167	9	5	−7	7	337	348	13
4	0	2	399	423	4	4	5	−10	133	135	−37	5	−14	1	103	106	−19	5	−7	8	189	190	9
4	0	3	314	334	6	4	5	−9	125	132	7	5	−14	2	116	118	8	5	−7	9	90	84	13
4	0	4	241	239	7	4	5	−8	172	174	5	5	−14	3	167	163	20	5	−6	−8	117	124	11
4	0	5	413	389	16	4	5	−7	191	52	−33	5	−14	4	212	200	17	5	−6	−7	131	130	16
4	0	6	308	309	6	4	5	−6	293	297	12	5	−14	5	138	137	22	5	−6	−5	240	247	14
4	0	7	209	197	25	4	5	−5	466	452	19	5	−14	6	112	104	−20	5	−6	−4	386	386	4
4	1	−10	126	127	11	4	5	−4	366	355	4	5	−14	7	112	106	17	5	−6	−3	210	203	11
4	1	−9	109	118	8	4	5	−3	280	272	20	5	−12	0	129	131	9	5	−6	−2	355	356	4
4	1	−8	247	229	−48	4	5	−2	239	230	5	5	−12	1	200	199	6	5	−6	−1	410	405	4
						4	5	−1	167	167	7	5	−11	−4	176	156	9	5	−6	0	527	520	11
4	1	−7	215	211	26	4	5	0	441	427	18	5	−11	−3	99	135	−31	5	−6	1	528	520	5
4	1	−6	441	449	13	4	5	1	357	368	14	5	−11	−2	107	109	−28	5	−6	2	399	425	8
4	1	−5	535	532	32	4	5	2	338	314	37	5	−11	−1	217	220	17	5	−6	3	164	188	8
4	1	−4	197	188	14	4	5	3	169	161	8	5	−11	0	261	255	5	5	−6	4	182	184	7
4	1	−3	229	246	9	4	5	4	155	159	20	5	−11	1	418	425	4	5	−6	5	474	500	24
4	1	−2	146	154	7	4	6	−10	97	99	−18	5	−11	2	298	315	6	5	−6	6	284	297	9
4	1	−1	573	558	17	4	6	−9	106	113	7	5	−11	3	127	137	20	5	−6	7	248	251	27
4	1	0	881	833	18	4	6	−8	167	167	−34	5	−11	4	168	170	10	5	−6	8	131	127	20
4	1	1	366	379	4	4	6	−7	170	181	5	5	−11	5	112	120	7	5	−5	−8	79	104	12
4	1	2	411	416	4	4	6	−6	318	322	6	5	−11	6	231	240	12	5	−5	−7	92	99	−27
4	1	3	238	238	14	4	6	−5	239	237	10	5	−11	7	188	187	11	5	−5	−5	293	300	18
4	1	4	387	377	4	4	6	−4	178	188	5	5	−11	8	147	137	19	5	−5	−4	398	382	8
4	1	5	371	373	19	4	6	−3	211	210	6	5	−10	−3	195	189	8	5	−5	−3	277	274	3
4	1	6	181	188	9	4	6	−2	232	231	14	5	−10	−2	221	217	7	5	−5	−2	300	299	3
4	1	7	125	132	11	4	6	−1	405	398	4	5	−10	−1	394	396	4	5	−5	−1	692	676	7
						4	6	0	389	369	4	5	−10	0	220	201	24	5	−5	0	629	622	6
4	2	−10	98	115	14	4	6	1	195	199	6	5	−10	1	345	357	3	5	−5	1	122	131	5
4	2	−9	147	154	6	4	6	2	172	180	10	5	−10	2	141	146	7	5	−5	2	390	407	8
4	2	−8	143	149	6	4	6	3	152	144	21	5	−10	3	116	106	12	5	−5	3	344	361	3
4	2	−7	312	323	16	4	7	−10	90	94	−37	5	−10	4	234	238	5	5	−5	4	473	485	5
4	2	−6	248	263	17	4	7	−9	70	110	18	5	−10	5	372	374	7	5	−5	5	382	398	11
4	2	−5	201	206	14	4	7	−8	106	106	−19	5	−10	6	269	265	16	5	−5	6	281	290	6
4	2	−4	337	329	3	4	7	−7	179	180	7	5	−10	7	175	177	5	5	−5	7	134	138	7

Table A5—*Continued.*

h	k	l	$10F_c$	$10F_c$	$10S_g$	h	k	l	$10F_o$	$10F_c$	$10S_g$	h	k	l	$10F_o$	$10F_c$	$10S_g$	h	k	l	$10F_o$	$10F_c$	$10S_g$
5	−5	8	154	136	14	5	0	2	184	206	4	5	5	−3	293	304	6	6	−12	1	163	152	18
5	−4	−9	178	57	−33	5	0	3	181	177	7	5	5	−2	262	266	3	6	−12	2	247	259	5
5	−4	−8	181	97	−33	5	0	4	323	337	13	5	5	−1	556	525	22	6	−12	3	59	83	12
5	−4	−6	315	314	22	5	0	5	341	323	31	5	5	0	226	219	5	6	−12	4	149	161	6
5	−4	−5	221	229	20	5	0	6	251	252	30	5	5	1	187	193	11	6	−12	5	247	228	12
5	−4	−4	280	288	8	5	1	−10	72	88	−21	5	5	2	128	133	8	6	−12	6	257	243	8
5	−4	−3	291	292	6	5	1	−9	103	119	9	5	5	3	160	159	−29	6	−12	7	184	181	6
5	−4	−2	502	502	10	5	1	−8	80	68	−29	5	6	−10	74	77	−52	6	−12	8	95	83	13
5	−4	−1	627	618	6	5	1	−7	297	315	21	5	6	−9	174	50	−33	6	−11	−4	141	139	7
5	−4	0	364	367	4	5	1	−6	284	288	6	5	6	−8	104	105	12	6	−11	−3	120	138	8
5	−4	1	322	312	3	5	1	−5	322	323	3	5	6	−7	155	161	6	6	−11	−2	120	123	8
5	−4	2	504	529	5	5	1	−4	315	296	6	5	6	−6	248	259	17	6	−11	−1	240	245	5
5	−4	3	406	425	4	5	1	−3	301	309	3	5	6	−5	201	181	4	6	−11	0	300	301	9
5	−4	4	501	535	10	5	1	−2	412	396	8	5	6	−4	281	265	14	6	−11	1	145	166	20
5	−4	5	171	171	24	5	1	−1	548	529	16	5	6	−3	258	253	23	6	−11	2	186	188	13
5	−4	6	255	267	5	5	1	0	384	390	4	5	6	−2	240	246	5	6	−11	3	250	250	12
5	−4	7	150	154	6	5	1	1	267	267	3	5	6	−1	241	241	12	6	−11	4	259	254	5
5	−4	8	195	170	16	5	1	2	284	312	6	5	6	0	143	137	6	6	−11	5	237	225	12
5	−3	−9	76	74	−17	5	1	3	328	343	13	5	6	1	172	175	7	6	−11	6	218	205	11
5	−3	−7	266	278	8	5	1	4	419	430	21	5	6	2	151	176	12	6	−11	7	69	82	−18
5	−3	−5	211	229	8	5	1	5	231	218	7	5	7	−9	97	83	13	6	−11	8	176	60	−33
5	−3	−4	251	258	5	5	1	6	131	116	8	5	7	−8	169	155	8	6	−10	−5	139	146	10
5	−3	−3	580	583	23	5	2	−10	86	62	13	5	7	−7	196	197	24	6	−10	−3	186	196	7
5	−3	−2	629	600	6	5	2	−9	120	118	7	5	7	−6	157	155	20	6	−10	−2	255	257	5
5	−3	−1	451	552	5	5	2	−8	125	126	18	5	7	−5	122	123	15	6	−10	−1	228	222	14
5	−3	0	274	275	3	5	2	−7	392	396	16	5	7	−4	163	170	5	6	−10	0	294	292	3
5	−3	1	543	542	5	5	2	−6	149	143	7	5	7	−3	179	186	11	6	−10	1	186	189	4
5	−3	2	375	407	4	5	2	−5	245	260	12	5	7	−2	290	285	12	6	−10	2	191	205	8
5	−3	3	341	370	7	5	2	−4	244	260	2	5	7	−1	128	130	6	6	−10	3	251	266	5
5	−3	4	411	428	8	5	2	−3	303	296	6	5	7	0	200	191	6	6	−10	4	298	294	9
5	−3	5	231	224	5	5	2	−2	662	651	53	5	7	1	165	173	20	6	−10	5	224	217	7
5	−3	7	246	221	39	5	2	−1	445	425	22	5	8	−9	135	121	11	6	−10	6	182	173	7
5	−3	8	244	228	−72	5	2	0	307	324	9	5	8	−8	145	114	9	6	−10	7	106	96	17
5	−2	−6	168	174	12	5	2	1	278	272	3	5	8	−7	101	103	9	6	−10	8	169	159	20
5	−2	−5	377	384	19	5	2	2	326	343	7	5	8	−6	114	92	15	6	−9	−6	126	130	9
5	−2	−4	381	384	8	5	2	3	358	375	4	5	8	−5	128	150	8	6	−9	−5	138	135	10
5	−2	−3	538	522	5	5	2	4	176	187	9	4	8	−4	206	209	33	6	−9	−3	164	183	7
5	−2	−2	581	582	6	5	2	5	140	139	13	5	8	−3	213	198	6	6	−9	−2	299	299	3

Table A5 —*Continued.*

h	*k*	*l*	$10F_o$	$10F_c$	$10S_g$	*h*	*k*	*l*	$10F_o$	$10F_c$	$10S_g$	*h*	*k*	*l*	$10F_o$	$10F_c$	$10S_g$	*h*	*k*	*l*	$10F_o$	$10F_c$	$10S_g$
5	−2	−1	283	291	6	5	3	−10	75	86	−14	5	8	−2	195	186	14	6	−9	−1	261	255	3
5	−2	0	150	160	4	5	3	−9	134	134	7	5	8	−1	117	110	−25	6	−9	0	157	165	6
5	−2	1	428	434	13	5	3	−8	220	229	11	5	9	−8	82	77	−13	6	−9	1	286	294	3
5	−2	2	596	630	6	5	3	−7	226	238	5	5	9	−7	91	91	10	6	−9	2	292	301	9
5	−2	3	483	499	5	5	3	−6	84	100	13	5	9	−6	105	115	8	6	−9	3	417	438	8
5	−2	4	213	219	13	5	3	−5	279	298	3	5	9	−5	157	150	8	6	−9	4	350	349	3
5	−2	5	332	346	3	5	3	−4	419	415	8	5	9	−4	187	178	11	6	−9	5	117	125	9
5	−2	6	196	200	8	5	3	−3	563	536	34	5	9	−3	129	136	21	6	−9	6	178	162	7
5	−2	7	258	234	8	5	3	−2	296	285	6	6	−15	1	104	93	12	6	−9	7	169	150	22
5	−1	−10	121	153	12	5	3	−1	169	170	8	6	−15	2	78	65	11	6	−9	8	213	214	6
5	−1	−9	136	140	9	5	3	0	227	227	11	6	−15	3	180	160	−31	6	−8	−7	114	124	−50
5	−1	−8	199	208	6	5	3	1	336	333	3	6	−15	4	176	152	7	6	−8	−6	182	68	−33
5	−1	−7	89	88	10	5	3	2	349	367	3	6	−15	5	170	136	7	6	−8	−5	181	176	7
5	−1	−6	281	282	8	5	3	3	237	236	28	6	−15	6	92	71	13	6	−8	−4	96	113	11
5	−1	−5	341	346	14	5	3	4	208	198	10	6	−14	−1	99	108	15	6	−8	−3	348	345	3
5	−1	−4	531	529	11	5	4	−10	110	120	−30	6	−14	0	98	104	15	6	−8	−2	315	323	13
5	−1	−3	308	306	3	5	4	−9	164	178	23	6	−14	1	117	115	8	6	−8	−1	226	222	5
5	−1	−2	244	249	2	5	4	−8	170	161	19	6	−14	2	165	148	12	6	−8	0	328	320	7
5	−1	−1	215	223	2	5	4	−7	151	158	15	6	−14	3	232	216	5	6	−8	1	413	415	4
5	−1	0	642	619	13	5	4	−6	222	211	4	6	−14	4	172	153	10	6	−8	2	439	466	4
5	−1	1	689	695	7	5	4	−5	343	335	10	6	−14	5	105	102	−29	6	−8	3	293	325	6
5	−1	2	546	561	5	5	4	−4	319	304	6	6	−14	6	101	78	14	6	−8	4	57	51	−20
5	−1	3	271	286	3	5	4	−3	129	120	6	6	−14	7	80	84	12	6	−8	5	213	219	11
5	−1	6	270	270	8	5	4	−2	110	107	7	6	−13	−2	150	151	9	6	−8	6	204	200	4
5	−1	7	216	185	26	5	4	−1	441	426	22	6	−13	−1	90	64	12	6	−8	7	281	268	14
5	0	−10	159	134	8	5	4	0	290	288	3	6	−13	0	166	172	10	6	−8	8	211	198	4
5	0	−9	72	100	12	5	4	1	458	466	14	6	−13	1	187	170	21	6	−7	−7	56	54	−22
5	0	−8	115	118	7	5	4	2	231	251	5	6	−13	2	235	239	19	6	−7	−6	119	123	15
5	0	−7	188	198	6	5	4	3	127	133	8	6	−13	3	182	168	15	6	−7	−4	320	320	3
5	0	−6	296	304	21	5	4	4	182	168	16	6	−13	4	98	97	7	6	−7	−3	410	407	20
5	0	−5	332	351	7	5	5	−10	146	134	−38	6	−13	5	79	80	−23	6	−7	−2	189	180	8
5	0	−4	401	396	8	5	5	−9	92	105	−17	6	−13	7	156	148	8	6	−7	−1	247	229	10
5	0	−3	156	162	3	5	5	−8	117	116	7	6	−12	−4	111	131	14	6	−7	0	383	405	4
5	0	−2	543	517	5	5	5	−7	119	125	6	6	−12	−3	148	142	9	6	−7	1	380	406	4
5	0	−1	477	471	10	5	5	−6	201	201	4	6	−12	−2	98	90	9	5	−7	2	207	220	4
5	0	0	759	735	8	5	5	−5	222	212	9	6	−12	−1	163	152	8	6	7	3	203	218	16
5	0	1	414	415	8	5	5	−4	170	164	12	6	−12	0	265	261	19	6	−7	4	221	221	4

Table A5—*Continued.*

h	k	l	$10F_c$	$10F_c$	$10S_g$	h	k	l	$10F_o$	$10F_c$	$10S_g$	h	k	l	$10F_o$	$10F_c$	$10S_g$	h	k	l	$10F_o$	$10F_c$	$10S_g$
6	−7	5	392	396	4	6	−2	−2	304	302	3	6	3	−8	103	113	7	7	−13	−2	85	44	9
6	−7	6	297	320	6	6	−2	−1	444	442	4	6	3	−7	112	111	7	7	−13	−1	149	158	9
6	−7	7	229	218	−38	6	−2	0	492	465	5	6	3	−6	217	220	26	7	−13	0	140	141	22
6	−7	8	80	84	12	6	−2	1	427	432	4	6	3	−5	256	266	20	7	−13	1	223	215	4
6	−6	−8	77	51	−16	6	−2	2	492	493	10	6	3	−4	312	320	28	7	−13	2	129	134	9
6	−6	−7	103	103	−17	6	−2	3	217	238	11	6	3	−3	295	288	12	7	−13	3	99	92	8
6	−6	−5	320	323	10	6	−2	4	175	158	−29	6	3	−2	73	62	9	7	−13	4	123	122	−21
6	−6	−4	287	273	9	6	−2	5	266	261	37	6	3	−1	310	300	9	7	−13	5	212	196	17
6	−6	−3	99	93	9	6	−2	6	257	245	31	6	3	0	438	437	9	7	−13	6	181	167	5
6	−6	−2	281	302	3	6	−1	−10	87	80	11	6	3	1	312	306	3	7	−13	7	157	147	6
6	−6	−1	209	227	19	6	−1	−9	69	80	12	6	3	2	180	190	9	7	−12	−4	122	109	7
6	−6	0	548	558	22	6	−1	−8	68	75	9	6	3	3	90	87	−36	7	−12	−3	87	92	10
6	−6	1	456	464	5	6	−1	−7	166	175	15	6	4	−10	120	97	−24	7	−12	−2	99	92	−16
6	−6	2	247	264	2	6	−1	−6	267	304	29	6	4	−9	106	112	16	7	−12	−1	215	211	15
6	−6	3	352	363	14	6	−1	−5	202	210	8	6	4	−8	79	77	−17	7	−12	0	164	168	8
6	−6	4	397	414	8	6	−1	−4	420	414	8	6	4	−7	104	126	−32	7	−12	1	206	205	6
6	−6	5	279	283	3	6	−1	−3	322	326	3	6	4	−6	228	243	23	7	−12	2	134	142	5
6	−6	6	268	250	5	6	−1	−2	369	335	7	6	4	−5	246	247	37	7	−12	3	177	165	9
6	−6	7	87	92	−18	6	−1	−1	537	540	11	6	4	−4	175	175	5	7	−12	4	265	251	5
6	−6	8	123	105	−29	6	−1	0	454	447	9	6	4	−3	193	184	4	7	−12	5	205	191	25
6	−5	−8	78	52	−14	6	−1	1	357	362	11	6	4	−2	271	269	8	7	−12	6	150	126	4
6	−5	−7	189	201	8	6	−1	2	135	134	5	6	4	−1	332	322	13	7	−12	7	99	90	9
6	−5	−6	268	271	5	6	−1	3	239	268	14	6	4	0	261	268	3	7	−11	−5	98	82	13
6	−5	−5	171	180	7	6	−1	4	293	285	6	6	4	1	166	164	12	7	−11	−4	106	122	16
6	−5	−4	217	229	4	6	−1	5	308	309	40	6	4	2	120	112	7	7	−11	−3	177	71	−33
6	−5	−3	219	241	13	6	−1	6	219	211	−52	6	4	3	185	203	9	7	−11	−1	209	206	6
5	−5	−2	346	357	10	6	0	−10	180	56	−33	6	5	−10	96	71	13	7	−11	0	261	249	21
6	−5	−1	708	700	7	6	0	−9	124	115	11	6	5	−9	176	30	−33	7	−11	1	193	197	25
6	−5	0	433	428	4	6	0	−8	117	114	−27	6	5	−8	114	128	16	7	−11	2	158	149	5
6	−5	1	370	360	4	6	0	−7	165	174	20	6	5	−7	159	165	6	7	−11	3	232	232	16
6	−5	2	203	214	4	6	0	−6	344	381	48	6	5	−5	195	191	6	7	−11	4	193	211	15
6	−5	3	367	374	4	6	0	−5	265	260	3	6	5	−4	127	136	6	7	−11	5	139	136	21
6	−5	4	411	424	16	6	0	−4	272	270	5	6	5	−3	197	204	26	7	−11	6	111	99	12
6	−5	5	135	144	5	6	0	−3	369	379	4	6	5	−2	275	252	11	7	−11	7	105	116	9
6	−5	6	225	208	18	6	0	−2	398	406	4	6	5	−1	225	236	20	7	−10	−5	69	77	−16
6	−5	7	184	179	6	6	0	−1	271	270	5	6	5	0	193	193	4	7	−10	−2	286	281	6
6	−5	8	160	169	−31	6	0	0	314	318	3	6	5	1	176	163	19	7	−10	−1	230	222	5
6	−4	−9	87	86	−14	6	0	1	258	257	5	6	5	2	180	183	18	7	−10	0	159	157	11

Table A5 –*Continued.*

h	*k*	*l*	$10F_c$	$10F_c$	$10S_g$	*h*	*k*	*l*	$10F_o$	$10F_c$	$10S_g$	*h*	*k*	*l*	$10F_o$	$10F_c$	$10S_g$	*h*	*k*	*l*	$10F_o$	$10F_c$	$10S_g$
6	−4	−8	120	130	16	6	0	2	233	243	16	6	6	−9	121	79	−32	7	−10	1	153	157	6
6	−4	−6	216	227	26	6	0	3	361	386	7	6	6	−8	154	161	−28	7	−10	2	243	247	5
6	−4	−5	147	166	10	6	0	4	309	306	15	6	6	−7	199	198	30	7	−10	3	210	217	19
6	−4	−4	188	189	4	6	0	5	240	248	38	6	6	−6	79	93	15	7	−10	4	224	227	4
6	−4	−3	506	499	5	6	1	−10	75	61	−19	6	6	−5	108	132	10	7	−10	5	227	218	7
6	−4	−2	382	375	8	6	1	−9	121	118	10	6	6	−4	141	145	20	7	−10	6	103	107	−20
6	−4	−1	460	457	9	6	1	−8	202	222	28	6	6	−3	197	199	6	7	−10	7	189	189	6
6	−4	0	180	193	5	6	1	−7	164	184	25	6	6	−2	280	271	6	7	−10	8	193	180	6
6	−4	1	351	356	4	6	1	−6	288	309	17	6	6	−1	168	165	27	7	−9	−6	216	47	−40
6	−4	2	329	345	3	6	1	−5	150	155	24	6	6	0	145	144	9	7	−9	−5	96	99	−20
6	−4	3	394	417	4	6	1	−4	179	190	21	6	7	−8	122	124	18	7	−9	−3	181	186	7
6	−4	4	307	315	9	6	1	−3	310	299	3	6	7	−7	101	97	−32	7	−9	−2	236	234	5
6	−4	5	248	239	12	6	1	−2	485	476	15	6	7	−5	180	166	5	7	−9	−1	212	221	13
6	−4	6	206	208	8	6	1	−1	250	228	15	6	7	−4	151	159	9	7	−9	0	181	179	7
6	−4	7	223	204	33	6	1	0	301	303	6	6	7	−3	217	209	4	7	−9	1	219	222	13
6	−3	−7	118	136	7	6	1	1	283	277	3	6	7	−2	158	153	13	7	−9	2	347	376	21
6	−3	−6	106	99	6	6	1	2	348	356	7	6	7	−1	118	103	11	7	−9	3	322	355	16
6	−3	−5	222	213	18	6	1	3	322	337	10	6	8	−7	181	58	−33	7	−9	4	124	124	6
6	−3	−4	226	224	11	6	1	4	248	241	25	6	8	−6	133	114	11	7	−9	5	226	217	5
6	−3	−3	575	580	23	6	1	5	108	114	−22	6	8	−5	151	142	−41	7	−9	6	202	183	10
6	−3	−2	242	471	12	6	2	−10	98	98	12	6	8	−4	156	157	9	7	−9	7	199	195	30
6	−3	−1	343	346	3	6	2	−9	93	128	−20	6	8	−3	133	125	−42	7	−9	8	118	133	−25
6	−3	0	376	370	4	6	2	−8	196	208	4	7	−15	0	94	63	13	7	−8	−7	77	34	11
6	−3	1	374	385	7	6	2	−7	120	128	6	7	−15	1	92	84	14	7	−8	−6	94	95	−19
6	−3	2	477	471	10	6	2	−6	86	102	−21	7	−15	2	121	113	−23	7	−8	−5	165	170	8
6	−3	3	377	412	4	6	2	−5	238	245	7	7	−15	3	180	165	5	7	−8	−3	301	303	12
6	−3	4	210	226	4	6	2	−4	317	324	19	7	−15	4	118	120	19	7	−8	−2	162	173	5
6	−3	5	270	262	24	6	2	−3	404	390	16	7	15	5	85	64	9	7	−8	−1	215	215	11
6	−3	6	190	195	−35	6	2	−2	362	371	33	7	−14	−1	79	72	11	7	−8	0	353	351	7
6	−3	7	189	189	11	6	2	−1	80	88	−21	7	−14	0	81	57	13	7	−8	1	264	276	3
6	−2	−9	115	129	12	6	2	0	363	362	4	7	−14	1	181	191	15	7	−8	2	381	413	4
6	−2	−8	141	130	11	6	2	1	300	291	6	7	−14	2	182	188	11	7	−8	3	131	133	5
6	−2	−7	61	36	−13	6	2	2	386	421	12	7	−14	3	129	115	13	7	−8	4	182	182	5
6	−2	−6	160	179	8	6	2	3	206	213	8	7	−14	4	90	84	13	7	−8	5	244	235	20
6	−2	−5	359	366	18	6	2	4	98	111	−32	7	−14	5	112	87	17	7	−8	6	269	242	19
6	−2	−4	368	384	26	6	3	−10	73	80	−18	7	−14	6	144	127	17	7	−8	7	171	155	7
6	−2	−3	286	304	20	6	3	−9	135	136	5	7	−13	−3	83	106	17	7	−7	−7	71	84	12

Table A5—*Continued.*

h	*k*	*l*	$10F_c$	$10F_c$	$10S_g$	*h*	*k*	*l*	$10F_o$	$10F_c$	$10S_g$	*h*	*k*	*l*	$10F_o$	$10F_c$	$10S_g$	*h*	*k*	*l*	$10F_o$	$10F_c$	$10S_g$
7	−7	−6	176	185	5	7	−3	6	226	227	20	7	2	2	182	179	7	8	−12	1	183	175	7
7	−7	−5	222	230	7	7	−2	−9	100	103	14	7	2	3	88	88	10	8	−12	2	130	124	8
7	−7	−4	293	309	9	7	−2	−8	212	53	−40	7	3	−9	89	99	−17	8	−12	3	209	189	4
7	−7	−3	131	141	18	7	−2	−7	233	268	28	7	3	−8	85	75	−28	8	−12	3	216	189	15
7	−7	−2	202	203	4	7	−2	−6	195	209	25	7	3	−7	102	108	10	8	−12	5	140	130	11
7	−7	−1	275	276	3	7	−2	−5	263	297	26	7	3	−6	237	254	38	8	−12	6	113	108	−40
7	−7	0	333	340	7	7	−2	−4	191	197	10	7	3	−5	190	188	9	8	−12	7	107	72	11
7	−7	1	337	343	10	7	−2	−3	147	149	7	7	3	−4	254	263	15	8	−11	−4	75	54	−16
7	−7	2	198	204	6	7	−2	−2	321	327	13	7	3	−3	136	137	11	8	−11	−3	181	168	9
7	−7	3	151	156	9	7	−2	−1	449	462	13	7	3	−2	154	157	5	8	−11	−2	187	199	−40
7	−7	4	392	402	8	7	−2	0	320	324	3	7	3	−1	228	229	5	8	−11	−1	181	172	7
7	−7	5	213	207	11	7	−2	1	270	269	3	7	3	0	230	223	9	8	−11	0	171	183	10
7	−7	6	230	219	5	7	−2	2	236	237	5	7	3	1	207	200	19	8	−11	1	155	153	−27
7	−7	7	116	117	12	7	−2	3	229	237	7	7	3	2	109	113	−27	8	−11	2	172	168	7
7	−6	−8	74	74	−15	7	−2	4	287	286	9	7	4	−9	59	46	−20	8	−11	3	256	252	5
7	−6	−5	251	266	5	7	−2	5	271	270	14	7	4	−8	82	72	−14	8	−11	4	89	87	−24
7	−6	−4	82	75	11	7	−2	6	164	162	7	7	4	−7	161	166	13	8	−11	5	175	161	14
7	−6	−3	138	140	11	7	−1	−9	95	84	12	7	4	−6	210	205	10	8	−11	6	88	82	−24
7	−6	−2	366	363	7	7	−1	−8	94	104	15	7	4	−5	125	143	−28	8	−11	7	147	134	24
7	−6	−1	330	339	13	7	−1	−7	250	279	37	7	4	−4	115	103	−27	8	−10	−5	64	83	−13
7	−6	0	287	283	14	7	−1	−6	133	134	−28	7	4	−3	100	97	6	8	−10	−3	246	237	7
7	−6	1	305	308	9	7	−1	−5	196	208	24	7	4	−2	309	301	9	8	−10	−3	145	237	26
7	−6	2	274	308	11	7	−1	−4	215	221	4	7	4	−1	207	206	10	8	−10	−2	182	184	7
7	−6	3	288	305	23	7	−1	−3	193	196	12	7	4	0	217	210	17	8	−10	−1	86	103	−18
7	−6	4	332	341	20	7	−1	−2	375	371	15	7	4	1	173	167	−34	8	−10	0	162	156	5
7	−6	5	248	242	5	7	−1	−1	387	379	4	7	5	−9	209	60	−40	8	−10	1	199	206	6
7	−6	6	141	126	7	7	−1	0	315	321	22	7	5	−8	128	128	9	8	−10	2	178	189	9
7	−6	7	128	136	22	7	−1	1	261	262	3	7	5	−7	162	164	13	8	−10	3	237	232	12
7	−5	−8	191	169	8	7	−1	2	180	179	9	7	5	−6	93	105	−17	8	−10	4	149	140	15
7	−5	−6	147	158	12	7	−1	3	304	327	15	7	5	−5	71	78	−12	8	−10	5	182	176	22
7	−5	−5	54	72	−12	7	−1	4	265	245	29	7	5	−4	183	185	4	8	−10	6	180	170	−30
7	−5	−4	159	161	16	7	−1	5	172	179	12	7	5	−3	223	222	22	8	−10	7	187	167	−34
7	−5	−3	267	269	5	7	0	−10	183	72	−1	7	5	−2	217	214	4	8	−9	−6	95	94	10
7	−5	−2	448	444	22	7	0	−9	91	96	−35	7	5	−1	171	177	14	8	−9	−5	121	157	−49
7	−5	−1	387	398	15	7	0	−8	162	166	18	7	5	0	118	112	−23	8	−9	−3	92	106	7
7	−5	0	219	239	4	7	0	−7	188	204	24	7	6	−8	101	121	−27	8	−9	−2	133	129	11
7	−5	1	317	320	16	7	0	−6	131	124	9	7	6	−7	103	96	8	8	−9	−1	148	127	6
7	−5	2	334	347	10	7	0	−5	163	167	16	7	6	−6	198	64	−33	8	−9	0	274	282	22

Table A5—*Continued.*

h	k	l	$10F_c$	$10F_c$	$10S_g$	h	k	l	$10F_o$	$10F_c$	$10S_g$	h	k	l	$10F_o$	$10F_c$	$10S_g$	h	k	l	$10F_o$	$10F_c$	$10S_g$
7	−5	3	384	394	15	7	0	−4	187	187	11	7	6	−5	139	139	7	8	−9	1	275	278	5
7	−5	4	200	212	4	7	0	−3	301	300	12	7	6	−4	182	183	5	8	−9	2	247	261	5
7	−5	5	195	178	8	7	0	−2	436	439	17	7	6	−3	170	170	22	8	−9	3	218	227	7
7	−5	6	157	162	17	7	0	−1	335	335	3	7	6	−2	96	105	9	8	−9	4	167	165	13
7	−5	7	165	163	7	7	0	0	108	116	6	7	6	−1	107	102	−25	8	−9	5	137	140	7
7	−4	−9	110	95	12	7	0	1	243	235	15	7	7	−7	68	46	−19	8	−9	6	215	201	9
7	−4	−8	147	162	7	7	0	2	296	296	12	7	7	−6	122	112	10	8	−9	7	139	127	−45
7	−4	−7	79	78	10	7	0	3	258	267	10	7	7	−5	149	132	6	8	−8	−7	95	95	9
7	−4	−6	50	46	−11	7	0	4	256	247	8	7	7	−4	135	142	11	8	−8	−5	123	121	−31
7	−4	−5	168	169	12	7	0	5	130	123	−25	7	7	−3	106	111	16	8	−8	−3	186	181	4
7	−4	−4	340	354	34	7	1	−10	90	83	11	8	−15	1	85	78	−36	8	−8	−2	111	102	6
7	−4	−3	423	429	21	7	1	−9	111	112	14	8	−15	2	181	179	9	8	−8	−1	334	347	7
7	−4	−2	377	391	15	7	1	−8	137	141	5	8	−15	3	128	116	−40	8	−8	0	278	292	8
7	−4	−1	96	99	10	7	1	−7	112	123	−35	8	−15	4	215	53	−40	8	−8	1	278	291	6
7	−4	0	365	353	4	7	1	−6	88	85	7	8	−14	−1	128	75	9	8	−8	2	142	156	−26
7	−4	1	376	375	8	7	1	−5	180	196	29	8	−14	0	167	150	7	8	−8	3	85	75	7
7	−4	2	374	391	15	7	1	−4	294	315	32	8	−14	1	177	157	11	8	−8	4	274	275	22
7	−4	3	249	254	5	7	1	−3	332	333	10	8	−14	2	121	125	19	8	−8	5	184	187	6
7	−4	4	165	186	18	7	1	−2	208	210	10	8	−14	3	66	71	−15	8	−8	6	187	181	6
7	−4	5	165	164	15	7	1	−1	285	283	11	8	−14	4	97	94	10	8	−8	7	131	116	−51
7	−4	6	213	219	6	7	1	0	109	110	5	8	−14	5	141	125	21	8	−7	−6	117	133	7
7	−3	−10	114	75	9	7	1	1	382	373	8	8	−14	6	153	136	−31	8	−7	−4	88	88	11
7	−3	−9	98	74	12	7	1	2	337	349	10	8	−13	−3	180	64	−33	8	−7	−3	141	155	21
7	−3	−8	73	61	−14	7	1	3	183	193	16	8	−13	−2	216	84	−40	8	−7	−2	219	219	4
7	−3	−7	90	95	11	7	1	4	82	108	13	8	−13	−1	166	151	7	8	−7	−1	352	360	28
7	−3	−6	196	197	16	7	2	−10	91	79	−45	8	−13	0	156	158	9	8	−7	0	210	223	6
7	−3	−5	336	361	30	7	2	−9	110	97	−34	8	−13	1	123	138	11	8	−7	1	172	175	10
7	−3	−4	374	392	22	7	2	−8	107	115	13	8	−13	2	75	89	−25	8	−7	2	144	148	9
7	−3	−3	196	207	8	7	2	−7	82	86	−19	8	−13	3	134	114	9	8	−7	3	297	326	3
7	−3	−2	152	139	5	7	2	−6	148	169	12	8	−13	4	196	178	24	8	−7	4	292	284	23
7	−3	−1	312	323	9	7	2	−5	248	253	30	8	−13	5	144	124	6	8	−7	5	229	218	23
7	−3	0	476	466	5	7	2	−4	261	266	8	8	−13	6	224	133	−183	8	−7	6	128	123	18
7	−3	1	360	372	4	7	2	−3	325	324	13	8	−12	−4	65	48	−15	8	−7	7	103	92	−21
7	−3	2	272	288	16	7	2	−2	89	95	9	8	−12	−3	93	87	12	8	−6	−8	143	135	10
7	−3	3	138	141	7	7	2	−1	320	311	6	8	−12	−2	158	147	8	8	−6	−7	90	100	9
7	−3	4	237	240	12	7	2	0	265	267	8	8	−12	−1	177	169	9	8	−6	−6	116	99	−24
7	−3	5	244	235	17	7	2	1	270	267	13	8	−12	0	137	127	8	8	−6	−5	68	89	11

Table A5—*Continued.*

h	k	l	$10F_c$	$10F_c$	$10S_g$	h	k	l	$10F_o$	$10F_c$	$10S_g$	h	k	l	$10F_o$	$10F_c$	$10S_g$	h	k	l	$10F_o$	$10F_c$	$10S_g$
8	−6	−4	76	41	10	8	−1	−4	202	216	22	8	6	−5	148	147	−40	9	−8	2	75	66	−21
8	−6	−3	327	350	43	8	−1	−3	266	275	32	8	6	−4	147	127	9	9	−8	3	158	161	16
8	−6	−2	354	367	32	8	−1	−2	304	322	15	9	−15	1	140	112	7	9	−8	4	219	219	20
8	−6	−1	329	344	33	8	−1	−1	187	187	4	9	−15	2	101	93	−44	9	−8	5	162	143	6
8	−6	0	183	178	4	8	−1	0	293	301	15	9	−15	3	214	48	−40	9	−8	6	126	124	−28
8	−6	1	169	179	17	8	−1	1	103	95	7	9	−14	−1	98	95	10	9	−7	−7	78	121	19
8	−6	2	328	347	26	8	−1	2	259	253	5	9	−14	0	131	124	8	9	−7	−6	82	61	13
8	−6	3	286	314	20	8	−1	3	242	234	5	9	−14	1	124	114	16	9	−7	−5	163	149	8
8	−6	4	159	166	13	8	−1	4	178	185	9	9	−14	2	67	71	−18	9	−7	−4	117	128	−29
8	−6	5	162	148	19	8	0	−9	109	110	9	9	−14	3	179	68	−33	9	−7	−3	208	208	27
8	−6	6	125	116	7	8	0	−8	97	104	11	9	−14	4	158	152	−27	9	−7	−2	281	307	31
8	−5	−7	180	44	−33	8	0	−7	100	114	17	9	−14	5	119	116	−33	9	−7	−1	132	142	−23
8	−5	−6	74	86	10	8	0	−6	118	143	−50	9	−13	−3	226	32	−40	9	−7	0	120	120	−22
8	−5	−5	125	150	15	8	0	−5	182	201	22	9	−13	−2	128	126	12	9	−7	1	74	49	−24
8	−5	−4	403	429	48	8	0	−4	189	202	23	9	−13	−1	181	166	11	9	−7	2	228	238	18
8	−5	−3	357	380	46	8	0	−3	308	322	28	9	−13	0	115	103	11	9	−7	3	281	283	8
8	−5	−2	239	240	17	8	0	−2	148	143	10	9	−13	1	89	74	−43	9	−7	4	209	225	19
8	−5	−1	123	126	5	8	0	−1	182	166	7	9	−13	2	110	119	8	9	−7	5	98	114	10
8	−5	0	131	137	5	8	0	0	188	192	17	9	−13	3	159	141	14	9	−7	6	117	119	8
8	−5	1	268	287	19	8	0	1	254	244	8	9	−13	4	123	129	9	9	−6	−7	114	118	19
8	−5	2	303	326	6	8	0	2	280	277	8	9	−13	5	143	120	13	9	−6	−6	83	80	−17
8	−5	3	248	261	5	8	0	3	158	167	8	9	−12	−4	88	58	13	9	−6	−5	146	137	19
8	−5	4	127	123	5	8	1	−9	104	103	9	9	−12	−3	156	140	9	9	−6	−4	169	192	29
8	−5	5	144	149	10	8	1	−8	136	134	5	9	−12	−2	167	154	7	9	−6	−3	201	221	−41
8	−5	6	219	196	13	8	1	−7	85	92	11	9	−12	−1	127	126	10	9	−6	−2	81	89	11
8	−4	−8	89	102	11	8	1	−6	127	134	11	9	−12	0	87	87	13	9	−6	−1	127	130	5
8	−4	−7	72	77	−31	8	1	−5	188	202	24	9	−12	1	111	97	10	9	−6	0	135	129	−23
8	−4	−6	259	284	21	8	1	−4	147	156	−31	9	−12	2	183	167	20	9	−6	1	309	319	31
8	−4	−5	213	230	28	8	1	−3	214	204	−35	9	−12	3	192	194	25	9	−6	2	358	383	36
8	−4	−4	235	245	16	8	1	−2	129	138	12	9	−12	4	114	101	−18	9	−6	3	166	171	7
8	−4	−3	186	202	19	8	1	−1	232	232	5	9	−12	5	126	122	9	9	−6	4	127	124	18
8	−4	−2	143	44	−27	8	1	0	248	256	10	9	−12	6	82	77	−15	9	−6	5	93	101	−27
8	−4	−1	148	155	10	8	1	1	256	247	8	9	−11	−5	77	81	−24	9	−5	−7	145	130	9
8	−4	0	379	387	30	8	1	2	153	154	12	9	−11	−4	149	132	9	9	−5	−6	176	29	−33
8	−4	1	387	407	35	8	1	3	129	121	18	9	−11	−3	185	165	−69	9	−5	−5	146	174	−37
8	−4	2	212	224	6	8	2	−9	92	67	12	9	−11	−2	115	115	13	9	−5	−4	150	181	26
8	−4	3	162	169	6	8	2	−8	103	89	−23	9	−11	−1	77	69	−12	9	−5	−3	120	110	18
8	−4	4	178	169	5	8	2	−7	212	61	−40	9	−11	0	136	138	−29	9	−5	−2	150	141	24

Table A5—*Continued.*

h	*k*	*l*	$10F_c$	$10F_c$	$10S_g$	*h*	*k*	*l*	$10F_o$	$10F_c$	$10S_g$	*h*	*k*	*l*	$10F_o$	$10F_c$	$10S_g$	*h*	*k*	*l*	$10F_o$	$10F_c$	$10S_g$
8	−4	5	257	251	5	8	2	−6	142	146	14	9	−11	1	141	143	16	9	−5	−1	275	292	27
8	−4	6	177	168	28	8	2	−5	198	203	14	9	−11	2	239	237	12	9	−5	0	298	300	27
8	−3	−9	137	126	−51	8	2	−4	164	164	5	9	−11	3	131	129	−36	9	−5	1	304	312	21
8	−3	−8	109	89	17	8	2	−3	159	169	14	9	−11	4	111	110	14	9	−5	2	123	124	6
8	−3	−7	62	66	−11	8	2	−2	174	177	10	9	−11	5	108	96	−20	9	−5	3	135	122	5
8	−3	−6	220	256	35	8	2	−1	225	236	9	9	−11	6	134	116	−23	9	−5	4	103	100	8
8	−3	−5	132	129	−24	8	2	0	217	207	26	9	−10	−4	149	151	10	9	−5	5	208	201	31
8	−3	−4	133	137	5	8	2	1	175	171	7	9	−10	−3	87	78	12	9	−4	−8	74	36	−35
8	−3	−3	140	137	4	8	2	2	129	121	16	9	−10	−2	89	104	10	9	−4	−7	168	63	−30
8	−3	−2	276	289	17	8	3	−9	209	43	−40	9	−10	−1	100	91	−28	9	−4	−6	124	117	6
8	−3	−1	328	327	13	8	3	−8	175	59	−33	9	−10	0	179	185	21	9	−4	−5	181	178	16
8	−3	0	371	384	19	8	3	−7	152	160	14	9	−10	1	252	258	5	9	−4	−4	167	178	10
8	−3	1	238	242	5	8	3	−6	148	153	7	9	−10	2	177	181	5	9	−4	−3	142	158	21
8	−3	2	165	159	10	8	3	−5	161	167	18	9	−10	3	105	89	7	9	−4	−2	218	224	28
8	−3	3	215	236	26	8	3	−4	112	102	−28	9	−10	4	190	182	6	9	−4	−1	278	292	17
8	−3	4	237	227	21	8	3	−3	99	105	15	9	−10	5	136	135	11	9	−4	0	172	173	10
8	−3	5	216	213	6	8	3	−2	257	249	26	9	−10	6	162	157	6	9	−4	1	222	218	13
8	−2	−9	179	34	−33	8	3	−1	197	193	4	9	−9	−6	193	89	−33	9	−4	2	81	224	15
8	−2	−8	185	85	−33	8	3	0	158	156	6	9	−9	−4	96	89	−45	9	−4	3	179	186	20
8	−2	−6	179	201	−35	8	3	1	157	128	9	9	−9	−3	64	60	−13	9	−4	4	230	226	21
8	−2	−5	165	170	5	8	4	−8	117	119	−33	9	−9	−2	174	161	7	9	−4	5	204	180	6
8	−2	−4	141	153	7	8	4	−7	135	135	−23	9	−9	−1	203	219	4	9	−3	−8	60	49	−18
8	−2	−3	188	183	4	8	4	−6	185	87	−33	9	−9	0	248	258	−46	9	−3	−7	153	145	6
8	−2	−2	402	420	24	8	4	−5	94	87	−18	9	−9	1	210	220	31	9	−3	−6	156	155	14
8	−2	−1	189	186	4	8	4	−4	108	83	11	9	−9	2	152	176	21	9	−3	−5	143	156	16
8	−2	0	345	354	3	8	4	−3	212	220	19	9	−9	3	137	131	12	9	−3	−4	128	153	23
8	−2	1	163	169	5	8	4	−2	230	222	25	9	−9	4	159	159	6	9	−3	−3	78	95	−19
8	−2	2	219	228	7	8	4	−1	110	114	15	9	−9	6	128	123	8	9	−3	−2	291	315	29
8	−2	3	235	227	7	8	4	0	93	97	−22	9	−8	−7	101	91	15	9	−3	−1	276	280	22
8	−2	4	209	207	13	8	5	−8	75	90	−16	9	−8	−6	135	107	9	9	−3	0	107	109	−20
8	−2	4	132	207	9	8	5	−7	63	56	−12	9	−8	−5	80	85	−14	9	−3	1	184	180	7
8	−2	7	140	82	8	8	5	−6	65	60	−18	9	−8	−4	131	122	7	9	−3	2	205	196	12
8	−1	−9	102	64	12	8	5	−5	98	99	−18	9	−8	−3	125	136	6	9	−3	3	200	196	12
8	−1	−8	138	136	18	8	5	−4	198	211	8	9	−8	−2	240	247	−45	9	−3	4	209	193	6
8	−1	−7	173	172	19	8	5	−3	175	165	12	9	−8	−1	260	274	29	9	−2	−9	210	40	−40
8	−1	−6	89	104	17	8	5	−2	115	106	−27	9	−8	0	222	228	22	9	−2	−8	107	119	19
8	−1	−5	120	129	6	8	6	−6	121	112	−22	9	−8	1	151	163	11	9	−2	−7	138	142	12

Table A5—*Continued.*

h	k	l	$10F_c$	$10F_c$	$10S_g$	h	k	l	$10F_o$	$10F_c$	$10S_g$	h	k	l	$10F_o$	$10F_c$	$10S_g$	h	k	l	$10F_o$	$10F_c$	$10S_g$
9	−2	−6	70	94	−16	10	−13	−1	92	86	9	10	−6	−4	161	161	16	10	1	−7	92	101	16
9	−2	−5	107	107	12	10	−13	0	174	58	−33	10	−6	−3	141	150	6	10	1	−6	108	98	12
9	−2	−4	153	174	15	10	−13	1	70	58	−13	10	−6	−2	169	178	−36	10	1	−5	67	95	−16
9	−2	−3	277	290	33	10	−13	2	122	118	18	10	−6	−1	160	166	−37	10	1	−4	92	66	−31
9	−2	−2	187	190	19	10	−13	3	184	174	9	10	−6	0	262	277	16	10	1	−3	87	100	13
9	−2	−1	203	196	12	10	−13	4	95	81	−18	10	−6	1	211	217	17	10	1	−2	151	144	18
9	−2	0	112	104	−18	10	−12	−3	141	123	10	10	−6	2	73	82	−33	10	1	−1	163	165	10
9	−2	1	178	172	7	10	−12	−2	84	62	13	10	−6	3	72	65	−25	10	2	−7	95	88	−15
9	−2	2	254	247	13	10	−12	−1	169	51	−30	10	−6	4	101	97	16	10	2	−6	80	76	−37
9	−2	3	185	187	13	10	−12	0	122	106	−23	10	−5	−7	57	53	−22	10	2	−5	89	52	12
9	−2	4	132	132	8	10	−12	1	185	155	28	10	−5	−6	221	104	−40	10	2	−4	89	101	−37
9	−1	−9	101	96	−27	10	−12	2	176	175	−32	10	−5	−5	203	204	24	10	2	−3	156	141	23
9	−1	−8	106	103	8	10	−12	3	120	113	7	10	−5	−4	172	180	29	10	2	−2	149	140	7
9	−1	−7	88	92	14	10	−12	4	113	92	10	10	−5	−3	80	82	10	11	−13	−1	83	39	13
9	−1	−6	103	117	8	10	−12	5	73	61	−17	10	−5	−2	173	188	−34	11	−13	0	77	65	11
9	−1	−5	124	134	11	10	−11	−4	193	93	−33	10	−5	−1	102	104	12	11	−13	1	122	115	−31
9	−1	−4	192	211	6	10	−11	−3	93	97	−21	10	−5	0	241	258	22	11	−13	2	156	140	6
9	−1	−3	218	217	35	10	−11	−2	207	48	−40	10	−5	1	77	59	−19	11	−13	3	186	54	−33
9	−1	−2	60	68	−13	10	−11	−1	168	164	8	10	−5	2	100	105	9	11	−12	−3	84	57	13
9	−1	−1	162	162	5	10	−11	0	159	150	22	10	−5	3	161	160	26	11	−12	−2	68	47	−18
9	−1	0	199	198	18	10	−11	1	167	169	7	10	−5	4	171	183	7	11	−12	−1	81	74	−14
9	−1	1	213	218	6	10	−11	2	149	131	−35	10	−4	−8	63	47	−18	11	−12	0	138	128	17
9	−1	2	218	214	7	10	−11	3	74	43	−13	10	−4	−7	121	133	16	11	−12	1	127	121	8
9	−1	3	131	146	18	10	−11	4	127	100	−33	10	−4	−6	143	160	7	11	−12	2	72	64	−14
9	0	−9	107	91	9	10	−11	5	102	106	−32	10	−4	−5	79	93	10	11	−12	3	182	47	−33
9	0	−8	229	65	−40	10	−10	−5	113	111	12	10	−4	−4	54	56	−16	11	−11	−4	83	58	−15
9	0	−7	97	62	−41	10	−10	−4	97	80	13	10	−4	−3	69	95	−18	11	−11	−3	176	31	−33
9	0	−6	147	145	6	10	−10	−3	72	101	−16	10	−4	−2	193	191	−36	11	−11	−2	81	90	11
9	0	−5	105	109	16	10	−10	−2	120	110	14	10	−4	−1	184	187	24	11	−11	−1	113	114	9
9	0	−4	170	181	17	10	−10	−1	160	161	10	10	−4	0	200	193	4	11	−11	0	116	108	8
9	0	−3	138	137	17	10	−10	0	140	136	6	10	−4	1	102	92	−28	11	−11	1	108	86	10
9	0	−2	152	162	6	10	−10	1	140	137	8	10	−4	2	159	163	22	11	−11	2	80	64	−17
9	0	−1	180	168	5	10	−10	2	87	73	−36	10	−4	3	179	176	5	11	−11	3	100	90	−31
9	0	0	208	201	6	10	−10	3	137	138	19	10	−3	−8	99	100	−27	11	−11	4	147	128	7
9	0	1	244	231	5	10	−10	4	152	135	15	10	−3	−7	92	113	16	11	−10	−4	63	29	−14
9	0	2	137	131	−39	10	−10	5	172	165	−28	10	−3	−6	167	49	−30	11	−10	−3	96	55	−32
9	1	−9	66	41	−18	10	−9	−5	103	92	−54	10	−3	−5	92	101	9	11	−10	−2	116	126	16
9	1	−8	178	44	−33	10	−9	−4	167	60	−30	10	−3	−4	61	59	−16	11	−10	−1	105	115	−38

Table A5 *Continued.*

h	*k*	*l*	$10F_c$	$10F_c$	$10S_g$	*h*	*k*	*l*	$10F_o$	$10F_c$	$10S_g$	*h*	*k*	*l*	$10F_o$	$10F_c$	$10S_g$	*h*	*k*	*l*	$10F_o$	$10F_c$	$10S_g$
9	1	−7	81	82	−23	10	−9	−3	101	103	8	10	−3	−3	232	246	−41	11	−10	0	130	113	−25
9	1	−6	131	134	10	10	−9	−2	173	147	17	10	−3	−2	194	202	8	11	−10	1	209	67	−40
9	1	−5	157	157	6	10	−9	−2	153	147	−31	10	−3	−1	149	142	6	11	−10	2	138	123	10
9	1	−4	189	185	6	10	−9	0	136	143	14	10	−3	0	92	106	−21	11	−10	3	136	134	11
9	1	−3	98	85	10	10	−9	1	95	100	−23	10	−3	1	137	131	16	11	−10	4	146	149	23
9	1	−2	172	153	9	10	−9	2	132	140	22	10	−3	2	198	206	8	11	−9	−5	179	49	−33
9	1	−1	217	205	28	10	−9	3	170	165	−31	10	−3	3	167	174	7	11	−9	−4	214	61	−40
9	1	0	200	195	6	10	−9	4	148	151	10	10	−2	−8	113	122	−36	11	−9	−3	134	133	8
9	1	1	137	145	7	10	−9	5	130	125	−21	10	−2	−7	57	40	−20	11	−9	−2	135	118	7
9	2	−8	180	71	−33	10	−8	−6	81	104	17	10	−2	−6	182	58	−33	11	−9	−1	156	156	6
9	2	−7	153	140	−45	10	−8	−5	209	27	−40	10	−2	−5	111	123	13	11	−9	0	179	58	−33
9	2	−6	141	140	13	10	−8	−4	134	134	12	10	−2	−4	139	134	6	11	−9	1	131	129	8
9	2	−5	131	115	9	10	−3	−3	174	171	5	10	−2	−3	224	221	25	11	−9	2	188	175	6
9	2	−4	89	101	9	10	−8	−2	151	163	23	10	−2	−2	89	85	−14	11	−9	3	131	129	−36
9	2	−3	89	109	−18	10	−8	−1	82	104	9	10	−2	−1	141	128	8	11	−9	4	113	88	8
9	2	−2	146	156	7	10	−8	0	77	106	12	10	−2	0	161	156	8	11	−8	−6	79	23	−14
9	2	−1	219	218	7	10	−8	1	123	121	20	10	−2	1	207	197	6	11	−8	−5	103	91	16
9	2	0	139	134	17	10	−8	2	157	154	−27	10	−2	2	163	160	15	11	−8	−4	124	125	14
9	3	−8	141	114	10	10	−8	3	218	223	7	10	−1	−8	59	43	−20	11	−8	−3	148	141	7
9	3	−7	117	120	−27	10	−8	4	162	161	16	10	−1	−7	71	30	−15	11	−8	−2	106	98	8
9	3	−6	79	69	−14	10	−8	5	56	84	−22	10	−1	−6	69	83	−17	11	−8	−1	126	120	−20
9	3	−5	90	68	11	10	−7	−7	54	27	−22	10	−1	−5	162	154	23	11	−8	0	85	82	10
9	3	−4	64	81	−16	10	−7	−6	127	118	10	10	−1	−4	153	155	18	11	−8	1	180	180	11
9	3	−3	156	160	6	10	−7	−5	93	78	−33	10	−1	−3	140	121	20	11	−8	2	95	87	9
9	3	−1	105	102	13	10	−7	−4	178	87	−33	10	−1	−2	137	133	−50	11	−8	3	112	109	8
9	3	2	195	145	12	10	−7	−4	100	87	8	10	−1	−1	137	139	7	11	−7	−6	66	80	−13
9	4	−7	199	37	−33	10	−7	−3	167	180	−36	10	−1	0	150	145	22	11	−7	−5	125	99	10
9	4	−6	92	58	12	10	−7	−2	50	76	−18	10	−1	1	179	157	5	11	−7	−4	131	128	14
9	4	−5	103	74	10	10	−7	−1	82	88	−29	10	0	−8	77	21	−17	11	−7	−3	111	93	9
9	4	−4	152	165	9	10	−7	0	200	197	18	10	0	−7	109	87	14	11	−7	−2	86	90	13
9	4	−3	138	149	19	10	−7	1	223	224	27	10	0	−6	119	130	−25	11	−7	−1	118	123	8
10	−14	−1	125	102	−26	10	−7	2	275	277	8	10	0	−5	154	147	6	11	−7	0	41	55	−25
10	−14	0	126	100	11	10	−7	3	134	156	−31	10	0	−4	101	99	11	11	−7	1	181	191	18
10	−14	1	83	67	−13	10	−7	5	121	94	13	10	0	−3	73	89	14	11	−7	2	125	90	6
10	−14	2	39	34	−25	10	−6	−7	67	26	−12	10	0	−2	139	129	7	11	−7	3	91	84	−25
10	−14	3	148	134	9	10	−6	−6	76	89	20	10	0	−1	120	119	11	11	−6	−6	89	75	14
10	−13	−2	136	129	11	10	−6	−5	178	58	−33	10	0	0	142	146	10	11	−6	4	139	147	7

Table A5—*Continued.*

h	k	l	$10F_c$	$10F_c$	$10S_g$	h	k	l	$10F_o$	$10F_c$	$10S_g$	h	k	l	$10F_o$	$10F_c$	$10S_g$	h	k	l	$10F_o$	$10F_c$	$10S_g$
11	−6	−3	177	23	−33	11	−3	−4	146	144	7	12	−11	−1	109	98	10	12	−7	0	142	128	19
11	−6	−2	95	104	12	11	−3	−3	137	144	11	12	−11	0	111	91	−37	12	−7	1	137	118	−25
11	−6	−1	144	143	6	11	−3	−2	130	116	19	12	−11	1	179	37	−33	12	−6	−5	91	99	−24
11	−6	0	170	166	27	11	−3	−1	105	104	14	12	−11	2	83	74	−14	12	−6	−4	77	20	−13
11	−6	1	181	171	9	11	−3	0	117	116	−29	12	−10	−3	147	129	7	12	−6	−3	108	99	8
11	−6	2	104	90	8	11	−3	1	136	143	11	12	−10	−2	90	84	10	12	−6	−2	130	115	14
11	−6	3	91	98	−28	11	−2	−7	182	30	−33	12	−10	−1	175	48	−33	12	−6	−1	134	125	21
11	−5	−7	104	82	13	11	−2	−6	97	79	−32	12	−10	0	81	81	−18	12	−6	0	125	121	11
11	−5	−6	90	108	15	11	−2	−5	114	114	8	12	−10	1	88	52	14	12	−6	1	179	45	−33
11	−5	−5	93	90	13	11	−2	−4	161	170	19	12	−10	2	128	120	8	12	−5	−6	81	64	11
11	−5	−4	66	53	−19	11	−2	−2	87	49	−15	12	−9	−4	88	86	−25	12	−5	−5	179	44	−33
11	−5	−3	100	100	14	11	−2	−1	130	135	−39	12	−9	−3	92	78	9	12	−5	−4	190	36	−33
11	−5	−2	134	131	9	11	−2	0	121	119	7	12	−9	−2	67	75	−22	12	−5	−3	132	136	−53
11	−5	−1	202	193	6	11	−1	−7	99	78	9	12	−9	−1	69	51	−11	12	−5	−2	103	110	17
11	−5	0	140	140	7	11	−1	−6	116	92	−29	12	−9	0	90	102	−28	12	−5	−1	78	85	11
11	−5	1	170	42	−30	11	−1	−5	112	112	9	12	−9	1	123	108	11	12	−5	0	62	42	−19
11	−5	2	120	114	14	11	−1	−4	98	52	11	12	−9	2	111	93	8	12	−4	−6	203	23	−37
11	−4	−7	95	109	−20	11	−1	−3	65	58	−16	12	−8	−5	40	74	−29	12	−4	−5	180	50	−33
11	−4	−6	76	85	−17	11	−1	−2	109	103	−30	12	−8	−4	93	87	−18	12	−4	−4	131	114	10
11	−4	−5	170	20	−30	11	−1	−1	136	141	11	12	−8	−3	85	59	13	12	−4	−3	114	112	13
11	−4	−4	96	88	12	11	0	−6	96	80	14	12	−8	−2	89	82	10	12	−4	−2	83	90	−16
11	−4	−3	149	149	6	11	0	−5	75	58	−13	12	−8	−1	171	47	−30	12	−4	−1	177	36	−33
11	−4	−2	142	145	9	11	0	−4	82	59	9	12	−8	0	138	133	10	12	−4	0	92	84	−29
11	−4	−1	101	102	−16	11	0	−3	107	94	−18	12	−8	1	87	81	10	12	−3	−5	93	111	−32
11	−4	0	63	87	−15	11	0	−2	165	151	8	12	−8	2	108	93	17	12	−3	−4	74	95	−17
11	−4	1	109	127	10	12	−12	−1	102	83	−35	12	−7	−5	62	83	−21	12	−3	−3	91	68	12
11	−4	2	151	155	12	12	−12	0	135	123	−30	12	−7	−4	61	53	−19	12	−3	−2	54	36	−21
11	−3	−7	181	34	−33	12	−12	1	71	69	−17	12	−7	−3	66	56	−16	12	−3	−1	103	93	11
11	−3	−6	66	34	−15	12	−11	−3	73	66	−17	12	−7	−2	81	78	−19	12	−2	−4	181	53	−33
11	−3	−5	171	64	−30	12	−11	−2	121	112	18	12	−7	−1	112	107	−20	12	−2	−3	181	42	−33
13	−8	−2	77	47	−14	13	−8	−1	182	75	−33	13	−7	−2	82	88	−15						

Pergamon

PII: S0277–5387(97)00410–5

Polyhedron Vol. 17, No. 15, pp. 2563–2565, 1998
© 1998 Published by Elsevier Science Ltd
All rights reserved. Printed in Great Britain
0277–5387/98 $19.00+0.00

Transition metal-carbonyl labeling reagent containing iodoacetamido function: $CpFe(CO)_2$ [η^1-*N*(1)-4-iodoacetamidophthalimidato]-synthesis and reaction with the phenytoin and ethosuximide anions

Konrad Kowalski and Janusz Zakrzewski*

Department of Organic Chemistry, University of Łódź, 90-136 Łódź, Narutowicza 68, Poland

(Received 30 May 1997; accepted 1 October 1997)

Abstract—The first transition metal-carbonyl complex containing iodoacetamido function, $CpFe(CO)_2$[η^1-*N*(1)-4-iodoacetamidophthalimidato] was synthesized and used for labeling of two drugs: phenytoin and ethosuximide. © 1998 Published by Elsevier Science Ltd. All rights reserved

Keywords: metal-carbonyl; iodoacetamido; phenytoin anion; ethosuximide anion

Transition metal carbonyl complexes having substituents able to react selectively with functional groups present in molecules of biological and pharmacological interest, currently attract considerable interest as IR-detectable labeling reagents [1]. The detection of the bioconjugates is feasible in a pico- or subpicomole scale by virtue of very strong absorption bands corresponding to the ν(CO) modes, appearing at 2100–1850 cm^{-1} i.e. in the region which is generally free from other interferring absorptions, even in aqueous solutions and biological systems [2,3]. This approach was successfully applied for the labeling of haptens in immunoassays (CMIA-carbonylmetalloimmunoassay) [2], for labeling of steroid hormones for the study of hormone-receptor interaction [4], and labeling of oligonucleotides [5,6]. Most of the labeling procedures described up to now is based on organometallic complexes containing active *N*-hydroxysuccinimide ester function which reacts with the amino group present in the biomolecule and forming the amido bond. Another approach uses organometallic complexes having pyrylium system [7], or iminoester [8], as a reactive function (target function-NH_2).

We have recently reported the synthesis of $CpFe(CO)_2$(η^1-N-maleimidato), which contains a maleimide system reactive towards thiol groups and can be used for labeling of e.g. cysteine-containing peptides or proteins [9]. However, we have demonstrated that it can also label histidine and (in basic medium) lysine residues [10]. Another approach developed recently in our laboratory in collaboration with the Prof. Jaouen's group is the use of the $CpFe(CO)_2$– complexes of phthalimide containing in the 3- or 4-position isothiocyanato functions reactive towards amino groups [11].

In this communication we report the synthesis of the first metallocarbonyl marker containing the $CpFe(CO)_2$(η^1-N-phthalimidato) system and iodoacetamido group as the reactive function. This function is believed to be specific for thiols (cysteines), although it can also react with methionines (MeS-), histidines (imidazole) and lysines (NH_2) [12,13]. However, prompted by recent interest in the development of organometallic tracers for immunoassays of antiepileptic and sedative drugs [2,14,15], we decided to study the reactivity of our reagent toward anions of two important representants of this group of drugs: phenytoin (5,5-diphenylhydantoin) and ethosuximide (2-methyl-2-ethylsuccinimide).

We synthesized the bioconjugates of these products which are of interest as potential markers in carbonylmetalloimmunoassays (CMIA).

* Author to whom correspondence should be addressed.

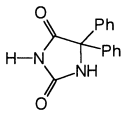

phenytoin

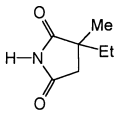

ethosuximide

Experimental

All reactions were carried out under argon. Dichloromethane was distilled from CaH_2. $CpFe(CO)_2[\eta^1$-*N*(1)-4-aminophthalimidato] (**1**) was prepared according to the earlier published procedure [11]. All reagents and other solvents (reagent grade) were used as received from Aldrich or Fluka. Column chromatographies were carried out using Kieselgel 60 (230–400 mesh ASTM) purchased by Merck. Instrumentation: IR-Specord 75 IR; ^{1}H NMR: Varian Gemini 200BB (200 MHz); FAB MS: Finnigan MAT 95. IR spectra were recorded in $CHCl_3$, ^{1}H-NMR in $CDCl_3$ and referenced to internal TMS, FAB spectra in m-nitrobenzyl alcohol matrices.

$CpFe(CO)_2(\eta^1$-*N*(1)-4-*iodoacetamidophthalimidato*) (**2**)

To a solution of **1** (310 mg, 0.92 mmol) in CH_2Cl_2 (5 ml) DCC (206 mg, 1.0 mmol) and iodoacetic acid (186 mg, 1.0 mmol) were added. After 1 h stirring at r.t. the solid formed was filtered off and the filtrate evaporated to dryness. Column chromatography (eluent $CHCl_3$) and crystallization (CH_2Cl_2-ether) gave **2** as yellow solid. Yield 386 mg (83%). IR (cm^{-1}): 2050 and 1995 cm^{-1} (Fe–CO), 1690 cm^{-1} (CO–amide), 1655 (CO–phthalimide), 1535 (amide-II). ^{1}H NMR ($CHCl_3$): 8.10, b, 1H, NH; 7.76, d ($J = 8.0$ Hz), 1H and 7.58, d ($J = 8.0$ Hz), 1H, H-5 and H-6; 7.69, s, 1H, H-3; 5.12, s, 5H, Cp; 3.90, s, 2H, CH_2. Residual ether (0.2 molecule) shows signals at 3.49, q and 1.22, t.

Analysis: Found: C, 40.61, H, 2.37; N, 5.83, I, 24.75. Calc. for $C_{17}H_{11}N_2O_5IFe \times 0.2\ C_4H_{10}O$: C, 40.35; H, 2.19; N, 5.54; I, 25.08.

Reaction of **2** *with Na-phenytoin*

A solution of **2** (102 mg, 0.20 mmol) and phenytoin (51 mg, 0.20 mmol) in 0.05 M NaOMe in MeOH (4 ml) was incubated at 50°C for 24 h, cooled to r.t. and poured to water (20 ml). The yellow precipitate was filtered off, dried under vacuum and recrystallized from CH_2Cl_2- pentane. Yield 107 mg (85%). IR (cm^{-1}): 2045, 1990 (Fe–CO); 1780, 1725 (phenytoin and amide CO); 1645 (phthalimide CO); ^{1}H-NMR: 9.11, bs, 1H (NH); 7.3–7.8, m, 13H (aromatic Hs); 5.07, s, 5H (Cp); 4.34, s, 2H (CH_2); FAB MS [positive ions, m/e (intensity)]: 631 (24%), M + H; 575 (56%), M + H-2CO. Elemental analysis: Found: C 61.08; H 3.72; N 8.82. Calc. for $C_{32}H_{22}N_4O_7Fe$: C 60.97; H 3.52; N 8.89.

Reaction of **2** *with Na-ethosuximide*

A solution of **2** (102 mg, 0.20 mmol) and ethosuximide (30 mg, 0.21 mmol) in 0.05 M NaOMe in MeOH (4 ml) was incubated at 50°C for 2 d, cooled to r.t., poured to water (20 ml) and extracted with dichloromethane (3×5 ml). The combined extracts were dried with sodium sulphate and evaporated to dryness to give yellow oil. The oil was dissolved in ether ($\sim$20 ml), diluted with hexanes and slowly concentrated *in vacuo* to give an yellow solid (53 mg, 51%). IR (cm^{-1}): 2045, 1990, (Fe–CO); 1775, 1720 (amide and succinimide CO); 1645 (phthalimide CO); ^{1}H-NMR: 8.32 bs, 1H, NH; 7.72, d ($J = 8$ Hz), 1H and 7.54, d ($J = 8$ Hz), 1H, H-5 and H-6; 7.67, s, 1H, H-3; 5.12, s, 5H, Cp; 4.38, s, 2H, $COCH_2$; 2.77, d ($J = 18$ Hz) 1H and 2.54, d ($J = 18$ Hz), 1H, succinimide ring CH_2, 1.82 m, 2H CH_2 (in Et); 1.38, s, 3H, Me; 0.94, t ($J = 7$ Hz), 3H, CH_3 (in Et); FAB MS [positive ions, m/e (intensity)]: 520 (26%), M + H; 464 (51%), M + H-2CO. Elemental analysis: Found: C 55.68; H 4.12; N, 8.32. Calc. for $C_{24}H_{21}N_3O_7Fe$: C 55.51; H 4.08; N, 8.09.

RESULTS AND DISCUSSION

Our results are summarized in Scheme 1.

We have found that readily accessible 4-aminophthalimidato complex **1** [11] readily reacts with iodoacetic acid and *N*,*N*′-dicyclohexylcarbodiimide (DCC) in dichloromethane at room temperature to give the 4-iodoacetamido derivative **2** in high yield. Its structure was confirmed by spectroscopic as well as elemental analyses data. The amino group in **1** can be therefore acylated under mild conditions and **1** is a potential labeling reagent for biomolecules containing carboxylic functions. This possibility, however, will be a subject of further studies.

The iodoacetamido complex **2** readily reacts with sodium salts of phenytoin and ethosuximide (prepared by dissolving of the corresponding NH acids in methanol containing the equimolar amount of sodium methoxide) to afford conjugates **3** and **4,** respectively. The structures of these complexes were confirmed by spectroscopic and elemental analysis data. Their FAB mass spectra (*meta*-nitrobenzyl alcohol as a matrix) display, in the positive ions mode, peaks corresponding to M + H and M + H-2CO ions and in the negative ions mode to M-H and M-H-2CO ions. ^{1}H NMR spectra of conjugates **3** and **4** show characteristic singlet of —$COCH_2N$— protons (4.44 ppm for **3** and 4.38 ppm for **4**), shifted downfield in comparison to the signal of the —$COCH_2I$ protons in **2** (3.90 ppm). The complexes **3** and **4** are yellow air-stable microcrystalline solids, soluble in polar organic

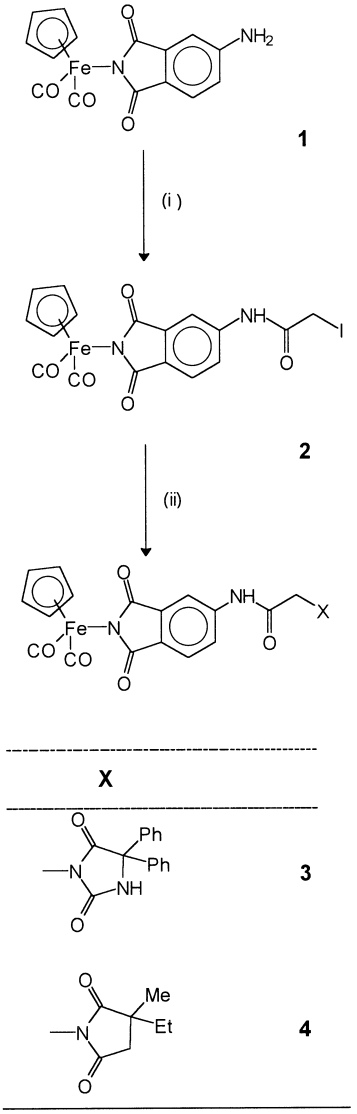

Scheme 1. (i) ICH_2COOH—DCC; (ii) phenytoin (ethosuximide)-CH_3ONa-CH_3OH.

solvents (ethanol, dimethylsulfoxide, dimethylformamide), in chloroform, and practically insoluble in water. Their IR spectra show very strong absorption bands at around 2050 cm^{-1} and 1990 cm^{-1} i.e. in the region where the detection is particularly sensitive [2,3].

Compound **2** as containing the iodoacetamido function is also a potential label for biomolecules containing HS-groups [12,13]. Feasibility of such labeling is currently under study in our laboratory.

Acknowledgement—This work was supported by a grant from the Polish State Committee for Scientific Research (KBN) : 3 T09A 008 08.

REFERENCES

1. Jaouen, G., Vessières, A. and Butler, I. S., *Acc. Chem. Res.*, 1993, **26,** 361.
2. Salmain, M., Vessières, A., Jaouen, G. and Butler, I. S., *Anal. Chem.*, 1991, **63,** 2323.
3. Varenne, A., Vessières, A., Salmain, M., Durand, S., Brossier, P. and Jaouen, G., *Anal. Biochem.*, 1996, **242,** 172.
4. Top, S., El Hafa, H., Vessières, A., Quivy, J., Vaissermann, J., Hughes, D. W., McGlinchey, M. J., Mornon, J.-P., Thoreau, E. and Jaouen, G., *J. Am. Chem. Soc.*, 1995, **117,** 8372.
5. Wang, Z., Roe, B. A., Nicholas, K. M. and White, R. L., *J. Am. Chem. Soc.*, 1993, **115,** 4399.
6. Dalla Riva Toma, J. M. and Bergstrom, D. E., *J. Org. Chem.*, 1994, **59,** 2418.
7. Malisza, K. L., Top, S., Vaissermann, J., Caro, B., Sénéchal-Tocquer, M.-C., Sénéchal, D., Saillard, J.-Y., Triki, S., Kahlal, S., Britten, J. F., McGlinchey, M. J. and Jaouen, G., *Organometallics*, 1995, **14,** 5273.
8. Blanalt, S., Salmain, M., Malezieux, B. and Jaouen, G., *Tetradron Lett.*, 1996, **37,** 6561.
9. Rudolf, B. and Zakrzewski, J., *Tetrahedron Lett.*, 1994, **35,** 9611.
10. Rudolf, B. and Zakrzewski, J., *J. Organomet. Chem.*, 1996, **522,** 313.
11. Kazimierczak, A., Zakrzewski, J., Salmain, M. and Jaouen, G., *Bioconjugate Chem.*, 1997, **8,** 489.
12. Lunblad, R., in *Proteins Labfax* (Edited by N. C. Price), pp. 287–298. Bios Scientific Publishers, Academic Press, San Diego (1996).
13. Brinkley, M., *Bioconjugate Chem.*, 1992, **3,** 2.
14. Varenne, A., Vessières, A., Salmain, M., Brossier, P. and Jaouen, G., *Immunoanal. Biol. Spec.*, 1994, **9,** 205.
15. Varenne, A., Vessières, A., Brossier, P. and Jaouen, G., *Res. Commun. Chem. Phatol. Pharmacol.*, 1994, **84,** 81.

Pergamon

PII : S0277–5387(97)00359–8

Polyhedron Vol. 17, No. 15, pp. 2567–2574, 1998
© 1998 Elsevier Science Ltd
All rights reserved. Printed in Great Britain
0277–5387/98 $19.00+0.00

Syntheses and characterization of diamine complexes of nickel(II) trifluoroacetate : thermochromism and X-ray single crystal structure analyses of $[Ni(pren)_2(CF_3CO_2)_2]$ and $[Ni(ipren)_2(CF_3CO_2)_2]$ (pren = N-propylethane-1,2-diamine and ipren = N-isopropylethane-1,2-diamine)

Debasis Das,[a] Golam Mostafa,[b] Ken-ichi Okamoto[c] and Nirmalendu Ray Chaudhuri[a]*

[a] Department of Inorganic Chemistry, Indian Association for the Cultivation of Science, Calcutta-700 032, India

[b] Department of Solid State Physics, Indian Association for the Cultivation of Science, Calcutta-700 032, India

[c] Department of Chemistry, University of Tsukuba, Tsukuba, Ibaraki-305, Japan

(Received 11 June 1997 ; accepted 15 August 1997)

Abstract—The complexes, $[NiL_2(CF_3CO_2)_2]$ [L = N-methylethane-1,2-diamine (meen), N-ethylethane-1,2-diamine (eten), N-propylethane-1,2-diamine (pren) and N-isopropylethane-1,2-diamine (ipren)] have been prepared and X-ray single crystal structures of $[Ni(pren)_2(CF_3CO_2)_2]$ **3** and $[Ni(ipren)_2(CF_3CO_2)_2]$ **4** are determined. Both **3** and **4** have slightly distorted *trans*-octahedral geometry with N_4O_2-chromophore around nickel(II). The crystals are stabilized by H-bonds and this interaction is higher in **4** due to close proximity of methyl H-atoms of isopropyl group with oxygen atoms of trifluoroacetate groups. The complexes **3** and **4** exhibit blue to light-violet, irreversible discontinuous thermochromism. $[Ni(meen)_2(CF_3CO_2)_2]$ **1** also shows thermochromism, blue-violet to blue but reverts on keeping in humid atmosphere. On the other hand, $[Ni(eten)_2(CF_3CO_2)_2]$ **2** undergoes decomposition without showing any phase transition. However, thermochromism here is considered to be due to a decreased in-plane ligand field strength resulting from the conformational changes in diamine chelate rings. © 1998 Elsevier Science Ltd. All rights reserved

Keywords: thermochromism ; N-propylethane-1,2-diamine ; N-isopropylethane-1,2-diamine ; X-ray single crystal analysis of nickel(II) ; nickel(II) trifluoroacetate ; conformational isomerism

Thermochromic phenomenon in diamine complexes of nickel(II) is well documented in the literature [1–12]. This usually takes place with (i) change in geometry/chromophore or (ii) retention of geometry/chromophore. The former is known from the inception of nickel-amine chemistry. It is observed that X-ray single crystal analyses are not usually essential to characterize the thermochromic isomers of the first kind as the routine physico-chemical measurements (magnetic susceptibility, electronic spectra etc.) are often enough to do the same and even help to interpret the mechanism of such thermochromism. On the other hand, thermochromism of the latter kind which was first reported by Pfeiffer *et al.* [13] in 1938, became popular in the early 1960s when some workers studied $M(diamine)_2X_2$ [M=Cu(II)/Ni(II) and X an anion]. It is evident that such thermochromism can only be characterized by X-ray single crystal analyses as in general the changes observed in magnetic, electronic

* Author to whom correspondence should be addressed.

spectral etc. measurements are not so detectable and the syntheses of suitable single crystals specially of high-temperature phase species are extremely difficult. However, Grenthe *et al.* [5] reported for the first time the X-ray single crystal analyses of both the low- and high-temperature phase species of bis-(*N*,*N*-diethylethane-1,2-diamine)copper(II) perchlorate and concluded that thermochromism of this kind was due to a decreased strength of in-plane ligand field, the mechanism which was first proposed by Hatfield *et al.* [14] in 1963. From the reports presented so far one can conclude that this type of thermochromism largely depends on the nature of the diamine as well as on the counter anion. Easily polarizable anions like I^-, Br^- etc. are observed to exhibit continuous thermochromism, whereas less easily polarizable anions like ClO_4^-, BF_4^- etc. show discontinuous thermochromism. However, studies on thermochromism with a less easily polarizable anion, $CF_3CO_2^-$ are scanty. Moreover, the thermochromic phenomena exhibited by nickel(II) complexes of $RNHCH_2CH_2NH_2$ (R = alkyl group) are not investigated systematically. In this context, studies of N-alkyl substituted diamine complexes of nickel(II) trifluoroacetate are relevant and here we report the syntheses and characterization of N-alkyl substituted diamine complexes of nickel(II) trifluoroacetate; X-ray single crystal structure analyses of $[NiL_2(CF_3CO_2)_2]$ (L = N-propyl/isopropylethane-1,2-diamine) and their thermochromism in the solid phase.

EXPERIMENTAL

Materials

High-purity N-methylethane-1,2-diamine (meen), N-ethylethane-1,2-diamine (eten), N-propylethane-1,2-diamine (pren) and N-isopropylethane-1,2-diamine (ipren) were purchased from Aldrich Chemical Company Inc. and used as received. All other chemicals were of analytical reagent grade.

Physical measurements

The thermal analyses (TG-DTA) were carried out using a Shimadzu DT-30 thermal analyser under a flow of nitrogen (flow rate : 30 $cm^3\ min^{-1}$). The sample (particle size of 150–200 mesh) was heated in a platinum crucible at a rate of 10°C min^{-1} with inert alumina as reference. The changes of phase transitions were calculated by a Perkin–Elmer DSC-7 differential scanning calorimeter using indium metal as calibrant (rate of heating/cooling, 10°C min^{-1}). Elemental analyses, IR-spectra (KBr, 4000–400 cm^{-1}), electronic spectra (Nujol mull), magnetic susceptibility and X-ray powder diffraction were done by a Perkin–Elmer 240C elemental analyser, a Perkin–Elmer IR 783, a Shimadzu UV 2100, an EG and G PAR 155 vibrating sample magnetometer and a Seifert XRD 3000P, respectively.

Syntheses of the complexes

$[Ni(meen)_2(CF_3CO_2)_2]$ **1** was prepared as reported earlier [15]. Analytical data were in well agreement with the previous report. All attempts to prepare single crystals suitable for X-ray analysis failed.

$[Ni(eten)_2(CF_3CO_2)_2]$ **2** was synthesized by adding the diamine (2 mmol) to nickel(II)trifluoroacetate hexahydrate dissolved in acetonitrile-butanol (1 : 1) mixture. The resulting solution was kept in a $CaCl_2$-desiccator and after a few days crystalline complex was separated out. It was filtered, washed with butanol and dried in a $CaCl_2$-desiccator. (Yield : 71% ; Found : C, 31.1 ; H, 5.2 ; N, 12.0 ; Ni, 12.7. Calc. for $C_{12}H_{24}N_4O_4F_6Ni$: C, 31.2 ; H, 5.2 ; N, 12.1 ; Ni, 12.7%) ; μ_{eff}, 3.11 B.M. ; λ_{max}(Nujol) 1088, 785, 565 and 352 nm). Here also no suitable single crystal for X-ray analysis was obtained.

$[Ni(pren)_2(CF_3CO_2)_2]$ **3** was prepared following the procedure adopted for complex **2** (Yield : 68% ; Found : C, 34.4 ; H, 5.7 ; N, 11.2 ; Ni, 12.0. Calc. for $C_{14}H_{28}N_4O_4F_6Ni$: C, 34.4 ; H, 5.7 ; N, 11.4 ; Ni, 12.0%) ; μ_{eff}, 3.14 B.M. ; λ_{max}(Nujol) 1135, 825, 562 and 358 nm. Single crystals suitable for X-ray analysis were obtained on crystallization of **3** from acetonitrile.

$[Ni(ipren)_2(CF_3CO_2)_2]$ **4** was obtained by adopting the same procedure as of complex **2** (Yield : 64% ; Found : C, 34.4 ; H, 5.7 ; N, 11.2 ; Ni, 12.0. Calc. for $C_{14}H_{28}N_4O_4F_6Ni$: C, 34.4 ; H, 5.7 ; N, 11.4 ; Ni, 12.0%) ; μ_{eff}, 3.13 B.M. ; λ_{max} (Nujol) 1167, 783, 578 and 383 nm. Single crystals suitable for X-ray measurement were prepared by following the procedure adopted for complex **3**.

Crystallography

Suitable single crystals of complexes **3** and **4** were mounted on a Rigaku/AFC 7 diffractometer. Setting angles for 25 accurately centred reflections were measured for both cases and lattice constants were obtained by least squares refinements. Crystal data were summarized in Table 1. Intensity data were collected using graphite monochromated Mo-K_α radiation ($\lambda = 0.7107$ Å) with ω-2θ scan mode. The stability of the crystal was measured during X-ray exposures by monitoring three standard reflections at a regular interval. In both cases all data were corrected for Lorentz and polarization effects. Empirical absorption corrections were made for both crystals using the ψ-scan method (T_{min}/T_{max} 0.857/0.999 for **3** and T_{min}/T_{max} 0.965/0.998 for **4**). The structures were solved by Patterson methods followed by Fourier syntheses. Anisotropic full-matrix least-squares refinements based on F were carried out on the non hydrogen atoms (TEXSAN) [16]. During the refinement both the crystal structures were found to be

Table 1. Crystallographic data for complexes **3, 3a, 4** and **4a**

	(**3**)	(**3a**)	(**4**)	(**4a**)
Molecular formula	X	X	X	X
Molecular weight	489.09	489.09	489.09	489.09
Crystal system	Monoclinic	Monoclinic	Monoclinic	Monoclinic
Space group	$P2_1/c$	$P2_1$	$P2_1/c$	$P2_1$
a (Å)	9.261(2)	8.52(1)	9.604(2)	8.89(2)
b (Å)	9.833(2)	10.99(2)	9.170(2)	8.75(2)
c (Å)	12.112(2)	10.84(2)	12.386(2)	12.84(3)
β (°)	102.20(1)	103.66(5)	94.11(1)	93.8(1)
v (Å^3)	1078.1(4)	986.3(4)	1087.9(3)	996.6(5)
Z	2	2	2	2
D_{calc} (mg m^{-3})	1.507	1.647	1.493	1.630
$F(000)$	508	508	508	508
Radiation	Mo-K_α	Cu–K_α	Mo-K_α	Cu–K_α
(λ, Å)	0.71073	1.5406	0.71073	1.5406
θ Range (°)	2.53–27.48	5.0–25.0	2.60–27.50	5.0–25.0
Crystal size (mm)	$0.5\times0.3\times0.2$	Powder	$0.35\times0.35\times0.35$	Powder
μ (mm^{-1})	0.977		0.968	
Transmission coefficent (max., min)	0.998, 0.965		0.999, 0.857	
Unique reflections	2622		2654	
Observed reflections				
$[I > 3(I)]$	1828		1656	
$R(F)$	0.039		0.0549	
$wR(F)$	0.0486		0.0356	
Goodness of fit	2.048		3.918	
Max. Δ/e.s.d.	0.03		0.124	
δ_{max}	0.23		0.68	
δ_{min}	−0.40		−0.73	
Weighting parameter (p)	0.00018		0.000	

$X = C_{14}H_{28}N_4O_4F_6Ni$; $R = \Sigma\|F_o| - |F_c\|/\Sigma|F_o|$; $wR = \Sigma w(F_o^2 - F_c^2)/\Sigma[w(F_o^2)^2]^{1/2}$,
$w = 1/[\sigma^2(F_o) + pF_o^2]$

disordered. In complex **3,** the three fluorine atoms of the trifluoroacetate group were distributed over a pair of three positions (F1, F2, F3; F1A, F2A, F3A) with equal site occupancy factor 0.5. In complex **4,** the following cases of disorder were observed: oxygen atom (O2) distributed over two positions O2 and O2A, with site occupancy ratio 0.75/0.25; the three fluorine atoms of the trifluoroacetate group distributed over two pairs of three positions (F1, F2, F3; F1A, F2A, F3A) with equal occupancy factor 0.5; each of the two diamine carbon atoms distributed over two positions (C2, C2A; C3, C3A) with site occupancy ratio 0.6/0.4 in each case. Hydrogen atoms were included in fixed calculated positions. Complex neutral scattering factors were used. All calculations were carried out using TEXSAN [16], PARST [17] and ORTEP-II [18] programs. Selected bond distances and angles are in Table 2.

Additional materials available from the Cambridge Crystallographic Data Centres comprises of lists of structure factors, all bond lengths and angles, coordinates and occupancy factors, thermal parameters and H-atom coordinates.

RESULTS AND DISCUSSION

The composition of the complexes were confirmed by elemental analyses. The complexes exhibit IR bands comparable to those of the diamine systems whose chelate character has been established by X-ray single crystal analyses [10,19]. The magnetic and electronic spectral data of the complexes are in good agreement with octahedral nickel(II), indicating that nickel(II) is surrounded by N_4O_2-chromophore in each complex. The Near-IR spectrum of each complex shows three bands suggesting D_{4h}-symmetry. Thus, the complexes are in the *trans*-configuration [20]. The solid state thermal property of $[Ni(meen)_2(CF_3CO_2)_2]$ **1** is found to be in good agreement with the work reported by us. Earlier [15], we omitted to observe the thermochromism, blue-violet-to-blue phenomenon associated with this phase transition. However, $[Ni(eten)_2(CF_3CO_2)_2]$ **2** upon heating does not show any phase transition before decomposition (initial temperature of decomposition, Ti = 122°C). On the other hand, blue complexes $[Ni(pren)_2(CF_3CO_2)_2]$ **3** and $[Ni(ipren)_2(CF_3CO_2)_2]$ **4** exhibit irreversible endo-

Table 2. Selected bond distances (Å) and angles (°) for complex **3** and **4**

	(3)	(4)
Ni···O1	2.088(3)	2.101(2)
Ni···N1	2.100(3)	2.089(2)
Ni···N2	2.109(4)	2.175(2)
N1···C1	1.475(5)	1.441(4)
C1···C2	1.516(6)	1.393(7)
C1···C2A		1.473(9)
N2···C2	1.506(5)	1.541(6)
N2···C2A		1.484(9)
N2···C3	1.466(5)	1.424(6)
N2···C3A		1.574(8)
O1···C6	1.227(5)	1.235(3)
O2···C6	1.230(5)	1.21(1)
O2A···C6		1.31(1)
C6···C7	1.486(7)	1.534(4)
O1···Ni···N1	93.7(1)	90.68(8)
O1···Ni···N2	89.5(1)	93.15(8)
N1···Ni···N2	83.9(1)	82.72(9)
Ni···O1···C6	131.8(3)	130.5(2)
Ni···N1···C1	108.0(3)	108.9(2)
Ni···N2···C2	105.6(3)	100.4(2)
Ni···N2···C3	120.1(3)	128.2(3)

thermic phase transition (86–112°C; $\Delta H = 13.2$ kJ mol^{-1} for **3** and 155–174°C; $\Delta H = 12.2$ kJ mol^{-1} for **4**) yielding light-violet species **3a** and **4a,** respectively (Figs 1 and 2). The species **3a** and **4a** retain their identity in solid state and revert only on crystallization from $CH_3OH/C_2H_5OH/CH_3CN$ etc. The complexes **3a** and **4a** on further heating undergo melting (190–200°C; $\Delta H = 23.6$ kJ mol^{-1} for **3a** and 208–216°C; $\Delta H = 21.8$ kJ mol^{-1} for **4a,** respectively) (Fig. 1). The melted species on cooling show exotherm with equal enthalpy changes as are observed during heating. Thus, the meltings are reversible in nature. It is evident from the thermal data that the temperature ranges and the value of enthalpy changes associated with phase transitions as well as melting for **3** and **4** have noticeable differences. This probably arises due to steric factors. However, the magnetic data of **3a** and **4a** do not differ from **3** and **4,** respectively. But there is a slight shift in the electronic band position on the thermochromic phase transitions to a shorter wavelength region [λ_{max}(Nujol) 1056, 818, 555 and 355 nm for **3a** and 1095, 765, 560 and 365 nm for **4a,** *vide supra*]. All these suggest that the *trans*-octahedral configuration is retained in **3a** and **4a**. Thus, it may be inferred that these phase transitions (**3** → **3a** and **4** → **4a**) are not associated with any change in geometry/chromophore around nickel(II). However, the IR-spectra of the pairs [(**3, 3a**) and (**4, 4a**)] show marked differences in the regions of 3300–3100, 3000–2800, 1400–1350, 1330–1000 and 1000–430 cm^{-1}, where the vibration of $\nu(NH_2)$, $\nu(CH_2)$, $\rho_w(CH_2)$, $\tau(NH_2)+\tau(CH_2)+\rho_w(NH_2)$ and $\rho_r(NH_2)+\nu$(M—N) appear. It is well documented that the five membered chelate rings formed by ethane-1,2-diamine (en) and its derivatives are not planar and due to this non-planarity they exist in either of two conformations delta (δ) or lambda (λ) in a chelate complex causing the existence of different conformational isomers [21]. As for example, in a *trans*-bis(en) complex, the (en) ring can form three conformational isomers $\delta\lambda$, $\delta\delta$ and $\lambda\lambda$ (of which the latter two are a mirror image to each other and identical in energy). We reported earlier two conformational isomers of $NiL_2(NCS)_2$ (L = *N,N′*-dimethylethane-1,2-diamine) [10] and characterized them by X-ray crystallography. They showed noticeable differences in IR-spectra in the regions as stated above. So it may be assumed that the members of the respective pair [(**3, 3a**) and (**4, 4a**)] are conformational isomers to each other.

The ORTEP views of the complexes **3** and **4** are given in Figs 3 and 4 showing the atom numbering scheme. Since the crystal structure of both the complexes are very similar, a general description of the structures is given. In both complex units of **3** and **4,** the nickel atom occupies a centre of inversion and displays slightly distorted octahedral coordination. Two trifluoroacetate groups are bonded to metal atom in *trans* positions. The four ligand nitrogen atoms (N1, N2 and their centrosymmetrically related ones) define the equatorial plane. The ligand moieties are monometallic, bidentate, resulting in a distorted octahedral coordination around Ni atom. The distortions of the coordination octahedra are due to the slight differences between equatorial Ni—N1 [2.100(3) Å for **3** and 2.089(2) Å for **4**] and Ni—N2 [2.109(4) Å for **3** and 2.175(2) Å for **4**] lengths as well as between endocyclic N1—Ni—N2 [83.9(1)° for **3** and 82.7(1)° for **4**] and exocyclic N1—Ni—N2 [96.1(1)° for **3** and 97.3(1)° for **4**] angles and slight deviation of the O1—Ni—O1* axis from orthogonality [range 86.3(1)° to 93.7(1)° for **3** and 86.9(1)° to 93.2(1)° for **4**] to equatorial plane. The Ni—N, Ni—O bond distances are consistent with the corresponding values of other analogous octahedrally coordinated Ni-complexes [10,22,23]. However, it is interesting to note that in complex **3** Ni—N2 distance is 2.109(4) Å, whereas, in complex **4** Ni—N2 distance is 2.175(2) Å. This reflects the differences in the electronic effects of the chain attached to metal atom via N2. The C—F distances and the large librational motion of F for both crystals call for comment. The mean C—F distance is 1.29(2) Å for complex **3** and 1.292(9) Å for **4**. Angles in CF_3 vary widely from the expected threefold symmetry. These values agree with CSD data base survey of trifluoroacetate group by Gleghorn *et al.* [24]. The large librational motion of F atom may be due to fairly free rotation of CF_3. In complex **3,** the five membered chelate rings display an open envelope geometry with the flap atom C2, 0.555(5) Å away from the least-square plane through the remaining endocyclic atoms. The chelate rings in complex **4** also

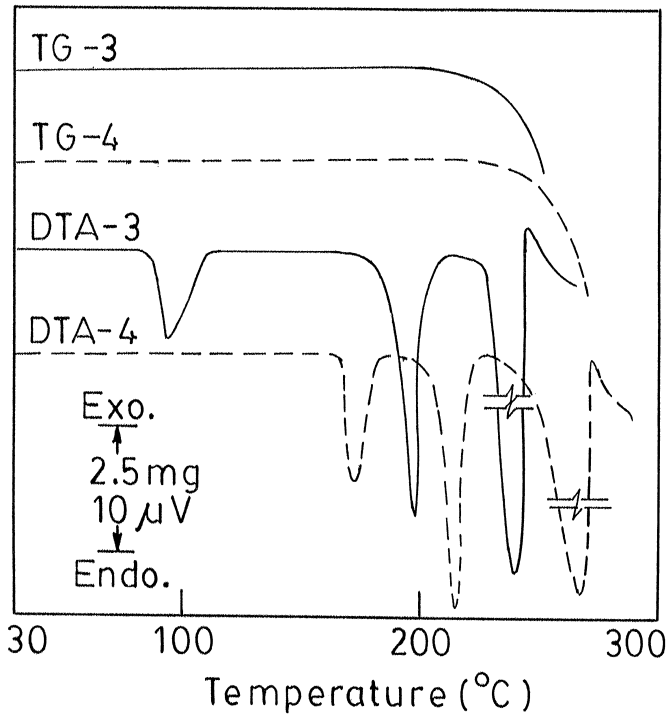

Fig. 1. TG-DTA curves for complex **3** (weight taken = 11.75 mg) (——) and complex **4** (weight taken = 11.45 mg) (- - - -).

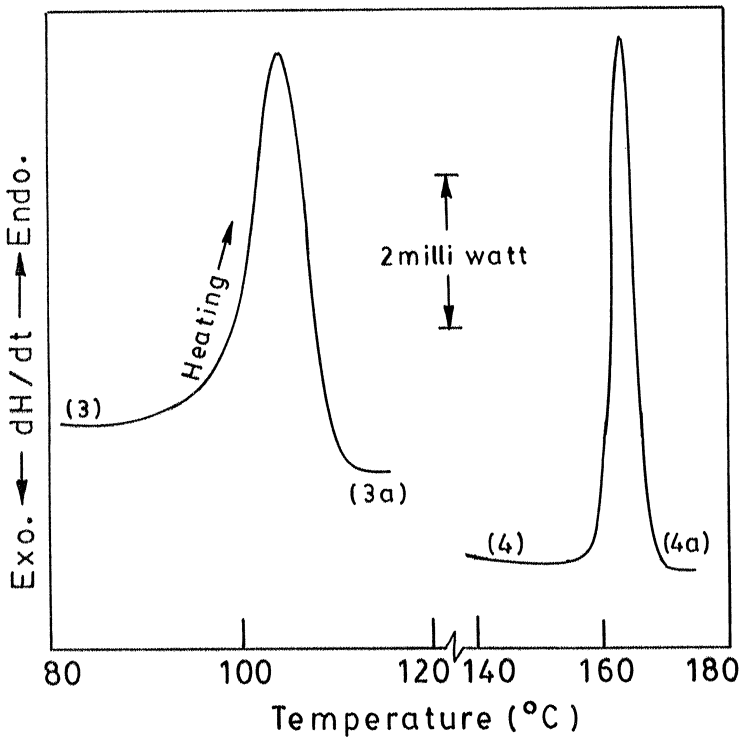

Fig. 2. DSC curves for complex **3** (weight taken = 7.85 mg) and complex **4** (weight taken = 7.65 mg).

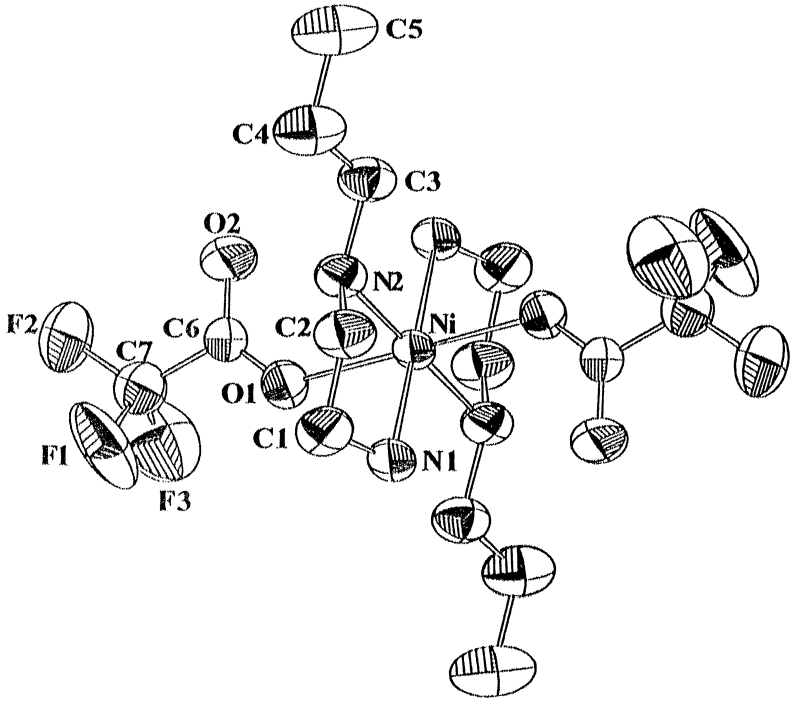

Fig. 3. An ORTEP[18] view of complex **3**.

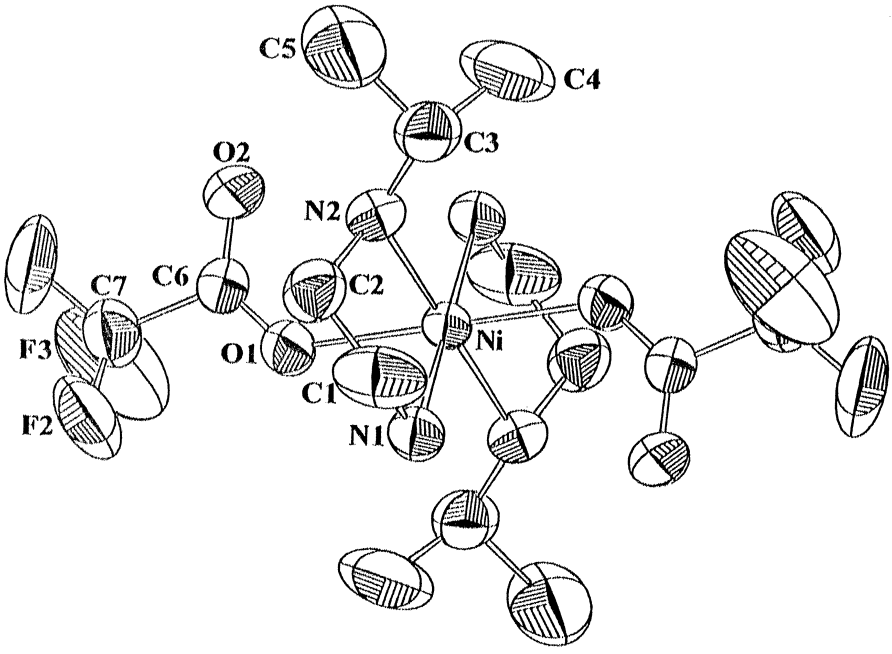

Fig. 4. An ORTEP[18] view of complex **4**.

display the pen envelope geometry with the flap atom C2 and C2A, 0.571(9) Å and 0.550(6) Å, respectively, away from the least square planes through the remaining atoms of the chelate rings. The dihedral angle of the planar parts of the two orientations of the chelate rings is 0.02°.

Crystal packing and hydrogen bonds

Both complexes **3** and **4** are stabilized mainly by intermolecular hydrogen bonds N—H···O which control the overall chelate ring conformations. The O2 atom of trifluoroacetate group of both **3** and **4** provides a potential hydrogen bond acceptor site (H···O2, 2.172(6) Å for **3** and 2.223(10) Å and H···O2A, 2.22(3) Å for **4**) in addition to amine N1 atoms. Other moderate intermolecular hydrogen bonds C4—H···O1, C4—H···N1, N2—H···O2 occur in complex **4**. Possible hydrogen bonds are listed in Table 3 with the widely accepted criteria that hydrogen bonds should be less than the sum of van der Waals radii of H and the acceptor atom.

The molecular packings of both crystals are dominated by strings of molecules along the *b* direction. The strings are held together by several intermolecular hydrogen bonding network. From the comparison of hydrogen bonding networks (Table 3) one may envisage that the hydrogen bonding system of complex **4** is much more extensive than that of complex **3**. This discrepancy is a consequence of bulky isopropyl groups in complex **4,** so that both C4 and C5 take part in hydrogen bonding. This may explain the higher temperature ranges for phase transition as well as melting exhibited by complex **4**.

Several attempts were made to obtain suitable single crystals of complexes **3a** and **4a** but they crystallized to **3** and **4,** respectively from solution. Thus we examined the complexes **3a** and **4a** by X-ray powder diffraction. Accurate d_{hkl} spacings (Å) were obtained from the powder patterns recorded on a Seifert XRD 3000P diffractometer at 30 kv and 30 mA with 2° min^{-1} scan rate. The initial cell parameters have been determined from powder diffraction data and accurate lattice parameters were obtained by least-squares refinements [25] (Table 1). Though it is difficult to comment on the mechanism of phase transition from X-ray powder data (deposited) the following observations are noteworthy. 0*k*0 data containing lines of both **3a** and **4a** show systematic absences with *k* odd but all *h*01 reflection types are present. The likely space group for both **3a** and **4a** is therefore $P2_1$. There are no drastic changes in the cell volume apart from a slight decrease (Table 1) and the systems remain monoclinic. Crystals of **3** and **4** with space group $P2_1/c$, $Z = 2$ and the molecules being centrosymmetric, the Ni-atoms assume the special positions. But with space group $P2_1$ the two molecules have to be distributed over two general equivalent positions.

Table 3. Hydrogen bonding geometry (Å, °)

Complex **3**			
D—H···A	D···A	H···A	<D—H···A
N1—H2···O2[1]	2.976(8)	2.172(6)	141.9(3)
N1—H1···O2[3]	3.018(6)	2.253(5)	136.8(2)
N2—H3···F2A[5]	3.34(4)	2.43(4)	161.6(9)
C1—H4···F2[7]	3.30(1)	2.56(1)	134.9(4)
C1—H5···F1[7]	3.49(2)	2.67(1)	145.4(4)
Complex **4**			
D—H···A	D···A	H···A	<D—H···A
N1—H2···O2[1]	3.000(10)	2.223(10)	138.5(3)
N1—H2···O2A[1]	3.02(3)	2.22(3)	142.3(8)
C4—H19···O1[1]	3.233(5)	2.434(2)	141.1(3)
C4—H17···N1(2)	3.448(7)	2.697(3)	136.6(4)
N2—H12···O2(2)	3.291(10)	2.520(9)	138.3(2)
C1—H5···O2(3)	3.216(9)	2.600(8)	122.8(3)
N1—H1···O2A(3)	3.09(3)	2.23(3)	149.7(7)
N1—H1···O2(3)	3.086(10)	2.329(10)	136.2(3)
C1—H4···F1A(4)	3.29(1)	2.56(1)	133.8(4)
C1—H4···F2(4)	3.28(1)	2.40(10)	153.4(3)
C2—H10···F3(5)	3.075(10)	2.459(8)	122.3(4)
C4—H20···F2A(6)	3.19(1)	2.48(1)	132.1(4)
C5—H25···F1(8)	3.38(2)	2.58(2)	142.0(5)

Symmetry codes:
(1) x,y,z; (2) $-x,-y,-z$; (3) $-x,+y-1/2,-z-1/2$; (4) $x,-y+1/2,+z-1/2$; (5) $x,+y-1,+z$; (6) $x,-y+1/2,+z+1/2$; (7) $x,-y+1/2,z-1/2$; (8) $-x+1,-y,-z$.

Then the molecules are no longer centrosymmetric. This may be explained as follows. In the lower temperature phase N—H···O and C—H···N bonds would be expected to hinder the bond rotation of trifluoroacetate group and the alkyl groups of the ligand moieties. In the transition to the high-temperature phases the H-bonds are weakened upon onset of hindered rotation and lead to a different molecular conformations. Due to the decrease of cell volume, the high-temperature molecular framework of both the crystals are more compact, making the transition irreversible.

CONCLUSIONS

The anion, $CF_3CO_2^-$, like other less easily polarizable anions ClO_4^-, BF_4^- etc. exhibits discontinuous thermochromism due to conformational changes of the diamine chelate rings. N-methylethane-1,2-diamine yields discontinuous thermochromism which is found to be time dependent reversible in nature, whereas N-propyl and N-isopropylethane-1,2-diamine exhibit irreversible thermochromism and N-ethylethane-1,2-dimine does not show any thermochromism likely to be due to overlapping with its decomposition temperature range. Thus, it may be concluded that steric and inductive effect exerted by *n*-propyl and isopropyl alkyl groups are optimum to exhibit irreversible discontinuous thermochromism in the nickel(II) trifluoroacetate system.

Acknowledgements—We thank Professor A. K. Pal, Department of Material Science, IACS, for electronic spectra and the Council of Scientific and Industrial Research (New Delhi) for financial support (NRC).

REFERENCES

1. Lifschitz, I., Bos, J. G. and Dijkema, K. M., *Z. Anorg. Allg. chem.* 1939, **242,** 97.
2. Ballhausen, C. J. and Liehr, A. D., *J. Am. Chem. Soc.* 1959, **81,** 538.
3. Nyburg, S. C. and Wood, J. S., *Inorg. Chem.* 1964, **3,** 468.
4. Kennedy, B. P. and Lever, A. B. P., *J. Am. Chem. Soc.* 1973, **95,** 6907.
5. Grenthe, I., Paoletti, P., Sandstrom, M. and Glikberg, S., *Inorg. Chem.* 1979, **18,** 2687.
6. Bloomquist, D. R. and Willett, R. D., *Coord. Chem. Rev.* 1982, **47,** 125.
7. Pylkki, R. J., Willett, R. D. and Dodgen, H. W., *Inorg. Chem.*,1984, **23,** 594.
8. De, G., Biswas, P. K. and Chaudhuri, Ray N., *J. Chem. Soc., Dalton Trans.* 1984, 2591.
9. Sone, K. and Fukuda, Y., *Inorganic Thermochromism*. Springer-Verlag, New York, 1987, p. 112.
10. Mukherjee, A. K., Mukherjee, M., Welch, A. J., Ghosh, A., De, G. and Chaudhuri, Ray N., *J. Chem. Soc., Dalton Trans.* 1987, 997.
11. Koner, S., Ghosh, A. and Chaudhuri, Ray N., *J. Chem. Soc., Dalton Trans.* 1990, 1563.
12. Das, D., Ghosh, A. and Chaudhuri, Ray N., *Polyhedron*, 1996, **15,** 3919.
13. Pfeiffer, P. and Glaser, H., *J. Prakt. Chem.*, 1938, **151,** 134.
14. Hatfield, W. E., Piper, T. S. and Klabunde, U., *Inorg. Chem.* 1963, **2,** 629.
15. Roy, S., Ghosh, A. and Chaudhuri, Ray N., *Thermochim. Acta* 1988, **136,** 191.
16. TEXSAN Crystal Structure Analysis Package, Molecular Structure Corporation, Houston, TX, 1985, 1992.
17. Nardelli, M., *Comput. Chem.* 1983, **7,** 95.
18. Johnson, C. K., ORTEP-II, Report ORNL-5138, Oak Ridge National Laboratory, Tennessee, 1976.
19. Nakamoto, K., *Infrared and Raman Spectra of Inorganic and Coordination Compounds*, 3rd edn. Wiley, New York, 1977, pp. 206–211 and references therein.
20. Lever, A. B. P., *Inorganic Electronic Spectroscopy*, 2nd edn. Elsevier, Amsterdam, 1984, ch. 6, pp. 507–520.
21. Corey, E. J. and Bailar, J. C. Jr., *J. Am. Chem. Soc.* 1959, **81,** 2620.
22. Pariya, C., Ghosh, S., Ghosh, A., Mukherjee, M., Mukherjee, A. K. and Chaudhuri, Ray N., *J. Chem. Soc. Dalton Trans.*, 1995, 337.
23. Pariya, C., Ghosh, S., Ghosh, A., Mukherjee, M., Mukherjee, A. K. and Chaudhuri, Ray N., *Polyhedron*, 1996, **15,** 1643.
24. Gleghorn, J. T. and Small, R. W. H., *Acta Cryst.* 1995, **B51,** 265.
25. Gabe, E. J., Le Page, Y., Charland, J. P., Lee, F. L. and White, P. S., *J. Appl. Cryst.* 1989, **22,** 384.

Pergamon

PII : S0277–5387(97)00188–5

Polyhedron Vol. 17, No. 15, pp. 2575–2580, 1998
© 1998 Elsevier Science Ltd
All rights reserved. Printed in Great Britain
0277–5387/98 $19.00+0.00

Hydrothermal synthesis and crystal structure of $(H_3NCH_2CH_2NH_3)[V(OH)(HPO_4)_2]\cdot H_2O$ with novel 1-D $\{V^{3+}—OH—V^{3+}\}$ polymeric chains

Yiping Zhang,[a,b] Christopher J. Warren,[a,1] Abraham Clearfield,[a]* Robert C. Haushalter[a,*,1]

[a] NEC Research Institute, 4 Independence Way, Princeton, NJ 08540, U.S.A.

[b] Department of Chemistry, Texas A&M University, College Station, TX 77843, U.S.A.

(Received 28 October 1996; accepted 5 May 1997)

Abstract—A new V^{III} vanadium phosphate, $(H_3NCH_2CH_2NH_3)[V(OH)(HPO_4)_2]\cdot H_2O$ (**1**), with a novel 1-D polymeric chain structure was prepared hydrothermally and its structure determined by X-ray diffraction. The structure consists of infinite $\{V(OH)(HPO_4)_2\}^{2-}$ chains, ethylenediammonium dications and lattice water molecules. The $\{V(OH)(HPO_4)_2\}^{2-}$ chains contain an infinite $\{V^{3+}—OH—V^{3+}\}$ backbone bridged by $(HPO_4)^{2-}$ groups. Each V^{3+} atom has a quite regular octahedral configuration containing four phosphate oxygens and two trans positioned OH groups. © 1998 Elsevier Science Ltd. All rights reserved

Keywords: vanadium phosphates; hydrothermal synthesis; X-ray crystal structure

The V/O/phosphate or arsenate system is dominated by three dimensional (3-D) and two dimensional (2-D) structures. Examples of lamellar vanadium phosphates include $VO(PO_4)\cdot 2H_2O$ [1], $VO(HPO_4)\cdot nH_2O$ [2,3], and a series compounds with the compositions of $M_{0.5}[VOPO_4]\cdot nH_2O$ [4–6] (M = Na, Ca, Sr, Pb, Co, Ni, Cu; $n = 2$, and M = K; $n = 1.5$). Among the known 3-D vanadium phosphates are the compounds $Ni_{0.5}[VOPO_4]\cdot 1.5H_2O$ [7], $Pb_{0.5}[VOPO_4]$ [8], and M_nVOPO_4 [9–15] (M = Li, Na, K, $n = 1$, and M = Ca, Ba; $n = 0.5$), while known examples of 1-D polymers of vanadium phosphates are provided by $NH_4(VO_2)(HPO_4)$ [15] and $VO(HPO_4)\cdot 4H_2O$ [16]. We have synthesized several novel vanadium phosphates with 2-D and 3-D framework structures through the introduction of organic templates or by the combination of both organic and inorganic cations in the reaction mixtures [17–20]. In addition, two organically templated 1-D vanadium arsenate polymers, $(H_2NC_4H_8NH_2)[(VO)_2(HAsO_4)_2(H_2AsO_4)_2]$ and $(H_3NCH_2CH_2NH_3)[V^{III}(HAsO_4)_2(H_2AsO_4)]\cdot H_2O$, have recently been isolated [21]. The structural diversity of the vanadium system results from the variation in the vanadium oxidation state and in the vanadium to phosphate or arsenate ratio. While V^{IV}-containing phosphates are very common, phosphates containing exclusively V^{III} are rare [22–25]. We report here the hydrothermal synthesis and single crystal structure of a V^{III} phosphate, $(H_3NCH_2CH_2NH_3)[V(OH)(HPO_4)_2]\cdot H_2O$ (**1**), which contains a novel polymeric chain structure.

EXPERIMENTAL

Synthesis of $(H_3N(CH_2)_2NH_3)[V(OH)(HPO_4)_2]\cdot H_2O$, (**1**)

The synthesis of the title compound was carried out in a polytetrafluoroethylene-lined stainless steel container under autogeneous pressure. The greenish plate-like crystals were obtained as a minor product ~5%) from hydrothermal reaction of VO_2, CuO, H_3PO_4, $H_2NCH_2CH_2NH_2$ and H_2O in a mole ratio of

* Authors to whom correspondence should be addressed.
[1] Present address: Symyx Technologies, 3100 Central Expressway, Santa Clara, CA 95051, USA.

1.0 : 0.7 : 6.9 : 3.6 : 265 at 160°C for 4 days with $(H_3N(CH_2)_2NH_3)_4[(V(H_2O)_2(VO)_6(OH)_2(HPO_4)_3(PO_4)_5]\cdot 3H_2O$ [26] as the major product. A higher yield of the title compound was obtained from the hydrothermal reaction of VO_2, H_3PO_4, $FeSO_4\cdot 7H_2O$, $H_2NCH_2CH_2NH_2$ and H_2O in the mole ratio of 1.0 : 7.3 : 0.5 : 3.7 : 256 at 160°C for 5 days. Under the latter reaction conditions, greenish needle-shaped crystals were isolated in about 50% yield based on vanadium. Small amounts of tiny black crystals (<5%), whose EDS analysis showed the presence of V (but not P), were also present as an impurity phase. Some of the needle-shaped crystals from this prep contained iron in varying amounts as indicated by EDS analysis, but there was no evidence of iron substitution at the vanadium sites in the final crystal structure solution. Although not completely understood, the presence of $FeSO_4\cdot 7H_2O$ seems to be necessary for the high yield synthesis of phosphate (**1**). Reactions done under similar conditions, but without $FeSO_4\cdot 7H_2O$, yielded different products.

Crystallography

A greenish plate-like crystal of the title compound having approximate dimensions of $0.2\times 0.2\times 0.05$ mm was mounted on a glass fiber. All measurements were made on a Rigaku AFC7R diffractometer with graphite monochromated Mo-K_α radiation and an 18 kW rotating anode generator. Cell constants and an orientation matrix for data collection, obtained from a least-squares refinement using the setting angles of 25 reflections in the range $20.53 \leqslant 2\theta \leqslant 26.78°$, corresponded to a triclinic cell. Based on the statistical analysis of intensity distribution, and the successful solution and refinement of the structure, the space group was determined to be $P\bar{1}$. The data were collected out to 60° in 2θ using the ω–2θ scan technique at a speed of 16°/min in ω. A total of 2223 reflections were measured of which 2022 were unique ($R_{int} = 0.039$). The intensities of three representative reflections were measured after every 150 reflections and remained constant throughout data collection. An empirical absorption correction based on ψ scans was applied to the data, and the data were corrected for Lorentz and polarization effects. The structure of (**1**) was solved by direct methods using the *teXsan* crystallographic software package from Molecular Structure Corporation [27]. All the non-hydrogen atoms were refined anisotropically, and no attempt was made to locate the hydrogen atoms. A high thermal parameter was observed for the water molecule in the structure of (**1**), and is likely indicative of partial occupancy. The final cycle of full-matrix least-squares refinement was based on 1329 observed reflections ($I \geqslant 3\sigma(I)$) and 157 variable parameters, and converged with unweighted and weighted agreement factors of $R = \Sigma\|F_o - |F_c\|/\Sigma|F_o| = 0.051$ and $R_w = (\Sigma\omega(|F_o| - |F_c|)^2/\Sigma\omega F_o^3)^{1/2} = 0.058$. Further details of the X-ray structural analysis are given in Table 1.

Table 1. Crystallographic data for $(H_3NCH_2CH_2NH_3)[V(OH)(HPO_4)_2]\cdot H_2O$

Empirical Formula	$VP_2O_{10}N_2C_2H_{15}$
F.W.	335.0
a (Å)	8.538(2)
b (Å)	9.835(3)
c (Å)	7.225(1)
α (°)	90.63(2)
β (°)	92.28(2)
γ (°)	65.43(2)
V (Å^3)	551.4(2)
Z	2
Space group	$P\bar{1}$
D_c (g/cm^3)	2.02
T (°C)	20 ± 1
λ (Mo-Kα) (Å)	0.7107
Trans. coeff.	0.897–0.994
No. reflections ($I \geqslant 3\sigma(I)$)	1329
No. Variables	157
R	0.051
R_w	0.058
Goodness of fit	1.19
Max. shift/error	0.02
Max. peak in final diff. map (e/Å^3)	0.94
Min. peak in final diff. map (e/Å^3)	−0.91

RESULTS AND DISCUSSION

Our continued investigation into the vanadium phosphate system has resulted in the synthesis of an unusual 1-D $\{V^{+3}—OH—V^{3+}\}$ polymeric chain material. The structure of $(H_3N(CH_2)_2NH_3)[V(OH)(HPO_4)_2]\cdot H_2O$ (**1**) consists of infinite $\{V(OH)(HPO_4)_2\}^{2-}$ chains, ethylenediammonium dications and lattice water molecules, which are all clearly visible in the unit cell view depicted in Fig. 1. The corner-shared hydroxide group (O(8)) is at nearly equal distances to the two V^{3+} centers with a V—O—V angle of 131.3(3)°, thus forming an infinite zig-zag {V—OH—V} chain which runs down the crystallographic c axis. As can also be seen in Fig. 1, there is an extensive hydrogen bonding scheme in this structure. The $\{V(OH)(HPO_4)_2\}^{2-}$ chains are hydrogen bonded to each other via the pendant P—OH groups along the crystallographic a axis with a short O(3)···O(6) contact of 2.605(8) Å. The lattice water molecule, O(10), is in contact with O(9) and the hydroxide group, [O(8)], with distances in the range of 2.77–2.86 Å. The chains are also hydrogen bonded to the NH_3^+ groups of the ethylenediammonium cations with all N···O distances less than 3 Å. Other bond distances and angles of interest can be found in Table 2.

The infinite $\{V(OH)(HPO_4)_2\}^{2-}$ chains of $(H_3N(CH_2)_2NH_3)[V(OH)(HPO_4)_2]\cdot H_2O$ (**1**) are more clearly depicted in Fig. 2. Each chain contains an

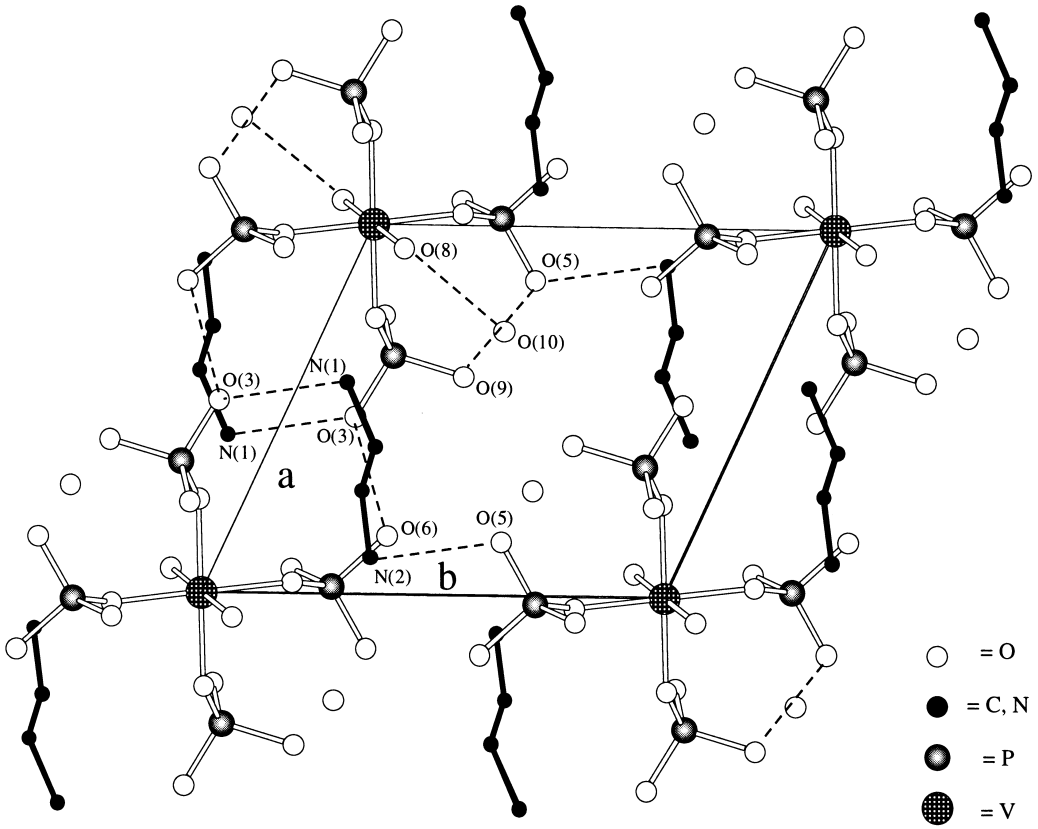

Fig. 1. A projection of the structure of $(H_3NCH_2CH_2NH_3)[V(OH)(HPO_4)_2]\cdot H_2O$ down the crystallographic c axis showing the ethylenediamine molecules, lattice water molecules, and the infinite chains of corner sharing VO_6 octahedra.

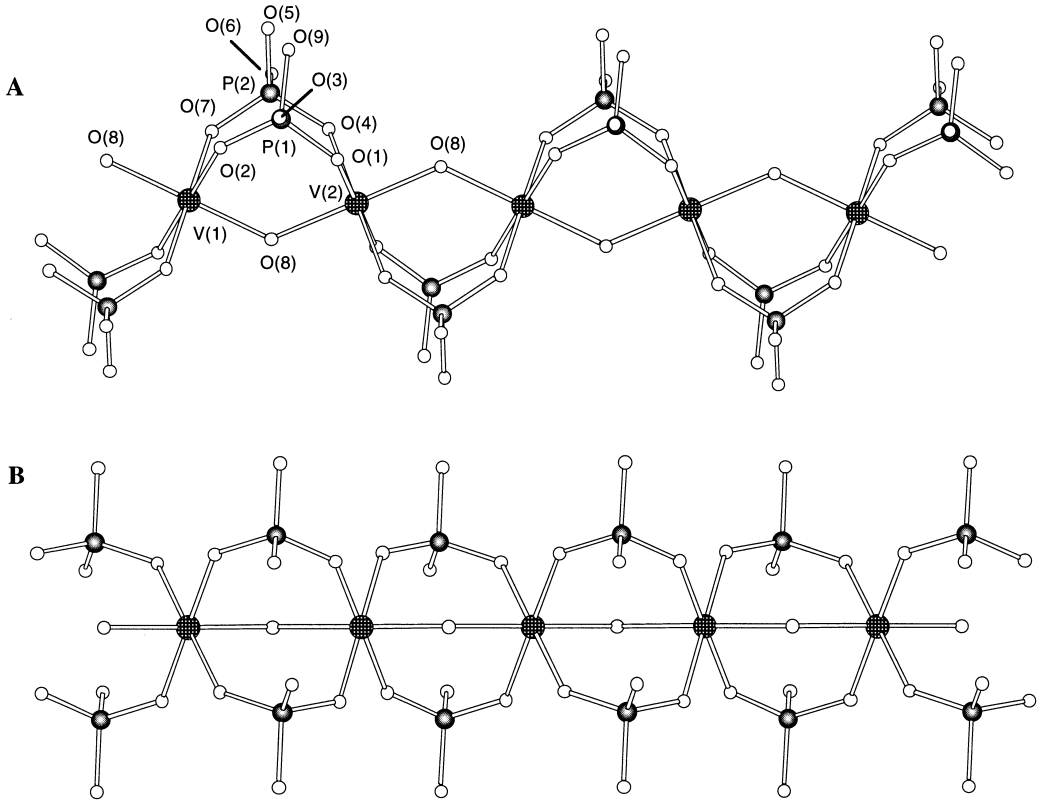

Fig. 2. Two perspective views of the polymeric chain of $\{V(OH)(HPO_4)_2\}^{2-}$ in the structure of $(H_3NCH_2CH_2NH_3)[V(OH)(HPO_4)_2]\cdot H_2O$.

Table 2. Selected bond lengths (Å) and angles (°) for $(H_3NCH_2CH_2NH_3)[V(OH)(HPO_4)_2]\cdot H_2O$

V(1)—O(2)	2.032(5)	P(1)—O(1)	1.517(5)
V(1)—O(2)A	2.032(5)	P(1)—O(2)	1.530(5)
V(1)—O(7)	2.016(5)	P(1)—O(3)	1.519(6)
V(1)—O(7)A	2.016(5)	P(1)—O(9)	1.573(6)
V(1)—O(8)	1.979(5)	P(2)—O(4)	1.528(5)
V(1)—O(8)A	1.979(5)	P(2)—O(5)	1.498(6)
V(2)—O(1)	2.014(5)	P(2)—O(6)	1.588(6)
V(2)—O(1)A	2.014(5)	P(2)—O(7)	1.521(5)
V(2)—O(4)	2.029(5)	N(1)—C(1)	1.50(1)
V(2)—O(4)A	2.029(5)	N(2)—C(2)	1.47(1)
V(2)—O(8)A	1.986(5)	C(1)—C(2)	1.51(1)
V(2)—O(8)C	1.986(5)		

O(2)A—V(1)—O(2)	180.0	O(1)A—V(2)—O(8)A	89.2(2)
O(2)A—V(1)—O(7)A	90.1(2)	O(4)—V(2)—O(4)A	180.0
O(2)A—V(1)—O(7)	89.9(2)	O(4)—V(2)—O(8)C	89.2(2)
O(2)A—V(1)—O(8)A	88.9(2)	O(4)—V(2)—O(8)A	90.8(2)
O(2)—V(1)—O(8)A	91.1(2)	O(4)A—V(2)—O(8)C	90.8(2)
O(2)—V(1)—O(7)A	89.9(2)	O(4)A—V(2)—O(8)A	89.2(2)
O(2)—V(1)—O(7)	90.1(2)	O(8)A—V(2)—O(8)C	180.0
O(2)—V(1)—O(8)A	91.1(2)	O(1)—P(1)—O(2)	111.0(3)
O(2)—V(1)—O(8)	88.9(2)	O(1)—P(1)—O(3)	111.3(3)
O(7)—V(1)—O(7)A	180.0	O(1)—P(1)—O(9)	109.6(3)
O(7)—V(1)—O(8)	89.4(2)	O(2)—P(1)—O(3)	110.3(3)
O(7)—V(1)—O(8)A	90.6(2)	O(2)—P(1)—O(9)	109.0(3)
O(7)A—V(1)—O(8)	90.6(2)	O(3)—P(1)—O(9)	105.4(3)
O(7)A—V(1)—O(8)A	89.4(2)	O(4)—P(2)—O(5)	112.8(3)
O(8)—V(1)—O(8)A	180.0	O(4)—P(2)—O(6)	107.1(3)
O(1)—V(2)—O(1)A	180.0	O(4)—P(2)—O(7)	111.1(3)
O(1)—V(2)—O(4)	92.4(2)	O(5)—P(2)—O(6)	102.9(3)
O(1)—V(2)—O(4)A	87.6(2)	O(5)—P(2)—O(7)	113.7(3)
O(1)—V(2)—O(8)C	89.2(2)	O(6)—P(2)—O(7)	108.6(3)
O(1)—V(2)—O(8)A	90.8(2)	V(1)—O(8)—V(2)	131.3(3)
O(1)A—V(2)—O(4)	87.6(2)	N(1)—C(1)—C(2)	108.9(7)
O(1)A—V(2)—O(4)A	92.4(2)	N(2)—C(2)—C(1)	109.4(7)
O(1)A—V(2)—O(8)C	90.8(2)		

infinite $\{V^{3+}—OH—V^{3+}\}$ backbone bridged by $(HPO_4)^{2-}$ groups. As can be seen in this figure, only two of the four oxygen atoms of each $(HPO_4)^{2-}$ group are bridged to two V^{3+} centers. Also, since each V^{3+} atom resides on an inversion center, it has a quite regular octahedral configuration containing four phosphate oxygens and two trans positioned OH groups. The six V—O bond distances for V(1) in the chains are in the range of 1.979(5)–2.032(5) Å, and the V—O bond distances for V(2) are in the range of 1.986(5)–2.029(5) Å. Such a regular octahedral coordination is indicative of V^{3+}, and this $+3$ oxidation state has in fact been confirmed by valence sum calculations.

It is interesting to note that the finite $\{V^{3+}—OH—V^{3-}\}$ chains in (**1**) are different from those in the structures of $(H_3NCH_2CH_2NH_3)[V^{III}(HAsO_4)_2(H_2AsO_4)]\cdot H_2O$ (**2**) and $(H_2C_4H_8NH_2)[(VO)_2(HAsO_4)_2(H_2AsO_4)_2]$ (**3**) [21]. While the infinite chains in arsenate (**2**) contain $V^{III}O_6$ octahedra bridged into 1-D chain *via* $(HAsO_4)$ and (H_2AsO_4) groups, these chains contain isolated VO_6 octahedra with no covalent $\{V—O—V\}$ intrachain connections. In (**2**), the two free vertices in the octahedra are compensated by two oxygen atoms from an additional bridging $\{AsO_4\}$ group. Similar chains to those in (**2**) are also found in the structure of a strontium vanadium phosphate $Sr_2[V^{III}(PO_4)_2(H_2PO_4)]$ [22]. The infinite chains in arsenate (**3**) are composed of corner sharing $V^{IV}O_6$ octahedra and $(HAsO_4)$ and (H_2AsO_4) tetrahedra. The backbone of these chains consists of $\{V^{4+}{=}O\cdots V^{4+}\}$ chains containing alternating short V=O vanadyl contacts of 1.627 Å and longer $V\cdots O$ distances of 2.248 Å *trans* to the vanadyl oxygen positions. Such corner sharing 1-D chains of $V^{IV}O_6$ octahedra are also found in the 3-D structures of $(NH_4)[(VO)(V_2O_3)(AsO_4)_2(HAsO_4)]$ [28] and $NH_4[VOPO_4]$ [29].

The $\{M^{3+}—OH—M^{3+}\}$ (M = Al, Fe) type chains found in (**1**) are fairly common in naturally occurring

minerals. Examples include sideronatrite $Na_2[Fe(SO_4)_2(OH)]\cdot 3H_2O$ [30], metasideronatrite $Na_2[Fe(SO_4)_2(OH)]$ [31], tancoite $LiNa_2H[Al(PO_4)_2(OH)]$ [32] and overite $Ca_2Mg_2[Al(PO_4)_2(OH)]_2\cdot 8H_2O$ [33]. The synthetic compound $Na_4[Al(PO_4)_2(OH)]$ [34] also contains chains of {Al—OH—Al} which are similar to those found in mineral tancoite.

Using the same organic template, ethylenediamine, but under different reaction conditions and with different vanadium sources, two open framework vanadium phosphates with very large tunnels in which protonated ethylenediamine molecules reside have been made [19,26]. In these reactions, ethylenediamine acts not only as a templating agent, but also as a reducing agent, which is responsible for the reduction of V^{5+} to V^{4+} under the hydrothermal conditions. In case of phosphate (**1**), however, it is not clear whether ethylenediamine is solely responsible for the reduction of V^{4+} to V^{3+}. Since EDS analysis showed that some of the crystal obtained from reactions with the presence of $FeSO_4\cdot 7H_2O$ contained small amounts of iron, it is possible that the presence of Fe^{2+} may have played a role in the reduction processes. Also, the fact that the content of iron differs from one crystal to another indicates that isomorphous substitution of iron for V^{3+} may have taken place. This kind of substitution is not unusual and has been observed in many compounds. In fact, the $\{Fe^{3+}—OH—Fe^{3+}\}$-type chains have been found in the layered structures of phosphate minerals like jahnsite. $CaMnMg_2[Fe(PO_4)_2(OH)]_2\cdot 8H_2O$ [35] and segelerite $Ca_2Mg_2[Fe(PO_4)_2(OH)]_2\cdot 8H_2O$ [33].

In summary, the isolation of $(H_3NCH_2CH_2NH_3)[V(OH)(HPO_4)_2]\cdot H_2O$ (**1**) provides another demonstration of the dramatic expansion of the structural and compositional range of the phosphate materials resulting from the incorporation of organic templates.

Acknowledgements—The work at Texas A&M University was supported by the National Science Foundation under grant No. DMR-9107715 for which grateful acknowledgement is made. We thank Professor A. K. Cheetham for providing us with the information on $Na_4[Al(PO_4)_2(OH)]$ before publication.

Supplementary materials available— Tables of atomic coordinates, bond lengths and angles, anisotropic displacement coefficients (16 pages), and observed and calculated structure factors (10 pages) for (**1**) are available on request.

REFERENCES

1. Tietze, H. R., *J. Austr. Chem.*, 1981, **34,** 2035.
2. Bail, A. L., Ferrey, G., Amoros, P. and Beltran-Porter, D., *Eur. Solid State Inorg. Chem.*, 1989, **26,** 419.
3. Johnson, J. W., Johnston, D. C., Jacobson, A. J. and Brody, J. F., *J. Am. Chem. Soc.*, 1984, **106,** 8123.
4. Wang, S. L., Kang, H. Y., Cheng, C. Y. and Lii, K. H., *Inorg. Chem.*, 1991, **30,** 3496.
5. Kang, H. Y., Lee, W. C., Wang, S. L. and Lii, K. H., *Inorg. Chem.*, 1992, **31,** 4743.
6. Lii, K. H., Wu, L. S. and Gau, H. M., *Inorg. Chem.*, 1993, **32,** 4153.
7. Lii, K. H. and Mao, L. F., *J. Solid State Chem.*, 1992, **96,** 436.
8. Grandin, A., Chardon, J., Borel, M. M., LeClaire, A. and Raveau, B., *Acta Crystallogr.*, 1992, **C48,** 1913.
9. Lii, K.-H., Li, C.-H., Chen, T.-M. and Wang, S.-L., *Z. Kristallorg.*, 1991, **197,** 67.
10. Lavrov, A. V., Nikolaev, V. P., Sadikov, G. G. and Poraikoshits, M. A., *Sov. Phys. Dokl. Engl. Ed.*, 1982, **27,** 680.
11. Lii, K. H., Li, C. H., Cheng, C. Y. and Wang, S. L., *J. Solid State Chem.*, 1991, **95,** 352.
12. Lii, K. H., Cheuh, B. R., Kang, H. Y. and Wang, S. L., *J. Solid State Chem.*, 1992, **99,** 72.
13. Phillips, M. L. F., Harrison, W. T. A., Gier, T. E., Stucky, G. D., Kulkarni, G. V. and Burdett, J. K., *Inorg. Chem.*, 1990, **29,** 2158.
14. Lii, K. H. and Tsai, H. J., *J. Solid State Chem.*, 1991, **90,** 291.
15. Amoros, P. and Bail, A. L., *J. Solid State Chem.*, 1992, **97,** 283.
16. Leonowicz, M. E., Johnson, J. W., Brody, J. F. Shannon, H. F. and Newsam, J. M., *J. Solid State Chem.*, 1985, **56,** 370.
17. Soghomonian, V., Haushalter, R., Chen, Q. and Zubieta, *J. Inorg. Chem.*, 1993, **33,** 1700.
18. Soghomonian, V., Chen, Q., Haushalter, R. C., Zubieta, J., O'Connor, C. J. and Lee, Y.-S., *Chem. Mater.*, 1993, **5,** 1690.
19. Soghomonian, V., Chen, Q., Haushalter, R. C. and Zubieta, J., *Angew. Chem. Int. Ed. Engl.*, 1993, **32,** 610.
20. Soghomonian, V., Haushalter, R. C., Chen, Q. and Zubieta, J., *Chem. Mater.*, 1994.
21. Haushalter, R., Meyer, L., Dhingra, S., Wang, Z., Thompson, M. and Zubieta, J., *Chem. Mater.*, 1994, **6,** 1463.
22. Lii, K.-H., Lee, T.-C., Liu, S.-N. and Wang, S.-L., *J. Chem. Soc., Dalton Trans*, 1993, 1051.
23. Haushalter, R. C., Wang, Z., Thompson, M. E. and Zubieta, J., *Inorg. Chem.*, 1993, **32,** 3700 and refs therein.
24. Lii, K.-H., Wen, N.-S., Su, C.-C. and Chen, B.-R., *Inorg. Chem.*, 1992, **31,** 439.
25. Vaughey, J.T., Harrison, W. T. A., Jacobson, A. J., Doshorn, D. P. and Johnson, J. W., *Inorg. Chem.*, 1994, **33,** 2482.
26. Zhang, Y., Clearfield, A. and Haushalter, R. C., *Chem. Mater.*, 1995, **7,** 1221.
27. teXsan: X-ray Structural Analysis Package. Molecular Structure Corporation, The Woodlands, TX, 1992 (revised).
28. Haushalter, R. C., Meyer, L., Dhingra, S., Thompson, M., Wang, Z. and Zubieta, J., *Inorg. Chim. Acta*, 1994, **218,** 59.
29. O'Connor, C. J., Soghomonian, V., Haushalter, R. C., Wang, Z. and Zubieta, J., *J. App. Phys.*, 1994, **75,** 5859.
30. Scordari, F., *Tschermaks Min. Petr. Mitt.*, 1981, **28,** 315.

31. Scordari, F. and Milella, G. N., *Jb. Min. Mh.*, 1982, 255.
32. Hawthorne, F. C., *Tschermaks Min. Petr. Mitt.*, 1983, **31,** 121.
33. Moore, P. B. and Araki, T., *Amer. Min.*, 1977, **62,** 692.
34. Attfield, M. P., Morris, R. E., Bursshtein, I., Campana, C. F. and Cheetham, A. K., *J. Solid State Chem.*, 1995, **118,** 412.
35. Moore, P. B. and Araki, T,, *Amer. Min.*, 1974, **59,** 964.

Pergamon

Polyhedron Vol. 17, No. 15, pp. 2581, 1998
© 1998 Elsevier Science Ltd
All rights reserved. Printed in Great Britain
0277–5387/98 $19.00 + 0.00

PII : S0277–5387(97)00437–3

BOOK REVIEW

Gmelin Handbook of Inorganic and Organometallic Chemistry, 8th Edition, Supplement Volume B 9. Ternary and Quaternary Si(H)F—O, Si(H)F—N, and SiF(—O)—N Compounds, Derivatives Substituted at O and N, and Fluorosilicate Salts of O- and N-Based Cations. Springer-Verlag, Berlin, 1997. 289 + xv pages. Price DM 1740. (ISBN 3-540-93750-1).

This volume is the third and last instalment of Gmelin Supplements dealing with silicon-fluorine compounds. Binary Si—F species were the subject of Volume B 7 and ternary Si—F—H compounds of Volume B 8. Now it is the turn of compounds which all contain silicon linked to fluorine and also to nitrogen, to oxygen or to both nitrogen and oxygen; such compounds which additionally have Si—H bonds are also included. This definition is taken to include not only adducts of Si—F_x species with N- and O-donors, such as $SiF_4 \cdot 2NH_3$, but also those salts in with an SiF_x^{n-} anion is associated with an ammonium or substituted ammonium cation, such as $(PhNH_3)_2^+(SiF_6)^{2-}$. Because of the classification system used in Gmelin, no compounds with Si—C bonds are included. This explanation of the actual contents may reassure those worried by the length of the volume's title. The literature coverage effectively dates from 1959 to 1995, although some papers published up to November 1996 have been considered; this represents commendably rapid publication, given the complexity of a book of this type.

Perhaps a volume of Gmelin does not always suggest itself as ideal bedtime reading, yet here may be found many intriguing nuggets of information and pointers to further research. For example, $(NH_4)_2SiF_6$ can be found as a crystalline mineral, resulting from volcanic activity or burning coal mines—unsuitable experimental conditions for the laboratory, however. Also a polymer of claimed composition $(FSiN)_x$, first prepared over 20 years ago, has recently appeared in a patent as a protective semiconducting layer in the manufacture of LCD devices. Another patent describes how a substituted pyridyldiazonium salt $(RN_2)_2SiF_6$ may be used in the synthesis of pharmaceuticals. The major areas of coverage relate to adducts of SiF_4 with N-bases, fluorosiloxanes such as $SiF_3O(SiF_2O)_nSiF_3$ ($n = 0, 1, 2, \ldots$), alkoxysilanes $SiF_n(OR)_{4-n}$ ($n = 1$–3), corresponding aminosilanes $SiF_n(NR^1R^2)_{4-n}$ ($n = 1$–3; R^1 = H or organyl), cyclosilazanes $[F_2SiNR]_2$, *Si*-fluorosilatranes, and salts of SiF_5^- and SiF_6^{2-} with $[(N\text{-Base})H]^+$ cations. Besides these main categories, however, there is a miscellany of other compounds, some of which were reported in the 1960s and 1970s and could helpfully be reinvestigated using modern techniques. The theoreticians have been active in this whole field, too; here there are calculations which provide structures, thermodynamic data, bond dissociation energies, and likely reaction paths for small molecules such as $F_2Si{=}O$, $FSi{\equiv}N$, and F_3SiNH and even large molecules like $H_3SiNSiF_2N(SiH_3)SiF_2$. Practical applications are not forgotten: the fluoroalkoxysilane $SiF(OC_2H_5)_3$, for instance, can act as a precursor for chemical vapour deposition of Si/O/F thin films, and also enters into sol-gel processes for making special glasses or preceramic polymers.

This volume is written by a group of Gmelin staff, together with U. Klingebiel (Göttingen), and edited overall by R. Haubold and F. Schröder. It fully maintains the high reputation of these volumes for meticulous accuracy, completeness and critical appraisal of the extensive literature.

B. J. AYLETT
Queen Mary and Westfield College
London E1 4NS, U.K.

Pergamon

PII: S00277-5387(98)00275-1

Polyhedron Vol. 17, No. 16, pp. 2583–2586, 1998
© 1998 Elsevier Science Ltd
All rights reserved. Printed in Great Britain
0277–5387/98 $19.00+0.00

Synthesis and structure of a homoleptic rhenium thiolate cluster

Wei-Wei Zhuang[a], David M. Hoffman[a]*, Dimitrios Lappas[b] and Jeremy Cohen[b]

[a]Department of Chemistry, University of Houston, Houston, TX 77204, U.S.A.

[b]Department of Chemistry, Harvard University, Cambridge, MA 02138, U.S.A.

(Received 22 March 1997; accepted 12 June 1997)

Abstract—Rhenium(III) chloride reacts with sodium isopropylthiolate to give the homoleptic rhenium thiolate cluster $Re_3(\mu\text{-}SPr^i)_3(SPr^i)_6$ in moderate yield. Proton and ^{13}C NMR spectra indicate the cluster has virtual C_s symmetry in solution due to the high barrier to inversion for the three-coordinate sulfur atoms at the bridging sites. The Re–Re bond distances are longer than those in analogous alkoxide clusters. © 1998 Elsevier Science Ltd. All rights reserved

Keywords: rhenium ; cluster ; thiolate.

INTRODUCTION

We recently reported the synthesis of the homoleptic rhenium alkoxide clusters $Re_3(\mu\text{-}OPr^i)_3(OPr^i)_6$ and $Re_3(\mu\text{-}OCH_2Bu^t)_3(OCH_2Bu^t)_6$ (**I**) [1–3]. Both act as

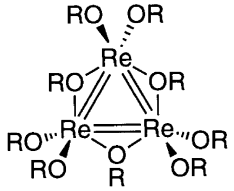

I

sources of terminal monohydride clusters, $Re_3(\mu\text{-}OR)_3H(OR)_5$, from which an extensive Re–H insertion chemistry can be generated [1–5]. The homoleptic neopentoxide cluster also reacts with ethyne to give $Re_3(\mu\text{-}HCCH)(\mu\text{-}OCH_2Bu^t)_2(OCH_2Bu^t)_7$, an unusual cluster in which the Re–Re multiple bonds appear to be involved in the Re–ethyne bonding [5, 6]. The extensive reactivity observed for the alkoxide clusters prompted us to attempt the synthesis of a thiolate analog. Surprisingly, the only structurally characterized homoleptic rhenium thiolate complexes in the literature are the trigonal prismatic chelate complexes $Re(SC(Ph)=C(Ph)S)_3$ and $[Re(MeC(CH_2S)_3)_2]^-$ [7, 8]. Other structurally characterized metal–organic rhenium compounds with exclusively sulfur coordination include $[Re(1,4,7\text{-trithiacyclononane})_2]^{2+}$ [9], $[Re(S)(SCH_2CH_2S)_2]^-$ [10], $[Re_2(\mu\text{-}S\text{-}S_2CNMe_2)_2(S_2CNMe_2)_3]^+$, $[Re(\eta^2\text{-}S_2CNMe_2)_4]^+$, and $[Re(\mu\text{-}S)(\eta^2\text{-}S_2CNBu^i_2)_2]_2$ [11].

We report here the synthesis, solution characterization and X-ray crystal structure determination of $Re_3(\mu\text{-}SPr^i)_3(SPr^i)_6$.

EXPERIMENTAL

All manipulations were carried out in a nitrogen-filled glove box or by using standard Schlenk techniques. Solvents were purified by standard techniques and then stored in the glovebox over molecular sieves until they were needed. Rhenium metal was purchased from Cleveland Refractory Metals and $Re_3(\mu\text{-}Cl)_3Cl_6(THF)_3$ was prepared as described in the literature [12–14]. Proton and ^{13}C NMR spectra were referenced internally to solvent proton and carbon-13 resonances, respectively. The spectra were collected on a 300-MHz instrument. Elemental analyses were performed by Oneida Research Services, Whitesboro, NY.

* Author to whom correspondence should be addressed.

Synthesis of $Re_3(\mu\text{-}SPr^i)_3(SPr^i)_6$

Sodium isopropylthiolate (1.6 g, 16 mmol) was added to a red solution of $Re_3Cl_9(THF)_3$ (2.0 g, 1.8 mmol) in THF (140 cm^3). The mixture was refluxed for 2 days, and the solvent was then removed under reduced pressure. The residue was extracted with hexanes ($5 \times 20\ cm^3$), and the extracts were combined and filtered through Celite. The filtrate was taken to dryness *in vacuo* and the residue was dissolved in a mixture of CH_2Cl_2 and CH_3CN (5:1). The solution was concentrated to about 5 cm^3 and the flask was then transferred to a freezer ($-35°C$) where red crystals formed over a period of 2 days (yield 0.65 g, 58%). Found: C, 26.4; H, 5.0. Calc. for $Re_3S_9C_{27}H_{63}$: C, 26.7; H, 5.1%.

^1H NMR ($CDCl_3$): δ 1.06 (d, 6, $J_{HH} = 6.9$ Hz, SCHMe_2), 1.09 (d, 6 $J_{HH} = 7.2$ Hz, SCHMe_2), 1.25 (d, 6, $J_{HH} = 6.9$ Hz, SCHMe_2), 1.31 (d, 6, $J_{HH} = 6.9$ Hz, SCHMe_2), 1.39 (d, 6, $J_{HH} = 6.9$ Hz, SCHMe_2), 1.50 (d, 6 $J_{HH} = 6.6$ Hz, SCHMe_2), 1.69 (d, 6, $J_{HH} = 6.6$ Hz, SCHMe_2), 1.75 (d, 6, $J_{HH} = 6.6$ Hz, SCHMe_2), 1.84 (d, 6, $J_{HH} = 6.6$ Hz, SCHMe_2), 3.27 (septet, 1 $J_{HH} = 6.6$ Hz, SC*H*Me_2), 3.84 (septet, 3, $J_{HH} = 6.6$ Hz, SC*H*Me_2), 4.01 (septet, 2, $J_{HH} = 6.6$ Hz, SC*H*Me_2), 4.50 (septet, 1, $J_{HH} = 6.6$ Hz, SC*H*Me_2), 4.57 (septet, 2 $J_{HH} = 6.6$ Hz, SC*H*Me_2), $^{13}C\{^1H\}$ NMR ($CDCl_3$): δ 25.6 (2, SCHMe_2), 25.9 (2, SCHMe_2), 26.7 (2, SCHMe_2), 27.4 (2, SCHMe_2), 28.0 (2, SCHMe_2), 28.3 (2, SCHMe_2), 28.4 (4, SCHMe_2), 28.7 (2, SCHMe_2), 32.5 (1, S*C*HMe_2), 37.5 (2, S*C*HMe_2), 38.0 (1, S*C*HMe_2), 44.2 (2, S*C*HMe_2), 44.3 (2, S*C*HMe_2), 47.1 (1, S*C*HMe_2). IR (Nujol, KBr, cm^{-1}): 1306 w, 1304 w, 1236 s, 1150 s, 1040 m, 984 w, 914 m, 799 w, 723 m, 594 w.

Crystal structure determination

The crystals for study were grown from a concentrated CH_2Cl_2/MeCN solution at $-35°C$ over a period of one month.

Crystal data. $C_{27}H_{63}S_9Re_3 \cdot CH_2Cl_2$, $M = 1319.97$, monoclinic, space group $P2_1/n$, $a = 13.327(3)$, $b = 16.868(6)$, $c = 21.352(6)$ Å, $\beta = 102.62(2)°$, $U = 4684$ Å^3, $T = -50°C$, Mo-K_α ($\lambda = 0.71073$ Å), $Z = 4$, $D_c = 1.87\ g\,cm^{-3}$, $F(000) = 2544$, $\mu = 83.61\ cm^{-1}$. Crystal size: $0.30 \times 0.50 \times 0.60$ mm.

Data collection. The magenta-colored irregular blocks were manipulated under mineral oil. Nicolet R3m/V diffractometer equipped with a low-temperature device, ω mode with scan width $\Delta\theta = 1.30 + (K\alpha_2 - K\alpha_1)°$, scan speed range 1.5–15.0° min^{-1}, graphite-monochromated Mo-K_α radiation; 6615 reflections measured ($4° \leqslant 2\theta \leqslant 45°$, h, k, $\pm l$), 4567 independent with $I > 3\sigma(I)$. Lorentz and polarization corrections were applied as well as semi-empirical absorption corrections based on psi scans of ten reflections having chi angles between 70 and 90°. Two standard reflections were measured every two hours or after every 100 data collected, and these showed no significant variation.

Structure solution and refinement. The Laue symmetry was determined to be 2/m and the space group was shown to be $P2_1/n$. The structure was solved by interpretation of the Patterson map, which revealed the positions of the three independent Re atoms. Remaining nonhydrogen atoms were found in subsequent difference Fourier syntheses. The hydrogen atoms were placed in calculated positions and constrained to riding motion, with a single variable isotropic temperature factor for all of them. Two of the isopropyl groups (C4 and C13) were found to be significantly disordered, and these were treated by substituting two ideal rigid bodies having 50% occupancy at each site and allowing them to rotate independently. Additionally, a heavily disordered molecule of methylene chloride solvent was located, and eventually it was refined as three ideal rigid bodies each having 1/3 occupancy. After all shift/esd ratios were less than 0.1 (except for the rigid bodies) convergence was reached with R, $R_w = 0.048$, 0.049. The weighting scheme was $w = [\sigma(F)]^{-2}$ (GOF = 2.18). No unusually high correlations were noted between any of the variables in the last cycle of full-matrix least squares refinement except between variables in the disordered methylene chloride solvent. The final difference density map showed a maximum peak of about 1.50 e/Å^3 located near Re. All calculations were made using Nicolet's SHELXTL PLUS (1987) package of programs [15].

Tables of final atomic coordinates, bond distances, bond angles, torsion angles, anisotropic thermal parameters, least-squares planes and calculated H-atom positions, as well as a packing diagram, have been deposited with the Editor.

RESULTS AND DISCUSSION

The halide $Re_3(\mu\text{-}Cl)_3Cl_6(THF)_3$ reacts with $NaSPr^i$ in refluxing THF to give $Re_3(\mu\text{-}SPr^i)_3(SPr^i)_6$ as red crystals in moderate yield after a workup that includes crystallization from CH_2Cl_2/MeCN. Attempted preparations of other derivatives, including phenyl thiolate and substituted phenyl thiolate derivatives, failed to give clean products.

The room temperature ^1H NMR spectrum of $Re_3(\mu\text{-}SPr^i)_3(SPr^i)_6$ consists of nine sharp equal-intensity doublets and five septets in a 3:2:2:1:1 ratio arising, respectively, from the methyl and methine protons. The septet of relative intensity 3 consists of two accidentally degenerate septets. Proton NMR spectra recorded for a toluene-d_8 solution at temperatures up to 90°C were not significantly different from room temperature spectra. These data are consistent with a static structure that has a bridging isopropyl groups locked into a configuration with one group antifacial to the other two (**II**). The same structure is observed in the solid state (see next page).

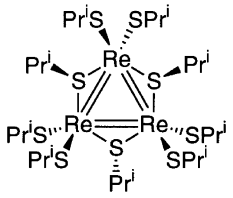

II

The bridging isopropyl thiolates are locked into one configuration as a consequence of the relatively large barrier to inversion at sulfur [16]. This is in contrast to the analogous isopropoxide cluster $Re_3(\mu\text{-}OPr^i)_3(OPr^i)_6$, which has rapid inversion at oxygen for the bridging alkoxide sites and a ^1H NMR spectrum consisting of only four peaks, two 2:1 methyl doublets and two 2:1 methine septets.

The high temperature stability of $Re_3(\mu\text{-}SPr^i)_3(SPr^i)_6$ in solution contrasts sharply with the behavior of $Re_3(\mu\text{-}OPr^i)_3(OPr^i)_6$. In solution, the homoleptic isopropoxide cluster exists in equilibrium with $Re_3(\mu\text{-}OPr^i)_3(H)(OPr^i)_5$ and free acetone even at room temperature ($K_{eq} = 6 \times 10^{-4}$ M at 23°C) [2]. The equilibrium presumably does not exist for $Re_3(\mu\text{-}SPr^i)_3(SPr^i)_6$ because the C═S bond in Me_2C═S is weaker than C═O in Me_2C═O [E(C═O) = 191 kcal/mol vs E(C═S) ≈ 137 kcal/mol] [17] and the difference in these bond energies is not compensated for by the stronger Re–OR bond in comparison to Re–SR. Also, greater stabilization is expected for release of Me_2C═O from the more sterically crowded alkoxide cluster in comparison to release of Me_2C═S from the thiolate cluster. The alkoxide cluster is more sterically crowded than the thiolate cluster because the Re–O and O–C bonds are shorter than the Re–S and S–C bonds.

To confirm the structure of $Re_3(\mu\text{-}SPr^i)_3(SPr^i)_6$ an X-ray crystallographic study was carried out. A thermal ellipsoid plot is shown in Fig. 1 and selected bond distances and angles are given in Table 1. The Re–Re bond distances [2.475(1)–2.494(1) Å] are significantly longer than the distances observed in trirhenium(III) clusters with alkoxide bridges, such as $Re_3(\mu\text{-}OCH_2Bu^t)_3(OCH_2Bu^t)_6$ [2.365(1)–2.372(1) Å] [3], and for the chloride-bridged Re–Re bonds in $Re_3(\mu\text{-}Cl)_3(OBu^t)_6$ [2.436(3)–2.439(3) Å] and $Re_3(\mu\text{-}Cl)(\mu\text{-menthoxo})_2Cl(menthoxo)_5$ [2.422(3) Å]. The Re–$S_{terminal}$ distances [av. 2.28 Å] are shorter than the Re–S_{bridge} distances [av. 2.40 Å], and both sets of distances are normal; for example, the Re–S distances [8, 10] in $[Re(MeC(CH_2S)_3)_2]^-$ and $[Re(S)(SCH_2CH_2S)_2]^-$ range from 2.285(2) to 2.345(5) Å and the Re–S_{bridge} distances in $[Re(\mu\text{-}SEt)Cl(3,6\text{-dithiaoctane})]_2$ are 2.330(6)–2.371(6) Å] [18].

The angles at sulfur for the terminal ligands, 113–121°, are normal [19]. The $S_{terminal}$–Re–$S_{terminal}$ angles are all very close to 124° but at each Re site one of the two terminal sulfurs is closer to being perpendicular to the Re_3 plane than the other. The most pronounced difference involves S(5) and S(6) for which the centroid [Re(1)–Re(2)]–Re(3)–S angles are 129.6 and 106.6°, respectively. The differences may be due to the configurations of the bridging thiolates. The isopropyl

Table 1. Selected bond distances (Å) and angles (°) for $Re_3(\mu\text{-}SPr^i)_3(SPr^i)_6$

Re(1)–Re(2)	2.487(1)	Re(3)–S(6)	2.274(4)
Re(2)–Re(3)	2.494(1)	Re(1)–S(7)	2.396(5)
Re(1)–Re(3)	2.475(1)	Re(2)–S(7)	2.417(5)
Re(1)–S(1)	2.270(4)	Re(1)–S(9)	2.404(5)
Re(1)–S(2)	2.303(5)	Re(3)–S(9)	2.379(5)
Re(2)–S(3)	2.289(5)	Re(2)–S(8)	2.395(5)
Re(2)–S(4)	2.267(5)	Re(3)–S(8)	2.437(5)
Re(3)–S(5)	2.293(5)		

Re(2)–Re(1)–S(1)	108.3(1)	Re(3)–Re(1)–S(1)	111.6(1)
Re(2)–Re(1)–S(2)	115.2(1)	Re(3)–Re(1)–S(2)	120.1(1)
Re(1)–Re(2)–S(3)	110.7(1)	Re(3)–Re(2)–S(3)	121.6(1)
Re(1)–Re(2)–S(4)	115.6(1)	Re(3)–Re(2)–S(4)	108.5(1)
Re(1)–Re(3)–S(5)	119.9(1)	Re(2)–Re(3)–S(5)	127.3(1)
Re(1)–Re(3)–S(6)	109.0(1)	Re(2)–Re(3)–S(6)	99.7(1)
S(1)–Re(1)–S(2)	123.7(2)	S(3)–Re(2)–S(4)	123.9(2)
S(5)–Re(3)–S(6)	123.8(2)	X(2/3)–Re(1)–S(1)[a]	113.3
X(1/2)–Re(3)–S(5)[a]	129.6	X(2/3)–Re(1)–S(2)[a]	122.4
X(1/2)–Re(3)–S(6)[a]	106.6	X(1/3)–Re(2)–S(3)[a]	120.4
Re(1)–S(1)–C(1)	120.9(6)	X(1/3)–Re(2)–S(4)[a]	115.6
Re(1)–S(2)–C(4)	120.7(10)	Re(3)–S(5)–C(13)	120.3(14)
Re(1)–S(2)–C(4′)	117.6(11)	Re(3)–S(5)–C(13′)	116.7(18)
Re(2)–S(3)–C(7)	114.2(6)	Re(3)–S(6)–C(16)	112.8(6)
Re(2)–S(4)–C(10)	115.9(7)		

[a] X(m/n) is the centroid of the Re(m)–Re(n) bond.

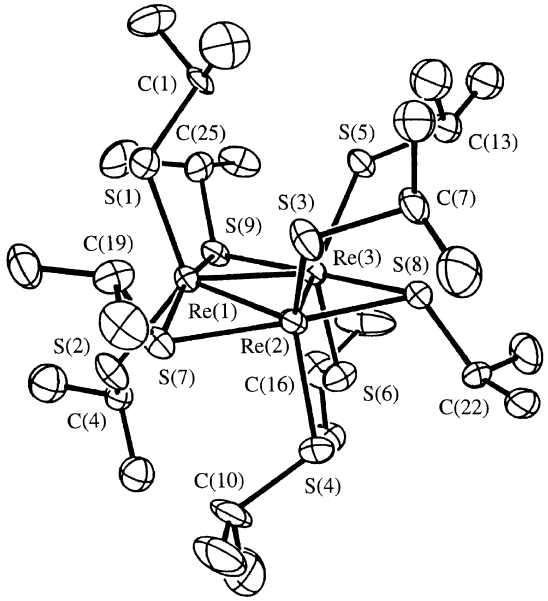

Fig. 1. Molecular structure of $Re_3(\mu\text{-}SPr^i)_3(SPr^i)_6$ (40% probability ellipsoids). Only one orientation of each disordered group is shown.

groups of the S(7) and S(9) bridging thiolates are bent to the same side of the Re_3 plane as the S(3) and S(5) terminal thiolates. This causes the terminal ligands to bend away from the Re_3 plane and consequently the S(4) and S(6) terminal ligands move towards being perpendicular to the plane. The positions of the S(4) and S(6) ligands apparently force the S(2) thiolate away from the plane, which in turn brings S(1) closer to the perpendicular position.

CONCLUSION

The halide $Re_3(\mu\text{-}Cl)_3Cl_6(THF)_3$ reacts with $NaSPr^i$ to give the homoleptic trirhenium(III) thiolate cluster $Re_3(\mu\text{-}SPr^i)_3(SPr^i)_6$ in moderate yield. In solution the cluster has virtual C_s symmetry because of the high barrier to inversion for the three-coordinate sulfurs at the bridging sites. The Re–Re bond distances are longer than those in analogous alkoxide clusters. $Re_3(\mu\text{-}SPr^i)_3(SPr^i)_6$ appears to be the first structurally characterized homoleptic rhenium thiolate cluster.

*Acknowledgements*Acknowledgement for support is made to the Robert A. Welch Foundation. We are grateful to Dr James Korp for his technical assistance with the X-ray crystallographic analysis.

REFERENCES

1. Hoffman, D. M., Lappas, D. and Wierda, D. A., *J. Am. Chem. Soc*., 1989, **111,** 1531.
2. Hoffman, D. M., Lappas, D. and Wierda, D. A., *J. Am. Chem. Soc*., 1989, **115,** 10538.
3. Zhuang, W. W., Truitt, B. E. and Hoffman, D. M., *Inorg. Chem*., 1997, **36,** 3330.
4. Hoffman, D. M., Lappas, D. and Wierda, D. A., *Organometallics*, 1997, **16,** 972.
5. Zhuang, W. W. and Hoffman, D. M., *Organometallics*, 1997, **16,** 3102.
6. Zhuang, W. W. and Hoffman, D. M., *J. Chem. Soc., Chem. Commun*., 1997, 295.
7. Eisenberg, R. and Ibers, J. A., *Inorg. Chem*., 1966, **5,** 411.
8. Blower, P. J., Dilworth, J. R., Hutchinson, J. P., Nicholson, T. and Zubieta, J., *J. Chem. Soc., Dalton Trans*., 1986, 1339.
9. Matondo, S. O. C., Mountford, P., Watkin, D. J., Jones, W. B. and Cooper, S. R., *J. Chem. Soc., Chem. Commun*., 1995, 161.
10. Blower, P. J., Dilworth, J. R., Hutchinson, J. P. and Zubieta, J. A., *Inorg. Chim. Acta*, 1982, **65,** L225.
11. Murray, H. H., Wei, L., Sherman, S. E., Greaney, M. A., Eriksen, K. A., Carstensen, B., Halbert, T. R. and Stiefel, E. I., *Inorg. Chem*., 1995, **34,** 841.
12. Lincoln, R., Wilkinson, G., Walton, R. A. and Wood, T. E., *Inorg. Synth*., 1980, **20,** 41.
13. Lincoln, R., Wilkinson, G., Walton, R. A. and Wood, T. E., *Inorg. Synth*., 1980, **20,** 44.
14. Mertis, K., Edwards, P. G., Wilkinson, G., Malik, K. M. A. and Hursthouse, M. B., *J. Chem. Soc., Dalton Trans*., 1981, 705.
15. Sheldrick, G. M., *SHELXTL PLUS*, Release 3.4 for the Nicolet R3m/v Crystallographic System, Nicolet Instrument Corp., Madison, 1987.
16. Albright, T. A., Burdett, J. K. and Whangbo, M. H., *Orbital Interactions in Chemistry*. Wiley-Interscience, Chichester, 1985, p. 143.
17. Huheey, J. E., *Inorganic Chemistry*, *Principles of Structure and Reactivity*, 3rd edn., Harper & Row, London, 1983, p. A-37.
18. Heyen, B. J. and Powell, G. L., *Inorg. Chem*., 1990, **29,** 4574.
19. Dilworth, J. R., Hu, J., Miller, J. R., Hughes, D. L., Zubieta, J. A. and Chen, Q., *J. Chem. Soc., Dalton Trans*., 1995, 3153.

Pergamon

PII : S0277–5387(97)00448–8

Polyhedron Vol. 17, No. 16, pp. 2587–2598, 1998
© 1998 Elsevier Science Ltd
All rights reserved. Printed in Great Britain
0277–5387/98 $19.00+0.00

The preparation, crystal structure and some reaction chemistry of Bromo(η^5-pentaphenylcyclopentadienyl)dicarbonylosmium(II), [Os(η^5-C_5Ph_5)$(CO)_2$Br]

L. D. Field,* T. W. Hambley, P. A. Humphrey, A. F. Masters* and P. Turner

School of Chemistry, The University of Sydney, NSW, 2006 Australia

(Received 24 July 1997 ; accepted 28 October 1997)

Abstract—The preparation and characterisation of [Os(η^5-C_5Ph_5)$(CO)_2$Br] (**1**) are described ; this complex is the first reported $C_5Ph_5^-$ derivative of osmium. A single crystal X-ray diffraction study of (**1**) (refined to $R = 0.040$, $R_w = 0.043$) is also reported. The related complexes, [Os{η^5-C_5Ph_4(p-^{t}BuC_6H_4)}$(CO)_2$Br] (**2**) and [Os{η^5-C_5(p-MeC_6H_4)$_5$}$(CO)_2$Br] (**3**), have also been prepared. Carbonyl substitution of (**1**) in tetrahydrofuran following treatment with Me_3NO afforded [Os(η^5-C_5Ph_5)(CO)(L)Br] (L = PMe_2Ph (**4**), $P(OEt)_3$ (**5**), $P(OCH_2)_3CCH_3$ (**6**) and ^{t}BuNC (**7**)). A single crystal X-ray diffraction study of (**6**) (refined to $R = 0.066$, $R_w = 0.073$) is described. © 1998 Elsevier Science Ltd. All rights reserved

Keywords: osmium ; cyclopentadienyl ; pentaphenylcyclopentadienyl ; crystal structure.

Relatively few cyclopentadienyl or substituted cyclopentadienyl complexes of osmium have been described and the number of structurally characterised derivatives is correspondingly small [1–22]. Previously, the half-sandwich compounds [Os(η^5-C_5H_5)$(CO)_2$Br] and [Os(η^5-C_5H_5)$(CO)_2$H] have been prepared from the reactions of $Os(CO)_4Br_2$ with $(C_5H_6)_2$ in decane and Tl(C_5H_5) in heptane, respectively [23]. In addition, [Os(η^5-C_5Me_5)$(CO)_2$Br] has been synthesised by reacting $Os(CO)_4Br_2$ with C_5Me_5H in decane [23] ; [Os(η^5-C_5Me_5)$(CO)_2$I] from a one-pot reaction of $Os_3(CO)_{12}$, I_2 and C_5Me_5H in benzene [6], and [Os(η^5-C_5Me_5)$(CO)_2$H] from $Os_3(CO)_{12}$ and C_5Me_5H in heptane [23]. More recently, [Os(η^5-C_5Me_5)Br(μ-Br)]$_2$ has been synthesized in good yield from H_2OsBr_6 and C_5Me_5H [20]. This dimer proved to be a convenient intermediate in the synthesis of a wide variety of [Os(C_5Me_5)L_n] complexes.

The formal oxidative addition of $C_5R_{5-n}H_nX$ (n = 0–5) to a transition metal precursor is an alternative synthetic route to cyclopentadienyl and substituted cyclopentadienyl complexes. This route has not been widely exploited because of the lack of ready availability of most of the necessary $C_5R_{5-n}H_nX$ precursors. However, 1-bromo-1,2,3,4,5-pentaarylcyclopentadienyl species are readily prepared in high yield and their reactions with organometallic precursors provide convenient routes to pentaarylcyclopentadienyl complexes [24–26]. A potentially wide range of ligands with varying electronic and steric properties is accessible in this way.

Although pentaphenylcyclopentadienyl complexes of many metals are known and several of these have been structurally characterised [27–56], no pentaphenylcyclopentadienyl complex of osmium has been reported.

Herein we describe the preparation of [Os(η^5-C_5Ph_5)$(CO)_2$Br] by the formal oxidative addition of C_5Ph_5Br to $Os_3(CO)_{12}$. The similar complexes [Os{η^5-C_5Ph_4(p-^{t}BuC_6H_4)}$(CO)_2$Br] and [Os{η^5-C_5(p-MeC_6H_4)$_5$}$(CO)_2$Br] have also been prepared. The crystal structure of [Os(η^5-C_5Ph_5)$(CO)_2$Br] and the preparation of several derivatives of the mono (pentaphenylcyclopentadienyl)osmium moiety are also reported.

RESULTS AND DISCUSSION

[Os(η^5-C_5Ph_5)$(CO)_2$Br] (**1**) was prepared by refluxing a mixture of $Os_3(CO)_{12}$ and C_5Ph_5Br in chloro-

* Author to whom correspondence should be addressed.

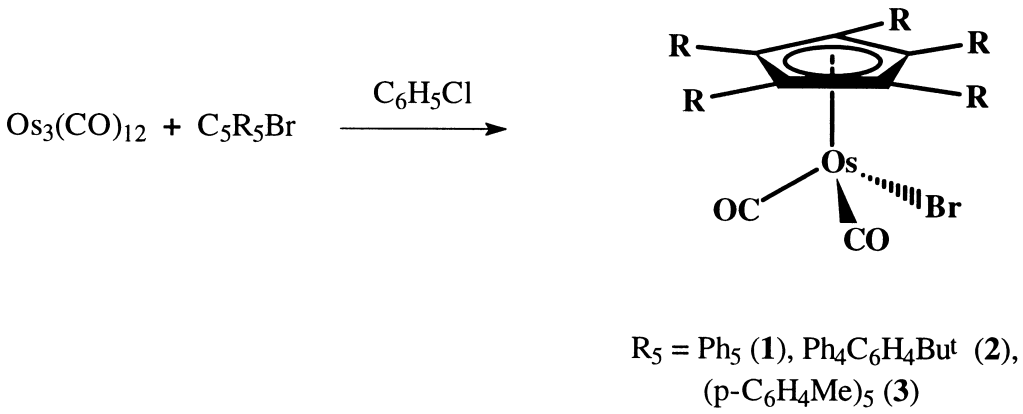

Scheme 1.

benzene. The complex was isolated as an air-stable pale yellow solid after purification on a silica gel column and crystallisation from dichloromethane/*n*-hexane, and was characterised by elemental analysis, and mass, infrared and ^{1}H and ^{13}C NMR spectra. Small amounts of the new complex [Os(η^5-C_5Ph_5)$(CO)_2$H] (similarly characterised), and of C_5Ph_5H and $Os_3(CO)_{10}Br_2$ were also obtained in variable amounts and were isolated after column chromatography of the reaction mixture. The analogous osmium compounds, [Os{η^5-C_5Ph_4(*p*-^{t}BuC_6H_4)}$(CO)_2$Br] (**2**) and [Os{η^5-C_5(*p*-MeC_6H_4)$_5$}$(CO)_2$Br] (**3**) have also been prepared by reacting the corresponding perarylcyclopentadienyl bromide with $Os_3(CO)_{12}$ in chlorobenzene (Scheme 1). Although the yields of (**2**) and (**3**) were considerably lower than that of (**1**), they have not been optimised. The analytical and spectroscopic data of (**1**)–(**3**) were consistent with the formulation of the products as [Os(η^5-ligand)$(CO)_2$Br]. The mass spectra of (**1**)–(**3**) show that the main fragmentation pathway is via the loss of the two carbonyl ligands although all exhibit an (often intense) ion assigned to [Os(ligand)$_2$ − H]$^+$.

A single crystal X-ray diffraction study of (**1**) was undertaken for comparison with those of the iron [30] and ruthenium [46] analogues. [Os(η^5-C_5Ph_5)$(CO)_2$Br] crystallises in the orthorhombic space group PBCA and is isostructural with [Fe(η^5-C_5Ph_5)$(CO)_2$Br] [30] and [Ru(η^5-C_5Ph_5)$(CO)_2$Br] [46]. The crystal structure of [Os(η^5-C_5Ph_5)$(CO)_2$Br] consists of discrete molecules in the solid state and no intermolecular contacts of significance were observed in the solid. The closest intermolecular contact is 3.44 Å between O(1) on molecule (x, y, z) and C(22) on molecule ($1/2-x$, $1/2+y$, $+z$). The closest intermolecular non-bonding approaches to osmium are greater than 4 Å. Final atomic positional coordinates, with estimated standard deviations, bond lengths and angles and anisotropic thermal parameters are deposited.* Selected interatomic bond distances and angles, with standard deviations derived from the refinement, are given in Tables 1 and 2. The atomic nomenclature is defined in Fig. 1. Figures 1 and 2 illustrate the molecular geometry viewed along, and perpendicular to, the normal to the C_5 plane of the $C_5Ph_5^-$ ligand, respectively.

The [Os(η^5-C_5Ph_5)$(CO)_2$Br] *molecule*

Coordination by the η^5 pentaphenylcyclopentadienyl group, the bromine atom and the two carbonyl groups creates a "piano stool" environment about the osmium atom. The Os-(ring centroid) distance is 1.90 Å and the average Os—C distance of 2.27 Å may be compared with 2.214 Å for [Os(η^5-

Table 1. Selected bond lengths (Å) for [Os(η^5-C_5Ph_5)$(CO)_2$Br] (**1**)

Atoms	*d*	Atoms	*d*
Os(1)—Br(1)	2.531(2)	Os(1)—C(1)	1.87(2)
Os(1)—C(2)	1.93(2)	Os(1)—C(3)	2.31(1)
Os(1)—C(4)	2.26(1)	Os(1)—C(5)	2.25(1)
Os(1)—C(6)	2.24(1)	Os(1)—C(7)	2.28(1)
O(1)—C(1)	1.09(2)	O(2)—C(2)	1.00(2)
C(3)—C(4)	1.48(2)	C(3)—C(7)	1.42(2)
C(4)—C(5)	1.45(2)	C(5)—C(6)	1.45(2)
C(6)—C(7)	1.47(2)	C(7)—C(8)	1.47(2)
C(3)—C(14)	1.45(2)	C(4)—C(20)	1.48(2)
C(5)—C(26)	1.48(2)	C(6)—C(32)	1.47(2)

* The atomic coordinates and thermal parameters have been submitted as supplementary material for deposition at the Cambridge Crystallographic Data Centre (see Deposition of crystallographic data).

Table 2. Selected bond angles (°) for [Os(η^5-C_5Ph_5)$(CO)_2$Br] (**1**)

Atoms	Angle	Atoms	Angle
C(1)—Os(1)—Br(1)	88.1(5)	C(2)—Os(1)—Br(1)	87.4(5)
C(1)—Os(1)—C(2)	88.6(7)	C(3)—Os(1)—Br(1)	95.1(3)
C(4)—Os(1)—Br(1)	105.1(3)	C(5)—Os(1)—Br(1)	141.0(3)
C(6)—Os(1)—Br(1)	156.1(3)	C(7)—Os(1)—Br(1)	118.4(3)
O(1)—C(1)—Os(1)	178(1)	O(2)—C(2)—Os(1)	177(1)
C(4)—C(3)—C(7)	107(1)	C(4)—C(5)—C(6)	109(1)
C(3)—C(4)—C(5)	107(1)	C(5)—C(6)—C(7)	106(1)
C(3)—C(7)—C(6)	109(1)	C(4)—C(3)—C(14)	124(1)
C(5)—C(6)—C(32)	127(1)	C(7)—C(3)—C(14)	127(1)
C(7)—C(6)—C(32)	125(1)	C(3)—C(4)—C(20)	122(1)
C(3)—C(7)—C(8)	122(1)	C(5)—C(4)—C(20)	128(1)
C(6)—C(7)—C(8)	126(1)	C(4)—C(5)—C(26)	123(1)
C(6)—C(5)—C(26)	126(1)	C(6)—C(32)—C(33)	118(1)
C(7)—C(8)—C(9)	118(1)	C(6)—C(32)—C(37)	121(1)
C(7)—C(8)—C(13)	124(1)	C(5)—C(26)—C(27)	117(1)
C(4)—C(20)—C(21)	119(1)	C(5)—C(26)—C(31)	123(1)
C(4)—C(20)—C(25)	123(1)	C(3)—C(14)—C(15)	120(1)
C(3)—C(14)—C(19)	120(1)		

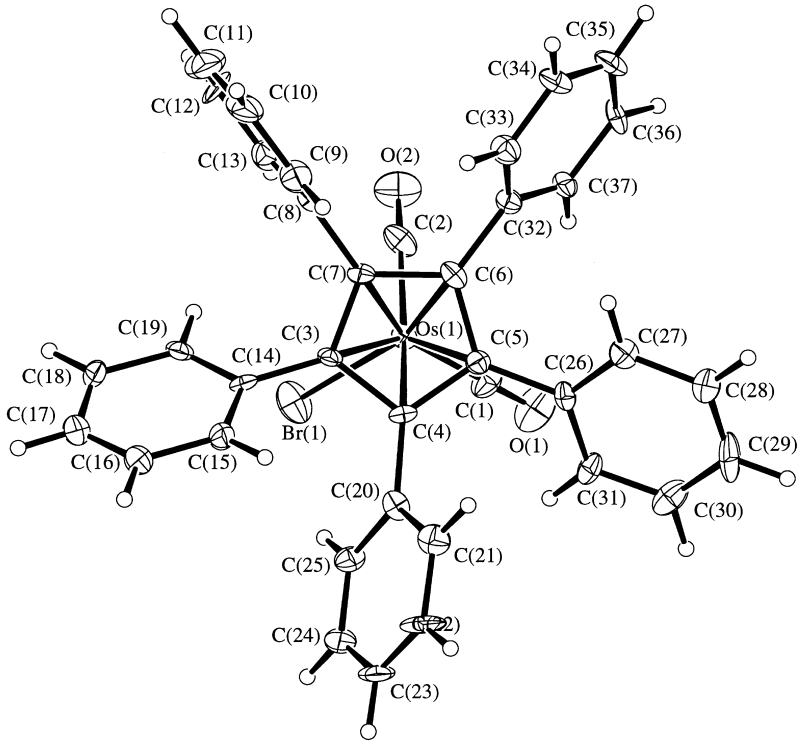

Fig. 1. ORTEP [69] (25% probability) illustration of the molecular structure of [Os(η^5-C_5Ph_5)$(CO)_2$Br] (**1**) showing the atom numbering. Viewed along the normal to the C_5Ph_5 plane.

C_5H_5)$(PPh_3)_2$Cl] [3], 2.177 Å for [Os(η^5-C_5H_5)$(PPh_3)_2$Br] [22], 2.25 Å for [Os(η^5-C_5H_5)$(PMe_3)_2(NO)]^+$ [1], 2.247 Å for [Os_2(η^5-$C_5Me_5)_2(CO)_2$(μ-H)$_2$] [2] and 2.223 and 2.261 Å for the two isomeric forms of [Os(η^5-C_5H_5)(η^2-CH_2═CH-$C_6H_4PPh_2$)Br] [4]. The Os—CO distances (1.87(2) and 1.93(2) Å) are indistinguishable and may be compared, for example, with a bond length of 1.833(9) Å in [Os_2($\eta^5C_5Me_5)_2(CO)_2$(μ-H)$_2$] [2], 1.879(5) Å in [Os(η^5-C_5Me_5)(CO)(PPh_3)(═C═C(^{t}Bu)H][BF_4] [6]

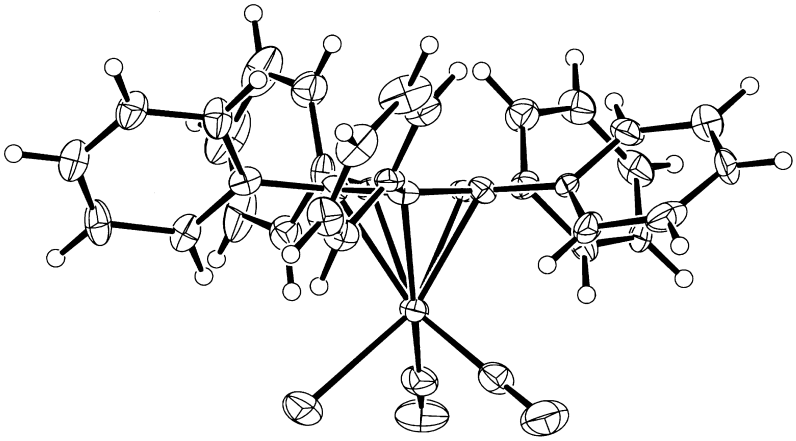

Fig. 2. ORTEP [69] (25% probability) illustration of the molecular structure of $[Os(\eta^5\text{-}C_5Ph_5)(CO)_2Br]$ (**1**) viewed perpendicular to the normal to the C_5Ph_5 plane.

and 1.919(14), 1.961(15) and 1.929(15) Å in $[Os(\eta^4\text{-}C_4Ph_4CO)(CO)_3]$ [57]. The C═O bond lengths in (**1**) are equivalent. The Os—Br distance is 2.530(2) Å and may be compared with values of 2.5438(9) Å for $[Os(\eta^5\text{-}C_5H_5)(PPh_3)_2Br]$ [22], 2.545(2) and 2.510(2) Å in two molecules of $[Os(\eta^5\text{-}C_5H_5)(\eta^2\text{-}CH_2{=}CH\text{-}C_6H_4PPh_2)Br]$ [4] and 2.559(1) Å for $[Os(\eta^5\text{-}C_5Me_5)Br(\mu\text{-}Br)]_2$ [20].

The C_5 nucleus of the pentaphenylcyclopentadienyl ligand is planar to within 0.02 Å. The C—C bond lengths of the C_5 ring range from 1.42(2)–1.48(2) Å, the average C—C bond length being 1.45 Å, which is consistent with C_5Ph_5 rings in other metal complexes. The *ipso*-carbon atoms of each of the phenyl rings are displaced slightly from the C_5 plane by between 0.07 and 0.25 Å, with the average distance being 0.16 Å. The *ipso*-carbon atoms of all phenyl rings are on the opposite side of the C_5 plane to the osmium atom. The phenyl rings are all also planar to within 0.02 Å and are canted at between 39.5 and 88.0° to the C_5 ring in a paddle wheel arrangement. The phenyl ring defined by C(8) is almost perpendicular to the C_5 ring.

Table 3 compares some bond length data determined for $[Os(\eta^5\text{-}C_5Ph_5)(CO)_2Br]$ and its iron (**8**) and ruthenium (**9**) analogues. As expected, it is evident that differences between the compounds of the three metals are generally small. For all three compounds the view of the coordination sphere of the metal as a distorted octahedron is supported by the angles subtended at the metal atom by the bromine atom and the two carbonyl carbon atoms (C(1)—M(1)—Br(1) = 86.6(1)°, 86.8(2)° and 88.1(5)°; C(1)—M(1)—C(2) = 89.8(2)°, 87.9(3)° and 88.6(7)°; C(2)—M(1)—Br(1) = 86.6(1)°, 85.5(3)° and 87.4(5)° for M = Fe (**8**), Ru (**9**) and Os (**1**), respectively). The average deviation of the phenyl rings from coplanarity with the C_5 ring is 59.9° in (**1**), which is similar to that of (**8**) (58.7°) [30] and (**9**) (62.0°) [46], while both (**8**) (87.4°) and (**9**) (87.4°) also contain a phenyl ring almost perpendicular to the C_5 ring.

Mono-carbonyl substitution of (**1**) in tetrahydrofuran using Me_3NO and appropriate ligands, L, afforded $[Os(\eta^5\text{-}C_5Ph_5)(CO)(L)Br]$ (L = PMe_2Ph (**4**), $P(OEt)_3$ (**5**), $P(OCH_2)_3CCH_3$ (**6**) and ^{t}BuNC (**7**)) (Scheme 2), which have been characterised by elemental analysis, and mass, infrared and ^{1}H and ^{31}P NMR

Table 3. Comparisons of selected metrical data between $[M(\eta^5\text{-}C_5Ph_5)(CO)_2Br]$ (M = Fe (**8**), Ru (**9**), Os (**1**))

Bond	Distance (Å)		
	Fe[30]	Ru[46]	Os[a]
M—CO	1.786(5), 1.812(5)	1.902(9), 1.930(9)	1.87(2), 1.93(2)
M—Br	2.424(1)	2.537(1)	2.530(2)
M—C(C_5 ring)	2.090(3)–2.165(4)	2.215(6)–2.304(6)	2.24(1)–2.31(1)
	2.125 av.	2.258 av.	2.27 av.
M—(C_5 ring plane)	1.738(5)	not given	1.90
C—C(C_5Ph_5)	1.420(5)–1.451(5)	1.411(8)–1.462(9)	1.42(2)–1.48(2)
	1.435 av.	1.441 av.	1.45 av.
C—O	1.052(6), 1.097(6)	1.024(8), 1.102(8)	0.99(2), 1.10(2)

[a] This work

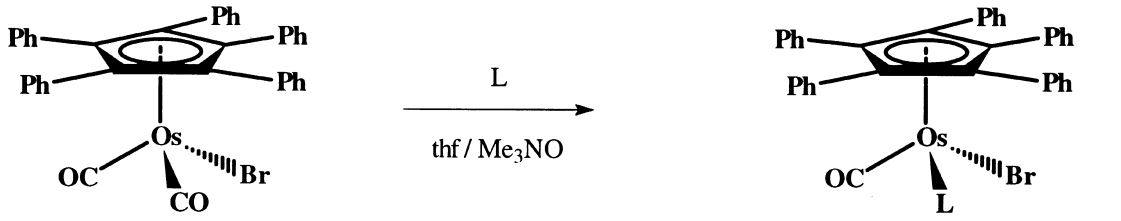

L = PMe_2Ph (**4**), $P(OEt)_3$ (**5**), $P(OCH_2)_3CCH_3$ (**6**), $CNBu^t$ (**7**)

Scheme 2.

spectra. The mass spectra of compounds (**4**)–(**7**) all exhibit a molecular ion, although the dominant ion is $[M\text{-CO-L}]^+$. A single CO stretching vibration is observed in the IR spectrum in CH_2Cl_2 solution. As observed in the solid state IR spectrum of $[Fe(\eta^5\text{-}C_5Ph_5)(CO)(PMe_3)Br]$ [58], the spectra of (**4**)–(**6**) in KBr show a splitting of the CO stretching absorptions observed in solution. This is thought to be due to the presence of two diastereoisomers derived from the opposite canting modes of the five phenyl groups around the C_5 rings [58]. The observation of one set of NMR signals in CD_2Cl_2 suggest, however, that in solution the five phenyl groups around the ring rotate rapidly on the NMR time scale. In none of these reactions, even when an excess of ligand and Me_3NO were used, did we observe the loss of two carbonyl ligands.

A single crystal X-ray diffraction study was undertaken on $[Os(\eta^5\text{-}C_5Ph_5)(CO)\{P(OCH_2)_3CCH_3\}Br]$. The compound crystallises in the monoclinic space group $P2_1/n$ (#14). The pentaphenylcyclopentadienyl ligand is once again coordinated in the η^5 mode with coordination completed by the $P(OCH_2)_3CCH_3$ ligand, one carbonyl ligand and the bromide ligand, the latter two of which are disordered between two sites. Final atomic positional coordinates, with estimated standard deviations, bond lengths and angles and anisotropic thermal parameters are deposited.* Selected interatomic bond distances and angles, with standard deviations from the refinement are given in Tables 4 and 5. The atomic nomenclature is defined in Fig. 3, which illustrates the molecular geometry viewed perpendicular to the normal to the C_5 plane of the $C_5Ph_5^-$ ligand.

Again no intermolecular contacts of significance were observed in the solid. The closest intermolecular contact is 3.13 Å between O(1a) on molecule (x, y, z) and C(29) on molecule ($-1/2-x$, $y-1/2$, $1/2-z$). The closest intermolecular non-bonding approaches to osmium are greater than 4 Å.

The $[Os(\eta^5\text{-}C_5Ph_5)(CO)\{P(OCH_2)_3CCH_3\}Br]$ *molecule*

The Os-(ring centroid) distance is 1.92 Å and the average Os—C distance is 2.28 Å. Disorder in the carbonyl and bromine ligands precludes any comment on the Os—CO bond distances and the C—O distances. The Os—Br distances appear to be shorter than that of (**1**).

The C_5 nucleus of the pentaphenylcyclopentadienyl ligand is planar to within 0.02 Å. The C—C bond lengths of the C_5 ring range from 1.43(1)–1.46(1) Å, the average being 1.45 Å. The *ipso*-carbon atom of each of the phenyl rings is displaced from the C_5 plane by between 0.11–0.35 Å, with the average being 0.18 Å. Again the *ipso* carbons of all phenyl rings are on the opposite side of the C_5 plane to the osmium atom. The phenyl rings are all planar to within 0.03 Å with normal dimensions and are canted at between 44.6 and 56.3° to the C_5 ring in the usual paddlewheel arrangement, with an average deviation from coplanarity of 52.6°.

EXPERIMENTAL

All manipulations were performed at atmospheric pressure under an atmosphere of dinitrogen by using conventional Schlenk techniques. Chlorobenzene (Merck) was dried, distilled and stored over calcium hydride. Tetrahydrofuran (thf) (Merck) was pre-dried over sodium wire and distilled from sodium benzophenone ketyl. *n*-Hexane (BDH) was distilled from sodium wire. Dichloromethane (Ajax) was distilled from calcium hydride. C_5Ph_5Br, [59] $C_5Ph_4(p\text{-}^tBuC_6H_4)Br$ [59] and $C_5(p\text{-}MeC_6H_4)_5Br$ [25] were prepared as described previously. $Os_3(CO)_{12}$ (Aldrich), $P(OEt)_3$ (Merck), PMe_2Ph (Fluka) and ^{t}BuNC (Aldrich) were used as received. Trimethylamine *N*-oxide dihydrate (Aldrich) was dehydrated by sublimation prior to use. Flash silica (240–400 mesh) was obtained

Table 4. Selected bond lengths (Å) for $[Os(\eta^5\text{-}C_5Ph_5)(CO)\{P(OCH_2)_3CCH_3\}Br]$ (**6**)

Atoms	*d*	Atoms	*d*
Os(1)—Br(1a)	2.422(5)	Os(1)—Br(1b)	2.504(2)
Os(1)—P(1)	2.239(3)	Os(1)—C(1a)	2.1292(5)
Os(1)—C(2)	2.27(1)	Os(1)—C(1b)	2.1213(5)
Os(1)—C(4)	2.28(1)	Os(1)—C(3)	2.28(1)
Os(1)—C(6)	2.255(9)	Os(1)—C(5)	2.288(9)
O(1a)—C(1a)	1.2496(1)	O(1b)—C(1b)	1.23
C(3)—C(4)	1.44(1)	C(2)—C(6)	1.43(1)
C(4)—C(5)	1.45(1)	C(5)—C(6)	1.45(1)
C(2)—C(3)	1.46(1)	C(2)—C(13)	1.47(1)
C(3)—C(19)	1.47(1)	C(4)—C(25)	1.49(1)
C(5)—C(31)	1.49(1)	C(6)—C(7)	1.46(1)
P(1)—O(2)	1.58(1)	P(1)—O(3)	1.588(9)
P(1)—O(4)	1.56(10)	O(4)—C(40)	1.44(2)
O(2)—C(38)	1.45(2)	O(3)—C(39)	1.48(2)
C(40)—C(37)	1.51(2)	C(38)—C(37)	1.44(2)
C(39)—C(37)	1.52(2)	C(37)—C(41)	1.55(2)

Table 5. Selected bond angles (°) for $[Os(\eta^5\text{-}C_5Ph_5)(CO)\{P(OCH_2)_3CCH_3\}Br]$ (**6**)

Atoms	Angle	Atoms	Angle
C(1b)—Os(1)—Br(1a)	82.3(2)	P(1)—Os(1)—Br(1a)	85.3(1)
C(1a)—Os(1)—Br(1b)	88.57(7)	P(1)—Os(1)—Br(1b)	85.49(9)
P(1)—Os(1)—C(1b)	86.80(8)	P(1)—Os(1)—C(1a)	74.31(7)
C(3)—Os(1)—Br(1a)	106.2(3)	C(4)—Os(1)—Br(1a)	141.5(3)
C(5)—Os(1)—Br(1a)	155.3(3)	C(6)—Os(1)—Br(1a)	118.6(3)
C(2)—Os(1)—Br(1a)	95.9(3)	C(3)—Os(1)—Br(1b)	103.5(3)
C(4)—Os(1)—Br(1b)	93.6(3)	C(5)—Os(1)—Br(1b)	117.5(2)
C(6)—Os(1)—Br(1b)	153.9(3)	C(2)—Os(1)—Br(1b)	139.7(3)
O(1b)—C(1b)—Os(1)	157.68(1)	O(1a)—C(1a)—Os(1)	154.13(1)
C(4)—C(3)—C(2)	105.8(8)	C(4)—C(5)—C(6)	107.3(8)
C(3)—C(4)—C(5)	109.6(8)	C(5)—C(6)—C(2)	107.6(8)
C(3)—C(2)—C(6)	109.6(9)	C(4)—C(3)—C(19)	126.9(8)
C(5)—C(6)—C(7)	127.6(9)	C(5)—C(4)—C(25)	124.1(9)
C(2)—C(6)—C(7)	124.0(9)	C(3)—C(4)—C(25)	126.1(9)
C(6)—C(2)—C(13)	126.3(9)	C(6)—C(5)—C(31)	126.7(8)
C(3)—C(2)—C(13)	123.7(9)	C(4)—C(5)—C(31)	124.2(8)
C(2)—C(3)—C(19)	126.7(9)	C(6)—C(7)—C(12)	120(1)
C(2)—C(13)—C(18)	120.5(10)	C(6)—C(7)—C(8)	122(1)
C(2)—C(13)—C(14)	121.5(10)	C(5)—C(31)—C(32)	121(1)
C(4)—C(25)—C(30)	119.7(10)	C(5)—C(31)—C(36)	120(1)
C(4)—C(25)—C(26)	120(1)	C(3)—C(19)—C(24)	119(1)
C(3)—C(19)—C(20)	121(1)	P(1)—O(4)—C(40)	116.5(9)
Os(1)—P(1)—O(2)	114.7(4)	P(1)—O(2)—C(38)	113(1)
Os(1)—P(1)—O(3)	116.0(4)	P(1)—O(3)—C(39)	115.6(9)
Os(1)—P(1)—O(4)	118.0(4)	C(38)—C(37)—C(41)	111(1)
O(2)—C(38)—C(37)	113(1)	C(40)—C(37)—C(41)	110(1)
O(3)—C(39)—C(37)	109(1)	C(39)—C(37)—C(41)	110(1)
O(4)—C(40)—C(37)	110(1)		

from Merck. Elemental analyses (C, H, N, Br) were performed by the Australian Microanalytical Service. Melting points were recorded on a Reichert hot platform in air and are uncorrected. Fourier transform infrared spectra were recorded on a Digilab FTS-40 spectrometer. ^1H and ^{13}C NMR spectra were recorded

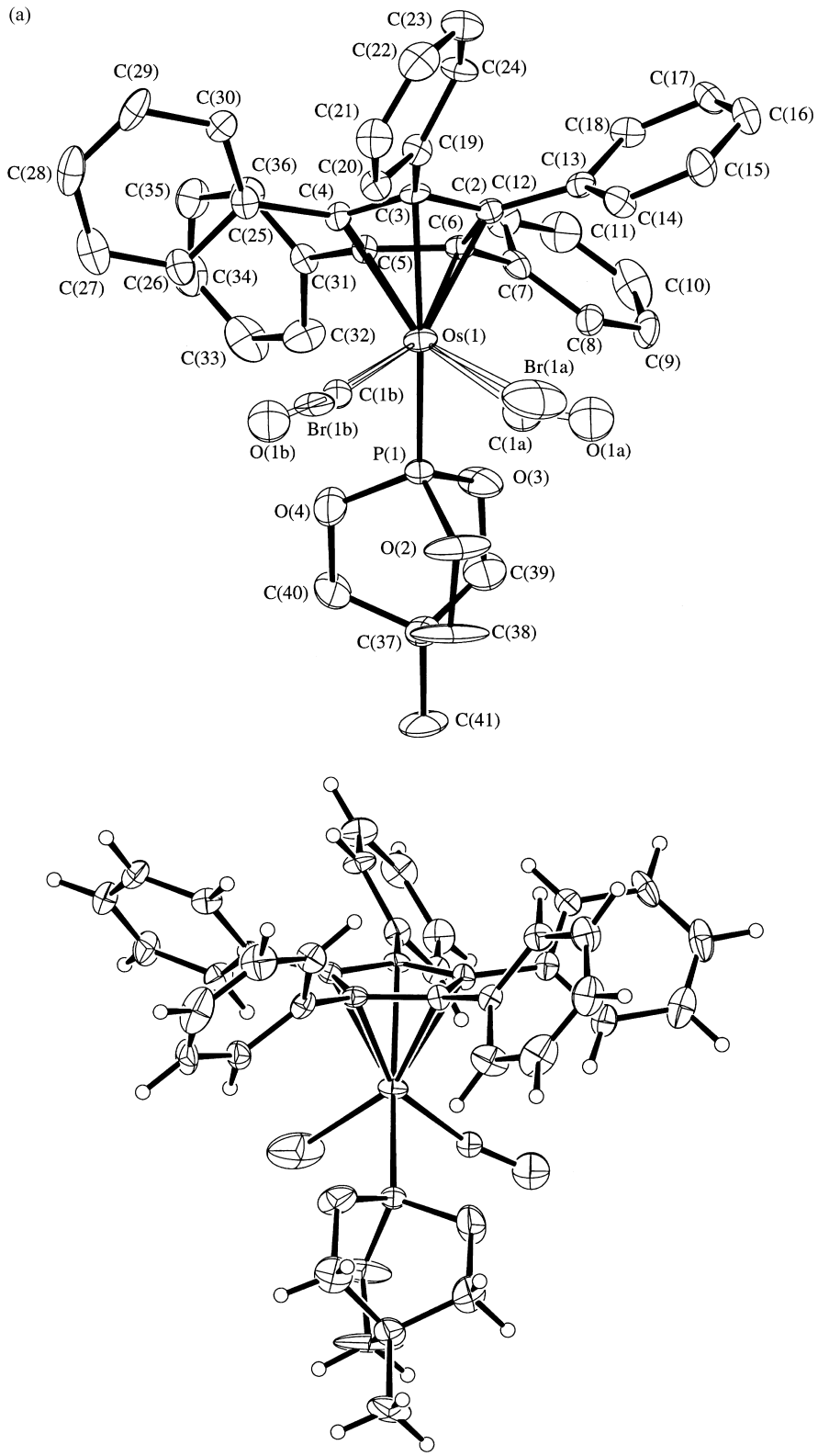

Fig. 3. ORTEP [69] (25% probability) illustration of the molecular structure of [Os(η^5-C_5Ph_5)(CO){P(OCH$_2$)$_3$CCH$_3$}Br] (**6**) viewed approximately perpendicular to the normal to the C_5Ph_5 plane (a) illustrating the disorder and (b) with the disorder now shown, for clarity.

on Bruker AC200F (^{1}H NMR 200.13 MHz, ^{13}C NMR 50.33 MHz) or Bruker AMX400 (^{1}H NMR 400.21 MHz) spectrometers. The spectra were referenced internally to TMS or to residual solvent resonances (CD_2Cl_2, ^{1}H δ 5.30 ppm, ^{13}C δ 53.8 ppm). ^{31}P NMR spectra were recorded on a Bruker AMX400 spectrometer operating at 162.0 MHz and were referenced with respect to 85% H_3PO_4 as standard reference, with an external reference of neat trimethylphosphite (δ 140.85 ppm). Electron impact mass spectra were obtained using a Kratos MS 9 geometry mass spectrometer with a direct insertion probe, a 280°C source temperature, 70 eV ionisation voltage and 4 kV acceleration voltage.

Preparation of [Os(η^5-C_5Ph_5)$(CO)_2$Br] (**1**)

A mixture of $Os_3(CO)_{12}$ (219 mg, 0.242 mmol) and C_5Ph_5Br (402 mg, 0.765 mmol) in chlorobenzene (90 ml) was heated at reflux for 18 h. The solvent was removed *in vacuo*, then column chromatography was performed. Elution with *n*-hexane afforded a small amount of $Os_3(CO)_{10}Br_2$. (Found: C 12.1, H < 0.1, Br 17.5. $C_{10}Br_2O_{10}Os_3$ requires C 11.9, Br 15.8%). IR (cyclohexane): *v* (CO) 2114 w, 2080 s, 2069 s, 2026 vs, 2012 s, 1993 w, 1989 w cm^{-1} [lit. [60]: *v* (CO) 2113 w, 2080 s, 2069 s, 2026 s, 2012 s, 1991 sh, 1987 w cm^{-1}]. A small amount of C_5Ph_5H (identified on the basis of IR (KBr) and m.p.) was similarly obtained by elution with 20% CH_2Cl_2/80% *n*-hexane. Elution with 30% CH_2Cl_2/70% *n*-hexane and evaporation to dryness (rotary evaporator) afforded a white solid which was crystallised from CH_2Cl_2/*n*-hexane to give colourless crystals of [Os(η^5-C_5Ph_5)$(CO)_2$H] m.p. > 140°C (dec.). (Found: C 64.3, H 3.6. $C_{37}H_{26}O_2Os$ requires C 64.2, H 3.8%). ^{1}H NMR ($CDCl_3$, 200.13 MHz): δ 7.10–7.03 (m, 25H, Ar-*H*), −13.19 (s, 1H, Os-*H*) ppm. Mass spectrum: EI (*m*/*e*) 694 ([*M*]$^+$, 100%). IR (KBr) ν_{max} 3110 vw, 3087 vw, 3061 w, 3040 vw, 3031 vw, 2077 w, 1998 vs, 1984 w, 1938 vs, 1907 w, 1734 vw, 1717 vw, 1700 vw, 1684 vw, 1653 w, 1602 w, 1577 w, 1559 w, 1540 w, 1505 w, 1457 vw, 1446 w, 1412 w, 1182 vw, 1157 vw, 1073 w, 1029 w, 922 vw, 803 w, 783 w, 758 w, 741 m, 709 (sh), 698 m, 607 w, 575 w, 562 w, 518 w, 509 w cm^{-1}. IR (CH_2Cl_2): *v* (Os—H) 2087 vs, *v* (CO) 2008 vs, 1945 vs, cm^{-1}. Further elution with 70% CH_2Cl_2/30% *n*-hexane afforded a yellow solution which after evaporation and crystallisation of the solid from CH_2Cl_2/*n*-hexane gave yellow crystals of [Os(η^5-C_5Ph_5)$(CO)_2$Br] (**1**) (365 mg, 65%) m.p. > 205°C (dec.). (Found: C 57.2, H 3.3, Br 10.5. $C_{37}H_{25}BrO_2Os$ requires C 57.6, H 3.3, Br 10.4%). ^{1}H NMR (CD_2Cl_2, 200.13 MHz): δ 7.25–7.00 (m, 25H, Ar-*H*) ppm. ^{13}C NMR (CD_2Cl_2, 50.33 MHz): δ 178.0 (*C*O), 132.9 (quaternary Ar-*C*), 129.7, 128.9, 128.3 (Ar-*C*H), 104.9 (Cp-*C*) ppm. Mass spectrum: EI (*m*/*e*) 1081 ([Os(η^5(C_5Ph_5)$_2$—H]$^+$, 3%), 772 ([*M*]$^+$, 1%), 744 ([*M*]—CO]$^+$, 1%), 716 ([*M*—2CO]$^+$, 100%), 446 (HC_5Ph_5, 12%), 445 (C_5Ph_5, 10%). IR (KBr) ν_{max}: 3111 vw, 3090 w, 3059 w, 3046 (sh), 2028 vs, 1973 vs, 1602 w, 1579 vw, 1502 w, 1446 w, 1419 w, 1398 vw, 1379 vw, 1184 vw, 1158 vw, 1076 w, 1030 w, 1002 vw, 921 vw, 841 vw, 802 w, 782 w, 767 vw, 738 m, 707 m, 697 m, 676 vw, 593 w, 581 w, 571 w, 562 w, 544 w, 518 vw, 501 vw, 493 vw, 465 w cm^{-1}. IR (CH_2Cl_2): *v* (CO) 2033 vs, 1978 vs cm^{-1}.

Preparation of [Os{η^5-C_5Ph_4(*p*-^{t}BuC_6H_4)}$(CO)_2$Br] (**2**)

A similar reaction of $Os_3(CO)_{12}$ (111 mg, 0.122 mmol) and C_5Ph_4(*p*-^{t}BuC_6H_4)Br (223 mg, 0.383 mmol) in chlorobenzene (50 ml) afforded after column chromatography, elution with 50% CH_2Cl_2/50% *n*-hexane and crystallisation from CH_2Cl_2/*n*-hexane, a pale yellow powder identified as [Os{η^5-C_5Ph_4(*p*-^{t}Bu-C_6H_4)}$(CO)_2$Br] (**2**) (110 mg, 36%) m.p. > 210°C (dec.). (Found: C 59.2, H 4.2, Br 9.9. $C_{41}H_{33}BrO_2Os$ requires C 59.5, H 4.0, Br 9.7%). ^{1}H NMR (CD_2Cl_2, 200.13 MHz): δ 7.25–6.90 (m, 24H, Ar-*H*), 1.24 (s, 9H, ^{t}Bu) ppm. Mass spectrum: EI (*m*/*e*) 1193 ([Os(C_5Ph_4(*p*-^{t}BuC_6H_4))$_2$—H]$^+$, 37%), 772 [*M*—2CO]$^+$, 100%). IR (KBr) ν_{max} 3110 vw, 3091 vw, 3058 w, 3042 (sh), 2965 w, 2936 vw, 2905 vw, 2870 vw, 2026 vs, 1971 vs, 1684 vw, 1653 vw, 1602 vw, 1578 vw, 1559 vw, 1540 vw, 1520 vw, 1506 vw, 1502 vw, 1473 vw, 1457 vw, 1441 w, 1420 vw, 1396 vw, 1364 vw, 1269 vw, 1200 vw, 1185 vw, 1120 vw, 1108 vw, 1076 vw, 1027 vw, 1018 vw, 919 vw, 842 w, 797 vw, 756 w, 749 w, 737 w, 705 m, 699 m, 596 w, 581 w, 569 w, 558 w, 547 w, 501 vw, 493 vw, 464 w cm^{-1}. IR (CH_2Cl_2): *v* (CO) 2033 vs, 1977 vs cm^{-1}.

Preparation of [Os{η^5-C_5(*p*-MeC_6H_4)$_5$}$CO)_2$Br] (**3**)

Similarly, reaction of a mixture of $Os_3(CO)_{12}$ (235 mg, 0.259 mmol) and C_5(*p*-MeC_6H_4)$_5$Br (460 mg, 0.772 mmol) in chlorobenzene (60 ml) afforded after column chromatography, elution with 70% CH_2Cl_2/30% *n*-hexane and crystallisation from CH_2Cl_2/*n*-hexane, a pale yellow powder identified as [Os{η^5-C_5(*p*-MeC_6H_4)$_5$}$(CO)_2$Br] (**3**) (60 mg, 9%) m.p. > 210°C (dec.) (Found: C 60.1, H 4.1. $C_{42}H_{35}BrO_2Os$ requires C 59.9, H 4.2%). ^{1}H NMR (CD_2Cl_2, 200.13 MHz): δ 6.90 (m, 20H, Ar-*H*), 2.27 (s, 15H, Me) ppm. Mass spectrum: EI (*m*/*e*) 1221 ([Os(C_5(*p*-MeC_6H_4)$_5$)$_2$—H]$^+$, 100%), 786 ([*M*—2CO]$^+$, 97%), 515 (C_5(*p*-MeC_6H_4)$_5$, 88%). IR (KBr) ν_{max} 3133 vw, 3089 (sh), 3057 w, 3034 w, 3023 w, 2969 (sh), 2952 (sh), 2923 w, 2864 w, 2732 vw, 2026 vs, 2022 (sh), 1973 vs, 1970 (sh), 1942 vw, 1613 vw, 1520 w, 1456 vw, 1450 vw, 1437 vw, 1406 vw, 1398 vw, 1379 vw, 1188 w, 1119 vw, 1039 vw, 1021 vw, 844 vw, 833 w, 820 w, 805 w, 749 w, 728 w, 701 w, 595 w, 578 w, 556 w, 532 w, 526 vw, 495 vw, 468 vw, 443 w cm^{-1}. IR (CH_2Cl_2): *v* (CO) 2030 vs, 1974 vs cm^{-1}.

Preparation of $[Os(\eta^5\text{-}C_5Ph_5)(CO)(PMe_2Ph)Br]$ (**4**)

A portion of Me_3NO (18 mg, 0.24 mmol) was added to a mixture of $[Os(\eta^5\text{-}C_5Ph_5)(CO)_2Br]$ (141 mg, 0.183 mmol) and PMe_2Ph (0.030 ml, 0.21 mmol) in thf (25 ml) giving a colour change from yellow to orange-yellow. After stirring at room temperature for 1 h spot TLC (CH_2Cl_2/*n*-hexane 1 : 1) and solution IR (CH_2Cl_2) showed that no starting material remained. The reaction mixture was evaporated *in vacuo* and then column chromatography was performed. Elution with 50% CH_2Cl_2/50% *n*-hexane afforded an orange solution which after evaporation and crystallisation of the solid from CH_2Cl_2/*n*-hexane afforded orange crystals of $[Os(\eta^5\text{-}C_5Ph_5)(CO)(PMe_2Ph)Br]$ (**4**) (135 mg, 84%) m.p. $> 250°C$ (dec.). (Found: C 59.7, H 4.1, Br 8.7. $C_{44}H_{36}BrOOsP$ requires C 59.9, H 4.1, Br 9.1%). ^1H NMR (CD_2Cl_2, 200.13 MHz): δ 7.71–7.61, 7.31–7.26 (2 × m, 5H, P-Ar-*H*), 7.15–6.85 (m, 25H, Ar-*H*), 2.04 (d, *J* (PH) = 10 Hz, 3H, Me), 1.97 (d, *J* (PH) = 10 Hz, 3H, Me) ppm. ^{31}P $\{^1H\}$ NMR (CD_2Cl_2, 162.0 MHz): δ 100.3 ppm. Mass spectrum: EI (*m*/*e*) 882 ($[M]^+$, 95%), 854 ($[M—CO]^+$, 62%), 716 ($[M—CO—PMe_2Ph]^+$, 100%), 138 (PMe_2Ph, 89%). IR (KBr) ν_{max} 3154 vw, 3106 vw, 3085 vw, 3058 (sh), 3053 w, 3039 vw, 3031 (sh), 3006 vw, 2988 vw, 2915 vw, 1928 s, 1919 vs, 1600 w, 1580 vw, 1502 w, 1481 vw, 1445 w, 1436 w, 1415 vw, 1378 vw, 1317 vw, 1298 vw, 1284 vw, 1265 vw, 1181 vw, 1154 vw, 1099 vw, 1076 w, 1028 w, 1004 vw, 944 w, 914 w, 842 w, 799 w, 782 w, 747 (sh), 740 m, 707 m, 701 s, 682 w, 620 vw, 598 w, 592 w, 565 w, 561 w, 550 w, 533 vw, 514 w, 493 w, 434 w cm^{-1}. IR (CH_2Cl_2): *v* (CO) 1928 vs cm^{-1}.

Preparation of $[Os(\eta^5\text{-}C_5Ph_5)(CO)\{P(OEt)_3\}Br]$ (**5**)

A similar reaction and workup of $[Os(\eta^5\text{-}C_5Ph_5)(CO)_2Br]$ (112 mg, 0.145 mmol), $P(OEt)_3$ (0.030 ml, 0.173 mmol) and Me_3NO (15 mg, 0.20 mmol) in thf (22 ml) afforded yellow crystals of $[Os(\eta^5\text{-}C_5Ph_5)(CO)\{P(OEt)_3\}Br]$ (**5**) (97 mg, 74%) m.p. $> 230°C$ (dec.). (Found: C 55.9, H 4.6, Br 9.2. $C_{42}H_{40}BrO_4OsP$ requires C 55.4, H 4.4, Br 8.8%). ^1H NMR (CD_2Cl_2, 400.21 MHz): δ 7.14–7.00 (m, 25H, Ar-*H*), 4.23–3.98 (m (32 peaks), 6H, CH_2), 1.07 (t, 2*J* (HH) = 7 Hz, 9H, CH_3) ppm. ^{31}P $\{^1H\}$ NMR (CD_2Cl_2, 162.0 MHz): δ 214.0 ppm. Mass spectrum: EI (*m*/*e*) 910 ($[M]^+$, 11%), 882 ($[M—CO]^+$, 6%), 716 ($[M—CO—P(OEt)_3]^+$, 100%). IR (KBr) ν_{max} 3110 vw, 3087 vw, 3057 w, 3041 vw, 3033 vw, 2977 w, 2928 vw, 2905 vw, 2867 vw, 1947 (sh), 1936 vs, 1890 vw, 1602 w, 1503 w, 1445 w, 1392 w, 1319 vw, 1286 vw, 1183 vw, 1159 w, 1093 w, 1061 w, 1028 s, 955 m, 936 w, 849 vw, 801 w, 783 w, 765 w, 744 m, 711 m, 703 s, 678 vw, 668 vw, 622 vw, 591 w, 565 w, 559 w, 549 w, 537 w, 517 w, 482 vw cm^{-1}. IR (CH_2Cl_2): *v* (CO) 1940 vs cm^{-1}.

Preparation of $[Os(\eta^5\text{-}C_5Ph_5)(CO)\{P(OCH_2)_3CCH_3\}Br]$ (**6**)

A mixture of $[Os(\eta^5\text{-}C_5Ph_5)(CO)_2Br]$ (228 mg, 0.295 mmol), $P(OCH_2)_3CCH_3$ (125 mg, 0.844 mmol) and Me_3NO (37 mg, 0.49 mmol) in thf (30 ml) was stirred at room temperature for 24 h after which time column chromatography was performed. Elution with 50% CH_2Cl_2/50% *n*-hexane, evaporation of the solvent and crystallisation of the solid from CH_2Cl_2/*n*-hexane afforded $[Os(\eta^5\text{-}C_5Ph_5)(CO)_2Br]$ (**1**) (80 mg, 35%). Subsequent elution with 100% CH_2Cl_2 and crystallisation of the solid from CH_2Cl_2/*n*-hexane afforded bright yellow crystals of $[Os(\eta^5\text{-}C_5Ph_5)(CO)\{P(OCH_2)_3CCH_3\}Br]$ (**6**) (128 mg, 49%) m.p. $> 270°C$. (Found: C 55.1, H 3.7, Br 9.4. $C_{41}H_{34}BrO_4OsP$ requires C 55.2, H 3.8, Br 9.0%). ^1H NMR (CD_2Cl_2, 200.13 MHz): δ 7.19–7.03 (m, 25H, Ar-*H*), 4.23 (d, *J* (PH) = 5 Hz, 6H, CH_2), 0.76 (s, 3H, CH_3) ppm. ^{31}P $\{^1H\}$ NMR (CD_2Cl_2, 162.0 MHz): δ 216.7 ppm. Mass spectrum: EI (*m*/*e*) 892 ($[M]^+$, 26%), 864 ($[M—CO]^+$, 11%), 716 ($[M—CO—P(OCH_2)_3CCH_3]^+$, 100%). IR (KBr) ν_{max} 3108 vw, 3085 vw, 3055 w, 3037 vw, 3031 (sh), 2966 vw, 2960 (sh), 2943 vw, 2884 w, 1960 vs, 1952 (sh), 1912 vw, 1601 w, 1579 vw, 1501 w, 1484 vw, 1463 w, 1445 w, 1415 vw, 1395 w, 1184 w, 1174 w, 1155 vw, 1075 w, 1030 s, 988 vw, 959 w, 928 w, 860 w, 802 w, 795 m, 788 m, 742 w, 711 w, 700 m, 658 m, 621 vw, 587 w, 561 w, 547 w, 524 w, 516 w, 498 vw, 417 w cm^{-1}. IR (CH_2Cl_2): *v* (CO) 1963 vs cm^{-1}.

Preparation of $[Os(\eta^5\text{-}C_5Ph_5)(CO)(CNBu^t)Br]$ (**7**)

To a mixture of $[Os(\eta^5\text{-}C_5Ph_5)(CO)_2Br]$ (128 mg, 0.166 mmol) and ^{t}BuNC (0.030 ml, 0.27 mmol) in thf (25 ml) was added Me_3NO (16 mg, 0.21 mmol), giving a colour change from pale yellow to orange-yellow. After stirring at room temperature for 1 h, the solution IR *v* (CO) (CH_2Cl_2) showed that no starting material remained. The reaction mixture was evaporated to dryness (*in vacuo*) and column chromatography was performed. Elution with 70% CH_2Cl_2/30% *n*-hexane afforded a yellow-orange solution which after evaporation and crystallisation of the solid from CH_2Cl_2/*n*-hexane gave yellow crystals of $[Os(\eta^5\text{-}C_5Ph_5)(CO)(CNBu^t)Br]$ (**7**) (124 mg, 90%) m.p. $> 240°C$ (dec.). (Found: C 59.9, H, 4.1, Br 9.7, N 1.8. $C_{41}H_{34}BrNOOs$ requires C 59.6, H 4.1, Br 9.7, N 1.7%). ^1H NMR (CD_2Cl_2, 200.13 MHz): δ 7.20–7.05 (m, 25H, Ar-*H*), 1.40 (s, 9H, ^{t}Bu) ppm. Mass spectrum. EI (*m*/*e*) 827 ($[M]^+$, 26%), 799 ($[M—CO]^+$, 6%), 771 ($[M—C(CH_3)_2CH_2]^+$, 10%), 743 ($[M—CNBu^t—H]^+$, 67%), 716 ($[M—CO—CNBu^t]^+$, 100%). IR (KBr) ν_{max} 3110 vw, 3087 vw, 3084 vw, 3056 w, 3037 vw, 3033 vw, 2984 w, 2937 vw, 2147 m, 2072 (sh), 2024 vw, 1954 vs, 1905 vw, 1602 w, 1504 w, 1473 w, 1457 w, 1445 w, 1419 w, 1398 w, 1370 w, 1232 w, 1206 w, 1183 w, 1074 w, 1029 w, 919

w, 802 w, 783 w, 739 m, 698 vs, 587 w, 567 s, 555 w, 541 vw, 517 vw, 464 w cm^{-1}. IR (CH_2Cl_2): *v* (CN) 2156 m, *v* (CO) 1960 vs cm^{-1}.

Structure determinations

(a) $[Os(\eta^5\text{-}C_5Ph_5)(CO)_2Br]$ (**1**). Primitive orthorhombic cell constants were obtained from a least-square refinement against the setting angles of 25 reflections in the range $16.18 < 2\theta < 24.08^\circ$ measured and refined on an Enraf-Nonius CAD-4 four-circle diffractometer, employing graphite monochromated Mo–K_α radiation. The intensities of three representative reflections measured every hour did not change significantly during the course of the data collection. An analytical absorption correction was applied to the data and the data were also corrected for Lorentz and polarisation effects. All calculations were performed using the teXsan [61] crystallographic software package. The structure was solved in the space group PBCA (#61) by direct methods [62] and expanded using Fourier techniques [63]. Non-hydrogen atom sites were modelled anisotropically and hydrogen parameters were included in the full matrix least squares refinement with calculated positions and group temperature factors. Neutral atom scattering factors were taken from Cromer and Waber [64]. Anomalous dispersion effects were included in the structure factor calculation [65], and the values for $\Delta f'$ and $\Delta f''$ were those of Creagh and McAuley [66]. The values for the mass attenuation coefficients are those of Creagh and Hubbel [67].

Crystal data for $[Os(\eta^5\text{-}C_5Ph_5)(CO)_2Br]$ (**1**)

$C_{37}H_{25}BrO_2Os$, M = 771.71, orthorhombic, space group, PBCA (#61), $a = 18.028(3)$, $b = 14.921(2)$, $c = 21.718(3)$ Å, $U = 5842(1)$ Å^3, $D_c(Z = 8) = 1.76$ g cm^{-3}, $F(000) = 2992$, μ (Mo–K_α) = 57.67 cm^{-1}. Specimen: yellow blade, $0.525 \times 0.125 \times 0.012$ mm. $N = 4162$, $N_{unique} = 3976$, $N_o = 2249$, range of *hkl* $0 \to 15$, $0 \to 18$, $0 \to 22$, $R_{merge} = 0.166$, $R = 0.040$, $R_w = 0.043$, residual extrema -1.15 and 1.01 eÅ^3, $T_{min,max} = 0.27, 0.86$.

(b) $[Os(\eta^5\text{-}C_5Ph_5)(CO)\{P(OCH_2)_3CCH_3\}Br]$ (**6**). Lattice parameters at 21°C were obtained from a least squares refinement to the setting angles of 25 reflections in the range $19.77 < 2\theta < 113.36^\circ$, measured and refined on a Rigaku AFC7R diffractometer, employing graphite monochromated CuKα radiation, generated from a direct drive rotating anode. Intensity data were collected with $\omega/2\theta$ scans to a maximum 2θ value of 120.1°, with a scan width of $(1.1 + 0.35 \tan\theta)^\circ$. An empirical absorption correction based on azimuthal scans of three reflections was applied to the data. The data were corrected for Lorentz and polarisation effects and a small correction for secondary extinction applied (coefficient = 1.11 $\times 10^{-6}$). All calculations were performed using the teXsan structure determination software package [61]. The structure was solved by direct methods [68] and extended with Fourier maps [63]. The refinement weighting scheme was based on counting statistics. Generally the non-hydrogen atoms were refined anisotropically, and the hydrogen atoms were included in the full matrix least squares refinement at calculated positions with group temperature factors. The carbonyl and bromide ligands were found to be site disordered. Although the carbonyl groups could be located they could not be successfully refined; possibly because of orientation disorder or a consequence of the site disorder. Neutral atom scattering factors were taken from Cromer and Waber [64]. Anomalous dispersion effects were included in the structure factor calculation [65], and the values for $\Delta f'$ and $\Delta f''$ were those of Creagh and McAuley [66]. The values for the mass attenuation coefficients are those of Creagh and Hubbel [67].

Crystal data for $[Os(\eta^5\text{-}C_5Ph_5)(CO)\{P(OCH_2)_3CCH_3\}Br]$ (**6**)

$C_{41}H_{34}BrO_4OsP$, M = 891.80, monoclinic, space group, $P2_1/n$ (#14), $a = 12.230(3)$, $b = 16.135(9)$, $c = 18.331(3)$ Å, $\beta = 101.63(2)$, $U = 3543(1)$ Å^3, $D_c(Z = 4) = 1.672$ g cm^{-3}, $F(000) = 1752$, μ (Cu-K_α) = 88.89 cm^{-1}. Specimen: yellow prism, $0.260 \times 0.250 \times 0.140$ mm. $N = 5787$, $N_{unique} = 5496$, $N_o = 4242$, range of *hkl* $0 \to 13$, $0 \to 18$, $-20 \to 20$, $R_{merge} = 0.0327$, $R = 0.066$, $R_w = 0.073$, residual extrema -2.75 and 2.31 eÅ^3, $T_{min,max} = 0.48, 0.98$.

CONCLUSION

The preparation and crystal structure of $[Os(\eta^5\text{-}C_5Ph_5)(CO)_2Br]$, the first osmium complex of the pentaphenylcyclopentadienyl ligand, has been described. This completes the preparation and characterisation of the iron-triad $[M(\eta^5\text{-}C_5Ph_5)(CO)_2Br]$ series of this ligand. The crystal structure of the osmium complex is isostructural with those of its iron and ruthenium analogues. The osmium complex is stable in air and readily undergoes monocarbonyl substitution with a variety of ligands. The crystal structure of one such resultant complex, $[Os(\eta^5\text{-}C_5Ph_5)(CO)\{P(OCH_2)_3CCH_3\}Br]$, is also reported.

Acknowledgements—We thank the Australian Research Council for financial support and Dr M. J. Aroney for the gift of $P(OCH_2)_3CCH_3$.

REFERENCES

1. Bruce, M. I., Tomkins, B., Wong, F. S., Skelton, B. W. and White, A. H., *J. Chem. Soc., Dalton Trans.*, 1982, 687.

2. Hoyano, J. K. and Graham, W. A. G., *J. Am. Chem. Soc.*, 1982, **104,** 3722.
3. Bruce, M. I., Williams, M. L., Patrick, J. M. and White, A. H., *Aust. J. Chem.*, 1983, **36,** 1353.
4. Bruce, M. I., Hambley, T. W., Snow, M. R. and Swincer, A. G., *J. Organomet. Chem.*, 1984, **273,** 361.
5. Gallop, M. A., Johnson, B. F. G., Lewis, J. and Raithby, P. R., *J. Chem. Soc., Chem. Commun.*, 1986, 706.
6. Pourreau, D. B., Geoffroy, G. L., Rheingold, A. L. and Geib, S. J., *Organometallics*, 1986, **5,** 1337.
7. Albers, M. O., Liles, D. C., Robinson, D. J., Shaver, A., Singleton, E., Wiege, M. B., Boeyens, J. C. A. and Levendis, D. C., *Organometallics*, 1986, **5,** 2321.
8. Droege, M. W., Harman, W. D. and Taube, H., *Inorg. Chem.*, 1986, **26,** 1309.
9. Boeyens, J. C. A., Levendis, D. C., Bruce, M. I. and Williams, M. L., *J. Cryst. Spectrosc.*, 1986, **16,** 519.
10. Droege, M. W. and Taube, H., *Inorg. Chem.*, 1987, **26,** 3316.
11. O'Hare, D., Green, J. C., Chadwick, T. P. and Miller, J. S., *Organometallics*, 1988, **7,** 1335.
12. Rybinskaya, M. I., Kreindlin, A. Z., Struchkov, Y. T. and Yanovsky, A. I., *J. Organomet. Chem.*, 1989, **359,** 233.
13. Lumme, P. O., Turpeinen, U., Kudinov, A. R. and Rybinskaya, M. I., *Acta Crystallogr. C* (*Cryst. Str. Comm.*), 1990, **46,** 1410.
14. Abel, E. W., Long, N. J., Osborne, A. G., Hursthouse, M. B. and Mazid, M. A., *J. Organomet. Chem.*, 1992, **430,** 117.
15. Turpeinen, U., Kreindlin, A. Z., Petrovskii, P. V. and Rybinskaya, M. I., *J. Organomet. Chem.*, 1992, **441,** 109.
16. Rottink, M. K. and Angelici, R. J., *J. Am. Chem. Soc.*, 1993, **115,** 7267.
17. Wang, W., Einstein, F. W. B. and Pomeroy, R. K., *Organometallics*, 1993, **12,** 3079.
18. Wang, W., Davis, H. B., Einstein, F. W. B. and Pomeroy, R. K., *Organometallics*, 1994, **13,** 5113.
19. Yamazaki, Y., Goto, M., Kobayashi, K., Ogawa, Y., Shimura, T., Oka, S. and Okuno, H., *Bioorg. Med. Chem. Lett.*, 1994, **4,** 483.
20. Gross, C. L., Wilson, S. R. and Girolami, G. S., *J. Am. Chem. Soc.*, 1994, **116,** 10294.
21. Goto, M., Yamazaki, Y., Honda, K. and Masaki, A., *Bull. Chem. Soc. Jpn*, 1995, **68,** 1305.
22. Bruce, M. I., Low, P. J., Skelton, B. W., Tiekink, E. R. T., Werth, A. and White, A. H., *Aust. J. Chem.*, 1995, **48,** 1887.
23. Hoyano, J. K., May, C. J. and Graham, W. A. G., *Inorg. Chem.*, 1982, **21,** 3095.
24. McVey, S. and Pauson, P. L., *J. Chem. Soc.*, 1965, 4312.
25. Field, L. D., Masters, A. F., Gibson, M., Latimer, D. R., Hambley, T. W. and Buys, I. E., *Inorg. Chem.*, 1993, **32,** 211.
26. Connelly, N. G. and Manners, I., *J. Chem. Soc., Dalton Trans.*, 1989, 283.
27. Thewalt, U. and Schmidt, G., *J. Organomet. Chem.*, 1991, **412,** 343.
28. Hoobler, R. J., Hutton, M. A., Dillard, M. M., Castellani, M. P., Rheingold, A. L., Rieger, A. L., Rieger, P. H., Richards, T. C. and Geiger, W. E., *Organometallics*, 1993, **12,** 116.
29. Hammack, D. J., Dillard, M. M., Castellani, M. P., Rheingold, A. L., Rieger, A. L., and Rieger, P. H., *Organometallics*, 1996, **15,** 4791.
30. Field, L. D., Hambley, T. W., Lindall, C. M. and Masters, A. G., *Polyhedron*, 1989, **8,** 2425.
31. Field, L. D., Hambley, T. W., Lay, P. A., Lindall, C. M. and Masters, A. F., *J. Chem. Soc., Dalton Trans.*, 1991, 1499.
32. Aroney, M. J., Buys, I. E., Dennis, G. D., Field, L. D., Hambley, T. W., Lay, P. A. and Masters, A. F., *Polyhedron*, 1993, **12,** 2051.
33. Schumann, H., Lentz, A., Weimann, R. and Pickardt, J., *Ang. Chem. Int. Ed. Engl.*, 1994, **33,** 1731.
34. Li, L., Decken, A., Sayer, B. G., McGlinchey, M. J., Brégaint, P., Thépot, J.-Y., Toupet, L., Hamon, J.-R. and Lapinte, C., *Organometallics*, 1994, **13,** 682.
35. Field, L. D., Gainsford, G. J., Hambley, T. W., Humphrey, P. A., Lindall, C. M., Masters, A. F., Pierre, T. G. S. and Webb, J., *Aust. J. Chem.*, 1995, **48,** 851.
36. Chambers, J. W., Baskar, A. J., Bott, S. G., Atwood, J. L. and Rausch, M. D., *Organometallics*, 1986, **5,** 1635.
37. Ficker, R., Hiller, W., Drobnik, S. and Lorenz, I. P., *Z. Krystallogr.*, 1996, **211,** 845.
38. Hoberg, H., Krause-Göing, R., Krüger, C. and Sekutowski, J. C., *Angew. Chem. Int. Ed. Engl.*, 1977, **16,** 183.
39. Huhn, M., Kläui, W., Ramacher, L., Herbst-Irmer, R. and Egert, E., *J. Organomet. Chem.*, 1990, **398,** 339.
40. Kläui, W., Huhn, M. and Herbst-Irmer, R., *J. Organomet. Chem.*, 1991, **415,** 133.
41. Matt, D., Huhn, M., Fischer, J., Cian, A. D., Kläui, W., Tkatchenko, I. and Bonnet, M. C., *J. Chem. Soc., Dalton Trans.*, 1993, 1173.
42. Matt, D., Huhn, M., Bonnet, M., Tkatchenko, I., Englert, U. and Kläui, W., *Inorg. Chem.*, 1995, **34,** 1288.
43. Field, L. D., Hambley, T. W., He, T., Humphrey, P. A., Lindall, C. M. and Masters, A. F., *Aust. J. Chem.*, 1996, **49,** 889.
44. Janiak, C., Schwichtenberg, M. and Hahn, F. E., *J. Organomet. Chem.*, 1989, **365,** 37.
45. Song, L.-C., Hu, Q.-M., Yang, J.-S., Cao, X.-C., Wang, R.-J. and Mak, T. C. W., *Inorg. Chim. Acta*, 1996, **245,** 109.
46. Slocum, D. W., Matusz, M., Clearfield, A., Peascoe, R. and Duraj, S., *J. Macromol. Sci. Chem.*, 1990, **27A,** 1405.
47. Adams, H., Bailey, N. A., Browning, A. F., Ramsden, J. A. and White, C., *J. Organomet. Chem.*, 1990, **387,** 305.
48. Behrens, U. and Edelmann, F., *Z. Naturforsch., B*, 1986, **41,** 1426.
49. Baghdadi, J., Bailey, N. A., Dowding, A. S. and White, C., *J. Chem. Soc., Chem. Commun.*, 1992, 170.
50. Ban, E., Cheng, P.-T., Jack, T., Nyburg, S. C. and Powell, J., *J. Chem. Soc., Chem. Commun.*, 1973, 368.
51. Jack, T. R., May, C. J. and Powell, J., *J. Am. Chem. Soc.*, 1977, **99,** 4707.

52. Connelly, N. G., Geiger, W. E., Orpen, A. G., Orsini, J. J. J. and Richarson, K. E., *J. Chem. Soc., Dalton Trans.*, 1991, 2967.
53. Tanase, T., Fukushima, T., Nomura, T., Yamamoto, Y. and Kobayashi, K., *Inorg. Chem.*, 1994, **33,** 32.
54. Heeg, M. J., Janiak, C. and Zuckerman, J. J., *J. Am. Chem. Soc.*, 1984, **106,** 4259.
55. Heeg, M. J., Herber, R. H., Janiak, C., Zuckerman, J. J., Schumann, H. and Manders, W. F., *J. Organomet. Chem.*, 1988, **346,** 321.
56. Yeh, W.-Y., Ho, C.-L., Chiang, M. Y. and Chen, I.-T., *Organometallics*, 1997, **16,** 2698.
57. Burke, M. R., Funk, T., Takats, J. and Day, V. W., *Organometallics*, 1994, **13,** 2109.
58. Brégaint, P., Hamon, J.-R. and Lapinte, C., *Organometallics*, 1992, **11,** 1417.
59. Field, L. D., Ho, K. M., Lindall, C. M., Masters, A. F. and Webb, A. G., *Aust. J. Chem.*, 1990, **43,** 281.
60. Deeming, A. J., Johnson, B. F. G. and Lewis, J., *J. Chem. Soc.* (*A*), 1970, 897.
61. Molecular Structure Corporation, TeXsan: Single Crystal Structure Analysis Software, Version 1.6, Molecular Structure Corporation, The Woodlands, TX, U.S.A., 1993.
62. Sheldrick, G. M., *SHELXS*-86. Oxford University Press, Oxford, U.K., 1985.
63. Beurskens, P. T., Admiraal, G., Beurskens, G., Bosman, W. P., de Gelder, R., Israel, R. and Smits, J. M. M., *The DIRDIF*-94 *Program System*. Technical Report. Crystallography Laboratory, University of Nijmegen, The Netherlands, DIRDIF-94, Nijmegen, 1994.
64. Cromer, D. T. and Waber, J. T., In *International Tables for X-Ray Crystallography*, Vol. IV, ed. J. A. Ibers and W. C. Hamilton, Kynock Press, Birmingham, U.K., 1974, p. 71.
65. Ibers, J. A. and Hamilton, W. C., *Acta Crystallogr.*, 1964, **17,** 781.
66. Creagh, D. C. and McAuley, W. J., In *International Tables for Crystallography*, Vol. C, ed. A. J. C. Wilson, Kluwer Academic Publishers, Boston, 1992, p. 219.
67. Creagh, D. C. and Hubbell, J. H., In *International Tables for Crystallography* Vol. C, ed. A. J. C. Wilson, Kluwer Academic Publishers, Boston, 1992, p. 200.
68. Altomare, A., Cascarano, M., Giacovazzo, C. and Guagliardi, A., *J. Appl. Cryst.*, 1993, **26,** 343.
69. Johnson, C. K., ORTEP, a Thermal Ellipsoid Plotting Program, Report ORNL-5138, Oak Ridge National Laboratories, Oak Ridge, TN, 1976.

Pergamon

PII: S0277–5387(97)00395–1

Polyhedron Vol. 17, No. 16, pp. 2599–2605, 1998
© 1998 Elsevier Science Ltd
All rights reserved. Printed in Great Britain
0277–5387/98 $19.00+0.00

Hydrothermal synthesis and characterization of an unusual polyoxovanadium borate cluster: structure of $Rb_4[(VO)_6\{B_{10}O_{16}(OH)_6\}_2]\cdot 0.5H_2O$

Christopher J. Warren,[a,†] Job T. Rijssenbeek,[a] David J. Rose,[b] Robert C. Haushalter[a†*] and Jon Zubieta[b*]

[a]NEC Research Institute, 4 Independence Way, Princeton, NJ 08540, U.S.A.

[b]Department of Chemistry, Syracuse University, Syracuse, NY 13244, U.S.A.

(Received 16 June 1997; accepted 24 September 1997)

Abstract—The hydrothermal reaction of $RbVO_3$, $(NH_4)_2B_4O_7\cdot 4H_2O$, ethylenediamine (en), and H_2O in a mole ratio of 1:8:2:135 heated at 170°C for 5 days produces pale green crystals of the novel polyoxovanadium borate cluster compound $Rb_4[(VO)_6\{B_{10}O_{16}(OH)_6\}_2]\cdot 0.5H_2O$ (**1**) which contains $[V_6B_{20}O_{38}(OH)_{12}]^{4-}$ clusters, each cluster comprising a nearly hexagonal ring of six *trans*-edge-sharing VO_5 square pyramids capped on each side by a $B_{10}O_{16}(OH)_6^{8-}$ triangle. The $[V_6B_{20}O_{38}(OH)_{12}]^{4-}$ clusters are separated in the solid state by Rb^+ cations. Magnetic susceptibility and valence sum calculations indicate that all six of the vanadium atoms in the cluster are in the 4+ oxidation state. © 1998 Elsevier Science Ltd. All rights reserved. © 1998 Elsevier Science Ltd. All rights reserved

Keywords: hydrothermal synthesis; polyoxovanadium borates; polyoxometalates; X-ray structures.

INTRODUCTION

The chemistry of polyoxometalates incorporates a rich and diverse agglomeration of compounds unique in their topological and electronic properties, making them applicable in fields ranging from analytical and clinical chemistry, to catalysis (including photocatalysis), biochemistry (electron transport inhibition), medicine (antitumoral and antiviral), and solid state devices [1]. Metal-metal interactions in the oxo clusters range from very weak (virtually none) to very strong (metal-metal bonding) and can be controlled by choice of metal (3d, 4d, 5d), electron population (degree of reduction), and extent of protonation. It has been observed that mixed-valence vanadates, in particular, show highly variable capacities for unpaired electrons, and many form clusters containing highly symmetrical core assemblies of VO_x units that can adopt quasi-spherical structures [2]. Although the chemistry of the polyoxovanadates (a subset of the polyoxometalates) is very diverse, only a few structural motifs, which are based largely on edge and corner sharing VO_5 square pyramids, are actually observed [3]. The polyoxovanadium borates (a subset of the polyoxovanadates) remain largely unexplored, and although a large number of borate mineral structures are known [4], synthetically prepared and structurally characterized examples are rare [5]. Having recently isolated the polyoxovanadium borates $(enH)(enH_2)_4[(VO)_{12}B_{17}O_{38}(OH)_8]\cdot H_2O$ (en = ethylenediamine) and $(enH_2)_5[(VO)_{12}O_6\{B_3O_6(OH)\}_6]\cdot H_2O$ [6], which were prepared by hydrothermal synthetic techniques, we were encouraged to further explore this potentially rich and structurally diverse system. We report herein the synthesis of a novel polyoxovanadium borate cluster species, $Rb_4[(VO)_6\{B_{10}O_{16}(OH)_6\}_2]\cdot 0.5H_2O$ (**1**), containing a hexavanadate core and polyborate ligands of unprecedented structure.

*Author to whom correspondence should be addressed.

†Current mailing address: SymyX Technologies, 3100 Central Expressway, Santa Clara, CA 95051, U.S.A.

EXPERIMENTAL

General

Compound (**1**) was prepared by the hydrothermal reaction of $RbVO_3$ (0.114 g) $(NH_4)_2B_4O_7 \cdot 4H_2O$ (1.30 g), ethylenediamine (0.074 g), and H_2O in a 1:8:2:135 molar ratio heated at 170°C for 5 days. The syntheses were conducted in 23 mL polytetrafluoroethylene-lined acid digestion bombs filled to ca. 8% at room temperature. In all cases, the borate was added first, followed by the vanadium source, water, and finally the amine. This preparation gave a nearly single phase of pale green plate-shaped crystals of $Rb_4[(VO)_6\{B_{10}O_{16}(OH)_6\}_2] \cdot 0.5H_2O$ (**1**) which were isolated in approximately 45% yield with a minor phase (ca. 1–2%) of orange crystals. An X-ray structural analysis of the orange crystals revealed that they contained the previously characterized $[(VO)_{12}O_6\{B_3O_6(OH)\}_6]^{10-}$ cluster [6]. The role of the ethylenediamine (en) in the preparation is currently under investigation as this species appears to be needed in the syntheses (perhaps to adjust the pH of the reactions which are typically in the 8–9 range) although it is not incorporated in the final structure. Indeed, experiments using equimolar amounts of 1,3-diaminopropane (DAP) in place of en resulted in nearly the same yield of (**1**), but if neither en nor DAP are used, no crystals are obtained [7].

Crystallography

A single crystal of (**1**) having approximate dimensions of $0.17 \times 0.12 \times 0.11$ mm was mounted on a glass fiber. A total of 14,207 reflections were collected on a Siemens SMART system equipped with a CCD detector at 293 K in the θ range of 2.08° to 28.25°, of which 5390 ($R_{int} = 0.0456$) were considered observed [($I \geq 3.0\sigma$ (I)] and 5384 were used in the final refinement. The structure was solved by direct methods and refined by full-matrix least-squares on F^2 using SHELXTL. All of the non-hydrogen atoms were refined with anisotropic displacement parameters. The Rb^+ atoms were disordered and refined with 50% occupancy factors. The final cycle of least-squares using 421 variable parameters converged with $R(R_w) = 0.0366(0.0472)$ and a goodness-of-fit value of 1.021. The largest (smallest) peak in the final difference map was 0.947(−0.582) eÅ^{-3}. Further details of the X-ray structural analysis are given in Table 1, and some selected bond lengths and angles are given in Table 2. A complete listing of atomic coordinates, thermal parameters and F_{obs}/F_{calc} values have been deposited at the Cambridge Crystallographic Data Centre.

Magnetic Susceptibility

Magnetic susceptibility measurements were done on a Quantum Design MPMS SQUID magnetometer.

Table 1. Crystallographic Data for $Rb_4[(VO)_6\{B_{10}O_{16}(OH)_6\}_2] \cdot 0.5H_2O$

Formula	$Rb_4V_6B_{20}O_{50.5}H_7$
FW	1678.28
Crystal Color, Habit	Green, Plate
a(Å)	11.9932(3)
b(Å)	12.74480(10)
c(Å)	14.9514(2)
β(°)	95.7320(10)
V(Å^3)	2273.85(4)
Z	2
Space Group	$P\,2_1/n$ (No.14)
D_{calc}(ġcm^{-3})	2.452
μ (mm^{-1})	5.574
Crystal Size (mm)	0.17x0.12x0.11
θ range for Data Collection (°)	2.08 to 28.25
No. of Data Collected	14207
Data $I \geq 3\sigma(I)$	5390
No. of Variables	420
Final R/R_w	0.0366/0.04572

The data from 100 to 300 K were fit to the Curie–Weiss law and gave an effective moment per vanadium atom of 1.71 μ_B. This agrees well with the theoretical value of 1.73 μ_B for a free spin d^1 (V^{4+}) system.

RESULTS AND DISCUSSION

The $V_6B_{20}O_{50}$ clusters in $Rb_4[(VO)_6\{B_{10}O_{16}(OH)_6\}_2] \cdot 0.5H_2O$ (**1**) can be visualized most easily as being composed of a nearly hexagonal ring of six *trans*-edge-sharing VO_5 square pyramids (Fig. 1) capped on each side by a $B_{10}O_{16}(OH)_6^{8-}$ triangle (Fig. 2). All six of the terminal vanadyl (V=O) groups in this hexagonal vanadate, whose toroid structure is unprecedented among polyoxometalate species, radiate outwardly from the cluster, and have V–O bond distances ranging from 1.612(2)–1.624(2) Å. The $B_{10}O_{16}(OH)_6^{8-}$ caps are composed of three fused $B_3O_5(OH)_3^{4-}$ FBB's (fundamental building blocks) [8] that share oxygen atoms with a central tetrahedral BO_4 group. This tetrahedral BO_4 group possesses a terminal B–O$^-$ bond that is collinear with the pseudo $\bar{3}$ axis of the cluster, and the two $B_{10}O_{16}(OH)_6^{8-}$ caps are related by twofold symmetry about one of the three two-fold axes bisecting the vanadium ring. Of the six-OH groups that radiate out from the triangular $B_{10}O_{16}(OH)_6^{8-}$ units, three are bonded to trigonal planar boron atoms and have B–O bond distances ranging from 1.385(4)–1.378(4) Å, while the other three (which were identified using valence bond calculations) [9] are shared between adjacent tetrahedral boron atoms having B–O bond distances ranging from 1.425(4)–1.439(4) Å. The central tetrahedral BO_4 group has three internal B–O bond distances of 1.495(4), 1.493(4), and 1.488(4) Å, and a significantly shorter terminal B–O bond distance of 1.424(4) Å

Table 2. Selected Bond Lengths (Å) and Bond Angles (°) in $Rb_4[(VO)_6\{B_{10}O_{16}(OH)_6\}_2]\cdot 0.5H_2O$

V(1)–O(1)	1.612(2)	V(1)–O(13)	1.944(2)
V(1)–O(4)	1.963(2)	V(1)–O(17)	1.967(2)
V(1)–O(8)	1.968(2)	V(1)–V(3)#1	3.0481(7)
V(1)–V(2)	3.0758(7)	V(2)–O(2)	1.624(2)
V(2)–O(8)	1.948(2)	V(2)–O(20)	1.952(2)
V(2)–O(11)	1.956(2)	V(2)–O(17)	1.960(2)
V(2)–V(3)	3.0139(7)	V(3)–O(3)	1.620(2)
V(3)–O(13)#1	1.951(2)	V(3)–O(20)	1.955(2)
V(3)–O(4)#1	1.960(2)	V(3)–O(11)	1.971(2)
V(3)–V(1)#1	3.0481(7)	O(4)–B(1)	1.466(4)
O(4)–V(3)#1	1.960(2)	O(5)–B(2)	1.425(4)
O(5)–B(1)	1.434(4)	O(6)–B(7)	1.357(4)
O(6)–B(1)	1.453(4)	O(7)–B(10)#1	1.493(4)
O(7)–B(6)#1	1.532(4)	O(7)–B(1)	1.536(4)
O(8)–B(2)	1.457(4)	O(9)–B(10)#1	1.487(4)
O(9)–B(3)	1.526(4)	O(9)–B(2)	1.542(4)
O(10)–B(8)	1.355(4)	O(10)–B(2)	1.464(4)
O(11)–B(3)	1.481(4)	O(12)–B(8)	1.366(4)
O(12)–B(3)	1.470(4)	O(13)–B(4)	1.467(4)
O(13)–V(3)#1	1.951(2)	O(14)–B(10)	1.495(4)
O(14)–B(5)	1.526(4)	O(14)–B(4)	1.529(4)
O(15)–B(9)	1.359(4)	O(15)–B(4)	1.469(4)
O(16)–B(4)	1.433(4)	O(16)–B(3)#1	1.439(4)
O(17)–B(5)	1.474(4)	O(18)–B(5)	1.429(4)
O(18)–B(6)	1.435(4)	O(19)–B(9)	1.371(4)
O(19)–B(5)	1.464(4)	O(20)–B(6)	1.477(4)
O(21)–B(7)	1.368(4)	O(21)–B(6)#1	1.463(4)
O(22)–B(7)	1.385(4)	O(23)–B(8)	1.384(5)
O(24)–B(9)	1.378(4)	O(25)–B(10)	1.424(4)
B(3)–O(16)#1	1.439(4)	B(6)–O(21)#1	1.463(4)
B(6)–O(7)#1	1.532(4)	B(10)–O(9)#1	1.487(4)
B(10)–O(7)#1	1.493(4)		
O(1)–V(1)–O(13)	106.86(11)	O(1)–V(1)–O(4)	110.04(11)
O(13)–V(1)–O(4)	77.03(9)	O(1)–V(1)–O(17)	107.38(11)
O(13)–V(1)–O(17)	91.67(9)	O(4)–V(1)–O(17)	142.57(9)
O(1)–V(1)–O(8)	111.87(11)	O(13)–V(1)–O (8)	141.25(9)
O(4)–V(1)–O(8)	90.84(9)	O(17)–V(1)–O(8)	75.82(9)
O(1)–V(1)–V(3)#1	118.72(9)	O(13)–V(1)–V(3)#1	38.57(6)
O(4)–V(1)–V(3)#1	38.98(6)	O(17)–V(1)–V(3)#1	118.16(7)
O(8)–V(1)–V(3)#1	117.16(6)	O(1)–V(1)–V(2)	120.05(g)
O(13)–V(1)–V(2)	117.48(7)	O(4)–V(1)–V(2)	117.36(7)
O(17)–V(1)–V(2)	38.35(6)	O(8)–V(1)–V(2)	38.00(6)
V(3)#1–V(1)–V(2)	121.16(2)	O(2)–V(2)–O(8)	109.81(11)
O(2)–V(2)–O(20)	108.42(11)	O(8)–V(2)–O(20)	141.72(9)
O(2)–V(2)–O(11)	108.27(11)	O(8)–V(2)–O(11)	90.94(9)
O(20)–V(2)–O(11)	78.91(9)	O(2)–V(2)–O(17)	109.52(11)
O(8)–V(2)–O(17)	76.47(9)	O(20)–V(2)–O(17)	89.21(9)
O(11)–V(2)–O(17)	142.22(9)	O(2)–V(2)–V(3)	119.80(9)
O(8)–V(2)–V(3)	117.28(7)	O(20)–V(2)–V(3)	39.56(6)
O(11)–V(2)–V(3)	40.04(6)	O(17)–V(2)–V(3)	116.02(7)
O(2)–V(2)–V(1)	120.30(9)	O(8)–V(2)–V(1)	38.47(6)
O(20)–V(2)–V(1)	116.05(7)	O(11)–V(2)–V(1)	117.43(7)
O(17)–V(2)–V(1)	38.53(6)	V(3)–V(2)–V(1)	119.89(2)
O(3)–V(3)–O(13)#1	109.74(11)	O(3)–V(3)–O(20)	109.95(11)
O(13)#1–V(3)–O(20)	140.31(9)	O(3)–V(3)–O(4)#1	108.20(11)
O(13)#1–V(3)–O(4)#1	76.93(9)	O(20)–V(3)–O(4)#1	90.58(9)
O(3)–V(3)–O(11)	109.69(11)	O(13)#1–V(3)–O(11)	88.56(9)
O(20)–V(3)–O(11)	78.48(9)	O(4)#1–V(3)–O(11)	142.06(9)
O(3)–V(3)–V(2)	121.66(9)	O(13)#1–V(3)–V(2)	114.74(7)
O(20)–V(3)–V(2)	39.48(6)	O(4)#1–V(3)–V(2)	116.92 (7)
O(11)–V(3)–V(2)	39.69(6)	O(3)–V(3)–V(1)#1	119.41(9)
O(13)#1–V(3)–V(1)#1	38.41(6)	O(20)–V(3)–V(1)#1	116.55(7)

continued

Table 2—*continued.*

O(4)#1–V(3)–V(1)#1	39.04(6)	O(11)–V(3)–V(1)#1	115.66(7)
V(2)–V(3)–V(1) #1	118.92(2)	B (1)–O(4)–V(3) #1	129.0 (2)
B(1)–O(4)–V(1)	124.4(2)	V(3)#1–O(4)–V(1)	101.98(10)
B(2)–O(5)–B(1)	117.6(2)	B(7)–O(6)–B(1)	121.2(3)
B(10)#1–O(7)–B(6)#1	122.5(2)	B(10)#1–O(7)–B(1)	122.1(2)
B(6)#1–O(7)–B(1)	114.7(2)	B(2)–O(8)–V(2)	128.2 (2)
B(2)–O(8)–V(1)	125.1(2)	V(2)–O(8)–V(1)	103.53 (10)
B(10)#1–O(9)–B(3)	122.2(2)	B(10)#1–O(9)–B(2)	122.5(2)
B(3)–O (9)–B (2)	115.3 (2)	B(8)–O(10)–B(2)	122.2 (3)
B(3)–O(11)–V(2)	128.1 (2)	B(3)–O(11)–V(3)	126.7 (2)
V(2)–O(11)–V(3)	100.27(9)	B(8)–O(12)–B(3)	120.7(3)
B(4)–O(13)–V(1)	126.9(2)	B(4)–(13)–V(3)#1	127.4(2)
V(1)–O(13)–V(3)#1	103.01(10)	B(10)–O(14)–B(5)	121.3(2)
B(10)–O(14)–B(4)	121.6(2)	B(5)–O(14)–B(4)	117.1(2)
B(5)–O(15)–B(4)	121.5(3)	B(4)–O(16)–B(3)#1	116.9(2)
B(5)–O(17)–V(2)	126.5(2)	B(5)–O(17)–V(1)	127.1(2)
V(2)–O(17)–V(1)	103.11(10)	B (5)–O(18)–B(6)	115.7 (2)
B(9)–O(19)–B(5)	121.1(3)	B(6)–O(20)–V(2)	126.4(2)
B(6)–O(20)–V(3)	128.0(2)	V(2)–O(20)–V(3)	100.96(10)
B(7)–O(21)–B(6)#1	120.9(3)	O(5)–B(1)–O(6)	108.5(2)
O(5)–B(1)–O(4)	112.3(3)	O(6)–B(1)–O(4)	111.9(3)
O(5)–B(1)–O(7)	108.9(2)	O(6)–B(1)–O(7)	108.1(2)
O(4)–B(1)–O(7)	107.0(2)	O(5)–B(2)–O(8)	112.2(3)
O(5)–B(2)–O(10)	110.1(2)	O(8)–B(2)–O(10)	111.2(2)
O(5)–B(2)–O(9)	108.4(2)	O(8)–B(2)–O(9)	107.7(2)
O(10)–B(2)–O(9)	107.0(2)	O(16)#1–B(3)–O(12)	111.3(3)
O(16)#1–B(3)–O(11)	111.3(2)	O(12)–B(3)–O(11)	109.6(2)
O(16)#1–B(3)–O(9)	108.3(2)	O(12)–B(3)–O(9)	108.0(2)
O(11)–B(3)–O(9)	108.2(2)	O(16)–B(4)–O(13)	112.1(2)
O(16)–B(4)–O(15)	111.7 (2)	O(13)–B(4)–O (15)	109.3(3)
O(16)–B(4)–O(14)	108.5(2)	O(13)–B(4)–O(14)	107.7(2)
O(15)–B(4)–O(14)	107.4(2)	O(18)–B(5)–O(19)	110.8(3)
O(18)–B(5)–O(17)	112.4 (3)	O(19)–B(5)–O (17)	108.6(2)
O(18)–B(5)–O(14)	109.8(2)	O(19)–B(5)–O(14)	107.5(2)
O(17)–B(5)–O(14)	107.5(2)	O(18)–B(6)–O(21)#1	110.0(2)
O(18)–B(6)–O(20)	112.1(2)	O(21)#1–B(6)–O(20)	109.9(3)
O(18)–B(6)–O(7)#1	108.5(2)	O(21)#1–B(6)–O(7)#1	108.7(2)
O(20)–B(6)–O(7)#1	107.5(2)	O(6)–B(7)–O(21)	124.4(3)
O(6)–B(7)–O(22)	119.4(3)	O(21)–B(7)–O(22)	116.2(3)
O(10)–B(8)–O(12)	124.3(3)	O(10)–B(8)–O(23)	119.4(3)
O(12)–B(8)–O(23)	116.3 (3)	O(15)–B(9)–O (19)	124.1(3)
O(15)–B(9)–O(24)	117.1(3)	O(19)–B(9)–O(24)	118.8(3)
O(25)–B(10)–O(9)#1	109.7(3)	O(25)–B(10)–O(7)#1	113.9(3)
O(9)#1–B(10)–O(7)#1	106.5(2)	O(25)–B(10)–O(14)	112.6(3)
O(9)#1–B(10)–O(14)	107.6(2)	O(7)#1–B(10)–O(14)	106.1(2)

Symmetry transformations used to generate equivalent atoms: #1 $-x, -y+1, -z$.

(which is consistent with its assignment as an O^- group). The assignment of the O^- group to the central tetrahedral boron atom (and not one of the trigonal boron atoms) is also reasonable given the fact that one would expect an oxygen atom bonded to a tetrahedral boron to be more acidic than an oxygen atom bonded to a corresponding trigonal boron. This assignment is also consistent with valence bond calculations [9], and the charge balancing requirements of the cluster.

As can be seen in Figs 3 and 4, the $[(VO)_6\{B_{10}O_{16}(OH)_6\}_2]^{4-}$ cluster, as a whole, displays approximate $\bar{3}$ symmetry about an axis running through the center of the vanadium ring perpendicular to the plane of the six vanadium atoms. The cluster has an approximate diameter of 6 Å (V–V) at the vanadium ring and a height of 5.9 Å (O–O of the nearest oxygens of the central boron in each cap). Unlike the previously characterized $V_{12}B_{17}O_{58}$ and $V_{12}B_{18}O_{60}$ clusters [6], which contain ethylenediamine template molecules and water molecules that reside between the clusters, the intercluster space in (**1**) is filled only with Rb^+ cations, and the intracluster space contains electron density corresponding to a partially occupied water molecule. In comparing the structures

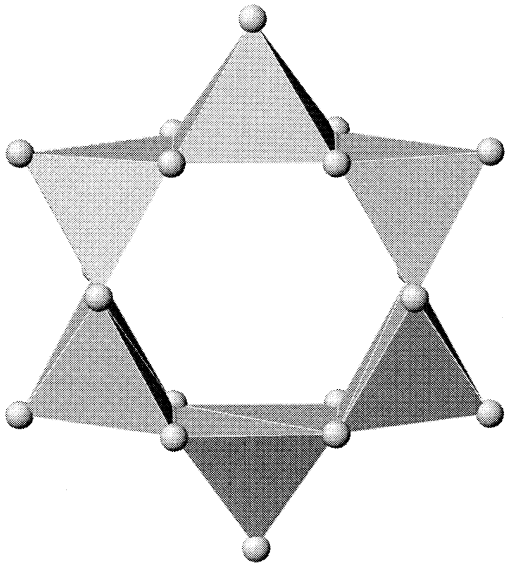

Fig. 1. A polyhedral representation of the hexagonal ring of six *trans*-edge-sharing VO_5 square pyramids present in the structure of (**1**).

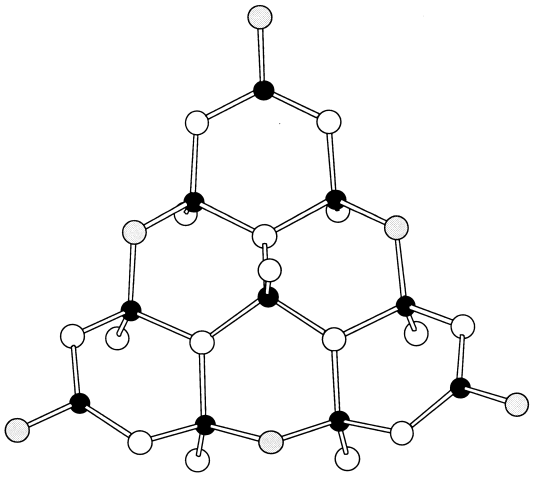

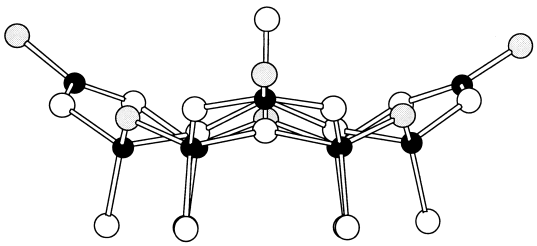

Fig. 2. Two views of the $B_{10}O_{16}(OH)_6^{8-}$ triangular polyborate caps that are present in the structure of (**1**). The central tetrahedral boron atom has a B–O$^-$ bond which is collinear with the pseudo $\bar{3}$ axis of the cluster, while the other six tetrahedral boron atoms have oxygen atoms pointing in the opposite direction that are part of the hexavanadate ring.

of these unusual polyoxovanadate borate clusters, it is interesting to note that each has a very specific polyborate ligand which is associated with a very specific vanadate moiety. The $V_{12}B_{18}O_{60}$ cluster, for example, comprises a puckered $B_{18}O_{36}(OH)_6$ ring sandwiched between two triangular rings of six alternating *cis* and *trans* edge-sharing vanadium atoms. The $V_{12}B_{17}O_{58}$ cluster, on the other hand, comprises a contorted vanadium oxide ring in which two semicircles of five *trans* edge-sharing VO_5 square pyramids interpenetrate forming clefts which are occupied by $B_8O_{17}(OH)_4$ and $B_9O_{18}(OH_4)$(enH) chains. Obviously,

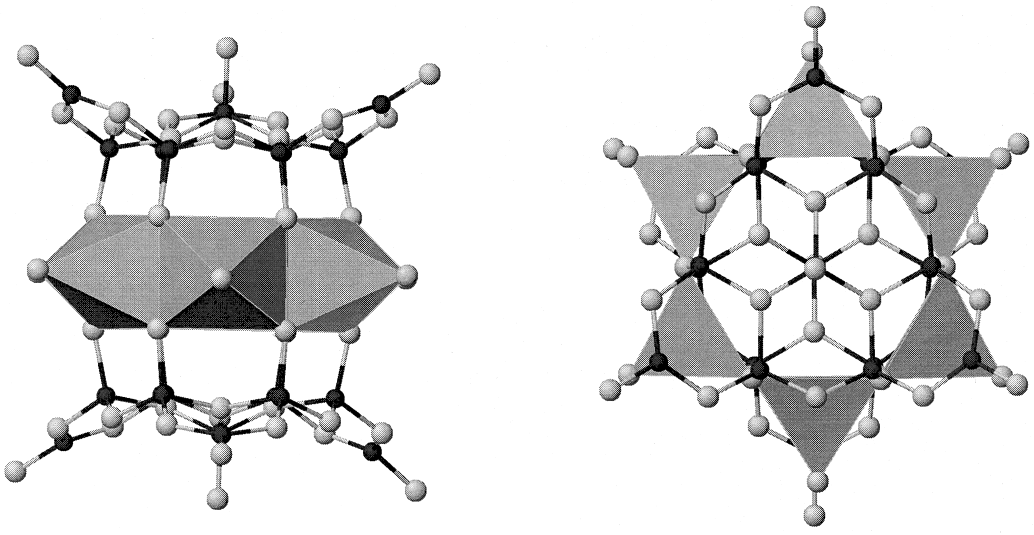

Fig. 3. Two views of the structure of the $[V_6B_{20}O_{38}(OH)_{12}]^{4-}$ cluster in $Rb_4[(VO)_6\{B_{10}O_{16}(OH)_6\}_2]\cdot 0.5H_2O$ (**1**).

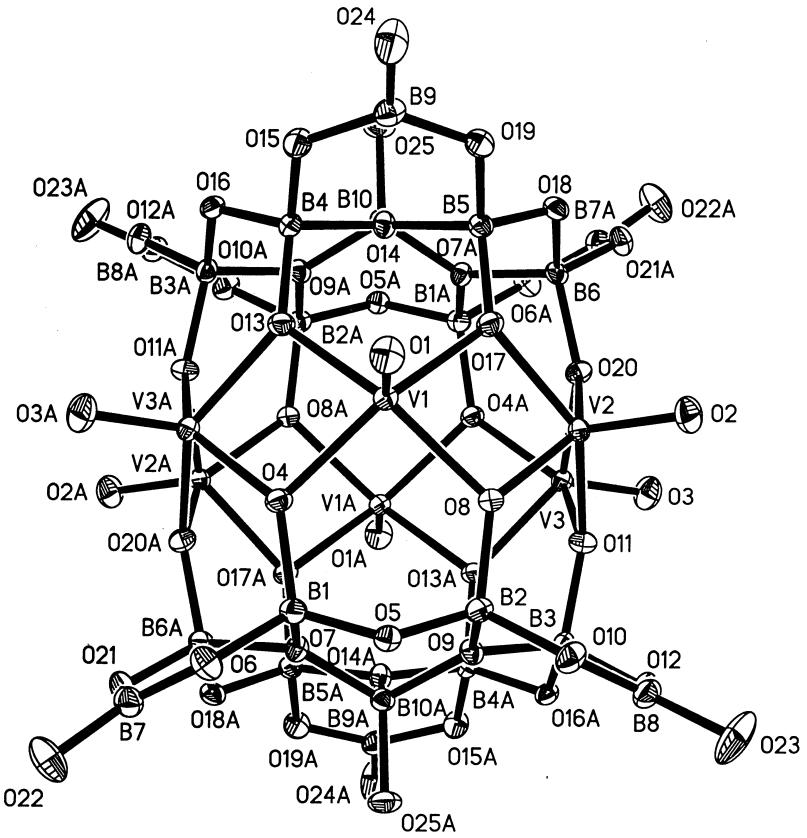

Fig. 4. ORTEP view of the structure of the $[V_6B_{20}O_{38}(OH)_{12}]^{4-}$ cluster in $Rb_4[(VO)_6\{B_{10}O_{16}(OH)_6\}_2]\cdot 0.5H_2O$ (**1**) showing the 50% probability thermal ellipsoids and atomic numbering scheme.

very sensitive relationships exist between the polyborate and vanadate moieties, and these relationships are clearly dependent on synthetic conditions which will require further study.

The +4 oxidation state of the vanadium atoms in (**1**) satisfies the charge requirements of the cluster and has been confirmed by valence bond calculations [9]. This oxidation state has also been verified by magnetic susceptibility experiments. The pale green color of the crystals also suggests that (**1**) contains only V^{IV}, and not mixed V^{IV}/V^{V} sites as are observed in the orange or dark red compounds containing $V_{12}B_{17}O_{58}$ and $V_{12}B_{18}O_{60}$, respectively.

The facile, high yield, synthesis of this and other structurally and compositionally unprecedented vanadium borate clusters [7] continues to point to hydrothermal synthesis as a particularly useful, and increasingly important, method for preparation of new compounds.

Acknowledgements—The work at Syracuse University was supported by NSF Grant CHE9617232. We thank Chris D.W. Jones for performing the magnetic susceptibility measurements.

REFERENCES

1. (a) Pope, M. T., *Heteropoly and Isopoly Oxometalates*, Springer Verlag, New York, 1983; (b) Day, V. W. and Klemperer, W. G., *Science*, 1985, **228**, 533.
2. (a) Day, V. W., Klemperer, W. G. and Maltbie, D. J., *J. Am. Chem. Soc.*, 1987, **109**, 2991; (b) Chen, Q., Liu, S. and Zubieta, J., *Inorg. Chem.*, 1989, **28**, 4433; (c) Day, V. W., Klemperer, W. G. and Yaghi, O. M., *J. Am. Chem. Soc.*, 1989, **111**, 5959; (d) Müller, A., Krickemeyer, E., Penk, H., Walberg, H.-J. and Bögge, H., *Angew. Chem. Int. Ed. Engl.*, 1987, **26**, 1045; (e) Johnson, G. K. and Schlemper, E. O., *J. Am. Chem. Soc.*, 1978, **100**, 3645; (f) Müller, A., Döring, J., Bögge, H. and Krickemeyer, E., *Chimica*, 1988, **42**, 300; (g) Müller, A., Penk, M., Rohfling, R., Krickemeyer, E. and Döring, J., *Angew. Chem. Int. Ed. Engl.*, 1990, **29**, 926; (h) Rehder, D., Priebsch, W. and von Oeynhausen, M., *Angew. Chem. Int. Ed. Engl.*, 1989, **28**, 1221.
3. Pope, M. T. and Müller, A., *Angew. Chem. Int. Ed. Engl.*, 1991, **30,** 34.
4. Burns, P. C., Grice, J. D. and Hawthorne, F. C., *Can. Mineral*, 1995, **33,** 1131 and references therein.
5. (a) Thompson, P. D. and Keszler, D. A., *Chem. Mater.*, 1994, **6**, 2005; (b) Cox, J. R., Keszler, D. A. and Huang, J., *Chem. Mater.*, 1994, **6**, 2008; (c) Behm, H., *Acta Crystallogr. Sect. C*, 1985, **41**, 642; (c) Behm, H., *Acta Crystallogr. Sect. C*, 1983, **39**,

20; (d) Christ, C. L. and Clark, J. R., *Phys. Chem. Minerals*, 1977, **2**, 59; (e) Heller, G. and Pickardt, J., *Z. Naturforsch.*, 1985, **40b**, 462; (f) Harrison, W. T. A., Gier, T. E. and Stucky, G. D., *Angew. Chem. Int. Ed. Engl.*, 1993, **32**, 724.
6. Rijssenbeek, J. T., Rose, D. J., Haushalter, R. C. and Zubieta, J., *Angew. Chem. Int. Ed. Engl.*, 1997, **36,** 1008.
7. Unpublished results.
8. Burns, P. C., *Can. Mineral.*, 1995, **33,** 1167.
9. Brown, I. D. and Wu, K. K., *Acta Crystallogr. Sect. B*, 1976, **32,** 1957.

Pergamon

PII : S0277–5387(97)00431–2

Polyhedron Vol. 17, No. 16, pp. 2607–2615, 1998
© 1998 Elsevier Science Ltd
All rights reserved. Printed in Great Britain
0277–5387/98 $19.00+0.00

Monomeric Cu(II) complexes with tetradentate bis(benzimidazole) ligand ; synthesis, EPR, spectral and electrochemical studies

Rajesh and Pavan Mathur*

Department of Chemistry, University of Delhi, Delhi—110 007, India

(Received 27 June 1997 ; accepted 21 October 1997)

Abstract—A series of 1 : 1 copper(II) complexes with the tetradentate ligand 1,2*bis* (2 benzimidazolyloxamethyl) benzene (L) have been prepared with stoichiometry of $Cu(L)X_2 \cdot nH_2O$ ($X = Cl^-$, NO_3^-, OAc^- and $HCOO^-$). X-band EPR spectra of the above complexes examined as a frozen DMSO/DMF solution indicate $g_\parallel > g_\perp > 2.0$ and show four or less than four $g_\parallel$ lines and a broadening of the $g_\perp$ component suggesting a lowered site symmetry for the copper(II) ion. The $g_\perp$ component of all the complexes show nitrogen superhyperfine structure. A clear five line pattern is found in the $g_\perp$ region with $B_N \simeq 15G \pm 1$ for $Cu(L)\ X_2 \cdot nH_2O$ complexes indicating that two nitrogen from the benzimidazole ring are coordinated to the central Cu^{II} in the equatorial basal plane while the other two positions in the sphere are occupied by the anionic ligand (X). Interestingly with ClO_4^- as the anion, a 1 : 2 complex results with stoichiometry of $[Cu(L)_2]\ (ClO_4)_2$.

The X-band EPR spectra of $[Cu(L)_2](ClO_4)_2$ complex shows a clear nine line SHF structure on the $g_\perp$ component indicating the presence of four nitrogen atoms coordinated to the central Cu^{II} atom ; this confirms the retention of two ligands around Cu^{II} in solution. Molecular orbital coefficients β_1 and β_1' have been evaluated from the expression used by Manoharan and Rogers. The trends of β_1 and β_1' indicate increasing electron delocalization on nitrogen atom as we change the exogenous ligand from formate/acetate-chloride to nitrate. The covalency parameter, α^2, has also been evaluated and reflects the decreasing trend of covalency in the order, nitrate > chloride ⩾ acetate > formate for complexes containing these ligands. This trend of order is in conformity with that obtained from MO coefficients. All the complexes exhibit a visible band with λ_{max} in the 625–690 nm region, in DMF ; suggesting a distorted geometry for copper(II) ion in the present series of complexes. Cyclic voltammetric studies of copper(II) complexes reveal that the $E_{1/2}$ for the Cu^{II}/Cu^{I} couple shifts to most negative value with $HCOO^-$ and OAc^- anionic ligands implying that these anion stabilize the Cu^{II} state whereas $E_{1/2}$ data for NO_3^- reveals that this anion destabilizes the Cu^{II} state. A plot of visible band energy vs $E_{1/2}$ shows that as the energy of the $d_{x^2-y^2}$ orbital decreases, an anodic shift in $Cu^{II} \rightarrow Cu^{I}$ reduction potential is observed. © 1998 Elsevier Science Ltd. All rights reserved

Copper in a biological system is utilized, primarily in redox reactions associated with the reduction of oxygen to water, and oxygenation reactions. A copper containing superoxide dismutase has the specific but important role of removing the highly reactive superoxide anion (dismutation), and in these oxygenation reactions copper is active as the biological catalyst in the reaction [1]. The second major biological role of copper is in the transport of copper around the human body controlling its uptake and excretion [2]. The uptake of copper(II) by brain tissue was found to be facilitated by complexation using histidine in a study of the uptake of complexed copper-67 by brain hypothalamic tissue [3].

Galactose oxidase, an extracellular enzyme secreted by the fungus Dactylum dendroides, is among the few known copper containing enzymes that have a built in secondary co-factor. The copper site has a square planar coordination, comprises one tyrosine oxygen atom, two histidine nitrogen atoms and an acetate oxygen atom, providing an N_2O_2 donor array to the copper site with an axial tyrosine [4,5].

Since protein structure imparts a distortion in coordination geometry around the metal ion, which is an important factor in controlling the redox properties of the particular protein and imidazole group of histidine being a ligand apparently present in many proteins [6–8] ; a logical step to synthetic models should be to

* Author to whom correspondence should be addressed.

design and synthesize ligands containing one or two imidazole groups and so might impose a distorted coordination around the Cu^{II}. In an effort to simulate low symmetry metal environment as can be imposed by the protein structure, numerous septadentate [9], hexadentate [10], tetradentate [11], and tridentate [12], benzimidazole based ligands have been utilized to synthesize model compounds.

For the present study we have synthesized a series of copper(II) complexes by utilizing a tetradentate 1,2*bis* (2 benzimidazolyloxamethyl) benzene (L) ligand. These complexes are expected to have the following: (a) having a nearly square planar ($Cu^{II}N_4$) and $Cu^{II}N_2O_2$ chromophore as is observed in the bovine dismutase and galactose oxidase; (b) having a high affinity for an exogenous ligand in the cupric; (c) exhibiting at least quasi-reversible redox behaviour. Earlier we have utilized this ligand to synthesize some manganese(III) complexes [13].

EXPERIMENTAL

Starting materials

1,2-Diaminobenzene was recrystallized before use. Solvents and reagents (A.R. Grade) were used without purification.

Synthesis of ligand 1,2bis(2-*benzimidazolyl oxa methyl*)*benzene* (*L*)

1,2 phenylene dioxy diacetic acid (20.3 g, 90 m mol) was combined with 1,2-diaminobenzene (19.5 g, 180 m mol) and powdered. The mixture was heated for 3 h at a temperature of 150–160°C on an oil bath until all effervescence ceased. The resulting red blue glasslike solid after cooling was powdered and was added to 4MHCl (250 cm^3). Upon scratching the sides of the flask a grey white precipitate was obtained. This was filtered out and washed by slurrying in acetone several times. The above hydrochloride was dissolved in distilled water (220 cm^3) and the resulting filtrate was then neutralized with 1 : 1 ammonia until a white precipitate was formed. The white precipitate was collected, washed with ether and dried over P_2O_5 *in vacuo* (yield 70%). The procedure is similar to that reported by Reed *et al.* [14]. The ligand was characterized by ^1H NMR.

^1H NMR L δ_H (DMSO-d_6); 12.6 (NH 2H,S), 7.6 (aArH 4H,m), 7.2 (bArH + cArH 6H,m), 7.0 (dArH 2H,S), 5.3 (Aliph. 4H,S).

Elemental analysis and UV spectra of the ligand are reported in Table 1.

Synthesis of complexes

The coordination compounds of general formulae $Cu(L)X_2 \cdot nH_2O$ ($X = Cl^-$, NO_3^-, OAc^- and $HCOO^-$) were prepared by dissolving the appropriate hydrated metal salt (1 m mol) in methanol (10 cm^3) and adding this solution to the ligand (1 m mol) in warm methanol (20 cm^3). The reaction mixture was then left stirring. After 1 h of stirring bluish green precipitates of the desired compounds were obtained. These were collected by filtration, washed with methanol and dried over P_2O_5 *in vacuo*. The $[Cu(L)_2](ClO_4)$ (**5**) was prepared by the similar procedure as above except that crystallized precipitate was obtained on slow evaporation of the reaction mixture upon standing at room temperature.

CAUTION: Although no accident occurred with the present copper(II) perchlorate complex during the experimental work, it should be remembered that perchlorates are potentially explosive.

Physical measurements

Elemental analyses were obtained from microanalytical laboratory of RSIC, University of Punjab, Chandigarh, India. Metal was estimated by shimadzu model AA 640-13 atomic absorbance spectrophotometer.

Infrared spectra of the samples in Nujol mulls were recorded on a Perkin–Elmer model 1710 FT-IR spectrometer, solution electronic spectra were obtained on a Perkin–Elmer DU-260 spectrophotometer, ^1H NMR spectra on a Bruker 300 MHz FT-NMR spectrometer and EPR spectra on a varian E 112 X-band

Table 1. Microanalytical data for the copper(II) complexes

Compound	Mol. formulae	Found (Calcd) % C	H	N	M
$L \cdot H_2O$	$C_{22}H_{18}N_4O_2 \cdot H_2O$	68.9(68.0)	5.0(5.1)	14.3(14.4)	—
$[Cu(L)Cl_2]H_2O$ (**1**)	$CuC_{22}H_{18}N_4O_2Cl_2 \cdot H_2O$	51.1(50.5)	2.8(3.8)	10.7(10.7)	13.0(12.2)
$[Cu(L)(NO_3)_2]$ (**2**)	$CuC_{22}H_{18}N_6O_8$	46.9(47.3)	2.9(3.2)	14.3(15.0)	11.0(11.5)
$[Cu(L)(OAc)_2]2H_2O$ (**3**)	$CuC_{26}H_{24}N_4O_6 \cdot 2H_2O$	53.3(53.1)	4.3(4.7)	9.5(9.5)	11.0(10.9)
$[Cu(L)(HCOO)_2]H_2O$ (**4**)	$CuC_{24}H_{20}N_4O_6 \cdot H_2O$	52.9(53.9)	3.9(4.0)	10.2(10.3)	12.0(11.8)
$[Cu(L)_2(ClO_4)_2]2H_2O$ (**5**)	$CuC_{44}H_{36}N_8O_{12} \cdot Cl_2 \cdot 2H_2O$	50.2(50.8)	3.6(3.8)	10.6(10.8)	6.0(6.4)

spectrometer calibrated with diphenyl picrylhydrazyl (dpph), at liquid nitrogen temperature (77 K).

Cyclic voltammetric (c.v.) measurements were carried out using a BAS model CV-50W electrochemical analysing system. A 3 : 7 DMSO : MeCN solvent system was employed for c.v. studies with 0.1 M $NaClO_4$ as supporting electrolyte. A three electrode configuration was used, comprising a Pt disc working electrode (~ 3.1 mm^2 area), Pt wire counter electrode and an $Ag/AgNO_3$ (0.01 M $AgNO_3 + 0.1$ M TBAP/MeCN) reference electrode. The electrode performance was monitored by observing the ferrocenium/ferrocene (Fc^+/Fc) couple in the above solvent system. Experiments were carried out at room temperature (25°C) under dry N_2.

RESULTS AND DISCUSSION

EPR spectroscopy

Figure 1a–c represents the X-band EPR spectra of copper(II) complexes at 77 K, examined as a frozen dimethyl formamide solution. In general the EPR spectra reveal the presence of a distorted tetragonal copper site in the complexes. This is evident from the trend of their respective $g_\parallel$ and $g_\perp$ values which in all cases show $g_\parallel > g_\perp > 2$ (Table 2). All the complexes show four or less than four $g_\parallel$ components and a broadening of $g_\perp$ component. Such a broadening [15] of $g_\perp$ component is indicative of lowered symmetry.

The EPR spectra of all the complexes show nitrogen superhyperfine structure in the perpendicular region, arising from the interaction of the copper(II) odd electron with nitrogen atom, as can be seen from their spectra in Fig. 1a–c. The clear five line pattern in the perpendicular region for $Cu(L)X_2 \cdot nH_2O$ ($X = Cl^-$, NO_3^-, OAc^- and $HCOO^-$) indicates that two imine nitrogen from the two benzimidazole rings are coordinated to Cu atom in the equatorial basal plane. The other two positions in the plane are occupied by the anionic ligand (X) as supported by the IR spectra and further by the crystal structure of a related compound Cu(L) Br_2 [L = 1,6*bis* (benzimidazole-2yl)-2,5 dioxahexane] where Cu atom is bounded strongly to two benzimidazole N atoms of benzimidazole ligand and two anionic Br atoms are bounded in the basal plane with a rhombus shape [16].

The spin Hamiltonian parameters of some $Cu(L)X_2 \cdot nH_2O$ ($X = NO_3^-, OAc^-, HCOO^-$) complexes are very similar to the EPR X-band spectral parameters observed for galactose oxidase ($g_\perp = 2.04$, $g_\parallel = 2.28$) [17]; this indicates that the above complexes may have potential relevance to mononuclear copper site in the galactose oxidase.

Cryogenic frozen EPR spectra of $[Cu(L)_2]$ $(ClO_4)_2$ complex shows superhyperfine structure (SHF) on the $g_\perp$ component, having a clear nine line pattern with $B_N \simeq 15\text{G} \pm 1$. The appearance of clear nine SHF lines on the perpendicular copper hyperfine component indicates the presence of four nitrogen atoms coordinated to Cu^{II} atom, thus confirming the retention of

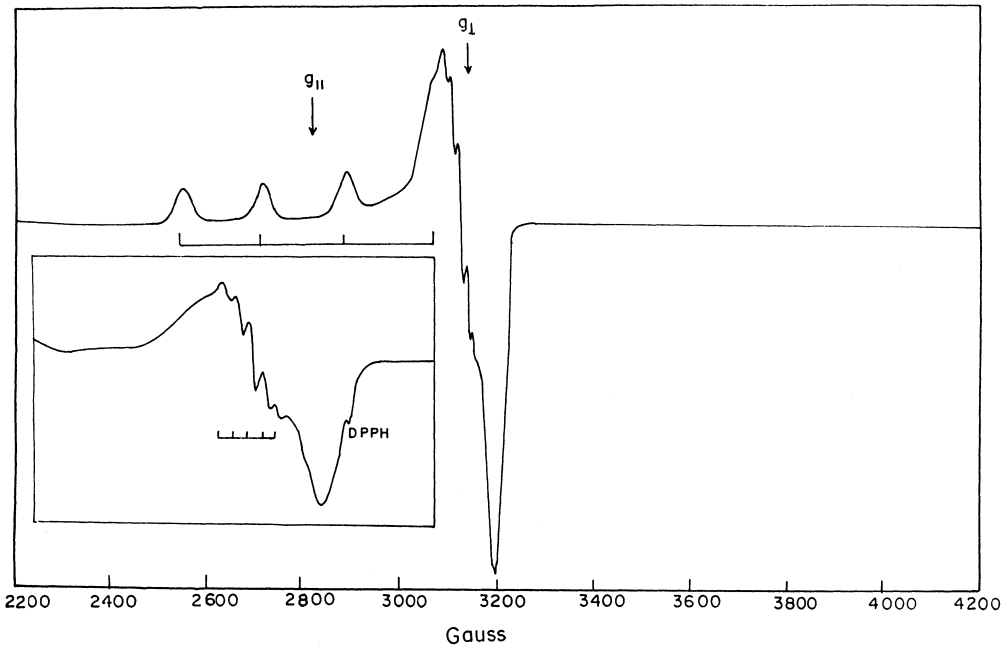

Fig. 1a. 2000 G Scan of frozen DMF solution of $Cu(L)(NO_3)_2$. Conditions: receiver gain = 2.0×10^2 G; microwave power 20 mW; microwave frequency 9.01 GHz; modulation amplitude 2.5 G; $T = 77$ K at X-band.

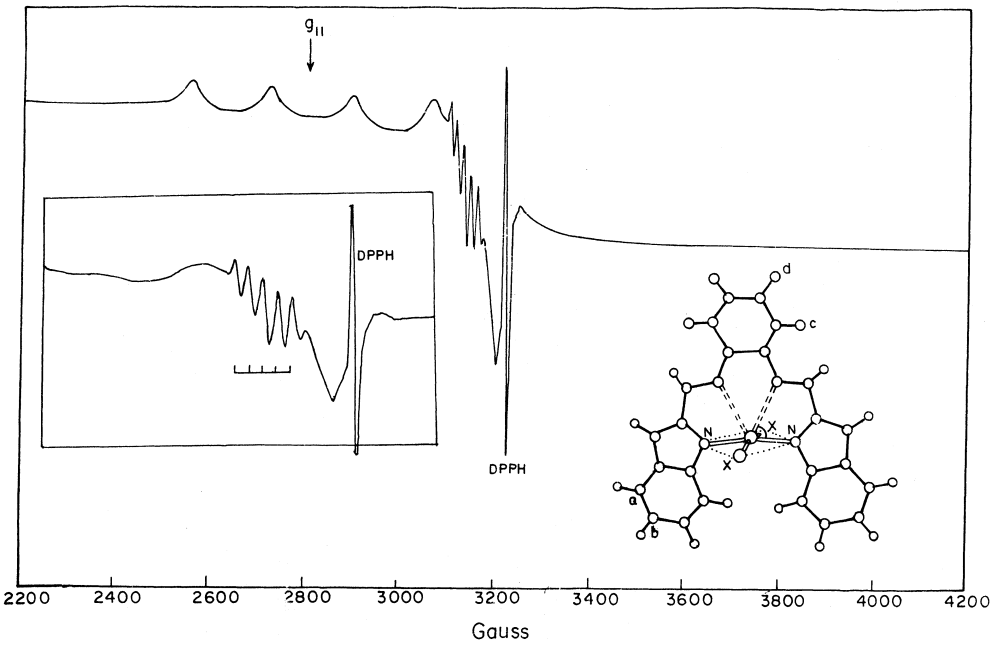

Fig. 1b. 2000 G Scan of frozen DMF solution of $Cu(L)(OAc)_2 \cdot H_2O$. Conditions: receiver gain = 5.0×10^3 G; microwave power 20 mW; microwave frequency 9.01 GHz; modulation amplitude 2.5 G; $T = 77$ K at X-band (figure in inset is proposed structure of $Cu(L)X_2$ ($X = OAc^-$)).

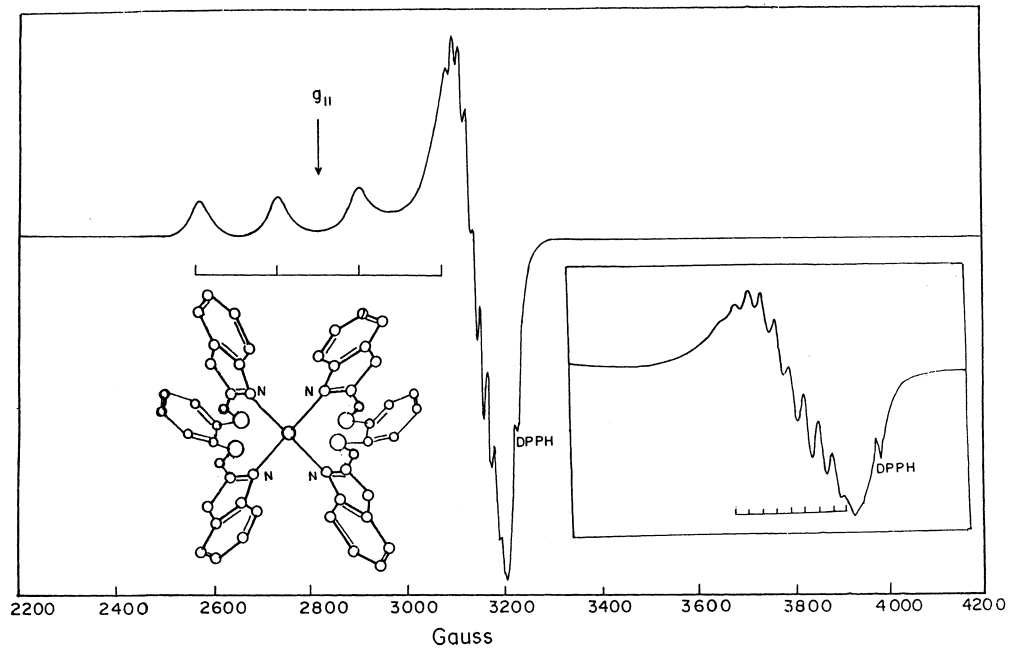

Fig. 1c. 2000 G Scan of frozen DMF solution of $[Cu(L)_2](ClO_4)_2$. Conditions: receiver gain = 4.0×10^2 G; microwave power 20 mW; microwave frequency 9.01 GHz; modulation amplitude 2.5 G; $T = 77$ K at X-band (figure in inset is proposed structure of $[Cu(L)_2](ClO_4)_2$).

Table 2. X-band EPR spectral data for copper(II) complexes at 77 K (values in gauss)

Complex	Medium	g_0	A_0	$g_\parallel$	$A_\parallel$	$g_\perp$	$A_\perp$	$g_\parallel/A_\parallel \times 10^4$	B_N	β_1'	β_1	α^2
$[Cu(L)Cl_2]H_2O$	DMSO	2.122	81	2.293	168.3	2.037	36.6	136	14.7	0.61	0.85	0.67
$[Cu(L)(NO_3)_2]$	DMF	2.122	82	2.282	170.0	2.042	36.6	134	15.5	0.62	0.84	0.61
$[Cu(L)(OAc)_2]2H_2O$	DMF	2.128	78	2.286	170.0	2.049	33.3	134	14.5	0.60	0.86	0.67
$[Cu(L)\ (HCOO)_2]H_2O$	DMF	2.126	80	2.286	170.0	2.049	33.3	134	14.5	0.60	0.86	0.68
$[Cu(L)_2](ClO_4)_2 \cdot 2H_2O$	DMF	2.120	83	2.278	171.6	2.042	40.0	132	14.7	0.61	0.85	0.65

$g_0 = 1/3(2g_\perp + g_\parallel)$, $A_0 = 1/3(2A_\perp + A_\parallel)$

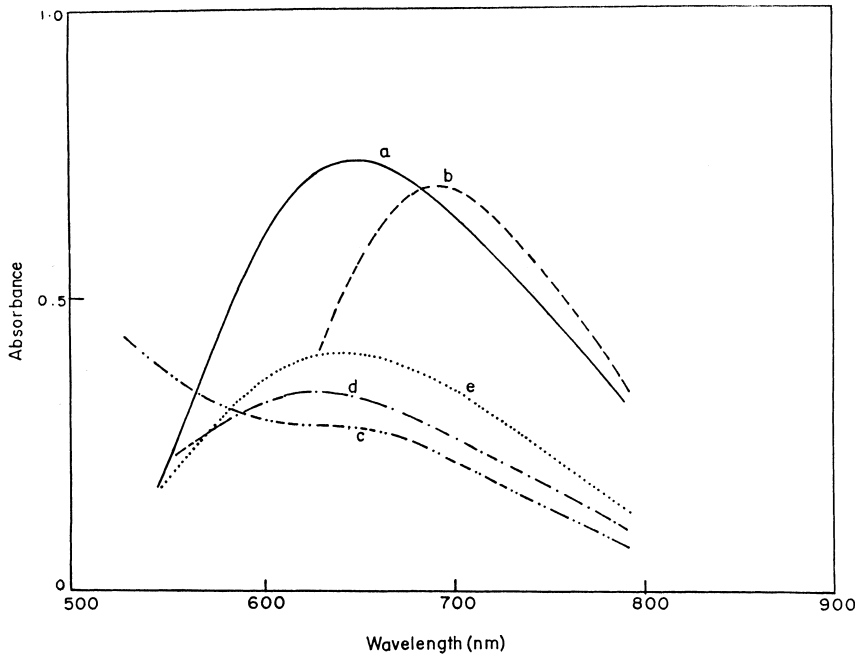

Fig. 2. Visible spectra of: (a) $Cu(L)Cl_2 \cdot H_2O$; (b) $Cu(L)(NO_3)_2$; (c) $Cu(L)(OAc)_2 \cdot 2H_2O$; (d) $Cu(L)(HCOO)_2 \cdot H_2O$; (e) $Cu(L)(ClO_4)_2$; all in DMF.

Table 3. Electronic spectral data for copper(II) complexes

Compound	Solvent	λ_{max}(nm) (ε, L mol^{-1} cm^{-1})
$L \cdot H_2O$	DMF	278(16,982), 282(15,849)
$[Cu(L)Cl_2]H_2O$ (**1**)	DMF	277(23,988), 281(19,498), 650(46.7)
$[Cu(L)(NO_3)_2]$(**2**)	DMF	272(20,417), 278(19,498), 690(29.5)
$[Cu(L)(OAc)_2]2H_2O$ (**3**)	DMF	275(25,118), 281(20,417), 635(31.6)
$[Cu(L)(HCOO)_2]H_2O$ (**4**)	DMF	275(22,908), 282(18,620), 625(27.5)
$[Cu(L)_2](ClO_4)_2 \cdot 2H_2O$ (**5**)	DMF	277(28,183), 280(24,547), 645(37.1)

two ligands around Cu in a square planar array in solution. The $g_\parallel$ and $A_\parallel$ values of the complex lies on the $g_\parallel$ vs $A_\parallel$ map [18] and is typical for planar CuN_4 chromophore [19]. The value of $g_\parallel/A_\parallel$ quotient 132.0 cm^{-1} supports the square planar geometry with no appreciable tetrahedral distortion [20–22].

We have made an attempt to calculate the MO coefficients for the b1g orbital, i.e. β_1 and also the ligand coefficient β_1' in the b1g MO, from the superhyperfine structure in the $g_\perp$ region. The SHF coupling constant (B_N) could be related to β_1' and the contribution from the 2*s* and 2*p* functions [23] (with $\phi^2(2s) = 33.4 \times 10^{24}$ cm^{-3} for the 2*s* function and $<r^{-3}>_p = 21.1 \times 10^{24}$ cm^{-3} for the 2*p* function following Maki and McGarvey [24]). Once β_1' is known, β_1 could be calculated by the relation $\beta_1^2 + \beta_1'^2 - 2\beta_1\beta_1' s = 1$ where *s* is the overlap integral. The values of β_1 and β_1' are in keeping with those calculated for Cu^{II} TPP complex, and provide proof that there is considerable covalent bonding particularly in plane σ bonding. The relative trend of β_1 and β_1' with respect to exogenous ligand (X = Cl^-, NO_3^-, OAc^-, $HCOO^-$) shows that there is greater unpaired electron delocalization on benzimidazole nitrogen atom as we move from formato/acetato-chloride to nitrato complex.

Electronic and electrochemistry

Figure 2 shows the electronic spectra of copper(II) complexes; their band positions and extinction coefficients are reported in Table 3. Several prominent bands are obtained in the UV region and are assigned to the benzimidazolyl group π-π^* transition. These bands show a slight blue shift in their respective complexes and support binding of the benzimidazolyl ring imine nitrogen to the metal centre, this being the preferred nitrogen atom for coordination [13–15,25]. New bands arise in the visible part of the spectrum in the region of 625–690 nm, and are assigned to *d-d* transition. The energy of the *d-d* transition suggests distorted tetragonal copper(II) complexes [15] and follows the order nitrate (**2**) <chloride (**1**) <acetate (**3**) <formate (**4**). A square N_2O_2 donor array is expected to produce a *d-d* transition in the region of 500–550 nm [26]; the considerably longer wavelength observed in our complexes is a clear indication of the weakened equatorial ligand field, due to the lowered basicity of the imine N-atom of the benzimidazole. We have calculated the covalency parameter, α^2, using a simple relationship: $g_\parallel = 2.0023 - 8\lambda\alpha^2/xy$ [27]. The smaller the value of α^2, the more the covalency of copper-ligand bond in the complex; thus on the basis of α^2 value, the order of decreasing covalency is nitrate > chloride $\geqslant$ acetate > formate for copper(II) complexes containing these ligands. This trend is in conformity with that obtained from MO coefficients.

The order of energies is in keeping with the above covalency order found from EPR parameters. The decreasing order of covalency reflects the increasing order of visible band energy, i.e. the higher the covalency, the lower the energy of the $d_{x^2-y^2}$ orbital and correspondingly the energy of the $d_{xy} \rightarrow d_{x^2-y^2}/d_{xz}, d_{yz} \rightarrow d_{x^2-y^2}$ transition is also lowered.

Figure 3a–d and Fig. 4 shows the cyclic voltammogram and differential pulse voltammogram of the copper(II) complexes taken in 3:7 DMSO: MeCN solvent system. The reversible one electron Fc^+/Fc couple in the above solvent system has an $E_{1/2}$ of 0.27 V vs $Ag/AgNO_3$. The electrode potentials of the copper(II) complexes are given in Table 4.

All complexes exhibit a quasi-reversible reduction wave in the range of +0.12V to −0.24V region, with peak to peak width much larger than that observed for the one electron couple Fc^+/Fc ion in the same solvent system. Larger peak width for the one-electron $Cu^{II} \rightarrow Cu^I$ couple in their respective complexes is not an uncommon observation [28]. We therefore assign this cathodic wave to the reduction of $Cu^{II} \rightarrow Cu^I$ couple. $E_{1/2}$ data for this couple (Table 4) indicates that the most negative potential is for formate/acetato complex followed by chloride and nitrato. We there-

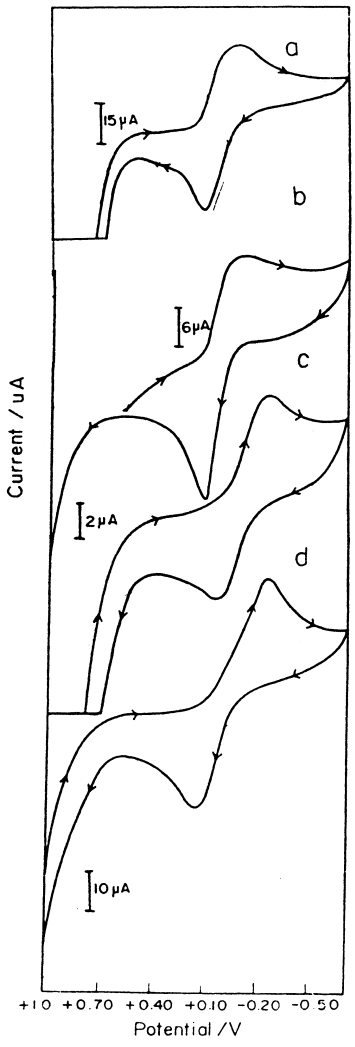

Fig. 3. CV spectra of: (a) $Cu(L)Cl_2 \cdot H_2O$; (b) $Cu(L)(NO_3)_2$; (c) $Cu(L)(HCOO)_2 \cdot H_2O$; (d) $Cu(L)(ClO_4)_2$; all in 3:7 DMSO: MeCN solvent: scan rate, 100 mV s^{-1}.

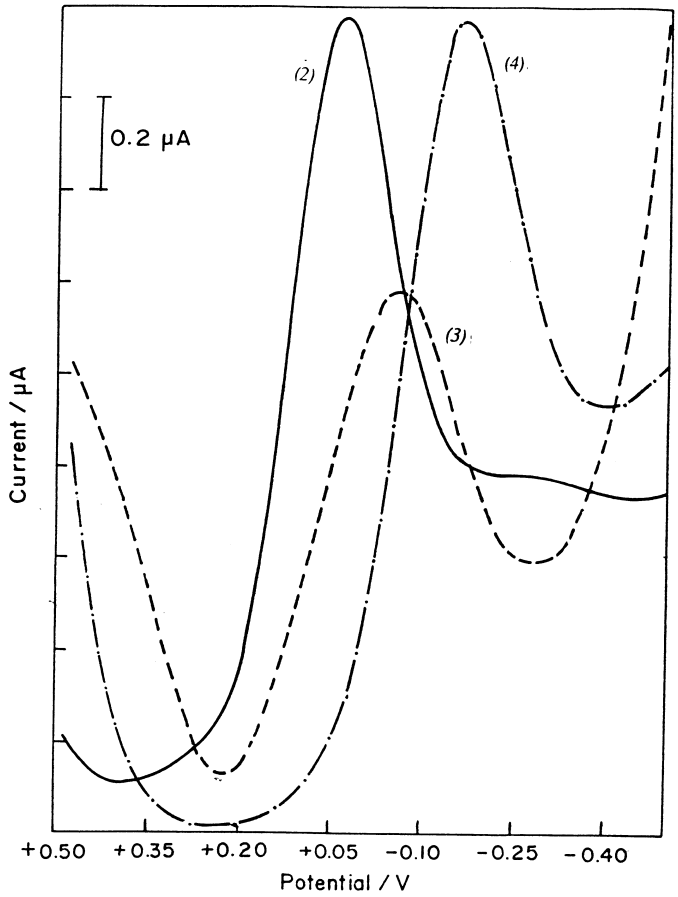

Fig. 4. Differential pulse voltammograms of $Cu(L)(NO_3)_2$ (**2**), $Cu(L)(OAc)_2 \cdot 2H_2O$ (**3**) and $Cu(L)(HCOO)_2H_2O$ (**4**). Sweep rate 100 mV s^{-1}, pulse amplitude 50 mV, pulse period 200 ms.

Table 4. Electrochemical data for copper(II) complexes at 298 K

Complex	E_{pc} (v)	E_{pa} (v)	$E_{1/2}$ (v)	i_{pa}/i_{pc}	DPV (v)
$[Cu(L)Cl_2]H_2O$ (**1**)	−0.026	+0.122	+0.048	1.1	−0.025
$[Cu(L)(NO_3)_2]$ (**2**)	−0.012	+0.118	+0.053	0.8	+0.046
$[Cu(L)(OAc)_2]2H_2O$ (**3**)	−0.187	+0.015	−0.086	0.9	−0.054
$[Cu(L)(HCOO)_2]H_2O$ (**4**)	−0.242	+0.012	−0.115	1.0	−0.157
$[Cu(L)_2](ClO_4)_2\ 2H_2O$ (**5**)	−0.235	+0.125	−0.055	0.8	—

fore conclude that the binding of the formato/acetate anion stabilizes the Cu^{II} centre, while the binding of the nitrate anion tends to stabilize the Cu^{I} state in comparison to the Cu^{II} state.

The stabilization of Cu^{II} state by exogenous ligand can be well understood by making a correlation between the covalency factor, α^2, *d-d* energy bands and redox potentials ($E_{1/2}$) in the respective complexes. An increase in covalency in the Cu^{II}—N equatorial bond leads to a decrease in repulsion between the $d_{x^2-y^2}$ orbital and the equatorial ligands, causing a concomitant decrease in the energy of this orbital and also an anodic shift in the $Cu^{II} \rightarrow Cu^{I}$ reduction potential [28]. This parameter will also be affected by other equatorial ligands (x) in the complexes. This is evident from a plot of *d-d* band energy (ν_{max}) vs $Cu^{II} \rightarrow Cu^{I}$ redox potential ($E_{1/2}$) (Fig. 5).

Infrared spectroscopy

In the IR spectra of the free ligand (in Nujol), a strong band in 1460 cm^{-1} is attributed to stretching

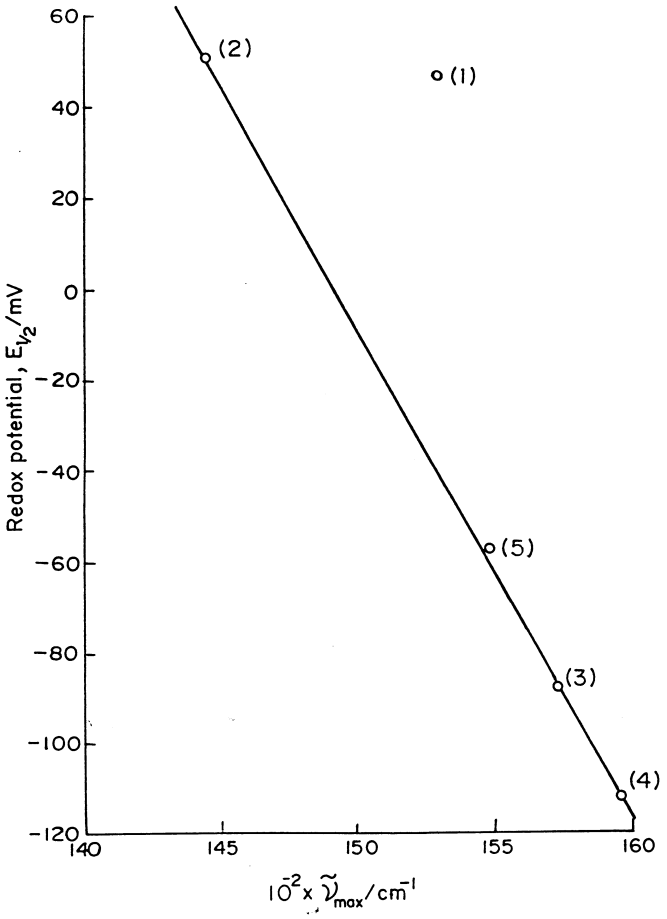

Fig. 5. Plot of visible band energy (ν_{max} cm^{-1}) vs redox potential $E_{1/2}$ (mV) for $Cu(L)Cl_2 \cdot H_2O$ (**1**), $Cu(L)(NO_3)_2$ (**2**), $Cu(L)(OAc)_2 \cdot 2H_2O$ (**3**), $Cu(L)(HCOO)_2 \cdot H_2O$ (**4**) and $Cu(L)_2(ClO_4)_2 \cdot 2H_2O$ (**5**).

mode for [—C═N—C═C—]. In the present case we find that the shift in 1460 cm^{-1} is 10–20 cm^{-1} for the copper complexes. This implies direct coordinates of all the imine nitrogen atoms to Cu^{II}. This is a preferred nitrogen atom for coordination as found in other metal complexes with benzimidazole [25]. The acetato and formato complexes show additional band at 1600–1610 cm^{-1} and 1320–1340 cm^{-1} respectively. These suggest the presence of coordinated acetate/formate and are assigned to a unidentate mode of binding of acetato/formato group [29]. In the nitrato complex new bands appear at 1420, 1320, and 1020 cm^{-1} are assigned to $\nu_{asym}(NO_2)$, $\nu_{sym}(NO_2)$ and $\nu_{asym}(NO)$ respectively, suggesting a unidentate mode of binding of nitrate group [30], whereas in the copper(II) perchlorate complex appearance of strong bands at 1080 and 910 cm^{-1}, suggests the presence of ionic perchlorate [31].

Acknowledgements—We thank the Regional Sophisticated Instrumentation Centre, IIT, Madras for the EPR facility. One of the authors (Rajesh) is thankful to UGC, India, for the award of Senior Research Fellowship (SRF). We are thankful to DST project SP/S1/FO3/93 for support.

REFERENCES

1. Corfield, P. W. R. and Shearer, H. M. M., *Acta crystallograph*, 1996, **21,** 957.
2. Sarkar, B., *Metal Ions in Biological Systems*, ed. H. Sigel Dekker. New York, 1973–81, p. 1.
3. Katz, B. M. and Barnea, A., *J. Biol. Chem.*, 1990, **258,** C140.
4. Ito, N., Phillips, S. E., Stevens, C., Ogel, Z. B., McPherron, M. J., Keen, T. N., Yadav, K. D. S. and Knowles, P. F., *Nature*, 1991, **350,** 87.
5. Ito, N., Phillips, S. E. W., Stevens, C., Ogel, Z. B., McPherron, M. L., Keen, T. N., Yadav, K. D. S. and Knowles, P. F., *J. Inorg. Biochem.*, 1991, **43,** 165.
6. Tweedle, M. F., Wilson, L. J., Garcia-Iniquiz, L., Babcock, G. T. and Palmer, G., *J. Biol. Chem.*, 1978, **253,** 8065.
7. Brown, J. M., Powers, L., Kincaid, B., Larrabee,

J. A. and Spiro, T. G., *J. Am. Chem. Soc*., 1980, **102,** 4210.
8. Larrabee, J. A. and Spiro, T. G., *J. Am. Chem. Soc*., 1980, **102,** 4217.
9. (a) Berends, H. P. and Stephan, D. W., *Inorg. Chem*., 1987, **26,** 749; (b) McKee, V., Zvagulis, M., Dagdigian, J. V., Patch, M. G., Reed, C., *J. Am. Chem. Soc*., 1984, **106,** 4765.
10. Hendriks, J. M. H., Briker, P. J. M. W. L., Jacobus, V. R., Verschoor, G. C. and Reedijk, J., *J. Am. Chem. Soc*., 1982, **104,** 3607.
11. Birker, P. J. M. W. L., Krebs, R. and Henkel, G., *Inorg. Chem*., 1982, **21,** 357.
12. (a) Berends, H. P. and Stephan, D. W., *Inorg. Chim. Acta*, 1984, **93,** 173; (b) Dagdigian, J. V. and Reed, C. A., *Inorg. Chem*., 1979, **18,** 3623.
13. Rajesh, Das, S. K. and Mathur, P., *Polyhedron*, 1997, **20,** 3511.
14. McKee, V., Zvagulis, M., Dagdigian, J. V., Patch, M. G. and Reed, C., *J. Am. Chem. Soc*., 1984, **106,** 4765.
15. Batra, G. and Mathur, P., *Inorg. Chem*., 1992, **31,** 1575.
16. Clegg, W. and Lockhart, J. C., *Polyhedron*, 1987, **6,** 1149.
17. (a) Solomon, E. I., Penfield, K. W. and Wilcox, D. E., *Struct. Bonding* (Berlin), 1983, **1,** 53; (b) Branden, R., Malmstrom, B. G. and Vanngard, T., *Eur. J. Biochem*., 1973, **36,** 195.
18. Peisach, J. and Blumberg, W. E., *Arch. Biochem. Biophys*., 1974, **145,** 691.
19. Addison, A. W., Carpenter, M., Lau, L. K. M. and Wicholas, M., *Inorg. Chem*., 1978, **17,** 1545.
20. Sakaguchi, U. and Addision, A. W., *J. Chem. Soc*., *Dalton Trans*., 1979, 600.
21. van Steenbergen, A. C., Bouwman, E., deGraff, R. A. G., Driessen, W. L., Reedijk, J. and Zanello, P. J., *J. Chem. Soc*., *Dalton Trans*., 1990, 3175.
22. Mathews, C. J., Clegg, W., Elsegood, M. R. J., Leese, T. A., Thorp, D., Thornton, P. and Lockhart, J. C., *J. Chem. Soc*., *Dalton. Trans*., 1996, 1531.
23. Manoharan, P. T. and Ragers, M. T., *Electron Spin Resonance of Metal Complexes*, ed. Teh Fu Yen. Plenum Press, New York, 1969.
24. Maki, A. H. and McGarvey, B. R., *J. Chem. Phys*., 1958, **29,** 1.
25. (a) Tripathi, A. K. and Mathur, P., *Polyhedron*, 1994, **13,** 1005; (b) Rajesh, Nohria, L. and Mathur, P., *Transition Metal Chemistry*, 1996, **21,** 524.
26. Hathaway, B. J., *J. Chem. Soc*., *Dalton. Trans*., 1196, 1972.
27. Grawford, T. H. and Dalton, J. O., *Arch. Biochem. Biophys*., 1969, **131,** 123.
28. (a) Palaniandavar, M., Pandiyan, T., Laxminarayanan, M. and Manohar, H., *J. Chem. Soc*., *Dalton. Trans*., 1995, 455: (b) Palaniandavar, M., Somasundaram, I., Lakshminarayanan, M. and Manohar, H., *J. Chem. Soc*., *Dalton. Trans*., 1996, 1333.
29. Nakamoto, K., *Infrared and Raman Spectra of Inorganic and Coordination Compounds*. John Wiley, New York, 1976, 232.
30. (a) Gatehouse, B. M., Livingstone, S. E. and Nyholm, R. S., *J. Chem. Soc*., 1957, 422; (b) Menage, S. and Quijr, L., *Inorg. Chem*., 1990, **29,** 4293.
31. Rosenthal, M. R., *J. Chem. Ed*., 1973, **50,** 331.

Pergamon

PII : S0277–5387(97)00454–3

Polyhedron Vol. 17, No. 16, pp. 2617–2622, 1998
© 1998 Elsevier Science Ltd
All rights reserved. Printed in Great Britain
0277–5387/98 $19.00+0.00

Solid state metathesis routes to Group IIIa nitrides : comparison of Li_3N, NaN_3, Ca_3N_2 and Mg_3N_2 as nitriding agents

I. P. Parkin* and A. M. Nartowski

Department of Chemistry, University College London, 20 Gordon Street, London WC1H OAJ, U.K.

(Received 15 July 1997 : accepted 31 October 1997)

Abstract—Reaction of MCl_3 (M = Sc, Y, La) with Li_3N, NaN_3, Ca_3N_2 and Mg_3N_2 at 380–800°C in sealed glass or Pyrex ampoules for 1–2 h produces MN in good yield. The metal nitrides were characterised by X-ray powder diffraction, electron probe analysis, FT-IR and microanalysis. Variations in reaction initiation temperatures, nitride composition and crystallinity were correlated with nitriding agent. © 1998 Elsevier Science Ltd. All rights reserved

Keywords: nitride ; solid-state ; metathesis.

Metal nitrides are man made materials that have found applications in a wide variety of industrial processes. Early transition metal nitrides are hard, refractory materials which show good electrical and thermal conductivity similar to metals but with better wear resistance. Titanium and zirconium nitride are used as hard phases in steel manufacture and also as coatings for tool bits [1]. Surprisingly, metal nitrides are also utilised in solar control coatings for windows where their particular reflectance and transmission properties can be used in environmental management [2]. Nitrides have also been used in high temperature crucibles, electronic circuits, catalysts and jewellery [3]. Nitrides of the Group I and II elements are salt like with metal cations and nitride anions [4]. Transition metal nitrides are interstitial compounds with nitrogen filling vacancies within a close packed metal lattice. The interstitial nature of the materials means that non-stoichiometries are common [5,6], for example, tantalum nitride has known phases from Ta_3N_5 to $TaN_{0.01}$.

Nitrides have been made by a number of methods. Conventionally combination of metal with ammonia, nitrogen or nitrogen/hydrogen mix has allowed nitride formation [7]. These routes can suffer from incomplete reaction and require prolonged elevated temperatures (1000°C). High temperature combination of the metal halide with ammonia has also yielded metal nitrides [8]. Disalvo and co workers have synthesised a range of new ternary metal nitrides by reactions in liquid sodium at 750°C [9]. Russian scientists have developed self propagating routes to metal nitrides by reacting metal powders with nitrogen under high pressure [10]. Kaner *et al.* [11,12] and ourselves [13–17] have shown that it is possible to form metal nitrides by solid state metathesis reactions (SSM) of anhydrous metal halides with lithium nitride and sodium azide eqn (1).

$$Li_3N + TiCl_3 \rightarrow TiN + 3\,LiCl \qquad (1)$$

These reactions are self propagating requiring no heat other than to initiate them. They are rapid (over in 2–3 s) with dramatically fast heating (up to 1400°C) and cooling rates. The reactions are very exothermic driven by the lattice energy of the coproduced lithium chloride. Removal of the coproduced chloride is relatively straight-forward simply by washing the product with water.

In this paper we outline the synthesis of Group IIIa nitrides using various nitriding sources. This was undertaken both to extend the range of metathesis reactions to Group IIIa nitrides and more importantly to see how changes in nitriding reagent altered ease of reaction initiation and product crystallinity and composition. The air sensitivity of the nitrides was also probed.

* Author to whom correspondence should be addressed.

EXPERIMENTAL

All reagent manipulations were carried out under nitrogen or argon atmospheres using either glove box or Schlenk line techniques. Glass ampoules (greater than 35 cm^3 internal volume) were annealed prior to use and thoroughly flame dried under vacuum. Anhydrous metal chlorides and NaN_3, Li_3N, Ca_3N_2 and Mg_3N_2 were obtained from Aldrich Chemical Co. and Strem chemicals and used as supplied. Methanol was dried over 3 Å molecular sieves and degassed with nitrogen prior to use. Infra-red spectra were recorded on a Nicolet 205 FT-IR spectrometer using KBr discs. Powder XRD measurements were performed on a Siemens Diffractometer D5000 in transmission mode using Ge monochromated Cu-$K_{\alpha 1}$ ($\lambda = 1.5406$ Å) radiation. SEM profiles and energy dispersive X-ray analyses (EXDA) were obtained on a Jeol JSM 820 instrument using a Kevex detector and software. EDXA was performed on various regions across the sample surface, using point analyses to determine regional homogeneity. Electron probe analysis were performed on a Jeol EMA microprobe. A Lenton Thermal Designs programmable tube furnace was used to initiate the bulk reactions. Point source reactions were initiated by electrically heated nicrome wire filament at 800°C. Microanalysis was determined by the departmental service at UCL.

Reaction of NaN_3 *with* MCl_3 (M = Sc, Y, La)

The same general reaction scale and procedure was utilised for all reactions outlined below for sodium azide and lanthanum trichloride.

Sodium azide (0.050 g, 0.77 mmol) and $LaCl_3$ (0.504 g, 0.22 mmol) were carefully ground together and sealed under vacuum in a large pyrex ampoule. The ampoule was placed into a tube furnace and the temperature ramped at 10°C per minute from room temperature until a reaction was observed (380°C) by a thermal flash and the appearance of material at the end wall of the ampoule. After cooling, the ampoule was broken open and the material was washed with methanol (4×7 ml) and dried *in vacuo*. The residual black materials were analysed by powder XRD (Table 1), SEM/EDXA and FT-IR. Microanalysis LaN ; calculated N = 9.1%, observed N = 5.8% (implying non-stoichiometry and formation of $LaN_{0.61}$; nitrogen stoichiometry as determined by electron probe indicated that the nitride products were in the range $MN_{0.9}$–$MN_{0.7}$ (M = Y, La) also indicating non-stoichiometry).

Reactions involving Ca_3N_2 and Mg_3N_2 with MCl_3 were conducted in quartz ampoules and the oven temperature raised up to 800°C maintained at this temperature for 1 h and allowed to cool to room temperature.

Reactions involving Li_3N and MCl_3 initiated at 500°C with an orange thermoflash. Reactions can be made to occur with these reagents at 400°C for 3 h, however a very poorly crystalline product is produced.

Isolated yields for the Li_3N, Mg_3N_2 and Ca_3N_2 reactions were typically 70–90%. Sodium azide reactions gave yields from 20–30%.

Filament initiation ; reactions did not initiate in the filament mode (nichrome wire, 800°C).

Caution! These reactions are extremely exothermic and can produce large quantities of nitrogen (especially the NaN_3 reactions). Large ampoules should be used to minimise the risk of pressure explosions and reactions should be conducted behind a safety screen.

RESULTS AND DISCUSSION

Synthesis and characterisation

Reactions of Group IIIa anhydrous chlorides with a number of different nitriding agents (Li_3N, Mg_3N_2, Ca_3N_2 and NaN_3) were investigated. Mixtures of the preground elements were heated in sealed glass or quartz ampoules. At certain temperatures (Table 1) a thermal flash was observed and the solid material was spread over the ampoule walls. In the Ca_3N_2 and Mg_3N_2 reactions the ampoules were heated further for 1 h at 750°C and then allowed to cool to room temperature. All reactions afforded a (dark) powder which was purified by washing with methanol and dried briefly *in vacuo*. Both the washed and as prepared powders were analysed by SEM/EDAX, X-ray powder diffraction, microanalysis, electron probe and FT-IR.

The as prepared materials showed by powder XRD a mixture of Group IIIa metal nitride and main Group chloride. Metal chloride was removed by trituration to leave just the diffraction patterns for either ScN, YN (Fig. 1) or LaN. Patterns indexed well and correlated with literature measurements [18]. However a small variation in the observed *a* parameter was noted depending on the nitriding source (Table 1). This may correspond to some nitrogen substoichiometry, especially as cubic transition metal nitrides are known to tolerate wide ranges in composition ($MN_{1.0}$–$MN_{0.7}$). Differences in the degree of crystallinity of the powders were noted dependent on nitriding agent. This is commented on below. SEM measurements of the as prepared powders revealed a smooth morphology, whilst EDAX showed the presence of Group IIIa metal, main group metal and chlorine (nitrogen was below the threshold of the EDAX system used). This corresponds to the formation of Group IIIa nitride with main group metal chloride on the surface. Trituration of the material produced small (ca 1 μm) aggregates with sharp angles and faces by SEM and only Group IIIa metal by EDAX. Surprisingly little variation in morphology was observed for different reaction temperatures (Table 1), although the highest temperature reactions did show slightly

Table 1. Reaction conditions and XRD data for the products from reactions of MCl_3 (M = Sc, Y, La) with Li_3N, NaN_3, Mg_3N_2 and Ca_3N_2

Reagents	Synthesis	Colour	Phase observed	Observed *a* parameter (Å)	Literature [18] *a* parameter (Å)
$Li_3N/ScCl_3$	Thermoflash 560°C	Dark brown	ScN	4.488	4.45
$NaN_3/ScCl_3$	Thermoflash at 380°C	Black	ScN	4.491	4.45
$Mg_3N_2/ScCl_3$	750°C 1h	Black	ScN	4.493	4.45
Li_3N/YCl_3	Thermoflash at 550°C	Black	YN	4.882	4.89
NaN_3/YCl_3	Thermoflash at 380°C	Grey/black	YN	4.894	4.89
Mg_3N_2/YCl_3	750°C 1h	Brown/red	YN	4.862	4.89
Ca_3N_2/YCl_3	750°C 1h	Brown	YN	4.897	4.89
$Li_3N/LaCl_3$	Thermoflash at 550°C	Black	LaN	5.295	5.30
$NaN_3/LaCl_3$	Thermoflash at 380°C	Black	LaN	5.277	5.30

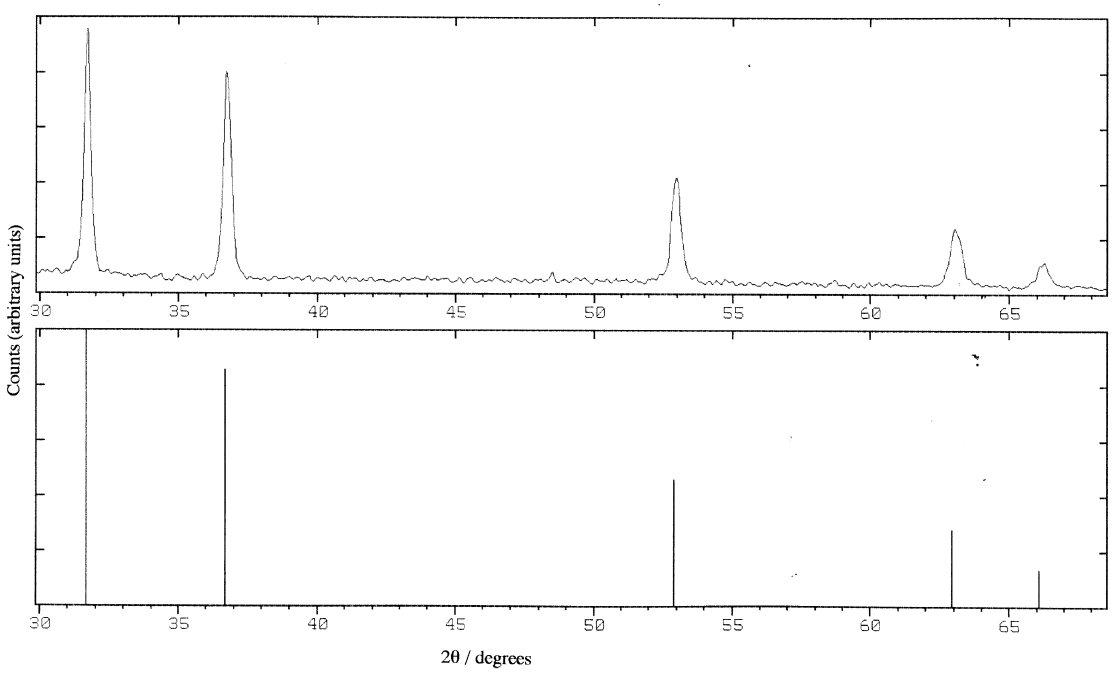

Fig. 1. Top trace; powder XRD pattern obtained from the reaction of Ca_3N_2 and YCl_3. Bottom trace; literature stick pattern for YN.

larger agglomerates after washing. Electron probe measurements showed predominantly the presence of metal and nitrogen with elemental ratios in the range $MN_{0.9}$–$MN_{0.7}$ across many surface spots. Notably little oxygen was detected, indicating that the products are not metal oxynitrides. FT-IR analysis of the nitride powders showed just a single broad absorption band centred at 650 cm^{-1} (LaN) corresponding to a metal nitrogen stretch [19]. Elemental combustion analysis also showed a nitrogen deficient nitride of formula $LaN_{0.61}$. This low value maybe due to the refractory nature of the nitride (making combustion analysis difficult). Although as stated above it is likely that the Group IIIa nitrides formed are sub-stoichiometric in nitrogen. It should also be noted that some nitrogen loss may occur prior to analysis (see later).

Overall the reactions can be summarised as indicated in eqns (2)–(5).

$$MCl_3 + 3NaN_3 \rightarrow MN + 3NaCl + 4N_2 \quad (M = Sc, Y, La) \quad (2)$$

$$MCl_3 + Li_3 \rightarrow MN + 3LiCl \quad (M = Sc, Y, La) \quad (3)$$

$$2MCl_3 + Ca_3N_2 \rightarrow 2MN + 3CaCl_2 \quad (M = Sc, Y, La) \tag{4}$$

$$2MCl_3 + Mg_3N_2 \rightarrow 2MN + 3MgCl_2 \quad (M = Sc, Y) \tag{5}$$

Initiation temperatures

Reactions with sodium azide all initiated at 380°C (NaN_3 dec 365°C) [19]. A bright white thermoflash occurred at the initiation temperature and the products were spread throughout the ampoule due to nitrogen evolution eqn 2. Crystallinity of the product was much lower than with other nitriding agents as the product is spread throughout the ampoule allowing for less self annealing. Reactions of other nitriding agents with anhydrous metal chlorides formed a partly fused solid, eqns 3–5. In general use of Li_3N produced the most crystalline product. In this case the reactions initiated at 550°C with an orange thermal flash and produced a dark partly fused product. It was possible to get a reaction between Li_3N and MCl_3 at 400°C below the thermal flash temperature if the reaction was left for 3 h, however the product was notably less crystalline and more unstable readily losing nitrogen. No reaction was observed between calcium or magnesium nitrides and Group IIIa metal halides at temperatures up to 600°C.

However heating to 750°C for 1 h in a quartz ampoule did promote reaction. In this case no thermoflash was observed and a darkening of the solid was noted at 700–750°C (Table 1). For comparable reactions calcium nitride tended to give more crystalline products than magnesium nitride.

The temperature required for initiation of the solid state metathesis reaction is very dependent on the nitriding reagent. This can be directly related to the ease in which the solid state diffusion barrier is overcome. Sodium azide decomposes at ca 365°C [12]. This allows the lowest temperature initiation of any of the nitriding agents studied. Presumably the sodium released on decomposition can react with chloride of the metal halide and allow partial reduction of the metal halide and formation of molten NaCl in which the reaction can propagate. This reaction is probably of the reduction-oxidation mechanism as described by Kaner [12]. Lithium nitride reactions were observed to initiate at ca 550°C with Group IIIa chlorides. This is below the melting points of both Li_3N (810°C) [12] and MCl_3 (850°C M = Sc, Y, La) [21]. Interestingly an early report noted that Li_3N starts to lose some nitrogen at 550°C prior to melting [22]. This temperature corresponds to the initiation temperatures observed. Thus either the partial loss of nitrogen is important in initiating the reaction, or at this temperature the rate of solid state diffusion between reacting grains (possibly promoted by some free Li generated on loss of nitrogen) has become sufficient for the exothermic combination reaction to become self propagating. The reactions of magnesium and calcium nitrides and MCl_3 do not show a thermal flash. Notably the decomposition points of Mg_3N_2 and Ca_3N_2 at 1500°C and 900°C [21] (note 1150°C is also quoted for Ca_3N_2 [22]) are above the decomposition points of the metal halides.

Thermodynamic considerations

Reactions of Group IIIa anhydrous chlorides and the various nitriding agents were studied by point source filament initiation. This was achieved by placing a glowing filament (800°C) onto a preground mixture of the reacting powders. No solid flame was observed and all the reactions failed to propagate. Some reaction was observed at the tip of the filament for the reactions involving sodium azide and lithium nitride, probably corresponding to partial reaction or decomposition. It has been shown previously [12,17] that the ease of reaction propagation can be related to $T_{ad,s}$ (the adiabatic reaction temperature for the reaction assuming salt formation only i.e. $LaCl_3 + Li_3N \rightarrow La + N + 3LiCl$) and the melting points of the co-produced metal halides. This model has been built up by empirical argument stating that the reaction can only propagate if sufficient reaction energy is available to melt the co-produced salt, the reaction proceeding between intervening layers with the melt; thereby overcoming the solid state diffusion barrier. In the reactions outlined for Group IIIa elements $T_{ad,s}$ for La and Y is below the melting point of the co-produced salts, the reaction between $ScCl_3$ and Li_3N is at the cross over point for propagation.

Heats of reaction for eqns 2–5 as assessed by Hess's Law show a decrease in exothermicity with nitriding agent in the order NaN_3, Li_3N, Ca_3N_2, Mg_3N_2 (ca -650 kJ mol^{-1} NaN_3 and $ScCl_3$ to -260 kJ mol^{-1} Mg_3N_2 and $LaCl_3$). The most exothermic reactions did not correspond to the most crystalline sample. However the Mg_3N_2 prepared nitrides showed the least crystallinity (ca 200 Å from the Scherrer equation [1]) and these reactions were also the least exothermic. The sodium azide prepared nitrides also showed limited crystallinity [1] (ca 250 Å) probably because of the excess gas produced in the reaction and spread of product within the ampoule, thus limiting self annealing [17]. The lithium nitride reactions showed the greatest crystallinity (ca 450 Å) [1] probably as a fused product was obtained and the reaction was also very exothermic. It may also be possible that the coproduced LiCl acts as a template for the formation of cubic nitrides [13,15].

Changes in nitridation

It was observed that the nitridation level of the metal nitrides was adversely effected by the use of vacuum drying. In the case of YN prepared from

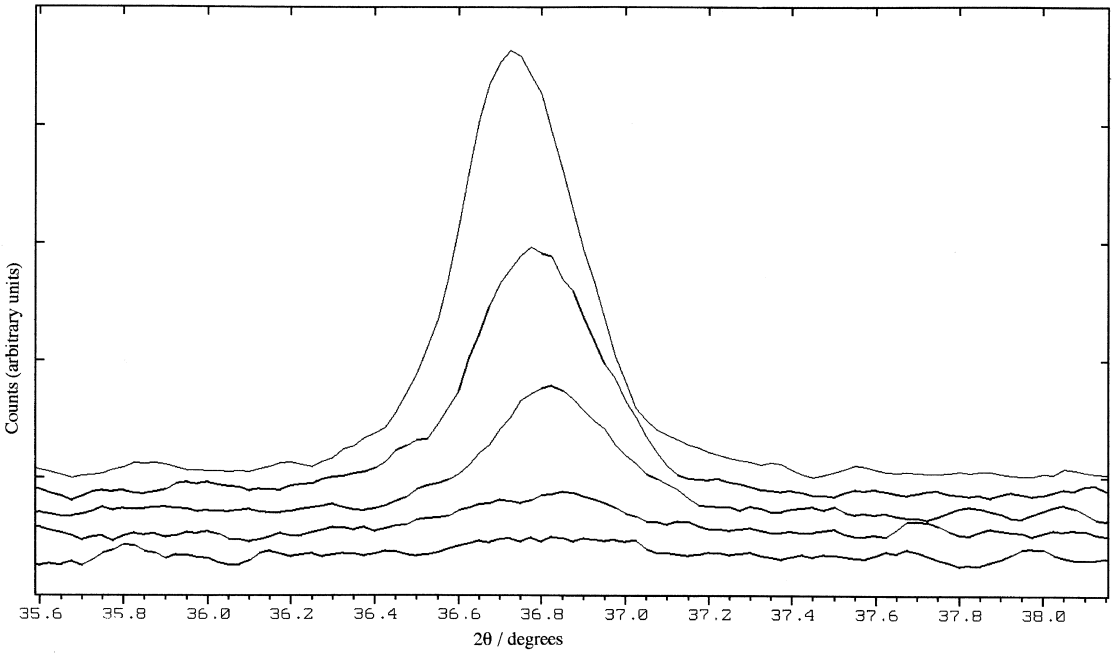

Fig. 2. Changes in the YN (1 1 1) reflection with time after storage in air (patterns recorded at 10 min intervals).

Ca_3N_2 and YCl_3 the *a*-parameter shifted from 4.897 Å to 4.886 Å, this was also accompanied by a change in colour from brown to navy green. Goldschmidt [23] determined that the lattice parameter is sensitive to degree of nitridation. The *a* value of cubic nitrides decreases as the amount of nitrogen in the product goes down, until a critical point is reached and the material ceases to have a cubic structure. Changes in nitride lattice parameter can often be correlated with Vegards law [24]. We would have liked to correlate the observed low levels of nitridation in the Group IIIa nitrides ($MN_{0.8}$ by electron probe) with the lower *a* parameter, however to our knowledge no Vegard like compositional range for Group IIIa nitrides has been published. However it is probably fair to note that a decrease in *a*-value corresponds to lower nitridation levels. Additionally a decrease in lattice parameter is noticed upon short vacuum drying of the product. It also appears that the loss of nitrogen from the structure *in vacuo* is fast initially at high levels of nitridation, but slows dramatically as the nitrogen content decreases.

Nitride samples prepared by SSM reactions also appear to be sensitive to the presence of oxygen, far more so than nitrides prepared by conventional means. This may be due to the high defect concentrations and relatively high surface areas generating quite a porous material. It was noted that diffraction peaks for YN when measured in air decreased in intensity with time for the same sample. A new set of diffraction lines appeared with oxidation corresponding to Y_2O_3, however these only grew in initially and did not continue to increase as the nitride peaks diminished. In addition to the nitride peaks going down in intensity they also shifted position (Fig. 2) ($a = 4.883$ Å over a period of 1 h in air) corresponding to loss of nitrogen. Such nitride materials must be handled and stored in a nitrogen atmosphere.

Attempts at forming solid solutions of Y_xSc_yN using mixtures of the metal chlorides and Li_3N were unsuccessful forming a mixtures of phases that could be assessed as the individual nitrides.

CONCLUSIONS

Reaction of Li_3N, Na_3N, Ca_3N_2 and Mg_3N_2 with anhydrous Group IIIa chlorides offer a convenient one step high yield route to metal nitrides MN. Crystallinity is dependent on the nitriding reagent with Li_3N and Ca_3N_2 producing the most crystalline products. Ease of reaction initiation is related to the ease in which the solid state diffusion barrier is overcome, this can be correlated to decomposition points of the nitride reagents. Group IIIa nitrides formed via SSM reactions are air and vacuum sensitive losing nitrogen.

Acknowledgements—I.P.P. and A.M.N. thank the EPSRC for Grant No. GR/L 06850. A. Craven and M. MacKenzie (Glasgow University) and P. Hatto (Multiarc U.K.) are thanked for useful discussions.

REFERENCES

1. Wells, A. F., *Structural Inorganic Chemistry*, 5th Edn. Oxford, London, 1984

2. Elger, G. W., Traut, D. E., Slavens, G. J. and Gerdeman, S. J., *Metall. Trans. B*, 1989, **20,** 493; Dowsen, D., Taylor, C. M. and Grodel, M. Eds, *Tribology Series* 17, Elsevier Science, Amsterdam, 1990, p. 81.
3. Bonnot, A. M., Belkier, H., Pailharey, D. and Marthiez, P., *Sol. Energy Mater.*, 1986, **13,** 339; Liu, J. S. and Ignatiev, A., *Sol. Energy Mater.*, 1986, **13,** 399; Haygarth, J. C., *Thin Solid Films*, 1980, **72,** 51.
4. Toth, L. E., *Transition Metal Carbides and Nitrides*, Chapters 1–3. Academic Press, New York, 1971.
5. Jones, K., in *Comprehensive Inorganic Chemistry*, ed. J. Bailar, H. J. Emeleus, R. Nyholm and A. F. Trotman Dickenson, Vol. 2. Pergamon, Oxford, 1973.
6. Vikar, A. V., Jackson, T. B. and Cutler, R. A., *J. Am. Ceram. Soc.*, 1980, **72,** 2031.
7. Koenig, V., *Surf. Coat. Technology*, 1987, **33,** 91.
8. Johansen, H. A., *Survey Prog. Chem.*, 1977, **8,** 57.
9. Clarke, S. J. and DiSalvo, F. J., *J. Sol. St. Chem.*, 1997, **129,** 144; Clarke, S. J. and DiSalvo, F. J., *Inorg. Chem.*, **36,** 1143; Clarke, S. J. and DiSalvo, F. J., *Curr. Op. Sol. St. Mat. Sci.*, 1996, **1,** 241.
10. Torbov, V. J., Chukalin, V. I. and Yarembash, E. J., *Inorg. Mater.*, 1970, **6,** 1559; Sheppard, L. M., *Adv. Mater. Proc.*, 1986, **2,** 25.
11. Rao, L. and Kaner, R. B., *Inorg. Chem.*, 1994, **33,** 3210; Gillan, E. G. and Kaner, R. B., *Inorg. Chem.*, 1994, **33,** 5693.
12. Gillan, E. G. and Kaner, R. B., *Chem. Mater.*, 1996, **8,** 333.
13. Fitzmaurice, J. C., Hector, A. L. and Parkin, I. P., *J. Chem. Soc., Dalton Trans.*, 1993, 2435.
14. Hector, A. L. and Parkin. I. P., *J. Chem. Soc. Chem. Commun.*, 1993, 1095.
15. Fitzmaurice, J. C., Hector, A. L., Rowley A. T. and Parkin, I. P., *Polyhedron*, 1994, **13,** 235.
16. Aguas, M., Ali, S., Parkin, I. P., Henshaw, G. and Hector, A. L., *Polyhedron*, 1997, in press.
17. Hector, A. L. and Parkin, I. P., *Chem. Mater.*, 1995, **7,** 1728; Hector, A. L. and Parkin, I. P., *Polyhedron*, 1995, **14,** 913.
18. PDF-2 database, International Center for Diffraction Data, Swartmore, PA, 19081, 1990.
19. Nakamoto, K., *Infra-red and Raman of Inorganic and Coordination Compounds*, 3rd edn. Wiley, New York, 1978.
20. *Handbook of Chemistry and Physics*, 55th edn. CRC Press, 1974.
21. Gallais, F. and Masdupuy, E., *Compt. Rend.*, 1948, **227,** 635.
22. Mellor, J. W., *Mellors Comprehensive Treatise on Inorganic and Theoretical Chemistry*, Vol VIII, Suppl. I, Nitrogen part I. Longmans, London, 1964, p. 161.
23. Goldschmidt, H. J., *Interstitial Alloys*. Butterworths and Co., London, 1967, p. 214.
24. Klug, H. P. and Alexander, L. E., *X-ray diffraction Procedure for Polycrystalline and Amorphous Materials*, 2nd edn. Wiley, New York, 1974.

Pergamon

PII : S0277–5387(97)00515–9

Polyhedron Vol. 17, No. 16, pp. 2623–2626, 1998
© 1998 Elsevier Science Ltd
All rights reserved. Printed in Great Britain
0277–5387/98 $19.00 + 0.00

COMMUNICATION

The first well characterized $Fe(phen)Cl_3$ complex : structure of aquo mono(1,10-phenanthroline)iron(III) trichloride : $[Fe(phen)Cl_3(H_2O)]$

Prasad Kulkarni,[a] Subhash Padhye[a]* and Ekkehard Sinn[b]

[a] Department of Chemistry, University of Poona, Poona-411 007, India

[b] School of Chemistry, University of Hull, Hull HU6 7RX, U.K.

(Received 26 August 1997 ; accepted 6 December 1997)

Abstract—The crystal structure of the neutral, *pseudo*-octahedral *mono* phenanthroline iron(III) complex $Fe(phen)Cl_3H_2O$ is reported, which surprisingly is the first well-characterized $Fe(phen)Cl_3$ complex (space group $P\bar{1}$; $a = 10.224(4)$ Å, $b = 10.603(3)$ Å ; $c = 6.628(2)$ Å ; $\alpha = 100.70(2)^\circ$, $\beta = 108.17(2)^\circ$, $\gamma = 92.06(2)^\circ$; $R = R_w = 0.033$). Of the three unidentate chloride ions, two are coplanar with phenanthroline ligand while the third is out of plane and is *trans* to the water molecule. The metal environment is distorted from regular octahedral due to the non-equivalent ligand donor set. The N–Fe–N bite angle of 75.6° is compressed below right-angular with a corresponding opening of the other bond angles around the iron in this plane. The Fe—Cl bonds are inequivalent, ranging from 2.25 to 2.35 Å, the axial Fe—Cl bond being elongated. The axial aquo group is tilted towards the phenanthroline ring, making an angle of 83.8° with N(1) and 81.8° with N(2), respectively. Comparison with the Mn(III) analog yields the effect of changing from a high spin d^5 to a high spin d^4 center. © 1997 Elsevier Science Ltd

Keywords: iron(III) ; phenanthroline ; DNA intercalator.

1,10-phenanthroline (phen) is a popular ligand, extensively studied for the DNA cleaving activity of its copper compounds [1] and the DNA intercalating properties of the ruthenium compounds [2]. The screw-chain structure of 1,10-phenanthroline · H_2O [3] forms via a H-bonding network. Phen complexes with many metals exhibiting 1 : 1, 1 : 2, and 1 : 3 metal to ligands stoichiometries. Numerous X-ray crystal structures have been reported for bis-phen [4–8] and tris-phen [9–12] complexes, while complexes containing a solitary phen ligand are scarce [14–16]. Attempts to prepare the species with the empirical formula $Fe(phen)Cl_3$ have been described [17–19] but the correct composition of the product has not been clearly established and several formulae have been proposed. For example, the action of phen on $FeCl_3$ in acetone was recently shown to yield $[Fe(phen)_2Cl_2][FeCl_4]$ [4].

EXPERIMENTAL

$Fe(phen)Cl_3 \cdot H_2O$ was prepared by mixing an aqueous solution of iron chloride with 1,10-phenanthroline solution in 10 M HCl in the mole ratio of 1 : 1 and recrystallizing the resulting compound from a water : methanol (1 : 1) mixture. The yield of the compound is very low. Elemental Analysis : Found C, 41.23% ; H, 2.76%, Fe, 14.84% ; Calcd C, 39.99% ; H, 2.80%, Fe, 15.49%.

Data collection and processing

Measurements were made as previously described [31] using a Rigaku AFC6S diffractometer with

* Author to whom correspondence should be addressed.

graphite monochromated MoKα radiation on a red crystal fragment of [Fe(phen)(H_2O)Cl_3], $C_{12}H_{10}ON_2FeCl_3$, dimensions $0.50 \times 0.40 \times 0.30$ mm, on a glass fibre. Cell dimensions were $a = 10.224(4)$ Å, $b = 10.603(3)$ Å; $c = 6.628(2)$ Å; $\alpha = 100.70(2)^\circ$, $\beta = 108.17(2)$, $\gamma = 92.06(2)^\circ$; V = 667.4(4) Å [3]. For Z = 2 and F.W. = 360.4, the calculated density is 1.79 g/cm [3]. Based on packing considerations, a statistical analysis of intensity distribution, and the structure solution, the space group was determined to be $P\bar{1}$. Data were collected at 20°C using ω–2θ scans. Scans of $(1.37 + 0.33 \tan\theta)^\circ$ were made at 4.0°/min (in ω). Stationary background counts were made on both sides of each reflection. Of the 3409 reflections collected, 3232 were unique ($R_{int.} = 0.043$); equivalent reflections were averaged. Of these, 2172 reflections and $F_0^2 > 3\ \sigma(F_0^2)$, where $\sigma(F_0^2)$ was estimated from counting statistics [31,32]. Lorentz-polarization and absorption [33] corrections were applied. The intensities of three standard reflections measured after every 150 reflections showed no greater variation than those expected from Poisson statistics.

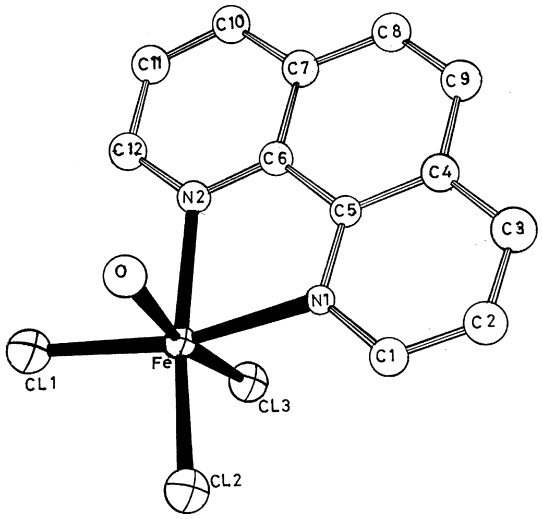

Fig. 1. Molecular structure of [Fe(phen)Cl_3(H_2O)]. Selected bond distances (Å): Fe—Cl(1) 2.282(1), Fe—Cl(2) 2.250(1), Fe—O 2.188(3), Fe—Cl(3) 2.342(1), Fe—N(1) 2.167(3), Fe—N(2) 2.182(3); bond angles (°): Cl(3)—Fe—O 169.13(7), Cl(2)—Fe—Cl(3) 98.71(5), O—Fe—N(1) 83.8(1), O—Fe—N(2) 81.8(1), N(1)—Fe—N(2) 75.6(1).

Structure solution and refinement

The metal and halogen position were determined from a 3-D Patterson which phased the data sufficiently to locate the other atoms from difference Fourier maps. Non-hydrogen atoms were refined anisotropically. Full-matrix least-squares refinement [34] using the TEXRAY [35] program set gave unweighted and weighted agreement factors of $R = (\Sigma||F_o| - |F_c||)/\Sigma|F_o| = 0.033$, $R_w = [(\Sigma w(|F_o| - |F_c|)^2/\Sigma w(F_o^2))]^{1/2} = 0.033$. The standard deviation of an observation of unit weight [36] was 1.66. The weighting scheme was based on counting statistics and included a factor ($p = 0.015$) to downweight the intense reflections. Neutral atom scattering factors were taken from Cromer and Waber [37]. Anomalous dispersion effects were included in F_{calc} [38], the values for $\Delta f'$ and $\Delta f''$ were those of Cromer [39].

RESULTS AND DISCUSSION

Here we report the crystal structure of [Fe(phen)Cl_3(H_2O)] which is a distorted octahedral compound an ORTEP [20] of which is shown in Fig. 1. The N_2Cl_2 equatorial plane exhibits slightly unequal bond distances for the Fe–N linkages at 2.167 and 2.182 Å. The shorter of these is balanced by a slightly longer (2.282 Å vs 2.250 Å) Fe—Cl bond on the opposite side. Metal ligand bond lengths can be used to determine the spin state and further that the effect of counterions is relatively small when a spin equilibrium is not present [21–30]. The comparison with the tris (phen) complex (Table 1) shows the present complex to be unambiguously high spin d^5. The iron–nitrogen distances observed in the present complex are significantly greater than those found for the tris phenanthroline compounds (Table 1) while the Fe—Cl distances are slightly greater than those in bis derivatives. The remaining chloro group is axial at a greater distance (Fe—Cl = 2.342 Å) compared with the 2.282 Å and 2.250 Å values for the in-plane Fe—Cl bonds. The aquo group, *trans* to the axial chloro group, at 2.188 Å and is slightly tilted away from the halogens and towards the plane of the phen ring, making angles of 83.82° and 81.8° with N1 and N2 atoms, respectively. The bond angle N1—Fe—N2 atoms is fairly compressed (75.6°) due to the constraint exercised by the solitary chelate ring and is compensated by opening of the other bond angles around iron in the N_2Cl_2 plane.

The molecules link together via a weak hydrogen bonding network. The coordinated water links to the axial chloride of the neighbouring molecule (3.265(3) Å progressing along the *b* axis), and also to an equatorial Cl(1) through the crystallographic inversion centre (3.258(3) Å progressing along the *a* axis). The closest Fe–Fe separation is 5.555(2) Å.

A manganese(III) analog of the present complex has been reported and this provides an opportunity to compare d^4 and d^5 configurations in the same ligand environment (Table 1). The overall average metal–ligand bonds are similar, 2.235 Å for Fe and 2.240 Å for Mn, the trend reflecting the expected slightly smaller size of the Fe^{3+} ion. However, the individual bonds show far greater differences. The manganese ion lies closer to the phen ligand, with Mn—N distances 2.067, 2.074 Å, vs 2.167, 2.182 Å for Fe, which opens up the N—Mn—N angle (79.8° vs 75.6° for Fe). The equatorial Mn—Cl bonds show the same trend at

Table 1. Summary of averaged bond distances and bond angles of some phen complexes

Compound	⟨M-N⟩ (Å)	M-Cl (Å)	N-M-N(°)	Spin state	Ref.
$[Fe(III)(phen)Cl_3H_2O]$	2.174(3)	2.276[b] 2.276[b]	75.6(1)	HS[d]	*a*
$[Fe(III)(phen)_2Cl_2][FeCl_4]$	2.250(11)	2.246(4)	—	HS[d]	4
$[Fe(III)(phen)_3](ClO4)_3]H_2O$	1.973(8)	—	83.0(3)	LS[e]	10
$[Mn(III)(phen)Cl_3(H_2O)]$	2.971(2)	2.233[b] 2.527[c]	79.82	HS[d]	14

[a] Present work.
[b] Equatorial.
[c] Axial.
[d] High spin.
[e] Low spin.

2.225, 2.240 Å vs 2.250, 2.282 Å for Fe. The most dramatic difference occurs in the axial bonds which show the manganese complex to be dramatically distorted in the Jahn-Teller sense : there is dramatic elongation in the bond to the axial oxygen (2.306 Å for Mn vs 2.189 Å for Fe) and the axial Cl (2.527 Å for Mn vs 2.306 Å for Fe).

Acknowledgements—PPK thanks CSIR for JRF while SP is grateful to British Council, Bombay, for the assistance under the Indo-British Link Program.

REFERENCES

1. Sigman, D., Graham, D. R., D'Aurora, V. and Stern, A. M., *J. Biol. Chem*., 1979, **254,** 12,269.
2. Mie, H. Y. and Barton, J. K., *J. Am. Chem. Soc*. 1986, **108,** 7414.
3. Tian, Y. P., Duan, C. Y., Xu, X. X. and You, X. Z., *Acta. Cryst*., 1995, **C51,** 2309.
4. Goodwin, H. J., McPartlin, M. and Goodwin, H. A., *Inorg. Chim. Acta*, 1977, **25,** L74.
5. Otieno, T., Bond, M., Morky, L. M., Walter, R. B. and Carrano, C. J., *J. Chem. Soc. Chem. Comm*., 1996, 37.
6. Li, J., Zou, J., Wu, M., Xu, Z., You, X. and Mak, T. C., *Polyhedron*, 1995, **14,** 3519.
7. Reddy, K. R. and Rajsekharan, M. V., *Polyhedron*, 1994, **13,** 765.
8. Holleman, S. R., Parker, O. J. and Breneman, G. L., *Acta Cryst*., 1994, **C50,** 867.
9. Anderson, P. O., *J. Chem. Soc*., *Dalton Trans*., 1973, 1237.
10. Baker, J., Engelhardt, L. M., Figgis, B. N. and White, A. H., *J. Chem. Soc*., *Dalton Trans*., 1975, 530.
11. Boys, D., Escobar, C. and Wittke, O., *Acta Cryst*., 1984, **C40,** 1359–1362.
12. Koh, L. L., Xu, Y., Hsieh, A. K., Song, B., Wu, F. and Ji, L., *Acta Cryst*., 1994, **C50,** 884.
13. Breneman, G. L. and Parker, O. JL., *Polyhedron*, 1993, **12,** 891.
14. Swarnabala, G., Reddy, K. R., Tirunagar, J., Rajsekharan, M. V., *Trans. Met. Chem*., 1994, **19,** 506.
15. Su, C.-C., Wu, S.-P., Wu, C.-Y. and Chang, T.-Y., *Polyhedron*, 1995, **14,** 267.
16. Simon, A., Morgenstern, G. and Albrecht, W. H., *Z. anorg. allg. Chem*., 1937, **230,** 225.
17. Harris, C. M. and Lockyer, T. N., *Chem and Ind*., 1968, 1231.
18. Berrett, R. R., Fitzsimmons, B. W. and Owusu, A. A., *J. Chem. Soc. A*, 1968, 1575.
19. Ghosh, S. N., *Ind. J. Chem*., 1975, **13,** 66.
20. Johnson, C. K., ORTEP II. Report ORNL-5138. Oak Ridge National Laboratory, Oak Ridge, Tennessee (1976).
21. Cukauskas, E. J., Deaver, B. S. Jr. and Sinn, E., *J. Chem. Phys*., 1977, **67,** 1257.
22. Sinn, E., Sim, P. G., Dose, E. V., Tweedle, M. F. and Wilson, L. J., *J. Am. Chem. Soc*., 1978, **100,** 3375.
23. Greenaway, A. M. and Sinn, E., *J. Am. Chem. Soc*., 1978, **100,** 8080.
24. Greenaway, A. M., Schrock, A. and Sinn, E., *Inorg. Chem*., 1979, **18,** 2692.
25. Sim, P. G. and Sinn, E., *J. Am. Chem. Soc*., 1981, **103,** 241.
26. Sim, P. G., Sinn, E., Petty, R. H., Merrill, C. L. and Wilson, L. J., *Inorg. Chem*., 1981, **20,** 1213.
27. Timken, M. D., Hendrickson, D. N. and Sinn, E., *Inorg. Chem*., 1985, **24,** 2947.
28. Addison, A. W., Burman, S., Wahlgren, C. G., Rajan, O. A., Rowe, T. M. and Sinn, E., *J. Chem. Soc*., *Dalton Trans*., 1987, 2621.
29. Magnetic Properties. Sinn, E. in *Encyclopaedia of Analytical Chemistry*, ed. A. Townsend. Academic Press, 1995, 2765.
30. Collison, D., Garner, D., McGrath, C. M., Mosselmans, J. F. W., Roper, M. D., Seddon, J. W. M., Sinn, E. and Young, N. A., *J. Chem. Soc*., *Dalton Trans*., 1997, 4371.
31. Backhouse, J. R., Lowe, H. M., Sinn, E., Suzuki, S. and Woodward, S., *J. Chem. Soc*., *Dalton Trans*., 1995, 1489.
32. Corfield, P. W. P., Doedens, R. J. and Ibers, J. A., *Inorg. Chem*., 1967, **6,** 197.

33. An empirical absorption correction, based on azimuthal scans of several reflections, was applied which resulted in transmission factors ranging from 0.84 to 1.10.
34. Least-Squares: Function minimized is $\Sigma w(|\mathrm{iF_o}|-|F_c|)^2$ where $w = 4F_o^2/\sigma^2(F_o^2)$; $\sigma^2(F_o^2) = [S^2(C+R^2B)+(pF_o^2)^2]/Lp^2$; S = Scan rate; C = Total Integrated Peak Count; R = Ratio of Scan Time to background counting time; p = p-factor; B = Total Background Count; Lp = Lorentz-polarization factor.
35. TEXSAN–TEXRAY Structure Analysis Package, Molecular Structure Corporation, 1985.
36. Standard deviation of an observation of unit weight: $[\Sigma w(|F_0|-|F_c|)^2/(No-Nv)]^{1/2}$ where No = number of observations, Nv = number of variables.
37. Cromer, D. T. and Waber, J. T., *International Tables for X-ray Crystallography*, Vol. IV. The Kynoch Press, Birmingham, U.K., Table 2.2A, 1974.
38. Ibers, J. A. and Hamilton, W. C., *Acta Cryst.*, 1964, **17,** 781.
39. Cromer, D. T., *International Tables for X-ray Crystallography*, Vol. IV. The Kynoch Press, Birmingham, U.K. Table 2.3.1, 1974.

Pergamon

PII : S0277–5387(98)00011–4

Polyhedron Vol. 17, No. 16, pp. 2627–2632, 1998
© 1998 Elsevier Science Ltd
All rights reserved. Printed in Great Britain
0277–5387/98 $19.00+0.00

Charge-compensated carbarhodaboranes. Synthesis and molecular structures of 3-L-3,3-$(I)_2$-4-SMe_2-3,1,2-*closo*-$RhC_2B_9H_{10}$, L = CO or PPh_3

Alan S. F. Boyd, Georgina M. Rosair, Franca B. H. Tiarks, Andrew S. Weller, Stephan K. Zahn and Alan J. Welch*

Department of Chemistry, Heriot-Watt University, Edinburgh EH14 4AS, U.K.

(Received 3 September 1997; accepted 5 January 1998)

Abstract—Reaction of 3,3-$(CO)_2$-4-SMe_2-3,1,2-*closo*-$RhC_2B_9H_{10}$ with iodine results in the formation of 3-(CO)-3,3-$(I)_2$-4-SMe_2-3,1,2-*closo*-$RhC_2B_9H_{10}$, **1**. Reaction between **1** and PPh_3 results in substitution of the carbonyl group to afford 3-PPh_3-3,3-$(I)_2$-4-SMe_2-3,1,2-*closo*-$RhC_2B_9H_{10}$, **2**. Both new compounds have been fully characterised by multinuclear NMR spectroscopy and also by a single crystal X-ray diffraction studies.
© 1998 Elsevier Science Ltd. All rights reserved

Keywords: carbaborane; rhodium; synthesis; structure.

We [1] and others [2], have recently been interested in the synthesis and chemistry of "charge-compensated" carbaboranes and carbametallaboranes derived from them, particularly those based upon [9-SMe_2-7,8-*nido*-$C_2B_9H_{10}]^-$, $[carb']^-$, and its derivatives. Such compounds are of interest due to the formal analogy that exists between the monoanionic $[carb']^-$ and $[\eta^5$-$C_5H_5]^-$, Cp^-, exemplified by, amongst others, the compounds *commo*-[3,3′-Fe-{4-SMe_2-1,2-$C_2B_9H_{10}\}_2$] [2c], an analogue of the ubiquitous organometallic species $FeCp_2$, 3-(η^5-C_5Me_5)-4-SMe_2-3,1,2-*closo*-$MC_2B_9H_{10}$, M = Fe [2d], Ru [1g], and 3,3,3-$(CO)_3$-4-SMe_2-3,1,2-*closo*-$MnC_2B_9H_{10}$ [1c], an analogue of $CpMn(CO)_3$. Although it has been shown [2c], for example, that *commo*-[3,3′-Fe-{4-SMe_2-1,2-$C_2B_9H_{10}\}_2$] can readily be oxidised to *commo*-[3,3′-Fe-{4-SMe_2-1,2-$C_2B_9H_{10}\}_2]^+$, paralleling the oxidation of ferrocene to ferrocinium, relatively little derivative chemistry of charge-compensated carbametalloboranes has so far been reported.

The compound $CpRhI_2(CO)$ has been known for nearly 30 years [3], being formed by simple oxidation of $CpRh(CO)_2$ with iodine. Moreover the carbonyl group of $CpRhI_2(CO)$ is readily displaced by phosphine ligands. We report here the synthesis, characterisation and reactivity of analogous compounds in which the cyclopentadienyl group had been replaced by the formally isolobal carb′ ligand.

EXPERIMENTAL

General

All experiments were carried out under a dry, oxygen-free dinitrogen atmosphere, with the new compounds reported being stable as solids to the ambient atmosphere and slightly sensitive as solutions. All solvents were stored over the appropriate drying agents and distilled immediately prior to use: CH_2Cl_2; CaH_2: 60–80°C light petroleum fraction; Na wire: diethylether; Na wire/benzophenone ketyl. Microanalyses were performed by the departmental service. The compound 3,3-$(CO)_2$-4-SME_2-3,1,2-*closo*-$RhC_2B_9H_{10}$ [1e] was prepared as previously described.

NMR spectroscopy

^1H NMR spectra were recorded on Brüker AC200 and DPX 400 (NOESY spectra) spectrometers. ^{11}B and ^{31}P spectra were recorded on the DPX 400 spectrometer. Unless otherwise stated, measurements were made at 297 K from $CDCl_3$ solutions. Proton chemical shifts are reported relative to residual protio solvent

* Author to whom correspondence should be addressed.

in the sample, ^{11}B shifts (at 128.4 MHz) are relative to external $BF_3 \cdot OEt_2$, and ^{13}P shifts (at 162.0 MHz) are relative to external H_3PO_4.

IR spectroscopy

IR spectra were recorded on a Nicolet Impact 400 spectrometer from CH_2Cl_2 solutions in 0.1 mm solution cells.

3-(CO)-3-$(I)_2$-4-SMe_2-3,1,2-*closo*-$RhC_2B_9H_{10}$, **1**. To a stirring, ice-cooled solution of 3,3-$(CO)_2$-4-SMe_2-3,1,2-*closo*-$RhC_2B_9H_{10}$ (0.055 g, 0.16 mmol) in Et_2O (15 cm^3) was added, dropwise over 10 min, a soln of iodine (0.045 g, 0.18 mmol). Over the addition period a fine black precipitate formed. The solution was warmed to room temperature, with stirring, over 30 min and then allowed to settle. The dark supernatant liquid was decanted via syringe, and the resulting solid washed with Et_2O (2×10 cm^3) and dried *in vacuo* to afford 0.063 g (68%) of black 3-(CO)-3-$(I)_2$-4-SMe_2-3,1,2-closo-$RhC_2B_9H_{10}$, **1**. Diffraction-quality crystals were obtained from the slow diffusion of a CH_2Cl_2 soln of **1** and light petroleum (1 : 4) at room temp. $C_5H_{16}B_9I_2ORhS$ requires C 10.4, H 2.79%. Found for **1** C 10.3, H 2.56%. IR (cm^{-1}): 2581 (*br m*, B-H), 2079 (*s*, CO). NMR (δ ppm): ^1H; 5.15 (*br s*, 1H, C_{cage}—H), 4.89 (*br s*, 1H, C_{cage}—H), 2.77 (*s*, 3H, SMe), 2.58 (*s*, 3H, SMe): $^{11}B\{^1H\}$; 11.84 (1B), 8.08 (1B), 1.13 (2B), −0.05 (1B), −5.18 (1B), −6.09 (1B), −8.83 (1B), −21.34 (1B).

3-PPh_3-3-$(I)_2$-4-SMe_2-3,1,2-*closo*-$RhC_2B_9H_{10}$, **2**. Compound **1** (0.070 g, 0.12 mmol) was dissolved in CH_2Cl_2 (15 cm^3) and PPh_3 (0.032 g, 0.12 mmol) added as a solid. The soln was stirred for 50 min after which time IR spectroscopy indicated that all of **1** had been consumed. The solvent was removed *in vacuo* and the resulting burgundy solid washed with Et_2O (15 cm^3) to afford 0.091 g (93%) of 3-PPh_3-3-$(I)_2$-4-SMe_2-3,1,2-*closo*-$RhC_2B_9H_{10}$, **2**. Crystals suitable for X-ray diffraction were obtained by slow diffusion of a concentrated CH_2Cl_2 soln of **2** and light petroleum (1 : 4) at 4°C. $C_{22}H_{31}B_9I_2PRhS$ requires C 32.5, H 3.85%. Found for **2** C 32.1, H 3.70%. IR (cm^{-1}): 2572 (*br*, B-H). NMR (δ ppm): ^1H; 7.95 (*m*, 2H, C_6H_5), 7.82 (*m*, 2H, C_6H_5), 7.71 (*m*, 2H, C_6H_5), 7.46–7.20 (*m*, 9H, C_6H_5), 5.62 (*br s*, 1H, C_{cage}—H), 2.78 (*s*, 3H, SMe), 2.58 (*s*, 3H, SMe), 2.26 (*br s*, 1H, C_{cage}—H): $^{11}B\{^1H\}$; 9.16 (1B), 8.10 (1B), 0.93 (1B), −2.37 (2B), −5.09 (1B), −12.21 (1B), −18.20 (2B): $^{31}P\{^1H\}$; 34.78 [*d*, *J*(RhP) 124 Hz].

Crystallographic studies

Measurements on single crystals of **1** and **2** were carried out at room temperature on a Siemens P4 diffractometer with graphite-monochromated Mo–K_α X-radiation ($\lambda = 0.71073$ Å) using ω scans. Crystallographic computing was performed using the XSCANS [4] and SHELXTL [5] systems, the latter on a Pentium 90 MHz PC.

Table 1 lists details of unit cell data, intensity data collection and structure refinement. The unit cell parameters and orientation matrix for data collection were determined by the least-squares refinement of the setting angles of 18 and 28 centred reflections, for **1** and **2** respectively, with 2θ ranging from 10.67–24.93° for **1** and 10.67–16.49 for **2**. Data were collected to 2θ max of 50° for **1** and 45° for **2**. Standard reflections were re-measured every 100 data and crystal decay detected (5 and 26% for **1** and **2** respectively) for which subsequent correction was made. Data were further corrected for absorption by psi scans. Both structures were solved by direct and difference Fourier methods and refined by full-matrix least-squares against F^2. Cage C atoms were identified by a combination of refined (as B) isotropic thermal parameters and interatomic distances. Phenyl and methyl H atoms were set in calculated positions, allowed to ride on their respective C atom, and cage B—H atoms were similarly treated. Cage C—H atoms were located in difference Fourier maps and refined subject to a fixed C—H distance of 1.15 Å. All H atoms were assigned (riding) isotropic thermal parameters set at $1.2 \times U_{iso}$ of the attached "heavy" atom, except for methyl H atoms ($1.5 \times U_{C\text{-methyl}}$). Refinement of the structure of compound **1** was routine, but the quality of the data for **2** did not justify anisotropic refinement of C or B atoms.

Complete atomic co-ordinates, thermal parameters and bond lengths and angles have been deposited with the Cambridge Crystallographic Data Centre. See Instructions for Authors, *Polyhedron*, 1998, Issue 1.

RESULTS AND DISCUSSION

Reaction between 3,3-$(CO)_2$-4-SMe_2-3,1,2-*closo*-$RhC_2B_9H_{10}$ and one equivalent of I_2 in ether solvent affords the new compound 3-(CO)-3,3-$(I)_2$-4-SMe_2-3,1,2-*closo*-$RhC_2B_9H_{10}$, **1,** as a black solid in good yield. The IR spectrum of compound **1** (in CH_2Cl_2) demonstrates that one carbonyl ligand has been lost in the reaction, since only a single CO stretching band is observed, at 2079 cm^{-1}. In **1** ν(CO) is 33 cm^{-1} to high frequency of that found in the precursor, reflecting the change from a formal Rh^I metal centre to a formal Rh^{III} centre and the change in the metal-ligand set. The ^1H NMR spectrum of **1** displays resonances due to the inequivalent cage-carbon bound hydrogen atoms as two, integral one, singlets, at 5.15 and 4.89 ppm, at unusually high frequency for a carbametallaborane [6], and shifted by ca 2 ppm to high frequency relative to the precursor [1e]. The inequivalent SMe groups are seen as the expected two, integral three, singlets at 2.77 and 2.58 ppm. The $^{11}B\{^1H\}$ NMR spectrum shows eight resonances between 11.84 and −21.34 ppm, in the ratio 1 : 1 : 2 : 1 : 1 : 1 : 1 : 1 (high frequency to low frequency), the integral two

Table 1. Crystallographic data for compounds **1** and **2**

	1	**2**
Formula	$C_5H_{16}B_9I_2ORhS$	$C_{22}H_{31}B_9I_2PRhS$
M	578.24	812.50
Crystal system	Monoclinic	Triclinic
Space group	$P2_1/n$	$P\bar{1}$
a (Å)	11.695(2)	9.815(2)
b (Å)	9.612(2)	10.515(2)
c (Å)	15.400(3)	14.572(3)
α (°)	90.0	77.64(3)
β (°)	99.75(3)	83.058(14)
γ (°)	90.0	81.861(13)
V (Å^3)	1706.1(6)	1447.9(50
Z	4	2
D_{calc}(Mg m^{-3})	2.251	1.864
μ (Mo–K_α) (mm^{-1})	4.722	2.863
F(000)	1064	780
$\theta_{orientation}$(°)	5.34–12.48	5.34–8.24
$\theta_{data\ collection}$(°)	2.03–25.00	1.44–22.50
hkl ranges	−1–13, −1–11, −18–18	−1–10, −11–11, −15–15
ω scan speeds (°min^{-1})	1.5–30.0	1.7–40.0
crystal decay (%) (corrected for)	4.8	26.2
data measured	3282	4717
unique data (used in refinement)	2615	3687
a	0.0865	0.0302
b	0	5.8336
R, wR_2 (all data)	0.0375, 0.0976	0.2491, 0.4673
observed data [$I > 2\sigma(I)$]	2337	2706
R, wR_2 (observed data)	0.0331, 0.0931	0.1396, 0.3415
S	1.100	1.152
variables	178	122
E_{max}, E_{min} (e Å^{-3})	1.03, −1.02	2.30, −2.39

Weight expression: $w^{-1} = [\sigma_c^2(F_o)^2 + (aP)^2 + bP]$ where $P = [0.333 \max\{F_o, 0\} + 0.667(F_o)^2]$

resonance representing a 1 + 1 coincidence. To confirm the molecular architecture of compound **1** a single-crystal diffraction study was undertaken.

Figure 1 shows a perspective view of compound **1,** demonstrating the atomic numbering scheme employed, whilst Table 2 gives selected interatomic distances and angles. Compound **1** displays the *closo*-MC_2B_9 molecular architecture predicted by empirical electron counting rules [7]. The $\{Rh(I)_2(CO)\}$ fragment is oriented such that the carbonyl group lies effectively *trans* to the cage carbon atoms, reflecting the fact that the frontier molecular orbitals of *nido*-C_2B_9 carbaborane ligands are localised on the facial boron atoms [8]. The rhodium atom is essentially *pseudo* octahedrally coordinated, I(1)—Rh(3)—I(2) 86.44(2)°, I(1)—Rh(3)—C(30) 88.8(2)°, and I(2)—Rh(3)—C(30) 82.9(2)°. Whilst the Rh—C(30) distance, 1.869(6) Å, is slightly longer than found in other formal Rh^{III}—CO species [9], it nevertheless lies within the range reported for other *closo* carbarhodaboranes bearing a carbonyl ligand [10]. The C_{cage}—C_{cage} connectivity, 1.591(8) Å, is essentially the

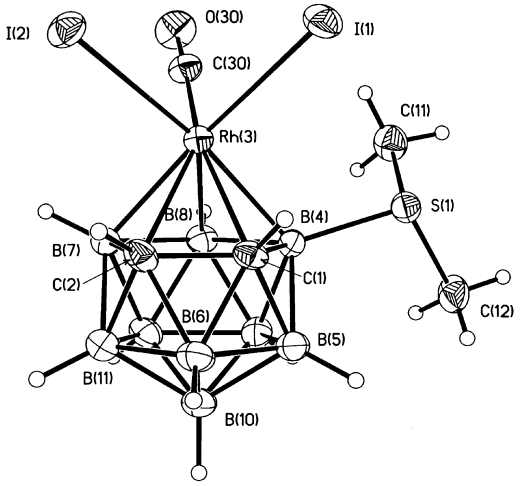

Fig. 1. Perspective view of compound **1** demonstrating the numbering scheme used. Thermal ellipsoids are drawn at the 40% probability level, except for H atoms which have an artificially small radius for clarity.

Table 2. Selected interatomic distances (Å) and angles (°) for **1**

Rh(3)—C(30)	1.869(6)	Rh(3)—B(7)	2.198(6)	Rh(3)—B(4)	2.202(6)
Rh(3)—B(8)	2.220(6)	Rh(3)—C(1)	2.237(6)	Rh(3)—C(2)	2.243(6)
Rh(3)—I(2)	2.7056(7)	Rh(3)—I(1)	2.7195(8)	S(1)—C(12)	1.796(6)
S(1)—C(11)	1.810(7)	S(1)—B(4)	1.918(6)	C(1)—C(2)	1.594(8)
C(1)—B(5)	1.692(9)	C(1)—B(6)	1.707(9)	C(1)—B(4)	1.742(8)
C(2)—B(11)	1.672(9)	C(2)—B(6)	1.707(10)	C(2)—B(7)	1.753(8)
B(4)—B(9)	1.755(8)	B(4)—B(5)	1.797(10)	B(4)—B(8)	1.805(8)
B(5)—B(6)	1.757(10)	B(5)—B(10)	1.778(10)	B(5)—B(9)	1.791(9)
B(6)—B(11)	1.777(10)	B(6)—B(10)	1.784(10)	B(7)—B(12)	1.784(10)
B(7)—B(11)	1.803(10)	B(7)—B(8)	1.821(9)	B(8)—B(12)	1.779(10)
B(8)—B(9)	1.781(10)	B(9)—B(12)	1.773(10)	B(9)—B(10)	1.778(11)
B(10)—B(11)	1.780(11)	B(10)—B(12)	1.784(11)	B(11)—B(12)	1.777(11)
C(30)—O(30)	1.128(8)				

C(30)—Rh(3)—B(7)	102.0(3)	C(30)—Rh(3)—B(4)	113.5(2)	O(30)—C(30)—Rh(3)	177.8(6)
B(7)—Rh(3)—B(4)	81.8(2)	B(7)—Rh(3)—B(8)	48.7(2)	B(4)—Rh(3)—B(8)	48.2(2)
B(7)—Rh(3)—C(1)	77.6(2)	B(4)—Rh(3)—C(1)	46.2(2)	B(8)—Rh(3)—C(1)	79.2(2)
B(7)—Rh(3)—C(2)	46.5(2)	B(4)—Rh(3)—C(2)	76.4(2)	B(8)—Rh(3)—C(2)	78.9(2)
C(1)—Rh(3)—C(2)	41.6(2)	C(30)—Rh(3)—I(2)	82.9(2)	C(30)—Rh(3)—I(1)	88.8(2)
I(2)—Rh(3)—I(1)	86.44(2)	C(12)—S(1)—C(11)	100.1(4)	C(12)—S(1)—B(4)	104.7(30
C(11)—S(1)—B(4)	103.1(3)	C(2)—C(1)—B(6)	62.1(4)	B(5)—C(1)—B(6)	62.3(4)
B(5)—C(1)—B(4)	63.0(4)	C(2)—C(1)—Rh(3)	69.4(3)	B(4)—C(1)—Rh(3)	65.8(3)
C(1)—C(2)—B(6)	62.3(4)	B(11)—C(2)—B(6)	63.4(4)	C(1)—C(2)—B(7)	112.2(4)
B(11)—C(2)—B(7)	63.5(4)	C(1)—C(2)—Rh(3)	69.0(3)	B(7)—C(2)—Rh(3)	65.4(3)
C(1)—B(4)—B(5)	57.1(4)	B(9)—B(4)—B(5)	60.5(4)	B(9)—B(4)—B(8)	60.0(4)
B(5)—B(4)—B(8)	109.3(4)	C(1)—B(4)—S(1)	119.8(4)	B(9)—B(4)—S(1)	118.9(4)
B(5)—B(4)—S(1)	109.6(4)	B(8)—B(4)—S(1)	130.7(4)	C(1)—B(4)—Rh(3)	67.9(3)
B(8)—B(4)—Rh(3)	66.5(3)	S(1)—B(4)—Rh(3)	114.7(3)	C(1)—B(5)—B(6)	59.3(4)
B(6)—B(5)—B(10)	60.6(4)	B(10)—B(5)—B(9)	59.8(4)	C(1)—B(5)—B(4)	59.8(4)
B(9)—B(5)—B(4)	58.6(4)	C(2)—B(6)—C(1)	55.6(4)	C(1)—B(6)—B(5)	58.5(4)
C(2)—B(6)—B(11)	57.4(4)	B(5)—B(6)—B(10)	60.3(4)	B(11)—B(6)—B(10)	60.0(4)
C(2)—B(7)—B(11)	56.1(3)	B(12)—B(7)—B(11)	59.4(4)	B(12)—B(7)—B(8)	59.1(4)
C(2)—B(7)—Rh(3)	68.1(3)	B(8)—B(7)—Rh(3)	66.3(3)	B(12)—B(8)—B(9)	59.7(4)
B(9)—B(8)—B(4)	58.6(3)	B(12)—B(8)—B(7)	59.4(4)	B(4)—B(8)—Rh(3)	65.4(3)
B(7)—B(8)—Rh(3)	65.0(3)	B(12)—B(9)—B(10)	60.3(4)	B(4)—B(9)—B(8)	61.4(4)
B(12)—B(9)—B(8)	60.1(4)	B(4)—B(9)—B(5)	60.9(4)	B(10)—B(9)—B(5)	59.8(4)
B(5)—B(10)—B(9)	60.4(4)	B(9)—B(10)—B(12)	59.7(4)	B(11)—B(10)—B(12)	59.8(4)
B(5)—B(10)—B(6)	59.2(4)	B(11)—B(10)—B(6)	59.8(4)	C(2)—B(11)—B(6)	59.2(4)
B(6)—B(11)—B(10)	60.2(4)	B(12)—B(11)—B(10)	60.2(4)	C(2)—B(11)—B(7)	60.5(4)
B(12)—B(11)—B(7)	59.8(4)	B(9)—B(12)—B(8)	60.2(4)	B(9)—B(12)—B(10)	60.0(4)
B(11)—B(12)—B(10)	60.0(4)	B(11)—B(12)—B(7)	60.9(4)	B(8)—B(12)—B(7)	61.5(4)

Table 3. Selected interatomic distances (Å) and angles (°) for **2**

Rh(3)—P(1)	2.310(11)	Rh(3)—I(1)	2.707(4)
Rh(3)—I(2)	2.729(4)	P(1)—C(21)	1.86(2)
P(1)—C(11)	1.877(14)	P(1)—C(31)	1.879(14)
S(1)—B(4)	1.89(5)	C(1)—C(2)	1.60(6)
B(7)—B(8)	1.88(6)		

P(1)—Rh(3)—I(1)	90.2(3)	P(1)—Rh(3)—I(2)	91.3(3)
I(1)—Rh(3)—I(2)	88.33(13)		

same length as that found in the precursor species 3,3-$(CO)_2$-4-SMe_2-3,1,2-*closo*-$RhC_2B_9H_{10}$ [1e], 1.596(4) Å, and in 3,3,3-$(CO)_3$-4-SMe_2-3,1,2-*closo*-$MnC_2B_9H_{10}$ [1c], 1.585(3) Å, whilst all other bond lengths and angles in the cage are in the ranges normally associated with such polyhedra.

The orientation of the SMe_2 ligand is conveniently measured by τ, the calculated torsion angle

C(1)—B(4)—S(1)—S(lone pair). In **1** τ is -25.5° (the minus sign representing a clockwise rotation about the S—B bond when viewed from S for the enantiomer shown in Fig. 1), at the upper end of the range generally found (ca -3° to -21°) in carb′H and its uncrowded derivatives [1a–1e], possibly due to a minimisation of steric interactions between I(1) and the methyl group C(11).

In $CpRhI_2(CO)$ the high value of ν(CO), 2065 cm^{-1} (Nujol), implies a relatively weakly bound CO ligand. Consistent with this, $CpRhI_2(CO)$ reacts with PPh_3, via loss of CO, to afford $CpRhI_2(PPh_3)$ [3]. Similarly, treatment of a CH_2Cl_2 soln of compound **1** with one equivalent of PPh_3 results in the disappearance of the CO stretch in the IR spectrum and the isolation of the new compound 3-(PPh_3)-3,3-$(I)_2$-4-SMe_2-3,1,2-*closo*-$RhC_2B_9H_{10}$, **2,** in good yield. The ^1H NMR spectrum of compound **2** shows resonances due to the triphenylphosphine ligand as an unusual set of three, integral two, multiplets, centred on 7.95, 7.82 and 7.71 ppm, and an integral nine multiplet, between 7.46 and 7.20 ppm. The cage-carbon hydrogen atoms are observed at 5.62 ppm and 2.26 ppm, the former frequency comparable to those in **1** but the latter shifted significantly to low frequency. Peaks due to the inequivalent SMe groups are essentially unchanged from their positions in **1**. In the $^{11}B\{^1H\}$ NMR spectrum there are seven resonances (1 : 1 : 1 : 2 : 1 : 1 : 2, high frequency to low frequency) between 9.16 and -18.20 ppm. In the $^{31}P\{^1H\}$ NMR spectrum is observed a doublet at 34.78 ppm with the expected rhodium coupling, J(RhP) 124 Hz.

To establish a firm stereochemistry for compound **2** a single crystal X-ray structural determination was performed. Unfortunately, and despite repeated recrystallisations, only small, weakly diffracting crystals of compound **2** could ever be obtained. Although the eventual structural solution is characterised by a relatively poor residual (conventional R factor ca 0.14) we are confident that the C_{cage} atoms identified in Fig. 2, a perspective view of a single molecule, are correctly positioned for the following reasons: the 1–2 distance is 1.60 Å, cf the 7–8 distance of 1.88 Å; all R indices and the goodness-of-fit parameter are worse if C(1) and C(2) are interchanged with B(7) and B(8); the PPh_3 ligand lies approximately *trans* to the C_{cage} positions in Fig. 2, as would be expected by analogy with the structure established for compound **1**. Steric crowding between the PPh_3 and SMe_2 units results in the latter adopting a conformation defined by $\tau = 77.7^\circ$, i.e. rotated ca 90° from its position in **1**.

A ^1H-^1H NOESY NMR experiment on compound **2** demonstrated that only one of the cage carbon hydrogen atoms, that which resonates at 5.62 ppm, shows a strong contact with (one of) the SMe signals, whilst the other, at 2.26 ppm, shows contact with the 5.62 ppm signal and with the three, integral two, aromatic signals. Thus the resonance at 5.62 ppm is ascribed to H(1) and that at 2.26 ppm to H(2). Overall this data implies that, whilst rotation of the Ph rings

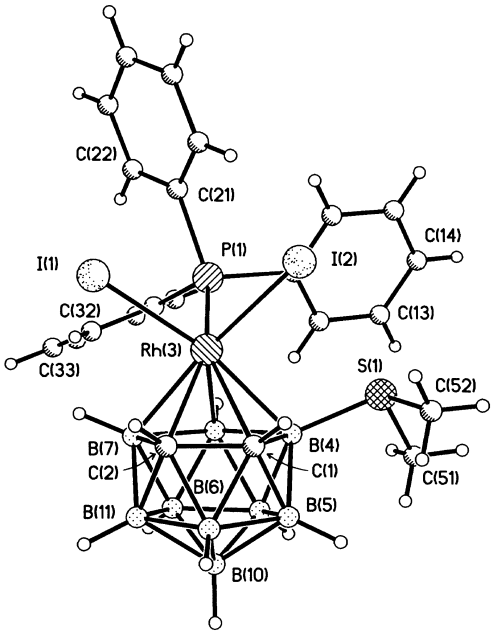

Fig. 2. Molecular structure and atomic numbering scheme for compound **2**.

about the P—C bonds must be rapid on the NMR timescale (affording equivalence of the *ortho* protons on each ring), rotation of the PPh_3 groups about the Rh-P bond is slow on the NMR timescale (three integral two signals observed) but rapid on the NOESY timescale [allowing each pair of *ortho* protons contact with H(2)]. Moreover, given the conformation of **2** determined crystallographically, some sort of dynamic process must be operating in solution that allows the *ortho* phenyl protons to contact with H(2). The factors affecting the rotation of metal-fragment vertices in carbametallaboranes have been discussed previously [11], and in the case of fragments of local C_s symmetry bound to asymmetric carbaborane cages large rotational barriers are generally observed. This might imply that in **2** the $\{RhI_2(PPh_3)\}$ fragment merely undergoes substantial libration about the Rh(3)···B(10) axis on the timescale of the NOESY experiment.

CONCLUSIONS

We have shown here that the chemistry of 3,3-$(CO)_2$-4-SMe_2-3,1,2-*closo*-$RhC_2B_9H_{10}$ parallels that of $CpRh(CO)_2$ in as much as both compounds undergo oxidation with elemental iodine to afford species in which one carbonyl ligand has been replaced by two iodide ligands. Additionally, reaction of this new bis-iodo-carbarhodaborane with triphenylphosphine results in substitution of the remaining carbonyl ligand by phosphine, again paralleling the behaviour of the analogous cyclopentadienyl compound.

Acknowledgements—We thank the EPSRC for support (G.M.R. and A.S.W.) and the Callery Chemical Company for continued support of our work through a generous gift of $B_{10}H_{14}$. F.B.H.T. and S.K.Z. are recipients of ERASMUS exchange scholarships from the Philipps University, Marburg, and S.K.Z. is additionally holder of a Studienstiftung des deutschen Volkes.

REFERENCES

1. (a) Cowie, J., Hamilton, E. J. M., Laurie, J. C. V. and Welch, A. J., *Acta Cryst*., 1988, **C44,** 1648; (b) Hamilton, E. J. M. and Welch, A. J., *Acta Cryst*., 1990, **C46,** 1228; (c) Cowie, J., Hamilton, E. J. M., Laurie, J. C. V. and Welch, A. J., *J. Organomet. Chem*., 1990, **394,** 1; (d) Hamilton, E. J. M. and Welch, A. J., *Polyhedron*, 1991, **10,** 471; (e) Douek, N. L. and Welch, A. J., *J. Chem. Soc., Dalton Trans*., 1995, 1917; (f) Rosair, G. M., Welch, A. J., Weller, A. S. and Zahn, S. K., *J. Organomet. Chem*., 1997, **536,** 299; (g) Rosair, G. M., Welch, A. J. and Weller, A. S., *Organometallics*, in press.
2. (a) Kang, H. C., Lee, S. S., Knobler, C. B. and Hawthorne, M. F., *Inorg. Chem*., 1991, **30,** 2024; (b) Mullica, D. F., Sappenfield, E. L., Stone, F. G. A. and Woollam, S. F., *Organometallics*, 1994, **13,** 157; (c) Yan, Y.-K., Mingos, D. M. P., Müller, T. E., Williams, D. J. and Kurmoo, M., *J. Chem. Soc., Dalton Trans*., 1994, 1735; (d) Yai, Y. K., Mingos, D. M. P., Muller, T. E., Williams, D. J. and Kurmoo, M., *J. Chem. Soc., Dalton Trans*., 1995, 2509; (e) Gomez-Saso, M., Mullica, D. F., Sappenfield, E. and Stone, F. G. A., *Polyhedron*, 1996, **15,** 793.
3. King, R. B., *Inorg. Chem*., 1996, **5,** 82.
4. XSCANS, data collection and reduction programme. Siemens Analytical Instruments, Inc., Madison, Wisconsin, U.S.A., 1994.
5. Sheldrick, G. M., SHELXTL. Siemens Analytical Instruments, Inc., Madison, Wisconsin, U.S.A., 1994.
6. δ C-*H* in carbametallaboranes is typically between 3.5 and 4.5 ppm in the absence of moderating influences such as the ring currents of phenyl rings.
7. Wade, K., *Adv. Inorg. Chem. Radiochem*., 1976, **18,** 1.
8. Mingos, D. M. P., Forsyth, M. I. and Welch, A. J., *J. Chem. Soc., Dalton Trans*., 1978, 1363.
9. (a) Gash, R. C., Cole-Hamilton, D. J., Whyman, R., Barbes, J. C. and Simpson, M. C., *J. Chem. Soc., Dalton Trans*., 1994, 1963; (b) Adams, H., Bailey, N. A., Mann, B. E., Manuel, C. P., Spencer, C. M. and Kent, A. G., *J. Chem. Soc., Dalton Trans*., 1988, 489.
10. (a) Teller, R. G., Weilczynski, J. J. and Hawthorne, M. F., *J. Chem. Soc., Chem. Commun*., 1979, 472; (b) Pilotti, M. U., Topaloglu, I. and Stone, F. G. A., *J. Chem. Soc., Dalton Trans*., 1991, 1355; (c) Carr, N., Gimeno, M. C., Goldberg, J. E., Pilotti, M. U., Stone, F. G. A. and Topaloglu, I., *J. Chem. Soc., Dalton Trans*., 1990, 2253.
11. Marder, T. B., Baker, R. T., Long, J. A., Doi, J. A. and Hawthorne, M. F., *J. Am. Chem. Soc*., 1981, **103,** 2988.

Pergamon

PII : S0277–5387(98)00009–6

Polyhedron Vol. 17, No. 16, pp. 2633–2638, 1998
© 1998 Elsevier Science Ltd
All rights reserved. Printed in Great Britain
0277–5387/98 $19.00 + 0.00

pH-Independent decomposition reactions of L-ascorbic acid in aqueous metal solutions. 2. Imaging by scanning tunneling microscopy

M. H. Zareie,[a] Y. Zencir,[b] C. Ünaleroğlu,[b] B. Zümreoğlu-Karan[b]* and E. Pişkin[a]

[a] Chemical Engineering Department and Bioengineering Division and [b] Department of Chemistry, Hacettepe University, Beytepe Campus, 06532 Ankara, Turkey

(Received 25 August 1997; accepted 5 January 1998)

Abstract—STM images of aqueous solutions of L-ascorbic acid containing Gd^{3+} ions at pH values of 2, 6 and 12 have been recorded periodically after drying the samples on gold coated mica. The results have revealed that the organisations of the AA molecules and metal ions show different features throughout the conversion of Gd-ascorbate complexes to Gd-oxalates. © 1998 Elsevier Science Ltd. All rights reserved

Keywords: STM; vitamin C; decomposition.

Vitamin C, being a constituent of the cell, and a good reductant, has momentous biological functions. The recent findings of Hallis *et al.* [1] on the antitumor activities of several platinum diammine ascorbate compounds and Cardin and Roy [2], on the anticancer properties of some organometallic titanium and tin ascorbate complexes have added more attention to the biochemistry of this sugar molecule.

The aqueous chemistry of L-ascorbic acid (AA) is of essential importance in understanding the characteristics of this water-soluble vitamin. Among the numerous reactions studied are those involving its efficient reduction of many transition metal ions and complexes at moderately low to low pH values [3–8]. In alkaline solutions, the rate of autooxidation of AA and the effect of catalytic impurities increase significantly [9]. It is also known that *in vitro* decomposition of dehydroascorbic acid (DHA), the stable oxidation product of AA, leads to the formation of CO_2, oxalic acid, trihydroxybutyric acid and other products, depending on the reaction conditions [10–12]. DHA, diketogulonic acid, ascorbate sulfate, oxalate, methyl ascorbate and 2-ketoascorbitol have been identified as the AA metabolites in human urine [13]. However, the chemical redox behavior, metabolism and enzymatic behavior, such as for ascorbate oxidase, of the acid are not fully realized and the research concerning particularly the degradation details are somewhat limited.

Recently, we reported the decomposition of AA in the presence of nonoxidizing metal ions from low to high pH values providing that the metal ions do not hydrolyze or precipitate extensively [14]. We studied with Co^{2+} and Gd^{3+} ions specifying transition and rare earth metals and observed the pH-independent formation of metal oxalates via ascorbate complexes by IR spectroscopic and X-ray crystallographic analyses. In this paper, we present the images of the interaction of AA with Gd^{3+} to gain a molecular-level structural information by Scanning Tunneling Microscopy (STM), which is a novel technique successfully employed for the examination of biological samples [15–20].

EXPERIMENTAL

General

Reactions were conducted in deionized/deoxygenated water at a AA to metal ratio of 10 : 2. 0.0013 g of AA (Merck) was dissolved in 95 ml of water and the pH of this solution was adjusted to the desired value (6 and 12) by the controlled addition of

* Author to whom correspondence should be addressed. Fax : (0312) 299 2163. E-mail : bkaran@eti.cc.hun.edu.tr

NaOH solution and to 2 by adding HCl. The solution containing Gd^{3+} was prepared by dissolving the appropriate quantity of $Gd(NO_3)_3 \cdot 6H_2O$ (prepared from Gd_2O_3) in 5 ml of water. Each experiment was started from freshly prepared solutions and oxygen-free conditions were provided by passing nitrogen gas through the system. The reaction mixtures obtained by the addition of the metal solution to the acid solutions at different pH values were kept at closed vessels and 10 μl samples were withdrawn for STM tests after each time interval.

STM studies

The STM used in this work was constructed in our laboratory [21]. Mechanically, it consists of two main modules : a scanner and a course positioner. The scanner part is constructed with a PZT tube (EBL #PZT-5H, Staveley Sensors Inc., CT) glued to an aluminum body. Electrical connections to the PZT are through a special connector. The tip holder is glued to the interior of the PZT tube but isolated electrically. The course positioner is magnetically driven slider which is fastened to the scanner. The whole system is mounted on a vibration isolation stage.

In order to obtain the STM images, 10 μl of AA solution (0.1 mg ml^{-1}) was deposited on the Au (111) which was grown epitaxially on mica [22]. The deposit was dried at room temperature under atmospheric pressure in a clean room with a relatively slow drying rate. The STM was operated in air at atmospheric pressure with a tip-to-substrate bias of 200–400 mV and a tunnelling current of 50 pA. Etched tips of Pt/Ir (80 : 20) wires (0.5 mm in diameter, Digital Instruments, Santa Barbara, CA) were used in constant current mode. The average sizes of the species have been determined by use of about 50 different STM images at a scan speed of image/1.40 s.

RESULTS AND DISCUSSION

Our previous findings had revealed that AA complexes with Co^{2+} and Gd^{3+} ions in aqueous solutions and these complexes subsequently decompose to the metal oxalates irrespective of the pH of the solution [14]. The acidity of the medium had almost no effect on the composition of the cobalt oxalates. In all investigated cases, providing pH > 3, the final products obtained with Co^{2+} had been defined as $CoC_2O_4 \cdot 2H_2O$, which were stable in solution but not in the solid state to accumulate X-ray data. On the other hand, the oxalates produced with Gd^{3+} had shown variations in their water content depending on the pH of the solution.

In this study, we attempted to correlate the structures of both vitamin C (Fig. 1). and its interaction with Gd^{3+} ions by a novel technique, the so-called "scanning tunnelling microscopy". A home-made STM was used, which was successfully employed in our previous studies for imaging of various biological molecules, e.g. nucleic acids [23], tRNA [24]. Gold coated mica was used as the basic substrate. Au (111) grown epitaxially on mica has atomically flat terraces and is a suitable substrate for organic material to be used under ambient conditions [25]. The direct tip-surface interaction is relatively weak and the structure of the substrate is not visible in the presence of the adsorbate. In order to eliminate the "gluing" effect, humidity of the STM chamber was kept around 35%, at which reliable images were taken, by a humidity control unit. For the same reason, and also to get images with high resolution, bias voltage was kept relatively high (in the range of 200–400 mV), and the tunneling current was 50 pA.

STM images under constant current mode permit topographic and the so-called "chemical contrast" images to be obtained. Figure 2 gives the STM micrographs of vitamin C on gold coated mica at a constant current mode. Figure 2(A) shows the two dimension image with scan area of 2×2.1 nm, the enlarged image given on the right hand corner more clearly shows the AA molecule. Figure 2(B) shows the three dimensional image of this molecule with scan area of 0.43×0.75 nm. STM images always involve both topographic and electronic contributions which can be difficult to separate and theoretical approaches are needed to relate the images to the structure of the molecule. We adopted the CACAO program to calculate the molecular orbitals of the isolated AA molecule [26]. Figure 3(A, B) shows the charge density contour plots that we obtained using this program. The energy gap between the HOMO and LUMO is 3.1 eV. The most significant contribution to the image is known to come from the frontier orbitals (HOMO and LUMO) for small molecules [27]. The experimental image of the AA molecule looks similar to the HOMO orbital and this is inconsistent with the fact that tunneling is through the unoccupied states with positive sample bias in the free molecule. Considering the possibility that AA molecule changes its geometrical structure on the Au layer due to a keto-enol tautomerism, calculations were also done for the corresponding enol tautomer. The contour plots are almost identical for both tautomeric forms concluding that the image corresponds to the HOMO orbital. The calculations were also repeated for the ascorbate anion and the same results were obtained. So, the missing agreement between the expected structure and the STM image is mainly due to the substrate effect. The interaction of the molecule with the surface states near the Fermi level might have caused shifts and broadenings in the energy levels. It is also possible that other orbitals neighbouring HOMO and LUMO contribute to the observed image. The topographic image is brighter in the vicinity of the carbon–carbon double bond because this bond is more readily conductive to tunneling current. The hydroxyl groups and the saturated aliphatic backbone are less conductive to tunneling and they give darker images.

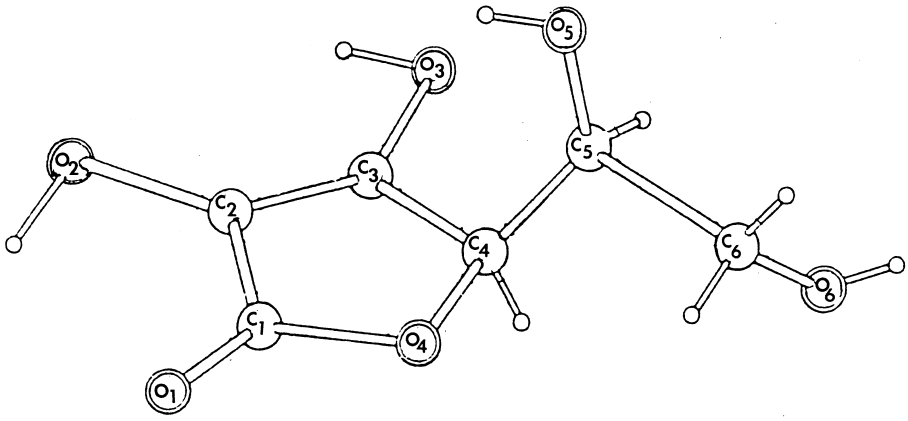

Fig. 1. L-ascorbic acid.

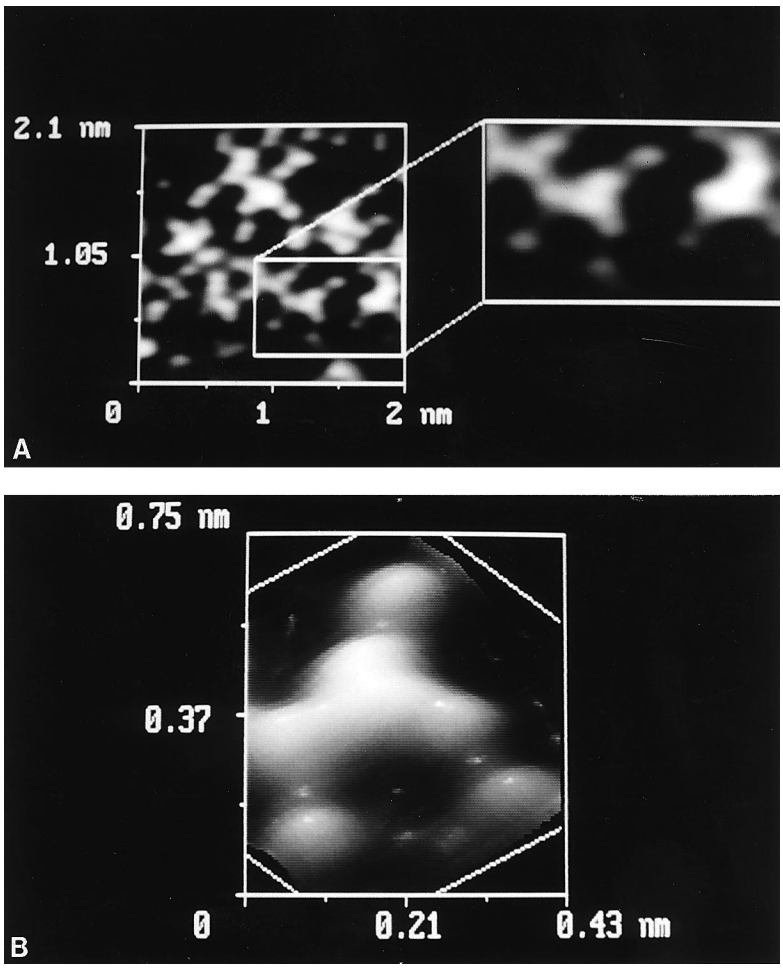

Fig. 2. Representative STM images of L-ascorbic acid on gold coated mica substrate. (A) Two dimensional image, scan area : 2×2.1 nm ; (B) Three dimensional image, scan area : 0.43×0.75 nm.

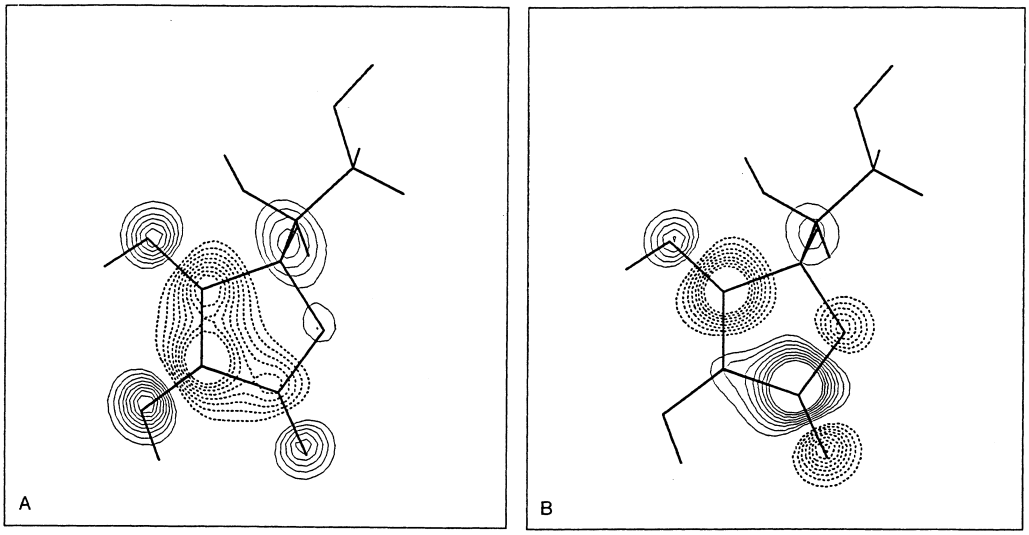

Fig. 3. (A) Contour plot of charge density of HOMO (B) Contour plot of the charge density of LUMO.

The results obtained by STM analysis of some biological molecules have been successfully used for direct comparison with the information provided by X-ray crystallography [28]. Since AA is well-characterized by X-ray [29], we attempted to correlate the topographic image with its X-ray data. The STM ring width of AA measured as approximately 4 Å is larger than that predicted by crystallography which is 2.2 Å. This disagreement is not very surprising since molecules can adopt various orientations and binding modes at the surfaces and the radius of the molecule is known to increase upon adsorption [30].

The images recorded periodically from solutions containing AA and Gd^{3+} ions at pH values of 2, 6 and 12 are given in Fig. 4. As shown in Fig. 4(A), the lighter parts that look like blobs indicate the Gd^{3+} ions with diameters of 2.5 ± 0.2 Å (experimental value is 2.5 Å) [31]. The gray (darker) parts indicate the AA molecules in contact with the metal ions. This image taken after two days in acid solutions shows the AA molecules organizing to some extent with some structural modifications. After four days (B), the vitamin molecules and Gd^{3+} ions seemed to be arranged in a periodic array with a 28.5 Å spacing between the rows. After twelve days of standing (C), a highly symmetrical polymeric structure was observed. Concerning our previous experimental results, we assume that this polymeric matrix corresponds to the oxalate structure.

Fig. 4(D) and Fig. 4(G) represent the images from solution of pH = 6 and 12, respectively, after two days from the start of the experiments. AA molecules came into sight as clusters with individual Gd^{3+} ions around. The micrographs taken in the following intervals Fig. 4(E, H), represented almost the same features. Figure 4(F, I) denote to the images obtained after twelve days which are notably different than the final image at pH = 2. A structural organization was not recognized in these samples prepared at high pH values. This is in agreement with our previous results that the stable, crystalline gadolinium oxalate could be obtained only at pH = 2. No significant change was noted in the images during the period between the fourth and twelfth days.

Image interpretation is still the most serious limitation on useful application of STM. However, our qualitative analysis agrees with the experimental results and this promotes us to propose the following mechanism. When AA molecules contact with the metal ions, the first interaction is supposed to occur over the ring part. AA coordinates metal ions forming chelates $[MHL^{+(n-1)}]$ at low and intermediate pH values and unprotonated chelates $[ML^{+(n-2)}]$ at high pH, however the complexes are suggested to be weak in aqueous solution [9]. It is quite reasonable to suggest that the lactone ring is opened to give chain-like structures and then the chains collapse and grow in an anisotropic way to build up the oxalate structures. Major variations in the ring stretching and deformation vibrations of the ascorbate complexes had been noted before in their IR spectra upon decomposition to the oxalates [14]. Nevertheless, evidence to the proposed decomposition scheme using the STM images is speculative and requires high resolution studies and advanced theoretical calculations.

CONCLUSIONS

There seems to be a commonality in the chemistry of decomposition of AA in the presence of nonoxidizing metals. The experimental results reveal that the decomposition products are metal oxalates irrespective of the pH of the solution. However, the path-

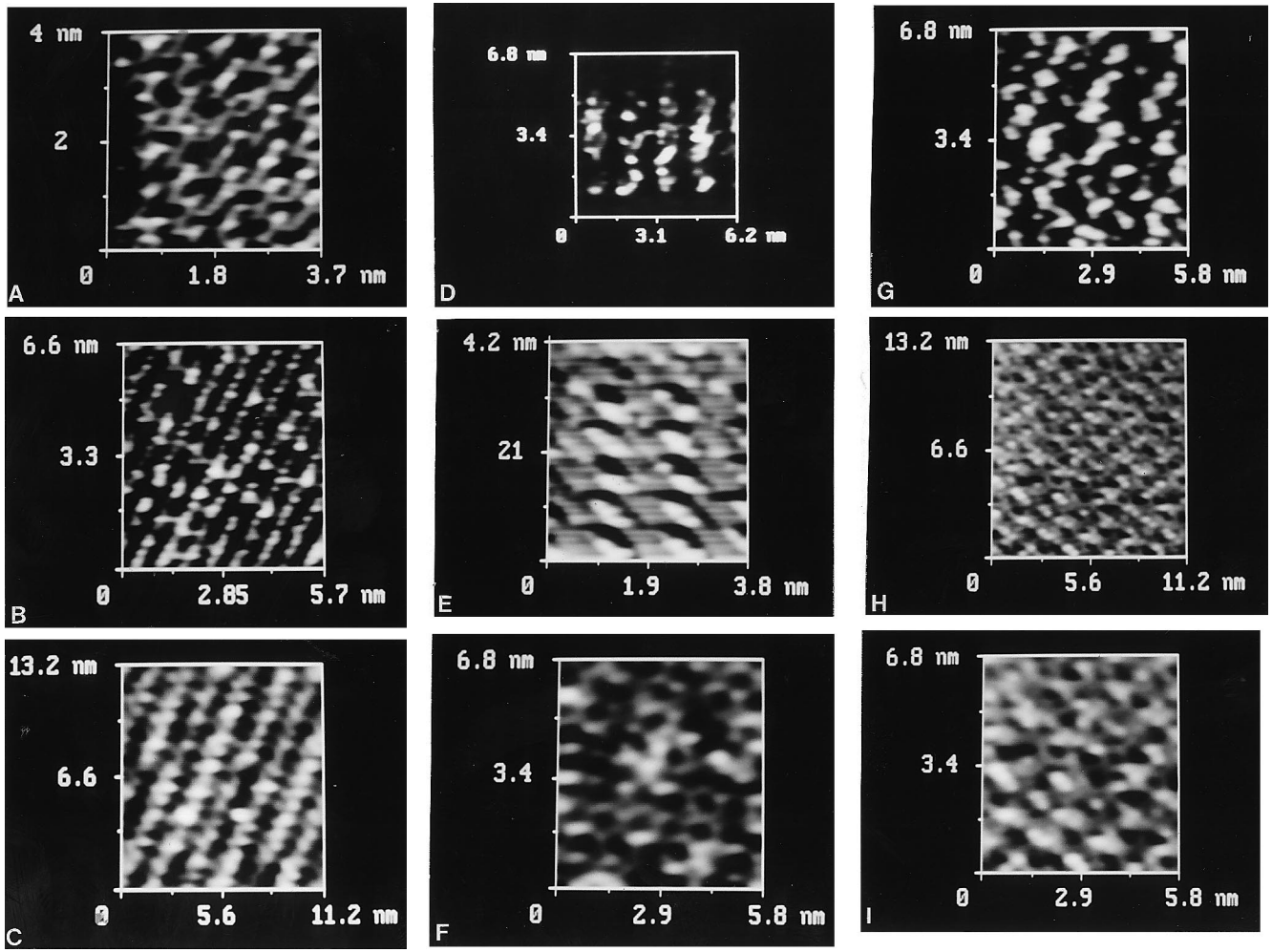

Fig. 4. Representative STM images of L-ascorbic acid solutions containing Gd^{3+} ions on gold coated mica substrate. (A, B, C) Images from solutions of pH = 2. (A) after two days, scan area : 3.7×4 nm, (B) after four days, scan area : 5.7×6.6 nm, (C) after twelve days, scan area : 11.2×13.2 nm. (D, E, F) Images from solutions of pH = 6. (D) after two days, scan area : 6.2×6.8 nm, (E) after four days, scan area : 3.8×4.2 nm, (C) after twelve days, scan area : 5.8×6.8 nm. (G, H, I) Images from solutions of pH = 12. (G) after two days, scan area : 5.8×6.8 nm, (H) after twelve days, scan area : 11.2×13.2 nm, (I) enlarged image of (H), scan area : 5.8×6.8 nm.

ways, the rate of decomposition and the structures of the final oxalates are governed by the pH to some extent. STM analyses have displayed that during the formation of the oxalate structures, the organization of the molecules at different pH values proceeds in different manners.

Acknowledgement—This work has been supported in part by the Turkish Scientific and Technological Research Council under the agreement no. TBAG 1311.

REFERENCES

1. Hallis, L. S., Amundsen, A. R. and Stern, E. W., *J. Amer. Chem. Soc.*, 1985, **107,** 274.
2. Cardin, C. J. and Roy, A., *Inorg. Chim. Acta*, 1985, **105,** L37–L39.
3. Dixon, D. A., Sadler, N. P. and Dasgupta, T. P., *J. Chem. Soc. Dalton. Trans.*, 1993, 3489.
4. Taqui Khan, M. M. and Shukla, R. S., *Polyhedron*, 1991, **10,** 2711.
5. Taqui Khan, M. M. and Martell, A. E., *J. Amer. Chem. Soc.*, 1968, **90 :22,** 6011.
6. Taqui Khan, M. M. and Martell, A. E., *ibid*, 1969, **91 :17,** 4668.
7. Taqui Khan, M. M. and Martell, A. E., *ibid*, 1967, **89 :16,** 4176.
8. Jameson, R. F. and Blackburn, N. J., *J. Inorg. Nucl. Chem.*, 1975, **37,** 809.
9. Martell, A. E. In *Ascorbic Acid Chemistry, Metabolism and Uses*, ed. P. A. Seib and B. M. Tolbert. Advances in Chemistry Series 200, American Chemical Society : Washington, D.C., 1989, pp. 152–156.
10. Finholt, P., Paulssen, R. B., Alsos, J. and Higuchi, T., *J. Pharm. Sci.*, 1965, **54,** 124.
11. Stearns, D. M. and Wetterhahn, K. E., *Chem. Res. Toxicol.*, 1994, **7,** 219.
12. Herbert, R. W., Hirst, E. L., Percival, E. G. V., Reynolds, R. J. W. and Smith, F., *J. Chem. Soc.*, 1933, 1270.
13. Omaye, S. T., Tillotson, J. A. and Sauberlich, H. E. In *Ascorbic Acid Chemistry, Metabolism and Uses*, ed. P. A. Seib and B. M. Tolbert. Advances in Chemistry Series 200, American Chemical Society : Washington D.C., 1989, pp. 317–334.
14. Ünaleroğlu, C., Zümreoğlu-Karan, B., Zencir, Y. and Hökelek, T., *Polyhedron*, 1997, **16,** 2155.
15. Wickramasinghe, H. K., *Scientific American*, 1989, 74.
16. Binnig, G. and Rohrer, H. In *Trends in Physics*, ed. J. Janta and J. Pantollick, 1984, 38.
17. Lindsay, S. M., Jing, T. W., Pan, J. and Vaught, A., *Nanobiology*, 1994, **3,** 17.
18. Hansma, H. G., Weisenhorn, A. L., Gould, S. A. C., Sinsheimer, R. L., Gaub, H. E., Stucky, G. D., Zaremba, C. M. and Hansma, P. K., *J. Vac. Sci. Technol.*, 1991, **9,** 1282.
19. Morris, V. J., *Prog. Biophys. Molec. Biol.*, 1994, **61,** 131.
20. Ikai, A., *Surf. Sci. R.*, 1996, **26,** 261–332.
21. Zareie, M. H., Thesis, Hacettepe University, Ankara, Turkey, 1995.
22. De Rose, J. A., Lampner, D. B. and Lindsay, S. M., *J. Vac. Sci. Tech.*, 1993, **A11,** 776.
23. Zareie, M. H., Erdem, G., Öner, C., Öner, R., Öğüş, A. and Pişkin, E., *Int. J. Biol. Macromol.*, 1996, **19,** 69.
24. Zareie, M. H., Pişkin, A. K., Verimli, R., Kansu, E. and Pişkin, E., *Nanobiology*, 1996, **4,** 101.
25. Wiesendanger, R., *Scanning Probe Microscopy and Spectroscopy*, 1994, Cambridge University Press, Cambridge, pp. 493–536.
26. Mealli, C. and Proserpio, D. M., *J. Chem. Educ.*, 1990, **67,** 401.
27. Richter, S. and Manassen, Y., *J. Phys. Chem.*, 1994, **98,** 2941.
28. Mosca, A., Pallieri, R., Arosio, P., Cricenti, A., Scarselli, A., Generosi, R., Selci, S. and Rovida, E., *J. Vac. Sci. Technol.*, 1994, **B12,** 1486.
29. Hvoslef, J., *Acta Crystallogr. Sect. B*, 1968, **24,** 23.
30. Sautet, P. and Bocquet, M.-L., *Israel J. Chem.*, 1996, **36,** 63.
31. Shannon, R. D., *Acta Crystallogr. Sec. A*, 1969, **32,** 751.

Pergamon

PII : S0277–5387(98)00020–5

Polyhedron Vol. 17, No. 16, pp. 2639–2646, 1998
© 1998 Elsevier Science Ltd
All rights reserved. Printed in Great Britain
0277–5387/98 $19.00+0.00

Structural variation and magnetic properties of tetrakis(μ_2-carboxylate)-bridged dicopper(II) complexes of betaines with different axial ligands

Xiao-Ming Chen,* Xiao-Long Feng,[a] Zhi-Tao Xu,[a] Xiao-Hong Zhang,[a] Feng Xue[b] and Thomas C. W. Mak[b]

[a] Department of Chemistry, Zhongshan University, Guangzhou 510275, P.R. China

[b] Department of Chemistry, The Chinese University of Hong Kong, Shatin, New Territories, Hong Kong

(Received 11 November 1997; accepted 6 January 1997)

Abstract—Three tetrakis(μ_2-carboxylate)-bridged dicopper(II) complexes of betaines, $[Cu_2(pybet)_4(H_2O)_2](NO_3)_2(ClO_4)_2\cdot 2H_2O$ (pybet = pyridinioacetate, $C_5H_5N^+CH_2CO_2^-$, pybet) (**1**), $[Cu_2(pybet)_4(H_2O)Cl](ClO_4)_3\cdot 2H_2O$ (**2**) and $[Cu_2(ppbet)_4Cl_2](ClO_4)_2$ (ppbet = pyridiniopropionate, $C_5H_5N^+CH_2CH_2CO_2^-$) (**3**), have been synthesized and characterized by X-ray crystallography. These complexes all comprise $[Cu_2(\mu_2\text{-carboxylate})_2]$ structures (Cu···Cu = 2.677(1)–2.760(1) Å) with each copper(II) atom being coordinated in a square-pyramidal CuO_4L environment, in which the axial ligands (L) are two aqua molecules (Cu—O = 2.093(2) Å), one aqua molecule and one chloride ion (Cu—O = 2.130(8), Cu—Cl = 2.358(4) Å) and, two chloride ions (Cu—Cl = 2.454(2) Å) in complexes **1, 2** and **3,** respectively. The intramolecular Cu···Cu distance may correlate to the mutual repulsion between the axial and basal metal-ligand bonds. Temperature-dependent magnetic susceptibility data of the powder samples of the complexes have been fitted, yielding the intramolecular coupling constant $2J$ values of -340, -321 and -301 cm^{-1} for **1, 2** and **3,** respectively. The magnitudes of $2J$ may be inversely correlated to the displacement of the metal atom from the basal plane. © 1998 Elsevier Science Ltd. All rights reserved

Keywords: copper(II); carboxylate; dimeric; crystal structure; magnetic properties.

Since the first report of the crystal structure of copper(II) acetate monohydrate, $[Cu_2(MeCO_2)_4(H_2O)_2]$ [1], a large number of copper(II) carboxylates of this type, generally formulated as $[Cu_2(RCO_2)_4L_2]$ (L denotes the axial ligand), have been structurally established [2–4] where the R groups include a variety of small and bulky organic groups [1–8]. The intramolecular Cu···Cu distance can vary from 2.563(4) Å in $[Cu_2(EtCO_2)_4(dioxane)_2]$ [9] to the longest 2.886(2) Å in $[Cu_2(F_3CCO_2)_4(quinoline)_2]$ [10]. On the other hand, anionic compounds are rarely established as the axial ligands in this type of dimeric compounds, two known complexes contain SCN^- anions [8]. While only one example of the two axial positions occupied by two different ligands has been very recently uncovered, in which the two axial ligands are one water and one methanol molecules [11].

More interesting is the fact that the nature of the structural variation and the magnetic properties is not yet clear and has provoked considerable controversy after the very extensive investigation. The structural results and magnetic studies have confirmed that the insensitivity of the coupling constants $2J$ to the Cu···Cu separation. Therefore the idea that the spin coupling exchange proceeds predominantly by the superexchange through the carboxylate bridges has become increasingly favoured [5,8,10,12]. Nevertheless, no concrete conclusion has been drawn for the magneto-structural relation [5,12].

Recently we took advantage of the zwitterionic characteristics of betaines to prepare metal carboxylate complexes containing anionic ligands [13]. Particularly, we have synthesized several dimeric copper(II) complexes of betaines, and exhibited the very important effect of the axial ligands on the Cu···Cu separations [14]. Encouraged by this fact, we have attempted to synthesize new dimeric copper(II) car-

* Author to whom correspondence should be addressed.

boxylate complexes containing different kind of carboxylate bridges as well as different kind of axial ligands to provide structural models of trivial differences for magneto-structural investigation, and we report herewith the syntheses, crystal structures and magnetic properties of three new dimeric copper(II) carboxylate complexes bridged by betaine derivatives, namely $[Cu_2(pybet)_4(H_2O)_2](NO_3)_2(ClO_4)_2 \cdot 2H_2O$ (pybet = pyridinioacetate, $C_5H_5N^+CH_2CO_2^-$, pybet) (**1**), $[Cu_2(pybet)_4(H_2O)Cl](ClO_4)_3 \cdot 2H_2O$ (**2**) and $[Cu_2(ppbet)_4Cl_2](ClO_4)_2$ (ppbet = pyridiniopropionate, $C_5H_5N^+CH_2CH_2CO_2^-$) (**3**), in which the axial ligands are two aqua ligand, one aqua and one chloride ligands and, two chloride ligands, respectively.

EXPERIMENTAL

Materials

Pyridinioacetate (pybet) and pyridiniopropionate (ppbet) were synthesized with the literature method [15]. All other reagents were commercially available and used as received.

Caution. Metal perchlorate containing organic ligands are potentially explosive. Only a small amount of material should be prepared and handled carefully.

Syntheses

$[Cu_2(pybet)_4(H_2O)_2](NO_3)_2(ClO_4)_2 \cdot 2H_2O$ (**1**). A mixt. of pybet (0.412 g, 3 mmol) and $Cu(NO_3)_2 \cdot 6H_2O$ (0.362 g, 1.5 mmol) was dissolved in distilled water (8 ml) and heated at 50°C for 10 min, an aq. soln (2 ml) of $NaClO_4 \cdot H_2O$ (0.106 g, 1.5 mmol) was then added with stirring for 20 min. The soln was allowed to evap. slowly at room temp. After about a week greenish blue polyhedral crystals began to appear, and the product was collected within one month in 70% yield (Found: C, 31.3; H, 3.5; N, 7.8. Calcd for $C_{28}H_{34}Cl_2Cu_2N_6O_{26}$ **1**: C, 31.4; H, 3.4; N, 7.9%). IR data (ν/cm^{-1}): 3409 s (br), 3135 m, 3085 m, 3057 m, 1637 s (br), 1489 s, 1384 vs, 1307 s (br), 1215 w, 1194 w, 1114 s, 1117 s, 1082 s, 983 w, 934 w, 828 w, 779 w, 716 m, 674 w, 625 m.

$[Cu_2(pybet)_4(H_2O)Cl](ClO_4)_3 \cdot 2H_2O$ (**2**). A mixt. of pybet (0.412 g, 3 mmol) and $CuCl_2 \cdot 2H_2O$ (0.256 g, 1.5 mmol) was dissolved in distilled water (8 ml) and heated at 60°C for 10 min, after that an aq. soln (2 ml) of $NaClO_4 \cdot H_2O$ (0.106 g, 1.5 mmol) was added with stirring for 20 min. The soln was allowed to evap. slowly at room temp. After about 4 days light blue polyhedral crystals began to appear. The product was collected within one week (50% yield) (Found: C, 31.3; H, 3.1; N, 5.1. Calcd for $C_{28}H_{32}Cl_4Cu_2N_4O_{23}$ **2**: C, 31.6; H, 3.2; N, 5.3%). IR data (ν/cm^{-1}): 3550 m (br), 3430 m (br), 3135 m, 3085 m, 2980 w, 1672 vs, 1637 vs, 1489 s, 1449 m, 1398 vs, 1314 m, 1222 m, 1194 m, 1145 vs, 1117 vs, 1084 vs, 967 w, 934 w, 850 w, 779 w, 716 s, 674 m, 625 s, 584 w. A small quantity of a deep blue crystalline compound was also isolated as a minor product, which has been carefully separated under microscope, and characterized as a monomeric complex $[Cu(pybet)_2(H_2O)_2Cl]ClO_4$, and the structure of which will be published elsewhere.

$[Cu_2(ppbet)_4Cl_2](ClO_4)_2$ (**3**). A mixt of ppbet (0.454 g, 3 mmol) and $CuCl_2 \cdot 4H_2O$ (0.256 g, 1.5 mmol) was dissolved in distilled water (8 ml) and heated at 60°C for 10 min, an aq. soln (2 ml) of $NaClO_4 \cdot H_2O$ (0.106 g, 1.5 mmol) was then added with stirring for 20 min. The soln was allowed to evap. slowly at room temp. After about 10 days greenish blue polyhedral crystals began to appear. The product was collected within one month, and the yield was 55% (Found: C, 38.2; H, 3.5; N, 5.4. Calcd for $C_{32}H_{36}Cl_4Cu_2N_4O_{16}$ **3**: C, 38.4; H, 3.6; N, 5.6%). IR data (ν/cm^{-1}): 3128 w, 3085 w, 2973 w, 2924 w, 2853 w, 1630 vs, 1581 w, 1489 s, 1433 s, 1405 s, 1306 w, 1328 w, 1300 m, 1215 w, 1160 m, 1096 vs, 990 w, 962 w, 878 w, 779 m, 681 s, 625 s, 596 m.

Physical measurements

The C, H and N microanalyses were carried out with a Perkin–Elmer elemental analyzer. The FT-IR spectra were recorded from KBr pellets in range of 4000–400 cm^{-1} on a Nicolet 5DX spectrometer.

Magnetic susceptibility measurements were carried out on microcrystalline samples in the temp. range 100–300 K and in an applied field of 1000 G with a Quantum Design MPMS SQUID magnetometer. The data were corrected for the diamagnetic contributions, which were estimated from the Pascal constants [16].

X-ray crystallography

A summary of selected crystallographic data for the three complexes is given in Table 1. Intensity data collections for complexes **1** and **3** were carried out on a Siemens P4 diffractometer using graphite-monochromated Mo–K_α (λ = 0.71073 Å) radiation at 294 K, while the intensity data for complex **2** were collected on an Enraf-Nonius CAD4 diffractometer using graphite-monochromated Mo–K_α radiation at 294 K. For all complexes, determinations of the crystal class, orientation matrix, and cell dimensions were performed according to the established procedures; the intensity data were collected using the ω-scan mode. The data processing was made with SHELXTL-PC program package [17] for complexes **1** and **3,** and with the NRCVAX program package [18] for complex **2**. Lp corrections and absorption corrections have been applied [19].

Most of the non-hydrogen atoms in the crystal structures were located with the direct methods of SHELXTL-PC program package and subsequent Fourier syntheses were used to derive the remaining non-hydrogen atoms. All the non-hydrogen atoms

Table 1. Crystallographic data

Complex	**1**	**2**	**3**
Formula	$C_{28}H_{36}Cl_2Cu_2N_6O_{26}$	$C_{28}H_{32}Cl_4Cu_2N_4O_{23}$	$C_{32}H_{36}Cl_4Cu_2N_4O_{16}$
M	1070.61	1063.47	1001.53
Colour and habit	light blue polyhedral	greenish blue polyhedral	green prismatic
Crystal system	orthorhombic	orthorhombic	orthorhombic
Space group	*Cmca* (No. 64)	*Pnma* (No. 62)	*Pbca* (No. 61)
Cell parameters			
a(Å)	23.249(2)	15.623(3)	15.319(3)
b(Å)	14.651(2)	23.756(5)	13.415(2)
c(Å)	12.129(4)	11.036(2)	19.391(2)
V(Å^3)	4131.4(12)	4095.9(14)	3984.8(10)
Z	4	4	4
F(000)	2184	2160	2040
D_{calc} (g cm^{-3})	1.721	1.725	1.669
Absorption Coef.	12.61 cm^{-1}	13.91 cm^{-1}	14.11 cm^{-1}
Crystal size	$0.24\times0.40\times0.50$ mm^3	$0.38\times0.38\times0.14$ mm^3	$0.34\times0.36\times0.42$ mm^3
2θ range	3 to 55°	2 to 50°	2 to 50°
Transmission factors	0.897/0.675	0.989/0.891	0.897/0.675
Unique data	2419	3704	3504
Obs. data [$I \geqslant 2\sigma(I)$]	1734	2092	2231
Parameters refined	171	283	262
R (R_w) value	0.0413 (0.0490)	0.0737 (0.0855)	0.0510 (0.0612)
Goodness-of-Fit	1.31	1.63	1.39
Weighting scheme	$w = 1/[\sigma^2(F)+0.004\|F\|^2]$	$w = 1/[\sigma^2(F)+0.001\|F\|^2]$	$w = 1/[\sigma^2(F)+0.0006\|F\|^2]$
$\Delta\rho_{max}/\Delta\rho_{min}$	0.44/−0.45 eÅ^{-3}	0.86/−1.28 eÅ^{-3}	0.74/−0.85 eÅ^{-3}

were refined anisotropically except the two-fold disordered oxygen atoms of one perchlorate anion in complex **2,** which were subjected to geometric restraints. Hydrogen atoms of water molecules were located from the difference maps; hydrogen atoms of the betaine ligands were generated geometrically (C—H 0.96 Å), assigned isotropic thermal parameters, and ride on their parent carbon atoms. All the hydrogen atoms were held stationary and included in the final stage of full-matrix least-squares refinement using SHELXTL-PC program package. Analytical expressions of neutral-atom scattering factors were employed, and anomalous dispersion corrections were incorporated [20]. The selected bond lengths and bond angles are listed in Table 2. Additional crystallographic data are available as supplementary materials.

RESULTS AND DISCUSSION

Crystal structures

The crystal structure of complex **1** contains discrete $[Cu_2(pybet)_4(H_2O)_2]^{4+}$ cations, nitrate and perchlorate anions, and lattice water molecules. The dimeric $[Cu_2(pybet)_4(H_2O)_4]^{4-}$ cation, as shown in Fig. 1, has a centrosymmetrically tetrakis(μ_2-carboxylate)-bridged structure, which is analogous to that of the copper(II) acetate complex [1]. In the dimeric cation, each copper(II) atom is coordinated in a distorted square-pyramidal environment by four oxygen atoms of the μ_2-carboxylate groups at the basal plane (mean Cu—O = 1.982 Å) and by an aqua ligand at the axial position with a markedly longer Cu—O distance of 2.093(3) Å. The Cu···Cu separation (2.677(1) Å) in the dimeric structure of complex **1** is very similar to the analogous complex containing the same dimeric cation [14], and slightly longer than that (2.614(3) Å) in the acetate complex [1]. The displacement of the metal atom from the basal plane in the square-pyramid (designated as δ hereafter) is 0.214 Å with the mean Cu—O—C angle being 121.2°.

Complex **2** is composed of a dinuclear $[Cu_2(pybet)_4(H_2O)Cl]^{3+}$ cation, perchlorate anions and lattice water molecules. The $[Cu_2(pybet)_4(H_2O)Cl]^{3+}$ cation, as illustrated in Fig. 2, has a similar tetrakis(μ_2-carboxylate)-bridged dinuclear structure as found for other compounds of the type of copper(II) acetate monohydrate [1]. Noteworthy is that the two axial positions of this dinuclear cation are occupied by one water molecule and one chloride ion, respectively. So far very few tetrakis(μ_2-carboxylate)-bridged dimeric or dinuclear copper(II) complexes with both of the axial positions ligated by anionic ligands, such SCN^- and Cl^-, have been documented [8, 14], and only one dinuclear copper(II) complex comprising two different axial ligands, namely one aqua and one methanol molecules, has been reported very recently [11]. No example of such tetrakis(μ_2-carboxylate)-bridged dicopper(II) complex composed of one neutral and

Table 2. Selected inter-atomic distances (Å) and bond angles (°)

Complex **1**			
Cu(1)···Cu(1a)	2.677(1)	Cu(1)—O(1w)	2.093(3)
Cu(1)—O(1)	1.976(2)	Cu(1)—O(2a)	1.972(2)
O(1)—C(1)	1.255(4)	O(2)—C(1)	1.249(4)
N(2)—O(3)	1.220(6)	N(2)—O(4)	1.248(5)
O(1w)—Cu(1)—O(1)	95.7(1)	O(1)—Cu(1)—O(1a)	88.2(1)
O(1w)—Cu(1)—O(2a)	96.7(1)	O(1)—Cu(1)—O(2a)	167.5(1)
O(1a)—Cu(1)—O(2a)	89.2(1)	O(2a)—Cu(1)—O(2b)	90.7(1)
Cu(1)—O(1)—C(1)	120.3(2)	C(1)—O(2)—Cu(1a)	124.1(2)
O(1)—C(1)—O(2)	127.9(3)	O(1)—C(1)—C(2)	118.2(3)
Complex **2**			
Cu(1)···Cu(2)	2.722(2)	Cu(1)—Cl(1)	2.358(4)
Cu(1)—O(11)	1.972(7)	Cu(1)—O(21)	2.007(7)
Cu(2)—O(1w)	2.130(8)	Cu(2)—O(12)	1.984(7)
Cu(2)—O(22)	1.970(7)	O(11)—C(11)	1.257(12)
O(12)—C(11)	1.226(12)	O(21)—C(21)	1.248(13)
O(22)—C(21)	1.251(13)		
Cl(1)—Cu(1)—O(11)	100.0(2)	Cl(1)—Cu(1)—O(21)	96.0(2)
O(11)—Cu(1)—O(21)	88.8(3)	O(11)—Cu(1)—O(11a)	90.4(4)
O(21)—Cu(1)—O(11a)	163.8(3)	O(21)—Cu(1)—O(21a)	87.5(4)
O(1w)—Cu(2)—O(12)	93.3(3)	O(1w)—Cu(2)—O(22)	98.2(3)
O(12)—Cu(2)—O(22)	88.8(3)	O(12)—Cu(2)—O(12a)	89.5(4)
O(22)—Cu(2)—O(12a)	168.5(3)	O(22)—Cu(2)—O(22a)	90.7(4)
Cu(1)—O(11)—C(11)	123.9(6)	Cu(2)—O(12)—C(11)	120.2(7)
Cu(1)—O(21)—C(21)	122.9(7)	Cu(2)—O(22)—C(21)	122.8(6)
O(11)—C(11)—O(12)	129.7(9)	O(21)—C(21)—O(22)	128.0(9)
Complex **3**			
Cu(1)···Cu(1a)	2.760(1)	Cu(1)—Cl(1)	2.454(2)
Cu(1)—O(11)	1.986(4)	Cu(1)—O(21)	1.996(4)
Cu(1)—O(12a)	1.974(4)	Cu(1)—O(22a)	1.971(4)
O(11)—C(11)	1.273(8)	O(12)—C(11)	1.234(7)
O(22)—C(21)	1.250(7)	O(21)—C(21)	1.257(8)
Cl(1)—Cu(1)—O(11)	100.7(1)	Cl(1)—Cu(1)—O(21)	91.2(1)
O(11)—Cu(1)—O(21)	90.5(2)	Cl(1)—Cu(1)—O(12a)	95.4(1)
O(11)—Cu(1)—O(12a)	163.7(2)	O(21)—Cu(1)—O(12a)	90.9(2)
Cl(1)—Cu(1)—O(22a)	104.1(1)	O(11)—Cu(1)—O(22a)	88.2(2)
O(21)—Cu(1)—O(22a)	164.6(2)	O(12a)—Cu(1)—O(22a)	86.2(2)
Cu(1)—O(11)—C(11)	119.8(4)	C(11)—O(12)—Cu(1a)	130.2(4)
Cu(1)—O(21)—C(21)	127.4(4)	C(21)—O(22)—Cu(1a)	122.3(4)
O(11)—C(11)—O(12)	125.3(6)	O(21)—C(21)—O(22)	125.5(6)

Symmetry codes: for **1,** (a) $-x, 1-y, -z$; (b) $-x, y, z$; (c) $x, 1-y, -z$; for **2** (a) $x, 0.5-y, z$; for **3,** (a) $2-x, -y, 1-z$.

one anionic axial ligands has been documented. Thus complex **2** may present a novel structural variety among the tetrakis(μ_2-carboxylate)-bridged copper(II) complexes. It is also of interest to compare the geometries of the two crystallographically independent copper(II) atoms in the dinuclear structure. The Cu(1) atom is ligated by a chloride atom at the axial position, the δ (0.279 Å), Cu—O—C (mean 123.4°), and Cu—O(basal) (mean 1.990 Å) values for the Cu(1) atom are significantly larger than the corresponding values (0.198 Å, 121.5, 1.977 Å) for the Cu(2) atom which is ligated by an aqua ligand at the axial position. These observations can be rationalized on the base that with ligation of a larger and anionic axial ligand Cl^-, there will be a greater repulsion between the Cu—Cl and Cu—O(basal) bonds resulting in larger Cl—Cu—O(basal) bond angles, ''moving'' of the Cu(1) atom toward the axial ligand, and/or lengthening the Cu—O(basal) bond distance [14]. Thus displacement of the Cu(1) atom from the basal plane of the square-pyramid is much greater than that of the Cu(2) atom.

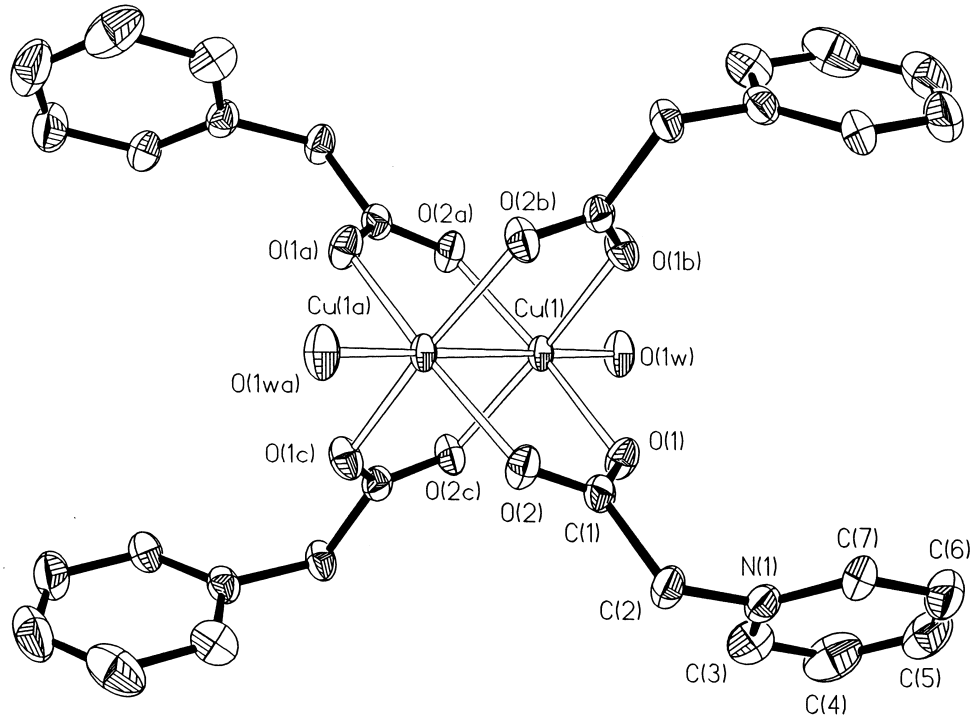

Fig. 1. ORTEP drawing (at 35% probability) of the dimeric cation in complex **1**. Symmetry codes are given in Table 2.

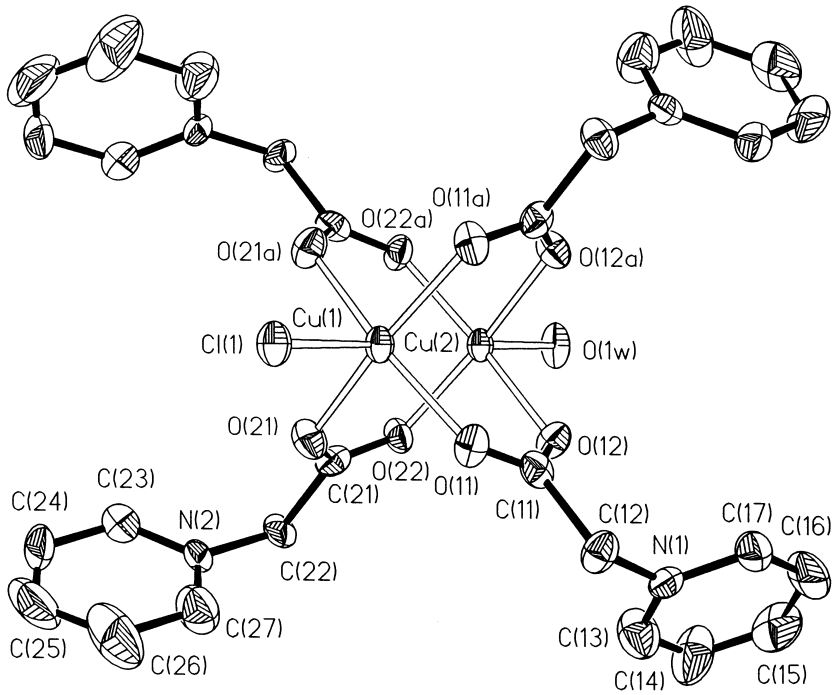

Fig. 2. ORTEP drawing (at 35% probability) of the dinuclear cation in complex **2**. Symmetry code: (a) x, $0.5-y$, z.

Complex **3** is composed of a dimeric $[Cu_2(ppbet)_4Cl_2]^{2+}$ cation and two perchlorate anions. The $[Cu_2(ppbet)_4Cl_2]^{4+}$ cation, as illustrated in Fig. 2, has a similar centrosymmetrically tetrakis(μ_2-carboxylate)-bridged dimeric structure as found for other compounds of the type of copper(II) acetate monohy-

drate. Since the axial positions are both occupied by chloride ligands, the greater repulsion between the Cu—Cl and Cu—O(basal) bonds in complex **3** affords larger Cl—Cu—O(basal) bond angles, a very large intramolecular Cu···Cu separation (2.760(1) Å), a larger δ (0.269 Å), a larger Cu—O(basal) bond lengths (mean 1.982 Å), as well as very large Cu—O—C angles (mean 124.9°). Similar tetrakis(μ_2-carboxylate)-bridged dimeric copper(II) complexes with both axial chloride ligands have been reported in our previous work, where the μ_2-carboxylate groups are betaine ($Me_3N^+CH_2CO_2^-$) and pybet [14].

Magnetic properties

Temperature-dependent magnetic susceptibility data for the three complexes have been measured from 300 K down to 100 K. The μ_{eff} values are plotted versus temp. in Fig. 4 for the three complexes. At room temp., the μ_{eff} values are ca 2.0 μ_B for these complexes. Upon cooling down from room temp., the μ_{eff} values decreases continuously for all three complexes, thus indicating a strong antiferromagnetic interaction between the copper(II) atoms in the dimeric or dinuclear structures. Assuming isotropic exchange, the exchange Hamiltonian is $H = -2JS_1 \cdot S_2$ with $S_1 = S_2 = 1/2$, and the magnetic susceptibility per cation is given by the eqn (1) [21]

$$\chi_M = \frac{2Ng^2\beta^2}{3kT}\left[1+\tfrac{1}{3}\exp\left(\frac{2J}{kT}\right)\right]^{-1}(1-\rho)+\frac{Ng^2\beta^2}{2kT}\rho \qquad (1)$$

where N, g, β, k are Avogadro's constant, g factor, Bohr magneton, and Boltzman constant, respectively and $2J$ is the exchange coupling constant. The best least-squares fitting results are illustrated in Fig. 4 and are listed in Table 3, exhibiting that the magnitudes of the intramolecular magnetic coupling are greater than 300 cm^{-1} for all three complexes, which are compatible to those found for the acetate analogues (-285 to -325 cm^{-1}) [2,3,22,23].

Discussion

We have suggested that [14], the Cu···Cu separation in the $[Cu_2(RCO_2)_4L_2]$ structures may be generally correlated to the electronic repulsion of the metal-ligand bonds, especially in the case of less sterically demanding ligands, and to the steric interaction between the bulky axial and bridging carboxylate ligands in the case of bulky ligands. Our current observations in this work are in accord with this assumption. With different axial ligands, we demonstrate the effect of the axial ligands on the geometrical variation such as the Cu···Cu separation and δ value. With one axial position occupied by chloride ligand in complex **2,** the Cu···Cu separation and mean δ value become larger in comparison to those in complex **1,** while these values are more larger in complex **3,** in which both axial positions are occupied by chloride ligands. Particularly, complex **2** is a nice example demonstrating the mutual repulsion between the axial and the basal coordination bonds. Hence we may conclude that the structural variation in the $[Cu_2(RCO_2)_4L_2]$ structures is mainly dictated by the mutual repulsion between the basal and axial metal-ligand bonds [14].

There have been several attempts to correlate the magnitudes of $2J$ with structural parameters in the $[Cu_2(RCO_2)_4L_2]$ structures, but no success has been achieved [2,3,5,11,12,21]. One may also notice that the ideal of the spin coupling by superexchange through the carboxylate bridges is favoured by both experimental [5,8,22,23] and theoretical [24] investigations.

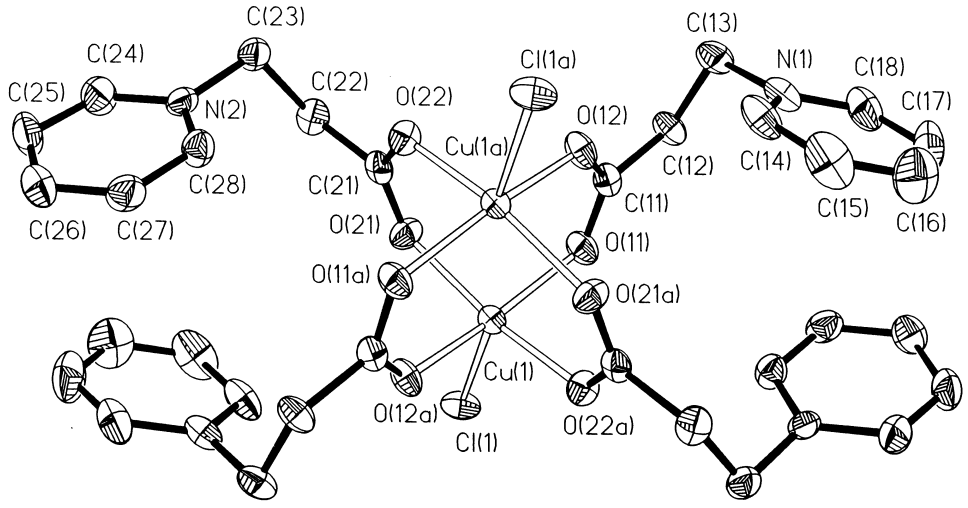

Fig. 3. ORTEP drawing (at 35% probability) of the dimeric cation in complex **3**.

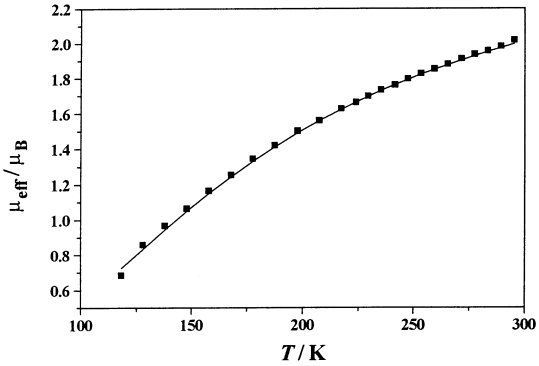

(*a*)

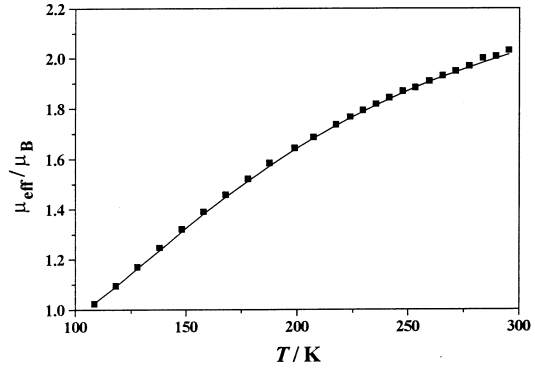

(*b*)

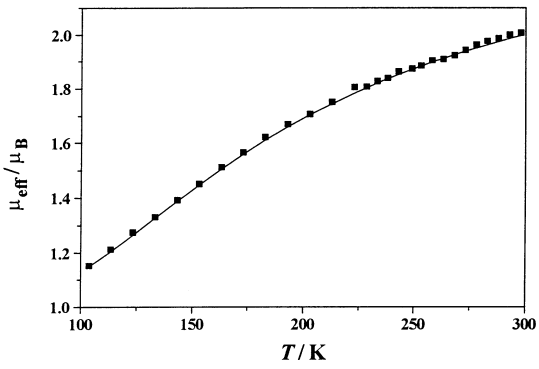

(*c*)

Fig. 4. Temperature-dependence of molar effective magnetic moment μ_{eff} for complexes **1** (a), **2** (b) and **3** (c). The solid lines represent the best theoretical fits (see Table 3).

Table 3. Parameters deduced from magnetic data

Complex	$2J$, cm^{-1}	g	ρ	10^3 R^a
1	340	2.23	3.0	8.7
2	321	2.19	5.5	4.9
3	301	2.05	4.9	6.0

[a] $R = [\Sigma(\chi_{obs}T - \chi_{obs}T)^2/(\chi_{obs}T)^2]^{1/2}$

Inspection of the structural data and the magnetic parameters for the three complexes (see Table 4) shows that the intramolecular coupling constants may apparently be correlated to the Cu···Cu distances, δ values or the mean Cu—O—C bond angles, and are not very sensitive to the Cu—O(basal) bond lengths. On the other hand, previous studies have shown that the direct interaction between the pair of copper(II) atoms should be very weak or even negligible [12]. Therefore it may be reasonable to correlate the magnetic coupling magnitudes to the δ values, since the δ value geometrically reflects both the Cu—O bond lengths and the O—Cu—L bond angles, and hence is indicative of the molecular orbital overlap between the metal atom and the carboxylate groups. As shown in Table 4, a smaller δ value represents a stronger magnetic coupling. It should be pointed out that due to lack of detailed structural parameters and/or magnetic results, we could not examine this deduction on other related quadruply μ_2-carboxylate-bridged dicopper(II) complexes.

Conclusion

This work presents three new dimeric (or dinuclear) copper(II) carboxylates, among which one has two aqua molecules, one has an aqua molecule and one chloride ion, and one has two chloride ions, as axial ligands, respectively. The structural variations in the dimeric structures may be correlated to the mutual repulsion of the basal and axial metal-ligand bonds in the square-pyramidal environment around the copper(II) atom. The current results demonstrate that the magnitudes of the intramolecular antiferromagnetic coupling between the two copper(II) atoms may be

Table 4. Comparison of the structural[a] and magnetic parameters

Complex	Cu···Cu(Å)	δ (Å)	Cu—O (Å)	Cu—O—C (°)	$2J$ (cm^{-1})
1	2.677(1)	0.214	1.974	120.3	−340
2	2.722(2)	0.238	1.980	122.5	−321
3	2.760(1)	0.269	1.982	124.9	−301

[a] mean values.

inversely correlated to the displacements of the metal atom from the basal plane.

Acknowledgements—This work was supported by the NSFC (29625102) and NSF of Guangdong, and a Hong Kong Research Grants Council Earmarked Grant No. CUHK 89/93E. We also thank Mr Shi-Yong Fang of Institute of Physics, Chinese Academy of Sciences for the magnetic measurements.

REFERENCES

1. van Niekerk, J. N. and Schoening, F. R. L., *Acta Crystallogr*., 1953, **6,** 227.
2. Doedens, R. J., *Prog. Inorg. Chem*., 1976, **21,** 209.
3. Catterick, J. and Thornton, P., *Adv. Inorg. Chem*., 1977, **21,** 291.
4. Melnik, M., *Coord. Chem. Rev*., 1982, **42,** 259.
5. Kato, M., *Coord. Chem. Rev*., 1988, **92,** 45.
6. Porter, L. C., Dickman, M. H. and Doedens, R. J., *Inorg. Chem*., 1986, **25,** 678.
7. Steward, O. W., McAfee, R. C., Chang, S.-C., Pisker, S. R., Schreiber, W. J., Jurry, C. F., Taylor, C. E., Pletcher, J. F. and Chen, C.-S., *Inorg. Chem*., 1986, **25,** 629.
8. Goodgame, D. M. L., Hill, N. J., Marsham, D. F. and Skapski, A. C., *Chem. Commun*., 1969, 629.
9. Borel, M. M. and Leclare, A., *Acta Crystallogr*., *Sect. A*, 1976, **32,** 1275.
10. Moreland, J. A. and Doedens, R. J., *J. Am. Chem. Soc*., 1975, **97,** 508.
11. Ueyama, N., Yamada, Y., Takeda, J., Okamura, T., Mori, W. and Nakamura, A., *J. Chem. Soc*., *Chem. Commun*., 1996, 1377.
12. Sapiña, F., Burgos, M., Escrivá, E., Folgado, J.-V., Beltrán, D. and Gómez-Romero, P., *Inorg. Chim. Acta*, 1994, **216,** 185.
13. (a) Chen, X.-M., Feng, X.-L., Yu, X.-L. and Mak, T. C. W., *Inorg. Chim. Acta*, 1997, **266,** 121; (b) Tong, Y.-X., Chen, X.-M. and Ng, S. W., *Polyhedron*, 1997, **26,** 3363, and references cited therein.
14. Chen, X.-M. and Mak, T. C. W., *Struct. Chem*., 1993, **4,** 247.
15. (a) Chen, X.-M. and Mak, T. C. W., *J. Chem. Soc*., *Dalton Trans*., 1992, 1585; (b) Chen, X.-M. and Mak, T. C. W., *J. Chem. Soc*., *Dalton Trans*., 1991, 3253.
16. Boudreaus, E. A. and Mulay, L. N., ed., *Theory and Applications of Molecular Paramagnetism*, Wiley, New York, 1976, p. 491.
17. Sheldrick, G. M., *SHELXTL-PC*, User's Manual. Siemens Analytical X-ray Instruments, Inc., Madison, Wisconsin, U.S.A., 1990.
18. Gabe, E. J., Le Page, Y., Charland, J.-P. and Lee, F. C., *J. Appl. Cryst*., 1989, **22,** 384.
19. North, A. C. T., Phillips, D. C. and Mathews, F. S., *Acta Crystallogr*., *Section A*, 1968, **24,** 351.
20. *International Tables for X-ray Crystallography*, Vol. 4, pp. 55, 99, 149, Birmingham, UK, 1974.
21. Journaux, Y., Slatten, J. and Kahn, O., *Inorg. Chem*., 1985, **24,** 4063.
22. Jotham, R. W., Kettle, S. F. A. and Marks, J. A., *J. Chem. Soc*., *Dalton Trans*., 1972, 428.
23. (a)Asakawa, T., Inoue, M., Hara, K. and Kabo, M., *Bull. Chem. Soc. Jpn*, 1972, **45,** 1054; (b) Zelonka, R. A. and Baired, M. C., *Inorg. Chem*., 1972, **11,** 134; (c) Beddoes, R. L., Connor, J. A., Dubowski, D., Jones, A. C., Mills, O. S. and Price, R., *J. Chem. Soc*., *Dalton Trans*., 1979, 781.
24. (a) Hay, P. J., Thibeault, J. C. and Hoffman, R., *J. Am. Chem. Soc*., 1975, **97,** 4884; (b) Harcourt, R. D., Skrezenek, F. L. and Maclagan, R. G. A. R., *J. Am. Chem. Soc*., 1986, **108,** 5403.

Pergamon

PII: S0277–5387(98)00023–0

Polyhedron Vol. 17, No. 16, pp. 2647–2653, 1998
© 1998 Elsevier Science Ltd
All rights reserved. Printed in Great Britain
0277–5387/98 $19.00+0.00

Syntheses, crystal structures and properties of two chloranilate-bridging dinuclear Mn(II) compounds with different lattice solvate molecules: $[Mn_2(TPA)_2(CA)](ClO_4)_2 \cdot 3H_2O$ and $[Mn_2(TPA)_2(CA)](ClO_4)_2 \cdot 2CH_3CN$ (TPA = tris(2-pyridylmethyl)amine; CA = dianion of chloranilic acid)

Dao Feng Xiang, Chun Ying Duan, Xiang Shi Tan, Yong Jiang Liu and Wen Xia Tang*

State Key Laboratory of the Coordination Chemistry, Coordination Chemistry Institute, Nanjing University, Nanjing 210093, P. R. China

(Received 24 October 1997: accepted 6 January 1998)

Abstract—Two chloranilate-bridging dinuclear Mn(II) compounds with different lattice solvate molecules, $[Mn_2(TPA)_2(CA)](ClO_4)_2 \cdot 3H_2O$ (compound **1**) and $[Mn_2(TPA)_2(CA)](ClO_4)_2 \cdot 2CH_3CN$ (compound **2**), were synthesized and their crystal structures were determined by single-crystal X-ray diffraction. In the cation $[Mn_2(TAP)_2(CA)]^{2+}$, each Mn^{2+} ion is coordinated by four nitrogen atoms from TPA and two oxygen atoms from chloranilate and the chloranilate bridges two Mn^{2+} ions in a bis bidentate fashion. The temperature-dependent magnetic susceptibility data of compound **1** were fitted based on $H = -JS_1S_2$, yielding the intramolecular coupling constant J value of -0.12 cm^{-1}. The electrochemical properties and catalase-like activity of compound **1** were studied. © 1998 Elsevier Science Ltd. All rights reserved

Keywords: manganese complexes; dinuclear complexes; crystal structures; magnetism; cyclic voltammetry; catalase activity.

The study of Manganese complexes with various nuclearities and various oxidation states has received considerable attention in the past few years. The research interests are mainly centred on two aspects, one is in the field of molecular magnetism aimed at the investigation of exchange-coupling interactions between adjacent metal ions in the polynuclear complexes of Mn, another is the endeavour to model the structures, properties and functions of the active sites of Mn-containing enzymes in biological systems, such as the oxygen-evolving complex of photosystem II, [1,2] manganese catalases [3,4], Mn-SOD and manganese ribonucleotide reductase [5].

Manganese catalases catalyse the disproportionation of hydrogen peroxide to dioxygen and water very efficiently and this process is important for cell detoxification. Manganese catalases all appear to have a binuclear manganese active site and it is generally believed that the disproportionation reaction is catalysed by the interconversion of the two oxidation states $Mn^{III}Mn^{III}$ and $Mn^{II}Mn^{II}$. However, the core structure in manganese catalases has not been established yet and the exact mechanism of H_2O_2 disproportionation is still unknown [6]. In order to gain insight into the structure and catalytic mechanism of manganese catalase, it is of value to synthesize and characterize dinuclear manganese complexes in various oxidation states to unravel the more complex behavior of the biological sites by serving as models of the structural, spectral, or functional properties [7–10].

* Author to whom correspondence should be addressed.

In this study on dinuclear manganese complexes we used tripod ligand TPA as ending ligand and chloranillic acid as bridging ligand and succeeded in synthesizing and characterizing compounds **1** and **2**. It is especially interesting that our efforts to synthesize the dinuclear manganese(III) complex is in vain, because the Mn(II) dimer is always obtained whether the starting material is divalent manganese salt or trivalent manganese salt. Chloranilic acid can be capable of bridging metal ions by their four, partically negatively charged oxygen atoms. Previous reports on oligomeric or polymeric Cu, Ni, Fe, Mo complexes bridged by the anion of chloranilic acid are known [11–14]. But no Mn complexes containing chloranilic acid ligand has been reported until now. Thus compounds **1** and **2** are the first examples of chloranilate-bridged manganese(II) complexes. The present work will report the syntheses and crystal structures of these two compounds, together with the magnetic properties, the electrochemical properties and the catalase-like activity of the compounds.

EXPERIMENTAL

Preparations

$TPA \cdot 3HClO_4$ was synthesized according to literature procedure [15]. Tetra-*n*-butylammonium perchlorate (TBAP) was twice recrystallized from absolute ethanol and dried *in vacuo* at 40°C prior to use. Acetonitrile (MeCN) was purified as previously described [16]. All other chemicals were purchased commercially and used as received.

$[Mn_2(TPA)_2(C_6Cl_2O_4)](ClO_4)_2 \cdot 3H_2O$ (compound **1**) was prepared by mixing $TPA \cdot 3HClO_4$ (0.118 g, 0.2 mmol) and Et_3N (0.081 g, 0.8 mmol) in 30 ml of methanol and $Mn(ClO_4)_2 \cdot 6H_2O$ (0.0724 g, 0.2 mmol) in 10 ml of methanol and after stirring for about 10 min, a methanolic solution (10 ml) of chloranilic acid (0.021 g, 0.1 mmol) was added to the reacting mixture. The resulting red solution was stirred for another half an hour and was then allowed to stand at room temperature. Dark red prismatic single crystals suitable for X-ray crystallography were obtained after ten days (0.07 g, yield 61%). Anal: Calcd for $C_{42}H_{42}Cl_4Mn_2N_8O_{15}$: C, 43.84; H, 3.68; N, 9.74; Mn, 9.55. Found: C, 43.72; H, 3.76; N, 9.84; Mn, 9.26%.

$[Mn_2(TPA)_2(C_6Cl_2O_4)](ClO_4)_2 \cdot 2CH_3CN$ (compound **2**) was prepared as follows. A methanolic solution (10 ml) of chloranilic acid (0.021 g, 0.1 mmol) was added to a stirring mixture of $TPA \cdot 3HClO_4$ (0.118 g, 0.2 mmol) in 20 ml of methanol and Et_3N (0.081 g, 0.8 mmol) and $Mn(CH_3COO)_2 \cdot 6H_2O$ (0.049 g, 0.2 mmol) in 10 ml of methanol. After stirring for half an hour the resulting red solution was allowed to stand at room temperature and one week later the black red microcrystalline material was obtained by filtration and then redissolved in MeCN. The black red single crystals were recovered by the vapour diffusion of Et_2O into the MeCN solution for several days (0.038 g, yield 32%). Anal: Calcd for $C_{46}H_{42}Cl_4Mn_2N_{10}O_{12}$: C, 46.88; H, 3.59; N, 11.89; Mn, 9.32. Found: C, 46.70; H, 3.52; N, 12.24; Mn, 9.25%.

CAUTION: Although we experienced no difficulties with the compounds isolated as their perchlorate salts, the unpredictable behaviour of perchlorate salts necessitates extreme caution in their handling.

Physical measurements

Elemental analyses were performed on a Perkin–Elmer 240c analytical instrument. Magnetic susceptibility data on powder samples were measured over a temperature range of 75–300 K at a measuring 6000 G by using a CAHN-2000 Faraday-type magnetometer. The apparatus was calibrated with $[Ni(en)_3]S_2O_3$ (en = ethylenediamine). Diamagnetic corrections were made using Pascal's constants. Electrochemical analysis by cyclic voltammetry were performed on a BAS-100B electrochemical analyzer, in conjunction with a conventional three-electrodes fitted with a purged dinitrogen gas inlet and outlet, a glassy-carbon working electrode, Ag/AgCl electrode as the reference electrode and a platinum auxiliary electrode. All electrochemical experiments were carried out under dry and purified dinitrogen atmosphere at 298 K. The Fc^+/Fc couple was used as an external standard ($E_{1/2} = 0.43$ V).

Crystal structure determination and refinement

The relevant crystal data and structural parameters for compounds **1** and **2** are summarized in Table 1. The intensities were collected at 294 K on a Siemens P_4 four-circle diffractometer with monochromated Mo–K_α ($\lambda = 0.71073$A) radiation using $\theta/2\theta$ scan mode with a variable scan speed 5.0–50.0° min^{-1} in ω. The data were corrected for Lorentz and polarization effects during data reduction using XSCANS [17].

The structure was solved by direct method and refined on F^2 by full-matrix least squares methods using SHELXTL version 5.0 [18]. The O atoms of perchlorate in compound **1** (sof (site occupancy factor) = 0.7 for O(11), O(12), O(13) and O(14); sof = 0.3 for O(11′), O(12′), O(13′) and O(14′)), as well as O(2w) (sof = 0.5) are found disordered. All the non-hydrogen atoms were refined anisotropically, except the water and perchlorate oxygen atoms in compound **1** which are isotropic. All the hydrogen atoms were placed in calculated positions (C—H, 0.96; N—H, 0.90 and O—H, 0.85Å) assigned fixed isotropic thermal parameters at 1.2 times the equivalent isotropic U of the atoms to which they are attached (1.5 times for the O—H and methyl groups) and allowed to ride on their respective parent atoms.

Table 1. Crystallographic data for compounds **1** and **2**

	1	**2**
Formula	$C_{42}H_{42}Cl_4Mn_2N_8O_{15}$	$C_{46}H_{42}Cl_4Mn_2N_{10}O_{12}$
M	1150.52	1178.58
Crystal size (mm)	$0.45 \times 0.35 \times 0.24$	$0.35 \times 0.32 \times 0.28$
Crystal system	monoclinic	triclinic
Space group	$C2/c$	$P\bar{1}$
a (Å)	27.016(3)	10.792(5)
b (Å)	11.1475(10)	11.114(3)
c (Å)	16.765(6)	11.552(4)
α (°)	90	86.62(2)
β (°)	93.406(12)	73.35(3)
γ (°)	90	73.51(3)
U (Å^3)	5040(2)	1272.4(8)
Z	4	1
D_{calc} (Mg m^{-3})	1.516	1.538
μ (mm^{-1})	0.786	0.778
$F(000)$	2352	602
Reflections	3974	5253
Unique reflections	3285	4478
Data/restraints/parameters	3282/18/312	4476/0/334
R, wR $[I > 2\sigma(I)]$	0.0547, 0.1459	0.0555, 0.1285
w^{-1}	$\sigma^2(F_o^2)$	$\sigma^2(F_o^2) + (0.0800P)^2 + 0.1300P^a$
Goodness of fit on F^2	1.129	1.013
ρ_{max}, ρ_{min}(eA^3)	0.522, −0.448	0.592, −0.397

[a] $P = (F_o^2 + 2F_c^2)/3$

The contributions of these hydrogen atoms were included in the structure-factors calculations.

All computations carried out on a PC-586 computer using the SHELXTL-PC Program Package [18]. Analytical expressions of neutral-atom scattering factors employed and anomalous dispersion corrections were incorporated [19].

RESULTS AND DISCUSSION

Structure description

ORTEP representations of the two compounds **1** and **2** are shown in Fig. 1 and Fig. 2, respectively. Selected bond distances and bond angles for **1** and **2** are listed in Table 2.

Compound **1** crystallizes in the monoclinic space group $C2/c$, and consists of discrete $[Mn_2(TPA)_2(CA)]^{2+}$ cations, two perchlorate and three lattice water molecules. The cation is centrosymmetric and the asymmetric unit thus consists of half of the cation. The chloranilate ligand bridges two Mn^{2+} ions in a bis bidentate fashion with fairly small chelating bond angles (73.84(6)° for O(1)—Mn(1)—O(2)). The Mn···Mn distance in the dimer is 8.151(6) Å. The C_6 ring entity is planar and the largest deviation of the atoms from the least-squares plane, defined by the ring atoms (C(19), C(20), C(21), C(19A), C(20A), C(21A) is 0.001(7) Å for C(21), C(21A). The largest deviation for the oxygen atoms is 0.054(7) Å for O(2). The Mn ions is protruding out by 0.317(5) Å of the defined plane. The C(19)—C(20) distance (1.542(3) Å) is comparable to C—C single bond length, whereas the significantly shorter C(20)—C(21) distance (1.411(4) Å) are close to a C=C double bond length. The C(19)—O(1) length and C(20)—O(2) length are 1.252(3) Å and 1.251(3) Å, respectively. These structural features of the bridging chloranilate ligand indicate it has a partially delocalized, quinoid structure which is true of the free dianion [20] and are similar to those for reported chloranilate-bridging dinuclear Cu(II) or Ni(II) complexes [21].

Six coordination of the manganese atom are completed by the four nitrogen atoms (N(1), N(2), N(3) and N(4) from TPA. The tripodal ligand TPA causes a characteristic coordination geometry in metal complexes. The Mn(1)—N(1) (amine) bond is the longest (2.358(2) Å) among the Mn(1)—N bonds. The bonds between Mn(1) and N (pyridine) atoms (N(2), N(3) and N(4)) lie in the range of 2.205(2)–2.242(2) Å and the average Mn—N (pyridine) bond length is 2.226(4) Å. The average N(amine)—Mn(1)—(pyridine) bond angle is 74.04(6)°. These observations agree well with those reported for other Mn(II) complexes of TPA [22]. The Mn—O lengths of 2.155(2) Å and 2.214(2) Å are similar to the Mn—O lengths of oxalate-bridged Mn(II) complexes [23]. The resulting manganese (II) coordination is quite severely distorted due to the

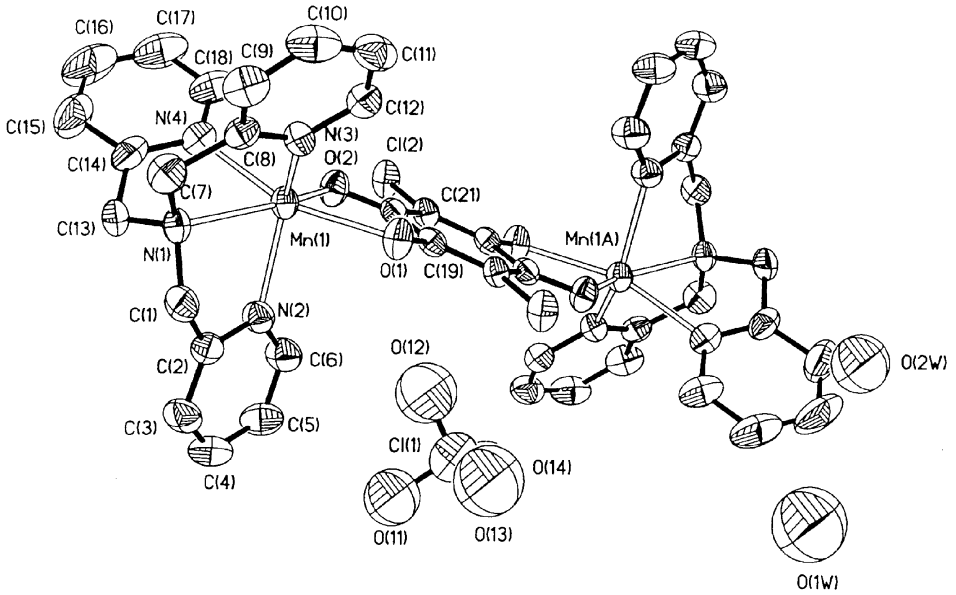

Fig. 1. Molecular structure and atom numbering of the cation of compound **1**. Thermal ellipsoids are drawn at the 30% probability level.

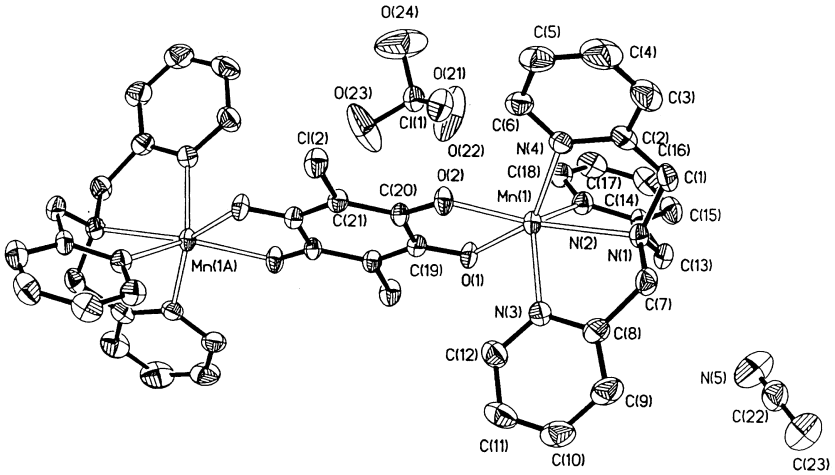

Fig. 2. Molecular structure and atom numbering of the cation of compound **2**. Thermal ellipsoids are drawn at the 30% probability level.

small bite angles formed by the TPA ligands and the chloranilate ligands. The perchlorate groups have their expected tetrahedral geometry.

Compound **2** crystallizes in the space group ($P\bar{1}$). Three lattice water molecules in compound **1** were replaced by two MeCN molecules. The cation also possess a center of symmetry. The C_6 entity of bridging chloranilate ligand is also planar and the largest deviation of the atoms from the least-squares plane, defined by the ring atoms C(19), C(20), C(21), C(19A), C(20A), C(21A)) is $-0.023(7)$ Å for C(21), C(21A). The largest deviation for the oxygen atoms is 0.054(7) Å for O(2). The Mn ion is 0.031(5) Å out of this plane and this deviation is much smaller than that in compound **1**. The Mn$\cdots$Mn separation is 8.231(7) Å. The Mn—N bond lengths and Mn—O bond lengths show little differences compared with those in compound **1**. (*cf.* Table 2) which confirm that Mn atoms in compound **2** are indeed divalent as in compound **1**. The chelating bond angles (72.65(12)° for O(1)—Mn(1)—O(2)) formed by the bridging chloranilate and the average N(1)(amine)—

Table 2. Selected bond lengths (Å) and angles (°) for compounds **1** and **2** with e.s.d.s. in parentheses

Mn(1)—N(1)	2.358(2)	2.366(4)
Mn(1)—N(2)	2.231(2)	2.228(4)
Mn(1)—N(3)	2.205(2)	2.223(4)
Mn(1)—N(4)	2.242(2)	2.290(4)
Mn(1)—O(1)	2.214(2)	2.241(3)
Mn(1)—O(2)	2.155(2)	2.149(3)
C(19)—C(20)	1.542(3)	1.525(6)
C(20)—C(21)	1.411(4)	1.384(6)
C(19)—O(1)	1.252(3)	1.255(5)
C(20)—O(2)	1.251(3)	1.256(5)
O(1)—Mn(1)—O(2)	73.84(6)	72.65(12)
O(1)—Mn(1)—N(1)	132.27(7)	137.94(13)
O(1)—Mn(1)—N(2)	85.79(7)	81.41(14)
O(1)—Mn(1)—N(3)	87.05(7)	92.3(2)
O(1)—Mn(1)—N(4)	154.25(8)	146.2(2)
O(2)—Mn(1)—N(1)	149.43(7)	147.11(13)
O(2)—Mn(1)—N(2)	96.22(8)	134.85(14)
O(2)—Mn(1)—N(3)	128.81(8)	97.7(2)
O(2)—Mn(1)—N(4)	83.26(8)	82.8(14)
N(1)—Mn(1)—N(2)	73.91(8)	72.81(14)
N(1)—Mn(1)—N(3)	75.00(8)	73.6(2)
N(1)—Mn(1)—N(4)	73.21(8)	72.8(2)
N(2)—Mn(1)—N(3)	129.86(8)	120.0(2)
N(2)—Mn(1)—N(4)	108.65(8)	101.1(2)
N(3)—Mn(1)—N(4)	98.63(8)	114.1(2)

Mn(1)—N(pyridine) bond angle (73.07(6)°) are both slightly smaller than the relevant angles (73.90(5)° and 74.05(6)°) in compound **1**.

Magnetic properties

Temperature dependent magnetic susceptibility for compound **1** have been measured down to 75 K and χ_M values are plotted vs temperature (Fig. 3), where χ_M is the molar magnetic susceptibility. The effective magnetic moment at 300.30 K is 8.34 B.M. which is close to the spin-only value of 8.36 B.M. expected for two uncoupled high-spin Mn^{II} ions. Upon cooling, the magnetic moment value decrease slowly from 8.34 B.M. at 300.2 K to 7.92 B.M. at 75 K, showing the presence of extremely weak antiferromagnetic exchange interaction. Assuming isotropic exchange, the exchange Hamiltonian is $H = -2JS_1 \cdot S_2$ with $S_1 = S_2 = 5/2$, and the magnetic susceptibility per mole of the dimer is given by eqn (1) [24]

$$\chi_M = 2Ng^2\beta^2/ kT[(e^x + 5e^{3x} + 14e^{6x} + 30e^{10x} + 55e^{15x})/ (1 + 3e^x + 5e^{3x} + 7e^{6x} + 9e^{10x} + 11e^{15x})] \quad (1)$$

where N, g, β, x are Avogadro's constant, g factor, Bohr magneton, and $x = J/kT$, respectively, and J is the exchange coupling constant for the manganese dimer. Using eqn (1), the least-squares fit to the magnetic susceptibility data gives the parameters: $g = 1.991$, $J = -0.12$ cm^{-1}. the discrepancy factor defined as $R = \Sigma(\chi_{calc} - \chi_{obs})^2]/\Sigma(\chi_{obs})^2$ is 1.5×10^{-4}. The magnetic susceptibility calculated by using the fit parameters is shown as the solid line in Fig. 3.

The magnetic exchange interaction through bridging chloranilate ligand is very weak. The J value is slightly smaller than those of other Mn^{II} complexes bridged by terephthalate, isophthalate or *trans* butaene diacid salt ligands ($J = -1.04$–-0.53) [25,26].

Cyclic voltammetry

Cyclic voltammogram of compound **1** in degassed and deaerated acetonitrile solution containing 0.1 mol cm^{-3} TBAP is shown in Fig. 4. Compound **1** undergo three quasireversible one-electron redox processes [27], suggesting the formation of $[Mn_2(TPA)_2(CA)]^{n+}$ species, with $n = 1$–4. The first quasireversible electron-transfer process ($E_{1/2} = -0.95$ V vs Ag/AgCl

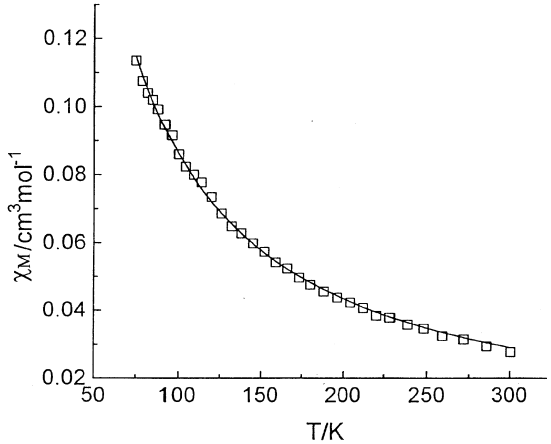

Fig. 3. The plot of X-T for compound **1**. The solid line represents best fit of data according to eqn (1).

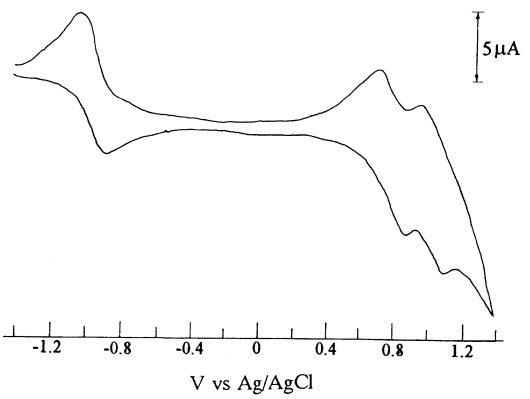

Fig. 4. Cyclic voltammogram of compound **1** in MeCN, 0.1 mol dm^{-3} TBAP. Scan rate is 0.1 V s^{-1}.

and $\Delta E = 100$ mV) which can be suggested to be associated with a ligand-centered electron-transfer reaction (CA^{2-}/CA^{3-}). Another two quasireversible one-electron redox processes observed at more positive potentials ($E_{1/2} = 0.8$ V vs Ag/AgCl and $\Delta E = 105$ mV; $E_{1/2} = 1.0$ V vs Ag/AgCl and $\Delta E = 100$ mV can be assigned to the couples, $Mn_2^{III}/Mn^{III}Mn^{III}$ and $Mn^{I}{}^{I}Mn^{III}/Mn^{II}Mn^{II}$. It is noticeable that the difference between the two redox steps is small (0.2 V), so that the disproportionation constant associated with the equilibrium

$$2[Mn_2(TPA)_2(CA)]^{3+} \leftrightharpoons [Mn_2(TPA)_2(CA)]^{4+} + [Mn_2(TPA)_2(CA)]^{2+} \quad (2)$$

is ca 10^{-3}. This result strongly suggested that the cation $[Mn_2(TPA)_2(CA)]^{3+}$ is not stable [28] and gives a reasonable explanation to the phenomenon observed that $[Mn_2(TPA)_2(CA)]^{2+}$ is obtained in spite of Mn(III) salt being used as starting material. The cyclic voltammetry of compound **2** was also measured and exact same C.V. diagram was obtained (not shown).

Reaction with hydrogen peroxide

Hydrogen peroxide decomposes catalytically in the presence of compound **1**. To a solid sample (10 mg, 8.7×10^{-3} mmol) of compound **1** was added aqueous H_2O_2 (7.9 M, 2 ml, 15.8 mmol). The mixture was stirred and thermostated at 25°C and the evolved O_2 was measured volumetrically [7]. The total amount of O_2 evolved corresponded to half the equivalent of H_2O_2 added, indicating that all the H_2O_2 disproportionated into O_2 and H_2O [eq. (3)]. The time courses of dioxygen

$$2H_2O_2 \rightarrow O_2 + 2H_2O \quad (3)$$

evolving are shown in Fig. 5. During the first minute of the reaction each mol of compound **1** disproportionated 890 mol of H_2O_2. This model catalyst is approximately five orders of magnitude less reactive than the metalloproteins from *L. plantarum* or *T. album* and is close to another model compound reported earlier [7,8]. Besides, we tested the catalase activity of manganese(II) perchlorate and manganese(III) acetate under the identical conditions as in the case of compound **1** (not shown). During the first minute of the reaction each mol of manganese(II) perchlorate and manganese(III) acetate can only disproportionate 0.12 and 1.16 mol of H_2O_2, respectively [8]. It is obvious that compound **1** can act as an effective catalyst for the disproportionation of H_2O_2.

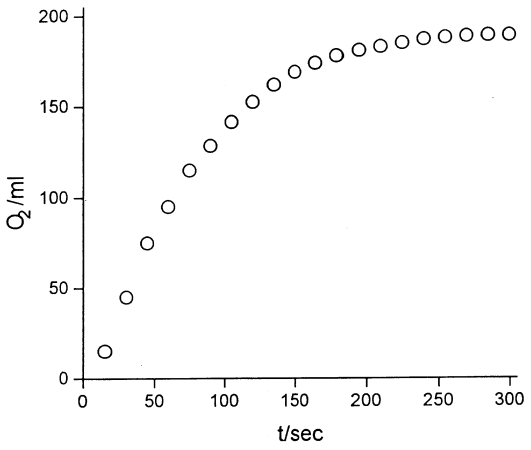

Fig. 5. Time course of dioxygen evolution in H_2O_2 disproportionation by compound **1**. Conditions: **1** (10 mg, 8.7×10^{-3} mmol), H_2O_2 (7.9 M, 2 ml, 15.8 mmol), at 298 K.

REFERENCES

1. Pecoraro, V. L., *Manganese Redox Enzymes*; VCH Publishers Inc, New York, 1992.
2. Dismukes, G. C., *Photochem. Photobiol.*, 1986, **43,** 99.
3. Fronko, R. M., Penner-Hahn, J. E. and Bender, C. J., *J. Am. Chem. Soc.*, 1988, **110,** 7554.
4. Allgood, G. S. and Perry, J. J., *J. Bacteriol*, 1986, **168,** 563.
5. Willing, A., Follman, H. and Auling, G., *Eur. J. Biochem.*, 1988, **170,** 603.
6. Waldo, G. S. and Penner-Hahn, J. E., *Biochemistry*, 1995, **34,** 1507.
7. Bossek, U., Saher, M., Weyhermüller, T. and Wieghardt, K., *J. Chem. Soc., Chem. Commun.*, 1992, 1780.
8. Larson, E. J. and Pecoraro, V. L., *J. Am. Chem. Soc.*, 1991, **113,** 7809.
9. Higuchi, C., Sakiyama, H., Õkawa, H., Isobe, R. and Fenton, D. E., *J. Chem. Soc., Dalton Trans.*, 1995, 4015.
10. Pessiki, P. J., Khangulov, S. V., Ho, D. M. and Dismukes, G. C., *J. Am. Chem. Soc.*, 1994, **116,** 891.
11. Tinti, F., Verdaguer, M., Kahn, O. and Savariault, J. -M., *Inorg. Chem.*, 1987, **26,** 2380.
12. Liu, S. C., Shaikh, S. N. and Zubieta, J., *J. Chem. Soc., Chem. Commun.*, 1988, 1017.
13. Wrobleski, J. T. and Brown, D. B., *Inorg. Chem.*, 1979, **18,** 498.
14. Decurtins, S., Schmalle, H. W., Zheng, L. M. and Ensling, Jügen, *Inorganica Chimica Acta*, 1996, **244,** 165.
15. Gafford, B. G. and Holwerda, R. A., *Inorg. Chem.*, 1989, **28,** 60.
16. Odonnel, J. F., Ayres, J. T. and Mann, C. K., *Analyt. Chem.*, 1965, **37,** 1161.
17. Siemens, XSCANS (*Version* 2.1), Siemens Analytical X-ray Instruments Inc. Madison, U.S.A., 1994.
18. Siemens, SHELXTL (*Version* 5.0), Siemens Industrial Automation Inc. Analytical Instrumentation, U.S.A., 1995.
19. *International Tables for X-ray Crystallography*, Vol. C, ed. A. J. C. Wilson, Kluwer Academic Publishers, Dordrecht, 1992, Tables 6.1.1.4, pp.

500–502 ; 4.2.6.8, pp. 219–22 and 4.2.4.2, pp. 193–199 respectively.
20. Andersen, E. K., *Acta Crystallogr*., 1967, **22,** 196.
21. Pierpont, C. G., Francesconi, L. C. and Hendrickson, D. N., *Inorg. Chem*., 1977, **16,** 2367.
22. Oshio, H., Ino, E., Mogi, I. and Ito, T., *Inorg. Chem*., 1993, **32,** 5697.
23. Deguenon, D., Bernardinelli, G., Tuchagues, J. - P. and Castan, P., *Inorg. Chem*., 1990, **29,** 3031.
24. Kahn, O., *Molecular Magnetism*, VCH publisher, Inc., New York, 1993.
25. Xiang Shin Tan, Dao Feng Xiang, Wen Xia Tang and Jie Sun, *Polyhedron*, 1997, **16,** 689.
26. Cano, J., Munno, G. D., Sanz, J., Ruizm, R., Lloret, F., Faus, J. and Julve, M., *J. Chem. Soc*., *Dalton. Trans*., 1994, 3465.
27. Caemelbecke, E. V., Kutner, W. and Kadish, K. M., *Inorg. Chem*., 1993, **32,** 438.
28. Dei, A., Gatteschi, D., Pardi, L. and Russo, U., *Inorg. Chem*., 1991, **30,** 2589.

Pergamon

PII : S0277–5387(98)00024–2

Polyhedron Vol. 17, No. 16, pp. 2655–2668, 1998
© 1998 Elsevier Science Ltd
All rights reserved. Printed in Great Britain
0277–5387/98 $19.00 + 0.00

Heterocyclic systems containing antimony (III)-VIII [1]. Hypervalency by intramolecular 1,5-chelation Sb···N in rings $RSb[(CH_2)_3]_2NR'$ (NR′ = NMe, NBz, NBu^i) and comparison to analogous compounds of As^{III}, Bi^{III}, Ge^{IV} and Sn^{IV}

Elmar Bräu,[a] Andrea Zickgraf,[a] Martin Dräger,[a]* Enrico Mocellin,[b]* Masaki Maeda,[c] Masashi Takahashi,[c] Masuo Takeda[c]* and Carlo Mealli[d]

[a] Institut für Anorganische Chemie und Analytische Chemie der Johannes Gutenberg-Universität, D-55099 Mainz, Germany

[b] School of Biological and Chemical Sciences, Faculty of Science and Technology, Deakin University, Geelong Victoria 3217, Australia

[c] Department of Chemistry, Faculty of Science, Toho University, Funabashi, Chiba 274, Japan

[d] Istituto per lo Studio della Stereochimica ed Energetica dei Composti di Coordinazione, C.N.R., I-50132 Firenze, Italia

(Received : 17 November 1997 ; accepted 6 January 1998)

Abstract—Eleven antimony compounds $RSb[(CH_2)_3]_2$ NR′ and eight germanium compounds $R_2Ge[(CH_2)_3]_2$ NR′ (some combinations of R = Cl, I, NCS, $OSiPh_3$, Ph, and NR′ = NMe, NBz, NBu^i) have been synthesized by diGrignard reactions and subsequent treatment with AgSCN, Ph_3SiONa or PhLi. The compounds were compared to 14 Sn, 1 As, 5 Sb and 4 Bi analogues taken from the literature. Evidence is provided for 1,5-chelation Sb···N via crystal structure determinations (5 + 1 (lit) Sb compounds), ^{13}C- and ^{29}Si-NMR chemical shifts, ^{121}Sb and ^{127}I Mössbauer data (11 and 3 Sb compounds, respectively), cyclic voltammetry (9 Sb compounds) and semi-empirical MO calculations on the Extended Hückel level (8 present compounds and 4 models). The ligand sequence (Cl < I < NCS) holds for an increasing approach N···Sb. The effect of electronegativity and the effect of *n*- or $\pi \rightarrow \sigma^*$ charge transfer into the LUMO at Sb are counteractive. The intramolecular donor strength increases in the following order : NBu^i < NBz < NMe. Simultaneously a decrease of the absolute value of the ^{121}Sb quadrupole coupling constant from Mössbauer spectroscopy occurs. The postulation of a control of the Sb···N chelation by frontier orbital interactions is supported by the CV results in CH_2Cl_2 at a Au/Hg electrode. It is proved by scan rate dependence that the observed reversible reduction/oxidation process is diffusion controlled, and by coulometry that the reduction takes place by transfer of one electron. © 1998 Elsevier Science Ltd. All rights reserved

Keywords: antimony ; hypervalency ; frontier orbitals ; Mössbauer spectroscopy ; cyclic voltammetry ; coulometry ; NMR.

Recently we have created a novel view about the bonding scheme of the long-known phenomenon of hypervalency at tin(IV) [2]. This view arose from systematic experimental investigations in some series of heterocycles which contained a potential intramolecular donor and the axial/equatorial ligands Cl, Br, I and Me [2]. The sequences of interaction (donor)···Sn showed that, with regard to the ligands

* Authors to whom correspondence should be addressed.

Scheme 1. Short notation for a compound: **number**(door/ligands); e.g. **1** (NMe/Cl_2) for the first compound.

NMe	NBz	NBu^i	NMe	NBz	NBu^i	NMe	NMe	NBz	NBu^i	NMe	NBz
Cl_2	Cl_2	Cl_2	Cl_2[d]	Cl_2[e]	Cl_2[e]	Cl_2[c]	Cl[c]	Cl[c]	Cl[c]	Cl[c]	Cl[c]
ClPh	ClPh		ClPh[e]	ClPh[e]	ClPh[e]		Br[c]			I[c]	I[c]
$(OSiPh_3)_2$			$(OSiPh_3)_2$[e]	$(OSiPh_3)_2$[e]	$(OSiPh_3)_2$[e]		I	I	I		
			Ph_2[e]	Ph_2[e]	Ph_2[e]		NCS	NCS	NCS		
			$(OSiPh_3)Ph$[e]	$(OSiPh_3)Ph$[e]			$OSiPh_3$	$OSiPh_3$	$OSiPh_3$		
								Ph	Ph		

[a] In addition data for **1** (O/Cl_2) and **1** (S/Cl_2) are given.
[b] In addition data for **4** (S/Cl) are given.
[c] See Ref. [6a].
[d] See Ref. [5].
[e] See Ref. [6b].

at Sn, their electronegativity and a $n \rightarrow \sigma^*$ charge transfer into the LUMO at Sn^{IV} are counteractive. The geometric impetus for this view came from the method of structure correlation of Bürgi and Dunitz [3a] and from papers of van Koten [3b], whereas the theoretical portions build on papers of Musher [3c] and of Noyori [3d].

In this work our ideas shall be extended to antimony(III) as a central atom, and the question of the influence of the lone pair of electrons in a ψ-trigonal bipyramidal geometry arises [4]. We synthesized a series of compounds **4** with Sb^{III} and, in addition, the compounds **1** with Ge^{IV} as a central atom (Scheme 1) [5–7]. Structural, spectroscopic and electrochemical data and semi-empirical MO calculations for these compounds will be compared to the analogous data of the rings **2, 3** and **5,** which contain Sn^{IV} [6b], As^{III} [6a] and Bi^{III} [6a] as central atoms (Scheme 1).

RESULTS

Synthetic aspects

The Cl_2, ClPh, Cl and I substituted heterocycles **1** and **4** were obtained by reaction of the diGrignard reagent $R'N[(CH_2)_3MgCl]_2$ with $GeCl_4$ [2d], $PhGeCl_3$, $SbCl_3$ or SbI_3. To obtain the NCS substituted compounds, $R'N[(CH_2)_3]_2SbI$ was reacted with AgSCN in CH_2Cl_2. The heterocycles substituted with ($OSiPh_3$) or Ph have been obtained from those with Cl_2 or Cl substitution by reaction with Ph_3SiONa in toluene or with PhLi in *n*-hexane.

Molecular structures

Five structure determinations have been carried out in this paper; the data for the compound **4** (NMe/Cl) were taken from Ref. [6a]. Bond distances at antimony and axial and equatorial bond angles are given in Table 1. The cores of all six molecular structures are similar. Figures 1 and 2 show exemplarily plots of the compounds **4** (NMe/NCS) and **4** (NBu^i/I).

In order to get an idea about the goodness of the ψ-trigonal bipyramidal geometry around antimony, angle differences have been included in Table 1. Distances between atoms of different kinds were transformed into Pauling bond orders BO [8] in order to obtain comparability. All six structures have similar conformations, and no short intermolecular contacts disturb the distances given in Table 1.

Spectroscopic data

Table 2 contains the ^{13}C NMR chemical shifts of the α-CH_2 groups in equatorial position at Ge, Sn [6b], As [6a], Sb, or Bi [6a] for all compounds of Scheme 1. In addition, the ^{29}Si NMR chemical shifts of the $OSiPh_3$ groups are given. A full set of the ^{13}C NMR chemical shifts of the compounds **1** and **4** has been deposited with the Editor as supplementary material.

Table 3 contains the ^{121}Sb and ^{127}I Mössbauer parameters of the compounds **4**. Figure 3 gives exemplarily the ^{121}Sb Mössbauer spectra of the compounds **4** (NMe/Cl,Br,I). The asymmetric shape of the

Table 1. Distances *d* and Pauling bond orders BO[a], axial and equatorial bond angles θ(ax) and θ(eq)[b] and difference of the angles $\Delta\theta$[c] for the heterocycles **4**[d] (e.s.d.s in parentheses)

Compound	Sb···N d(Å)	Sb···N BO	Sb—R(ax) d(Å)	Sb—R(ax) BO	θ(ax) (°)	θ(eq) (°)	$\Delta\theta$ (°)
4 (NMe/Cl)[e]	2.379(4)	0.446(6)	2.641(1)	0.457(2)	88.8(1),90.4(1)	100.3(2)	10.7
4 (NMe/I)	2.349(4)	0.494(9)	2.995(1)	0.423(2)	86.0(1),90.6(2)	101.8(2)	13.5
4 (NMe/NCS)[f]	2.324(14)	0.53(2)	2.25(2)	0.68(7)	85.7(6),85.7(6)	102.0(8)	16.3
4 (NBz/Cl)	2.405(5)	0.412(8)	2.616(2)	0.496(4)	89.3(2),93.5(2)	98.4(2)	7.0
4 (NBz/I)	2.391(7)	0.43(1)	2.982(1)	0.441(2)	87.8(3),91.3(2)	99.1(4)	9.6
4 (NBu^i/I)	2.420(5)	0.393(9)	2.994(1)	0.424(1)	88.3(2),89.6(2)	101.2(3)	12.3

[a]See Ref. [8].

[b]2 angles θ(ax): R(ax)—Sb—CH_2; 1 angle θ(eq): CH_2—Sb—CH_2.

[c]$\Delta\theta = \theta(\text{eq}) - (\Sigma\theta(\text{ax}))/2$; $\Delta\theta = 0°$ for a perfect ψ-tetrahedron; $\Delta\theta = 30°$ for a perfect ψ-trigonal bipyramid; cf the related $\Sigma\theta$ as a parameter for the goodness of a trigonal bipyramid [2a,b].

[d]Distance d(Sb—C) = 2.14–2.23 Å; conformations of the eight-membered rings: 5 × boat-chair, 1 × chair-chair (compound **4** (NMe/NCS)); no intermolecular distances shorter than 4.5 Å.

[e]See Ref. [6a].

[f]A disorder in the eight-membered ring and at the nitrogen atom of NCS (see Experimental) results in large e.s.d.s.

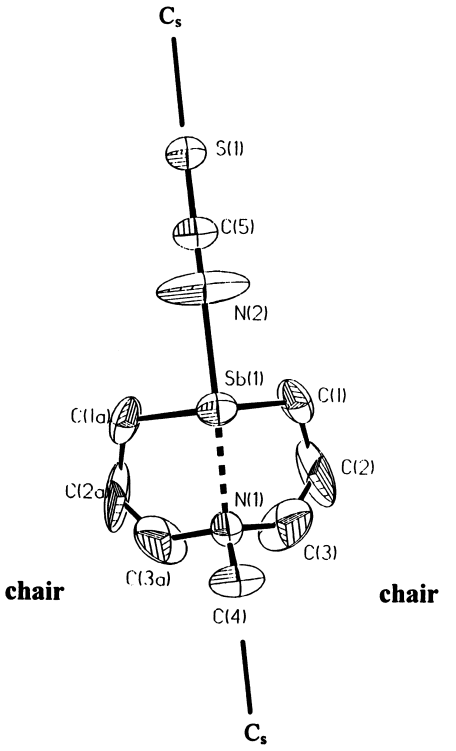

Fig. 1. Ortep plot of the compound **4** (NMe/NCS); thermal ellipsoids are at the 40% probability level. Partial disorder at C(2) and at N(2) (see Experimental). Hydrogen atoms are omitted for better clarity. The perfect C_s plane is outlined.

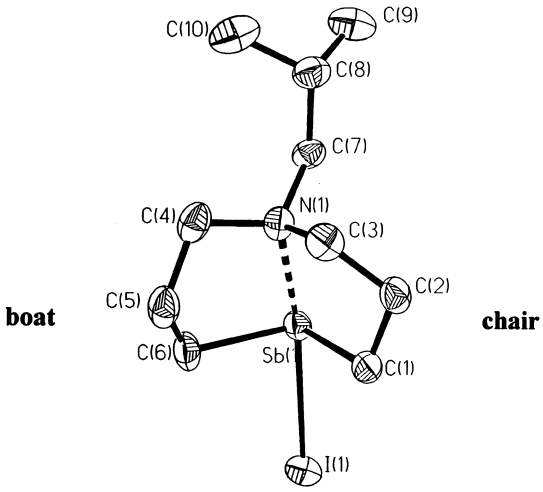

Fig. 2. Ortep plot of the compound **4** (NBu^i/I); thermal ellipsoids are at the 40% probability level. Hydrogen atoms are omitted for better clarity.

absorption peaks shows that the sign of the quadrupole coupling constant (e^2qQ) is obviously negative [12b].

Extended Hückel calculations

To support the bonding scheme of hypervalency which had been introduced in Ref. [2], semi-empirical MO calculations on the Extended Hückel level have been performed for the six compounds **4** whose geometry is known from the crystal structure analyses [13a,14]. Figure 4 shows in graphical form the energetical sequence of the MO's for the compound **4** (NMe/Cl) and the distribution of three filled and one empty orbital over the atoms of the molecule. Table 4 summarizes some typical results and contains also results for the compounds **1** (NBu^i/Cl_2) and **2** (NBu^i/

Table 2. ^{13}C NMR chemical shifts of the α-CH_2 group at Ge, Sn, As, Sb or Bi and ^{29}Si NMR chemical shifts of the —$OSiPh_3$ ligand (ambient temperature, $CDCl_3$ solution)

Compound	$\delta(^{13}C)$ (ppm)	Compound	$\delta(^{13}C)$ (ppm)
1 (NMe/Cl_2)	28.2	**2** (NBz/($OSiPh_3$)Ph)[e]	11.6
1 (NBz/Cl_2)	28.0	**3** (NMe/Cl)	34.6
1 (NBu^i/Cl_2)	22.4	**4** (NMe/Cl)	25.9
1 (NMe/ClPh)	11.1	**4** (NBz/Cl)	26.0
1 (NBz/ClPh)	11.0	**4** (NBu^i/Cl)	26.1
1 (NMe/($OSiPh_3$)$_2$)	14.0	**4** (NMe/Br)	25.4
1 (O/Cl_2)	31.9	**4** (NMe/I)	23.6
1 (S/Cl_2)	34.7	**4** (NBz/I)	22.4
2 (NMe/Cl_2)	22.3	**4** (NBu^i/I)	23.3
2 (NBz/Cl_2)	22.2	**4** (NMe/NCS)[a]	23.0
2 (NBu^i/Cl_2)	22.0	**4** (NBz/NCS)[a]	23.8
2 (NMe/ClPh)	14.5	**4** (NBu^i/NCS)[a]	24.6
2 (NBz/ClPh)	14.0	**4** (NMe/$OSiPh_3$)	25.0
2 (NBu^i/ClPh)	13.8	**4** (NBz/$OSiPh_3$)	24.4
2 (NMe/($OSiPh_3$)$_2$)	16.9	**4** (NBu^i/$OSiPh_3$)	24.2
2 (NBz/($OSiPh_3$)$_2$)	16.9	**4** (NBz/Ph)	14.8
2 (NBu^i/($OSiPh_3$)$_2$)	16.6	**4** (NBu^i/Ph)	14.8
2 (NMe/Ph_2)	8.7	**4** (S/Cl)	26.7
2 (NBz/Ph_2)	8.3	**5** (NMe/Cl)	46.6
2 (NBu^i/Ph_2)	8.1	**5** (NBz/Cl)	47.2
2 (NMe/($OSiPh_3$)Ph)[e]	12.1	**5** (NMe/I)	40.9
		5 (NBz/I)[f]	39.6

Compound	$\delta(^{29}Si)$[b](ppm)	Compound	$\delta(^{29}Si)$[b](ppm)
1 (NMe/($OSiPh_3$)$_2$)	−21.79[c]	**2** (O/($OSiPh_3$)$_2$)	−21.80[d]
2 (NMe/($OSiPh_3$)$_2$)	ax −24.61	**2** (NMe/($OSiPh_3$)Ph)[e]	−26.24
	eq −19.66	**2** (NBz/($OSiPh_3$)Ph)[e]	−25.98
2 (NBz/($OSiPh_3$)$_2$)	ax −24.29	**4** (NMe/($OSiPh_3$))	−24.40
	eq −19.51	**4** (NBz/($OSiPh_3$))	−23.78
2 (NBu^i/($OSiPh_3$)$_2$)	ax −24.59	**4** (NBu^i/($OSiPh_3$))	−24.21
	eq −19.42		

[a] $\delta(^{13}C)$ for NCS: **4** (NMe/NCS) 134.7, **4** (NBz/NCS) 133.1, **4** (NBu^i/NCS) 136.8 ppm. [b] $\delta(^{29}Si)$ for the compound $O(SiPh_3)_2$ −18.45 ppm. [c] One sharp signal. [d] One broad signal. [e] See Ref. [10]. [f] See Ref. [11].

Cl_2) [6c] with Ge and Sn as central atoms [13a,14]. In addition, Table 4 gives the results for the four hypothetical molecules $Cl_2Ge/SnBu^n{}_2$ and ClAs/$SbBu^n_2$, for which a perfect tetrahedral/ψ-tetrahedral geometry had been optimized by means of a force-field calculation prior to the Extended Hückel calculation [13b,14].

Cyclic voltammetry in CH_2Cl_2 *solution*

To get an experimental support of the calculated HOMO (lone pair σ) and LUMO (3-center $^3\sigma^*$) of Fig. 4, cyclic voltammetric experiments with nine from the sixteen available Sb compounds **4** have been performed [15]. After considerable optimization the proper conditions for reproducible results in both initial sweep directions (oxidative electron transfer from the HOMO into the reference electrode and reductive electron transfer from the reference electrode into the LUMO) were found. The results are summarized in Table 5, and two examples of the cyclic voltammograms obtained are shown in Fig. 5.

With regard to the initial anodic sweep direction, all nine investigated Sb compounds show an oxidative peak E_{ox} between +0.55 and +1.25 V. The peaks are generally small and broad. After inversion of the applied potential at +1.5 V, a decomposition of the compounds occurs in most cases. Only for **4** (NBz/I) (Fig. 5a) and for **4** (NBu^i/I) a quasi-reversible reduction peak E_{red} was found.

With regard to the initial cathodic sweep direction, three of the investigated Sb compounds (**4** (NBu^i/Cl), **4** (NBz/I) (borderline case, see footnote *d* of Table 5) and **4** (NMe/$OSiPh_3$)) decompose immediately under the influence of the reductive potential. The six other investigated compounds result in reversible cyclic voltammograms with $E_{red} - E_{ox}$ between 0.10 and 0.14

Table 3. ^{121}Sb and ^{127}I Mössbauer data (isomer shifts δ^a (mm s^{-1}), quadrupole coupling constants e^2qQ (mm s^{-1}), asymmetry parameters η, and half widths Γ (mm s^{-1}), and for ^{127}I outer electron configurations (electrons) and charges Z(I) (electrons) from a Townes-Dailey treatment[b]

	^{121}Sb			
Compound	δ^a	e^2qQ	η	Γ
4 (NMe/Cl)	−2.75	−28.2	0.65	2.59
4 (NBz/Cl)	−2.40	−28.4	0.66	2.53
4 (NBu^i/Cl)[c]	−2.27	−31.0	0.25	2.46
4 (NMe/Br)	−2.45	−28.6	0.57	2.51
4 (NMe/I)	−2.38	−26.9	0.74	2.61
4 (NBz/I)	−2.49	−27.8	0.66	2.65
4 (NBu^i/I)	−2.45	−29.9	0.47	2.85
4 (NMe/NCS)	−2.24	−30.7	0.66	2.45
4 (NBz/NCS)	−2.31	−31.1	0.57	2.41
4 (NBu^i/NCS)	−2.22	−31.6	0.58	2.33
4 (S/Cl)	−2.85	−27.6	0.64	2.59
	^{127}I[d]			
Compound	δ^a	e^2qQ[e]	Γ	Z(I)
4 (NMe/I)	−0.13	−12.1	2.86	−0.76
$5s/5p_x/5p_y/5p_z$			2.00/2.00/2.00/1.76	
4 (NBz/I)	−0.07	−12.8	2.64	−0.72
$5s/5p_x/5p_y/5p_z$			1.98/2.00/2.00/1.74	
4 (NBu^i/I)	−0.13	−12.5	2.59	−0.75
$5s/5p_x/5p_y/5p_z$			2.00/2.00/2.00/1.75	

[a]Relative to InSb and KI, both at 20K. [b]See Ref. [12a]. [c]Poor fit of the spectrum; the spectrum for a synthetically different batch was not better. [d]η fixed to 0.0. [e]1 mm s^{-1} corresponds to 46.46 MHz.

V (Fig. 5b). The voltammograms are comparable to those of the used standard ferrocene ($E_{red} - E_{ox} = 0.13$ V). The solution diffusion control of the process was established by measuring the peak currents for both reduction (i_c) and oxidation (i_a) for **4** (NMe/I) and **4** (NMe/NCS) and plotting i_c and i_a against the square root of the scan rate over three decades of speed (10–1000 mV s^{-1}) and using ferrocene as a standard [15a].

Bulk electrolysis in CH_2Cl_2 *solution*

To ascertain the number of electrons involved in the reversible redox process, controlled potential electrolysis (coulometry) [16b] was performed for the compound **4** (NMe/I). The results are given in Table 6. After extensive optimization of the experimental conditions (applied potential, cooling) it was concluded definitely that the process is a one-electron-transfer.

DISCUSSION

Investigation in the solid

The X-ray data of Table 1 demonstrate the order (1) for the intramolecular nucleophilic attack of the donor R′N at the σ-Lewis acidic Sb on a path to a four-electron three-center interaction R′N···Sb—R(ax).

$$d(\text{R′N}\cdots\text{SbCl}) > d(\text{R′N}\cdots\text{SbI}) > d(\text{R′N}\cdots\text{SbNCS}) \quad (1)$$

Geometrically, a continuous change from a ψ-tetrahedral three-coordination to a ψ-trigonal-bipyramidal four-coordination occurs. The order (1) is not governed by the electronegativity of the ligands R (influence of the HOMO). An enhanced $n \rightarrow \sigma^*$ or $\pi \rightarrow \sigma^*$ charge transfer from R(ax) into the LUMO of the π-acidic Sb promotes the path [2]. With regard to the HOMOs, the negative sign of the ^{121}Sb coupling constant e^2qQ (Table 3) suggests a larger population of

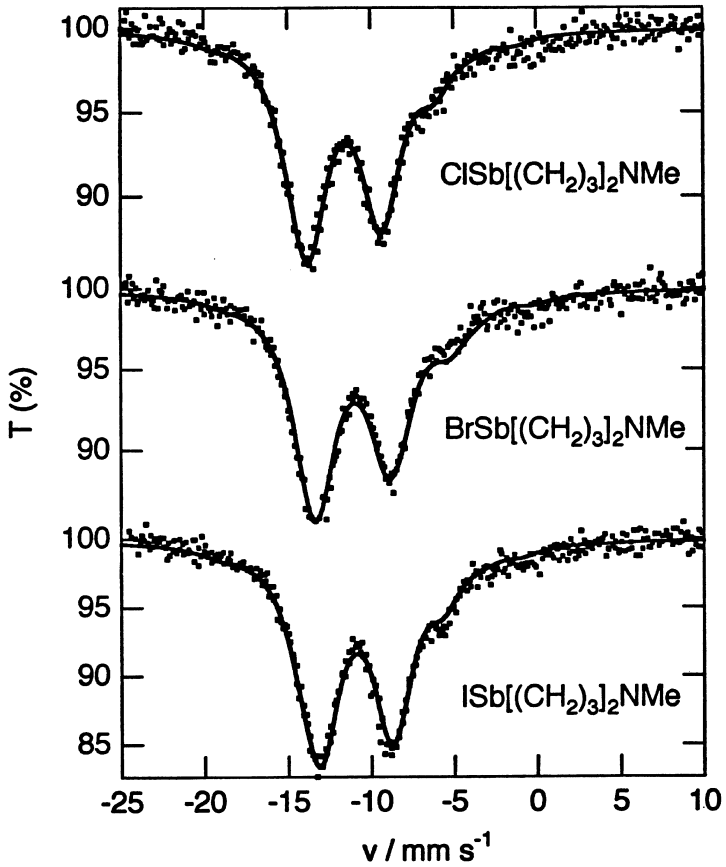

Fig. 3. ^{121}Sb Mössbauer spectra of the three compounds **4** (NMe/Cl,Br,I) at 20 K.

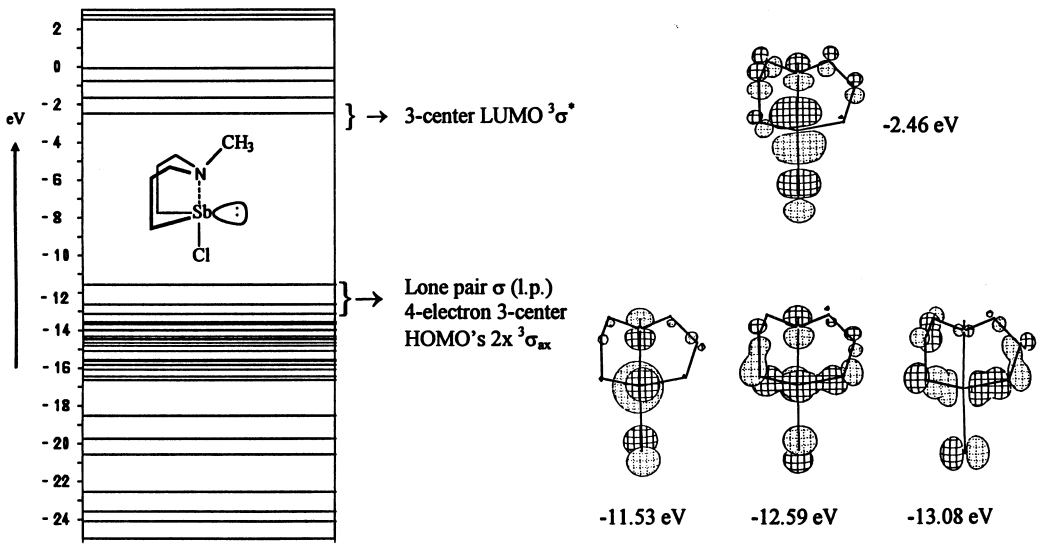

Fig. 4. Sequence of the Mo's for compound **4** (NMe/Cl) and CACAO-graphs [13a,14].

Table 4. LUMO and HOMO energies of **1, 2,** and **4** (geometry of the crystal structure determinations)[a] and for the compounds $Cl_2MBu^n_2$ (M = Ge, Sn) and $ClMBu^n_2$ (M = As, Sb) (tetrahedral/ψ-tetrahedral geometry)[b]

Compound	LUMO (eV)	HOMOs (eV) isolated				HOMOs (eV) at lower energy
1 (NBu^i/Cl_2)[c]	−0.856	−12.003	−12.369			< −13.1
2 (NBu^i/Cl_2)[c]	−0.855	−12.110	−12.261			< −13.0
4 (NMe/Cl)	−2.459	−11.528	−12.586	−13.082		< −13.5
4 (NMe/I)	−4.508	−11.544	−12.377	−12.582	−12.964	< −13.3
4 (NMe/NCS)	−2.339[d]	−11.556	−12.233	−12.610		< −13.2
4 (NBz/Cl)	−4.439[d]	−11.389	−12.295	−12.694	−12.789	< −13.0
4 (NBz/I)	−4.597[d]	−11.475	−12.219	−12.567		< −12.6
4 (NBu^i/I)	−4.869	−11.561	−12.227	−12.574	−12.848	< −13.2
$Cl_2GeBu^n_2$	0.530	−12.060				
$Cl_2SnBu^n_2$	0.562	−12.090				
$ClAsBu^n_2$	−0.291	−11.576				
$ClSbBu^n_2$	−1.370	−11.436				

[a] See Ref. [13 a, 14]. [b] See Ref. [13b, 14]. [c] See Ref. [6c]. [d] Coefficients at Sb; additional LUMOs at NCS (−6.50 and −6.54 eV: π^* (NCS)) and at benzyl (−8.07 and −8.20, −8.14 and −8.14 eV: π^* (phenyl)).

Table 5. Cyclic voltammetric peak potentials E_{ox} and E_{red}, ΔE and current ratios i_a/i_c vs. a Ag/AgCl reference electrode[a] in CH_2Cl_2 solution for the compounds **4** (3–8 mg/5 ml CH_2Cl_2) and for ferrocene as a controlling standard

Compound	E_{ox} (V)	E_{red} (V)	E_{ox} (V)	ΔE (V)	i_a/i_c
initial oxidative sweep direction[b]					
ferrocene	0.40	0.27		0.13	0.92
4 (NBz/I)	0.58	0.36		0.22	1.19
4 (NBu^i/I)	0.55	0.36		0.19	0.83
initial reductive sweep direction[c]					
4 (NMe/Cl)		−1.21	−1.11	0.10	0.89
4 (NMe/I)		−1.13	−1.03	0.10	0.98
4 (NBz/I)[d]		(−1.21	−1.00	0.21	1.18)
4 (NBu^i/I)		−1.11	−0.98	0.13	1.14
4 (NMe/NCS)		−1.17	−1.05	0.12	0.88
4 (NBz/NCS)		−1.09	−0.95	0.14	0.98
4 (NBu^i/NCS)		−1.14	−1.00	0.14	1.06

[a] Counter electrode Pt; scan rate 100 mV s^{-1}; evaluation of the voltammograms according to Ref. [16a].
[b] Working electrode Pt; sweep range 0.0 to +1.5 to −1.5 to 0.0 V.
[c] Working electrode Au/Hg; sweep range −0.2 to −1.7 (or −2.0) to −0.2 V.
[d] Scan rate 300 mV s^{-1}, at lower scan rates immediate decomposition; result not fully reproducible.

the antimony 5p electrons in the equatorial plane (6 electrons) compared to those in the axial direction (< 4 electrons).

With regard to the donor group R′N, Table 1 demonstrates the order (2) of increasing interaction, i.e. increasing σ-donor strength.

$$d(Bu^iN\cdots SbI) > d(BzN\cdots SbI) > d(MeN\cdots SbI) \quad (2)$$

The absolute value e^2qQ of ^{121}Sb (Table 3) decreases for all three investigated ligands, Cl, I and NCS, identically to order (2). This decrease suggests a simultaneous increase in the electron density of the axial three-center interaction R′N···Sb—R(ax).

In Fig. 6 the bond orders of the ligands at antimony BO(Sb—R(ax)) are plotted versus BO(Sb···N) for the five halide substituted cases. The familiar structural trans influence (shorter N···Sb and longer Sb—R(ax)) is valid for pairs of identical donor groups (NBz and NMe). It inverts or becomes zero at an interchange of the donor groups (NBu^i into NBz, NBz into NMe; compounds **4** (NBu^i/I) → **4** (NBz/I): d(Sb···N) 2.420 (5) → 2.391 (7) Å and d(Sb-I) 2.994 (1) → 2.982 (1) Å; for similar results in three series of tin compounds and in one series of silicon compounds

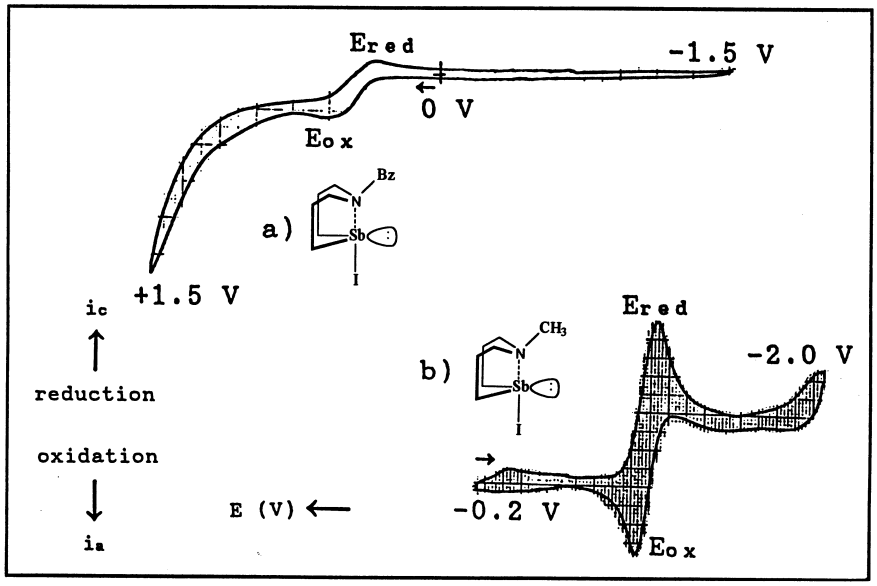

Fig. 5. Cyclic voltammograms of the compound **4** (NBz/I) a) (oxidative sweep direction, Pt electrode) and **4** (NMe/I) b) (reductive sweep direction, Au/Hg electrode).

Table 6. Controlled potential electrolysis of **4** (NMe/I) (30–40 mg/60 ml CH_2Cl_2) at $-10°C$

Reductive potential[a] (mV)	No. of electrons	Reductive potential[a] (mV)	No. of electrons
−1260	0.44	−1340	b
−1270	0.87	−1370	b
−1280	0.72	−1500	b,c
−1290	0.73	−1700	b,c
−1320	1.00		

[a] Ag/AgCl reference electrode different from that used in Table 5: CV peaks (scan rate 100 mV s^{-1}) for ferrocene E_{ox}/E_{red} +368/+190 mV, for **4**(NMe/I) E_{red}/E_{ox} −1309/−1122 mV.

[b] Decomposition into colorless, insoluble Sb(III) material; without cooling, elementary antimony precipitates.

[c] Amalgamation of the precipitated elementary antimony with the mercury pool cathode.

see Ref. [2d]). This behaviour supports the assumption of a charge flow from the ligands into the LUMO at Sb.

With regard to the charges on ^{127}I (Townes-Dailey treatment [12a] in Table 3), the order (3) mirrors the structural finding (4). Compounds with a longer Sb-I distance own a more negative charge on the iodine atom, i.e. the Sb-I bond seems to be more ionic.

$$|Z(I)|(MeN\cdots SbI) \geqslant |Z(I)|(Bu^tN\cdots SbI) > |Z(I)|(BzN\cdots SbI) \quad (3)$$

$$d(Sb—I)\,2.995(1) \geqslant d(Sb—I)\,2.994(1) > d(Sb—I)\,2.982(1)Å \quad (4)$$

HOMO and LUMO by cyclic voltammetry and coulometry

The oxidation of the compounds **4** at a positive potential is followed in most cases by decomposition. The two cases of quasi-reversible oxidation/reduction suggest that no full oxidation of Sb(III) to Sb(V)

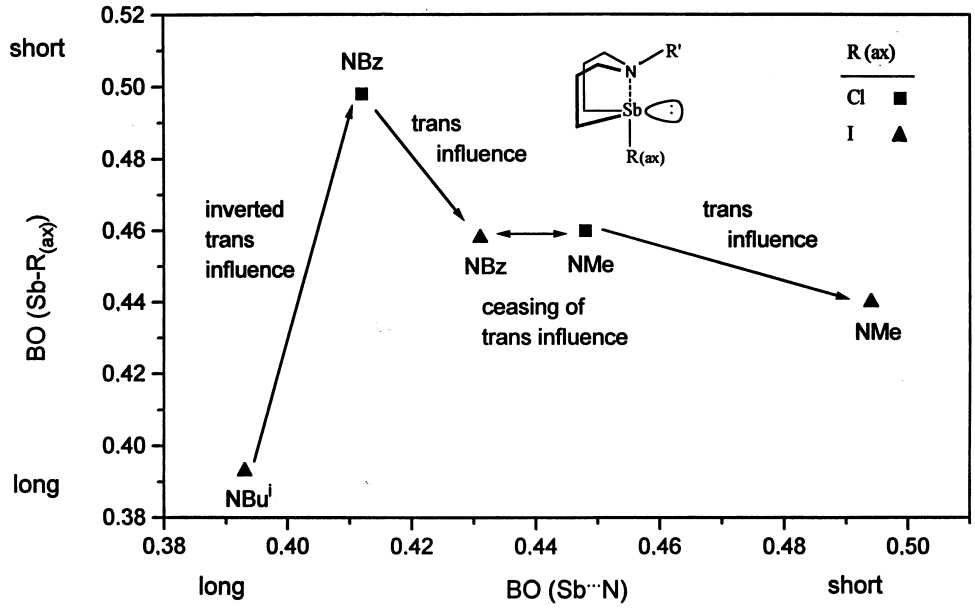

Fig. 6. Related *trans* bond orders of the four-electron three-center interaction N · · · Sb-Hal.

occurs. The signals are broad ; for a two-electron process narrow signals should be expected [15b].

The reversibility of the redox potentials E_{red} and E_{ox} in the reductive mode, the proof of a diffusion controlled molecular process in solution and the proof of a one-electron reduction for **4** (NMe/I) support experimentally the likelihood of a charge flow from the ligands into the LUMO mostly associated with the central Sb atom. The similarity of all CVs and their peak voltage positions indicate that for all these Sb compounds a transfer of one electron into an equivalent molecular orbital eventuates. Because of the extended time frame of the bulk electrolysis compared to the cyclic voltammetry in the former, restricted experimental conditions are involved while in the latter no such decomposition occurred due to the brevity of the experiment.

In view of the qualitative nature of the kinetically controlled method cyclic voltammetry [17], and with regard to the approximations of the Extended Hückel method, no direct numerical comparison of the potentials of Table 5 (units V) to the calculated LUMO energies of Table 4 (units eV) can be made.

^{13}C NMR *chemical shifts in* $CDCl_3$ *solution*

Figure 7 summarizes the chemical shifts of the α-methylene groups in the rings of Scheme 1. The overall sequences of the ^{13}C deshielding ($CH_2Ge \geqslant CH_2Sn$ and $CH_2Bi > CH_2As > CH_2Sb$) suggest sequences of electronegativity of the central atoms ($EN(Ge) \geqslant EN(Sn)$ and $EN(Bi) > EN(As) > EN(Sb)$), respectively (for a detailed discussion of this aspect see Ref. [6a]). For each element individually, the ligand Ph induces a distinct up-field shift. The special kind of donor group NR′ has no influence on $\delta(^{13}C)$.

For the three Sb—NCS compounds $\delta(^{13}C)$ is slightly deshielded (= 135 ppm) in comparison to Me—NCS (= 128.5 ppm [18]). This deshielding is in accordance with the assumed charge-giving power of the isothiocyanate ligand into the LUMO at Sb. On the other hand, the bonding isomerism Sb—NCS (compound **4** (NMe/NCS), is confirmed also for the two other compounds ($\delta(^{13}C$(Et—SCN) 112 ppm [18]).

^{29}Si NMR *chemical shifts in* $CDCl_3$ *solution*

The values of $\delta(^{29}Si)$ for the (—$OSiPh_3$) ligand in the compounds **1, 2, 4** and in the tetrahedral analogue $Ph_3SiOSiPh_3$ are sterically determined : −18.5, −19.5 and −(24 to 26) ppm for the ligand in tetrahedral, equatorial and axial trigonal bipyramidal position, respectively. In two cases, the (—$OSiPh_3$) ligands exchange at room temperature on the NMR time scale. With regard to axial (—$OSiPh_3$) bound to Sn or Sb, no difference in $\delta(^{29}Si)$ exists.

EXPERIMENTAL

General considerations

The starting ligands $R'N[(CH_2)_3Cl]_2$ and the related diGrignard reagents were prepared as described previously [6a]. Grignard iniators were CCl_4 for the chlorine substituted compounds and I_2 for the iodine

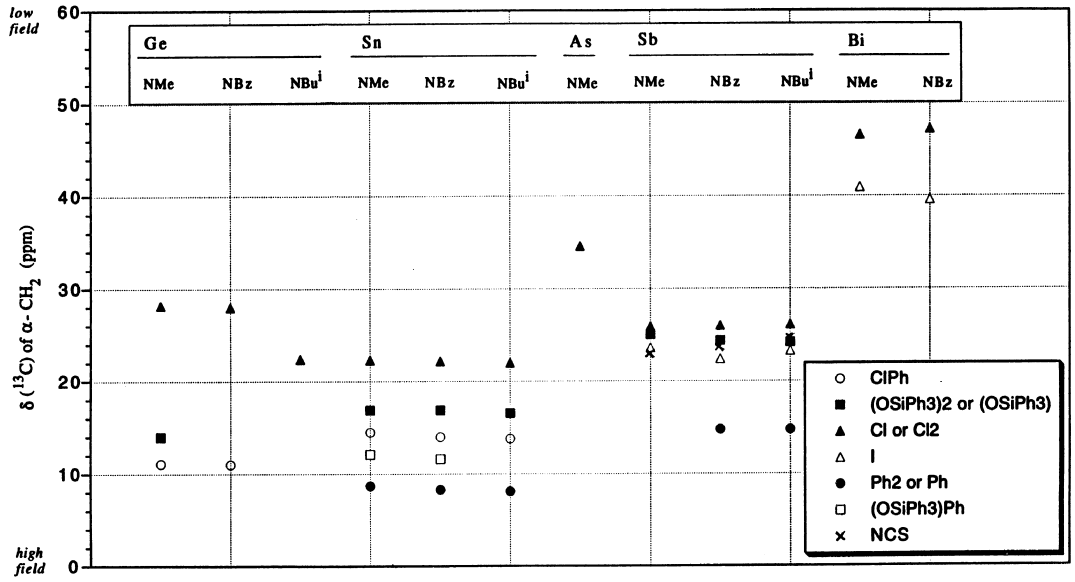

Fig. 7. Sequence of $\delta(^{13}C)$ for the equatorial α-methylene groups in the rings **1** to **5** in $CDCl_3$ solution.

substituted ones. The reagent AgSCN was precipitated from an aqueous solution of KSCN with $AgNO_3$, washed with cold acetone and dried *in vacuo*. The reagent Ph_3SiONa was obtained by reaction of Ph_3SiOH with sodium in toluene. Melting points were determined in glass capillaries in a Kofler block. Elemental analyses were carried out by the Microanalytical Laboratory of the Institut für Organische Chemie, Universität Mainz. NMR spectra were recorded on a Bruker WP-80/DS spectrometer (^{13}C/20.15, ^{29}Si/15.92 MHz; solvent $CDCl_3$; ambient temperature; external standard $SiMe_4$). Mass spectra were recorded using a Finnigan 8230 spectrometer.

Preparations of **1** *and* **4**

The syntheses of the Cl substituted compounds were carried out as described previously [6a]. Detailed procedures follow for the compounds **4** (NMe/I) and **4** (NBz/NSC). Under the exclusion of light and air and under vigorous stirring, 0.08 mol of the diGrignard reagent $MeN[(CH_2)_3MgCl]_2$ in 150 ml THF and 0.08 mol SbI_3 as a solid were added simultaneously into 1.5 l toluene (three-necked 2 l flask) over a period of 1.5 h. Stirring was continued at room temperature for 24 h. The dark-reddish reaction mixture was filtered twice to remove MgI_2. The solvent was removed under vacuum and moderate temperature, and the crude product was recrystallized from ethanol. A colorless solid was obtained. A suspension of 0.005 mol of freshly prepared and dried AgSCN and 0.005 mol **4** (NBz/I) were stirred in 150 ml CH_2Cl_2 for 24 h at room temperature. The reaction mixture was filtered off and the solvent removed under vacuum. The resulting crude product was recrystallized from ethanol to obtain a colorless solid. Table 7 summarizes the yields and the analytical data for the 19 synthesized compounds. For some of the Ge compounds **1** the analytical data are not satisfying. All these compounds **1** were obtained in low yields and the separation from oligomeric by-products was difficult. Repeated chromatographic purifications resulted in no better analytical data. Nevertheless, the identities of the compounds are not in doubt. The compound **1** (O/Cl_2) was not obtained in a pure state at all.

Mössbauer spectroscopy

^{121}Sb Mössbauer spectra were measured with an Austin Science S-600 Mössbauer spectrometer using a $Ca^{121m}SnO_3$ source (16 MBq) and a pure germanium detector [19a]. ^{127}I Mössbauer spectra were recorded in the same way as described previously by using a $Mg_3{}^{127m}TeO_6$ source instead of a $Zn^{127m}Te$ source [19b]. The Mössbauer source (1.6 GBq) was prepared by a high flux neutron irradiation of $Mg_3{}^{126}TeO_6$ (193 mg) at a reactor core of JRR-3M of the Japan Atomic Energy Research Institute. Both the corresponding sources and the samples [(15 mg Sb)/cm^2 or (30 mg I)/cm^2 were kept at 20 K in a cryostat incorporating a closed-cycle refrigerator [19c]. The Doppler velocity was measured with an Austin Science LC-9 laser interferometer and calibrated by measuring the ^{57}Fe Mössbauer spectrum of an iron foil at 20 K using a $^{57}Co(Rh)$ source. The spectra were fitted to twelve-line quadrupole-split lines by using a transmission integral method [19d].

Table 7. Preparation and analytical data for **1**[a] and **4**[a]

Compound	Method yield (%)	Formula M_r	mp (°C) M/e[b] (%)	Anal. found (calcd) %C	%H	%N	%Hal
1 (NMe/Cl_2)	diGrignard	$C_7H_{15}Cl_2NGe$	110	33.22	5.94	5.44	—
	15	256.72	257[c] (100)	(32.72)	(5.84)	(5.45)	(27.66)
1 (NBz/Cl_2)	diGrignard	$C_{13}H_{19}Cl_2NGe$	188	47.35	5.86	4.22	—
	10	332.82	331 (8)	(46.87)	(5.71)	(4.21)	(21.33)
1 (NBu^i/Cl_2)	diGrignard	$C_{10}H_{21}Cl_2NGe$	114	39.02	6.84	4.63	—
	3	298.79	299 (7)	(40.13)	(7.02)	(4.68)	(23.75)
1 (S/Cl_2)	diGrignard	$C_6H_{12}Cl_2SGe$	134	26.34	4.33		—
	12	259.74	260 (3)	(27.72)	(4.62)		(27.34)
1 (NMe/ClPh)	diGrignard	$C_{13}H_{20}ClNGe$	105	50.84	6.54	4.33	—
	14	298.37	299 (8)	(52.28)	(6.70)	(4.69)	(11.90)
1 (NBz/ClPh)	diGrignard	$C_{19}H_{25}ClNGe$	181	58.94	6.52	3.63	—
	12	375.48	341[d] (3)	(60.72)	(6.66)	(3.72)	(9.45)
1 (NMe/$OSiPh_3)_2$)	Ph_3SiONa	$C_{43}H_{45}NOSi_2Ge$	149	70.92	6.30	1.64	
	24	719.77	463[e] (24)	(71.68)	(6.25)	(1.94)	
4 (NMe/I)	diGrignard	$C_7H_{15}INSb$	207	23.40	4.38	3.85	33.34[i]
	31	361.86	234[f] (100)	(23.23)	(4.18)	(3.87)	(35.07)
4 (NBz/I)	diGrignard	$C_{13}H_{19}INSb$	224	35.91	4.30	3.16	28.11[i]
	35	437.96	310[f] (100)	(35.65)	(4.37)	(3.20)	(28.98)
4 (NBu^i/I)	diGrignard	$C_{10}H_{21}INSb$	138	29.80	5.43	3.42	31.02[j]
	23	403.94	404 (0.5)	(29.73)	(5.42)	(3.47)	(31.42)
4 (NMe/$OSiPh_3$)	Ph_3SiONa	$C_{25}H_{30}NOSiSb$	192	56.63	6.23	2.81	
	56	510.35	509 (95)	(58.84)	(5.92)	(2.74)	
4 (NBz/$OSiPh_3$)	Ph_3SiONa	$C_{31}H_{34}NOSiSb$	97	63.98	5.96	2.27	5.00[h]
	59	586.45	585[g] (100)	(63.49)	(5.84)	(2.39)	(4.79)
4 (NBu^i/$OSiPh_3$)	Ph_3SiONa	$C_{28}H_{36}NOSiSb$	101	60.42	6.37	2.43	
	28	552.44	553[g] (100)	(60.88)	(6.57)	(2.54)	
4 (NMe/NCS)	AgSCN	$C_8H_{15}N_2SSb$	200	32.75	5.19	9.52	
	82	293.03	292 (2)	(32.79)	(5.16)	(9.56)	
4 (NBz/NCS)	AgSCN	$C_{14}H_{19}N_2SSb$	154	45.32	5.12	7.49	
	75	369.13	368[g] (2)	(45.55)	(5.19)	(7.59)	
4 (NBu^i/NCS)	AgSCN	$C_{11}H_{21}N_2SSb$	98	38.90	6.65	8.00	
	49	335.11	336[g] (2)	(39.43)	(6.32)	(8.36)	
4 (NBz/Ph)	PhLi	$C_{19}H_{24}NSb$	138	58.60	6.22	3.52	
	75	388.16	388 (100)	(58.79)	(6.23)	(3.61)	
4 (NBu^i/Ph)	PhLi	$C_{16}H_{26}NSb$	oil	54.67	6.93	4.14	
	47	349.10	349 (100)	(55.05)	(6.56)	(4.01)	

[a] Compound **1**(O/Cl_2) could not be obtained in a pure state; for the compounds **4**(NMe/Cl, NBz/Cl, NBu^i/Cl, NMe/Br and S/Cl) see Ref. [6a]. [b] EI mass spectra: M^+. [c] FI mass specrum. [d] M^+—(Cl). [e] M^+—($OSiPh_3$). [f] M^+—(I). [g] FD mass spectrum. [h] Si by X-ray fluorescence analysis. [i] Contaminated by some Cl from the Grignard reagent. [j] Traces of Cl, see X-ray crystallography.

Electrochemistry

The CV measurements of Table 5 were performed with a BAS CV 27 Voltammograph coupled with a Houston Instruments Series 2000 Omnigraph X-Y recorder. The scan rate dependence and the coulometry were done with a BAS 100 B/W electrochemical analyser coupled to a PC.

Conventional disk gold electrodes (2.5 mm diameter) were amalgamated by dipping in triple distilled mercury until a good coating of mercury completely covered the gold surface, and used immediately. To renew the Au surface, the electrode was dipped in nitric acid and washed with water, polished on a cloth pad which was exclusively used for these electrodes and then again washed with water, acetone and finally with dry CH_2Cl_2, and the Hg amalgamating procedure was repeated. Auxiliary electrodes were of 1 mm diameter Pt wire. Reference electrodes were Ag/AgCl filled with CH_2Cl_2 (saturated LiCl) and were separated from the test solution by a fritted salt bridge containing CH_2Cl_2 and the electrolyte. Measurements were made in a conventional three electrode cell, from quiescent solutions blanketed with N_2, which were previously sparged with dry high purity N_2.

The bulk electrolysis was performed in a cylindrical glass cell equipped with a separate fritted anode compartment (Pt basket anode) and a magnetically stirred

Table 8. Summary of crystal data, intensity data collection (Mo radiation, ambient temperature) and refinement for the compounds **4**

	4(NMe/I)	**4**(NMe/NCS)	**4**(NBz/Cl)	**4**(NBz/I)	**4**(NBu^i/I)
Crystal system	monoclinic	orthorhombic	monoclinic	monoclinic	triclinic
Space group	$P2_1/n$ (no 14)	Pnam (no 62)	C_2/c (no 15)	$C2/c$ (no 15)	$P\bar{1}$ (no 2)
a (Å)	7.583 (2)	11.249 (2)	24.137 (5)	25.085 (5)	7.597 (2)
b (Å)	10.755 (2)	13.102 (3)	9.920 (2)	10.181 (2)	8.040 (2)
c (Å)	13.546 (3)	7.788 (2)	11.691 (2)	11.559 (2)	11.940 (2)
β (°)	93.06 (3)		98.88 (3)	98.76 (3)	75.52 (3), 84.06 (3), 78.37 (3)
V (Å^3)	1103 (1)	1148 (1)	2766 (1)	2918 (1)	691 (1)
Z	4	4	8	8	2
F (000)	672	576	1376	1664	384
D_{calcd}	2.179	1.696	1.664	1.994	1.943
D_{exptl} (g cm^{-3})	2.182	1.686	1.621	1.980	1.871
sin Θ_{max}/λ (Å^{-1})	0.5723	0.5000	0.4539	0.6388	0.7035
refl : meas	3521	1949	3118	3780	4297
indep (int R)	3134 (0.017)	1790	2438 (0.030)	3499 (0.025)	4015 (0.017)
no. of variables (ratio rflns/var)	93 (25.2)	66 (14.7)	147 (11.9)	147 (15.9)	120 (24.3)
R	0.0325	0.0802	0.0315	0.0477	0.0570

mercury pool cathode. The solution was continually sparged with N_2 during the coulometric measurement. The electrolysis was stopped if no further current decrease occurred (15 to 5% of the initial current, about 1 h).

The CH_2Cl_2 (anal. gr. BDH) was passed through activity 1 alumina which had been previously preheated to 600°C. The supporting electrolyte, Bu$^n{}_4$NPF$_6$, was stored over P_2O_5 for 48 h prior to usage and solutions of this in CH_2Cl_2 (0.1 M) were made up just prior to the measurements. Ferrocene (Riedel-de Haën) was used as a standard.

X-ray crystallography

Colorless single crystals were obtained from ethanol (**4**(NMe/I, NMe/NCS, NBu^i/I, NBz/Cl)) or from ethanol/toluene 1 : 1 (**4**(NBz/I)). A summary of the crystal data, of the intensity data collections and of the refinements is given in Table 8. The densities were determined by flotation in aqueous polytungstate solution. The quality of the crystals was examined by Laue exposures. Integrated intensities were measured by means of $\omega/2\theta$ scans on an Enraf-Nonius CAD4 diffractometer. The structures were solved by Patterson syntheses and completed by Fourier syntheses (program package SHELXTL). The refinements resulted in good convergences and in even distributions of the variances. Hydrogen atoms were calculated and refined as riding on their carbon atoms. Two atoms of the compound **4** (NMe/NCS) are severely disordered (N(2) and the ring atom C(2)); all attempts to resolve this disorder failed. The space group is unambiguously Pnam (no. 62 : C_s symmetric molecule). Refinements in the space group Pna2$_1$ resulted in a severely distorted molecule and in many correlations. The crystal of **4** (NBu^i/I) contained traces of Cl from the Grignard reagent (residual 4.0 e$^-$/Å^3, D_{calcd}/D_{exptl} 1.94/1.87 g cm^{-3}, the analytical iodine content in Table 7 is low) which crystallographically could not be refined. Details of crystal data and structure determinations, ORTEP views, tables of positional and thermal parameters, bond lengths, bond angles and torsion angles have been deposited with the Editor as supplementary material.

CONCLUSIONS

All experimental data (structure determinations, Mössbauer spectroscopy, electrochemistry, NMR spectroscopy) and the Extended Hückel calculations are in a rough agreement with the assumed bonding scheme of hypervalency: four-electron three-center interaction and its main control by a partial charge transfer from the ligands into the three-center LUMO. In view of the fact that the Extended Hückel method is a very first approximation, a state of the art ab initio calculation is needed for a fully consistent interpretation of the experimental findings. Such calculations are in preparation.

Acknowledgements—We gratefully acknowledge Prof. Alan Bond, Monash University, Melbourne, Australia, for his supporting electrochemical discussions. We are grateful for financial assistance from the Deutsche Forschungsgemeinschaft, Bonn, Germany, from the Fonds der Chemischen Industrie, Frankfurt/Main, Germany, and by Grants-in-Aid for Scientific Research (No. 06453053) from the Min-

istry of Education, Science and Culture of the Japanese Government.

REFERENCES

1. Part 7: Hoffmann, H. M. and Dräger, M., *J. Organomet. Chem.*, 1987, **329,** 51.
2. (a) Kolb, U., Beuter, M. and Dräger, M., *Inorg. Chem.*, 1994, **33,** 4522; (b) Kolb, U., Beuter, M., Gerner, M. and Dräger, M., *Organometallics*, 1994, **13,** 4413; (c) Kolb, U., Dräger, M., Dargatz, M. and Jurkschat, K., *Organometallics*, 1995, **14,** 2827; (d) Beuter, M., Kolb, U., Zickgraf, A., Bräu, E., Bletz, M. and Dräger, M., *Polyhedron*, 1997, **16,** 4005; (e) Zickgraf, A., Beuter, M., Kolb, U., Dräger, M., Tozer, R., Dakternieks, D. and Jurkschat, K., *Inorg. Chim. Acta*, in press.
3. Bürgi, H.-B. and Dunitz, J. D., *Structure Correlation*, eds. VCH, Weinheim, 1994; (b) van Koten, G., Jastrzebski, J. T. B. H., Noltes, J. G., Pontenagel, W. M. G. F., Kroon, J. and Spek, A. L., *J. Am. Chem. Soc.*, 1978, **100,** 5020; (c) Musher, J. I., *Angew. Chem.*, 1969, **81,** 68; *Angew. Chem. Int. Ed. Engl.*, 1969, **8,** 54; (d) Suzuki, M., Son, I.-H., Noyori, R. and Masuda, H., *Organometallics*, 1990, **9,** 3043.
4. Cf an updated view on the long-known model of VSEPR: Gillespie, R. J. and Robinson, E. A., *Angew. Chem.*, 1996, **108,** 539; *Angew. Chem. Int. Ed. Engl.*, 1996, **35,** 477.
5. The compound **2** (NMe/Cl_2) of Scheme 1 has been synthesized as the first compound of this class: Jurkschat, K. and Tzschach, A., *J. Organomet. Chem.*, 1984, **272,** C13. For further analogues and homologues see: (a) M = Sn: Jurkschat, K., Schilling, J., Mügge, C., Tzschach, A., Meunier-Piret, J., van Meerssche, M., Gielen, M. and Willem, R., *Organometallics*, 1988, **7,** 38; (b) M = Si: Jurkschat, K., Mügge, C., Schmidt, J. and Tzschach, A., *J. Organomet. Chem.*, 1985, **287,** C1; (c) M = P: Wilbrandt, D., Jurkschat, K. and Meunier-Piret, J., *Phosphorus, Sulfur, Silicon*, 1991, **61,** 261; cf also: Toto, S. D., Arbuckle, B. W., Bharadwaj, P. K., Takahashi Doi, J. and Musker, W. K., *Phosphorus, Sulfur, Silicon*, 1991, **56,** 27.
6. (a) Five of the Sb compounds **4** and the five As and Bi compounds **3** and **5** of Scheme 1 have been described in a previous paper: Bräu, E., Falke, R., Ellner, A., Beuter, M., Kolb, U. and Dräger, M., *Polyhedron*, 1994, **13,** 365; (b) the data for the fourteen Sn compounds **2** were taken from Ref. [2d]; (c) the crystal structure data for the compounds **1** (NBu^i/Cl_2) and **2** (NBu^i/Cl_2) were taken from Ref. [2d].
7. Much work has also been done previously on the analogous compound series $R_2M/RM[SCH_2CH_2]_2X$. (a) M = Ge: Dräger, M., *Z. Anorg. Allg. Chem.*, 1976, **423,** 53; (b) M = Sn [2a,b]: Tzschach, A. and Jurkschat, K., *Comments Inorg. Chem.*, 1983, **3,** 35; Jung, O.-S., Jeong, J. H. and Sohn, Y. S., *Organometallics*, 1991, **10,** 761; Cea-Olivares, R., Loleli, V., Hernandez-Ortega, S. and Haiduc, I., *Polyhedron*, 1995, **14,** 747;(c) M = Pb: Dräger, M. and Kleiner, N., *Angew. Chem.*, 1980, **92,** 950; *Angew. Chem. Int. Ed. Engl.*, 1980, **19,** 923; (d) M = As: Cea-Olivares, R., Estrada, M. R., Espinosa-Perez, G., Haiduc, I., Garcia, P. G. Y., Lopez-Cardoso, M., Lopez-Vaca, M. and Cotero-Villegas, A.-M., *Main Group Chem.*, 1995, **1,** 159; (e) M = Sb: Cea-Olivares, R., Munoz-Hernandez, M.-A., Hernandez-Ortega, S. and Silvestru, C., *Inorg. Chim. Acta*, 1995, **236,** 31; (f) M = Bi: Agocs, L., Burford, N., Cameron, T. S., Curtis, J. M., Richardson, J. F., Robertson,K. N. and Yhard, G. B., *J. Am. Chem. Soc.*, 1996, **118,** 3225.
8. Pauling bond order $BO = 10^{-[1.41*\ (d\text{-}d(\text{standard}))]}$ [2,9]. Single bond standard distances d(Sb—N/O/Cl/I/C) = 2.13/2.04/2.40/2.74/2.19 Å. Sum of radii without correction for electronegativity: O'Keeffe, M. and Brese, N. E., *J. Am. Chem. Soc.*, 1991, **113,** 3226.
9. Pauling, L., *The Nature of the Chemical Bond*, 3rd edn., Ch. 7, Cornell University Press, Ithaca, NY, 1960.
10. Gerner, M. and Dräger, M., unpublished data.
11. Falke, R. and Dräger, M., unpublished data.
12. (a) Ikezawa, H., Takahashi, M., Takeda, M. and Ito, Y., *Bull. Chem. Soc. Japan*, 1993, **66,** 1959; (b) Stevens, J. G., Trooster, J. M., Meinema, H. A. and Noltes, J. G., *Inorg. Chem.*, 1981, **20,** 801; Takeda, M., Takahashi, M., Yanagida, Y., Kojima, S. and Akiba, K.-Y., *Chem. Soc. Japan, Chem. Lett.*, 1993, 2037.
13. (a) Program CACAO (Computer Aided Composition of Atomic Orbitals): Mealli, C. and Proserpio, D. M., *J. Chem. Educ.*, 1990, **67,** 399; (b) Program HYPERCHEM: Hyperchem. Inc., 419 Philip Street, Waterloo, Ontario, Canada, 1994.
14. Extended Hückel parameters H_{ii} (eV)/exponent: C(2s −21.40/1.625, 2p −11.40/1.625); H(1s −13.60/1.300); As (4s −16.22/2.23, 4p −12.16/1.89); Cl (3s −26.30/2.183, 3p −14.20/1.733); Ge (4s −16.00/2.160, 4p −9.00/1.850); N (2s −26.00/1.950, 2p −13.40/1.950); S (3s −20.0/2.122, 3p −13.3/1.827); Sb (5s −18.80/2.323, 5p −11.70/1.999); Sn (5s −16.16/2.120, 5p −8.32/1.820). Compilation by: Alvarez, S., *Table of Parameters for Extended Hückel Calculations*, Barcelona, 1985.
15. (a) For a recent concise introduction to cyclic voltammetry see: Brett, C. M. A. and Oliveira Brett, A. M., *Electrochemistry*, Ch. 9, Oxford University Press, Oxford, New York, Tokyo, 1993; (b) much cyclic voltammetric work has been done on transition metals: Noel, M. and Vasu, K. I., *Cyclic voltammetry and the frontiers of electrochemistry*, Aspect Publ., London, 1990; (c) for cyclic voltammetry on organic antimony compounds see: Dessy, R. E., Chivers, T. and Kitching, W., *J. Am. Chem. Soc.*, 1966, **88,** 467.
16. (a) Kissinger, P. T. and Heineman, W. R., eds., *Laboratory Techniques in Electroanalytical Chemistry*, Marcel Dekker Inc., New York, Basel, 1984, p. 88; (b) Bard, A. J. and Faulkner, L. R., *Electrochemical Methods*, Ch. 10, Wiley & Sons, New York, 1980.

17. Kissinger, P. T. and Heineman, W. R., *J. Chem. Educ.*, 1983, **60,** 703.
18. Kalinowski, H.-O., Berger. S. and Braun, S., ^{13}C-*NMR-Spektroskopie*, Thieme Verlag, Stuttgart, New York, 1984, p. 228.
19. (a) Takeda, M., *Radioisotopes*, 1985, **34,** 628; Takeda, M., Takahashi, M., Ohyama, R. and Nakai, I., *Hyperfine Int.*, 1986, **28,** 741; (b) Ikezawa, H., Takahashi, M., Takeda, M., Takano, T. and Ito, Y., *Radioisotopes*, 1990, **39,** 212; (c) Takano, T., Ito, Y. and Takeda, M., *Radioisotopes*, 1980, **29,** 29; (d) Shenoy, G. K., Friedt, J. M., Maletta, H. and Ruby, S. L. In *Mössbauer Effect Methodology*, Vol. 9, ed. I. J. Gruverman, C. W. Seidel and D. K. Dieterly, Plenum Press, New York, 1974, p. 277.

Pergamon

PII : S0277–5387(98)00028–X

Polyhedron Vol. 17, No. 16, pp. 2669–2677, 1998
© 1998 Elsevier Science Ltd
All rights reserved. Printed in Great Britain
0277–5387/98 $19.00+0.00

Synthesis, characterization, magnetic and electrochemical studies of homo- and hetero-dinuclear complexes of a macrocyclic ligand with dissimilar compartments

Sasankasekhar Mohanta,[a]* Sujoy Baitalik,[b] Sujit K. Dutta[b] and Bibhutosh Adhikary[c]

[a] Department of Chemistry, University College of Science, 92 A.P.C. Road, Calcutta 700 009, India

[b] Department of Inorganic Chemistry, Indian Association for the Cultivation of Science, Calcutta 700 032, India

[c] Department of Chemistry, Bengal Engineering College (Deemed University), Shibpur, Howrah 711 103, India

(Received 8 October 1997 : accepted 9 January 1998)

Abstract—A series of mononuclear complexes $[M(H_2L)](ClO_4)_2$ (**1**–**6**) [M = Mg^{II}, Cu^{II}, Ni^{II}, Co^{II}, Fe^{II}, Mn^{II}], homo-/hetero-dinuclear complexes $[M_ALM_B](ClO_4)_2$ (**7**–**11**) [$M_A = M_B = Cu^{II}$, Ni^{II}; $M_A = Ni^{II}$, $M_B = Cu^{II}$, Co^{II}; $M_A = Mn^{II}$, $M_B = Cu^{II}$], and a tetranuclear complex $[\{Ni^{II}LFe^{III}(H_2O)\}_2(\mu\text{-}O)](ClO_4)_4$ (**12**) derived from an asymmetric tetraiminodiphenol macrocyclic ligand H_2L have been synthesized and characterized. The dinucleating ligand is formally the condensation product of 2 equiv. of 2,6-diformyl-4-methylphenol and 1 equiv. each of 1,2-diaminoethane and 1,3-diaminopropane. In the complexes $[Ni(H_2L)](ClO_4)_2$ (**3**), $[NiLCu](ClO_4)_2$ (**9**) and $[NiLCo(H_2O)_2](ClO_4)_2$ (**10**), the Ni^{2+} ion is located at the site having the ethylene chain and has a square planar geometry, while the second metal centre in **9** or **10** is either of square planar or pseudo octahedral geometry. The nickel(II) centre continguous to the propylene chain in $[NiLNi(H_2O)_2](ClO_4)_2$ (**8**), however, has octahedral configuration. Variable-temperature magnetic susceptibility data for $[MnLCu(H_2O)](Cl)(ClO_4)$ (**11**) reveal antiferromagnetic spin-exchange interaction ($\mathbf{H} = -2J\ S_1 \cdot S_2$) with $J = -31$ cm^{-1}. The cyclic voltammograms of $[CuLCu](ClO_4)_2 \cdot 2H_2O$ (**7**) and $[NiLNi(H_2O)_2](ClO_4)_2$ (**8**) show the occurrence of two stepwise reduction couples $M^{II}M^{II}/M^{II}M^{I}$ and $M^{II}M^{I}/M^{I}M^{I}$ and the corresponding comproportionation constants are 2.4×10^{12} and 1.7×10^{4}, respectively. The heterodinuclear complexes also undergo stepwise reduction, e.g. $[NiLCu]^{2+}$ with $E^1_{1/2} = -0.25$ V and $E^2_{1/2} = -1.45$ V, and $[NiLCo(H_2O)_2]^{2+}$ with $E^1_{1/2} = -1.10$ V and $E^2_{1/2} = -1.30$ V. In the hetero-tetranuclear complex $[\{Ni^{II}LFe^{III}(H_2O)\}_2(\mu\text{–}O)](ClO_4)_4$ (**12**) the electron transfer reactions take place in three steps at −0.04, −0.40 and −1.20 V. © 1998 Elsevier Science Ltd. All rights reserved

Keywords: macrocylic complexes; phenolate bridged Schiff base; homo- and hetero-dinuclear complexes; dissimilar dicompartmental complexes; magnetochemistry; electrochemistry.

Studies on dinuclear metal complexes of Schiff base type dicompartmental tetraazadiphenol macrocyclic ligands have contributed significantly to the understanding of chemical behaviour of coupled systems [1–15]. Recently [16–20] there has been increasing attention in homo- and hetero-dinuclear complexes with different donor compartments to understand mutual influence of two metal ions upon their physiochemical properties. Metal complexes of dinucleating macrocyclic ligands with dissimilar coordination sites are of special importance because of their unprecedented electronic, magnetic and redox

* Author to whom correspondence should be addressed.

properties. Furthermore, it is possible to control properties of such systems by matching the size of the ligand hole and metal ions. Of particular interest is studying the effect of cavity size of the ligand compartment on redox potential of the complexes and stability of mixed-valence species.

The dinucleating macrocycles derived from 2 : 2 condensation of 2,6-diformyl-4-methyphenol and 1,3-diaminopropane was first studies by Pilkington and Robson [21]. Nag *et al.* [20] and Okawa *et al.* [16] have reported the synthesis of tetraaminodiphenol macrocylic ligands with different lateral chains. Herein, we report the synthesis, spectroscopic, magnetic properties and electrochemistry of homo- and hetero-dinuclear metal complexes having asymmetric compartments derived from a precursor magnesium complex $[Mg(H_2L)](NO_3)_2 \cdot 2H_2O$ (**1**).

EXPERIMENTAL

Materials

All reagents and solvents were purchased from commercial sources and used as such unless stated otherwise. 2,6-diformyl-4-methylphenol was obtained as described in the literature [22].

Preparation of the complexes

All the cobalt(II), iron(II) and manganese(II) complexes were prepared under oxygen-free dry nitrogen. The solvents were thoroughly degassed before use.

$[Mg(H_2L)](NO_3)_2 \cdot 2H_2O$ (**1**). This compound was prepared by slight modification of the method reported earlier [20a]. To a boiling solution of a mixture of $Mg(NO_3)_2 \cdot 6H_2O$ (2.56 g, 10 mmol), $Mg(OAc)_2 \cdot 4H_2O$ (2.14 g, 10 mmol) and 2,6-diformyl-4-methylphenol (3.28 g, 20 mmol) in methanol (150 cm^3) was added a solution (50 cm^3) of 1,2-diaminoethane (0.6 g, 10 mmol) over a period 2 h. After additional reflux for 1 h, a second solution (50 cm^3) of 1,3-diaminopropane (0.74 g, 10 mmol) in methanol was added again over a period of 2 h. The solution was refluxed for a total period of 6 h, which on concentration on a rotary evaporator gave orange-red crystals of the magnesium iminomethyl-diprotonated complex. This was filtered off and air dried. Yield : 5.25 g, 92%.

General procedure for the synthesis of the complexes $[M(H_2L)](ClO_4)_2$ (**2**–**6**) [M = Cu^{II}, Ni^{II}, Co^{II}, Fe^{II} or Mn^{II}].

A solution of complex **1** (0.57 g, 1 mmol) and the metal salt $M(ClO_4)_2 \cdot xH_2O$ (2 mmol) in methanol (30 cm^3) was stirred for 10 min, during which time the compound was separated as microcrystals. This was collected by filtration, washed with methanol and air dried. Yield : 70–80%.

$[CuLCu](ClO_4)_2 \cdot 2H_2O$ (**7**). A suspension of $[Cu(H_2L)](ClO_4)_2$ (**2**) (0.33 g, 0.5 mmol), $Cu(ClO_4)_2 \cdot 6H_2O$ (0.18 g, 0.5 mmol) and Et_3N (0.101 g, 1 mmol) in methanol (30 cm^3) was stirred for ca. 0.5 h when a clear green solution was obtained. The solution was kept at room temperature for overnight period, during which time green crystals deposited. The compound was recrystallized from MeOH–MeCN (1 : 1) mixture ; Yield : 0.34 g, 90%.

$[NiLNi(H_2O)_2](ClO_4)_2$ (**8**). To a solution of $[Ni(H_2L)](ClO_4)_2$ (**3**) (0.32 g, 0.5 mmol) in acetonitrile (50 cm^3) were added $Ni(ClO_4)_2 \cdot 6H_2O$ (0.18 g, 0.5 mmol) and Et_3N (0.101 g, 1 mmol) and refluxed for 0.5 h. The deep red solution was rotary evaporated to ca 20 cm^3, which on cooling (5°C) deposited bright red crystals. These were collected by filtration and recrystallized from MeOH ; Yield : 0.30 g, 82%.

$[NiLCu](ClO_4)_2$ (**9**). To a solution of **3** (0.32 gm, 0.5 mmol) in acetonitrile (50 cm^3) were successively added a solution of $Cu(ClO_4)_2 \cdot 6H_2O$ (0.185 gm 0.5 mmol) in methanol (10 cm^3) and Et_3N (0.101 gm 1 mmol). The solution was stirred at room temperature for 0.5 h and allowed to undergo slow evaporation. The brown crystalline compound that deposited on standing was filtered and washed with cold MeOH ; Yield : 0.24 gm 68%.

$[NiLCo(H_2O)_2](ClO_4)_2$ (**10**). To a boiling solution of **3** (0.32 gm, 0.5 mmol) in acetonitrile (40 cm^3) were added sequentially $Co(ClO_4)_2 \cdot 6H_2O$ (0.18 g, 0.5 mmol) and Et_3N (0.101 g, 1 mmol). After refluxing for 0.5 h, part of the solvent (ca 20 cm^3) was removed in a stream of nitrogen and the solution kept in a refrigerator for several hours. The orange crystalline compound that deposited was collected by filtration and washed with MeOH ; Yield : 0.23 g, 62%.

$[Mn(H_2O)LCu(Cl)](ClO_4)$ (**11**). $[Mn(H_2L)(H_2O)_2](ClO_4)_2$ (**6**) (0.30 g, 0.5 mmol) in 1 : 1 MeCN–MeOH (30 cm^3) solution was first treated with a solution of $CuCl_2 \cdot 2H_2O$ (0.085 g, 0.5 mmol) in methanol (10 cm^3) and then Et_3N (0.101 g, 1 mmol). The solution was stirred for 1 h, concentrated (ca 10 cm^3) and cooled. The product that deposited in crystalline form was collected by filtration and dried in vacuum ; Yield : 0.19 g, 60%.

$[\{Ni^{II}LFe^{III}(H_2O)\}_2(\mu\text{-}O)](ClO_4)_4 \cdot 2H_2O$ (**12**). A mixture of **3** (0.65 g, 1 mmol), $Fe(ClO_4)_2 \cdot 6H_2O$ (0.36 g, 1 mmol) and Et_3N (0.202 g, 2 mmol) in acetonitrile (70 cm^3) was kept exposed to air and refluxed for 1 h. The deep red solution was filtered, concentrated (ca 30 cm^3) and set aside for several hours. The compound that deposited as red crystal was filtered and recrystallized from acetonitrile ; Yield : 0.48 g, 65%.

CAUTION! All the perchlorate salts reported here are potentially explosive and therefore should be handled with care.

Physical measurements

IR spectra were recorded on a Perkin–Elmer 783 spectrophotometer using KBr discs. Electronic spec-

tra were obtained with Shimadzu UV-160 and Hitachi U 3400 spectrophotometers over the UV–vis and near IR regions. The electrochemical data were obtained with a BAS 100B assembly (BAS) comprising a glassy carbon or a Pt working electrode, a Pt auxiliary electrode and a Ag-AgCl reference electrode. The concentration of the supporting electrolyte tetraethylammonium perchlorate (TEAP) was maintained to 0.1 mol dm^{-3}. The reference electrode was separated from the bulk solution with a salt bridge having a Vycor plug. IR compensation was achieved before each CV was recorded. The ferrocene/ferrocenium couple was used to monitor the reference electrode and was observed at 0.36 V. Room temperature and variable-temperature magnetic susceptibility measurements were made with a PAR model 155 vibrating sample magnetometer employing $[HgCo(NCS)_4]$ as a calibrant. Carbon, hydrogen and nitrogen analysis were carried out on a Perkin–Elmer 240 C elemental analyzer.

RESULTS AND DISCUSSION

Synthesis

The asymmetric macrocyclic magnesium complex $[Mg(H_2L)](NO_3)_2 \cdot 2H_2O$ (**1**) was synthesized by the sequential addition of 1 equiv. each of 1,2-diaminoethane and 1,3-diaminopropane to a boiling methanol solution containing $Mg(NO_3)_2 \cdot 6H_2O$, $Mg(OAc)_2 \cdot 4H_2O$ and 2,6-diformyl-4-methylphenol (2 equiv.) over a period of several hours. The conversion of the Mg-complex (**1**) to the mononuclear complexes $[M(H_2L)](ClO_4)_2$ (**2**–**6**; M = Cu^{II}, Ni^{II}, Co^{II}, Fe^{II} and Mn^{II}) by transmetallation reaction was achieved in good yield. The homo- and hetero-dinuclear complexes (**7**–**11**) were obtained by reacting an appropriate mononuclear complex with its complimentary metal salt and triethylamine. However, when $[Ni(H_2L)](ClO_4)_2$ was reacted with $Fe(ClO_4)_2 \cdot 6H_2O$ in open air a heterotetranuclear complex $[\{Ni^{II}LFe^{II}(H_2O)\}_2(\mu\text{-}O)](ClO_4)_4$ (**12**) was obtained. The formation of the different types of metal complexes are illustrated in Scheme 1.

Characterization

The analytical data of the compounds (Table 1) are consistent with the proposed compositions. The characteristic band(s) due to $\nu_{C=N}$ in all the complexes are observed between 1640 and 1620 cm^{-1}. Moreover, all the dinuclear complexes (**7**–**11**) show a group of structured bands in the range 1100–1200 cm^{-1}, and at ca 630 cm^{-1} due to either metal-bound or hydrogen bonded perchlorates.

Magnetic properties

The room temperature magnetic moments of the complexes are given in Table 1. The diamagnetic behaviour of the mononuclear nickel(II) complex **3** is indicative of the square-planar geometry of the metal ion. The location of the low-spin nickel(II) centre in the smaller ligand compartment provided by the —$(CH_2)_2$— chain in preference to that having the —$(CH_2)_3$— chain can be concluded on the basis of earlier studies [16a,20a]. In retrospect, this also leads to conclude that the magnesium ion in the precursor complex **1** is positioned in the smaller ligand compartment.

The room temperature diamagnetic nature of the dicopper(II) complex **7** is indicative of strong intramolecular antiferromagnetic spin-exchange interaction. The magnetic moment of the dinickel(II) complex $[NiLNi(H_2O)_2](ClO_4)_2$ (**8**) at room temperature (3.18 μ_B) is consistent with the value expected for a combination of a low-spin ($S = 0$) and a high-

Table 1. Analytical data and magnetic moments for the complexes

Complex	Analyses : Found (Calcd.) C	H	N	μ_{eff}(298 K), B.M.
1 $[Mg(H_2L)](NO_3)_2 \cdot 2H_2O$	47.8(48.0)	5.2(5.2)	14.9(14.6)	
2 $[Cu(H_2L)](ClO_4)_2$	42.6(42.3)	4.1(4.0)	9.1(8.6)	1.69
3 $[Ni(H_2L)](ClO_4)_2$	42.8(42.6)	3.9(4.0)	8.4(8.6)	diamagnetic
4 $[Co(H_2L)(H_2O)_2](ClO_4)_2$	40.8(40.3)	4.2(4.4)	8.4(8.2)	2.50
5 $[Fe(H_2L)(H_2O)_2](ClO_4)_2$	39.9(40.5)	3.7(4.4)	8.1(8.2)	5.72
6 $[Mn(H_2L)(H_2O)_2](ClO_4)_2$	40.2(40.6)	4.1(4.4)	8.1(8.2)	6.00
7 $[CuLCu](ClO_4)_2 \cdot 2H_2O$	37.0(36.8)	3.7(3.7)	7.6(7.5)	diamagnetic
8 $[NiLNi(H_2O)_2](ClO_4)_2$	37.3(37.3)	3.9(3.8)	7.6(7.6)	3.18
9 $[NiLCu](ClO_4)_2$	39.1(38.9)	3.4(3.4)	7.9(7.9)	1.75
10 $[NiLCo(H_2O)_2](ClO_4)_2$	37.7(37.3)	3.6(3.8)	7.9(7.6)	4.84
11 $[MnLCu(H_2O)](Cl)(ClO_4)$	41.5(41.8)	3.7(3.9)	8.3(8.4)	5.66
12 $[\{NiLFe(H_2O)\}_2(\mu\text{-}O)](ClO_4)_4 \cdot 2H_2O$	37.2(37.0)	3.8(3.7)	7.5(7.5)	2.07

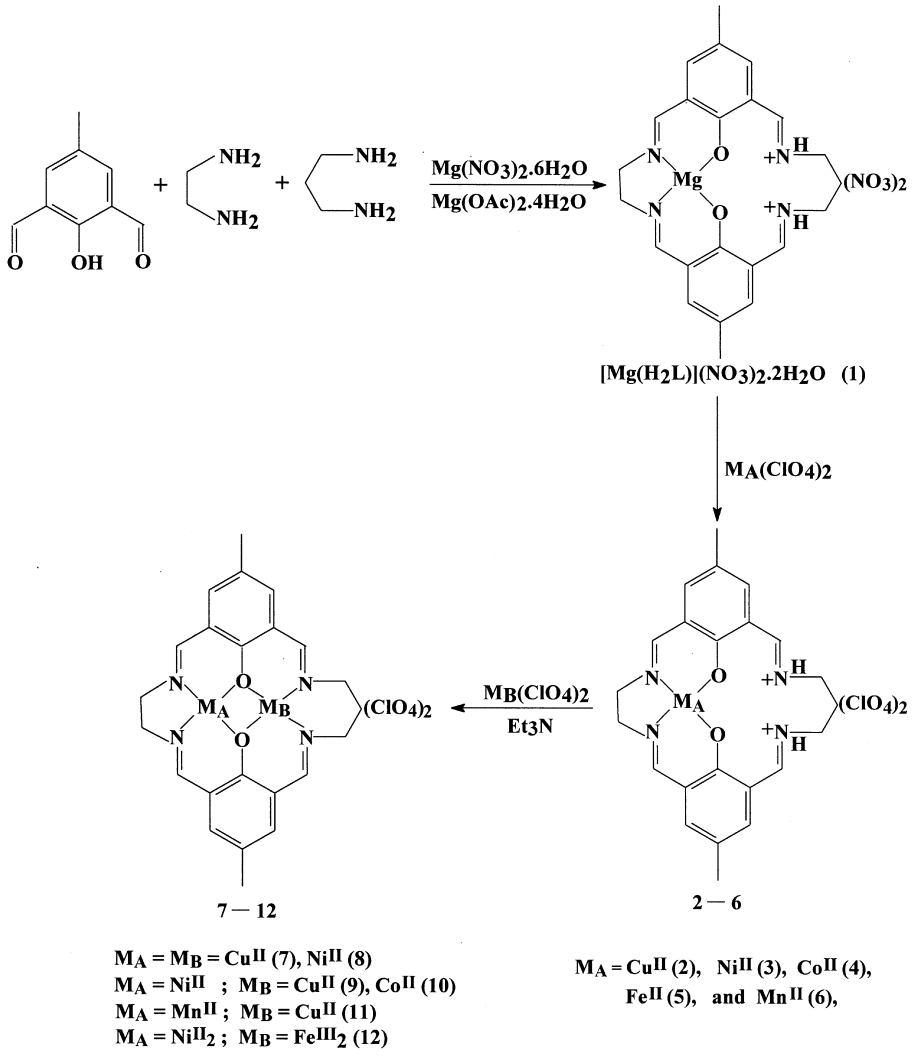

Scheme 1.

spin ($S = 1$) nickel(II) centers. It should be noted that similar magnetic behaviour was observed for the structurally characterized analogous dinickel(II) complex [20a] derived from the saturated macrocyclic ligand version of H_2L. The room temperature magnetic moment of the heterodinuclear $Ni^{II}Cu^{II}$ complex **9** (1.75 μ_B) is again in agreement with the value expected for a compound in which the nickel(II) ion is spin-paired. In the case of $Ni^{II}Co^{II}$ complex **10,** however, the observed moment (4.84 μ_B) is considerably higher than the expected value (3.87 μ_B for $S = 2$ and $g = 2.0$), presumably due to the significant contribution of orbital magnetic moment of the cobalt(II) centre. The tetranuclear complex $[\{NiL\text{-}Fe(H_2O)\}_2(\mu\text{-}O)](ClO_4)_4$ (**12**), on the other hand, shows a magnetic moment 2.07 μ_B (at 300 K), which is indicative of a strong intramolecular (Fe^{III}—O—Fe^{III}) antiferromagnetic spin-exchange interaction.

Variable temperature magnetic susceptibility measurement has been carried out for the $Mn^{II}Cu^{II}$ complex **11** between the temperature range 85 and 293 K (Fig. 1). The susceptibility data have been analyzed using the isotropic Heisenberg-Dirac-van Vleck model with the spin Hamiltonian $\mathbf{H} = -2JS_1 \cdot S_2$. Nonlinear least-squares fitting of the theoretical expression (1)

$$\chi_M = \frac{N\beta^2 g^2}{kT}\left[\frac{10 + 28e^{6J/kT}}{5 + 7e^{6J/kT}}\right] \qquad (1)$$

to the experimental data has been made by varying J and g. In eqn (1) the symbols have their usual meanings. Since the measurements were limited up to 85 K, additional terms due to temperature independent paramagnetism and contribution of the mononuclear paramagnetic impurity were not considered. The room temperature magnetic moment of **11** is lower than the spin-only value and decreases with decreasing temperature. The observed behaviour is indicative of

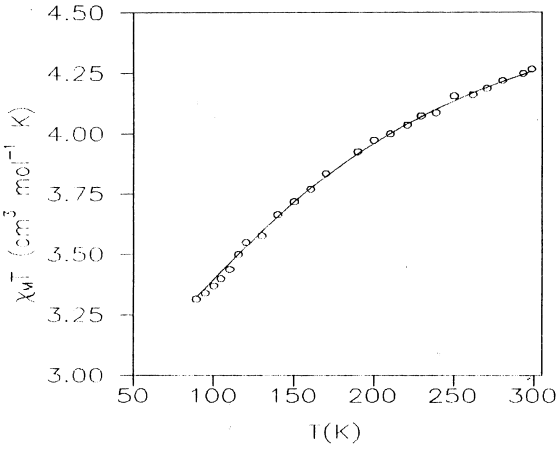

Fig. 1. Thermal variations of the product of the molar magnetic susceptibility with temperature (o) for the complex **11**. The solid lines represent the calculated values using the best-fit parameters given in the text.

intramolecular antiferromagnetic spin exchange interaction. Figure 1 shows that the $\chi_M T$ vs T data for complex **11** can be satisfactorily fitted to eqn (1) with $J = -31$ cm^{-1} and $g = 2.04$. The exchange integral of **11** is similar to the values ($-J = 30$–36 cm^{-1}) reported for several $Cu^{II}Mn^{II}$ complexes derived from related macrocyclic ligands [13c,23].

Electronic spectra

The electronic spectral data for the complexes are given in Table 2. The mononuclear complexes (**2**–**6**) show the azomethine π–π^* band at ca 410 nm whereas for the dinuclear complexes (**7**–**11**) it occurs at shorter wavelengths (360–385 nm). Furthermore, the extinction coefficients of the π–π^* band of the dinuclear complexes **7**–**11** (9000–10000 dm^3 mol^{-1} cm^{-1}) are significantly lower than those of the mononuclear complexes (13000–14000 dm^3 mol^{-1} cm^{-1}). This probably indicates that the uncoordinated protonated azomethine moieties act as a strong chromphore.

Table 2. Electronic spectral data for the complexes

Complex	UV–vis $\lambda_{max(nm)}/\varepsilon$(M^{-1} cm^{-1})
2 $[Cu(H_2L)](ClO_4)_2$	565(206), 390(13725), 255(50575
3 $[Ni(H_2L)](ClO_4)_2$	530(sh), 415(14575), 315(8780)
4 $[Co(H_2L)(H_2O)_2](ClO_4)_2$	560(sh), 410(13050)
5 $[Fe(H_2L)(H_2O)_2](ClO_4)_2$	390(11160)
6 $[Mn(H_2L)(H_2O)_2](ClO_4)_2$	520(sh), 400(12780)
7 $[CuLCu](ClO_4)_2 \cdot 2H_2O$	565(205), 360(11,125)
8 $[NiLNi(H_2O)_2](ClO_4)_2$	990(10), 525(sh), 385(9760)
9 $[NiLCu](ClO_4)_2$	670(49), 375(9770)
10 $[NiLCo(H_2O)_2](ClO_4)_2$	960(10), 540(sh), 380(9880)
11 $[MnL(H_2O)Cu(Cl)](ClO_4)$	540(145), 365(12810)
12 $[\{NiLFe(H_2O)\}_2(\mu\text{-}O)](ClO_4)_4 2H_2O$	655(38), 370(9150)

The dicopper(II) complex (**7**) exhibit a copper-based d–d band in the visible region at ca 560 nm. The spectral feature of the dinickel(II) complex (**8**) shows three bonds at ca 990, 525 and 385 nm, which can be attributed to the octahedral nickel(II) centre with the transitions due to $^3A_{2g} \rightarrow {}^3T_{2g}$, $^3A_{2g} \rightarrow {}^3T_{1g}$ and $^3A_{2g} \rightarrow {}^3T_{1g}(P)$, respectively. The extinction coefficient of the band at 385 nm ($\varepsilon = 9760$ M^{-1} cm^{-1}) indicates that the $^3A_{2g} \rightarrow {}^3T_{1g}(P)$ transition must be admixed with the intraligand π–π^* transition. In the visible range the $Ni^{II}Cu^{II}$ complex (**9**) exhibits a d–d band due to the copper(II) centre at 670 nm, while in the $Ni^{II}Co^{II}$ complex (**10**) two d–d bands are observed at ca 960 and 540 nm due to the octahedral cobalt(II) centre. It may be noted that in square planar mononuclear nickel(II) complex only an ill-defined shoulder is observed at ca 530 nm, which apparently gets obscured in the heterodinuclear complexes **8**–**10**. Finally, the $Mn^{II}Cu^{II}$ complex (**11**) which shows a band at 540 nm ($\varepsilon = 145$ M^{-1} cm^{-1}) is clearly due to the d–d transition of the copper(II) centre because spin-forbidden d–d transition due to manganese will be too weak.

Electrochemistry

The electrochemical properties of the complexes have been studies by cyclic voltammetric and differential pulse voltammetric measurements. For oxidation acetonitrile solution and a Pt electrode was used, while for reduction DMSO solution and a glassy carbon electrode was used. The electrochemical data of the complexes are given in Table 3.

Of the five mononuclear complexes **2**–**6,** $[Cu(H_2L)](ClO_4)_2$ (**2**) and $[Ni(H_2L)](ClO_4)_2$ (**3**) do not show any electrochemical response during oxidation up to 1.5 V. On the other hand, the complexes of cobalt(II), iron(II) and manganese(II) undergo nearly reversible or quasireversible oxidation reaction. In the case of $[Co(H_2L)(H_2O)_2](ClO_4)_2$ (**4**) the Co^{II}/Co^{III} couple has the $E_{1/2}$ value of -0.03 V whose peak to peak separation (ΔE_p) increases from 140 to 200 mV with the increase of scan rate from 50 to 500 mV s^{-1}. The behaviour of $[Mn(H_2L)(H_2O)_2](ClO_4)_2$ (**6**) is quite similar to that of **4** with $E_{1/2} = -0.00$ V and ΔE_p changes from 120 to 180 mV as the scan rate (v) is varied from 50 to 500 mV s^{-1}. By contrast, the variation of ΔE_p for $[Fe(H_2L)(H_2O)_2(ClO_4)_2$ (**5**) occurs in a narrow range 70–90 mV from $v = 50$–500 mV s^{-1}, and the $E_{1/2}$ of the Fe^{II}/Fe^{III} couple occurs at -0.20 V. The facile oxidation of the iron(II) complex at a negative potential is noteworthy. The criteria

Table 3. Electrochemical data for the complexes[a]

Complex	Oxidation		Reduction				
	$E^1_{1/2}$(V)	ΔE^1_p(mV)	E_{pc}[a]	$E^1_{1/2}$(V)	ΔE^1_p(mV)	$E^2_{1/2}$(V)	ΔE^1_p(mV)
3			−0.95[b]				
4	−0.03	60	−1.0[b]				
5	−0.20	75					
6	−0.00	143					
7				−0.40	70	−1.15	85
8				−0.95	75	−1.20	140
9				−0.25	60	−1.45	60
10				**−1.10**	**70**	**−1.30**	**75**
12			−0.04[b]	−0.40[b]	−1.20[b]		

[a] Scan rate, 100 mV s^{-1}.
[b] Irreversible peak potential from DPV.

of quasireversibility viz (i) a linear relation between current height (i_{pa} or i_{pc}) and square root of scan rate (v); (ii) the ratio of i_{pa} to i_{pc} almost unity; and (iii) the invariance of $E_{1/2}$ with variation of scan rate have been verified for all the three compounds. Furthermore, one electron transfer that occurs during oxidation $M^{2+} = M^{3+} + e^-$ has been established by coulometric measurements carried at a potential more positive to $E_{1/2}$ by 0.2 V.

As compared to oxidation, the electrochemical reduction of the mononuclear complexes lack well defined features. They either undergo irreversible reduction or following electron transfer dissociation of the metal ion from the macrocyclic ring takes place. Thus, while **3** and **4** get irreversibly reduced at −0.95 and −1.0 V, respectively, the behaviour of complexes **2, 5,** and **6** are complicated by demetallation.

The cyclic voltammogram of [CuL-Cu]$(ClO_4)_2 \cdot 2H_2O$ (**7**) exhibits two redox couples at −0.40 and −1.15 V with their peak to peak separation (ΔE_p at $v = 100$ mV s^{-1}) of 70 and 85 mV, respectively, indicating that both the couples are practically reversible in nature. Differential pulse voltammetric measurements also revealed the occurrence of two waves with equal pulse heights at the indicated potentials. Coulometric analyses have established that each of the redox couples are associated with one electron transfer process, that is, $Cu^{II}Cu^{II}/Cu^{II}Cu^{I}$ and $Cu^{II}Cu^{I}/Cu^{I}Cu^{I}$. The wave at −0.40 V seems to be due to the reduction of the Cu^{II} centre located at the —$(CH_2)_3$— chain and the wave at −1.15 V to the reduction of the Cu^{II} centre located at the —$(CH_2)_2$— site. This assignment seems reasonable [24] because the greater flexibility of the —$(CH_2)_3$— chain (with respect to the more rigid —$(CH_2)_2$— chain) makes it easier for the copper(II) ion go get reduced and undergo reorganization to the pseudotetrahedral geometry of copper(I).

It is of interest to compare the redox potentials $E^1_{1/2}$ and $E^2_{1/2}$ of the present dicopper(II) complex (designated as *2*,*3*-derivative for the lateral chains —$(CH_2)_2$— and —$(CH_2)_3$—) with the analogous (*2*, *2*) [−0.55 and −1.10 V] and (*3*, *3*) [−0.50 and −0.95 V] macrocyclic complexes [24]. Clearly, the $E^1_{1/2}$ value of the (*2*, *3*) complex (−0.40 V) is greater than those of the (*2*, *2*) [−0.55 V] and (*3*, *3*) [−0.50 V] complexes, whereas the $E^2_{1/2}$ value of the (*2*, *3*) [−1.15 V] is lower than those of the (*2*, *2*) [−1.10V] and (*3*, *3*) [−0.95 V] complexes. The easier reduction of the first copper(II) centre in the (*2*, *3*) complex indicates greater stability of its mixed-valence species. The equilibrium constants (K_c) for the comproportionation reaction $2M^{II}M^{I} = M^{II}M^{II} + M^{I}M^{I}$ is obtained using eqn (2)

$$K_c = 10^{\Delta E/0.059} \quad (2)$$

where $\Delta E = [E^1_{1/2} - E^2_{1/2}]$ in volt. The values of K_c are: 2.4×10^{12} (for *2*, *3*), 3.8×10^9 (for *2*, *2*) and 5.1×10^7 (for *3*, *3*) [24].

Figure 2 shows that the two nickel(II) centres in $[NiLNi(H_2O)_2](ClO_4)_2$ (**8**) undergo stepwise reduction. In the first step one electron transfer reaction of $Ni^{II}Ni^{II}$ to $Ni^{II}Ni^{I}$ takes place almost reversibly since for this couple i_{pc}/i_{pa} ratio remains unity and ΔE_p varies only to a small extent from 70 to 110 mV with the increase of scan rate from 50 to 500 mV s^{-1}, while the $E_{1/2}$ value (−0.95 V) remains unchanged. Moreover, the linear dependence of i_{pc} on $\sqrt{v}$ has been observed. By comparison to the reduction potential ($E_{pc} = -0.95$ V) of the mononuclear nickel(II) complex (**3**), the first electron transfer reaction in **8** can be attributed to the square-planar nickel(II) site. The second couple involving $Ni^{II}Ni^{I}/Ni^{I}Ni^{I}$ is quasireversible in nature with $E_{1/2} = -1.20$ V and $\Delta E_p = 140$ mV at $v = 100$ mV s^{-1}. However, as may be noted in Fig. 2, in the case of the reoxidation peak relative to the most cathodic step is rather high and the ratio of i_{pc} to i_{pa} is ca 0.8. When the scan rate is

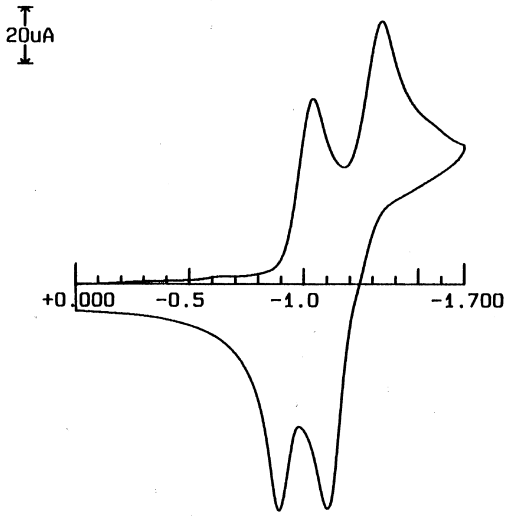

Fig. 2. Cyclic voltammogram of **8** in CH_3CN with a glassy carbon electrode at a scan rate of 100 mV s^{-1}. Concentration of the complex: 1.0×10^{-3} mol dm^{-3}; concentration of supporting electrolyte $[Et_3N](ClO_4)$: 0.1 mol dm^{-3}.

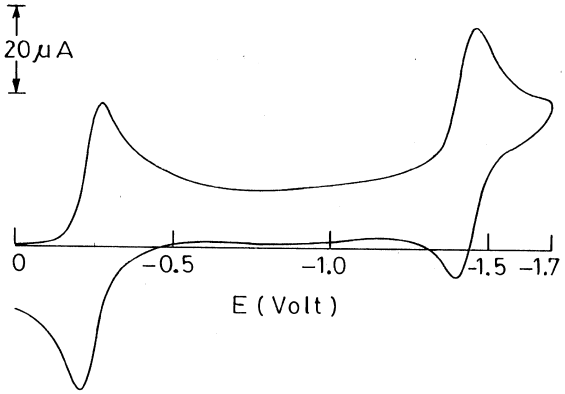

Fig. 3. Cyclic voltammogram of **9** in CH_3CN with a glassy carbon electrode at a scan rate of 100 mV s^{-1}. Concentration of the complex: 1×10^{-3}; concentration of supporting electrolyte $[Et_4N](ClO_4)$: 0.1 mol dm^{-3}.

increased, the augmentation in height of the anodic peak occurs to a greater extent relative to that of the cathodic peak. This indicates that the reduced $Ni^{I}Ni^{I}$ species is weakly adsorbed on the electrode surface [25]. From the difference in potentials ($\Delta E_{1/2}$) of the two redox couples in **8** (0.25 V) the comproportionation constant K_c is estimated to be 1.7×10^4.

The electrochemistry of the heterodinuclear [NiL-Cu]$(ClO_4)_2$ complex **9** (Fig. 3) shows two well-separated reversible redox couples with their $E_{1/2}$ values of -0.25 and -1.45 V. For each couples ΔE_p value (60 mV) remains invariant with the change of scan rate. The first redox couple is evidently due to Cu^{II}/Cu^{I} [13,26], while the second is due to Ni^{II}/Ni^{I} [13b,16d]. It may be noted that in **9** the $E^1_{1/2}$ value for the copper(II) centre is shifted to a more positive potential (-0.25 V) relative to that of **7** (-0.40 V), while the value of $E^2_{1/2}$ for the nickel(II) centre is more negative in **9** (-1.45 V) relative to that of **8** (-1.20 V). The observed differences in potentials of the heterodinuclear complex *vis-à-vis* the homodinuclear complexes must be related to their structures. Although crystallographic data for these complexes are not available at this stage, it is reasonable to assume that in the $Ni^{II}Cu^{II}$ complex (**9**) the square-planar nickel(II) centre located at the smaller cavity has shorter Ni—O and Ni—N distances relative to the Cu—O and Cu—N distances located at the larger cavity. As a result, the nickel(II) centres is more electron-rich compared to copper(II) centre. Consequently, it will be easier to add an electron to the copper(II), while it will be more difficult to reduce the nickel(II) centre.

Figure 4 shows the cyclic voltammogram of the heterodinuclear $Ni^{II}Co^{II}$ complex (**10**) which undergoes stepwise reversible reductions at potentials -1.10 V ($\Delta E_p = 70$ mV at $v = 100$ mv s^{-1}) and -1.30 V ($\Delta E_p = 75$ mV at $v = 100$ mv s^{-1}). By taking into consideration the reduction potentials of the relevant mononuclear complexes **3** or **4,** the redox couple at -1.10 V for **10** is tentatively assigned to Ni^{II}/Ni^{I} and the other couple at -1.30 V to Co^{II}/Co^{I}.

The oxo-bridged $Ni^{II}_2Fe^{III}_2$ complex (**12**) exhibits complex electrochemical responses in the potential range 0.2 to -1.17 V. Figure 5 shows three stepwise reductions at the potentials -0.04, -0.40 and -1.20 V, of which the first and second steps are one electron transfer processes whereas the third one is a two electron transfer reaction. The differential pulse voltammogram shows that the height of third step is almost double of the other two steps. The ΔE_p value for the third couple ($\Delta E_p = 75$ mV at $v = 100$ mV s^{-1}) is indicative of a quasireversible electron transfer process. In the light of a previous study [27] the overall electron transfer reactions may be tentatively considered in the following way

$$Ni^{II}Fe^{III}—O—Fe^{III}Ni^{II} \xrightarrow[-0.04\,V]{e^-} Ni^{II}Fe^{II}—OH—Fe^{III}Ni^{II}$$

$$e- \Big| \; -0.40\,V \downarrow$$

$$2Ni^{I}Fe^{II} \underset{-1.20\,V}{\overset{2e^-}{\rightleftharpoons}} 2Ni^{II}Fe^{II}$$

Acknowledgements—Thanks to Prof. K. Nag (Indian Association for the Cultivation of Science) for helpful suggestions and laboratory facilities.

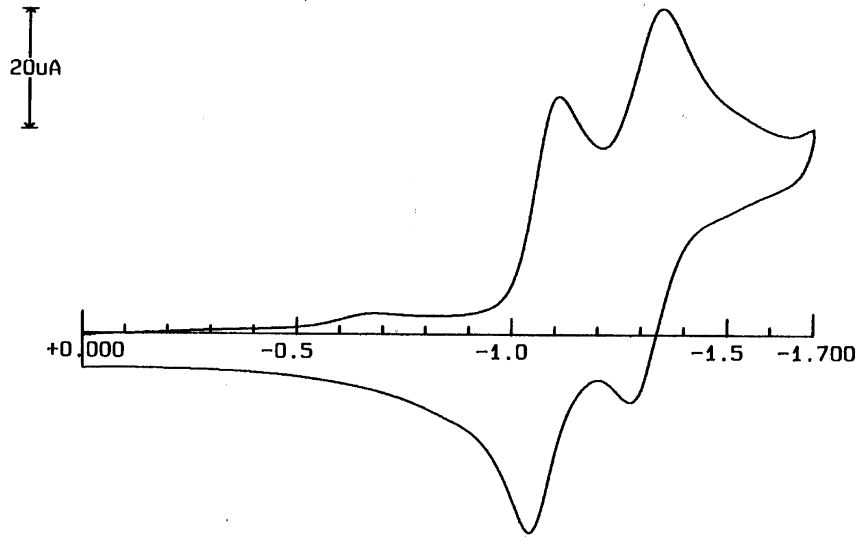

Fig. 4. Cyclic voltammogram of **10** in CH_3CN with a glassy carbon electrode at a scan rate of 100 mV s^{-1}. Concentration of the complex: 1×10^{-3} mol dm^{-3}; concentration of supporting electrolyte $[Et_4N](ClO_4)$: 0.1 mol dm^{-3}.

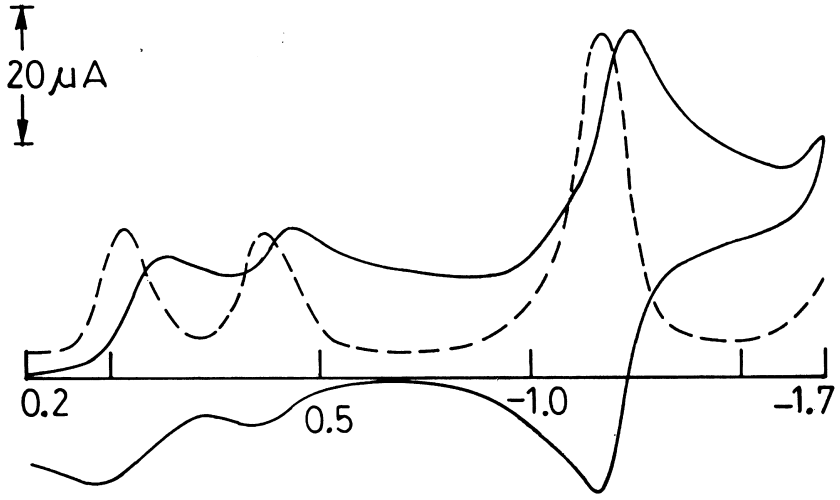

Fig. 5. Cyclic voltammogram of **12** in CH_3CN with a glassy carbon electrode at a scan rate of 100 mV s^{-1}. Concentration of the complex: 1×10^{-3}; concentration of supporting electrolyte $[Et_4N](ClO_4)$: 0.1 mol dm^{-3}. Differential pulse voltammogram (- - -) of **12** at a scan rate of 100 mV s^{-1}.

REFERENCES

1. Casellato, U., Vigato, P. A., Fenton, D. E. and Vidali, M., *Chem. Soc. Rev.*, 1979, **8,** 199.
2. Zanello, P., Tamburini, S., Vigato, P. A. and Mazzochin, G. A., *Coord. Chem. Rev.*, 1987, **77,** 165.
3. Vigato, P. A., Tamburini, S. and Fenton, D. E., *Coord. Chem. Rev.*, 1990, **106,** 25.
4. Groh, S. E., *Isr. J. Chem.*, 1976/77, **15,** 277.
5. Cairns, C. J. and Busch, D. H., *Coord. Chem. Rev.*, 1986, **69,** 1.
6. Addison, A. W., *Inorg. Nucl. Chem. Lett.*, 1976, **12,** 899.
7. Downward, A. J., McKee, V. and Tandon, S. S., *Inorg. Chim. Acta.*, 1990, **173,** 181.
8. (a) Hoskins, B. F. and Williams, G. A., *Aust. J. Chem.*, 1975, **28,** 2607; (b) Hoskins, B. F., Robson, R. and Williams, G. A., *Inorg. Chim. Acta.*, 1976, **16,** 121.
9. (a) Atkins, A. J., Blake, A. J. and Schroder, M., *J. Chem. Soc., Chem. Commun.*, 1993, 353; *ibid* 1993, 1662; (b) Atkins, A. J., Black, D., Blake, A. J., Marin-Becerra, A., Parsons, S., Ruiz-Rami-

rez, L. and Schroder, M., *J. Chem. Soc., Chem. Commun*., 1996, 457.
10. (a) Caselato, U., Fregora, D., Sitram, S., Tamburini, S. and Vigato, P. A., *Inorg. Chim. Acta*., 1985, **110,** 181; (b) Caselato, U., Guerriero, P., Tamburini, S. and Vigato, P. A., *Inorg. Chim. Acta*., **119,** 215.
11. McKee, V. and Tandon, S. S., *J. Chem. Soc., Dalton Trans*, 1991, 221.
12. Fraser, C., Johnston, L., Rheingold, A. L., Haggerty, B. S., Williams, G. K., Whelar, J. and Bosnich, B., *Inorg. Chem*., 1992, **31,** 1835.
13. (a)Gague, R. R., Koval, C. A., Smith, T. J., Cimolino, M. C., *J. Am. Chem. Soc*., 1979, **101,** 4571; (b) Gagne, R. R., Sprio, C. L., Smith, T. J., Hamann, C. A., Thies, W. R. and Shiemke, A. K., *J. Am. Chem. Soc*., 1981, **103,** 4073; (c) Lambert, S. L., Spiro, C. L., Gagne, R. R. and Hendrickson, D. N., *Inorg. Chem*., 1982, **21,** 68.
14. (a) Long, R. C. and Hendrickson, D. N., *J. Am. Chem. Soc*., 1983, **105,** 1513; (b) Lambert, S. L. and Hendrickson, D. N., *Inorg. Chem*., 1979, **18,** 2683.
15. (a) Nag, K., *Proc. Indian Acad. Sci.* (*Chem. Sci.*), 1990, **102,** 269; (b) Mandal, S. K. and Nag, K., *J. Org. Chem*., 1986, **51,** 3900; (c) Mondal, S. K., Thompson, L. K., Nag, K., Charland, J.-P. and Gabe, E. J., *Inorg. Chem*., 1987, **26,** 1391; (d) Mandal, S. K., Adhikary, B. and Nag, K., *J. Chem. Soc., Dalton Trans.* 1986, 1175; (e) Mandal, S. K., Thompson, L. K., Newlands, M. J., Biswas, A. K., Adhikary, B., Nag, K., Gabe, E. J. and Lee, F., *Can. J. Chem*., 1989, **67,** 662; (f) Nanda, K. K., Das, R., Newlands, M. J., Hynes, R., Gabe, E. J. and Nag, K., *J. Chem. Soc., Dalton Trans*., 1992, 897; (g) Das, R., Nanda, K. K., Mukherjee, A. K., Mukherjee, M., Heliwell, M. and Nag, K., *J. Chem. Soc., Dalton Trans*., 1993, 2241; (h) Nanda, K. K., Das, R., Thompson, L. K., Venketsubramanian, K. and Nag, K., *Inorg. Chem*., 1994, **33,** 5934; (i) Dutta, S. K., Werner, R., Florke, U., Mahanta, S., Nanda, K. K., Haase, W. and Nag, K., *Inorg. Chem*., 1996, **35,** 2292; (j) Mohanta, S., Nanda, K. K., Ghosh, S., Mukherjee, M., Helliwell, M. and Nag, K., *Inorg. Chem*., 1995, **34,** 2861.
16. (a) Okawa, H. and Kida, S., *Bull Chem. Soc. Jpn*., 1972, **45,** 1759; (b) Tadokoro, M., Okawa, H., Matsumoto, N., Koikawa, M., Kida, S., *J. Chem. Soc., Dalton Trans*., 1991, 1657; (c) Tadokoro, M., Sakiyama, H., Matsumoto, N., Kodera, M., Okawa, H. and Kida, S., *J. Chem. Soc., Dalton Trans*., 1992, 313; (d) Okawa, H., Nishio, J., Ohba, M., Tadokoro, M., Matsumoto, N., Koikawa, M., Kida, S. and Fenton, D. E., *Inorg. Chem*., 1993, **32,** 2949; (e) Ohtsuka, S., Kodera, M., Motoda, M., Ohba, M. and Okawa, H., *J. Chem. Soc., Dalton Trans*., 1995, 2599; (f) Yonemura, M., Matsumura, Y., Ohba, M., Okawa, H. and Fenton, D. E., *Chem. Lett*., 1996, 601; (g) Yonemura, M., Matsumura, Y., Furutachi, H., Ohba, M., Okawa, H. and Fenton, D. E., *Inorg. Chem*., 1997, **36,** 2711; (h) Furutachi, H. and Okawa, H., *Inorg. Chem*., 1997, **36,** 3911.
17. Cabbines, D. K. and Margerum, D. W., *J. Am. Chem. Soc*., 1969, **91,** 6450.
18. Endicott, J. F. and Durham, B., In *Coordination Chemistry of Macrocyclic Compounds*, ed. G. A. Melson, Plenum Press, New York, 1979, 393.
19. Birkelbach, F., Winter, M., Florke, U., Haupt, H.-J., Butzlaff, C., Lengen, M., Bill, E., Trautwein, A., Wieghardt, K. and Chaudhuri, P., *Inorg. Chem*., 1994, **33,** 3990.
20. (a) Nanda, K. K., Das, R., Venkatsubramanian, K., Paul, P. and Nag, K., *J. Chem. Soc., Dalton Trans*., 1993, 2515; (b) Nanda, K. K., Dutta, S. K., Baitalik, S., Venkatsubramanian, K., Nag, K., *J. Chem. Soc., Dalton Trans*., 1995, 1239.
21. Pilkington, N. H. and Robson, R., *Aust. J. Chem*., 1970, **23,** 2225.
22. Ulleman, F. and Brittner, K., *Chem. Ber*., 1909, **42,** 2539.
23. (a) Torihara, N., Okawa, H. and Kida, S., *Chem. Lett*., 1978, 185; (b) Kahn, O., Tola, K. and Coudanne, H., *Chem. Phys*., 1979, **42,** 355.
24. (a) Mandal, S. K. and Nag, K., *J. Chem. Soc., Dalton Trans*., 1984, 2141; (b) Mohanta, S. K., Nanda, K. K., Werner, R., Haase, W., Mukherjee, A. K., Dutta, S. K. and Nag, K., *Inorg. Chem*., 1997, **36,** 4656.
25. Bard, A. J. and Faulkner, L. R., In *Electrochemical Methods Fundamental and Application*., John Wiley & Sons, Inc., 1980.
26. Mondal, S. K. and Nag, K., *J. Chem. Soc., Dalton Trans*., 1983, 2429.
27. Dutta, S. K., Werner, R., Flörke, U., Mohanta, S., Nanda, K. K., Haase, W. and Nag, K., *Inorg. Chem*., 1997, **36,** 2292.

Pergamon

PII: S0277–5387(98)00030–8

Polyhedron Vol. 17, No. 16, pp. 2679–2685, 1998
© 1998 Elsevier Science Ltd
All rights reserved. Printed in Great Britain
0277–5387/98 $19.00 + 0.00

Crystal and molecular structure of $Mn[(OPPh_2)_2N]_3 \cdot CH_2Cl_2$, a new monomeric manganese(III) complex stabilized by oxygen chelating ligands

Noe Zuniga-Villareal,*[a] Marisol Reyes Lezama,[a] Simón Hernandez-Ortega[a] and Cristian Silvestru[b]

[a] Instituto de Química, Universidad Nacional Autónoma de México, Ciudad Universitaria, Coyoacán, 04510 México, D.F., Mexico

[b] Facultatea de Chimie, Universitatea "Babeş-Bolyai", RO-3400 Cluj-Napoca, Roumania

(Received 20 October 1997; accepted 12 January 1998)

Abstract—The reaction between $[Mn(CO)_5]Br$ and $Na[(OPPh_2)_2N]$ in argon atmosphere affords the preparation of $Mn(CO)_4[(OPPh_2)_2N]$ as a white powder. During attempts to grow X-ray diffraction quality crystals the tetracarbonylmanaganese(I) complex was oxidized and deep purplish-blue crystals were isolated. An X-ray diffractometry analysis has revealed the identity of the new product, i.e. the manganese(III) derivative, $Mn[(OPPh_2)_2N]_3 \cdot CH_2Cl_2$. The compound crystallizes in the triclinic space group *P*-1 and the crystal contains discrete, monomeric molecules of $Mn[(OPPh_2)_2N]_3$. The imidodiphosphinato groups are coordinated through both oxygen atoms of a ligand moiety to the central manganese atom. The resulted coordination octahedron exhibits a tetragonally elongated distortion as reflected by the Mn—O bond lengths [av. 2.130(16), 1.945(6) Å] and *cis* O—Mn—O bond angles [endocyclic (av.) 90.5(0.6)°; exocyclic (range) 87.2(0.1)–92.7(0.1)°]. The structure of the title compound is compared with those of other monomeric manganese(III) derivatives containing MnO_6 cores with various degrees of distortion. © 1998 Elsevier Science Ltd. All rights reserved

Keywords: manganese(III) complexes; imidodiphosphinato.

Recently we have described the synthesis and the molecular structure of the monomeric complex $Mn(CO)_4[(SPPh_2)_2N]$ [1]. Our interest in the investigation of metal complexes containing such ligands prompted us to attempt the preparation of the dioxo analog in order to establish structural changes which might be produced by changes in the chalcogen atoms attached to phosphorus. Several previous studies using phosphorus ligands have proved that modification in the organic groups or chalcogen atoms at phosphorus may result in dramatic structural changes [2] not only in the case of Main Group metal compounds [e.g. lead compounds, $Pb(S_2PR_2)_2$ [3,4], inorganic and organoantimony(III) and antimony(V) compounds [5], but also for transition metal compounds [e.g. $Ni[(SPR_2)_2N]_2$, R = Me [6], Ph [7,8] exhibit a tetrahedral NiS_4 core, $Ni[(SPMe_2)(SPPh_2)N]_2$, has a square-planar NiS_4 core [8], while the dinuclear $\{Ni_2[(OPPh_2)_2N]_4(H_2O)\}$ contains two different octahedral NiO_6 cores [9].

We wish to report here the molecular structure of the manganese(III) complex, $Mn[(OPPh_2)_2N]_3 \cdot CH_2Cl_2$, produced via aerial oxidation during recrystallization of the product isolated by reacting $[Mn(CO)_5]Br$ and $Na[(OPPh_2)_2N]$. It should be noted that the oxygen-donor ligands are known to stabilize manganese(III) species [10].

EXPERIMENTAL

$[Mn(CO)_5]Br$ [11] was obtained according to literature. IR spectra were obtained in KBr disk (4000–200 cm^{-1}) using a Perkin–Elmer 283B spectrometer. ^1H, ^{13}C and ^{31}P NMR spectra were recorded using Varian

* Author to whom correspondence should be addressed.

Gemini 200 and Varian VXR 300S instruments. The chemical shifts are reported in ppm relative to TMS and H_3PO_4 85%, respectively.

Preparation of tetraphenylimidodiphosphinic acid, $(OPPh_2)_2HN$ [12]

A slight excess of H_2O_2 30% (14 ml) was added dropwise to a suspension of $(PPh_2)_2NH$ (20 g, 0.05 mol) in 200 ml THF, and the reaction mixture was stirred over night. The resulting white, solid product was filtered, washed with THF and dried in air. Yield: 21 g (97%), m.p. = 275–277°C (lit. [12] 268–269°C). IR (KBr, cm^{-1}): ν(PO) 1120 s, 1105 s; $\nu_{as}(P_2NH)$ 920 s. ^{1}H NMR ($CDCl_3$, 200 MHz): 7.35 m (3H, C_6H_5-meta + para), 7.80 ddd [2H, C_6H_5-ortho, ^3J(PH) 12.8, ^3J(HH) 7.5, ^4J(HH) 1.5 Hz]. ^{13}C NMR ($CDCl_3$, 50 MHz): 128.24 m [C_m, ^3J(PC) 13.0 Hz], 131.96 s (C_p), 131.96 m [C_o, ^2J(PC) 10.9 Hz], 134.33 d [C_i, ^1J(PC) 101.6 Hz]. ^{31}P NMR ($CDCl_3$, 121.4 MHz): 19.4 s.

Preparation of sodium tetraphenylimidodiphosphinate, $Na[(OPPh_2)_2N]$ [13]

$(OPPh_2)_2NH$ (4.5 g, 10.8 mmol) and NaOMe (0.6 g, 11 mmol) in 100 ml ethanol were stirred for 6 h, at room temperature. The insoluble solid product was filtered, and the solvent was removed from the clear filtrate in a rotary evaporator to dryness. The remaining white solid was extracted several times in a Soxhlet apparatus using MeCN as solvent. The white crystals of the title compound which deposited from the MeCN extract were filtered and dried *in vacuo*. Yield: 3.3 g (70%), m.p. = 335–338°C. IR (KBr, cm^{-1}): $\nu_{as}(P_2N)$ 1260 vs, 1220 vs; ν(PO) 1140 vs, 1120 s. ^{1}H NMR (CD_3OD, 300 MHz): 7.18 m (3H, C_6H_5-meta + para), 7.72 ddd (2H, C_6H_5-ortho, ^3J(PH) 12.3, ^3J(HH) 7.7, ^4J(HH) 1.9). ^{13}C NMR (CD_3OD, 75 MHz): 128.52 m [C_m, ^3J(PC) 12.7 Hz], 130.64 s (C_p), 132.50 t [C_o, ^2J(PC) 9.8 Hz], 140.86 d [C_i, ^1J(PC) 134.5 Hz]. ^{31}P NMR (CD_3OD, 121.4 MHz): 11.3 s.

Reaction of $[Mn(CO)_5]Br$ *with* $Na[(OPPh_2)_2N]$

A stoichiometric amount of $Na[(OPPh_2)_2N]$ (1.1 g, 2.55 mmol) was added to a solution of $[Mn(CO)_5]Br$ (0.7 g, 2.55 mmol) in 100 ml anhydrous THF. The reaction mixture was stirred under reflux until the IR spectrum of the crude solution remained unchanged in the region characteristic for CO stretching vibrations. After 0.5 h the formation of a white solid was noted. The NaBr was filtered off and the removal of the solvent from the clear filtrate under vacuum resulted in an oily product. Recrystallization of this material from a THF/*n*-hexane (1 : 1) solvent mixture resulted in isolation of $Mn(CO)_4[(OPPh_2)_2N]$ as a white solid. Yield: 0.53 g (36%), m.p. = 170–175°C (dec.). IR (KBr, cm^{-1}): $\nu_{as}(P_2N)$ 1243 vs; ν(PO) 1126 vs, 1097 s; ν(CO) 2035 vs, 2008 vs, 1983 vs, 1924 vs.

X-ray crystal determination of $Mn[(OPPh_2)_2N]_3$

Empirical formula $C_{72}H_{60}N_3O_6P_6Mn{\cdot}CH_2Cl_2$, M = 1388.9, triclinic, $a = 13.572(1)$, $b = 13.852(1)$, $c = 18.761(2)$ Å, $\alpha = 95.44(2)$, $\beta = 98.50(2)$, $\gamma = 97.08(2)^\circ$, $U = 3438.7(5)$ Å^3, $F(000) = 1436$, $Z = 2$, $D_C = 1.341$ g cm^{-3}, space group P-1, μ(Cu–K_α) = 4.031 mm^{-1}, crystal size $0.28 \times 0.26 \times 0.24$ mm.

Purplish blue prisms of $Mn[(OPPh_2)_2N]_3$. [Anal. Calc. for $C_{72}H_{60}N_3O_6P_6Mn{\cdot}CH_2Cl_2$: C, 63.1; H, 4.5; N, 3.0; Found: C, 62.8; H, 4.4; N, 2.8%; ES (CH_2Cl_2, cm^{-1}): 32,570, 18,250] were obtained from CH_2Cl_2/*n*-hexane solution. Data were collected at room temperature (293 K) on a Siemens P4/PC four-circle diffractometer with parallel-graphite crystal monochromator (Cu–K_α radiation, $\lambda = 1.54178$ Å), for 9660 reflections of which 9194 were independent reflections [$R_{int} = 6.20\%$] and 7287 ($F^2 > 2.0\sigma(F^2)$) were used in the full-matrix least-squares refinement with the SHELXL-97 program system [14]. The structure was solved by Patterson methods [15] and difference Fourier synthesis revealed the positions for the other non-hydrogen atoms. All non-hydrogen atoms were refined anisotropically, and hydrogen atoms were calculated as a riding model with isotropic U. Semi-empirical absorption correction was applied based on ψ-scan (transmission: min. 0.0128, max. 0.7645). The CH_2Cl_2 solvent molecule was distorted and was modeled [14] in two positions for each atom; the site occupation factors were 0.30/0.70 for C(1a)/C(1b), Cl(1)/Cl(1a) and Cl(2)/Cl(2a), respectively. The final R values are $R_1 = \Sigma|F_o - F_c|/|\Sigma|F_o| = 6.24\%$ and $wR_2 = [\Sigma(w|F_o - F_c|)^2/\Sigma w|F_0|^2]^{1/2} = 15.83\%$ with weights $w^{-1} = \sigma^2(F_o^2) + (0.1003P)^2 + 2.8031P$, where $P = (F_o^2 - 2F_c^2)/3$; goodness-of-fit 1.009. The residual electron density from a final difference Fourier synthesis was in the range of 0.523, -0.753 eÅ^{-3}.

RESULTS AND DISCUSSION

The tetraphenylimidodiphosphinic acid and its sodium salt were prepared using previously described procedures [12,13], and were characterized by IR and multinuclear NMR spectroscopy. The resonance signals observed in the ^{1}H and ^{13}C NMR spectra of both compounds exhibit the expected pattern due to the proton–proton and proton–phosphorus, and carbon–phosphorus couplings, respectively. A significant increase in the ^1J(PC) coupling constant from 101.6 Hz in the free acid to 134.5 Hz in the sodium salt was noted. In addition, when the ^{13}C NMR spectrum of $Na[(OPPh_2)_2N]$ was recorded in DMSOd_6, the resonance for the *ipso* carbon was further split due to the coupling to the second phosphorus atom of the ligand unit [^1J(PC) = 129.0 Hz, ^3J(PC) = 4.3 Hz]. However, ^{31}P NMR spectra show only one broad resonance for

both phosphorus atoms, in the sodium salt the signal being shifted about 10 ppm to lower field due to delocalization of the electrons over the OPNPO fragment.

The carbonylmanganese(I) complex, $Mn(CO)_4[(OPPh_2)_2N]$, was prepared by methatesis according to eq (1) and isolated as a white solid:

$$[Mn(CO)_5]Br + Na[(OPPh_2)_2N] \rightarrow Mn(CO)_4[(OPPh_2)_2N] + CO + NaBr \quad (1)$$

Its IR spectrum shows a strong absorption assigned to $\nu_{as}(P_2N)$ stretching vibration at about 1243 cm^{-1} which is consistent with the coordination of the ligand in its deprotonated form (cf $\nu_{as}(P_2NH)$ 920 cm^{-1} in $(OPPh_2)_2NH$, and $\nu_{as}(P_2N)$ 1260, 1220 cm^{-1} in $Na[(OPPh_2)_2N]$). In the carbonyl stretching region the expected four bands were observed (2035 vs, 2008 vs, 1983 vs, 1924 vs cm^{-1}, in KBr pellet, and 2051 vs, 2012 vs, 1980 m, and 1932 m cm^{-1}, in *n*-hexane solution), corresponding to non-degenerate ν(CO) vibrations $(2A_1 + B_1 + B_2)$ [16]. This behavior is characteristic of psuedooctahedral complexes with a carbonyl C_{2v} local symmetry, and is consistent with the coordination of the imidodiphosphinato ligand through both oxygen atoms.

A monomeric structure (**a**) might be proposed for this carbonylmanganese complex in solid state, similar to that established for the dithio analog [1]. However, a dimeric structure of type (**b**) cannot be ruled out.

Several attempts to grow X-ray quality crystals of $Mn(CO)_4[(OPPh_2)_2N]$ were performed using $CHCl_3$/hexane and CH_2Cl_2/hexane solutions but always decomposition of the starting material was achieved. The initial colorless solution became violet within few days and deposited purplish-blue crystals of the manganese(III) complex $Mn[(OPPh_2)_2N]_3$ (as proved by X-ray diffractometry—see below) together with an amorphous brown solid (probably MnO_2). The decomposition process might be described by eqn (2):

$$3\,Mn(CO)_4[(OPPh_2)_2N] + 2\,O_2 \rightarrow Mn[(OPPh_2)_2N]_3 + 2\,MnO_2 + 12\,CO \quad (2)$$

Attempts to obtain the same manganese(III) compound by oxidizing the manganese(II) complex, $Mn[(OPPh_2)_2N]_2$ [17], with hydrogen peroxide both in water suspension or chloroform solution have failed. No color change was observed when air was bubbled about out 6 h through a $CHCl_3$ solution of $Mn[(OPPh_2)_2N]_2$. However after a long period of time during which the solvent was slowly evaporated a purplish-blue solid was finally obtained. This was soluble in chloroform and was proved to be the corresponding manganese(III) complex. The compound was very stable and no decomposition was observed after several weeks in open atmosphere.

Table 1 contains selected bond distances and angles in $Mn[(OPPh_2)_2N]_3$ and Fig. 1 shows the ORTEP-like view [15] of the molecular structure with the atom numbering scheme.

The crystal contains discrete molecules of the manganese(III) complex, in which the imidodiphosphinato ligands act as bidentate moieties. As expected the PNP fragment, which in the free acid has a linear orientation, becomes now angular [av. 124.6(6)°] to allow the coordination of both oxygen atoms to the metal. Although significant differences in the manganese–oxygen bond lengths are noted (see below), the corresponding phosphorus–oxygen distances are equivalent [av. 1.518(9) Å] as are the phosphorus–nitrogen bonds [av. 1.587(7) Å]. These values might be considered of intermediate magnitude between single and double phosphorus–oxygen [cf $Ph_2P(=S)OMe$ [18]: P—O 1.60(2) Å; $Ph_3P(=O)$ [19]: P=O 1.487(2) Å] and phosphorus-nitrogen bonds [cf $Me—S—PPh_2=N—Ph_2P=S$ [20]: P—N 1.610(4), P=N 1.568(4) Å]. However the considerable double bond character of both bond types is evident.

The six-membered MnO_2P_2N inorganic rings thus formed are not planar despite the averaging in bond lengths due to some delocalization of π-electrons over the OPNPO fragment. They exhibit a twisted boat conformation as reflected by the torsion angles and the deviations from the MnO_2 planes within a MnO_2P_2N ring, respectively (Table 2).

For 6-coordinate complexes the octahedral geometry is the most common. However in many cases different degrees of distortion from the octahedron have been established [21], and this is the case for various manganese(III) complexes with chelating oxo ligands, MnL_3, resulting in a MnO_6 core (Fig. 2). A first type of distortion is the tetragonal distortion, that is either elongation or compression along one of the fourfold rotational axes of the octahedron, resulting in a reduction of symmetry from O_h to D_{4h}. This is the case of the previously reported β- and γ-forms of Mn(acetilacetonato)$_3$ and the distortion has been

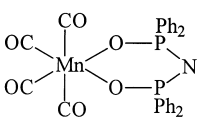

a

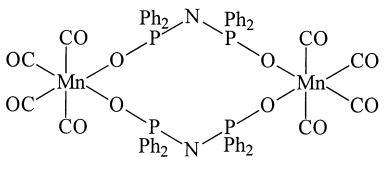

b

Table 1. Selected bond distances (Å) and angles (°) in $Mn[(OPPh_2)_2N]_3$

Mn(1)—O(1)	2.141(3)			*cis*-O—Mn—O angles	
Mn(1)—O(2)	1.953(3)	O(1)—Mn(1)—O(2)	89.9(1)	O(2)—Mn(1)—O(6)	92.0(1)
Mn(1)—O(3)	1.941(3)	O(1)—Mn(1)—O(3)	92.7(1)	O(3)—Mn(1)—O(4)	91.2(1)
Mn(1)—O(4)	1.939(3)	O(1)—Mn(1)—O(4)	88.4(1)	O(3)—Mn(1)—O(5)	87.9(1)
Mn(1)—O(5)	2.118(3)	O(1)—Mn(1)—O(6)	88.9(1)	O(4)—Mn(1)—O(5)	92.4(1)
Mn(1)—O(6)	1.950(3)	O(2)—Mn(1)—O(3)	87.2(1)	O(4)—Mn(1)—O(6)	89.7(1)
		O(2)—Mn(1)—O(5)	89.2(1)	O(5)—Mn(1)—O(6)	90.4(1)
				trans-O—Mn—O angles	
		O(1)—Mn(1)—O(5)	178.9(1)	O(3)—Mn(1)—O(6)	178.2(1)
		O(2)—Mn(1)—O(4)	177.6(1)		
P(1)—O(1)	1.513(3)	O(1)—P(1)—N(1)	117.7(2)	Mn(1)—O(1)—P(1)	124.0(2)
P(2)—O(2)	1.514(3)	O(2)—P(2)—N(1)	117.9(2)	Mn(1)—O(2)—P(2)	131.2(2)
P(1)—N(1)	1.588(4)				
P(2)—N(1)	1.595(4)	P(1)—N(1)—P(2)	123.9(2)		
P(3)—O(3)	1.520(3)	O(3)—P(3)—N(2)	116.6(2)	Mn(1)—O(3)—P(3)	131.1(2)
P(4)—O(4)	1.530(3)	O(4)—P(4)—N(2)	116.4(2)	Mn(1)—O(4)—P(4)	130.1(2)
P(3)—N(2)	1.584(4)				
P(4)—N(2)	1.584(4)	P(3)—N(2)—P(4)	124.9(2)		
P(5)—O(5)	1.505(3)	O(5)—P(5)—N(3)	117.8(2)	Mn(1)—O(5)—P(5)	128.5(2)
P(6)—O(6)	1.524(3)	O(6)—P(6)—N(3)	117.3(2)	Mn(1)—O(6)—P(6)	129.3(2)
P(5)—N(3)	1.592(4)				
P(6)—N(3)	1.576(4)	P(5)—N(3)—P(6)	124.9(3)		

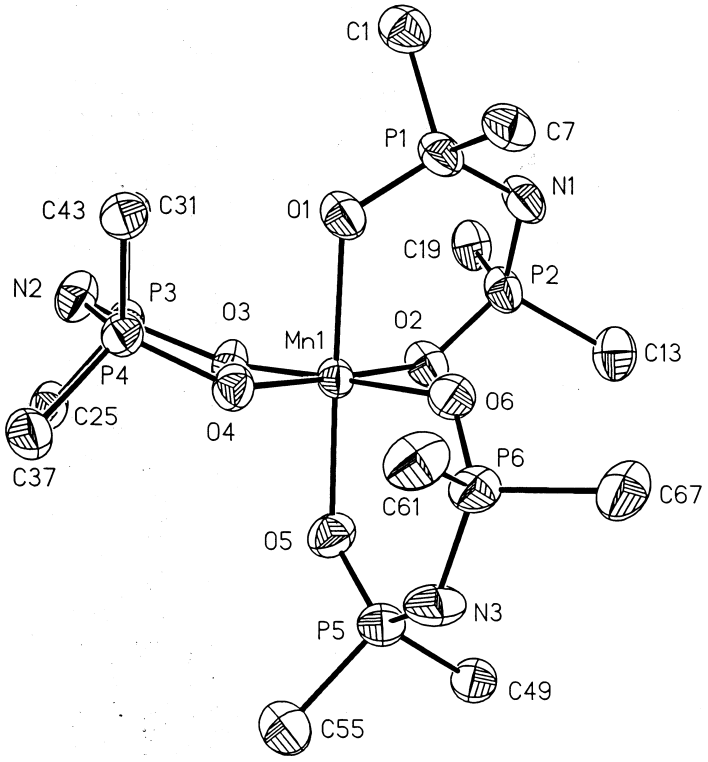

Fig. 1. Three dimensional representation of the molecular structure of $Mn[(OPPh_2)_2N]_3$ (for clarity only *ipso* carbons attached to phosphorus atoms are shown).

Table 2. Torsion angles (°) and least-square planes (deviations, Å) in $Mn[(OPPh_2)_2N]_3$

N(1)P(1)O(1)Mn(1)	27.5	N(2)P(3)O(3)Mn(1)	−12.5	N(3)P(5)O(5)Mn(1)	9.6
O(1)P(1)N(1)P(2)	11.2	O(3)P(3)N(2)P(4)	−11.9	O(5)P(5)N(3)P(6)	−22.5
O(2)P(2)N(1)P(1)	−26.6	O(4)P(4)N(2)P(3)	8.1	O(6)P(6)N(3)P(5)	3.1
N(1)P(2)O(2)Mn(1)	0.3	N(2)P(4)O(4)Mn(1)	20.7	N(3)P(6)O(6)Mn(1)	33.4
O(1)Mn(1)O(2)P(2)	25.9	O(3)Mn(1)O(4)P(4)	−33.3	O(5)Mn(1)O(6)P(6)	−36.7
O(2)Mn(1)O(1)P(1)	−40.1	O(4)Mn(1)O(3)P(3)	29.1	O(6)Mn(1)O(5)P(5)	14.0

Mn(1)O(1)O(2) plane		Mn(1)O(3)O(4) plane		Mn(1)O(5)O(6) plane	
P(1)	−0.809	P(3)	0.556	P(5)	0.287
P(2)	−0.498	P(4)	0.643	P(6)	0.707
N(1)	−1.155	N(2)	0.988	N(3)	0.866

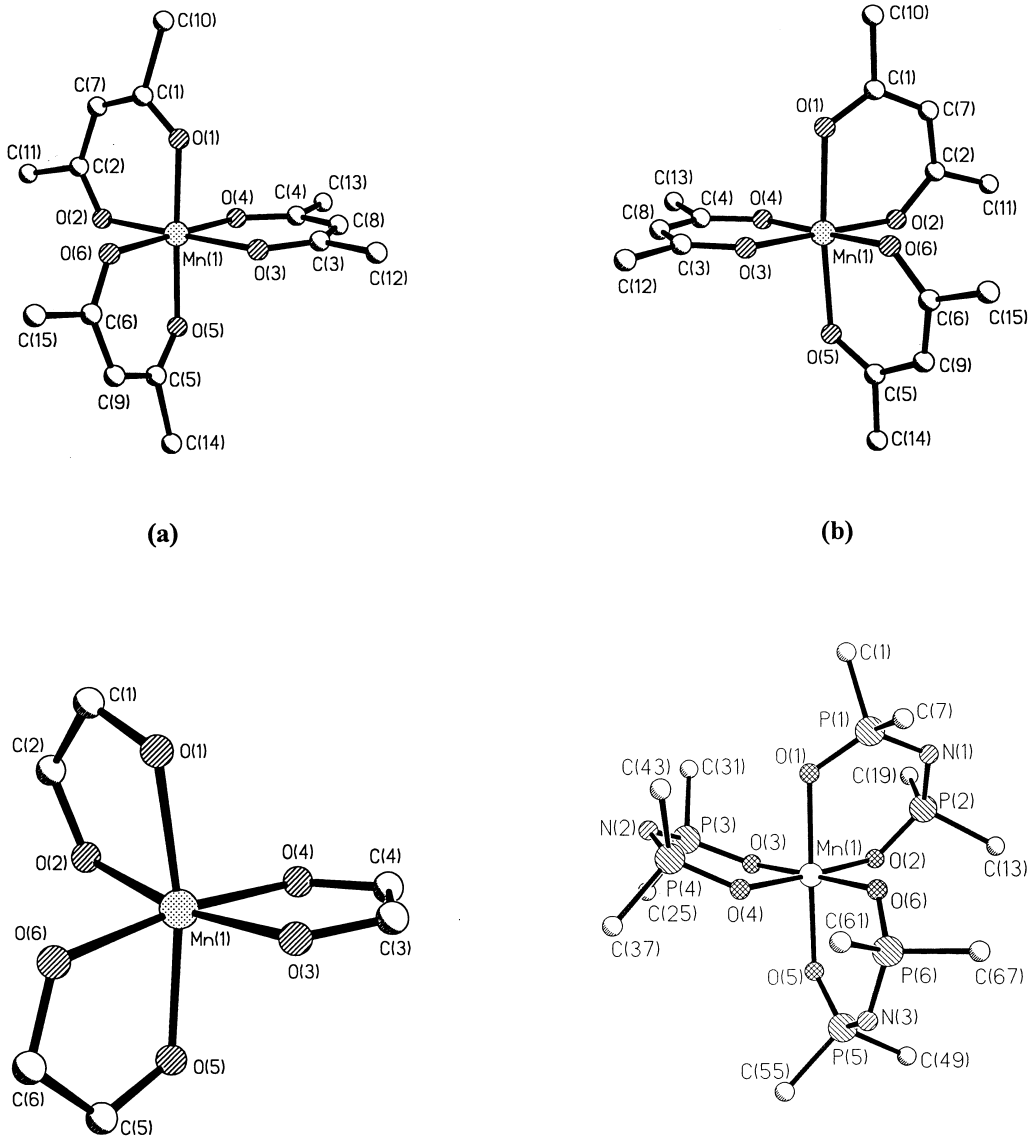

Fig. 2. MnO_6 cores in (**a**) β-$Mn[(OCMe)_2CH]_3$, (**b**) γ-$Mn[(OCMe)_2CH]_3$, (**c**) $Mn[O_2C_7H_5]_3$ (molecule **2**), (**d**) $Mn[(OPPh_2)_2N]_3$ [for clarity only carbons attached to oxygen and phosphorus atoms are shown in (**c**) and (**d**), respectively].

Table 3. Comparative structural data in $Mn[(OPPh_2)_2N]_3$ and related MnO_6 core-containing derivatives[a]

	$Mn[(OPPh_2)_2N]_3$ [this work]	β-$Mn[(OCMe)_2CH]_3$ [22]	γ-$Mn[(OCMe)_2CH]_3$ [23]	$Mn[O_2C_7H_5]_3$ [24][b]	
				molecule **1**	molecule **2**
MnO_6 core geometry[c]	tetragonally elongated MnO_6 distortion	tetragonally compressed MnO_6 distortion	tetragonally elongated MnO_6 distortion	tetragonally elongated MnO_6 distortion	orthorhombic MnO_6 distortion
b (Å)[d]	1.42	1.41	1.40	1.27	1.27
θ (degree)[e]	29.1	30.1	29.6	24.5	24.5
Mn—O (average)	1.946(7) 2.130(16)	1.944(18) 2.000(16)	1.935(5) 2.111(2)	1.942(15) 2.127(24)	1.944(7) 1.990(4) 2.052(16)
O···O bite (average)	2.85(7)	2.79(2)	2.80(4)	2.56(5)	2.54(3)
O—Mn—O (endocyclic, average)	90.5(0.6)	89.6(0.5)	89.2(1.5)	79.2(1.5)	79.0(1.9)
O—Mn—O (endocyclic, *cis*, range)	87.2(0.1)–92.7(0.1)	88.8(0.3)–91.7(0.3)	87.5(0.1)–92.5(0.1)	86.8(0.6)–104.1(0.6)	90.0(0.6)–97.4(0.6)
O—Mn—O (endocyclic, *trans*, range)	117.6(0.1)–178.9(0.1)	178.0(0.4)–179.0(0.4)	174.6–178.9[e]	162.9(0.6)–173.5(0.6)	169.1(0.6)–171.4(0.6)
Mn—O—X (average)	129.0(2.7)	127.2(0.4)	127.1(1.4)	115.0(4.1)	115.4(2.0)

[a] Esds for average bond length are calculated from the equation $\sigma = \left\{\left[\sum_{i=1}^{i=N}(x_i - x)^2/(N-1)\right]\right\}^{1/2}$, where x_i is ith bond length and x is the mean of the N equivalent bond lengths. An analogous formula is used for the calculation of esds for average bond angles [25].

[b] $O_2C_7H_5$ = tropolonato.

[c] TD = tetrahedral, SP = square-planar.

[d] Normalized bite of the bidentate ligand [21].

[e] Twist angle between the upper and lower triangular faces of the MnO_6 octahedron [20].

[e] Calculated from published atomic coordinates.

discussed in connection with the Jahn-Teller effect. The title compound, $Mn[(OPPh_2)_2N]_3$, exhibits a similar tetragonal elongation of the MnO_6 octahedral core (for comparative molecular parameters see Table 3): the axial Mn—O bond distances [av. 2.130(16) Å] are about 0.18 Å longer than the equatorial Mn—O bond distances [av. 1.946(7) Å]. The distortion of the oxygen atom arrangement around the metal is also reflected in the magnitude of the O—Mn—O angles. An elongation or compression along one of the three-fold rotational axes of the octahedron might also be expected and results in a trigonal antiprism (D_{3h}). The Mn(tropolonato)$_3$ complex shows an unusual feature, i.e. there are two crystallographically independent molecules: one is tetragonal elongated, while the other one was described as orthorhombical distorted with three pairs of different Mn—O distances [24]. It should be mentioned here that Keppert has considered an orthorhombical distortion of β-$Mn[(OCMe)_2CH]_3$, while the two independent molecules in the unit cell of the Mn(tropolonato)$_3$ complex were both described as exhibiting different degrees of tetragonal elongation (4% and 10%) [21].

Another possibility of distorsion might be considered for complexes containing MX_6 cores the coordination polyhedron being intermediate between a perfect octahedral symmetry and a trigonal prismatic coordination. For M(bidentate ligand)$_3$ complexes this type of distortion is completely defined by the normalized bite of the bidentate ligand b and the twist angle θ between two opposite triangular faces [21]: the shorter the bite distance, the smaller the twist angle. For manganese(III) complexes containing bidentate dioxo ligands (Table 3), if any Jahn-Teller distortions are ignored and the O—Mn—O bond angles are averaged assuming a three fold axis, then the calculated values of b and θ are consistent with the repulsion-energy calculations [21]. The flexibility of the OPNPO skeleton can allow smaller or larger O···O bite values as required by the coordination geometry around the metal atom. Therefore the tetragonal elongation observed in the case of $Mn[(OPPh_2)_2N]_3$ adds further evidence that the distortion of the molecular structure of Mn(III) complexes is due to the Jahn-Teller effect.

Acknowledgements—C.S. acknowledges a visiting fellowship grant from CONACYT and UNAM. N.Z.-V. also acknowledges financial support from CONACYT.

REFERENCES

1. Zuniga-Villarreal, N., Silvestru, C., Reyes Lezama, M., Hernandez-Ortega, S. and Alvarez Toledano, C., *J. Organomet. Chem.*, 1995, **496,** 169.
2. Haiduc, I., Sowerby, D. B. and Lu, S.-F., *Polyhedron*, 1995, **14,** 3389.
3. Ebert, K. H., Breunig, H. J., Silvestru, C., Stefan, I. and Haiduc, I., *Inorg. Chem.*, 1994, **33,** 1695 and references cited therein.
4. Silvestru, C., Haiduc, I., Cea-Olivares, R. and Hernandez-Ortega, S., *Inorg. Chim. Acta*, 1995, **233,** 151.
5. Silvestru, C. and Haiduc, I., *Coord. Chem. Rev.*, 1996, **147,** 117.
6. Churchill, M. R., Crooke, J., Fennessey, J. P. and Wormald, J., *Inorg. Chem.*, 1971, **10,** 1031.
7. Bhattacharyya, P., Novosad, J., Phillips, J., Slawin, A. M. Z., Williams, D. J. and Woollins, J. D., *J. Chem. Soc., Dalton Trans.*, 1995, 1607.
8. Rösler, R., Silvestru, C., Espinosa-Perez, G., Haiduc, I. and Cea-Olivares, R., *Inorg. Chim. Acta*, 1996, **241,** 47.
9. Silvestru, C., Rösler, R. and Toscano, R. A., unpublished results.
10. Greenwood, N. N. and Earnshaw, A., *Chemistry of the Elements*. Pergamon Press, Oxford, 1990, p. 1228.
11. Quick, M. H. and Angelici, R. J., *Inorg. Synth.*, 1979, **19,** 160.
12. Wang, F. T., Najdzionek, J., Leneker, K. L., Wasserman, H. and Braitsch, D. M., *Synth. React. Inorg. Met.-Org. Chem.*, 1978, **8,** 119.
13. Day, R. O., Holmes, R. R., Schmidpeter, A., Stoll, K. and Howe, L., *Chem. Ber.*, 1991, **124,** 2443.
14. Sheldrick, G. M., Crystal Structure Refinement Ver. SHELXL-97, *Inst. Anorg. Chem.*, Gottingen, Germany, 1997.
15. Sheldrick, G. M., SHELXL/PC User's Manual Siemens Analytical X-Ray, Inc., Madison, WI, 1990.
16. Orgel, L. E., *Inorg. Chem.*, 1962, **1,** 25.
17. Szekely, I., Drake, J. E. and Silvestru, C., *Phosphorus, Sulfur and Silicon*, 1997, in press.
18. Lepicard, G., de Saint-Giniez-Liebig, D., Laurent, A. and Rerat, C., *Acta Crystallogr.*, 1969, **B25,** 617.
19. Baures, P. W. and Silverton, J. V., *Acta Crystallogr.*, 1990, **C46,** 715.
20. Silvestru, C., Rösler, R. and Espinosa-Perez, G., unpublished work.
21. Kepert, D. L., *Progr. Inorg. Chem.*, 1977, **23,** 1.
22. Fackler, Jr. J. P. and Avdeef, A., *Inorg. Chem.*, 1974, **13,** 1864.
23. Stults, B. R., Marianelli, R. S. and Day, V. W., *Inorg. Chem.*, 1979, **18,** 1853.
24. Avdeef, A., Costamagna, J. A. and Fackler, Jr. J. P., *Inorg. Chem.*, 1979, **13,** 1854.
25. Churchill, M. R., Cooke, J., Wormald, J., Davison, A. and Switkes, E. S., *J. Am. Chem. Soc.*, 1969, **91,** 6518.

Pergamon

PII : S0277–5387(98)00034–5

Polyhedron Vol. 17, No. 16, pp. 2687–2692, 1998
© 1998 Elsevier Science Ltd
All rights reserved. Printed in Great Britain
0277–5387/98 $19.00+0.00

Carboxylate shift in one dimension polymeric chain complexes $[Cu(dien)(OAc)]_n(ClO_4)_n$. Syntheses, crystal structure and spectroscopic study on isomer

Bao-Hui Ye,[a,*] Liang-Nian Ji,[a] Feng Xue[b] and Thomas C. W. Mak[b]

[a] Chemistry Department, Zhongshan University, Guangzhou, 510275, P.R. China

[b] Chemistry Department, The Chinese University of Hong Kong, Shatin, New Territories, Hong Kong

(Received 13 November 1997; accepted 11 January 1998)

Abstract—Two one dimension copper(II) polymer chain complexes with an identical molecular formula, $[Cu(dien)(OAc)]_n(ClO_4)_n$, but different stuctural features were synthesized through the reaction of $Cu_2(OAc)_4 \cdot 2H_2O$ with $M(dien)_2(ClO_4)_2$ ($M = Cu^{2+}$, Ni^{2+} and Zn^{2+}; dien = diethylenetriamine). In complex **1,** the geometry at each Cu(II) ion is a distorted octahedron (4+2) (D. K. Towle, *et al*. *Inorg*. *Chem*. 1988, **27,** 394–399); while in complex **2,** that is pentacoordinate and best described as a distorted trigonal bipyramid. The acetate groups act as monodentate bridging mode in **1,** but as single *syn-anti* bridging fashion (Cu—O = 2.008(10) and 2.062(11) Å) in **2**. These provide a good example for the suggested pathway in the "carboxylate shift". The isomer can also be diagnosed by FT-IR and FT-Raman spectroscopies, and X-ray powder diffraction. © 1998 Elsevier Science Ltd. All rights reserved

Keywords: copper complex; diethylenetriamine; acetate; coordination polymer; carboxylate shift; one dimension.

A plethora of dinuclear or polynuclear carboxylates of a variety of transition metal ions have been prepared and structurally characterized in recent years. The increasing interest in this coordination chemistry is due to several reasons. Firstly, the carboxylate groups from aspartate and glutamate side chains play a crucial role as ligands in many metalloenzymes involving mono- or polymetallic active sites [1], and the synthesis and characterization of discrete dinuclear and polynuclear carboxylates is one of the major objectives of bioinorganic model chemistry [2]. Secondly, carboxylate metal complexes are good catalyst in some reactions and widely applied in industrial and laboratorial catalyses [3]. Thirdly, carboxylate anions have a versatile coordination behavior, generating various and sometimes surprising molecular architectures [4]. Lastly, polynuclear carboxylates are very good candidates for the investigation of exchange-coupling interactions between adjacent metal ions [5].

Though a number of carboxylate-bridged copper(II) complexes have been synthesized and characterized, only a few mono(μ-carboxylate)-bridged copper(II) chain complexes were obtained [6]. Of these few examples, the geometry at each Cu(II) ion in the chain complex $[Cu(dien)(OAc)]_n(ClO_4)_n$ (**1**) is a distorted 4+2 octahedron [6a]. Every Cu(II) ion is connected to two others in the chain through acetate bridges, and the acetate groups act as monodentate bridging mode which is an important intermediate between other carboxylate binding modes [1b,7]. The movement from monodentate bridging to other binding modes is termed the "carboxylate shift" [7]. This phenomenon could be kinetically important in carboxylate containing metalloproteins.

Such observations have prompted us to further investigate the "carboxylate shift" from the monodentate bridging to other binding fashion using the diethylenetriamine as a tridentate ligand in the synthesis of carboxylate Cu(II) complexes. In this paper, we report the syntheses and structural characterization of two one dimension polymer chain com-

* Author to whom correspondence should be addressed.

plexes with an identical molecular formula $[Cu(dien)(OAc)]_n(ClO_4)_n$. They are good example for the suggested pathway in the "carboxylate shift" [1b].

EXPERIMENTAL

Starting materials were purchased from commercial sources and were used without further purification. The complex $[Cu(dien)_2](ClO_4)_2$, $[Zn(dien)_2](ClO_4)_2$ and $[Ni(dien)_2](ClO_4)_2$ were preparated according to the procedure described [8]. (**CAUTION**: No problems were encountered during the preparation of the perchlorate derivatives described above. However, suitable care and precautions must be taken when handling such potentially explosive compounds.) Elemental analyses (C, H and N) were performed on a Perkin–Elmer 240Q Elemental analyzer. FT-IR spectra were recorded on a Bruker IFS-66 spectrometer as KBr pellets (4000–400 cm^{-1}). FT-Raman spectra were collected on a Brucker RFS-100 spectrometer with an excited source 1064 nm. UV–visible spectra were measured on a Milton Roy Spectronic 3000 spectrophotometer in methanol solution at room temperature. X-ray powder diffraction was recorded by a Philips MPD-1880I diffractiometer at room temperature using Cu–K_α (1.540562 Å) radiation, 40 kV anodic voltage and 50 mA current. The samples were scanned for 2θ angles from 4 to 64° at a scanning rate of 0.02° per min.

Synthesis

Hexacoordinated $[Cu(dien)(OAc)]_n(ClO_4)_n$ (**1**). Method A. $Cu_2(OAc)_4 \cdot 2H_2O$ (0.199 g, 0.5 mmol) was added to a methanol solution (20 ml, methanol : water = 9 : 1) containing $Cu(dien)_2(ClO_4)_2$ (0.468 g, 1 mmol) with stirring. The solution was stirred at 50°C for 3 h. A blue precipitate was produced, filtered off after cooling to room temperature and washed with ethanol and acetone and dried in air. The blue colour product was recrystallined with water and methanol. Yield: 0.62 g, 95.0%. Found: C, 22.31; H, 3.43; N, 12.75%. Calc. for $C_6H_{11}N_3O_6ClCu$: C, 22.15; H, 3.38; N, 12.92%. FT-IR data (cm^{-1}): 3222 m, 3130 s, 2937 m, 1603 vs, 1572 vs, 1430 m, 1402 vs, 1335 m, 1144–1086 vs, 1034 m, 687 m, 636 m, 626 s. FT-Raman data (cm^{-1}): 1601 w, 1563 w, 1464 s, 1257 m, 1144 m, 1122 m, 932 vs, 914 m, 625 m, 463 vs, 388 m, 348 w, 320 m, 276 m, 224 s. Electronic spectrum in water, λ_{max}, nm (ε, M^{-1} cm^{-1}): 610 (195), 246(3400). A single crystal suitable for X-ray analysis was obtained by slow evaporating a methanol and water mixture solution of compound **1**.

Method B. $Cu_2(OAc)_4 \cdot 2H_2O$ (0.199 g, 0.5 mmol) was added to a stirring methanol solution (20 ml, methanol : water = 3 : 1) containing $Ni(dien)_2(ClO_4)_2$ (0.462 g, 1 mmol). The solution was stirred at 50°C for 5 h. A blue precipitate was produced, filtered off after cooling to room temperature and washed with ethanol and acetone and dried in air. The product was recrystallined with water and methanol. Yield: 0.28 g, 86.1%. The product was identified by FT-IR spectra (*vide infra*).

Pentacoordinated $[Cu(dien)(OAc)]_n(ClO_4)_n$ (**2**). Method A. Complex **1** (0.325 g, 1 mmol) and $NaOAc \cdot 3H_2O$ (0.136 g, 1mmol) were added to an ethanol solution (30 ml, ethanol : water = 1 : 1), and the solution was stirred at 60°C for 5 h. The solution was filtered off, and the filtrate was stayed in air to evaporate slowly to get crystals. The pale blue crystals were collected, washed with cold ethanol-diethyl ether (1 : 1) and dried in air. Yield: 0.13 g, 40%. Found: C, 22.42; H, 3.50; N, 12.80%. Calc. for $C_6H_{11}N_3O_6ClCu$: C, 22.15; H, 3.38; N, 12.92%. FT-IR data (cm^{-1}): 3317 s, 3262 s, 2923 m, 1608 m, 1562 vs, 1458 m, 1427 s, 1338 w, 1142–1065 vs, 1014 m, 938 s, 675 m, 633 s, 627 s, 507 m. FT-Raman data (cm^{-1}): 1602 w, 1471 s, 1458 s, 1254 m, 1128 m, 1063 m, 959 m, 931 vs, 911 m, 625 m, 457 m, 423 m, 304 w, 229 w. Electronic spectrum in water, λ_{max}, nm (ε M^{-1} cm^{-1}): 613 (176), 249 (3350). A single crystal suitable for X-ray analysis was obtained by slow evaporating a methanol and water mixture solution of compound **2**.

Method B. $Cu_2(OAc)_4 \cdot 2H_2O$ (0.199 g, 0.5 mmol) was added with stirring to an ethanol solution (20 ml ethanol : water = 1 : 1) containing $Zn(dien)_2(ClO_4)_2$ (0.469 g, 1 mmol). The solution was stirred at 60°C for 5 h. The solution was filtered off after cooling to room temperature. The blue precipitate was washed with cool ethanol and acetone and dried in air. Yield: 0.15 g, 46.1%. The product was identified by FT-IR spectra (*vide infra*), and it displays an almost same spectrum of hexacoordinate **1**. The filtrate was stayed in air to evaporate the solvent to get crystals after 3 days. The product was collected by filter, washed with cold ethanol-diethyl ether (1 : 1) and dried in air. Yield: 0.1 g, 30.7%. The identification of the product was deduced by FT-IR spectra comparison with method A (*vide infra*).

Crystallographic measurements and structure resolution

Crystal data for **2**: $C_6H_{11}ClN_3O_6Cu$, orthorhombic, space group *P*nma, $a = 8.3130(10)$, $b = 8.642(2)$, $c = 17.727(2)$ Å, $V = 1273.6(3)$ $Å^3$, $Z = 4$, $D_{calc} = 1.670$ Mg/m^3, $\mu = 1.943$ mm^{-1}, $T = 294$ K.

A pale blue single crystal of complex **2** having approximate dimension of $0.08 \times 0.25 \times 0.30$ mm was mounted on a glass fiber and placed on a Siemens R3m/V diffractometer using graphite-monochromated Mo–K_α X-radiation ($\lambda = 0.71073$ Å). Cell constants and orientation matrix for data collection, obtained from a least-squares refinement using the setting angles of 25 carefully centered reflections with $12 \leqslant 2\theta \leqslant 23°$. 1201 independent reflections were collected in the range $7.0 \leqslant 2\theta \leqslant 45.0°$ ($0 \leqslant h \leqslant 9$,

$0 \leqslant k \leqslant 10$, $0 \leqslant l \leqslant 20$) with the variable-speed ω-scan technique. Crystal stability was monitored by recording three check reflections at intervals of 97 data measurements, and no significant variation was detected. The structure was solved by direct methods using the SHELXTL-PC program package [9]. All the non-hydrogen atoms were refined anisotropically. Hydrogen atoms of the ligands were generated in their idealized positions (C—H = 0.96 Å), assigned isotropic thermal parameters. The structure was refined in full-matrix least-squares where the function minimized was $\Sigma w(F_o - F_c)^2$ and the weighting scheme $w = [\sigma^2 (F) + 0.0001F^2]^{-1}$. The final cycle of refinement was based on 807 observed reflections and 92 variable parameters and converged with unweighted and weighted agreement factors of $R = \Sigma([F_o] - [F_c])/\Sigma[F_c] = 0.0712$ and $R_w = [\Sigma w(F_o - F_c)^2/\Sigma w(F_o)^2]^{1/2} = 0.0780$, GOF = 0.92. The largest difference peaks and hole were 1.14 and -0.71 eÅ^{-3}, respectively. The unit cell of **1**: monoclinic, space group $P2_1/n$ with $a = 10.124(2)$ Å, $b = 8.082(3)$ Å, $c = 15.512(2)$ Å, $\beta = 99.02\ (2)^\circ$, $V = 1254.6$ Å^3, $Z = 4$, and is the same as the reported [6a], and its structure was not refined.

RESULTS AND DISCUSSION

Syntheses and spectra properties

The synthesis of the complex formulated as $[Cu(dien)(OAc)]_n(ClO_4)_n$ was first reported by Towle and his coworker in 1988 [6a], because of its interesting magnetic properties. The present syntheses differ from that reported and result in the formation of a novel isomer. The reactions of the copper(II) acetate with $M(dien)_2(ClO_4)_2$ ($M = Cu^{2+}$, Ni^{2+} and Zn^{2+}) were carried out in methanol-water solution, and a dark blue polymer copper(II) complex $[Cu(dien)(OAc)]_n(ClO_4)_n$, **1,** was precipitated from the solution. On the other hand, the filtrate of the reaction solution from $Zn(dien)_2(ClO_4)_2$ and $Cu_2(OAc)_4 \cdot 2H_2O$ was left in air to evaporate the solvent and pale blue crystals were obtained. These observations have prompted us to further examine what differences in their geometries and how we can obtain the desired product under the reaction conditions. We notice that the counterion ClO_4^- is essential to obtain the desired product under this reaction condition. Efforts to obtain a polymeric structure analogous to **1** or **2** using Cl^- anion displacing the counterion ClO_4^- was not successful. We have tried to expand this synthetic procedure to prepare other polymer compounds containing Zn^{2+} or Ni^{2+} ion. We found that an isostructural complex $[Zn(dien)(OAc)]_n(ClO_4)_n$ was produced, however, trying to prepare an analogous complex containing Ni^{2+} ion was not successful under this condition [10].

Complexes **1** and **2** display quite different on their FT-IR and FT-Raman spectra, though they have an identical molecular formula. The IR spectra of both complexes **1** and **2** exhibit very strong bands around 1100 and 625 cm^{-1}, which were assigned to $v_3(T_2)$ and $v_4(T_2)$ modes of the uncoordinated perchlorate anion. The v(NH) stretching vibration in the free dien ligand at 3360 and 3295 cm^{-1} bands were assigned to primary and second amine groups, respectively, which were down-shift to 3317 and 3262 cm^{-1} for **2,** 3222 and 3130 cm^{-1} for **1,** respectively. These shifts are strong evidence that the ligand is coordinated in a tridentate mode [11]. A number of geometric isomers of hexacoordinate dien complexes $M(dien)L_3$ have been prepared and the ligand conformation has been studied by IR spectroscopy. It has been concluded that the facial (*fac*) and meridional (*mer*) isomers for monodien complexes may be distinguished by their IR spectra [11,12]. The presence of a band at ca 933 cm^{-1} in the recorded spectrum is taken as evidence for the *fac* conformation of dien [12b]. However, the spectrum of complex **2** displays an intense peak at 938 cm^{-1} while it is absent in complex **1**. Thus, our results also seem to support that this band could be used as a diagnostic tool for the dien conformation. On the other hand, the v(COO) stretching vibrations also display significant differences in the spectra of **1** and **2**. The v_{as}(COO) and v_s(COO) bands are located at 1572 and 1402, and 1562 and 1427 cm^{-1} in the spectra of **1** and **2,** respectively. The difference values of v_{as}(COO) and v_s(COO) are 170 and 137 cm^{-1} for **1** and **2,** respectively. These are consistent with the geometries of acetate groups adopted as monodentate bridging mode in **1** and *syn-anti* mode in **2** [13].

Complex **1** shows a band at 1563 cm^{-1} in FT-Raman spectrum; however, this peak was absent in complex **2**. But the strong band at 1464 cm^{-1} in **1** was split into a doublet at 1471 and 1459 cm^{-1} with 12 cm^{-1} apart in **2**. These were also strong evidence that the acetate groups adopted as distinct fashions in **1** and **2,** consistenting with the results from FT-IR and single crystal diffraction experiments. X-ray powder diffraction experiments also display significant differences between **1** and **2** (seen Fig. 1).

Crystal structure

The crystal structure of **2** reveal that the complex has an extended structure, forming infinite μ-OAc chain. A labelled diagram is shown in Fig. 2. Selected bond distances and angles are collected in Table 1. The Cu(II) ions are connected through single *syn-anti* acetate bridges, forming infinite zig-zag chains running along the *a* crystallographic axis. The average distance between the two chains is 9.953 Å. Though a number of copper(II)-carboxylate complexes were prepared, complexes exhibiting a single *syn-anti* carboxylate bridge are not very common in the literature [6], due to the fact that the *anti* lone pair of the carboxylate groups have a lower basicity than the *syn* ones [14].

The geometry of each copper(II) ion is five coor-

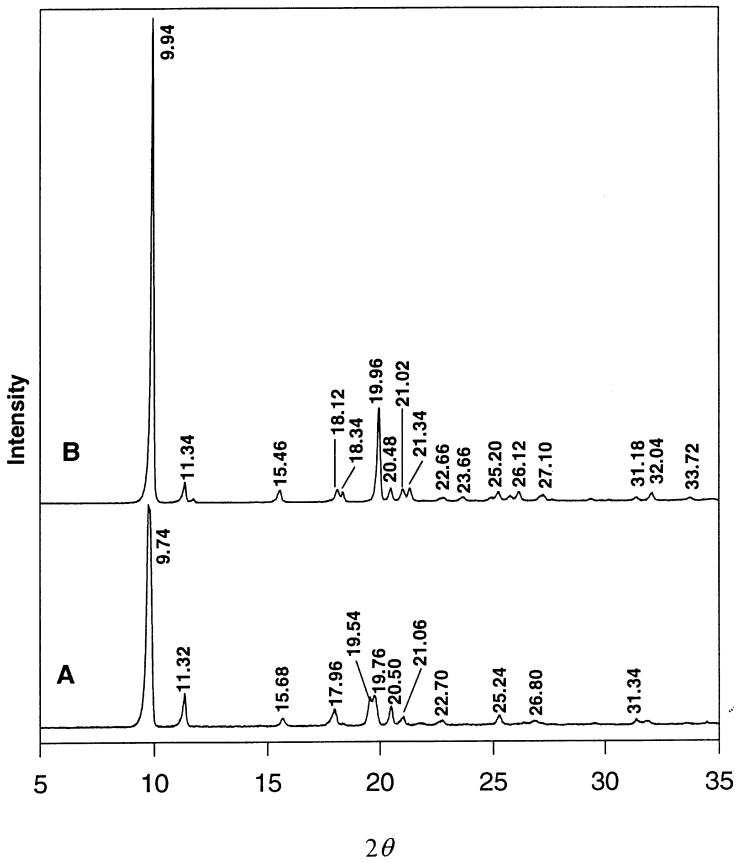

Fig. 1. X-ray powder patters for (A) complex **2** and (B) complex **1** at room temperature with 0.02° per min rate using Cu–K_α (1.540562 Å) radiation, 40 kV anodic voltage and 50 mA current.

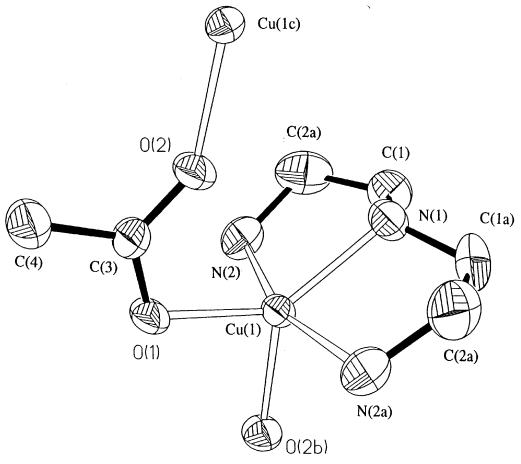

Fig. 2. ORTEP view of $[Cu(dien)(OAc)](ClO_4)$, showing 40% probability thermal ellipsoids and atoms labels.

dinate with C_{2v} symmetry, the structure being best described as a distorted trigonal bipyramid in which N(2) and N(2a) are axial while N(1), O(1) and O(2) are in the trigonal plane. As expected for a trigonal bipyramid, Cu(II) ion lies in the trigonal plane (average deviation from the four-atom plane is 0). This plane is coplanar with the two adjacent carboxylate planes, and perpendicular with the plane consisting of three nitrogen atoms and Cu(II) (the largest deviation from the four-atom plane is 0.075 Å). The principal distortion from trigonal pyramidal geometry is the angles in the trigonal plane; in the idealized case these should all be 120°, but in complex **2** they range from 93.3(3)–139.2(6)°. Obviously, there is an alternate description of the complex **2** as a distorted tetragonal pyramid, where one oxygen atom from the acetate is axial while the other oxygen atom from another acetate and the three nitrogen atoms from the dien ligand are equatorial. But the distortions from idealized tetragonal pyramidal geometry are severe. The structure of the infinite chain resembles those found in $[Cu(dien)(HCOO)]_n(HCOO)_n$ [6b] and $[Cu(1,1\text{-}Me_2\text{-}dien)(OAc)]_n(ClO_4)_n$ [6e], which contain similar carboxylate bridges. It is interesting that there are several differences between the molecular structure of **2** and **1,** although they have an identical molecular formula $[Cu(dien)(OAc)]_n(ClO_4)_n$. In complex **1,** the coor-

Table 1. Selected bond distances (Å) and angles (°) of **2**

Cu(1)—N(1)	2.098(15)	Cu(1)—N(2)	2.140(9)
Cu(1)—O(1)	2.008(10)	Cu(1)—N(2A)	2.140(9)
Cu(1)—O(2B)	2.062(11)	C(3)—O(1)	1.250(21)
C(3)—O(2)	1.232(20)		

N(1)—Cu(1)—N(2)	80.9(3)	N(1)—Cu(1)—O(1)	139.2(6)
N(2)—Cu(1)—O(1)	98.9(3)	N(1)—Cu(1)—N(2A)	80.9(3)
N(2)—Cu(1)—N(2A)	160.8(6)	O(1)—Cu(1)—N(2A)	98.9(3)
N(1)—Cu(1)—O(2B)	127.5(6)	N(2)—Cu(1)—O(2B)	93.2(3)
O(1)—Cu(1)—O(2B)	93.3(5)	N(2A)—Cu(1)—O(2B)	93.2(3)
C(4)—C(3)—O(1)	117.7(16)	C(4)—C(3)—O(2)	123.0(17)
O(1)—C(3)—O(2)	119.3(14)		

Symmetry code, A: $x, 0.5-y, z$; B: $0.5+x, y, 0.5-z$; C: $-0.5+x, y, 0.5-z$.

dination around the Cu(II) ion is a distorted octahedron (4+2), due to the implication of both *syn* and *anti* lone pairs of the bridging oxygen atom [6a]. The coordination mode of the acetate groups in **1** can best be described as monodentate bridging, the "dangling" oxygen [1b] occupying one of the equatorial positions at 1.972(4) Å. In complex **2,** however, the distances between O(2b) (*anti*) and two neighbouring Cu(II) ions within the chain are 2.062(11) and 2.701 Å, whereas in **1** they are 2.403(4) and 2.646(4) Å [6a]. As a consequence, the Cu···Cu distance in **2** (4.440 Å) is significantly longer than that found in **1** (4.210 Å). The differences between **1** and **2** arise mainly from the coordination modes adopted by the acetate groups. These can be realized through the "carboxylate shift" (see Scheme 1). In complex **1,** the acetate groups act as monodentate bridging mode which would be considered as an important intermediate towards other carboxylate binding modes [1b]. The *syn* electron pair of the second carboxylate oxygen, called the "dangling" oxygen atom, would play an important role by interacting with one of the bridged metallic centers. The gradual change from monodentate bridging to other binding modes was termed the "carboxylate shift" [1b]. The shift from monodentate bridging to the classical *syn-syn* bidentate bridging would occur through *syn-anti* bidentate bridging attachment of the carboxylate ligand, such as observed in complex **2**.

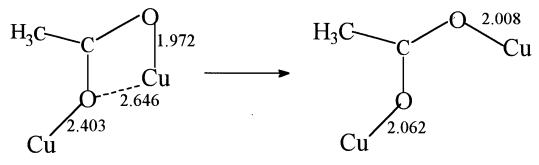

1
Monodentate bridge

2
Syn-anti bridge

Scheme 1. The carboxylate shift from monodentate bridge (**1**) to *syn-anti* bridge (**2**) with different Cu—O distances (angstrom).

Therefore, the different geometries of acetate groups adopted in **1** and **2** illustrate well the suggested pathway in the "carboxylate shift".

Supplementary materials—List of atomic coordinates and isotropic temperature factors, anisotropic temperature factors, hydrogen coordinates, bond distances and angles, and observed and calculated amplitudes have been deposited with the Cambridge Crystallographic Data Center.

Acknowledgements—We gratefully acknowledge financial support from Zhongshan University.

REFERENCES

1. (a) Holm, R. H., Kennepohl, P. and Solomon, E. I., *Chem. Rev.*, 1996, **96,** 2239; (b) Rardin, R. L. Tollman W. B. and Lippard, S. J., *New J. Chem.*, 1991, **15,** 417; (c) Wilcox, D. E., *Chem. Rev.*, 1996, **96,** 2435.
2. (a) Feig, A. L. and Lippard, S. J., *Chem. Rev.*, 1994, **94,** 759; (b) Que Jr. L. and True, A. E., *Prog. Inorg. Chem.*, 1990, **37,** 97; (c) Christou, G., *Acc. Chem. Res.*, 1989, **22,** 328; (d) Halcrow M. A. and Christou, G., *Chem. Rev.*, 1994, **94,** 2421; (e) Wieghardt, K., *Angew. Chem. Int. Ed. Engl.*, 1989, **28,** 1153; (f) Lippard, S. J., *Angew. Chem. Int. Ed. Engl.*, 1988, **27,** 344.
3. Mehrotra, R. C. and Bohra, R., *Metal Carboxylates*, Academic, New York 1983.
4. Hathaway, B. J., In *Comprehensive Coordination Chemistry*, **Vol. 2,** ed. G. Wilkinson, R. D. Gillard and J. A. McCleverty, Pergamon Press, Oxford, 1987, p. 413.
5. Kahn, O., *Molecular Magnetism*, VCH, New York, 1993; *Adv. Inorg. Chem.*, 1996, **43,** 179; Murray, K. S., *Adv. Inorg. Chem.*, 1996, **43,** 261.
6. (a) Towle, D. K., Hoffmann, S. K., Hatfielf, W. E., Singh, P. and Chaudhuri, P., *Inorg. Chem.*, 1988, **27,** 394; (b) Davey, G. and Stephens, F. S., *J. Chem. Soc.* (*A*), 1971, 103; (c) Hatfield, W. E., Helms, J. H., Rohrs, B. R. and Haar, L. W., *J. Am. Chem. Soc.*, 1986, *108,* 542; (d) Coughlin, P. K. and Lippard, S. J., *J. Am. Chem. Soc.*, 1984,

106, 2328; (e) Rochon, F. D., Melanson, R. and Andruh, M., *Polyhedron*, 1996, **15,** 3075.
7. Rardin, R. L., Bino, A., Poganiuch, P., Tolman, W. B., Liu, S. and Lippard, S. J., *Angew. Chem. Int. Ed. Engl.*, 1990, **29,** 812.
8. Curtis, N. F. and Powell, H. K. J., *J. Chem. Soc.* (*A*), 1968, 3069.
9. Sheldrick, G. M., SHELXTL-PC, *Program System for X-ray Crystal Structure Determination*, Siemen Analytic Instruments, Inc., Karlsruhe, Germany, 1990.
10. Ye, B.-H. and Chen, X.-M., unpublished result.
11. (a) Trendafilova, N., Nikolov, D. S., Bauer, G. and Kellner, R., *Inorg. Chim. Acta*, 1993, **210,** 77; (b) Allmann, R., Krestl, M., Bolos, C., Manoussakis, G. and Nikolov, G. S., *Inorg. Chim. Acta*, 1990, **175,** 255.
12. (a) Mukherjee, A. K., Koner, S., Ghosh, A., Chaudhuri, N. R., Mukherjee M. and Welch, A. J., *J. Chem. Soc. Dalton Trans.*, 1994, 2367; (b) Schmidtke, H.-H. and Garthhof. D., *Inorg. Chim. Acta*, 1968, **2,** 357.
13. Deacon, G. B. and Phillips, R. J., *Coord. Chem. Rev.*, 1980, **33,** 227.
14. Gandour, R. D., *Bioorg. Chem.*, 1981, **10,** 169; Wiberg, K. B. and Laidig, K. E., *J. Am. Chem. Soc.*, 1987, **109,** 5935.

Pergamon

PII : S0277–5387(98)00036–9

Polyhedron Vol. 17, No. 16, pp. 2693–2697, 1998
© 1998 Elsevier Science Ltd
All rights reserved. Printed in Great Britain
0277–5387/98 $19.00+0.00

The bidentate bonding mode of *bis*[2-oximinocyanacetamidato(2-)-*N*,*N*]nickelate(II) anion towards tetraphenylantimony(V) : unusually long Sb—O contact

Andrei A. Mokhir,[a] Rosario Vilaplana,[b] Francisco Gonzalez-Vilchez,[b,*] Igor Olegovich Fritsky,[a,*] Konstantin V. Domasevitch[a] and Nickolai M. Dudarenko[a]

[a] Department of Chemistry, Shevchenko University, Kiev 252033, Ukraine

[b] Departamento de Quimica Inorganica, Facultad de Quimica, Universidad de Sevilla, Aptdo. 553, 41071 Sevilla, Spain

(Received 2 June 1997 ; accepted 12 January 1998)

Abstract—The heteronuclear complex of tetraphenylantimony(V) with anion of *bis*(oximino-cyanoacetamidato(2-)-*N*,*N*)nickelate(II) $[(Ph_4Sb)_2\{Ni(NCC(NO)C(O)NH)_2\}]$ **1** was synthesized and investigated by single crystal X-ray analysis. **1** was isolated as a result of the reaction between tetraphenylantimony(V) chloride and nickel(II) complex with (hydroximino)cyanoacetamide (H_2aco) $Na_2\{Ni(aco)_2\}$ obtained by reaction of $Ni(Haco)_2$ with NaOH. The crystal comprises heterometal centrosymmetric molecules $(Ph_4Sb)_2\{Ni(aco)_2\}$. The Ni atom is in a slightly distorted square planar surrounding formed by the four nitrogen atoms of deprotonated hydroximino and amide groups (Ni—N_{oxime} 1.890(4), Ni—N_{amide} 1.862(4) Å). The ligands are situated in *trans* positions with respect to each other. The coordination environment of the antimony atom in the Ph_4Sb^+ cation is somewhat distorted trigonal bipyramidal [SbC_4O], Sb—C_{eq} 2.084(5)–2.108(5) Å. All angles C_{eq}—Sb—O_{ax} are less than 90°. Ph_4Sb^+ coordinates to the oxygen atom of C═O group (Sb—O 2.647(3) Å). The geometrical parameters of the CNO group indicate that it exists in the nitroso-form. © 1998 Elsevier Science Ltd. All rights reserved

Keywords: heteronuclear complex ; oximes ; tetraphenylantimony(V) ; nickel(II) complex ; crystal structure.

The last decade is marked by the increasing interest to the design and synthesis of new homo- and heteropolynuclear metal assemblies. These compounds often possess unusual structural, spectral and magnetic properties and represent an evident interest in the field of molecular electronics and magnetism. Bi- and polynuclear metal complexes were also successfully used in bioinorganic chemistry as models of active centers of some metalloproteins (*e.g.*, superoxidedismutase) [1]. Another possible application of the mentioned compounds in this field is connected with their bioactivity which may be quite different as compared to that indicated by mononuclear complexes. The compounds containing potentially anti-cancer ions : diorganotin(IV) [2], organoantimony(V) [3], platinum(II), palladium(II) [4–6], ruthenium(III,IV) [7,8] together with 3d-metals ions having remarkable biological activity [9] are of special interest.

One possible approach for synthesis of heteropolynuclear complexes with desirable structure is usage of mononuclear complexes as ligands. The suitable ligands for obtaining of such "building blocks" should form rather stable mononuclear complexes and not undergo the rearrangement of the coordination sphere upon interaction with the additional metal ions. Chelating ligands possessing strong field donor groups such as oxamide derivatives [10] and dioximes [11] were used for these purposes. Earlier we reported the oxime analogues of aminoacids and peptides which were shown to be specific and efficient

* Authors to whom correspondence should be addressed.

ligands for Cu^{2+} and Ni^{2+} ions [12,13]. These ligands contain adjacent oxime and amide groups and was established to form stable anionic complexes with ($[MN_4]$, $2N_{oxime}$, $2N_{amide}$) coordination (M=Cu^{2+}, Ni^{2+}) at pH 7 and higher. These species can form additional coordination bonds by means of the oxygen atoms of oxime (C=NO) and carbamoyl (C=O) group. The former coordination mode is the most likely and was observed recently in homobinuclear complexes of (hydroximino)propanamide (H_2pox): $[Cu\{Cu(Hpox)(pox)\}]^{+}$[11] and (hydroximino)cyanacetamide (H_2aco): $[Cu\{Cu(aco)_2\}]$[12] formed in aqueous solution, while the latter one was not known up to date.

In this work the crystal and molecular structure of the first heteronuclear complex containing doubly deprotonated (hydroximino)cyanacetamide $[(Ph_4Sb)_2[Ni(aco)_2]$ is reported.

EXPERIMENTAL

All chemicals were commercial products of reagent grade and used without further purification. Ni(H-aco)$_2 \cdot 2H_2O$ was synthesized according to [14].

^{13}C and 1H NMR spectra were recorded on a JEOL-400 GSX FT-NMR spectrometer. UV–VIS spectra were obtained on a Cary-14 spectrometer. IR spectra were recorded on a 2020 Galaxy Series FT-IR spectrometer.

Synthesis of $[(Ph_4Sb)_2\{Ni(NCC(NO)C(O)NH)_2\}]$ **1**

To the suspension of 0.103 g (0.323 mmol) of Ni(H-aco)$_2 \cdot 2H_2O$ in 25 ml of water 0.16 ml of 2M NaOH solution was added. The obtained mixture was heated at 80°C upon continuous stirring until complete dissolution of solid. 0.301 g of Ph_4SbCl (0.626 mmol) was added to the resulting solution, and the formed precipitate after 2 h was filtered off and washed with a small amount of ice water. The product **1** may be purified by recrystallization from water or acetonitrile. Yield: 0.282 g (76.5%). Found: C, 55.9; H, 3.1; N, 7.8; Ni, 5.5. Calc. for $C_{54}H_{42}N_6O_4NiSb_2$: C, 56.2; H, 2.9; N, 7.5; Ni, 5.9 %. ^{1}H NMR ($CDCl_3$), ppm δ 7.696 (d, $J = 7.2$ Hz, 16H), 7.496 (m, 24H), 3.010 (s, 2H); ^{13}C NMR ($CDCl_3$), ppm δ 170.0167 (**C**(O)NH_2), 135.36, 133.57, 131.62, 129.88 (Ph), 124.57 (**C**≡N), 113.34 (**C**NO); UV–vis, cm^{-1} 17600 ($\varepsilon = 130$), 18800 ($\varepsilon = 70$); IR, cm^{-1} ν(C≡N) 2199, ν(C=O) 1561, ν(N—O) 1163.

The crystal suitable for X-ray analysis was obtained by slow isothermal (298 K) evaporation of acetonitrile solution of **1**.

Crystallographic data collection and structure determination

Crystal data and experimental details are presented in Table 1. The accurate unit cell parameters and the orientation matrix were calculated from the setting angles of 24 reflections using the least-square technique. Intensities were collected using an Enraf-Nonius CAD-4 diffractometer in the ω-2θ scan mode using graphite-monochromated Cu–K_α radiation. The intensities of three standard reflections, monitored every 100 intensity scans showed no evidence of crystal decay. Corrections for Lorentz and polarization effects as well as an empirical correction for absorption using DIFABS [15] were applied; minimum and maximum absorption corrections were 0.974 and 1.020.

The structure was solved by direct methods using SHELXS-86 [16] and refined by full-matrix, least-squares on all F_o^2 using SHELXL-93 [17]. Neutral atom scattering factors and anomalous dispersion terms used in the refinement were taken from reference [18], real and imaginary components of anomalous dispersion were included for all non-H atoms. The position of the N—H hydrogen atom was determined from difference Fourier synthesis and refined in isotropic approximation. The C—H hydrogen atoms of the phenyl groups were added at calculated positions and included in the calculation of structure factors as the fixed contributions. Correction for extinction was taken into account in the course of refinement. A weighting scheme of the form $w = 1/\sigma^2(F_o^2) + (0.0813xP)^2 + 3.35\ P$ [where P is defined as $(F_o^2 + 2F_c^2)/3$] was applied. Observed and calculated structure factors, anisotropic thermal parameters, atomic coordinates, full list of interatomic distances, bond angles and torsion angles are given in supplementary material. The selected bond distances and angles are listed in Table 2.

RESULTS AND DISCUSSION

The crystal comprises centrosymmetric molecules $(Ph_4Sb)_2\{Ni(aco)_2\}$ having no close contacts between each other (Fig. 1). The closest intermolecular contacts in the crystal packing are 3.565(3) Å (C(12)—O(1) $(1-x,1-y,-z)$) that is equal to the sum of the Van der Waals radii [19].

In the complex anion the nickel atom occupies a center of symmetry. The coordination environment of the central atom is slightly distorted square planar formed by the four nitrogen atoms belonging to the deprotonated hydroximino and amide groups. The ligands are two-charged anions of (hydroximino)cyanacetamide. They are situated in *trans* position with respect to each other. The Ni—N(oxime) and Ni—N(amide) distances are 1.890(4) and 1.862(4) Å, respectively. The angular distortions around the Ni atom are connected with formation of five-members chelate ring: the bite angle N(1)—Ni—N(2) is decreased to 83.7(2)°, the N(1)—Ni—N(2)$(-x+2, -y+2, -z)$ angle is increased to 96.3(2)°. The mentioned chelate ring is in fact planar.

Table 1. Crystal data and structure refinement for $[((C_6H_5)_4Sb)_2\{Ni(aco)_2\}]$

Empirical formula	$C_{54}H_{42}N_6O_4NiSb_2$
M	1141.14
Temperature (K)	293(2)
Wavelength Å	1.54178
Crystal system	monoclinic
Space group	$P2_1/n$
a(Å)	8.853(2)
b(Å)	9.748(2)
c(Å)	27.167(5)
β(°)	96.29(3)
U(Å^3)	2330.4(8)
Z	2
D_c (Mg m^{-3})	1.626
μ (mm^{-1})	10.032
F(000)	1140
Crystal size (mm)	$10 \times 25 \times 30$
θ range(°)	3.27–57.94
Range hkl	−9 to 9, 0 to 10, 0 to 29
Reflections collected	3253
Independent reflections (R_{int})	3253
Data/parameters	3253/305
Goodness-of-fit on F^2	1.087
Final R indices [$I > 2\sigma(I)$]	$R_1^a = 0.0387$, $wR_2^b = 0.1099$
R indices (all data)	$R_1^a = 0.0434$, $wR_2^b = 0.1176$
Max. Δ/σ/Å	0.006
Max., min. electron density (e Å^{-3})	1.026, −0.631

[a] $R_1 = \Sigma(F_o - F_c)/\Sigma F_o$
[b] $wR_2 = \{\Sigma[w(F_o^2 - F_c^2)^2]/\Sigma[w(F_o^2)^2]\}^{1/2}$

Table 2. Selected bond lengths (Å) and angles (°) $[(Ph_4Sb)_2\{Ni(aco)_2\}]$

Sb—C(10)	2.084(5)	O(1)—N(1)	1.268(6)
Sb—C(4)	2.102(5)	O(2)—C(1)	1.269(6)
Sb—C(16)	2.108(5)	N(1)—C(2)	1.327(7)
Sb—C(22)	2.120(5)	N(2)—C(1)	1.309(7)
Sb—O(2)[b]	2.647(3)	N(3)—C(3)	1.140(7)
Ni—N(2)	1.862(4)	C(1)—C(2)	1.472(7)
Ni—N(1)	1.890(4)	C(2)—C(3)	1.422(8)
C(10)—Sb—C(4)	116.5(2)	O(1)—N(1)—C(2)	122.1(5)
C(10)—Sb—C(16)	120.9(2)	O(2)—C(1)—N(2)	128.9(5)
C(4)—Sb—C(16)	113.9(2)	O(2)—C(1)—C(2)	120.2(4)
C(10)—Sb—C(22)	100.6(2)	N(2)—C(1)—C(2)	110.8(4)
C(4)—Sb—C(22)	100.8(2)	N(1)—C(2)—C(3)	120.4(5)
C(16)—Sb—C(22)	98.3(2)	N(1)—C(2)—C(1)	115.2(4)
C(10)—Sb—O(2)[b]	77.6(2)	C(3)—C(2)—C(1)	124.4(4)
C(4)—Sb—O(2)[b]	82.3(2)	N(3)—C(3)—C(2)	178.0(6)
C(16)—Sb—O(2)[b]	80.6(2)		
C(22)—Sb—O(2)[b]	176.9(2)		
N(2)[a]—Ni—N(1)	96.3(2)		
N(2)—Ni—N(1)	83.7(2)		

Symmetry transformations used to generate equivalent atoms:
[a] $-x+2, -y+2, -z$;
[b] $x-1, y-1, z$.

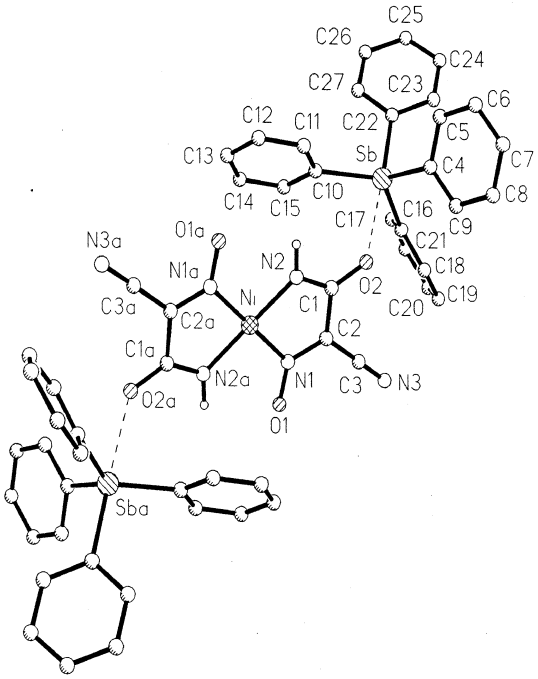

Fig. 1. Structure and numbering scheme for complex **1**.

The antimony atom of Ph_4Sb^+ cation is in somewhat distorted trigonal bipyramidal surrounding. Equatorial positions are occupied by the carbon atoms of phenyl rings which are situated in the most sterically favorable propeller-like conformation and slightly inclined to the oxygen atom occupying the axial position. All the angles C_{eq}—Sb—O_{ax} are less than 90° (Table 2). The second apical position is occupied by the carbon atom of the phenyl ring, the Sb—C_{ax} distance is slightly increased as compared to Sb—C_{eq} (2.120(5) Å, Table 2). According to relative electronegativity of oxygen and carbon atoms, the oxygen atom of carbamoyl group occupies the axial position. The distance Sb—O(2) ($x-1$, $y-1$, z) 2.647(3) Å is relatively long, which indicates its ionic character. For comparison, the distances Sb—O observed in five-coordinated tetraphenylantimony(V) complexes lie in the range 2.20–2.35 Å [20]; the longest Sb—O contact reported for tetraphenylstibonium benzenesulfonate monohydrate 2.506 Å [21]. Such elongation of the Sb—O bond length in (1) leads to an increase of the tetrahedral distortion in the Ph_4Sb moiety; C_{eq}—Sb—O_{ax} 77.6(2)–82.3(2)° for **1,** 80.59(7)–84.76(7)° for Ph_4Sb(Haco) and 82.8(2)–86.6(2)° for Ph_4Sb(dco) [22].

Ph_4Sb^+ coordinates to oxygen atom of C═O group forming O═C—C═N(oxime) bridges between two metal centers. As a result the electron density in the frame of the ligand is significantly disturbed. Thus the C═O and C═N(oxime) bond lengths (Table 2) are increased as compared to the values observed in $\{(H_3C)_4N)_2[Cu(aco)_2]\}$ [13] (1.237(3) and 1.302(3) Å, respectively), whereas the C—N(amide) and N—O bond lengths (Table 2) are decreased (in $\{(H_3C)_4N)_2[Cu(aco)_2]\}$ [13] 1.313(3) and 1.289(3).

The angular parameters of the present ligand are similar to those observed for the other ligands having deprotonated oxime and amide groups [12,13]. The geometrical parameters of CNO group (Table 2) indicate that this moiety exists in the nitroso-form.

Acknowledgments—This work was partially supported by NATO (Grant for I.O.F. within the Program "Expert Visits"), by Soros International Science Foundation (Individual grant for A.A.M. [1] PSU063071) and CICYT (SAF94-0467). We also thank Dr. Edward B. Rusanov for collection of X-ray data.

REFERENCES

1. Cowan, J. A., *Inorganic Biochemistry*: *An Indroduction*, VCH Publishers, Inc., New York. 1993.
2. Gielen, M., Willem, R., Bouhdid, A., Devos, D., Kuiper C. M., Veerman G. and Peters G. J., *Oncology Reports*, 1996, **3,** 583.
3. Silvestru, C., Haiduc, L., Tiekink, E. R. T., Devos, D., Biesemans, M., Willem, R. and Gielen, M., *Applied Organomet. Chem.*, 1995, **9,** 597.
4. Clarke, M. G., in Platinum, Gold and Other Metal Chemotherapeutic Agents, *American Chemical Society Symposium Series* 209, ed. S. J. Lippard, Washington, DC, 1983, 335.
5. Cavallo, L., Cini, R., Kobe, J., Marzilli, L. G. and Natile, G., *J. Chem. Soc., Dalton Trans.*, 1991, 1867.
6. van Beusichem, M. and Farrell, N., *Inorg Chem.*, 1992, **31,** 634.
7. Vilaplana, R. A., Gonzalez-Vilchez, F., Gutierrez-Puebla, E. and Ruiz-Valero, C., *Inorg. Chim. Acta*, 1994, **224,** 15.
8. Mei, H. E. and Barton, J. K., *Proc. Natl. Acad. Sci. U.S.A.*, 1985, **85,** 1339.
9. Sadler, P. J., *Adv. Inorg. Chem.*, 1996, **36,** 1.
10. (a) Mathoniere, C., Kahn, O., Daran, J. C., Hilbig, H. and Kohler, F. H., *Inorg. Chem.*, 1993, **32**(19), 4057; (b) Lloret, F., Julve, M., Ruiz, R., Journaux, Y., Nakatani, K., Kahn, O. and Sletten, J., *Inorg. Chem.*, 1993, **32**(1), 27.
11. (a) Ruiz, R., Sanz, J., Cervera, B., Lloret, F., Julve, M., Bois, C., Faus, J. and Munoz, M. C., *J. Chem. Soc., Dalton Trans.*, 1993, **10,** 1623; (b) Ruiz, R., Sanz, J., Lloret, F., Julve, M., Faus, J., Bois, C. and Munoz, M. C., *J. Chem. Soc., Dalton Trans.*, 1993, **20,** 3035; (c) Lloret, F., Ruiz, R., Cervera, B., Castro, I., Julve, M., Faus, J., Real, J. A., Sapina, F., Journaux, Y., Colin, J. C. and Verdaguer, M., *J. Chem. Soc., Chem. Commun.*, 1994, **22,** 2615.
12. Sliva, T. Yu., Kowalik-Jankowska, T., Amirkhanov, V. M., Glowiak, T., Onindo, C. O., Fritsky, I. O. and Kozlowski, H., *J. Inorg. Biochem.*, 1997, **65,** 287.
13. Sliva, T. Yu., Duda, A. M., Glowiak, T., Fritsky, I. O., Amirkhanov, V. M., Mokhir, A. A. and Kozlowski, H., *J. Chem. Soc., Dalton Trans.*, 1997, 273.

14. Skopenko, V. V., Zub, Yu. L., Lampeka, R. D., Bel'skii, V. K. and Zavodnik, V. E., *Dopov. Akad. Nauk Ukr. RSR*, *Ser. B*, 1983, **4,** 60.
15. Walker, N. and Stuart, D., *Acta Crystallogr., Sect. A*, 1983, **39,** 158.
16. Sheldrick, G. M., *Acta crystallogr., Sect A*, 1990, **46,** 467.
17. Sheldrick, G. M., *SHELXL* 93, University of Gottingen, 1993
18. *International Tables for Crystallography*, Vol. C., Kluwer, Dordrecht, Netherlands, 1992, Tables 4.2.6.8. and 6.1.1.4.
19. Batsanov, S. S., *Zh. Neorg. Khim.* (*Russ*), 1991, **36,** 3015.
20. (a) Kopf, J., Vetter, G. and Klar, G., *Z. Anorg. Allg. Chem.*, 1972, **409,** 285; (b) Ferguson, G., Hawley, D. M., *Acta Crystallogr., Sect. B*, 1974, **30,** 103; (c) Bone, S. P., Sowerby, D. B., *Phosphorus, Sulfur, and Silicon*, 1989, **45,** 23.
21. Ruther, R., Huber, F. and Preut, H., *J. Organomet. Chem.*, 1985, **21,** 295.
22. Domasevich, K. V., Chernega, A. N., Lindeman, S. V. and Struchkov, Yu. T., *Zh. Neorg. Khim.* (*Russ*), 1995, **40,** 426.

Pergamon

PII : S0277–5387(98)00039–4

Polyhedron Vol. 17, No. 16, pp. 2699–2711, 1998
© 1998 Elsevier Science Ltd
All rights reserved. Printed in Great Britain
0277–5387/98 $19.00+0.00

Spin crossover in substituted *N*,*N*′-ethylenebis(salicylidenamine) iron(III) complexes : variable temperature EPR and X-ray structures of [Fe(5-CH_3O-SALEN)$(Im)_2$]Y, where Y = ClO_4^- and Cl^-

Mohan M. Bhadbhade and D. Srinivas*

Sophisticated Analytical Instruments Laboratory, Central Salt and Marine Chemicals Research Institute, Gijubhai Badheka Marg, Bhavnagar 364 002, India

(Received 24 October 1997 ; accepted 23 January 1998)

Abstract—The spin state of iron(III) in substituted *N*,*N*′-ethylenebis(salicylidenaminato) complexes of type [Fe(5-X-salen)L_2]Y, where X = CH_3O, H and Cl, L = Im and 2-MeIm and Y = Cl^-, ClO_4^- and BPh_4^- was determined using X-ray structures, magnetic susceptibility and variable temperature EPR studies. X-ray data of [Fe(5-CH_3O-salen)$(Im)_2$]Y, where Y = ClO_4^- (**1**) and Cl^- (**2**) are as follows : **1**, $C_{24}H_{26}N_6O_8ClFe$, monoclinic $P2_1/n$, a = 10.516(4) Å, b = 13.752(3) Å, c = 19.227(3) Å, β = 102.14(2)°, V = 2718(11) Å^3, Z = 4, R = 0.097 (R_w = 0.084) ; **2**, $C_{24}H_{26}N_6O_4ClFe$, monoclinic $P2_1/n$, a = 11.709(3) Å, b = 12.746(2) Å, c = 17.388(4) Å, β = 106.15(2)°, V = 2493(15) Å^3, Z = 4, R = 0.062 (R_w = 0.065). Metal-ligand bond distances are consistent with a HS state for iron(III) which has a tetragonally distorted octahedral geometry. Imidazole planes are coplanar and bisect the N—Fe—O bond angle in **2** while they are oriented by 77.3° apart in **1** almost coinciding with the N—Fe—O direction. Counterions showed significant effect on the overall molecular geometry and FeN_2C_2 ring. Methanolic solutions of all the complexes showed spin crossover whereas only salen and 5-Cl-salen complexes exhibited this phenomenon in solid state. EPR investigations revealed, for the first time, two types of interconvertible low spin species (LS1 and LS2) in solution ; the former was characterized by an almost axial g tensor with lower g anisotropy (2.238–1.937) while the latter with a rhombic tensor with larger g anisotropy (2.382–1.911). Ground state wave functions and distortion parameters were calculated. Structure-spin state-reactivity correlations are proposed. © 1998 Elsevier Science Ltd. All rights reserved

Keywords: Iron(III) complexes ; salen ; spin crossover ; structures ; EPR.

Spin crossover in iron complexes has been extensively studied to understand the mechanisms and various factors influencing the phenomenon, to explore its implications in metalloproteins e.g., myoglobin, hemoglobin and cytochromes and to examine the spin state-reactivity correlation [1–5]. Recently, molecules with labile electronic ground state are attracting more attention due to their potential application as sensors and memory devices [6,7]. Factors like substitution, axial ligands, counterions, solvent of crystallization etc, influence the nature of spin state crossover [5,8]. Interestingly, the orientation of axial imidazole and pyridine ligands in porphyrinato complexes also control the electronic ground state [4,9]. Variable temperature X-ray structural studies have revealed that the electron transfer rate is coupled to intermolecular solid state effects and the onset of dynamic motions of a solvent molecule in the lattice. The dynamic disorders in the lattice lead to rapid spin interconversion rates and reversible abrupt transition while static order leads to slow rates and gradual spin crossover behavior [10].

Spin crossover in salen type complexes was observed initially by Nishida *et al.* [11] and later Kennedy and co-workers have reported a detailed study

*Author to whom all correspondence should be addressed : Special Instruments Laboratory, National Chemical Laboratory, Pune 411 008, India.

on the influence of uncoordinated anion on the spin state interconversion dynamics [12]. With a view to understand further the structure-spin state-reactivity correlations we report here structure and variable temperature ESR investigations on some Fe(III) substituted quadridentate salen complexes of type [Fe(5-X-salen)L_2]Y, where X = CH_3O, H and Cl; L = substituted imidazole (Im) and Y = Cl^-, ClO_4^- and BPh_4^-. Ligand field strength is systematically varied by introducing varying donacity substituents in salen as well as in axial imidazole ligands.

EXPERIMENTAL

Synthesis

The Schiff base ligands, *N*,*N*′-ethylenebis(5-methoxysalicylidenamine) (5-CH_3O-salenH_2), *N*,*N*′-ethylenebis(salicylidenamine) (salenH_2) and *N*,*N*′-ethylenebis(5-chlorosalicylidenamine) (5-Cl-salenH_2), were prepared as condensation products of the respective aldehyde (2 mmol) and en (1 mmol) in absolute alcohol [13]. Iron(III) complexes with these ligands, Fe(5-X-salen)Cl were prepared following the method of Gerloch *et al*. [14].

[Fe(5-X-salen)L_2]Cl

The complexes were synthesized by adding the ethanolic soln (10 ml) of axial ligand L (Im or 2-MeIm, 5 mmol) in small frs to a hot suspension of Fe(5-X-salen)Cl in ethanol (1 mmol, 25 ml). The reaction mixt was refluxed for ~1 h under inert atmosphere, filtered and kept for slow evaporation. Microcrystals were obtained overnight.

[Fe(5-X-salen)L_2]Y

The complexes with counterion Y (ClO_4^- or BPh_4^-) were prepared by adding freshly prepared $NaClO_4$ and $NaBPh_4$ (1 mmol) in ethanol to the above hot ethanolic solns of [Fe(5-X-salen)L_2]Cl. Microcrystals were obtained overnight by slow evaporation.

In the case of salen and 5-Cl-salen the products were isolated by using a rotary evaporator as slow evaporation always yielded products contaminated with an orange red μ-oxo compound. **Caution!** Perchlorato salts can potentially explode during drying and grinding, so proper care should be exercised while handling such compounds. So far we have not experienced any problems during sample preparation.

Physical measurements

Microanalyses of complexes were done using a CHN Carlo Erba 1106 elemental analyzer. The IR spectra were measured for KBr pellets (1% *w*/*w*) at 298 K on a Carl Zeiss Specord M-80 spectrophotometer. Electronic spectra were recorded for ethanolic solns on a Shimadzu UV–vis spectrophotometer in the range 200–1100 nm. Magnetic susceptibilities of the complexes were measured by the Faraday method; $Hg[Co(SCN)_4]$ was used as a calibrant. Effective magnetic moments (μ_{eff}) were calculated after applying diamagnetic correction.

EPR investigations were carried out on a Bruker ESP 300 X-band spectrometer with a 100 kHz field modulation. DPPH was used as a field marker ($g = 2.0036$). Samples were taken in quartz tubes as glass tubes in general contained iron(III) ion impurity which gave signal at $g \cong 4.2$ overlapping with the compound signals. The spectra were measured in the temperature range 77–298 K for both polycrystalline samples and solns. Measurements at 77 K were performed using a quartz inserting Dewar while variable temperature studies were done with a Bruker ER4111 set-up.

X-ray crystallography

Crystallographic data for complexes **1** and **2** are summarized in Table 1. Both the structures were solved by the heavy-atom method and refined by the full-matrix least-squares procedure as described in Table 1. The oxygen atoms of perchlorate ion in complex **1** show very high thermal anisotropic vibrations, a possible factor for a rather high R value for this complex. Hydrogen atom positions were mostly obtained from difference Fourier synthesis, a few (belonging to the methyl group) were fixed stereochemically at appropriate geometries. The H-atoms were included only for the structure factor calculation and were not refined in the least-squares. All computations were performed on a PDP-11/73 computer using the Structure Determination Package (SDP) available from Enraf-Nonius [16].

Analysis of EPR data

The EPR spectra for Fe(III) complexes have been extensively studied by several workers [17]. The spectrum for a high spin complex ($t_{2g}^3\ e_g^2$, $S = 5/2$) is described by the following spin Hamiltonian.

$$\mathcal{H} = D[S_z^2 - S(S+1)/3 + (E/D)(S_x^2 - S_y^2)] + \beta_e \mathrm{H}.g.S \quad (1)$$

Here D and E are the tetragonal and rhombic zero-field splitting parameters for $^6A_{1g}$. If the electron Zeeman energy is greater than the zero-field terms, one observes resonances from all the $(2S+1)$ fine structure levels at free spin g value. On the other hand, if $D > g\beta_e$H and the system is tetragonal ($E = 0$), the three Kramers' doublets are well separated and only transitions are allowed within the ground state doublet $|\pm 1/2>$ resulting in resonances at $g\perp \cong 6.0$ and $g\| \cong 2.0$. However, in the case of extreme rhombic

Table 1. Summary of crystallographic data

Experimental values	**1**	**2**
Molecular formula	$C_{24}H_{26}N_6O_8FeCl$	$C_{24}H_{26}N_6O_4FeCl$
Molecular weight	617.8	553.8
Space group	Monoclinic, $P2_1/n$	Monoclinic, $P2_1/n$
Cell parameters		
a (Å)	10.516(4)	11.709(3)
b (Å)	13.752(3)	12.746(2)
c (Å)	19.227(3)	17.388(4)
β (°)	102.14(2)	106.15(2)
Z	4	4
V (Å^3)	2718(11)	2493(15)
No. of reflection used and θ range (°) used for unit cell parameters	20, 15–25	25, 18–25
Radiation used, λ (Å)	Cu–K$_\alpha$, 1.5418	Cu–K$_\alpha$, 1.5418
D_{calc} (g cm^{-3})	1.504	1.473
Absorption Coeff, μ (cm^{-1})	58.7	62.2
Temperature (K)	295	295
Colour and description	brown plates	brown plates
Crystal dimensions (mm)	$0.20\times0.12\times0.10$	$0.40\times0.32\times0.24$
Diffractometer	Enraf-Nonius CAD-4	Enraf-Nonius CAD-4
Scan mode	$\omega/2\theta$	$\omega/2\theta$
Absorption correction [15]	empirical	empirical
Transmission min, max	73.9, 99.95	59.5, 99.7
Measured reflections	4517	4202
Observed reflections $I > 3\sigma(I)$	2001	2800
θmax (°)	65	65
h_{min}, h_{max}	0, 12	0, 13
k_{min}, k_{max}	0, 16	0, 14
I_{min}, I_{max}	−22, 22	−20, 19
No. of intensity control reflections, frequency and variation	3, 1 h, nil	3, 1 h, nil
No. of orientation control reflections, frequency and variation	3, every 200 reflns., nil	3, every 200 refln, nil
Refinement on	$\|F\|$	$\|F\|$
Final R	0.097	0.062
Weighted R	0.084	0.065
Reflections used	2001	2800
No. of parameters in least-squares	361	325
Hydrogen atom positions	not refined	not refined
$(\Delta/\sigma)_{max}$	0.09	0.02
Weighting scheme	$1/\sigma(F)^2$	$1/\sigma(F)^2$
$\Delta\rho_{max}$ (e/Å^3)	1.09	0.51
$\Delta\rho_{min}$ (e/Å^3)	−0.75	−1.03
Extinction correction	not applied	not applied
Source of atomic scattering factors	International Tables for X-ray crystallography, Vol. IV, Kynoch Press, Birmingham	

symmetry ($E/D = 1/3$) the resonances corresponding to each doublet occur at

$$E_3 : g_x \cong g_y \cong 0.6, g_z \cong 9.6 \quad \text{highly anisotropic}$$

$$E_2 : g_x = g_y = g_z \cong 4.286 \quad \text{almost isotropic}$$

$$E_1 : g_x = g_z \cong 0.6, g_y \cong 9.6 \quad \text{highly anisotropic}$$

Inclusion of cubic field terms further deviate these values. In the case of polycrystalline samples the spectrum corresponds to an ensemble average of all the orientations and consists a strong signal at $g \cong 4.3$.

In the case of low spin Fe(III) complexes, if the appropriate one electron orbitals for the t_{2g}^5 configuration ($S' = 1/2$) are employed with the following Hamiltonian

$$\mathscr{H} = \zeta 1.s - \Delta[1_z^2 - 1(1+1)/3] - V(1_+^2 + 1_-^2)/2 \quad (2)$$

then a set of three secular equations result for the ground state Kramers' doublet [18]. Here ζ is the one electron spin-orbit coupling constant, Δ is the axial distortion and V is the low symmetry rhombic distor-

tion. The secular equations can be solved to give wave functions which upon application of a Zeeman Hamiltonian operator gives the following expressions for the g values.

$$g_z = -2[a^2 - b^2 + c^2 + K(a^2 - c^2)]$$
$$g_x = 2[2ac - b^2 + \sqrt{2}Kb(c - a)]$$
$$g_y = -2[2ac + b^2 + \sqrt{2}Kb(c + a)] \quad (3)$$

Here K is the orbital reduction parameter or covalency parameter; a, b and c are the MO coefficients describing the ground state Kramers' doublet

$$\psi = a|+1^+> + b|\xi^-> + c|-1^+>$$
$$\psi' = a|-1^-> - b|\xi^+> + c|+1^-> \quad (4)$$

where $|+1>$, $|-1>$ and $|\xi>$ $\{= (|+2> - |-2>)/\sqrt{2}\}$ are the one electron orbitals. A computer program was written to evaluate a, b, c and K by least squares fitting the experimental g values to the above g value expressions and the normalization condition given by eqn (5)

$$a^2 + b^2 + c^2 = 1 \quad (5)$$

In addition the energy separations of the three Kramers' doublets of $^2T_{2g}$ ($\Delta E_1/\lambda$ and $\Delta E_2/\lambda$) and distortion parameters (Δ/λ and V/λ) were obtained by solving the secular equations. In the absence of information about the sign and orientation of g values, as usually happens for powder samples, 48 combinations were considered. The best fit values were selected on the basis of physically reasonable values of K, Δ and V. These values for all the complexes are listed in Table 3.

RESULTS AND DISCUSSION

Spectral characterization

The IR spectra for solids showed intense peaks in the range 1608–1650 cm^{-1} attributable to the stretching modes of azomethine and phenyl groups. Upon complexation these peaks shifted to lower frequency side by ~ 10 cm^{-1}, compared to that for free ligands. The absence of a broad band around 3460 cm^{-1} due to ν(O—H) indicated the coordination of salen as a dianionic ligand. The presence of axial ligands was confirmed by their characteristic peaks. Perchlorate ion gave strong peaks around 1148, 1116, 1086 and 630 cm^{-1}. Methanolic solutions of the complexes showed intense charge transfer bands of ligand origin in the UV-visible spectra around 249, 305 and 375 nm. In the case of the complexes with 5-CH_3O-salen, moderately intense bands were observed additionally at 450 and 567 nm due to MLCT transitions. However, for salen and 5-Cl-salen these bands have shifted to ~ 460 nm revealing the effect of substituents on the ligand field strength.

Effects of counterion and substitution on the chelate geometry. Structures of [Fe(5-CH_3O-salen)$(Im)_2$]Y, *where* Y = ClO_4^- (**1**) *and* Y = Cl^- (**2**)

ORTEP [19] views of **1** and **2** are shown in Fig. 1 along with the atom numbering. Selected bond distances and angles are given in Table 2. The Fe atom is in a tetragonally distorted octahedral coordination in **1**, with the Fe—O bond distances being the shortest (1.923(6), 1.869(6) Å), Fe—N(salen) distances being intermediate (2.109(7), 2.117(6) Å) and axial Fe—N(Im) being the longest (2.15(1), 2.21(1) Å). The Fe—N(salen) and Fe—O distances are comparable with those of the high spin complex [Fe(salen)$(Im)_2$]PF_6 [12]. The five membered FeN_2C_2 (ethylenediamine) ring has the *meso* conformation in **1** with the displacements of atoms C8 and C9 being 0.25 Å and 0.40 Å from the FeN_2 plane, in opposite directions. The planar sal1 and sal2 units are symmetrically bent in opposite directions form the N_2O_2 plane, making almost equal angles (~ 13–14°) with it. The overall conformation of **1** is very much like the one observed for [Fe(salen)$(Im)_2$]PF_6 complex [12]. This type of conformation is observed to lock up the Fe atom in a high spin state, which is indeed the case with complex **1** in solid state.

The Fe—O distances in **2** are identical (1.913(4), 1.914(3) Å), Fe—N(Im) distances are much shorter (2.112(7), 2.132(7) Å) compared to **1** and Fe—N-(salen) distance (Fe—N2 = 2.150(4) Å) is the longest in the Fe-coordination polyhedron reflecting a weaker coordination probably due to the thermal agitation of the ring atoms. The conformation of salen framework in **2** shows a marked difference from that of **1**. Here, the ethylenediamine ring appears to be planar as opposed to the *meso* form in **1**. However, rather long thermal ellipsoids (Fig. 1) of carbon atoms C8 and C9 with their longest axes perpendicular to the FeN_2 plane indicate a disorder of C8 and C9 implying the equilibrium of the two opposite *meso* conformations, whether it is static or dynamic in nature cannot be resolved by one temperature X-ray structure alone. Similar observation has also been reported for Co(II) complexes [20]. This makes the overall conformation (Fig. 2) of the molecule quite different from **1**. The sal1 and sal2 units are bent towards the same side with respect to the N_2O_2 plane by unequal amounts (13.1° and 6.99°, respectively), giving a shallow "umbrella like" shape to the molecule.

The complex molecule adopts two different conformations as seen best in Fig. 2, which could be attributed to the presence of different anions resulting in different packing forces. The extreme influence of the anions on the solid state conformations is seen in the case of [Fe(salen)$(Im)_2$]Y structures; the molecule has a "stepped" conformation exhibiting spin tran-

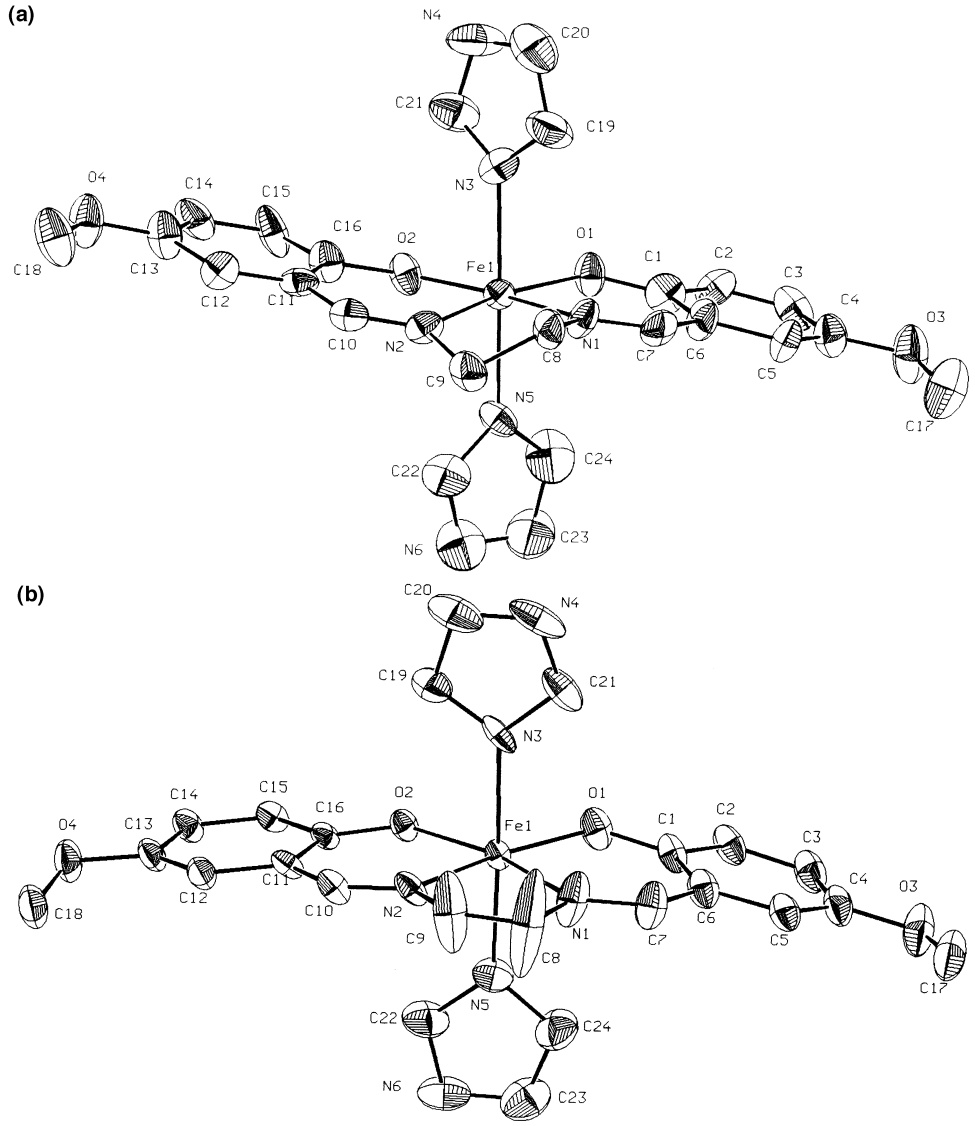

Fig. 1. Molecular Structure (ORTEP diagrams) of the cation $[Fe(5\text{-}CH_3O\text{-}salen)]^+$ in (a) **1**, Y = ClO_4^-, 50% probability surfaces and (b) **2**, Y = Cl^-, 40% probability surfaces.

sition (ST) behavior when Y = ClO_4^- whereas the molecule is planar showing no ST when Y = PF_6^- [12].

The orientation of the imidazole rings in **1** and **2** is best seen looking approximately down in the perpendicular direction to the FeN_2 plane of 5-CH_3O-salen (fig. 3). In **1**, the imidazoles are aligned almost along the O—Fe—N bond directions, thus making an angle of 77.3° with each other. In **2**, both the planes of imidazole rings are almost along the direction bisecting the O—Fe—N angles, the angle between the planes is 175.1°. In **1**, the imidazole ring containing N4 does not show any H-bonding interaction of N—H···O type with ClO_4^- oxygens, the other imidazole ring N5, C22, N6, C23, C24 shows a weak (N6H)···O5 hydrogen bond (3.08 Å, 128°) whereas in **2**, both the imidazole N—H make good H-bonding interactions with the Cl^- anion (N4—H···Cl1 = 3.15 Å, 158°; N6—H···Cl1 = 3.08 Å, 142°).

Spin crossover in polycrystals-magnetism and EPR studies

All the complexes are paramagnetic and μ_{eff} values at 298 K vary in the range 5.54–5.96 μ_B corresponding to a high spin electronic ground state with five unpaired electrons. The salen and 5-Cl-salen complexes with Cl^- and ClO_4^- ions however, showed interesting spectral changes due to spin crossover as the temperature was lowered to 77 K. A typical variation for polycrystals of $[Fe(salen)(2\text{-}MeIm)_2]ClO_4$ is depicted in Fig. 4. In fact, several resonances were observed at

Table 2. Bond lengths (Å) and angles (°) e.s.d.'s in parentheses

	Complex **1**	Complex **2**
FE1—O1	1.923(6)	1.913(4)
FE1—O2	1.869(6)	1.914(3)
FE1—N1	2.109(7)	2.117(5)
FE1—N2	2.117(6)	2.150(4)
FE1—N3	2.21(1)	2.132(7)
FE1—N5	2.15(1)	2.112(7)
O1—C1	1.30(1)	1.307(5)
O2—C16	1.38(1)	1.306(3)
O3—C4	1.36(1)	1.375(6)
O3—C17	1.43(2)	1.43(1)
O4—C13	1.34(1)	1.369(5)
O4—C18	1.44(1)	1.412(8)
N1—C7	1.28(1)	1.283(6)
N1—C8	1.468(9)	1.442(9)
N2—C9	1.51(1)	1.450(7)
N2—C10	1.27(1)	1.255(5)
N3—C19	1.34(2)	1.380(6)
N3—C21	1.30(2)	1.337(7)
N4—C20	1.34(3)	1.343(9)
N4—C21	1.32(2)	1.320(7)
N5—C22	1.29(2)	1.347(9)
N5—C24	1.35(2)	1.408(6)
N6—C22	1.29(2)	1.327(7)
C1—C2	1.43(1)	1.425(6)
C1—C6	1.36(1)	1.412(7)
C2—C3	1.34(2)	1.387(6)
C3—C4	1.41(2)	1.396(8)
C4—C5	1.37(1)	1.375(7)
C5—C6	1.43(1)	1.384(6)
C6—C7	1.46(1)	1.439(7)
C8—C9	1.51(2)	1.282(9)
C10—C11	1.42(1)	1.455(6)
C11—C12	1.37(1)	1.405(5)
C11—C16	1.39(1)	1.404(5)
C12—C13	1.45(1)	1.364(6)
C13—C14	1.40(1)	1.414(7)
C14—C15	1.34(1)	1.382(5)
C15—C16	1.41(1)	1.418(5)
C19—C20	1.37(2)	1.36(1)
C23—C24	1.33(3)	1.32(1)
O1—FE1—O2	107.5(3)	110.0(2)
O1—FE1—N1	87.9(3)	87.4(2)
O1—FE1—N2	164.6(3)	163.8(3)
O1—FE1—N3	90.9(3)	90.9(2)
O1—FE1—N5	89.4(3)	92.0(2)
O2—FE1—N1	164.5(3)	162.6(3)
O2—FE1—N2	87.8(3)	86.0(2)
O2—FE1—N3	88.1(3)	90.7(2)
O2—FE1—N5	91.0(3)	89.7(2)
N1—FE1—N2	77.0(3)	76.7(2)
N1—FE1—N3	89.1(3)	89.4(2)
N1—FE1—N5	91.7(3)	89.3(2)
N2—FE1—N3	91.5(3)	85.9(2)
N2—FE1—N5	88.5(3)	91.0(2)
N3—FE1—N5	179.1(3)	176.8(3)
FE1—O1—C1	130.6(7)	131.4(3)
FE1—O2—C16	131.4(6)	133.9(3)

Table 2—*continued.*

	Complex **1**	Complex **2**
C4—O3—C17	117(1)	116.3(6)
C13—O4—C18	117(1)	115.8(5)
FE1—N1—C7	124.6(6)	126.2(4)
FE1—N1—C8	116.0(6)	114.0(4)
C7—N1—C8	119.3(8)	119.8(5)
FE1—N2—C9	113.7(5)	112.5(3)
FE1—N2—C10	126.3(6)	127.8(3)
C9—N2—C10	120.0(7)	119.7(4)
FE1—N3—C19	127.2(8)	129.3(3)
FE1—N3—C21	122.7(8)	127.1(3)
C19—N3—C21	110(1)	103.7(4)
C20—N4—C21	109(2)	109.8(6)
FE1—N5—C22	129.2(8)	127.3(4)
FE1—N5—C24	128.0(9)	130.2(4)
C22—N5—C24	103(1)	102.5(5)
C22—N6—C23	105(2)	107.7(6)
O1—C1—C2	117.9(9)	119.1(4)
O1—C1—C6	126(1)	125.0(4)
C2—C1—C6	115.7(9)	116.0(4)
C1—C2—C3	123(1)	121.3(5)
C2—C3—C4	121(1)	120.7(5)
O3—C4—C3	117(1)	116.6(5)
O3—C4—C5	124(1)	124.5(5)
C3—C4—C5	120(1)	118.9(5)
C4—C5—C6	118.1(9)	121.1(5)
C1—C6—C5	123.3(9)	121.9(4)
C1—C6—C7	122.0(9)	121.9(4)
C5—C6—C7	114.8(8)	116.2(5)
N1—C7—C6	126.4(9)	125.8(5)
N1—C8—C9	107.5(8)	118.1(7)
N2—C9—C8	106.5(7)	117.8(6)
N2—C10—C11	125.4(8)	124.5(4)
C10—C11—C12	115.7(8)	116.2(3)
C10—C11—C16	124.3(9)	123.1(3)
C12—C11—C16	120.0(8)	120.7(3)
C11—C12—C13	120.1(8)	121.6(4)
O4—C13—C12	125.5(9)	125.7(4)
O4—C13—C14	117.4(9)	115.6(4)
C12—C13—C14	117.0(9)	118.8(4)
C13—C14—C15	123(1)	120.4(4)
C14—C15—C16	119(1)	121.4(3)
O2—C16—C11	122.4(8)	124.0(3)
O2—C16—C15	116.8(9)	118.8(3)
C11—C16—C15	120.6(9)	117.1(3)
N3—C19—C20	106(1)	110.9(5)
N4—C20—C19	107(2)	104.7(6)
N3—C21—N4	109(1)	110.9(5)
N5—C22—N6	115(1)	111.9(6)
N6—C23—C24	106(2)	108.2(8)
N5—C24—C23	111(2)	109.8(7)

ambient temperatures with g values being 19.26, 10.72, 8.29, 7.14, 4.32, 3.7, 3.43 and 2.87. As discussed in the experimental section (*vide supra*), higher limit of g for high spin species in a rhombically distorted zero-field (if $D \geqslant 0.15\ cm^{-1}$) is ~ 10. The signals with $g \sim 19.26$

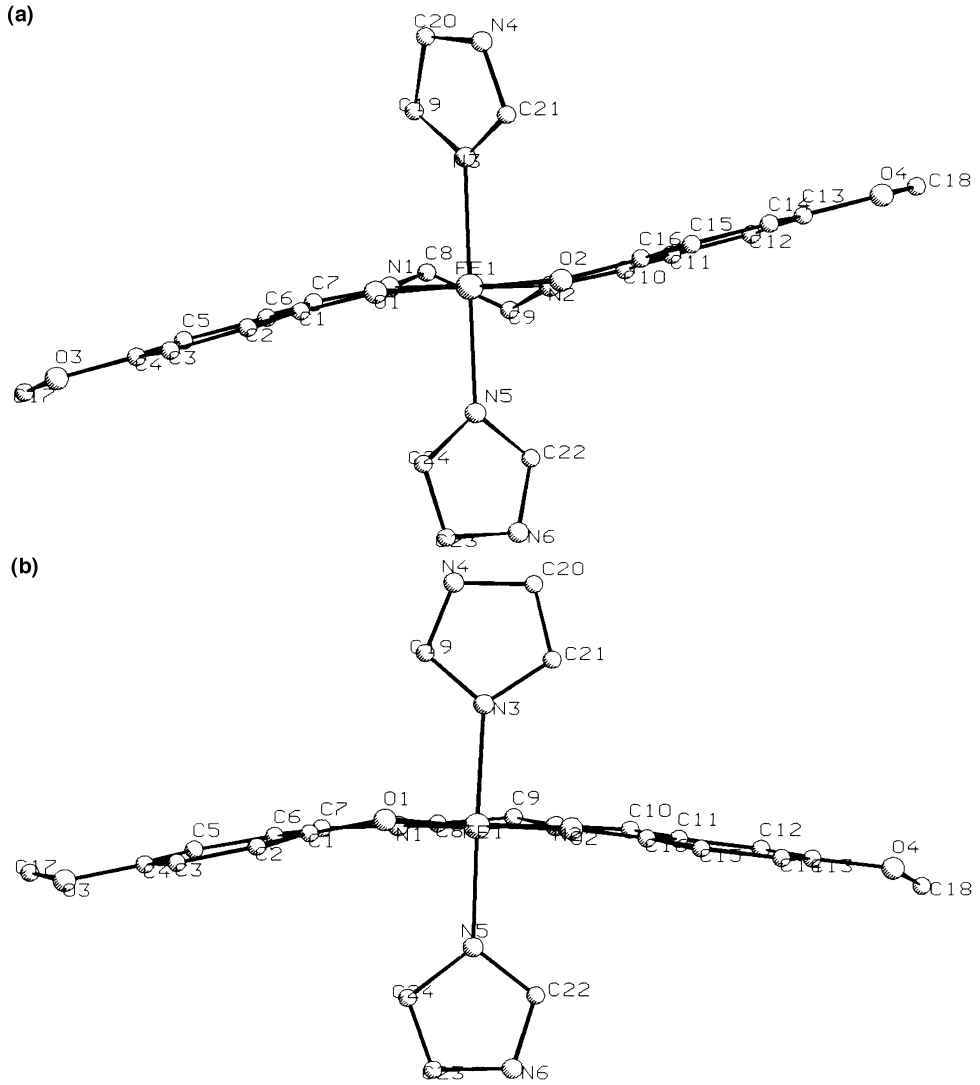

Fig. 2. Diagrams showing the effect of counterion on the conformational flexibility of 5-CH_3O-salen moiety in (a) **1** and (b) **2**.

and 10.72, prevalent only at ambient temperatures, cannot be accounted for an isolated high spin ferric ion but are attributed to those originating through exchange interactions between weakly antiferromagnetically coupled nearest neighbors [21]. As the temperature of the sample was lowered the intensity of these signals decreased and around 230 K a new signal ($g \sim 2.1$) appeared, the intensity of which increased with further lowering of temperature. Finally, an axial spectrum was observed at 77 K with $g\| = 2.107$ and $g\perp = 2.067(3)$ corresponding to a low spin configuration for Fe(III). But for complexes with Im as an axial ligand, the low spin species was characterized by a rhombic spectrum. Complexes with BPh_4^- as the counter anion showed two resonances ($g \sim 8.6$ and 4.3) at 298 K. However, at 77 K additional weak signals appeared around $g \sim 2$ corresponding to spin equilibrium ($5/2 \rightleftharpoons 1/2$). It is important to note that the observation of distinct high and low spin resonances implies that the spin state conversion rates are slower than the EPR time scale ($\sim 10^{10}$ s^{-1}).

Unlike those of salen and 5-Cl-salen, the complexes with 5-CH_3O-salen showed very broad signals in the range 800–4000 G at 298 K. Cooling the sample to 77 K has moderately reduced the line widths. These features indicate that 5-CH_3O-salen complexes are of high spin type throughout the temperature range and are consistent with the structural parameters. X-ray structure of **2** indeed revealed the intermolecular interactions through counterion (Cl^-) making N3(H)—Cl—(H)N6 bonds. We believe that these H-bonds are probably the pathway for exchange interactions resulting in broad signals.

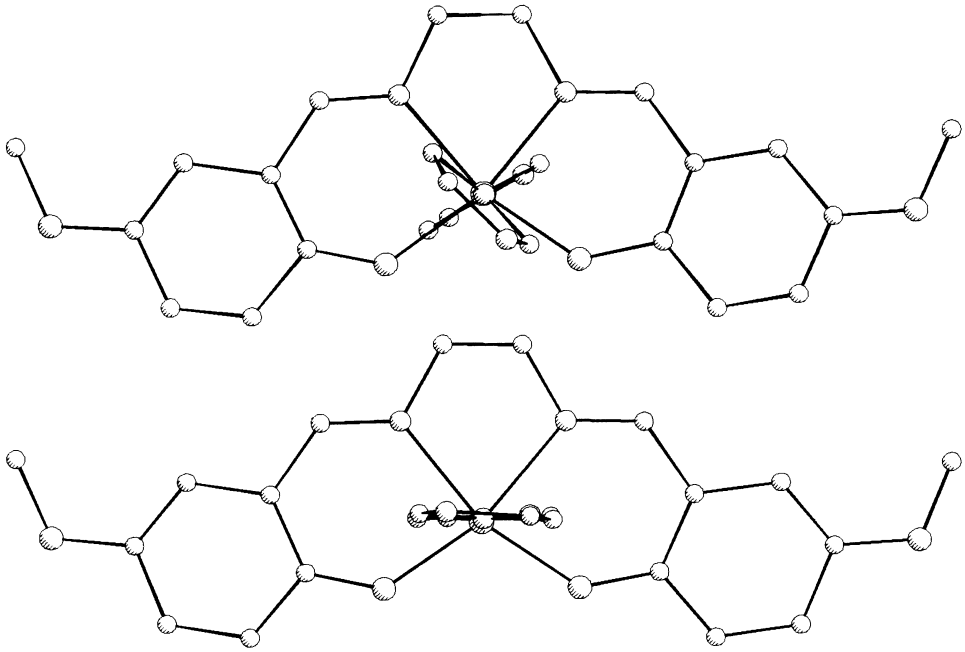

Fig. 3. Projections of the cations in (a) **1** and (b) **2** down the imidazole N3—N5 direction showing the differences in imidazole orientation.

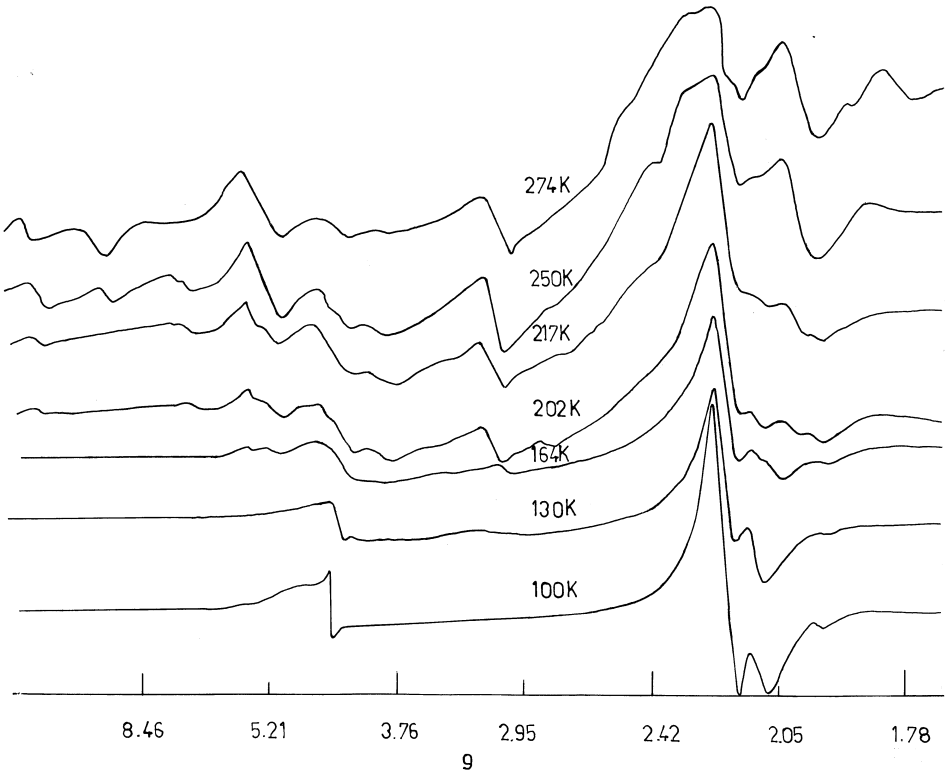

Fig. 4. Variable temperature EPR spectra for polycrystals of $[Fe(salen)(2\text{-}MeIm)_2](ClO_4)$. Experimental conditions 9.47 GHz microwave frequency, 2 mW power, 3.15-G modulation and 2×10^4 gain.

EPR of solutions

Methanolic and DMF solutions of the complexes did not show EPR at ambient temperatures, probably due to short electron spin lattice relaxation times. However, upon cooling a sharp signal due to high spin state (at $g \cong 4.3$) and around 220 K, a signal for a low spin state (at $g = 2.1$) appeared. As the temperature was further lowered the intensity of the signal due to low spin state gradually increased while that of high spin state decreased. For salen and 5-Cl-salen complexes the spectrum at 77 K could be attributed solely to a low spin state (Fig. 5). Spin crossover in these complexes is gradual and complete. 5-CH_3O-salen complexes are high spin in solid state whereas their methanolic solutions exhibit spin crossover behavior. The spectrum at 77 K (Fig. 5) contains signals due to both high and low spin states. In other words, spin crossover in 5-CH_3O-salen complexes is not complete above 77 K. It is clear from Fig. 5 that the intensity ratio of HS to LS state signals varies linearly with the donacity of the substituents in the order $CH_3O > H > Cl$.

Variable temperature spectra for Salen and 5-Cl-salen complexes with Im as axial ligand and Cl^- and ClO_4^- as counterions showed the presence of two types of low spin (LS1 and LS2) species. Around 220 K, methanolic solutions showed an almost "axial" spectrum with g anisotropic being 2.22–1.95 corresponding to LS1. As the temperature was lowered, the intensity of signals for LS1 decreased and a rhombic type spectrum with higher g anisotropy (2.44–1.89) corresponding to LS2 appeared. The intensity of signals for the latter species increased with further lowering of temperature. The transition from LS1 to LS2 is reversible and Fig. 6 depicts the variable temperature spectra for [Fe(5-Cl-salen)$(Im)_2$]Cl. As far as we are aware, this is the first report showing the existence of two types of low spin species.

Complexes with 2-MeIm as axial ligand showed spectra characteristic of LS1 species only. The intensity ratio of the HS to LS signals at 77 K varied with counter ions in the order $BPh_4^- > ClO_4^- > Cl^-$. While the methanolic solutions of the complexes exhibited spin crossover behavior, their DMF solutions were high spin throughout the temperature range. It may be possible that the highly coordinating solvents may not allow changes in the chelate conformation and restrict the breathing modes of the salen ligand responsible for the spin crossover phenomenon. Indeed such solvent and Schiff base interactions were observed in our earlier studies on Cu(II) complexes [22] and by others [23]. The g values for low spin state are listed in Table 3.

Methanolic solutions of the complexes showed remarkable thermochromism, with the colour changing from reddish brown to bluish violet or green. Interesting to note that reddish brown is associated

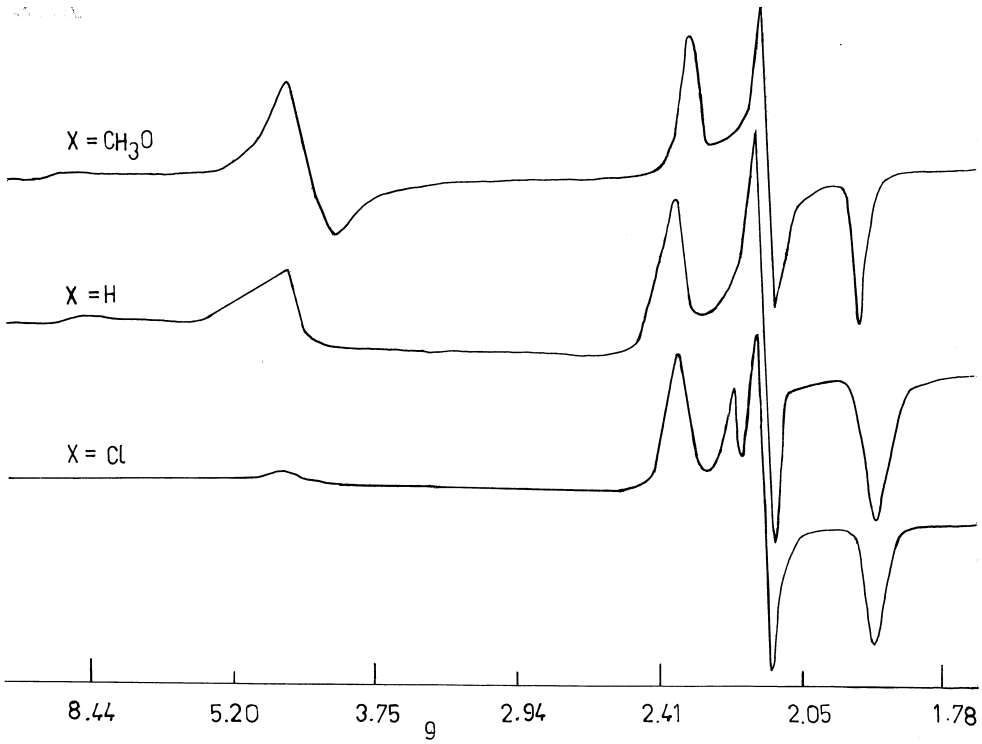

Fig. 5. Effect of substituent (X) on the X-band EPR spectra for frozen methanol solutions of [Fe(5-X-salen)$(Im)_2$](ClO_4) at 77 K. Experimental conditions: 9.45 GHz microwave frequency, 2 mW power, 2.5-G modulation and 4×10^4 gain.

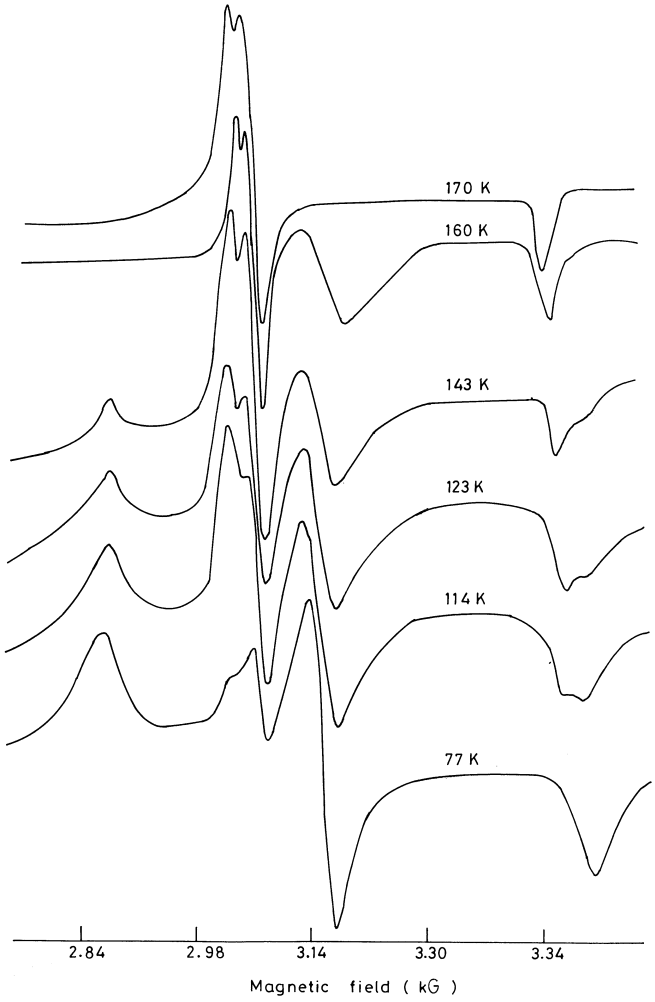

Fig. 6. Variable temperature X-band EPR spectra for methanol solution of [Fe(5-Cl-salen)(Im)$_2$]Cl showing a gradual transition of low spin LS1 to LS2 state. Experimental conditions: 9.45 GHz microwave frequency, 2 mW power, 2.5-G modulation and 4×10^4 gain.

Table 3. EPR g values, MO coefficients for the ground state Kramers' doublet, distortion parameters and excitation energies for [Fe(5-X-salen)L$_2$]Y complexes in low spin electronic state

Complex	g_x	g_y	g_z	a	b	c	K	Δ/λ	V/λ	$\Delta E_1/\lambda$	$\Delta E_2/\lambda$
[Fe(salen)(Im)$_2$]Cl	2.376	2.143	1.915	0.199	0.992	0.040	0.871	7.178	−5.201	4.169	9.678
[Fe(salen)(Im)$_2$]ClO$_4$	2.382	2.144	1.911	0.112	0.992	0.048	0.866	7.015	−5.089	4.052	9.456
[Fe(salen)(Im)$_2$]BPh$_4$[a]	2.238	2.211	1.937	0.105	0.994	0.005	0.832	7.112	−0.713	6.095	7.534
	2.441	2.148	1.894	0.132	0.990	0.047	0.905	6.664	−5.248	3.587	9.166
[Fe(salen)(2-MeIm)$_2$]Cl	2.236	2.207	1.936	0.107	0.994	0.005	0.815	7.041	−0.763	6.009	7.479
[Fe(salen)(2-MeIm)$_2$]ClO$_4$	2.237	2.211	1.937	0.106	0.994	0.005	0.830	7.108	−0.687	6.097	7.522
[Fe(salen)(2-MeIm)$_2$]BPh$_4$	2.238	2.211	1.938	0.105	0.995	0.005	0.839	7.175	−0.721	6.160	7.602
[Fe(5-CH$_3$O-salen)(Im)$_2$]Cl	2.313	2.213	1.925	0.113	0.993	0.017	0.910	6.792	−2.167	5.246	7.838
[Fe(5-CH$_3$O-salen)(Im)$_2$]ClO$_4$	2.333	2.134	1.939	0.100	0.994	0.038	0.907	8.456	−6.065	5.084	11.408
[Fe(5-CH$_3$O-salen)(Im)$_2$]BPh$_4$	2.337	2.134	1.922	0.115	0.993	0.037	0.819	7.317	−5.045	4.399	9.747
[Fe(5-CH$_3$O-salen)(2-MeIm)$_2$]ClO$_4$	2.222	2.199	1.949	0.094	0.996	0.004	0.859	7.906	−0.738	6.925	8.357
[Fe(5-Cl-salen)(Im)$_2$]Cl[a]	2.367	2.143	1.917	0.118	0.992	0.039	0.864	7.206	−5.112	4.246	9.664
	2.237	2.202	1.934	0.109	0.994	0.007	0.797	6.926	−0.905	5.853	7.414

[a] Two types of low spin species LS1 and LS2.

with the HS state while bluish violet to LS1 and green to LS2 states. Such colour isomerism with spin crossover was also observed in some related Fe(III) complexes and this phenomenon probably associates with changes in the ligand geometry.

Ground state wave function, distortion parameters and excitation energies for low spin configuration

The EPR data for the low spin configurations (Table 4) were least squares fitted to the g value expressions given by eqns (5)–(7) and the MO coefficients for the ground state Kramers' doublet (a, b and c), orbital reduction parameter (K), distortion parameters (axial, Δ and rhombic, V) and energy separations of the two excited doublets are listed in Table 3. It is obvious that the ground state has a "predominant" d_{xy} character with a little admixture from the d_{xz} and d_{yz} orbitals ($b > a$ and c). The orbital reduction parameter (K) varies in accordance with the donacity of the substituent in the order 5-CH_3O > H > Cl and suggests more covalent bonding in salen and 5-Cl-salen complexes compared to 5-CH_3O-salen complexes. The V/Δ values, a measure of rhombicity, are higher for 5-Cl-salen and salen than for 5-CH_3O-salen complexes. A considerable variation in these values is observed for LS1 and LS2 configurations (LS2 > LS1). Taking the value of spin-orbit coupling constant (λ) to be 460 cm^{-1} for a free Fe(III) ion, the separation of the two excited Kramers' doublets (ΔE_1 and ΔE_2) were calculated to lie in the range 1485–2736 and 2800–4774 cm^{-1}, respectively. These values indicate that the three doublets are well separated and resonances occur from the ground state Kramers' doublet only. Interestingly X-ray structures indicate that Fe—N and Fe—O bond distances are shorter for spin crossover $[Fe(salen)(Im)_2](ClO_4)$ [12] compared to $[Fe(5\text{-}CH_3O\text{-salen})(Im)_2]Y$, where $Y = ClO_4^-$ (**1**) and Cl^- (**2**) and complement the EPR results confirming higher covalency for salen than for 5-CH_3O-salen.

Structure-spin state-reactivity correlations

For complexes with ligand field strength in the crossover region, a change in the physical parameters (temperature, pressure etc.) alters the molecular geometry and thereby causes spin state conversion. According to Scheidt and Reed [4] upon crossover from a HS to a LS state the iron atom in porphyrin complexes moves more into the plane of the macrocyclic ligand and Fe—N bond lengths decrease from ~2.14 Å for a high spin to ~1.99 Å for a low spin configuration; as a consequence of this the size of the porphyrin core reduces. Kennedy *et al.* have reported similar structural changes in Fe—N bond lengths for a related $[Fe(salen)(Im)_2](ClO_4)$ complex [12] and Hendrickson *et al.* [10] for $[Fe(3\text{-OEt-salAPA})_2]ClO_4 \cdot C_6H_6$, where 3-OEt-salAPA = Schiff base condensate of 3-ethoxysalicylaldehyde and N-(3-aminopropyl)aziridine. X-ray structural data and molecular geometries of various related Fe(III) Schiff base complexes are listed in Table 5. These results and those of our on analogous Cu(II) complexes [22] reveal that salen ligand is conformationally flexible like the heme environment in metalloproteins and adopts an overall "stepped, umbrella or planar" conformation. Also the FeN_2C_2 ring containing the ethylene back-

Table 4. Structural parameters of some related high spin and low spin Fe(III) quadridentate Schiff base complexes

Complex[a]	Temp. K	Fe—N1 Å	Fe—N2 Å	Fe—O1 Å	Fe—O2 Å	Fe—ax1 Å	Fe—ax2 Å	Spin state, overall ligand geometry and FeN_2C_2 conformation[c]
$Fe(acen)(Im)_2BPh_4$	298	1.892	1.906	1.912	1.928	1.983	1.997	LS, stepped, envelope [25]
$K[Fe(acen)(CN)_2] \cdot 2H_2O$[b]	298	1.916	1.921	1.915	1.922	1.984	2.011	LS, stepped, envelope [26]
		1.918	1.919	1.934	1.937	1.989	2.005	
$Fe(salen)(Im)_2ClO_4$	298	2.051	2.083	1.885	1.917	2.141	2.151	ST, stepped, envelope [12]
	120	1.905	1.921	1.885	1.921	1.990	1.993	
$Fe(salen)(Im)_2BPh_4$	298	2.055	2.089	1.897	1.906	2.117	2.128	SE, stepped, envelope [12]
$Fe(salen)(Im)_2PF_6$	298	2.125	2.146	1.894	1.913	2.153	2.153	HS, planar, gauche [12]
$Fe(salen)(Im)_2ClO_4 \cdot H_2O$	298	2.105	2.130	1.906	1.928	2.137	2.148	HS, umbrella, planar [25]
$Fe(salen)(Im)(NCS) \cdot 0.5MeOH$[b]	298	2.108	2.125	1.907	1.928	2.149	2.085	HS, planar gauche [27]
		2.091	2.093	1.888	1.926	2.145	2.106	
$Fe(3\text{-}CH_3Osalen)(5\text{-PhIm})(H_2O)$	298	2.060	2.082	1.880	1.891	2.132	2.205	HS, planar, gauche [21]
$Fe(5\text{-}CH_3Osalen)(Im)_2Cl$	298	2.110	2.129	1.911	1.910	2.140	2.145	HS, umbrella, planar
$Fe(5\text{-}CH_3Osalen)(Im)_2ClO_4$	298	2.134	2.145	1.896	1.911	2.157	2.162	HS, planar, gauche [25]
$Fe(saloph)(Im)_2BPh_4$	298	2.108	2.143	1.883	1.910	2.158	2.172	HS, planar

[a] acen = *N,N′*-ethylenebis(acetylactonylidenaminato); saloph = *N,N′-O*-phenylenebis(salicylidenaminato).
[b] Two crystallographically independent molecules in the asymmetric unit.
[c] ST = spin transition, SE = spin equilibrium, HS = high spin and LS = low spin.

bone takes up geometries like "envelope, planar or *meso*" conformations. X-ray structures in the present investigation indicate a considerable effect of the counterion on ligand geometry. The chloro complex (**2**) has an "umbrella" type overall chelate conformation with a "planar" geometry for FeN_2C_2 whereas the perchlorato complex (**1**) possesses an overall "planar" conformation with a "*meso*" arrangement for the FeN_2C_2 ring. The bond lengths of Fe—N(salen/Im) and Fe—O fall within the range for high spin complexes consistent with EPR results for solid complexes. The comparative study (Table 4) clearly indicates and agrees well with the report by Kennedy *et al*. [12] that the "envelope" geometry is essential for spin crossover while "*meso*" is for high spin configuration. Probably shortening of Fe—N bonds without much alterations in the geometry of the molecule is possible only with the "stepped" conformation. Although 5-CH_3O-salen complexes are high spin in solid state, their methanolic solutions exhibit spin crossover behavior. This observation suggests that in solid state the molecule is fixed in a high spin type "umbrella or planar" geometry due to packing or intermolecular interactions while in solutions it undergoes conformational changes to a "stepped" conformation with a certain degree of "envelope" geometry for the FeN_2C_2 ring which is responsible for spin crossover.

The axial ligands (Im) in **1** and **2** adopt two types of conformations "syn" for (Cl^-) and "gauche" (for ClO_4^-), but their orientations unlike for porphyrin complexes [4,9] have little effect on the spin state of Fe(III). However, the "syn" orientation results in higher symmetry at the site of Fe(III) and an axial spectrum for LS1. Steric hindrance due to CH_3 groups in complexes with 2-MeIm probably allows only the "syn" arrangement for the axial ligands whereas in complexes with Im, the axial ligands undergo orientational changes with lowering of temperature resulting in a "gauche" arrangement corresponding to LS2 and a rhombic EPR spectrum (Table 3). Effect of solvent on spin crossover suggests that DMF molecules probably involve in H-bonding interactions with the Schiff base ligand and does not allow the molecules to take up the "stepped" conformation responsible for spin transition. These results reveal that a flexible ligand geometry providing required ligand field strength is essential for the central metal ion Fe(III) to exhibit spin crossover behavior.

During the preparation it was observed that the spin crossover complexes 5-Cl-salen and salen were highly reactive towards molecular oxygen and readily forms orange red μ-oxo Fe(III) species. It is pertinent to note that a similar reactivity towards molecular oxygen also by Co(II) [24,26], Ni(III) [28] and Mn(II) [29] salen type complexes. Interestingly the bioinorganic catalysts, hemoproteins involved in several physiological functions also exhibit conformational flexibility of the surrounding protein macrostructure *vis-a-vis* labile spin states. All these factors tempt us to conclude that there exists an interesting correlation between the structure-spin state and functionality of the molecules. The energy liberated by electronic structural rearrangement would enhance the functionality of spin crossover complexes.

CONCLUSIONS

Substituents on salen ligand and counterion showed significant effect on the chelate geometry, spin state and reactivity of iron(III) in [Fe(5-X-salen)$(Im)_2$]Y complexes. A "stepped" conformation for salen is essential for spin crossover. Finally, it is believed that spin crossover associated with changes in the chelate conformation aids the reactivity of the molecules.

Acknowledgements—The authors acknowledge Dr S. D. Gomkale Acting Director for encouragement.

Supplementary material available— Listing of positional and thermal parameters of all the atoms, bond distances and angles, F_o/F_c values and packing diagrams for complexes. Ordering information is given on any current masthead page.

REFERENCES

1. Gutlich, P., *Struct. Bonding* (*Berlin*), 1981, **44,** 83.
2. Konig, E., Ritter, G. and Kulshreshtha, S. K., *Chem. Rev*., 1985, **85,** 219.
3. Bacci, M., *Coord. Chem. Rev*., 1985, **85,** 219.
4. Scheidt, W. R. and Reed, C. S., *Chem. Rev*., 1981, **81,** 543.
5. Tuftlund, H., *Coord. Chem. Rev*., 1989, **94,** 67.
6. Yoshizawa, K., Miyajima, H. and Yamabe, T., *J. Phys. Chem*., 1997, **101B,** 4383.
7. Sato, O., Einaga, Y., Iyoda, T., Fujishima, A. and Hashimoto, K., *J. Phys. Chem*., 1997, **101,** 3903.
8. Federer, W. D. and Hendrickson, D. N., *Inorg. Chem*., 1984, **23,** 3861 and 3870.
9. Safo, M. K., Ann Walker, F., Raitsimring, A. M., Walters, W. P., Dolata, D. P., Debrunner, P. G. and Scheidt, W. R., *J. Am. Chem. Soc*., 1994, **115,** 7760.
10. Timken, M. D., Strouse, C. E., Soltis, S. M., Daverio, S. A., Hendrickson, D. N., Abdel-Mawgoud, A. M. and Wilson, S. R., *J. Am. Chem. Soc*., 1986, **108,** 395.
11. Nishida, Y., Oshi, S. and Kida, S., *Chem. Lett*., 1975, 79.
12. Kennedy, B. J., McGrath, A. C., Murray, K. S., Skelton, B. W. and White, A. H., *Inorg. Chem*., 1987, **26,** 483.
13. Calderazzo, F., Floriani, C., Henzi, R. L. and Eplattenier, F., *J. Chem. Soc. A*, 1969, 1378.
14. Gerloch, M., Lewis, J., Mabbs, F. E. and Richards, A., *J. Chem. Soc. A*, 1968, 112.
15. North, A. C. T., Phillips, D. C. and Mathews, F. S., *Acta Crystallogr*., 1968, **A24,** 351.
16. Frenz, B. A. and Associates, *SDP Structure Determination Package*, College Station, TX and Enraf Nonius, Delft, The Netherlands, 1985.
17. Castner, Jr., T., Newell, G. S., Holton, W. C. and Slichter, C. P., *J. Chem. Phys*., 1960, **32,** 668.
18. Bohan, T. L., *J. Magn. Reson*., 1971, **26,** 109.

19. Johnson, C. K., *ORTEP*: *Report ORNL*-3794, Oak Ridge National Laboratory, Oak Ridge, TN, 1976.
20. Calligaris, M., Nardin, G. and Randaccio, L., *J. Chem. Soc*., *Dalton Trans*., 1974, 1903.
21. Kennedy, B. J., Brain, G., Horn, E., Murray, K. S. and Snow, M. R., *Inorg. Chem*., 1985, **24,** 1647.
22. Bhadbhade, M. M. and Srinivas, D., *Inorg. Chem*., 1993, **32,** 5458.
23. Baker, E. N., Hall, D. and Waters, T. N., *J. Chem. Soc. A*, 1970, 400 and 406.
24. Jones, R. D., Summerville, D. A. and Basolo, F., *Chem. Rev*., 1979, **79,** 139.
25. Wang, X., Pennington, W. T., Ankers, D. C. and Fanning, J. C., *Polyhedron*, 1992, **11,** 2253.
26. Nishida, Y., Kino, K. and Kida, S., *J. Chem. Soc*., *Dalton Trans*., 1987, 1157.
27. Kennedy, B. J., Murray, K. S., Zwack, P. R., Horn, E., Snow, M. R. and Tiekink, E. R. T., *Proc. Indian Acad. Sci*. (*Chem. Sci*.), 1987, **98,** 99.
28. Castro, B. D. and Freire, C., *Inorg. Chem*., 1990, **29,** 5113.
29. Dailey, G. C., Horitz, C. P. and Lisele, C. A., *Inorg. Chem*., 1992, **31,** 5325.

Pergamon

Polyhedron Vol. 17, No. 16, pp. 2713–2718, 1998
© 1998 Elsevier Science Ltd
All rights reserved. Printed in Great Britain
0277–5387/98 $19.00+0.00

PII: S0277–5387(98)00040–0

Copper(II) complexes of two new oxamidate bis-tetradentate Schiff-base ligands

Jose M. Dominguez-Vera,* Natividad Galvez, Jose M. Moreno and Enrique Colacio

Departamento de Química Inorgánica, Facultad de Ciencias, Universidad de Granada, 18071 Granada, Spain

(Received 17 November 1997; accepted 21 January 1998)

Abstract—Two novel symmetrical bis-tetradentate Schiff base ligands, H_2L^1 and H_4L^2, have been prepared from the condensation of *N*,*N*′-bis(3-aminopropyl)oxamide with pyridine-2-carbaldehyde and pyrrol-2-carbaldehyde, respectively. The ligands react with copper(II) nitrate in basic medium to yield the dinuclear complexes $[Cu_2L^1](NO_3)_2$ and $[Cu_2L^2]$. $[Cu_2L^1](NO_3)_2$ reacts with sodium azide to yield the neutral dinuclear complex $[Cu_2L^1(N_3)_2]$, which was structurally characterized by X-ray diffraction. The complex crystallizes in the monoclinic system, space group $P2_1/c$ with cell constants: $a = 7.916(2)$ Å, $c = 20.110(4)$ Å, $\beta = 95.20(3)^\circ$, $V = 1255.4(4)$ Å^3, $Z = 2$. The structure consists of neutral quasi-planar centrosymmetric dinuclear copper(II) molecules, where two crystallographically equivalent copper(II) ions are bridged by an oxamidate group in *trans* conformation, resulting in a copper-copper distance of 5.271 Å. Each copper(II) ion occupies the N_3O inner site of the doubly-deprotonated L^1 ligand with bond distances of ca 2.0 Å, whereas a nitrogen atom from the azide group completes the coordination polyhedron with a longer bond distance of 2.340(4) Å. All the dinuclear complexes exhibited strong antiferromagnetic exchange interaction. The magnetic data were analyzed by using the Bleaney-Bowers equation ($H = -JS_1S_2$) leading to singlet-triplet energy values (J) of 425.5 cm^{-1} for $[Cu_2L^1](NO_3)_2$, 427.9 cm^{-1} for $[Cu_2L^2]$ and 424.1 cm^{-1} for $[Cu_2(L^1)(N_3)_2]$. These J values are a consequence of the ability of the oxamidate-bridge to propagate the antiferromagnetic exchange interaction between metal ions which allow a large overlap of the $d_{x^2-y^2}$ magnetic orbitals centered on each copper(II) ion. © 1998 Elsevier Science Ltd. All rights reserved

Keywords:

N,*N*′-bis(substituted)oxamides (scheme) have played a key role in the design of polymetallic ligands due to their versatility and remarkable ability to mediate strong exchange interactions when acting as bridging ligands between paramagnetic centers. The versatility of these ligands is based on (i) the wide variety of derivatives which can be prepared by changing the substituents of the amino groups, thus leading to different chelate rings and/or donor atoms and (ii) their easy *cis-trans* conformational isomerization.

Most *N*,*N*′-bis(substituted)oxamides reported up to date contain an amino moiety (primary, secondary to tertiary) as a terminal group X and an aliphatic chain of two or three carbon atoms. From this type of ligands, a lot of structures, including di- [1–13], tri [13], tetra- [14] and infinite polynuclear [1,15] copper(II) complexes have been reported and their magnetic properties studied. When X is NH_2, it has been recently shown that the oxamide reacts with aldehydes, such as salicylaldehyde [16] or imidazole-2-carbaldehyde [17] to yield new binucleating ligands. This latter fact adds a new perspective that increases the interest of this type of ligands, since by choosing the appropriate aldehyde reagent, one can obtain new polynucleating ligands designed for particular problems.

Following this line, condensation of *N*,*N*′-bis(3-aminopropyl)oxamide with pyridine-2-carbaldehyde or pyrrol-2-carbaldehyde leads to two new symmetric ligands, H_2L^1 and H_4L^2 (scheme). In both ligands, the *trans* conformation become more likely due to steric hindrance from the pyridyl or pyrrol groups. In the *trans* conformation, both ligands display two identical

* Author to whom correspondence should be addressed.

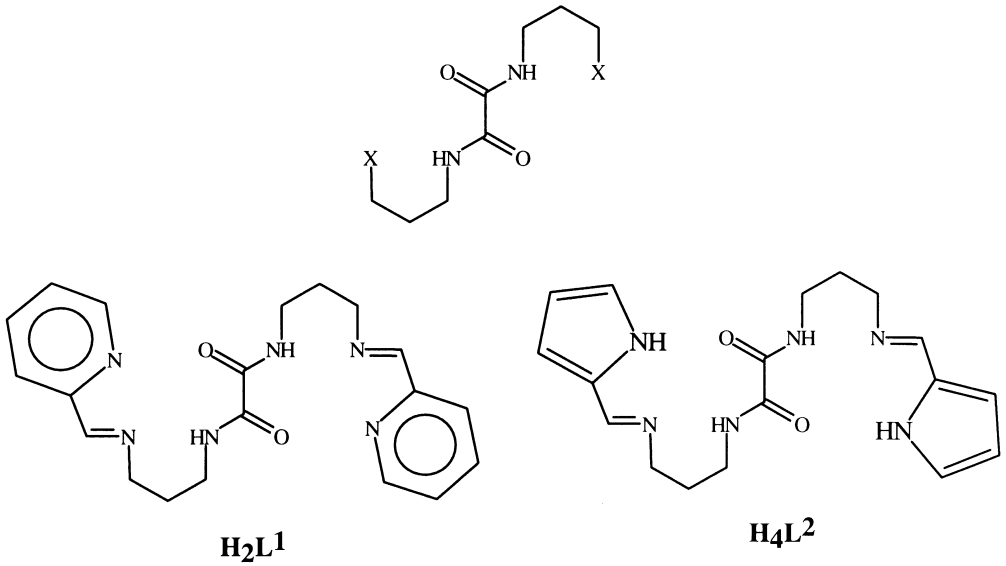

H_2L^1 H_4L^2

Scheme 1.

N_3O coordination sites and then, the ligand can simultaneously accommodate two copper(II) ions. In fact, H_2L^1 and H_4L^2 readily react with copper(II) nitrate hydrate to afford homodinuclear complexes of formula $[Cu_2L^1](NO_3)_2 \cdot 2H_2O$ and $[Cu_2L^2] \cdot 2H_2O$, respectively. In the complex $[Cu_2L^1](NO_3)_2 \cdot 2H_2O$, each copper(II) ion can accept one donor atom in axial position. Thus, by reaction of $[Cu_2L^1](NO_3)_2 \cdot 2H_2O$ with sodium azide we succeeded in obtaining the neutral dinuclear complex $[Cu_2L^1(N_3)_2]$, which was structurally characterized by X-ray diffraction. All the dinuclear complexes exhibited strong antiferromagnetic exchange interaction.

EXPERIMENTAL

Preparation of the ligands

N,*N*′-bis(3-aminopropyl)oxamide (hereafter H_2oxpn) was prepared as previously reported [17]. H_2L^1 and H_4L^2 were synthesized by following a general procedure we recently reported [17]. Pyridine-2-carbaldehyde or pyrrol-2-carbaldehyde was directly added to a methanolic suspension of H_2oxpn. After one hour of heating at 50°C, the resulting yellow soln was kept at 0°C for one day. H_2L^1 and H_4L^2 were obtained in good yield as yellow pale and white powders, respectively. Analytical data (C, H, N) were according to the anhydrous ligands. ^{1}H NMR [$(CD_3)_2SO$] of H_2L^1: δ 1.84 (q, 4H, CCH_2C), δ 3.23 (m, 4H, CH_2NH), δ 3.63 (t, 4H, NCH_2), δ 7.44 (dd, 2H, CH), δ 7.85 (pst, 2H, CH), δ 7.97 (psd, 2H, CH), δ 8.33 (s, 2H, HC═N), δ 8.62 (psd, 2H, CH) and δ 8.80 (t, 2H, NH). ^{1}H NMR [$(CD_3)_2SO$] of H_4L^2: δ 1.77 (q, 4H, CCH_2C), δ 3.23 (m, 4H, CH_2NH), δ 3.48 (t, 4H, NCH_2), δ 6.11 (m, 2H, CH), δ 6.43 (dd, 2H, CH), δ 6.85 (pst, 2H, CH), δ 8.06 (s, 2H, HC═N), δ 8.97 (t, 2H, NH).

Preparation of the complexes

$[Cu_2L^1](NO_3)_2 \cdot 2H_2O$. H_2L^1 (2 mmol, 760 mg) was dissolved in 50 ml of a methanol/water (4 : 1) mixt. containing potassium hydroxide (4 mmol, 224 mg). Then, solid copper nitrate hydrate (4 mmol, 750 mg) was directly added with stirring. After a few minutes a dark-blue soln was obtained, which was filtered to remove any amount of insoluble material. Slow evaporation at room temp. afforded green crystals which were filtered off, washed with methanol and diethyl ether and air-dried; yield 78% (Found: C, 36.1; H, 4.1; N, 16.6. Calc. for $C_{20}H_{26}N_8O_{10}Cu_2$: C, 36.1; H, 3.9; N, 16.8).

$[Cu_2L^2] \cdot 2H_2O$. H_4L^2 (2 mmol, 708 mg) was dissolved in 50 ml of methanol containing potassium hydroxide (8 mmol, 448 mg). Addition of any copper(II) salt (2 mmol) such as nitrate, acetate or chloride leads after a few minutes of stirring to the precipitation of the complex as a brown powder, which was filtered off, washed with methanol and diethyl ether and air-dried; yield 70%. (Found: C, 42.0; H, 4.4; N, 16.3. Calc. for $C_{18}H_{22}N_6O_4Cu_2$: C, 42.1; H, 4.3; N, 16.4).

Both complexes $[Cu_2L^1](NO_3)_2 \cdot 2H_2O$ and $[Cu_2L^2] \cdot 2H_2O$ can also be prepared from the condensation of the complex $[Cu_2(trans\text{-oxpn})(NO_3)_2]$ [1] with pyridine-2-carbaldehyde or pyrrol-2-carbaldehyde, respectively in basic medium.

$[Cu_2(L^1)(N_3)_2]$. Sodium azide (3 mmol, 195 mg) was added to a methanolic soln of $[Cu_2L^1](NO_3)_2 \cdot 2H_2O$ (1 mmol, 665 mg). The resulting blue soln was filtered to remove any amount of insoluble material and

allowed to stand at room temp. After one day, blue crystals suitable for X-ray diffraction were obtained in good yield, 76%. (Found : C, 40.9 ; H, 3.5 ; N, 28.6. Calc. for $C_{20}H_{20}N_{12}O_2Cu_2$: C, 40.9 ; H, 3.4 ; N, 28.6).

Physical measurements

Elemental analyses were carried out at the Technical Services of the University of Granada on a Fisons-Carlo Erba analyzer model EA 1108. IR spectra were recorded on a Perkin–Elmer 983 G spectrometer using KBr pellets and NMR spectra, ^{1}H, on a Bruker AM-300 using dmso-d_6 as solvent. Variable-temperature magnetic susceptibility data were collected on powdered samples of the compounds with use of a pendulum type magnetometer (MANICS DSM8) equipped with a helium continuous flow cryostat working in the temperature ranges 300–4 K for $[Cu_2(L^1)(N_3)_2]$ and $[Cu_2L^2]\cdot 2H_2O$ and 300–60 K for $[Cu_2L^1](NO_3)_2\cdot 2H_2O$ with a Drusch EAF 164E electromagnet. The magnetic field was approximately 15,000 G. Data were corrected for the diamagnetism of the ligands using Pascal's constants.

X-Ray data collection and structure determination of the complex $[Cu_2(L^1)(N_3)_2]$

Single crystal data collection was performed at 293 K with a Siemens R3m/V diffractometer using graphite monochromatized Mo–K_α ($\lambda = 0.71073$ Å) radiation. A prismatic blue crystal of dimensions $0.28 \times 0.40 \times 0.24$ mm was used.

The unit cell parameters were calculated by least-squares refinement of 25 well centred reflections in the range $15 < 2\theta < 45°$. A total of 4193 reflections ($5 < 2\theta < 60°$) were collected and of those 2399 unique reflections with $I > 2.5\sigma(Io)$ were considered as observed. The data were corrected for Lorentz-polarization effects and for absorption (empirical Ψ scan). Crystallographic data are listed in Table 1.

The structure was solved by direct methods and subsequent Fourier syntheses with the SHELXTL-PC V.5 program [18]. All non-hydrogen atoms were refined anisotropically, except the C(10) atom which was refined isotropically in two disordered positions. The hydrogen atoms were generated at their ideal positions and included in the calculations riding on their carrying atoms. Neutral atomic scattering and dispersion factors were those included in the SHELXTL-PC package.

Table 1. Crystal data and structure refinement for $[Cu_2L^1(N_3)_2]$

Empirical formula	$C_{20}H_{22}N_{12}O_2Cu_2$
Formula weight	589.58
Temperature (K)	293(2)
Wavelength (Å)	0.71073
Crystal system	Monoclinic
Space group	$P2_1/c$
a(Å)	7.916(2)
b(Å)	7.919(2)
c(Å)	20.110(4)
β(°)	95.20(3)
V (Å^3)	1255.4(4)
Z	2
D (g/cm^3)	1.560
Absorption coefficient	1.737 mm^{-1}
F(000)	600
Crystal size (mm)	$0.28 \times 0.40 \times 0.24$
2θ range for data collection (°)	5.16–60.06
Limiting indices	$-1 \leftarrow h \leftarrow 8$ $-1 \leftarrow k \leftarrow 11$ $-28 \leftarrow l \leftarrow 28$
Reflections collected	4193
Independent reflections	3102 [$R_{int} = 0.0438$]
Refinement method	Full-matrix least-squares on F^2
Data/restraints/parameters	2399/0/173
Goodness-of-fit on F^2	1.028
Final R indices [$I > 2.5\sigma(Io)$]	$R_1 = 0.0674$, $wR_2 = 0.1706$
R indices (all data)	$R_1 = 0.1011$, $wR_2 = 0.2382$
Largest diff. peak and hole (e Å^{-3})	1.134 and -1.681

RESULTS AND DISCUSSION

The ability of H_2oxpn to react with imidazole-2-carbaldehyde has been recently shown [17]. In this paper we extend such method with other aldehyde reagents in order to prepare two new bis-tetradentate schiff-base ligands. The ligands H_2L^1 and H_4L^2 are easily obtained by condensation of one mol of H_2oxpn with two moles of pyridine-2-carbaldehyde or pyrrol-2-carbaldehyde, respectively. ^{1}H NMR spectroscopy provides a good characterization of both ligands. The assignments (see experimental section) are based on the chemical shift, intensity and multiplicity values and they are supported by comparison between themselves with literature data for similar compounds [16,17].

The complexes $[Cu_2L^1](NO_3)_2\cdot 2H_2O$ and $[Cu_2L^2]\cdot 2H_2O$ can be prepared either from the respective ligands, by direct reaction with copper(II) nitrate or by making use of the template effect, by reacting the complex $[Cu_2(trans\text{-oxpn})(NO_3)_2]$ [1] with pyridine-2-carbaldehyde or pyrrol-2-carbaldehyde. In this second way, as for other similar reactions previously reported [17], a basic medium is needed to carry out the formation of the Schiff-base.

The IR spectra of both ligands show the characteristic sharp and intense ν(N—H) vibrations at 3303 and 3298 cm^{-1} and ν(C═O) amide bands at 1653 and 1648 cm^{-1} for H_2L^1 and H_4L^2, respectively. In addition, for H_4L^2, a small band corresponding to the ν(N—H) of the pyrrol ring is observed at 3190 cm^{-1}.

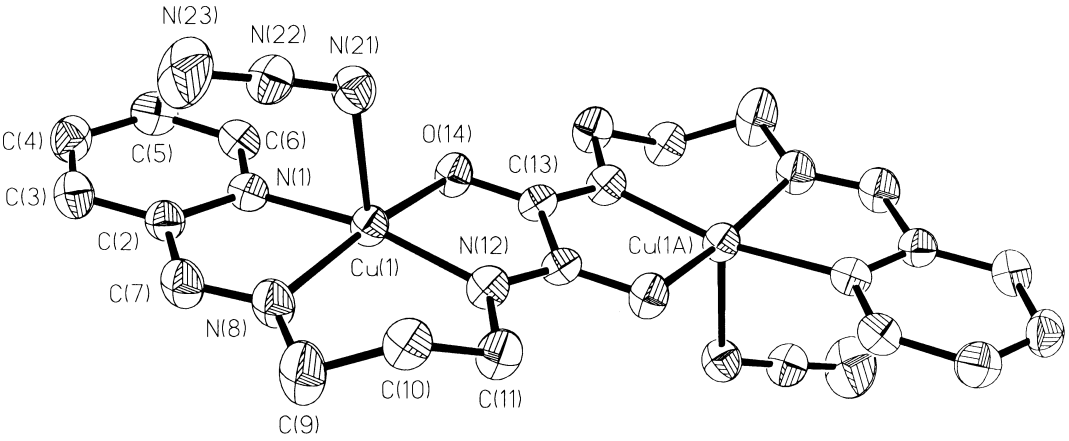

Fig. 1. A perspective view of the dinuclear $[Cu_2L^1(N_3)_2]$ molecule.

Likewise, a comparative study of the IR spectra of the ligands and their complexes reveals some details of the coordinating behaviour of the H_2L^1 and H_4L^2 ligands. Thus, in the IR spectra of all the copper(II) complexes NH absorption are absent, which confirms that the oxamidate group in H_2L^1 and the oxamidate and pyrrol groups in H_4L^2 coordinate the copper(II) ion in a deprotonated form. Moreover, the IR spectra of the copper(II) complexes of H_2L^1exhibit bands of the corresponding copper salt anion. These spectral features are in accord with the molecular structure proposed for $[Cu_2L^1](NO_3)_2 \cdot 2H_2O$ and $[Cu_2L^2] \cdot 2H_2O$, in which two copper(II) ions occupy the two symmetric N_3O inner sites of the di- and tetradeprotonated L^1 and L^2 ligands, respectively.

In $[Cu_2L^1](NO_3)_2 \cdot 2H_2O$, each copper(II) ion can accept one donor atom, such as the nitrogen atom from an azide anion, giving rise to the neutral complex $[Cu_2L^1(N_3)_2]$, that can be obtained as blue crystals suitable for X-ray diffraction. The structure of this complex consists of neutral centrosymmetric dinuclear copper(II) molecules. A perspective view of the molecular structure together with the atomic numbering scheme is shown in Fig. 1. Selected intramolecular bond distances and angles are listed in Table 2.

Within the dinuclear molecules, the crystallographically equivalent copper(II) ions are bridged by an oxamidate group in *trans* conformation, resulting in a copper-copper distance of 5.271 Å. A centre of inversion is located at the middle of the C(13)—C(13)^{i} bond of the oxamidate group (i: $-x$, $-y$, $-z+1$). Each copper(II) ion occupies the N_3O inner site of the doubly-deprotonated L^1 ligand with bond distances of ca 2.0 Å. The N(21) atom from the azide group completes the coordination polyhedron. The copper ion environment can be considered as CuN_4O square-pyramidal, $\tau = 0.02$ (according to the procedure proposed by Addison *et al.* [19], τ is 1 for the regular trigonal bipyramid and 0 for the square pyramid), with the basal plane defined by the N_3O coordination site of L^1 and the apical position being occupied by the azide N(21) atom at a longer bond distance of 2.340(4) Å. The coordination basal plane is almost

Table 2. Selected bond lengths (Å) and angles (°) for $[Cu_2L^1(N_3)_2]$

Cu(1)—N(12)	1.971(4)	Cu(1)—O(14)	1.999(3)
Cu(1)—N(8)	2.017(4)	Cu(1)—N(1)	2.023(4)
Cu(1)—N(21)	2.340(4)	N(21)—N(22)	1.199(6)
N(22)—N(23)	1.155(7)		

N(12)—Cu(1)—O(14)	84.93(13)	N(12)—Cu(1)—N(8)	95.5(2)
O(14)—Cu(1)—N(8)	168.2(2)	N(12)—Cu(1)—N(1)	167.43(14)
O(14)—Cu(1)—N(1)	96.20(14)	N(8)—Cu(1)—N(1)	80.9(2)
N(12)—Cu(1)—N(21)	100.7(2)	O(14)—Cu(1)—N(21)	101.48(14)
N(8)—Cu(1)—N(21)	90.0(2)	N(1)—Cu(1)—N(21)	91.34(14)
N(22)—N(21)—Cu(1)	114.4(3)	N(23)—N(22)—N(21)	176.9(5)

planar with maximum deviation of 0.0076 Å for the atom N(8). As usual in this geometry, the copper(II) ion deviates (0.2085 Å) from the coordination basal plane toward the apical position.

The bis-tetradentate behaviour of the ligand gives rise to one six- and two five-membered chelate rings on each copper(II) ion. The coordination basal plane and the oxamidate bridging group are almost planar and form a dihedral angle of 8.8°. The deviation of the copper(II) ion from the $C_2N_2O_2$ plane is very small (0.0139 Å), so that the dinuclear $[Cu_2L^1]^{2+}$ skeleton is not far from planarity.

The azide fragment is quasi-linear, with a N(21)—N(22)—N(23) angle of 176.9(5)°, and asymmetric with N(21)—N(22) and N(22)—N(23) distances of 1.199(6) and 1.155(7) Å, respectively. The angle Cu—N(21)—N(22) is of 114.4(3)° which agrees with a sp^2-hybridization of the N(21) atom.

There are no hydrogen bonds or close contacts between the dinuclear molecules, indicating that these are well isolated in the structure.

Magnetic properties

The temperature dependence of the χT product per copper atom for $[Cu_2L^1](NO_3)_2\cdot 2H_2O$, $[Cu_2L^2]\cdot 2H_2O$ and $[Cu_2L^1(N_3)_2]$ are shown in Fig. 2. The room-temperature χT values for the three compounds are lower than that expected for non-interacting copper(II) ions (0.375 $cm^3\ mol^{-1}$ K with $g = 2.0$). This fact together with the decreasing of χT with T over the explored temperature range, clearly indicate that strong antiferromagnetic exchange couplings operate between copper(II) ions in the three compounds.

In keeping with their dinuclear structures, the magnetic data of the complexes were analyzed by the Bleaney-Bowers equation ($H = -JS_1S_2$). A parameter, ρ, was included into the equation to consider the mononuclear magnetic impurity and in the case of the complex $[Cu_2L^1(N_3)_2]$, a Weiss constant, θ, was also included to take phenomenologically into account the decrease of χT at low temperature. The g values were those obtained from the polycrystalline EPR spectra at room temperature. The best fit of the magnetic data by this equation was found with $J = 425.5\ cm^{-1}$, $g = 2.05$, $\rho = 5.8\%$ for $[Cu_2L^1](NO_3)_2\cdot 2H_2O$, $J = 427.9\ cm^{-1}$, $g = 2.04$ and $\rho = 6.1$ for $[Cu_2L^2]\cdot 2H_2O$ and $J = 424.1\ cm^{-1}$, $g = 2.09$, $\rho = 2.1$ and $\theta = -9.2$ K for $[Cu_2L^1(N_3)_2]$.

The singlet-triplet energy values (J) obtained are close to other structurally characterized *trans*-oxamidate-bridged dinuclear copper(II) complexes [1–8] and they are a consequence of the ability of the oxamidate-bridge to propagate the antiferromagnetic exchange interaction between metal ions, which allows a large overlap of the $d_{x^2-y^2}$ magnetic orbitals centered on each copper(II) ion [20]. The high bridging site planarity also contribute to the large J values observed for these complexes.

Acknowledgements—J.-M.D.-V., J.-M.M. and E.C. are grateful to the Dirección General de Investigación Científica y Técnica for financial support (project PB94-0764).

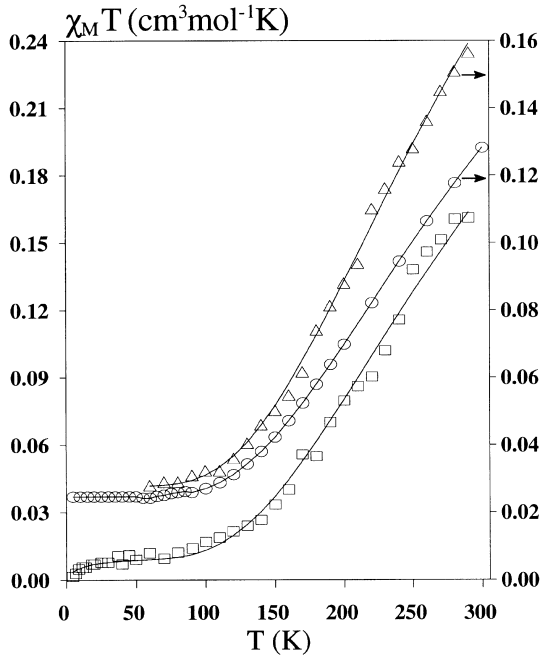

Fig. 2. Temperature dependences of χT per copper(II) atom for $[Cu_2L^1](NO_3)_2\cdot 2H_2O$ (Δ), $[Cu_2L^2]\cdot 2H_2O$ (○) and $[Cu_2L^1(N_3)_2]$ (□). Solid lines were generated from the corresponding best-fit magnetic parameters.

REFERENCES

1. Sanz, J. L., Cervera, B., Ruiz, R., Bois, C., Faus, J., Lloret, F. and Julve, M., *J. Chem. Soc., Dalton Trans.*, 1996, 1359.
2. Lloret, F., Julve, M., Faus, J., Ruiz, R., Castro, I., Mollar, M. and Philoche-Levisalles, M., *Inorg. Chem.*, 1992, **31,** 784.
3. Chen, Z. N., Tang, W. X. and Yu, K. B., *Polyhedron*, 1994, **13,** 783.
4. Real, J. A., Mollar, M., Ruiz, R., Faus, J., Lloret, F., Julve, M., Philoche-Levisalles, M., *J. Chem. Soc., Dalton Trans.*, 1993, 1483.
5. Chen, Z. N., Wang, J. L., Qiu, J., Miao, F. M. and Tang, W. X., *Inorg. Chem.*, 1995, **34,** 2255.
6. Real, J. A., Ruiz, R., Faus, J., Lloret, F., Julve, M., Yournaux, Y., Philoche-Levisalles, M. and Bois, C., *J. Chem. Soc., Dalton Trans.*, 1994, 3769.
7. Lloret, F., Julve, M., Real, J. A., Faus, J., Ruiz, R., Mollar, M., Castro, I. and Bois, C., *Inorg. Chem.*, 1992, **31,** 2956.
8. Chen, Z. N., Qiu, J., Wu, Z. K., Fu, D. G., Yu, K. B., Tang, W. X., *J. Chem. Soc., Dalton Trans.*, 1994, 1923.
9. Journaux, Y., Sletten, J. and Kahn, O., *Inorg. Chem.*, 1985, **24,** 4063.
10. Zhang, Z. Y., Liao, D. Z., Jiang, Z. H., Hao, S.

Q., Yao, X. K., Wang, H. G. and Wang, G. L., *Inorg. Chim. Acta*, 1990, **173,** 201.
11. Escuer, A., Vicente, R., Ribas, J., Costa, R. and Solans, X., *Inorg. Chem.*, 1992, **31,** 2627.
12. Mathoniere, C., Kahn, O., Davan, J. C., Hilbig, H. and Koler, F. H., *Inorg. Chem.*, 1993, **32,** 4057.
13. Journaux, Y., Sletten, J. and Kahn, O., *Inorg. Chem.*, 1986, **25,** 439.
14. Lloret, F., Journaux, Y. and Julve, M., *Inorg. Chem.*, 1990, **29,** 3967.
15. (a) Chen, Z. N., Qiu, J., Tang, W. X. and Yu, K. B., *Inorg. Chim. Acta*, 1994, **171,** 224; (b) Bencini, A., Benelli, C., Fabretti, A. C., Franchini, G. and Gatteschi, D., *Inorg. Chem.*, 1986, **25,** 1063; (c) Chen, Z. N., Liu, S. X., Qiu, J., Wang, Z. M., Huang, J. L. and Tang, W. X., *J. Chem. Soc., Dalton Trans.*, 1994, 2989; (d) Chen, Z. N., Fu, D. G., Yu, K. B. and Tang, W. X., *J. Chem. Soc., Dalton Trans.*, 1994, 1917.
16. Laurent, J.-P., Costes, J.-P. and Pradie, G., *Inorg. Chim. Acta*, 1993, **213,** 57.
17. Dominguez-Vera, J. M., Galvez, N., Colacio, E., Cuesta, R., Costes, J.-P. and Laurent, J.-P., *J. Chem. Soc., Dalton Trans.*, 1996, 861.
18. SHELXTL-PC V.5 Release 5. Siemens. Analytical X-Ray Instruments. Madison, WI, 1995.
19. Addison, A. W., Burke, P. J. and Henrick, H., *Inorg. Chem.*, 1982, **21,** 60.
20. Kahn, O., *Angew. Chem. Int. Ed. Engl.*, 1985, **24,** 834.

Pergamon

PII : S0277–5387(98)00042–4

Polyhedron Vol. 17, No. 16, pp. 2719–2726, 1998
© 1998 Elsevier Science Ltd
All rights reserved. Printed in Great Britain
0277–5387/98 $19.00 + 0.00

Interaction of $[(dien)Cu(ONO_2)]NO_3$ and [(dien)Cu(Br)]Br with guanosine and adenine. Crystal structure of $[(dien)Cu(Guo\text{-}N^7)(ONO_2)]NO_3$

C. A. Bolos,*[a] P. C. Christidis[b] and S. T. Triantafyllou[b]

[a] Department of General and Inorganic Chemistry, Lab. of Inorganic Chemistry, Aristotle University, Thessaloniki 54006, Greece

[b] Laboratory of Applied Physics, Aristotle University, Thessaloniki, 54006, Greece

(Received 26 November 1997; accepted 21 January 1998)

Abstract—The reaction of $[(dien)Cu(ONO_2)]NO_3$ and [(dien)CuBr]Br with Guanosine(Guo) gave the compounds $[(dien)Cu(Guo\text{-}N^7)(ONO_2)]NO_3$ [dien = diethylenetriamine and [(dien)Cu(Guo)(Br)]Br, respectively. The reaction of $[(dien)Cu(ONO_2)]NO_3$ with Adenine(A) afforded the compound $[(dien)Cu(A)(ONO_2)]NO_3$. The complexes have been characterized by elemental analyses, molar conductance and magnetic measurements, as well as by electronic and IR spectral studies. According to the spectral data the ligands (Guo and A) bind to the copper atom via N^7. The crystal structure of the $[(dien)Cu(Guo\text{-}N^7)(ONO_2)]NO_3$ complex has been determined by X-ray diffraction. Copper(II) is five coordinated with three nitrogen atoms from the dien molecule [2.015(6) Å, 2.007(4) Å, 2.038(6) Å], the N^7 atom from guanosine [2.006(4) Å] and an oxygen atom from a nitrato group [2.251(6) Å]. The five donor atoms form a distorted square pyramid with the four nitrogen atoms on its basal plane and the oxygen atom at the apical position. All the complexes are electrolytes as indicated by their molar conductance in methanol or water. The magnetic moments are consistent with monomeric copper(II) units. © 1998 Elsevier Science Ltd. All rights reserved

Keywords: Copper(II) complexes; dien; guanosine; adenine; crystal structure; absolute configuration.

The antitumour activity of inorganic compounds was reported more than 25 years ago [1]. It is well known that the most famous antitumour drug *cis*-DDP reacts with cellular components such as DNA and proteins [2,3]. The formation of metal complex-DNA adduct is expected to have a significant impact on the biological function of DNA. NMR and X-ray structural studies showed that the metals prefer as binding sites on DNA the N^7 atoms of guanine and adenine [4,5], the N^1 atom of adenine [6,7] and the N^3 atom of cytosine [8]. In some cases the preference of the metals for other coordination sites of the bases, is governed by the reaction conditions [9, 10], such as solvent, pH, etc; it is also associated with the stronger basicity of certain nitrogen atoms, the hydrogen bonds, the steric hindrance and unpredictable factors.

Although the Pt(II) complexes seem to be the major pharmacological tool in chemotherapy, some inorganic compounds of Re [11], Ru [12], Rh [13], Cu(I) and Cu(II) [14] have also been documented to exhibit carcinostatic activity. These metal centres with polyamine ligands, could be the key for future studies, owing to their lower toxicity to humans as compared to that of platinum [15, 16].

In a previous study [17] we found that the antiproliferative activity of copper(II) compounds with triamines (dien, dpt and their derivatives) is related with their electronic structure and is independent of the additional counter-ion (e.g. NO_3^-, SO_4^{2-}, etc.). Taking into account that the square planar or square pyramidal Cu(II) compounds exhibit the tendency for axial ligation [18] and in order to extend our knowledge on the coordination chemistry of the above complexes, we carried out reactions of $[(dien)Cu(ONO_2)]NO_3$ and [(dien)Cu(Br)]Br with DNA com-

* Author to whom correspondence should be addressed.

ponents, such as guanosine and adenine and studied the reaction products. The results of this work are presented in this paper.

EXPERIMENTAL

Starting materials

Adenine and guanosine were purchased from P-L Biochemicals Inc., copper(II) nitrate trihydrate and copper(II) bromide were obtained from Merck Chemicals and used as received. [(dien)Cu(ONO_2)]NO_3 and [(dien)Cu(Br)]Br were prepared as previously described elsewhere [19,20]. The solvents were reagent grade and were used without further purification.

Preparation of complexes

The new complexes were prepared by mixing a methanolic suspension of guanosine and a methanolic or aqueous solution of [(dien)Cu(ONO_2)]NO_3 or [(dien)Cu(Br)]Br in 1 : 1 molar ratio. The same products were also formed in a different molar ratio (1 : 2).

Compound **1**. [(dien)Cu(Guo-N^7)(ONO_2)]NO_3 (**1**) was prepared by mixing a methanolic suspension of guanosine (2 mmol in 20 cm^3 of MeOH) and a methanolic solution of [(dien)Cu(ONO_2)]NO_3 compound (2 mmol in 10 cm^3 of MeOH). The reaction mixture became clear after 1 h stirring at 45°C, and it was then left for slow evaporation at room temperature. After 10 days blue crystals formed. The crystals were isolated by filtration and dried under vacuum. The yield of the reaction was 65%.

Anal. (**1**) Calcd for $C_{14}H_{26}N_{10}O_{11}Cu$: C, 29.29; H, 4.57; N, 24.49; Cu, 11.07. Found: C, 29.35; H, 4.55; N, 24.45; Cu, 11.08. UV–vis bands; 596 nm ($\log\varepsilon = 1.93$), 266 nm ($\log\varepsilon = 3.97$) (MeOH), 613 nm ($\log\varepsilon = 1.93$), 208 nm ($\log\varepsilon = 4.58$), 250 ($\log\varepsilon = 4.54$), 274 sh, (in H_2O), $\Lambda\mu = 130$ μS cm^{-1} (in MeOH), $\Lambda\mu = 242$ μS cm^{-1} (in H_2O).

Compound **2**. The [(dien)Cu(Guo-N^7)Br]Br (**2**) compound was prepared by the reaction of [(dien)Cu(Br)]Br with guanosine. An aqueous solution of [(dien)Cu(Br)]Br (2 mmol in 3 cm^3 H_2O) was mixed with a suspension 2 mmol of guanosine in methanol (20 cm^3). The Guo reacted slowly with [(dien)Cu(Br)]Br and after 2 h stirring a light blue solid was formed. The solid was isolated by filtration and recrystallized from water-methanol (1 : 1). The yield of the reaction was 52%.

Anal. (**2**) Calcd for $C_{14}H_{26}N_8O_5Br_2Cu$: C, 27.57; H, 4.27; N, 18.38; Cu, 10.43. Found: C, 27.60; H, 4.25; N, 18.40; Cu, 10.40. UV–vis bands; 608 nm, 276 nm, 254 nm, 209 nm (MeOH), 619 nm ($\log\varepsilon = 1.86$), 282 nm ($\log\varepsilon = 3.34$), 227 nm ($\log\varepsilon = 3.35$) (in H_2O), $\Lambda\mu = 240$ μS cm^{-1} (H_2O), $\Lambda\mu = 128$ μS cm^{-1} (MeOH).

Compound **3**. [(dien)Cu(A)(ONO_2)]NO_3 (**3**) was prepared by mixing a methanolic suspension of adenine (2 mmol in 20 cm^3 of MeOH) and a methanolic solution of [(dien)Cu(ONO_2)]NO_3 (2 mmol in 10 cm^3 of MeOH). The resulting mixture was refluxed for 1 h and cooled at room temperature. The light blue product was isolated by filtration, washed with diethylether and dried under vacuum. The yield of the reaction was 70%.

Anal. (**3**) Calcd for $C_9H_{18}N_{10}O_6Cu$: C, 25.38; H, 4.23; N, 32.89; Cu, 14.93. Found: C, 25.40; H, 4.23; N, 32.77; Cu, 14.89. UV–vis bands; 619 nm ($\log\varepsilon = 1.99$), 259 nm ($\log\varepsilon = 4.41$), 216 ($\log\varepsilon = 4.38$) (MeOH), 622 nm ($\log\varepsilon = 1.83$), 259 nm ($\log\varepsilon = 4.45$), 208 nm ($\log\varepsilon = 4.64$) (in H_2O), $\Lambda\mu = 207$ μS cm^{-1} (in H_2O), 120 μS cm^{-1} (in MeOH).

Physical methods

C, H and N microanalyses were carried out with a Perkin–Elmer 2400 elemental analyser and copper was determined by atomic absorption spectroscopy. IR spectra were recorded with a Perkin–Elmer 1650 FT-IR instrument in the 200–4000 cm^{-1} region, using KBr pellets and calibrated against polystyrene. Electronic spectra were obtained in solution on a Shimadzu UV-160A spectrophotometer in the 200–1100 nm region. Molar conductivities were run on a WTW conductivity bridge and a calibrated dip type cell. Magnetic susceptibilities of powdered samples were determined by employing the Faraday method with a home-made balance against $Hg[Co(SCN)_4]$ as a calibrant. Diamagnetic corrections were estimated from Pascal constants.

X-ray structure determination of [(dien)Cu(Guo-N^7)(ONO_2)]NO_3

A blue crystal prism of dimensions $0.63 \times 0.22 \times 0.18$ mm was mounted on a modernized Philips PW1100 single-crystal diffractometer. Cell parameters were calculated by least squares refinement of the setting angles of 29 reflections [$25.09° < 2\theta < 31.34°$, Mo–$K_\alpha$ radiation]. From systematic absences the space group $P2_12_12_1$ was unequivocally determined. Intensity data were collected up to $2\theta = 55°$ with graphite monochromated Mo–K_α radiation using the learnt profile method [21] (scintillation counter, $2\theta/\omega$ scan mode, three standard reflections monitored every 120 min). Two independent sets of reflections were measured, which were corrected for Lorentz and polarization effects but not for absorption. They were finally reduced to 2987 unique ones of which 2458 were considered as observed [$F_o > 4\sigma(F_o)$] and were used in the subsequent calculations. Crystal data for [(dien)Cu(Guo-N^7)(ONO_2)]NO_3 are given in Table 2. For the solution, refinement and analysis of the structure the PC version of the XTAL 3.2 system of crystallographic programmes was used [22].

The structure was solved by direct methods and difference Fourier syntheses. Neutral atomic scattering factors and anomalous dispersion corrections were taken from Ref. [23]. The structure refinement was performed by the full-matrix least-squares method, in which the function minimized was $\Sigma w(F_o - F_c)^2$. All hydrogen atoms, except H(O5A) (see Fig. 1), could be located in a difference Fourier map. Non-hydrogen and hydrogen atom parameters were refined in alternate cycles. In the final stage of refinement anisotropic displacement parameters were introduced for all the non-hydrogen atoms and isotropic ones for the hydrogen atoms. Also, bond length restraints for the hydrogen atoms attached to the nitrogen atoms of the dien group were applied. Atoms H1(C5A) and H2(C5A), which showed a tendency to move to chemically unrealistic positions, were kept fixed. The weighting scheme used was $w = 1/\sigma^2(F_o)$, where $\sigma^2(F_o) = \sigma^2(F_{statistics}) + \sigma^2(F_{mod})$ and $\sigma^2(F_{mod})$ is the so called "ignorance factor" [22]. An extinction correction was deemed as not necessary. At convergence R was 0.049 and Rw 0.036. A separate refinement of the enantiomorph structure resulted in final R and Rw values of 0.060 and 0.041, respectively. The application of the $\mathscr{R}$ test [24] indicates that the first enantiomorph is correct at a significance level much lower than 0.005.

RESULTS AND DISCUSSION

The reaction of [(dien)Cu(ONO$_2$)]NO$_3$ with guanosine(Guo) and adenine(A) yielded coloured, air stable, microcrystalline or crystalline compounds of the general formula [(dien)CuBX)]X; [B = guanosine(Guo), adenine(A) and X = NO$_3$, Br]. The complexes **1** and **3** are soluble in methanol and water, whereas the [(dien)Cu(Guo)(Br)]Br is soluble in water and slightly soluble in methanol. The prepared complexes are all insoluble in common organic solvents and their elemental analysis fit the proposed stoichiometry well. The magnetic moments of the Cu(II) complexes, at room temperature, were found to be 1.73–1.85 BM (Table 1). These values are in accordance with the d^9 electronic configuration of copper(II) and confirm the monomeric nature of the compounds under investigation. The $\Lambda\mu$ values of all complexes in methanol and water are indicative of 1 : 1 and 2 : 1 electrolytes, respectively [25]. The conductivities of the complexes were again measured after 24 and 48 h.

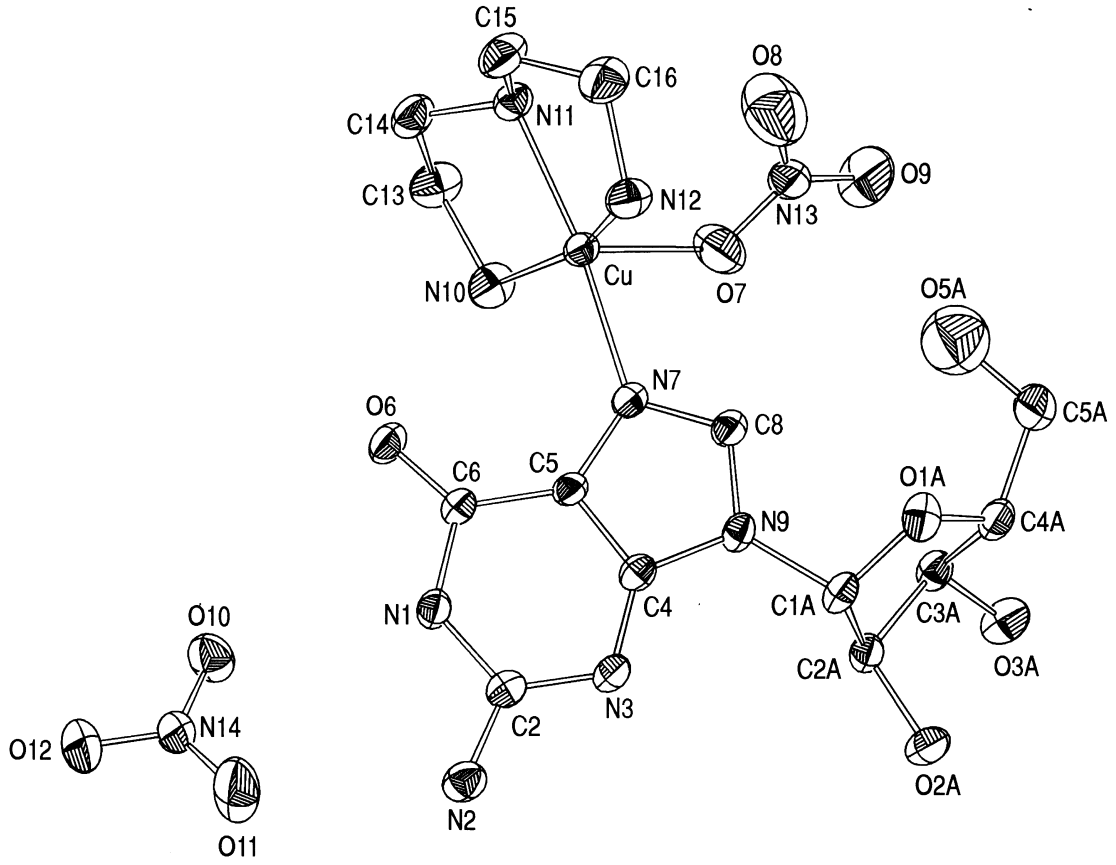

Fig. 1. ORTEP plot of the symmetric unit of the structure of [(dien)Cu(Guo-N^7)(ONO$_2$)](NO$_3$) with the atomic numbering scheme. Hydrogen atoms are omitted for clarity and atomic thermal ellipsoids are at 30% probability level.

Table 1. Selected bands (cm^{-1}) of the IR spectral data and magnetic moments of the Cu(II) complexes

Compound	ν_s(N—H) ν_{as}(N—H) ν(O—H)	ν(C═O) ν(C═N)	NO_3	ν(Cu—N)	ν(Cu—O)	μ_{eff} (BM)
$[Cu(dien)(ONO_2)]NO_3$	3282		1750			
	3250		1444	470	398	1.85
	3233		1384			
	3160					
Guanosine	3469	1733, 1693				
	3319	1641, 1625				
	3215	1608				
$[(dien)Cu(Gua)(ONO_2)]NO_3$ **1**	3423, 3312	1685, 1646	1750	458	370	1.73
	3199, 3113	1619,	1403			
		1587,	1384			
		1539, 1494				
$[(dien)CuBr_2]$	3277, 3232	1578		447	388	
	3137	1471				
[(dien)Cu(Guo)Br]Br **2**	3453, 3280	1690, 1620				
	3250, 3155	1608, 1587		439		1.78
		1534, 1488				
Adenine	3294	1672, 1602				
	3116	1500				
$[(dien)Cu(A)(ONO_2)]No_3$ **3**	3396, 3300	1656, 1593	1750	451	341	1.73
	3239, 3201	1567, 1511	1411			
	3144	1489	1384			

The results were almost identical suggesting that the complexes are stable in solution. Attempts to react $[(dien)Cu(ONO_2)]NO_3$ with guanine or adenosine failed to give the expected product. Also, the reactions of [(dien)Cu(Br)]Br with the previous ligands plus adenine were not successful.

IR spectral studies

The most important IR bands of the ligands and their complexes are displayed in Table 1. In the infrared spectra of the ligands guanosine, adenine and the starting complexes $[(dien)Cu(ONO_2)]NO_3$ and [(dien) Cu(Br)]Br, the medium intensity bands in the 3350–3100 cm^{-1} range, could be assigned to primary and secondary amino groups, respectively. Some of these bands are shifted upon complexation to higher and some others to lower frequencies. Although these shifts are strong evidence that the dien ligand is coordinated in a tridentate mode, an accurate assignment of these bands seems to be impossible, since some of them are obscured by others coming from guanosine or adenine. In the IR spectra of **1** and **2** complexes, the bands 3423 and 3453 cm^{-1} are attributed to the ν(O—H) vibration of the sugar moiety and are shifted to lower frequencies by 46 and 16 cm^{-1}, respectively. This shift may be due to the effect of hydrogen bonding between the protons of O—H groups and the counterions (NO_3^-) for **1** and Br^- for **2**. The band assigned as $\nu(C^6{=}O^6)$ for guanosine (1732 cm^{-1}), upon coordination shows a negative shift of 58 and 42 cm^{-1} for **1** and **2,** respectively. Considering that the $C^6{=}O^6$ group does not participate in coordination via its oxygen atom or in any other mode, the observed shift of the respective band is probably attributed to a rearrangement of the intraligand hydrogen bonding of the ligands, caused by the metallation of N^7. Support for the above argument is provided by the X-ray data (*vide infra*). The strong $\nu(C{=}N^7)$ bands of the ligands occurring at 1693 (Guo) and 1672 (A) cm^{-1}, appear at 1619, 1620 and 1656 cm^{-1} in the spectra of the respective complexes **1, 2, 3,** i.e. they are all shifted to lower wave numbers. The observed negative shifts strongly suggest that coordination of the ligands to the copper(II) atom occurs via the N^7, in agreement with its marked basicity [26]. In the IR spectra of **1** and **3** complexes, the weak band at ca 1750 cm^{-1} and the strong bands at 1410 and 1384 cm^{-1} indicate the existence of a free [27] NO_3^- and a unidentate [28] nitrato group, respectively. This observation is in accordance with molar conductivities and X-ray data. Finally, the weak or medium intensity bands in the regions 461–439 and 390–332 cm^{-1} are due to the stretching vibrations of Cu—N and Cu—O bonds, respectively [29]. These bands, as expected, shift to lower wave numbers by 19–8 cm^{-1} for Cu—N and 28–10 cm^{-1} for Cu—O bonds, in respect to those of the starting material $[(dien)Cu(ONO_2)]NO_3$. Finally,

Table 2. Crystal data and refinement results for [(dien)Cu(Guo-N^7)(ONO$_2$)]NO$_3$

Empirical formula	$C_{14}H_{26}N_{10}O_{11}Cu$
Formula weight	573.96
Crystal system	Orthorhombic
Space group	$P2_12_12_1$
a (Å)	7.2453(6)
b (Å)	10.0485(7)
c (Å)	31.0598(16)
V (Å^3)	2261.3(3)
Z	4
F(000)	1180
D_{meas} (mg m^{-3})	1.68 (flotation in $CH_3I/CHCl_3$ mixture)
D_{calc} (mg m^{-3})	1.686
μ (mm^{-1}) (for Mo–K_α)	1.04
λ (Mo–K$_\alpha$) (Å)	0.71069
Total reflections measured	6715
Unique reflections	2987
Observed unique reflections [$F_o > 4\sigma(F_o)$]	2458
No. of parameters	417
R(%)[a]	4.9
R_w(%)[b]	3.6
S[c]	0.993
(shift/error)$_{max}$	0.33 (for the non-hydrogen atoms)
(shift/error)$_{max}$	1.1 (for the hydrogen atoms)
$(\Delta\rho)_{max}$ (e Å^{-3})	1.3
$(\Delta\rho)_{min}$ (e Å^{-3})	−0.4

[a] $R = \Sigma\|\|F_o| - |F_c\|| / \Sigma|F_o|$,
[b] $R_w = [\Sigma_w(|F_o| - |F_c|)^2 / \Sigma w|F_o|^2]^{1/2}$
[c] $S = [\Sigma w(|F_o| - |F_c|)^2 / (N_{ref}\text{-}N_{param})]^{1/2}$

the complex **2** displays a single band at 284 cm^{-1}, which is due to the Cu—Br stretching vibration.

In view of our IR, magnetic and conductivity data, it can be concluded that the metal in compounds **1** and **3** is five coordinated, the four coordination sites being occupied by nitrogen atoms [three from dien and one from guanosine (**1**) or adenine (**3**)] and the fifth one by one oxygen atom from the nitrato group. The complex **2** is also five coordinated with the three nitrogen atoms of dien and the N^7 atom from guanosine, while the fifth site is occupied by the bromine atom.

Electronic spectral studies

The electronic spectra of the complexes taken in methanol and water were recorded between 1100 nm and 200 nm. The bands in the UV–vis spectra of the new complexes may be related either to the ligands guanosine, adenine or to the starting materials [(dien)Cu(ONO$_2$)]NO$_3$ and [(dien)Cu(Br)]Br. The band at 615 nm and 618 nm of the starting materials [(dien)Cu(ONO$_2$)]NO$_3$ and [(dien)Cu(Br)]Br, respectively can be considered as a crystal field band on the basis of its low intensity. It is very broad and possibly represents a spectral envelope covering several *d-d* transitions [30]. The bands of **1, 2** and **3** in methanol, occurring at 596–608 nm region, are shifted to higher energies as compared to the analogous ones of the starting materials. It is reasonable to assume that the ligands (guanosine and adenine) influence appreciably the energy levels of *d* orbitals of the metal ion. This *d-d* separation is the result of transformation of [CuN_3O_2] and [CuN_3Br] chromophores of [(dien)Cu(ONO$_2$)]NO$_3$ and [(dien)Cu(Br)]Br to [CuN_4O] and to [CuN_4Br], respectively in the new complexes. Furthermore, the crystal field bands of **1, 2** and **3** complexes in aqueous solution are shifted to lower energies, implying ligand (NO_3, Br) replacement by one or two water molecules. The above change in the coordination sphere is further supported by molar conductivity measurements, indicating transformation from 1 : 1 (methanol) to 2 : 1 electrolytes (water). The intense absorption band at 251 nm of the [(dien)Cu(ONO$_2$)]NO$_3$ complex is tentatively attributed to a $\pi^* \leftarrow n$ intraligand transition. This band also occurs in the spectra of **1** and **3** complexes, but is slightly shifted towards lower energy. The bands at 254 nm and 260 nm in the spectra of the free guanosine and adenine, respectively, is attributed to an intraligand transition of $\pi^* \leftarrow \pi$ type, located possibly on the C=N group. This band is shifted to higher wave numbers, in the **1, 2** and **3** complexes, a fact further supporting the idea of the coordination of the guanosino and adenosino ligands via the N^7.

Crystal structure of [(dien)Cu(Guo-N^7)(ONO_2)]NO_3

An ORTEP view of the asymmetric unit of the structure of [(dien)Cu(Guo-N^7)(ONO_2)]NO_3 is shown in Fig. 1, while selected bond lengths and angles along with the established hydrogen bonds are given in Table 3.

Copper is bonded to the Guo ligand through N(7) and to the dien ligand through N(10), N(11) and N(12) with the terminal atoms N(10) and N(12) being in *trans* position to each other. Moreover, one of the NO_3 groups is linked to copper through O(7), thus completing a distorted square pyramidal (SP) arrangement with O(7) occupying its apex and with atoms N(7), N(10), N(11) and N(12) lying on the basal plane. The compound may be thus formulated as $[(dien)Cu(Guo\text{-}N^7)(ONO_2)]^+(NO_3)^-$. The same atomic arrangement around the copper atom may

Table 3. Selected bond lengths (Å) and angles (deg) in [(dien)Cu(Guo-N^7)(ONO_2)]NO_3

Cu—N(7)	2.006(4)	N(7)—Cu—N(10)	96.0(2)
Cu—N(10)	2.015(6)	N(7)—Cu—N—N(11)	169.9(2)
Cu—N(11)	2.007(4)	N(7)—Cu—N—N(12)	91.9(2)
Cu—N(12)	2.038(6)	N(7)—Cu—N—O(7)	83.4(2)
Cu—O(7)	2.251(6)	N(10)—Cu—N(11)	85.0(3)
		N(10)—Cu—N—N(12)	162.9(2)
C(13)—N(10)	1.496(9)	N(10)—Cu—N—O(7)	85.9(2)
C(13)—C(14)	1.507(9)	N(11)—Cu—N(12)	84.7(2)
C(14)—N(11)	1.46(1)	N(11)—Cu—N—O(7)	106.7(2)
C(15)—N(11)	1.481(8)	N(12)—Cu—O(7)	110.2(2)
C(15)—C(16)	1.50(1)		
C(16)—N(12)	1.49(1)	C(13)—N(10)—Cu	108.1(4)
		C(14)—C(13)—N(10)	108.4(5)
C(8)—N(7)	1.313(7)	C(13)—C(14)—N(11)	106.9(5)
C(18)—N(9)	1.362(7)	C(14)—N(11)—Cu	106.8(4)
C(4)—N(9)	1.380(8)	C(14)—N(11)—C(15)	114.5(5)
C(4)—C(5)	1.383(7)	C(15)—N(11)—Cu	109.0(4)
C(5)—N(7)	1.381(7)	C(16)—C(15)—N(11)	107.5(5)
C(5)—C(6)	1.416(8)	C(15)—C(16)—N(12)	109.1(6)
C(6)—N(1)	1.379(7)	C(16)—N(12)—Cu	108.3(5)
C(6)—O(6)	1.235(7)		
C(2)—N(1)	1.388(7)	C(5)—N(7)—C(8)	106.3(4)
C(2)—N(2)	1.314(8)	C(4)—C(5)—N(7)	109.4(5)
C(2)—N(3)	1.331(8)	C(4)—C(5)—C(6)	119.2(5)
C(4)—N(3)	1.349(7)	C(5)—C(4)—N(3)	128.1(5)
		C(5)—C(4)—N(9)	105.5(5)
C(1A)—N(9)	1.485(7)	N(7)—C(8)—N(9)	111.5(5)
C(1A)—C(2A)	1.528(7)	C(4)—N(9)—C(8)	107.3(4)
C(1A)—O(1A)	1.403(8)	C(5)—C(6)—N(1)	111.7(5)
C(2A)—C(3A)	1.520(8)	C(2)—N(1)—C(6)	125.7(5)
C(2A)—O(2A)	1.421(6)	N(1)—C(2)—N(3)	122.7(5)
C(3A)—C(4A)	1.522(9)	C(2)—N(3)—C(4)	112.6(4)
C(3A)—O(3A)	1.442(6)		
C(4A)—C(5A)	1.52(1)	C(2A)—C(1A)—O(1A)	108.0(4)
C(4A)—O(1A)	1.451(7)	C(1A)—C(2A)—C(3A)	101.1(4)
C(5A)—O(5A)	1.30(1)	V(2A)—C(3A)—C(4A)	102.4(4)
		C(3A)—C(4A)—O(1A)	103.9(5)
		C(1A)—O(1A)—C(4A)	109.9(4)
		C(4A)—C(5A)—O(5A)	111.0(1)

Hydrogen bonds	D—H (Å)	H···A (Å)	D···A (Å)	D—H···A (Å) (°)
N1—H(N1)···O10[a]	0.72(7)	2.13(7)	2.849(8)	171(7)
N2—H1(N2)···O9[b]	0.71(4)	2.43(5)	2.92(1)	128(5)
N2—H1(N2)···O3A[d]	0.71(4)	2.68(7)	3.190(8)	131(5)
N2—H2(N2)···O11[a]	0.92(7)	2.01(7)	2.93(1)	174(6)
O2A—H(O2A)···O7[d]	0.97(9)	1.85(8)	2.811(7)	170(8)
O2A—H(O2A)···N13[d]	0.97(9)	2.69(10)	3.635(8)	164(7)
O3A—H(O3A)···N3[c]	0.81(10)	2.05(10)	2.802(6)	154(10)

Symmetry operations: [a] $x+1, y, z$; [b] $x+1, y+1, z$; [c] $1-x; -1/2+y, 1/2-z$; [d] $1-x, 1/2+y, 1/2-z$.

be described as distorted trigonal bipyramidal (TBP) with atoms N(7) and N(11) at axial positions. The degree of distortion of the coordination polyhedron from the ideal SP arrangement may be defined as $\tau = (\beta - \alpha)/60$ [31]. For an ideal square pyramid it is $\alpha = \beta = 180^\circ$ and $\tau = 0$, while for an ideal trigonal bipyramid it is $\beta = 180^\circ$, $\alpha = 120^\circ$ and $\tau = 1$. In our case is $\alpha = 162.9^\circ$, $\beta = 169.9^\circ$ and $\tau = 0.12$, which indicates a geometry very close to square pyramidal. The maximum deviation from the best plane through the four basal atoms occurs for N(11) [0.061(9) Å], while the metal atom is 0.213(1) Å distant from that plane. The geometry of the dien moiety is as expected [32,19,33]. The N^PCuN^S valence angles (N^P from primary and N^S from secondary amino group) are lower than 90° [85.0(3)° and 84.7(2)°] and N^PCuN^P is much lower than 180° [162.9(2)°], indicating a slight strain in the coordinated dien ligand.

The pyrimidine and imidazole rings of the Guo group are planar within experimental error ($3\sigma_{combined}$) forming an angle of 1.3(2)° between them, so that the whole purine nucleus appears essentially as planar. This value is substantially smaller than the corresponding ones of similar compounds, e.g. 4.0° in the complex of cadmium(II) with guanosine 5′-phosphate [34]. The best plane through the purine ring makes an angle of 66.0(1)° with the basal plane of the copper coordination polyhedron. This value may be compared with the corresponding values of 63.4° for [Pd(diethylenetriamine)(guanosine)]$(ClO_4)_2$ [33], of 65.9° for $\{[(dien)Pt]_2G\text{-}N^1,N^7)\}(ClO_4)_3 \cdot 2H_2O$ (Pt1 coordination plane) [35] and of 61.7° and 69.6° for *cis*-$[(NH_3)_2Pt(U\text{-}N^3(G\text{-}N^1,N^7)Pt(dien)](ClO_4)$. $2.5H_2O$ (coordination planes of Pt1 and Pt2, respectively [35]). The geometry of the purine ring is as expected, with the bond lengths lying in the range 1.313(7)–1.383(7) Å for the imidazole and 1.331(8)–1.416(8) Å for the pyrimidine rings, respectively, while the corresponding valence angles ranges are 105.5(5)°–111.5(5)° and 111.7(5)°–128.1(5)°. The general observation that the internal ring angle at N(1) is greater than at N(3), the latter having no extra-annular attachment, is also confirmed by the present study [33,36]. The deviations of the substituents N(2) and O(6) from the purine best plane are significant [0.08(1) Å and 0.065(7) Å, respectively], which may be attributed to the involvement of these atoms in the hydrogen bonding system of the structure (see Table 3).

The valence angles in the ribose ring are close to tetrahedral values ranging between 101.1(4)° and 109.9(4)°. Atoms C(1A), C(2A), C(4A) and (O(1A) are coplanar within experimental error, while C(3A) is 0.584(9) Å distant from that plane, on the same side as C(5A) and N(9). This corresponds to the C(3A) *endo* conformation. The angle formed by the ribose and purine rings is 105.7(2)° The orientation of the C(5A)—O(5A) bond relative to the ribose ring is *gauche-gauche*, the torsional angles $\phi_{O\text{–}O}$ and $\phi_{C\text{–}O}$ being −47(1)° and 68.4(9)° respectively.

Both NO_3 groups have normal geometry, the mean N—O distances being 1.204(6) Å and 1.221(5) Å, and the mean O—N—O valence angles being 120.0(5)° and 120.0(4)° for the coordinated and the uncoordinated NO_3 groups, respectively.

As can be seen from Table 3, hydrogen bonding plays a predominant role in the stabilization of the structure. Intermolecular hydrogen bonds occur between neighbour [(dien)Cu(Guo-N^7)(ONO_2)]$^+$ cations as well as between [(dien)Cu(Guo-N^7)(ONO_2)]$^+$ cations and (NO_3^- anions. Furthermore, three intramolecular hydrogen bonds [N(10)—H(10)···O(6), N(12)—H(12)···O(8) and O(5A)—H(O5A)···O(1A)] are possible, as can be deduced from the short donor-acceptor contact distances 3.098(8) Å, 3.21(1) Å and 2.666(1) Å, respectively. The shortening of the C(5A)—O(5A) bond distance to 1.30(1) Å may be attributed to the latter mentioned hydrogen bond [37,38].

CONCLUSION

In conclusion, the present study showed that the reaction of [(dien)CuX]X, (X = NO_3, Br) with guanosine or adenine (B) gave compounds of the general formula [(dien)CuBX]X. In all these compounds, spectral data indicated that the ligands bind to the copper atom through N7. This has also been confirmed in one case, [(dien)Cu(Guo)(ONO_2)]NO_3, by X-ray analysis. Lastly, the inability of [(dien)Cu(ONO_2)]NO_3 complex to react with guanine and adenosine and that of [(dien)Cu(Br)]Br complex with guanine, adenine and adenosine, which may be due to their electronic and molecular parameters, should indicate lower anticancer activity than that of diethylenetriamine-Pt complexes.

REFERENCES

1. Rosenberg, B., Van Camp, L., Trosko, J. E. and Mansour, V. H., *Nature*, 1969, **222,** 385.
2. Lippert, B., *Prog. in Inorg. Chem.*, 1989, **37,** 1.
3. (a) Basile, L. A. and Barton, J. K., *Met. Ions in Biol. Systems*, 1989, **25,** 31; (b) Aletras, V., Hadjiliadis, N., Lymberopoulou-Karaliota, A., Rombeck, I. and Lippert, B., *Inorg. Chim. Acta*, 1994, **227,** 17.
4. Reedijk, J., Fichtinger-Schepman, A. M. J., van Oosterom, A. T. and van de Putte P., *Struct. Bonding*, 1987, **67,** 53.
5. Sherman, S. E. and Lippard, S. J., *Chem. Rev.*, 1987, **87,** 1153.
6. Beyerle-Pfnür, R., Braun, B., Faggiani, R., Lippert, B. and Lock, C. J. L., *Inorg. Chem.*, 1985, **24,** 4001.
7. Arpalathi, J. and Lehikoinen, L., *Inorg. Chim. Acta*, 1989, **159,** 115.
8. Scheller, K. H. and Sigel, H., *J. Am. Chem. Soc.*, 1983, **105,** 5891.
9. Raudaschl-Sieber, G., Marzilli, L. G., Lippert, B. and Shinozuka, K., *Inorg. Chem.*, 1985, **24,** 989.
10. Frommer, G., Mutakainen, I., Pesh, F. J., Hillg-

eris, E. C., Preut, H. and Lippert, B., *Inorg. Chim. Acta*, 1992, **197,** 243.
11. Dimitrov, N. V. and Eastland, G. W., *Curr. Chemother., Proc. Int. Congr. Chemother., 10th*, 1978, **2,** 1319.
12. Keppler, B. K., Henn, M., Juhl, U. M., Berger, M. R., Neibl, R. E. and Wagner, F. E., *Prog. Clin. Biochem. Med.*, 1989, **10,** 41.
13. Howard, R. A., Kimball, A. P. and Bear, J. L., *Cancer Res.*, 1979, **39,** 2568.
14. Scarcia, V., Furlani, A., Pilloni, G., Longato, B. and Corain, B., *Inorg. Chim. Acta*, 1997, **254,** 199.
15. Seiler, H. G., Sigel, H. and Sigel, A., *Handbook on Toxicity of Inorganic Compounds*, Marcel Dekker, Inc., New York, 1988.
16. Navarro-Ranninger, C., Amo Ochoa, P., Pérez, J. M., González, V. M., Masaguer, J. R. and Alonso, C., *J. of Inroganic Biochemistry*, 1994, **53,** 177.
17. Bolos, C. A., Nikolov, G. St., Ecateriniadou, L., Kortsaris, A. and Kyriakidis, D. A., Unpublished results.
18. Bacci, M., *New J. Chem.*, 1993, **17,** 67.
19. Allmann, R., Krestl, M., Bolos, C., Manoussakis, G. and Nikolov, G. St., *Inorg. Chim. Acta*, 1990, **175,** 255.
20. Bew, M. J., Hathaway, B. J. and Fereday, R. J., *J. C. S. Dalton*, 1972, 1229.
21. Clegg, W., *Acta Cryst.*, 1981, **A37,** 22.
22. Hall, S. R., Flack, H. D. and Stewart, J. M. ed. *XTAL* 3.2 *Reference Manual*. Universities of Western Australia, Geneva and Maryland. *Lamb : Perth*, 1992.
23. *International Tables for X-ray Crystallography*, Vol. IV, Kynoch, Birmingham, UK, 1974.
24. Hamilton, W. C., *Acta Cryst.*, 1965, **18,** 502.
25. Geary, W. J., *Coord. Chem. Rev.*, 1971, **7,** 81.
26. Reedijk, J., *Inorg. Chim. Acta*, 1992, **198–200,** 873.
27. Lever, A. B., Mantovani, E., Ramaswamy, B. S., *Can. J. Chem.*, 1971, **49,** 1957.
28. Curtis, N. F. and Curtis, Y. M., *Inorg. Chem.*, 1965, **4,** 804.
29. Díaz, G., Diez, S., López, L., Muñoz, R., Campos-Vellete, M., Manríquez, V. and Wittke, O., *Vibrational Spectroscopy*, 1993, **6,** 37.
30. Bray, K. L. and Drickamer, H. G., *J. Phys. Chem.*, 1989, **93,** 7604.
31. Addison, A. W., Rao, T. N., Reedijk, J., van Rijn, J. and Verschoor, G. C., *J. Chem. Soc., Dalton Trans.*, 1984, 1349.
32. Stephens, F. S., *J. Chem. Soc.* (*A*), 1969, 2493.
33. Rochon, F. D., Kong, P. C., Coulomb, B. and Melanson, R., *Can. J. Chem.*, 1980, **58,** 381.
34. Aoki, K., *Acta Cryst.*, 1976, **B32,** 1454.
35. Frommer, G., Schöllhorn, H., Thewalt, U. and Lippert, B., *Inorg. Chem.*, 1990, **29,** 1417.
36. Singh, C., *Acta Cryst.*, 1965, **19,** 861.
37. Cygler, M., Przybylska, M. and Edwards, O. E., *Acta Cryst.*, 1982, **B38,** 479.
38. Jeffrey, G. A., Ruble, J. R., McMullan, R. K., De Frees, D. J., Binkley, J. S. and Pople, J. A., *Acta Cryst.*, 1980, **B36,** 2292.

Pergamon

PII : S0277–5387(98)00055–2

Polyhedron Vol. 17, No. 16, pp. 2727–2732, 1998
© 1998 Elsevier Science Ltd
All rights reserved. Printed in Great Britain
0277–5387/98 $19.00 + 0.00

Some water-soluble organometallic complexes of group 10 transition metal(II) ions with 1,3,5-triaza-7-phosphaadamantane (TPA). Syntheses, characterization and reactivity. The crystal and molecular structure of $[Ni(CN)_2(TPA)_3] \cdot 4.3H_2O$

Elmer C. Alyea,* George Ferguson and Shanmugaperumal Kannan

Department of Chemistry and Biochemistry, University of Guelph, Guelph, Ontario, Canada N1G 2W1

(Received 5 January 1998 : accepted 15 January 1998)

Abstract—The 1,3,5-triaza-7-phosphaadamantane [TPA] complexes of the type $[MCl_2(TPA)_2]$ (where M = Ni, Pd, Pt), $[Ni(CN)_2(TPA)_3]$ and $[PtCl(TPA)_3](BPh_4)$ have been synthesized and characterized by ^1H, $^{31}P\{^1H\}$ NMR, Laser-Raman spectroscopy and elemental analyses. The reactivity of the complexes $[MCl_2(TPA)_2]$ with water to produce the oxide of TPA follows the order Pt > Pd > Ni. The structure of the complex $[Ni(CN)_2(TPA)_3] \cdot 4.3H_2O$ was determined by single crystal X-ray diffraction methods. The structure determination shows that the nickel atom has a trigonal-bipyramidal geometry with the cyanide ligands in the apical positions. © 1998 Elsevier Science Ltd. All rights reserved

Keywords: group 10 complexes ; 1,3,5-triaza-7-phosphaadamantane ; crystal structure.

Considerable attention has been focused in recent years on the complexes of the water-soluble air-stable phosphine 1,3,5-triaza-7-phosphaadamantane [TPA] with transition metal ions [1,2]. Studies by Darensbourg and co-workers have shown that certain rhodium and ruthenium complexes have high catalytic activity towards the hydrogenation of olefins and the conversion of unsaturated aldehydes to saturated aldehydes or unsaturated alcohols in aqueous two-phase solvent systems [1]. Furthermore, the small steric size, greater basicity and non-ionic nature of TPA makes it an attractive alternative to the commonly employed sulphonated phosphines such as tris-*meta*-sulphonatophenylphosphine(TPPTS) [1f,3]. Hence, since group 10 complexes are well established as homogeneous hydrogenation catalysts, it is of great interest to also develop the chemistry of TPA with these metal ions. Although we explored the synthesis of Ni, Pd and Pt complexes in an earlier preliminary survey of TPA metal complexation behaviour [2a], to this date only two papers concerning group 10 complexes of TPA have been reported ; they describe the crystal structures of $[Pt(TPA)_3Cl]Cl \cdot MeOH \cdot H_2O$ [2c] and *trans*-$[Pt(TPA)_2(CN)_2$ [4]. In continuation of our research on the chemistry of transition metal ions with this interesting ligand [2], we report here the syntheses and characterization of some complexes of the TPA ligand with group 10 metals, including the X-ray structural determination of a pentacoordinate nickel cyanide complex.

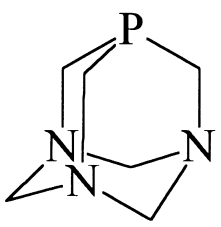

* Author to whom correspondence should be addressed. E-mail address : Alyea@chembio.uoguelph.ca

RESULTS AND DISCUSSION

The reaction of TPA with $NiCl_2 \cdot 2H_2O$, $Na_2[Ni(CN)_4]$, $PdCl_2$ or $MCl_2(PhCN)_2$ (M = Pd or Pt) yielded molecular complexes of the type $[MCl_2(TPA)_2]$ (where M = Ni, Pd, Pt), $[Ni(CN)_2(TPA)_3]$ or $[(PtCl(TPA)_3)]Y$ (Where M = Pt, Y = Cl or BPh_4). Most of the syntheses were effected in methanolic solution because of the unexpectedly [1,2] low solubility of the complexes in water and their reactivity with water (*vide infra*). NMR spectroscopic data were therefore collected for dimethylsulphoxide (DMSO) solutions.

The Laser Raman spectra of the complexes $[MX_2(TPA)_2]$ (M = Ni, Pd or Pt) show that the complexes exist exclusively in the *cis* isomeric form. The $^{31}P\{^1H\}$ NMR spectra of these square-planar complexes show single broad resonances for the nickel(II) (also variable with concentration and time) and palladium(II) complexes and a sharper resonance with the expected Pt-195 satellites for the platinum(II) complex. The ^1J(Pt-P) value shows that the chlorine atom is *trans* to the phosphine group as its magnitude (3305 Hz) confirms the *cis*- nature of the complexes. Broadening of the $^{31}P\{^1H\}$ NMR signal occurred when excess TPA was added to a solution of the palladium complex, indicating that phosphine exchange was responsible for the broadness of the resonance. Decomposition of the complexes in the presence of water was also evident, as will be discussed later.

The $^{31}P\{^1H\}$ NMR spectrum of the complex $[PtCl(TPA)_3]BPh_4$ in CH_3CN/D_2O solution shows two resonances (1 : 2 ratio) with platinum satellites. The coupling constant of ^1J(Pt—P) = 3300 Hz (for the smaller peak) corresponds to the TPA trans to the chlorine atom whereas the other value of ^1J(Pt—P) = 2211 Hz corresponds to a TPA trans to another TPA group. In the case of $[Ni(CN)_2(TPA)_3]$, the $^{31}P\{^1H\}$ NMR spectrum in CD_3OD/H_2O solution showed a broad peak at −49.1 ppm together with a weak sharp one at −1.7 ppm that shows the presence of some TPA oxide.

The $^{31}P\{^1H\}$ NMR spectra of the complexes $[Ni(CN)_2(TPA)_3]$ and $[PtCl(TPA)_3]BPh_4$ in DMSO-d_6 display broad peaks (with the disappearance of satellites for the platinum complex). In the former case, the peak due to TPA oxide is more intense than it was in CD_3OD/H_2O solution. These observations may be a consequence of coordination of DMSO with the nickel or platinum atoms giving a hexacoordinated nickel(II) complex $[Ni(CN)_2(TPA)_3(DMSO)]$ or pentacoordinated $[PtCl(DMSO)(PTA)_3(BPh_4)$ or tetracoordinated $[Pt(DMSO)(TPA)_3]Cl(BPh_4)$ platinum(II) complexes. Due to the small size of the TPA ligand (the Tolman cone angle is only 102°), these solvated complexes might easily exchange the coordinated DMSO with free DMSO and exhibit fluxionality and/or TPA exchange leading to the observed broad $^{31}P\{^1H\}$ peak with the disappearance of satellites. In contrast, as mentioned above, the corresponding palladium and platinum complexes *cis*-$[PdCl_2(TPA)_2]$ and *cis*-$[PtCl_2(TPA)_2]$ show sharper $^{31}P\{^1H\}$ NMR spectra under similar conditions, indicating that there is no coordination of DMSO with the central metal ion that might lead to TPA exchange or fluxionality. The structure determination of crystals of the $[PdCl_2(TPA)_2]$ complex prepared in aqueous solution [method (a)] has shown that the asymmetric unit contains two molecules of the square-planar complex linked by a water molecule of solvation [2g].

The ^1H NMR spectra of all the complexes show the expected peaks and integrations [1,2]. The —CH_2— protons nearer to the phosphorus atom are much more deshielded than the —CH_2— protons nearer to the nitrogen atoms. This confirms the coordination of the phosphorus atom rather than any nitrogen atom of the TPA ligand; in contrast, it was shown earlier that one (only) nitrogen atom of TPA is more readily protonated, with the pK_a being near 6.0 [2d].

The red colored $[NiCl_2(TPA)_2]$ complex is insoluble in most organic solvents (sparingly soluble in DMSO, giving a very broad ^1H or $^{31}P\{^1H\}$ NMR spectrum) but dissolves readily in water giving first a dark blue color, then immediately turning to an orange color, and finally giving a colorless solution. This solution on slow evaporation yielded colorless crystals of TPA oxide. The ^1H NMR spectra of the complexes $[NiCl_2(TPA)_2]$, $[PdCl_2(TPA)_2]$ and $[PtCl_2(TPA)_2]$ in water observed over different intervals show that all three complexes undergo reaction with water and give TPA oxide. This observation is similar to that reported for a Rh(I)—TPA complex $[RhCl(TPA)_3]$ [1f]. For the present group 10 complexes we observed, on a qualitative basis only, that the reactivity follows the order Pt > Pd > Ni and that the formation of TPA oxide is very much less when an excess of free TPA is in solution.

In order to probe the probable mechanism and to isolate any resulting species after the reaction, the $[PtCl_2(TPA)_2]$ complex was dissolved in a CH_2Cl_2/methanol (20 ml) solution, to which 10 ml of water was added, and the solution was kept to allow slow evaporation during a few weeks. The resulting crystalline product was filtered off, washed with water (to remove a soluble compound identified by NMR and IR spectroscopy as TPA oxide) and analyzed by a single crystal X-ray diffraction analysis. The preliminary X-ray data showed that the isolated complex was $[PtCl(TPA)_3]Cl$, previously characterized by crystallography [2c]. As suggested for a Rh-TPA complex [1f], the probable mechanism for this reaction involving group 10 metal ions may be the oxidative addition of water to form an hydriohydroxo M(IV) species, which allows TPA to be oxidized; subsequent TPA and chloride exchange could then lead to the isolated products of TPA oxide and $[MCl(TPA)_3]Cl$. The observed relative rate of the reaction agrees well with the order of the M^{2+}/M^{4+} oxidation potentials of these ions, i.e. the tendency for oxidative addition, though other mechanisms (especially for Ni) can not

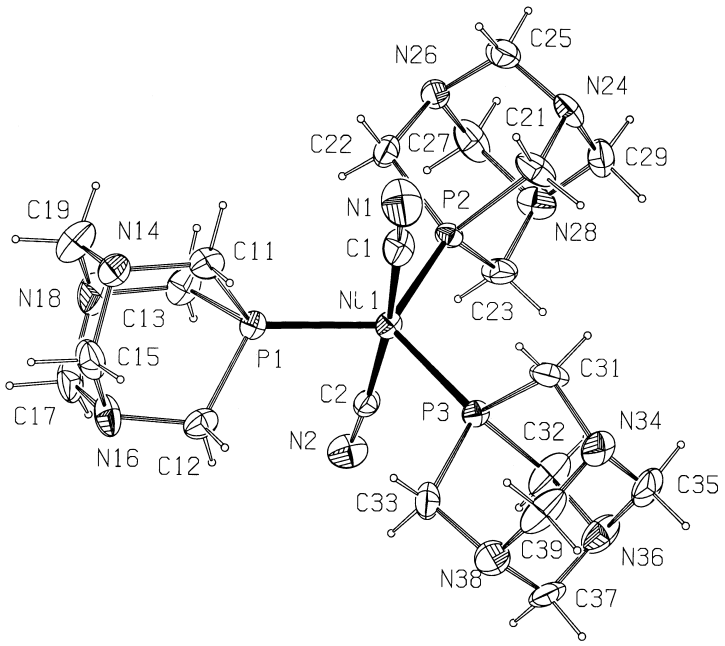

Fig. 1. A view of the $[Ni(CN)_2(TPA)_2]$ molecule showing our numbering scheme. Anisotropic displacement ellipsoids are drawn at the 30% level.

be ruled out. The propensity of group 10 metal ions to form tris-TPA complexes may be a strong factor in lowering the barriers to TPA oxidation. In a separate experiment, $[PtCl(TPA)_3]BPh_4$ was readily isolated in high yield (Experimental); the corresponding palladium complex apparently formed as a yellow complex (giving two very broad ^{31}P NMR signals in D_2O) but its purification was not pursued due to its ease of decomposition.

Structure of $[Ni(CN)_2(TPA)_3]$,4.3(H_2O); (**1**),4.3 (H_2O)

An ORTEP plot of (**1**) is shown in Fig. 1; selected dimensions are given in Table 1. The nickel atom is bonded to three equatorial TPA ligands and two axial cyanide groups giving a trigonal bipyrimidal geometry. A search of the April 1997 release of the Cambridge Structural Database [5] revealed several

Table 1. Selected dimensions for $[Ni(CN)_2(TPA)_2]$ bond lengths (Å) and angles (°)

Ni1—C1	1.868(15)	P1—C11	1.834(13)
Ni1—C2	1.841(14)	P1—C12	1.806(16)
Ni1—P1	2.197(3)	P1—C13	1.843(11)
Ni1—P2	2.234(3)	C1—N1	1.117(17)
Ni1—P3	2.227(3)	C2—N2	1.156(16)
C1—Ni1—C2	173.3(6)	P3—Ni1—P1	122.56(13)
P1—Ni1—C2	85.8(4)	P2—Ni1—C2	93.7(4)
P1—Ni1—C1	87.6(4)	P2—Ni1—C1	91.0(5)
P3—Ni1—C2	90.8(4)	P1—Ni1—P2	122.07(13)
P3—Ni1—C1	91.6(4)	P2—Ni1—P3	115.37(12)

X-ray analyses for $Ni(CN)_2(PR_3)_3$ species. Those complexes involving $PPh(OEt)_2$ [6], $C_{13}H_{11}P$ (5-methyl-dibenzophosphole) [7] and $P(CH_2OH)Ph_2$ [8] were best described as having square-pyramidal geometries, while those with $PPhMe_2$ [9] and $C_{14}H_{13}P$ (5-ethyl-dibenzophosphole) [7] as the phosphine ligands had geometries that were closer to being trigonal-bipyramidal in shape. Comparison of the structural data shows clearly that the present TPA species has a structure only slightly distorted from the ideal trigonal-bipyramidal shape.

The Ni—P bond distances in **1** (ave. 2.226(3) Å) are not significantly different from each other or from those found in $[Ni(CN)_2(PPhMe_2)_3$ (**2**) (ave. 2.235(3) Å) [9] and in $[Ni(CN)_2(C_{14}H_{13}P)_3$ (**3**) (ave. 2.253 Å) [7]. Similarly, the Ni—CN bond distances of 1.852(15) and 1.855(15) Å in **1** are comparable to those in **2** (1.836(11) and 1.860(12) Å) and in **3** (1.820 and 1.855 Å). The C—Ni—C bond angle in **1** is significantly less, at 173.6(6)°, than those found in **2** (176.5(4)°) and **3** (176.7)°. This angle departs considerably from 180° for analogous $Ni(CN)_2(PR_3)_3$ species with greater distortions toward the square-pyramidal shape; for example, C—Ni—C is 163.8(4) for the species with $P(CH_2OH)Ph_2$ [8]. Another indication of distortion is the range of C—Ni—P angles. These are 86.0(4)–91.4(4)° in **1,** 88.6(3)–92.4(3)° in **2** and 85.8–93.7° in **3**, signifying that these three complexes undergo similar small distortions. This is not surprising even though the phosphines differ considerably in their cone angles because steric hindrance is minimized with all three phosphine ligands occupying equatorial sites. In **1** the presence of water molecules in the crystal lattice may contribute to the small observed distortions from idealized trigonal-pyramidal geometry. As observed in previous TPA structures [1], extensive hydrogen-bonding occurs between the water molecules and nitrogen atoms of various TPA ligands. No H atoms were located on water molecules (some of which are disordered with partial occupancy) but the various O···N distances (supplementary material) are in the ranges normally associated with O—H···N hydrogen bonds. Other bond distances and angles observed in **1** for the TPA ligands are comparable to those previously reported [1,2,4].

EXPERIMENTAL

$NiCl_2 \cdot 2H_2O$, $NiCl_2 \cdot 6H_2O$, NaCN, $PdCl_2$ and $PtCl_2$ were obtained from commercial sources. The $[PdCl_2(CH_3CN)_2]$, $[PdCl_2(PhCN)_2]$, $[PtCl_2(PhCN)_2]$ [10] and TPA [11] were prepared according to the reported methods. All the solvents were distilled and dried prior to use. The $^{31}P\{^1H\}$ NMR spectra were recorded on a Varian Unity-400 MHz instrument operating at 161.8 MHz whereas ^1H NMR spectra were recorded on a Varian-Gemini-200 spectrometer operating at 200 MHz. The chemical shifts are relative to external 85% H_3PO_4 and internal chloroform or DMSO peaks respectively for the $^{31}P\{^1H\}$ and ^1H resonances. The IR spectra were recorded on a Nicolet DXC-20 FTIR instrument using KBr discs (4000–400 cm^{-1}). The Raman spectra were recorded on a Bruker FRA 106 FT-Raman module interfaced to a Bruker IFS-66 FT-IR bench; the incident radiation was at 943.4 nm.

Synthesis of $[NiCl_2(TPA)_2] \cdot 2H_2O$

To a methanolic solution of $NiCl_2 \cdot 2H_2O$ (106 mg, 0.64 mmol), a methanolic solution of TPA (200 mg, 1.28 mmol) was added under a nitrogen atmosphere. The solution immediately turned to a dark blue color and on stirring, deposited a red colored powder leaving a colorless solution. The red powder was filtered, washed with methanol and dried (50 mg, 18%; Anal: Calcd for $C_{12}H_{24}H_6P_2NiCl_2 \cdot 2H_2O$: C, 30.4; H, 5.8; N, 17.5. Found: C, 30.0; H, 5.9; N, 17.6. mp, 220°C (dec); ^1H NMR (δ ppm, DMSO): very broad (4.1–5.2); Laser Raman (ν_{Ni-Cl}): 272, 305 cm^{-1}).

The supernatant on slow evaporation yielded colorless crystals (120 mg; $^{31}P\{^1H\}$ NMR (δ ppm, CD_3OD/H_2O): −1.2; ^1H NMR (δ ppm, D_2O): 3.85 (d, ^2J(P—H) = 10 Hz, PCH_2, 6H); 4.15 (q, NCH_2, 6H, ^2J(H—H) 14 Hz).

Synthesis of $[Ni(CN)_2(TPA)_3] \cdot 4.3H_2O$

To an aqueous solution of $NiCl_2 \cdot 6H_2O$ (200 mg, 0.83 mmol), NaCN (82 mg, 1.67 mol) solid was added and stirred for 10 min. To this suspension, excess of TPA (450 mg, 2.8 mmol) was added and the clear red solution was stirred for 30 min. The solution was evaporated in vacuum, and the residue washed with methanol, filtered off and dried. It was recrystallized from a water/ethanol mixture. Since the crystallized product was contaminated with some TPA-oxide (colorless crystals), the red coloured crystals of the titled compound were picked out from the mixture. (Mp, 230°C (dec); FTIR (ν in cm^{-1}): 3565 [br, NH, OH, st]; 2096 [CN, st]; 1613 [br, NH, OH, bend]: $^{31}P\{^1H\}$ NMR (δ ppm): (CD_3OD/H_2O): −49.1; (DMSO): very broad spectrum at −49.7; ^1H NMR (δ ppm, CD_3OD): 4.23 (br, PCH_2, 18H); 4.62 (m, NCH_2, 18H).

Synthesis of cis- $[PdCl_2(PTA)_2]$

Method (*a*). To a water solution of TPA (excess) (543 mg, 3.4 mmol), $PdCl_2$ solid (104 mg, 0.587 mmol) was added and the mixture was stirred for 10 min. By that time all the $PdCl_2$ dissolved to give a clear greenish yellow solution. After filtration, the solution on slow evaporation yielded a greenish yellow crystalline product (Yield: 250 mg, 87%), mp 235°C (dec): Anal: Calcd for $C_{12}N_{24}N_6P_2PdCl_2 \cdot 0.5\ H_2O$: C, 28.79,; H, 5.03; N, 16.79. Found: C, 28.8; H, 4.9; N,

16.7. Laser Raman (ν_{Pd-Cl}): 273, 302 cm^{-1}; $^{31}P\{^1H\}$ (δ ppm, DMSO): −18.3; ^1H (δ ppm, DMSO); 4.35–4.55 (m, PCH_2, NCH_2).

Method (*b*). To a hot acetonitrile solution of $[PdCl_2(CH_3CN)_2]$ (202 mg, 0.77 mmol), a water/methanol solution of TPA (300 mg, 1.9 mmol) was added and stirred for 3 h. The greenish yellow colored product that had precipitated was filtered off and dried (Yield 250 mg, 66%). $^{31}P\{^1H\}$ NMR (δ ppm, DMSO): −18.5.

Method (*c*). To a dichloromethane solution of $[PdCl_2(PhCN)_2]$ (170 mg, 0.44 mmol), a water/methanol solution of TPA (157 mg, 1.0 mmol) was added and stirred for 2 h. The resulting precipitate was filtered and washed with methanol and dried (Yield: 160 mg, 74%). $^{31}P\{^1H\}$ NMR (δ ppm, DMSO): −18.1.

Synthesis of cis-$[PtCl_2(TPA)_2]$

To a dichloromethane solution of $[PtCl_2(PhCN)_2]$ (300 mg, 0.64 mmol), a methanolic solution of TPA (200 mg, 1.28 mmol) was added and stirred for 3 h. The resulting colorless precipitate was filtered, washed with methanol and dried (Yield: 300 mg, 81%, mp,

Table 2. Summary of crystal data, data collection[a], structure solution and refinement details[b]

Empirical formula	$C_{20}H_{36}N_{11}NiP_3.4.3(H_2O)$
Molar mass	659.5
Color, habit	yellow, lath
Crystal size (mm)	$0.42 \times 0.26 \times 0.12$
Crystal system	monoclinic
a (Å)	9.883(2)
b (Å)	7.7165(15)
c (Å)	19.750(3)
α (°)	90
β (°)	95.690(16)
γ (°)	90
V (Å^3)	1498.7(5)
Space group	$P2_1$
Z	2
F (000)	681
d_{calc} (g cm^{-3})	1.442
μ (mm^{-1})	0.86
Temp (K)	294(1)
Unit-cell reflections (θ-range°)	7.8 14.2
Max. θ(°) for reflections	24.93
hkl range of reflections	−11 11; 0.9; 0, 23
Decay in 3 standard reflections	14%
Reflections measured	2984
Unique reflections	2828
R_{int}	0.021
Reflections with $I > 2\sigma(I)$	1864
Absorption correction type	psi-scans
Min. max. abs. corr.	0.5384, 0.7849
Refinement on	F^2
Solution method	Patterson heavy atom
H-atom treatment	riding
No. of variables in L.S. weights:	357
k in $w = 1/(\sigma_2 F_o^2 + k)$	$(0.1117P)^2$ $[P = (F_o^2 + 2F_c^2)/3]$
R, R_w, GOF	0.067, 0.1830, 0.982
Flack parameter	−0.02(5)
Density range in final Δ-map(e Å^{-3})	−0.80 to 0.98
Final shift/error ratio	0.00

[a] Data collection on a Nonius CAD4 diffractometer with graphite monochromatized Mo–K_α radiation (λ 0.7107 Å).

[b] All calculations were done on a Silicon Graphics 4D-35TG computer system with the NRCVAX system of programs (Gabe, E. J., Le Page, Y., Charland, J-P., Lee, F. L. and White, P. S., *J. Appl. Cryst.*, 1989, **22,** 384–389) for refinement with observed data on F, or with SHELXL-97 (Sheldrick, G. M., 1997) for refinement with all data on F^2.

240°C (dec); Anal: Calcd for $C_{12}H_{24}N_6P_2PtCl_2$: C, 24.8; H, 4.2; N, 14.5. Found: 25.1; H, 4.3; N, 14.7; Laser Raman (ν_{Pt-Cl}): 306, 326 cm^{-1}; $^{31}P\{^1H\}$ NMR (δ ppm, $CDCl_3/CH_3OH$): −53.0, ^1J(Pt—P) = 3305 Hz; (DMSO): −47.54, ^1J(Pt—P)3302 Hz; ^1H NMR (δ ppm, DMSO): 4.34 (br, PCH_2, 12H); 4.21 (br, NCH_2, 12H).

Synthesis of $[PtCl(TPA)_3](BPh_4)$

To a dichloromethane solution of $[PtCl_2(PhCN)_2]$ (200 mg, 0.43 mmol), $NaBPh_4$ in methanol (290 mg, 0.85 mmol) was added and the solution was stirred for 3 h. To this clear solution TPA in methanol (266 mg, 1.69 mmol) was added and the solution stirred for a further 5 h. The solvent was removed *in vacuo*, the residue extracted with acetonitrile and the solution filtered. To the filtrate a few drops of ethanol were added and the solution was kept aside for crystallization. The solution on slow evaporation yielded the colorless crystalline product. (Yield: 380 mg, 88%); mp, 230°C (dec);Anal: Calcd for $C_{42}H_{56}P_3N_9PtClB$: C, 49.4; H, 5.5; N, 12.3%. Found: C, 50.7; H, 5.5; N, 12.3%; $^{31}P\{^1H\}$ NMR (δ in ppm, Ch_3CN/D_2O): −51.5, ^1J(Pt—P) = 2215 Hz; −48.0, ^1J(Pt—P) = 3347 Hz; (DMSO): −50.5 (v broad); ^1H NMR (DMSO-d_6): 4.42 (br, PCH_2); 4.48 (br, NCH_2); 6.7–7.17 (m, BPh_4).

Crystallography

Details of the cell data, data collection and refinement for $[Ni(CN)_2(TPA)_2]\cdot 4.3H_2O$ are summarized in Table 2. There was 14% decay of standard intensities during data collection and this was allowed for by appropriate scaling. In the final refinement cycles, all non-H atoms except those of the partially occupied water molecules (O4, O51, O52) were allowed anisotropic displacement parameters; water O atoms O4, O51, O52 were refined isotropically. All H atoms on the TPA ligands were treated as riding atoms. The final positional and displacement parameters, structure factors, full list of dimensions involving all non-H atoms have been deposited with the Cambridge Crystallographic Data Centre and are also available from the authors in CIF format.

CONCLUSIONS

The reaction of the small water-soluble phosphine TPA with group 10 metal(II) chlorides yielded the corresponding *cis*-$[MCl_2(TPA)_2]$ complexes. These complexes are unstable (except in the presence of excess of TPA) in water producing TPA oxide, apparently via a $[MCl(TPA)_3]$ cation intermediate, in the reactivity order of Pt > Pd > Ni. The complex $[Ni(CN)_2(TPA)_3]\cdot 4.3H_2O$ was shown to have a slightly distorted *trans*-trigonal bipyramidal geometry by X-ray analysis.

Acknowledgements—ECA and GF thank NSERC (Canada) for research grants.

REFERENCES

1. (a) DeLerno, L. R., Trefonas, L. M., Darensbourg, M. Y. and Majeste, R. J., *Inorg. Chem.*, 1976, **15,** 816; (b) Darensbourg, D. J., Joo, F., Kannisto, M., Katho, A. and Reibenspies, J. H., *Organometallics*, 1992, **11,** 1990; (c) Darensbourg, D. J., Joo, F., Kannisto, M., Katho, A., Reibenspies, J. H. and Daigle, D. J., *Inorg. Chem.*, 1994, **33,** 200; (d) Fackler, Jr, J. P., Staples, R. J. and Assefa, Z., *J. Chem. Soc. Chem. Commun.*, 1994, 431; (e) Assefa, Z., McBurnett, B. G., Staples, R. J., Fackler, Jr, J. P., Assmann, B., Angermaier, K. and Schmidbaur, H., *Inorg. Chem.*, 1995, **34,** 75; (f) Darensbourg, D. J., Stafford, N. W., Joo, F. and Reibenspies, J. H., *J. Organomet. Chem.*, 1995, **99,** 488.
2. (a) Alyea, E. C. and Fisher, K. J., Third Chemical Congress of North America, June 5–10, 1988, Toronto, Canada, INORG. ABS., 172 and 420; (b) Alyea, E. C., Fisher, K. J. and Johnson, S., *Can. J. Chem.*, 1989, **67,** 1319; (c) Muir, M. M., Muir J. A., Alyea, E. C. and Fisher, K. J., *J. Cryst. Spect. Res.*, 1993, **23,** 745; (d) Fisher, K. J., Alyea, E. C. and Shahnazarian, N., *Phosphorus, Sulphur, Silicon, Relat. Elem.*, 1990, **48,** 37; (e) Alyea, E. C., Fisher, K. J. Foo, S. and Philip, B., *Polyhedron*, 1993, **12,** 484; (f) Alyea, E. C., Ferguson, G. and Kannan, S., *Polyhedron*, 1997, **16,** 3533; (g) Alyea, E. C., Ferguson, G. and Kannan, S., *J. Chem. Soc. Chem. Commun.*, 1998, 345.
3. Kalch, P. and Monteil, F., *Adv. Organometal. Chem.*, 1992, **34,** 219.
4. Assefa, Z., McBurnett, B. G., Staples, R. J. and Fackler, Jr, J. P., *Acta. Cryst.*, 1995, **C51,** 1742.
5. Allen, F. R. and Kennard, O., *Chem. Des. Autom. News*, 1993, **8,** 131.
6. Stalick, J. K. and Ibers, J. A., *Inorg. Chem.*, 1969, **8,** 1084.
7. Allen, D. W., Mann, F. G., Millar, I. T., Powell, H. M. and Watkin, D., *J. Chem. Soc. Chem. Commun.*, 1969, 1004.
8. Hope, H., Olmstead, M. M., Power, P. P. and Viggiano, M., *Inorg. Chem.*, **23,** 326.
9. Stalick, J. K. and Ibers, J. A., *Inorg. Chem.*, 1969, **8,** 1090.
10. Hartley, F. R., *The Chemistry of Platinum and Palladium.*, John Wiley and Sons, New York, 1973.
11. Daigle, D. J., Pepperman, A. B. and Vail, S. L., *J. Heterocycl. Chem.*, 1974, **11,** 407.

Pergamon

PII: S0277–5387(98)00056–4

Polyhedron Vol. 17, No. 16, pp. 2733–2738, 1998
© 1998 Elsevier Science Ltd
All rights reserved. Printed in Great Britain
0277–5387/98 $19.00+0.00

New mono- and di-nuclear mixed complexes of cyanides and 2,3-bis(2′-pyridyl)pyrazine with ruthenium

Mónica E. García Posse, Florencia Fagalde, Mónica M. Vergara and Néstor E. Katz*

Instituto de Química Física, Facultad de Bioquímica, Química y Farmacia, Universidad Nacional de Tucumán, Ayacucho 491, (4000) San Miguel de Tucumán, Argentina

(Received : 9 July 1997 ; accepted 15 January 1998)

Abstract—The synthesis and spectroscopic, electrochemical and emissive properties of a new mononuclear mixed complex, of formula $[Ru(dpp)(CN)_4]^{2-}$ (dpp = 2,3-bis(2′-pyridyl)pyrazine are reported. The spectroscopic (IR, UV-visible, and emission) results demonstrate that dpp has a π-acceptor capacity intermediate between bpy and bpz (bpy = 2,2′-bipyridine, bpz = 2,2′-bipyrazine), when coordinated to ruthenium cyanides. The redox potential of the Ru^{II}/Ru^{III} couple and the observed luminiscence at room temperature imply its possible use as a photosensitizer. Since dpp has also the extra ability, when compared to bpy, to form supramolecular complexes, new dinuclear complexes with dpp bridging $Ru(CN)_4{}^{n-}$ (n = 1,2) moieties can also be obtained. The corresponding mixed-valent complex, $[(CN)_4Ru^{II}(dpp)Ru^{III}(CN)_4]^{3-}$, has the characteristics of a Class (II) species, as disclosed by the weak interaction between both metallic centres. © 1998 Elsevier Science Ltd. All rights reserved

Keywords: polypyridine complexes ; dpp ; ruthenium ; π-backbonding ; mixed valence.

Polypyridyl complexes of ruthenium(II) have been extensively investigated due to their interest in photocatalysis and energy conversion [1–3]. The prototype of all inorganic photosensitizers, the ion $Ru(bpy)_3{}^{2+}$ (bpy = 2,2′-bipyridine) presents severe photochemical drawbacks, since the presence of low-lying *d-d* excited states gives rise to photodecomposition [4–6]. Thus, the use of auxiliary non-chromophoric ligands with strong ligand fields, such as cyanide groups, is necessary to inhibit these undesirable side reactions in the design of new photosensitizers, such as $[Ru(bpy)(CN)_4]^{2-}$ [7], $[Fe(bpz)(CN)_4]^{2-}$ [8], $[Os(bpy)(CN)_4]^{2-}$ and $[Ru(bpz)(CN)_4]^{2-}$ (bpz = 2,2′-bipyrazine) [9]. In this work, we report the synthesis and structural properties of the new mononuclear complex $[Ru(dpp)(CN)_4]^{2-}$ (dpp = 2,3-bis(2′-pyridyl)pyrazine) and some dinuclear complexes derived from it. We aim to compare the π-backbonding ability of the ligands bpy, bpz and dpp, shown in Scheme 1, in the same chemical environment. Both bpz and dpp have the additional capacity (absent in bpy) to incorporate other metallic centres by coordinating through their remote N atoms, so that supramolecular systems can be obtained [10–23].

EXPERIMENTAL

Syntheses

$Na_2[Ru(dpp)(CN)_4].4H_2O$ (**I**). It was prepared in a similar way to that previously described for the corresponding complex of bpz [9]. 0.5 g of $K_4[Ru(CN)_6].3H_2O$ and 0.25 g of dpp were dissolved in a 3 : 1 v/v mixture of H_2O/MeOH (34 cm^3). The solution was irradiated under constant stirring with a UV lamp at λ = 254 nm for 52 h, and then filtered. The filtrate was evaporated to dryness. The violet solid was dissolved in 11 cm^3 of water and filtered to eliminate the excess of dpp. Upon addition of MeOH (200 cm^3), the unreacted $K_4[Ru(CN)_6]$ was separated

* Author to whom correspondence should be addressed.

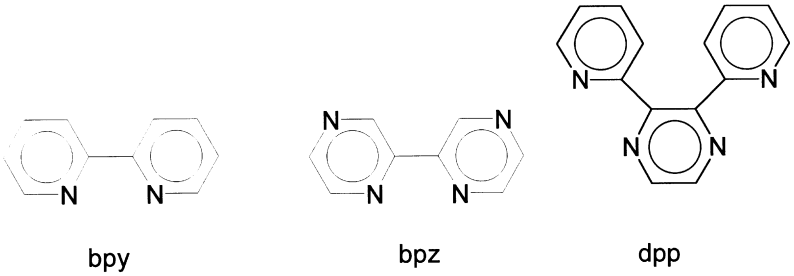

Scheme 1.

from the mixture and the filtrate was evaporated to dryness. The solid was redissolved in 10 cm^3 of water, reprecipitated with 200 cm^3 of acetone, filtered off and dried *in vacuo* over P_4O_{10}. The solid was then sorbed onto an SP-Sephadex A-25 column and eluted with 0.2 M NaI, rotoevaporated to 8 cm^3, cooled to room temperature, and precipitated with EtOH (100 cm^3). The orange powder was filtered, washed with EtOH and dried *in vacuo* over P_4O_{10}. Yield: 80 mg (13%). Anal. Calcd: C, 38.78; H, 3.26; N, 20.10%. Found: C, 38.41; H, 3.75; N, 21.43%.

$Na_4[(CN)_4Ru(dpp)Ru(CN)_4].4NaI.12H_2O$ (**II**). This complex was obtained as a by-product of the synthesis of **I**. It was eluted from the Sephadex column with 0.4 M NaI, rotoevaporated, cooled to room temperature, and precipitated with acetone (100 cm^3). It was then filtered off, washed with acetone and dried *in vacuo* over P_4O_{10}. Yield: 32 mg (4%). Anal. Calcd: C, 17.02; H, 2.21; N, 10.82%. Found: C, 16.48; H, 2.53; N, 11.32%. The tetrabutylammonium salts of (**I**) and (**II**) were obtained by exchanging Na^+ ions by Bu_4N^+ ions in a SP-Sephadex C-25 column previously equilibrated with $Bu_4{}^nNBr$.

Materials, instrumentation and techniques

MeCN was distilled from $KMnO_4$ and dried over molecular sieves. *Tetrakis*(*n*-butyl)ammonium hexafluorophosphate (TBAH) was recrystallized four times from EtOH and dried at 150°C for 72 h. All other chemicals were reagent grade and used without further purification.

Chemical analyses were performed at INQUIMAE (University of Buenos Aires, Argentina).

IR spectra were recorded as KBr or CsI pellets on a Perkin-Elmer 983G spectrophotometer. UV–vis spectra were obtained with a Shimadzu UV-160A spectrophotometer. Electrochemical measurements were performed with an EQMAT-Sl potentiostat in a standard H-type three-electrode cell with platinum wires as working and auxiliary electrodes and Ag/AgCl (3 M) as a reference electrode. Emission spectra were obtained with a Shimadzu RF-5301 PC spectrofluorometer at room temperature (23 ± 1°C). Emission quantum yields were determined by comparing the integrated emission spectra of the complexes relative to that of an isoabsorbative solution of $Ru(bpy)_3{}^{2+}$ ($\varphi_{em} = 0.042$).

RESULTS AND DISCUSSION

Figure 1 shows the IR spectrum of (**I**). Four bands are observed in the cyanide stretching frequency (ν_{CN}) zone, as expected for a cyanometalate of C_{2v} symmetry [8]. As shown in Table 1, the values of ν_{CN} for this complex are intermediate between those of the corresponding complexes of bpy and bpz. Since these frequencies are sensitive to the extent of $d_\pi(Ru) \rightarrow \pi^*(CN)$ backbonding and considering the competition between the cyanide groups and the polypyridyl ligand for the π-electron density of Ru, the following order of π-acceptor capacity towards the $Ru(CN)_4{}^{2-}$ moiety is disclosed:

$$bpy < dpp < bpz.$$

In complex (**II**), only 3 bands are detected in the ν_{CN} zone (at 2097, 2064 and 2047 cm^{-1}), as expected from the higher symmetry of a dinuclear species. These values are similar to those of (**I**), indicating small interaction between both metallic centres in (**II**).

Figure 2 shows the UV–vis spectrum of (**I**) in aqueous solution. Ligand(dpp)-centered π-π^* transitions are observed at 248, 272 and 302 nm. Three metal-to-ligand charge-transfer transitions (MLCT) are observed at 220 nm [$d_\pi(Ru) \rightarrow \pi^*(CN)$], 380 nm, [$d_\pi(Ru) \rightarrow \pi_2^*(dpp)$] and 447 nm [$d_\pi(Ru) \rightarrow \pi_1^*(dpp)$]. The energy value for the lowest-lying MLCT excited state ($E_{op} = 2.77$ eV) is intermediate between those

Table 1. Values of ν_{CN}(in cm^{-1}), for the Na^+ salts of $[(Ru(L)(CN)_4]^{2-}$ ions

L	ν_1	ν_2	ν_3	ν_4	Ref.
bpy	2092	2060	2048	2035	9
dpp	2098	2067	2062	2046	this work
bpz	2105	2073	2066	2052	9

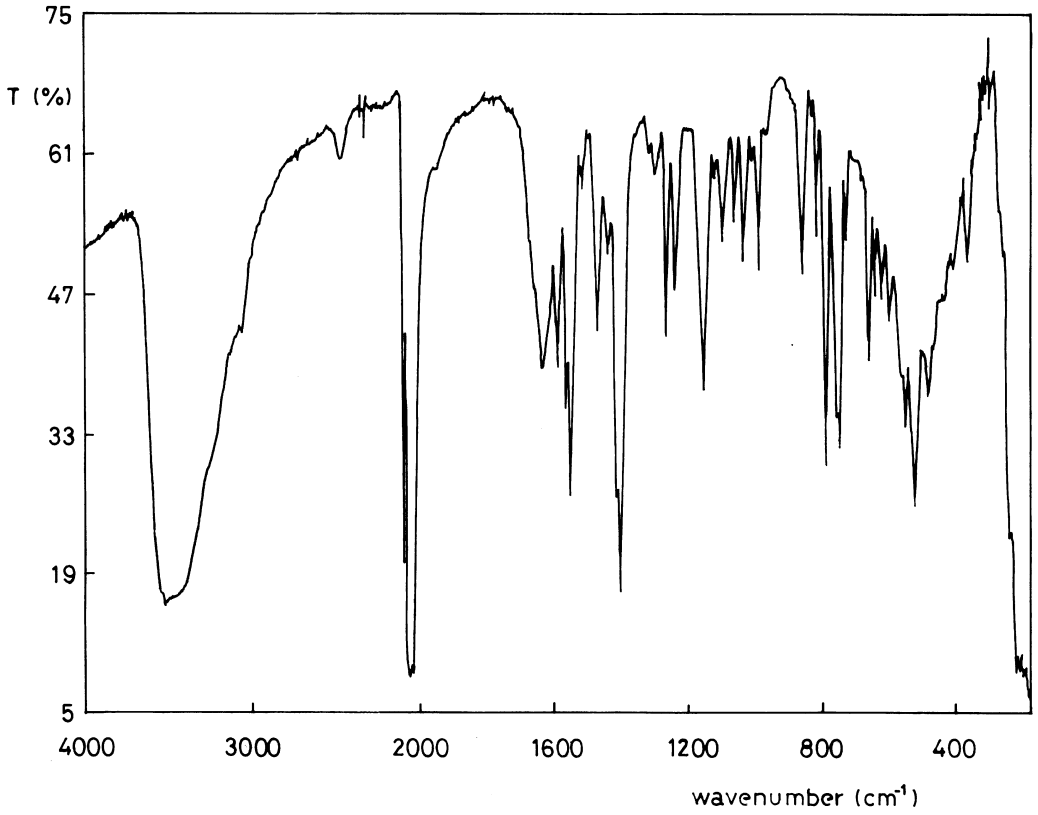

Fig. 1. IR spectrum of $Na_2[Ru(dpp)(CN)_4].4\ H_2O$ (as a KBr pellet).

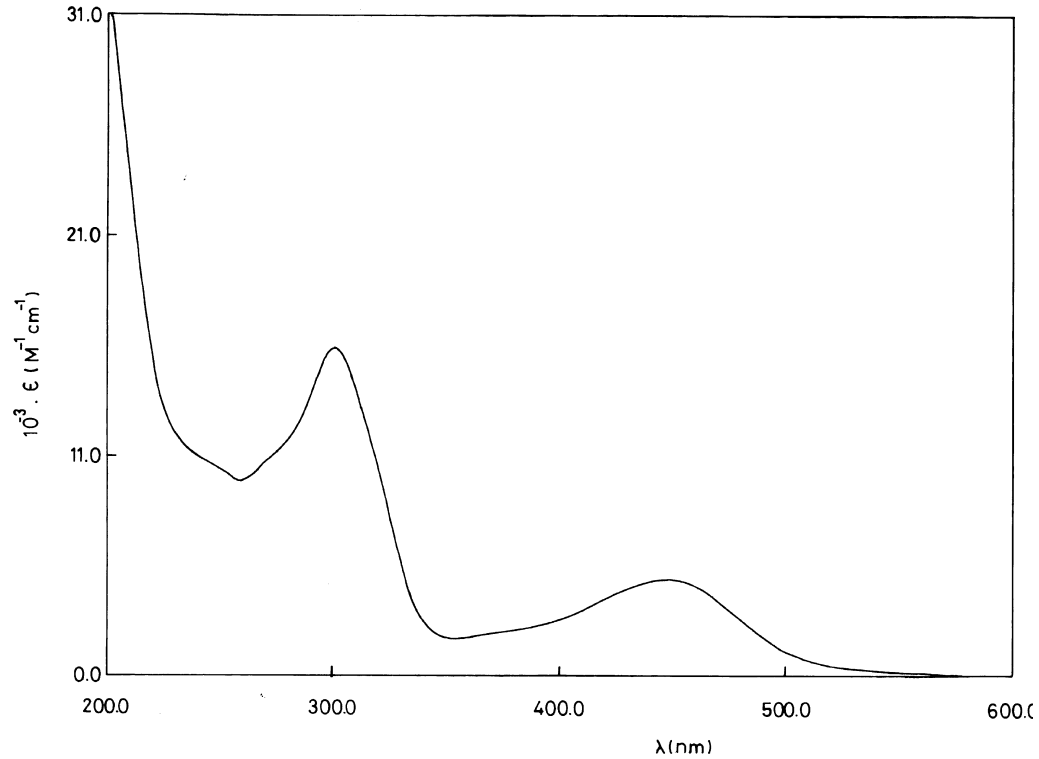

Fig. 2. UV–vis spectra in aqueous solution of $[Ru(dpp)(CN)_4]^{2-}$.

corresponding to the bpy (3.10 eV) and bpz (2.68 eV) complexes of $Ru(CN)_4^{2-}$ [7,9], in agreement with the IR results, since these energy values connote the extent of $Ru \rightarrow L$ π-backbonding (with L = polypyridyl ligand). On the other hand, this value of E_{op} for complex (**I**) is higher than the corresponding values for $[Ru(dpp)(bpy)_2]^{2+}$ (2.58 eV) and $[Ru(dpp)(NH_3)_4]^{2+}$ (2.27 eV) [10,12], indicating that the extent of π-backbonding Ru $\rightarrow$ dpp is strongly diminished when cyanides are used as co-ligands. For the Bu_4N^+ salt of (**I**), spectra in different solvents can be obtained. The correlation between E_{op} for the MLCT $d_\pi(Ru) \rightarrow \pi_1^*(dpp)$ and the acceptor number (AN) of the solvent, as shown in Fig 3, is similar to those encountered in analogous complexes [9], and can be accounted for by the specific interactions of the electron-donating cyanides with the solvents.

Complex (**II**) has a value of $\lambda_{max} = 474$ nm, corresponding to the MLCT transition of minimum energy. The small shift in E_{op}, when compared to the mononuclear species (**I**) ($\Delta E_{op} = 0.14$ eV) is equivalent to introducing a weak electron-withdrawing substituent in the periphery of dpp; this small interaction can be attributed to steric restrictions in the bridging ligand [10].

Figure 4 shows a spectrophotometric titration of complex (**II**) performed by adding stoichiometric amounts of $S_2O_8^{2-}$ in $HOAc/AcO^-$ aqueous buffer. A new band is observed at $\lambda_{max} \approx 1100$ nm, corresponding to a metal-to-metal charge transfer (MMCT) transition in the mixed-valent complex $[(CN)_4Ru^{II}(dpp)Ru^{III}(CN)_4]^{3-}$. The electronic coupling is rather weak ($H_{AB} \approx 550$ cm^{-1}), pointing to a Class (II) species [24]. By contrast, no MMCT band was detected for the mixed-valent analogue $[(bpy)_2Ru(dpp)Ru(bpy)_2]^{5+}$, a fact explained by the little metal-metal interaction appearing in this latter complex as a consequence of the steric constraints imposed by the dpp bridging ligand [10]. We conclude that steric effects are less demanding when replacing bipyridines by cyanides as co-ligands.

The redox potentials determined by cyclic voltammetry are typical for cyanometalates [9]. In the Bu_4N^+ salt of the mononuclear complex $[Ru(dpp)(CN)_4]^{2-}$, the Ru^{III}/Ru^{II} redox potential is $E_{ox} = 0.44$ V (vs $Ag^+/AgCl$, in MeCN, 0.1 M TBAH), while the ligand reduction potential appears at $E_{red} = -1.59$ V (in the same conditions). The difference $E_{ox} - E_{red}$ is lower than the corresponding values for the bpy and bpz analogues [9]. For complex (**II**), two oxidative waves are observed, as expected for both Ru^{III}/Ru^{II} couples, with a difference in redox potentials of 0.23 V (in aqueous solution). This value indicates that the coupling of both metallic centers in this dinuclear species is intermediate between that of $[(NH_3)_4Ru(dpp)Ru(NH_3)_4]^{4+}$ ($\Delta E_{1/2} = 0.36$ V) and that of $[(bpy)_2Ru(dpp)Ru(bpy)_2]^{4+}$ ($\Delta E_{1/2} = 0.19$ V) [10,12]. This last result is consistent with the detection of a MMCT band in the mixed-valent derivative of (**II**).

Complex (**I**) emits in aqueous solution at room temperature. Figure 5 shows the emission spectra at

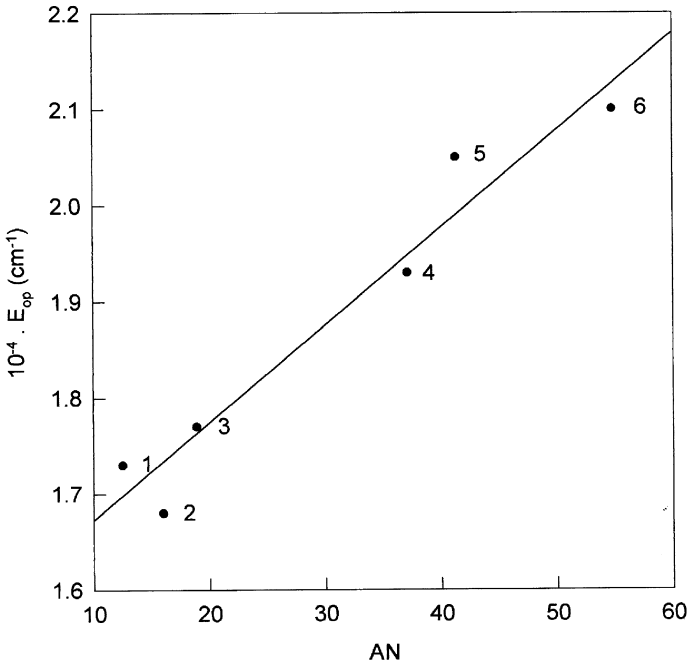

Fig. 3. Plot of E_{op} for the lowest-lying MLCT in $[Ru(dpp)(CN)_4]^{2-}$ vs the solvent acceptor number (AN). **1** = acetone; **2** = *N*,*N*-dimethylformamide; **3** = acetonitrile; **4** = ethanol; **5** = methanol; **6** = water.

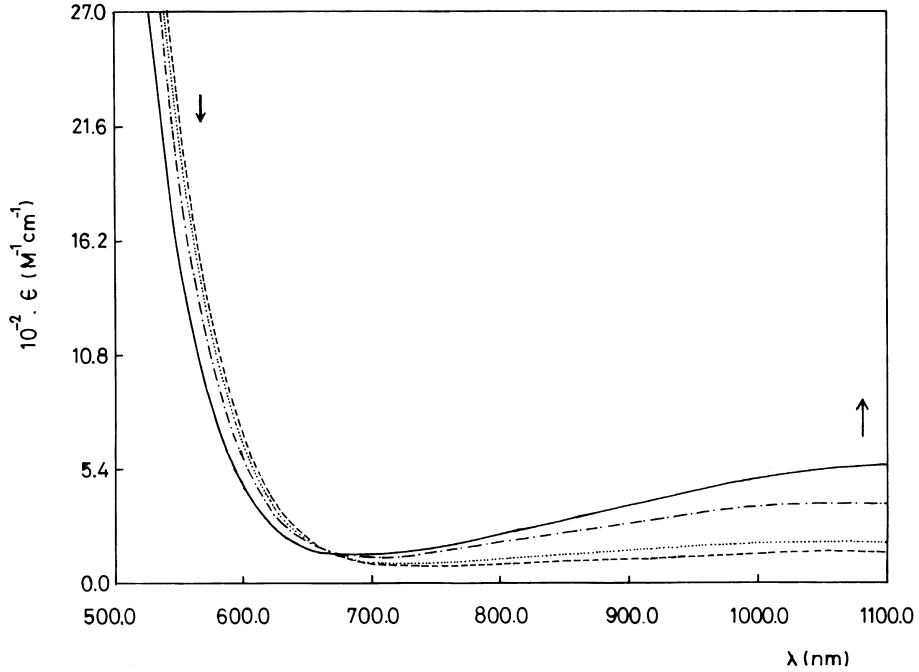

Fig. 4. Visible spectrophotometric titration of $[(CN)_4Ru^{II}(dpp)Ru^{III}(CN)_4]^{4-}$ with increasing amounts of $S_2O_8^{2-}$, in water, at pH = 4.

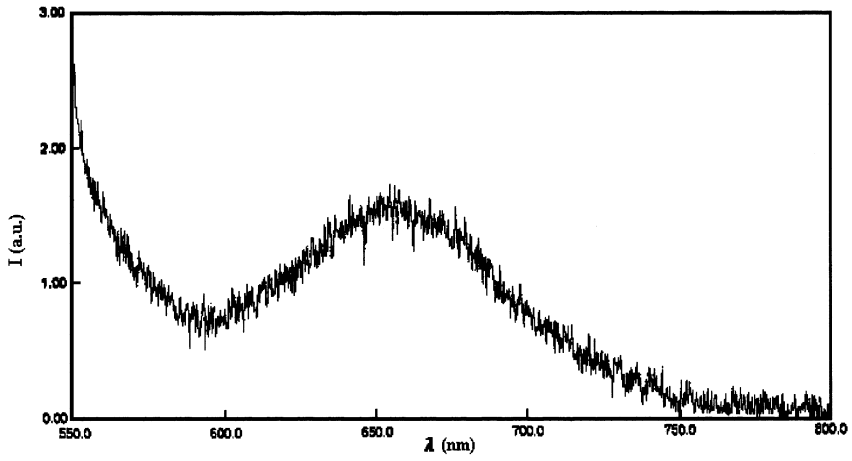

Fig. 5. Emission spectrum of $[Ru(dpp)(CN)_4]^{2-}$ in aqueous solution (λ_{ex} = 450 nm).

λ_{ex} = 450 nm. The obtained value of $\lambda_{em} = (652 \pm 2)$ nm is almost solvent independent and the corresponding energy value (E_{em} = 1.91 eV) is intermediate between those of the analogous complexes of bpy (E_{em} = 2.03 eV [7]) and bpz (E_{em} = 1.76 eV [9]), in agreement with the IR and UV–vis results. The quantum yield is $\phi_{em} < 0.001$. We can then deduce that complex (**I**) can be used as a photosensitizer in aqueous solution. Complex (**II**) does not emit in water at room temperature, contrasting to the behaviour of $[(bpy)_2Ru(dpp)Ru(bpy)_2]^{4+}$, which is emissive at room temperature [10]. This result points to a stronger metal-metal interaction in the complex described in this work as compared to $[(bpy)_2Ru(dpp)Ru(bpy)_2]^{4+}$, in accord with their optical and electrochemical properties.

It can be concluded that the new mono- and di-nuclear mixed complexes of dpp and ruthenium cyanides synthesized and characterized in this work allow us to classify dpp as a ligand whose electronic π-accepting ability is intermediate between bpy and bpz. While the mononuclear complex $[Ru(dpp)(CN)_4]^{2-}$

can be used as a photosensitizer in aqueous solution, the electronic interactions disclosed in the dinuclear species $[(CN)_4Ru(dpp)Ru(CN)_4]^{4-}$ seem to be lower than those found in similar bpz-bridged complexes [25], but stronger than in $[(bpy)_2Ru(dpp)Ru(bpy)_2]^{4+}$ [10]. The electronic coupling between metallic centers can thus be tuned by using bridging ligands with some steric restrictions, such as dpp, and co-ligands with no steric constraints, such as cyanides.

Acknowledgements—We thank Consejo Nacional de Investigaciones Científicas y Técnicas (CONICET, Argentina) Agencia Nacional de Promoción Científica y Tecnológica (ANPCyT, Argentina), Consejo de Investigaciones de la Universidad Nacional de Tucumán (CIUNT, Argentina) and Fundación Antorchas (Argentina) for financial help. N.E.K. and F.F. are Members of the Research Career (CONICET).

REFERENCES

1. Sutin, N. and Creutz, C., *Pure Appl. Chem.*, 1980, **52,** 2717.
2. Kalyanasundaram, K., *Coord. Chem. Rev.*, 1982, **46,** 159.
3. (a) Juris, A., Balzani, V., Barigelletti, F., Campagna, S., Belser, P. and Von Zelewsky, A., *Coord. Chem. Rev.*, 1988, **84,** 85; (b) Meyer, T. J., *Acc. Chem. Res.*, 1989, **22,** 163.
4. Pinnick, D. and Durham, B., *Inorg. Chem.*, 1984, **23,** 1440.
5. Kober, E. M., Marshall, J. L., Dressick, W. J., Sullivan, B. P., Caspar, J. V. and Meyer, T. J., *Inorg. Chem.*, 1985, **24,** 2755.
6. Lumpkin, R. S., Kober, E. M., Worl, L. A., Murtaza, Z. and Meyer, T. J., *J. Phys. Chem.*, 1990, **94,** 239.
7. Bignozzi, C. A., Chiorboli, C., Indelli, M. T., Rampi Scandola, M. A., Varani, G. and Scandola, F., *J. Am. Chem. Soc.*, 1986, **108,** 7872.
8. Katz, N. E., *An. Asoc. Quim. Argent.*, 1991, **79,** 67.
9. García Posse, M. E., Katz, N. E., Baraldo, L. M., Polonuer, D., Colombano, C. and Olabe, J. A., *Inorg. Chem.*, 1995, **34,** 1830.
10. Braunstein, C. H., Baker, A. D., Strekas, T. C. and Gaffney, H. D., *Inorg. Chem.*, 1984, **23,** 857.
11. Toma, H. E., Auburn, P. R., Dodsworth, E. S., Golovin, M. N. and Lever, A. B. P., *Inorg. Chem.*, 1987, **26,** 4257.
12. Ruminski, R. R., Cockroft, T. and Shoup, M., *Inorg. Chem.*, 1988, **27,** 4026.
13. Kalyanasundaram, K. and Nazeeruddin, Md. K., *Chem. Phys. Lett.*, 1989, **158,** 45.
14. Baiano, J. A., Carlson, D. L., Wolosh, G. M., DeJesus, D. E., Knowles, C. F., Szabo, E. G. and Murphy, W. R., Jr., *Inorg. Chem.*, 1990, **29,** 2327.
15. (c) Balzani, V. and Scandola, F., *Supramolecular Photochemistry*, Ellis Horwood Ltd, Chichester, 1991.
16. Serroni, S., Denti, G., Campagna, S., Juris, A., Ciano, M. and Balzani, V., *Angew. Chem. Int. Ed. Engl.*, 1992, **31,** 1493.
17. Nazeeruddin, M. K., Grätzel, M., Kalyanasundaram, K., Girling, R. B. and Hester, R. E., *J. C. S. Dalton*, 1993, 321.
18. Richter, M. M. and Brewer, K. J., *Inorg. Chem.*, 1993, **32,** 5762.
19. Yam, V. W. W., Lee, V. W. M. and Cheung, K. K., *J. C. S. Chem. Commun.*, 1994, 2075.
20. DuPreez, J. G. H., Gerber, T. I. A. and Jacobs, R., *J. Coord. Chem.*, 1994, **33,** 147.
21. Granifo, J., *Polyhedron*, 1994, **13,** 713.
22. Molnar, S. M., Jensen, G. E., Vogler, L. M., Jones, S. W., Laverman, L., Bridgewater, J. S., Richter, M. M. and Brewer, K. J., *J. Photochem. Photobiol. A*, 1994, **80,** 315.
23. Lee, Y. F., Kirchhoff, J. R., Berger, R. M. and Gosztola, D., *J. C. S. Dalton*, 1995, 3677.
24. Creutz, C., *Progr. Inorg. Chem.*, 1983, **30,** 1.
25. Fagalde, F. and Katz, N. E., work in progress.

Pergamon

PII : S0277–5387(98)00062–X

Polyhedron Vol. 17, No. 16, pp. 2739–2749, 1998
© 1998 Elsevier Science Ltd
All rights reserved. Printed in Great Britain
0277–5387/98 $19.00+0.00

Kinetics and mechanism of the oxidation of D-galactono-1,4-lactone by Cr^{VI} and Cr^{V}†

S. Signorella,[a] M. Santoro,[a] C. Palopoli,[a] C. Brondino,[b] J. M. Salas-Peregrin,[c] M. Quiroz[c] and L. F. Sala[a]*

[a] Departamento de Química, Facultad de Ciencias Bioquímicas, y Farmacéuticas, UNR, Suipacha 531, 2000 Rosario, Argentina,

[b] Instituto de Desarrolo Tecnológico para la Industria Química, Güemes 3450, 3000 Santa Fe, Argentina,

[c] Departamento de Química Inorgánica, Facultad de Ciencias, Universidad de Granada, Fuentenueva s/n, 18071 Granada, España

(Received 21 January 1998 ; accepted in revised form 26 January 1998)

Abstract—The oxidation of D-galactono-1,4-lactone by Cr^{VI} yields D-lyxonic acid, carbon dioxide and Cr^{3+} as final products when an excess of sugar acid over Cr^{VI} is used. The redox reaction occurs through $Cr^{VI} \rightarrow Cr^{III}$ and $Cr^{VI} \rightarrow Cr^{V} \rightarrow Cr^{III}$ paths. The complete rate law for the Cr^{VI} oxidation reaction is expressed by $-d[Cr^{VI}]/dt = (k_0 + k_H\,[H^+])\,[gal][Cr^{VI}]$, where $k_0 = (31 \pm 3) \times 10^{-4}\ M^{-1}\ s^{-1}$ and $k_H = (99 \pm 5) \times 10^{-4}\ M^{-2}\ s^{-1}$, at 40°C. Cr^{V} is formed in a rapid step by reaction of the $CO_2^{\cdot-}$ radical with Cr^{VI}. Cr^{V} reacts with the substrate faster than does Cr^{VI}. The Cr^{V} oxidation follows the rate law: $-d[Cr^{V}]/dt = (k'_0 + k'_H\,[H^+])\,[gal]$, where $k'_0 = (15 \pm 2) \times 10^{-3}\ M^{-1}\ s^{-1}$ and $k'_H = (34 \pm 4) \times 10^{-3}\ M^{-2}\ s^{-1}$, at 40°C. The EPR spectra show that several intermediate $[Cr(O)(gala)_2]^-$ linkage isomers are formed in rapid pre-equilibria before the redox steps.
© 1998 Elsevier Science Ltd. All rights reserved

Keywords: galactonolactone ; chromium ; oxidation ; kinetics ; mechanism ; Cr^{V} ; Cr^{VI}.

Hexavalent chromium, in many different compounds, is a well established carcinogen and mutagen [1–5]. The observation of Cr^{V} and Cr^{IV} intermediates in the selective oxidation of organic substrates by Cr^{VI} and their implication in the mechanism of Cr-induced cancers [6–8] has generated a considerable amount of interest in their chemistry and biochemistry [9–12]. The biological reduction of Cr^{VI} to lower states has been observed with a wide variety of naturally occurring cellular reductants [13–15]. Ligands that possess two oxygen atoms able to form five-membered rings about the metal ion, such as 1,2-diols and α-hydroxyacids, are effective as non enzymatic reductants and complexation agents towards hypervalent chromium and can stabilise the labile oxidation states of chromium [12, 16–19]. For this reason sugars, or their derivatives, may play an important role in the chemistry of Cr^{VI}. Aldonic acids (or their lactones) have been found as metabolic intermediates in animals and plants, as products of the action of micro-organisms on carbohydrates and as constituents of acidic polysaccharides [20]. Cr^{VI} oxidation of α-hydroxyacids has been extensively studied [21–29]. These oxidations may yield products coming from either C—C [21–22,25–27,29] or C—H [23–24,28,29] cleavage, depending on the particular molecular characteristics of the organic substrate, through mechanisms involving either two-electron or three-electron initial oxidation of substrate by Cr^{VI}. Polyhydroxyacids offer additional binding sites to form the Cr^{VI} (Cr^{V}) ester precursor of slow electron-transfer steps and provide helpful information about stereoelectronic effects affecting the reaction course [28]. In previous work we have found that the number and arrangement of hydroxyl groups of aldoses affect the Cr^{VI} and Cr^{V} oxidation rates and mechanism [30–34]. At present, we are interested in correlating the stereochemistry of aldonic acids with their ability for reducing and co-

* Author to whom correspondence should be addressed. e-mail : inquibir@satlink.com

† The present work was presented at the X Meeting on Physical-Chemistry, Tucumán, Argentina, April 21, 1997.

ordinating Cr^{VI} and Cr^{V}, as well as determining the preferred donor sites of these polyhydroxyacids. In this paper we report our results on the chromic oxidation of D-galactono-1,4-lactone (Scheme 1) and we present structural evidences for the intermediate Cr^{V} complexes formed in acid and neutral aqueous solutions.

EXPERIMENTAL

Materials

D-Galactono-1,4-lactone (Sigma grade), D-gluconic acid (Sigma grade), potassium dichromate (BDH), sodium perchlorate (Fluka grade), acrylonitrile (Aldrich grade) and perchloric acid (P. A. Merck) were used without further purification. Water was purified by deionisation, followed by double distillation from a potassium permanganate solution. $Na[Cr(O)(ehba)_2]\cdot H_2O$ was synthesised from 2-ethyl-2-hydroxybutanoic acid (Aldrich grade) and sodium dichromate (Merck) in acetone (Merck, A. R. grade) according to the literature method [35].

The stability of the organic substrate under conditions used in the kinetic studies was tested. The acid (gala) : lactone (galL) proportion of the reductant in the starting solution was calculated by optical rotation measurements at given hydrogen ion concentrations [36] and the composition of the substrate solution at different perchloric acid concentrations is shown in Table 1. The equilibrated solutions are stable over the time required for the kinetic measurements. In the text that follow gal refers to the total reductant concentration ([gal] = [galL] + [gala]).

For experiments performed in the 2–8 pH range, the pH of the solutions was adjusted by addition of 0.5 M NaOH and 0.5 M $HClO_4$.

Spectrophotometric measurements

Most kinetics measurements were made at 350 nm, by monitoring the absorbance changes on a Guilford Response II spectrophotometer with fully thermostated cell compartments. Mixtures of sodium perchlorate and perchloric acid were used to maintain a constant ionic strength (I) of 1.0 M. Reactant solutions were previously thermostated and transferred into a cell of 1 cm path length immediately after mixing and disappearance of Cr^{VI} was followed until at least 80% conversion. Experiments were performed at 40°C unless otherwise mentioned. In most experiments the concentration of Cr^{VI} was kept constant at 3.6×10^{-4} M while the gal concentration was varied from 0.018 to 0.122 M. The first-order dependence of the rate upon $[Cr^{VI}]$ was verified. The pseudo-first-order rate constants were calculated at various $[Cr^{VI}]_0$, but at constant temperature, $[gal]_0$, $[H^+]$ and I. As expected on the basis of a $-d(\ln[Cr^{VI}])dt = k_{obs}$ rate law where $k_{obs} = f([gal][H^+])$, k_{obs} was found to be essentially constant with increasing $[Cr^{VI}]_0$.

Cr^{V} was monitored by following the absorbance growth and decay at 750 nm of mixtures of Cr^{VI} (3.6×10^{-3} M) and excess gal (0.18–0.57 M) at fixed perchloric acid concentrations. The formation of Cr^{III} was monitored at 570 nm ($[Cr^{VI}]_0 = 1.8\times10^{-2}$ M and ratios of gal to Cr^{VI} from 10 : 1 to 20 : 1, at $[HClO_4]$ in the 0.25–0.75 M range). At the end of the reaction the two *d–d* bands ascribed to Cr^{III} were observed at

Table 1. Proportion of D-galactonolactone (galL) and D-galactonic acid (gala) in the starting solution[a]

[HClO4]/M	$10^2\ C_T$[b]/M	R[c]	galL (%)	gala (%)
0.25	6.60	−0.760	78.9	21.1
0.38	5.00	−0.539	72.2	27.8
0.50	5.45	−0.584	71.6	28.4
0.63	5.14	−0.578	76.4	23.6
0.75	5.06	−0.573	77.1	22.9
0.90	6.29	−0.660	82.0	18.0
1.00	5.58	−0.682	85.3	14.7

[a] Values used in calculations: molar rotations: −13.84 (galL); −2.84 (gala), +0.805 (gal^-); $K = [H^+][gal^-]/([gala]+[galL]) = 2.25\times10^{-5}$.

[b] $C_T = [gala]+[galL]+[gal^-]$, where gal^- refers to galactonate and represents <0.02% of C_T.

[c] Optical rotation.

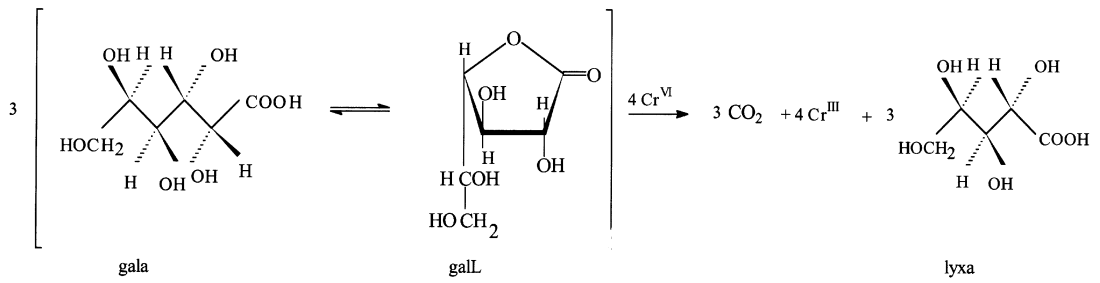

Scheme 1.

$\lambda_{max} = 410$ ($\varepsilon = 33$) and 566 nm ($\varepsilon = 27.5$ dm^3 mol^{-1} cm^{-1}) ([$HClO_4$] = 0.25 M). Both, visible and UV spectral maxima and intensities, are in close agreement (*vide infra*) with those observed for the acid solutions of the K[Cr(OH)(gala)(lyxa)] (lyxa = D-lyxonic acid) ternary complex, independently synthesised [37] according to a literature method [38]. These *d–d* bands changed with time toward bands of lower intensity at $\lambda_{max} = 408$ ($\varepsilon = 19.7$) and 573 nm ($\varepsilon = 15$ dm^3 mol^{-1} cm^{-1}), characteristic of the $[Cr(H_2O)_6]^{3+}$ ion.

Products analysis

Under the conditions used in the kinetic measurements (ratios of gal to Cr^{VI} from 50 : 1 to 340 : 1), qualitative identification of D-lyxonic acid as the reaction product was carried out by paper chromatography. D-lyxonic acid was identified against an authentic sample using *n*-butanol/acetic acid/water (4 : 1 : 5) as eluent. Paper chromatograms were visualised by two kinds of development reagents : a three-stage dip of silver nitrate, sodium hydroxide and sodium thiosulphate [39] and *p*-anisidine reagent [40]. D-lyxonic acid identification as the only reaction product was also made by ^{13}C NMR. A mixture of gal (7.64×10^{-3} mmol) and potassium dichromate (1.66×10^{-3} mmol) in 1 M $HClO_4$ (10 cm^3) was allowed to react at 40°C. After the reaction had proceeded to completion the mixture was stirred with a Dowex 50W-X8 cation exchange resin until all the Cr^{III} was removed from the solution and a concentrated sample was analysed by ^{13}C NMR. Lyxonic acid and unreacted galL and gala were identified by comparing against authentic samples.

Under all these experimental conditions (large to moderate excess of organic substrate) a quantitative yield of carbon dioxide was observed.

The presence of free radicals was tested for in the reaction of gal with Cr^{VI}. A solution of potassium dichromate (4×10^{-4} mmol) in 2 cm^3 of 0.5 M $HClO_4$ was added to a mixture of 4×10^{-2} mmol gal and acrylonitrile (0.25 cm^3) in 0.5 M $HClO_4$ (0.25 cm^3) at 40°C. After 1 h a white precipitate appeared. Control experiments (without potassium dichromate or reductant present) did not show the formation of a precipitate. Besides, the addition of an excess of acrylonitrile on the reaction mixture results in the complete suppression of the carbon dioxide evolution.

EPR spectroscopy

The EPR spectra were obtained on a Bruker ESP 300 spectrometer. The microwave frequency was generated with a Bruker 04 ER (9–10 GHz) and measured with a Racal-Dana frequency meter. The magnetic field was measured with a Bruker NMR-probe gaussmeter. A least-squares EPR spectrum-fitting program, e23new, was used to estimate the spectral parameters and relative concentrations of the Cr^{V} complexes, using Lorentzian line shapes [41,42].

RESULTS AND DISCUSSION

Rate studies

The absorbance vs time curves at 350 nm exhibit a monotonic decrease of absorbance which cannot be described by a single exponential decay. At this wavelength, kinetic traces show an initial deviation from first-order decay over short time periods. These kinetic profiles could be adequately described by the set of consecutive first-order reactions of Scheme 2 :

It is known that Cr^{V} species absorb strongly at 350 nm and may superimpose Cr^{VI} absorbance yielding the wrong interpretation of spectrophotometric absorbance decay values [29]. Thus, considering the Cr^{V} absorption superimposition, the absorbance at 350 nm, at any time during the reaction, is given by

$$Abs^{350} = \varepsilon^{VI}[Cr^{VI}] + \varepsilon^{V}[Cr^{V}] \quad (1)$$

Combining the eqn (1) with rate expressions [43] derived from scheme 2, yields :

$$Abs^{350} = Abs_0 e^{-k6t} + k_6 \varepsilon^{V}[Cr^{VI}]_0 (e^{-k5t} - e^{-2k6t})/(2k_6 - k_5) \quad (2)$$

In this equation, ε^{V} refers to the molar absorptivity of Cr^{V} at 350 nm and was assumed to be the same as for the complex $[Cr^{V}(O)(ehba)_2]^-$ [35]. Parameters k_6 and k_5 refer to the rate of disappearance of Cr^{VI} and Cr^{V}, respectively, and were evaluated from a non-linear iterative computer fit of eqn (2). It must be noted that in eqn (2), k_6 appears in the numerator of the pre-exponential term and $2k_6$ appears in the denominator and in the exponential terms because, according to the proposed reaction scheme, only half of the Cr^{VI} reaches Cr^{III} through a Cr^{V} intermediate.

Figure 1(a) shows a typical curve for one run at 350 nm and the curve fit according to eqn (2). The calculated kinetic parameters, k_6 and k_5, for various concentrations of gal at fixed concentrations of $HClO_4$, are summarised in Table 2. In multiple measurements, the reproducibility of the two rate constants is better than 10%.

Values of k_5 and k_6 may also be obtained from absorbance data at 750 nm. At this wave length, only Cr^{V} absorbs and the experimentally observed intermediate Cr^{V} growth and decay curve could be fitted by eqn (3)

$$Abs^{750} = k_6[Cr^{VI}]_0 \varepsilon^{V}(e^{-k5t} - e^{-2k6t})/(2k_6 - k_5) \quad (3)$$

where ε^{V} refers here to Cr^{V} molar absorptivity at 750 nm. A good fit of data is obtained with $\varepsilon^{V} = 38$ M^{-1} cm^{-1} [26], as shown in Fig. 1(b). Since at least tenfold higher initial Cr^{VI} and gal concentrations were necessary to follow absorbance changes at 750 nm, $k_5/10$ and $2k_6/10$ values calculated by eqn (3) are coincident

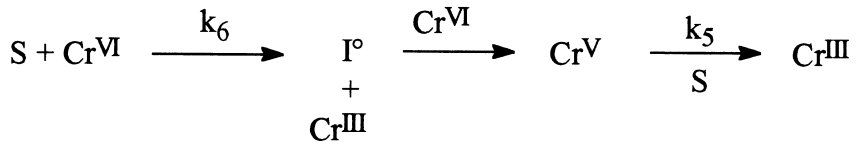

Scheme 2. S = organic substrate; I° = intermediate radical

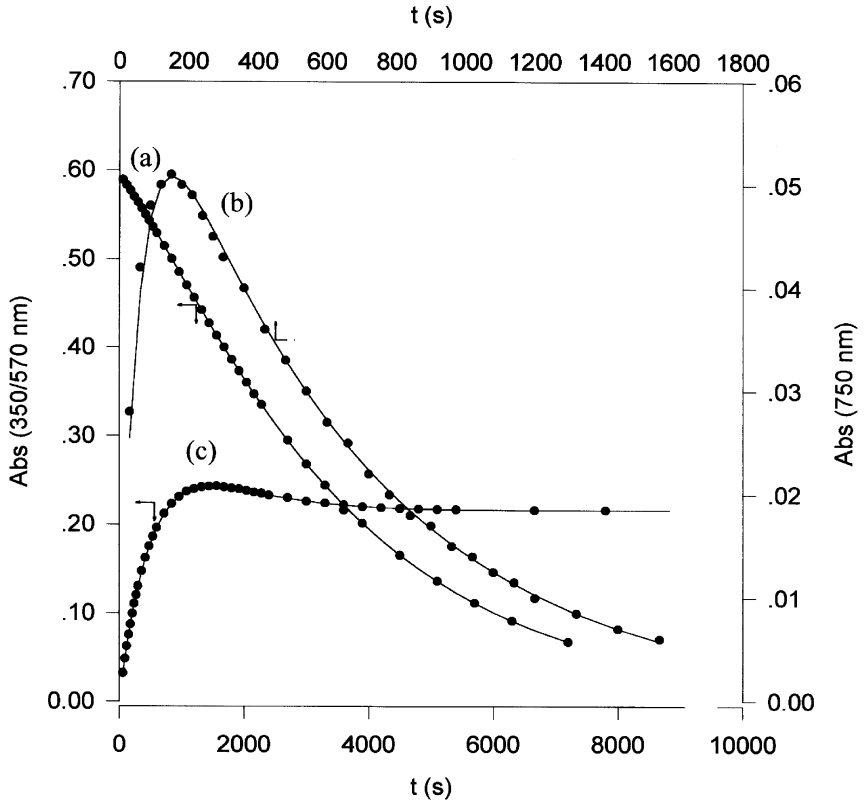

Fig. 1. Absorbance vs time curves for the chromic oxidation of gal, $I = 1$M, $T = 40^{\circ}$C at (a) 350 nm, $[Cr^{VI}] = 3.6 \times 10^{-4}$ M, $[gal] = 3.6 \times 10^{-2}$ M, $[H^+] = 0.38$ M; (b) 750 nm, $[Cr^{VI}] = 3.6 \times 10^{-2}$ M, $[gal] = 3.6 \times 10^{-1}$ M, $[H^+] = 0.38$ M; (c) 570 nm, $[Cr^{VI}] = 1.8 \times 10^{-2}$ M, $[gal] = 1.8 \times 10^{-1}$ M, $[H^+] = 0.75$ M.

Table 2. Observed pseudo-first-order rate constants (k_6 and k_5) for different concentrations of $HClO_4$ and organic substrate. $T = 40^{\circ}$C; $[Cr^{VI}]_0 = 3.6 \times 10^{-4}$ M; $I = 1$ M

[gal]/M	$2k_6$ (s^{-1}) and k_5 (s^{-1}) for $[HClO_4]$/M of									
	0.25		0.38		0.50		0.75		1.00	
	$10^4 2k_6$	$10^4 k_5$	$10^4 2k_6$	$10^4 k_5$	$10^4 2k_6$	$10^4 k_5$	$10^4 2k_6$	$10^4 k_5$	$10^4 2k_6$	$10^4 k_5$
0.018	0.90	4.00	1.39	5.30	1.61	6.1	1.98	7.20	2.41	8.91
0.036	1.88	6.29	2.78	10.7	3.12	12.6	4.10	14.4	4.70	17.5
0.050	2.50	10.5	3.82	15.2	—	17.0	5.18	20.6	6.48	24.8
0.057	—	—	4.39	17.6	4.61	18.9	—	—	—	—
0.072	3.70	15.6	5.00	20.7	6.22	24.1	8.01	29.6	9.42	33.9
0.086	—	—	—	—	—	—	9.30	33.7	—	—
0.093	—	—	—	—	—	—	—	—	12.2	45.8
0.108	5.39	21.0	7.71	32.1	8.71	36.8	10.9	42.1	—	—
0.122	6.61	26.1	8.78	36.2	9.99	41.0	12.6	46.6	15.6	58.2

with those obtained from eqn (2), when the same gal/Cr^{VI} ratio and [$HClO_4$] were employed. For gal and Cr^{VI} concentrations used in the kinetic measurements, either at 350 or 750 nm, the calculated maximum Cr^{V} concentrations ($[Cr^{V}]_{max}$) represent up to 8% of the total chromium concentration.

The Cr^{III} formation was followed at 570 nm. At this wave length, changes in Cr^{III} concentration can be described by the pair of consecutive reactions shown in the Scheme 3 and the experimental absorbance can be fitted by eqn (4)

$$\begin{aligned} Abs^{570} &= Abs([Cr^{III}]) + Abs(Cr^{3+}) \\ &= [Cr^{VI}]_0 k_1 (e^{-k1t} - e^{-k3t})(\varepsilon_1^{III} - \varepsilon_2^{III})/ \\ &\quad (k_3 - k_1) + Abs_\infty (1 - e^{-k1t}) \end{aligned} \quad (4)$$

where k_1 and k_3 refer to the rates of Cr^{VI} and [Cr^{III}] disappearance, and ε_1^{III}, ε_2^{III} are the molar absorptivities of the Cr^{III} complex formed at the end of the redox reaction and $[Cr(H_2O)_6]^{3+}$, respectively. A typical fit of experimental data at 570 nm by using eqn (4) is shown in Fig. 1(c). Here, we have considered that the rate of Cr^{III} complex formation equals the rate of Cr^{VI} decay, without taking into account Cr^{V}. This is consistent with the observation of an isosbestic point at 525 nm under conditions employed to follow Cr^{III} at 570 nm (Fig. 2) and the low $[Cr^{V}]_{max}$ (up to 8%) observed at 750 nm (Fig. 1), for the same oxidant and reductant concentration range. Values of k_1 calculated by eqn (4) are coincident with $2k_6$ values obtained by using either eqn (2) or (3). On the other hand, k_3 depends strongly on [H^+] and a more detailed study is required for the complete description of the hydrolysis mechanism.

Cr^{VI} *oxidation of gal*

In the proton concentration range studied, plots of $2k_6$ vs [gal] gave good straight lines from which values of k were determined (Table 3). A plot of k vs [H^+] gave a straight line with a positive intercept, showing that the second-order rate constant may be expressed as consisting of an acidity independent and an acidity dependent term:

$$k = k_0 + k_H[H^+] \quad (5)$$

where $k_0 = (31 \pm 3) \times 10^{-4}$ M^{-1} s^{-1} and $k_H = (99 \pm 5) \times 10^{-4}$ M^{-2} s^{-1}

The complete rate law is then given by

$$-d[Cr^{VI}]/dt = 2k_6[Cr^{VI}]_T = (k_0 + k_H[H^+])[gal][Cr^{VI}]_T \quad (6)$$

where $[Cr^{VI}]_T$ represents the total Cr^{VI} concentration.

The two terms in the rate law (eqn (6)) results from the fact that there are at least two transition states, differing in composition but similar in energy, through which the reduction of Cr^{VI} can proceed. Thus, the oxidation of gal by Cr^{VI} should occur through two parallel slow steps leading to the redox products. Besides, in the range of substrate concentrations employed, only substrate first-order dependence was observed and D-lyxonic acid and carbon dioxide were the only detected reaction products, clearly showing that the C—C scission is preferred to the C—H cleavage at the α-carbon. A mechanism taking account of these facts is proposed in Scheme 4.

In this mechanism we have assumed that the open carboxylic acid is the reactive form of the organic substrate. This assumption is based on previous findings showing the enhanced ability of hydroxyacids to bind Cr^{VI} and Cr^{V} [13,25–28]. In any case, a possible mechanism involving the lactone may not be discarded. However, if the lactone was the reactive form of the organic reductant, co-ordination of Cr^{VI} should be favoured at a pair of adjacent hydroxyl groups of the molecule [44]. The intermediate complex formed in this way might be present in the equilibrium mixture but should not be a direct precursor of the slow redox steps. Opening of the lactone ring and rearrangement should be required for the slow electron transfer steps to take place within a complex with the carboxylate bound to Cr^{VI}. On the other hand, in the [H^+] range studied, Cr^{VI} exists mainly as $Cr_2O_7^{=}$ [45,46]. Thus, the first step of the proposed mechanism may be interpreted as the formation of a monochelate with gala acting as a bidentate ligand bound to Cr^{VI} at Cl—O and C2—O to yield the anionic species A^{2-}. This intermediate, or its monoprotonated form (AH^-), may decompose to the products. The rate law corresponding to this mechanism may be expressed as in eqn (7):

$$-d[Cr^{VI}]/dt = (k_1K_1 + k_2K_1K_2[H^+])[gala][Cr^{VI}] \quad (7)$$

Equation (7) may be expressed as a function of the total organic substrate concentration as in eqn (8):

$$-d[Cr^{VI}]/dt = (k_1K_1 + k_2K_1K_2[H^+])[gal]K_h[Cr^{VI}]/(1 + K_h) \quad (8)$$

We propose that redox paths, involving either A^{2-} or AH^- intermediate complexes, are three electron steps, just as observed for the chromic oxidation of mandelic [25], 2-hydroxy-3-methylbutanoic [21] and D-ribonic [22] acids, and Cr^{III} is formed with the oxidation products. The alternative path corresponding to the sequence $Cr^{VI}/Cr^{IV}/Cr^{III}$ was discarded on the basis of the complete CO_2 suppression after addition of excess

$$Cr^{VI} \xrightarrow{k_1} [Cr^{III}] \xrightarrow{k_3} Cr^{3+}$$

Scheme 3. [Cr^{III}] = Cr^{III}-gala-lyxa ternary complex

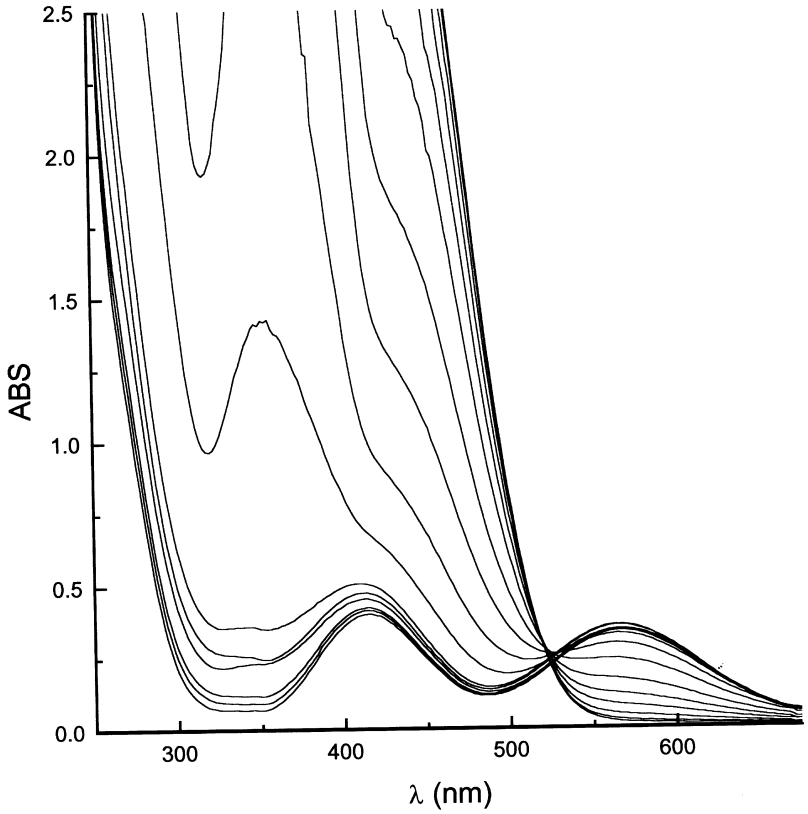

Fig. 2. Time evolution of the UV–vis spectrum of a mixture of gal (0.75 M) and Cr^{VI} (1.8×10^{-2} M). [$HClO_4$] = 0.5 M; $T = 25^{\circ}C$, over a period of ca 45 min.

Table 3. Values of k and k' for different [$HClO_4$]

[$HClO_4$/M	0.25	0.38	0.5	0.75	1.0
$10^3\,k/M^{-1}\,s^{-1}$	5.20	7.24	8.22	10.5	12.9
$10^3\,k'/M^{-1}\,s^{-1}$	20.6	29.7	33.8	39.2	48.2

acrylonitrile on the reaction mixture and the fact that the 2-ketoacid was not observed over the whole set of conditions used here. Besides, Cr^{II} formation was not proposed since CrO_2^{2+}, which is taken as evidence that Cr^{II} is an intermediate product of the reaction, was not observed as we did for the oxidation of homoserine by Cr^{VI} [24]. $CO_2^{\cdot-}$ radicals formed in the slow steps may react with Cr^{VI} in a subsequent fast step to yield Cr^{V} and carbon dioxide. Polymerisation after addition of acrylonitrile support the formation of these radicals. Cr^{V} can further oxidise gala as will now be discussed.

Cr^{V} *oxidation of gal*

At the [$HClO_4$] used in the kinetics measurements, the reaction of Cr^{VI} with excess gal generates an EPR spectrum dominated by a single detectable signal at $g_{iso} = 1.9781$ (Fig. 3 Inset) with the four weak ^{53}Cr (9.55% abundance, $I = 3/2$) hyperfine peaks at 18 G spacing, typical of five-co-ordinate oxochromate(V) complexes [47,48].

The rate of formation and disappearance of the intermediate Cr^{V} calculated from the peak-to-peak heights (and/or areas) of the EPR signals as a function of time (Fig. 3) are consistent with values obtained from the spectrophotometric measurements. The delayed t_{max} observed by this technique, account for the lower temperature (25°C, instead of 40°C) used in the EPR measurements.

In the 0.25–1 M proton concentration range, plots of k_5 vs [gal] gave good straight lines from which values of k' were determined (Table 3). A plot of k' vs [H^+] gave a straight line with a positive intercept, showing that the second-order rate constant may be expressed as consisting of an acidity independent and an acidity dependent term. The rate constant for the disappearance of Cr^{V} then may be expressed as:

$$k_5 = (k'_0 + k'_H[H^+])[gal] \quad (9)$$

where $k'_0 = (15 \pm 2) \times 10^{-3} M^{-1} s^{-1}$

and $k'_H = (34 \pm 4) \times 10^{-3} M^{-2} s^{-1}$ (10)

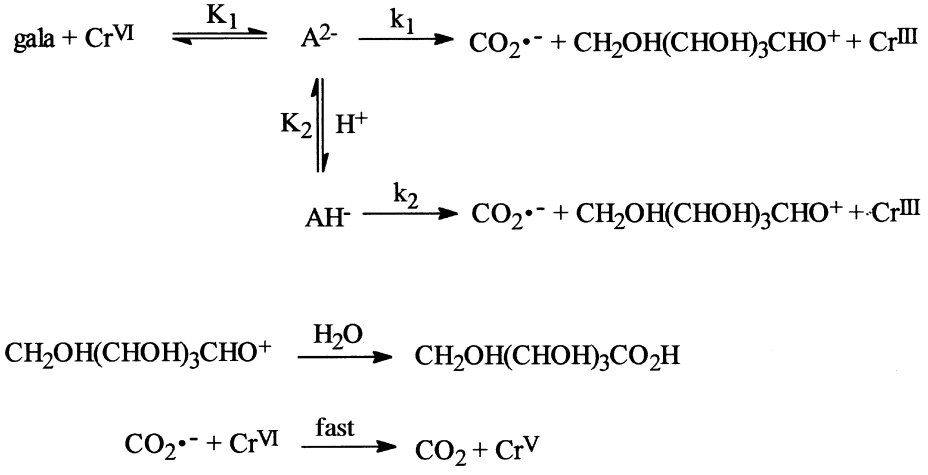

Scheme 4. $A^{2-} = [(galaH_{-2})(O)_2(OH_2)CrOCrO_3]^{2-}$

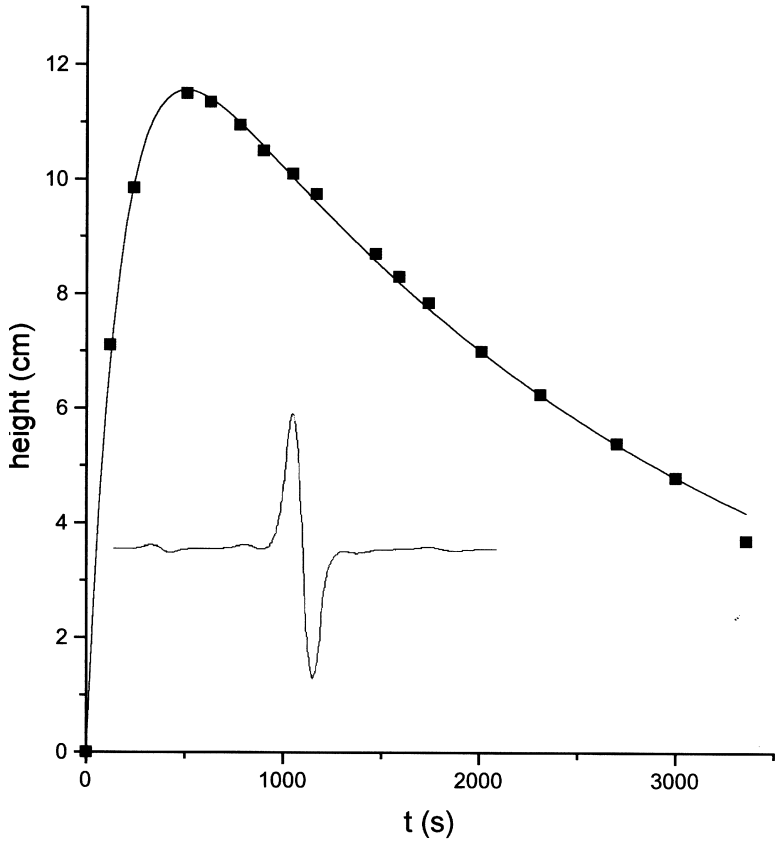

Fig. 3. Peak-to-peak heights of Cr^{V} EPR signals vs time. [gal] = 0.144 M; $[Cr^{VI}] = 3.6 \times 10^{-3}$ M; $[H^+] = 0.5$ M; $I = 1$ M; $T = 25°C$. $T_{max} = 508$ s. Inset: EPR signal recorded at $t = 15$ min.

This means that the Cr^{V} intermediate decays to the product directly or through an acid-catalysed step. Since the latter is of the same order as the non-catalysed step, at low acid concentration (i.e. neutral pH) the oxidation occurs mainly through the non-acid-catalysed path. In this way, the intermediate Cr^{V} is consumed faster than observed for the reaction of Cr^{VI} with sugars for which the non-acid catalysed path is extremely slow and the Cr^{V} intermediates remain in solution after several weeks [30–32].

A mechanism taking into account the structural evidence for the Cr^V intermediate complex and the kinetics results is given in Scheme 5.

In this mechanism, only one of the two gala molecules involved in the Cr^V complex formation is oxidised to D-lyxonic acid through the two-electron intramolecular redox path, in accordance with the observed first-order rate on [gala]. Possibly, several linkage isomers might be formed by co-ordination of gala with Cr^{VI} via any pair of properly disposed hydroxyl group (see discussion below). However, since D-lyxonic acid is the only reaction product observed in the solution, the Cr^V complex, precursor of the redox steps, must be one with at least one gala molecule bound to Cr^V at the carboxylate group. Besides, the g_{iso} and A_{iso} values observed for the Cr^V intermediate are close to those of $[Cr(O)(ehba)_2]^-$. Since the g_{iso} and, specially, A_{iso} values are very sensitive to the Cr^V co-ordination environment, our assumption seems to be a reasonable one.

It must be noted that, in Scheme 5, the two-electron substrate C—C cleavage affords formic acid. However, under our experimental conditions, we have never detected formic acid. This fact may be explained if, under conditions used here, formic acid is oxidised faster than gal. Effectively, Cr^{VI} oxidation of formic acid to carbon dioxide is faster than gal oxidation [49], affording the observed quantitative yield of carbon dioxide.

The proton superhyperfine (shf) coupling has been shown to be useful in determining the binding of 1,2-diolate moieties of sugars to the Cr^V centre [30,44]. We found that performing the reaction at pH > 2, the single broad (linewidth ~ 2 G) signal observed at higher $[H^+]$ sharpens and the shf pattern resolves, thus providing new insights about the gala co-ordination sites.

The reaction of Cr^{VI} with an excess of 5–20 times of gal, in the 2–6 pH range, at 25°C, results in the formation of a Cr^V EPR spectrum which is a composite of at least two EPR signals at $g_1 = 1.9781$ and $g_2 = 1.9788$. The relative proportion of the signals depends on the pH, but is independent of the gal/Cr^{VI} ratio employed and the reaction time (the signals were deconvoluted by fitting the spectra by Lorentzian derivatives). Figure 4(a) shows the spectrum of a reaction mixture at pH = 5 with the simulated spectrum, for which a g_1/g_2 ratio = 0.41 was obtained. The best fit of the spectrum yields the spectral parameters summarised in Table 4. The g_{iso} values obtained for the two signals are those expected for five-co-ordinate oxochromate(V) complexes; while the different shf patterns indicate that they are linkage isomers [50]. In this way, the shf splitting of the signal at g_1 arises from the coupling of two equivalent protons and may be attributed to a complex with two ligand molecules bound to Cr^V at Cl—O/C2—O. The shf splitting of the signal at g_2 may be assumed to arise from two different binding modes of the two ligand molecules co-ordinated to Cr^V, via a 1,2-diolate and the α-hydroxocarboxylate donor sites, respectively. In the oxidation of D-gluconic acid (glca) with Cr^{VI}, in this pH range, only one species is detected. Interestingly, the g_{iso} value (1.978) and the shf pattern (Fig. 5) reveal the same chelation mode of glca as for gala in the complex giving rise to the signal at g_2. For the same gal/Cr^{VI} ratios, in the 6–8 pH range, the spectra are dominated by a signal at 1.9795 with a shf splitting value of 0.92 G. The g_{iso} and shf pattern clearly indicate that CrO^{3+} co-ordinates two gala molecules via a 1,2-diolate moiety and that the shf structure derives from the coupling with the four equivalent protons. In this pH range, the minor signal ($g_{iso} = 1.978$) can be attributed to the isomer with the ligand acting through a 1,2-diolate and the α-hydroxocarboxylate donor sites. Figure 4(b) shows the spectrum of a reaction mixture at pH = 7.4 with the simulated spectrum, for which the major Cr^V species represents the 92% of the Cr^V in solution.

A last point to consider is that, at each pH, the

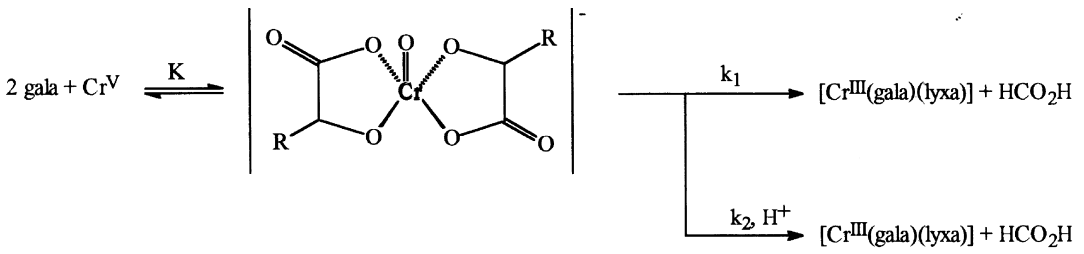

$$[Cr^{III}(gala)(lyxa)] \longrightarrow Cr^{3+} + gala + lyxa$$

Scheme 5. R = $CH_2OH(CHOH)_3$

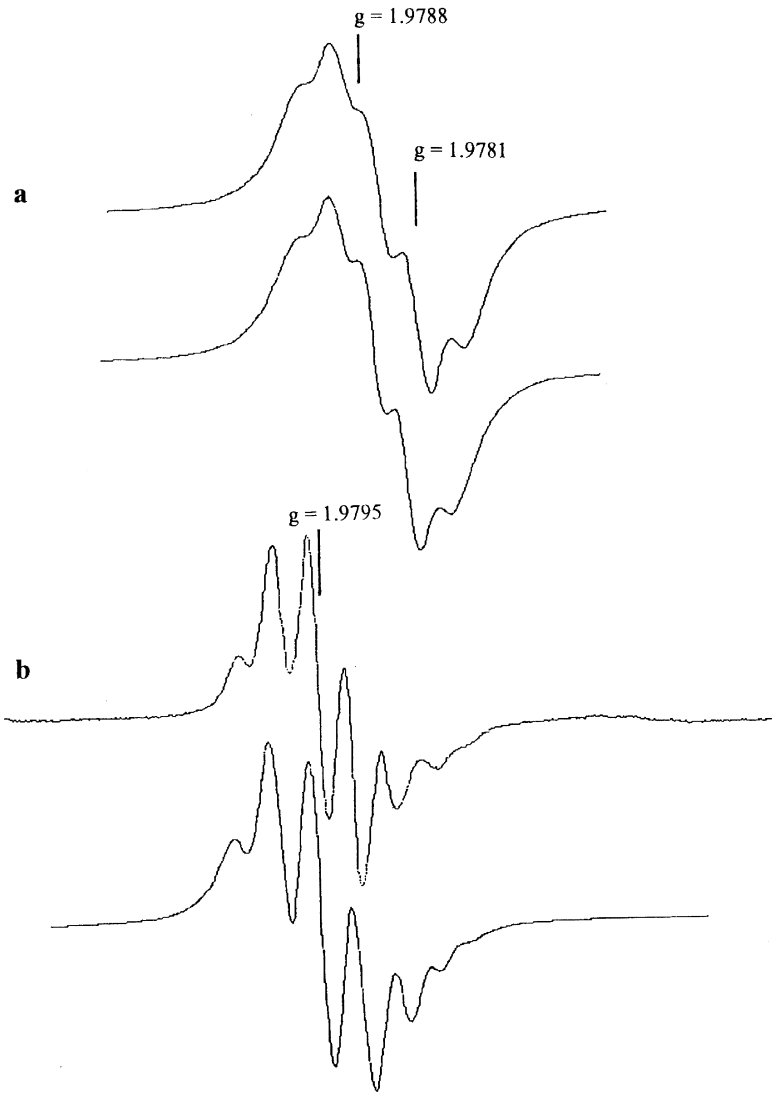

Fig. 4. X-band EPR signal of a mixture of gal and Cr^{VI} (5 : 1 mole ratio) at (a) pH = 5.4, 2 h after mixing, (b) pH = 7.4, 1 day after mixing, and the corresponding simulated spectra (linewidth = 0.8 and 0.6 G, respectively) ; $T = 25^{\circ}C$, modulation amplitude = 0.63 G, centre field = 3555 G ; frequency = 9.84 GHz.

Table 4. EPR spectral parameters

	g_{1iso} (m)	a_{1iso}/G	g_{2iso} (m)	a_{2iso}/G
[H+] > 0.1 M	1.9781	—		
pH = 2–6	1.9781 (t)	0.75	1.9788 (dt)	0.75, 0.92
pH = 6–8	1.9795 (quint)	0.92	1.978 (dt)	0.7, 0.9

m = multiplicity ; t = triplet ; dt = double-triplet ; quint = quintet

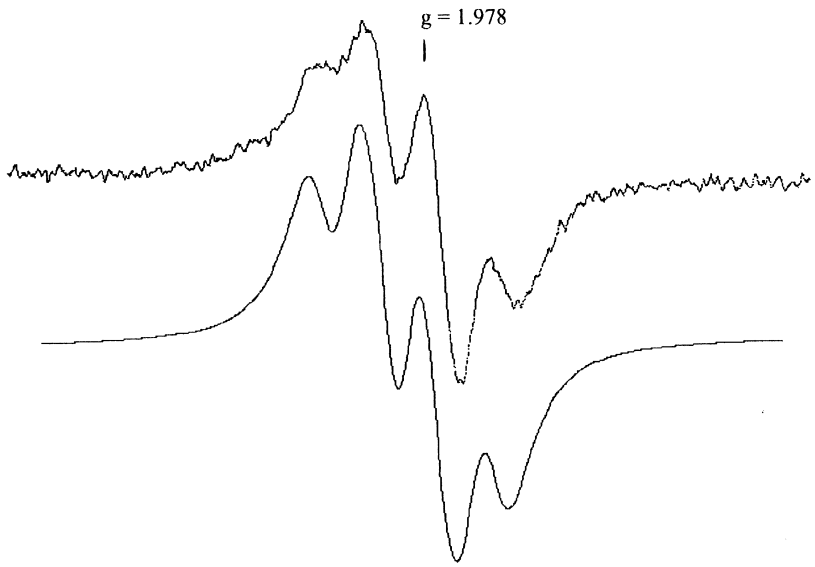

Fig. 5. X-band EPR signal of a mixture of D-gluconic acid and Cr^{VI} (10 : 1 mole ratio) at pH = 4, 1 day after mixing and the corresponding simulated spectrum (linewidth = 0.55); $T = 25°C$; modulation amplitude = 0.515 G; centre field = 3530 G; frequency = 9.77 GHz.

relative proportion of the intermediate Cr^{V} complexes remains constant over the reaction time, meaning that these Cr^{V} intermediates are in rapid equilibria compared to the time scale of their subsequent reduction to Cr^{III}.

Acknowledgements—We thank the National Research Council of Argentina (CONICET), The Third World Academy of Sciences (TWAS), the National University of Rosario, Antorchas Foundation and The International Foundation for Sciences (IFS) for financial support. We thank Prof. Brumby and Prof. Lay for providing us with the e23new Program.

REFERENCES

1. O'Brien, P. and Wang, G., *Polyhedron*, 1993, **12,** 1409.
2. Cohen, M., Kagacin, B., Klein, C. and Costa, M., *Crit. Rev. Toxicol.*, 1993, **23,** 255.
3. Ramana, V. and Sastry, K., *J. Inorg. Biochem.*, 1994, **56,** 87.
4. Katz, S. and Salem, H., *The Biological and Environmental Chemistry of Chromium*, VCH Publishers. Inc., New York, 1994.
5. Casadevall, M. and Kortenkamp, A., *Carcinogenesis*, 1994, **15,** 407.
6. Farrell, R., Judd, R., Lay, P., Dixon, N. and Baker, R., *A. Bonin. Chem. Res. Toxicol.*, 1989, **2,** 227.
7. Moghaddas, S., Gelerinter, E. and Bose, R., *J. Inorg. Biochem.*, 1995, **57,** 135.
8. Luo, H., Lu, Y., Mao, Y., Shi, X. and Dalal, N., *J. Inorg. Biochem.*, 1996, **64,** 25.
9. Cieslak-Golonka, M., *Polyhedron*, 1996, **15,** 3667.
10. Mitewa, M. and Bontchev, R., *Coord. Chem. Rev.*, 1985, **61,** 214.
11. Gould, E., *Coord. Chem. Rev.*, 1994, **135/136**, 651.
12. Zhang, L. and Lay, P., *J. Am. Chem. Soc.*, 1996, **118,** 12624.
13. Stearns, D. and Wetterhahn, K., *Chem. Res. Toxicol.*, 1994, **7,** 219.
14. Jannette, K., *J. Am. Chem. Soc.*, 1982, **104,** 874.
15. O'Brien, P., Barrett, J. and Swanson, F., *Inorg. Chim. Acta*, 1985, **108,** L19.
16. Krumpolc, M., de Boer, B. and Rocek, J., *J. Am. Chem. Soc.*, 1978, **100,** 145.
17. Brauer, S. and Wetterhahn, K., *J. Am. Chem. Soc.*, 1991, **113,** 3001.
18. Goodgame, D., Hayman, P. and Hathaway, D., *Polyhedron*, 1982, **1,** 497.
19. Goodgame, D. and Joy, M., *J. Inorg. Biochem.*, 1986, **26,** 219.
20. Pigman, W. and Horton, D., *The Carbohydrates. Chemistry and Biochemistry*, Vol. 1B. Academic Press Inc., New York, 1980.
21. Signorella, S., García, S. and Sala, L., *Polyhedron*, 1992, **11,** 1391.
22. Signorella, S., García, S. and Sala, L., *Polyhedron*, 1997, **16,** 701.
23. Signorella, S., Santoro, M., Mulero, M. and Sala, L., *Can. J. Chem.*, 1994, **72,** 398.
24. Palopoli, C., Signorella, S. and Sala, L., *New J. Chem.*, 1997, **21,** 343.
25. Ip, D. and Rocek, J., *J. Am. Chem. Soc.*, 1979, **101,** 6311.
26. Krumpolc, M. and Rocek, J., *J. Am. Chem. Soc.*, 1977, **99,** 137.
27. Ramesh, S., Mahapatro, S., Lui, J. and Rocek, J., *J. Am. Chem. Soc.*, 1981, **103,** 5172.
28. Srinivasan, K. and Rocek, J., *J. Am. Chem. Soc.*, 1978, **100,** 2789.

29. Haight, G., Jwisich, G., Kelso, M. and Merril, P., *Inorg. Chem.*, 1985, **24,** 2740.
30. Sala, L., Signorella, S., Rizzotto, M., Frascaroli, M. and Gandolfo, F., *Can. J. Chem.*, 1992, **70,** 2046.
31. Signorella, S., Rizzotto, M., Daier, V., Frascaroli, M., Palopoli, C., Martino, D., Bousseckson, A. and Sala, L., *J. Chem. Soc., Dalton Trans.*, 1996, 1607.
32. Rizzotto, M., Signorella, S., Frascaroli, M., Daier, V. and Sala, L., *J. Carbohyd. Chem.*, 1995, **14,** 45.
33. Sala, L., Palopoli, C. and Signorella, S., *Polyhedron*, 1995, **14,** 1725.
34. Rizzotto, M., Frascaroli, M., Signorella, S. and Sala, L., *Polyhedron*, 1996, **15,** 1517.
35. Krumpolc, M. and Rocek, J., *Inorg. Synth.*, 1980, **20,** 63.
36. Dutta, S. K., *Indian J. Chem.*, 1975, **13,** 980.
37. Signorella, S., Santoro, M., Moreno, V., Salas-Peregrin, J. M. and Sala, L. to be submitted for publication at *Polyhedron*.
38. Kaiwar, S. P., Raghavan, M. S. and Rao, P., *J. Chem. Soc., Dalton Trans.*, 1995, 1569.
39. Travelyan, W., Proctor, D. and Harrison, J., *Nature*, 1950, **166,** 44.
40. Haugh, L., Jones, J. and Wadman, N., *J. Chem. Soc.*, 1950, 1702.
41. Brumby, S., *Appl. Spectrosc.*, 1992, **46,** 176.
42. Beckwith, A. L. and Brumby, S., *J. Magn. Reson.*, 1987, **73,** 252.
43. Wilkins, R. G., *The Study of Kinetics and Mechanism of Reactions of Transition Metal Complexes*, Allyn and Bacon, Boston, 1974, pp. 20–23.
44. Branca, M., Dessi, A., Kozlowski, H., Micera, G. and Swiatek, J., *J. Inorg. Biochem.*, 1990, **39,** 217.
45. Cieslak-Golonka, M., *Coord. Chem. Rev.*, 1991, **109,** 223.
46. Poulopoulo, V., Vrachnou, E., Koinis, S. and Katakis, D., *Polyhedron*, 1997, **16,** 521.
47. Barr-David, G., Charara, M., Codd, R., Farrel, R., Irwin, J., Lay, P., Brambley, R., Brumby, S., Ji, J. and Hanson, G., *J. Chem. Soc., Faraday Trans.*, 1995, **91,** 1207.
48. Farrel, R., Judd, R. and Lay, P., *Inorg. Chem.*, 1989, **28,** 3401.
49. Arias, C. and Pérez-Benito, J., *Collect. Czech. Chem. Commun.*, 1992, **57,** 1821.
50. Brambley, R., Ji, J., Judd, R. and Lay, P., *Inorg. Chem.*, 1990, **29,** 3089.

Pergamon

PII : S0277–5387(98)00063–1

Polyhedron Vol. 17, No. 16, pp. 2751–2757, 1998
© 1998 Elsevier Science Ltd
All rights reserved. Printed in Great Britain
0277–5387/98 $19.00 + 0.00

Spectral and structural studies of metal complexes of 1-phenylglyoxal bis{N(3)-diethylthiosemicarbazone}

Alfonso Castiñeiras,[a] Elena Bermejo,[a] Douglas X. West,*[b] Ayman K. El-Sawaf[b] and John K. Swearingen[b]

[a] Departamento de Química Inorgánica, Universidad de Santiago de Compostela, Santiago de Compostela, Spain

[b] Department of Chemistry, Illinois State University, Normal, Illinois 61790-4160 U.S.A.

(Received 21 January 1998; accepted 26 January 1998)

Abstract—Nickel(II), copper(II) and palladium(II) complexes of 1-phenylglyoxal bis{N(3)-diethylthiosemicarbazone}, H_2Pg4DE, have been prepared, studied spectroscopically and their crystal structures solved. H_2Pg4DE and the three complexes have been characterized by IR, electronic, ^{1}H NMR (Ni, Pd) and ESR (Cu) spectra. Upon formation of these complexes, loss of the N(2)H hydrogens from both thiosemicarbazone moieties occurs, and the ligands coordinate to the metal centers as dianionic, tetradentate N_2S_2 ligands. The nickel(II) and copper(II) complexes, [M(Pg4DE)], coordinate in the expected 5-5-5-chelate ring system, but [Pd(Pg4DE)] coordinates with 5-6-4-membered chelate rings. The thiosemicarbazone moiety attached to the phenyl keto carbon in [Pd(Pg4DE)] forms the 4-membered chelate ring coordinating via N(2) rather than the azomethine nitrogen, N(1). © 1998 Elsevier Science Ltd. All rights reserved

Keywords: 1-phenylglyoxal; bis(thiosemicarbazone); nickel(II); copper(II); palladium(II); N(3)-diethylthiosemicarbazone.

The synthesis and spectral characterization of metal complexes with 1-phenylglyoxal bis{N(3)-substituted thiosemicarbazone} ligands have been reported previously [1]. The copper(II) and nickel(II) complexes of the bis{N(3)-methyl-, N(3)-dimethyl- and piperidylthiosemicarbazones} were included in that study. Because of the antitumor activity of α-diketone and α-ketoaldehyde bis(thiosemicarbazones) [2], as well as their metal complexes [3], and the considerable dependence of the biological activity on the nature of the N(3)-substituent attached to the thiosemicarbazone moiety in other series of thiosemicarbazones [4], a series of copper(II) and nickel(II) complexes of 2,3-butanedione [5], pyruvaldehyde [6] and glyoxaldehyde [7] bis{N(3)-substituted thiosemicarbazones} have also been studied. We have now prepared and spectrally characterized 1-phenylglyoxal bis{N(3)-diethylthiosemicarbazone}, H_2Pg4DE, and its nickel(II), copper(II) and palladium(II) complexes. The crystal structures of the three complexes have been solved and are included here. Because of the bulkiness of the phenyl group, the two thiosemicarbazone moieties may not be on opposite sides of the carbon-carbon backbone, as was found with 2,3-butanedione thiosemicarbazones [5]. Thus, they are shown on the same side of the carbon-carbon backbone for H_2Pg4DE in Fig. 1.

* Author to whom correspondence should be addressed.

EXPERIMENTAL

Preparation of phenylglyoxal bis{N(3)-diethylthiosemicarbazone}

1-Phenylglyoxal bis{N(3)-diethylthiosemicarbazone}, H_2Pg4DE, was obtained by stirring 1-phenylglyoxal monohydrate (Aldrich) and N(3)-diethylthiosemicarbazide for several hours in a molar ratio of 1 : 2 in absolute ethanol with a few drops of concentrated sulfuric acid added to catalyze the reaction. N(3)-diethylthiosemicarbazide was prepared by the

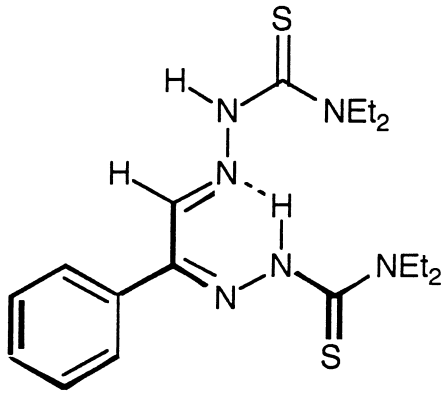

Fig. 1. Intramolecularly hydrogen bonded H_2Pg4DE.

method described by Scovill [8]. H_2Pg4DE has been characterized by IR, UV–vis, ^1H and ^{13}C NMR spectra and has a melting point of 158–159°C.

Preparation of metal complexes

The metal complexes were prepared by refluxing a solution of H_2Pg4DE and an equimolar amount of the metal acetate (Ni, Cu) in ethanol for 4–5 h (aqueous-methanol mixture of K_2PdCl_4 with triethylamine added for the preparation of [Pd(Pg4DE)]. The resulting solids, which formed on cooling, were filtered, washed with diethyl ether and dried at 35°C. Found: Calcd for [Ni(Pg4DE)]·$1/2H_2O$: %C = 47.0 (47.2); %H = 5.5 (5.9) and %N = 18.3 (18.3); for [Cu(Pg4DE)]·H_2O: %C = 45.7 (45.8); %H = 5.3 (6.0).

Partial elemental analyses were performed by National Chemical Consulting, Inc. of Tenafly, NJ. The magnetic susceptibilities were measured with a Johnson Matthey Magnetic Susceptibility balance. Infrared spectra were recorded with Perkin–Elmer 783 and Bruker Model IFS 66V Spectrometers using Nujol mulls between Csl plates; electronic spectra were acquired as Nujol mulls impregnated on filter paper and as dimethylsulfoxide (DMSO) solutions in 1 cm cells with a Perkin–Elmer 330 spectrometer and NMR spectra were obtained with a Varian 300 MHz Gemini spectrometer using d^6-DMSO as the solvent with tetramethylsilane as reference. ESR spectra were recorded with a Varian E104 Spectrometer in an insert Dewar with DPPH as reference.

X-ray data collection and reduction

A brown prismatic crystal of [Ni(Pg4DE)], a violet prismatic crystal of [Cu(Pg4DE)] and a garnet prismatic crystal of [Pd(Pg4DE)] were mounted on a glass fiber and used for data collection. Cell constants and an orientation matrix for data collection were obtained by least-squares refinement of the diffraction data from 25 reflections in the range $5.563° < \theta < 11.993°$, $21.424° < \theta < 42.274°$ and $8.817° < \theta < 18.090°$ for [Ni(Pg4DE)], [Cu(Pg4DE)] and [Pd(Pg4DE)], respectively, with an ENRAF-NONIUS MACH3 automatic diffractometer [9]. Data were collected at 293° using Mo–K_α radiation ($\lambda = 0.71073$ Å) for [Ni(Pg4DE)] and [Pd(Pg4DE)] and Cu–K_α ($\lambda = 1.54184$ Å) for [Cu(Pg4DE)] and the ω scan technique, and the data corrected for Lorentz and polarization effects [10]. An empirical absorption correction was made [11].

Structure solution and refinement

The structure was solved by direct-methods [12], which revealed the position of all non-hydrogen atoms, and refined on F^2 by a full-matrix least-squares procedure using anisotropic displacement parameters [13]. The hydrogen atoms were located in their calculated positions (C—H, 0.93–0.97 Å) and refined using a riding model. Atomic scattering factors were taken from the *International Tables for X-ray Crystallography* [14]. Molecular graphics are from ZORTEP [15]. A summary of the crystal data, experimental details and refinement results are listed in Table 1.

RESULTS AND DISCUSSION

NMR results

The ^1H and ^{13}C NMR spectral results are shown in Table 1 for both H_2Pg4DE and the metal complexes, [Ni(Pg4DE] and [Pd(Pg4DE)]. Because the two thiosemicarbazone moieties are attached to carbon centers with different environments, the ^1H resonances for the individual hydrogens are different in the two moieties. For H_2Pg4DE one of the N(2)Hs is found at $\delta = 12.898$ and the other at $\delta = 10.784$. The former, based on X-ray crystal studies of related bis(thiosemicarbazones) of 1-phenylglyoxal [16], is attached to the "phenyl arm" which is hydrogen bonding to the azomethine nitrogen of the "aldehyde arm" as depicted in Fig. 1. In d^6-DMSO the "phenyl arm" N(2)H is found at $\delta = 13.151$ and the "aldehyde arm" at $\delta = 10.990$ with a weaker resonance at 11.200, which is likely due to the aldehyde arm's N(2)H hydrogen bonding with DMSO. Both N(2)Hs are lost on formation of the nickel(II) and palladium(II) complexes {and copper(II) complex} so that neither spectrum has resonances at low field.

The aldehyde hydrogen attached to C(11) (*vide infra*) shifts up field from $\delta = 8.310$ in the spectrum of H_2Pg4DE to $\delta = 7.256$ and 7.135 in the spectra of [Ni(Pg4DE)] and [Pd(Pg4DE)], respectively. The greater covalency of the C—H bond accompanies the donation of electron density by the azomethine nitrogen to the metal centers. Two resonances are assignable to the ethyl group's CH_2 protons because of the two different thiosemicarbazone moieties. The shifts

Table 1. ^{1}H NMR (δ), IR (cm^{-1}) and UV–vis (cm^{-1}) data for H_2Pg4DE, [Ni(Pg4DE)], [Cu(Pg4DE)] and [Pd(Pg4DE)]

Compound	H_2Pg4DE	[Ni(Pg4DE)]	[Cu(Pg4DE)]	[Pd(Pg4DE)]
N(2)*H*	12.898 10.784	—	—	—
*H*C(aldehyde)	8.310	7.256	—	7.135
NCH_2	3.858 3.697	3.601 3.504	—	3.697 3.645
NCH_2CH_3	1.219	1.277 1.184	—	1.323 1.230
ν(C═N)	1546, 1540 s, sh	1538 s	1540 s	1540 s
ν(C═S)	793 w	744 w	757 m	702 w
ν(MN)		439 m 428 sh	458 s, b	449 m 436 m
ν(MS)		395 sh 389 m	357 s 337 sh	373 m 364 sh
π–π*	40,320 (4.340)[a]	40,000 (4.629)	40,980 (4.014)	40,980 (4.507)
n–π* and	31,650 sh	34,480 (4.461)	34,970 sh	34,970 (4.463)
S–M(II) C.T.	28,410 (4.359)	28,740 sh	31,650 (4.374)	30,860 sh
	22,830 sh	23,920	27,030 sh	26,460 sh
	18,590 sh			22,830 sh
d–d		17,990 sh	19,230 sh	19,920 sh
bands[b]		16,390 (3.605)	17,300 (3.812)	18,590 sh
				16,230 sh
				14,790 (3.266)

[a] Numbers in parentheses are log ε; [b] the intensity of these bands indicates that some n–π* charge transfer and/or intraligand character must also be involved, particularly since H_2Pg4DE has a band at 18,590 cm^{-1}.

on coordination are not as great as the aldehyde hydrogen because of their greater distance from the coordinating thiolato sulfurs. Even smaller shifts of the ethyl groups' CH_3 protons occurs on coordination. The magnetic susceptibility for the violet [Cu(Pg4DE)] is 1.73 B.M., which is consistent with minimal spin orbit coupling of the unpaired electron, as well as weak/no coupling between copper(II) centres.

Crystal structures of [*Ni*(*Pg*4*DE*)], [*Cu*(*Pg*4*DE*)] *and* [*Pd*(*Pg*4*DE*)]

The crystal data for [Ni(Pg4DE)], [Cu(Pg4DE)] and [Pd(Pg4DE)] are shown in Table 2, selected bond lengths in Table 3 and selected bond angles in Table 4. A complete list of bond distances and angles, as well as the positional parameters, equivalent isotropic temperature factors and lists of F_o/F_c values are included in the supplementary material deposited with the Editor. Perspective views of [Ni(Pg4DE)], [Cu(Pg4DE)] and [Pd(Pg4DE)] are shown in Figs 2, 3 and 4, respectively.

Based on other thiosemicarbazones [17] the mode of coordination for [Ni(Pg4DE)] and [Cu(Pg4DE)] is as expected with the two azomethine nitrogens and the two thiolato sulfurs bonding, on loss of N(2)H from both moieties, to give approximately planar, 4-coordinate complexes. The M—S bonds for these two complexes {and for [Pd(Pg4DE)]} are significantly longer than the M—N bonds so that the coordination geometry about the metal ions is more rectangular than square; the *cis* bond angles in [Cu(Pg4DE)] range from 81.12(14)°, N(21)—Cu—N(11) to 108.36(5)°, S(1)—Cu—S(2). Also, the bonds within the two thiosemicarbazone moieties of [Ni(Pg4DE)] and [Cu(Pg4DE)] have different distances which are conveniently listed in Table 5. Significant differences are found for both Ni, Cu—N and Ni, Cu—S for the two moieties with the "phenyl arm" having the longer Ni, Cu—N bond, but the shorter Ni, Cu—S bond. In the thiosemicarbazone moieties of [Ni(Pg4DE)] there are significant differences for the N—N, the N═C and C—N bonds along the thiosemicarbazone moiety, but not for C═N where the two moieties would be expected to be most different. The bond angles involving the nickel(II) center are not significantly different among the two moieties, nor are there significant difference in the bond angles within the two moieties. Surprisingly, the bond distances and angles for the two arms of [Cu(Pg4DE)] are not very different.

In contrast the two "arms" of [Pd(Pg4DE)] coordinate in a different manner; the "aldehyde arm" coordinates in the expected fashion like both arms of [Ni(Pg4DE)] and [Cu(Pg4DE)], but the "phenyl arm" coordinates via the thioamide nitrogen, rather than the azomethine nitrogen, forming a four-membered chelate ring with the thiolato sulfur donor. Thus, the coordination about the nickel and copper in their complexes is 5-5-5 in terms of the number of atoms in the three chelate rings, but for [Pd(Pg4DE)] it is 5-6-4. This results in the coordination for [Pd(Pg4DE)] being even less square than [Ni(Pg4DE)] and [Cu(Pg4DE)]; the *cis* bond angles range from 70.3(3)°, N(21)—Pd—S to 110.94(11)°, S(1)—Ni—S(2). However, the N(21)—M—S(1) trans angle is 178.7(3)° for [Pd(Pg4DE)], but 166.69(11)° for [Cu(Pg4DE)] and 171.4(3)° for [Ni(Pg4DE)].

Table 2. Crystal data and structure refinement for phenylglyoxal bis{N(4)-diethylthiosemicarbazone}nickel(II), -copper(II) and -palladium(II), [Ni(Pg4DE)], [Cu(Pg4DE)] and [Pd(Pg4DE)], respectively

Empirical formula	$C_{18}H_{26}N_6NiS_2$	$C_{18}H_{26}N_6CuS_2$	$C_{18}H_{26}N_6PdS_2$
Formula weight	449.28	454.11	496.97
Temperature (K)	293(2)	292(2)	293(2)
Crystal system	Monoclinic	Monoclinic	Orthorhombic
Space group	$C2/c$	$C2/c$	$Pcan$
a(Å)	29.51(2)	29.252(2)	8.6157(13)
b(Å)	8.7308(12)	8.9001(5)	20.055(3)
c(Å)	20.362(2)	20.2689(18)	24.944(20
β(°)	124.80(4)	124.675(5)	
V(Å^3)	4308(2)	4339.7(6)	4310(2)
Z	8	8	8
D_{calcd} (Mg/m^3)	1.380	1.390	1.532
Absorption coeff.	1.109 mm^{-1}	3.334 mm^{-1}	1.070 mm^{-1}
F(000)	1888	1896	2032
Crystal size (mm)	$0.25\times0.15\times0.15$	$0.25\times0.25\times0.15$	$0.10\times0.25\times0.35$
Θ range for data collection (°)	2.44–22.76	3.67–74.25	2.57–22.64
Index ranges	$-26\leqslant h\leqslant 32$, $-9\leqslant k\leqslant 0$, $-22\leqslant l\leqslant 0$	$-36\leqslant h\leqslant 32$, $0\leqslant k\leqslant 11$, $-20\leqslant l\leqslant 25$	$-10\leqslant h\leqslant 0$, $-23\leqslant k\leqslant 0$, $0\leqslant l\leqslant 29$
Reflections collected	3023	4503	3633
Independent reflections	2921 [$R_{int}=0.0464$]	4414 [$R_{int}=0.0268$]	3633 [$R_{int}=0.0000$]
Absorption correction	Empirical	Semi-empirical	Empirical
Max. and min. transmission	1.000 and 0.316	0.980 and 0.756	1.000 and 0.244
Refinement method	Full-matrix least-squares on F^2	Full-matrix least-squares on F^2	Full-matrix least-squares on F^2
Data/parameters	2921/248	4414/273	3633/208
Goodness-of-fit on F^2	1.011	1.034	1.005
Final R indices [$I>2\sigma(I)$]	$R_1=0.0608$, $wR_2=0.1307$	$R_1=0.0520$, $wR_2=0.1374$	$R_1=0.0609$, $wR_2=0.1491$
R indices (all data)	$R_1=0.2286$, $wR_2=0.1904$	$R_1=0.1078$, $wR_2=0.1650$	$R_1=0.2053$, $wR_2=0.2134$
Largest diff. peak and hole (eÅ^3)	0.472 and −0.389	0.590 and −0.458	0.863 and −0.597

Table 3. Selected bond distances (Å) for [Ni(Pg4DE)], [Cu(Pg4DE)] and [Pd(Pg4DE)]

Bond	[Ni(Pg4DE)]	[Cu(Pg4DE)]	[Pd(Pg4DE)]
M—N(21)	1.840(7)	1.932(4)	1.966(8)
M—N(11)	1.906(8)	1.979(3)	1.968(8)
M—S(1)	2.130(3)	2.2088(14)	2.257(3)
M—S(2)	2.151(3)	2.2348(13)	2.344(43)
S(1)—C(12)	1.736(9)	1.750(4)	1.736(12)
S(2)—C(22)	1.733(11)	1.747(5)	1.736(11)
N(11)—C(11)	1.319(9)	1.308(5)	1.310(11)
N(11)—N(12)	1.304(9)	1.361(5)	1.340(10)
N(12)—C(12)	1.405(10)	1.341(5)	1.332(12)
N(13)—C(12)	1.334(11)	1.341(5)	1.339(14)
N(13)—C(15)	1.503(11)	1.480(6)	1.520(14)
N(13)—C(13)	1.508(12)	1.526(8)	1.716(16)
N(21)—C(21)	1.293(9)	1.290(5)	1.302(11)
N(21)—N(22)	1.358(9)	1.358(5)	1.364(9)
N(22)—C(22)	1.336(10)	1.341(6)	1.322(11)
N(23)—C(22)	1.309(11)	1.322(6)	1.347(12)
N(23)—C(25)	1.471(11)	1.454(6)	1.494(12)
N(23)—C(23)	1.580(15)	1.589(14)	1.606(16)

Table 4. Selected bond angles (°) for [Ni(Pg4DE)], [Cu(Pg4DE)] and [Pd(Pg4DE)]

Angle	[Ni(Pg4DE)]	[Cu(Pg4DE)]	[Pd(Pg4DE)]
N(21)—M—N(11)	82.6(4)	81.12(14)	94.4(3) {N(12)}
N(21)—M—S(1)	171.4(3)	166.69(11)	178.7(3)
N(11)—M—S(1)	88.9(3)	85.80(11)	84.4(2)
N(21)—M—S(2)	87.2(3)	84.81(11)	70.3(3)
N(11)—M—S(2)	169.7(3)	165.70(11)	164.6(3)
S(1)—M—S(2)	101.33(11)	108.36(5)	110.94(11)
C(12)—S(1)—M	93.7(4)	94.97(16)	78.1(4)
C(22)—S(2)—M	94.5(4)	95.13(16)	94.6(4)
C(11)—N(11)—M	115.6(7)	115.2(3)	103.0(7) {C(12)—N(12)—Pd}
N(12)—N(11)—M	123.3(7)	122.5(2)	129.1(7)
C(11)—N(11)—N(12)	121.1(9)	122.3(3)	118.7(8)
N(11)—N(12)—C(12)	109.5(9)	111.0(3)	127.9(9)
C(12)—N(13)—C(15)	120.7(9)	122.1(4)	117.1(11)
C(12)—N(13)—C(13)	121.7(9)	120.5(4)	124.5(10)
C(15)—N(13)—C(13)	117.2(9)	117.4(5)	116.5(10)
N(12)—C(12)—N(13)	115.1(9)	116.7(4)	126.4(11)
N(12)—C(12)—S(1)	124.5(9)	125.7(4)	125.0(9)
N(13)—C(12)—S(1)	120.4(9)	117.6(3)	108.6(8)
C(21)—N(21)—M	114.8(7)	114.4(3)	120.5(7)
N(22)—N(21)—M	124.9(6)	124.7(3)	123.5(6)
C(21)—N(21)—N(22)	120.3(8)	120.9(4)	116.0(8)
N(21)—N(22)—C(22)	109.4(8)	111.0(4)	111.2(9)
C(22)—N(23)—C(25)	125.0(9)	125.1(5)	123.1(9)
C(22)—N(23)—C(23)	119.7(9)	118.5(5)	123.3(90
C(25)—N(23)—C(23)	115.0(9)	115.8(5)	112.5(9)
N(22)—C(22)—N(23)	116.3(10)	117.2(5)	115.6(10)
N(22)—C(22)—S(2)	124.0(8)	124.4(4)	126.1(9)
N(23)—C(22)—S(2)	119.7(8)	118.4(5)	118.2(8)

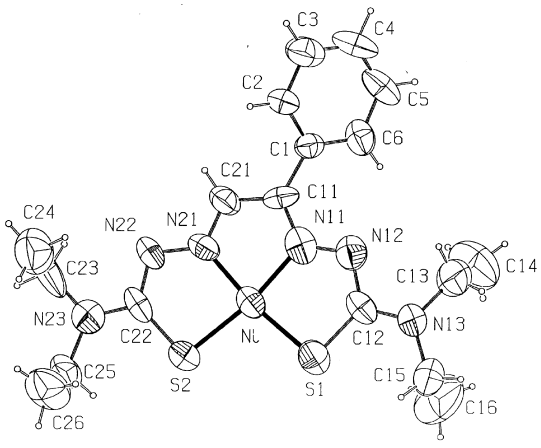

Fig. 2. A perspective view of [Ni(Pg4DE)].

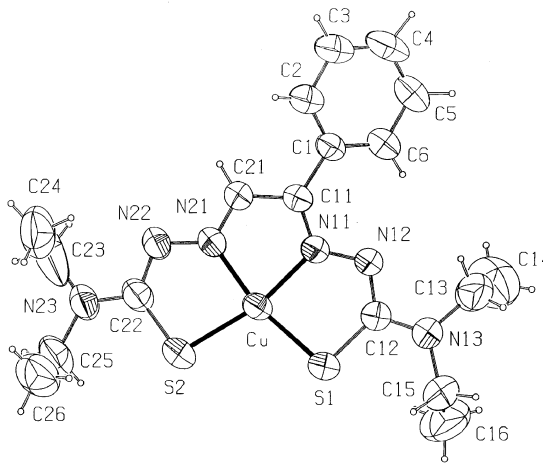

Fig. 3. A perspective view of [Cu(Pg4DE)].

In addition, the two "arms" of [Pd(Pg4DE)] would be expected to have different bond distances and angles between their thiosemicarbazone moieties, as well as in coordination to the palladium(II) center. Somewhat surprisingly the two Pd—N bonds are not significantly different, but the two Pd—S bonds, 2.257(3) for the "phenyl arm" and 2.344(3) for the "aldehyde arm" are very different. In the two thiosemicarbazone moieties of [Pd(Pg4DE)], the greatest difference occurs for the N—N bond, but its difference is nearly equal to the combination of estimated standard deviations. The bond angles involving sulfur coordination as well as the thiosemicarbazone moiet-

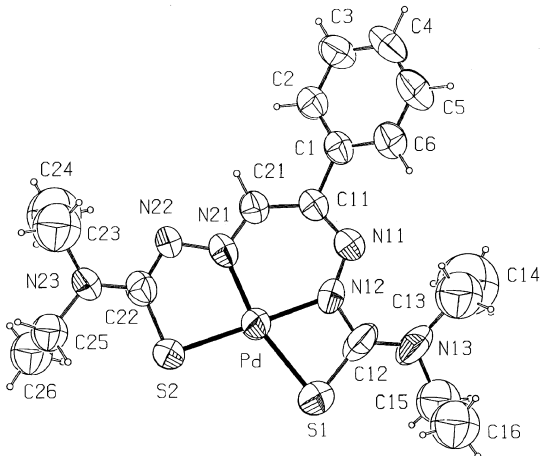

Fig. 4. A perspective view of [Pd(Pg4DE)].

ies, however, do show significant differences with the largest being as follows (phenyl arm listed first): Pd—S—C, 78.1(4)°, 94.6(4)°; N—N—C(S), 127.9(9)°, 111.2(9)°; N—C(S)—NEt_2, 126.4(11)°, 115.6(10)° and S—C—NEt_2, 108.6(8)°, 118.2(8)°. The latter two bond angle comparisons show that the NEt_2 function's position in the two "arms" is rather different. Even though the chelate ring sizes are different, the N(12)—C(12)—S(1) angle of 125.0(9)° of the phenyl arm (i.e., 4-membered chelated ring) and the corresponding N(22)—C(22)—S(2) bond angle, 126.17(9)° (i.e., 5-membered chelated ring), are within combined estimated standard deviations.

As would be expected, the metal-ligand bond distances are significantly longer for [Pd(Pg4DE)] than for [Ni(Pg4DE)], and those of [Cu(Pg4DE)] are more similar to [Pd(Pg4DE)]. Also, a comparison of the bond distances of the "aldehyde arms" of the three complexes shows that they are not significantly different. There is somewhat more variation in the bond angles of [Pd(Pg4DE)] compared to [Ni(Pg4DE)] and [Cu(Pg4DE)]: C(21)—N(21)—Pd is 120.5(7)° compared to ca 114.6°; C(21)—N(21)—N(22) is 116.0(4)° for [Pd(Pg4DE)] compared to ca 120.6° and C(25)—N(23)—C(23) is 112.5(9)° for [Pd(Pg4DE)] compared to ca 115.4°.

For [Ni(Pg4DE)] there is only a very small mean plane deviation of 0.0186 Å for the donor atom plane, S1—N11—N21—S2, and the two nitrogens deviate from the plane to the greatest extent {i.e., N11 = −0.0208(31) Å and N21 = 0.0214(32) Å}. There is even less deviation from planarity of the planes involving the thiosemicarbazone moieties, and these planes are almost coplanar with the S1—N11—N21—S2 plane, the angles for the various planes being in the 1–2° range. For [Cu(Pg4DE)] there is a somewhat larger mean plane deviation of 0.0390 Å for the donor atom plane, S1—N11—N21—S2, and again the two nitrogens deviate from the plane to the greatest extent {i.e., N11 = −0.0447(17) Å and N21 = 0.0455(18) Å}. The planes involving the thiosemicarbazone moieties are again nearly coplanar with the S1—N11—N21—S2 plane, the angles for the various planes being in the 1–2° range. For [Pd(Pg4DE)], S1—N11—N21—S2 has a mean plane deviation of 0.199 with the two nitrogens showing the largest deviation. The angles with the thiosemicarbazone moiety planes are less than 1°.

IR, UV–vis and ESR spectral results

The assignments of IR spectral bands useful for determining the bis(thiosemicarbazone's) mode of coordination are listed in Table 1. The ν(C=N) bands of H_2Pg4DE (1546, 1540 cm^{-1}) shift to slightly lower

Table 5. A comparison of the bond distances (Å) and angles (°) of the two thiosemicarbazone moieties of [Ni(Pg4DE)], [Cu(Pg4DE)] and [Pd(Pg4DE)]

Compound	Arm	C=N	N—N	N—C	C—S	C—N	M—N	M—S
[Ni(Pg4DE)]	H	1.293(9)	1.358(9)	1.336(10)	1.733(11)	1.309(11)	1.840(7)	2.151(3)
[Ni(Pg4DE)]	Ph	1.319(9)	1.304(9)	1.405(10)	1.736(9)	1.334(11)	1.906(8)	2.130(3)
[Cu(Pg4DE)]	H	1.290(5)	1.358(5)	1.341(6)	1.747(5)	1.322(6)	1.932(4)	2.2348(13)
[Cu(Pg4DE)]	Ph	1.308(5)	1.361(5)	1.341(5)	1.750(4)	1.341(5)	1.979(3)	2.088(14)
[Pd(Pg4DE)]	H	1.302(11)	1.364(9)	1.322(11)	1.736(11)	1.347(12)	1.966(8)	2.344(3)
[Pd(Pg4DE)]	Ph	1.310(11)	1.340(10)	1.332(12)	1.736(12)	1.332(12)	1.968(8)	2.257(3)
		C—N—N	N—N—C	N—C—S	N—C—N	S—C—N	M—N—C(N)	M—S—C
[Ni(Pg4DE)]	H	120.3(8)	109.4(8)	124.0(8)	116.3(10)	119.7(8)	114.8(7)	94.5(4)
[Ni(Pg4DE)]	Ph	121.1(9)	109.5(9)	124.5(9)	115.1(9)	120.4(9)	115.6(7)	93.7(4)
[Ni(Pg4DE)]	H	120.9(4)	111.0(4)	124.4(4)	117.2(5)	118.4(5)	114.4(3)	95.13(16)
[Ni(Pg4DE)]	Ph	122.3(3)	111.0(3)	125.7(4)	116.7(4)	117.6(3)	115.2(3)	94.97(16)
[Pd(Pg4DE)]	H	116.0(4)	111.2(9)	126.1(9)	115.6(10)	118.2(8)	120.5(7)	94.6(4)
[Pd(Pg4DE)]	Ph	118.7(8)	127.9(9)	125.0(9)	126.4(11)	108.6(8)	103.0(7)[a]	78.1(4)

[a] M—N—N for the "phenyl arm".

frequencies in the spectra of the complexes indicating coordination of the azomethine nitrogen {N(1)}. A second band due to ν\{C(3)=N(2)\} (which formally becomes a double bond in the complexes) is often observed in this same range in the complexes' spectra, but is not resolved in these spectra. The uncomplexed H_2Pg4DE's spectrum shows the thioamide IV band, which possesses considerable contribution from ν(CS), at 793 cm^{-1}. This band, which is a single band in the spectra of H_2Pg4DE and its complexes, shifts to lower energy by 50–90 cm^{-1} on coordination in agreement with previous studies [5–7]. Bands in the 350 cm^{-1} region are assigned to ν(M—S) and those in the 450–470 cm^{-1} region to ν(M—N) vibrations, supporting the coordination of the ligands as tetradentate N_2S_2 chelating agents [18].

Also included in Table 1 are the band maxima of solution ($CHCl_3$) electronic transitions for H_2Pg4DE and its complexes. The high energy π–π* transition (ca 40,000 cm^{-1}) is not significantly altered on complex formation except that the molar absorptivity is larger in the complexes because of overlap of the blue shifted n–π* transition, which also has a higher molar absorptivity in the spectra of the complexes. The two n–π* transitions at 31,650 and 28,410 cm^{-1} primarily associated with the azomethine functions of the two thiosemicarbazone moieties are shifted to higher energy for the complexes and merged into one band at about 34,500 cm^{-1}. The thioamide functions cause the lower energy bands in the spectrum of H_2Pg4DE, and these also shift to higher energy (ca 27,000 cm^{-1}) in the spectra of the three metal complexes. Bands below 25,000 cm^{-1} in their spectra are assignable to S–M(II) charge transfer bands [19], and the bands below 20,000 cm^{-1} also probably possess some charge transfer character since the molar absorptivities are in excess of 10^3.

The powder ESR spectrum of [Cu(Pg4DE)] at room temperature does not allow resolution of the lowest field feature, which often occurs for copper(II) centers having one or more soft donors such as sulfur. At liquid nitrogen temperature the $g_\parallel$ feature appears to be at 2.118 and $g_\perp = 2.038$ resulting in a g_{av} of 2.065 which is comparable to recently studied bis(thiosemicarbazone) complexes of copper(II) [1,5–7]. The familiar 4-line pattern due to copper(II) hyperfine occurs in DMF solution with 5 lines in 1 : 2 : 3 : 2 : 1 ratio due to nitrogen superhyperfine (2 nearly equivalent nitrogens) resolved on the two highest field hyperfine lines. The ESR solution parameters are $g_o = 2.058$, A_o(Cu) = 88 G and A(N) = 15 G. The frozen DMF solution ESR clearly shows the first two parallel features and the third parallel is at essentially the same field as the perpendicular feature. The frozen solution parameters are as follows: $A_\parallel = 195$ G, $g_\parallel = 2.109$, $g_\perp = 2.025$ and $g_{av} = 2.053$. The region of the spectrum containing the third parallel feature and the perpendicular feature is nicely resolved (>11 lines) and has a splitting of ca 17 G. Assuming $2A_\perp + A_\parallel/3 = 76$ G should be about the same as A_o (solution), 88 G, suggests that the splitting is better assigned to nitrogen superhyperfine than $A_\perp$(Cu).

REFERENCES

1. Beraldo, H., Ives, J. S., Kaisner, S. B., Turner, J. D., Billeh, I. S. and West, D. X., *Transition Met. Chem.*, 1997, **22,** 459.
2. Petering, H. G., Buskirk, H. H. and Underwood, G. E., *Cancer Res.*, 1964, **24,** 367.
3. Van Giessen, G. J., Crim, J. A., Petering, D. H. and Petering, H. G., *J. Natl. Cancer Inst.*, 1973, **51,** 139.
4. Liberta, A. E. and West, D. X., *Biometals*, 1992, **5,** 121.
5. West, D. X., Ives, J. S., Bain, G. A., Liberta, A. E., Valdés-Martínez, J., Ebert, K. H. and Hernández-Ortega, S., *Polyhedron*, 1997, **16,** 1895.
6. Beraldo, H. and West, D. X., *Transition Met. Chem.*, 1997, **22,** 294.
7. Beraldo, H., Boyd, L. P. and West, D. X., *Transition Met. Chem.*, in press.
8. Scovill, J. P., *Phosphorus, Sulfur and Silicon*, 1991, **60,** 15.
9. ENRAF-NONIUS, *CAD4-Express Software*, Version 5.1, 1995. Enraf-Nonius Delft, The Netherlands.
10. Spek, A. L., *HELENA. A Program for data reduction of CAD4 data*, 1993, University of Utrecht, The Netherlands.
11. Walker, N. and Stuart, D., *Acta Cryst.*, 1983, **A39,** 158.
12. Sheldrick, G. M., *Acta Cryst.*, 1990, **A46,** 467.
13. Sheldrick, G. M., *SHELXL93. Program for the Refinement of Crystal Structures*, University of Göttingen, Germany, 1993.
14. *International Table for X-ray Crystallography*, Vol. C., Kluwer Academic Publishers, Dordrecht, The Netherlands, 1995.
15. Zsolnai, L., *ZORTEP. A Program for the Presentation of Thermal Ellipsoids*, University of Heidelberg, German, 1994.
16. Castiñeiras, A., Bermejo, E. and West, D. X., unpublished results.
17. West, D. X., Padhye, S. B. and Sonawane, P. B., *Structure and Bonding*, 1991, **76,** 1.
18. Ali, M. A., Haroon, C. M., Nazimuddin, M., Majumbder, S. M. M., Tarafder, M. T. H. and Khair, M. A., *Transition Met. Chem.*, 1992, **17,** 133.
19. Downes, J. M., Whelan, J. and Bosnich, B., *Inorg. Chem.*, 1981, **20,** 1081.

Pergamon

PII : S0277–5387(98)00064–3

Polyhedron Vol. 17, No. 16, pp. 2759–2764, 1998
© 1998 Elsevier Science Ltd
All rights reserved. Printed in Great Britain
0277–5387/98 $19.00+0.00

New dithiocarbamate compounds of manganese carbonyl and a zinc polymer

Richard D. Adams* and Mingsheng Huang

Department of Chemistry and Biochemistry, University of South Carolina, Columbia, SC 29208, U.S.A.

(Received 13 November 1997; accepted 26 January 1998)

Abstract—The reaction of $[EtO_2CN{=}CS_2C\{N(H)CO_2Et\}\{S_2CN(H)CO_2Et\}]$, **1** with $Mn_2(CO)_9NCMe$ yielded the dithiocarbamate complex $Mn(CO)_4[S_2CN(H)CO_2Et]$, **2** which was characterized structurally in the form of its phosphine derivative $Mn(CO)_3(PMe_2Ph)[S_2CN(H)CO_2Et]$, **3**. Compound **3** was found to contain a chelating dithiocarbamato ligand with a *cis*-positioned phosphine ligand. Compound **1** also reacts with zinc acetylacetonate to yield the zinc dithiocarbamate complex $Zn(\mu\text{-}S,S\text{-}S_2CN(H)CO_2Et)(\mu\text{-}O,S\text{-}S_2CN(H)CO_2Et)$, **4**. Compound **4** forms a helical polymer in the solid state with the zinc ions linked by bridging dithiocarbamate ligands. Compound **1** appears to be a good source of the ethoxycarbonylthiocarbamate ligand. © 1998 Elsevier Science Ltd. All rights reserved

Keywords: dithiocarbamate ligand; manganese; zinc; polymer.

We have recently obtained the new compound $\{EtO_2CN{=}CS_2C[N(H)CO_2Et][S_2CN(H)CO_2Et]\}$, **1** from the reaction of water with ethoxycarbonylisothiocyanate [1]. Compound **1** can be viewed as an adduct of a dimer **A** of the isothiocyanate

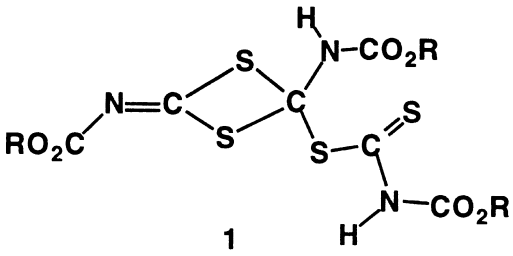

1

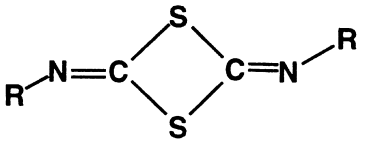

A

and the dithiocarbamic acid, EtO_2CNHCS_2H. Isothiocyanates are effective ligands for the transition metals [2,3]. They have been shown to coordinate in η^2-C—S, **B** and bridging μ-η^2-C—S, **C** and μ-η^3-N—C—S, **D** bonding modes between two metal atoms. Dithiocarbamate anions are also good ligands for the transition metals and a large number of complexes have been made by employing them [4].

In this report we describe reaction of the compound **1** with $Mn_2(CO)_9(MeCN)$ and zinc acetylacetonate. We have found that compound **1** readily transfers its dithiocarbamate grouping to the metal atoms to yield new metal compounds.

EXPERIMENTAL

Unless specified otherwise, all reactions were performed under an atmosphere of nitrogen. All solvents were appropriately dried and degassed prior to use. Zinc acetylacetonate was purchased from Strem and was used without further purification. TLC separations were performed in air by using silica gel (60 Å, F_{254}) on plates (Whatman, 0.25 mm). Elemental analyses were performed by Desert Analytics, Tucson, AZ. Mass spectra were carried out on a VG Model

* Author to whom correspondence should be addressed.

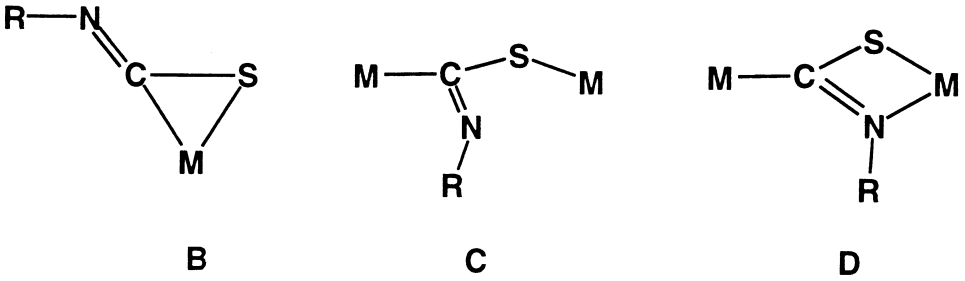

B C D

70SQ mass spectrometer (direct inlet, electron impact ionization). {$EtO_2CN{=}CS_2C[N(H)CO_2Et][S_2CN(H)CO_2Et]$}, **1** which contains one equivalent of cocrystallized $EtO_2CN{=}C{=}S$ was prepared as previously described [1]. $Mn_2(CO)_9(MeCN)$ was prepared by the reported method [5].

Reaction of **1** *with* $Mn_2(CO)_9(MeCN)$

An 89.0 mg amount (0.159 mmol) of **1** · ($EtO_2CN{=}C{=}S$) was added to a soln of a 25.0 mg amount (0.062 mmol) of $Mn_2(CO)_9(MeCN)$ in 10 ml of hexane. The mixt was stirred at room temp. for 4 days. The volatiles were removed under vacuum, and the residue was separated by TLC using a 3/1 hexane/CH_2Cl_2 solvent mixt. This yielded $Mn_2(CO)_{10}$, (1.7 mg) and yellow $Mn(CO)_4[S_2CN(H)CO_2Et]$, **2** (18.6 mg, 45% yield). Spectral data for **2**: IR (ν_{CO} in hexane, cm^{-1}): 2092 (m), 2014 (s), 2003 (s), 1966 (s), 1777 (w, br), 1759 (w, br). ^1H NMR (δ in C_6D_6, ppm): 7.45 (s, br, 1H, NH), 3.63 (q, $^3J_{H-H} = 7.2$ Hz, 2H, OCH_2Me), 0.73 (t, $^3J_{H-H} = 7.1$ Hz, 3H, CH_3). MS: parent ion m/e = 331 plus ions corresponding to the loss of each of the four carbonyl ligands.

Reaction of **2** *with* PMe_2Ph

A 19.1 mg amount (0.058 mmol) of **2** and 9.0 ml amount (0.116 mmol) of dimethylphenylphosphine were dissolved in 25 ml of hexane. The soln was heated to reflux for 30 min. After the solvent was removed via rotary evaporation, the residue was separated by TLC using a 1/1 hexane/CH_2Cl_2 solvent mixt. This yielded a yellow band of $Mn(CO)_3(PMe_2Ph)[S_2CN(H)CO_2Et]$, **3** (22.1 mg, 87% yield). Spectral data for **3**: IR (ν_{CO} in hexane, cm^{-1}): 2026 (vs), 1947 (s), 1917 (s), 1773 (w, br), 1751 (w, br). ^1H NMR (δ in $CDCl_3$, ppm): 8.05 (s, br, 1H, NH), 7.42 (m, 5H, C_6H_5), 4.20 (q, $^3J_{H-H} = 7.0$ Hz, 2H, OCH_2Me), 1.82 (d, $^3J_{H-H} = 8.1$ Hz, 6H, $P(CH_3)_2$), 1.29 (t, $^3J_{H-H} = 7.0$ Hz, 3H, OCH_2CH_3). Anal: Calc. (found): C, 40.82 (40.77); H, 3.88 (3.51); N, 3.17 (3.20).

Preparation of $Zn(S_2CNHCO_2Et)_2$, **4**

(a) To a 15 ml three necked flask was added a 50.0 mg amount (0.089 mmol) of **1** · ($EtO_2CN{=}C{=}S$), a 50.0 mg amount (0.186 mmol) of $Zn(acac)_2$ and 5 ml of CH_2Cl_2. The mixt was stirred at room temperature for 18 h. The mixt was filtered and washed with 2×0.5 ml of ethylacetate. The filtrate and the washings were combined and the solvent removed. The resulting residue was separated by TLC using silica gel thin plates without fluorescent indicator and a 1/3 hexane/CH_2Cl_2 solvent mixt. This yielded 11.2 mg of Zn (μ-*S*,*S*-$S_2CN(H)CO_2Et$)(μ-*O*,*S*-$S_2CN(H)CO_2Et$), **4** (57% yield based on **1**). Spectra data for **4**: ^1H NMR (δ in $CDCl_3$, ppm): 9.05 (s, br, 2H, NH), 4.30 (q, $^3J_{H-H} = 7.1$ Hz, 4H, OCH_2Me), 1.33 (t, $^3J_{H-H} = 7.1$ Hz, 6H, CH_3). Anal: Calcd (found): C, 24.40 (24.45); H, 3.07 (2.86); N, 7.11 (7.01).

(b) A 30.0 mg amount (0.054 mmol) of **1** · ($EtO_2CN{=}C{=}S$) was dissolved in a minimum amount of CH_2Cl_2. The soln was loaded on TLC plates (silica gel with Zn_2SiO_4 fluorescent indicator). A pale yellow band was eluted with a 3/1 CH_2Cl_2/hexane solvent mixt to yield 4.8 mg of **4** (45% yield).

Crystallographic analyses

Crystals of **3** suitable for X-ray diffraction analysis were obtained by slow evaporation of solvent from a hexane soln at $-4°C$. Crystals of **4** suitable for X-ray diffraction analysis were obtained by slow evaporation of solvent from a 1/3 acetone/acetonitrile soln at 25°C. The crystals used in intensity measurements were mounted in thin-walled glass capillaries. Diffraction measurements for **3** were made on a Rigaku AFC6S fully automated four-circle diffractometer using graphite-monochromated Mo–K_α radiation. Diffraction measurements for **4** were made on a Rigaku AFC5R fully automated four-circle diffractometer using graphite-monochromated Cu–K_α radiation. The unit cells were determined and refined from 15 randomly selected reflections obtained by using the AFC6S or AFC5R automatic search, center,

Table 1. Crystal data for compounds **3** and **4**

Compound	**3**	**4**
Formula	$MnS_2PO_5NC_{15}H_{17}$	$ZnS_4O_4N_2C_8H_{12}\cdot MeCN$
Formula weight	441.33	434.87
Crystal system	Monoclinic	Monoclinic
a (Å)	11.599(2)	14.743(2)
b (Å)	10.694(1)	7.941(1)
c (Å)	16.403(2)	15.305(1)
β (°)	96.57(1)	91.20(1)
V (Å^3)	2021.1(4)	1791.4(3)
Space group	$P2_1/c$ (#14)	$P2_1/c$ (#14)
Z value	4	4
ρ_{calc} (g/cm^3)	1.45	1.61
μ(Mo–K_α) (cm^{-1})	9.61	64.31 (Cu–K_α)
$2\Theta_{max}$ (°)	48	120
No. obs. ($I > 3\sigma$)	2609	2011
No. variables	231	208
Goodness of fit (GOF[a])	2.58	2.56
Max shift in final cycle	0.02	0.05
Residuals[a]: R; R_w	0.034; 0.040	0.043; 0.048
Abs. cor.	Difabs	empirical
Transmis coeff max/min	1.00/0.76	1.00/0.37
Largest residual pk (e/Å^3)	0.32	0.78

[a] $R = \Sigma_{hkl}(\|F_{obs}| - |F_{calc}\|)/\Sigma_{hkl}|F_{obs}|$; $R_w = [\Sigma_{hkl}w(|F_{obs}| - |F_{calc}|)^2/\Sigma_{hkl}wF^2_{obs}]^{1/2}$, $w = 1/\sigma^2(F_{obs})$; GOF $= [\Sigma_{hkl}w(|F_{obs}| - |F_{calc}|)^2/(n_{data} - n_{vari})]^{1/2}$.

index, and least-squares routines. Crystal data, data collection parameters, and results of these analyses are listed in Table 1. All data processing was performed on a Silicon Graphics Indigo^2 computer by using the TEXSAN structure solving program library obtained from the Molecular Structure Corp., The Woodlands, TX. Neutral atom scattering factors were calculated by the standard procedures [6a]. Anomalous dispersion corrections were applied to all non-hydrogen atoms [6b]. Lorentz-polarization (Lp) and absorption corrections were applied in each analysis. Full matrix least-squares refinements minimized the function: $\Sigma_{hkl}w(|F_o| - |F_c|)^2$, where $w = 1/\sigma(F)^2$, $\sigma(F) = \sigma(F_o^2)/2F_o$, and $\sigma(F_o^2) = [\sigma(I_{raw})^2 + (0.02\cdot I_{net})^2]^{1/2}/\mathrm{Lp}$.

Compounds **3** and **4** crystallized in the monoclinic crystal system. The patterns of systematic absences observed during the collection of intensity data identified the space group uniquely as $P2_1/c$ for compounds **3** and **4**. For **3** the hydrogen atom (H) on the nitrogen atom N was located and refined with isotropic thermal parameters. The positions of all other hydrogen atoms were calculated by assuming idealized geometries with all C—H distances at 0.95 Å. Their contributions were added to the structure factor calculations, but their positions were not refined. For **4** the hydrogen atoms H(1) and H(2) on the nitrogen atoms N(1) and N(2) were located and refined with isotropic thermal parameters. The positions of all other hydrogen atoms were calculated by assuming idealized geometries with all C—H distances at 0.95 Å. Their contributions were added to the structure factor calculations, but their positions were not refined. One equivalent of MeCN from the crystallization solvent was found cocrystallized in the lattice. This was included in the calculations and was satisfactorily refined with 100% occupancy.

RESULTS AND DISCUSSION

When compound **1** was allowed to react with $Mn_2(CO)_9(MeCN)$ in a hexane soln at 25°C for 4 days, the compound **2** was formed in 45% yield. A manganese pentacarbonyl grouping was eliminated in the process, presumably as $HMn(CO)_5$. $HMn(CO)_5$ is relatively unstable and was not recovered from the reaction. The formula of compound **2** was established by a combination of IR, ^{1}H NMR, mass spectral and elemental analyses. The structure proposed for **2** is based largely on a single crystal X-ray diffraction analysis of the PMe_2Ph derivative *fac*-$Mn(CO)_3$(P-Me_2Ph)[$S_2CN(H)CO_2Et$], **3** that was obtained by the reaction of **2** with PMe_2Ph. Compound **3** is obtained in 87% yield after 30 min at reflux in a hexane soln, eqn (1).

Compound **3** was characterized crystallographically and an ORTEP diagram of the molecular structure is shown in Fig. 1. Compound **3** is a six coordinate complex. It contains three COs, one PMe_2Ph and one $S_2CN(H)CO_2Et$ ligand. The three CO ligands are arranged in a *fac*-form. This is consistent with three strong absorptions in the IR spectrum in solution, 2026 (vs), 1947 (s), 1917 (s) cm^{-1}. The dithio-

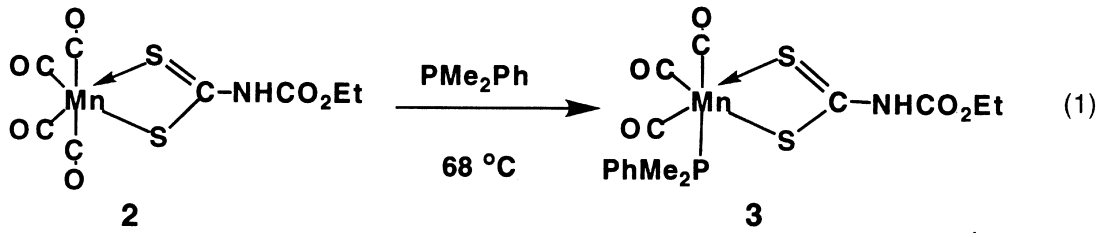

(1)

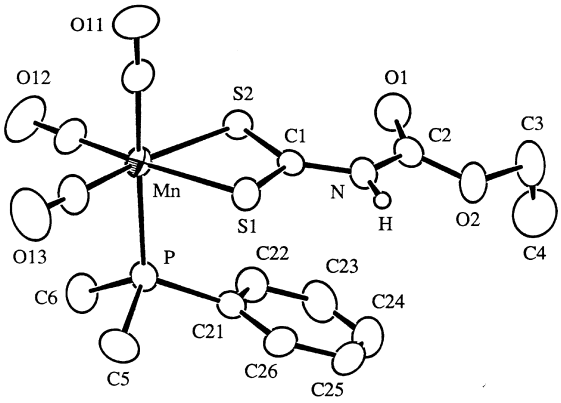

Fig. 1. An ORTEP diagram of $Mn(CO)_3(PMe_2Ph)(S_2CNHCO_2Et)$, **3**. Selected interatomic distances (Å) and angles (°) are: Mn—S(1) = 2.3882(8), Mn—S(2) = 2.3851(9), Mn—P = 2.3554(9), S(1)—C(1) = 1.704(3), S(2)—C(1) = 1.678(3), C(1)—N = 1.363(4), C(2)—N = 1.390(4), C(2)—O(1) = 1.191(4), C(2)—O(2) = 1.337(4); S(1)—C(1)—S(2) = 114.2(2), N(1)—C(1)—S(1) = 118.9(2), N(1)—C(1)—S(2) = 126.8(2), C(1)—N(1)—C(2) = 127.1(3).

carbamato ligand is chelated to the metal atom via the two sulfur atoms. The Mn—S distances are essentially identical, Mn—S(1) = 2.3882(8) Å, Mn—S(2) = 2.3851(9) Å, and are similar to those found in the related complex $Mn(CO)_3(PPh_3)(S_2CNMe_2)$, **5,** 2.373–2.385 Å [7]. The carbon–sulfur distances are very similar in length C(1)—S(1) = 1.704(3) Å, C(1)—S(1) = 1.678(3) Å and are similar to those found in compound **5,** 1.646–1.706 Å. The hydrogen atom on the nitrogen atom was located crystallographically and its resonance was observed in the ^1H NMR spectrum as a broad singlet at $\delta = 8.05$ ppm.

We anticipate that the formation of **2** has occurred by the transfer of the dithiocarbamate ion from **1** to the $Mn_2(CO)_9(NCMe)$ through cleavage of the carbon–sulfur bond and a nucleophilic displacement of the NCMe ligand from the manganese complex by the dithiocarbamate. Although this could occur via a mechanism involving radicals, we prefer a mechanism based on two electron processes as shown in the Scheme which culminates with a protonation of a transient $Mn(CO)_5$ anion formed by cleavage of the Mn—Mn bond to yield $HMn(CO)_5$.

Compound **1** was also found to react with $Zn(acac)_2$ in CH_2Cl_2 solvent at 25°C over a period of 18 h to produce a new compound $Zn(\mu\text{-}S,S\text{-}S_2CN(H)CO_2Et)(\mu\text{-}O,S\text{-}S_2CN(H)CO_2Et)$, **4** in 57% yield. It is even formed (45% yield) simply by eluting **1** over TLC plates containing the $Zn_2(SiO_4)$ fluorescent indicator. Compound **4** was characterized by a single-crystal X-ray diffraction analysis. The compound exists in a polymeric form in the solid state. An ORTEP diagram showing a portion of one polymeric chain of the structure is shown in Fig. 2. The ZnSCS linkage of the polymer is indicated by the solid bonds. In compound **4,** one dithiocarbamato ligand is chelated to the zinc atom via the two sulfur atoms S(1) and S(2). This ligand is not involved in the polymeric linkage. The Zn—S(1) distance of 2.671(2) Å is significantly longer than the Zn—S(2) distance, 2.345(2) Å. This may be related to the coordination geometry and bonding about the zinc ion, see below. The polymeric chain is formed via the coordination of the second dithiocarbamate ligand. The sulfur atom S(4) is bonded to one zinc atom, Zn—S(4) = 2.342(2) Å, while the other sulfur atom S(3) is bonded to another zinc atom, Zn*—S(3) = 2.326(2) Å. This coordination leads to the formation of an helical infinite chain along *b*-direction of the unit cell. In addition, the carbonyl oxygen atom O(3) of the carboxylate group is also coordinated to zinc. This results in the formation of a six membered metallocycle, Zn—S(3)—C(3)—N(2)—C(4)—O(3). The zinc atom has a five-coordinate distorted trigonal bipyramidal geometry. The equatorial sites are occupied by the sulfur atoms S(2), S(3) and S(4). The axial sites are occupied by the atoms S(1) and O(3). Both zinc-ligand axial bonds are unusually long, Zn—S(1) = 2.671(2) Å and Zn—O(3) = 2.154(2) Å. Zinc has been found in distorted trigonal bipyramidal environments in the related five coordinate dithiocarbamate complexes $Zn(S_2CNEt_2)_2$ [8] and $Zn(py)(S_2CNMe_2)_2 \cdot 0.5C_6H_6$ [9]. In both cases the axial Zn—S bond distances are significantly longer than the equatorial Zn—S bond distances. The Zn—O(3) bond distance is significantly longer than those found in related carboxylate complexes $[NBu^n_4[Zn(S_2CNEt_2)_2(O_2CMe)]$, 1.979(6) Å [10] and $Zn(O_2CCH_2CH_3)_2$, 1.95 Å [11]. In the solid state, the two dithiocarbamato ligands in **4** are inequi-

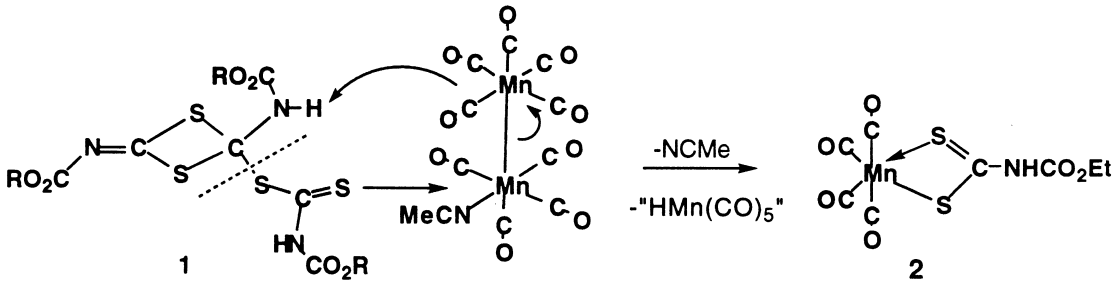

Scheme 1.

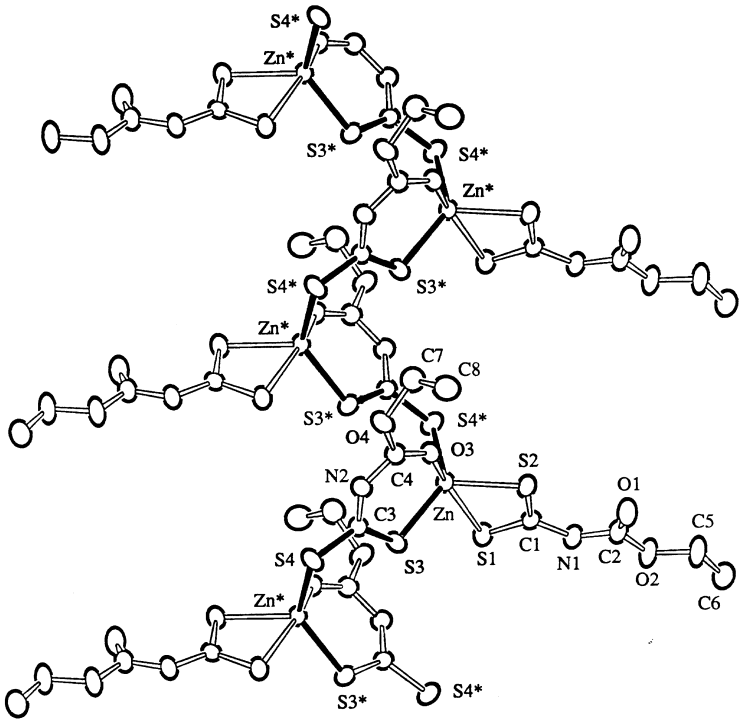

Fig. 2. An ORTEP diagram showing a portion of the polymeric chain Zn(μ-*S*,*S*-$S_2CN(H)CO_2Et$)(μ-*O*,*S*-$S_2CN(H)CO_2Et$), **4**. The connectivity of the ZnSCS polymer is indicated by the solid bonds. Selected interatomic distances (Å) and angles (°) are: Zn—S(1) = 2.671(2), Zn—S(2) = 2.3451(2), Zn—S(3) = 2.326(2), Zn—S(4) = 2.342(2), Zn—O(3) = 2.154(4), S(1)—C(1) = 1.678(6), S(2)—C(1) = 1.704(5), S(3)—C(3) = 1.682(5), S(4)—C(3) = 1.691(5), C(1)—N(1) = 1.371(7), C(2)—N(1) = 1.405(7), C(3)—N(2) = 1.365(7), C(4)—N(2) = 1.379(7), C(4)—O(3) = 1.212(6); S(1)—Zn—S(2) = 71.64(5), S(1)—Zn—S(3) = 90.06(5), S(1)—Zn—S(4) = 90.63(5), S(1)—Zn—O(3) = 161.4(1), S(2)—Zn—S(3) = 121.43(6), S(2)—Zn—S(4) = 107.28(6), S(2)—Zn—O(3) = 94.4(1), S(3)—Zn—S(4) = 107.68(7), S(3)—Zn—O(3) = 86.9(1), S(4)—Zn—O(3) = 105.6(1), S(1)—C(1)—S(2) = 121.3(3), S(3)—C(1)—S(4) = 121.9(3).

valent, however, only one set of resonances for the ethyl groups and only one for the hydrogen atom bonded to two nitrogen atoms, 9.05 (s, br, 2H, NH), are observed in the ^{1}H NMR spectrum in solution. This suggests that compound **4** depolymerizes when dissolved in chloroform solvent, and the two dithiocarbamato ligands are either structurally equivalent or are dynamically averaged on the NMR time scale in solution. Other zinc dithiocarbamates, $Zn(S_2CNEt_2)_2$ [8] and $Zn(S_2CNMe_2)_2$ [12] have been found to form dimeric units in solid state, but they exist in monomeric forms in solution.

The formation of compound **4** also appears to be the result of transfer of the dithiocarbamate grouping of **1** to a zinc ion. Zinc and other dithiocarbamates have been used for a variety of purposes ranging from

pesticides to rubber vulcanization accelerators [13]. In summary it appears that **1,** which is very easily obtained from ethoxycarbonylisothiocyanate, is a convenient source of the ethoxycarbonyldithiocarbamate.

Supplementary material: Tables of final atomic positional parameters, bond distances, bond angles and anisotropic thermal parameters are available for the structural analysis of **3** and **4** (11 pages) have been deposited with the Cambridge Crystallographic Data Centre. Support for an upgrade of the NMR facilities at the University of South Carolina was provided by an NSF ARI grant, Grant No. CHE-9601723.

Acknowledgments—These studies were supported by the Division of Chemical Sciences of the Office of Basic Energy Sciences of the U.S. Department of Energy. The authors wish to thank Prof. F. A. Cotton and Dr Lee Daniels for measurement of the diffraction intensity data for compound **4**.

REFERENCES

1. Adams, R. D. and Huang, M., *Eur. J. Org. Chem.*, in press.
2. (a) Werner, H., *Coord. Chem. Rev.*, 1982, **43,** 165; (b) Bertleff, W. and Werner, H., *Chem. Ber.*, 1982, **115,** 1012; (c) Itoh, K., Matsuda, L., Ueda, F., Ishii, Y. and Ibers, J. A., *J. Am. Chem. Soc.*, 1977, **99,** 2118; (d) Bianchini, C., Masi, D. and Meli, A., *J. Organomet. Chem.*, 1983, **247,** C29.
3. Adams, R. D. and Huang, M., *Organometallics*, 1996, **15,** 3644.
4. (a) Coucouvanis, D., *Prog. Inorg. Chem.*, 1979, **26,** 301; (b) Coucouvanis, D., *Prog. Inorg. Chem.*, 1970, **11,** 233.
5. Koelle, U., *J. Organomet. Chem.*, 1978, **155,** 53.
6. (a) *International Tables for X-ray Crystallography*, Vol. IV. Kynoch Press, Birmingham, England, 1975, Table 2.2b, pp. 99–101; (b) *Ibid.*, Table 2.3.1, pp. 149–150.
7. Dean, W. K. and Moncrief, J. W., *J. Coord. Chem.*, 1976, **6,** 107.
8. Bonamica, M., Mazzone, G., Vaciago, A. and Zambonelli, L., *Acta Cryst.*, 1965, **19,** 898.
9. Fraser, K. A. and Harding, M., *Acta Cryst.*, 1967, **22,** 75.
10. McCleverty, J. A., Spencer, N., Bailey, N. A. and Shackleton, S., *J. Chem. Soc., Dalton Trans.*, 1980, 1939.
11. Goldschmied, E. and Rae, A. D., *Acta Cryst.*, 1977, **B33,** 2117.
12. Klug, H. P., *Acta Cryst.*, 1966, **21,** 536.
13. (a) McCleverty, J. A., Morrison, N., Spencer, N., Ashworth, C. C., Bailey, N. A., Johnson, M. R., Smith, J. M. A., Tabbiner, B. A., Taylor, C. R. and Shackleton, S., *J. Chem. Soc., Dalton Trans.*, 1980, 1945; (c) Ashworth, C. C., Bailey, N. A., Johnson, M. R., McCleverty, J. A., Morrison, N. and Tabbiner, B. A., *J. Chem. Soc., Chem. Comm.*, 1976, 743.

Pergamon

PII : S0277–5387(98)00065–5

Polyhedron Vol. 17, No. 16, pp. 2765–2772, 1998
© 1998 Elsevier Science Ltd
All rights reserved. Printed in Great Britain
0277–5387/98 $19.00+0.00

Formation of 2-pyridinyl-2-oxazolines in the coordination sphere of copper(II) and cobalt(II). The crystal structure of bromo-bis[(2-(2-pyridinyl)-4,4-bis(hydroxymethyl)-2-oxazoline)] copper(II) bromide hemihydrate

P. Segl'a,[a]* M. Jamnický,[b] M. Koman[a] and T. Glowiak[c]

[a] Department of Inorganic Chemistry, Slovak Technical University, 812 37 Bratislava, Slovak Republic

[b] Department of Ceramics, Glass and Cements, Slovak Technical University, 812 37 Bratislava, Slovak Republic

[c] Institute of Chemistry, University of Wroclaw, F. Joliot-Curie 14, 50 383 Wroclaw, Poland

(Received 2 December 1997; accepted 3 February 1998)

Abstract—The reaction of pyridine-2-carbonitrile (2-CNpy) with 2-amino-2-hydroxymethyl-1,3-propanediol (AL^1), 2-amino-2-methyl-1,3-propanediol (AL^2) and 2-amino-2-methyl-1-propanol(AL^3) in ethanolic solutions of Cu(II) and Co(II) salts led to the formation of solid complexes containing 2-(2-pyridinyl)-4,4-bis (hydroxymethyl)-2-oxazoline (pyoxaL^1), 2-(2-pyridinyl)-4-hydroxymethyl-4-methyl-2-oxazoline (pyoxaL^2) and 2-(2-pyridinyl)-4,4-dimethyl-2-oxazoline (pyoxaL^3), respectively. Their stereochemistry and the mode of ligand coordination have been determined by spectral, magnetic and conductometric measurements. The crystal structure of [CuBr(2-(2-pyridinyl)-4,4-bis(hydroxymethyl)-2-oxazoline)$_2$]Br·0.5H_2O was determined by X-ray diffraction technique. The influence of Cu(II) and Co(II) salts on the formation of 2-pyridinyl-2-oxazolines is briefly compared with that of Ni(II) salts. © 1998 Elsevier Science Ltd. All rights reserved

Keywords: 2-pyridinyl-2-oxazoline; nucleophilic reaction; copper(II) complexes; cobalt(II) complexes; crystal structure.

The activation of molecules containing the nitrile group upon their coordination to a metal atom has been exploited in addition reactions of nucleophiles such as water, alcohols and amines yielding amide [1,2], iminoether [3,4] or amidine [3,5] complexes. The reaction of pyridine-2-carbonitrile with water or an alcohol in the presence of some metal(II) salts leads to the formation of complexes which contain pyridine-2-carboxamide or O-alkylpyridine-2-carboximidate [6–11]. However, several nickel(II) complexes of 2-pyridinyl-2-oxazolines have been isolated [12] from the aqueous or ethanolic solutions of pyridine-2-carbonitrile in the presence of some amino alcohols (Scheme 1).

This paper describes the synthesis and the structural characterization of some copper(II) and cobalt(II) solid complexes which contain 2-pyridinyl-2-oxazolines (denoted as pyoxaL^1, pyoxaL^2 and pyoxaL^3). These complexes were prepared by the reaction of pyridine-2-carbonitrile with 2-amino-2-hydroxymethyl-1,3-propanediol, 2-amino-2-methyl-1,3-propanediol, or 2-amino-2-methyl-1-propanol in the presence of Cu(II) or Co(II) salts. Dry or wet ethanol was usually used as a solvent. The X-ray crystal structures of [CuCl(pyoxaL^1)$_2$]Cl·0.5H_2O [13] and [CuBr(pyoxaL^3)$_2$]Br·H_2O [14] have been recently determined. In order to help solve the problem of oxazoline ring coordination in complexes with

* Author to whom correspondence should be addressed.

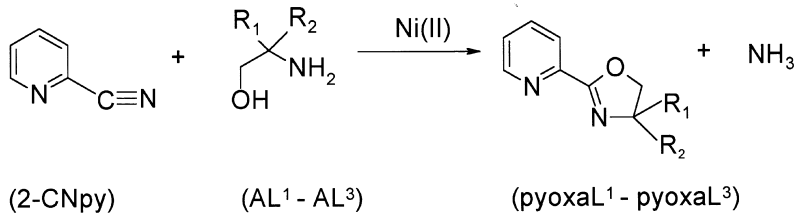

AL^1, $pyoxaL^1$: $R_1 = R_2 = CH_2OH$
AL^2, $pyoxaL^2$: $R_1 = CH_2OH$, $R_2 = CH_3$
AL^3, $pyoxaL^3$: $R_1 = R_2 = CH_3$

Scheme 1. Formation of 2-pyridinyl-2-oxazolines [12].

pyoxaL, the crystal structure of complex $[CuBr(pyoxaL^1)_2]Br \cdot 0.5H_2O$ was also solved in our research.

EXPERIMENTAL

Chemical reagents

All the chemicals used were of reagent grade. Hydrates and anhydrous copper(II) and cobalt(II) salts were prepared according to previously described procedures [15,16]. Ethanol was dried by the standard method [17]. Solid pyridine-2-carbonitrile (2-CNpy) was purified by distillation under reduced pressure. 2-Amino-2-hydroxymethyl-1,3-propanediol (AL^1), 2-amino-2-methyl-1,3-propanediol (AL^2) and 2-amino-2-methyl-1-propanol (AL^3) were used without further purification.

Analysis and physical measurements

Copper and cobalt were determined by EDTA titration; carbon, hydrogen and nitrogen by micro-analytical methods (Carlo Erba Instruments EA 1108).

Magnetic moments were measured with a Gouy balance for the powdered solid at 293 K. Electronic spectra of the powdered samples in Nujol mulls and diffuse reflectance spectra in MgO were recorded at room temperature on a Specord M40 and a Magna 750 spectrophotometer, respectively. A Radelkis OK 104 conductometer was used for conductivity measurements of complexes (concentration 1.0×10^{-3} M) in acetonitrile, nitromethane and nitrobenzene at 298 K. Analytical data, magnetic moments, electronic spectral data and molar conductivity values of complexes are given in Tables 1 and 4. IR spectra were recorded on a Philips Analytical PU 9800 FTIR spectrometer at room temperature with 4 cm^{-1} resolution. The spectra of solid samples were obtained in mulls (Nujol and hexachlorobutadiene) as well as in KBr pellets (1 wt%).

X-ray structure determination

Crystallography. The diffraction intensities for complex $[CuBr(pyoxaL^1)_2]Br \cdot 0.5H_2O$ (complex **IV**) were collected with a KUMA KM 4 diffractometer using a graphite-monochromated Mo-K_α radiation. A summary of crystal, experimental and refinement data are listed in Table 2. The space group $C2/c$ was assumed throughout the structure analysis and was confirmed by the successful refinement of the structure. All data were collected at room temperature with a variable-speed ω–2θ scan technique to a maximum 2θ value 54.28°. The unit-cell parameters were derived from least-squares refinement of 25 well-centered reflections. The intensities of three representative reflections, which were measured after 100 reflections, remained constant throughout data collection. Lorentz and polarization corrections were applied, but not absorption. For the determination of the structure a total of 4353 reflections were measured of which 3851 reflections were unique with $F_o \geqslant 4\sigma(F)$.

Structure solution and refinement. The positions of copper and bromine atoms were located from the Patterson method by program SHELXS-86 (Sheldrick, 1985) [18] and the remaining non-hydrogen atoms were located subsequently via Fourier methods [19]. All non-hydrogen atoms were refined anisotropically. Hydrogen atoms, except those in water, were placed in geometrically calculated positions. Atomic scattering factors were taken from *International Tables for X-ray Crystallography* [20]. Selec-

Table 1. Analytical data[a]

No.	Complex	Calculated (%) Found (%)			
		M	C	H	N
I	$[CuCl(pyoxaL^1)_2]Cl \cdot 0.5H_2O$	11.4	42.9	4.5	10.0
		11.4	42.8	4.4	10.0
II	$[CuCl(pyoxaL^2)_2]Cl \cdot 0.5H_2O$	12.0	45.5	4.8	10.6
		12.0	45.2	4.8	10.6
III	$[CuCl(pyoxaL^3)_2]Cl \cdot H_2O$	12.6	47.6	5.2	11.1
		12.3	47.2	5.2	11.3
IV	$[CuBr(pyoxaL^1)_2]Br \cdot 0.5H_2O$	9.8	37.0	3.9	8.6
		9.7	37.1	3.9	8.6
V	$[CuBr(pyoxaL^2)_2]Br$	10.5	39.5	4.0	9.2
		10.2	39.1	4.0	9.1
VI	$[CuBr(pyoxaL^3)_2]Br \cdot H_2O$	10.7	40.5	4.4	9.4
		10.6	40.7	4.4	9.4
VII	$[CoCl_2(pyoxaL^1)_2]$	10.8	44.0	4.4	10.3
		10.7	43.6	4.5	10.1
VIII	$[CoBr_2(pyoxaL^1)_2]$	9.3	37.8	3.8	8.8
		9.1	37.5	3.8	9.2
IX	$[Co(H_2O)_2(pyoxaL^1)_2](ClO_4)_2$	8.3	33.8	4.0	7.9
		8.1	33.4	3.6	7.7
X	$[Co(NCS)_2(pyoxaL^1)_2]$	10.0	44.7	4.1	14.2
		10.2	44.4	4.2	14.4
XI	$[Co(NCS)_2(pyoxaL^2)_2]$	10.5	47.2	4.3	15.0
		10.7	47.0	4.3	14.9
XII	$[Co(NCS)_2(pyoxaL^3)_2]$	11.2	50.1	4.6	15.9
		10.9	49.7	4.5	15.9

[a] Microanalysis results obtained with maximum deviations: M, ±0.3; C, ±0.4; H, ±0.4; N, ±0.4.

ted interatomic distances and angles are listed in Table 3. Additional data for the structure are included in the Supplementary material available (see later).

Preparation of complexes

Most of the complexes were formed in reaction mixtures containing metal(II) salts, pyridine-2-carbonitrile, amino alcohols and ethanol (dry or wet). The complex $[Co(NCS)_2(pyoxaL^1)_2]$ (**X**) was, however, prepared in ethanolic as well as in aqueous solutions. On the other hand, complex $[Co(H_2O)_2(pyoxaL^1)_2](ClO_4)_2$ (**IX**) can only be prepared in an aqueous solution of appropriate reagents.

The complexes can be obtained in high yields (from 65% to 80%) under mild reaction conditions. Reaction mixtures were first heated at 330 K for 20 min or under reflux for several hours and then slowly cooled to room temperature. While some complexes started to precipitate during heating of mixtures, the others deposited from final solutions over several minutes or days. Some special conditions used in investigated complexes are described in the following text.

Copper(II) complexes

For the synthesis of all complexes, anhydrous copper(II) salts and ethanol as a solvent were used. To achieve higher yields and well-shaped crystalline products, however, wet ethanol appears to be more suitable for the preparation of complexes **I**–**VI**.

$[CuCl(pyoxaL^1)_2]Cl \cdot 0.5H_2O$ (**I**),

$[CuCl(pyoxaL^2)_2]Cl \cdot 0.5H_2O$ (**II**) and

$[CuCl(pyoxaL^3)_2]Cl \cdot H_2O$ (**III**).

A filtered solution of copper(II) chloride (5 mmol) in ethanol (40 cm^3) was mixed with an ethanolic solution (20 cm^3) containing pyridine-2-carbonitrile and an appropriate amino alcohol in equimolar quantities (10 mmol). The mixture was heated for 20 min at about 330 K. Immediately formed precipitates were gradually dissolved to produce the final reaction solutions. Blue-green complexes **I** and **II** started to crystallize from these solutions after several days. When the final reaction solution prepared from amino alcohol AL^3 was cooled to room temperature, a powder-like green compound with a composition close to $[CuCl_2(NH_3)_2]$

Table 2. Crystal data and structure refinement for $[CuBr(pyoxaL^1)_2]Br \cdot 0.5H_2O$ (complex **IV**)

Crystal data	Complex **IV**
Empirical formula	$C_{20}H_{25}Br_2CuN_4O_{6.5}$
Formula weight (g mol^{-1})	648.80
Crystal dimensions (mm)	$0.20 \times 0.30 \times 0.30$
Crystal system	Monoclinic
Space group	$C2/c$
Z	8
Unit cell dimensions from 25 reflections (°)	$8.20 \leqslant 2\theta \leqslant 19.40$
a (Å)	18.308(4)
b (Å)	16.646(3)
c (Å)	17.454(3)
β (°)	115.25(3)
V (Å^3)	4811.0(9)
D_{calcd} (Mg m^{-3})	1.792
Linear absorption coefficient (μ) (mm^{-1})	4.28
Standard reflections	3 measured every 100
Number of data collected	4353
Observed reflections with $F_o \geqslant 4\sigma(F)$	3851
Number of parameters refined	304
$R = \Sigma(\|F_o\| - \|F_c\|)/\Sigma\|F_o\|$	0.0536
$R_2 = \Sigma(\|F_o\| - \|F_c\|)^2/\Sigma\|F_o\|^2]^{1/2}$	0.1538
$w^{-1} = \sigma^2(F_o) + 0.003090\ (F_o)^2$	
Maximum shift/error	0.001
Largest diff. peak and hole (e Å^{-3})	$0.97/-1.03$

Table 3. Selected interatomic distances (Å) and angles (°) for $[CuBr(pyoxaL^1)_2]Br \cdot 0.5H_2O$ (complex **IV**)

Cu—N(1)	2.018(4)	Cu—N(3)	2.001(4)
Cu—N(2)	2.093(4)	Cu—N(4)	2.201(5)
Cu—Br(1)	2.403(1)		
N(1)—Cu—N(3)	176.5(2)	N(1)—Cu—N(2)	81.3(2)
N(3)—Cu—N(2)	96.4(2)	N(1)—Cu—N(4)	98.4(2)
N(3)—Cu—N(4)	79.4(2)	N(2)—Cu—N(4)	98.8(2)
N(1)—Cu—Br(1)	92.8(1)	N(3)—Cu—Br(1)	90.6(1)
N(2)—Cu—Br(1)	147.1(1)	N(4)—Cu—Br(1)	114.1(1)

was first obtained in a small amount. After standing the filtrate for several weeks, during which time most of the solvent evaporated, acetone (1 : 1) was added to the resulting oil and blue green crystals of complex **III** were obtained. All of the solid complexes **I**–**III** were collected by filtration, washed with ethanol and finally, dried *in vacuo*.

$[CuBr(pyoxaL^1)_2]Br \cdot 0.5H_2O$ (**IV**), $[CuBr(pyoxaL^2)_2]Br$ (**V**) and $[CuBr(pyoxaL^3)_2]Br \cdot H_2O$ (**VI**)

Ethanolic solutions of reagents were prepared in the same way as described above. However, the reaction mixtures were refluxed for 1h, 3h and 6h, respectively, for the preparation of complexes **IV, V** and **VI**. Well-shaped green crystals of complexes **IV, V** and **VI** were obtained when the resulting solutions were left to crystallize at room temperature for several days.

Cobalt(II) complexes

To prepare pure solid complexes **VII**–**XII** in good yields it was necessary to use various solvents (water, dry or wet ethanol). Anhydrous cobalt(II) salts, except of $Co(ClO_4)_2 \cdot 6H_2O$, were used for the synthesis of the appropriate complexes.

$[CoCl_2(pyoxaL^1)_2]$ (**VII**) and

$[CoBr_2(pyoxaL^1)_2]$ (**VIII**).

Complexes **VII** and **VIII** were prepared in dry ethanolic solutions by the reaction of equimolar quantities of 2-CNpy and AL^1 (10 mmol) with 5 mmol of $CoCl_2$ and $CoBr_2$, respectively.

The mixture was heated under reflux for 3 h. Both complexes started to deposit during refluxing the reaction solutions. Pink crystals were filtered, washed with dry ethanol and finally dried *in vacuo*.

$[Co(H_2O)_2(pyoxaL^1)_2](ClO_4)_2$ (**IX**) and

$[Co(NCS)_2(pyoxaL^1)_2]$ (**X**).

Both complexes were prepared in the similar way as described above, but as a solvent water was used. The reaction mixture was refluxed only for 1 h. While pink complex **X** was precipitated upon being heated under reflux, pink crystals of complex **IX** were deposited after several hours from the filtrate.

Complex **X** can also be prepared in wet ethanolic solution.

$[Co(NCS)_2(pyoxaL^2)_2]$ (**XI**) and

$[Co(NCS)_2(pyoxaL^3)_2]$ (**XII**).

Pink complexes **XI** and **XII** were prepared only when wet ethanol was used. The other reaction conditions for the production of both solid complexes were identical with those of complex **X** synthesis.

RESULTS AND DISCUSSION

Synthesis

The reaction of 2-CNpy with amino alcohol (AL^1–AL^3) in ethanolic solution of Cu(II) and Co(II) salts leads to the formation of solid complexes containing respective 2-pyridinyl-2-oxazolines ($pyoxaL^1$–$pyoxaL^3$) in good yields. To achieve higher yields and well-shaped crystalline product, however, wet ethanol appears to be more suitable for the preparation of Cu(II) complexes (**I**–**VI**). Only perchlorato (**IX**) and thiocyanato (**X**) Co(II) complexes with $pyoxaL^1$ were prepared in aqueous solution by the analogous reaction of 2-CNpy with AL^1 as described [12] for the preparation of all Ni(II) complexes. All other pure Co(II) complexes (**VII, VIII, XI** and **XII**) were synthesized only from dry ethanolic solution. Study of the different reaction products formed by the reaction of 2-CNpy with AL^1, as well as by the hydrolysis of $pyoxaL^1$ in aqueous solution of Ni(II), Co(II) and Cu(II) salts, is in progress and will be reported [21] later.

Crystal structure description of complex **IV**

Composition and structure of two prepared bromo copper(II) complexes, namely $[CuBr(pyoxaL^1)_2]Br \cdot 0.5H_2O$ (**IV**) and $[CuBr(pyoxaL^3)_2]Br \cdot H_2O$ (**VI**) [14], were determined by single crystal X-ray diffraction technique. The crystal structure of the complexes consists of $[CuBr(pyoxaL)_2]^+$ (where pyoxaL is equal to $pyoxaL^1$ or $pyoxaL^3$) cations, Br^- counter-anions and water of crystallization linked by hydrogen-bonding interactions. Perspective view and atomic numbering of $[CuBr(pyoxaL^1)_2]^+$ are shown in Fig. 1. Selected bond distances and angles for cation are listed in Table 3. Moreover, the X-ray crystal structure of the chloro complex $[CuCl(pyoxaL^1)_2]Cl \cdot 0.5H_2O$ (**I**) has been previously determined [13] and is very similar to that of bromo complex **IV**. The copper(II) atom is five-coordinated. The molecules of 2-pyridinyl-2-oxazoline are coordinated to copper(II) atom via the N1 and N3 (the nitrogen atom of the pyridine ring) as well as via the N2 and N4 (the nitrogen atom of the oxazoline ring) as *N*,*N*-coordinated chelates. Formation of other five-membered chelate ring (contain hydroxymethyl group in 4 position of the oxazoline ring) by coordination of the oxygen atom of hydroxymethyl group is not observed in any case. The fifth coordination site of the copper(II) atom is occupied by the halogenide anion. The value of τ parameter for complexes **I, IV** and **VI** ($\tau = 0.48$) shows that the coordination polyhedron around Cu(II) is best described as an intermediate between trigonal bipyramidal and square pyramidal [22]. This finding is in good agreement with interpretation of their electronic spectra (see later).

The Cu—Br(1) interatomic distances in the coordination polyhedron of bromo complexes **IV** (2.401 Å) and **VI** (2.403 Å) are nearly equal. The average value of bond distances Cu—N(1) and Cu—N(3) (nitrogen atoms of pyridine ring) for complex **IV** (Table 3) is 2.010 Å. Similarly, the average value of bond distances Cu—N(2) and Cu—N(4) (nitrogen atoms of the oxazoline ring) is 2.147 Å. Therefore, the bond distances of copper(II) atom to nitrogen atoms

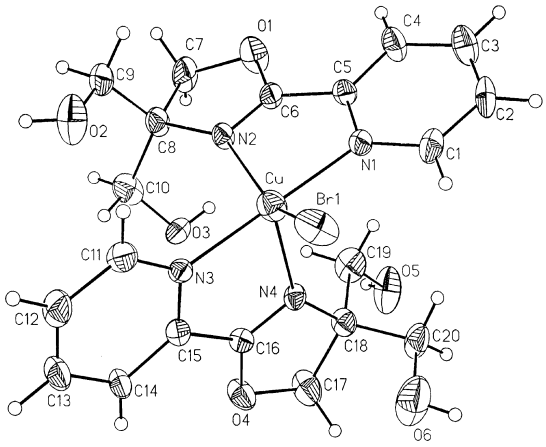

Fig. 1. PLUTO plot of $[CuBr(pyoxaL^1)_2]^+$ cation in complex **IV** (thermal ellipsoids are shown at 50% probability level).

of the oxazoline ring are rather longer than bond distances to nitrogen atom of pyridine rings. The Cu—N bond distances in bromo complex **VI** and chloro complex **I** are in the same range as for complex **IV**. The angle between five-membered planar chelate ring formed by Cu—N1—C5—C6—N2 and Cu—N3—C15—C16—N4 atoms for [CuBr(pyoxaL^1)$_2$]Br·0.5H$_2$O (**IV**) is equal to 89.2(1)°.

Stereochemistry of complexes

All of the complexes contain two molecules of *N*,*N*-coordinated 2-pyridinyl-2-oxazoline ligands (see IR spectra). In agreement with this finding and based on the values of magnetic moments, molar conductivities and electronic spectral data (Table 4), the composition and stereochemistry were assigned to the complexes under investigation.

Copper(II) complexes. Molar conductivity values in nitromethane and in acetonitrile show that all of the copper complexes are univalent compounds [23], i.e. one halogenide anion is coordinated to the central atom (copper has coordination number five), the other acts as a counter-ion. The main reasons for some lower value (in acetonitrile for chloro and nitrobenzene for bromo complexes) would seem to be solvent interactions and the low ionic mobilities of some of the ions involved [23].

For five coordinate copper(II) complexes there are two extreme structures, the square pyramid and the trigonal bipyramid, but not unexpectedly, many distorted intermediates are known. Copper(II) complexes (**I**–**VI**) exhibit peaks in electronic spectra extending from 9000 to 13,500 cm^{-1} (usually, the higher peak maximum energy, the higher molar absorptivity), which is rather typical for square pyramidal Cu(II) complexes. However, the reflectance

Table 4. Magnetic moments, electronic spectral data and molar conductivities of complexes

No.	Complex	μ_{ef} (BM)		Maxima of absorption band[a] (cm^{-1})		Λ_m[b] (Ω^{-1} cm^2 mol^{-1})	Λ_m[c,d] (Ω^{-1} cm^2 mol^{-1})
I	[CuCl(pyoxaL^1)$_2$]Cl·0.5H$_2$O	1.88		13400 9300	28000 sh	43	67[c]
II	[CuCl(pyoxaL^2)$_2$]Cl·0.5H$_2$O	1.90		13300 9400	29000 sh	68	63[c]
III	[CuCl(pyoxaL^3)$_2$]Cl·H$_2$O	1.90		13500 9000	28000 sh	60	65[c]
IV	[CuBr(pyoxaL^1)$_2$]Br·0.5H$_2$O	1.89		13400 9600	26000 sh	122	10[d]
V	[CuBr(pyoxaL^2)$_2$]Br	1.89		13300 9300	26000 sh	155	15[d]
VI	[CuBr(pyoxaL^3)$_2$]Br·H$_2$O	1.90		13500 9200	25000 sh	155	27[d]
VII	[CoCl$_2$(pyoxaL^1)$_2$]	4.94	8200 br	20200 19100 18300 sh		7	0[d]
VIII	[CoBr$_2$(pyoxaL^1)$_2$]	4.78	7900 br	19800 18800 18000 sh		68	0[d]
IX	[Co(H$_2$O)$_2$(pyoxaL^1)$_2$](ClO$_4$)$_2$	4.78	9700 br	21100 19200 sh		303	45[d]
X	[Co(NCS)$_2$(pyoxaL^1)$_2$]	4.80	9500 br	20100 21300 sh 18600 sh		42	1[d]
XI	[Co(NCS)$_2$(pyoxaL^2)$_2$]	4.91	9300 br	20000 21500 sh 18400 sh		50	0[d]
XII	[Co(NCS)$_2$(pyoxaL^3)$_2$]	4.76	9200 br	20200 21500 sh 18500 sh		65	1[d]

[a] sh, shoulder; br, broad.
[b] In acetonitrile.
[c] In nitromethane.
[d] In nitrobenzene.

electronic spectra do not allow us to safely distinguish the regular square pyramids from the regular trigonal bipyramids and the data should be interpreted with care [24]. The suggested composition and stereochemistry of these complexes, namely

$[CuCl(pyoxaL^1)_2]Cl \cdot 0.5H_2O$ [**I**] [13],

$[CuBr(pyoxaL^1)_2]Br \cdot 0.5H_2O$ (**IV**) and

$[CuBr(pyoxaL^3)_2]Br \cdot H_2O$ [**VI**] [14]

are also in a good agreement with their crystal structure determined by single crystal X-ray diffraction.

Cobalt(II) complexes. The electronic spectra of cobalt(II) complexes (**VII**–**XII**) contain a broad band in the near infrared region from 7900 to 9700 cm^{-1}. Second band, present in the visible near 20,000 cm^{-1}, has a shoulder or fine structure to it. Therefore, the electronic spectra of cobalt(II) complexes are clearly consistent with a tetragonally distorted octahedral structure [24]. Similarly, the magnetic moments values of these complexes are within the range usually found for distorted octahedral cobalt(II) complexes [15]. The molar conductivities of all complexes (except of **IX**) in acetonitrile and nitrobenzene are typical for those of non-electrolytes [23]. Molar conductivities for complex **IX** in acetonitrile as well as in nitrobenzene suggest that compound **IX** is a 1 : 2 electrolyte with non-coordinated perchlorate anions [23].

IR spectra

The IR spectra of 2-pyridinyl-2-oxazolines under study ($pyoxaL^1$–$pyoxaL^3$) and their Ni(II) complexes have been published [12]. The IR spectral data of all complexes **I**–**XII** that are diagnostic of the coordinating groups are available as supplementary material. Now the crystal and molecular structure of complexes **I, IV** and **VI** fully confirms the formation of the new organic ligand, i.e. the conversion of the nitrile to the 2-oxazoline. Thus both the knowledge of the crystal structure of complexes **I, IV** and **VI** and IR spectral data confirm *N*,*N*-coordination of 2-pyridinyl-2-oxazolines molecules in all solid complexes. The IR spectra of the other complexes, when compared with those of complexes **I, IV** and **VI,** provide evidence that all the complexes contain *N*,*N*-coordinated 2-pyridinyl-2-oxazolines molecules as the only organic ligands.

Thiocyanate complexes **X**–**XII** show a very strong and broad band in the region 2090–2070 cm^{-1}. The position of this band due to $\nu(C{\equiv}N)$ indicates the presence of monodentate NCS groups which are coordinated through the nitrogen atoms only [25].

The coordination mode of the perchlorate groups in solid complex **IX** was established mainly on the basis of their IR spectra. The spectrum of complex show a very broad band with maximum at about 1080 cm^{-1} which correspond to the non-coordinated perchlorate group [25].

Supplementary material available—The atomic positional parameters and isotropic thermal parameters, anisotropic thermal parameters, H atom parameters, observed and calculated structure factors, equations of planes and full listings of bond distances and angles for complex **IV** have been deposited with the Editor as supplementary data. Atomic coordinates have also been deposited with the Cambridge Crystallographic Data Centre.

Acknowledgements—This work was financially supported by Grant no. 201/5195/95 of the Ministry of Education of the Slovak Republic. The authors would also like to acknowledge Dr. J. Šima (from the Department of Inorganic Chemistry, STU) for helpful discussions.

REFERENCES

1. Belakon, Y. N., Tarasov, V. I., Savel'eva, T. F., Vitt, S. V., Paskonova, E. A., Dotdayev, S. Ch., Borisov, Y. A., Struchkov, Y. T., Batasanov A. S. and Belikov, V. M. *Inorg. Chem*., 1988, **27,** 4046.
2. Creaser, I. I., Harrowfield, J. MacB., Keene F. R. and Sargeson, A. M., *J. Am. Chem. Soc*., 1981, **103,** 3559.
3. Paul, P. and Nag, K., *Inorg. Chem*., 1987, **26,** 1586.
4. Potts, R. A., Gaj, D. L., Schneider, W. F., Dean, N. S., Kampf, J. W. and Oliver, J. P., *Polyhedron*, 1991, **10,** 1631.
5. Uguagliati, P., Belluco, U., Michelin, R. A. and Guerriero, P., *Inorg. Chim. Acta*, 1984, **81,** 61.
6. Barnard, P. F. B., *J. Chem. Soc. A*, 1969, 2140.
7. Suzuki, S., Nakahara, M. and Watanabe, K., *Bull. Chem. Soc. Jpn*., 1973, **46,** 2792.
8. Segl'a, P. and Jamnický, M., *Inorg. Chim. Acta*, 1988, **146,** 93.
9. Katritzky, A. R. and Offerman, R. J., *J. Fluor. Chem*., 1989, **44,** 121.
10. Byers, P., Drew, M. G. B., Hudson, M. J., Isaacs, N. S. and Upadhaya, A., *Polyhedron*, 1994, **13,** 345.
11. Jamnický, M., Segl'a P. and Koman, M., *Polyhedron*, 1995, **14,** 1837.
12. Segl'a, P. and Jamnický, M., *Inorg. Chim. Acta*, 1993, **205,** 221.
13. Koman, Segl'a, P., Jamnický M. and Glowiak, T., *Z. Krist*., 1996, in print.
14. Koman, Segl'a, P., Jamnický, M. and Glowiak, T., *Z. Krist*., 1997, in print.
15. Nichols, D., in *Comprehensive Inorganic Chemistry*, Vol. 24, 2nd edn, ed. J. C. Bailar, Jr, Pergamon, Oxford, 1975, Ch. 41, pp. 1068 and 1124.
16. Masey, A. G., in *Comprehensive Inorganic Chemistry*, Vol. 17, 2nd edn, ed. J. C. Bailar, Jr, Pergamon, Oxford, 1975, Ch. 27, p. 41.
17. Vogel, A. I., *Practical Organic Chemistry*, 3rd edn, ELBS and Longman, London, 1965, p. 163.
18. Sheldrick, G. M., SHELXS-86. *Crystallographic Computing*, Vol. 3, Oxford University Press, 1985, pp. 175–189.
19. Sheldrick, G. M., SHELXL 93. *Program for Refinement of Crystal Structures*. University of Göttingen, Germany, 1994.

20. *International Tables for X-ray Crystallography*, Vol. 4, Kynoch Press, Birmingham, 1974.
21. Segl'a, P. and Jamnický, M., unpublished work.
22. Addison, A. W., Rao, T. N., Reedijk, R., Rijn, J. and Verschoor, G. C., *J. Chem. Soc., Dalton Trans.*, 1984, 1349.
23. Geary, W. J., *Coord. Chem. Rev.*, 1971, **7,** 81.
24. Lever, A. B. P., *Inorganic Electronic Spectroscopy*, 2nd edn, Elsevier, Amsterdam, 1984, pp. 480 and 554.
25. Nakamoto, K., *Infrared and Raman Spectra of Inorganic and Coordination Compounds*, Wiley, New York, 1986, pp. 139, 206, 251 and 282.

Pergamon

PII: S0277-5387(98)00058-8

Polyhedron Vol. 17, No. 17, pp. 2773–2774, 1998
© 1998 Elsevier Science Ltd
All rights reserved. Printed in Great Britain
0277-5387/98 $19.00+0.00

Foreword

The word "cluster" takes on many implications in various areas of chemistry. To the inorganic chemist the definition most commonly recognized was provided by F. A. Cotton some three decades ago: "a finite group of metal atoms that are held together mainly or at least to a significant extent, by bonds directly between metal atoms, even though some nonmetal atoms may also be intimately associated with the cluster" [1]. A word is but a word and in any language its meaning is continually changing, being influenced by its heritage and its common usage and so an inorganic chemist of 1998 would, if composing a dictionary, have to extend the meaning of cluster to include complexes where metal ions contained within an aggregate show strong cooperative electronic or magnetic interactions. This extension of Cotton's original definition has been modified by its common usage in bioinorganic chemistry. Metalloenzymes that have strongly coupled metal centers, such as the Fe_4S_4 cubanes, are referred to as clusters. However, *the moving finger writes and having writ moves on* and so from bioinorganic "clusters" have emerged abiological clusters. These have neither biological relevance nor metal-metal bonds but show fascinating magnetic properties—single molecular magnets. So in the current language of inorganic chemistry a "cluster" may take on many meanings but it is still distinct from a polynuclear aggregate such as a polyoxometallate or polymeric alkoxide of aluminum or yttrium. Inorganic clusters may be neutral molecules, complex ions or may exist as subunits in extended lattice structures.

In organometallic chemistry the beginning of cluster chemistry can be traced to that of metal carbonyl chemistry with the early work of Dewar [2] ($Fe_2(CO)_9$, $Fe_3(CO)_{12}$) and Mond [3] ($Co_2(CO)_8$) which was followed by the pioneering work of the great German chemist Walter Hieber [4]. The field of metal carbonyl cluster chemistry did not fully flourish until the advent of routine ^{13}C NMR spectroscopy and single crystal X-ray diffraction by automated diffractometers. This led to the general recognition of so many issues that we now take for granted: fluxionality and stereochemical non-rigidity; ligands such as carbide and hydride; unique modes of ligand binding and, indeed, hydrocarbyl ligands that could not be supported by a single metal center. The field developed so fast with each new finding fueling further intensive study. The concepts of organometallic surface chemistry became intertwined with cluster chemistry and heterogeneous catalysis [5]. The range of ligands supporting organometallic cluster chemistry became more and more extensive: cyclopentadienes, tertiary phosphines, alkoxides, thiolates, halides [6]. Complementary ligands such as π-donors and π-acceptors were shown to relate early and late transition metal cluster compounds through isolobal relationships [7]. As the size of some metal clusters increased, they impinged on colloidal and nanoparticles. When would the size of a metal cluster be large enough that certain metallic properties would persist in the cluster?

With this brief and simplistic background, it has been my pleasure to edit this symposium-in-print which traverses a wide variety of topics in the general field of inorganic cluster chemistry. It is also particularly appropriate to do so in the year that Lord Lewis enters his eighth decade, for without any doubt his group at Cambridge will long be remembered for their pioneering work on high nuclearity clusters. Professor Lewis' work, spanning now over four decades, has contributed greatly to numerous areas of inorganic chemistry and he and his coworkers, in particular, Brian Figgis and Malcolm Gerloch, also pioneered the field of ligand field theory and magnetism. It thus seems particularly appropriate that this special issue on clusters and magnetism within clusters is effectively a tribute to Jack Lewis as a man who has given so much to chemistry and, at the same time, has given so much of himself in the service of science and higher education. He has been and still is an ambassador for chemistry and science in the public arena and in setting public policy on environmental matters.

On behalf of the chemical community, I express our genuine appreciation and admiration for his achievements to date and, on this the celebration of his 70th birthday, wish him well in all his endeavors in the coming years.

Malcolm H. Chisholm
Indiana University

REFERENCES

1. Cotton, F. A., *Quarterly Review* (*Chem. Soc. London*), 1966, **20,** 389.
2. Dewar J. and Jones, H. O., *Proc. R. Chem.* (*London*), 1905, **A76,** 558; Dewar, J. and Jones, H. O., *Proc. R. Soc.* (*London*), 1907, **A79,** 66.

3. Mond, L., Hirtz, H. and Coop, M. D., *J. Chem. Soc.*, 1910, 997.
4. Hieber, W., *Adv. Organometal. Chem.*, 1970, **8,** 1.
5. Muetterties, E. L., *Bull. Soc. Chim. Belg.*, 1975, **84,** 959.
6. *The Chemistry of Metal Cluster Complexes*, ed. D. F. Shriver, H. D. Kaesz and R. D. Adams. VCH Publishers, Inc., 1990; *Early Transition Metal Clusters with π-Donor Ligands*, ed. M. H. Chisholm. VCH Publishers, 1995.
7. Hoffmann, R., *Angew. Chem. Int. Edit. Engl.*, 1982, **21,** 711; Chisholm, M. H., Clark, D. L., Hampden-Smith, M. J. and Hoffman, D. M., *Angew, Chem. Int. Edit. Engl.*, 1989, **28,** 432.

Pergamon

PII: S0277-5387(97)00318-5

Polyhedron Vol. 17, No. 17, pp. 2775–2780, 1998
© 1998 Elsevier Science Ltd
All rights reserved. Printed in Great Britain
0277-5387/98 $19.00+0.00

New compounds with extended structure lattices from the reactions of cuprous iodide with cyclic polydisulfides†

Richard D. Adams*, Mingsheng Huang and Sherida Johnson

Department of Chemistry and Biochemistry, University of South Carolina, Columbia, SC 29208, U.S.A.

(Received 23 May 1997; accepted 3 July 1997)

Abstract—The reactions of CuI with 1,2,5,6-tetrathiacyclooctane, **1** $\overline{SCH_2CH_2SSCH_2CH_2S}$ and 1,2,5,6,9,10-hexathiacyclododecane, **2** $\overline{SCH_2CH_2SSCH_2CH_2SSCH_2CH_2S}$ in acetonitrile solvent have yielded the new compounds $[Cu_2I_2(\mu\text{-}\overline{SCH_2CH_2SSCH_2CH_2S})]_\infty$, **3** and $[CuI(\mu\text{-}\overline{SCH_2CH_2SSCH_2CH_2SSCH_2CH_2S}]_\infty$, **4** in yields of 75 and 61%, respectively. Both products were characterized crystallographically. Compound **3** contains a network of CuI double chains with step ladder-like structures. The chains are linked by bridging η^2-tetrathiacyclooctane ligands to form 2-dimensional sheets through coordination of the disulfide groups to the copper atoms. Compound **4** contains isolated Cu_2I_2 groups which are linked by two bridging η^2-hexathiacyclododecane ligands to form 1-dimensional chains along the crystallographic *b*-direction. © 1998 Elsevier Science Ltd

Keywords: cyclic polydisulfides; copper iodide.

In recent studies we have shown that the thiirane complex $W(CO)_5(\overline{SCH_2CH_2})$ is an effective catalyst for the transformation of thiirane into cyclic polydisulfides, eq. (1) [1]. 1,2,5,6-tetrathiacyclooctane, **1** $\overline{SCH_2CH_2SSCH_2CH_2S}$ and 1,2,5,6,9,10-hexathiacyclododecane, **2** $\overline{SCH_2CH_2SSCH_2CH_2SSCH_2CH_2S}$ are the principal products. Polythioether macrocycles have been demonstrated to be an important class of ligands [2], but the coordination properties of cyclic polydisulfides have not yet been investigated.

Coordination complexes of simple aliphatic organic disulfides have been prepared with copper [3], rhenium [4], silver [5], mercury [6] and manganese [7] without inducing rupture of the disulfide S—S bond. However, the reaction of **1** with $Ru_3(CO)_{12}$ leads to the formation of two isomers of $Ru_3(CO)_7(\mu\text{-}SCH_2CH_2S)_2$ which contain bridging ethanedithiolate ligands formed by cleavage of both of the disulfide S—S bonds [8]. In an effort to prepare complexes of **1** and **2** without cleavage of the S—S bond, we proceeded to investigate their reactions with CuI. We have observed the formation of two new compounds that exhibit interesting extended structures in the solid state that are created by the formation of bridging ligands involving η^2-coordination of the cyclic disulfides. The results of this study are reported herein.

EXPERIMENTAL

General data

Reagent grade acetonitrile was used as purchased. All reactions were performed in air. The products do not appear to be air sensitive. The cyclic disulfides **1** and **2** were prepared by our previously reported procedure [1]. CuI was purchased from Strem and was used without further purification. ^{1}H NMR spectra were taken at 300 MHz on a Bruker AM-300 spectrometer. Elemental analyses were performed by Desert Analytics, Tucson, AZ.

Synthesis of $[(CuI_2(\mu\text{-}\overline{SCH_2CH_2SSCH_2CH_2S}))]_\alpha$, **3**

A solution of 114.0 mg (0.60 mmol) of CuI in 10 cm^3 of acetonitrile was combined with a solution of

* Author to whom correspondence should be addressed.

† Dedicated to Lord Lewis on the occasion of his 70th birthday.

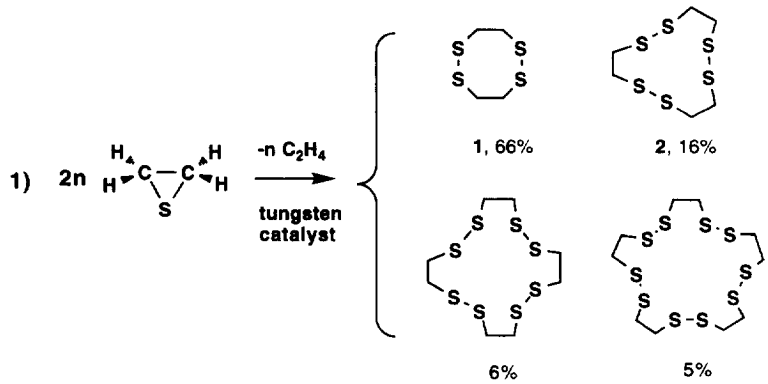

50.0 mg (0.27 mmol) of **1** in 5 cm^3 of acetonitrile in a small vial. The solution was stirred at room temperature for 1 h and then filtered to remove any undissolved particles. The filtrate was allowed to stand at room temperature in open air for 3 days. 123.1 mg of colorless crystals of $[Cu_2I_2(\overline{SCH_2CH_2SSCH_2CH_2S})_\infty]$, **3** formed and was collected (yield 75% based on **1**). Spectral data for **3**: ^1H NMR (δ in CD_3CN, ppm): 3.14 (s, 8H, $4CH_2$). Anal. calc (found): C, 8.55 (8.50); H, 1.27 (1.43).

Synthesis of $[CuI(\mu\text{-}\overline{SCH_2CH_2SSCH_2CH_2SSCH_2CH_2S})]_\infty$, **4**

A solution of 31.0 mg (0.16 mmol) of CuI in 12 cm^3 of acetonitrile was combined with a solution of 13.0 mg (0.047 mmol) of **2** in 10 cm^3 of CH_2Cl_2 in a small vial. The mixture was stirred at room temperature for 30 min and then filtered to remove any undissolved particles. The filtrate was allowed to stand at room temperature in open air for 3 days. 27.0 mg of colorless crystals of $[CuI(\mu\text{-}\overline{SCH_2CH_2SSCH_2CH_2SSCH_2CH_2S}]_\infty$, **4** formed and was collected (yield 61% based on the **2**). Spectral data for **4**: ^1H NMR (δ in CD_3CN, ppm): 3.21 (s, 12H, $6CH_2$). Anal. calc (found): C, 15.43 (15.40); H, 2.59 (2.36).

Crystallographic analyses

Crystals of **3** and **4** suitable for X-ray diffraction analysis were obtained simply by slow evaporation of solvent from solutions of CuI and the appropriate ligand, **1** or **2**, in acetonitrile solvent at 25°C. The crystals used in intensity measurements were mounted in thin-walled glass capillaries. Diffraction measurements were made on a Rigaku AFC6S fully automated four-circle diffractometer using graphite-monochromated Mo-K_α radiation. The unit cells were determined and refined from 15 randomly selected reflections obtained by using the AFC6S automatic search, center, index, and least-squares routines. Crystal data, data collection parameters, and results of these analyses are listed in Table 1. All data processing was performed on a Silicon Graphics Indigo^2 computer by using the TEXSAN structure solving program library obtained from the Molecular Structure Corp., The Woodlands, TX. Neutral atom scattering factors were calculated by the standard procedures [9a]. Anomalous dispersion corrections were applied to all non-hydrogen atoms [9b]. Lorentz-polarization (Lp) and absorption corrections were applied in each analysis. Full matrix least-squares refinements minimized the function: $\Sigma_{hkl}w(|F_o|-|F_c|)^2$, where $w = 1/\sigma(F)^2$, $\sigma(F) = \sigma(F_o^2)/2F_o$, and $\sigma(F_o^2) = [\sigma(I_{raw})^2 + (0.02I_{net})^2]^{1/2}/\text{Lp}$.

Compound **3** crystallized in the triclinic crystal system. The space group $P\bar{1}$ was assumed and confirmed by the successful solution and refinement of the structure. The structure was solved by a combination of direct methods (MITHRIL) and difference Fourier syntheses. All nonhydrogen atoms were refined with anisotropic thermal parameters. The positions of all hydrogen atoms were calculated by assuming idealized geometries with all C—H distances at 0.95 Å. Their contributions were added to the structure factor calculations, but their positions were not refined.

Compound **4** crystallized in the monoclinic crystal system. The patterns of systematic absences observed during the collection of intensity data were consistent with either of the space groups $C2/c$ or Cc. The structure was solved and successfully refined in the higher symmetry centrosymmetric space group $C2/c$. The structure was solved by a combination of direct methods (MITHRIL) and difference Fourier syntheses. All nonhydrogen atoms were refined with anisotropic thermal parameters. The positions of all hydrogen atoms were calculated by assuming idealized geometries with all C—H distances at 0.95 Å. Their contributions were added to the structure factor calculations, but their positions were not refined.

RESULTS AND DISCUSSION

When a solution of CuI and **1** in acetonitrile was allowed to evaporate in the open air, the compound

Table 1. Crystallographic data for compounds **3** and **4**

Compound	**3**	**4**
Formula	$Cu_2I_2S_4C_4H_8$	$CuIS_6C_6H_{12}$
Crystal system	Triclinic	Monoclinic
a (Å)	8.827(2)	22.091(8)
b (Å)	9.745(2)	9.770(3)
c (Å)	8.033(2)	16.791(6)
α (°)	96.31(2)	
β (°)	111.22(2)	129.78(2)
γ (°)	108.01(2)	
V (Å^3)	593.0(3)	2785(2)
Space group	$P\bar{1}$ (#2)	$C2/c$ (#15)
Z value	2	8
ρ_{calc} (g/cm^3)	3.17	2.23
μ (Mo-K_α) (cm^{-1})	94.45	46.48
Temperature (°C)	20	20
$2\Theta_{max}$ (°)	50.0	45.0
No. Obs. ($I > 3\sigma$)	1821	1325
No. Variables	109	128
Goodness of Fit (GOF)[a]	2.36	1.59
Max shift in final cycle	0.00	0.01
Residuals: R[a], R_W[a]	0.029; 0.038	0.027; 0.028
Abs. Cor.	Difabs	Difabs
Transmission coeff., Max/Min	1.00/0.58	1.00/0.56
Largest peak in Final Diff. Map (e$^-$/Å^3)	1.27	0.47

[a] $R = \Sigma_{hkl}(||F_{obs}| - |F_{calc}||)/\Sigma_{hkl}|F_{obs}|$, $R_W = [\Sigma_{hkl}w(|F_{obs}| - |F_{calc}|)^2/\Sigma_{hkl}wF_{obs}^2]^{1/2}$, $w = 1/\sigma^2(F_{obs})$; GOF $= [\Sigma_{hkl}w(|F_{obs}| - |F_{calc}|)^2/(n_{obs} - n_{vari})]^{1/2}$.

$[Cu_2I_2(\overline{SCH_2CH_2SSCH_2CH_2S})]_\infty$, **3** was formed in a crystalline form in a 75% yield. The crystals which formed were suitable for single crystal X-ray diffraction analysis and the product was therefore promptly characterized by this method. An ORTEP drawing of a section of the solid state structure of **3** is shown in Fig. 1. Selected interatomic distances and angles are listed in Tables 2 and 3, respectively. The solid state structure of **3** consists of a double chain arrangement of CuI in a 'step ladder-like' structure that runs parallel to the a-axis of the unit cell. Each copper atom is coordinated to three iodide ligands in the chain and one sulfur atom of one disulfide group of the $\overline{SCH_2CH_2SSCH_2CH_2S}$ ligand. The second disulfide group is coordinated by one of its sulfur atoms to the copper atom of a neighboring CuI double chain. This pattern is repeated indefinitely along the length of the chain. Moreover, the chains are linked in such a way as to form a 2-dimensional sheet. The Cu(1)—S(1) distance is slightly longer than the Cu(2)—S(3) distance, 2.374(2) *vs* 2.342(2) Å. The difference must

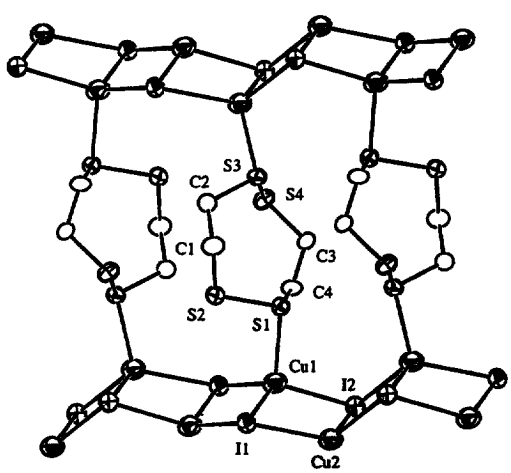

Fig. 1. An ORTEP diagram showing several repeating units of solid state structure of $Cu_2I_2(\mu\text{-}S_4C_4H_8)$, **3**. The atoms comprising one asymmetric crystal unit are labeled.

Table 2. Intramolecular distances for compound **3**[a]

I(1)—Cu(1)	2.603(1)	S(1)—S(2)	2.048(2)
I(1)—Cu(1)*	2.764(1)	S(1)—C(4)	1.821(7)
I(1)—Cu(2)	2.675(1)	S(2)—C(1)	1.818(7)
I(2)—Cu(1)	2.649(1)	S(3)—S(4)	2.061(3)
I(2)—Cu(2)	2.630(1)	S(3)—C(2)	1.831(7)
I(2)—Cu(2)*	2.746(1)	S(4)—C(3)	1.813(6)
Cu(1)—S(1)	2.374(2)	C(1)—C(2)	1.52(1)
Cu(2)—S(3)*	2.342(2)	C(3)—C(4)	1.51(1)

[a] Distances are in angstroms (Å). Estimated standard deviations in the least significant figure are given in parentheses.

Table 3. Intramolecular bond angles for compound **3**[a]

Cu(1)—I(1)—Cu(1)*	64.96(4)	I(2)—Cu(2)—I(2*	100.50(3)
Cu(1)—I(1)—Cu(2)	67.06(3)	I(2)—Cu(2)—S(3)	113.55(6)
Cu(1)—I(1)—Cu(2)*	115.93(4)	I(2)—Cu(2)—S(3*	105.58(6)
Cu(1)—I(2)—Cu(2)	67.06(3)	Cu(1)—S(1)—S(2)	97.72(9)
Cu(1)—I(2)—Cu(2)*	105.65(4)	Cu(1)—S(1)—C(4)	97.7(2)
Cu(2)—I(2)—Cu(2)*	79.50(3)	S(2)—S(1)—C(4)	106.5(2)
I(1)—Cu(1)—I(1)*	115.04(4)	S(1)—S(2)—C(1)	105.9(2)
I(1)—Cu(1)—I(2)	113.40(4)	Cu(2)—S(3)—S(4)	104.4(1)
I(1)—Cu(1)—S(1)	108.46(6)	Cu(2)—S(3)—C(2)	105.6(2)
I(1)—Cu(1)—I(2)*	110.81(4)	S(4)—S(3)—C(2)	107.0(2)
I(1)*—Cu(1)—S(1)	103.15(6)	S(3)—S(4)—C(3)	104.9(2)
I(2)—Cu(1)—S(1)	104.91(5)	S(2)—C(1)—C(2)	116.6(5)
I(1)—Cu(2)—I(2)	111.65(4)	S(3)—C(2)—C(1)	116.8(5)
I(1)—Cu(2)—I(2)*	112.19(4)	S(4)—C(3)—C(4)	117.3(5)
I(1)—Cu(2)—S(3)	112.60(6)	S(1)—C(4)—C(3)	118.4(5)

[a] Angles are in degrees (°). Estimated standard deviations in the least significant figures are given in parentheses.

be attributed to packing effects. Each copper ion has an approximate tetrahedral geometry. The conformation of the $\overline{SCH_2CH_2SSCH_2CH_2S}$ ligand has a crown type structure which differs from that of the free molecule which has been described as a 'twist-boat-chair' [10]. There are many examples of ladder-like CuX double chain structures in the literature [11], but there are very few in which the chains are linked together to form 2-dimensional sheets [12]. The reaction of CuI with EtSSEt has been reported to yield the complex CuI(μ-η^2-EtSSEt) that contains isolated CuI double chains in which the η^2-EtSSEt ligand bridges adjacent Cu atoms in the same chain [3].

When **3** is dissolved in CD_3CN, only one resonance is observed in the ^1H NMR spectrum at $\delta = 3.14$ ppm. This is not consistent with the solid state structure. This resonance is not significantly different from that of the free molecule **1**; therefore, it is concluded that the $\overline{SCH_2CH_2SSCH_2CH_2S}$ ligand is displaced from the copper atoms when **3** is dissolved.

When a solution of CuI and **2** in acetonitrile was allowed to evaporate in the open air, the compound **4** was formed in a crystalline form in a 61% yield. The crystals which formed were suitable for single crystal X-ray diffraction analysis and the product was thus characterized by this method. An ORTEP drawing of a section of the solid state structure of **4** is shown in Fig. 2. Selected interatomic distances and angles are listed in Tables 4 and 5, respectively. The solid state structure of **4** consists of isolated Cu_2I_2 groups which are linked by two bridging η^2-hexathiacyclododecane ligands to form 1-dimensional chains that run parallel to the crystallographic *b*-direction of the unit cell. The two independent copper atoms lie on special positions on the *b*-axis and the chain has a 2-fold rotational symmetry. Each copper atom is coordinated to two iodide ligands in the chain and two sulfur atoms: one from a disulfide group of two separate

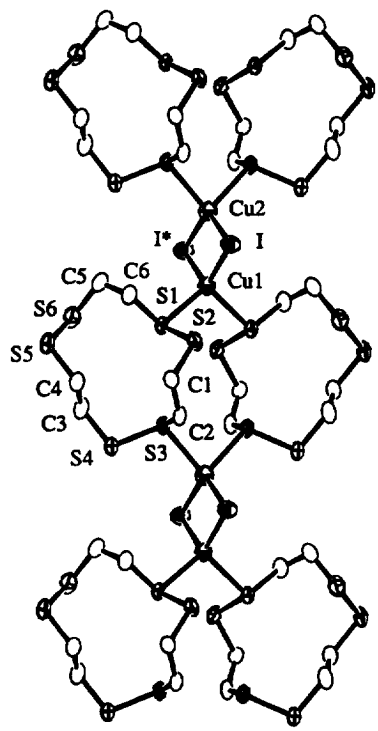

Fig. 2. An ORTEP diagram showing several repeating units of solid state structure of CuI(μ-$S_6C_6H_{12}$), **4**. The atoms comprising one asymmetric crystal unit plus one symmetry equivalent iodide ligand I* are labeled.

$\overline{SCH_2CH_2SSCH_2CH_2SSCH_2CH_2S}$ ligands. A second disulfide group is coordinated by one of its sulfur atoms to the copper atom of an adjacent Cu_2I_2 group. The Cu—S distances are similar to those in **3**: Cu(1)—S(1) = 2.379(2) Å and Cu(2)—S(3) = 2.433(2)Å. Each copper ion has an approximate tetra-

Table 4. Intramolecular distances for compound **4**[a]

I—Cu(1)	2.621(1)	S(3)—C(2)	1.84(1)
I—Cu(2)	2.585(1)	S(4)—C(3)	1.83(1)
Cu(1)—Cu(2)	2.795(2)	S(5)—S(6)	2.027(3)
Cu(1)—S(1)	2.379(2)	S(5)—C(4)	1.816(8)
Cu(2)—S(3)*	2.433(2)	S(6)—C(5)	1.81(1)
S(1)—S(2)	2.055(4)	C(1)—C(2)	1.514(9)
S(1)—C(6)	1.818(6)	C(3)—C(4)	1.50(1)
S(2)—C(1)	1.817(6)	C(5)—C(6)	1.52(2)
S(3)—S(4)	2.043(3)		

[a] Distances are in angstroms (Å). Estimated standard deviations in the least significant figure are given in parentheses.

hedral geometry, but the two copper atoms are different. As can be seen in the figure, Cu(2) is coordinated to the two sulfur atoms of the S_2 grouping, S(3) and S(3*), that lie closest to the Cu—Cu axis, while Cu(1) is coordinated to the two sulfur atoms of the S_2 grouping, S(1) and S(1*), that lie farther from the Cu—Cu axis. As a result, the S(3)—Cu(2)—S(3*) angle is much smaller than the S(1)—Cu(1)—S(1*) angle, 85.87(9) *vs* 101.24(9)°. These distortions produce an opposite but smaller counter effect on the I—Cu—I angles, that is, the I—Cu(2)—1* angle is significantly larger than the I—Cu(1)—1* angle, 116.32(5) *vs* 113.80(5)°. The conformation of the ring of the $\overline{SCH_2CH_2SSCH_2CH_2SSCH_2CH_2S}$ ligand is similar to that of the free molecule [13], except for some minor twisting in the conformation at the sites of coordination. There are a number of reports of ligated CuI dimers in the literature [14], but there are a very few examples of chain structures formed by the head-to-tail ligation of dimeric CuI groupings by bidentate ligands [12a,15]. CuX dimers form 1-dimensional chains with tetrahydrothiophene by using the sulfur atom as a single atom bridge [16].

When **4** is dissolved in CD_3CN, only one resonance is observed in the ^1H NMR spectrum at $\delta = 3.21$ ppm. This is not consistent with the solid state structure. This resonance is not significantly different from that of the free molecule **2**, and therefore, as with **3**, it is concluded that the $\overline{SCH_2CH_2SSCH_2CH_2SSCH_2CH_2S}$ ligand in **4** is displaced from the copper atoms when the compound is dissolved.

Two new compounds, **3** and **4**, were obtained from reactions of CuI with the cyclic disulfides **1** and **2**, respectively. Each case only one of the two sulfur atoms in the disulfide group is engaged in coordination to copper. Interestingly, in both cases the cyclic disulfide ligands have adopted bridging bidentate coordination modes by employing coordination of two disulfide groupings. In **3** the copper iodide assembled itself in the well known double chain, step-ladder structure. The interesting feature of the solid state structure is that the bridging disulfide ligands serve as links between the chains together to form 2-dimensional sheets.

For **4** the copper iodide formed in groups no larger than dimers, Cu_2I_2. The dimers are then linked by two bridging ligands of **2** to form 1-dimensional chains. At this time, one can only speculate as to why the two different structural types have formed from these two similar ligands. Steric bulk and geometry of the ligands are two factors which distinguish them. For example, for **1** the disulfide groups lie on opposite sides of the ring. It is easy to arrange a regular repeating pattern of the ligands in a way that can allow a chain of copper atoms to be coordinated to one of the disulfide groups and a second chain to be coordinated to the second disulfide group, etc. to form a sheet. Seemingly, it would be possible to arrange an extended lattice of two bridged CuI chains by using **2** as well, but extending this into a sheet would be more difficult and would probably require considerable folding which might be energetically unfavorable.

Table 5. Intramolecular bond angles for Compound **4**[a]

Cu(1)—I—Cu(2)	64.94(4)	Cu(2)*—S(3)—S(4)	108.21(9)
I—Cu(1)—I*	113.80(5)	Cu(2)*—S(3)—C(2)	97.9(2)
I—Cu(1)—S(1)	107.76(5)	S(4)—S(3)—C(2)	106.3(2)
I*—Cu(1)—S(1)	112.82(4)	S(3)—S(4)—C(3)	104.4(3)
S(1)—Cu(1)—S(1)*	101.24(9)	S(6)—S(5)—C(4)	105.1(2)
I—Cu(2)—I*	116.32(5)	S(5)—S(6)—C(5)	104.8(3)
I—Cu(2)—S(3)*	113.22(5)	S(2)—C(1)—C(2)	115.2(5)
I*—Cu(2)—S(3)*	112.22(4)	S(3)—C(2)—C(1)	118.0(5)
S(3)—Cu(2)—S(3)*	85.87(9)	S(4)—C(3)—C(4)	114.3(5)
Cu(1)—S(1)—S(2)	92.84(8)	S(5)—C(4)—C(3)	114.4(5)
Cu(1)—S(1)—C(6)	104.5(2)	S(6)—C(5)—C(6)	116.7(5)
S(2)—S(1)—C(6)	103.0(3)	S(1)—C(6)—C(5)	111.1(5)
S(1)—S(2)—C(1)	105.2(2)		

[a] Angles are in degrees (°). Estimated standard deviations in the least significant figure are given in parentheses.

Acknowledgements—These studies were supported by the Division of Chemical Sciences of the Office of Basic Energy Sciences of the U.S. Department of Energy. Support for an upgrade of the NMR facilities at the University of South Carolina was provided by an NSF ARI grant, Grant No. CHE-9601723.

REFERENCES

1. Adams, R. D., Yamamoto, J. H., Holmes, A. and Baker, B. J., *Organometallics*, **16,** 1430, (1997).
2. Cooper, S. R., in *Crown Compounds: Toward Future Applications*, Ch. 15, S. R. Cooper, Ed.; VCH Publishers, New York (1992); (b) Cooper, S. R. and Rawle, S C., *Struc. and Bonding*, 1990, **72,** 1; (c) Blake, A. J. and Schröder, M., *Adv. Inorg. Chem.*, 1990, **35,** 1.
3. Boorman, P. M., Kerr, K. A., Kidd, R. A., Moynihan, K. J. and Valentine, K. A., *J. Chem. Soc., Dalton Trans.*, 1982, 1401.
4. (a) Bernal, I., Atwood, J. L., Calderazzo, F. and Vitali, D., *Isr. J. Chem.*, 1977, **15,** 153; (b) Bernal, I., Atwood, J. L., Calderazzo, F. and Vitali, D., *Gazz. Chem. Ital.*, 1976, **106,** 971.
5. Roesky, H. W., Gries, T., Jones, P. G., Weber, K.-L. and Sheldrick, G. M., *J.Chem. Soc., Dalton Trans.*, 1984, 1781.
6. Boorman, P. M., Merrit, C. L., Nandana, W. A. S. and Richardson, J. F., *J. Chem. Soc., Dalton Trans.*, 1986, 1251.
7. Braunwarth, H., Lau, P., Huttner, G., Minelli, M., Gunauer, D., Zsolnai, L., Jibril, I. and Evertz, K., *J. Organomet. Chem.*, 1991, **411,** 383.
8. Adams, R. D. and Yamamoto, J. H., *J. Cluster Sci.*, 1996, **7,** 643.
9. (a) *International Tables for X-ray Crystallography*; Table 2.2B, pp. 99–101. Vol. IV, Kynoch Press, Birmingham, England, (1975); (b) *Ibid.*, Table 2.3.1, pp 149–150.
10. Goodrow, M. H., Olmstead, M. M. and Musker, W. K., *Tetrahedron Lett.*, 1982, **23,** 3231.
11. (a) Healy, P. C., Kildea, J. D., Skelton, B. W. and White, A. H., *Aus. J. Chem.*, 1989, **42,** 79; (b) Healy, P. C., Kildea, J. D., Skelton, B. W. and White, A. H., *Aus. J. Chem.*, 1989, **42,** 93; (c) Jasinski, J. P., Rath, N. P. and Holt, E. M., *Inorg. Chim. Acta*, 1985, **97,** 91; (d) Massaux, M., Bernard, M. J. and LeBihan, M. T., *Bull. Soc. Fr. Miner. Crist.*, 1969, **92,** 118; (e) Massaux, M., Bernard, M. J. and LeBihan, M. T., *Acta Cryst. Sect. B*, 1971, **27,** 2419; (f) Massaux, M. and LeBihan, M. T., *Acta Cryst. Sect. B*, 1976, **32,** 1586; (g) Bolte, M. and Massaux, M., *Inorg. Chim. Acta*, 1981, **52,** 191; (h) Campbell, J. A., Raston, C. L. and White, A. H., *Aus. J. Chem.*, 1977, **30,** 1937; (i) Engelhardt, L. M., Healy, P. C., Kildea, J. D. and White, A. H., *Aus. J. Chem.*, 1989, **42,** 185; (j) Strähle, J., Hiller, W., Eitel, E. and Oelkrug, D., *Z. Krist.*, 1980, **153,** 277.
12. (a) Munakata, M., Kuroda-Sowa, T., Maelawa, M., Honda, A. and Kitagawa, S., *J. Chem. Soc., Dalton Trans.*, 1994, 2771; (b) Brown, I. D. and Dunitz, J. D., *Acta Cryst.*, 1960, **13,** 28.
13. Goodrow, M. H., Musker, W. K. and Olmstead, M. M., *Acta Cryst.*, 1986, **C42,** 255; (b) Norén, B. and Oskarsson, Å., *Acta Chim. Scand.*, 1987, **A41,** 12.
14. (a) Dyaspm, J. C., Engelhardt, L. M., Healy, P. C. and White, A. H., *Aus. J. Chem.*, 1984, **37,** 2201; (b) Gill, J. T., Mayerle, J. J., Welcker, P. S., Lewis, D. F., Ucko, D. A., Barton, D. J., Stowens, D. and Lippard, S. J., *Inorg. Chem.*, 1976, **15,** 1155; (c) Albano, V. G., Bellon, P. L., Ciani, G. and Manassero, M., *J. Chem. Soc., Dalton Trans.*, 1972, 171.
15. Brunn, K., Endres, H. and Weiss, J., *Z. Naturforsch.*, 1988, **43b,** 224.
16. Maelger, H., Olbrich, F., Kopf, J., Abeln, D. and Weiss, E., *Z. Naturforsch.*, 1992, **47b,** 1276.

Pergamon

PII: S0277-5387(97)00470-1

Polyhedron Vol. 17, No. 17, pp. 2781–2793, 1998
© 1998 Elsevier Science Ltd
All rights reserved. Printed in Great Britain
0277-5387/98 $19.00+0.00

From end-on coordination of acetonitrile molecules to crosswise bridging; formation of iminophosphino and acetamidate ligands in a dimolybdenum complex by further reactions with nucleophiles†

F. Albert Cotton,[a]* Lee M. Daniels,[a] Carlos A. Murillo[a,b]* and Xiaoping Wang[a]

[a] Laboratory for Molecular Structure and Bonding, Department of Chemistry, Texas A&M University, P.O. Box 300012, College Station, TX 77842-3012, U.S.A.

[b] Department of Chemistry, University of Costa Rica, Ciudad Universitaria, Costa Rica

(Received 22 September 1997; accepted 12 November 1997)

Abstract—Three complexes from the reaction of bis(diphenylphosphino)ethane (dppe), water and acetonitrile have been structurally characterized. Reaction of the quadruply M—M bonded complex $[Mo_2(CH_3CN)_8(ax\text{-}CH_3CN)][BF_4]_4$ (**1a**), with dppe produces $[Mo_2(\mu,\eta^2\text{-}CH_3CN)(\mu,\eta^1\text{-}NC(CH_3)P(Ph_2)CH_2CH_2PPh_2)(CH_3CN)_7][BF_4]_4$ (**2**), in which an acetonitrile molecule is bound to both Mo atoms in a perpendicular mode. A new chelating ligand, namely $NC(CH_3)P(Ph_2)CH_2CH_2PPh_2$, is formed by coupling of a dppe to an acetonitrile molecule. It bridges both Mo atoms with its **N** atom and chelates to one of the Mo atoms with both **N** and **P** atoms. When a trace amount of water is introduced into **2** at low temperature, the compound $[Mo_2(\mu,\eta^2\text{-}CH_3CNBF_3)(\mu,\eta^1\text{-}N(H)COCH_3)(CH_3CN)_8][BF_4]_3$ (**3**), is obtained. It has a crosswise bridging acetonitrile moiety; the nitrogen atom of this bridging acetonitrile is also coordinated to a BF_3 group in the solid state. An acetamidate ligand, instead of the coupled dppe group, bonds to both Mo atoms symmetrically using only the N atom. Hydrogen bonding is observed between the amide NH group and one F atom of one of the BF_4^- counteranions. Both compounds **2** and **3** have edge-sharing bioctahedra and elongated Mo—Mo distances. By adding an excess of water to the solution of **2**, complex $[Mo_2(\mu\text{-}N(H)COCH_3)_2(CH_3CN)_4][BF_4]_2$ (**4**) is produced. The crystal structure of **4** shows two *cis* bridging acetamidate ligands. The N and O atoms of each acetamido group coordinate to the Mo atoms and they are evenly distributed on two positions. The results are rationalized as nucleophilic attacks of dppe or water molecules on coordinated acetonitrile ligands on the dimolybdenum complexes. © 1998 Elsevier Science Ltd. All rights reserved

Keywords: dimolybdenum compounds; crosswise bridging; iminophosphine; acetamidate; crystal structure.

Among the large family of metal to metal bonded complexes of molybdenum [1], dinuclear complexes in which all the ligands coordinated to the $[Mo_2]^{4+}$ core are labile are rare, although there are a few [2]. Several years ago we reported an efficient synthesis of an acetonitrile complex of this type, namely, $[Mo_2(CH_3CN)_8(ax\text{-}CH_3CN)_2][BF_4]_4 \cdot 2CH_3CN$ [3], $\mathbf{1} \cdot 2CH_3CN$ and anticipated its use in the preparation of other molybdenum compounds [4]. However, the isolated products are extremely dependent on the reaction conditions. We have observed recently not only ligand substitution reactions, but also transformations of the nitrile molecules. In two cases, products having perpendicular bridging (**I**) instead of end-on coordination (**II**) of acetonitrile molecules have been observed, namely, $[Mo_2(\mu,\eta^2\text{-}CH_3CN)(\mu\text{-dppa})(\mu\text{-}NC(CH_3)P(C_6H_5)_2NP(C_6H_5)_2)(CH_3CN)_5][BF_4]_3$ and $[Mo_2(\mu,\eta^2\text{-}CH_3CN)(\mu\text{-}O)(\mu\text{-dppa})_2(CH_3CN)_4][BF_4]_2$, where dppa is bis(diphenylphosphino)amine [5]. The first compound of any kind with a crosswise bridging acetonitrile ligand $W_2Cl_4(\mu\text{-dppm})_2(\mu,\eta^2\text{-}$

* Authors to whom correspondence should be addressed.

† Dedicated to Lord Lewis on the occasion of his 70th birthday.

CH_3CN), had been reported only about a year earlier by Eglin and coworkers [6]. Though nitrile complexes of this kind are still uncommon, isostructural and isoelectronic alkyne complexes are well established [7].

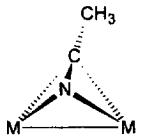

crosswise bridging

I

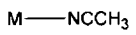

end-on coordination

II

In addition to the formation of a crosswise bridging acetonitrile molecule, the reaction of **1** with dppa led to another unusual result: a deprotonated dppa became linked to one acetonitrile molecule, as shown in Scheme 1. This dppa—CH_3CN coupled ligand (**III**) is monoanionic. It forms a six-membered ring with one of the Mo atoms as the result of a nucleophilic attack of the phosphine on the acetonitrile molecule.

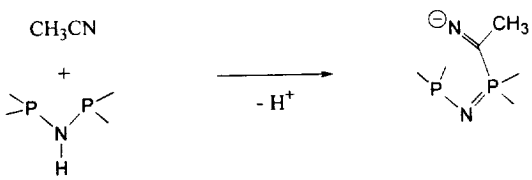

III

A practical problem with compound $\mathbf{1}\cdot 2CH_3CN$ is that it easily loses some acetonitrile and is thus difficult to handle in the crystalline form. Here we first report the structure of a more stable crystalline form of this compound, namely $[Mo_2(CH_3CN)_8(ax\text{-}CH_3CN)][BF_4]_4$ (**1a**). We have also characterized three compounds obtained from the reaction of **1a** with nucleophiles. With dppe, a dimolybdenum complex $[Mo_2(\mu,\eta^2\text{-}CH_3CN)(\mu\text{-}NC(CH_3)P(C_6H_5)_2CH_2CH_2P(C_6H_5)_2)(CH_3CN)_7][BF_4]_4$ (**2**), is produced. It contains a μ,η^2-CH_3CN ligand perpendicular to the metal-metal bond, and a new chelating ligand NC$(CH_3)P(Ph)_2CH_2CH_2\mathbf{P}(Ph)_2$ (**IV**) as well, which is formed by linking of dppe to acetonitrile, as shown in Scheme 2. When a trace amount of water is added to **2** at low temperature, the compound $[Mo_2(\mu,\eta^2\text{-}CH_3CNBF_3)(\mu,\eta^1\text{-}N(H)COCH_3)(CH_3CN)_8][BF_4]_3$ (**3**), is formed. Compound **3** has a BF_3 group bound to the N atom of the crosswise bridging μ,η^2-CH_3CN ligand. In addition, there is an acetamidate ligand, CH_3CONH^-, bridging both Mo atoms through the amide N atom in a μ,η^1 coordination mode. The bridging CH_3CNBF_3 ligand in **3** can also dissociate partially in solution to give $[Mo_2(\mu,\eta^2\text{-}CH_3CN)(\mu,\eta^1\text{-}N(H)CO\text{-}CH_3)(CH_3CN)_8][BF_4]_3$, (**3a**), and BF_3. When more than one equivalent of water is present, further hydrolysis of acetonitrile gives two acetamidate ligands and the complex $[Mo_2(\mu\text{-}N(H)COCH_3)_2(CH_3CN)_4][BF_4]_2$ (**4**) is formed. In this compound an Mo_2^{4+} core is supported by two acetamido ligands that bind in the previously known syn way [1] with the remaining four positions occupied by CH_3CN molecules.

EXPERIMENTAL

Materials and methods

All operations were carried out under an argon atmosphere using standard Schlenk or drybox techniques. Solvents were purified by conventional methods and distilled under nitrogen from CaH_2 or Na/K, as appropriate. Published procedures were used to synthesize **1** in amorphous form by drying it under vacuum [3]. Single crystals of $[Mo_2(CH_3CN)_8(ax\text{-}CH_3CN)][BF_4]_4$ (**1a**) were obtained by slow diffusion of a layer of toluene into an acetonitrile solution. Other chemicals, including dppe were purchased from Aldrich and were used as received. Infrared spectra were recorded in the range 4000–400 cm^{-1} on a Perkin–Elmer 16-PC spectrophotometer using KBr pellets. Nuclear magnetic resonance spectra were recorded on a Unity plus 300 spectrometer at 300 MHz for ^1H, 282 MHz for ^{19}F, and 121.4 MHz for ^{31}P. Reference standards were: ^1H, CH_3CN (1.95 ppm); ^{19}F, CCl_3F (0.00 ppm); ^{31}P, H_3PO_4 (0.00 ppm).

Preparation of $[Mo_2(\mu,\eta^2\text{-}CH_3CN)(\mu\text{-}NC(CH_3)P(C_6H_5)_2CH_2CH_2P(C_6H_5)_2)(CH_3CN)_7][BF_4]_4$ (**2**)

A mixture of **1a** (0.23 g, 0.25 mmol) and dppe (0.10 g, 0.25 mmol) was dissolved in acetonitrile (20 cm^3) to give a bright blue solution. After the solution was stirred for a few minutes, it turned dark green. Stirring was continued for 2 h and then toluene (20 cm^3) was injected underneath the resulting solution. Slow diffusion of the two layers gave green crystals of $[Mo_2(\mu,\eta^2\text{-}CH_3CN)(\mu\text{-}NC(CH_3)P(C_6H_5)_2CH_2CH_2P(C_6H_5)_2)(CH_3CN)_7][BF_4]_4\cdot 3$toluene, $\mathbf{2}\cdot 3$toluene, which were separated by filtration. Yield: 0.080 g, 20%. Another crop of **2**, namely $\mathbf{2}\cdot CH_3CN$, was isolated by layering the concentrated filtrate with diethylether (20 cm^3). Yield: 0.138 g, 41%. ^1H-NMR (300 MHz, CD_3CN, 20.0°C) δ (ppm): 7.12–8.14 (m, 20H, aromat. H), 3.63 (s, 3H, bridging CH_3CN), 3.35, 2.75 (m, 4H, coupled CH_3CN-dppe C_2H_4), 2.29 (s, 3H, coupled CH_3CN-dppe CH_3), 1.95 (s, terminal $NCCH_3$); $^{31}P\{^1H\}$-NMR (121.4 MHz, CD_3CN, 20.0°C) δ (ppm): 16.06, 13.96; $^{19}F\{^1H\}$-NMR (282.2 MHz, CD_3CN, 20.0°C) δ (ppm): −150.17 (NMR lines are generally broad.); IR (KBr) (cm^{-1}): 2963 (m), 2925 (m), 2320 (m), 2292 (m), 1638 (m), 1522 (w), 1485 (w), 1438 (m), 1370 (w), 1300 (w), 1262 (m), 1083 (vs), 803 (m), 742 (w), 693 (w).

Preparation of $[Mo_2(\mu,\eta^2\text{-}CH_3CNBF_3)(\mu\text{-}N(H)CO\text{-}CH_3)(CH_3CN)_8][BF_4]_3$ (**3**)

A mixture of **1a** (0.23 g, 0.25 mmol) and dppe (0.10 g, 0.25 mmol) was dissolved in acetonitrile (15 cm^3).

Table 1. Crystal data and structure refinement for **1a**, **2**·CH_3CN, **3**·$2CH_3CN$ and **4**·$2CH_3CN$

Compound	**1a**	**2**·CH_3CN	**3**·$2CH_3CN$	**4**·$2CH_3CN$
Formula	$C_{18}H_{27}B_4F_{16}Mo_2N_9$	$C_{46}H_{54}B_4F_{16}Mo_2N_{10}P_2$	$C_{24}H_{37}B_4F_{15}Mo_2N_{12}O$	$C_{16}H_{26}B_2F_8Mo_2N_8O_2$
Formula weight	908.61	1348.05	1029.78	727.95
Space group	*I*4	$P\bar{1}$	$P2_1$	*Aba*2
a(Å)	12.307(1)	11.515(4)	12.8560(8)	18.002(3)
b(Å)	12.307(1)	11.528(3)	11.979(1)	16.023(4)
c(Å)	11.692(1)	23.098(8)	14.441(1)	19.565(5)
α(°)	90	101.17(3)	90	90
β(°)	90	98.55(1)	102.798(5)	90
γ(°)	90	102.98(2)	90	90
V(Å^3)	1770.9(3)	2871(2)	2168.7(3)	5643(2)
Z	2	2	2	8
D_{calc} (g/cm^3)	1.704	1.559	1.577	1.714
Absorption coefficient (mm^{-1})	0.819	0.587	0.679	0.971
Radiation (Mo–K_α), Å	0.71073	0.71073	0.71073	0.71073
Temperature (K)	213(2)	213(2)	213(2)	213(2)
R indices [$I > 2\sigma(I)$] R_1, wR_2	0.049, 0.112	0.053, 0.119	0.038, 0.094	0.055, 0.144
R indices (all data) R_1, wR_2	0.057, 0.132	0.069, 0.133	0.041, 0.097	0.063, 0.149
Quality-of-Fit indicator	1.071	1.083	1.073	1.033

[a] $R_1 = \Sigma\|F_o| - |F_c\|/\Sigma|F_o|$.

[b] $wR_2 = [\Sigma w(F_o^2 - F_c^2)^2/\Sigma w(F_o^2)^2]^{1/2}$; $w = 1/\sigma^2(F_o^2) + (a \cdot p)^2 + b \cdot p$, $p = [\text{Max}(F_o^2 \text{ or } 0) + 2(F_c^2)]/3$. $a = 0.093$, $b = 0.0$ for **1**, $a = 0.040$ and $b = 16.1$ for **2**; $a = 0.045$ and $b = 5.06$ for **3**; $a = 0.11$ and $b = 9.8$ for **4**.

[c] Quality-of-fit $= w(|F| - |F|)^2/(N_{obs} - N_{parameters})^{1/2}$.

The solution was stirred for 1 h. At this stage, one equivalent of H_2O in 10 cm^3 acetonitrile (made by adding 4.5×10^{-2} cm^3 H_2O to 100 cm^3 CH_3CN) was added with a syringe and stirring was ceased after 30 min. Toluene (20 cm^3) was then injected underneath the resulting solution. Slow diffusion of the two solvent layers at −20°C gave purple crystals of $[Mo_2(\mu,\eta^2\text{-}CH_3CNBF_3)(\mu\text{-}N(H)COCH_3)(CH_3CN)_8][BF_4]_3 \cdot 2CH_3CN$, **3**·$2CH_3CN$. Yield: 0.257 g, 25%. ^{1}H-NMR (300 MHz, CD_3CN, 20.0°C) δ (ppm) 9.81 (br, 1H, acetamido NH), 3.37 (s, 3H, bridging $N(BF_3)CCH_3$), 2.81 (s, 3H, acetamido CH_3), 1.95 (s, terminal CH_3CN); $^{19}F\{^1H\}$-NMR (282.2 MHz, CD_3CN, 20.0°C) δ (ppm): −138.90 (br, bridging CH_3CNBF_3), −150.27 (s, BF_4^-); IR (KBr) (cm^{-1}): 3387 (s), 2317 (m), 2290 (m), 1375 (vw), 1701 (sh), 1636 (m), 1370 (m), 1300 (w), 1216 (m), 1084 (vs), 694 (w), 534 (m), 521 (m).

Preparation of $[Mo_2(\mu\text{-}N(H)COCH_3)_2(CH_3CN)_4][BF_4]_2$ (**4**)

A bright blue solution was obtained after **1a** (0.24 g, 0.26 mmol) and dppe (0.11g, 0.27 mmol) were dis solved in acetonitrile (20 cm^3). It became dark green after being stirred for 1 h. At this stage, H_2O (1.0×10^{-2} cm^3, 5.5 mmol) was added by a microsyringe. The green solution was stirred until the color changed to red, in about 10 h. Toluene (20 cm^3) was then injected underneath the resulting solution, and slow diffusion of the two layers at room temperature gave crystals of $[Mo_2(\mu\text{-}N(H)C(O)CH_3)_2(CH_3CN)_4][BF_4]_2 \cdot 2CH_3CN$, **4**·$2CH_3CN$. Yield: 0.153 g, 81%. ^{1}H-NMR (300 MHz, CD_3CN, 20.0°C) δ (ppm): 7.69 to 7.19 (br, 2H, bridging acetamidate NH), 2.13 (s, 6H, bridging acetamido ligands CH_3), 1.95 (s, terminal CH_3CN); $^{19}F\{^1H\}$-NMR (282.2 MHz, CD_3CN, 20.0°C) δ (ppm): −150.57 (s, BF_4^-); IR (KBr) (cm^{-1}): 3425 (m), 2939 (m), 2321 (m), 2292 (m), 1658 (s), 1578 (m), 1437 (m), 1262 (w), 1066 (vs), 804 (w), 748 (w), 697 (m), 521 (m).

Crystallographic studies

Crystals of each compound, **1a**, **2**·CH_3CN, **3**·$2CH_3CN$, and **4**·$2CH_3CN$, were mounted on the tips of glass fibers and cooled under a nitrogen stream on the Nonius FAST area-detector diffractometer at −60°C. Unit cell dimensions were obtained by indexing 250 strong reflections in the 2θ range of 18.0° to 41.8° and confirmed by taking axial images. Details of the use of the FAST diffractometer in our laboratory have been previously described [8]. The highly redundant data sets were corrected for Lorentz and polarization effects. The absorption corrections were based on fitting a function to the empirical transmission surface as sampled by the multiple equivalent measurements inherent in area detector data [9].

In each case the structure was solved by direct methods and refined using the SHELXTL programs

Table 2. Selected bond lengths [Å] and angles [°] for **1**

Mo(1)—Mo(2)	2.180(1)	Mo(2)—N(2)	2.12(1)
Mo(1)—N(1)	2.12(1)	Mo(2)—N(3)	2.36(1)
N(1)—C(1)	1.09(2)	C(1)—C(11)	1.44(3)
N(2)—C(2)	1.19(2)	C(2)—C(21)	1.42(3)
N(3)—C(3)	1.17(1)		

N(1)#2—Mo(1)—N(1)	159.0(5)	N(1)#1—Mo(1)—N(1)	88.1(1)
N(1)—Mo(1)—N(1)#3	88.1(1)	N(1)—Mo(1)—Mo(2)	100.5(3)
N(2)#2—Mo(2)—N(2)	161.9(9)	N(2)#1—Mo(2)—N(2)	88.6(1)
N(2)—Mo(2)—Mo(1)	99.0(4)	N(2)£2—Mo(2)—N(2)#3	88.6(1)
N(2)—Mo(2)—N(3)	81.0(4)	N(2)#1—Mo(2)—N(3)	81.0(4)
C(1)—N(1)—Mo(1)	174(2)	C(2)—N(2)—Mo(2)	178(2)

Symmetry transformations used to generate equivalent atoms: #1 $-y+2, x, z$, #2 $-x+2, -y+2, z$, #3 $y, -x+2, z$.

[10]. Disorder of the BF_4^- ions was encountered during structural refinement for **1a**, **2**·CH_3CN and **4**·$2CH_3CN$. Atoms of the disordered anions were refined isotropically. Final residuals and figures of merit and other crystallographic details for all structures are reported in Table 1.

The structure of the $[Mo_2(CH_3CN)_8(ax\text{-}CH_3CN)]^{4+}$ core of **1a** was refined anisotropically and all hydrogen atoms were placed in calculated positions. Careful consideration was given to the choice of the chiral space group *I*4. The molecule is incompatible with any other space group, but there was some evidence that the crystals were enantiomeric twins. Inclusion of the inversion twin law in the refinement resulted in successful refinement of the model. Selected bond distances and angles are listed in Table 2.

Two crystalline forms for compound **2** have been obtained. Crystals of the toluene solvate, **2**·3toluene, were very thin plates, from which only a weak data set was collected.* Crystals of the acetonitrile solvate, **2**·CH_3CN, were of better quality for single crystal X-ray analysis. During refinement, one of the four independent phenyl groups of the dppe ligand was found to be disordered with the two orientations being slightly displaced from each other and having occupancies of 0.7 and 0.3. Displacement parameters in the disordered group were refined isotropically. Hydrogen atoms were included in calculated positions. Selected bond distances and angles are listed in Table 3.

Compound **3**·$2CH_3CN$ crystallized in the chiral monoclinic space group $P2_1$. The absolute structure of **3**·$2CH_3CN$ was determined from the Flack parameter [$x = -0.13(5)$] [11]. All non-hydrogen atoms of the metal complex were refined with anisotropic displacement parameters, and hydrogen atoms were included in calculated positions. Selected bond distances and angles are listed in Table 4.

Compound **4**·$2CH_3CN$ crystallizes in the centered orthorhombic space group *Aba*2. Both acetamido ligands are disordered; the O and N atoms are best refined as distributed evenly on each side of the monoanionic ligand. Hydrogen atoms were included in calculated positions during final refinement. Selected bond distances and angles for **4**·$2CH_3CN$ are listed in Table 5.

Other crystallographic data, including that for **2**·3toluene, are given as supplementary material. Supplementary data have been deposited with the Cambridge Crystallographic Data Centre.**

RESULTS AND DISCUSSIONS

Compound **1a**

Published procedures [3b] were used to prepare **1** as an amorphous powder material. It was then recrystallized by allowing toluene to diffuse into a concentrated acetonitrile solution giving a nonaacetonitrile species (**1a**) instead of the crystalline decaacetonitrile complex reported earlier [3].

A perspective view of the $[Mo_2(CH_3CN)(ax\text{-}CH_3CN)]^{4+}$ core of compound **1a** is shown in Fig. 1. It consists of a discrete $[Mo_2]^{4+}$ unit with Mo—Mo distance of 2.180(1) Å. Both Mo atoms and the axially coordinated CH_3CN ligand reside on a crystallo-

*Compound **2**·3toluene crystallizes in orthorhombic space group $P2_12_12$ with the following unit cell parameters: $a = 22.710(3)$ Å, $b = 25.976(5)$ Å, $c = 11.4213(8)$ Å, $V = 6738(2)$ Å^3, and $Z = 4$. Data were collected on a Nonius FAST area detector system with Mo–K_α radiation. Because the data set had a low data to parameter ratio, (4.2 : 1 for $I > 2\sigma(I)$), we did not attempt a complete refinement of the structure. However, the chemical composition was clear from the preliminary study. Further crystal data and atomic coordinates for **2**·3toluene have been deposited with the Cambridge Crystallographic Data Centre.

Supplementary material available: Table of positional parameters for **1a, **2**·CH_3CN, **2**·3toluene, **3**·$3CH_3CN$, **4**·$2CH_3CN$, full tables of displacement parameters and molecular dimensions (50 pages).

Table 3. Selected bond lengths (Å) and angles (°) for **2**·CH_3CN

Mo(1)—Mo(2)	2.488(1)	Mo(2)—C(91)	2.096(6)
Mo(1)—N(1)	2.192(5)	P(1)—C(1)	1.836(6)
Mo(1)—N(2)	2.150(6)	C(1)—C(2)	1.550(9)
Mo(1)—N(3)	2.227(6)	P(2)—C(2)	1.825(6)
Mo(2)—N(4)	2.198(5)	P(1)—C(11P)	1.810(6)
Mo(2)—N(5)	2.214(6)	P(1)—C(21P)	1.839(6)
Mo(2)—N(6)	2.150(6)	P(2)—C(31P)	1.798(6)
Mo(2)—N(7)	2.126(6)	P(2)—C(41P)	1.805(7)
Mo(2)—N(8)	2.049(5)	P(2)—C(81)	1.826(6)
Mo(2)—N(9)	2.113(5)	N(8)—C(81)	1.305(8)
Mo(1)—N(8)	2.034(5)	C(81)—C(82)	1.500(8)
Mo(1)—N(9)	2.122(5)	N(9)—C(91)	1.269(8)
Mo(1)—C(91)	2.099(6)	C(91)—C(92)	1.514(9)
Mo(1)—P(1)	2.566(2)		

Mo(1)—N(8)—Mo(2)	75.1(2)	Mo(2)—N(9)—Mo(1)	72.0(2)
C(1)—C(2)—P(2)	120.1(4)	C(81)—N(8)—Mo(2)	139.0(4)
C(1)—P(1)—C(21P)	104.9(3)	C(11P)—P(1)—Mo(1)	120.6(2)
C(1)—P(1)—Mo(1)	107.6(2)	N(8)—C(81)—P(2)	119.0(4)
C(11P)—P(1)—C(1)	105.1(3)	C(11P)—P(1)—C(21P)	102.5(3)
C(2)—P(2)—C(81)	112.7(3)	C(2)—C(1)—P(1)	115.6(4)
C(21P)—P(1)—Mo(1)	114.7(2)	C(31P)—P(2)—C(41P)	107.7(3)
C(31P)—P(2)—C(2)	107.5(3)	C(41P)—P(2)—C(2)	110.0(3)
C(31P)—P(2)—C(81)	107.3(3)	C(41P)—P(2)—C(81)	111.3(3)
C(81)—N(8)—Mo(1)	145.8(4)	C(91)—N(9)—Mo(2)	71.8(3)
C(82)—C(81)—P(2)	115.3(4)	C(92)—C(91)—Mo(1)	135.9(5)
C(91)—N(9)—Mo(1)	71.5(4)	N(9)—C(91)—C(92)	136.2(6)
N(8)—C(81)—C(82)	125.7(6)	C(92)—C(91)—Mo(2)	137.5(5)
N(9)—C(91)—Mo(1)	73.5(4)	Mo(2)—C(91)—Mo(1)	72.8(2)
N(9)—C(91)—Mo(2)	73.2(4)		

Table 4. Selected bond lengths (Å) and angles (°) for **3**·$2CH_3CN$

Mo(1)—Mo(2)	2.4697(7)	Mo(2)—N(9)	2.095(7)
Mo(1)—N(1)	2.177(7)	Mo(1)—N(10)	2.100(6)
Mo(1)—N(2)	2.121(6)	Mo(1)—C(91)	2.096(6)
Mo(1)—N(3)	2.164(5)	Mo(2)—C(91)	2.094(7)
Mo(1)—N(4)	2.120(6)	N(9)—C(91)	1.30(1)
Mo(2)—N(5)	2.179(8)	C(91)—C(92)	1.501(9)
Mo(2)—N(6)	2.149(6)	N(10)—C(101)	1.428(9)
Mo(2)—N(7)	2.191(6)	C(101)—C(102)	1.50(1)
Mo(2)—N(8)	2.123(6)	N(9)—B(1)	1.59(1)
Mo(1)—N(9)	2.089(6)	N(10)—F(6)	2.98(1)
Mo(2)—N(10)	2.103(6)	H(10)···F(6)	2.069(9)

Mo(1)—N(9)—Mo(2)	72.3(2)	N(9)—C(91)—C(92)	133.7(6)
Mo(1)—N(10)—Mo(2)	72.0(2)	N(10)—C(101)—C(102)	115.9(7)
Mo(2)—C(91)—Mo(1)	72.2(2)	N(10)—H(10)—F(6)	174.6(3)
C(91)—N(9)—B(1)	130.2(6)	C(101)—N(10)—H(10)	111.3(4)
O(1)—C(101)—N(10)	122.2(7)	O(1)—C(101)—C(102)	121.9(7)

graphic four-fold axis. The two crystallographically independent bond distances between the Mo atoms and the equatorial N atoms are 2.12(1) Å, while that for the axially coordinated N atom is 2.36(1) Å. The structure of **1a** is quite similar to that of **1** [3a] except for the absence of one axial CH_3CN molecule. In the case of **1** the Mo—N distances were 2.13 Å (mean) and 2.600 Å for the equatorial and axial ones, respectively.

The ^1H NMR spectrum of **1a** in CD_3CN shows only one peak at 1.95 ppm; which is an indication that the

Table 5. Selected bond lengths (Å) and angles (°) for **4**·2CH_3CN

Mo(1)—Mo(2)	2.144(2)	Mo(1)—N(1)	2.07(1)
Mo(1)—O(2)	2.07(1)	Mo(1)—N(3)	2.15(2)
Mo(1)—N(5)	2.16(1)	Mo(2)—O(1)	2.09(1)
Mo(2)—N(2)	2.08(1)	Mo(2)—N(4)	2.15(2)
Mo(2)—N(6)	2.17(1)	O(1)—C(1)	1.33(2)
N(1)—C(1)	1.23(2)	O(2)—C(3)	1.25(2)
N(2)—C(3)	1.27(2)		

O(2)—Mo(1)—N(1)	88.3(4)	O(2)—Mo(1)—Mo(2)	91.4(3)
N(1)—Mo(1)—Mo(2)	91.6(3)	O(2)—Mo(1)—N(3)	164.9(5)
N(1)—Mo(1)—N(3)	86.6(5)	N(1)—Mo(1)—N(5)	168.4(5)
Mo(2)—Mo(1)—N(3)	102.9(4)	Mo(2)—Mo(1)—N(5)	99.9(3)
O(2)—Mo(1)—N(5)	89.8(5)	N(2)—Mo(2)—O(1)	90.2(4)
N(3)—Mo(1)—N(5)	92.3(5)	O(1)—Mo(2)—Mo(1)	90.0(3)
N(2)—Mo(2)—Mo(1)	90.8(3)	O(1)—Mo(2)—N(4)	90.8(5)
N(2)—Mo(2)—N(4)	166.8(5)	Mo(1)—Mo(2)—N(4)	102.3(4)
O(1)—Mo(2)—N(6)	168.4(4)	N(2)—Mo(2)—N(6)	89.9(4)
Mo(1)—Mo(2)—N(6)	101.6(3)	N(4)—Mo(2)—N(6)	86.5(5)
C(1)—O(1)—Mo(2)	118(1)	C(1)—N(1)—Mo(1)	121(1)
C(3)—O(2)—Mo(1)	117(1)	C(3)—N(2)—Mo(2)	116.5(9)
N(1)—C(1)—O(1)	119(1)	N(1)—C(1)—C(2)	121(2)
O(1)—C(1)—C(2)	120(2)	O(2)—C(3)—N(2)	124(1)
C(5)—N(3)—Mo(1)	169(1)	O(2)—C(3)—C(4)	116(2)
N(2)—C(3)—C(4)	120(1)		

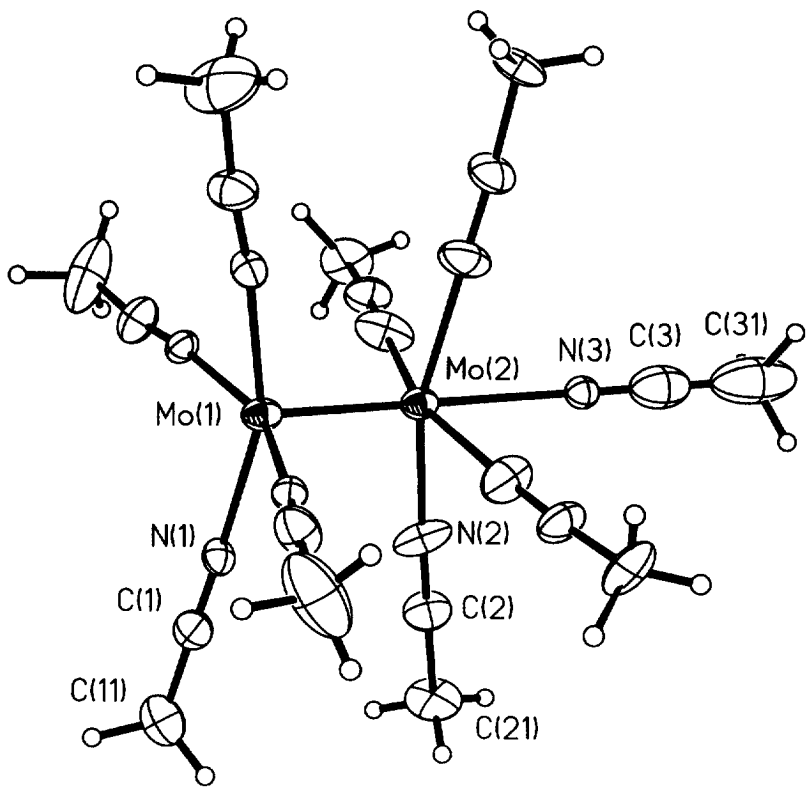

Fig. 1. The $[Mo_2(CH_3CN)_8(ax\text{-}CH_3CN)]^{4+}$ cation in **1a**. Thermal displacement ellipsoids are shown at the 30% probability level; hydrogen atoms are omitted.

CH_3CN ligands are labile and undergo rapid exchange with the solvent; a similar result was previously observed for complex **1** [3a]. In solution **1a** is very sensitive to its environment. It is important that only freshly distilled acetonitrile be used for the reactions, otherwise decomposition of **1a** gives a brown solution in less than one day.

Compound **2**

The reaction of **1a** with bis(diphenylphosphino)ethane, dppe, in acetonitrile at room temperature produces compound **2** (eqn (1)).

$$[Mo_2(CH_3CN)_8(ax\text{-}CH_3CN)][BF_4]_4 + dppe \xrightarrow[CH_3CN]{} [Mo_2(\mu,\eta^2\text{-}CH_3CN)(\mu\text{-}NC(CH_3)PPh_2\text{-}CH_2CH_2PPh_2)(CH_3CN)_7][BF_4]_4 \quad (1)$$

The reaction takes place quickly as an obvious color change from bright blue to dark green occurs within a few minutes.

The bonding of the newly formed ligand **IV** is unusual. It forms a seven-membered ring with one of the Mo atoms. Though the $NC(CH_3)P(Ph_2)CH_2CH_2PPh_2$ ligand itself is neutral, formally there is a partial charge distribution that makes the coupled phosphorus atom P(2) of dppe positive (i.e. it is effectively quaternized) and the acetonitrile nitrogen atom N(8) negative. As shown in Table 3, the bonds from the formally charged P atom to its adjacent atoms are about 0.01 to 0.03 Å shorter than those for the phosphine atom P(1). Thus the CH_3CN-dppe coupled ligand **IV** can be considered as consisting of a four electron donor imino group bridging the Mo atoms. As shown in Fig. 2, atom N(8) bridges both Mo atoms with Mo—N distances of 2.034(5) Å and 2.049(5) Å with a very acute Mo(1)—N(8)—Mo(2) angle of 75.1(2)°. This seven membered ring differs from that of the previously reported dppa compound [5], where a nitrogen to phosphorus double bond produces a coplanar six membered ring. Nevertheless, they are chemically related as shown in Scheme 3.

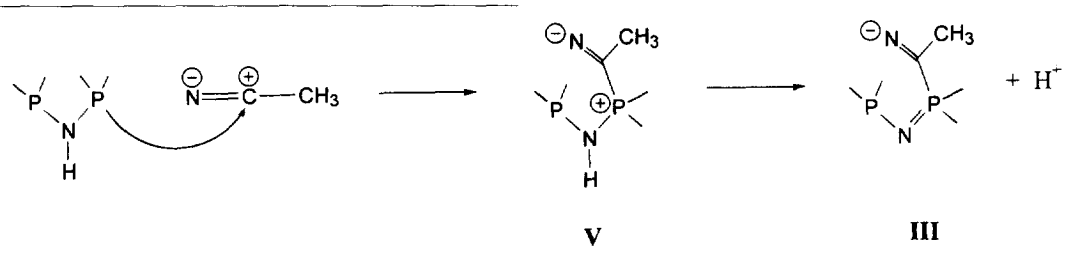

V **III**

The structure of the cation in $2 \cdot CH_3CN$ is shown in Fig. 2. Two important features merit comment. First, there is a μ,η^2-CH_3CN ligand which is perpendicular to the Mo—Mo bond. This coordination mode is well known for alkyne complexes but there are only a few examples for nitrile compounds [5]. Coordination of the CH_3CN molecule to the dinuclear system increases the N—C bond distance to 1.269(8) Å and decreases the N—C—CH_3 angle to 136.2(6)°. Second, a new chelating ligand $NC(CH_3)P(Ph_2)CH_2CH_2PPh_2$, **IV**, is formed as shown in Scheme 2. One of the P atoms of the dppe group is bonded to the carbon atom of an acetonitrile molecule; the formal oxidation state of this P atom changes from +3 to +5.

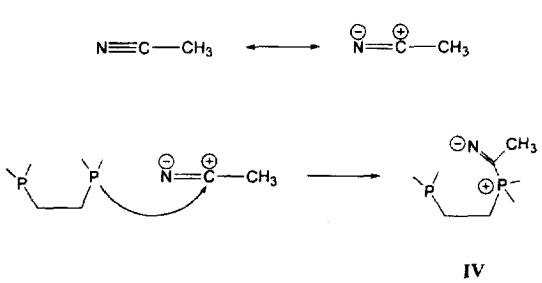

IV

The monoanionic CH_3CN-dppa coupled ligand **III** is formed by deprotonation of the neutral intermediate **V**, which is less stable than that formed by dppe and CH_3CN. The dimolybdenum unit changes from a paddlewheel structure in the starting material to an edge-sharing one in **2**. As a consequence the Mo—Mo distance increases from 2.180(1) to 2.488(1) Å, which is in the range found for double bonded edge-sharing dimolybdenum compounds [12].

Spectroscopic data are also consistent with the formation of **2**. The methyl group of the μ,η^2 acetonitrile molecule shows a peak at 3.63 ppm in ^1H NMR. The complex multiplets centered at 3.35 and 2.75 ppm are in agreement with the unsymmetrical environment of the C_2H_4 group in the coupled CH_3CN-dppe ligand **IV**; a singlet at 2.29 ppm corresponds to the CH_3 group of the CH_3CN-dppe ligand. The $^{31}P\{^1H\}$ NMR spectrum of compound **2** shows two signals of equal intensity at 16.06 and 13.96 ppm which is consistent with the two P atoms of the modified dppe moiety being chemically different. The $^{19}F\{^1H\}$ NMR spectrum exhibits a single peak for the BF_4^- counter anions at −150.17 ppm. An IR band at 1638 cm^{-1} is assigned to the μ,η^2-CH_3CN ligand; the terminal acetonitrile stretching vibrations are at 2317

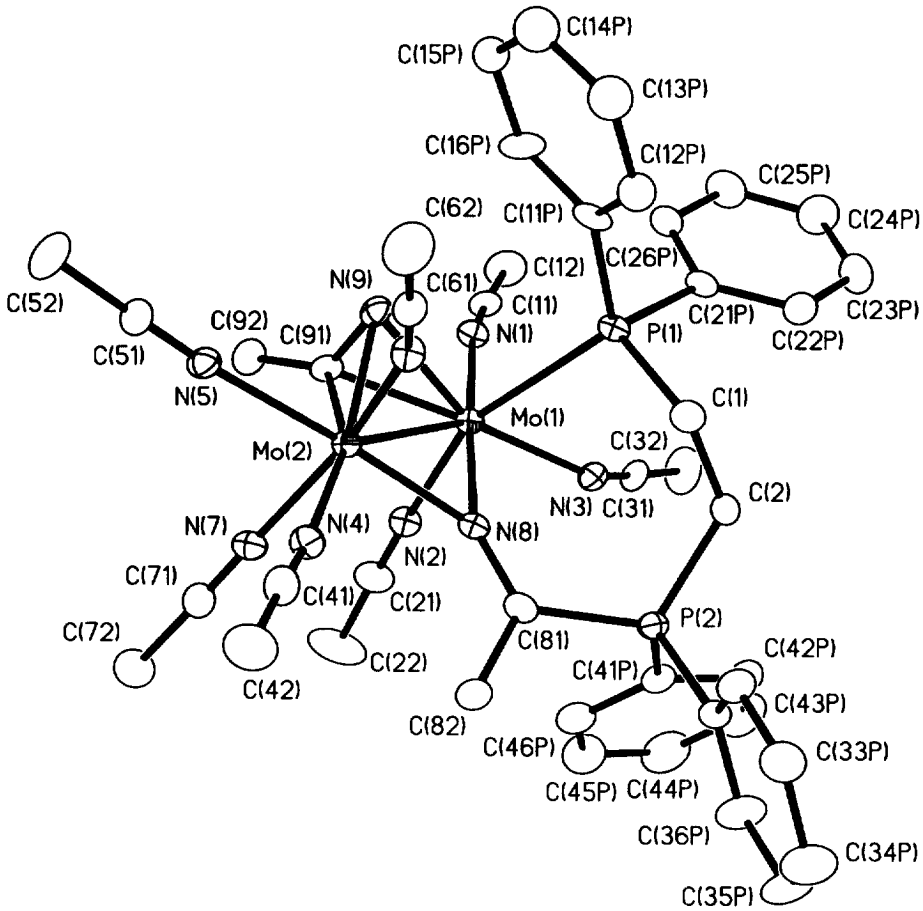

Fig. 2. The $[Mo_2(\mu,\eta^2\text{-}CH_3CN)(\mu\text{-}NC(CH_3)P(C_6H_5)_2CH_2CH_2P(C_6H_5)_2)(CH_3CN)_7]^{4+}$ cation in compound **2** · CH_3CN. Atoms are represented by their thermal displacement ellipsoids at the 30% probability level; hydrogen atoms are omitted.

and 2290 cm^{-1}. All of the features are fully consistent with the solid state structure.

Solutions of compound **2** are extremely sensitive to impurities. Thus, it is critical that freshly distilled acetonitrile be used for the reaction in order to isolate the described product. If even traces of water are present, decomposition of **2** occurs and the color of the reaction solution changes from green to purple. Materials isolated from such a reaction mixture show a broad signal at 9.8 ppm in the ^1H NMR, which is consistent with the existence of an amido NH group. Unfortunately, crystals of the isolated purple material are badly twinned preventing a detailed investigation of the solid-state structure [13], and we have made no further attempt to characterize this substance. Further comments on it will be found in the section entitled Conclusions.

Compound **3**

To understand the chemistry of the highly reactive CH_3CN-dppe coupled compound **2**, the result of careful, deliberate hydrolysis of **2** was studied. When a trace amount of water is introduced into the reaction system at low temperature, a reaction takes place that leads to the formation of an isolable acetamidate-coordinated compound **3** (eqn (2)).

$$[Mo_2(\mu,\eta^2\text{-}CH_3CN)(\mu\text{-}NC(CH_3)PPh_2CH_2CH_2PPh_2)(CH_3CN)_7][BF_4]_4 + H_2O \xrightarrow[CH_3CN]{} [Mo_2(\mu,\eta^2\text{-}CH_3CNBF_3)(\mu\text{-}N(H)COCH_3)(CH_3CN)_8][BF_4]_3 + HF + dppe \quad (2)$$

The structure of the cation of **3** · $2CH_3CN$ is shown in Fig. 3. There is a bridging acetonitrile moiety perpendicular to the M—M bond. A BF_3 group is also bound to the N atom of the bridging acetonitrile with a B—N distance of 1.59(1) Å. The crosswise bridged acetonitrile moiety has an N—C distance of 1.30(1) Å and an N—C—CH_3 angle of 133.7(6)° similar to that in **2**. Introducing a trace amount of water forms the acetamidate ligand $^-HNCOCH_3$; no coupling is

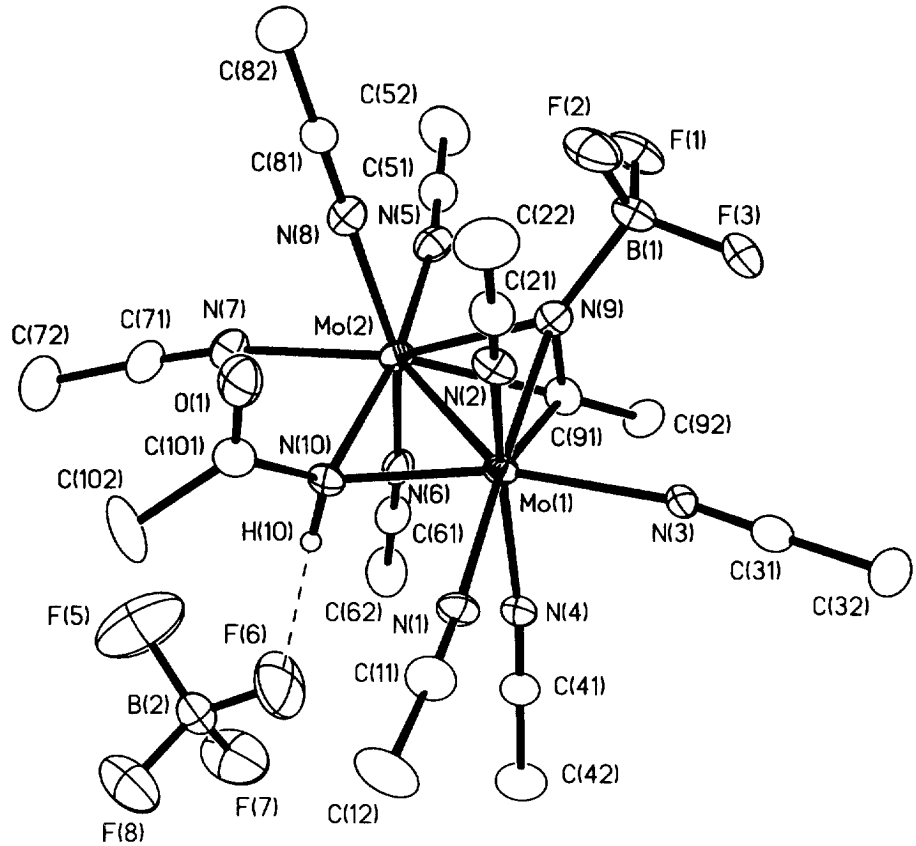

Fig. 3. The cation in $3 \cdot 2CH_3CN$, together with one hydrogen-bonded BF_4^- ion. Atoms are represented by their thermal displacement ellipsoids at the 30% probability level; hydrogen atoms are omitted.

observed. The N atom of the acetamidate ligand binds to both Mo atoms with Mo—N distances of 2.100(6) and 2.103(6) Å. The existence of an amidate NH^- group also leads to hydrogen bonding to one of the BF_4^- counter anions, as shown in Fig. 3. The N(10)—F(6) distance is 2.98(1) Å and the N(10)—H(10)—F(6) angle is 174.6(3)°. It is interesting to notice that the monodentate resonance form **VIa** (Scheme 4) is stabilized in this compound instead of the bidentate form **VIb**, in which the electronic structure of the ligand is delocalized.

The proton NMR spectrum for **3**, Fig. 4(a), shows

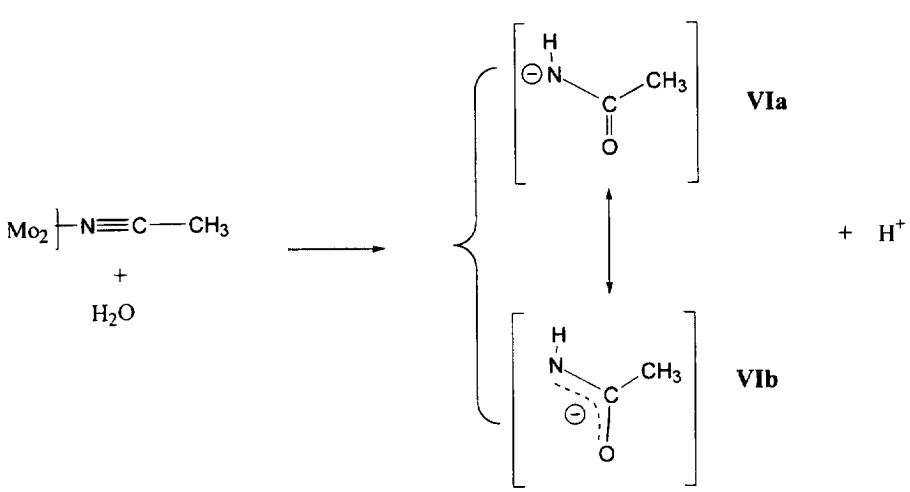

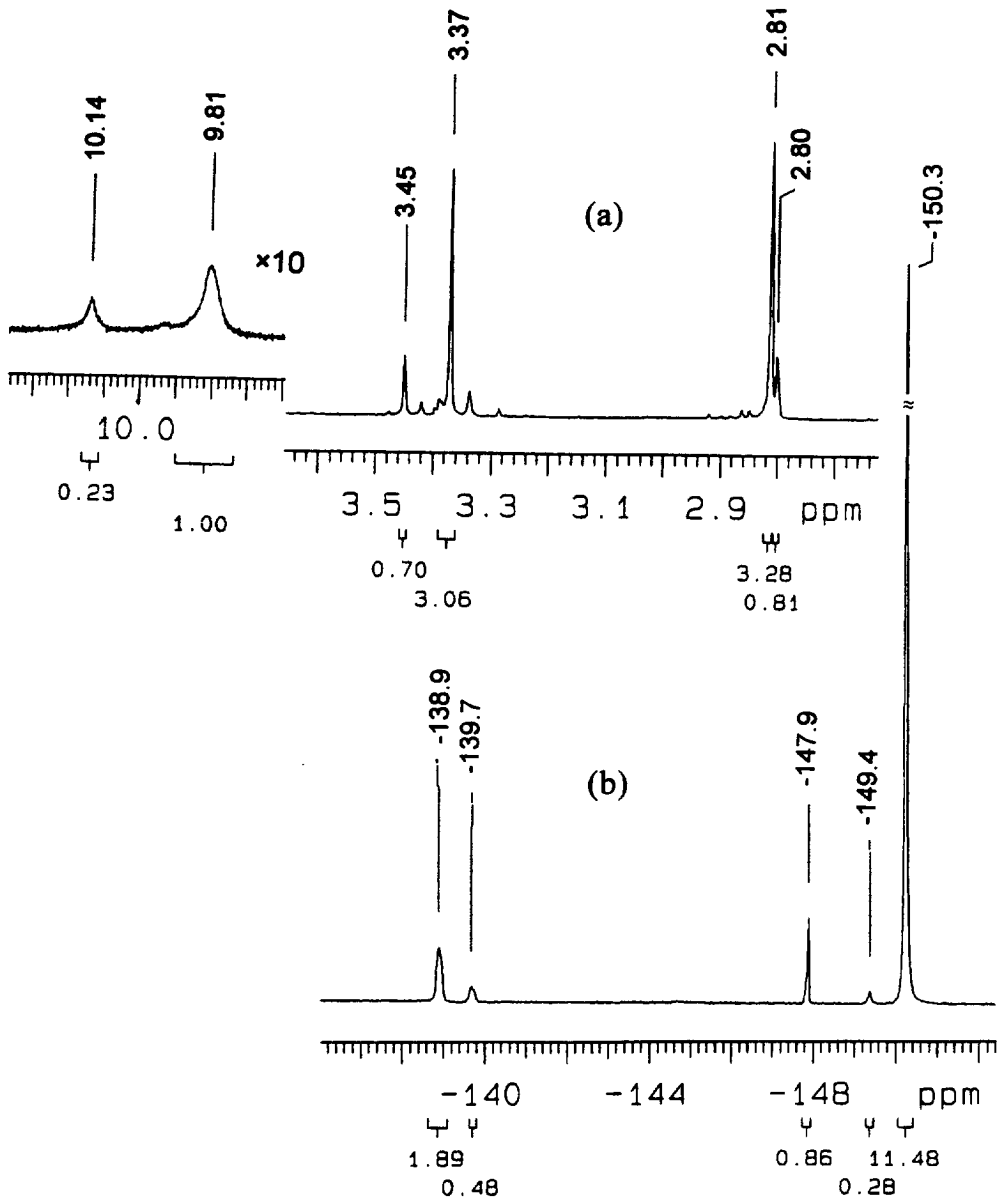

Fig. 4. (a) Proton NMR spectrum of **3** in CD_3CN showing the existence of two sets of N—H and CH_3 groups. One set of resonances with higher intensities corresponds to the bridging CH_3CNBF_3 and acetamidate ligands in **3**; the other set is for the bridging CH_3CN and acetamidate ligands in **3a**. (b) The $^{19}F\{^1H\}$ NMR spectrum of **3** in CD_3CN.

that the molecule persists in solution but that it partly dissociates to release the BF_3 group, giving **3a**. For **3** and **3a** there are broad signals at 9.81 and 10.14 ppm due to the N—H protons, with an intensity ratio of about 4 : 1. Upfield, in the aliphatic C—H region there are signals at 2.81 ppm for the amidate CH_3 group and 3.37 ppm for the CH_3 group in CH_3CNBF_3 in **3**. Signals that correspond to the amidate and μ,η^2—CH_3CN groups in **3a** are seen at 3.45 and 2.80 ppm, respectively at about 0.25 the intensity.

Turning now to the ^{19}F spectrum, Fig 4(b), we found a strong signal at −150.3 ppm for the BF_4^- ions. The peaks at −138.9 and −139.7 can be assigned to the BF_3 moieties, the former ones bound in the μ,η^2—CH_3CNBF_3 group and the latter being free CH_3CNBF_3 molecules arising from the dissociation. The assignments of the signals at −147.9 and −149.4 ppm are uncertain. A possible assignment of the signal at −147.9 is to $B_2F_7^-$ [14]. If this is correct, we get a fairly good fit to the relative intensities. The intensity of the signal would be apportioned in a prorata way to its formal components, $BF_3 + BF_4^-$. Thus the "total" BF_3 intensity would be 1.89 + 0.48 + 0.37 = 2.74 and the "total" BF_4^- inten-

sity would be 11.48+0.49 = 11.97. The ratio 11.97/2.74 = 4.37 is in fair agreement with the ideal ratio of 4.0.

The formation of acetamide by hydrolysis of coordinated acetonitrile is well known [15].

Compound **4**

Compound **4** is formed by adding an excess of water to the acetonitrile solution of **1a** and dppe. As the reaction proceeds, the color of the mixture changes gradually from green to purple to red (eqn (3)).

$$[Mo_2(CH_3CN)_8(ax\text{-}CH_3CN)][BF_4]_4 + 2H_2O \xrightarrow[CH_3CN]{dppe} [Mo_2(\mu\text{-}N(H)COCH_3)_2(CH_3CN)_4][BF_4]_2 + 2HBF_4 \quad (3)$$

Compound $4 \cdot 2CH_3CN$ has a paddlewheel structure with two bidentate amidate ligands *cis* to each other as shown in Fig. 5. Though it is possible that a *trans* isomer may be produced from the hydrolysis of **1a**, it is not seen in the solid state. In this bisacetamidate-bridged complex, the positions of the N and O atoms are best described as evenly occupied by both N and O atoms. This disorder could be due to "head to tail" (**VIIa**) or "head to head" molecules (**VIIb**) pointing in both directions or to a random mixture of "head to tail" and "head to head" molecules. The X-ray results do not discriminate among these possibilities. Perhaps a disorder of "head to tail" molecules is most likely.

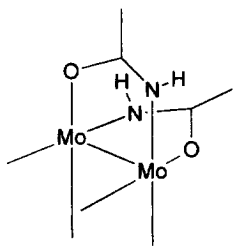

VIIa

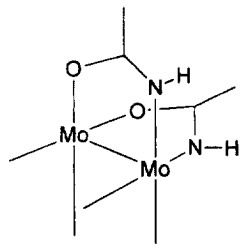

VIIb

Distances from the O or N atoms of the acetamidate ligands to the Mo atoms are in the range of 2.07(1) to

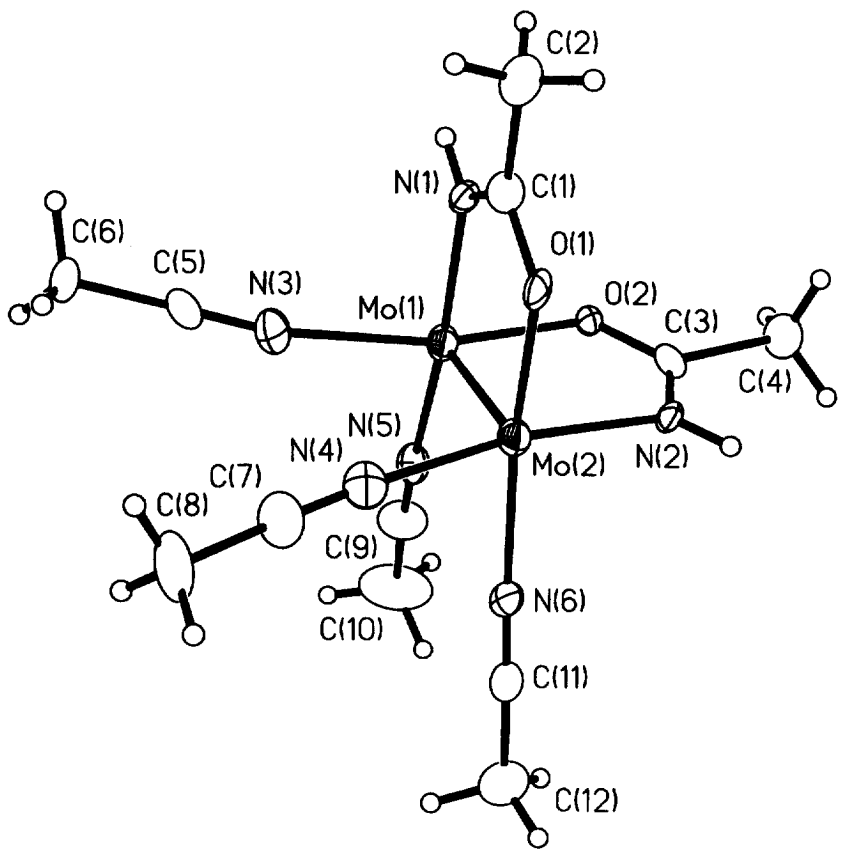

Fig. 5. The cation in $4 \cdot 2CH_3CN$. Atoms are represented by their thermal displacement ellipsoids at the 30% probability level. Hydrogen atoms are drawn as spheres of arbitrary size.

2.09(1) Å. The Mo—Mo bond distance is 2.144(2) Å; it is shorter than that of the starting material $[Mo_2(CH_3CN)_8(ax\text{-}CH_3CN)][BF_4]_4$ (**1a**) and similar to that of the closely related bisacetate acetonitrile cation $[Mo_2(O_2CCH_3)_2(CH_3CN)_4]^{2+}$, in which the Mo—Mo distance is 2.133 Å [16].

Both acetamidate ligands adopt the delocalized electron structure **VIb** shown in Scheme 4, as they are bidentate. The fact that **4** exhibits only a broad peak at 2.13 ppm for the acetamidate CH_3 group in the ^1H NMR spectrum is in agreement with the observation that only the *cis* isomer exists in the solid state. The broad signals that appear between 7.69 and 7.19 ppm for the amido NH groups of the bridging acetamidate ligands might indicate the coexistence of "head to tail" or "head to head" configurations in the *cis* isomer. The $^{19}F\{^1H\}$ NMR spectrum of **4** has a single resonance at −150.57 ppm for the BF_4^- ions. The existence of two BF_4^- counteranions in the crystal structure of **4** also implies that the Mo atoms are in an oxidation state of +2.

CONCLUSIONS

The genesis of this work was the observation made many years ago in this laboratory that treatment of a solution of **1** with a phosphine (with the intention, originally, of simply replacing coordinated CH_3CN ligands by phosphines) led to the formation of a purple product. Crystals of this purple product have been obtained several times, but the structure was not cleanly determined because of disorder and/or twinning. This crystallographic problem has never been overcome.

As far as could be determined, the purple product consists of a tetrapositive dimolybdenum cation with an edge-sharing bioctahedral structure and four BF_4^- ions. The eight terminal ligands in this cation are clearly seen as end-coordinated CH_3CN molecules, but the bridging ligands could not be cleanly resolved. No phosphine is present in this product. The present investigation was undertaken to see what leads up to this purple product, and we have, indeed, gained much insight into that aspect of the chemistry.

Three dimolybdenum compounds that contain ligands which result from the transformation of acetonitrile molecules have been prepared and structurally characterized. The common feature of these ligands is that they result from nucleophilic attacks on the cyanide carbon atom of the acetonitrile by phosphine and water. Depending on the reaction conditions, crosswise bridging acetonitrile, coupled CH_3CN-dppe, μ,η^1 and μ,η^2 coordinated acetamidate ligands have been observed.

The single crystal X-ray structures of compounds **2** and **3** confirmed an edge-sharing bioctahedral geometry. The bonding of the crosswise bridging acetonitrile molecules to the Mo atoms in both compounds are similar: the bridging acetonitrile ligands bend upon coordination and their C—N distances are close to the ideal value for sp^2-hybridized carbon atoms. In compound **3**, the bridging acetonitrile ligand also coordinates to a BF_3 molecule which is labile and can dissociate in acetonitrile solution to produce **3a**.

In addition to the formation of bridging acetonitrile molecules, there is a CH_3CN-dppe coupled chelating ligand $NC(CH_3)P(Ph_2)\,CH_2CH_2PPh_2$ in compound **2**. Although the ligand is neutral, there is a formally localized negative charge on the N atom and a positive charge on the neighboring P atom. According to the valence structure, this negatively charged N atom can be considered as a four electron donor. The difference between the coupled CH_3CN-dppe ligand and the previously reported coupled CH_3CN-dppa ligand is that the amine NH group in dppa can be readily deprotonated to give a monoanionic ligand. These two compounds provide examples of nucleophilic attacks by phosphine molecules on a nitrile carbon atom.

Hydrolysis then produces acetamidate ligands, which coordinate in a manner that depends on reaction conditions. By introducing a trace amount of water to a cold solution of compound **2**, compound **3** is obtained. When two equivalents of water are added at ambient temperature, compound **4** is isolated in which neither coupled dppe nor a bridging acetonitrile ligand is observed. Instead, there are two acetamidate ligands bridging both Mo atoms in **4**.

We now believe that the purple compound is an intermediate between **2** and/or **3** and the ultimate hydrolysis product **4**, but exactly what it is still remains uncertain.

Acknowledgments—We are grateful to the Robert A. Welch Foundation for their financial support of this work.

REFERENCES

1. Cotton, F. A. and Walton, R. A., Muliple Bonds Between Metal Atoms, 2nd edn, Oxford University Press, Oxford, 1993, Chapter 3.
2. (a) Comrie, A. G., McVitie, A. and Peacock, R. D., *Polyhedron*, 1994, **13,** 193; (b) Bino, A., Cotton, F. A. and Fanwick, P. E., *Inorg. Chem.*, 1979, **18,** 3558; (c) Cotton, F. A., Troup, J. M., Webb, T. R., Williamson D. H. and Wilkinson, G., *J. Am. Chem. Soc.*, 1974, **96,** 3824.
3. (a) Cotton, F. A. and Wiesinger, K. J., *Inorg. Chem.*, 1991, **30,** 871; (b) Cotton, F. A. and Wiesinger, K. J., *Inorg. Synth.*, 1992, **29,** 134.
4. Cotton, F. A., Eglin, J. L. and Wiesinger, K. J., *Inorg. Chim. Acta*, 1992, **195,** 11.
5. Cotton, F. A. and Kuhn, F. E., *J. Am. Chem. Soc.*, 1996, **118,** 5826.
6. Eglin, J. L., Hines, E., Valente, E. J. and Zubkowski, J. D., *Inorg. Chim. Acta*, 1995, **229,** 113.
7. Amouri, H. E. and Gruselle, M., *Chem. Rev.*, 1996, **96,** 1077.
8. Bryan, J. C., Cotton, F. A., Daniels, L. M., Haef-

ner, S. C. and Sattelberger, A. P., *Inorg. Chem.*, 1995, **34,** 1875.
9. Blessing, R. H., *Acta Cryst.*, 1995, **A51,** 33.
10. SHELXTL V.5, Siemens Industrial Automation, Madison, WI, 1990.
11. Flack, H. D., *Acta Cryst.*, 1983, **A39,** 876.
12. Cotton, F. A., Maloney. D. J. and Su, J., *Inorg. Chim. Acta*, 1995, **236,** 21.
13. Cotton, F. A., Daniels, L. M. and Wiesinger, K. J. Unpublished results.
14. The $B_2F_7^-$ ion has been reported. See for example, Harris, J. J., *Inorg. Chem.*, 1966, **5,** 1627.
15. (a) Erxleben, A. and Lippert, B., *J. Chem. Soc., Dalton Trans.*, 1996, 2329 and references therein; (b) Erxleben, A., Mutikainen, I. and Lippert, B., *J. Chem. Soc., Dalton Trans.*, 1994, 3667; (c) Cini, R., Fanizzi, F. P., Intini, F. P., Maresca, L. and Natile, G., *J. Am. Chem. Soc.*, 1993, **115,** 5123; (d) Fanizzi, F. P., Intini, F. P., Maresca, L. and Natile, G., *J. Chem. Soc., Dalton Trans.*, 1990, 1019; (e) Rochon, F. D., Kong, P. C. and Melanson, *Inorg. Chem.*, 1990, **29,** 1325; (f) Maresca, L., Natile, G., Intini, F. P., Gasparini, F., Tiripicchio, A. and Tiripicchio-Camellini, M., *J. Am. Chem. Soc.*, 1986, **108,** 1180; (g) Storhoff, B. N. and Lewis, H. C., *Coord. Chem. Rev.*, 1977, **23,** 1; (h) Gillard, R. D. and Wilkinson, G., *J. Chem. Soc.*, 1964, 2835.
16. Cotton, F. A., Reid, A. R. and Schwotzer, W., *Inorg. Chem.*, 1985, **24,** 3965.

Pergamon

PII: S0277-5387(97)00484-1

Polyhedron Vol. 17, No. 17 pp. 2795–2802, 1998
© 1998 Elsevier Science Ltd
All rights reserved. Printed in Great Britain
0277–5387/98 $19.00+0.00

Reactions of $Ru_5(\mu_5\text{-}C_2)(\mu\text{-}SMe)_2(\mu\text{-}PPh_2)_2(CO)_{11}$ with $Co_2(CO)_8$: X-ray structures of $Co_2Ru_6(\mu_7\text{-}C_2)(\mu_3\text{-}SMe)(\mu\text{-}PPh_2)_2(\mu\text{-}CO)_4(CO)_{13}$ and $Co_4Ru_5(\mu_8\text{-}C_2)(\mu_3\text{-}SMe)_2(\mu\text{-}PPh_2)_2(\mu\text{-}CO)_7(CO)_{11}$†

Chris J. Adams,[a] Michael I. Bruce,*[a] Brian W. Skelton[b] and Allan H. White[b]

[a] Jordan Laboratories, Department of Chemistry, University of Adelaide, Adelaide, South Australia 5005

[b] Department of Chemistry, University of Western Australia, Nedlands, Western Australia 6907

(Accepted 19 November 1997)

Abstract—Reactions between $Ru_5(\mu_5\text{-}C_2)(\mu\text{-}SMe)_2(\mu\text{-}PPh_2)_2(CO)_{11}$ (**1**) and $Co_2(CO)_8$ give the octanuclear cluster $Co_2Ru_6(\mu_7\text{-}C_2)(\mu_3\text{-}SMe)_2(\mu\text{-}PPh_2)_2(\mu\text{-}CO)_4(CO)_{13}$ (**4**) and the nonanuclear $Co_4Ru_5(\mu_8\text{-}C_2)(\mu_3\text{-}SMe)_2(\mu\text{-}PPh_2)_2(\mu\text{-}CO)_7(CO)_{11}$ (**5**), both characterised by single crystal X-ray structure determinations. The core of **4** consists of a Co_2Ru_3 square pyramid sharing a basal edge with a $CoRu_3$ square; the seventh Ru atom bridges the outer edge of the square pyramid. In **5**, two of the metal atoms are disordered (M = Co/Ru = 1 : 1). In this complex, two square pyramids (Co_2MRu_2 and Co_2M_2Ru) share a non-bonded edge [3.22 Å], with the ninth atom (Ru) bridging an outer edge. In both complexes, the μ_3-SMe groups and three of the Ru atoms they bridge form an almost planar $SRuSRu_2$ ring. The C_2 ligands hold the two square faces at dihedral angles of 85.75(3) (**4**), 87.8° (**5**) and are attached to seven metal atoms in **4**, eight metal atoms in **5**. © 1998 Elsevier Science Ltd. All rights reserved

Keywords: cobalt; ruthenium; carbido cluster; crystal structure.

Earlier, we have described reactions of the open cluster $Ru_5(\mu_5\text{-}C_2)(\mu\text{-}SMe)_2(\mu\text{-}PPh_2)_2(CO)_{11}$ (**1**) with iron and ruthenium carbonyls to give the hexa- and heptanuclear clusters $MR\mu_5(\mu_6\text{-}C_2)(\mu\text{-}SMe)_2(\mu\text{-}PPh_2)_2(CO)_{14}$ (**2**) and $M_2Ru_5(\mu_6\text{-}C_2)(\mu_3\text{-}SMe)_2(\mu\text{-}PPh_2)_2(\mu\text{-}CO)(CO)_{15}$ (**3**) (M = Fe, Ru) (Scheme 1) [1]. In these reactions, the C_2 ligand acts as a centre around which further metal atoms may be added and it also serves to hold apart the square faces of the clusters. At the time of our communication [1], we also reported briefly on one of the products obtained from similar reactions of **1** with $Co_2(CO)_8$. This paper describes these reactions in detail together with the structures of the two heteronuclear complexes obtained.

RESULTS AND DISCUSSION

The reaction between **1** and $Co_2(CO)_8$ was carried out in toluene for 2 h at 110°C in a Carius tube. The black solution was separated into a major and a minor product by preparative thin-layer chromatography followed by crystallisation from methanol-dichloromethane. The two complexes were characterised by single crystal X-ray structure determinations as $Co_2Ru_6(\mu_7\text{-}C_2)(\mu_3\text{-}SMe)_2(\mu\text{-}PPh_2)_2(\mu\text{-}CO)_4(CO)_{13}$ (**4**) (black, 60% yield) and $Co_4Ru_5(\mu_8\text{-}C_2)(\mu_3\text{-}SMe)_2(\mu\text{-}PPh_2)_2(\mu\text{-}CO)_7(CO)_{11}$ (**5**) (orange, 32% yield) (Scheme 2).

Molecular structure of $Co_2Ru_6(\mu_7\text{-}C_2)(\mu_3\text{-}SMe)_2(\mu\text{-}PPh_2)_2(\mu\text{-}CO)_4(CO)_{13}$ (**4**)

Figure 1 shows a plot of a molecule of **4** and selected bond parameters are given in Table 1 The Co_2Ru_6

* Author to whom correspondence should be addressed.

† Dedicated to Professor Lord Lewis on the occasion of his 70th birthday.

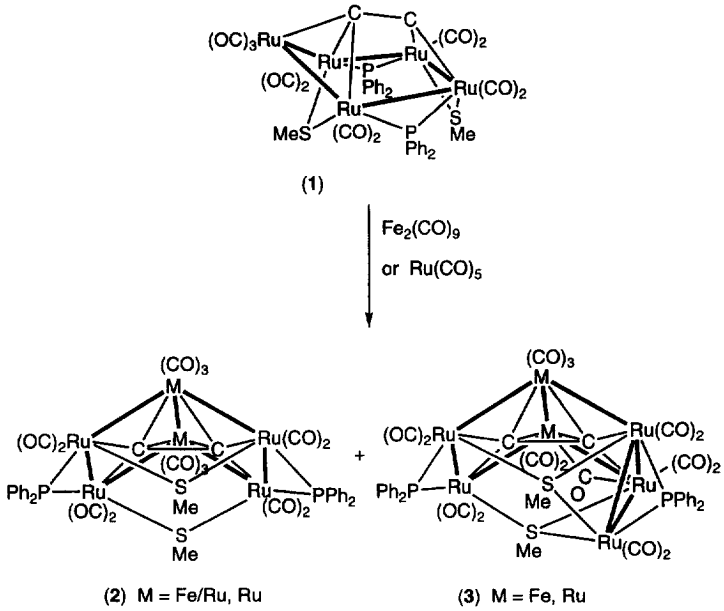

Scheme. 1.

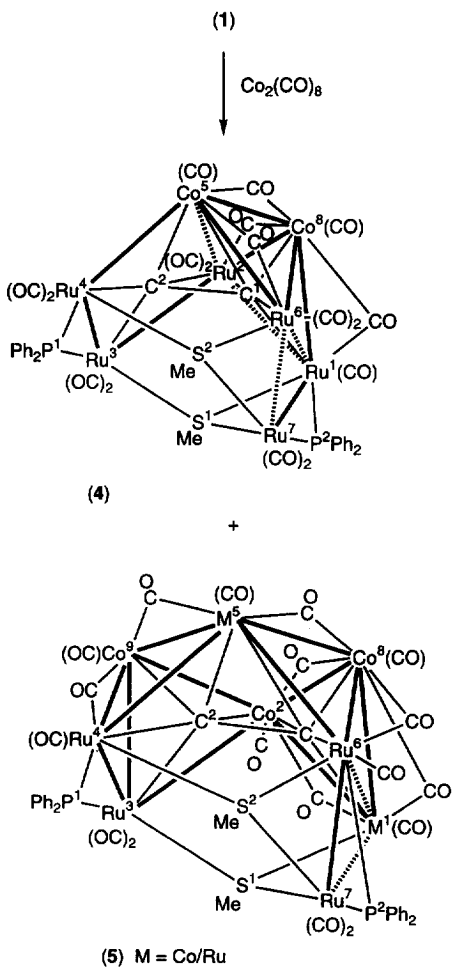

Scheme. 2.

core consists of a permetallabicyclo[2.2.0]hexane skeleton, of which the outer Ru(1)—Ru(6) edge is bridged by Ru(7), with a geometry resembling that found for complexes **3**. The central hinge atoms are Co(5) and Ru(2). The eighth atom, Co(8), caps the square face [Co(5)Ru(1,2,6)] containing the non-bridged outer edge. The C_2 ligand [C(1)—C(2) 1.36(2) Å] links the two square faces and is also close enough to the capping Co(8) atom for there to be a significant bonding interaction with C(1). Only the edge-bridging Ru(7) atom is not attached to the C_2 ligand. The two SMe groups bridge non-bonded Ru···Ru vectors [Ru—S 2.412–2.416(3) and 2.431–2.458(3) Å], while the PPh_2 ligands bridge Ru(1)—Ru(7) and Ru(3)—Ru(4) edges [Ru—P 2.295–2.348(4) Å]. Atoms S(1)Ru(3,4)S(2)Ru(7) form a nearly planar ring [χ^2 2654; maximum deviation, S(1) 0.131(3) Å] as found in complexes **3**. There are also 17 carbonyl groups which complete the coordination of the various metal atoms; of these, four are found associated with the Co(5)—Co(8) [CO(53), bridging], Co(8)—Ru(1) [CO(12), semi-bridging], Co(8)—Ru(2) [CO(23), bridging] and Co(5)—Ru(6) [CO(52), bridging] edges.

The metal–metal bond distances fall into the following groups. The unique Co(5)—Co(8) distance is 2.517(3) Å, which may be compared with the Co—Co separation in $Co_2(CO)_8$ (2.52 Å) [2]. There are two cobalt–ruthenium separations longer than 2.9 Å [Co(5)—Ru(2), Co(8)—Ru(6)] and four others are between 2.610(2) [Co(8)—Ru(2)] and 2.867(2) Å [Co(8)—Ru(1)]. Typical Co—Ru separations are found in $Co_2Ru(\mu\text{-CO})(CO)_{10}$ [2.720(5) Å] [3], $Co_2Ru(\mu_3\text{-}RC_2R')(\mu\text{-CO})(CO)_8$ [non-bridged 2.699(1), 2.690(6) Å; CO-bridged 2.591(2), 2.568(1) Å for R, R′ = H, Bu^t and Ph, Ph, respectively] [4], and

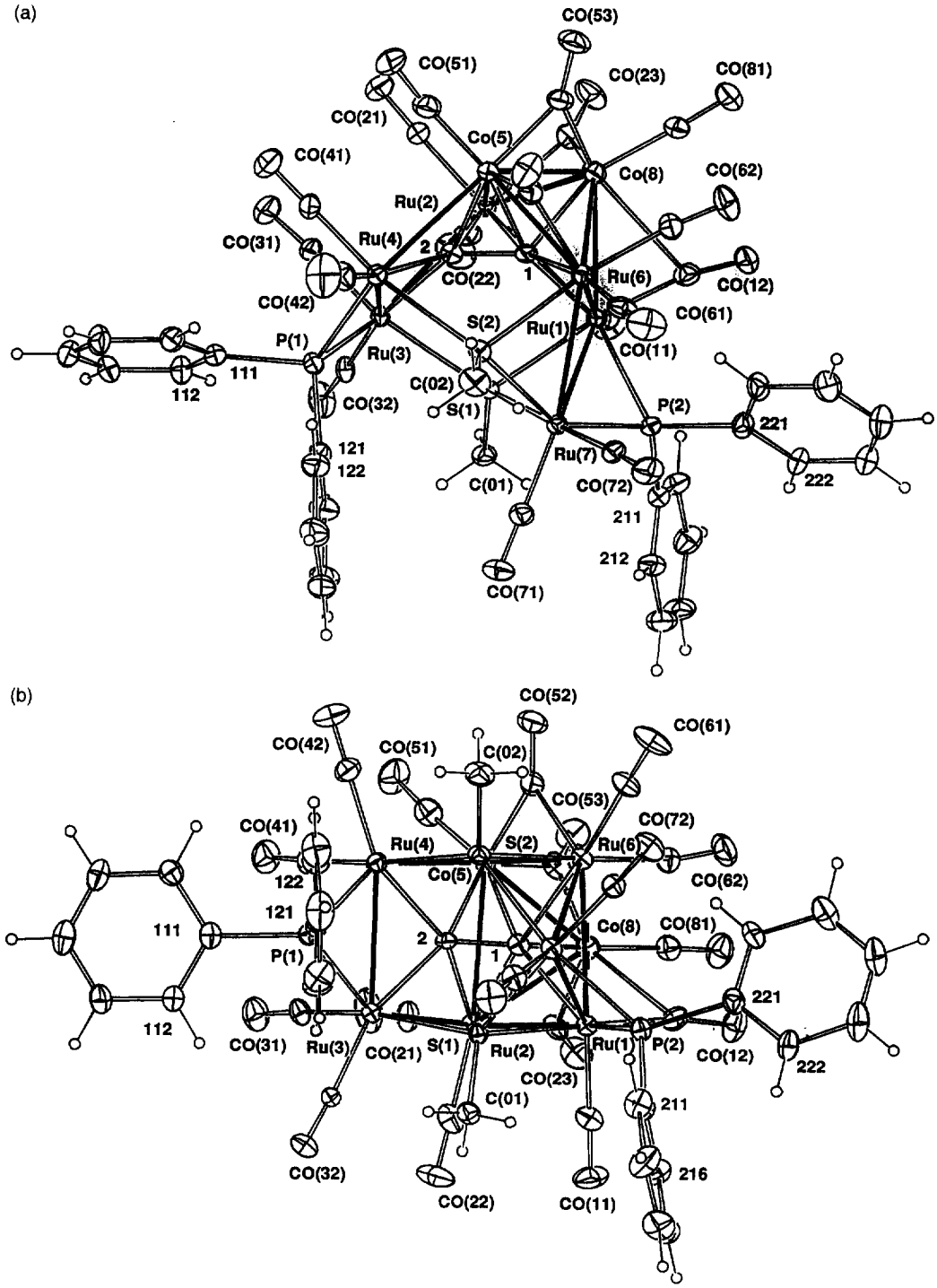

Fig. 1. Plots of two orientations of a molecule of $Co_2Ru_6(\mu_7\text{-}C_2)(\mu_3\text{-}SMe)_2(\mu\text{-}PPh_2)_2(\mu\text{-}CO)_4(CO)_{13}$ (**4**), showing the atom numbering scheme. In this figure and Fig. 2, non-hydrogen atoms are shown with 20% thermal envelopes; hydrogen atoms have arbitrary radii of 0.1 Å.

$Co_2Ru_3(\mu_5\text{-}PhC_2C_2Ph)(\mu\text{-}CO)_2(CO)_{12}$ [2.587, 2.598(1) Å, CO-bridged; 2.643, 2.730(1) Å, non-bridged] [5]. Three Ru—Ru separations are between 2.841(2) [Ru(3)—Ru(4)] and 2.952(2) Å [Ru(1)—Ru(7)] and three exceed 3.0 Å [Ru(1)—Ru(2,6) and Ru(6)—Ru(7)].

The interactions of the C_2 ligand with the metal atoms are similar to those found for carbido clusters,

Table 1. Selected bond parameters for $Co_2Ru_6(\mu_7\text{-}C_2)(\mu_3\text{-}SMe)_2(\mu\text{-}PPh_2)_2(\mu\text{-}CO)_4(CO)_{13}$ (**4**) and $Co_4Ru_5(\mu_8\text{-}C_2)(\mu_3\text{-}SMe)_2(\mu\text{-}PPh_2)_2(\mu\text{-}CO)_7(CO)_{11}$ (**5**). Where two values are given (for a mixed Co/Ru site), the first value is for the Co component

	4	**5**		**4**	**5**
Bond lengths (Å)					
M(1)—Ru(2)	3.046(1)	2.67(2), 2.63(1)	Ru(3)—P(1)	2.302(4)	2.300(9)
M(1)—Ru(6)	3.168(2)	3.12(2), 3.06(1)	Ru(4)—P(1)	2.295(2)	2.250(8)
M(1)—Ru(7)	2.952(2)	3.04(2), 3.09(1)	Ru(1)—P(2)	2.348(3)	—
M(1)—Co(8)	2.867(2)	2.80(2), 2.69(1)	Ru(6)—P(2)	—	2.369(8)
Ru(2)—Ru(3)	2.908(2)	—	Ru(7)—P(2)	2.311(4)	2.283(8)
Co(2)—Ru(3)	—	2.926(6)	M(1)—C(1)	2.16(1)	2.11(3), 2.05(3)
Ru(2)—M(5)	3.097(2)	—	Ru(2)—C(1)	2.200(9)	—
Co(2)—M(5)	—	3.22(2), 3.253(8)	Co(2)—C(1)	—	2.05(2)
Ru(2)—Co(8)	2.610(2)	—	M(5)—C(1)	2.05(1)	2.13(3), 2.19(2)
Co(2)—Co(8)	—	2.551(6)	Ru(6)—C(1)	2.185(9)	2.20(2)
Co(2)—Co(9)	—	2.619(6)	Co(8)—C(1)	2.039(8)	1.94(3)
Ru(3)—Ru(4)	2.841(2)	2.841(3)	Ru(2)—C(2)	2.15(1)	—
Ru(3)—Co(9)	—	2.860(4)	Co(2)—C(2)	—	2.06(3)
Ru(4)—M(5)	2.857(2)	2.84(3), 2.908(9)	Ru(3)—C(2)	2.137(8)	2.21(2)
Ru(4)—Co(9)	—	2.689(5)	Ru(4)—C(2)	2.12(1)	2.10(3)
M(5)—Ru(6)	2.719(2)	2.88(2), 2.920(9)	M(5)—C(2)	2.040(8)	2.09(3), 2.16(2)
M(5)—Co(8)	2.517(3)	2.61(3), 2.61(1)	Co(9)—C(2)	—	1.94(2)
M(5)—Co(9)	—	2.59(2), 2.609(9)	C(1)—C(2)	1.36(2)	1.41(4)
Ru(6)—Ru(7)	3.061(1)	2.920(3)			
Ru(6)—Co(8)	2.973(2)	2.811(5)	M(5)—C(52)	1.89(1)	2.02(4), 1.99(3)
M(1)—S(1)	2.416(3)	2.30(3), 2.39(1)	Ru(6)—C(52)	2.08(1)	—
Ru(3)—S(1)	2.437(3)	2.471(8)	Ru(2)—C(23)	2.06(1)	—
Ru(7)—S(1)	2.414(2)	2.398(7)	Co(2)—C(23)	—	1.87(3)
Ru(4)—S(2)	2.458(3)	2.451(7)	Co(8)—C(23)	1.96(1)	—
Ru(6)—S(2)	2.412(3)	2.430(8)	M(5)—C(53)	1.92(1)	1.76(5), 1.74(4)
Ru(7)—S(2)	2.431(4)	2.416(7)	Co(8)—C(53)	1.92(1)	—
Bond angles (°)					
M(1)—Ru(2)—M(5)	85.14(5)	—	Ru(3)—Ru(2)—M(5)	86.31(5)	—
M(1)—Co(2)—M(5)	—	89.5–91.6(5)	Ru(3)—Co(2)—M(5)	—	87.3(5), 88.5(2)
Ru(2)—M(5)—Ru(6)	96.52(6)	—	M(1)—Ru(6)—Ru(7)	56.55(4)	60.4(4), 62.2(2)
Co(2)—M(5)—Ru(6)	—	87.0(6), 85.7(2)	M(1)—Ru(7)—Ru(6)	63.56(4)	63.1(4), 61.1(2)
M(1)—Ru(6)—M(5)	89.46(5)	88.5–89.8(4)	Ru(6)—M(1)—Ru(7)	59.89(4)	56.5(4), 56.7(2)
Ru(2)—M(1)—Ru(6)	88.76(5)	—	Ru(3)—S(1)—Ru(7)	127.7(1)	128.2(3)
Co(2)—M(1)—Ru(6)	—	92.8(6), 95.0(3)	Ru(4)—Ru(3)—S(1)	98.30(8)	96.3(2)
Ru(2)—Ru(3)—Ru(4)	92.61(4)	—	Ru(3)—Ru(4)—S(2)	94.60(9)	97.0(2)
Co(2)—Ru(3)—Ru(4)	—	90.7(1)	Ru(4)—S(2)—Ru(7)	129.8(1)	128.0(3)
Ru(3)—Ru(4)—M(5)	92.31(5)	96.9(5), 97.4(2)	M(1)—S(1)—Ru(3)	111.76(8)	106.9(6), 105.8(4)
Ru(2)—M(5)—Ru(4)	88.46(4)	—	Ru(4)—S(2)—Ru(6)	103.50(8)	110.2(3)
Co(2)—M(5)—Ru(4)	—	85.0(6), 83.3(2)			
Dihedral angles for **4**:					
Ru(2)Ru(3)Ru(4)M(5)/M(1)Ru(2)M(5)Ru(6)				85.75(3)	
M(1)Ru(2)M(5)Ru(6)/M(1)Ru(6)Ru(7)				56.81(4)	
Dihedral angles for **5**:					
Co(2)Ru(3)Ru(4)M(5)/M(1)Co(2)M(5)Ru(6)				87.4(1)	
M(1)Co(2)M(5)Ru(6)/M(1)Ru(6)Ru(7)				57.1(1)	
For **4**, angles of C(1)—C(2) vector with mean planes of					
Ru(2)Ru(3)Ru(4)M(5)	43.08(2)				
M(1)Ru(2)M(5)Ru(6)	42.72(2)				
For **5**, angles of C(1)—C(2) vector with mean planes of					
Co(2)Ru(3)Ru(4)M(5)	42.8(1)				
M(1)Co(2)M(5)Ru(6)	45.1(1)				

Table 2. Crystal data and refinement details for **4** and **5**

Compound	**4**	**5**
Formula	$C_{45}H_{26}Co_2O_{17}P_2Ru_6S_2 \cdot CH_2Cl_2$	$C_{46}H_{26}Co_4O_{18}P_2Ru_5S_2$
MW	1774.0	1733.9
Crystal system	Monoclinic	Monoclinic
Space group	$P2_1/c$, No. 14	$P2_1/c$
a (Å)	12.466(5)	22.41(1)
b (Å)	33.824(7)	11.662(4)
c (Å)	16.230(6)	20.908(3)
β (°)	126.78(3)	98.59(5)
U (Å^3)	5481	5402
Z	4	4
D_{calc} (g cm^{-3})	2.15	2.13
$F(000)$	3416	3344
Crystal size (mm)	$0.07 \times 0.09 \times 0.51$	$0.08 \times 0.16 \times 0.25$
A^* (min, max)	1.21, 1.43	1.47, 1.68
μ (cm^{-1})	24.8	27.7
$2\theta_{max}$ (°)	50	50
N	9626	8651
N_o	6665	4095
R	0.047	0.085
R_w	0.050	0.088

e.g. Ru—C 2.12(1)–2.200(9) Å and Co—C 2.039(8)–2.05(1) Å, which may be compared with values of about 2.04 Å for the Ru—C(carbide) bonds in $Ru_5C(CO)_{15}$ [6] and of about 1.87(2) Å for the stronger Co—C(carbide) bonds in (trigonal prismatic) $[NEt_4]_2[Co_6C(CO)_{13}]$ [7].

Molecular structure of $Co_4Ru_5(\mu_8\text{-}C_2)(\mu_3\text{-}SMe)_2(\mu\text{-}PPh_2)_2(\mu\text{-}CO)_7(CO)_{11}$ (**5**).

The structure of **5** was reported briefly in our original communication [1], but no extended discussion of the molecular structure has been given until now. Figure 2 gives a plot of a molecule of **5** and selected bond distances and angles are collected in Table 1. The metal cluster consists of two edge-sharing square pyramids, which are also linked by the C_2 ligand in the same fashion as found for **4**. In this complex, atoms Co(8) and Co(9) cap the square faces on opposite sides to the C_2 ligand. Both of these metal atoms are within bonding distance [1.94(3) Å] of the appropriate carbon atoms, with separations which more closely resemble those found for other Co—C(carbide) distances [7].

Disorder is found in the two atom sites M(1,5), with M(1) and M(5) refining to 1/1 Co/Ru in each case. It is interesting that whereas the disorder found in the $FeRu_5$ and Fe_2Ru_5 complexes (**2-Fe** and **3-Fe**) involves the hinge atoms [1], in the present structure only one such atom [M(5)] is disordered, with M(1) being in the opposite corner across the square base. Atom Ru(7) bridges the M(1)—Ru(6) edge. The two SMe groups are in the μ_3 bridging mode, linking atoms M(1)—Ru(3)—Ru(7) and Ru(4)—Ru(6)—Ru(7); here the S(1)Ru(3)Ru(4)S(2)Ru(7) ring is also nearly planar [χ^2 250; maximum deviation, S(1) 0.127(9) Å]. The two PPh_2 ligands bridge Ru(3)—Ru(4) and Ru(6)—Ru(7). Of the 18 carbonyl groups, seven are found bridging various Co—Ru and Ru—Ru bonds.

The spectroscopic properties of the two complexes are in accord with their solid-state structures. The IR ν(CO) spectra contain both terminal and bridging CO absorptions. The ^{1}H NMR spectrum of **4** contains a singlet at δ 1.74 and a doublet at δ 2.85 from the SMe groups, the ^{31}P coupling to the latter signal suggesting that it arises from SMe(2). For **5**, both SMe groups give rise to singlets at δ 1.87 and 1.93. We did not record a ^{13}C NMR spectrum for **4** because of its low solubility; that for **5** contains a low-field resonance at δ 254.9 which is coupled to one of the ^{31}P nuclei, and assigned to the carbons of the C_2 ligand.

These two clusters have interesting electron counts, which can be related in part to the unusual metal separations found in the core; the dicarbon ligand is considered to be a six-electron donor. The skeleton may be derived from a trigonal prism by breaking two M—M bonds to give the permetallabicyclohexane structure. For **4**, where one square is capped by Co and one edge is bridged by Ru, the cluster condensation rules of Mingos [9] predict a C.V.E. count of 118 [square (64) + square pyramid (74) − edge (34) + triangle (48) − edge (34) = 118], or four fewer than found [2 × Co (18) + 6 × Ru (48) + 17 × CO (34) + 2 × SMe (10) + 2 × PPh_2 (6) + C_2 (6) = 122]. For **5**, in which both squares are open [no M—M bond is assumed between M(2) and Co(5) (3.22 Å), as sup-

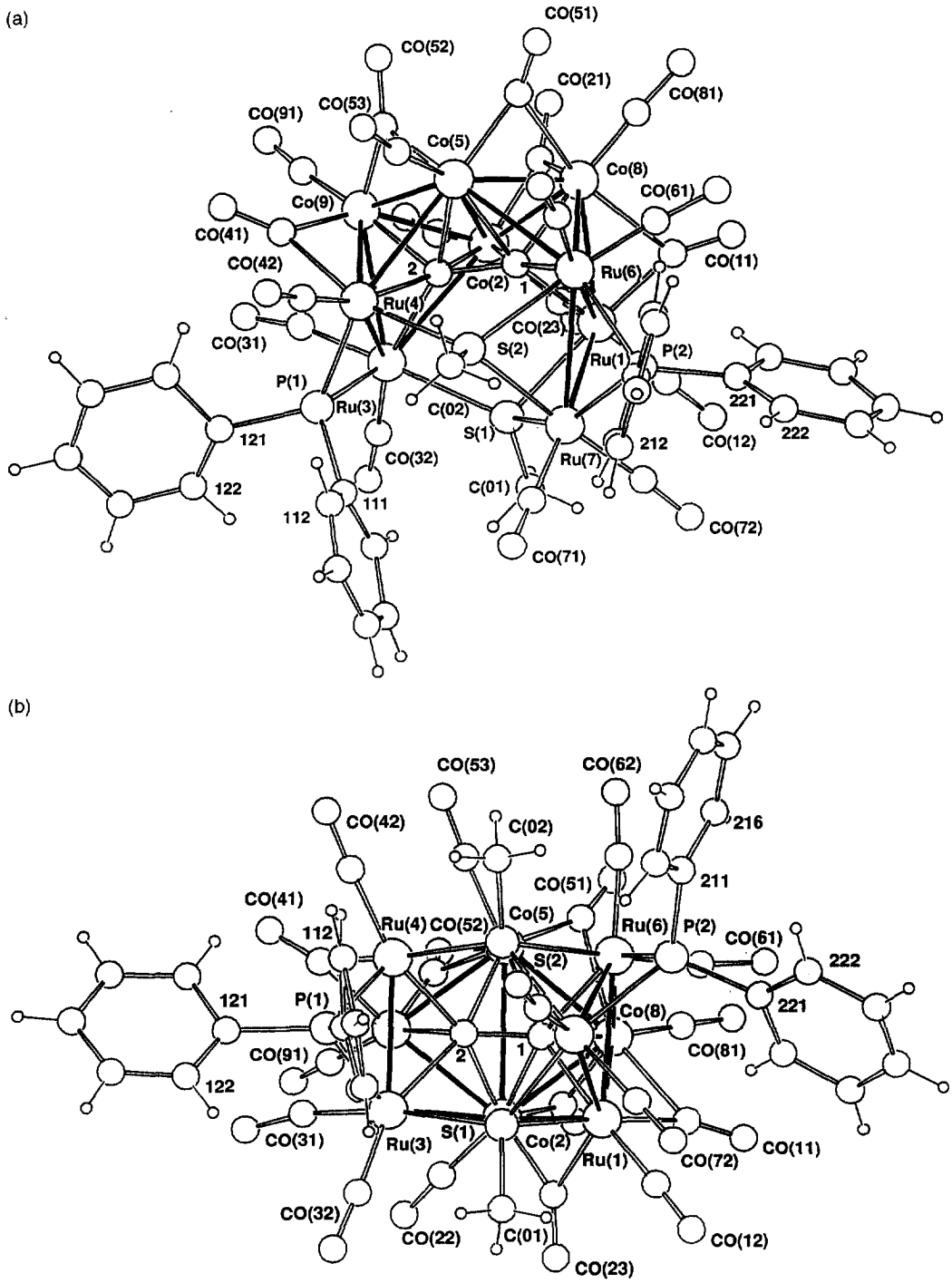

Fig. 2. Plots of two orientations of a molecule of $Co_4Ru_5(\mu_8\text{-}C_2)(\mu_3\text{-}SMe)_2(\mu\text{-}PPh_2)_2(\mu\text{-}CO)_7(CO)_{11}$ (**5**), showing the atom numbering scheme.

ported by EH MO calculations (see below)] and capped by Co atoms, with an edge bridged by the fifth Ru atom, the expected C.V.E. count is 130 [2 × open square pyramid (152) − 2 × shared atoms (36) + triangle (48) − edge (34) = 130]. The observed C.V.E. count for **5** is 134 [4 × Co (36) + 5 × Ru (40) + 18 × CO (36) + 2 × SMe (10) + 2 × PPh_2 (6) + C_2 (6) = 134], which is four more than expected, as found for **4**.

Detailed consideration of these molecular structures shows that several of the M—M separations are longer than 3.0 Å. In these clusters the excess of electron density is considered to be accommodated in

M—M anti-bonding orbitals, delocalised over several metal centres, as found with earlier examples of 50 C.V.E trinuclear clusters [10]. This is confirmed by EH MO calculations in the case of **5**, for instance, which indicate that molecular orbitals in the HOMO region are rather heavily weighted towards the metal atoms (>85%) and slightly M—M anti-bonding [8]. Rather weak M—M overlap populations are computed for **5** overall compared with those computed in smaller M_nC_2 species which obey the Mingos rules [8]. Note that the overlap population for the $M(2)\cdots Co(5)$ separation is slightly negative (−0.01), clearly indicating no bonding interaction. A small but still significant HOMO/LUMO gap (0.60 eV) is calculated for **5**. Further, the interactions of the C_2 ligand with the capping Co atoms weaken the electron density in the C—C bond, leading to a lengthening of this bond [cf 1.36 Å in **4** (with one capping Co), further lengthened to 1.41 Å in **5** (two capping Co atoms)]. This is reflected in the atomic net charges, which show that the two carbons in **5** are less negatively charged than in smaller M_nC_2 species (−1.7/−0.19 vs −0.32 in complex **2-Fe**, for instance) [8].

The C_2 ligand appears to be too large to fit into a trigonal prism, so that the open arrangements found in **4** and **5** (which can be derived from a trigonal prism by cleavage of two M—M bonds) are the most suitable. Larger clusters containing a fully encapsulated C_2 ligand have been described, such as $[NEt_4]_2[Co_6Ni_2(C_2)(\mu\text{-}CO)_8(CO)_8]$ [11] and $[PPh_4]_2[Co_3Ni_7(C_2)(\mu\text{-}CO)_{10}(CO)_6]$ [12]. However, the role of the bridging SMe groups in preventing the clusters in **4** and **5** from closing further cannot be discounted.

The mechanism of formation of **4** and **5** is not easy to discern. We note that there is a good mass balance in its reaction, a total isolated yield of 92% of the two complexes being obtained. Formally, addition of the $Co(CO)_3$ fragment to **1** may proceed in a manner similar to that proposed for the formation of **3** and **4** [13]. However, an additional reaction involving some disproportionation of the ruthenium cluster must occur to allow the sixth Ru atom to be incorporated into **4**.

CONCLUSION

Reactions of **1** with metal substrates have proved to be a rich source of unusual cluster architectures as a result of the C_2 ligand acting as a partial template around which the novel cores can be constructed. In addition, the ability of the SMe groups to act as μ_2 or μ_3 bridging units gives a facility for incorporation of extra metal atoms. Our original MO calculations [14] pointed to localisation of a high lying MO on one of the bridging SMe groups of **1**. The potential for this group to enter into further reactions has been amply demonstrated by the formation of larger clusters such as **2–5**, and points to further exciting chemistry to be derived from **1**.

EXPERIMENTAL

General conditions

All reactions were carried out under dry, high purity nitrogen using standard Schlenk techniques. Solvents were dried and distilled before use. Elemental analyses were by the Canadian Microanalytical Service, Delta, B.C., Canada V4G 1G7. Preparative T.L.C. was carried out on glass plates (20 × 20 cm) coated with silica gel (Merck 60 GF_{254}, 0.5 mm thick).

Reagents. Complex **1** was prepared as described earlier [15]. $Co_2(CO)_8$ (Strem) was used as received.

Instrumentation. IR: Perkin–Elmer 1700X FT IR; 683 double beam, NaCl optics; NMR: Bruker CXP300 or ACP300 (^{1}H NMR at 300.13 MHz, ^{13}C NMR at 75.47 MHz). FAB MS: VG ZAB 2HF (FAB MS, using 3-nitrobenzyl alcohol as matrix, exciting gas Ar, FAB gun voltage 7.5 kV, current 1 mA, accelerating potential 7 kV).

Reaction of **1** *with* $Co_2(CO)_8$

A solution of **1** (75 mg, 0.051 mmol) and $Co_2(CO)_8$ (300 mg, 0.88 mmol) in toluene (10 ml) was heated in a Carius tube at 110°C for 22 h. Solvent was removed and the residue purified by preparative T.L.C. (light petroleum/acetone 10/3).

The major black band (R_f 0.3) was recrystallised from CH_2Cl_2/MeOH to yield black crystals of $Co_2Ru_6(\mu_7\text{-}C_2)(\mu_3\text{-}SMe)_2(\mu\text{-}PPh_2)_2(\mu\text{-}CO)_4(CO)_{13}$ (**4**) (52 mg, 60%). Anal. Found: C, 31.83; H, 1.57%; M, 1690, (mass spectrometry). $C_{45}H_{26}Co_2O_{17}P_2Ru_6S_2$. Calcd C, 32.00; H, 1.55%; M, 1690. IR: ν(CO) (cyclohexane) 2066 m, 2040 s, 2029 vs, 2007 m, 2001 m, 1983 m, 1974 m, 1965 w, 1960 w, 1854 m, 1827 w cm^{-1}. ^{1}H NMR ($CDCl_3$): δ 1.74 (3H, s, SMe), 2.85 (3H, d, J_{HP} 1.7 Hz, SMe), 6.73–7.91 (20H, m, Ph). FAB MS (m/z): 1690 M^+; 1662–1186, $[M-n\text{CO}]^+$ (n = 1–17).

An orange band (R_f 0.6) was recrystallised (CH_2Cl_2/MeOH) to give orange crystals of $Co_4Ru_5(\mu_8\text{-}C_2)(\mu_3\text{-}SMe)_2(\mu\text{-}PPh_2)_2(\mu\text{-}CO)_7(CO)_{11}$ (**5**) (24 mg, 32%). Anal. Found: C, 31.75; H, 1.58%; M, 1735 (mass spectrometry). $C_{46}H_{26}Co_4O_{18}P_2Ru_5S_2$. Calcd C, 31.83; H, 1.50%; M, 1735. IR (cyclohexane): ν(CO) 2065 m, 2041 vs, 2031 s, 2024 s, 2010 m, 2006 (sh), 1995 m, 1988 (sh), 1976 m, 1968 w, 1962 (sh), 1950 vw, 1876 m, 1856 m, 1843 w, 1839 (sh), 1832 w, 1824 w, 1816 (sh) cm^{-1}. ^{1}H NMR ($CDCl_3$): δ 1.71, 2.81 (2 × 3H, s, SMe), 6.85–7.68 (20H, m, pH). FAB MS (m/z): 1735, M^+; 1707–1231, $[M-n\text{CO}]^+$ (n = 1–18).

CRYSTALLOGRAPHY

Unique data sets were measured at ca 295 K within the specified $2\theta_{max}$ limits using an Enraf-Nonius CAD4 diffractometer ($2\theta/\theta$ scan mode; mono-

chromatic Mo–K_α radiation, λ 0.7107$_3$ Å); N independent reflections were obtained, N_o with $I > 3\sigma(I)$ being considered "observed" and used in the full matrix least squares refinement after gaussian absorption correction. Anisotropic thermal parameters were refined for the non-hydrogen atoms; $(x, y, z, U_{iso})_H$ were included constrained at estimated values. Conventional residuals R, R' on $|F|$ are quoted, statistical weights derivative of $\sigma^2(I) = \sigma^2(I_{diff}) + 0.0004\sigma^4(I_{diff})$ being used. Computation used the XTAL 2.6 program system [16] implemented by S. R. Hall; neutral atom complex scattering factors were employed. Pertinent results are given in the figures and tables.

Abnormal features/variations in procedure

(**4**). The solvent molecule as modelled had very high "thermal motion".

(**5**). Possibly consequent on mixed site occupancy in M(1,5), data were weaker and more limited in extent than in **4**, supporting meaningful anisotropic thermal parameter refinement for Ru, Co, S, P only.

Acknowledgements—We thank the Australian Research Council for financial support and Johnson Matthey Technology Centre of a generous loan of $RuCl_3 \cdot nH_2O$. Continuing discussions with Professor J.-F. Halet, Université de Rennes 1, France, are acknowledged.

REFERENCES

1. Adams, C. J., Bruce, M. I., Skelton, B. W. and White, A. H., *J. Chem. Soc., Chem. Commun.*, 1993, 446.
2. (a) Sumner, G. G., Klug, H. P. and Alexander, L. E., *Acta Crystallogr.*, 1964, **17,** 732; (b) Leung, P. C. and Coppens, P., *Acta Crystallogr.*, 1983, **B39,** 535.
3. Roland, E. and Vahrenkamp, H., *Chem. Ber.*, 1985, **118,** 1133.
4. Roland, E., Bernhardt, W. and Vahrenkamp, H., *Chem. Ber.*, 1985, **118,** 2858.
5. Bruce, M. I., Zaitseva, N. N., Skelton, B. W. and White, A. H., *Polyhedron*, 1995, **14,** 2647.
6. (a) Farrar, D. H., Jackson, P. F., Johnson, B. F. G., Lewis, J., Nicholls, J. N. and McPartlin, M., *J. Chem. Soc., Chem. Commun.*, 1981, 415; (b) Johnson, B. F. G., Lewis, J., Nichols, J. N., Puga, J., Raithby, P. R., Rosales, M. J., McPartlin, M. and Clegg, W., *J. Chem. Soc., Dalton Trans.*, 1983, 277.
7. Albano, V. G., Braga, D. and Grepioni, F., *Acta Crystallogr.*, 1989, **B45,** 60.
8. Frapper, G., Halet, J.-F. and Bruce, M. I., *Organometallics*, 1997, **16,** 2590.
9. Mingos, D. M. P., *J. Chem. Soc., Chem. Commun.*, 1983, 706.
10. Halet, J.-F., *Coord. Chem. Rev.*, 1995, **142,** 637.
11. (a) Arrigoni, A., Ceriotti, A., Della Pergola, R., Longoni, G., Manassero, M., Masciocchi, N. and Sansoni, M., *Angew. Chem.*, 1984, **96,** 290; (b) *Angew. Chem., Int. Ed. Engl.*, 1984, **23,** 322.
12. (a) Arrigoni, A., Ceriotti, A., Della Pergola, R., Longoni, G., Manassero, M. and Sansoni, M., *J. Organomet. Chem.*, 1985, **296,** 243; (b) Longoni, G., Ceriotti, A., Della Pergola, R., Manassero, M., Perego, M., Piro, G. and Sansoni, M., *Phil. Trans. R. Soc. London*, 1982, **A308,** 47.
13. Adams, C. J., Bruce, M. I., Liddell, M. J., Skelton, B. W. and White, A. H., *J. Organomet. Chem.*, 1997, in press.
14. Adams, C. J., Bruce, M. I., Liddell, M. J., Skelton, B. W. and White, A. H., *J. Chem. Soc., Chem. Commun.*, 1992, 1314.
15. (a) Adams, C. J., Bruce, M. I., Skelton, B. W. and White, A. H., *J. Chem. Soc., Chem. Commun.*, 1992, 26; (b) *J. Chem. Soc., Dalton Trans.*, 1997, 2937.
16. Hall, S. R. and Stewart, J. M., ed., *The XTAL 2.6 Reference Manual.* Universities of Western Australia and Maryland, 1992.

Pergamon

PII: S0277-5387(97)00509-3

Polyhedron Vol. 17, No. 17, pp. 2803–2815, 1998
© 1998 Elsevier Science Ltd
All rights reserved. Printed in Great Britain
0277-5387/98 $19.00+0.00

Structural and bonding trends in rhenium carbonyl cluster chemistry: metal–metal and metal–ligand bond lengths and calculated strengths*

Katherine M. Hillary, Andrew K. Hughes, Karen L. Peat and Ken Wade†

Department of Chemistry, University Science Laboratories, South Road, Durham, DH1 3LE, U.K.

(Received 6 October 1997; accepted 24 November 1997)

Abstract—The published Re—Re bond lengths, d(Re—Re), of neutral and anionic rhenium carbonyl clusters, including those containing hydride ligands and core carbon atoms, $[Re_x(CO)_yH_z]^{c-}$ and $[Re_xC(CO)_yH_z]^{c-}$, have been converted into rhenium–rhenium bond enthalpies, E(Re—Re), using $E(Re—Re) = A\,d(Re—Re)^{-4.6}$ where $A = 2.118 \times 10^{13}$ for d(Re—Re) in picometres and E(Re—Re) in kJ mol^{-1}. Values for the total metal–metal bond enthalpies, ΣE(Re—Re), have been calculated for each cluster. Trends in ΣE(Re—Re) are explored as a function of the cluster nuclearity, x, and the number of electrons donated by the ligands. Trends in ΣE(Re—Re) are also explored as a function of the number of electron pairs involved in cluster bonding, determined by both localised (EAN) and delocalised (PSEPT) models. For the rhenium clusters containing core carbon atoms the total metal–metal bond enthalpy is consistently higher than for other species of similar electron counts, indicating that the metal atoms in such clusters are pulled closer together by the core carbon atoms, which have an effective radius of ca 0.622 Å. Moreover, the addition and removal of ligands from core carbon clusters does not alter ΣE(Re—Re) as greatly as in smaller clusters devoid of core atoms. The $[ReH(CO)_4]_n$ ($n = 2, 3, 4$) clusters are compared and contrasted with the isolobal cycloalkanes, $(CH_2)_n$, and the requirements of octahedral $Re(CO)_4X_2$ fragments and bent Re—H—Re 3c—2e bonds are shown to favour the 6-membered $(ReH)_3$ ring as the strain-free ring. © 1998 Elsevier Science Ltd. All rights reserved

Keywords: rhenium; carbonyls; clusters; bond-enthalpies; bond-lengths.

Many fundamental and commercially important reactions of small organic molecules (CO, H_2, alkenes) are catalysed by metal surfaces, and there is a need to understand the thermodynamics and kinetics of these processes. Whilst the overall reaction may involve the conversion of one organic species into another, and the thermodynamics of such species are well understood, the thermodynamics of individual steps at a metal surface are less well defined. Metal carbonyl clusters containing hydride ligands are models of CO and H_2 on metal surfaces, and studies of the thermodynamics of $M_x(CO)_yH_z$ clusters will lead to data for M—CO and M—H bond energies which can be applied to metal-surface processes. In the present paper we focus on the ways in which the attachment of carbonyl and hydride ligands to small rhenium clusters affects the metal–metal bonding therein, as revealed by a detailed study of their metal–metal distances.

In two recent papers [1,2], we have explored the implications of a relationship, $E = A\,d^{-k}$, between the length (d) and strength (E) of metal–metal bonds in transition metal carbonyl clusters, in conjunction with the available experimental thermodynamic data, and shown how one could assess the relative thermodynamic stabilities of osmium carbonyl clusters, $Os_x(CO)_y$, and their hydride and anionic derivatives, from their structures. Our approach assigned bond enthalpies, E(Os—Os), to the individual pairwise (though not necessarily electron pairwise) metal–metal bonding interactions they contained. For the binary osmium carbonyls, we found that the osmium–

* Dedicated to Lord (Jack) Lewis, one of the great pioneers of metal carbonyl cluster chemistry, on the occasion of his 70th birthday.

† Author to whom correspondence should be addressed.

carbonyl bond enthalpy, E(M—CO), increased slightly, but consistently, as the cluster nuclearity, x, increased, and as the proportion of ligand molecules to metal atoms, y/x, decreased [1]. In examining a wider range of osmium carbonyl clusters, including neutral and anionic species containing hydride ligands, we explored trends in the total metal–metal bond enthalpy, ΣE(Os—Os), as a function of ligand to metal ratio, number of hydride ligands, and the number of electrons formally available to bond the metal atoms [2]. We also estimated limiting values for Os—H bond enthalpies, and drew attention to a relationship between cluster nuclearity and the Os—C and CO bond lengths.

We are now extending the application of our bond length–bond enthalpy relationship to other metals, with the aims of exploring the validity of this relationship, and of utilising the total metal–metal bond enthalpies of clusters to explore and illustrate trends in cluster bonding and geometry. We are also attempting to elucidate values for bond enthalpies E(M—CO) and E(M—H) for a wide range of transition metals. The metal—metal bond enthalpy of the binary rhenium carbonyl, $Re_2(CO)_{10}$, was discussed by us previously [3]. In the current work we consider a wide range of carbonyl clusters of rhenium, including some containing interstitial carbon atoms.

Rhenium clusters pose some contrasts with those of osmium, although the differences between the clusters of these two metals are not as great as those between osmium and other metals. Since rhenium has one electron fewer than osmium, the ligands in a cluster need to provide relatively more electrons in order to achieve electronic saturation. However, this can be difficult without causing steric congestion. As a result, there are few very high nuclearity rhenium clusters, and the majority of pentanuclear and larger clusters contain interstitial carbon atoms, which provide four electrons to the cluster electron count without occupying surface coordination sites. In common with the carbonyl clusters of osmium, the clusters of rhenium tend to have terminal carbonyl ligands. The need to achieve electronic saturation without reaching coordinative saturation means that there are many rhenium clusters which contain formal Re—Re double bonds, a feature to which we shall return. There are series of rhenium clusters having different electron counts for the same number of metal atoms, also a series of similar composition, $[HRe(CO)_4]_n$, but differing nuclearity, n, and these provide opportunities to explore and illustrate trends in the metal–metal bonding.

The basis of our approach is that the metal–metal bonds in metal carbonyl clusters resemble those in the bulk metal sufficiently to permit use of the same bond length–bond enthalpy relationship. The metal–metal bonds in question are relatively weak, much weaker than the metal–ligand bonds, which is why adsorption of ligands such as carbon monoxide molecules on metal surfaces can cause drastic rearrangement of the metal surface atoms [4]. However, despite the relative softness of the metal–metal bonding potential energy well, we consider the use of the bond length–bond enthalpy relationship to be justified, particularly because we focus on the total bond enthalpy, ΣE(M—M), rather than on individual bonds. We feel that the important feature of our method is that we use a single parameter to characterise all the small bond length changes which accompany a chemical change (protonation, ligand addition) to a cluster, and in the case of large clusters this single parameter is easier to interpret than a list of many bond lengths.

RESULTS AND DISCUSSION

It is the basis of our method that the length, d, and enthalpy, E, of individual M—M bonds are described by $E = Ad^{-k}$, where $k = 4.6$ for all transition metals, and the constant A is determined from the atomisation enthalpy and the interatomic distances in the bulk metal. For rhenium $A = 2.118 \times 10^{13}$ for d in picometres and E in kJ mol^{-1}. As in our earliest papers [3,5], we include only nearest neighbour (polyhedron edge) interactions in calculating the total metal–metal bond enthalpy, ΣE(Re—Re) for the Re clusters considered here.

For the crystallographically characterised neutral binary osmium carbonyls we were able to estimate the gas-phase enthalpies of formation from the enthalpy of disruption to gaseous metal atoms and CO, the enthalpy of atomisation of the bulk metal, and the enthalpy of formation of carbon monoxide [1]. This method is based on a knowledge of the experimental enthalpies of formation of some simple binary carbonyls including $Os_3(CO)_{12}$ and $Re_2(CO)_{10}$ [6]. To extend such a study to clusters containing hydride ligands it would be necessary to include E(M—H) terms, and for a cluster containing an interstitial carbon atom, we require knowledge of the enthalpy change associated with the release of a carbon atom from such a site, or of the relationship between M—C distances and associated E(M—C) bond enthalpies. Studies are in progress to investigate these relationships [7]. For the present we consider only the total rhenium–rhenium bond enthalpy, ΣE(Re—Re), for clusters containing interstitial atoms as a function of the electrons they contribute, and investigate patterns and trends in this parameter.

Three main ways of predicting or rationalising the shapes of metal clusters have been explored. One, the treatment of metal clusters as fragments of the bulk metal [8], has evident merit for large clusters, although it is exceedingly difficult to estimate the ligand-bonding capacity of the metal atoms on the fragment surfaces and anyway rhenium is not known to generate high nuclearity clusters. A second approach is to assume that each metal atom obeys the 18 electron rule, by using all nine valence shell orbitals either to bond ligands, to accommodate lone pair electrons,

or to participate in 2-centre 2-electron metal–metal bonds. This approach works well for small clusters such as $[Re_4(CO)_{16}]^{2-}$, indeed for rationalising the metal networks in most of the carbonyls of rhenium, but has limited use for certain important species such as $[Re_6H_7(CO)_{18}]^-$, for which there is an electron pair too many to explain the 12 edges of the octahedron as 2c2e bonds. The 2c2e approach to cluster electron counting, though often helpful in understanding connectivities, is not readily able to predict cluster geometries. The third method of treating the bonding in osmium carbonyl and similar metal clusters, Polyhedral Skeletal Electron Pair Theory, PSEPT [9], exploits the analogy with borane clusters [10]. This too assumes that each metal atom uses all nine valence shell atomic orbitals, six for bonding to carbonyl ligands or accommodating lone pair electrons, the remaining three orbitals being available for metal–metal bonding use. This approach allows many structures to be rationalised or even predicted, including some important systems that appear anomalous in localised bond terms, like the octahedral cluster referred to above. However, it should be noted that PSEPT classifies as skeletal electron pairs some electrons that contribute little or not at all to the actual metal–metal bonding, even though the presence of these (effectively lone pair) electrons does influence the molecular shape. In our discussion of metal–metal bond energies below, we draw attention to some of these features, and analyse the effectiveness with which the available electrons, counted by each of these latter two schemes, are used for metal–metal bonding.

Since the important features of the clusters that we wish to discuss, apart from the metal–metal bond distances, are their polyhedral shapes, the structures of the rhenium carbonyl clusters discussed here are presented in figures in a way that draws attention to the polyhedral shape defined by the metal atoms, the numbers of bonding contacts (polyhedron edge lengths) therein, the numbers and distribution of the carbonyl ligands, and the locations of bridging carbonyl ligands and hydrides. All of these clusters have been structurally characterised by diffraction techniques, the majority using X-ray diffraction, so although the hydrogen atoms have not been located directly, their positions have been deduced by potential energy calculations [11].

Figure 1 shows the structurally characterised examples of neutral rhenium carbonyls, $[Re_x(CO)_y]$, rhenium carbonyl anions, $[Re_x(CO)_y]^{c-}$, and both neutral and anionic rhenium carbonyl hydride clusters, $[Re_x(CO)_yH_z]^{c-}$. We indicate in Table 1 the total metal–metal bond enthalpies, $\Sigma E(Re—Re)$, calculated for these clusters using eqn (1), including all first coordination sphere contacts. The Table also shows the number of skeletal electron pairs according to PSEPT (S_p), the number of electron pair bonds according to a localised (18 electron or EAN) bond model (S_{lb}), and the total metal–metal bond enthalpy per osmium, per PSEPT electron pair and per localised electron pair bond. Several of the anionic rhenium clusters have been characterised as salts with more than one counter-ion. These are indicated in the Table, and the data for only one of these salts are discussed in later sections. The salt $[Re_4H_4(CO)_{15}][NEt_4]_2$ has been crystallographically characterised in three polymorphs, described as Forms I, II and III in Ref. 12. These three polymorphs give very similar $\Sigma E(Re—Re)$ values, as indicated in the Table.

The most informative way to represent the total metal–metal bond enthalpy is to plot the total metal–metal bond enthalpy per rhenium atom, $\Sigma E(Re—Re)/x$, as a function of the number of ligand electrons per rhenium atom, as shown in Fig. 2. As in the case of similar graphs plotted for osmium and rhodium clusters, the data in Fig. 2 fall on or close to a curve, which can be approximately fitted by a second order polynomial showing that the metal–metal bonding becomes stronger as the clusters become larger and the ratio of ligand electrons to metal atoms becomes smaller. The data for Re are more scattered than those for Os and Rh, and large rhenium clusters are only known with multiple hydride ligands, which utilise some of the metal–metal bonding electrons for M—H—M bonding and so reduce the value of $\Sigma E(Re—Re)$. Both of these factors mean that a fit to the data in Fig. 2 extrapolates to give a value for the atomisation enthalpy of bulk Re metal (when the number of electrons per metal equals seven) which is lower than the experimental value (770 kJ mol^{-1}).

We have included examples of crystallographically characterised rhenium carbonyl clusters containing interstitial carbon atoms. Their structures are shown in Fig. 3. We have chosen at this stage to consider only clusters containing interstitial atoms entirely surrounded by metal atoms, where it is clear that all the valence shell electrons of the interstitial atom are involved in cluster bonding. We wish to exclude from the current discussion clusters where heteroatoms bridge surface metal atoms, when some of the valence electrons may be counted as lone pairs. The $[Re_5C(CO)_{16}H]^{2-}$ cluster has been included, since all the valence electrons of the carbon atom are involved in cluster bonding. Table 2 lists the rhenium clusters containing interstitial carbon atoms which have been examined in this study, along with the $\Sigma E(Re—Re)$ value, and the total number of ligand electrons donated to the cluster, where the core carbon atom contributes all of its four valence electrons to the cluster electron count. In the PSEPT bonding model all of the rhenium carbide clusters in the current work formally contain seven skeletal electron pairs, and are thus based on the *nido* square pyramid for the Re_5 cluster, or the *closo* octahedron for Re_6 clusters, with the addition of capping atoms in the case of Re_7 and Re_8 clusters. Figure 2 includes these core carbide systems.

In Fig. 2, the core carbon containing clusters fall on a line approximately parallel with, but above, the line through the non core carbon clusters. This indi-

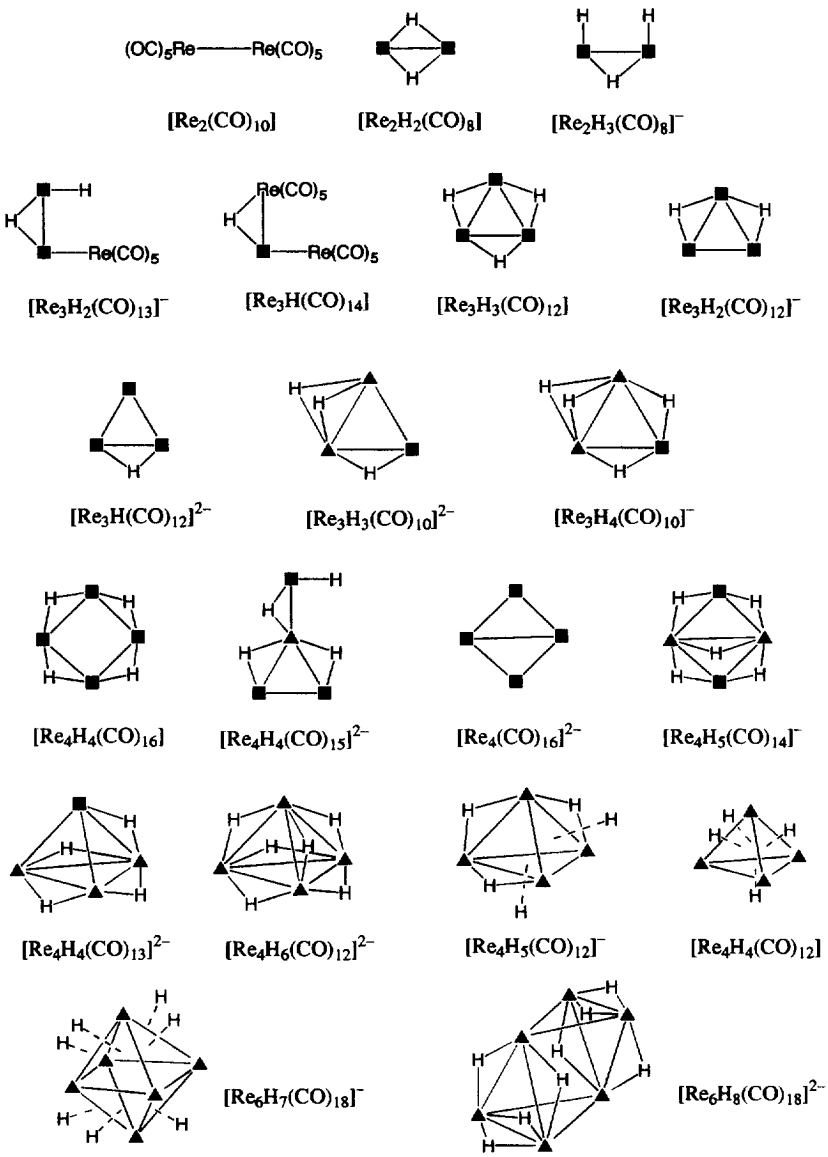

Fig. 1. The structures of the rhenium carbonyl clusters discussed in this work. Lines are drawn to indicate connectivity, and do not imply the presence of single bonds. The following symbols are used: ■ = $Re(CO)_4$; ▲ = $Re(CO)_3$. Hydride and bridging carbonyl ligands are drawn explicitly, dashed lines are drawn to face-bridging hydrides.

cates that the metal–metal bonding in the core carbon clusters is stronger than the metal–metal bonding in non core carbon clusters. This trend can be interpreted by considering the structural and electronic effects of introducing a core atom into a rhenium cluster. As indicated in the introduction, there are no examples of large rhenium clusters such as $[Re_6(CO)_{21}]^{2-}$ that do not contain either hydride or core carbon ligands, but if we consider the hypothetical octahedral cluster $[Re_6(CO)_{21}]^{2-}$, and assume that the Re—Re distances will be of the same length or shorter than those in $Re_2(CO)_{10}$ [3.042 Å, E(Re—Re) = 80 kJ mol^{-1}], then the total metal–metal bond enthalpy, ΣE(Re—Re) for $[Re_6(CO)_{21}]^{2-}$ will be $\geqslant$960 kJ mol^{-1}. Replacement of two CO ligands by a core carbon atom gives the known $[Re_6C(CO)_{19}]^{2-}$ cluster, which has ΣE(Re—Re) = 1015 kJ mol^{-1}. This suggests that in the case of octahedral rhenium clusters the introduction of a core carbon atom pulls the rhenium atoms closer together, increasing metal–metal bonding. The transformation of $[Re_6(CO)_{21}]^{2-}$ into $[Re_6C(CO)_{19}]^{2-}$ removes two ligands from the crowded outside of the cluster, and compensates for the electron count by adding a core carbon atom.

The mean Re—Re distance in $[Re_6C(CO)_{19}]^{2-}$ is 3.006 Å, implying a radius for the rhenium atoms of

Table 1. The rhenium carbonyl clusters studied not containing core carbon atoms, listing their CSD code, the number of valence shell electrons, number of PSEPT electron pairs (S_p), number of localised 2c2e bonds (S_{lb}) according to the EAN model, the total metal–metal bond enthalpy, the number of valence electrons per metal atom and the total metal–metal bond enthalpy per metal atom, per PSEPT electron pair and per localised bond pair

CSD Code	Formula	Valence electrons	PSEPT electron pairs	S_{lb}	ΣE(Re—Re) (kJ mol^{-1})	Valence electrons per Re	ΣE(Re—Re) per Re atom	ΣE(Re—Re) per S_p	ΣE(Re—Re) per S_{lb}	Notes
FIZTIR	$Re_2H_3(CO)_8^-$	34	5	1	59.1	17	29.55	11.8	59.1	1
FUZTOJ	$Re_2(CO)_{10}$	34	5	1	80.1	17	40.05	16.0	80.1	
JIHGAI	$Re_2H_2(CO)_8$	32	4	2	103.6	16	51.8	25.9	51.8	2
KEYZAP	$Re_3H(CO)_{14}$	50	7	2	127.6	16.67	42.53	18.2	63.8	
	$Re_3H_2(CO)_3^-$	50	7	2	132	16.67	44	18.9	66.0	
JIHGAI	$Re_3H_3(CO)_{12}$	48	6	3	179.5	16	59.83	29.9	59.8	
TPARCH	$Re_3H_2(CO)_{12}^-$	48	6	3	212	16	70.67	35.3	70.7	
EAHRFC	$Re_3H(CO)_{12}^{2-}$	48	6	3	237.5	16	79.17	39.6	79.2	
JIHGEM	$Re_4H_4(CO)_{16}$	64	8	4	182.2	16	45.55	22.8	45.5	
DEBVOV	$Re_3H_4(CO)_{10}^-$	46	5	4	248.1	15.33	82.7	49.6	62.0	3
	$Re_3H_3(CO)_{10}^{2-}$	46	5	4	280.6	15.33	93.53	56.1	70.1	
EAREHC01	$Re_4H_4(CO)_{15}^{2-}$	64	8	4	264.3	16	66.07	33.0	66.1	4
DOKTIG	$Re_4H_5(CO)_{14}^-$	62	7	5	304.4	15.5	76.11	43.5	60.9	
EAMCRE	$Re_4(CO)_{16}^{2-}$	62	7	5	422.3	15.5	105.58	60.3	84.5	5
TMBTRE	$Re_4H_6(CO)_{12}^{2-}$	60	6	6	404.9	15	101.23	67.5	67.5	6
KUWVED	$Re_4H_4(CO)_{13}^{2-}$	60	6	6	452.5	15	113.13	75.4	75.4	7
FENNER	$Re_4H_5(CO)_{12}^-$	58	5	7	494.3	14.5	123.57	98.9	70.6	8
FUZHAJ	$Re_4H_4(CO)_{12}$	56	4	8	586.9	14	146.73	146.7	73.4	
	$Re_6H_8(CO)_{18}^{2-}$	88	8	10	620.6	14.67	103.43	77.6	62.1	9
LEYRAI	$Re_6H_7(CO)_{18}^-$	86	7	11	774.5	14.33	129.08	110.6	70.4	

1. Two molecules in the asymmetric unit, ΣE(Re—Re) = 57.2 kJ mol^{-1} for the second molecule.

2. Data are for $[Re_2H_2(CO)_8]$ co-crystallised with $[Re_3H_3(CO)_{12}]$. An older structure of $[Re_2H_2(CO)_8]$ gives ΣE(Re—Re) = 100.4 kJ mol^{-1}.

3. Data for $[Ph_3PNPPh_3][Re_3H_4(CO)_{10}]$; $[Et_4N][Re_3H_4(CO)_{10}]$ gives ΣE(Re—Re) = 243.2 kJ mol^{-1}.

4. Three polymorphs of $[Re_4H_5(CO)_{15}][NEt_4]_2$ are known, data are given for Form II (EAREHC02), for Form I (EAREHC01) ΣE(Re—Re) = 268.0 kJ mol^{-1}; for Form III (EAREHC) ΣE(Re—Re) = 264.9 kJ mol^{-1}.

5. Although the structure of $[Re_4(CO)_{16}][Et_4N]_2 \cdot 0.5\{(NEt_4)[trans\text{-}ReH_2(CO)_4]\}$ is disordered, the structure is of better quality than $[Bu_4N]_2[Re_4(CO)_{16}]$, for which ΣE(Re—Re) = 431.4 kJ mol^{-1}.

6. Data are for $[BzMe_3N]_2[Re_4H_6(CO)_{12}]$; $(Ph_4As)_2[Re_4H_6(CO)_{12}]$ gives ΣE(Re—Re) = 403.0 kJ mol^{-1}.

7. Data for $[Ph_4As]_2[Re_4H_4(CO)_{13}]$; for $(Et_4N)_2[Re_4H_4(CO)_{13}]$ ΣE(Re—Re) = 449.1 kJ mol^{-1}.

8. Two half-molecules in the asymmetric unit, ΣE(Re—Re) = 489.5 kJ mol^{-1} for other half molecule.

9. $[Re(CO)_3(DMF)_3][Re_3H_4(CO)_9]$ exists as a monomer in solution, the solid-state structure contains the $[Re_6H_8(CO)_{18}]^{2-}$ ion, data are given for the dimer. The three Re—Re bonds of the Re_3 fragment give ΣE(Re—Re) = 222.6 kJ mol^{-1}.

1.503 Å and a radius for the core carbon atom of 1.503×0.414 Å = 0.622 Å, which is rather smaller than the single bond covalent radius of carbon (0.77 Å). Mason has correlated the effective carbon radius for a number of core-carbon metal clusters with the ^{13}C NMR chemical shift [13], and interpreted the strongly deshielded shifts in terms of a "compression" of the interstitial carbon atoms. We note that density-functional theory calculations by Kaupp have proposed an alternative interpretation [14]. Our bond-enthalpy data do not suggest that the core carbon atom is "compressed" to fit into the hole in an octahedral rhenium cluster such as $[Re_6C(CO)_{19}]^{2-}$. Instead we suggest that it should be regarded as a $C^{\delta+}$ ion, with a radius $\leqslant$0.622 Å, which pulls the metal atoms towards it. Furthermore, the idea of a strong "pull" between core carbon atom and the surrounding metal atoms equates to a strong metal-carbon bond enthalpy. We will explore likely values for E(M—C) bond enthalpies in a future paper.

For the clusters in Table 1 the total metal–metal bond enthalpy per localised bond pair ranges from 45 to 85 kJ mol^{-1}. Such a wide range of values indicates that it would be difficult to interpret the thermodynamics of these clusters with a model using a single value for the metal–metal bond enthalpy in rhenium clusters. For the core carbon-containing clusters, the total metal–metal bond enthalpy per localised bond pair covers a very much narrower range of values, providing a further illustration of the influence of the core carbon atoms "pulling" the metal atoms together, giving a metal–metal bond enthalpy which is influenced much less by the ligands around the cluster.

For all of the rhenium carbonyl clusters, we have

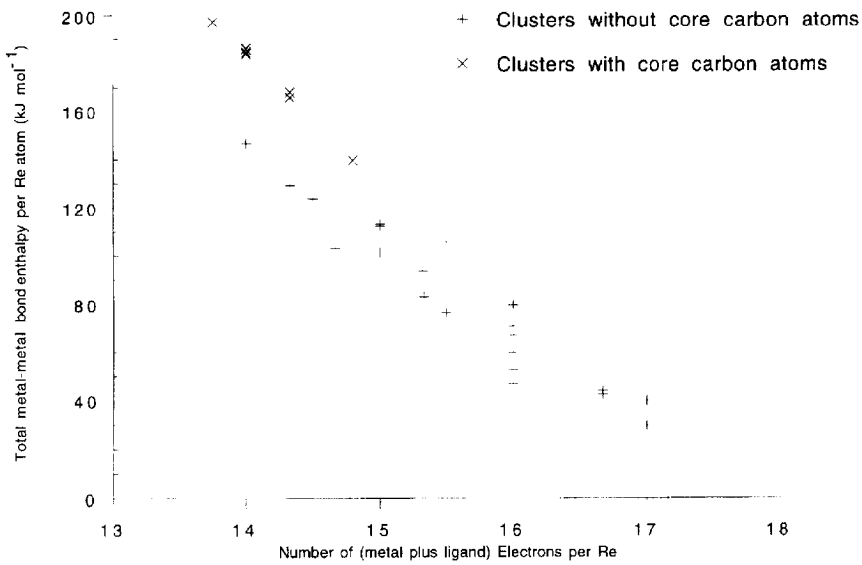

Fig. 2. Plot of total metal–metal bond enthalpy per metal atom as a function of the number of electrons for rhenium carbonyl clusters.

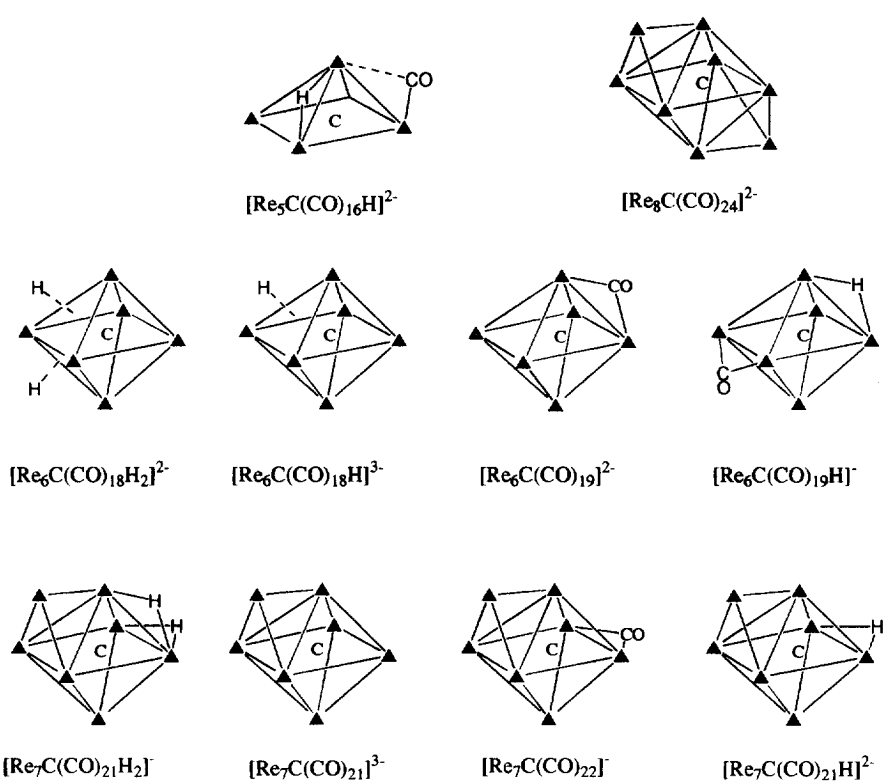

Fig. 3. The structures of the core carbon containing rhenium carbonyl clusters discussed. Lines are drawn to indicate connectivity, and do not imply the presence of single bonds. The following symbols are used : ■ = $Re(CO)_4$; ▲ = $Re(CO)_3$. Hydride and bridging carbonyl ligands are drawn explicitly ; dashed lines are drawn to face-bridging hydrides.

Table 2. The rhenium carbonyl core carbon clusters studied, listing their CSD code, formula, the number of valence shell electrons, the number of localised 2c2e bonds according to the EAN model (S_{1b}), the total metal–metal bond enthalpy and the number of valence shell electrons per metal atom and total metal–metal bond enthalpy per metal atom, per PSEPT electron pair ($S_p = 7$ for all these clusters) and per localised bond pair

CSD code	Formula	Valence electrons	S_{1b}	ΣE(Re—Re) (kJ mol^{-1})	Valence electrons per Re	ΣE(Re—Re) per Re atom	ΣE(Re—Re) per S_p	ΣE(Re—Re) per S_{1b}	Notes
FUDJUJ	$[Re_5C(CO)_{16}H]^{2-}$	74	8	697.8	14.8	139.6	99.7	87.2	
BUHLIZ	$[Re_6C(CO)_{18}H_2]^{2-}$	86	11	995	14.33	165.8	142.1	90.5	
HIGJUC	$[Re_6C(CO)_{18}H]^{3-}$	86	11	1008	14.33	168.0	144.0	91.6	
VOSLIY	$[Re_6C(CO)_{19}H]^{-}$	86	11	1008.2	14.33	168.0	144.0	91.7	
VOSLEU	$[Re_6C(CO)_{19}]^{2-}$	86	11	1015	14.33	169.2	145.0	92.3	1
SEWPOZ	$[Re_7C(CO)_{21}H_2]^{-}$	98	14	1287	14	183.9	183.9	91.9	
FOFFIP	$[Re_7C(CO)_{22}]^{-}$	98	14	1291	14	184.4	184.4	92.2	
GEGFUT	$[Re_7C(CO)_{21}H]^{2-}$	98	14	1300	14	185.7	185.7	92.9	2
BEJBOH	$[Re_7C(CO)_{21}]^{3-}$	98	14	1302	14	186	186.0	93.0	
BEVDIP	$[Re_8C(CO)_{24}]^{2-}$	110	17	1576	13.75	197	225.1	92.7	
DUKBOA	$\{Re_7C(CO)_{21}[Au[(PPh_3)]\}^{2-}$	98	14	1274	14	182.0	182.0	91.0	

1. Data are taken for one of the molecules in the asymmetric unit of VOSLEU, $[Re_6C(CO)_{19}][Ph_4P]_2$; for the other molecule ΣE(Re—Re) = 1008 kJ mol^{-1}; for JOCXAA, $[Re_6C(CO)_{19}][Ph_3PNPPh_3]_2$ ΣE(Re—Re) = 1036.6 kJ mol^{-1}.

2. Data are taken for GEGFUT, $[Re_7C(CO)_{21}H][Et_4N]_2$; for GEGAA, $[Re_7C(CO)_{21}H][Et_4N][C_7H_7]$, ΣE(Re—Re) = 1287 kJ mol^{-1}.

explored correlations between the total metal–metal bond enthalpy and the number of skeletal electron pairs formally available to bond the metal atoms, using a delocalised (PSEPT = Polyhedral Skeletal Electron Pair Theory) bonding model. Table 3 presents the total metal–metal bond enthalpy per PSEPT skeletal electron pair, tabulated as a function of the number of skeletal electron pairs and the cluster structural type (capped-*closo*, *closo*, *nido*, *arachno*, or *hypho*). The metal–metal bond enthalpy per skeletal electron pair increases as the cluster structural type becomes less open (upwards in Table 3), and the available electrons are used for metal–metal bonding, rather than as metal-based lone pairs. Within a given cluster structural type, the metal–metal bond enthalpy increases as the number of skeletal electron pairs or vertices increases.

There are two features of rhenium carbonyl cluster chemistry which we wish to explore using the total

Table 3. Total metal–metal bond enthalpy per PSEPT skeletal electron pair, ΣE(Re—Re)/S_p in kJ mol^{-1}, tabulated as a function of structural type and the number of skeletal pairs according to PSEPT

	4 pairs		5 pairs		6 pairs		7 pairs		8 pairs	
dicapped *closo*							$[Re_5C(CO)_{24}]^{2-}$	225.1		
capped *closo*	$[Re_4H_4(CO)_{12}]$	146.7					$[Re_7C(CO)_{21}]^{3-}$	186.0		
							$\{Re_7C(CO)_{21}H\}^{2-}$	185.7		
							$[Re_7C(CO)_{22}]$	184.4		
							$[Re_7C(CO)_{21}H_2]^{-}$	183.9		
closo			$[Re_4H_4(CO)_{12}]^{-}$	98.9			$[Re_6C(CO)_{19}]^{2-}$	145.0		
							$[Re_6C(CO)_{19}H]^{-}$	144.0		
							$[Re_6C(CO)_{18}H]^{3-}$	144.0		
							$[Re_6C(CO)_{18}H_2]^{2-}$	142.1		
							$[Re_6H_7(CO)_{18}]^{-}$	110.6		
nido	$[Re_2H_2(CO)_8]$	25.9	$[Re_3H_3(CO)_{10}]^{2-}$	56.1	$[Re_4H_4(CO)_{13}]^{2-}$	75.4	$[Re_5C(CO)_{16}H]^{2-}$	99.7	$[Re_6H_8(CO)_{18}]^{2-}$	77.6
			$[Re_3H_4(CO)_{10}]$	49.6	$[Re_4H_6(CO)_{12}]^{2-}$	67.5				
arachno			$[Re_2H_3(CO)_8]^{-}$	11.8	$[Re_3H(CO)_{12}]^{2-}$	39.6	$[Re_4(CO)_{16}]^{2-}$	60.3		
			$[Re_2(CO)_{10}]$	16	$[Re_3H_2(CO)_{12}]$	35.3	$[Re_4H_5(CO)_{14}]$	43.5		
					$[Re_3H_3(CO)_{12}]$	29.9				
hypho							$[Re_3H_2(CO)_{13}]^{-}$	18.9	$[Re_4H_4(CO)_{15}]^{2-}$	33.0[a]
							$[Re_3H(CO)_{14}]$	18.2	$[Re_4H_4(CO)_{16}]$	22.8

[a] The structure of $[Re_4H_4(CO)_{16}]$ is a square of Re atoms, the $[Re_4H_4(CO)_{15}]^{2-}$ cluster has the alternative spiked triangle geometry.

metal–metal bond enthalpy to quantify structural changes. The first is the presence of series of clusters which have the same empirical formula, namely the $[ReH(CO)_4]_n$ (n = 2–4) series, which are three of the clusters which have 16 valence electrons per metal (or nine ligand electrons per metal), the other examples being $[Re_4H_4(CO)_{15}]^{2-}$, $[Re_3H_2(CO)_{12}]^-$ and $[Re_3H(CO)_{12}]^{2-}$, the latter two being obtained by successive deprotonations of $[ReH(CO)_4]_3$. The second feature is the presence of two series of clusters containing three and four metal atoms, with varying electron counts, and hence structures which vary between very open clusters and unsaturated closed clusters.

As in our previous discussion of hydride-containing osmium carbonyl clusters, we note that the "hydride" ligand in a general mono-hydride cluster $[Re_xH(CO)_y]^{c-}$ can be formally regarded as an H^+ ion protonating the hydride-free $[Re_x(CO)_y]^{(c+1)-}$ cluster. Terminal hydrides may be regarded as resulting from the protonation of metal-based lone pairs, whereas (μ_2-H) ligands may be regarded as resulting from protonation of a 2c2e metal–metal bond, converting the two centre Re—Re bond pair into a three-centre two-electron Re(μ-H)Re system. Triply-bridging hydride ligands on a cluster face result from the protonation of a three-centre two-electron Re_3 bond. In such a formalism, the doubly hydride-bridged bonds of $[Re_2H_2(CO)_8]$ can be regarded as resulting from the addition of two H^+ ions to $[Re_2(CO)_8]^{2-}$ (cf B_2H_6 derivable from $[B_2H_4]^{2-}$: these systems are both analogues of C_2H_4). Each protonation converts one electron pair of the double bond into a three-centre two-electron bond*.

The photochemical and thermal interconversion of the three rhenium clusters $[ReH(CO)_4]_n$ (n = 2–4) has been described together with their solid-state structures, and these clusters have been described as organometallic analogues of the $(CH_2)_n$ molecules ethene, cyclopropane and cyclobutane, possessing respectively four, six and eight skeletal electron pairs according to PSEPT, although the analogy also holds in a localised bond description. In fact, given the presence of bridging hydrides in these rhenium clusters, they might be better described as analogues of B_2H_6, B_3H_9 and B_4H_{12}, though the latter boranes are only postulated as reactive intermediates in borane reactions. The anionic spiked-triangular cluster $[Re_4H_4(CO)_{15}]^{2-}$ is formally an analogue of methylcyclopropane; the spiked triangle presents a structure with four Re—Re bonds, three of which are protonated/bridged by hydride ligands, the final hydride is terminally located on the spike atom. Studies of the thermochemistry of cyclopropane, cyclobutane and cyclopentane show that these cycloalkanes have a measurable ring-strain [15], associated with their bond angles deviating from the ideal tetrahedral angle (109°) since their structures require eclipsed C—C—C fragments, with bond angles of 60°, 90° and 108°, respectively. Cyclohexane is strain-free, since the chair conformation allows staggered bonds and angles of 109°. In contrast, the structures of the cyclic rhenium clusters $[ReH(CO)_4]_n$ (n = 3 and 4) are based on octahedral metal fragments, and so the preferred angle for a strain-free structure would appear to be 90°. A further feature is that three centre two electron M—H—M bonds are bent at the hydrogen. Figure 4 shows the equatorial projections (the axial CO ligands are omitted) of the hypothetical hydride-free clusters $[Re_3(CO)_{12}]^{3-}$ and $[Re_4(CO)_{12}]^{4-}$ constructed using strictly octahedral metal geometries. For the cluster $[Re_3(CO)_{12}]^{3-}$, (a), the Re_3 ring will be strained, since the Re—Re—Re angles will be 60° rather than 90°, but the protonation to form $[Re_3H_3(CO)_{12}]$ (b), with bent 3c—2e bonds will relieve the strain. By contrast, for the cluster $[Re_4(CO)_{12}]^{4-}$ a square geometry, (d), would be strain-free, and the addition of four protons along the Re—Re edges to give bent at hydrogen 3c—2e bonds will introduce strain, minimised by placing two protons inside the ring and two outside, (e). The published structure of $[Re_4H_4(CO)_{16}]$ resembles (e). Although the hydrogen atoms were not located in electron density maps, their locations were deduced from potential energy calculations. The crystal structure of $[Re_4H_4(CO)_{16}]$ does present the short and long non-bonded carbonyl contacts suggested by Fig. 4e. The conclusion that can be drawn is that the combination of octahedral metal coordination and bent 3c—2e bonds makes the $[Re_3H_3(CO)_{12}]$ cluster strain-free, whilst the non-bonded contacts in $[Re_4H_4(CO)_{16}]$ make this a strained ring. This conclusion is borne out by the fact that the total metal–metal bond enthalpy for the four bonds of $[Re_4H_4(CO)_{16}]$ (182 kJ mol^{-1}) is barely greater than that for the three bonds of $[Re_3H_3(CO)_{12}]$ (179.5 kJ mol^{-1}). There are thus different trends in ring-strain as a function of ring size in the $(CH_2)_n$ and $[ReH(CO)_4]_n$ systems, a consequence of the differences between tetrahedral and octahedral coordination together with the nonlinear nature of M—H—M bonds.

Progressive deprotonation of $[Re_3H_3(CO)_{12}]$ would be expected to introduce progressively greater ring-strain, so reducing ΣE(Re—Re) for this trinuclear cluster, whereas deprotonation of $[Re_4H_4(CO)_{16}]$ would be expected to increase ΣE(Re—Re) as ring strain, and non-bonded repulsions are reduced. A corollary is that $[Re_4H_4(CO)_{16}]$ should be a stronger Brönsted acid than $[Re_3H_3(CO)_{12}]$.

It is worth noting that $[Re_4H_4(CO)_{15}]^{2-}$ has the spiked triangular skeleton that is more suited to its degree of protonation than a square skeleton would be.

The total metal–metal bond enthalpies for the rhenium carbonyl clusters containing three and four rhenium atoms are presented in Tables 4 and 5 listed according to the number of cluster valence electrons.

*Many textbooks and papers draw a structure for complexes such as $[Re_2H_2(CO)_8]$ with a double bond and two bridging hydrides, which is misleading.

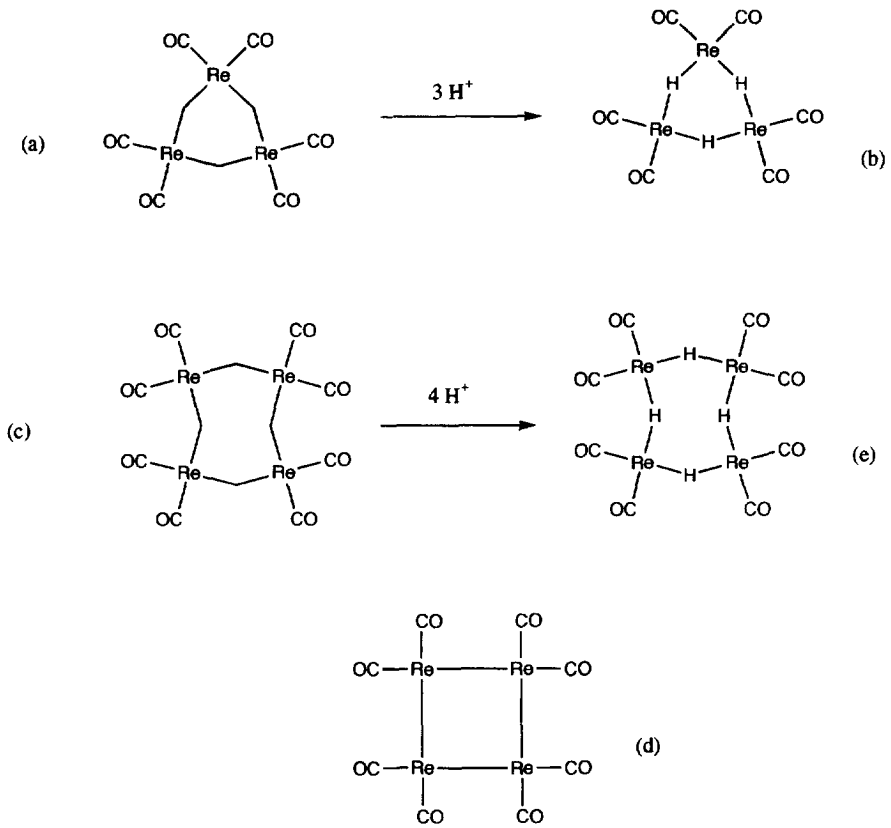

Fig. 4. The clusters $[Re_3(CO)_{12}]^{3-}$ and $[Re_4(CO)_{16}]^{4-}$ constructed using octahedral metal fragments, with all angles 90°. As shown, addition of protons forming bent Re—H—Re bonds gives the known $[Re_3H_3(CO)_{12}]$ and $[Re_4H_4(CO)_{16}]$ clusters. Only the equatorial planes of the clusters are drawn, the axial carbonyl ligands are omitted.

Table 4. The Re_3 clusters studied in this work and the calculated total metal–metal bond enthalpy, ΣE(Re—Re) in kJ mol^{-1}, for each cluster, tabulated as a function of electron count, and the departure of cluster formula from the parent $[Re_3H_3(CO)_y]$ clusters. Those parent clusters in italics are not structurally known, but are included for the purposes of constructing the table. Values in parentheses are the total metal–metal bond enthalpy per localised bond electron pair, $\Sigma E(Re—Re)/S_{lb}$

	5 skeletal electron pairs 46 valence electrons 4M—M bonds	6 skeletal electron pairs 48 valence electrons 3 M—M bonds	7 skeletal electron pairs 50 valence electrons 2 M—M bonds
$-H_2+CO$			$[Re_3H(CO)_{14}]$ 127.6(63.8)
$-2H^+$		$[Re_3H(CO)_{12}]^{2-}$ 237.5(79.2)	
$-H+$		$[Re_3H_2(CO)_{12}]^-$ 212(70.7)	$[Re_3H_2(CO)_{13}]^-$ 132(66.0)
Parent	*$[Re_3H_3(CO)_{11}]$*	$[Re_3H_3(CO)_{12}]$ 179.5(59.8)	*$[Re_3H_3(CO)_{13}]$*
$-CO+2e^-$	$[Re_3H_3(CO)_{10}]^{2-}$ 280.6(70.2)		
$-CO+H^-$	$[Re_3H_4(CO)_{10}]^-$ 248.1(62.0)		

The Tables show the equivalent number of PSEPT skeletal electron pairs and number of formal Re—Re bonds required to satisfy the 18 electron rule. The structures of the clusters are presented in the form of the connectivities and bond orders of the underlying metal cores, although the clusters are more delocalised than the representation given by the figures, thus, there are two bonds of formal bond order 1.5 in $[Re_4H_5(CO)_{12}]^-$, but the bonds in $[Re_4H_4(CO)_{12}]$ all have the same bond order. The vertical layout of the

Table 5. The Re_4 clusters studied in this work and their calculated total metal–metal bond enthalpies, $\Sigma E(Re—Re)$ in kJ mol^{-1}, tabulated as a function of electron count and the departure of the cluster molecular formula from the parent $[Re_4H_4(CO)_y]$ clusters. Those clusters in italics are not structurally known, but are included for purpose of constructing the table. Values in parentheses are the total metal–metal bond enthalpy per localised bond electron pair, $\Sigma E(Re—Re)/S_{lb}$

Ligands added to/removed from parent cluster	4 PSEPT pairs 56 valence electrons 8 M—M bonds	5 PSEPT pairs 58 valence electrons 7 M—M bonds	6 PSEPT pairs 60 valence electrons 6 M—M bonds	7 PSEPT pairs 62 valence electrons 5 M—M bonds	8 PSEPT pairs 64 valence electrons 4 M—M bonds
$-2H^+ - H_2 + CO$				$[Re_4(CO)_{16}^{2-}]$ 422.3(84.5)	
$-CO + 2e$			$[Re_4H_4(CO)_{13}^{2-}]$ 452.5(75.4)		$[Re_4H_4(CO)_{15}^{2-}]$ 264.3(66.1)
Parent	$[Re_4H_4(CO)_{12}]$ 586.9(73.4)	*$[Re_4H_4(CO)_{13}]$*	*$[Re_4H_4(CO)_{14}]$*	*$[Re_4H_4(CO)_{15}]$*	$[Re_4H_4(CO)_{16}]$ 182.2(45.6)
$-CO + H^-$		$[Re_4H_5(CO)_{12}]$ 494.3(70.6)	*$[Re_4H_5(CO)_{13}^-]$*	$[Re_4H_5(CO)_{14}]$ 304.4(60.9)	
$-2CO + 2H$			$[Re_4H_6(CO)_{12}^{2-}]$ 404.9(67.5)		

data for the Re_3 clusters is centred about the $[Re_3H_3(CO)_y]$ ($y = 11$–13) clusters, only one of which is known, with vertical steps representing the formal reactions shown at the left. The Re_4 clusters are presented as based on $[Re_4H_4(CO)_y]$ ($y = 12$–16), although only the most open cluster, $[Re_4H_4(CO)_{16}]$, and the most closed example, $[Re_4H_4(CO)_{12}]$, are known. For both the Re_3 and Re_4 series there is the expected trend for the total metal–metal bond enthalpy to decrease as the number of skeletal electron pairs increases and the cluster becomes more open. For the Re_4 clusters there is a steady trend in the total metal–metal bond enthalpy of the most hydride-rich clusters. When presented as a function of the number of formal localised Re—Re bonds, as in Table 1, it becomes clear that the total metal–metal bond enthalpy per formal metal–metal bond is also not constant, indicating that any analysis of the thermodynamics of metal carbonyl clusters using a model which has fixed metal–metal bond enthalpies will be flawed.

There are three classes of clusters which are related by reactions which formally involve the loss or gain of ligands. Thus there are pairs of rhenium carbonyl clusters which are related by the addition or loss of a proton, there are also pairs of clusters which are formally related by the reductive elimination of H_2 followed by the addition of CO to maintain the same number of electrons, and there are clusters where formally a CO ligand is removed and two electrons added. These cluster interconversion reactions are listed in Table 6 together with the total metal–metal bond enthalpies of the pairs of clusters, and the change in $\Sigma E(Re—Re)$ for the formal reaction. A number of features can be noted from the data in Table 6. All ligand interchange reactions involving clusters containing interstitial carbon atoms result in much smaller changes in the metal–metal bonding enthalpies than similar reactions involving clusters which do not contain interstitial atoms. This suggests that the metal–metal bond distances in core carbon containing clusters are not very sensitive to ligand exchange, and may be largely determined by the bonding or steric requirements of the core carbon atom. The addition of a proton to the small clusters produces a loss in metal–metal bonding between 25 and 32 kJ mol^{-1}, all three examples involving the protonation of a metal–metal bond pair. The loss in metal–metal bonding will be compensated for by the E(cluster-H) bond enthalpy (on which there are at present no thermochemical experimental data). Similarly, replacement of two hydride ligands (as H_2) by CO produces a gain in metal–metal bonding as 3c—2e Re—H—Re bonds are replaced by two centre Re—Re and Re—CO bonds.

The gold phosphine fragment, $Au(PPh_3)^+$, is isolobal with the proton, so the mixed-metal rhenium gold cluster $\{Re_7C(CO)_{21}[Au(PPh_3)]\}^{2-}$ is a direct analogue of $[Re_7C(CO)_{21}H]^{2-}$. The total metal–metal bond enthalpy for the gold cluster is 28 kJ mol^{-1} less than the metal–metal bond enthalpy of $[Re_7C(CO)_{21}]^{3-}$, indicating that some metal–metal bonding is lost on introduction of the gold vertex, which is presumably compensated for by Re—Au bonding. However, whilst the hydride ligand in $[Re_7C(CO)_{21}H]^{2-}$ bridges an edge, the gold fragment in $\{Re_7C(CO)_{21}[Au(PPh_3)]\}^{2-}$ is located in a triply bridging mode on the face opposite the capping Re atom.

Earlier we discussed the replacement of two CO ligands in the hypothetical $[Re_6(CO)_{21}]^{2-}$ by a core

Table 6. Pairs of rhenium carbonyl clusters which are related by addition and removal of ligands and or electrons. In each case the total metal–metal bond enthalpy for each cluster pair is given, together with the change in total metal–metal bond enthalpy for the reaction. All enthalpies in kJ mol^{-1}

cluster pair	ΣE(Re—Re)	Δ[ΣE(Re—Re)]
(a) Addition of a proton ($+H^+$)		
$[Re_3H_3(CO)_{10}]^{2-} \rightarrow [Re_3H_4(CO)_{10}]^-$	280.6 → 248.1	−32.5
$[Re_3H(CO)_{12}]^{2-} \rightarrow [Re_3H_2(CO)_{12}]^-$	237.5 → 212	−25.5
$[Re_3H_2(CO)_{12}]^- \rightarrow [Re_3H_3(CO)_{12}]$	212 → 179.5	−32.5
$[Re_6C(CO)_{19}]^{2-} \rightarrow [Re_6C(CO)_{19}H]^-$	1015 → 1008	−7
$[Re_6C(CO)_{18}H]^{3-} \rightarrow [Re_6C(CO)_{18}H_2]^{2-}$	1008 → 995	−13
$[Re_7C(CO)_{21}]^{3-} \rightarrow [Re_7C(CO)_{21}H]^{2-}$	1302 → 1300	−2
$[Re_7C(CO)_{21}H]^{2-} \rightarrow [Re_7C(CO)_{21}H_2]^-$	1300 → 1287	−13
(b) Reductive elimination of H_2 followed by addition of a CO ligand ($-H_2+CO$)		
$[Re_4H_6(CO)_{12}]^{2-} \rightarrow [Re_4H_4(CO)_{13}]^{2-}$	404.9 → 452.5	+47.6
$[Re_6C(CO)_{18}H_2]^{2-} \rightarrow [Re_6C(CO)_{19}]^{2-}$	995 → 1015	+20
$[Re_7C(CO)_{21}H_2]^- \rightarrow [Re_7C(CO)_{22}]^-$	1287 → 1291	+4
(c) Replacement of a CO ligand by two electrons ($-CO+2e^-$)		
$[Re_4H_4(CO)_{16}] \rightarrow [Re_4H_4(CO)_{15}]^{2-}$	182.2 → 264.3	+82.1
$[Re_7C(CO)_{22}]^- \rightarrow [Re_7C(CO)_{21}]^{3-}$	1291 → 1302	+11

carbon to give $[Re_6C(CO)_{19}]^{2-}$, and estimated the total metal–metal bond enthalpy of $[Re_6(CO)_{21}]^{2-}$ to be $\geqslant 960$ kJ mol^{-1}. Alternatively removal of one H^+ [$\Delta\Sigma$(Re—Re) = 30 kJ mol^{-1}] and replacement of three H_2 groups by CO ligands [$\Delta\Sigma$(Re—Re) $\geqslant 3 \times 40$ kJ mol^{-1}] will convert $[Re_6H_7(CO)_{18}]^-$ [ΣE(Re—Re) = 774.5 kJ mol^{-1}] into $[Re_6(CO)_{21}]^{2-}$ giving an alternative estimate of ΣE(Re—Re) $\geqslant 925$ kJ mol^{-1} for $[Re_6(CO)_{21}]^{2-}$.

The highly unsaturated cluster $[Re_3H_4(CO)_9]^-$ is interesting in that it formally contains two Re—Re double bonds (which are protonated) [16] and is thus an analogue of the unknown cyclopropadiene. Although conductivity data indicate that this cluster exists as a monomer in solution, in the solid state the electronic unsaturation is relieved by the formation of a dimer $[Re_6H_8(CO)_{18}]^{2-}$, the structure of which is a trigonal antiprism, or octahedron elongated along one of the S_3 axes. The four Re—Re bonds which are broken on converting the dimer into the monomer provide a metal–metal bond enthalpy of 175 kJ (mol of dimer)$^{-1}$. This substantial bond enthalpy is lost on forming the monomer in solution, suggesting that dissociation of the dimer is likely to be a process favoured by entropy, and the likelihood that the three Re—Re bonds in the monomer are shorter, and stronger, than the same bonds in the solid-state dimer. In analysing the data, we have considered this cluster in its dimeric form, and the data in Fig. 2 relate to $[Re_6H_8(CO)_{18}]^{2-}$.

CONCLUSIONS

We have shown that the total metal–metal bond enthalpy of a rhenium carbonyl cluster provides a single parameter to characterise the metal–metal bonding. Changes in bond lengths on the addition of protons and carbonyl ligands can be quantified through the total metal–metal bond enthalpy. We have investigated trends in the metal–metal bond enthalpy of rhenium carbonyl clusters as a function of the number of electrons available for bonding in both localised (18 electron or EAN) and delocalised (PSEPT) bonding models. For rhenium clusters containing core carbon atoms the metal–metal bond enthalpy is higher than for clusters with similar electron counts devoid of core carbon atoms, and we interpret this as a consequence of the attractive pull of a cationic core carbon, $C^{\delta+}$, on its surrounding metal atoms. A core carbon atom apparently requires less space (radius 0.622 Å) than octahedral rhenium carbonyl clusters held together by seven skeletal electron pairs would normally make available.

EXPERIMENTAL

Fractional atomic coordinates for $[Re_2(CO)_{10}]$ [17], $[Re_2H_3(CO)_8][Et_4N]$ [18], $[Re_3H(CO)_{14}]$ [19], $[Re_3H(CO)_{12}][Et_4N]_2$ [20], co-crystallised $[Re_2H_2(CO)_8]$ $[Re_3H_3(CO)_{12}]$ [21], $[Re_4H_4(CO)_{16}]$ [21], $[Re_3H_2(CO)_{12}][Ph_4As]$ [22], $[Re_4H_5(CO)_{14}][Et_4N]$ [23], $[Re_3H_4(CO)_{10}][Ph_3PNPPh_3]$ [24], $[Re_4H_6(CO)_{12}][BzMe_3N]_2$ [25], $[Re_4H_4(CO)_{13}][Ph_4As]_2$ [26], $[Re_4(CO)_{16}][Bu_4N]_2$ [27], $[Re_4H_5(CO)_{12}][Et_4N]$ [28], $[Re_6H_7(CO)_{18}][Et_4N]$ [29], $[Re_4H_4(CO)_{12}]$ [30], $[Re_6C(CO)_{18}H][Et_4N]_3$ [31], $[Re_5C(CO)_{16}H][Et_4N]_2$ [32], $[Re_7C(CO)_{21}H][Et_4N]_2$ and $[Re_7C(CO)_{21}H]$ $[Et_4N][C_7H_7]$ [33], $[Re_7$

$C(CO)_{21}H_2][Et_4N]$ [34], $[Re_7C(CO)_{21}][Ph_4P]_3$ [35], $[Re_6C(CO)_{19}H][Et_4N]$. CH_2Cl_2 [36], $[Re_6C(CO)_{19}][Ph_4As]_2$ [36], $[Re_7C(CO)_{22}]$ $[Et_4N]$ [37] and $\{Re_7C(CO)_{21}[Au(PPh_3)]\}[Ph_4As]_2$ [38] were retrieved from the Cambridge Structural Database [CSD April 1997 release, version 5.11 on the University of Durham UNIX network) [39] using QUEST and metal–metal distances were evaluated using BABEL [40]. The fractional atomic coordinates for Forms I and II of $[Re_4H_4(CO)_{15}][Et_4N]_2$ were retrieved from the CSD [12], the Re—Re bond lengths of Form III were also retrieved from Ref. 12. Fractional atomic coordinates for $[Re_2H_2(CO)_8]$ [41], $[Re_4(CO)_{16}][Et_4N]\cdot 0.5\{[NEt_4]$-*trans*-$ReH_2(CO)_4\}$ [20], $[Re_3H_4(CO)_{10}][Et_4N]$ [43], and $[Re_3H_3(CO)_{10}][NEt_4]_2$ [43], $[Re_4H_6(CO)_{12}]$ $[Ph_4As]_2$ [44], $[Re_4H_4(CO)_{13}][Et_4N]_2$ [45], $[Re_6C(CO)_{18}H_2][MePh_3P]_2$ [46], $[Re_6C(CO)_{19}]$ $[Ph_3PNPPh_3]_2$ [47], and $[Re_8C(CO)_{24}][Et_4N]_2$ [48], are not available in either the CSD or the Inorganic Crystal Structure Datafile (ICSD) or in the original publications, and metal–metal distances were retrieved directly from figures or tables in the publications. The structures of $[Re_3H_2(CO)_{13}][NEt_4]$ [49], and $[Re(CO)_3$ $(DMF)_3]_2[Re_3H_4(CO)_9]_2$ [15] were published whilst this work was in progress, and data is not available from the CSD at the time of writing this manuscript; for these clusters metal–metal distances were retrieved from the publications.

Kaleidagraph running on a Mac LCII was used to draw Fig. 2, relating the total Re—Re bond enthalpy per metal atom $\Sigma E(Re—Re)/x$, to the number of ligand electrons per metal atom.

The Re—Re distances used in this work are without e.s.d.s since they were derived from fractional atomic coordinate data available from the Cambridge Structural Database which does not contain e.s.d.s, and in many cases complete lists of Re—Re distances are not available in the original publication, so we are unable to extract e.s.d.s from that source; as indicated previously [1], we feel that the crystallographic contribution to the errors in $\Sigma E(Re—Re)$ is less than 1 kJ mol^{-1}. In contrast the e.s.d.s on M—C and C—O distances are typically larger, reflecting the lighter atomic masses of these elements and libration of carbonyl ligands, and mean that any attempt to estimate Re—C and C—O bond enthalpies from current crystallographic data will result in large estimated errors.

Acknowledgements—We wish to acknowledge the use of the EPSRC's Chemical Database at Daresbury [50].

REFERENCES

1. Hughes, A. K., Peat, K. L. and Wade, K., *J. Chem. Soc., Dalton Trans.*, 1996, 4639.
2. Hughes, A. K., Peat, K. L. and Wade, K., *J. Chem. Soc., Dalton Trans.*, 1997, 2139.
3. Housecroft, C. E., O'Neill, M. E., Wade, K. and Smith, B. C., *J. Organomet. Chem.*, 1981, **213,** 35.
4. Martin, R., Gardiner, P. and Bradshaw, A. M., *Surface Science*, 1995, **342,** 69.
5. (a) Housecroft, C. E., Wade, K. and Smith, B. C., *J. Chem. Soc., Chem. Commun.*, 1978, 765; (b) Housecroft, C. E., Wade, K. and Smith, B. C., *J. Organomet. Chem.*, 1979, **170,** C1.
6. (a) Connor, J. A., *Top. Curr. Chem.*, 1977, **71,** 71; (b) Connor, J. A., Skinner, H. A. and Virmani, Y., *Faraday Symp. Chem. Soc.*, 1973, **8,** 18.
7. Hughes, A. K., Johnson, A. L. and Wade, K., unpublished results.
8. (a) Muetterties, E. L., Rhodin, T. N., Band, E., Brucker, C. F. and Pretzer, W. R., *Chem. Rev.*, 1979, **79,** 91; (b) Albert, M. R. and Yates, J. T., *The Surface Scientist's Guide to Organometallic Chemistry*, American Chemical Society, Washington, 1987.
9. Wade, K., *Adv. Inorg. Chem. Radiochem.*, 1976, **18,** 1.
10. Housecroft, C. E. and Wade, K., *Gazz. Chim. Ital.*, 1980, **110,** 87.
11. Orpen, A. G., *J. Chem. Soc., Dalton Trans.*, 1980, 2509.
12. EAREHC01/02, Ciani, G., Albano, V. G. and Immirzi, A., *J. Organomet. Chem.*, 1976, **121,** 237.
13. Mason, J., *J. Am. Chem. Soc.*, 1991, **113,** 24.
14. Kaupp, M. *J. Chem. Soc., Chem. Commun.*, 1996, 1141.
15. Cohen, N. and Benson, S. W., *Chem. Rev.*, 1993, **93,** 2419.
16. Horng, H. C., Cheng, C. P., Yang, C. S. and Lee, G.-H., *Organometallics*, 1996, **15,** 2543.
17. FUZTOJ, Churchill, M. R., Amoh, K. N. and Wasserman, H. J., *Inorg. Chem.*, 1981, **20,** 1609.
18. FIZTIR, Beringhelli, T., D'Alfonso, G., Ghidorsi, L., Ciani, G., Sironi, A. and Molinari, H., *Organometallics*, 1987, **6,** 1365.
19. KEYZAP, Chang, C. S., Cheng, C. P., Guo, L. W. and Wang, Y., *J. Chin. Chem. Soc. (Taipei)*, 1989, **32,** 17.
20. EAHRFC EAMCRE, Ciani, G., D'Alfonso, G., Freni, M., Romiti, P. and Sironi, A., *J. Organomet. Chem.*, 1978, **157,** 199.
21. JIHGAI JIHGEM, Masciocchi, N., Sironi, A. and D'Alfonso, G., *J. Am. Chem. Soc.*, 1990, **112,** 9395.
22. TPARCH, Churchill, M. R., Bird, P. H., Kaesz, H. D., Bau, R. and Fontal, B., *J. Am. Chem. Soc.*, 1968, **90,** 7135.
23. DOKTIG, Beringhelli, T., Ciani, G., D'Alfonso, G., De Malde, V., Sironi, A. and Freni, M., *J. Chem. Soc., Dalton Trans.*, 1986, 1051.
24. DEBVOV, Beringhelli, T., Ciani, G., D'Alfonso, G., Molinari, H. and Sironi, A., *Inorg. Chem.*, 1985, **24,** 2666.
25. TMBTRE, Ciani, G., Sironi, A. and Albano, V. G., *J. Organomet. Chem.*, 1977, **136,** 339.
26. KUWVED, Beringhelli, T., D'Alfonso, G., Minoja, A. P., Ciani, G. and Sironi, A., *J. Organomet. Chem.*, 1992, **440,** 175.
27. BATCRE10, Churchill, M. R., and Bau, R., *Inorg. Chem.*, 1968, **7,** 2606.
28. FENNER, Beringhelli, T., D'Alfonso, G., Ciani, G. and Molinari, H., *J. Chem. Soc., Chem. Commun.*, 1987, 486.

29. LEYRAI, Yang, C. S. and Cheng, C. P., *J. Chem. Soc., Dalton Trans.*, 1994, 2011.
30. FUZHAJ, Wilson, R. D. and Bau, R., *J. Am. Chem. Soc.*, 1976, **98,** 4687.
31. HIGJUC, Shapley, J. R., Rheingold, A. L., Allen, M. B., unpublished results.
32. FUDJUJ, Henly, T. J., Wilson, S. R. and Shapley, J. R., *Organometallics*, 1987, **6,** 2618.
33. GEGFUT and GEGGAA, Beringhelli, T., D'Alfonso, G., Ciani, G., Sironi, A. and Molinari, H., *J. Chem. Soc., Dalton Trans.*, 1988, 1281.
34. SEWPOZ, Beringhelli, T., D'Alfonso, G., Ciani, G., Sironi, A. and Molinari, H. *J. Chem. Soc., Dalton Trans.*, 1990, 1901.
35. BEJBOH, Ciani, G., D'Alfonso, G., Freni, M., Romiti, P. and Sironi, A., *J. Chem. Soc., Chem. Commun.*, 1982, 339.
36. VOSLIY VOSLEU, Beringhelli, T., D'Alfonso, G., Molinari, H. and Sironi, A., *J. Chem. Soc., Dalton Trans.*, 1992, 689.
37. FOFFIP, Beringhelli, T., D'Alfonso, G., de Angelis, M., Ciani, G. and Sironi, A., *J. Organomet. Chem.*, 1987, **322,** C21.
38. DUKBOA, Henly, T. J., Shapley, J. R. and Rheingold, A. L., *J. Organomet. Chem.*, 1986, **310,** 55.
39. Allen, F. H. and Kennard, O., *Chemical Design Automation News*, 1993, **8,** 1 & 31–37.
40. BABEL, Walters, P. and Stahl, M., Department of Chemistry, University of Arizona, 1994.
41. Bennett, M. J., Graham, W. A. G., Hoyano, J. K. and Hutcheon, W. L., *J. Am. Chem. Soc.*, 1972, **94,** 6232.
42. EAHDRE, Ciani, G., D'Alfonso, G., Freni, M., Romiti, P., Sironi, A. and Albinati, A., *J. Organomet. Chem.*, 1977, **136,** C49.
43. Bertolucci, A., Freni, M., Romiti, P., Ciani, G., Sironi, A. and Albano, V. G., *J. Organomet. Chem.*, 1976, **113,** C61.
44. Kaesz, H. D., Fontal, B., Bau, R., Kirtley, S. W. and Churchill, M. R., *J. Am. Chem. Soc.*, 1969, **91,** 1021.
45. HCREEA, Bertolucci A., Ciani, G., Freni, M., Romiti, P., Albano, V. G. and Albinati, A., *J. Organomet. Chem.*, 1976, **117,** C37.
46. BUHLIZ, Ciani, G., D'Alfonso, G., Romiti, P., Sironi, A. and Freni, M. *J. Organomet. Chem.*, 1983, **244,** C27.
47. JOCXAA, Hsu, G., Wilson, S. R. and Shapley, J. R., *Inorg. Chem.*, 1991, **30,** 3881.
48. BEVDIP, Ciani, G., D'Alfonso, G., Freni, M., Romiti, P. and Sironi, A., *J. Chem. Soc., Chem. Commun.*, 1982, 705.
49. Bergano, M., Beringhelli, T., D'Alfonso, G., Ciani, G., Moret, M. and Sironi, A., *Organometallics*, 1996, **15,** 3876.
50. Fletcher, D. A., McMeeking, R. F. and Parkin, D., *J. Chem. Inf. Comput. Sci.*, 1996, **36,** 746.

Pergamon

PII: S0277-5387(97)00529-9

Polyhedron Vol. 17, No. 17, pp. 2817–2827, 1998
© 1998 Elsevier Science Ltd
All rights reserved. Printed in Great Britain
0277-5387/98 $19.00+0.00

Amphiphilic organoruthenium oxomolybdenum and oxovanadium clusters†

Georg Süss-Fink,[a]* Laurent Plasseraud,[a] Vincent Ferrand,[a] Sandrine Stanislas,[a] Antonia Neels,[a] Helen Stoeckli-Evans,[a] Marc Henry,[b] Gabor Laurenczy[c] and Raymond Roulet[c]

[a] Institut de Chimie, Université de Neuchâtel, Avenue de Bellevaux 51, CH-2000 Neuchâtel, Switzerland

[b] Laboratoire de Chimie Moleculaire de l'Etat Solide, Université Louis Pasteur, Institut Le Bel, 4 rue Blaise Pascal, F-67070 Strasbourg Cedex, France

[c] Institut de Chimie Minérale et Analytique, Université de Lausanne-BCH, CH-1015 Lausanne, Switzerland

(Received 27 September 1997; accepted 3 December 1997)

Abstract—*Para*-cymene ruthenium dichloride dimer reacts in aqueous solution with sodium molybdate or sodium vanadate to give the amphiphilic clusters $[(\eta^6\text{-}p\text{-}MeC_6H_4iPr)_4Ru_4Mo_4O_{16}]$ (**1**) and $[(\eta^6\text{-}p\text{-}MeC_6H_4iPr)_4Ru_4V_6O_{19}]$ (**4**) respectively. The analogous reaction of hexamethylbenzene ruthenium dichloride dimer with sodium vanadate gives $[(\eta^6\text{-}C_6Me_6)_4Ru_4V_6O_{19}]$ (**5**). The mixed-metal clusters $[(\eta^6\text{-}p\text{-}MeC_6H_4iPr)Ru(\eta^5\text{-}C_5Me_5)_3Rh_3Mo_4O_{16}]$ (**2**) and $[(\eta^6\text{-}p\text{-}MeC_6H_4iPr)_2Ru_2(\eta^5\text{-}C_5Me_5)_2Rh_2Mo_4O16]$ (**3**) are accessible from a mixture of *para*-cymene ruthenium dichloride dimer and pentamethylcyclopentadienyl rhodium dichloride dimer with sodium molybdate in aqueous solution. The crystal structure analyses of **1** and **4** reveal different framework geometries of the metal oxygen skeletons. ^{17}O NMR spectroscopy and partial charge calculations confirm the presence of three different types of oxygen atoms in **1**. © 1998 Elsevier Science Ltd. All rights reserved

Keywords: arene; ruthenium; molybdenum; vanadium; oxo clusters; X-ray structure.

The past two decades have witnessed a steadily growing interest in molecules containing both, organometallic groups and oxometallic entities [1]. Such clusters are accessible by metathesis reaction between an organometallic halide and an oxometallic anion.

$$(\eta^5\text{-}C_5H_5)TiCl_3 + [H_3PW_{11}O_{39}]^{4-} \rightarrow [(\eta^5\text{-}C_5H_5)Ti(PW_{11}O_{39})]^{4-} + 3HCl$$

Since the discovery of $[(\eta^5\text{-}C_5H_5)Ti(PW_{11}O_{39})]^{4-}$ in 1978 by W. G. Klemperer and co-workers [2], a large number of organometallic oxide complexes have been prepared, in particular by W. G. Klemperer [3], K. Isobe [4] and R. G. Finke [5]. This type of compound contains soft as well as hard metal centers and hydrophobic as well as hydrophilic ligands. The combination of low- and high-valent transition metals and the amphiphilic character predispose these molecules also as homogeneous catalysts for oxidation reactions; the catalytic potential of these compounds has been reviewed recently [6]. Furthermore organometallic oxo clusters provide molecular models for heterogeneous catalysts derived from organometallic complexes adsorbed at metal oxide surfaces [7].

Recently, in a preliminary communication, we reported the neutral amphiphilic cluster $[(\eta^6\text{-}p\text{-}MeC_6H_4iPr)_4Ru_4Mo_4O_{16}]$ (**1**) which was found to present a unique framework geometry [8]. In this paper we extend our study to hexamethylbenzene ruthenium and pentamethylcyclopentadienyl rhodium units as well as to vanadate. Thus, the synthesis and characterisation of $[(\eta^6\text{-}p\text{-}MeC_6H_4iPr)Ru(\eta^5\text{-}C_5Me_5)_3$

† Dedicated to The Lord Lewis of Newnham—mentor, inspirer and friend.

* Author to whom correspondence should be addressed.

$Rh_3Mo_4O_{16}$] (**2**) [(η^6-*p*-$MeC_6H_4iPr)_2Ru_2(\eta^5$-$C_5Me_5)_2Rh_2Mo_4O_{16}$] (**3**), [(*p*-$MeC_6H_4iPr)_4Ru_4V_6O_{19}$] (**4**) and [($\eta^6$-$C_6Me_6)_4Ru_4V_6O_{19}$] (**5**) are reported; in addition we describe the characterisation of the three different types of oxygen atoms in **1** by ^{17}O NMR spectroscopy and by electron-density calculations.

RESULTS AND DISCUSSION

The *para*-cymene complex [(η^6-*p*-$MeC_6H_4iPr)_2Ru_2Cl_4$] reacts with Na_2MoO_4 in aqueous solution at room temperature to give the neutral organoruthenium oxomolybdenum cluster [(η^6-*p*-$MeC_6H_4iPr)_4Ru_4Mo_4O_{16}$] (**1**) only. Complex **1** is sparingly soluble in water and aromatic hydrocarbons, and well soluble in polar organic solvents such as dichloromethane or methanol.

$$2[(\eta^6\text{-}p\text{-}MeC_6H_4iPr)_2Ru_2Cl_4] + 4Na_2MoO_4 \rightarrow [(\eta^6\text{-}p\text{-}MeC_6H_4iPr)_4Ru_4Mo_4O_{16}] + 8NaCl \quad (1)$$

Single-crystal X-ray structure analysis of **1**·2 C_6H_5Me (orange, rod-like crystals) revealed the molecule to contain a unique $Ru_4Mo_4O_{12}$ framework which can be described as a central Mo_4O_4 cube with four folded ORuO flaps resembling the sails of a windmill. The molecular structure of **1** is depicted in Fig. 2. Important bond lengths and angles are presented in Table 1. The distortion [Mo(2)—O(2)—Mo(1) 106.04(12)°, O(12)—Mo(1)—O(2) 71.37(10)°] with respect to the idealized cubic representation is due to the geometry of the oxygen atoms of the central cube which is more tetrahedral than octahedral. Eight of the twelve framework oxygen atoms are doubly bridging, while four are quadruply bridging. Each ruthenium atom is coordinated to an η^6-*p*-cymene ligand [Ru(1)—C6 ring centroid 1.627 Å], and each molybdenum atom carries a terminal oxo ligand [Mo(1)—O(7) 1.706(3) Å].

A calculation of the charge distribution in **1**, based on the application of the partial charge model [9], to the structural data of **1** gave the following results: The partial charge on the four ruthenium atoms is +1.093, and on the four molybdenum atoms +1.737, reflecting the electronegativity difference between ruthenium and molybdenum. The four *p*-cymene ligands have a partial charge of −0.412, whereas there is a clear differentiation of the different oxo ligands: The terminal oxo ligands (O_4, O_7, O_8 and O_{14}) have a partial charge of −0.492, the doubly bridging oxo ligands (O_1, O_3, O_5, O_6, O_{10}, O_{11}, O_{13} and O_{16}) −0.578, and the quadruply bridging oxo ligands (O_2, O_9, O_{12} and O_{15}) −0,769. Thus, the electronic density driven from the metal atoms has flown mainly onto oxo atoms, but also onto the aromatic ligands. It is interesting to note the strong discrimination among the oxygen atoms due to their relative structural environment, with the lowest electronic structural density found on the terminal oxygen atoms.

The three different types of oxygen atoms in **1** are also confirmed by ^{17}O NMR spectroscopy: A sample of **1**, enriched in ^{17}O, prepared from enriched Na_2MoO_4, gives rise to three completely resolved signals, in addition to the signal of the MoO_4^{2-} anion at δ 748 ppm. These signals can be easily assigned on the basis of a qualitative correlation between the shift of ^{17}O signal and the decreasing number of metal centres bound to the oxygen atom [10]. Thus, the signal at δ 783 ppm corresponds to the four terminal (μ_1) oxygen atoms in **1**, while the eight doubly bridging (μ_2) and the four quadruply bridging (μ_4) oxygen atoms give rise to a resonance at δ 21 and −7 ppm, respectively.

Sodium molybdate reacts with a 1:1 mixture of *para*-cymene ruthenium dichloride dimer and pentamethylcyclopentadienyl rhodium dichloride dimer

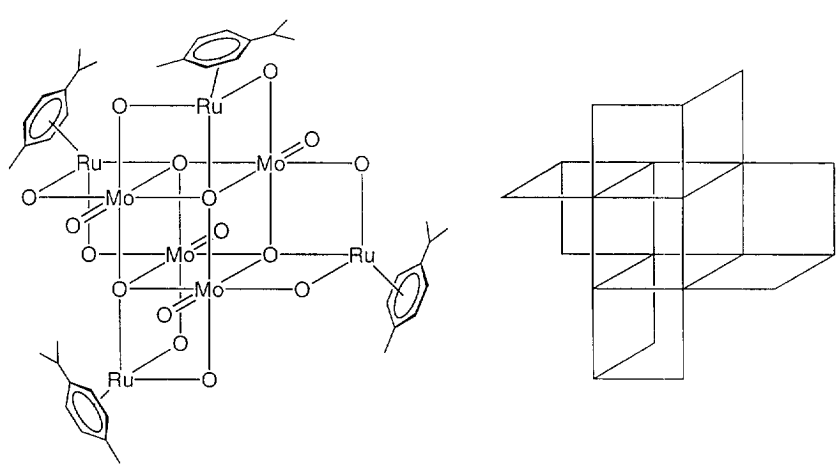

Fig. 1. Molecular representation of [(η^6-*p*-$MeC_6H_4iPr)_4Ru_4Mo_4O_{16}$] (**1**).

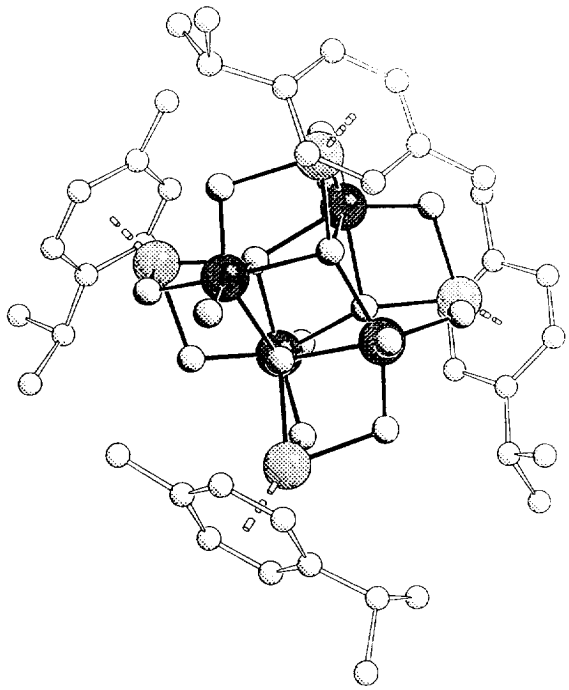

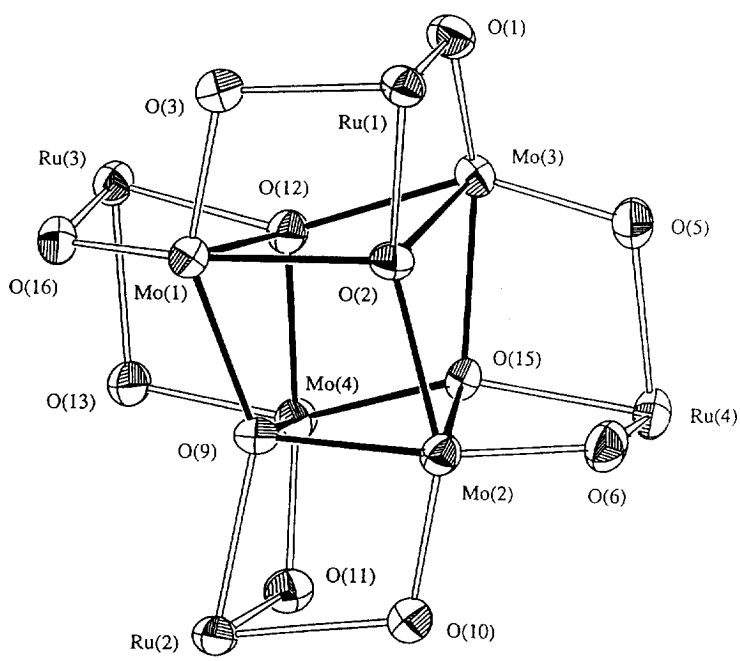

Fig. 2. Molecular structure of $[(\eta^6\text{-}p\text{-}MeC_6H_4iPr)_4Ru_4Mo_4O_{16}]$ (**1**). (a) Hydrogen atoms and two toluene molecules have been omitted for clarity. (b) $Ru_4Mo_4O_{12}$ framework with labelling scheme.

Table 1. Selected bond lengths (Å) and angles (°) for $[(\eta^6\text{-}p\text{-}MeC_6H_4iPr)_4Ru_4Mo_4O_{16}]$ (**1**)

Ru(1)—O(1)	2.088(3)
Ru(1)—O(2)	2.089(3)
Mo(1)—O(2)	2.122(3)
Mo(1)—O(3)	1.804(3)
Ru(1)—O(3)	2.094(3)
Mo(1)—O(7)	1.706(3)
Mo(1)—O(9)	2.073(3)
Mo(1)—O(12)	2.365(3)
Mo(1)—O(16)	1.798(3)
Mo(2)—O(2)—Mo(1)	106.04(12)
Mo(1)—O(9)—Ru(2)	145.40(14)
Mo(3)—O(12)—Mo(1)	105.31(11)
O(10)—Ru(2)—O(11)	80.53(12)
O(7)—Mo(1)—O(16)	103.93(14)
O(9)—Mo(1)—O(12)	72.20(10)
O(2)—Mo(1)—O(12)	71.37(10)

in aqueous solution to yield a mixture of mixed ruthenium-rhodium complexes, from which $[(\eta^6\text{-}p\text{-}MeC_6H_4iPr)Ru(\eta^5\text{-}C_5Me_5)_3Rh_3Mo_4O_{16}]$ (**2**) and $[(\eta^6\text{-}p\text{-}MeC_6H_4iPr)_2Ru_2(\eta^5\text{-}C_5Me_5)_2Rh_2Mo_4O_{16}]$ (**3**) can be isolated by thin-layer chromatography.

$$1/2[(\eta^6\text{-}p\text{-}MeC_6H_4iPr)_2Ru_2Cl_4] + 3/2[(\eta^5\text{-}C_5Me_5)_2Rh_2Cl_4] + 4Na_2MoO_4Na_2 \rightarrow [(\eta^6\text{-}p\text{-}MeC_6H_4iPr)Ru(\eta^5\text{-}C_5Me_5)_3Rh_3Mo_4O_{16}] + 8NaCl \quad (2)$$

$$[(\eta^6\text{-}p\text{-}MeC_6H_4iPr)_2Ru_2Cl_4] + [(\eta^5\text{-}C_5Me_5)_2Rh_2Cl_4] + 4Na_2MoO_4Na_2 \rightarrow [(\eta^6\text{-}p\text{-}MeC_6H_4iPr)_2Ru_2(\eta^5\text{-}C_5Me_5)_2Rh_2Mo_4O_{16}] + 8NaCl \quad (3)$$

The two mixed ruthenium-rhodium clusters **2** and **3** have a very similar infrared spectrum which, however, differs significantly from that of **1** but resembles the Mo—O absorption pattern of the known [4a] rhodium cluster $[(\eta^5\text{-}C_5Me_5)_4Rh_4Mo_4O_{16}]$. Both **2** and **3** show two strong bands at 925, 898 cm^{-1} and 927, 901 cm^{-1} respectively, which can be assigned to the vibrations of the terminal Mo=O bonds. Characteristic absorptions at 689, 642, 584, 538 cm^{-1} (**2**) and 692, 641, 587, 538 cm^{-1} (**3**) are attributed to the Mo—O vibrations of the internal oxygen atoms, in line with the assignment proposed by K. Isobe *et al.* for $[(\eta^5\text{-}C_5Me_5)_4Rh_4Mo_4O_{16}]$ [4a]. On the basis of the infrared spectra, it can be concluded that the mixed ruthenium-rhodium clusters **2** and **3** do not adopt the structure of the windmill-like ruthenium cluster **1**, but the triple cube-like structure of the rhodium cluster $[(\eta^5\text{-}C_5Me_5)_4Rh_4Mo_4O_{16}]$. Accordingly, the ^1H NMR spectrum of **2** shows a 1 : 3 ratio of the *p*-cymene and pentamethylcyclopentadienyl signals. However, there are three possibilities of replacing two $(C_5Me_5)Rh$ units in $[(\eta^5\text{-}C_5Me_5)_4Rh_4Mo_4O_{16}]$ by two $(\eta^6\text{-}p\text{-}MeC_6H_4iPr)Ru$ fragments, so that three isomers can be expected for **3**. Indeed, the ^1H NMR spectrum reveals **3** to be a mixture of at least two isomers, because, instead of one CH_3 doublet of the isopropyl substituent of the *p*-cymene ligand, two doublet signals centrered at $\delta = 1.38$ and 1.37 ppm are observed.

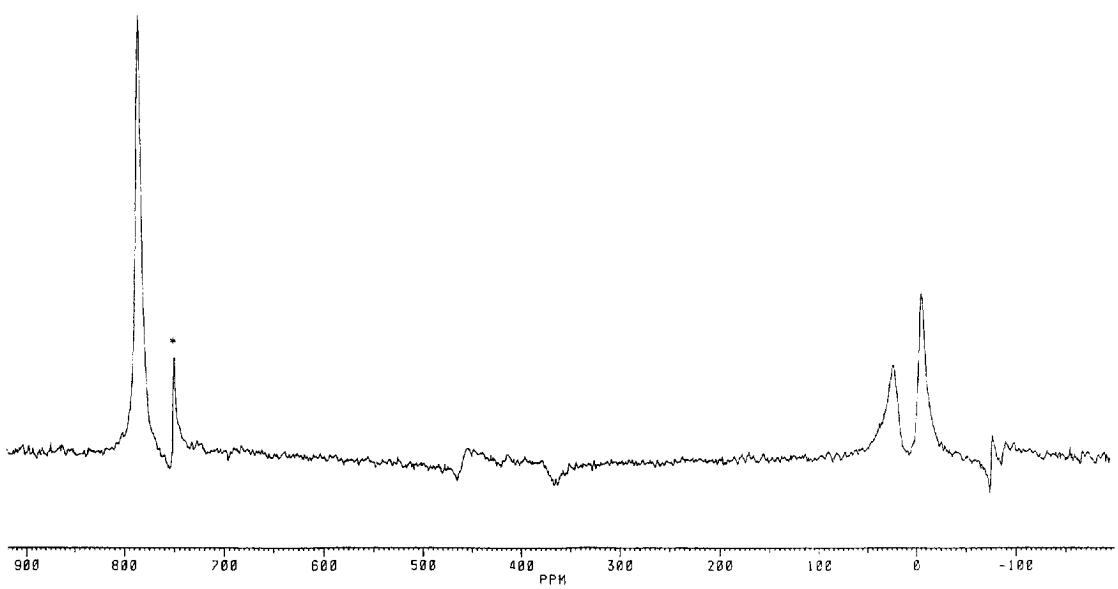

Fig. 3. ^{17}O NMR spectrum of $[(\eta^6\text{-}p\text{-}MeC_6H_4iPr)_4Ru_4Mo_4O_{16}]$ (**1**) in $CDCl_3$ (*excess of MoO_4^{2-}).

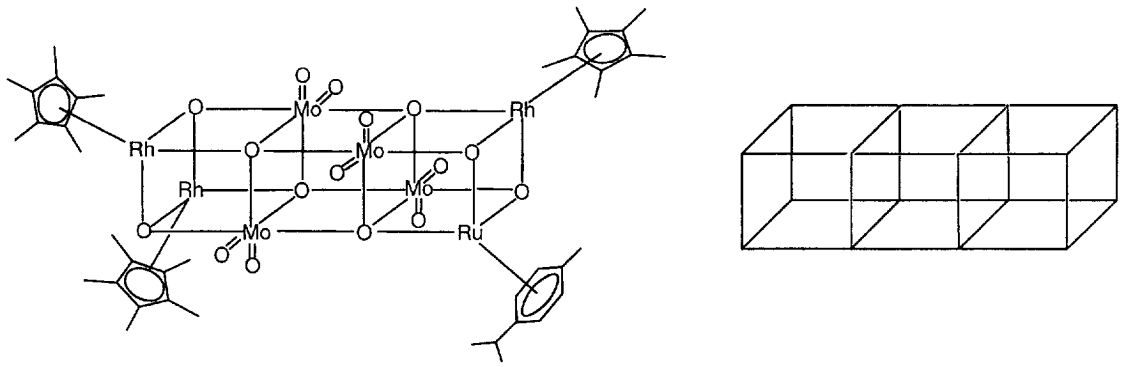

Fig. 4. Proposed molecular representation of $[(\eta^6\text{-}p\text{-}MeC_6H_4iPr)Ru(\eta^6\text{-}C_5Me_5)_3Rh_3Mo_4O_{16}]$ (**2**) with the triple-cube geometry of the $RuRh_3Mo_4O_8$ framework.

With sodium vanadate, *p*-cymene ruthenium dichloride dimer reacts in aqueous solution to give organoruthenium oxovanadium cluster $[(\eta^6\text{-}p\text{-}MeC_6H_4iPr)_4Ru_4V_6O_{19}]$ (**4**). Complex **4** is also soluble in both, dichloromethane and water.

$$2[(\eta^6\text{-}p\text{-}MeC_6H_4iPr)_2Ru_2Cl_4] + 6NaVO_3 + H_2O \rightarrow [(\eta^6\text{-}p\text{-}MeC_6H_4iPr)_4Ru_4V_6O_{19}] + 6NaCl + 2HCl \quad (4)$$

The ^1H NMR spectrum of **4** shows the four *p*-cymene ligands to be equivalent, since there is only one set of signals for the methyl, isopropyl and aromatic protons with correct integral ratio. In the IR spectrum of **4**, the absorptions at 1089, 1037, and 944 cm^{-1} correspond to the stretching vibration of the terminal V=O bonds. Bands at 677 and 568 cm^{-1} can be assigned to the vibrations of bridging (μ_3) oxygen atoms, while an absorption at 493 cm^{-1} is attributed to the vibration of a central (μ_6) oxygen atom.

The structure analysis of a single crystal of **4** reveals a $Ru_4V_6O_{13}$ framework which can be described as a quadruple-cube with a μ_6-oxygen atom at the centre. This structure can be derived from that of the hypothetical $V_6O_{19}^{8-}$ anion, isostructural with the well-known $Nb_6O_{19}^{8-}$ [11], $Ta_6O_{19}^{8-}$ [12], $Mo_6O_{19}^{2-}$ [13] and $W_6O_{19}^{2-}$ [14] anions. It is also found in the known clusters $[(C_5Me_5)_4Rh_4V_6O_{19}]$ and $[(C_5Me_5)_4Ir_4V_6O_{19}]$ reported by K. Isobe *et al.* [4c,15]. The structure of **4** is shown in Fig. 5. Selected bond distances and angles are listed in Table 4. The cluster presents a quadruple-cube framework that contains four RuV_3O_4 cubic units alternatively fitted through V—O bonds at the three edges of the cube. The central oxygen atom of the V_6O_{19} group is common to all four RuV_3O_4 units, thus all oxygen atoms of the V_6O_{19} group, except for the terminal oxygen atom, participate in the quadruple-cube cluster. Each vanadium atom carries a terminal oxygen atom [O(6)—V(4) 1.607(4) Å], and each ruthenium atom is coordinated to a η^6-*p*-cymene ligand. In an alternative view, **4** can be considered as comprising one $V_6O_{19}^{8-}$ unit and four $(\eta^6\text{-}p\text{-}MeC_6H_4iPr)Ru^{2+}$ groups, sitting on alternating faces of the octahedron formed by the hexavanadate unit through oxygen bridges. The vanadium atoms can be described as octahedrally coordinated. The ruthenium atom in the $(\eta^6\text{-}p\text{-}MeC_6H_4iPr)Ru^{2+}$ group is bound to three adjacent bridging O atoms [Ru(4)—O(8) 2.103(4) Å].

Whereas sodium molybdate does not react with the hexamethylbenzene analogue $[(\eta^6\text{-}C_6Me_6)_2Ru_2Cl_4]$ to give a complex analogous to **1**, sodium vanadate reacts to give $[(\eta^6\text{-}C_6Me_6)_4Ru_4V_6O_{19}]$ (**5**), analogous to **4**. Like **4**, complex **5** is soluble in both water and organic solvents, but it forms blue crystals, while **4** has a violet colour. The IR, MS and ^1H NMR data of **5** suggest the compound to have the same structure as the *p*-cymene analogue **4**.

EXPERIMENTAL

The following chemicals were purchased from commercial sources and used without further purification: $RuCl_3 \cdot n\ H_2O$ (Johnson Matthey); $RhCl_3 \cdot 3H_2O$ (Métaux Précieux); (R)-(−)-5-Isopropyl-2-methyl-1,3-cyclo-hexadiene (Merck); hexamethyldewarbenzene (Aldrich); hexamethylbenzene (Lancaster), $Na_2MoO_4 \cdot 2\ H_2O$ (Fluka); $NaVO_3$ (Fluka). The organic solvents were refluxed over appropriate desiccants, distilled, and saturated with nitrogen. The bidistilled water degassed and saturated with N_2 prior to use. The ^1H NMR spectra were recorded on a Varian Gemini 200 BB instrument. ^{17}O NMR spectra were measured on a Bruker AM 360 spectrometer working at 48.82 MHz and using 10 mm o.d. sample tubes, the solvent was CD_2Cl_2. Total spectral width of 55.6 kHz with 8 K data points for the FIDs (10^4–10^5 transients added) were used. ^{17}O chemical shift were measured with respect to bulk water (external reference, 0 ppm). To flatten the baseline larger pre-scan-delay values (DE) were used causing some first order phase errors. The IR spectra were recorded on a Perkin–Elmer FTIR 1720 X spectrophotometer (4000–400 cm^{-1}) as KBr pellets. The mass spectra (FAB)

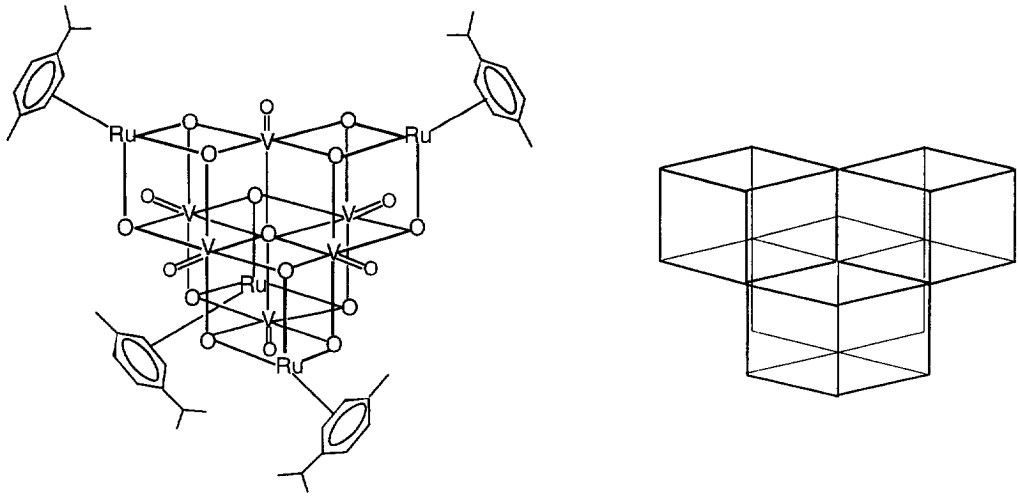

Fig. 5. Molecular representation of $[(\eta^6\text{-}p\text{-}MeC_6H_4iPr)_4Ru_4V_6O_{19}]$ (**4**).

were performed by Prof. Titus A. Jenny, University of Fribourg. Microanalytical data were obtained from the Mikroelementaranalytisches Laboratorium ETH Zürich. The starting materials $[(\eta^6\text{-}p\text{-}MeC_6H_4iPr)_2Ru_2Cl_4]$ [16], $[(\eta^6\text{-}C_6Me_6)_2Ru_2Cl_4]$ [16] and $[(\eta^5\text{-}C_5Me_5)_2Rh_2Cl_4]$ [17] were synthesised according to the literature procedures.

Preparation of $[(\eta^6\text{-}p\text{-}MeC_6H_4iPr)_4Ru_4Mo_4O_{16}]$ (**1**)

A suspension of $[(p\text{-}MeC_6H_4iPr)_2Ru_2Cl_4]$ (200 mg, $3.27 \cdot 10^{-4}$ mol) in 20 cm^3 of water was added dropwise to an aqueous solution (10 cm^3) of $Na_2MoO_4 \cdot 2H_2O$ (790 mg, $3.3 \cdot 10^{-3}$ mol). The mixture was stirred for 4 h at 25°C. After evaporation of the water, the product was extracted with CH_2Cl_2 (20 cm^3) and dried over $MgSO_4$. (**1**) was recrystallised from a mixture of dichloromethane and toluene (1:1) to give analytically pure orange crystals (155 mg, 60% yield). IR (KBr): ν[cm^{-1}] = 921, 874 (terminal oxygen atom); 785, 739, 642 and 602 (bridging oxygen atom). MS (FAB+): *m/z*: 1581 (^{101}Ru, ^{96}Mo). ^{1}H NMR (200 MHz, CD_2Cl_2): δ = 1.39 (d, 6H, $CH(CH_3)_2$), 2.27 (s, 3H, $C_6H_4CH_3$), 2.97 (sp, ^{1}H, $CH(CH_3)_2$), 5.30 (d, 2H, C_6H_4), 5.37 (d, 2H, C_6H_4). Found: C, 30.33; H 3.51. Calc. for $C_{40}H_{56}Mo_4O_{16}Ru_4$: C, 30.39; H, 3.57%.

Preparation of $[(\eta^6\text{-}p\text{-}MeC_6H_4iPr)Ru(\eta^5\text{-}C_5Me_5)_3Rh_3Mo_4O_{16}]$ (**2**) and $[(\eta^6\text{-}p\text{-}MeC_6H_4iPr)_2Ru_2(\eta^5\text{-}C_5Me_5)_2Rh_2Mo_4O_{16}]$ (**3**)

$[(\eta^5\text{-}C_5Me_5)_2Rh_2Cl_4]$ (200 mg, $3.24 \cdot 10^{-4}$ mol) and $[(\eta^6\text{-}p\text{-}MeC_6H_4iPr)_2Ru_2Cl_4]$ (200 mg, $3.27 \cdot 10^{-4}$ mol) were suspended in 50 cm^3 of water and treated with an aqueous solution of $Na_2MoO_4 \cdot 2H_2O$ (1.57 *g*, $6.5 \cdot 10^{-3}$ mol) in 20 cm^3 of water. The mixture was stirred for 12 h. The resulting red-orange solution was extracted with 30 cm^3 of dichloromethane, then the organic layer was collected and dried with $MgSO_4$, giving a crude red-orange powder product on evaporation of the solvent. The crude product was dissolved in a minimum of dichloromethane and separated by thin-layer chromatography on silica (CH_2Cl_2/acetone/methanol, 5:10:3). The products **2** and **3** were isolated from the two main bands by elution with CH_2Cl_2/aceton/methanol (5:10:3) and evaporation to dryness after filtration of $MgSO_4$. (a) $[(\eta^6\text{-}p\text{-}MeC_6H_4iPr)Ru(\eta^5\text{-}C_5Me_5)_3Rh_3Mo_4O_{16}]$ (**2**): IR (KBr): ν[cm^{-1}] = 925, 898 (terminal oxygen atom); 689, 642, 584 and 538 (bridging oxygen atom). MS (FAB+): *m/z*: 1590 (^{101}Ru, ^{103}Rh, ^{96}Mo). ^{1}H NMR (200 MHz, CD_2Cl_2): δ = 1.38 (d, 6H, $CH(CH_3)_2$), 1.68 (s, 45H, C5(CH_3)$_5$), 2.25 (s, 3H, C_6H_4CH3), 2.99 (sp, ^{1}H, $CH(CH_3)_2$), 5.31 (d, 2H, C_6H_4), 5.37 (d, 2H, C_6H_4). Found: C, 35.22; H 4.36. Calc. for $C_{40}H_{59}Mo_4O_{16}RuRh_3 \cdot 2C_6H_12$: C, 35.45; H, 4.97% (20% yield). (b) $[(\eta^6\text{-}p\text{-}MeC_6H_4iPr)_2Ru_2(\eta^5\text{-}C_5Me_5)_2Rh_2Mo_4O_{16}]$ (**3**): IR (KBr): ν[cm^{-1}] = 927, 901 (terminal oxygen atom); 692, 641, 587 and 538 (bridging oxygen atom). MS (ES): $[M+H]^+$ = 1588 (^{101}Ru, ^{103}Rh, ^{96}Mo) ^{1}H NMR (200 MHz, CD_2Cl_2): δ = 1.38, 1.37 (2 doublets, 12H, $CH(CH_3)_2$), 1.67 (s, 30H, $C_5(CH_3)_5$), 2.25 (s, 6H, $C_6H_4CH_3$), 2.99 (sp, 2H, $CH(CH_3)_2$), 5.35 (m, 8H, C_6H_4). Found: C, 32.57; H, 3.81. Calc. for $C_{40}H_{58}Mo_4O_{16}Ru_2Rh_2 \cdot C_6H_{12}$: C, 33.03; H, 4.34% (15% yield).

Preparation of $[(\eta^6\text{-}p\text{-}MeC_6H_4iPr)_4Ru_4V_6O_{19}]$ (**4**)

A suspension of $[(p\text{-}C_6H_4iPrMe)_2Ru_2Cl_4]$ (200 mg, $3.27 \cdot 10^{-4}$ mol) in 20 cm^3 of water was added dropwise to an aqueous solution (35 cm^3) of $NaVO_3$ (398 mg, $3.27 \cdot 10^{-3}$ mol). The mixture was stirred for 4 h at 25°C. After evaporation of the water, the solid was extracted with CH_2Cl_2 (20 cm^3). The dichloromethane solution was dried over $MgSO_4$, and evaporated to

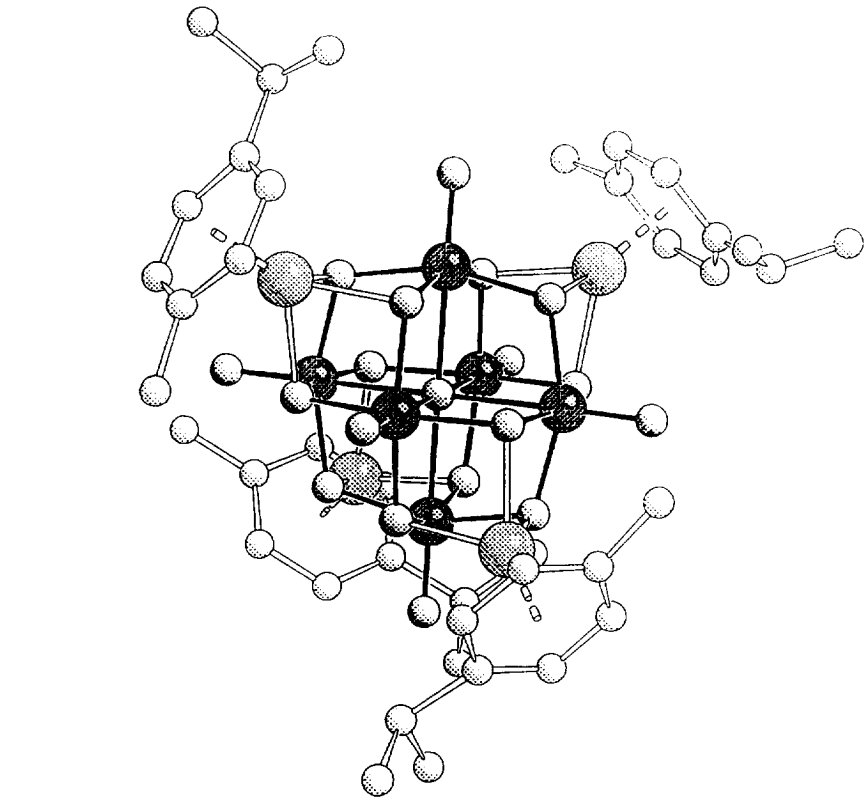

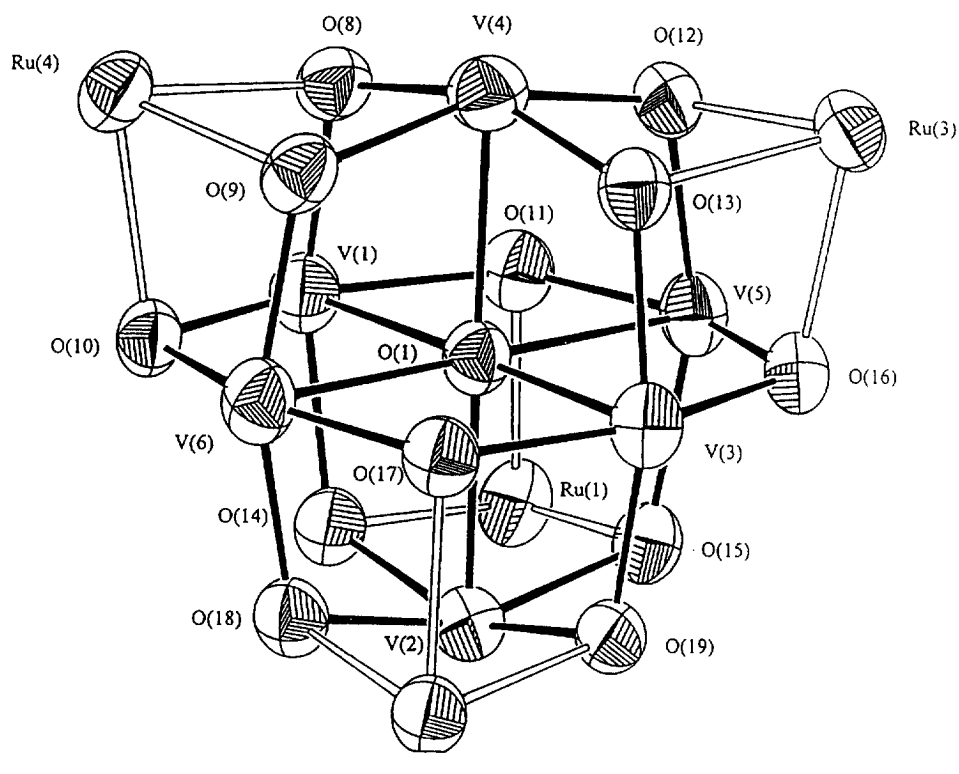

Fig. 6. Molecular structure of $[(\eta^6\text{-}p\text{-}MeC_6H_4iPr)_4Ru_4V_6O_{19}]$ (**4**). (a) Hydrogen atoms and two water molecules have been omitted for clarity. (b) $Ru_4V_6O_{13}$ framework with labelling scheme.

Table 2. Selected bond lengths (Å) and angles (°) for $[(\eta^6\text{—}p\text{—}MeC_6H_4iPr)_4Ru_4V_6O_{19}]$ (**4**)

Ru(1)—O(11)	2.082(4)	V(1)—O(7)	1.607(4)	V(4)—O(1)	2.240(4)	V(6)—O(1)	2.235(4)
Ru(4)—O(8)	2.103(4)	V(1)—O(8)	1.905(4)	V(4)—O(6)	1.607(4)	V(6)—O(3)	1.610(4)
Ru(4)—O(9)	2.108(4)	V(1)—O(10)	1.922(4)	V(4)—O(8)	1.928(4)	V(6)—O(9)	1.890(4)
Ru(4)—O(10)	2.103(4)	V(1)—O(11)	1.912(4)	V(4)—O(9)	1.924(4)		
V(1)—O(1)	2.232(4)	V(2)—O(1)	2.239(4)	V(5)—O(11)	1.916(4)		
V(1)—O(1)—V(6)	90.27(13)	V(1)—O(1)—V(2)	89.86(14)	V(6)—O(1)—V(2)	90.24(14)	V(1)—O(1)—V(4)	90.40(14)
V(6)—O(1)—V(4)	90.34(13)	V(2)—O(1)—V(4)	179.4(2)	V(1)—O(1)—V(3)	179.8(2)	V(6)—O(1)—V(3)	89.81(14)
V(6)—O(1)—V(5)	179.5(2)	V(1)—O(8)—Ru(4)	96.6(2)	V(4)—O(8)—Ru(4)	97.0(2)	V(6)—O(9)—V(4)	112.6(2)
V(6)—O(9)—Ru(4)	95.5(2)	V(4)—O(9)—Ru(4)	96.9(2)	V(6)—O(10)—V(1)	111.3(2)	V(6)—O(10)—Ru(4)	95.0(2)
V(1)—O(10)—Ru(4)	96.1(2)	O(7)—V(1)—Ru(4)	93.7(2)	Ru(3)—V(4)—Ru(4)	174.08(4)	O(3)—V(6)—O(9)	101.7(2)
O(3)—V(6)—O(10)	101.3(2)	O(9)—V(6)—O(10)	86.9(2)	O(3)—V(6)—O(18)	101.0(2)	O(9)—V(6)—O(18)	157.3(2)
O(10)—V(6)—O(18)	89.4(2)	O(3)—V(6)—O(17)	100.5(2)	O(9)—V(6)—O(17)	90.3(2)	O(10)—V(6)—O(17)	158.2(2)
O(3)—V(6)—O(1)	179.2(2)	O(9)—V(6)—O(1)	78.9(2)	O(10)—V(6)—O(1)	79.3(2)	O(18)—V(6)—O(1)	78.4(2)
O(17)—V(6)—O(1)	79.0(2)	O(10)—Ru(4)—O(8)	76.49(14)	O(10)—Ru(4)—O(9)	76.8(2)	O(8)—Ru(4)—O(9)	76.0(2)

dryness to give the product as a dark purple powder (199 mg, 78% yield). **4** was recrystallised from a mixture of cyclohexane and toluene (1 : 1) to give purple crystals. IR (KBr): $\nu[cm^{-1}] = 1089, 1037, 944$ (terminal oxygen atom), 677, 568 (bridging oxygen atom), 493 (central oxygen atom). MS (FAB+): *m/z*: 1551 (^{101}Ru, ^{51}V). ^1H NMR (200 MHz, CD_2Cl_2): $\delta = 1.43$ (d, 6H, $CH(CH_3)_2$), 2.40 (s, 3H, $C_6H_4CH_3$), 3.09 (sp, ^1H, $CH(CH_3)_2$), 5.75 (d, 2H, C_6H_4), 5.81 (d, 2H, C_6H_4). Found: C, 31.05; H, 3.60. Calc. for $C_{40}H_{56}O_{19}Ru_4V_6$: C, 30.98; H, 3.64%.

Preparation of $[(\eta^6\text{-}C_6Me_6)_4Ru_4V_6O_{19}]$ **(5)**

A suspension of $[(\eta^6\text{-}C_6Me_6)_2Ru_2Cl_4]$ (100 mg, $1.49 \cdot 10^{-4}$ mol) in 25 cm^3 of water was added dropwise to an aqueous solution (20 cm^3) of $NaVO_3$ (181 mg, $1.49 \cdot 10^{-3}$ mol). The mixture was stirred for 4 h at 25 C. After evaporation of the water, the solid was extracted with CH_2Cl_2 (20 cm^3). The dichloromethane solution was dried over $MgSO_4$, and evaporated to dryness to give the product as a dark blue powder (95 mg, 68% yield). IR (KBr): $\nu[cm^{-1}] = 1075, 1024, 939$ (terminal oxygen atom), 675, 567 (bridging oxygen atom), 492 (central oxygen atom). ^1H NMR (200 MHz, CD_2Cl_2): $\delta = 2.29$ (s, 18H, $C_6(CH_3)_6$), MS (FAB+): *m/z*: 1663 (^{101}Ru, ^{51}V). Found: C, 31.11; H, 3.97. Calc. for $C_{48}H_{72}O_{19}Ru_4V_6 \cdot 4CH_2Cl_2$: C, 31.19; H, 4.03%.

^{17}O-enrichment procedure

A solution of $Na_2MoO_4 \cdot 2\ H_2O$ (395 mg, 1.63 10^{-3} mol) in 1 cm^3 of 10% enriched $H_2{}^{17}O$ (Yeda, Israel) was heated to 90°C for 3 h with stirring and cooled to 25°C. To the resulting solution, containing ^{17}O-enriched MoO_4^{2-}, 200 mg ($3.27 \cdot 10^{-4}$ mol) of $[(\eta^6\text{-}p\text{-}MeC_6H_4iPr)_2Ru_2Cl_4]$ were added, then the mixture was heated to 95°C with vigorous stirring during 3 h. Then the solvent was removed, the residual orange solid was extracted with dichloromethane (25 cm^3) and crystallised from a mixture of dichloromethane and toluene (1 : 1).

X-ray structure determination of **1** *and* **4**

Suitable crystals of **1** and **4** were obtained as indicated in the synthetic section. Selected experimental crystallographic details of the structure determination of **1** and **4** are given in Tables 3 and 4. For **1**, single-crystal X-ray diffraction data were collected at −50 C on a Stoe-Siemens AED2 4-circle diffractometer using Mo–K_α graphite monochromated radiation ($\lambda = 0.71073$ Å; $\omega/2\theta$ scans), whereas for **4**, the X-ray diffraction data were collected at room temperature on a Stoe Imaging Plate Diffractometer System (Stoe and Cie 1995) equipped with a one-circle goniometer and a graphite Mo–K_α monochromated

Table 3. Crystallographic and refinement data for $\mathbf{1} \cdot 2(CH_3C_6H_5)$

Compound	**1**
Crystal habit	Red-orange rod
Crystal size (mm)	$0.57 \times 0.27 \times 0.17$
Empirical Formula	$C_{40}H_{56}Mo_4O_{16}Ru_4 \cdot 2CH_3C_6H_5$
Formula Weight (g mol^{-1})	1765.30
Temperature (K)	223
Crystal system	Triclinic
Space group	$P\bar{1}$
a (Å)	13.846(2)
b (Å)	15.210(2)
c (Å)	16.104(1)
α (°)	88.12(1)
β (°)	78.94(1)
γ (°)	65.47(1)
U (Å^3)	3023.7(6)
Z	2
D_{calc} (g cm^{-3}	1.939
Diffractometer	Stoe-Siemens AED2 4-circle
Radiation	Mo-K_α graphite monochromated
λ (Å)	0.71073
Scan type	ω-2θ
Absorption coefficient (Mo-K_α, mm^{-1})	1.659
F(000)	1736
θ Scan range(°)	$2.01 \leqslant \theta \leqslant 25.50$
h, k, l ranges	$-16 \leqslant h \leqslant 16, -18 \leqslant k \leqslant 18, 0 \leqslant l \leqslant 19$
Reflections collected	11234
Independent reflections	11234
Reflections observed [$I > 2\sigma(I)$]	9940
Data/restraints/parameters	11234/0/717
$R_1[I > 2\sigma(I)]/R_1$(all data)[a]	0.0324/0.0404
$wR_2[I > 2\varepsilon(I)]/wR_2$(all data)[b]	0.0701/0.0736
Goodness of fit on F^2[c]	1.118
Largest diff. Peak and hole (e Å^3)	0.749 and −0.580
Empirical Absorption coorection	Empirical [DIFABS]
Transmission factors: min/max	0.667/1.248

[a] $R_1 = \Sigma \| F_o | - | F_c \| / \Sigma | F_o |$.
[b] $wR_2 = [\Sigma w(F_o^2 - F_c^2)^2 / \Sigma w(F_o)^4]^{1/2}$.
[c] $S = [\Sigma w(F_o^2 - F_c^2)^2 / (n-p)]^{1/2}$ (n = number of reflections, p = number of parameters).

radiation ($\lambda = 0.71073$ Å, φ oscillation). Data were collected in one stage: 120 exposures (3 min per exposure) were obtained at 80 mm with $0 \leqslant \varphi \leqslant 120°$ and with the crystal oscillated through 1° in φ. The structure of **1** was solved by Patterson methods and that of **4** by direct methods using the program SHELXS 86 [18]. For both compounds, **1** and **4**, the structure refinement, using weighted full-matrix least-square on F^2, was carried out using the program SHELXL 93 [19]. During the refinement of **1**, two molecules of toluene were located. Two partially occupied H_2O positions were found for **4** (occupancies 0.33 and 0.5). For compound **1**, an empirical absorption correction was applied using DIFABS (PLATON) [20]. Non-H atoms were refined anisotropically, and hydrogen atoms were included in calculated positions and refined as riding atoms using the SHELXL 93 default parameters. The figures were drawn using the programs ZORTEP [21] (thermal ellipsoides, 50% probability level) and SCHAKAL [22]. Complete tables of bond lengths and angles and lists of thermal parameters have been deposited at the Cambridge Crystallographic Data Centre, 12 Union Road, Cambridge CB2 1EZ (U.K.).

Application of the partial charge model

The partial charge model [9] was applied to the crystallographic data of **1**, using the following parametrization: Electronegativities (Mulliken scale, values in eV): $\chi(H) = 7.176$; $\chi(C, sp^2) = 8.876$; $\chi(C, sp^3) = 8.148$; $\chi(O) = 9.630$; $\chi(Ru) = 4.11$ and $\chi(Mo) = 8.876$. Atomic sizes (covalent radii in Å): $r(H) = 0.37$; $r(C) = 0.77$; $r(O) = 0.73$; $r(Ru) = 1.25$; $r(Mo) = 1.30$. Total electrical charge = 0.0 (neutral complex). The program calculated the minimum interatomic distance to be 0.94

Table 4. Crystallographic and refinement data for **4**·0.83 H_2O

Compound	**4**
Crystal habit	dark-brown block
Crystal size (mm)	$0.38 \times 0.34 \times 0.23$
Empirical Formula	$C_{40}H_{56}O_{19}Ru_4V_6 \cdot 0.83H_2O$
Formula Weight (g mol^{-1})	1565.78
Temperature (K)	293(2)
Crystal system	Cubic
Space group	$Pa\bar{3}$
a (Å)	31.753(2)
b (Å)	31.753(2)
c (Å)	31.753(2)
α (°)	90
β (°)	90
γ (°)	90
U (Å^3)	32016(3)
Z	24
D_{calc} (g cm^{-3})	1.949
Diffractometer	Stoe Imaging Plate Diffractometer System (IPDS)
Radiation	Mo–K_α
λ (Å)	0.71073
Scan type	φ oscillation scans
Absorption coefficient (Mo–K_α, mm^{-1})	2.166
F(000)	18488
θ Scan range(°)	$1.81 \leqslant \theta \leqslant 24.08$
h, k, l ranges	$-36 \leqslant h \leqslant 36, -36 \leqslant k \leqslant 23, -36 \leqslant l \leqslant 31$
Reflections collected	119211
Independent reflections	8432
Reflections observed [$I > 2\sigma(I)$]	5677
Data/restraints/parameters	8428/0/646
$R_1[I > 2\sigma(I)]/R_1$(all data)[a]	0.0366/0.0602
$wR_2[I > 2$[gkS1]$(I)]/wR_2$(all data)[b]	0.0964/0.1076
Goodness of fit on F^2[c]	0.906
Largest diff. Peak and hole (e Å^3)	1.033 and −0.534

[a] $R_1 = \Sigma \| F_o | - | F_c \| / \Sigma | F_o |$.
[b] $wR_2 = [\Sigma w(F_o^2 - F_c^2)^2 / \Sigma w(F_o)^4]^{1/2}$.
[c] $S = [\Sigma w(F_o^2 - F_c^2)^2 / (n-p)]^{1/2}$ (n = number of reflections, p = number of parameters).

Å, the mean electronegativity to be 8.03 eV, the dipolar moment to be 0.07 D and the electrostatic balance to be −127.7 eV.

Acknowledgements—This work was supported by the Fonds National Suisse de la Recherche Scientifique (Grant 20-46592.96). A generous loan of ruthenium trichloride hydrate from the Johnson Matthey Technology Centre is gratefully acknowledged.

REFERENCES

1. Day, V. W. and Klemperer, W. G., *Science*, 1985, **228,** 533.
2. Ho, R. K. C. and Klemperer, W. G., *J. Am. Chem. Soc.*, 1978, **100,** 6772.
3. (a) Chae, H. K., Klemperer, W. G. and Day V. W., *Inorg. Chem.*, 1989, **28,** 1424; (b) Chae, H. K., Klemperer, W. G., Paez Loyo, D. E., Day, V. W. and Ebersbacher T. A., *Inorg. Chem.*, 1991, **31,** 3187; (c) Klemperer, W. G. and Marquart, T. A., *Coord. Chem. Rev.*, 1993, **128,** 209.
4. (a) Hayashi, Y., Toriumi, K. and Isobe, K., *J. Am. Chem. Soc.*, 1988, **110,** 3666; (b) Do, Y., You, X.-Z., Zhang, C., Ozawa, Y. and Isobe, K., *J. Am. Chem. Soc.*, 1991, **113,** 5892; (c) Hayashi, Y., Ozawa, Y. and Isobe, K., *Inorg. Chem.*, 1991, **30,** 1025; (d) Park, T. J., Nishioka, T., Suzuki, T. and Isobe, K., *Bull. Chem. Soc. Jpn.*, 1994, **67,** 1968.
5. (a) Lin, Y., Nomiya, K. and Finke R. G., *Inorg. Chem.*, 1993, **32,** 6040; (b) Trovarelli, A. and Finke, R. G., *Inorg. Chem.*, 1993, **32,** 6034; (c) Pohl, M. and Finke R. G., *Organometallics*, 1993, **12,** 1453; (d) Rapko, B. M., Pohl, M. and Finke, R. G., *Inorg. Chem.*, 1994, **33,** 3625; (e) Pohl, M., Lyon, D. K., Mizuno, N., Nomiya, K. and Finke, R. G., *Inorg. Chem.*, 1995, **34,** 1413; (f) Nomiya, K., Nozaki, Ch., Kaneko, M., Finke, R. G. and Pohl, M., *J. Organomet. Chem.*, 1995, **505,** 23; (g) Pohl, M., Lin, Y., Weakley, T. J. R., Nomiya, K., Kaneko, M., Weiner, H. and Finke, R. G., *Inorg. Chem.*, 1995, **34,** 767.
6. Hill, C. L. and Prosser-McCartha, C. M., *Coord. Chem. Rev.*, 1995, **143,** 407.

7. Ichikawa, M., Pan, W., Imada, Y., Yamaguchi, M., Isobe, K. and Shido, T., *J. Mol. Catal.*, 1996, **107,** 23.
8. Süss-Fink, G., Plasseraud, L., Ferrand, V. and Stoeckli-Evans, H., *J. Chem. Soc., Chem. Commun.* 1997, in press.
9. Henry, M., *Top. Mol. Organ. Eng.*, 1997, **15,** 273.
10. Filowitz, M., Klemperer, W. G., Messerle, L. and Shum, W., *J. Am. Chem. Soc.*, 1976, **98,** 2345.
11. Lindqvist, I., *Arkiv. Kemi.*, 1952, **5,** 247.
12. Lindqvist, I. and Aronsson, B., *Arkiv. Kemi.*, 1954, **7,** 49.
13. Nagano, O. and Sasaki, Y., *Acta. Cryst.*, 1979, **B35,** 2387.
14. Fuchs, J., Freiwald, W. and Hartl, H., *Acta. Cryst.*, 1978.
15. Hayashi, Y., Ozawa, Y. and Isobe, K., *Chem. Lett.*, 1989, 425.
16. Bennett, M. A., Huang, T.-N., Matheson, T. W. and Smith, A. K., *Inorg. Synth.*, 1982, **21,** 74.
17. Booth, B. L., Haszeldine, R. N. and Hill, M., *J. Chem. Soc. (A).*, 1969, 1299.
18. Sheldrick, G. M., SHELXL 86. *Acta Crystallogr., Sect. A.*, 1990, **46,** 467.
19. Sheldrick, G. M., SHELXL 93, A Program for Crystal Structure Refinement; University of Göttingen, Göttingen, Germany, 1993.
20. Spek, A. L., *Acta Crystallogr., Sect. A.*, 1990, **46,** C 34.
21. Zsolnai, L., Pritzkow, H., ZORTEP: University of Heidelberg, Heidelberg, Germany, 1994 (a modified version of ORTEP (for PC) by Johnson, C. K., Oak Ridge National Laboratory, Oak Ridge, TN).
22. Keller, E., SCHAKAL 92/V256, A Fortran Program for The Graphical Representation of Molecular and Crystallographic Models, University of Freiburg, Freiburg, Germany, 1992.

Pergamon

PII: S0277-5387(97)00535-4

Polyhedron Vol. 17, No. 17, pp. 2829–2856, 1998
© 1998 Elsevier Science Ltd
All rights reserved. Printed in Great Britain
0277-5387/98 $19.00+0.00

Structural systematics in penta- and hexanuclear metal clusters containing carbocyclic ligands†

Paul R. Raithby* and Gregory P. Shields

Department of Chemistry, Lensfield Road, Cambridge CB2 1EW, U.K.

(Received 3 October 1997; accepted 16 December 1997)

Abstract—This article describes the structural chemistry of penta- and hexanuclear ruthenium and osmium carbonyl clusters which contain one or more arene (η^6-Ar) or cyclopentadienyl (η^5-Cp) groups, and compares and contrasts their structures with those of related binary carbonyl and carbonyl hydride clusters. The pentanuclear structures described are based on the trigonal bipyramidal metal framework, or on frameworks derived from this by the cleavage of one or more metal–metal edges. The steric and electronic factors which determine the position of the M(η^6-Ar) or M(η^5-Cp) units in the framework are discussed. For the hexanuclear clusters two basic metal core geometries are observed, the bicapped tetrahedron, comprising three fused tetrahedra, and the octahedron. The two series of compounds exhibit quite different structural chemistries. The bicapped tetrahedral structures exhibit quite extensive isomerism for the carbocyclic ligand substituted complexes, the positions of the M(η^6-Ar) or M(η^5-Cp) being dependent on both steric and electronic factors. For the octahedral carbocyclic ligand substituted complexes isomerism is less prevalent, but an analysis of the ligand polyhedra in these systems shows that low energy transformations, consistent with the fluxional properties of these complexes, are possible. The metal core geometries and ligand polyhedral geometries of related series of hexanuclear clusters are analysed statistically using half-normal probability plots and scatter plots. © 1998 Elsevier Science Ltd. All rights reserved

Keywords: osmium; ruthenium; carbocyclic ligands; X-ray structures; statistical analysis.

The last four decades have seen the development of cluster chemistry from its infancy to one of the major areas of research within the discipline of "organometallic chemistry" [1]. Lewis and his co-workers have been instrumental in the expansion of the subject, from early studies, which confirmed the existence of metal–metal bonds between transition metals [2], to the recent characterisation of high nuclearity metal clusters which form the link between conventional organometallic complexes and the bulk metal [3].

One of the key areas of transition metal cluster research has concerned the nature of the interaction between the metal cluster core and arene and cyclopentadienyl ligands. These carbocyclic ligands are of great importance in many catalytic processes, and establishing the nature of the bonding between the carbocyclic ring and the surface of the metal catalyst is fundamental to the understanding of the reaction [4]. Cluster complexes, which can be probed by conventional spectroscopic and structural techniques, are useful as models for investigating these processes. In 1968, Lewis and Johnson synthesised $Ru_6C(CO)_{14}(\eta^6$-$C_6H_3Me_3)$, the first structurally characterised cluster to exhibit the η^6-bonding mode for the arene [5], and in 1985 they reported the synthesis and characterisation of the clusters $Os_3(CO)_9(\mu_3$-$\eta^2:\eta^2:\eta^2$-$C_6H_6)$ and $Ru_6C(CO)_{14}(\mu_3$-$\eta^2:\eta^2:\eta^2$-$C_6H_6)$ [6], in which an arene ring lies parallel to a triangular face of the cluster; a bonding mode predicted for the interaction of an arene ring with the Rh{111} surface of the bulk metal. These and related studies have led to the development of an extensive chemistry of this class of complex which has been the subject of several recent reviews [7].

The arene and cyclopentadienyl-substituted clusters may be prepared by a number of synthetic routes. These include: (i) the coupling of a mononuclear carbocyclic metal-containing cation, a capping reagent, with a pre-formed anionic carbonyl cluster [8]; (ii) the thermolysis or pyrolysis of a carbocyclic

* Author to whom correspondence should be addressed.

† Dedicated to Professor Lord Lewis on the occasion of his 70th birthday, with sincere thanks for his support and friendship over the years.

compound with a binary carbonyl complex [6,9]; and (iii) the reaction of the carbocyclic ligand with an Me_3NO-activated cluster which leads to the transfer of the ligand to the cluster [10].

The carbocycle-substituted clusters have been shown by crystallographic studies to adopt a range of metal framework geometries and ligand distributions. The structures have been interpreted both in terms of the established electron counting rules, such as the Effective Atomic Number Rule (E.A.N.) [11] and the Polyhedral Skeletal Electron Pair Theory (P.S.E.P.T.) [12], and in terms of the Ligand Polyhedral Model (L.P.M.) [13]. The electron counting rules deal only with the metal framework geometry, in either a predictive or interpretative mode, and give no guide to the distributions of the ligands around the cluster core. In contrast, the L.P.M. approach considers the cluster in terms of a metal core enclosed in a polyhedron of carbonyl ligands, the arrangement of which is dependent on their mutual non-bonded interactions, and little information can be gleaned concerning the metal core geometry. The role of the intermolecular interactions in the crystal packing arrangements of arene-substituted clusters has also been investigated, with particular reference to arene-arene π-stacking [14] and C(arene)—H $\cdots$ O(carbonyl)/M—H $\cdots$ O(carbonyl) hydrogen bonding [15]. Such interactions will perturb the ligand polyhedron and hence, indirectly, the metal core structure, since the metal–metal bonding interactions are relatively "soft", i.e. not strongly distance dependent.

These approaches to rationalizing the structures of carbocycle-substituted clusters are complementary, but do not give the complete picture regarding the structure and reactivity of these complexes. In this review, where we concentrate on the extensive chemistry of penta- and hexanuclear osmium and ruthenium carbocycle clusters, we aim to consider both the steric and electronic components that determine the structures of this class of complex, including the nature of the reaction by which they were formed, and draw general conclusions concerning the structures adopted.

We commence our study by considering pentanuclear clusters which contain a terminally bound carbocyclic ligand, and compare them with related binary carbonyls and binary carbonyl hydrides. These clusters may be considered as the simplest case, where a carbocyclic-substituted metal complex caps a preformed tetrahedral metal cluster core, and forms the first series of compounds where not all the metal atoms form the same number of connections to the other metal atoms in the core. In the trigonal bipyramid, the five-vertex deltahedron (a polyhedron with all triangular faces), the two apical metal atoms have a metal connectivity of (3) while the equatorial ones have a metal connectivity of (4) as shown in Fig. 1.

We then expand the study to consider hexanuclear systems, and emphasise the structural differences between the series of clusters which have metal core structures based on fused tetrahedral and on octahedral geometries.

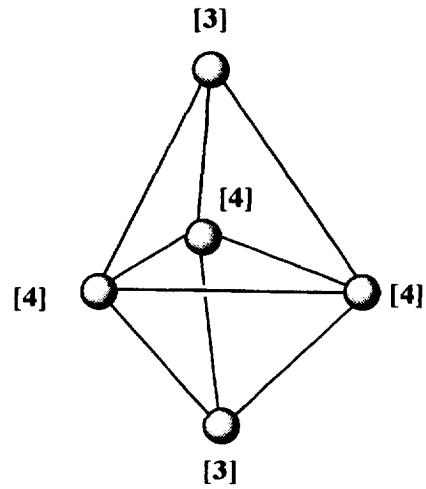

Fig. 1. Metal–metal connectivities in the trigonal bipyramid.

OBSERVATIONS AND DISCUSSION

Trigonal bipyramidal clusters

The archetypal pentanuclear cluster with a trigonal bipyramidal metal core is $Os_5(CO)_{16}$ **1** [16,17] (Fig. 2a). The two apical Os atoms are connected to three equatorial Os atoms and to three terminal carbonyls. Two of the equatorial Os atoms are connected to two equatorial and two axial Os atoms and to three carbonyls, while one equatorial Os atom is connected to two axial and two equatorial Os atoms and to *four* carbonyls [18]. The two carbonyl groups in the equatorial plane bonded to the latter Os atom form very asymmetric ("incipient") bridges to the other two equatorial Os atoms, while the two axial carbonyls are linear. The Os—Os bond lengths involving the eight co-ordinate, formally $20e^-$ metal centre are considerably longer (by ca 0.1 Å) than the other Os—Os distances in the cluster. This observation may be attributed to steric or electronic effects, or both. Mingos and Evans [19] have shown that the replacement of one $Os(CO)_3$ by an $Os(CO)_4$ unit in an electron-precise or deltahedral cluster does not change the electron count, but is accompanied by a decrease in the M—M bond strength due to differences in the frontier orbitals of the two units. The carbonyl ligand polyhedron, expressed in Föppl notation, is essentially 1 : 6 : 3(3) : 3 in form, one of several found to have approximately equal lowest energy, although it is distorted quantitatively due to the asphericity of the trigonal bipyramidal metal core [20].

Metal–metal bond lengths for all the trigonal bipyramidal structures discussed in this section are presented in Table 1. A common numbering scheme, as illustrated in the table, is adopted in which the two

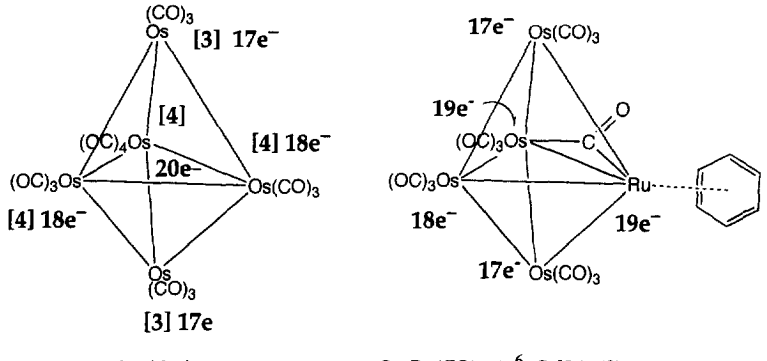

$Os_5(CO)_{16}$ **(1)** (a)

$Os_4Ru(CO)_{13}(\eta^6\text{-}C_6H_6)$ **(2)** (b)

Fig. 2. The structures of clusters **1** and **2**.

Table 1. Bond lengths (Å) in trigonal bipyramidal clusters

	M1—M2	M1—M3	M1—M4	M2—M3	M2—M4	M3—M4	M2—M5	M3—M5	M4—M5
$Os_5(CO)_{16}$ **1**	2.738(3)	2.764(3)	2.869(3)	2.748(4)	2.867(3)	= M2—M3 = M1—M3 = M1—M2 = M1—M4			
$Os_4Ru(CO)_{13}(\eta^6\text{-}C_6H_6)$ **2**	2.703(2)	2.821(2)	2.792(2)	2.775(2)	2.786(2)	2.799(2)	2.728(2)	2.781(2)	2.780(2)
$[HOs_5(CO)_{15}]^-$ **3**	2.710(4)	2.872(4)	2.852(4)	2.833(4)	2.831(4)	2.867(4)	2.732(4)	2.829(4)	2.843(4)
$H_2Os_5(CO)_{12}(\eta^6\text{-}C_6H_5Me)$ **8**	2.765(4)	2.835(4)	2.797(4)	2.795(4)	2.814(4)	2.827(4)	2.780(4)	2.805(3)	2.809(4)
$HOs_5(CO)_{12}(C_6H_6)(AuPPh_3)$ **10**	2.780(2)	2.807(2)	2.767(3)	2.892(2)	2.791(2)	2.854(2)	2.742(2)	2.904(2)	2.756(2)
$HOs_5(CO)_{15}AuPPh_3$ **11**	2.750(1)	2.868(1)	2.852(1)	2.890(1)	2.855(1)	2.888(1)	2.728(1)	3.072(2)	8.828(1)
$H_4Os_4Ru(CO)_{11}(\eta^6\text{-}C_6H_6)$ **12**	2.863(3)	2.806(2)	2.756(3)	2.887(2)	2.885(3)	2.803(3)	2.857(2)	2.804(2)	2.744(3)
$H_4Os_5(CO)_{11}(\eta^6\text{-}C_6H_6)$ **13**	2.868(3)	2.808(2)	2.743(2)	2.888(2)	2.874(2)	2.796(2)	2.872(2)	2.814(2)	2.753(2)
$HOs_4(CO)_{13}RuCp$ **15a**	2.770(1)	2.792(1)	2.986(2)	2.754(1)	2.824(2)	2.858(2)	2.727(1)	2.737(2)	2.876(2)
15b	2.776(1)	2.789(1)	2.982(2)	2.756(1)	2.801(2)	2.868(2)	2.741(2)	2.735(2)	2.880(2)
$HOs_4(CO)_{13}RuCp(AuPPh_3)$ **16**	2.797(2)	2.764(3)	2.764(2)	2.827(3)	2.814(3)	2.850(3)	2.799(2)	2.872(3)	2.746(2)
$Os_3(CO)_{11}Ru_2Cp_2$ **17**	2.777(1)	= M1—M2	2.762(3)	2.787(2)	2.825(2)	= M2—M4	2.794(2)	= M2—M5	2.691(3)

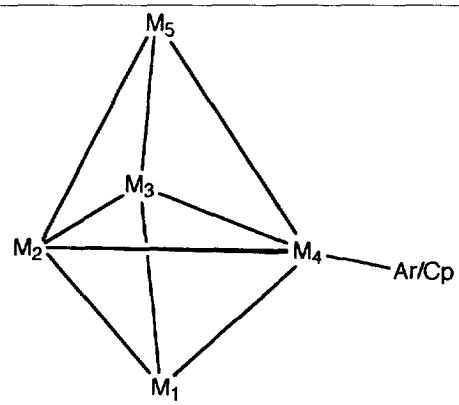

axial sites are denoted M_1 and M_5, and the equatorial carbocyclic ligand-substituted site is denoted M_4.

The mixed-metal cluster $Os_4Ru(CO)_{13}(\eta^6\text{-}C_6H_6)$ **2** may be synthesised via the ionic coupling reaction shown in eqn (1) [21,22]:

$$[Os_4(CO)_{13}X]^- \xrightarrow{K^+/Ph_2CO^-} [Os_4(CO)_{13}]^{2-} \quad X = Cl, Br, I$$

$$\xrightarrow{[Ru(C_6H_6)(MeCN)_3]^{2+}} Os_4(CO)_{13}Ru(C_6H_6) \quad (1)$$

The molecular structure (Fig. 2b) has approximate C_s symmetry with one CO ligand bridging the equatorial edge between the Ru and an Os centre. The shortest bonds are between the formally $17e^-$ axial Os and $18e^-$ equatorial Os vertices. In the equatorial plane the shortest edge is the Os—Os bond and the longest the carbonyl bridged Os—Ru edge, although the differences are only the order of 0.02 Å or less, and the capping group is bonded essentially symmetrically. There is no structural evidence for an isomer with the Ru in the axial position, only the thermodynamic

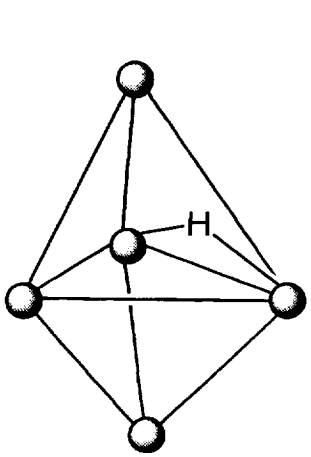

$Os_5(CO)_{15}]^-$ (3)

Fig. 3. The molecular structure of the anion 3.

product with the arene in the equatorial position is observed. The greater donor character of the metal-arene M(η^6-Ar) [Ar = arene] or M(η^5-Cp) [Cp = η^5-C_5H_5] fragment compared to an $M(CO)_3$ or $M(CO)_4$ unit enhances electron donation from the formally $20e^-$ to the $17e^-$ sites, stabilising the cluster, and hence, where steric constraints permit, the M(η^6-Ar) or M(η^5-Cp) group should occupy the "electron rich" centre. The replacement of an $M(CO)_3$ or $M(CO)_4$ fragment by an M(η^6-Ar) or M(η^5-Cp) fragment is always associated with the presence of a bridging CO group, bridging the M(η^6-Ar) or M(η^5-Cp) fragment and an adjacent metal. The bridging CO is better able to distribute the addition electron density in the cluster core which originates from the "electron rich" M(η^6-Ar)/M(η^5-Cp) fragment.

The dihydrido cluster $H_2Os_5(CO)_{15}$ has not been characterised crystallographically, although the related dianion $[HOs_5(CO)_{15}]^-$ **3** [23] has been studied as its PPN^+ [$PPN^+ = [N(PPh_3)_2]^+$] salt [24]. The anion (Fig. 3) has ideal C_{2v} symmetry, although the metal core is somewhat distorted from this. The μ-H ligand bridges an equatorial edge, and this Os—Os edge is the longest metal–metal contact in the structure, between the Os atoms of highest connectivity. As in $Os_5(CO)_{16}$ **1**, the axial-equatorial distances between $Os(CO)_3$ units are the shortest in the structure. Other distances are comparable, given the deviations of ca 0.04 Å between chemically equivalent distances, indicating considerable deformation of the soft metal core with intermolecular interactions.

The arene derivatives have been prepared by the reaction of the reduction product of $H_2Os_4(CO)_{13}$ with K^+/Ph_2CO^- with $[M(\eta^6\text{-}C_6H_6)(MeCN)_3]^{2+}$ (M = Ru, Os) or $Os(\eta^6\text{-}C_6H_5Me)(CF_3SO_3)_2$ (Scheme 1) [25]. In each case, the initial kinetic products $H_2Os_4(CO)_{12}M(\eta^6\text{-Ar})$ [M = Ru, Ar = C_6H_6 **4**, M = Os, Ar = C_6H_6 **5**, Ar = C_6H_5Me **6**] are unstable and a structure with the arene in an axial site, i.e. a simple face-capping product, has been postulated [25]. The Os complexes **5** and **6** convert, at room temperature, to the equatorial isomers **7** and **8**, respectively, in ca 40% yield. The crystal and molecular structure of **8** has been determined, and the $Os(C_6H_5Me)$ group occupies an equatorial site in the trigonal bipyramid (Fig. 4). The hydride ligands bridge two adjacent axial-equatorial edges. These are the shortest in the metal core, involving the formally $17e^-$, equatorial Os atom bound to only two terminal CO ligands, while the longest edge Os—Os is bridged by a carbonyl ligand which is again associated with the arene-substituted metal centre.

Two possible mechanisms for the formation of the equatorial isomers **7** and **8** exist. The first involves the "clipping" of the M(η^6-Ar) fragment onto a face of the pre-formed metal tetrahedron, to give the axial isomer, followed by a Berry pseudo-rotation mech-

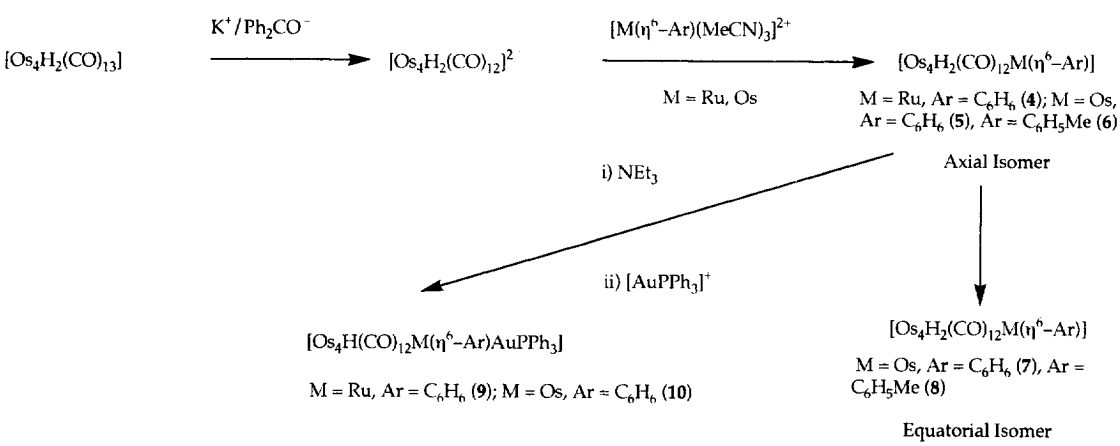

Scheme 1.

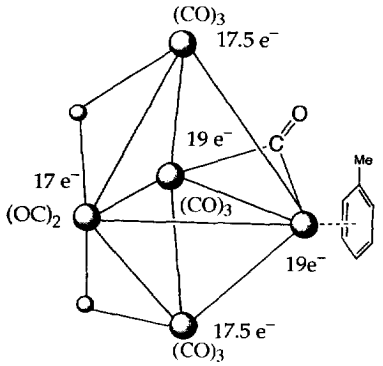

$H_2Os_5(CO)_{12}(C_6H_5Me)$ (**8**)
equatorial isomer

Fig. 4. The molecular structure of the equatorial isomer of **8**.

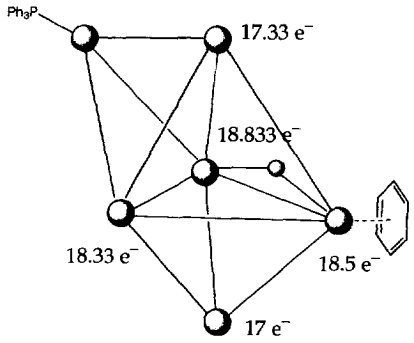

$Os_5H(CO)_{12}(C_6H_6)(AuPPh_3)$ (**10**)

Fig. 6. The molecular structure of **10**.

anism involving a trigonal bipyrimidal-square based pyramid-trigonal bipyramid cluster rearrangement to give the observed equatorial isomer (Fig. 5). This type of mechanism has been suggested in order to account for the formation of related thermodynamic products in other systems [26]. The second mechanism would involve the opening out of one edge of the metal tetrahedron, and the insertion of the M(η^6-Ar) fragment into that edge to form the trigonal bipyramid to give the isomer with the M(η^6-Ar) unit in the equatorial site. In view of the observation of the clusters **4**, **5** and **6**, although not their complete characterisation, it is probable that the first mechanism is the correct one for both the hydrido and non-hydrido clusters.

Deprotonation of initial axial products **4** and **5** with NEt_3 followed by ionic coupling with excess $[AuPPh_3]^+[NO_3]^-$ produces $HOs_4M(CO)_{12}(\eta^6\text{-}C_6H_6)AuPPh_3$ (M = Ru **9**, Os **10**) (Scheme 1) which have similar IR and ^1H NMR spectra [26]. The solid state structure of **10** (Fig. 6) has the Os(η^6-Ar) group in the electronically and sterically (with respect to $AuPPh_3$) favoured equatorial site; it is unclear whether this results from a metal core rearrangement in the anion or in the final product. The parent cluster $HOs_5(CO)_{15}AuPPh_3$ **11** [27] has a similar $AuPPh_3$-capped trigonal bipyramidal geometry and the hydride ligand also bridges an equatorial edge.

However, the M—M bond distances differ significantly in detail between the structures of **10** and **11**. All bonds involving the arene-substituted Os atom in **10** are substantially shorter by (0.03 Å or more) than the corresponding distances for the $Os(CO)_3$ group in **11** and the H-bridged bond is shorter than the Au-bridged bond in **10** whereas they are approximately equal in **11**. The $AuPPh_3$ moiety caps asymmetrically in each. Whilst some of these differences can be attributed to the greater donor ability of the Os(η^6-Ar) group as compared to $Os(CO)_3$, some may be a consequence of distortions imposed on the metal core by intermolecular interactions.

Tetra-hydrido clusters may also be prepared by the similar ionic coupling route (eqn (2)) [28]:

$$Os_4H_4(CO)_{12} \xrightarrow{K^+/Ph_2CO^-} [Os_4H_4(CO)_{11}]^{2-}$$

$$\xrightarrow[M=Ru,Os]{[M(C_6H_6)(MeCN)_3]^{2+}} H_4Os_4(CO)_{11}M(C_6H_6) \quad (2)$$

M = Ru **12**, Os **13**

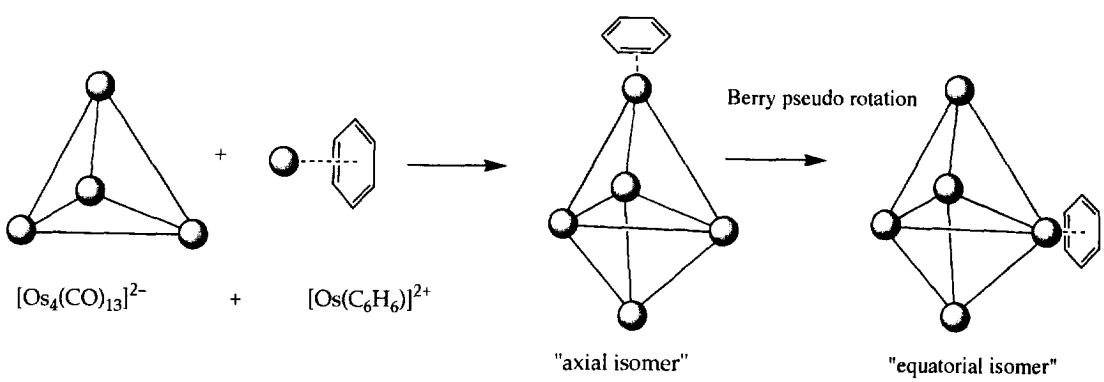

Fig. 5. A possible mechanism for the formation of clusters **7** and **8**.

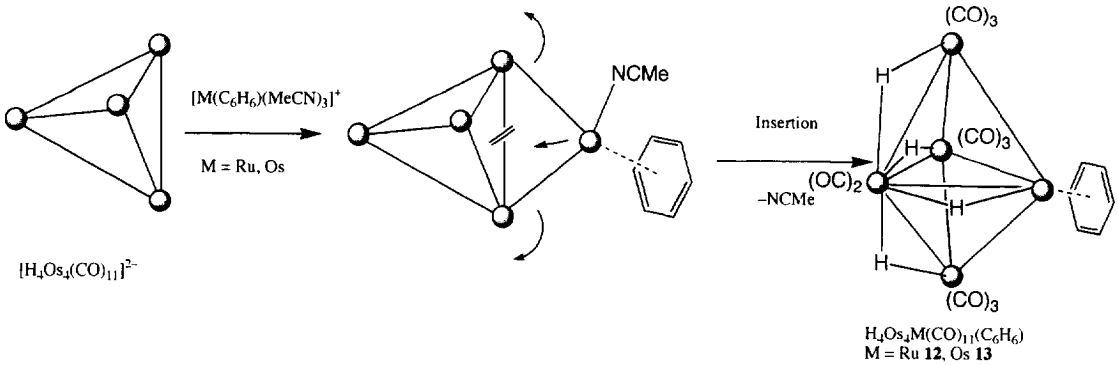

Fig. 7. A possible mechanism for the formation of **12** and **13**.

In this reaction there was no evidence for the existence of axially-capped derivatives and both $H_4Os_4M(CO)_{11}(\eta^6\text{-}C_6H_6)$ [M = Ru **12**, Os **13**] have the benzene ligand in the favoured equatorial site in the solid state. Clusters **12** and **13** are isomorphous and their core bond lengths are similar, with no clear trends apparent on substituting Os with Ru. With regard to the formation of **12** and **13**, an edge-bridged tetrahedral intermediate which retains one acetonitrile ligand has been postulated, the $M(\eta^6\text{-Ar})$ unit then inserts into the edge-bridged Os—Os bond with loss of MeCN to generate the product (Fig. 7) [28,29]. In contrast to the di-hydrido structure **8**, the longest axial-equatorial bonds in **12** and **13** are those bridged by hydrides, as the equatorial Os atom coordinated to two terminal carbonyls is now ten-coordinate and has a higher formal electron count. Similarly, the unbridged equatorial edge is the shortest, the presence of the equatorial ligands causing the $Ru(\eta^6\text{-}C_6H_6)$ unit to bond asymmetrically in the equatorial plane. The M—Os(axial) bonds involving the $M(\eta^6\text{-}C_6H_6)$ unit are the shortest axial-equatorial distances (cf **10**).

Cyclopentadienyl-substituted pentanuclear clusters are also known, and the $[Os_4RuCp(CO)_{13}]^-$ anion **14** has been synthesised in a similar manner to $Os_4(CO)_{13}Ru(\eta^6\text{-}C_6H_6)$ **2** using $[RuCp(MeCN)_3]^+$ as the capping group. It has not been characterised in the solid state, although spectroscopic data are consistent with a structure similar to that of **2** [21]. The anion **14** may also be produced by deprotonation of $HOs_4(CO)_{13}RuCp$ **15**, which is formed when $[RuCp(MeCN)_3]^+$ is treated with $[Os_4(CO)_{13}Cl]^-$ in the absence of an additional reducing agent [18,30]. In the solid state, the cluster has the expected trigonal bipyramidal metal core with the Cp-bound Ru atom in an electronically favoured equatorial site, and coordinated to a semi-bridging CO ligand (Fig. 8). The bond parameters in **15** follow the same trends as those in $H_2Os_5(CO)_{12}(\eta^6\text{-}C_6H_5Me)$ **8**. The two independent molecules in the asymmetric unit of **15** have similar bond parameters; the longest distances involve the Ru atom, which has the highest connectivity and electron count. The semi-bridged edge is longer than other

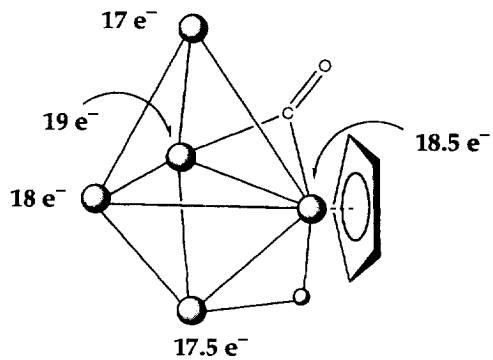

$HOs_4(CO)_{13}Ru(C_5H_5)$ **(15)**

Fig. 8. The molecular structure of **15**.

Ru—Os equatorial edges, an effect more marked than in **8**, i.e. the cap is less symmetric.

The anion **14** may be capped with $[AuPPh_3]^+[NO_3]^-$ to produce the cluster $Os_4(CO)_{13}RuCp(AuPPh_3)$ **16** (Fig. 9) which has a similar structure to the $AuPPh_3$-capped, arene-substituted clusters **9** and **10** [21]. It is interesting to note that in both the case of **16** and of the gold-containing, arene-substituted clusters the "$AuPR_3$" fragment clips on to a triangular face of the preformed Os_5 or Os_4Ru cluster, and there is no indication of the core rearrangement that must take place when either the $M(\eta^6\text{-Ar})$ or $M(\eta^5\text{-Cp})$ fragment is added to the tetrahedral Os_4 unit. In **16** the $AuPPh_3$ group caps asymmetrically, in a manner dissimilar to that in either **10** or **11**. This capping Au atom has the effect of increasing axial-equatorial distances, whereas the absence of a μ-H decreases the coordination number of the Ru atom such that its bonds are much shorter than those in $HOs_4(CO)_{13}RuCp$ **15**, and are comparable to the unbridged Os—Os axial-equatorial distances.

Having seen that metal framework rearrangements occur when an $M(\eta^5\text{-Cp})$ or an $M(\eta^6\text{-Ar})$ fragment is added to a tetrahedral cluster core, and that in the final

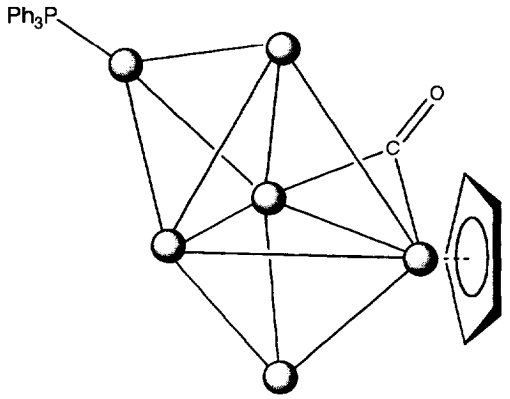

$Os_4(CO)_{13}Ru(Cp)AuPPh_3$ **(16)**

Fig. 9. The molecular structure of **16**.

product obtained from these syntheses the trigonal bipyramidal metal core always has the M(η^5-Cp) or M(η^6-Ar) unit occupying an equatorial site, it is of interest to see what core geometry is obtained if two carbocyclic-substituted metal units are added to a trinuclear cluster core.

Bicapped clusters derived from trinuclear precursors may be prepared readily. If the dianion $[Os_3(CO)_{11}]^{2-}$ is reacted with two equivalents of $[RuCp(MeCN)_3]^+[PF_6]^-$, $Os_3(CO)_{11}Ru_2Cp_2$ **17** is produced (Fig. 10). Alternatively, deprotonation of $Os_3RuH(CO)_{11}Cp$ followed by addition of one equivalent of the capping reagent is equally effective [21,30,31]. Cluster **17** has crystallographic C_s symmetry in the solid state and the metal framework is again a trigonal bipyramid. However, in this case, while one of the Ru(η^5-Cp) units occupies the favoured "electron rich" equatorial site, as seen for the mono-carbocyclic ligand-substituted systems, the second Ru(η^5-Cp) unit occupies an axial site. Another important feature of the structure is that it has two μ_3-CO ligands which cap the two $OsRu_2$ triangular faces of the trigonal bipyramid. In this bonding mode CO ligands are better π-acceptors than terminal or μ_2-CO ligands and serve to reduce electron density on the metal core introduced by two adjacent Ru(η^5-Cp) units. This feature perhaps balances out the additional electron density being pushed into the cluster core by the Ru(η^5-Cp) fragment occupying an electronically less favoured axial site. There is no evidence for cluster rearrangement since the product could be derived by repeated capping of the triangular precursor (as could an axial-axial isomer, although the equatorial position is the preferred site, since, as has been discussed previously, the enhanced electron-donating ability of Cp ligands, compared to carbonyl groups, enhancing donor bonds to the axial sites). The Ru—Ru bond is shortest metal–metal contact in the structure, and Ru—Os bonds are generally longer than Os—Os bonds.

Edge-bridged and spiked tetrahedral clusters

Two crystallographic modifications of $H_2Os_5(CO)_{16}$ **18,** both of which have the edge-bridged tetrahedral metal core (Fig. 11) and essentially similar bond lengths have been studied; one has crystallographic C_s symmetry (II) [32,33]. The longest edges are those bridged by hydrido ligands, each having three terminal CO ligands associated with each Os atom, and distances to the edge bridging Os atom are longer than the other unbridged edges. Selected bond lengths for all the structurally characterised edge-bridged and spiked tetrahedral clusters discussed in this section are listed in Table 2; a common numbering scheme for the metal core is adopted, as illustrated in Table 2, with the edge-bridging metal atom denoted M_5.

The clusters $Os_4MH_2(CO)_{13}(\eta^6\text{-}C_6H_6)$ [M = Ru **19,** Os **20**] with an edge-bridged tetrahedral metal core, with benzene bound to the edge-bridging metal, are produced by CO scavenging from the initially produced trigonal bipyramidal axial isomers of $Os_4MH_2(CO)_{12}(\eta^6\text{-}C_6H_6)$ [M = Ru **4,** Os **5**] in yields of 15% and 40%, respectively [25]. This demonstrates that the trigonal bipyramidal cluster is activated to nucleophilic substitution by arenes in axial sites compared to $H_2Os_5(CO)_{15}$ [34]. The Ru complex **19** has

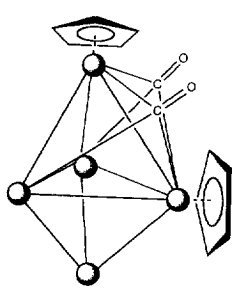

$[Os_3(CO)_9(\mu_3\text{-}CO)_2Ru_2(C_5H_5)_2]$ **(17)**

Fig. 10. The molecular structure of **17**.

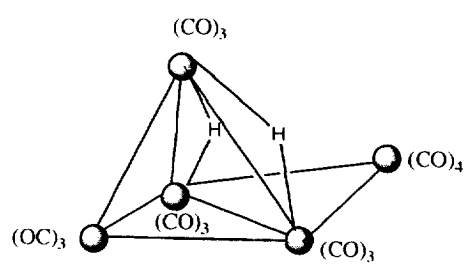

$H_2Os_5(CO)_{16}$

Fig. 11. The molecular structure of $H_2Os_5(CO)_{16}$.

Table 2. Bond lengths (Å) in edge-bridged and spiked tetrahedral clusters

	M1—M2	M1—M3	M2—M3	M1—M4	M2—M4	M3—M4	M1—M5	M2—M5	C(H)—M5
$H_2Os_5(CO)_{16}$ **18I**	2.796(5)	2.969(5)	2.955(5)	2.845(5)	2.843(5)	2.787	2.893(5)	2.893(5)	—
18II	2.811(1)	2.953(1)	= M1—M3	2.8405(9)	= M1—M4	2.780(1)	2.906(1)	= M1—M5	—
$H_2Os_4Ru(CO)_{13}(C_6H_6)$ **19**	2.753(2)	2.962(2)	2.962(2)	2.819(2)	2.835(2)	2.779(2)	2.828(3)	2.841(3)	2.22(4) – 3.31(4)
$H_4Os_5(CO)_{12}(C_6H_6)$ **22**	2.813(2)	2.974(2)	2.963(2)	2.919(2)	2.804(2)	2.793(2)	2.929(2)	2.849(2)	2.17(5) – 2.34(5)
$H_2Os_4(CO)_{13}RhCp$ **23**	2.758(1)	2.954(1)	2.941(1)	2.824(1)	2.837(1)	2.786(1)	2.770(1)	2.789(1)	2.19(1) – 2.26(1)
$H_2Os_4(CO)_{13}RhCp^*$ **24**	2.7707(5)	2.9451(4)	= M1—M3	2.8278(4)	= M1—M4	2.7856(5)	2.8129(6)	= M1—M5	2.199(6) – 2.294(9)
$H_2Os_5(C_6H_6)(CO)_{12}$ PPh_2Me **25**	2.775(3)	2.973(3)	2.958(3)	2.845(3)	2.792(3)	2.793(3)	2.878(3)	2.801(2)	2.18(4) – 2.35(5)
$H_3Os_4Ru(C_6H_5)(CO)_{12}$ PPh_2Me **27**	2.959(2)	2.811(2)	2.970(2)	2.770(2)	2.789(2)	2.833(2)	3.006(3)	—	—
$H_3Os_4Ru(C_6H_5)(CO)_{12}$ $P(OMe)_3$ **28**	2.954(3)	2.808(3)	2.969(3)	2.751(3)	2.800(3)	2.847(3)	2.990(5)	—	—
$HOs_3Ru_2Cp(C_5H_4)(CO)_{11}$ $P(OMe)_3$ **29**	2.955(1)	2.927(1)	2.877(1)	2.7905(9)	2.7480(8)	2.893(1)	2.816(1)	—	2.18(4) – 2.32(4)

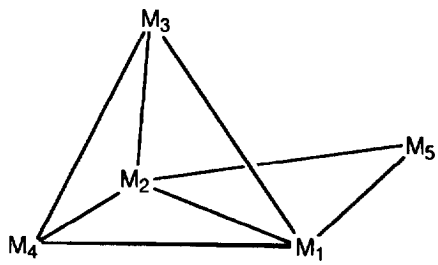

been characterised structurally (Fig. 12), and has bond lengths which are similar to those in $H_2Os_5(CO)_{16}$ **18** except that the Ru—Os bridge bonds are shorter, and the Os—Os bridged edge is substantially so (by ca 0.05 Å). This suggests that the benzene ligand increases the M—M bond strength on the bridged edge (or reduces crowding) as in $HOs_5(CO)_{15}AuPPh_3$ **11** vs $HOs_5(CO)_{12}(\eta^6\text{-}C_6H_6)AuPPh_3$ **10**.

Similarly, reaction of **4** and **5** with H_2 is accompanied by edge cleavage and the generation of $H_4Os_4M(CO)_{12}(\eta^6\text{-}C_6H_6)$ (M = Ru **21**, Os **22**) (Fig. 13) [26]. The pentaosmium compound **22** had been characterised previously as a product of the capping of $[Os_4H_4(CO)_{11}]^{2-}$ with $Os(\eta^6\text{-}C_6H_6)(MeCN)_3$, accompanied by CO scavenging [28]. It was suggested that **22** was formed from an MeCN-substituted edge-bridged intermediate, as the equatorial benzene cluster $H_4Os_5(CO)_{11}(\eta^6\text{-}C_6H_6)$ **13** is inactive towards CO addition and **22** could not be decarbonylated to give **13**. This indicates that equatorial arene substitution deactivates trigonal bipyramidal clusters to nucleophilic addition since the greater donor ability of the arene increases the electron density on the axial metal atoms. In the solid state, it can be seen, by reference to Table 2, that the hydrido-bridged edges in **22**

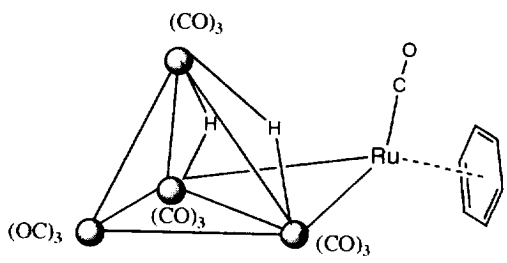

$H_2Os_4Ru(CO)_{13}(C_6H_6)$ **(19)**

Fig. 12. The molecular structure of **19**.

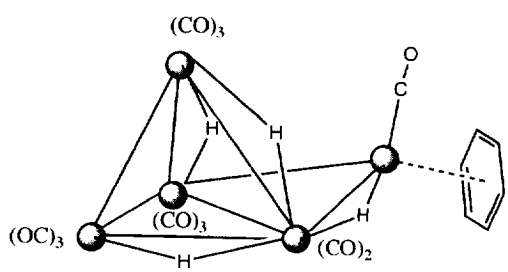

$H_4Os_5(CO)_{12}(C_6H_6)$ **(22)**

Fig. 13. The molecular structure of **22**.

involving M_2 are shorter than the corresponding edges in $H_2Os_5(CO)_{16}$ **18,** whilst those involving M_1 are longer. This is probably a consequence of reduced steric crowding at M_2 which bears only two CO ligands, as in the trigonal bipyramidal cluster $H_2Os_5(CO)_{12}(\eta^6\text{-}C_6H_5Me)$ **8**.

A Rh(CO)Cp*-bridged cluster [Cp* = η^5-C_5Me_5] has been synthesised by a similar route (eqn (3)) [35]:

$$Os_4H_4(CO)_{12} \xrightarrow{K^+/Ph_2CO^-} \begin{matrix}[Os_4H_4(CO)_{11}]^{2-} \\ + \\ [Os_4H_2(CO)_{12}]^{2-}\end{matrix} \xrightarrow{[RhCp^*(MeCN)_3]^{2+}} Os_4H_2(CO)_{13}RhCp^* \quad (3)$$

24

The edge-bridged tetrahedral core in $H_2Os_4(CO)_{13}RhCp^*$ **24** has crystallographic C_s symmetry (Fig. 14). The Cp analogue **23** had been prepared previously as a minor product (3.5% yield) in the thermolysis of $H_2Os_3(CO)_{10}$ and $CpRh(CO)_2$ [36]. The bond lengths in **23** and **24** (Table 2) are broadly similar to those in $H_2Os_4Ru(CO)_{13}(\eta^6\text{-}C_6H_6)$ **19,** although the bonds to edge-bridging rhodium atoms are shorter.

Similar edge-bridged tetrahedral structures have been suggested as the initial products of the reaction of $H_2Os_4(CO)_{12}M(\eta^6\text{-}C_6H_6)$ [M = Ru **4,** Os **5**] with phosphines and phosphites. In the reaction of **5** with PPh_2Me, substitution occurs at an equatorial site on the tetrahedron, adjacent to the edge-bridging $Os(CO)(C_6H_6)$ group, to yield $H_2Os_5(\eta^6\text{-}C_6H_6)(CO)_{12}PPh_2Me$ **25** (Fig. 15) [25]. Consideration of IR and ^1H NMR spectral data indicate that the $P(OMe)_3$ derivative is structurally analogous to **25** [25]. The phosphine has an edge-lengthening effect in **25** compared to $H_2Os_4Ru(CO)_{13}(\eta^6\text{-}C_6H_6)$ **19.** Most notably the *cis* Os—Os edge involving the edge-bridging Os atom is considerably longer (by ca 0.08 Å) than the other bond to the edge-bridging Os atom which is supported by an incipient CO bridge (Fig. 15).

For the axial isomer of $H_2Os_4Ru(CO)_{13}(\eta^6\text{-}C_6H_6)$ **4,** spectroscopic data suggest that the initial products are different from those obtained with **5,** with substitution occurring preferentially at the Ru centre **26** [25,37].

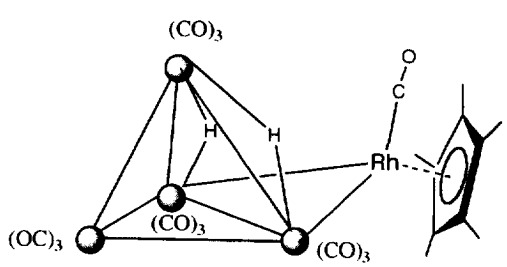

Fig. 14. The molecular structure of **24**.

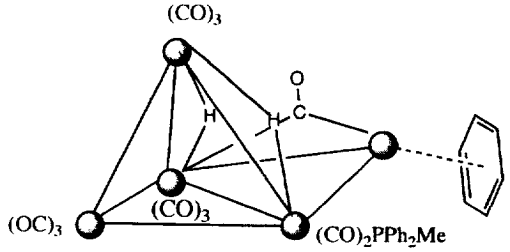

Fig. 15. The molecular structure of **25**.

These products are unstable and convert irreversibly to the clusters $H_2Os_4Ru(CO)_{12}(\eta^6\text{-}C_6H_6)(PPh_2Me)$ **27** and $H_2Os_4Ru(CO)_{12}(\eta^6\text{-}C_6H_6)(P\{OMe\}_3)$ **28,** respectively, in which orthometallation of the benzene ring and metal–metal bond cleavage has occurred to provide a spiked tetrahedral core geometry (Fig. 16). This transformation may be induced by the bulk and σ-donor properties of the phosphine at the Ru centre and the C—H cleavage driven by the formation of additional M—H and M—C bonds. Both complexes have similar core geometries in the solid state (Table 2), and three hydride ligands bridge the longest edges, of which the spike bond is the longest. The PPh_3 derivative and toluene analogue of **27** have been prepared and characterised spectroscopically, and the ^1H NMR spectrum suggests that the methyl group is *para* to the orthometallated carbon of the arene ring [26]. A similar orthometallation of a Cp ligand occurs in the related reaction (eqn (4)) [21]:

$$Os_3(CO)_{11}P(OMe)_3 \xrightarrow{K^-/Ph_2CO^-} [Os_3(CO)_{10}P(OMe)_3]^{2-} \xrightarrow{[RuCp(MeCN)_3]^+} Os_3Ru_2Cp_2(CO)_{11}P(OMe)_3 \xrightarrow{\downarrow heat, 2h} HOs_3Ru_2Cp(C_5H_4)(CO)_{11}P(OMe)_3 \; \mathbf{29} \quad (4)$$

In this instance, thermal activation is required to affect orthometallation. The final product **29** has been characterised structurally (Fig. 17, Table 2). In this cluster, the orthometalled cyclopentadienyl ring is π-bonded to the capping Ru(3) atom with C(1) bridging the spiked edge, Ru(5) possessing an η^5-Cp ligand. The geometry about the triply-bridging carbon atom C(1) is more asymmetric than in the arene-substituted clusters, with the shortest bond to the spike atom Ru(5) and longest to Os(1), such that the π-bond to Ru(3) is shorter than the latter. The spiked edge is also bridged, essentially symmetrically, by a CO ligand rather than a hydride as in **27** or **28** and the Os(1)—Ru(5) distance is thus considerably shorter (by ca 0.2 Å). The spike bond is bent towards Os(3) and Os(4) compared to geometry of **27** or **28** in order to accommodate the different position of the carbocyclic ligand, although the Ru(5)—Os(1)—Os(2) angle is essentially unchanged. Attempts to synthesise

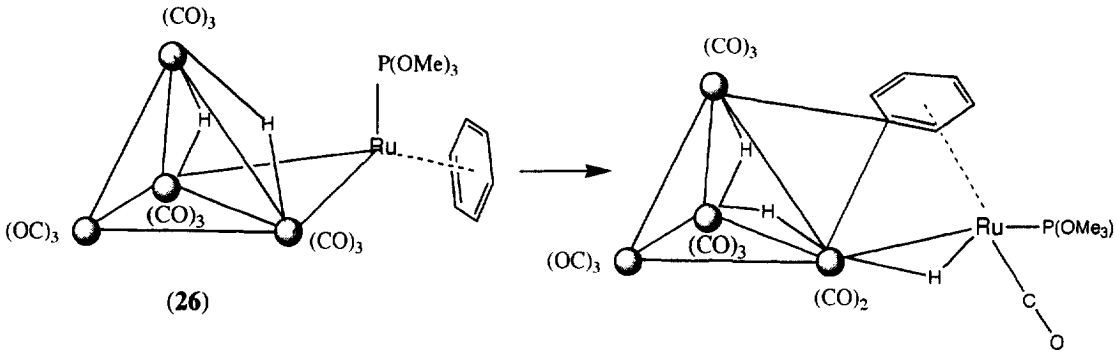

Fig. 16. The formation of **28** from **26**.

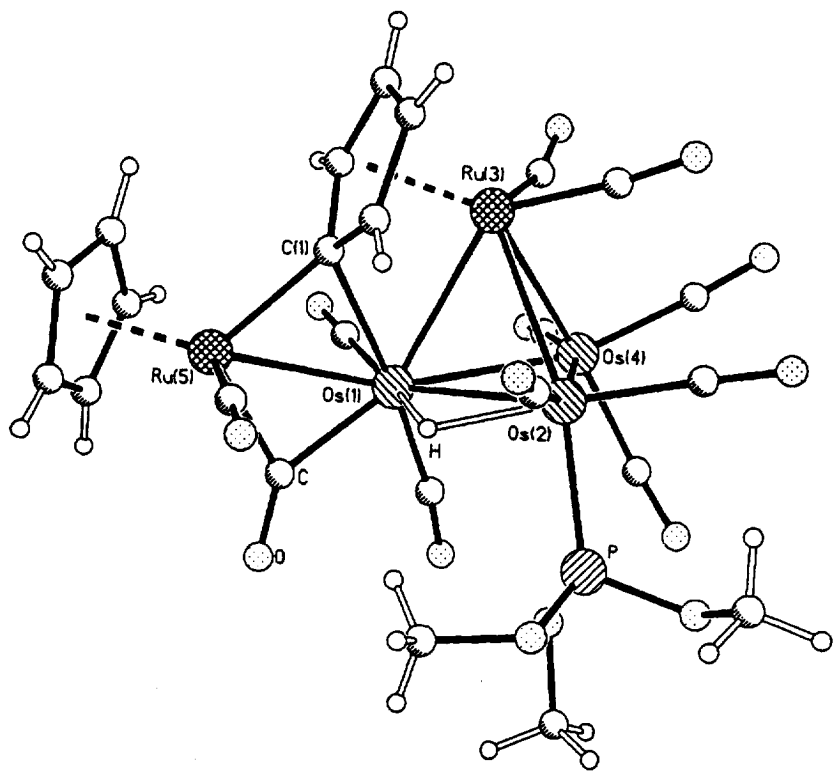

Fig. 17. The molecular structure of **29**.

the PPh_3 derivative by a similar route failed to produce an analogous complex [21].

The isolation of the spiked tetrahedral clusters **27–29**, when stabilised by strongly electron donating phosphines or phosphites, may suggest that these are intermediates either for the metal framework rearrangements postulated for the formation of the trigonal bipyramidal pentanuclear clusters, described above, or for carbocyclic ring migration over the cluster surface. However, the reaction chemistry of these systems does not lead either to the formation of trigonal bipyramidal clusters, or to clusters in which the arene or cyclopentadienyl ring has migrated from one metal to another.

Bicapped and bis *edge-bridged tetrahedral clusters*

The archetypal bicapped tetrahedral cluster $Os_6(CO)_{18}$ **30** [16] has been characterised in the solid state alone [38] and as a $CHCl_3$ solvate (in which there are some solvent-carbonyl interactions) [39]. Each

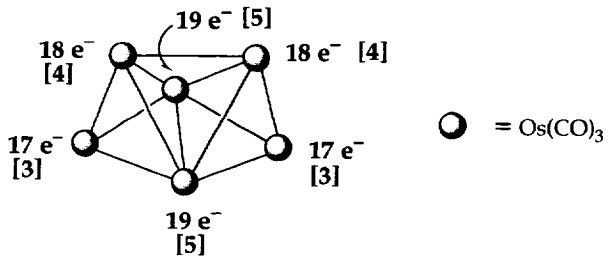

$Os_6(CO)_{18}$ **(30)**

Fig. 18. The metal–metal connectivities and the metal atom electron counts in **30**.

metal has three terminal CO ligands, giving formal electron counts of 17, 18 and 19e⁻ for (3), (4) and (5) metal-connected vertices, respectively (Fig. 18). The (4)–(4) and (5)–(5) distances are shortest, i.e. those between metals of the same formal electron count [38]. Large variations, due to intermolecular interactions, in chemically equivalent distances prevent elucidation of trends in the other Os—Os lengths. The carbonyl polyhedron around the aspherical metal core is shown in Fig. 19 for the solvate **30**·$CHCl_3$; the ligand arrangement is somewhat distorted from ideal C_{2v} symmetry. As with the pentanuclear clusters, selected bond parameters for the bicapped tetrahedral clusters discussed in this section are presented in Table 3, and follow a common numbering scheme as illustrated by the diagram in Table 3.

Whilst the $Ru_6(CO)_{18}$ is unknown, the related cluster $(\mu_3\text{-H})_2Ru_6(CO)_{17}$ **31** (Fig. 20) has been characterised structurally [40]. It has two faces bridged by H ligands and one (somewhat asymmetric) bridging carbonyl between the two four-connected (4) vertices. The pattern of bond lengths is clearer and follows the trend M(4)—M(4) < M(4)—M(3) < M(5)—M(5) < M(5) —M(3) < M(4)—M(5), where shortening of M(4)—M(3) and M(4)—M(4) connections is attributable to reduced steric crowding and μ-CO on the M(4)—M(4) edge. The lengthening of M(4)—M(5) edges with respect to M(3)—M(5) edges is related to the presence of face-bridging hydrides.

Bicapped tetrahedral clusters in which three carbonyl ligands are replaced, formally, by an arene ligand may be produced by the ionic coupling reaction (eqn (5)) [41,42]:

$$[Os_5(CO)_{15}]^{2-} \xrightarrow{[M(\eta^6\text{-}C_6H_6)(MeCN)_3]^{2+}[BF_4]_2^-} [Os_5(CO)_{15}M(\eta^6\text{-}C_6H_6)]$$

$$\{M = Os\ \mathbf{32}, Ru\ \mathbf{33}\}$$

$$\xrightarrow{[Os(\eta^6\text{-}C_6H_5CH_3)(CF_3SO_3)_2]} [Os_6(CO)_{15}(\eta^6\text{-}C_6H_6)]\ \mathbf{34} \quad (5)$$

For these arene-substituted clusters there is good evidence that more than one isomer exists but one isomer has been crystallised and structurally characterised for **32**–**34**. Whereas the arene is bound to a metal atom in an 18e⁻ (4) site in $Os_6(CO)_{15}(\eta^6\text{-}C_6H_6)$ **32**, it adopts

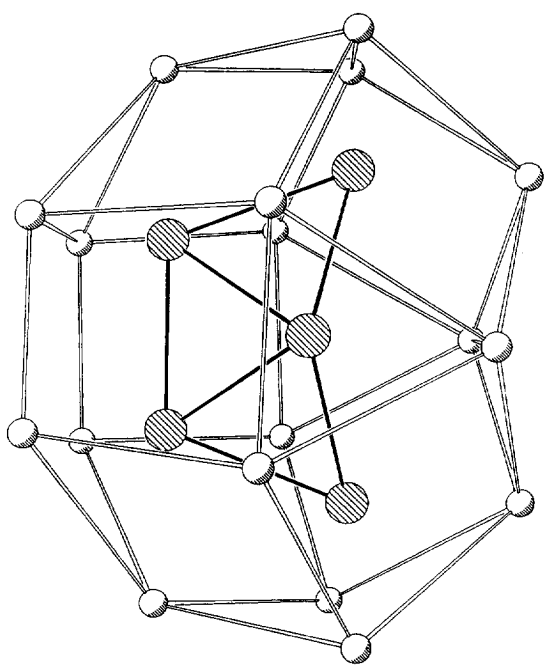

Fig. 19. The carbonyl polyhedron and the metal framework in **30** viewed down the central metal–metal bond.

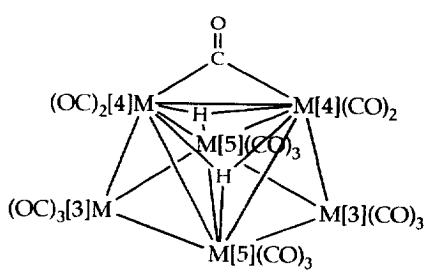

$H_2Ru_6(CO)_{17}$ **(31)**

Fig. 20. The molecular structure of **31**.

Table 3. Bond distances (Å) and angles (°) in bicapped tetrahedral clusters

	M1—M2	M1—M3	M1—M4	M1—M5	M1—M6	M2—M3	M2—M4
$Os_6(CO)_{18}$ **30**	2.757(1)	2.802(1)	2.806(1)	2.829(1)	2.800(1)	2.808(1)	2.789(1)
$Os_6(CO)_{18}$ **30** · $CHCl_3$	2.7605(11)	2.8137(12)	2.8313(11)	2.8050(12)	2.8006(11)	2.7875(11)	2.8159(12)
$H_2Ru_6(CO)_{17}$ **31**	2.753(1)	2.999(1)	2.999(1)	2.833(1)	2.833(1)	3.009(1)	2.993(1)
$Os_6(CO)_{15}(C_6H_6)$ **32**	2.759(2)	2.757(3)	2.803(3)	2.823(3)	2.821(2)	2.767(2)	2.788(3)
$Os_5(CO)_{15}Ru(C_6H_6)$ **33**	2.753(6)	2.753(6)	2.859(6)	2.975(6)	2.824(6)	2.845(7)	2.716(6)
$Os_6(CO)_{15}(C_6H_5Me)$ **34**	2.757(3)	2.757(3)	2.867(3)	2.990(3)	2.842(3)	2.868(3)	2.716(3)
$Os_5(CO)_{15}RhCp^*$ **36**	2.733(2)	2.771(2)	2.771(2)	2.784(3)	2.788(2)	2.765(2)	2.762(2)
$Os_5(CO)_{15}RuCp(AuPPh_3)$ **38a**	2.7695(14)	2.953(2)	2.9184(13)	2.931(2)	2.918(2)	2.837(2)	2.8044(14)
38b	2.7500(13)	3.0308(14)	2.8939(12)	2.917(2)	2.937(2)	2.874(2)	2.8509(13)
$Os_6(CO)_{12}(C_6H_6)_2$ **39**	2.770(1)	2.741(2)	2.859(2)	2.924(2)	2.860(2)	2.791(2)	2.672(2)
$Os_5Ru(CO)_{12}(C_6H_6)_2$ **40**	2.7620(9)	2.7365(9)	2.8561(9)	2.9241(14)	2.8642(9)	2.7748(8)	2.6740(9)
$Os_4Ru_2(CO)_{12}(C_6H_6)_2$ **41**	2.7570(11)	2.7327(12)	2.866(2)	2.933(2)	2.8559(12)	2.7778(11)	2.684(2)
$Os_6(CO)_{12}(C_6H_6)(C_6H_5Me)$ **42**	2.7823(11)	2.7425(11)	2.8546(12)	2.9180(11)	2.8763(11)	2.7830(11)	2.6691(12)

	M2—M5	M2—M6	M3—M4	M3—M5	M4—M6	M2—C1	M5—C1	M2—C1—O	M5—C1—O	M4—C(H) M5—C(H)
30	2.816(1)	2.836(1)	2.732(1)	2.780(1)	2.806(1)	—	—	—	—	—
30	2.8249(11)	2.7890(12)	2.7395(11)	2.7829(12)	2.8043(12)	—	—	—	—	—
31	2.851(1)	2.850(1)	2.643(1)	2.690(1)	2.708(1)	—	—	—	—	—
32	2.797(2)	2.810(3)	2.706(2)	2.802(3)	2.720(3)	—	—	—	—	2.19(3)–2.26(3)
33	2.599(10)	2.780(6)	2.807(6)	2.906(10)	2.772(6)	1.91	2.40(9)	171(6)	115	—
										2.25(6)–2.32(6)
34	2.560(3)	2.772(3)	2.796(3)	2.886(3)	2.772(3)	2.04(5)	2.11(5)	146(5)	137(4)	—
										2.16(5)–2.24(5)
36	2.712(2)	2.794(2)	2.709(2)	2.848(3)	2.758(2)	—	—	—	—	—
										2.13(2)–2.18(3)
38a	2.668(3)	2.765(2)	2.715(2)	2.763(2)	2.761(2)	1.93(4)	2.23(3)	154(3)	126(3)	—
										2.14(4)–2.26(4)
38b	2.729(2)	2.7963(14)	2.683(2)	2.745(2)	2.706(2)	1.95(3)	2.40(3)	156(3)	127(2)	—
										2.13(3)–2.20(3)
39	2.587(2)	2.722(2)	2.757(2)	2.880(2)	2.712(2)	2.02(3)	2.10(3)	144(2)	137(3)	2.22(3)–2.31(3)
										2.19(4)–2.28(4)
40	2.6015(13)	2.7230(10)	2.7449(10)	2.864(2)	2.7112(9)	2.01(2)	2.12(2)	148(1)	135(1)	2.20(2)–2.31(20
										2.17(2)–2.25(2)
41	2.597(2)	2.1784(13)	2.760(2)	2.870(2)	2.721(2)	1.99(2)	2.09(2)	146(2)	135(2)	2.16(3)–2.28(3)
										2.06(3)–2.21(2)
42	2.5881(11)	2.7065(12)	2.7629(11)	2.8882(14)	2.7150(13)	2.07(2)	2.10(2)	141(2)	142(2)	2.20(3)–2.27(3)
										2.19(3)–2.29(3)

	Au—M1	Au—M3	Au—M4	M3—C2 M3—C3	M5—C2 M4—C3	M2—C2—O M2—C3—O	M5—C2—O M4—C3—O
$Os_5(CO)_{15}RuCpAuPPh_3$ **38a**	2.792(2)	2.8872(14)	2.8795(14)	2.08(3)	2.05(4)	138(3)	138(3)
				2.58(3)	1.82(4)	121(3)	165(3)
$Os_5(CO)_{15}RuCpAuPPh_3$	2.7881(14)	2.8653(14)	2.898(2)	2.06(3)	2.01(3)	138(2)	137(2)
38b							
				2.34(3)	1.92(3)	131(3)	151(3)

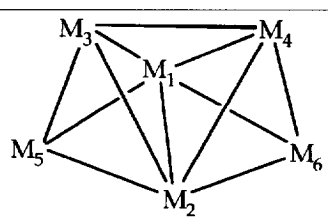

the $17e^-$ (3) site in **33** and **34** (Fig. 21). Electronic factors would be expected to favour the sites in the order (5) > (4) > (3) with respect to metal–metal connectivity (since, at a simplistic level, the presence of better donor ligands in sites of higher formal electron count will enhance the strength of the formal donor bonds). However, the reverse would be expected on steric grounds, i.e. (3) > (4) > (5). Thus the observed geometries are a compromise between these two opposing influences. For **33** and **34,** solution studies identify the existence of a (4) substituted isomer which does not interconvert with the (3) isomer in the temperature range studied; there is also some evidence for a second isomer of **32** ((3)) in solution in addition to the major (45%) (4) product [30]. Only one isomer of $Os_6(CO)_{15}(\eta^6\text{-}C_6H_3Me_3)$ **35** is found in solution, with the bulky mesitylene ligand in the sterically-favoured (3) site [43]. The precise details of the mechanism leading to the (4) isomers remain unclear, although ^{13}C labelling experiments suggest that the related "capping" of $[Os_{15}(CO)_{15}]^{2-}$ with $[Ru(CO)_3(MeCN)]^{2+}$ proceeds via an edge-cleavage process [43]. Alternatively, $Os_6(CO)_{15}(\eta^6\text{-}C_6H_6)$ **34** may be synthesised in low yield from the reaction of $Os_6(CO)_{18}$ with three equivalents of Me_3NO in the presence of benzene.

Metal core geometries of the (3) isomers of **33** and **34** are strictly comparable in the solid state, given relatively large E.S.D.s for the Ru compound **33** (Table 3). The most striking feature of these molecules is the short metal–metal bond (ca 2.6 Å) which is associated with a semi-bridging CO ligand that is coordinated to the arene-substituted metal atom. The latter is more incipient in character in **33,** which has been attributed to the decreased electronegativity of Ru cf Os [42], but this may not be significant given the relatively poor quality of the Ru structure. This shortening is accompanied by considerable lengthening of the other bonds to arene-substituted metal (Table 3) compared to those in $Os_6(CO)_{18}$ **30**. The central tetrahedron is also twisted, such that M_1—M_3 and M_2—M_4 are shorter and M_1—M_4 and M_2—M_3 are longer (see labelling scheme in Table 3); this twist is associated with an elongation of the (4)—(4) bond M_3—M_4. This may be a consequence of intramolecular distortions in the ligand polyhedron introduced by the semi-bridging CO ligand or subtle changes in the electronic distribution in the molecule. Distances in $Os_6(CO)_{15}(\eta^6\text{-}C_6H_6)$ **32** do not differ as much from the $Os_6(CO)_{18}$ **30,** although there is a significant shortening of the M_3—M_4 and, especially, M_4—M_6 (by 0.09 Å) bonds; these changes are accompanied by small (ca 0.025 Å) decreases in distances M_2—M_3 and M_1—M_3.

If the capping reaction with $[Os_5(CO)_{15}]^{2-}$ is repeated using $[RhCp^*(MeCN)_3]^{2+}$ as the cationic reagent, three isomers are obtained from the one reaction [41]. The isomer that is produced in highest yield has been characterised structurally as $[Os_5Rh(CO)_{15}Cp^*]$ **36,** with the $Rh(\eta^5\text{-}C_5Me_5)$ group occupying one of the 17 electron, (3) connectivity centres; the sterically favoured product. The three isomers interconvert readily (on the ^1H NMR time scale) and samples of each revert to a mixture of isomers [41,44]. It is probable that the other isomers are (4) and (5) substituted products [41] and it is possible that the (5) isomer opens out to give the *bis* edge-bridged tetrahedral structure with $\mu_4\text{-}\eta^2$-CO ligands as in the Ru_5Rh analogue, $Ru_5(CO)_{12}(\mu\text{-}CO)(\eta^2\text{-}\mu_4\text{-}CO)_2RhCp^*$ **46** (Fig. 26) [45].

The anion $[Os_5(CO)_{15}RuCp]^-$ **37** may be prepared in a similar manner by the reaction of $[RuCp(MeCN)_3]^+$ with $[Os_5(CO)_{15}]^{2-}$ [30,46]. The ^1H NMR spectrum shows two singlets in the Cp region indicating that two isomers (probably with the RuCp in the (3) and (4) positions) are present in solution. Addition of one equivalent of $[AuPPh_3]^+[NO_3]^-$ yields the Au-capped species $Os_5(CO)_{15}RuCp(AuPPh_3)$ **38** [21] which has been studied crystallographically (Fig. 22). The asymmetric unit comprises two independent molecules, which although similar differ subtly in their ligand arrangements. These differences are reflected in variations in corresponding bond lengths (some of more than 0.05 Å) which are highly significant statistically, whereas the differences in light atom positions are of marginal significance.

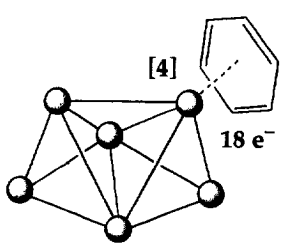

$[Os_5(CO)_{15}Os(\eta^6\text{-}C_6H_6)]$ (**32**)

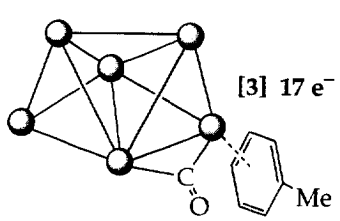

$[Os_5(CO)_{15}Ru(\eta^6\text{-}C_6H_6)]$ (**33**)

& $[Os_5(CO)_{15}Os(\eta^6\text{-}C_6H_5Me)]$ (**34**)

Fig. 21. The molecular structures of **32, 33** and **34**.

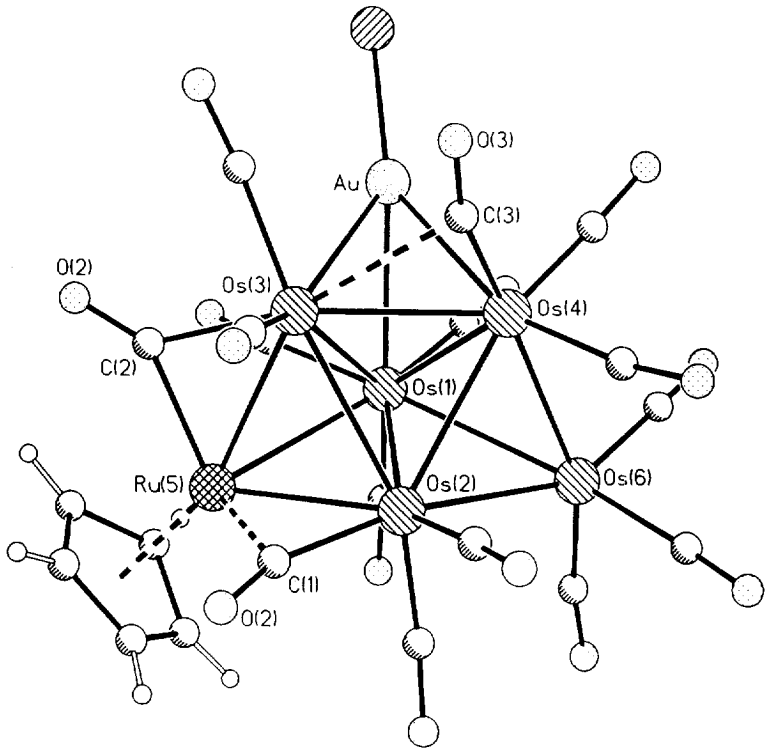

Fig. 22. Molecular structure of **38** with the phenyl rings omitted for clarity.

The reaction could be considered as a simple face-capping addition of the $[AuPPh_3]^+$ cation to the anion $[Os_5(CO)_{15}RuCp]^-$ **37**, since the RuCp moiety in $Os_5(CO)_{15}RuCp(AuPPh_3)$ **38** adopts the (3) position. However, ^1H and ^{31}P NMR spectra demonstrate the existence of other isomers in solution, which may have different positions of the Ru or Au centres (or both) compared to the solid-state structure [21]. The Au ligand caps one of the (5)(4)(4) faces Os(1)—Os(3)—Os(4) asymmetrically, with a considerably shorter bond to Os(1) in both independent molecules; this causes an elongation of the Os(1)—Os/Ru(3) and Os(1)—Os(4) bonds to distances of ca 2.9 Å or greater. The addition of the Au atom on this face necessitates a rearrangement of the ligand polyhedron around the Os(3)—Os(4) edge; one of the CO ligands forming a bridge to Ru(5) and another semi-bridging from Os(4) to Os(3). In both molecules, the Os(3)—Os(4) bond is ca 0.15–0.20 Å shorter than the other edges capped by the Au atom.

Having seen that it is possible to obtain the three possible isomers of the bicapped tetrahedral structures via the capping of dianionic pentanuclear clusters with dicationic mononuclear metal carbocyclic ligand fragments, it is logical to attempt to obtain bicapped tetrahedral structures in which two metal arene/cyclopentadienyl units replace two metal tricarbonyl units, and to investigate which isomers predominate in this situation. *Bis*-arene clusters $Os_4MM'(CO)_{12}(\eta^6\text{-Ar})(\eta^6\text{-Ar}')$ [Ar = Ar′ = C_6H_6, M = M′ = Os **39**; M = Os, M′ = Ru **40**; M = M′ = Ru **41**; Ar = C_6H_6, Ar′ = C_6H_5Me, M = M′ = Os **42**] may be prepared from the axially-substituted pentanuclear intermediates $H_2Os_4(CO)_{12}M(\eta^6\text{-Ar})$ (M = Ru **4**, Os **5**) by deprotonation and subsequent capping with dicationic reagents [25,47]. In all the structurally characterised products **39–42**, one arene ligand substitutes in a (3) and the other in a (4) site (Fig. 23), and there is no evidence for (4), (4) or (3), (3) isomers in solution or in the solid state. The (4), (4) isomer may be disfavoured electronically (too much electron density on adjacent metal atoms) and/or sterically. The isomer of $Os_5Ru(CO)_{12}(\eta^6\text{-}C_6H_6)_2$ **40** with Ru in the (3) position and Os in (4) position is produced irrespective of

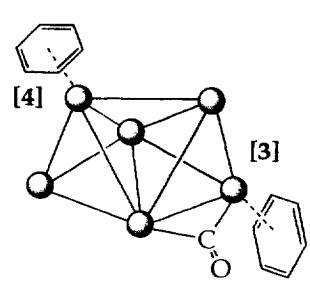

$[Os_4(CO)_{12}MM'(arene)(arene')]$ **(39–42)**

Fig. 23. The structures of clusters **39–42**.

whether the Ru(η^6-Ar) fragment originates from the cluster anion or the capping anion. The toluene ligand occupies a (3) site in **42,** probably for steric reasons. Since simple capping products ((3), (3)) are not observed, metal core rearrangement must occur to generate the thermodynamically favoured product. It should be noted that rearrangement of the pentanuclear anion would not be sufficient to account for the formation of **40** by both routes. No evidence was found for arene migration in these studies, the arene remaining bound to the capping metal atom where this could be distinguished, i.e. in **40** and **41**.

The bond lengths in all four compounds are similar, and the *bis*(benzene) compounds **39–41** are isomorphous. Given that a series of closely related, independently measured structures is available, it is instructive to compare the bond parameters across the series by analytical methods. This can be achieved by means of a half-normal probability plot which shows whether systematic differences exist between the sets of parameters being compared [48]. In the case of the series of arene-substituted clusters, comparison of coordinates on half-normal probability plots (Fig. 24) indicates that there are significant differences in dimensions of the metal–metal core at level of nominal E.S.D.s, reflecting subtle differences in electronic behaviour of Os and Ru in these systems. However, CO and arene ligand positions are consistent with random error underestimated by factors of ca 1.5–1.6, indicating that the limited precision of light atom positions precludes detailed structural investigation of differences in the ligand polyhedra.

Distances involving the capped metal atom M(5) in compounds **39–42** (Table 4) have a similar asymmetry to those in **33** and **34** and the geometry of the semi-bridging CO is strictly comparable to that in **34,** although elongation of the M_1—M_5 bond is less marked. The same shortening of the M_6—M_4 edge is apparent as in $Os_6(CO)_{15}(\eta^6\text{-}C_6H_6)$ **32**; M_3—M_4 is longer than in either **30** or **32** but shorter than in **33–38**. The central tetrahedron is twisted as in **33–34,** although bonds to M_2 are considerably shorter (by $\geqslant 0.04$ Å). Similarly, M_2—M_6 is shorter than in either the (3) or (4) mono-arene isomers and may reflect, in part, reduced crowding with μ-CO at M_2. It should be noted that these changes will not be independent of each other, as changes in electron distribution and the ligand polyhedron will influence the entire cluster core.

Whilst the isomer with Cp or arene in the (5) site are unknown, compounds formally derived from this in which the metal core has opened out to provide a *bis* edge-bridged structure have been observed (Fig. 25). These contain carbonyl ligands in the uncommon μ_4-η^2-CO bonding mode, with the C=O π-bond donating two electrons to the bridging metal atoms after having "inserted" into the M_1—M_5 and M_1—M_6 bonds.

The $Ru_6(CO)_{15}(\eta^6\text{-}C_6Me_6)$ **43** and $Ru_6(CO)_{15}(\eta^6\text{-}1,3,5\text{-}Me_3C_6H_3)$ **44** clusters with this geometry are produced in the thermolysis of the respective arene with $Ru_3(CO)_{12}$ [49,50,51]. The central core structures are very similar (Table 4 and Fig. 25), with the shortest bond being M_3—M_4 which bears a μ-CO ligand. Within the central tetrahedron, the next shortest bonds are M_2—M_3 and M_2—M_4, between metal atoms with the (5) and (4) metal–metal connections. Edge bridge bonds to the (4) metals, M_3 and M_4 are shorter than those to M_2 which has connections to five metal atoms. Thermolysis of $Ru_3(CO)_{12}$ with cyclohexene leads to ring closure and production of an η^5-C_5H_4Me ligand which is bound to the apical atom M_1 in a similar structure **45,** although replacement of a $6e^-$ with a $5e^-$ donor is accompanied by a contract of the bonds to M_1 [52]. A μ_3-H ligand caps the basal face of the tetrahedron, causing these bonds to be elongated.

The heterometallic cluster $Ru_5(CO)_{15}RhCp^*$ **46** has been synthesised recently via an ionic coupling reaction accompanied by loss of $Ru(CO)_3$ group, as shown in (eqn (6)) [45]:

$$[Ru_6(CO)_{18}]^{2-} \xrightarrow[-\text{"}[Ru(CO)_3]\text{"}]{[RhCp^*(MeCN)_3]^{2+}} Ru_5(CO)_{12}(\mu\text{-}CO)(\eta^2\text{-}\mu_4CO)_2RhCp^* \quad (6)$$

The crystal structure comprises two independent molecules of $Ru_5(CO)_{15}RhCp^*$ **46** (Fig. 26) in the asymmetric unit, each lying on a mirror plane. Bond lengths in the metal core and those involving μ_4-CO ligands are broadly similar to those in **43–44**. The opening of the structure may serve to decrease steric congestion at the formally $19e^-$ site and/or reduce electron density at this site with the formation of face-capping CO ligands with enhanced π-acceptor character [45]. However, the fact that this type of structure is observed does suggest that "electron rich" donor groups, such as RhCp*, would be expected to occupy the $19e^-$ site.

Octahedral clusters

Theoretically, clusters based on an octahedral core could be formed by the ionic coupling of an anionic square-based pyramidal cluster with a cationic metal fragment. Such ionic coupling has been achieved when the square based pyramidal dianion is stabilised by a semi-interstitial carbido ligand, as in the anion $[Ru_5C(CO)_{14}]^{2-}$. However, unlike all the previous examples discussed for penta- and hexanuclear clusters, all six metal sites in the octahedral are electronically equivalent, with the same number of metal connections, and the opportunity for isomerism, in terms for the ligand positions, is severely limited. Again, unlike the bicapped tetrahedral clusters, there are not the appropriate number of electrons to describe the octahedral core geometries, even formally, in terms of localised two-centre two-electron metal–metal bonds, but applying Wade's Rules, all the octahedral carbo-

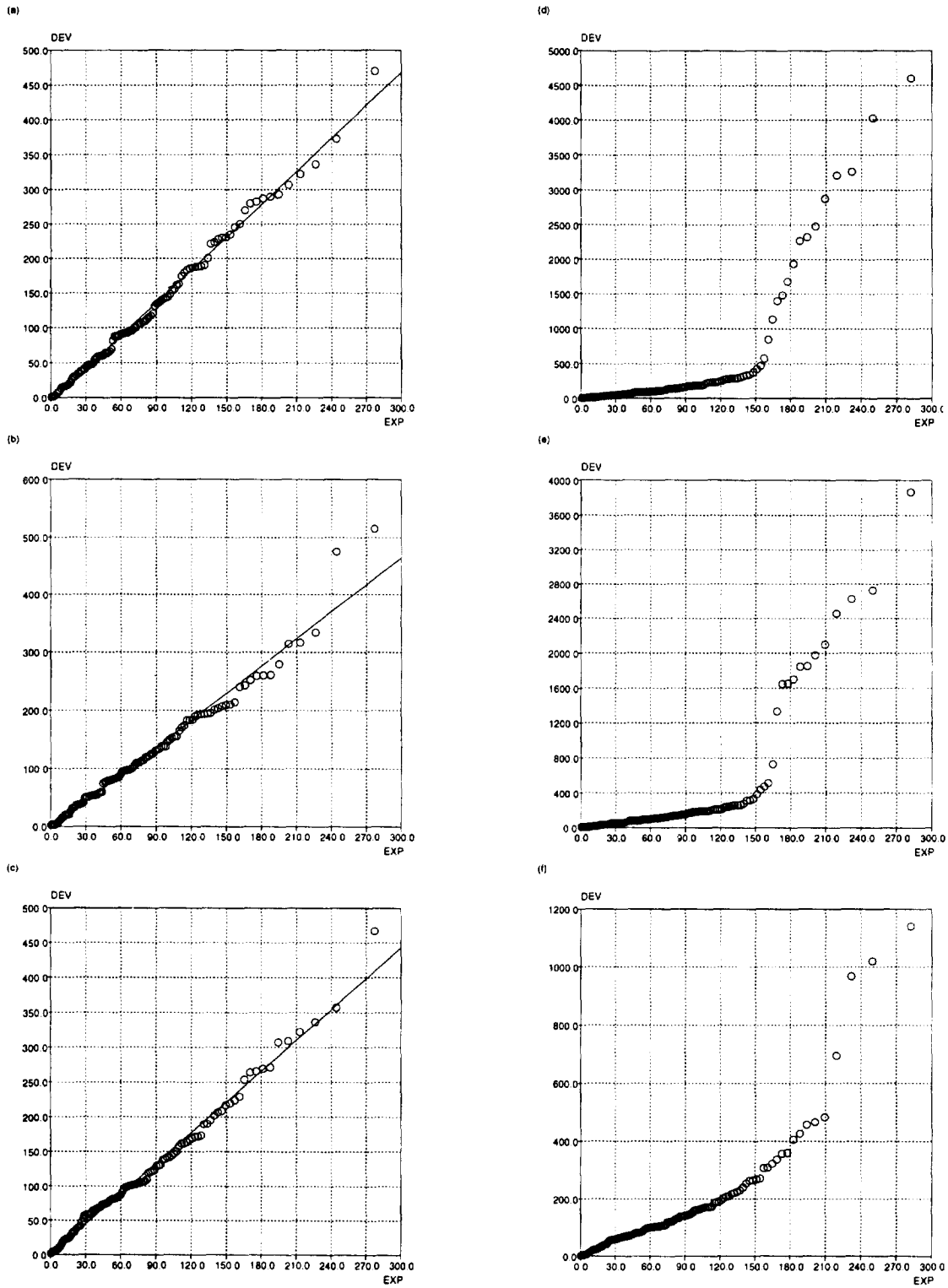

Fig. 24. Half-normal probability plots for coordinates of **39–40** (a, d), **39–41** (b, e), **40–41** (c, f) for light atoms alone (a–c) and all atoms (d–f).

Table 4. *Bis* edge-bridged tetrahedral clusters

	M1—C1 M1—C2	M2—C1 M2—C2	M3—C1 M4—C2	M5—C1 M5—C2	M5—O1 M6—O2	C1—O1 C2—O2	M3—C3 M4—C3
$Ru_6(CO)_{15}(\eta^6\text{-}C_6Me_6)$ **43**	1.957(6)	2.168(6)	2.170(6)	2.296(6)	1.267(7)	1.267(7)	—
$Ru_6(CO)_{15}(\eta^6\text{-}C_6H_3Me_3)$ **44**	1.969(9)	2.187(7)	2.169(9)	2.270(8)	1.245(11)	1.245(11)	2.091(11)
	1.969(7)	2.169(8)	2.159(8)	2.277(7)	1.265(9)	1.265(9)	2.153(8)
$HRu_6(CO)_{15}(\eta^5\text{-}C_5H_4Me)$ **45**	1.936(9)	2.219(9)	2.267(8)	2.290(2)	1.232(10)	1.232(10)	2.126(10)
$Ru_6(CO)_{15}RhCp^*$ **46a**	1.995(9)	2.158(10)	2.158(9)	2.241(9)	1.252(11)	1.252(11)	2.142(14)
46b	2.000(10)	2.167(10)	2.154(9)	2.255(9)	1.244(11)	1.244(11)	2.129(14)

	M1—M2	M1—M3	M1—M4	M2—M3	M2—M4	M2—M5	M2—M6	M3—M4	M3—M5	M4—M6
43	2.796(1)	2.823(1)	= M1—M3	2.721(1)	= M2—M3	2.839(1)	= M2—M5	2.645(1)	2.780(1)	= M3—M5
44	2.783(1)	2.843(1)	2.820(1)	2.733(1)	2.740(1)	2.839(1)	2.842(1)	2.628(1)	2.785(1)	2.776(1)
45	2.759(2)	2.780(1)	= M1—M3	2.884(1)	= M2—M3	2.843(1)	= M2—M5	2.717(2)	2.777(1)	= M3—M5
46a	2.769(2)	2.823(1)	= M1—M3	2.766(1)	= M2—M3	2.850(1)	= M2—M5	2.636(2)	2.787(1)	= M3—M5
46b	2.762(2)	2.803(1)	= M1—M3	2.764(1)	= M2—M3	2.841(1)	= M2—M5	2.639(2)	2.784(1)	= M3—M5

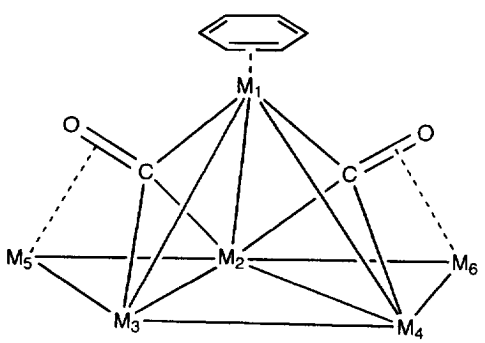

Fig. 25. The metal numbering and the ligand arrangement in *bis*-edge bridged tetrahedral clusters.

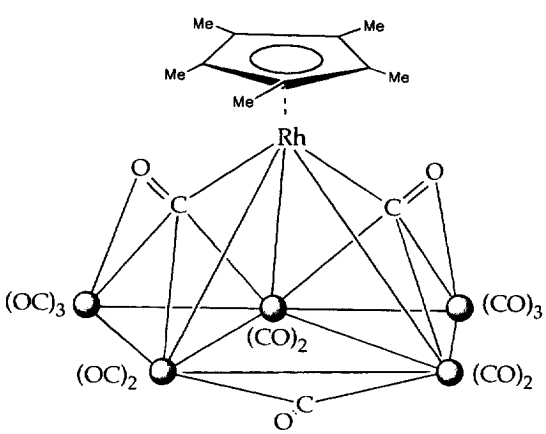

(46)

Fig. 26. The molecular structure of **46**.

cyclic ligand-substituted clusters have seven electron pairs for cluster framework bonding.

Since the structural chemistry of the central octahedral core of octahedral metal carbonyl clusters is fairly straightforward much attention has been focused on polymorphism and intermolecular interactions in Ru_6C systems [53,54,55], with packing energies being estimated for different arrangements. These species are characterised by a relatively flexible ligand polyhedron (which may be attributed to the inherent asymmetry in an $Ru_6(CO)_{17}$ structure with six metal vertices and 17 ligands, there being no unique low-energy manner in which to arrange them). It has been remarked previously [55,56,57] that the observed structures represent different compromises between conformational energies and crystal energy, i.e. the potential energy surface is relatively flat and conformation can be controlled at the intermolecular level [55]. Furthermore, there is a great variation in metal–metal bond lengths in different polymorphs and between crystallographically independent molecules in the lattice, i.e. M—M bonds are "soft" and adaptable to the electronic and steric demands of the ligands and packing arrangements [55]. This is expected because there is a greater delocalisation of the bonding electron density in the O_h core than in the lower symmetry (C_{2v}) bicapped tetrahedral systems, and the bonding in the octahedron cannot be rationalised in terms of a localised bonding description.

This flexibility should allow a greater part of the ligand conformational surface to be investigated, since it allows more local minima to be observed in the solid state. However, these polyhedra themselves have not been investigated in any detail previously, although three possible conformers were identified for $Ru_6C(CO)_{17}$ **47**, those with $(CO)_3$ units *cis-cis*, *cis-trans* and *trans-trans*

to the most symmetric bridging CO ligand (Fig. 27) [55]. In the two polymorphs reported [55,58], I is essentially *cis-trans* (I) while II has 11/2 molecules in the asymmetric unit, one on a 2-fold axis, with approximately *cis-cis* arrangements (IIA and IIB).

The ligand polyhedra are shown in Fig. 28, the carbonyl ligands being represented by the centroid of the C—O bond. I has an essentially 3 : 4 : 3 : 4 : (3) polytopal form (Fig. 28a) based on a tricapped trapezoidal prism with two triangles above and below the trapezoidal faces. In the solid state structure, the upper *trans* triangle (shaded spheres) is tilted with respect to the trapezoidal face (dotted spheres) and the *trans* CO ligand (denoted t) causes a significant lengthening of the uncapped rectangular face. A bridging CO ligand on an adjacent molecule "locks" into the irregular pentagonal hole thus generated in the ligand polyhedron [55]. The C_2-symmetric molecules IIb also pack in a similar "head-to-tail" manner, into the uncapped square face. The $(CO)_3$ units deviate subtly from an ideal *cis* arrangement, in that the CO ligands associated with the uncapped edges are twisted such that one CO (denoted a) lies over one of the long edges of the trapezia (black spheres), interactions with the semi-bridging CO ligands causing a complementary tilt of the central triangle (denoted b and t) (Fig. 28b). This provides two voids in the coordination polyhedron, which may interlock with the other (crystallographically independent) molecules. In IIa (Fig. 28c), one $(CO)_3$ group is in the symmetric *cis* conformation whilst the other is twisted as in IIb. In both the "*cis-cis*" variants, the bridging CO ligand is in a six-connected environment in the ligand polyhedron.

One way to display and compare ligand polyhedra is to produce a plot in which the positions of the centroids of the carbonyl ligands are converted to spherical polar coordinates, which are defined in terms of two angles θ and ϕ, and show the orientation of the ligands with respect to a common origin. These conformations for the polymorphs of **47** are represented in the symmetry-expanded spherical polar coordinate plot (Fig 29) which shows the angular disposition of the centroids of the C—O bonds with respect to the centroid of the Ru_6 octahedron as defined in Section 4.2 (each circle representing the position of a carbonyl ligand in one of the polymorphic structures). It can be seen that there is little variation in the positions of the bridging and semi-bridging CO ligands in the equatorial plane (these lying at positions close to ϕ 0°, 120° and 240° for the *cis-cis* form), whilst a preferred orientation for the $M(CO)_3$ units (circles lying close to the centre of the plot) is not apparent.

Mono-arene derivatives which contain an octahedral metal core may be prepared by a variety of routes. In addition to ionic coupling, these routes include the thermolysis of the arene with $Ru_3(CO)_{12}$ and reaction of $Ru_6C(CO)_{17}$ **47** with 1,3 or 1,4 hexadiene in presence of excess Me_3NO, and these methods of synthesis are summarised in a recent review [59]. Two polymorphs of $Ru_6C(CO)_{14}(\eta^6\text{-}1,4\text{-}C_6H_4Me_2)$ **48** have been synthesised recently by a different route [60].

Scatter plots can be used to show that the carbonyl ligands in the polymorphs of **48** adopt similar arrangements to those in $Ru_6C(CO)_{17}$ **47**, by comparison of Fig. 30 to Fig. 29, in particular the central 4 : 3 : 4 unit is maintained. The variations in the precise positions of the CO ligands in this central girdle of the ligand polyhedron may be attributed to differences in the nature of the arene and orientation of the terminal $M(CO)_3$ unit. These three ligands show no clear orientational preference, as in **47**. This has important consequences for the interpretation of fluxional processes in these molecules since it indicates that the $M(CO)_3$ unit could rotate independently of the other 14 CO ligands; whilst perturbing them to some extent, a complete polytopal rearrangement would not be required.

Scatter plots can also be used to analyse the orien-

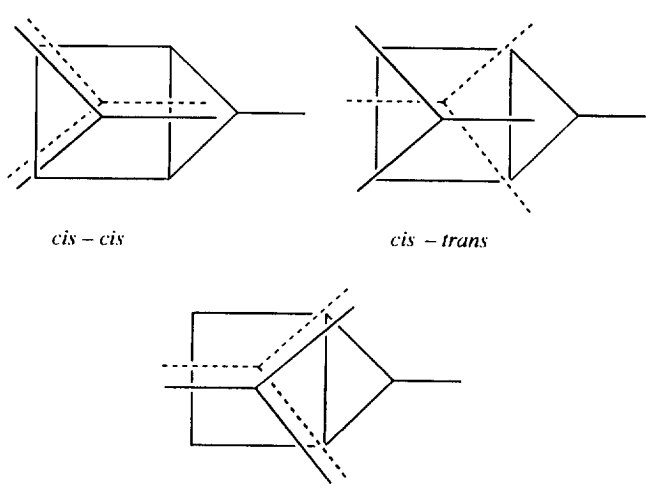

Fig. 27. The possible carbonyl arrangements in polymorphs of **47**.

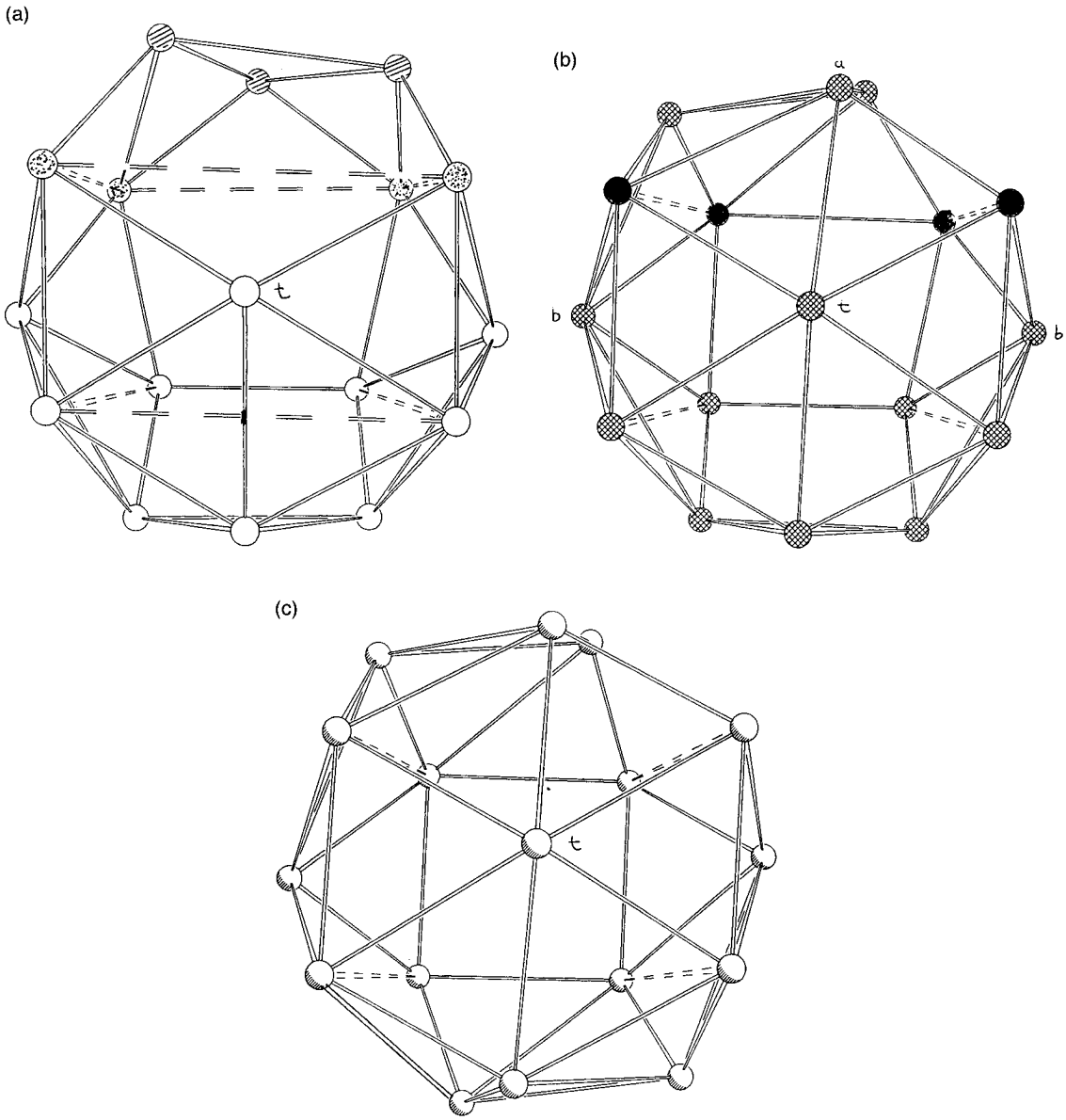

Fig. 28. The ligand polyhedra in the polymorphs of **47**. (a) I, (b) IIb, (c) IIa.

tation of the arene rings with respect to the carbonyl polyhedron. With three substituents in the 1,3,5 positions on the benzene ring in $Ru_6C(CO)_{14}(C_6H_3R_3)$ [$C_6H_3Me_3$ **49** [54,58], $C_6H_3Et_3$ **50** [53]], one substituent lies parallel to the bridging CO ligand (0° position in ϕ) and the other two over the long sides of the trapezoidal face ($\pm 120°$ positions), minimising ligand–ligand interactions (Fig. 30b). Similar orientations are observed with 1,3-xylene (**51**): in one of the crystallographically independent molecules, and in the co-crystal with $[Ru_6C(CO)_{11}(\eta^6\text{-}1,3\text{-}C_6H_4Me_2)_2]$ **61,** one Me group is parallel to the μ-CO ligand, whereas in the other independent molecule, both Me groups are in the $\pm 120°$ positions [52,61]. In $Ru_6C(CO)_{14}(\eta^6\text{-}C_6H_5Me)$ **52** [62] and $Ru_6C(CO)_{14}(\eta^6\text{-}C_6H_5\{(CH_2)_2Ph\})$ **53** [63], the α-carbon lies parallel to the bridging CO (0° position) whilst with η^6-biphenyl the free Ph is in the 120° orientation [63]. With such bulky ligands, intermolecular interactions will be even more important in determining the conformation, given difficulties in ensuring an efficient packing motif.

A quite different orientation is displayed by *para*-substituted arenes, as exemplified by the *p*-xylene polymorphs **49** I and **49** II. The structure of **49** I was determined at room temperature and shows high thermal motion in some of the CO ligands which was modelled as two-fold disorder (Fig. 31, the dotted spheres and the dashed lines showing the second orientation). The carbonyl polyhedron of **49** II, determined at 153 K, is not disordered thermally. Scatter plots show that in both

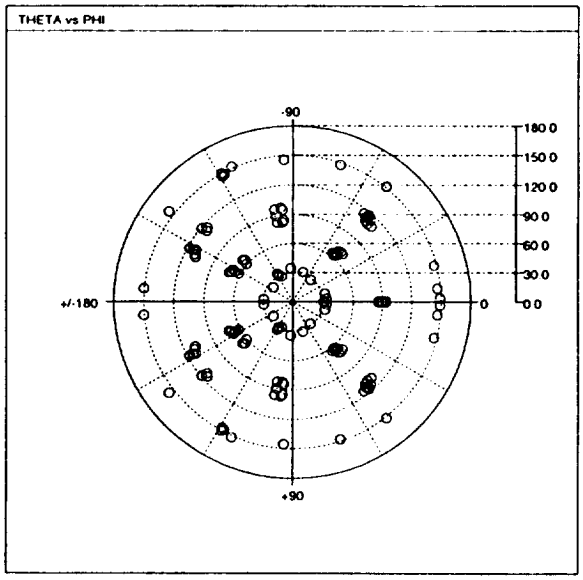

Fig. 29. Polar scatterplot of CO centroid distribution in the polymorphs of **47**.

polymorphs, the Me groups lie parallel to the bridged Ru—Ru edge (90° positions) such that the C_6 ring is rotated by 30° compared to those in **50–54**.

The arene conformation in $Ru_6C(CO)_{14}(\eta^6\text{-}1,4\text{-}C_6H_4Ph_2)$ **54** [64] is similar (although somewhat twisted) and the single CH_2Ph subsistent in $Ru_6C(CO)_{14}\{\eta^6\text{-}C_6H_5(CH_2Ph)\}$ **55** adopts the same position [63]. The benzene ligand in $Ru_6C(CO)_{14}(\eta^6\text{-}C_6H_6)$ **56**, which would not be expected to have a strong orientational preference, has one H aligned approximately parallel to the bridging CO [65]. The preference for substituents to adopt 0°, ±90° and ±120° is a common feature of all these clusters (Fig. 30b), the reluctance of the substituents to lie over the short edge of the trapezium (180° position) being due to the steric crowding with the two CO ligands at these vertices. In these structures, the carbido C atom is displaced from the centroid of the Ru_6 octahedron (mean 0.084(6) Å) towards the arene-bonded vertex to compensate for the greater donor ability of the arene [54,62].

Capping of $[Ru_5C(CO)_{14}]^{2-}$ with one equivalent of the monocation $[RuCp(MeCN)_3]^+[PF_6]^-$ produces the octahedral anion $[Ru_6C(CO)_{14}Cp]^-$ **57** as one product which has been characterised structurally as the $[(Ph_3P)_2N]^+$ salt [30,66]. The structure of this anion is similar to that of the arene complexes and the related cluster $[Ru_6C(CO)_{14}(\eta^5\text{-}C_5H_4PPh_3)]$ **58** [67]. The carbonyl polyhedra of **57** and **58** are similar, showing a similar scatter plot distribution (Fig. 30a), and scatter plots of the Cp rings show that they are tilted in both complexes away from the semi-bridging CO as this ligand occupies the position at θ and ϕ of zero (as defined earlier) (Fig. 32a).

Similarly, coupling of $[Ru_5C(CO)_{14}]^{2-}$ with $[RhCp^*(MeCN)_3]^{2+}$ yields the octahedral cluster $Ru_5RhCp^*(CO)_{14}$ **59** [68,69]. As in the homonuclear mono(arene) structures, the carbido C atom is displaced slightly toward the carbocycle-bound metal atom (by ca 0.01 Å). Although this displacement is not highly significant statistically, it is apparent in two independent determinations of this structure [68,69], and has also been observed in the structure determinations for all the arene-substituted Ru_6C cores [61–64]. The carbonyl ligand arrangement is similar to that in **48–58**; the orientation of the Cp* ligand (Fig. 32b) differs from that of the Cp ligand in complexes **57** and **58** by comparison to the orientation shown in the scatter plot for these complexes (Fig. 32a).

So far, only mono-carbocyclic-substituted octahedral carbonyl clusters have been considered. With di-substituted octahedral clusters isomers are again possible. *Bis*(arene) octahedral clusters exhibited three principal coordination modes: *cis*-η^6,η^6; $\eta^6,\mu_3\text{-}\eta^2:\eta^2:\eta^2$ and *trans*-η^6,η^6 (Fig. 33), but the structural chemistry of these systems has not yet been extensively exploited [59]. On steric grounds, with the arene rings at opposite ends of the cluster, the *trans*-η^6,η^6 coordination mode is the most common. The CO distribution is similar to that in $Ru_6C(CO)_{17}$ **47** in the *trans*-η^6,η^6 only, the central 4 : 3 : 4 layers being maintained (Fig. 34a). In some examples, the central triangle is tilted and the short edges of the trapezia are mutually skewed (Fig. 34b); such an arrangement maintains C_2 symmetry although the mirror planes are lost. This effect can also be seen in the polar scatter plot (Fig. 35a), angle ϕ for the CO ligands at $\phi \approx \pm 150°$ spanning a 30° range.

In the *bis*(mesitylene) cluster $Ru_6C(CO)_{11}(\eta^6\text{-}C_6H_3Me_3)_2$ **60** [70,71], the methyl groups adopt the same configuration as in **49** and are mutually staggered; the CO polyhedron adopts the less twisted form (Fig. 34a). The mixed arene cluster $Ru_6C(CO)_{11}(\eta^6\text{-}1,3\text{-}C_6H_4Me_2)(\eta^6\text{-}C_6H_5Me)$ **61** is similar [72], with an Me

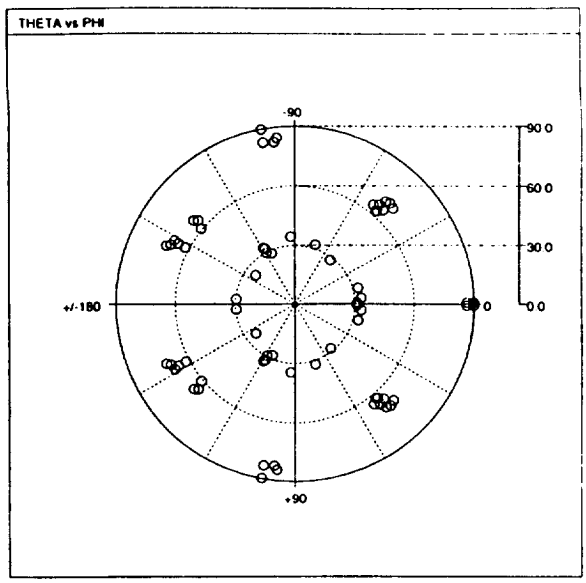

(a)

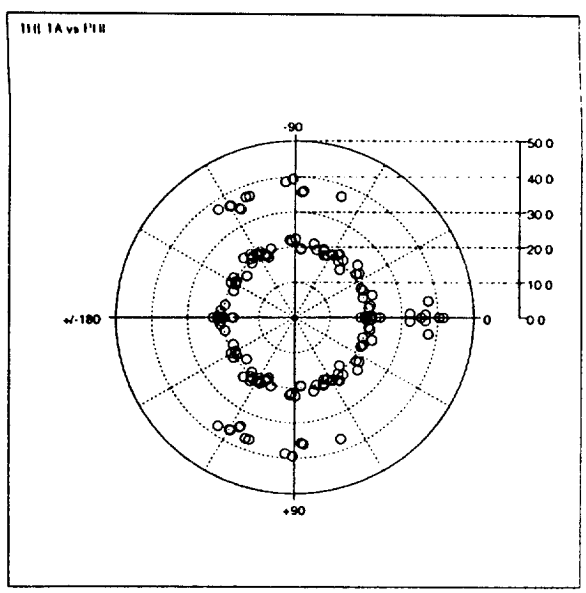

(b)

Fig. 30. Polar scatterplots of (a) CO centroid distribution in molecules of **48**–**58** and (b) arene ligand orientations (C atom positions) in **48**–**56**.

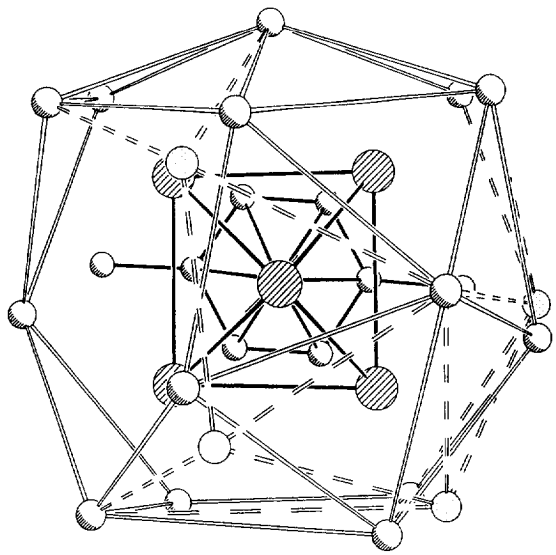

Fig. 31. Interlocking ligand polyhedra showing the disorder in **48**I.

group of each arene lying parallel to μ-CO ligand ($\phi = 0°$ position). Whereas in the co-crystal of $Ru_6C(CO)_{11}(\eta^6\text{-}1,3\text{-}Me_2C_6H_4)_2$ **62** with **51** all methyl groups are mutually staggered, the structure of **62** alone has crystallographic C_2 symmetry and the CO ligands adopt the more twisted arrangement (Fig. 34b) with only the Me groups at 0° being staggered [61]. This serves to decrease the distance between the CO ligands and H atoms of the methyl groups, consistent with some intramolecular attraction.

The *bis*(benzene) complex **63** [73] has the same CO arrangement and precise C_2 symmetry; benzene ligands are twisted slightly from staggered conformation, concomitant with distortion of CO arrangement. It is apparent from Fig. 35b that substituents on the arene adopt the $\phi = 0°$, $\pm 120°$ positions, no examples with *para* substituents having been characterised structurally.

CONCLUSIONS

From the range of structures reviewed above it is apparent that metal clusters, where the metal framework structures can, at least formally, be rationalised in terms of localised bonding schemes (those penta- and hexanuclear clusters based on fused tetrahedral metal core geometries), do exhibit a structural chemistry which retains remnant of localised metal–metal bonding. In cation/anion coupling reactions between tetrahedral cluster anions and mononuclear carbocyclic-coordinated metal cations the resulting pentanuclear clusters offer more than one possible site for the cationic capping group to attach itself to the cluster. In trigonal bipyramidal structures, the carbocyclic ligand-coordinated metal unit occupies the $20e^-$ equatorial site, i.e. the thermodynamic product with the "electron-rich" group in the site of higher metal coordination number, and this product may be thought to be produced by a metal framework rearrangement. Generally, the "electron rich" metal is associated with (semi-)bridging CO or H ligands. The initial kinetic product may be the simple axially-capped derivative in some cases, although these are susceptible to nucleophilic attack to generate edge-bridged structures, in which the metal arene or metal cyclopentadienyl fragment invariably adopts the bridging site. When phosphines are present, such edge-bridged structures may rearrange to spike-tetrahedral clusters in which orthometallation of the arene or cyclopentadienyl ligand has occurred.

By contrast, coupling reactions between tetrahedral cluster anions and $[AuPR_3]^+$ fragments, give products in which the gold-containing fragment just clips on to an edge or a face of the existing metal carbonyl polyhedron, and no metal framework rearrangement necessarily occurs.

Three distinct sites with formal electron counts of 17, 18 and $19e^-$ are available for substitution in bicapped tetrahedral clusters. No clear preferences emerge, since steric and electronic factors are opposed, and several isomers exist for a number of compounds in solution. The presence of the arene has a greater effect on the geometry of the metal core in the (3) $17e^-$ isomers, one bond to this cap being shortened significantly and associated with a semi-bridging carbonyl interaction. Where two arene fragments are present, one adopts a $17e^-$ and the other an $18e^-$ site, presumably for steric reasons. No clusters with an arene or Cp ligand in the $19e^-$ site are known. However, when good electron donor fragments, such as "$Ru(C_6H_3Me_3)$" or "$Rh(C_5Me_5)$" are introduced into the cluster, the core opens

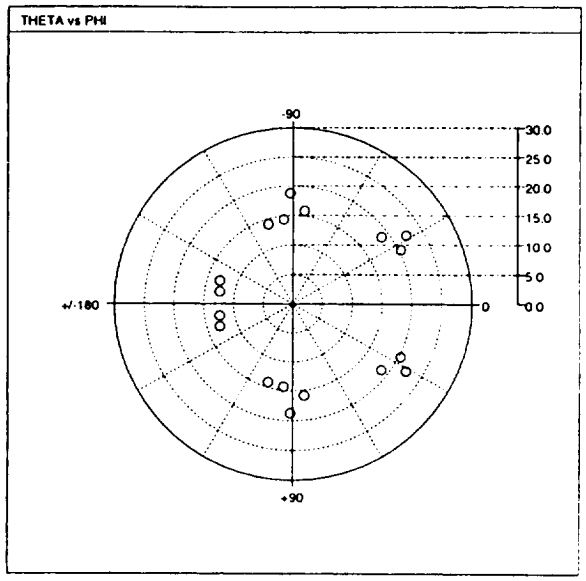

(a)

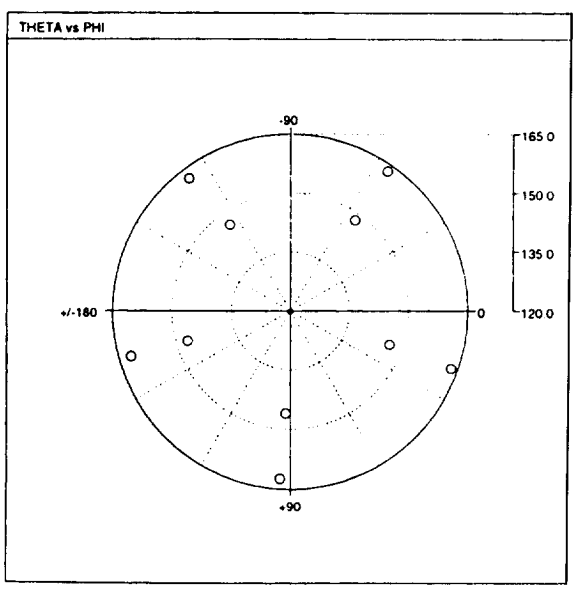

(b)

Fig. 32. Polar scatterplot of Cp ligand orientations in (a) **57**–**58** and (b) **59**.

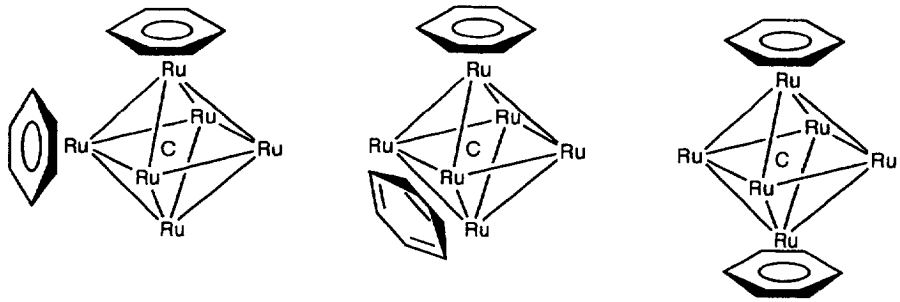

Fig. 33. Coordination modes in *bis*(arene) octahedral clusters.

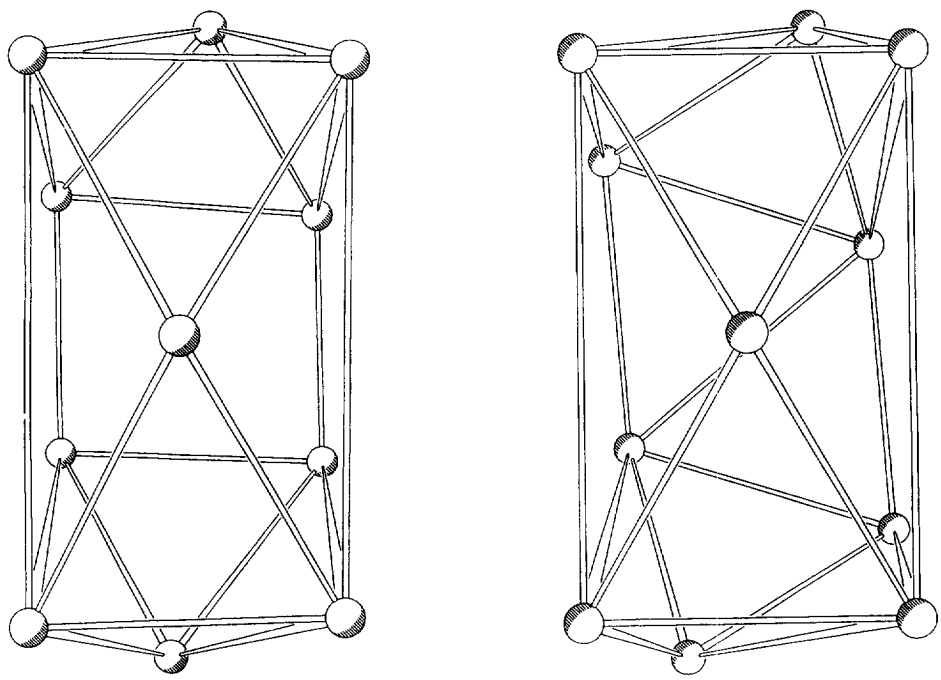

Fig. 34. (a) C_{2v} and (b) C_2 carbonyl ligand arrangements in **60–63**.

out to a *bis* edge-bridged tetrahedral arrangement with two μ_2-η^4-CO ligands, and the "electron rich" metal-carbocyclic ligand fragment occupies the previously $19e^-$ site.

The M_6 octahedral clusters exhibit delocalised metal framework bonding, and coupling reactions between metal–arene and metal–cyclopentadienyl cationic fragments and carbido-stabilised square-base pyramidal cluster anions afford simple octahedral coupled products. The octahedral carbido clusters that have been structurally studied display essentially the same ligand arrangement which is highly flexible. This is reflected in the M—M distances which follow no clear trend. Since, in an octahedron all the metal sites are equivalent, there are no favoured positions for the metal carbocyclic ligand units in the mono-substituted clusters. The orientational preferences of arene ligands with different substituents may be rationalised by analysing the CO ligand polyhedra. One clear electronic effect in these structures is the tendency for the interstitial carbido ligand to be displaced towards the arene-bearing metal vertex and is reminiscent of the behaviour of the alkyne-bridged tetranuclear clusters [74].

Half-normal probability plots for isomorphous structures demonstrate that while errors in light-atom positions are too large to make any comparison of their positions, differences in metal coordinates are significant. However, the significance of M—M bond distances will

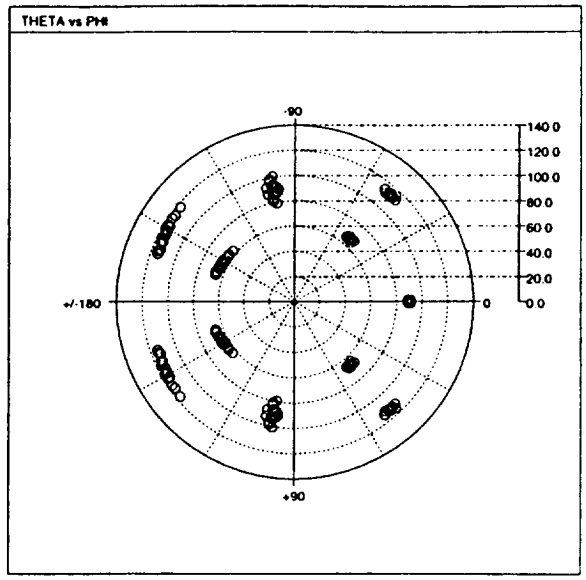

(a)

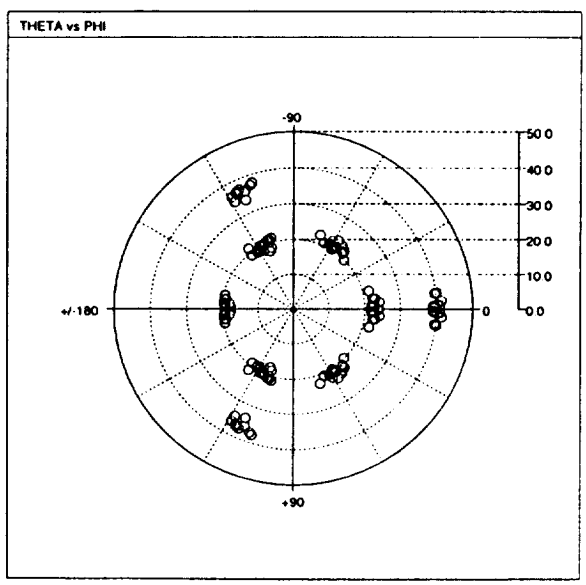

(b)

Fig. 35. Polar scatter plots of (a) CO distribution and (b) arene orientation in **60–63**.

also be dependent on the accuracy and precision of the unit cell parameters, the uncertainties in which may be seriously underestimated in some cases [75]. Furthermore, comparison of differences in chemically-equivalent M—M bond distances, within the same molecule or between independent molecules in the same or different crystal structures using the χ^2 test, indicates that they are significant at the 99% probability level, based on the nominal E.S.D.s. In the solid state, these differences reflect the softness of the M—M parameters and may be attributed to a variety of intra- and intermolecular interactions, and give cause for caution in their interpretation.

METHODOLOGY

Half-normal probability plots

Atomic coordinates and E.S.D.s were obtained from the original refinements where these had been performed in the Department of Chemistry, Uni-

versity of Cambridge. Otherwise, coordinates were downloaded from the CSD and E.S.D.s were entered manually from the original publications (although coordinate E.S.D.s have been stored in the CSD from a certain date, it is not possible to obtain them using the currently available software). The deviations $|\delta_i|$ were calculated by a FORTRAN-77 program written by the author, incorporating an ordering subroutine based on the delayed-exchange shellsort [76] procedure. The expected order statistics were derived using subroutine G01DAF in the NAG FORTRAN library [77]. The actual and expected order statistics, scaled by a factor of 100, were output in the form of a CSD.tab file [78] and imported into the program VISTA [79] for scatter plotting and gradient calculation. In some cases, E.S.D.s were only available to one significant figure; the consequent rounding errors being manifested as undulations on the half-normal plots.

Polar scatter plots for Ru_6C *clusters*

Atomic coordinates were obtained from the original refinements, where these were available, or from the CSD. The Ru_6 octahedra were fitted by a least-squares procedure to an ideal O_h geometry (Fig. 36) with Ru—Ru bond lengths of 2.89 Å (mean length in 2 polymorphs of $Ru_6(CO)_{17}$) using the program XP [80] and mass-weighted centroids of the C—O bonds calculated. The x axis was taken as bisecting the Ru—Ru bond bridged most symmetrically by a CO ligand and the coordinates of the metal and ligand atoms were output as Cartesian coordinates. The deviation of the carbido C atom from the centroid of the ideal octahedron and the spherical polar coordinates of the CO centroids, C atoms in arene/Cp rings and α C atom of any substituents were calculated using a program developed by the author for the purpose and exported in .tab format. The coordinates of the $Ru_6(CO)_{17}$ and $Ru_6(CO)_{11}L_2$ structures were four-fold permuted to take into account their ideal C_{2v} symmetry, whereas the $Ru_6(CO)_{14}L$ structures were two-fold permuted to represent their ideal $C_{s(v)}$ symmetry. Histograms and polar scatter plots were produced using the program VISTA.

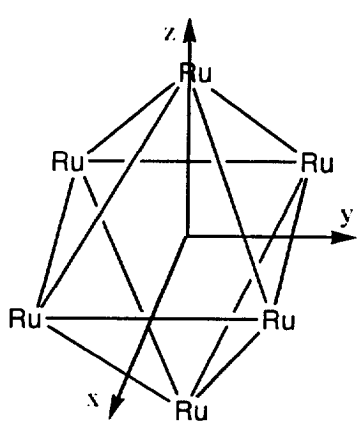

Fig. 36. Reference Ru_6 octahedral geometry showing the orientation of the Cartesian axes.

Acknowledgements—We are grateful to the E.P.S.R.C. for financial support (to G.P.S.) and to the Cambridge Crystallographic Data Centre for both a grant (to G.P.S.) and for assistance with the analysis of the data.

REFERENCES

1. (a) Johnson, B. F. G., ed., *Transition Metal Clusters*. Wiley Interscience, Chichester, 1980; (b) Mingos, D. M. P. and Wales, D. J., *Introduction to Cluster Chemistry*. Prentice-Hall International Editions, New York, 1990; (c) Shriver, D. J., Kaesz, H. D. and Adams, R. D., *The Chemistry of Metal Cluster Complexes*. VCH Publishers Inc., Weinheim, 1990; (d) Lewis, J. and Raithby, P. R., *J. Organomet. Chem.*, 1995, **500,** 227.
2. Johnson, B. F. G. and Lewis, J., *Adv. Inorg. Chem. Radiochem.*, 1981, **24,** 225.
3. Beswick, M. A., Lewis, J., Raithby, P. R. and Ramirez de Arellano, M. C., *Angew. Chem., Int. Ed. Engl.*, 1997, **36,** 291.
4. Johnson, B. F. G., Lewis, J., Housecroft, C. E., Gallop, M. A., Martinelli, M., Braga, D. and Grepioni, F., *J. Mol. Catal.*, 1992, **74,** 61.
5. Mason, R. and Robinson, W. R., *J. Chem. Soc., Chem. Commun.*, 1968, 468.
6. Goméz-Sal, M. P., Johnson, B. F. G., Lewis, J., Raithby, P. R. and Wright, A. H., *J. Chem. Soc., Chem. Commun.*, 1985, 1682.
7. (a) Wadepohl, H., *Angew. Chem., Int. Ed. Engl.*, 1992, **31,** 247; (b) Johnson, B. F. G., *J. Organomet. Chem.*, 1994, **475,** 31.
8. (a) Lewis, J., Li, C.-K., Raithby, P. R. and Wong, W.-T., *J. Chem. Soc., Dalton Trans.*, 1993, 999; (b) Lewis, J., Morewood, C. A., Raithby, P. R. and Ramirez de Arellano, M. C., *J. Chem. Soc., Dalton Trans.*, 1996, 4509.
9. Adams, C. J., Bruce, M. I., Skelton, B. W. and White, A. H., *J. Cluster Sci.*, 1994, **3,** 419.
10. (a) Blake, A. J., Dyson, P. J., Johnson, B. F. G., Martin, C. M., Nairn, J. G. M., Parisini, E. and Lewis, J., *J. Chem. Soc., Dalton Trans.*, 1993, 981; (b) Edwards, A. J., Gallop, M. A., Johnson, B. F. G., Köhler, J. U., Lewis, J. and Raithby, P. R., *Angew. Chem., Int. Ed. Engl.*, 1994, **33,** 1093.
11. (a) Wade, K., *Transition Metal Clusters*, ed. B. F. G. Johnson. Wiley Interscience, Chichester, 1980; (b) Owen, S. M., *Polyhedron*, 1988, **7,** 253.
12. (a) Wade, K., *Adv. Inorg. Chem. Radiochem.*, 1976, **18,** 1; (b) Mingos, D. M. P., *Nature Phys. Sci. (London)*, 1972, **236,** 99.
13. Benfield, R. E. and Johnson, B. F. G., *Transition Met. Chem.*, 1981, **6,** 131.
14. (a) Braga, D. and Grepioni, F., *Organometallics*, 1991, **10,** 2563; (b) Braga, D., Dyson, P. J., Grepioni, F., Johnson, B. F. G. and Calhorda, M., J., *Inorg. Chem.*, 1994, **33,** 3218; (c) Braga, D., Grepioni, F., Johnson, B. F. G., Chen, H. and

Lewis, J., *J. Chem. Soc., Dalton Trans.*, 1991, 2559; (d) Braga, D., Grepioni, F., Martin, C. M., Parisini, E., Dyson, P. J. and Johnson, B. F. G., *Organometallics*, 1994, **13,** 2170.
15. (a) Braga, D. and Grepioni, F., *J. Chem. Soc., Dalton Trans.*, 1993, 1223; (b) Braga, D., Grepioni, F., Sabatino, P. and Desiraju, G. R., *Organometallics*, 1994, **13,** 3532; (c) Braga, D., Grepioni, F., Byrne, J. J. and Calhorda, M. J., *J. Chem. Soc., Dalton Trans.*, 1995, 3287.
16. Eady, C. R., Johnson, B. F. G. and Lewis, J., *J. Organomet. Chem.*, 1972, **37,** C39.
17. Eady, C. R., Johnson, B. F. G. and Lewis, J., *J. Chem. Soc., Dalton Trans.*, 1975, 2606.
18. Reichert, B. E. and Sheldrick, G. M., *Acta Cryst.*, 1977, **B33,** 173.
19. Mingos, D. M. P. and Evans, D. G., *Organometallics* 1983, **2,** 435.
20. (a) Johnson, B. F. G. and Benfield, R. E., *J. Chem. Soc., Dalton Trans.*, 1978, 1554; (b) *ibid.*, 1980, 1743.
21. Buntem, R., Ph.D. Thesis, University of Cambridge, 1995.
22. Buntem, R., Lewis, J., Raithby, P. R. and Ramirez de Arellano, M. C., manuscript in preparation.
23. Eady, C. R., Guy, J. J., Johnson, B. F. G., Lewis, J., Malatesta, M. C. and Sheldrick, G. M., *J. Chem. Soc., Chem. Comm.*, 1976, 807.
24. Guy, J. J. and Sheldrick, G. M., *Acta Cryst.*, 1978, **B34,** 1722.
25. Al-Mandhary, M. R. A., Ph.D. Thesis, University of Cambridge, 1994.
26. Johnson, B. F. G., Martin, C. M., Blake, A. J., Reed, D., Braga, D. and Grepioni, F., *J. Chem. Soc., Dalton Trans.*, 1996, 2165.
27. Johnson, B. F. G., Khattar, R., Lewis, J. and Raithby, P. R., *J. Chem. Soc., Dalton Trans.*, 1989, 1421.
28. Lewis, J., Li, C.-K., Ramirez de Arellano, M. C., Raithby, P. R. and Wong, W. T., *J. Chem. Soc., Dalton Trans.*, 1993, 1359.
29. Braga, D., Grepioni, F., Calhorda, M. J. and Veiros, L. F., *Organometallics*, 1995, **14,** 1992.
30. Morewood, C. A., Ph.D. Thesis, University of Cambridge, 1996.
31. Morewood, C. A., Lewis, J., Raithby, P. R. and Ramirez de Arellano, M. C., manuscript in preparation.
32. Guy, J. J. and Sheldrick, G. M., *Acta Cryst.*, 1978, **B34,** 1725.
33. Leong, W.-K., Einstein, F. B. W. and Pomeroy, R. K., *Acta Cryst.*, 1996, **C52,** 1607.
34. John, G. R., Johnson, B. F. G., Lewis, J., Nelson, W. J. H. and McPartlin, M., *J. Organomet. Chem.*, 1979, **171,** C14.
35. Clegg, W., Nahar, S. and Raithby, P. R., unpublished work.
36. Colombie, A., McCarthy, D. A., Krause, J., Leh-Yeh Hsu, Wen-Liang Hsu, Deng-Yang Jan and S. G. Shore, *J. Organomet. Chem.*, **383,** 421.
37. Al-Mandhary, M. R. A., Lewis, J. and Raithby, P. R., *J. Organomet. Chem.*, 1997, **530,** 247.
38. Mason, R., Thomas, K. M. and Mingos, D. M. P., *J. Am. Chem. Soc.*, 1973, **95,** 3802.
39. Blake, A. J., Johnson, B. F. G. and Nairn, J. G. M., *Acta Cryst.*, 1994, **C50,** 1052.
40. McCarthy, D. A., Krause, J. A. and Shore, S. G., *J. Am. Chem. Soc.*, 1990, **112,** 8587.
41. Henderson, R. K., Jackson, P. A., Johnson, B. F. G., Lewis, J. and Raithby, P. R., *Inorg. Chim. Acta*, 1992, **198–200,** 393.
42. Lewis, J., Li, C.-K., Morewood, C. A., Ramirez de Arellano, M. C., Raithby, P. R. and Wong, W.-T., *J. Chem. Soc., Dalton Trans.*, 1994, 2159.
43. Ward, G. N., Ph.D. Thesis, University of Cambridge, 1995.
44. Jackson, P. A., Ph.D. Thesis, University of Cambridge, 1989.
45. Davies, J. E., Nahar, S., Raithby, P. R. and Shields, G. P., *J. Chem. Soc., Dalton Trans.*, 1997, 13.
46. Lewis, J., Morewood, C. A., Raithby, P. R. and Ramirez de Arellano, M. C., *J. Chem. Soc., Dalton Trans.*, 1996, 4509.
47. Lewis, J., Li, C.-K., Al-Mandhary, M. R. A. and Raithby, P. R., *J. Chem. Soc., Dalton Trans.*, 1993, 1915.
48. Abrahams, S. C. and Keve, E. T., *Acta Crystallogr., Sect. A*, 1971, **27,** 157.
49. Anson, C. E., Bailey, P. J., Conole, G., Johnson, B. F. G., Lewis, J., McPartlin, M. and Powell, H. R., *J. Chem. Soc., Chem. Commun.*, 1989, 442.
50. Bailey, P. J., Duer, M. J., Johnson, B. F. G., Lewis, J., Conole, G., McPartlin, M., Powell, H. R. and Anson, C. E., *J. Organomet. Chem.*, 1990, **383,** 441.
51. Blake, A. J., Dyson, P. J., Ingham, S. L., Johnson, B. F. G. and Martin, C. M., *Inorg. Chim. Acta*, 1995, **240,** 29.
52. Ingham, S. L., Johnson, B. F. G., Martin, C. M. and Parker, D., *J. Chem. Soc., Chem. Comm.*, 1995, 159.
53. Braga, D., Grepioni, F., Parisini, E., Dyson, P. J., Blake, A. J. and Johnson, B. F. G., *J. Chem. Soc., Dalton Trans.*, 1993, 2951.
54. Braga, D., Grepioni, F., Johnson, B. F. G., Chen, H. and Lewis, J., *J. Chem. Soc., Dalton Trans.*, 1991, 2559.
55. Braga, D., Grepioni, F., Dyson, P. J., Johnson, B. F. G., Frediani, P., Bianchi, M. and Piacenti, F., *J. Chem. Soc., Dalton Trans.*, 1992, 2565.
56. Braga, D. and Grepioni, F., *Acta Cryst.*, 1989, **B45,** 378.
57. Albano, V. G. and Braga, D., *Accurate Molecular Structures*, ed. A. Domenicano and I. Harghittay. Oxford University Press, 1991.
58. Sirigu, A., Bianchi, M. and Benedetti, E., *J. Chim. Soc., Chem. Comm.*, 1969, 596.
59. Braga, D., Dyson, P. J., Grepioni, F. and Johnson, B. F. G., *Chem. Rev.*, 1994, **94,** 1585.
60. Wadepohl, H., Pritzkow, H., Bochert, T. and Lewis, J., submitted for publication.
61. Braga, D., Grepioni, F., Martin, C. M., Parisini, E., Dyson, P. J. and Johnson, B. F. G., *Organometallics*, 1994, **13,** 2170.
62. Farrugia, L. J., *Acta Cryst.*, 1988, **C44,** 997.
63. Blake, A. J., Johnson, B. F. G., Reed, D. and Shepherd, D. S., *J. Chem. Soc., Dalton Trans.*, 1995, 843.
64. Borchert, T., Lewis, J., Pritzkow, H., Raithby, P. R. and Wadepohl, H., *J. Chem. Soc., Dalton Trans.*, 1995, 1061.

65. Dyson, P. J., Johnson, B. F. G., Lewis, J., Martinelli, M., Braga, D. and Grepioni, F., *J. Am. Chem. Soc.*, 1993, **115,** 9062.
66. Lewis, J., Morewood, C. A., Raithby, P. R. and Ramirez de Arellano, M. C., *J. Chem. Soc., Dalton Trans.*, in press.
67. Blake, A. J., Johnson, B. F. G., Parsons, S. and Shephard, D. S., *J. Chem. Soc., Dalton Trans.*, 1995, 495.
68. Bailey, P. J., Blake, A. J., Dyson, P. J., Johnson, B. F. G., Lewis, J. and Parisini, E., *J. Organomet. Chem.*, 1993, **454,** 175.
69. Adatia, T., McPartlin, M., Morris, J., Curtis, H. and Lewis, J., *Acta Cryst.*, 1994, **C50,** 1233–1235.
70. Braga, D., Grepioni, F., Righi, S., Johnson, B. F. G., Bailey, P. J., Dyson, P. J., Lewis, J. and Martinelli, M., *J. Chem. Soc., Dalton Trans.*, 1992, 2121.
71. Braga, D., Grepioni, F., Righi, S., Dyson, P. J., Johnson, B. F. G., Bailey, P. J. and Lewis, J., *Organometallics*, 1992, **11,** 4042.
72. Dyson, P. J., Johnson, B. F. G., Braga, D., Grepioni, F., Martin, C. M. and Parisini, E., *Inorg. Chem. Acta*, 1995, **235,** 413.
73. Adams, R. D. and Wengan Wu, *Polyhedron*, 1992, **11,** 2123.
74. Raithby, P. R. and Rosales, M. J., *Adv. Inorg. Chem. Radiochem.* 1985, **29,** 169.
75. Martín, A. and Orpen, A. G., *J. Am. Chem. Soc.*, 1996, **118,** 1464.
76. Main, P., personal communication, University of York, 1985.
77. NAG FORTRAN Library Mark 16, NAG Limited, Oxford, U.K., 1994.
78. Cambridge Crystallographic Data Centre, *CSDS User Manuals*, Vol. 3, 1992.
79. Cambridge Crystallographic Data Centre, *CSDS User Guide—VISTA Version* 2.0, 1995.
80. XP Molecular Graphics Program, Siemens Analytical X-Ray Instruments Inc., Madison, WI, 1990.

Pergamon

PII: S0277-5387(98)00016-3

Polyhedron Vol. 17, No. 17, pp. 2857–2863, 1998
© 1998 Elsevier Science Ltd
All rights reserved. Printed in Great Britain
0277–5387/98 $19.00+0.00

H-motion in $H_4Ru_4(CO)_{12-x}L_x$ ($x = 0, 1$; $L = P(OMe)_3$) from solid state NMR studies†

R. A. Harding,[a] H. Nakayama,[a]‡ T. Eguchi,[a] N. Nakamura,[a]‡ B. T. Heaton[b]* and A. K. Smith[b]§

[a] Department of Chemistry, Graduate School of Science, Osaka University, Toyonaka, Osaka 560, Japan

[b] Department of Chemistry, University of Liverpool, Liverpool, L69 7ZD U.K.

(Received 8 October 1997; accepted 17 December 1997)

Abstract—Variable temperature, MAS and wide-line solid state NMR measurements have been carried out on $H_4Ru_4(CO)_{12}$ and $H_4Ru_4(CO)_{11}\{P(OMe)_3\}$. The variation of spin-lattice relaxation time (T_1) and linewidth at half intensity ($\Delta\nu_{1/2}$) of the hydride resonance with temperature for both samples are very similar and suggests that a common hydride movement occurs with $E_a = 17 \pm 2$ kJ mol^{-1}. We attribute this movement to a 2-site H-flip about H-occupied Ru—Ru edges which preserves the site symmetry of the crystals. © 1998 Elsevier Science Ltd. All rights reserved

Keywords: cluster carbonyls; solid state NMR; hydride; ruthenium.

There is now a large number of transition metal carbonyl clusters containing hydride ligands but the *exact* H-location in the solid state is difficult without the benefit of a neutron diffraction structure [1]. It is sometimes possible in solution to obtain the limiting low temperature spectrum which can distinguish between terminal, edge-, face-bridging, pseudo-interstitial and interstitial site occupancy when the metal has a spin (e.g. ^{103}Rh [2–4]) or through other two bond spin-spin coupling data as exemplified by $H_4Ru_4(CO)_{11}\{P(OMe)_3\}$, *vide infra* [5]. In solution, H is notoriously labile and variable temperature NMR measurements show that it can undergo a variety of fluxional processes including migration within the metallic skeleton [4] and migration over the periphery of the metallic skeleton [2,5]. Comparative H-migrational studies between the behaviour found in the solid state and in solution are much less numerous. However, initial comparative studies on $H_2Ru_2Rh_2(CO)_{12}$ [6], $[H_xRh_{13}(CO)_{24}]^{(5-x)-}$ ($x = 2, 3$) [6] and $H_4Ru_4(CO)_{12}$ [7] in all cases suggest that there is much more restricted H-movement in the solid compared to the solution state. Following our recent work on $H_2Ru_2Rh_2(CO)_{12}$ [6], and in order to gain further insight into H-migration in tetranuclear carbonyl clusters in the solid state, we now report solid state NMR measurements on $H_4Ru_4(CO)_{12-x}L_x$ ($x = 0$, 1; $L = P(OMe)_3$) which give an activation energy for H-motion in $H_4Ru_4(CO)_{12}$ that is significantly different to the previously reported value [7].

The structures of $H_4M_4(CO)_{12-x}L_x$ (M = Ru, Os; $x = 0$–4; L = PR_3 or $P(OR)_3$) have been reviewed [8]. For this series of compounds, neutron diffraction data is only available on $H_4Os_4(CO)_{11}\{P(OMe)_3\}$ [9] and $H_4Ru_4(CO)_8\{P(OMe)_3\}_4$ [10]. In both cases the hydrides occupy the four long edges of the M_4-tetrahedron and HYDEX [11] has been used to indirectly locate the hydrides from X-ray diffraction studies of related clusters. In this family of derivatives, all adopt a pseudo-D_{2d} H_4M_4-core (see Fig. 1) and progressive carbonyl substitution by other ligands occurs on different metals *trans* to the non-H-bridged metal–metal vector and *transoid* to each other in a step-wise

† This paper is dedicated to Professor Lord Lewis FRS for his outstanding contributions to inorganic chemistry and particularly his contributions to furthering the greater understanding of metal carbonyl clusters.

* Author to whom correspondence should be addressed.

‡ Present address: Kobe Pharmaceutical University, Japan.

§ Present address: CPE, Lyon, France.

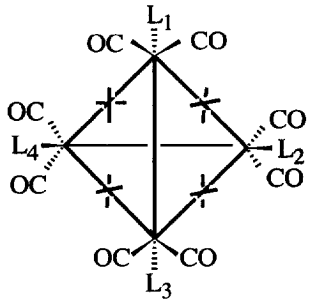

$L_1 = L_2 = L_3 = L_4 = CO$

$L_1 = P(OMe)_3$; $L_2 = L_3 = L_4 = CO$

$L_1 = L_2 = P(OMe)_3$; $L_3 = L_4 = CO$

$L_1 = L_2 = L_3 = P(OMe)_3$; $L_4 = CO$

$L_1 = L_2 = L_3 = L_4 = P(OMe)_3$

Fig. 1. Substitution pattern in $H_4Ru_4(CO)_{12}$ by P-donor ligands (L). $\times = \mu$-H.

manner. In all these cases, the carbonyls are approximately ccp and each of the CO's in the $M(CO)_3$ unit is oriented over a M_3-face (see Fig. 2).

Solution NMR studies show that there is rapid intramolecular hydrogen-exchange for the substituted derivatives $H_4Ru_4(CO)_{12-x}\{P(OMe)_3\}_x$ ($x = 1, 2, 3, 4$) [5]. Thus, at room temperature, there is only one hydride chemical shift with a time-averaged coupling to phosphorus; on cooling to 149 K, the monosubstituted cluster has two equally intense hydride resonances at -17.55 ppm (singlet) and -18.10 ppm (doublet) (^2J(P—H) 12.5 Hz) which is entirely consistent with the solid state neutron diffraction structure of the analogous cluster, $H_4Os_4(CO)_{11}\{P(OMe)_3\}$ [9]. The activation energy for the H-exchange over the Ru_4-tetrahedron in $H_4Ru_4(CO)_{11}\{P(OMe)_3\}$ in solution is 14.2 kJ mol^{-1} and involves concerted H-movement from occupied to unoccupied Ru—Ru edges [13]. Solution measurements on $H_4Ru_4(CO)_{12}$ show that there is just one ^{13}C resonance (198.0 ppm) and one ^1H resonance (-17.98 ppm) down to 153 K and recently variable temperature ^{13}C-$\{^1H\}$ CP/MAS, ^1H MAS and ^1H wide-line NMR spectra of $H_4Ru_4(CO)_{12}$ have been reported [7]. These data were used to obtain an activation energy (67.2 ± 8 kJ mol^{-1}) for a motional process which does not involve the carbonyl ligands and was attributed to a dynamic process involving either the H_4Ru_4-core as a whole about the approximate C_2 axis which incorporates the midpoints of the non H-bridged Ru—Ru edges or a concerted motion of the hydrides over the surface of the Ru_4-tetrahedron between the four equivalent positions. From their T_1 data, Aime *et al.* [7] report the value of E_a of 59.2 kJ mol^{-1} but our calculations using their data shows that the value of E_a should be 32.3 kJ mol^{-1}. In order to resolve this discrepancy, we have repeated the solid state NMR measurements on $H_4Ru_4(CO)_{12}$. In addition, we now also report analogous measurements on $H_4Ru_4(CO)_{11}\{P(OMe)_3\}$.

RESULTS AND DISCUSSION

Variable temperature solid state ^1H NMR measurements have been carried out on $H_4Ru_4(CO)_{12-x}L_x$ ($x = 0, 1$; L = $P(OMe)_3$) together with ^{13}C CP/MAS measurements on the unsubstituted derivative. Room temperature ^{31}P-$\{^1H\}$ MAS measurements on H_4Ru_4

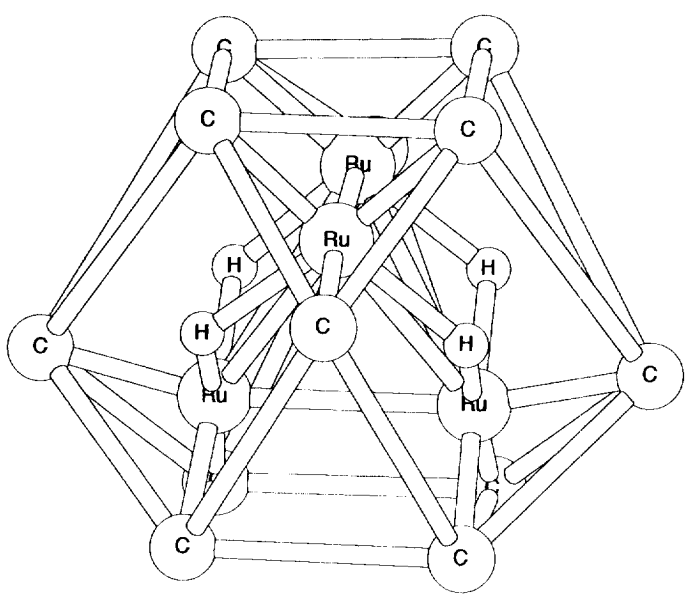

Fig. 2. Schematic representation of the H_4Ru_4-group within the CO-polyhedron of $H_4Ru_4(CO)_{12}$.

$(CO)_{11}\{P(OMe)_3\}$ have also been carried out and the spectrum consists of a single ^{31}P resonance at $\delta_{iso} = 145.7$ ppm with spinning sidebands. The observed spectrum can be simulated by using the parameters of $\delta_{11} = 256$, $\delta_{22} = 205$, and $\delta_{33} = -24$ ppm, and is entirely consistent with the presence of a single isomer (see Fig. 1) analogous to $H_4Os_4(CO)_{11}\{P(OMe)_3\}$ characterized by neutron diffraction [9]. Our room temperature ^{13}C CP/MAS NMR measurements on $H_4Ru_4(CO)_{12}$ are entirely in agreement with those reported previously [7] but our T_1 and wide-line ^1H NMR measurements on $H_4Ru_4(CO)_{12}$ differ significantly from those reported previously [7]. In addition, we now also report new ^1H NMR measurements on $H_4Ru_4(CO)_{11}\{P(OMe)_3\}$.

Variable temperature ^1H MAS spectra of $H_4Ru_4(CO)_{12}$ are shown in Fig. 3. The peaks between 0–5 ppm are due to residual solvent (octane and dichloromethane) and the centre of the hydride resonance appears at ca -18 ppm. It is to be noted that the relative ratio of solvent : hydride is much lower in our spectra than found previously [7] thus allowing us to obtain better data from wide-line measurements, *vide infra*. In agreement with earlier ^1H MAS measurements [7], there is only one hydride resonance. The observed sharpening of this peak above room temperature corresponds to the line-narrowing of the wide-line spectra as shown in Fig. 3 (at 200 MHz : 290 to ca 350 K; at 270 MHz [7]: 310 to ca 360 K). Crystallographically [12], because of the slight distortion of the Ru_4-core from T_d symmetry, we could expect up to four hydride resonances in the solid state but, in wide-line NMR measurements these resonances will be severely broadened due to dipole-dipole interactions. Thus, the lack of variation in $\Delta\nu_{1/2}$ of the hydride resonance at low temperature is consistent with the rigid-lattice structure but at higher temperatures some H-movement must occur in the solid state and, in order to obtain the activation energy (E_a) for this motion without MAS effects, we have measured wide-line ^1H NMR spectra (Fig. 4). Below 280 K, we can recognize the typical powder pattern (so-called "Pake doublets"), in which the peak separation is approximately given by [14,15]

$$\Delta\nu_{p-p} \approx \frac{3}{4\pi}\gamma^2 h d^{-3}. \quad (1)$$

Using eqn (1) and d(H—H) = 2.8 Å (obtained using HYDEX [11]) we obtain $\Delta\nu_{p-p} = 16.4$ kHz compared

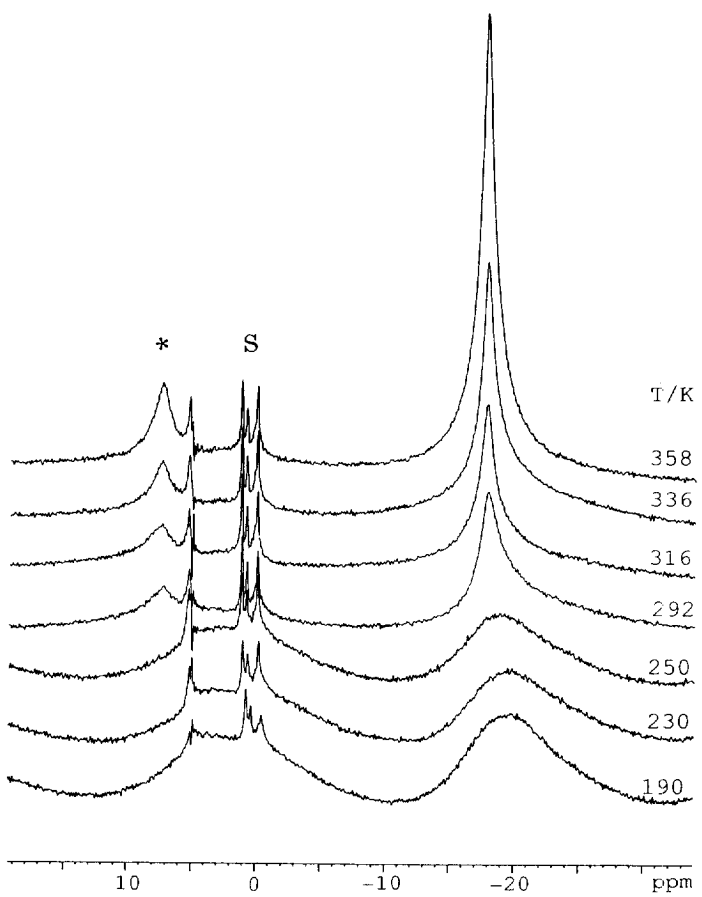

Fig. 3. Variable-temperature ^1H MAS NMR of $H_4Ru_4(CO)_{12}$ at a spinning rate of 5 kHz. * : sideband, S : solvent.

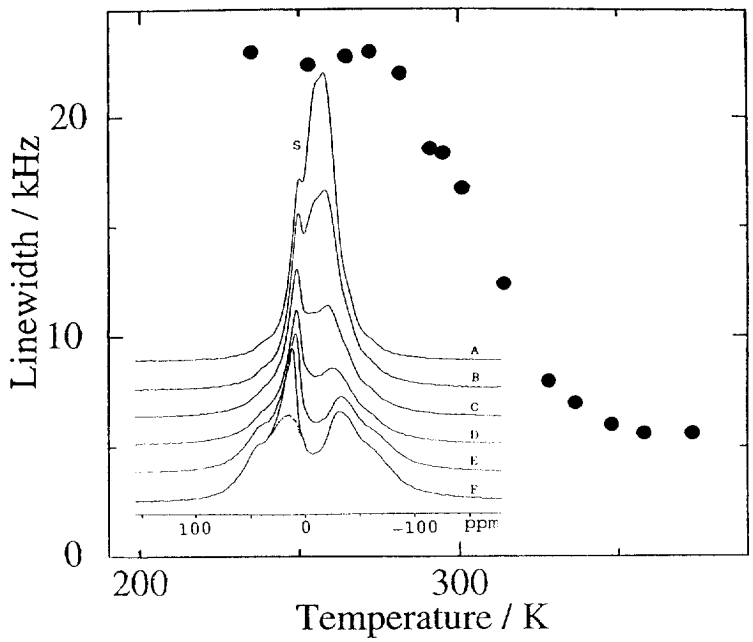

Fig. 4. Temperature dependence of the linewidth ($\Delta\nu_{1/2}$) of wide-line ^{1}H NMR spectra for $H_4Ru_4(CO)_{12}$. The spectra in the insert were measured at (A) 336, (B) 328, (C) 314, (D) 301, (E) 280, (F) 230 K, respectively. S: solvent.

with the peak-to-peak width, 14.5 ± 1.5 kHz, in the observed spectrum at 230 K (Fig. 4). It is, therefore, obvious that below 280 K $\Delta\nu_{1/2}$ assumes the rigid lattice value (23 kHz) which is much larger than the one (12 kHz) reported by Aime *et al.* [7]. Above 280 K, a distinct narrowing of the resonance was observed. The variation in $\Delta\nu_{1/2}$ of the hydride resonance with temperature allows us to calculate an activation energy of $E_a = 18.5 \pm 2$ kJ mol^{-1} which is much smaller than previously reported (75.1 kJ mol^{-1}) [7].

Figure 5 shows the temperature variation in the spin-lattice relaxation time (T_1) at 200 MHz for solid $H_4Ru_4(CO)_{12-x}L_x$ ($x = 0, 1$; L = $P(OMe)_3$) together with the data from previous measurements at 270 MHz on $H_4Ru_4(CO)_{12}$ [7]. These data and the variation in $\Delta\nu_{1/2}$ with temperature as described above indicate that the correlation time τ_c of the hydride motion in all these samples must be in the slow-motion region where $\omega_0\tau_c \gg 1$. It is interesting to compare our T_1 values for $H_4Ru_4(CO)_{12}$ with those reported in Ref. 7: as the dipolar T_1 is proportional to ω_0^2 in the slow-motion region, the T_1 values measured at 270 MHz must be longer than those measured at 200 MHz if there is no specific relaxation mechanism at high frequency. However, inspection of Fig. 5 shows that this is obviously not the case. It is possible that this results from an averaging of the intrinsic hydride relaxation with the very short relaxation of a large amount of solvent protons present in Aime *et al.*'s sample [7]; this would result in a shorter T_1 reported in Ref. 7 compared to the T_1 observed in the present study.

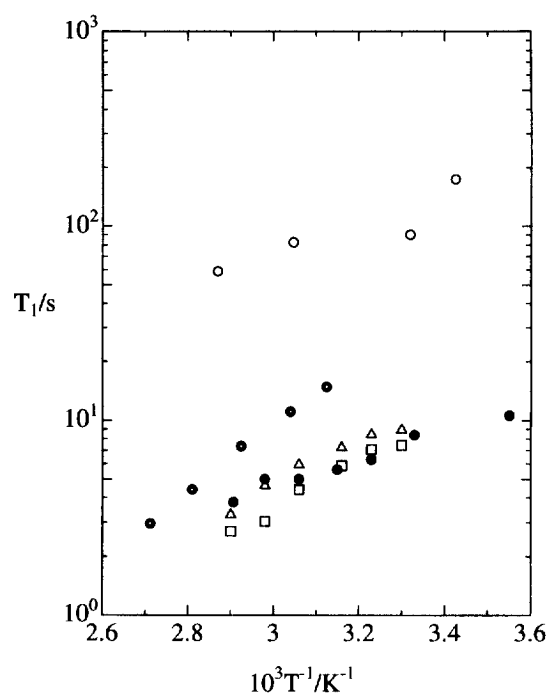

Fig. 5. Temperature dependence of the ^{1}H spin-lattice relaxation time (T_1) for: ○ $H_4Ru_4(CO)_{12}$ (from wide-line measurements); ◎ $H_4Ru_4(CO)_{12}$ (from wide-line measurements) [7]; ● $H_4Ru_4(CO)_{11}\{P(OMe)_3\}$ (from hydride resonance); □ $H_4Ru_4(CO)_{11}\{P(OMe)_3\}$ (from CH_3 resonance); △ $H_4Ru_4(CO)_{11}\{P(OMe)_3\}$ (from wide-line measurements).

We calculate E_a to be 16.1 ± 0.5 kJ mol^{-1} using our static T_1 data for $H_4Ru_4(CO)_{12}$ as shown in Fig. 5; this is in close agreement with the value calculated from the variation in $\Delta\nu_{1/2}$ with temperature, *vide supra* but significantly different from that reported by Aime *et al.* [7] ($E_a = 59.2$ kJ mol^{-1}); our recalculation, using their data, shows that their value of E_a should be 32.3 kJ mol^{-1} which is still much larger than the E_a value obtained from our measurements (see Table 1).

We have also measured the temperature dependence of the wide-line ^{1}H NMR spectra for the monosubstituted derivative [see Fig. 6(a)]. In this case, although $\Delta\nu_{1/2}$ of the hydride resonance was expected to change with temperature, it was not possible to obtain quantitative linewidth variations at half height for the hydride resonance because of the close proximity of the intense resonance from the phosphite ligand and residual solvent. However, comparison of the lineshape at 145 K with that at 344 K shows that there is some evidence for motional narrowing.

Figure 6(b) shows the variable temperature ^{1}H MAS spectra of $H_4Ru_4(CO)_{11}\{P(OMe)_3\}$ which consists of a broad and intense resonance due to the methyl groups at ca 3 ppm together with a high field resonance at -18 ppm due to the hydrides. In contrast to the solution NMR spectrum at low temperature [13], the hydride resonance consists of a single broad line due to the dipolar couplings of the four inequivalent hydrides (chemical shift difference is probably less than 0.6 ppm) in the solid state. Analysis of the lineshape reveals that there is a slight variation in the hydride resonance from 180 to 355 K when compared with the unsubstituted cluster (see Fig. 3). In other words, motional narrowing in the monosubstituted cluster occurs at a higher temperature than that observed for the unsubstituted cluster.

The T_1 values for both the hydride and methyl resonances, obtained with MAS, show a similar temperature dependence between 300 and 345 K (see Fig. 5). The hydride T_1 in $H_4Ru_4(CO)_{11}\{P(OMe)_3\}$ is shorter than in $H_4Ru_4(CO)_{12}$ as a result of the dipolar coupling between the hydrides and methyl protons, but the temperature dependence of the hydride T_1 gives a similar value of E_a (15.8 ± 0.5 kJ mol^{-1}) to those we obtained for $H_4Ru_4(CO)_{12}$ over the same temperature range. Usually at room temperature the correlation time of the CH_3-reorientation with such an activation energy is considered to be in the fast-motion region where $\omega_0\tau_c \ll 1$ [16.17]. Thus, it is probable that the same type of hydride motion with similar values of E_a (17 ± 2 kJ mol^{-1}) takes place in both unsubstituted and monosubstituted clusters, although the correlation times for this motion are different for both compounds.

Previous work on $H_2Ru_2Rh_2(CO)_{12}$ shows that the lowest activation energy H-movement in solution involves the Ru—H—Rh hydrogen moving to the unoccupied Ru—Rh vector [18]. In order for this to occur, the hydrogen on the Ru—Rh vector must initially flip about this edge so that it changes from being coplanar with the Ru—Rh_2-face to become coplanar with the Ru_2Rh-face (see Fig. 7 in Ref. 6), before traversing the $RuRh_2$-face to the previously unoccupied Ru—Rh edge. Solid state NMR studies on $H_2Ru_2Rh_2(CO)_{12}$ show that the H-movement is much more restricted than in solution [6]. In order to account for the low value of E_a (ca 1 kJ mol^{-1}) *and* the T_1 value for $H_2Ru_2Rh_2(CO)_{12}$ in the solid state, it has been suggested that both these values can be accommodated by a H-movement which only involves a flip-flop about the occupied Ru—Rh edge (see Fig. 7) [6]. Such ideal extreme positions have been suggested to be adopted in transition metal hydride clusters [19] and a flip-flop about a single Ru—Rh edge would give rise to a flipping angle of the H—H vector of $<$ca 16°. It is suggested that our present solid state NMR data can be accommodated by a similar H-movement involving all the H's in $H_4Ru_4(CO)_{12}$. This would give rise to an extreme fluctuation of the H—H vector of $<$ca 32° and calculations, using d(H—H) = 2.8 Å and the same procedure as reported previously [6], gives a minimum T_1 value of 6.6 s at 200 MHz. However, since this calculation neglects the variation in d(H—H) and the inter-H—H-vector interaction, the value of T_1 (min) could be even shorter for this H-flipping model which is consistent with the data reported in Fig. 5. If the concerted motion pro-

Table 1. Values of E_a for H-migration in $H_4Ru_4(CO)_{12-x}L_x$ ($x = 0$, 1; L = $P(OMe)_3$) and $H_2Ru_2Rh_2(CO)_{12}$ in the solid state—see text for explanation

	E_a/kJ mol^{-1}		Ref.
	$\Delta\nu_{1/2}$	T_1	
$H_4Ru_4(CO)_{12}$	75.1	59.2	7
		32[a]	7[a]
	18.5 ± 2	16.1 ± 0.5	This work
$H_4Ru_4(CO)_{11}\{P(OMe)_3\}$		15.8 ± 0.5	This work
$H_2Ru_2Rh_2(CO)_{12}$		ca 1	6

[a] Recalculation using the T_1 data from Ref. 7.

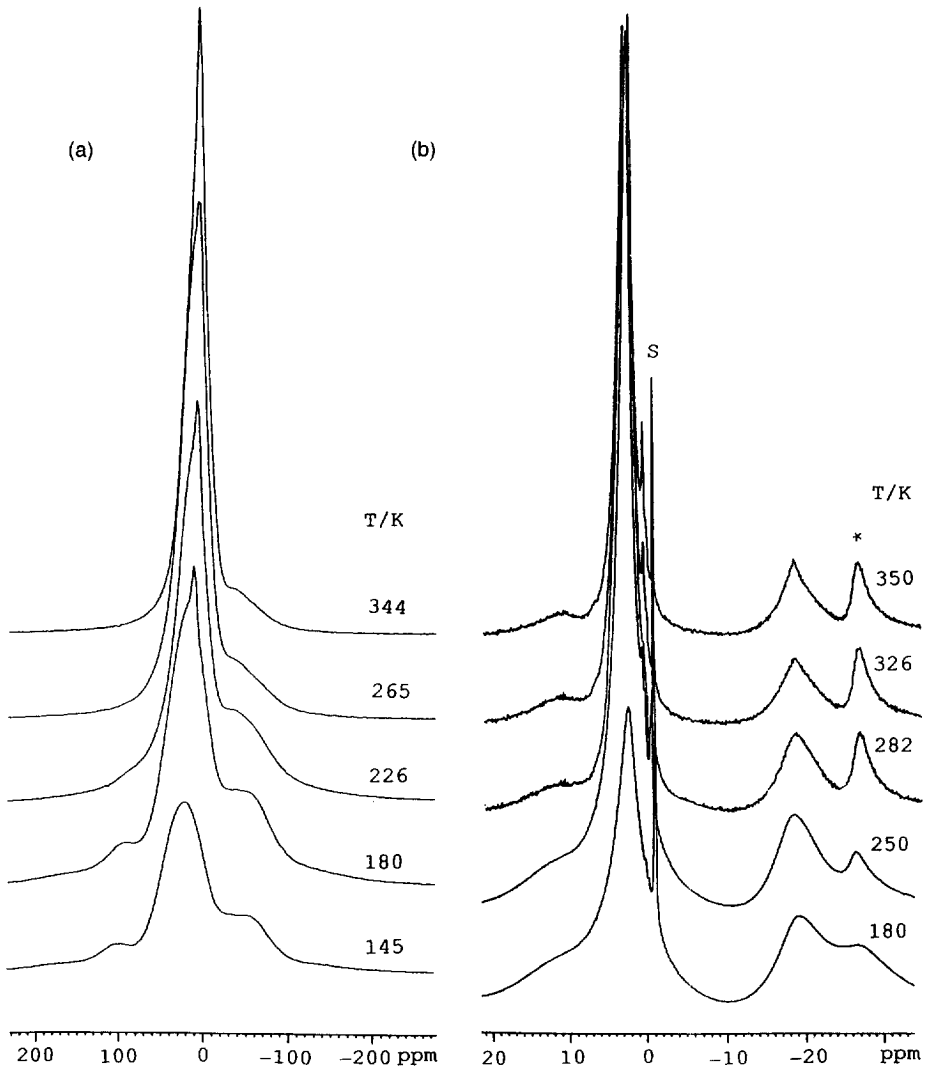

Fig. 6. (a) Variable-temperature wide-line ^1H NMR spectra and (b) ^1H MAS NMR spectra of $H_4Ru_4(CO)_{11}\{P(OMe)_3\}$ at a spinning rate of 5.8 kHz. (The hydride resonance was not well resolved at 5 kHz). *: sideband, S: solvent.

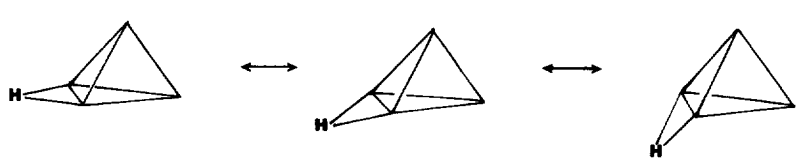

Fig. 7. Extreme H-positions, which are coplanar with adjacent M_3-triangles, after flipping about an edge in a M_4-tetrahedron [18].

posed by Aime *et al.* [7] is considered, the calculated T_1 (min) would be much shorter (<1.5 s) which is inconsistent with the available T_1 data. Because of the similar value of E_a found for H-movement in both the unsubstituted and monosubstituted clusters, it seems probable that a similar H-movement is involved in both clusters although it is presently not possible to be sure whether *all* the hydrides in $H_4Ru_4(CO)_{11}L$ ($L = P(OMe)_3$) are involved. Nevertheless, it is worth noting that a H-flipping mechanism might induce the phase transition found for $H_4Ru_4(CO)_{11}\{P(OMe)_3\}$ [10].

It is concluded that $H_4Ru_4(CO)_{12-x}L_x$ ($x = 0, 1$; $L = P(OMe)_3$) both undergo the same type of hydride motion (2-site flip about the occupied edge) in the solid state and the following summarises the supporting evidence:

(1) The values of E_a from our temperature dependent wide-line measurements involving T_1 and $\Delta\nu_{1/2}$ are in close agreement and the similarity of E_a (17 ± 2 kJ mol^{-1}) suggests a common mechanism for the H-movement.

(2) The calculated T_1 (min) value for the H-movement involving H-flipping about an edge is in the same region as that experimentally observed in $H_4Ru_4(CO)_{12}$.

(3) The value for the concerted hydride motion from occupied to unoccupied edges was found to be 14.2 kJ mol^{-1} [13] and for an analogous motion in the solid state, would be expected to be much higher than the value of E_a found in the present solid state NMR measurements.

EXPERIMENTAL

Solid state NMR measurements were carried out on a Bruker DSX200 spectrometer operating at 200 MHz using a 7 mm diameter rotor for MAS experiments and using a sealed 5 mm diameter glass ampoule for wide-line measurements. ^1H T_1 values were obtained using the inversion recovery technique. The ^1H and ^{31}P-$\{^1H\}$ chemical shifts were referenced to TMS and H_3PO_4 85% aq. solution respectively. The temperature of the MAS probe was calibrated by the method reported previously [20] and the wide-line probe was calibrated using a CA thermocouple before the NMR measurements were carried out.

$H_4Ru_4(CO)_{12}$ and $H_4Ru_4(CO)_{11}\{P(OMe)_3\}$ were prepared as described previously [21,22] and recrystallised from dichloromethane/octane. Prior to NMR measurements all samples were dried for a minimum of 12 h under high vacuum (10^{-3} mm Hg) at a temperature of 70°C. Purity of all samples was checked by IR and solution ^1H NMR before and after NMR measurements.

When the solvent was not completely removed from $H_4Ru_4(CO)_{11}\{P(OMe)_3\}$, a very sharp component of the hydride resonance appeared above room temperature which was observed to be reversible on cooling. This narrow component has a much shorter T_1 (ca 1.2 s at 345 K) than the broad component. We also found that the relative intensity of this narrow component decreases after heating the sample several times. The appearance of this very sharp resonance is typical of the isotropically averaged "solution-state behaviour" of molecules; we propose that this arises due to a process which is as yet not well understood but may involve the partial dissolution of the compound in the residual solvent trapped in the crystal lattice.

Acknowledgment—We thank the Japan Society for the Promotion of Science, the Royal Society, the British Council and the Daiwa Foundation for financial support and B.T.H. thanks the Leverhulme Foundation for the award of a Research Fellowship.

REFERENCES

1. Bau, R., Drabnis, M. H., Garlaschelli, L., Klooster, W. T., Xie, Z., Koetzle, T. F. and Martinengo, S., *Science*, 1997, **275,** 1099.
2. Heaton, B. T., Strona, L., Martinengo, S., Strumolo, D., Goodfellow, R. J. and Sadler, I. H., *J. Chem. Soc., Dalton Trans.*, 1982, 1499.
3. Bordoni, S., Heaton, B. T., Seregni, C., Strona, L., Goodfellow, R. J., Hursthouse, M. B., Thornton-Pett, M. and Martinengo, S., *J. Chem. Soc., Dalton Trans.*, 1988, 2103.
4. Allevi, C., Heaton, B. T., Seregni, C., Strona, L., Goodfellow, R. J., Chini, P. and Martinengo, S., *J. Chem. Soc., Dalton Trans.*, 1986, 1375.
5. Knox, S. A. R. and Kaesz, H. D., *J. Am. Chem. Soc.*, 1971, **93,** 4594.
6. Eguchi, T., Heaton, B. T., Harding, R. A., Miyagi, K., Longoni, G., Nahring, J., Nakamura, N., Nakayama, H., Pakkanen, T. A., Pursiainen, J. and Smith, A. K., *J. Chem. Soc., Dalton Trans.*, 1996, 625.
7. Aime, S., Gobetto, R., Orlandi, A., Groombridge, C. J., Hawkes, G. E., Mantle, M. D. and Sale, K. D., *Organometallics*, 1994, **13,** 2375.
8. Bau, R. and Teller, R. G., *Structure and Bonding*, 1981, **44,** 1.
9. Wei, C.-Y., Garlaschelli, L., Bau, R. and Koetzle, T. F., *J. Organomet. Chem.*, 1981, **213,** 63.
10. Orpen, A. G. and McMullan, R. K., *J. Chem. Soc., Dalton Trans.*, 1983, 463.
11. Orpen, A. G., *J. Chem. Soc., Dalton Trans.*, 1980, 2509.
12. Wilson, R. D., Wu, S. M., Love, R. A. and Bau, R., *Inorg. Chem.*, 1978, **17,** 1171.
13. Kaesz, H. D., *Chem. Brit.*, 1973, **9,** 344.
14. Abragam, A., *The Principles of Nuclear Magnetism.* Chap. VII, Oxford, 1961.
15. Nicol, A. T. and Vaughan, R. W., Transition metal hydrides, *ACS Adv. Chem. Ser.*, 1978, **167,** 248.
16. Eguchi, T. and Chihara, H., *J. Magn. Reson.*, 1988, **76,** 143.
17. Eguchi, T., Harding, R. A., Heaton, B. T., Longoni, G., Miyagi, K., Nähring, J., Nakamura, N., Nakayama, H. and Smith, A. K., *J. Chem. Soc., Dalton Trans.*, 1997, 479.
18. Pursiainen, J., Pakkanen, T. A., Heaton, B. T., Seregni, C. and Goodfellow, R. J., *J. Chem. Soc., Dalton Trans.*, 1986, 681.
19. Churchill, M. R. and Hollander, F. J., *Inorg. Chem.*, 1979, **18,** 161.
20. Bulechi, A. and Burum, D. P., *J. Magn. Reson., A*, 1995, **116,** 215.
21. Bruce, M. I. and Williams, M. L., *Inorg. Synth.*, 1989, **26,** 262.
22. Kaesz, H. D. and Knox, S. A. R., *J. Am. Chem. Soc.*, 1971, **93,** 4595.

Pergamon

PII: S0277-5387(98)00031-X

Polyhedron Vol. 17, No. 17, pp. 2865–2875, 1998
© 1998 Elsevier Science Ltd
All rights reserved. Printed in Great Britain
0277-5387/98 $19.00+0.00

High nuclearity iridium clusters derived from the transformation of $[Ir_4(CO)_{11}(PPh_2Cl)]$ on silica gel and the thermolysis of $[HIr_4(CO)_{10}(\mu\text{-}PPh_2)]$; synthesis and characterization of $[Ir_6(\mu\text{-}CO)(CO)_{12}(\mu\text{-}PPh_2)_2]$, $[Ir_7(\mu\text{-}CO)(CO)_{13}(\mu\text{-}PPh_2)(\mu_3\text{-}PPhC_6H_4)]$ and $[Ir_8(\mu\text{-}CO)_2(CO)_{14}(\eta^1\text{-}Ph)(\mu\text{-}PPh_2)(\mu_4\text{-}PPh)]$†

Maria Helena de Araujo,[a] Maria D. Vargas,[a]* Dario Braga[b] and Fabrizia Grepioni[b]

[a] Instituto de Química, Universidade Estadual de Campinas, CP 6154, Campinas, 13083-970, SP, Brazil

[b] Dipartimento di Chimica "G. Ciamician", Universitá degli Studi di Bologna, Via Selmi 2, 40126, Bologna, Italy

(Received 10 October 1997; accepted 30 December 1997)

Abstract—The monosubstituted compound $[Ir_4(CO)_{11}(PPh_2Cl)]$ reacts on silica gel to give $[HIr_4(CO)_{10}(\mu\text{-}PPh_2)]$ and the novel compounds $[Ir_4(CO)_{11}(PPh_2OH)]$ and $[Ir_6(\mu\text{-}CO)(CO)_{12}(\mu\text{-}PPh_2)_2]$ whose relative yields (up to 75, 10 and 40%, respectively) depend on cluster loading and the polarity of the eluent. The molecular structure of the hexanuclear compound was established by an X-ray analysis and consists of an octahedron of iridium atoms with two diphenylphosphido groups symmetrically bridging two non consecutive edges. Thermolysis of $[HIr_4(CO)_{10}(\mu\text{-}PPh_2)]$ in THF results in the formation of the same hexanuclear compound (up to 40%), together with $[Ir_7(\mu\text{-}CO)(CO)_{13}(\mu\text{-}PPh_2)(\mu_3\text{-}PPhC_6H_4)]$ (10%) and $[Ir_8(\mu\text{-}CO)_2(CO)_{14}(\eta^1\text{-}Ph)(\mu\text{-}PPh_2)(\mu_4\text{-}PPh)]$ (40%), depending on the reaction conditions; their molecular structures were determined by X-ray analyses. The heptanuclear compound exhibits a capped octahedral metal frame with a diphenylphosphido and a phenyl orthometallated phosphido ligands bridging two opposite equatorial edges of the octahedron; the octanuclear cluster exhibits a fused octahedron-square based pyramid metal atom arrangement with the phosphinedene ligand bonded to the square face of the pyramid and the phosphido group to one of the edges of the octahedron. Possible mechanisms for the formation of these high nuclearity clusters are discussed. © 1998 Elsevier Science Ltd. All rights reserved

Keywords: high nuclearity clusters; iridium; synthesis; thermolysis.

Surface mediated cluster synthesis has emerged in recent years as an extremely efficient and selective alternative to the established synthetic routes [1] involving vacuum pyrolysis, thermolysis and reduction of preformed carbonyls [2]. The selectivity of surface mediated syntheses is controlled by the choice of the inorganic oxide that plays the role of the solvent in conventional syntheses. A number of high nuclearity iridium clusters, which were previously obtained from the reduction of $[Ir_4(CO)_{12}]$, e.g. $[Ir_6(CO)_{15}]^{2-}$ [3,4], $[Ir_8(CO_{22}]^{2-}$ [5], have been produced by reductive carbonylation of $[Ir_4(CO)_{12}]$ adsorbed on MgO surfaces [6,7]. Similarly, neutral carbonyl Ir, Rh, Os and Ru clusters have been synthesized from the reductive carbonylation of supported halide precursors on SiO_2 [1].

Transformations of cluster compounds on silica gel

* Author to whom correspondence should be addressed.

† Dedicated to Prof. the Lord Lewis for his outstanding contribution to chemistry and for his enthusiastic support to the younger generation.

or alumina during purification have been described [8] and are certainly much more common than suggested by literature reports. To our knowledge, however, not a single case involving cluster build-up has been reported so far. This report describes our studies involving the synthesis and transformation of $[Ir_4(CO)_{11}(PPh_2Cl)]$ on silica gel plates to give the novel compound $[Ir_6(\mu\text{-}CO)(CO)_{12}(\mu\text{-}PPh_2)_2]$, and an alternative route to this compound and to $[Ir_7(\mu\text{-}CO)(CO)_{13}(\mu\text{-}PPh_2)(\mu_3\text{-}PPhC_6H_4)]$ (10%) and $[Ir_8(\mu\text{-}CO)_2(CO)_{14}(\eta^1\text{-}Ph)(\mu\text{-}PPh_2)\text{-}(\mu_4\text{-}PPh)]$ (up to 40%), via thermolysis of $[HIr_4(CO)_{10}(\mu\text{-}PPh_2)]$.

RESULTS AND DISCUSSION

Synthesis and characterisation of $[Ir_4(CO)_{11}(PPh_2Cl)]$, **3a**

The cluster compound $[Ir_4(CO)_{12}]$, **1**, reacts with equivalent amounts of Bu_4NBr and PPNCl in refluxing THF to yield $Bu_4N[Ir_4(CO)_{11}Br]$, **2a**, and $PPN[Ir_4(CO)_{11}Cl]$, **2b**, respectively, in quantitative yields [9]. The reactions of **2a** and **2b** with 1 equivalent of PPh_2Cl in CH_2Cl_2 or acetone at room temperature lead to an immediate colour change from orange to yellow, and formation of $[Ir_4(CO)_{11}(PPh_2Cl)]$, **3a**, as evidenced by IR and ^{31}P NMR spectroscopies. If these reaction mixtures are left stirring, however, precipitation of **1** starts to occur, after 10 min. These reactions were monitored by $^{31}P\{^1H\}$ NMR spectroscopy in $CH_2Cl_2/CDCl_3$, for 4 h under atmospheres of Ar and CO. The spectra of the mixtures under Ar, just after the addition of PPh_2Cl to **2a** and **2b**, showed only a very strong peak at δ 35.2 (s) attributed to **3a** and a weak broad peak at δ −33.3, attributed to $[Ir_4(CO)_{10}(PPh_2Cl)_2]$, **4**. A decrease in the concentration of **3a**, concomitant with an increase in that of **4**, was noted during the first hour, but no substantial change was evidenced during the next 3 h. Furthermore, no additional peaks were observed in the spectra of the supernatants of either reaction mixtures. Under an atmosphere of CO, the process occurred more rapidly, and the $^{31}P\{^1H\}$ NMR spectra of the supernatants of both reaction mixtures showed only the presence of **4**, after 30 min. Further precipitation of **1** and darkening of the solutions were observed after longer periods of time, in the absence of CO, due to the decomposition of **4** into unidentified species.

In order to investigate whether the presence of PPNCl or Bu_4NBr was necessary for the formation of **1** and **4**, pure samples of **3a** were left stirring in $CH_2Cl_2/CDCl_3$ under Ar and under CO for 4 h, during which time precipitation of **1** was not noted and the $^{31}P\{^1H\}$ NMR spectrum of **3b** stayed unchanged. It is well known that PPNCl catalyses CO substitution by nucleophiles in ruthenium carbonyl clusters [10]. In our case, however, the halide seems to be catalysing the substitution, not only of a CO, but also of a PPh_2Cl ligand, according to the following equations:

$$[Ir_4(CO)_{11}(PPh_2Cl)],\mathbf{3a} + X^- \rightarrow \text{“}[Ir_4(CO)_{10}(PPh_2Cl)X]^-\text{”} + CO$$

$$[Ir_4(CO)_{11}(PPh_2Cl)],\mathbf{3a} + X^- \rightarrow \text{“}[Ir_4(CO)_{11}X]^-\text{”} + PPh_2Cl$$

$$\text{“}[Ir_4(CO)_{10}(PPh_2Cl)X]^-\text{”} + PPh_2Cl \rightarrow [Ir_4(CO)_{10}(PPh_2Cl)_2],\mathbf{4} + X^-$$

$$\text{“}[Ir_4(CO)_{11}X]^-\text{”} + CO \rightarrow [Ir_4(CO)_{12}],\mathbf{1} + X^-$$

$$X = Br^- \text{ or } Cl^-$$

The process is driven by the precipitation of **1** and occurs, most probably, as a result of the high lability of the PPh_2Cl ligand. By comparison, reaction of the analogous compound $[Ir_4(CO)_{11}(PPh_2Me)]$ with PPNCl occurs only under much harsher conditions (THF, reflux, 3 h), to yield $PPN[Ir_4(CO)_{10}(PPh_2Me)Cl]$, and is readily reversed in the presence of CO, without formation of **1** [11]. In fact, labilization of ligands other than CO in the presence of halides has not yet been observed in tetranuclear iridium systems.

Study of the behaviour of **3a** *on TLC plates*

Purification of **3a** by TLC was only possible if performed under specific conditions, such as very low cluster loading, quick elution of the compound and extraction from the plates, as soon as it separates out from the base line. Under the chromatographic conditions normally employed for the purification of the PR_3, PR_2H and PRH_2 derivatives of **1** [12a] (~20 mg of the compound per plate, CH_2Cl_2 : hexane 1 : 4 as eluent), the mixture reacted on the silica gel to give three products, which separated out, and whose yields (based on **1**) were extremely sensitive to cluster loading and to the polarity of the eluent. Low cluster loading (10 mg/plate) and solvent polarity (CH_2Cl_2/hexane 1.5 : 8.5) yielded the novel yellow compound $[Ir_4(CO)_{11}(PPh_2OH)]$, **3b** (10%) and the known orange species $[HIr_4(CO)_{10}(\mu\text{-}PPh_2)]$ [12b], **5** in high yields (75%). This compound was previously obtained from $[Ir_4(CO)_{10}(PPh_2H)]$, **3c**, upon deprotonation and protonation of the resulting anion $[Ir_4(CO)_{10}(\mu\text{-}PPh_2)]^-$, in 85% yield, based on **1**. High cluster loading (40 mg/plate) and solvent polarity (CH_2Cl_2/hexane 3 : 7), however, resulted in the darkening of the reaction mixture on the plates and separation of **5** (10%), **3b** (10%) and of the dark brown species $[Ir_6(\mu\text{-}CO)(CO)_{12}(\mu\text{-}PPh_2)_2]$, **6** (40%), see Scheme 1.

Interestingly, compounds **3b**, **5** and **6** were formed in small amounts, when an excess silica gel for TLC was added to solutions of **3a** in $CH_2Cl_2/CDCl_3$, both

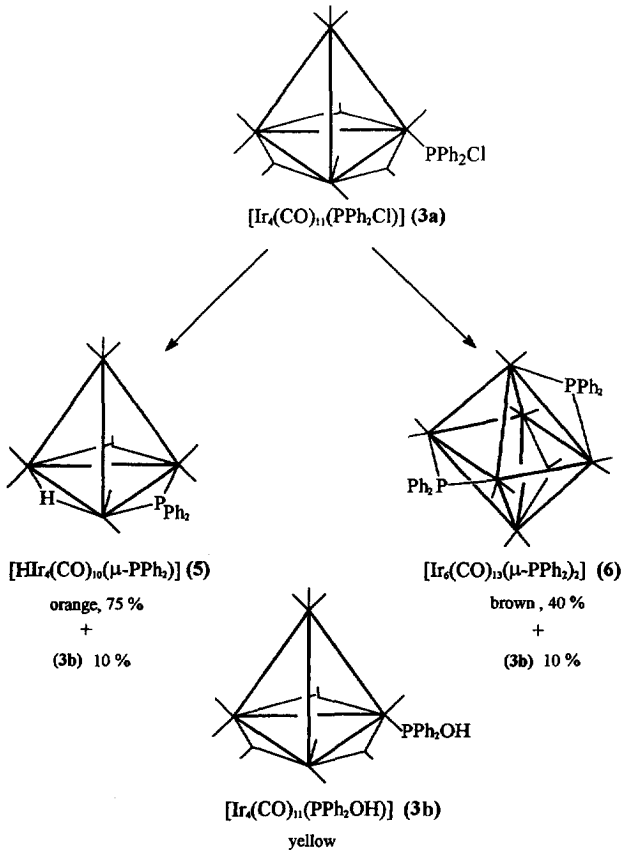

Scheme 1.

in the presence and in the absence of PPNCl or Bu_4NBr, and the mixtures were left stirring under Ar or in air for 1 h, as shown by ^{31}P NMR spectroscopy.

Quantitative formation of **3b** was shown to occur, by ^{31}P NMR spectroscopy, upon addition of degassed water to a solution of **3a** in $CH_2Cl_2/CDCl_3$. Furthermore, this compound is stable on TLC plates, and therefore, it must result from the reaction of **3a** with the silica gel surface water. This process is related to the previously reported hydrolysis of the aminophosphinidene ligand of $[Ru_4(CO)_{12}(\mu_3\text{-}P(NPr^i_2)_2)]$ absorbed onto silica that yields $[Pr^i_2NH_2]$ $[Ru_4(CO)_{12}(\mu_3\text{-}P{=}O)]$, possibly via formation of the hydroxyphosphinidene cluster $[Ru_4(CO)_{12}(\mu_3\text{-}POH)]$ [13].

The transformation of **3a** into **5** and **6** has not been investigated under conditions that would discount the importance of the water and oxygen in their formation, so we can only speculate about the possible reactions of **3a** on the silica gel surface that might be involved in the formation of these species. Thus, electrophilic attack of the silanol group at the P—Cl bond of the PPh_2Cl coordinated ligand in **3a** and elimination of HCl would result in the formation of the $[Ir_4(CO)_{11}(PPh_2OSi{\equiv})]$ species. Also, oxidative addition of surface silanol groups at an Ir—Ir bond, as with $[M_3(CO)_{12}]$ (M = Ru and Os), from which $[(\mu\text{-}H)M_3(CO)_{10}OSi{\equiv}]$ are formed on silica surface [14], would result in species such as $[(\mu\text{-}H)Ir_4(CO)_{10}(OSi{\equiv})(PPh_2Cl)]$. Both reactions are favoured on highly hydroxilated surfaces. In addition, oxidation of these species and of **3a** (and possibly **4**) may also occur, with the generation of reactive fragments, whose combination would be favoured by the high cluster concentration on the plates, to generate the hexanuclear cluster **6**.

Characterisation of $[Ir_4(CO)_{11}(PPh_2OH)]$, **3b**

The formulation of compound **3b** was based on spectroscopic and analytical data (see Table 1), as crystals suitable for an X-ray analysis could not be obtained. The hydroxil proton of **3b** appears at δ 3.1, $J_{P,H}$ = 13 Hz in the ^1H NMR spectrum, at 233 K. The $^{31}P\{^1H\}$ NMR spectrum of **3b** in CD_2Cl_2, at 295 K, consists of a broad singlet at δ 72.3. On cooling to 233 K, two signals are resolved at δ 68.8 and 65.5 in the

Table 1. ^{1}H and $^{31}P\{^{1}H\}$ NMR spectra of compounds **3b** and **6–8**

Compounds	$^{31}P\{^{1}H\}$	^{1}H
$[Ir_4(CO)_{11}(PPh_2OH)]$ **3b**[a]	68.8, 65.2 (s, 1 : 0.03)	3.1 (d, J_{P-H} 13) 7.6–7.5 (Ph, m)
$[Ir_6(\mu\text{-CO})(CO)_{12}(\mu\text{-}PPh_2)_2]$ **6**[b]	127.7 s	7.6–7.2 (Ph, m)
$[Ir_7(\mu\text{-CO})(CO)_{13}(\mu\text{-}PPh_2)(\mu_3\text{-}PPhC_6H_4)]$ **7**[c]	152.7 d, 253.6 d, $^{3}J_{P-P}$ 4	7.6–6.7 (Ph, m)
$[Ir_8(\mu\text{-CO})_2(CO)_{14}(\eta^1\text{-Ph})(\mu\text{-}PPh_2)(\mu_4\text{-}PPh)]$ **8**[c]	191.1 d, 47.0 d, $^{3}J_{P-P}$ 63	7.7–6.9 (Ph, m)

Chemical shifts in ppm, coupling constants in Hz.
[a] −40°C in CD_2Cl_2,
[b] 25 to −90°C in CD_2Cl_2,
[c] 25°C in $CDCl_3$.

intensity ratio 1 : 0.03. These data indicate that **3b** exists in solution in the form of two inter-converting isomers which, by analogy with the $[Ir_4(CO)_{11}L]$ (L = PPh_3, PPh_2Me, PMe_3), compounds, are the C_{3v}axial and C_{3v}radial isomers [15].

Although to our knowledge this is the first report of a phosphinous acid derivative R_2POH stabilized by a carbonyl cluster, PH_2OH itself and some of its derivatives have been stabilized previously by P-complexation to "$W(CO)_5$" [16].

X-ray molecular structure of $[Ir_6(\mu\text{-CO})(CO)_{12}(\mu\text{-}PPh_2)_2]$, **6**

Compound **6** was characterized by analytical and spectroscopic methods (see Table 1 and Experimental) and by an X-ray analysis. Crystals of **6** suitable for X-ray crystallography were obtained from CH_2Cl_2/hexane. A perspective view of **6** is shown in Fig. 1, together with the labeling scheme. Selected bond distances and angles of **6** are listed in Table 2. The molecule contains an Ir_6 octahedral core, with eleven Ir—Ir bond distances falling in a fairly narrow range [from 2.729(1) to 2.791(1) Å]. Two diphenylphosphido ligands symmetrically bridge two non-consecutive edges belonging to two different equators of the octahedral frame. P—Ir bond distances average to 2.294(4) and 2.281(4) Å for the P(1)Ph_2 and P(2)Ph_2 ligands, respectively. Interestingly, the Ir—Ir edge, which is bridged by the closest PPh_2 group also shows the shortest metal-metal bond distance in the octahedron frame. Twelve CO ligands are terminally bound, two on each metal vertex, while the thirteenth CO group symmetrically bridges one edge of the octahedron equator not substituted by the PPh_2 ligands.

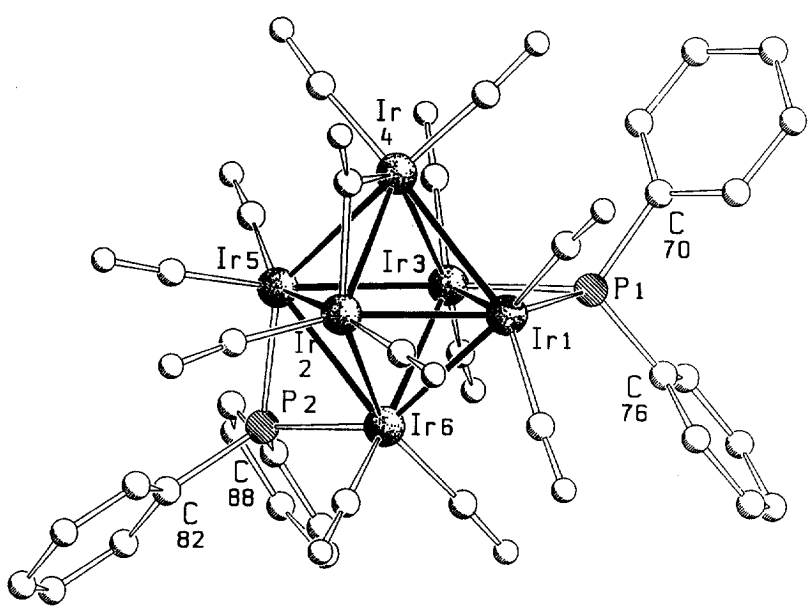

Fig. 1. Molecular structure of $[Ir_6(\mu\text{-CO})(CO)_{12}(\mu\text{-}PPh_2)_2]$, **6**.

Table 2. Relevant bond lengths [Å] for **6**, **7** and **8**

6		**7**		**8**	
Ir(1)—Ir(2)	2.736(1)	Ir(1)—Ir(4)	2.728(4)	Ir(1)—Ir(2)	2.755(2)
Ir(1)—Ir(3)	2.756(1)	Ir(1)—Ir(3)	2.788(4)	Ir(1)—Ir(3)	2.845(2)
Ir(1)—Ir(4)	2.792(1)	Ir(1)—Ir(7)	2.792(5)	Ir(1)—Ir(4)	2.797(2)
Ir(1)—Ir(6)	2.781(1)	Ir(1)—Ir(6)	2.811(5)	Ir(1)—Ir(5)	2.735(2)
Ir(2)—Ir(4)	2.751(1)	Ir(1)—Ir(2)	2.840(4)	Ir(1)—Ir(7)	2.770(2)
Ir(2)—Ir(5)	2.839(1)	Ir(2)—Ir(7)	2.712(5)	Ir(1)—Ir(8)	2.820(2)
Ir(2)—Ir(6)	2.791(1)	Ir(2)—Ir(5)	2.747(5)	Ir(2)—Ir(3)	2.799(2)
Ir(3)—Ir(4)	2.775(1)	Ir(2)—Ir(3)	2.817(4)	Ir(2)—Ir(5)	2.746(2)
Ir(3)—Ir(5)	2.778(1)	Ir(2)—Ir(4)	2.828(4)	Ir(3)—Ir(4)	2.787(2)
Ir(3)—Ir(6)	2.782(1)	Ir(3)—Ir(7)	2.632(5)	Ir(4)—Ir(5)	2.810(2)
Ir(4)—Ir(5)	2.762(1)	Ir(3)—Ir(5)	2.721(5)	Ir(4)—Ir(6)	2.711(2)
Ir(5)—Ir(6)	2.729(1)	Ir(3)—Ir(6)	2.729(5)	Ir(4)—Ir(7)	2.752(2)
		Ir(4)—Ir(6)	2.758(4)	Ir(5)—Ir(6)	2.752(2)
Ir(1)—P(1)	2.291(4)	Ir(4)—Ir(5)	2.866(4)	Ir(5)—Ir(8)	2.743(2)
Ir(3)—P(1)	2.297(4)	Ir(5)—Ir(6)	2.741(4)	Ir(6)—Ir(7)	2.817(2)
Ir(5)—P(2)	2.282(4)			Ir(6)—Ir(8)	2.752(2)
Ir(6)—P(2)	2.279(4)	Ir(2)—P(1)	2.27(2)	Ir(7)—Ir(8)	2.763(2)
		Ir(5)—P(1)	2.28(2)		
P(1)—C(70)	1.811(9)	Ir(1)—P(2)	2.33(2)	Ir(2)—P(1)	2.400(9)
P(1)—C(76)	1.830(9)	Ir(6)—P(2)	2.26(2)	Ir(3)—P(1)	2.408(9)
P(2)—C(82)	1.838(9)	Ir(4)—C(117)	2.17(3)	Ir(4)—P(1)	2.261(10)
P(2)—C(88)	1.818(10)			Ir(5)—P(1)	2.346(9)
		P(1)—C(100)	1.80(4)	Ir(6)—P(2)	2.277(9)
mean Ir—C(t)	1.86(2)	P(1)—C(106)	1.80(4)	Ir(8)—P(2)	2.266(9)
mean Ir—C(b)	2.06(2)	P(2)—C(112)	1.76(3)	Ir(3)—C(90)	2.06(4)
mean C—O	1.13(2)	P(2)—C(118)	1.79(4)		
				P(1)—C(96)	1.80(2)
		mean Ir—C(t)	1.84(4)	P(2)—C(102)	1.80(2)
		mean Ir—C(b)	1.99(10)	P(2)—C(108)	1.82(2)
		mean C—O	1.18(4)	C(90)—C(95)	1.41(5)
				C(90)—C(91)	1.44(5)
				C(91)—C(92)	1.28(6)
				C(92)—C(93)	1.50(6)
				C(93)—C(94)	1.31(6)
				C(94)—C(95)	1.37(6)
				mean Ir—C(b)	2.03(3)
				mean Ir—C(t)	1.87(3)
				mean C—O	1.13(4)

Cluster **6** possesses 86 valence electrons, and exhibits a remarkably similar molecular geometry to those of the dianionic $[Ir_6(\mu\text{-}CO)_3(CO)_{12}]^{2-}$ [17] and the monoanionic $[Ir_6(\mu\text{-}CO)_2(CO)_2(\mu\text{-}PPh_2)]^-$ [18] clusters. The latter compound was recently obtained from the oxidation of $[Ir_6(\mu\text{-}CO)_3(CO)_{12}]^{2-}$ with $[FeCp_2]^+$ in the presence of PPh_2H, followed by deprotonation of the coordinated phosphine. Two of the three bridging CO ligands in the dianionic compound are formally replaced by two 3-electron donor PPh_2 groups in **6**, whilst $[Ir_6(\mu\text{-}CO)_2(CO)_{12}(\mu\text{-}PPh_2)]^-$ results, formally, from the replacement of one μ-CO in the dianion by a μ-PPh_2 fragment. The steric arrangement of the remaining twelve CO ligands does not differ substantially in the three species. Average Ir—Ir bond distances compare well in **6**, $[Ir_6(\mu\text{-}CO)_2(CO)_{12}(\mu\text{-}PPh_2)]^-$ and $[Ir_6(\mu\text{-}CO)_3(CO)_{12}]^{2-}$ [av. Ir—Ir 2.776(1), 2.776(1) and 2.773(1) Å, respectively] and so do the metal-carbon bond lengths [av. $Ir—C_{(COt)}$ 1.86(2), 1.87(2) and 1.86(2); $Ir—C_{(COb)}$ 2.06(2), 2.05(2) and 2.04(2), respectively].

In spite of the lack of symmetry of compound **6** in the solid state, the $^{31}P\{^1H\}$ NMR spectrum showed a singlet at δ 127.7 from 295 to 183 K which indicates that it is fluxional at those temperatures.

Thermolysis of $[HIr_4(CO)_{10}(\mu\text{-}PPh_2)]$, **5**

In order to find out whether compound **6** would also be formed under thermolytic conditions, compound **5** was heated in THF under reflux. After 12 h, three compounds were isolated in sufficient yields to be fully characterized by analytical and spectroscopic data

and by X-ray analyses: compound **6** (40%), $[Ir_7(\mu\text{-}CO)_2(CO)_{12}(\mu\text{-}PPh_2)(\mu_3\text{-}PPhC_6H_4)]$, **7** (10%) and $[Ir_8(\mu\text{-}CO)(CO)_{15}(\eta^1\text{-}Ph)(\mu\text{-}PPh_2)(\mu_4\text{-}PPh)]$ **8**, (18%), in addition to starting material **5** (18%). Heating compound **5** for an additional 12 h period did not lead to the formation of other products, but resulted in an increase in the yield of the octanuclear cluster **8** (40%) and a decrease in that of the hexanuclear compound **6** (14%), whilst that of **7** (10%) remained unchanged; some starting material **5** (9%) was also recovered under these conditions. Furthermore, thermolysis of **5** in THF for longer periods of time, or in refluxing toluene for 12 h led to larger amounts of decomposition material on the base line of the TLC plates.

Formation of **6** might be rationalized in terms of condensation of **5** with a reactive unsaturated hydrido-phosphido fragment with loss of H_2 and CO (See Scheme 2). Considering that heating compound **6** under reflux in THF for 12 h does not lead to cluster build up, it is possible that compounds **7** and **8** might result from further condensation of a monomeric and a dimeric unsaturated fragments, respectively, with **6**, accompanied by orthometallation and cleavage of a $P—C_{Ph}$ bond, respectively.

Formation of high nuclearity clusters from other phosphido compounds, such as $[HRu_3(CO)_{10}(\mu\text{-}PPh_2)]$, $[HRu_3(CO)_9(\mu\text{-}PPh_2)]$ [19,20], $[H_2Ru_3(CO)_8(\mu\text{-}PPh_2)_2]$ [20] and $[H_3Ru_3(CO)_7(\mu\text{-}PPh_2)_3]$ [20], has been shown to occur previously. Also in these cases, products resulting from the activation of $P—C_{Ph}$ and orthometallation were isolated. It is interesting, however, that heating $[HM_3(CO)_{10}(\mu\text{-}PPh_2)]$ (M = Ru [20] and Os [21]) under mild conditions leads to the formation of the unsaturated compound $[HRu_3(CO)_9(\mu\text{-}PPh_2)]$ and of the orthometallated product $[H_2Os_3(CO)_9(\mu\text{-}PPhC_6H_4)]$, respectively, whilst even under mild conditions, compound **5** undergoes cluster build up.

X-ray molecular structure of $[Ir_7(\mu\text{-}CO)(CO)_{13}(\mu\text{-}PPh_2)(\mu_3\text{-}PPhC_6H_4)]$, **7**

The molecular structure of **7** is shown in Fig. 2. Selected bond distances are listed in Table 2. The molecule possesses 98 valence electrons, and exhibits a capped octahedron arrangement of iridium atoms, with fifteen Ir—Ir bond distances falling in the range

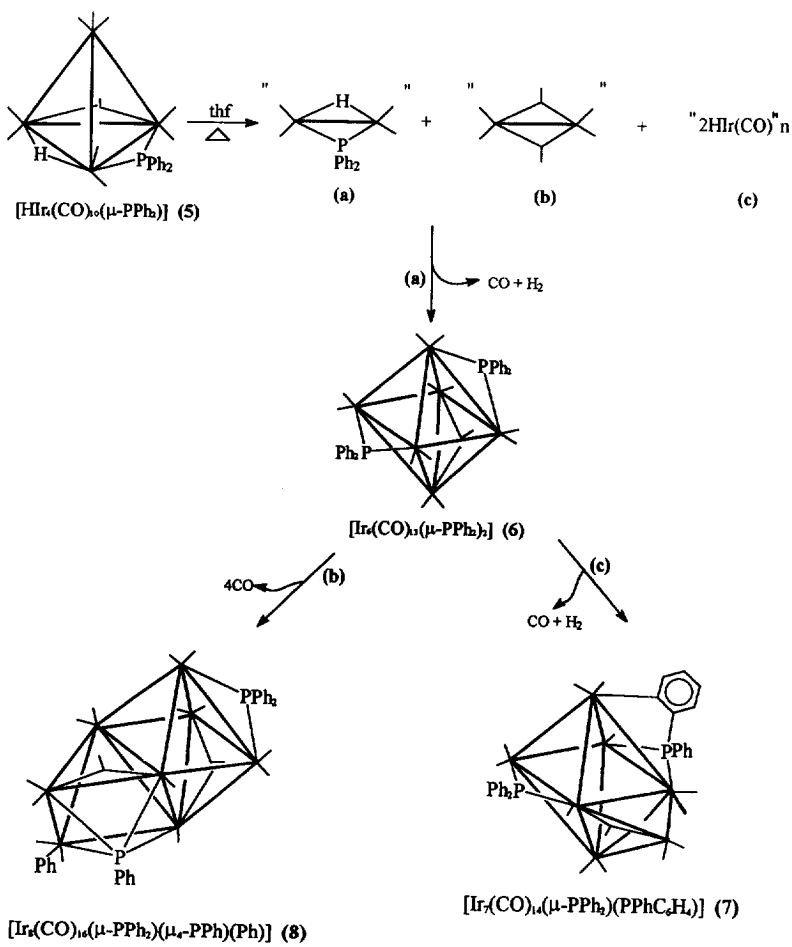

Scheme 2.

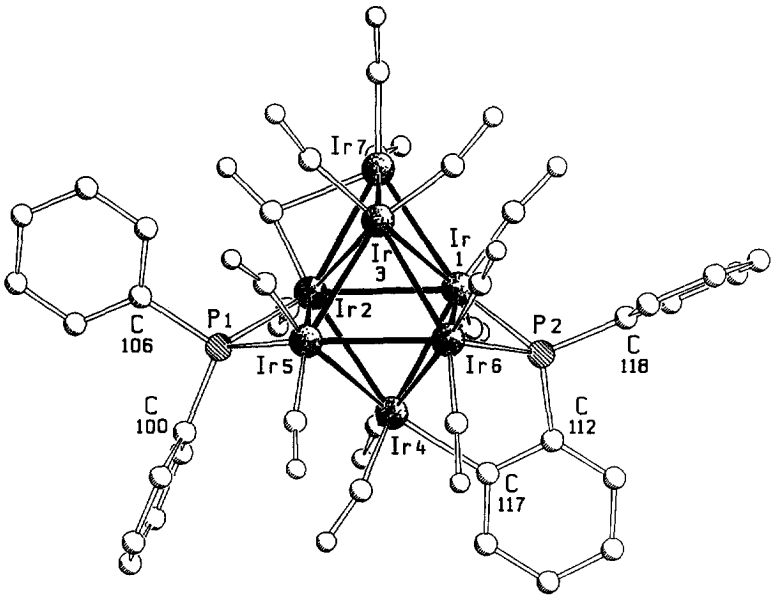

Fig. 2. Molecular structure of $[Ir_7(\mu\text{-CO})(CO)_{13}(\mu\text{-PPh}_2)(\mu_3\text{-PPhC}_6H_4)]$, **7**.

from 2.632(5) to 2.866(4) Å. A diphenylphophido and a phenyl orthometallated phosphido ligands bridge two opposite equatorial edges of the octahedron. Thirteen CO ligands are terminally bound, two on six metal vertex and one on the seventh metal atom, while the fourteenth CO group symmetrically bridges the edge formed by the capping iridium atom and the iridium atom bearing only one terminal CO. The only other known heptanuclear iridium cluster, $[Ir_7(\mu\text{-CO})(CO)_{11}(C_8H_{12})(C_8H_{11})(C_8H_{10})]$, which was obtained from the reaction of **1** with 1,5-cyclooctadiene in refluxing chorobenzene [22], exhibits a similar metal framework arrangement. The steric arrangement of the thirteen CO ligands does not differ substantially in the two species. Average Ir—Ir bond distances compare well in **7** and $[Ir_7(\mu\text{-CO})(CO)_{11}(C_8H_{12})(C_8H_{11})(C_8H_{10})]$ [av. Ir—Ir 2.767(5), and 2.763(1) Å, respectively] and the same can be said for the metal-carbon bond lengths [av. Ir—$C_{(CO_t)}$ 1.84(4) and 1.86(5); Ir—$C_{(CO_b)}$ 1.99(10) and 2.04(4), respectively].

X-ray molecular structure of $[Ir_8(\mu\text{-CO})_2(CO)_{14}(\eta^1\text{-Ph})(\mu\text{-PPh}_2)(\mu_4\text{-PPh})]$, **8**

Compound **8** was formulated on the basis of analytical and spectroscopic data (see Table 1 and Experimental) but an X-ray analysis experiment was necessary to establish its structure unambiguously. The molecular structure of **8** is shown in Fig. 3, together with the labeling scheme. Selected bond distances are listed in Table 2. The metal arrangement can be described as a fused polyhedron, formed by an octahedron and a square based pyramid (atoms Ir1—Ir5) sharing a triangular face. Ir—Ir bond distances range from 2.711(2) to 2.845(2) Å. The μ-PPh_2 ligand symmetrically bridges one of the edges of the octahedron. A second PPh_2 ligand has undergone P—C bond cleavage; the two resulting fragments, *viz* the phenyl ligand and the phenyl phosphinedene, bind in η^1-fashion to one of the basal atoms and in μ_4-fashion the four basal atoms of the square based pyramid, respectively. A similar kind of μ_4-coordination of a PPh ligand, which donates four electrons to the metal frame, has previously been observed in the pentanuclear iridium compounds $[Ir_5(\mu\text{-CO})_2(CO)_7L(\eta^5\text{-}C_5Me_5)(\mu_4\text{-PPh})]$ (L = CO, PPh_3) [23]. Fourteen carbonyls are terminally bound to the iridium atoms, while the remaining two CO ligands symmetrically bridge one of the basal square pyramids and one of the octahedron edges. The only two other octanuclear iridium clusters whose structures have been determined to date are $[Ir_8(CO)_{22}]^-$ [24] and $[Ir_8Au_2(CO)_{20}(PhPPPh)(PEt_3)]$ [25], which exhibit *bis*-tetranuclear frameworks linked by an Ir—Ir bond and by the PhPPPh ligand, respectively.

EXPERIMENTAL

General procedures and materials

Iridium trichloride (Johnson and Matthey), PPNCl and Bu_4NBr (Aldrich), diphenyl phosphine and chlorodiphenyl phosphine (Strem Chemicals) were used as purchased. The compounds $[Ir_4(CO)_{12}]$ **1** [26], $[Ir_4(CO)_{11}(PPh_2H)]$ **3c**, $[HIr_4(CO)_{10}(\mu\text{-PPh}_2)]$ **5** [12], $Bu_4N[Ir_4(CO)_{11}Br]$ **2a** and $PPN[Ir_4(CO)_{11}Cl]$ **2b** [9] were prepared by literature methods. Manipulations

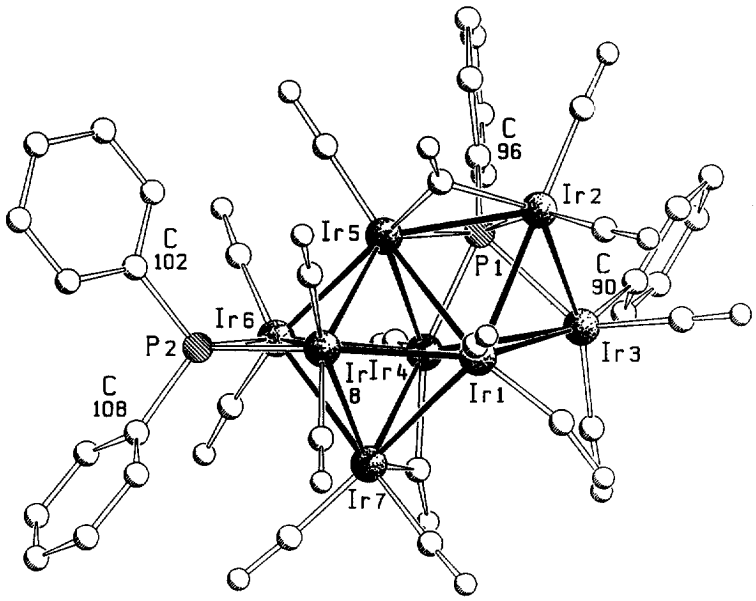

Fig. 3. Molecular structure of $[Ir_8(\mu\text{-}CO)_2(CO)_{14}(\eta^1\text{-}Ph)(\mu\text{-}PPh_2)(\mu_4\text{-}PPh)]$, **8**.

were performed in Schlenk tubes, under an atmosphere of dry Ar, unless otherwise specified. Solvents were dried as previously described [12] and freshly distilled under Ar and degassed before use. Preparative TLC was carried out in air by using *ca* 2 mm thick glass-backed silica gel plates (20 × 20 cm) prepared from silica GF_{254} Type 60, Fluka, and the compounds extracted from the silica with dichloromethane. All substituted Ir_4 cluster compounds were stored under an inert atmosphere for they were found to be slightly air sensitive in the solid state. FAB-MS were obtained on a VG AutoSpec using p-nitrobenzyl alcohol as a matrix at the University of Sussex, U.K. IR spectra on a JASCO IR 700 between 2200 and 1600 cm^{-1} using CaF_2 cells. ^1H and ^{31}P $\{^1H\}$ NMR data were obtained on a Bruker AC 300 instrument, using deuterated solvents as lock and reference [^1H $SiMe_4$; ^{31}P 85% H_3PO_4 (external)]. Microanalyses were performed at the Instituto de Química, UNICAMP, Brazil.

Preparation of $[Ir_4(CO)_{11}(PPh_2Cl)]$, **3a**

An orange solution of $PPN[Ir_4(CO)_{11}Cl]$ **2b** (37.1 mg, 0.023 mmol) in CH_2Cl_2 (2 cm^3) was cooled to −30°C and treated with PPh_2Cl (4.1 μl, 0.023 mmol). The yellow reaction mixture was warmed to 25°C. Quick purification of the reaction mixture by TLC, using CH_2Cl_2/hexane (3:7) as eluent, taking care to load each plate with a maximum of 3 mg of **3a**, and extracting the yellow compound from the plates, just after it had separated out from the base line, gave pure **3a** (17.3 mg, 60%), IR (ν_{CO} hexane): 2084 s, 2052 vs, 2040 vs, 2030 vs, 1955 m, 1885 w, 1845 m and 1824 m, cm^{-1}. Use of $Bu_4N[Ir_4(CO)_{11}Br]$ **2a**, instead of **2b**, gave similar yields of **3a**, under the same conditions.

Investigation of the stability of **3a** *in the presence of* PPNCl *or* Bu_4NBr

An orange solution of $PPN[Ir_4(CO)_{11}Cl]$ **2b** (148.5 mg, 0.09 mmol) in CH_2Cl_2 (5 cm^3) was cooled to −30°C and treated with PPh_2Cl (16.6 μl, 0.09 mmol). Quick warming of the reaction mixture to 20°C was followed by addition of 0.5 cm^3 of $CDCl_3$. A ^{31}P $\{^1H\}$ NMR spectrum was recorded immediately, and every 30 min thereafter. After 10 min stirring at room temperature **1** started to precipitate, and was decanted, before each sampling. Same procedure was followed in the reaction of $Bu_4N[Ir_4(CO)_{11}Br]$, **2a** with PPh_2Cl.

Investigation of the stability of **3a** *in the absence of* PPNCl *or* Bu_4NBr

Solutions of pure **3a** (20 mg, 0.016 mmol) in CH_2Cl_2:$CDCl_3$ (0.8 cm^3:0.5 cm^3) were left stirring under Ar and under CO for 4 h. No precipitation of **1** was observed and the ^{31}P $\{^1H\}$ NMR spectra of both solutions showed only the presence of **3a**.

Reaction of $[Ir_4(CO)_{11}(PPh_2Cl)]$ **3a** *on TLC plates*

Method 1: Low cluster loading (10 mg/plate), CH_2Cl_2/hexane (1.5:8.5), yielded the orange species **5** (83.5 mg, 75%), the yellow compound $[Ir_4(CO)_{11}(PPh_2OH)]$ **3b** (11.5 mg, 10%); R_f 0.79, IR (ν_{CO} hexane): 2084 s, 2052 vs, 2014 vs, 1974 vs, 1880 w,

1845 m and 1823 m cm^{-1} and the brown compound $[Ir_6(\mu\text{-}CO)(CO)_{12}(\mu\text{-}PPh_2)_2]$ **6** (8.5 mg, 5%) R_f 0.64, IR (ν_{CO} hexane): 2078 s, 2050 vs, 2040 vs, 2020 wsh, 2010 s, 1993 s, 1957 w and 1842 s cm^{-1}. Found: C, 23.2; H, 0.8. Calc. for $C_{37}H_{20}O_{13}P_2Ir_6$: C, 23.5; H, 1.0%. *Method* 2: High cluster loading (40 mg/plate), CH_2Cl_2/hexane (3:7), resulted in the separation of compounds **5** (11 mg, 10%), **3b** (11.5 mg, 10%) and **6** (68 mg, 40%).

Reactions of **3a** *with silica gel*

The following reactions were monitored by $^{31}P\{^1H\}$ NMR spectroscopy, after stirring for 1 h at 25°C under (a) Ar and (b) air. Addition of silica gel for TLC (excess, approximately 50 mg) to three solutions containing **3a** (20 mg, 0.016 mmol) and PPNCl (1 equiv.), **3a** and Bu_4NBr (1 equiv.) or pure **3a** in CH_2Cl_2: $CDCl_3$ (2 cm^3: 1 cm^3) led to the formation of compounds **3b, 5** and **6** in trace amounts.

Reaction of **3a** *with* H_2O

Addition of H_2O (50 μl, 2.85 mmol) to a solution of **3a** (10 mg, 0.008 mmol) in CH_2Cl_2: $CDCl_3$ (4 cm^3: 1 cm^3) led to quantitative formation of $[Ir_4(CO)_{11}(PPh_2OH)]$ **3b,** confirmed by $^{31}P\{^1H\}$ NMR spectroscopy.

Thermolysis of **5**

A solution of compound **5** (100 mg, 0.08 mmol) in THF (20 cm^3) was heated under reflux for 12 h. The solvent was evaporated, the mixture was dissolved in CH_2Cl_2 (2 cm^3) and purified by TLC with CH_2Cl_2/hexane (1:5) as eluent, to yield: compounds **6** (R_f 0.51, 60 mg, 40%); $[Ir_7(\mu\text{-}CO)_2CO)_{12}(\mu\text{-}PPh_2)(\mu_3\text{-}PPhC_6H_4)]$ **7** (R_f 0.58, 17 mg, 10%), IR (ν_{CO} hexane): 2074 m, 2046 s, 2040 vs, 2022 m, 2006 w, 1993 w and 1850 w, cm^{-1}; and $[Ir_8(\mu\text{-}CO)(CO)_{15}(\eta^1\text{-}Ph)(\mu\text{-}PPh_2)(\mu_4\text{-}PPh)]$ **8** (R_f 0.40, 28 mg, 15%): IR (ν_{CO} hexane): 2076 s, 2048 vs, 2038 vs, 2008 m, 1991 m, 1955 m and 1840 s, cm^{-1}; Found: C, 20.2; H, 0.6. Calc. for $C_{40}H_{20}O_{16}P_2Ir_8$: C, 20.4; H, 0.8%. FAB-MS m/z = 2362 (=M) [M-n(CO)] (n = 1–16); three brown species (R_f 0.24, 0.29, 0.62) in minute amounts and unreacted **5** (18 mg, 18%).

The thermolysis of compound **5** was repeated (a) under the same conditions but for 24 h, and gave the same three products, **6** (10 mg, 14%), **7** (8 mg, 10%) and **8** (37 mg, 40%), and unreacted **5** (4 mg, 9%); (b) in toluene under reflux for 12 h, and produced the

Table 3. Crystal data and details of measurements for compounds **6, 7** and **8**

Compound	**6**	**7**	**8**
Formula	$C_{37}H_{20}Ir_6O_{13}P_2$	$C_{38}H_{19}Ir_7O_{14}P_2$	$C_{40}H_{20}Ir_8O_{16}P_2$
Formula weight	1875.67	2092.87	2340.10
Crystal system	Triclinic	Triclinic	Monoclinic
Space group	$P\bar{1}$	$P\bar{1}$	$P2_1/c$
a (Å)	13.090 (2)	9.874 (8)	19.394 (7)
b (Å)	15.707 (3)	11.347 (4)	13.427 (5)
c (Å)	10.665 (3)	19.332 (6)	20.681 (9)
α (°)	103.52 (2)	93.88 (3)	90
β (°)	92.19 (2)	92.66 (4)	117.06 (3)
γ (°)	77.420 (10)	90.10 (4)	90
V (Å^3)	2080.6 (8)	2159 (2)	4796 (3)
T (K)	293 (2)	293 (2)	293 (2)
D_{calcd} (mg m^{-3})	2.994	3.220	3.241
Z	2	2	4
F (000)	1676	1856	4136
λ (Mo–K_α), Å	0.71069	0.71069	0.71069
Absorption coefficient (mm^{-1})	18.59	20.88	21.47
Psi-scan correction			
min.–max. transmission	0.61—1.00	0.48–1.00	0.56–1.00
θ range (°)	3–25	3–25	3–25
Reflections collected	6922	7767	7935
Independent reflections	6290	7525	7673
Independent reflections with $I > 2\sigma(I)$	4439	3146	4547
No. of refined parameters	356	315	360
R_1 (on F, $I > 2\sigma(I)$)	$R_1 = 0.0459$	$R_1 = 0.1195$	$R_1 = 0.0703$
wR_2 (on F^2, all data)	$wR_2 = 0.1474$	$wR_2 = 0.3704$	$wR_2 = 0.2264$

same products **6** (23 mg, 30%), **7** (5 mg, 6%) and **8** (27 mg, 32%), and unreacted **5** (4 mg, 9%).

Thermolysis of $[Ir_6(\mu\text{-}CO)(CO)_{12}(\mu\text{-}PPh_2)_2]$, **6**. A solution of compound **6** (20 mg, 0.01 mmol) in THF (10 cm^3) was heated under reflux for 12 h. The reaction was monitored by IR spectroscopy, which showed no changes in the ν_{CO} region. The solvent was evaporated, the mixture was dissolved in CH_2Cl_2 (1 cm^3) and purified by TLC with CH_2Cl_2/hexane (1.5:8.5) as eluent. Only compound **6** (16 mg, 84%) was recovered from the plates, which showed also some decomposition material on the base line.

Crystal structure determination. Crystal data and details of measurements for compounds **6, 7** and **8** are summarized in Table 3. Diffraction intensities were collected at room temperature on an Enraf-Nonius CAD-4 diffractometer equipped with a graphite monochromator (Mo–K_α, $\lambda = 0.71069$ Å). Intensity data were reduced to F_o^2. Crystals were obtained from CH_2Cl_2/hexane by slow evaporation. The structures were solved by direct methods, followed by least-squares refinements. For all calculations the crystallographic programs SHELX86 [27a] and SHELXL93 [27b] were used. Empirical absorption correction was applied for the three compounds by azimuthal scanning of reflections with $\chi > 80°$. Ir and P atoms and CO groups in **6**, Ir, P and O atoms in **7** and **8** were refined anisotropically. All phenyl rings (except for the orthometallated ring in **8**) were refined as rigid groups. Due to the scarce quality of data, constraints were applied for compound **7** on refining Ir—C_{CO} and C—O distances. The hydrogen atoms were added in calculated positions (C_{sp}^2—H 0.93 Å) and refined "riding" on the corresponding C atoms. For graphical representations the program SCHAKAL92 [27c] was used.

Acknowledgements—We thank FAPESP, PADCT and CNPq of Brazil (M.H.A. and M.D.V.) and the Ministero della Universitá e della Ricerca Scientifica e Tecnologica of Italy (D.B. and F.G.) for research grants, Johnson and Matthey plc for their generous loan of $IrCl_3$ and Prof. J. F. Nixon for the FAB-MS at the University of Sussex.

Supplementary material available—Complete listings of fractional atomic coordinates, anisotropic thermal parameters and bond lengths and angles.

REFERENCES

1. Roberto, D., Cariati, E., Ugo, R. and Psaro, R., *Inorg. Chem.*, 1996, **35,** 2311.
2. Vargas, M. D. and Nicholls, J. N., *Adv. Inorg. Chem. Radiochem.*, 1986, **30,** 123.
3. Demartin, F., Manassero, M., Sansoni, M., Garlaschelli, L., Martinengo, S. and Canziani, F., *J. Chem. Soc., Chem. Commun.*, 1980, 133.
4. Stevens, R. A., Liu, P. C. C. and Gladfelter, W. L., *J. Organomet. Chem.*, 1985, **287,** 133.
5. Angoletta, M., Malatesta, L. and Caglio, G., *J. Organomet. Chem.*, 1975, **97,** 99.
6. Maloney, S. D., Kelley, M. J., Koningsberger, D. C. and Gates, B. C., *J. Phys. Chem.*, 1991, **95,** 9406.
7. Maloney, S. D., Kelley, M. J. and Gates, B. C., *J. Organomet. Chem.*, 1992, **435,** 377.
8. (a) Lu, K.-L., Chen, C.-J., Lin, Y.-W., Gau, H.-M., Hong, F.-E. and Wen, Y.-S., *Organometallics*, 1993, **12,** 2188; (b) Gervasio, G. and Sappa, E., *J. Organomet. Chem.*, 1995, **498,** 73 and references therein; (c) Gervasio, G., Marabello, D. and Sappa, E., *J. Chem. Soc., Dalton Trans.*, 1997, 1851 and references therein.
9. Ciani, G., Chini, P., Martinengo, S., Manassero, M., Sironi, A. and Canziani, F., *J. Organomet. Chem.*, 1978, **152,** C35.
10. Rivomanana, S., Lavigne, G., Lugan, N. and Bonnet, J.-J., *Organometallics*, 1991, **10,** 2285.
11. Vargas, M. D., unpublished results.
12. (a) Mann, B. E., Vargas, M. D., Khattar, R., *J. Chem. Soc., Dalton Trans.*, 1992, 1725; (b) Livotto, F. S., Raithby, P. and Vargas, M. D., *J. Chem. Soc., Dalton Trans.*, 1993, 1797.
13. (a) Corrigan, J. F., Doherty, S., Taylor, J. and Carty, A. J., *J. Am. Chem. Soc.*, 1994, **116,** 9799; (b) Wang, W., Corrigan, J. F., Doherty, S., Enright, G. D., Taylor, J. N. and Carty, A. J., *Organometallics*, 1996, **15,** 2770.
14. Basset, J. M. and Choplin, A., *J. Mol. Catal.*, 1993, **21,** 95.
15. Ros, R., Scrivanti, A., Albano, V. G. and Garlaschelli, L., *J. Chem. Soc., Dalton Trans.*, 1986, 2411.
16. (a) Mercier, F. and Matthey, F., *J. Chem. Soc., Chem. Commun.*, 1984, 782; (b) Mercier, F., Matthey, F., Afiong-Akpan, C. and Nixon, J. F., *J. Organomet. Chem.*, 1988, **348,** 361.
17. Demartin, F., Manassero, M., Sansoni, M., Garlaschelli, L. and Martinengo, S., *J. Chem. Soc., Chem. Commun.*, 1980, 903.
18. Della Pergola, R., Brivio, E., Garlaschelli, L., Masciocchi, N. and Manassero, M., *J. Cluster Sci.*, 1994, **5,** 363.
19. (a) MacLaughlin, S. A., Taylor, N. J. and Carty, A. J., *Organometallics*, 1984, **3,** 392; (b) ibid, *Can. J. Chem.*, 1982, **60,** 87; (c) ibid, *Inorg. Chem.*, 1983, **22,** 1409; (d) van Gastel, F., Taylor, N. J. and Carty, A. J., *J. Chem. Soc., Chem. Commun.*, 1987, 1049; (e) ibid, *Inorg. Chem.*, 1989, **28,** 85. a20. Field, J. S., Haines, J. and Mulla, F., *J. Organomet. Chem.*, 1990, **389,** 227.
21. Colbran, S. B., Irele, P. T., Johnson, B. F. G., Lahoz, F. J., Lewis, J. and Raithby, P. R., *J. Chem. Soc., Dalton Trans.*, 1984, 2723.
22. (a) Pierpont, C. G., *Inorg. Chem.*, 1979, **18,** 2972; (b) Pierpont, C. G., Stuntz, G. F. and Shapley, J. R., *J. Am. Chem. Soc.*, 1978, 100, 616.
23. Khattar, R., Naylor, S., Vargas, M. D., Braga, D. and Grepioni, F., *Organometallics*, 1990, **9,** 645.
24. (a) Demartin, F., Manassero, M., Sansoni, M., Garlaschelli, L., Raimondi, C., Martinengo, S. and Canziani, F., *J. Chem. Soc., Chem. Commun.*, 1981, 528; (b) Angoletta, M., Malatesta, L. and Caglio, G., *J. Organomet. Chem.*, 1975, **94,** 99.

25. Nicholls, J. N., Raithby, P. R. and Vargas, M. D., *J. Chem. Soc., Chem. Commun.*, 1986, 16.
26. Whyman, R., *J. Chem. Soc., Dalton Trans.*, 1972, 2294.
27. (a) Sheldrick, G. M., *Acta Crystallogr.*, 1990, **A46**, 467; (b) Sheldrick, G. M., *SHELXL92, Program for Crystal Structure Determination*, University of Göttingen, Göttingen, Germany, 1993; (c) Keller, E., *SCHAKAL92 Graphical Representation of Molecular Models*, University of Freiburg, Germany, 1992.

Pergamon

PII: SO277-5387(98)00018-7

Polyhedron Vol. 17, No. 17, pp. 2877–2887, 1998
© 1998 Elsevier Science Ltd
All rights reserved. Printed in Great Britain
0277-5387/98 $19.00+0.00

C-C coupling reactions on a flexible Ru_3Pt framework: X-ray crystal structures of $Ru_3Pt[\mu_4\text{-}C(Bu^t)C(H)C\{C(Bu^t)\}\{C(H)C(Bu^t)\}]\{\mu\text{-}\sigma\text{-}\pi\text{-}C(H)=C(H)(Bu^t)\}(CO)_7(dppe)$, $Ru_3Pt[\mu_3\text{-}C(Bu^t)CC(Bu^t)CH_2](CO)_8(dppe)$ and $Ru_3Pt\{\mu_4\text{-}C(Ph)CCC(H)(Bu^t)\}(\mu_4\text{-}Te)(\mu\text{-}TePr^i)(CO)_6(dppe)$‡

Louis J. Farrugia*, Neil MacDonald and Robert D. Peacock

Department of Chemistry, University of Glasgow, Glasgow G12 8QQ, UK

(Received 9 October 1997: accepted 2 January 1998)

Abstract—Reaction of $Ru_3Pt(\mu\text{-}H)\{\mu_4\text{-}C{\equiv}C(Bu^t)\}(CO)_9(dppe)$ (**1**) with excess $HC{\equiv}CBu^t$ afforded three C-C coupled products, $Ru_3Pt[\mu_4\text{-}C(Bu^t)C(H)C\{C(Bu^t)\}\{C(H)C(Bu^t)\}]\{\mu\text{-}\sigma\text{-}\pi\text{-}C(H)=C(H)(Bu^t)\}(CO)_7(dppe)$ (**3**), and an inseparable mixture of the *trans*- and *gem*-isomers of $Ru_3Pt[\mu_3\text{-}C(Bu^t)CC(Bu^t)\cdot CH_2](CO)_8(dppe)$ **4a**. Single crystal X-ray structure determinations of **3** and ***gem*-4a** were undertaken. Cluster **3** contains an Ru_3Pt chain-skeleton with three metal-metal bonds and incorporates three molecules of $HC{\equiv}CBu^t$ as a σ-π-vinyl ligand and an unusual C-C coupled ligand. Cluster ***gem*-4a** contains a tetrahedral Ru_3Pt skeleton with a C-C coupled vinyl-alkyne ligand. Reaction of **1** with $HC{\equiv}CR$, R=Ph and $SiMe_3$ gave similar products **4b** and **4c** respectively, with evidence for all three possible isomers *cis*-, *trans*-, and *gem*, while reaction of **1** with $PhC{\equiv}CPh$ gave the expected *cis*-, *trans* mixture of isomers of **4d**. Treatment of **1** with $Pr^iTeC{\equiv}CPh$ afforded two isomers of $Ru_3Pt\{\mu_4\text{-}C(Ph)CCC(H)(Bu^t)\}(\mu_4\text{-}Te)(\mu\text{-}TePr^i)(CO)_6(dppe)$ (**5**) as an inseparable mixture. A single crystal X-ray structure determination of the isomer ***trans*-5** was undertaken. The Ru_3Pt skeleton consists of a distorted square plane with a μ_4-capping tellurium atom. The C-C coupled ligand μ_4-$C(Ph)CCC(H)(Bu^t)$ is bonded in an unusual fashion to all four metal atoms, and can be thought of as a metallated vinyl-alkyne.
© 1998 Elsevier Science Ltd. All rights reserved

Keywords: ruthenium-platinum cluster; alkynyl ligand; acetylide ligand; C-C coupling reaction, tellurium; telluro-alkyne; crystal structure.

The hydrido-alkynyl cluster $Ru_3Pt(\mu\text{-}H)\{\mu_4\text{-}C{\equiv}C(Bu^t)\}(CO)_9(L_2)$ (**1**, L_2 = dppe), containing a spiked-triangular metal skeleton, undergoes an interesting tautomerisation to the vinylidene cluster $Ru_3Pt\{\mu_4\text{-}C{=}CH(Bu^t)\}(CO)_9(L_2)$ (**2**, L_2 = dppe) which has a butterfly metal skeleton [1]. This reaction is reversible, and shows an inverse kinetic isotope effect, and the first order rate constant also shows a marked dependence on the nature of the chelating diphosphine L_2 [2,3]. The H-atom migration between the Ru-Ru bond and the vinylidene CH position has been shown to be intra-molecular [1,2], and the change in geometry of the metal skeleton has been followed directly using EXAFS [4]. In view of the continuing interest in C_2 chemistry in metal clusters [5], and of earlier studies on C-C coupling reactions of alkynes at metal clusters [6], we report herein some reactions of **1** with alkynes. Aspects of this work have been previously communicated in a review [7].

* Author to whom correspondence should be addressed.

‡ This article is dedicated to Lord Lewis on the occasion of his 70th birthday.

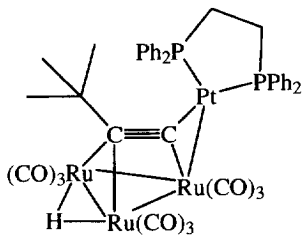

1

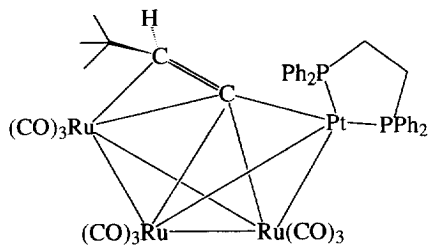

2

EXPERIMENTAL

All reactions were carried out under nitrogen using Schlenk tube techniques and freshly distilled dried solvents as previously reported [1]. The complex $Ru_3Pt(\mu\text{-}H)\{\mu_4\text{-}C{\equiv}C(Bu^t)\}(CO)_9(dppe)$ (**1**) was prepared in situ, as previously described [1]. All the alkynes, except $Pr^iTeC{\equiv}CPh$, were obtained from Aldrich Chemicals, and used as received. The literature route [8] was used to prepare $Pr^iTeC{\equiv}CPh$, which was stored in the dark at 5°C.

Reactions of $Ru_3Pt(\mu\text{-}H)\{\mu_4\text{-}C{\equiv}C(Bu^t)\}(CO)_9(dppe)$ (**1**) *with* $RC{\equiv}CR^1$

(*a*) R = Bu^t, R^1 = H. To a solution of 0.262 g (0.213 mmol) of **1** in 20 ml THF was added a large excess of $HC{\equiv}CBu^t$ (0.2 ml, 1.6 mmol). The resulting orange solution was heated under gentle reflux for a period of 16 hours, after which time the colour changed to deep red. The solvent was removed *in vacuo* and chromatography (Florisil, 2·20 cm column, hexanes/CH_2Cl_2 mixtures as eluant) of the red solid residue afforded two bands. The first band (total weight 0.086 g) was bright red and contained complex **3** $Ru_3Pt[\mu_4\text{-}C(Bu^t)C(H)C\{C(Bu^t)\}\{C(H)C(Bu^t)\}]\{\mu\text{-}\sigma\text{-}\pi\text{-}C(H){=}C(H)(Bu^t)\}(CO)_7(dppe)$, and the essentially inseparable, non-interconverting *gem* and *trans*-isomers of complex **4a** $Ru_3Pt[\mu_3\text{-}C(Bu^t)CCC(Bu^t)](CO)_8(dppe)$. The second orange-red band (0.107 g, 41%) contained cluster **2**. Fractional recrystallisation of the first band from hot n-octane gave yellow crystals (0.008 g, 3%) of complex **3**, and an inseparable red crystalline mixture (~0.05 g) of the isomers of **4a**. The two isomers are formed in equal proportions. The relative proportions could be changed on further fractional recrystallisation, but we were unable to obtain spectroscopically pure bulk samples of either isomer. A few crystals of pure *gem*-**4a** were obtained, and examined by X-ray crystallography. The spectroscopic assignments were made on the basis of examining several samples with differing relative concentrations of the two isomers. A ^{31}P NMR spectrum of the crystal sample from the X-ray analysis was used to confirm the relative assignments of the isomers, and to demonstrate that the crystal sample was representative of the bulk sample. Satisfactory microanalyses were obtained for **3** and for all the isomer mixtures of **4**. Only those resonances which could be unambiguously assigned to individual isomers are listed below.

Spectroscopic data for **3**. IR (cyclo-C_6H_{12}) ν(CO) 2050 (s), 2009 (m), 2000 (s), 1976 (s), 1969 (m), 1932 (w), 1925 (w) cm^{-1}. ^1H NMR ($CDCl_3$, 298 K) 8.37 [d, 1H, H (10), J(H-H) = 13.6 Hz], 8.10–7.03 [m, 20H, Ph], 6.55 [s, 1H, H (15), J(P-H) = 11 Hz], 4.27 [d, 1H, H (11), J(H-H) = 13.6 Hz], 1.35 [s, 9H, Bu^t] 1.29 [s, 9H, Bu^t], 0.97 [s, 9H, Bu^t], 0.22 [s, 9H, Bu^t]. ^{31}P NMR ($CDCl_3$, 298 K) δ 51.9 [d, 1P, J(P-P) = 10.3, J(Pt-P) = 2304 Hz], 50.6 [d, 1P, J(P-P) = 10.3, J(Pt-P) = 3136 Hz]. The signal for H (17) could not be unambiguously assigned, and is presumably obscured by other resonances. In view of the shorter distance between P1 and the Pt atom (see Table 2), the ^{31}P resonance at δ 50.6 with the largest J(Pt-P) is tentatively assigned to this phosphorus atom.

Spectroscopic data for gem-**4a**. ^1H NMR ($CDCl_3$, 298 K) δ 8.13–7.10 [m, 20H, Ph], 3.30 [s, 1H, C=C(H)], 1.60 [s, 9H, Bu^t], 0.99 [s, 9H, Bu^t], 0.78 [s, 1H, C=C(H)]. ^{31}P NMR ($CDCl_3$, 298 K) δ 56.4 [d, 1P, J(P-P) = 28.5, J(Pt-P) = 3541 Hz], 43.4 [d, 1P, J(P-P) = 28.5, J(Pt-P) = 2540 Hz]. In view of the shorter distance between P1 and the Pt atom (see Table 3), the ^{31}P resonance at δ 56.4 with the largest J(Pt-P) is tentatively assigned to this phosphorus atom.

Spectroscopic data for trans-**4a**. ^1H NMR ($CDCl_3$, 298 K) δ 8.10–7.03 [m, 20H, Ph], 4.05 [dd, 1H, C=C(H), J(H-H) = 10, J(P-H) = 1.5 Hz], 2.72 [d, 1H, C=C(H), J(H-H) = 10 Hz]. ^{31}P NMR ($CDCl_3$, 298 K) δ 58.9 [d, 1P, J(P-P) = 27, J(Pt-P) = 3539 Hz], 43.8 [d, 1P, J(P-P) = 27, J(Pt-P) = 2520 Hz].

(*b*) R = Ph, R^1 = H. A solution of 0.236 g (0.19 mmol) of **1** in 20 ml THF was treated with 0.2 ml (1.8 mmol) of $PhC{\equiv}CH$. After heating under gentle reflux for 17 h, workup as before afforded a bright red band (0.114 g) containing three compounds inseparable by chromatography, *trans*-**4b**, *gem*-**4b** and *cis*-**4b** in the ratio 50 : 32 : 18 respectively on the basis of integration of the ^{31}P NMR peaks.

Spectroscopic data for gem-**4b**. ^1H NMR ($CDCl_3$, 298 K) δ 8.20–6.15 [m, 25H, Ph], 3.42 [s, 1H, C=C(H)], 3.24–1.92 [m, 4H, CH_2], 1.34 [s, 9H, Bu^t], 0.78 [s, 1H, C=C(H)]. ^{31}P NMR ($CDCl_3$, 298 K) δ

57.5 [d, 1P, J(P-P) = 28, J(Pt-P) = 3531 Hz], 44.4 [d, 1P, J(P-P) = 28, J(Pt-P) = 2524 Hz].

Spectroscopic data for trans-**4b**. ^{1}H NMR ($CDCl_3$, 298 K) δ 7.77–6.86 [m, 25H, Ph], 4.80 [d, 1H, C=C(H), J(H-H) = 9.2 Hz], 3.24 [d, 1H, C=C(H), J(H-H) = 9.2 Hz], 3.14–1.68 [m, 4H, CH_2], 1.55 [s, 9H, Bu^t]. ^{31}P NMR ($CDCl_3$, 298 K) δ 61.3 [d, 1P, J(P-P) = 26, J(Pt-P) = 3549 Hz], 45.7 [d, 1P, J(P-P) = 26, J(Pt-P) = 2523 Hz].

Spectroscopic data for cis-**4b**. ^{1}H NMR ($CDCl_3$, 298 K) δ 8.02–6.28 [m, 25H, Ph], 5.24 [d, 1H, C=C(H), J(H-H) = 7 Hz], 4.36 [d, 1H, C=C(H), J(H-H) = 7 Hz], 3.19–2.10 [m, 4H, CH_2], 1.70 [s, 9H, Bu^t]. ^{31}P NMR ($CDCl_3$, 298 K) δ 58.2 [d, 1P, J(P-P) = 31, J(Pt-P) = 3522 Hz], 46.7 [d, 1P, J(P-P) = 31, J(Pt-P) = 2573 Hz].

(*c*) R = Me_3Si, R^1 = H. A solution of 0.137 g (0.11 mmol) of **1** in 20 ml THF was treated with 0.2 ml (0.14 g, 1.4 mmol) of $Me_3SiC{\equiv}CH$. After heating under gentle reflux for 14 h, workup as before afforded three bands. The second red band afforded a bright red solid (0.056 g) containing three compounds inseparable by chromatography, *gem*-**4c**, *trans*-**4c** and *cis*-**4c** in the ratio 46 : 43 : 11 respectively on the basis of integration of the ^{31}P NMR peaks. In addition cluster **2** (third band) and $Ru_3(\mu$-H)(C≡CBu^t)(CO)$_9$ (first band) were also isolated.

Spectroscopic data for gem-**4c**. ^{1}H NMR ($CDCl_3$, 298 K) δ 8.22–6.76 [m, 20H, Ph], 3.24–1.93 [m, 4H, CH_2], 3.14 [s, 1H, C=C(H)], 1.54 [s, 9H, Bu^t], 0.98 [s, 1H, C=C(H)], −0.02 [s, 9H, Me_3 Si]. ^{31}P NMR ($CDCl_3$, 298 K) δ 57.1 [d, 1P, J(P-P) = 28, J(Pt-P) = 3539 Hz], 44.3 [d, 1P, J(P-P) = 28, J(Pt-P) = 2529 Hz].

Spectroscopic data for trans-**4c**. ^{1}H NMR ($CDCl_3$, 298 K) δ 8.24–6.18 [m, 20H, Ph], 4.04 [dd, 1H, C=C(H), J(H-H) = 11.3, J(P-H) = 1 Hz], 3.27–1.99 [m, 4H, CH_2], 1.55 [s, 9H, Bu^t], 1.38 [d, 1H, C=C(H), J(H-H) = 11.3 Hz])], 0.03 [s, 9H, Me_3Si]. ^{31}P NMR ($CDCl_3$, 298 K) δ 59.1 [d, 1P, J(P-P) = 27, J(Pt-P) = 3538 Hz], 44.4 [d, 1P, J(P-P) = 27, J(Pt-P) = 2530 Hz].

Spectroscopic data for cis-**4c**. ^{1}H NMR ($CDCl_3$, 298 K) δ 1.06 [s, 9H, Bu^t], 0.03 [s, 9H, Me_3Si]. ^{31}P NMR ($CDCl_3$, 298 K) δ 60.5 [d, 1P, J(P-P) = 26, J(Pt-P) = 3554 Hz], 45.7 [d, 1P, J(P-P) = 26, J(Pt-P) = 2522 Hz].

(*d*) R = R^1 = Ph. To a solution of 0.105 g (0.11 mmol) of **1** in 20 ml THF was added 0.23 mmol of PhC≡CPh. After heating under gentle reflux for 17 h, workup as before afforded a single red band, giving a bright red solid (0.085 g) containing two compounds inseparable by chromatography, *cis*-**4d** and *trans*-**4d** in the ratio 91 : 9 respectively on the basis of integration of the ^{31}P NMR peaks.

Spectroscopic data for trans-**4d**. ^{1}H NMR ($CDCl_3$, 298 K) δ 7.98–6.49 [m, 30H, Ph], 4.8 [s, 1H, C=C(H)], 3.15–1.64 [m, 4H, CH_2], 1.41 [s, 9H, Bu^t], 1.38 [d, 1H, C=C(H), J(H-H) = 11.3 Hz])],0.03 [s, 9H, Me_3Si]. ^{31}P NMR ($CDCl_3$, 298 K) δ 57.8 [d, 1P, J(P-P) = 34, J(Pt-P) = 3460 Hz], 44.2 [d, 1P, J(P-P) = 34, J(Pt-P) = 2580 Hz].

Spectroscopic data for cis-**4d**. ^{1}H NMR ($CDCl_3$, 298 K) δ 8.02–6.46 [m, 30H, Ph], 3.19–1.60 [m, 4H, CH_2], 3.10 [s, 1H, C=C(H)], 1.22 [s, 9H, Bu^t]. ^{31}P NMR ($CDCl_3$, 298 K) δ 57.0 [d, 1P, J(P-P) = 28, J(Pt-P) = 3532 Hz], 44.2 [d, 1P, J(P-P) = 28, J(Pt-P) = 2535 Hz].

(*e*) R = TePr^i, R^1 = Ph. To a solution of 0.097 g (0.10 mmol) of **1** in 20 ml THF was added 0.54 mmol of Pr^{i}TeC≡CPh. After heating under gentle reflux for 18 h the solution became deep red-purple. Workup as before afforded, in addition to unreacted alkyne and cluster **2**, a purple-red band. On recrystallisation of this band from hexanes/CH_2Cl_2, a dark red crystalline solid (0.026 g) was obtained, which contained two compounds inseparable by chromatography, *trans*-**5** and (tentatively) *cis*-**5** in the ratio 85 : 15 respectively on the basis of integration of the ^{31}P NMR peaks. A ^{31}P spectrum of the sample used for X-ray crystallography was used for the relative assignments of the isomers.

Spectroscopic data for trans-**5**. ^{1}H NMR ($CDCl_3$, 298 K) δ 8.18–6.42 [m, 25H, Ph], 5.67 [s, 1H, C=C(H)], 3.28–2.15 [m, 4H, CH_2], 2.88 [septet, 1H, $CHMe_2$ J(H-H) = 7 Hz] 1.52 [d, 6H, $CHMe_2$, J(H-H) = 7Hz], 1.35 [s, 9H, Bu^t]. ^{31}P NMR ($CDCl_3$, 298 K) δ 47.0 [d, 1P, J(P-P) = 10, J(Pt-P) = 4767 Hz], 25.1 [d, 1P, J(P-P) = 10, J(Pt-P) = 2614 Hz]. In view of the shorter distance between P1 and the Pt atom (see Table 4), the resonance at δ 47.0 with the largest J(Pt-P) is tentatively assigned to this phosphorus atom.

Spectroscopic data for cis-**5**. ^{31}P NMR ($CDCl_3$, 298 K) δ 44.0 [d, 1P, J(P-P) = 9, J(Pt-P) = 4739 Hz], 23.7 [d, 1P, J(P-P) = 9, J(Pt-P) = 2573 Hz].

Crystallographic studies on 3, gem-**4a** *and* trans-**5**

Single crystals of suitable size were attached to glass fibres using acrylic resin, and mounted on a goniometer head in a general position. Data were collected in bisecting mode using graphite monochromated X-radiation (λ = 0.71073 Å) on an Enraf-Nonius CAD4 diffractometer. All data sets were collected at ambient temperature (nominally 293 K). Details of data collection procedures and structure refinements are given in Table 1. Unit cell dimensions were determined by refinement of the setting angles of 25 reflections. Standard reflections were measured every 2 h during data collection, and an interpolated correction was applied to the reflection data where necessary. Lorentz-polarisation corrections, and absorption corrections by the method of Stuart and Walker [9] were also applied. The structures were solved by direct methods (MITHRIL [10]) and subsequent electron density difference Fourier maps. Anisotropic thermal parameters were used for all non-H atoms in complexes **3** and *trans*-**5**, and for the Pt, Ru, P and O atoms in

Table 1. Experimental details of the crystallographic studies

Compound number	**3**	*gem*-**4a**	*trans*-**5**
Compound formula	$C_{57}H_{64}O_7P_2PtRu_3$	$C_{46}H_{44}O_8P_2PtRu_3$	$C_{49}H_{46}O_6P_2PtRu_3Te_2$
Compound colour	Yellow	Red	Red
M_r	1421.32	1285.05	1546.30
Space group	$P2_1/n$	$P\bar{1}$	$C2/c$
Crystal system	Monoclinic	Triclinic	Monoclinic
a (Å)	11.670(4)	13.155(8)	24.183(3)
b (Å)	26.582(9)	14.373(4)	19.502(5)
c (Å)	20.698(5)	16.701(7)	25.080(4)
α (°)		68.89(2)	
β (°)	96.19(3)	85.81(5)	116.56(1)
γ (°)		64.30(4)	
V (Å^{-3})	6383(3)	2641(2)	10580(3)
θ range for cell	11.6–13.9	11.2–13.5	11.4–13.3
Z	4	2	8
D_{calc} (g cm^{-3})	1.479	1.616	1.942
$F(000)$	2808	1248	5856
μ(Mo-K_α) (cm^{-1})	29.74	35.86	46.61
Scan mode	$\omega/2\theta$	$\omega/2\theta$	$\omega/2\theta$
θ range (°)	2.1–22.5	2.1–22.5	2.3–25.0
Crystal size (mm)	0.5 × 0.2 × 0.2	0.8 × 0.4 × 0.4	0.5 × 0.25 × 0.2
No. of data collected	9287	7235	9512
No. of unique data	8349	6876	9277
hkl (range)	0→12; −1→28; −22→22	0→14; −13→15; −17→17;	0→28; 0→23; −29→26
R_{int}	0.0458	0.0626	0.047
Standard reflections	(3 12 4)(5 −12 6)	(1 −7 −3)(5 7 2) (1 −6 −2)	(−7 −9 6)(−5 −3 −9)
No. of data in refinement	8349	6876	9277
No. of refined parameters	595	269	513
Final $R[I > 2\sigma(I)]$(all data)	0.063(0.116)	0.086(0.126)	0.040(0.096)
$R_w^2[I > 2\sigma(I)]$(all data)	0.160(0.198)	0.234(0.270)	0.093(0.103)
Goodness of fit S	1.041	1.122	0.985
Weighting parameters A and B	0.1051, 0.0	0.1349, 52.7633	0.0413, 0.0
Largest remaining feature in electron	1.22(max)	2.81(max)	1.08(max)
density map (eÅ^{-3})	−1.49(min)	−3.11(min)	−0.77(min)
Shift/esd in last cycle (max)	0.031	0.001	0.002

$R = \Sigma(|F_o| - |F_c|)/\Sigma(F_o)$; $wR2 = \{\Sigma(w(F_o^2 - F_c^2)^2)/\Sigma(w(F_o^2)^2)\}^{1/2}$.
$R_{int} = \Sigma|F_o^2 - F_o^2(\text{mean})|/\Sigma F_o^2$ (summation is carried out only where more than one symmetry equivalent is averaged).
Weight $W = [\sigma^2(F_o^2) + (AP)^2 + BP]^{-1}$ where $P = [F_o^2/3 + 2F_c^2/3]$.

gem-**4a**. Hydrogen atoms were included in calculated positions with C-H = 0.96 Å, except for some of the hydrogens bonded to the coordinated carbons of the organo-ligands. Those on carbons C10, C11, C15 and C17 in cluster **3**, and on C13 in *trans*-**5** were included in calculated positions assuming sp^2 hybridisation at these centres. Those on C11 in *gem*-**4a** were observed from Fourier maps and were included at the observed positions. They were allowed to ride on the carbon atom C11 during refinement. The crystal quality for **3** and particularly *gem*-**4a** was poor, and this is reflected in the final residuals. In view of this, isotropic rather than anisotropic thermal parameters were used for the C-atoms in *gem*-**4a**. Nevertheless, the main structural features of all clusters were clearly defined by the X-ray analyses. Calculations using PLATON [11] showed that all three crystals displayed voids in the lattice, presumably containing solvent molecules. Although weak peaks were observed in the Fourier maps close to these voids, indicative of disordered, partially occupied solvent molecules, in no case was it possible to refine any realistic solvent molecules. For this reason, the SQUEEZE procedure of van de Sluis and Spek [12] was used to model this aspect of the electron density. Refinement (SHELXL-97 [13]) was by full-matrix least-squares on F^2, using all the unique data and the weighting scheme $W = [\sigma^2(F_o)^2 + (AP)^2 + BP]^{-1}$ where $P = [F_o^2/3 + 2F_c^2/3]$. All calculations were carried out on a Pentium P120 PC, and ORTEP [14] thermal ellipsoid plots were obtained using the program ORTEP-3 for Windows [15].

RESULTS AND DISCUSSION

The reaction of the hydrido-alkynyl cluster $Ru_3Pt(\mu\text{-H})\{\mu_4\text{-C}{\equiv}\text{C(Bu}^t\text{)}\}\text{-(CO)}_9\text{(dppe)}$ (**1**) with

excess HC≡CBu^t afforded on workup a modest yield of a bright red solid which contained three complexes which proved inseparable by chromatography. Under the conditions of the experiment cluster **1** slowly tautomerises to the vinylidene cluster $Ru_3Pt\{\mu_4$-C=CH-(Bu^t)$\}(CO)_9$(dppe) (**2**) [1–3], and in a test reaction cluster **2** was found to react with HC≡CBu^t in an identical fashion to **1**. It is not clear whether **1** or **2** (or indeed both) are the reactive clusters, since the reaction is reversible [1–3], but in all experiments reported here, the more readily available cluster **1** was used.

Fractional recrystallisation of the bright red solid from hot n-octane allowed the isolation of a small sample of pure yellow $Ru_3Pt[\mu_4$-C(Bu^t)C(H)C{C(Bu^t)}{C(H)C(Bu^t)}]$\{\mu$-σ-π-C(H)≡C(H)(Bu^t)$\}(CO)_7$(dppe) (**3**), but we were unable to obtain pure samples of the isomers of red $Ru_3Pt\{\mu_3$-C(Bu^{2t})CC(Bu^t)CH$_2$$\}(CO)_8$(dppe) **4a**. The complexes were characterised by spectroscopic means, and for complexes **3** and the *gem*-isomer of **4a** also by single crystal X-ray diffraction. The relative proportions of the two isomers of **4a** could be changed somewhat by fractional crystallisation. This was most easily followed by ^{31}P NMR spectroscopy, where the signals from both isomers were clearly distinguished. Most of the ^{1}H resonances from both isomers could be identified, though due to signal overlaps, not all expected resonances could be unambiguously assigned.

An ORTEP [14] view of the molecular structure of **3** is shown in Fig. 1, with important metrical parameters given in Table 2. The cluster contains an Ru_3Pt chain, with three metal-metal bonds. The Pt atom is formally a 16-electron centre, and is coordinated to the dppe ligand, to one Ru atom [Ru-Pt = 2.730(2)Å), and is σ-bonded to C14. A complex C-C coupled ligand C(Bu^t)C(H)C{C(Bu^t)}{C(H)C(Bu^t)} is bonded to all four metal atoms. The carbon atoms C14=C15 act as a σ-π-vinyl ligand across the Pt-Ru1 vector, and hence are formally doubly bonded. The C14=C15 distance of 1.45(3) Å indicates a degree of π-delocalisation with the ruthena-cyclopentadienyl group, which comprises the ring of atoms Ru3=C20=C16=C17=C18. The six central C-atoms C14=C18 and C20 and the ruthenium atom Ru3 are virtually coplanar, the maximum deviation from their mean plane being 0.05(2) Å for C16. The carbons C10, C11, C15 and C17 each bear one hydrogen atom. The central ruthenium atoms Ru1 and Ru2 carry two terminal CO ligands each, and are bridged by the C10=C11 atoms of a second σ-π-vinyl ligand CH=CH(Bu^t). The Ru2 atom is bonded to all four atoms C16=C17=C18=C20, with marginally shorter distances to the inner carbons C16 and C17. The terminal ruthenium atom Ru3 bears three terminal CO ligands.

The μ_4-C(Bu^t)C(H)C{C(Bu^t)}{C(H)C(Bu^t)} ligand is derived either by C-C coupling of two HC≡CBu^t groups with the original alkynyl ligand in **1** (or the vinylidene ligand in **2**) or of three HC≡CBu^t molecules with each other. Since the Bu^t substituents on the alkyne and alkynyl ligands are identical, it is

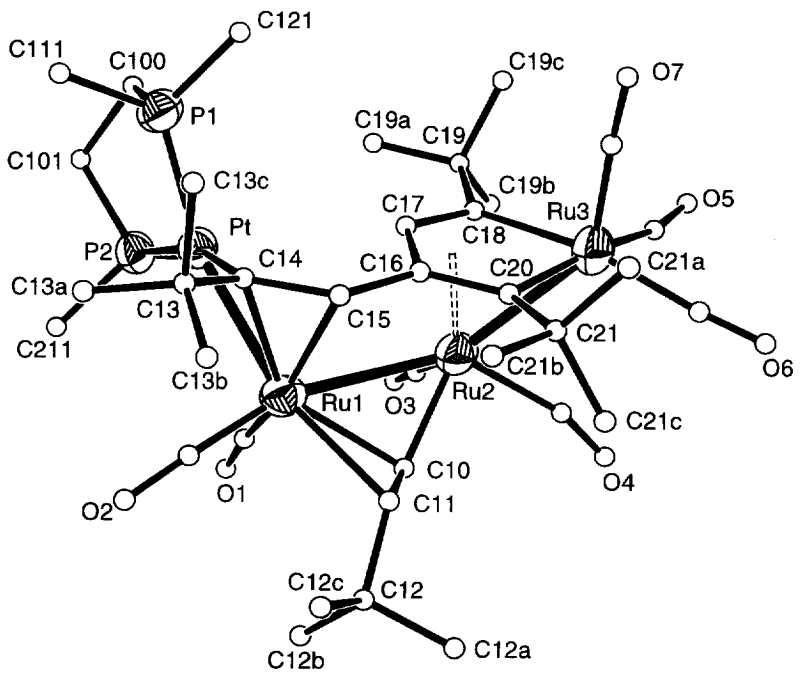

Fig. 1. Molecular structure and atomic labelling scheme for $Ru_3Pt[\mu_4$-C(Bu^t)C(H)C{C(Bu^t)}{C(H)C(Bu^t)}]$\{\mu$-σ-π-C(H)≡C(H)(Bu^t)$\}(CO)_7$(dppe) (**3**). Thermal ellipsoids are drawn at the 50% probability level, and C and O atoms are drawn as spheres of arbitary radius.

Table 2. Important bond lengths [Å] and bond angles (°) for $Ru_3Pt[\mu_4\text{-}C(Bu^t)C(H)C\{C(Bu^t)\}\{C(H)C(Bu^t)\}]\{\mu\text{-}\sigma\text{-}\pi\text{-}C(H)\equiv C(H)(Bu^t)\}(CO)_7(dppe)$ (**3**)

Pt—Ru1	2.730(2)	Ru2—C17	2.248(16)
Ru1—Ru2	2.921(2)	Ru2—C18	2.349(18)
Ru2—Ru3	2.720(2)	Ru2—C20	2.334(17)
Pt—P1	2.249(4)	Ru3—C18	2.096(17)
Pt—P2	2.305(4)	Ru3—C20	2.135(19)
Pt—C14	2.035(15)	C10—C11	1.34(2)
Ru1—C10	2.209(14)	C14—C15	1.45(2)
Ru1—C11	2.413(18)	C15—C16	1.45(2)
Ru1—C14	2.322(17)	C16—C17	1.44(2)
Ru1—C15	2.341(15)	C16—C20	1.39(2)
Ru2—C10	2.077(15)	C17—C18	1.42(2)
Ru2—C16	2.270		
Ru2—C10—C11	128.5(13)	C15—C16—C20	130.0(15)
C10—C11—C12	124.5(19)	C16—C17—C18	120.8(15)
Pt—C14—C15	122.4(14)	C17—C18—Ru3	111.0(13)
C14—C15—C16	134.5(14)	C16—C20—Ru3	114.7(12)
C15—C16—C17	116.4(14)		

not possible to distinguish these possibilities. Unfortunately, we are unable to isolate any analogs of **3** using alkyne reagents with differing substituents (see below). Nevertheless, it is clear that a total of three $HC\equiv CBu^t$ molecules have been incorporated into the cluster. A search of the Cambridge Crystallographic DataBase revealed that the connectivity of the μ_4-$C(Bu^t)C(H)C\{C(Bu^t)\}\{C(H)C(Bu^t)\}$ ligand in cluster **3** is unique. There are numerous examples of metallocyclopentadienyl units coordinated to a second metal atom (i.e. the so called ferrole structure), but very few with ligating substituents on the 1-, or 2-positions. One rare example is $Ru_3(CO)_8$ [RCC(Ph)(Ph)CR] [R = C(H)=C(H)(Ph)] reported by Koridze *et al.* [16] where one of the 1-vinyl groups is coordinated to an Ru atom.

The total cluster valence electron (CVE) count in cluster **3** is 64, assuming the μ_4-$C(Bu^t)C(H)C\{C(Bu^t)\}\{C(H)C(Bu^t)\}$ ligand acts as a 9-electron donor. This is consistent with the presence of three metal-metal bonds and a 16-electron Pt centre [17].

The cluster $Ru_3Pt\{\mu_3\text{-}C(Bu^t)CC(Bu^t)CH_2\}(CO)_8$ (dppe) *gem*-**4a** was also characterised by X-ray crystallography. An ORTEP [14] view of the molecular structure is shown in Fig. 2, with important metrical parameters given in Table 3. The cluster contains a tetrahedral Ru_3Pt arrangement, with rather unsymmetrical Pt-Ru distances [2.697(3)–2.982(3) Å]. The dppe ligand remains coordinated to the Pt atom. This atom is on the opposite side of the Ru_3 triangle to the hydrocarbyl ligand, with which it forms no bonds. This is in contrast to the situation found in **1** and **2** [1,2], where the hydrocarbyl ligand is bonded to all four metals. Ruthenium atoms Ru1 and Ru2 each bear three CO ligands, the carbonyl CO(6) being semi-bridging towards the Pt atom [Ru2=C6 = 2.02(3), Pt=C6 = 2.31(3) Å]. The ruthenium atom Ru3 bears two terminal CO ligands, and is also coordinated to the allylic C_3 fragment C11=C12=C13.

The μ_3-$C(Bu^t)CC(Bu^t)CH_2$ ligand coordinated to the three Ru atoms is the result of a head-to-tail C-C coupling of the original alkynyl (or vinylidene) ligand with one molecule of $HC\equiv CBu^t$. One possible description of this ligand is that of a vinyl substituted alkyne $(Bu^t)C\equiv C{=}C(Bu^t){=}CH_2$, with the alkyne component coordinated to the Ru_3 in the classic $\{\mu_3\text{-}\eta^2\text{-}(\|)\}$-mode [6a], and with the vinyl group η^2-coordinated to Ru3. This would give carbons C13 and C14 an *sp* hybridisation, with sp^2 hybridisation for carbons C12 and C11. The angles at these carbons (see Table 2), and the C-C distances of C11=C12 = 1.44(4), C12=C13 = 1.35(3), C13=C14 = 1.49(3) Å indicate that this is a simplification. All three distances are intermediate between single and double bonds. Alternatively, one may view the C11=C12=C13 section as an allyl group, which is metallated at the carbons C13 and C14. An identical ligand, coordinated in an identical fashion, has been previously reported by Aime *et al.* [18a] in the cluster $Ru_3(CO)_6\{\mu_3\text{-}C(Bu^t)CC(Bu^t)CH_2\}\{\mu_3\text{-}C(H)C(Bu^t)COC(Bu^t)CH]$ (this compound exists as two isomers [18b]), and by Gervasio *et al.* [19] in the cluster $Ru_3(CO)_5\{\mu_3\text{-}C(Bu^t)CH_2\}\{\mu_3\text{-}C(H)C(Bu^t)COC(Bu^t)CHC(Bu^t)CH]$. A closely related species is $Ru_3(CO)_7\{\mu_3\text{-}C(Bu^t)CC(Ph)CH(Ph)\}(C_2Ph_2)$[20].

The total CVE count in cluster **4a** is 60, assuming that the μ_3-$C(Bu^t)CC(Bu^t)CH_2$ ligand acts as a 6-electron donor. This is consistent with the presence of six metal-metal bonds and an 18-electron Pt centre [17]. The ^{31}P NMR data indicates that the two P atoms are inequivalent, which is consistent with the crystal structure. There was no evidence for exchange broad-

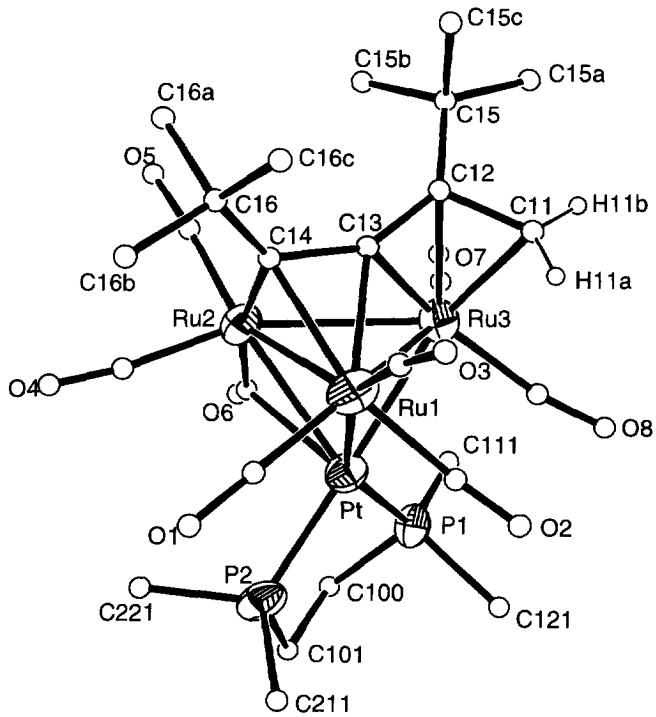

Fig. 2. Molecular structure and atomic labelling scheme for $Ru_3Pt\{\mu_3\text{-}C(Bu^t)CC(Bu^t)CH_2\}(CO)_8(dppe)$ (*gem*-**4a**). Thermal ellipsoids are drawn at the 50% probability level, and C, O and H atoms are drawn as spheres of arbitary radius.

Table 3. Important bond lengths (Å) and bond angles (°) for $Ru_3Pt\{\mu_3\text{-}C(Bu^t)CC(Bu^t)CH_2\}(CO)_8(dppe)$ (*gem*-**4a**)

Pt—Ru1	2.892(2)	Ru2—Ru3	2.903(3)
Pt—Ru2	2.771(3)	Ru2—C13	2.52(2)
Pt—Ru3	2.697(3)	Ru2—C14	2.14(2)
Pt—P1	2.281(5)	Ru3—C11	2.25(3)
Pt—P2	2.306(7)	Ru3—C12	2.25(2)
Pt—C6	2.31(3)	Ru3—C13	2.11(2)
Ru1—Ru2	2.802(3)	C11—C12	1.44(4)
Ru1—Ru3	2.768(3)	C12—C13	1.35(3)
Ru1—C13	2.23(2)	C13—C14	1.49(3)
Ru1—C14	2.24(2)	C14—C16	1.44(3)
Ru2—C6	2.02(3)	C12—C15	1.48(4)
C16—C14—C13	130(2)	C13—C12—C11	115(2)
C14—C13—C12	148(2)	C15—C12—C11	110(3)
Ru2—C14—C13	86.1(12)		
Ru3—C13—C14	131.6(15)		

ening at room temperature, indicating that any rotation of the Pt(dppe) fragment [2] was slow on the NMR timescale. The values of $J(^{195}Pt\text{-}P)$ for the high and low frequency ^{31}P resonances are in the narrow ranges of 3535 ± 15 Hz and 2550 ± 30 Hz respectively for all the derivatives **4** and their isomers (see Experimental Section). In conjunction with the similarity of chemical shifts, this proves very strong evidence that they all have closely similar structures.

There are potentially three isomers of **4a** (shown in the Scheme), depending on the stereo-geometry of the H atoms in the C-C coupled ligand, namely *gem*-**4a** observed in the crystal structure, *trans*-**4a** and *cis*-**4a**. The first isomer arises from a "head-to-tail" C-C coupling, while the latter two result from a "head-to-head" coupling. Only two isomers were observed for **4a**, the second isomer being assigned to *trans*-**4a** on the basis of the significant H-H coupling. The lack of

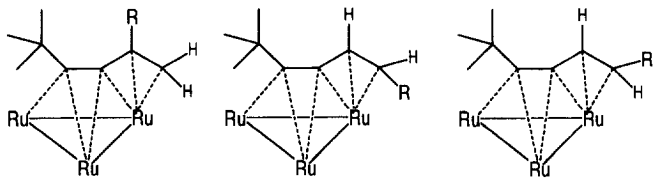

Scheme 1.

observable quantities of *cis*-**4a** is attributed to the steric bulk of the Bu^t group, which would cause unacceptable steric strain were it substituted in the position of H11a, see Fig. 2 and the space-fill view in Fig. 3.

Reactions of **1** with PhC≡CH and $Me_3SiC{\equiv}CH$ gave mixtures of three inseparable isomers of **4b** and **4c** respectively, which had closely similar ^{31}P NMR spectra. The Ph and $SiMe_3$ groups are evidently less sterically demanding than the Bu^t group in these compounds, since the cis isomers are also formed, albeit in minor proportions. It is somewhat surprising that the $SiMe_3$ derivative forms a cis isomer, but this is attributed to the expected larger C-Si distance as compared with the corresponding C-C distance (~1.85 versus 1.54 Å), which means that the bulky methyl groups are further from the terminal C-atom (C11 in Fig. 2). No evidence for analogs of compound **3** was obtained for these alkynes. Reaction of **1** with PhC≡CPh afforded two isomers of **4d**, as expected, with the Ph groups cis (main isomer) and trans. Again, the ^{31}P NMR spectra were very similar to the above mentioned derivatives.

We have previously reported [3] that the reaction of **1** with the phosphino-alkyne $Ph_2PC{\equiv}CPPh_2$ afforded modest yields of the two phosphido species, $Ru_3Pt(\mu_4\text{-}C{\equiv}CBu^t)(\mu\text{-}PPh_2)(CO)_7(dppe)$ and $Ru_3Pt\{\mu\text{-}C{\equiv}C(H)Bu^t\}(\mu\text{-}PPh_2)_2(CO)_7(dppe)$, the former being characterised by an X-ray structure. We did not isolate any C-C coupled products from this reaction. In view of the extensive cluster chemistry of phosphino-alkynes, often involving P=C bond cleavage, [21] it was decided to investigate the reactivity of **1** with a related telluro-alkyne ligand $Pr^tTeC{\equiv}CPh$.

The synthesis of a series of alkyltelluro-alkynes was reported by Comasseto and Dabdoub [8], though very little coordination chemistry of these potentially interesting ligands has been reported. Apart from a few simple coordination complexes [22], we are only aware of one crystallographically characterised cluster complex containing such a ligand, *viz* $Co_2(CO)_6[C_6Me_3H_2$-

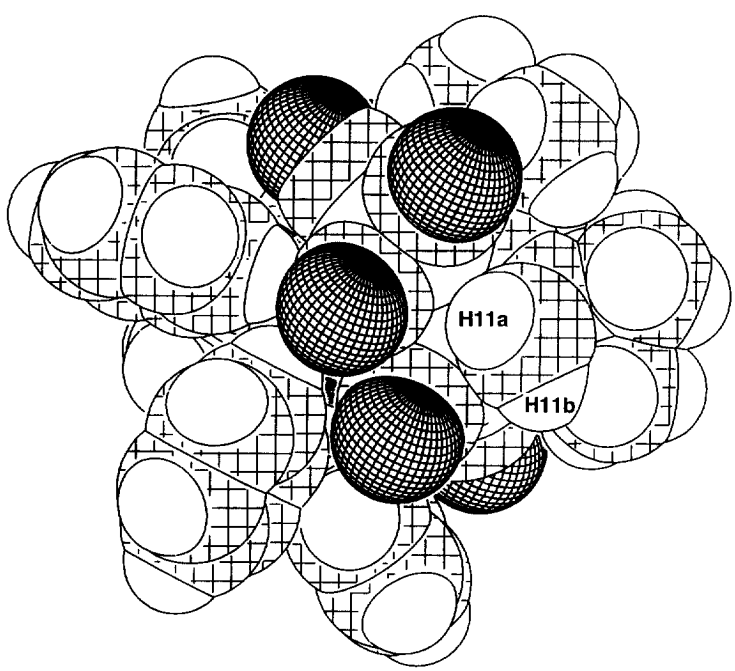

Fig. 3. Space-fill view of $Ru_3Pt\{\mu_3\text{-}C(Bu^t)CC(Bu^t)CH_2\}(CO)_8(dppe)$ (*gem*-**4a**). C atoms are shown as cross-hatched, O atoms are net-shaded globes and H atoms have no shading.

$TeC{\equiv}CSiMe_3$} [23]. The reaction of **1** with excess $Pr^iTeC{\equiv}CPh$ afforded modest yields of a crystalline mixture of two complexes in the ratio 85 : 15 which proved inseparable by chromatography. A single crystal X-ray structure of the major component showed it to have the composition $Ru_3Pt\{\mu_4\text{-}C(Ph)CCC(H)(Bu^t)\}(\mu_4\text{-}Te)(\mu\text{-}TePr^i)(CO)_6(dppe)$ (*trans*-**5**). In view of the similarity of the ^{31}P NMR spectra of both compounds (see Experimental Section), we tentatively assign the minor component as the isomer *cis*-**5**, with the alternate stereo-geometry at C13. Due to the small quantities available, we have not examined this minor product in any more detail.

The molecular structure of *trans*-**5** is shown in Fig. 4, and important bond lengths and angles are given in Table 4. The complex retains the Ru_3Pt skeleton, with four metal-metal bonds, though the Pt=Ru3 distance of 3.1289(9) Å is somewhat longer than Pt=Ru1 = 2.9834(9) Å, and is best considered as a weak interaction. The metal skeletal geometry is a distorted square plane. If the μ_4-Te atom is treated as a 6-electron donor, and each M=C interaction as a σ-interaction, this results in an 18-electron count at each metal atom, and a CVE count of 66. This is consistent with three metal-metal bonds. The alternate treatment of the μ_4-Te atom as a 4-electron donor, giving a CVE count of 64, with four metal-metal bonds and an 18-electron Pt centre is also reasonable. It is probably preferable to treat the μ_4-Te atom as a part of the cluster core. Cluster *trans*-**5** has 8 skeletal electron pairs and may be viewed as an arachno-pentagonal bipyramid, which is consistent with the long Pt=Ru3 bond. A few similar examples [24] of clusters containing the μ_4-Te atom are known. The cluster $Fe_2Ru_2(\mu_4\text{-}Te)_2(CO)_{11}$ [24b] provides an interesting comparison with *trans*-**5**, in that treating the μ_4-Te atoms as formal 6-electron donors gives a CVE count of 66, and the Fe=Fe distance of 2.872(4) Å is substantially longer than is normal for an Fe=Fe bond.

The μ_4-C(Ph)CCC(H)(Bu^t) ligand is derived from a heat to tail C-C coupling of the alkynyl ligand in **1** (or the vinylidene ligand in **2**) with a C≡CPh group resulting from cleavage of the ligand $Pr^iTeC{\equiv}CPh$. It may be thought of as a coordinated vinyl-alkyne, where the C_1 atom of the vinyl group (C12 in Fig. 4) is metallated. The bonding of the resultant C_4 fragment to a tetra-metallic skeleton is unique, though it is related to the bonding of the diyne in $Ru_4(CO)_{10}(\mu_4\text{-}PR)\{\mu_4\text{-}RC{\equiv}C{=}C{\equiv}CR\}$ (**6a** R = C≡CBu^t, R = Bu^t [25a], **6b** R = Me_3Si, R = Me [25b]. In *trans*-**5** the C_4 ligand is a 7-electron donor, while the diyne ligand in **6** is an 8-electron donor. In both cases the formalism describing the nature of the C_4 ligands is clearly simplistic, as may be judged from the C=C bond lengths. In both complexes *trans*-**5** and **6**, the central C=C bond is the shortest one, and Carty and coworkers [25a] have suggested the diyne ligand in **6a** may be considered as a bis(alkylidyne) dicarbide. The formation of the C-C coupled ligand in *trans*-**5** may be a further example of the activating influence of

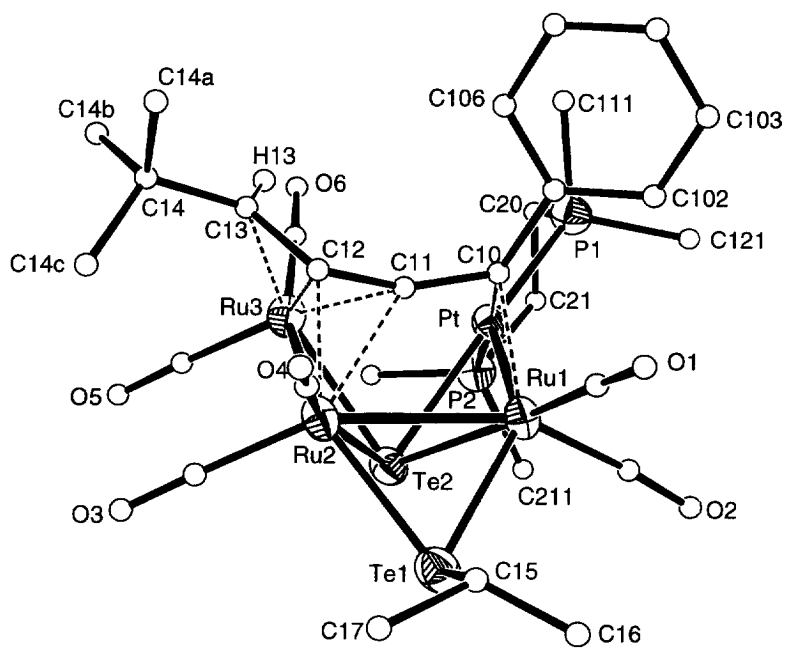

Fig. 4. Molecular structure and atomic labelling scheme for $Ru_3Pt\{\mu_4\text{-}C(Ph)CCC(H)(Bu^t)\}(\mu_4\text{-}Te)(\mu\text{-}TePr^i)(CO)_6(dppe)$ (*trans*-**5**). Thermal ellipsoids are drawn at the 50% probability level, and C, O and H atoms are drawn as spheres of arbitary radius.

Table 4. Important bond lengths (Å) and bond angles (°) for $Ru_3Pt\{\mu_4$-C(Ph)CCC(H)(Bu^t)$\}$ (μ_4-Te)(μ-TePr^i)(CO)$_6$(dppe)(*trans*-**5**)

Pt—Ru1	2.9834(9)	Ru2—Ru3	2.800(1)
Pt—Ru3	3.1289(9)	Ru2—Te1	2.665(1)
Pt—Te2	2.715(1)	Ru2—Te2	2.811(1)
Pt—P1	2.258(3)	Ru2—C11	2.337(10)
Pt—P2	2.305(2)	Ru2—C12	2.112(10)
Pt—C10	2.133(9)	Ru3—Te2	2.686(1)
Ru1—Ru2	2.849(1)	Ru3—C11	2.267(10)
Ru1—Te1	2.644(1)	Ru3—C12	2.132(9)
Ru1—Te2	2.749(1)	Ru3—C13	2.220(10)
Ru1—C10	2.181(9)	C10—C101	1.493(10)
C10—C11	1.397(13)	C11—C12	1.321(13)
C12—C13	1.422(14)	C13—14	1.511(15)
C101—C10—Pt	128.4(6)	C11—C12—C13	128.7(10)
C101—C10—Ru1	124.1(6)	C11—C12—Ru2	82.3(6)
C101—C10—C11	119.4(7)	C11—C12—Ru3	78.2(6)
C10—C11—C12	159.3(9)	C12—C13—C14	131.6(11)
C10—C11—Ru2	133.8(7)		
C10—C11—Ru3	123.6(7)		

main group elements [see reference 25b and references therein]. A related metallated alkynyl fuctionalised vinylidene ligand bonded to an Ru_2Pt cluster in $Ru_2Pt(CO)_6(\mu$-$PPh_2)(\mu_3$-C=C=C≡CBu^t) has also been reported recently [26].

CONCLUSIONS

Cluster **1** (or **2** or both) readily react with a variety of alkynes to undergo C-C coupling reactions under mild conditions. Modest to reasonable yields of these products were obtained. In cases where isomers of the C-C coupled ligand are possible, all isomers were observed except for **4a**. The Ru_3Pt skeleton remains intact throughout these reactions, although the number of metal-metal bonds in the products differs. These reactions provide further evidence for the flexibility of the metal skeleton in platinum-containing cluster compounds [7,17].

Supplementary material—Tables of atomic coordinates and equivalent isotropic thermal parameters, anisotropic thermal parameters and a complete listing of bond lengths and bond angles for complexes **3**, *gem*-**4a** and *trans*-**5**. Tables of observed and calculated structure factors are available from LJF on request.

Acknowledgements—Financial support from the EPSRC towards the purchase of a diffractometer is greatly appreciated. The University of Glasgow is also thanked for a studentship for NM.

REFERENCES

1. Ewing, P. and Farrugia, L. J., *Organometallics*, 1989, **8**, 1246.
2. Farrugia, L. J., McDonald, N. and Peacock, R. D., *J. Clust. Sci.*, 194, **5**, 341.
3. Farrugia, L. J., McDonald, N. and Peacock, R. D., *J. Chem. Soc., Chem. Commun.*, 1991, 163.
4. Dent, A. J., Farrugia, L. J., Orpen, A. G. and Stratford, S. E., *J. Chem. Soc., Chem. Commun.*, 1992, 1456.
5. Bruce, M. I., *J. Clust. Sci.*, 1997, **8**, 293, and refs therein.
6. (a) Raithby, P. R. and Rosales, M. J., *Adv. Inorg. Radiochem.*, 1985, **29**, 169. (b) Sappa, E., *J. Clust. Sci.*, 1994, **5**, 211. (c) Sappa, E., Tiripicchio, A. and Braunstein, P., *Chem. Rev.*, 1983, **83**, 203.
7. Farrugia, L. J., *J. Clust. Sci.*, 1992, **3**, 361.
8. Dabdoub, M. J. and Comasseto, J. V., *Organometallics*, 1988, **7**, 84.
9. Walker, N. and Stuart, D., *Acta. Crystallogr., Sect. A.*, 1983, **A39**, 158.
10. Gilmore, C. J., *J. Appl. Cryst.*, 1984, **17**, 42.
11. Spek, A. L., *Acta. Crystallogr., Sect. A.*, 1990, **A46**, C34.
12. Sluis, P. v. d. and Spek, A. L., *Acta Crystallogr., Sect. A.*, 1990, **A46**, 194.
13. Sheldrick, G. M.: SHELXL97, Program for crystal structure refinement, University of Gôttingen, 1997.
14. Burnett, M. N. and Johnson, C. K.: ORTEP-III, Program for thermal ellipsoid plots, Oak Ridge National Laboratory, Oak Ridge, Tennessee, ORNL-6895, 1996.
15. Farrugia, L. J., *J. Appl. Cryst.*, 1997, **30**, 565.
16. Koridze, A. A., Zdanovich, V. I., Dolgushin, F. M., Yanovsky, A. I., Struchkov, Yu. T. and Petrovsk, P. V., *Izv. Akad. Nauk., Ser. Khim.*, 1994, 2049.
17. Farrugia, L. J., *Adv. Organometallic Chem.*, 1990, **31**, 301.
18. (a) Aime, S., Gervasio, G., Milone, L., Sappa, E. and Franchini-Angela, M., *Inorg. Chim. Acta.*,

1978, **27,** 145. (b) Gervasio, G., Aime, S., Milone, L., Sappa, E. and Franchini-Angela, M., *Transition Met. Chem.*, 1976, **1,** 96.
19. Gervasio, G., Sappa, A., Manotti-Lanfredi, A. M. and Tiripicchio, A., *Inorg. Chim. Acta*, 1983, **68,** 171.
20. Sappa, E., Manotti-Lanfredi, A. M., Predieri, G. and Tiripicchio, A., *Inorg. Chim. Acta*, 1982, **61,** 217.
21. (a) Carty, A. J., *Pure Appl. Chem.*, 1982, **54,** 113. (b) Carty, A. J., *Adv. Chem., Ser.*, 1982, **196,** 163.
22. (a) Plate, M., Hofacker, P., Massa, W., Schwartz, B., Neumuller, B. and Dehnicke, K., *Z. Naturforsch., Teil B*, 1993, **48,** 1105. (b) Plate, M., Wocadlo, S., Massa, W., Dehnicke, K. and Krautscheid, H., *Z. Anorg. Allg. Chem.*, 1995, **621,** 388. (c) Plate, M., Dehnicke, K., Magull, J., Goesmann, H. and Fenske, D., *Z. Anorg. Allg. Chem.*, 1995, **621,** 393.
23. Keller, H., Daran, J. C. and Lang, H., *J. Organomet. Chem.*, 1994, **482,** 63.
24. (a) Mathur, P., Thimmappa, B. H. S. and Rheingold, A. L., *Inorg. Chem.*, 1990, **29,** 4658. (b) Mathur, P., Mavunkal, I. J., Rugmini, V. and Mahon, M. F., *Inorg. Chem.*, 1990, 4838.
25. (a) Bobbie, B. J., Taylor, N. J. and Carty, A. J., *J. Chem. Soc., Chem. Commun.*, 1991, 1511. (b) Corrigan, J. F., Docherty, S., Taylor, N. J. and Carty, A. J., *Organometallics*, 1993, **12,** 1365.
26. Blenkiron, P., Enright, G. D. and Carty, A. J., *J. Chem. Soc., Chem. Commun.*, 1997, 483.

Pergamon

PII: S0277-5387(98)00017-5

Polyhedron Vol. 17, No. 17, pp. 2889–2897, 1998
© 1998 Elsevier Science Ltd
All rights reserved. Printed in Great Britain
0277-5387/98 $19.00+0.00

Structural characterization of [Crypt221-Na]$_2$[$H_2Ru_4(CO)_{12}$] and [Crypt222-K]$_2$[$Ru_4(CO)_{13}$]

Robert Suter, Alak A. Bhattacharyya, L.-Y. Hsu, Jeanette A. Krause Bauer and Sheldon G. Shore*

Department of Chemistry, The Ohio State University, Columbus, OH 43210

(Received 6 November 1997; accepted 5 January 1998)

Abstract—The structures of [Crypt221-Na]$_2$[$H_2Ru_4(CO)_{12}$] and [Crypt222-K]$_2$[$Ru_4(CO)_{13}$] were determined from single crystal X-ray diffraction studies. A survey of the structures of tetranuclear carbonyl clusters of the Group 8 metals and their conjugate bases is presented. The cluster core of $[H_2Ru_4(CO)_{12}]^{2-}$ is a tetrahedron of Ru atoms with three edge bridging carbonyls arranged around the base. Two single edge bridging hydrogens reside between the apical Ru atom and two basal Ru atoms. Two terminal carbonyls are bound to each basal Ru atom and three terminal carbonyls are bound to the apical Ru atom. The apical Ru atom has three terminal carbonyls bound to it. In addition, two singly bridging hydrogens occur between apical and basal rutheniums. The $[Ru_4(CO)_{13}]^{2-}$ dianion structure consists of a tetrahedral Ru_4 core with three edge bridging carbonyls arranged around the base. Two semi-edge bridging carbonyls reside between the apical and two basal Ru atoms. Crystal data for [Crypt221-Na]$_2$[$H_2Ru_4(CO)_{12}$]: space group $P\bar{1}$, $a = 13.718(2)$ Å, $b = 20.997(6)$ Å, $c = 10.344(1)$ Å, $\alpha = 97.02(2)^\circ$, $\beta = 92.81(1)^\circ$, $\gamma = 77.80(2)^\circ$, $V = 2889.56$ Å^3. Crystal data for [Crypt222-K]$_2$[$Ru_4(CO)_{13}$]: space group $P2_1/c$, $a = 11.221(3)$ Å, $b = 22.951(6)$ Å, $c = 25.219(6)$ Å, $\beta = 97.61(2)^\circ$, V = 6427.74 Å^3. © 1998 Elsevier Science Ltd. All rights reserved

While homonuclear and heteronuclear tetrahedral carbonyl hydride clusters of the iron subgroup and their conjugate anion Brönsted bases have been reported, gaps still remain with respect to structural information regarding arrangements of carbonyl groups as a function of charge on the cluster. In this respect we are interested in ligand arrangements in ruthenium carbonylate anions that were prepared earlier in this laboratory [1–3] as part of a program to develop systematic syntheses of such cluster complexes. The anion $[H_2Ru_4(CO)_{12}]^{2-}$ [1] is conveniently prepared by deprotonating $H_4Ru_4(CO)_{12}$ with KH (Reaction (1)). IR spectra and ^{13}C NMR spectra indicate that this anion contains bridging carbonyls and a structure was proposed [1]. Since the molecular structures of its conjugate Brönsted acids $H_4Ru_4(CO)_{12}$ [4], $[H_3Ru_4(CO)_{12}]^-$ [5,6], and its osmium cluster counterpart $[H_2Os_4(CO)_{12}]^{2-}$ [7] possess only terminal carbonyl groups, it was of interest to determine the solid state structure of $[H_2Ru_4(CO)_{12}]^{2-}$ to determine if the spectroscopic data accurately reflect the disposition of the carbonyl ligands.

$$H_4Ru_4(CO)_{12} + 2KH \xrightarrow{THF} K_2[H_2Ru_4(CO)_{12}] + 2H_2 \quad (1)$$

The anion $[Ru_4(CO)_{13}]^{2-}$ [2] is prepared by the stoichiometric reduction of $Ru_3(CO)_{12}$ according to the reaction shown below (Reaction (2)). This anion is highly fluxional in solution.

$$Ru_3(CO)_{12} + 3/2K(C_6H_5)_2CO \xrightarrow{THF} 3/4K_2[Ru_4(CO)_{13}] + 9/4CO \quad (2)$$

IR spectra suggest the presence of bridging carbonyls. Carbon-13 NMR spectra over the temperature range 20°C to −138°C display only a single resonace at 223.5 ppm, intermediate for bridge and terminal carbonyls. The conjugate acids of $[Ru_4(CO)_{13}]^{2-}$,

* Author to whom correspondence should be addressed.

Dedication: To Lord Jack Lewis, a true scholar and gentleman.

$[HRu_4(CO)_{13}]^-$ [8] and $H_2Ru_4(CO)_{13}$ [9] contain one edge-bridging and two semibridging carbonyls, respectively. It was of interest to determine the structure of $[Ru_4(CO)_{13}]^{2-}$ in order to learn how the carbonyl ligands are disposed with increasing charge in the sequence $H_2Ru_4(CO)_{13}$, $[HRu_4(CO)_{13}]^-$, and $[Ru_4(CO)_{13}]^{2-}$. Furthermore, it was of interest to compare the structure of $[Ru_4(CO)_{13}]^{2-}$ with that of the known structure of $[Fe_4(CO)_{13}]^{2-}$ [10,11], especially since the structure of $[HFe_4(CO)_{13}]^-$ [12] differs markedly from that of $[HRu_4(CO)_{13}]^-$.

In the present report, we provide structural details for the $[H_2Ru_4(CO)_{12}]^{2-}$ and $[Ru_4(CO)_{13}]^{2-}$ anions based upon X-ray diffraction analyses and we summarize available crystallographic results on the structures of tetrahedral homonuclear and heteronuclear clusters of the iron subgroup.

EXPERIMENTAL

Materials

All manipulations were carried out on a standard high vacuum line or in a glovebox. Solvents were dried and degassed according to standard procedures [13]. $Na_2H_2Ru_4(CO)_{12}$ and $K_2Ru_4(CO)_{13}$ were prepared by the literature methods [1,2]. Kryptofix-2.2.2 and Kryptofix-2.2.1 were purchased from MCB Manufacturing Chemists Inc. and used as received.

$[Crypt222\text{-}K]_2[Ru_4(CO)_{13}]$. Kryptofix-2.2.2 (13 mg, 0.035 mmol, 12% molar excess) and $K_2Ru_4(CO)_{13}$ (13 mg, 0.015 mmol) were combined in a 10 ml flask under a dry, oxygen-free atmosphere. Dry THF (4 ml) was condensed into the flask and stirred for 4 hrs. The solution was then filtered to yield very fine red crystals of $[Crypt222\text{-}K]_2[Ru_4(CO)_{13}]$. Additional crystals suitable for X-ray analysis were obtained from the filtrate after 24 h at room temperature.

$[Crypt221\text{-}Na]_2[H_2Ru_4(CO)_{12}]$. $[Crypt221\text{-}Na]_2[H_2Ru_4(CO)_{12}]$ was prepared in analogous fashion as that described above using Kryptofix-2.2.1 and $Na_2[H_2Ru_4(CO)_{12}]$.

X-ray crystallography

For X-ray examination and data collection, each crystal was sealed in a glass capillary and mounted on a goniometer head. All X-ray data were collected on an Enraf-Nonius CAD4 diffractometer with graphite-monochromated Mo-K_α radiation. Unit cell parameters and standard deviations were obtained by least squares refinement from 24 reflections, well-distributed in reciprocal space and lying in the 2θ range 20–30°. Intensity data were collected at 25°C in the ω-2θ scan mode for the range $4 \leqslant 2\theta \leqslant 50°$. Six standard reflections were monitored and showed no significant decay. The data were corrected for Lorentz and polarization effects. The intensities were also corrected for absorption by using an empirical method based upon measured ψ scans.

The structures were solved using a combination of direct methods for $[Crypt222\text{-}K]_2[Ru_4(CO)_{13}]$ or the Patterson function for $[Crypt221\text{-}Na]_2[H_2Ru_4(CO)_{12}]$, difference Fourier and least squares refinement on F using SDP (Structure Determination Package) [14]. A final difference Fourier synthesis showed no significant features. Table 1 summarizes the crystallographic data for $[Crypt221\text{-}Na]_2[H_2Ru_4(CO)_{12}]$ and $[Crypt222\text{-}K]_2[Ru_4(CO)_{13}]$.

RESULTS

Structure of $[H_2Ru_4(CO)_{12}]^{2-}$.

The molecular structure of $[H_2Ru_4(CO)_{12}]^{2-}$ is shown in Fig. 1. Interatomic distances and angles are collected in Tables 2 and 3, respectively.

The Ru_4 core of the $[H_2Ru_4(CO)_{12}]^{2-}$ cluster is a tetrahedron with three edge-bridging carbonyls arranged around the base. Two terminal carbonyls are bound to each basal Ru atom while the apical Ru(4) binds to three terminal carbonyls. Although not located directly in the structure determination, two singly bridging hydrogens that span the Ru(1)—Ru(4) and Ru(3)—Ru(4) bonds are inferred as indicated by the long Ru—Ru distances (ave. 2.973 Å) compared to the Ru(2)—Ru(4) bond length of 2.820(1) Å. "Long" Ru—Ru distances that are hydrogen bridged (2.92–2.93 Å) and "short" Ru-Ru distances that are not hydrogen bridged (2.80 Å) have been observed in $[H_3Ru_4(CO)_{12}]^-$, the isomer of C_2 symmetry, for which the bridge hydrogens were located [5]. Other examples: $H_4Ru_4(CO)_{12}$ [4] and $H_2Ru_4(CO)_{13}$ [9] also have "long" and "short" Ru-Ru distances, with the long distances inferring the presence of bridge hydrogens and the short distances unbridged.

Carbonyl bridged Ru—Ru distances in $[H_2Ru_4(CO)_{12}]^{2-}$ are on the average 2.770 Å. The terminal carbonyls on the Ru(4) apex are staggered with respect to the three cluster faces with the common vertex Ru(4). The carbonyl that is staggered with respect to the Ru(1)—Ru(3)—Ru(4) face has a Ru(4)—C(43) distance of 1.917(3) Å and M—Ru(4)—C(43) angles where (M=Ru(1) or Ru(3) $\approx$ 113.5°) that are longer and more obtuse, respectively, than the remaining carbonyls on Ru(4) which have Ru—C distances of 1.88—1.89 Å and angles of 84.6–97.7°. This effect is attributed to the presence of hydrogen atoms that are situated along the Ru(4)—Ru(3) and Ru(4)—Ru(1) edges of the Ru(1)—Ru(4)—Ru(3) face.

Structure of $[Ru_4(CO)_{13}]^{2-}$. The molecular structure of $[Ru_4(CO)_{13}]^{2-}$ is shown in Fig. 1. Interatomic distances and angles are given in Tables 4 and 5, respectively. The $[Ru_4(CO)_{13}]^{2-}$ anion structure is based on a tetrahedral Ru_4 core. The apical ruthenium Ru(3) is

Table 1. Crystal data for $[Crypt222\text{-}K]_2[Ru_4(CO)_{13}]$ and $[Crypt221\text{-}Na]_2[H_2Ru_4(CO)_{12}]$

	$[Crypt222\text{-}K]_2[Ru_4(CO)_{13}]$	$[Crypt221\text{-}Na]_2[H_2Ru_4(CO)_{12}]$
Formula	$Ru_4K_2O_{25}N_4C_{49}H_{72}$	$Ru_4Na_2O_{22}N_4C_{44}H_{66}$
Color, habit	Dark red plate	Red needle
Size (mm)	$0.20 \times 0.70 \times 0.75$	$0.35 \times 0.38 \times 0.70$
Crystal system	Monoclinic	Triclinic
Space group	$P2_1/c$	$P\bar{1}$
Z	4	2
a (Å)	11.221(3)	13.718(2)
b (Å)	22.951(6)	20.997(6)
c (Å)	25.219(6)	10.344(1)
α (°)		97.02(2)
β (°)	97.61(2)	92.81(1)
γ (°)		77.80(2)
V (Å^3)	6427.74	2889.56
Min/max T (%)	99.98/70.24	99.97/92.59
No. unique reflns	10,868	10,752
No. reflns > 3σ(I)	7998	8697
R_f	0.042	0.029
wR	0.060	0.035

$R_f = \Sigma(|F_o| - |F_c|)/\Sigma|F_o|$
$wR = \Sigma w^{1/2}(|F_o| - |F_c|)/\Sigma w^{1/2}|F_o|$

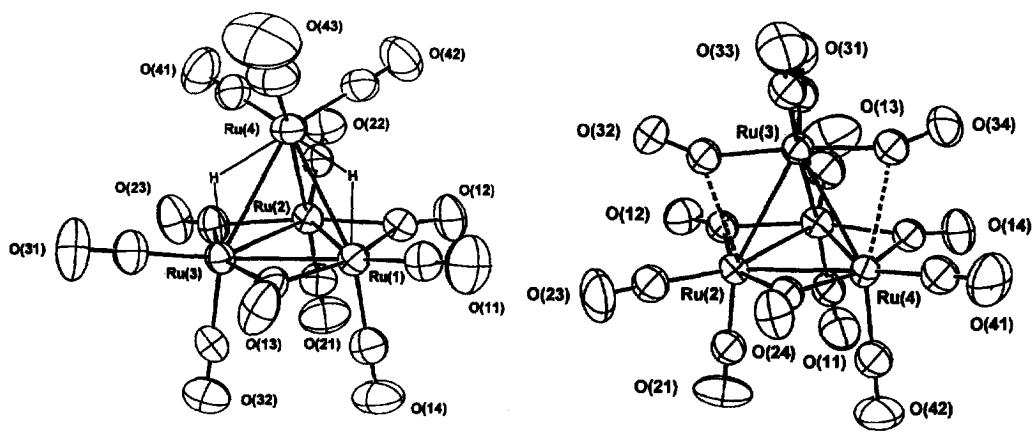

$[H_2Ru_4(CO)_{12}]^{2-}$ $[Ru_4(CO)_{13}]^{2-}$

Fig. 1. X-ray structures of $[Ru_4(CO)_{13}]^{2-}$ and $[H_2Ru_4(CO)_{12}]^{2-}$.

bound to four carbonyls, two of which are semibridging to the basal rutheniums Ru(2) and Ru(4). Distances of these ruthenium atoms to the carbonyl carbons are Ru(2)...C(32)=2.439(4) Å and Ru(4)...C(34)=2.592(4) Å, while the ruthenium–carbonyl bond angles are Ru(3)—C(32)—O(32)=153.6(4)° and Ru(3)—C(34)—O(34)=160.1(4)°. The semibridging carbonyls in the parent cluster, $H_2Ru_4(CO)_{13}$, have similar bonding distances and angles (2.31–2.47 Å, 144–154°) [9]. The distances of the Ru(3) atom to the carbons of the semibridging carbonyls are significantly longer than the distances of the Ru(3) atom to the terminal carbonyls: Ru(3)—C(32)=1.959(4) Å and Ru(3)—C(34)=1.941(4) Å as compared to Ru(3)—C(31)=1.882(5) Å and Ru(3)—C(33)=1.870(4) Å. Each basal ruthenium of the $[Ru_4(CO)_{13}]^{2-}$ anion has two terminal carbonyls bonded to it and is edge-bridged to each of the other rutheniums *via* a slightly asymmetric carbonyl bridge.

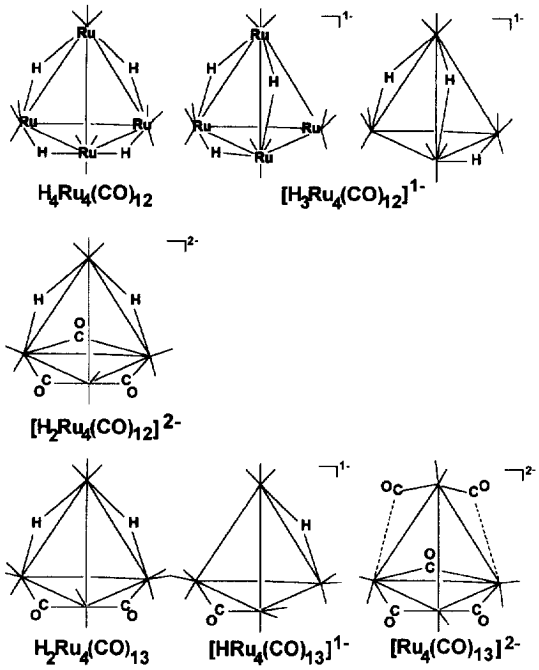

Fig. 2. Comparison of structures of $H_4Ru_4(CO)_{12}$ and $H_2Ru_4(CO)_{13}$ and their conjugate bases.

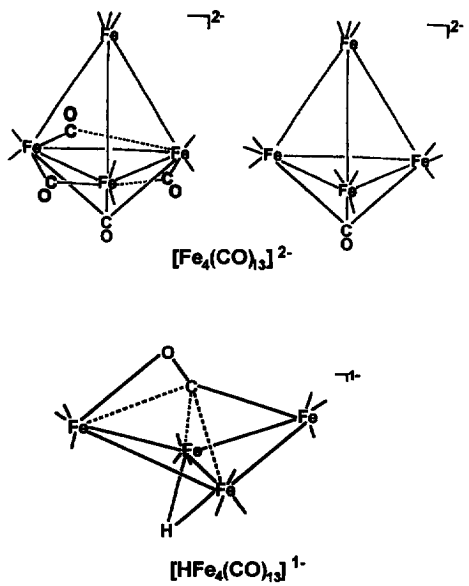

Fig. 3. Comparison of the structures of $[Fe_4(CO)_{13}]^{2-}$ and $[HFe_4(CO)_{13}]^{-}$.

The basal Ru—Ru bond lengths average 2.779 Å while the apical Ru bonds are somewhat longer (ave. 2.864 Å). Similar values are observed for the carbonyl bridged Ru—Ru and unbridged Ru—Ru distances in $[H_2Ru_4(CO)_{12}]^{2-}$ and $[HRu_4(CO)_{13}]^{-}$ [8].

Table 2. Selected bond distances (Å) for [Crypt221-Na]$_2$[$H_2Ru_4(CO)_{12}$]

(a) Ru—Ru distances			
Ru(1)—Ru(2)	2.763(1)	Ru(2)—Ru(3)	2.785(1)
Ru(1)—Ru(3)	2.762(1)	Ru(2)—Ru(4)	2.820(1)
Ru(1)—Ru(4)	2.976(1)	Ru(3)—Ru(4)	2.970(1)
(b) Ru—$C_{terminal}$ distances			
Ru(1)—C(11)	1.872(3)	Ru(3)—C(31)	1.866(3)
Ru(1)—C(14)	1.864(3)	Ru(3)—C(32)	1.855(3)
Ru(2)—C(21)	1.862(3)	Ru(4)—C(41)	1.883(3)
Ru(2)—C(22)	1.860(2)	Ru(4)—C(42)	1.886(3)
		Ru(4)—C(43)	1.917(3)
(c) Ru—C_{bridge} distances			
Ru(1)—C(12)	2.115(2)	Ru(2)—C(23)	2.068(3)
Ru(1)—C(13)	2.124(2)	Ru(3)—C(13)	2.102(2)
Ru(2)—C(12)	2.123(3)	Ru(3)—C(23)	2.150(2)
(d) C—O distances			
C(11)—O(11)	1.139(3)	C(23)—O(23)	1.170(3)
C(12)—O(12)	1.166(3)	C(31)—O(31)	1.150(3)
C(13)—O(13)	1.166(3)	C(32)—O(32)	1.138(3)
C(14)—O(14)	1.140(3)	C(41)—O(41)	1.159(3)
C(21)—O(21)	1.148(3)	C(42)—O(42)	1.153(3)
C(22)—O(22)	1.153(3)	C(43)—O(43)	1.130(3)

Table 3. Selected bond angles (°) for [Crypt221-Na]$_2$[$H_2Ru_4(CO)_{12}$]

(a) Ru—Ru—Ru angles			
Ru(2)—Ru(1)—Ru(3)	60.54(1)	Ru(1)—Ru(3)—Ru(2)	59.75(1)
Ru(2)—Ru(1)—Ru(4)	58.72(1)	Ru(1)—Ru(3)—Ru(4)	62.42(1)
Ru(3)—Ru(1)—Ru(4)	62.23(1)	Ru(2)—Ru(3)—Ru(4)	58.56(1)
Ru(1)—Ru(2)—Ru(3)	59.71(1)	Ru(1)—Ru(4)—Ru(2)	56.87(1)
Ru(1)—Ru(2)—Ru(4)	64.41(1)	Ru(1)—Ru(4)—Ru(3)	55.35(1)
Ru(3)—Ru(2)—Ru(4)	64.01(1)	Ru(2)—Ru(4)—Ru(3)	57.43(1)
(b) Ru—Ru—C angles			
Ru(2)—Ru(1)—C(11)	151.02(7)	Ru(1)—Ru(3)—C(13)	49.54(6)
Ru(2)—Ru(1)—C(12)	49.44(7)	Ru(1)—Ru(3)—C(23)	107.16(7)
Ru(2)—Ru(1)—C(13)	109.33(7)	Ru(1)—Ru(3)—C(31)	153.80(8)
Ru(2)—Ru(1)—C(14)	97.80(8)	Ru(1)—Ru(3)—C(32)	97.70(8)
Ru(3)—Ru(1)—C(11)	144.40(7)	Ru(2)—Ru(3)—C(13)	109.24(6)
Ru(3)—Ru(1)—C(12)	109.98(7)	Ru(2)—Ru(3)—C(23)	47.43(7)
Ru(3)—Ru(1)—C(13)	48.84(7)	Ru(2)—Ru(3)—C(31)	142.28(8)
Ru(3)—Ru(1)—C(14)	98.33(8)	Ru(2)—Ru(3)—C(32)	100.18(8)
Ru(4)—Ru(1)—C(11)	113.19(8)	Ru(4)—Ru(3)—C(13)	85.46(7)
Ru(4)—Ru(1)—C(12)	80.78(7)	Ru(4)—Ru(3)—C(23)	80.45(7)
Ru(4)—Ru(1)—C(13)	84.95(6)	Ru(4)—Ru(3)—C(31)	112.35(9)
Ru(4)—Ru(1)—C(14)	154.28(9)	Ru(4)—Ru(3)—C(32)	155.69(8)
Ru(1)—Ru(2)—C(12)	49.19(6)	Ru(1)—Ru(4)—C(41)	139.00(9)
Ru(1)—Ru(2)—C(21)	107.21(8)	Ru(1)—Ru(4)—C(42)	97.68(8)
Ru(1)—Ru(2)—C(22)	142.58(8)	Ru(1)—Ru(4)—C(43)	113.6(1)
Ru(1)—Ru(2)—C(23)	109.67(7)	Ru(2)—Ru(4)—C(41)	84.63(9)
Ru(3)—Ru(2)—C(12)	108.90(6)	Ru(2)—Ru(4)—C(42)	85.79(9)
Ru(3)—Ru(2)—C(21)	108.76(8)	Ru(2)—Ru(4)—C(43)	169.1(1)
Ru(3)—Ru(2)—C(22)	142.17(8)	Ru(3)—Ru(4)—C(41)	93.81(9)
Ru(3)—Ru(2)—C(23)	49.97(7)	Ru(3)—Ru(4)—C(42)	141.80(9)
Ru(4)—Ru(2)—C(21)	84.51(7)	Ru(3)—Ru(4)—C(43)	113.5(1)
Ru(4)—Ru(2)—C(22)	96.05(8)	Ru(4)—Ru(2)—C(43)	85.58(8)
(c) C—Ru—C angles			
C(11)—Ru(1)—C(12)	103.5(1)	C(22)—Ru(2)—C(23)	99.5(1)
C(11)—Ru(1)—C(13)	96.7(1)	C(13)—Ru(3)—C(23)	156.65(9)
C(11)—Ru(1)—C(14)	92.4(1)	C(31)—Ru(3)—C(31)	106.0(1)
C(12)—Ru(1)—C(13)	158.6(1)	C(13)—Ru(3)—C(32)	91.7(1)
C(12)—Ru(1)—C(14)	91.6(1)	C(23)—Ru(3)—C(31)	96.6(1)
C(13)—Ru(1)—C(14)	94.5(1)	C(23)—Ru(3)—C(32)	93.5(1)
C(12)—Ru(2)—C(21)	92.8(1)	C(31)—Ru(3)—C(32)	91.7(1)
C(12)—Ru(2)—C(22)	100.1(1)	C(41)—Ru(4)—C(42)	92.4(1)
C(12)—Ru(2)—C(23)	158.85(9)	C(41)—Ru(4)—C(43)	102.9(1)
C(21)—Ru(2)—C(22)	93.2(1)	C(42)—Ru(4)—C(43)	101.7(1)
C(21)—Ru(2)—C(23)	94.0(1)		
(d) Ru—C—Ru angles			
Ru(1)—C(12)—Ru(2)	81.37(9)	Ru(2)—C(23)—Ru(3)	82.60(9)
Ru(1)—C(13)—Ru(3)	81.62(8)		
(e) Ru—C—O angles			
Ru(1)—C(11)—O(11)	177.4(2)	Ru(3)—C(31)—O(31)	177.5(3)
Ru(1)—C(14)—O(14)	179.0(2)	Ru(3)—C(32)—O(32)	179.2(3)
Ru(2)—C(21)—O(21)	177.7(3)	Ru(4)—C(41)—O(41)	179.8(3)
Ru(2)—C(22)—O(22)	178.6(2)	Ru(4)—C(42)—O(42)	178.3(3)
		Ru(4)—C(43)—O(43)	179.1(4)
Ru(1)—C(12)—O(12)	138.5(2)	Ru(2)—C(23)—O(23)	141.9(2)
Ru(1)—C(13)—O(13)	137.8(2)	Ru(3)—C(13)—O(13)	140.6(2)
Ru(2)—C(12)—O(12)	140.0(2)	Ru(3)—C(23)—O(23)	135.4(2)

Table 4. Selected bond distances (Å) for $[Crypt222\text{-}K]_2[Ru_4(CO)_{13}]$

(a) Ru—Ru distances			
Ru(1)—Ru(2)	2.777(1)	Ru(2)—Ru(3)	2.864(1)
Ru(1)—Ru(3)	2.859(1)	Ru(2)—Ru(4)	2.764(1)
Ru(1)—Ru(4)	2.797(1)	Ru(3)—Ru(4)	2.867(1)
(b) Ru—$C_{terminal}$ distances			
Ru(1)—C(11)	1.850(4)	Ru(3)—C(31)	1.882(5)
Ru(1)—C(13)	1.853(5)	Ru(3)—C(33)	1.870(4)
Ru(2)—C(21)	1.842(4)	Ru(4)—C(41)	1.856(5)
Ru(2)—C(23)	1.873(5)	Ru(4)—C(42)	1.855(5)
(c) Ru—C_{bridge} and Ru—$C_{semibridge}$ distances			
Ru(1)—C(12)	2.098(4)	Ru(2)—C(32)	2.439(4)
Ru(1)—C(14)	2.106(4)	Ru(3)—C(32)	1.959(4)
Ru(2)—C(12)	2.153(4)	Ru(3)—C(34)	1.941(4)
Ru(2)—C(24)	2.146(4)	Ru(4)—C(34)	2.592(4)
Ru(4)—C(14)	2.173(4)	Ru(4)—C(24)	2.087(4)
(d) C—O distances			
C(11)—O(11)	1.157(5)	C(31)—O(31)	1.157(5)
C(12)—O(12)	1.159(4)	C(32)—O(32)	1.166(5)
C(13)—O(13)	1.159(6)	C(33)—O(33)	1.137(5)
C(14)—O(14)	1.160(5)	C(34)—O(34)	1.160(5)
C(21)—O(21)	1.149(5)	C(41)—O(41)	1.155(5)
C(23)—O(23)	1.152(5)	C(42)—O(42)	1.135(5)
C(24)—O(24)	1.163(5)		

DISCUSSION

Figure 2 depicts schematic arrangements of carbonyl groups and hydrogens in the known structures of $H_4Ru_4(CO)_{12}$ and $H_2Ru_4(CO)_{13}$ and their conjugate bases $[H_3Ru_4(CO)_{12}]^-$, $[H_2Ru_4(CO)_{12}]^{2-}$, $[HRu_4(CO)_{13}]^-$, and $[Ru_4(CO)_{13}]^{2-}$. In the series defined by $H_4Ru_4(CO)_{12}$ [4], the removal of one proton results in the formation of two structurally identified isomers [5,6] of $[H_3Ru_4(CO)_{12}]^-$ which differ solely by the placement of bridging hydrogen atoms. The removal of a second proton results in the formation of $[H_2Ru_4(CO)_{12}]^{2-}$. In this case the three terminal carbonyls have moved to edge-bridging sites. This structure is consistent with that proposed earlier by Inkrott and Shore [1] based upon NMR and IR spectra. This difference in carbonyl arrangement in $[H_2Ru_4(CO)_{12}]^{2-}$ compared to $H_4Ru_4(CO)_{12}$ and $[H_3Ru_4(CO)_{12}]^-$ is believed to be due to the larger negative charge on the dianion and reflects a mode of averaging charge distribution in the cluster framework. Chini [15] found a linear relationship between the fractions of terminal carbonyl groups and the average negative charge per carbonyl group for a series of isoelectronic octahedral carbonyl rhodium clusters. It appears that the ability of carbonyl ligands to disperse electron density on a metal cluster decreases in the order face-bridging > edge-bridging > terminal [15,16].

Table 6 compares the known structures of tetrahedral clusters of the Group 8 metals of the type $H_{4-n}M_4(CO)_{12}^{-n}$ ($n = 0, 1, 2$). All of the Ru_4 and Os_4 clusters are essentially isostructural with the exception of $[H_2Ru_4(CO)_{12}]^{2-}$ and $[H_2Os_4(CO)_{12}]^{2-}$ [7] which reflects the well-known fact that the tendency for carbonyls to occupy bridging sites diminishes down the Fe, Ru, Os group. While two isomers [5,6] of $[H_3Ru_4(CO)_{12}]^-$ have been structurally identified (Figure 2) only the structure of C_2 symmetry has been positively identified for $[H_3Os_4(CO)_{12}]^-$ [5].

Table 6 also compares the known structures of tetrahedral clusters of the Group 8 metals that have 13 carbonyls. The arrangements of carbonyl groups on the metal cores of the $[Ru_4(CO)_{13}]^{2-}$ and $[Fe_4(CO)_{13}]^{2-}$ are markedly different. In the case of the ruthenium cluster anion there are two semibridging carbonyls from the apical Ru atom to the basal Ru atoms and three bridging carbonyls around the base. In the case of the iron cluster with a PPN^+ counterion [10] (Fig. 3) a carbonyl group caps the basal Fe_3 triangle. The remaining 12 carbonyls in this anion are in terminal positions (Fe—C . . . Fe=2.67–2.82 Å, Fe—C—O=169–171°). On the other hand with a $[Fe(py)_6]^{2+}$ cation [11], three of the terminal carbonyls on the Fe_3 basal triangle move to semibridging positions (Fe—C . . . Fe = 2.24–2.33 Å, Fe—C—O = 151–158°), but the capping carbonyl remains in place.

In the case of the $[Ru_4(CO)_{13}]^{2-}$ dianion, we observed no significant difference in its structure when the counter ion is $[Crypt222\text{-}K]^+$ or $[PPh_4]^+$. The $[PPh_4]^+$ salt has a similar structure wherein the three basal edge-bridging carbonyls and the two apical semibridging carbonyls are maintained [17].

A further point of interest is that while the structure of $[Fe_4(CO)_{13}]^{2-}$ [10,11] and $[Ru_4(CO)_{13}]^{2-}$ have similar metal cores and differ principally in the fact that $[Fe_4(CO)_{13}]^{2-}$ contains a face-capping carbonyl group, the $[HFe_4(CO)_{13}]^-$ [12] and $[HRu_4(CO)_{13}]^-$ [8] ions have markedly different metal cores. A tetrahedral Ru_4 core exists in $[HRu_4(CO)_{13}]^-$ while a "butterfly" Fe_4 core accompanied by an oxocarbonyl bridge occurs in $[HFe_4(CO)_{13}]^-$.

Crabtree and Lavin [18] expanded upon the structural analyses of semibridging carbonyl bond angles first considered by Curtis [19]. At that time, however, structures for only three tetranuclear carbonyl clusters of the iron sub-group were known. We have examined the M_1CO (denoted as θ) and CM_1M_2 (denoted as ψ) angles for the clusters in the present study and from structures reported since Crabtree and Lavin's work was published. In general, the results reported here fall in the ranges of angles assigned by Crabtree and Lavin [18] to terminal ($\psi > 70°$, $\theta > 165°$), semibridging ($\psi \approx 50$–$75°$, $\theta \approx 145$–$165°$), edge-bridging ($\psi \approx 49°$, $\theta \approx 138°$) carbonyls.

Acknowlegement—We thank the National Science Foundation for support of this work.

Table 5. Selected bond angles (°) for [Crypt222-K]$_2$[$Ru_4(CO)_{13}$]

(a) Ru—Ru—Ru angles			
Ru(2)—Ru(1)—Ru(3)	61.05(1)	Ru(1)—Ru(3)—Ru(2)	58.06(1)
Ru(2)—Ru(1)—Ru(4)	59.45(1)	Ru(1)—Ru(3)—Ru(4)	58.47(1)
Ru(3)—Ru(1)—Ru(4)	60.92(1)	Ru(2)—Ru(3)—Ru(4)	57.66(1)
Ru(1)—Ru(2)—Ru(3)	60.89(1)	Ru(1)—Ru(4)—Ru(2)	59.92(1)
Ru(1)—Ru(2)—Ru(4)	60.63(1)	Ru(1)—Ru(4)—Ru(3)	60.61(1)
Ru(3)—Ru(2)—Ru(4)	61.24(1)	Ru(2)—Ru(4)—Ru(3)	61.10(1)
(b) Ru—Ru—C angles			
Ru(2)—Ru(1)—C(11)	101.4(1)	Ru(1)—Ru(3)—C(31)	72.5(2)
Ru(2)—Ru(1)—C(12)	50.1(1)	Ru(1)—Ru(3)—C(32)	94.3(1)
Ru(2)—Ru(1)—C(13)	144.9(2)	Ru(1)—Ru(3)—C(32)	176.8(1)
Ru(2)—Ru(1)—C(14)	109.5(1)	Ru(1)—Ru(3)—C(33)	89.0(1)
Ru(3)—Ru(1)—C(11)	157.5(1)	Ru(2)—Ru(3)—C(31)	116.4(2)
Ru(3)—Ru(1)—C(12)	83.6(1)	Ru(2)—Ru(3)—C(32)	57.1(1)
Ru(3)—Ru(1)—C(13)	107.4(2)	Ru(2)—Ru(3)—C(33)	125.2(1)
Ru(3)—Ru(1)—C(14)	87.3(1)	Ru(2)—Ru(3)—C(34)	119.4(1)
Ru(4)—Ru(1)—C(11)	98.7(1)	Ru(4)—Ru(3)—C(31)	124.4(2)
Ru(4)—Ru(1)—C(12)	109.5(1)	Ru(4)—Ru(3)—C(32)	114.0(1)
Ru(4)—Ru(1)—C(13)	147.8(2)	Ru(4)—Ru(3)—C(33)	122.6(1)
Ru(4)—Ru(1)—C(14)	50.2(1)	Ru(4)—Ru(3)—C(34)	61.7(1)
Ru(1)—Ru(2)—C(12)	48.3(1)	Ru(1)—Ru(4)—C(14)	48.2(1)
Ru(1)—Ru(2)—C(21)	93.6(1)	Ru(1)—Ru(4)—C(24)	109.6(1)
Ru(1)—Ru(2)—C(23)	155.3(1)	Ru(1)—Ru(4)—C(41)	145.8(1)
Ru(1)—Ru(2)—C(24)	108.5(1)	Ru(1)—Ru(4)—C(42)	103.4(2)
Ru(3)—Ru(2)—C(12)	82.5(1)	Ru(2)—Ru(4)—C(14)	107.9(1)
Ru(3)—Ru(2)—C(21)	152.5(1)	Ru(2)—Ru(4)—C(24)	50.2(1)
Ru(3)—Ru(2)—C(23)	118.5(1)	Ru(2)—Ru(4)—C(41)	151.3(2)
Ru(3)—Ru(2)—C(24)	78.3(1)	Ru(2)—Ru(4)—C(42)	94.8(2)
Ru(4)—Ru(2)—C(12)	109.0(1)	Ru(3)—Ru(4)—C(14)	85.8(1)
Ru(4)—Ru(2)—C(21)	98.4(1)	Ru(3)—Ru(4)—C(24)	79.1(1)
Ru(4)—Ru(2)—C(23)	143.2(1)	Ru(3)—Ru(4)—C(41)	114.0(1)
Ru(4)—Ru(2)—C(24)	48.3(1)	Ru(3)—Ru(4)—C(42)	155.1(2)
(c) C—Ru—C angles			
C(11)—Ru(1)—C(12)	95.8(2)	C(31)—Ru(3)—C(32)	92.9(2)
C(11)—Ru(1)—C(13)	95.0(2)	C(31)—Ru(3)—C(33)	105.1(2)
C(11)—Ru(1)—C(14)	85.8(2)	C(31)—Ru(3)—C(34)	95.1(2)
C(12)—Ru(1)—C(13)	97.9(2)	C(32)—Ru(3)—C(33)	87.9(2)
C(12)—Ru(1)—C(14)	159.5(2)	C(32)—Ru(3)—C(34)	171.9(2)
C(13)—Ru(1)—C(14)	102.3(2)	C(33)—Ru(3)—C(34)	89.1(2)
C(12)—Ru(2)—C(21)	87.7(2)	C(14)—Ru(4)—C(24)	157.7(2)
C(12)—Ru(2)—C(23)	107.3(2)	C(14)—Ru(4)—C(41)	99.5(2)
C(12)—Ru(2)—C(24)	155.8(2)	C(14)—Ru(4)—C(42)	97.0(2)
C(21)—Ru(2)—C(23)	88.9(2)	C(14)—Ru(4)—C(41)	101.6(2)
C(21)—Ru(2)—C(24)	102.6(2)	C(24)—Ru(4)—C(42)	90.1(2)
C(23)—Ru(2)—C(24)	94.9(2)	C(41)—Ru(4)—C(42)	90.0(2)
(d) Ru—C—Ru angles			
Ru(1)—C(12)—Ru(2)	81.6(2)	Ru(2)—C(32)—Ru(3)	80.4(2)
Ru(1)—C(14)—Ru(4)	81.6(2)	Ru(3)—C(34)—Ru(4)	77.0(1)
Ru(2)—C(24)—Ru(4)	81.5(2)		
(e) Ru—C—O angles			
Ru(1)—C(11)—O(11)	174.6(4)	Ru(3)—C(31)—O(31)	166.9(5)
Ru(1)—C(12)—O(12)	141.4(4)	Ru(3)—C(32)—O(32)	153.6(4)
Ru(1)—C(13)—O(13)	177.9(6)	Ru(3)—C(33)—O(33)	175.1(5)
Ru(1)—C(14)—O(14)	141.3(4)	Ru(3)—C(34)—O(34)	160.1(4)
Ru(2)—C(12)—O(12)	136.9(4)	Ru(4)—C(14)—O(14)	136.9(4)
Ru(2)—C(21)—O(21)	175.8(4)	Ru(4)—C(24)—O(24)	140.6(3)
Ru(2)—C(23)—O(23)	175.3(4)	Ru(4)—C(41)—O(41)	177.8(4)
Ru(2)—C(24)—O(24)	137.9(3)	Ru(4)—C(42)—O(42)	174.2(5)
Ru(2)—C(32)—O(32)	125.9(3)	Ru(4)—C(34)—O(34)	122.8(3)

Table 6. Comparison of the known structures of the tetranuclear cluster series

Cluster	Terminal	Semibridge	Edge–bridge	Face–cap	Ref.
$[Crypt222\text{-}K]_2[Ru_4(CO)_{13}]$	8	2	3		This work
$[PPh_4]_2[Ru_4(CO)_{13}]$	8	2	3		[17]
$[Fe(py)_6]_2[Fe_4(CO)_{13}]$	9	3		1	[11]
$[PPN]_2[Fe_4(CO)_{13}]$	12			1	[10]
$PPN[HRu_4(CO)_{13}]$	12		1		[8]
$PPN[HOs_4(CO)_{13}]$	12		1		[20]
$[Me_3NCH_2Ph][HFe_4(CO)_{13}]$	12		1		[12]
$PPN[HFeRu_3(CO)_{13}]$	11	2			[21]
$PPN[HFeOs_3(CO)_{13}]$	11	2			[22]
$PPN[HFe_2Ru_2(CO)_{13}]$	12		1		[21]
$H_2Ru_4(CO)_{13}$	11	2			[9]
$H_2Os_4(CO)_{13}$	11	2			[23]
$H_2FeRu_3(CO)_{13}$	11	2			[24]
$H_2FeOs_3(CO)_{13}$	11	2			[25]
$H_2Fe_2Ru_2(CO)_{13}$	11	2			[26]
$H_2RuOs_3(CO)_{13}$	11	2			[27,28]
$[Crypt221\text{-}Na]_2[H_2Ru_4(CO)_{12}]$	9		3		This work
$[PPN]_2[H_2Os_4(CO)_{12}]$	12				[7]
$PPN[H_3Ru_4(CO)_{12}]$	12				[5,6]
$PPN[H_3Os_4(CO)_{12}]$	12				[5]
$[Me_4N][H_3Os_4(CO)_{12}]$	12				[29]
$[Ph_4As][H_3RuOs_3(CO)_{12}]$	12				[27]
$H_4Ru_4(CO)_{12}$	12				[4]
$H_4Os_4(CO)_{12}$	12				[30]

REFERENCES

1. (a) Inkrott, K. E. and Shore, S. G., *Inorg. Chem.*, 1979, **18,** 2817; (b) Inkrott, K. E. and Shore, S. G., *J. Am. Chem. Soc.*, 1978, **100,** 3954.
2. (a) Bhattacharyya, A. A., Nagel, C. C. and Shore, S. G., *Organometallics*, 1983, **2,** 1187; (b) Nagel, C. C. and Shore, S. G., *J. Chem. Soc., Chem. Commun.*, 1980, 530.
3. Bhattacharyya, A. A. and Shore, S. G., *Organometallics*, 1983, **2,** 1251.
4. Wilson, R. D., Wu, S. M., Love, R. A. and Bau, R., *Inorg. Chem.*, 1978, **17,** 1271.
5. McPartlin, M. and Nelson, W. J. H., *J. Chem. Soc., Dalton. Trans.*, 1986, 1557.
6. Jackson, P. F., Johnson, B. F. G. and Lewis, J., *J. Chem. Soc., Chem. Commun.*, 1978, 920.
7. Johnson, B. F. G., Lewis, J., Raithby, P. R., Sheldrick, G. M. and Süss, G., *J. Organomet. Chem.*, 1978, **162,** 179.
8. Jensen, J. A., Fjare, D. E. and Gladfelter, W. L., *Inorg. Chem.*, 1983, **22,** 1250.
9. Yawney, D. B. W. and Doedens, R. J., *Inorg. Chem.*, 1972, **11,** 838.
10. van Buskirk, G., Knobler, C. B. and Kaesz, H. D., *Organometallics*, 1985, **4,** 149.
11. Doedens, R. J. and Dahl, L. F., *J. Am. Chem. Soc.*, 1966, **88,** 4847.
12. Manassero, M., Sansoni, M. and Longoni, G., *J. Chem. Soc., Chem. Comm.*, 1976, 919.
13. Shriver,D. F. and Drezdzon, M. A., *The Manipulation of Air-Sensitive Compounds*, 2nd Edition, New York : John Wiley and Sons, 1986.
14. SDP (Structure Determination Package) developed by B. A. Fenz and Associates, Inc.
15. (a) Chini, P., Longoni, G. and Albano, V. G., *Adv. Organomet. Chem.*, 1976, **14,** 285; (b) Chini, P. and Heaton, B. J., *Top. Curr. Chem.*, 1977, **71,** 1
16. (a) Johnston, R. D., *Adv. Inorg. Chem. Radiochem.*, 1970, **13,** 471; (b) King, R. B., *Prog. Inorg. Chem.*, 1972, **15,** 235.
17. Payne, M., Hsu, L.-Y. and Shore, S. G., unpublished results.
18. Crabtree, R. H. and Lavin, M., *Inorg. Chem.*, 1986, **25,** 805.
19. Klingler, R. J., Butler, W. H. and Curtis, M. D., *J. Am. Chem. Soc.*, 1978, **100,** 5034.
20. Dawson, P. A., Johnson, B. F. G., Lewis, J., Kaner, D. A. and Raithby, P. R., *J. Chem. Soc., Chem. Comm.*, 1980, 961.
21. Takasagaw, F., Fumagalli, A., Koetzle, T. F., Steinmetz, G. R., Rosen, R. P., Gladfelter, W. L., Geoffroy, G. L., Bruck, M. A. and Bau, R., *Inorg. Chem.*, 1981, **20,** 3823.
22. Eadie, D. T., Holden, H. D., Johnson, B. F. G. and Lewis, J., *J. Chem. Soc., Dalton. Trans.*1984, 301.
23. Krause, J. A., Siriwardane, U., Salupo, T. A., Wermer, J. R., Knoeppel, D. W. and Shore, S. G. *J. Organomet. Chem.*, 1993, **454,** 263.
24. (a) Gilmore, C. J. and Woodward, P. J., *J. Chem. Soc. (A)*, 1971, 3453; (b) Gilmore, C. J. and Woodward, P. J., *J. Chem. Soc., Chem. Comm.*, 1970, 1463; (c) Hsu, L.-Y., Bhattacharyya, A. A. and Shore, S. G. *Acta Cryst.*, 1984, **C40,** 722.

25. Churchill, M. R., Bueno, C., Hsu, W. L., Plotkin, J. S. and Shore, S. G., *Inorg. Chem.*, 1982, **21,** 1958.
26. Venäläinen, T. and Pakkanen, T. A., *J. Organomet. Chem.*, 1986, 316, 183.
27. Rheingold, A. L., Gates, B. C., Scott, J. P. and Budge, J. R., *J. Organomet. Chem.*, 1987, **331,** 81.
28. Siriwardane, U., Hsu, L.-Y., Krause, J., Wermer, J. and Shore, S. G., unpublished results.
29. Johnson, B. F. G, Lewis, J., Raithby, P. R. and Zuccaro, C., *Acta Cryst.*, 1978, **B34,** 3765.
30. Johnson, B. F. G, Lewis, J., Raithby, P. R. and Zuccaro, C., *Acta Cryst.*, 1981, **B37,** 1728.

Pergamon

PII: S0277-5387(98)00032-1

Polyhedron Vol. 17, No. 17, pp. 2899–2905, 1998
© 1998 Elsevier Science Ltd
All rights reserved. Printed in Great Britain
0277-5387/98 $19.00+0.00

The synthesis and characterisation of some water soluble ruthenium and osmium clusters and a preliminary study of their use as catalysts in the water gas shift reaction

Daren J. F. Bryce,[a] Paul J. Dyson,[a]* Brian K. Nicholson[b] and David G. Parker[c]

[a] Department of Chemistry, Imperial College of Science, Technology and Medicine, South Kensington, London, SW7 2AY, U.K.

[b] Department of Chemistry, University of Waikato, Hamilton, New Zealand

[c] ICI Group R & T Affairs, PO Box 90, Wilton Centre, Middlesbrough, Cleveland, TS90 8JE, U.K.

(Received 15 October 1997; accepted 5 January 1998)

Abstract—The clusters $Ru_3(CO)_{12}$, $Ru_6C(CO)_{17}$, $H_4Ru_4(CO)_{12}$ and $H_2Os_3(CO)_{10}$ react with the phosphine, $P(m\text{-}C_6H_4SO_3Na)_3$, to afford water soluble clusters which are catalyst precursors in the water gas shift reaction. Electrospray mass spectrometry provides an excellent means of characterising the clusters in solution from their negative ion spectra. © 1998 Elsevier Science Ltd. All rights reserved

Keywords: clusters; phosphine; water soluble; ruthenium; osmium

There has been considerable interest over the last two decades in conducting organometallic reactions in an aqueous environment. This is partly because water is cheap and environmentally friendly, but also from a synthetic viewpoint, biphasic catalytic processes can be performed which allows separations to be achieved with considerable ease [1]. In this respect, much effort has been devoted to the synthesis of water soluble mononuclear catalysts and this area has been recently reviewed [2]. The most noteworthy complex of this type is perhaps the rhodium adduct $Rh(H)CO\{P(m\text{-}C_6H_4SO_3Na)_3\}_3$ which is employed in a biphasic system catalysing the conversion of propene to *n*-butyraldehyde [3], although a number of other catalytic systems have also been developed [4].

While cluster compounds are known to be effective catalysts for a large number of processes [5], the area of water soluble clusters is poorly developed. Süss-Fink and his coworkers have prepared several tetraruthenium-tetraarene clusters including the 58 electron species $[H_4Ru_4(\eta\text{-}C_6H_6)_4]^{2+}$ [6]. This cluster has been shown to catalyse the hydrogenation of various arenes to give the corresponding cyclohexanes under biphasic conditions [7].

There has also been a preliminary report describing the synthesis of several water soluble carbonyl clusters with the water soluble phosphine, $P(m\text{-}C_5H_4SO_3Na)_3$, but their use as catalysts was not investigated [8]. Since the reactivity of transition metal carbonyl clusters towards phosphine ligands is a mature area we decided to prepare further clusters, including some with hydride ligands, with the water soluble phosphine $P(m\text{-}C_6H_4SO_3Na)_3$. In this paper we describe the results of this study which includes their synthesis, characterisation, stability and catalytic activity in the water gas shift reaction. This is an important reaction in industry and if successful, could be used in biphasic hydrogenation reactions using water as the source of H_2 gas.

RESULTS AND DISCUSSION

The reaction of $Ru_3(CO)_{12}$ with one to three equivalents of the water soluble phosphine, $P(m\text{-}C_6H_4SO_3Na)_3$, in methanol for 2 h affords $Ru_3(CO)_{11}\{P(m\text{-}C_6H_4SO_3Na)_3\}$ **1**, $Ru_3(CO)_{10}\{P(m\text{-}$

* Author to whom correspondence should be addressed.

$C_6H_4SO_3Na)_3\}_2$ **2** and $Ru_3(CO)_9\{P(m\text{-}C_6H_4SO_3Na)_3\}_3$ **3** in quantitative yield (Scheme 1). In a related reaction, $Ru_6C(CO)_{17}$ was heated under reflux in methanol containing one equivalent of $P(m\text{-}C_6H_4SO_3Na)_3$ to afford $Ru_6C(CO)_{16}\{P(m\text{-}C_6H_4SO_3Na)_3\}$ **4** in quantitative yield (Scheme 2). The hydride cluster $H_4Ru_4(CO)_{12}$ has been reacted with one, two and four equivalents of $P(m\text{-}C_6H_4SO_3Na)_3\}$ to afford $H_4Ru_4(CO)_{11}\text{-}\{P(m\text{-}C_6H_4SO_3Na)_3\}$ **5**, $H_4Ru_4(CO)_{10}\{P(m\text{-}C_6H_4SO_3Na)_3\}_2$ **6** and $H_4Ru_4(CO)_8\{P(m\text{-}C_6H_4SO_3Na)_3\}_4$ **7** in high yield (Scheme 3). The unsaturated 46 electron hydride cluster $H_2Os_3(CO)_{10}$ undergoes addition reactions with phosphine ligands and also reacts with methanol [9]. Therefore, $H_2Os_3(CO)_{10}$ and $P(m\text{-}C_6H_4SO_3Na)_3$ were stirred in equimolar quantities in refluxing propanone for 2 h to afford $H_2Os_3(CO)_{10}\{P(m\text{-}C_6H_4SO_3Na)_3\}$ **8** in 43% yield (Scheme 4). The lower yield obtained from this reaction is attributed to the poor solubility of the phosphine ligand in the solvent and extending the reaction time did not improve the yield. Clusters **1–8** are all highly soluble in water and slightly soluble in methanol at room temperature. In deoxygenated water they are stable for several days but when exposed to air they slowly decompose. As solid materials they are stable for prolonged periods even when precautions to exclude air or moisture are not taken.

Compounds **1–8** were characterised by spectroscopy and full details are given in the experimental section. Clusters **1–3** have been reported previously and spectroscopic data is in good agreement with that obtained earlier [8]. Microanalytical data was obtained on all the compounds but was not very informative. It would appear that methanol and/or water contaminates the sample and even after prolonged periods under vacuum not all the solvent could be removed. Mass spectra were obtained using fast atom bombardment (FAB) ionisation in both positive and negative modes, and electrospray techniques (ESMS) to compare the older FAB method with the newer ESMS method which has only recently been applied to organometallic systems [10]. ESMS is particularly appropriate for ionic species such as those

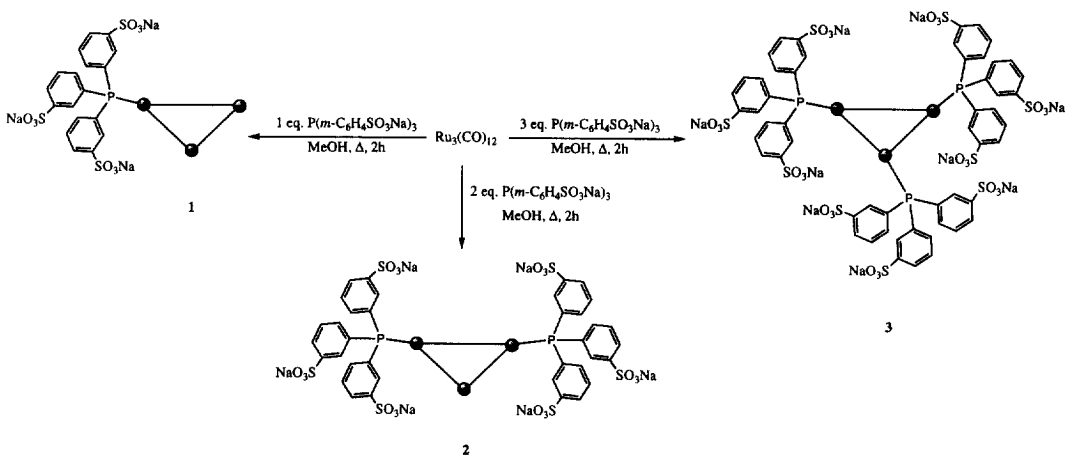

Scheme 1. The synthesis of **1**, **2** and **3**; CO ligands have been omitted for clarity.

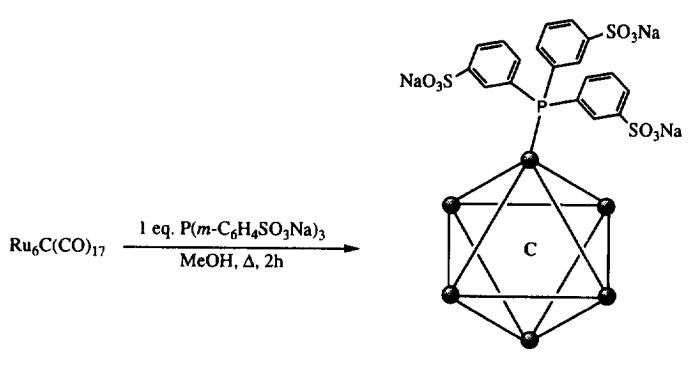

Scheme 2. The synthesis of **4**; CO ligands have been omitted for clarity.

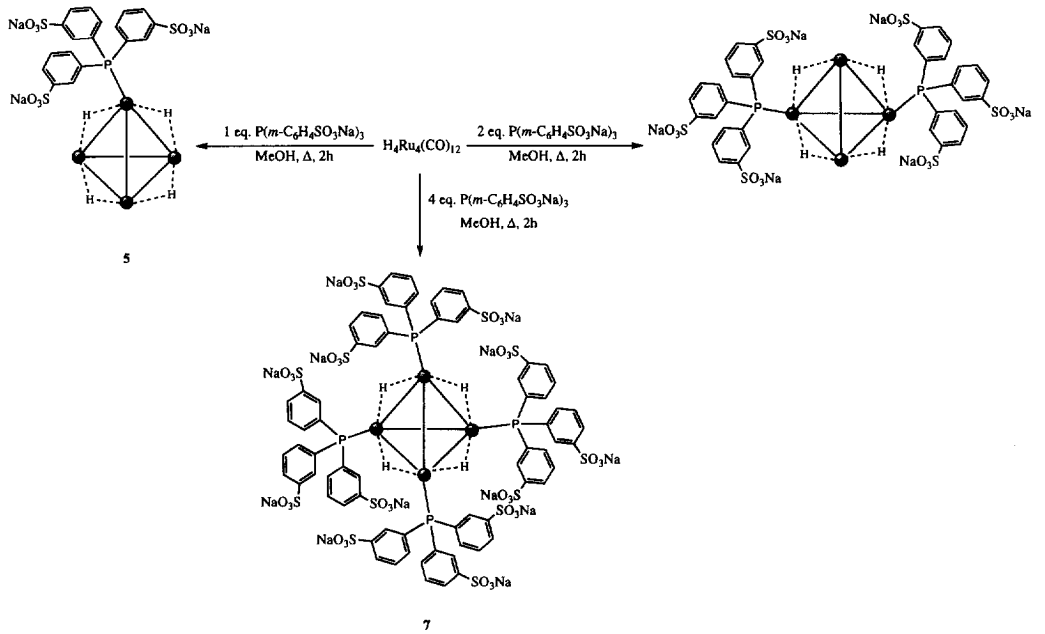

Scheme 3. The synthesis of **5**, **6** and **7**; CO ligands have been omitted for clarity.

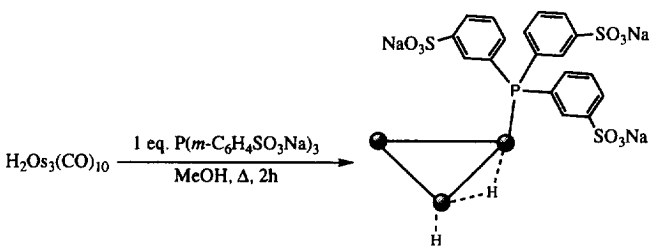

Scheme 4. The synthesis of **8**; CO ligands have been omitted for clarity.

examined here and can be readily recorded from aqueous solutions. The ligand itself has been examined previously and gives clear peaks in the negative ion mode assignable to $[P(m\text{-}C_6H_4SO_3)_3Na_2]^-$, $[P(m\text{-}C_6H_4SO_3)_3Na]^{2-}$ and $[P(m\text{-}C_6H_4SO_3)_3]^{3-}$ [11]. However ESMS of complexes or clusters incorporating this ligand do not appear to have been reported before.

With FAB mass spectrometry it was only possible to obtain spectra for the mono-phosphine derivatives (**1**, **4**, **5** and **8**) as the more highly substituted clusters did not contain peaks at higher masses. In positive mode peaks were observed which either corresponded to the intact parent ion or that in which one carbonyl loss had taken place. In addition, peaks which may be assigned to further carbonyl loss and cluster fragmentation were also observed. Only **4** gave a negative mode spectrum corresponding to the intact parent cluster in which one sodium ion was lost. This was followed by peaks corresponding to the sequential loss of some of the carbonyl groups and peaks corresponding to lower nuclearity fragments were also observed.

Generally the ESMS spectra were more useful for characterisation and showed common features. As an illustration, we discuss the spectra of $Ru_6C(CO)_{16}\{P(m\text{-}C_6H_4SO_3Na)_3\}$ **4**, recorded with water as the mobile phase. At low cone voltages (10 V) there were essentially two peaks, one centred at m/z 523 which can be assigned to $[Ru_6C(CO)_{16}\{P(m\text{-}C_6H_4SO_3)_3\}]^{3-}$, and one centred about m/z 795 which is assigned to $[Ru_6C(CO)_{16}\{P(m\text{-}C_6H_4SO_3)_3 + Na]^{2-}$. In each case the assignment was confirmed by a comparison of the simulated isotope pattern with that recorded at high resolution (see inset, Fig. 1). As the cone voltage was increased, leading to more vigorous collisions in the source, a third peak at m/z at 1612 appeared, corresponding to $[Ru_6C(CO)_{16}\{P(m\text{-}C_6H_4SO_3)_3\} + 2Na]^-$, but this was always weak. At

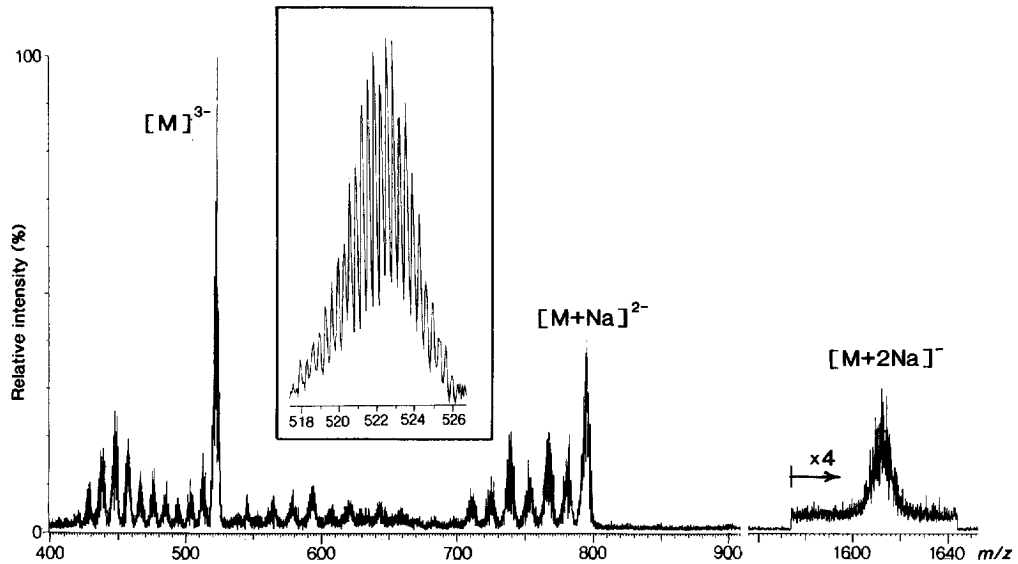

Fig. 1. The negative ion electrospray mass spectrum of $Ru_6C(CO)_{16}\{P(m\text{-}C_6H_4SO_3Na)_3\}$ **4** in aqueous solution, recorded with cone voltage of 40 V to induce some fragmentation. Peaks are assigned with [M] = $[Ru_6C(CO)_{16}\{P(m\text{-}C_6H_4SO_3)_3\}]^{3-}$. The charges on the ions are apparent from the separation in the isotope pattern (the inset is an enlargement of the peak at m/z 520, with mass separation of 0.33 mass units) and by the mass differences associated with CO loss (9.3 for the 3-ion and 14 for the 2-ion). The weak peaks between 540 and 660 mass units appear to arise from an impurity in the sample as they cannot be assigned as fragmentation ions.

the same time fragmentation by CO loss occurred from the 2− and 3− peaks. This is illustrated in Fig. 1, recorded at intermediate cone voltages. One interesting observation is that under these conditions the amount of fragmentation is markedly different for the different ions; the 1− ion at *m/z* 1612 shows no detectable fragmentation, the 2− ion at *m/z* 795 is flanked by peaks corresponding to the loss of up to six CO ligands, whereas the 3− ion at *m/z* 523 shows associated fragmentation peaks with up to ten CO groups eliminated. The reverse might have been expected since CO ligands are expected to be more tightly bound in species with higher negative charge, although in this case most of the charge is probably localised on the phosphine ligand. Presumably the higher charged species travel at higher velocity as they are accelerated across the skimmer cone voltage difference leading to more energetic collisions and hence greater fragmentation. A similar effect has been found with Cd-thiolate clusters [12]. Adding extra Na^+ ions to the solution under analysis had little effect on the relative amounts of the ions $[Ru_6C(CO)_{16}\{P(m\text{-}C_6H_4SO_3)_3\}+n\text{Na}]^{(3-n)-}$, but added Cs^+ suppressed the $[Ru_6C(CO)_{16}\{P(m\text{-}C_6H_4SO_3)_3\}+\text{Na}]^{2-}$ peak in favour of a $[Ru_6C(CO)_{16}\{P(m\text{-}C_6H_4SO_3)_3\}+\text{Cs}]^{2-}$ signal at *m/z* 849.5. Clearly ESMS could be used conveniently to assess the relative ion-pairing abilities of different cations with these cluster anions.

The spectra recorded for $H_4Ru_4(CO)_{11}\{P(m\text{-}C_6H_4SO_3Na)_3\}$ **5** followed the same pattern, with clear $[H_4Ru_4(CO)_{11}\{P(m\text{-}C_6H_4SO_3)_3\}]^{3-}$ and $[H_4Ru_4(CO)_{11}\{P(m\text{-}C_6H_4SO_3)_3\}+\text{Na}]^{2-}$ peaks dominating the spectra at lower cone voltages and these with their CO-loss analogues at higher voltages. No $[H_4Ru_4(CO)_{11}\{P(m\text{-}C_6H_4SO_3)_3\}+2\text{Na}]^-$ was observed at all for this example.

The doubly substituted species $Ru_3(CO)_{10}\{P(m\text{-}C_6H_4SO_3Na)_3\}_2$ **2** was expected to give higher charged ions, potentially up to 6−. At low cone voltages the peaks observed were assigned to [**2**-2Na]$^{2-}$, [**2**-3Na]$^{3-}$, [**2**-4Na]$^{4-}$, and [**2**-5Na]$^{5-}$, with the 4− ion being dominant. The fully dissociated 6− ion apparently has too high a charge density to be detected. The isotope patterns for the 4− and 5− ions could not be fully resolved but the charges on the anions were clear from the spacing between the CO-loss species (7 and 5.6 mass units respectively) at higher cone voltages. Even at the lowest cone voltages CO-loss species were observed for the 4− and 5− ions, confirming the observation that fragmentation increases for the higher charged species. As noted above, no sensible FAB mass spectra signals at all could be obtained for this cluster.

For $Ru_3(CO)_9\{p(m\text{-}C_6H_4SO_3Na)_3\}_3$ **3**, even higher-charged species are potentially possible. The ESMS spectrum of this cluster was less clean, but peaks corresponding to [**3**-4Na]$^{4-}$ and [**3**-3Na]$^{5-}$ were the main ones observed. There were competing signals from the disubstituted cluster **1**, but whether these arose from an impurity in the sample or from rearrangement in the spectrometer is not clear. The corresponding spectra of the samples were also recorded using MeOH as mobile phase, but there were no significant differences to those obtained from aqueous solutions.

For all of these examples, the overall quality of the ESMS spectra and the observation of a series of ions from varying degrees of association with Na^+ cations makes this the method of choice for analysing the $\{P(m\text{-}C_6H_4SO_3Na)_3\}$-substituted clusters.

The ^1H NMR clusters **1–8** showed multiplet resonances typical of phenyl ring protons between 7.2 and 8.2 ppm. In addition, clusters **5–8** afforded multiplet resonances at negative δ values due to the presence of hydride ligands. These were quite complicated signals and since the spectra were recorded in D_2O it was not possible to lower the temperature. The $^{31}P\text{-}\{^1H\}$ NMR spectra of clusters **1–4** and **8** all contained one singlet resonance in the region 34.5–37.3 ppm. The tetraruthenium clusters all gave rise to more than one resonance with the peaks lying in a slightly larger range, *viz.* 35.5–46.5 ppm. Clearly, this data is not very informative and as such the ESMS was the most useful technique available for the characterisation of these clusters.

It has not been possible to obtain single crystals of **1–8** suitable for X-ray diffraction studies. The structures shown in the Schemes for the $\{P(m\text{-}C_6H_4SO_3Na)_3\}$-containing clusters are based on those identified by single crystal X-ray diffraction analyses for related PPh_3 and other simple phosphine derivatives, as in most cases the IR spectra of the $\{P(m\text{-}C_6H_4SO_3Na)_3\}$ and PPh_3 or other simple phosphine species are quite similar [13].

The precursor clusters $Ru_3(CO)_{12}$, $H_4Ru_4(CO)_{12}$ and $H_2Os_3(CO)_{10}$ have all been shown to catalyse the water gas shift reaction (i.e. the conversion of H_2O and CO to H_2 and CO_2) [14]. We decided to test the water soluble derivatives of these aforementioned clusters, *viz.* **3, 7** and **8,** as potential catalysts in this process (see experimental for details). All these clusters were found to catalyse the formation of CO_2 and H_2. However, on recovery of the clusters after two cycles, only $H_4Ru_4(CO)_8\{P(m\text{-}C_6H_4SO_3Na)_3\}_4$ **7** remained unchanged. As yet it has not been possible to fully characterise the materials recovered from these reactions although the compound derived from cluster **3** which did not originally contain a hydride ligand was found to have peaks indicative of hydrides in the ^1H NMR spectrum.

EXPERIMENTAL

The synthesis of clusters was conducted under an atmosphere of nitrogen gas using degassed solvents. *Tris*-(3-sulphonatophenyl)phosphine tetrahydrate trisodium salt, $P(m\text{-}C_6H_4SO_3Na)_3 \cdot 4H_2O$, was purchased from Strem Chemicals and used as received. The clusters $Ru_3(CO)_{12}$ [15], $Ru_6C(CO)_{17}$ [16], $H_4Ru_4(CO)_{12}$ [17] and $H_2Os_3(CO)_{10}$ [17] were prepared according to the literature methods. The preparation of $Ru_3(CO)_{11}\{P(m\text{-}C_6H_4SO_3Na)_3\}$ and $Ru_3(CO)_{10}\{P(m\text{-}C_6H_4SO_3Na)_3\}_2$ have been reported previously using a method similar to that described herein [8]. Infrared spectra were recorded as KBr discs using a Mattson Research Series 1 FTIR instrument. $^{31}P\text{-}\{^1H\}$ and ^1H NMR spectra were recorded on a JEOL JNM-EX270 FT NMR instrument. FAB mass spectra were obtained using a Micromass autospec instrument. ESMS spectra were recorded on a VG Platform II mass spectrometer using water as the mobile phase at a flow rate of 0.1 ml min^{-1}. Nitrogen was used as the nebulising and drying gas. Samples were introduced as aqueous solutions, and spectra were recorded with skimmer cone voltages between 10 and 50 V. Theoretical isotope patterns were calculated using the *Isotope* program [18]. Values for *m/z* given in the experimental section are for the most intense isotopomer.

Preparation of $Ru_3(CO)_{11}\{P(m\text{-}C_6H_4SO_3Na)_3\}$ **1**

The cluster $Ru_3(CO)_{12}$ (60 mg) and $P(m\text{-}C_6H_4SO_3Na)_3$ (57 mg, 1 mol equiv.) was heated under reflux in methanol (20 ml) for 2 h during which time the reaction mixture turned deep red in colour. The solvent was removed under reduced pressure to afford a red solid which was washed with hexane (2×10 ml) and dried under vacuum. The compound was characterised by spectroscopy as $Ru_3(CO)_{11}\{P(m\text{-}C_6H_4SO_3Na)_3\}$ **1** (120 mg, quantitative yield). Compound **1** is soluble in water and stable for several days.

Spectroscopic data for **1**. IR: (KBr disc) ν_{CO}, 2102 (m), 2052 (s), 2009 (vs), 1957 (m, sh) cm^{-1}; $^{31}P\text{-}\{^1H\}$ NMR: (D_2O) 34.7 (s) ppm; ^1H NMR: (D_2O) 7.5–8.1 (m) ppm; FAB^+ mass spectrum: 1180 $[1]^+$. The spectroscopic data is in good agreement with that previously reported.

Preparation of $Ru_3(CO)_{10}\{P(m\text{-}C_6H_4SO_3Na)_3\}_2$ **2**

The cluster $Ru_3(CO)_{12}$ (100 mg) and $P(m\text{-}C_6H_4SO_3Na)_3$ (190 mg, 2 mol equiv.) was heated under reflux in methanol (20 ml) for 2 h during which time the reaction mixture turned deep red in colour. The solvent was removed under reduced pressure to afford a red solid which was washed with hexane (2×10 ml) and dried under vacuum. The compound was characterised by spectroscopy as $Ru_3(CO)_{10}\{P(m\text{-}C_6H_4SO_3Na)_3\}_2$ **2** (298 mg, quantitative yield). Compound **2** is soluble in water and stable for several days.

Spectroscopic data for **2**. IR: (KBr disc) ν_{CO}, 2072 (w), 2060 (w), 2047 (m), 2034 (s), 2024 (s), 1990 (s), 1968 (s), 1950 (m) cm^{-1}; $^{31}P\text{-}\{^1H\}$ NMR: (D_2O) 36.9 (s) ppm; ^1H NMR: (D_2O) 7.5–8.1 (m) ppm; FAB^+ and FAB^- mass spectra did not afford peaks which could be assigned to the cluster. ESMS spectrum (cone voltage 10 V) *m/z* 837 (3%) $[\mathbf{2}\text{-}2Na]^{2-}$, 550 (30%) $[\mathbf{2}\text{-}3Na]^{3-}$, 407 (100%) $[\mathbf{2}\text{-}4Na]^{4-}$, and 321 (25%) $[\mathbf{2}\text{-}5Na]^{5-}$.

Preparation of $Ru_3(CO)_9\{P(m\text{-}C_6H_4SO_3Na)_3\}_3$ **3**

The cluster $Ru_3(CO)_{12}$ (70 mg) and $P(m\text{-}C_6H_4SO_3Na)_3$ (200 mg, 3 mol equiv.) was heated under reflux in methanol (20 ml) for 2 h during which time the reaction mixture turned deep red in colour. The solvent was removed under reduced pressure to afford a red solid which was washed with hexane (2 × 10 ml) and dried under vacuum. The compound was characterised by spectroscopy as $Ru_3(CO)_9\{P(m\text{-}C_6H_4SO_3Na)_3\}_3$ **3** (242 mg, quantitative yield). Compound **3** is soluble in water and stable for several days.

Spectroscopic data for **3**. IR: (KBr disc) ν_{CO}, 2053 (s), 2017 (s, sh), 1995 (vs), 1943 (s), 1907 (m) cm^{-1}; $^{31}P\text{-}\{^1H\}$ NMR: (D_2O) 37.3 (s) ppm; ^1H NMR: (D_2O) 7.2–8.1 (m) ppm; FAB^+ and FAB^- mass spectra did not afford peaks which could be assigned to the cluster and the ESMS spectra were less clean than for other examples but peaks at *m/z* 542 $[\mathbf{3}\text{-}4Na]^{4-}$ and 429 $[\mathbf{3}\text{-}5Na]^{5-}$ were clear.

Preparation of $Ru_6C(CO)_{16}\{P(m\text{-}C_6H_4SO_3Na)_3\}$ **4**

The cluster $Ru_6C(CO)_{17}$ (50 mg) and $P(m\text{-}C_6H_4SO_3Na)_3$ (33 mg, 1 mol equiv.) was heated under reflux in methanol (20 ml) for 2 h. The solvent was removed under reduced pressure to afford a red solid which was washed with hexane (2 × 10 ml) and dried under vacuum. The compound was characterised by spectroscopy as $Ru_6C(CO)_{16}\{P(m\text{-}C_6H_4SO_3Na)_3\}$ **4** (77 mg, quantitative yield). Compound **4** is soluble in water and stable for several days.

Spectroscopic data for **4**. IR: (KBr disc) ν_{CO}, 2090 (m), 2055 (s, sh), 2023 (vs), 1986 (m, sh), 1838 (w) cm^{-1}; $^{31}P\text{-}\{^1H\}$ NMR: (D_2O) 36.2 (s) ppm; ^1H NMR: (D_2O) 7.7–8.2 (m) ppm; FAB^- mass spectrum: *m/z* 1613 $[\mathbf{4}\text{-}Na]^-$. ESMS (cone voltage 12 V) *m/z* 1612 (4%) $[\mathbf{4}\text{-}Na]^-$, *m/z* 795 (20%) $[\mathbf{4}\text{-}2Na]^{2-}$, *m/z* 522 (100%) $[\mathbf{4}\text{-}3Na]^{3-}$. (See also Fig. 1 for the spectrum at higher cone voltages).

Preparation of $H_4Ru_4(CO)_{11}\{P(m\text{-}C_6H_4SO_3Na)_3\}$ **5**

The cluster of $H_4Ru_4(CO)_{12}$ (39 mg) and $P(m\text{-}C_6H_4SO_3Na)_3$ (32 mg, 1 mol equiv.) was heated under reflux in methanol (20 ml) for 2 h during which time the reaction mixture became deep red in colour. The solvent was removed under reduced pressure to afford an orange-brown solid which was washed with hexane (2 × 10 ml) and dried under vacuum. The compound was characterised by spectroscopy as $H_4Ru_4(CO)_{11}\{P(m\text{-}C_6H_4SO_3Na)_3\}$ **5** (65 mg, 89% yield). Compound **5** is soluble in water and stable for several days.

Spectroscopic data for **5**. IR: (KBr disc) ν_{CO}, 2098 (m), 2070 (s), 2059 (vs), 2024 (s), 2017 (s), 1997 (m), 1958 (m) cm^{-1}; $^{31}P\text{-}\{^1H\}$ NMR: (D_2O) 41.0 (s, 1P), 46.5 (s, 1P) ppm; ^1H NMR: (D_2O) 7.2–8.1 (m), −31.0–−32.5 (m) ppm; FAB^+ mass spectrum: *m/z* 1284 $[\mathbf{5}]^+$. ESMS (cone voltage 10 V) *m/z* 620 (8%) $[\mathbf{5}\text{-}2Na]^{2-}$, *m/z* 406 (100%) $[\mathbf{5}\text{-}3Na]^{3-}$, (cone voltage 20 V) *m/z* 620 (30%) $[\mathbf{5}\text{-}2Na]^{2-}$, *m/z* 405.7 (100%) $[\mathbf{5}\text{-}3Na]^{3-}$, *m/z* 396.3 (80%) $[\mathbf{5}\text{-}CO\text{-}3Na]^{3-}$, *m/z* 387 (70%) $[\mathbf{5}\text{-}2CO\text{-}3Na]^{3-}$, *m/z* 377.7 (70%) $[\mathbf{5}\text{-}3CO\text{-}3Na]^{3-}$, *m/z* 368.3 (35%) $[\mathbf{5}\text{-}4CO\text{-}3Na]^{3-}$.

Preparation of $H_4Ru_4(CO)_{10}\{P(m\text{-}C_6H_4SO_3Na)_3\}_2$ **6**

The cluster $H_4Ru_4(CO)_{12}$ (32 mg) and $P(m\text{-}C_6H_4SO_3Na)_3$ (53 mg, 2 mol equiv.) was heated under reflux in methanol (20 ml) for 2 h during which time the reaction mixture became deep red in colour. The solvent was removed under reduced pressure to afford an orange-brown solid which was washed with hexane (2 × 10 ml) and dried under vacuum. The compound was characterised by spectroscopy as $H_4Ru_4(CO)_{10}\{P(m\text{-}C_6H_4SO_3Na)_3\}_2$ **6** (82 mg, 95% yield). Compound **6** is soluble in water and stable for several days.

Spectroscopic data for **6**. IR: (KBr disc) ν_{CO}, 2093 (w), 2059 (vs), 2107 (vs), 1996 (s), 1970 (m) cm^{-1}; $^{31}P\text{-}\{^1H\}$ NMR: (D_2O) 36.3 (s, 3P), 44.0 (s, 1P) ppm; ^1H NMR: (D_2O) 7.2–8.0 (m), −32.0–−33.0 (m) ppm; FAB^+ and FAB^- mass spectra did not afford peaks which could be assigned to the cluster.

Preparation of $H_4Ru_4(CO)_8\{P(m\text{-}C_6H_4SO_3Na)_3\}_4$ **7**

The cluster $H_4Ru_4(CO)_{12}$ (25 mg) and $P(m\text{-}C_6H_4SO_3Na)_3$ (83 mg, 4 mol equiv.) was heated under reflux in methanol (20 ml) for 2 h during which time the reaction mixture became deep red in colour. The solvent was removed under reduced pressure to afford an orange-brown solid which was washed with hexane (2 × 10 ml) and dried under vacuum. The compound was characterised by spectroscopy as $H_4Ru_4(CO)_8\{P(m\text{-}C_6H_4SO_3Na)_3\}_4$ **7** (75 mg, 75% yield). Compound **7** is soluble in water and stable for several days.

Spectroscopic data for **7**. IR: (KBr disc) ν_{CO}, 2080 (w), 2065 (m), 2059 (m), 2021 (s), 1967 (m) cm^{-1}; $^{31}P\text{-}\{^1H\}$ NMR: (D_2O) 35.5 (s, 1P), 36.9 (s, 2P), 39.1 (s, 1P) ppm; ^1H NMR: (D_2O) 7.4–8.0 (m), −31.7–−32.8 (m) ppm; FAB^+ and FAB^- mass spectra did not afford peaks which could be assigned to the cluster.

Preparation of $H_2Os_3(CO)_{10}\{P(m\text{-}C_6H_4SO_3Na)_3\}$ **8**

The cluster $H_2Os_3(CO)_{10}$ (50 mg) and $P(m\text{-}C_6H_4SO_3Na)_3$ (35 mg, 1 mol equiv.) was heated under reflux in acetone (20 ml) for 2 h during which time the reaction mixture changed from purple to an orange-brown colour. The solvent was removed under reduced pressure to afford an orange-brown solid which was washed with hexane (2 × 10 ml) and dried under vacuum. The compound was characterised by

spectroscopy as $H_2Os_3(CO)_{10}\{P(m\text{-}C_6H_4SO_3Na)_3\}$ **8** (50 mg, 43% yield). Compound **8** is soluble in water and stable for several days.

Spectroscopic data for **8**. IR: (KBr disc) ν_{CO}, 2082 (m), 2052 (s, sh), 2017 (vs), 2009 (vs), 1984 (s, sh), 1950 (m, sh) cm^{-1}; $^{31}P\text{-}\{^1H\}$ NMR: (D_2O) 34.5 (s) ppm; ^1H NMR: (D_2O) 7.4–8.2 (m), −31.5–−32.5 (m) ppm; FAB^- *m/z* 1373 [**8**-Na-CO]$^-$.

Catalytic runs

In a typical experiment the cluster (ca 25 mg) was dissolved in degassed water (30 ml) and placed in an autoclave under an atmosphere of CO. The solution was heated under reflux for 5 h and the gas tested qualitatively for the presence of CO_2. The autoclave was recharged with CO and heated under reflux for a further 12 h. The gas was again qualitatively tested for CO_2 after this time. The solvent was removed under reduced pressure and the cluster recovered.

Acknowledgements—We would like to thank the Royal Society for a University Research Fellowship (PJD) and ICI (Wilton) for financial support (DJFB). A grant from the New Zealand Lotteries Board for the electrospray mass spectrometer is acknowledged. We thank Priya Suman (IC) for running the NMR spectra and Dr W. Henderson (UW) for helpful comments.

REFERENCES

1. Horváth, I. T., *J. Mol. Catal A: Chem.*, 1997, **116,** 1.
2. (a) Herrmann, W. A. and Kohlpainter, C. W., *Angew. Chem. Int. Ed. Engl.*, 1993, **32,** 1524; (b) Joó, F. and Kathó, Á., *J. Mol. Catal A: Chem.*, 1997, **116,** 3.
3. Cornils, B., Hibbel, J., Konkol, W., Lieder, B., Much, J., Schmid, V. and Wiebus, E., (Ruhrchemie AG), DE-B 3234701, 1982, *Chem. Abstr.*, 1984, **100,** 194 022k.
4. For recent examples see, (a) Hernandez, M. and Kalck, P., *J. Mol. Catal A: Chem.*, 1997, **116,** 117 and 131.
5. Whyman, R., In *Transition Metal Clusters*, ed. Johnson, B. F. G. John Wiley and Sons, Chichester, 1980.
6. Süss-Fink, G., Meister, A. and Meister, G., *Coord. Chem. Rev.*, 1995, **143,** 97.
7. Plasseraud, L. and Süss-Fink, G., *J. Organomet. Chem.*, 1997, **539,** 163.
8. Fontal, B., Orlewski, J., Santini, C. C. and Basset, J. M., *Inorg. Chem.*, 1986, **25,** 4321.
9. Deeming, A. J. and Hasso, S., *J. Organomet. Chem.*, 1976, **114,** 313.
10. For examples see, (a) Colton, R., D'Agostino, A. and Traeger, J. C., *Mass Spectrom. Rev.*, 1995, **14,** 79; (b) Hop, C. E. C. A. and Bakhtiar, R., *J. Chem. Educ.*, 1996, **73,** A162; (c) Henderson, W., Nicholson, B. K. and McCaffrey, L. J., *Polyhedron*, to be submitted.
11. Henderson, W. and Olsen, G., *Polyhedron*, in press.
12. Lover, T., Henderson, W., Bowmaker, G. A., Seakins, J. M. and Cooney, R. P., *Inorg. Chem.*, 1997, **36,** 3711.
13. Related phosphine derivatives for the cluster reported herein based on the Ru_3, Ru_6C, H_4Ru_4 and H_2Os_3 cluster units are, (a) Foulds, G. A., Johnson, B. F. G. and Lewis, J., *J. Organomet. Chem.*, 1985, **296,** 147; (b) Brown, S. C., Evans, J. and Webster, M., *J. Chem. Soc., Dalton Trans.*, 1981, 2263; (c) Wilson, R. D., Wu, S. M., Love, R. A. and Bau, R., *Inorg. Chem.*, 1978, **17,** 1271; (d) see Ref. 9.
14. Kang, H.-C., Mauldin, C. H., Cole, T., Slegeir, W., Cann, K. and Pettit, R., *J. Am. Chem. Soc.*, 1977, **99,** 8323.
15. Johnson, B. F. G., Lewis, J. and Kilty, P. A., *J. Chem. Soc. (A)*, 1968, 2859.
16. Johnson, B. F. G., Lewis, J., McPartlin, M., Nelson, W. J. H., Sankey, S. W. and Wong, K., *J. Organomet. Chem.*, 1980, **191,** C3.
17. *Inorganic Synthesis* Vol. 28, ed. Angelici, R. J. John Wiley and Sons, N.Y., 1990.
18. Arnold, L. J., *J. Chem. Educ.*, 1992, **69,** 811.

Pergamon

PII: S0277-5387(98)00038-2

Polyhedron Vol. 17, No. 17, pp. 2907–2919, 1998
© 1998 Elsevier Science Ltd
All rights reserved. Printed in Great Britain
0277-5387/98 $19.00+0.00

Structural studies on substituted pentaruthenium carbido carbonyl clusters†

Robert A. Burrow, David H. Farrar*, Jianbin Hao, Alan Lough, Ophyr Mourad, Anthony J. Poë* and Ying Zheng

Lash Miller Chemical Laboratories, University of Toronto, 80 St. George Street, Toronto, Ontario, Canada M5S 3H6

(Received 27 October 1997; accepted 13 January 1998)

Abstract—The structures of $[Ru_5C(CO)_{14}L]$, where L = $P(4\text{-}C_6H_4OMe)_3$, **2a**, $P(4\text{-}C_6H_4F)_3$, **2b**, and PCy_3, **2c**, and of $[Ru_5C(CO)_{13}(etpb)_2]$ (etpb = $P(OCH_2)_3CEt$)), **3**, have been determined. The Ru—Ru and Ru—P bond distances of the $[Ru_5C(CO)_{15-n}L_n]$ clusters, **2a, 2b, 2c, 3**, $[Ru_5C(CO)_{14}(PPh_3)]$, and $[Ru_5C(CO)_{13}(PPh_3)_2]$, were analyzed and the results are compared with those reported elsewhere for the unsubstituted parent cluster, and for the clusters $[Ru_3(CO)_{12-n}L_n]$, $n = 1$ or 2. The Ru_5 clusters all maintain the square pyramidal arrangement of the parent cluster and the general arrangement of the ligands. The average Ru—Ru distances are remarkably constant but individual Ru—Ru distances vary widely. A clear feature is that the lengths of the Ru—Ru bonds in the basal plane that are *cis* to the axial Ru—P bonds are longer than any of the other Ru—Ru distances in all the $[Ru_5C(CO)_{15-n}L_n]$ clusters except **3**. The distance lengthens slightly with increasing cone angle of the substituent P-donor ligand but this effect may be at least partly due to crystal packing effects. The Ru—P distances in the Ru_5 and Ru_3 clusters increase significantly with increasing ligand cone angle and net electron donicity. The two effects cannot easily be separated due to the general correlation of the donicity and size of the P-donor ligands and both effects may apply. A distinctive feature of these changes in bond lengths is that they do not depend on whether $n = 1$ or 2, showing that the substituent effects are localized. The carbido atom out-of-plane distance increases in an approximately linear fashion with the basicity of the P-donor ligand.
© 1998 Elsevier Science Ltd. All rights reserved

Keywords: pentaruthenium complexes; carbonyl complexes; carbido clusters, P-donor substituent complexes; cluster complexes; X-ray crystal structure.

The reaction chemistry of $[Ru_5C(CO)_{15}]$, **1**, has been extensively studied since the cluster was first reported in 1973 [1]. Most reactions of **1** begin by the direct substitution of a CO ligand although this step is sometimes promoted by Me_3NO [2]. The substitution of the CO ligands in **1** by P-donor ligands has been reported and the structures of some of the derivatives have been characterized by X-ray crystallography [3].

The single crystal X-ray structure for the parent cluster $[Ru_5C(CO)_{15}]$, **1** has been reported [3b]. The five Ru atoms in **1** form the corners of a square pyramid, consistent with the prediction from cluster electron counting rules for a *nido*-octahedral structure [4]. The apical Ru atom is bound to four other Ru atoms, and the basal Ru atoms to three others. The carbido atom is situated equidistantly from the four basal Ru atoms and is slightly (0.11(2) Å) below the basal plane. The CO ligands surround the framework with three ligands terminally bound to each Ru atom. Studies of the adduct $[Ru_5C(CO)_{15}(NCMe)]$, formed when **1** is dissolved in acetonitrile, have shown that the addition of a ligand to **1** results in a structural change of the Ru_5 core to an *arachno*-pentagonal-bipyramid [3b]. The reaction of **1** with PPh_3 gives a substituted complex, $[Ru_5C(CO)_{14}(PPh_3)]$, in which a carbonyl ligand on one of the basal Ru atoms is replaced by the PPh_3 ligand [3b]. In the presence of an excess of PPh_3, two carbonyl ligands on opposite basal Ru atoms are replaced giving $[Ru_5C(CO)_{13}(PPh_3)_2]$.

* Authors to whom correspondence should be addressed.

† Dedicated to Jack Lewis on the occasion of his 70th birthday.

Kinetic studies on the substitution of a CO ligand in **1** by P-donor ligands shows a marked difference in the mechanism between smaller incoming nucleophiles and the larger ones [5a]. The substitution reactions of **1** with the smaller phosphine and phosphite nucleophiles proceed through two observable steps, and kinetic parameters were determined for both. The first step proceeds very quickly with an associative rate law characterized by a linear dependence of k_{obs} on the concentration of the incoming nucleophile. The carbonyl stretches in the infrared spectrum of the product of this first step have a similar pattern to the known acetonitrile adduct $[Ru_5C(CO)_{15}(NCMe)]$ [3b]. A second, much slower step, to form the monosubstituted product follows a dissociative rate law for which the rate law is independent of the concentration of the incoming nucleophile. For the larger nucleophiles, the initial adduct is not detected. Instead, the substitution reaction proceeds by a single observable step that follows an associative rate law with a first order dependence on the concentration of the incoming nucleophile.

The kinetic studies clearly demonstrate the important effects of the nature of the phosphorus donor nucleophile on the substitution reactions of **1**. The structures of a series of phosphine or phosphite substituted clusters, $[Ru_5C(CO)_{14}L]$ and $[Ru_5C(CO)_{13}L_2]$, were determined to complement the kinetic studies [5]. The trends of the bond distances in the core of these substituted clusters, when compared with the steric and electronic parameters of the ligands, can possibly give insight into the nature of the dynamic behaviour of these clusters.

RESULTS AND DISCUSSION

The structures of $[Ru_5C(CO)_{14}L]$, where L = $P(4\text{-}C_6H_4OMe)_3$, **2a**, $P(4\text{-}C_6H_4F)_3$, **2b**, and PCy_3, **2c**, and $[Ru_5C(CO)_{13}(etpb)_2]$, (etpb = $P(OCH_2)_3CEt$)) **3**, have been determined. Table 1 summarizes the crystallographic information. Atomic parameters for **2a**, **2b**, **2c** and **3** have been deposited as supplementary material. The molecular structures are depicted in Figs 1 through 7. The X-ray structure determinations for **2a**, **2b** and **3** were straightforward and for these three structures all non-H atoms were refined with anisotropic thermal parameters. The structure of **2c** was difficult to solve and refine, due to poor crystal mosaicity resulting in weak X-ray data, and the unusually large number of molecules in the asymmetric unit. Consequently, all the C atoms in **2c** were refined isotropically to increase the data to parameter ratio.

In the crystal structures, the Ru metal skeleton of the substituted clusters $[Ru_5C(CO)_{15-n}L_n]$ ($n = 1, 2$) **2a**, **2b**, **2c**, **3**, $[Ru_5C(CO)_{14}(PPh_3)]$, and $[Ru_5C(CO)_{13}(PPh_3)_2]$, are similar to that of the parent cluster $[Ru_5C(CO)_{15}]$ (see Table 2). Thus, the square pyramidal cluster framework is able to accommodate a vast range of sizes of ligands bound to the basal Ru atoms—from the small CO ligand to the bulky PCy_3—without any significant distortion of its basic geometry. The three ligands bound to the basal Ru atoms are all disposed in the same way in one axial and two equatorial positions, the latter being fairly symmetrical with respect to each of the Ru^a—Ru^b bonds, and the P-donor substituents are always in axial positions. (Ru^a and Ru^b are apical and basal Ru atoms, respectively.) There are therefore always two Ru^b—Ru^b bonds that are *cis* to each substituent. The three CO ligands attached to the apical Ru atom are necessarily less symmetrically bound because this Ru atom is connected to four basal metal atoms. One of the Ru^a—CO^b bonds always lies roughly above one of the Ru^a—Ru^b bonds while the other two are almost symmetrically disposed on either side of the Ru^a—Ru^b bond "*trans*" to the first and are roughly eclipsed with respect to the two equatorial CO ligands attached to the Ru^b atom. In no case are carbonyl ligands seen to adopt the "semi-bridging" arrangement reported in the related $[Ru_3(CO)_{10}(PPh_3)_2]$ cluster [6]. There are no discernable systematic differences in Ru—CO bond lengths between the unsubstituted cluster and any of the substituted ones showing that such substituent effects are dissipated over the whole of the cluster rather than being evident in any specific Ru—CO bond. This is also indicated by the small range of C—O stretching frequencies found in a large variety of substituted clusters. Thus plots of corresponding values of ν_{co} against χ [7a,8] are closely linear for all bands with gradients of only 0.1–0.2 [5a,9] in contrast to gradients of ca. 1 and 2 for the complexes $[Ru(CO)_4L]$ and $[Ru(CO)_3L_2]$, respectively [10]. (χ is a measure of the net electron donicity of the ligands based on the values of the C—O stretching frequencies in the complexes $[Ni(CO)_3L]$.) However, the Ru—P distances, presented in Table 3, vary widely from 2.217(3) Å to 2.407(9) Å.

If the arrangement of the ligands described above were completely symmetrical it would be expected that there would be three types of Ru^a—Ru^b bond in the parent cluster: one that is eclipsed by an Ru^b—CO bond, another "*trans*" to that bond and two "*cis*" to it. However, in most cases there are four quite distinct Ru^a—Ru^b bond lengths (Table 2), even in the unsubstituted cluster, and it seems likely that crystal packing effects lower the symmetry of all the individual molecules. The ranges of Ru^a—Ru^b bond lengths, presented in Table 2 and shown graphically in Fig. 8, do vary substantially, even within otherwise identical molecules. Thus the range in **2c**, II is only 0.049(6) Å whereas it is 0.177(6) Å in **2c**, III, indicating the ease of deformation of the framework. The Ru^b—Ru^b bond lengths show a comparable variation.

Since the X-ray crystallography data are sparse for the P-donor substituted clusters $[Ru_5C(CO)_{15-n}L_n]$, structural parameters of the related clusters $[Ru_3(CO)_{12-n}L_n]$, $n = 1$ or 2, will be considered as well [6,11] (Table 4). The Ru_3 metal framework is closely related to the triangular face of the Ru_5C cluster but

Table 1. Summary of X-ray experimental data

Compound	**2a**	**2b**	**2c**	**3**
Empirical formula	$C_{36}H_{21}O_{17}PRu_5$	$C_{33}H_{12}F_3O_{14}PRu_5$	$C_{33}H_{33}O_{14}PRu_5$	$C_{26}H_{22}O_{19}P_2Ru_5$
M	1261.8	1225.7	1189.9	1205.7
Crystal colour, shape	red needles	red needles	deep red needles	red needles
Approx. crystal size (mm)	0.10 × 0.10 × 0.20	0.10 × 0.15 × 0.25	0.10 × 0.15 × 0.50	0.10 × 0.20 × 0.50
Crystal system	triclinic	monoclinic	orthorhombic	monoclinic
Space group	$P\bar{1}$ (No. 2)	$P2_1/n$(No. 13 alt.)	$P2_12_12_1$ (No. 19)	$P2_1/n$ (No. 13 alt.)
a (Å)	11.276(2)	12.252(5)	17.487(3)	19.919(4)
b (Å)	12.865(3)	18.512(5)	23.208(4)	17.947(3)
c (Å)	16.187(3)	16.602(5)	29.474(4)	21.441(4)
α (°)	104.35(3)	90	90	90
β (°)	90.03(3)	94.44(2)	90	104.97(2)
γ (°)	111.48(3)	90	90	90
V (Å^3)	2106.0(11)	3754(2)	11961(3)	7404(4)
Z	2	4	12	8
2θ range of centering refs. (°)	28.9–35.7	24.1–31.9	27.9–30.7	22.5–27.9
D_x (mg m^{-3})	1.990	2.169	1.982	2.163
F(000)	1216	2336	6936	4640
μ (Mo–K_α) (mm^{-1})	1.860	2.089	1.953	2.156
Indices	h −14–14	h −14–14	h0–21	h −23–22
	k −16–15	k0–21	k0–28	k0–21
	l0–20	l0–19	l0–35	l0–25
2θ range (°)	2.6–54.0	2.2–50.0	2.2–51.0	2.0–50.0
Scan range	0.60° + 0.35° × tan θ	0.60° + 0.35° × tan θ	0.60° + 0.35° × tan θ	0.80° + 0.35° × tan θ
Prescan speed (° min^{-1})	5.49	5.49	5.49	8.24
Scan speed (° min^{-1})	0.92–5.49	1.83–5.49	1.03–5.49	1.65–8.24
Variation of standards	0.951–1.018	0.969–1.004	0.990–1.011	0.960–1.025
Min., max. trans. coeffs./abs. correction	0.3658, 0.8709	0.6174, 0.8564	0.3203, 0.8650	0.5662, 0.8522
No. data collected, suitable	9377, 9162	7221, 7035	12104, 12029	13916, 13361
No. unique data (R_{int})	9162	6571 (0.0348)	11987	12984 (0.0238)
Extinction correction parameter	0.0024(2)	0.00011(4)	0.000003(2)	0.000024(5)
Weighting scheme parameters	0.0457, 1.32	0.0365, 4.24	0.0276, 0.00	0.0242, 15.49
No data used	9142	6570	9016	12981
Final R_1, wR_2	0.0261, 0.0749	0.0369, 0.0756	0.0762, 0.0721	0.0487, 0.0797
Final $R1_1$, wR_2 (all data)	0.0761, 0.1770	0.0803, 0.0947	0.1969, 0.0997	0.1590, 0.1047
Goodness of fit	1.088	1.058	0.979	1.005
No. variables (obs./variables)	542 (16.9)	509 (12.9)	939 (9.6)	949 (13.7)
$(\Delta/\sigma)_{max}$, $(\Delta/\sigma)_{average}$	0.003, 0.000	−0.001, 0.000	−0.022, 0.001	0.081, 0.001
$\Delta\rho_{min}$, $\Delta\rho_{max}$ (eÅ^{-3})	−0.768, 0.673	−0.692, 0.563	−1.053, 1.552	−0.838, 0.887

any substituents are situated in the Ru_3 plane rather than axially as in the Ru_5 clusters. This has the result that there are two sorts of Ru—Ru bonds when one Ru atom has a substituent attached, i.e. one *trans* to the substituent and another *cis* to it. The Ru—Ru and Ru—P bond lengths [6,11] of the P-donor substituted Ru_3 clusters are very similar to those of the corresponding Ru_5C clusters. A study of the variation of the Ru—Ru and Ru—P bond lengths within some of the Ru_3 clusters listed in Table 8 has been published [11b]. The results suggested that the length of the Ru—Ru bonds *cis* to the phosphorus ligand correlated with the ligand cone angles in a non-linear fashion, whereas the Ru—P bond lengths correlated linearly with substituent cone angles.

Ru—Ru *bonds*

The total variation of the Ru—Ru bond lengths in the $[Ru_5C(CO)_{15-n}L_n]$ (n = 0–2) clusters is quite large. The difference between the shortest and longest Ru—Ru distances listed in Table 2 is 0.199(5) Å, the shortest being a Ru^a—Ru^b in **2c,** III, and the longest a Ru^b—Ru^bL bond in **2c,** II and $[Ru_5C(CO)_{14}PPh_3]$. If all the Ru—Ru bonds in the substituted clusters are treated as random variations of a single bond length then the average of the 72 values is 2.8400(50) Å compared with an average of the unsubstituted clusters of 2.8404(66) Å. This shows that, if there are any changes in some of the bond lengths caused by substitution, they essentially cancel each other out. If

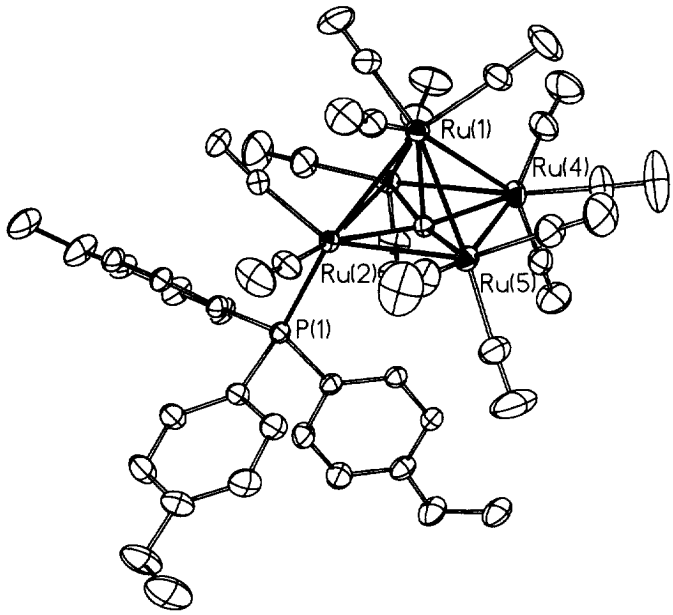

Fig. 1. ORTEP diagram for $[Ru_5C(CO)_{14}P(4\text{-}C_6H_4OMe)_3]$, **2a**, with 25% ellipsoids; the H atoms on the phenyl and methyl groups were omitted for clarity.

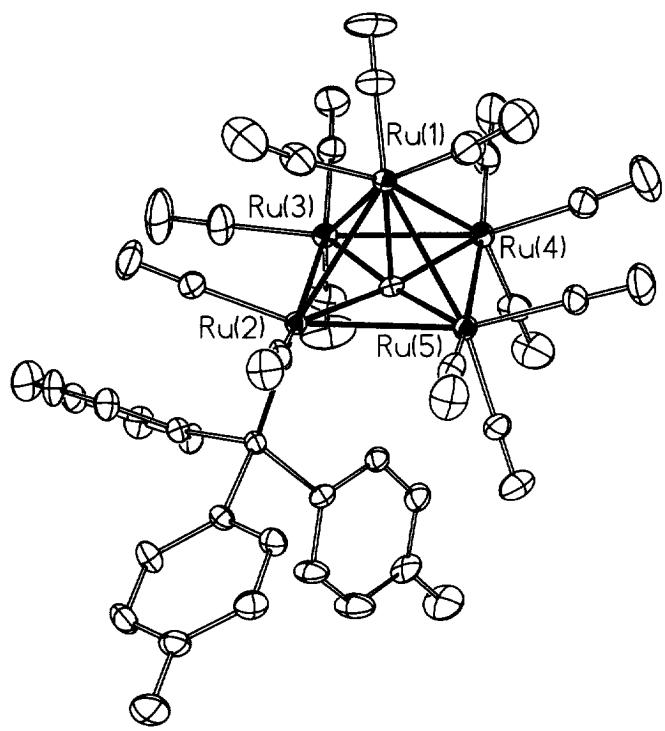

Fig. 2. ORTEP diagram for $[Ru_5C(CO)_{14}P(4\text{-}C_6H_4F)_3]$, **2b**, with 25% ellipsoids; the H atoms on the phenyl groups were omitted for clarity.

the Ru—Ru distances of each cluster are averaged, the largest variation between clusters is only 0.013 Å which again suggests that there are compensating effects of lengthening and shortening of bonds. Introduction of a large P-donor substituent might be expected to cause an expansion of the framework of the cluster due to the expansion of the ligand envelope. Metal–metal bonds are generally weaker than the

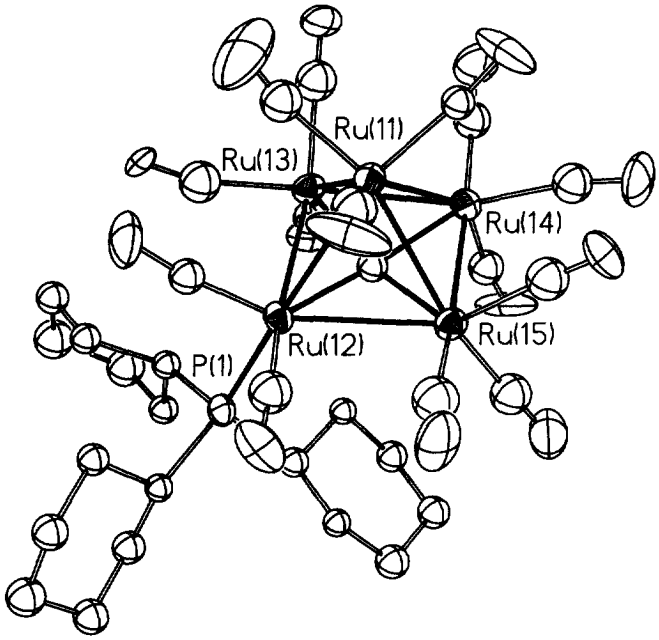

Fig. 3. ORTEP diagram for $[Ru_5C(CO)_{14}P(C_6H_{11})_3]$, **2c**, molecule I, with 25% ellipsoids; the H atoms were removed for clarity.

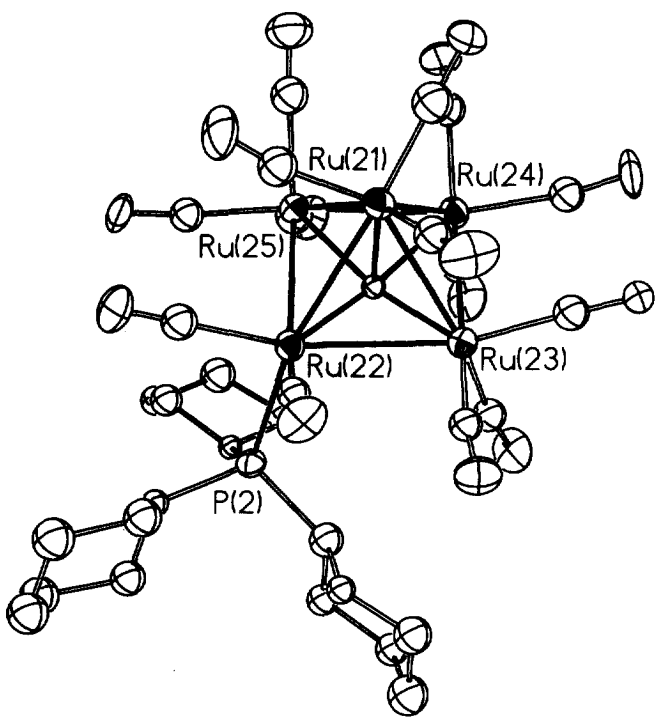

Fig. 4. ORTEP diagram for $[Ru_5C(CO)_{14}P(C_6H_{11})_3]$, **2c**, molecule II, with 25% ellipsoids; the H atoms were omitted for clarity.

metal–CO bonds; the estimated contribution to the enthalpy of disruption of the $[Ru_3(CO)_{12}]$ cluster (into Ru and CO) has been estimated to be 117 kJ mol^{-1} for each Ru—Ru bond and 172 kJ mol^{-1} for each Ru—CO bond [12]. Thus, as a small carbonyl ligand is replaced by a larger P-donor ligand, the ligand

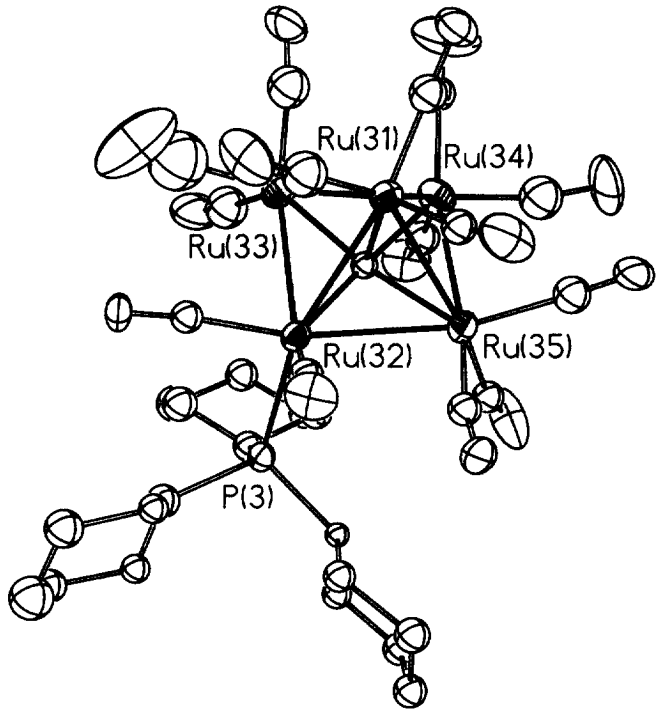

Fig. 5. ORTEP diagram for $[Ru_5C(CO)_{14}P(C_6H_{11})_3]$, **2c**, molecule III, with 25% ellipsoids; the H atoms were removed for clarity.

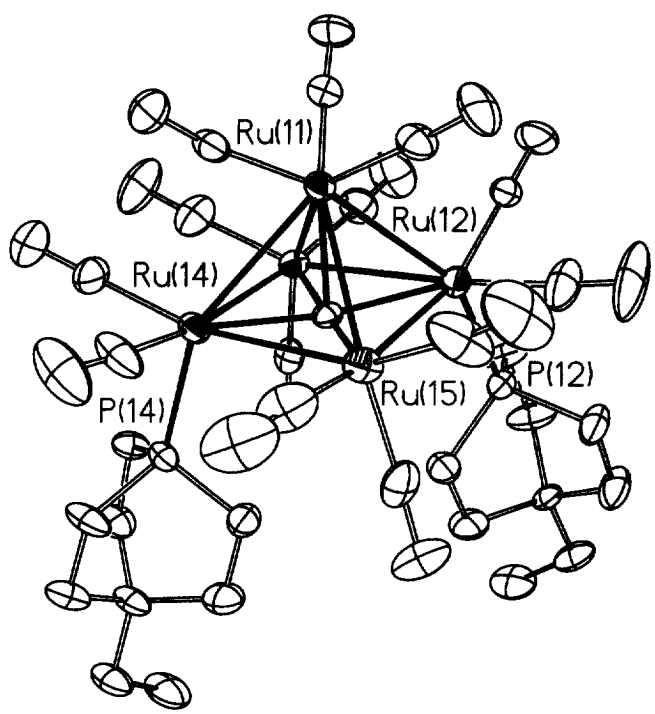

Fig. 6. ORTEP diagram for $[Ru_5C(CO)_{13}(P(OCH_2)_3CEt)_2]$, **3**, molecule I, with 25% ellipsoids; the H atoms were removed for clarity.

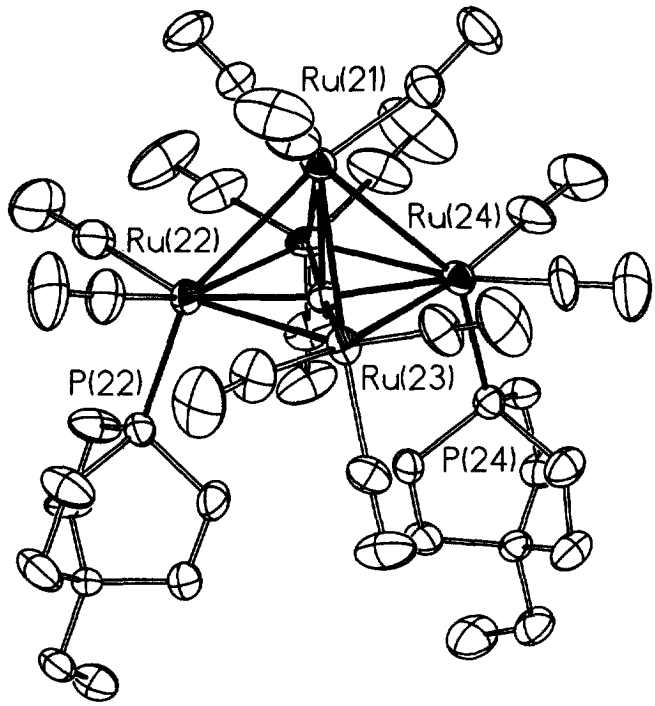

Fig. 7. ORTEP diagram for $[Ru_5C(CO)_{13}(P(OCH_2)_3CEt)_2]$, **3**, molecule II, with 25% ellipsoids; the H atoms were removed for clarity.

sphere would be expected to expand and the metal atoms would be correspondingly pulled apart. However, the average Ru—Ru distance within the clusters varies considerably less than the individual Ru—Ru distances, and this suggests that any expansion must be localized and is being counterbalanced by shortening elsewhere. It seems most likely that the expansion involves Ru—Ru bonds that are near the P-donor ligand. It is clear from Fig. 8, however, that the shortest Ru^b—Ru^bL bond is as long or much longer than the longest of any of the other distances in the same type of cluster so it is only the Ru^b—Ru^bL distances in the monosubstituted clusters and in $[Ru_5C(CO)_{13}(PPh_3)_2]$ that are being selectively lengthened. This effect is less pronounced in $[Ru_5C(CO)_{13}(etpb)_2]$ where the Ru^b—Ru^bL distances overlap with the others.

These observations were confirmed by a statistical analysis of the variation in Ru—Ru distances in both the Ru_5 and Ru_3 clusters which was approached in several stages [13]. (Details of the statistical procedures are given in the Supplementary Pages.) Firstly, the average Ru—Ru bond length was plotted against the separate stereo-electronic parameters for the phosphorus ligands. The ligand size was described by Tolman's cone angle θ [7] and the electronic donicity of the ligand was characterized by Tolman's χ parameter [7a], as modified by Bartik *et al.* [8] (see above). The resulting plots showed no obvious correlations. This was confirmed with a regression analysis; all correlations for average Ru—Ru bond distance against steric and electronic parameters had a $p > 0.05$ and usually $p > 0.35$ for both the F test of the analysis of the variation and for the probability of the t statistic. (p represents the probability that the correlation can be rejected.) The effect of the substitution of one or two carbonyl ligands with P-donor ligands shows no overall effect on the average Ru—Ru distance within the cluster.

Secondly, the effect of the P-donor ligand on the neighbouring Ru—Ru bonds in Ru_5C clusters was analyzed. The Ru—Ru bonds were grouped into Ru^a—Ru^b and Ru^b—Ru^b bonds which were subdivided according to whether the Ru atom had an attached P atom (Ru^a—Ru^bL or Ru^b—Ru^bL) or not (see Table 2). There were then four groups since no P atoms are bound to an apical Ru atom. The Ru—Ru bond distances were compared against each other using a one way analysis of variance. The test suggested that the groups were not equivalent. The groups were then compared against each other by the F-test for equivalence of variance and students' t-test for the equivalence of means. The statistical tests show conclusively that the basal Ru—Ru bond in which a P-donor ligand is bound to one of the Ru atoms (i.e. the Ru^b—Ru^bL bond) is longer than the others, which are statistically equivalent to each other. The lengthening of this Ru—Ru distance shows that the presence of the P-donor ligand only affects the Ru—Ru distance in the bond *cis* to the substituent. The other Ru—Ru

Table 2. The Ru—Ru bond lengths (Å) of the monosubstituted and disubstituted complexes $[Ru_5C(CO)_{14}L]$ and $[Ru_5C(CO)_{13}L_2]$

Complex	Ru—Ru bond distance (Å)			
	Ru^a—Ru^b	Ru^a—Ru^bL	Ru^b—Ru^b	Ru^b—Ru^bL
$[Ru_5C(CO)_{14}P(C_6H_4OMe\text{-}4)_3]$, **2a**	2.8436(8)	2.7980(7)	2.8466(10)	2.8498(1)
	2.8253(14)		2.8347(9)	2.9389(10)
	2.7841(11)			
$[Ru_5C(CO)_{14}P(C_6H_4F\text{-}4)_3]$, **2b**	2.8345(11)	2.8263(13)	2.8460(11)	2.8795(10)
	2.7966(11)		2.8502(10)	2.8868(11)
	2.8403(11)			
$[Ru_5C(CO)_{14}PCy_3]$, **2c**, I	2.768(4)	2.863(3)	2.788(4)	2.897(4)
	2.825(4)		2.827(4)	2.930(4)
	2.776(4)			
$[Ru_5C(CO)_{14}PCy_3]$, **2c**, II	2.813(4)	2.831(3)	2.806(4)	2.895(4)
	2.815(4)		2.799(4)	2.940(4)
	2.791(4)			
$[Ru_5C(CO)_{14}PCy_3]$, **2c**, III	2.741(4)	2.856(4)	2.854(5)	2.918(4)
	2.818(5)		2.825(5)	2.881(4)
	2.776(6)			
$[Ru_5C(CO)_{13}(P(OCH_2)_3CEt)_2]$, **3**, I	2.8401(12)	2.7811(12)		2.8451(12)
	2.8614(14)	2.8162(13)		2.8708(14)
				2.8469(12)
				2.8541(13)
$[Ru_5C(CO)_{13}(P(OCH_2)_3CEt)_2]$, **3**, II	2.8545(13)	2.7918(12)		2.8675(13)
	2.8136(13)	2.8395(14)		2.8725(14)
				2.8288(13)
				2.8455(14)
$[Ru_5C(CO)_{14}PPh_3]$[c]	2.800(1)	2.813(1)	2.830(1)	2.940(2)
	2.830(1)		2.815(1)	2.892(1)
	2.819(1)			
$[Ru_5C(CO)_{13}(PPh_3)_2]$[c]	2.804(2)	2.787(2)		2.919(2)
	2.815(2)	2.832(2)		2.899(2)
				2.845(2)
				2.864(2)
$[Ru_5C(CO)_{15}]$, I[c]	2.853(2)		2.836(2)	
	2.829(2)		2.843(2)	
	2.804(2)		2.858(3)	
	2.800(2)		2.882(2)	
$[Ru_5C(CO)_{15}]$, II[c]	2.811(2)		2.838(2)	
	2.872(2)		2.847(2)	
	2.800(2)		2.859(2)	
	2.838(2)		2.876(2)	

[a] Apical Ru atom bonded to 3 CO ligands and 2 Ru atoms.

[b] Basal Ru atom bonded to 3 CO ligands and 3 Ru atoms (labeled Ru) or 2 CO ligands, 1 phosphorus ligand and 3 Ru atoms (labeled RuL).

[c] From Ref. 3b.

distances then must all shorten, on average, by approximately an equal amount, although individually the shortening will be quite small.

To see if the lengthening of the Ru^b—Ru^bL distance in the Ru_5 clusters, and the *cis* Ru—Ru distance in the Ru_3 clusters, depends on the nature of the P-donor ligands, the Ru^b—Ru^bL and *cis* Ru—RuL distances were plotted against the steric and electronic parameters of the substituents. All plots showed a wide scatter of the bond distances around the lines but trends can be seen. Generally, the Ru—Ru distances increase with increasing net electron donicity of the ligands (decreasing χ) and increase with increasing size (θ) of the substituent, the gradients of the linear least squares plots being $-(1.9 \pm 0.4) \times 4^{-4}$ Å cm and $(7.3 \pm 1.7) \times 10^{-3}$ Å deg^{-1}, respectively. The *F*-statistics are (1,41)23.6 and (1,43)19.4, respectively. The R^2 values are both very low (0.31 and 0.37) and this shows that features other than the electronic and steric properties of the individual substituents are accounting for 60–70% of the variations. These are likely to be due to intermolecular packing forces since the molecules generally packed in different ways for each structure. However, both correlations are nevertheless

Table 3. The Ru—P bond distance (Å) of the monosubstituted and disubstituted complexes, $[Ru_5C(CO)_{14}L]$ and $[Ru_5C(CO)_{13}L_2]$

Complex	L	θ_L(°)	Ru—P
3	$P(OCH_2)_3CEt$	101	2.235(3)
			2.243(3)
			2.218(3)
			2.217(3)
2a	$P(C_6H_4OMe\text{-}4)_3$	145	2.3624(10)
2b	$P(C_6H_4F\text{-}4)_3$	145	2.350(2)
$[Ru_5C(CO)_{14}PPh_3]$[a]	PPh_3	145	2.376(3)
$[Ru_5C(CO)_{13}(PPh_3)_2]$[a]	PPh_3	145	2.377(3)
			2.363(2)
2c	PCy_3	170	2.407(9)
			2.382(8)
			2.398(9)

[a] From Ref. 3b.

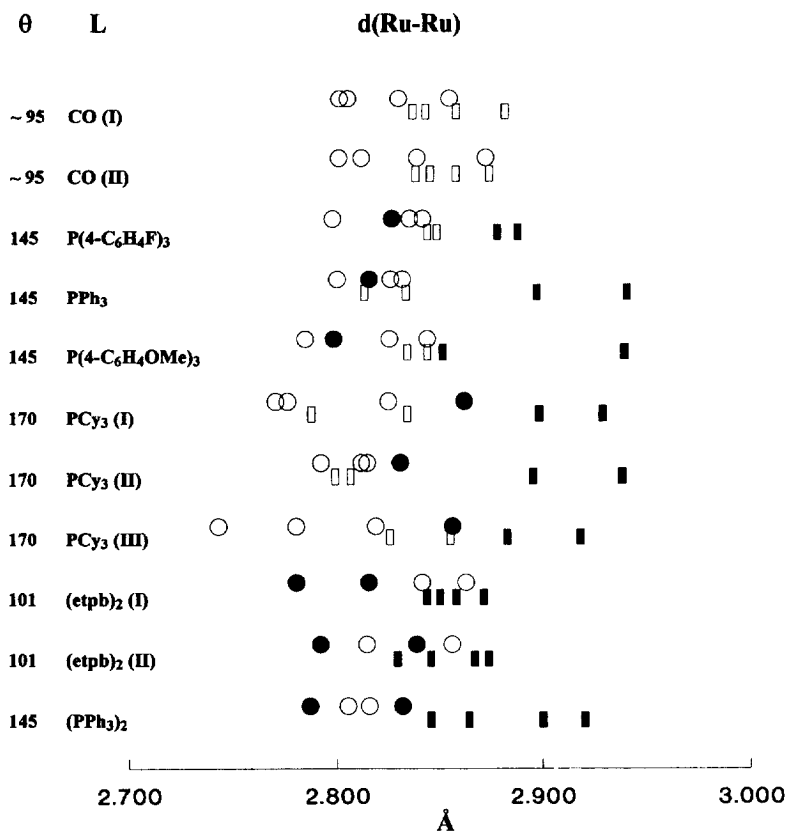

Fig. 8. Ru–Ru distances in the clusters $[Ru_5C(CO)_{15-n}L_n]$ ($n = 0-2$). ○: Ru^a–Ru^b; ●: Ru^a–Ru^bL; □: Ru^b–Ru^b; ■: Ru^b–Ru^bL

statistically significant at $p \ll 0.05$ for both the F test of the analysis of the variation, and the t statistic, so the contribution of the electronic and/or steric effects to the trends is well established. The reason for the dual correlation may be that the electronic parameters correlate with the cone angles with $p \ll 0.05$, as the smaller ligands tended to be less basic. In an attempt to differentiate between the steric and electronic effects the compounds containing phosphine ligands with phenyl and substituted phenyl groups ($\theta = 145°$) were

Table 4. The Ru—Ru and Ru—P bond distances (Å) of the monosubstituted complexes $[Ru_3(CO)_{11}L]$ and disubstituted complexes $[Ru_3(CO)_{10}L_2]$ for comparative purposes

Complex	L	θ_L (°)	*cis* Ru—Ru	Ru—P	Ref
$[Ru_3(CO)_{11}L]$	$P(OCH_2)_3CEt$	101	2.829(2)	2.238(1)	7a
	$P(OMe)_3$	107	2.8883(3)	2.2750(7)	7b
	$P(OCH_2CF_3)_3$	≈110	2.862(1)	2.254(1)	7a
	$PPh(OMe)_2$	115	2.872(1)	2.287(1)	7a
	$P(OPh)_3$	130	2.852(1)	2.256(2)	7c
	PEt_3	132	2.9078(2)	2.3489(5)	7b
	$PPh_2(CCPh)$	≈134	2.858(1)	2.342(1)	7d
	PPh_3	145	2.907(3)	2.380(6)	7e
	PCy_3	170	2.902(2)	2.425(3)	7f
			2.920(2)	2.420(3)	
$[Ru_3(CO)_{10}L_2]$	$P(OMe)_3$	107	2.859(1)	2.330(1)	7f
			2.845(1)	2.265(2)	
	$PPh(OMe)_2$	115	2.865(1)	2.295(1)	7g
	PPh_3	145	2.842(4)	2.344(7)	7g
			2.873(3)	2.393(7)	
			2.838(4)	2.370(7)	
			2.881(3)	2.367(7)	
			2.833(3)	2.357(6)	6
			2.823(3)	2.363(7)	
			2.873(3)	2.378(6)	
			2.863(3)	2.377(7)	
$[Ru_3(CO)_{10}(L_2)]$	$((EtO)_2P)_2O$	≈112	2.8131(9)	2.253(2)	7h
				2.254(2)	
	$(Ph_2P)_2C{=}CH_2$	≈120	2.836(1)	2.331(1)	7e
				2.316(1)	
	$(Ph_2P)_2CH_2$	121	2.834(1)	2.322(2)	7i
				2.334(2)	
	$Ph_2PCH_2CH_2PPh_2$	125	2.856(1)	2.330(2)	7j
				2.330(2)	

selected and the Ru^b—Ru^bL distances of these Ru_5 clusters were plotted against the electronic parameter. The plots show no trend and a regression analysis shows no correlation. Unfortunately the range of basicities and number of ligands involved were both small but the result suggests that the changes in the Ru^b—Ru^bL distances (and possibly also the *cis* Ru—Ru distances) may depend more on the size of the ligands than on their basicity. If the lengthening of the Ru^b—Ru^bL distances is related to the size of the P-donor ligand, it might be expected that increasing the size of the P-donor ligand also would increase the angle between the Ru—P vector and the plane defined by the four basal Ru atoms. This is observed although the variation within chemically equivalent values, in **2c** and **3**, is large (~6°). The angles between the Ru—P vectors and the planes defined by the four basal Ru atoms in **2c** are over 10° larger than the corresponding angles in **3**. Since the size and shape of the P-donor ligands could influence the packing of the lattice even the statistically significant increase in the Ru^b—Ru^bL distance with cone angle might be accounted for by lattice effects if these were systematic enough, i.e. the trends would not be properties of the individual molecules. In this connection it should be noted that the trends observed include examples of both bis and mono substituted clusters. For instance the Ru^b—Ru^bL lengths are very close for the mono and *bis* PPh_3 clusters which shows that the effects of the substituents are limited to the neighbouring Ru—Ru bonds. If the P-donor ligands caused a general expansion of the cluster then it would have been expected that two substituents would have a greater influence than one. Also there are two Ru—Ru bonds that are lengthened by each substituent in the Ru_5 clusters whereas only one is lengthened by the Ru_3 clusters. In spite of these differences the correlations are still highly significant.

Ru—P *bonds*

The Ru—P bonds in Tables 3 and 4 were analyzed in the same manner as the Ru—Ru bonds, and the situation is considerably clearer. The bond lengths vary significantly more than the Ru—Ru distances discussed above and the Ru—P bond lengths correlate extremely well with both the θ and χ parameters of

the ligands individually, the lengths increasing with increasing size (by $(2.58 \pm 0.14) \times 10^{-3}$ Å deg^{-1} with $R^2 = 0.92$ and $F(1,29)^* = 321$) and net electron donicity of the P-donor ligands (by $-(6.1 \pm 0.5) \times 10^{-3}$ Å cm with $R^2 = 0.87$ and $F(1,27) = 181$) so the putative lattice effects contribute a great deal less to the variations in these bond lengths. Again the size and basicity effects cannot be easily partitioned and, indeed, both could affect the Ru—P distance. Larger P-donors could well have longer Ru—P bonds for steric reasons, but it is also true that the smaller ligands are generally phosphites. These are believed to be π-acids as well as σ-donors while the larger ligands are only σ-donors [4], and the smaller ligands could be more strongly bonded and shorter as a result. The correlation with χ would not otherwise make sense since more strongly σ-donating P-donors would be expected to be more strongly bound and shorter so that the correlation would be opposite to that expected. The possibility that electronic effects could influence the Ru—P distance has been demonstrated by Giering *et al.* [14]. They noted in a study of steric and electronic effects on Fe—P bond lengths in the complexes [(η-Cp)(L)(CO)FeCOMe] and [(η-Cp′)(L)(CO)FeCOMe] (Cp′ = MeC_5H_4) that the least basic P-donors, which they concluded to be π-acceptors, fell into a group with Fe—P distances that were shorter by about 0.1 Å than those in the complexes containing ligands that they classified as pure σ donors. However, the plot of Ru—P distances against χ does show a monotonic decrease and the ligands are not grouped in the manner noted for the Fe—P distances [14]. It should also be noted that the changes in the Ru—P bond lengths are the same irrespective of whether there are one or two substituents present, and this reemphasizes the fact that the effects of different substituents within the ligand envelope are localized.

The problem of correlations between the χ and θ parameters of the P-donor ligands was reduced, as before, by using the data for ligands with a constant θ ($\theta = 145°$). A $p > 0.05$ of the F- and t-tests for the linear least squares fit was obtained, and consequently no trend of the Ru—P distance with the value of χ is evident. This suggests that the substantial variations in the Ru—P lengths are more likely to be influenced by the ligand size though the qualifications noted above are equally applicable here.

Carbido atom out-of-plane distance

The distance that the carbido atom lies below the plane formed by the four basal Ru atoms varies by about 0.12 Å and appears to depend on the basicity of the P donors (Table 5). Theoretical calculations [15] on the cluster $[Fe_5C(CO)_{15}]$ predict that, if it were to gain two electrons, the carbido atom should move to the vertex position, about 0.84 Å below the plane. The carbido atom would then be required to donate only two electrons to the total of skeletal bonding electrons. Similarly, as the P-donor ligands donate more electron density to the Ru_5 framework, the carbido atom could move further from the basal plane to compensate for the extra electron density in the metal framework. To examine this hypothesis, the carbido out-of-plane distance is plotted in Fig. 9 against the net electron donicity of the ligands as measured by the value of $\delta(^{13}CO)$, the chemical shift of the ^{13}C atom in the complexes $[Ni(CO)_3L]$ referenced to that in $[Ni(CO)_4]$ [16]. Choice of this parameter rather than χ allows the data for the parent cluster to be included. The data for the monosubstituted clusters fall on a line that also goes close to the point for the parent cluster, and the point for the bis-substituted PPh_3 cluster would also fall on the line if the net electron donicity of the pair of ligands were assumed simply to be twice that indicated by the $\delta(^{13}CO)$ value for PPh_3. However, the data for the two forms of the *bis*-etpb cluster both lie below the line, even before an increased electron donicity due to the presence of two ligands is allowed for, and they are both less than the value for the parent cluster. Nevertheless the expected general trend with net electron donicity seems to be reasonably well established.

CONCLUSION

The Ru—Ru and Ru—P bond distances of the $[Ru_5C(CO)_{15-n}L_n]$ clusters were analyzed and the results combined with those reported for the clusters $[Ru_3(CO)_{12-n}L_n]$ [6,11]. The largest effect is the significant and linear increase of ca 0.2 Å in the Ru—P bond lengths with increasing basicity and/or size of the P-donor ligands. The effects of size and basicity

Table 5. The distance the carbido atom lies out of the plane of the four basal Ru atoms from the X-ray data for the $[Ru_5C(CO)_{15-n}L_n]$ complexes

Complex	Distance
$[Ru_5(C)(CO)_{14}P(C_6H_4OMe\text{-}4)_3]$, **2a**	0.170(3)
$[Ru_5(C)(CO)_{14}P(C_6H_4F\text{-}4)_3]$, **2b**	0.140(6)
$[Ru_5(C)(CO)_{13}(P(OCH_2)_3CEt)_2]$, **3**	0.113(8)
	0.127(9)
$[Ru_5(C)(CO)_{14}PCy_3]$, **2c**	0.190(26)
	0.194(23)
	0.172(26)
$[Ru_5(C)(CO)_{15}]^a$	0.130
$[Ru_5(C)(CO)_{14}PPh_3]^a$	0.172
$[Ru_5(C)(CO)_{13}(PPh_3)_2]^a$	0.228

[a] Calculated from coordinate data from Ref. 3b.

*Two "outlying" data points were omitted from the analysis.

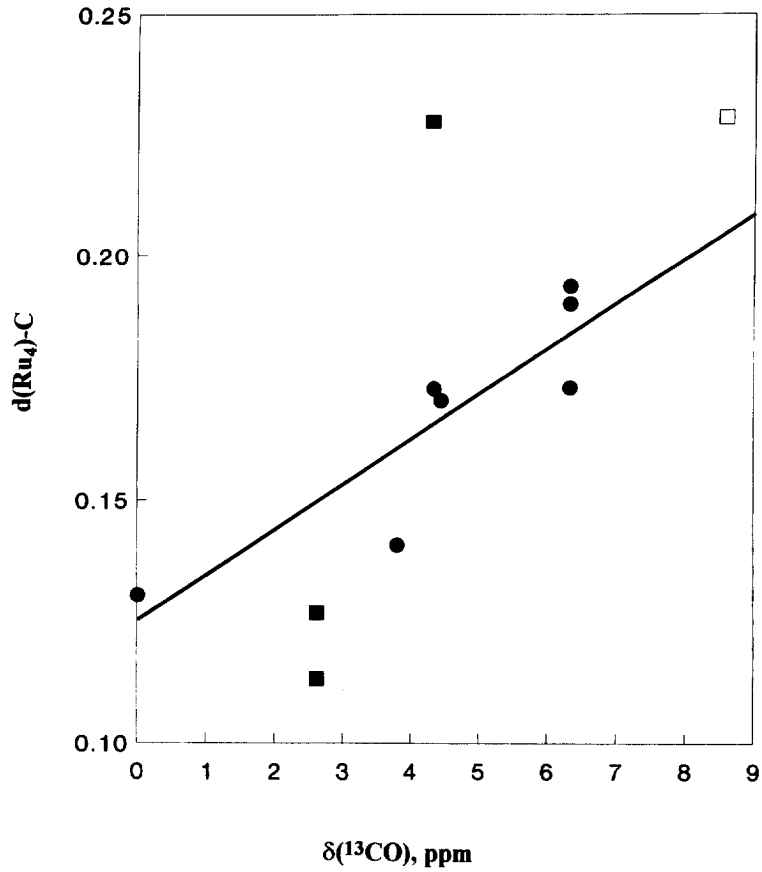

Fig. 9. Effect of net electron donicity of L (L = CO or P-donor ligands) on the distance that the C atom lies below the basal Ru_4 plane. ●: unsubstituted or monosubstituted clusters; ■: disubstituted clusters; □: the disubstituted cluster with L = PPh_3 and twice as much net electron donicity allowed for as in the monosubstituted PPh_3 substituted cluster.

cannot easily be separated, due to the correlation of the basicity and size parameters for most of the P-donor ligands, and both effects may be important. The Ru—Ru bonds are also significantly longer when a P-donor ligand is attached to one of the Ru atoms (a basal one) in all the $[Ru_5C(CO)_{15-n}L_n]$ clusters (except when L = etpb), and the Ru—Ru bonds *cis* to the Ru—P bonds are longer than the other Ru—Ru distances in the Ru_3 clusters. However, the dependence of these Ru—Ru bond distances on the nature of the P-donor substituents is quite small and can account for only 30–40% of the variations in the bond lengths. It seems probable that lattice effects account for the remaining 60–70% of the differences between the substituted and parent clusters. The effects on the Ru—Ru and Ru—P distances are not affected by whether there are one or two substituents present so the effects appear to be localized close to the substituents. As in the parent cluster, the carbido atoms in all the substituted Ru_5 clusters lie below the plane defined by the four basal Ru atoms and the extent of this distortion appears to be determined usually by the degree of electron donation from the substituents.

EXPERIMENTAL

The compound **2a, 2b, 2c** and **3** were prepared by literature methods [3b,5] and crystals were grown by slow evaporation of 1 : 1 hexane : CH_2Cl_2 solutions. Table 1 details the experimental data for the single crystal X-ray solution and refinement for the structures.

Accurate cell dimensions and crystal orientation matrix were determined on an Enraf-Nonius CAD-4 diffractometer by a least squares treatment of the setting angles of 25 high angle reflections [17]. Intensities of reflections were collected with variable scan speeds and widths of the ω-2θ type scans by using graphite monochromatized Mo–K_α radiation (0.70930 Å), at a temperature of 293(2) K. A scan of 25% of the full range on either side of each reflection was used for the background measurement. Three standard reflections were collected every 120 min to check the crystal orientation and intensity of the reflections. A linear correction was applied to correct for the variation of the standards. The structures were solved by direct methods [18]. Refinements were by full-matrix least-

squares calculations on F^2 using all data, initially with isotropic and then anisotropic thermal parameters for non-hydrogen atoms; the carbon atoms for **2c** were refined isotropically due to the low value of the data to parameter ratio. In the final rounds of calculations, the hydrogen atoms were positioned on geometric grounds (C—H 0.96 Å for —CH_3 groups, C—H 0.97 Å for CH_2 groups and 0.93 Å for aryl CH groups) and included as riding atoms in the structure factor calculation with refinement rotation of the methyl groups where possible; the isotropic displacement coefficients were refined on a per group basis. The refinement minimized $wR_2 = [\Sigma w(F_o^2 - F_c^2)^2]/[\Sigma w(F_o^2)^2]$ for all reflections where $w = 1/[\sigma^2(F_o^2) + (aP)^2 + bP]$, where a and b are the first and second weighting scheme parameters, respectively and $P = [(\text{the maximum of } 0 \text{ or } F_o^2)/3 + 2F_c^2/3]$. The extinction coefficient, χ, where $F^* = F_c[1 + (\chi \times F_c^2 \times \lambda^3)/(1000 \times \sin 2\theta)]^{-1/4}$ was used. The data sets were corrected for absorption using a semi-empirical approach [19]. The absolute configuration for the non-centrosymmetric space group in the structure of **2c** was confirmed by the Flack parameter which refined to a value of $-0.2(1)$ [20]. Scattering factors for neutral atoms were used as stored in the programs. All calculations were carried out on a personal computer with SHELXTL PC, version 4.2 [18].

Acknowledgements—Are made to the Natural Sciences and Engineering Research Council (NSERC), Canada, for provision of equipment and operating funds, and one of us (O.M.) thanks NSERC for the award of a Summer Research Bursary.

REFERENCES

1. Eady, C. R., Johnson, B. F. G., Lewis, J. and Matheson, T., *J. Organometal Chem.*, 1973, **57,** C82.
2. Braga, D., Sabatino, P., Dyson, P. J., Blake, A. J. and Johnson, B. F. G., *J. Chem. Soc., Dalton Trans.*, 1994, 393.
3. (a) Farrar, D. H., Jackson, P. F., Johnson, B. F. G., Lewis, J., Nicholls, J. N. and McPartlin, M., *J. Chem. Soc., Chem. Commun*, 1981, 415; (b) Johnson, B. F. G., Lewis, J., Nicholls, J. N., Puga, J., Raithby, P. R., Rosales, M. J., McPartlin, M. and Clegg, W., *J. Chem. Soc., Dalton Trans.*, 1983, 277; (c) Evans, J., Gracey, B. P., Gray, L. R. and Webster, M., *J. Organomet. Chem*, 1982, **240,** C61.
4. Mingos, D. M. P. and Johnston, R. L., *Struct. Bond.*, 1987, **68,** 29.
5. (a) Farrar, D. H., Poë, A. J. and Zheng, Y., *J. Am. Chem. Soc.*, 1994, **116,** 6252; (b) Farrar, D. H., Hao, J., Mourad, O. and Poë, A. J., *Organometallics*, 1997, **16,** 5015.
6. Chin-Choy, T., Keder, N. L., Stucky, G. D. and Ford, P. C., *J. Organomet. Chem.*, 1988, **346,** 225.
7. (a) Tolman, C. A., *Chem. Rev.*, 1977, **77,** 313; (b) Tolman, C. A., *J. Am. Chem. Soc.*, 1970, **92,** 2956.
8. Bartik, T., Himmler, T., Schulte, H.-G. and Seevogel, K., *J. Organomet. Chem.*, 1984, **272,** 29.
9. Zheng, Y., Ph.D. thesis, University of Toronto, 1993.
10. Chen, L. and Poë, A. J., *Inorg. Chem.*, 1989, **28,** 3641.
11. (a) Bruce, M. I., Liddell, M. J., Hughes, C. A., Skelton, B. W. and White, A. H., *J. Organomet. Chem.*, 1988, **347,** 157; (b) Brodie, N. M. J., Chen, L., Poë, A. J. and Sawyer, J. F., *Acta Cryst.*, 1989, **C45,** 1314; (c) bin Shawkataly, O., Teoh, S.-G., and Fun, H.-K., *Z. Kristallographie*, 1991, **194,** 193; (d) Carty, A. J., MacLaughlin, S. A. and Taylor, N. J., *J. Organomet. Chem.*, 1981, **204,** C27; (e) Forbes, E. J., Goodhand, N., Jones, D. L. and Hamor, T. A., *J. Organomet. Chem.*, 1979, **183,** 143; (f) Bruce, M. I., Matisons, J. G., Skelton, B. W. and White, A. H., *J. Chem. Soc., Dalton Trans.*, 1983, 2375; (g) Bruce, M. I., Liddell, M. J., Hughes, C. A., Patrick, J. M., Skelton, B. W. and White, A. H., *J. Organomet. Chem.*, 1988, **347,** 181; (h) Cabeza, J. A., Riera, V., Jeannin, Y. and Miguel, D., *Inorg. Chim. Acta*, 1990, **168,** 77; (i) Coleman, A. W., Jones, D. F., Dixneuf, P. H., Brisson, C., Bonnet, J.-J. and Lavigne, G., *Inorg. Chem.*, 1984, **23,** 952; (j) Bruce, M. I.. Hambley, T. W., Nicholson, B. K. and Snow, M. R., *J. Organomet. Chem.*, 1982, **235,** 83.
12. Connor, J. A., *Topics Current Chem.*, 1977, **71,** 71.
13. Snedecor, G. W. and Cochran, W. G., *Statistical Methods*, 8th edn, Iowa State University Press, Iowa, 1989.
14. Liu, H.-Y., Eriks, K., Prock, A. and Giering, W. P., *Organometallics*, 1990, **9,** 1758.
15. Halet, J.-F., Saillard, J.-Y., Lissillour, R., McGlinchey, M. J. and Jaouen, G., *Organometallics*, 1985, **5,** 139.
16. Bodner, G. M., May, M. P. and McKinney, L. E., *Inorg. Chem.*, 1980, **19,** 1951.
17. CAD4F and SDP-Plus User's Manuals, Enraf-Nonius, Delft, 1982.
18. SHELXTL PC, Version 4.1, Siemens Analytical Instruments, U.S.A., 1990.
19. Sheldrick, G. M., SHELXA-90, University of Göttingen, Germany, 1990.
20. Flack, H. D., *Acta Cryst.*, 1983, **A39,** 876.

Pergamon

PII: S0277-5387(98)00037-0

Polyhedron Vol. 17, No. 17, pp. 2921–2930, 1998
© 1998 Elsevier Science Ltd
All rights reserved. Printed in Great Britain
0277-5387/98 $19.00+0.00

Homometallic octahedral boride cluster chemistry: Reactions of $[Ru_6(CO)_{17}B]^-$ with PPh_3 and $P(OMe)_3$, and the crystal structure of $[Ru_6(CO)_{16}\{P(OMe)_3\}B(AuPPh_3)]$†

Catherine E. Housecroft,*[a] Arnold L. Rheingold,*[b] Anne Waller[c] and Glenn P. A. Yap[b]

[a] Institut für Anorganische Chemie, Spitalstrasse 51, CH-4056 Basel, Switzerland

[b] Department of Chemistry, University of Delaware, Newark, DE 19716, U.S.A.

[c] Department of Chemistry, University of Cambridge, Lensfield Road, Cambridge CB2 1EW, U.K.

(Received 14 October 1997; accepted 14 January 1998)

Abstract—The reaction between $[(PPh_3)_2N][Ru_6(CO)_{17}B]$ and PPh_3 leads to the formation of $[(PPh_3)_2N][Ru_6(CO)_{16}(PPh_3)B]$, the yield being dependent on reaction conditions. Treatment of $[Ru_6(CO)_{16}(PPh_3)B]^-$ with CF_3CO_2H or Ph_3PAuCl gives $[HRu_6(CO)_{16}(PPh_3)B]$ or $[Ru_6(CO)_{16}(PPh_3)B(AuPPh_3)]$ respectively; the latter cluster can also be prepared by PPh_3-for-CO substitution starting from $[Ru_6(CO)_{17}B(AuPPh_3)]$. When $[(PPh_3)_2N][Ru_6(CO)_{17}B]$ is treated with $P(OMe)_3$, followed by the addition of Ph_3PAuCl, the cluster $[Ru_6(CO)_{16}\{P(OMe)_3\}B(AuPPh_3)]$, **4** is obtained, but reaction of $[(PPh_3)_2N][Ru_6(CO)_{16}\{P(OMe)_3\}B]$ with CF_3CO_2H results in cleavage of one methoxy group and the formation of $[Ru_6(CO)_{16}\{\mu\text{-}P(OMe)_2\}B]$. Whereas multi-phosphine substitution in $[Ru_6(CO)_{17}B]^-$ was not achieved when the Lewis base was PPh_3, up to four $P(OMe)_3$ ligands could be introduced. An X-ray crystal structure determination of **4** confirms the retention of the octahedral Ru_6-cluster core with an interstitial boron atom; the gold(I) phosphine unit bridges an Ru—Ru edge causing significant elongation of the latter, and the $P(OMe)_3$ substituent occupies a terminal site on a ruthenium centre remote from the gold(I) fragment. © 1998 Elsevier Science Ltd. All rights reserved

Keywords: boride; cluster; phosphine; phosphite; ruthenium.

Our studies of the reactivity of boride-containing homometallic ruthenium clusters with phosphines and phosphites have been confined to compounds containing three (triangular framework) or four (butterfly framework) metal centres [1–3]. The substitution behaviour of $[HRu_4(CO)_{12}BH_2]$ is significantly influenced by the nature of the Lewis base, and (for the range of ligands studied) high degrees of substitution were only achieved with the tertiary phosphite $P(OMe)_3$ [2]. In each of the homometallic ruthenaboranes studied, the boron atom was exposed, either residing in a vertex site or in a semi-interstitial position, and was attached to two or more H atoms.

In the present paper we extend our studies to the cluster $[Ru_6(CO)_{17}B]^-$, the conjugate acid $[HRu_6(CO)_{17}B]$ has been structurally characterized [4,5] and possesses an octahedral framework containing an interstitial boron atom. In the lower nuclearity clusters, some competition between B and Ru sites of attack are possible and have been observed [1]; this was also the case in the related ferraborane $[HFe_3(CO)_9BH_2R]^-$ (R = H; CH_3) [6,7]. The interstitially sited B atom in $[Ru_6(CO)_{17}B]^-$ is shielded from attack and substitution chemistry is expected to involve the ruthenium-bound carbonyl ligands. The anion $[Ru_6(CO)_{17}B]^-$ is isoelectronic with the neutral carbido cluster $[Ru_6(CO)_{17}C]$ for which both mono- and disubstituted PPh_3 derivatives have been reported [8]. With $P(OMe)_3$, up to four CO ligands in $[Ru_6CO)_{17}C]$ have been replaced [9], a result that parallels our

* Author to whom correspondence should be addressed.

† This paper is dedicated to Jack Lewis on the occasion of his 70th birthday.

observation of multi-substitution by $P(OMe)_3$ in $[HRu_4(CO)_{12}BH_2]$ [2]. The aims of the present study were to explore the reactivity of $[Ru_6(CO)_{17}B]^-$ towards PPh_3 and $P(OMe)_3$, and to investigate the effects of protonation of the anionic products and the reactions of the latter with [PhPAuCl].

EXPERIMENTAL

General data

Fourier-transform NMR spectra were recorded on a Bruker WM 250 spectrometer, ^1H shifts are reported with respect to δ 0 for Me_4Si, ^{11}B NMR with respect to δ 0 for $F_3B \cdot OEt_2$ and ^{31}P NMR with respect to δ 0 for 85% H_3PO_4; downfield chemical shifts are positive. Solution infrared spectra were recorded on a Perkin–Elmer FT 1710 spectrophotometer, and fast ion bombardment (FIB) and fast atom bombardment (FAB) mass spectra using Kratos instruments (3-NBA matrix = 3-nitrobenzyl alcohol).

All reactions were carried out under argon by using standard Schlenk methods. Solvents were pre-dried and distilled under N_2. Separations were achieved by using thin layer plate chromatography with Kieselgel 60-PF-254 (Merck). PPh_3 and $P(OMe)_3$ were used as received (Aldrich); $[Ph_3PAuCl]$ [10], $[(Ph_3P)_2N][Ru_6(CO)_{17}B]$ [11] and $[Ru_6(CO)_{17}B(AuPPh_3)$ [11] were prepared according to literature methods. Yields were somewhat variable and typical values (with respect to starting cluster) are given.

Preparation of $[(Ph_3P)_2N][Ru_6(CO)_{16}(PPh_3)B]$, $[(Ph_3P)_2N][1]$

In a typical reaction, $[(Ph_3P)_2N][Ru_6(CO)_{17}B]$ (33 mg, 0.020 mmol) was dissolved in CH_2Cl_2 (5 ml), and to this was added PPh_3 (26 mg, 0.1 mmol). The solution was stirred at room temperature and was monitored by spot TLC until there was no apparent change in the number and relative quantities of the compounds present. The reaction time was 3 hr; solvent was removed *in vacuo*, and the products (two fractions) were separated by TLC (2 : 1 CH_2Cl_2 : hexane). The first fraction (orange, 5%) was unreacted $[(Ph_3P)_2N][Ru_6(CO)_{17}B]$, and the second (brown, $\approx$90%) was identified as $[(Ph_3P)_2N][Ru_6(CO)_{16}(PPh_3B]$, $[(Ph_3P)_2N][\mathbf{1}]$. If the stoichiometry is altered to 1 : 2 (cluster : phosphine), the yield of $[(Ph_3P)_2N][\mathbf{1}]$ is $\approx$70%, and in a 1 : 1 reaction, the yield falls to $\approx$35%. Photolysis of the CH_2Cl_2 solution containing a 1 : 5 cluster : PPh_3 mixture resulted in a greater product distribution (see text). $[Ph_3P)_2N][\mathbf{1}]$: ^1H NMR ($CDCl_3$, 298 K): δ 7.3–7.7 (m, Ph); ^{11}B NMR ($CDCl_3$ 298 K): δ 196.0, $^{31}P\{^1H\}$ NMR (CD_2Cl_2, 185 K): δ 53.2 (1P, PPh_3), 21.0 (2P, cation). IR (CH_2Cl_2) ν(CO) 2058 m, 2025 s, 1999 vs, 1945 w cm^{-1}. MS (negative FIB): 1328 (P^-) with 2 CO loses, 1066 (P^-—PPh_3) with 3 CO losses.

Preparation of $[HRu_6(CO)_{16}(PPh_3)B]$

$[(Ph_3P)_2N][\mathbf{1}]$ (34 mg, 0.018 mmol) was dissolved in CH_2Cl_2 (5 ml) and 5 μl CF_3CO_2H was added. The solution was stirred at room temperature and the reaction was monitored by IR spectroscopy. After 10 min, solvent was removed *in vacuo*, and the products were separated by TLC (2 : 1 hexane : CH_2Cl_2). One fraction eluted and $[HRu_6(CO)_{16}(PPh_3)B]$ was isolated in $\geqslant$95% yield. ^1H NMR ($CDCl_3$, 298 K): δ 7.5–7.8 (m, Ph), −17.5 (s, Ru—H—Ru); ^{11}B NMR ($CDCl_3$, 298 K): δ 195.0; $^{31}P\{^1H\}$ NMR ($CDCl_3$, 298 K): δ 35.9. IR (CH_2Cl_2) ν(CO) 2087 w, 2052 vs, 2026 s, 2000 w sh, 1974 w sh cm^{-1}. MS (positive FAB): 1330 (P^+) with 3 to 15 CO losses.

Preparation of $[Ru_6(CO)_{16}(PPh_3)B(AuPPh_3)]$. Method 1

$[(Ph_3P)_2N][\mathbf{1}]$ (35 mg, 0.018 mmol) was dissolved in CH_2Cl_2 (5 ml) and to this were added solid $[Ph_3PAuCl]$ (18 mg, 0.036 mmol) and $Tl[PF_6]$ (4 mg, 0.01 mmol). The solution was stirred for 1 h at room temperature and then solvent was removed *in vacuo*. Product separation by TLC (2 : 1 hexane : CH_2Cl_2) gave one predominant orange-brown fraction identified as $[Ru_6(CO)_{16}(PPh_3)B(AuPPh_3)]$ (90% yield). ^1H NMR ($CDCl_3$, 298 K): δ 7.3–7.8 (m, Ph); ^{11}B NMR ($CDCl_3$, 298 K): δ 195. 9; $^{31}P\{^1H\}$ NMR ($CDCl_3$, 298 K): δ 71 (1P, $AuPPh_3$), 42 (1P, $RuPPh_3$). IR (CH_2Cl_2) ν(CO) 2071 m, 2030 vs, 1993 m, 1978 w sh, 1950 w sh, 1854 w, 1825 w cm^{-1}. MS (positive FIB): 1787 (P^+) with 16 CO losses.

Preparation of $[Ru_6(CO)_{16}(PPh_3)B(AuPPh_3)]$. Method 2

$[Ru_6(CO)_{17}B(AuPPh_3)$ [11] (104 mg, 0.067 mmol) was dissolved in CH_2Cl_2 (5 ml) and to this was added PPh_3 (88 mg, 34 mmol). The solution was stirred at room temperature for 1 h, solvent was removed *in vacuo*, and the products were separated by TLC (2 : 1 CH_2Cl_2 : hexane). One major fraction (orange-brown) was collected and identified as $[Ru_6(CO)_{16}(PPh_3)B(AuPPh_3)]$ yield $\approx$70%) with the same spectroscopic signatures as the product formed from method 1.

Preparation of $[(Ph_3P)_2N][Ru_6(CO)_{16}\{P(OMe)_3\}B]$, $[(Ph_3P)_2N][\mathbf{2}]$

In a typical reaction, $[(Ph_3P)_2N][Ru_6(CO)_{17}B]$ (33 mg, 0.020 mmol) was dissolved in CH_2Cl_2 (5 ml), and to this was added $P(OMe)_3$ (2 μl, 0.02 mmol). The reaction was monitored by IR spectroscopy, and after 10 min, the most intense absorption had shifted to 1999 cm^{-1}. Solvent was removed *in vacuo* and products were separated by TLC (2 : 1 CH_2Cl_2 : hexane).

Only one fraction eluted (orange-brown, typically ≈60% yield) and was identified as $[(Ph_3P)_2N][Ru_6(CO)_{16}\{P(OMe)_3\}B]$. ^1H NMR ($CDCl_3$, 298 K): δ 7.4–7.7 (m, Ph), 3.6 (d, J_{PH} 12 Hz, Me); ^{11}B NMR ($CDCl_3$, 298 K): δ 197.2; $^{31}P\{^1H\}$ NMR ($CDCl_3$, 298 K): δ 150.3 (1P, $P(OMe)_3$), 21.0 (2P, cation). IR (CH_2Cl_2) ν(CO) 2060 m, 2026 s, 2001 vs, 1914 m cm^{-1}. MS (negative FIB): 1190 (P^-) with 9 CO losses.

Preparation of $[Ru_6(CO)_{16}\{\mu\text{-}P(OMe)_2\}B]$, **3**. Method 1

$[(Ph_3P)_2N][\mathbf{2}]$ (21 mg, 0.012 mmol) was dissolved in CH_2Cl_2 (5 ml) and CF_3CO_2H (5 μl) was added. The solution was stirred for 5 min during which time it became red; IR spectroscopic monitoring indicated that the reaction was complete within this period. The solvent was removed *in vacuo* and the products were separated by TLC (2:1 hexane:CH_2Cl_2). One red-orange fraction eluted, and was identified as $[Ru_6(CO)_{16}\{\mu\text{-}P(OMe)_2\}B]$ (≥95% yield). ^1H NMR ($CDCl_3$, 298 K): δ 3.8 (d, J_{PH} 13 Hz, Me); ^{11}B NMR ($CDCl_3$, 298 K): δ 193.3; $^{31}P\{^1H\}$ NMR ($CDCl_3$, 298 K): δ 357.7. IR (CH_2Cl_2) ν(CO) 2089 w, 2080 m, 2065 m, 2055 s, 2039 vs, 2025 m sh, 1989 m cm^{-1}. MS (negative FIB): 1190 (P^-) with 9 CO losses.

Preparation of $[Ru_6(CO)_{16}\{\mu\text{-}P(OMe)_2\}B]$, **3**. Method 2

The advantage of this method over method 1 is that it does not involve the isolation of the intermediate anion **2**. In a typical reaction, $[(Ph_3P)_2N][Ru_6(CO)_{17}B]$ (98 mg, 0.06 mmol) was dissolved in CH_2Cl_2 (5 ml), and to this was added $P(OMe)_3$ (7μl, 0.06 mmol). The solution was stirred at room temperature, and IR spectroscopic monitoring showed the reaction to be complete in 10 min; the strongest absorption had shifted to 1996 cm^{-1}. Trifluoroacetic acid (10 μl) was added to the solution; it was stirred for 5 min at room temperature, after which time the strongest absorption in the IR spectrum had shifted to 2065 cm^{-1}. Solvent was removed *in vacuo* and the products were separated by TLC (2:1 hexane:CH_2Cl_2). The first (orange, 15%) fraction was $[H_2Ru_4(CO)_{13}]$, identified by its IR spectrum [12]; the second (red-orange, 30%)band was compound **3**, and the final fraction (brown, 40%) was unreacted $[(Ph_3P)_2N][Ru_6(CO)_{17}B]$.

Preparation of $[Ru_6(CO)_{16}\{P(OM)_3\}B(AuPPh_3)]$, **4**

In a typical reaction, $[(Ph_3P)_2N][Ru_6(CO)_{17}B]$ (49 mg, 0.03 mmol) was dissolved in CH_2Cl_2 (5 ml), and to this was added $P(OMe)_3$ (3.5 μl, 0.03 mmol). The solution was stirred at room temperature and the reaction monitored by IR spectroscopy; the strongest absorption shifted to 1998 cm^{-1}. After 10 min, $[Ph_3PAuCl]$ (30 mg, 0.06 mmol) and $Tl[PF_6]$ (4 mg, 0.01 mmol) were added, and the solution was stirred at room temperature for 30 min. Solvent was then removed *in vacuo*, and products were separated by TLC (2:1 hexane:CH_2Cl_2). Three fractions eluted the first band was non-boron containing and was not characterized further. The second and third fractions were $[Ru_6(CO)_{17}B(AuPPh_3)]$ [11] (orange, ≈15%), and $[Ru_6(CO)_{16}\{P(OMe)_3\}B(AuPPh_3)]$ (red, ≈40%) respectively. ^1H NMR ($CDCl_3$, 298 K): δ 7.4–7.7 (m, Ph, 15H), 3.6 (d, J_{PH} 12 Hz, Me, 9H); ^{11}B NMR ($CDCl_3$, 298 K): δ 195.6; $^{31}P\{^1H\}$ NMR ($CDCl_3$, 298 K): δ 140.8 (1P, $P(OMe)_3$), 72.2 (1P, $AuPPh_3$). IR (CH_2Cl_2) ν(CO) 2055 m, 2032 vs, 1989 s, 1983 s cm^{-1}. MS (positive FIB): 1651 (P^+) with 15 CO losses.

Preparation of $[Ru_6(CO)_{14}\{P(OMe)_3\}_3B(AuPPh_3)]$

In a typical reaction, $[(Ph_3P)_2N][Ru_6(CO)_{17}B]$ (38 mg, 0.023 mmol) was dissolved in CH_2Cl_2 (5 ml), and to this was added $P(OMe)_3$ (6μl, 0.058 mmol). The solution was stirred at room temperature and the reaction monitored by IR spectroscopy; after 10 min, the strongest absorption had shifted to 1986 cm^{-1} and the spectrum showed no further changes. $[Ph_3PAuCl]$ (23 mg, 0.046 mmol) and $Tl[PF_6]$ (4 mg, 0.01 mmol) were added to the reaction mixture, and the solution was stirred for 30 min. Solvent was then removed *in vacuo*, and the products were separated by TLC (1:1 hexane:CH_2Cl_2). Two fractions eluted; the first was identified as $[Ru_6(CO)_{16}\{P(OMe)_3\}B(AuPPh_3)]$ (≈10%) and the second fraction was $[Ru_6(CO)_{14}\{P(OMe)_3\}_3B(AuPPh_3)]$ (orange-brown, ≈80%). ^1H NMR ($CDCl_3$, 298 K): δ 7.4–7.7 (m, Ph, 15H), 3.6 (d, J_{PH} 11 Hz, Me, 9H), 3.5 (d, J_{PH} 12 Hz, Me, 18H); ^{11}B NMR ($CDCl_3$, 298 K): δ 197.8; $^{13}P\{^1H\}$ NMR ($CDCl_3$, 298 K): δ 144.4 (2P, $P(OMe)_3$), 137.0 (1P, $P(OMe)_3$), 69.9 (1P, $AuPPh_3$). IR (CH_2Cl_2) ν(CO) 2055 m, 2032 vs, 1989 s, 1983 s cm^{-1}. MS (positive FIB): 1841 (P^+) with 14 CO losses.

Preparation of $[Ru_6(CO)_{13}\{P(OMe)_3\}_4B(AuPPh_3)]$

$[(Ph_3P)_2N][Ru_6(CO)_{17}B]$ (49 mg, 0.03 mmol) was dissolved in CH_2Cl_2 (5 ml), and to this was added $P(OMe)_3$ (14 μl, 0.12 mmol). The solution was stirred, and the reaction monitored by IR spectroscopy; the reaction was deemed complete after 30 min, when the strongest absorption had shifted to 1976 cm^{-1} and showed no further change. $[Ph_3PAuCl]$ (30 mg, 0.06 mmol) and $Tl[PF_6]$ (4 mg, 0.01 mmol) were added, the solution was stirred for 30 min, and then solvent was removed *in vacuo*. Separation by TLC (1:2 hexane:CH_2Cl_2) yielded one major fraction, identified as $[Ru_6(CO)_{13}\{P(OMe)_3\}_4B(AuPPh_3)]$ (red-brown, ≈80%). ^1H NMR ($CDCl_3$, 298 K): δ 7.4–7.7 (m, Ph, 15H), 3.6 (d, J_{PH} 11 Hz, Me, 18H), 3.7 (d, J_{PH} 11 Hz, Me, 18H); ^{11}B NMR ($CDCl_3$, 298 K): δ 196.2; $^{31}P\{^1H\}$ NMR ($CDCl_3$, 298 K): δ 141.2 (2P,

$P(OMe)_3$), 137.5 (2P, $P(OMe)_3$), 68.0 (1P, $AuPPh_3$). IR (CH_2Cl_2) ν(CO) 2096 m, 2026 m, 1997 s sh, 1983 vs cm^{-1}. MS (positive FAB): 1937 (P^+) with 1 CO loss.

Crystal structure determination of **4**

Crystals suitable for X-ray diffraction were grown from a concentrated CH_2Cl_2 solution layered with hexane. Crystallographic data for $[Ru_6(CO)_{16}\{P(OMe)_3\}B(AuPPh_3)]$, **4**, are collected in Table 1. Crystals (deep red plates) were photographically characterized and determined to belong to the triclinic crystal system. The centrosymmetric alternative was initially selected and this choice was supported by the results of refinement. An empirical correction for absorption was applied to the diffraction data ($T_{max/min} = 1.41$). The structure was solved by direct methods, completed from difference Fourier maps, and refined with anisotropic thermal parameters for all non-hydrogen atoms. Hydrogen atom locations were idealized. All computations used SHELXTL 4.2 software (G. Sheldrick, Siemens XRD, Madison, WI).

RESULTS AND DISCUSSION

Triphenylphosphine substitution

The reaction of $[Ru_6(CO)_{17}B]^-$ with PPh_3 was initially performed with the reagents in a 1 : 1 molar ratio. After one hour, $\approx$65% of $[Ru_6(CO)_{17}B]^-$ remained unreacted; only one new product was obtained and was identified as the monosubstituted product $[Ru_6(CO)_{16}(PPh_3)B]^-$, **1**. The FIB mass spectrum showed a parent ion at m/z 1328 and the isotopic distribution was in accord with the proposed formulation. The presence of one PPh_3 ligand was confirmed by the appearance in the ^{31}P NMR spectrum at 185 K of a singlet at δ 53.2 with a relative integral of half that of the signal assigned to the $[(Ph_3P)_2N]^+$ counter-ion; at 298 K, only the signal due to the cation was resolved. The ^{11}B NMR spectrum of $[(Ph_3P)_2N][\mathbf{1}]$ exhibited a broadened singlet at δ 196.0, shift which is characteristic of a boron atom encapsulated within an octahedral Ru_6-cage [13]. The yield of **1** can be increased to $\approx$70% by lengthening the reaction period to 2 h, or by altering the ratio of $[Ru_6(CO)_{17}B]^-$: PPh_3 to 1 : 5 and with a reaction time of 3 h (yield $\geq$90%). In each case, there was no evidence for the substitution of more than one CO ligand by PPh_3. In an attempt to facilitate multisubstitution, we photolysed the reaction mixture, irradiation with a mercury high-pressure lamp for 2 h, and using a 1 : 5 cluster : ligand ratio. Under these conditions, a range of products, most in very low yield, was formed; no attempt was made to characterize these compounds. The two main products of the photolysis reaction were $[(Ph_3P)_2N][\mathbf{1}]$ (35% yield) and a neutral material which was tentatively formulated from mass spectrometric data as a mixture of $[HRu_7(CO)_{19}B]$ and $[HRu_7(CO)_{18}(PPh_3)B]$. The +FAB mass spectrum showed two sets of fragmentation patterns arising from parent ions at m/z 1253 and 1484. Attempts to further separate these materials were unsuccessful; the mixture showed one broad signal in the ^{11}B NMR spectrum, at δ 191 indicative of an octahedral Ru_6B-environment, and the ^{31}P NMR spectrum exhibited a singlet at δ 27. In the ^1H NMR spectrum of the mixture, signals assigned to the Ph groups were observed (δ 7.3–7.8) but no highfield resonances due to metal-bound H atoms could be resolved. With the formulations of $[HRu_7(CO)_{19}B]$ and $[HRu_7(CO)_{18}(PPh_3)B]$, the products are 98 electron clusters, consistent with capped octahedral Ru_7-frameworks. Among homometallic ruthenium clusters, this geometry has been crystallographically confirmed for the 98 electron clusters $[HRu_7(CO)_{20}]^-$ [14] and $[HRu_7(CO)_{19}(\mu\text{-}CNMe_2]^-$ [15]. Interestingly, our attempts to achieve an analogous cluster expansion reaction using $[Ru_6(CO)_{17}B]^-$ as the starting material, in the absence of PPh_3 but under the same photolytic conditions as described above, were unsuccessful.

Anion **1** protonates readily when treated with CF_3CO_2H, and the conversion to $[HRu_6(CO)_{16}(PPh_3)B]$ is essentially quantitative (Fig. 1). In the mass spectrum of this product, the parent ion and its isotopic distribution are consistent with the formulation. Upon protonation, the shift in the ^{11}B NMR signal is negligible (δ 196.0 to 195.0) indicating that the octahedral cage around the boron atom is

Table 1. Crystallographic data for $[Ru_6(CO)_{16}\{P(OMe)_3\}B(AuPPh_3)]$, **4**

Formula	$C_{37}H_{24}AuBO_{19}P_2Ru_6$
Formula weight	1648.70
Crystal system	triclinic
Space group	$P\bar{1}$
a (Å)	10.124(6)
b (Å)	12.777(6)
c (Å)	19.163(6)
α (°)	108.73(4)
β (°)	97.56(4)
γ (°)	90.50(4)
V (Å^3)	2323(2)
Z	2
D_x (g cm^{-3})	2.356
μ(Mo–K$_\alpha$), cm^{-1}	51.8
Temperature (K)	298
Diffractometer	Siemens P4 (graphite monochromator)
2θ range (°)	4–55 ($\pm h$, $\pm k$, $\pm l$)
Reflections (collected, indpt)	10644, 10351, 4458)
$R(F)$, $R(wF^2)$, [a](%)	3.81, 7.64
GOF	1.04
N_o/N_v	17.4
Max. peak (e Å^{-3})	0.913

[a] Quantity minimized = $R(F) = \Sigma\Delta/\Sigma(F_o)$; $R(wF^2) = \Sigma[w(F_o^2 - F_c^2)^2]/\Sigma[w(F_o^2)^2]^{1/2}$ $\Delta = |F_o - F_c|$

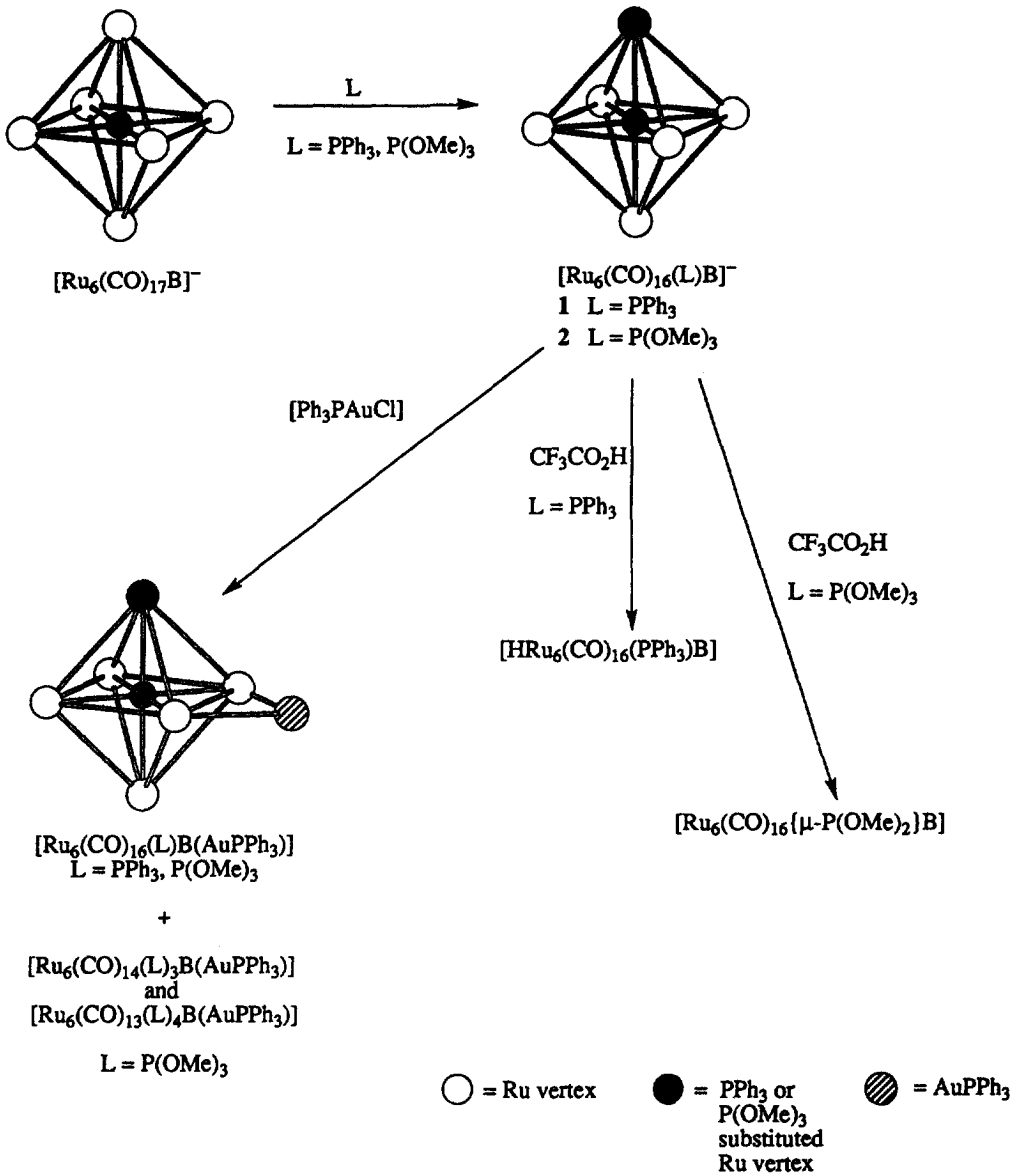

Fig. 1. Reaction scheme for substitution reactions of $[Ru_6(CO)_{17}B]^-$ with PPh_3 and $P(OMe)_3$, and subsequent reactions with CF_3CO_2H and $[Ph_3PAuCl]$.

retained. In the ^{31}P NMR spectrum of the product, the loss of the resonance due to $[(Ph_3P)_2N]^+$ is consistent with the formation of a neutral species; a singlet, observed at δ 35.9, was assigned to the ruthenium-bound PPh_3 ligand. In the ^1H NMR spectrum, the presence of the metal-bound hydride was confirmed by the appearance of a highfield singlet (δ −17.5), and the lack of ^{31}P-^1H spin-spin coupling indicated that the H and P atoms were not attached to the same Ru atom. We propose that the H atom bridges an Ru—Ru edge (as in $[HRu_6(CO)_{17}B]$ [4,5], and is remote from the ruthenium atom carrying the PPh_3 ligand.

Reactions of metal cluster anions with gold(I) phosphine fragments are well established pathways to heterometallic clusters [16], and the relative ease with which these derivatives often crystallize makes them useful targets for study. Anion **1** reacts with an excess of $[Ph_3PAuCl]$ in the presence of $Tl[PF_6]$ to give an orange-brown product in high yield. The parent ion in the mass spectrum suggested the formulation $[Ru_6(CO)_{16}(PPh_3)B(AuPPh_3)]$; in the ^{31}P NMR spectrum, two singlets of relative intensities 1 : 1 were observed. On going from **1** to $[Ru_6(CO)_{16}(PPh_3)B(AuPPh_3)]$, the ^{11}B NMR signal shows virtually no change in chemical shift, in keeping with there being no disruption of the octahedral Ru_6B-core. From the spectroscopic data, it is not possible

to give an unambiguous structural assignment for $[Ru_6(CO)_{16}(PPh_3)B(AuPPh_3)]$, but by analogy with the $P(OMe)_3$ analogue discussed below, we propose a structure as represented in Fig. 1. We have previously reported details of the compounds $[Ru_6(CO)_{17}B(AuPR_3)]$ (R = Ph or 2-MeC_6H_4) [11]; the gold(I) phosphine unit bridges an edge of the octahedral Ru_6-cage and this further supports the structural proposal in Fig. 1.

The compound $[Ru_6(CO)_{16}(PPh_3)B(AuPPh_3)]$ can also be prepared by replacing a CO ligand in $[Ru_6(CO)_{17}B(AuPPh_3)]$ by triphenylphosphine. The IR and NMR spectroscopic properties of this product are identical to those of that obtained from anion **1**, confirming that the same isomer is formed preferentially in both reaction paths.

Trimethylphosphite substitution: monosubstitution

In contrast to the predictable behaviour of the triphenylphosphine system described above, reaction of $[(Ph_3P)_2N][Ru_6(CO)_{17}B]$ with $P(OMe)_3$ followed by protonation or treatment with $[Ph_3PAuCl]$ provided contrasting results. The reaction between equimolar equivalents of $[(Ph_3P)_2N][Ru_6(CO)_{17}B]$ and $P(OMe)_3$ led to the formation of $[(Ph_3P)_2N][Ru_6(CO)_{16}\{P(OMe)_3\}B]$, $[(Ph_3P)_2N]$[**2**] as expected. Mass spectrometric data were in accord with the formulation, and the ^{31}P NMR spectrum exhibited two singlets (relative intensities 1:2), the chemical shifts of which were consistent with a terminally bound $P(OMe)_3$ group (δ 150.3) and $[(Ph_3P)_2N]^+$ (δ 21.0). In the ^1H NMR spectrum, in addition to Ph resonances, a doublet at δ 3.6 (J_{PH} = 12 Hz) was assigned to the Me groups of $P(OMe)_3$. There was no significant change in the signal in the ^{11}B NMR spectrum on going from $[Ru_6(CO)_{17}B]^-$ to **2**, indicating retention of the octahedral metal framework around the boron atom.

Anion **2** reacts with CF_3CO_2H under the same conditions that facilitated the conversion of **1** to its conjugate acid. However, simple protonation does not occur. The ^{31}P NMR spectroscopic signature of the product was particularly revealing, with the appearance of a downfield signal at δ 357.7. This is characteristic of a bridging phosphido group and suggested that reaction with CF_3CO_2H had resulted in the conversion of the terminal $P(OMe)_3$ ligand to a μ-$P(OMe)_2$ unit (Fig. 1). This was supported by a parent ion at m/z 1190 in the mass spectrum, and the product was formulated as $[Ru_6(CO)_{16}\{\mu\text{-}P(OMe)_2\}B]$. The ^{11}B NMR spectroscopic resonance indicated that the octahedral Ru_6B-core was not disrupted during the reaction, and in the ^1H NMR spectrum, only a doublet (δ 3.8, J_{PH} 13 Hz) was observed, in keeping with the fact that protonation was not accompanied by the formation of a direct Ru—H interaction. It is assumed that the MeO group cleaved from the $P(OMe)_3$ ligand leaves as MeOH (eqn (1)). The cluster conversion proceeds without a change to the electron count since the two electrons contributed by the terminal $P(OMe)_3$ ligand and the single electron provided by the charge are replaced by three electrons contributed by the bridging $P(OMe)_2$ group. Unfortunately, X-ray quality crystals could not be obtained to permit crystallographic confirmation of the formation of the phosphido derivative.

$$[Ru_6(CO)_{16}\{P(OMe)_3\}B]^- + H^+ \rightarrow [Ru_6(CO)_{16}\{\mu\text{-}P(OMe)_2\}B] + MeOH \quad (1)$$

These results are in contrast to the reaction between $[Ru_3(CO)_{10}\{P(OMe)_3\}_2]$ and CF_3CO_2H which leads to $[HRu_3(CO)_{10}\{P(OMe)_3\}_2]^+$ [17]. Although, the conversions of a terminal $P(OMe)_3$ ligand to μ_4-P(OMe) and bridging $OP(OMe)_2$ or OP(OMe)$OP(OMe)_2$ groups have previously been thermally promoted [18–20], the facile manner in which **2** converts to $[Ru_6(CO)_{16}\{\mu\text{-}P(OMe)_2\}B]$ upon protonation appears to be a novel observation. A related reaction has been reported by Süss-Fink and coworkers; the phosphido derivative $[Ru_3(CO)_9(PPh_3)(\mu\text{-}PPh_2)]^-$ was isolated as a product of the reaction between $[HRu_3(CO)_{11}]^-$ and PPh_3, and ^1H NMR spectroscopic data suggested that the reaction proceeded by the formation of $[HRu_3(CO)_{10}(PPh_3)]^-$ followed by $[HRu_3(CO)_9(PPh_3)_2]^-$ with consequent elimination of C_6H_6 [21].

The 1:1 reaction of $[(Ph_3P)_2N][Ru_6(CO)_{17}B]$ with $P(OMe)_3$ followed by the addition of an excess of $[Ph_3PAuCl]$ gave the expected product $[Ru_6(CO)_{16}\{P(OMe)_3\}B(AuPPh_3)]$, **4**, as well as $[Ru_6(CO)_{17}B(AuPPh_3)]$ which clearly arose from direct combination of $[Ph_3PAuCl]$ with $[(Ph_3P)_2N][Ru_6(CO)_{17}B]$. Spectroscopic and mass spectrometric data for **4** were consistent with this formulation, and the boron-containing octahedral Ru_6-core suggested by the ^{11}B NMR spectroscopic shift (δ 195.6) was confirmed by the results of an X-ray structure determination.

Crystal structure of $[Ru_6(CO)_{16}\{P(OMe)_3\}B(AuPPh_3)]$

The structure of compound **4** is shown in Fig. 2a and a view of the cluster core showing the site of substitution is given in Fig. 2b. Selected bond distances and angles are listed in Table 2. The ruthenium atoms define a distorted octahedron, with the edge bridged by the gold(I) phosphine unit being significantly longer (3.299(2) Å) than the other eleven edges (see Table 2). The edge-bridging site adopted by the $AuPPh_3$ unit mimics that found for the $AuP(C_6H_4\text{-}2\text{-}Me)_3$ group in $[Ru_6(CO)_{17}B\{AuP(C_6H_4\text{-}2\text{-}Me)_3\}]$ [11]: here too, the bridged Ru—Ru edge is elongated (3.241(1) Å) but in both $[Ru_6(CO)_{17}B\{AuP(C_6H_4\text{-}2\text{-}Me)_3\}]$ and **4**, the long edges should be considered to contain ruthenium atoms within

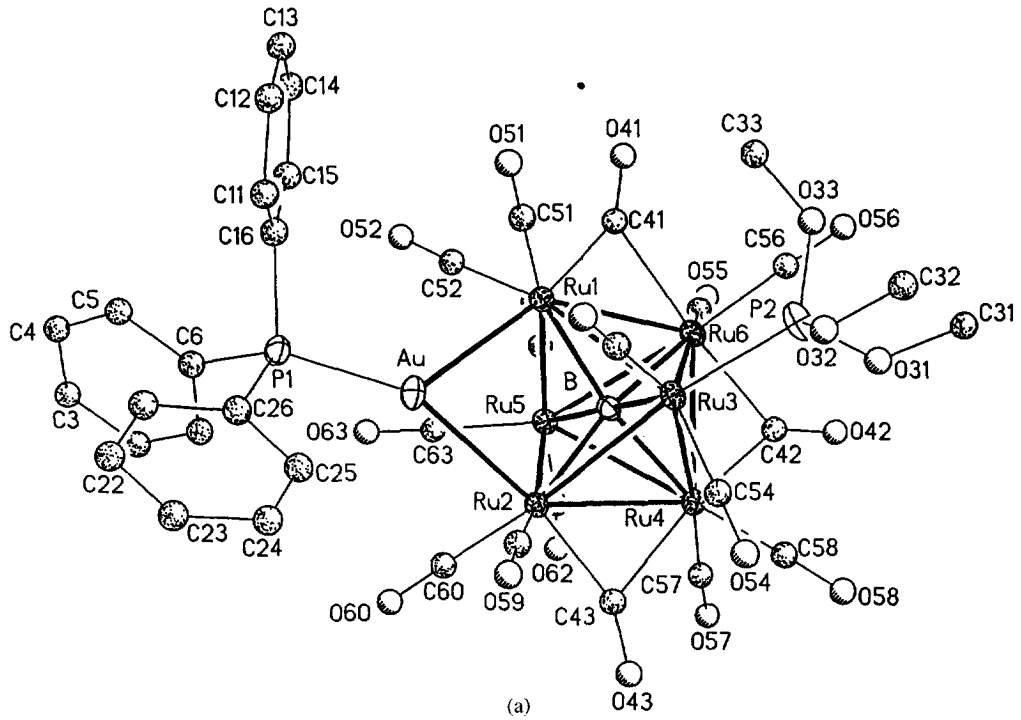

(a)

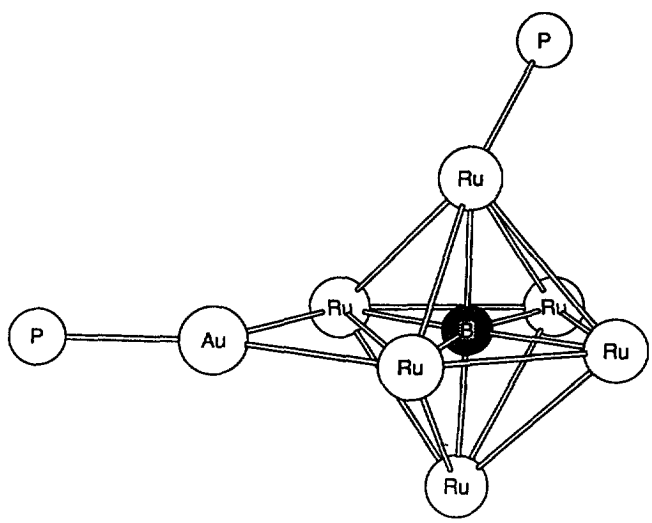

(b)

Fig. 2. (a) The molecular structure of compound **4**, in an orientation that clearly illustrates the elongation of the edge Ru(1)—Ru(2); (b) a view of the cluster core including the P atoms of the $AuPPh_3$ and $P(OMe)_3$ groups.

bonding contact in order that the 86-electron Ru_6-core is consistent with the expected octahedral cage. The boron atom in **4** lies centrally within the Ru_6-cage, with Ru—B distances in the range 2.057(7) to 2.140(7) Å, the longer distances being associated with the two Ru atoms lying in the Ru_4Au equatorial plane but being remote from the gold atom. The $P(OMe)_3$ ligand occupies a terminal site, attached to an apical ruthenium atom (Ru(3)—P(2) = 2.260(2) Å); additionally, atom Ru(3) bears two terminal CO ligands, and the related ruthenium atom, Ru(5), bears three terminal carbonyls. Each ruthenium atom in the equatorial plane carries two terminal CO groups; of the remaining CO ligands, one is fully bridging along Ru(4)—Ru(6) (Ru(4)—C(42) = 2.015(7) and Ru(6)—C(42) = 2.118(7) Å), while edges Ru(1)—Ru(6) and Ru(2)—Ru(4) carry semi-bridging CO ligands (Ru(1)—C(41) = 1.981(7), Ru(6)—C(41) = 2.258(7), Ru(2)—C(43) = 1.960(7) and Ru(4)—C(43) = 2.316(7) Å).

Table 2. Selected bond distances and angles for $[Ru_6(CO)_{16}\{P(OMe)_3\}B(AuPPh_3)]$, **4**

Bond distances (Å)			
Au—P(1)	2.304(2)	Au—Ru(2)	2.734(1)
Au—Ru(1)	2.835(2)	Ru(1)—Ru(6)	2.860(1)
Ru(1)—Ru(3)	2.959(2)	Ru(1)—Ru(5)	2.876(2)
Ru(1)—Ru(2)	3.299(2)	Ru(2)—Ru(4)	2.875(1)
Ru(2)—Ru(5)	2.896(2)	Ru(2)—Ru(3)	2.910(2)
Ru(3)—Ru(4)	2.961(2)	Ru(3)—Ru(6)	3.076(2)
Ru(4)—Ru(6)	2.800(2)	Ru(4)—Ru(5)	3.014(1)
Ru(5)—Ru(6)	2.948(2)	Ru(1)—B	2.067(7)
Ru(2)—B	2.072(7)	Ru(3)—B	2.057(7)
Ru(4)—B	2.124(7)	Ru(3)—P(2)	2.260(2)
Ru(5)—B	2.094(7)	Ru(6)—B	2.140(7)
Bond angles (°)			
P(1)—Au—Ru(2)	155.56(5)	P(1)—Au—Ru(1)	131.78(5)
Ru(2)—Au—Ru(1)	72.63(4)	Au—Ru(1)—Ru(6)	137.64(3)
Au—Ru(2)—Ru(4)	139.63(3)	Ru(1)—B—Ru(4)	167.7(4)
Ru(2)—B—Ru(6)	167.9(4)	Ru(3)—B—Ru(5)	177.3(4)

Trimethylphosphite substitution: multisubstitution

The substitution behaviour of $P(OMe)_3$ in ruthenium carbonyl clusters has previously provided examples of relatively high degrees of substitution, for example in $[Ru_3(CO)_{12}]$ [22], $[H_4Ru_4(CO)_{12}]$ [23–25], $[HRu_4(CO)_{12}BH_2]$ [2], $[Ru_6(CO)_{17}C]$ [9] and $[HRu_3(CO)_{10}(NO)]$ [26]. One contributing factor is the relatively small cone angle of $P(OMe)_3$ (107°) compared with, for example, PPh_3 (145°) [27].

The reaction of $[(Ph_3P)_2N][Ru_6(CO)_{17}B]$ with 2.5 molar equivalents of $P(OMe)_3$ resulted in the formation of a product mixture, the IR spectrum of which contained a strong absorption at 1986 cm^{-1}, i.e. at lower wavenumber than the strongest absorption in the IR spectrum of $[Ru_6(CO)_{16}\{P(OMe)_3\}B]^-$ (2001 cm^{-1}). This observation suggested that a higher degree of substitution had been achieved. After the addition of $[Ph_3PAuCl]$ to the reaction mixture, two products were isolated: $[Ru_6(CO)_{16}\{P(OMe)_3\}B(AuPPh_3)]$ and $[Ru_6(CO)_{14}\{P(OMe)_3\}_3B(AuPPh_3)]$ were formulated on the basis of mass spectrometric and multinuclear NMR spectroscopic data. There was no evidence for $[Ru_6(CO)_{15}\{P(OMe)_3\}_2B(AuPPh_3)]$ being an isolable product. Three signals (relative integrals 2:1:1) were observed in the ^{31}P NMR spectrum of $[Ru_6(CO)_{14}\{P(OMe)_3\}_3B(AuPPh_3)]$, and that at δ 69.9 (relative integral 1) was assigned to the $AuPPh_3$ unit. Consistent with the remaining two ^{31}P NMR spectroscopic signals (the chemical shifts of which indicated terminally bound $P(OMe)_3$ ligands), the ^1H NMR spectrum showed two doublets (J_{PH} 11 and 12 Hz) of relative integrals 1:2. Two possible arrangements for the three $P(OMe)_3$ ligands, which take into account steric effects, are shown schematically in Fig. 3a and 3b. Although our data do not allow these two ligand dispositions to be distinguished, the arrangement shown in Fig. 3b has been proposed in the related carbido species $[Ru_6(CO)_{14}\{P(OMe)_3\}_3C]$ [9].

With a four-fold excess of $P(OMe)_3$, tetrasubstitution in $[Ru_6(CO)_{17}B]^-$ was achieved and the addition of $[Ph_3PAuCl]$ to the crude reaction mixture led to the formation of $[Ru_6(CO)_{13}\{P(OMe)_3\}_4B(AuPPh_3)]$ in ≈80% yield. The parent envelope in the mass spectrum was consistent with this formation, and the ^{31}P NMR spectrum exhibited signals in the 2:2:1; the latter signal (δ 68.0) was assigned to the $AuPPh_3$ group, while the remaining signals (δ 141.2 and 137.5) were indicative of terminally bound $P(OMe)_3$ ligands. Two equal intensity doublets in the ^1H NMR spectrum (δ 3.6 and 3.7) were assigned to the phosphite methyl groups. The most likely arrangement of the four $P(OMe)_4$ ligands is depicted in Fig. 3c, and is in keeping with the addition of a fourth ligand to either of the possible isomers proposed for $[Ru_6(CO)_{14}\{P(OMe)_3\}_3B(AuPPh_3)]$.

CONCLUSIONS

The borido anion $[Ru_6(CO)_{17}B]^-$ undergoes substitution with both PPh_3 and $P(OMe)_3$. Whereas monosubstitution of triphenylphosphine appears to be the limiting degree of reaction, up to four CO ligands can be replaced by $P(OMe)_3$ under facile reaction conditions. Protonation of $[Ru_6(CO)_{16}(PPh_3)B]^-$ is readily achieved, but treatment of $[Ru_6(CO)_{16}\{P(OMe)_3\}B]^-$ with H^+ results in the cleavage of one OMe group and the conversion of the terminal $P(OMe)_3$ ligand into a bridging $P(OMe)_2$ group.

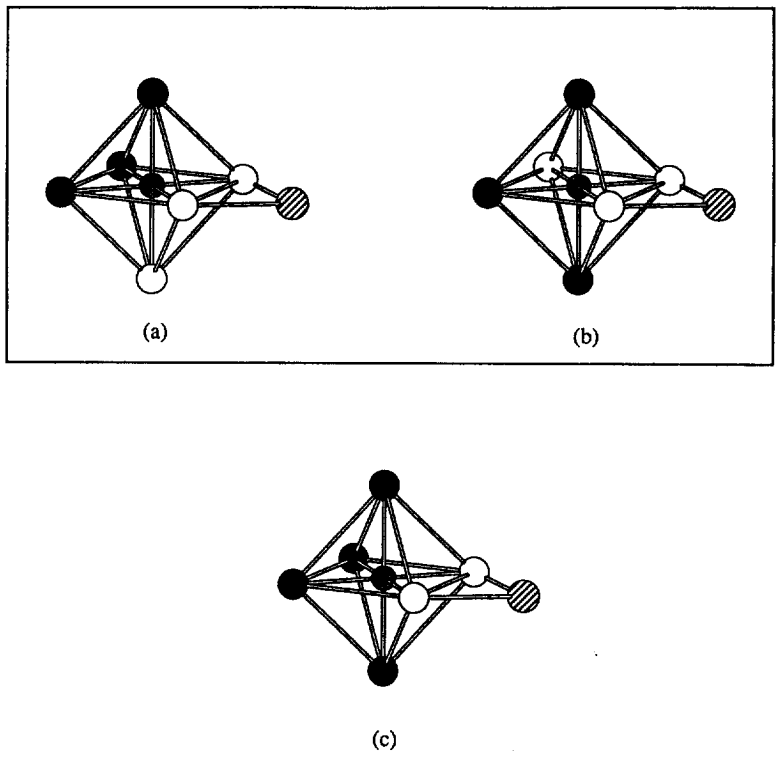

Fig. 3. Proposed arrangements of $P(OMe)_3$ ligands in (a) and (b) $[Ru_6(CO)_{14}\{P(OMe)_3\}_3B(AuPPh_3)]$, and (c) $[Ru_6(CO)_{13}\{P(OMe)_3\}_4B(AuPPh_3)]$.

Reactions of $[Ru_6(CO)_{16}(PPh_3)B]^-$ or $[Ru_6(CO)_{16}\{P(OMe)_3\}B]^-$ with $[Ph_3PAuCl]$ proceed as expected to produce $[Ru_6(CO)_{16}(PPh_3B(AuPPh_3)]$ or $[Ru_6(CO)_{16}\{P(OMe)_3\}B(AuPPh_3)]$ respectively. Crystallographic and ^{11}B NMR spectroscopic data provide evidence for the retention of the octahedral cluster core throughout the various transformations explored.

Acknowledgements—We thank the donors of the Petroleum Research Fund, Administered by the American Chemical Society for support for this work (Grant 25533-AC3), the EPSRC (studentship to A.W.), and the National Science Foundation for a grant (CHE 9007852) towards the purchase of a diffractometer at the University of Delaware.

REFERENCES

1. Housecroft, C. E., Matthews, D. M., Edwards, A. J. and Rheingold, A. L., *J. Chem. Soc., Dalton Trans.*, 1993, 2727.
2. Draper, S. M., Housecroft, C. E., Humphrey, J. S. and Rheingold, A. L., *J. Chem. Soc., Dalton Trans.*, 1995, 3789.
3. Housecroft, C. E., Humphrey, J. S. and Rheingold, A. L., *Inorg. Chim. Acta*, 1997, **259**, 85.
4. Hong, F.-E., Coffy, T. J., McCarthy, D. A. and Shore, S. G., *Inorg. Chem.*, 1989, **28**, 3284.
5. Draper, S. M., Housecroft, C. E., Keep, A. K., Matthews, D. M., Song, X. and Rheingold, A. L., *J. Organomet. Chem.*, 1992, **423**, 241.
6. Housecroft, C. E. and Fehlner, T. P., *Inorg. Chem.*, 1986, **25**, 404.
7. Housecroft, C. E. and Fehlner, T. P., *J. Am. Chem. Soc.*, 1986, **108**, 4867.
8. Johnson, B. F. G., Lewis, J., Wong, K. and McPartlin, M., *J. Organomet. Chem.*, 1980, **185**, C17.
9. Brown, S. C., Evans, J. and Webster, M., *J. Chem. Soc., Dalton Trans.*, 1982, 2263.
10. Mann, F. G., Wells, A. F. and Purdie, D. J., *J. Chem. Soc.*, 1937, 1828.
11. Housecroft, C. E., Matthews, D. M., Waller, A., Edwards, A. J. and Rheingold, A. L., *J. Chem. Soc., Dalton Trans.*, 1993, 3059.
12. Johnson, B. F. G., Johnston, R. D., Lewis, J., Robinson, B. H. and Wilkinson, G., *J. Chem. Soc. (A)*, 1968, 2856.
13. Housecroft, C. E., *Coord. Chem. Rev.*, 1995, **143**, 297 and references therein.

14. Housecroft, C. E., Rheingold, A. L. and Song, X., *Inorg. Chem.*, 1992, **31,** 4023.
15. Adams, R. D., Babin, J. E. and Tanner, J. T., *Organometallics*, 1988, **7,** 2027.
16. See for example: Salter, I. D., *Adv. Organomet. Chem.*, 1989, **29,** 249.
17. Kabir, S. E., Miah, A., Uddin, K. and Deeming, A. J., *J. Organomet. Chem.*, 1994, **476,** 121.
18. Fernandez, J. M., Johnson, B. F. G., Lewis, J. and Raithby, P. R., *Acta Crystallogr., Sect. B.*, 1979, **35,** 1711.
19. Fernandez, J. M., Johnson, B. F. G., Lewis, J., Raithby, P. R. and Sheldrick, G. M., *Acta Crystallogr., Sect. B*, 1978, **34,** 1994.
20. Orpen, A. G. and Sheldrick, G. M., *Acta Crystallogr., Sect. B*, 1978, **34,** 1992.
21. Gremaud, G., Jungbluth, H., Stoeckli-Evans, H. and Süss-Fink, G., *J. Organomet. Chem.*, 1990, **388,** 351.
22. Bruce, M. I., Liddell, M. J., Shawkataly, O. bin., Bytheway, I., Skelton, B. W. and White, A. H., *J. Organomet. Chem.*, 1989, **369,** 217.
23. Knox, S. A. R. and Kaesz, H. D., *J. Am. Chem. Soc.*, 1071, **93,** 4594.
24. Bruce, M. I., Kehoe, D. C., Matisons, J. G., Nicholson, B. K., Rieger, P. H. and Williams, M. L., *J. Chem. Soc., Chem. Commun.*, 1982, 442.
25. Orpen, A. G. and McMullan, R. K., *J. Chem. Soc., Dalton Trans.*, 1983, 463.
26. Johnson, B. F. G., Raithby, P. R. and Zuccaro. C., *J. Chem. Soc., Dalton Trans.*, 1980, 99.
27. Tolman, C. A., *Chem. Rev.*, 1977, **77,** 313.

Pergamon

PII: S0277-5387(98)00079-5

Polyhedron Vol. 17, No. 17, pp. 2931–2935, 1998
© 1998 Elsevier Science Ltd
All rights reserved. Printed in Great Britain
0277-5387/98 $19.00+0.00

A study of the photochemical reaction between $W_2(OCH_2{}^tBu)_6$ and P_4. Characterization of the phosphido cluster $W_4(P)_2(OCH_2{}^tBu)_{10}$†

Malcolm H. Chisholm, Kristen Folting and Manfred Scheer‡*

Department of Chemistry and Molecular Structure Center, Indiana University, Bloomington, IN 47405, U.S.A.

(Received 26 November 1997; accepted 1 February 1998)

Abstract—The photochemical reaction between $W_2(OCH_2{}^tBu)_6$ and P_4 has been studied by NMR spectroscopy in toluene-d_8 and those reactions have been complemented by studies on the bench top. A complex sequence of reactions is implicated by the formation of a variety of products, one of which has been observed previously in the thermal reaction between $W_2(OCH_2{}^tBu)_6L_2$ where L = py and $HNMe_2$ and P_4, namely $W_3(\mu_3\text{-}P)(OCH_2{}^tBu)_9$, while others must arise from degradation of OR ligands. A new compound $W_4(\mu_3\text{-}P)_2(\mu\text{-}OCH_2{}^tBu)_4(OCH_2{}^tBu)_6$ has been isolated and characterized. Crystal data at −165°C: $a = 19.955(4)$, $b = 25.222(3)$, $c = 12.775(2)$ Å, $Z = 4$ and space group *Pcab*. The centrosymmetric structure consists of a distorted rhombus of metal atoms having two different W—W edge distances 2.6938(8) and 2.7981(8) Å and a bonding W—W distance of 2.692(1) Å between the back-bone W atoms of the planar W_4 butterfly. The outer or wing-tip tungsten atoms are in a square based pyramidal environment with respect to the PWO_4 moiety with the W—P bond in the apical position. The O_4 basal plane involves two terminal and two bridging OR groups. The internal or back-bone tungsten atoms are also five coordinate, P_2WO_3, where two bridging OR groups occupy axial and the two W—P bonds and one W—OR terminal group occupy equatorial sites of a trigonal bipyramid. The cluster geometry is compared with those seen for $W_3(\mu_3\text{-}X)(OR)_9$, where X = CCH_3 and P, $W_4(O^iPr)_{12}$ and $W_4(OEt)_{16}$. The latter contains a central centrosymmetric W_4^{16-} cluster as does the present compound and the presence of the distorted rhomboidal geometry observed in both is proposed to arise from a second order Jahn-Teller distortion. © 1998 Elsevier Science Ltd. All rights reserved

Keywords: tungsten; alkoxide; phosphide; cluster.

Previous work in this laboratory has shown that the thermal reaction between P_4 and $W_2(OCH_2{}^tBu)_6(L)_2$, where L = a labile neutral ligand such as $HNMe_2$ or pyridine, has led to the isolation and characterization of the compounds $(\eta^3\text{-}P_3)W(OR)_3L^1$ and $W_3(\mu_3\text{-}P)(OR)_9$.[2] Although it is possible to consider the formation of these two compounds by a reaction sequence wherein an initially formed tetranuclear $W_4(OR)_{12}(\mu\text{-}P_4)$ complex undergoes a disproportionation to give $W_3(\mu_3\text{-}P_3)(OR)_9$ and $(\eta^3\text{-}P_3)W(OR)_3$, we suggested that another reaction pathway was possible, namely one wherein a reactive $(RO)_3W{\equiv}P$ moiety was formed [along with $(\eta^3\text{-}P_3)W(OR)_3$] and that this underwent a conproportionation reaction of the type shown in eqn 1 [2].

$$(RO)_3W{\equiv}P + W_2(OR)_6 \rightarrow W_3(\mu_3\text{-}P)(OR)_9 \quad (1)$$

While we had no direct evidence for a reactive intermediate of the form $(RO)_3W{\equiv}P$ the conproportionation reaction of $(RO)_3W{\equiv}CMe$ with $M_2(OR)_6$ to give $M_2W(\mu\text{-}CMe)(OR)_9$ (M = Mo, W) were known [3] as were related reactions involving $(RO)_4W{=}E$ and $W_2(OR)_6$ to give $(RO)_{10}W_3(\mu_3\text{-}E)$ where E = O [4] and NH [5]. Subsequent to this work $L_3Mo{\equiv}P$ complexes were isolated from reactions between L_3Mo and P_4 by Cummins *et al.* [6] [L = $N(^tBu\text{-}d_6)(3,5\text{-}Me_2C_6H_3)$] and related $W{\equiv}P$

* Author to whom correspondence should be addressed.

† Dedicated to Lord Lewis on the occasion of his 70th birthday.

‡ Present address: Prof. Dr Manfred Scheer, University of Karlsruhe, Institute of Inorganic Chemistry, D-76128 Karlsruhe, Germany.

bonded complexes were prepared by Schrock and coworkers [7] employing the use of the bulky quadridentate trianionic ligand $N(CH_2CH_2NSiMe_3)_3^{3-}$.

We report here our studies of the reactions between P_4 and $W_2(OCH_2{}^tBu)_6$ in toluene under photolysis. Photolysis is known to lead to fragmentation of P_x moieties bound to metal atoms [8] and thus we expected that these reactions might proceed differently from those described earlier where the reactions were driven by heat.

RESULTS AND DISCUSSION

Syntheses and spectroscopic studies

The reaction between P_4 and $W_2(OCH_2{}^tBu)_6$ in toluene-d_8 under photolysis was carried out in a water cooled bath with the photolysis coming from the use of a Hanova Hg lamp. The reaction was monitored by $^{31}P\{^1H\}$ and ^1H NMR spectroscopy with time. These studies were complemented by bench top photolysis reactions in toluene. A number of products were seen to be formed in these reactions and the separation of the products proved exceptionally difficult. Column chromatography employing silica gel, which so commonly enjoys great success in metal carbonyl cluster chemistry, is not possible for these alkoxide clusters since Si—OH bonds present in the silica lead to permanent adsorption and subsequent decomposition of the clusters in the column. Silation of the silica with $(Me_3Si)_2NH$ does not prove to inhibit the decomposition. Consequently, we needed to rely on product analysis by spectroscopy (NMR) and by fractional crystallizations employing hydrocarbon solvents.

A major product in the reaction was the known compound $W_3(\mu_3\text{-}P)(\mu\text{-}OCH_2{}^tBu)_3(OCH_2{}^tBu)_6$ which was readily identifiable by $^{31}P\{^1H\}$ and ^1H NMR spectroscopy [2]. Notably, under photolytic conditions, no $(\eta^3\text{-}P_3)W(OCH_2{}^tBu)_3$ was observed [1]. Other products of ligand redistribution that were observed (and characterized) were $W_3(\mu_3\text{-}O)(OCH_2{}^tBu)_{10}$ and $W_3(\mu_3\text{-}O)(OCH_2{}^tBu)_9(O^tBu)$ [9]. Presumably here the oxo group arises from decomposition of alkoxide ligands and the structure of $W_3(\mu_3\text{-}O)(OCH_2{}^tBu)_{10}$ was seen to be akin to that previously reported for the related isopropoxide [10]. The occurrence of $W_3(\mu_3\text{-}O)(OCH_2{}^tBu)_9(O^tBu)$ reflects the presence of a rogue O^tBu ligand, present as a result of incomplete alcoholysis in the preparation of $W_2(OCH_2{}^tBu)_6$ from $W_2(O^tBu)_6$ and neopentanol.

By $^{31}P\{^1H\}$ NMR spectroscopy three other compounds were present in significant concentrations. One is possibly a P_6 complex (based on ^{31}P chemical shift) [11] which could have the form $(RO)_xW(\mu_1\text{-}\eta^6\text{-}P_6)W(OR)_x$. Regrettably we were unable to obtain this complex in single crystalline form. It is known that $Cp^*Mo(CO)_2(\eta^3\text{-}P_3)$ is converted by photolysis to $Cp^*Mo(\mu_1\text{-}\eta^6\text{-}P_6)MoCp^*$, for example [12]. This could explain the absence of $(\eta^3\text{-}P_3)W(OCH_2{}^tBu)_3$ in our photolysis. Furthermore, a singlet at 42.4 ppm with a $J_{W\,P}$ of 63 Hz is detected, so that—in comparison to other P_2 ligand complexes [13]—one could speculate on the existence of a $W_2(OR)_x(\mu,\eta^2\text{-}P_2)$ complex. The third compound, as we show below, is $W_4(\mu_3\text{-}P)_2(OCH_2{}^tBu)_{10}$. This compound must be formed by sacrificial OR group transfer—a process necessary to account for the formation of $W_3(\mu_3\text{-}O)(OCH_2{}^tBu)_{10}$.

$W_4(\mu_3\text{-}P)_2(OCH_2{}^tBu)_{10}$

An ORTEP drawing of the centrosymmetric $W_4(\mu_3\text{-}P)_2(OCH_2{}^tBu)_{10}$ molecule is given in Fig. 1 where the central $W_4P_2O_{10}$ core is numbered. A view perpendicular to that shown in Fig. 1 is given in Fig. 2. From these two views one can see that there is a central rhomboidal W_4 unit, or a flattened butterfly. The two μ_3-P ligands cap opposite triangular faces and each W atom is five coordinate with respect to ligand bonding. The outer W atoms, or wing-tip W atoms, W(1), are in a square based pyramid environment with the μ-P ligand in an apical position and the two terminal and two bridging OR ligands in the basal plane. The hinge or back-bone W atoms, W(2) are in a distorted trigonal bipyramidal environment with two bridging OR groups axial and the two μ-P and one terminal OR group in equatorial sites. Selected bond distances and angles are given in Tables 1 and 2, respectively.

The coordination about W(1) is similar to that seen in $W_3(\mu_3\text{-}P)(\mu\text{-}OCH_2{}^tBu)_3(OCH_2{}^tBu)_6$ [2] and one of the wing-tip Mo atoms in the butterfly Mo_4-complex anion $Mo_4(\mu_3\text{-}P)(OCH_2{}^tBu)_{10}^-$ [14]. By comparing these phosphido capped triangles it is also worthy to note that the M—M distances all fall within a narrow range from 2.7 to 2.8 Å. However, the oxidation states of the metal atoms and hence the electron count for cluster M—M bondings is different. For example, in $W_3(\mu_3\text{-}P)(OCH_2{}^tBu)_9$ and $Mo_4(\mu_3\text{-}P)(OCH_2{}^tBu)_{10}$ the oxidation state of the metal atoms is +4 and +3, respectively, and in the present complex of the formula $W_4(\mu_3\text{-}P)_2(OR)_{10}$ the central W_4^{16+} core gives W(4+) atoms. In this regard it is noteworthy that the planar rhomboidal structure is also seen in $W_4(OEt)_{16}$ [15] and in $W_4(O^iPr)_{12}$ [16] which represent clusters having W atoms in the +4 and +3 oxidation states, respectively. In each of these W_4 planar and centrosymmetric structures [$W_4(OEt)_{16}$, $W_4(O^iPr)_{12}$ and $W_4(P)_2(OCH_2{}^tBu)_{10}$] we observe two sets of edge distances differing by ca 0.1 Å. In other words the D_{2d} symmetrical structure with an M_4 diamond distorts to generate a C_{2h} structure with alternating short and long edges. The bonding in $W_4(O^iPr)_{12}$ [16] and $W_4(OEt)_{16}$ [17] have been investigated by computational methods and in both instances the distortion has been correlated with a second order Jahn-Teller effect. It seems that the same must be true in the present case for the W_4^{16+} core but calculations have as yet not been performed.

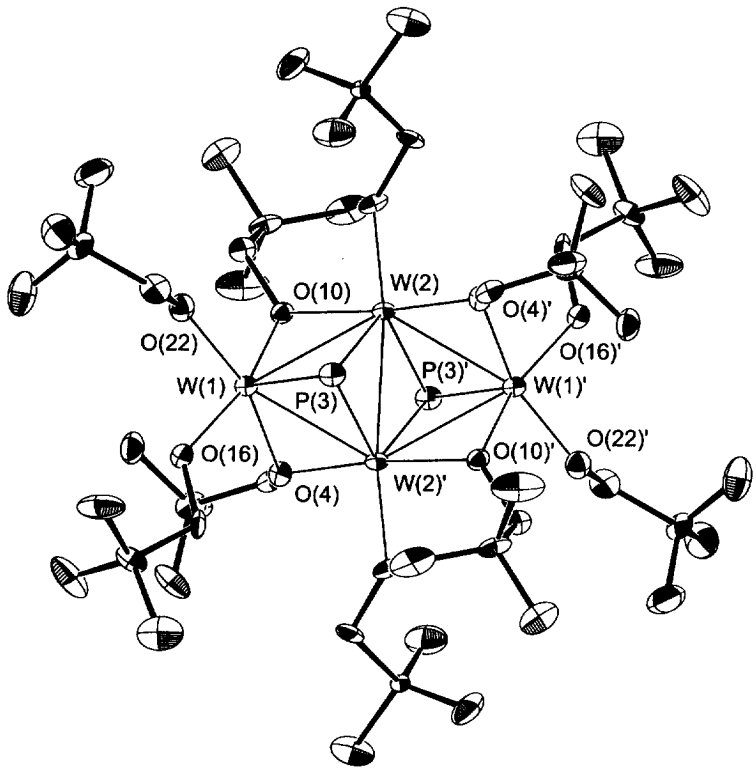

Fig. 1. An ORTEP drawing of the centrosymmetrical $W_4(\mu_3\text{-}P)_2(\mu\text{-}OCH_2{}^tBu)_4(OCH_2{}^tBu)_6$ molecule giving the atom number system used in the tables. This view emphasizes the rhomboidal W_4 unit and the two capping μ_3-P ligands.

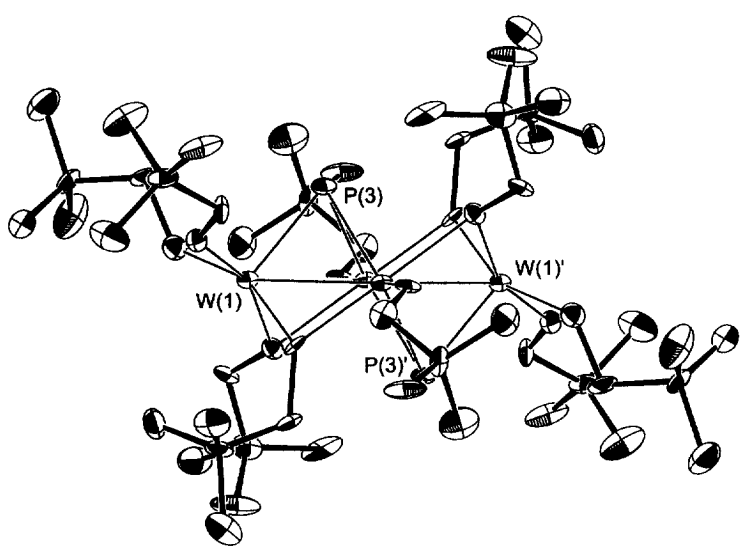

Fig. 2. An ORTEP view of the molecular structure of $W_4(\mu_3\text{-}P)_2(\mu\text{-}OCH_2{}^tBu)_4(OCH_2{}^tBu)_6$ viewed parallel to the W_4 plane. The square based pyramidal geometry of the wing-tip W atoms, W(1) and W(1)′ is clearly evident from this view.

Table 1. Selected Bond Distances (Å) for $W_4(P)_2(O\text{-}CH_2{}^tBu)_{10}$

W(1)—W(2)′	2.6938(8)
W(1)—W(2)	2.7981(8)
W(1)—P(3)	2.292(4)
W(1)—O(4)	2.062(8)
W(1)—O(10)	2.030(9)
W(1)—O(16)	1.904(9)
W(1)—O(22)	1.896(9)
W(2)—W(2)′	2.6924(11)
W(2)—P(3)	2.377(4)
W(2)—P(3)′	2.484(4)
W(2)′—P(3)	2.484(4)
W(2)—O(4)′	2.057(9)
W(2)—O(10)	2.193(9)
W(2)—O(28)	1.931(8)

Table 2. Selected bond angles (°) for $W_4(P)_2(OCH_2{}^tBu)_{10}$

W(2)′—W(1)—W(2)	58.676(23)
W(2)′—W(1)—P(3)	59.10(9)
W(2)—W(1)—P(3)	54.60(9)
W(2)′—W(1)—O(4)	49.08(25)
W(2)—W(1)—O(4)	93.88(24)
W(2)′—W(1)—O(10)	91.76(24)
W(2)—W(1)—O(10)	51.06(24)
W(2)′—W(1)—O(16)	101.46(26)
W(2)—W(1)—O(16)	150.06(27)
W(2)′—W(1)—O(22)	154.0(3)
W(2)—W(1)—O(22)	101.3(3)
P(3)—W(1)—O(4)	107.03(27)
P(3)—W(1)—O(10)	104.41(25)
P(3)—W(1)—O(16)	96.7(3)
P(3)—W(1)—O(22)	96.4(3)
O(4)—W(1)—O(10)	89.8(3)
O(4)—W(1)—O(16)	86.5(4)
O(4)—W(1)—O(22)	156.5(4)
O(10)—W(1)—O(16)	158.8(4)
O(10)—W(1)—O(22)	86.0(4)
O(16)—W(1)—O(22)	89.1(4)
W(1)′—W(2)—W(1)	121.324(23)
W(1)′—W(2)—W(2)′	62.598(24)
W(1)—W(2)—W(2)′	58.726(23)
W(1)′—W(2)—P(3)′	52.36(9)
W(1)′—W(2)—P(3)	96.71(9)
W(1)—W(2)—P(3)′	91.68(9)
W(1)—W(2)—P(3)	51.80(9)
W(1)′—W(2)—O(4)′	49.23(23)
W(1)—W(2)—O(4)′	138.47(24)
W(1)′—W(2)—O(10)	133.76(22)
W(1)—W(2)—O(10)	46.05(24)
W(1)—W(2)—O(28)	125.73(27)
W(1)—W(2)—O(28)	112.94(27)
W(2)′—W(2)—P(3)′	54.51(9)
W(2)′—W(2)—P(3)	58.27(9)
W(2)′—W(2)—O(4)′	97.16(25)
W(2)′—W(2)—O(10)	88.32(23)
W(2)—W(2)—O(28)	171.65(27)
P(3)—W(2)—P(3)′	112.78(9)
P(3)′—W(2)—O(4)′	100.55(25)
P(3)—W(2)—O(4)′	87.13(25)
P(3)′—W(2)—O(10)	81.70(24)
P(3)—W(2)—O(10)	96.76(25)
P(3)′—W(2)—O(28)	129.53(26)
P(3)—W(2)—O(28)	117.10(27)
O(4)′—W(2)—O(10)	174.4(3)
O(4)′—W(2)—O(28)	89.3(4)
O(10)—W(2)—O(28)	85.3(3)
W(1)—P(3)—W(2)′	68.54(10)
W(1)—P(3)—W(2)	73.61(10)
W(2)—P(3)—W(2)′	67.22(9)
W(1)—O(4)—W(2)′	81.7(3)
W(1)—O(4)—C(5)	126.5(8)
W(2)′—O(4)—C(5)	129.9(8)
W(1)—O(10)—W(2)	82.9(3)
W(1)—O(10)—C(11)	127.4(8)
W(2)—O(10)—C(11)	127.3(7)
W(1)—O(16)—C(17)	131.0(8)
W(1)—O(22)—C(23)	130.5(9)
W(2)—O(28)—C(29)	139.7(8)

EXPERIMENTAL SECTION

General

All solvents were dried, degassed and stored under N_2. All synthetic and handling procedures were carried out in a purified N_2 atmosphere using Schlenk techniques. P_4 was obtained from commercial sources and used after sublimation. The tungsten starting complex $[W_2(OCH_2{}^tBu)_6]$ was prepared from $[W_2(OCH_2{}^tBu)_6]$ and $^tBuCH_2OH$ as described in the literature [18]. ^{31}P NMR spectra were recorded on a Nicolet NT-360 (146.185 MHz) and the ^1H NMR data were obtained on a Bruker AM-500 (500.136 MHz).

Reaction of $W_2(OCH_2{}^tBu)_6$ *with* P_4*–Isolation of* $W_4(\mu_3\text{-}P)_2(\mu\text{-}OCH_2{}^tBu)_4(OCH_2{}^tBu)_6$

707 mg (0.79 mmol) $[W_2(OCH_2{}^tBu)_6]$ and 98.6 mg P_4 (0.79 mmol) in 150 ml toluene were radiated for 2 h in a UV apparatus (medium pressure mercury lamp, Hanovia 450-W) under internal water cooling to 15°C. The solvent was completely removed in vacuum. The resulting brown solid was purified from unreacted P_4 by sublimation of the latter in vacuum (10^{-3} Torr) at a bath temperature of 50°C. The ^{31}P NMR spectra of the crude reaction mixture revealed four phosphorus containing main products at 274.3 ppm ($J_{W\text{-}P} = 46$ Hz; ≈ 20 Mol.−%P), 224.8 ppm ($J_{W\text{-}P} \approx 60$ Hz, broad unresolved satellites; ≈ 5 Mol.−%P), 42.4 ppm ($J_{W\text{-}P} = 63$ Hz; ≈ 16 Mol.−%P) and −245.5 ppm ($J_{W\text{-}P} \approx 71$ Hz; ≈ 59 Mol.−%P). The residue was solved in 10 ml toluene. Fractional crystallization at 5°C give first 75 mg (10%) of $[W_3(\mu_3\text{-}P)(\mu\text{-}OCH_2{}^t\text{-}Bu)_3(OCH_2{}^tBu)_6]$ and after removal 20 mg (3%) of $[W_4(\mu_3\text{-}P)_2(\mu\text{-}OCH_2{}^tBu)_4(OCH_2{}^tBu)_6]$. Both other compounds could not be separated by fractional crystallization due to their low stability over a longer

Table 3. Crystal data for $W_4(P)_2(OCH_2{}^tBu)_{10}$

Empirical formula	$C_{50}H_{110}O_{10}P_2W_4$
Space group	*Pcab*
T (°C)	−165
a (Å)	19.955(3)
b (Å)	25.222(3)
c (Å)	12.775(2)
Z	4
V (Å^3)	6429.45
D_{calcd} (g/cm^3)	1.724
Wavelength (Å^3)	0.71069
$R(F)$	0.0527
$R_W(F)$	0.0505
Goodness of fit for the last cycle	1.543
Maximum Δ/σ for last cycle	0.04

$R(F) = \Sigma||F_o|-|F_c||/\Sigma|F_o|$;
$Rw(F) = \{\Sigma w(|F_o|-|F_c|)^2/\Sigma wF_o^2\}^{1/2}$;
$R_W(F) = \{\Sigma w(|F_o|-|F_c|)^2/N_{obs}-N_{variables}\}^{1/2}$.

period in the solvent. ^1H (C_6D_6, 23°C): —CH_2 region δ 4.91, 4.71, 4.52 (d, 4:8:8H, J = 10 Hz), CH_3 region (1.08, 1.12, 1.22 (s, 18:36:36H). $^{31}P\{^1H\}$ (C_6D_6, 23°C): 224.8 ppm ($J_{W-P} \approx 60$ Hz, broad unresolved satellites).

Crystallographic studies. General operating procedures and listing of programs have been given [10]. A summary of crystal data for $W_4(P)_2(OCH_2{}^tBu)_{10}$ is given in Table 3.

Acknowledgements—We thank the National Science Foundation for financial support. M.S. thanks the Alexander von Humboldt Foundation for a Feodor-Lynen-Fellowship.

REFERENCES

1. Chisholm, M. H., Huffman, J. C. and Pasterczyk, J. W., *Inorganica Chim. Acta*, 1987, **133,** 17.
2. Chisholm, M. H., Folting, K. and Pasterczyk, J. W., *Inorg. Chem.*, 1988, **27,** 3057.
3. (a) Chisholm, M. H., Hoffman, D. M. and Huffman, J. C., *Inorg. Chem.*, 1984, **23,** 3683; (b) Chisholm, M. H., Folting, K., Heppert, J. A., Hoffman, D. M. and Huffman, J. C., *J. Am. Chem. Soc.*, 1985, **107,** 1234.
4. (a) Chisholm, M. H., Cotton, F. A., Fang, A. and Kober, E. C., *Inorg. Chem.*, 1984, **23,** 749; (b) Chisholm, M. H., Folting, K., Huffman, J. C. and Kober, E. C., *Inorg. Chem.*, 1985, **24,** 241; (c) Chisholm, M. H., Folting, K., Eichhorn, B. W. and Huffman, J. C., *J. Am. Chem. Soc.*, 1987, **109,** 3146.
5. Chisholm, M. H., Hoffman, D. M. and Huffman, J. C., *Inorg. Chem.*, 1985, **24,** 796.
6. (a) Laplaza, C. E., Davis, W. M. and Cummins, C. C., *Angew. Chemie Intl. Edit. Engl.*, 1995, **34,** 2042; (b) Laplaza, C. E., Johnson, M. J. A., Peters, J. C., Odom, A. L., Kim, E., Cummins, C. C., George, G. N. and Pickering, I. J., *J. Am. Chem. Soc.*, 1996, **118,** 8623.
7. (a) R. R. Schrock, N. C. Zanetti and Davis, W. N., *Angew. Chemie Inlt. Edit. Engl.*, 1995, **34,** 2044; (b) Johnson-Carr, J. A., Nanetti, N. C., Schrock, R. R. and Hopkins, M. D., *J. Am. Chem. Soc.*, 1996, **118,** 11305.
8. (a) Scheer, M. and Becker, U., *Chem. Ber.*, 1996, **129,** 1307; (b) Scheer, M. and Becker, U., *J. Organometal. Chem.*, 1997, 545–546, 451.
9. Crystal data for $W_3(\mu_3\text{-}O)(OCH_2{}^tBu)_{10}$ at −168°C: a = 19.234(6) Å, b = 35.635(12) Å, c = 19.106(6) Å, Z = 8, in space group *Pnac* and for $W_3(\mu_3\text{-}O)(OCH_2{}^tBu)_9(\mu_3\text{-}O{}^tBu)$ at −150°C: $a = b$ = 18.901(5) Å, c = 11.708(3) Å, γ = 120.0° and space group P_{321}. Full details are available through the Internet at url http:www.iumsc.indiana.edu. For $W_2(P)_2(OCH_2{}^tBu)_{10}$ request MSC Report No. 93017; for $W_3(O)(OCH_2{}^tBu)_{10}$ request MSC Report No. 93090 and for $W_3(O)(OCH_2{}^tBu)_9(O{}^tBu)$ request MSC Report No. 92287.
10. Chisholm, M. H., Folting, K., Huffman, J. C. and Kirkpatrick, C. C., *Inorg. Chem.*, 1984, **23,** 1021.
11. $\delta(^{31}P) = -245.5$ ppm ($J_{W-P} = 71$ Hz; ratio P:W = 3:1).
12. Jutzi, P. and Kross, R., *Chem. Ber.*, 1988, **103,** 1399.
13. (a) Scherer, O. J., Sitzmann, H. and Wolmerhäuser, G., *J. Organometal. Chem.*, 1984, **268,** C4; (b) Scherer, O. J., Schwalb, J., Swarowsky, H., Wolmershäuser, G., Kaim, W. and Groß, R., *Chem. Ber.*, 1988, **121,** 443; (c) Chisholm, M. H., Folting, K., Huffman, J. C. and Koh, J. J., *Polyhedron*, 1985, **4,** 893.
14. Budzichowski, T. A., Chisholm, M. H., Folting, K., Streib W. E. and Scheer, M., *Inorg. Chem.*, 1996, **35,** 3659.
15. Chisholm, M. H., Huffman, J. C. and Leonelli, J., *J. C. S. Chem. Comm.*, 1981, 270.
16. Chisholm, M. H., Clark, D. L., Folting, K., Huffman, J. C. and Hampden-Smith, M. J., *J. Am. Chem. Soc.*, 1987, **6,** 1747.
17. Cotton, F. A. and Fang, A., *J. Am. Chem. Soc.*, 1982, **104,** 113.
18. (a) Chisholm, M. H., Cotton, F. A., Murillo, C. A. and Reichert, W. W., *Inorg. Chem.*, 1977, **16,** 1801; (b) Akiyama, M., Chisholm, M. H., Cotton, F. A., Extine, M. W., Haitko, D. A., Little, D. and Fanwick, P. E., *Inorg. Chem.*, 1979, **18,** 2266; (c) Chisholm, M. H., Folting, K., Hammond, C. E., Hampden-Smith, M. J. and Moodley, K. G., *J. Am. Chem. Soc.*, 1989, **111,** 5300.

Pergamon

PII: S0277-5387(98)00067-9

Polyhedron Vol. 17, No. 17, pp. 2937–2955, 1998
© 1998 Elsevier Science Ltd
All rights reserved. Printed in Great Britain
0277-5387/98 $19.00+0.00

Dehydration, hydration and substitution reactions of the hydrido acetylide complexes $HRu_3(CO)_9\{C_2CR(OH)R'\}$.* X-ray structures and NMR fluxionality of $HRu_3(CO)_7(dppm)\{C_2CMe(OH)Ph\}$ and $HRu_3(CO)_7(dppm)\{C_2C(=CH_2)Ph\}$

Giuliana Gervasio, Roberto Gobetto, Philip J. King, Domenica Marabello and Enrico Sappa†

Dipartimento di Chimica IFM, Università di Torino, Via Pietro Giuria 7, I-10125 Torino, Italy

(Received 17 October 1997; accepted 8 February 1998)

Abstract—The complexes $HRu_3(CO)_9\{C_2CR(OH)R'\}$ (**1**) have been obtained by reaction, in hydrocarbon solution, of $Ru_3(CO)_{12}$ with propargyl alcohols of general formula $HC_2CR(OH)R'$. In contrast, reaction of $Ru_3(CO)_{12}$ with the alcohols (R = R′ = Me; R = Me, R′ = Ph) in CH_3OH/KOH solution leads to formation of the corresponding allenylidene complexes $HRu_3(CO)_9\{HC_2C(R)R'\}$ (**2**). The ^1H and ^{13}C NMR fluxional behaviour of the complexes are discussed. The acetylide clusters are stable species and lose water only under drastic conditions (i.e. in the presence of strong acids or on TLC silica), to form vinylacetylide or allenylidene derivatives according to the nature of the acetylide substituents. The reverse hydration reactions occur with some difficulty.

The chiral cluster $HRu_3(CO)_9\{C_2CMe(OH)Ph\}$ (**1d**) reacts with dppm forming the "bridged" complex $HRu_3(CO)_7(dppm)\{C_2CMe(OH)Ph\}$ (**3**) which exists both in the solid state and in solution as two diastereoisomeric pairs of enantiomers. The X-ray structure and the NMR fluxionality of complex **3** is discussed. Protonation of complex **3** leads to loss of water and formation of $HRu_3(CO)_7(dppm)\{C_2C(=CH_2)Ph\}$ (**4**), the X-ray structure of which is also discussed. © 1998 Elsevier Science Ltd. All rights reserved

Propargyl alcohols have been used as synthons in organic reactions promoted by metal complexes since Reppe's time [1] and in recent times their synthetic potential has been extensively exploited [2]. For example, $HC_2CMe_2(OH)$ is a low cost starting material for the synthesis of both aryl- and diaryl-acetylenes [3] and of carbamates [4]. Propargyl alcohols have also been used in organic syntheses promoted by mononuclear ruthenium complexes [5], in olygomerization reactions [6] and, last but not least, $HC_2CR(OH)R'$ ligands have been used to form chiral $Co_2(CO)_6$(alkyne) derivatives [7].

Reactions of propargyl alcohols with metal carbonyl clusters have previously been reported and some examples will be discussed in this paper; for instance, with $M_3(CO)_{12}$ (M=Ru, Os) the ligands $HC_2CR(OH)R'$ undergo oxidative addition to form the hydrido-acetylide complexes $HM_3(CO)_9\{C_2CR(OH)R'\}$ (**1**) [8].

We have undertaken a systematic study of the reactions of propargyl alcohols with $Ru_3(CO)_{12}$ in either hydrocarbon or CH_3OH/KOH solutions; new complexes have been obtained together with improved yields of some known derivatives. Protonation (dehydration) and hydration reactions were performed on some of the products and followed using NMR spectroscopic techniques. Further, we have attempted to correlate the yields, protonation behaviour and acetylide ^{13}C NMR data with the donor properties of the cluster-bound ligands.

* R = R′ = Me, Ph; R = Me, R′ = Ph, Et, Pr^n.

† Author to whom correspondence should be addressed.

The chiral complex $HRu_3(CO)_9\{C_2CMe(OH)Ph\}$ (**1d**) has been reacted with dppm to give the "bridged" species $HRu_3(CO)_7(dppm)\{C_2CMe(OH)Ph\}$ (**3**). The solid state structure of monosubstituted **3** has been determined by X-ray diffraction while the fluxional nature of the complex has been investigated using multinuclear NMR spectroscopic techniques.

Protonation of **3** results in loss of water and formation of $HRu_3(CO)_7(dppm)\{C_2C[=CH_2)Ph\}$ (**4**), the structure of which has been confirmed using X-ray diffraction techniques.

EXPERIMENTAL

General materials and analysis of products

$Ru_3(CO)_{12}$ and alkynes are commercial products and were used as supplied. The propargyl alcohol $HC_2C(Ph)_2OH$ was synthesized using a slightly modified literature method [9] and characterized by ^1H and ^{13}C NMR spectroscopy [10].

Unless stated otherwise, the reactions were performed in conventional three-necked flasks equipped with gas inlet, reflux condenser and oil check valve. Analytically pure heptane, benzene, toluene or methanol were used as solvents, under dry nitrogen atmosphere. The reaction mixtures, filtered under N_2, were brought to small volume under reduced pressure and purified by means of preparative TLC plates (Kieselgel PF, Merck; eluants light petroleum 40–70°C and diethyl ether in variable v/v proportions according to the alkyne substituents). The products collected were crystallized, where possible, from heptane, heptane/$CHCl_3$, heptane/toluene or hexane/CH_2Cl_2 mixtures kept at low temperature for several days.

The products were analyzed by means of an F & M, C, H, N analyzer and a Perkin–Elmer AAS; some analyses were performed by F. Pascher Laboratories (Bonn, Germany). Satisfactory elemental analyses were obtained for all the complexes. The IR spectra were registered on a Perkin–Elmer 580 instrument using heptane or cyclohexane as solvent. The ^1H, $^{31}P\{^1H\}$ and $^{13}C\{^1H\}$ NMR data were collected on JEOL JNM 270/89 and EX 400 instruments and, unless otherwise specified, the spectra were run at room temperature, using $CDCl_3$ as solvent [11]. The EI and CI mass spectra were recorded with a Finnigan-Mat TSQ-700 mass spectrometer (Servizio di Spettrometria di Massa, Dipartimento di Scienza e Tecnologia del Farmaco, Università di Torino).

Reaction of $Ru_3(CO)_{12}$ with propargyl alcohols and related ligands, in hydrocarbon solvents

Complexes $HRu_3(CO)_9\{C_2Me(OH)R\}$ (R = Me, **1b**; R = Ph, **1d**; R = Et, **1e**) were obtained as previously reported [12,13] in 8%, 45% and 18% yields respectively.

Reaction with 2-diphenyl-1-propyn-2-ol $\{HC_2CPh_2(OH)\}$. A suspension of 400 mg (0.63 mmol) of $Ru_3(CO)_{12}$ and 700 mg (3.36 mmol) of ligand was heated at reflux in toluene for 4 min. A clear brown solution was obtained; TLC purification showed the presence of $Ru_3(CO)_{12}$ (5 mg, 1%), complex **1c** (100 mg, 21%), an orange product (complex **1c'**, 20 mg [15]) and decomposition. The reaction was repeated in refluxing benzene (10 min) with the same substrate/cluster ratio leading to an increase in the yield of **1c** to 200 mg (45%).

Complex **1c**. IR (ν_{CO}): 2101 w, 2075 s, 2055 s, 2025 vs, 1991 m, cm^{-1}. ^1H NMR [14]. ^{13}C NMR: (−40°C): 80.0, 105.9, 125.1, 127.6, 128.4, 145.7, 169.3, 186.6 s, 188.5 s, 192.8 s, 196.8 s, 199.1 s. EI mass spectrum. $P^+ = 768$ *m/z*, loss of 9 carbonyls and corresponding doubly charged ions.

Reaction with 3-methyl-1-hexyn-3-ol, $\{HC_2CMe(OH)Pr^n\}$. To a toluene suspension of 400 mg (0.63 mmol) of $Ru_3(CO)_{12}$ was added 1.0 cm^3 (6.4 mmol ca) of liquid alkyne and the mixture heated at reflux for 2 min. The orange-yellow solution was purified by TLC; small amounts of unreacted parent carbonyl, complex **1f** (80 mg, 20%), and considerable decomposition products were obtained.

Complex **1f**. IR: 2100 m, 2074 vs, 2058 vs, 2026 vs (b), 1991 m–s (b), cm^{-1}. ^1H NMR: 1.91 m (CH_2, Pr^n); 1.68 s (OH); 1.65 s (Me); 1.55 m (CH_2, Pr^n); 1.00 t (CH_3, Pr^n); −20.87 s (hydride). EI mass spectrum: P^+ 670 *m/z*, loss of 9 carbonyls.

Reaction with 1-pentyn-3-ol, $\{HC_2C(H)(OH)Et\}$. Treatment of a toluene solution of 0.5 g (0.79 mmol) of $Ru_3(CO)_{12}$ with 1.0 cm^3 (ca 9.5 mmol) of liquid alkyne and heating of the mixture at reflux for 5 min, gave a yellow-brown suspension; TLC showed the presence of a yellow (**Bg**) and a whitish-yellow (**Ag'**, ca 20%) product along with a red residue (ca 70%) [15].

Reaction with 3-methyl-1-butyne, $\{HC_2CMe_2H\}$. To a toluene suspension of 400 mg (0.63 mmol) of $Ru_3(CO)_{12}$ was added 0.6 cm^3 (ca 7.3 mmol) of liquid alkyne and the mixture heated at reflux for 2 min; after TLC purification. complex **1h** (60 mg, 15%) and several decomposition products were isolated.

Complex **1h**. IR: 2099 m, 2082 s, 2076 s, 2050 vs, 2024–2010 vs (b), 1994 m, cm^{-1}. ^1H NMR: 2.91 m (C—H), 1.12 d (CH_3), −20.95 s (hydride). EI mass spectrum: P^- 626 *m/z*, loss of 9 carbonyls.

Reaction with $\{HC_2C(=CH_2)CH_3\}$ [*isopropenylacetylene*]. A suspension of 400 mg of $Ru_3(CO)_{12}$ (0.62 mmol) and 0.5 cm^3 of alkyne (ca 7.6 mmol) in toluene was heated at reflux for 4 min. TLC separation showed the presence of yellow $HRu_3(CO)_9\{C_2C(=CH_2)CH_3\}$ (**1j**) (85 mg, 21%), orange-yellow $Ru_2(CO)_6L_2$ (**Aj**) (ca 20%) and orange $Ru_3(CO)_8L_2$ (**Cj**) [15].

Complex **1j**. ^1H NMR. [11] EI mass spectrum: P^+ 624 *m/z*, loss of 9 carbonyls.

Reaction of $Ru_3(CO)_{12}$ *with* $HC_2CR(OH)R'$ (R = R′ = Me; R = Me, R′ = Ph) *in* MeOH/KOH *solution*

To a methanolic solution (100 cm^3) of $Ru_3(CO)_{12}$ (200 mg; 0.32 mmol) was added 40 cm^3 of aqueous 1 M KOH solution and the mixture stirred until all of the ruthenium carbonyl was dissolved. A methanolic solution (15 cm^3) of either $HC_2Me(OH)Ph$ (462 mg; 3.20 mmol) or $HC_2CMe_2(OH)$ (2.5 cm^3; 28.5 mmol) was added to the mixture and the whole stirred for 2.5 h. After this time the solution was acidified by addition of H_2SO_4, the mixture filtered and the solid and liquid phases extracted separately with $CHCl_3$. Combination of the two fractions followed by TLC purification, eluting with pentane, led to isolation of yellow $HRu_3(CO)_9\{HC_2C(Me)Ph\}$ (**2c**), in 20% yield, or $HRu_3(CO)_9\{HC_2C(Me)Me\}$ (**2b**), in 35% yield respectively.

Complex **2c**. IR: 2094 m, 2083 s, 2065 s, 2060 m, 2053 w, 2043 s, 2038 w, 2028 s, 2021 s, 2010 s, 2001 m, 1991 m, 1989 m–sh, cm^{-1}. ^1H NMR: major isomer (−40°C), 8.45 s (1H, J = 1.86 Hz), 7.85–7.20 m (Ph), 2.22 s (Me); −20.20 s (hydride, J = 1.86 Hz). Minor isomer (−40°C); 8.57 s (1H); 7.85–7.20 m (Ph); 2.63 s (Me); −20.20 s (hydride).

Complex **2b**. IR: 2094.2 m, 2085.1 m, 2070.1 s, 2066.8 s, 2052.7 s, 2042.3 s, 2017.0 s, 2008.6 s, 2001.0 s, 1990.7 m, 1985.7 m–sh, cm^{-1}. ^1H NMR (CD_2CL_2) (−40°C); 8.13 d (1H, J = 1.86 Hz); 2.13 s (Me); 1.82 s (Me); −20.52 d (1H, J = 1.86 Hz).

Protonation, dehydration and hydration reactions in solution or on TLC plates

The protonation reactions of complexes **1b, 1c,** and **1d** were followed by NMR; these reactions were carried out via dropwise addition of concentrated H_2SO_4 (96%) to a $CDCl_3$ solution of the complex in a NMR tube. In some instances CF_3COOH was used [13] instead of sulphuric acid. The reactions were followed as a function of either time or concentration of H_2SO_4 and the yields of the products were evaluated by integration of the relevant NMR signals. Where possible, the nature of the products was confirmed by synthesizing them independently (e.g. complex **1j**). In some instances, the protonation reactions were performed in normal reaction vessels in order to isolate the products.

Protonation of $HRu_3(CO)_9\{C_2CMe_2(OH)\}$ (**1b**). Addition of three drops of H_2SO_4 resulted (after 10 min) in formation of the dehydration product $HRu_3(CO)_9\{C_2C(=CH_2)Me\}$ (**1j**) in 10% yield. The yield of **1j** was seen to increase slowly to a maximum of about 25% after 30 min. On leaving the mixture to stand for 12 h, however, total decomposition of the complex was found to have occurred.

Protonation of $HRu_3(CO)_9\{C_2CMe(OH)Ph\}$ (**1d**). Addition of 3 drops of H_2SO_4 resulted in the immediate formation of $HRu_3(CO)_9\{C_2C(=CH_2)Ph\}$ in 10% yield. After 20 min the yield reached ca 80% and after 30 min the reaction was nearly complete. It is worthy of note that, after 30 min, a hydridic signal at δ −11.3 (the intensity of which remained constant throughout the reaction) was observed; this may be due to the presence of $Ru_3(H)(OH)(C{=}C{=}C(Me)Ph)$ in the solution [16]. After protonation, TLC purification showed the presence of a yellow band which was collected and characterized as $HRu_3(CO)_9\{C_2(=CH_2)Ph\}$ (**1k**) [13].

Protonation of $HRu_3(CO)_9\{C_2CPh_2(OH)\}$ (**1c**). Addition of 50 μl of H_2SO_4 resulted in formation of a small amount (about 15%) of the corresponding dehydration product $Ru_3(H)(OH)(CO)_9(C{=}C{=}CPh_2)$ [16] (suggested by a decrease in the intensity of the OH signal at δ 2.64 and appearance of a hydridic signal at δ −11.37); no increase in the yield was noted after 15 min. Addition of a further 50 μl of acid resulted in the immediate formation of the allenylidene $Ru_3(H)(OH)(CO)_9(C{=}C{=}CPh_2)$ in 100% yield. Further addition of 50 μl of acid resulted in decomposition (gradual disappearance of the hydridic signal).

Dehydration—hydration reactions on TLC plates. These reactions are skimpily described in Ref. [17].

Synthesis and reactivity of $HRu_3(CO)_7(dppm)\{C_2CMe(OH)Ph\}$ (**3**) *and related compounds*

Reaction of $HRu_3(CO)_9[C_2Me(OH)Ph]$ *with dppm and* $Me_3NO\cdot 2H_2O$. $Ru_3(CO)_{12}$ (200 mg, 0.29 mmol), dppm (0.30 g, 0.78 mmol) and $Me_2NO\cdot 2H_2O$ (a few crystals) were dissolved in toluene (100 cm^3) and heated at reflux for 1 min during which time a colour change from yellow to red was observed. TLC, eluting with diethyl ether: petroleum ether (1:5), showed the presence of two bands; the first, yellow, provided $HRu_3(CO)_7(dppm)\{C_2C(Me)(Ph)OH\}$ (**3**) (70 mg, 24%, yellow crystals) and the second, red, provided an orange powder (70 mg), tentatively identified as $HRu_3(CO)_5(dppm)_2\{C_2CMe(OH)Ph\}$ (**D**).

Complex **3**. IR: 2064 vs, 2011 vs, 1995 vs, 1980 m, 1960 m, cm^{-1}.

^1H NMR ($CDCl_3$, −40°C): 8.21–6.47 m (Ph); 4.43 q (CH^a, J = 14 Hz); 4.29 q ($CH^{a'}$, J = 14 Hz); 3.41 q (CH^b, J = 14 Hz); 3.32 q ($CH^{b'}$, J = 14 Hz); 1.77 s (OH); 1.73 s (Me); −19.92 d (μ-H, J = 35 Hz); −20.04 d (μ-H, J = 35 Hz).

^{31}P NMR ($CDCl_3$, 0°C): 36.22 d (P^a, J = 53 Hz); 35.74 d ($P^{a'}$, J = 55 Hz); 30.27 d (P^b, J = 52 Hz); 29.60 d ($P^{b'}$, J = 52 Hz).

^{13}C NMR ($CDCl_3$, −20°C): 188.36 dd (d^1,$d^{1'}$); 191.45 d (d,d^1); 198.03 dd (a^1,$a^{1'}$); 199.00 dd (a,a′); 201 s (c,c′); 206.7 t (b,b′) [18].

Complex **D**. IR: 2061 m, 2052 m, 1998 s, 1975 m, cm^{-1}.

^1H NMR (−40°C): 7.84–6.09 m (Ph); 4.40 q

(CH_2), 3.35 q, 3.18 q (CH_2); 3.25 s (OH); 1.23 s (CH_3); −19.8/−20.5 dd (hydride).

^{31}P NMR (−40°C): 33.26, 33.01, 32.74, 32.48 q (J = 39.7, 44.2, 41.8); 19.91, 19.67 d (J = 39.7), 19.57, 19.33 d (J = 35.7) 24.67, 24.13 d (J = 86.9), 24.03, 23.68 q (J = 66.5).

Reaction of $Ru_3(CO)_{10}$(dppm) *with* $HC_2CMe(OH)Ph$ *in hydrocarbons.* A toluene solution (75 cm^3) of $Ru_3(CO)_{10}$(dppm) [19] (200 mg, 0.21 mmol) and $HC_2CMe(OH)Ph$ (120 mg, 0.82 mmol) was heated at reflux for 3 min: no colour change of the solution was observed. TLC purification, eluting with 50% diethyl ether, allowed the isolation of an orange band which ^1H NMR spectroscopy showed to be the starting complex.

Protonation of $HRu_3(CO)_7$(dppm){$C_2CMe(OH)Ph$} (**3**). Treatment of a $CDCl_3$ solution of complex **3** with 3 drops of H_2SO_4 led to formation of $HRu_3(CO)_7$(dppm){$C_2C(=CH_2)Ph$} (**4**). Purification of the complex was effected through chromatography on TLC plates, eluting with diethyl ether: petroleum ether (1 : 1) to give a yellow band (complex **4**).

Complex **4**. IR: 2007 s, 1983 s, 1975 s, 1945 s, 1932 s, 1889 w, cm^{-1}.

^1H NMR: 7.77–6.70 mm (Ph): 5.67 s (=CH_2); 4.37 q, 3.44 q (CH_2, dppm), 1.56 s (Me); −19.39, −19.47 d (hydride).

X-ray analyses of complexes **3** *and* **4**

Crystals of complex **3** were obtained by slow diffusion of hexane into a toluene solution of the complex. Crystals of complex **4** were formed through slow evaporation of dichloromethane at −20°C from a dichloromethane/hexane solution of the complex.

The data were collected on a Siemens P4 diffractometer using graphite-monochromated Mo–K_α radiation, in θ–2θ (complex **3**) and ω (complex **4**) scan mode, with a scan range of 2.2° (**3**) and 1.6° (**4**). The range of scan speed was 4–20° min^{-1}. Two standard reflections were measured every 50 reflections and they showed no decay. Cell constants were obtained from a least-squares refinement based on the setting angles of 35 reflections in the range $20° \leqslant 2\theta \leqslant 30°$. Empirical absorption corrections were performed for **3** and **4** according to the method of Ref. [20].

The structures were solved by direct methods and refined using the program SHELXTL PLUS (PC version 5.03).

Crystal data and refinement parameters are collected in Table 1.

The substitution of two equatorial CO groups by dppm on the two enantiomers of **1d,** deriving from the chiral alcohol, gives rise in complex **3** to a further asymmetry of the cluster and, consequently, to two pairs of enantiomers. During the refinement of complex **3** two diastereoisomers appeared superimposed in the asymmetric unit: they differ only in the chirality of the asymmetric C(10) and consequently in the orientation of its substituents. The two fragments corresponding to *R*- and *S*-C(10) were refined with occupancy factor 0.5. All non-hydrogen atoms, excluded those with occupancy factor 0.5, were anisotropically refined for both complexes.

The hydride atom was located for both complexes on the last Fourier difference maps and its refinement gave good results, obviously with high uncertainty; the other hydrogen atoms (except those of the OH groups which were not included, and those of C(11) of complex **4,** which were located on the experimental peaks) were calculated and refined according to the "riding" model, even if many of them appeared in the Fourier difference maps.

The weighting scheme was: $w = 1/[\sigma^2(F_o^2) + (0.0329 \cdot P)^2 + 1.30 \cdot P]$, $P = [\max(F_o^2) + 2F_c^2]/3$ for complex **3** and: $w = 1/[\sigma^2(F_o^2) + (0.0228 \cdot P)^2 + 2.27 \cdot P]$, $P = [\max(F_o^2) + 2F_c^2]/3$ for complex **4**. Tables of atomic coordinates and displacement parameters, lists of observed and calculated structure factors and complete lists of bond lengths and angles have been deposited with the Editor; atomic coordinates have been left with the Cambridge Crystallographic Data Centre.

RESULTS AND DISCUSSION

Synthesis of complexes $HRu_3(CO)_9${$C_2CR((OH)R'$} (**1**)

We obtained complexes **1** through a direct synthetic pathway consisting of oxidative addition of the propargyl ligands to $Ru_3(CO)_{12}$ as previously described for the range of alcohols $HC_2RR'(OH)$ [R = R′ = Me; R = Me, R′ = Et; R = Me, R′ = Ph) [13]; medium-low yields of complexes **1** were reported for M = Ru and higher yields for M = Os. For osmium it has also been shown that intact alcohols can coordinate first in a "parallel" fashion before undergoing oxidative addition to form complexes **1** [12].

Complexes **1** can also be obtained indirectly through C—C bond cleavage of diols to give complexes **1** and ketones [21]. Further, it has been shown that neither alkynes nor propargyl alcohols having hydrogen alpha to the alkyne C—C bond form complexes of type **1** [22] but instead lead to the formation of hydrido-allenyl or -allyl derivatives [23]. In accordance with this we have found during the course of our studies that no complexes of type **1** were isolated from reaction of $Ru_3(CO)_{12}$ with the series of alcohols $HC_2CR(OH)H$ (R = Me, Et, Ph). All of the complexes **1** reported or discussed in this paper are collected, along with their yields, in Table 2.

The yields of complexes **1a**–**1j** vary considerably according to the nature of the alkyne employed in the reaction and do not seem to bear any relation to the σ-Taft values. One general trend, however, is the increase in the yields of the complexes **1** when either

Table 1. Crystal data and structure refinement parameters for complexes **3** and **4**

Identification code	**3**	**4**
Empirical formula	$C_{42}H_{32}O_8P_2Ru_3$	$C_{42}H_{30}O_7P_2Ru_3$
Formula weight	1029.82	1011.81
Temperature	293 K	293 K
Wavelength	0.71073 Å	0.71073 Å
Crystal system	Triclinic	Monoclinic
Space group	$P\bar{1}$	$P2_1/c$
a (Å)	11.515(2)	11.617(2)
b (Å)	12.787(2)	12.608(2)
c (Å)	14.439(3)	27.515(4)
α (°)	68.54(1)	
β (°)	88.17(1)	91.961(12)
γ (°)	88.83(1)	
V (Å^3)	1977.5(6)	4027.6(10)
Z	2	4
D_{calcd} (g/cm^3)	1.728	1.669
Absorption coefficient (mm^{-1})	1.264	1.238
$F(000)$	1018	2000
Crystal size; color	0.30 × 0.22 × 0.12 mm; yellow	0.32 × 0.42 × 0.74 mm; yellow
θ range for data collection (°)	1.52 to 30.04	1.48 to 30.01
Limiting indices	$-16 \leqslant h \leqslant 16$, $-16 \leqslant k \leqslant 18$, $0 \leqslant l \leqslant 20$	$-16 \leqslant h \leqslant 16$, $0 \leqslant k \leqslant 17$, $0 \leqslant l \leqslant 38$
Reflections collected	12060	11990
Independent reflections	11520 [$R_{(int)} = 0.0295$]	11693 [$R_{(int)} = 0.0295$]
Absorption correction	Semi-empirical from psi-scans	Semi-empirical from psi-scans
Max. and min. transmission	0.58 and 0.31	0.23 and 0.19
Refinement method	Full-matrix least-squares on F^2	Full-matrix least-squares on F^2
Data/restraints/parameters	11517/15/491	11672/0/491
Goodness-of-fit on F^2	1.044	1.102
Final R indices [$I > 2\sigma(I)$]	$R_1 = 0.0406$, $wR_2 = 0.0766$	$R_1 = 0.0349$, $wR_2 = 0.0652$
R indices (all data)	$R_1 = 0.0727$, $wR_2 = 0.0917$	$R_1 = 0.0589$, $wR_2 = 0.0797$
Extinction coefficient		0.00377(8)
Largest diff. peak and hole (eA^{-3})	0.751 and −0.565	0.443 and −0.374

$R_1 = \Sigma \| F_o | - | F_c \| / \Sigma | F_o |$
$wR_2 = [\Sigma[w(F_o^2 - F_c^2)^2] / \Sigma[w(F_o^2)^2]]^{1/2}$
Goodness-of-fit $= [\Sigma[w(F_o^2 - F_c^2)^2] / (n-p)]^{1/2}$

strong electron donor (i.e. those alkynes with highly positive σ-Taft values) or acceptor (i.e. those with highly negative σ-Taft values) ligands are present on the alkyne (although it should be noted that this rule does not apply to those alkynes having H alpha to the C≡C bond which, as mentioned above, do not give complexes of type **1**).

The ^{13}C NMR data for the acetylide units in complexes **1a**–**1j** (and related clusters) are presented in Table 3 [28–36]. The assignments are based on data in the literature [24–27].

In principle, the chemical shifts of the C_α and C_β should be affected directly by the electron donating ability of the acetylide substituents and the presence of substituents on the cluster frame.

Previously, it has been proposed that changes in the chemical shifts (δ) of the acetylide carbons may be associated with a change in their charges, although the observed chemical shifts are also dominated by paramagnetic terms of the screening constants. Further, it was suggested that the sum $\delta(C_\alpha) + \delta(C_\beta)$ ($\Delta+$) reflects any charge changes in the triple bond, while the difference $\delta(C_\alpha) - \delta(C_\beta)$ ($\Delta-$) can be used as a measure of the charge polarization in the triple bond [27].

For complexes **1** the $\Delta+$ and $\Delta-$ values show only slight differences from each other and are not sensibly affected by either different acetylide substituents or substitution of other ligands for CO, thus suggesting considerable "electronic rigidity" of the cluster frames. However, some small but regular trends can be discerned. For example, when metal fragments replace the bridging hydride group or when COs are substituted by Group XV donor ligands (in particular arsine and stibine) the $\Delta+$ values are always greater than that of $HRu_3(CO)_9(C_2Bu^t)$ (**1a**, arbitrarily taken as a reference) [8]. Further, the $\Delta-$ values are greater for the propargyl alcohols derivatives than for com-

Table 2. Yields of complexes **1** and σ-Taft values of the alkyne substituents

Complex	Alkyne substituents {$HC_2C(R)(R')R''$} R	R′	R″	σ-Taft[a]	Yields of complexes **1** %
1c	OH	Ph	Ph	+1.200	21–45
1d	OH	Ph	Me	+0.600	45
1b	OH	Me	Me	0	8
1e	OH	Me	Et	−0.100	18
1f	OH	Me	Pr^n	−0.115	20
	OH	H	Me	+0.490	0
	OH	H	Ph	+1.090	0
1h	H	Me	Me	−0.115[b]	20
1a	Me	Me	Me	−0.300[c]	80
1j	—	$=CH_2$	Me		21

[a] As the sum of the separate substituents.
[b] As Pr^i.
[c] As Bu^t.

plex **1a**; in particular, complexes **1c** and **1d** bearing phenyl groups give rise to higher values of $\Delta-$ than the other propargyl alcohols.

Protonation (dehydration) and attempted hydration reactions of complexes **1**

The behaviour observed for propargyl alcohols at an $M_3(CO)_{12}$ [M = Ru, Os] centre contrasts strongly with that seen at a tri-iron centre. The reactions of $Fe_3(CO)_{12}$ lead not to complexes of type **1** but, instead, facile dehydration of the ligands occurs in one or two different ways. The first requires the loss of the alcoholic OH and of a hydrogen from a methyl group on the same carbon atom, leading to a vinylacetylide or "ene-yne" ligand (route A). The second process (route B) requires loss of the OH and of the terminal alkynic hydrogen thus forming allenylidene derivatives. These two routes may occur competitively [37].

Table 3. ^{13}C NMR chemical shifts of the acetylide carbons in complexes $HRu_3(CO)_9\{C_2R\}$ and related derivatives

Complex	(d)C_α	(d)C_β	d+d	d−d	Ref.
$HRu_3(CO)_9(C_2Bu^t)$	164.2	110.6	274.8	53.6	28
		Propargyl alcohol derivatives			
$HRu_3(CO)_9\{C_2CMe_2OH\}$ (**1b**)	165.4	105.4	270.8	60.0	t.w.
$HRu_3(CO)_9\{C_2CMeEtOH\}$ (**1e**)	167.1	105.5	272.6	61.6	t.w.
$HRu_3(CO)_9\{C_2CMePr^nOH\}$ (**1f**)	166.7	105.5	272.2	61.2	t.w.
$HRu_3(CO)_9\{C_2CMePhOH\}$ (**1d**)	168.9	107.9	276.0	61.0	t.w.
$HRu_3(CO)_9\{C_2CPh_2OH\}$ (**1e**)	169.6	106.7	276.3	62.9	t.w.
$HRu_3(CO)_9\{C_2CMe_2(H)\}$ (**1h**)	163.6	103.7	267.3	59.9	t.w.
$HRu_3(CO)_9\{C_2C(CH_2)CH_3\}$ (**1j**)	163.6	103.1	266.7	60.5	t.w.
		Hydride substitution products			
$(XM)Ru_3(CO)_9(C_2Bu^t)$					
$XM = Cu(PPh_3)$	174.9	121.4	286.3	53.5	29
$XM = Ag(PPh_3)$	173.0	118.9	291.3	54.1	30
$XM = Au(PPh_3)$	172.2	120.7	292.2	51.5	31
		Monophosphine substituted products			
$HRu_3(CO)_8(L)(C_2Bu^t)$					
$L = PPh_2(OEt)$	165.7	112.2	277.9	53.5	32
$L = \{PMe_2Ph\}$	163.7	112.6	276.3	51.1	33
$L = (PPh_3)$	166.9	112.2	279.1	54.7	t.w.
$L = (AsPh_3)$	168.8	113.7	282.5	54.5	t.w.
$L = (SbPh_3)$	168.3	113.8	282.1	54.5	t.w.
$L = PPh_2C_2Ph$	166.9	110.5	277.4	56.4	34
		Diphosphine substituted products			
$HRu_3(CO)_7(L)(C_2Bu^t)$					
L = dppm	163.3	109.6	272.9	53.7	35
L = arphos	165.9	114.3	280.2	51.6	36
L = arphos	163.7	116.0	279.7	47.7	36
L = dppe	162.0	116.0	278.0	46.0	36

(d)$C_\alpha = \delta C_\alpha$; (d)$C_\beta = \delta C_\beta$; d+d = $\delta C_\alpha + \delta C\beta$; d−d = $\delta C_\alpha - \delta C_\beta$.

In addition, for the alkyne $HC_2CMe(OH)Ph$ "deoxygenation" of the ligand has also been observed [38]. Examples of routes A and B are given in Fig. 1a.

Propargyl alcohols do not readily undergo dehydration at an Ru_3 centre, the process only being effected under harsh reaction conditions (e.g. protonation with strong acids as discussed below). Some protonation reactions, using CF_3COOH, have been reported. For example, complexes **1d** and **1e** form eneyne ligands via "route A" [13] in yields of 20 and 55% respectively. In contrast, protonation of $HM_3(CO)_9\{C_2CPh_2(OH)\}$ allowed isolation (in the case of M = Os) of the allenylidene species $HM_3(CO)_9(OH)(C{=}C{=}CPh_2)$ which was proposed to be an intermediate in the dehydration of the parent complex via route B (see Fig. 1b). In the case of M = Ru, the corresponding allenylidene species could not be isolated but was intimated by the presence of signals in the ^1H NMR spectrum at 7.5 (10 H, m) and −11.27 (1H, s) ppm [16].

In this context it is interesting to note that reaction of ROH with $Cp^*WRe_2(CO)_9[C_2C(=CH_2)Me]$, containing a cluster bound isopropenyl-acetylide, has been shown to lead to the allenylidene complex $Cp^*WRe_2(CO)_8(\mu\text{-OMe})$ $(C{=}C{=}CMe_2)$ bearing a μ-OR moiety on an open cluster edge [39].

The protonation reactions described below were followed using ^1H NMR spectroscopic techniques varying either the reaction time or amount of acid added (see experimental section for details). The ^1H NMR data for the parent complexes and the dehydration products are presented in Table 4 together with the yields of the products (deduced through integration of the ^1H NMR resonances).

For complexes **1d** and **1c** when the concentration on acid was kept constant the yields of the protonated products increased steadily with time until the reaction was complete. In both cases, however, leaving the acidified solutions to stand at room temperature overnight resulted in decomposition of the products. Interestingly, for complex **1b** the yield was seen to reach a maximum of 25% after 30 min and then gradually decrease as the product started to decompose.

For each of the complexes **1b, 1c,** and **1d** the product yields were found to increase when the amount of acid used was increased. This observation is in accordance with the protonation mechanisms reported for surface reactions which are thought to proceed via direct attack of H^+ at the OH site of the alcohol [40].

There are several literature reports on the effect of supports in promoting hydration/dehydration reactions [41]. In particular, splitting and addition of

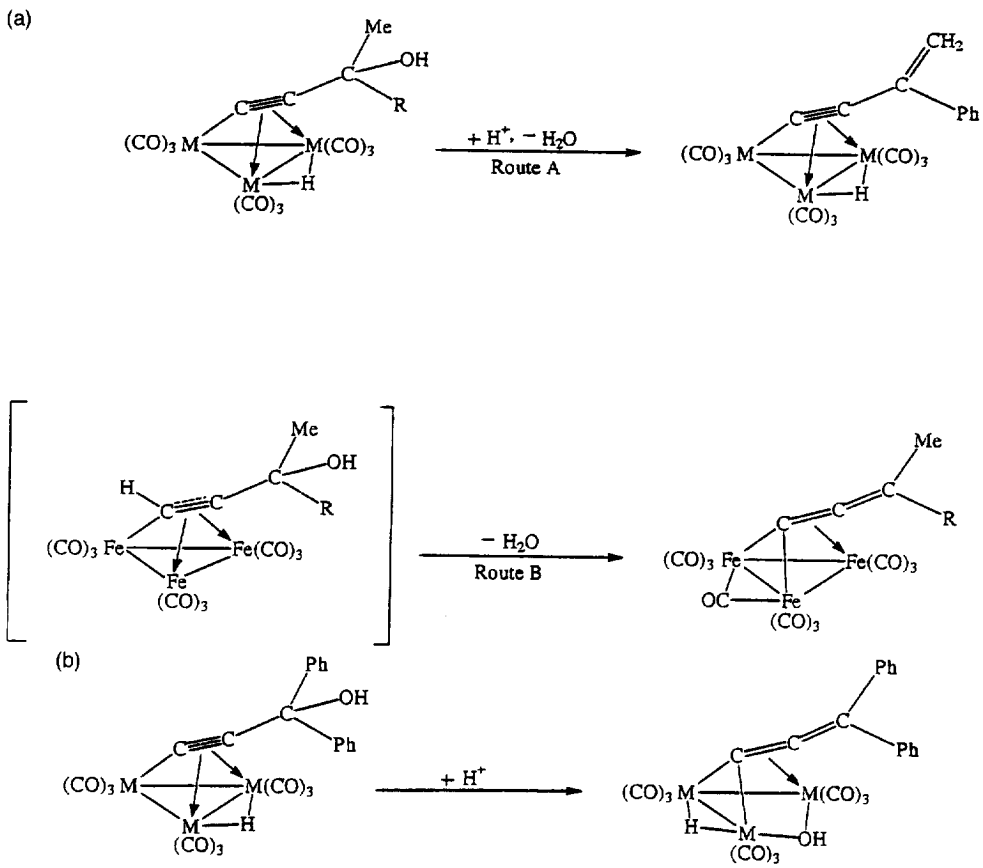

Fig. 1. Dehydration modes of propargyl alcohols at $M_3(CO)_{12}$ centres.

Table 4. ^{1}H NMR data for the dehydrated compounds and parent clusters

Complex	Me	Ph	$=CH_2$	OH	μ-H
[M]{$C_2CMe_2(OH)$} (**1b**)	1.60 (s, 6H)	—	—	1.55 (s, 1H)	−21.02 (s, 1H)
[M]{$C_2C(=CH_2)Me$} (**1j**)	2.19 (s, 3H)	—	5.33 (d, 1H)–5.26 (3, 1H)		−20.82 (s, 1H)
[M]{$C_2CMe(OH)Ph$} (**1d**)	2.08 (s, 3H)	7.18–7.64 (m, Ph)	5.72 (d, 1H)–5.61 (d, 1H)	2.14 (s, 1H)	−21.08 (s, 1H)
[M]{$C_2C(=CH_2)Ph$} (**1k**)	—	7.27–7.64 (m, Ph)		—	−20.83 (s, 1H)
[M]{$C_2CPh_2(OH)$} (**1c**)	—	7.77–7.24 (m, Ph)	—	2.64 (s, 1H)	−21.11 (s, 1H)
[M]*{$C=C=CPh_2$}	—	—	—	—	−11.27 (s, 1H)

[M] = $HRu_3(CO)_9$
[M]* = $HRu_3(CO)_9(\mu$-OH).

water [42] or of methanol [43] to ene-yne or allenylidene tri-iron derivatives occurs very easily on TLC silica.

In stark contrast to the above, the behaviour of complex **1d** on TLC silica plates indicates that the inorganic oxide has a very low hydration activity. Thus, adsorption of complex **1d** onto a TLC silica plate and heating in oven at 100°C for 15 min produced only trace amounts of the corresponding dehydration product $HRu_3(CO)_9[C_2C(=CH_2)Ph]$. Further, the failure of complex **1j** to react with "wet" TLC plates at room temperature, or a silica/water slurry at 55°C (see Ref. [17]) suggests that hydration of these complexes does not occur easily on silica. Hydration of **1j** to give $HRu_3(CO)_9(C_2CMe_2OH)$ (**1b**) was only effected under harsh reaction conditions (i.e. addition of acid to a chloroform solution of the complex followed by addition of water) and in low yield (< 10%).

In general, it would appear that dehydration of complexes **1** containing a methyl substituent on the same carbon as the OH unit leads to formation of the corresponding ene-yne product. However, during the protonation reactions described above, resonances in the ^{1}H NMR spectra were observed at about −11 ppm suggesting, perhaps, the formation of allenylidene products in minor yields (cf the hydride resonance seen for $HRu_3(CO)_9(OH)(C=C=CPh_2)$ at −11.27 ppm) [16]. Relationships between ene-ynes and allenylidene ligands have been demonstrated for dimolybdenum complexes [44]. In addition, as previously discussed, $Os_3(CO)_9(\mu$-CO)(HC≡CCMe$_2$OH) (containing a "parallel" alkyne unit) can either undergo oxidative addition forming complexes of type **1**, or can be protonated using CF_3COOH to form $HOs_3(CO)_9[C_2C(=CH_2)Me]$ via an allenylidene intermediate [12].

A summary of the synthetic pathways to complexes **1** and of the dehydration (rehydration) reactions is given in Scheme 1 below.

Most complexes of type **1** show fluxional behaviour of the carbonyls at room temperature [45]. Complex **1d** is no exception, however, a discussion of its fluxionality will be presented in a future publication.

Synthesis of complexes $HRu_3(CO)_9[HC_2C(Me)R]$ (**2**)

While reaction of $Ru_3(CO)_{12}$ with the propargyl alcohols $HC_2C(Me)_2OH$ and $HC_2C(Me)(OH)Ph$, in hydrocarbon solvents, led to formation of the corresponding alkylidine species $HRu_3(CO)_9[C_2C(Me)(OH)R]$ (**1b** R = Me, **1d** R = Ph), reaction of $Ru_3(CO)_{12}$ with the same alcohols in MeOH/KOH solution gave instead the allenylidene complexes $HRu_3(CO)_9[HC_2CMe_2]$ (**2b**) and $HRu_3(CO)_9[HC_2C(Me)(Ph)]$ (**2c**).

Characterization of the new complexes was relatively straightforward through comparison of the ^{1}H NMR and IR spectroscopic data with those of the directly analogous species $HRu_3(CO)_9[MeC_2CMe_2]$ [46] and $HRu_3(CO)_9[(C_2H_5)C_2C(Me)H]$ [23a].

The mechanism of the reaction is unclear. However, in keeping with the results seen earlier for the protonation of complexes **1b, 1d** etc, it may be that the loss of the OH group from the propargyl alcohol moiety is effected during acidification of the reaction mixture by addition of H_2SO_4 (see experimental section). A tempting alterative hypothesis (suggested by referees) could be the following; it is known that, under basic conditions, $Ru_3(CO)_{12}$ gives as the main product the anion $[HRu_3(CO)_{11}]^-$ [47]. This could react with the alkynes to form the allenyl complexes eventually via $H(\mu$-OH)$Ru_3(CO)_9$(allene) intermediates.

^{1}H NMR fluxionality of complexes **2**

The low temperature limiting ^{1}H NMR spectrum of **2b**, recorded at −40°C, shows two sharp resonances for the inequivalent methyl groups of the allenylidene ligand (see Fig. 2). At room temperature, however, the signals have started to broaden and col-

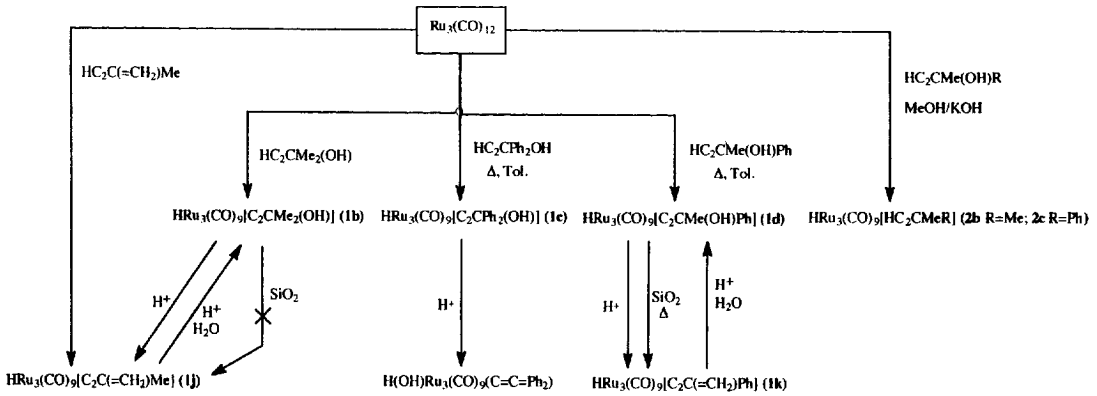

Scheme 1

lapse into the baseline indicating that some fluxional process is occurring.

Variable temperature ^1H and ^{13}C NMR studies have been carried out by Aime *et al.* [46] into the fluxionality of the related species $HRu_3(CO)_9[MeC_2CMe_2]$ and $HOs_3(CO)_9[MeC_2CMe_2]$ which both show identical behaviour in the ^1H NMR spectrum to complex **2b**. They proposed a mechanism for the fluxional process (see Fig. 2) in which the hydride migrates from the Ru(1)—Ru(2) edge to the Ru(1)—Ru(3) edge while the allenylidene unit undergoes a "wagging" motion, pivoting about the C(2) carbon, allowing the two methyl groups attached to C(3) to be seen as a single sharp resonance in the ^1H NMR spectrum at higher temperatures.

Interestingly, the ^1H NMR spectrum of complex **2c** at $-40°C$ shows it to exist as a mixture of two isomers in a ratio of ca 3 : 1. The fact that the same is not true for complex **2b** suggests that the isomerism is due to the presence of two different groups (methyl and phenyl) on the C(3) carbon of the allenylidene ligand and that the isomers differ only in the orientation of these two substituents (see below).

If this is the case then the fluxional process described above should allow interconversion between the two isomers to occur and, indeed, ^1H NMR spectrum of **2c** at room temperature shows broadening of the signals for the unique proton, the methyl and the hydride groups of each isomer (see Fig. 2).

Synthesis of $HRu_3(CO)_7(dppm)\{C_2C(Me)(OH)Ph\}$ **(3)**

It is perhaps surprising to note that substitution of cluster carbonyls on complex **1d** for dppm occurs under thermal conditions, without loss of water or re-orientation of the acetylide unit, to give $HRu_3(CO)_7(dppm)\{C_2C(Me)(OH)Ph\}$ **(1)** (see Scheme 2).

Re-orientation of alkynes on addition or removal of carbonyls from a complex has been observed in the past. For example, Lavigne and co-workers have shown that the complex $Ru_3(CO)_7(\mu\text{-}CO)(dppm)\{C_2Ph_2\}$, having an alkyne bound in a parallel fashion, loses CO reversibly to yield the perpendicular bound alkyne complex $Ru_3(CO)_7(dppm)\{C_2Ph_2\}$ [48]. Further, Smith *et al.*, have synthesized the complex $Os_3(CO)_7(dppm)\{C_2Ph_2\}$, having a perpendicular alkyne, which can also undergo reversible addition of CO resulting in a parallel arrangement of the alkyne on the complex [49].

Interestingly, attempts at preparing complex **3** from reaction of $Ru_3(CO)_{10}(dppm)$ with $HC_2CMe(OH)Ph$ were unsuccessful; it may be that the already coordinated dppm does not favour oxidative addition of the alkyne. The structure of complex **3** has been determined by X-ray crystallography and is discussed later.

Protonation of complex **3**. Complex **3** has been protonated following the same procedure used for complexes **1**. Loss of water, via route A, to give $HRu_3(CO)_7(dppm)\{C_2C(=CH_2)Ph\}$ **(4)** was observed but no other major structural changes could be detected. The solid state structure of **4** has also been obtained through a single crystal X-ray analysis and is discussed in the following section along with that of complex **3**.

X-ray structures of $HRu_3(CO)_7(dppm)\{C_2C(Me)(OH)Ph\}$ **(3)** *and* $HRu_3(CO)_7(dppm)\{C_2C(=CH_2)Ph\}$ **(4)**

The structures of two superimposed diastereoisomers of complex **3** and the structure of complex **4** are shown in Figs 3 and 4 respectively. Relevant bond lengths and angles are reported in Table 5.

The framework of both clusters **3** and **4** consist of a triangle of ruthenium atoms, with Ru(1) and Ru(2) coordinated to two carbonyl groups and Ru(3) to three carbonyl groups. The Ru(1)—Ru(2) edge of the cluster is bridged by a dppm ligand held in an equatorial position and tilted towards the acetylide ligand, the angle between the Ru_3 and the Ru(1)P(1)P(2)Ru(2) planes being 15° **(3)** and 17° **(4)**, while

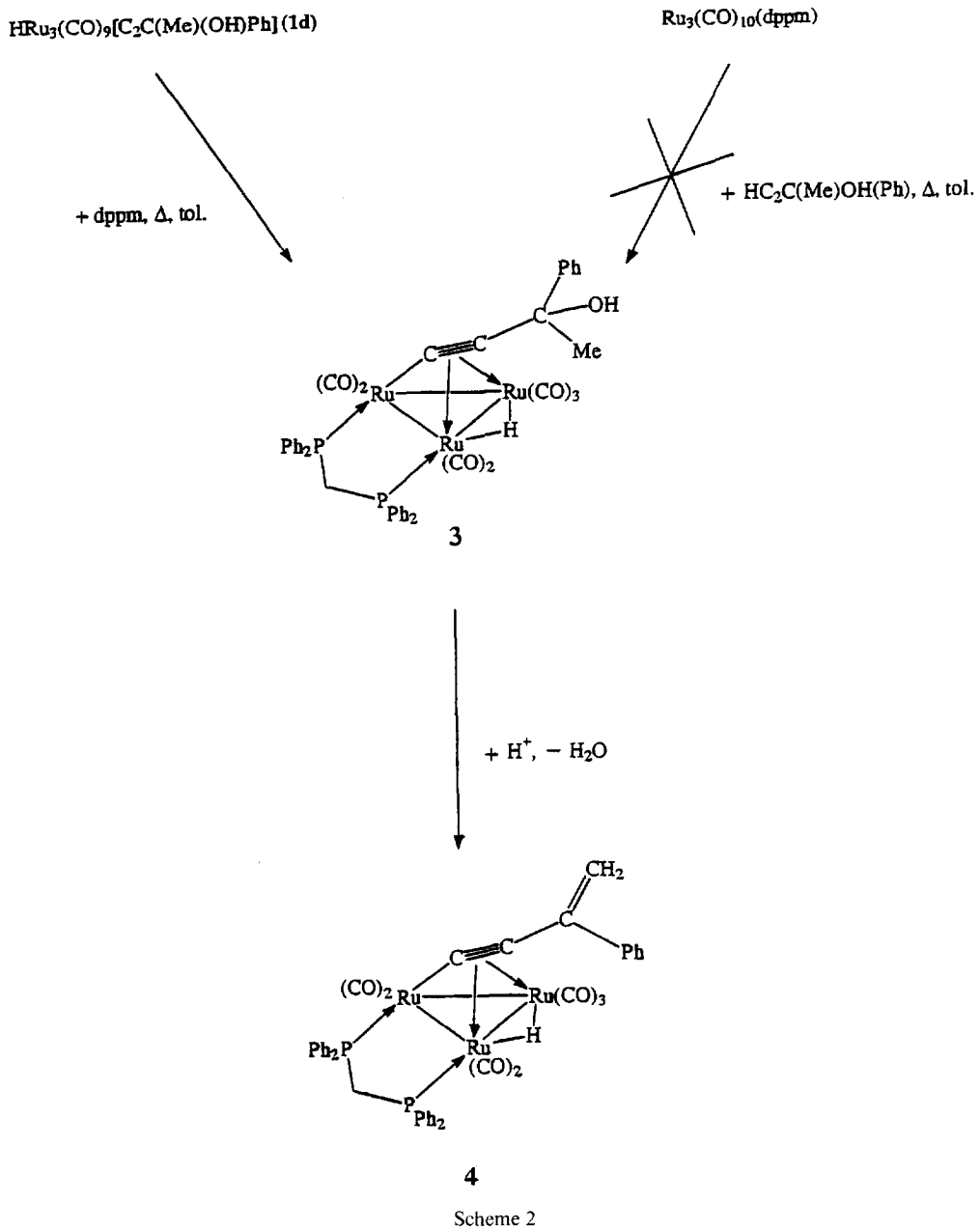

Scheme 2

the methylene group of the dppm molecule is out of the plane. A bridging hydride spans the Ru(2)—Ru(3) edge and is in a niche formed by the carbonyl groups (having a mean distance of 2.49 Å from the C atoms for both compounds). The hydride lies in the plane formed by the atoms C(3)C(4)C(5) and C(7) (having a mean deviation from the plane of 0.056 Å (**3**) and 0.038 Å (**4**)) but at an angle of 39° (**3**) and 38° (**4**) from the Ru_3 plane. The presence of the hydride atom causes a great tilt of the CO(6) group trans to it (26° with respect to the Ru_3 plane as opposed to the 0–14° range for the other equatorial CO groups); this arrangement of carbonyls leads to an octahedral coordination about Ru(2) and Ru(3) (if the Ru(2)—Ru(3) bond is not taken into account).

The acetylide is coordinated in a "perpendicular" fashion to all three metal atoms and is positioned across the Ru(2)—Ru(3) edge.

For complex **3** it is noteworthy that, in the solid state, two pairs of enantiomers (A/C and B/D) can be detected (see Scheme 5). These differ in orientation of the acetylide ligand with respect to the dppm unit (e.g.

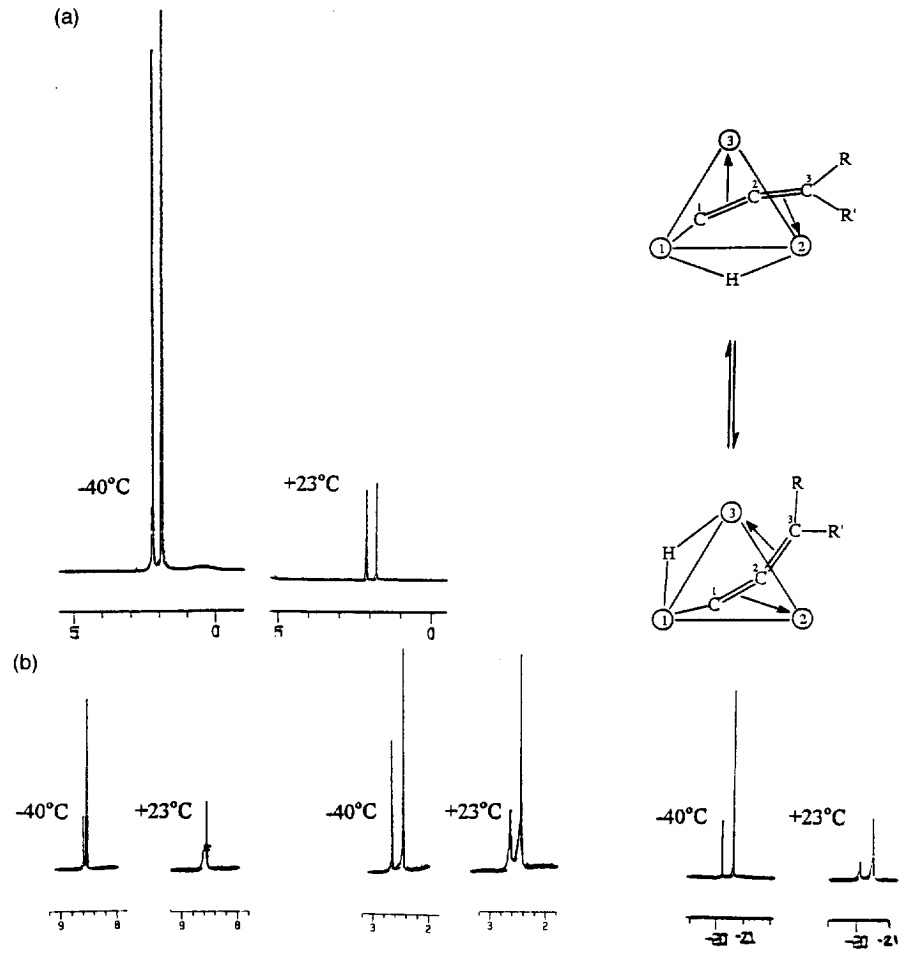

Fig. 2. (a) Variable temperature ^1H NMR spectra of $HRu_3(CO)_9(HC_2CMe_2)$ (**2b**) in CD_2Cl_2 solution; methyl region only; (b) Variable temperature ^1H NMR spectra of $HRu_3(CO)_9(HC_2CMe(Ph))$ (**2c**) in $CDCl_3$ solution; HC=C, methyl and hydride regions only.

pairs A/D and C/B) and in the chirality of C(10) (e.g. pairs A/B and C/D).

It appears that the phenyl group is always held away from the dppm ligand, presumably for steric reasons.

The complex $HRu_3(CO)_7(dppm)\{C_2Bu^t\}$ (**3a**) has been studied previously [35] using X-ray crystallography and has a structure similar to that of **3**. The main difference between **3** and **3a** stems from the fact that, whereas, complex **3a** exists as a mixture of two enantiomers due to the chirality induced on the metal frame by the dppm substitution, complex **3** contains, in addition, a chiral ligand giving rise to two pairs of enantiomers (four diastereoisomers).

Like complexes **3** and **4**, the t-butyl species **3a** has found to have the dppm bound in an equatorial manner to the cluster and so it seems likely that this is the arrangement most favoured for complexes of type **1**. This contrasts with the behaviour seen for dppe and other chelating ligands which may also give axial and/or chelated derivatives [36] but agrees well with the fact that these types of complexes have not previously been isolated from reaction of dppm with triruthenium acetylide derivatives [35,48].

Some important bonding parameters for the clusters **1a, 1k, 3, 3a, 4** and the chelate derivative $HRu_3(CO)_7(bpcd)\{C_2Bu^t\}$ (**3b**) (bpcd = 4,5-bis(diphenylphosphino)-4-cyclopenten-1,3-dione) [50], are presented in Table 6 below.

From the data listed in Table 6, one can see that the dppm substitution has no effect on the mean cluster dimensions; as expected, the Ru(1)—C(8) σ-bond is always significantly shorter than the other Ru-acetylide bonds. A close inspection of the data of Table 6 shows that the majority of the differences are within the e.s.d. values, thus rendering them insignificant. It seems, therefore, that the Ru_3C_2 core of the alkylidene clusters is "rigid" *vis-a-vis* substitution of dppm for CO; this agrees well with the ^{13}C NMR and σ-Taft data discussed earlier for these types of complexes.

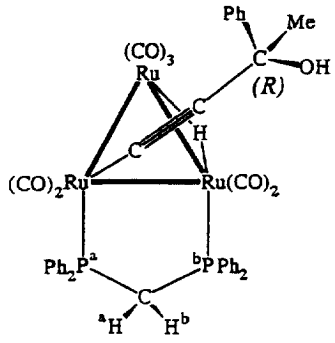

A

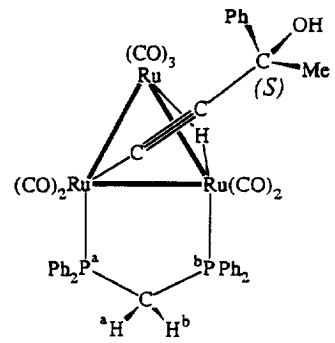

B

m ——— m

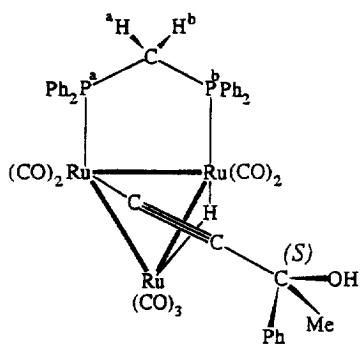

C

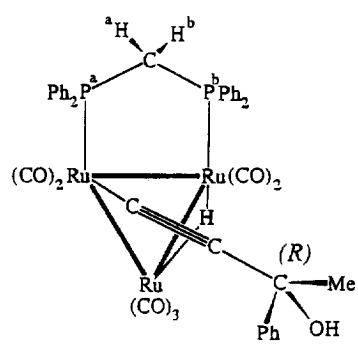

D

Scheme 3

Fluxionality of complexes **3** *and* **4**

Complex **3** can exist as a mixture of two enantiomers due to the chirality of the cluster induced by the dppm group. In addition, the presence of a chiral centre on the acetylide unit allows each of the enantiomers to exist as two diastereoisomers having either an *R*- or *S*-configuration of the ligand chiral centre. These two centres of chirality on the cluster give rise to two sets of signals on the NMR spectra, each set corresponding to one of the two enantiomeric pairs of isomers. Thus, in the low temperature limiting ^{1}H NMR spectrum of **3** signals are observed in the hydride region at δ −19.31 (d, μ-H) and −19.35 (d, μ-H′) and in the methylene region at δ 3.41 (q, CH^a) and 4.43 (q, CH^b) and δ 3.32 (q, Ch$^{a'}$) and 4.29 (q, CH$^{b'}$) (see Fig. 5). This is in contrast with the analogous complex $HRu_3(CO)_7(dppm)\{C_2Bu^t\}$ (**3a**) which possesses only one centre of chirality (that on the cluster) and shows only one set of resonances in the ^{1}H NMR spectrum (i.e. having a doublet for the hydride group and two quartets corresponding to the inequivalent protons of the methylene group). Similarly, in the ^{31}P NMR spectrum of **3**, recorded at 0°C, four AB type resonances (corresponding to P^a, P$^{a'}$, P^b and P$^{b'}$) are seen as opposed to the two AB type resonances that were observed for complex **3a** at this temperature.

Variable temperature NMR studies on complex **3a** have shown it to undergo a fluxional process at higher temperatures [35]. The same process is found to occur for complex **3** and is best described as "rotation of the propargyl alcohol moiety concurrent with hydride migration" and leads to equivalence of P^a and P^b and Ru_1 and Ru_2, and so loss of the dppm induced chirality of the cluster (see Scheme 6).

Thus, in the hydride region of the ^{1}H NMR, as the temperature is increased from −80°C, the two

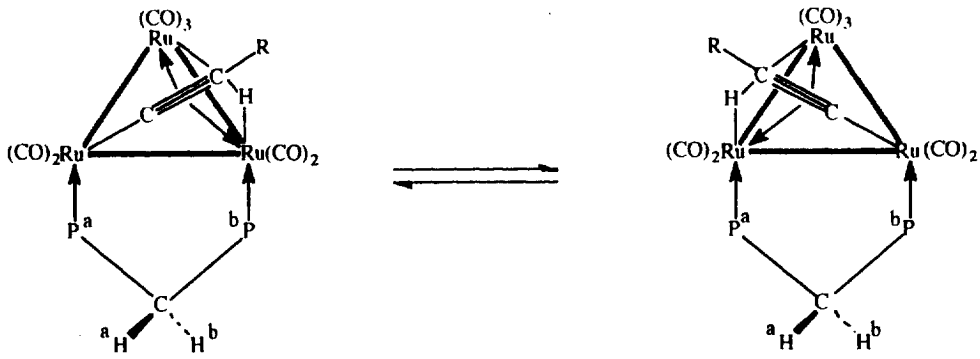

3 [R = C(Ph)(Me)OH]

3a [R = Bu^t]

4 [R = $C(=CH_2)Ph$]

Scheme 4

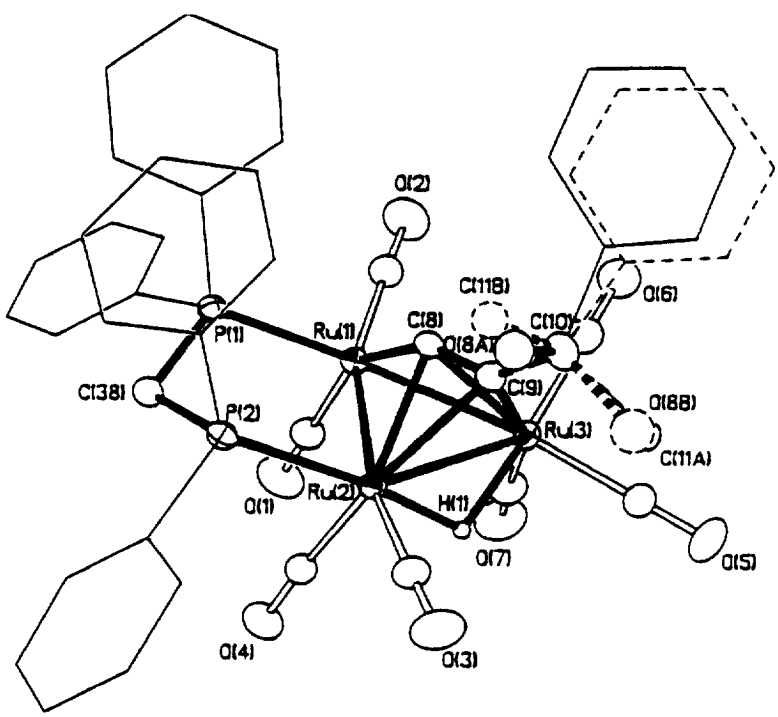

Fig. 3. Molecular structure of $HRu_3(CO)_7(dppm)(C_2CPh(OH)Me)$ (**3**) showing labelling scheme.

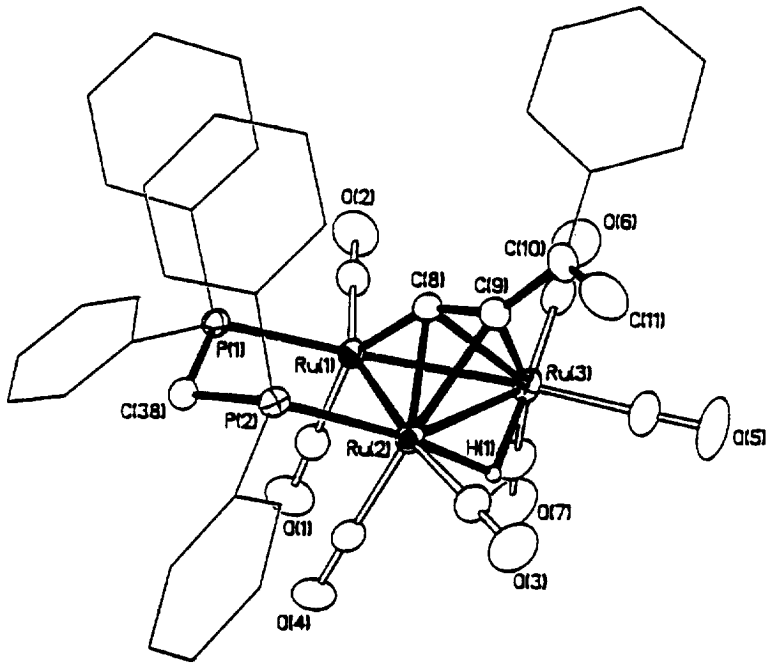

Fig. 4. Molecular structure of $HRu_3(CO)_7(dppm)(C_2C(=CH_2)Ph)$ (**4**) showing labelling scheme.

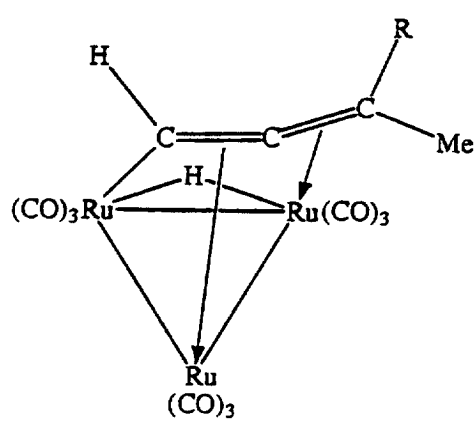

2b R = Me
2c R = Ph

Scheme 5

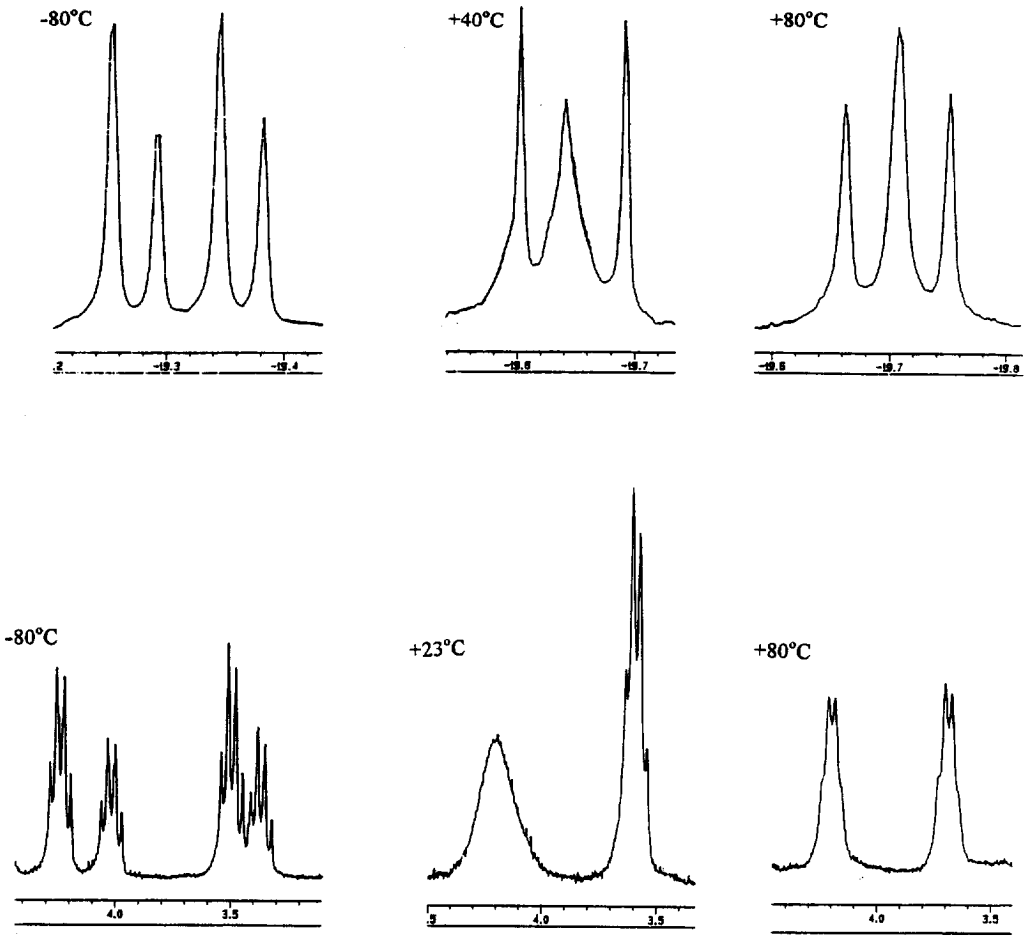

Fig. 5. Variable temperature ^1H NMR spectra of $HRu_3(CO)_7(dppm)(C_2CPh(OH)Me)$ (**3**) in d^8-toluene; methylene and hydride regions only.

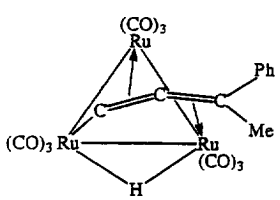

2c

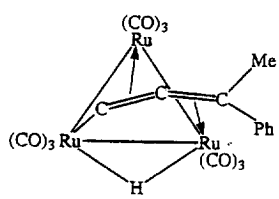

2c'

Scheme 6

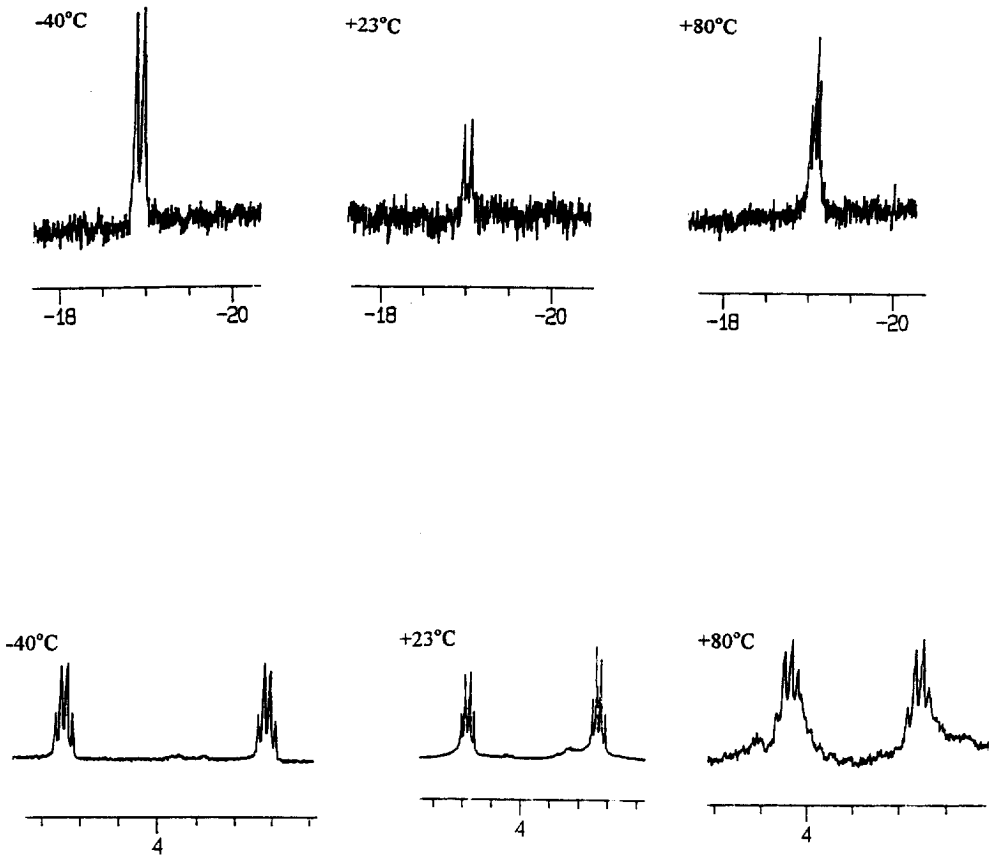

Fig. 6. Variable temperature ^{1}H NMR spectra of $HRu_3(CO)_7(dppm)(C_2C(=CH_2)Ph)$ (**4**) in d^8-toluene; methylene and hydride regions only.

doublets start to merge together as the chirality of the cluster is lost. At 40°C the remaining doublet has started to collapse into the baseline until at 80°C a triplet is observed corresponding to the A_2X system expected when rapid interconversion of the isomers is occurring on the NMR timescale.

Interestingly, for the methylene protons of the dppm ligand warming the solution leads to coalescence of the signals due to protons H^a and $H^{a'}$ and H^b and $H^{b'}$ until at 80°C two quartets are observed for the inequivalent protons H^a and H^b. That the fluxional process does not lead to equivalence of protons H^a and H^b confirms that the dppm ligand stays rigidly anchored to the Ru^1—Ru^2 edge throughout.

As expected, in the ^{31}P NMR spectrum the resonances start to coalesce and collapse into the baseline on warming until, at 58°C, the two phosphorous atoms appear as one broad hump centred at about 27 ppm suggesting that they are becoming chemically equivalent. Unfortunately, a higher temperature spectrum was not obtained.

The same fluxional process as described above for complexes **3** and **3a** is also found to occur for complex **4**. However, as complex **4** was obtained through dehydration of the propargyl alcohol unit of **3** the chirality of the acetylide ligand is lost and so the variable temperature NMR data mirror exactly those of complex **3a**. Thus, in the low temperature limiting ^{1}H NMR spectrum (−80°C) the hydride proton is observed as a doublet at δ −20.25 and the methylene protons H^a and H^b as quartets at δ 4.37 and 3.32 respectively (see Fig. 6).

On raising the temperature the doublet for the hydride tends to a triplet (A_2X system at 80°C) while the resonances for the methylene protons remain unchanged suggesting, once again, that the dppm ligand remains rigid throughout the fluxional process.

Comparable behaviour to that discussed above for complex **3** has been reported for the complex $(CpCo)_3$(1,1-diphenylethane) $[HC(Ph)_2CH_3]$ where one phenyl group is coordinated facially to the trico-

Table 5. Selected bond lengths [Å] and angles [°] for complex **3** and **4**

Complex	**3**	**4**
Ru(1)—C(8)	1.961(3)	1.949(3)
Ru(1)—P(1)	2.2855(10)	2.2925(8)
Ru(1)—Ru(2)	2.8016(7)	2.7994(5)
Ru(1)—Ru(3)	2.7854(6)	2.8023(4)
Ru(2)—C(8)	2.203(3)	2.200(3)
Ru(2)—C(9)	2.259(3)	2.239(3)
Ru(2)—P(2)	2.3422(10)	2.3261(8)
Ru(2)—Ru(3)	2.8083(6)	2.7936(5)
Ru(3)—C(8)	2.222(3)	2.214(3)
Ru(3)—C(9)	2.251(3)	2.271(3)
C(8)—C(9)	1.314(5)	1.315(4)
C(9)—C(10)	1.520(5)	1.464(4)
C(10)—O(8A)	1.427(7)	
C(10)—O(8B)	1.433(7)	
C(10)—C(39B)	1.522(7)	
C(10)—C(39A)	1.537(7)	
C(10)—C(11A)	1.582(8)	1.315(5)
C(10)—C(11B)	1.627(8)	
P(1)—C(38)	1.832(3)	1.838(3)
P(2)—C(38)	1.844(3)	1.836(3)
P(1)—Ru(1)—Ru(2)	95.72(3)	95.01(2)
Ru(3)—Ru(1)—Ru(2)	60.35(2)	59.828(12)
P(2)—Ru(2)—Ru(1)	90.23(3)	91.03(2)
Ru(1)—Ru(2)—Ru(3)	59.540(14)	60.138(9)
P(2)—Ru(2)—H(1)	166.0(14)	169.0(14)
Ru(1)—Ru(3)—Ru(2)	60.11(2)	60.034(11)
C(6)—Ru(3)—H(1)	175.5(14)	176.1(14)
C(9)—C(8)—Ru(1)	151.9(3)	153.2(2)
C(8)—C(9)—C(10)	146.3(3)	145.6(3)
O(8A)—C(10)—C(9)	113.5(4)	
O(8B)—C(10)—C(9)	113.7(4)	
O(8A)—C(10)—C(11A)	113.2(5)	
C(9)—C(10)—C(11A)	101.9(4)	
O(8B)—C(10)—C(11B)	111.5(5)	
C(9)—C(10)—C(11B)	106.3(4)	122.5(3)
C(38)—P(1)—Ru(1)	110.11(12)	110.48(9)
C(38)—P(2)—Ru(2)	111.06(11)	110.55(9)
P(1)—C(38)—P(2)	111.8(2)	112.2(2)

Table 6. Comparison of structural parameters of complexes $HRu_3(CO)_7(dppm)\{C_2CCH_3(OH)Ph\}$ (**3**) and $HRu_3(CO)_7(dppm)(C_2C{=}CH_2Ph)$ (**4**) with those of $HRu_3(CO)_7(dppm)(C_2Bu^t)$ (**3a**), of chelate $HRu_3(CO)_7(bpcd)(C_2Bu^t)$[a] (**3b**), of $HRu_3(CO)_9(C_2Bu^t)$ (**1a**) and of $HRu_3(CO)_9(C_2C{=}CH_2Ph)$ (**1k**)

Bond distances	(3)	(3a)	(3b)	(1a)	(4)	(1k)
Ru(1)—Ru(2)	2.8016(7)	2.783(4)	2.833(1)	2.795(3)	2.7994(5)	2.810(2)
Ru(1)—Ru(3)	2.7854(6)	2.781(3)	2.841(1)	2.799(3)	2.8023(4)	2.812(2)
Ru(2)—Ru(3)	2.8083(6)	2.787(5)	2.802(1)	2.792(3)	2.7936(5)	2.791(2)
Ru(1)—C(8)	1.961(3)	1.964(9)	1.949(9)	1.947(3)	1.949(3)	1.904(14)
Ru(2)—C(8)	2.203(3)	2.197(7)	2.232(9)	2.207(3)	2.200(3)	2.190(15)
Ru(3)—C(8)	2.222(3)	2.215(10)	2.220(9)	2.214(3)	2.214(3)	2.178(15)
Ru(2)—C(9)	2.259(3)	2.309(7)	2.27(1)	2.268(3)	2.239(3)	2.276(14)
Ru(3)—C(9)	2.251(3)	2.286(10)	2.26(1)	2.271(3)	2.271(3)	2.188(14)
C(8)—C(9)	1.314(5)	1.285(12)	1.34(1)	1.315(3)	1.315(4)	1.272(22)
Ru(1)—P(1)	2.286(1)	2.226(4)	2.274(3)	—	2.2925(8)	—
Ru(2)—P(2)	2.343(1)	2.303(4)	2.268(3)[b]	—	2.3261(8)	—
Ru(2)—H	1.74(4)	—	—	1.789(5)	1.73(4)	1.7
Ru(3)—H	1.77(4)	—	—	1.796(5)	1.72(4)	1.7
Ref.	this work	36	50	8b (neutron)	this work	13

For atomic numbering scheme see Figs 3 and 4.
[a] bcpd = 4,5-bis(diphenylphosphino)-4-cyclopenten-1,3-dione
[b] Ru(1)—P(2)

balt centre and the remaining —C(H)(Ph)CH_3 unit is chiral [51].

Acknowledgements—A Royal Society of Chemistry European Exchange Fellowship (to P.J.K.) is gratefully acknowledged.

REFERENCES

1. Castiglioni, G. L., Fumagalli, C. and Vaccari, A., *Chim. E. Ind. (Milan)*, 1996, **78,** 575 and references therein.
2. Tedeschi, R. J., *Acetylene-based Chemicals from Coal and other Natural Resources*, M. Dekker, New York, 1982.
3. (a) Sabourin, E. T. and Onopchenko, A., *J. Org. Chem.*, 1983, **48,** 5135; (b) Carpita, A., Lessi, A. and Rossi, R., *Synthesis*, 1984, 571.
4. Kim, T-J., Kwon, K-H., Kwon, S-C., Baeg, J-O., Shim, S-C. and Lee, D-H., *J. Organomet. Chem.*, 1990, **389,** 205.
5. Bruneau, C. and Dixneuf, P. H., *J. Chem. Soc., Chem. Commun.*, 1997, 507 and references therein.
6. Hartmann, W. and Singer, H., *J. Mol. Catal.*, 1988, **48,** 81.
7. Bradley, D. H., Khan, M. A. and Nicholas, K. M., *Organometallics*, 1989, **8,** 554.
8. The first complex with this structure obtained in high yields (ca 80%) was $HRu_3(CO)_9(C_2Bu^t)$, complex **1a**. (a) Synthesis: Sappa, E., Gambino, O., Milone, L. and Cetini, G., *J. Organomet. Chem.*, 1972, **39,** 169; (b) Structure: Catti, M., Gervasio, G. and Mason, S. A., *J. Chem. Soc., Dalton Trans.*, 1977, 2260. This complex is therefore used, in the present paper, for comparison with the propargyl alcohol derivatives.
9. Midland, R. M., *J. Org. Chem.*, 1975, **40,** 2250.
10. ^1H NMR (CH_2Cl_2): δ 7.75–7.22 mm (Ph); 3.01 s (H), 2.9 s (OH). On addition of THF the signal at 2.9 ppm is displaced at 4.50 s and shows some broadening. This allowed us to attribute the signal at 2.9 ppm to the OH and that at 3.01 ppm to the alkyne hydrogen. ^{13}C NMR: 74.3 s, 75.6 s, 86.5 s (C_β, alkyne), 125.9–131.1 (Ph), 164.8 (C_α, alkyne).
11. The ^1H and ^{13}C NMR data relevant for the discussion of the reactivity or fluxionality of several complexes are given in the results and discussion section or in Tables 2 and 4 and, therefore, are not listed in the experimental section.
12. Aime, S. and Deeming, A. J., *J. Chem. Soc., Dalton Trans.*, 1981, 828.
13. Ermer, S., Karpelus, R., Miura, S., Rosenberg, E., Tiripicchio, A. and Manotti Lanfredi, A. M., *J. Organomet. Chem.*, 1980, **187,** 81.
14. Complex **1c′**: IR (ν_{CO}): 2096 m, 2057 s, 2032 s, 2014 w, 1866 m, cm^{-1}. ^1H NMR: δ 8.51 s, 7.83–7.16 mm (Ph); 6.30 s; 1.57 s; −21.12 s (hydride). EI MS: $P^+ = 768$ *m/z* loss of 9 CO and doubly charged ions [see **1c**]. Tentatively identified as $H_2Ru_3(CO)_9[HC_2C(OH)Ph_2]$, $P^+ = 770$ *m/z*.
15. "Side reactions" occurring during the synthesis of complexes **1** often lead to metallacyclic complexes of the general formula $Ru_2(CO)_6(alkyne)_2$ formed through coupling of two alkynes (complexes A) or of one intact and one dehydrated propargyl

alcohol (complexes B). Other metallacyclic products include those of general formula $Ru_3(CO)_8(alkyne)_2$ (complexes C). Spectroscopic data for complexes of type A, B, or C obtained during the course of this work are given below.

Complex **Bg**: ^1H NMR: δ 11.4 s (H—C), 7.40 s (C—H), 3.05 qq (CH_2), 1.58 s (CH_3/OH), 1.26 m (CH_3/OH), 0.99 m (OH). EI-MS: $P^+ = 522$ *m/z* $[Ru_2(CO)_6X_2–H_2O]$.

Complex **Ag**: IR: 2079 ms, 2048 vs, 1997 s (b), cm^{-1}. ^1H NMR: δ 6.87 d ($J = 3.49$), 6.62 d ($J = 2.8$) (external Hs); 4.53 d ($J = 4.9$), 4.07 d (internal Hs); 1.93 s, 1.89 s (OH), 1.80 qq, 1.01 tt (Et). ^{13}C NMR: δ 32.8 d (CH_3, CH_2): 74.5 s, 79.6 s (C—OH); 98.4 s, 134.5 s, 141.7 s, 178.6 s (Cs of metallacycle); 194.9, 195.6, 196.4, 196.6, 198.7 {3 non equivalent and 3 equivalent COs}. EI-MS: $P^+ = 540$ *m/z*, loss of six CO $[Ru_2(CO)_6X_2$, isomers?].

Complex **Aj**: IR: 2083 s, 2053 vs, 2013 vs, 1996 s, 1987 m–s, cm^{-1}. ^1H NMR: δ 6.24 s (2H), 4.87 s, 4.71 s (CH_2), 1.90 s (CH_3). EI-MS: P^+ *m/z* = 504, loss of 6 CO, then complex fragmentation.

Complex **Cj**: IR: 2062 m–s, 2024 vs, 2000 ms, 1976 m–s, 1881 m, cm^{-1}. ^1H NMR: δ 8.87 s, 7.01 s, 5.48 s, 5.21 m, 3.40 s, 2.45 s, 2.02 s (CH_3). EI-MS: P^+ *m.z* = 664, loss of 8 CO and correspondingly doubly charged ions.

16. Aime, S., Deeming, A. J., Hursthouse, M. B. and Baker-Dirks, J. D. J., *J. Chem. Soc., Dalton Trans.*, 1982, 1625.
17. A chloroform solution of **1d** was deposited on a dry TLC plate at room temperature and then heated at 100°C for 15 min, after which time a mixture of parent **1d** and of the dehydration product $HRu_3(CO)_9\{C_2C(=CH_2)Ph\}$ in a ratio of ca 60 : 1 was obtained. Chromatography of complex **1j** on wet TLC plates, resulted in unaltered **1j**. Complex **1j** was dissolved in hexane and a slurry of silica and D_2O added; the suspension was heated at 55°C for 1 h, after which time only starting **1j** was recovered. To a chloroform solution of **1j** four drops of H_2SO_4 was added, then water; after 30 min, small amounts of the hydration product **1b** were obtained.
18. Throughout the NMR data the "superscript" refers to the two possible (*R* and *S*) configurations of the chiral propargyl alcohol ligand, see results and discussion section.
19. Bruce, M. I., Hambley, T. W., Nicholson, B. K. and Snow, M. R., *J. Organomet. Chem.*, 1982, **235,** 83.
20. North, A. C. T., Phillips, D. C., Mathews, F. S., *Acta Crystallogr.*, 1968, **A24,** 351.
21. Aime, S., Milone, L. and Deeming, A. J., *J. Chem. Soc., Chem. Commun.*, 1980, 1168.
22. Aime, S., Tiripicchio, A., Tiripicchio Camellini, M. and Deeming, A. J., *Inorg. Chem.*, 1981, **20,** 2027.
23. (a) Allenyl derivatives: Gervasio, G., Osella, D. and Valle, M., *Inorg. Chem.*, 1976, **15,** 1221; (b) Allyl derivatives: Evans, M., Hursthouse, M., Randall, E. W., Rosenberg, E., Milone, L. and Valle, M., *J. Chem. Soc., Chem. Commun.*, 1972, 545.
24. Rosenberg, D. and Drenth, W., *Tetrahedron*, 1971, **27,** 3893.
25. Sappa, E., *J. Cluster, Sci.*, 1994, **5,** 211 and references therein.
26. Sappa, E., *J. Organomet. Chem.*, 1978, **323,** 83.
27. Carty, A. J., Cherkas, A. A. and Randall, L. M., *Polyhedron*, 1988, **7,** 1045.
28. Aime, S., Gambino, O., Milone, L., Sappa, E. and Rosenberg, E., *Inorg. Chim. Acta*, 1975, **15,** 53.
29. Brice, R. A., Pearson, S. C., Salter, I. D. and Henrick, K., *J. Chem. Soc., Dalton Trans.*, 1986, 2181.
30. Adatia, T., McPartlin, M. and Salter, I. D., *J. Chem. Soc., Chem. Commun.*, 1988, 2889.
31. Braunstein, P., Predieri, G., Tiripicchio, A. and Sappa, E., *Inorg. Chim. Acta*, 1982, **63,** 113.
32. Carty, A. J., MacLaughlin, S. A., Taylor, N. J. and Sappa, E., *Inorg. Chem.*, 1981, **20,** 4437.
33. Farrugia, L. J. and Rae, S. E., *Organometallics*, 1992, **11,** 196.
34. Sappa, E., Pasquinelli, G., Tiripicchio, A. and Tiripicchio Camellini, M., *J. Chem. Soc., Dalton Trans.*, 1989, 601.
35. Predieri, G., Tiripicchio, A., Vignali, C. and Sappa, E., *J. Organomet. Chem.*, 1988, **342,** C33.
36. Sappa, E., Predieri, G., Tiripicchio, A. and Vignali, C., *J. Organomet. Chem.*, 1989, **378,** 109.
37. Sappa, E., Predieri, G., Tiripicchio, A. and Ugozzoli, F., *Gazz. Chim. Ital.*, 1995, **125,** 51.
38. Gervasio, G. and Sappa, E., *Organometallics*, 1993, **12,** 1458.
39. Peng, J-J., Horng, K-M., Cheng, P-S., Chi, Y., Peng, S-M. and Lee, G-H., *Organometallics*, 1994, **13,** 2365.
40. Tanabe, K., Misono, M., Ono, Y. and Hattori, H., In "*New Solid Acids and Bases*", *Studies in Surface Science and Catalysis*, Vol. 51, ed. B. Delmon and J. T. Yates, Elsevier, Tokyo, 1989.
41. Deabate, S., King, P. J. and Sappa, E., manuscript in preparation.
42. Gervasio, G. and Sappa, E., *J. Organomet. Chem.*, 1995, **498,** 73.
43. Gervasio, G., Marabello, D. and Sappa, E., *J. Chem. Soc., Dalton Trans.*, 1997, 1851.
44. (a) Froom, S. F. T., Green, M., Mercer, R. J., Nagle, K. R., Orpen, A. G. and Schwiegk, S., *J. Chem. Soc., Chem. Commun.*, 1986, 1666; (b) Froom, S. F. T., Green, M., Mercer, R. J., Nagle, K. R., Orpen, A. G. and Rodrigues, R. A., *J. Chem. Soc., Dalton Trans.*, 1991, 3171.
45. Rosenberg, E., Aime, S., Milone, L., Sappa, E., Tiripicchio, A. and Manolti Lanfredi, A. M., *J. Chem. Soc., Dalton Trans.*, 1981, 2023.
46. Aime, S., Dastru, W., Gobetto, R., Milone, L. and Viale, A., *J. Chem. Soc., Chem. Commun.*, 1997, 361 and references therein.
47. Aime, S., Gobetto, R., Osella, D., Milone, L. and Rosenberg, E., *Organometallics*, 1982, **1,** 640.
48. Rivomanana, S., Mongin, C. and Lavigne, G., *Organometallics*, 1996, **15,** 1195.
49. (a) Clucas, J. A., Dolby, P. A., Harding, M. M. and Smith, A. K., *J. Chem. Soc., Chem. Commun.*, 1987, 1829; (b) Harding, R. A. and Smith, A. K., *J. Chem. Soc., Dalton Trans.*, 1996, 117.
50. Shen, H., Williams, T. J., Bott, S. G. and Richmond, M. G., *J. Organomet. Chem.*, 1995, **505,** 1.
51. Wadepohl, H., *Angew. Chem. Int. Ed. Engl.*, 1992, **31,** 247.

Pergamon

PII: S0277-5387(98)00068-0

Polyhedron Vol. 17, No. 17, pp. 2957–2970, 1998
© 1998 Elsevier Science Ltd
All rights reserved. Printed in Great Britain
0277-5387/98 $19.00+0.00

Heterometallic octahedral boride cluster chemistry: reactions of $[Rh_2Ru_4(CO)_{16}B]^-$ with PPh_3 and $P(OMe)_3$, and the crystal structures of $[Rh_2Ru_4(CO)_{16}B(AuPPh_3)]$ and $[Rh_2Ru_4(CO)_{14}(PPh_3)_2B(AuPPh_3)]$

Andrew D. Hattersley,[a] Catherine E. Housecroft,*[b] Louise M. Liable-Sands,[c] Arnold L. Rheingold*[c] and Anne Waller[a]

[a] Department of Chemistry, University of Cambridge, Lensfield Road, Cambridge CB2 1EW, U.K.

[b] Institut für Anorganische Chemie, Spitalstrasse 51, CH-4056 Basel, Switzerland

[c] Department of Chemistry, University of Delaware, Newark, DE 19716, U.S.A.

(Received 8 November 1997: accepted 11 February 1998)

Abstract—The reaction between $[(PPh_3)_2N][Rh_2Ru_4(CO)_{16}B]$ and five-fold excess of PPh_3, followed by addition of Ph_3PAuCl leads to the formation of $[Rh_2Ru_4(CO)_{15}(PPh_3)B(AuPPh_3)]$ and $[Rh_2Ru_4(CO)_{14}(PPh_3)_2B(AuPPh_3)]$. Phosphorus-31 NMR spectroscopic data were in accord with substitution at the Rh centres; and X-ray diffraction study of $[Rh_2Ru_4(CO)_{14}(PPh_3)_2B(AuPPh_3)]$ showed that the Rh atoms occupied *cis*-sites in the octahedral Rh_2Ru_4-cage. The reaction between $[(PPh_3)_2N][Rh_2Ru_4(CO)_{16}B]$ and a five-fold excess of PPh_3, followed by addition of CF_3CO_2H yielded $[HRh_2Ru_4(CO)_{15}(PPh_3)B]$, $[HRh_2Ru_4(CO)_{14}(PPh_3)_2B]$ and $[HRh_2Ru_4(CO)_{13}(PPh_3)_3B]$, their formations being dependent on reaction conditions. Treatment of $[(PPh_3)_2N][Rh_2Ru_4(CO)_{16}B]$ and $P(OMe)_3$ (1 : 1) followed by Ph_3PAuCl leads to the formation of $[Rh_2Ru_4(CO)_{16}B(AuPPh_3)]$ (for which an X-ray structural determination has been carried out), $[Rh_2Ru_4(CO)_{15}\{P(OMe)_3\}B(AuPPh_3)]$ and $[Rh_2Ru_4(CO)_{14}\{P(OMe)_3\}_2B(AuPPh_3)]$. By altering the cluster : phosphite ratio to 1 : 3, the major product was $[Rh_2Ru_4(CO)_{13}\{P(OMe)_3\}_3B(AuPPh)_3)]$. The addition of CF_2CO_2H in place of Ph_3PAuCl to the crude products of the reaction between $[(PPh_3)_2N][Rh_2Ru_4(CO)_{16}B]$ and $P(OMe)_3$ promoted cleavage of the P—O bond and results in the formation of $[Rh_2Ru_4(CO)_{14}\{P(OMe)_3\}\{\mu\text{-}P(OMe)_2\}B]$ and $[Rh_2Ru_4(CO)_{13}\{P(OMe)_3\}_2\{\mu\text{-}P(OMe)_2\}B]$. Products have been characterized by IR and multi-nuclear NMR spectroscopies and mass spectrometry, and evidence for *cis-trans* isomerization of the Rh_2Ru_4-framework is presented. © 1998 Elsevier Science Ltd. All rights reserved

Keywords: Boride; cluster.

We have recently reported the results of a study of the reactions of the homometallic boride cluster anion $[Ru_6(CO)_{17}B]^-$ with PPh_3 and $P(OMe)_3$ and the subsequent reactions of the phosphine or phosphite substituted products with sources of Ph_3PAu^+ or H^+ [1]. In the present paper, we describe a complementary study which focuses on the reactivity of the heterometallic cluster $[Rh_2Ru_4(CO)_{16}B]^-$. The metal cluster core of this anion exhibits two isomers in which the Rh atoms are either adjacent (*cis* isomer) or apart (*trans* isomer), the latter being the preferred species [2]. We were interested in investigating how replacement of CO for phosphine or phosphite ligands might influence this *cis-trans* isomer distribution, and how the reactivity behaviour of $[Rh_2Ru_4(CO)_{16}B]^-$ differed from that of $[Ru_6(CO)_{17}B]^-$; for example, we were unable to introduce more than one PPh_3 group into $[Ru_6(CO)_{17}B]^-$, and, whereas $[Ru_6(CO)_{16}(PPh_3)B]^-$ protonated on an Ru—Ru edge, treatment of $[Ru_6(CO)_{16}\{P(OMe)_3\}B]^-$ with acid resulted in the cleavage

* Author to whom correspondence should be addressed.

of one methoxy group and the formation of $[Ru_6(CO)_{16}\{\mu\text{-}P(OMe)_2\}B]$ [1].

EXPERIMENTAL

General data

Fourier-transform NMR spectra were recorded on a Bruker WM 250 spectrometer; ^1H shifts are reported with respect of δ 0 for Me_4Si, ^{11}B NMR with respect to δ 0 for $F_3B \cdot OEt_2$, and ^{31}P NMR with respect to δ 0 for 85% H_3PO_4; downfield chemical shifts are positive. Solution infrared spectra were recorded on a Perkin-Elmer FT 1710 spectrophotometer, and fast ion bombardment (FIB) and fast atom bombardment (FAB) mass spectra using Kratos instruments (3-NBA matrix = 3-nitrobenzyl alcohol). The isotopic patterns of the parent peaks reported were consistent with simulated isotope distributions.

Reactions were carried out under argon using standard Schlenk techniques. Solvents were pre-dried and distilled under N_2. Separation involved thin layer plate chromatography using Kieselgel 60-PF-254 (Merck). PPh_3 and $P(OMe)_3$ were used as received (Aldrich); $[Ph_3PAuCl]$ [3], and $[(Ph_3P)_2N][Rh_2Ru_4(CO)_{16}B]$ [2] were prepared according to literature procedures. Typical yields (with respect to starting cluster) from a series of reactions are given; yields tend to be variable.

Preparations of $[Rh_2Ru_4(CO)_{15}(PPh_3)B(AuPPh_3)]$ *and* $[Rh_2Ru_4(CO)_{14}(PPh_3)_2B(AuPPh_3)]$

In a typical reaction, $[(Ph_3P)_2N][Rh_2Ru_4(CO)_{16}B]$ (10 mg, 6.2 μmol) was dissolved in CH_2Cl_2 (3 ml) and to this solution was added PPh_3 (8.2 mg, 31 mmol). The solution was stirred at room temperature for 17 h, after which time $[Ph_3PAuCl]$ (an excess, ≈ 10 μmol) was added. The solution was stirred for 30 min, and then solvent was removed *in vacuo*. The products were separated by TLC (hexane: CH_2Cl_2 4:5); two green fractions were eluted, but the lower one converted quantitatively to another green fraction during elution. The first fraction (50%) was identified as $[Rh_2Ru_4(CO)_{15}(PPh_3)B(AuPPh_3)]$; the second (final $r_f \approx 0.7$, 45%) was $[Rh_2Ru_4(CO)_{14}(PPh_3)_2B(AuPPh_3)]$.

$[Rh_2Ru_4(CO)_{15}(PPh_3)B(AuPPh_3)]$. ^1H NMR (CD_2Cl_2, 298 K): δ 7.3–7.6 (m, Ph); ^{11}B NMR (CD_2Cl_2, 298 K); δ 199.1; $^{31}P\{^1H\}$ NMR (CD_2Cl_2): δ 70.9 (1P, s), 32.5 (1P, d, J_{RhP} 195 Hz); IR (CH_2Cl_2) ν(CO) 2071 w, 2038 vs, 2022 m sh, 1990 w, 1873 w, 1847 w cm^{-1}. MS (positive FAB): $^{12}C_{51}{}^1H_{30}{}^{197}Au{}^{11}B{}^{16}O_{15}{}^{31}P_2{}^{103}Rh_2{}^{101}Ru_4$ 1762 (P^+).

$[Rh_2Ru_4(CO)_{14}(PPh_3)_2B(AuPPh_3)]$. ^1H NMR (CD_2Cl_2, 298 K): δ 7.3–7.7 (m, Ph); ^{11}B NMR (CD_2Cl_2, 298 K): δ 188.5; $^{31}P\{^1H\}$ NMR (CD_2Cl_2): δ 65.9 (1P, s), 38.5 (2P, d, J_{RhP} 142 Hz); IR (CH_2Cl_2) ν(CO) 2055 w, 2034 vs, 1998 vs, 1942 w, 1832 w cm^{-1}. MS (positive FAB): $^{12}C_{68}{}^1H_{45}{}^{197}Au{}^{11}B{}^{16}O_{14}{}^{31}P_3{}^{103}Rh_2{}^{101}Ru_4$ 1996 (P^+).

Preparations of $[HRh_2Ru_4(CO)_{14}(PPh_3)_2B]$ *and* $[HRh_2Ru_4(CO)_{13}(PPh_3)_3B]$

In a typical reaction, $[(Ph_3P)_2N][Rh_2Ru_4(CO)_{16}B]$ (129 mg, 0.08 mmol) was dissolved in CH_2Cl_2 (10 ml) and to this solution was added solid PPh_3 (105 mg, 0.40 mmol). The solution was stirred at room temperature for 17 h, after which time the strongest absorption in the IR spectrum had shifted to 2009 cm^{-1}. CF_3CO_2H (10 μl) was added to the stirring solution and after 15 min, the strongest absorption in the IR spectrum had shifted to 2029 cm^{-1}. Solvent was removed *in vacuo*, and the products separated by TLC (hexane: CH_2Cl_2 2:1). The first fraction (orange, 25%) was identified as $[HRh_2Ru_4(CO)_{14}(PPh_3)_2B]$ and the second (orange-brown, 60%) as $[HRh_2Ru_4(CO)_{13}(PPh_3)_3B]$. A third fraction (red) was isolated in low yield and could not be sufficiently characterized.

$[HRh_2Ru_4(CO)_{14}(PPh_3)_2B]$. ^1H NMR ($CDCl_3$, 298 K): δ 7.3–7.7 (m, Ph), −14.9 (s, Ru—H—Ru); ^{11}B NMR ($CDCl_3$, 298 K): δ 186.5; $^{31}P\{^1H\}$ NMR ($CDCl_3$): δ 36.6 (d, J_{RhP} 150 Hz); IR (CH_2Cl_2) ν(CO) 2068 m, 2042 vs, 2022 s, 1992 m, 1845 w cm^{-1}. MS (positive FAB): $^{12}C_{50}{}^1H_{31}{}^{11}B{}^{16}O_{14}{}^{31}P_2{}^{103}Rh_2{}^{101}Ru_4$ 1538 (P^+) with 12 CO losses.

$[HRh_2Ru_4(CO)_{13}(PPh_3)_3B]$. IR ($CH_2Cl_2$) ν(CO) 2054 m, 2029 vs, 2009 s, 1958 m, 1833 w cm^{-1}. MS (positive FAB): 1774 (P^+) with 3 to 6 CO losses. The NMR spectroscopic data showed the presence of two isomers (see text):

Isomer **I**. ^1H NMR ($CDCl_3$, 298 K): δ 7.3–7.7 (m, Ph), −14.2 (d, J_{PH} 20 Hz, Ru—H—Ru); ^{11}B NMR ($CDCl_3$, 298 K): δ 188.6; $^{31}P\{^1H\}$ NMR ($CDCl_3$): δ 38.4 (1P, s), 33.9 (2P, d, J_{RhP} 154 Hz).

Isomer **II**. ^1H NMR ($CDCl_3$, 298 K): δ 7.3–7.7 (m, Ph), −15.3 (br, Ru—H—Ru); ^{11}B NMR ($CDCl_3$, 298 K): δ 194.5; $^{31}P\{^1H\}$ NMR ($CDCl_3$): δ 37.5 (1P, s), 36.8 (2P, d, J_{RhP} 153 Hz).

Preparation of $[HRh_2Ru_4(CO)_{15}(PPh_3)B]$

$[(Ph_3P)_2N][Rh_2Ru_4(CO)_{16}B]$ (48 mg, 0.03 mmol) was dissolved in CH_2Cl_2 (5 ml) and to this solution was added PPh_3 (8 mg, 0.03 mmol). The solution was stirred at room temperature and was monitored by IR spectroscopy; after 15 min the strongest absorption in the spectrum had shifted to 2010 cm^{-1}. CF_3CO_2H (5 μl) was added to the stirring solution and after 5 min, the IR spectrum exhibited the strongest carbonyl absorption at 2050 cm^{-1}. Solvent was removed *in vacuo*, and the products separated by TLC (hexane: CH_2Cl_2 2:1). Two fractions were eluted, the first (orange-brown, 50%) was $[HRh_2Ru_4(CO)_{15}(PPh_3)B]$ and the second $[HRh_2Ru_4(CO)_{14}(PPh_3)_2B]$ (30%).

$[HRh_2Ru_4(CO)_{15}(PPh_3)B]$. IR ($CH_2Cl_2$) ν(CO) 2087 m, 2050 vs, 1995 m, 1852 w cm^{-1}. MS (positive

FIB): $^{12}C_{33}{}^{1}H_{16}{}^{11}B^{16}O_{15}{}^{31}P^{103}Rh_2{}^{101}Ru_4$ 1301 (P^+) with 10 CO losses. The NMR spectroscopic data showed the presence of two isomers (see text).

Isomer **I**. ^{1}H NMR ($CDCl_3$, 298 K): δ 7.4–7.7 (m, Ph), −15.6 (td, J_{RhH} 13, J_{PH} 4Hz, Rh—H—Rh); ^{11}B NMR ($CDCl_3$, 298 K): δ 192.7 (triplet, J_{RhB} 30 Hz); $^{31}P\{^1H\}$ NMR ($CDCl_3$): δ 28.9 (dd, $^1J_{RhP}$ 148 Hz, $^2J_{RhP}$ 31 Hz).

Isomer **II**. ^{1}H NMR ($CDCl_3$, 298 K): δ 7.4–7.7 (m, Ph), −14.9 (s, Ru—H—Ru); ^{11}B NMR ($CDCl_3$, 298 K): δ 187.7; $^{31}P\{^1H\}$ NMR ($CDCl_3$): δ 36.7 (dd, $^1J_{RhP}$ 176 Hz, $^2J_{RhP}$ 31 Hz).

Preparations of $[Rh_2Ru_4(CO)_{16}B(AuPPh_3)]$, *cis- and trans-*$[Rh_2Ru_4(CO)_{15}\{P(OMe)_3\}B(AuPPh_3)]$ *and* $[Rh_2Ru_4(CO)_{14}\{P(OMe)_3\}_2B(AuPPh_3)]$

In a typical reaction, $[(Ph_3P)_2N][Rh_2Ru_4(CO)_{16}B]$ (48 mg, 0.03 mmol) was dissolved in CH_2Cl_2 (5 ml) and to this solution was added $P(OMe)_3$ (3.5 mmol, 0.03 mmol). The solution was stirred at room temperature for 15 min, the time taken for the strongest absorption in the IR spectrum to shift to 2009 cm^{-1}. Solid $[Ph_3PAuCl]$ (30 mg, 0.06 mmol) and $TlPF_6$ (4 mg, 0.01 mmol) were then added, and the solution stirred for 30 min; solvent was then removed *in vacuo*. Separation by TLC (hexane:CH_2Cl_2 1:1) gave four fractions; the first (green, 30%) was identified as $[Rh_2Ru_4(CO)_{16}B(AuPPh_3)]$ [2], the second (brown, 20%) was *cis*-$[Rh_2Ru_4(CO)_{15}\{P(OMe)_3\}B(AuPPh_3)]$, the third (green, 20%) was *trans*-$[Rh_2Ru_4(CO)_{15}\{P(OMe)_3\}B(AuPPh_3)]$, and the final band (brown, 20%) *cis*-$[Rh_2Ru_4(CO)_{14}\{P(OMe)_3\}_2B(AuPPh_3)]$. This latter compound was unstable with respect to (relatively slow) conversion into the green *trans*-isomer (see text).

cis-$[Rh_2Ru_4(CO)_{15}\{P(OMe)_3\}B(AuPPh_3)]$. This was unstable with respect to conversion to *trans*-$[Rh_2Ru_4(CO)_{15}\{P(OMe)_3\}B(AuPPh_3)]$, and could only be partially characterized: IR (CH_2Cl_2) ν(CO) 2070 m, 2032 vs, 1989 m, 1856 w cm^{-1}.

trans-$[Rh_2Ru_4(CO)_{15}\{P(OMe)_3\}B(AuPPh_3)]$. Two inseparable isomers: IR (CH_2Cl_2) ν(CO) 2056 m, 2038 vs, 1988 m, 1850 w cm^{-1}. MS (positive FAB): $^{12}C_{36}{}^{1}H_{24}{}^{197}Au^{11}B^{16}O_{18}{}^{31}P_2{}^{103}Rh_2{}^{101}Ru_4$ 1624 (P^+) with 13 CO losses.

Isomer **I**. ^{1}H NMR ($CDCl_3$ 298 K): δ 7.3–7.7 (m, Ph), 3.6 (d, J_{PH} 11 Hz); ^{11}B NMR ($CDCl_3$, 298 K): δ 200.6; $^{31}P\{^1H\}$ NMR ($CDCl_3$): δ 70.6 (1P, s), 133.9 (1P, s).

Isomer **II**. ^{1}H NMR ($CDCl_3$, 298 K): δ 7.3–7.7 (m, Ph), 3.7 (d, J_{PH} 11 Hz); ^{11}B NMR ($CDCl_3$, 298 K): δ 195.8; $^{31}P\{^1H\}$ NMR ($CDCl_3$): δ 67.5 (1P, s), 134.5 (1P, s).

cis-$[Rh_2Ru_4(CO)_{14}\{P(OMe_3\}_2B(AuPPh_3)]$. Two inseparable isomers: IR (CH_2Cl_2) ν(CO) 2058 m, 2021 vs, 2016 vs, 1839 m cm^{-1}.

Isomer **I**. ^{1}H NMR ($CDCl_3$, 298 K): δ 7.4–7.7 (m, Ph), 3.6 (d, J_{PH} 12 Hz); ^{11}B NMR ($CDCl_3$, 298 K): δ 187.0; $^{31}P\{^1H\}$ NMR ($CDCl_3$): δ 68.0 (s), 129.1 (d, J_{RhP} 227 Hz).

Isomer **II**. ^{1}H NMR ($CDCl_3$, 298 K): δ 7.4–7.7 (m, Ph), 3.8 (d, J_{PH} 12 Hz); ^{11}B NMR ($CDCl_3$, 298 K): δ 194.6; $^{31}P\{^1H\}$ NMR ($CDCl_3$): δ 68.0 (s), 134.5 (s).

trans-$[Rh_2Ru_4(CO)_{14}\{P(OMe)_3\}_2B(AuPPh_3)]$. ^{1}H NMR ($CDCl_3$, 298 K): δ 7.4–7.7 (m, Ph, 15H), 3.5 (d, J_{PH} 13 Hz, 18H); ^{11}B NMR ($CDCl_3$, 298 K): δ 201.6; $^{31}P\{^1H\}$ NMR ($CDCl_3$): δ 70.8 (s, 1P), 129.8 (s, 2P); IR (CH_2Cl_2) ν(CO) 2057 s, 2024 vs, 2002 vs, 1859 w, 1836 w cm^{-1}; MS (positive FAB): $^{12}C_{38}{}^{1}H_{33}{}^{197}Au^{11}B^{16}O_{20}{}^{31}P_3{}^{103}Rh_2{}^{101}Ru_4$ 1720 (P^+) with 11 CO losses.

Preparation of $[Rh_2Ru_4(CO)_{13}\{P(OMe)_3\}_3B(AuPPh_3)]$.

$[(Ph_3P)_2N][Rh_2Ru_4(CO)_{16}B]$ (80 mg, 0.05 mmol) was dissolved in CH_2Cl_2 (5 ml) and to this solution was added $P(OMe)_3$ (16 mmol, 0.15 mmol). The solution was stirred at room temperature for 10 min, after which time the strongest absorption in the IR spectrum had shifted to 1987 cm^{-1}. Solid $[Ph_3PAuCl]$ (49 mg, 0.10 mmol) and $TlPF_6$ (4 mg, 0.01 mmol) were added, and the solution stirred for 30 min; solvent was then removed *in vacuo*. Separation by TLC (hexane:CH_2Cl_2 2:1) gave four fractions; the two bands (brown) with lowest r_f values were not sufficiently well characterized for identification. The first fraction (brown, 20%) was identified as *cis*-$[Rh_2Ru_4(CO)_{13}\{P(OMe)_3\}_3B(AuPPh_3)]$ and the second (green, 30%) as *trans*-$[Rh_2Ru_4(CO)_{13}\{P(OMe)_3\}_3B(AuPPh_3)]$.

cis-$[Rh_2Ru_4(CO)_{13}\{P(OMe)\}_3B(AuPPh_3)]$. ^{1}H NMR ($CDCl_3$, 298 K): δ 7.4–7.7 (m, Ph, 15H), 3.6 (d, J_{PH} 12 Hz, 18H), 3.7 (d, J_{PH} 12 Hz, 9H); ^{11}B NMR ($CDCl_3$, 298 K): δ 188.7; $^{31}P\{^1H\}$ NMR ($CDCl_3$): δ 66.9 (s, 1P), 132.6 (d, J_{RhP} 236 Hz, 2P), 135.4 (s, 1P); IR (CH_2Cl_2) ν(CO) 2059 m, 2042 m, 1997 vs cm^{-1}; MS (positive FAB): $^{12}C_{40}{}^{1}H_{42}{}^{197}Au^{11}B^{16}O_{22}{}^{31}P_4{}^{103}Rh_2{}^{101}Ru_4$ 1816 (P^+) with 3 to 8 CO losses.

trans-$[Rh_2Ru_4(CO)_{13}\{P(OMe)_3\}_3B(AuPPh_3)]$. ^{1}H NMR ($CDCl_3$, 298 K): δ 7.4–7.7 (m, Ph, 15H), 3.4–3.8 (m, 27H); ^{11}B NMR ($CDCl_3$, 298 K): δ 203.2; $^{31}P\{^1H\}$ NMR ($CDCl_3$): δ 70.8 (s, 1P), 130.8 (s, 1P), 131.5 (s, 1P), 133.9 (d, J_{RhP} 324 Hz, 1P); IR (CH_2Cl_2) ν(CO) 2058 m, 2044 m, 1994 vs, 1846 w, 1821 w cm^{-1}; MS (positive FAB): $^{12}C_{40}{}^{1}H_{42}{}^{197}Au^{11}B^{16}O_{22}{}^{31}P_4{}^{103}Rh_2{}^{101}Ru_4$ 1816 (P^+) with 9 CO losses.

Preparations of $[Rh_2Ru_4(CO)_{14}\{P(OMe)_3\}\{\mu\text{-}P(OMe)_2B]$ *and* $[Rh_2Ru_4(CO)_{13}\{P(OMe)_3\}_2\{\mu\text{-}P(OMe)_2\}B]$

In a typical reaction, $[(Ph_3P)_2N][Rh_2Ru_4(CO)_{16}B]$ (56 mg, 0.035 mmol) was dissolved in CH_2Cl_2 (5 ml) and to this solution was added $P(OMe)_3$ (8 μl, 0.07 mmol). The solution was stirred at room temperature for 10 min, the time taken for the strongest absorption

in the IR spectrum to shift to 1998 cm^{-1}. CF_3CO_2H (5 μl) was added to the stirring solution and after 5 min, the strongest absorption in the IR spectrum had shifted to 2034 cm^{-1}. Solvent was removed *in vacuo*, and the products separated by TLC (hexane : CH_2Cl_2 1 : 1). Three fractions were eluted, leaving a brown residue on the baseline, identified as unreacted $[(Ph_3P)_2N][Rh_2Ru_4(CO)_{16}B]$. The first and third fractions were $[Rh_2Ru_4(CO)_{14}\{P(OMe)_3\}\{\mu\text{-}P(OMe)_2\}B]$ (orange-brown, 40%) and $[Rh_2Ru_4(CO)_{13}\{P(OMe)_3\}_2\{\mu\text{-}P(OMe)_2\}B]$ (orange, 10%). The second fraction, present in low yield, eluded full characterization.

$[Rh_2Ru_4(CO)_{14}\{P(OMe)_3\}\{\mu\text{-}P(OMe)_2\}B]$. Two inseparable isomers: IR (CH_2Cl_2) ν(CO) 2075 m, 2035 vs, 2015 s sh, 1971 m, 1872 w cm^{-1}. MS (positive FAB): $^{12}C_{19}{}^{1}H_{15}{}^{11}B^{16}O_{19}{}^{31}P_2{}^{103}Rh_2{}^{101}Ru_4$ 1230 (P^+) with 9 CO losses.

Isomer **I**. ^{1}H NMR ($CDCl_3$, 298 K): δ 3.66 (d, J_{PH} 13 Hz), 3.74 (d, J_{PH} 13 Hz); ^{11}B NMR ($CDCl_3$, 298 K): δ 190.3; $^{31}P\{^1H\}$ NMR ($CDCl_3$): δ 125.8 (dd, $^1J_{RhP}$ 243, $^2J_{RhP}$ 32 Hz, 1P), 352.5 (d, J_{RhP} 65 Hz, 1P).

Isomer **II**. ^{1}H NMR ($CDCl_3$ 298 K): δ 3.68 (d, J_{PH} 13 Jz), 3.69 (d, J_{PH} 13 Hz); ^{11}B NMR ($CDCl_3$, 298 K): δ 194.7 (dd, J_{RhB} 39, 21 Hz); $^{31}P\{^1H\}$ NMR ($CDCl_3$): δ 130.9 (dd, J_{RhP} 259, J_{PP} 65 Hz, 1P), 331.0 (dd, J_{RhP} 130, J_{PP} 65 Hz, 1P).

$[Rh_2Ru_4(CO)_{13}\{P(OMe)_3\}_2\{\mu\text{-}P(OMe)_2\}B]$. ^{1}H NMR ($CDCl_3$, 298 K): δ 3.65 (d, J_{PH} 12 Hz), 3.69 (d, J_{PH} 12 Hz), 3.71 (d, J_{PH} 12 Hz); ^{11}B NMR ($CDCl_3$, 298 K): δ 191.0; $^{31}P\{^1H\}$ NMR ($CDCl_3$): δ 126.8 (dd, J_{RhP} 227, $^2J_{RhP}$ 35 Hz, 1P), 129.2 (dd, $^1J_{RhP}$ 243, $^2J_{RhP}$ 35 Hz, 1P), 354.7 (d, J_{RhP} 54 Hz, 1P); IR (CH_2Cl_2) ν(CO) 2059 m, 2018 vs 1956 m sh, 1848 w cm^{-1}; MS (positive FAB): $^{12}C_{21}{}^{1}H_{24}{}^{11}B^{16}O_{21}{}^{31}P_3{}^{103}Rh_2{}^{101}Ru_4$ 1326 (P^+) with 8 CO losses.

Crystal structure determinations of $[Rh_2Ru_4(CO)_{16}B(AuPPh_3)]$ *and* $[Rh_2Ru_4(CO)_{14}(PPh_3)_2B(AuPPh_3)]$

Crystallographic data are collected in Table 1. Crystals were photographically characterized and determined to belong to the monoclinic crystal system. For the *I*-centred monoclinic, the centrosymmetric alternative was initially selected, and this choice was supported by the results of refinement. Empirical corrections for absorption were applied to the diffraction data. The structures were solved by direct methods, completed from difference Fourier maps, and refined with anisotropic thermal parameters for all non-hydrogen atoms. Hydrogen-atom locations were idealized. All computations used SHELXTL 4.2 software (G. Sheldrick, Siemens XRD, Madison, WI).

RESULTS AND DISCUSSION

The starting cluster anion for the reactions described in this paper was $[Rh_2Ru_4(CO)_{16}B]^-$, and it is important to note that the octahedral cage exists in both the *trans* and *cis* forms (with respect the Rh positions), with the former being the preferred species in solution [2]. The structure of the *trans*-isomer has been confirmed by an X-ray diffraction study [4]. Thus, in any reaction of $[Rh_2Ru_4(CO)_{16}B]^-$, products may arise from the reaction of either isomer. In the discussion that follows, isomerism in respect of the

Table 1. Crystallographic data for $[Rh_2Ru_4(CO)_{14}(PPh_3)_2B(AuPPh_3)]$ and $[Rh_2Ru_4(CO)_{16}B(AuPPh_3)]$

Formula	$C_{68}H_{45}AuBO_{14}P_3Rh_2Ru_4$	$C_{34}H_{15}AuBO_{16}PRh_2Ru_4$
Formula weight	1996.8	1528.3
Crystal colour, habit	red-brown block	red block
Crystal system	monoclinic	monoclinic
Space group	$P2_1/n$	$I2/a$
a(Å)	13.306(6)	13.837(3)
b(Å)	27.024(10)	18.537(4)
c(Å)	19.429(9)	34.117(8)
β(°)	105.86(3)	92.18(2)
V(Å^3)	6720(4)	8744(4)
Z	4	8
D_x(g cm^{-3})	1.974	2.322
μ(Mo–K_α(cm^{-1})	37.1	55.2
T(K)	298	257
Diffractometer	Siemens P4 (graphite monochromator)	Siemens P4 (graphite monochromator)
2θ range(°)	4–48($\pm h$, $+k$, $+l$)	4–42($\pm h$, $+k$, $+l$)
Reflections (collected, indpt)	10917, 6764	4779, 4690
$R(F)$, $R(wF^2)$[a](%)	5.01, 5.87	4.69, 10.73
GOF	1.14	0.93
Max. peak(e Å^{-3})	0.99	1.761

[a] Quantity minimized = $R(F) = \Sigma\Delta/\Sigma(F_o)$; $R(wF^2) = \Sigma[w(F_o^2 - F_c^2)^2]/\Sigma[w(F_o^2)^2]^{1/2}$ $\Delta = |F_o - F_c|$

Rh_2Ru_4 will be termed "cage-isomerism" to distinguish it from isomers arising from substitution of the PPh_3 or $P(OMe)_3$ ligands.

Reaction of $[Rh_2Ru_4(CO)_{16}B]^-$ *with 5-fold* PPh_3 *and excess* Ph_3PAuCl. The reaction between $[(PPh_3)_2N][Rh_2Ru_4(CO)_{16}B]$ and a five-fold excess of PPh_3, followed by addition of an excess of Ph_3PAuCl yielded two green products, and during TLC separation, the lower fraction quantitatively converted to a new green compound. The mass spectrum of the first fraction was consistent with this being a monophosphine substitution product of $[Rh_2Ru_4(CO)_{16}B]^-$ with the addition of an $AuPPh_3$ fragment, i.e. $[Rh_2Ru_4(CO)_{15}(PPh_3)B(AuPPh_3)]$. This was supported by the $^{31}P\{^1H\}$ NMR spectrum which exhibited two signals in a 1 : 1 ratio; the singlet at δ 70.9 was assigned to the gold-bound PPh_3 group and a doublet at δ 3.25 (J 195 Hz) showed that the phosphine ligand had substituted at a Rh site (^{103}Rh, 100%, $I = \frac{1}{2}$). Although spectroscopic data indicate that only one cage-isomer is formed, it was not possible to confirm whether this was the *trans* or *cis* arrangement.

Mass spectrometric data for the second isolated product of the reaction indicated the formation of $[Rh_2Ru_4(CO)_{14}(PPh_3)_2B(AuPPh_3)]$, and the $^{31}P\{^1H\}$ NMR spectrum was consistent with this. Two signals in a 1 : 2 ratio were observed; a singlet at δ 65.9 was assigned to the $AuPPh_3$ group and a doublet at δ 38.5 (2P, J 142 Hz) revealed that both phosphine ligands were attached to rhodium. As in the monosubstituted case, spectroscopic data for $[Rh_2Ru_4(CO)_{14}(PPh_3)_2B(AuPPh_3)]$ indicated that only one cage-isomer was present in solution. Crystals suitable for an X-ray diffraction study were grown away from dichloromethane layered with hexane.

Crystal structure of $[Rh_2Ru_4(CO)_{14}(PPh_3)_2B(AuPPh_3)]$

Figure 1 shows the molecular structure of $[Rh_2Ru_4(CO)_{14}(PPh_3)_2B(AuPPh_3)]$, and selected bond distances and angles are given in Table 2. The presence of the phosphorus atoms (and using the ^{31}P NMR spectroscopic data described above) allow us to effectively label the Rh centres, thereby overcoming the problem of distinguishing the Rh and Ru atoms by X-ray crystallographic methods. The Rh atoms are mutually *cis* in an octahedral Rh_2Ru_4 cage, with the boron atom being fully interstitial (a fact that is also evident from the down field shift of δ 188.5 in the ^{11}B NMR spectrum). The gold(I) phosphine unit adopts an Ru—Ru edge-bridging position, with the Au and P atoms lying in the plane containing the Rh(1), Rh(2), Ru(1) and Ru(4) atoms. In related structures we have observed both edge-bridging and face-capping environments for AuL fragments [2,5], but the most relevant comparison is between the arrangements in $[Rh_2Ru_4(CO)_{14}(PPh_3)_2B(AuPPh_3)]$ and $[Ir_2Ru_4(CO)_{16}B\{AuP(C_6H_{11})_3\}]$ [2]. Both have the heteroatoms in adjacent sites in the octahedral framework, but in $[Ir_2Ru_4(CO)_{16}B\{AuP(C_6H_{11})_3\}]$, the $AuP(C_6H_{11})_3$] fragment bridges the Ir—Ir edge, whereas in $[Rh_2Ru_4(CO)_{14}(PPh_3)_2B(AuPPh_3)]$, $AuPPh_3$ bridges an Ru—Ru edge. In the iridium case however, we proposed [2] that a *trans* → *cis* isomerism of the Ir_2Ru_4 cage accompanied the addition of the $[AuP(C_6H_{11})_3]^+$ electrophile. In the reaction sequence for the preparation of $[Rh_2Ru_4(CO)_{14}(PPh_3)_2B(AuPPh_3)]$, phosphine substitution occurs prior to the addition of $AuPPh_3$, and it is likely that steric factors play in role directing the gold(I) unit to the ruthenium-centred site. However, it remains unproven at what stage in the reaction the dominance of a *cis*-Rh_2Ru_4 cage (in contrast to the starting anion $[Rh_2Ru_4(CO)_{16}B]^-$) prevails. The conversion observed on the TLC plate is, of course, a possibility, but it would seem more likely that this takes place in concert with the addition of Ph_3PAuCl, and that the former is a more facile process, perhaps associated with a rearrangement involving the gold fragment on the surface of the Rh_2Ru_4-framework. We report the solid state structure of $[Rh_2Ru_4(CO)_{16}B(AuPPh_3)]$ later in this paper.

Reaction of $[Rh_2Ru_4(CO)_{16}B]^-$ *with 5-fold* PPh_3 *and* CF_3CO_2H

The isolobal analogy between $[AuL]^+$ and H^+ has been exploited in cluster chemistry for many years [6,7]. The aim of carrying out the reaction of $[Rh_2Ru_4(CO)_{16}B]^-$ with a five-fold excess of PPh_3 followed by acidification was to compare as parallel a reaction as possible with that described above. Mass spectrometric data suggested that the products isolated from the reaction were $[HRh_2Ru_4(CO)_{14}(PPh_3)_2B]$ and $[HRh_2Ru_4(CO)_{13}(PPh_3)_3B]$. The ^{11}B and ^{31}P NMR spectra of $[HRh_2Ru_4(CO)_{14}(PPh_3)_2B]$ were consistent with the presence of one cage-isomer, and one arrangement of the PPh_3 ligands; a doublet (J 150 Hz) in the $^{31}P\{^1H\}$ NMR spectrum indicated that both PPh_3 groups were rhodium-bound. A singlet at δ −14.9 in the ^1H NMR spectrum showed the presence of a ruthenium-attached hydrido ligand. Two possible structures can be proposed for $[HRh_2Ru_4(CO)_{14}(PPh_3)_2B]$ with the Rh atoms either *trans* or *cis*; however, the similarity between the ^{11}B NMR chemical shifts [8] for $[HRh_2Ru_4(CO)_{14}(PPh_3)_2B]$ and $[Rh_2Ru_4(CO)_{14}(PPh_3)_2B(AuPPh_3)]$ strongly suggest that the Rh_2Ru_4 arrangements are the same and hence we propose that $[HRh_2Ru_4(CO)_{14}(PPh_3)_2B]$ is the *cis*-isomer with the hydrido ligand occupying the same site as the $AuPPh_3$ group in $[Rh_2Ru_4(CO)_{14}(PPh_3)_2B(AuPPh_3)]$ (Fig. 1).

The NMR spectroscopic data for $[HRh_2Ru_4(CO)_{13}(PPh_3)_3B]$ were consistent with the presence of two isomers, **I** and **II**, and we were able to separate these by thin layer chromatography. The ^{11}B NMR spectrum showed two broad signals at δ 188.6 (isomer

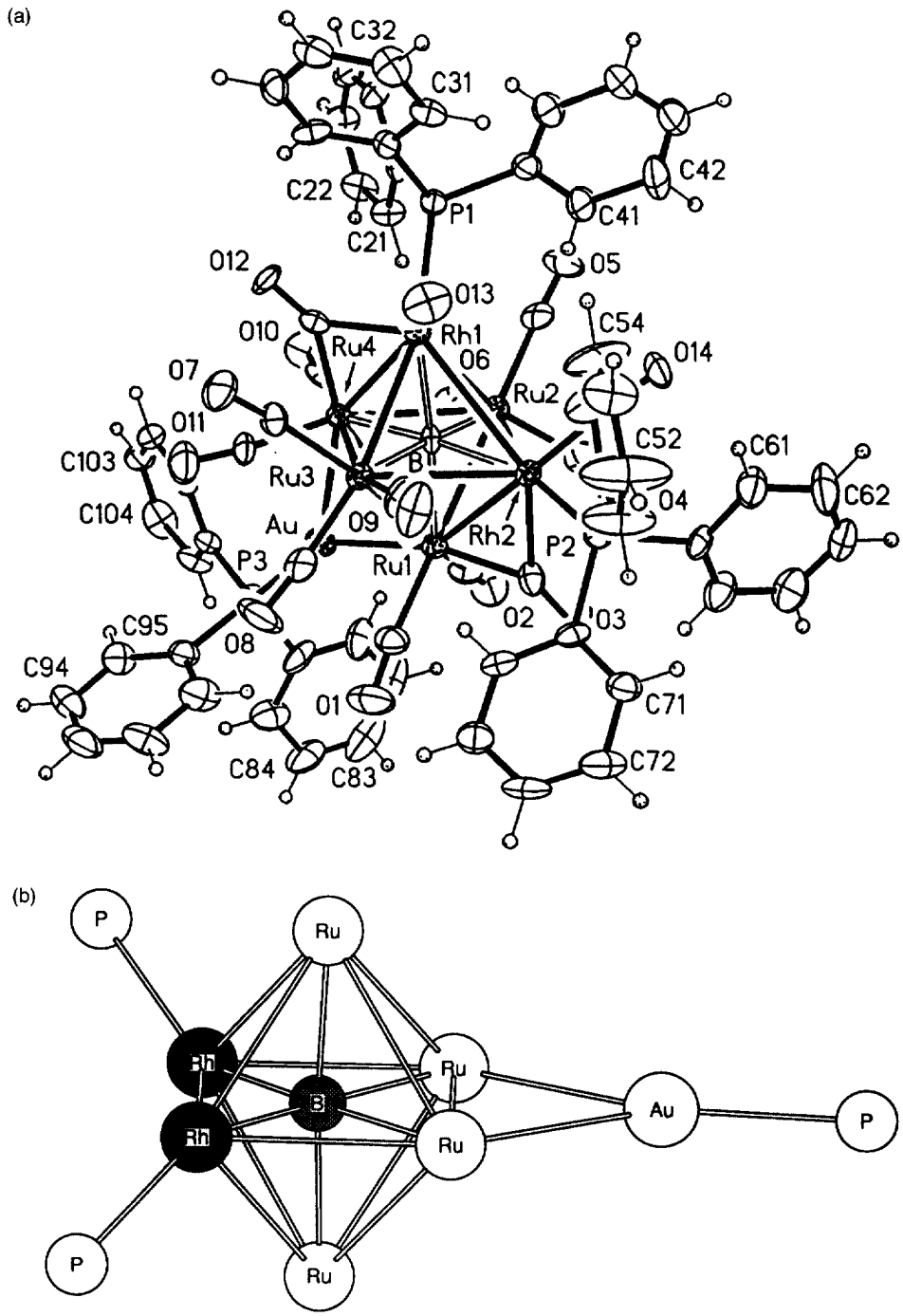

Fig. 1. (a) The molecular structure of $[Rh_2Ru_4(CO)_{14}(PPh)_3B(AuPPh_3)]$; (b) the $Rh_2Ru_4P_2B(AuP)$ core of $[Rh_2Ru_4(CO)_{14}(PPh)_3B(AuPPh_3)]$.

I) and 194.5 (isomer **II**) in a ratio $\approx 3:1$, while the $^{31}P\{^1H\}$ NMR spectrum exhibited four signals, which, on the ground of relative integrals, could be assigned as a singlet (1P) and doublet (2P, J_{RhP} 154 Hz) for isomer **I**, and a singlet (1P) and doublet (2P, J_{RhP} 153 Hz) for isomer **II**. In the highfield part of the ^1H NMR spectrum, two signals in a ratio $\approx 3:1$ were observed, a doublet at $\delta -14.2$ (J_{PH} 20 Hz) and a broad singlet at $\delta -15.3$ assigned to isomers **I** and **II** respectively. In proposing structures of isomers **I** and **II**, we have made the assumption that the trisubstituted derivative arises by PPh_3 substitution on the disubstituted product and that no skeletal rearrangement takes place. Figure 2 shows structures which are consistent with

Table 2. Selected bond distances and angles for $[Rh_2Ru_4(CO)_{14}(PPh_3)_2B(AuPPh_3)]$

Bond distances (Å)			
Au—P(3)	2.290(4)	Au—Ru(1)	2.764(1)
Au—Ru(4)	2.788(1)	Ru(1)—Ru(2)	2.686(2)
Ru(1)—Ru(3)	3.021(1)	Ru(1)—Ru(4)	3.011(2)
Rh(1)—Rh(2)	3.223(1)	Ru(1)—Rh(2)	2.834(2)
Ru(2)—Rh(1)	3.083(1)	Ru(2)—Rh(2)	2.863(2)
Ru(2)—Ru(4)	3.009(1)	Ru(3)—Ru(4)	2.873(2)
Ru(3)—Rh(1)	2.866(2)	Ru(3)—Rh(2)	3.074(1)
Ru(4)—Rh(1)	2.812(2)	Rh(1)—P(1)	2.373(4)
Rh(2)—P(2)	2.355(4)	Ru(1)—B	2.15(2)
Ru(2)—B	2.09(1)	Ru(3)—B	2.08(1)
Ru(4)—B	2.11(1)	Rh(1)—B	2.06(2)
Rh(2)—B	2.09(1)		
Bond angles (°)			
P(3)—Au—Ru(1)	148.4(1)	P(3)—Au—Ru(4)	145.7(1)
Ru(1)—Au—Ru(4)	65.7(1)	Ru(2)—Rh(1)—P(1)	107.5(1)
Ru(2)—Rh(2)—P(2)	160.1(1)	Ru(3)—Rh(1)—P(1)	162.6(1)
Ru(3)—Rh(2)—P(2)	110.4(1)	Ru(2)—B—Ru(3)	175.9(8)
Ru(4)—B—Rh(2)	173.5(8)	Ru(1)—B—Rh(1)	174.5(7)

the spectroscopic data for isomers **I** and **II** of $[HRh_2Ru_4(CO)_{13}(PPh_3)_3B]$. The presence of the bulky triphenylphosphine ligands should hinder cage-isomerization; however, our observations that both $[Rh_2Ru_4(CO)_{14}\{P(OMe)_3\}_2B(AuPPh_3)]$ and $[Rh_2Ru_4(CO)_{13}\{P(OMe)_3\}_3B(AuPPh_3)]$ undergo *cis* → *trans* cage-isomerization (see later) underline the fact that caution in making an assumption about cage-rearrangement is needed and in the absence of crystallographic data, we emphasize that these structures are likely, they are not unique possibilities.

Reaction of $[Rh_2Ru_4(CO)_{16}B]^-$ *with an equivalent of* PPh_3 *followed by* CF_3CO_2H

In an attempt to facilitate monosubstitution in $[Rh_2Ru_4(CO)_{16}B]^-$, we carried out a 1:1 reaction between this anion and PPh_3 with vastly reduced reaction time, followed by protonation. The desired product $[HRh_2Ru_4(CO)_{15}(PPh_3)B]$ was obtained in ≈50% yield, and its formation was accompanied by that of $[HRh_2Ru_4(CO)_{14}(PPh_3)_2B]$. The formulation of $[HRh_2Ru_4(CO)_{15}(PPh_3)B]$ was indicated by the mass spectrum of the compound, but solution NMR spectroscopic data showed the presence of two isomers (**I** and **II**); these were inseparable by TLC. The ^{11}B NMR spectrum exhibited two signals at δ 192.7 (with resolved ^{103}Rh—^{11}B coupling of 30 Hz) and 187.7, the former being more intense. The ^{31}P NMR spectrum of the isomer mixture showed two doublets of doublets, consistent with Rh—P bond formation in each isomer: isomer **I**, $^1J_{RhP}$ 148 Hz, $^2J_{RhP}$ 31 Hz, and isomer **II**, $^1J_{RhP}$ 176 Hz, $^2J_{RhP}$ 31 Hz. The fact that a ^2J coupling was observed indicated that the rhodium atoms were adjacent to each other, confirming a *cis*-Rh_2Ru_4 core. Two highfield signals in the ^1H NMR spectrum (δ −15.6 and −14.9 for isomers **I** and **II**, respectively) were indicative of protonation on the metal cage. For isomer **I**, a triplet of doublets was observed due to coupling to two ^{103}Rh centres (J 13 Hz) and to one ^{31}P nucleus, the value of 4 Hz being characteristic of a *cis* P—M—H arrangement. The hydride signal for isomer **II** was a singlet indicating an Ru—H—Ru environment, remote from the phosphine ligand. Figure 3 shows the proposed structures for the two isomers of $[HRh_2Ru_4(CO)_{15}(PPh_3)B]$; that for **I** is clearly assigned from the NMR spectroscopic data, while for isomer **II**, the particular edge chosen for the placement of the bridging hydrido ligand is not definitive.

Reaction of $[Rh_2Ru_4(CO)_{16}B]^-$ *with an equivalent of* $P(OMe)_3$ *followed by* Ph_3PAuCl

Our previous studies of the reactivity of $[Ru_6(CO)_{17}B]^-$ with $P(OMe)_3$ followed by treatment with either Ph_3PAuCl or acid had given contrasting results, with the proposed formation of a phosphido bridge in the second case [1]. We were therefore interested to investigate parallel reactions with $[Rh_2Ru_4(CO)_{16}B]^-$. As the discussion that follows shows, substitution by $P(OMe)_3$ appears to have the effect of giving species in which *cis* → *trans* isomerization of the Rh_2Ru_4 framework occurs relatively slowly.

The 1:1 reaction of $[Rh_2Ru_4(CO)_{16}B]^-$ with $P(OMe)_3$ yielded mono- and disubstitution products in addition to unreacted cluster anion. Each was isolated as the triphenylphosphine gold(I) derivative. The chromatographic separation of the products gave $[Rh_2Ru_4(CO)_{16}B(AuPPh_3)]$ as the first fraction; we return to this compound in the next section. The

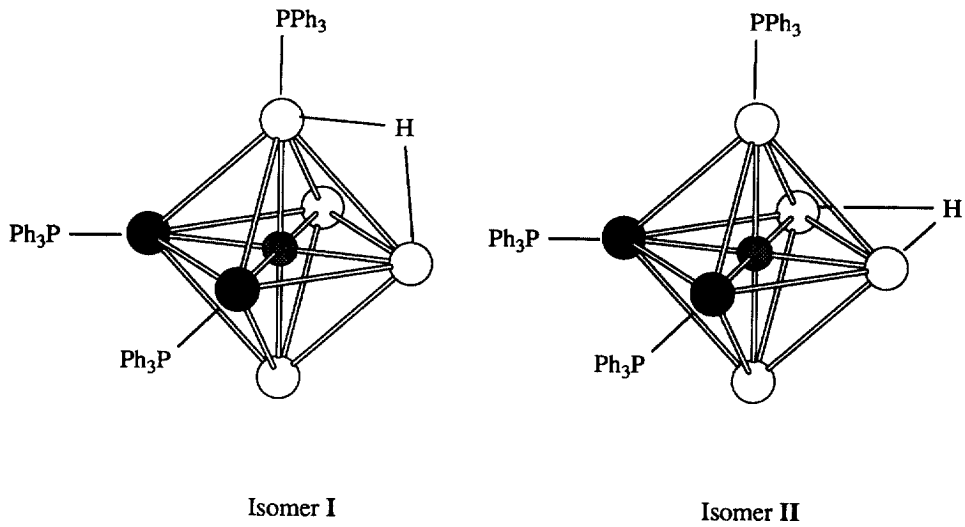

Isomer I Isomer II

● = Rh ○ = Ru

Fig. 2. The proposed structures of isomers **I** and **II** of $[HRh_2Ru_4(CO)_{13}(PPh_3)_3B]$, made with the assumption that the Rh atoms are mutually *cis* (see text).

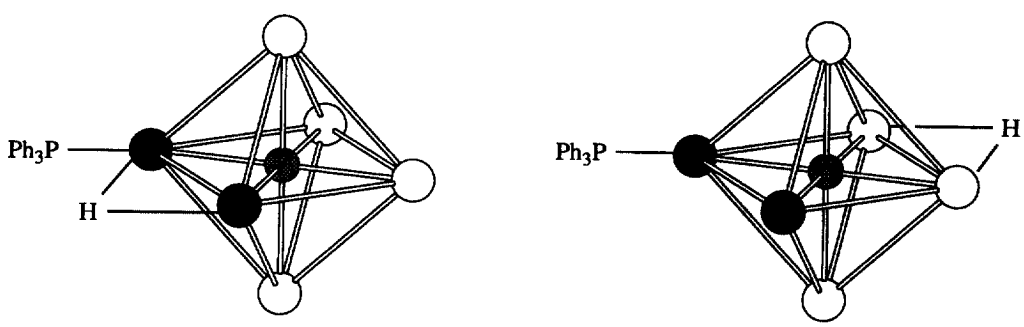

Isomer I Isomer II

● = Rh ○ = Ru

Fig. 3. The proposed structures of isomers **I** and **II** of $[HRh_2Ru_4(CO)_{15}(PPh_3)B]$.

second (brown) and third (green) fractions were identified as *cis*- and *trans*-$[Rh_2Ru_4(CO)_{15}\{P(OMe)_3\}B(AuPPh_3)]$ respectively. Over a period of time, the brown product converted quantitatively to the green compound, reminiscent of the *cis* → *trans* cage-isomerisms observed for related clusters [2]. The rate of isomerization was sufficiently rapid that the *cis*-isomer could not be well characterized. The mass spectrum of the green isomer was consistent with the formulation $[Rh_2Ru_4(CO)_{15}\{P(OMe)_3\}B(AuPPh_3)]$, but solution spectroscopic data showed the presence of two (inseparable by TLC) isomers. The ^{11}B NMR spectrum of the mixture exhibited two signals at δ 200.6 and 195.8 (relative integrals 3:2, assigned to isomers **I** and **II** respectively); although not unambiguous, these particularly downfield shifts (compared with ^{11}B shifts in the earlier discussions) are consistent with a *trans*-arrangement of the Rh_2Ru_4 cage [8]. Four singlets were observed in the $^{31}P\{^1H\}$ NMR spectrum, two were assigned to gold-bound PPh_3 groups and two to ruthenium-bound $P(OMe)_3$ ligands. Their relative integrals allowed assignments to appropriate isomers (see experimental section). The ^1H NMR spectroscopic data were consistent with the presence of two isomers, but provided no further structural information. Given that the data suggest (i) the Rh_2Ru_4 octahedral cage is retained in both isomers, (ii) that the Rh atoms are *trans* to each other, and (iii) that the $P(OMe)_3$ group is attached to a ruthenium atom, isomerism must be due to the location of the $AuPPh_3$ group. Since our previous studies of Rh_2Ru_4 and Ir_2Ru_4 borides, (supported by crystallographic data), have evidenced different bonding modes (edge-bridging, face-capping, association with Ru and/or rhodium or iridium) [2,5, this work], it is not possible to speculate on the distinction between isomers **I** and **II** of *trans*-$[Rh_2Ru_4(CO)_{15}\{P(OMe)_3\}B(AuPPh_3)]$ and we have not been able to obtain X-ray quality crystals to aid structural assignments.

The final fraction to be isolated was brown in colour, but on storage in either the solid state or in solution, underwent quantitative conversion to a green compound, suggesting a *cis* → *trans* cage-isomerization. However, this isomerization was sufficiently slow that both isomers could be independently characterized by mass spectrometry and IR and NMR spectroscopies. The mass spectra of both green and brown compounds were consistent with the formulation $[Rh_2Ru_4(CO)_{14}\{P(OMe)_3\}_2B(AuPPh_3)]$. The spectroscopic characteristics of the green compound indicated a single species, with the significantly downfield ^{11}B NMR shift of δ 201.6 consistent with a *trans*-arrangement of Rh atoms. The $^{31}P\{^1H\}$ spectrum exhibited singlets in a ratio 1:2, assigned to gold- and ruthenium-bound phosphorus atoms respectively. One doublet (for the methyl protons) in the ^1H NMR spectrum is also consistent with equivalent $P(OMe)_3$ groups. Two possible structures for *trans*-$[Rh_2Ru_4(CO)_{14}\{P(OMe)_3\}_2B(AuPPh_3)]$ are shown in Fig. 4; one has an edge-bridging $AuPPh_3$ unit. Alternatively, the gold(I) phosphine unit could be face-capping over one of the Ru_2Rh faces remote from the $RuP(OMe)_3$ units; this would give a structure analogous to that of $[Rh_2Ru_4(CO)_{16}B\{AuP(C_6H_{11})_3\}]$ which has been crystallographically confirmed [2]. A structure with the $P(OMe)_3$ ligands attached to *trans* rather than *cis* Ru atoms is also possible, but is considered less likely.

We now return to *cis*-$[Rh_2Ru_4(CO)_{14}\{P(OMe)_3\}_2B(AuPPh_3)]$, from which *trans*-$[Rh_2Ru_4(CO)_{14}\{P(OMe)_3\}_2B(AuPPh_3)]$ is formed. The spectroscopic data for the *cis*-isomer showed the presence of two structural isomers, **I** and **II** (inseparable by TLC), present in a 2:1 ratio respectively. In the $^{31}P\{^1H\}$ spectrum of the isomer mixture, only one signal was observed for the $AuPPh_3$ unit (δ 68.0), suggesting very similar environments in each isomer. The $P(OMe)_3$ ligands are attached to ruthenium in isomer **I** (^{31}P singlet) and to rhodium in isomer **II** (^{31}P, doublet, J_{RhP} 227 Hz). This observation is significant because it means that for isomer **II**, *cis* → *trans* cage-isomerization is accompanied by phosphite migration from rhodium to ruthenium. The structures that we propose for isomers **I** and **II** of *cis*-$[Rh_2Ru_4(CO)_{14}\{P(OMe)_3\}_2B(AuPPh_3)]$ are shown in Fig. 4b.

Crystal structure of $[Rh_2Ru_4(CO)_{16}B(AuPPh_3)]$

We have previously reported the synthesis and spectroscopic characterization of $[Rh_2Ru_4(CO)_{16}B(AuPPh_3)]$ [2]. The isolation of this compound in the present work gave crystals (grown from a CH_2Cl_2 solution layered with hexane) which were suitable for single crystal structural analysis. The molecular structure of $[Rh_2Ru_4(CO)_{16}B(AuPPh_3)]$ is shown in Fig. 5, and selected bond distances and angles are listed in Table 3. The results of the determination confirm the presence of the octahedral metal core around an interstitial boron atom. The structure is analogous to that found for $[Rh_2Ru_4(CO)_{16}B\{Au\{C_6H_{11})_3\}]$ [2]; as in that structure, it is not possible to unambiguously distinguish between Ru and Rh atoms by single-crystal X-ray diffraction techniques. However, in low oxidation state metal carbonyl clusters, the connectivity number of ruthenium to the CO ligands is generally greater than that of rhodium, and rhodium centres are more likely to be associated with bridging CO ligands than are ruthenium atoms. The allocation of the rhodium atoms in a *trans*-arrangement as shown in Fig. 5 follows from these guidelines. The gold(I) phosphine fragment caps the Ru(1)Ru(4)Rh(1)-face; the eight faces of the *trans*-Rh_2Ru_4 octahedron are, of course, equivalent.

Preparation and characterization of $[Rh_2Ru_4(CO)_{13}\{P(OMe)_3\}_3B(AuPPh_3)]$

Trisubstitution by $P(OMe)_3$ in $[Rh_2Ru_4(CO)_{16}B]^-$ was achieved by using a 1:3 stoichiometry, and neutral products were isolated after the addition of

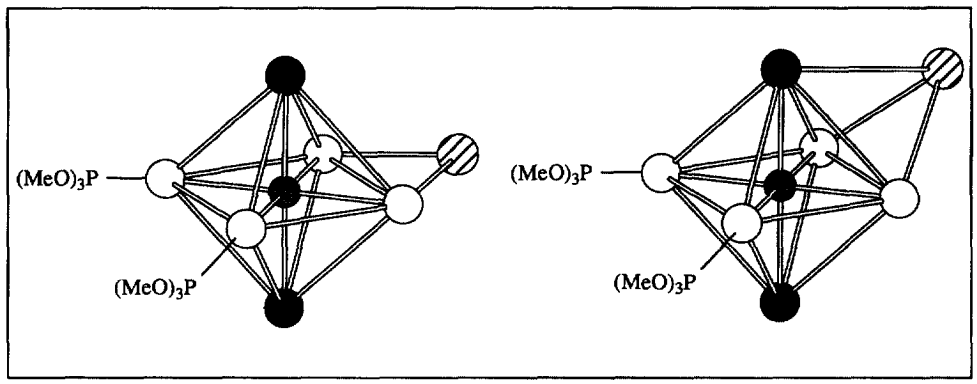

(a)

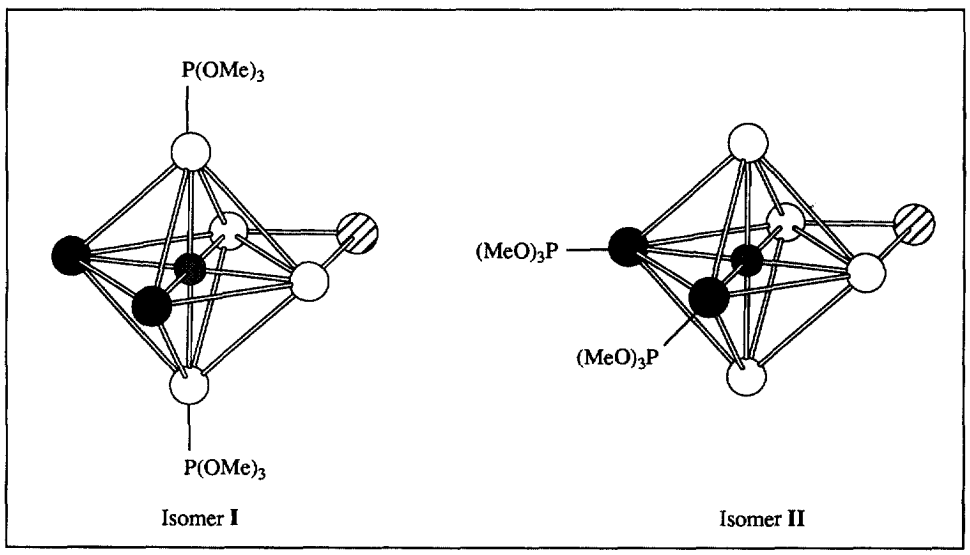

(b)

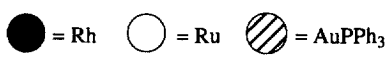

Fig. 4. (a) Two possible structures for *trans*-$[Rh_2Ru_4(CO)_{14}\{P(OMe)_3\}_2B(AuPPh_3)]$; both are consistent with spectroscopic data; (b) proposed structures for isomers **I** and **II** of *cis*-$[Rh_2Ru_4(CO)_{14}\{P(OMe)_3\}_2B(AuPPh_3)]$.

$[Ph_3PAuCl]$. An extended reaction time was not required and 50% conversion to $[Rh_2Ru_4(CO)_{13}\{P(OMe)_3\}_3B(AuPPh_3)]$ (present as two cage isomers) was achieved in 10 min; two unidentifiable products were also formed. Mass spectrometric data for the two products isolated showed them both to be consistent with the formulation $[Rh_2Ru_4(CO)_{13}\{P(OMe)_3\}_3B(AuPPh_3)]$. The ^{11}B NMR spectrum of each compound exhibited one peak, but the different chemical shift values (δ 203.2 and 188.7) suggested that the products were *trans*- and *cis*-cage isomers, respectively. This was further supported by the fact that, over a period of days, the compound with δ ^{11}B 188.7 converted to that with δ ^{11}B 203.2. Significantly, this isomerization process was slower than that observed for *cis* → *trans* $[Rh_2Ru_4(CO)_{14}\{P(OMe)_3\}_2B(AuPPh_3)]$. Both isomers of $[Rh_2Ru_4(CO)_{13}\{P(OMe)_3\}_3B(AuPPh_3)]$ could therefore be spectroscopically characterized without problems associated with isomerization. The $^{31}P\{^1H\}$ NMR spectrum of *cis*-$[Rh_2Ru_4(CO)_{13}\{P(OMe)_3\}_3B(AuPPh_3)]$ showed, in addition to a signal at δ 66.9 assigned to the PPh_3 group, a double (J_{RhP} 236 Hz) and a singlet with relative integrals of 2:1. In the $^{31}P\{^1H\}$ NMR spectrum of *trans*-$[Rh_2Ru_4(CO)_{13}\{P(OMe)_3\}_3B(AuPPh_3)]$, three singlets and a doublet were observed; the singlet at δ 70.8 was assigned to the $AuPPh_3$ groups, and the lower field singlets (1:1, δ

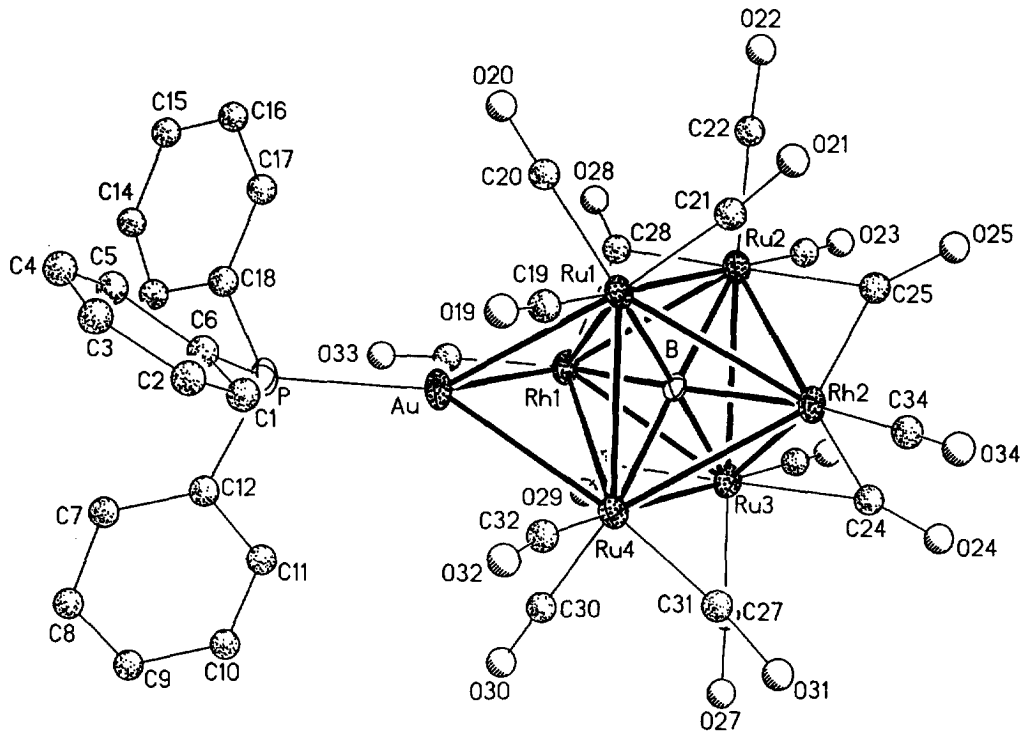

Fig. 5. The molecular structure of $[Rh_2Ru_4(CO)_{16}B(AuPPh_3)]$; phenyl H atoms are omitted.

Table 3. Selected bond distances and angles for $[Rh_2Ru_4(CO)_{16}B(AuPPh_3)]$

Bond distances			
Au—P	2.324(4)	Au—Ru(1)	2.821(2)
Au—Ru(4)	2.854(2)	Au—Rh(1)	2.797(2)
Ru(1)—Ru(2)	2.957(2)	Ru(1)—Ru(4)	2.916(2)
Ru(1)—Rh(1)	3.164(2)	Ru(1)—Rh(2)	3.010(2)
Ru(2)—Rh(1)	2.829(2)	Ru(2)—Rh(2)	2.808(2)
Ru(2)—Ru(3)	3.031(2)	Ru(3)—Ru(4)	2.952(2)
Ru(3)—Rh(1)	2.808(2)	Ru(3)—Rh(2)	2.815(2)
Ru(4)—Rh(1)	3.153(2)	Ru(4)—Rh(2)	2.995(2)
Ru(1)—B	2.10(2)	Ru(2)—B	2.09(2)
Ru(3)—B	2.10(2)	Ru(4)—B	2.10(2)
Rh(1)—B	2.09(2)	Rh(2)—B	2.05(2)
Bond angles (°)			
P—Au—Ru(1)	142.7(1)	P—Au—Ru(4)	148.8(1)
P—Au—Rh(1)	131.1(1)	Ru(1)—Au—Ru(4)	61.85(4)
Ru(1)—Au—Rh(1)	68.56(4)	Rh(1)—Au—Ru(4)	67.8(4)
Ru(1)—B—Ru(3)	177.0(10)	Ru(2)—B—Ru(4)	176.8(10)
Rh(1)—B—Rh(2)	165.4(9)		

130.8 and 131.5) denoted the presence of two inequivalent ruthenium-bound $P(OMe)_3$ ligands. The doublet (δ 133.9, J_{RhP} 324 Hz) showed that the third $P(OMe)_3$ was attached to rhodium. The proposed structures for *cis*- and *trans*-$[Rh_2Ru_4(CO)_{13}\{P(OMe)_3\}_3B(AuPPh_3)]$ are shown in Fig. 6; edge-bridging sites are shown for the gold(I) phosphine units, but we have not been able to obtain X-ray quality crystals of either isomer to confirm this. Even in the absence of definitive crystallographic data, the ^{31}P NMR spec-

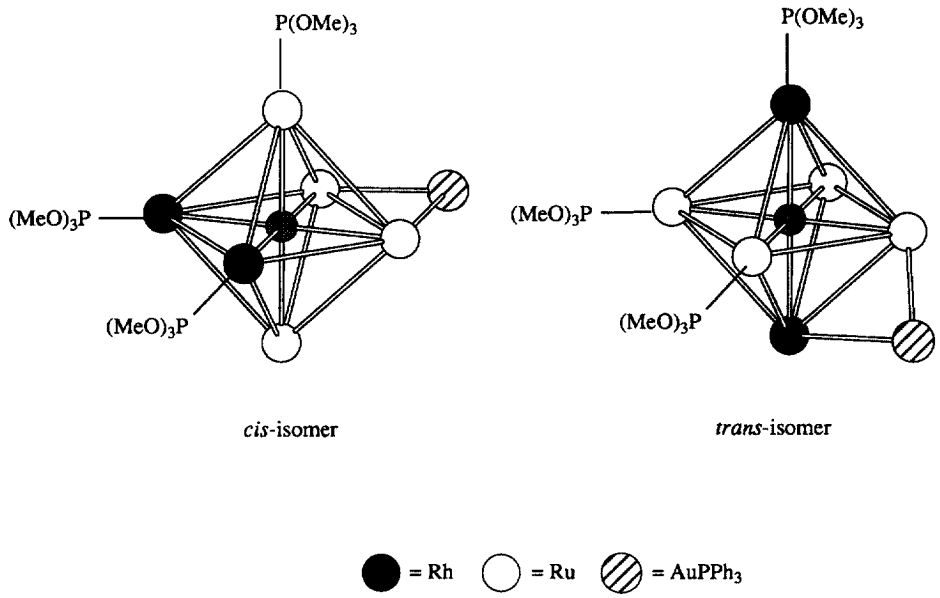

Fig. 6. The proposed structures for *cis*- and *trans*-$[Rh_2Ru_4(CO)_{13}\{P(OMe)_3\}_3B(AuPPh_3)]$.

troscopic results clearly reveal that *cis* → *trans* cage isomerism is accompanied by migration of one $P(OMe)_3$ ligand from rhodium to ruthenium.

The reaction of $[Rh_2Ru_4(CO)_{16}B]^-$ *with* $P(OMe)_3$ *followed by protonation*

The results of our investigations into the reaction of $[Ru_6(CO)_{17}B]^-$ with $P(OMe)_3$ followed by protonation were consistent with the initial substitution of one CO by $P(OMe)_3$ followed by cleavage of one methoxy group and the formation of $[Ru_6(CO)_{16}\{\mu\text{-}P(OMe)_2\}B]$. However, we were unable to confirm this by the determination of the solid state structure of the latter compound [1]. As the discussion below shows, similar results have now been obtained with $[Rh_2Ru_4(CO)_{16}B]^-$.

The reaction of $[Rh_2Ru_4(CO)_{16}B]^-$ with a two-molar equivalent of $P(OMe)_3$, followed by protonation with CF_3CO_2H, gave two isolable products, the mass spectra of which were consistent with the formula $[Rh_2Ru_4(CO)_{14}\{P(OMe)_3\}\{P(OMe)_2\}B]$ and $[Rh_2Ru_4(CO)_{13}\{P(OMe)_3\}_2\{P(OMe)_2\}B]$. The fact that each $P(OMe)_2$ group is in a bridging mode is supported by characteristic shifts in the ^{31}P NMR spectrum of each compound (see below) and is consistent with electron-counting schemes for the compounds in which the $P(OMe)_2$ group contributes three electrons. The ^{11}B NMR spectrum of $[Rh_2Ru_4(CO)_{14}\{P(OMe)_3\}\{\mu\text{-}P(OMe)_2\}B]$ showed two signals, δ 190.3 (isomer **I**) and 194.7 (isomer **II**) with relative integrals 3 : 1, indicative of two isomers, and this was consistent with both the $^{31}P\{^1H\}$ NMR and ^1H NMR spectroscopic data. Based upon signal integrals, the signals in the $^{31}P\{^1H\}$ NMR spectrum could be assigned to individual. For isomer **I**, the observation of a doublet of doublets (δ 125.8, $^1J_{RhP}$ 243, $^2J_{RhP}$ 32 Hz) and a lowfield doublet (δ 352.5, J_{RhP} 65 Hz) was interpreted in terms of a rhodium-bound, terminal $P(OMe)_3$ group and a Ru—Rh, edge-bridging $P(OMe)_2$ group. Moreover, the fact that $^2J\,^{103}Rh—^{31}P$ coupling was observed for the terminal phosphite ligand implied that the two Rh atoms in the metal cage were mutually *cis*. From our experience with these species, it is reasonable to assume that isomer **II** also possesses a *cis*-arrangement of Rh atoms in the metal cage; isomers **I** and **II** were inseparable by TLC, and there was no spectroscopic evidence for their interconversion. The $^{31}P\{^1H\}$ NMR spectrum of isomer **II**, exhibited two doublets of doublets. The higher field signal (δ 130.9) showed couplings of 259 Hz (characteristic of a rhodium-bound, terminal $P(OMe)_3$ ligand) and 65 Hz. The lower field signal (δ 331.0) exhibited couplings of 130 Hz (assigned to $^{103}Rh—^{31}P$ coupling) and 65 Hz. The common coupling (65 Hz) was assigned to $^{31}P—^{31}P$ spin-spin coupling, implying that the two phosphorus atoms were attached to the same Rh centre. Proposed structures for isomers **I** and **II** are shown in Fig. 7a.

Spectroscopic data showed that the second product of the reaction, $[Rh_2Ru_4(CO)_{13}\{P(OMe)_3\}_2\{P(OMe)_2\}B]$, existed in one structural form. The $^{31}P\{^1H\}$ NMR spectrum exhibited three signals (equal relative integrals), two (doublets of doublets) due to terminal $P(OMe)_3$ ligands (δ 126.8 and 129.2), and one (a doublet) due to a bridging $P(OMe)_2$ group (δ 354.7). The observation of $^2J_{RhP}$ coupling for the terminal ligands, suggested that the rhodium atoms in

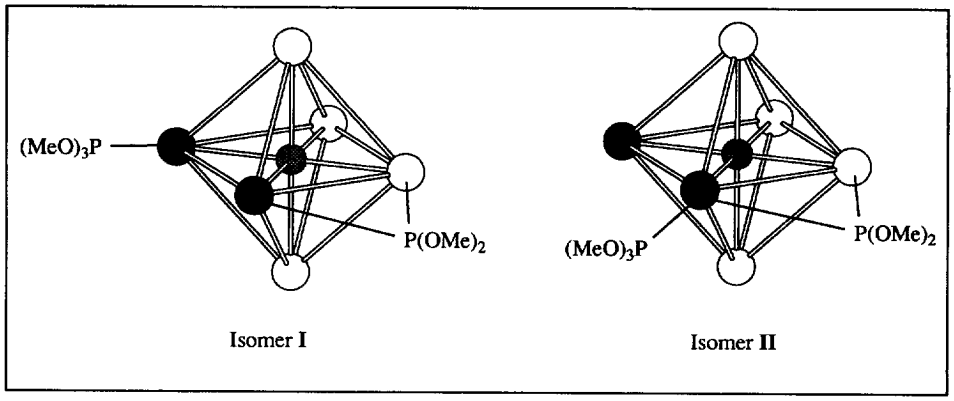

(a)

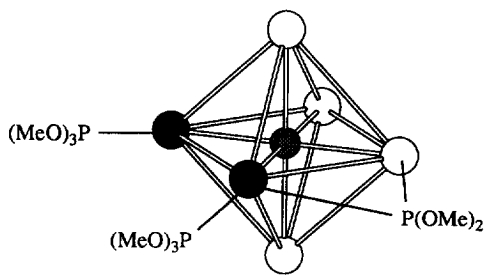

(b)

● = Rh ○ = Ru

Fig. 7. (a) The proposed structures of isomers **I** and **II** of $[Rh_2Ru_4(CO)_{14}\{P(OMe)_3\}\{P(OMe)_2\}B]$; (b) the proposed structure of $[Rh_2Ru_4(CO)_{13}\{P(OMe)_3\}_2\{P(OMe)_2\}B]$.

the cage were mutually *cis*, and the data are in accord with the structure shown in Fig. 7b. In this case, no $^{31}P_{terminal}$—$^{31}P_{bridge}$ coupling was observed. However, values of J depend upon the relative orientations of the ligands [9] and it is reasonable that the coupling was too small to be resolved.

Neither *cis*-$[Rh_2Ru_4(CO)_{14}\{P(OMe_3\}\{\mu\text{-}P(OMe)_2\}B]$ nor *cis*-$[Rh_2Ru_4(CO)_{13}\{P(OMe)_3\}_2\{P(OMe)_2\}B]$ showed a tendency for conversion to the *trans*-isomers over a period of storage of several days.

CONCLUSIONS

The behaviour of $[Rh_2Ru_4(CO)_{16}B]^-$ towards PPh_3 or $P(OMe)_3$ followed by protonation or reaction with Ph_3PAuCl shows general similarities to that of the homometallic boride $[Ru_6(CO)_{17}B]^-$ [1]. In particular, terminal $P(OMe)_3$ in the anionic cluster can be readily converted to a μ-$P(OMe)_2$ group by protonation with trifluoroacetic acid, presumably through loss of MeOH. We have previously commented upon related reactions: protonation of $[Ru_3(CO)_{10}\{P(OMe)_3\}_2]$ by CF_3CO_2H which gives $[HRu_3(CO)_{10}\{P(OMe)_3\}_2]^+$ [10] rather than a $P(OMe)_2$ bridge, thermally promoted conversions of terminal $P(OMe)_3$ to μ_4-P(OMe), bridging $OP(OMe)_2$ or $OP(OMe)OP(OMe)_2$ [11–13], and the formation of $[Ru_3(CO)_9(PPh_3)(\mu\text{-}PPh_2)]^-$ from $[HRu_3(CO)_{11}]^-$ and PPh_3 [14].

As anticipated, the presence of the heterometals in $[Rh_2Ru_4(CO)_{16}B]^-$ complicates the picture with respect to the behaviour of $[Ru_6(CO)_{17}B]^-$, but at the same time "labels" two sites in the cage with respect to the other four. Some general observations are that: (i) PPh_3 substitutes for CO at rhodium rather than ruthenium; (ii) introduction of two PPh_3 ligands (at Rh) is possible, whereas attempts to introduce two PPh_3 ligands into $[Ru_6(CO)_{17}B]^-$ failed [1]; (iii) cage isomerization (*cis* → *trans* Rh_2Ru_4) becomes less facile

across the series $[Rh_2Ru_4(CO)_{16-x}\{P(OMe)_3\}_xB(AuPPh_3)]$ for $x = 1$ to 3; (iv) migration of $P(OMe)_3$ from Rh to Ru accompanies *cis* → *trans* cage rearrangement in $[Rh_2Ru_4(CO)_{16-x}\{P(OMe)_3\}_xB(AuPPh_3)]$, $x = 2$ or 3.

Acknowledgements—We thank the donors of the Petroleum Research Fund, administered by the American Chemical Society for support of this work (Grant #25533–AC3), the EPSRC (to A.D.H. and A.W.), and the National Science Foundation for a grant (CHE 9007852) towards the purchase of a diffractometer at the University of Delaware.

REFERENCES

1. Housecroft, C. E., Rheingold, A. L., Waller, A. and Yap, G. P. A., *Polyhedron*, 1998, in press.
2. Galsworthy, J. R., Hattersley, A. D., Housecroft, C. E., Rheingold, A. L. and Waller, A., *J. Chem. Soc., Dalton Trans.*, 1995, 549.
3. Mann, F. G., Wells, A. F., and Purdie, D. J., *J. Chem. Soc.*, 1937, 1828.
4. Galsworthy, J. R., Housecroft, C. E. and Rheingold, A. L., *J. Chem. Soc., Dalton Trans.*, 1994, 2359.
5. Hattersley, A. D., Housecroft, C. E. and Rheingold, A. L., *J. Cluster Sci.*, 1997, **8,** 329.
6. Hall, K. P. and Mingos, D. M. P., *Prog. Inorg. Chem.*, 1984, **32,** 237.
7. Salter, I. D., *Adv. Organomet. Chem.*, 1989, **29,** 249.
8. *cis* to *trans*-isomerism in Rh_2Ru_4B or Rh_2Fe_4B cages is accompanied by a shift in the ^{11}B NMR signal to lower field: for Rh_2Ru_4B see Ref. [2] and for Rh_2Fe_4B, see Khattar, R., Puga, J., Fehlner, T. P. and Rheingold, A. L., *J. Am. Chem. Soc.*, 1989, **111,** 1877.
9. See for example: Heaton, B. T., Longetti, L., Mingos, D. M. P., Brient, C. E., Minshall, P. C., Theobald, B. R. C., Garlaschelli, L. and Sartorelli, U., *J. Organomet. Chem.*, 1981, **213,** 333.
10. Kabir, S. E.,Miah, A., Uddin, K. and Deeming, A. J., *J. Organomet. Chem.*, 1994, **476,** 121.
11. Fernandez, J. M., Johnson, B. F. G., Lewis, J. and Raithby, P. R., *Acta Crystallogr., Sect. B*, 1979, **35,** 1711.
12. Fernandez, J. M., Johnson, B. F. G., Lewis, J., Raithby, P. R. and Sheldrick, G. M., *Acta Crystallogr., Sect. B*, 1978, **34,** 1994.
13. Orpen, A. G. and Sheldrick, G. M., *Acta Crystallogr., Sect. B*, 1978, **34,** 1992.
14. Gremaud, G., Jungbluth, H., Stoeckli-Evans, H. and Süss-Fink, G., *J. Organomet. Chem.*, 1990, **388,** 351.

Pergamon

PII: S0277-5387(98)00099-0

Polyhedron Vol. 17, No. 17, pp. 2971–2974, 1998
© 1998 Elsevier Science Ltd
All rights reserved. Printed in Great Britain
0277-5387/98 $19.00+0.00

Oxide bridged early–late metal organometallics: the synthesis of complexes with W–O–Ru and W–O–P bridges‡

John H. Yamamoto,[a] Gary D. Enright[a] and Arthur J. Carty[a,b*]

[a]Steacie Institute for Molecular Sciences, National Research Council of Canada, 100 Sussex Drive, Ottawa, Ontario, Canada K1A OR6

[b]Department of Chemistry, University of Ottawa, Ottawa, Ontario, Canada K1N 6N5

(Received 19 December 1997)

Abstract—Reaction of the tungsten oxo acetylide complex $Cp^*W(O)_2CCPh$ with $Ru_4(CO)_{12-13}[PN(^iPr)_2]$ affords two oxo bridged metal clusters η^5-$Cp^*p^*W(\mu\text{-}O)Ru_4(CO)_9(\mu\text{-}CO)[\mu_3\text{-}\eta^2\text{-}OPN(^iPr)_2](\mu_4\text{-}\eta^2\text{-}CCPh)$ **2** and η^5-$Cp^*p^*W(\mu\text{-}O)_2Ru_4(CO)_{10}[\mu_3\text{-}PN(^iPr)_2](\mu_5\text{-}\eta^2\text{-}CCPh)$ **3**. X-ray analysis shows that **2** has a single W–O–Ru oxide bridge and contains a bridging diisopropylaminophosphinidoxo ligand while in **3** both oxide ligands bridge W–Ru bonds. © 1998 Elsevier Science Ltd. All rights reserved

Keywords: Phosphinidoxo; oxo; acetylide; ruthenium; tungsten

The oxide (=O) group is normally considered to be a hard ligand in organometallic chemistry, principally associated with early, high oxidation state metal fragments [1]. However, recent developments suggest that oxides can play an important role as interfacial ligands, bridging early–high and late–low oxidation state metal centers to form mixed metal oxide clusters which may serve as models for oxide supported platinum metal catalysts [2, 3]. In this communication we report the synthesis of two new oxide bridged early–late organometallic clusters, one of which has W–O–Ru and W–O–P interactions and contains the rare phosphinidoxo ligand RPO [4], the other having two oxide ligands bridging Ru–W bonds.

A potentially powerful methodology for constructing oxide bridged mixed metal clusters consists of delivering an early metal oxo compound bearing an unsaturated hydrocarbyl ligand to a late metal which has a high affinity for unsaturated hydrocarbyl groups. Using this strategy, reaction of η^5-$Cp^*W(O)_2CCPh$ ($Cp^*=C_5Me_5$)(13.0 mg, 0.029 mmol) [5] in refluxing hexane for 3 h with the nido 62e-phosphinidene cluster $Ru_4(CO)_{13}[PN(^iPr)_2]$ **1** (25.0 mg, 0.028 mmol) [6], known to strongly coordinate acetylenes, afforded two new complexes η^5-$Cp^*W(\mu\text{-}O)Ru_4(CO)_9(\mu\text{-}CO)[\mu_3\text{-}\eta^2\text{-}OPN(^iPr)_2](\mu_4\text{-}\eta^2\text{-}CCPh)$ **2** [7] and η^5-$Cp^*W(\mu\text{-}O)_2Ru_4(CO)_{10}[\mu_3\text{-}PN(^iPr)_2](\mu_5\text{-}\eta^2\text{-}CCPh)$ **3** [8] in 57% and 32% yield respectively.

The molecular structure of **2** [9] (Fig. 1) consists of an almost planar Ru_4 butterfly (dihedral angle of 177.43°) with the Cp^*WC_2Ph fragment coordinated as a 6e-donor to the Ru(2)Ru(3)Ru(4) triangle as a μ_3-η^2-$\parallel$-acetylene and with the tungsten atom asymmetrically bridging the Ru(1)–Ru(2) bond (Ru(1)–W = 2.9248(3); Ru(2)–W = 2.7823(3)). The most interesting features of the cluster are associated with the oxide ligands derived from the $Cp^*W(O)_2$ moiety. One oxygen atom, O(2) acts as a bridge between tungsten and the phosphorus atom of the phosphinidene of **1** forming a μ_3-η^2 diisopropylaminophosphinidoxo $[O{=}PN(^iPr)_2]$ ligand on the Ru(1)–Ru(2)–W face. The P–O(2) bond length (1.570(1) Å) is comparable to that in the μ-diphenylphosphidoxo cluster $Fe_3(CO)_9(\mu_3\text{-}\eta^2\text{-}C_2{}^t\text{Bu})(\mu\text{-}OPPh_2)$ (P–O = 1.539(2) Å) [4] and in $Fe_3(CO)_{10}(\mu_3\text{-}O{=}P^t\text{Bu})$ (P–O = 1.532(4) Å) [4] and only slightly longer than the P=O distance in phosphine oxide complexes [10]. Although many examples of terminal phosphine oxides, μ–O=PR_2 (phosphidoxo) [11] and most recently, PO (phosphorus

* Corresponding author.

‡ Dedicated to the Lord Jack Lewis on the occasion of his 70th birthday.

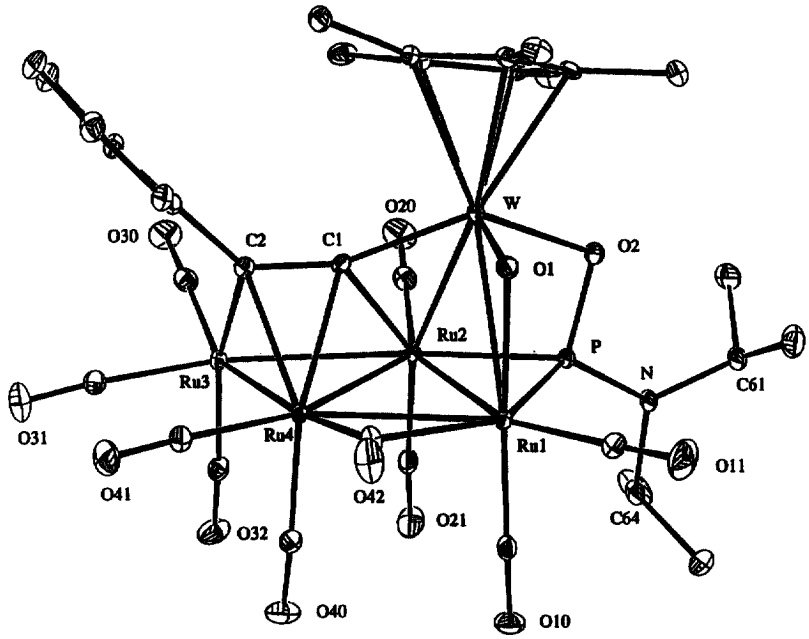

Fig. 1. An ORTEP diagram of η^5-Cp*W(μ-O)Ru$_4$(CO)$_9$(μ-CO)(μ_3-η^2-OPN(^{i}Pr)$_2$)(μ_4-η^2-CCPh) **2** showing 30% probability thermal ellipsoids. Hydrogen atoms were omitted for clarity. Selected bond lengths not mentioned in the text (Å): W–Ru(1) = 2.9248(3), W–Ru(2) = 2.7823(1), Ru(1)–Ru(2) = 2.8428(4), Ru(1)–Ru(4) = 2.8306(4), Ru(2)–Ru(3) = 2.8802(4), Ru(2)–Ru(4) = 2.7587(4), Ru(3)–Ru(4) = 2.6882(4) and Angles (°) O(1)–W–O(2) = 96.5(1), N–P–O(2) = 106.1(1).

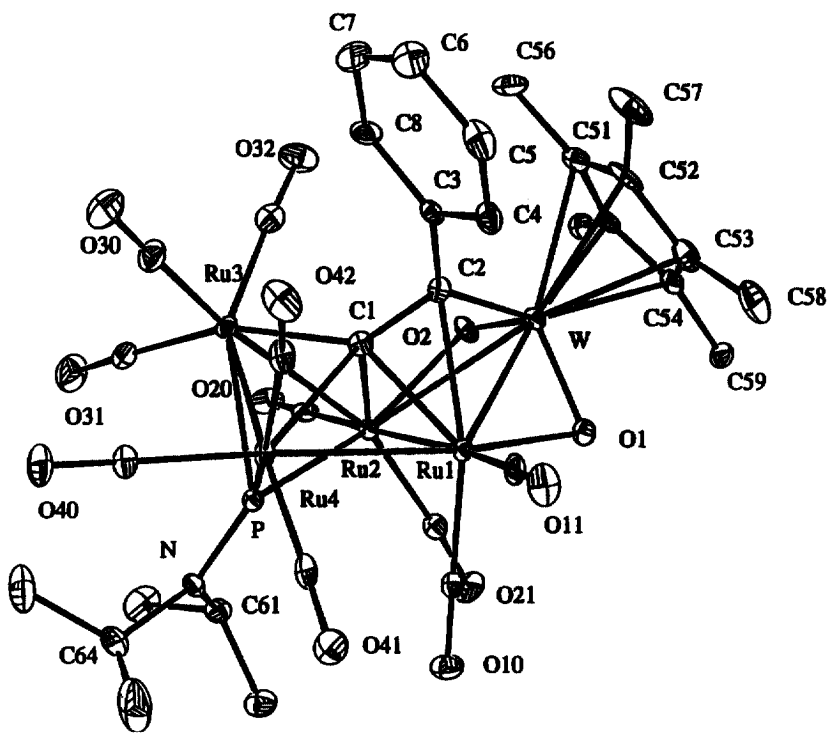

Fig. 2. An ORTEP diagram of η^5-Cp*W(μ-O)$_2$Ru$_4$(CO)$_{10}$(μ_3-PN(^{i}Pr)$_2$)(μ_5-η^2-CCPh) **3** showing 30% probability thermal ellipsoids. Hydrogen atoms were omitted for clarity. Selected bond lengths not mentioned in the text (Å): W–Ru(1) = 2.6910(5), W–Ru(2) = 3.0467(5), Ru(1)–Ru(2) = 2.8154(7), Ru(1)–Ru(4) = 2.8661(6), Ru(2)–Ru(3) = 2.7786(6), Ru(3)–Ru(4) = 2.8393(7) and Angles (°) O(1)–W–O(2) = 111.0(2).

monoxide) complexes [6] are known, clusters with oxidised phosphinidene ligands μ-O=PR are very rare. The only other examples are the $Fe_3(CO)_{10}(\mu_3$-O=PR) (R=^{t}Bu, ^{i}Pr) compounds synthesised in very low yields by Huttner and co-workers [4]. Together with the long W–O(2) distance (2.07(2) Å) indicative of a W–O single bond, the P=O bond length in **2** suggests a P=O→W interaction. Cluster **2** also has a W–O(1)–Ru(1) bridge (W–O(1) = 1.759(2); Ru(1)–O(1) = 2.227(2) Å) but, in this case, the oxide is double bonded to the tungsten atom and the interaction is best described as W=O→Ru. In this model tungsten is in a +4 oxidation state and one of the original oxo ligands has transferred to and oxidised the phosphinidene ligand. Overall **2** is electron precise (76 e-, 7 M–M).

In the second cluster **3** [12] (Fig. 2) the $Cp^*W(O)_2C_2Ph$ fragment is attached to a non-planar arrangement of four ruthenium atoms (4 Ru–Ru) via a μ_5-acetylide, two W–Ru bonds and two W–O–Ru oxide bridges. From the W–O and Ru–O bond lengths (W–O(1) = 1.815(4); W–O(2) = 1.783(4); Ru(1)–O(1) = 2.147(4); Ru(2)–O(2) = 2.191(4) Å), the metal–oxide interactions are best represented as W=O→Ru in both cases. In this case the tungsten atom is formally in a +6 oxidation state. Complex **3** is the first example of an early–late metal organometallic cluster with two oxide bridges to ruthenium [13].

In the tungsten oxo acetylide **1** and in the cluster **2** the alkynyl ligand is bound to tungsten via the Cα carbon atom. However in the conversion of **2** to **3** an apparent rotation of the alkynyl group has occurred such that in **3** Cβ, the carbon atom bearing the phenyl group, is attached to the tungsten atom. Although phenyl group migrations are known in organometallic chemistry [14], a reorientation of the acetylide on the cluster framework, similar to the rearrangement observed in other alkynyl clusters [15] is more likely.

On refluxing in heptane, **3** is converted solely to **2** whereas **2** remains unchanged under identical conditions. (Scheme 1). Thus **3**, with two W–O–Ru bridges is the kinetic product of the reaction of $Cp^*W(O)_2C_2Ph$ with **1** and **2** which formally results from oxidation of a phosphinidene ligand by a tungsten oxo functionality is the thermodynamic product. The high stability of complexes such as **2** in solution and in the solid state suggests, *inter alia* that oxide ligands may support novel combinations of early and late metals in disparate oxidation states and that oxidation of organophosphorus ligands may serve as a mechanism to reduce or mediate formal oxidation state differences between metal centers in clusters.

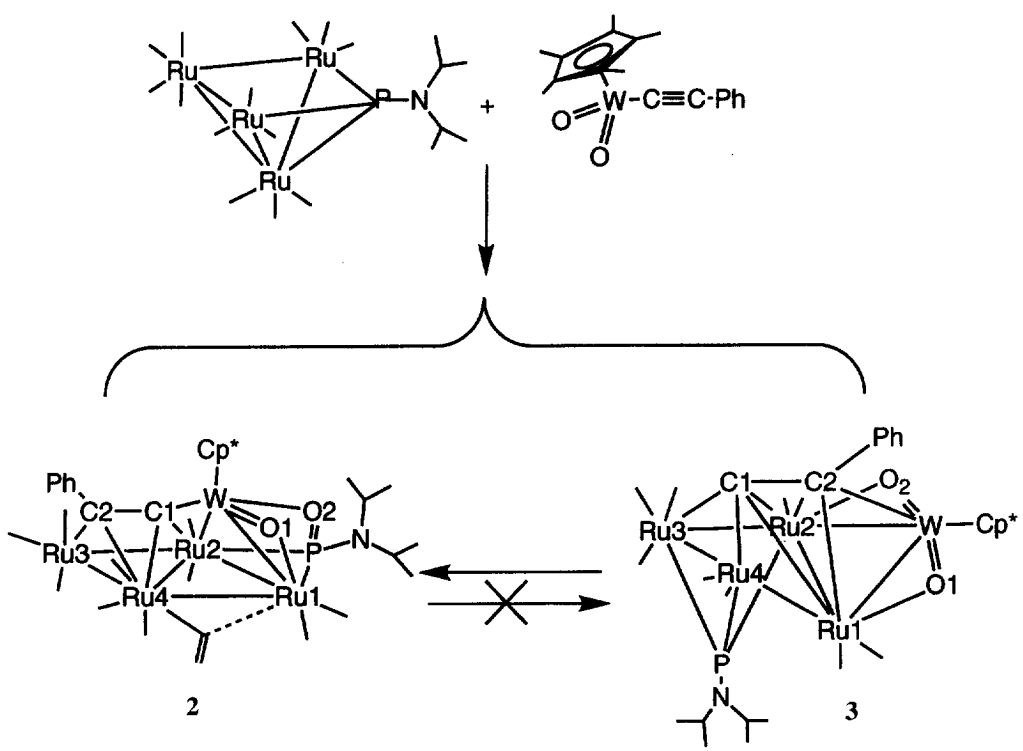

Scheme 1. *Synopsis* The new mixed early–late metal oxide bridged clusters $Cp^*W(\mu\text{-}O)Ru_4(CO)_9(\mu\text{-}CO)[\mu_3\text{-}\eta^2\text{-}OPN(^iPr)_2](\mu_4\text{-}\eta^2\text{-}CCPh)$ **2** and $Cp^*W(\mu\text{-}O)_2Ru_4(CO)_9[\mu_3\text{-}PN(^iPr)_2)(\mu_5\text{-}\eta^2\text{-}CCPh)$ **3** have been synthesised via the strategy of delivering an early metal oxo acetylide $Cp^*W(O)_2CCPh$ to a late metal alkyne acceptor $Ru_4(CO)_{13}(\mu_3\text{-}PN(^iPr)_2)$. Crystal structures reveal two W–O–Ru bridges in **3**, a single W–O–Ru Interaction in **2** and a novel W–O–P bridge to a μ_3-η^2-phosphinidoxo (O=PPh) ligand in **2**. The metals in **2** and **3** exist in disparate oxidation states.

In summary, new types of stable oxide bridged mixed metal organometallic clusters can be accessed via reaction of high oxidation state oxo acetylides with late metal carbonyl complexes. We are currently examining the potential of this methodology for the introduction of oxide ligands into other mixed oxidation state organometallic clusters and for the generation of new "oxidised" phosphido supporting ligands.

Supplementary material available

Texts describing the experimental details for complexes **2–3**, full details of crystal structure analyses including tables of bond distances and angles, atomic coordinates, anisotropic thermal parameters (23 pages). Ordering information is given on any current masthead page.

Acknowledgements—This work was supported by grants from the National Research Council of Canada and the Natural Sciences and Engineering Research Council of Canada (to A. J. C.). We are very grateful to Professor Y. Chi for a sample of $Cp^*W(O)_2C_2Ph$.

REFERENCES

1. (a) Schauer, C. K., Voss, E. J., Sabat, M. and Shriver, D. F. *J. Am. Chem. Soc.*, 1989, **111**, 7662. (b) Chi, Y., Hwang, L.-S., Lee, G.-H. and Peng, S.-M. *J. Chem. Soc., Chem. Commun.*, 1988, 1456. (d) Bottomley, F. and Sutin, L. *Adv. Organomet. Chem.*, 1988, **28**, 339. (e) Xiao, J., Vittal, J. J., Puddephatt, R. J., Manojlovic-Muir, L. and Muir, K. W. *J. Am. Chem. Soc.*, 1993, **115**, 7882. (f) Herrmann, W. A., Roesky, P. W., Wang, M. and Scherer, W. *Organometallics*, 1994, **13**, 4531. (e) Ichikawa, M. *Adv. Catal.*, 1992, **38**, 283.
2. Xiao, J. and Puddephatt, R. J., *Coord. Chem. Rev.*, 1995, **143**, 457.
3. Blenkiron, P., Carty, A. J., Peng, S.-M., Lee, G.-H., Su, C.-J., Shiu, C.-W. and Chi, Y., *Organometallics*, 1997, **16**, 519.
4. Buchholz, D., Huttner, G. and Imhof, W., *J. Organomet. Chem.*, 1990, **388**, 307.
5. Shiu, C.-W., Su, C-J., Pin, C.-W., Chi, Y., Peng, P. S.-M. and Lee, G.-H., *J. Organomet. Chem.*, 1997, **545–546**, 151.
6. Wang, W., Corrigan, J. F., Doherty, S., Enright, G. D., Taylor, N. J. and Carty, A. J., *Organometallics*, 1996, **15**, 2770.
7. Spectral data for **2**: IR (ν(CO) in C_6H_{14}) 2065(s); 2027(s); 2015(vs); 2001(m); 1981(m); 1965(w); 1960(vw) IR (CH_2Cl_2) 2060(s); 2022(vs); 2009(s); 2194(m); 1976(m); 1957(w); 1985(w) ^{1}H NMR ($CDCl_3$) δ: 7.80 (1H, d, $J_{H-H}=7.9$ Hz); 7.49 (1H, dd, $J_{H-H}=6.7$, $J_{H-H}=7.9$); 7.20 (1H, dd, $J_{H-H}=7.9$ Hz, $J_{H-H}=7.4$ Hz); 7.20 (1H, dd, $J_{H-H}=6.7$ Hz, $J_{H-H}=7.9$ Hz); 6.78 (1H, d, $J_{H-H}=7.4$ Hz); 3.88 (1H, q, $J_{H-H}=6.8$); 3.75 (1H, q, $J_{H-H}=6.8$); 2.00 (s, 15H); 1.43 (6H, d, $J_{H-H}=6.8$), 1.37 (6H, d, $J_{H-H}=6.8$) ^{31}P NMR ($CDCl_3$) δ: 248(s) Anal. Calcd. for **2**: C, 32.11, H, 2.70, N, 1.10% Found: C, 31.40, H, 2.61, N, 1.36%.
8. Spectral data for **3**: IR (ν(CO) in C_6H_{14}) 2071(s); 2036(s); 2021(vs); 2006(s); 1986(m); 1966(w); 1949(m) IR (CH_2Cl_2) 2070(m); 2036(s); 2016(vs); 2002(m); 1994(m); 1958(w); 1939(w) ^{1}H NMR ($CDCl_3$) δ: 8.55 (1H, d, $J_{H-H}=7.6$ Hz); 7.59 (1H, dd, $J_{H-H}=6.9$, $J_{H-H}=7.4$); 7.19 (2H, m); 6.19 (1H, d, $J_{H-H}=7.4$ Hz); 3.92 (2H, m); 1.83 (s, 15H); 1.30 (d, 12H $J_{H-H}=6.83$) ^{31}P NMR ($CDCl_3$) δ: 356 (bs) Anal. Calcd. for 3: C, 31.92, H, 2.60, N, 1.13% Found: C, 31.81, H, 2.35, N, 1.21%.
9. Crystal data for **2**: dark red crystals, $WRu_4PO_{12}NC_{34}H_{34}$, $M_r=1267.73$, monoclinic, space group $P2_1/n$, $a=13.0014(2)$, $b=21.4552(3)$, $c=14.7878(3)$ Å, $\beta=107.96(1)°$, $V=3024.1(1)$ Å^3, $Z=4$, $D_{calcd}=2.15$ mg/m^3, $\mu=4.53$ mm^{-1}, Mo–Kα $\lambda=0.70930$Å, F(000)=2403.27, $T=123$ K, Siemens SMART CCD, crystal size $0.20\times0.20\times0.20$ mm, $2\theta_{max}=57.5°$, 27,168 reflections measured, 10,104 unique reflections, 8,270 observed reflections ($I\geq2.5\sigma$(I)), semi-empirical absorption correction (transmission factors = 1.000–0.5494). Structure solution by direct methods, refinement on F^2 with anisotropic thermal parameters for all non-hydrogen atoms. Final R and Rw 0.036, 0.042. NRCVAX computer programs.
10. De Wet, J. F., Caire, M. R. and Gellatly, B. J., *Acta Cryst.*, 1978, **B34**, 762.
11. (a) Fogg, D. E. and Carty, A. J. *Polyhedron*, 1987, **7**, 2285. (b) Fogg, D. E., Taylor, N. J., Meyer, A. and Carty, A. J. *Organometallics*, 1986, **6**, 2252.
12. Crystal data for **3**: dark orange crystals, $WRu_4PO_{12}NC_{34}H_{34}CH_2Cl_2$, $M_r=1352.67$, triclinic, space group $P\bar{1}$, $a=11.2133(6)$, $b=12.0983(6)$, $c=16.9326(8)$ Å, $\alpha=73.04(1)$, $\beta=87.20(1)$, $\gamma=74.75(1)°$, $V=2118.87(3)$ Å^3, $Z=2$, $D_{calcd}=2.12$ mg/m^3, $\mu=4.35$ mm^{-1}, Mo–Kα $\lambda=0.70930$ Å, F(000)=1283.66, $T=123$ K, Siemens SMART CCD, crystal size $0.03\times0.15\times0.20$ mm, $2\theta_{max}=57.5$, 17,866 reflections measured, 10,556 unique reflections, 8203 observed reflections ($I>2.5\sigma$(I)), semi-empirical absorption correction (transmission factors = 0.4923–0.3422). Structure solution by direct methods, refinement on F^2 with anisotropic thermal parameters for all non-hydrogen atoms. Final R and Rw 0.036, 0.042. NRCVAX computer programs.
13. Bottomley, F. and Sutin, L., *Advances in Organomet. Chem.*, 1988, **28**, 339.
14. a) Blenkiron, P., Enright, G. D., Taylor, N. J. and Carty, A. J. *Organometallics*, 1996, **15**, 2855. b) Bly, R. S., Zhong, Z., Kane, C. and Bly, R. K. *Organometallics*, 1994, **13**, 899 and references therein.
15. Su, P.-C., Chiang, S.-J., Chang, L.-L., Chi, Y., Peng, S.-M. and Lee, G.-H., *Organometallics*, 1995, **14**, 4844.

Pergamon

PII: S0277-5387(98)00100-4

Polyhedron Vol. 17, No. 17, pp. 2975–2984, 1998
© 1998 Elsevier Science Ltd
All rights reserved. Printed in Great Britain
0277-5387/98 $19.00+0.00

The solution dynamics of adduct formation and electronic communication between ligand and metal core in electron deficient quinoline triosmium clusters‡

Avi Bar Din[a], Brian Bergman[a], Edward Rosenberg[a,*], Ryan Smith[a], Walter Dastru'[b], Roberto Gobetto[b], Luciano Milone[b] and Alessandra Viale[b]

[a]Department of Chemistry, The University of Montana, Missoula, MT 59812, U.S.A.

[b]Dipartimento di Chimica IFM, Universitá di Torino, 10125 Torino, Italy

(Received 31 October 1997; accepted 14 March 1998)

Abstract—The coordination of ammonia and of aliphatic amines (RNH_2(R = Et, n-Bu, s-Bu, t-Bu, cyclohexyl) and Et_2NH) to the electron deficient clusters $Os_3(CO)_9(\mu_3\text{-}\eta^2\text{-}C_9H_6N)(\mu\text{-}H)$ (**1**) and $Os_3(CO)_9(\mu_3\text{-}\eta^2\text{-}XC_9H_5N)(\mu\text{-}H)$ (X = 5-NH_2, **4**; 3-NH_2, **5**; 6-NH_2, **6**; 5-Br, **7**; 5-CH_3, **8**) has been studied. The initially formed adducts of the amines with **1** gradually isomerize to give a mixture of two isomers whose ratio varies with the cluster, the solvent and the amine. Studies of the variation of the isomer ratio with temperature yield ΔH° and ΔS° values for the isomer equilibrium. The primary cause of the change in the isomer ratio is the variation in ΔS° which is rationalized as being due to solvation effects. The overall structure of the two isomers is assigned on the basis of NMR measurements to one where the amine occupies an axial position on the cluster and where the hydride and quinoline ring bridge different edges of the cluster. The equilibrium constant for amine complex formation is primarily determined by the steric bulk of the amine. The amine substituted complex **4** shows absolutely no tendency to coordinate amines and this is ascribed to relief of the electron deficiency at the metal core by the mesomeric effects of the *para*-amino group. The isomeric **5** and **6**, however, do undergo coordination of amines at the metal core. The 5-methyl substituted complex **8** does not complex amine either. Compounds **1**,**4**–**8** all undergo simple protonation with both coordinating (CF_3CO_2H) and non-coordinating acids (HBF_4) to give cationic dihydrido complexes whose solution structures are elucidated by NMR techniques. The chemistry of these electron deficient clusters is compared with related $\mu_3\text{-}\eta^2$ imidoyl complexes and can be understood in terms of the Hammett equation, at least for protonation. © 1998 Elsevier Science Ltd. All rights reserved

Keywords: Amines; clusters; Osmium; Quinolines.

INTRODUCTION

We recently reported the synthesis and reactivity of a novel class of electron deficient triosmium clusters $Os_3(CO)_9(\mu_3\text{-}\eta$ [2]-$C_9H_6N)(\mu\text{-}H)$ (**1**) from the reaction of quinoline with $Os_3(CO)_{10}(CH_3CN)_2$ followed by thermolysis or photolysis of the initially formed decacarbonyl eq. (1) [1–3]. This type of compound can be synthesized in good yield with a wide range of substituents in the quinoline ring [1, 4].

The reaction of these complexes with soft nucleophiles such as phosphines results in ligand addition at the metal core along with rearrangement eq. (2) [1, 3]. On the other hand, reaction with hydride [1] or carbanions [4] results in nucleophilic attack at the 5-position of the quinoline ring. Subsequent protonation leads to a nucleophilic addition product eq. (3) [4] and hydride abstraction from the intermediate anion effects overall nucleophilic substitution eq. (4) [4]. In light of this diverse reactivity, we thought it would be useful to study the reactivity of **1** with amines

* Author to whom correspondence should be addressed.

‡ Dedicated, with respect and admiration to Professor Jack Lewis on the occasion of his 70th birthday.

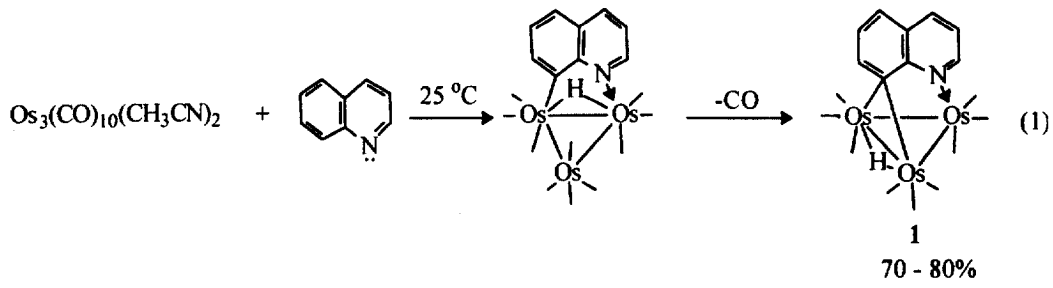

(1)

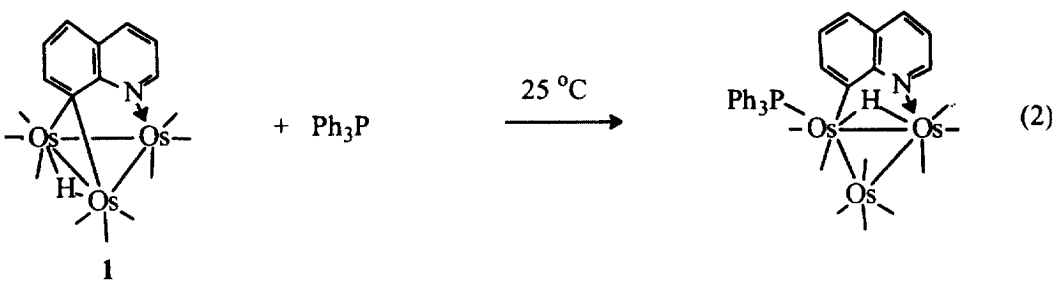

(2)

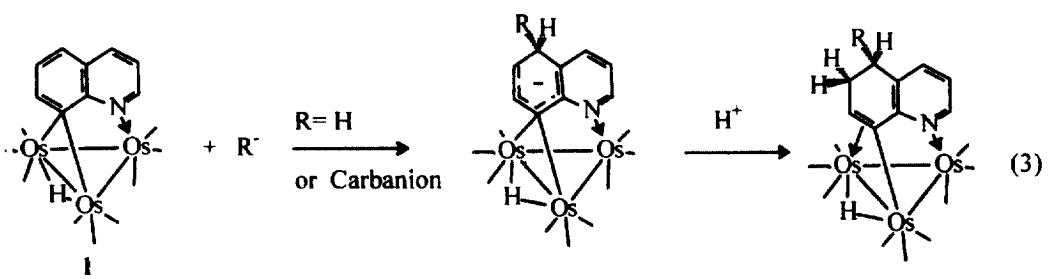

(3)

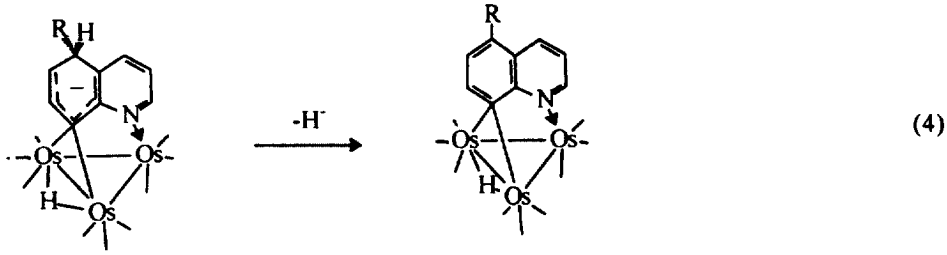

(4)

and carboxylic acids which are intermediate in nucleophilicity relative to phosphines and carbanions.

We recently completed detailed studies of the reaction of these ligands with the electron precise, but quite reactive μ_3 imidoyl complexes of the type, $Os_3(CO)_9(\mu_3\text{-}\eta^2\text{-}C{=}N(\text{-}CH_2\text{-})_3(\mu\text{-}H)$, where coordination was highly selective for primary amines and where the formation of two axially coordinated isomers, $Os_3(CO)_9(\mu\text{-}\eta^2\text{-}C{=}N(\text{-}CH_2\text{-})_3(\mu\text{-}H)L$ (**2** and **2'**) was observed eq. (5) [5]. The neutral adduct $Os_3(CO)_9(\mu\text{-}\eta^2\text{-}C{=}N(\text{-}CH_2\text{-})_3(\mu\text{-}H)_2(CF_3CO_2)$ (**3**), was the main product of the reaction of trifluoroacetic acid with the μ_3-imidoyl complexes but a small amount of a monoprotonated species was observed to be in equilibrium with the adduct eq. (6). In the case of non-coordinating anions such as BF_4^-, only simple protonation was observed [6, 7].

We report here the results of studies on the coor-

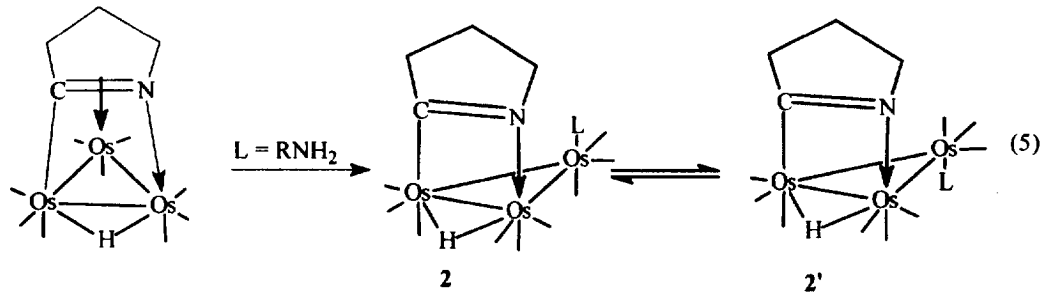

(5)

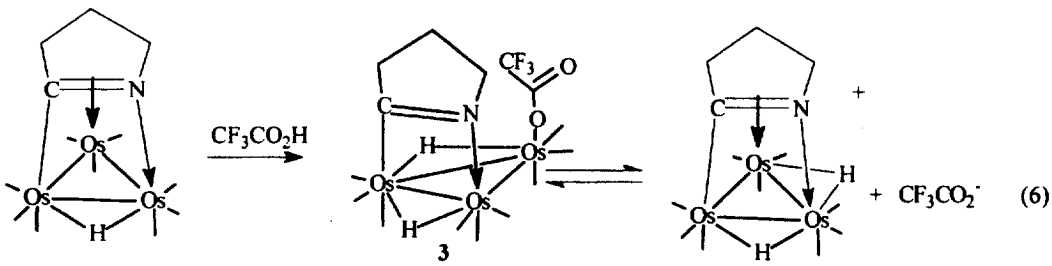

(6)

dination chemistry of ammonia, aliphatic amines, and protic acids with **1**, in an attempt to define the stereodynamics of its coordination sites and how these differ from those observed in **2** and **3** (eqs. (5–6)). One of our research goals in developing the chemistry of complexes such as **1** was to understand the degree of electronic communication between the quinoline ring and the metal core. Our initial efforts in this area have resulted in the synthesis of the compounds $Os_3(CO)_9(\mu_3\text{-}\eta^2\text{-}XC_9H_5N)(\mu\text{-}H)$ (X = 5-NH_2, **4**; 3-NH_2, **5**; 6-NH_2, **6**; 5-Br, **7**; 5-CH_3, **8**). We report here our initial results on the synthesis of these compounds according to the methods outlined in eqs. (1–4). Studies of their reactivity reveal the extraordinary impact of the electron deficient bonding mode of the cluster on the substituent in the 5-position and *vice versa*.

RESULTS AND DISCUSSION

Reactions with amines

The addition of a large excess (50 fold) of ammonia and various aliphatic amines to **1** results in an instant color change from green to orange and in the appearance of two new hydride peaks in the ^1H NMR in the range of −12 to −14 ppm (Table 1). The resonance at higher field (isomer I) is invariably in greater intensity (except in the case of NH_3) and the lower field resonance (isomer II) gradually increases in intensity until a final ratio (I/II), in the range of 0.5 to 4.8, is reached which does not change further (Table 1).

The ^{13}C NMR ($CDCl_3$, −60°C) of a ^{13}CO enriched sample of **1** treated with excess ammonia shows two sets of nine carbonyls (I: 187.3, 185.5, 185.6, 180.4, 179.8, 178.8 ($^2J^{13}C\text{-}^1H = 14$ Hz), 177.3($^2J^{13}C\text{-}^1H = 9$ Hz), 176.7, 176.2 ppm; II: 187.3, 186.7, 184.6, 182.0, 180.8, 177.8($^2J^{13}C\text{-}^1H = 12.5$ Hz), 177.5 ($^2J^{13}C\text{-}^1H = 9.6$ Hz), 176.8, 176.2 ppm). Significantly, the spectrum shows no resonances with ^{13}C satellites that, if present are indicative of a large *trans*-carbonyl coupling associated with the presence of an $Os(CO)_4$ group [5]. The previously reported amine complexes of triosmium clusters, **2** and **2'**, invariably have the amine (or ammonia) in an axial position eq. (5) [5]. Based on these facts alone, we can propose two alternative structures for the set of isomers formed from the interaction of amines with **1** eq. (7). One set has the hydride and the quinoline ring sharing a common edge while the amine occupies either axial site on the third, unbridged osmium atom (structures **A**, **A'**, eq. (7)). This structure is directly analogous to that observed related to μ_3 imidoyl complexes, **2** and **2'**, for which solid state structures are available eq. (5) [5].

On the other hand, coordination of the amine at the electron deficient osmium edge of **1** could lead to a structure where the quinoline ring and the hydride are on different edges with the amine occupying an axial position on the osmium atom bridged by the hydride but not by the quinoline ring structures **B**, **B'**, eq. (7)). This type of structure has been observed in the case of one imidoyl complex bearing ethyl and propyl groups on the imidoyl carbon and nitrogen atoms respectively eq. (8) [8]. We have also obtained indirect evidence for this structural type as a short-lived intermediate from the selective incorporation of

Table 1. Chemical Shifts (ppm) and Isomer Ratios for Amine Adducts of $Os_3(CO)_9(\mu_3\text{-}\eta^2\text{-}C_9H_6N)(\mu\text{-}H)$, **1**.[1]

	Isomer I	Isomer II	Solvent	Temperature	I/II
NH_3	−13.65 ppm	−13.05	$CDCl_3$	RT	0.5
	−13.40	−12.70	acetone	RT	1.3
$EtNH_2$	−13.66	−13.06	$CDCl_3$	RT	1.3
	−13.43	−12.77	acetone	−40°C	3.8
Et_2NH[a]	−13.80	—	$CDCl_3$	RT	—
t-$BuNH_2$	−14.12	−13.56	$CDCl_3$	−40°C	7.4
s-$BuNH_2$[b]	−13.59/	−12.97/	$CDCl_3$	−40°C	3.3
	−13.62	−13.00			
n-$BuNH_2$	−13.39	−12.76	$CDCl_3$	RT	2.8
$CyNH_2$	−13.61	−13.03	$CDCl_3$	RT	3.1
	−13.46	−12.81	acetone	RT	4.8

[a] only one isomer observed
[b] four hydride resonances observed

carbon monoxide into **1** [3]. In the case of phosphines reacting with **1**, such an intermediate is probably the initial product as well but goes on to rearrange as shown above eq. (2) [1, 3].

The initial formation of one isomer followed by the gradual appearance of a second has been shown to be an intermolecular process for the related μ_3-imidoyl complexes [5]. It would appear that this is also the case for **1** reacting with amines since the overall behavior of **1** towards amines is so similar [5]. The question of the structure of the amine adducts of **1** (**A** or **B**) still remains unanswered in the absence of a solid state structure.

The change in longitudinal relaxation time (T_1) of hydrides in metal clusters induced by proximal ligand protons can be used to qualitatively assess the distance between these two types of hydrogens [9]. Thus, for $Os_3(CO)_{10}(\mu\text{-}\eta^2\text{-}C_9H_6N)(\mu\text{-}H)$ (**9**) the T_1 of the hydride is 7.0 s while for **1** it is 4.0 s (Figure 1). We can attribute the shorter relaxation time in **1** to the proximity of the hydrogen of C(7) to the μ-hydride. If the amine adducts of **1** have a structure identical to their μ_3-imidoyl analogs then the T_1 of the μ-hydride would be expected to have a relaxation time similar to **9**. In fact, the T_1 of the ammonia adduct of **1** is 1.4 s which is consistent with a structure where the ammonia protons are proximal to the hydride; i.e., the structure resulting from addition of the ligand to the carbon bridged edge of the cluster without further rearrangement (structure **B**, eq. (7)).

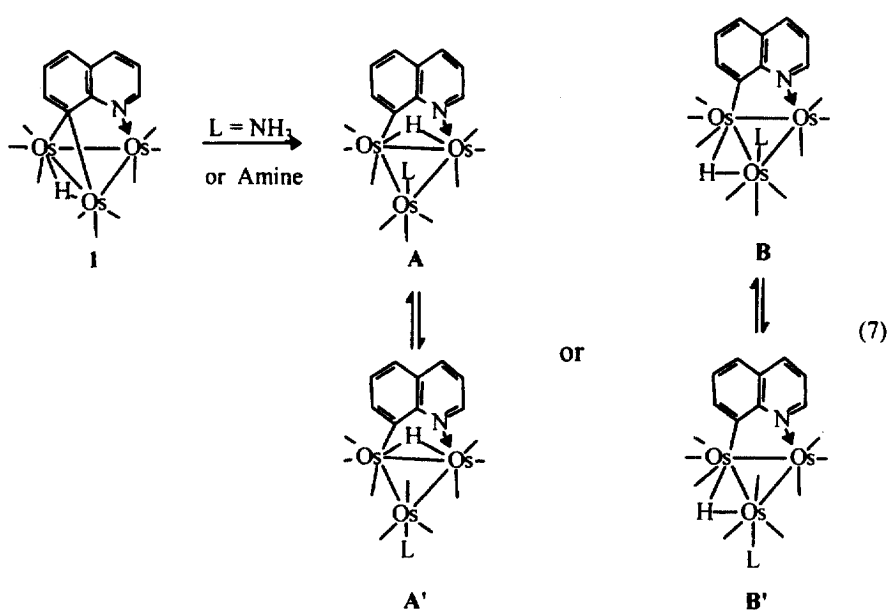

(7)

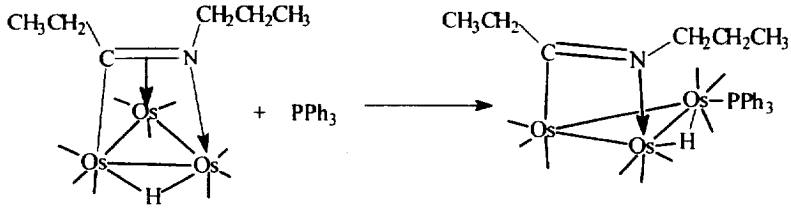

9

$T_1 = 7$ s

1

$T_1 = 4$ s

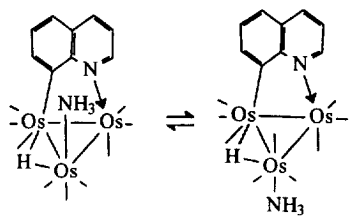

B B'

$T_1 = 1.4$ s

Scheme 1.

This suggested structure is further supported by the ^{1}H NMR data obtained for the s-butyl adduct **1**. Here, four hydride resonances are observed. This is undoubtedly due to the presence of diastereomers induced by the presence of the chiral center on the s-butyl amine. In the structure proposed based on the T_1 measurements (structure B, eq. (7)), the environment on the osmium atom bound to the amine is quite asymmetric owing to the presence of the bridging hydride on one of the two edges of the triangle associated with the amine coordinated osmium atom. In the case of the structure adopted by the μ_3-imidoyl amine adducts (**2** and **2'** eq. (5)), the localized environment on the amine bound nitrogen is more symmetric and indeed only two hydride resonances are observed for the s-butyl complex [5].

Finally, the structure proposed is most consistent with a reversible amine coordination based on the principle of least motion since only the motion of the C(8) carbon pivoting on the coordinated nitrogen is required to reform **1** from its corresponding amine adduct. This motion is related to the reversible coordination of the C=N bond observed in the μ_3- to μ- to μ_3-imidoyl interconversions [5].

In our previous study of the imidoyl amine adducts, the initially formed isomer has the amine on the same face of the osmium triangle as the pyrrolidine ring (i.e., *syn*-) [5]. This isomer is more favored for the bulkier amines and this also appears to be the trend for the amine complexes of **1** Table 1. In fact, for the secondary amine Et_2NH only one isomer with a hydride chemical shift similar to the proposed *syn*-isomer is observed Table 1. Our initial thought for the imidoyl series was that the strictly sigma-bond framework of the pyrrolidine ring was less bulky than the carbonyl ligands which have π-electrons [5]. In light of the isomer ratios observed for the amine complexes of **1**, this cannot be the case since the quinoline ring also has π-electron density. Yet, the *syn*-isomer is still favored for bulkier ligands and the *anti*-isomer for the least bulky (ammonia). In order to further investigate this point, we measured the effect of temperature and solvent on the isomer ratio for three amine adducts of **1**. There are two obvious trends in the data (Table 2). First, it can be seen that the population of the *syn*-isomer is enhanced in the more polar solvent acetone Table 2. This, of course, is sensible in light of the expected greater polarity of the Os–

Table 2. ΔH° (kJ/mol) and ΔS° (J/mol K) for Amine Adducts of $Os_3(CO)_9(\mu_3\text{-}\eta^2\text{-}C_9H_6N)(\mu\text{-}H)$, **1**[a2]

	k(I/II) 273 K	k(I/II) 298 K	ΔH° kJ/mol	ΔS° J/mol K	solvent
NH_3	0.52	0.49	-0.85 ± 0.19	-8.44 ± 0.77	$CDCl_3$
NH_3	1.55	1.33	-2.15 ± 0.75	-4.38 ± 2.9	Acetone
NH_2Et	1.22	1.34	3.35 ± 0.48	13.9 ± 1.8	$CDCl_3$
NH_2Et	4.0	3.85	2.20 ± 0.74	19.7 ± 2.9	Acetone
$CycNH_2$	3.45	3.07	-0.95 ± 0.54	6.76 ± 2.2	$CDCl_3$
$CycNH_2$	5.12	4.81 (extr.)	-1.44 ± 0.27	8.21 ± 1.1	Acetone

[a] Values and errors obtained by taking the least squares fit to the function $\ln I/II = \Delta H^\circ - T\Delta S^\circ$ for at least ten temperatures between 233 and 298 K.

N bonds with the quinoline and amine relative to the Os–CO bonds. Overall, the ΔH° values hover around zero, ranging from -3 to $+2$ kJ/mole. The most significant differences between compounds and between solvents are in the ΔS° Table 2. Significantly, the ammonia complex is the only one with a negative ΔS°. This indicates that solvation, not steric effects, can account for the observed differences in the isomer ratios. Apparently, the more polar *syn-* isomers lead to more disordered solute–solvent interactions and this effect is enhanced by the presence of non-polar substituents on the amine. That the larger cyclohexyl group shows a less positive ΔS° than the ethyl group is difficult to rationalize but may relate to the mobility of this ligand in the adduct.

The trends in the equilibrium constants for the formation of amine complexes with **1** follow the trends observed for the related μ_3 imidoyl species, *n*-Bu > *s*-Bu > *t*-Bu. The absolute values for the equilibrium constants for **1** however, are much greater being 44.4, 2.7, and 0.39; and 1.25, 0.37, and 0.005 for **1** and the μ_3-imidoyls respectively [5]. This undoubtedly reflects the greater electron deficiency for the 46e$^-$ cluster relative to the reactive but electron-precise μ_3-imidoyls.

In order to assess the impact of an electron donating group on the coordination chemistry observed for **1**, we undertook the synthesis of the 3-, 5- and 6-amino analogs of **1**. The synthesis of these complexes proceeded in a straightforward manner. Significantly, the 5-amino derivative, $Os_3(CO)_9(\mu_3\text{-}\eta^2\text{-}5\text{-}NH_2C_9H_5)(\mu\text{-}H)$ (**4**) formed directly, at ambient temperatures, without requiring thermal or photochemical decarbonylation eq. (9) [1–3]. This undoubtedly reflects the impact of the strong π-electron donor in a position *para-* to the incipient three center, two electron band. The 3- and 6-amino derivatives **5** and **6** did require the usual decarbonylation procedure (eqs. (10–11)). In all of these reactions (eqs. (9–11)) no detectable competition for coordination of the quinoline nitrogen by the aniline amino groups is seen but the yields of **5** and **6** were significantly lower than for **4** and **1**.

The reaction of **4** with *n*-$BuNH_2$ in both CD_2Cl_2 and CD_3OD showed no sign of complex formation even in the presence of a 100-fold excess of *n*-$BuNH_2$. This can be attributed to the electron donating ability of the amino group which funnels electron density down to the electron deficient C(8)–Os_2 bonding framework by conventional benzenoid resonance.

The 3- and 6-amino derivatives **5** and **6** do coordinate *n*-$BuNH_2$, as **1**. The formation constants are of the same order of magnitude as for **1**, with **6** showing a significantly larger formation constant than **5** or **1** (Table 3). As for **1**, isomer I, presumably the more polar isomer is favored with the equilibrium ratios of I/II being two to three times larger than for **1** Table 3. One might have expected the K_f for **6** to be less than that of **5** since the electron donating amino group is on the carbocyclic ring, albeit in the meta position. Clearly, the magnitude of K_f and the I/II ratio depend on a subtle combination of factors which cannot be delineated at this time. The one firm conclusion that can be drawn from these studies is the profound influence that substitution at the 5-position of the quinoline ring has on the electron density at the metal core. This is born out by our studies of the $Os_3(CO)_9(\mu_3\text{-}\eta^2\text{-}(5\text{-}Br)C_9H_5N)(\mu\text{-}H)$ [4] (**7**) where the electron withdrawing bromine in the 5-position gives the largest K_f of all the derivatives of **1** investigated so far. In the case of $Os_3(CO)_9(\mu_3\text{-}\eta^2\text{-}(5\text{-}CH_3)C_9H_5N)(\mu\text{-}H)$ [4] (**8**), where there is only a weakly electron donating group in the 5-position amine complex formation was also not observed even in the presence of a large excess of n-$BuNH_2$.

Reactions with protic acids

In order to further probe the electron distribution in **1** and **4–8** we investigated their reactions with CF_3CO_2H and HBF_4. Addition of a six-fold excess of CF_3CO_2H to a CD_2Cl_2 solution of **1** results in complete conversion to a deep orange solution which exhibits two hydride resonances at -13.66 and -11.61 ppm in a 1:1 ratio. The aromatic resonances are all shifted downfield with respect to **1**. An equilibrium constant for protonation was calculated from a titration of **1** with CF_3CO_2H (Table 4). The ^{13}C-

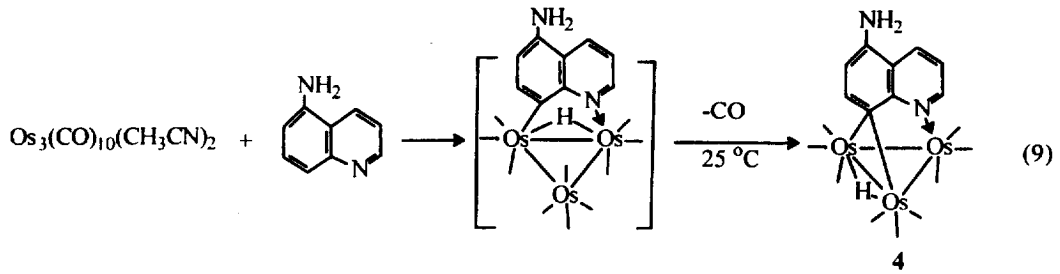

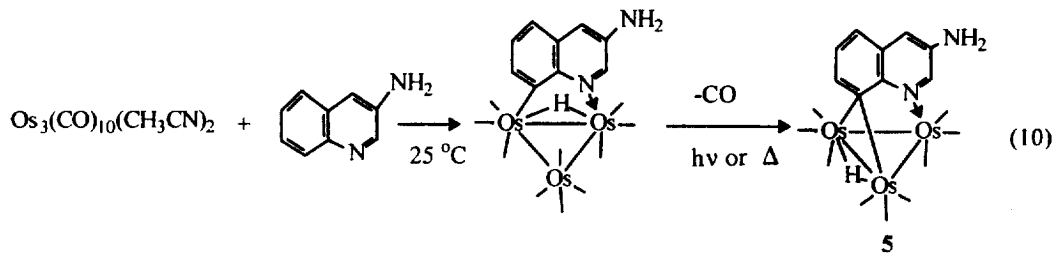

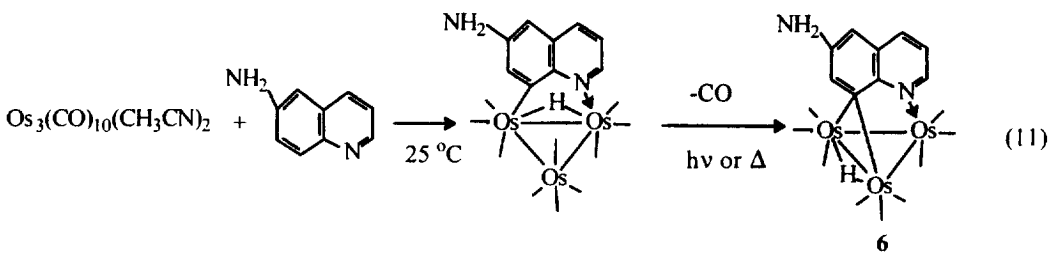

Table 3. Equilibrium Constants and Isomer Ratios for n-BuNH$_2$ Complexes of Electron Deficient Quinoline Clusters[a3]

Compound	K_{FORM}	I/II	δ hydride I(II)	Solvent
1	44.4	2.8	−13.39(−12.76)	$CDCl_3$
5	53.9	7.3	−13.42(−12.81)	CD_2Cl_2
6	66.7	4.6	−13.42(−12.79)	CD_2Cl_2
7	94.5	1.2	−13.47(−12.90)	$CDCl_3$

[a] ±10% at 22°C

NMR (CD_2Cl_2) of a ^{13}CO sample of **1** in the presence of the same excess gives a ^{13}C NMR in the carbonyl region showing nine resonances at 180.65, 175.20, 172.50, 172.45, 171.01, 167.93, 166.52, 159.84, and 159.99 ppm. The two resonances at 159.84 and 158.99 ppm appear as doublets of doublets in the proton coupled spectrum ($^2J^{13}C\text{-}^1H = 13.74$, 4.58 and 13.73, 6.10 Hz respectively) while the two at 180.65 and 172.45 ppm appear as doublets ($^2J^{13}C\text{-}^1H = 9.15$ and 7.63 Hz). Protonation with the non-coordinating acid, HBF_4 yields the virtually identical ^1H Table 4 and ^{13}C NMR (CD_2Cl_2) data (180.61, 175.78, 172.92, 172.36, 171.43, 168.13, 166.71, 159.94, 158.85 ppm with an identical coupling pattern). These data are consistent with simple protonation to give a dihydride cation eq. (12) as opposed to acid adduct formation

Table 4. Protonation Equilibria for Electron Deficient Quinoline Triosmium Clusters[a4]

Compound	K_{eq}	Acid	δ hydrides	Solvent
1	0.12	CF_3CO_2H	−13.66 −11.61	$CDCl_3$
1	12.2	HBF_4	−13.70 −11.65	$CDCl_3$
4	20.8	CF_3CO_2H	−14.35 −12.60	$CDCl_3$
5	0.72	CF_3CO_2H	−13.81 −11.73	$CDCl_3$
6	1.88	CF_3CO_2H	−13.72 −11.70	$CDCl_3$
7	0.05	CF_3CO_2H	−13.78 −11.50	$CDCl_3$
8	1.19	CF_3CO_2H	−14.00 −12.15	$CDCl_3$

[a] Measured by ^1H NMR ±10% at +22°C

eq. (6). The equilibrium constant for formation of the cation is considerably larger for the stronger acid, HBF_4 Table 4. The observation of well resolved carbonyl–hydride couplings indicates that the protonated species is rigid on the NMR time scale while the hydrides in the related cationic μ_3-imidoyl species are fluxional at ambient temperatures.

that the partially averaged acid/amine resonance is found between **5** and **6** ppm, suggesting a higher degree of amine protonation. The protonation equilibrium values (Table 4) obtained from these experiments are consistent with **4** having the greatest influence on the electron density at the metal core. A Hammett plot of the equilibrium data using standard

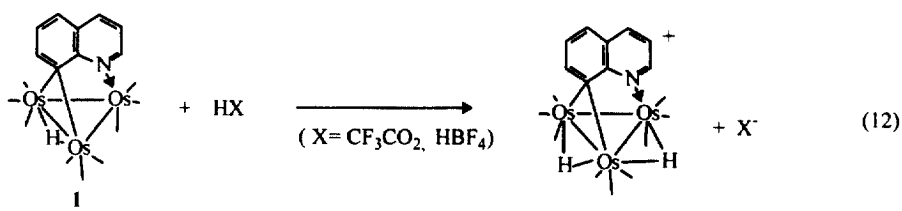

1 (12)

The protonation of **4** with aliquots of CF_3CO_2H reveals that the 5-amino derivative is considerably more basic at the metal core than **1** Table 4. After the first aliquot (slightly in excess of 1 equivalent) is added, **4** is completely converted to the dihydride cation and the resonance at 5.60 ppm attributable to the amino resonance is no longer observed. Instead, a broad resonance at 7.82 ppm is observed which is attributable to a partially averaged signal of the CF_3CO_2H and the amino group of **4**. The CF_3CO_2H proton resonance is observed at 8.00 ppm in the presence of **1**. As more CF_3CO_2H is added to the solution of **4**, the acid amine resonance shifts to lower fields and sharpens somewhat indicating more rapid exchange between the amine and the acid. Significantly, the amine resonances for **5** and **6** are found at considerably higher fields than for **4** at 4.14 and 4.79 ppm respectively. On treatment with CF_3CO_2H, the same overall behavior as for **4** is observed for **5** and **6** except

values of σ[10] yields a reasonably good straight line with a correlation coefficient of 0.93 and ρ value of −0.13 (Figure 1).

CONCLUSIONS

The electron deficient μ_3-η^2-quinoline triosmium clusters exhibit behavior towards amines similar to the related μ_3-η^2 pyrrolidine triosmium clusters [5]. Both show initial formation of a single isomer which then equilibrates to a mixture of two complexes. The equilibrium constants in both series depend on the steric bulk of the amine with the overall magnitudes being much greater for the quinoline series. Based on the NMR evidence accumulated to date, the actual structure of the amine–quinoline adducts is different from that of the imidoyls. However, definitive conclusions about the actual structures must await solid

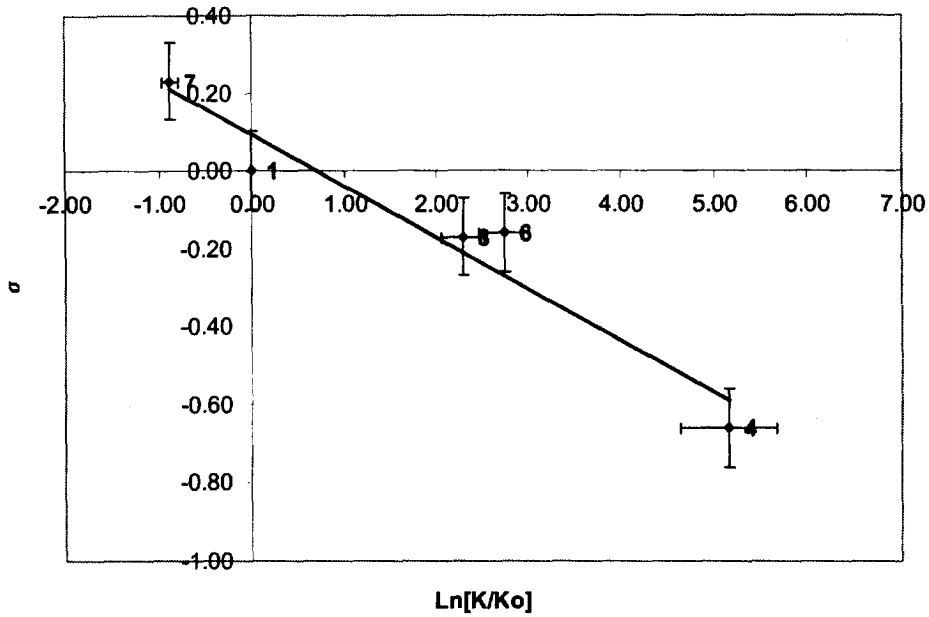

Fig. 1. Hammett, σ/ρ Plot of the Protonation Equilibria for Compounds **1**, **4**–**8** reacting with CF_3CO_2H (error bars for the σ values are from reference [10] and are $\pm 10\%$ for the K_{eq} values).

state structural determinations which have been difficult to obtain owing to the instability of the adducts as crystalline solids.

In sharp contrast to the μ_3-η^2-imidoyl clusters, the μ_3-η^2-quinoline clusters do not form acid adducts but simply undergo protonation in the presence of CF_3CO_2H.

The most interesting aspect of these studies is the profound influence that substituents in the 5-position have on the electronic properties of the metal core. That the simple free energy relationship normally applied to organic reactions can be used to rationalize the relationship between substitution on the carbocyclic ring and protonation at the metal core is reassuring in that it says that the relatively complex interactions (from an orbital point of view) between an organic moiety and two metal atoms can be understood in terms of a traditional physical organic chemistry model. The isomer I and II populations and the somewhat higher value of K_f for the 6-amino quinoline derivative, are less well understood, but seem to be dominated by solvation effects, at least from the data gathered so far.

EXPERIMENTAL

General: Compounds **1** [1], **7** [11] **8** [4], and 5-amino quinoline [11] and 5-bromo quinoline [11] were synthesized by known literature procedures. 3-Amino quinoline and 6-amino quinoline were purchased from Aldrich Chemical Co. and used as received. Methylene chloride was distilled from calcium hydride before use. Acetone-d_6, methylene chloride-d_2, and methanol-d_4 were purchased from Aldrich in single sample ampules and used as received. Chloroform-d_1 was dried over molecular sieves before use. NMR spectra were recorded on Jeol EX-400 or Varian Unity Plus 400 NMR spectrometers. Samples for T_1 measurement were previously degassed by three freeze thaw cycles. The non selective inversion recovery pulse sequence was used to obtain T_1 values. Infrared spectra were recorded on a Perkin–Elmer 1600 spectrometer and elemental analyses were performed by Schwarzkopf Microanalytical Laboratories, Woodside, New York.

Preparation of $Os_3(CO)_9(\mu_3\text{-}\eta^2\text{-}(5\text{-}NH_2)C_9H_5N)(\mu\text{-}H)$ ***4***. $Os_3(CO)_{10}(MeCN)_2$ (0.250 g, 0.268 mmol) was dissolved in CH_2Cl_2 (150 mL) and 5-amino quinoline (0.080 g, 0.5 mmol) was added. The reaction mixture was stirred for 16 h at room temperature. The resulting deep green solution was separated and filtered through a 14″ silica gel column eluted with hexane/CH_2Cl_2 (70:30), giving two bands. The first yellow band was a mixture of the isomers $Os_3(CO)_{10}(\mu\text{-}\eta^2\text{-}(5\text{-}NH_2)C_9H_5N)(\mu\text{-H})$ (less than 10%). The second fraction yielded (0.223 g, 0.219 mmol, 82.1% overall from $Os_3(CO)_{10}(CH_3CN)_2$) of the green major product, **4**, $Os_3(CO)_9(\mu_3\text{-}\eta^2\text{-}(5\text{-}NH_2)C_9H_5N)(\mu\text{-H})$ which gave green crystals from hexane/CH_2Cl_2 at -20C.

Analytical and spectroscopic data for $[Os_3(CO)_9(\mu_3\text{-}\eta^2\text{-}(5\text{-}NH_2)C_9H_5N)(\mu\text{-}H)]$ ***4***. Anal. calcd for $C_{18}H_8N_2O_9Os_3$: C, 22.38, H, 0.78; N, 2.76. Found: C, 22.37; H, 0.75; N, 2.83. IR (ν(CO) in hexane): 2080w, 2069m, 2040s, 2013s, 1981s, 1967w cm^{-1}. ^{1}H-NMR at 400 MHz in $CDCl_3$: δ 9.25 (dd, H(2)), 7.07 (t, H(3)), 8.00 (dd, H(4)), 8.16 (dd, H(6), 6.43 (d, H(7)), 5.60 (broad singlet, NH_2), -13.01 (s, hydride).

Synthesis of $Os_3(CO)_9(\mu_3\text{-}\eta^2\text{-}(n\text{-}X)C_9H_5N)(\mu\text{-}H)$, **5** (n = 3, $X = NH_2$), **6** (n = 6, $X = NH_2$), **7** (n = 5, $X = Br$). $Os_3(CO)_{10}(CH_3CN)_2$ (0.250–0.500 g, 0.27–0.54 mmol) was dissolved in 150–200 mL CH_2Cl_2 and a two-fold molar excess of the substituted quinoline was added by syringe. The solution was stirred for 16–20 h and then filtered through a small silica gel column to remove excess ligand and a small amount of brown decomposition product. The yellow methylene chloride solution was then photolyzed using a Rayonet photochemical reaction chamber equipped with 300 nm lamps for 2–4 h or until the infrared spectrum showed essentially complete conversion to the green nonacarbonyl derivative. The green methylene solution was then concentrated and purified by thin layer chromatography using 1:1 hexane/methylene chloride (for **5** and **6**) or 7:3 hexane/methylene chloride (for **7**). Yields for **5** and **6** ranged from 50–60% while those for **7** were 80–85%.

Analytical and spectroscopic data for $Os_3(CO)_9(\mu_3\text{-}\eta^2(3\text{-}NH_2)C_9H_5N)(\mu\text{-}H)$ **5**. Calculated for $C_{18}H_8N_2O_9Os_3$: C, 22.38; H, 0.78; N, 2.76. Found: C, 22.12; H, 1.02; N, 2.84. IR(ν(CO) in CH_2Cl_2): 2076w, 2050s, 2017s, 1989m, br cm^{-1}. ^1H NMR at 400 MHz in Acetone-d_6: δ 9.31(d, 1H), 8.68(dd, 1H), 8.61(dd, 1H), 7.41(d, 1H), 7.30(dd, 1H), 4.14(s, br, 2H), −12.23(s, 1H).

Analytical and spectroscopic data for $Os_3(CO)_9(\mu_3\text{-}\eta^2\text{-}(6\text{-}NH_2)C_9H_5N)(\mu\text{-}H)$ **6**. Calculated for $C_{18}H_8N_2O_9Os_3$: C, 22.38; H, 0.78; N, 2.76. Found: C, 22.49, H, 0.86; N, 2.71. IR (ν(CO) in CH_2Cl_2): 2076w, 2041s, 2018s, 1988m, br, 1973w, br cm^{-1}. ^1H NMR at 400 MHz in $CDCl_3$: δ 8.92(dd, 1H), 7.83(d, 1H), 7.79(dd, 1H), 7.36(d, 1H), 6.97(dd, 1H), 4.79(s, br 2H), −12.23(s, 1H).

Spectroscopic and analytical data for $Os_3(CO)_9(\mu_3\text{-}\eta^2\text{-}(5\text{-}Br)C_9H_5N)$ **7**. Calculated for $C_{18}H_6NO_9BrOs_3$: C, 20.97; H, 0.48, N, 1.36. Found: C, 20.84; H, 0.38; N, 1.37; IR(ν(CO) in CH_2Cl_2): 2077m, 2050s, 2020s, 1990s, 1977w, 1952w cm^{-1}. ^1H NMR at 400 MHz in $CDCl_3$: δ 9.32(dd, 1H), 8.49(dd, 1H), 8.39(d, 1H), 7.46(d, 1H), 7.19(dd, 1H), −12.07(s, 1H).

Evaluation of isomer ratios and equilibrium constants. Compounds **1** or **4–8**, were weighed directly into flame dried NMR tubes in 9–11 mg samples (~0.01 mmol). 0.60 mL of the NMR solvent was then added by syringe, followed by syringe addition of 2–20 μL of the amine or acid. The NMR tube was then capped and shaken and the proton or ^{13}C NMR monitored for at least 24 h after which time no further changes in the spectra were observed. The isomer ratios and equilibrium constants were evaluated by integration of the appropriate resonances. For formation constants, the equilibrium expression was:

$$K_f(\text{L/mol}) = \frac{[\text{cluster}-\text{amine adduct}]}{[\text{cluster}][\text{amine}]}$$

in most cases the equilibrium constant was evaluated at several concentrations of added amine and an average value is reported in Table 3. For the protonation equilibrium, the expression used was:

$$K_p = \frac{[\text{clusterH}^+][X^-]}{[\text{cluster}][HX]}$$

Again, the value of the equilibrium constant was evaluated at several acid concentrations in most cases.

Acknowledgements. We gratefully acknowledge the National Science Foundation CHE 9625367 (E. Rosenberg), the Consiglio Nazionale Ricerche (CNR, L. Milone), the Ministry of Education (L. Milone), the University of Montana (E. Rosenberg), and the University of Turin (E. Rosenberg and L. Milone) and the CNR Programma di Scambi Internazionali (E. Rosenberg).

REFERENCES

1. Rosenberg, E., Kabir, S. E., Kolwaite, D. S., Hardcastle, K. I., Cresswell, W. and Grindstaff, J., *Organometallics*, 1995, **14,** 3611.
2. Rosenberg, E., Kolwaite, D. S., Kabir, S. E., Hardcastle, K. I., McPhillips, T. and Duque, R., Day, M., *Organometallics*, 1996, **15,** 1979.
3. Rosenberg, E., Kolwaite, D.S., Arcia, E., Hardcastle, K.I., Ciurash, J., Duque, R., Gobetto, R., Milone, L., Osella, D., Botta, M., Dastru', W., Viale, A., Fiedler, J., *Organometallics*, 1998, **17,** 415.
4. Rosenberg, E., Bergman, B., Hardcastle, K.I., Visi, Mondana, Ciurash, Joana, 1998 (submitted).
5. Rosenberg, E., Kabir, S. E., Day, M., Wolf, E., McPhillips, T. and Hardcastle, K. I., *Organometallics*, 1995, **14,** 721.
6. Rosenberg, E., Hardcastle, K. I., Kabir, S. E., Milone, L., Gobetto, R., Botta, M., Nishimura, N. and Yin, M., *Organometallics*, 1995, **14,** 3068.
7. Rosenberg, E., Day, M., Espitia, D., Kabir, S. E., Day, M., Hardcastle, K. I. and Irving, M., *J. Cluster Sci.*, 1994, **5,** 481.
8. Rosenberg, E., Hardcastle, K. I., Kabir, S. E., Gobetto, R., Milone, L. and Osella, D., *Organometallics*, 1991, **10,** 3550.
9. Aime, S., Gobetto, R. (to be published).
10. Hammett, L. P., *Physical Organic Chemistry*, 2nd edn. McGraw–Hill, New York, 1970.
11. Bradford, L., Elliot, T. J. and Rowe, F. M., *J. Amer. Chem. Soc.*, 1947, **69,** 437.

Pergamon

PII: S0277-5387(98)00101-6

Polyhedron Vol. 17, No. 17, pp. 2985–2991, 1998
© 1998 Elsevier Science Ltd
All rights reserved. Printed in Great Britain
0277–5387/98 $19.00+0.00

In situ infrared spectroelectrochemical studies of $[Ru_6C(CO)_{17}]$ and $[Ru_6C(CO)_{16}]^{2-}$: the redox induced conversion of carbon monoxide to carbon dioxide*

Robin J. H. Clark[a], Paul J. Dyson[b], David G. Humphrey[a,*] and Brian F. G. Johnson[c]

[a] Christopher Ingold Laboratories, University College London, 20 Gordon Street, London, WC1H 0AJ, U.K.

[b] Department of Chemistry, Imperial College of Science, Technology and Medicine, South Kensington, London, SW7 2AY, U.K.

[c] University Chemical Laboratories, Lensfield Road, Cambridge, CB2 1EW, U.K.

(Received 20 January 1998)

Abstract—Cyclic voltammetry and *in situ* infrared spectroelectrochemistry and have been used to investigate the redox behaviour of $[Ru_6C(CO)_{17}]$ and $[NBu_4]_2[Ru_6C(CO)_{16}]$. Under strictly anaerobic conditions, the electrochemical reduction of $[Ru_6C(CO)_{17}]$ yields only $[Ru_6C(CO)_{16}]^{2-}$. However, in the presence of O_2, the reduction of $[Ru_6C(CO)_{17}]$ produces 1.1–1.3 mole of CO_2 per mole of cluster, in addition to $[Ru_6C(CO)_{16}]^{2-}$ and some cluster degradation products. Re-oxidation of electrogenerated $[Ru_6C(CO)_{16}]^{2-}$ results in the re-formation of $[Ru_6C(CO)_{17}]$. The conditions under which oxidation of chemically prepared $[Ru_6C(CO)_{16}]^{2-}$ leads to the formation of $[Ru_6C(CO)_{17}]$ have also been established. The oxidation of $[NBu_4]_2[Ru_6C(CO)_{16}]$ in the absence of a CO-source gives only ill-defined products, as does oxidation in the presence of CO_2, such that $[Ru_6C(CO)_{16}]^{2-}$ does not scavenge CO from other cluster molecules to form $[Ru_6C(CO)_{17}]$. The oxidation of a CO-saturated solution of $[NBu_4]_2[Ru_6C(CO)_{16}]$ produces near quantitative yields of $[Ru_6C(CO)_{17}]$. Mechanisms have been proposed to account for these interconversions.

The activation of polynuclear transition metal carbonyl clusters by oxidation or reduction has proven to be an effective means of initiating a variety of chemical reactions, and as a consequence clusters of this type have been the subject of extensive electrochemical investigations [1–9]. In the case of the hexanuclear carbide-centred octahedral cluster $[Ru_6C(CO)_{17}]$, two-electron reduction is known to induce ligand dissociation, producing $[Ru_6C(CO)_{16}]^{2-}$ which retains the octahedral $\{Ru_6C\}$ core geometry [10–12]. Recently, whilst reinvestigating the redox chemistry of $[Ru_6C(CO)_{17}]$ in non-aqueous media, CO_2 was observed to form, in addition to $[Ru_6C(CO)_{16}]^{2-}$, upon *reduction* of this cluster at a platinum electrode. The conversion of CO to CO_2 is a process that has attracted some attention within the chemical literature. This conversion can be achieved by a number of methods, including both homogeneous and heterogeneous catalysis§ [13–16] stoichiometric reaction of certain carbonyl and molecular oxygen complexes [17–20] electrochemical oxidation of adsorbed CO [21], and the action of oxygen-transfer reagents on transition metal carbonyl complexes [22]. The formation of CO_2 upon reduction of $[Ru_6C(CO)_{17}]$ was discovered when the electrolysis was performed in an infrared reflection-absorption spectroscopic (IRRAS) cell, which

* This paper is dedicated to Sir Jack Lewis on the occasion of his 70th birthday.

† Present address: Department of Chemistry, Monash University, Wellngton Road, Clayton, Victoria 3168, Australia. Author to whom correspondence should be addressed.

§ The water gas shift reaction is a well known example, where CO and H_2O are converted to CO_2 and H_2. See [13–15].

permits direct spectroscopic analysis of the redox products as they are formed. The details of this cell have been reported previously [23, 24] This observation prompted a detailed investigation of the redox behaviour of $[Ru_6C(CO)_{17}]$ and $[NBu_4]_2[Ru_6C(CO)_{16}]$ by voltammetric and infrared (IR) spectroelectrochemical techniques, in an effort to understand the apparent redox-activated transformation of coordinated CO to CO_2. The results from these studies are described herein.

EXPERIMENTAL

$[Ru_6C(CO)_{17}]$ and $[NBu_4]_2[Ru_6C(CO)_{16}]$ were prepared by standard procedures [11]. Voltammetric measurements were performed as described previously [25], using a Pt bead working electrode, Pt wire auxiliary electrode and a Ag/AgCl reference electrode, for which the ferrocene/ferrocenium couple was measured at +0.55 V. Infrared (IR) spectroelectrochemical measurements were conducted using an IRRAS cell [23, 24]. Freshly distilled solvents were used throughout with $[NBu_4][PF_6]$ electrolyte previously dried at 100°C under vacuum.

RESULTS AND DISCUSSION

2.1. *Reduction of* $[Ru_6C(CO)_{17}]$ *in the presence (or absence) of* O_2

Previous electrochemical studies of $[Ru_6C(CO)_{17}]$ have shown that this complex can be reduced in an irreversible two-electron process that leads to the formation of $[Ru_6C(CO)_{16}]^{2-}$ [12]. Cyclic voltammetry (CV) of $[Ru_6C(CO)_{17}]$ in 0.5 mol dm^{-3} $[NBu_4][PF_6]$ in CH_2Cl_2 (*vs.* Ag/AgCl reference electrode) confirmed these results. The irreversible reduction of $[Ru_6C(CO)_{17}]$, observed at $E_{pc} = -0.48$ V, gives rise to another irreversible process, at $E_{pa} = +0.52$ V, which can be attributed to the oxidation of $[Ru_6C(CO)_{16}]^{2-}$ (see below).

Through a series of IR spectroelectrochemical experiments, it has been established that the formation of CO_2 is dependent upon the presence of O_2 in solution, since the reduction of $[Ru_6C(CO)_{17}]$ under strictly anaerobic conditions yields $[Ru_6C(CO)_{16}]^{2-}$, with no CO_2 detected. The changes in the IR difference spectrum accompanying reduction in the absence of O_2 are shown in Fig. 1. The ν_{CO} bands for $[Ru_6C(CO)_{17}]$ at 2068 and 2048 cm^{-1} grow at negative absorbance, indicating depletion of the parent complex in the thin-layer, whilst new bands at 1978, 1918 and 1782 cm^{-1} grow at positive absorbance. The latter bands can be assigned to $[Ru_6C(CO)_{16}]^{2-}$, in accord with the voltammetric experiment. Free CO is thought to be produced when $[Ru_6C(CO)_{17}]$ is reduced under these conditions, although it was not detected (ν_{CO} expected at $\approx$2140 cm^{-1}) [26]. Low concentrations of free CO in solution are reportedly difficult to observe by IR spectroscopy due to the low absorption coefficient for ν_{CO} [26, 27].

O_2 itself does not react with the parent cluster $[Ru_6C(CO)_{17}]$ under the conditions of the voltammetric and spectroelectrochemical experiments, since the IR spectrum of a solution of $[Ru_6C(CO)_{17}]$ in 0.5 mol dm^{-3} $[NBu_4][PF_6]$ in CH_2Cl_2 remains unchanged in the presence of O_2. The CV of $[Ru_6C(CO)_{17}]$ in 0.5 mol dm^{-3} $[NBu_4][PF_6]$ in CH_2Cl_2 in the presence of O_2 is shown in Fig. 2(a). The CV is qualitatively similar to that recorded in the absence of O_2, the only differences being that the irreversible reduction wave at $E_{pc} = -0.48$ V is broadened somewhat and the magnitude of the peak current for the $[Ru_6C(CO)_{16}]^{2-}$ oxidation wave ($E_{pa} = +0.52$ V) is significantly reduced, indicating a diminished yield of this latter species on the CV timescale. The IR spectral changes accompanying the reduction of $[Ru_6C(CO)_{17}]$ in the presence of O_2 are shown in Fig. 3. Aside from the conversion of $[Ru_6C(CO)_{17}]$ to $[Ru_6C(CO)_{16}]^{2-}$, the reduction is accompanied by the formation of CO_2, as shown by the growth of the band in the IR spectrum at 2339 cm^{-1} [28].[4]* The voltammetry and spectroelectrochemistry of $[Ru_6C(CO)_{17}]$, both in the presence and absence of O_2, are unchanged at low temperature (210 K) and are similar in other solvents, *i.e.* acetonitrile and tetrahydrofuran.

QUANTIFICATION OF AMOUNT OF CO_2 FORMED

The quantity of CO_2 formed upon reduction of $[Ru_6C(CO)_{17}]$ can be established directly from the IR spectroelectrochemical experiments, using the ν_{CO} and ν_{CO_2} absorption coefficients for $[Ru_6C(CO)_{17}]$ and CO_2 respectively (Table 1) [29]. Qualitatively, the amount of CO_2 generated increases with increasing concentration of O_2, to a maximum level which corresponds to 1.1–1.3 mole of CO_2 per mole of cluster reduced, *i.e.* solutions pre-saturated with O_2 prior to electrolysis produce between 1.1–1.3 equivalents of

* The reduction of $[Ru_6C(CO)_{17}]$ on a preparative scale is most conveniently achieved using KOH/MeOH as the reductant. In this case the process is thought to involve the nucleophilic addition of OH^- to a CO ligand, forming a carboxylic acid intermediate, followed by the expulsion of CO_2 and then removal of H^+ by OH^- to form $[Ru_6C(CO)_{16}]^{2-}$. The possibility that adventitious H_2O is involved in the ligand transformation rather than O_2 is discounted since the concentration of H_2O (aside from being very low) will be approximately the same for all experiments. If adventitious H_2O were involved in the reaction, then CO_2 would still be liberated, even in the absence of O_2. The solvent/electrolyte solution is prepared in an identical manner just prior to each experiment, using freshly distilled solvent and electrolyte dried under high vacuum. Under these conditions, and with thorough purging of the cell, CO_2 is not liberated upon reduction of the cluster. Only upon the addition of O_2 was CO_2 observed to form.

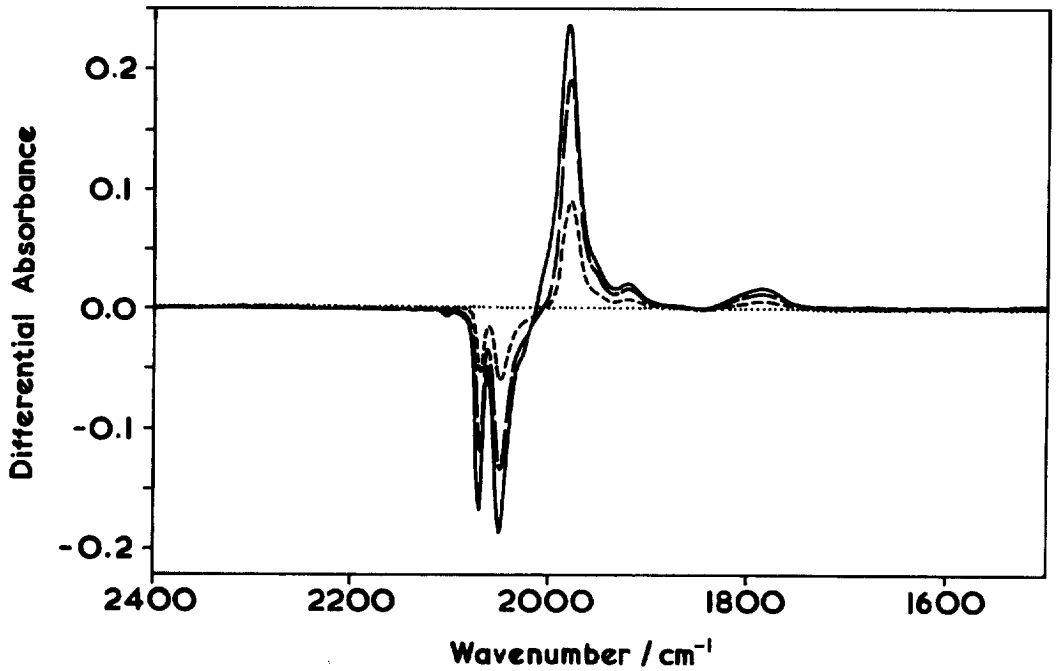

Fig. 1. Changes in the IR difference spectrum accompanying the reduction of $[Ru_6C(CO)_{17}]$ in an IRRAS cell in 0.5 mol dm^{-3} $[NBu_4][PF_6]$ in CH_2Cl_2 at room temperature. Following collection of the initial spectrum of $[Ru_6C(CO)_{17}]$, the potential of the Pt mirror working electrode (E_{app}) is stepped to −0.6 V and single scan spectra (1.0 cm^{-1} resolution) are then collected as a function of time. All spectra are ratioed against the initial $[Ru_6C(CO)_{17}]$ spectrum, such that the first spectrum prior to electrolysis is given by the horizontal line at zero absorbance. Those features that grow at negative absorbance correspond to the consumption of the parent complex, whilst those that grow at positive absorbance indicate formation of the redox product.

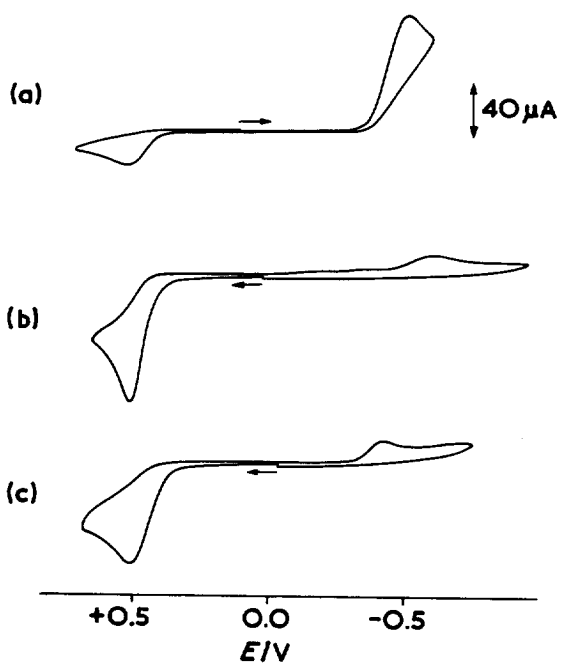

Fig. 2. Cyclic voltammetry in 0.5 mol dm^{-3} $[NBu_4][PF_6]$ in CH_2Cl_2 of (a) $[Ru_6C(CO)_{17}]$ in the presence of O_2, (b) $[NBu_4]_2$ $[Ru_6C(CO)_{16}]$ (c) $[NBu_4]_2[Ru_6C(CO)_{16}]$ in the presence of CO.

CO_2. The formation of greater than one equivalent of CO_2, in cases where the O_2 concentration is relatively high, indicates that the reduction of $[Ru_6C(CO)_{17}]$ in the presence of O_2 to form $[Ru_6C(CO)_{16}]^{2-}$ and CO_2 does not occur stoichiometrically. The conversion of additional CO groups of the active $\{Ru_6C\}$ species to CO_2 necessitates the formation of cluster degradation products and therefore less $[Ru_6C(CO)_{16}]^{2-}$. Comparing the final $[Ru_6C(CO)_{16}]^{2-}$ spectrum shown in Fig. 3 with that of chemically prepared $[Ru_6C(CO)_{16}]^{2-}$ (*e.g.* the first spectrum in Fig. 4) indicates the presence of additional carbonyl-containing species with ν_{CO} in the region 2000–2080 cm^{-1}. These features are attributed to CO-deficient $\{Ru_mC(CO)_n\}$ degradation products. In accord with these observations, the amount of $[Ru_6C(CO)_{16}]^{2-}$ formed, as compared with $[Ru_6C(CO)_{17}]$ initially present, is somewhat variable, depending upon the concentration of O_2 in solution.

REFORMATION OF $[Ru_6C(CO)_{17}]$

The spectral changes accompanying the re-oxidation of $[Ru_6C(CO)_{16}]^{2-}$, electrogenerated in the IRRAS cell as described above, occur in two distinct phases. The initial phase of the electrolysis involves the consumption of $[Ru_6C(CO)_{16}]^{2-}$ as shown by the collapse of the bands at 1978, 1918 and 1782 cm^{-1}, and

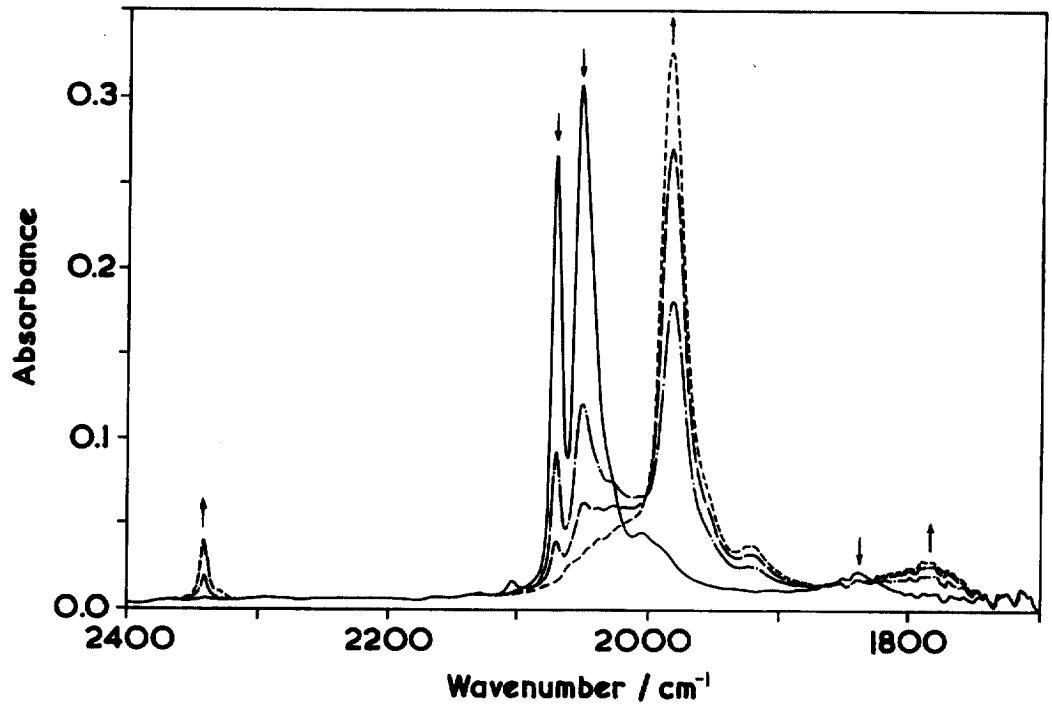

Fig. 3. IR spectral changes accompanying the reduction of $[Ru_6C(CO)_{17}]$ in an IRRAS cell in 0.5 mol dm^{-3} $[NBu_4][PF_6]$ in CH_2Cl_2 at room temperature, in the presence of O_2.

Table 1. Infrared band maxima and absorption coefficients.

Species	band maxima/cm^{-1} (absorption coefficient/ dm^3 mol^{-1} cm^{-1})
$[Ru_6C(CO)_{17}]$[a]	2068[b] (11000), 2048[b] (12000) 1840[c]
$[Ru_6C(CO)_{16}]^{2-}$ [a]	1978[b](22600), 1918[b], 1782[c]
CO_2	2339 (1300)[d]

[a] Measured in 0.5 mol dm^{-3} $[NBu_4][PF_6]$ in CH_2Cl_2.
[b] Terminal ν_{CO}
[c] Bridging ν_{CO} [d] Reference [30].

the formation of a species with $\nu_{CO} \approx 2030$–$2025\,cm^{-1}$. With most of the $[Ru_6C(CO)_{16}]^{2-}$ cluster consumed, the second phase of spectral changes occurs. The band(s) at ≈ 2030– $2025\,cm^{-1}$ decrease in intensity, ultimately producing a spectrum with sharp bands at 2068 and 2048 cm^{-1}, signifying the reformation of a considerable quantity of the parent cluster, $[Ru_6C(CO)_{17}]$.

The nature of the intermediate with $\nu_{CO} \approx 2030$–$2025\,cm^{-1}$ is of considerable interest, although its precise identity is uncertain. When the spectroelectrochemical experiment is conducted in tetrahydrofuran, similar spectral changes are observed, although the intermediate is distinctly more stable under these conditions. In this case it is proposed that an $[Ru_6C(CO)_{16}L]$ species is formed, where L is a weakly bound solvent molecule. For those experiments carried out in dichloromethane, where the solvent/electrolyte combination is considered to be non-coordinating medium, the stabilisation of a $[Ru_6C(CO)_{16}L]$ species may arise through an intermolecular interaction between two cluster molecules, or through the reorganisation of carbonyl ligands, *e.g.* end-bound CO (2 electron donor) becoming side-bound (4 electron donor). Another alternative for the intermediate species is the 84 electron-precise octahedral cluster $[Ru_6C(CO)_{16}]$, although given that the two-electron oxidation of $[Ru_6C(CO)_{16}]^{2-}$ is irreversible, even at low temperature (see below), this seems unlikely. The source of CO required for the reformation of $[Ru_6C(CO)_{17}]$, is discussed below.

OXIDATION OF $[Ru_6C(CO)_{16}]^{2-}$ IN THE ABSENCE OF POTENTIAL LIGANDS

Given the observation that the oxidation of electrogenerated $[Ru_6C(CO)_{16}]^{2-}$ leads to the reformation of a considerable amount of the starting cluster $[Ru_6C(CO)_{17}]$, the redox behaviour of chemically prepared $[NBu_4]_2[Ru_6C(CO)_{16}]$ was examined inde-

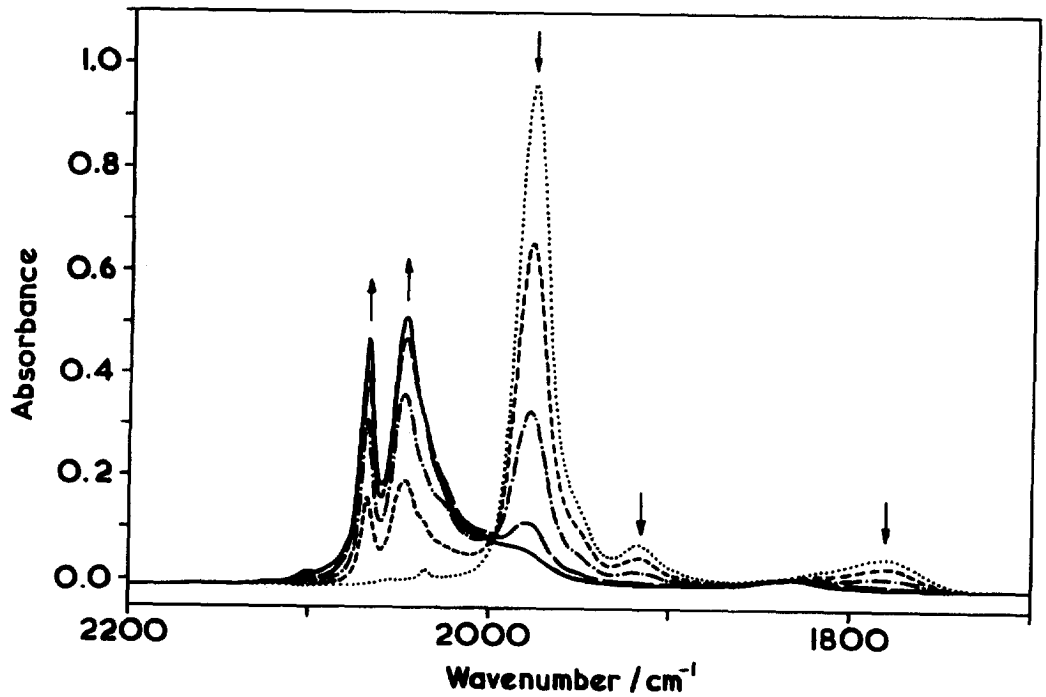

Fig. 4. IR spectral changes accompanying the oxidation of $[NBu_4]_2[Ru_6C(CO)_{16}]$ in an IRRAS cell in 0.5 mol dm^{-3} $[NBu_4][PF_6]$ in CH_2Cl_2 at room temperature, in the presence of CO.

pendently. The CV of $[NBu_4]_2[Ru_6C(CO)_{16}]$, dissolved in 0.5 mol dm^{-3} $[NBu_4][PF_6]$ in CH_2Cl_2, is shown in Fig. 2(b). An irreversible wave at $E_{pa} = +0.52$ V corresponds to the two-electron oxidation of $[Ru_6C(CO)_{16}]^{2-}$ [5] [12].* On the return scan several processes are detected in the region 0– −0.6 V, the most pronounced of which is that with $E_{pc} = -0.59$ V (*cf.* $E_{pc} = -0.48$ V for $[Ru_6C(CO)_{17}]$), in consequence of which $[Ru_6C(CO)_{17}]$ does not appear to re-form on the time-scale of the CV experiment. The species giving rise to the processes detected between 0– −0.6 V form as a result of oxidation of $[Ru_6C(CO)_{16}]^{2-}$, since they are not observed if the scan is switched prior to the irreversible wave with $E_{pa} = +0.52$ V. The CV of $[Ru_6C(CO)_{16}]^{2-}$ was also examined at low temperature (≈213 K), where the oxidation remained irreversible.

The oxidation of $[NBu_4]_2[Ru_6C(CO)_{16}]$ in the IRRAS cell, under conditions identical to those used in the voltammetric experiment, reveals a rapid series of spectral changes showing consumption of the parent cluster $[Ru_6C(CO)_{16}]^{2-}$ and the formation of product(s) with ν_{CO} in the region ≈2030–2025 cm^{-1}. With time, the ν_{CO} bands at 2030–2025 cm^{-1} also collapse, giving rise to a broad, ill-defined band(s) in the region 2110–2030 cm^{-1} with a maximum at ≈2082 cm^{-1}. At no stage of the electrolysis is there any evidence for the formation of $[Ru_6C(CO)_{17}]$, although a small quantity of this cluster may not necessarily be detected, given that the ν_{CO} bands diagnostic of $[Ru_6C(CO)_{17}]$ could be concealed under the broad band centred at 2082 cm^{-1}.

OXIDATION OF $[Ru_6C(CO)_{16}]^{2-}$ IN THE PRESENCE OF CO_2

The behaviour of $[Ru_6C(CO)_{16}]^{2-}$ in the presence of CO_2 was also examined by CV and IR spectroelectrochemistry. The CV of $[NBu_4]_2[Ru_6C(CO)_{16}]$ in 0.5 mol dm^{-3} $[NBu_4][PF_6]$ in CH_2Cl_2, pre-saturated with CO_2, is essentially identical to that recorded in the absence of CO_2. Upon oxidation of this solution in the IRRAS cell, those bands due to $[Ru_6C(CO)_{16}]^{2-}$ collapse with the growth of a slightly broad band at ≈2030–2025 cm^{-1}, during which time the intensity of the band due to CO_2 was unchanged. A further series of spectral changes occur with time, with the band(s) at ≈2030–2025 cm^{-1} decreasing in intensity and ultimately producing a spectrum with bands at 2158 and 2079 cm^{-1}. During the latter phase of the electrolysis some CO_2 is consumed, concomitant with the appearance of weak bands at 1714, 1587 and 1553 cm^{-1}. Although the product(s) of the oxidation of

* If the switching potential is made more positive, a further process is observed with $E_{pa} = +0.75$ V. This process, which has some reversibility in that there is evidence for a return wave ($i_{pc}/i_{pa} < 1.0$), arises as a consequence of oxidation of $[Ru_6C(CO)_{16}]^{2-}$, and may well be associated with the intermediate detected spectroscopically with $\nu_{CO} \approx 2030$–2025 cm^{-1}.

$[Ru_6C(CO)_{16}]^{2-}$ in the presence of CO_2 remain unidentified, in the context of this work the experiment serves to show that dissolved CO_2 does not function as a source of CO for the re-formation of $[Ru_6C(CO)_{17}]$ upon oxidation of electrogenerated $[Ru_6C(CO)_{16}]^{2-}$.

OXIDATION OF $[Ru_6C(CO)_{16}]^{2-}$ IN THE PRESENCE OF CO

The $[Ru_6C(CO)_{16}]^{2-}$ cluster is known to bind certain ligands upon oxidation to form clusters of general formula $[Ru_6C(CO)_{16}L]$ [12, 30]. The CV of $[NBu_4]_2[Ru_6C(CO)_{16}]$ in $0.5\,mol\,dm^{-3}$ $[NBu_4][PF_6]$ in CH_2Cl_2, pre-saturated with CO, is shown in Fig. 2(c). The irreversible oxidation at $E_{pa} = +0.52$ V gives rise to a product wave at $E_{pc} = 0.48$ V, which is consistent with the formation of $[Ru_6C(CO)_{17}]$. The oxidation of this solution in the IRRAS cell produces the spectral changes shown in Fig. 4. Those ν_{CO} bands due to $[Ru_6C(CO)_{16}]^{2-}$ at 1978, 1918 and 1782 cm^{-1} collapse with the growth of bands at 2068 and 2048 cm^{-1}, these being characteristic of $[Ru_6C(CO)_{17}]$. Under these experimental conditions, *i.e.* dry, non co-ordinating solvent and excess of CO, the conversion of $[Ru_6C(CO)_{16}]^{2-}$ to $[Ru_6C(CO)_{17}]$ appears to be quantitative, with no evidence for the production of other carbonyl-containing species. $[Ru_6C(CO)_{17}]$ has also previously been prepared, in nearly quantitative yield, by chemical oxidation of $[Ru_6C(CO)_{16}]^{2-}$ in a solution saturated with CO [31].

It is notable that the oxidative conversion of $[Ru_6C(CO)_{16}]^{2-}$ to $[Ru_6C(CO)_{17}]$ occurs quite quickly, and that there is no spectral evidence for the reaction proceeding *via* a long-lived intermediate, by contrast with the oxidations of electrogenerated $[Ru_6C(CO)_{16}]^{2-}$ or chemically prepared $[Ru_6C(CO)_{16}]^{2-}$. The spectral changes shown in Fig. 4 also give a good indication of the anticipated intensity ratios of ν_{CO} bands for the clean, stoichiometric interconversion of $[Ru_6C(CO)_{16}]^{2-}$ and $[Ru_6C(CO)_{17}]$. A comparison of Fig. 3 and Fig. 4 clearly shows that the reduction of $[Ru_6C(CO)_{17}]$ in the presence of O_2 does not produce a stoichiometric equivalent of $[Ru_6C(CO)_{16}]^{2-}$.

PROPOSED MECHANISM

A mechanism proposed to account for these observations is presented in Fig. 5. The reduction of $[Ru_6C(CO)_{17}]$ first gives the radical-anion $[Ru_6C(CO)_{17}]^{-\cdot}$. This species is probably present in low concentration only, given that the second reduction of the overall two-electron process is likely to be thermodynamically *easier* than the first. Whilst there is no IR spectral evidence for the formation of this thermodynamically unstable species, a previous study has reported its epr spectrum [32]. In the absence of O_2, $[Ru_6C(CO)_{17}]^{-\cdot}$ is reduced further to $[Ru_6C(CO)_{17}]^{2-}$, which is followed by chemical reaction involving CO ejection from the electron-rich cluster $[Ru_6C(CO)_{17}]^{2-}$ to yield $[Ru_6C(CO)_{16}]^{2-}$. Overall, the formation of $[Ru_6C(CO)_{16}]^{2-}$ from $[Ru_6C(CO)_{17}]$ under anaerobic conditions can be described in terms of the Testa and Reinmuth notation [33] as an EEC reaction. Should the $\{Ru_6C\}$ core of the proposed 87 and 88 electron intermediates ($[Ru_6C(CO)_{17}]^{-\cdot}$ and $[Ru_6C(CO)_{17}]^{2-}$ respectively) retain the octahedral geometry of $[Ru_6C(CO)_{17}]$, then $[Ru_6C(CO)_{17}]^{-\cdot}$ and $[Ru_6C(CO)_{17}]^{2-}$ are anticipated to be short-lived. In the presence of O_2 a somewhat different route is proposed. The first intermediate is likely to be the same as that formed under anaerobic conditions, *viz.* the radical-anion $[Ru_6C(CO)_{17}]^{-\cdot}$. Localisation of the odd electron onto a C-atom of a carbonyl ligand would render the radical ·CO group reactive towards O_2, thereby generating first a peroxy-carbonate ligand, $\cdot C(O)_2O$, which then undergoes decomposition either *via* a bimolecular interaction or *via* rearrangement through a carbonato ligand to generate CO_2 and $[Ru_6C(CO)_{16}]^{2-}$ (ECC). The radical-anion $[Ru_6C(CO)_{17}]^{-\cdot}$, although only present in low concentrations, is clearly highly reactive because small amounts of CO_2 are formed upon reduction of $[Ru_6C(CO)_{17}]$ unless extreme care is taken to exclude O_2, an efficient radical scavenger.

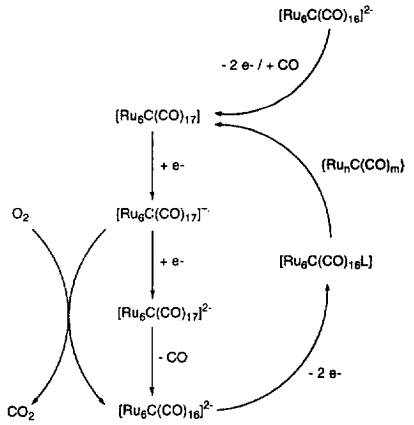

Fig. 5. Proposed Mechanisms. $\{Ru_mC(CO)_n\}$ refers to the cluster degradation products, formed during the initial reduction of $[Ru_6C(CO)_{17}]$ in the presence of O_2.

Through the experiments conducted with $[NBu_4]_2[Ru_6C(CO)_{16}]$, it can be concluded that the re-formation of $[Ru_6C(CO)_{17}]$ upon oxidation of electrogenerated $[Ru_6C(CO)_{16}]^{2-}$ does not occur through scavenging of CO from other $[Ru_6C(CO)_{16}]^{2-}$ species, nor through extraction of CO from CO_2. Instead, it is likely that the cluster degradation products, present in low concentration from the initial reduction of $[Ru_6C(CO)_{17}]$, are the source of CO.

The reaction of O_2 with a polynuclear carbonyl complex is not without precedent. In earlier work with the cluster anion, $[(\mu\text{-H})Os_3(CO)_{11}]^-$, it was dem-

onstrated that the reaction with O_2 led to the formation of the peroxy-formyl anion $[(\mu\text{-H})Os_3(CO)_{10}(\mu\text{-}CO_3)]^-$ which, in the presence of suitable electrophiles such as $[Os_6(CO)_{18}]$, yield CO_2-linked clusters [34]. The proposed peroxy-carbonate intermediate in the present system is clearly closely related to the osmium compound, $[(\mu\text{-H})Os_3(CO)_{10}(\mu\text{-}CO_3)]^-$.

Acknowledgements—The authors thank The Royal Society for a University Research Fellowship (PJD) and the Ramsay Memorial Fellowships Trust for a British Ramsay Memorial Fellowship (DGH).

REFERENCES

1. Dessy, R. E. and Bares, L. A., *Acc. Chem. Res.*, 1972, **5,** 415.
2. Meyer, T. J., *Prog. Inorg. Chem.*, 1975, **19,** 1.
3. Lemoine, P., *Coord. Chem. Rev.*, 1982, **47,** 55.
4. Geiger, W. E., *Prog. Inorg. Chem.*, 1985, **33,** 275.
5. Geiger, W. E. and Connelly, N. G., *Adv. Organomet. Chem.*, 1985, **24,** 87.
6. Lemoine, P., *Coord. Chem. Rev.*, 1988, **83,** 169.
7. Drake, S. R., *Poyhedron*, 1990, **9,** 455.
8. Arce, A. J., Bates, P. A., Best, S. P., Clark, R. J. H., Deeming, A. J., Hursthouse, M. B., McQueen, R. C. S. and Powell, N. I., *J. Chem. Soc., Chem. Commun.*, 1988, 478.
9. Best, S. P., Clark, R. J. H., Deeming, A. J., McQueen, R. C. S., Powell, N. I., Acuna, C. and de Sanctis, Y., *J. Chem. Soc., Dalton Trans.*, 1991, 1111.
10. Braga, D., Grepioni, F., Dyson, P. J., Johnson, B. F. G., Frediani, P., Bianchi, M. and Piacenti, F., *J. Chem. Soc., Dalton Trans.*, 1992, 2565.
11. Johnson, B. F. G., Lewis, J., Sankey, S. W., Wong, K., McPartlin, M. and Nelson, H. J. W., *J. Organomet. Chem.*, 1980, **191,** C3.
12. Drake, S. R., Johnson, B. F. G. and Lewis, J., *J. Chem. Soc., Dalton Trans.*, 1989, 243.
13. Laine, R. M., Rinker, R. G. and Ford, P. C., *J. Am. Chem. Soc.*, 1977, **99,** 252.
14. Cheng, C. H., Hendriksen, D. E. and Eisenberg, R., *J. Am. Chem. Soc.*, 1977, **99,** 2791.
15. Kang, H., Mauldin, C. H., Cole, T., Slegeir, W. and Cann, K., Pettit, R., *J. Am. Chem. Soc.*, 1977, **99,** 8323.
16. Ford, P. C. and Rokicki, A., *Adv. Organomet. Chem.*, 1988, **28,** 139.
17. Mercer, G. D., Shing Shu, J., Rauchfuss, T. B. and Roundhill, D. M., *J. Am. Chem. Soc.*, 1975, **97,** 1967.
18. Mercer, G. D., Beaulieu, W. B. and Roundhill, D. M., *J. Am. Chem. Soc.*, 1977, **99,** 6551.
19. Roundhill, D. M., Dickson, M. K., Dixit, N. S. and Sudha-Dixit, B. P., *J. Am. Chem. Soc.*, 1980, **102,** 5538.
20. Kubota, M., Rosenberg, F. S. and Sailor, M. J., *J. Am. Chem. Soc.*, 1985, **107,** 4558.
21. Edens, G. J., Hamelin, A. and Weaver, M. J., *J. Phys. Chem.*, 1996, **100,** 2322.
22. Shvo, Y. and Hazum, E., *J. Chem. Soc., Chem. Comm.*, 1974, 336.
23. Best, S. P., Clark, R. J. H., Cooney, R. P. and McQueen, R. C. S., *Rev. Sci. Instrum.*, 1987, **58,** 2071.
24. Best, S. P., Ciniawsky, S. A. and Humphrey, D. G., *J. Chem. Soc., Dalton Trans.*, 1996, 2945.
25. Clark, R. J. H. and Humphrey, D. G., *Inorg. Chem.*, 1996, **35,** 2053.
26. Christensen, P. A., Hamnett, A., Muir, A. V. G. and Freeman, N. A., *J. Electroanal. Chem.*, 1990, **288,** 197.
27. Yamaguchi, Y., Frisch, M., Gaw, J., Schaefer, H. F. and Binkley, J. S., *J. Chem. Phys.*, 1986, **84,** 2262.
28. Christensen, P., Hamnett, A., Muir, A. V. G. and Timney, J. A., *J. Chem. Soc., Dalton Trans.*, 1992, 1455.
29. Haines, R. J., Wittrig, R. E. and Kubiak, C. P., *Inorg. Chem.*, 1994, **33,** 4723.
30. Drake, S. R., Johnson, B. F. G. and Lewis, J., *J. Chem. Soc., Chem. Comm.*, 1988, 1033.
31. Hayward, C. T. and Shapley, J. R., *Inorg. Chem.*, 1982, **21,** 3816.
32. Peake, B. M., Robinson, B. H., Simpson, J. and Watson, D. J., *J. Chem. Soc., Chem. Comm.*, 1974, 945.
33. Testa, A. C. and Reinmuth, W. H., *Anal. Chem.*, 1961, **33,** 1320.
34. Cathey, C. J., Johnson, B. F. G., Lewis, J., Raithby, P. R. and Wong, W. T., *J. Organomet. Chem.*, 1993, **450,** C12.

Pergamon

PII: S0277-5387(98)00103-X

Polyhedron Vol. 17, No. 17, pp. 2993–3004, 1998
© 1998 Elsevier Science Ltd
All rights reserved. Printed in Great Britain
0277-5387/98 $19.00+0.00

Labile SR′C(O)CRCH-bridged dicobalt complexes; synthesis, structures and ^{13}CO labelling studies

Gráinne Conole,[a] Maggie Kessler,[a] Martin J. Mays,[b]* Giles E. Pateman[b] and Gregory A. Solan[b]

[a]School of Applied Chemistry, University of North London, Holloway Road, London, N7 8DB, U.K.

[b]Department of Chemistry, Lensfield Road, Cambridge CB2 1EW, U.K.

(Received 15 September 1997; accepted 28 February 1998)

Abstract—Three alkyne-bridged dicobalt carbonyl complexes, $[Co_2(\mu\text{-RCCH})(CO)_6]$ (R = H **1a**, Me **1b**, CH_2OH **1c**) have been reacted with $Ph_2P(SPh)$ and with the new thiophosphine ligands, $Ph_2P(SR')$ (R′ = Bu^n, Bu^t), to give, initially, both mono-substituted $[Co_2(\mu\text{-RCCH})(CO)_5\{PPh_2(SR')\}]$ [(R′ = Ph; R = H **2a**, Me **2b**, CH_2OH **2c**), (R′ = Bu^n; R = H **3a**, Me **3b**, CH_2OH **3c**), (R′ = Bu^t; R = H **4a**, Me **4b**)] and bis-substituted $[Co_2(\mu\text{-RCCH})(CO)_4\{PPh_2(SPh)\}_2]$ [(R′ = Ph; R = H **5a**, Me **5b**, CH_2OH **5c**), (R′ = Bu^n; R = H **6a**, Me **6b**, CH_2OH **6c**), (R′ = Bu^t; R = H **7a**, Me **7b**)] products. Thermolysis of complexes **2–4** gives $[Co_2(\mu\text{-}PPh_2)\{\mu\text{-SR′C(O)CRCH}\}(CO)_4]$ [(R′ = Ph; R = H **8a**, Me **8b**, CH_2OH **8c**), (R′ = Bu^n; R = H **9a**, Me **9b**), (R′ = Bu^t; R = H **10a**, R = Me **10b**)] in which sulphur–phosphorus bond cleavage and sulphur–carbon bond formation at the dicobalt centre have occurred to generate SR′C(O)CRCH ligands incorporated into 5-membered ring metallacycles. The transformations are regiospecific with the bulky substituents (R = H) in all cases being located adjacent to the CO moiety of the metallacycle. Treatment of the complex $[Co_2(\mu\text{-}PPh_2)\{\mu\text{-SPhC(O)CHCH}\}(CO)_4]$ **8a** with ^{13}CO and monitoring of the reaction via $^{13}C\text{-}\{^1H\}$-NMR spectroscopy reveals the formation of a selectively labelled species, $[Co_2(\mu\text{-}PPh_2)\{\mu\text{-SPh}^{13}C(O)CHCH\}(^{13}CO)_2(CO)_2]$, in which the ketonic bridging carbonyl signal has been enhanced, while only two of the four signals due to the terminal carbonyl groups have been similarly enhanced. The mechanistic implications of this labelling study are discussed and pathways postulated for the reversible fragmentation of the SR′C(O)CRCH-bridged dicobalt systems. Single crystal X-ray diffraction studies have been performed on $[Co_2(\mu\text{-HCCH})(CO)_4\{PPh_2(SBu^n)\}_2]$ **6a**, revealing axially substituted thiophosphine groups and on $[Co_2(\mu\text{-}PPh_2)\{\mu\text{-SBu}^nC(O)CHCH\}(CO)_4]$ **9a**, in which an almost planar Co–S–C–C=C metallacycle-coordinated to the other cobalt is observed. © 1998 Elsevier Science Ltd. All rights reserved

Keywords: dicobalt; labile; metallacycle; thiolate; phosphide; regioselectivity; labelling.

INTRODUCTION

Bimetallic transition metal complexes in which the metal centres are spanned by linked alkyne and carbonyl groups [μ-C(O)CRCR] have been thoroughly studied and a number of different bonding modes have been reported [1–3]. A common observation with these complexes is of the ease with which the alkyne–CO link can be cleaved, often to generate alkyne-bridged bimetallic species [2]. Notably, in the case of $[Rh_2(\mu\text{-CO})\{\mu\text{-C(O)CPhC}(C_6F_5)\}(\eta^5\text{-}C_5Me_5)_2]$, an equilibrium exists in the solid and in solution, with the isomeric alkyne-bridged species $[Rh_2\{\mu\text{-CPhC}(C_6F_5)\}(CO)_2(\eta^5\text{-}C_5Me_5)_2]$ [3].

As a consequence of our studies on the reactions of alkyne-hexacarbonyldicobalt complexes with ligands capable of undergoing intra-ligand bond cleavage, we have prepared a series of dicobalt complexes involving the C(O)CRCR structural motif incorporated into more elaborate bridging systems [4–7]. For example, dicobalt complexes with bridging ligands which incorporate linked alkyne, carbonyl and phosphide groups can be prepared from the reaction of $[Co_2(\mu\text{-CRCR})$

* To whom correspondence should be addressed.

$(CO)_6]$ **1** (R = H, alkyl, aryl or CO_2Me) with diphosphane, $Ph_2P(PPh_2)$, the ordering of the linked groups being influenced by the nature of the R groups [6]. As part of a preliminary communication, we reported that the reaction of $[Co_2(\mu\text{-HCCH})(CO)_6]$ **1a** with the thiophosphine, $Ph_2P(SPh)$, affords, as the sole product, $[Co_2(\mu\text{-}PPh_2)\{\mu\text{-SPhC(O)CHCH}\}(CO)_4]$ **8a**, in which the thiolate rather than the phosphide fragment is linked to the ketonic carbon of the C(O)CHCH moiety [7]. In order to examine the generality and regioselectivity of this reaction, we have sought to explore the role of the substituents on both the alkyne and on the thiolate group (Scheme 1). In addition, we describe the results of ^{13}CO labelling experiments undertaken in order to examine the rigidity of the bridging SRC(O)CRCR ligand in these dicobalt systems.

RESULTS AND DISCUSSION

Preparation of $Ph_2P(SR')$ ($R' = Bu^n$, Bu^t)

Two new thiophosphine ligands, $Ph_2P(SBu^n)$ and $Ph_2P(SBu^t)$, have been prepared in high yield from the reactions of the corresponding sodium thiolates with chlorodiphenylphosphine in THF (see Experimental). The FAB mass spectra of the compounds show their molecular ion peaks while the $^{31}P\text{-}\{^1H\}$ NMR spectra display resonances for the respective diphenylphosphide phosphorus atoms.

Reactions of **1** *with* $Ph_2P(SR')$

The reactions of $[Co_2(\mu\text{-RCCH})(CO)_6]$ (R = H **1a**, Me **1b**, CH_2OH **1c**) with $Ph_2P(SR')$ ($R' = Ph$, Bu^t, Bu^n) in toluene at 293 K afford $[Co_2(\mu\text{-RCCH})(CO)_5\{PPh_2(SR')\}]$ [($R' = Ph$; R = H **2a**, Me **2b**, CH_2OH **2c**), ($R' = Bu^n$; R = H **3a**, Me **3b**, CH_2OH **3c**), ($R' = Bu^t$; R = H **4a**, Me **4b**)] and $[Co_2(\mu\text{-RCCH})(CO)_4\{PPh_2(SR')\}_2]$ [($R' = Ph$; R = H **5a**, Me **5b**, CH_2OH **5c**), ($R' = Bu^n$; R = H **6a**, Me **6b**, CH_2OH **6c**, ($R' = Bu^t$; R = H **7a**, Me **7b**)] (Scheme 1). All of the complexes have been characterised by mass spectrometry, IR, ^1H, ^{31}P and ^{13}C NMR spectroscopy (see Table 1 and Experimental). In addition, the structure of complex **6a** has been the subject of an X-ray diffraction study.

The spectroscopic properties of the mono-substituted species, **2**, **3** and **4**, in solution are consistent with those found for analogous alkyne bridged dicobalt pentacarbonyl complexes with other phosphine substituents [8]. The $^{31}P\text{-}\{^1H\}$ NMR spectrum in each

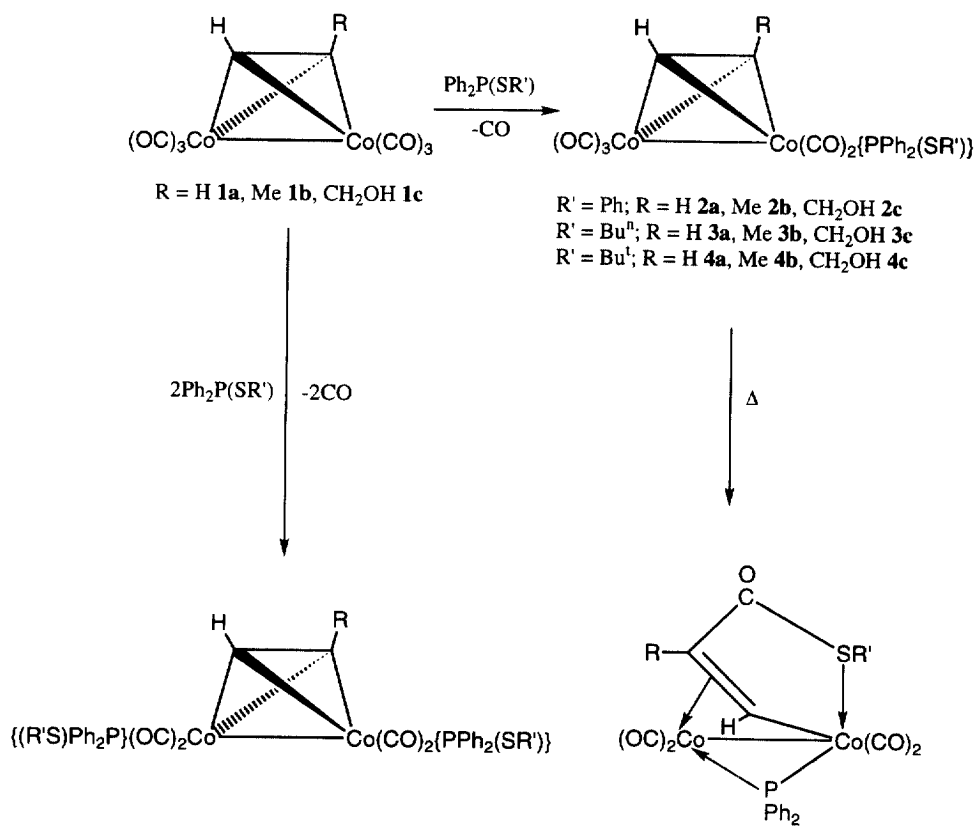

Scheme 1. Products from the reaction of **1** with $Ph_2P(SR')$.

Table 1. Infrared, ^{1}H and ^{31}P NMR data for complexes **2–10**

Compound	ν(CO) (cm^{-1})[a]	^{1}H NMR (δ)[b]	^{31}P NMR (δ)[c]
2a	2068s, 2018s, 1999m, 1978m	7.7–6.9[m, 15H, Ph], 5.00[s, br, 2H, C*H*]	−47.7[s, *P*Ph_2(SPh)]
2b	2065s, 2014vs, 2006vs, 1993m, 1975w	7.5–7.0[m, 15H, Ph], 5.10[s, br, 1H, C*H*], 1.93[s, 3H, Me]	−48.1[s, *P*Ph_2(SPh)]
2c	2025s, 2056s, 2025vs, 1999w	7.7–6.9[m, 15H, Ph], 5.19[dd, ^{3}J(PH) 4.5, 1H, C(CH_2OH)C*H*], 4.39[t, ^{3}J(HH) 6, 1H, C(CH_2O*H*)CH], 3.63[d, ^{3}J(HH) 6, 2H, C(CH_2OH)CH]	−49.9[s, PPh_2(SPh)]
3a	2068s, 2015s, 2010s, 1973m	7.8–7.2[m, 10H, Ph], 5.28[d, ^{3}J(PH) 2.9, 2H, C*H*CH], 2.55–0.7[m, 9H, Bu^n]	−59.9[s, *P*Ph_2(SBu^n)]
3b	2063s, 2011vs, 2005vs, 1992m, 1967w	7.9–7.2[m, 10H, Ph], 5.12[d, ^{3}J(PH) 3.4, 1H, C*H*], 2.41[s, 3H, Me], 2.8–0.7[m, 9H, Bu^n]	−60.6[s, *P*Ph_2(SBu^n)]
3c	2096s, 2056s, 2027vs, 2000w	not recorded	−61.0[s, *P*Ph_2(SBu^n)]
4a	2067s, 2016vs, 2009vs, 1973w	7.8–7.0[m, 10H, Ph], 5.24[d, ^{3}J(PH) 3.0, 2H, C*HCH*], 1.4[s, 9H, Bu^t]	−66.1[s, *P*Ph_2(SBu^t)]
4b	2064s, 2013vs, 2006vs, 1992m, 1967w	7.7–7.1[m, 10H, Ph], 5.16[d, ^{3}J(PH) 3.7, 1H, C*H*], 2.47[s, 3H, Me], 1.37[s, 9H, Bu^t]	−66.1[s, *P*Ph_2(SBu^t)]
5a	2032s, 1990sh, 1980s, 1957w,	7.7–7.0(m, 30H, Ph), 4.25[t, ^{3}J(PH) 3.2, 2H, C*H*], 4.34[dd, ^{3}J(PH) 5.1, 1H, C(O)C*H*CH]	−49.0[s, 2*P*PH_2(SPh)]
5b	2027s, 1977s, 1954w,	8.0–6.9[m, 3OH, Ph], 4.26[d, ^{3}J(PH) 3.1, 1H, C*H*], 1.33[s, 3H, Me]	−48.7[s, 2*P*PH_2(SPh)]
5c	2035s, 1986s	7.7–6.9[m, 30H, Ph], 4.36[dd, ^{3}J(PH) 4.1, ^{3}J(PH) 3.9, 1H, C(CH_2OH)C*H*], 3.92[m, 2H, C(CH_2OH)CH]	−50.6[s, 2*P*Ph_2(SPh)]
6a	2031s, 1988vs, 1978vs, 1954w	7.7–6.9[m, 20H, Ph], 4.59[t, ^{3}J(PH) 3.4, 2H, C*HCH*], 2.5–0.7[m, 9H, Bu^n]	−60.7[s, 2*P*PH_2(SBu^n)]
6b	2018s, 1974vs, 1954m	7.9–7.0[m, 20H, Ph], 4.49[s, br, C*H*], 2.13[m, 3H, Me], 2.8–0.7[m, 9H, Bu^n]	−60.3[s, 2*P*PH_2(SBu^n)]
6c	2095m, 2056vs, 2027vs	7.8–7.2[m, 20H, Ph], 4.59[dd, ^{3}J(PH) 4.1, ^{3}J(PH) 3.9, 1H, C(CH_2OH)C*H*], 3.92[m, 2H, C(CH_2OH)CH], 2.8–0.7 [m, 9H, Bu^n]	−62.5[s, 2*P*Ph_2(SBu^n)]
7a	2019s, 1997vs, 1977m	7.8–7.0[m, 20H, Ph], 4.60[s, br, 2H, C*HCH*], 1.37[s, 9H, Bu^t]	−66.1[s, 2*P*Ph_2(SBu^t)]
7b	2016s, 1992m, 1970m	not recorded	−66.3[s, 2*P*Ph_2(SBu^t)]
8a	2054m, 2018s, 2012sh, 1980m, 1722w	7.8–7.3[m, 15H, Ph], 6.25[dd, ^{3}J(PH) 19.5, ^{3}J(HH) 4.5, 1H, C(O)CHC*H*], 4.34[dd, ^{3}J(PH) 5.1, 1H, C(O)C*H*CH]	43.0[s, μ-*P*Ph_2]
8b	2052m, 2014s, 1977s, 1688w	7.8–7.3[m, Ph, 15H], 6.20[d, ^{3}J(PH) 19.4, 1H, C(O)MeC*H*], 1.80[d, ^{4}J(PH) 4.0, 3H, C(O)C*Me*CH]	50.8[s, br, μ-PPh_2]
8c	2056m, 2017s, 1979m, 1677w	8.1–7.1[m, Ph, 15H], 6.27[d, ^{3}J(PH) 19.3, 1H, C(O)C(CH_2OH)C*H*], 4.10[dd, ^{3}J(PH) 14.0, ^{3}J(HH) 6.8, 2H, CH_2O*H*], 2.53[t, ^{3}J(HH) 6.8, 1H, CH_2O*H*]	49.4[s, μ-*P*Ph_2]
9a	2049m, 2014s, 1972m, 1654w	7.8–7.3[m, 10H, Ph], 6.12[dd, ^{3}J(PH) 19.6, ^{3}J(HH) 4.4, 1H, C(O)CHC*H*] 4.32 [dd, ^{3}J(PH) 5.2, ^{3}J(HH) 4.4, 1H, C(O)C*H*CH], 2.8–0.7[m, 9H, Bu^n]	17.8[s, μ-*P*Ph_2]
9c	2052m, 2013s, 1967m, 1655w	7.9–7.2[m, 10H, Ph], 6.11[d, ^{3}J(PH) 19.1, 1H, C(O)C(CH_2OH)C*H*], 4.13[s, br, 2H, CH_2OH], 2.8–0.7[m, 9H, Bu^n]	12.8[s, μ-*P*Ph_2]
10a	2047m, 2017s, 1982s, 1714m	not recorded	21.2[s, μ-*P*Ph_2]
10b	2045m, 2016s, 1983m, 1713m	7.7–7.1[m, 10H, Ph], 6.07[d, ^{3}J(PH) 20.0, 1H, C(O)CMeC*H*], 1.74[d, ^{4}J(PH) 3.5, 3H, C(O)C*Me*CH], 1.27[s, 9H, Bu^t]	18.1[s, μ-*P*Ph_2]

[a] Recorded in *n*-hexane solution.

[b] ^{1}H chemical shifts (δ) in ppm relative to $SiMe_4$ (0.0 ppm), coupling constants in Hz in $CDCl_3$ at 293 K.

[c] ^{31}P chemical shifts (δ) in ppm relative to external $P(OMe)_3$ (0.0 ppm) (upfield shifts negative), {^{1}H}-gated decoupled, measured in $CDCL_3$ at 293 K.

case shows the presence of a terminal $Ph_2P(SPh)$ ligand as a broad singlet resonance, assignable to the phosphorus atom of the ligand bound directly to a quadrupolar ^{59}Co atom. In the ^{13}C-$\{^1H\}$ NMR spectra, two carbonyl resonances of intensity ratio 3:2 suggest that the three carbonyl ligands residing on the unsubstituted cobalt are fluxional at room temperature on the NMR timescale and that the carbonyl ligands on the phosphine-substituted cobalt are either fluxional or are both coordinated pseudo-equatorially with the $Ph_2P(SR')$ group in a pseudo-axial position. X-ray studies of other reported alkyne-bridged pentacarbonyl–phosphinedicobalt complexes do show a preference for the phosphine ligands to be coordinated pseudo-axially [8].

The molecular structure of the bis-substituted complex $[Co_2(\mu\text{-HCCH})(CO)_4\{PPh_2(SBu^n)\}_2]$ **6a** complex has been determined by a single crystal X-ray diffraction study. The structure is illustrated in Fig. 1; Table 2 lists selected bond distances and angles.

The Co–Co bond [2.457(1) Å] in **6a** is bridged by an acetylene unit which lies almost perpendicular to the cobalt–cobalt bond [C(1)–Co(1)–Co(2) 50.5(2), C(1)–Co(2)–Co(1) 50.9(2), C(2)–Co(1)–Co(2) 51.3(2), C(2)–Co(2)–Co(1) 50.6(2)°]. Each cobalt atom is further bonded by two carbonyl ligands and a thiophosphine ligand which bonds *via* the phosphorus atom to complete a distorted octahedral arrangement about both metal centres. The two thiophosphine groups are orientated in a "sawhorse" configuration about the cobalt–cobalt bond occupying pseudo-axial sites on each each metal centre [Co(1)–P(1) 2.175(2) Å, P(1)–Co(1)–Co(2) 150.70(5)°; Co(2)–P(2) 2.169(2) Å, P(2)–Co(2)–Co(1) 147.82(5)°]. The configuration of $[Co_2(\mu\text{-HCCH})(CO)_4\{PPh_2(SBu^n)\}_2]$ **6a** is similar to that observed for the related complexes $[Co_2(\mu\text{-PhCCH})(CO)_4\{PPh_2(SPh)\}_2]$ [9] and $[Co_2(\mu\text{-HCCH})(CO)_4(PMe_3)_2]$ [10] with the phosphorus-containing ligands occupying pseudo-axial sites despite the resulting greater steric interactions with the bridging alkynes.

The spectroscopic properties of **6a** and the other bis-substituted complexes, **5–7**, are similar to those reported for analogous bis-substituted triorganophosphine complexes [8, 11]. The ^{31}P-$\{^1H\}$ NMR spectrum, in each case, exhibits one broad signal due to the phosphorus atoms being equivalent and directly coordinated to quadrupolar ^{59}Co atoms. In the complexes containing a symmetrical alkyne bridge (**5a**, **6a**, **7a**), one terminal carbonyl resonance is observed in the ^{13}C-$\{^1H\}$ NMR spectra. However, in the ^{13}C-$\{^1H\}$ NMR spectra of complexes containing an unsymmetrical alkyne bridge (**5b**, **5c**, **6b**, **6c**, **7b**), two terminal peaks are observed implying, either that the CO groups on each substituted cobalt atom are non-fluxional on the NMR timescale at room temperature, or that there is a fluxional process which leaves the CO groups inequivalent, such as the trigonal twist process which has been suggested elsewhere for related complexes [6].

Syntheses and properties of $[Co_2(\mu\text{-PPh}_2)\{\mu\text{-SR'C(O)CRCH}\}(CO)_4]$ **8–10**

Syntheses. The thermolysis of $[Co_2(\mu\text{-RCCH})(CO)_5\{PPh_2(SR')\}]$ [(R' = Ph; R = H **2a**, Me **2b**, CH_2OH **2c**), (R' = Bu^n; R = H **3a**, Me **3b**), (R' = Bu^t; R = H **4a**, Me **4b**)] in toluene at 313 K gives, in addition to the starting material, the complexes $[Co_2(\mu\text{-PPh}_2)\{\mu\text{-SR'C(O)CRCH}\}(CO)_4]$ [(R' = Ph; R = H **8a**, Me **8b**, CH_2OH **8c**), (R' = Bu^n; R = H **9a**, Me **9b**), (R' = Bu^t; R = H **10a**, R = Me **10b**)] in moderate yields (Scheme 1). These complexes have been characterised by ^1H, ^{13}C, ^{31}P NMR and IR spectroscopy, and by mass spectrometry and micro-

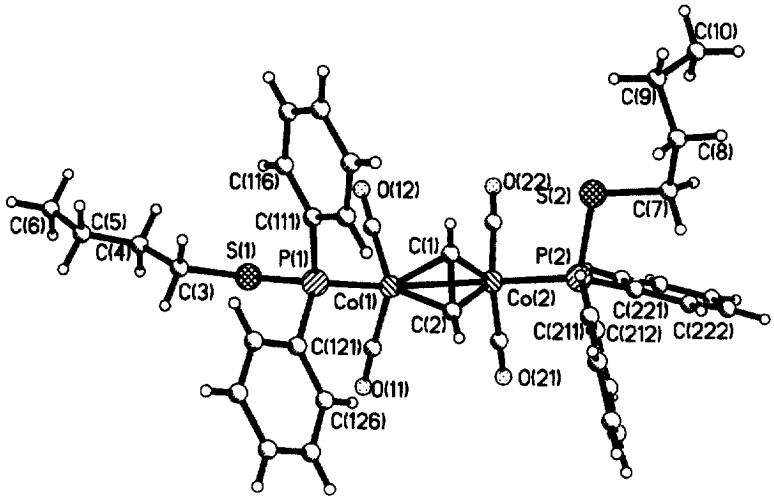

Fig. 1. Molecular structure of $[Co_2(\mu\text{-HCCH})(CO)_4\{PPh_2(SBu^n)\}_2]$ **6a** including the atom numbering scheme.

Table 2. Selected bond lengths (Å) and angles (°) for $[Co_2(\mu\text{-HCCH})(CO)_4\{PPh_2(SBu^n)\}_2]$ **6a**

Co(1)–Co(2)	2.457(1)	Co(1)–P(1)	2.175(2)
Co(2)–P(2)	2.169(2)	Co(1)–C(1)	1.946(6)
Co(1)–C(2)	1.939(6)	Co(2)–C(1)	1.934(6)
Co(2)–C(2)	1.959(6)	C(1)–C(2)	1.298(8)
P(1)–S(1)	2.072(2)	P(2)–S(2)	2.075(2)
S(1)–C(3)	1.809(6)	S(2)–C(7)	1.802(6)
Co(1)–C(11)	1.780(7)	Co(1)–C(12)	1.780(7)
Co(2)–C(21)	1.771(7)	Co(2)–C(22)	1.780(7)
Co(2)–C(1)–Co(1)	78.5(2)	Co(1)–C(2)–Co(2)	78.1(2)
C(2)–Co(1)–C(1)	39.0(2)	C(1)–Co(2)–C(2)	39.0(2)
C(1)–Co(1)–Co(2)	50.5(2)	C(2)–Co(1)–Co(2)	51.3(2)
C(1)–Co(2)–Co(1)	50.9(2)	C(2)–Co(2)–Co(1)	50.6(2)
P(1)–Co(1)–Co(2)	150.70(5)	P(2)–Co(2)–Co(1)	147.82(5)
S(1)–P(1)–Co(1)	105.21(8)	S(2)–P(2)–Co(2)	107.23(8)
	range: Co–C–O	177.4(6)–179.4(6)	

analysis. Complex **9a** has been the subject of a single crystal X-ray diffraction study.

Characterisation. The molecular structure of complex $[Co_2(\mu\text{-}PPh_2)\{\mu\text{-}SBu^nC(O)CHCH\}(CO)_4]$ **9a**, including the atom numbering scheme, is illustrated in Fig. 2. Table 3 lists selected bond distances and angles.

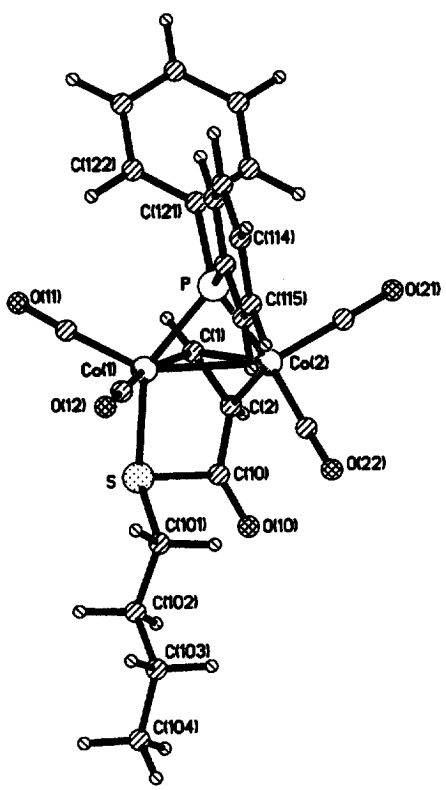

Fig. 2. Molecular structure of $[Co_2(\mu\text{-}PPh_2)\{\mu\text{-}SBu^n\text{-}C(O)CHCH\}(CO)_4]$ **9a** including the atom numbering scheme.

The single cobalt–cobalt bond [2.477(1) Å] is bridged by a diphenylphosphido group and the flyover ring [μ-SBu^{n}C(O)CHCH]. The latter is coordinated *via* S(1) and C(1) to Co(1) to form an almost planar [max. deviation from plane by C(1) 0.28 Å], five-membered metallacyclic ring [Co(1)–S–C(10)–C(2)=C(1)], in which the carbon–carbon double bond is π-coordinated to Co(2) *via* C(1) and C(2). The [μ-SBu^n-C(O)CHCH] ligand is attached to Co(1) such that S(1) and C(1) lie pseudo-*trans* and pseudo-*cis*, respectively, relative to the bridging phosphido group. The [μ-SBu^{n}C(O)CHCH] ligand is arranged in a similar manner to that of [μ-PPh_2C(O)CHCH] in $[Co_2(\mu\text{-}PPh_2)\{\mu\text{-}PPh_2C(O)CHCH\}(CO)_3(PPh_3)]$ [6] and shows very little structural deviation from the related complex, $[Co_2(\mu\text{-}PPh_2)\{\mu\text{-}SPhC(O)CHCH\}(CO)_4]$ **8a**, reported in an earlier communication [7]. The phosphido group bridges the two metal centres asymmetrically with Co(1)–P [2.202(2) Å] being considerably longer than Co(2)–P [2.136(2) Å]. This is presumably due to the better π-donation from Co(2) into the d-orbitals of the phosphorus [Co(2), zero oxidation state; Co(1), oxidation state II].

The spectroscopic properties of the metallacyclic ring complexes **8**–**10** are all very similar and, on this basis, can be considered to have related structures. In their IR spectra (in hexane), in addition to terminal ν_{CO} bands, weak bands at lower wavenumber (*region*: 1722–1653 cm^{-1}) corresponding to the presence of the inserted carbonyl in the [μ-SR′*C(O)*CRCH moiety] are observed.

The NMR spectra are particularly informative about the conformation of **8**–**10**. In the $^{31}P\text{-}\{^1H\}$ NMR spectra, one broad singlet resonance (*region*: 12.8–50.8 ppm), typical of a phosphido ligand bridging a single metal–metal bond [12] is observed for each complex. Similarly, in the ^1H NMR spectra, the orientation of the unsymmetrical olefinic moieties within the five-membered rings can be established unequivocally. When the olefinic moiety has only H sub-

Table 3. Selected bond lengths (Å) and angles (°) for $[Co_2(\mu\text{-}PPh_2)\{\mu\text{-}SBu^nC(O)CHCH\}(CO)_4]$ **9a**

Co(1)–Co(2)	2.477(1)	Co(1)–P	2.202(2)
Co(2)–P	2.136(2)	Co(1)–S	2.258(2)
S–C(10)	1.880(8)	C(10)–C(2)	1.436(10)
C(1)–C(2)	1.402(9)	Co(1)–C(1)	1.973(7)
Co(2)–C(1)	1.928(7)	Co(2)–C(2)	2.099(7)
Co(1)–C(11)	1.785(8)	Co(1)–C(12)	1.779(8)
Co(2)–C(21)	1.748(7)	Co(2)–C(22)	1.782(8)
Co(2)–C(1)–Co(1)	78.8(2)	Co(2)–P–Co(1)	69.6(1)
C(1)–C(2)–C(10)	120.7(7)	C(2)–C(1)–Co(1)	117.0(5)
C(10)–S–Co(1)	97.0(2)		
	range: Co–C–O	176.5(7)–177.6(7)	

stituents (**8a**, **9a**, **10a**) then, in addition to phosphido and thiolate group resonances, two signals both taking the form of double doublets and integrating as one proton each are seen. The downfield signal (*ca.* δ 6.2) is assigned to the [μ-SR′C(O)CHC*H*] protons, with the more upfield signal (*ca.* δ 4.3) being assigned to the [μ-SR′C(O)C*H*CH] protons. The spectra of the complexes containing an unsymmetrical olefinic fragment within the μ-SR′C(O)CRCH ligand [(R′ = Ph; R = Me **8b**, CH_2OH **8c**), (R′ = Bu^n; R = Me **9b**, CH_2OH **9c**), (R′ = Bu^t; R = Me **10b**)] display, in addition to the phosphido, thiolate and R′ group resonances, one further signal at *ca.* δ 6.2 taking the form of a doublet and integrating as one proton. The observation of only one olefinic hydrogen signal implies that the transformation is regiospecific, with the position of the signal indicating that the olefinic carbon to which the hydrogen is attached is σ-bonded to one of the cobalt atoms. It is noteworty that regiospecificity is not observed in the related thermolytic reaction of $[Co_2(\mu\text{-CRCH})(CO)_6]$ (R = Me **1b**, CH_2OH **1c**) with $Ph_2P(PPh_2)$ in which an approximately 1:1 mixture of $[Co_2(\mu\text{-}PPh_2)\{\mu\text{-}PPh_2C(O)CRCH\}(CO)_4]$ and $[Co_2(\mu\text{-}PPh_2)\{\mu\text{-}PPh_2C(O)CHCR\}(CO)_4]$ is obtained, although in this instance these are not the major products of the reactions [6].

In the $^{13}C\text{-}\{^1H\}$ NMR spectra of complexes **8–10**, in addition to upfield peaks corresponding to the olefinic carbon atoms, clearly identifiable signals are observed at lower fields for the terminal carbonyl [*range*: δ 207.8–198.8] groups and for the C(O) moieties [*range*: δ 184.2–178.8] of the bridging ligands. In most cases, all four of the terminal CO groups give rise to distinct resonances, suggesting the carbonyl ligands are non-equivalent at room temperature.

^{13}CO *labelling studies.* The facility with which the C(O)–CRCR link can be cleaved in a number of bimetallic complexes [1, 2] has prompted us to examine the possibility of similar cleavage within the SR′C(O)CRCH ligand using complex **8a** as a representative example.

Figure 3(a) shows the carbonyl region of the $^{13}C\text{-}\{^1H\}$ NMR spectrum at room temperature of ^{13}CO enriched **8a** $[Co_2(\mu\text{-}PPh_2)\{\mu\text{-}SPh^{13}C(O)CHCH\}(^{13}CO)_4]$, prepared by the reaction of a ^{13}CO enriched sample of **1a** with $Ph_2P(SPh)$. The enrichment is non-selective and five signals are seen; the four more downfield broader signals [δ 206.4, 202.3, 201.8, 198.9] correspond to the carbonyl groups bound to the quadrupolar cobalt atoms, while the sharper singlet resonance at δ 184.2 is due to the C(O) group incorporated into the bridging ligand. In Fig. 3(b) the ^{13}CO spectrum of complex **8a**, enriched by treating **8a** with ^{13}CO at 293 K, is shown. Two significant points emerge from a study of this latter spectrum: (i) the observed ^{13}CO enrichment of the ketonic C(O) group shows that this group exchanges rapidly with ^{13}CO gas at room temperature and (ii) only two of the four terminal carbonyl groups exchange. Accordingly the complex may be formulated as $[Co_2(\mu\text{-}PPh_2)\{\mu\text{-}SPh^{13}C(O)CHCH\}(^{13}CO)_2(CO)_2]$.

The substitution by ^{13}CO gas of the ketonic carbonyl group in solution at room temperature implies that, remarkably under these mild conditions, **8a** readily and reversibly undergoes both olefin–carbonyl and sulphur–carbonyl bond cleavage since these are both necessary for the labelling process. Scheme 2 shows a series of equilibria, the existence of which could account for the labelling process. Although we were unable to detect in solution by NMR spectroscopy any of the postulated intermediate species **A**, **B** or **C**, related complexes containing the proposed or similar bridging ligands have been isolated and shown to undergo carbonylation and/or decarbonylation reactions. Thus, examples of the reversible coupling of alkynes with CO groups on bimetallic centres have been well documented [1, 2, 3] although rare in dicobalt chemistry [13]. Dixneuf *et al.* have demonstrated the reversible decarbonylation reaction of the phosphide-containing metallacyclic ring species $[RuCo(\mu\text{-}CO)\{\mu\text{-}PPh_2C(O)CRCR'\}(CO)_5]$ to give $[RuCo(\mu\text{-}CO)\{\mu\text{-}PPh_2CRCR'\}(CO)_5]$ [14] which presumably proceeds via a similar set of equilibria. It should be noted that intermediate species **C** is not required for ^{13}CO exchange to take place but stable complexes containing a PhSCRCR bridging ligand are known

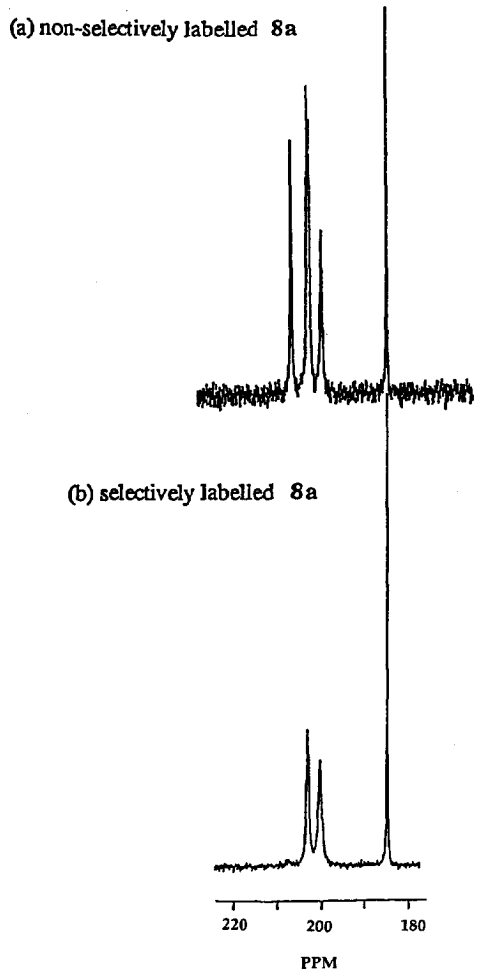

Fig. 3. Carbonyl regions of the ^{13}C-{^1H} NMR spectra of (a) non-selectivity labelled $[Co_2(\mu\text{-}PPh_2)\{\mu\text{-}SPH^{13}C(O)CHCH\}(^{13}CO)_4]$ **8a** and (b) selectively labelled $[Co_2(\mu\text{-}PPh_2)\{\mu\text{-}SPh^{13}C(O)CHCH\}(^{13}CO)_2(CO)_2]$ **8a**.

[15] and it seems likely that intermediate **B**, if it is formed, would be in equilibrium with a further intermediate of this type.

The other observation concerning the labelling, namely that only two of the four terminal carbonyl ligands in **8a** become labelled, is more difficult to explain and it is not clear which two are labelled. Two possible assigments are shown in Scheme 3; in (i) labelling of two carbonyl groups at one metal centre is proposed and in (ii) labelling has occurred at the axial sites of each metal centre. The observed spectra do not permit a distinction between these assignments. It is noteworthy, however, that substitution of carbonyl groups by phosphites or phosphines in complexes possessing the $(OC)_2Co\text{–}Co(CO)_2$ skeleton display a preference for sites axial to the metal–metal bond [4, 6, 7] and it may be that the ^{13}CO substitution favours only the axial sites.

CONCLUSIONS

In all cases, the reactions of thiophosphines with alkyne–hexacarbonyldicobalt complexes proceed by initial coordination of the intact $Ph_2P(SR')$ ligand, followed by phosphorus–sulphur bond cleavage and subsequent coupling of the thiolate fragment with a coordinated CO and CRCH group on the dicobalt complex. The transformations are regiospecific, such that the bulky substituent on the olefinic group is positioned adjacent to the ketonic group. In no case does the generated phosphide fragment couple with the alkyne or the CO groups, instead preferring to adopt a bridging mode between the metal centres. This result may be contrasted with the corresponding reactions of related molybdenum–cobalt alkyne-bridged systems which react with $Ph_2P(SR')$ to give products in which the PPh_2 fragment is linked to the alkyne moiety while the thiolate fragment bridges the metal centres [15]. This difference may be kinetic or thermodynamic in origin but the ready rearrangement of the SPhC(O)CHCH-bridged complex to a $PPh_2CHCHC(O)$-bridged species on bis-phosphine substitution [7], suggests that any kinetic barriers are low. This suggestion is supported by the results from the ^{13}CO labelling of **8a**, which shows that the SR′C(O)CRCH ligand fragments readily and reversibly under mild conditions. In the absence of phosphines therefore, the preference for the SR′ group to be coupled to the organic moiety and for the Ph_2P

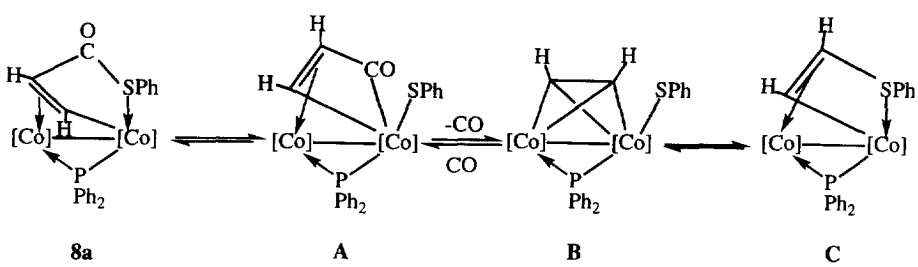

Scheme 2. A possible pathway to account for the ^{13}CO labelling of the ketonic carbonyl group in **8a**. Terminal carbonyl groups have been omitted for clarity.

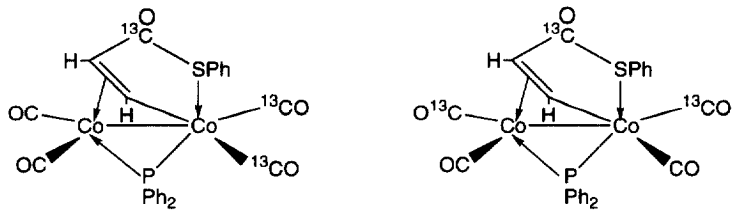

Scheme 3. Two possible assignments for the selectively ^{13}CO labelled terminal carbonyl groups in **8a**.

group to bridge the two metal centres is probably thermodynamically determined.

EXPERIMENTAL

All reactions were carried out under a nitrogen atmosphere using standard Schlenk techniques. Solvents were distilled under nitrogen from appropriate drying agents and degassed prior to use. Preparative thin-layer chromatography (TLC) was carried out on commercial Merck plates with a 0.25 mm layer of silica, or on 1 mm silica plates prepared at the University Chemical Laboratory, Cambridge. Column chromatography was performed on Kieselgel 60 (70–230 mesh) or (230–400 mesh). Products are given in order of decreasing R_f values.

The instrumentation used to obtain spectroscopic data has been described previously [17]. Unless otherwise stated, all reagents were obtained from commercial suppliers and the compounds $[Co_2(\mu\text{-RCCH})(CO)_6]$ (R = H **1a**, Me **1b**, CH_2OH **1c**) and $Ph_2P(SPh)$ were prepared by literature methods [18, 19, 20].

Synthesis of the ligands $Ph_2P(SR')$ ($R' = Bu^n$ *or* Bu^t)

To a solution of NaH (2.00 g, 0.08 mol) in THF (200 cm^3), was added R'SH ($R' = Bu^n$ or Bu^t, 8.8 cm^3, 0.08 mol) and the solution was left to stir. After 2 h, Ph_2PCl (15.0 cm^3, 0.08 mol) was added and the mixture was stirred for a further 3 h. The solvent was removed under reduced pressure and the residue was dissolved in hot toluene and filtered. Removal of the toluene from the filtrate gave $Ph_2P(SBu^n)$ (20.20 g, 92%) as a clear liquid, while pure $Ph_2P(SBu^t)$ (20.03 g, 92%) could be obtained by recrystallisation of the residue from hexane. Compound $Ph_2P(SBu^n)$: fast atom bombardment (FAB) mass spectrum, *m/z* 274 (M^+). ^1H NMR: δ 2.80[m, 2H, CH_2-S], 1.69[m, 2H, CH_2CH_2S], 1.49[m, 2H, $CH_2CH_2CH_2S$] and 0.95[m, 3H, $CH_3CH_2CH_2CH_2S$]. ^{31}P-{^1H} NMR: δ −113.0. ^{13}C-{^1H} NMR: δ 142–128[m, Ph], 32.5[s, CH_2S], 32.3[s, CH_2CH_2S], 20.0[s, $CH_2CH_2CH_2S$] and 11.1[s, $CH_3CH_2CH_2CH_2$]. Compound $Ph_2P(SBu^t)$: FAB mass spectrum, *m/z* 274 (M^+). ^{31}P-{^1H} NMR: δ −130.5.

Reactions of $[Co_2(\mu\text{-CRCH})(CO)_6]$ **1** *with* $Ph_2P(SR')$

(i) To a solution of $[Co_2(\mu\text{-HCCH})(CO)_6]$ **1a** (1.00 g, 3.21 mmol) in toluene (50 cm^3) was added $Ph_2P(SR')$ ($R' = Ph$, 0.944 g, 3.21 mmol; Bu^n, 0.881 g, 3.21 mmol; Bu^t, 0.881 g, 3.21 mmol) in toluene (50 cm^3). The solutions were stirred at 298 K for 24 h and, after removal of the solvent under reduced pressure, the mixtures were adsorbed onto a minimum amount of silica, added to the top of chromatography columns and purified by eluting with hexane–dichloromethane (10:1). This gave, in addition to a small amount of unreacted starting material, orange $[Co_2(\mu\text{-CHCH})(CO)_5\{PPh_2(SR')\}]$ [$R' = Ph$ **2a** (1.149 g, 62%); $R' = Bu^n$ **3a** (1.075 g, 60%); $R' = Bu^t$ **4a** (1.038 g, 58%)] and orange crystalline $[Co_2(\mu\text{-CHCH})(CO)_4\{PPh_2(SR')\}_2]$ [$R' = Ph$ **5a** (0.379 g, 14%); $R' = Bu^n$ **6a** (0.387 g, 15%); $R' = Bu^t$ **7a** (0.390 g, 15%)]. Complex **2a**: FAB mass spectrum, *m/z* 578 (M^+) and M^+-*n*CO (*n* = 1–5). ^{13}C NMR ($CDCl_3$, 293 K, ^1H composite pulse decoupled): δ 204.1(s, 2CO), 201.5(s, 3CO), 136–127(m, Ph) and 70.6(s, 2*C*H). Complex **5a**: FAB mass spectrum, *m/z* 844 (M^+) and M^+-*n*CO (*n* = 1–4). ^{13}C NMR ($CDCl_3$, 293 K, ^1H composite pulse decoupled): δ 206.0(s, 4CO), 136–128(m, Ph) and 70.9(s, 2*C*H). Complex **3a** (Found: C, 49.7; H, 3.8. $C_{23}H_{21}Co_2PSO_5$ requires C, 49.5; H, 3.8): FAB mass spectrum, *m/z* 558 (M^+) and (M^+-*n*CO) (*n* = 1–5). NMR ($CDCl_3$); ^{13}C(^1H composite pulse decoupled), δ 204.5[s, 2CoCO], 201.8[s, 3CoCO], 135–127[m, Ph], 70.7[s, *C*HCH], 32.4[s, CH_2], 31.7[s, CH_2], 21.7[s, CH_2] and 13.4[s, CH_3]. Complex **6a** (Found: C, 56.6; H, 5.0. $C_{38}H_{40}Co_2P_2S_2O_4$ requires C, 56.7; H, 5.0): FAB mass spectrum, *m/z* 804 (M^+) and (M^+-*n*CO) (*n* = 1–4). NMR ($CDCl_3$); ^{13}C(^1H composite pulse decoupled), δ 206.0[s, 4CoCO], 134–128[m, Ph], 70.7[s, *C*HCH], 32.5[s, CH_2], 32.0[s, CH_2], 22.7[s, CH_2] and 13.5[s, CH_3]. Complex **4a**: FAB mass spectrum, *m/z* 558 (M^+) and (M^+-*n*CO) (*n* = 1–5). NMR ($CDCl_3$); ^{13}C(^1H composite pulse decoupled), δ 205.0[s, 2CoCO], 201.9[s, 3CoCO], 137–127[m, Ph], 71.7[s, *C*HCH] and 32.6[s, Bu^t]. Complex **7a**: FAB mass spectrum, *m/z* 804 (M^+) and (M^+-*n*CO) (*n* = 1–4). NMR ($CDCl_3$); ^{13}C(^1H composite pulse decoupled), δ 206.1[s, 2CoCO], 205.9[s, 2CoCO], 135–127[m, Ph], 72.0[s, *C*HCH] and 32.5[s, Bu^t].

(ii) To a solution of $[Co_2(\mu\text{-MeCCH})(CO)_6]$ **1b** (1.00 g, 3.07 mmol) in toluene (50 cm^3) was added $Ph_2P(SR')$ (R′ = Ph, 0.902 g, 3.07 mmol; Bu^n, 0.841 g, 3.07 mmol; Bu^t, 0.841 g, 3.07 mmol) in toluene (50 cm^3). The solutions were stirred at 298 K for 24 h and after removal of the solvent under reduced pressure, the mixtures were adsorbed onto a minimum amount of silica, added to the top of chromatography columns and purified by eluting with hexane–dichloromethane (10:1). This gave, in addition to a small amount of unreacted starting material, orange $[Co_2(\mu\text{-CMeCH})(CO)_5\{PPh_2(SR')\}]$ [R′ = Ph **2b** (1.117 g, 63%); R′ = Bu^n **3b** (0.913 g, 52%); R′ = Bu^t **4b** (0.842 g, 48%)] and orange crystalline $[Co_2(\mu\text{-CMeCH})(CO)_4\{PPh_2(SR')\}_2]$ [R′ = Ph **5b** (0.342 g, 13%); R′ = Bu^n **6b** (0.352 g, 14%); R′ = Bu^t **7b** (0.251 g, 10%)]. Complex **2b** (Found: C, 52.8; H, 3.4; P, 5.3. $C_{26}H_{19}Co_2PSO_5$ requires C, 52.7; H, 3.2; P, 5.2): FAB mass spectrum, m/z 592 (M^+) and (M^+-nCO) (n = 1–5). NMR ($CDCl_3$); $^{13}C\{^1H$ composite pulse decoupled), δ 205.2[s, CoCO], 204.0[s, CoCO], 202.3[s, 3CO], 136–128[m, Ph], 89.8[s, *C*Me], 72.9[s, *C*H] and 19.4[s, Me]. Complex **5b**: FAB mass spectrum, m/z 858 (M^+) and (M^+-nCO) (n = 1–4). NMR ($CDCl_3$); $^{13}C\{^1H$ composite pulse decoupled), δ 206.2[s, 2CoCO], 205.9[s, 2CoCO], 136–127[m, Ph], 86.3[s, *C*Me], 72.5[s, *C*H] and 18.0[s, Me]. Complex **3b**: FAB mass spectrum, m/z 572 (M^+) and (M^+-nCO) (n = 1–5). NMR ($CDCl_3$); $^{13}C\{^1H$ composite pulse decoupled), δ 207.0[s, CoCO], 206.0[s, CoCO], 202.3[s, 3CoCO], 135–125[m, Ph], 88.8[s, *C*Me], 72.8[s, *C*H], 32.4[s, CH_2], 31.7[s, CH_2], 21.7[s, CH_2], 19.5[s, Me] and 13.4[s, CH_2CH_3]. Complex **5b**: FAB mass spectrum, m/z 818 (M^+) and (M^+-nCO) (n = 1–4). NMR ($CDCl_3$); $^{13}C\{^1H$ composite pulse decoupled), δ 206.0[s, 2CoCO], 205.9[s, 2CoCO], 136–128[m, Ph], 88.4[s, *C*Me], 72.1[s, *C*H], 32.3[s, CH_2], 31.9[s, CH_2], 21.8[s, CH_2], 18.1[s, Me] and 13.4[s, CH_2CH_3]. Complex **4b**: FAB mass spectrum, m/z 572 (M^+) and (M^+-nCO) (n = 1–5). NMR ($CDCl_3$); $^{13}C\{^1H$ composite pulse decoupled), δ 205.5[s, CoCO], 204.5[s, CoCO], 202.0[s, 3CoCO], 135–128[m, Ph], 89.0[s, *C*Me], 73.0[s, *C*H], 52.7[s, $C(CH_3)$], 32.6[s, $C(CH_3)_3$] and 19.3[s, Me]. Complex **7b**: FAB mass spectrum, m/z 818 (M^+) and (M^+-nCO) (n = 1–4).

(iii) To a solution of $[Co_2\{\mu\text{-}(CH_2OH)CCH\}(CO)_6]$ **1c** (1.00 g, 2.92 mmol) in toluene (50 cm^3) was added $Ph_2P(SR')$ (R′ = Ph, 0.860 g, 2.92 mmol; R′ = Bu^n, 0.801 g, 2.92 mmol) in toluene (50 cm^3). The solutions were stirred at 298 K for 24 h and after removal of the solvent under reduced pressure, the mixtures were adsorbed onto a minimum amount of silica, added to the top of chromatography columns and purified by eluting with hexane–ethylacetate (10:1). This gave, in addition to a small amount of unreacted starting material, orange $[Co_2\{\mu\text{-}(CH_2OH)CCH\}(CO)_5\{PPh_2(SR')\}]$ [R′ = Ph **2c** (1.134 g, 64%); R′ = Bu^n 3c (1.064 g, 62%)] and orange crystalline $[Co_2\{\mu\text{-}(CH_2OH)CCH\}(CO)_4\{PPh_2(SR')\}_2]$ [R′ = Ph **5c** (0.434 g, 17%); R′ = Bu^n **6c** (0.438 g, 18%)]. Complex **2c**: FAB mass spectrum, m/z 608 (M^+) and (M^+-nCO) (n = 1–5). NMR ($CDCl_3$); $^{13}C\{^1H$ composite pulse decoupled), Δ 205.7[s, br, 2CoCO], 205.1[s, 3CoCO], 135–128[m, Ph], 92.9[s, *C*(CH_2OH)CH], 70.1[s, C(CH_2OH)*C*H] and 62.8[s, C(*C*H_2OH)CH]. Complex **5c**: FAB mass spectrum, m/z 874 (M^+) and (M^+-nCO) (n = 1–4). NMR ($CDCl_3$); $^{13}C\{^1H$ composite pulse decoupled), δ 205.2[s, 2CoCO], 201.9[s, 2CoCO], 135–128[m, Ph], 91.2[s, *C*(CH_2OH)CH], 69.7[s, C(CH_2OH)*C*H] and 61.9[s, C(*C*H_2OH)CH]. Complex **3c**: FAB mass spectrum, m/z 588 (M^+) and (M^+-nCO) (n = 1–5). NMR ($CDCl_3$); $^{13}C\{^1H$ composite pulse decoupled), δ 206.0[s, CoCO], 203.5[s, CoCO], 201.0[s, 3CoCO], 134–128[m, Ph], 92.4[s, *C*(CH_2OH)CH], 70.8[s, C(CH_2OH)*C*H], 63.0[s, C(*C*H_2OH)CH], 32.4[s, CH_2], 31.7[s, CH_2], 21.7[s, CH_2] and 13.4[s, CH_3]. Complex **6c**: FAB mass spectrum, m/z 834 (M^+) and (M^+-nCO) (n = 1–4). NMR ($CDCl_3$); $^{13}C\{^1H$ composite pulse decoupled), δ 206.0[s, br, 4CoCO], 135–128[m, Ph], 92.0[s, *C*(CH_2OH)CH], 70.0[s, C(CH_2OH)*C*H], 62.9[s, C(*C*H_2OH)CH], 32.5[s, CH_2], 31.8[s, CH_2], 21.8[s, CH_2] and 13.4[s, CH_3].

Syntheses of $[Co_2(\mu\text{-}PPh_2)\{\mu\text{-}SR'C(O)CRCH\}(CO)_4]$ **8–10**

(i) Solutions of $[Co_2(\mu\text{-CHCH})(CO)_5\{PPh_2(SR')\}]$ (R′ = Ph **2a**, 0.289 g, 0.50 mmol; R′ = Bu^n **3a**, 0.300 g, 0.54 mmol; R′ = Bu^t **4a**, 0.300 g, 0.54 mmol) in toluene (50 cm^3) were thermolysed at 313 K for 5–8 h. After removal of the solvent under reduced pressure, the mixtures were purified using preparative TLC with hexane–dichloromethane (6:1) as eluent to give, in addition to a small amount of unreacted starting material, the red crystalline complexes $[Co_2(\mu\text{-}PPh_2)\{\mu\text{-}SR'C(O)CHCH\}(CO)_4]$ [R′ = Ph **8a** (0.173 g, 60%); R′ = Bu^n **9a** (0.168 g, 56%); R′ = Bu^t **10a** (0.159 g, 53%)]. Complex **8a** (Found: C, 51.6; H, 3.2; P, 5.5. $C_{25}H_{17}Co_2O_5PS$ requires C, 51.9; H, 3.0; P, 5.4): FAB mass spectrum, m/z 578 (M^+) and M^+-nCO (n = 1–5). ^{13}C NMR ($CDCl_3$, 293 K, ^1H composite pulse decoupled): δ 206.4(s, CO), 202.3(s, CO), 201.8(s, CO), 198.9(s, CO), 181.7[s, SPh*C*(O)CHCH], 142–128(m, Ph), 124.0[d, br, ^2J(PC) 30, SPhC(O)CH*C*H] and 63.1[s, br, SPhC(O)*C*HCH]. Complex **9a** (Found: C, 49.5; H, 3.8. $C_{23}H_{21}Co_2O_5PS$ requires C, 49.5; H, 3.8): FAB mass spectrum, m/z 558 (M^+) and M^+-nCO (n = 1–4). ^{13}C NMR ($CDCl_3$, 293 K, ^1H composite pulse decoupled): δ 206.6(s, CoCO), 202.9(s, CoCO), 202.0(s, CoCO), 199.0(s, CoCO), 184.2[s, SBu^n*C*(O)CHCH], 141–128(m, Ph), 124.0[d, ^2J(PC) 34, SBu^{n}C(O)CH*C*H], 62.7[s, SBu^{n}C(O)*C*HCH], 29.7[s, CH_2], 29.4[s, CH_2], 21.9[s, CH_2] and 13.6[s, CH_3]. Complex **10a**: FAB mass spectrum, m/z 558 (M^+) and M^+-nCO (n = 1–4).

(ii) Solutions of $[Co_2(\mu\text{-CMeCH})(CO)_5\{PPh_2(SR')\}]$ (R′ = Ph **2b**, 0.289 g, 0.50 mmol; R′ = Bu^n **3b**, 0.300 g, 0.54 mmol; R′ = Bu^t **4b**, 0.300 g, 0.54 mmol) in toluene

($50\,cm^3$) were thermolysed at 313 K for 5–8 h. After removal of the solvent under reduced pressure, the mixtures were purified using preparative TLC with hexane–dichloromethane (6:1) as eluent to give, in addition to a small amount of unreacted starting material, the red crystalline complexes $[Co_2(\mu\text{-}PPh_2)\{\mu\text{-}SR'C(O)CMeCH\}(CO)_4]$ [R′ = Ph **8b** (0.173 g, 60%); R′ = Bu^n **9b** (0.168 g, 56%; R′ = Bu^t **10b** (0.159 g, 53%)]. Complex **8b** (Found: C, 52.4; H, 3.4; P, 5.4. $C_{26}H_{19}Co_2O_5PS$ requires C, 52.7; H, 3.2; P, 5.2): FAB mass spectrum, *m/z* 592 (M^+) and M^+-*n*CO (*n* = 1–5). ^{13}C NMR ($CDCl_3$, 293 K, ^1H composite pulse decoupled): δ 207.8(s, CoCO), 202.7(s, CoCO), 202.0(s, CoCO), 199.4(s, CoCO), 178.8[s, SPh*C*(O)CMeCH], 142–127[m, Ph and SPhC(O)C-MeCH], 78.9[s, br, SPhC(O)*C*MeCH] and 23.6[s, Me]. Complex **9b**: FAB mass spectrum, *m/z* 572 (M^+) and M^+-*n*CO (*n* = 1–4). ^{13}C NMR ($CDCl_3$, 293 K, ^1H composite pulse decoupled): δ 207.4(s, CoCO), 207.0(s, 2CoCO), 198.8(s, CoCO), 181.3[s, SBu^n-*C*(O)CMeCH], 141–128(m, Ph), 126.6[d, ^2J(PC) 33, SBu^{n}C(O)CMe*C*H], 70.6[s, SBu^{n}C(O)*C*MeCH], 29.7[s, CH_2], 29.4[s, CH_2], 21.9[s, SBu^{n}C(O)C*Me*CH], 21.7[s, CH_2] and 13.6[s, CH_3]. Complex **10b**: FAB mass spectrum, *m/z* 572 (M^+) and M^+-*n*CO (*n* = 1–4).

(iii) Solutions of $[Co_2\{\mu\text{-}(CH_2OH)CCH\}(CO)_5\{PPh_2(SR')\}]$ (R′ = Ph **2a**, 0.289 g, 0.50 mmol; R′ = Bu^n **3a**, 0.300 g, 0.54 mmol; R′ = Bu^t **4a**, 0.300 g, 0.54 mmol) in toluene ($50\,cm^3$) were thermolysed at 313 K for 5–8 h. After removal of the solvent under reduced pressure, the mixtures were purified using preparative TLC with hexane–dichloromethane (6:1) as eluent to give, in addition to a small amount of unreacted starting material, the red crystalline complexes $[Co_2(\mu\text{-}PPh_2)\{\mu\text{-}SR'C(O)C(CH_2OH)CH\}(CO)_4]$ [R′ = Ph **8c** (0.173 g, 60%); R′ = Bu^n **9c** (0.168 g, 56%)]. Complex **8c** (Found: C, 50.9; H, 3.4. $C_{26}H_{19}Co_2O_6PS$ requires C, 51.3; H, 3.1): FAB mass spectrum, *m/z* 608 (M^+) and M^+-*n*CO (*n* = 1–4). ^{13}C NMR ($CDCl_3$, 293 K, ^1H composite pulse decoupled): δ 206.5(s, CoCO), 201.8(s, 2CoCO), 198.9(s, CoCO), 180.5[s, SPh*C*(O)C(CH_2OH)CH], 142–128[m, Ph], 126.2[d, ^2J(PC) 33 SPhC(O)C-(CH_2OH)*C*H], 66.3[s, SPhC(O)C(*C*H_2OH)CH] and 63.4[s, SPhC(O)*C*(CH_2OH)CH]. Complex **9c**: FAB mass spectrum, *m/z* 588 (M^+) and M^+-*n*CO (*n* = 1–4). ^{13}C NMR ($CDCl_3$, 293 K, ^1H composite pulse decoupled): δ 207.0(s, CoCO), 204.0(s, CoCO), 202.0(s, CoCO), 200.0(s, CoCO), 183.3[s, SBu^n-*C*(O)C(CH_2OH)CH], 142–128(m, Ph), 128.3[d, ^2J(PC) 33, SBu^{n}C(O)C(CH_2OH)*C*H], 66.5[s, SBu^n-C(O)C(*C*H_2OH)CH], 64.9[s, SBu^{n}C(O)*C*(CH_2OH)CH], 29.7[s, CH_2], 29.0[s, CH_2], 21.9[s, CH_2] and 13.5[s, CH_3].

Isotopic labelling experiments

Isotopic enrichment of **1a**. Complex $[Co_2(\mu\text{-}HCCH)(CO)_6]$ **1a** (1.00 g, 3.21 mmol) was dissolved in toluene ($50\,cm^3$). The solution was degassed under reduced pressure, back-filled with an atmosphere of ^{13}CO and left to stir at 293 K for 24 h. The reaction mixture was filtered and the solvent removed under reduced pressure to give the isotopically labelled species $[Co_2(\mu\text{-}HCCH)(^{13}CO)_n(^{12}CO)_n]$ (*n* = 1–6). NMR evidence shows a degree of enrichment >90% had been achieved.

Preparation of non-selectively labelled **8a**. The non-selectively labelled complex $[Co_2(\mu\text{-}PPh_2)\{\mu\text{-}SPh^{13}C(O)CHCH\}(^{13}CO)_4]$ **8a** was prepared using the procedure outlined in parts (b) and (c) above, starting from an isotopically enriched sample of **1a**.

Preparation of selectively labelled **8a**. Complex $[Co_2(\mu\text{-}PPh_2)\{\mu\text{-}SPhC(O)CHCH\}(CO)_4]$ **8a** (0.200 g, 0.35 mmol) was dissolved in toluene ($50\,cm^3$). The solution was degassed under reduced pressure, back-filled with an atmosphere of ^{13}CO and left to stir at 293 K for 24 h. The reaction mixture was filtered and the solvent removed under reduced pressure to give the selectively labelled species $[Co_2(\mu\text{-}PPh_2)\{\mu\text{-}SPh^{13}C(O)CHCH\}(^{13}CO)_2(CO)_2]$. NMR evidence shows a degree of enrichment of the labelled carbonyl groups to be >90%.

Crystal structure analysis of complexes **6a** *and* **9a**

Crystal data for $[Co_2(\mu\text{-}HCCH)(CO)_4\{PPh_2(SBu^n)\}_2]$ **6a**. $C_{38}H_{40}Co_2O_4P_2S_2$, M = 804.62, triclinic, space group $P\bar{1}$ (no. 2), a = 10.634(2), b = 13.563(3), c = 13.864(3) Å, α = 74.16(2), β = 82.46(2), γ = 81.26(2)°, U = 1892.8(7) Å^3, D_c = 1.412 g cm^{-3}, Z = 2, μ(Mo-K_α) = 11.0 cm^{-1}, $F(000)$ = 832.

Data collection for **6a**. An orange crystal of size 0.06 × 0.46 × 0.48 mm was used in data collection. Intensity data were collected on a Siemens R3m/V diffractometer at 295 K, using ω-2θ scan mode with graphite monochromated Mo-K_α radiation (λ = 0.71073 Å). No significant drift was encountered during data collection. 13271 reflections ($-12 \le h \le 12$, $-15 \le k \le 15$, $-16 \le l \le 16$) were collected in the range θ 1.5–25.0° with a scan width of 1.20°, to give 6636 (R_{int} = 0.0640) independent reflections with $I/\sigma(I) > 2.0$.

Structure solution and refinement for **6a**. All intensity data were corrected for Lorentz polarisation effects, and absorption corrections by the ψ-scan method; minimum and maximum transmission factors 0.3161 and 0.3804. Computations were performed using the SHELTXL PLUS package [21]. The structure was solved by a combination of Patterson synthesis (Co atoms) and Fourier-difference techniques. The structure was refined by full matrix least squares with all atoms assigned anisotropic displacement parameters [22]. Hydrogen atoms were placed in idealised positions and allowed to ride on the relevant carbon atoms. Residual electron densisty found after all atoms had been assigned, was successfully attributed to disorder of the butyl fragment of one of the PPh_2(S-

Bu^n) ligands and this was included in the final refinement. In the final cycles of refinement, a weighting scheme of the form $\omega^{-1}=\sigma^2(F)+0.010F^2$ gave satisfactory agreement analysis. The refinement converged to $R=0.0553$, w$R=0.1088$ and a goodness of fit = 1.002, with a final shift/esd of 0.019 and a residual electronic density of less than 1 e Å^{-3}.

Crystal data for [$Co_2(\mu$-$PPh_2)\{\mu$-SBu^n C(O)CHCH$\}(CO)_4$] **9a**. $C_{23}H_{21}Co_2O_5PS$, $M=558.29$, orthorhombic, space group $P2_12_12_1$, $a=10.240(3)$, $b=10.612(4)$, $c=22.160(4)$ Å, $U=2408.1(6)$ Å^3, $D_c=1.540$ g cm^{-3}, $Z=4$, μ(Mo–K_α) = 10.6 cm^{-1}, $F(000)=1136$.

Data collection for **9a**. A red crystal of size $0.25\times0.34\times0.29$ mm was used in data collection. Intensity data were collected on a 4 circle Philips diffractometer at 295 K, using ω-2θ scan modewith graphite monochromated Mo–K_α radiation ($\lambda=0.71073$ Å). No significant drift was encountered during data collection. 2438 reflections ($0\le h\le14$, $0\le k\le14$, $0\le l\le29$) were collected in the range θ 3–25°, with a scan width of 0.70°. Equivalent reflections were merged to give 1972 ($R_{int}=0.0644$) independent reflections with $I/\sigma(I)>3.0$.

Structure solution and refinement of **9a** [23]. The fractional coordinates of the metal atoms were obtained from a Patterson synthesis; remaining non-hydrogen atoms were located from subsequent Fourier-difference syntheses. The hydrogen atoms of this structure were included in geometrically idealised postions and constrained to ride on the relevant carbon atoms in calculated positions of C–H 1.080 Å with fixed thermal parameters of 0.08 Å^2, but were not refined. After initial refinement with isotropic thermal parameters for all atoms, empirical absorption correction were applied [24]. In the final stages of full matrix refinement the two metal atoms, the S and P atoms on the bridging ligands and the atoms of the CO groups were treated as anisotropically vibrating atoms. The final shift/esd was 0.032 and there was a residual electronic density of less than 1 e Å^{-3}. Refinement converged with reliability factors of $R=0.039$ and Rw = 0.042 and with weights of $1/\sigma^2F_o$ assigned to individual reflections [23].

Additional material, available from the Cambridge Crystallographic Data Centre, comprises H-atom coordinates, thermal parameters and remaining bond lengths and angles.

Acknowledgements—We thank the EPSRC (G. E. P. and G. A. S.) for financial support.

REFERENCES

1. (a) Checuti, M. J., Grant, B. E., Fanwick, P. E., *Organometallics*, 1995, **14**, 2937; (b) Checuti, M. J., Eigenbrot, C., Green, K. A., *Organometallics*, 1987, **6**, 2298; (c) Checuti, M. J., Grant, B. E., Fanwick, P. E., *Organometallics*, 1996, **15**, 4389; (d) Boag, N. M., Goodfellow, R. J., Green, M., Hessner, B., Howard, J. A. K., Stone, F. G. A., *J. Chem. Soc., Dalton Trans.*, 1983, 2585; (e) Gracey, B. P., Knox, S. A. R., Macpherson, K. A., Orpen, A. G., Stobart, S. R., *J. Chem. Soc., Dalton Trans.*, 1985, 1935; (f) Wong, A., Pawlick, R. V., Thomas, C. G., Leon, D. R., Liu, L.-K., *Organometallics*, 1991, **10**, 530; (g) Hogarth, G., Kayser, F., Knox, S. A. R., Morton, D. A. V., Orpen, A. G., Turner, M. L., *J. Chem. Soc., Chem. Commun.*, 1988, 358; (h) Fontaine, X. L. R., Jacobsen, G. B., Shaw, B. L., Thornton-Pett, M., *J. Chem. Soc., Dalton Trans.*, 1988, 741; (i) Dickson, R. S., Gatehouse, B. M., Nesbit, M. C., Pain, G. N., *J. Organomet. Chem.*, 1981, **215**, 97.
2. (a) Finnimore, S. R., Knox, S. A. R., Taylor, G. E., *J. Chem. Soc., Dalton Trans.*, 1982, 1783; (b) Dyke, A. F., Knox, S. A. R., Morris, M. J., Naish, P. J., *J. Chem. Soc., Dalton Trans.*, 1983, 1417.
3. Dickson, R. S., Evans, G. S. and Fallon, G. D., *Aust. J. Chem.*, 1985, **38**, 273.
4. (a) Martín, A., Mays, M. J., Raithby, P. R., Solan, G. A., *J. Chem. Soc., Dalton Trans.*, 1993, 1789; (b) Caffyn, A. J. M., Martín, A., Mays, M. J., Raithby, P. R., Solan, G. A., *J. Chem. Soc., Dalton Trans.*, 1994, 609.
5. Caffyn, A. J. M., Mays, M. J., Solan, G. A., Braga, D., Sabatino, P., Tiripicchio, A., Tiripicchio-Camellini, M., *Organometallics*, 1993, **12**, 1876.
6. (a) Caffyn, A. J. M., Braga, D., Sabatino, P., Conole, G., McPartlin, M., Powell, H. R., *J. Chem. Soc., Dalton Trans.*, 1991, 3103; (b) Caffyn, A. J. M., Mays, M. J., Solan, G. A., Conole, G., Tiripicchio, A., *J. Chem. Soc., Dalton Trans.*, 1993, 2345.
7. Edwards, A. J., Martín, A., Mays, M. J., Raithby, P. R. and Solan, G. A., *J. Chem. Soc., Chem. Commun.*, 1992, 1416.
8. (a) Bradley, D. H., Khan, M. A., Nicholas, K. M., *Organometallics*, 1989, **8**, 554; (b) Bradley, D. H., Khan, M. A., Nicholas, K. M., *Organometallics*, 1992, **11**, 2598; (c) Cragg, R. H., Jeffery, J. C., Went, M. J., *J. Chem. Soc., Dalton Trans.*, 1991, 137; (d) Caffyn, A. J. M., Mays, M. J., Conole, G., McPartlin, M., Powell, H. R., *J. Organomet., Chem.*, 1992, **436**, 83.
9. Solan, G. A., PhD Thesis. University of Cambridge, 1993.
10. Bonnet, J. J. and Mathieu, R., *Inorg. Chem.*, 1978, **17**, 1973.
11. Chia, L. S., Cullen, W. R., Franklin, M. and Manning, A. R., *Inorg, Chem.*, 1975, **14**, 2521.
12. Carty, A. J., *Adv. Chem. Ser.*, 1982, **196**, 163.
13. (a) Hermann, W. A., Bauer, C., Weichmann, J., *J. Organomet. Chem.*, 1983, **243**, C21; (b) Pályi, G., Varadi G., Márko, L., in *Stereochemistry of Organometallic and Inorganic Compounds*, vol. 1, ed. I. Bernal. Amsterdam, 1986, pp. 358–410.
14. Regragui, R., Dixneuf, P. H., Taylor, N. J., Carty, A. J., *Organometallics*, (a) 1984, **3**, 814; (b) 1990, **9**, 2234.
15. (a) Rumin, R., Guernou, K., Petillon, F. Y., Muir, K. W., *J. Chem. Soc., Dalton Trans.*, 1997, 1381; (b) Mays, M. J., Pateman, G. E., Solan, G. A., unpublished results.
16. (a) Martín, A., Mays, M. J., Raithby, P. R., Solan,

G. A., *J. Chem. Soc., Dalton Trans.*, 1993, 1431; (b) Ingham, S. L., Mays, M. J., Raithby, P. R., Solan, G. A., Sundavadra, B. V., Conole, G., Kessler, M., *J. Chem. Soc., Dalton Trans.*, 1994, 3607.
17. Caffyn, A. J. M., Mays, M. J. and Raithby, P. R., *J. Chem. Soc., Dalton Trans.*, 1991, 2349.
18. Sternberg, H. W., Greenfield, H., Friedel, R. A., Wotiz, J., Markby, R. and Wender, I., *J. Am. Chem. Soc.*, 1954, **76,** 1457.
19. Sternberg, H. W. and Greenfield, H., *J. Am. Chem. Soc.*, 1956, **78,** 120.
20. Job, B. E., Mclean, R. A. N. and Thompson, D. T., *J. Chem. Soc., Chem. Commun.*, 1966, 895.
21. SHELX PLUS program version 4.0. Siemens Analytical X-Ray Instruments, Madison, WI, 1990.
22. Cooper, M. K., Guerney, P. J. and McPartlin, M., *J. Chem. Soc., Dalton Trans.*, 1982, 757.
23. Sheldrick, G. M., *SHELX* 76 *program for crystal structure determination.* University of Cambridge, 1976.
24. Walker, N. and Stuart, D., DIFABS program, *Acta Crystallogr.*, 1968, **24,** 158 Sect A.

Pergamon

PII: S0277-5387(98)00104-1

Polyhedron Vol. 17, No. 17, pp. 3005–3020, 1998
© 1998 Elsevier Science Ltd
All rights reserved. Printed in Great Britain
0277-5387/98 $19.00+0.00

Manganese carboxylate clusters: from structural aesthetics to single-molecule magnets[1]

Guillem Aromí,[a] Sheila M. J. Aubin,[b] Milissa A. Bolcar,[a] George Christou,[a]* Hilary J. Eppley,[a] Kirsten Folting,[a] David N. Hendrickson,[b] John C. Huffman,[a] Rachel C. Squire,[a] Hui-Lien Tsai,[b] Sheyi Wang[a] and Michael W. Wemple[a]

[a]Department of Chemistry and Molecular Structure Center, Indiana University, Bloomington, IN 47405-4001, U.S.A

[b]Department of Chemistry, University of California at San Diego, La Jolla, CA 92093, U.S.A

(Received 13 February 1998)

Abstract—An overview is provided of some recent developments in manganese carboxylate cluster chemistry. A variety of synthetic methodologies are described together with the structures of the resultant products, which span metal nuclearities of 4 to 18 and oxidation states of II to IV, including mixed-valency. The spins of the ground states of these products are often large and sometimes abnormally large, and in certain cases when this is coupled to a sufficiently large magnetoanisotropy, the clusters function as single-molecule magnets i.e., they can be magnetized by an external magnetic field below a critical temperature. These complexes display hysteresis in magnetization *vs.* magnetic field studies, and clear evidence for quantum tunnelling of magnetization. Such results establish single-molecule magnetism as a new magnetic phenomenon, and one that holds great promise for next-century technological applications. © 1998 Elsevier Science Ltd. All rights reserved

INTRODUCTION

Over the last decade or so, manganese carboxylate cluster chemistry has proved to be a rich source of a variety of polynuclear species. To date, metal nuclearities of up to 18 have been encountered in discrete form, and the Mn oxidation states have spanned the range II–IV, including mixed valency. The metal ions are invariably bridged by combinations of O^{2-}, HO^- and RO^- ions, and occasionally by one or both oxygen atoms of carboxylate groups. The stimuli for these studies have been varied and have included (i) the search for models of Mn-containing proteins and enzymes, in which Mn nuclearities up to 4 have been identified [1]; and (ii) the realization that Mn clusters often possess large (and occasionally abnormally large) values of ground state spin (S) [2], leading to a desire to understand the factors that yield this property and, in turn, stimulating the development of synthesis methodologies that might yield such species on a regular basis.

In a previous report during the early years of our efforts in Mn carboxylate chemistry [3], we described how the trinuclear, oxide-centered complexes $[Mn_3O(O_2CR)_6L_3]^z$ ($z = 0$, Mn^{II}, $2Mn^{III}$; $z = +1$, $3Mn^{III}$) were an excellent starting point for the synthesis of species with nuclearities up to 12. In the intervening years, a number of new synthesis procedures have been developed, several of which will be summarized herein. We shall also describe the magnetic properties of selected species and show how the high spin value exhibited by some of them leads to these complexes displaying the new magnetic phenomenon of single-molecule magnetism, which was indeed initially identified in Mn carboxylate chemistry. For

[1] Dedicated to Professor Jack Lewis on the occasion of his 70th birthday.

* Author to whom correspondence should be addressed.

consistency with the theme of this Symposium-in-Print, we shall only describe complexes with nuclearities $\geqslant 4$.

SYNTHETIC METHODS

Aggregation of $[Mn_4O_2]^{8+}$ *butterfly complexes*

One family of complexes that had been frequently encountered in earlier work was that containing a $[Mn_4O_2]^{8+}$ core with a planar or butterfly-like Mn_4 unit and μ_3-O^{2-} ions. Thus, the species $[Mn_4O_2(O_2CR)_7(L\text{-}L)_2]^z$ had been prepared and characterized, and contain peripheral ligation provided by bridging RCO_2^- and chelating L-L (bipyridyl (bpy) [4], or the anions of picolinic acid (pic^-) [5], 8-hydroxyquinoline (hqn^-) [6], 2-hydroxymethylpyridine (hmp^-) [6] or dibenzoylmethane (dbm^-) [7]. These complexes were studied in detail by a variety of methods but did not represent good starting points to higher nuclearity species until the related complex $(NBu^n_4)[Mn_4O_2(O_2CPh)_9(H_2O)]$ (**1**; $4Mn^{III}$) was synthesized (Fig. 1) [7, 8]: the anion contains a $[Mn_4O_2]^{8+}$ butterfly unit with only H_2O and $PhCO_2^-$ peripheral groups, and it has consequently proven a superb stepping stone to other species. A few examples of its use for this purpose will be described.

Addition of Me_3SiCl destabilizes **1** by carboxylate abstraction and causes a nuclearity change to yield $(NBu^n_4)[Mn_8O_6Cl_6(O_2CPh)_7(H_2O)_2]$ (**2**; $8Mn^{III}$) [7, 9], whose anion is shown in Fig. 2. Such a transformation must clearly involve a complicated series of fragmentation/aggregation steps and equilibria, and the formation and isolation of **2** is undoubtedly facilitated by its low solubility that causes it to crystallize from solution. This is a common theme in many syntheses of higher nuclearity Mn species, and also rationalizes the often observed sensitivity of the product identity to the exact reaction conditions (i.e., carboxylate, solvent, etc.) which likely alter the relative solubilities of solution species in equilibrium. The structure of

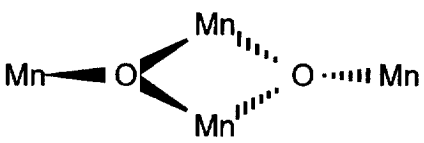

planar

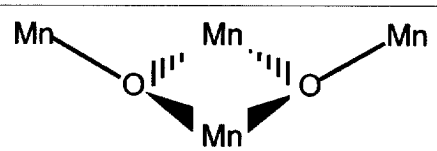

butterfly

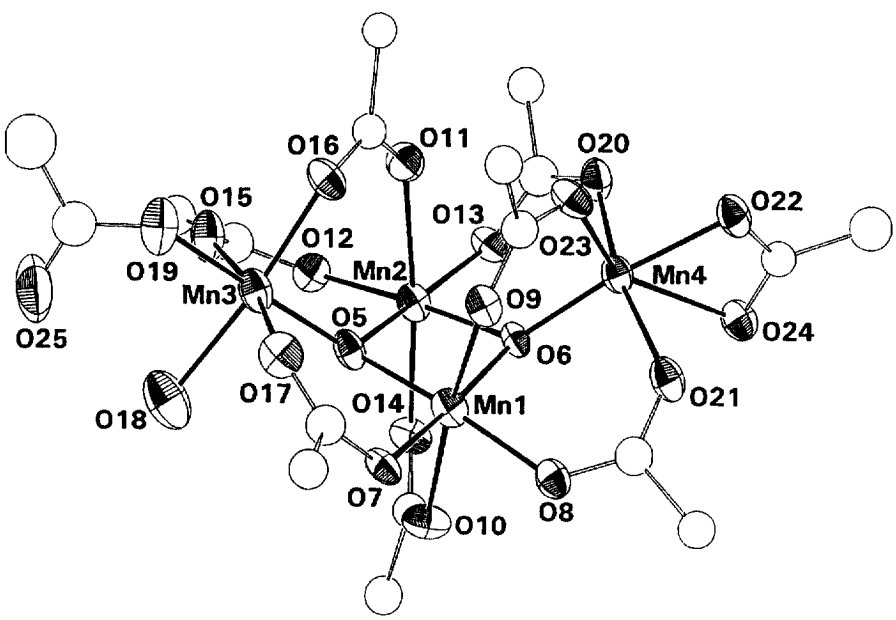

Fig. 1. The structure of the $[Mn_4O_2(O_2CPh)_9(H_2O)]^-$ anion of complex **1**.

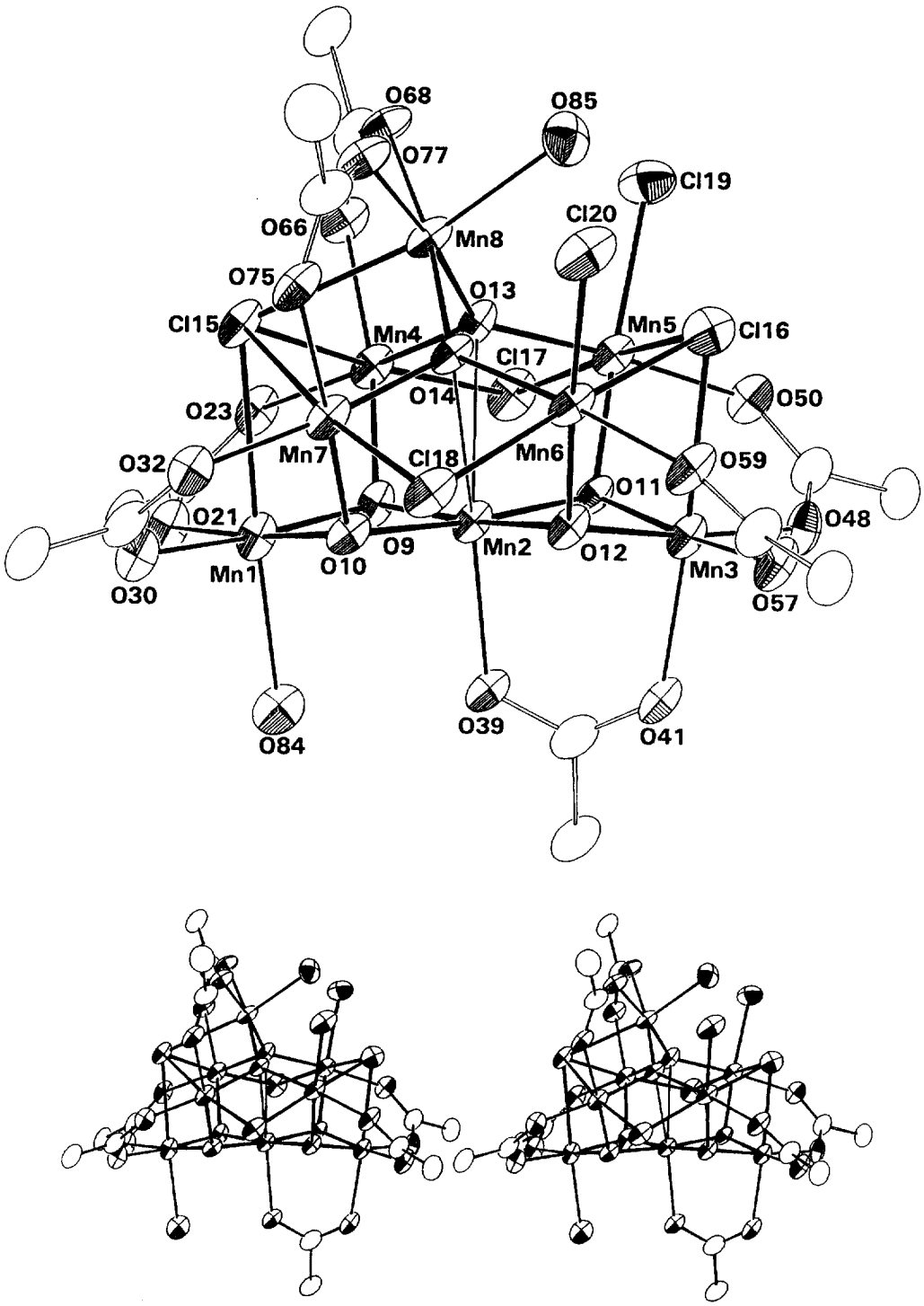

Fig. 2. The structure of the $[Mn_8O_6Cl_6(O_2CPh)_7(H_2O)_2]^-$ anion of complex **2**.

2 consists of two body-fused butterfly units sharing central Mn(2), and an eighth metal atom, Mn(8), is held to the four wingtip Mn atoms by oxide bridges O(13) and O(14).

Another way of destabilizing complex **1** to aggregation is addition of benzoyl peroxide $(PhCO_2)_2$, which again gives a higher nuclearity product $[Mn_9Na_2O_7(O_2CPh)_{15}(MeCN)_2]$ (**3**; $9Mn^{III}$) [9] but no increase in the Mn oxidation level (of the isolated product, at least). The structure (Fig. 3) again comprises two body-fused butterfly units as in **2**, but now with two additional Mn atoms attached to the wingtip

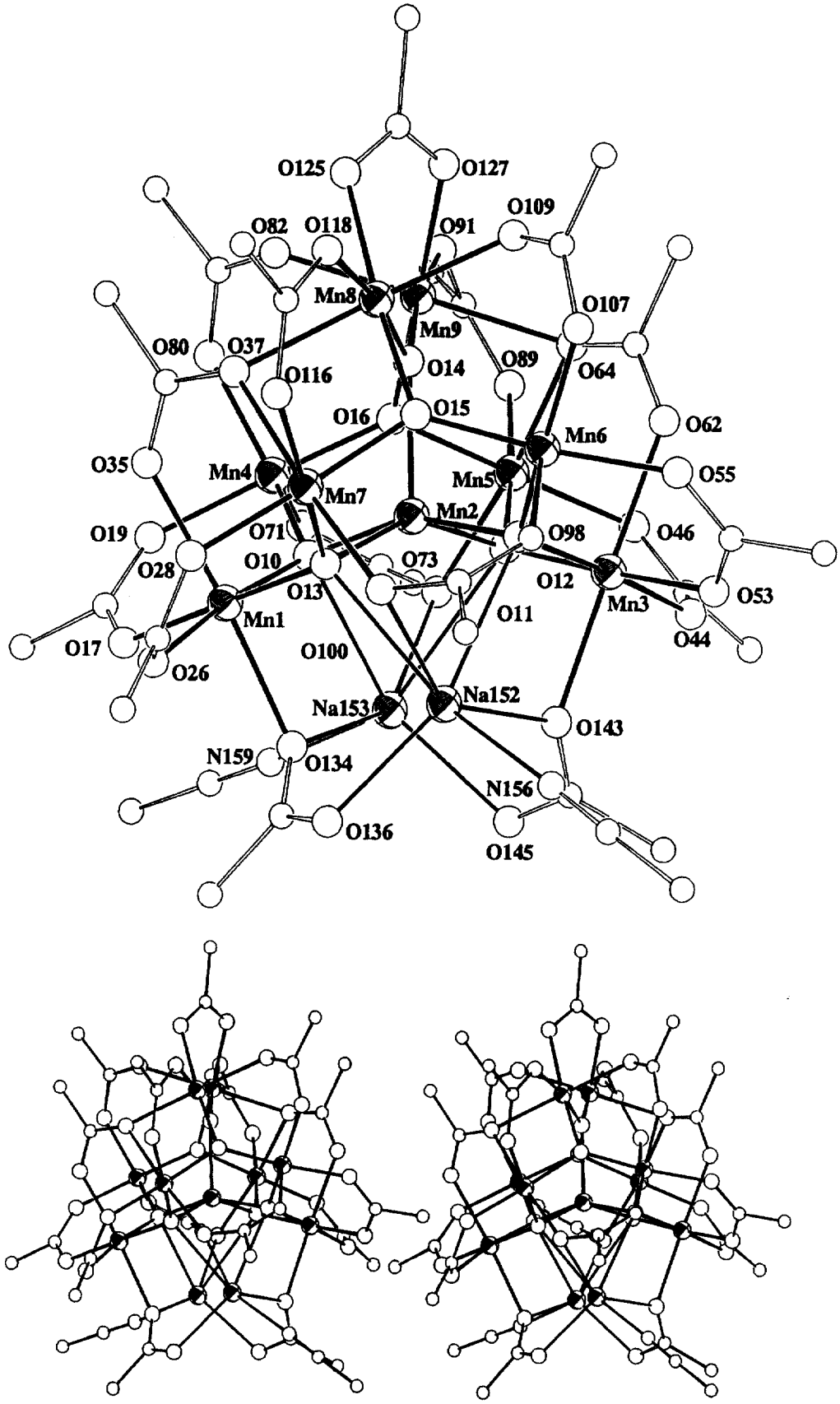

Fig. 3. The structure of $[Mn_9Na_2O_7(O_2CPh)_{15}(MeCN)_2]$ (**3**).

positions by three O^{2-} ions O(14)–O(16). The Na^+ ions are intimately attached to the $[Mn_9O_7]$ unit and the system is best described as a mixed-metal cluster. A related complex with the same core structure but without Na^+ ions, $[Mn_9O_7(O_2CPh)_{13}(py)_2]$, has been made by Armstrong and coworkers [10].

The reactions of complex **1** with appropriate dicarboxylates was envisaged as a potential way of bringing two or more $[Mn_4O_2]$ units into close proximity and thereby possibly triggering aggregation into a higher nuclear product. Two particularly interesting successes of this strategy can be described. The reaction of **1** with 2,2-diethylmalonate (Et_2mal^{2-}) gives $(NBu^n_4)_2[Mn_8O_4(O_2CPh)_{12}(Et_2mal)_2(H_2O)_2]$ (**4**; $2Mn^{II}$, $6Mn^{III}$) [8] whose structure (Fig. 4) clearly demonstrates that its $[Mn_8O_4]$ core can be described as two linked $[Mn_4O_2]$ butterfly units. The Et_2mal^{2-} groups provide additional inter-butterfly linkages and thus no doubt contribute to the formation and stabilization of an octanuclear species, presumably by initially forming a species in which two separate $[Mn_4O_2]$ complexes are bridged by a Et_2mal^{2-} group. In contrast, the reaction of complex **1** with KH(phth) (phth = phthalate) causes a transformation to the octadecanuclear cluster $[K_4Mn_{18}O_{16}(O_2CPh)_{22}(phth)_2(H_2O)_4]$ (**5**; $18Mn^{III}$) [11] shown in Fig. 5. This remarkable structure can nevertheless be considered as the result of the linkage of several $[Mn_4O_2]$ units, and the two $phth^{2-}$ groups are μ_4 and bridge a total of six Mn^{III} ions between them, no doubt a contributing factor to the high nuclearity of the product.

A final example of a high nuclearity product from a $[Mn_4O_2]$ complex is provided by the dissolution of $[Mn_4O_2(O_2CPh)_6(MeCN)_2(pic)_2]$ in Me_2NCOMe (DMA); black crystals of $[Mn_{10}O_8(O_2CPh)_6(pic)_8]$ (**6**; $10Mn^{III}$) slowly form (Fig. 6) [12]. This interesting transformation only occurs in DMA and is presumably caused by the good donor solvent destabilizing the $[Mn_4O_2]$ species to aggregation by partial or complete displacement of one or more carboxylate groups; again the low solubility of the product undoubtedly assists attainment of pure material.

Controlled potential electrolysis

The previous observation in our group that $[Mn_4O_2(O_2CMe)_6(py)_2(dbm)_2]$ ($4Mn^{III}$) would disproportionate to $[Mn_4O_3X(O_2CMe)_3(dbm)_3]$ ($X = Cl^-$ or Br^-; $3Mn^{III}$,Mn^{IV}) on treatment with

$$3[Mn_4O_2]^{8+} + 2X^- \rightarrow 2[Mn_4O_3X]^{6+} + 2Mn^{2+} + 2Mn^{3+} \quad (1)$$

Me_3SiX in CH_2X_2 (eq. (1)) [8, 13] prompted an investigation of the electrochemical oxidation of selected $[Mn_4O_2]^{8+}$ species as a potentially useful method of forming similar or related products. Controlled potential electrolysis (CPE) of $[Mn_4O_2(O_2CMe)_6(py)_2(dbm)_2]$ at 0.84 V *vs.* ferrocene in the presence of dbmH gave $[Mn_4O_3(O_2CMe)_4(dbm)_3]$ (**7**; $3Mn^{III}$, Mn^{IV}) [14]. Similarly, the CPE of $(NBu^n_4)[Mn_4O_2(O_2CPh)_7(dbm)_2]$ at 0.65 V gave $[Mn_4O_3(O_2CPh)_4(dbm)_3]$ (**8**; $3Mn^{III}$, Mn^{IV}) [15]. In both cases, the one-electron oxidation of the $[Mn_4O_2]^{8+}$ core has triggered incorporation of a third O^{2-} group, presumably from H_2O, and a change to a $[Mn_4(\mu_3\text{-}O)_3(\mu_3\text{-}O_2CR)]^{6+}$ core. This is summarized for **8** in eq. (2); a related equation summarizes the formation of **7**. The structures of **7**

$$[Mn_4O_2(O_2CPh)_7(dbm)_2]^- + dbmH - e^- + H_2O \rightarrow [Mn_4O_3(O_2CPh)_4(dbm)_3] + 3PhCO_2H \quad (2)$$

and **8** (Figs 7 and 8) are similar to those of $[Mn_4O_3X(O_2CMe)_3(dbm)_3]$ in possessing a trigonal pyramidal core with O^{2-} ions on three faces and the basal face of $3Mn^{III}$ ions capped by a μ_3-X^- or RCO_2^- ion. The R = Me (**7**) and Ph (**8**) species differ slightly, however, in that the former has a $\eta^1,\mu_3 - MeCO_2^-$ and the latter a $\eta^2,\mu_3 - PhCO_2^-$, the difference being assigned to the larger size of Ph *vs.* Me causing steric problems with the dbm Ph groups in a η^1, μ_3-bridging mode for the R = Ph case.

Access to complex **7** in particular has allowed site-selective ligand substitution reactions at the $\mu_3 - MeCO_2^-$ position to be developed, a process facilitated by the $\mu_3 - MeCO_2^-$ group lying at the intersection of the three Mn^{III} Jahn–Teller elongation axes and thus being more weakly bound and more susceptible to electrophilic attack by trimethylsilyl or related reagents than the other ligands in the molecule. Crystallographically confirmed products are shown in Fig. 9 [13–17], and others are currently being characterized.

Comproportionation reactions

A useful way of obtaining Mn_x products at the ~III oxidation level is the comproportionation between a Mn^{II} source and MnO_4^-. This was the original method used by Lis to access the dodecanuclear complex $[Mn_{12}O_{12}(O_2CMe)_{16}(H_2O)_4]\cdot 2H_2O\cdot 4MeCO_2H$ (**9**; $8Mn^{III}$, $4Mn^{IV}$) [18], the complex which has since initiated the field of Single-Molecule Magnetism (*vide infra*). Thus, the reaction of $Mn(O_2CMe)_2\cdot 4H_2O$ and $KMnO_4$ in 60% (v/v) $MeCO_2H/H_2O$ gives **9** *via* the comproportionation summarized in eq. (3). From **9** can now be made a variety of derivatives by

$$44Mn^{2+} + 16Mn^{7+} \rightarrow 5[Mn_{12}]^{40+} \quad (3)$$

ligand substitution reactions with other carboxylic acids eq. (4) [19, 20]; the R = Ph complex [19] is shown in Fig. 10. All these Mn_{12} complexes are trapped-valence and contain a central

$$[Mn_{12}O_{12}(O_2CMe)_{16}(H_2O)_4] + 16RCO_2H \rightarrow [Mn_{12}O_{12}(O_2CR)_{16}(H_2O)_4] + 16MeCO_2H \quad (4)$$

$[Mn^{IV}_4O_4]$ cubane around which is a non-planar ring

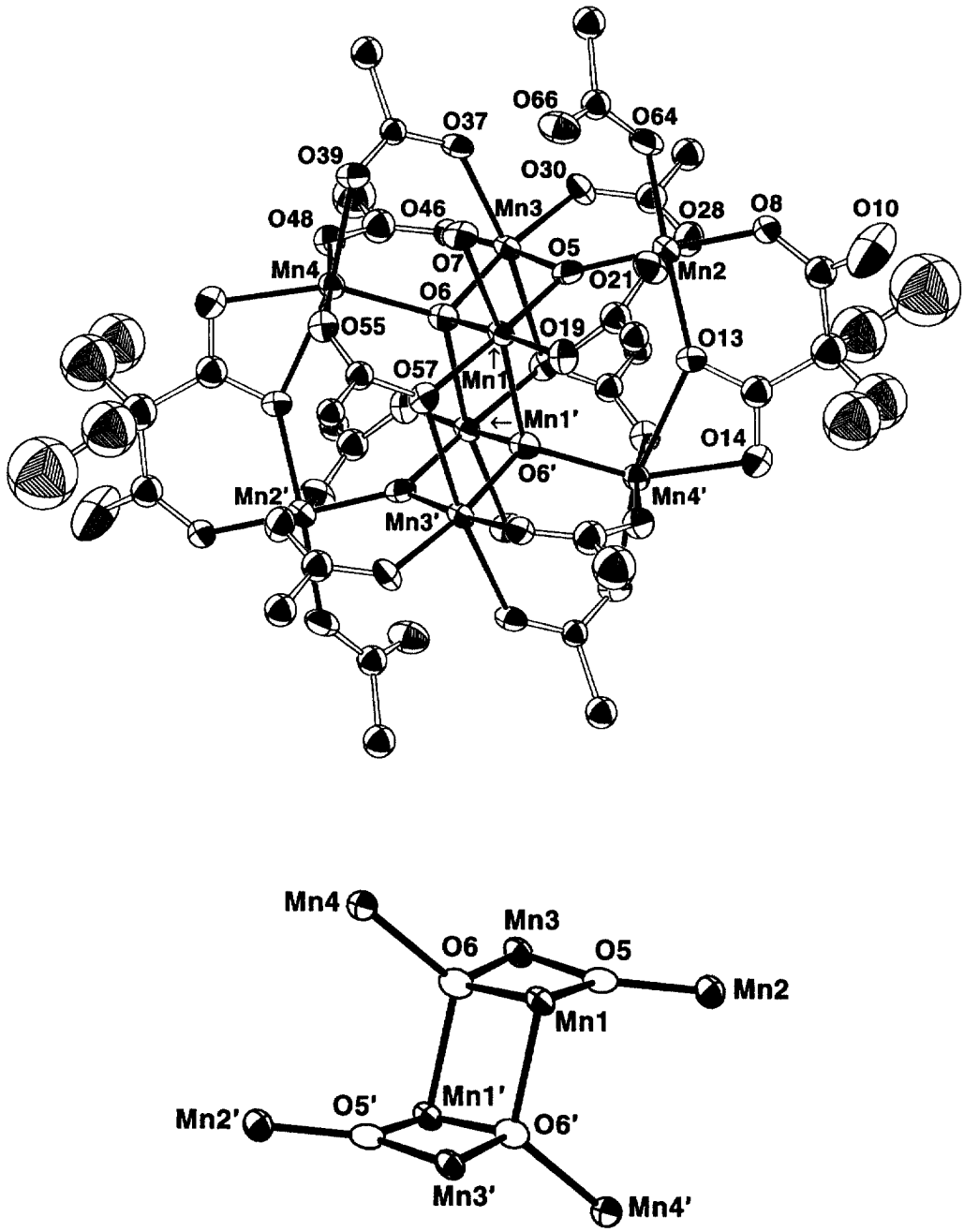

Fig. 4. The structure of $[Mn_8O_4(O_2CPh)_{12}(Et_2mal)_2(H_2O)_2]^{2-}$ anion and its $[Mn_8O_4]^{14+}$ core; the Mn^{II} ions are Mn4 and Mn4′.

of Mn^{III} ions held to the central cubane by eight O^{2-} ions.

The $[Mn_{12}O_{12}(O_2CR)_{16}(H_2O)_4]$ complexes display a reversible one-electron reduction in the 0.00 to 0.50 V *vs.* ferrocene range, and this has allowed [20] isolation and characterization of the one-electron reduced clusters from reductions with I^-. Thus, for example, $(PPh_4)[Mn_{12}O_{12}(O_2CEt)_{16}(H_2O)_4]$ (**10**) can be prepared *via* eq. (5), a method that can readily be extended to other carboxylates [20].

$$[Mn_{12}] + PPh_4I \rightarrow (PPh_4)[Mn_{12}] + 1/2I_2 \qquad (5)$$

The comproportionation method has recently been employed to access a new Mn_7 complex. Treatment of $MnCl_2 \cdot 4H_2O$ with 2-hydroxymethylpyridine (hmpH) and NEt_4MnO_4 leads to $(NEt_4)[Mn_7(OH)_3Cl_3(hmp)_9]$

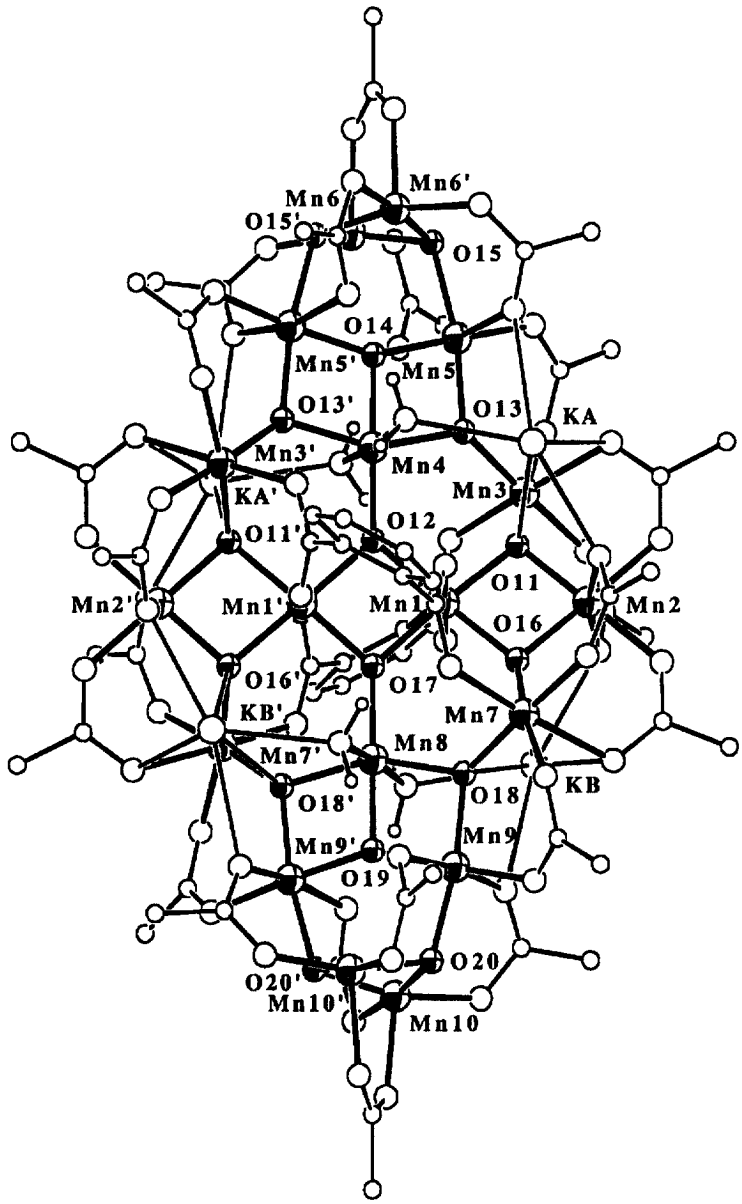

Fig. 5. The structure of $[K_4Mn_{18}O_{16}(O_2CPh)_{22}(phth)_2(H_2O)_4]$ **5**; the K^+ ions are labeled as KA and KB.

$(Cl)(MnCl_4)$ (**11**) [21], the Mn_7 anion of which (Fig. 11) contains $4Mn^{II}$, $3Mn^{III}$, the Mn^{III} ions being easily identified from structural parameters and Jahn–Teller distortions as Mn(2), Mn(4) and Mn(6). Use of $MnBr_2{\cdot}4H_2O$ leads to the corresponding Br derivative, which is isostructural. Interestingly, the reaction of hmpH with the Mn^{III} species $[Mn_3O(O_2CMe)_6(py)_3](ClO_4)$ leads to $[Mn_{10}O_4(OH)_2(O_2CMe)_8(hmp)_8](ClO_4)_4$ (**12**) [22], the cation of which (Fig. 12) is related to, but nevertheless distinctly different from that of **11**. Both **11** and **12** contain almost planar Mn_x cores held together by bridging O^{2-}/OH^- ions, with peripheral ligation provided by bridging hmp^- and (for **12**) $MeCO_2^-$ groups.

MAGNETIC PROPERTIES

Ground state spin value

It has become evident over the course of the last several years that small values of spin, S, in the ground states of Mn carboxylate clusters are almost the exception rather than the rule [2]. For example, in Table 1 are listed the S values for the Mn_x carboxylate species mentioned in this paper, and although clusters with $S = 0$ are present, noteworthy is the significant number of large S values in this list: for calibration, the largest S for a molecular species is currently the $S = 33/2$ for one of the clusters in cocrystallized Fe_{17}

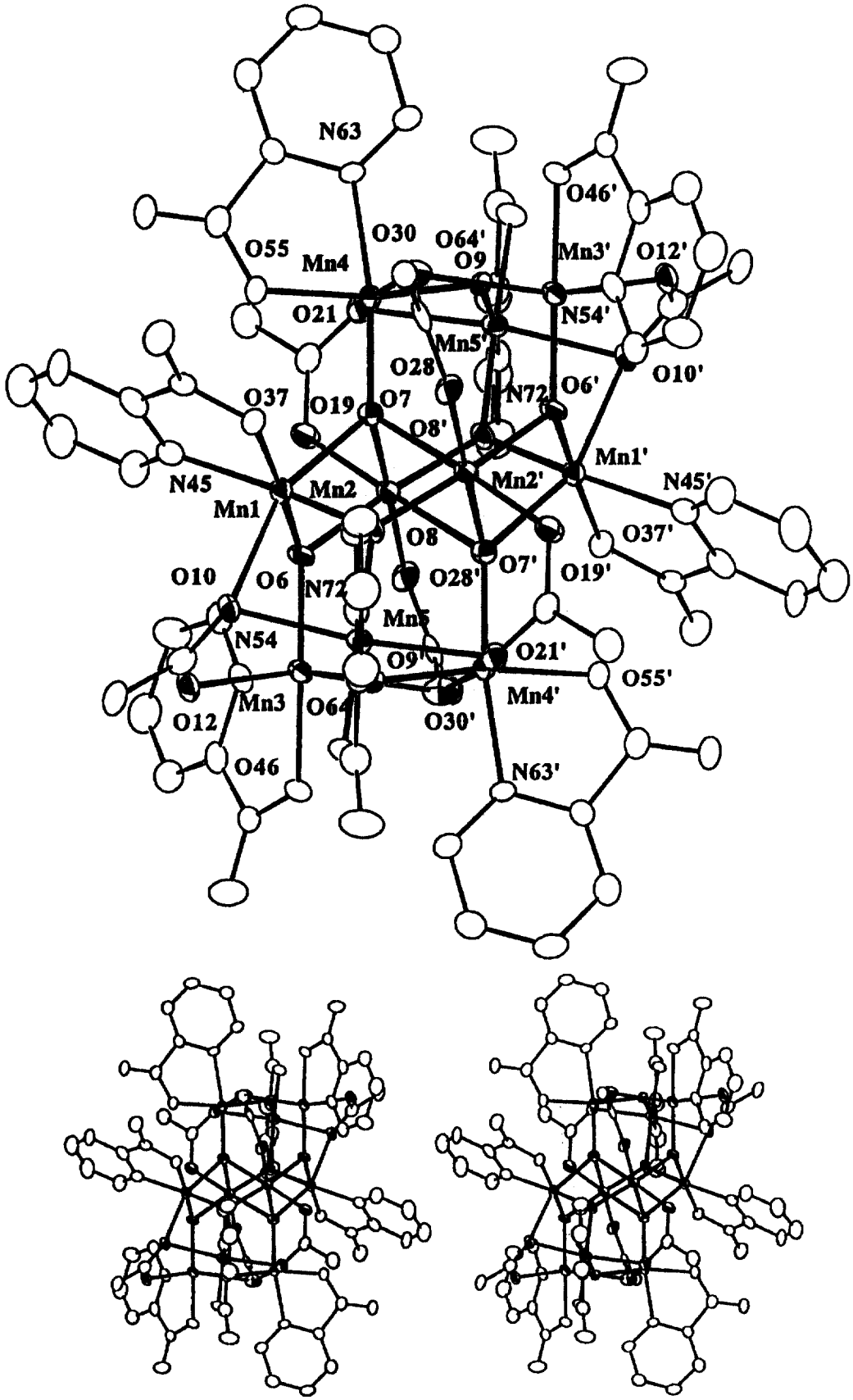

Fig. 6. The structure of $[Mn_{10}O_8(O_2CPh)_6(pic)_8]$ (**6**).

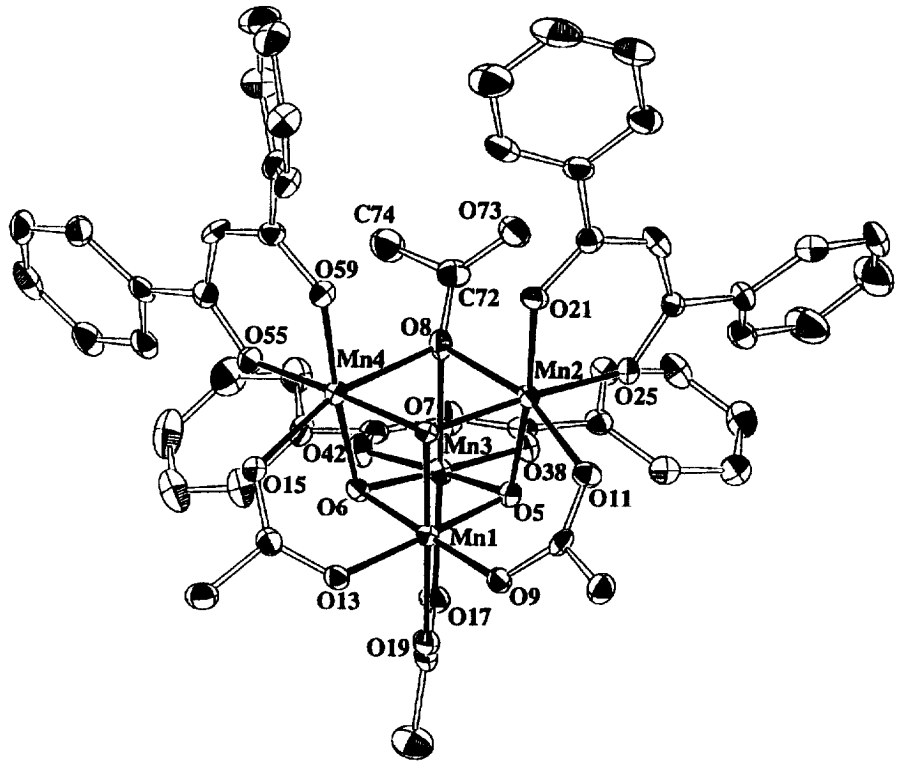

Fig. 7. The structure of $[Mn_4O_3(O_2CMe)_4(dbm)_3]$ (7).

and Fe_{19} units [23]. The origin of the large S value is a result of the presence of (at least some) ferromagnetic exchange interactions and/or spin frustration [24, 25] effects arising from the presence in certain topologies of competing exchange interactions. The latter prevent (frustrate) the preferred spin alignments that would otherwise normally yield low spin species.

For smaller clusters such as some of those in Table 1, the individual pairwise exchange parameters can be

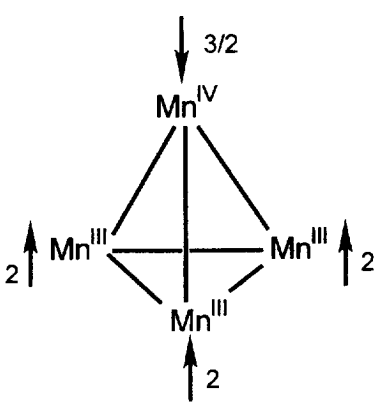

determined by fitting experimental molar magnetic susceptibility (χ_m) *vs.* T data to the appropriate theoretical equation derived for that topology and metal oxidation state(s) using the Kambe vector coupling methods [26]. In those cases, the ground state S value may be readily rationalized. In other clusters, their complexity (size, symmetry) precludes such an analysis and only the value of the ground state may be obtained (*via* magnetization *vs.* field studies). An example of the former is found in the $[Mn_4O_3X]^{6+}$ species, which contain a $3Mn^{III},Mn^{IV}$ pyramid of C_{3v} symmetry [13]. The Mn^{III}/Mn^{III} exchange interactions (J_{33}) are ferromagnetic ($+5$ to $+10\,cm^{-1}$) and the Mn^{III}/Mn^{IV} interactions (J_{34}) are antiferromagnetic (-20 to $-30\,cm^{-1}$), and the alignment of the individual Mn^{III} and Mn^{IV} spins (2 and 3/2, respectively) in the ground state are as shown, giving the molecular spin as $S = 6-3/2 = 9/2$, as is found experimentally.

An example of the latter approach is provided by the $[Mn_{12}O_{12}(O_2CR)_{16}(H_2O)_4]$ clusters, which have $S = 10$ ground states, except for a few, such as the R = Et species, which have $S = 9$ [19, 20]. The ground state may be rationalized as resulting from ferromagnetic exchange interactions within the central $[Mn_4O_4]$ cubane and antiferromagnetic interactions between central Mn^{IV} and outer Mn^{III} ions (although none of the J values are actually known). This predicts a ground state of $S = 16-6 = 10$ since all the Mn^{IV} and Mn^{III} spins would be parallel and antiparallel, respectively. For complexes **2–6**, even this level of rationalization is not possible given the complex Mn_x topology. Many competing exchange interactions of comparable magnitude and resultant spin frustration effects are undoubtedly present, and the observed

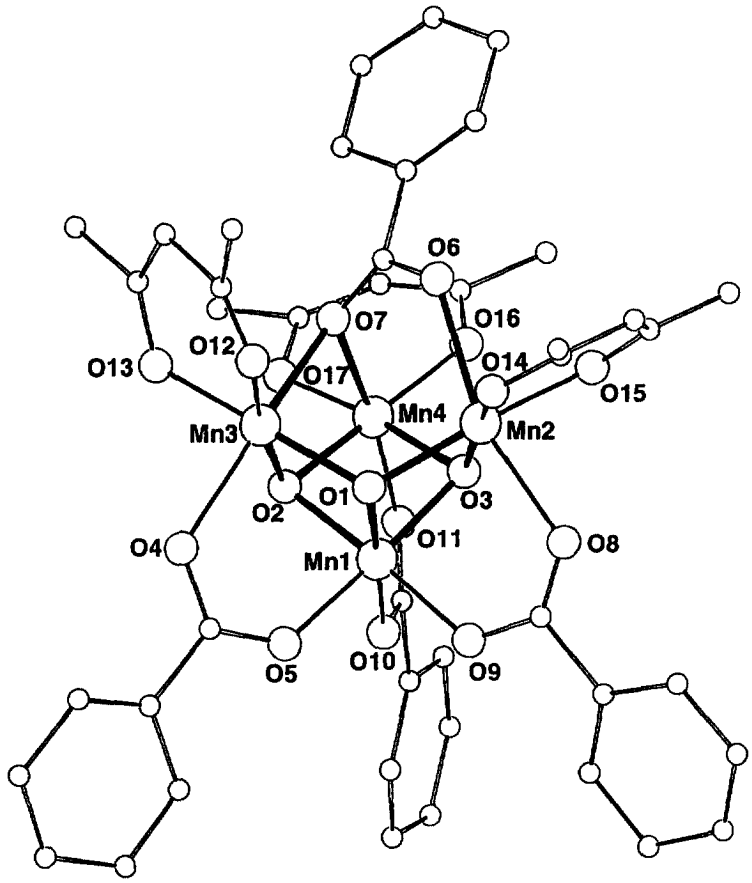

Fig. 8. The structure of $[Mn_4O_3(O_2CPh)_4(dbm)_3]$ (**8**).

ground states must therefore be a delicate balance of several factors. The latter makes it extremely difficult, in general, to predict in advance what the ground state might be of a new structural type, although some rationalization of the measured value is usually possible with hindsight, and this can still be a very useful level of understanding to possess.

A case in point is provided by complex **11** [21], whose ground state $S = 10$ or 11 may be rationalized as due to competition between the various pairwise exchange interactions which all involve Mn^{II}/Mn^{II} (J_{22}) or Mn^{II}/Mn^{III} (J_{23}) pairs and are thus all expected

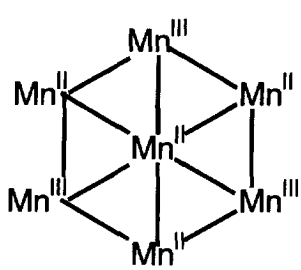

to probably be antiferromagnetic and very weak (and therefore of comparable magnitude). In particular, competition between J_{io} and J_{oo} (o = outer, i = inner), the former comprising both J_{22} and J_{23} and the latter only J_{23}, clearly prevents all spins aligning in an antiparallel arrangement. The resultant spin frustration thus gives a high spin ground state whose precise value must therefore be due to the relative magnitudes of the J values. The interesting prediction that follows from this argument is that removal of the central Mn should give a non-frustrated system with antiparallel spin alignments around the hexagonal ring and a $S = 15/2 - 6 = 3/2$ ground state. Such a $[Mn^{II}_3Mn^{III}_3]$ cyclic species is not yet available to test this prediction but we note that $[Fe_6Na(OMe)_{12}(dbm)_6]^+$ has a hexagonal ring of Fe^{III} ions, a central Na^+, and a $S=0$ ground state, as expected for a non-frustrated, antiferromagnetically-coupled system [27].

Single-molecule magnetism

In 1993, it was discovered that the $[Mn_{12}O_{12}(O_2CMe)_{16}(H_2O)_4]\cdot 2H_2O\cdot 4MeCO_2H$ (**9**) complex could function as a nanoscale magnet [19, 28]. This initiated the field of molecular nanomagnetism and such a molecule has since been termed a single-molecule mag-

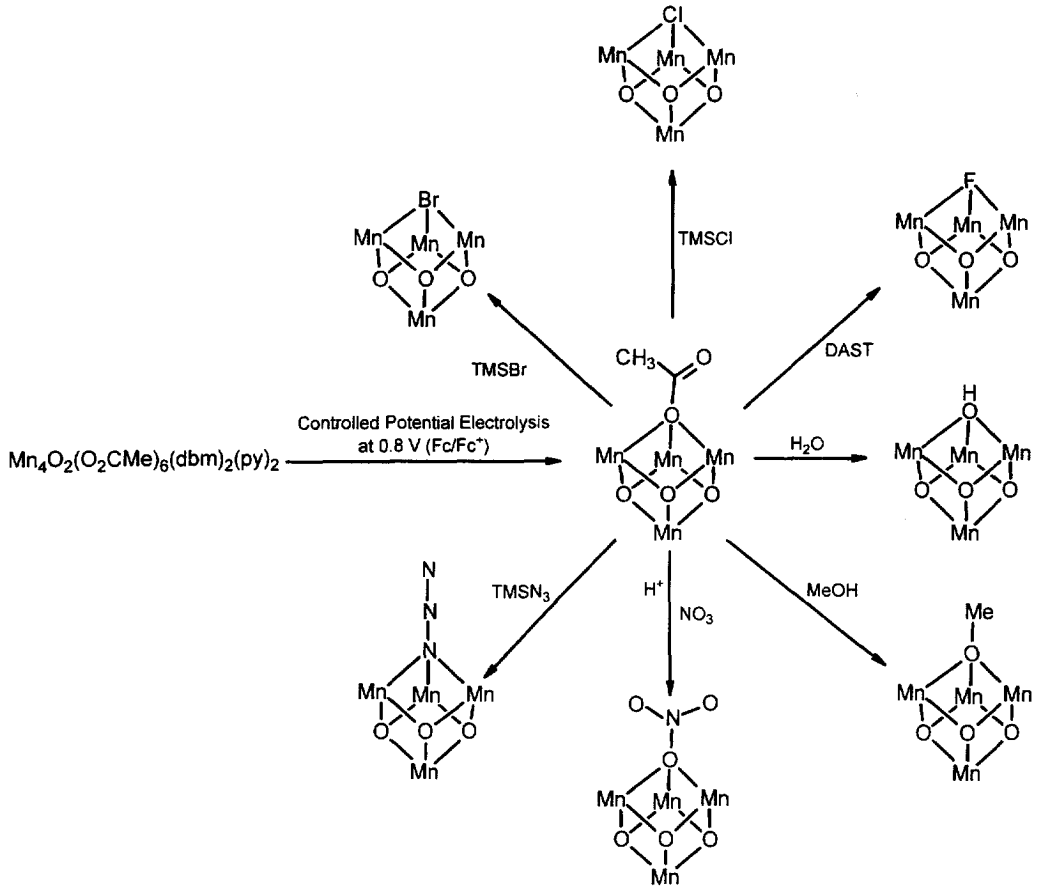

Fig. 9. Variation of X in structurally-characterized $[Mn_4O_3X]^{6+}$-containing products obtained from complex **7**. DAST is Et_2NSF_3; TMS is trimethylsilyl.

net (SMM) [29]. Nanoscale magnetic particles (nanomagnets) are typically of size 20–200 nm and are usually obtained by fragmenting bulk ferro- or ferrimagnets such as magnetite (Fe_3O_4), but this approach gives a distribution of particle sizes that complicates size *vs.* property studies and precludes a uniform response to an external influence such as an applied magnetic field. The discovery of SMMs in metal cluster chemistry represented an exciting breakthrough for a number of reasons: (i) metal clusters are normally prepared by solution methods and, once purified, such samples are composed of species of a

Table 1. state spin (S) values[1]

Complex[a]	Ox. state	S
$Mn_4O_3X(O_2CR)_3dbm)_3]$ (**7**,**8**)	$3Mn^{III}$, Mn^{IV}	9/2
$[Mn_7(OH)_3Cl_3(hmp)_9]^{2+}$ (**11**)	$4Mn^{II}$, $3Mn^{III}$	10 or 11
$[Mn_8O_6Cl_6(O_2CPh)_7(H_2O)_2]^-$ (**2**)	$8Mn^{III}$	11
$[Mn_8O_4(O_2CPh)_{12}(Et_2mal)_2(H_2O)_2]^{2-}$ (**4**)	$2Mn^{II}$, $6Mn^{III}$	3
$[Mn_9Na_2O_7(O_2CPh)_{15}(MeCN)_2]$ (**3**)	$9Mn^{III}$	4
$[Mn_{10}O_8(O_2CPh)_6(pic)_8]$ (**6**)	$10Mn^{III}$	0
$[Mn_{10}O_4(OH)_2(O_2CMe)_8(hmp)_8]^{4+}$	$10Mn^{III}$	0
$[Mn_{12}O_{12}(O_2CR)_{16}(H_2O)_4]$ (**9**)	$8Mn^{III}$, $4Mn^{IV}$	9 or 10
$[Mn_{12}O_{12}(O_2CR)_{16}(H_2O)_4]^-$ (**10**)	Mn^{II}, $7Mn^{III}$, $4Mn^{IV}$	19/2
$[K_4Mn_{18}O_{16}(O_2CPh)_{22}(phth)_2(H_2O)_4]$ (**5**)	$18Mn^{III}$	0

[a]For salts, only the Mn_x-containing ion is shown.

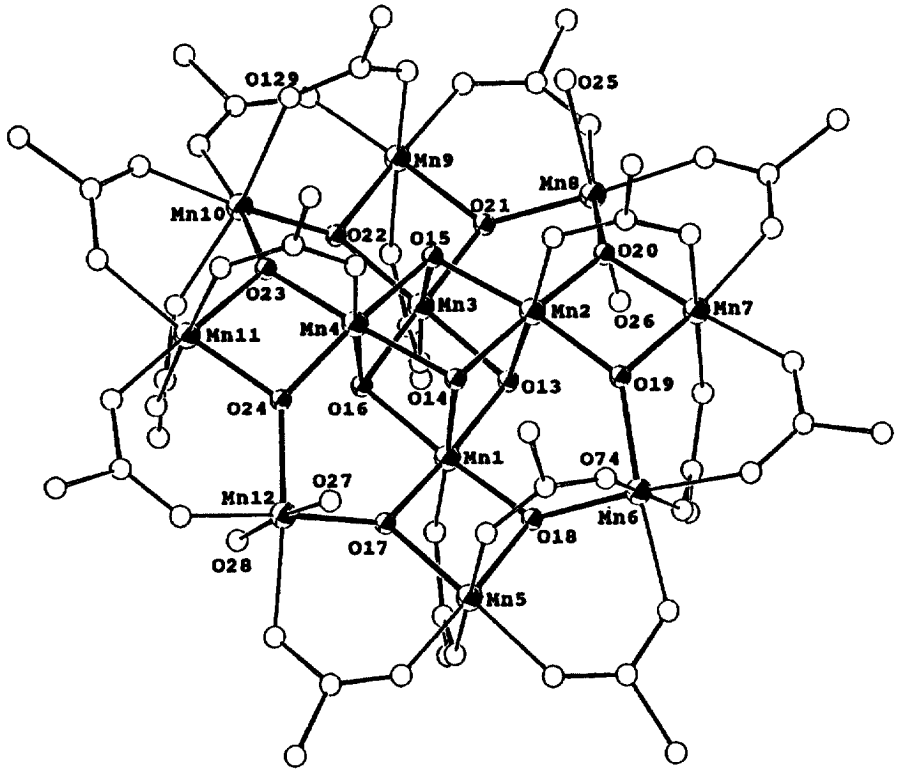

Fig. 10. The structure of $[Mn_{12}O_{12}(O_2CPh)_{16}(H_2O)_4]$; for clarity, only the *ipso* carbon atom of each Ph ring is shown.

single, sharply-defined size; (ii) they are readily amenable to variation in peripheral carboxylate ligation (small *vs.* bulky, hydrophilic *vs.* hydrophobic, etc.); (iii) they are normally soluble in common solvents providing advantages in potential applications, e.g., thin film formation (and removal); and (iv) they are, in fact, of sub-nanoscale dimensions—the $[Mn_{12}O_{12}]$ core of **9** has an approximate volume of only 0.1 nm^3. Points (i) and (iii) are major advantages of SMMs over conventional nanoscale magnetic particles, and point (iv) holds the promise of access to the ultimate high density memory device. Including the carboxylates, the volume of **9** is very approximately 2 nm^3, with a shape that can be described as a disc of circular surface area $\sim 2\,nm^2$ and thickness ~ 1 nm. Close packing could fit $\sim 5 \times 10^{13}$ clusters on a 1 cm^2 computer chip, at least four or five orders of magnitude greater than the highest density possible to date.

The SMM behavior of **9** and other carboxylate derivatives studied more recently is due to a combination of a large ground state spin S and negative magnetoanisotropy as gauged by a negative zero-field splitting parameter D. As a result, there is a significantly large barrier for the reorientation of the cluster's magnetization vector. Thus, if an applied magnetic field is used to orient all the molecular magnetization vectors in one direction, the temperature lowered below a critical (or "blocking") temperature (~ 3 K), and the field switched off, the magnetization vectors remain aligned and the sample is thus magnetized. The time scale of the magnetization relaxation is greater than two months.

More recently [20], the ionic species $(PPh_4)[Mn_{12}O_{12}(O_2CEt)_{16}(H_2O)_4]$ **10** and other carboxylate derivatives (such as the benzoate) have also been found to be SMMs, thus extending this new magnetic phenomenon to ionic species (i.e., "single-ion magnetism", although this alternate term has not been employed to date).

A characteristic signature of a magnet is hysteresis in the magnetization *vs.* magnetic field response, and representative examples are shown in Figs 13 and 14 for complex **10** [20, 30] and $[Mn_{12}O_{12}(O_2CC_6H_4\text{-}p\text{-}Me)_{16}(H_2O)_4]$ [31], respectively. Hysteresis of magnetization is clearly evident, confirming magnetic bistability and the appropriateness of the SMM description, but these figures also show two additional features that represent the focus of intense study at the present time. Considering Fig. 13 first, there are clear signs of steps on the hysteresis loop at regular intervals of magnetic field. Such steps were first seen for the $MeCO_2^-$ complex **9** [32] and are a signature of quantum tunnelling of the magnetization (QTM) i.e., instead of the cluster's magnetization relaxing from,

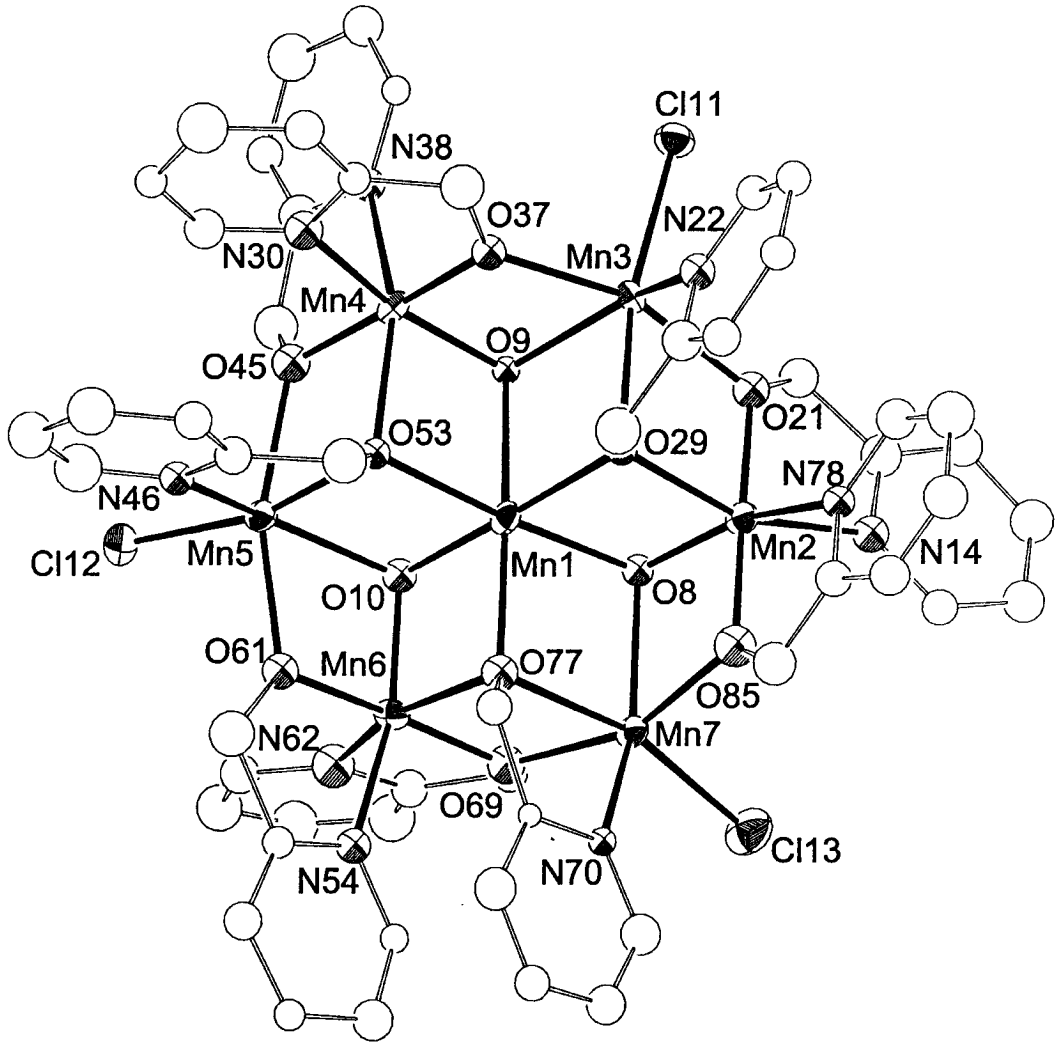

Fig. 11. The $[Mn_7(OH)_3Cl_3(hmp)_9]^{2+}$ cation of complex **11**.

say, "spin up" to "spin down" by going over the reorientation barrier, it instead tunnels through the barrier; more detailed discussion and analysis of the step behavior are available elsewhere [31–34]. In essence, these nanoscale clusters straddle the classical/quantum interface and thus allow study of how quantum mechanical behavior at the macroscopic scale underlies classical behavior at the macroscopic scale.

The hysteresis loops in Fig. 14 again show steps but also demonstrate a remarkable sensitivity of the hysteresis and QTM behavior to subtle differences resulting from two different crystal forms of the complex i.e., the $3H_2O$ solvate (space group $I2/a$) and the $HO_2CC_6H_4$-*p*-Me solvate (space group $C2/c$) [31]. The two crystal forms show significantly different step sizes, particularly the first step at zero field, which suggests that environmental differences in the two complexes have profound effects on the QTM rates. We have also found similar changes when the identity of the carboxylate is altered [34]. Such a significant sensitivity of the quantum behavior to readily-altered macroscopic parameters is important to understand and control, since this is likely to be important in future technological applications of SMMs.

One way to consider the Mn_{12} SMMs is as extremely small pieces of a metal oxide stabilized and solubilized by the carboxylate ligands. It is often contemplated how small a piece of a 3D extended solid such as a metal oxide can become and still retain the essential properties of the bulk material. With respect to magnetic properties, it would appear that as few as 12 metal ions in the $[Mn_{12}O_{12}]$-containing complexes will suffice! It should be added that the $[Mn_{12}O_{12}]$ core is not an exact, repeating unit within a known Mn oxide. In fact, an even smaller molecule can also be a SMM.

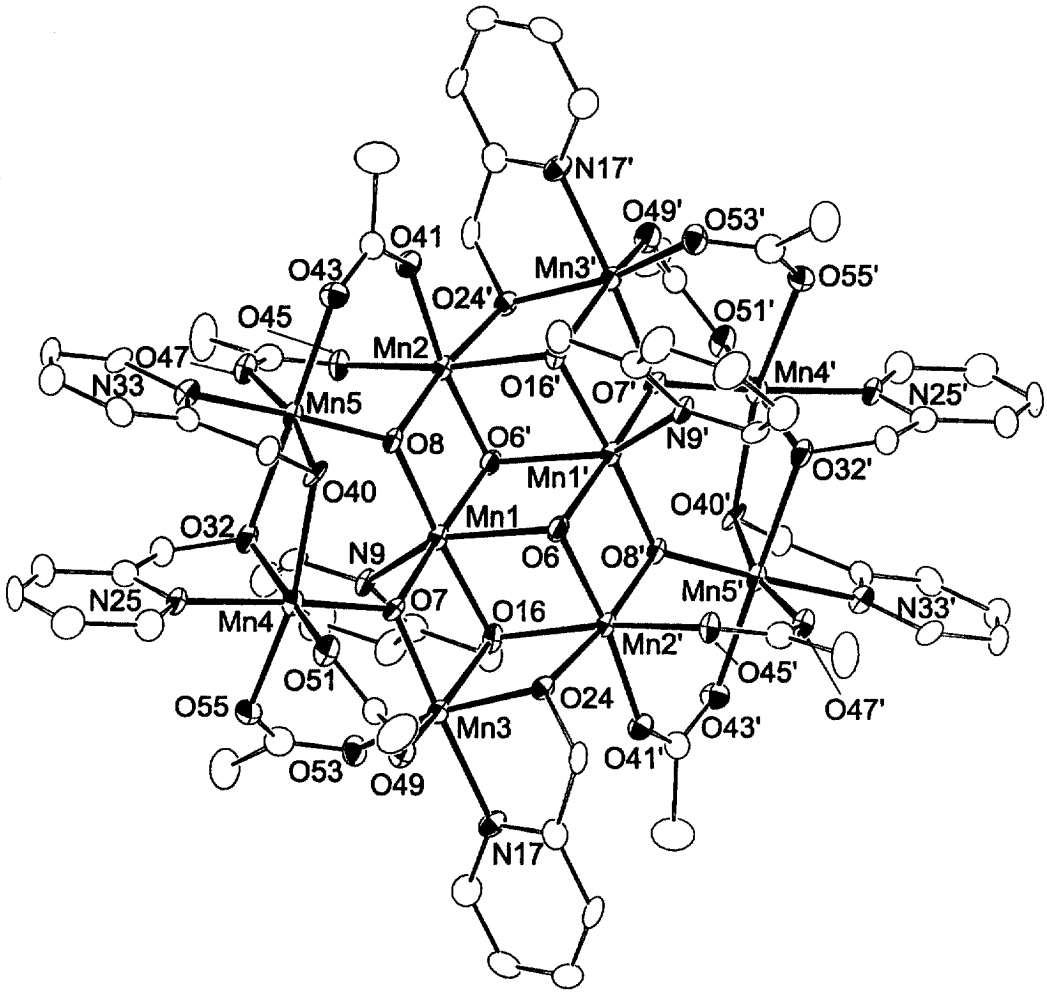

Fig. 12. The $[Mn_{10}O_4(OH)_2(O_2CMe)_8(hmp)_8]^{4+}$ cation of **12**.

The $[Mn_4O_3X]^{6+}$-containing clusters such as **7** have also been found to be SMMs, as reflected in the slow relaxation of magnetization [29], and the appearance [35] of a hysteresis loop *and* steps characteristic of QTM (Fig. 15). Lower temperatures are required, which is consistent with the smaller ground state spin of $S = 9/2$ for these clusters, as well as smaller D values than for the Mn_{12} species. Nevertheless, it firmly demonstrates that there is essentially no size minimum for the occurrence of SMM behavior; the $[Mn_4O_3X]$ core has a volume of $\sim 0.01\ nm^3$.

CONCLUSIONS

Manganese carboxylate cluster chemistry has proven to be an area that has something for everyone, from synthetic chemistry and structural aesthetics to high-spin ground states and novel magnetic properties. The SMM behavior could not of course have been anticipated, and this area is thus a perfect example of a curiosity-driven line of "pure" research that leads to results of potentially major technological application. The temperatures required for SMM behavior in this first generation of examples are very low (< 3 K) but in this regard the field is at the same stage as superconductivity was when it was discovered in elemental mercury at liquid helium temperatures i.e., the important point is the establishment of the phenomenon and it will be up to future efforts in the field of SMMs to push the critical temperature to higher, more useful values. Other examples of SMMs both outside and within Mn chemistry are being reported [36, 37], but they are all like the $[Mn_4O_3X]$ species in requiring lower temperatures than the $[Mn_{12}O_{12}]$ complexes. However, the search has only just begun.

Acknowledgements—This research was supported by the U.S. National Science Foundation and National Institutes of Health.

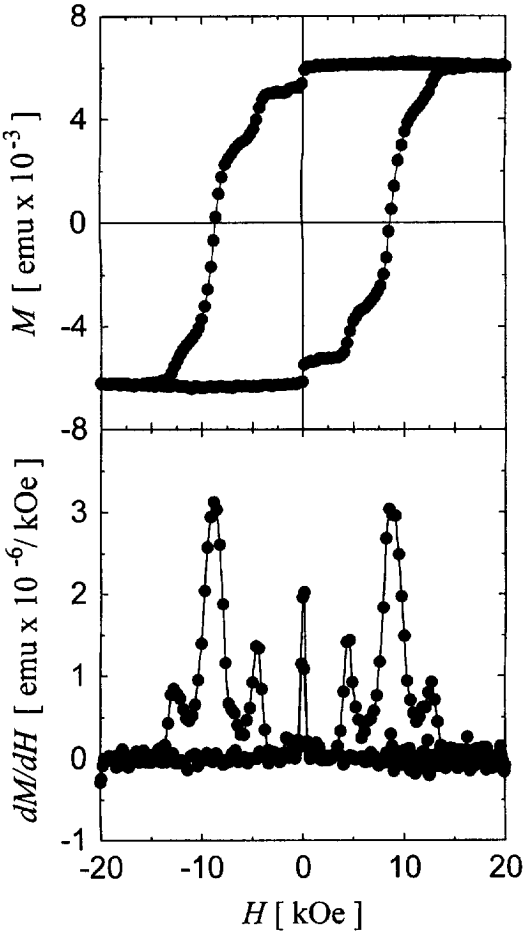

Fig. 13. (top) Magnetization hysteresis loop at 1.85 K for oriented crystals of $(PPh_4)[Mn_{12}O_{12}(O_2CEt)_{16}(H_2O)_4]$ (**10**); and (bottom) plot of the first derivative of the hysteresis loop emphasizing the positions of the steps.

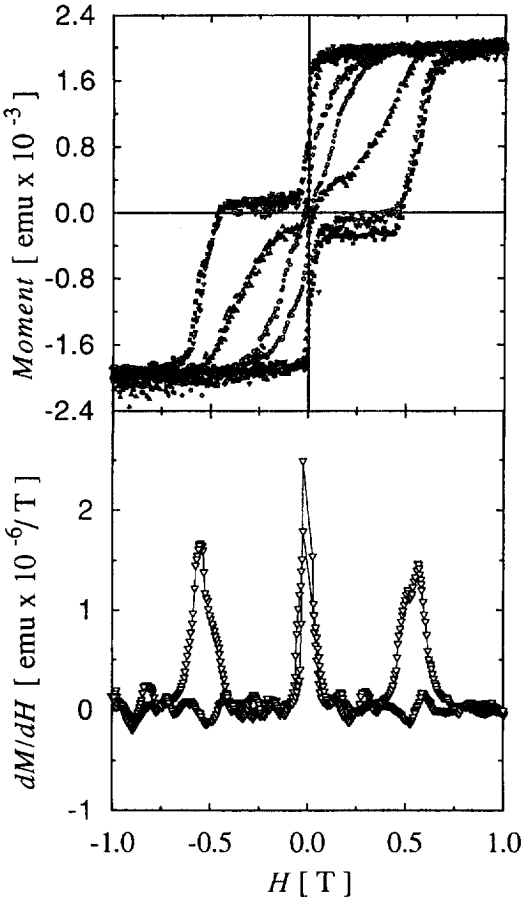

Fig. 15. (top) Magnetization hysteresis loop for oriented crystals of $[Mn_4O_3Cl(O_2CMe)_3(dbm)_3]$ at 0.426 (■), 0.53 (▽), 0.706 (△), and 0.90 K (○); and (bottom) the first derivative of the hysteresis loop.

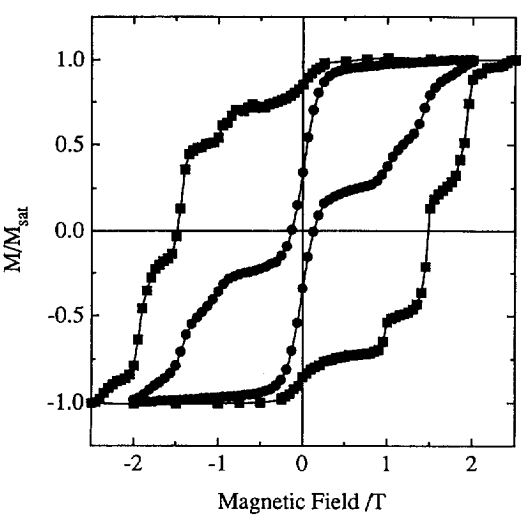

Fig. 14. Magnetization hysteresis loops at 1.90 K for oriented crystals of $[Mn_{12}O_{12}(O_2CC_6H_4\text{-}p\text{-}Me)_{16}(H_2O)_4]$ as the $3H_2O$ (■) or $HO_2CC_6H_4\text{-}p\text{-}Me$ (●) solvates.

REFERENCES

1. (a) Yachandra. V. K., Sauer K. and Klein M. P., *Chem. Rev.* 1996, **96**, 2927. (b) Debus, J. R., *Biochim. Biophys. Acta* 1992, **1102**, 269.
2. Christou, G., in *Magnetism a Supramolecular Function*: ed. Kahn, O., NATO ASI Series; Kluwer, Dordrecht, The Netherlands, 1996, pp. 383–410.
3. Christou, G., *Acc. Chem. Res.*, 1989, **22,** 328.
4. Vincent, J. B., Christmas, C., Chang, H.-R., Li, Q., Boyd, P. D. W., Huffman, J. C., Hendrickson, D. N. and Christou, G., *J. Am. Chem. Soc.*, 1989, **111,** 2086.
5. Libby, E., McCusker, J. K., Schmitt, E. A., Folting, K., Hendrickson, D. N. and Christou, G., *Inorg. Chem.*, 1991, **30,** 3486.
6. Bouwman, E., Bolcar, M. A., Libby, E., Huffman, J. C., Folting, K. and Christou, G., *Inorg. Chem.*, 1992, **31,** 5185.
7. Wang, S., Huffman, J. C., Folting, K., Streib, W. E., Lobkovsky, E. B. and Christou, G., *Angew. Chem. Int. Ed. Engl.*, 1991, **30,** 1672.

8. (a) Wang, S., Folting, K., Streib, W. E., Schmitt, E. A., McCusker, J. K., Hendrickson, D. N. and Christou, G., *Angew. Chem. Int. Ed. Engl.*, 1991, **30**, 305. (b) Wemple, M. W., Tsai, H.-L., Wang, S., Claude, J.-P., Streib, W. E., Huffman, J. C., Hendrickson D. N. and Christou, G., *Inorg. Chem.*, 1996, **35**, 6437.
9. Tsai, H.-L., Wang, S., Folting, K., Streib, W. E., Hendrickson, D. N. and Christou, G., *J. Am. Chem. Soc.*, 1995, **117**, 2503.
10. Low, D. W., Eichhorn, D. M., Draganescu, A. and Armstrong, W. H., *Inorg. Chem.*, 1991, **30**, 878.
11. (a) Squire, R. C., Aubin, S. M. J., Folting, K., Streib, W. E., Hendrickson, D. N. and Christou, G., *Angew. Chem. Int. Ed. Engl.*, 1995, **34**, 887. (b) Squire, R. C., S. M. J. Aubin, Folting, K., Streib, W. E., Christou, G. and Hendrickson, D. N., *Inorg. Chem.*, 1995, **34**, 6463.
12. Eppley, H. J., Aubin, S. J. M., Streib, W. E., Bollinger, J. C., Hendrickson, D. N. and Christou, G., *Inorg. Chem.*, 1997, **36**, 109.
13. a) Wang, S., Tsai, H.-L., Streib, W. E., Christou, G. and Hendrickson, D. N., *J. Chem. Soc., Chem. Commun.*, 1992, 1427. (b) Wang, S., Tsai, H.-L., Folting, K., Streib, W. E., Hendrickson, D. N. and Christou, G., *Inorg. Chem.*, 1996, **35**, 7578.
14. Wemple, M. W., Adams, D. M., Folting, K., Hendrickson, D. N. and Christou, G., *J. Am. Chem. Soc.*, 1995, **117**, 7275.
15. Wang, S., Tsai, H.-L., Hagen, K. S., Hendrickson, D. N. and Christou, G., *J. Am. Chem. Soc.*, 1994, **116**, 8376.
16. Aromí, G., Folting, K., Huffman J. C. and Christou, G., (results to be published).
17. Aromí, G., Wemple, M. W., Aubin, S. M. J., Folting, K., Hendrickson, D. N. and Christou, G., *J. Am. Chem. Soc.*, (submitted for publication).
18. Lis, T., *Acta Cryst.*, 1980, **B36**, 2042.
19. Sessoli, R., Tsai, H.-L., Schake, A. R., Wang, S., Vincent, J. B., Folting, K., Gatteschi, D., Christou, G. and Hendrickson, D. N., *J. Am. Chem. Soc.*, 1993, **115**, 1804.
20. Eppley, H. J., Tsai, H.-L., de Vries, N., Folting, K., Christou, G. and Hendrickson, D. N., *J. Am. Chem. Soc.*, 1995, **117**, 301.
21. Bolcar, M. A., Aubin, S. M. J., Folting, K., Hendrickson, D. N. and Christou, G., *Chem. Commun.*, 1997, 1485.
22. Bolcar, M. A., Folting K. and Christou, G., (results to be published).
23. Powell, A. K., Heath, S. L., Gatteschi, D., Pardi, L., Sessoli, R., Spina, G., Del Giallo, F. and Pieralli, F., *J. Am. Chem. Soc.*, 1995, **117**, 2491.
24. To accommodate the comments of Kahn[25], expressions such as "spin frustration degeneracy" will be employed to describe the special case where competing exchange interactions lead to a degenerate ground state. In accord with our practice to date, we shall use "spin frustration" to describe the more general case where competing exchange interactions of comparable magnitude lead to the preferred spin alignments being prevented (frustrated).
25. Kahn, O., *Chem. Phys. Lett.*, 1997, **265**, 109.
26. Kambe, K., *J. Phys. Soc. Jpn.*, 1950, **5**, 48.
27. Caneschi, A., Cornia, A. and Lippard, S. J., *Angew. Chem. Int. Ed. Engl.*, 1995, **34**, 467.
28. Sessoli, R., Gatteschi, D., Caneschi, A. and Novak, M. A., *Nature*, 1993, **365**, 141.
29. Aubin, S. M. J., Wemple, M. W., Adams, D. M., Tsai, H.-L., Christou, G. and Hendrickson, D. N., *J. Am. Chem. Soc.*, 1996, **118**, 7746.
30. Aubin, S. M. J., Spagna, S., Eppley, H. J., Sager. R. E., Christou, G. and Hendrickson, D. N., *Chem. Commun.*, 1998, 803.
31. *Aubin, S. M. J., Sun, Z., Guzei, I. A., Rheingold, A. L., Christou, G. and Hendrickson, D. N., Chem. Commun.*, 1997, 2239.
32. Friedman, J. R., Sarachik, M. P., Hernandez, J. M., Zhang, X. X., Tejada, J., Molins, E. and Ziolo, R., *J. Appl. Phys.*, 1997, **81**, 3978.
33. (a) Tejada, J., Ziolo R. F. and Zhang, X. X., *Chem. Mater.*, 1996, **8**, 1784. (b) Thomas, L., Lionti, F., Ballou, R., Gatteschi, D., Sessoli R. and Barbara, B., *Nature*, 1996, **383**, 145.
34. Ruiz, D., Sun, Z., Albela, B., Folting, K., Ribas, J., Christou, G. and Hendrickson, D. N., *Angew. Chem. Int. Ed. Engl.*, 1998, **37**, 300.
35. Aubin, S. M. J., Dilley, N. R., Wemple, M. W., Maple, M. B., Hendrickson, D. N. and Christou, G., *J. Am. Chem. Soc.*, 1998, **120**, 839.
36. (a) Sun, Z., Grant, C. M., Castro, S. L., Hendrickson, D. N. and Christou, G., *Chem. Commun.*, 1998, 721. (b) Castro, S. L., Sun, Z., Grant, C. M., Bollinger, J. C., Hendrickson D. N. and Christou, G., *J. Am. Chem. Soc.*, 1998, **120**, 2977.
37. Barra, A. L., Debrunner, P., Gatteschi, D., Schultz, C. E. and Sessoli, R., *Europhys. Lett.*, 1996, **35**, 133.

Pergamon

PII: S0277-5387(98)00130-2

Polyhedron Vol. 17, No. 17, pp. 3021–3029, 1998
© 1998 Elsevier Science Ltd
All rights reserved. Printed in Great Britain
0277-5387/98 $19.00+0.00

Synthesis, spectroscopy and crystal structures of $[Au_2\{\mu\text{-}Ph_2PN(Et)PPh_2\}_2][SbF_6]_2$ and $[Au_3Cl_2\{\mu\text{-}Ph_2PN(Et)PPh_2\}_2]PF_6$*

John S. Field,[a,†] Judith Grieve,[a] Raymond J. Haines,[a] Noellene May[a] and Mthembeni M. Zulu[b,‡]

[a] Department of Chemistry, University of Natal, Private Bag X01, Scottsville, Pietermaritzburg, Republic of South Africa 3209

[b] Department of Chemistry, University of Zululand, Private Bag X1001, Kwadlangezwa, Republic of South Africa 3886

(Received 24 November 1997; accepted 29 March 1998)

Abstract—Treatment of $[Au(MeCN)_2]SbF_6$ in acetonitrile with bis(diphenylphosphino)ethylamine (dppa) afforded a colourless crystalline material characterised as $[Au_2(\mu\text{-dppa})_2][SbF_6]_2$. An X-ray diffraction study confirmed that the two ligands bridge the two gold atoms with a Au···Au separation of 2.838(2) Å. The electronic absorption spectrum exhibits a band at 298 nm (ϵ_{max}, *ca.* 17000 $dm^3\,mol^{-1}\,cm^{-1}$) attributable to a $p_\sigma \Leftarrow d_\sigma^*$ transition. The compound luminesces strongly in acetonitrile (λ_{max} = 500 nm). Treatment of $HAuCl_4.2H_2O$ with 2,2′-thioethanol in methanol followed by the ligand afforded a colourless crystalline material characterised as $[Au_3Cl_2(\mu\text{-dppa})_2]PF_6$. A crystal structure determination revealed a cation of C_2 symmetry, comprising a bent chain of three gold atoms (Au···Au···Au = 167.5(8)°, Au···Au = 3.037(1) Å), with each pair of adjacent gold atoms bridged by a diphosphazane ligand and with the coordination at the outer gold atoms completed by a chloride ligand. This compound luminesces extremely weakly in acetonitrile but does emit strongly at 485 nm when irradiated in the solid state. The luminescence displayed by both compounds is attributed to the presence of a substantial intramolecular interaction between the gold atoms, but ligand effects appear to be more important in determining the emissive energies. © 1998 Elsevier Science Ltd. All rights reserved

Homoleptic digold(I) complexes, in which the gold atoms are bridged by two symmetric diphosphine ligands and in which each gold atom is two-coordinate, have been shown to be photoluminescent [1]. The best studied examples are salts of the dppm (dppm = $Ph_2PCH_2PPh_2$) ligand-bridged digold(I) cation, $[Au_2(\mu\text{-dppm})_2]^{2+}$. The BF_4^- salt is strongly phosphorescent in acetonitrile solution, the emission being observed at 593 nm at room temperature with a lifetime of 21 μs and a quantum yield of 0.31 [2]. The ClO_4^- salt also exhibits phosphorescence at room temperature in acetonitrile solution, but at 570 nm with a lifetime of 18 μs and a quantum yield of 0.15 [3, 4]. The room temperature emission spectrum of the BH_3CN^- salt has been recorded in the solid state, since this species decomposes on irradiation in solution; emission occurs at 490 nm in this case [2, 5]. In contrast, mononuclear bisphosphine complexes such as $[Au(PPh_3)_2]BPh_4$ are not luminescent [6]. This has led to the conclusion that the loss of centrosymmetric structure, brought about by the presence of an Au···Au interaction in the dinuclear species, is in some way responsible for the luminescence displayed by compounds of this type [6]. However, the intermetallic separation does not appear to play a significant role in determining the energy of the emission. For instance, Fackler *et al.* have shown that there is no direct correlation between the Au···Au separation and the emission wavelength (recorded in the solid state) for the following series of luminescent ligand-bridged digold(I) compounds: $[Au_2(\mu\text{-dppm})_2][BH_3CN]_2$, $[Au_2(\mu\text{-dppm})_2]Cl_2$, $[Au(CH_2)_2PPh_2]_2$, $[n\text{-}Bu_4N]_2$

* (Dedicated to our friend and colleague, Jack Lewis, on the occasion of his 70th birthday)

† Author to whom correspondence should be addressed.

‡ The late.

$[Au(S_2C{=}C(CN)_2)]_2$, $[Au(CH_2P(S)Ph_2)]_2$, and $[Au(S_2CNEt_2)]_2$ [2]. It has been suggested that this lack of correlation may be as a consequence of the HOMO having some ligand character and not being a purely metal orbital, with ligand changes affecting the energy of the HOMO, either directly or indirectly [2]. This being the case, the emissive properties of diphosphine ligand-bridged digold(I) complexes of the $[Au_2(\mu\text{-dppm})_2]^{2+}$ type may be more the property of the diphosphine ligand and, in particular, of the AuP_2 unit rather than of the intergold separation [1]. The diphosphazane ligand $Ph_2PN(Et)PPh_2$ (dppa) is closely related to the dppm ligand, the only difference being the presence of an ethylamino, rather than a methylene group, between the two phosphorus atoms. It was therefore of interest to compare the structure and emissive properties of the diphosphazane ligand-bridged chromophore, $[Au_2(\mu\text{-dppa})_2]^{2+}$, with those of the $[Au_2(\mu\text{-dppm})_2]^{2+}$ species. Accordingly, the SbF_6^- salt of the $[Au_2(\mu\text{-dppa})_2]^{2+}$ cation has been synthesised, its structure determined by means of X-ray diffraction, and its absorption and emission spectra in acetonitrile recorded.

Trigold(I) complexes stabilised by bidentate bridging ligands have received less attention, especially with regard to their photophysical properties. However, the syntheses and crystal structures of the $[AuCl(C_6F_5)_3]^-$ and chloride salts of the $[Au_3Cl_2(\mu\text{-dppm})_2]^+$ cation have been reported [7, 8]. In contrast to $[Au_2(\mu\text{-dppm})_2]^{2+}$, this cation does not appear to luminesce in solution, the authors only reporting the existence of an intense emission at 485 nm in the solid state for the chloride salt [8].

To establish whether $[Au_3Cl_2(\mu\text{-dppa})_2]^+$ has similar luminescent properties, its synthesis as the hexafluorophosphate salt was effected and its crystal structure and emission properties determined.

RESULTS AND DISCUSSION

Treatment of an acetonitrile solution of $[Au(MeCN)_2]^+$ with a molar equivalent of the solid $Ph_2PN(Et)PPh_2$ (dppa) ligand afforded a yellow solution from which $[Au_2(\mu\text{-dppa})_2][SbF_6]_2$ could be isolated in good yield as a colourless microcrystalline solid by precipitation with diethylether. Elemental analysis, the infrared spectrum recorded as a KBr pellet and the ^1H NMR spectrum are all consistent with the formulation of the compound as $[Au_2(\mu\text{-dppa})_2][SbF_6]_2$, as subsequently confirmed by means of a single crystal structure determination (see below). The $^{31}P\{^1H\}$ NMR spectrum recorded in CD_3CN exhibits a single sharp peak at 100.25 ppm, indicative of a phosphorus atom bonded to a gold atom; the phosphorus atoms of the free ligand resonate at 60.60 ppm. Interestingly, the phosphorus atoms of the diphosphazane ligand are considerably deshielded relative to those of the dppm ligand, the latter resonating at *ca.* 35 ppm in $[Au_2(\mu\text{-dppm})_2][ClO_4]_2$ [4]. This is to be expected in view of the stronger electron-withdrawing properties of the ethylamino as opposed to the methylene group. The compound is stable in the solid state but, if left to stand in solution in the presence of oxygen, it slowly degrades.

The procedure used for the preparation of $[Au_3Cl_2(\mu\text{-dppa})_2]PF_6$ is similar to one of two methods employed by Lin *et al.* for the preparation of $[Au_3Cl_2(\mu\text{-dppm})_2]Cl$ [8]. Thus, the compound is obtained in good yield by reacting $HAuCl_4.2H_2O$ with 2,2′-thioethanol in methanol before treating it with a slight excess of ligand. Isolation of the compound as a colourless microcrystalline solid was achieved by addition of NH_4PF_6 and crystallisation from the methanol solution. Elemental analysis, the infrared spectrum recorded as a KBr pellet and the ^1H NMR spectrum are all consistent with the formulation of the compound as $[Au_3Cl_2(\mu\text{-dppa})_2]PF_6$, as subsequently confirmed by means of a single crystal structure determination (see below). The $^{31}P\{^1H\}$ NMR spectrum recorded in CD_3CN exhibits a well-defined AA′BB′ pattern with the multiplets centred at 103.61 and 83.11 ppm. Such a pattern is also observed for the $[Au_3Cl_2(\mu\text{-dppm})_2]^+$ cation in its $[AuCl(C_6F_5)_3]^-$ salt [7]. On the other hand the $^{31}P\{^1H\}$ spectrum for the chloride salt is complicated by an exchange process driven by the reaction of the chloride counterion with the trinuclear gold cation. In this case, a AA′BB′ pattern is only observed in the presence of added $AgBF_4$, *i.e.*, when the potentially coordinating chloride counterion is replaced by the non-coordinating tetrafluoroborate anion [8]. As expected, the phosphorus atoms in the diphosphazane ligand-bridged trigold cation are deshielded relative to those in the analogous dppm ligand-bridged species; Uson *et al.* report an AA′BB′ pattern for $[Au_3Cl_2(\mu\text{-dppm})_2][AuCl(C_6F_5)_3]$ with the multiplets centred at 37.1 and 29.0 ppm [7]. As with the dinuclear diphosphazane ligand-bridged species, the trinuclear complex $[Au_3Cl_2(\mu\text{-dppa})_2]PF_6$ is stable in the solid state but, if left to stand in solution in the presence of oxygen, it slowly degrades.

Crystal structure and photophysical properties of $[Au_2(\mu\text{-dppa})_2][SbF_6]_2$

Crystals of the compound consist of well-separated $[Au_2(\mu\text{-dppa})_2]^{2+}$ cations and SbF_6^- anions, there being no unusual intermolecular contact distances. Figure 1 shows an ORTEP drawing of the cation, while selected interatomic distances and angles for the cation are given in Table 1.

The two gold atoms are bridged by the two diphosphazane ligands such that there is a crystallographically imposed centre of symmetry midway between them. The coordination at each gold atom is only approximately linear, as evidenced by a P(1)–Au–P(2′) angle of 167.5(8)°. As illustrated in Fig. 1, the deviation from linearity apparently results from

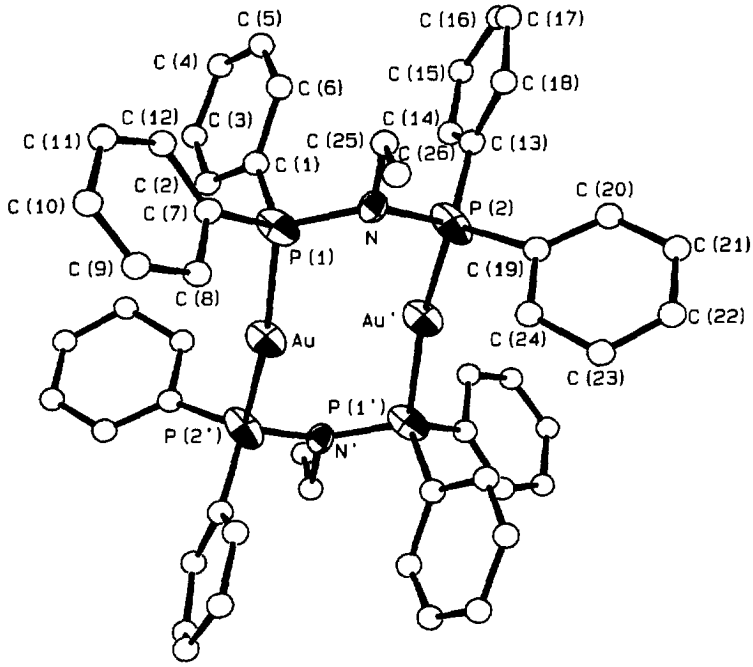

Fig. 1. ORTEP drawing of the $[Au_2(\mu\text{-dppa})_2]^{2+}$ cation in $[Au_2(\mu\text{-dppa})_2][SbF_6]_2$. The carbon atoms are drawn as spheres of arbitrary radius and the remaining atoms as 20% probability ellipsoids.

Table 1. Selected interatomic distances (Å) and angles (°) for $[Au_2(\mu\text{-dppa})_2][SbF_6]_2$

Au···Au′	2.838(2)	Au–P(1)	2.313(6)
Au–P(2′)	2.298(5)	P(1)–N	1.70(2)
P(1)–C(1)	1.75(3)	P(1)–C(7)	1.79(3)
P(2)–C(13)	1.75(3)	P(2)–C(7)	1.79(3)
P(2)–C(19)	1.82(3)	P(2)–C(19)	1.82(3)

P(1)–Au–P(2′)	167.5(7)	Au–P(1)–N	115.4(8)
Au–P(1)–C(1)	106.4(10)	Au–P(1)–C(7)	114.3(9)
N–P(1)–C(1)	110.1(13)	N–P(1)–C(7)	104.7(12)
C(1)–P(1)–C(7)	106(2)	Au′–P(2)–N	111.3(8)
Au′–P(2)–C(13)	115.5(9)	Au′–P(2)–C(19)	105.6(9)
N–P(2)–C(13)	107.5(12)	N–P(2)–C(19)	105.4(12)
C(13)–P(2)–C(19)	111.2(14)	P(1)–N–P(2)	117.0(11)
P(1)–N–C(25)	121.5(7)	P(2)–N–C(25)	116.9(7)

the two gold atoms being pulled towards each other by a substantial Au···Au interaction. This is reflected in an Au···Au distance of 2.838(2) Å that is significantly shorter than the Au···Au distances in $[Au_2(\mu\text{-dppm})_2][BH_3CN]_2{\cdot}2CH_2Cl_2$ (2.982 Å) [9], $[Au_2(\mu\text{-}Me_2PCH_2PMe_2)_2][ClO_4]_2$ (3.028 Å) [10], $[Au_2(\mu\text{-}Me_2PCH_2PMe_2)_2]Br_2{\cdot}H_2O$ (3.023 Å) [10], $[Au_2(\mu\text{-}Me_2PCH_2PMe_2)_2]Cl_2{\cdot}H_2O$ (3.010 Å) [11] and $[Au_2(\mu\text{-}Cy_2PCH_2PCy_2)_2][PF_6]_2$ (2.935 Å) [12]. It is also shorter than the Au···Au distance of 2.962 Å reported for $[Au_2(\mu\text{-dppm})_2]Cl_2$, but this comparison is not strictly valid since the gold atoms in the latter compound are formally three-coordinate, due to the close approach of the chloride anions [13]. In fact, the core structure of the $[Au_2(\mu\text{-dppa})_2]^{2+}$ cation is very similar in all respects to that observed for the other digold(I) ligand bridged species listed above, there being no evidence of a tendency for the gold atom to become three-coordinate by associating with the fluoride of the SbF_6^- anion. There is a slight twisting of the bridging ligands about the Au···Au vector, as reflected by a P(1)–Au···Au′–P(2) torsion angle of 12.4°. The Au–P bond lengths of 2.314(5) and 2.297(5) Å are somewhat shorter than the value of 2.400 Å given for eight compounds of the closely related dppm ligand with gold [14], but are very similar to the Au–P distance of

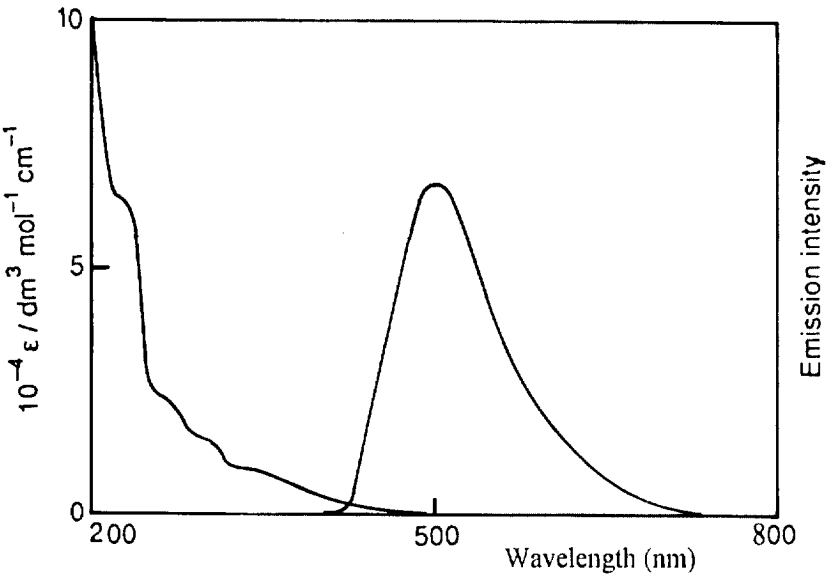

Fig. 2. Absorption and emission (340 nm excitation) spectra in CH_3CN of $[Au_2(\mu\text{-dppa})_2][SbF_6]_2$.

2.314(2) Å in $[Au_2(\mu\text{-}Cy_2PCH_2PCy_2)_2]^{2+}$ [12] and the Au–P distances of 2.311(4) and 2.317(4) Å in $[Au_2(\mu\text{-dppm})_2][BH_3CN]_2\cdot 2CH_2Cl_2$ [9].

The room temperature UV/vis absorption spectrum of $[Au_2(\mu\text{-dppa})_2][SbF_6]_2$ in acetonitrile is shown in Fig. 2. A very intense absorption band is observed as a shoulder at 226 nm which can be attributed to transitions within the phenyl rings [2]. Also observed are bands at 267 nm (ϵ_{max}, *ca.* 23000 dm^3 mol^{-1} cm^{-1}) and at 298 nm (ϵ_{max}, *ca.* 17000 dm^3 mol^{-1} cm^{-1}) while some lower energy and weaker absorptions are observed in the region 330–370 nm. Thus, the bands in the 250–400 nm region appear at positions very similar to those observed in the absorption spectrum of $[Au_2(\mu\text{-dppm})_2][ClO_4]_2$ recorded in acetonitrile [4], but with differences in the relative intensities of the bands and a generally lower resolution of the peaks in the absorption spectrum of $[Au_2(\mu\text{-dppa})_2][SbF_6]_2$. On this basis, we tentatively assign the absorption band at 298 nm to the spin-allowed $p_\sigma \Leftarrow d_\sigma^*$ transition, the equivalent band in the dppm-bridged cation being at 290 nm for the ClO_4^- salt [4] and at 293 nm for the BF_4^- salt [2]. Figure 2 also shows the emission spectrum of the $[Au_2(\mu\text{-dppa})_2]^{2+}$ cation measured at room temperature in acetonitrile, an intense and asymmetric emission band being observed at 500 nm. Thus, the $[Au_2(\mu\text{-dppm})_2]^{2+}$ and $[Au_2(\mu\text{-dppa})_2]^{2+}$ chromophores have in common the fact that they both emit strongly on irradiation in solution. This is unusual, as most ligand-bridged digold(I) species do not generally emit in solution, only displaying luminescence in the solid state [2]. For example, the diphosphine ligand-bridged species $[Au_2(\mu\text{-}Cy_2PCH_2PCy_2)_2]^{2+}$ does not emit at room temperature, only luminescing at 489 nm in the solid state at 77 K [12].

The emission maximum of 500 nm, recorded at room temperature in acetonitrile for the $[Au_2(\mu\text{-dppa})_2]^{2+}$ cation, occurs at a considerably lower wavelength, compared to the wavelengths recorded for the emission maxima observed under the same conditions for the $[Au_2(\mu\text{-dppm})_2]^{2+}$ cation; these occur at 570 and 593 nm for the ClO_4^- [3, 4] and BF_4^- salts [2] respectively. The difference of 23 nm in the emission wavelengths for the latter two salts has been ascribed to medium effects [1], but these seem unlikely to account for the decrease in emission wavelength of $\geqslant 70$ nm observed for the dppa ligand-bridged species. The emissive state for the dppm ligand-bridged cation is generally accepted as being phosphorescent [2–4], with the excited state being assigned as either $^3A_u(d\sigma^*)(p\sigma)$ [2–4] or $^3B_{1u}(d\delta^*)(p\sigma)$ [3, 4]. Assuming that one of these two assignments also applies to the dppa ligand-bridged chromophore, the expectation would be that a *decrease* in the Au···Au distance would lead to an increase in the interaction between the gold atoms and, hence, an *increase* in the emission wavelength. Exactly the opposite trend is observed when the Au···Au distances of the two cations are compared. Thus, although the Au···Au distance of 2.838(2) Å observed for $[Au_2(\mu\text{-dppa})_2]^{2+}$ is significantly shorter than the value of 2.982(2) Å reported for the BH_3CN^- salt of the $[Au_2(\mu\text{-dppm})_2]^{2+}$ cation [9], the wavelength of the emission is substantially *shorter*. It seems certain that effects intrinsic to the bridging ligands are responsible for the large difference in emission energy observed for the $[Au_2(\mu\text{-dppm})_2]^{2+}$ and $[Au_2(\mu\text{-dppa})_2]^{2+}$ chromophores. Such an effect could be caused by replacing a CH_2 group in the dppm ligand with an electron-withdrawing N(Et) group to give the dppa ligand,

resulting in less electron density on the donor phosphorus atoms in the dppa as compared to the dppm ligand. However, we are not in a position to quantify such an effect on the relative energies of the HOMO and LUMO in species of this type and, hence, to fully explain the differences in emission energy.

Crystal structure and photophysical properties of $[Au_3Cl_2(\mu\text{-}dppa)_2]PF_6$

Crystals of the compound consist of well-separated $[Au_3Cl_2(\mu\text{-dppa})_2]^+$ cations and PF_6^- anions, there being no unusual intermolecular contact distances. Figure 3 shows an ORTEP drawing of the cation while selected interatomic distances and angles for the cation are given in Table 2.

The cation comprises a bent chain of three gold atoms, each pair of adjacent gold atoms being bridged by a diphosphazane ligand and with the coordination at the two outer gold atoms being completed by a chloride ligand. Overall, the cation has C_2 symmetry. The deviation of the chain of gold atoms from linearity is reflected by a Au(2)···Au(1)···Au(2′) angle of 163.8(2)°. This is in marked contrast to the arrangement of gold atoms in $[Au_3Cl_2(\mu\text{-dppm})_2]^+$, where the Au···Au···Au angles are 74.2 and 74.6° for the $[AuCl(C_6F_5)_3]^-$ and Cl^- salts respectively [7, 8]. Each diphosphazane ligand is considerably twisted, as reflected by a P(1)–Au(1)···Au(2)–P(2) torsion angle of 46.9°. The equivalent torsion angles in the dppm-bridged trigold(I) cation are somewhat smaller, being 15.4 and 26.7° in the $[AuCl(C_6F_5)_3]^-$ salt and 23.6° in the chloride salt. It has been previously shown that diphosphazane ligands are very flexible in terms of twisting about the metal–metal vector which they bridge [15] and it may be that this is, in some way, responsible for the adoption of a near linear arrangement of gold atoms in the $[Au_3Cl_2(\mu\text{-dppa})_2]^+$ cation. The central gold atom is symmetrically coordinated by the phosphorus atoms of *trans* disposed diphosphazane ligands with a P(1)–Au(1) P(1′) angle of 175.4(6)°. The outer two gold atoms are asymmetrically coordinated, being bonded to the phosphorus atom of a diphosphazane ligand and to a chloride ligand; the P(2)–Au(2)–Cl angle of 177.1(1)° shows only a small deviation from linearity. The Au(1)···Au(2) distance of 3.037(1) Å is somewhat shorter than the Au···Au distances observed for the $[Au_3Cl_2(\mu\text{-dppm})_2]^+$ cation, these being 3.067 and 3.164 Å for the $[AuCl(C_6F_5)_3]^-$ salt and 3.076 Å for the chloride salt [7, 8]. This trend is consistent with the shorter Au···Au distance observed for the $[Au_2(\mu\text{-dppa})_2]^{2+}$ cation as compared to that reported for the $[Au_2(\mu\text{-dppm})_2]^{2+}$ cation (see above). The Au(1)–P(1) bond length of 2.313(2) Å is significantly longer than the Au(2)–P(2) bond length of 2.228(2) Å, presumably because of the greater *trans* influence of the diphosphazane as opposed to the chloride ligand. As might be expected, the Au–P(1) distance of 2.313(2) Å agrees well with that of 2.316 Å found for $[Au(PMePh_2)_2]^+$ [16] since, in both cases, the gold atom is symmetrically coordinated by phosphorus donor

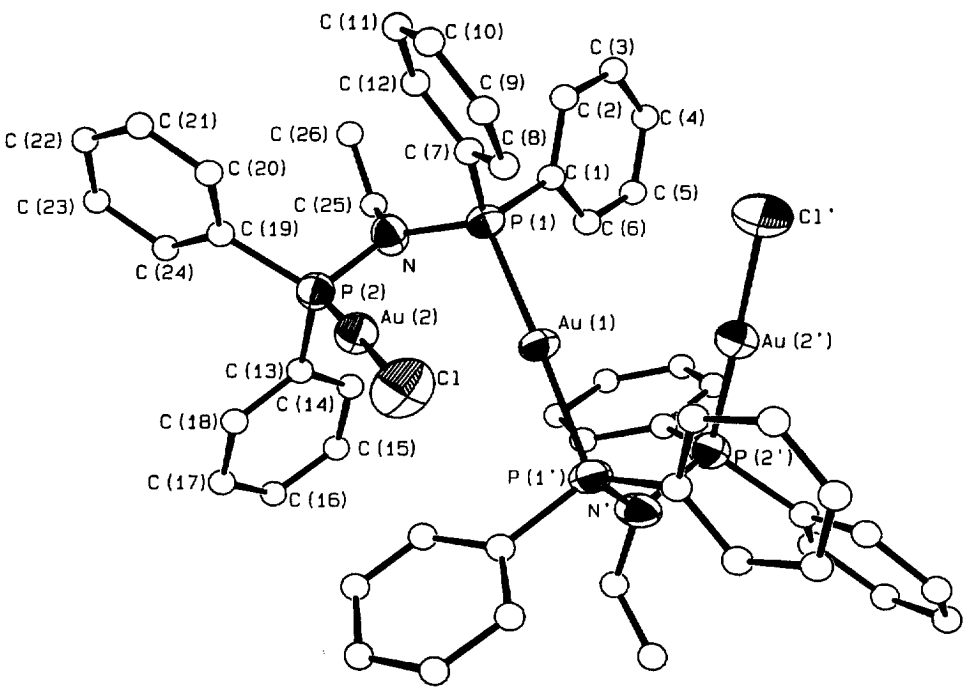

Fig. 3. ORTEP drawing of the $[Au_3Cl_2(\mu\text{-dppa})_2]^{2+}$ cation in $[Au_3Cl_2(\mu\text{-dppa})_2]PF_6$. The carbon atoms are drawn as spheres of arbitrary radius and the remaining atoms as 50% probability thermal ellipsoids.

Table 2. Selected interatomic distances (Å) and angles (°) for $[Au_3Cl_2(\mu\text{-dppa})_2]PF_6$

Au(1)···Au(2)	3.037(1)	Au(1)–P(1)	2.313(2)
Au(2)–Cl	2.282(2)	Au–P(2)	2.228(2)
P(1)–N	1.709(6)	P(1)–C(1)	1.807(7)
P(1)–C(7)	1.797(7)	P(2)–N	1.683(6)
P(2)–C(13)	1.780(13)	P(2)–C(19)	1.809(7)
N–C(25)	1.490(9)		

Au(2)···Au(1)···Au(2′)	163.8(2)	P(1)–Au(1)–P(1′)	175.4(6)
P(2)–Au(2)–Cl	177.1(1)	Au(1)–P(1)–N	109.4(2)
Au(1)–P(1)–C(1)	112.8(2)	Au(1)–P(1)–C(7)	113.3(2)
N–P(1)–C(1)	104.5(3)	N–P(1)–C(7)	107.6(3)
C(1)–P(1)–C(7)	108.7(3)	Au(2)–P(2)–N	110.8(2)
Au(2)–P(2)–C(13)	110.4(2)	Au(2)–P(2)–C(19)	116.7(2)
N–P(2)–C13	107.7(3)	N–P(2)–C(19)	104.5(3)
C(13)–P(2)–C(19)	106.2(3)	P(1)–N–P(2)	117.5(3)
P(1)–N–C(25)	123.3(5)	P(2)–N–C(25)	119.1(5)

ligands. Similarly, the Au(2)–P(2) distance of 2.228(2) Å corresponds closely with the Au–P distance of 2.238(5) Å in [ClAu(dppm)AuCl] [17] since the coordination environments of the gold atoms are the same. The Au(2)–Cl bond length of 2.282(2) Å is very similar to that observed in [ClAu(dppm)AuCl] [17] (2.288 Å) and those reported for the $[Au_3Cl_2(\mu\text{-dppm})_2]^+$ cation of 2.288 and 2.301 Å in the $[AuCl(C_6F_5)_3]^-$ salt and 2.290 Å in the chloride salt. In summary, although the arrangements of the gold atoms in $[Au_3Cl_2(\mu\text{-dppm})_2]^+$ and $[Au_3Cl_2(\mu\text{-dppa})_2]^+$ cations are different, the immediate coordination environments of the gold atoms are very similar.

The room temperature UV/vis absorption spectrum of $[Au_3Cl_2(\mu\text{-dppa})_2]PF_6$ in acetonitrile is shown in Fig. 4. The band at 230 nm, which is observed as a shoulder on the very intense peak in the ultraviolet region, can be attributed to transitions within the phenyl rings [2]. Also observed are a band at 295 nm ($\epsilon_{max} = ca.$ 20000 $dm^3 mol^{-1} cm^{-1}$) and a relatively weak absorption centred at 357 nm. The band at 295 nm is in a very similar position to that at 298 nm observed in the UV/vis spectrum of $[Au_2(\mu\text{-dppa})_2][SbF_6]_2$ measured in acetonitrile Fig. 2. On this basis, and for the same reasons as those discussed above, it is also tentatively assigned to a $p\sigma \Leftarrow d\sigma^*$

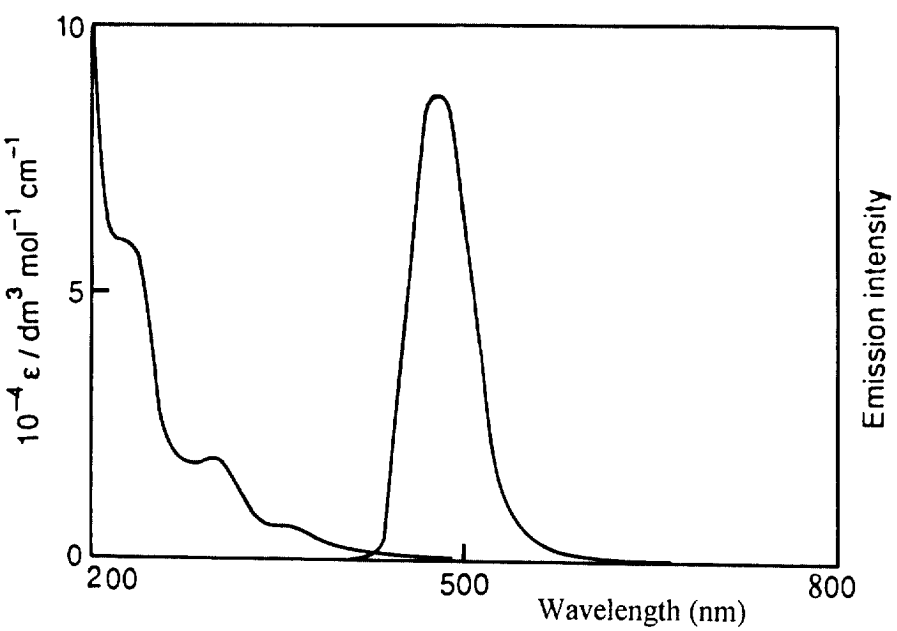

Fig. 4. Absorption in CH_3CN and solid state emission (340 nm excitation) spectra of $[Au_3Cl_2(\mu\text{-dppa})_2]PF_6$.

transition. Irradiation of an acetonitrile solution of $[Au_3Cl_2(\mu\text{-dppa})_2]PF_6$ at 340 nm only affords a very weak and indistinct emission band centred at about 560 nm. On the other hand, a powdered sample of the compound exhibits an intense blue emission as shown in Fig. 4 ($\lambda_{max} = 475$ nm). This emission is slightly blue-shifted compared to the emission maximum of 485 nm recorded in the solid state for $[Au_3Cl_2(\mu\text{-dppm})_2]Cl$ [8]. The origin of the emission is uncertain. However, solid $[AuCl(PPh_3)]$ has only a slight bluish-white emission, due to π–π^* transitions in the phenyl rings and bis(phosphine)gold(I) complexes such as $[Au(PPh_3)_2]BPh_4$ do not emit at all, neither in solution nor in the solid state [6]. It would therefore appear that the intramolecular gold–gold interactions present in the trinuclear $[Au_3Cl_2(\mu\text{-L-L})_2]^{2+}$ cations (L-L = dppm or dppa) are, in some way, responsible for the intense emission observed in the solid state for these compounds.

EXPERIMENTAL

General considerations

All manipulations were performed under nitrogen using a combination of vacuum and Schlenk techniques. Solvents were purified and degassed by standard procedures [18]. Infrared data were recorded as KBr pellets on a Shimadzu FTIR-4300 spectrophotometer. ^1H NMR spectra were recorded on a Varian Gemini-200 spectrometer with chemical shifts referenced to $SiMe_4$. $^{31}P\{H\}$ NMR spectra were recorded on a Varian FT80A spectrometer, chemical shifts being quoted relative to 85% H_3PO_4 (external, ^{31}P). Absorption spectra were recorded on a Shimadzu UV-2101PC UV-vis scanning spectrophotometer. Emission spectra were obtained on a Shimadzu RF-5000 recording spectrofluorophotometer. The C, H, and N analyses were performed by Galbraith Laboratories of Knoxville, Tennessee. The ligand $Ph_2PN(Et)PPh_2$ was prepared by a slight modification of the literature method [19].

Synthesis of $[Au_2(\mu\text{-dppa})_2][SbF_6]_2$

Excess gold powder (0.238 g, 1.208 mmol) was added with stirring to a solution of $NOSbF_6$ (0.134 g, 0.504 mmol) in acetonitrile (*ca.* 10 cm^3) at room temperature. Stirring was continued overnight to allow oxidation of gold to gold(I). The excess gold powder was removed by filtration through glass microfibre filter paper affording a clear colourless solution. Solid $Ph_2PN(Et)PPh_2$ (0.208 g, 0.504 mmol) was added with stirring following which the ligand dissolved and the solution turned yellow. After *ca* 1 h, the volume of the solution was reduced *in vacuo* and diethylether added. The product, which separated from the solution as a colourless microcrystalline solid, was isolated by filtration, washed with diethylether and dried *in vacuo*. Yield: *ca.* 0.77 g (90%). Found: C, 36.7; H, 2.9; N, 1.7; Calc. for $C_{52}H_{50}Au_2F_{12}N_2P_4Sb_2$: C, 36.9; H, 3.0; N, 1.6%. IR data (KBr pellet, cm^{-1}): 658 (vs) (SbF_6^-). ^1H NMR (CD_3CN): δ 7.64 (m, 40H, C_6H_5); 3.12 (q, 4H, CH_2); 0.35 (t, 6H, CH_3). $^{31}P\{^1H\}$ NMR (CD_3CN): δ 100.25.

Synthesis of $[Au_3Cl_2(\mu\text{-dppa})_2]PF_6$

Thiodiglycol (2,2′-thiodiethanol) (*ca.* 0.2 cm^3) was added, with stirring, to an orange-coloured solution of $HAuCl_4.2H_2O$ (0.211 g, 0.560 mmol) in methanol (*ca.* 15 cm^3) at room temperature. A slight excess of solid $Ph_2PN(Et)PPh_2$ (0.232 g, 0.560 mmol) was then added with stirring. After a period of *ca.* 30 min the ligand had dissolved to afford a solution of red-brown colour which subsequently turned yellow. After standing overnight, the solution became colourless. An excess of solid NH_4PF_6 (0.185 g, 1.140 mmol) was added and the solution stirred for 3–4 h. During this time, the product precipitated from the solution as a colourless microcrystalline solid. This was isolated by filtration through glass microfibre paper, washed with water followed by ether and finally dried *in vacuo*. Yield: *ca.* 0.70 g (80%). Found: C, 38.5; H, 3.2; N, 1.8; Calc. for $C_{52}H_{50}Au_3Cl_2F_6N_2P_5$: C, 38.3; H, 3.1; N, 1.7%. IR data (KBr pellet, cm^{-1}): 840 (vs) (PF_6^-). ^1H NMR (CD_3CN): δ 7.64 (m, 40H, C_6H_5); 3.12 (q, 4H, CH_2); 0.35 (t, 6H, CH_3). $^{31}P\{^1H\}$ NMR (CD_3CN): δ 103.61 and 83.11 (AA′BB′ pattern).

X-ray structure determinations of $[Au_2(\mu\text{-dppa})_2][SbF_6]_2$ *and* $[Au_3Cl_2(\mu\text{-dppa})_2]PF_6$

Crystal data, data collection and refinement parameters for $[Au_2(\mu\text{-dppa})_2][SbF_6]_2$ and $[Au_3Cl_2(\mu\text{-dppa})_2]PF_6$ are given in Table 3. Single crystals of the former compound were grown by slow diffusion of diethylether into a solution of the compound in dichloromethane, while single crystals of the latter compound were grown by slow diffusion of diethylether into an acetonitrile solution of the compound. Weissenberg photographs of the $[Au_2(\mu\text{-dppa})_2][SbF_6]_2$ crystals showed that the reflections were generally weak and rather diffuse, but repeated attempts to grow crystals which gave a better-defined diffraction pattern were unsuccessful. Diffractometer data were collected at 295 K with a Nonius CAD4 diffractometer using graphite monochromated Mo–$K\alpha$ radiation ($\lambda = 0.71073$ Å). Lattice parameters were obtained from the least-squares refinement of the setting angles of 25 reflections with $\theta > 12°$. Reflection intensities were measured by the variable-speed ω-2θ method in the range $3 \leqslant 2\theta \leqslant 46°$. Examination of three standard reflections, monitored after every 60 min, showed no evidence for crystal deterioration for either compound. Both data sets were corrected for Lorentz-polarisation effects and were also corrected for absorption using the psi-scan method [20]

Table 3. Crystal and intensity collection data and details of refinement for $[Au_2(\mu\text{-dppa})_2][SbF_6]_2$ and $[Au_3Cl_2(\mu\text{-dppa})_2]PF_6$

	$[Au_2(\mu\text{-dppa})_2][SbF_6]_2$	$[Au_3Cl_2(\mu\text{-dppa})_2]PF_6$
Formula	$C_{52}H_{50}Au_2F_{12}N_2P_4Sb_2$	$C_{52}H_{50}Au_3Cl_2F_6N_2P_5$
Formula weight	1646.37	1633.07
Crystal size (mm)	$0.40\times0.25\times0.15$	$0.28\times0.25\times0.22$
Crystal system	Monoclinic	Monoclinic
a (Å)	12.160(4)	22.969(4)
b (Å)	19.782(6)	15.781(3)
c (Å)	11.395(4)	16.916(3)
β (°)	99.29(3)	117.86(2)
V (Å^3)	2705(2)	5420(2)
Z	2	4
Radiation, λ (Å)	0.71073	0.71073
Space group	$P2_1/c$	$C2/c$
ρ(calc.) (g cm^{-3})	2.02	2.00
μ(Mo–$K\alpha$) (cm^{-1})	67.61	86.26
Unique intensities	2410 [$I>3\sigma(I)$]	3257 [$I>3\sigma(I)$]
Weighting scheme	$1/[\sigma^2(F)+0.0028F^2]$	$1/[\sigma^2(F)+0.0009F^2]$
No. of parameters	332	321
$R=\Sigma(F_o-F_c)/\Sigma F_o$	0.099	0.028
$R_w=\Sigma_w^{1/2}(F_o-F_c)/\Sigma_w^{1/2}F_o$	0.110	0.034
$(\Delta/\sigma)_{max}$	0.055	0.057
$\Delta\rho_{max}$ (eÅ^{-3})	4.18 (*ca.* 1 Å from Au)	1.10

(maximum and minimum transmission factors are 0.9999, 0.8936 and 0.9987, 0.8416 for $[Au_2(\mu\text{-dppa})_2][SbF_6]_2$ and $[Au_3Cl_2(\mu\text{-dppa})_2]PF_6$ respectively).

The structures of $[Au_2(\mu\text{-dppa})_2][SbF_6]_2$ and $[Au_3Cl_2(\mu\text{-dppa})_2]PF_6$ were solved by standard Patterson methods using the program SHELXS 86 [21] and subsequently completed by Fourier recycling and refinement using the program SHELX 76 [21]. The full-matrix least-squares refinements were based on $|F_o|$. The ethyl groups of the diphosphazane ligands in $[Au_2(\mu\text{-dppa})_2][SbF_6]_2$ are disordered such that they are not precisely related by the centre of symmetry midway between the two gold atoms. Various models for the disorder were tested but none gave a satisfactory solution. In the end, restrictions were placed on the N–C and C–C bond lengths with the methylene and methyl hydrogens not being included in the refinement. All the non-H atoms were assigned anisotropic temperature factors and the H-atoms a single common isotropic temperature factor; the latter were placed in calculated positions, except for the NEt hydrogens as noted above. Neutral-atom scattering factors were used with corrections for anomalous dispersion [22].

CONCLUSION

Two diphosphazane ligand-bridged complexes of gold have been synthesised, their crystal structures determined and their spectroscopic properties investigated, these being $[Au_2\{\mu\text{-}Ph_2PN(Et)PPh_2\}_2][SbF_6]_2$ and $[Au_3Cl_2\{\mu\text{-}Ph_2PN(Et)PPh_2\}_2]PF_6$. The cations of these compounds have in common Au···Au distances which are sufficiently short to indicate a substantial interaction between the gold atoms. This interaction is believed to be, in some way, responsible for the luminescence exhibited by the compounds, in solution for the dinuclear species and in the solid state for the trinuclear complex. However, we have not been able to establish a correlation between the Au···Au separation and the energy of the emission and, thus, conclude that the emission wavelength is determined more by the properties of the ligand. This conclusion is borne-out by a comparison of the emission properties of the diphosphazane ligand-bridged compounds with those reported for salts of the bis(diphenylphosphino)methane ligand-bridged cations, $[Au_2(\mu\text{-}Ph_2PCH_2PPh_2)_2]^{2+}$ and $[Au_3Cl_2(\mu\text{-}Ph_2PCH_2PPh_2)_2]^+$.

Acknowledgements—We thank the University of Natal and the South African Foundation for Research Development for financial support. The assistance of Elena I. Lakoba and Campbell J. Parry is gratefully acknowledged.

REFERENCES

1. Roundhill, D. M., *Photochemistry and Photophysics of Metal Complexes*. Plenum Press, New York, (1994), Chapter 4, pp. 138–140.
2. King, C., Wang, J.-C., Khan, M. N. I. and Fackler, J. P., *Inorg. Chem.*, 1989, **28**, 2145.
3. Che, C. M., Kwong, H. L., Yam, V. W. W. and Cho, K. C., *J. Chem. Soc., Chem. Commun.*, 1989, 885.

4. Che, C. M., Kwong, H.-L. and Poon, C.-K., *J. Chem. Soc. Dalton Trans.*, 1990, 3215.
5. King, C., Khan, M. N. I., Staples, R. J. and Fackler, J. P., *Inorg. Chem.*, 1994, **33,** 3848.
6. King, C., Khan, M. N. I., Staples, R. J. and Fackler, J. P., *Inorg. Chem.*, 1992, **31,** 3236.
7. Uson, R., Laguna, A., Laguna, M., Fernandez, E., Villacampa, M. D., Jones, P. G. and Sheldrick, G. M., *J. Chem. Soc., Dalton Trans.*, 1983, 1679.
8. Lin, I. J. B., Hwang, J. M., Feng, D.-F., Cheng, M. C. and Wang, Y., *Inorg. Chem.*, 1994, **33,** 3467.
9. Khan, M. D. I., King, C., Heinrich, D. D., Fackler, J. P. and Porter, L. C., *Inorg. Chem.*, 1989, **28,** 2150.
10. Jaw, H.-R. C., Savas, M. M., Rogers, R. D. and Mason, W. R., *Inorg. Chem.*, 1989, **28,** 1028.
11. Kozelka, J., Oswald, H. R. and Dubler, E., *Acta Crystallogr.*, 1986, **C42,** 1007.
12. Schaefer, W. P., Marsh, R. E., McCleskey, T. M. and Gray, H. B., *Acta Crystallogr.*, 1991, **C47,** 2553.
13. Schmidbauer, H., Wohlleben, A., Schubert, U., Frank, A. and Huttner, G., *Chem. Ber.*, 1997, **110,** 2751.
14. Orpen, A. G., Brammer, L., Allen, F. H., Kennard, O., Watson, D. G. and Taylor, R., *J. Chem. Soc., Dalton Trans.*, 1989, S1–S83.
15. de Leeuw, G., Field, J. S. and Haines, R. J., *J. Organometal. Chem.*, 1989, **359,** 245.
16. Guy, J. J., Jones, P. G. and Sheldrick, G. M., *Acta Crystallogr., Sect. B*, 1976, **32,** 1937.
17. Schmidbauer, H., Wohlleben, A., Wagner, F., Orama, O. and Huttner, G., *Chem. Ber.*, 1977, **110,** 1748.
18. Perrin, D. D., Amarego, W. L. F. and Perrin, D. R. *Purification of Laboratory Chemicals*, 2nd edn., Pergamon, New York (1980).
19. Ewart, G., Lane, A. P., McKechnie, J. and Payne, D. S., *J. Chem. Soc.*, 1964, 1543.
20. *North, A. C. T., Philips, D. C. and Mathews, F. A., Acta Crystallogr., Sect. A*, 1968, **24,** 35.
21. Sheldrick, G. M., *SHELXS* 86. Program for Crystal Structure Determination. University of Göttingen (1986); *SHELX* 76. Program for Crystal Structure Determination and Refinement. University of Cambridge (1976).
22. *International Tables for X-ray Crystallography*, Kynoch Press, Birmingham, Vol. 4, pp. 99 & 148.

Pergamon

PII: S0277-5387(98)00161-2

Polyhedron Vol. 17, No. 17, pp. 3031–3043, 1998
© 1998 Elsevier Science Ltd
All rights reserved. Printed in Great Britain
0277-5387/98 $19.00+0.00

Synthesis, structure and magnetic properties of $[Cu_5(bta)_6L_4]$ (bta = benzotriazolate; L = β-diketonate) Clusters

Mark Murrie,[a] David Collison,[a] C. David Garner,[a]* Madeleine Helliwell,[a] Peter A. Tasker[b] and Scott S. Turner[c]

[a] Department of Chemistry, The University of Manchester, Manchester, M13 9PL U.K.

[b] Zeneca Specialties, Blackley, Manchester, M9 3DA U.K.

[c] The Royal Institution of Great Britain, London, W1X 4BS U.K.

(Received 22 January 1998)

Abstract—Reaction of $[CuL_2]$ (LH: tfpbdH = 4,4,4-trifluoro-1-phenyl-1,3-butanedione; tropH = tropolone; or acacH = acetylacetone; Ph/Me-pdH = 1-phenyl-1,3-butanedione; Ph/Ph-pdH = 1,3-diphenyl-1,3-propanedione; or C_4H_3S/CF_3-pdH = 4,4,4-trifluoro-1-(2-thienyl-1,3-butanedione)) with benzotriazole (btaH) in CH_2Cl_2 yields the corresponding compound $[Cu_5(bta)_6L_4]$ (L = tfpbd, **1**; trop, **2**; acac, **3**; (Ph/Me-pd) **4**; (Ph/Ph-pd) **5**; (C_4H_3S/CF_3-pd) **6**). The structures of **1** and **2** have been determined by single crystal X-ray diffraction revealing a distorted tetrahedral arrangement of four Cu(II) centered on a fifth Cu(II). Each of the six bta ligands spans an edge of the Cu_4 tetrahedron and is ligated to the central Cu through its central nitrogen. Solid-state magnetic susceptibility studies from 2–300 K have been accomplished for **1**, **2** and **3** and reveal a weak antiferromagnetic intramolecular interaction between the five Cu(II) centres. The tridentate (μ_3-bridging) bonding motif of bta is well suited for the formation of a protective monolayer of bta^- ions on oxidised copper surfaces. Furthermore, the flexibility in this mode of coordination exhibited by bta^- ions, as manifest within the structures of **1**, **2**, and **3** (the structure of which was determined previously), is advantageous and would allow benzotriazolate to adapt to the various surface topographies which could well be presented by lightly oxidized copper surfaces. © 1998 Elsevier Science Ltd. All rights reserved

Keywords: benzotriazole; β-diketonates; copper complexes; corrosion; crystal structures; magnetic properties.

INTRODUCTION

Specific ligands have been found to inhibit the corrosion of particular metals; benzotriazole (btaH) and substituted benzotriazoles are well established corrosion inhibitors for copper and its alloys [1]. It has been postulated that copper oxide films are prerequisites for successful corrosion inhibition [2] and practical use of btaH as a corrosion inhibitor involves application to copper surfaces which have undergone some degree of oxidation. We have investigated the mode of interaction of btaH with lightly oxidized copper surfaces by studying the coordination chemistry of this pro-ligand with complexes of Cu(II) bound to oxygen-donor ligands.

$[Cu_5(bta)_6(acac)_4]$, first reported by Marshall [3], is an attractive analogue for the structure of species formed by btaH in forming the protective barrier on the surface of copper and its alloys. Treatment of a CH_2Cl_2 solution of $[Cu(acac)_2]$ with solid btaH in a 1:5 ratio, followed by slow evaporation of the solvent yielded green, prismatic crystals of $[Cu_5(bta)_6(acac)_4].0.5CH_2Cl_2$. The structure of this cluster, wherein each bta ligand forms three η^1 Cu–N bonds in an "arrowhead" structural motif [4], is in accord with a

* Correspondence and proofs: Professor C. David Garner, FRS, Department of Chemistry, The University of Manchester, Manchester M13 9PL (UK).

model of the interaction of btaH with metal or metal oxide surfaces proposed on the basis of single crystal, UHV surface studies [5]. This relatively simple synthetic route to $[Cu_5(bta)_6(acac)_4]$ has permitted variation of the copper-containing starting material to produce other examples of this structural motif, as described herein. These systems allow further exploration of copper-bta interactions in an oxygen-rich metal environment. Not only are these clusters relevant to the corrosion inhibitive properties of btaH but also they are of chemical interest in their own right.

EXPERIMENTAL

General

All chemicals were reagent grade and were used as received. All preparations were carried out in air at ambient temperature.

Synthesis of $[CuL_2]$ (*L* = *tfpbd, trop, acac, (Ph/Me-pd), (Ph/Ph-pd), and* $(C_4H_3S/CF_3$-*pd)*

These compounds were prepared by an adaptation of a method described by Fernelius and Bryant [6] and crystallized from hot $CHCl_3$. Each compound had satisfactory elemental analysis (C,H,Cu) and the expected IR (KBr disk) and UV/Vis (CH_2Cl_2) spectroscopic properties.

Synthesis of $[Cu_5(bta)_6L_4]$ (*L* = *tfpbd* (*1*), *trop* (*2*), *acac* (*3*), *(Ph/Me-pd)* (*4*), *(Ph/Ph-pd)* (*5*), *and* $(C_4H_3S/CF_3$-*pd)* (*6*))

A solution of benzotriazole (0.143 g, 1.2 mmol) in CH_2Cl_2 (10 cm^3) was added to a solution of $[CuL_2]$ (1.0 mmol) in CH_2Cl_2 (75 cm^3). The resulting deep green solution was stirred for 2 h. at room temperature and the solvent left to evaporate in air. The resulting solid was crystallized by careful layering of a concentrated CH_2Cl_2 (or, for **4** $CHCl_3$) solution with a co-solvent (**1**, petroleum ether (40/60); **2**, **6** cyclohexane; **3**, **4** EtOH; **5** Et_2O) (1:4, v/v).

Microanalyses were carried out by the Microanalytical Laboratory of the Chemistry Department, The University of Manchester. IR spectra were recorded as KBr disks on an ATI Mattson Genesis Series FTIR spectrometer. UV/Vis spectra were recorded using a Varian Cary 1E UV/Vis spectrophotometer. Magnetic susceptibility measurements were performed on a Quantum Design MPMS-7 SQUID magnetometer at a field strength of 100 G (0.01 T) and over a temperature range of 2–300 K. Volume susceptibilities were measured on randomly oriented polycrystalline materials of **1** (23.6 mg), **2** (22.9 mg) and **3** (25.9 mg).

1. Analysis: Calc. for $C_{76}H_{48}N_{18}Cu_5F_{12}O_8$, C 48.4; H 2.6; N 13.4; Cu 16.8. Found C 48.4; H 2.8; N 13.2; Cu 16.2%. IR: (KBr disk)/cm^{-1} 1609s, 1575s, 1532w, 1490w, 1459w, 1434w, 1320m, 1294s, 1191m, 1143m, 1098w, 1080w, 1026w, 999w, 949w, 788w, 765w, 745m. UV/Vis: (CH_2Cl_2) λ/nm (ϵ/$dm^3\,mol^{-1}\,cm^{-1}$) 674 (480), 336 (6.3×10^4), 276 (8.9×10^4). MS: (+FAB) m/z (% intensity) 1769 (11%, Molecular ion (M)-bta), 1554 (12), 1339 (5), 1219 (11), 1004 (7), 789 (98), 608 (64).
2. Analysis: Calc. for $C_{64}H_{44}N_{18}Cu_5O_8$, C 50.9; H 2.9; N 16.7; Cu 21.0. Found C 51.8; H 3.1; N 17.0; Cu 20.0%. IR: (KBr disk)/cm^{-1} 1592s, 1515s, 1432s, 1409s, 1366s, 1274w, 1254w, 1225m, 1205w, 997w, 877w, 788w, 741m. UV/Vis: (CH_2Cl_2) λ/nm (ϵ/$dm^3\,mol^{-1}\,cm^{-1}$) 677 (640), 388 (2.4×10^4), 332 (7.1×10^4), 245 (1.2×10^5). MS: (+FAB) m/z (% intensity): 1391 (19%, M-bta), 1270 (10), 1151 (10), 1031 (12), 910 (9), 789 (85), 608 (56).
3. Analysis: Calc. for **3**.CH_2Cl_2 $C_{57}H_{54}N_{18}Cl_2Cu_5O_8$, C 45.4; H 3.6; N 16.7; Cu 21.1. Found C 43.6; H 2.9; N 16.7; Cu 21.7%. (KBr disk)/cm^{-1} 1590s, 1515s, 1426m, 1388s, 1270m, 1210m, 1187m, 1022w, 995w, 927w, 787m, 745s. UV/Vis: (CH_2Cl_2) λ/nm (ϵ/$dm^3\,mol^{-1}\,cm^{-1}$) 663 (480), 301 (5.4×10^4), 275 (8.3×10^4). MS: (+FAB) m/z (% intensity): 1305 (17%, M-bta), 1206 (9), 1105 (5), 987 (7), 888 (5), 789 (100), 608 (64).
4. Analysis: Calc. for **4**.CH_3Cl.EtOH $C_{79}H_{67}N_{18}Cl_3Cu_5O_9$, C 51.7, H 3.7, N 13.7, Cu 17.3%. Found: C 51.2, H 3.4, N 13.5, Cu 16.5%. IR (KBr disk)/cm^{-1} 1592s, 1563s, 1513s, 1487m, 1451m, 1383s, 1309w, 1272w, 1210w, 1183w, 997w, 788w, 747m, 713w, 691w. UV/Vis (CH_2Cl_2) λ/nm (ϵ/$dm^3\,mol^{-1}\,cm^{-1}$): 659 (500), 335 (4.8×10^4), 273 (8.4×10^4). MS (+FAB) m/z (% intensity): 1553 (10%, M-bta), 1392 (5), 1229 (2), 1111 (5), 950 (6), 789 (100), 608 (69).
5. Analysis: Calc. for **5**.$2CH_2Cl_2$ $C_{98}H_{72}N_{18}Cl_4Cu_5O_8$, C 56.3, H 3.5, N 12.1, Cu 15.2%. Found: C 56.0, H 3.5, N 11.5, Cu 15.0%. IR (KBr disk)/cm^{-1}: 1594m, 1548s, 1520s, 1478m, 1452m, 1381s, 1316w, 1272w, 1221w, 1183w, 1069w, 1025w, 998w, 945w, 788w, 746m, 722w, 689w. UV/Vis (CH_2Cl_2) λ/nm (ϵ/$dm^3\,mol^{-1}\,cm^{-1}$): 659 (460), 363 (6.0×10^4), 273 (1.0×10^5). MS (+FAB): m/z (% intensity): 1801 (5%, M-bta), 1578 (4), 1354 (trace), 1235 (4), 1014 (6), 789 (100), 608 (86).
6. Analysis: Calc. for **6**.CH_2Cl_2 $C_{69}H_{42}N_{18}Cl_2Cu_5F_{12}O_8S_4$, C 41.5, H 2.1, N 12.6, Cu 15.9%. Found: C 42.8, H 2.1, N 12.7, Cu 15.5%. IR (KBr disk)/cm^{-1}: 1600s, 1581s, 1537s, 1504m, 1440m, 1409s, 1359m, 1351m, 1312s, 1253m, 1232m, 1195s, 1144s, 1083w, 1067m, 939w, 790m, 745m, 724m, 689w. UV/Vis (CH_2Cl_2) λ/nm (ϵ/$dm^3\,mol^{-1}\,cm^{-1}$): 673 (470), 348 (7.7×10^4), 277 (8.5×10^4). MS (+FAB) m/z (% intensity): 1794 (22%, M-bta), 1573 (10), 1351 (2), 1231 (9), 1010 (5), 789 (95), 608 (100).

Crystallography

The crystallographic data for the structural determinations of **1** and **2** are summarized in Table 1; the X-ray structural determination of **3** has been previously published [4]. A single crystal of **1** or **2** was mounted in a glass capillary in the presence of some of the mother liquor. Data collection was carried out using a Rigaku AFC5R diffractometer which utilized graphite monochromated CuK_α radiation ($\lambda = 1.54178$ Å). The data were corrected for absorption [7], Lorentz-polarisation effects and, for **2**, a small linear intensity decay. The structures were solved by standard direct methods [8] and all refinements were performed using the teXsan crystallographic software package [9].

The asymmetric unit of **1**.$(C_6H_{14})_2C_6H_{12}$ consists of half a molecule, the second half being generated by rotation about a 2-fold axis. Also present are two solvent fragments considered to originate from the petroleum ether (40/60) used in the crystallization which were included as one hexane molecule and half a cyclohexane molecule, the second half being generated by inversion. The non-hydrogen atoms, except for carbon (C19–C38) atoms in the four bidentate oxygen donors, were refined anisotropically. A view of the $[Cu_5(bta)_6(tfpbd4]$ cluster of **1**, as viewed along the crystallographic two fold axis, is given in Fig. 1.

The asymmetric unit of **2**.H_2O consists of two $[Cu_5(bta)_6(trop)_4]$ and two H_2O molecules. In the second copper-containing molecule, one of the $C_7H_5O_2$ groups showed some disorder with two positions being identified for O10. Due to the large number of parameters involved in this structure, each molecule was refined separately. The non-hydrogen atoms, except for O17 and O18 of the water molecules, were refined anisotropically. A view of one of the copper clusters of **2**, with the carbon atoms of tropolonate omitted for clarity, is given in Fig. 2.

For both crystal structure determinations, the hydrogen atoms were included in calculated positions with fixed isotropic thermal parameters. Selected bond lengths, bond angles, non-bonding distances and non-bonding angles for the $[Cu_5(bta)_6(\beta\text{-diketonate})_4]$ cluster of **1**.$(C_6H_{14})_2C_6H_{12}$ and **2**.H_2O are presented in Tables 2 and 3, respectively.

RESULTS AND DISCUSSION

The previously employed synthetic methodology for the synthesis of $[Cu_5(bta)_6L_4]$ clusters [3, 4] has

Table 1. Crystallographic data for $[Cu_5(bta)_6(tfpbd)_4].(C_6H_{14})_2C_6H_{12}$ (**1**.$(C_6H_{14})_2C_6H_{12}$) and $[Cu_5(bta)_6(trop)_4].H_2O$ (**2**.H_2O)

Compound	**1**.$(C_6H_{14})_2C_6H_{12}$	**2**.H_2O
Empirical Formula	$C_{94}H_{88}N_{18}Cu_5F_{12}O_8$	$C_{64}H_{46}N_{18}Cu_5O_9$
Formula Weight	2143.55	1528.92
Crystal colour, Habit	Green, Plate	Green, Prismatic
Crystal dimensions (mm)	$0.25 \times 0.20 \times 0.05$	$0.35 \times 0.37 \times 0.20$
Crystal system	Monoclinic	Monoclinic
a/Å	20.424(7)	22.223(4)
b/Å	17.042(8)	13.198(4)
c/Å	28.51(1)	22.505(6)
β/deg.	91.26(3)	104.21(2)
V/Å^3	9921(7)	6399(5)
Space group	C2/c (#15)	$P2_1$ (#4)
Z	4	4
D_{calc}/gcm^{-3}	1.435	1.569
μ/cm^{-1}	18.76	23.72
Temperature/K	294	294
Scan Type	$\omega/2\theta$	$\omega/2\theta$
Scan Rate/deg.min^{-1}	8.0	16.0
Scan Width/deg.	$1.31 + 0.30\tan\theta$	$1.10 + 0.30\tan\theta$
$2\theta_{max}$/deg.	120.2	120.2
Decay	—	−17.00% decline
No. of reflections measured	7911	10300
No. observations ($I > 3.00\sigma(I)$)	2536	7735
No. of variables	474	855
Residuals: R[a]; R_w[b]	0.069, 0.069	0.049, 0.054
Goodness of fit indicator	1.82	1.58

[a] $R = \Sigma\|\|F_o\| - |F_c\|\|/\Sigma|F_o|$

[b] $R_w = [(\Sigma w(|F_o| - |F_c|)^2/\Sigma wF_o^2)]^{1/2}$

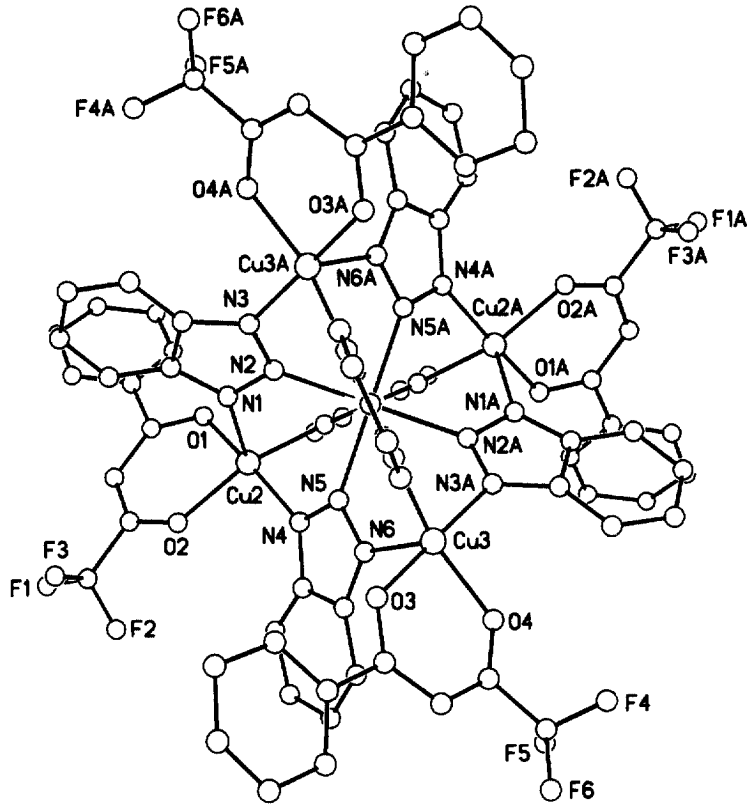

Fig. 1. PLUTO diagram of $[Cu_5(bta)_6(tfpbd)_4]$ (**1**) showing all non-hydrogen atoms; for clarity, all atoms are not labelled.

been improved by the use of a stoichiometric amount of btaH in the preparation of the complexes **1**–**6**, resulting in the isolation of crystalline products in good yield.

The crystal and molecular structures of 1 and 2

As previously seen for **3** [4], the pentanuclear Cu(II) assemblies of **1** and **2** (see Figs. 1 and 2, respectively) each consist of a distorted tetrahedral arrangement of four Cu(II) centred on the fifth (see Figs. 3 and 4). Each benzotriazolate anion spans an edge of the tetrahedron and is ligated to the central Cu(II) *via* its central nitrogen atom. The coordination sphere at each apical Cu(II) is completed by a bidentate β-diketonate ligand. The central Cu(II) has a tetragonally distorted (4+2) octahedral coordination geometry, with (see Tabs. 2 and 3) average distances of Cu–N_{ax} = 2.29 Å, Cu–N_{eq} = 2.08 Å for **1** and Cu–N_{ax} = 2.41 Å, Cu–N_{eq} = 2.04 Å for **2**. Each apical Cu(II) is in an approximately square-based pyramidal $(Cu(N_2O_2)_{eq}(N)_{ax})$ environment, bound to three benzotriazolate nitrogen atoms and two oxygen atoms of the bidentate donor molecule. Average distances defining the geometry at the apical copper ions are Cu–N_{eq} = 1.97, Cu–N_{ax} = 2.20 and Cu–O = 1.94 Å for **1** and Cu–N_{eq} = 2.00, Cu–N_{ax} = 2.23 and Cu–O = 1.94 Å for **2**.

The distortion of the Cu^{II}_4 tetrahedral array can be measured by considering the Cu···Cu separations of the apical Cu(II) ions. For the Cu(II) bridged by axial benzotriazolate anions, (see Fig. 3), the average distance between apical coppers is 5.82 Å for **1** and 5.74 Å for **2**. This distance increases to *ca.* 6.05 Å for the Cu(II) bridged by equatorial benzotriazolate anions in **1** and *ca.* 6.16 Å for **2** and is accompanied by an increase in the $Cu_{(apical)}Cu_{(central)}Cu_{(apical)}$ bond angle (see Tabs. 2 and 3). The dihedral angles between opposite $Cu_{(apical)}Cu_{(central)}Cu_{(apical)}$ planes in **1** are 90.4° in the axial direction and 83.1 and 86.0° between planes in the equatorial direction. The corresponding angles in the two distinct molecules in the asymmetric unit of **2** are 90.6, 82.4 and 82.9° (Cu1–Cu5) and 90.1, 82.3 and 82.4° (Cu6–Cu10).

There are significant structural variations within each Cu^{II}_3–bta moiety of the structures **1**, **2** and **3**. The angles of inclination of the bta^- ions have been assessed by calculating the angle between the plane of the bta and that of the corresponding $Cu_{(apical)}Cu_{(central)}Cu_{(apical)}$ plane (Tab. 4). For the two axial bta^- ions of **1**, the angle is either 0 or 1.4°, whereas two of the equatorial bta^- ions are bonded at an angle of 7.9° and the other two at an angle of

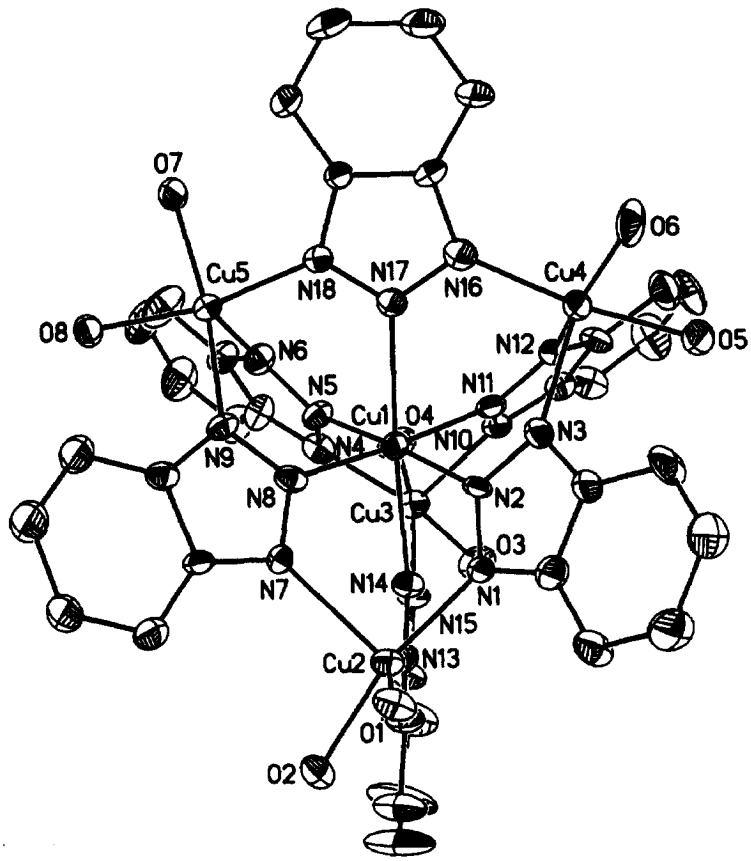

Fig. 2. ORTEP diagram showing the non-hydrogen atoms of $[Cu_5(bta)_6(trop)_4]$ (**2**); for clarity, the C atoms are not labelled and 30% probability thermal ellipsoids are given.

16.8°. This indicates that the two axial bta^- ions are bonded in a more upright orientation. In **2** the angle is 4.1 or 3.4° (Cu1–Cu5) and 4.3 or 2.9° (Cu6–Cu10) in the axial direction and in the equatorial direction the angle is 5.4, 7.4, 9.7 or 12.2° (Cu1–Cu5) and 3.0, 9.2, 12.1, 13.0° (Cu6–Cu10). The more irregular bonding of the equatorial bta^- ions could result from the square-based pyramidal geometry at the apical Cu(II). Thus, the longer Cu–N bond of the $(Cu(N_2O_2)_{eq}(N)_{ax})$ environment is found within each $Cu^{II}{}_3-bta_{eq}$ moiety and this asymmetry is reflected in the tilting of the bta^- ions. This situation does not occur in **3** since one of the longer Cu–N bonds is located in the $Cu^{II}{}_3-bta_{eq}$ moiety (Cu4, Cu1, Cu5).

Mass spectrometry

The $[Cu_5(bta)_6L_4]$ compounds were found to be amenable to characterisation by positive ion fast atom bombardment (+FAB) mass spectrometry and all exhibited a characteristic fragmentation pattern (Fig. 5). No parent ion was seen and, in each case, the first ion detected was $[Cu_5(bta)_5L_4]^+$. Each of these cluster cations fragment by losing two of the bidentate oxygen chelates, then a second bta, followed by the loss of the two remaining oxygen chelates. All of the mass spectra exhibited a characteristic "fingerprint" peak at $m/z = 789$, assigned to $[Cu_5(bta)_4]^+$. Loss of bta from this latter ion produced a second fingerprint peak at $m/z = 608$, corresponding to $[Cu_4(bta)_3]^+$. Other, less intense, peaks were present in each mass spectrum indicating other fragmentation routes; *e.g.*, a small peak was sometimes observed corresponding to the production of the $[Cu_5(bta)_6L_3]^+$.

Thus, in these mass spectra one of the tridentate μ_3-bridging bta is the first ligand to be lost by the cluster. With reference to the structural information available for these pentanuclear copper(II) clusters, the initial loss of bta may be explained by considering the Cu–N bonding at the central Cu(II) which is in a tetragonal ligand field-consistent with a Jahn-Teller distortion producing an elongation of the two Cu–N bonds to the axial bta. This lengthening of the bond between

Table 2. Selected intramolecular dimensions of $1.(C_6H_{14})_2C_6H_{12}$.

Bond	Distance/Å †	Bond	Distance/Å †		
Cu1–N2	2.09(1)	Cu2–N1	2.19(1)		
Cu1–N2A	2.09(1)	Cu2–N4	1.99(1)		
Cu1–N5	2.06(1)	Cu2–N8	1.98(1)		
Cu1–N5A	2.06(1)	Cu3–O3	1.93(1)		
Cu1–N7	2.31(2)	Cu3–O4	1.94(1)		
Cu1–N9	2.26(2)	Cu3–N3A	1.99(1)		
Cu2–O1	1.951(9)	Cu3–N6	2.20(1)		
Cu2–O2	1.956(9)	Cu3–N10	1.97(1)		
Atoms	Angle/° †	Atoms	Angle/° †	Atoms	Angle/° †
N1–Cu1–N9	180.0(7)	N8–Cu2–N4	90.5(5)	N10–Cu3–N3A	91.3(5)
N2–Cu1–N2A	172.0(7)	N4–Cu2–O2	88.3(5)	N3A–Cu3–O4	90.7(5)
N5A–Cu1–N5	171.7(7)	O2–Cu2–O1	90.4(4)	O4–Cu3–O3	89.5(4)
N2–Cu1–N5	89.9(5)	O1–Cu2–N4	170.6(5)	O3–Cu3–N3A	175.3(5)
N5–Cu1–N2A	90.7(5)	O2–Cu2–N8	158.4(5)	O4–Cu3–N10	156.9(5)
N7–Cu1–N5	85.8(4)	N1–Cu2–O1	96.2(4)	N6–Cu3–O3	94.9(4)
N7–Cu1–N2	94.0(4)	N1–Cu2–N8	100.6(5)	N6–Cu3–N10	100.5(5)
N9–Cu1–N5	94.2(4)	N1–Cu2–N4	93.2(5)	N6–Cu3–N3A	89.7(5)
N9–Cu1–N2	86.0(4)	N1–Cu2–O2	101.0(4)	N6–Cu3–O4	102.5(5)
O1–Cu2–N8	87.2(4)	O3–Cu3–N10	86.7(5)		
Atom1-Atom2	Distance/Å †	Atom1-Atom2	Distance/Å †		
Cu1–Cu2	3.662(3)	Cu2–Cu3	6.056(4)		
Cu1–Cu2A	3.662(3)	Cu2–Cu2A	5.797(5)		
Cu1–Cu3	3.654(3)	Cu3–Cu2A	6.038(4)		
Cu1–Cu3A	3.654(3)	Cu3–Cu3A	5.847(5)		
Cu2–Cu3A	6.038(4)	Cu2A–Cu3A	6.056(4)		
Atoms	Angle/° †	Atoms	Angle/° †		
Cu2A–Cu1–Cu3	111.25(6)	Cu2A–Cu1–Cu3A	111.76(5)		
Cu2–Cu1–Cu2A	104.7(1)	Cu3–Cu1–Cu3A	106.3(1)		
Cu2–Cu1–Cu3	111.76(5)	Cu2–Cu1–Cu3A	111.25(6)		

† Estimated standard deviations in the least significant figure are given in parentheses.

the central Cu(II) and the central nitrogen atoms, from *ca.* 2.0 Å in the equatorial direction to *ca.* 2.4 Å in the axial direction, suggests that the axial bta ligands are more weakly bound than the equatorial ones.

IR spectroscopy

The IR spectra of the $[Cu_5(bta)_6L_4]$ compounds in KBr discs are dominated by bands attributable to the bidentate oxygen chelate and contain strong absorptions between *ca.* 1500 and 1600 cm^{-1} attributable to C···C and C···O stretching modes [10]. The coordinated benzotriazole in these complexes is considered responsible for the two bands at *ca.* 788 and 745 cm^{-1}; the stronger (at 745 cm^{-1}) is assigned as a C–H out-of-plane vibration and the weaker to a vibration involving both benzene and triazole in-plane bending [11].

UV/Vis spectroscopy

The $[Cu_5(bta)_6L_4]$ compounds, dissolved in CH_2Cl_2, exhibit a broad absorption profile in the visible region of the electromagnetic spectrum centred on *ca.* 670 nm (ε *ca.* 500 $dm^3\,mol^{-1}\,cm^{-1}$). This absorption accounts for the green colour of the compounds and is considered to arise from *d–d* transitions within each cluster.

The UV region of the spectra of the compounds $[Cu_5(bta)_6L_4]$ (where L = β-diketonates) contain two strong absorptions: the more intense band was observed at *ca.* 275 nm (ϵ *ca.* 8×10^4 to 1×10^5 $dm^3\,mol^{-1}\,cm^{-1}$) and the other between 300–

Table 3. Selected intramolecular dimensions of **2**.H_2O

Bond	Distance/Å †	Bond	Distance/Å †
Cu1–N2	2.041(8)	Cu3–N4	2.012(9)
Cu1–N5	2.040(9)	Cu3–N10	2.225(8)
Cu1–N8	2.044(9)	Cu3–N15	1.973(8)
Cu1–N11	2.026(8)	Cu4–O5	1.936(9)
Cu1–N14	2.417(8)	Cu4–O6	1.906(7)
Cu1–N17	2.385(8)	Cu4–N3	2.224(8)
Cu2–O1	1.945(8)	Cu4–N12	2.003(9)
Cu2–O2	1.958(6)	Cu4–N16	1.97(1)
Cu2–N1	2.011(7)	Cu5–O7	1.934(7)
Cu2–N7	2.264(8)	Cu5–O8	1.942(8)
Cu2–N13	1.990(9)	Cu5–N6	2.242(9)
Cu3–O3	1.935(8)	Cu5–N9	2.025(7)
Cu3–O4	1.939(9)	Cu5–N18	1.975(8)

Bond	Distance/Å †	Bond	Distance/Å †
Cu6–N20	2.043(9)	Cu8–N24	2.254(9)
Cu6–N23	2.073(9)	Cu8–N30	1.962(7)
Cu6–N26	2.003(7)	Cu8–N31	2.023(9)
Cu6–N29	2.401(8)	Cu9–O13	1.946(8)
Cu6–N32	2.060(7)	Cu9–O14	1.946(8)
Cu6–N35	2.452(8)	Cu9–N21	2.194(8)
Cu7–O9	1.956(9)	Cu9–N33	2.039(9)
Cu7–O10B	1.92(3)	Cu9–N34	1.978(9)
Cu7–N19	2.095(8)	Cu10–O15	1.936(8)
Cu7–N25	2.15(1)	Cu10–O16	1.939(7)
Cu7–N28	1.972(9)	Cu10–N22	1.984(9)
Cu8–O11	1.945(8)	Cu10–N27	2.291(9)
Cu8–O12	1.938(6)	Cu10–N36	1.992(8)

Atoms	Angle/° †	Atoms	Angle/° †	Atoms	Angle/° †
N11–Cu1–N5	89.0(3)	O2–Cu2–N13	91.4(3)	O6–Cu4–N3	110.7(4)
N11–Cu1–N8	176.1(3)	O2–Cu2–N1	165.9(3)	O5–Cu4–N16	171.6(3)
N11–Cu1–N2	91.8(3)	O2–Cu2–N7	100.4(3)	O5–Cu4–N12	88.7(3)
N11–Cu1–N17	87.7(3)	N13–Cu2–N1	94.4(3)	O5–Cu4–N3	94.7(3)
N11–Cu1–N14	89.9(3)	N13–Cu2–N7	95.7(3)	N16–Cu4–N12	95.6(3)
N5–Cu1–N8	89.4(3)	N1–Cu2–N7	91.8(3)	N16–Cu4–N3	92.3(3)
N5–Cu1–N2	176.1(3)	O3–Cu3–O4	81.4(3)	N12–Cu4–N3	92.8(3)
N5–Cu1–N17	93.4(3)	O3–Cu3–N15	90.6(3)	O7–Cu5–O8	81.1(3)
N5–Cu1–N14	89.5(3)	O3–Cu3–N4	162.4(3)	O7–Cu5–N9	167.4(4)
N8–Cu1–N2	90.1(3)	O3–Cu3–N10	105.2(3)	O7–Cu5–N6	101.2(3)
N8–Cu1–N17	88.9(3)	O4–Cu3–N15	162.2(3)	O7–Cu5–N18	89.8(3)
N8–Cu1–N14	93.6(3)	O4–Cu3–N4	88.1(3)	O8–Cu5–N9	92.1(3)
N2–Cu1–N17	90.4(3)	O4–Cu3–N10	101.4(3)	O8–Cu5–N6	97.6(3)
N2–Cu1–N14	86.7(3)	N15–Cu3–N4	95.4(3)	O8–Cu5–N18	165.4(3)
N17–Cu1–N14	176.3(3)	N15–Cu3–N10	96.0(3)	N9–Cu5–N6	90.2(3)
O1–Cu2–O2	80.7(3)	N4–Cu3–N10	90.6(3)	N9–Cu5–N18	94.5(3)
O1–Cu2–N13	160.3(3)	O6–Cu4–O5	81.0(3)	N6–Cu5–N18	95.4(3)
O1–Cu2–N1	89.6(3)	O6–Cu4–N16	92.2(3)		
O1–Cu2–N7	103.5(3)	O6–Cu4–N12	155.0(4)		

Atoms	Angle/° †	Atoms	Angle/° †	Atoms	Angle/° †
N26–Cu6–N20	88.1(3)	O10B–Cu7–O9	80(1)	O13–Cu9–O14	81.6(3)
N26–Cu6–N32	176.0(4)	O10B–Cu7–N28	90.7(9)	O13–Cu9–N34	167.8(3)
N26–Cu6–N23	91.8(3)	O10B–Cu7–N19	123(1)	O13–Cu9–N33	89.1(3)
N26–Cu6–N29	92.7(3)	O10B–Cu7–N25	144(1)	O13–Cu9–N21	92.1(3)
N26–Cu6–N35	92.6(3)	O9–Cu7–N28	170.8(4)	O14–Cu9–N34	90.1(4)
N20–Cu6–N32	88.5(3)	O9–Cu7–N19	89.7(4)	O14–Cu9–N33	159.3(3)
N20–Cu6–N23	179.9(3)	O9–Cu7–N25	91.8(4)	O14–Cu9–N21	107.7(3)

continued

Table 3—*continued.*

Atoms	*Angle*/° †	Atoms	Angle/° †	Atoms	Angle/° †
N20–Cu6–N29	89.8(3)	N28–Cu7–N19	93.5(4)	N34–Cu9–N33	95.9(4)
N20–Cu6–N35	94.1(4)	N28–Cu7–N25	96.8(4)	N34–Cu9–N21	98.9(3)
N32–Cu6–N23	91.6(3)	N19–Cu7–N25	91.4(3)	N33–Cu9–N21	90.0(3)
N32–Cu6–N29	89.3(3)	O12–Cu8–O11	82.4(3)	O15–Cu10–O16	80.8(3)
N32–Cu6–N35	85.6(3)	O12–Cu8–N30	170.5(3)	O15–Cu10–N22	157.2(4)
N23–Cu6–N29	90.3(3)	O12–Cu8–N31	87.8(3)	O15–Cu10–N36	93.7(3)
N23–Cu6–N35	85.8(4)	O12–Cu8–N24	95.0(3)	O15–Cu10–N27	107.6(3)
N29–Cu6–N35	86.7(3)	O11–Cu8–N30	92.0(3)	O16–Cu10–N22	89.7(3)
O10–Cu7–O10B	26(1)	O11–Cu8–N31	161.1(3)	O16–Cu10–N36	172.7(4)
O10–Cu7–O9	79.3(7)	O11–Cu8–N24	103.2(3)	O16–Cu10–N27	92.8(3)
O10–Cu7–N28	93.6(7)	N30–Cu8–N31	95.3(3)	N22–Cu10–N36	93.8(3)
O10–Cu7–N19	148.2(7)	N30–Cu8–N24	93.7(3)	N22–Cu10–N27	93.3(3)
O10–Cu7–N25	118.5(6)	N31–Cu8–N24	93.7(3)	N36–Cu10–N27	93.5(3)
Atom1-Atom2	Distance/Å †	Atom1-Atom2	Distance/Å †		
Cu1–Cu2	3.688(2)	Cu6–Cu7	3.6802(7)		
Cu1–Cu3	3.711(2)	Cu6–Cu8	3.6746(7)		
Cu1–Cu4	3.701(2)	Cu6–Cu9	3.6778(9)		
Cu1–Cu5	3.684(2)	Cu6–Cu10	3.7013(7)		
Cu2–Cu3	5.761(2)	Cu7–Cu8	5.730(1)		
Cu2–Cu4	6.154(3)	Cu7–Cu9	6.162(1)		
Cu2–Cu5	6.184(3)	Cu7–Cu10	6.287(1)		
Cu3–Cu4	6.179(2)	Cu8–Cu9	6.020(1)		
Cu3–Cu5	6.156(3)	Cu8–Cu10	6.142(2)		
Cu4–Cu5	5.757(2)	Cu9–Cu10	5.715(2)		
Atoms	Angle/° †	Atoms	Angle/° †		
Cu2–Cu1–Cu3	102.28(4)	Cu7–Cu6–Cu8	102.35(1)		
Cu2–Cu1–Cu4	112.82(5)	Cu7–Cu6–Cu9	113.76(2)		
Cu2–Cu1–Cu5	114.07(4)	Cu7–Cu6–Cu10	116.80(1)		
Cu3–Cu1–Cu4	112.96(4)	Cu8–Cu6–Cu9	109.93(1)		
Cu3–Cu1–Cu5	112.71(5)	Cu8–Cu6–Cu10	112.76(2)		
Cu4–Cu1–Cu5	102.44(5)	Cu9–Cu6–Cu10	101.50(2)		

† Estimated standard deviations in the least significant figure are given in parentheses.

360 nm (ϵ *ca.* 5×10^4 to 8×10^4 $dm^3 mol^{-1} cm^{-1}$) depending on the nature of L. Each of these absorptions was usually accompanied by a low energy shoulder. The UV spectrum of bta^- (1.5×10^{-3} M btaH in an $NaOH/H_2O$ solution at pH = *ca.* 10) contains an absorption at 275 nm (ϵ = *ca.* 8.7×10^3 dm^3 mol^{-1} cm^{-1}), in agreement with the results reported by Xu *et al.* who assigned this absorption as a π–π^* transition in bta^- on the basis of the results of CNDO calculations [12].

Therefore, we assign the absorption of the band at *ca.* 275 nm in the UV spectra of the $[Cu_5(bta)_6L_4]$ compounds as a π-π^* transition of the bta ligands. The UV spectrum of $[Cu(acac)_2]$ (5.5×10^{-4} M in CH_2Cl_2) contains two absorptions at 245 and 296 nm ($\epsilon = 1.9 \times 10^4$ and 1.4×10^4 $dm^3 mol^{-1} cm^{-1}$, respectively). Investigation of the UV spectra of Cu(II) β-diketonates by Singh and Sahai led to the assignment of the former absorption as a L→M charge-transfer transition and the latter as a ligand π-π^* transition [13]. Therefore, the absorption at 300–360 nm is assigned as a π-π^* transition of L and the position of this band varies, as expected, with the nature of L. Thus, substitution of Me in L shifts the absorption from 301 nm (L = acac) to 335 nm (L = Ph/Me-pd), 336 nm (L = Ph/CF_3-pd), 363 nm (L = Ph/Ph-pd) and 348 nm (L = C_4H_3S/CF_3-pd), variations which parallel those observed in the spectra of $[CuL_2]$ compounds [13].

The UV spectrum of **2** contains absorptions at 245 and 332 nm and a broad absorption between 360 and 400 nm ($\epsilon = 1.2 \times 10^5$, 7.1×10^4 and 2.4×10^4 dm^3 mol^{-1} cm^{-1}, respectively). These absorptions, apart from the shoulder at *ca.* 275 nm, are also seen at lower intensity, in the UV spectrum of $[Cu(trop)_2]$ (3.4×10^{-4} M in CH_2Cl_2), λ/nm (ϵ/dm^3 mol^{-1} cm^{-1}) 390 (4.2×10^3), 332 (1.2×10^4), 251 (2.1×10^4). A shoulder was seen at *ca.* 275 nm which may cor-

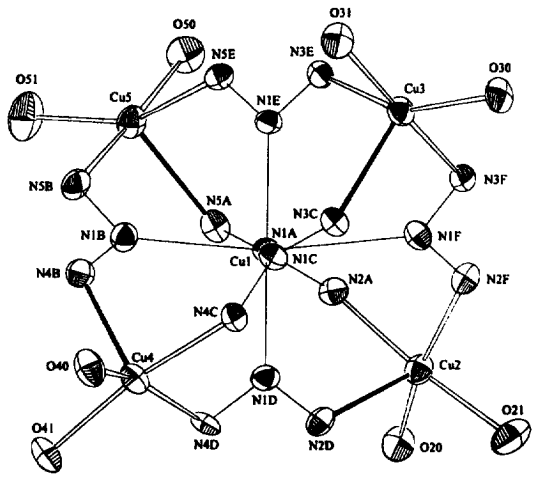

$[Cu_5(bta)_6(acac)_4]$

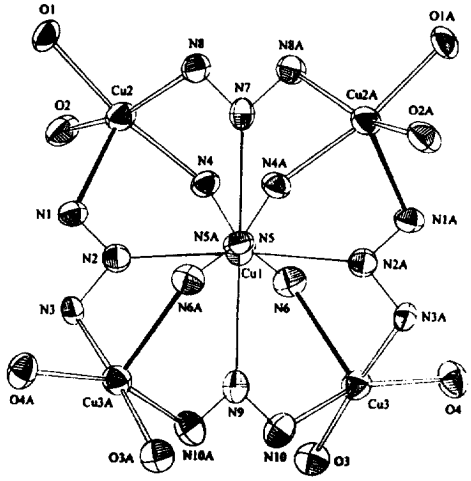

$[Cu_5(bta)_6(tfpbd)_4]$

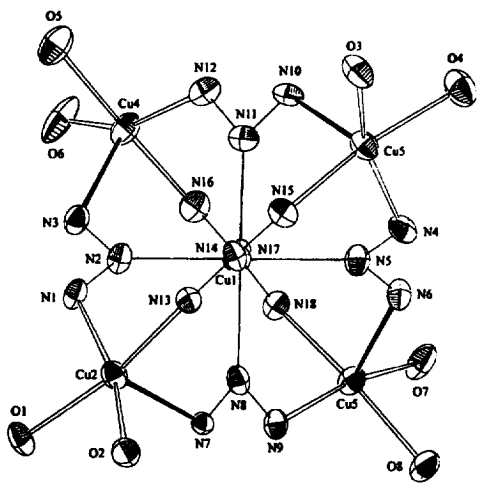

$[Cu_5(bta)_6(trop)_4]$ (Cu1-Cu5)

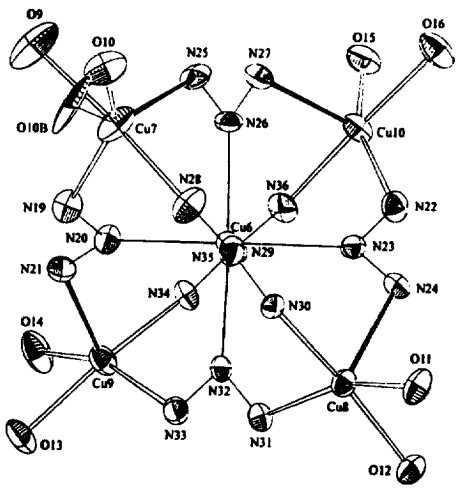

$[Cu_5(bta)_6(trop)_4]$ (Cu6-Cu10)

Fig. 3. The $Cu_5\{N_3\}_6\{O_2\}_4\}$ core of $[Cu_5(bta)_6L_4]$ (L = acac (**3**), tfpbd (**1**) trop (**2**)) highlighting the square-based pyramidal $(Cu(N_2O_2)_{eq}(N)_{ax})$ environment with Cu–$(N)_{ax}$ bonds shown in bold.

respond to the π-π^* transition of the bta ligands for $[Cu_5(bta)_6L_4]$ (where L = β-diketonate) (see above).

Magnetic properties

The experimental data were corrected for inherent diamagnetism using Pascal's constants [14] and for the temperature independent paramagnetism (TIP) of 60×10^{-6} cm^3 mol^{-1} arising from four antiferromagnetically coupled Cu atoms [15]. TIP can arise in overall spin singlet systems resulting from mixing of the ground state wave function with non-thermally populated excited states [14]. The corrected $\chi_m T$ versus T plots for all three compounds exhibits the same general behaviour (as illustrated in Fig. 6). At high temperatures the curves have positive gradients. The $\chi_m T$ values at 300 K shown in Table 5 are comparable to the paramagnet limit of five isolated S = 1/2 spins (0.46875g^2 cm^3 K mol^{-1}). $\chi_m T$ decreases with a decreasing temperature, indicating that the antiferromagnetic contributions become more rel-

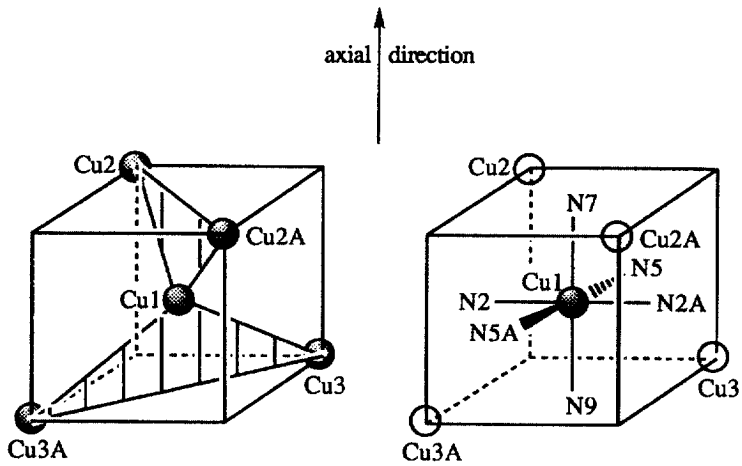

Fig. 4. Schematic diagram showing the Cu^{II}_5 arrangement and atom labelling in $[Cu_5(bta)_6(tfpbd)_4]$ (**1**) the bta^- ions bonded to Cu1 *via* N7 and N9 are termed axially bonded and the bta^- ions bonded to Cu1 *via* N2, N2A, N5 and N5A are termed equatorially bonded.

Table 4. Angles(°)[a] between the plane of the bta^- anion and the corresponding Cu(apical)Cu(central)Cu(apical) plane of **1**, **2** and **3**

Compound		θ^b	θ^b.	θ	θ	θ	θ
$[Cu_5(bta)_6(tfpbd)_4]$	**1**	0	1.4	7.9	7.9	16.8	16.8
$[Cu_5(bta)_6(trop)_4]$ (Cu1-Cu5)	**2**	3.4	4.1	5.4	7.4	9.7	12.2
$[Cu_5(bta)_6(trop)_4]$ (Cu6-Cu10)	**2**	2.9	4.3	3.0	9.2	12.1	13.0
$[Cu_5(bta)_6(acac)_4]$	**3**[4]	9.8	15.2	3.1	13.5	14.4	27.7

[a]The calculations were performed using the programme XPMA on a Silicon Graphics workstation.
[b]Axial bta^- ions.

evant as thermal randomising energy is removed from the system. The $\chi_m T$ value for each of the compounds at 2 K equates to an $S = 1/2$ ground state. Plots of $1/\chi_m$ versus T give curves which could be fitted to a Curie–Weiss expression in the high temperature region (50–300 K). A least-squares fit gives the Weiss constants shown in the Table 5.

Magnetic modelling For the purposes of modelling the magnetic properties of the $[Cu_5(bta)_6L_4]$ systems, the geometry of the Cu_5 cluster was assumed to be that of a regular tetrahedron (T_d symmetry) with four equivalent spins at the vertices and an additional body-centred spin (Fig. 7). This geometry gives the energy levels:

$$E(S_{1234},S_T) = -J_1S_T(S_T+1)+J_1S_0(S_0+1) + (J_1-J_2)S_{1234}(S_{1234}+1)+4J_2S(S+1)$$

where: S_{1234} = algebraic sum of the spins for the outer Cu sites; S_T = total algebraic sum of all spins; S_0 = cen-

Table 5. Magnetic data observed, and magnetic parameters obtained, for **1**, **2** and **3**

Compound	J_1/cm^{-1}	J_2/cm^{-1}	g	$\chi_m T$ at 300 K/cm^3 K mol^{-1}	Weiss constant
1	−7.0	−7.3	2.39	2.61	−29.2
2	−6.5	−6.4	2.23	2.18	−19.9
3	−9.5	−9.4	2.14	2.00	−33.4

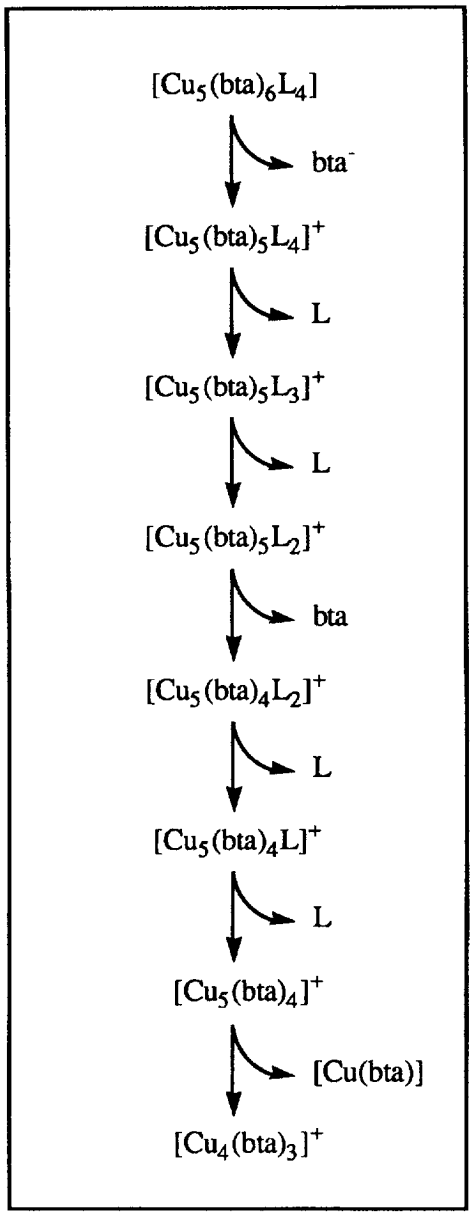

Fig. 5. Schematic diagram showing the observed fragmentation pattern of $[Cu_5(bta)_6L_4]$ under +FAB.

tral spin quantum number; J_1 = coupling constant between the central and outlying spins; J_2 = coupling constant between the outlying Cu sites [16]. The energy levels are applied to the Van Vleck equation summed over all possible combinations of the five spin sites.

$$\chi_m T = \frac{Ng^2\beta^2}{3k} \times \frac{\sum_{S_T} S_T(S_T+1)(2S_T+1)\exp(-E(S_T)/kT)}{\sum_{S_T}(2S_T+1)\exp(-E(S_T)/kT)}$$

Thus,

$$\chi_m T = (0.12505g^2)\frac{N}{D}$$

where:-

$$N = 52.5\exp([2J_1+3J_2]/kT) + 45\exp([J_1-J_2]/kT) + 3\exp(-3J_2/kT) + 15\exp([-3J_1+3J_2]/kT) + 4.5\exp([-2J_1-J_2]/kT)$$

$$D = 6\exp([2J_1+3J_2]/kT) + 12\exp([J_1-J_2]/kT) + 4\exp(-3J_2/kT) + 4\exp([-3J_1+3J_2]/kT) + 6\exp([-2J_1-J_2]/kT)$$

A least-squares fitting of this expression for $\chi_m T$ to the experimental results, using the Levenberg–Marquardt algorithm, gave the J_1, J_2 and g values presented in Table 5; these parameters were allowed full freedom in the model. The refined g-values are in the range 2.14 to 2.39 and are as expected for Cu^{II} centres, thereby giving added confidence to the use of this simple magnetic coupling model. Similar fits to the experimental data were also obtained for $J_1 \approx 3$ and $J_2 \approx 10$ cm^{-1} with a lower g-value; these were discounted because the fit at low temperatures (< 50 K) was significantly inferior to that with the values quoted above. Furthermore, the calculated g-values for these curves were lower than expected for spin-orbit coupled Cu(II). The values of J_1 and J_2 in Table 5 are low and this is not unexpected since most of the Cu(II)–Cu(II) couplings occur by a route which involves an axial and an equatorial nitrogen atom and, therefore, is quite long. $[Ni_5(OH)(bta)_5(acac)_4(H_2O)_4]$ [17] has a similar molecular structure to that of the compounds reported herein with bta ligands spanning five of the six edges of a Ni^{II}_4 tetrahedron centred on the fifth Ni^{II}. Magnetic studies have shown that the coupling constants between the Ni^{II} centres at the corners of the tetrahedron (J_2) are $-5\,cm^{-1}$ and $-10.7\,cm^{-1}$; the coupling constant between the central Ni^{II} and the outer Ni^{II} atoms (J_1) is $-6.1\,cm^{-1}$. These values are similar to those reported for the pentanuclear Cu^{II}-bta compounds described herein and indicate that the bta ligand propagates very weak antiferromagnetic exchange.

CONCLUSIONS

The tridentate (μ_3-bridging) bonding motif of bta^- ions is well suited for the formation of a protective monolayer on lightly oxidised copper surfaces. The flexibility in this mode of coordination exhibited within the clusters of **1**, **2**, and **3** is advantageous and would allow benzotriazolate to adapt to the various surface topographies which could well be presented by "real" oxidized copper surfaces.

Acknowledgements—We are grateful for the financial support of The University of Manchester, Zeneca Specialties and The Royal Society. We also thank Professor P. Day of

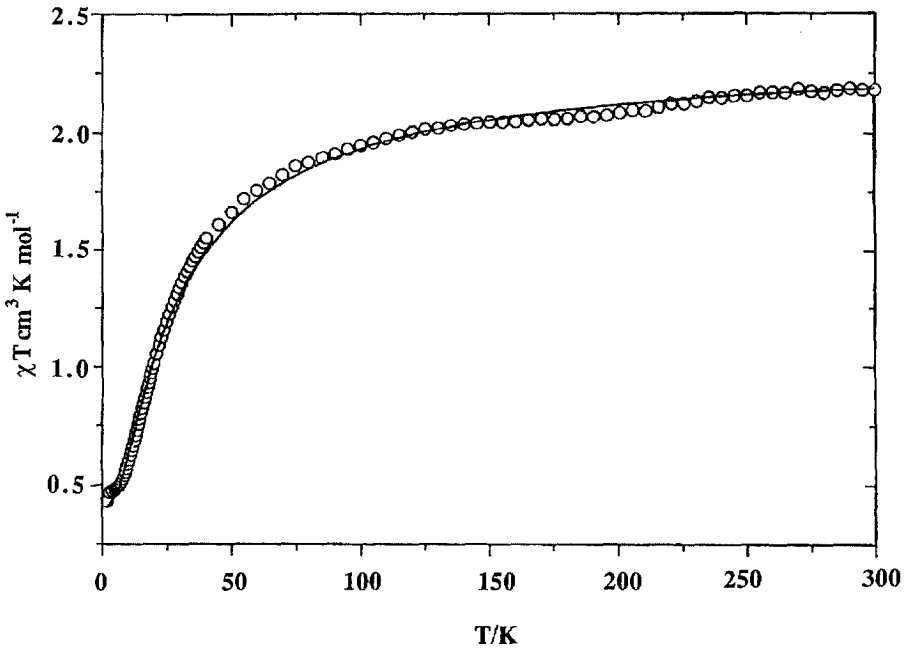

Fig. 6. Plot of $\chi_m T$ versus T over the temperature range 300–2 K for **2**; T is in degrees Kelvin and χ_m is the molar magnetic susceptibility.

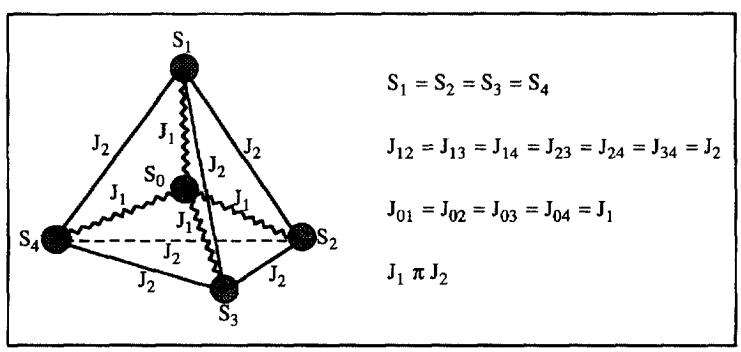

Fig. 7. The tetrahedral configuration of four equivalent spins and an additional central spin with isotropic exchange interactions used to fit the magnetic susceptibility data (see Fig. 6).

the Royal Institution of Great Britain for allowing access to a SQUID magnetometer.

REFERENCES

1. Dugdale, I. and Cotton, J. B., *Corros. Sci.*, 1963, **3,** 69.
2. Chadwick, D. and Hashemi, T., *Corros. Sci.*, 1978, **18,** 39.
3. Marshall, J. H., *Inorg. Chem.*, 1978, **17,** 3711.
4. Handley, J., Collison, D., Garner, C. D., Helliwell, M., Docherty, R., Lawson, J. R. and Tasker, P. A., *Angew. Chem. Int. Ed. Engl.*, 1993, **32,** 1036.
5. Walsh, J. F., PhD Thesis, The University of Manchester, 1995.
6. Fernelius, W. C. and Bryant, B. E., *Inorg. Synth.*, 1957, **5,** 105.
7. Walker, N. and Stuart, D., *DIFABS, Acta. Cryst.*, 1983, **A39,** 158.
8. Sheldrick, G. M., SHELXS-86, Crystallographic Computing 3, Oxford University Press, 1985, 175–189; P. T. Beurskens, DIRDIF, Technical Report 1984/1, Crystallography Laboratory, Toernooiveld, 6525 Ed Nijmegen, Netherlands.

9. teXsan: Crystal structure analysis package, Molecular Structure Corporation, 1985.
10. Nakamoto, K., *Infrared Spectra of Inorganic and Coordination Compounds*, 2nd edn., Wiley-Interscience, New York, 1970, p. 249.
11. Nonnenmacher, G. and Mecke, R., *Spectrochim. Acta.*, 1961, **17,** 1049.
12. Xu, Z., Lau, S. and Bohn, P. W., *Langmuir*, 1993, **9,** 993.
13. Singh, P. R. and Sahai, R., *J. Indian Chem. Soc.*, 1969, **46,** 945.
14. Carlin, R. L., *Magnetochemistry*, Springer–Verlag, 1986.
15. Bürger, K-S., Chaudhuri, P. and Wieghardt, K., *J. Chem. Soc., Dalton Trans.*, 1996, 247.
16. Berlorizky, E. and Fries, P. H., *J. Chim. Phys.*, 1993, **90,** 1077.
17. Bakalbassis, E. G., Diamantopoulou, E., Perlepes, S. P., Raptopoulou, C. P., Tangoulis, V., Terzis, A. and Zafiropoulos, T. F., *J. Chem. Soc., Chem. Commun.*, 1995, 1347.

Pergamon

PII: S0277-5387(98)00025-4

Polyhedron Vol. 17, No. 18, pp. 3047–3051, 1998
© 1998 Elsevier Science Ltd
All rights reserved. Printed in Great Britain
0277-5387/98 $19.00+0.00

Synthesis and structure of bis[2,2′-methylenebis(2,4-di-*t*-butylphenoxo)]niobium chloride

Lee Higham, Mark Thornton-Pett and Manfred Bochmann*

School of Chemistry, University of Leeds, Leeds LS2 9JT, U.K.

(Received 24 October 1997; accepted 5 January 1998)

Abstract—The addition of Li_2MTP [$MTPH_2$ = 2,2′-methylenebis(2,4-di-*t*-butylphenol)] to a suspension of $NbCl_5$ in toluene in either 1 : 1 or 2 : 1 ratios leads to the formation of a red powdery product from which deep red crystalline $NbCl(MTP)_2$ (**1**) can be obtained by sublimation. The structure of **1** was determined by single crystal X-ray diffraction. The compound is monomeric in the solid state, with a trigonal-bipyramidal $NbClO_4$ core and the chloride ligand in an equatorial position. The reaction of **1** with methyllithium affords yellow $NbMe(MTP)_2$. © 1998 Elsevier Science Ltd. All rights reserved

Keywords: aryloxide complex; chelate complex; niobium; alkylation.

Aryloxide ligands of varying degrees of steric hindrance are well known to be able to stabilise early transition metals in a range of oxidation states and ligand environments. Examples include dimeric compounds of the type $Nb_2(OR)_{10}$ (R = Me [1], 4-MeC_6H_4 or 3,5-$Me_2C_6H_3$ [2]), as well as monomeric Nb(V) complexes with bulkier aryl substituents such as R = 2,6-$Me_2C_6H_3$. The niobium and tantalum complexes possess an extensive organometallic chemistry including their application as hydrogenation catalysts [3–5]. Early transition metal complexes with chelating aryloxide ligands are less well investigated but have received attention as alternatives to cyclopentadienyl ligands in homogenous polymerisation catalysts. For example, Miyatake *et al.* [6] reported that TiX_2(TBP) (X = Cl, OPr^i) activated with methylaluminoxane polymerised ethene with good activities. Related titanium and zirconium complexes were reported by Schaverien *et al.* [7] who found moderate polymerisation activity coupled with usually comparatively broad polymer molecular weight distributions. Other examples were provided by Floriani *et al.* [8] and Zubieta *et al.* [9] who isolated complexes such as $TiCl_2$(MMBP) and V(O)Cl (MMBP). A recent more systematic study of TiX_2(O—X—O)/MAO catalysts has highlighted the importance of the nature of X on the performance of such compounds as polymerisation catalysts [10].

As part of our interest in chelating ligands in Cp-free homogeneous alkene polymerisation systems [11] we became interested in the synthesis of complexes of the type (O—O)$NbCl_3$ and (O—O)$_2$NbCl (O—O = chelating bisphenolate). The recent report by Chisholm *et al.* [12] on related titanium, zirconium and tantalum complexes of the $[MMPB]^{2-}$ ligand prompts us to report the reaction of $NbCl_5$ with the chelating phenoxide ligand $[MTP]^{2-}$.

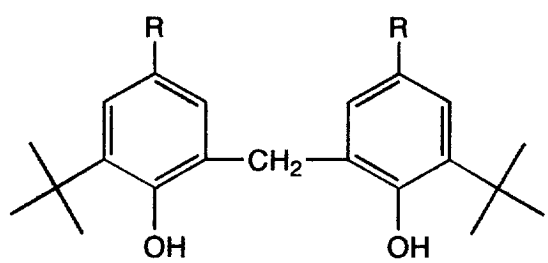

$MMBPH_2$, R = Me

$MTPH_2$, R = CMe_3

* Author to whom correspondence should be addressed.

RESULTS AND DISCUSSION

Syntheses

In an attempt to prepare (MTP)$NbCl_3$, a suspension of $NbCl_5$ in toluene was treated at −78°C with a toluene solution of Li_2[MTP]. A viscous red solution resulted; there was no apparent further change on warming to room temperature. Filtration from precipitated LiCl and evaporation of the solvent left a red powder which, according to ^{1}H NMR data, contained coordinated MTP as well as free $MTPH_2$. Both the complex and the free ligand show similar solubility properties, being very soluble in diethyl ether but sparingly soluble in light petroleum, and efforts to achieved purification by recrystallisation were unsuccessful. Mass spectrometry indicated, however, that in spite of the chosen Nb/MTP ratio of 1:1 a volatile 1:2 complex of composition NbCl(MTP)$_2$ had been formed.

A crystalline product was obtained by the slow sublimation of the crude product through a plug of glass wool at 175 C/0.01 mm Hg. Some $MTPH_2$ sublimed as an off-white band. On raising the temperature to 275 C this was followed by the formation of dark-red crystalline blocks NbCl(MTP)$_2$ (**1**). The same product was obtained from the reaction of $NbCl_5$ and Li_2[MTP] in a 1:2 stoichiometry. Attempts to improve on the synthesis by varying the solvent were not successful. From THF solutions a yellow crystalline product was obtained which rapidly lost solvent of crystallisation and could not be fully characterised.

Compound **1** was characterised by single crystal X-ray diffraction. An ORTEP diagram is shown in Fig. 1. Selected bond distances and angles are collected in Table 1. The complex possesses trigonal-bipyramidal geometry, with an equatorial Cl ligand. Variable temperature NMR data indicate that this structure remains unchanged in solution; no interchange is observed between the diastereotopic hydrogen atoms of the bridging methylene group. In the solid state,

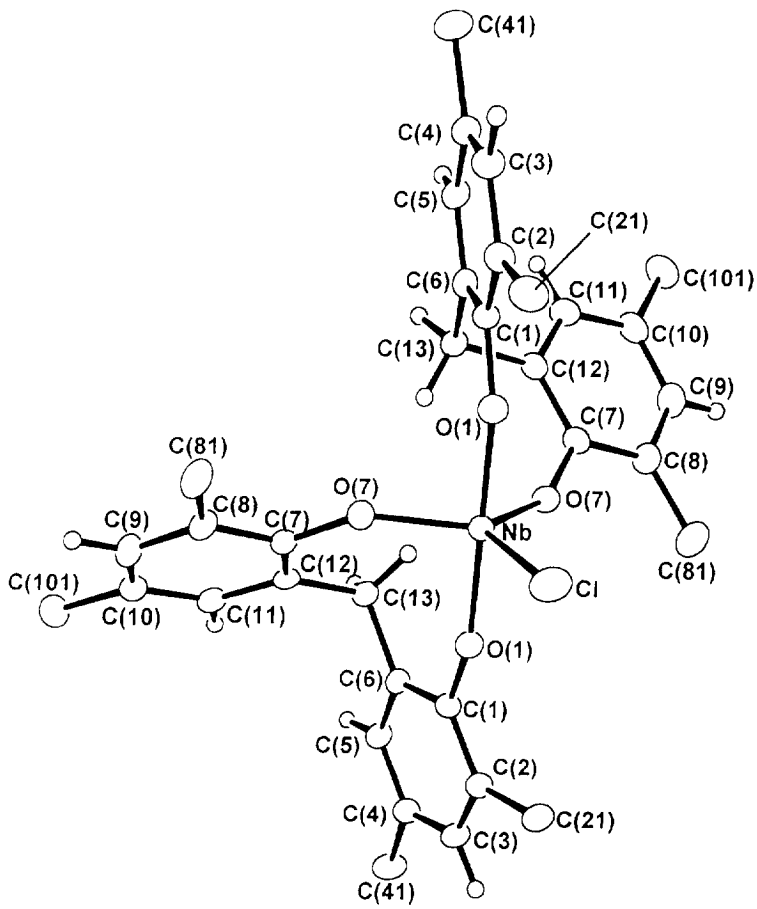

Fig. 1. ORTEP-type [20] diagram of the crystal structure of NbCl(MTP)$_2$. Thermal ellipsoids are shown at the 40% probability level. The molecule possesses crystallographic C_2 symmetry such that the C_2 axis runs along the Nb—Cl bond vector. In the interests of clarity, the methyl groups of the *t*-butyl substituents have been omitted.

Table 1. Selected interatomic distances (Å) and angles between interatomic vectors (°) for $NbCl(MTP)_2$ (**1**)

Nb—O(7)	1.8770(14)	Nb—O(1)	1.897(2)
Nb—Cl	2.3357(9)		
O(1)—C(1)	1.370(3)	C(1)—C(6)	1.399(30
C(1)—C(2)	1.408(3)	C(2)—C(3)	1.392(3)
C(2)—C(21)	1.539(3)	C(3)—C(4)	1.395(3)
C(4)—C(5)	1.393(3)	C(4)—C(41)	1.534(3)
C(5)—C(6)	1.384(3)	C(6)—C(13)	1.520(3)
O(7)—C(7)	1.382(3)	C(7)—C(12)	1.390(3)
C(7)—C(8)	1.409(3)	C(8)—C(9)	1.390(3)
C(8)—C(81)	1.541(3)	C(9)—C(10)	1.395(3)
C(10)—C(11)	1.387(3)	C(10)—C(101)	1.542(3)
C(11)—C(12)	1.393(3)	C(12)—C(13)	1.520(3)
O(7)—Nb—O(7*)	118.30(9)	O(7*)—Nb—O)(1)	89.67(6)
O(7)—Nb—O(1)	90.36(6)	O(1*)—Nb—O(1)	179.93(2)
O(7)—Nb—Cl	120.85(4)	O(1)—Nb—Cl	89.97(4)
C(1)—O(1)—Nb	157.58(13)	C(7)—O(7)—Nb	149.23(13)
O(1)—C(1)—C(6)	117.3(2)	C(7)—C(7)—C(12)	119.8(2)
O(1)—C(1)—C(2)	120.9(2)	O(7)—C(7)—C(8)	118.2(2)
C(5)—C(6)—C(13)	120.1(2)	C(11)—C(12)—C(13)	118.1(2)
C(1)—C(6)—C(13)	120.8(2)	C(7)—C(12)—C(13)	123.6(2)
c(12)—C(13)—C(6)	114.2(2)		

Atoms marked * are related to their unmarked equivalents by the symmetry operator $-x$, y, $1/2+z$.

the (non-bonding) distance between the metal centre and one of these methylene-hydrogens (H13b) is 2.78 Å, while the other (H13b) is more remote, 4.34 Å.

The chloride ligand is in an equatorial position. The Nb—Cl distance of 2.3357(9) Å is slightly longer than the distances to terminal chloride ligands in Nb_2Cl_{10} [2.250(6) and 2.302(5) Å] [13] but significantly shorter than Nb—Cl bond lengths in the octahedral complex. $NbCl_3(OPr^i)_2\{O{=}P(NMe_2)_3\}$ [*trans*: 2.401(4) and 2.415 Å; *cis*: 2.452(3) Å] [14]. The Nb—O distances are typical for terminal alkoxo ligands in 5- and 6-coordinate niobium alkoxides; some comparative values are given in Table 2. Each chelate ring occupies an axial and an equatorial position of the NbO_4Cl core, with O—Nb—O angles of very close to 90° between the axial and equatorial oxygen atoms, while the O(1)—Nb—O(1*) moiety is strictly linear, 179.93(2)°.

In spite of the fact that the chelate rings might be expected to induce some angular distortions, the angles between the equatorial ligand atoms deviate only slightly from the ideal value of 120°, with

Table 2. Nb—O distancesin niobium alkoxides

Compound	Structure	$Nb—O_{eq}$	$Nb—O_{ax}$	Ref.
$Nb_2(OMe)_{10}$	Octahedral	1.880(7).	1.902(5)	[1b]
		1.912(8)	1.903(5)	
$NbCl_3(OPr^i)_2 \cdot OP(NMe_2)_3$	Octahedral	1.801(8)[a]	1.811(6)[b]	[14]
$Nb(OC_6H_3Me_2)_5$	*tbp*	1.890(2)	1.901(2)	[2]
		1.910(2)	1.903(2)	
$[Nb(OC_6H_3Me_2)_6]$	Octahedral		1.95(1) av.	[2]
$Nb^{II}(OC_6H_4Me)_2 \cdot (dmpe)_2$[c]	Octahedral		2.023(3)	[2]
$Nb(=NMe)(OAr)_3 \cdot NHMe_2$[d]	*tbp*	1.940(4)	1.958(4)	[16]
		1.965(5)		

[a] *Trans* to $OP(NMe_2)_3$.
[b] *Trans* to Cl.
[c] dmpe = $Me_2PCH_2CH_2PMe_2$.
[d] Ar = 2,6-$Ph_2C_6H_3$.

O(7)—Nb—O(7*) of 118.30(9)° and O(7)—Nb—Cl of 120.85(4)°. There is therefore no indication for ring strain in the 8-membered chelate rings. The Nb—O—C angles of, on average, 153.4° are significantly larger than tetrahedral, a typical feature in aryloxide complexes of electron deficient metals and are consistent with the partial M—O double bond character in these compounds, although these angles can vary significantly and those found in **1** are substantially larger than corresponding angles in related titanium and zirconium complexes [12].

There are a number of niobium and tantalum complexes with chelating ligands which adopt a similar structure, although in these cases the chelate ring formation is the result of C—H activation of ortho-substituents of the aryl rings. Pertinent examples are the Nb(V) alkyl (C—O)Nb(OAr)$_3$ [C—O = $OC_6H_4CMe_2CH_2-$] [3c] and a series of tantalum compounds such as (C—O)$_2$TaCl [15] and (C—O)$_2$TaMe [3b] (C—O = $-OC_6H_2X-2-Bu^t-6-CMe_2CH_2-$; X = H, Bu^t).

Complex **1** reacts with methyllithium in diethyl ether at −78°C to give (MTP)$_2$NbMe (**2**) as a yellow microcrystalline powder. The compound was characterised spectroscopically, and attempts to obtain X-ray quality crystals were unsuccessful. Characteristic are the set of two doublets for the bridging CH_2 group which are found in the ^{1}H NMR spectrum at δ 3.65 and 4.85, compared to chemical shifts of δ 3.50 and 5.42 in **1**, indicative of a structure very similar to that of **1**. The compound is sensitive to hydrolysis, with the evolution of methane, to give as yet uncharacterised products. Work exploring the reactivity of **1** and **2** is in progress.

CONCLUSION

Chelating aryloxo ligands strongly favour the formation of 2:1 complexes of the type (O—O)$_2$NbX, while 1:1 compounds (O—O)NbX$_3$ could not be isolated. The five-coordinate species strictly adhere to a trigonal-bipyramidal geometry. Fluxional processes which would lead to an interchange of the hydrogen atoms of the methylene groups in the two MTP ligands were not observed.

EXPERIMENTAL

All manipulations were carried out under a dry nitrogen atmosphere using vacuum line techniques. Solvents were dried over sodium (toluene), sodium-potassium alloy [diethyl ether, light petroleum (bp. 40–60°C)] or sodium-benzophenone (THf). Deuterated solvents were degassed by several free-thaw cycles and stored over 4A molecular sieve. NMR spectra were recorded on a Bruker DPX300 instrument. $NbCl_5$ was used as supplied. 2,2′-Methylenebis-(4,6-di-*t*-butylphenol) ($MTPH_2$) was prepared following a literature procedure [17].

Bis[2,2′-*methylenebis*(4,6-*di-t-butylphenoxo*)] *niobium chloride* (**1**).

A solution of $MTPH_2$ (6.86 g, 166 mmol) in toluene (100 cm^3) was cooled to −78°C and treated dropwise with *n*-butyllithium (13 cm^3, 1.6 M, 32 mmol). The solution was allowed to warm to room temperature, stirred for 1 h, and then transferred by cannula into a second flask containing niobium pentachloride (2.2 g, 8 mmol) in toluene (50 cm^3) at −78°C. The mixture turned red and was warmed to room temperature. Stirring was continued for 3 h. A white precipitate of LiCl was allowed to settle, and the somewhat viscous supernatant was filtered off. The filtrate was evaporated to dryness, leaving a dark-red powder, the NMR spectrum of which showed the presence of some free $MTPH_2$. Since both the niobium product and $MTPH_2$ are very soluble in diethylether and light petroleum and no purification could be achieved by recrystallisation, the solid product was transferred to a long sublimation tube, covered with a plug of glass wool and heated in a tube furnace to 175°C under reduced pressure (10^{-2} mm Hg). An off-white band of $MTPH_2$ appeared at the top of the sublimation tube. On raising the temperature to 275°C dark-red prisms of **1** were deposited half-way up the tube; these were collected (2.2 g, 2.27 mmol, 28%). ^{1}H NMR (C_6D_6, 25°C, δ): 7.31 (s, 8 H, Ar), 5.42 (d, 2 H, $^2J_{HH}$ = 14 Hz, CH*H*), 3.50 (d, 2 H, $^2J_{HH}$ = 14 Hz, C*H*H), 1.50 (s, 36 H, CMe_3), 1.30 (s, 36 H, CMe_3). ^{13}C NMR (C_6D_6, 25°C, δ): 158.6 (*ipso*-C), 145.7 (*p*-C), 137.9 (*o*-C), 135.9 (*o*-C), 125.2 (*m*-C), 122.4 (*m*-C), 35.9 (*C*Me$_3$), 35.6 (t, $^1J_{CH}$ = 127 Hz, CH_2), 34.6 (*C*Me$_3$), 31.5 (C*Me*$_3$), 30.4 (C*Me*$_3$). Anal. Found: C, 71.7; H, 8.8; Cl, 3.9. Calc. for $C_{58}H_{84}ClNbO_4$: C, 71.6; H, 8.7; Cl, 3.6%.

Bis[2,2′-*methylenebis*(4,6-*di-t-butylphenoxo*)] *methylniobium* (**2**).

A solution of **1** (0.9 g, 0.92 mmol) in diethylether (20 cm^3) was cooled to −78°C, and methyllithium (0.63 cm^3, 1.6 M, 0.92 mmol) was added via syringe. The reaction was allowed to warm slowly to room temperature. The colour changed from deep red to orange-yellow, and a white precipitate of LiCl formed. The filtrate was evaporated and the residue dissolved in light petroleum, and filtered again,leaving more LiCl. Concentration of the supernatant gave a yellow powder (0.70 g, 0.73 mmol, 88%). ^{1}NMR (C_6D_6, 25°C, δ): 7.34 (s, 8 H, Ar), 4.85 (s, 2 H, CH*H*), 3.65 (s, 2 H, C*H*H), 2.44 (s, 3 H, Nb-CH_3), 1.58 (s, 36 H, CMe_3), 1.32 (s, 36 H, CMe_3). ^{13}C NMR (C_6D_6, 25°C, δ): 157.9 (*ipso*-C), 143.5 (*p*-C), 136.3 (*o*-C), 134.6 (*o*-C), 125.1 (*m*-C), 122.0 (*m*-C), 53.8 (Nb-Me), 38.1 (CH_2), 35.6 (*C*Me$_3$), 34.3 (*C*Me$_3$), 31.8 (C*Me*$_3$), 30.5 (C*Me*$_3$). Anal. Found: C, 72.8; H, 8.6. Calc. for $C_{59}H_{87}O_4Nb$: C, 74.3; H, 9.2%.

X-ray crystallography

All crystallographic measurements were carried out at 160 K on a Stoe STADI4 4-circle diffractometer operating in the ω-θ scan mode using graphite monochromated Cu–K_α radiation ($\lambda = 1.54184$ Å). Cell dimensions were refined from the values of 40 reflections (together with their Friedel opposites) measured at $\pm 2\theta$ in order to minimise systematic error. Crystal data: $C_{58}H_{84}ClNbO_4$, red prism, $0.60 \times 0.44 \times 0.33$ mm, monoclinic, space group $C2/c$, $a = 14.7009(11)$, $b = 15.603(2)$, $c = 24.928(2)$ Å, $\beta = 98.093(8)°$, $Z = 4$, $V = 5661.1(11)$ Å^3. A total of 8915 reflections were measured in the range $3.58 \leqslant \theta \leqslant 64.55$ [$-17 \leqslant h \leqslant 17$, $-18 \leqslant k \leqslant 18$, $-26 \leqslant l \leqslant 28$] of which 4627 were unique ($R_{int} = 0.0402$). Data were corrected for absorption empirically using azimuthal ψ-scans (maximum and minimum transmission factors 0.675 and 0.506 respectively). The structure, which possesses crystallographic C_2 symmetry, was solved by heavy-atom methods using SHELXS-86 [18] and was refined by full-matrix least-squares (against all the unique F^2 data) using SHELXL-93 [19]. Non-hydrogen atoms were refined with anisotropic displacement parameters including those of a *t*-butyl substituent which was disordered over two positions; hydrogen atoms were constrained to idealised positions using a riding model with free rotation for methyl groups and fixed isotropic displacement parameters. Final $wR_2 = \{\Sigma[w(F_o^2 - F_c^2)^2]/\Sigma(F_o^2)^2]\}^{1/2} = 0.0890$, conventional $R = 0.0331$ for F values of 4512 reflections with $F_o^2 > 2\sigma(F_o^2)$. Weighting scheme $w = [\sigma^2(F_o^2) + (0.0409P)^2 + 8.5311P]^{-1}$ where $P = (F_o^2 + 2F_c^2)/3$, goodness of fit = 1.060 for all F^2 values and 334 parameters. Maximum and minimum residual electron density 0.47 and -0.89 eÅ^{-3} respectively.

Crystallographic data (consisting of atomic coordinates and full lists of bond lengths and angles) for the structure reported in this paper has been deposited with the Cambridge Crystallographic Data Centre. Copies of the data can be obtained free of charge on application to The Director, CCDC, 12 Union Road, Cambridge CB2 1EZ, U.K. (fax: Int. code +(1223) 336-033; e-mail: teched@chemcrys.cam.ac.uk).

Acknowledgements—This work was supported by the Engineering and Physical Sciences Research Council. L. H. thanks the University of Leeds for a studentship.

REFERENCES

1. (a) Bradley, D. C. and Holloway, C. E., *J. Chem. Soc., A*, 1968, 219; (b) Pinkerton, A. A., Schwarzenbach, D., Hubert-Pfalzgraf, L. F. and Riess, J. G., *Inorg. Chem.*, 1976, **15,** 1196.
2. Coffindaffer, T. W., Steffey, B. D., Rothwell, I. P., Folting, K., Huffman, J. C., Streib, W. E., *J. Am. Chem. Soc.*, 1989, **111,** 4772.
3. (a) Rothwell, I. P., *Polyhedron*, 1985, **4,** 177; (b) Chamberlain, L. R., Rothwell, I. P. and Huffman, J. C., *J. Am. Chem. Soc.*, 1986, **108,** 1502; (c) Yu, J. S., Fanwick, P. E. and Rothwell, I. P., *J. Am. Chem. Soc.*, 1990, **112,** 8171.
4. Allen, K. D., Bruck, M. A., Gray, S. D., Kingsborough, R. P., Smith, D. A., Weller, K. J. and Wigley, D. E., *Polyhedron*, 1995, **14,** 3315.
5. Rothwell, I. P., *Chem. Commun.*, 1997, 1331, and references therein.
6. Miyatake, T., Mizunuma, K. and Kakugo, M., *Makromol. Chem., Macromol. Symp.*, 1993, **66,** 203.
7. Van der Linden, A., Schaverien, C. J., Meijboom, N., Ganter, C. and Orpen, A. G., *J. Am. Chem. Soc.*, 1995, **117,** 3008.
8. (a) Floriani, C., Corazzo, F., Lesueur, W., Chiesi-Villa, A. and Guastini, C., *Angew. Chem. Int. Ed. Engl.*, 1989, **28,** 66; (b) Corazzo, F., Floriani, C., Chiesi-Villa, A. and Guastini, C., *Inorg. Chem.*, 1991, **30,** 145.
9. Tuscano, P. J., Schemerhorn, E. J., Dettelbacher, C., Macherone, D. and Zubieta, J., *J. Chem. Soc., Chem. Commun.*, 1991, 933.
10. (a) Fokken, S., Spaniol, T. P., Kang, H. C., Massa, W. and Okuda, J., *Organometallics*, 1996, **15,** 5069; (b) Sernetz, F. G., Mülhaupt, R., Fokken, S. and Okuda, J., *Macromolecules*, 1997, **30,** 1562.
11. Male, N. A. H., Thornton-Pett, M. and Bochmann, M., *J. Chem. Soc., Dalton Trans.*, 1997, 2487.
12. Chisholm, M. H., Huang, J. H., Huffman, J. C., Streib, W. E. and Tiedtke, D., *Polyhedron*, 1997, **16,** 2941.
13. Zalkin, A. and Sands, D. E., *Acta Crystallogr.*, 1958, **11,** 615.
14. Hubert-Pfalzgraf, L. G., Pinkerton, A. A. and Riess, J. G., *Inorg. Chem.*, 1978, **17,** 663.
15. Steffey, B. D., Chamberlain, L. R., Chestnut, R. W., Chebi, D. E., Fanwick, P. E. and Rothwell, I. P., *Organometallics*, 1989, **8,** 1419.
16. Chestnut, R. W., Fanwick, P. E. and Rothwell, I. P., *Inorg. Chem.*, 1988, **27,** 752.
17. Odorisio, P. A., Pastor, S. D., Spivack, J. D., Bins, V. and Rodebaugh, R. K., *Phosphorus and Sulfur*, 1984, **19,** 285.
18. Sheldrick, G. M., *Acta Crystallogr., Sect A*, 1990, **46,** 467.
19. Sheldrick, G. M., SHELXL-93, Program for refinement of crystal structures, University of Göttingen, 1993.
20. McArdle, P., *J. Appl. Crystallogr.*, 1995, **28,** 65.

Pergamon

PII: S0277-5387(98)00013-8

Polyhedron Vol. 17, No. 18, pp. 3053–3058, 1998
© 1998 Elsevier Science Ltd
All rights reserved. Printed in Great Britain
0277-5387/98 $19.00+0.00

Mixed-ligand complexes of three valent lanthanide ions with acetylacetone and some organic unsaturated acids

V. T. Panyushkin,* N. V. Achrimenko and A. S. Khachatrian

Department of Chemistry, Kuban State University, Krasnodar 350040, Russia

(Received 24 June 1997; accepted 7 January 1998)

Abstract—The complexation in ternary systems Ln-L-A (Ln—lanthanide ions Ln(III); L—acrylic, methacrylic, maleic acids; A—acetylacetone) have been investigated by pH-potentiometric titration technique and by NMR spectra lineshape analysis on the base of quantum-mechanical formalism of spin density matrix. Stability constants, NMR spectra, paramagnetic shifts, relaxation times and lifetimes of mixed-ligand complexes were determined. General conformities of the complexation according to the lanthanide row were revealed. The dependences of complex compounds stability on the lanthanide ionic radius are explained by joint influence of electrostatic and steric effects. © 1998 Elsevier Science Ltd. All rights reserved

Keywords: mixed-ligand complexes; lanthanide ions; acetylacetone; organic unsaturated acids.

Crystal mixed-ligand complex compounds of lanthanides with acetylacetone and acrylic, methacrylic, maleic and fumaric acids of the composition $LnLA_2 \cdot H_2O$ (Ln(III)—Pr, Nd, Sm, Eu, Tb, Ho, Er, Yb; A—acetylacetone, L—unsaturated acids) have been synthesised earlier [1].

The aim of this work is the investigation of the composition and stability of mixed-ligand lanthanide complexes with acetylacetone and some organic unsaturated acids in aqueous medium by means of potentiometric titration and spectroscopic analysis of NMR line shape. The combination of two above-mentioned methods is interesting as far as NMR method enables us to determine the dynamics of the complexation process which is not available by potentiometric titration. So, having presumed some complexation model in NMR method we can approve the model if the results of two methods are proved to be similar. Moreover, a lot of publications on lanthanides complexation during the past years are focused more on X-ray structures. However, it is obvious that complex forms in solutions may be quite different.

RESULTS AND DISCUSSION

Such mixtures as organic acid—$LnCl_3$; acetylacetone—organic acid; acetylacetone—organic acid—$LnCl_3$ were titrated for determination of mixed-ligand complex stability constants.

The titration curves of ternary systems Ln-L-A (Ln—lanthanide ion Ln(III); L—acrylic, methacrylic, maleic acids; A—acetylacetone) are coincided with the titration curves of binary systems Ln-L at pH ~ 3.5–5.0, that confirms existence of binary lanthanide complexes with organic acids LnL at low pH values. Considerable divergence of titration curves is observed at pH ~ 5–8. The drop of buffer region of titration curves in ternary systems Ln-L-A witnesses the formation of mixed-ligand compounds.

Thus, stepwise rare earth metal complex formation with acetylacetone and unsaturated acids can be described by the following equations (the charges are omitted):

$$Ln + L \rightleftarrows LnL \quad (1)$$

$$LnL + A \rightleftarrows LnLA \quad (2)$$

$$LnLA + A \rightleftarrows LnLA_2 \quad (3)$$

The pH values of hydroxo species indicate the formation of mixed-ligand complex compounds in ternary systems Ln-L-A also (Table 1). It is interesting to note, that pH of the hydroxo species formation is higher in ternary systems than in binary ones. Saturation of lanthanide ions coordination sphere in pres-

* Author to whom correspondence should be addressed.

Table 1. pH values of different complexes formation in the systems Ln-L-A

Complex	pH of complex formation	pH of hydroxocomplex formation
LnA_3	4.0–7.0	7.5–7.7
	Acrylic acid	
LnL	3.5–4.5	6.0–6.5
$LnLA_2$	5.0–7.5	7.8–8.0
	Methacrylic acid	
LnL	3.5–4.5	5.9 6.3
$LnLA_2$	5.0–7.5	7.7–8.0
	Maleic acid	
LnL	4.3–5.2	6.2 6.5
$LnLA_2$	5.5–8.0	>8.0

ence of mixed-ligand complex formation should interfere the formation of hydroxo species [2].

Reagent ratio in initial solutions was maintained constant ($C_{Ln}:C_L:C_A = 1:1:2$) in all studied systems, because the increase of C_L and C_A up to 3 and 5 accordingly did not lead to titration curves shape change.

The usage of diluted solutions prevented the formation of polymeric particles in investigated systems Ln-L-A [2]. The selected reagent ratio also prevented the formation of complexes LnL_2^+ and LnL_3 in given systems.

The ternary systems were also studied by NMR spectra lineshape function analysis [3–5], which based on quantum-mechanical method of spin density matrix [6]. Concentration reagent ranges in NMR investigation were selected by mathematical model on the base of appreciative stability constants values of binary complexes [7]. Reagent ratio was selected so that binary complex formation was enabled to neglect.

In development of spin density matrix formalism for the systems with three-positional ligand exchange, which can be accompanied by mixed-ligand LnLA and $LnLA_2$ complex formation, in work [8] the conditions which enable us to neglect the other complex formation in ternary systems were defined.

The description of NMR signal lineshape of isolated acetylacetone protons, which take place in three positional ligand exchange, must be examined. The condition of free A molecule in solution is described by spin density matrix $\rho^{(1)}$, but internal coordination sphere of paramagnetic ion—by spin density matrixes $\rho^{(2)}$ and $\rho^{(3)}$ in mixed-ligand complexes LnLA and $LnLA_2$ accordingly. We assumed, that spins in each molecule interact to each other inside one molecule only, and the interaction with the other nuclei of surrounding molecules and with paramagnetic centre may be taken into consideration by according relaxation parameters.

Under the assumption complex formation equilibria are given by:

$$\rho^{(2)} \leftarrow \rho^{(1)} \rightarrow \rho^{(3)} \quad \rho^{(1)} \leftarrow \rho^{(2)} \rightarrow \rho^{(3)} \quad \rho^{(1)} \leftarrow \rho^{(3)} \rightarrow \rho^{(2)} \tag{4}$$

The equations of spin density matrix motion in examined systems Ln-L-A in case of three-positional ligand exchange under the stable conditions are given by:

$$\frac{\rho^{(3)}-\rho^{(1)}}{\tau_{13}} + \frac{\rho^{(2)}-\rho^{(1)}}{\tau_{12}} + 2\pi i[\rho^{(1)}, \hat{H}^{(1)}] - \frac{\rho^{(1)}}{T_2^{(1)}} = 0$$

$$\frac{\rho^{(3)}-\rho^{(2)}}{\tau_{23}} + \frac{\rho^{(1)}-\rho^{(2)}}{\tau_{21}} + 2\pi i[\rho^{(2)}, \hat{H}^{(2)}] - \frac{\rho^{(2)}}{T_2^{(2)}} = 0$$

$$\frac{\rho^{(2)}-\rho^{(3)}}{\tau_{32}} + \frac{\rho^{(1)}-\rho^{(3)}}{\tau_{31}} + 2\pi i[\rho^{(3)}, \hat{H}^{(3)}] - \frac{\rho^{(3)}}{T_2^{(3)}} = 0$$

where τ_{ij} is the lifetime of i condition as related to transition to j condition, $T_2^{(i)}$—spin-spin relaxation time of nucleus to i condition.

Acetylacetone NMR signal lineshape in system Ln-L-A can be described by the following equation:

$$S(v) = \mathrm{Im}(P_A\rho_{12}^{(1)} + P_{LnLA}\rho_{12}^{(2)} + 2P_{LnLA_2}\rho_{12}^{(3)}) \tag{5}$$

where P_A, P_{LnLA}, P_{LnLA_2} are molar fractions of the according conditions.

NMR spectra lineshape depends on average lifetime values, as well as the resonance frequencies and relaxation times of examined ligand and complex nucleus. Correlation times τ_{ij} in the pseudo-first order reaction approximation are connected to each other by the equations:

$$\tau_{12}^{-1} = \tau_{21}^{-1} K_{LnLA}^{Ln}[Ln][L]; \quad \tau_{13}^{-1} = \tau_{32}^{-1} K_{LnLA_2}^{LnLA}[LnLA]$$

$$\tau_{23}^{-1} = \tau_{32}^{-1} K_{LnLA_2}^{LnLA}[L]; \quad \tau_{31} = \tau_{32}$$

Thus, the problem of theoretical NMR spectra calculation of acetylacetone, taking part in exchange (4), reduces to the solution of linear equations system with complex coefficients.

Iteration procedure of theoretical NMR spectra to experimental ones allows us to define the set of independent parameters that have influence on spectra shape. They are: NMR signals chemical shifts of acetylacetone methyl-protons (Table 2), relaxation times (Table 3) and stability constants of mixed-ligand complexes (Table 4).

Twenty to twenty five experimental S(v), values were used for optimisation of line shape for each NMR signal. The calculation of stability constants, chemical shifts, lifetimes and relaxation times were carried out by use of the program for theoretical NMR spectra calculation according to Binsch algorithm [6], which was supplied with minimising procedure on

Table 2. NMR paramagnetic shifts (ppm) of acetylacetone methyl protons in LnLA and $LnLA_2$

Ln	Acr LnLA	Acr $LnLA_2$	Met LnLA	Met $LnLA_2$	Mal LnLA	Mal $LnLA_2$
Pr	−2.52±0.13	−2.27±0.11	−3.15±0.09	−2.69±0.11	−2.31±0.10	−2.10±0.08
Nd	−1.14±0.06	−1.03±0.07	−1.37±0.08	−1.24±0.09	−1.02±0.10	−0.95±0.09
Sm	0.13±0.01	0.17±0.02	0.18±0.02	0.25±0.03	0.12±0.02	0.16±0.03
Eu	1.26±0.05	1.41±0.11	1.50±0.07	1.68±0.11	1.13±0.05	1.27±0.06
Gd	0.29±0.02	0.48±0.03	0.36±0.02	0.51±0.02	0.14±0.03	0.37±0.04
Tb	−8.31±0.07	−7.54±0.05	−9.12±0.02	−8.83±0.02	−7.46±0.01	−6.69±0.03
Ho	−4.95±0.08	−4.46±0.09	−5.81±0.05	−5.35±0.04	−4.45±0.09	−4.02±0.08
Er	5.19±0.06	5.81±0.02	6.23±0.04	6.97±0.02	4.68±0.05	5.23±0.04
Yb	4.75±0.03	5.32±0.04	5.62±0.05	5.95±0.06	4.29±0.03	4.77±0.02

Table 3. Relaxation times T_2 ($\times 10^2$) of acetylacetone methyl protons in LnLA and $LnLA_2$

Ln	Acr LnLA	Acr $LnLA_2$	Met LnLA	Met $LnLA_2$	Mal LnLA	Mal $LnLA_2$
Pr	6.56±0.33	6.68±0.32	5.92±0.24	5.94±0.23	6.18±0.25	6.34±0.20
Nd	5.87±0.35	5.95±0.24	4.62±0.23	5.07±0.20	5.49±0.27	5.80±0.23
Sm	5.09±0.33	5.40±0.22	4.38±0.26	4.82±0.28	4.96±0.30	5.26±0.26
Eu	6.03±0.24	6.15±0.18	5.20±0.26	5.67±0.34	5.76±0.35	6.09±0.25
Gd	1.25±0.10	1.93±0.15	1.48±0.12	1.65±0.13	1.09±0.10	1.70±0.13
Tb	3.34±0.17	3.57±0.29	2.64±0.13	2.90±0.23	2.95±0.22	3.01±0.21
Ho	4.01±0.20	4.42±0.22	3.17±0.13	3.23±0.23	3.54±0.25	3.79±0.23
Er	4.12±0.25	4.20±0.21	3.25±0.16	3.38±0.17	3.63±0.18	3.82±0.19
Yb	2.97±0.18	3.27±0.20	2.35±0.17	2.59±0.16	2.61±0.18	2.84±0.14

least squares method. There is good agreement between the calculated lineshapes and the experimental NMR spectra. The error does not exceed 1%.

Obtained values of mixed-ligand lanthanide complexes stability constants by pH-potentiometric titration and NMR data are summarised in Table 4. The accuracy in determination of complex stability constants does not exceed ±0.02–0.19 logarithmic units. Results obtained by both methods coincide with accuracy up to 10%.

The dependencies of mixed-ligand stability constants on lanthanide's ionic radius (r) are presented on Fig. 1. The violation of monotonous change of $\lg\beta$ for mixed-ligand complexes might be due to stereochemical effects, covalent investment, structural changes in compounds along lanthanide row [4]. Slowing-down of increase in stability constants in cerium group at praseodymium–neodymium ($4f^3$–$4f^4$ configurations) and insignificant decrease of stability constants in yttrium group at erbium ($4f^{11}$ configuration) were observed within the general increase in complex stability with the decrease of lanthanide ionic radius. That variation in stability constants of binary and mixed-ligand complexes might be due to tetrad-effect [9,10].

Exceedingly high stability of lanthanide mixed-ligand complexes with maleic acid can be connected with strongly marked "chelate effect", which is due to entropy increase in system at ousting of water molecules by ligand from metal ion coordination sphere. Since maleic acid acts as bidentate ligand in complexes, "chelate effect" is more significant than in the case of monodentate binding acrylic and methacrylic acids. Moreover, the connection between complex stability and acidic properties of ligands (L) in these cases seems to be possible, which are increased as following: methacrylic < acrylic < maleic.

Complex stability of lanthanides with acetylacetone and unsaturated acids is less than stability of rare earth metal acetylacetonates in general. That fact can be connected with electrostatic and statistical effects [9,11].

Such destabilisation is explained by smaller compatibility of different ligands in coordination sphere of lanthanide ion and by lower symmetry of complexes when mixed-ligand compounds formation is taken place.

The diagrams of complex particles distribution as pH changes in ternary systems Ln-L-A, when mixed-ligand complexes were formed, have been plotted with the use of experimental values of complex stability constants.

Table 4. Stability constants of lanthanide mixed ligand complexes with acetylacetone and unsaturated acids

Ln	Ln lgKLnAcr	LnAcr lgKLnAcrA	LnAcrA lgKLnAcrA2	Ln lgKLnMet	LnMet lgKLnMetA	LnMetA lgKLnMetA2	Ln lgKLnMal	LnMal lgKLnMalA	LnMalA lgKLnMalA2
Pr	2.16±0.02	5.19±0.08	3.78±0.07	2.33±0.03	5.17±0.06	3.72±0.06	3.62±0.03	4.42±0.08	3.89±0.04
Nd	2.20±0.04	5.33±0.07	4.04±0.08	2.35±0.02	5.32±0.08	3.86±0.06	3.79±0.06	4.50±0.07	4.17±0.05
Sm	2.23±0.07	5.86±0.04	4.43±0.09	2.40±0.04	5.82±0.06	4.23±0.06	3.83±0.05	5.05±0.08	4.01±0.08
Eu	2.15±0.06	5.75±0.07	4.37±0.03	2.41±0.05	5.67±0.02	3.90±0.09	3.74±0.05	4.96±0.08	4.27±0.09
Gd	2.08±0.03	5.72±0.17	4.33±0.08	2.39±0.03	5.66±0.09	3.87±0.10	3.68±0.04	4.90±0.07	4.06±0.10
Tb	2.06±0.04	5.77±0.16	4.46±0.09	2.35±0.03	5.74±0.08	4.06±0.13	3.64±0.07	5.07±0.06	4.35±0.07
Ho	1.98±0.03	5.92±0.12	4.48±0.06	2.32±0.02	5.89±0.08	4.26±0.09	3.54±0.06	5.16±0.10	4.45±0.07
Er	1.96±0.05	5.89±0.11	4.42±0.09	2.29±0.02	5.89±0.06	4.39±0.09	3.51±0.03	5.11±0.09	4.46±0.09
Yb	2.09±0.06	5.95±0.09	4.53±0.08	2.33±0.04	6.00±0.10	4.52±0.06	3.53±0.03	5.33±0.08	4.35±0.10

The following reactions may be proceeded in examining systems (the charges are omitted):

$$Ln + L \rightleftarrows LnL$$

$$Ln + A \rightleftarrows LnA$$

$$LnA + A \rightleftarrows LnA_2$$

$$LnA_2 + A \rightleftarrows LnA_3$$

$$LnL + A \rightleftarrows LnLA$$

$$LnLA + A \rightleftarrows LnLA_2$$

from which that system of equations can be composed:

$$[LnL] = \beta^{Ln}_{LnL}[Ln][L]$$

$$[LnA] = \beta^{Ln}_{LnA}[Ln][A]$$

$$[LnA_2] = \beta^{Ln}_{LnA_2}[Ln][A]^2$$

$$[LnA_3] = \beta^{Ln}_{LnA_3}[Ln][A]^3$$

$$[LnLA] = \beta^{Ln}_{LnL}K^{LnL}_{LnLA}[Ln][L][A]$$

$$[LnLA_2] = \beta^{Ln}_{LnLA_2}[Ln][L][A]^2$$

$$C_L = [HL] + [L] + [LnL] + [LnLA] + [LnLA_2]$$

$$C_A = [HA] + [A] + [LnA] + 2[LnA_2] + 3[LnA_3] + [LnLA] + 2[LnLA_2]$$

$$C^{Ln} = [Ln] + [LnL] + [LnA] + [LnA_2] + [LnA_3] + [LnLA] + [LnLA_2]$$

The solution of this equation's system was held according to composed program. Plots of complex particles' distribution in ternary system Nd-L-A (L-acrylic acid) are presented in Fig. 2, which show that maintenance of binary acetylacetonates is negligible (<10%). Therefore, competitive reactions of lanthanide acetylacetonates complex formation do not occur actually under chosen experimental conditions ($C^{Ln}:C_L:C_A = 1:1:2$).

EXPERIMENTAL

Initial rare-earth metal chlorides were synthesised according to procedure [12] by dissolving corresponding lanthanide oxides in concentrated hydrochloric acid (P.C.) followed by the water evaporation. The stock solutions of 0.1 M of rare earth metal chlorides were prepared and their metal contents were estimated by complexometric titration with EDTA and xylenol orange as an indicator. Acetylacetone, acrylic, methacrylic acids were refluxed with reflux condenser at vacuum of $2 \cdot 10^3$ Pa. Maleic acid was recrystallised from water solution. All solutions were prepared in double-distilled carbonate free water. The solution of 1 M potassium hydroxide free of carbonates was used as a titrant. An I-130 digital pH-meter with glass elec-

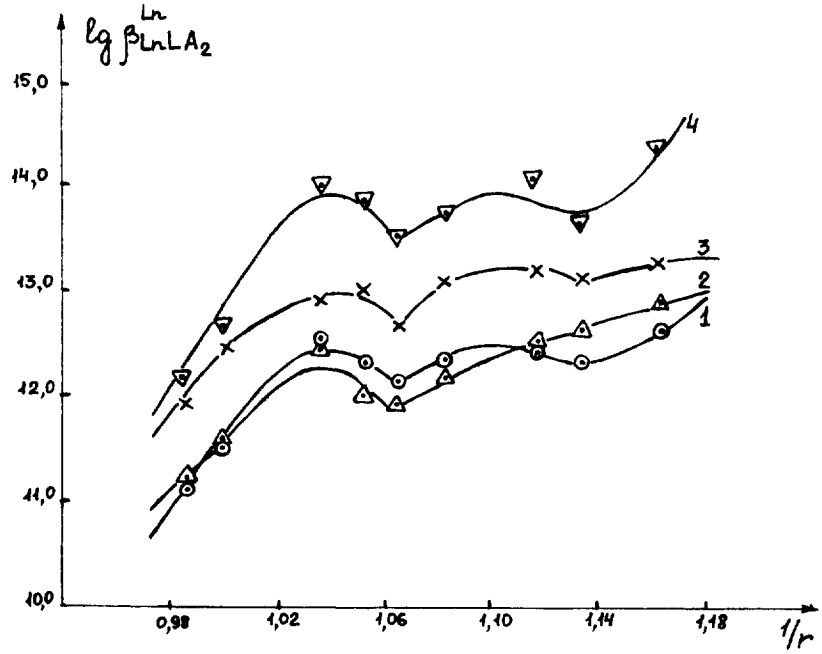

Fig. 1. Dependence of lanthanide mixed ligand complexes stability constants on rare earths ionic radius (1—acrylic, 2—methacrylic, 3—maleic, 4–LnA_3). The r (Ln^{3+}) values were taken from [7].

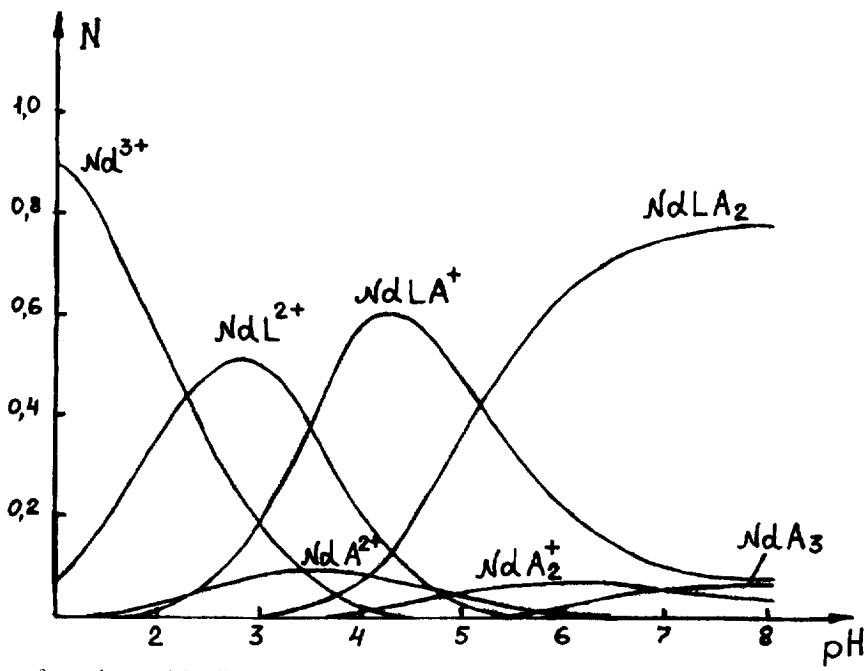

Fig. 2. Diagram of complex particles distribution with pH in ternary system neodimium chloride–acetylacetone–acrylic acid. $C_{Nd}:C_L:C_A = 1:1:2$, N—molar fraction of complexes.

trode and chlorine-silver electrode as comparative electrode were used for pH-titrations with accuracy of measurement ± 0.005 pH units. All pH-measurements of solutions were carried out at 25 ± 0.5° C.

The proton-ligand formation constants of acetylacetone and organic acids were determined by using Irving-Rossotti approach [13,14]. The calculations of rare-earth metal complex stability constants were per-

formed by Bjerrum [15,16] and Irving-Rossotti approach with the help of titration curves of such mixtures: organic acid-$LnCl_3$; acetylacetone-organic acid; acetylacetone-organic acid-$LnCl_3$ with the help of our developed computer program "Complex" with data calculation according to the least squares method.

The NMR spectra were obtained with 300 MHz Unity 300 spectrometer. Complex solutions were prepared in D_2O, TMS was used as an external standard.

REFERENCES

1. Panyushkin, V. T. and Achrimenko, N. V., *J. General Chem. (in Russian)*, 1994, **64**(3), 515.
2. Verma, Sangeeta and Saxena, M. C., *J. Electrochem. Soc. India*, 1990, **39**(2), 75–79.
3. Panyushkin, V. T., Vashyk, A. V. and Shumkin, A. M., *Theoretical and experimental chem. (in Russian)*, 1991, **27**(6), 745.
4. Panyushkin, V. T., Spectrochemistry of coordination compounds of rare-earth elements, (in Russian). Rostov-Don, Rostov University, 1984, 7–23.
5. Panyushkin, V. T., Shumkin, A. M. and Byiklisky, V. D., *Theoretical and experimental chem. (in Russian)*, 1983, **19**(2), 252.
6. Binsch, G. A., *J. Amer. Chem. Soc.*, 1969, **91**(6), 1304.
7. Yotcimirsky, K. B. and Kostromina, N. A., *Chemistry of rare-earth elements compounds (in Russian) Kiev*, 1996, 157–160.
8. Khachatrian, A. S., Vashyk, A. V. and Panyushkin, V. T., *J. General Chem. (in Russian)*, 1995, **65**(7), 1088–1091.
9. Verma, Sangeeta, Saxena, M. C., *Indian J. Chem.*, 1988, **27A,** 1068–1072.
10. Limaye, S. N. and Saxena, M. C., *J. Indian Chem. Soc.*, 1990, **67,** 66–68.
11. Limaye, S. N. and Saxena, M. C., *J. Indian Chem. Soc.*, 1984, **61**(10), 842–846.
12. Serebryannikov, V. V., The syntheses of the rare-earth elements compounds. Tomsk University, Tomsk, 1983.
13. Irving, H. M. and Rossotti, H. S., *J. Chem. Soc.*, 1954, 2904–2910.
14. Chidambaram, M. V. and Bhattacharya, P. K., *J. Inorg. Chem.*, 1970, **32,** 3271–3279.
15. Rossotti, F. and Rossotti, H., The determination of stability constants and other equilibrium constants in solutions. New York, Toronto, London, 1961.
16. Bjerrum, J., Metal Amine Formation in aqueous solutions. Haase, Copenhagen, 1941, Chap. 4.

Pergamon

PII: S0277-5387(98)00061-8

Polyhedron Vol. 17, No. 18, pp. 3059–3070, 1998
© 1998 Elsevier Science Ltd
All rights reserved. Printed in Great Britain
0277-5387/98 $19.00+0.00

Palladium(II) complexes of hybrid phosphine—phosphine oxide ligands

Randy J. Coyle,[a] Yuri L. Slovokhotov,[b]* Mikhail Yu. Antipin[b] and Vladimir V. Grushin[a]†*

[a]Department of Chemistry, Wilfrid Laurier University, Waterloo, Ontario, Canada N2L 3C5

[b]Institute of Organo-Element Compounds, Russian Academy of Sciences, 28 Vavilov St., B-334, Moscow, 117813, Russia

(Received 20 October 1997; accepted 28 January 1998)

Abstract—Complexes of the type $[L_2PdCl_2]$, where L = $Ph_2PCH_2P(O)Ph_2$ (dppmO), $Ph_2P(CH_2)_2P(O)Ph_2$ (dppeO), $Ph_2P(CH_2)_3P(O)Ph_2$ (dpppO), $Ph_2P(CH_2)_4P(O)Ph_2$ (dppbO), and $Ph_2PC_5H_4FeC_5H_4P(O)Ph_2$ (dppfcO), were prepared in high yield from $Na_2[PdCl_4]$ and 2 equiv. of the corresponding L in dichloromethane-methanol. All complexes, except for $[(dppfcO)_2PdCl_2]$, can exist as the *cis* and *trans* isomers, or mixtures of both, with the *cis*/*trans* ratio decreasing in media of low polarity. The ferrocene containing complex, $[(dppfcO)_2PdCl_2]$, appeared to be exclusively *trans* in both the solid state and solution, as established by single crystal X-ray diffraction of its 1 : 3 benzene solvate. The ion exchange extraction of dichloromethane solutions of $[(dppmO)_2PdCl_2]$ and $[(dppeO)_2PdCl_2]$ with aqueous $NaBF_4$ furnished the corresponding cationic *P,O*-chelates, *cis*-$[(dppmO)_2Pd]^{2+}$ $(BF_4^-)_2$ and *cis*-$[(dppeO)_2Pd]^{2+}$ $(BF_4^-)_2$. Alternatively, these cations can be generated by the reaction between the chloro complexes, $[(dppmO)_2PdCl_2]$ and $[(dppeO)_2PdCl_2]$, with Ag^+. Single crystal X-ray diffraction of *cis*-$[(dppeO)_2Pd]^{2+}$ $(BF_4^-)_2$ revealed distinct conformations (a puckered chair and a distorted sofa) for the two chelate rings situated around each Pd atom. A polymeric, poorly soluble material, $\{[(dpppO)_2Pd]^{2+}$ $(BF_4^-)_2\}_n$, was isolated from the reaction between $[(dppO)_2PdCl_2]$ and $AgNO_3$/$NaBF_4$, with both coordinated and free phosphoryl groups being present in the product (IR). In dilute solutions of the $\{[(dpppO)_2Pd]^{2+}$ $(BF_4^-)_2\}_n$, depolymerization occurred, giving rise to the monomeric cationic chelate, *cis*-$[(dpppO)_2Pd]^{2+}$ $(BF_4^-)_2$. © 1998 Published by Elsevier Science Ltd. All rights reserved

Keywords: bis-phosphine mono-oxides; palladium; chelates.

The coordination chemistry of bis-phosphine monoxides (BPMOs) of the general formula R_2P-X-$P(O)R_2$, where *X* = any divalent group, e.g. $(CH_2)_n$, is still insufficiently explored. Although some BPMO complexes with various metals have been reported [1–15], very little is known about palladium derivatives of BPMOs. Only two BPMO complexes of Pd have been described in the literature. One of them, $[(dppeO)_2PdCl_2]$ (dppeO = $Ph_2P(CH_2)_2P(O)Ph_2$), has been successfully used in catalyst [10]. However, no experimental procedure for the synthesis of this complex has been communicated. The other complex, $[(dppmO)_2PdCl_2]$ (dppmO = $Ph_2PCH_2P(O)Ph_2$), has been reported [6,13] but not characterized by any spectral or structural means. It is worth noting that studying solution behavior of such complexes is important because of their intriguing catalytic activity [10] and potential use in synthesis [13]. In the present paper we report, for the first time, the detailed preparation, full characterization, and some chemical reactions of a series of palladium complexes containing monoxides of bis(diphenylphosphino)methane (dppmO), 1,2-bis(diphenylphosphino)ethane (dppeO), 1,3-bis(diphenylphosphino)propane (dpppO), 1,4-bis(diphenylphosphino)butane (dppbO), and 1,1′-bis(diphenylphosphino)ferrocene (dppfcO).

* To whom correspondence should be addressed.
† Present address: E. I. Du Pont de Nemours and Co. Inc., Central Research and Development E328/306, Experimental Station, Wilmington, Delaware 19880-0328, U.S.A.

RESULTS AND DISCUSSION

Synthesis of $[L_2PdCl_2]$ (L = dppmO, dppeO, dpppO, dppbO, *and* dppfcO)

Adding methanolic $Na_2[PdCl_4]$ to a dichloromethane solution of a BPMO, L, (ca 2.1 equiv.) resulted in the formation of the corresponding $[L_2PdCl_2]$ in nearly quantitative yield (eqn (1)). The isolation and purification (if necessary) of the complexes is described in the Experimental Section.

$$Na_2[PdCl_4] + 2L \longrightarrow [L_2PdCl_2] + 2NaCl \quad (94\text{-}99\%) \quad (1)$$

All five compounds are stable crystalline solids which can be stored at room temperature in air for months with no sign of decomposition. All of them are soluble in dichloromethane and chloroform, slightly soluble in benzene, and insoluble in ether and alkanes. The complexes of dppmO and dppeO are soluble in methanol, whereas those containing dpppO and dppbO are only sparingly soluble in this solvent. The dppfcO complex was found to be insoluble in alcohols.

Solution behavior of $[L_2PdCl_2]$ (L = dppmO, dppeO, dpppO, dppbO, *and* dppfcO)

Like many square-planar Pd^{II} compounds of the general formula $[L_2PdCl_2]$ [16], complexes with L = dppmO, dppeO, dpppO, and dppbO exist in solution as mixtures of *cis* and *trans* isomers (eqn (2), Table 1). At room temperature, the isomers seem to equilibrate much more readily (seconds) than their monodentate tertiary phosphine counterparts. This remarkably facile *cis–trans* isomerization is likely due to the presence of the phosphoryl groups, whose oxygen atoms are capable of intramolecularly coordinating to the metal center. Clearly, this effect is similar to the free-ligand catalysis in the *cis–trans* isomerization reactions of Pd(II) and Pt(II) complexes [16]. As described below, firm evidence was obtained for such weak and reversible Pd—O interactions.

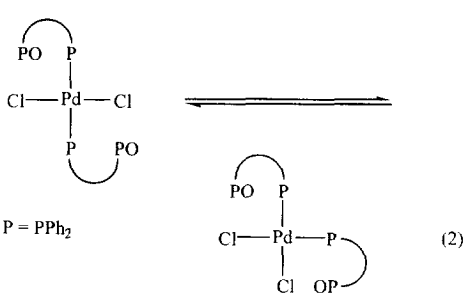

(2)

Structures of the isomers and their distribution in various solvents were studied by ^1H and ^{31}P NMR techniques. To assure reliable ^{31}P NMR integration measurements, the spectra of the first few samples were run with delay times D_1 = 1, 3, and 5 s. Since no changes in the integration ratios were noticed, the rest of the spectra were obtained with D_1 = 1 s. As anticipated [16], the *cis/trans* ratio for the equilibrated mixtures increased with solvent polarity (see Table 1).

$[(dppmO)_2PdCl_2]$. No NMR spectral characterization of this complex has appeared in the literature. According to our ^{31}P NMR data (Table 1), $[(dppmO)_2PdCl_2]$ in benzene is exclusively *trans*, whereas in methanol it is mostly *cis*, with the *cis–trans* ratio being 95 : 5. The resonances of both isomers are clearly seen in the ^{31}P NMR spectra obtained in CH_2Cl_2 and $CHCl_3$, solvents of intermediate polarity in comparison with benzene and MeOH. The small ^{31}P–^{31}P coupling constants did not allow us to immediately assign the observed resonances to the corresponding isomers. However, the proper assignment of the lines is easily made by comparison of the spectra of $[(dppmO)_2PdCl_2]$ with those of its dppeO analogue (see Table 1 and text below). In line with this assignment of the ^{31}P resonances are the patterns observed in the ^1H NMR spectra of the dppmO complex. The ^1H NMR spectrum of the $[(dppmO)_2PdCl_2]$ in $CDCl_3$, where the complex is 90% *trans* according to the ^{31}P NMR data, contains a doublet of virtual triplets ($J_{P\,H}$ = 11.4 Hz; $^2J_{P\,H}+{}^4J_{P\,H}$ = 7.4 Hz) at 3.9 ppm and a shoulder at 3.8 ppm due to the minor amount of the *cis* isomer. In methanol-d_4, the *cis* geometry prevails (ca 95%) and the resonance from the methylene protons appears at 4.3 ppm as a doublet of doublets with $J_{P\,H}$ = 13.5 and 10.5 Hz. This pattern was observed only for the freshly prepared sample, since the acidic CH_2 protons of the complex were found to undergo facile H/D exchange with the CD_3OD solvent. As a result, the methylene resonance soon began to diminish in intensity while transforming into a complex multiplet, and eventually disappeared altogether after a few days. As the H/D exchange occurred, a number of isotopomers (30.3–30.9 ppm) of varying intensities were observed for the P—Pd resonance in the ^{31}P NMR spectrum, due to the molecules containing the CH_2, CHD, and CD_2 groups.

$[(dppeO)_2PdCl_2]$. The ^{31}P NMR spectrum of a solid formulated as $[(dppeO)_2PdCl_2]\cdot 2H_2O$ was reported [3] to exhibit one singlet at 34.45 ppm. In another paper [10], two resonances (20.14 and 33.09 ppm) were observed in the ^{31}P NMR spectrum of $[(dppeO)_2PdCl_2]$ in chloroform-*d*, but no information was provided on the multiplicity of these signals. We found that solutions of $[(dppeO)_2PdCl_2]$ in chloroform-*d* contain both the *cis* and *trans* isomers, as can be clearly seen from the ^{31}P NMR spectrum. The *trans* isomer exhibits a doublet of doublets at 19.9 ppm for the P atom coordinated to the metal with $^3J_{P\,P}$ = 28.4 Hz and $^5J_{P\,P}$ = 25.9 Hz, and a virtual triplet at 33.2 ppm for the phosphoryl group with $^3J_{P\,P}+{}^5J_{P\,P}$ = 54.0 Hz. This spectral pattern exhibiting the remarkable long-range coupling is perfectly consistent with the *trans* geometry. Two doublets at 30.4 and 32.8 ppm ($J_{P\,P}$ = 56.1 Hz) were also found in the spectrum, obviously due to the *cis* isomer. Essentially the same pattern was observed for solutions of [(dppe-

Table 1. ^{31}P NMR data for palladium complexes of the type $[L_2PdCl_2]$ in different solvents

L	Solvent	Geometry	^{31}P NMR, δ P—Pd	P=O	*trans* : *cis*
dppmO	Benzene	*trans*	11.8	26.6	100 : 0
		cis	None	None	
	Chloroform	*trans*	11.8	24.4	90 : 10
		cis	22.5	24.9	
	Dichloromethane	*trans*	11.8	24.2	65 : 35
		cis	21.5	25.0	
	Methanol	*trans*	12.0	44.1	5 : 95
		cis	30.6	44.1	
dppeO	Benzene	*trans*	19.9	29.7	100 : 0
		cis	None	None	
	Chloroform	*trans*	19.9	33.2	85 : 15
		cis	30.4	32.8	
	Dichloromethane	*trans*	19.7	31.5	85 : 15
		cis	29.3	31.2	
	Methanol	*trans*	20.3	37.5	60 : 40
		cis	31.0	38.0	
dpppO	Benzene	*trans*	Insoluble		—
		cis	in benzene		
	Chloroform	*trans*	16.3	32.2	85 : 15
		cis	30.7	32.4	
	Dichloromethane	*trans*	16.2	30.8	80 : 20
		cis	28.5	30.7	
	Methanol	*trans*	16.9	37.6	55 : 45
		cis	30.7	38.0	
dppbO	Benzene	*trans*	16.8	28.4	100 : 0
		cis	None	None	
	Chloroform	*trans*	16.7	32.5	85 : 15
		cis	28.4	32.2	
	Dichloromethane	*trans*	16.7	30.9	80 : 20
		cis	27.6	30.9	
	Chloroform/methanol 1 : 10	*trans*	17.8	37.2	45 : 55
		cis	29.6	37.5	
dppfcO	Benzene	*trans*	15.2	25.5	—
		cis	None	None	
	Chloroform	*trans*	15.1	28.4	—
		cis	None	None	
	Dichloromethane	*trans*	15.3	27.4	—
		cis	None	None	
	Methanol	*trans*	Insoluble		—
		cis	in methanol		

$O)_2PdCl_2]$ in dichloromethane. It is worth noting that the coupling constant measured for the *cis* isomer is close to the values of 47.3–48.1 Hz obtained for the free ligand [17]. As anticipated, only the *trans* isomer was found in benzene solutions of the complex, whereas both the *cis* and *trans* isomers were present when methanol was used as the solvent (Table 1). The portionwise addition of water to the methanol solution lead to a noticeable increase in the *cis–trans* ratio.

$[(dpppO)_2PdCl_2]$ *and* $[(dppbO)_2PdCl_2]$. As the number of methylene groups separating the P^{III} and P^{V} atoms increases, the spectral behavior of the corresponding Pd complexes becomes less distinct. In fact, the ^{31}P NMR spectral patterns for the $[(dpppO)_2PdCl_2]$ and $[(dppbO)_2PdCl_2]$ are very similar, displaying almost identical parameters (Table 1). The chemical shift values provide information for the easy and unambiguous assignment of the resonances. Because of poor solubility no ^{31}P NMR spectra were obtained for solutions of $[(dpppO)_2PdCl_2]$ in benzene and $[(dppO)_2PdCl_2]$ in methanol. However, both isomers of $[(dppbO)_2PdCl_2]$ in approximately equal quantities were observed in a 1 : 10 chloroform–methanol solution of the complex.

$[(dppfcO)_2PdCl_2]$. Like the two preceding complexes, $[(dppfcO)_2PdCl_2]$ is a new compound. The ^{31}P NMR spectra of this complex suggest that in

benzene, chloroform, and dichloromethane it exists as only one isomer. In line with this is the ^{1}H NMR spectrum of the complex (see Experimental Section). Virtual insolubility of the $[(dppfcO)_2PdCl_2]$ in polar media, methanol included, prevented its characterization by NMR in such solvents.

As clearly seen from the above data, for the complexes $[L_2PdCl_2]$, where L = dppmO, dppeO, dpppO, and dppbO, the existence of both *cis* and *trans* isomers was reliably established by ^{31}P and ^{1}H NMR techniques. This was not the case, however, with the dppfcO complex, for which only one isomer was found to exist in various solvents. Due to the steric bulk of dppfcO ligand the *trans* geometry for the $[(dppfcO)_2PdCl_2]$ seemed to be more plausible. This conjecture was examined by X-ray analysis of the compound.

Single crystal X-ray diffraction study of $[(dppfcO)_2PdCl_2]$

As a new compound [18], the dppfcO ligand has been characterized by elemental analysis and NMR spectral data [19]. Although we had attempted a single crystal X-ray diffraction study of dppfcO twice, crystallographic disorder did not allow us to obtain accurate molecular parameters of the ligand. X-ray quality crystals of $[(dppfcO)_2PdCl_2]$ were obtained by diluting its saturated dichloromethane solution with benzene which caused slow precipitation of the complex as a 1 : 3 benzene solvate. Crystallographic parameters, data collection, and structure refinement summary are presented in Table 2. Table 3 lists the most important bond lengths and bond angles for the complex. As anticipated, the complex has a centrosymmetric *trans*-structure (Fig. 1) with almost ideal square-planar configuration around the Pd atom. One of the solvate benzene molecules occupies a general position in the crystal, whereas the second one lies on the center of symmetry. Both disubstituted ferrocene units possess slightly twisted conformation, often called "skew rings", which is dictated by steric requirements of diphenylphosphino and diphenylphosphoryl groups. The pseudo torsion angle P(1)–ring 1(center)–ring 2(center)–P(2) is equal to 133.7 , whereas at the ideal eclipsed conformation of the rings in ferrocene this angle is 144 . Both P(1) and P(2) slightly deviate from the mean planes of the corresponding 5-membered rings by 0.036 and 0.022 Å, respectively. The interplanar angle between the rings is 4.1 .

Although the dppfcO ligand is certainly bulkier than dppeO or PPh_3, the Pd—Cl and the Pd—P bond distances in $[(dppfcO)_2PdCl_2]$ are only slightly longer than those of *trans*-$[(dppeO)_2PdCl_2]$[11] and *trans*-$[(Ph_3P)_2PdCl_2$ [21,22]. Thus, the Pd—Cl bond length of 2.306 (1) Å was found in $[(dppfcO)_2PdCl_2]$, whereas the values of 2.292(1) Å [11] and 2.281–2.296(1) [21,22] have been reported for the dppeO [11] and triphenylphosphine [21,22] counterparts. The Pd—P bond in the dppfcO complex (2.347(1) Å) is ca 0.01 and 0.02 Å longer than those in the *trans*-$[L_2PdCl_2]$, where L = PPh_3 [21,22] and dppeO [11], respectively. This elongation may be due to the presence of the electron-rich, bulky ferrocene substituents on the coordinated phosphorus atoms. Among other features of the molecular geometry of the $[(dppfcO)_2PdCl_2] \cdot 3C_6H_6$ it is worth noting the small difference between the C—P (phosphine) and C—P (phosphoryl) bond lengths of 1.804–1.837(5) and 1.795–1.815(5) Å, respectively. No shortened intramolecular or intermolecular contacts were found in the structure of the complex.

Cationic palladium bis-chelates, $[(BPMO)_2Pd]^{2+}$

The literature [10–12] data and the data described above provide no firm evidence for any coordination of the phosphoryl group oxygen atoms to the metal center in complexes of the general formula $[(BPMO)_2PdCl_2]$ in the solid state or in solution. It was proposed [10] that such interactions between the phosphoryl oxygen atoms and the metal center might be responsible for the unique regioselectivity observed in the hydroxycarbonylation reaction of olefins catalyzed by $[(dppeO)_2PdCl_2]$. Higgins, Shaw, and Taylor [6] demonstrated that $[(dppmO)_2PdCl_2]$ can be forced to lose the chloro ligands when treated with 2 equiv. of $AgNO_3$. According to their ^{31}P NMR data, the resulting cationic complex, $[(dppmO)_2Pd]^{2+}$, is a *cis*-chelate with both oxygens of the phosphoryl groups coordinated to the metal [6]. Because of the ability of Ag^+ to trap Cl^- efficiently this result should not be regarded as evidence for the existence of equilibrium 3, either.

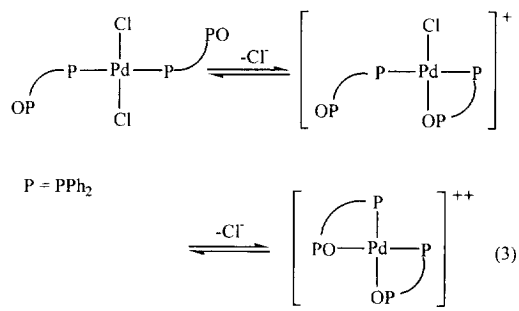

(3)

First evidence for equilibrium 3 was found in our work. Washing a dichloromethane solution of $[(dppmO)_2PdCl_2]$ with a few portions of 40% aqueous $NaBF_4$ at room temperature lead to the quantitative (^{31}P NMR) formation of $[(dppmO)_2Pd]$ $(BF_4)_2$ which was subsequently isolated in 74% yield. The ^{31}P NMR characterises of this complex were identical to those described for the cationic species obtained by the reaction between $[(dppmO)_2PdCl_2]$ and $AgNO_3$ [6]. The synthesis of $[(dppeO)_2Pd]$ $(BF_4)_2$ from the corresponding neutral dichloride and $NaBF_4$ was carried out in the same manner, furnishing the cationic complex in 96% isolated yield (eqn (4)).

Table 2. Crystallographic data for $[(dppfcO)_2PdCl_2]\cdot 3C_6H_6$ and $[(dppeO)_2Pd](BF_4)_2$

	$[(dppfcO)_2PdCl_2]\cdot 3C_6H_6$	$[(dppeO)_2Pd](BF_4)_2$
Empirical formula	$C_{86}H_{74}Cl_2Fe_2O_2P_4Pd$	$C_{52}H_{48}B_2F_8O_2P_4Pd$
Formula weight	1552.3	1108.8
Temperature (K)	153(2)	293(2)
Wavelength (Å)	0.71073	0.71073
Crystal system	monoclinic	monoclinic
Space group	$P = 2_1/c$	$P2_1/c$
a (Å)	13.710(3)	19.187(8)
b (Å)	10.566(2)	13.549(5)
c (Å)	25.170(6)	20.125(8)
β (°)	95.29(2)	93.72(5)
Z	2	4
V (Å^3)	3630(1)	5221(4)
D_{calcd} (g/cm^3)	1.420	1.411
Absorption coefficient	0.85 min^{-1}	0.545 mm^{-1}
$F(000)$	1596	2256
Crystal size (mm)	$0.4\times0.3\times0.2$	$0.3\times0.2\times0.2$
Θ range (°)	2.09–25.9	4.0–21.9
Reflections collected	6728	5878
Independent reflections	6420 ($R_{int} = 0.056$)	5668 ($R_{int} = 0.121$)
Refinement method	Full-matrix L.S. on F^2	Full-matrix L.S. on F^2
Data/restrains/parameters	6389/0/439	5076/0/620
Goodness of fit on F^2	1.061	1.146
Final R indices ($I>2\sigma(I)$)	$R_1 = 0.051$; $wR_2 = 0.097$	$R_1 = 0.118$; $wR_2 = 0.263$

Table 3. Selected bond lengths (Å) and angles (°) in the crystal structure of $[(dppfcO)_2PdCl_2]\cdot 3C_6H_6$

Pd(1)—Cl(1)	2.306(1)	Pd(1)—P(1)	2.347(1)
Fe(1)—C(1)	2.044(5)	Fe(1)—C(2)	2.051(5)
Fe(1)—C(3)	2.060(5)	Fe(1)—C(4)	2.061(5)
Fe(1)—C(5)	2.033(5)	Fe(1)—C(6)	2.069(5)
Fe(1)—C(7)	2.046(5)	Fe(1)—C(8)	2.041(4)
Fe(1)—C(9)	2.027(5)	Fe(1)—C(10)	2.057(5)
P(1)—C(1)	1.804(5)	P(1)—C(11)	1.822(5)
P(1)—C(17)	1.837(5)	P(2)—O(1)	1.487(3)
P(2)—C(8)	1.795(5)	P(2)—C(23)	1.815(5)
P(2)—C(29)	1.807(5)	C(1)—C(2)	1.439(6)
C(1)—C(5)	1.446(7)	C(2)—C(3)	1.412(7)
C(3)—C(4)	1.419(7)	C(4)—C(5)	1.426(7)
C(6)—C(7)	1.431(7)	C(6)—C(10)	1.411(7)
C(7)—C(8)	1.443(7)	C(8)—C(9)	1.431(6)
C(9)—C(10)	1.418(6)		
Cl(1)—Pd(1)—P(1)	93.17(5)	Cl(1)—Pd(1)—P(1)	86.83(5)
C(1)—P(1)—C(11)	105.8(2)	C(1)—P(1)—C(17)	101.2(2)
C(11)—P(1)—C(17)	103.5(2)	C(1)—P(1)—Pd(1)	115.8(2)
C(11)—P(1)—Pd(1)	106.3(2)	C(17)—P(1)—Pd(1)	122.5(2)
O(1)—P(2)—C(8)	116.0(2)	O(1)—P(2)—C(29)	113.2(2)
C(8)—P(2)—C(29)	103.9(2)	O(1)—P(2)—C(23)	110.8(2)
C(8)—P(2)—C(23)	104.5(2)	C(29)—P(2)—C(23)	107.7(2)
C(2)—C(1)—C(5)	107.3(4)	C(2)—C(1)—P(1)	126.2(4)
C(5)—C(1)—P(1)	126.4(4)	C(3)—C(2)—C(1)	107.6(4)
C(2)—C(3)—C(4)	109.4(4)	C(3)—C(4)—C(5)	107.7(4)
C(4)—C(5)—C(1)	107.8(4)	C(10)—C(6)—C(7)	107.9(4)
C(6)—C(7)—C(8)	107.7(4)	C(9)—C(8)—C(7)	107.3(4)
C(9)—C(8)—P(2)	126.9(4)	C(7)—C(8)—P(2)	125.8(4)
C(10)—C(9)—C(8)	108.0(4)	C(6)—C(10)—C(9)	109.1(4)

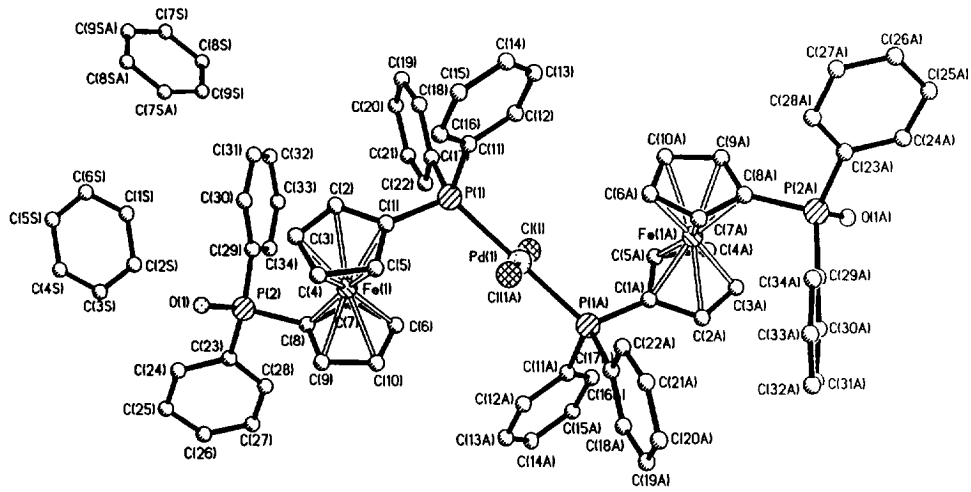

Fig. 1. Molecular structure of *trans*-$[(dppfcO)_2PdCl_2]$ with adopted numbering scheme. Hydrogen atoms are omitted for clarity.

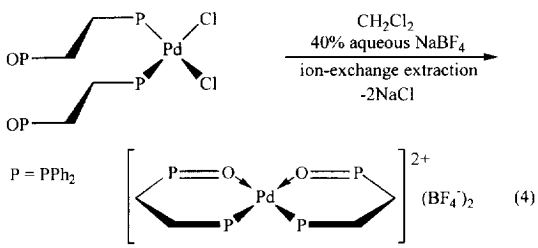

Both tetrafluoroborates, $[(dppeO)_2Pd]$ $(BF_4)_2$ and $[(dppmO)_2Pd]$ $(BF_4)_2$, are air-stable crystalline compounds soluble in dichloromethane and acetone, slightly soluble in chloroform, but insoluble in water, ether, and hydrocarbon solvents. Taking into account the poor affinity of the tetrafluoroborate anion for palladium(II) [23], it is reasonable to conclude that an intramolecular replacement of the chloro ligands by an oxygen of the coordinated BPMO takes place, followed by Cl^-/BF_4^- ion exchange.

The structure of the cationic bis-chelate, $[(dppeO)_2Pd]$ $(BF_4)_2$, was established by a single crystal X-ray diffraction study. Selected crystallographic data obtained, including experimental and structure refinement details, are given in Table 2. Some molecular geometry parameters are summarized in Table 4 and a general view of the dication is presented in Fig. 2. Although crystal disorder of the BF_4 anions and the single crystal's insufficient quality lowered accuracy of the structural results, the *cis* structure of the cation, $[(dppeO)_2Pd]^{2+}$, in the solid state was established beyond any doubt. The Pd atom and the four atoms constituting the first coordination sphere (P(1), P(2), O(1), and O(2)) are coplanar within 0.018 Å. However, a noticeable distortion from the ideal square-planar configuration is observed in the crystal structure, the O—Pd—O and P—Pd—P bond angles being 84.4(4)° and 97.3(2)°, respectively. It is remarkable that the two six-membered metallacycles appear to be in different conformations in the crystal state. For the PdP(1)C(49,50)P(2)O(1) ring a puckered chair conformation was established; the metal, oxygen, and both carbon atoms were coplanar within 0.011 Å, whereas P(1) and P(2) deviated from the plane by +0.84 and −0.70 Å, respectively. A distorted sofa conformation was observed for the other ring, PdP(3)C(51,52)P(4)O(2), with C(51) deviating by 0.77 Å from the mean plane formed by the other five atoms which are coplanar within 0.06 Å. It is worth noting the significant difference in the Pd—O—P bond angles, 124.1(6)° for Pd—O(1)—P(2) and 143.9(6)° for Pd—O(2)—P(4). Interestingly, the Pd—O bond distances (2.088(12) and 2.119(10) Å) are either comparable with or substantially shorter than the values reported for the Pd—O bond lengths in various palladium complexes containing hydroxo (2.07–2.28 Å) [24] and carboxylato (2.12–2.17 Å) [25] ligands. This suggests that the Pd—O coordination bonds are of considerable strength, despite the fact that they are *trans* to phosphine ligand whose *trans*-influence is normally significant. The Pd—P bond distances (2.240(4) and 2.247(5) Å) in the chelate are similar to those in *cis*-$[(dmpmO)_2PdCl_2]$ (2.254(1) and 2.248(1) Å) [12] but shorter by 0.08–0.09 Å than the Pd—P bond length in *trans*-$[(dppeO)_2PdCl_2]$ (2.327(1) Å) [11]. The Pd—P and Pd—O bond lengths measured suggest that the dication $[(dppeO)_2Pd]^{2+}$ is remarkably stable.

Among other structural characteristics of the chelate are shortened (3.27–3.28 Å) intramolecular C···C contacts due to the stacking interaction between the almost parallel C(1)—C(6) and C(31)—C(36) phenyl rings. Also, strong distortions are observed in the tetrahedral environment of P(1) and P(3), due to steric hindrance. Thus, Pd—P(1)—C(1) and Pd—P(3)—

Table .. Selected bond lengths (Å) and angles (°) in the crystal structure of $[(dppeO)_2Pd]\ (BF_4^-)_2$

Pd—O(2)	2.088(12)	Pd—O(1)	2.119(10)
Pd—P(3)	2.240(4)	Pd—P(1)	2.247(5)
P(1)—C(7)	1.79(2)	P(1)—C(1)	1.79(2)
P(1)—C(49)	1.86(2)	P(2)—O(1)	1.509(11)
P(2)—C(50)	1.77(2)	P(2)—C(13)	1.79(2)
P(2)—C(19)	1.83(2)	P(3)—C(51)	1.80(2)
P(3)—C(25)	1.81(2)	P(3)—C(31)	1.86(2)
P(4)—O(2)	1.537(12)	P(4)—C(37)	1.77(2)
P(4)—C(43)	1.80(2)	P(4)—C(52)	1.81(2)
C(49)—C(50)	1.53(2)	C(51)—C(52)	1.55(3)
O(2)—Pd—O(1)	84.4(4)	O(2)—Pd—P(3)	88.8(3)
O(1)—Pd—P(3)	173.1(3)	O(2)—Pd—P(1)	173.8(3)
O(1)—Pd—P(1)	89.6(3)	P(3)—Pd—P(1)	97.3(2)
C(7)—P(1)—C(1)	109.1(8)	C(7)—P(1)—C(49)	105.7(8)
C(1)—P(1)—C(49)	98.1(8)	C(7)—P(1)—Pd	108.9(6)
C(1)—P(1)—Pd	122.7(6)	C(49)—P(1)—Pd	110.9(6)
O(1)—P(2)—C(50)	112.1(7)	O(1)—P(2)—C(13)	110.6(7)
C(50)—P(2)—C(13)	108.2(9)	O(1)—P(2)—C(19)	109.3(7)
C(50)—P(2)—C(19)	109.4(9)	C(13)—P(2)—C(19)	107.1(8)
C(51)—P(3)—C(25)	105.9(9)	C(51)—P(3)—C(31)	103.5(9)
C(25)—P(3)—C(31)	106.2(9)	C(51)—P(3)—Pd	109.6(6)
C(25)—P(3)—Pd	110.5(6)	C(31)—P(3)—Pd	120.1(7)
O(2)—P(4)—C(37)	110.2(8)	O(2)—P(4)—C(43)	108.0(7)
C(37)—P(4)—C(43)	107.7(8)	O(2)—P(4)—C(52)	111.6(8)
C(37)—P(4)—C(52)	108.2(8)	C(43)—P(4)—C(52)	111.2(8)
P(2)—O(1)—Pd	124.1(6)	P(4)—O(2)—Pd	143.9(6)
C(50)—C(49)—P(1)	118.1(12)	C(49)—C(50)—P(2)	112.9(12)
C(52)—C(51)—P(3)	118.0(13)	C(51)—C(52)—P(4)	112.6(13)

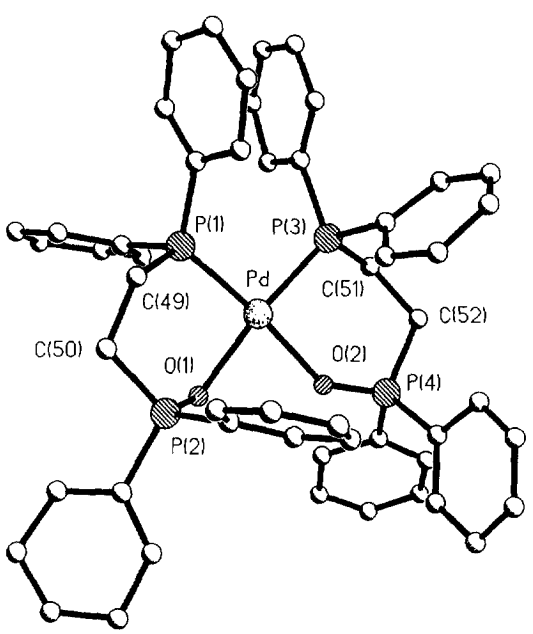

Fig. 2. Molecular structure of *cis*-$[(dppeO)_2Pd]^{2+}$ with adopted numbering scheme for the metallacycle atoms. Hydrogen atoms are omitted for clarity.

C(31) bond angles are increased to 122.7(6) and 120.1(7) degrees, whereas adjacent C(1)—P(1)—C(49) and C(25)—P(3)—C(31) bond angles are diminished to 98.1(8) and 103.5(8) degrees, respectively. On the contrary, P(2) and P(4) of the phosphoryl groups form tetrahedral bond angles of the almost ideal value, varying in the range of 107.1(8) to 112.1(7)°.

According to the room temperature ^{31}P NMR data, the $[(dppeO)_2Pd]\ (BF_4)_2$ remains *cis* in dichloromethane or methanol solutions, with both chelate rings undergoing conformational changes which are fast on the NMR time scale. Two sharp doublets of doublets at 36.5 and 48.2 ppm with $J_{P,P} = 10$ and 3 Hz were observed in the ^{31}P NMR spectrum of $[(dppeO)_2Pd]^{2+}$ in aqueous methanol, indicating that the geometry around the metal center is *cis*.

The dpppO counterpart of $[(dppeO)_2Pd]^{2+}$ and $[(dppmO)_2Pd]^{2+}$ was prepared by the reaction between $[(dpppO)_2PdCl_2]$ and $AgNO_3$ in dichloromethane/water, followed by the treatment of the reaction mixture with 40% $NaBF_4$ in water. Two broadened singlet resonances were observed in the ^{31}P NMR spectrum of the organic phase, with the chemical shifts of 30 ($\Delta\nu_{1/2} = 40$ Hz) and 55 ($\Delta\nu_{1/2} = 100$ Hz) ppm being indicative of a *P,O*-coordination mode for the dpppO ligands, as expected.

However, once precipitated by adding ether to the organic layer of the reaction mixture, the $[(dpppO)_2Pd]$ $(BF_4)_2$ appeared to be very poorly soluble in common organic solvents, dichloromethane and acetone included. In spite of this remarkably low solubility of the isolated crystalline compound, its ^{31}P NMR spectrum in CH_2Cl_2 was measured, exhibiting two *sharp doublets* ($J_{P\,P} = 7$ Hz) with virtually the same chemical shifts (30.4 and 55.6 ppm) as those observed before the complex was isolated. It is conceivable that in the concentrated solution formed upon reacting $[(dpppO)_2PdCl_2]$ with Ag^+ and then BF_4^-, the structure of the species obtained is somewhat different from that of the complex which has been isolated and consequently redissolved. The identical ^{31}P NMR chemical shifts suggest that both the P and O centers participate in coordinative interactions with the metal [6,14]. On the other hand, intermolecular Pd—O interactions of the type Pd—P—CH_2—CH_2—CH_2—PO—Pd might be pictured for the concentrated solution of the complex, resulting in the formation of oligometric/polymeric chains (Fig. 3). Facile ligand exchange in the oligomer is likely to be responsible for the line broadening in the ^{31}P NMR spectrum of the concentrated solution. It is noteworthy that the PO—Pd resonance was noticeably broader than the P—Pd signal, suggesting that the exchange processes involving the oxygen centers may be faster than those resulting in the cleavage and formation of the P—Pd bonds. In contrast, dilute solutions of the isolated complex contain the monomeric cation, $[(dpppO)_2Pd]^{2+}$, as indicated by the ^{31}P NMR data (see above).

Clearly, intramolecular vs intermolecular O—Pd coordination modes in the $[(dpppO)_2Pd]^{2+}$ system are strongly influenced by concentration effects which were not observed for the $[(dppmO)_2Pd]^{2+}$ and $[(dppeO)_2]^{2+}$ complexes. Furthermore, in the solid state both $[(dppmO)_2Pd]^{2+}$ and $[(dppeO)_2Pd]^{2+}$ are monomeric chelates, according to the solubility, X-ray, and also IR data. The IR spectra (KBr) of their tetrafluoroborate salts exhibited strong bands at 1102–1129 cm^{-1} due to the coordinated phosphoryl oxygens and no peaks in the range of 1180–1200 cm^{-1} where "free" phosphoryl P=O bonds normally absorb [6,14,15]. At the same time, two groups of bands were observed in the IR spectrum of the solid $[(dpppO)_2Pd]$ $(BF_4)_2$, at 1123–1105 cm^{-1} and 1195–1175 cm^{-1}. The former was obviously due to PO groups coordinated with the metal, whereas the latter pointed to the presence of free phosphoryls in the sample. It is clear that in order to contain both types of the phosphoryl groups while retaining square-planar geometry at the Pd centers, the solid $[(dpppO)_2Pd]$ $(BF_4)_2$ must possess polymeric or macrocyclic structure and should rather be formulated as $\{[(dpppO)_2Pd]$ $(BF_4)_2\}_n$. This is consistent with the ^{31}P NMR data obtained for the concentrated solution of oligomeric $[(dpppO)_2Pd]$ $(BF_4)_2$, prepared upon the exhaustive dechlorination of the $[(dpppO)_2PdCl_2]$ with Ag^+ (see above). The remarkable difference in the structure and behaviour of the three cationic complexes is definitely due to the substantial decrease in the magnitude of the chelate effect when going from the 5- and 6-membered metallacyles ($[(dppmO)_2Pd]^{2+}$ and $[(dppeO)_2Pd]^{2+}$, respectively) to the analogous, but much less stable, 7-membered rings ($[(dpppO)_2Pd]^{2+}$ [26]. For the same reason, the "silverless" synthesis of $[(dpppO)_2Pd]$ $(BF_4)_2$ from the corresponding dichloride requires many more ion-exchange extractions with aqueous $NaBF_4$, as compared with the above described similar preparation of $[(dppmO)_2Pd]$ $(BF_4)_2$ and $[(dppeO)_2Pd]$ $(BF_4)_2$. For instance, after a dichloromethane solution of $[(dpppO)_2PdCl_2]$ had been thoroughly washed with 40% aqueous $NaBF_4$ 12 times, the conversion to $[(dpppO)_2Pd]$ $(BF_4)_2$ was still incomplete (^{31}P NMR).

Attempted syntheses of $[(dppfcO)_2Pd]^{2+}$ and $[(dppbO)_2Pd]^{2+}$ from the corresponding dichloro complexes and aqueous $NaBF_4$ or $AgNO_3/NaBF_4$ were unsuccessful, and a complex mixture of unidentified products was obtained in both cases (^{31}P NMR). The metallacycles formed by the dppbO and dppfcO ligands are apparently too large in size to be

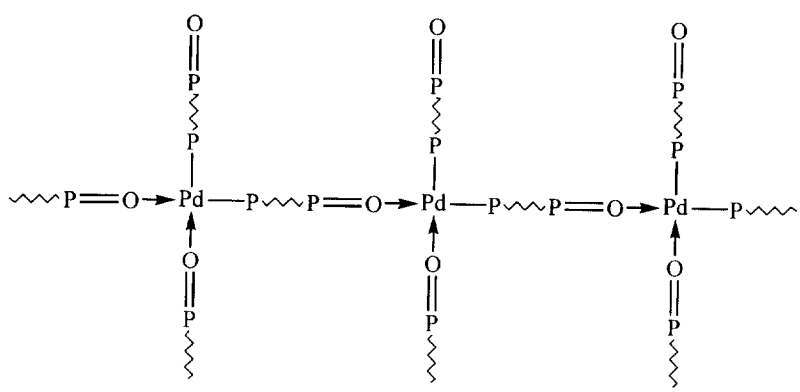

Fig. 3. Proposed structure for the $\{[(dpppO)_2Pd]^{2+}\}_n$ oligomer containing both coordinated and free phosphoryl groups.

sufficiently stable for successful isolation and characterization of the corresponding Pd chelates. Most likely, the generated compounds exist as mixtures of oligomeric species.

EXPERIMENTAL

NMR spectra were recorded on a Varian VXR-200 spectrometer. Chemical shifts are reported relative to TMS (^{1}H) and 85% H_3PO_4 (^{31}P). The BPMO ligands may be synthesized by the procedures reported in the literature [1b,3,6,27]. The phosphorus ligands, dppmO, dppeO, dpppO, dppbO, and dppfcO used in this work were prepared by the selective catalytic mono-oxidation of the corresponding bis-phosphines [18]. All other chemicals were purchased from Organometallics, Aldrich, and Strem and used as received. The synthesis, isolation, and purification of all complexes were conducted in air.

$[(dppmO)_2PdCl_2]$

A solution of $Na_2[PdCl_4]$ obtained by dissolving $PdCl_2$ (265 mg; 1.50 mmol) and NaCl (180 mg; 3.10 mmol) in hot methanol (20 ml) was added dropwise to a vigorously stirred solution of dppmO (1.459 g; 3.65 mmol) in CH_2Cl_2 (20 ml). The mixture was taken to dryness (rotary evaporation) and the residue was extracted with CH_2Cl_2 (30 ml). The dichloromethane solution was filtered, reduced in volume to ca 15 ml, diluted with ether (portionwise, 4 × 15 ml), and left at −15°C overnight. The yellow precipitate was separated, washed with ether, and dried under vacuum. The yield of $[(dppmO)_2PdCl_2]$ was 1.460 g (99%). The ^{31}P and ^{1}H NMR spectra of this complex in both chloroform-*d* and methanol-d_4 are described in the text and Table 1. In the ^{1}H NMR spectra, aromatic protons of the complex resonate as multiplets at 6.9–8.0 ppm and 7.0—8.0 ppm in $CDCl_3$ and CD_3OD, respectively.

$[(dppeO)_2PdCl_2]$

A solution of $Na_2[PdCl_4]$ obtained by dissolving $PdCl_2$ (498 mg; 2.81 mmol) and NaCl (361 mg; 6.22 mmol) in warm methanol (50 ml) was added dropwise to a vigorously stirred solution of dppeO (2.614 g; 6.23 mmol) in CH_2Cl_2 (30 ml). The mixture was evaporated to dryness and the residue was extracted with CH_2Cl_2. The combined dichloromethane extracts were filtered, reduced in volume, and treated with ether. The yellow precipitate was separated, washed with ether, and dried under vacuum. The yield of $[(dppeO)_2PdCl_2]$ was 2.677 g (95%). ^{1}H NMR ($CDCl_3$), δ: 2.6 (m, 8H, CH_2); 7.0–7.9 (m, 40H, C_6H_5).

$[(dpppO)_2PdCl_2]$

A solution of $Na_2[PdCl_4]$ obtained by dissolving $PdCl_2$ (520 mg; 2.94 mmol) and NaCl (385 mg; 6.64 mmol) in hot methanol (40 ml) was added dropwise to a vigorously stirred solution of dpppO (2.779 g; 6.49 mmol) in CH_2Cl_2 (30 ml). The mixture was taken to dryness (rotary evaporation) and the residue was extracted with CH_2Cl_2 (200 ml; the complex is only moderately soluble in dichloromethane [28]). The combined dichloromethane extracts were filtered, reduced in volume, and treated with ether to give a yellow microcrystalline solid which was separated, washed with ether, and dried under vacuum. The yield of $[(dpppO)_2PdCl_2]\cdot H_2O$ was 3.057 g (98%). Anal: Calcd for $C_{54}H_{54}Cl_2O_3P_4Pd$ ($C_{54}H_{52}Cl_2O_2P_4Pd\cdot H_2O$): C, 61.6; H, 5.2. Found: C, 61.7; H, 4.9. ^{1}H NMR ($CDCl_3$), δ: 1.8 (m, 4H, CCH_2C); 2.4 (m, 4H, CH_2PPd); 2.6 (m, 4H, CH_2PO); 7.0–7.8 (m, 40H, C_6H_5).

$[(dppbO)_2PdCl_2]$

A solution obtained by dissolving $PdCl_2$ (213 mg; 1.20 mmol) and NaCl (130 mg; 2.24 mmol) in hot methanol (50 ml) was added dropwise to a vigorously stirred solution of dppbO (1.216 g; 2.75 mmol) in CH_2Cl_2 (30 ml) [28]. Evaporation of the mixture gave a yellow oil which was dissolved in CH_2Cl_2 and the resulting solution was filtered, reduced in volume to ca 5 ml, and treated with ether (20 ml) to precipitate the complex. The crude solid product thus obtained (contaminated with ca 5% dppbO; ^{31}P NMR) was dissolved in dichloromethane (10 ml), the mixture was diluted with benzene (ca 30 ml), and the resulting yellow solution was slowly reduced in volume to ca 10 ml (rotary evaporation at room temperature). Upon standing for a few hours, yellow crystals of analytically and spectroscopically pure $[(dppbO)_2PdCl_2]\cdot 2C_6H_6$ precipitated, which was separated, washed with small quantities of benzene, and dried. The yield was 1.443 g (98%). Anal: Calcd for $C_{68}H_{68}Cl_2O_2P_4Pd$ ($C_{56}H_{56}Cl_2O_2P_4Pd\cdot 2C_6H_6$): C, 67.0; H, 5.6. Found: C, 67.4; H, 5.7. ^{1}H NMR ($CDCl_3$), δ: 1.6 (m, 8H, $C(CH_2)_2C$); 2.2 (m, 4H, CH_2PPd); 2.4 (m, 4H, CH_2PO); 7.1–7.8 (m, 40H + 12H, $C_6H_5 + C_6H_6$); an intense singlet at 7.3 ppm was observed due to the benzene present in the solid.

trans-$[(dppfcO)_2PdCl_2]$

A mixture of $PdCl_2$ (207 mg; 1.17 mmol) and NaCl (139 mg; 2.39 mmol) was stirred with methanol (40 ml) at ca 50°C until the solids dissolved. The resulting brown solution of $Na_2[PdCl_4]$ was added dropwise to a stirring solution of dppfoO [18,19] (1.477 g; 2.6 mmol) in CH_2Cl_2 (20 ml). After the dark red mixture was evaporated to dryness the residue was extracted

with CH_2Cl_2 (first 20 ml, then 4 × 5 ml), and the combined extracts were filtered, reduced in volume to ca 10 ml, and diluted with ether (portionwise, 4 × 5 ml). The orange-red crystals were separated, washed with ether, and dried. The yield of the *trans*-[(dppfcO)$_2$PdCl$_2$]·CH_2Cl_2 was 1.544 g (94%). Anal: Calcd for $C_{69}H_{58}Cl_4Fe_2O_2P_4Pd$ ($C_{68}H_{56}Cl_2Fe_2O_2P_4Pd \cdot CH_2Cl_2$): C, 59.1; H, 4.2. Found: C, 59.6; H, 4.2. ^{1}H NMR ($CDCl_3$), δ: 4.3 (s, 2H, C_5H_4); 4.4 (s, 2H, C_5H_4); 4.6 (s, 2H, C_5H_4); 4.9 (s, 2H, C_5H_4); 7.2–7.8 (m, 40H, C_6H_5).

cis-[(dppmO)$_2$Pd] (BF_4)$_2$

A solution of [(dppmO)$_2$PdCl$_2$] (202 mg; 0.21 mmol) in CH_2Cl_2 (5 ml) was vigorously stirred with 40% aqueous $NaBF_4$ (10 ml) for 15 min. The aqueous layer was separated by a pipette, another 10 ml of 40% $NaBF_4$ were added to the dichloromethane solution, and the mixture was stirred for another 15 min. This procedure was repeated five times. The organic phase was separated, filtered through cotton, and evaporated. The solid residue was recrystallized twice from CH_2Cl_2/ether to give 166 mg (74%) of white *cis*-[(dppmO)$_2$Pd] (BF_4)·H_2O. Anal: Calcd for $C_{50}H_{46}B_2F_8O_3P_4Pd$ ($C_{50}H_{44}B_2F_8O_2P_4Pd \cdot H_2O$): C, 54.7; H, 4.2. Found: C, 54.9; H, 4.2. ^{1}H NMR (acetone-d_6), δ: 4.8 (dd, 4H, $J_{P\,H}$ = 9.8 and 13.8 Hz, CH_2); 7.2–8.0 (m, 40H, C_6H_5). ^{31}P NMR (acetone-d_6), δ: 36.2 (d, 2P, $J_{P\,P}$ = 5.3 Hz, PPd); 59.7 (d, 2P, $J_{P\,P}$ = 5.3 Hz, POPd). IR (KBr), cm^{-1}: 1129, 1102 (PO).

cis-[(dppeO)$_2$Pd] (BF_4)$_2$

A solution of [(dppeO)$_2$PdCl$_2$] (204 mg; 0.21 mmol) in CH_2Cl_2 (5 ml) was vigorously stirred with 40% aqueous $NaBF_4$ (10 ml) for 15 min. The aqueous layer was separated by a pipette, another 10 ml of 40% $NaBF_4$, were added to the dichloromethane solution, and the mixture was stirred for another 15 min. This procedure was repeated five times. The organic phase was separated, filtered through cotton, and evaporated. The solid residue was recrystallized from CH_2Cl_2/ether (twice) and dried under vacuum to give 215 mg (96%) of pale-yellow *cis*-[(dppeO)$_2$Pd] (BF_4)$_2$. Anal: Calcd for $C_{52}H_{48}B_2F_8O_2P_4Pd$: C, 56.3; H, 4.4. Found: C, 56.1; H, 4.3. ^{1}H NMR (acetone-d_6), δ: 3.2 (m, 8H, CH_2); 7.2–8.2 (m, 40H, C_6H_5). ^{31}P NMR (MeOH), δ: 36.5 (dd, 2P, $J_{P\,P}$ = 10.0 Hz and 3.0 Hz, PPd); 48.2 (dd, 2P, $J_{P\,P}$ = 10.0 Hz and 3.0 Hz, POPd). ^{31}P NMR (acetone-d_6), δ: 37.8 (dd, 2P, $J_{P\,P}$ = 8.5 Hz and 4.6 Hz, PPd); 47.9 (dd, 2P, $J_{P\,P}$ = 8.5 H and 4.6 Hz, POPd). IR (KBr), cm^{-1}: 1125, 1103 (PO).

[(dpppO)$_2$Pd] (BF_4)$_2$

A solution of $AgNO_3$ (0.43 g; 2.5 mmol) in water (2 ml) was added to a vigorously stirred suspension of [(dpppO)$_2$PdCl$_2$] (1.00 g; 0.97 mmol) in CH_2Cl_2 (8 ml), causing an immediate precipitation of AgCl. Water (5 ml) and CH_2Cl_2 (7 ml) were added, and the mixture was stirred for another 5 min. The organic phase was separated, and the aqueous suspension of AgCl was washed with CH_2Cl_2 several times. The combined dichloromethane solutions were vigorously stirred with 40% $NaBF_4$ (2 × 20 ml, 30 min each), separated, filtered, reduced in volume, and treated with ether. The light-yellow precipitate was washed with ether and dried under vacuum. The yield of the cationic complex was 0.84 g (76%). Anal: Calcd for $C_{54}H_{52}B_2F_8O_2P_4Pd$: C, 57.0; H, 4.6. Found: C, 56.5; H, 4.6. ^{1}H NMR (acetone-d_6), δ: 2.8 (m, 4H, CH_2); 3.0 (m, 4H, CH_2); 3.2 (m, 4H, CH_2); 7.1–7.9 (m, 40H, C_6H_5). ^{31}P NMR (CH_2Cl_2), δ: 30.4 (d, 2P, $J_{P\,P}$ = 7.0 Hz, PPd); 55.6 (d, 2P, $J_{P\,P}$ = 7.0 Hz, POPd). IR (KBr), cm^{-1}: 1195, 1188, 1175, 1123, 1105 (PO).

X-ray diffraction studies

X-ray diffraction data were obtained with a Siemens P3/PC four-circle diffractometer with Mo–K_α-radiation and a graphite monochromator ($\theta/2\theta$ scan method) at 153 K and room temperature for single crystals of *trans*-[(dppfcO)$_2$PdCl$_2$] and *cis*-[(dppeO)$_2$Pd] (BF_4)$_2$, respectively. The diffraction quality of all examined crystal samples of the cationic complex was rather poor, displaying broad reflection peaks and irregular twinning. As all attempts to cool the samples led to an increase in the diffraction profiles, data collection was performed at room temperature. An empirical absorption correction was applied for the *trans*-[(dppfcO)$_2$PdCl$_2$], but not for the [(dppeO)$_2$Pd] (BF_4)$_2$ because of insufficient diffraction data quality. The structures were solved by direct methods and refined by the least squares techniques in the anisotropic (isotropic for disordered BF_4 anions) approximation. All H atoms were placed in geometrically calculated positions and included into refinement using a riding motion model. A PC SHELX PLUS program package was used for all calculations. Rotational disorder of the BF_4^- anions was detected in the difference Fourier maps for the cationic chelate, and therefore additional orientations of these anions were taken into account in the final refinement.

Acknowledgement—DuPont and the Science and Technology Endowment Program (STEP) Council at Wilfrid Laurier University are gratefully acknowledged for support.

Supporting information available—Full details of the X-ray diffraction studies of *trans*-[(dppfcO)$_2$PdCl$_2$] and *cis*-[(dppeO)$_2$Pd] (BF_4)$_2$, including crystallographic data, data collection, structure solution and refinement, ORTEP drawings, full tables of non-hydrogen atom coordinates with isotropic displacement parameters, full tables of bond lengths and bond angles, hydrogen atom coordinates, tables of anisotropic displacement parameters (22 pages), and two X-ray structure files in the CIF format. Ordering information is given on any current masthead page.

REFERENCES

1. (a) Grim, S. O. and Mitchell, J. D., *Synth. React. Inorg. Met.-Org. Chem.*, 1974, **4,** 221; (b) Grim, S. O., Satek, L. C., Tolman, C. A. and Jesson, J. P., *Inorg. Chem.*, 1975, **14,** 656; (c) Grim, S. O. and Mitchell, J. D., *Inorg. Chem.*, 1977, **16,** 1762; (d) Grim, S. O., Smith, P. H., Colquhoun, I. J. and McFarlane, W., *Inorg. Chem.*, 1980, **19,** 1395; (e) Grim, S. O. and Walton, E. D., *Inorg. Chem.*, 1980, **19,** 1982; (f) Colquhoun, I. J., Grim, S. O. and McFarlane, W., *Inorg. Chem.*, 1981, **20,** 2516.
2. Uson, R., *J. Chem. Soc., Dalton Trans.*, 1979, 73.
3. Kabachnik, M. I., Medved', T. Ya., Pisareva, S. A., Ignat'eva, T. I., Lomakina, L. N., Kozachenko, A. G., Matrosov, E. I., Petrovskii, P. V. and Komarova, M. P., *Izv. Akad. Nauk SSSR, Ser. Khim.*, 1980, 673; *Bull Acad. Sci. USSR, Div. Chem. Sci. (English Transl.)* 1980, 495.
4. Hall, S. R., Skelton, B. W. and White, A. H., *Aust. J. Chem.*, 1983, **36,** 267.
5. Wegman, R. W., Abatjoglou, A. G. and Harrison, A. M., *J. Chem. Soc., Chem. Commun.*, 1987, 1891.
6. Higgins, S. J., Shaw, B. L. and Taylor, R., *J. Organomet. Chem.*, 1987, **325,** 285.
7. Berry, D. E., Browning, J., Dixon, K. R. and Hilts, R. W., *Can. J. Chem.*, 1988, **66,** 1272.
8. Bond, A. M., Colton, R. and Pangiotidou, P., *Organometallics* 1988, **7,** 1767.
9. Bakar, M. A., Hills, A., Hughes, D. L. and Leigh, G. J., *J. Chem. Soc., Dalton Trans.*, 1989, 1417.
10. Terekhova, M. I., Kron, T. E., Bondarenko, N. A., Petrov, E. S. and Tsvetkov, E. N., *Izv. Akad. Nauk SSSR, Ser. Khim.*, 1991, 2003; *Bull. Acad. Sci. USSR, Div. Chem. Sci. (English Transl.)* 1991, 1555.
11. Kron, T. E., Sobolev, A. N., Terekhova, M. I., Bondarenko, N. A., Petrov, E. S. and Tsvetkov, E. N., *Koord. Khim.*, 1992, **18,** 103; *Coord. Chem. (English Transl.)* 1992, **18,** 89.
12. Davies, J. A., Pinkerton, A. A. and Vilmer, M., *Acta Cryst. C.*, 1992, **48,** 1027.
13. Visseaux, M., Dormond, A. and Baudry, D., *Bull. Soc. Chim. Fr.*, 1993, **130,** 173.
14. Blagborough, T. C., Davis, R. and Ivison, P., *J. Organomet. Chem.*, 1994, **467,** 85.
15. Al-Jibori, S. A., Kalay, Z. M. and Al-Allaf, T. A. K., *Transition Metal Chem.*, 1994, **19,** 293.
16. Anderson, G. K. and Cross, R. J., *Chem. Soc. Rev.*, 1980, **9,** 185.
17. (a) Berners-Rice, S. J., Johnson, R. J., Mirabelli, C. K., Faucette, L. F., McCabe, F. L. and Sadler, P. J., *Inorg. Chem.*, 1987, **26,** 3383; (b) Mason, M. R. and Verkade, J. G., *Organometallics*, 1992, **11,** 2212; (c) Grushin, V. V., 1995, unpublished results.
18. Prepared by the recently developed, novel catalytic method for the synthesis of BPMOs: Grushin, V. V., unpublished results (1995–1996); Patent application has been filed.
19. (a) Spectral and analytical data for dppfcO: ^{1}H NMR ($CDCl_3$, 20°C), δ: 4.0 (m, 2H, Cp); 4.2 (m, 2H, Cp); 4.4 (m, 2H, Cp); 4.6 (m, 2H, Cp); 7.1–7.7 (m, 20H, Ph). ^{13}C NMR ($CDCl_3$, 20°C), δ: 72.9 (s, C_5H_4); 73.0 (s, C_5H_4); 73.1 (s, C_5H_4); 73.2 (s, C_5H_4); 73.3 (d, $J_{P\text{-}C}$ = 1.7 Hz, C_5H_4); 73.5 (d, $J_{P\text{-}C}$ = 1.7 Hz, C_5H_4); 128.2 (d, $J_{P\text{-}C}$ = 11.0 Hz, m-C_6H_5PCp); 128.4 (d, $J_{P\text{-}C}$ = 16.7 Hz, m-$C_6H_5P(O)Cp$); 131.3 (s, p-C_6H_5PCp); 131.4 (s, p-$C_6H_5P(O)Cp$); 131.4 (d, $J_{P\text{-}C}$ = 9.7 Hz, o-C_6H_5PCp); 133.4 (d, $J_{P\text{-}C}$ = 19.7 Hz, o-$C_6H_5P(O)Cp$); 134.5 (d, $J_{P\text{-}C}$ = 105.6 Hz, q-C_6H_5PCp); 138.8 (d, $J_{P\text{-}C}$ = 10.8 Hz, q-$C_6H_5P(O)Cp$). ^{31}P NMR ($CDCl_3$, 20°C), δ: −16.7 (s, 1P, $CpPPh_2$); 28.5 (s, 1P, $CpP(O)Ph_2$). Anal: Calcd for $C_{68}H_{58}Fe_2O_3P_4$ ($C_{34}H_{28}FeOP_2 \cdot 0.5H_2O$): C, 70.5; H, 5.0. Found: C, 70.7; H, 5.0; (b) Although dppfcO itself is a new compound, its rhenium [19c] and tungsten [19d] complexes have been reported and structurally characterized. The Re and W complexes were obtained by the oxidation of the corresponding dppfc metal derivatives with H_2O_2; (c) Hor, T. S. A., Chan, H. S. O., Tan, K.-L., Phang, L.-T., Yan, Y. K., Liu, L.-K. and Wen, L.-K., *Polyhedron*, 1991, **10,** 2437; (d) Hsu, S. C. N., Yeh, W.-Y. and Chiang, M. Y., *J. Organomet. Chem.*, 1995, **492,** 121.
20. Ebsworth, E. A. V., Rankin, D. W. H. and Cradock, S., *Structural Methods in Inorganic Chemistry*. Blackwell Scientific Publications, Oxford, 1987.
21. (a) Ferguson, G., McCrindle, R., McAlees, A. J. and Parvez, M., *Acta Crystallogr. B*, 1982, **38,** 2679; (b) Kitano, Y., Kinoshita, Y., Nakamura, R. and Ashida, T., *Acta Crystallogr. C*, 1983, **39,** 1015.
22. Bertseh-Frank, B. and Frank, W., *Acta Crystallogr. C*, 1996, **52,** 328.
23. (a) A weak solid state Pd···FBF_3 interaction (2.235(5) Å) has been reported [23b]; (b) Rheingold, A. L., Wu, G. and Heck, R. F., *Inorg. Chim. Acta*, 1987, **131,** 147.
24. (a) Gilje, J. W. and Roesky, H. W., *Chem. Rev.*, 1994, **94,** 895 and references cited therein; (b) Grushin, V. V. and Alper, H., *Organometallics*, 1993, **12,** 1890; (c) Driver, M. S. and Hartwig, J. F., *J. Am. Chem. Soc.*, 1996, **118,** 4206; (d) Kuznetsov, V. F., Bensimon, C., Facey, G. A., Grushin, V. V. and Alper, H., *Organometallics*, 1997, **16,** 97.
25. (a) Oldham, C. In *Comprehensive Coordination Chemistry*, Vol. 2, Chapter 15.6, ed. G. Wilkinson. Pergamon Press, Oxford, 1987, p. 435 and references cited therein; (b) Barnard, C. F. G. and Russell, M. J. H. In *Comprehensive Coordination Chemistry*, Vol. 5, Chapter 51, ed. G. Wilkinson. Pergamon Press, Oxford, 1987, p. 1099 and references cited therein; (c) Ruiz, J., Cutillas, N., Torregrosa, J., Garcia, G., López, G., Chaloner, P. A., Hitchcock, P. B. and Harrison, R. M., *J. Chem. Soc., Dalton Trans.*, 1994, 2353; (d) Grushin, V. V., Bensimon, C. and Alper, H., *Organometallics*, 1995, **14,** 3259; (e) Grushin, V. V. and Alper, H., *J. Am. Chem. Soc.*, 1995, **117,** 4305.
26. Cotton, F. A. and Wilkinson, G., *Advanced Inorganic Chemistry*, 5th edn. John Wiley and Sons, New York, 1988.
27. (a) Seyferth, D., US Patent 3,426,021, 1969; (b) Abatjoglou, A. G. and Kapicak, L. A., US Patent

4,429,161, 1984. (c) Bondarenko, N. A., Rudomino, M. V. and Tsvetkov, E. N., *Izv. Akad. Nauk SSSR, Ser. Khim.*, 1990, 2180; *Synthesis* 1991, 125; (d) Brock, S. L. and Mayer, J. M., *Inorg. Chem.*, 1991, **30,** 2138.

28. It is worth noting that the solubility of dpppO in CH_2Cl_2 and $CHCl_3$ is much higher than that of dppbO, whereas the solubility of $[(dpppO)_2PdCl_2]$ in these solvents is noticeably lower than that of $[(dppbO)_2PdCl_2]$.

Pergamon

PII: S0277-5387(98)00074-6

Polyhedron Vol. 17, No. 18, pp. 3071–3082, 1998
© 1998 Elsevier Science Ltd
All rights reserved. Printed in Great Britain
0277-5387/98 $19.00+0.00

Synthesis, spectroscopic, photophysical and electrochemical properties of cyano-bridged copper(I)–ruthenium(II) complexes

Sudhir Ranjan and S. K. Dikshit*

Department of Chemistry, Indian Institute of Technology, Kanpur, (U.P.) 208016, India.

(Received 20 August 1997; accepted 12 February 1998)

Abstract—Complexes of the formula [(N–N)Cu($AsPh_3$)CN] (N–N = 2,2′–bipyridine, 1,10–phenanthroline) have been synthesized. $Ru(bpy)_2Cl_2.2H_2O$ and [(η^5–cp)$Ru(PPh_3)_2Cl$] react with [(N–N)Cu($AsPh_3$)CN] to give cyano-bridged compounds. IR spectral studies in the low frequency region (700–50 cm^{-1}) and 4000–400 cm^{-1} region reveal cyano bridging in the complexes. Luminescence measurements suggest oxidation of metal centres (Cu^I–Cu^{II} and Ru^{II}–Ru^{III}) on excitation at a charge transfer band. This has been substantiated with electrochemical studies of complexes which exhibit quasi-reversible reductions viz. Ru^{III}/Ru^{II} and Cu^{II}/Cu^I. The deposition of metallic copper is also observed at a potential of −1.55 V. Based on these data, a mechanism for photo-redox reaction of complexes has been presented. The properties of these bimetallic complexes are compared with those of parent complexes. © 1998 Elsevier Science Ltd. All rights reserved. © 1998 Elsevier Science Ltd. All rights reserved

Keywords: synthesis; binuclear complexes; FTIR, quasi-reversible; luminescence; electron-transfer.

Solar energy is the largest energy source available to mankind but its utilization in comparison to its availability is negligible. The design of suitable chromophores to be used as sensitizers in this process is one of the aims of co-ordination chemists [1]. Mononuclear and binuclear Ru^{II} polypyridine complexes show remarkable sensitizing properties [2, 3]. Such systems are also involved in electron-transfer and energy transfer processes [4]. In recent years much work has been done on cyanobridged homo and hetero/polynuclear complexes [5] to explore the various photophysical properties, including sensitization.

There are some reports on heteronuclear cyanide [6] bridged complexes containing Ru^{II} and other metal centres. We have been interested in the properties of cyano bridged bimetallic complexes and our earlier studies on these systems have highlighted some of the interesting properties [7]. In continuation, in this paper we wish to report the electrochemical, photophysical and spectral studies on a variety of cyano-bridged Cu^I–Ru^{II} complexes. The stimulation for photophysical studies of bridged systems is based on the fact that Cu^I complexes independently exhibit luminescence [8].

* Author to whom correspondence should be addressed. E-mail: skd@iitk.ernet.in

1. EXPERIMENTAL

^1H NMR spectroscopy was carried out on a Bruker WP-80 and a Bruker DRX300 spectrometer in the range 0–10 ppm (δ) using TMS as an internal calibrant. A COSY two-dimensional experiment was carried out on the Bruker DRX 300. ^{13}C NMR spectroscopy was carried out on a Bruker WP-80 and a Bruker DRX300 spectrometer. IR spectra were recorded on a Shimadzu IR 420 Spectrophotometer as KBr pellets in the 4000–400 cm^{-1} range, FTIR spectra on a Perkin–Elmer FTIR 1700X Spectrophotometer in Nujol mull with polyethylene plates in the range 700–50 cm^{-1}. UV–Vis spectra were carried out on a Shimadzu double beam UV-160 spectrophotometer in acetonitrile. Melting points were obtained on a Fisher-John melting point apparatus and are uncorrected. Conductivity measurements were carried out in acetonitrile on a Toshniwal Conductivity Bridge. Microanalyses were performed at the RSIC, CDRI, Lucknow, India.

Emission spectra were recorded on a Perkin–Elmer

Luminescence Spectrophotometer LS50B. Correction of the luminescence intensity profile was performed by fluorescence data manager software. Luminescence quantum yields ϕ_s were evaluated by comparing areas under the corrected luminescence spectra on an energy scale and by using the following equation:

$$\frac{\phi_s}{\phi_r} = \frac{F_s.A_r}{F_r.A_s}$$

where the F_s and F_r are the integrated fluorescence intensities of the sample and $[Ru(bpy)_3]^{2+}$. A_s and A_r are the absorbance of the sample and $[Ru(bpy)_3]^{2+}$ at excitation of same wavelength. ϕ_r for $[Ru(bpy)_3]^{2+}$ is taken as 0.028.

For the lifetime measurements a coherent synchronously pumped cavity dumped dye laser (702-1) pumped by a coherent CW mode-locked Nd:YAG laser (Antares 76s) was used. The fundamental laser light at 600 nm was frequency doubled to produce exciting light at 300 nm. The emissions were detected at a magic angle of 54.7° polarisation using a Hamamatsu MCP photomultiplier tube (2809U). The response time of the setup is 50–60 ps.

The FAB mass spectra were recorded on a JEOL SX 102/DA-6000 system using Xenon (6 kV, 100 mA) as the FAB gas and *m*-nitrobenzyl alcohol as a matrix.

Cyclic voltammograms were recorded on a Bio-Analytical System-27 electrochemical analyser, utilizing a three electrode configuration, consisting of a glassy carbon working electrode, Pt wire auxiliary electrode and Ag/AgCl reference electrode. An omnigraphic model 100X-Y recorder was used to record the current-voltage output.

$RuCl_3.xH_2O$ was obtained from Loba Chemie and triphenylarsine, 2,2′-bipyridine and 1, 10-phenanthroline from E-Merck and used as received; Acetonitrile (Qualigens) used in electrochemical and spectroscopic studies was dried over molecular sieves. All other chemicals used were either AnalaR grade or chemically pure. Manipulations were invariably performed under oxygen free dry nitrogen atmosphere using standard schelnk line and other techniques [9]. The solvents were dried using standard procedures before use.

$Ru(bpy)_2Cl_2.2H_2O$ [10] and $[(\eta^5-cp)Ru(PPh_3)_2Cl]$ [11] were prepared according to methods in literature. CuCN, $Cu(AsPh_3)_2CN$ and their substituted analogues were prepared by modifying the literature procedures [7, 12].

1.1. *Syntheses*

1.1.1. *Cyanobis-(triphenylarsine)copper(I)*; $[Cu(AsPh_3)_2CN]$ [**1**] To a suspension of CuCN (0.895 g, 0.01 mole) in chloroform (50 cm^3) was added a solution of triphenylarsine (12.258 g, 0.04 mole) in chloroform (70 cm^3), and the reaction mixture was stirred constantly for an hour. During the course of the reaction the desired complex was precipitated. The volume of the reaction mixture was reduced in a rotatory evaporator. While removing the solvent, a white precipitate dissolved and a thick viscous liquid appeared. It was cooled and then treated with benzene (40 cm^3) which resulted in superfine white crystals. These were then filtered and washed with dry ether and then dried *in vaccuo*.

1.1.2. *Cyanobipyridine(triphenylarsine)copper(I)*; $Cu(AsPh_3)(bpy)CN$ [**2**] To a suspension of $Cu(AsPh_3)_2(CN)$ (0.701 g, 1 mmol) in benzene (30 cm^3) was added a solution of bipyridine (0.156 g, 1 mmol) in benzene (30 cm^3) with constant stirring. The resulting yellow solution was refluxed for 2–3 hours. The clear solution thus obtained was cooled, the volume was reduced to half and excess petroleum ether (60–80° C) was added, which resulted in the precipitation of a pale-yellow compound. It was filtered, washed several times with petroleum ether and dried *in vaccuo*. It was recrystalized from a $CHCl_3$–xylene mixture (1:1).

1.1.3. *Cyano1,10–phenanthroline(triphenylarsine) copper[I]*; $[Cu(AsPh_3)(phen)CN]$ [**3**] To a suspension of $Cu(AsPh_3)_2CN]$ (0.701 g, 1 mmol) in benzene (30 cm^3) was added a solution of 1,10. phenanthroline (0.198 g, 1 mmol) in benzene (30 cm^3) with constant stirring. Immediately an orange–red precipitate appeared, the resulting mixture was refluxed for an hour. After cooling, excess petroleum ether (60–80° C, 100 cm^3) was added to ensure complete precipitation of the complex. The complex was centrifuged and washed several times with petroleum ether and dried *in vaccuo*. It was recrystalized from a $CHCl_3$–xylene mixture (1:1).

1.1.4. *Bis–(triphenylarsine)copper(I)*(μ–cyano)-chlorobis–(2,2′–bipyridine)ruthenium(II)hexafluorophosphate; $[((AsPh_3)_2Cu–CN–Ru(bpy)_2Cl]PF_6$.[**4**] A mixture of $[Cu(AsPh_3)_2CN]$ (0.701 g, 1 mmol) and $Ru(bpy)_2Cl_2.2H_2O$ (0.512 g, 1 mmol) was suspended in ethanol (50 cm^3) and the suspension was refluxed for an hour. The solution was cooled and filtered. A highly concentrated solution of NH_4PF_6 in water (0.0064 g in 1 cm^3) was added, which caused the immediate precipitation of a complex. The precipitate was washed thoroughly with water and then with ether, and dried over P_4O_{10} for several hours. It was recrystalized from a $CHCl_3$–CH_3CN mixture (1:1).

1.1.5. *Bis–(triphenylarsine)copper(I)*(μ–cyano)-cyclopentadienylbis–(triphenylphosphine)rutherium (II)hexafluorophosphate; $[(AsPh_3)_2Cu–CN–Ru(\eta^5–cp)(PPh_3)_2]PF_6$ [**5**] $[Cu(AsPh_3)_2CN]$ (0.701 g, 1 mmol) and $(\eta^5-cp)Ru(PPh_3)_2Cl]$ (0.725 g, 1 mmol) were taken in methanol (50 cm^3) and the mixture was stirred vigorously. NH_4PF_6 (0.174 g, 1.2 mmol) was added to this solution and refluxed for an hour, which upon cooling gave a pale yellow precipitate. The solvent was evaporated to dryness *in vaccuo* and the residue was extracted with a small amount of dichloromethane and filtered. On addition of excess petroleum ether (60–80 C), a complex precipitated, which was centrifuged and washed several times with

petroleum ether and dried in vaccuo. It was recrystalized from $CHCl_3$.

1.1.6. *(1,10-Phenanthroline)(triphenylarsine) copper(I)*(μ-cyano)chlorobis-(2,2′-bipyridine)ruthenium(II)hexafluorophosphate; [(phen)($AsPh_3$)Cu-CN-Ru(bpy)$_2$Cl]PF_6 [6] [Cu($AsPh_3$)(phen)CN] (0.179 g, 0.2 mmol) and Ru(bpy)$_2Cl_2.2H_2O$ (0.104 g, 0.2 mmol) were dissolved in a 1:1 mixture of water and ethanol (50 cm^3), and the solution was refluxed for 5 hours. The resulting solution was cooled and filtered. To this filtrate was added a concentrated aqueous solution of NH_4PF_6 (0.0064 g/cm^3). A precipitate of maroon colour immediately appeared, which was centrifuged and washed several times with ether and dried over P_4O_{10} for several hours *in vaccuo*. It was recrystalized from a $CHCl_3$–CH_3CN mixture (1:1).

1.1.7. *(2,2′-Bipyridine)(triphenylarsine)copper(I)*(μ-cyano)chlorobis-(2,2′-bipyridine) ruthenium(II) hexafluorophosphate; [(bpy)($AsPh_3$)Cu-CN-Ru(bpy)$_2$ Cl]PF_6.[7] The same as in Section 1.1.6, except [Cu($AsPh_3$)(bpy)CN] was used in place of [Cu(As Ph_3)(phen)CN].

2. RESULTS AND DISCUSSION

The analytical data for the complexes are given in Table 1, which are consistent with the stoichiometries proposed. The conductivity data of the complexes [**1**], [**2**], and [**3**] show a non-electrolytic nature, whereas other cation complexes are 1:1 electrolytes [13]. All the complexes are diamagnetic at room temperature.

FAB mass spectral data are assigned in Table 2. The molecular ion peak usually is of a low intensity. All the complexes show a M–PF_6 peak. Other isotopic peaks are also observed and appear as bands. Some of these are summarized in Table 2. The variation in the m/z values is mainly due to presence of the heavier atom isotopes of ruthenium (96-104), Cu(63,65) and Cl(35,37). In Complex [**5**], M-PF_6 shows large variation. This may be due to the presence of seventy-eight carbon atoms. The effect diminishes as the number of carbons decreases in other complexes. The peak at m/z = 123.5 [**5**] indicates dissociation of $AsPh_3$ and facile rearrangement of counter anion at copper centre to produce neutral complex. This is also observed in complex [**7**].

Table 1. Analytical and Physical data of the Complexes

Complex	Colour	Analysis Found (Calc) (%)			mp*a* /t C	Yield*b* (%)	Ω^{-1} cm^2 mol^{-1} Conductivity
		C	H	N			
[Cu($AsPh_3$)$_2$CN] [**1**]	White	63.21 (63.30)	4.22 (4.30)	1.97 (1.99)	182	87.7	
[Cu($AsPh_3$)(bpy)CN] [**2**]	Dark yellow	63.0 (63.10)	4.10 (4.17)	7.60 (7.61)	200 (d)	74.0	
[Cu($AsPh_3$)(phen)CN] [**3**]	Dark Orange	64.40 (64.46)	3.80 (3.99)	7.25 (7.29)	220 (d)	87.7	
[$AsPh_3$)$_2$Cu(μ-CN)Ru(bpy)$_2$Cl]PF_6.[**4**]	Orange red	52.62 (52.82)	3.51 (3.50)	5.40 (5.40)	177 (d)	81.2	126.8
[($AsPh_3$)$_2$Cu(μ-CN)Ru(η^5-cp) (PPh_3)$_2$]PF_6 [**5**]	Light yellow	60.70 (60.7)	4.20 (4.21)	1.10 (0.9)	136 (d)	63.3	154.4
[(phen)[($AsPh_3$)$_2$Cu(μ-CN)Ru(bpy)$_2$Cl]PF_6 [**6**]	Maroon	52.20 (52.30)	3.30 (3.30)	8.30 (8.38)	184 (d)	72.2	158.0
[(bpy)[($AsPh_3$)$_2$Cu(μ-CN)Ru(bpy)$_2$Cl]PF_6.[**7**]	Orange red	51.2 (51.35)	3.0 (3.05)	8.50 (8.55)	198 (d)	60.7	138.0

a d denotes decomposition temperature.
b based on Copper compounds 1, 2, and 3 and on Ruthenium for the other compounds.

2.1. *IR spectra*

The υ_{CN} stretching frequency data of the complexes [**1**]–[**7**] are given in Table 3. For complex [**1**], υ_{CN} at 2130 cm^{-1} (lit. value [14] 2125 cm^{-1}) indicates that the CN group is terminal. Lowering of υ_{CN} in complexes [**2**] and [**3**] may be due to an increase in coordination number [7, 15]. Further lowering of υ_{CN} stretching on bridging in complexes [**4**]–[**7**] is due to enhanced π-back donation from ruthenium and copper [7].

IR spectral data in the low frequency region of

Table 2. FAB Mass Spectra

Complex	m/z, found (Calc.) {r.a}*a*	Assignments
[5]	1541 (1541){10}	$[^{65}Cu–CN–^{104}Ru]PF_6$
	1536 (1536){3}	$[^{63}Cu–CN–^{101}Ru]PF_6$
	1409 (1396){8}	$[^{65}Cu–CN–^{104}Ru]^+$
	1405 (1391){3}	$[^{63}Cu–CN–^{101}Ru]^+$
	1235 (1235){12}	$[(PF_6)^{65}Cu–CN–^{104}Ru]$
[6]	1175 (1175){6}	$[^{65}Cu–CN–^{104}Ru(^{37}Cl)]PF_6$
	1170 (1170){4}	$[^{63}Cu–CN–^{101}Ru(^{37}Cl)]PF_6$
	1168 (1168){5}	$[^{63}Cu–CN–^{101}Ru(^{35}Cl)]PF_6$
	1030 (1030){7}	$[^{65}Cu–CN–^{104}Ru(^{37}Cl)]^-$
	1025 (1025){12}	$[^{63}Cu–CN–^{101}Ru(^{37}Cl)]^-$
	1023 (1023){10}	$[^{63}Cu–CN–^{101}Ru(^{35}Cl)]^-$
[7]	1151 (1151){3}	$[^{65}Cu–CN–^{104}Ru(^{37}Cl)]PF_6$
	1146 (1146){4}	$[^{63}Cu–CN–^{101}Ru(^{37}Cl)]PF_6$
	1144 (1144){4}	$[^{63}Cu–CN–^{101}Ru(^{35}Cl)]PF_6$
	1006 (1006){19}	$[^{65}Cu–CN–^{104}Ru(^{37}Cl)]^-$
	1001 (1001){17}	$[^{63}Cu–CN–^{101}Ru(^{37}Cl)]^+$
	999 (999) {21}	$[^{63}Cu–CN–^{101}Ru(^{35}Cl)]^+$
	838 (838){19}	$[PF_6)^{63}Cu–CN–^{101}Ru(^{35}Cl)]$

a r.a. stands for relative abundance.

Table 3. IR, FTIR and NMR Spectral data

Complex	IR Spectra (cm−1)					NMR Spectra (δ ppm)	
	υ_{CN} *a*	υ_{Cu-AS} *b*	δ_{Cu-CN} *b*	υ_{Cu-C} *b*	υ_{Ru-N} *b*	^1H	^{13}C
[1]	2130	282	314	364	—	7.40*d* (S, 30H)	128–135*c* (phenyl) 137.0 (CN)
[2]	2115	—			—	—	—
[3]	2110	—	—	—	—	—	—
[4]	2080	295 (*m*)	319 (*sh*)	352 (*sh*)	334 (*s*)	—	123.7–157.3*c* (bpy, phenyl)
[5]	2060	288 (*m*)	300 (*w*)	347 (*sh*)	—	7.09–7.37*d* (m, 60H) 4.43[d] (s, cp)	128.5–137.5[d] 85.9 (cp)
[6]	2090	292 (*s*)	309 (*w*)	363 (*m*)	331 (*m*)	—	—
[7]	2100	290 (*w*)	311 (*vw*)	362 (*vw*)	331 (*m*)	—	—

a in KBr pellets
b in polyethylene plates
c recorded at 300 MHz in DMSO-d_6 and
d recorded at 80 MHz in $CDCl_3$.
The ^{13}C NMR of bridging cyano group was not observed.
m stands for medium, *s* sharp, *sh* shoulder, *w* weak, *vw* very weak.

complexes [1]–[7] are given in Table 3. A representative FTIR spectra of complexes [1], [4] and [5] are shown in Fig. 1. The characteristics υ_{Ru-N}, υ_{Cu-C}, υ_{Cu-As} and δ_{Cu-CN} have been assigned according to literature data [16–22]. We find that similar spectral patterns also appear for new cyano bridged complexes. It is seen that some of the ligand vibrations which do not appear in the free ligand are activated by complex formation [20]. The splitting of some asymmetric bands are ascribed to lattice effect [22].

2.2. *NMR spectra*

The ^1H NMR and ^{13}C NMR spectral data are given in Table 3. The proton NMR of complex [5] having

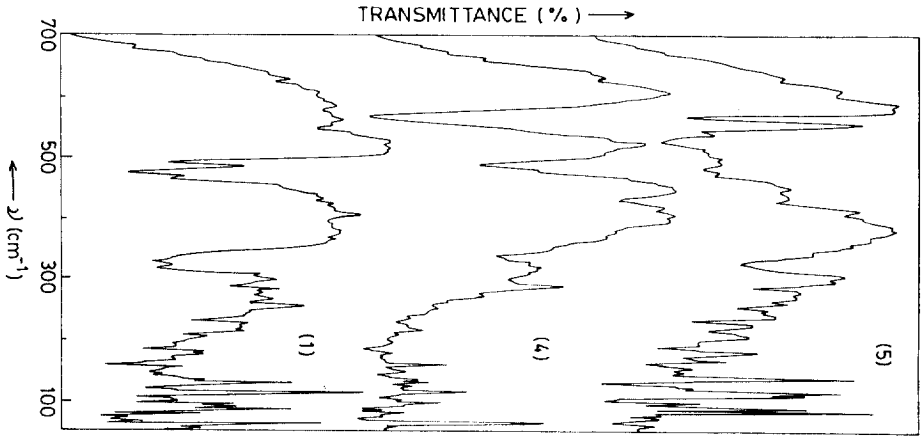

Fig. 1. Low Frequency IR spectra between 700 and 50 cm^{-1} of complexes [1], [4] and [5].

η^5–cp group shows a sharp singlet signal at 4.43 ppm (δ). The cp peak of a complex shifts slightly to higher δ in comparison to the parent complex $[(\eta^5-cp)Ru(PPh_3)_2Cl]$ [23]. The shift in δ value of cp protons in this complex suggests that the complex must be cationic in nature [24]. The proton signals of the phenyl groups appear in the region 7.0–8.0 as a broad multiplet [7].

Compound [4], [Fig. 2(a)], shows a complex pattern of resonance for which reliable assignment is not possible. To solve this problem spectra are assigned on the basis of a COSY two-dimensional experiment. Compound [4] is warmed to 120°C for a few minutes and then cooled before the spectrum was recorded. Two doublets are exhibited in the low-field area of the NMR spectrum and are found to be similar to the spectra reported in the literature [25, 26], whereas a multiplet is also observed in the region 7.0–8.8 ppm(δ) which cannot be assigned specifically [Fig. 2(b)]. These doublets are assigned as H^6 of bpy (A) and bpy (B) at 10.02 and 9.52 ppm (δ), respectively [Fig. 2(b)]. Appearance of these signals is due to different spatial interaction of the chloride ligand [26]. On further heating for one hour the spectra was recorded by suppressing phenyl protons. The spectrum indicated that the above multiplet has also fragmented into sharp signals [27] [Fig. 2(c)].

The ^{13}C NMR spectra of complex [1] exhibit NMR signals in the expected region of the phenyl group [28]. But in the case of complex [5], these signals were complicated and could not be specifically assigned. Nevertheless it can be said that the peak observed at 85.9 ppm (δ) for the cp group bound to ruthenium falls in the expected region [29].

2.3. *UV–Vis spectra*

Ground state absorption properties are summarised in Table 4, and the spectra of mononuclear and hetrobinuclear complexes are illustrated in Fig. 3. All the spectra were recorded in acetonitrile solution at room temperature. In cyanobridged complexes [4], [6] and [7] five bands are observed. These bands are characteristic bands of the $Ru(bpy)^{2+}_2$ chromophores [10, 30, 31]. Bands at 245, 246 and 244 nm in these complexes [4], [6] and [7] respectively are assigned as $\pi\rightarrow\pi^*$ (bpy) intraligand transition and $\pi\rightarrow\pi^*$ (phenyl) $AsPh_3$ transitions.

Small blue shifts are observed in comparison to $Ru(bpy)_2Cl_2.2H_2O$. A similar pattern of shifting has been observed for bands in the 280–290 nm range, which are characteristic of ligand-centred (LC) $\pi\rightarrow\pi^*$ (bpy) transitions. Assignment of bands at 346 nm [$d\pi(Ru)\rightarrow\pi^*$ (bpy)] and at 480 nm [$d\pi(Ru)\rightarrow\pi^*$ (bpy)] in complex [4] as metal-to-ligand charge transfer (MLCT) is based on literature reports [10, 30, 31]. Comparing these bands to corresponding values of $Ru(bpy)_2Cl_2.2H_2O$ ($\lambda_{max}=382$ nm and 551 nm), we infer that when the CN- ligand is attached to the $Ru(bpy)^{2+}_2$ moiety, there is an appreciable decrease in Ru→bpy π-backbonding. In this complex due to strong backbonding from Ru(II) to the cyano group, blue shift is observed, which is possible only when d-orbitals are increasingly stabilised. These bands predict the possibility of CN–Ru interaction. High energy bands, λ_{max} at 210 nm in [4], 213 nm in [6] and 209 nm in [7], are characteristics of [$d\pi(Ru)\rightarrow\pi^*(CN)$] MLCT transitions [32]. Thus, a possible explanation for the spectroscopic behaviour could be based on the fact that there are two types of Ru→Ligand MLCT transitions, one involving a terminal bpy ligand and the other involving a bridging CN- ligand. This has been supported by electrochemical results.

The absorption characteristics of [5] are similar to those of the well known analogue [7], $[(PPh_3)_2Cu-CN-Ru(\eta^5-cp)(PPh_3)_2]PF_6$. The MLCT transitions at 357.0 nm of complex $[(\eta^5-cp)Ru(PPh_3)_2Cl]$ is blue shifted which indicates the

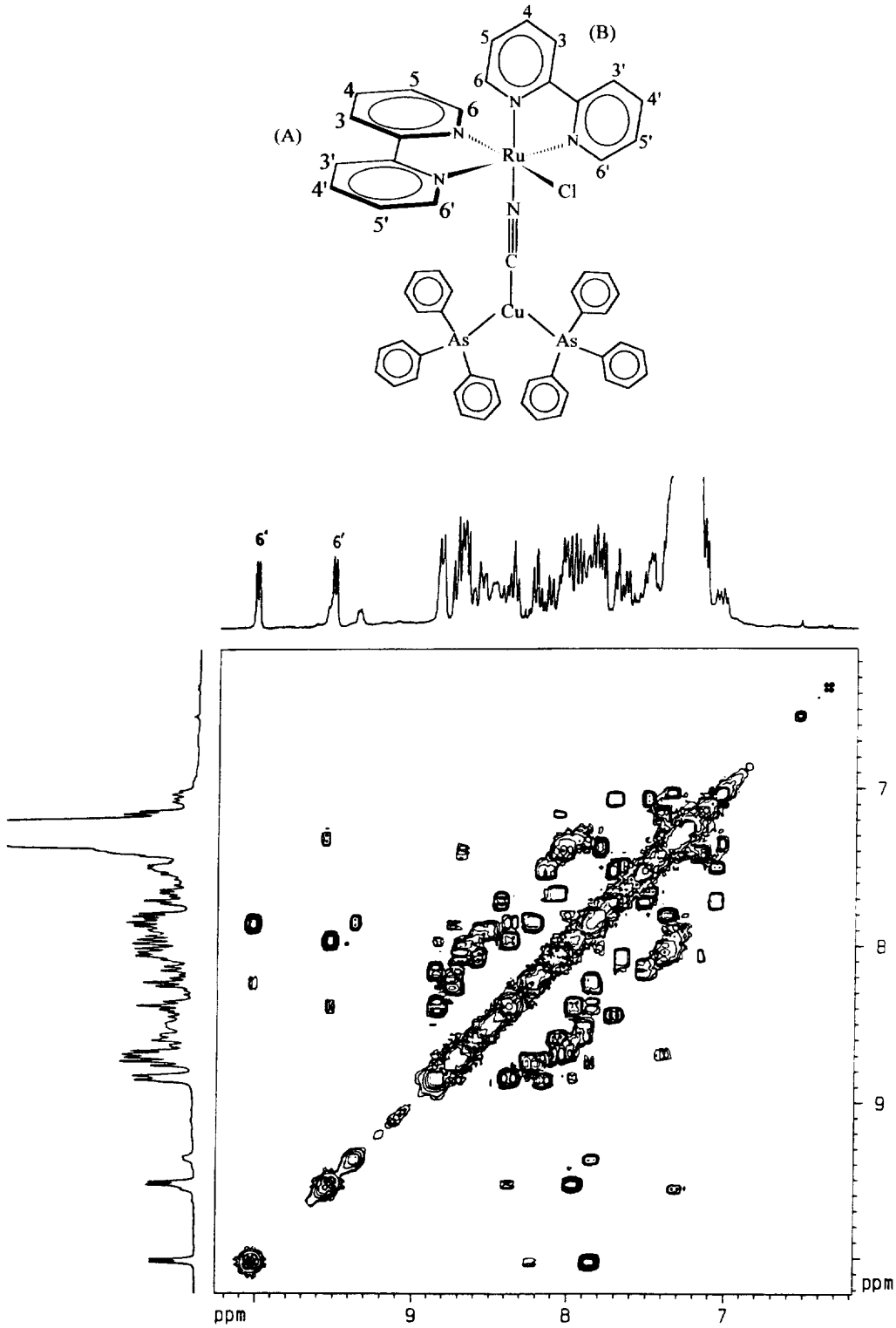

Fig. 2. a) The structure of $[(AsPh_3)_2Cu–CN–Ru(bpy)_2Cl]^+$ and the numbering of protons of bpy ligands A and B in different environment.b) 300 MHz COSY ^{2}D-NMR spectrum of **[4]** recorded in DMSO-d^6. Assignment of the multiplet in the range 7.5-8.8 could not be made because of the complexity of the multiplet.c) 300 MHz COSY ^{2}D-NMR spectrum of **[4]** recorded in DMSO-d^6. Assignment of all protons are given as follows: bpy (A); **6′** (10.02), **5′** (7.85), **4′** (8.23), **3′** (8.75), **3** (8.68), **4** (8.06), **5** (7.14), **6** (7.80), and bpy (B); 6′ (9.52), 5′ (7.98), 4′ (8.40), 3′ (8.83), 3 (8.68), 4(8.06), 5 (7.42), 6 (7.95) {ppm(δ)}.

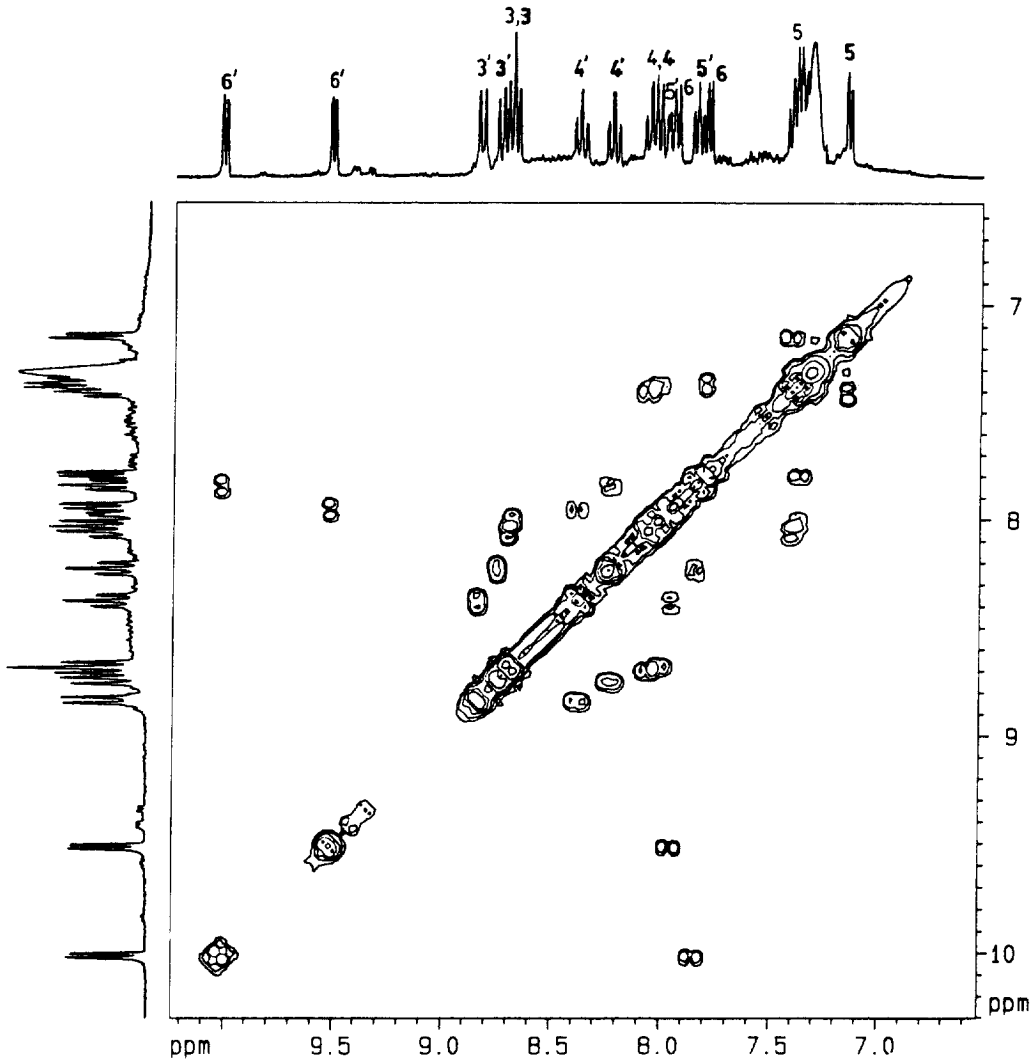

Fig. 2 — *continued.*

increasing stabilisation of ruthenium d-orbitals by backbonding from the ruthenium to the cyanide group. On bridge formation the MLCT transition at 246 nm in the complex becomes broad and appears as a shoulder. Such shifting is also observed in complexes [4]–[7], and is in good agreement with the shifting of υ_{CN} to low energy IR spectra. Complexes [2] and [3] give absorption bands at 357.5 nm and 363 nm respectively which are assigned as MLCT transitions and other bands are intraligand transitions [33]. The band at 269.0 nm of complex [3] appears as a shoulder on the band at 285.0 nm of complex [6]. Similarly the band at 284.0 nm of complex [2] appears as a shoulder on the band at 289.0 nm of complex [7]. No shoulder is observed in the electronic spectra of complex [4] because the band at 246.0 nm of [1] gets buried at the same λ_{max}.

2.4. *Electrochemical properties*

The electrochemical behaviour of a heterobinuclear cyano bridged system has been discussed previously [6], where ruthenium is one of the metal centres. Fig. 4 shows the voltammogram (*vs* Ag–AgCl in acetonitrile) of [6], at a scan rate of 100 mV/sec. $E_{1/2}$ values were obtained from the formula $E_{1/2}=\frac{E_{pa}+E_{pc}}{2}$. All of the waves with δE_p which are close to the values of δE_p for $[Ru(bpy)_3]^{2+}$ ($E_{1/2}=1.40$ V Vs Ag/AgCl [34], $\delta E_p=90$–120 mV at a scan rate of 100 mV/sec) are reversible. All the other waves can be regarded as quasi-reversible. This compound shows two quasi-reversible responses at 0.76 V ($E_{pa}=0.78$ V and $E_{pc}=0.73$ V) and 1.27 V ($E_{pa}=1.30$ V and $E_{pc}=1.24$ V) which are attributed to the processes

Table 4. Absorption spectral data

Complex	UV-Vis Bands[a]	
	λ_{max} (nm) $\{10^{-4}\ \epsilon\ dm^3\ mol^{-1}\ cm^{-1}\}$	Assignment
[1]	246 (4.59)	CT
	218 (7.18)	
[2]	357.5 (*sh*) (1.5)	CT
	284 (2.52)	
	223 (6.52)	
[3]	363.0 (*sh*) (1.3)	CT
	269 (5.69)	
	226 (8.38)	
[4]	482 (1.27)	$d\pi(Ru)\rightarrow\pi^*$ (bpy) CT
	346 (1.37)	$d\pi(Ru)\rightarrow\pi^*$ (bpy) CT
	288 (5.79)	$\pi\rightarrow\pi^*$(bpy) CT
	245 (2.18)	$\pi\rightarrow\pi^*$(bpy) IL
	210 (3.55)	
[5]	266 (*sh*) (4.86)	CT
	223 (13.37)	
[6]	480 (1.32)	$d\pi(Ru)\rightarrow\pi^*$ (bpy) CT
	346 (1.47)	$d\pi(Ru)\rightarrow\pi^*$ (bpy) CT
	285 (6.33)	$\pi\rightarrow\pi^*$(bpy) IL
	246 (2.52)	$\pi\rightarrow\pi^*$(bpy) IL
[7]	484 (0.98)	$d\pi(Ru)\rightarrow\pi^*$ (bpy) CT
	346 (1.05)	$d\pi(Ru)\rightarrow\pi^*$ (bpy) CT
	289 (4.70)	$\pi\rightarrow\pi^*$(bpy) IL
	244 (1.33)	$\pi\rightarrow\pi^*$(bpy) IL
	209 (1.34)	

[a] recorded in acetonitrile solution. *sh* denotes shoulder.

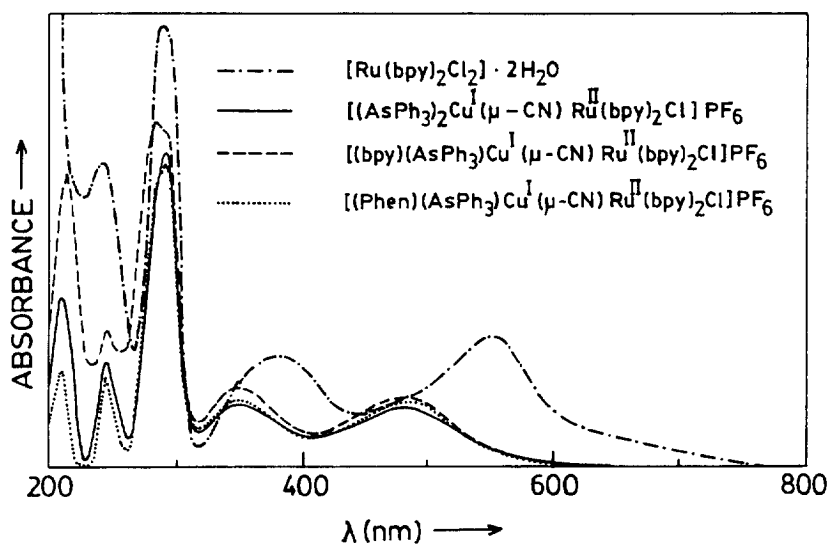

Fig. 3. The electronic (UV-Vis) spectra of complexes [4], [6], [7] and $[Ru(bpy)_2Cl_2]2H_2O$.

$Cu^I\rightarrow Cu^{II}$ and $Ru^{II}\rightarrow Ru^{III}$ corresponding to a phenanthroline bound copper metal centre and a bipyridine bound ruthenium metal centre respectively. The latter is consistent with literature values [32, 33]. The $E_{1/2}$ value for ligand reduction appears at -1.18 V which can be assigned to a copper bound phenanthroline reduction. Thus, the given ligand system can also stabilize the dinuclear cyano bridged com-

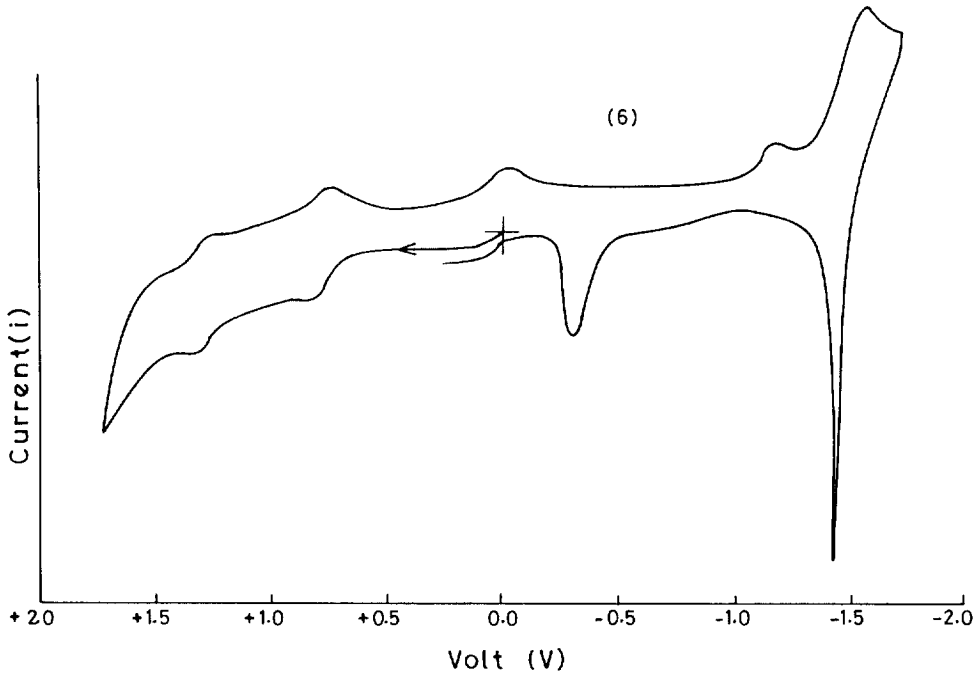

Fig. 4. Cyclic Voltammogram of complex [6] (vs Ag–AgCl in acetonitrile; 0.1 mol/dm^3 tetrabutylammonium hexafluorophosphate and scan rate 100 mV/sec; 25°C).

plexes in a higher oxidation state i.e., the Cu^{II}–CN–Ru^{III} form. Such a mechanism depends on the ability of the cyanide ligand to act as a conducting bridge and, moreover, it involves intramolecular electron transfer.

There is one irreversible reductive wave with $E_{red} = -1.55$ V attributable to the process $Cu^{I} \rightarrow Cu^{0}$ [35]. This shows the deposition of copper metal at the electrode. It is believed that the $E_{1/2}$ value for bipyridine ligand reduction has merged with Cu^{I}/Cu^{0} reduction value. The other $E_{1/2}$ value does not occur due to the narrow window range. A comparison of electrochemical data and previous investigations carried out on complexes of this type, has shown that Cu^{+} is oxidised at a potential less positive than Ru^{2+}, and Cu^{II} is interacting with Ru^{II} through a cyanide bridge. Complex [7] shows similar behaviour.

2.5. *Luminescence properties*

Room temperature emission band maxima, lifetimes and luminescence quantum yields are reported in Table 5. Representative luminescence spectra are shown in Fig. 5. The absorption spectra of cyano-bridged complexes are dominated by the $Ru(bpy)^{2+}_3$ chromophoric unit and the contribution of $[Cu(AsPh_3)(NN)]^{+}$ is negligible. Upon excitation performed at ~480 nm, these complexes exhibit emission band maxima at ~642 nm and are tentatively assigned as metal-to-ligand charge transfer transitions [36]. Besides these bands, emission bands appear at ~525–545 nm. The assignment of these electronic excited states poses an interesting problem. Probably the emission occurs from a copper sub-unit. Copper(I) centre, a d^{10} system is very electron rich in nature and can be stabilised by lignads having π-acid character, viz. PPh_3, bpy, phen, CO, CN- etc. Complexes having general formula $[Cu(PPh_3)_2(NN)]^{+}$, are known to exhibit emission properties both at low and room temperature. McMillin *et al* [33, 37], observed emissions at 608 and 575 nm in $[Cu(PPh_3)_2(phen)]^{+}$ and 620 nm in $[Cu(PPh_3)_2(bpy)]^{+}$. These emissions were tentatively assigned as metal-to-ligand charge transfers. However, a metal-centred $d \rightarrow s$ orbital transition was not ruled out. Moreover, there is extensive literature on the emission of poly nuclear copper(I) complexes. In the tri-nuclear copper(I) complex $[Cu_3(dpmp)_2(MeCN)_2(\mu-Cl)_2]^{+}$, where dpmp is bis(diphenylphosphinomethyl)methyl phosphine, an emission at 560 nm was assigned as a metal-centered $3d^9 4s^1 \rightarrow 3d^{10}$ transition [38]. In the bi-nuclear copper(I) complex $[PPh_3Cu_2Cl_2(py)]$ a similar type of assignment has been made by Jink *et al.*[39]. However, the possibility of a CT excited state was also predicted.

The emission bands at ~525–545 nm in the complexes [4], [6] and [7] have been assigned, based on a literature assignment of analogous compounds and our experimental observation. The complex [4] undergoes bi-exponential decay showing lifetimes at 0.201 ns ($A_1 = 0.67$) and 2.59 ns ($A_2 = 0.33$), [Fig. 6]. This confirms the presence of two species in the excited state, namely the copper and ruthenium sub-units.

Table 5. Luminescence Properties at 298 K

Complex	λ^{a}_{em}(nm)	τ (ns)	ϕ	K_r (s^{-1})	K_{nr} (s^{-1})
[4]	642	0.201	6.7×10^{-3}	33×10^{6}	4.9×10^{9}
[6]	644	0.118	7.5×10^{-4}	6.3×10^{6}	8.4×10^{9}
[7]	641	0.110	1.5×10^{-4}	1.3×10^{6}	9.0×10^{9}

a denotes Ru→bpy MLCT excited states, other λ_{em} values are ~525–545 nm for [4], [6] and [7] are assigned as metal-centered and metal-to-ligand charge transfer excited states.

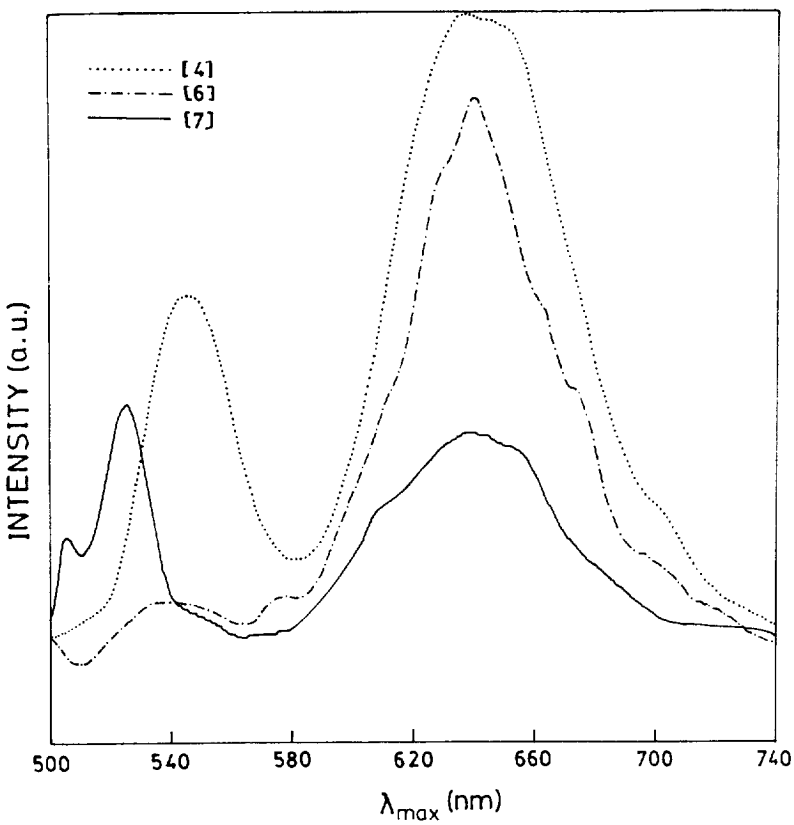

Fig. 5. Luminescence spectra of complexes [4], [6] and [7]; excitation were performed at $\lambda_{abs} \approx 480$ nm.

Hence the 525–545 nm emission bands have been assigned tentatively as metal-to-ligand charge transfers and metal-centred transitions. Thus the bridging between copper and ruthenium moieties introduces a new high energy state in the system. This proves that both the copper and ruthenium metal centres are emitters. It follows that energy transfer occurs from the ruthenium to the copper sub-unit due to ligand dissociation and the solvent (CH_3CN) takes the place of the copper coordination site [40]. Latimer type diagram of the complex [6] illustrate this inter-relationship using excited state redox potential in Fig. 7 in which oxidation of Cu(I) to Cu(II) occurs readily and hence the excited states of Cu(I)–polypyridyl sub-unit are potentially strongly reductant [33].

On the basis of the above facts, lifetimes and emission intensities decrease in the order $(AsPh_3)_2 >$ (phen)$(AsPh_3) >$ (bpy)$(AsPh_3)$ when $\lambda_{em} \approx 640$ nm, suggesting that non-radiative decay processes increase in efficiency along the same sequence and are significantly more effective in the bipyridine complex. These processes are also due to the favourable energetics of the bipyridine ligand bound to copper. The observation shows that the quantum efficiency of electron transfer is limited by the competing non-radiative decay process, which is quite rapid ($\approx 10^{9}$ s^{-1}).

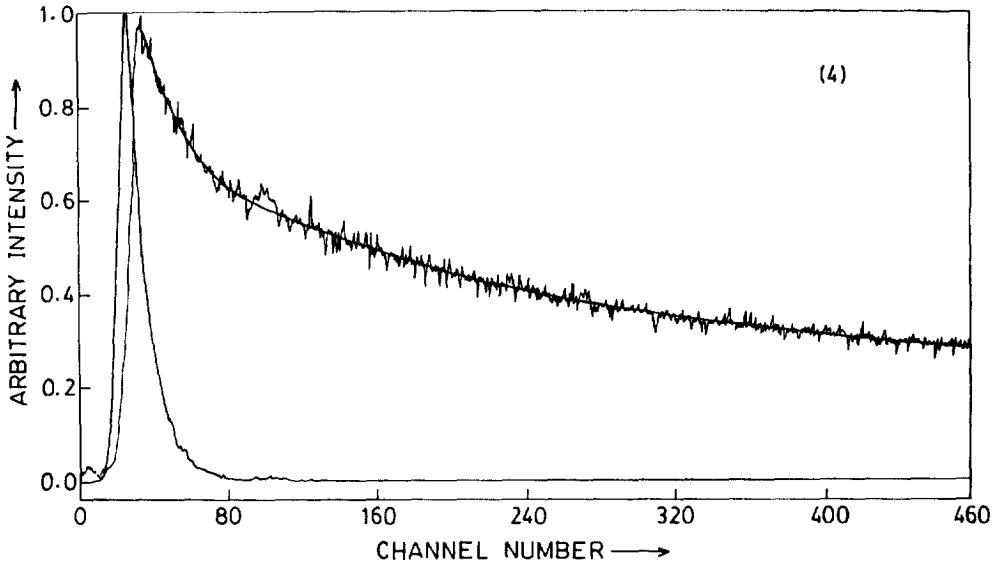

Fig. 6. Fluorescence decay curve of complex [4] at emission wavelength of 642 nm.

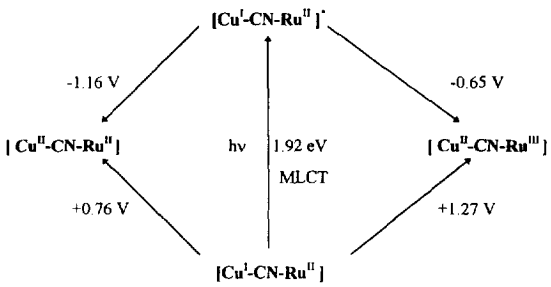

Fig. 7. Latimer type diagram showing ground and excited state potential of [6].

3. CONCLUSION

These studies show that the $[Ru(bpy)_2Cl]^+$ chromophore bound to copper moieties through a CN bridge cannot be easily functionalised. These moieties are redox active and ligand substitution usually causes a small change in excited state energy, but they can significantly change the excited state lifetime and the excited state redox potential. These excitations in the $[Ru(bpy)_2Cl]^+$ chromophore play a major role in determining the occurrence of specific intramolecular electron transfer processes.

Though the complexes exhibit relatively short lifetimes, compared to analogous complexes at room temperature, their desired properties may lead to the simple preparation of photochemical devices [41]. Studies in these directions are in progress.

Acknowledgements—The authors are grateful to Prof. T. K. Chandrashekar, Department of Chemistry, Indian Institute of Technology (Kanpur, India) and Prof. K. Bhattacharya and his group, Department of Physical Chemistry, Indian Association for the Cultivation of Science (Calcutta, India) for the use of the luminescence spectrophotometer and the lifetime measurement apparatus respectively. We gratefully acknowledge I.I.T. Delhi, India for the low frequency IR Spectra and Cyclic voltammogram data. The authors are grateful to Mr. H. M. Guniyal, CDRI, RSIC, Lucknow, for recording the ^{2}D–NMR spectrum.

REFERENCES

1. (a) Balzani, V., Moggi, L., Monfrin, M. F., Bolletta, F., Gleria, M., *Science*, 1975, **189**, 852; (b) Balzani, V., Bolletta, F., Gandolfi, M. and Maestri, M., *Top. Curr. Chem.*, 1978, **75**, 1; (c) Sutin, N. and Creutz, C., *Pure Appl. Chem.*, 1980, **52**, 2717; (d) Kalyanasundaram, K., *Coord. Chem. Rev.*, 1982, **46**, 159.
2. (a) Balzani, V., Barigelletti, F. and Cola, L. D., *Top. Curr. Chem.*, 1990, **158**, 31; (b) Kalyanasundaram, K., *Photochemistry of Polypyridine and Porphyrin Complexes*. Academic Press, New York, 1992, p. 105.
3. (a) Denti, G., Campagna, S., Sabatino, L., Serroni, S., Ciano, M. and Balzani, V., *Inorg. Chem.*, 1990, **29**, 4751; (b) Fagalde, F. and Katz, N. E., *J. Chem. Soc., Dalton Trans.*, 1993, 571.
4. (a) Scandola, F., Indelli, M. T., Chiorbolli, C., Bignozzi, A., *Top. Curr. Chem.*, 1990, **158**, 73 and refs therein; (b) Denti, G., Serroni, S., Campagna, S., Ricevuto, V., Juris, A., Ciano, M. and Balzani, V., *Inorg. Chim. Acta*, 1992, **198-200**, 507; (c) Denti, G., Campagna, S., Serroni, S., Ciano, M. and Balzani, V., *J. Am. Chem. Soc.*, 1992, **114**, 2944; (d) Bardwell, D. A., Barigelletti, F., Cleary, R. L., Flamigni, L., Guardigli, M., Jeffery, J. C. and Ward, M. D., *Inorg. Chem.*, 1995, **34**, 2438.
5. (a) Scandola, F., Bignozzi, C. A., Chiorboli, C.,

Indelli, M.T., Rampi, M.A., *Coord. Chem. Rev.*, 1990, **97**, 299 and refs. therein; (b) Bignozzi, C. A. and Scandola, F. A., *Inorg. Chem.*, 1984, **23**, 1540; (c) Carriedo, G. A., Connelly, N. G., Crespo, M. C., Duarmby, I. C., Riera, V. and Worth, G. H., *J. Chem. Soc., Dalton Trans.*, 1991, 315; (d) Darensbourg, D. J., Yoder, J. C., Holtcamp, M. W., Klausmeyer, K. K. and Reibenspies, J. H., *Inorg. Chem.*, 1996, **35**, 4764.

6. (a) Baird, G. J., Davies, S. G., Moon, S. D., Simpson, S. J. and Jones, R. H., *J. Chem. Soc. Dalton Trans.*, 1985, 1479; (b) Christofides, A., Connelly, N. G., Lawson, H. J., Loyns, A. C., Orpen, A. G., Simmonds, M. O. and Worth, G. H., *J. Chem. Soc. Dalton. Trans.*, 1991, 1595; (c) Laidlaw, W. M. and Denning, R. G., *J. Chem. Soc. Dalton. Trans.*, 1994, 1987; (d) Laidlaw, W. M. and Denning, R. G., *Polyhedron*, 1994, **13**, 1880 and 2337.
7. Singh, R. and Dikshit, S. K., *Polyhedron*, 1993, **12**, 1697.
8. Kutal, C., *Coord. Chem. Rev.*, 1990, **99**, 213 (and refs therein).
9. Singh, R. and Dikshit, S. K., *Chem. Educ.*, 1992, **9**, 51.
10. Sulivan, B. P., Salmon, D. J. and Meyer, T. J., *Inorg. Chem.*, 1978, **17**, 3334.
11. Bruce, M. I., Hameister, C., Swincer, A. G. and Wallis, R. C., *Inorg. Synth.*, 1982, **21**, 78.
12. Reichle, W. T., *Inorg. Chim. Acta.*, 1971, **5**, 325.
13. Geary, W. J., *Coord. Chem. Rev.*, 1971, **7**, 81.
14. Cooper, D. and Plane, R. A., *Inorg. Chem.*, 1966, **5**, 2209.
15. Nakamoto, K., *Infrared and Raman Spectra of Inorganic and Coordination Comounds*, John Wiley, New York, 1986, 278.
16. (a) Whiffen, D. H., *J. Chem. Soc.*, 1956, 1350 (b) Shobatake, K., Postmus, C., Ferraro, J. R. and Nakamoto, K., *Appl. Spectrosc.*, 1969, **23**, 12. (c) Jones, A. G. and Powell, D. B., *Spectrochim. Acta*, 1974, **30A**, 563. (d) Haines, R. J. and Dupreez, A. L., *J. Organomet. Chem.*, 1975, **84**, 357; Lippincott, E. R. and Welson, R. D., *Spectrochim. Acta*, 1958, **10**, 307. (e) Edwards, H. G. M., Lewis, T. R. and Turner, P. H., *Inorg. Chim. Acta*, 1994, **216**, 191.
17. Konya, K. and Nakamoto, K., *Spectrochim. Acta*, 1973, **29A**, 1965.
18. Percy, G. C. and Thornton, D. A., *J. Mol. Struct.*, 1972, **14**, 313.
19. Wilde, R. E., Srinivasan, T. K. K., *J. Inorg. Nucl. Chem.*, 1974, **36**, 323.
20. Saito, Y., Takemoto, J., Hutchinson, B. and Nakamoto, K., *Inorg. Chem.*, 1972, **11**, 2003.
21. Staniewicz, R. J., Hendriker, D. G. and Griffiths, P. R., *Inorg. Nucl. Chem. Lett.*, 1977, **13**, 467.
22. (a) Mackey, K. M., Sowerby, D. B., Young, W. C., *Spectrochim. Acta*, 1968, **24A**, 611; (b) Jones, L. H., *J. Chem. Phys.*, **29**, 1958, 463.
23. (a) Wilezewski, T., Bochenska, M. and Niernet, J. F., *J. Organomet. Chem.*, 1981, **215**, 87; (b) Blackmore, T., Bruce, M. I. and Stone, F. G. A., *J. Chem. Soc. (A).*, 1971, 2376.
24. Prasad, R., Mishra, L. and Agarwala, U.C., *Ind. J. Chem.*, 1991, **30A**, 45<comment>also 162 and refs. therein.
25. (a) Constable, E. C. and Holmes, J. M., *Inorg. Chim. Acta.*, 1987, **126**, 195; (b) Kelly, J. M., O'Connell, C. M. and Vos, J. G., *J. Chem. Soc. Dalton Trans.*, 1986, 253.
26. Heijden, M., Van Vliet, P. M., Haasnoot, J. G. and Reedijk, J., *J. Chem. Soc., Dalton Trans.*, 1993, 3675.
27. Birchel, J. D., O'Donoghue, T. D. and Wood, J. R., *Inorg. Chim. Acta*, 1979, **37**, L461.
28. Singh, R. and Dikshit, S. K., *Polyhedron*, 1995, **14**, 1799 (and refs. therein).
29. Bruce, M. I., Catlow, A., Humphery, M. G., Coutsantonis, G. A., Snow, M. R. and Tiekink, E. R. T., *J. Organomet. Chem.*, 1988, **388**, 59.
30. Fergusson, J. E. and Harris, G.M., *J. Chem. Soc. (A)*, 1966, 1293.
31. Bryant, G. M., Fergusson, J. E. and Powell, H. K. G., *Aust. J. Chem.*, 1971, **24**, 257.
32. Cutin, E. H. and Katz, N. E., *Polyhedron*, 1993, **12**, 955.
33. Rader, A., McMillin, D. R., Buckner, T., Matthews, G., Casadonte, J., Lengel, K., Whittaker, B., Darmon, M. and Lytle, E., *J. Am. Chem. Soc.*, 1981, **103**, 3906.
34. Brauenstein, C. H., Baker, A. D., Strekas, T. C. and Gafney, H. D., *Inorg. Chem.*, 1984, **23**, 857.
35. Hadjikakou, S. K., Akrivos, P. D., Karagiannidis, P. and Papadopoulos, N., *Polyhedron*, 1995, **14**, 2999.
36. Nakamaru, K., *Bull. Chem. Soc. Jpn.*, 1982, **55**, 2697.
37. (a) Buckner, M. T., Matthews, T. J., Lytle, F. E. and McMillin, D. R., *J. Am. Chem. Soc.*, 1979, **101**, 7863; (b) Blasse, G. and McMillin, D. R., *Chem. Phys. Lett.*, 1980, **70**, 1.
38. Li, D., Yip, H. K., Che, C. M., Zhou, Z. Y., Mak, T. C. W. and Liu, S. T., *J. Chem. Soc., Dalton Trans.*, 1992, 2445.
39. Henry, M., Wotton, J. L., Khan, S. I. and Zink, J. I., *Inorg. Chem.*, 1997, **36**, 796.
40. Kalyanasundaram, K., *Photochemistry of Polypyridine and Porphyrin Complexes*, Academic Press, New York, 1992, p. 293.
41. Balzani, V., Moggi, L. and Scandola, F., *Supramolecular Photochemistry*, Riedel, The Netherland, 1987.

Pergamon

PII: S0277-5387(98)00073-4

Polyhedron Vol. 17, No. 18, pp. 3083–3088, 1998
© 1998 Elsevier Science Ltd
All rights reserved. Printed in Great Britain
0277-5387/98 $19.00+0.00

Rhodium(I) complexes of the dppn ligand, 3,6-bis(2′-pyridyl)pyridazine and X-ray structure of $[Rh(CO)(dppn)(PPh_3)](PF_6)$

Noureddine Rahmouni,[a,c] Ali A. Bahsoun,[a] Marie-Thérèse Youinou,[a] John A. Osborn,[a]* Jean Fischer[b] and Aziz Ezzamarty[c]

[a] Laboratoire de Chimie des Métaux de Transition et de Catalyse

[b] Laboratoire de Cristallochimie et Chimie Structurale, URA 424 C.N.R.S., Institut Le Bel, Université Louis Pasteur, 4 rue Blaise Pascal, 67000 Strasbourg, France

[c] Laboratoire de Catalyse, Université Hassan II, Faculté des Sciences Ain Chok, B.P. 5366, Maârif, Casablanca, Maroc

(Received 19 September 1997: accepted 12 February 1998)

Abstract—The reaction of the 3,6-bis(2′-pyridyl)pyridazine(dppn) ligand, with one and two equivalents of $[Rh(CO)_2S_n](PF_6)$, (s = THF), yields respectively the mononuclear complex $[Rh(CO)_2(dppn)](PF_6)$ **1** and the binuclear complex $[Rh_2(CO)_4(dppn)](PF_6)_2$ **3**. Furthermore, the reaction of **1** with PPh_3 results in a substitution reaction to give $[Rh(CO)(dppn)(PPh_3)_2](PF_6)$ **2**. The unsaturated complex **3** reacts with the monodentate phosphine PPh_3 to yield a mixture of the known compound $[Rh(CO)_2(PPh_3)_2](PF_6)$ and of the mononuclear $[Rh(CO)(dppn)(PPh_3)](PF_6)$ **4**, the crystal structure of which was established by X-ray diffraction. Moreover, **3** reacts with the bis(diphenylphosphino)methane(dppm) ligand in a 1 : 2 ratio to form the binuclear A-frame complex $[Rh_2(CO)_2(dppn)(\mu\text{-dppm})_2](PF_6)_2$ **5**. However, the reaction of **3** with excess dppm (1 : 4 ratio) gives the known complex $[Rh(CO)(dppm)_2](PF_6)$ **6**. © 1998 Elsevier Science Ltd. All rights reserved

Keywords: 3,6-bis(2′-pyridyl)pyridazine; bis(diphenylphosphino)methane; triphenylphosphine; carbonyl; rhodium; X-ray structure.

The heterocyclic 3,6-bis(2′-pyridyl)pyridazine ligand, hereafter dppn, is interesting in that it provides two adjacent chelating sites which are able to coordinate transition metals at an internuclear distance of approximately 3.5 Å. This can allow the two metals to interact via ligand bridges or electronically across the dppn planar framework. Such properties have been exploited in several ways to synthesise, for example: (i) a binuclear Ni(II) complex [1] in which the magnetic properties denote the presence of an exchange interaction between the two metal centres; (ii) several binuclear Cu(II) complexes [2] such as $[Cu_2(\mu\text{-}OH)Cl_3(H_2O)(dppn)]$, for which structural studies show that the hydroxy ligand bridges the two metal centres with a Cu(II) to Cu(II) separation of 3.376 Å. In $[Cu_2(\mu\text{-}OH)Br_3(dppn)]_n$, a polymeric stacking of binuclear units joined through bromide ligands is found; (iii) certain heterobinuclear complexes using two separate steps with a sequential addition of one equivalent of each of metal complexes [3]; (iv) a tetranuclear Cu(I) grid-like complex, $[Cu_4(dppn)_4]^{4+}$. It was seen that when one tetrahedral metal ion is incorporated into the dppn ligand, self-assembly of the monometallic units is possible to yield a complex in which the four copper atoms are coplanar and spanned by four dppn ligands. The X-ray structure determination shows that pairs of the quasi-planar dppn ligands align in parallel above and below the rhombic array of Cu_4 [4]. This principle has subsequently been expanded to the synthesis of a variety of fascinating self-assembled structures [5].

The presence of two metals held in close proximity is conceptually of great interest in homogeneous catalysts for several reasons. For example, a substrate may be activated by a simultaneous interaction with both

* Author to whom correspondence should be addressed.

metal centres. Alternatively, the two metals could serve to activate selectively different substrates, but their proximity would allow further interactions between the activated molecules. Heterobimetallic systems may be of particular interest for this type of reactivity.

In this paper we present the synthesis and characterisation of mononuclear and binuclear cationic Rh(I) complexes of the dppn ligand. Further reactions of the dirhodium complex of dppn with PPh_3 and $CH_2(PPh_2)_2$ were also studied. The single crystal X-ray structure of a monomeric dppn derivative of Rh(I) is also described.

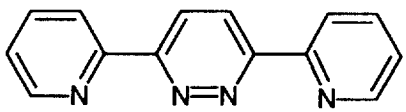

dppn

EXPERIMENTAL

General

All reactions were carried out under an atmosphere of prepurified nitrogen or argon using standard Schlenk techniques or performed in a Vacuum Atmospheres Corporation glove box. Solvents such as Et_2O. THF and hydrocarbons were distilled from sodium and benzophenone and CH_2Cl_2 from CaH_2 under nitrogen. The 3,6-bis(2′-pyridyl)pyridazine(dppn)[6] and bis(diphenylphosphino)methane(dppm) ligands [7] as well as $[Rh(CO)_2Cl]_2$ [8] were prepared according to literature procedures. $RhCl_3 \cdot 3H_2O$. $AgPF_6$ and PPh_3 were respectively purchased from Johnson Matthey and Strem Chemicals and used as supplied.

IR spectra were recorded on a Perkin–Elmer 597 instrument. NMR spectra were run on a Bruker SY 200 spectrometer. Solvent peaks (^1H, ^{13}C NMR) served as internal references with the data fitted relatively to TMS. $^{31}P\{^1H\}$ NMR spectra were referenced to external 85% H_3PO_4 with downfield chemical shifts reported as positive. Attempts to record the mass spectra of these compounds by spectroscopic methods were unsuccessful.

Preparation of $[Rh(CO)_2(dppn)](PF_6)$ **1**

A solution of $[Rh(CO)_2S_n](PF_6)$(S = THF) prepared from a 2:1 reaction mixture of $AgPF_6$(0.215 mg, 0.850 mmol) and $[Rh(CO)_2Cl]_2$ (0.165 mg, 0.425 mmol) in THF (10 cm^3) was added dropwise to a solution of dppn (0.200 g, 0.850 mmol) in benzene (10 cm^3). The yellow-green precipitate which formed rapidly was separated and washed successively with THF (2 cm^3) and CH_2Cl_2(2 cm^3)(Yield: 85%). IR (Nujol mull, cm^{-1}) ν_{CO} 2100 (s), 2050 (s); ν_{P-F} 840 (br, s), 560 (s); $\nu_{(C=C\text{ or }C=N)}$ 1600 (mw), 1590 (w). Anal: Calcd for $C_{16}H_{10}N_4O_2F_6PRh$: C, 35.71; H, 1.87; N, 10.44; Rh, 19.12. Found: C, 36.54; H, 1.52; N, 9.58; Rh, 18.13.

Preparation of $[Rh(CO)(dppn)(PPh_3)_2](PF_6)$ **2**

Complex **1** (0.100 g, 0.185 mmol) in acetone (5 cm^3) was added to an acetone solution (5 cm^3) of PPh_3 (0.097 g, 0.370 mmol). The light brown precipitate was filtered, washed several times with Et_2O (3 × 5 cm^3) and dried under vacuum (Yield: 85%). IR (Nujol mull, cm^{-1}) ν_{CO} 1940. $^{31}P(^1H)$ NMR, ($(CD_3)_2CO$, δ_{ppm}), 41 (d, $I = 2$, $^1J_{Rh-P} = 113$ Hz, PPh_3), −143 (hept, $I = 1$, PF_6^-). Anal: Calcd for $C_{51}H_{40}N_4OF_6P_3Rh$: C, 59.20; H, 3.90; N, 5.41. Found: C, 58.15; H, 3.93; N, 5.41.

Preparation of $[Rh_2(CO)_4(dppn)](PF_6)_2$ **3**

A solution of dppn (0.100 g, 0.425 mmol) in benzene (5 cm^3) was added to a yellow solution of $[Rh(CO)_2S_n](PF_6)$(0.850 mmol) in THF (5 cm^3). The compound **3** precipitated out as an orange microcrystalline compound which was filtered and washed with THF (2 cm^3) and then CH_2Cl_2 (2 cm^3)(Yield: 90%). IR (Nujol mull, cm^{-1}) ν_{CO} 2100 (s), 2050 (s); ν_{P-F} 840 (br, s), 560 (s); $\nu_{(C=C\text{ or }C=N)}$ 1600 (mw). ^1H NMR ($(CD_3)_2CO$, δ_{ppm}) H arom: 9.35 (s, 2H), 9.22 (d, 2H), 8.89 (d, 2H), 8.67 (t, 2H), 8.16 (t, 2H). Anal: Calcd for $C_{18}H_{10}N_4O_4F_{12}P_2Rh_2$: C, 25.68; H, 1.20; N, 6.65; P, 7.36; Rh, 24.44. Found: C, 26.35; H, 1.28; N, 6.25; P, 7.25; Rh, 23.26.

Preparation of $[Rh(CO)(dppn)PPh_3)](PF_6)$ **4**

A solution of PPh_3 (0.093 g, 0.356 mmol) in CH_2Cl_2 (5 cm^3) was added dropwise to a slurry of the dimer **3** (0.100 g, 0.119 mmol) in CH_2Cl_2 (5 cm^3) under vigorous stirring for 1 h. The deep red solution was filtered over celite and evaporated to dryness. After recrystallisation from CH_2Cl_2/hexane, a mixture of yellow crystals of the known complex $[Rh(CO)_2(PPh_3)_2](PF_6)$ [9] and of red crystals of $[Rh(CO)(dppn)(PPh_3)](PF_6)$ **4** was obtained. For **4**: IR (Nujol mull, cm $^{-1}$) ν_{CO} 2000 (s); $^{31}P\{^1H\}$ NMR ($(CD_3)_2CO/CH_2Cl_2$, δ_{ppm}), 42.24 (d, $I = 1$, $J_{Rh-P} = 150$ Hz, PPh_3), −142 (hept, $I = 1$, PF_6^-). X-ray quality crystals of **4**·$(CH_3)_2CO$ were obtained from a 1:1 mixture of acetone/ethanol.

Preparation of $[Rh_2(CO)_2(dppn)(\mu\text{-dppm})_2](PF_6)_2$ **5**

To a suspension of **3** (0.100 g, 0.119 mmol) in CH_2Cl_2 (5 cm^3) was added dropwise a solution of dppm (0.091 g, 0.237 mmol) in CH_2Cl_2 (5 cm^3). The

reaction mixture was allowed to stir for 2 h during which a deep green colour developed. The green precipitate which formed after addition of Et_2O (40 cm^3) was filtered off, washed successively with C_6H_6 and Et_2O and dried under vacuum (Yield: 90%). IR (Nujol mull, cm^{-1}), besides specific absorptions due to dppn and PF_6^-, ν_{CO} 2000 (vs). $^{31}P\{^1H\}$ NMR (CD_2Cl_2, δppm), 24.5 (m, $I = 4$) and −143 (hept, $I = 2$). ^1H NMR (CD_2Cl_2, δ_{ppm}), 9.4–8 and 7.6–6.8 (m, H arom), 4.03 (m, —CH_2). Anal: Calcd for $C_{66}H_{54}N_4O_2F_{12}P_6Rh_2$: C, 50.99; H, 3.50; N, 3.60; P, 11.97; Rh, 13.24. Found: C, 49.50; H, 3.65; N, 3.70; P, 12.14; Rh, 12.80.

Reaction of **3** *with an excess of dppn to give* $[Rh(CO)(dppm)_2](PF_6)$ **6**

A solution of dppm (0.182 g, 0.473 mmol) in CH_2Cl_2 (5 cm^3) was added to a slurry of the dimer **3** (0.100 g, 0.119 mmol) in CH_2Cl_2 (5 cm^3). The mixture was stirred for 2 h at room temperature and the solvent evaporated to dryness under vacuum. A yellow product **6** was extracted with ether (Yield: 90%). IR (Nujol mull, cm^{-1}) ν_{CO} 1945 (s). $^{31}P\{^1H\}$ NMR (CD_2Cl_2, δ_{ppm}) −19.5 (d, $I = 4$, $J_{Rh-P} = 103$ Hz, dppm), and −143 (hept, $I = 1$, PF_6^-). ^1H NMR ($(CD_3)_2CO$, δ_{ppm}) 7.2–7.5 (m, H arom.), 4.5 ppm (m, —CH_2). Anal: Calcd for $C_{51}H_{44}OF_6P_5Rh$: C, 58.62; H, 4.21; P, 14.85; Rh, 9.86. Found: C, 58.24; H, 4.08; P, 14.13; Rh, 9.84.

X-ray crystal structure analysis of $[Rh(CO)(dppn)(PPh_3)](PF_6)\cdot$*acetone*, **4**·acetone

Suitable red single crystals for **4**·acetone were obtained by recrystallisation from an acetone-ethanol mixture at room temperature. One single crystal was cut out from a cluster of deep red crystals and mounted on a rotation-free goniometer head. A systematic search in reciprocal space using a Enraf-Nonius CAD4–F automatic diffractometer showed that crystals of **4**·acetone belong to the triclinic system. Quantitative data were obtained at room temperature. All experimental parameters used are given in Table 1. The resulting data set was transferred to a VAX computer, and for all subsequent calculations the Enraf-Nonius Molen package was used [10]. Three standard reflections were measured every hour during the entire data period showed no significant trend. The raw data were converted to intensities and corrected for Lorentz and polarisation factors. Absorption corrections derived from the Φ scans of 4 reflections were applied. The structure was solved using the heavy atom method. After refinement of the heavy atoms, a difference-Fourier map revealed maxima of residual electronic density close to the positions expected for hydrogen atoms; they were introduced in structure factor calculations by their computed coordinates (C—H = 0.95 Å) and isotropic temperature factors

Table 1. X-ray experimental data for **4**·acetone

Formula	$C_{33}H_{25}N_4OPRh \cdot PF_6 \cdot OC(CH_3)_2$
Molecular weight	830.5
Colour	red
Crystal system	triclinic
a (Å)	13.321(4)
b (Å)	13.405(4)
c (Å)	10.603(3)
α (°)	97.72(2)
β (°)	111.26(2)
γ (°)	84.75(2)
V (Å^3)	1746.6
Z	2
D_{calc} (g cm^{-3})	1.579
Wavelength (Å)	0.7107
μ (cm^{-1})	6.396
Space group	$P\bar{1}$
Diffractometer	Nonius CAD4-F
Crystal size (mm)	0.23 × 0.28 × 0.35
T (K)	293
Radiation	Mo–K_α graphite monochromated
Mode	$\theta/2\theta$
Scan speed	variable
Scan width (°)	$1.00 + 0.34 \times \mathrm{tg}(\theta)$
Octants	$\pm h \pm k + l$
θ min/max (°)	2/23
Number of data colleted	4885
Number of data with $I > 3\sigma(I)$	3166
Number of variables	460
Abs min/max	0.73/1.09
$R(F)$	0.043
$R_w(F)$	0.056
p	0.08
Largest peak in final diff. (e Å^{-3})	0.10
GOF	1.095

such as B(H) = 1.3 Beqv(C) Å^2 but not refined. Full least squares refinements: $\sigma^2(F^2) = \sigma^2$ counts $+ (pI)^2$. A final difference map revealed no significant maxima. The scattering factor coefficients and anomalous dispersion coefficients come respectively from [11]. Table 1 lists experimental details and final results.

RESULTS AND DISCUSSION

The deep yellow-green compound. $[Rh(CO)_2(dppn)](PF_6)$ **1**, was obtained in high yield by the reaction of equimolar amounts of $[Rh(CO)_2(THF)_n](PF_6)$ and dppn [6]. The IR spectrum of **1** displays two strong absorptions at 2100 and 2050 cm^{-1}, typical of terminal *cis* carbonyl ligands and similar to those reported for the analogous 2,2′-bipyridine of *o*-phenenthroline carbonyl complexes of Rh(I)[12,13]. Hence one chelating site of the dppn ligand is coordinated to the Rh(I) centre completing the square planar configuration for **1**. The reaction of **1** with PPh_3 (1 : 2 mol ratio) gives a brick red complex

which analyses as $[Rh(CO)(dppn)(PPh_3)_2](PF_6)$ **2**. The $^{31}P\{^1H\}$ NMR spectrum shows a doublet at 41 ppm [^1J(Rh—P) = 113 Hz] which suggests a trigonal bipyramid configuration for the pentacoordinated Rh(I) derivative [13] with two axial PPh_3 ligands and an equatorial CO ligand which is also revealed by the presence of a strong absorption band at 1940 cm^{-1} in the IR spectrum.

When two equivalents of $[Rh(CO)_2(THF)_n](PF_6)$ are added to one equivalent of dppn in a THF/C_6H_6 mixture, an orange dimeric complex **3**, corresponding to $[Rh_2(CO)_4(dppn)](PF_6)_2$, is obtained. Its ^1H NMR spectrum shows five aromatic resonances of equal intensity as one singlet, two doublets and two triplets indicating that both coordination sites of the dppn ligand are occupied by Rh(I) ions. Also, the IR spectrum in the carbonyl region shows only two terminal ν_{CO} absorptions at 2100 and 2050 cm^{-1}. Hence we can propose the symmetric binuclear structure shown in Scheme 1.

However, one Rh(I) in **3** can be relatively easily removed by ligands such as phosphines (Scheme 1). Treatment of **3** with PPh_3 gives $[Rh(CO)_2(PPh_3)_2](PF_6)$ [9] and $[Rh(CO)(dppn)(PPh_3)](PF_6)$ **4**, the formation of which can be followed by ^{31}P NMR. We have structurally characterised **4**·$(CH_3)_2CO$ by X-ray diffraction (Fig. 1), which enables us in part to understand the instability of the binuclear unit. The distorted square planar Rh(I) cation is quasi-symmetrically coordinated to the two nitrogen atoms (N1 and N12) by one chelating site of the dppn ligand. The two Rh—N distances (Rh—N1 = 2.090 (5) Å) and Rh—N12 = 2.096 (5) Å and the Rh—CO of 1.833 (7) Å as well as the Rh—P of 2.267 (2) Å are within the range of expected bond lengths for this type of Rh(I) cation. Selected bond distances and angles are given in Table 2. The unexpected feature of this structure is the coordination of PPh_3 to Rh(I) in a *trans* position to N12 of the pyridyl arm and *cis* to the *N*-pyridazine, whereas simple steric considerations might have placed the PPh_3 *cis* to N12. The result is that the phenyl groups of the phosphine block the free chelating site of dppn which may be responsible for the loss of Rh(I) from this site. We therefore sought to stabilise the bimetallic unit in **3** by use of the bis(diphenylphosphino)methane ligand (dppm), which is well known to form binuclear A-Frame structures (Scheme 2).

Treatment of the unsaturated dimer **3** with dppm in CH_2Cl_2 (1 : 2 molar ratio) gives a deep green compound isolated in reasonable yield, which analyses as $[Rh_2(CO)_2(dppn)(dppm)_2](PF_6)_2$ **5**. Its IR spectrum in Nujol mull displays a very strong absorption ν_{CO} at 2000 cm^{-1}), characteristic of terminal carbonyls, as well as absorption bands due to the coordinated ligands dppn and dppm and to the PF_6^- anion. The $^{31}P\{^1H\}$ NMR spectrum shows one signal due to coordinated dppm at δ = 24.5 ppm(m), indicating that **5** possesses only equivalent phosphorus environments, while the ^1H NMR spectrum reveals the presence of a symmetrically coordinated dppn. Therefore the spectroscopic features indicate the formation of a classical

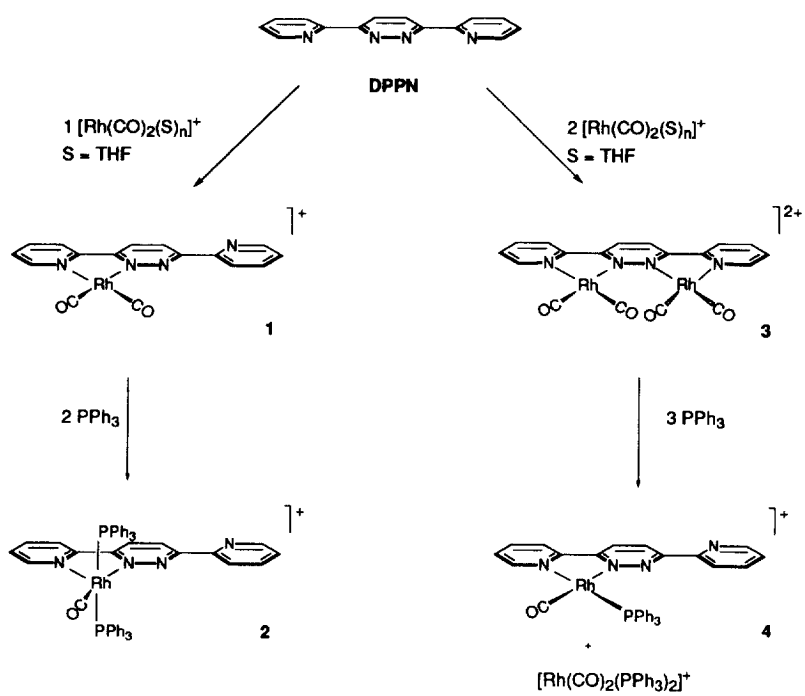

Scheme 1.

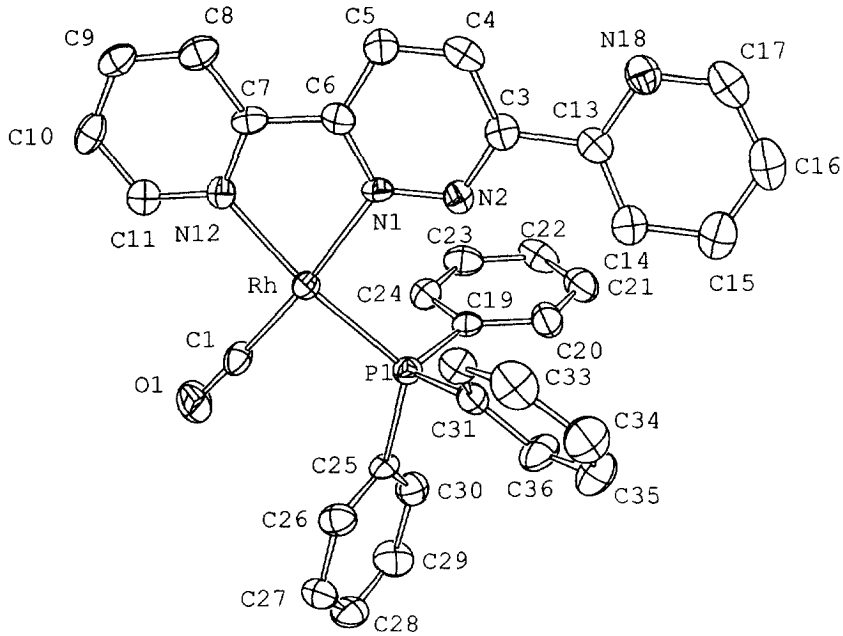

Fig. 1. Ortep plot of one molecule of **4**·acetone showing the numbering scheme used. Ellipsoids are scaled to enclose 50% of the electronic density. Hydrogen and solvate atoms are omitted for clarity.

Table 2. Selected bond lengths (Å) and angles (°) for [Rh(CO)(dppn)(PPh_3)](PF_6)·acetone

Rh—C1	1.833(7)	C8—C9	1.387(9)
Rh—N1	2.090(5)	C7—N12	1.353(7)
Rh—N12	2.096(5)	C9—C10	1.367(9)
Rh—P1	2.267(2)	C10—C11	1.377(9)
C1—O1	1.141(7)	C11—N12	1.341(8)
N1—N2	1.346(7)	C13—C14	1.375(9)
N1—C6	1.344(7)	C13—N18	1.338(8)
N2—C3	1.325(8)	C14—C15	1.395(9)
C3—C4	1.409(9)	C15—C16	1.36(1)
C3—C13	1.491(9)	C16—C17	1.38(1)
C4—C5	1.346(9)	C17—N18	1.330(9)
C5—C6	1.402(8)	P1—C19	1.841(7)
C6—C7	1.468(8)	P1—C25	1.823(6)
C7—C8	1.382(8)	P1—C31	1.832(6)
C1—Rh—N1	174.5(2)	N12—Rh—P1	172.7(1)
C1—Rh—N12	97.0(2)	Rh—C1—O1	177.4(6)
C1—Rh—P1	89.6(2)	N1—C6—C7	115.5(5)
N1—Rh—N12	77.5(2)	C6—C7—N12	115.1(5)
N1—Rh—P1	95.9(1)		

A-frame type structure as in **5a** with two bridging dppm units occupying mutually *trans* positions at the two Rh(I) centres and with the tetradentate dppn ligand as third bridge. Each Rh(I) would then possess a $18e^-$ configuration with a trigonal bipyramidal geometry (TBP) based on the CO ligand and a chelating site of the dppn ligand in the equatorial plane.

However we cannot exclude two other structural possibilities where only either the central pyridazine or the two pyridine end groups are coordinated to rhodium, as in **5b** and **5c** respectively; both Rh(I) atoms would then possess a $16e^-$ configuration. Such structures gain support from preliminary studies which show that this complex reacts rapidly with CO and H_2, more typical of an unsaturated Rh(I) centre. Further studies of this compound and its reactivity are in progress.

Finally, we found that the reaction of four equivalents of dppm with complex **3** in CH_2Cl_2 occurs with the total displacement of the dppn ligand, yielding a complex **6** having an analogous formulation to that already synthesised by another route $[Rh(CO)(dppm)_2]^+$[14]. Its spectroscopic features, including the IR spectrum (ν_{CO} at 1945 cm^{-1}) and the $^{31}P\{^1H\}$ NMR data in CD_2Cl_2 ($\delta = -19.5$ ppm (d), with $^1J_{Rh-P} = 103$ Hz), are closely similar to those previously reported.

CONCLUSION

The 3,6-bis(2′-pyridyl)pyridazine ligand, which possesses two contiguous binding sites for metal ions, has been found to form both mononuclear and binuclear complexes with Rh(I). However, the binuclear compounds were found to be relatively lab-

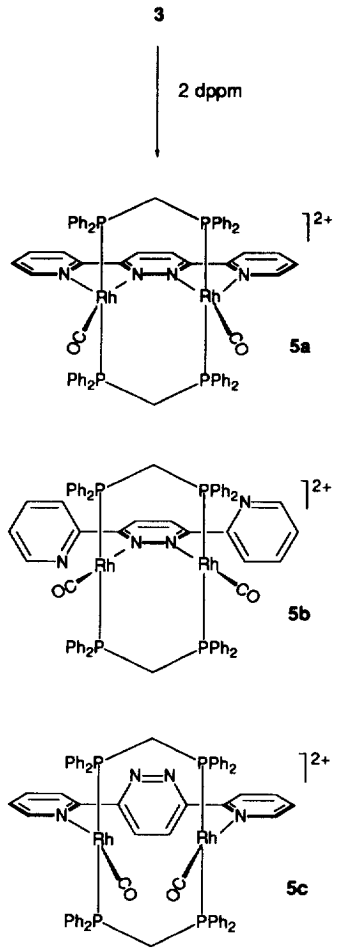

Scheme 2.

ile but their stability could be increased, in part, by the binding of further bridging ligands such as dppm.

Acknowledgements—We thank Dr Rafaël Sablong and Régis Gauvin for helpful discussions, the C.N.R.S. for financial support and the Moroccan Government for a research leave accorded to Noureddine Rahmouni.

REFERENCES

1. Ball, P. W. and Blake, A. B., *J. Chem. Soc. (A)*, 1969, 1415.
2. Ghedini, M., De Munno, G., Denti, G., Manotti-Lanfredi, A. M. and Tiripicchio, A., *Inorg. Chim. Acta*, 1982, **57,** 87; Dapporto, P., De Munno, G., Sega, A. and Mealli, C., *Inorg. Chim. Acta*, 1984, **83,** 171.
3. Ghedini, M., Neve, F., Morazzoni, F. and Oliva, C., *Polyhedron*, 1985, **4,** 497; Tiripicchio, A., Manotti-Lanfredi, A. M., Ghedini, M. and Neve, F., *J. Chem. Soc, Chem. Commun.*, 1983, 97.
4. Youinou, M.-T., Rahmouni, N., Fischer, J. and Osborn, J. A., *Angew. Chem., Int. Ed. Engl.*, 1992, **31,** 733.
5. Baxter, P. N. W., Lehn, J.-M., Fischer, J. and Youinou, M.-T., *Angew. Chem., Int. Ed. Engl.*, 1994, **33,** 2284; Warrener, R. N., Elsey, G. M., Sankar, I. V., Butler, D. N., Pekos, P. and Kennard, C. H. L., *Tetrahedron Lett.*, 1994, **35,** 6745.
6. Butte, W. A. and Case, F. H., *J. Org. Chem.*, 1961, **26,** 4690.
7. Sommer, K., *Z. Anorg. Allg. Chem.*, 1970, **376,** 37.
8. McCleverty, J. A. and Wilkinson, G., *Inorg. Synth.*, 1966, **VIII,** 211.
9. Hieber, W. and Frey, V., *Chem. Ber.*, 1966, **99,** 2614.
10. Fair, C. F. In *MolEN: An Interactive Intelligent System for Structure Analysis*, Nonius, Delf, The Netherlands, 1990.
11. Cromer, D. T. and Waber, J. T., *International Tables for X-ray Crystallography*, Vol. IV, The Kynoch Press, Birmingham, England, 1974, Table 2.2b; Table 2.3.1.
12. Reddy, G. K. N. and Susheelamma, C. H., *J. Chem. Soc., Chem. Commun.*, 1970, 54.
13. Cocevar, C., Mestroni, G. and Camus, A., *J. Organomet. Chem.*, 1972, **35,** 389.
14. Pignolet, L. H., Doughty, D. H., Nowicki, S. C. and Casalnuovo, A. L., *Inorg. Chem.*, 1980, **19,** 2172.

Pergamon

PII: S0277-5387(98)00072-2

Polyhedron Vol. 17, No. 18, pp. 3089–3100, 1998
© 1998 Elsevier Science Ltd
All rights reserved. Printed in Great Britain
0277-5387/98 $19.00+0.00

Ruthenium complexes of 2,2′:6′,2″:6″,2‴:6‴,2⁗-quinquepyridine (qpy) and its derivatives

Edwin C. Constable,*[a] and Juliet V. Walker[b]

[a] Institut für Anorganische Chemie, Spitalstrasse 51, CH-4056 Basel, Switzerland

[b] University Chemical Laboratory, Lensfield Road, Cambridge CB2 1EW, U.K.

(Received 29 January 1998; accepted 12 February 1998)

Abstract—Ruthenium(II) complexes of 2,2′:6′,2″:6″,2‴:6‴,2⁗-quinquepyridine ligands have been prepared and two series of complexes have been isolated. The first series consists of dinuclear double helical species of stoichiometry $[Ru_2L_2Cl_2][PF_6]_2$ in which one ruthenium centre is coordinated to two 2,2′:6′,2″-terpyridine domains of two 2,2′:6′,2″:6″,2‴:6‴, 2⁗-quinquepyridine ligands and the second is coordinated to the remaining 2,2′-bipyridine domains of ligands together with two chloride ligands. The second series consists of mononuclear $[RuL_2][PF_6]_2$ complexes which may be viewed as *prehelicates*. In essence they exhibit the same structural features as $[Ru_2L_2Cl_2][PF_6]_2$ with the exception that the $RuCl_2$ unit has been removed. The $[RuL_2][PF_6]_2$ complexes also exhibit a novel type of conformational isomerism leading to extremely interesting NMR behaviour. © 1998 Elsevier Science Ltd. All rights reserved

Keywords: double-helicates; ruthenium complexes; metallosupramolecular chemistry; X-ray structure.

Self assembling supramolecules have attracted considerable recent attention and those processes in which the assembly is directed by metal-ligand interactions have proved to be particularly versatile and facile [1,2]. We and others have investigated the structural requirements of ligands which give rise to helical co-ordination compounds [3] and have demonstrated that the oligopyridines and molecules containing oligopyridine metal-binding domains are of particular utility for the assembly of multiple-helical species [4,5]. Our interest lies in the development of the co-ordination chemistry of the higher oligopyridines as the organic components of helical supramolecular systems. In previous papers in this series we have discussed the co-ordination behaviour of 2,2′:6′,2″:6″,2‴:6‴,2⁗-quinquepyridine (qpy) and a number of its derivatives with a variety of transition metal ions [6–21]. Following our initial studies, other authors have also discussed aspects of the co-ordination chemistry of qpy and substituted derivatives [22–32]. In this paper we report our detailed studies of ruthenium complexes of qpy ligands.

* Author to whom correspondence should be addressed.

EXPERIMENTAL

Infrared spectra were recorded on Perkin-Elmer 1710, Philips PU9624 or Mattson Genesis Fourier-transform spectrophotometers with samples in compressed KBr discs. Proton NMR spectra were recorded on Brüker WM250, AM400 or Varian Gemini 300 MHz spectrometers. Fast atom bombardment (FAB) and electron-impact (EI) mass spectra were recorded on Kratos MS-50, Kratos MS-890, VG 70-250 or Kratos MS-902 spectrometers; for FAB or FIB spectra the sample was loaded using acetonitrile as a solvent and 3-nitrobenzyl alcohol as supporting matrix. Time of flight (Maldi) spectra were recorded using a PerSeptive Biosystems Voyager-RP Biospectrometry Workstation. Electrochemical measurements were performed with an Amel model 553 potentiostat connected to an Amel model 567 function generator and an Amel model 560/A interface or an Echo Chemie Autolab PGSTAT 20 system using platinum bead or glassy carbon working and auxiliary electrodes with an Ag/AgCl electrode as reference. The experiments were conducted using purified acetonitrile as solvent and freshly recrystallised 0.1 M $[Bu^n4N][BF_4]$ or $[Bu^n4N][PF_6]$ as supporting elec-

trolyte; ferrocene was added at the end of each experiment as an internal reference. The ligands 2,2′:6′,2″:6″,2‴:6‴,2⁗-quinquepyridine (qpy), 4′4‴-diphenyl-2,2′:6′,2″:6″,2‴:6‴,2⁗-quinquepyridine (dpqpy), and 4′,4‴-bis(4-chlorophenyl)-2,2′:6′,2″:6″,2‴:6‴,2⁗-quinquepyridine (dcqpy) were prepared as previously described [16]. All other chemicals were used as supplied. Hydrated ruthenium trichloride was purchased from Oxchem.

$[Ru_2L_2Cl_2][PF_6]_2$ (L = *qpy*, *dpqpy*, *dcqpy*)

The appropriate ligand (0.1 mmol) was added to a solution of commercial $RuCl_3 \cdot 3H_2O$ (0.20 g, 0.1 mmol) in ethane-1,2-diol (30 cm^3) containing *N*-ethylmorpholine (2 drops). The mixture was then heated to reflux for 45 min, after which time t.l.c. analysis showed a major red-purple spot. The reaction mixture was then filtered to remove any solids to give a clear red-purple solution. The solutions were then concentrated *in vacuo* and the products precipitated by the addition of methanolic ammonium hexafluorophosphate and water. The red-purple precipitates were then collected (yield ~ 40%) by filtration and recrystallised from methanol.

$[Ru_2(qpy)_2Cl_2][PF_6]_2$. Red-purple microcrystals. (Found: C, 44.3; H, 2.7; N, 10.4% $C_{50}H_{34}N_{10}Ru_2Cl_2P_2F_{12}$ requires C, 44.9; H, 2.6; N, 10.5%). IR (KBr): 1647 w, 1637 m, 1618 m, 1602 m, 1560 w, 1541 w, 1458 m, 1410 w, 1385 s, 1082 w, 1043 w, 1014 w, 847 s, 773 m, 559 s cm^{-1}. Mass spectrum (FAB) *m/z* 1193 $\{Ru_2(qpy)_2Cl_2(PF_6)\}$, 1048 $\{Ru_2(qpy)_2Cl_2\}$.

$[Ru_2(dpqpy)_2Cl_2][PF_6]_2$. Red-purple microcrystals. (Found: C, 54.0; H, 3.4; N, 8.3% $C_{74}H_{50}N_{10}Ru_2Cl_2P_2F_{12}$ requires C, 54.1; H, 3.1; N, 8.5%). IR (KBr): 1635 m, 1610 s, 1473 m, 1456 m, 1437 m, 1412 s, 1385 s, 1090 w, 1080 w, 1032 m, 1018 m, 845 s, 766 s, 557 s cm^{-1}. Mass spectrum (FAB) *m/z* 1501 $\{Ru_2(dpqpy)_2Cl_2(PF_6)\}$, 1352 $\{Ru_2(dpqpy)_2Cl_2\}$.

$[Ru_2(dcqpy)_2Cl_2][PF_6]_2$. Red-purple microcrystals. (Found: C, 50.9; H, 3.0; N, 8.4% $C_{74}H_{46}N_{10}Ru_2Cl_6P_2F_{12}$. MeCN requires C, 50.1; H, 2.7; N, 8.5%). IR (KBr): 1662 w, 1655 m, 1635 s, 1610 s, 1558 w, 1541 s, 1522 w, 1497 s, 1471 m, 1458 m, 1448 w, 1437 m, 1417 s, 1398 m, 1385 s, 1093 m, 1012 m, 847 s, 557 m cm^{-1}. Mass spectrum (FAB) *m/z* 1634 $\{Ru_2(dcqpy)_2Cl_2(PF_6)\}$, 1489 $\{Ru_2(dcqpy)_2Cl_2\}$.

$[RuL_2][PF_6]_2$, (L = *qpy*, *dpqpy*, *dcqpy*)

The appropriate ligand (0.2 mmol) was added to a solution of $RuCl_3 \cdot 3H_2O$ (0.020 g, 0.1 mmol) in *N*,*N*-dimethylformamide (DMF) (30 cm^3) containing *N*-ethylmorpholine (2 drops). The mixture was left to stand for 1.5 h during which time a green colour developed after which it was heated to reflux for 45 min. After this period, t.l.c. analysis showed one major orange spot. The mixture was then filtered and the clear orange filtrate was concentrated and methanolic ammonium hexafluorophosphate and water added. The orange precipitate was collected by filtration and dissolved in hot methanol. Upon cooling a small amount of purple $[Ru_2L_2Cl_2][PF_6]_2$ was precipitated and removed by filtration; the addition of a few drops of methanolic ammonium hexafluorophosphate to the orange filtrate and reduction in volume *in vacuo* gave the orange products in ~40% yield.

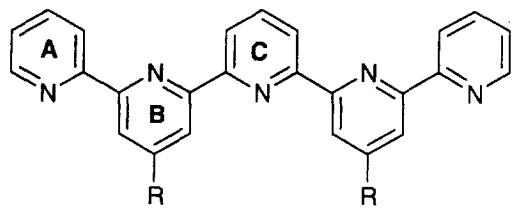

	R
qpy	H
dpqpy	Ph
dcqpy	4-(4-ClC_6H_4)
tbqpy	4-$^tBuC_6H_4$
dtqpy	4-MeC_6H_4

dfqpy

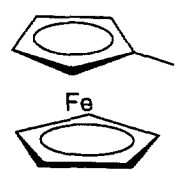

$[Ru(qpy)_2][PF_6]_2$. Orange-red crystals. (Found: C, 47.6; H, 3.4; N, 10.9% $C_{50}H_{34}N_{10}RuP_2F_{12} \cdot 5.5H_2O$ requires C, 47.5; H, 3.6; N 11.1%). IR (KBr): 1633 w, 1619 w, 1606 s, 1581 m, 1569 m, 1560 w, 1471 w, 1458 s, 1429 s, 1410 m, 1385 s, 1097 w, 1029 w, 845 s, 771 m, 557 m. cm^{-1}. Mass spectrum (FAB) *m/z* 1022 $\{Ru(qpy)_2(PF_6)\}$, 877 $\{Ru(qpy)_2\}$.

$[Ru[dpqpy)_2][PF_6]_2$. Orange-red powder, IR (KBr): 1610 s, 1585 m, 1566 w, 1541 m, 1473 w, 1456 m, 1437 m, 1414 s, 1385 m, 1084 m, 1034 m, 1003 w, 845 s, 796 w, 766 s, 698 w, 557 s cm^{-1}. Mass spectrum (FAB) *m/z* 1324 $\{Ru(dpqpy)_2(PF_6)\}$, 1180 $\{Ru[dpqpy)_2\}$.

$[Ru(dcqpy)_2][PF_6]_2$. Orange-red microcrystals, IR (KBr): 1635 w, 1608 s, 1597 m, 1568 m, 1558 m, 1541 m, 1496 m, 1473 m, 1442 m, 1442 m, 1417 m, 1400 m, 1385 w, 1093 w, 1012 w, 841 s, 785 m, 752 w 557 s cm^{-1}. Mass spectrum (FAB) *m/z* 1462 $\{Ru(dcqpy)_2(PF_6)\}$, 1317 $\{Ru(dcqpy)_2\}$.

RESULTS AND DISCUSSION

2,2′:6′,2″:6″,2‴:6‴,2⁗-quinquepyridine complexes

2,2′:6′,2″:6″,2‴:6‴,2⁗-quinquepyridine is a versatile ligand which forms a wide range of mono-helical and multi-helical complexes upon coordination to appropriate transition metal ions. Detailed studies of the behaviour of qpy ligands with a range of metal ions have led to an understanding of the interplay between the ligand donor properties and the size and electronic requirements of the metal centre. The bulk of the studies reported have been concerned with labile metal centres which allow self-assembly processes to dictate the structure of the final product. However, the useful redox, photochemical and photophysical properties of ruthenium(II) oligopyridine complexes have prompted us [17,21] and others [25] to investigate the co-ordination behaviour of qpy ligands with this less labile metal centre.

Reactions of $RuCL_3$ with qpy ligands

The simplest ruthenium complex containing a qpy ligand would be the ruthenium(III) 1:1 adduct with ruthenium trichloride [Ru(L-*N*,*N*′,*N*″)Cl_3](here and throughout L denotes 2,2′:6′,2″:6″,2‴:6‴,2⁗-quinquepyridine or a substituted derivative). We have made a number of attempts to prepare species of this stoichiometry from the reaction of commercial ruthenium trichloride with a variety of qpy ligands under a range of conditions. Our studies are uniformly disappointing and may be summarised as having one of two results. When mild reaction conditions are used (methanol or ethanol as solvent) with the less soluble qpy ligands (qpy, dpqpy, dtqpy, dcqpy), essentially no reaction is observed. This almost certainly reflects the insolubility of the ligands in the protic reaction solvents. In contrast, if solubilised ligands were used (tbqpy, dfqpy) or if less soluble ligands were reacted under forcing conditions (hot DMF or ethane-1,2-diol solvent) mixtures of various ruthenium(II) compounds (see later) were obtained.

Accordingly, we decided to investigate the direct formation of ruthenium(II) complexes from the reactions of ruthenium trichloride with the ligands under reductive conditions., Once again, we found that the less soluble ligands did not react with ruthenium trichloride under mild conditions (refluxing methanol or ethanol containing *N*-ethylmorpholine). In contrast, dark coloured reaction solutions were obtained from the solubilised ligands in alcoholic solvents or upon reaction of all of the ligands in hot DMF or ethane-1,2-diol containing *N*-ethylmorpholine. We concentrate now on the reactions of qpy, dcqpy and dpqpy which may be regarded as typical in their co-ordination behaviour. Thin layer chromatographic (t.l.c.) analysis of the dark-coloured reaction mixtures (silica, 1:7 saturated aqueous KNO_3 solution: acetonitrile) indicated the presence of variable amounts of two close-running orange-red and red-purple products in each case.

Attempts to purify the orange-red and red-purple products by column chromatography (silica) using a variety of mobile phases met with mixed success. The R_f values of the two products are very similar and, although clean fractions could be obtained from the fore-run and the tail, complete separation of the bands was only rarely and irreproducibly achieved. As a result, pure red-purple and orange-red products could only be obtained in very low yields by chromatographic methods. However, we also noted that the red-purple products were significantly less soluble in cold methanol than the orange-red ones and that recrystallisation from methanol yielded the pure red-purple species. From the mother liquor, it was possible to isolate the pure orange-red species by chromatography.

Eventually we found reaction conditions which resulted in large excesses of one of the two products. After 2 h at reflux in ethane-1,2-diol, 1:1 mixtures of ruthenium trichloride and the qpy ligand yielded orange solutions which were shown by t.l.c. to contain predominantly the orange-red product. In contrast, reaction in DMF at room temperature for 1.5 h yielded a deep green solution. Subsequent heating of this green solution to reflux for 45 min gave a purple solution that was shown by t.l.c. to contain only the red-purple product. For each ligand, pure orange-red and red-purple compounds were isolated as their hexafluorophosphate salts after recrystallisation from methanol. Representative microanalytic results are given in the experimental section, although we repeat our previous comments that combustion analysis of ruthenium complexes of the higher oligopyridines frequently gives results with unacceptably low carbon figures.

The red-purple $[Ru_2L_2Cl_2][PF_6]_2$ complexes

In each case, the FAB mass spectra of the red-purple compounds exhibited peaks corresponding to $\{Ru_2L_2Cl_2(PF_6)\}^+$ and $\{Ru_2L_2Cl_2\}^+$ and microanalysis indicated a formulation $[Ru_2L_2Cl_2][PF_6]_2$. Assuming two six co-ordinate ruthenium(II) centres, a total of twelve donor atoms are required. The mass spectrometric results strongly suggest a dimeric formulation and, as we have previously discussed, such a formulation results in a dinuclear double-helical complex with qpy ligands. However, two double-helical structures are possible, as shown in Fig. 1. In one, the two ruthenium centres are equivalent and each is in a N_5Cl environment whilst in the other, one ruthenium is in a N_6 environment whilst the other has a N_4Cl_2 donor set. Electrochemical studies proved to be useful in distinguishing between these possibilities. For each of the compounds, the cyclic voltammogram of an acetonitrile solution exhibits processes in the

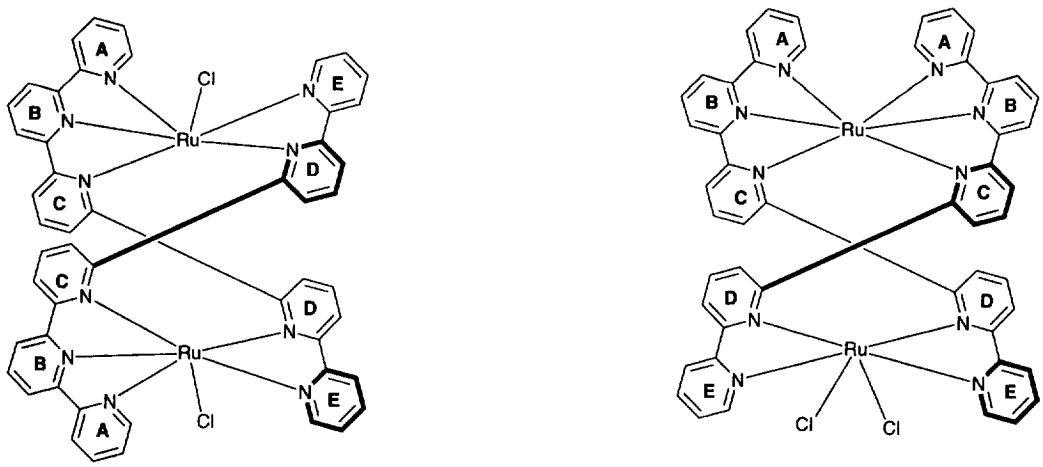

I II

Fig. 1. Possible structures of the complex $[Ru_2L_2Cl_2]^{2+}$.

region of +1.0 V (all potentials quoted vs $F_cF_c^+$: L = qpy, +1.1 V; L = dpqpy, +0.98 V; L = dcqpy, +0.99 V) together with additional processes in the ranges 0.70–0.72 V (L = qpy, +0.70 V; L = dpqpy, +0.74 V; L = dcqpy, +0.72 V) and 0.55–0.58 V (L = qpy, +0.58 V; L = dpqpy, +0.58 V; L = dcqpy, +0.55 V). The +1.00 V process is typical of a $\{Ru(tpy)_2\}$ centre whilst the process at +0.50 V is typical of a RuN_4Cl_2 centre [33]. We have previously shown that electrochemical oxidation of ruthenium(II) chloro complexes in acetonitrile leads to chloride loss and the formation of acetonitrile complexes, and we assign the +0.70 V process, which builds up with time, to a $RuN_4Cl(MeCN)$ centre [21]. In addition, each of the complexes exhibits reductions in the range −1.59 to −1.63 V and −1.76 to −1.80 V. These electrochemical data are only consistent with structure II in Fig. 1.

Further confirmation of the assignment of structure II to the complexes came from their ^1H NMR spectra, data for which are presented in Table 1. In both structures I and II, all of the pyridine rings of each ligand are non-equivalent and 17 resonances are expected in each case for the complex with qpy. The most noticeable features are doublets shifted to high and to low field of the bulk of the resonances; a typical spectrum for the complex $[Ru_2(dcqpy)_2Cl_2][PF_6]_2$ is presented in Fig 2. The following discussion will concentrate on the parent $[Ru_2(qpy)_2Cl_2][PF_6]_2$ complex. The coupling constants (5–6 Hz) unambiguously establish that both of these shifted resonances may be assigned to H^6 of a terminal pyridine ring. As mentioned earlier, the terminal pyridine rings of a given ligand are inequivalent in both of the possible structures presented in Fig. 1 although the large difference in chemical shifts argues indirectly in favour of structure II. The spectra were fully assigned by means of COSY (Fig. 3) and NOE experiments at 250, 400 and 500 MHz which lead to the assignments presented in Table 1. The unambiguous assignment to structure II follows from the H^6 resonances. The strong downfield shifting is a characteristic of H^{6A} of a 2,2′-bipyridine unit in which

Table 1. ^1H NMR spectroscopic data for CD_3CN solutions of the complexes $[Ru_2L_2Cl_2][PF_6]_2$ (L = qpy, dpqpy or dcqpy)

	L = qpy	L = Ph_2qpy	L = cp_2qpy
6A	6.13	6.19	6.17
5A	6.98	6.97	6.98
4A	7.68	7.7	7.68
3A	8.12	8.26	8.22
3B	8.28	8.53	8.51
4B	8.03	—	—
5B	8.32	8.63	8.59
5C	7.09	7.28	7.26
4C	7.54	7.52	7.53
3C	8.12	8.31	8.28
5D	7.33	7.93	7.91
4D	7.62	—	—
3D	7.33	7.8	7.75
6E	9.43	9.48	9.46
5E	7.60	7.08	7.11
4E	8.19	8.02	8.02
3E	8.39	8.60	8.59
ortho[a]		8.19	8.18
meta[a]		7.8	7.81
para[a]		7.7	—
ortho[b]		7.75	7.81
meta[b]		7.6	7.62
para[b]		7.6	—

[a] Aromatic ring attached to ring B.
[b] Aromatic ring attached to ring D.

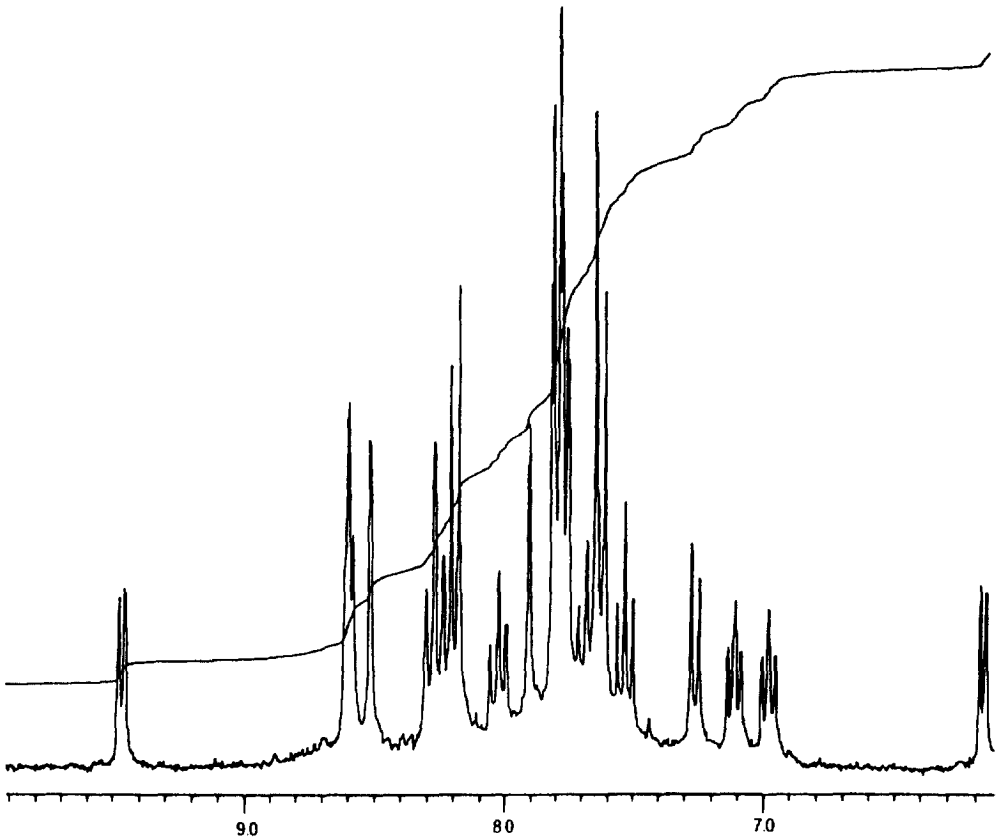

Fig. 2. 400 MHz ^{1}H NMR spectrum of a CD_3CN solution of $[Ru_2(dcqpy)_2Cl_2][PF_6]_2$.

ring A is *cis* and ring D is *trans* to a Ru—Cl bond (cf. δ 10.20 in $[Ru(tpy)(bpy)Cl]^+$). The upfield-shifted H^6 may also be unambiguously assigned to H^{6A} by comparison with the spectra of the $[Ru_2L(tpy)Cl][PF_6]_3$ complexes reported earlier [21]. The spectra of the complexes with the substituted ligands are exactly analogous, and the NMR experiments allow the unambiguous assignment of the structure $[Ru_2(\mu\text{-}\kappa^3N,N',N'':\kappa N''',N'''',\text{-L})_2Cl_2][PF_6]_2$ with a *cis* arrangement of the chloride ligands as presented in Fig. 1. Further support for the assignment of these structures to the complexes comes from the unambiguous solid state determination of the structure of the complex $[Ru_2(qpy)_2(O_2CCO_2)][CF_3SO_3]_2 \cdot 6H_2O$ which was prepared from $Ru_2(qpy)_2Cl_2][PF_6]_2$ [25]. In the complex cation $[Ru_2(qpy)_2(O_2CCO_2)]^{2+}$ the general double-helical dinuclear configuration of structure II is adopted, with the sties of the two chloride ligands being occupied by a didentate oxalate group.

The orange-red $[RuL_2][PF_6]_2$ *complexes*

We now turn to the orange-red compounds. The mass spectra of these compounds exhibit intense peaks corresponding to $\{RuL_2(PF_6)\}^+$ and $\{RuL_2\}^+$ whilst the microanalysis was consistent with a formulation $[RuL_2][PF_6]_2$. Each qpy ligand possesses a total of five nitrogen donors and ruthenium(II) centres are almost invariably six co-ordinate. We have shown previously, that if oligopyridine ligand arrays present more than six donors, that the consequence is the formation of complexes containing hypodentate ligands in which one or more pyridine is not +0.98 V together with reductions in the range −1.6 to −1.9 V. The +1.00 V process is typical of a $\{Ru(tpy)_2\}$ centre and is also remarkably consistent with the process assigned to the RuN_6 centre in the $[Ru_2L_2Cl_2][PF_6]_2$ compounds [33].

There are a three possible structures for such complexes, as shown in Fig. 4. In each structure, the two ligands present a tridentate tpy domain to the metal. In structure III, the two ligands are equivalent and a terminal tpy domain of each is involved, leaving a non-coordinated bpy domain. In structure IV, the two ligands are also equivalently partitioned, and each has two non-coordinated terminal pyridine residues. Finally, in structure V, one ligand has a non-coordinated bpy domain the other has two non-coordinated pyridine residues [34–36].

All of the chromatographic techniques that we used indicated that single isomers of the $[RuL_2][PF_6]_2$ compounds were formed. In particular, we expected dra-

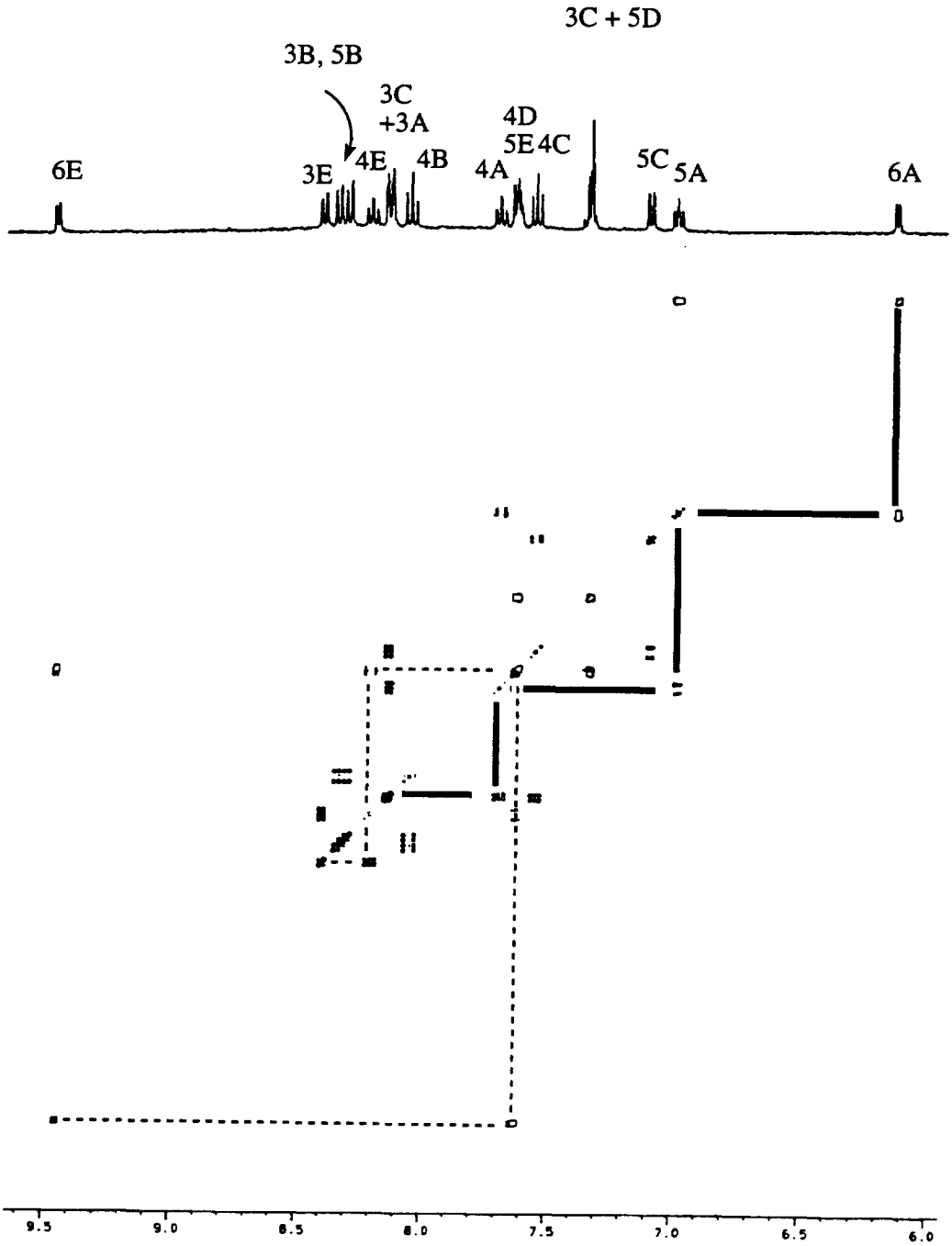

Fig. 3. 400 MHz ^{1}H COSY spectrum of $[Ru_2(qpy)_2Cl_2][PF_6]_2$ showing the connectivity of the two terminal rings and the assignment of the remaining resonances.

matically different behaviour on chromatography between complexes with four terminal pyridine rings non-coordinated and those with non-coordinated bpy domains. We also note, that 6,6″-diaryl-2,2′:6′,2″-terpyridine ligands exhibit severe steric interactions between the aryl groups and the complexes are significantly destabilised and also only formed in forcing conditions. These latter observations suggest that partitioning the ligand into a tpy and a bpy domain is more likely than the partitioning into a tpy and two pyridine domains. Structure IV is the most symmetrical of the various possibilities. The two ligands

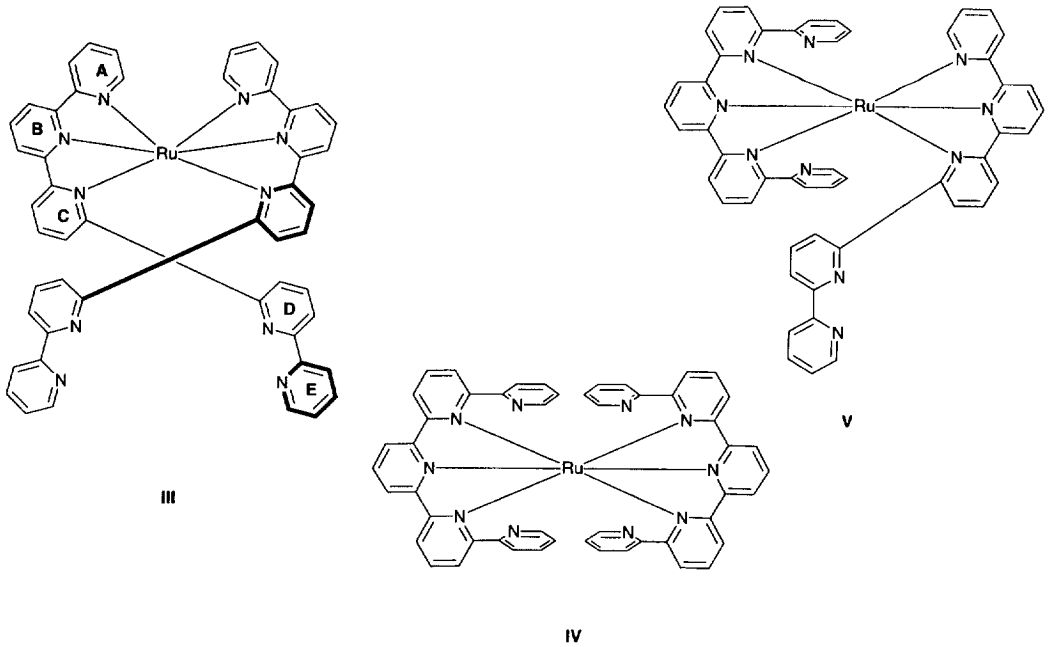

Fig. 4. Possible structures of the complex cations $[RuL_2]^{2+}$

are equivalent and each ligand is symmetrical about the central ring. Accordingly, structure IV would give rise to nine resonances for $[Ru(qpy)_2][PF_6]_2$. The 500 MHz ^1H COSY NMR spectrum of a CD_3CN solution of $[Ru(qpy)_2][PF_6]_2$ and is presented in Fig. 5. Without further analysis, it is immediately evident that the complexity of the spectra is not consistent with the symmetrical structure IV. This latter statement relies upon our previous comment that we are confident that only one of the structures III, IV or V is present.

Detailed analysis of this spectrum and the corresponding spectra for the complexes with dpqpy and dcqpy suggested that more than 17 (for qpy), 21 (for dpqpy) and 19 (for dcqpy) proton environments were present. We begin with a consideration of the spectrum of $[Ru(qpy)_2][PF_6]_2$. The most obvious feature is a low-field doublet at δ 8.9 with a coupling constant of 5.7 Hz which must be assigned to H^6 proton of a non coordinated ring. The COSY spectrum establishes the connectivity of this resonance (of intensity 1H) to three resonances of intensity 1/3 H at δ 7.6, 7.57 and 7.56. Subsequent analysis of the spectrum establishes the presence of three sub-spectra of very closely related compounds. The three subspectra consist of five separate connectivity systems in each case, although many of the expected 51 resonances are coincident and the connectivity is established through ^4J couplings. As was discussed earlier, the chromatographic behaviour argued strongly against the presence of mixtures of structures III, IV and V and the presence of a single H^6 proton of a non-coordinated ring is consistent only with structure III. Apparently three very similar isomers of structure III are present.

We have previously shown that in *N,N'*-bonded complexes of 6-phenyl-2,2';-bipyridine such as $[Ru(bpy)_2(Hpbpy)]^{2+}$ (Hpbpy = 6-phenyl-2,2'-bipyridine), the non-coordinated phenyl ring is stacked with one of the pyridine rings of a bpy ligand and cannot rotate freely about the interannular C—C bond to its directly bonded bipyridine unit [37]. We have also shown that related effects occur with hypodentate oligopyridine complexes [34–36]. Accordingly, each of the qpy ligands in $[Ru(qpy)_2][PF_6]_2$ can exist in two configurations related by the orientation of the non-coordinated bpy unit with respect to the coordinated tpy unit. This is illustrated for an archetypal $[Ru(qpy)(tpy)]^{2+}$ system in Fig. 6. In Fig. 6a, the non-coordinated bpy unit is oriented so that it faces forward and in Fig. 6b the corresponding isomer with it facing to the back is presented. The two cannot be interconverted without free rotation about the bond between the bpy and tpy components. If this were to occur, there would be serious steric interactions between the bpy unit and the other tpy ligand. Figure 6 also emphasises that in the parent $[Ru(qpy)(tpy)]^{2+}$ system, the two forms a and b are related as enantiomers. Figure 6c also introduces a notation which will simplify subsequent discussion . The tpy ligand is rotated so that it lies behind the plane of the paper and is represented as a hatched bar. The qpy ligand is oriented so that it lies in front of the plane of the paper and with the nitrogens of the terminal rings aligned vertically. The twisting about the C—C bond

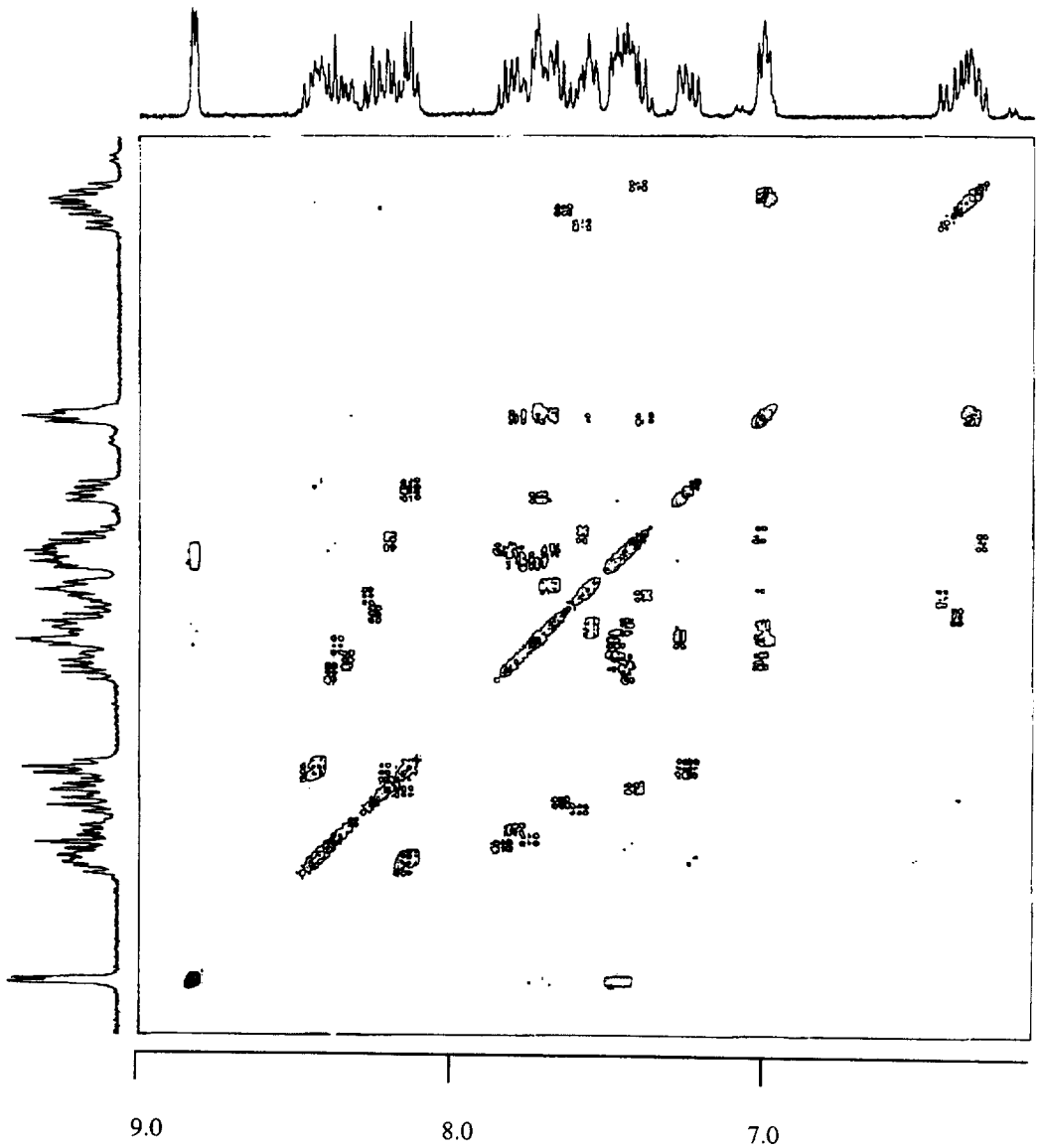

Fig. 5. 500 MHz ^{1}H COSY spectrum of $[Ru(qpy)_2][PF_6]_2$.

between the tpy and bpy domains of the qpy ligand is such that the two are near orthogonal. The qpy ligand is represented in solid black. Free rotation about the C—C bond of the two rings of the bpy domain is assumed.

The situation is more complicated when two such qpy ligands are present. Using the notation introduced in Fig. 6c, with the hatched ligand lying behind the plane of the paper, it is apparent that six isomers can exist, consisting of three enantiomeric pairs of conformers. Furthermore, these conformers cannot interconvert if free rotation about the bond between the tpy and bpy domains of each ligand is not possible. On the basis of this treatment we predict the three closely related species which occur in the spectrum of $[Ru(qpy)_2][PF_6]_2$ when it adopts the parent structure III. To conclude the discussion of the qpy complex, the experimental spectra are fully consistent with the presence of three conformers of structure III. The final assignments are given in Table 2, in which the sub-spectra IIIa, IIIb and IIIc are listed. The correlation of the individual rings to the individual sub-spectra is arbitrary—in other words, whilst the connectivity within the AIIIa ring of the BIIIa ring is absolutely certain, we do not know whether the AIIIa ring is bonded to the sub-spectrum for BIIIa, BIIIb or BIIIc nor can we, despite numerous attempts to deconvolute the high field NOESY spectra, unambiguously correlate the three sub-spectra a, b and c with the conformers α, β and γ.

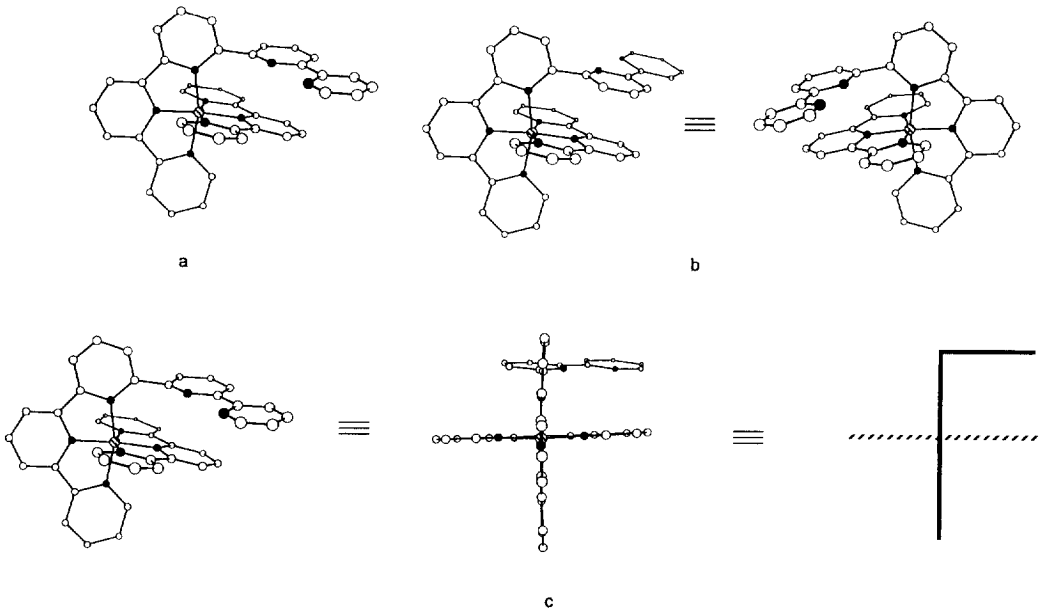

Fig. 6. Possible conformers of the complex cation $[Ru(tpy)(qpy)]^{2+}$. (a) One of the possible conformers is converted into (b) the other by rotation about the C—C bond between coordinated and non-coordinated rings. The new conformer is an enantiomer of the original conformer a. (c) A simple notation to describe the conformers of the $[Ru(tpy)(qpy)]^{2+}$ cation.

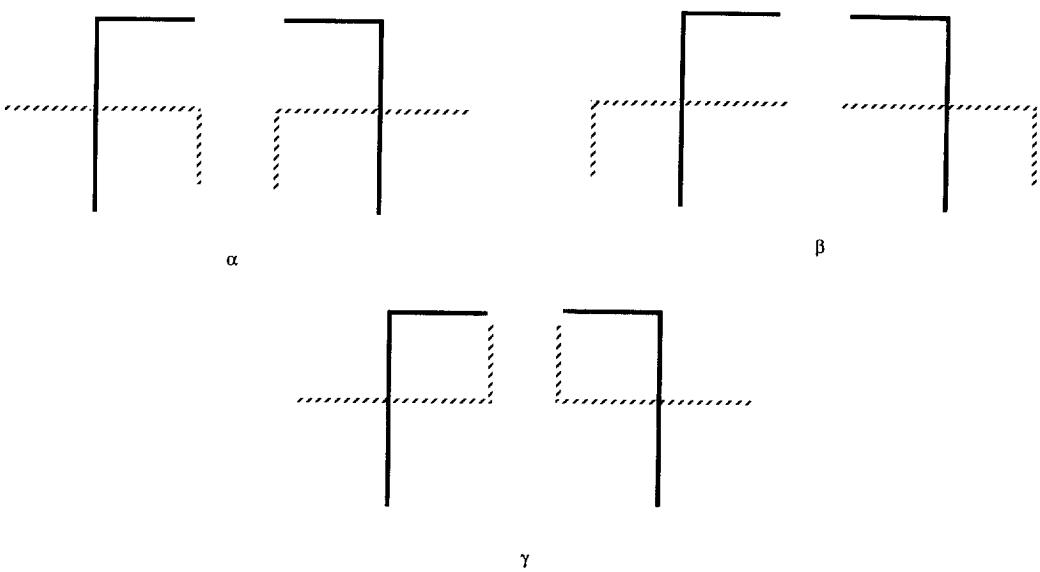

Fig. 7. Possible conformers of the complex cation $[Ru(qpy)_2]^{2+}$.

The introduction of additional substituents introduces more complexities to the system. Once again, all of the chromatographic analysis is consistent with the presence of just one of the isomers III, IV and V and a similar analysis to that discussed above leads to the conclusion that structure III represents the gross connectivity within the molecule. However, the presence of the additional aryl groups in the 4′ and 4‴-positions introduces new conformational possibilities. Returning to a simple model, Fig. 8a illustrates the effect of the introduction of a single phenyl substituent in a $[(4'\text{-Phqpy})(tpy)Ru]^{2+}$ complex. It is immediately apparent from Fig. 8a that the terminal non-coordinated pyridine ring and the aryl ring are spatially similar and that a conformer of type 8b will also exist. Figure 8c extends the earlier notation introducing a

Table 2. ^{1}H NMR spectroscopic data for CD_3CN solutions of the complexes $[RuL_2][PF_6]_2$ (L = qpy, dpqpy)

	L = dpqpy				L = qpy		
	S1	S2	S3	S4	S1	S2	S3
6	6.55	6.60	6.65	6.65	6.45	6.45	6.45
5	7.1	7.1	7.1	7.1	7.15	7.15	7.15
4	7.7	7.7	7.7	7.7	7.52	7.8	7.9
3	8.1	8.0	8.1	8.2			
5′	8.65	8.6	8.55	8.5	8.41	8.42	8.44
4′	—	—	—	—	7.95	7.85	7.90
3′	8.1	8.0	8.25	8.2	7.55	7.6	7.57
5″		7.2	7.2	7.2	7.35	7.4	7.4
4″		7.8	7.6	7.6	8.2	8.2	8.2
3″		8.0	8.0	7.8	8.5	8.5	8.5
5‴	8.65	8.55	8.55	8.55	8.3	8.3	8.35
4‴	–	—	—	—	7.5	7.75	7.7
3‴	7.0	7.0	6.9	6.6	6.45	6.52	6.55
6⁗	9.1	9.0	8.7	8.6	8.9	8.9	8.9
5⁗	7.7	7.6	7.55	7.52	7.6	7.57	7.57
4⁗		7.8	7.85	7.95	7.82	7.78	
3⁗		8.0	7.5			7.7	7.7

*Labels S1, S2, S3 and S4 only relate to the sub-spectra. They are not assigned unambiguously to the appropriate conformers in Figs 7 and 9.

dotted bar to represent the additional aryl ring. Moving directly to complexes with two substituted ligands, it follows that a total of three conformers are possible, each existing as a pair of enantiomers, as shown in Fig. 9. In the case of the α conformer, the two ligands are magnetically non-equivalent (most easily seen by considering the neighbours of the dotted aryl ring in Fig. 9) and will give rise to a separate sub-spectrum for each ligand. Accordingly, we predict a total of four sub-spectra corresponding to the three conformers α, β and γ from $[Ru(dpqpy)_2]^{2+}$ and it is extremely gratifying to find that the COSY spectrum reveals exactly this. Chemical shifts for the various sub-spectra, labelled a, b, c and d are presented in Table 2. Once again, the same provisos as discussed above for $[Ru(qpy)_2][PF_6]_2$ apply.

In conclusion, the ^{1}H NMR spectra of the $[RuL_2][PF_6]_2$ compounds are extremely complicated, but are fully compatible with the presence of only structure III complexes but with a number of non-interconverting conformers present in solution. Structure III is essentially very closely related to the structure II which was established for the $[RuL_2Cl_2][PF_6]_2$ complexes with the exception that the $RuCl_2$ unit is not present. This suggested that the $[RuL_2][PF_6]_2$ complexes could be viewed as precursors to $[RuL_2Cl_2][PF_6]_2$. The reaction of the $[RuL_2][PF_6]_2$ complexes with ruthenium trichloride in ethanol results in the quantitative conversion to $[RuL_2Cl_2][PF_6]_2$. Accordingly, we view these species as *prehelicates* or precursor complexes for the dinuclear double helicates.

CONCLUSIONS

We have shown that 2,2′:6′,2″:6″,2‴:6‴,2⁗-quinquepyridine ligands form mononuclear and dinuclear

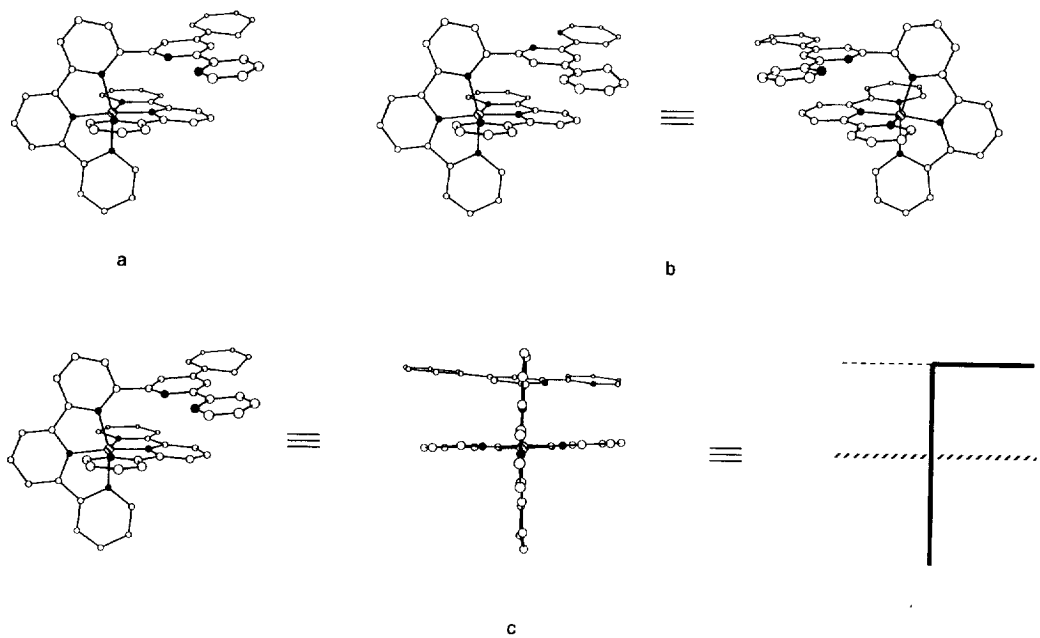

Fig. 8. (a, b) Possible conformers of the complex cation $[Ru(tpy)(4'\text{-Phqpy})]^{2+}$. (c) A simple notation to describe the conformers of the $[Ru(tpy)(4'\text{-Phqpy})]^{2+}$ cation.

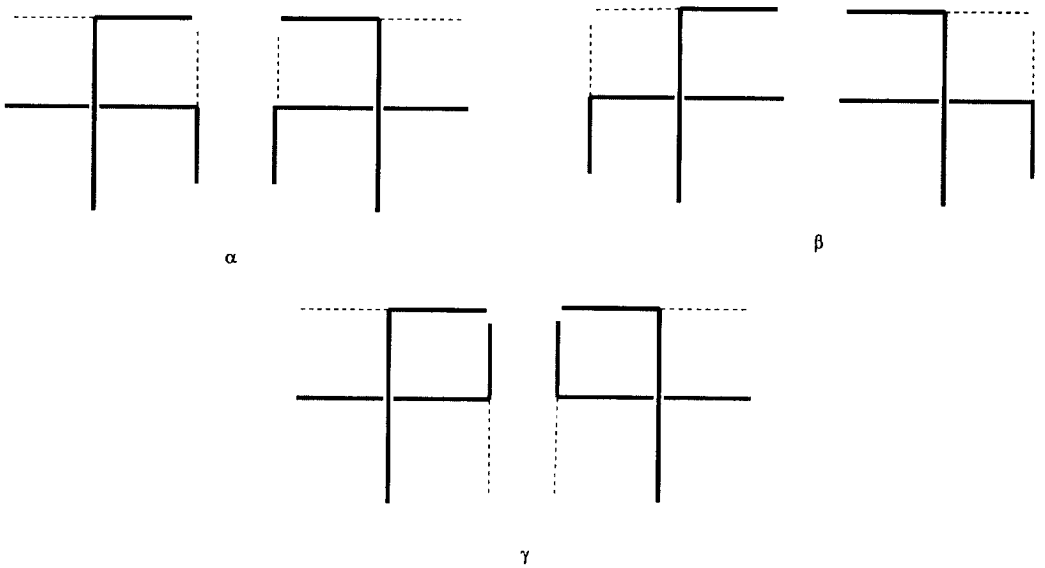

Fig. 9. Possible conformers of the complex cation $[Ru(dpqpy)_2]^{2+}$. The two ligands in the α conformer are magnetically non-equivalent.

ruthenium(II) complexes. The mononuclear complexes may be viewed as *prehelicates* in that they have a double helical ligand array with two non-coordinated bpy domains preorganised for coordination to a second metal centre. The dinuclear complexes are true double helicates and incorporate two six coordinate metal centres. We are currently investigating the extent of conformational effects in other hypodentate ligand systems are assessing the use of the *prehelicates* in the formation of heterodinuclear complexes.

Acknowledgements—We should like to thank the Schweizerischer Nationalfonds zur Förderung der wissenschaftlichen Forschung, the EPSRC (U.K.), the European Community (associated contract CEC ERBCHRXCT 940492/A2) and the University of Basel for support.

REFERENCES

1. Lehn, J-M., *Supramolecular Chemistry*, VCH, Weinheim, 1995.
2. Constable, E. C., *Metals and Ligand Reactivity*, VCH, Weinheim, 1995; Constable, E. C., *Chem. Ind.*, 1994, 56; Mascal, M., *Contemp. Org. Synth.*, 1994, 31; Balzani, V., *Tetrahedron*, 1992, **48**, 10443.
3. Constable, E. C. In *Comprehensive Supramolecular Chemistry*, Vol. 9, ed. J.-M. Lehn, Pergamon, Oxford, 1996, p. 213; Piguet, C., Bernardinelli, G. and Hopfgartner, G., *Chem. Rev*, 1997, **97**, 2005; Constable, E. C. and Smith, D. R. In *The Polymeric Materials Encyclopedia*, CRC Press, Boca Raton, 1996, p. 4237.
4. Constable, E. C., *Tetrahedron*, 1992, **48**, 10013
5. Constable, E. C., *Prog. Inorg. Chem.*, 1994, **42**, 67.
6. Constable, E. C., Lewis, J. and Schröder, M., *Polyhedron*, 1982, **1**, 311.
7. Constable, E. C., Drew, M. G. B. and Ward, M. D., *J. Chem. Soc., Chem. Commun.*, 1987, 1600.
8. Barley, M., Constable, E. C., Corr, S. A., McQueen, R. C. S., Nutkins, J. C., Ward, M. D. and Drew, M. G. B., *J. Chem. Soc., Dalton Trans.*, 1988, 2655.
9. Constable, E. C., Drew, M. G. B., Forsyth, G. and Ward, M. D., *J. Chem. Soc., Chem. Commun.*, 1988, 1450.
10. Constable, E. C., Ward, M. D., Drew, M. G. B. and Forsyth, G. A., *Polyhedron*, 1989, **8**, 2551.
11. Constable, E. C., Elder, S. M., Healy, J., Ward, M. D. and Tocher, D. A., *J. Am. Chem. Soc.*, 1990, **112**, 4590.
12. Constable, E. C., Elder, S. M., Raithby, P. R. and Ward, M. D., *Polyhedron*, 1991, **10**, 1395.
13. Constable, E. C., Elder, S. M., Walker, J. V., Wood, P. D. and Tocher, D. A., *J. Chem. Soc., Chem. Commun.*, 1992, 229.
14. Constable, E. C., Walker, J. V., Tocher, D. A. and Daniels, M. A. M., *J. Chem. Soc., Chem. Commun.*, 1992, 768.
15. Constable, E. C. and Walker, J. V., *J. Chem. Soc., Chem. Commun.*, 1992, 884.
16. Constable, E. C., Daniels, M. A. M., Drew, M. G. B., Tocher, D. A., Walker, J. V. and Wood, P. D., *J. Chem. Soc., Dalton Trans.*, 1993, 1947.
17. Constable, E. C., Martínez-Máñez, R., Cargill Thompson, A. M. W. and Walker, J. V., *J. Chem. Soc., Dalton Trans.*, 1994, 1585.
18. Constable, E. C., Edwards, A. J., Raithby, P. R. and Walker, J. V., *Angew Chem. Int. Ed. Engl.*, 1993, **32**, 1465.
19. Constable, E. C., Edwards, A. J., Raithby, P. R.,

Smith, D. R., Walker, J. V. and Whall, L., *Chem. Commun.*, 1996, 2551.
20. Constable, E. C., Neuberger, M., Whall, L. A. and Zehnder, M., *New J. Chem.*, in press.
21. Cathey, C. J., Constable, E. C., Hannon, M. J., Tocher, D. A. and Ward, M. D., *J. Chem. Soc., Chem. Commun.*, 1990, 621.
22. Ho, P. K. K., Peng, S. M., Wong, K. Y. and Che, C. M., *J. Chem. Soc., Dalton Trans.*, 1996, 1829.
23. Ho, P. K. K., Cheung, K. K., Peng, S. M., Wong, K. Y. and Che, C. M., *J. Chem. Soc., Dalton Trans.*, 1996, 1411.
24. Fu, X. J., Sun, J., Li, Q., Chen, Y., Dai, W. N., Wang, D. F., Mak, T. C. W., Tang, W. X. and Hu, H. W., *J. Chem. Soc., Dalton Trans.*, 1996, 2309.
25. Ho, P. K. K., Cheung, K. K. and Che, C. M., *Chem. Commun.*, 1996, 1197.
26. Potts, K. T., Keshavarz-K, M., Tham, F. S., Abruna, H. D. and Arana, C. R., *Inorg. Chem.*, 1993, **32,** 4436.
27. Potts, K. T., Keshavarz-K, M., Tham, F. S., Abruna, H. D. and Arana, C. R., *Inorg. Chem.*, 1993, **32,** 4422.
28. Potts, K. T., *Bulletin Des Societes Chimiques Belges*, 1990, **99,** 741.
29. Gheysen, K. A., Potts, K. T., Hurrell, H. C. and Abruna, H. D., *Inorg. Chem.*, 1990, **29,** 1589.
30. Dai, W. N., Hu, H. W., Wei, X. D., Zhu, S. M., Wang, D. F., Yu, K. B., Dalley, N. K. and Kou, X. L., *Polyhedron*, 1997, **16,** 2059.
31. Fu, Y. J., Li, Q., Zhou, Z. Y., Dai, W. N., Wang, D. F., Mak, T. C. W., Hu, H. W. and Tang, W. X., *Chem. Commun.*, 1996, 1549.
32. Fu, Y. J., Sun, J., Li, Q., Chen, Y., Dai, W. N., Wang, D. F., Mak, T. C. W., Tang, W. X. and Hu, H. W., *J. Chem. Soc., Dalton Trans.*, 1996, 2309.
33. Juris, A., Balzani, V., Barigelletti, F., Campagna, S., Belser, P. and Von Zelewsky, A., *Coord. Chem. Rev.*, 1988, **84,** 85.
34. Chotalia, R., Constable, E. C., Hannon, M. J. and Tocher, D. A., *J. Chem. Soc. Dalton Trans.*, 1995, 3571.
35. Constable, E. C., Hannon, M. J., Cargill Thompson, A. M. W., Tocher, D. A. and Walker, J. V., *Supramol. Chem.*, 1993, **2,** 243.
36. Constable, E. C. and Cargill Thompson, A. M. W., *Inorg. Chim. Acta*, 1994, **223,** 177.
37. Constable, E. C. and Hannon, M. J., *Inorg. Chim. Acta*, 1993, **211,** 101.

Pergamon

PII: S0277-5387(98)00070-9

Polyhedron Vol. 17, No. 18, pp. 3101–3109, 1998
© 1998 Elsevier Science Ltd
All rights reserved. Printed in Great Britain
0277-5387/98 $19.00+0.00

Structural organisation of [Ni(II)—Me(II)—Dtc] (Me = Zn, Cd, Hg) Dithiocarbamate complexes: ESR, ^{13}C and ^{15}N CP/MAS NMR studies

Alexander V. Ivanov,[a] Tatyana Rodyna[b] and Oleg N. Antzutkin*[c]

[a] Amur Integrated Research Institute, Far Eastern Branch of Russian Academy of Sciences, 675000 Blagoveschensk, Russia

[b] Department of Chemistry, Amur State University, 675027 Blagoveschensk, Russia

[c] Division of Inorganic Chemistry, Luleå University of Technology, S-971 87 Luleå, Sweden

(Received 13 October 1997; accepted 13 February 1998)

Abstract—Magnetically diluted systems of dithiocarbamate complexes of the type $^{63,65}Cu$/[Ni(II)—Me(II)—Dtc] (Me = Zn, Cd, Hg; Dtc = MDtc (dimethyl-) or EDtc (diethyldithiocarbamate)), which model the structural heterogeneity on the local, molecular and supramolecular levels, have been prepared and studied by means of ESR and solid state ^{13}C and ^{15}N CP/MAS NMR spectroscopy.

Three possible structures of these dithiocarbamate complexes were unambiguously identified in the composition of the samples under investigation: (i) the mononuclear square-planar, $Ni(Dtc)_2$; (ii) dinuclear with non-planar molecular configurations, $Me_2(Dtc)_4$ and (iii) heteropolynuclear complexes with a common composition of $Me_2(Dtc)_4 \cdot nNi(Dtc)_2$ (n = 1–4; Me = Zn, Cd, Hg). The latter is a newly proposed type of structure of dithiocarbamate complexes in the matrix of the model systems. © 1998 Elsevier Science Ltd. All rights reserved

Keywords: dithiocarbamate complexes; structure; heteropolynuclear compounds; magnetically diluted systems; ESR spectroscopy; ^{13}C and ^{15}N CP/MAS NMR spectroscopy.

Dithiocarbamates play an important role in inorganic chemistry and technology, in rubber chemistry as vulcanizing agents, in the froth flotation process of sulphide minerals, in agriculture as fungicides and pesticides, in medicine as radioprotectors and for the treatment of the chronic alcoholism, as antioxidants and lubricants etc. Therefore studies of these compounds have attracted interest for about one hundred years.

Depending on experimental preparation conditions, some dithiocarbamate complexes of transition metals can adopt both mono- and binuclear types of molecular structures [1]. Monomeric molecules are square-planar while the dimeric species have non-planar configurations of the coordination polyhedra of the central atom (distorted tetrahedral, or trigonally-bipyramidal, or square-pyramidal). It is known that nickel(II) complexes have mononuclear square-planar molecular structures, $Ni(Dtc)_2$ [2–8], while zinc(II) [9–13], cadmium(II) [14,15] and mercury(II) [16] complexes have dimeric non-planar molecular configurations $Me_2(Dtc)_4$.

Depending on a sample preparation procedure interesting possibilities for structural organizations of these substances occur when both mono- and dinuclear complexes are present simultaneously: (i) Uniform distribution of monomeric and dimeric molecules (a "molecular mixture"); (ii) Phase microheterogeneity, when each species forms local spatial domains with a homogeneous molecular composition; (iii) Intermediate, between "i" and "ii".

In our previous publications [17–20] we have prepared copper(II)-doped samples of various dithiocarbamate complexes and studied their structural

* Author to whom correspondence should be addressed.

features by means of ESR spectroscopy. Unusual ESR spectra have been detected in samples consisting of both structural types discussed above. We have suggested that in many cases not only purely mononuclear or/and binuclear molecules, but also a new structural type could be identified. However, we failed to prepare this new structural model in the single crystal state and to elucidate its structure by means of X-ray diffraction data analysis: Two components (Ni and Zn; Ni and Cd; Ni and Hg) crystallize separately forming local spatial domains with a homogeneous molecular composition. Therefore, only indirect spectroscopic methods can be used to characterize this new structural type.

In this article we report the preparation procedure and spectroscopic ESR and solid state ^{13}C and ^{15}N CP/MAS NMR studies of dithiocarbamate complexes: [Ni(II)—Me(II)—Dtc](Me = Zn, Cd, Hg) which model this new structural situation. The main structural peculiarity of these dithiocarbamates is a simultaneous presence of both mononuclear and dinuclear molecules. In the present article we confirm the identification of a new structural type of dithiocarbamate complexes in the [Ni(II)—Me(II)—Dtc] systems and propose its molecular structure.

EXPERIMENTAL

Preparation of model systems

All chemicals were commercial materials and were used without further purification. Dimethyl- and diethyldithiocarbamate complexes of Ni, Zn, Cd and Hg were prepared according to the literature [2–16].

The model systems [Ni(II)—Me(II)—Dtc] were prepared at 363 K by mixing water solutions of nickel(II) salts and zinc(II), cadmium(II) or mercury(II) salts (with concentrations C = 0.5 M and experimental ratios Ni : Me = 1 : 9–9 : 1) with an excess (~10%) of sodium dimethyldithiocarbamate (MDtc) dihydrate, $Na(CH_3)_2NC(S)S \cdot 2H_2O$, or sodium diethyldithiocarbamate (EDtc) trihydrate, $Na(C_2H_5)_2NC(S)S \cdot 3H_2O$, as the ligands in aqueous solution. The full coagulation and final ageing were carried out at room temperature or at 363 K. Then the prepared dark green precipitates were collected, filtered off, washed with water and dried *in vacuo* over phosphorus pentoxide in a desiccator.

The above dithiocarbamate complexes and model systems are diamagnetic and small amounts of copper(II) (Cu : [Ni + Me] = 1 : 1000) were therefore added as spin-labels for ESR studies. Copper(II) salts with natural isotopic abundance and also isotopically highly enriched samples (^{65}Cu −99.2 at.%; ^{63}Cu −99.95 at.%) were used in the synthesis.

Physical measurements

ESR measurements were made at 298 and 77 K on a "RadioPAN" ESR spectrometer SE/X-2544 working at ~9.5 GHz. First and second derivatives of ESR signals were recorded, as well as the second derivative of the second harmonic (corresponding to the third derivative). The latter considerably improves the resolution of ESR spectra [21]. A microwave frequency was measured with microwavemeter MCM-101. The magnetic field was calibrated and measured using the NMR-gaussmeter JTM-246. The uncertainty of measurements was ±0.003 for g-values, and ±2% for the anisotropic hyperfine coupling (h.f.c.) constants: A_1^{Cu}, A_2^{Cu} and A_3^{Cu} (given in Gauss (G)).

Solid state natural abundance ^{13}C magic-angle-spinning (MAS) NMR spectra were recorded on a Chemagnetics Infinity CMX-200 (B_0 = 4.70 T) spectrometer using cross-polarization (CP) from the protons together with proton decoupling [22]. The ^{13}C operating frequency was 50.35 MHz. The proton $\pi/2$ pulse duration was 3.8 μs, CP mixing time 2 ms and the nutation frequency of protons during decoupling $\omega_{nut}/2\pi$ = 88 kHz. For different samples from 1536 to 18,432 transients with a relaxation delay of 2 s were accumulated. Powder samples (ca. 50 mg) were packed into zirconium dioxide standard double bearing 4.0 mm rotor systems. The spinning frequencies for all samples were 4000 and/or 6000 Hz and stabilized to ±3 Hz using an inbuilt stabilization device. All ^{13}C chemical shift data were externally referenced to the least shielded resonance of solid adamantane at 38.56 ppm relative to tetramethylsilane [23].

Natural abundance ^{15}N CP/MAS NMR spectra were recorded on a Chemagnetics Infinity CMX-360 (B_0 = 8.46 T) spectrometer. The ^{15}N operating frequency was 36.48 MHz. The proton $\pi/2$ pulse duration was 3.2 μs, CP mixing time 3.5 ms and the nutation frequency of protons during decoupling was 50 kHz. A total of 17,600 transients, spaced by relaxation delays of 2 s, were accumulated. Powder samples (ca. 350 mg, 7.5 mm rotors) were spun at the spinning frequencies of 6000 Hz. ^{15}N isotropic chemical shifts are given with respect to NH_4Cl powder (0 ppm, externally referenced) [24,25]. The drift of the ^{15}N frequency (B_0—drift) was 0.016 Hz h^{-1}.

All solid state ^{13}C and ^{15}N CP/MAS NMR spectra were recorded at room temperature (ca. 300 K).

RESULTS AND DISCUSSION

ESR measurements

Figure 1 shows ESR spectra (first derivative) of magnetically diluted systems of diethyldithiocarbamate Ni and Zn complexes. Minute quantities (Cu : Me = 1 : 1000) of the copper isotopes, ^{63}Cu or ^{65}Cu, were used as spin-labels for ESR measurements. As we already reported, copper(II) can substitute Ni(II), Zn(II), Cd(II) and Hg(II) in dimethyl-, diethyl-, dibutyl-, pentamethylene-, hexamethylene- and morpholinedithiocarbamate complexes without considerable distortions of an original structure of

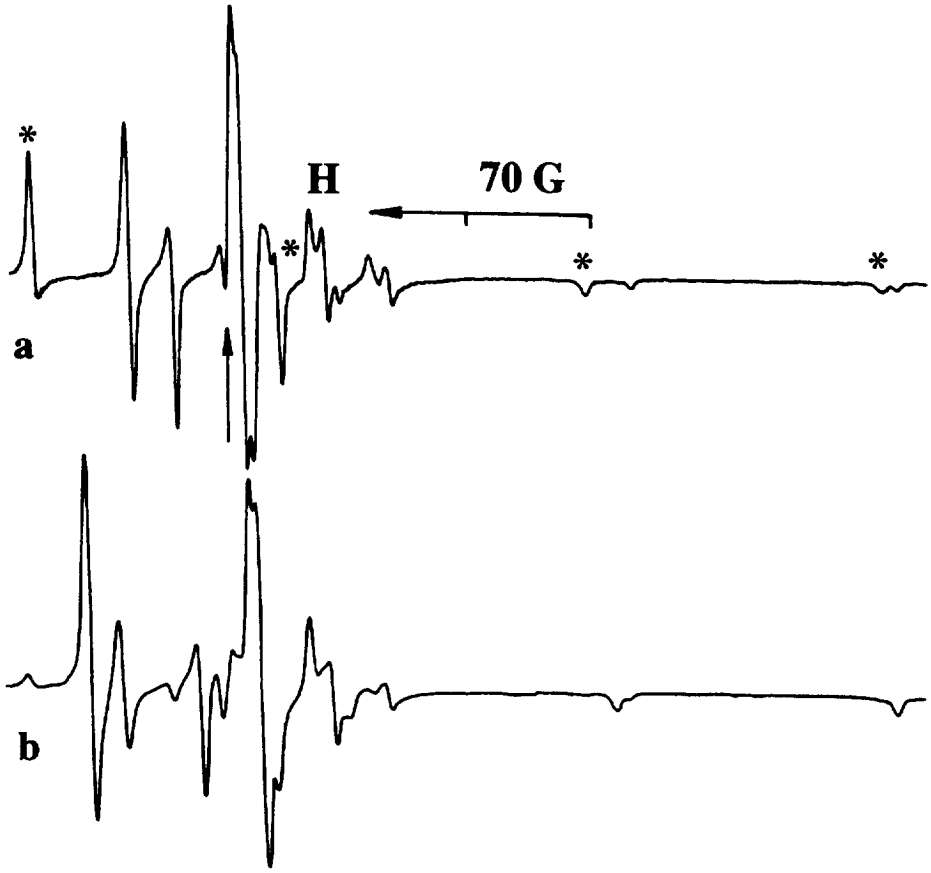

Fig. 1. ESR spectra of magnetically diluted systems with ratio Ni : Zn = 1 : 1 and ^{63}Cu : Me = 1 : 1000: (a) a mechanical mixture of ^{63}Cu(II)/[Ni(II)-EDtc] and ^{63}Cu(II)/[Zn(II)-EDtc]. Both the square-planar CuS_4 and the trigonal-bipyramidal CuS_5 chromophores are present. ESR components of the parallel orientation corresponding to the mononuclear complex (structural state **I**) are shown by asterisks (*). The other components correspond to the dinuclear complex (structural state **II**). The vertical arrow shows the position of DPPH signal; (b) ^{63}Cu(II)/[Ni(II)-Zn(II)-EDtc]. The square-pyramidal chromophore CuS_5 (structural state **III**) is dominated.

undoped complexes [17–20]. Therefore ESR signals from copper(II) can reveal structural features of these systems.

Figure 1a shows ESR spectrum of the mechanical mixture of ^{63}Cu(II)/[Ni(II)-EDtc] and ^{63}Cu(II)/[Zn(II)-EDtc]with the ratio of the metals Ni : Zn = 1 : 1. It is known that the dithiocarbamate nickel(II) complexes adopt the square-planar molecular structures[2–8] (structural state **I**), while Zn(II)-EDtc molecules are predominantly in the dinuclear states with a distorted trigonal bipyramidal or a distorted tetrahedral configurations of coordination polyhedra of the central atom [9–13] (structural state **II**). Therefore well-resolved hyperfine structures from both structural states of copper(II) are present simultaneously in the ESR spectrum. For each copper(II)-doped complex there is a quartet of resonance lines due to the hyperfine interaction of the unpaired electron with the ^{63}Cu or ^{65}Cu nuclear spin ($I = 3/2$) in each of the three principal orientations of the hyperfine coupling tensor. ESR parameters for various dithiocarbamate complexes, i.e. three different components of both g- and A-tensors, are summarized in Table 1. In this table data for dimethyldithiocarbamate complexes and for complexes of other metals (Cd, Hg) are also given (ESR spectra not shown).

Both g- and A-tensors of the first structural state (**I**) are almost axially symmetric with large parallel and small perpendicular components. However, there is a slight rhombicity of the ESR parameters in the xy-plane. This type of anisotropy reflects a slight unequivalence of Me—S chemical bonds which can be connected with a small rhombic distortion of a square-planar chromophore. As we reported earlier ESR parameters of the structural state **I** are extreme compared to copper(II) complexes with S-homogeneous coordination spheres [21]. Namely, g_1, g_2 and g_3 have minimal while A_1^{Cu}, A_2^{Cu} and A_3^{Cu} constants maximal possible values. These features are characteristic for the square-planar chromophores CuS_4. Therefore, both the character of experimental spectra

Table 1. ESR parameters of paramagnetic compounds in Cu(II)/[(Ni(II)-Me(II)-Dtc] (Me = Zn, Cd, Hg) systems

Complex	g_1	A_1^{Cu}*	g_2	A_2^{Cu}*	g_3	A_3^{Cu}*	Position	Type of geometry
Cu/Ni(MDtc)$_2$	2.084	162/173	2.024	42/45	2.020	39/42	I	Square-planar
CuZn(MDtc)$_4$	2.107	137/146	2.029	20/21	2.029	20/21	II	Tetrahedral
CuZn$_2$(MDtc)$_6$	2.089	152/162	2.027	37/40	2.027	37/40	III	Square-pyramidal
Cu/Ni(EDtc)$_2$	2.084	163/173	2.024	42/45	2.020	39/42	I	Square-planar
CuZn(EDtc)$_4$	2.107	147/158	2.032	31/33	2.023	6.5/7.0	II	Trigonally-bipyramidal
CuZn$_2$(EDtc)$_6$	2.098	154/165	2.029	36/39	2.029	36/39	III	Square-pyramidal
Cu/Ni(EDtc)$_2$	2.084	162/173	2.024	42/45	2.020	39/42	I	Square-planar
CuMe(EDtc)$_4$ (Me = Cd, Hg)	2.103	150/160	2.030	29/31	2.030	29/31	II	Square-pyramidal
CuCd$_2$(EDtc)$_6$	2.097	155/166					III	Square-pyramidal
CuHg$_2$(EDtc)$_6$	2.097	153/164	2.027	34/36	2.027	34/36	III	Square-pyramidal
Cu(EDtc)$_2$L**	2.102	155/166	2.028	38	2.028	38		Square-pyramidal
Cu(EDtc)$_2$L'**	2.104	150/161	2.030	37	2.030	37		Square-pyramidal

* A^{Cu}-values are given for $^{63}Cu/^{65}Cu$.

** Data from Ref. [28] for square-pyramidal adducts of bis-(diethyldithiocarbamato)copper(II) with axial coordination of organic sulphur bases (L-O-butyl-*N*-methyl- or O-butyl-*N*,*N*-diethylthionocarbamate; L'-cyclic organic sulphides: 2-methyltetrahydrothiophene, 2-hexylthiane, 3-amylthiane). Experimental conditions: toluene glasses at 77 K.

and ESR parameters can be used in the identification of the structural state **I**, Cu(Dtc)$_2$, with the square-planar mononuclear geometry (Scheme 1).

ESR-parameters of the second structure (II) reflect non-planar configurations of copper(II) coordination polyhedra: distorted tetrahedral, distorted trigonally-bipyramidal or distorted square-pyramidal (see Table 1) [17,18]. The stabilization of paramagnetic chromophores with unusual types of geometry: tetrahedral CuS_4, square-pyramidal and trigonally-bipyramidal CuS_5 can be explained by a formation of heterodinuclear complexes—CuMe(Dtc)$_4$ (Me = Zn, Cd, Hg) by means of a chemical interaction between the paramagnetic component and the diamagnetic matrix [26] The molecular structures of the corresponding zinc(II), cadmium(II), mercury (II) [9–16] and copper(II) [27] dithiocarbamate complexes are very similar. X-ray diffraction data show that all complexes are binuclear with two dithiocarbamate-bridged ligands. Scheme 2 shows the molecular structure of these heterobinuclear complexes.

Figure 1b shows ESR spectrum of a model Cu(II)/[Ni(II)-Zn(II)-EDtc] system with the Ni:Zn ratio 1:1. Components of the hyperfine structure corresponding to the square-planar molecules almost

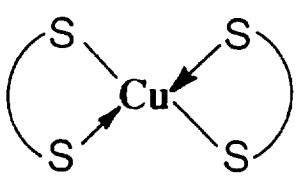

Scheme 1. The main fragment of the molecular structure of mononuclear square-planar complexes: Cu(Dtc)$_2$.

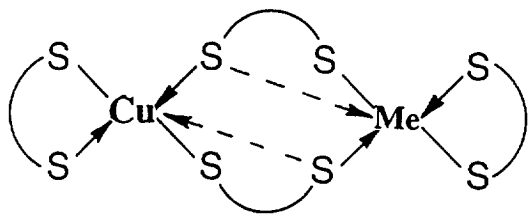

Scheme 2. The main fragment of the molecular structure of heterodinuclear dithicarbamate complexes: CuMe(Dtc)$_4$ (Me = Zn, Cd, Hg).

vanish in spite of the equal experimental ratio of the Ni and Zn metals. Instead, a high intensity "intermediate" ESR signal and the components of a moderate intensity from the dimeric form appear in the spectrum. Moreover, it was established that the "intermediate" is not an independent signal. It is a "satellite" of the signal of the dinuclear form. In fact it is not possible to observe the "intermediate" signal without the signal of a dinuclear complex in the experimental ESR spectra. This "intermediate" signal is assigned here to a new structural state (**III**) of copper(II) in the composition of magnetically diluted systems Cu/[Ni(II)-Me(II)-Dtc]. It is also tabulated in Table 1. A pertinent question arises, since nickel(II) and zinc(II) dithiocarbamate complexes adopt two different types of molecular structures, the mononuclear square-planar and the dinuclear with non-planar configurations respectively, what is a new structural state (**III**) detected in the model systems Cu(II)/[Ni(II)-Me(II)-Dtc]?

The third structural position of copper(II) is characterized by ESR parameters, which are typical for molecules with axial symmetry (see Table 1). Both

hyperfine coupling constants and g-values of the structural state **III** are very close to those formed by square-pyramidal adducts of bis(diethyldithiocarbamato) copper(II) with axially coordinated molecules of organic sulphur bases, $Cu(EDtc)_2L$, which have a homogeneous coordination sphere of sulphur atoms [28] (see Table 1). Therefore, it can be proposed that copper(II) in the structural state **III** forms the square-pyramidal chromophore CuS_5. The main reason for this deviation from the square-planar polyhedron towards the square-pyramidal one is the coordination of the terminal sulphur atom of the dinuclear molecule, $Me_2(Dtc)_4$, to the axial position of the mononuclear molecule—$Cu(Dtc)_2$ (Scheme 3).

Experimental data show that the square-planar structure of mononuclear complexes cannot be realized in the model systems [Ni(II)-Me(II)-Dtc]. This is because of a partial coordination unsaturation of copper(II) in $Cu(Dtc)_2$ in combination with a neighbouring environment of dimeric non-planar molecules $Me_2(Dtc)_4$. In this situation copper(II) occupies a new magnetic and structural position (**III**) which is readily revealed by ESR. One can also say that the formation of a new chemical bond is equivalent to the formation of a heterotrinuclear complex.

Important structural information can also be derived from the ratio of signal intensities of states **III** and **II**. For magnetically diluted trinuclear complexes a theoretical ratio of signal intensities **III/II** must be equal to 1:2 in accordance with a probability of a substitution of metal atoms by copper(II) in the "mononuclear" and "dinuclear" parts of trinuclear complexes. But in experimental spectra this ratio can vary from 1:2 to 2:1. This can be explained by a formation of new chemical bonds between a dinuclear and several mononuclear molecules: two (1:1), three (3:2) or four (2:1). Therefore, in principal, polynuclear complexes $Me_2(Dtc)_4 \cdot nNi(Dtc)_2$ (n = 1–4; Me = Zn, Cd, Hg) can be formed with almost identical ESR parameters of all square-pyramidal coordination polyhedrons in the corresponding copper(II)-doped systems.

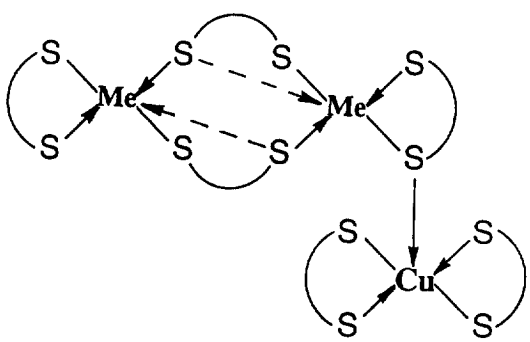

Scheme 3. The main fragment of the molecular structure of trinuclear complexes: $Cu(Dtc)_2$ $Me_2(Dtc)_4$ (Me = Zn, Cd, Hg)

^{13}C and ^{15}N CP/MAS NMR measurements

In order to confirm the above conclusions and establish further information the model systems were also studied by means of solid state ^{13}C and ^{15}N CP/MAS NMR spectroscopy. Figure 2a shows ^{13}C NMR spectrum of bis(diethylditiocarbamato) nickel(II). There are three resonances which can be assigned to the three inequivalent ^{13}C sites of ligands: methyl, methylene and dithiocarbamate groups: CH_3—, —CH_2— and =NC(S)S—. Both chemical shifts and the corresponding ratios of integral intensities (2:2:1) were used in the assignment. Note that chemical shifts of these three resonances are in accordance with data for natrium diethyldithiocarbamate

Fig. 2. The 50.35 MHz ^{13}C CP/MAS NMR spectra of the following complexes: (a) $Ni(EDtc)_2$; (b) $Zn_2(EDtc)_4$; (c) the model system [Ni(II)-Zn(II)-EDtc]. The experimental ratio Ni:Zn = 1:1. The MAS frequency was 4 kHz.

powder (Table 2). Experimental splittings of the asymmetric doublets for methylene and dithiocarbamate groups (85 and 70 Hz, respectively) arise from the incomplete suppression of the dipolar interaction between ^{13}C ($I = 1/2$) and quadrupolar nucleus ^{14}N ($I = 1$) by the MAS experiment [29,30]. Figure 3a shows ^{15}N NMR spectrum of the nickel(II) complex. The single resonance reflects undoubtedly the magnetic equivalence of dithiocarbamate ligands. Both ^{13}C and ^{15}N NMR measurements of bis(diethylditiocarbamato)nickel(II) agree well with X-ray diffraction data showing the mononuclear centrosymmetrical molecule with two structurally equivalent chelating diethyldithiocarbamate ligands [8].

Figures 2b and 3b show ^{13}C and ^{15}N CP/MAS spectra of the dinuclear zinc(II) complex. Each of the three corresponding ^{13}C resonances (methyl, methylene and dithiocarbamate groups) and ^{15}N resonance are split distinctly in doublets. These splittings reflect a structural difference between pairs of diethyldithiocarbamate ligands in the zinc(II) complex. Indeed, there are two groups of ligands with heterogeneous structural functions in the dinuclear zinc(II) diethyldithiocarbamate as is also confirmed by X-ray data analysis [10]. Each of two terminal ligands form the four-membered chelate ring (as in the nickel(II) complex) and two bridged ligands are coordinated by two zinc atoms and form an extensive eight-membered ring.

In order to assign ^{13}C and ^{15}N resonances to the terminal or to the bridged ligands, dithiocarbamate N—C interatomic distances were examined in both nickel(II) and zinc(II) complexes. The X-ray data analysis shows that the dithiocarbamate group is planar practically in all known transition metal complexes [2–16]. This is due to a considerable contribution of the double-bond character to single bonds in the =NC(S)S— group. The double-bond contribution varies from small values for relatively ionic compounds [31,32] to rather large values for mainly covalent complexes [2–16]. In the latter case a considerable δ^+ charge is localized on the nitrogen atom, while a δ^- charge is delocalized on the four-membered metallochelate ring CS_2Me (Scheme 4).

It is known that an admixture of the sp^2-hybridized state leads simultaneously to the decrease of both the N—C interatomic distance and the degree of shielding of the nitrogen nucleus by electrons. Table 3 shows N—C and C—S interatomic distances in relevant complexes obtained from X-ray data analysis [8,10,33]. From these data we can conclude that the largest carbon-nitrogen partial-double-bond character is at the bridged dithiocarbamate ligands of the $Zn_2(EDtc)_4$ complex. It corresponds to the largest deshielding of nitrogen nucleus and to the largest ^{15}N chemical shift value (δ = 149.8 ppm.). The other resonance can be assigned to the ^{15}N sites at the therminal ligands (δ = 136.8 ppm, see Fig. 3b).

Table 2. ^{13}C and ^{15}N chemical shifts of diethyldithiocarbamate complexes (from TMS and NH_4Cl)

Complex	Chemical Shifts (ppm)				
	=NC(S)S—	—CH_2—	—CH_3	=N—	
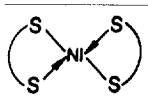	204.2 (70)*	46.2 (85)*	12.8	139.4	
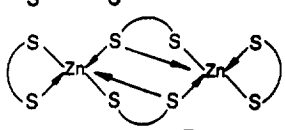	202.1 (72)* 199.5 (70)*	49.7 50.6	12.7 14.5	136.8 149.8	(terminal) (bridged)
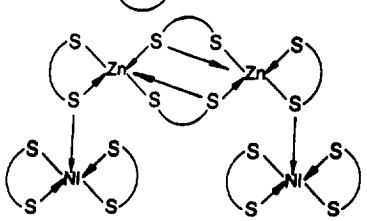	201.8	50.4	12.4	136.5	(terminal)
	199.5	50.4	14.5	149.5	(bridged)
	205.8 (82)*	43.9	12.4	131.6 133.9	
Na(EDtc)	206.5	48.6	13.2	139.0	

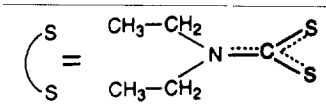

* ^{13}C–15N asymmetric doublets (in Hz).

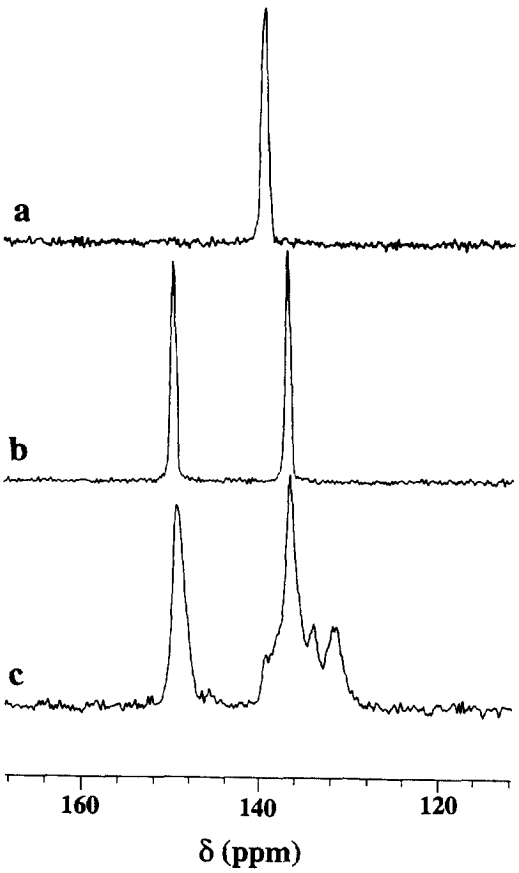

Fig. 3. The 36.48 MHz ^{15}N CP/MAS NMR spectra of $Ni(EDtc)_2$ (a), $Zn_2(EDtc)_4$ (b), and [Ni(II)-Zn(II)-EDtc](c) complexes. The MAS frequency was 6 kHz.

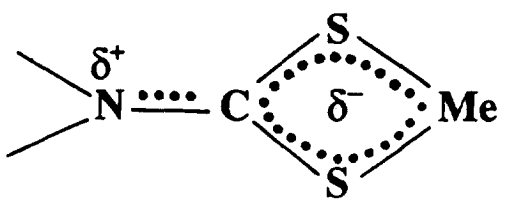

Scheme 4. The charge distribution in a dithiocarbamate group with the N—C partial-double-bond character.

Since the surplus charge δ^- is delocalized at the four-membered chelate ring CS_2Zn, the largest shielding of the ^{13}C sites is expected at the dithiocarbamate groups with the shortest N—C bond, i.e. at the bridged ligands of the $Zn_2(EDtc)_4$ complex. Owing similar arguments, we can assign the ^{13}C resonance at $\delta = 199.5$ ppm to the N—C site of the bridged ligands. It is also expected that the electron density is displaced from carbon atoms of methylene and methyl groups to the nitrogen atom which has the surplus charge δ^+. Therefore ^{13}C resonances at $\delta = 50.6$ and 14.5 ppm can be assigned to the methylene and methyl sites at the bridged ligands respectively.

The nickel(II) complex has an intermediate value for the N—C bond length and therefore also for an admixture of the sp^2-hybridized state at the nitrogen atom. Indeed, the ^{15}N chemical shift value for the nickel(II) complex is equal to 139.4 ppm which is between two ^{15}N resonances of the dinuclear zinc(II) complex. However, ^{13}C chemical shift value for the dithiocarbamate site at the nickel(II) complex fall out of these empirical correlations. In order to explain this an influence of the second factor, namely C—S bond lengths, was examined. Both C—S chemical bonds in the $Ni(EDtc)_2$ molecule are very short (see Table 3). Therefore, sulphur atoms which have a relatively high electronegative character cause an additional (compared to the zinc(II) complex) displacement of the electron density from the dithiocarbamate carbon atom, i.e. cause an additional deshielding of this site.

Even though the empirical correlations between chemical shifts and electron densities can be established for complexes discussed above, we stress here that theoretical calculations of chemical shifts are needed for more detailed structural elucidations. There has been recent progress in establishing correlations between calculated chemical shift values and structure both in small molecules and macromolecules such as peptides and proteins [34].

Figures 2c and 3c show ^{13}C and ^{15}N CP/MAS spectra of the model system [Ni(II)-Zn(II)-EDtc] (with Ni : Zn = 1 : 1) which consists of polynuclear complexes (**III**). It can be seen that both ^{13}C and ^{15}N sites of the "dinuclear" part of this polynuclear complex have chemical shifts which are very close to those of the corresponding sites of the zinc(II) complex (see Table 2). However, two new ^{13}C (see Fig. 2c) and two new ^{15}N resonances (Fig. 3c) of the above model system can not be assigned neither to the pure nickel(II) nor to the zinc(II) complexes. These four new resonances were assigned to ^{13}C and ^{15}N sites of dithiocarbamate groups and to ^{13}C sites of the methylene groups of diethyldithiocarbamate ligands in the square-planar molecules which are coordinated to the sulphur atoms in the terminal ligands of the dinuclear zinc(II) complex (see Table 2). It is known that an additional coordination of an electron donor atom to the axial position of a square-planar transition metal dithiocarbamates yields a decrease of the nitrogen-carbon partial-double-bond character and, as result of that, a displacement of the electron density from the carbon to the nitrogen atom in the metallochelate ring [35]. In our case the coordination of the sulphur atom to the axial position of the $Ni(EDtc)_2$ molecule leads to an increase of the ^{13}C chemical shift (by 1.6 ppm) and to a decrease of ^{15}N ones (by 6.7 ppm, in average) at the =NC(S)S— site. A decrease of the nitrogen δ^+ charge results in an enhanced shielding of methylene ^{13}C nuclei and therefore the decrease of the chemical shift (by 2.3 ppm) of these sites.

It is important to note the appearance of the two

Table 3. The interatomic distances in =NC(S)S— group of diethyldithiocarbamate compounds

Complex	$Ni(EDtc)_2$ [8]	$Zn_2(EDtc)_4$ [10]		$Na(EDtc)$ [33]
Distance N—C, Å:	1.324 (3)	1.340 (13) (terminal)	1.310 (12) (bridged)	1.339 (4)
Distance C—S, Å:	1.714 (3)	1.722 (10) (terminal)	1.723 (10) (bridged)	1.713 (3)
	1.715 (3)	1.725 (10)	1.737 (9)	1.729 (3)

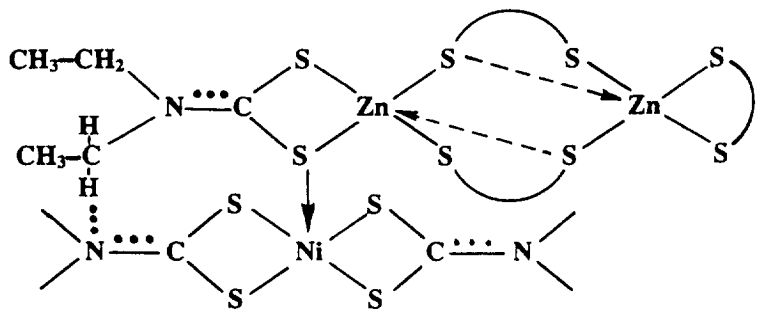

Scheme 5. Scheme of interaction between "dinuclear" and "mononuclear" parts in the polynuclear complexes.

structurally unequivalent ^{15}N sites (131.6 and 133.9 ppm) of the "nickel part" of the heteropolynuclear complex. This means that nitrogen atoms of the two dithiocarbamate ligands have different electronic environments. The most probable explanation for this structural unequivalence is the formation of a hydrogen bond between one of nitrogen atoms of the Ni(II) complex and a methylene group of the terminal ligand of the dinuclear molecule (Scheme 5).

The result of this interaction is the increase of ^{15}N chemical shift by 2.3 ppm which reflects the decrease of shielding of the corresponding nitrogen atom compared to the other one. The hydrogen bond formation is sterically allowed since the four-membered chelate ring of the dinuclear Zn(II) molecule is perpendicular to the plane of the square-planar Ni(II) complex. The other nitrogen atom of the "nickel part" of the heteropolynuclear complex is in a different environment, since the dinuclear molecule is non-planar. The dihedral angle between planes of the eight- and four-membered chelate rings is close to 90 .

CONCLUSIONS

Dithiocarbamate complexes of the type [Ni(II)-Me(II)-Dtc] (Me = Zn, Cd, Hg; Dtc = MDtc (dimethyl-) or EDtc (diethyldithiocarbamate)), which model a structural heterogeneity on the local, molecular and supramolecular levels, have been prepared and studied by means of ESR and solid state ^{13}C and ^{15}N CP/MAS NMR spectroscopy.

Three possible structures of these dithiocarbamate complexes were unambiguously identified: (i) the mononuclear square-planar, $Ni(Dtc)_2$; (ii) dinuclear with non-planar molecular configurations, $Me_2(Dtc)_4$ and (iii) polynuclear (supramolecular) complexes with a common composition of $Me_2(Dtc)_4 \cdot nNi(Dtc)_2$ (n = 1–4; Me = Zn, Cd, Hg). The latter is a newly proposed type of structure of dithiocarbamate complexes in the matrix of the model systems. It was established that the simultaneous presence of mononuclear and dinuclear molecules of dithiocarbamates in the prepared samples can lead to the formation of the heteropolynuclear complexes.

Acknowledgements—We acknowledge valuable discussions with Professor A. Lund, Department of Physics and Measurement Technology, Linköping University, Sweden. One of the authors (A.V.I.) is grateful to the Swedish Institute, to the Institute of Physical, Inorganic and Structural Chemistry (Stockholm University) and to the Center of Fundamental Nature Sciences at the Ministry of Comprehensive and Professional Education of the Russian Federation (St Petersburg State University), grant 95-0-9.3-35, for financial support. The CMX 360 spectrometer was purchased with a grant from Swedish Council for Planning and Coordination of Research (FRN).

REFERENCES

1. Boyd, P. D. W., Mitra, S., Raston, C. L., Rowbottom, G. L. and White, A. H., *J. Chem. Soc., Dalton Trans.*, 1981, **1**, 13.
2. Bonamico, M., Dessy, G., Mariani, C., Vaciago, A. and Zambonelli, L., *Acta Crystallogr.*, 1965, **19**, 619.
3. McConnell, J. F. and Kastalsky, V., *Acta Crystallogr.*, 1967, **22**, 853.
4. Starykova, Z. A., Shugam, E. A., Agre, V. M.

and Oboznenko, U. V., *Kristallografiya*, 1972, **17,** 111.
5. Martin, J. M., Newman, P. W. J., Robinson, B. W. and White, A. H., *J. Chem. Soc., Dalton Trans.*, 1972, **20,** 2233.
6. Newman, P. W. J. and White, A. H., *J. Chem. Soc., Dalton Trans.*, 1972, **20,** 2239.
7. Newman, P. W. J., Raston, C. L. and White, A. H., *J. Chem. Soc., Dalton Trans.*, 1973, **13,** 1332.
8. Selvaraju, R. and Panchanatheswaran, K., *Acta Crystallogr.*, 1995, **C51,** 606.
9. Bonamico, M., Dessy, G., Mazzone, G., Mugnoli, A., Vaciago, A. and Zambonelli, L., *Atti. Accad. Lincei*, 1963, **35,** 338.
10. Bonamico, M., Mazzone, G., Vaciago, A. and Zambonelli, L., *Acta Crystallogr.*, 1965, **19,** 898.
11. Klug, H. P., *Acta Crystallogr.*, 1966, **21,** 536.
12. Zvonkova, Z. V., Khvatkyna, A. N. and Ivanova, N. S., *Kristallografiya*, 1967, **12,** 1065.
13. Agre, V. M. and Shugam, E. A., *Zh. Strukt. Khim.*, 1972, **13,** 660.
14. Shugam, E. A. and Agre, V. M., *Kristallografiya*, 1968, **13,** 253.
15. Shugam, E. A. and Agre, V. M., *Kristallografiya*, 1972, **17,** 303.
16. Iwasaki, H., *Acta Crystallogr.*, 1973, **B29,** 2115.
17. Ivanov, A. V., Solozhenkin, P. M., Khamkar, M. Z., Klyashtorny, V. B. and Shvengler, Ph. A., *Koord. Khim.*, 1989, **15,** 1223.
18. Ivanov, A. V. and Solozhenkin, P. M., *Dokl. Akad. Nauk SSSR*, 1990, **311,** 392.
19. Ivanov, A. V., *Koord. Khim.*, 1991, **17,** 382.
20. Ivanov, A. V., Mitrofanova, V. I. and Rodina, T. A., *Russ. J. Inorg. Chem.*, 1997, **42,** 570.
21. Ivanov, A. V. and Solozhenkin, P. M., *Russ. J. Inorg. Chem.*, 1990, **35,** 871.
22. Pines, A., Gibby, M. G. and Waugh, J. S., *J. Chem. Phys.*, 1972, **56,** 1776.
23. Earl, W. L. and VanderHart, D. L., *J. Magn. Reson.*, 1982, **48,** 35.
24. Ratcliffe, C. I., Ripmeester, J. A. and Tse, J. S., *Chem. Phys. Lett.*, 1983, **99,** 177.
25. Mason, J., in *Encyclopedia of Nuclear Magnetic Resonance* Vol. 5, ed. D. M. Grant and R. K. Harris, John Wiley and Sons Ltd, N.Y., 1996, pp. 3222.
26. Al'tshuler, S. A., Kirmse, R. and Solov'ev, B. E., *J. Phys.*, 1975, **C8,** 1907.
27. Bonamico, M., Dessy, G., Mugnoly, A., Vaciago, A. and Zambonelli, L., *Acta Crystallogr.*, 1965, **19,** 886.
28. Solozhenkin, P. M., Ivanov, A. V., Kopytsia, N. I. and Shvengler, Ph. A., *Dokl. Akad. Nauk Tadzh. SSR*, 1983, **26,** 633.
29. Hexem, J. G., Frey, M. H., and Opella, S. J., *J. Chem. Phys.*, 1982, **77,** 3847.
30. Harris, R. K., Jonsen, P. and Packer, K. J., *Magn. Reson. Chem.*, 1985, **23,** 565.
31. Wahlberg, A., *Acta Crystallogr.*, 1978, **B34,** 3822.
32. Wahlberg, A., *Acta Chem. Scand.*, 1976, **A30,** 614.
33. Mereiter, K., Preisinger, A., Mikenda, W. and Steidl, H. *Inorg. Chim. Acta*, 1985, **98,** 71.
34. deDios, A. C. and Oldfield, E., *Solid State Nucl. Magn. Reson.*, 1996, **6,** 101.
35. Higgins, G. M. C. and Saville, B., *J. Amer. Chem. Soc.*, 1963, **3,** 2812.

Pergamon

PII: S0277-5387(98)00076-X

Polyhedron Vol. 17, No. 18, pp. 3111–3119, 1998
© 1998 Elsevier Science Ltd
All rights reserved. Printed in Great Britain
0277-5387/98 $19.00+0.00

Conductometric and spectroscopic investigations on the reactions between *N*-methylthiazolidine-2(3H)-selone (1) and *N*-methylbenzothiazole-2(3H)-selone (2) with Br_2

Massimiliano Arca,[a] Francesco Demartin,[b] Francesco A. Devillanova,[a]* Alessandra Garau,[a] Francesco Isaia,[a] Vito Lippolis,[a] Silvia Piludu[a] and Gaetano Verani[a]

[a] Dipartimento di Chimica e Tecnologie Inorganiche e Metallorganiche, Università di Cagliari, Via Ospedale 72, I-09124, Cagliari, Italy

[b] Dipartimento di Chimica Strutturale e Stereochimica Inorganica e Centro CNR, Università di Milano, Via G. Venezian 21, I-20133, Milano, Italy

(Received 17 December 1997: accepted 18 February 1998)

Abstract—The formation of the compounds $C_4H_7Br_2NSSe$ (**3**), $(C_4H_7BrNS)_2[SeBr_6]$ (**4**) and $C_8H_7Br_2NSSe$ (**5**) from the reaction of the title selenium donors (**1** and **2**) with molecular dibromine in CH_2Cl_2 and MeCN solutions has been investigated by ^{77}Se and ^{13}C NMR, UV-visible spectroscopies and by conductometric measurements. In the conductometric titrations of **1** or **2** with dibromine, the very low values of conductivity recorded up to the 1 : 1 Br_2/**1**(**2**) molar ratio indicate the formation of the non-conducting hypervalent selenium compounds **3** and **5**, as confirmed by UV–visible and NMR spectroscopies. Above this ratio, **1** and **2** behave differently; in fact, for both of them the conductivity values increase on increasing the amount of added dibromine, but the values recorded for **1**, that are much higher than those for **2**, are time-dependent. This indicates a kinetic transformation of **1** that has been shown to lead to the previously characterized **4**. © 1998 Elsevier Science Ltd. All rights reserved

Keywords: *N*-methylthiazolidine-2(3H)-selone; *N*-methylbenzothiazole-2(3H)-selone; hypervalent selenium compounds with bromine; hexabromoselenate(2-); conductometric measurements; ^{77}Se and ^{13}C NMR and UV–visible spectroscopies.

In our investigations on the donor/acceptor interactions between heterocycles containing thionic and selonic groups and dihalogens or interhalogens [1–6], we have found that, besides the donor/acceptor adducts, a large variety of products can be obtained and that X-ray crystal structure determination plays a crucial role in their characterization. As a development of our research in this field, we have recently reported the results obtained by reacting *N*-methyl-1,3-thiazolidine-2(3H)-selone (**1**) and *N*-methylbenzothiazole-2(3H)-selone (**2**) with molecular dibromine in CH_2Cl_2 solution [6] (Scheme 1). Whatever the reagent molar ratio, **2** gives the hypervalent compound $C_8H_7Br_2NSSe$ (**5**), which bears the Br—Se—Br linear group. **1** gives the hypervalent compound $C_4H_7Br_2NSSe$ (**3**) when the reaction is carried out in 1 : 1 Br_2/**1** molar ratio, while by using the 2 : 1 or higher reagent molar ratios, the ionic compound $2[C_4H_7BrNS]^+ [SeBr_6]^{2-}$ (**4**) is obtained. Compounds **4** and **5** were characterized by X-ray crystal structure determination [6].

Since **4** represents the unique case reported in literature where oxidation of the selenium of a selonic group leads to hexabromoselenate(2-), we thought of investigating its formation in CH_2Cl_2 as well as MeCN solution by UV–visible, ^{77}Se and ^{13}C NMR, and conductometric titration techniques.

* Author to whom correspondence should be addressed.

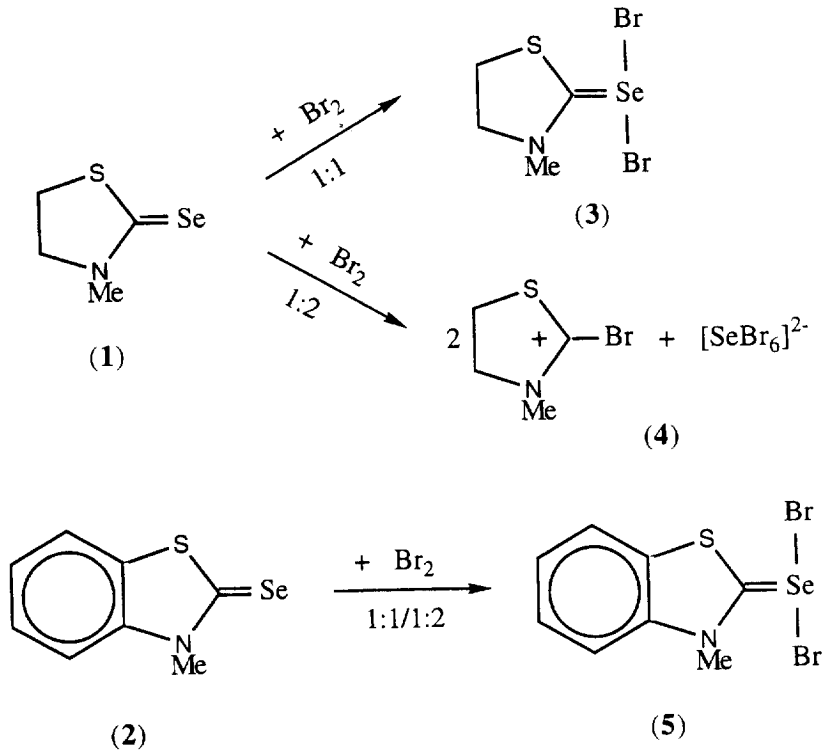

Scheme 1.

EXPERIMENTAL

Materials

N-methyl-1,3-thiazolidine-2(3H)-selone (**1**) was synthesized according to the procedure reported in Ref. [7]. *N*-methylbenzothiazole-2(3H)-selone (**2**), dibromine and the solvents (CH_2Cl_2 and MeCN) were purchased from Aldrich and used without further purification.

Conductometric titrations

Conductometric titrations were carried out at $T = 298$ K in CH_2Cl_2 solution in a standard-thermostatted cell with a Model 120 Microprocessor Conductivity Meter Analytical Control. The k cell (1.23 cm^{-1}) was determined by measuring at $T = 298$ K the conductivity of three bidistilled water solutions of KCl (0.1, 0.01 and 0.001 mol dm^{-3} respectively) previously kiln-dried for 12 h. Conductivity was recorded after 5 minutes from each Br_2 addition in order to allow the stabilization of the temperature. In the titration of **1**, since conductivity showed a continuous increase with time, the conductivity values were also recorded after 10 minutes from each addition. The CH_2Cl_2 solutions of Br_2 were titrated with a standard aqueous $Na_2S_2O_3$ solution (0.100 mol dm^{-3}) according to traditional methods.

Kinetic measurements and data treatment

The kinetic measurements ($T = 298$ K, CH_2Cl_2 solution, [**1**] = $1 \cdot 10^{-2}$ mol dm^{-3}) have been carried out in *pseudo*-first order conditions (large excess of dibromine) by mixing pre-thermostatted solutions of the reagents and recording the changes of conductivity with time. Straight lines have ben obtained by reporting $\ln(\sigma_t - \sigma_t)/(\sigma_t - \sigma_0)$ vs time (σ_0 and σ_t are the conductivity values in μS cm^{-1} at time 0 and ∞ respectively).

Ultraviolet spectra

Spectrophotometric measurements were carried out in CH_2Cl_2 and in MeCN solutions by using a Varian model Cary 5 UV–vis–NIR spectrophotometer equipped with a temperature controller accessory and connected with an IBM Personal System 2 Type 8513 TKQ S/N 55-DMR89. For both **1** and **2**, the spectra of 9 different solutions, with a Br_2/donor molar ratio ranging from 0.3 to 6 were recorded in the range 200–400 nm at the temperature of $T = 298$ K. Because of

the kinetic process for the reaction between **1** and Br_2, the spectra of their mixtures were recorded immediately after mixing the pre-thermostatted solutions of the reagents.

^{77}Se and ^{13}C NMR measurements

^{77}Se and ^{13}C NMR spectra were recorded at a temperature of 293 K by a Varian Unity 300 MHz spectrometer. Chemical shifts are quoted relative to Me_2Se ($\delta = 0$) for the ^{77}Se nucleus and TMS or DMSO-d_6, as the external reference, for the ^{13}C nucleus. For **1**, several solutions having the same donor concentration ($2.7 \cdot 10^{-2}$ mol dm^{-3}) and increasing amounts of dibromine (maximum value $[Br_2]/[\mathbf{1}]$ molar ratio 6) were prepared and their NMR spectra recorded some hours afterwards mixing the reagents. ^{77}Se spectra of compounds **3**, **4** and **5**, which have low solubility in CH_2Cl_2, were only recorded in MeCN solution at a concentration of approximately $2.7 \cdot 10^{-2}$ mol dm^{-3}.

RESULTS AND DISCUSSION

Depending on the reagent molar ratios, the reactions of *N*-methyl-1,3-thiazolidine-2(3H)-selone (**1**) and *N*-methylbenzothiazole-2(3H)-selone (**2**) with molecular dibromine in CH_2Cl_2 solution give the solid products, **3**, **4** and **5** [6, 8]. In fact, using a Br_2/donor 1 : 1 molar ratio, both donors yield the hypervalent selenium compounds **3** and **5**, bearing the Br—Se—Br linear group; with a 2 : 1 molar ratio, **2** gives **5** again, and **1** gives **4**.

In order to understand the different reactivity of **1** and **2** towards Br_2 and to ascertain whether **4** exists in solution or is formed only during the crystallization process, we prepared several solutions of **1** and **2** and Br_2 in different stoichiometric ratios and recorded their conductivities, ultraviolet absorption spectra and ^{77}Se and ^{13}C NMR chemical shifts.

Conductometric measurements

The conductometric titrations of **1** and **2** with Br_2, carried out in CH_2Cl_2 solution, show that the conductivity up to the 1 : 1 Br_2/**1**(**2**) molar ratio is constant and very low, for **2** lower than for **1** by about one order of magnitude. This indicates the formation of non-conducting species, which are very likely to be the hypervalent selenium compounds **3** and **5**.

Above the 1 : 1 molar ratio, **1** and **2** behave differently: while for **2**, conductivity does not vary after each addition of the Br_2 solution, for **1** it changes with time, and the drift continues beyond the titration until **4** starts precipitating. Moreover, the conductivity values for **2** still remain lower than for **1**.

It is important to remark once more that in the first part of the titration of **1** (up to the 1 : 1 Br_2/**1** molar ratio) the conductivity values are very low (but still higher than for **2**) and do not change in time; the low conductivity values indicate that the non-conducting species should be in equilibrium with some ions, and that this equilibrium should be almost completely shifted to the left (for **2** more than for **1**), towards the hypervalent compounds.

We have also carried out kinetic measurements, by recording the increase of the conductivity values in time (Fig. 1). In particular, six kinetic measurements ($T = 298$ K, $[\mathbf{1}] = 1 \cdot 10^{-2}$ mol dm^{-3}) have been carried out in *pseudo*-first order conditions, using concentrations of Br_2 from 30 to 80 times higher than that of **1**. In these conditions, the straight lines of $\ln(\sigma_t - \sigma_t)/(\sigma_t - \sigma_0)$ vs time (see Fig. 1) indicate that the reaction is of the first-order with respect to **1**. The k_{obs} are independent on the bromine concentration and a constant value of $(5.8 \pm 0.3) \cdot 10^{-4}$ s^{-1} is obtained for all kinetic experiments.

The conductometric results might be explained by hypothesizing the hypervalent selenium compounds in equilibrium with $[>CSeBr]^+$ and Br^- ions during the first part of the titration (Br_2/donor < 1 : 1) (see Scheme 2). The very low conductivity values recorded in this part of the titration for both **1** and **2** should be due to this equilibrium, which is prevalently shifted to the left. The addition of further amounts of dibromine (Br_2/donor > 1 : 1) shifts this equilibrium to the right as a consequence of the formation of the Br_3^- anion (step 3) and increases the conductivity values.

Under this hypothesis, it is possible to account for the different reactivity of **1** and **2** towards Br_2. In fact, the cation deriving from **2** should be more stable than that derived from **1**, because of a more efficient delocalization of the positive charge on the aromatic ring [9]. This justifies the fact that only compound **5** was obtained in the solid state [6] for both 1 : 1 and 2 : 1 Br_2/**2** molar ratios. In the case of **1**, further reactions lead to the formation of the ionic compound **4**. This causes an increase of the number of conducting species in time and, as a consequence, total conductivity increases.

Ultraviolet measurements

In order to support this hypothesis independently, we recorded the ultraviolet spectra of authentic samples of **1**–**5** dissolved in MeCN (Table 1), and of several mixtures of **1** (or **2**) and Br_2 in MeCN (see Figs 2 and 3). Since no kinetics occurs in the reaction between Br_2 and **2**, we start first with this case. Up to the 1 : 1 Br_2/**2** molar ratio (curves 1–4 of Fig. 3) the spectra show: (i) a decrease in the band at about 350 nm (which is the most intense of **2**); (ii) an increase in the absorption at around 235 nm (which is the most intense of **5**); and (iii) the presence of an isosbestic point at 329 nm; this should agree with an equilibrium between the two species **2** and **5**. However, a careful examination of the curves shows that other species in low concentrations (such as Br_3^- and $[>CSeBr]^+$)

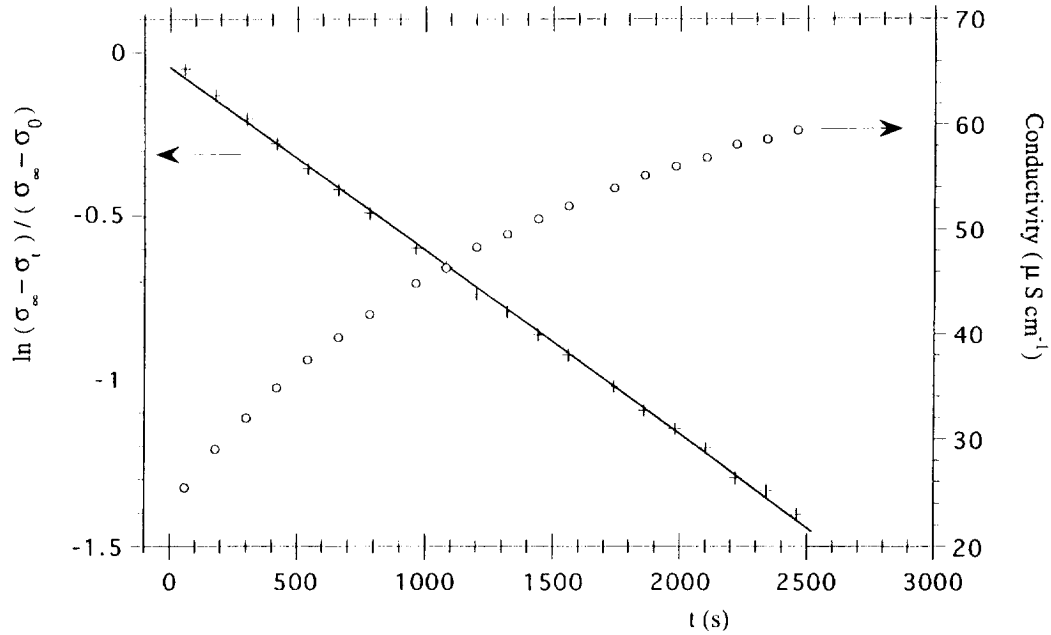

Fig. 1. Conductivity values (o; scale on the right) of the reaction between **1** and Br_2, recorded as a function of time (T = 298 K; CH_2Cl_2 solution; [**1**] = $1 \cdot 10^{-2}$ mol dm^{-3}; [Br_2]/[**1**] molar ratio = 50). The straight line obtained by reporting $\ln(\sigma_\infty - \sigma_t)/(\sigma_\infty - \sigma_0)$ (+; scale on the left) vs time has a slope of $5.6 \cdot 10^{-4}$ s^{-1} (correlation coefficient = 0.999) (σ_∞ and σ_0 are the conductivities at times ∞ and 0 respectively.

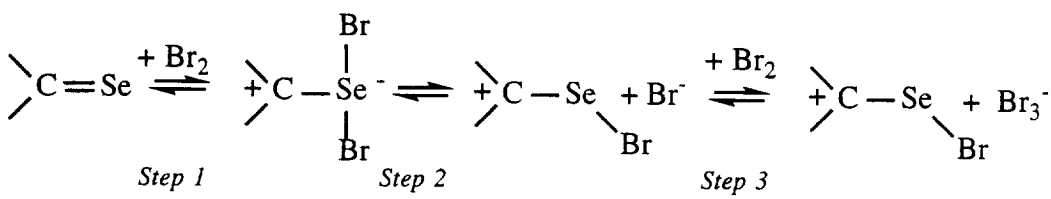

Scheme 2.

Table 1. UV–visible absorptions of all the species involved in the equilibria of **1** and **2** with Br_2 (log ε in parentheses) in MeCN

Compound	Absorption bands (nm)
1	227(3.73)253(3.68)302(4.01)
3	230(4.57)281(4.26)
4	204(4.48)216(4.40)270(4.90)
2	351(4.50)388(3.36)
5	200(4.41)236(4.50)306(4.05)
Br_3^-	269(4.75)[a]
Br_2	268(2.16)393(2.19)

[a] This value was measured on a freshly prepared solution of tetrabutylammonium tribromide ($4.0 \cdot 10^{-5}$ mol dm^{-3}) and is very close to the value of 4.74 reported by A. I. Popov [11].

should be present and might be responsible for the irregular trend around 260 cm^{-1}. By increasing the amount of Br_2 (curves 5–9), the spectra mainly show a continuous increase in the intensity of the band around 270 nm, due to the Br_3^- anion [11], as shown in step 3. As can be seen from an examination of the curves 6–9, the absorbance at 236 cm^{-1} does not increase any further above the 3 : 1 Br_2/**2** molar ratios, indicating that **2** has completely reacted to give **5**.

The spectra of freshly prepared mixtures of **1** and dibromine in MeCN solution were recorded immediately after temperature stabilization and look quite different. Again, the first four spectra (curves 1–4) show an increase in the absorption at around 230 nm (hypervalent selenium compound **3**), but neither a regular decrease of the band at 302 nm (which is the most intense of **1**) nor the presence of isosbestic points.

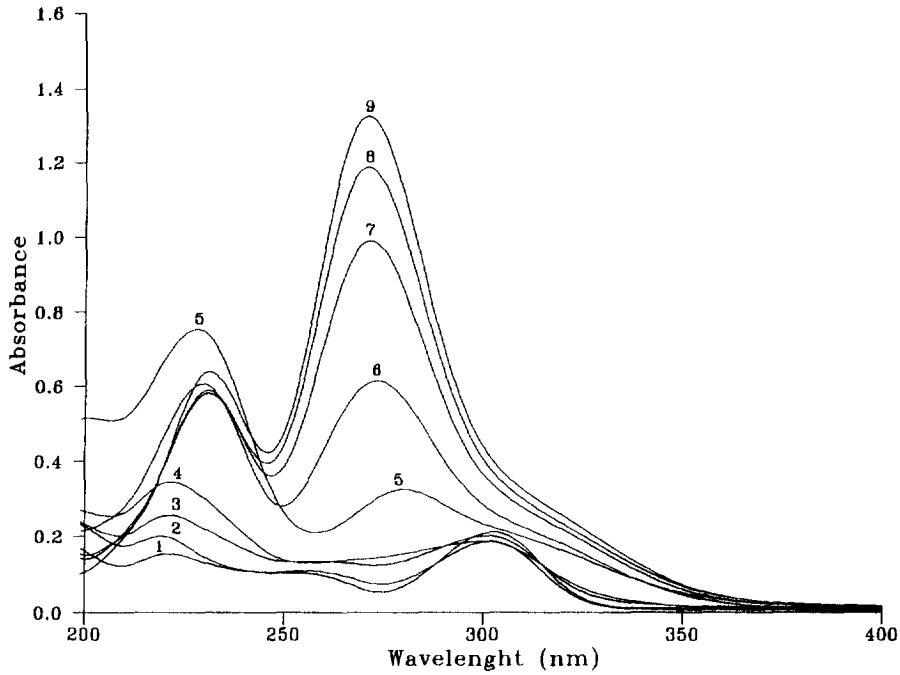

Fig. 2. Spectra of nine solutions having a constant concentration of **1** [$2.1 \cdot 10^{-5}$ mol dm^{-3}] and increasing amounts of Br_2 ($T = 298$ K; MeCN). The $[Br_2]/[\mathbf{1}]$ molar ratios are 0.24, 0.48, 0.71, 0.95, 2.02, 2.98, 4.05, 5.00 and 5.95 for 1–9 respectively.

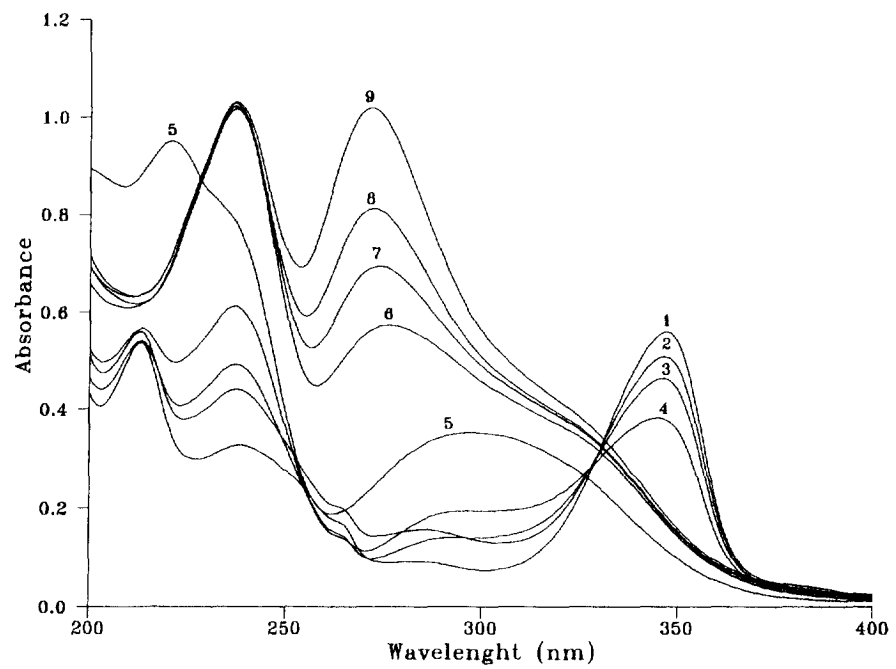

Fig. 3. Spectra of nine solutions having a constant concentration of **2** [$2.28 \cdot 10^{-5}$ mol dm^{-3}] and increasing amounts of Br_2 ($T = 298$ K; MeCN). The $[Br_2]/[\mathbf{2}]$ molar ratios are 0.27, 0.55, 0.68, 0.96, 1.92, 3.01, 3.97, 4.8 and 6.03 for 1–9 respectively. The spectra 1–4 show the presence of an isosbestic point at 329 nm.

The kinetic process and the presence of more than two species in solution should be responsible for this. For mixtures having Br_2/**1** molar ratios higher than 1 : 1 (curves 5–9), a band at around 270 nm, similar to that found in the case of **2**, increases on increasing Br_2 concentration, but in this case the band has a much higher intensity than the other bands in the spectrum, agreeing with the fact that both the Br_3^- and $SeBr_6^{2-}$ anions have very strong absorptions at this wavelength (see Table 1). Also these results confirm Scheme 2 and indicate the formation of **4** in solution on addition of Br_2 to **1** beyond the 1 : 1 Br_2/**1** molar ratio.

^{13}C and ^{77}Se NMR spectra

The titration of **1** with Br_2 has also been monitored by recording the ^{77}Se NMR chemical shifts of their mixtures in CH_2Cl_2 and MeCN solutions at the end of the reaction (Fig. 4) [12]. In both the solvents, the ^{77}Se NMR chemical shifts move to higher fields in presence of an equimolar amount of Br_2, from 420.4 to 374.5 ppm in CH_2Cl_2 and from 399.0 to 387.0 in MeCN, indicating shielding of the selenium atom. These values are very close to that recorded for an authentic sample of **3** (379.8 ppm) in MeCN (Fig. 4) [13]. All this indicates that **3** is forming during the first step of the titration in both solvents. By increasing the amount of added Br_2, the signal moves towards lower fields in both solvent, but, in MeCN solution, the ^{77}Se NMR chemical shifts (▲ in Fig. 4) show more deshielding with respect to that found in CH_2Cl_2 solution (+ in Fig. 4). The titration of **1** with Br_2 was also monitored by recording the ^{13}C NMR chemical shifts of C(4), C(5) and the methyl group (Fig. 5). The addition of Br_2 up to the 1 : 1 molar ratio linearly shifts the signals to low fields, indicating an increase in overall deshielding of the pentaatomic ring. After the 1 : 1 molar ratio, the signals of the carbons remain unchanged. This behaviour is quite different from that observed for the ^{77}Se chemical shifts. The comparison of the ^{13}C NMR spectra of **3** and **4** solves this puzzle. Apart from a signal at 167.6 ppm detected only for the $C_4H_7BrNS^+$ cation of **4** and attributed to the C(2) carbon atom, the values of all the other carbon resonances (61.3, 41.2, 31.1 ppm for **3** and 63.3, 43.3, 31.4 ppm for **4**) are very close. Then, the transformation of **3** into the $C_4H_7BrNS^+$ cation cannot be followed by the changes of the chemical shifts of the carbons, but by the changes of the conductivity values since it brings to charged species.

However, if **4** is forming during the kinetic process for a Br_2/**1** molar ratio higher than 1 : 1, as indicated

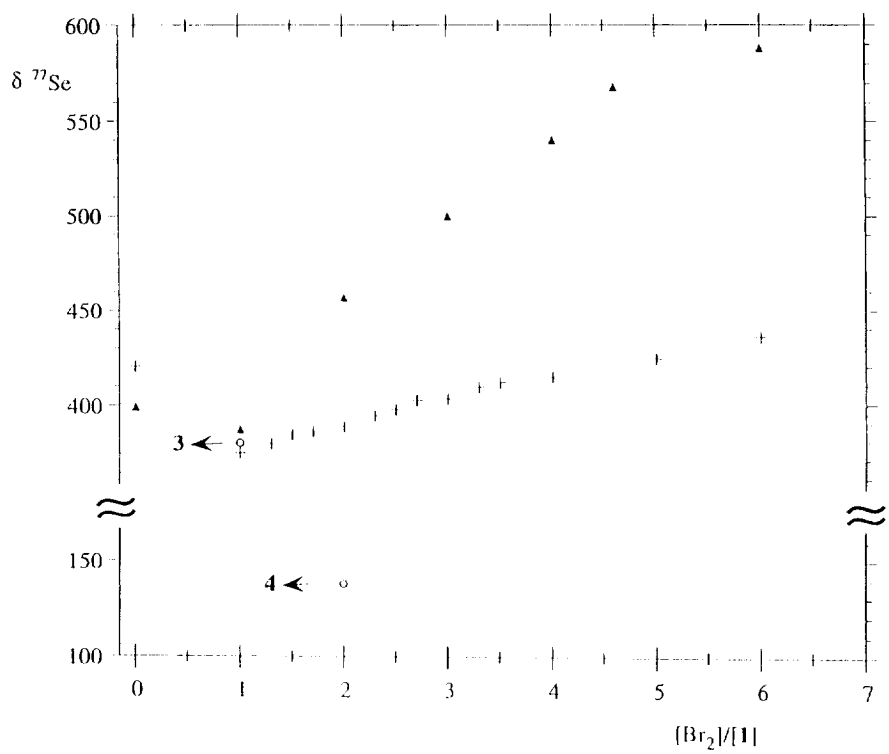

Fig. 4. ^{77}Se NMR chemical shifts of mixtures **1** and Br_2 in CH_2Cl_2 (+) and in MeCN (▲) as a function of $[Br_2]/[\mathbf{1}]$ molar ratios. The values recorded on authentic samples of **3** and **4** (o), dissolved in MeCN, are also reported. The value for **4** is reported at 2 on the abscissa, since **4** contains four bromine atoms for each pentaatomic ring. No values are reported in the first part of the titration for molar ratios intermediate between 0 and 1, since the ^{77}Se signal has not been detected.

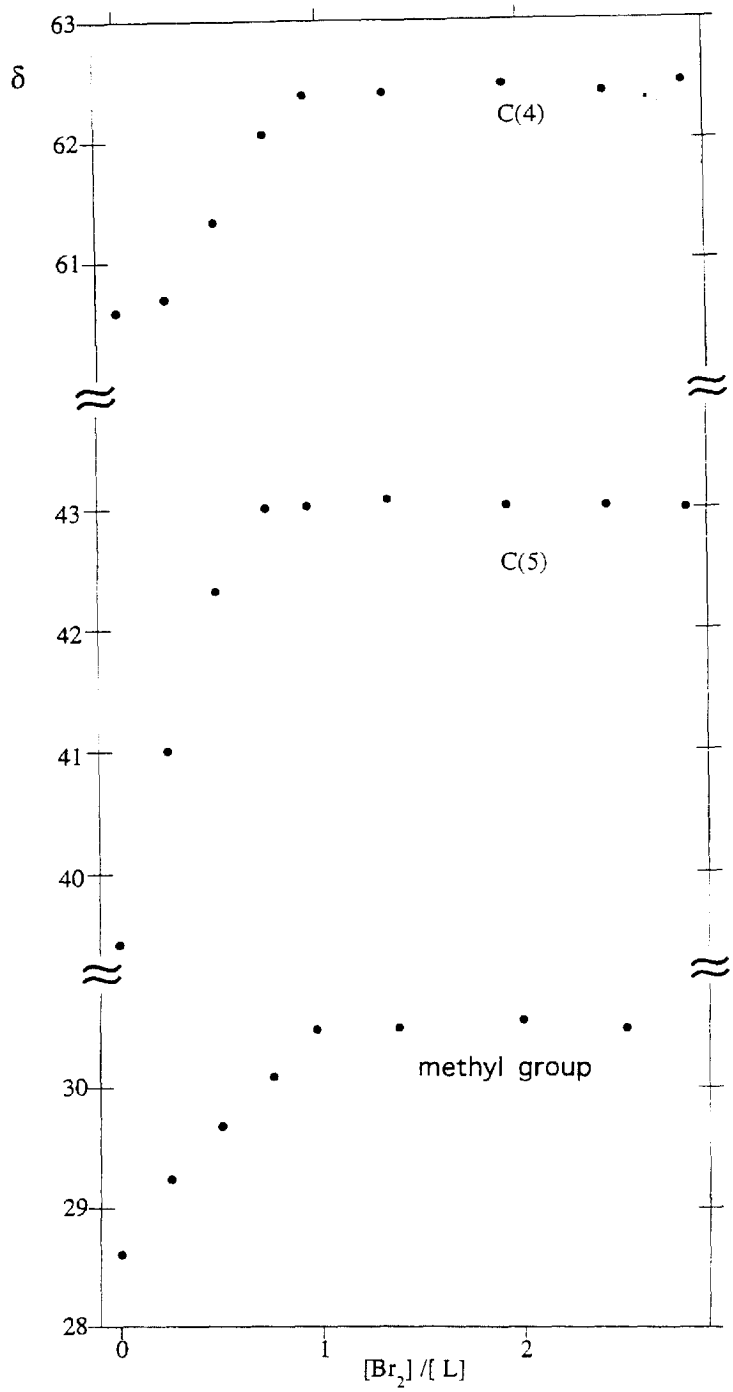

Fig. 5. ^{13}C NMR chemical shifts of C(4), C(5) and of the methyl group for mixtures of **1** [$2.7 \cdot 10^{-2}$ mol dm^{-3}] and Br_2 in CH_2Cl_2 as a function of $[Br_2]/[\mathbf{1}]$ molar ratios.

by conductometric measurements and UV–visible spectra, why does the ^{77}Se signal move in opposite direction compared with the value of 138.09 ppm (see Fig. 4) recorded in MeCN for pure **4**? [14]. This fact seems to be in contrast with the formation of $SeBr_6^{2-}$ ion in solution. In order to clarify this point and elucidate the stoichiometry of the reaction, in a typical experiment carried out in CH_2Cl_2 solution, we recorded the ^{77}Se NMR spectrum on the filtered solution after precipitation of **4**. A signal at 1368 ppm, which is not very different from the value of 1496 ppm reported for pure $SeBr_2$ [15], has been detected [16].

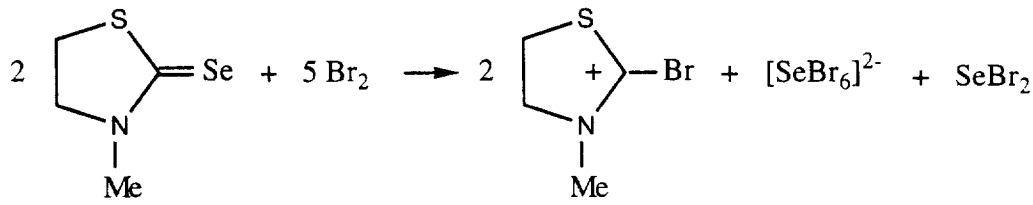

Scheme 3.

From this, it seems very likely that the reaction is that reported in Scheme 3 and the ^{77}Se NMR signal detected during the titration is mediated on the different selenium compounds present in solution. The value of 1368 ppm, which is different from that reported for $SeBr_2$, can easily be explained by taking into account further possible equilibria involving $SeBr_2$, bromide and $[SeBr_6]^{2-}$ ions.

In order to confirm this, an authentic sample of **4**, dissolved in MeCN, was reacted with approximately an equivalent amount of $SeBr_2$, obtained *in situ* by $SeBr_4$ and metallic selenium [15]. A signal of 373.5 ppm was detected for the mixture. The closeness of this value to those recorded during the titration confirms that it is precisely the $[SeBr_6]^{2-}$ ion that is forming in solution. The different values of the ^{77}Se NMR chemical shift of $[SeBr_6]^{2-}$, detected in presence and without $SeBr_2$, are the key to give a final explanation of all experimental data.

CONCLUSIONS

In this paper we investigate the different reactivity of **1** and **2** in the reaction with dibromine, using conductometric measurements, the UV–visible and ^{77}Se and ^{13}C NMR spectroscopies. The two donors give the corresponding 10-Se-3 [17] hypervalent compounds **3** and **5** by oxidative addition of Br_2 as a unique compound for the Br_2/**1**(or **2**) molar ratios $\leqslant 1:1$; this is in good agreement with conductometric and spectrophotometric measurements. In both cases, conductometric measurements show no formation of dications as intermediates in the oxidation reaction, unlike what has recently been found by us [9] for some 1,3-dimethylimidazoline-2-selone derivatives. For higher Br_2/**1**(or **2**) molar ratios, **1** and **2** behave very differently: **2** always gives the same hypervalent selenium compound **5**, while **1** gives the very unusual *N*-methyl-2-bromothiazolidium hexabromoselenate(2-) (**4**). In this case, the conductometric measurements have shown a measurable kinetic process of formation of **4**. The comparative spectrophotometric studies carried out on the two substrates in the same conditions, have allowed us to identify the different stability of the $[>CSeBr]^+$ cation [4], generated in the equilibrium reaction between the hypervalent compounds and Br_2, as the reason for the different behaviour of the two substrates. Finally, ^{77}Se NMR measurements have allowed to identify $SeBr_2$ as the species formed parallelly to **4**. According to the view that **3** and the cation of **4** may be regarded as adducts of nucleophilic carbene ligands (thiazolin-2-ylidene C_4H_7NS) with the acceptors $SeBr_2$ (**3**) and Br^+ (cation of **4**), it is interesting to point out that both groups affect the ^{13}C chemical shifts of the pentaatomic ring in the same manner.

Acknowledgements—We thank the Regione Autonoma della Sardegna and MURST 40% for their support to this research.

REFERENCES

1. Bigoli, F., Pellinghelli, A. M., Deplano, P., Devillanova, F. A., Lippolis, V., Mercuri, M. L. and Trogu, E. F., *Gazz. Chim. It.*, 1994, **124**, 445.
2. Demartin, F., Deplano, P., Devillanova, F. A., Isaia, F., Lippolis, V. and Verani, G., *Inorg. Chem.*, 1993, **32**, 3694.
3. Cristiani, F., Demartin, F., Devillanova, F. A., Isaia, F., Lippolis, V. and Verani, G., *Inorg. Chem.*, 1994, **33**, 6315.
4. Demartin, F., Devillanova, F. A., Isaia, F., Lippolis, V. and Verani, G., *Inorg. Chim. Acta.*, 1997, **255**, 203.
5. Bigoli, F., Demartin, F., Deplano, P., Devillanova, F. A., Isaia, F., Lippolis, V., Mercuri, M. L., Pellinghelli, A. M. and Trogu, E. F., *Inorg. Chem.*, 1996, **35**, 3194.
6. Devillanova, F. A., Deplano, P., Isaia, F., Lippolis, V., Mercuri, M. L., Piludu, S., Verani, G. and Demartin, F., *Polyhedron*, 1998, **17**, 305.
7. Cristiani, F., Devillanova, F. A. and Verani, G., *J. Chem. Soc., Perkin Trans. II*, 1977, 324.
8. **3**, **5** and the cation of **4** may be regarded as adducts of nucleophilic carbene ligands (thiazolin-2-ylidene C_4H_7NS and benzothiazol-2-ylidene C_8H_7NS) with the acceptors $SeBr_2$ (**3** and **5**) and Br^+ (cation of **4**).
9. In a recent paper [Bigoli, F., Deplano, P., Devillanova, F. A., Lippolis, V., Mercuri, M. L., Pellinghelli, A. M. and Trogu, E. F., *Eur. J. Inorg. Chem.*, 1998, **1**, 137, analogous titrations carried out on some imidazoline-2-selone derivatives have shown that conductivity values increase on addition of Br_2, reach a maximum for the 0.5 : 1 Br_2/imidazoline molar ratio, and subsequently decrease to the 1 : 1 molar ratio. Above the 1 : 1 molar ratio, conductivity increases and, as found

for **2**, is time independent. In those cases, it was shown that the reactions involve the formation of dications containing the Se—Se bridge as intermediates in the formations of the hypervalent 10-Se-3 selenium compounds. In the present case, however, the observed trends in the conductivity exclude the formation of the corresponding dications of **1** and **2** on the way to **3** and **5**. Very recently, S. Husebye [10] reported a scheme to collect the wide variety of compounds formed in reaction between chalcogen ligands and halogens, and showed different possible pathways for the formation of dications and hypervalent selenium compounds. On the basis of the results obtained with the imidazoline-2-selone derivatives, that scheme should be enlarged at least to include the direct formation of hypervalent selenium compounds from dications by addition of dihalogens.

10. Rudd, M. D., Lindeman, S. V. and Husebye, S., *Acta Chem. Scand.*, 1997, **51,** 689.
11. Popov, A. I. and Swensen, R. F., *J. Am. Chem. Soc.*, 1955, **77,** 3724.
12. Analogous titrations of **2** with Br_2 have not been carried out because of its low solubility.
13. The stability of the MeCN solutions of **3** and **4** have been checked by FT-Raman spectroscopy; moreover, the solids recovered by evaporation of the solvent after the NMR measurements were identical to the starting compounds as proved by FT-Raman, FT-IR spectra and CHNS analyses.
14. The ^{77}Se chemical shift of $[C_4H_7BrNS]_2[SeBr_6]$ has been recorded in MeCN solution for solubility reasons.
15. Baumgart, F., Jensen, D. and Steudel, R., *Polyhedron*, 1990, **9,** 1199.
16. It is not possible to carry out analogous experiments in MeCN solution, since compound **4** is soluble. In this case, the ^{77}Se NMR signal moves towards lower fields reaching a value of about 600 ppm at the end of the titration.
17. Perkins, C. W., Martin, J. C., Arduengo, A. J., Lau, W., Alegrie, A. and Kochi, J. K., *J. Am. Chem. Soc.*, 1980, **102,** 7753.

Pergamon

PII: S0277-5387(98)00096-5

Polyhedron Vol. 17, No. 18, pp. 3121–3130, 1998
© 1998 Elsevier Science Ltd
All rights reserved. Printed in Great Britain
0277-5387/98 $19.00+0.00

Molecular structures of $[(^tBu)_2Ga(\mu\text{-}O_2CPh)]_2$, $[(^tBu)_2Ga(\mu\text{-}O_2CC_6H_4\text{-}3\text{-}CN)]_2$, and $[(^tBu)_2Ga(\mu\text{-}SC_6H_5)]_2$: The efficacy of oxygen and sulfur donor ligands for binding GaAs and GaS surfaces

Andrea Keys,[a] Simon G. Bott[b]* and Andrew R. Barron[a]*

[a]Department of Chemistry, Rice University, Houston, Texas, 77005, U.S.A.

[b]Department of Chemistry, University of Houston, Houston, Texas, 77204, U.S.A.

(Received 15 December 1997; accepted 18 February 1998)

Abstract—The reaction of $Ga(^tBu)_3$ with 1 molar equivalent of a carboxylic acid yields the carboxylate bridged dimeric compounds, $[(^tBu)_2Ga(\mu\text{-}O_2CR)]_2$, where R = Ph (**1**), C_6H_4-3-CN (**2**), and C_6H_4-3-Br (**3**), respectively. Similarly, reaction of $Ga(^tBu)_3$ with HSPh yields the thiolate bridged compound, $[(^tBu)_2Ga(\mu\text{-}SPh)]_2$ (**4**). The molecular structures of compounds **1**, **2**, and **4** have been determined by X-ray crystallography. The Ga···Ga and Ga-ligand inter-atomic distances for these compounds, as well as group 15 and 16 donor bridging ligands, are compared to the values for the surface of GaAs and cubic-GaS in order to determine their suitability as linkage groups for self-assembled monolayers. © 1998 Elsevier Science Ltd. All rights reserved.

Keywords: gallium; carboxylate; thiolate; gallium arsenide; gallium sulfide

INTRODUCTION

There has been increasing interest in the development of chemical sensors with enhanced sensitivity and selectively. Important applications for such sensors include clinical chemistry, such as alternative site and critical care measurements [1], environmental detection of hazardous and mutagenic substances [2], and in-line monitors for the food production industry [3]. Requirements for such sensors are their ability to provide a rapid and reversible response, parts per billion (ppb) level detection, compact packaging for *in-situ* detection, performance in either gaseous or liquid media, highly sensitive (molecular) detection, and low cost. The overall requirements for a selective ion or molecular sensor are an indicator molecule that reversibly interacts with a target molecule with a high degree of specificity (e.g., Fig. 1) and the presence of some detectable property that changes when the target molecule has interacted. A wide variety of changes and therefore suitable detection methods have been employed, including electrochemical methods [4], optical [5, 6], photoelectronic [7, 8], thermal [9], and electronic [10]. With regard to electronic detection one such device is the chemFET (chemically sensitive field effect transistor) in which the flow of electrons in the channel is controlled by the absorption of a target molecule into a chemically sensitive membrane [11]. However, this membrane has a drawback in its affinity for water and other chemical species that interfere with its function. Additionally, the SiO_2 dielectric layer is porous which allows for the diffusion of water through to the channel thus destroying the device. Ideally, in order to realize a chemFET the gate dielectric would need to be chemically stable, compatible with commercial production techniques in a close-packed arrangement to avoid contamination, and be able to be chemically modified. We have recently reported that through the use of cubic-GaS (c-GaS)

* Authors to whom correspondence should be addressed. http://pchem1.rice.edu/~arb/Barron.html.

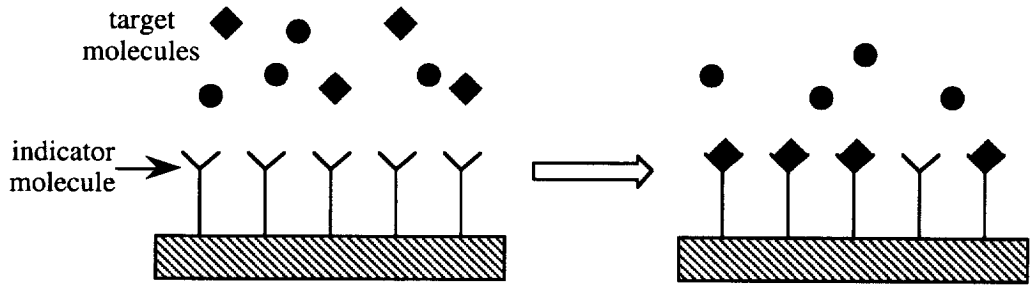

Fig. 1. Schematic representation of the selective interaction between a surface bound indicator molecule and a target molecule.

as the gate dielectric it is possible to fabricate a GaAs analog to the MOSFET (metal oxide semiconductor field effect transistor); a field effect transistor with an insulating sulfide heterojunction (FETISH) [12]. In contrast to SiO_2, c-GaS is non-porous and is chemically resistant to oxidation. Thus, we have proposed that a chemically responsive FETISH (chem-FETISH) should offer significant advantages over the traditional chem-FET.

The simplest method of fabricating a chem-FETISH would be to attach indicator molecules to the surface of the c-GaS gate dielectric. These could be bound via a spacer unit through chemical modification of the surface, e.g., Fig. 2. One key component is the use of a suitable linkage unit which will covalently bind to the surface and be stable in various solvent media. While suitable surface linkage moieties have been identified for such materials as gold [13], alumina [14], and zirconium oxide [15], there is little precedent for GaAs and none for c-GaS.

We have previously demonstrated that the strong binding of carboxylate groups to aluminum oxide surfaces is due to the topotactic nature of the reaction, i.e., no reconstruction (bulk reorganization) of the Al-O framework is required for the carboxylate group to bind to the surface [16]. We were able to show through the synthesis and characterization of model compounds that the carboxylate ligand is ideally suited to binding two aluminum atoms with a Al···Al distance of 3.11–4.46 Å, which encompasses the most accessible Al···Al distance present on the surface of aluminum oxides (3.70 Å). We propose to employ the same concept in rationalizing the best linkage units for binding to c-GaS (and GaAs). In this regard a variety of model compounds have been synthesized, and along with other model compounds previously reported [17–19], their Ga-to-Ga and Ga-to-ligand distances were compared to those of c-GaS and GaAs.

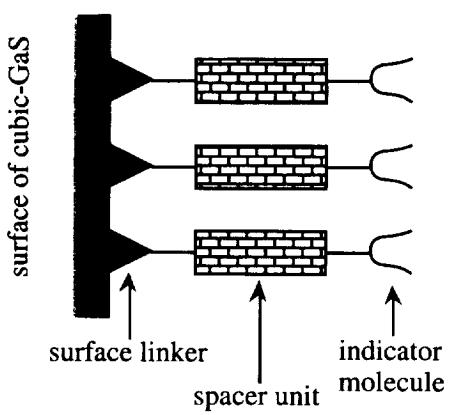

Fig. 2. Schematic representation of a sensor self-assembled monolayer (SAM) on c-GaS.

RESULTS AND DISCUSSION

Carboxylates

As noted in the Introduction we have previously shown that carboxylates are ideal ligands for complexation to aluminum oxide surfaces due to the topotactic nature of the reaction and the strength of the subsequent complex [16]. Since c-GaS and GaAs readily form native oxide layers through atmospheric oxidation/hydrolysis, a carboxylate linkage group is possible via the reaction of the surface with RCO_2H.

The reaction of $Ga(^tBu)_3$ [20, 21], with one molar equivalent of a carboxylic acids yields the di-*tert*-butylgallium carboxylates $[(^tBu)_2Ga(\mu\text{-}O_2CR)]_2$, eq. (1).

$$Ga(^tBu)_3 + RCO_2H \rightarrow {}^1/_2[(^tBu)_2Ga(\mu-O_2CR)]_2 + {}^tBuH \quad (1)$$

$$R = Ph(\mathbf{1}),\quad C_6H_4-3-CN(\mathbf{2}),\quad C_6H_4-3-Br(\mathbf{3})$$

In the case of compounds **2** and **3** the termini employed were chosen to provide suitable probes for XPS and/or IR characterization of surfaces. The ^1H and ^{13}C NMR spectroscopy and mass spectrometry of compounds **1**–**3** are consistent with dimeric structures, which have been confirmed for compounds **1** and **2** by X-ray crystallography.

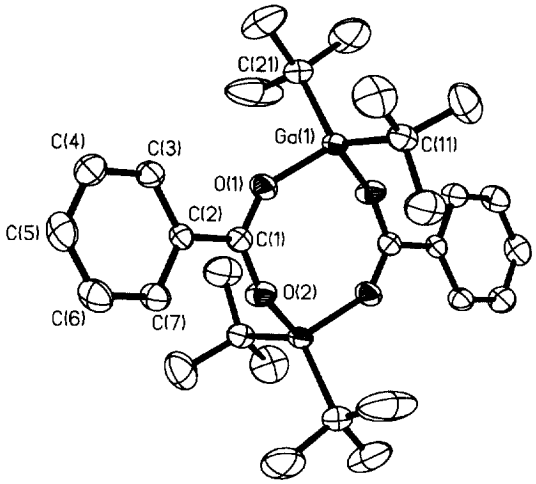

Fig. 3. The molecular structure of $[(^tBu)_2Ga(\mu\text{-}O_2CPh)]_2$ (**1**). Thermal ellipsoids are shown at the 30% level and hydrogen atoms are omitted for clarity.

The molecular structures of $[(^tBu)_2Ga(\mu\text{-}O_2CPh)]_2$ (**1**) and $[(^tBu)_2Ga(\mu\text{-}O_2CC_6H_4\text{-}3\text{-}CN)]_2$ (**2**) are shown in Fig. 3 and Fig. 4; selected bond lengths and angles are given in Tab. 1. The structures of both compounds consists of centro-symmetric dimers of two '$Ga(^tBu)_2$' units bridged by two carboxylate groups. This is consistent with other alkyl Group 13 carboxylates as shown from IR and Raman spectroscopy, mass spectrometry, and molecular weight measurements [22]. Additionally, the structure of compound **1** is isomorphous with its aluminum analog [16]. The Ga–O bond lengths to the carboxylate ligands in these dimeric systems [Ga–O = 1.957(3)–1.960(3) Å] are comparable to the bridging carboxylate interactions with the four-coordinate gallium in the polymeric $[MeGa(\mu\text{-}O_2CMe)_2]_x$ [1.899(3)–1.942(4) Å] [23], but significantly shorter than those observed in $Rb[(Me_3Ga)_2(\mu\text{-}O_2CMe)_2]$ [2.068(8), 2.070(8) Å] [24]. The carboxylate's O–C bond lengths in both compounds are similar (see Tab. 1), indicative of a symmetrically bound acid group that is unaffected by the carboxylate organic substituents. The bond lengths and angles within the carboxylate unit are typical of such moieties [25].

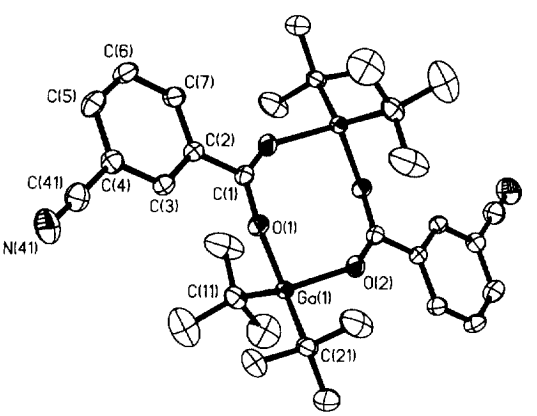

Fig. 4. The molecular structure of $[(^tBu)_2Ga(\mu\text{-}O_2CC_6H_4\text{-}3\text{-}CN)]_2$ (**2**). Thermal ellipsoids are shown at the 30% level and hydrogen atoms are omitted for clarity.

The $Ga_2O_4C_2$ cycles in $[(^tBu)_2Ga(\mu\text{-}O_2CR)]_2$ are examples of eight-membered ring compounds of the group 13 metals [18, 26]. The eight membered $Ga_2O_4C_2$ rings in compounds **1** and **2** adopt a chair-like structure, see Fig. 5. A similar confirmation is adopted by the aluminum carboxylates, $[(^tBu)_2Al(\mu\text{-}O_2CR)]_2$ [16]. The puckering of the $Ga_2O_4C_2$ ring may be considered to be as a result of folding of the eight-membered ring along the two inter-ligand O···O vectors. The extent of folding (θ_{ring}) is defined as the angle between the GaO_2 planes and the O_4C_2 plane. For the aluminum carboxylates, $[(^tBu)_2Al(\mu\text{-}O_2CR)]_2$, the geometrical result of the planar $Al_2O_4C_2$ core is that the Al···Al intra-molecular distance is maximized, and consequently so are the inter-substituent distances (i.e., $^tBu\cdots R$), resulting in a correlation between θ_{ring} and the steric bulk of the carboxylate substituent (**R**) as defined by Tolman's cone angle (θ) [27]. In this regard, the agreement in the θ_{ring} for the $Ga_2O_4C_2$ ring: $\theta_{ring} = 155.2°$ (**1**) and 154.1° (**2**) is consistent with the similarity of the steric bulk of the carboxylate groups in compounds **1** and **2**.

Benzenethiolate

The reaction of $Ga(^tBu)_3$ with one molar equivalent of PhSH yields the di-*tert*-butylgallium thiolate, eq. (2).

$$Ga(^tBu)_3 + RSH \rightarrow {}^1/_2[(^tBu)_2Ga(\mu\text{-}SR)]_2 + {}^tBuH \quad (2)$$
(4)

The molecular structure of one of the independent molecules of $[(^tBu)_2Ga(\mu\text{-}SPh)]_2$ (**4**) is shown in Fig. 6; selected bond lengths and angles are given in Tab. 2.

The Ga–S and Ga–C bond distances are within the range expected (Ga–S = 2.33–2.46 Å [28–31], Ga–C = 1.96–2.16 Å [25]). Furthermore, within each independent molecule the two Ga–S distances to each sulfur are essentially the same, suggesting the presence of a symmetrically bridging thiolate ligand. As has been reported for Group 13 thiolate [32, 33] selenolate [34, 35] and tellurolate [36] compounds the geometry about the sulfur is pyramidal (i.e., Fig. 7), i.e., Σ(X-E-X) = 333(2)°, not planar as is found in their oxygen analogs $[(^tBu)_2M(\mu\text{-}OR)]_2$ [17]. As consequence of the non-planar geometry of the sulfur there is significant distortion of the gallium center from ideal tetrahedral, with a distinct asymmetry in the C–Ga–S angles, see Fig. 7.

Table 1. Selected bond lengths (Å) and angles (°) for $[(^tBu)_2Ga(\mu\text{-}O_2CPh)]_2$ (**1**) and $[(^tBu)_2Ga(\mu\text{-}O_2CC_6H_4\text{-}3\text{-}CN)]_2$ (**2**).

	$[(^tBu)_2Ga(\mu\text{-}O_2CPh)]_2$	$[(^tBu)_2Ga(\mu\text{-}O_2CC_6H_4\text{-}3\text{-}CN)]_2$
Ga(1)–O(1)	1.942(4)	1.957(3)
Ga(1)–O(2)	1.948(3)	1.960(3)
Ga(1)–C(11)	1.988(6)	1.987(5)
Ga(1)–C(21)	1.982(6)	1.985(4)
O(1)–C(1)	1.252(6)	1.262(5)
O(2)–C(1′)	1.240(4)	1.232(3)
N(41)–C(41)		1.131(8)
O(1)–Ga(1)–O(2)	106.2(1)	104.3(1)
O(1)–Ga(1)–C(11)	107.1(2)	108.4(2)
O(1)–Ga(1)–C(21)	102.1(2)	102.5(2)
O(2)–Ga(1)–C(11)	106.5(2)	106.3(2)
O(2)–Ga(1)–C(21)	103.1(2)	102.6(2)
C(11)–Ga(2)–C(21)	129.9(2)	130.2(2)
Ga(1)–O(1)–C(1)	142.2(4)	139.5(3)
Ga(1)–O(2)–C(1′)	142.3(3)	143.2(2)

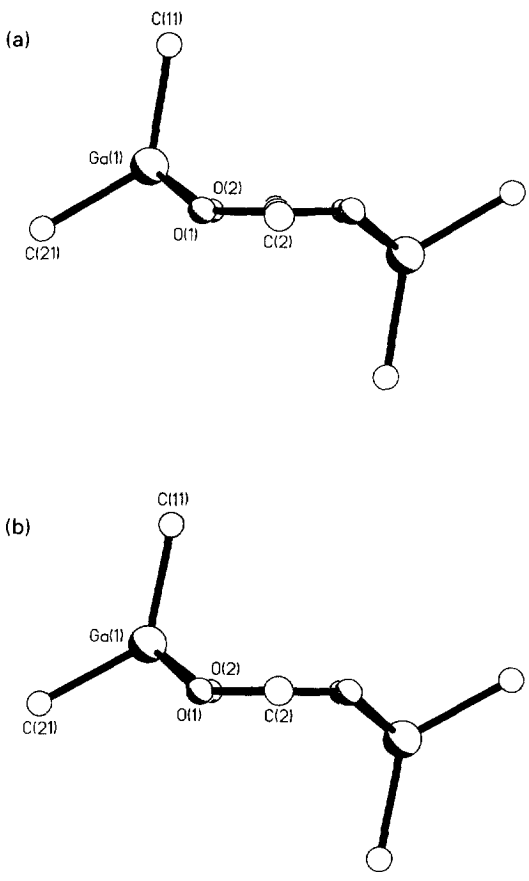

Fig. 5. The eight membered cyclic core of (a) $[(^tBu)_2Ga(\mu\text{-}O_2CPh)]_2$ (**1**) and (b) $[(^tBu)_2Ga(\mu\text{-}O_2CC_6H_4\text{-}3\text{-}CN)]_2$ (**2**) demonstrating the chair-like conformation of the $Ga_2O_4C_2$ cycles.

Model compounds for surface binding to c-GaS and GaAs

Both c-GaS and GaAs have *fcc*-Zinc Blende structures and although both {100} and {111} oriented crystals are employed in GaAs devices, the Ga···Ga distances are irrespective of orientation. Thus, for simplicity only the {100} face will be considered.

Complexation of any ligand to either a c-GaS or GaAs surface may occur via monodentate terminal, bidentate (e.g., bridging), or multidentate (e.g., cap-

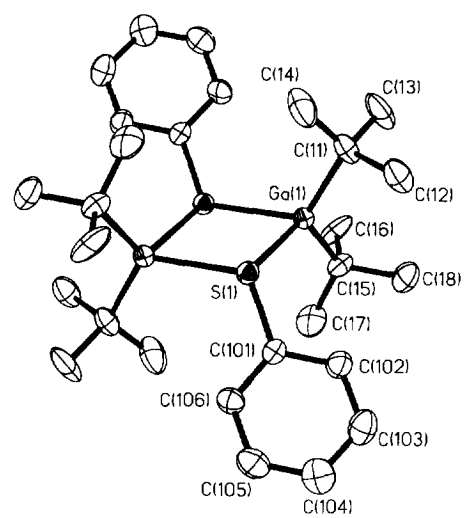

Fig. 6. The molecular structure of one of the independent molecules of $[(^tBu)_2Ga(\mu\text{-}SPh)]_2$ (**4**). Thermal ellipsoids are shown at the 30% level and hydrogen atoms are omitted for clarity.

Table 2. Selected bond lengths (Å) and angles (°) for $[(^tBu)_2Ga(\mu\text{-}SPh)]_2$ (**4**).

Molecule 1		Molecule 2	
Ga(1)–S(1)	2.421(2)	Ga(2)–S(2)	2.431(2)
Ga(1)–S(1′)	2.445(2)	Ga(2)–S(2′)	2.431(2)
Ga(1)–C(11)	2.006(7)	Ga(2)–C(21)	2.003(6)
Ga(1)–C(15)	1.996(5)	Ga(2)–C(25)	2.005(7)
S(1)–C(101)	1.783(5)	S(2)–C(201)	1.774(6)
S(1)–Ga(1)–S(1′)	82.33(4)	S(2)–Ga(2)–S(2′)	81.80(3)
S(1)–Ga(1)–C(11)	103.9(2)	S(2)–Ga(2)–C(21)	103.0(2)
S(1)–Ga(1)–C(15)	117.4(2)	S(2)–Ga(2)–C(25)	118.4(2)
C(11)–Ga(1)–C(15)	124.4(3)	C(21)–Ga(2)–C(25)	123.8(2)
Ga(1)–S(1)–Ga(1′)	97.67(6)	Ga(2)–S(2)–Ga(2′)	98.20(5)
Ga(1)–S(1)–C(101)	116.3(2)	Ga(2)–S(2)–C(201)	118.1(2)
Ga(1′)–S(1)–C(101)	119.1(2)	Ga(2′)–S(2)–C(201)	117.3(2)

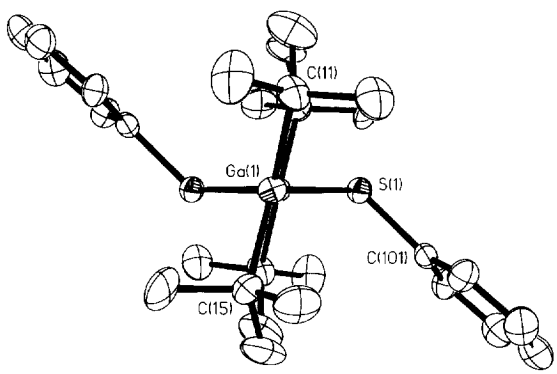

Fig. 7. Molecular structure of $[(^tBu)_2Ga(\mu\text{-}SPh)]_2$ (**4**) viewed along the Ga(1)–Ga(1′) vector, showing the distortion about the gallium centers.

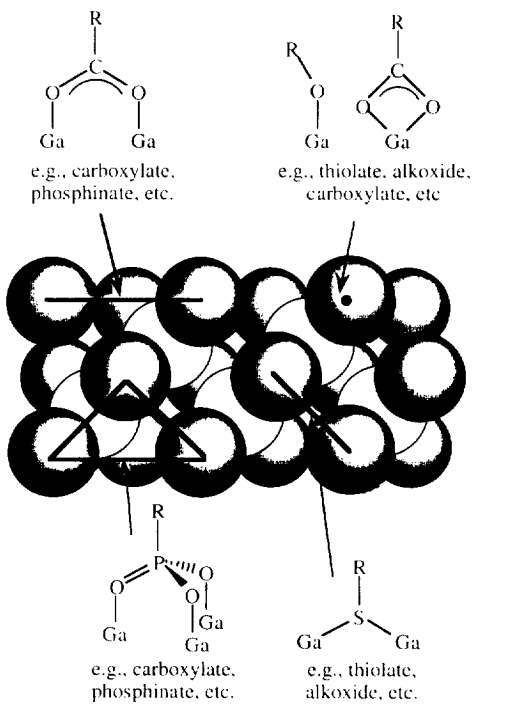

Fig. 8. A representation of the {100} surfaces of a *fcc*-lattice (e.g., GaAs and c-GaS), showing the possible sites for bridging ligands.

ping) ligation. Each of these binding modes is depicted schematically in Fig. 8. Terminal and chelating coordination should be independent of the structure of the surface, however, we have shown that the stability of bridging (and presumably capping) ligands is dependent on the distance over which they bridge [16]. A consideration of the possible Ga···Ga distances on the {100} face of c-GaS shows that two inter-gallium distances are possible, 3.89 and 5.50 Å [37]. Similarly, for GaAs these distances are 3.997 and 5.653 Å [38]. Table 3 summarizes the Ga-X and Ga···Ga distances observed for compounds **1**, **2** and **4** as well as those in complexes of selected Group 15 and 16 donor ligands. A graphical representation is given in Fig. 9, from which it can be seen that while carboxylate ligands are ideal for alumina surfaces they are not suitable for c-GaS and GaAs. In contrast, ER (E = S, Se, Te), ER_2 (E = P, As) and $O_{4-n}PR_2$ (n = 1, 2) all form complexes in which the Ga···Ga distance covers a range including those required to bind to the (100) surface of both GaAs and c-GaS. In fact, the thiolate ligand is nearly ideal to act as a bridging ligand across the Ga···Ga distance of either the (100) or (111) faces and it is interesting to speculate, with hindsight, that this observation provides a rationalization for the suitability of thiols to form self assembled monolayers on GaAs [39]. We propose that the reaction of thiols with the surface of c-GaS or GaAs be considered a topotactic reaction, since no reconstruction (bulk reorganization) of the Ga-E (E = S, As) framework is

Table 3. Summary of the Ga···Ga and Ga-X distances observed for gallium compounds with Group 15 and 16 donor ligands in comparison to GaAs and c-GaS.

Compound	Ga···Ga (Å)	Ga···X (Å)	References
c-GaS	3.89, 5.50	2.38	[37]
GaAs	3.997, 5.653	2.448	[38]
$[R_2Ga(OR')]_2$	2.97–3.35	1.95–1.97	[17, 40]
$[R_2Ga(SR')]_2$	2.94–3.68	2.26–2.46	[28–30, 41] this work
$[R_2Ga(SR')]_3$	3.46–3.79	2.34	[42]
$[R_2Ga(SR')]_4$	4.27–4.35	2.39	[43]
$[R_2Ga(SeR')]_2$	3.50	2.49–2.50	[44]
$[R_2Ga(TeR')]_2$	3.68	2.74–2.76	[34]
$[R_2Ga(NR'_2)]_2$	2.83–2.93	2.00–2.12	[45–51]
$[R_2Ga(NR'_2)]_3$	2.97–3.4	1.92–2.20	[52]
$[R_2Ga(PR'_2)]_2$	3.49–3.64	2.39–2.51	[53–55]
$[R_2Ga(PR'_2)]_3$	3.94–4.33	2.40–2.45	[56–58]
$[R_2Ga(AsR'_2)]_2$	3.71–3.81	2.47–2.58	[59, 60]
$[R_2Ga(AsR'_2)]_3$	3.81–4.04	2.43–2.45	[61]
$[R_2Ga(O_2CR)]_2$	4.35–4.68	1.957	[23] this work
$[R_2Ga(S_2CNR'_2)]_2$		2.379–2.46	[62]
$[R_2Ga(O_2PR'_2)]_2$	4.50	1.93–1.95	[18, 63]
$[R_2Ga(O_3PR'GaR_2)]_2$	4.76–6.00	1.88–1.91	[19]

required for the ligand to bind. Our surface binding studies will be reported elsewhere.

EXPERIMENTAL

All operations were carried out using Schlenk techniques or in an argon atmospheric VAC glovebox. ^1H and ^{13}C NMR analysis was carried out on a Bruker WM-250 MHz spectrometer. Mass spectrometry was performed using a Finnegan MAT95 mass spectrometer with an electron beam energy of 70 eV for EI mass spectra. IR analysis was carried out on Nicolet 760 and Perkin Elmer 1600 FT-IR spectrometers using Nujol mulls. The synthesis of $Ga(^tBu)_3$ was carried out by literature methods [20, 21]. The carboxylic acids were purchased from Aldrich and used without further purification.

$[(^tBu)_2Ga(\mu\text{-}O_2CPh)]_2$ (*1*)

A solution of benzoic acid (0.51 g, 4.2 mmol) was slurried in hexane (10 cm^3) and to this was added a solution of $Ga(^tBu)_3$ (0.80 g, 3.3 mmol) in hexane (10 cm^3). This addition was done slowly dropwise with continuous stirring. The reactant mixture became warm throughout the addition, and the solution appeared to be clear afterward, with only a small amount of white powder left at the bottom of the flask. The reaction mixture was allowed to stir for 40 h., and the resultant slurry was filtered. The volatiles were removed from the filtrate to reveal a white powder. Recrystallization in toluene gave small, block crystals. Yield *ca.* 80%. Mp: 203–205°C. EI-MS (*m/z*; %) 449 ($2M^+ - {}^t$Bu-OCPh + H, 5), 304 (M^+, 12), 247 (M^+-^{t}Bu, 40), 191 (M^+-2 ^{t}Bu, 100), 105 (COPh, 40), 57 (^{t}Bu, 60). IR (cm^{-1}): 1624 (w), 1609 (m), 1570 (m), 1410 (m), 1260 (w), 1176 (s), 1098 (w), 1069 (s), 1028 (s), 1012 (m), 821 (m), 716 (m), 685 (s). ^1H NMR (δ, $CDCl_3$) 8.17 [2H, d, $J(H-H) = 7.5$ Hz, o−CH], 7.63 [1H, t, $J(H-H) = 7.5$ Hz, p−CH], 7.50 [2H, t, $J(H-H) = 7.5$ Hz, m−CH], 1.10 [18H, s, $C(CH_3)_3$]. ^{13}C NMR (δ, $CDCl_3$): 222.2 (CO_2), 132.8 (*o*-CH), 130.7 (*m*-CH), 128.8 (*p*-CH), 30.1 [$C(CH_3)_3$], 25.0 [$C(CH_3)_3$].

$[(^tBu)_2Ga(\mu\text{-}O_2CC_6H_4\text{-}3\text{-}CN)]_2$ (*2*)

To a suspension of 3-cyanobenzoic acid (0.5 g, 2.08 mmol) in hexane (10 cm^3) was added $Ga(^tBu)_3$ (0.30 g, 2.04 mmol) *via* syringe, with no evidence of gas evolution. After stirring overnight, all volatiles were removed from the clear solution under vacuum leaving a white powder. Recrystallization in toluene gave clear, needle-like crystals. Yield: *ca.*, 70%. Mp: 203–205°C. EI-MS (*m/z*, %) 449 ($2M^+$-Ga-2^{t}Bu-CN, 100), 273 (M^+-$CH_2{=}CMe_2$, 20), 216 (M^+-2 $CH_2{=}CMe_2$, 20), 147 ($HO_2CC_6H_4CN$, 30), 102 (C_6H_4CN, 30), 57 (^{t}Bu, 90). IR (cm^{-1}): 2970 (s), 2858 (w), 2233 (m, ν C≡N), 1629 (m), 1572 (m), 1004 (m),

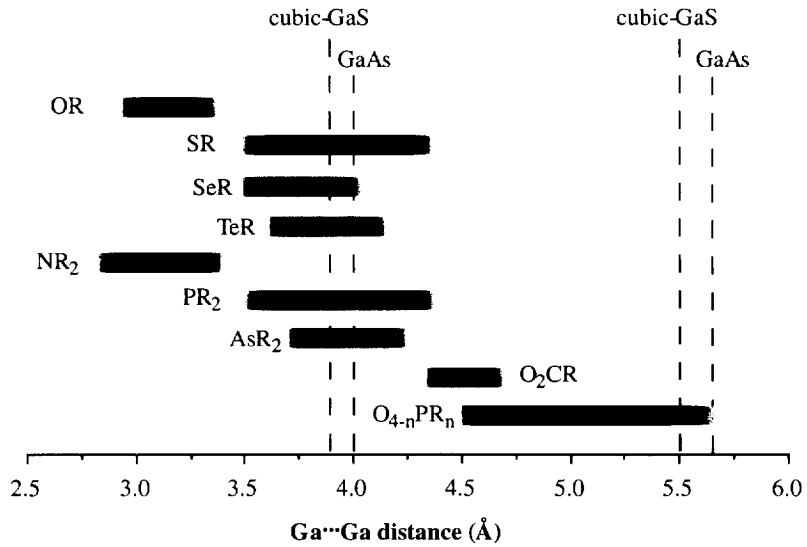

Fig. 9. Graphical representation of the Ga···Ga distance (Å) for selected Group 15 and 16 donor ligands in bridging complexes in comparison to c-GaS and GaAs.

917 (m), 758 (m). ^{1}H NMR (δ, $CDCl_3$): 8.36 (1H, s, 2−CH), 8.32 [1H, d, J(H−H) = 7.7 Hz, 6−CH], 7.92 [1H, d, J(H−H) = 7.7 Hz, 4−CH], 7.66 [1H, t, J(H−H) = 7.7 Hz, 5−CH], 1.09 [18H, s, $C(CH_3)_3$]. ^{13}C NMR (δ, C_6D_6): 137.0 (1−C), 134.1 (2−CH), 133.9 (4−CH), 130.0 (6−CH), 30.4 [$C(CH_3)_3$], 25.7 [$C(CH_3)_3$].

$[(^tBu)_2Ga(\mu\text{-}O_2CC_6H_4\text{-}3\text{-}Br)]_2$ (**3**)

To a solution of 3-bromobenzoic acid (0.81 g, 4.0 mmol) in hexane (10 cm^3), was added $Ga(^tBu)_3$ (1.0 g, 4.2 mmol) *via* syringe. The mixture was refluxed for 1.5 h. and allowed to cool to room temperature and stir for 3 h. All volatiles were removed under vacuum leaving a white powder. Yield *ca.* 80%. Mp: 202–204°C. EI-MS (*m/z*, %) 384 (M^+, 100), 200 ($O_2CC_6H_4Br$, 100), 183 (COC_6H_4Br, 60), 155 (C_6H_4Br, 35) 57 (^{t}Bu, 38). IR (cm^{-1}): 1613 (m), 1560 (m), 1550 (m), 1408 (s), 1271 (s), 1260 (s), 1105 (w), 1066 (s), 1012 (s), 939 (w), 901 (s), 869 (s), 817 (m), 760 (s), 707 (s), 650 (m). ^{1}H NMR (δ, C_6D_6): 8.51 (1H, s, 2−CH), 8.04 [1H, d, J(H−H) = 7.5 Hz, 6−CH], 7.21 [1H, d, J(H−H) = 7.5 Hz, 4−CH], 6.66 [2H, t, J(H−H) = 7.5 Hz, −CH], 1.26 [18H, s, $C(CH_3)_3$]. ^{13}C NMR (δ, C_6D_6): 136.7 (3−CH), 133.6 (2−CH), 130.4 (4−CH), 129.1 (6−CH), 122.9 (5−CH), 30.1 [$C(CH_3)_3$], 25.3 [$C(CH_3)_3$].

$[(^tBu)_2Ga(\mu\text{-}SPh)]_2$ (**4**)

To a solution of PhSH (0.50 g, 4.54 mmol) in hexane (10 cm^3), cooled to −78°C, was added $Ga(^tBu)_3$ (1.20 g, 5.0 mmol). No evidence of gas evolution was observed, and solution was allowed to warm to room temperature and stir overnight. Removal of the volatiles from the resulting clear solution under vacuum gave a white powder. Recrystallization from toluene giving colorless crystals. Yield: *ca.* 75%. Mp: 204–205°C. MS (EI, *m/z*:, %): 583 ($2M^+$-H, 2), 527 ($2M^+$-^{t}Bu, 4), 292 (M^+, 10), 235 (M^+-^{t}Bu, 62), 179 (M^+-2^{t}Bu, 75), 69 (Ga, 78), 57 (^{t}Bu, 100). IR (cm^{-1}): 1567 (m), 1168 (s), 1086 (s), 1009 (s), 810 (s), 732 (m), 682 (s). ^{1}H NMR (δ, C_6D_6): 7.46 [2H, d, J(H−H) = 7.4 Hz, o−CH], 6.95 [2H, t, J(H−H) = 7.4 Hz, m−CH], 6.85 [1H, d, J(H−H) = 7.4 Hz, p−CH], 1.38 [18H, s, $C(CH_3)_3$]. ^{13}C NMR (δ, C_6D_6): 131.8 (o−CH), 129.6 (m−CH), 126.6 (p−CH), 31.2 [$C(CH_3)_3$].

Crystallographic studies

Crystals of compounds **1**, **2** and **4** were sealed in a glass capillary under argon and mounted on the goniometer of a Enraf-Nonius CAD-4 automated diffractometer. Data collection and cell determinations were performed in a manner previously described [64], using the $\theta/2\theta$ scan technique. Pertinent details are given in Tab. 4. The structures were solved by direct methods (SHELX86) [65]. The models were refined using full-matrix least squares techniques. Ga, N, and O atoms were refined anisotropically for compound **2**, while all non-hydrogen atoms were refined anisotropically for compound **1** and **4**. Hydrogen atoms were included and constrained to 'ride' upon the appropriate atoms [d(C-H) = 0.95 Å, U(H) = 1.3 B_{eq}(C)]. All computations other than those specified were performed using MolEN [66]. A summary of cell parameters, data collection, and structure solution is

Table 4. Summary of X-ray Diffraction Data.

Compound	$[(^tBu)_2Ga(\mu\text{-}O_2CPh)]_2$ (**1**)	$[(^tBu)_2Ga(\mu\text{-}O_2CC_6H_4\text{-}3\text{-}CN)]_2$ (**2**)	$[(^tBu)_2Ga(\mu\text{-}SPh)]_2$ (**4**)
empir. formula	$C_{30}H_{46}Ga_2O_4$	$C_{32}H_{44}Ga_2N_2O_4$	$C_{28}H_{46}Ga_2S_2$
cryst size, mm	$0.21\times0.65\times0.85$	$0.15\times0.64\times0.68$	$0.35\times0.39\times0.42$
cryst system	triclinic	monoclinic	triclinic
space group	$P\bar{1}$	$P2_1/a$	$P\bar{1}$
a, Å	8.4728(8)	8.4092(9)	10.701(2)
b, Å	9.409(1)	21.823(2)	11.444(1)
c, Å	11.050(2)	9.4331(8)	13.571(2)
α, deg	70.64(1)		88.360(9)
β, deg	75.22(1)	93.031(8)	67.80(1)
γ, deg	86.83(1)		88.84(1)
V, Å^3	803.2(2)	1728.7(3)	1531.9(3)
Z	1	2	2
D(calcd), g/cm^3	1.261	1.268	1.271
μ, cm^{-1}	17.0	15.85	18.97
temp, K	298	298	298
2θ range, deg	3.0–50.0	2.0–50.0	2.0–44.0
no. collected	2816	3320	3750
no. ind	2816	3110	3750
no. obsd	$2320(\lvert F_o\rvert > 6.0\sigma\lvert F_o\rvert)$	$2298(\lvert F_o\rvert > 6.0\sigma\lvert F_o\rvert)$	$2874(\lvert F_o\rvert > 6.0\sigma\lvert F_o\rvert)^2$
weighting scheme	$w^{-1} = 0.04(\lvert F_o\rvert)^2 + \sigma(\lvert F_o\rvert)^2$	$w^{-1} = 0.04(\lvert F_o\rvert)^2 + \sigma(\lvert F_o\rvert)^2$	$w^{-1} = 0.04(\lvert F_o\rvert)^2 + \sigma(\lvert F_o\rvert)^2$
R	0.0430	0.0337	0.0346
R_w	0.0490	0.0401	0.0404
largest diff peak, eÅ^{-3}	0.86	0.35	0.48

given in Table. 4. Scattering factors were taken from reference [67].

Acknowledgements—Financial support for this work is provided by the National Science Foundation and the Office of Naval Research. The authors acknowledge the assistance of Dr. N. McMahon (Rice University) for mass spectrometry measurements.

REFERENCES

1. Home, P. D. and Alberti, K. G. M. M., *Biosensors: Fundamentals and Applications*, Chapter 36, Ed. Turner, A. P. F., Karube, I. and Wilson, G. S., Oxford University Press, New York, 1988.
2. Tran-Minh, C., *Ion-Selective Electrode Rev.*, 1985, **7**, 41.
3. Mason, O., *J. Assoc. Off. Anal. Chem.*, 1983, **66**, 981.
4. Guilbault, G. G., *Analytical Uses of Immobilized Enzymes*, Marcel Dekker, New York, 1984.
5. Zusman, R., Rottman, C., Ottolenghi, M. and Avnir, D., *J. Non-Cryst. Solids*, 1990, **122**, 107.
6. Dunn, B. and Zink, J. I., *J. Mater. Chem.*, 1991, **1**, 903.
7. Winder, E. J., Moore, D. E., Neu, D. R., Ellis, A. B., Geisz, J. F. and Kuech, T. F., *J. Cryst. Growth*, 1995, **148**, 63.
8. Geisz, J. F., Kuech, T. F. and Ellis, A. B., *J. Appl. Phys.*, 1995, **77**, 1233.
9. Mosbach, K. and Danielsson, B., *Anal. Chem.*, 1981, **57**, 83A.
10. (a) Murakami, T. I., *Anal. Lett.*, 1986, **19**, 1973. (b) Gotoh, M., Tamiya, E., Karube, I. and Kagawa, Y., *Anal. Chim. Acta*, 1986, **187**, 287.
11. (a) Bergveld, P., *IEEE Trans. Biomedical Eng.*, 1970, **17**, 70. (b) Moss, D., Janata, J. and Johnson, C. C., *Anal. Chem.*, 1975, **47**, 2238.
12. (a) Jenkins, P. P., MacInnes, A. N., Tabib-Azar, M. and Barron, A. R., *Science*, 1994, **263**, 1751. (b) Barron, A. R., *Mat. Res. Soc., Symp. Proc.*, 1996, **410**, 23.
13. (a) Folkers, J. P., Laibinis, P. E. and Whitesides, G. M., *Langmuir*, 1992, **8**, 1330. (b) Carey, R. I., Folkers, J. P. and Whitesides, G. M., *Langmuir*, 1994, **10**, 228.

14. Allara, D. L. and Nuzzo, R. G., *Langmuir*, 1985, **1,** 45.
15. Bell, C. M., Yang, H. C. and Mallouk, T. E., in *Materials Chemistry*, Eds. Interante, L. V., Casper, L. A. and Ellis, A. B., ACS, Washington DC, 1995.
16. Bethley, C. E., Aitken, C. L., Koide, Y., Harlan, C. J., Bott, S. G. and Barron, A. R., *Organometallics*, 1997, **16,** 329.
17. Cleaver, W. M., Barron, A. R., McGuffey, A. R. and Bott, S. G., *Polyhedron*, 1994, **13,** 2831.
18. Landry, C. C., Hynes, A., Barron, A. R., Haiduc, I. and Silvestru, C., *Polyhedron*, 1996, **15,** 391.
19. Keys, A., Bott, S. G. and Barron, A. R., *J. Chem. Soc., Chem. Commun.*, 1996, 2339.
20. Kovar, R. A., Derr, H., Brandau, D. and Callaway, J. O., *Inorg. Chem.*, 1975, **14,** 2809.
21. Schwering, H.-U., Jungk, E. and Weidlein, J., *J. Organomet. Chem.*, 1975, **91,** C4.
22. (a) Eisch, J. J., in, *Comprehensive Organometallic Chemistry*, Wilkinson, G., Stone, F. G. A. and Abel, E. W., Eds. Pergamon Press, Oxford, 1988, **1**, Chapter 6. (b) Weidlein, J., *Z. Anorg. Allgem. Chem.*, 1970, **378**, 245. (c) Pietrzykowski, A., Pasynkiewicz, S. and Poplawska, J., *Main Group Metal Chem.*, 1996, **18**, 651. (d) Zenina, G. V., Sheverdina, N. I. and Kocheskov, K. A., *Proc. Acad. Sci. USSR Engl. Trans.*, 1970, **195**, 786.
23. Hausen, H. D., Sille, K., Weidlein, J. and Schwarz, W., *J. Organomet. Chem.*, 1978, **160,** 411.
24. Zaworotko, M. J., Rogers, R. D. and Atwood, J. L., *Organometallics*, 1982, **1,** 1179.
25. Haaland, A., *Coordination Chemistry of Aluminum*, Ed. Robinson, G. H., Chapter 1, VCH, New York, 1993, p. 1.
26. (a) Haiduc, I., *The Chemistry of Inorganic Ring Systems*, Wiley, Chichester, 1970, **II**(7), 1018. (b) Cesari, M. and Cucinella, S., in, *The Chemistry of Inorganic Homo- and Heterocycles*, Eds. Haiduc, I. and Sowerly, D. B., Academic Press, New York, 1987, **2**, 167. (c) Oliver, J. P., Kumar, R. and Taghiof, M., in *Coordination Chemistry of Aluminum*, Ed. Robinson, G. H., VCH, New York, 1993, Chapter 5, p. 167. (d) Hausen, H. D., Gerstner, F. and Schwarz, W., *J. Organomet. Chem.*, 1978, **145**, 277. (e) Hahn, F. E. and Schneider, B., *Z. Naturforsch. B.*, 1990, **45**, 134. (f) Klemp, A., Uson, I., Ahlemann, J.-T., Belgardt, T., Storre, J., Roesky, H. W., *Main Group Chem.*, 1997, **1**, 27.
27. Tolman, C. A., *Chem. Rev.*, 1977, **77,** 313.
28. Boardman, A., Jeffs, S. E., Small, W. H. and Worrall, I. J., *Inorg. Chim. Acta*, 1985, **99,** L39.
29. Hoffmann, B. G. and Burschka, C., *J. Organomet. Chem.*, 1984, **267,** 229.
30. Hendershot, D. G., Kumar, R., Barber, M. and Oliver, J. P., *Organometallics*, 1991, **10,** 1917.
31. Ruhlandt-Senge, K. and Power, P. P., *Inorg. Chem.*, 1993, **32,** 3478.
32. Hoffmann, G. G. and Fisher, R., *Phosphorus, Sulfur and Silica*, 1989, **41,** 97.
33. Nomura, R., Inazawa, S., Kanaya, K. and Matsuda, H., *Polyhedron*, 1989, **8,** 763.
34. Banks, M. A., Beachley, O. T. Jr., Gysling, H. J. and Luss, H. R., *Organometallics*, 1990, **9,** 1979.
35. Uhl, W., Layh, M., Becker, G., Kinkhammer, K. W. and Hildenbrand, T., *Chem. Ber.*, 1992, **125,** 1547.
36. Bochmann, M., *Chem. Vap. Deposition*, 1996, **2,** 85.
37. MacInnes, A. N., Power, M. B. and Barron, A. R., *Chem. Mater.*, 1992, **4,** 11.
38. Mullins, J. B., Straughan, B. W., Driscoll, C. M. H., Willoughby, A. F. W., *Inst. Phys. Conf. Ser.*, 1975, **24,** 275.
39. Lunt, S. R., Santangelo, P. G. and Lewis, N. S., *J. Vac. Sci. Technol. B.*, 1991, **8,** 2256.
40. Dembowski, U., Pape, T., Herbst-Irmer, R., Pohl, E., Roesky, H. W. and Sheldrick, G. M., *Acta Cryst.*, 1993, **C49,** 1309.
41. (a) Ghazi, S. U., Heeg, M. J. and Oliver, J. P., *Inorg. Chem.*, 1994, **33**, 4517. (b) Hoffmann, B. G. and Burschka, C., *Agnew. Chem., Int. Ed. Engl.*, 1985, **24**, 970. (c) Maelia, L. E. and Koch, S. A., *Inorg. Chem.*, 1986, **25**, 1896.
42. Boardmann, A., Jeffs, S. E., Small, R. W. H. and Worrall, I. J., *Inorg. Chim. Acta*, 1984, **83,** L39.
43. Taghiof, M., Heeg, M. J., Bailey, M., Dick, D. G., Kumar, R., Hendershot, D. G., Rahbarnoohi, H. and Oliver, J. P., *Organometallics*, 1995, **14,** 2903.
44. Kumar, R., Kick, D. G., Ghazi, S. U., Taghiof, M., Heeg, M. J. and Oliver, J. P., *Organometallics*, 1995, **14,** 1601.
45. Lee, B., Pennington, W. T., Robinson, G. H. and Rogers, R. D., *J. Organomet. Chem.*, 1990, **396,** 269.
46. Herberich, G. E., Englert, U. and Posselt, D., *J. Organomet. Chem.*, 1993, **461,** 21.
47. Lorberth, O. T. Jr., Dorn, R., Massa, W. and Wocadlo, S., *Z. Naturforsch.*, 1993, **48b,** 224.
48. Beachley, O. T. Jr., Noble, M. J., Churchill, M. R. and Lake, C. H., *Organometallics*, 1992, **11,** 1051.
49. Park, J. T., Kim, Y. and Kim, K., Kim, Y., *Organometallics*, 1992, **11,** 3320.
50. Atwood, J. L., Bott, S. G., Jones, C. and Raston, C. L., *Inorg. Chem.*, 1991, **30,** 4868.
51. Nutt, W. R., Blanton, J. S., Kroh, F. O. and Odom, J. D., *Inorg. Chem.*, 1989, **28,** 2224.
52. Harrison, W., Storr, A. and Trotter, J., *J. Chem. Soc. Dalton Trans.*, 1972, 1554.
53. (a) Banks, M. A., Beachley, O. T. Jr., Buttrey, L. A., Churchill, M. R. and Fettinger, J. C., *Organometallics*, 1991, **10**, 1901. (b) Beachley, O. T. Jr., Maloney, J. D. and Rogers, R. D., *Organometallics*, 1993, **12**, 229.
54. Lee, K. E., Higa, K. T., Nissan, R. A. and Butcher, R. J., *Organometallics*, 1992, **11,** 2816.
55. Hoffmann, G. G., Fischer, R., Schubert, U. and Hirle, B., *J. Organomet. Chem.*, 1992, **441,** 7.
56. (a) Beachley, O. T. Jr., Royster, T. L. Jr., Arhar, J. R. and Rheingold, A. L., *Organometallics*, 1993, **12**, 1976. (b) Beachley, O. T. Jr., Maloney, J. D. and Rogers, R. D., *J. Organomet. Chem.*, 1993, **449**, 69.
57. Cowley, A. H., Jones, R. A., Mardones, M. A. and Nunn, C. M., *Organometallics*, 1991, **10,** 1635.
58. Elms, F. M., Koutsantonis, G. A. and Raston, C. L., *J. Chem. Soc., Chem. Commun.*, 1995, 1669.

59. (a) Wells, R. L., Purdy, A. P., Higa, K. T., McPhail, A. T. and Pitt, C. G., *J. Organomet. Chem.*, 1987, **325**, C7. (b) Wells, R. L., Purdy, A. P., McPhail, A. T. and Pitt, C. G., *J. Organomet. Chem.*, 1986, **308**, 281. (c) Purdy, A. P., Wells, R. L., McPhail, A. T. and Pitt, C. G., *Organometallics*, 1987, **6**, 2099. (d) Wells, R. L., McPhail, A. T., Pasterczyk, J. W. and Alvanipour, A., *Organometallics*, 1992, **11**, 226.
60. Pazik, J. C., George, C. and Berry, A., *Inorg. Chim. Acta*, 1991, **187**, 207.
61. Wells, R. L., Purdy, A. P., McPhail, A. T. and Pitt, C. G., *J. Organomet. Chem.*, 1988, **354**, 287.
62. Dymock, K., Palenik, G. J., Slezak, J., Raston, C. L. and White, A., *J. Chem. Soc., Dalton Trans.*, 1976, 28.
63. *Browning, D. J., Corker, J. M. and Webster, M., Acta Cryst.*, 1996, **C52**, 882.
64. Mason, M. R., Smith, J. M., Bott, S. G. and Barron, A. R., *J. Am. Chem. Soc.*, 1993, **115**, 4971.
65. SHELX86-Sheldrick, G. M., in *Crystallographic Computing*, Sheldrick, G. M., Kruger, C., Goddard, R., Eds. Oxford University Press, 1985, pp. 184-189.
66. MolEN-Enraf-Nonius. MolEN, An interactive Structure Solution Procedure, Enraf-Nonius, Delft, Netherlands, 1990.
67. *International Tables for X-Ray Crystallography*, Kynoch Press, Birmingham, 1974, vol. 4.

Pergamon

PII: S0277-5387(98)00077-1

Polyhedron Vol. 17, No. 18, pp. 3131–3135, 1998
© 1998 Elsevier Science Ltd
All rights reserved. Printed in Great Britain
0277-5387/98 $19.00+0.00

Anatase to rutile transformation in sol-gel titania by modification of precursor

C. Suresh, V. Biju, P. Mukundan and K. G. K. Warrier*

Structural Ceramics Unit, Regional Research Laboratory (CSIR), Trivandrum-695019, India

(Received 2 December 1997; accepted 18 February 1998)

Abstract—The effect of pH on the formation of high temperature phases in titanium oxide, derived by hydrolysis of modified titanium isopropoxide has been reported. The anatase to rutile phase transformation is delayed in the case of acetic acid modified gel precursor at pH 3 and 4, showing the presence of anatase phase even at 1000°C. On the other hand, in the sample precursor prepared at pH 6, anatase to rutile transformation is complete at 800°C, under identical conditions of heat treatment. The transformation has been followed by thermal analysis and X-ray powder diffraction data. Impedance spectroscopy has been attempted as a useful and effective tool in identifying the anatase and rutile phases as well as transformation temperatures. © 1998 Elsevier Science Ltd. All rights reserved

Keywords: sol-gel titania; impedance spectroscopy; anatase; rutile phases; transformation termperatures.

Titania has been well recognised as a pigment in paints, as a filler material and also in enamels and glazes for ceramics [1,2]. More recently the application of titania has spread to catalysts, catalyst supports and membranes [3–7]. Suitably modified titania has also been found to respond electrically in different humidity environments and has therefore found application as humidity sensors [8,9]. However these applications demand high purity titania with controlled particle size, definite phase composition and surface properties. Sol-gel methods have been widely investigated with advantage over conventional methods in controlling the properties of titania [10,11]. Further, titania normally undergoes anatase-rutile phase transformation in the temperature range 600–700°C [12]. For high temperature applications of titania as catalyst, membranes and sensors, a stable anatase phase is necessary [1,2]. Usually this is achieved to some extent by incorporating other metal oxides as dopants in small quantities. Y_2O_3 and SiO_2 have been found to shift the anatase-rutile transformation to higher levels [13,14]. Modifying the precursor characteristics by involving different solvents and by introducing gel modifiers [15,16] have been the other approaches attempted earlier to arrive at titania having specific properties. However, there has been no systematic data reported on the effect of pH condition in presence of modifiers on precursor and subsequent phase development on calcination. The anatase-rutile transformation is usually detected using X-ray powder diffraction analysis. Differential thermal analysis of the precursor gel has limited success in detecting this transformation since energy change involved is very small. Therefore other simple techniques where the change can be detected in bulk would be more useful. Sensitive electrical measurements can be effectively employed to characterise the phase change in TiO_2. Conventional electrical measurements are time consuming and limited to certain fixed frequencies but the impedance spectral method has been found to cover a large range of frequencies. This method has been successfully applied earlier to analyse doped and undoped zinc oxide varistors [16], solid state powder reactions of oxide superconductors [17] and also to study the role of microstructure in the electrical behaviour of sensor materials based on anatase [18].

Titania powders were prepared by sol-gel process in this study with acetic acid as a modifier at different pH conditions. The phase transformation during heat treatment was investigated by impedance spectroscopic measurements and the data are compared with those obtained from thermal analysis and X-ray powder diffraction. Impedance spectral measurement carried out on bulk samples is a novel and effective tool for detecting the anatase-rutile transformation,

* Author to whom correspondence should be addressed.

which has also been found to be dependent on the pH of the precursor.

EXPERIMENTAL

The titania samples were prepared by hydrolysis of titanium isopropoxide (Aldrich Chemicals, U.S.A.). In a typical experiment, 25 ml titanium isopropoxide was dissolved in 48 ml acetic acid (S.D. Fine Chemicals, India) and was stirred for 0.5 h. To this solution 150 ml double distilled water was added dropwise under continuous stirring for 1 h. The pH was adjusted to 3 by adding 10% ammonium hydroxide. The mixture was heated to 70°C in an air oven to get a gel. Similar procedures were followed to prepare titania samples at pH values 4, 5, and 6.

Thermal analysis of the gels were carried out in flowing nitrogen gas (DTA/TGA Shimadzu 50H) at a rate of 10°C/min. The IR spectra of gels dried at 80°C was recorded in Nicolet Impact 400 D FTIR Spectrometer in the range 4000–500 cm^{-1}as powders dispersed in KBr pellets. The dried gels were further calcined at 400, 600, 800 and 1000°C for 3 h, and X-ray powder diffraction patterns were recorded in a Philips Diffractometer PW 1710. The gels prepared at pH 4 and 6 were pelletised and heated at 400, 600, 800 and 1000°C and the parallel surfaces were coated with silver on to which copper leads were attached. Impedance spectral measurements on these samples were carried out using HP 4192A Impedance analyser and data measured were analysed using EQUIVCRT software.

RESULTS AND DISCUSSIONS

X-ray powder diffraction results are given in Table 1. Samples heated at 400°C show only anatase at all pH conditions. The same trend continues up to 600°C. When heated at 800°C samples at pH 3 and 4 show presence of anatase and traces of rutile, but the intensity of anatase peaks are greater in samples prepared at pH 3 and 4 than at 5. For the samples prepared at pH 6, only rutile phase is present (Fig. 1A and 1B). Samples prepared at pH 3 and 4 heat treated at 1000°C still show the presence of anatase phase but those prepared at pH 5 and 6 show rutile phase only.

Table 1. Crystalline phases determined by powder XRD for materials heated to different temperatures

Temp. C	Phases identified by XRD pH3	pH4	pH5	pH6
1000	A	A	R	R
	R	R		
800	A	A	A	
	R	R	R	R
600	A	A	A	A
400	A	A	A	A

A-Anatase, R-Rutile.

The thermogravimetric curves of gels prepared at pH 4 and 6 (Fig. 2) indicates nearly identical pattern of decomposition with a total loss of 25.81 and 35.54% respectively. The decomposition is nearly complete below 400°C. Greater weight loss in the sample prepared at pH 6 indicates the presence of a larger amount of hydroxyls in the gel as free water, since the low temperature decomposition curve has larger weight loss as compared to the sample prepared at pH 4. Further, the thermogravimetric curve of the precursor at pH 4 indicates a larger loss above 300°C, which is due to the larger amount of bonded hydroxyls. Differential thermal analysis curves of the gels prepared at pH 4 and 6 are shown in Fig. 3. The endothermic peak below 100°C which is assigned to the expulsion of free water from the gel, is more prominent in the sample prepared at pH 6. This is in conformation with the TGA analysis which shows a greater weight loss ~ 14% in the sample prepared at pH 6 as compared to the weight loss ~ 8% in the sample prepared at pH 4 up to 100°C. An endothermic peak at 266°C, which is prominent in the DTA curve of gel prepared at pH 4, is associated with the removal of water from the gel network. However this peak is very weak for the sample prepared at pH 6 indicating a lesser amount of bound water in the gel due to a more open structure at higher pH. The broad exothermic peak around 350°C present in the DTA curves of both the samples correspond to the removal of organics. The exothermic peak indicates the onset of anatase phase formation near 400°C in both the samples. It also appears that the formation of anatase for gel prepared at pH 4 is extended over a larger range of temperature compared to its counterpart at pH 6.

Analysis of the infra red spectra of the dried gels was done based on the results published earlier [19,20]. Bands corresponding to 1384 and 1407 cm^{-1} in the spectra of samples prepared at pH 3 and 4 are due to free acetic acid present in the system and these bands are not present in samples at pH 5 and 6. The band corresponding to 1530 cm^{-1} is due to the chelated acetate group [20] which is strong at pH 3 and weakens with increasing pH and no such band is observed in samples prepared at pH 6 (Fig. 4). This indicates that as the pH of the precursor increases the chelating effect of acetic acid decreases. The bands at 2913, 3103, 2990 and 3107 cm^{-1} are due to $-CH_3$ and $-CH_2$-stretching. The peaks corresponding to 653, 650, 673 and 676 cm^{-1} in the spectra of samples prepared at pH 3, 4, 5 and 6 respectively are due to Ti—O stretching vibration [19]. The shifting of the peak corresponding to Ti—O stretching to a higher wavenumber side with an increase of pH indicates an increase in the strength of Ti—O bond. It could be

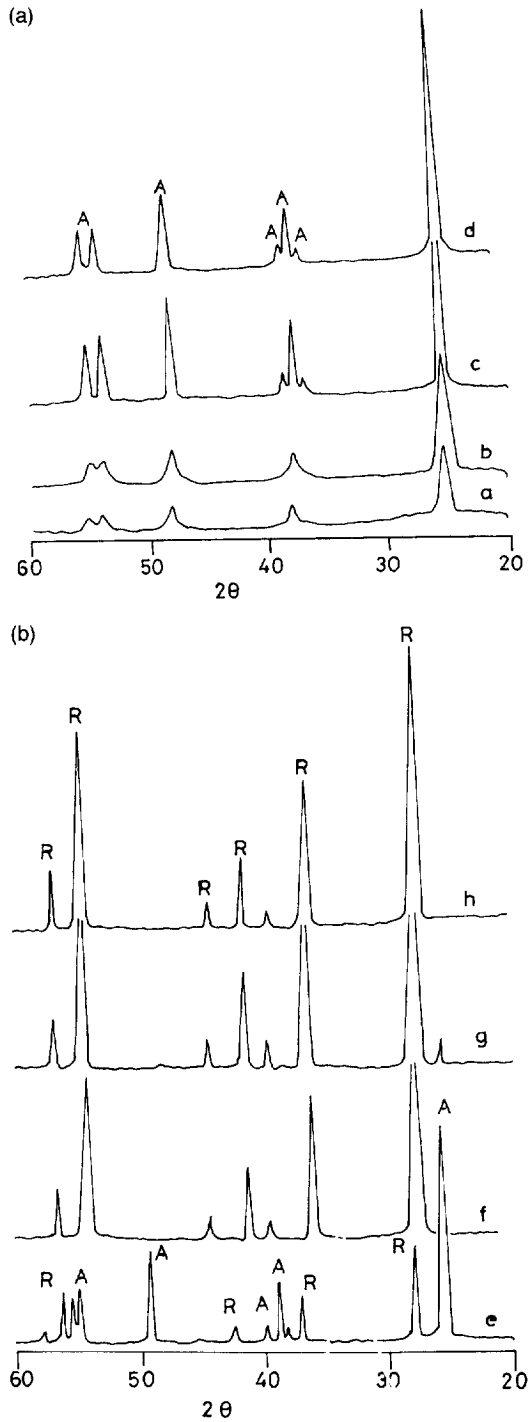

Fig. 1. A. XRD Patterns of samples calcined at (a) pH 4 400°C; (b) pH 6 400°C; (c) pH4 600°C; (d) pH6 600°C, A. Anatase. B. XRD Patterns of samples calcined at (e) pH4 800°C; (f) pH 6 800°C; (g) pH 4 1000°C; (h) pH 6 1000°C. A, Anatase; R. Rutile.

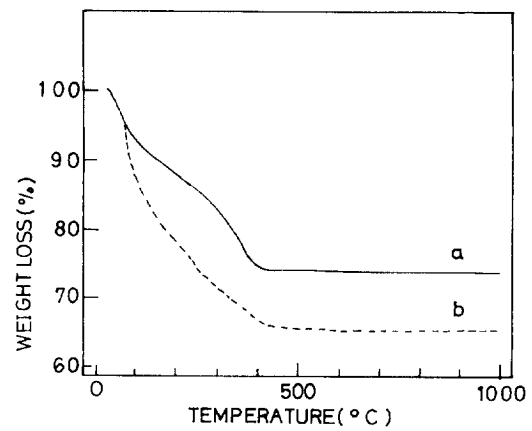

Fig. 2. TGA Curves of gels prepared at (a) pH4; (b) pH6.

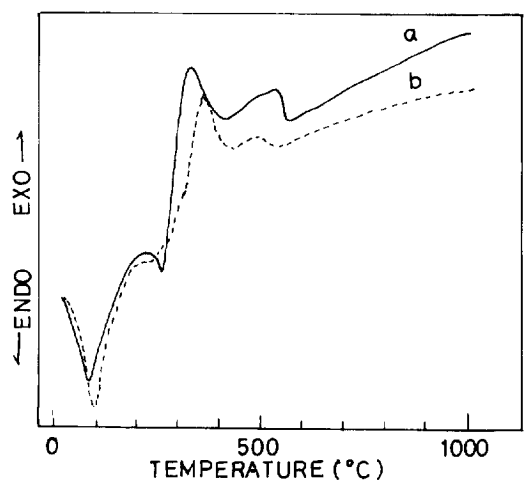

Fig. 3. DTA Curves of gels prepared at (a) pH4; (b) pH6.

concluded that the extent of chelation of acetate group decreases with an increase of pH.

The room temperature impedance measurements indicate that in all the samples, irrespective of pH, the bulk resistance increases with increase in calcination temperature. Impedance curves of the calcined gels prepared at pH 4 and pH 6 are presented in (Fig. 5) and the resistivity values measured on the same samples are shown in Table 2. At 400°C, the impedance curves of both the samples are similar. This is in conformation with the X-ray powder diffraction results. However, at 600°C, the impedance curves, as well as resistivity values show marked differences between samples at pH 4 and 6 even though the X-ray powder diffraction patterns are identical. The greater bulk resistivity value for the samples at pH 6 is due to the starting of anatase to rutile transformation which is beyond the detection limits of X-ray powder diffraction. This conclusion is based on our earlier studies [13,21], which indicated that anatase has a preferentially conducting and rutile insulating nature. The relatively low value of the bulk resistivity for the sample prepared at pH 4 indicates that anatase to rutile

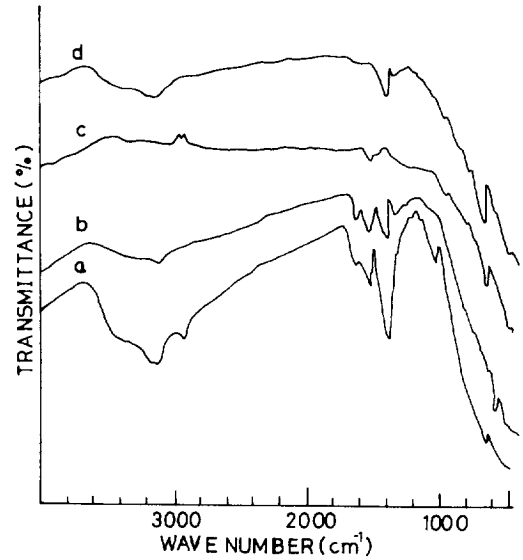

Fig. 4. FTIR Spectra of gels prepared at (a) pH3; (b) pH4; (c) pH5; (d) pH6.

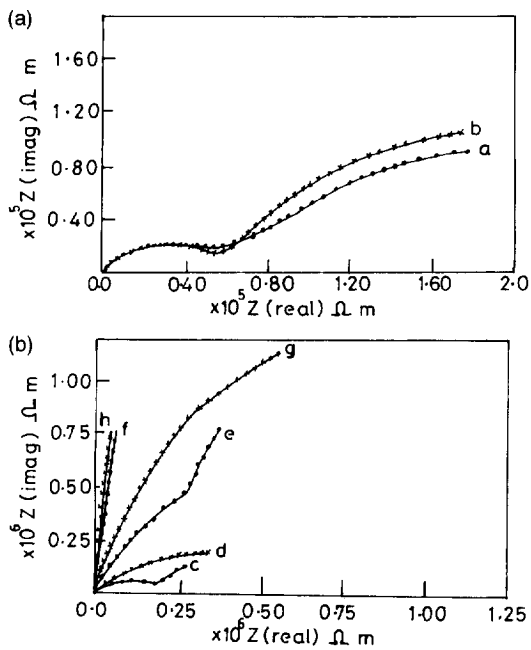

Fig. 5. A. Impedance spectra of calcined samples at (a) pH4 400°C; (b) pH6 400°C. B. Impedance spectra of calcined samples at (c) pH4 600°C; (d) pH6 600°C; (e) pH4 800°C; (f) pH6 800°C; (g) pH4 1000°C; (h) pH6 1000°C.

transformation has not yet started. At 800°C the samples prepared at pH 6 is highly resistive. This shows the presence of only rutile phase which is in conformation with X-ray powder diffraction analysis. The bulk resistivity of the samples prepared at pH 4 and calcined at 800°C is relatively low due to the low concentration

Table 2. Resistivity values of the samples calcined at different temperatures

	Resistivity (ohm-m) of the samples calcined at			
	400°C	600°C	800°C	1000°C
pH4	6.89×10^4	2.25×10^5	2.19×10^6	3.37×10^6
pH6	6.81×10^4	5.62×10^5	1.04×10^7	1.85×10^7

of rutile phase. The bulk resistivity of the samples calcined at 1000°C is very high. This is due to the rutile phase present. The greater value of bulk resistivity for the sample prepared at pH 6 is due to presence of only rutile phase. For the sample prepared at pH 4 the bulk resistivity is comparatively less due to the presence of appreciable quantities of anatase phase, easily detected by X-ray powder diffraction patterns which causes considerable decrease in resistivity values.

Acetic acid used here is to modify the hydrolysis and condensation reactions in the precursor gels since gel modifiers are known to control the size and shape of pore distributions [22]. As the pH is increased the chelated acetate group becomes weak facilitating early hydrolysis to form high temperature phases.

At low pH, condensation reaction is slow compared to hydrolysis because of charge-charge repulsion between protonated hydrated metal cations which allows branching to occur before particle growth to produce strongly cross linked gel. Further, increase in pH may alter the highly cross linked network structure. This is clearly seen from FTIR results where the bands corresponding to chelated acetate group that are strong at pH 3 becomes weaker with increase of pH and nearly disappears at pH 6. The gel having polymeric chains with little branching and cross linking, and also a smaller void region, is structurally weak and thus collapses rapidly on calcination [22]. Hence the strengthening of the gel network by modification through acetic acid and the associated structural changes have been evident in extending the anatase rutile transformation to higher temperatures. Thus the present study indicates that control of the precursor structure could be quite effective in increasing the stability of anatase phase, which is an important requirement for many of the high temperature applications of titania.

CONCLUSION

This study has shown the strong dependence of precursor history on the formation characteristics of various high temperature phases in sol-gel titania. Acetic acid in the pH range up to 4 is a very effective modifier to extend the thermal stability of anatase phase by about 100°C, compared to unmodified one. This approach has been significant since it may help to a considerable extent, in dispensing with the con-

ventional use of oxide dopants. Further, the use of impedance spectral measurement is seen to be a very simple tool to identify the anatase-rutile transformation in bulk specimens and the results are confirmed by X-ray powder diffraction data. Thus a novel approach is presented where on one hand, suitably modified gel precursor could be a simple source for anatase titania stable at high temperature which, on the other, could further be detected by a simple technique of impedance spectroscopy.

Acknowledgement—Among the authors, (C.S.) is grateful to STEC, Government of Kerala, India and (V.B.) to CSIR, Goverment of India, for financial support in the form of junior research fellowship.

REFERENCES

1. Hadjiivanov, K. I. and Klissurski, D. G., *Chem Soc. Rev.*, 1996, **25,** 61.
2. Hoffman, M. R., Martin, S. T., Choi, W. and Bahnemann, D. W., *Chem. Rev.*, 1995, **95,** 69.
3. Ball, P., *Nature*, 1995, **377,** 290.
4. Kumar, K. N. P., Keizer, K. and Burggraf, A. J., *J. Mat. Sci. Lett.*, 1994, **13,** 59.
5. Muneer, M., Philip, R. and Das, S., *Res. Chem. Intermed.*, 1997, **23,** 233.
6. Dagan, G. and Tomkiewiez, M., *J. Phys. Chem.*, 1993, **97,** 12651.
7. Fan, F. F., Liu, H. Y. and Brad, A. J., *J. Phys. Chem.*, 1985, **89,** 4418.
8. Gusmano, G., Montesperelli, G., Nunziante, P. and Traversa, E., *Br. Ceram. Trans.*, 1993, **92,** 104.
9. Cantalini, C. and Pelino, M., *J. Am. Ceram. Soc.*, 1992, **75,** 546.
10. Komarneni, S., Roy, R. and Breval, E., *J. Am. Ceram. Soc.*, 1985, **68,** C-41.
11. Keddie, J. L., Bran, P. V. and Giannelis, E. M., *J. Am. Ceram. Soc.*, 1996, **77**.
12. Kumar, K. N. P., Keizer, K., Burggraff, A. J., Okubo, T., Nagomoto, H. and Morooka, S., *Nature*, 1992, **358,** 48.
13. Ghosh, S. K., Vasudevan, A. K., Rao, P. P., Anilkumar, G. M., Krishnapriya, G., Damodaran, A. D. and Warrier, K. G. K., *J. Mat. Sci.*, (Communicated).
14. Anderson, C. and Brad, A. J., *J. Phys. Chem., B*, 1997, **101,** 2611.
15. Livage, J., *Mat. Res. Proc.*, 1986, **73,** 717.
16. Sharma, P. K. and Rahman, A., *J. Mat. Sci.*, 1996, **31,** 773.
17. Cooper, E. A., Mason, T. O., Biznek, M. E., Balachandran, U., *J. Am. Ceram. Soc.*, 1990, **73,** 154.
18. Azad, A. M., Younkman, L. B. and Akbar, S. A., *J. Am. Ceram. Soc.*, 1994, **77,** 481.
19. Joe, I. H., Vasudevan, A. K., Aruldhas, G., Damodaran, A. D. and Warrier, K. G. K., *J. Sol. State Chem.*, 1997, **131,** 18.
20. Doeuff, S., Henry, M., Sanchs, C. and Livage, J., *J. Non. Cryst. Solids* 1987, **89,** 206.
21. Vasudevan, A. K., Rao, P. P., Ghosh, S. K., Anilkumar, G. M., Damodaran, A. D. and Warrier, K. G. K., *J. Mat. Sci. Lett.*, 1997, **16,** 8.
22. Kung, H. H., and Ko, E. I., *The Chem. Engg. Journal*, 1996, **64,** 203.

Pergamon

PII: S0277-5387(98)00078-3

Polyhedron Vol. 17, No. 18, pp. 3137–3144, 1998
© 1998 Elsevier Science Ltd
All rights reserved. Printed in Great Britain
0277-5387/98 $19.00+0.00

Platinum(II) and palladium(II) complexes derived from the anion of sulfathiazole [4-amino-N-(thiazol-2-yl)benzenesulfonamide, stzH]; crystal structure of *cis*-$[Pt(stz)_2(PPh_3)_2]\cdot 3CHCl_3$

William Henderson,* Louise J. McCaffrey, Maarten B. Dinger and Brian K. Nicholson

Department of Chemistry, University of Waikato, Private Bag 3105, Hamilton, New Zealand

(Received 10 October 1997; accepted 18 February 1998)

Abstract—Reaction of the complexes *cis*-$[PtCl_2L_2]$ [L = PPh_3 or L_2 = 1,1′-bis(diphenylphosphino)ferrocene (dppf)], or $[PdCl_2(phen)]$ [phen = 1,10-phenanthroline] with two mole equivalents of sulfathiazole (stzH) in methanol with excess triethylamine yields the complexes *cis*-$[M(stz)_2L_2]$ in good yields. The complexes have been characterised by elemental microanalysis, together with infrared, ^1H and ^{31}P NMR spectroscopies. A single-crystal X-ray structure determination on the complex *cis*-$[Pt(stz)_2(PPh_3)_2]$ **3a** shows that both stz ligands coordinate via the thiazole nitrogen atoms. Using positive-ion electrospray mass spectrometry (ESMS) all complexes yield strong molecular ions $[M+H]^+$ at low cone voltages. At higher cone voltages, loss of one stz ligand occurs, giving $[L_2M(stz)]^+$ ions. The complex *cis*-$[PtCl(stz)(PPh_3)_2]$ **4** was also prepared using a 1:1 mole ratio of reactants. Functionalisation of both primary arylamine groups of **3a** can be accomplished using either acetic anhydride or trifluoroacetic anhydride, in pyridine solvent, and the derivatives **5** were characterised by ^{31}P NMR spectroscopy, elemental analysis and ESMS. © 1998 Elsevier Science Ltd. All rights reserved

Keywords: platinum; palladium; sulfathiazole; electrospray; crystal structure.

Sulfonamide compounds, including sulfanilamide **1** and sulfathiazole **2** have been long known for their antibacterial properties [1]. The presence of relatively acidic N—H protons in these compounds (activated by the adjacent electron-withdrawing sulfonyl moiety) suggested that these sulfa drugs should readily form complexes with platinum group metal complexes, bonding as their monoanions. Metal complexes of such ligands are of importance since the polymeric silver(I) complex of the related compound sulfadiazine, which contains silver–amide linkages, is widely used clinically for the treatment of severe burns [2]. We are interested in the general properties of platinum-group metal–amide complexes [3], particularly for ligands which have biological activity [4,5]. Studies on metal complexes of sulfa drugs is an area which has attracted interest in recent years. While a number of complexes of first-row transition metals have been described [6–8], few platinum or palladium complexes of sulfathiazole have been reported. However, some complexes of platinum(II) have been found to be effective bactericides against sulfa-drug resistant bacteria [9], and a platinum(II) complex of the related sulfa drug sulfadiazine has been found to show antitumour activity [10]. A palladium(II) complex of sulfathiazole has been used in the quantitative analysis of the ligand [11] and stability constants for a number of metal complexes, including palladium(II) have been determined [12]. Platinum and palladium complexes of other sulfonamide ligands are known [13,14].

In this paper we describe the synthesis of some new platinum(II) and palladium(II) derivatives containing

*Author to whom correspondence should be addressed. Fax: 0064 7 838 4219. E-mail: w.henderson@waikato.ac.nz.

deprotonated sulfathiazole ligands. The application of electrospray mass spectrometry to the study of this type of complex is also described.

RESULTS AND DISCUSSION

Syntheses and X-ray crystal structure

Reaction of the complexes *cis*-$[PtCl_2L_2]$ [L = PPh_3 or L_2 = 1,1′-bis(diphenylphosphino)ferrocene (dppf)], or $[PdCl_2(phen)]$ [phen = 1,10-phenanthroline] with two mole equivalents of sulfathiazole (stzH) **2** with excess triethylamine in hot methanol yields, after precipitation with water, filtration, washing and drying, the complexes *cis*-$[M(stz)_2L_2]$ (**3a–c**). The complexes are air-stable solids, poorly soluble in chlorinated organic solvents, and insoluble in water. However they are generally more soluble in dimethyl sulfoxide, allowing partial NMR characterisation of the complexes. Electrospray mass spectrometry was also used to characterise these complexes, this being a particularly useful technique for the analysis of complexes of low solubility, and where the reaction centre (in this case the NH_2 groups) is remote from the metal centre. The attempted synthesis of **3a** using milder reaction conditions (excess triethylamine in refluxing dichloromethane for 4 h) gave a mixture of **3a** and the mono stz complex **4**, identified by $^{31}P-\{^1H\}$ NMR spectroscopy. Subsequent reaction of *cis*-$[PtCl_2(PPh_3)_2]$ with one equivalent of stzH in CH_2Cl_2–MeOH with triethylamine gave crude complex **4** in 76% yield. The product also contained a small amount of **3a**.

The NH_2 groups of the platinum complex **3a** can be acetylated (acetic anhydride/pyridine) or trifluoroacetylated (trifluoroacetic anhydride/pyridine) to give the derivatised products **5a** and **5b**, respectively. Attempted sulfonylation of **3a** using *p*-toluenesulfonyl chloride in pyridine gave a mixture of products, as shown by ESMS (see below). The derivatised products **5** are somewhat more soluble in dichloromethane and chloroform than **3a**.

Unambiguous characterisation of the complexes **3–5** by NMR spectroscopy (*vide infra*) was not easily achieved, and thus a single-crystal X-ray diffraction study was carried out on one derivative. The majority of the complexes did not crystallise well, however crystals of **3a** suitable for a structure determination were obtained on allowing a saturated chloroform solution to stand at room temperature for several weeks. Figure 1 shows the molecular structure together with the atom numbering scheme, and the caption gives selected bond lengths and angles.

The complex contains the expected approximately square-planar platinum(II) centre, with two stz ligands coordinated through their thiazole nitrogen atoms, in a *cis*-arrangement. The structure determination is the first of a platinum-group metal sulfathiazole complex bonded via the thiazole nitrogen.

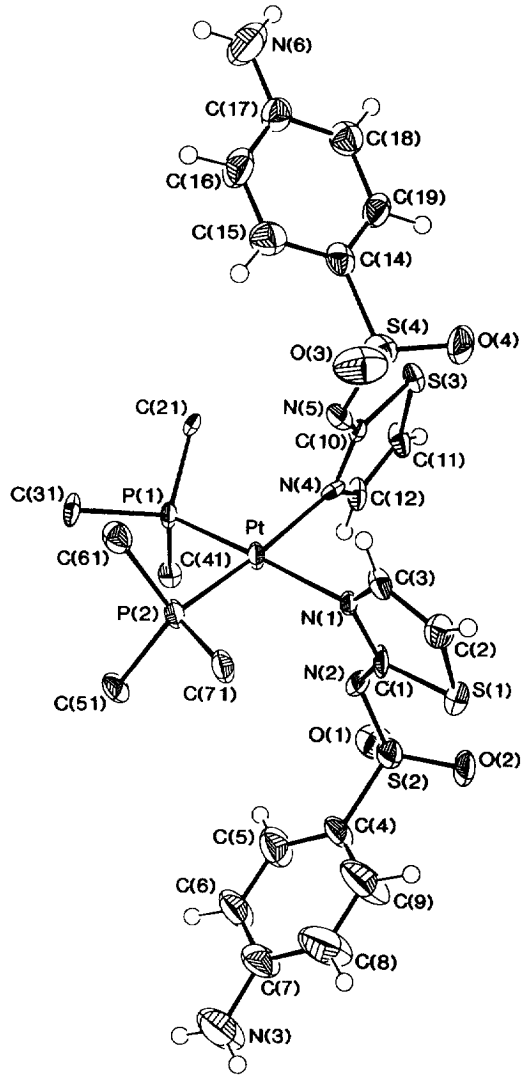

Fig. 1. Molecular structure of the complex *cis*-$[Pt(stz)_2(PPh_3)_2]$ **3a**, showing the atom numbering scheme. Only the phosphorus-bonded triphenylphosphine carbon atoms are shown for clarity, and the three chloroform molecules of solvation have also been omitted.
Selected bond lengths (Å) *and angles* (°): Pt(1)—N(4) 2.095(7); Pt(1)—N(1) 2.110(7); Pt(1)—P(2) 2.278(2); Pt(1)—P(1) 2.290(2); N(1)—C(1) 1.349(13); N(1)—C(3) 1.358(13); N(4)—C(10) 1.346(12); N(4)—C(12) 1.385(12); N(4)—Pt(1)—N(1) 85.0(3); N(1)—Pt(1)—P(2) 90.9(2); N(4)—Pt(1)—P(1) 89.5(2); P(2)—Pt(1)—P(1) 96.33(9).

There are only three other reported structures of transition-metal (copper and zinc) complexes containing solely thiazole nitrogen bonded stz ligands [7,8]. The thiazole moieties are roughly perpendicular to the platinum coordination plane, as shown in Fig. 2, resulting in a *trans*-disposition of the remainder of the stz ligands, presumably to minimise steric interactions. The coordination plane is twisted so that the

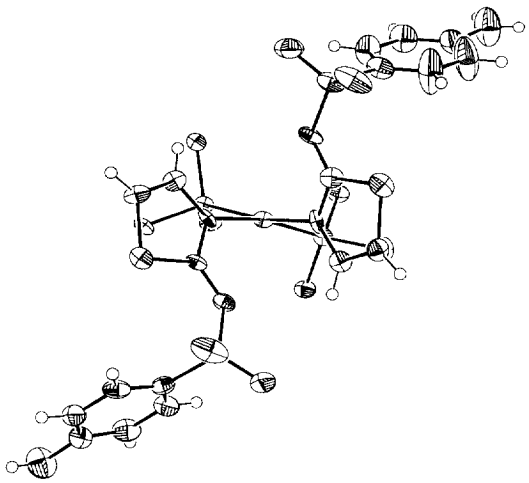

Fig. 2. View of complex **3a** along the N—Pt—N plane, showing the coordination of the thiazole moieties perpendicular to the platinum coordination plane, resulting in the disposition of the bulk of the stz ligands above and below the plane.

N—Pt—N plane is at 14.2° to the P—Pt—P one (Fig. 2).

NMR spectroscopy

The $^{31}P-\{^1H\}$ NMR spectra of the phosphine complexes **3a** and **3b** show a single resonance, consistent with two equivalent phosphine ligands. The values of $^1J(Pt,P)$ are indicative of the presence of phosphine ligands *trans* to relatively low *trans*-influence nitrogen donor ligands. Thus, for the triphenylphosphine complex **3a**, the value of $^1J(Pt,P)$ is 3444 Hz, which is in the range expected for nitrogen donor ligands, and compares well with the $^1J(Pt,P)$ values of 3054, 3454 and 3284 Hz found for the amide complexes *cis*-$[Pt(NCH_2CH_2CO)_2(PPh_3)_2]$ [5], $[Pt\{NHS(O)_2NH\}(PPh_3)_2]$ [13] and the isatin-derived complex *cis*-$[Pt(isat)_2(PPh_3)_2]$ (isatH = isatin, indole-2,3-dione) [15], respectively.

The ^1H and $^{13}C-\{^1H\}$ NMR spectra of the phosphine complexes **3a** and **3b** are relatively uninformative, due to the large number of overlapping signals in the aromatic region. However, unam-

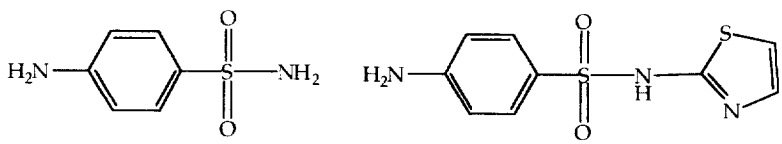

1 **2**

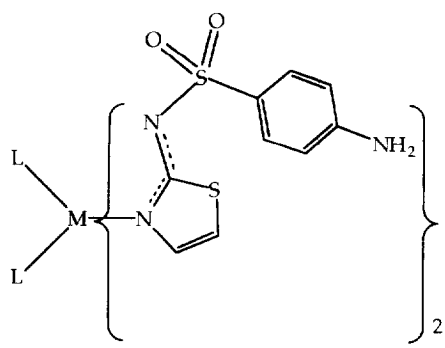

Complex	M	L or L_2
3a	Pt	PPh_3
3b	Pt	dppf
3c	Pd	phen

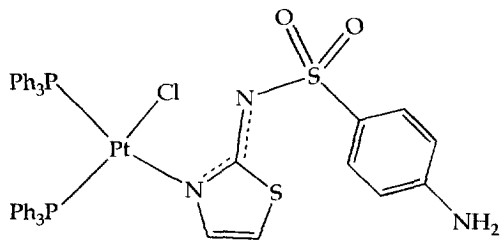

4

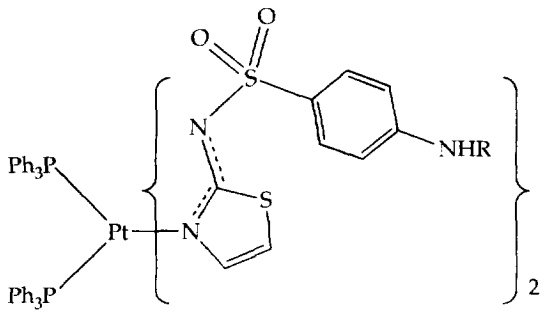

5a: R = $C(O)CH_3$
5b: R = $C(O)CF_3$
5c: R = $S(O)_2C_6H_4Me$-*p*

biguous NMR assignment of the complex **3a** was achieved using HMBC [Heteronuclear Multiple Bond Correlation (long-range ^{13}C-^1H correlation, optimised for ^2J and ^3J coupling)] and HMQC [Heteronuclear Multiple Quantum Correlation (short-range ^{13}C-^1H, optimised for ^1J coupling)] inverse 2D experiments. The aromatic region of the ^1H NMR spectrum of **3a** is illustrated in Fig. 3. The assignment of hydrogen atoms 2″ and 3″ (which cannot be easily distinguished by standard methods) was made using known assignments of the thiazole group in the literature [16]. No $^2J_{C,Pt}$ or $^3J_{C,Pt}$ couplings could be observed for this complex, even with overnight acquisition periods on a relatively concentrated solution. The addition of D_2O to a d_6-DMSO solution of compound **3a** resulted in complete exchange of the NH_2 protons at δ 5.64, confirming their assignment.

Complex **4** gives the expected AB pattern in the ^{31}P NMR spectrum, with resonances at δ 13.4 and 5.2, showing coupling of ^{195}Pt of 3850 and 3254 Hz, respectively, consistent with PPh_3 ligands *trans* to chloride and *N*-donor ligands. For the related complex *cis*-[PtCl(debarb)$(PPh_3)_2$] (debarb = anion of 5,5-diethylbarbituric acid) comparable values of ^1J(Pt,P) of 3950 and 3337 Hz were observed for the phosphines *trans* to chloride and amide ligands [4]. The difference in coupling constants is larger for the asymmetric complex **4** when compared to the symmetrical species *cis*-[$PtCl_2(PPh_3)_2$] [^1J(Pt,P) 3673 Hz] and the complex **3a** [^1J(Pt,P) 3444 Hz], and this effect has been reported previously [15,17].

The ^{31}P NMR spectra of the derivatised complexes **5** show little change in the ^1J(Pt,P) coupling constant [**5a** 3449 Hz, **5b** 3450 Hz] from the parent complex **3a** [3444 Hz]. This is not unexpected given the remoteness of the reactive site from the Pt—P moiety.

Electrospray mass spectrometry

The sulfathiazole complexes **3**–**5** have been investigated by electrospray mass spectrometry (ESMS). This relatively new technique, which was originally developed by Fenn and co-workers for the analysis of large biomolecules, is finding increased use in the characterisation of inorganic complexes [18]. ESMS is particularly well-suited for complexes having only low solubilities and volatilities, such as those described in this paper. Additionally, the rather complicated ^1H and ^{13}C NMR spectra yielded by such complexes containing multiple aromatic ring systems, coupled with remote NH_2 functional groups, makes a simple mass spectrometric technique the method of choice for the initial characterisation of complexes of this type.

ESMS data for complexes **3**–**5** are summarised in Table 1, and the complex *cis*-[$Pt(stz)_2(PPh_3)_2$] **3a** is taken as a representative example for the purposes of the following discussion. At a cone voltage of 20 V the complex yields a strong protonated ion peak $[M+H]^+$ at *m/z* 1229. Excellent agreement was observed between the observed and calculated isotope distribution patterns. Additional small peaks were observed due to $[M+Na]^+$ and $[M+K]^+$, formed from traces of the alkali metal cations present in the system. Such adducts from trace cations are well-known in electrospray mass spectra. No higher aggregates of the type $[2M+H]^+$ or $[3M+H]^+$ were observed. Upon increasing the cone voltage to 30 V, an additional species, having major peaks at *m/z* 973 and 974 is observed, and is assigned to the species $[Pt(stz)(PPh_3)_2]^+$, i.e. $[M-stz]^+$, formed by loss of a sulfathiazole anion ligand. Upon further increasing the cone voltage, the relative proportion of the $[M-stz]^+$ species increases at the expense of $[M+H]^+$ and $[M+Na]^+$. At still higher cone voltages, the species $[(o\text{-}C_6H_4PPh_2)Pt(PPh_3)]^+$ (*m/z* 718), containing an orthometallated PPh_3 ligand, and its solvated analogue $[(o\text{-}C_6H_4PPh_2)Pt(PPh_3)(NCCH_3)]^+$, are observed. We have previously observed such cyclometallation in studies of a wide range of platinum(II) complexes [4,5,15].

The other stz complexes show generally similar ESMS behaviour to the triphenylphosphine complex

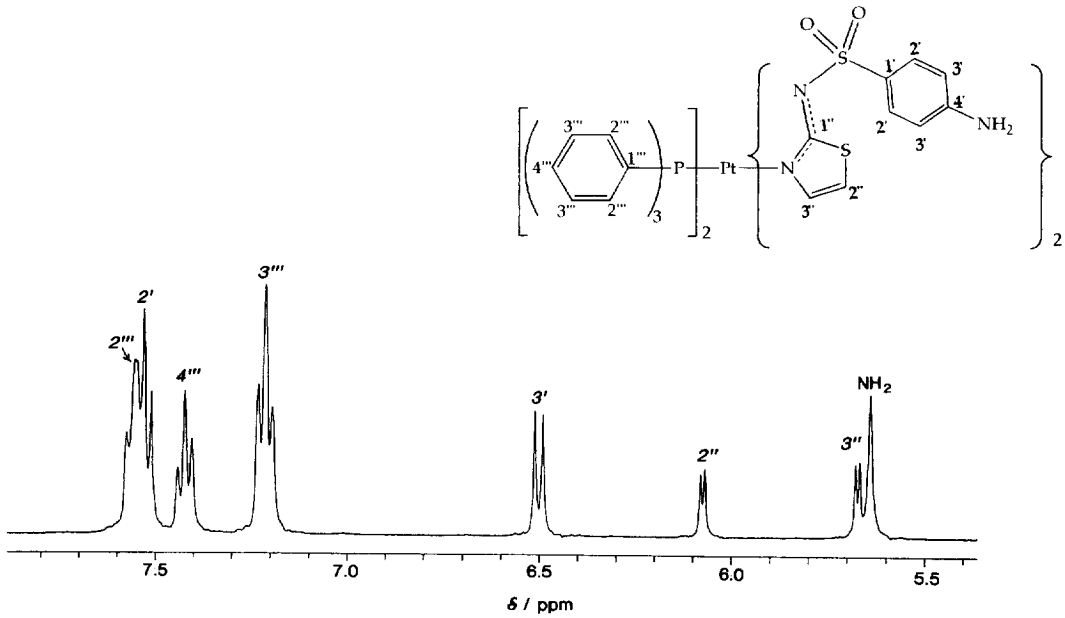

Fig. 3. ^{1}H NMR spectrum (400 MHz, d_6-DMSO solution) of the aromatic region of the platinum–triphenylphosphine complex *cis*-[Pt(stz)$_2$(PPh$_3$)$_2$] **3a**, showing the assignment of the various aromatic and NH_2 protons. The inset shows the atom numbering scheme.

Table 1. Electrospray mass spectrometric data for the sulfathiazole complexes

Complex	Cone voltage	Major observed ions (m/z, %)[a]
3a	20	$[M+H]^+$ (1229, 100%), $[M+Na]^+$ (1251, 9%), $[M+K]^-$ (1267, 1%)
	40	$[M-stz]^+$ (973/974, 100%), $[M+H]^+$ (1229, 21%), $[M+Na]^-$ (1251, 28%), $[M+K]^-$ (1267, 2%)
	80	$[(o\text{-}C_6H_4PPh_2)Pt(PPh_3)]^+$ (718, 100%), $[(o\text{-}C_6H_4PPh_2)Pt(PPh_3)(NCCH_3)]^+$ (759, 17%), $[M-stz]^+$ (973/974, 90%), $[M+H]^+$ (1229, 2%), $[M+Na]^-$ (1251, 9%)
	140	$[(o\text{-}C_6H_4PPh_2)Pt(PPh_3)]^+$ (718, 100%), $[(o\text{-}C_6H_4PPh_2)Pt(PPh_3)(NCCH_3)]^+$ (759, 10%), $[M-stz]^+$ (973/974, 39%)
3b	20	$[M+H]^+$ (1258, 100%), $[M+Na]^+$ (1280, 5%)
	60	$[M-stz]^+$ (1003, 1004, 100%), $[M+H]^+$ (1258, 5%), $[M+Na]^+$ (1280, 5%)
4[b]	20	$[M-stz]^+$ (974), $[M-stz+NH_3]^+$ (991), $[M+H]^+$ (1010)
	40	$[M-stz]^+$ (974)
5a	20	$[M-stzAc]^-$ (1015, 5%), $[M+H]^+$ (1313, 100%)
	50	$[M-stzAc]^-$ (1015, 100%), $[M+H]^+$ (1313, 18%)
5b	20	$[M+H]^+$ (1422, 100%)
	50	$[M-stzCOCF_3]^+$ (1069, 100%), $[M+H]^+$ (1422, 100%)

[a] Identification of ions is by means of the most intense peak or peaks in the isotope distribution pattern.
[b] Weak ions also observed due to the small amount of impurity **3a** present in this sample.

3a. All complexes yield a strong $[M+H]^+$ molecular ion, though different propensities to form the $[M(stz)L_2]^+$ ion were observed. The observation of $[M-stz]^+$ ions up to high cone voltage suggests that the platinum-amide bond in the monocationic species possess considerable stability, though cyclometallation of the PPh_3 ligands provides an apparent route for fragmentation. In contrast, loss of the first stz^- ligand appears to provide an alternative ionisation process (to protonation) at moderate cone voltages.

For complex **4** containing one chloride and one stz ligand, the ESMS spectrum of a freshly prepared solution showed a large $[M+H]^+$ peak at m/z 1010. The presence of both multi-isotopic platinum and di-isotopic chlorine leads to a highly distinctive isotope

distribution pattern for this species, and excellent agreement was found between observed and calculated patterns. The aromatic amine group present in the complex is expected to be the most basic in the complex, and is thus the likely site of protonation.

The acetylated complex **5a** shows a strong $[M+H]^+$ ion at *m/z* 1313 in the 20 V ESMS spectrum, confirming acetylation of both primary amine groups. When the cone voltage is increased to 50 V, one of the acetylated sulfathiazole ligands (stzAc) is lost, giving $[M-stzAc]^+$ (*m/z* 1015) as the base peak, thus paralleling the behaviour of the parent **3a**. Identical behaviour was shown by the trifluoroacetylated complex **5b**. However, the product (**5c**) from the attempted reaction of **3a** with *p*-toluenesulfonyl chloride (Tol-SO_2Cl) in pyridine was shown by ESMS to be a mixture of products, with both mono- and di-sulfonylated complexes giving their respective $[M+H]^+$ ions in the 20 V positive-ion spectrum. The major peak, at *m/z* 1207, is assigned as $[Pt(stz\text{-}SO_2Tol)(pyridine)(PPh_3)_2]^+$ apparently formed by loss of one stz ligand and coordination of a pyridine ligand, the solvent used in the synthesis of this product. However, $^{31}P\text{-}\{^1H\}$ NMR of this mixture of products yielded only a single resonance [δ 2.7, ^1J(PtP) 3450], suggesting that the neutral complexes **3a** and **5c** (and the mono-derivatised complex) have a lower ionisation efficiencies than the cationic $[Pt(stz\text{-}SO_2Tol)(pyridine)(PPh_3)_2]^+$. The NH_2 group is located some distance from the PPh_3 ligands, and ^{31}P NMR is therefore insensitive to changes at this position. Despite the lack of success of the synthesis of **5c**, the study demonstrates that ESMS provides a valuable characterisation technique for rapid identification of reaction products in this system, where ^1H and ^{13}C NMR is of limited diagnostic value.

In conclusion, a number of platinum(I) and palladium(II) complexes containing deprotonated sulfathiazole ligands have been prepared; a structure determination of the bis(triphenylphosphine) platinum complex **3a** shows the ligands to be coordinated through the thiazole nitrogen atoms. Electrospray mass spectrometry is demonstrated to be a useful technique for investigating the chemistry of this class of compound.

EXPERIMENTAL

The compound $[PdCl_2(phen)]$ [19] was synthesised via the literature procedure. The complexes *cis*-$[PtCl_2(PPh_3)_2]$ and $[PtCl_2(dppf)]$ were prepared by ligand substitution [20] of the cyclo-octa-1,5-diene (cod) ligand of the complex $[PtCl_2(cod)]$ [21]. The following compounds were either prepared via the literature procedure or used as supplied from commercial sources: PPh_3 (Pressure Chemical Company), dppf and trifluoroacetic anhydride (Aldrich), sulfathiazole **2** and *p*-toluenesulfonyl chloride (BDH). Methanol was of LR grade and used without any prior purification, while triethylamine was distilled from KOH pellets prior to use.

Melting points were recorded on a Reichert hot-stage apparatus and are uncorrected. Elemental analyses were performed by the Campbell Microanalytical Laboratory, University of Otago. IR spectra were recorded as KBr disks on a Perkin-Elmer 1600 Series or BioRad FTS-40 FTIR spectrophotometers. $^{31}P\text{-}\{^1H\}$ NMR spectra were recorded (unless otherwise stated) in $CDCl_3$ solution, to which ca 20% of DMSO was added, either on a JEOL JNM-FX90 spectrometer, at 36.23 MHz, or on a Bruker AC300P spectrometer at 121.51 MHz. Spectra were recorded with external 85% H_3PO_4 as the reference (δ 0.0). ^1H NMR spectra were recorded in d_6-DMSO solution on a Bruker DRX spectrometer at 400.13 MHz, or on a Bruker AC300P instrument at 300.13 MHz, chemical shifts being relative to $SiMe_4$ (δ 0.0). $^{13}C\text{-}\{^1H\}$ NMR spectra were recorded on a Bruker AC300P spectrometer at 75.47 MHz.

Electrospray mass spectra were obtained in positive-ion mode with a VG Platform II mass spectrometer, with MeCH–H_2O (1 : 1) as the mobile phase. Cone voltages were typically varied from 10 to 100 V, in order to investigate the effect of higher voltages on fragmentation of the parent ions. Excellent agreement between observed and calculated isotope distribution patterns was observed for all major ions. Theoretical isotope patterns were calculated using the *Isotope* program [22].

Melting point, microanalytical and IR spectroscopic data for complexes **3**–**5** are presented in Table 2.

Synthesis of cis-$[Pt(stz)_2(PPh_3)_2]$ **3a**

A suspension of *cis*-$[PtCl_2(PPh_3)_2]$ (200 mg, 0.253 mmol) and stzH **2** (133 mg, 0.521 mmol) was heated to reflux in methanol (20 cm^3) with triethylamine (0.4 cm^3) for 1.5 h to give a white suspension. The mixture was cooled and water (30 cm^3) added. The product was filtered, washed with water (5 cm^3) and dried *in vacuo* to yield **3a** (260 mg, 84%). NMR: $^{31}P\text{-}\{^1H\}$ (121.5 MHz), δ 3.48 [s, ^1J(Pt,P) 3444]. $^{13}C\text{-}\{^1H\}$: ($CDCl_3$) δ 168.5 (s, 1″), 151.4 (s, C-4′), 133.8 (d, C-2‴, 6‴), 133.2 (s, C-2″), 131.1 (d, C-4‴), 130.2 (s, C-1′), 128.3 (d, C-3‴, 5‴), 127.4 (d, C-2′, 6′), 126.9 [s, (dd, second-order, $^1J_{C,P}$ 68.53, $^3J_{C,P}$ 5.87), C-1‴], 112.3 (d, C-3′,5′), 105.8 (d, C-3″).

Synthesis of cis-$[Pt(stz)_2(dppf)]$ **3b**

A suspension of $[PtCl_2(dppf)]$ (101 mg, 0.123 mmol) and stzH **2** (63 mg, 0.247 mmol) in methanol (30 cm^3) with triethylamine (1 cm^3) was refluxed for 1.5 h. The yellow suspension was cooled to room temperature, and the product filtered, washed with methanol (5 cm^3) and dried *in vacuo* to give **3b** (118

Table 2. Melting point, microanalytical[a] and IR spectroscopic data for the sulfathiazole complexes **3–5**

Complex	m.pt. (°C)	Microanalytical data C	H	N	IR ν_{max} (cm^{-1})
3a	>230	52.6(52.8)	3.7(3.8)	6.9(6.8)	1452 (vs), 1130 (s), 1090 (s)
3d	>230	49.6(49.7)	3.5(3.5)	6.8(6.7)	1452 (vs), 1129 (s), 1089 (s), 688 (s)
3f	>230	45.2(45.3)	3.0(3.0)	14.3(14.1)	1597 (s), 1450 (vs), 1414 (s), 1327 (s), 1297 (s), 1267 (vs), 1171 (s), 1123 (vs), 1090 (vs), 1074 (vs), 935 (vs), 714 (s), 683 (vs), 654 (s), 569 (vs)
4	n.d.	52.3(53.6)	3.8(3.8)	4.1(4.2)	1459 (vs), 1132 (s), 1089 (s), 692 (s), 550 (s), 529 (s)
5a	>230	53.3(53.1)	4.1(3.8)	6.9(6.4)	1452 (vs), 1137 (s), 1090 (s)
5b	195–200	48.8(49.1)	3.2(3.1)	6.0(5.9)	1730 (s), 1452 (vs), 1290 (s), 1165 (vs), 1091 (vs), 942 (s), 689 (vs)

[a] Calculated values are given in parentheses.
n.d.: This sample was of low purity (^{31}P NMR) and melting point was therefore not determined.

mg, 76%). ^{31}P-$\{^1H\}$ NMR (121.5 MHz), δ 3.8 [s, ^1J(Pt,P) 3535].

Synthesis of [Pd(stz)$_2$(phen)] **3c**

The complex [PdCl$_2$(phen)] (125 mg, 0.350 mmol) with stzH **2** (179 mg, 0.701 mmol) in methanol (30 cm^3) with added triethylamine (1 cm^3) was refluxed for 16 h to give an orange suspension. Complex **3c** was filtered off, washed with methanol (5 cm^3), acetone (5 cm^3) and dried *in vacuo* to give an orange powder (244 mg, 88%).

Synthesis of cis-[PtCl(stz)(PPh$_3$)$_2$] **4**

To a solution of *cis*-[PtCl$_2$(PPh$_3$)$_2$] (143 mg, 0.181 mmol) and stzH **2** (47 mg, 0.184 mmol) in methanol (10 cm^3) and dichloromethane (20 cm^3) was added triethylamine (1 cm^3), and the mixture stirred overnight at room temperature. The resulting colourless solution was rotary evaporated to dryness at 40°C to afford a white solid, which was found to be complex **4**, with a small quantity (ca 3%) of the bis(stz) complex **3a**. The solid was washed with isopropanol (20 cm^3) to remove triethylammonium chloride, and dried *in vacuo* to give crude **4** (139 mg, 76%). ^{31}P-$\{^1H\}$ NMR (36.2 MHz), δ 13.4 [s, ^1J(Pt,P) 3850, ^2J(P,P) 17] and 5.2 [s, ^1J(Pt,P) 3254].

Reaction of ***3a*** *with acetic anhydride, trifluoroacetic anhydride and* p-*toluenesulfonyl chloride*

General method. To a stirred solution of complex **3a** (ca 150 mg, 0.122 mmol) in pyridine (5 cm^3) was added acetic anhydride or trifluoroacetic anhydride (40 drops) or *p*-toluenesulfonyl chloride (100 mg), and stirred for 60 min. The mixture was poured onto crushed ice and allowed to warm to room temperature. The resulting solid was filtered, washed with water (10 cm^3) and ether (10 cm^3) and dried *in vacuo*.

Complex **5a**. Reaction of **3a** (164 mg, 0.133 mmol) with acetic anhydride gave **5a** (108 mg, 62%) as a white powder. ^{31}P-$\{^1H\}$ NMR (121.5 MHz), δ 3.3 [^1J(Pt,P) 3449].

Complex **5b**. Reaction of **3a** (160 mg, 0.130 mmol) with trifluoroacetic anhydride gave **5b** (129 mg, 70%) as a pale pink powder. ^{31}P-$\{^1H\}$ NMR (121.5 MHz, $CDCl_3$), δ 2.2, ^1J(Pt,P) 3450.

Complex **5c**. Reaction of **3a** (154 mg, 0.125 mmol) with *p*-toluenesulfonyl chloride gave **5b** (96 mg) as a white powder, which was shown to be a mixture of products by ESMS. ^{31}P-$\{^1H\}$ NMR (121.5 MHz, $CDCl_3$) showed a single major peak at δ 2.7 [^1J(Pt,P) 3450].

Crystal structure determination of **3a**

Crystals of **3a** suitable for an X-ray structure determination were obtained by allowing a saturated $CHCl_3$ solution of the complex to stand at 4°C for several weeks. Unit cell dimensions and intensity data were obtained on a Seimens SMART diffractometer. The data collection nominally covered over a hemisphere of reciprocal space, by a combination of three sets of exposures: each set had a different ϕ angle for the crystal and each exposure covered 0.3° in ω. The crystal to detector distance was 5.0 cm. The data set was corrected using SADABS [23], including an empirical absorption correction ($T_{max,min}$ 0.83, 0.39).

Crystal data. $C_{54}H_{46}N_6O_4P_2S_4Pt.3CHCl_3$, Mr = 1586.34 (including solvent of crystallisations), triclinic, $P\bar{1}$, a = 11.0997(1), b = 14.7197(2), c = 21.3011(2) Å, α = 78.349(1), β = 77.424(1), γ = 71.016(1)°, U = 3179.43(6) Å^3, D_{calcd} 1.657 g cm^{-3}, Z = 2, $F(000)$ = 1580, Mo—K_α X-rays (λ = 0.71073 Å), μ(Mo-K_α) = 2.82 mm^{-1}, crystal 0.40 × 0.11 × 0.10 mm^3.

A total of 31,057 reflections in the range $2° < \theta < 28°$ were collected at 203 K, with 13,802 unique (R_{int} 0.087). The structure was solved by Patterson methods (SHELXS-96 [24]) and developed routinely. One of the three $CHCl_3$ molecules in the lattice was partially disordered with two of the chlorine atoms each distributed over two sites, while another showed high temperature factors suggesting at least partial disorder/occupancy. In the final cycles of least-squares refinement based on F^2 (SHELXL-96 [24]) all non-hydrogen atoms were anisotropic and hydrogen atoms were included in calculated positions. The refinement converged with $R_1 = 0.0854$ for 9727 data with $I > 2\sigma(I)$, 0.1230 for all data, $wR_2 = 0.1950$ $\{w = [\sigma^2(F_o^2) + 0.1143P^2]^{-1}$ where $P = (F_o^2 + 2F_c^2)/3\}$ and GoF 1.047. A final difference map showed somewhat large residual features of +7.21 and −3.66 e Å^{-3}, within 1 Å of the platinum atom, which could not be improved upon by reprocessing the data. This, together with the higher than usual *R* factors, suggests that the data were not of the best quality, a problem exacerbated by the disorder in the $CHCl_3$ molecules in the crystal. Detailed discussion of bond parameters is therefore deemed inappropriate.

Further details of the structure investigation, together with lists of final atomic coordinates, thermal parameters, and complete bond distances and angles, and structure factors may be obtained from the Cambridge Crystallographic Data Centre, or from the authors on request.

Acknowledgements—The University of Waikato and the New Zealand Lottery Grants Board are acknowledged for financial support. We also thank Johnson Matthey PLC for a generous loan of platinum, Assoc. Prof. C. E. F. Rickard and A. G. Oliver (University of Auckland) for collection of the X-ray data set, and Wendy Jackson and Amu Upreti for technical assistance.

REFERENCES

1. Selinger, B., *Chemistry in the Marketplace*, 4th edn. Harcourt Brace Jovanovich, Sydney, 1989; Behnisch, R., *Discoveries in Pharmacology*, Vol. 3, ed. Parnham, M. J. and Bruinvels, J. Elsevier, New York, 1986, pp. 225–275.
2. Sadler, P. J., *Adv. Inorg. Chem.*, 1991, **36,** 1.
3. Henderson, W., Nicholson, B. K. and Oliver, A. G., *J. Chem. Soc. Dalton Trans.*, 1994, 1831; Henderson, W., Nicholson, B. K. and Oliver, A. G., *Polyhedron*, 1994, **13,** 3099; Henderson, W., Fawcett, J., Kemmitt, R. D. W., Proctor, C. and Russell, D. R., *J. Chem. Soc., Dalton Trans.*, 1994, 1836; Dinger, M. B., Henderson, W., Nicholson, B. K. and Wilkins, A. L., *J. Organomet. Chem.*, 1966, **526,** 303.
4. Fawcett, J., Henderson, W., Kemmitt, R. D. W., Russell, D. R. and Upreti, A., *J. Chem. Soc., Dalton Trans.*, 1996, 1897.
5. Henderson, W. and Sabat, M., *Polyhedron*, 1997, **16,** 1663.
6. Casanova, J., Alzuet, G., Latorre, J. and Borrás, J., *Inorg. Chem.*, 1997, **36,** 2052 and references therein; Casanova, J., Alzuet, G., Borras, J., Lattore, J., Sanau, M. and Garcia-Granda, S., *J. Inorg. Biochem.*, 1995, **60,** 219; Bult, A., *Pharm. Weekbl*, 1976, **111,** 385.
7. Casanova, J., Alzuet, G., Borras, J. and Carugo, O., *J. Chem. Soc., Dalton Trans.*, 1996, 2239.
8. Casanova, J., Alzuet, G., Ferrer, S., Borras, J., Garcia-Granda, S. and Perez-Carreno, E., *J. Inorg. Biochem.*, 1993, **51,** 689.
9. Yamashita, S., Japanese Patent 7,920,121, 1979; *Chem. Abstr.*, 1979, **91,** 813.
10. Pasini, A. and Zunino, F., *Angew. Chem. Int. Ed. Engl.*, 1987, **26,** 615; Pasini, A., Bersanetti, E., Zunino, F. and Savi, G., *Inorg. Chim. Acta*, 1983, **80,** 99.
11. Agrawal, Y. K., Menon, S. K. and Giridhar, R., *Anal. Lett.*, 1987, **20,** 829.
12. Agrawal, Y. K., Giridhar, R. and Menon, S. K., *J. Pharm. Sci.*, 1987, **76,** 903.
13. Parkin, I. P. and Woollins, J. D., *J. Chem. Soc., Dalton Trans.*, 1990, 519.
14. Kemmitt, R. D. W., Mason, S., Moore, M. R. and Russell, D. R., *J. Chem. Soc., Dalton Trans.*, 1992, 409; Corradi, A. B., Gozzoli, E., Menabue, L., Saladini, M., Battaglia, L. P. and Sgarabotto, P., *J. Chem. Soc., Dalton Trans.*, 1994, 273; Corradi, A. B., *Coord. Chem. Rev.*, 1992, **117,** 45; Schaad, D. R. and Landis, C. R., *Organometallics*, 1992, **11,** 2024.
15. Law, J. M., Henderson, W. and Nicholson, B. K., *J. Chem. Soc., Dalton Trans.*, 1997, 4587.
16. Kalinowski, H., Berger, S. and Braun, S., *Carbon-13 NMR Spectroscopy*. John Wiley and Sons, 1988.
17. Andrews, M. A., Gould, G. L., Klooster, W. T., Koenig, K. S. and Voss, E. J., *Inorg. Chem.*, 1996, **35,** 5478.
18. Colton, R., D'Agostino, A. and Traeger, J. C., *Mass Spectrum Rev.*, 1995, **14,** 79; Hop, C. E. C. A. and Bakhtiar, R., *J. Chem. Educ.*, 1996, **73,** A162.
19. Wimmer, F. L., Wimmer, S. and Castan, P., *Inorg. Synth.*, 1992, **29,** 185.
20. Oliver, D. L. and Anderson, G. K., *Polyhedron*, 1992, **11,** 2415.
21. McDermott, J. X., White, J. F. and Whitesides, G. M., *J. Am. Chem. Soc.*, 1976, **98,** 6521.
22. Arnold, L. J., *J. Chem. Educ.*, 1992, **69,** 811.
23. Blessing, R. H., *Acta Cryst.*, 1995, **A51,** 33.
24. Sheldrick, G. M., SHELX-96, Programs for solving and refining crystal structures. University of Göttingen, 1996.

Pergamon

PII: S0277-5387(98)00089-8

Polyhedron Vol. 17, No. 18, pp. 3145–3151, 1998
© 1998 Elsevier Science Ltd
All rights reserved. Printed in Great Britain
0277-5387/98 $19.00+0.00

Palladium(I) phosphido-bridged dinuclear derivatives with phosphite ligands

Piero Leoni[a,b,*], Stefano Papucci[a] and Marco Pasquali[a]

[a] Dipartimento di Chimica e Chimica Industriale, Università di Pisa, I-56126 Pisa, Italy

[b] Scuola Normale Superiore, Piazza dei Cavalieri, I-56126 Pisa, Italy

(Received 2 December 1997; accepted 24 February 1998)

Abstract—New mono-phosphido-bridged cationic derivatives of dipalladium(I) have been prepared by reacting $[Pd_2(\mu-PBu^t_2)(PPh_3)_3]BF_4$ (**2**)BF_4, with $P(OR)_3$ (R = Me, Et, Ph). Under a large excess of the entering phosphite, all the PPh_3 molecules terminally bonded to the central $Pd_2(\mu-PBu^t_2)$ core can be substituted, yielding $[Pd_2(\mu-PBu^t_2)\{P(OR)_3\}_4]BF_4$, [(**4a**)$BF_4$, R = Me; (**4b**)$BF_4$, R = Et and (**4c**)$BF_4$, R = Ph]. The intermediate mixed-ligand complex $[Pd_2(\mu-PBu^t_2)(PPh_3)\{P(OPh)_3\}_2]BF_4$, (**5**)$BF_4$, was isolated in the reaction with $P(OPh)_3$. Moreover, the reactions of the new complexes with CO, isoprene and CS_2 were investigated and compared to the corresponding reactions of the phosphine-substituted complexes. © 1998 Elsevier Science Ltd. All rights reserved

Keywords: dinuclear; phosphido-bridges; palladium(I); phosphite; cationic.

The chemistry of phosphido-bridged palladium(I) dinuclear derivatives was rather unexplored until a few years ago [1]. Our group is involved in a systematic study of this field [2–7], and has shown that the secondary phosphine-bridged $[Pd_2(\mu-PBu^t_2)(\mu-PBu^t_2H)(PBu^t_2H)_2]BF_4$, (**1**)$BF_4$ [3], can be employed as the precursor of a series of mono-phosphido-bridged cationic derivatives of general formula $[Pd_2(\mu,PBu^t_2)(PR_3)_n]BF_4$, [4] with n depending on the steric demand of the phosphine ligand ($n=3$, R = Ph [(**2**)BF_4]; $n=4$, R = Me [(**3a**)BF_4], R = Et [(**3b**)BF_4] or $R_3 = Cy_2H$, [(**3c**)BF_4]; see Scheme 1). Both (**1**)BF_4 and its derivatives with other phosphines have shown an interesting reactivity; they can be used as a source of still rare examples of terminally bonded Pd(I) carbonyls [3b, 5] or show cooperation of the two metal centers in the coordination of polyunsaturated molecules as isoprene [5, 6] or CS_2 [4b, 7]. We now report the synthesis of new members of this family, bearing phosphites terminally bonded to the central $[Pd_2(\mu-PBu^t_2)]^+$ core, and compare their reactivity with that given by their phosphine analogues.

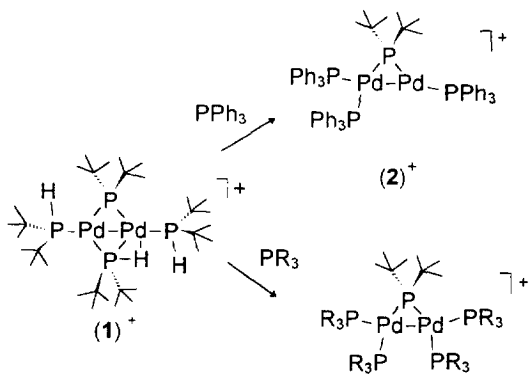

Scheme 1

EXPERIMENTAL

General and instrumental

All reactions were performed under an atmosphere of purified nitrogen or carbon monoxide by using standard Schlenck techniques. Solvents were dried by

* Address to whom correspondence should be addressed.

standard procedures and distilled under nitrogen prior to use. Deuterated solvents were used as purchased and stored on molecular sieves under an inert atmosphere. $[Pd_2(\mu-PBu^t_2)(PPh_3)_3]BF_4$, **(2)**$BF_4$, was prepared as previously described [4b]. IR spectra were recorded with a Perkin-Elmer FT-IR 1725X spectrophotometer and NMR spectra with a Varian Gemini 200BB spectrometer, frequencies were referenced to the residual signal of the deuterated solvent (^1H, ^{13}C) and to external 85% H_3PO_4 (^{31}P). The progress of the reactions was monitored by means of $^{31}P\{^1H\}$ NMR spectroscopic analyses of small samples of a reaction mixture, after adding a few drops of C_6D_6 for the lock signal capture and the field homogeneity optimization operations.

Preparation of $[Pd_2(\mu-PBu^t_2)\{P(OMe)_3\}_4]BF_4$, ***(4a)****BF*$_4$. Trimethyl phosphite (0.16 mL, 1.44 mmol) was added to a red acetone (10 mL) solution of **(2)**BF_4 (179 mg, 0.145 mmol). The solution turned quickly orange; after 15 min most of the solvent was evaporated and *n*-hexane (20 mL) was added, causing the precipitation of a yellow powder which was filtered off, washed with *n*-hexane, and *vacuum* dried (95 mg, 70% yield).

Elem. Anal. Calcd for $C_{20}H_{54}BF_4P_5Pd_2$: C, 25.5, H, 5.78. Found: C, 25.6, H, 5.80%. $^{31}P\{^1H\}$ NMR ($CDCl_3$, 298 K): δ (ppm) 345.5 (tm, $^2J_{PP} \approx 282$, 46 Hz, $\mu-PBu^t_2$), 136.2 (dm, $^2J_{PP} \approx 280$ Hz, $P(OMe)_3$ *trans* to μ-P), 127.2 (m, $P(OMe)_3$ *cis* to μ-P). ^1H NMR ($CDCl_3$, 298 K): δ (ppm) 3.65 (m, 36 H, OCH_3), 1.35 (d, $^3J_{HP} = 14.2$ Hz, 18 H, $PC(CH_3)_3$). IR (Nujol, KBr): 1028 s, br (ν_{BF}) cm^{-1}.

Preparation of $[Pd_2(\mu-PBu^t_2)\{P(OEt)_3\}_4]BF_4$, ***(4b)****BF*$_4$. Triethyl phosphite (0.37 mL, 2.16 mmol) was added to a red acetone (15 mL) solution of **(2)**BF_4 (266 mg, 0.216 mmol). The solution turned quickly orange; after 30 min most of the solvent was evaporated after which *n*-hexane (25 mL) was added, causing the precipitation of a yellow powder. The suspension was left overnight at -30 C, the solid filtered off, washed with *n*-hexane, and *vacuum* dried (158 mg, 66% yield).

Elem. Anal. Calcd for $C_{32}H_{78}BF_4O_{12}P_5Pd_2$: C, 34.6, H, 7.09. Found: C, 34.8, H, 6.99. $^{31}P\{^1H\}$ NMR (Acetone-d_6, 298 K): δ (ppm) 345.6 (tm, $^2J_{PP} \approx 280$, 50 Hz, $\mu-PBu^t_2$), 137.2 (dm, $^2J_{PP} \approx 280$ Hz, $P(OEt)_3$ *trans* to μ-P), 123 (m, $P(OEt)_3$ *cis* to μ-P). ^1H NMR ($CDCl_3$, 298 K): δ (ppm) 3.9 (br s, 24 H, OCH_2CH_3), 1.3 (overlapping m, 54 H, $OCH_2CH_3 + PC(CH_3)_3$). IR (Nujol, KBr): 1034 s, br (ν_{BF}) cm^{-1}.

Preparation of $[Pd_2(\mu-PBu^t_2)\{P(OPh)_3\}_4]BF_4$, ***(4c)****BF*$_4$. Triphenyl phosphite (1.71 mL, 6.52 mmol) was added to a red CH_2Cl_2 (15 mL) solution of **(2)**BF_4 (80 mg, 0.065 mmol). The color of the solution turned quickly orange; after 15 min 2/3 of the solvent were evaporated and Et_2O (20 mL) was added, causing the precipitation of an orange powder which was filtered, washed with Et_2O, and *vacuum* dried (88 mg, 80% yield).

Elem. Anal. Calcd for $C_{80}H_{78}BF_4O_{12}P_5Pd_2$: C, 57.0, H, 4.66. Found: C, 57.6, H, 4.66. $^{31}P\{^1H\}$ NMR ($CDCl_3$, 298 K): δ (ppm) 360.0 (tt, $^2J_{PP} \approx 240$, 46 Hz, $\mu-PBu^t_2$), 118.0 (dm, $^2J_{PP} = 240$ Hz, $P(OPh)_3$ *trans* to μ-P), 103 (m, $P(OPh)_3$ *cis* to μ-P). ^1H NMR ($CDCl_3$, 298 K): δ (ppm) 7.2 (m, 60 H, OC_6H_5), 1.3 (d, $^3J_{HP} = 15$ Hz, 18 H, $PC(CH_3)_3$). IR (Nujol, KBr): 1055 s, br (ν_{BF}) cm^{-1}.

Preparation of $[Pd_2(\mu-PBu^t_2)(PPh_3)\{P(OPh)_3\}_2]BF_4$, ***(5)****BF*$_4$. Triphenyl phosphite (4.07 mL, 15.5 mmol) was added to a red CH_2Cl_2 (10 mL) solution of **(2)**BF_4 (327 mg, 0.26 mmol). The color of the solution turned quickly orange; after 15 min most of the solvent was evaporated and Et_2O (30 mL) was added, causing the precipitation of an orange powder which was filtered, washed with Et_2O, and *vacuum* dried (220 mg, 64% yield).

Elem. Anal. Calcd for $C_{62}H_{63}BF_4O_6P_4Pd_2$: C, 56.1, H, 4.78. Found: C, 58.5, H, 5.05. $^{31}P\{^1H\}$ NMR (acetone-d_6, 298 K): δ (ppm) 374.2 (ddd, $^2J_{PP} = 195$, 102, 70 Hz, $\mu-PBu^t_2$), 124.2 (ddd, $^2J_{PP} = 102$, 37 Hz, $^3J_{PP} = 363$ Hz, $P(OPh)_3$), 113.6 (ddd, $^2J_{PP} = 70$, 14 Hz, $^3J_{PP} = 363$ Hz, $P(OPh)_3$), 26.8 (ddd, $^2J_{PP} = 195$, 37 Hz, $^3J_{PP} = 14$ Hz), the spectrum shows other minor signals (see Results and Discussion) due to other compounds which justify the low purity found in elemental analysis, attempted purification by column chromatography led to decomposition. ^1H NMR ($CDCl_3$, 298 K): δ (ppm) 7.1 (m, 45 H, $PC_6H_5 + OC_6H_5$), 1.4 (d, $^3J_{HP} = 14.6$ Hz, 18 H, $PC(CH_3)_3$). IR (Nujol, KBr): 3040 ($\nu_{=CH}$), 1588, 1486 ($\nu_{C=C}$), 1055 s, br (ν_{BF}) cm^{-1}.

Reactions of ***(4a,b)****BF*$_4$ with CS_2 A 10-fold excess of CS_2 was added by syringe to a $CDCl_3$ solution (0.5 mL) of **(4a)**BF_4 (15 mg, 0.0159 mmol) or **(4b)**BF_4 (18 mg, 0.0162 mmol). The orange solutions turned quickly yellow and were analyzed by $^{31}P\{^1H\}$ NMR spectroscopy (see Results and Discussion).

Reactions of ***(4a,b)****BF*$_4$ with isoprene A 10-fold excess of isoprene was added by syringe to a $CDCl_3$ solution (0.5 mL) of **(4a)**BF_4 (16 mg, 0.017 mmol) or **(4b)**BF_4 (19 mg, 0.0171 mmol). The orange solutions turned quickly yellow and were analyzed by $^{31}P\{^1H\}$ NMR (see Results and Discussion).

Reactions of ***(4a,b)****BF*$_4$ with *CO* Carbon monoxide was bubbled into orange $CDCl_3$ solutions of complex **(4a)**BF_4 or **(4b)**BF_4 (*ca* 30 mg/mL). A faint bleaching of the starting colour was observed and the solutions were analyzed by $^{31}P\{^1H\}$ NMR spectroscopy which exhibited only the resonances of the reagents. The IR spectra of the solutions exhibited medium-weak ν_{CO} absorptions around 2070 cm^{-1}.

RESULTS AND DISCUSSION

The unsaturated triphenylphosphine derivative $[Pd_2(\mu-PBu^t_2)(PPh_3)_3]BF_4$, **(2)**$BF_4$ [4b], proved to be a suitable precursor to phosphite substituted complexes. When acetone or methylene chloride solu-

tions of (**2**)BF_4 were reacted at room temperature with an excess of the appropriate phosphite, the corresponding persubstituted derivatives (eq 1) were formed and isolated as yellow microcrystalline solids in satisfactory to good yields (67–80%). The reactions were fast and clean when at least a 10-fold excess of the alkyl phosphite was employed; in the case of triphenyl phosphite a higher excess of the ligand was necessary. The new complexes analyzed nicely for the composition $[Pd_2(\mu-PBu^t_2)\{P(OR)_3\}_4]BF_4$, [(**4a**)$BF_4$, R = Me; (**4b**)$BF_4$, R = Et and (**4c**)$BF_4$, R = Ph] and, as inferred by the analysis of ^{31}P NMR spectra (see below), retain the usual [4a] structure exhibited by the analogous phosphine derivatives, with two palladium centers in a distorted square planar geometry sharing a bridging phosphido ligand and the metal-metal bond.

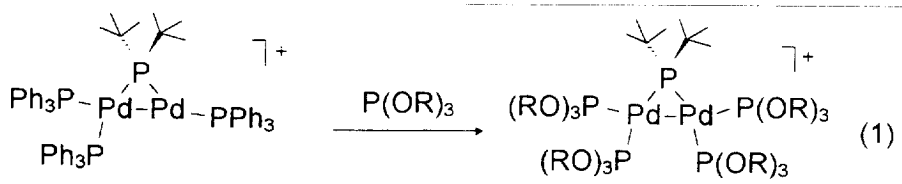

(**2**)$^+$

(**4a**)$^+$: R = Me
(**4b**)$^+$: R = Et
(**4c**)$^+$: R = Ph

The $^{31}P\{^1H\}$ NMR spectrum of (**4b**)BF_4 is shown in Scheme 1, with the numbering scheme.

This particular framework of phosphorus atoms (Pd_2P_5 planar core with C_{2v} symmetry) constitutes an AA′BB′X spin system where A and B are, respectively, the P-nuclei *trans* and *cis* to X, the bridging phosphorus. Due to the magnetic non-equivalence of the couples AA′ and BB′, the spectrum cannot be interpreted with simple first order approximations, and can be quite complex. In general, the lines within the multiplets are no longer directly correlated to the values of $^2J_{AX}$, $^2J_{BX}$ and $^2J_{AB}$, but to combinations of these coupling constants and of $^3J_{AA'}$, $^3J_{BB'}$ and $^3J_{AB'}$. When the differences (in Hertz) between the values of δ_A, δ_B and δ_X are much larger than coupling constants values, as in the case of the phosphine derivatives [4a], the spectrum is still relatively simple and easily simulated. The large downfield shift of δ_A and δ_B which occurs when phosphites are employed in place of the phosphines (around 100 ppm) approaches them to δ_X; the spin system is better defined as AA′BB′C and give rise to an extreme complication of the spectra; none of the nine independent variables of the spin system can be easily extracted from the spectrum. Due to this difficulty only some spectral features were reproduced in the simulation with a satisfactory approximation. This is particularly true for the low

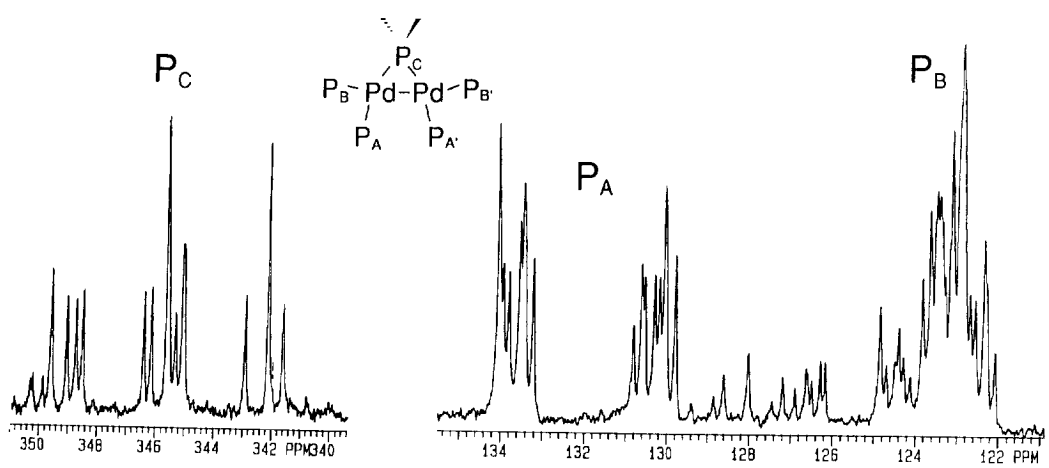

Fig. 1. $^{31}P\{^1H\}$ NMR spectrum (acetone-d_6, 293 K) of $[Pd_2(\mu-PBu^t_2)\{P(OEt)_3\}_4]BF_4$ (**4b**)BF_4, with the numbering scheme.

field signal due to μ-P, which highly resembles the signal given by the corresponding phosphorus [4a] of $[Pd_2(\mu-PBu^t_2)(PR_3)_4]BF_4$ (R = Me, Et), and allows an approximate evaluation of δ_C, $^2J_{AC}$ and $^2J_{BC}$, respectively found at *ca* 345.5 ppm, 282 and 46 Hz for (**4a**)BF_4, *ca* 345.6 ppm, 280 and 50 Hz for (**4b**)BF_4 and *ca* 360 ppm, 240 and 46 Hz for (**4c**)BF_4. These values confirm the approximately planar disposition of the $Pd_2(\mu$-P)P_4 core, with two *pseudo-trans* and two *pseudo-cis* (compared to μ-P) phosphite ligands.

^{1}H NMR spectra are easily interpreted and give the expected integral ratio between the various types of nuclei.

With lower $P(OR)_3$/(**2**)BF_4 ratios we observed the formation of mixtures of products arising from the progressive stepwise substitution of the three triphenylphosphine molecules contained in (**2**)$^+$. The number of observed intermediates, of general formula $[Pd_2(\mu-PBu^t_2)(PPh_3)_{(3-n)}\{P(OPh)_3\}_n]BF_4$, is generally high, since different geometrical isomers were observed for a given value of n. Therefore very complex mixtures were formed in most cases but one. In fact, when (**2**)BF_4 was reacted with a 10-fold excess of $P(OPh)_3$ one of these intermediates can be isolated sufficiently pure and readily identified as $[Pd_2(\mu-PBu^t_2)(PPh_3)\{P(OPh)_3\}_2]BF_4$, (**5**)$BF_4$. Its $^{31}P\{^1H\}$ NMR spectrum is quite simple and shows a doublet of doublets of doublets ($^2J_{PP}$ = 195, 70, 102 Hz) at 374.2 ppm for the bridging phosphide (P_1); the remaining three P nuclei give resonances at 26.8 ppm (ddd, J_{PP} = 195, 37, 14 Hz), assigned to the phosphorus (P_2) of a PPh_3 molecule(for its high field position) *trans* to μ-P (for the large J_{PP} = 195) and at 124.2 (J_{PP} = 363, 37, 102 Hz) and 113.6 (J_{PP} = 363, 70, 14 Hz), respectively assigned to P_3 of the phosphite on the tricoordinated palladium center and to P_4 of the phosphite *cis* to the phosphine molecule.

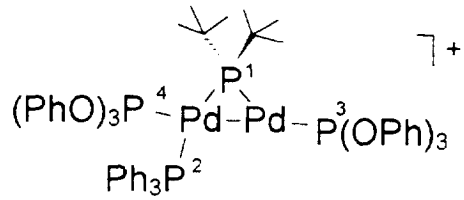

(**5**)$^+$

The assignment of the latter two resonances has been made by considering that the coupling to P_1 should be minor (70 Hz) when the angle P–Pd–P1 approaches 90° (P_4), and increase (102 Hz) when this angle becomes wider (P_3). Larger values of J_{PP} were observed for phosphite-phosphite or phosphite-phosphine couples with respect to the corresponding phosphine-phosphine couples of the structurally related cation (**2**)$^+$. The exceedingly high value of $^3J_{P3P4}$ = 363 Hz is probably due to a nearly linear dis-

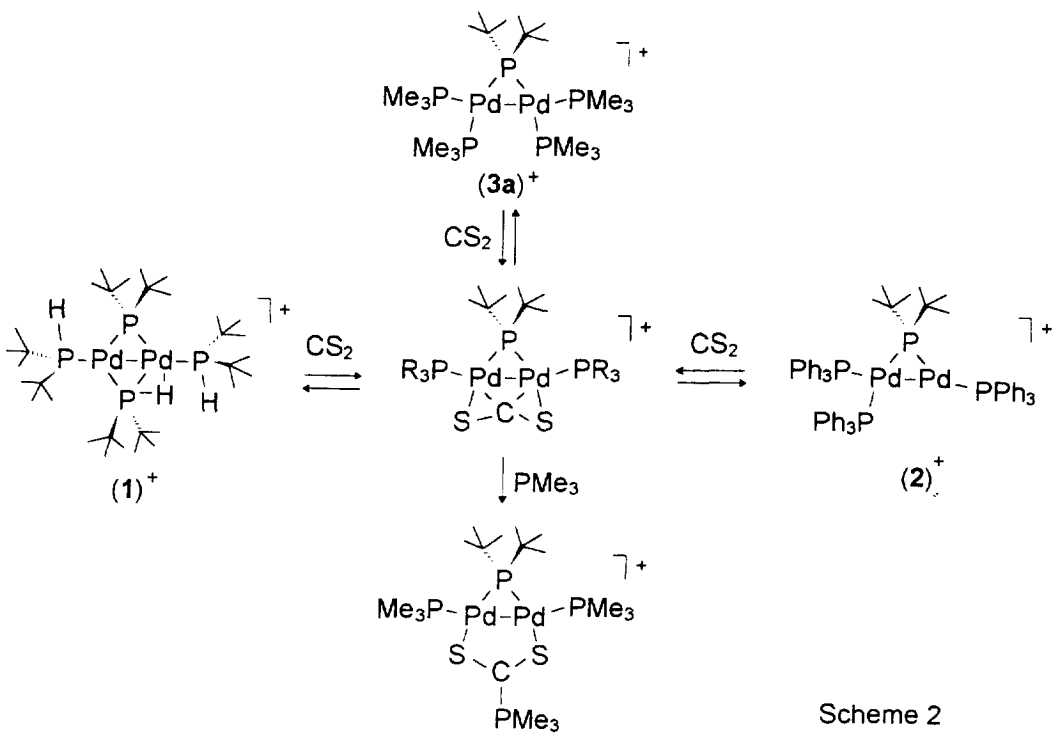

Scheme 2

position of the $(PhO)_3P$–Pd–Pd–$P(OPh)_3$ fragment; the corresponding constant was found at 135 Hz in $(\mathbf{2})^+$ [4b].

The purity of the samples of $(\mathbf{5})BF_4$ is not high (*ca* 80%) and small amounts of other intermediates were observable in the spectrum but not identified due to severe overlapping of the weak signals. Well separated signals were observed only in the phosphide region, where two weak ddd appear at 369.8 ($^2J_{PP}$ = 155, 52, 98 Hz) and 355.5 ppm ($^2J_{PP}$ = 220, 75, 61 Hz) suggesting for these derivatives the same type of skeleton assigned to $(\mathbf{5})^+$.

Reactivity of the cations $(\mathbf{4a,b})^+$. The availability of the new complexes allowed us to investigate the influence of the substitution with phosphites on the reactivity of this class of derivatives. We decided to use as tests the reactions with CS_2, isoprene and carbon monoxide, which had previously been investigated for the corresponding phosphine substituted derivatives [3b, 4–7].

Reactions with CS_2. We knew that carbon disulfide reacts with the cations $(\mathbf{1})^+$-$(\mathbf{3})^+$ yielding the corresponding adducts (see Scheme 2) [4b]; these exhibited an unprecedented coordination mode of the CS_2 molecule, with a central planar $Pd_2P_3(CS_2)$ core. One or two phosphine molecules are displaced from the starting complex; in one case (PMe_3) this can behave as a nucleophile toward the metal bonded carbon disulfide molecule [8].

An orange $CDCl_3$ solution of the alkyl phosphite derivatives $(\mathbf{4a})BF_4$ or $(\mathbf{4b})BF_4$ turns immediately yellow when reacted with a 10-fold excess of CS_2. The $^{31}P\{^1H\}$ NMR spectra of the solutions show that in both cases the same type of equilibrium given by the cations $(\mathbf{1})^+$ and $(\mathbf{2})^+$ has established, yielding the CS_2 adducts $(\mathbf{6a})BF_4$ and $(\mathbf{6b})BF_4$ (eq 2). The spectra of these species are very simple, as those given by the corresponding phosphine derivatives [4b], and consist of a high field triplet and a low field doublet coupled by a small $^2J_{PP(cis)}$; these parameters were found at 417.6, 130.1 ppm and 27 Hz for $(\mathbf{6a})BF_4$ and 354.2, 133.5 ppm and 24 Hz for $(\mathbf{6b})BF_4$.

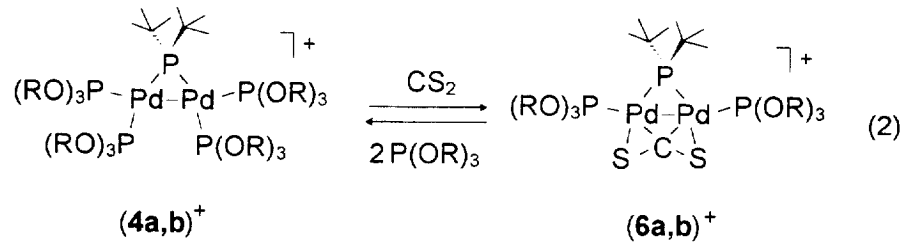

$(\mathbf{4a,b})^+$ $(\mathbf{6a,b})^+$ (2)

A significant difference between the reactions given by $(\mathbf{4a})BF_4$ and $(\mathbf{4b})BF_4$ concerns the position of the equilibrium. In the former case this is shifted toward the reagents: with also larger amounts of CS_2 the resonances of the cation $(\mathbf{4a})^+$ are well visible in the spectrum, although severely broadened by exchange processes. On the contrary, the reaction with $(\mathbf{4b})BF_4$ is shifted toward $(\mathbf{6b})BF_4$ and, with a 10-fold excess of CS_2, the resonances assigned to $(\mathbf{4b})^+$ have nearly completely disappeared from the spectrum.

Reactions with isoprene. Isoprene is another potentially bidentate ligand which was shown to react with the phosphine cations $(\mathbf{1})^+$ – $(\mathbf{3})^+$ yielding the corresponding isoprene derivatives $[Pd_2(\mu\text{-}PBu^t_2)(\mu,\eta^2,\eta^2\text{-isoprene})(PR_3)_2]^+$, as BF_4 or triflate salts [5, 6]. The cooperation between the two metal centers in the coordination of the bidentate ligand was demonstrated also in these cases. The diene molecule, with the two double bonds in a *trans* configuration, was in fact shown to simultaneously coordinate to both metals of the $[Pd_2(\mu\text{-}PBu^t_2)(PR_3)_2]^+$ fragment. The same type of reaction is given by the phosphite cations $(\mathbf{4a})^+$

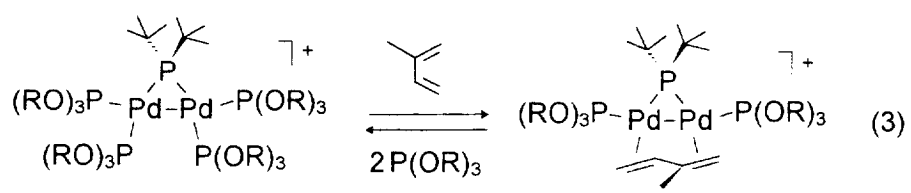

(3)

$(\mathbf{7a})^+$: R = Me
$(\mathbf{7b})^+$: R = Et

and $(\mathbf{4b})^+$ (eq. 3). In fact, after the addition of a 10:1 molar excess of isoprene, a $CDCl_3$ solution of $(\mathbf{4a})BF_4$ (or $(\mathbf{4b})BF_4$) exhibited in the $^{31}P\{^1H\}$ NMR spectrum new resonances assigned to the diene derivatives $(\mathbf{7a})BF_4$ and $(\mathbf{7b})BF_4$, together with the resonances of the starting complexes, considerably broadened. Analogously to the reactions with CS_2 described above, the equilibrium (eq. 3) is greatly shifted to the left when the phosphite is $P(OMe)_3$ and to the right when the phosphite is $P(OEt)_3$. As shown earlier for the corresponding phosphine complexes, the spectrum of $(\mathbf{7a})^+$ (or $(\mathbf{7b})^+$) is due to an ABX spin system, where X is the bridging phosphorus and A and B are the similar, but unequivalent, phosphite P-nuclei (δ_A, δ_B, δ_X and $J_{AX} \approx J_{BX}$ were respectively found at 134.2, 132.8, 381.9 ppm and 53 Hz for $(\mathbf{7a})BF_4$ and at 129.2, 127.4, 379.9 ppm and 51 Hz for $(\mathbf{7b})BF_4$).

Reactions with CO Carbon monoxide was bubbled into orange solutions of complexes $(\mathbf{4a,b})BF_4$. An immediate, hardly perceptible, bleaching of the solutions, together with the appearance of weak to medium ν_{CO} absorptions around 2070 cm^{-1} in the IR spectra, was observed. The $^{31}P\{^1H\}$ NMR spectra of the solutions exhibited broad signals practically in the same positions of those due to the starting materials. These results can be explained by the substitution of a phosphite ligand by a CO molecule, giving $[Pd_2(\mu-PBu^t_2)(CO)\{P(OR)_3\}_3]BF_4$ [$(\mathbf{8a})BF_4$, R = Me; $(\mathbf{8b})BF_4$, R = Et], as shown in eq. 4.

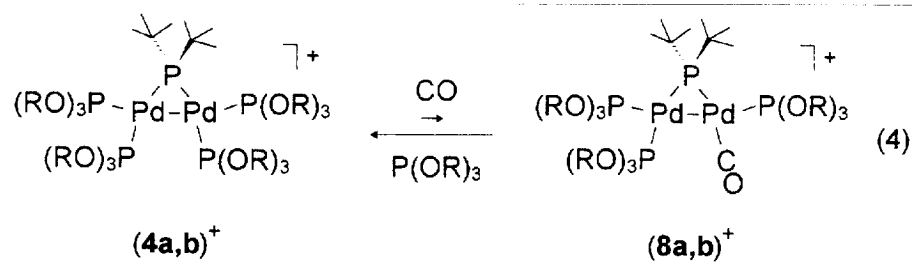

Equilibrium 4 should be far shifted to the left since the NMR resonances are not significantly shifted with respect to those of $(\mathbf{4a,b})BF_4$; their severe broadening is assignable either to the rate of the direct and forward reactions of eq. 4 or to exchange equilibria between coordinated and released $P(OR)_3$ molecules. An equilibrium analogous to that shown in eq. 4 was observed when studying the reaction of the trimethylphosphine derivative $(\mathbf{3a})BF_4$ with carbon monoxide, yielding $[Pd_2(\mu-PBu^t_2)(CO)(PMe_3)_3]BF_4$, this equilibrium is completely shifted to the right under 1 Atm of CO, but is easily reverted by reducing P_{CO} [5].

CONCLUSIONS

The new complexes $(\mathbf{4a–c})BF_4$, with a central $Pd_2(\mu-PBu^t_2)$ core binding four terminal phosphite ligands have been prepared in good yields and purity. At least with the phosphites employed in this work, electronically unsaturated derivatives bearing only three phosphite ligands proved to be too unstable to be isolated or even observed as transient species. The corresponding derivatives bearing phosphine ligands were shown to be isolable when the bulkier phosphines [as in complex $(\mathbf{2})BF_4$] are employed, or when at least one of the phosphines is secondary, and can saturate the electronic deficiency of the tricoordinated palladium center by donating the electrons of the P-H bond [as in the phosphine-bridged $(\mathbf{1})BF_4$]. It was instead possible to isolate, although not pure, a stable derivative with three mixed phosphine-phosphite terminal ligands, complex $(\mathbf{5})BF_4$. This is probably stable due to the presence of a PPh_3 molecule, bulkier than $P(OPh)_3$, which was in fact found to be adjacent to the unsaturated palladium center.

The results observed by studying the reactivity of $(\mathbf{4a,b})BF_4$ parallel those reported previously for their phosphine analogues, in fact both react with CO, CS_2 and isoprene equilibrating, respectively, with the corresponding derivatives $(\mathbf{6–8a,b})BF_4$.

As expected, the reactivity of these systems is highly dependent upon the dimensions of the ligands, since equilibria involving the trimethyl phosphite derivative $(\mathbf{4a})BF_4$, compared to those involving the triethyl phosphite analogue $(\mathbf{4b})BF_4$, are much more shifted towards the reactants. Since solution NMR spectra showed that the reactivity of the phosphite complexes towards CO, CS_2 and isoprene does not differ significantly from that of the phosphine derivatives we did not proceed further in the isolation of the products of these reactions.

Acknowledgements—Financial support from the 'Ministero della Ricerca Scientifica e Tecnologica' (MURST) and the Consiglio Nazionale delle Ricerche (CNR, Rome) is gratefully acknowledged.

REFERENCES

1. (a) Hayter, R. G. and Humiec, F. S., *Inorg. Chem.*, 1963, **2**, 306. (b) Brandon, J. B. and Dixon, K. R., *Can. J. Chem.*, 1981, **59**, 1188. (c) Arif, A. M.,

Heaton, D. E., Jones, R. A. and Nunn, C. M., *Inorg. Chem.*, 1987, **26**, 4228.
2. (a) Sommovigo, M., Pasquali, M., Leoni, P., Braga, D. and Sabatino, P., *Chem. Ber.*, 1991, **124**, 97. (b) Leoni, P., Sommovigo, M., Pasquali, M., Sabatino, P. and Braga, D., *J. Organomet. Chem.*, 1992, **423**, 263.
3. (a) Albinati, A., Lianza, F., Pasquali, M., Sommovigo, M., Leoni, P., Pregosin, P. S. and Ruegger, H., *Inorg. Chem.*, 1991, **30**, 4690. (b) Leoni, P., Pasquali, M., Sommovigo, M., Laschi, F., Zanello, P., Albinati, A., Lianza, F., Pregosin, P. S. and Rüegger, H., *Organometallics*, 1993, **12**, 1702.
4. (a) Leoni, P., Pasquali, M., Sommovigo, M., Albinati, A., Lianza, F., Pregosin, P. S. and Rüegger, H., *Organometallics*, 1994, **13**, 4017. (b) Leoni, P., Pasquali, M., Pieri, G., Albinati, A., Pregosin, P. S. and Rüegger, H., *Organometallics*, 1995, **14**, 3143.
5. Leoni, P., Pasquali, M., Sommovigo, M., Albinati, A., Pregosin, P. S. and Rüegger, H., *Organometallics*, 1996, **15**, 2047.
6. Leoni, P., Pasquali, M., Sommovigo, M., Albinati, A., Lianza, F., Pregosin, P. S. and Rüegger, H., *Organometallics*, 1993, **12**, 4503.
7. Leoni, P., Pasquali, M., Fadini, L., Albinati, A., Hofmann, P. and Metz, M., *J. Am. Chem Soc.*, 1997, **119**, 8625.
8. Leoni P. and Pasquali, M., unpublished results.

Pergamon

PII: S0277-5387(98)00091-6

Polyhedron Vol. 17, No. 18, pp. 3153–3160, 1998
© 1998 Elsevier Science Ltd
All rights reserved. Printed in Great Britain
0277-5387/98 $19.00+0.00

Synthesis and characterization of oxo-rhenium(V) complexes with monodentate $P(OCH_3)_3$ and bidentate $[OC(CH_3)_2C(CH_3)_2O]POC(CH_3)_2C(CH_3)_2OP[OC(CH_3)_2C(CH_3)_2O]$ phosphite ligands

Tadeusz Glowiak, Witold K. Rybak* and Anna Skarżyńska

Faculty of Chemistry, University of Wroclaw, 14 Joliot-Curie Str., 50-383 Wroclaw, Poland

(Received 6 January 1998; accepted 26 February 1998)

Abstract—The reactions of $ReOCl_3(Me_2S)(OPPh_3)$ with monodentate $P(OMe)_3$ (P) and bidentate $(OCMe_2CMe_2O)POCMe_2CMe_2OP(OCMe_2CMe_2O)$, (P–P) phosphites afford *fac*-$ReOCl_3P_2$ (**1**) and *fac*-$ReOCl_3$(P–P) (**2**) respectively. Both blue–violet **1** and **2** have been characterized by NMR, IR and UV–Vis spectroscopies as well as by X-ray crystallography. Crystal data of $ReOCl_3P_2$ (**1**): crystal class triclinic, space group $P\bar{1}$ (No 2), $a=8.558(2)$, $b=8.921(2)$, $c=12.617(3)$ Å; $\alpha=74.42(3)$, $\beta=81.81(3)$, $\gamma=63.43(1)$; $V=829.6(3)$ Å^3, $Z=2$. Crystal data of $ReOCl_3$(P–P) (**2**): monoclinic, space group $P2_{1/n}$, ($P2_{1/c}$ No 14), $a=9.615(2)$, $b=16.424(3)$, $c=17.395(3)$ Å; $\beta=99.81(3)$; $V=2706.8(9)$ Å^3, $Z=4$. There is 72:28 orientational disorder in **2** between the mutually *trans*-oxo and chloride ligands. In both **1** and **2**, the rhenium atoms are six coordinate with triply bonded terminal oxo ligands (**1** Re–O = 1.654(4) Å). (**2** Re–O = 1.692(15) Å) and chlorides in facial arrangements. © 1998 Elsevier Science Ltd. All rights reserved

Keywords: oxo-rhenium; phosphite ligands; crystal structures; orientational disorder.

The chemistry of the phosphite metal complexes is still less recognized than that of respective phosphine congeners also including rhenium compounds [1]. A great variety of the electronic and steric properties [2, 3] of readily accessible phosphite ligands make them attractive to examine the influence of these properties on the structure and reactivity of the metal phosphite complexes [4]. There are rather few oxo-rhenium(V) complexes containing phosphite ligands, exemplified by $ReOX_3(PPh_3)L$ where X=Cl or Br; L=$[P(OMe)_3]$, $[P(OCH_2)_3CMe]$ or $[P(OCH_2)_3CEt]$ [5](a) and $ReOCl_3[P(OEt)_3]_2$ [5](b). $ReOCl_2[P(O)(OMe)_2](PPh_3)_2$ complex, containing phosphonato ligand which derives from phosphite has also been obtained [5](c). Nevertheless, there has been no information about the synthesis and geometry of oxo-rhenium(V) complexes of the $ReOCl_3P_2$ or $ReOCl_3$(P–P) type (where P and P–P indicate mono and bidentate phosphite ligands respectively). However, the analogs of phosphine complexes are well described [6]. In the present paper, we report on the synthesis and structural characterization of oxo-rhenium(V) complexes containing phosphite ligands: $P(OMe)_3$ (P) and chelating sterically encumbered $(OCMe_2CMe_2O)POCMe_2CMe_2OP(OCMe_2CMe_2O)$ (P–P) [7] (abbreviated also as pinacop) [4](c). While the phosphine congeners of $ReOCl_3P_2$ complexes usually adopt *trans-mer* geometry [6], both phosphite analogs exhibit the *cis-fac* arrangement of the ligands. These complexes are most interesting, especially because of their potential catalytic properties in the oxygen atom transfer (OAT) [8] or olefin metathesis reactions [9].

EXPERIMENTAL

All preparations were performed in an dry, oxygen-free argon atmosphere using the conventional Schlenk technique. Solvents were carefully dried and deoxygenated by standard methods [10]. $ReOCl_3(PPh_3)_2$ [11]

*Corresponding author. Tel.: (4871)204-254; Fax: (4871)204-420; E-mail: rybak@ichuwr.chem.uni.wroc.pl

and $ReOCl_3(Me_2S)$-$(OPPh_3)$ [12, 13] were obtained according to the procedures previously described. Trimethyl phosphite (Fluka) was distilled in vacuo from CaH_2 and stored in argon. The known method [4](c) was used for the preparation of bidentate phosphite ligand pinacop: $(OCMe_2CMe_2O)POCMe_2CMe_2OP(OCMe_2CMe_2O)$. The IR and FIR measurements were made in KBr pellets or in Nujol with Nicolet FTIR Impact 400 or Brucker IFS 113V. Spectra of ^1H, ^{13}C and ^{31}P NMR were obtained on a Brucker AMX (300 MHz for H NMR). The chemical shifts, δ, are given in ppm towards the TMS and H_3PO_4, respectively, using deuterated solvents as lock and reference. UV–VIS spectra in CH_2Cl_2 solution were obtained on HP 8452A. Elemental analyses were performed on a Perkin–Elmer 2400 CHN in the Laboratory of Elemental Analyses of our Department. Molecular weights were measured in dichloromethane solutions using the Molecular Weight Apparatus Model 115 (Perkin Elmer). The physical data for the complexes here obtained are reported in the experimental or results and discussion segments herewith.

fac-$ReOCl_3[P(OMe)_3]_2$ (**1**)

A mixture of $ReOCl_3(Me_2S)(OPPh_3)$ (0.64 g, 1 mmol), THF (40 cm^3) and $P(OMe)_3$ (0.35 cm^3, 3 mmol) was stirred in a slow stream of argon at room temperature until the starting rhenium compound reacted (30 min) and the navy-blue solution appeared. The volatile components of the homogeneous reaction mixture were stripped in vacuo. The dry residue was extracted with diethyl ether. The blue solid of **1** and a yellow solution containing $ReCl_3[P(OMe_3]_3$ as a by-product were obtained. Pure **1** was recrystallized from dichloromethane/ethyl ether solution as blue–violet crystals, in yield, 80% (0.44 g). These crystals were found to be suitable for X-ray structure determination. Anal. for $C_6H_{18}O_7Cl_3P_2Re$ (mol.wt.calc.: 556.9, found: 550); calc: C, 12.93; H, 3.23%; Found: C, 12.94; H, 2.90%; ^1H NMR (CD_2Cl_2, 25 C): δ 3.93 (d, $J_{PH} = 7.0$ Hz, CH_3). $^{31}P\{^1H\}$ NMR (CD_2Cl_2, 25 C): δ (*vs.* H_3PO_4) 61.35s. IR(KBr, cm^{-1}) 1170m, 1040br.vs, ν(C–O–P) 980s ν(Re–O). FIR (nujol, cm^{-1}) 326vs, 296vs, 270sh, 234m ν(Re–Cl) and ν(Re–P).

fac-$ReOCl_3$*pinacop* (**2**)

Here we report on the details of synthesis of **2** [14], which provided crystals suitable for X-ray structure determination. A mixture of $ReOCl_3(Me_2S)(OPPh_3)$ (0.68 g, 1 mmol) and pinacop ligand (0.4 g, 1 mmol) in toluene (40 cm^3) was stirred and boiled, until the starting rhenium compound reacted (2 h) and the blue solid obtained. The crude solid was recrystallized from absolute ethanol which afforded blue–violet crystals of **2** (86% yield). Anal. for $C_{18}H_{36}O_7Cl_3P_2Re$ (mol.wt.calc.: 718.5, found: 800); calc: C, 30.07; H, 5.04%; Found: C, 29.58; H, 4.95%. ^1H NMR (CD_2Cl_2, 25 C): δ 1.57, 1.60, 1.63, 1.64, 1.65, 1.73 (s's, 1 each, CH_3). $^{13}C\{^1H\}$ NMR (CD_2Cl_2, 25 C): δ 25.1, 25.14, 25.79, 25.86, 26.11, 26.54 (s's, CH_3), 90.16, 91.92, 93.19 (s's, CCH_3). IR (KBr, cm^{-1}) 1140vs, 1040vs 1000s, ν(C–O–P) 980s ν(Re–O). FIR (nujol, cm^{-1}) 329vs, 300vs, 284s, 220m ν(Re–Cl) and ν(Re–P).

Crystal structure determination of complexes **1** *and* **2**

Table 1 summarizes the relevant data for the structure analyses. The diffraction data were collected on a Kuma KM-4, computer controlled, κ-axis diffractometer which was equipped with graphite monochromated MoKα radiation. The stability of intensities was monitored by the measurement of three standards every 100 reflections. Intensity data were corrected for Lorentz and polarization effects. The structures were solved with the heavy atom method, using SHELXS-86, and later refined by the full matrix, least square method using SHELXL-93 procedures [15]. Since **2** was found to be axially disordered, both orientations as well as the occupancy ratio were refined independently. All hydrogen atoms in both compounds were positioned based on the idealized geometry of the methyl group.

RESULTS AND DISCUSSION

Synthesis and characterization of the oxo-rhenium(V) complexes

A simple ligand substitution reaction of the labile compound $ReOCl_3(Me_2S)$-$(OPPh_3)$ [12] affords the preparations of complexes $ReOCl_3P_2$ (**1**) and $ReOCl_3P$–P (**2**), according to Scheme 1, where P=$P(OMe)_3$ and P–P=pinacop=$(OCMe_2CMe_2O)P$–$OCMe_2CMe_2OP(OCMe_2CMe_2O)$.

Complex **1** can be obtained at room temperature in THF solution. **2** can also be afforded at ambient temperature in THF solution. However, the ease of its separation from the reaction mixture was the reason for using the boiling toluene solution. In the previous attempts for preparation of **1**, using $ReOCl_3(PPh_3)_2$ as a starting compound, $ReOCl_3(PPh_3)[P(OMe)_3]$ has been obtained instead [5](a). The blue–violet oxo-rhenium complexes **1** and **2** are readily soluble in CH_2Cl_2, sparingly in ethanol or toluene and insoluble in ethyl ether. **1** and **2** are stable, both in solution and solid state, in the presence of dry air. Table 2 summarizes the spectroscopic data of several oxo-rhenium(V) complexes containing phosphorus ligands. Complexes **1** and **2** display two weak absorptions in the visible region of the electronic spectra, which are assigned to nd-π^*d transitions. A similar absorption maximum show complexes with the oxo-metal arrangement and 4–5d^2 electronic configuration [16]. The energetically higher and more intensive bands in UV correspond to CT transitions. The IR

Table 1. Crystallographic experimental data of complexes **1** and **2**

	1	**2**
Empirical formula	C6H18Cl3O7P2Re	C18H36Cl3O7P2Re
Formula weight	556.69	718.96
Temperature (K)	293(2)	293(2)
Wavelength (Å)	0.71069	0.71069
Crystal system	triclinic	monoclinic
Space group	$P\bar{1}$ (No 2)	$P2_{1/n}$ ($P2_{1/c}$ No 14)
a (Å)	8.558(2)	9.615(2)
b	8.921(2)	16.424(3)
c	12.617(3)	17.395(3)
α (°)	74.42(3)	90
β	81.81(3)	99.81(3)
γ	63.43(3)	90
Volume (Å^3)	829.6(3)	2706.8(9)
Z	2	4
Cell measurement refl. number	25	25
Cell measurement θ range (°)	$25.6 \leq 38.4$	$20.5 \leq 30.2$
Density (calculated) (Mg/m^3)	2.229	1.764
Density (measured)	2.233	
Crystal size (mm)	$0.20 \times 0.20 \times 0.30$	$0.2 \times 0.2 \times 0.2$
Absorption coefficient (cm^{-1})	80.19	49.37
$F(000)$	532	1424
Data collection method	$\omega - 2\theta$ scan	$\omega - 2\theta$ scan
θ range for data collection (°)	2.62 to 27.62	2.27 to 25.67
Index ranges h, k, l	$0 \rightarrow 11$ $-9 \rightarrow 11$ $-16 \rightarrow 16$	$0 \rightarrow 11$ $0 \rightarrow 20$ $-21 \rightarrow 20$
Collected independent reflections	3832	3687
No of observed reflections [$I > 4\sigma(I)$]	3419	3687
No of parameters varied	179	292
GOF	1.168	1.085
Final R and wR$^a_2$ indices	$R_1 = 0.0241$ $wR_2 = 0.0660$	$R_1 = 0.0469$ $wR_2 = 0.1086$
Largest diff. peak and hole (e.Å^{-3})	1.212 and -1.055	2.17 and -1.43

[a] Weighting Scheme: calc $w = 1/[\sigma^2(F_O^2) + (aP)^2 + bP]$. $P = (F_O^2 + 2F_C^2)/3$, the a and b values for the two compounds are: **1**, $a = 0.0269$, $b = 3.3239$; **2**, $a = 0.0531$, $b = 0$.

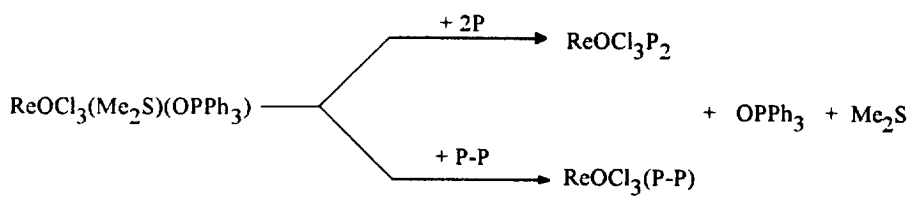

Scheme 1.

Table 2. Spectroscopic data of oxo-rhenium(V) complexes.

Complex	UV-VIS λ_{max}, nm (ϵ, M^{-1}cm^{-1})	IR ν(Re–O), cm^{-1}	FIR ν(Re–Cl)(Re–P), cm^{-1}	^{31}P {H} NMR ppm
fac-ReOCl$_3$[P(OMe)$_3$]$_2$ (**1**)	750(21), 565(54), 297(6100)	980vs	326vs, 296vs, 270sh, 234m	61.35s
fac-ReOCl$_3$(pinacop) (**2**)	750(17), 560(51), 298(4940) [14]	980[a]	329vs, 300vs, 284s, 220m	61.7s [14]
fac-ReOCl$_3$[P(OEt)$_3$]$_2$ [5](b)	765(20), 565(56), 300(5500)	975vs	322vs, 296vs, 280s, 236m	57.42s
cis-ReOCl$_3$(PEt$_2$Ph)$_2$ [6]	590(50), 365(1300), 301(3900), 252(10300)	977vs	322vs, 295s, 276s, 225m	

[a] Evaluated as result of substraction spectra of **2** and ReCl$_3$(pinacop)[P(OMe)$_3$] obtained in oxygen transfer reaction with P(OMe)$_3$.

spectra of **1** and **2** show bands characteristic for coordinated phosphite ligands and strong bands corresponding to ν(Re–O) stretching vibrations in the range 950–1000 cm^{-1}. In the spectrum of **2**, the band at 980 cm^{-1} is obscured by a very intensive ligand absorption. FIR spectra in the range of ν(Re–Cl) stretching vibrations (200–400 cm^{-1}) show four bands. But in the same region, ν(Re–P) vibrations also occur [17]. This precludes unequivocal assignment of ν(Re–Cl) stretches and the anticipation of geometry of **1** and **2**. The ^1H and ^{31}P NMR spectra of **1** and **2** are more informative. The spectra of **1** show a doublet in ^1H NMR at δ 3.93, $^3J(PH) = 7.0$ Hz and one singlet in $^{31}P\{^1H\}$ NMR δ 61.35, indicating the equivalence of both phosphite ligands. Two possible arrangements *cis-fac* and *trans-mer* are consistent with these data. The ^1H NMR spectra of **2**, obtained at low temperature (213 K), exhibit ten signals of nonequal intensity which are due to twelve unequivalent methyl groups, Fig. 1. As the temperature is raised these signals broaden and coalesce to give, at room temperature, six single sharp resonances at δ 1.57, 1.6, 1.63, 1.64, 1.65, 1.73 ppm, indicating that the species is fluxional on the ^1H NMR time scale. The variable temperature ^1H NMR spectra shown in Fig. 1 reveal a rather complicated pattern. Hence, it appears that, in our system, there are several dynamic processes exhibiting different coalescence temperatures for chelating metallacycle and two phosphorus cycles. This is consistent with the molecular C_1 symmetry of **2** in solution and expected *cis-fac* geometry of the donor atoms with phosphorus placed mutually in *cis* positions. Thus, this obviously rules out both *cis-mer* and *trans-mer* arrangements. The striking similarity of the spectroscopic data in Table 2 points to the *cis-fac* geometry for both **1** and **2**, as well as other complexes from the Table. The *cis-fac* geometry was also found for some other oxo-rhenium(V) complexes containing less sterically demanding phosphine ligands [6]. Interestingly, phosphine oxo-rhenium(V) complexes, $ReOCl_3P_2'$ (where $P' = PEt_3$ and PEt_2Ph), exist in two geometric forms or isomerize readily from *cis-fac* to *trans-mer*. By contrast, phosphite complexes **1** and previously obtained $ReOCl_3[P(OEt)_3]_2$ [5](b) do not undergo isomerization, even under vigorous conditions (in boiling toluene for 24 h). It may suggest that other bisphosphite oxo-rhenium complexes should be available, preferably in *cis-fac* geometry. Presumably, the reason for this is in the origin of a better π-acceptor capability of phosphite *vs.* phosphine ligands [2, 3]. Both **1** and **2** readily undergo reduction with $P(OMe)_3$ to corresponding rhenium(III) complexes *via* common oxygen atom transfer reaction [8]. Furthermore, the phosphite oxo-rhenium compounds, **1** and **2**, appear quite inert to the substitution reactions. This is in agreement with the inertness of isostructural *cis*-$ReOCl_3(CNCMe_3)_2$ in substitution reactions [12]. Indeed, **1** and **2** do not react noticeably either with pyridine or methanol under mild reaction conditions. The analogous phosphine complexes are rather labile, e.g., *trans*-$ReOCl_3(PPh_3)_2$ in reaction with pyridine or methanol yields either $ReOCl_3py_2$ or $ReOCl_2(OMe)(PPh_3)_2$, respectively.

Crystal structure determination

It has recently been suggested that the *cis-fac* geometry of Chatt's blue $ReOCl_3(PEt_2Ph)_2$ compound is responsible for the unusually long Re–O bond, 1.869(11) Å, resulting from "*trans*-influence isomerism" [18]. It is worthwhile to note that there is no response in decrease of ν(Re–O) stretches in the IR spectra of the latter compound, as one may expect, for a long Re–O bond. There are many controversies concerning the structure and composition of Chatt's "violet complex" formulated as *trans*-$ReOCl_3(PEt_2Ph)_2$ [6](a)[19]. Mentioned above, the "*trans*-influence isomerism" of Chatt's blue *cis* isomer [18] as well as the blue–violet colour of both our complexes prompted us to undertake X-ray crystal structure determination of **1** and **2**.

A view of the molecular structure of complex **1**, along with the atom labeling scheme used in the crystal structure determination, is shown in Fig. 2. Selected bond distances and angles are given in Table 3. Complex **1** has a distorted octahedral geometry with the central rhenium atom bonded to one terminal oxygen atom, two mutually *cis* phosphite phosphorus and three chlorides in facial arrangement. The Re–O_t bond length of 1.654(4) Å is in the usual range of multiply bonded mono-oxo group [20]. A considerable *trans*-influence exerted by the Re=O fragment, lengthens the Re–Cl_1 bond by ca. 0.04 Å, in comparison to Re–Cl_2 and Re–Cl_3 distances, and bends away *cis* chloride ligands, yielding obtuse bond angles O_t–Re–Cl_2 and O_t–Re–Cl_3 above 100°. No extraordinary structural features, either unusual length of the Re–O_t bond or crystallographic disorder for **1** has been found. By contrast, compound **2** exhibits remarkable orientational crystallographic disorder which, when not recognized, led to unusual and erroneous results. Thus, the Re–O_t bond was unusually long at 1.891(9) Å, and the Re–Cl_1 bond *trans* to terminal oxygen atom O_t was shortened at 2.276(5) Å. Other relevant rhenium–donor atom distances for this false model were in their usual ranges (Re–Cl_2 = 2.351(4), Re–Cl_3 = 2.348(4), Re–P_1 = 2.410(4), Re–P_2 = 2.405(4) Å). Furthermore, a large difference of electron densities in proximity to rhenium atoms (peak/hole = 6.72/−5.81 e$Å^3$) also suggested the disordered structure of **2**. The structure of **2**, with the atom labeling scheme used in the structure determination, is shown in Fig. 3. In the crystal state, **2** shows molecular symmetry near C_1. Some molecules in the crystal adopt an orientation inverted by 180° to the one adopted by the majority as is shown in Fig. 4. This is manifested by virtual lengthening of the Re–O_t bond to an extent depending on the occupancies of the two

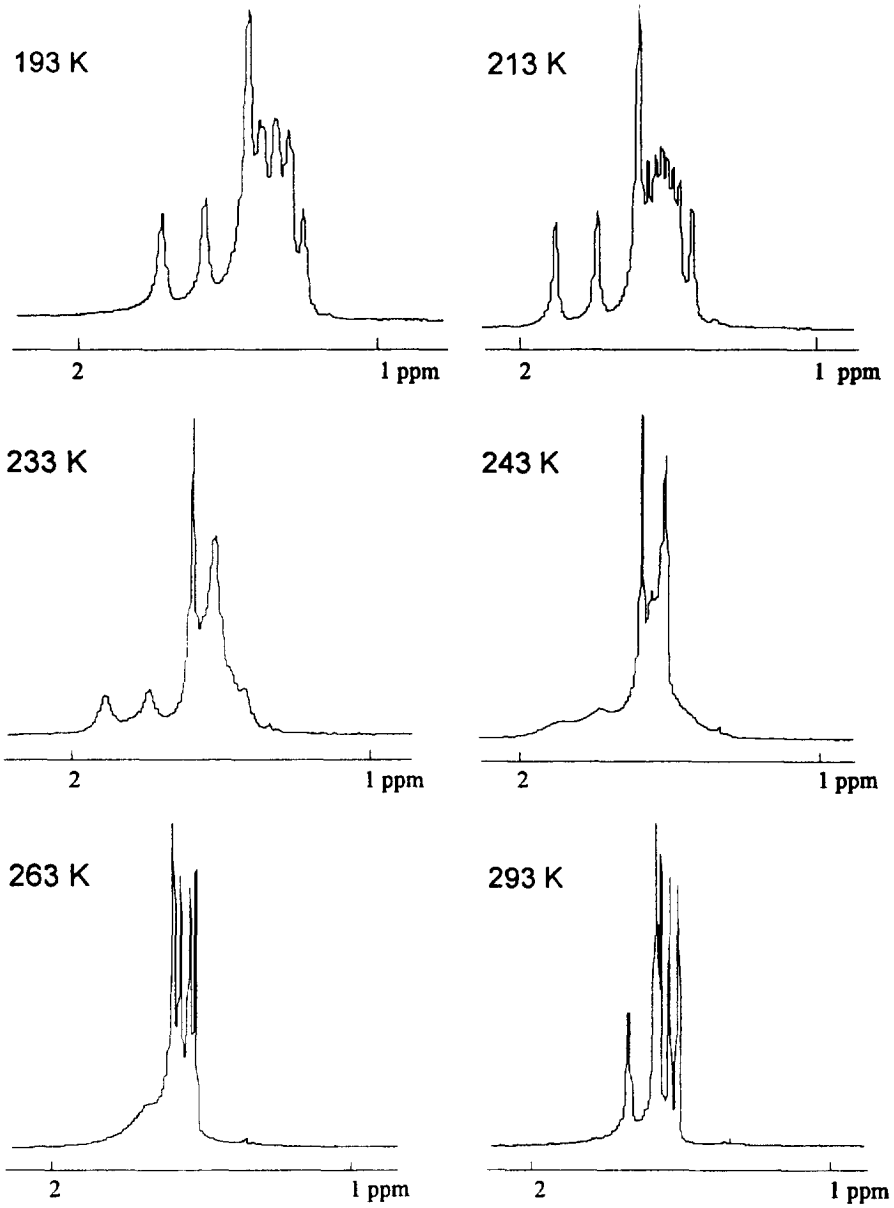

Fig. 1. Selected variable temperature ^{1}H NMR spectra of compound $ReOCl_3$pinacop (**2**)

orientations. The distance between disordered rhenium atom (Re_1–Re_2) is 0.505(6) Å, yet between disordered O_t–Cl_1, it is equal to 0.378(19) Å. The discerning data refinements gave the occupancy ratio 72:28 for the two vertical orientations. Finally, the separation of one orientation from another provides a correct set of structural parameters for **2** and its molecular structure. Selected bond distances and angles are given in Table 3. The seven membered ring COPRePOC is puckered and adopts a distorted chair conformation with two bridging phosphite oxygen atoms in opposite apical positions. In solution, a certain flexibility of the ring can be expected. Apart from orientational disorder and symmetry features, the molecular structure of **2** is quite similar to that of **1**. The Re–O_t bond length of 1.692(15) Å fits well to the triple rhenium oxygen bond distances [21]. A weak *trans*-influence, if any, is more likely pronounced by obtuse bond angles (O_t–Re–Cl_2 105.2° and O_t–Re–Cl_3 105.8) than by Re–Cl bond distances. Examples of other transition metal-oxo complexes that were suspected for unusually long Re–O bond or bond-stretch isomerism and appeared to be crystallographically disordered have been recently reviewed [22].

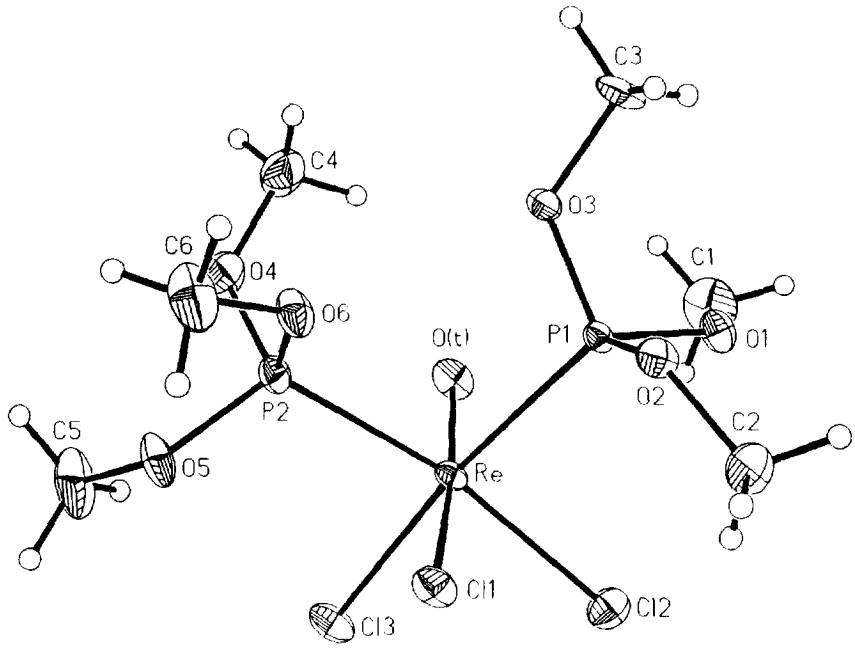

Fig. 2. Molecular structure of $ReOCl_3[P(OMe)_3]_2$ (**1**)

Table 3. Selected bond lengths (Å), bond angles and torsion angles (deg) for (**1**) and (**2**)

$ReOCl_3[P(OMe)_3]_2$ (**1**)			
Re–O(t)	1.654(3)	Re–Cl(3)	2.367(1)
Re–Cl(1)	2.413(1)	Re–P(1)	2.415(1)
Re–Cl(2)	2.372(2)	Re–P(2)	2.411(2)
O(t)–Re–Cl(3)	100.2(1)	Cl(2)–Re–Cl(1)	87.55(7)
O(t)–Re–Cl(2)	104.2(2)	P(2)–Re–Cl(1)	77.23(6)
Cl(3)–Re–Cl(2)	85.88(7)	O(T)–Re–P(1)	85.4(2)
O(t)–Re–P(2)	91.4(2)	Cl(3)–Re–P(1)	172.50(5)
Cl(3)–Re–P(2)	90.30(6)	Cl(2)–Re–P(1)	87.91(6)
Cl(2)–Re–P(2)	164.37(6)	P(2)–Re–P(1)	94.58(5)
O(T)–Re–Cl(1)	165.4(2)	Cl(1)–Re–P(1)	86.41(5)
Cl(3)–Re–Cl(1)	89.12(5)		
P(2)ReP(1)O(3)	−36.6(2)	ReP(1)O(3)C(3)	−169.9(4)
P(1)ReP(2)O(6)	−31.8(2)	ReP(2)O(6)C(6)	−148.0(6)
$ReOCl_3$(pinacop) (**2**)			
Re–O(t)	1.692(15)	Re–Cl(3)	2.346(5)
Re–Cl(1)	2.396(6)	Re–P(1)	2.409(4)
Re–Cl(2)	2.369(5)	Re–P(2)	2.409(4)
O(t)–Re–Cl(3)	105.8(5)	Cl(2)–Re–Cl(1)	92.3(3)
O(t)–Re–Cl(2)	105.2(5)	P(2)–Re–Cl(1)	79.9(2)
Cl(3)–Re–Cl(2)	85.9(2)	O(T)–Re–P(1)	82.7(5)
O(t)–Re–P(2)	84.2(5)	Cl(3)–Re–P(1)	171.2(3)
Cl(3)–Re–P(2)	87.2(2)	Cl(2)–Re–P(1)	89.6(2)
Cl(2)–Re–P(2)	169.6(3)	P(2)–Re–P(1)	96.1(1)
O(T)–Re–Cl(1)	156.8(4)	P(1)–Re–Cl(1)	82.3(2)
Cl(3)–Re–Cl(1)	90.3(3)		
P(2)ReP(1)O(3)	−29.2	ReP(1)O(3)C(7)	85.7
P(1)ReP(2)O(6)	−3.9	ReP(2)O(6)C(10)	62.4
P(1)O(3)C(7)C(10)	−103.2	P(2)O(6)C(10)C(7)	−93.8
O(3)C(7)C(10)O(6)	76.7		

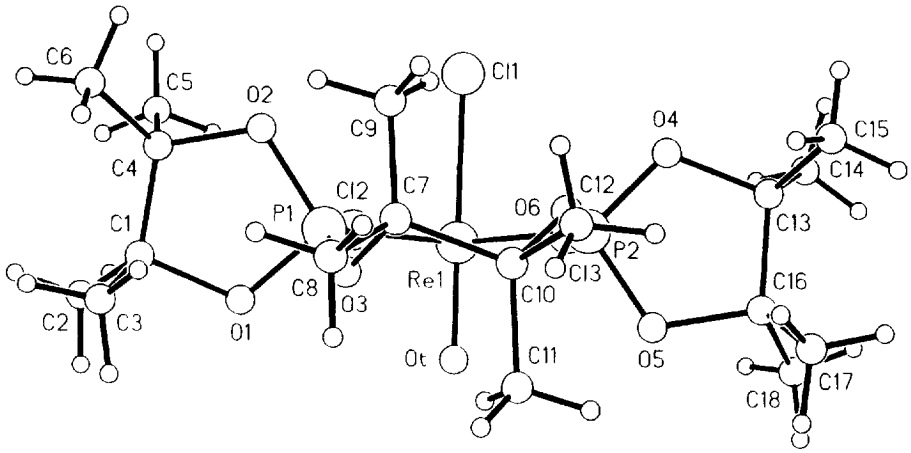

Fig. 3. Molecular structure of $ReOCl_3$pinacop (**2**)

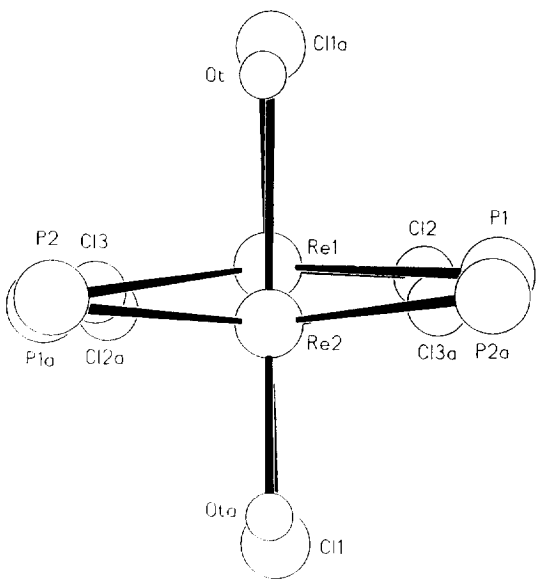

Fig. 4. View of disordered structure of (**2**)

This study has demonstrated that phosphite ligands may promote coordination chemistry distinct from that exhibited by phosphine congeners. This diversity was revealed in the geometry of quite inert *cis-fac*-$ReOCl_3P_2$ (**1** and **2**) complexes.

Supplementary material available

Tables of bond distances and angles, calculated positions, anisotropic thermal and isotropic hydrogen parameters for complexes **1** and **2** in both occupancies (24 pages), tables of observed and calculated structure factors (16 pages). Ordering information is given on any current masthead page.

Acknowledgements—We gratefully acknowledge the support for this work through the grant from KBN (Grant No. 2.P303.156.04).

REFERENCES

1. (a) Conner, K. A. and Walton, R. A. in *Comprehensive Coordination Chemistry*, ed. G. Wilkinson, R. D. Gillard and J. A. McCleverty, Pergamon Press, Oxford, Vol. 4, p. 125, 1987; (b) Vites, J. C., Lynam, M. M., *Coord. Chem. Rev.*, 1994, 131, 127; (c) Vites, J. C., Lynam, M. M., *Coord. Chem. Rev.*, 1995, 142, 1.
2. Tolman, C. A., *Chem. Rev.*, 1977, **77**, 313.
3. Rachman, M. M., Lin, H. Y., Prock, A. and Giering, W. P., *Organometallics*, 1987, **6**, 650.
4. (a) Choi, H. W. and Muetterties, E. L. *J. Am. Chem. Soc.*, 1982, 104, 153; (b) Brill, T. B. and London, S. J., *Chem. Rev.*, 1984, 84, 577; (c) Bleeke, J. R., Donaldson, A. J. and Peng, W. Y., *Organometallics*, 1988, 7, 33; (d) Trzeciak, A. M. and Ziolkowski, J. J., *J. Mol. Catal.*, 1988, 48, 319.
5. (a) Johnson, N. P. and Pickford, M. E. L., *J. Chem. Soc. Dalton*, 1976, 950; (b) Rhodes, L. F., Caulton, K. G., Rybak, W. K. and Ziolkowski, J. J. *Polyhedron*, 1986, 5, 1891; (c) Fernanda, M., Carvalho, N. N., Pombeiro, A. J. L., Hughes, D. L. and Richards, R. L., *J. Organomet. Chem.*, 1987, 335, C23.
6. (a) Chatt, J. and Rowe, G. A., *J. Chem. Soc.*, 1962, 4019; (b) Johnson, N. P., Lock, C. J. L., Wilkinson, G., *J. Chem. Soc.*, 1964, 1054; (c) Fergusson, J. E. and Heveldt, P. F., *J. Inorg. Nucl. Chem.*, 1976, 38, 2231.
7. Burgada, R., Germa, H., Willson, M. and Mathis, F., *Tetrahedron*, 1971, **27**, 5833.
8. (a) Rouschias, G., *Chem. Rev.*, 1974, 74, 531; (b) Holm, R. H., *Chem. Rev.*, 1987, 87, 1401; (c) Enemark, J. H. and Young, G. G., *Adv. Inorg. Chem.*, 1994, 40, 1; (d) Woo, L. K., *Chem. Rev.*, 1993, 93, 1125.

9. Rybak, W. K. and Ziolkowski, J. J., *J. Mol. Catal.*, 1987, **42,** 347.
10. Perrin, D. D. and Armarego, W. L. F., *Purification of Laboratory Chemicals*, 3rd ed. Pergamon Press, Oxford, 1988.
11. Parshall, W., *Inorg. Synth.*, 1977, **17,** 110.
12. Bryan, J. C., Stenkamp, R. E., Tulip, T. H. and Mayer, J. M., *Inorg. Chem.*, 1987, **26,** 2283.
13. Grove, D. E. and Wilkinson, G., *J. Chem. Soc. (A)*, 1966, **0,** 1224.
14. Rybak, W. K. and Zagiczek, A., *J. Coord. Chem.*, 1992, **26,** 79.
15. (a) Sheldrick, G. M., *Acta Crystal.*, 1990, A46, 467; (b) SHELX93 *Program for Refinement of Crystal Structures.* University of Goetingen, Germany, 1994.
16. (a) Lever, A. B. P., *Inorganic Electronic Spectroscopy*, 2nd ed. Elsevier Amsterdam, 1984; (b) Baluka, M., Hanuzza, J., Jezowska-Trzebiatowska, B., *Bull. Acad. Pol. Sci. Ser. Chim.*, 1972, 20, 20.
17. Nakamoto, K., *Infrared Spectra of Inorganic and Coordination Compounds*, 4th ed. Wiley Interscience, New York, 1986.
18. Sergienko, V. S. and Porai-Koshits, M. A., *Dokl. Akad. Nauk SSSR*, 1989, **309,** 903.
19. (a) Chatt, J., Garforth, J. D., Donaldson, N. P., Rowe, G. A., *J. Chem. Soc. (A)*, 1964, 601; (b) Sacerdoti, M., Bertolasi, V., Gilli, G., Duatti, A., *Acta Crystallogr.*, 1982. B38, 96; (c) Mayer, J. M., *Chemtracts: Inorg. Chem.*, 1991, 3, 115.
20. Mayer, J. M., *Inorg. Chem.*, 1988, **27,** 3899.
21. Nugent, W. A., *Metal–Ligand Multiple Bonds.* Wiley, New York, 1988.
22. (a) Parkin, G., *Acc. Chem. Res.*, 1992, 25, 455; (b) *Chem. Rev.*, 1993, 93, 887.

Pergamon

PII: S0277-5387(98)00090-4

Polyhedron Vol. 17, No. 18, pp. 3161–3166, 1998
© 1998 Elsevier Science Ltd
All rights reserved. Printed in Great Britain
0277-5387/98 $19.00+0.00

Synthesis, characterization and DNA binding study of Co(III) polypyridyl mixed-ligand complexes

Xiao-Feng He,[a] Lei Wang,[a] Han Chen,[a] Lin Xu[b] and Liang-Nian Ji[a,*]

[a]Department of Chemistry, Zhongshan University, Guangzhou, 510275, P.R. China

[b]Institute of entomology and state key laboratory for Biological control, Zhongshan University, Guangzhou, 510275, P.R. China

(Received 21 November 1997; accepted 26 February 1998)

Abstract—Two complexes $[Co(phen)_2TATP]^{3+}$ and $[Co(bipy)_2TATP]^{3+}$, where TATP is the planar ligand 1,4,8,9-tetra-aza-triphenylene, were synthesized and characterized. The binding of Co(III) polypyridyl mixed-ligand complexes to calf thymus DNA was investigated using absorption spectroscopy, fluorescence spectroscopy, viscosity measurement, and DNA cleavage assay. The absorption spectroscopic studies showed that the two new complexes $[Co(phen)_2TATP]^{3+}$ and $[Co(bipy)_2TATP]^{3+}$ exihibited apparently higher intercalating efficiency to DNA base pairs than $[Co(phen)_3]^{3+}$ and $[Co(bipy)_3]^{3+}$. The fluorescence of DNA helix was quenched by Co(III) complexes very strongly. From the viscosity experiment, we inferred that the binding of $[Co(phen)_3]^{3+}$ to DNA may be not by classical intercalation. When irradiated at 302 nm, $[Co(phen)_2TATP]^{3+}$ induced single-strand scissions and $[Co(bipy)_2TATP]^{3+}$ induced double-strand scissions in supercoiled DNA.
© 1998 Elsevier Science Ltd. All rights reserved

Keywords: Co(III) mixed-ligand complex; DNA; voltammetry; spectroscopy; viscosity; cleavage.

Considerable attention has been given to the design of small molecules that bind to DNA with site selectivity so as to develop new therapeutics and chemical probes for nucleic acid sites and structure, as well as novel diagnostic agents targeted to double-helical DNA [1]. Small molecules serve as analogues in studies of protein-nucleic acid recognition, provide site-specific reagents for molecular biology, and yield rationales for new drug design. The effect of size, shape, hydrophobicity and charge on the binding of the complex to DNA has been analyzed by changing the type of heteroaromatic ligand or metal center.

In the past decades, the interaction of Ru(II) polypyridyl coordination compounds have been studied extensively as structural probes and mediators of DNA cleavage reaction [2–4]. We have chosen to concentrate this work on complexes of Co(III), which have not received as much attention as the Ru(II) systems but possess the same interesting characteristics of metallointercalation and DNA cleaving properties [5–8]. In this paper, two Co(III) complexes, $[Co(phen)_2TATP](ClO_4)_3 \cdot 2H_2O$ and $[Co(bipy)_2TATP](ClO_4)_3 \cdot 3H_2O$ have been synthesized and identified the mode of binding with B-DNA by use of absorption spectroscopy, fluorescence spectroscopy, viscosity measurements, and DNA cleavage assay. The results should be valuable in understanding the mode of the complexes binding to DNA, as well as laying the foundation for the design of new probes for helical conformations and antitumor drugs.

EXPERIMENTAL

Materials and methods

All starting materials were commercially available and of analytical grade quality. TATP [9], cis-$[Co(phen)_2Cl_2]Cl \cdot 3H_2O$ [10], cis-$[Co(bipy)_2Cl_2]Cl \cdot 3H_2O$ [11], $[Co(phen)_3]Cl_3$ and $[Co(bipy)_3]Cl_3$ [12] were prepared and purified by methods described pre-

* Author to whom correspondence should be addressed.

viously, where bipy, phen and TATP stand for 2,2′-bipyridine, phenanthroline and 1,4,8,9-tetra-aza-triphenylene, respectively. The structures of ligands are showed in Fig. 1.

All the experiments involving the interaction of the Co(III) complexes with DNA were conducted in a pH 7.2 Tris buffer containing 5 mM tris (hydroxymethyl)aminomethane (Tris), 50 mM NaCl in doubly distilled water. Solution of calf thymus DNA gave ratios of UV absorbance at 260 nm and 280 nm, A_{260}/A_{280}, of ca. 1.8 ~ 1.9, indicating that the DNA was sufficiently free of protein [13]. DNA concentration per nucleotide was determined by $\epsilon_{260} = 6600\ M^{-1}cm^{-1}$ [14].

Cyclic voltammetry was performed by a Princeton Applied Research (PAR) Model 175 universal programmer with a three electrode system: the Au disk electrode (d = 4.0 mm) as the working electrode, saturated calomel electrode (SCE) as the reference electrode and Pt wire as the counter electrode. Supporting electrolytes were Tris buffer (pH = 7.2). Before each experiment, the supporting electrolytes were deaerated *via* purging pure N_2 for 15 min and nitrogen atmosphere was kept over the solution during the experiments.

The ^{1}HNMR spectra were recorded on a Bruker AM × 500 HNMR, Me_4Si as internal reference. IR spectra were recorded on Nicolet 170X-FT spectrophotometer with KBr pellets. UV spectra were obtained on a Shimadzu MPS-2000 UV-vis spectraphotometer. The fluorescence intensity measurements were carried out by a Shimadzu RF-5000 spectrofluorimeter.

Viscosity experments used a Ubbelodhe viscometer, immersed in a thermostated water bath maintained at 28(±0.1)°C. Data were presented as $(\eta/\eta)^{1/3}$ *versus* the concentration of Co(III) complexes, where η is the viscosity of DNA in the presence of complexes and η is the viscosity of DNA alone. Viscosity values were calculated from the observed flow times of DNA-containing solutions (t), corrected for the flow time of buffer alone (t), $\eta = t - t$ [15].

Photoactivated cleavage of 100 μM pBR322 DNA with 20 μM Co(III) complexes after irradiation at 302 nm (10 W-UV lamp) in 10 μL of 50 mM Tris, 18 mM NaCl, and pH 7.0 solution. Samples were subjected to electrophoresis on 0.8% agarose gels followed by staining with ethidium bromide. The photographs under UV light were taken.

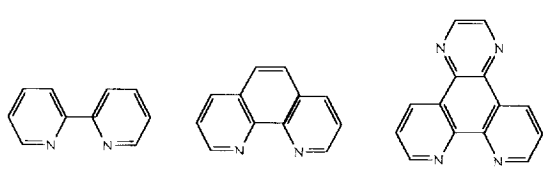

Fig. 1. Structures of the ligands.

Synthesis of $[Co(phen)_2TATP](ClO_4)_3 \cdot 2H_2O$

A mixture of cis-$[Co(phen)_2Cl_2]Cl \cdot 3H_2O$ (0.54 g, 0.001 mol) and TATP (0.26 g, 0.0011 mol) in water-methanol (20 cm^3, 1:1, v:v) was warmed on a water bath below 60°C for 2.5 hours. After filtration, the filtrate was treated with excess 8 M $NaClO_4$ solution, an orange precipitate formed. The precipitate was chromatographed over neutral Al_2O_3 column using a mixture of acetonitrile and toluene (1:1, v:v) solution as eluent to obtain a yellow solution. After concentration, a yellow solid was precipitated by adding ether into the solution. The precipitate was washed with ether and then dried under vacuum. Yield 44%. Anal. Calcd for $C_{38}H_{28}N_8CoCl_3O_{14}$: C, 46.29; H, 2.86; N, 11.36. Found: C, 46.25; H, 2.37; N, 11.27 (%). IR data (cm^{-1}): 1518 s, 1384 m, 1082 vs, 850 s, 723 s, 632 vs. UV λmax nm (log ε): 272.7 (4.85);217.7 (5.03). ^{1}HNMR (500 MHz, CD_3CN):δ 9.88(*t*, 2H), 9.46(*s*, 2H), 9.20(*t*, 2H), 8.60 (*d*, 2H), 8.16(*dd*, 2H), 7.99(*t*, 2H), 7.86(*t*, 2H), 7.72(*d*, 2H).

Synthesis of $[Co(bipy)_2TATP](ClO_4)_3 \cdot 3H_2O$

$[Co(bipy)_2TATP](ClO_4)_3 \cdot 3H_2O$ was prepared in a similar way with $[Co(phen)_2TATP](ClO_4)_3 \cdot 2H_2O$ Yield 35%. The eluent is acetonitrile and toluene (2:1, v:v) solution. Anal Calcd for $C_{34}H_{30}N_8CoCl_3O_{15}$: C, 42.71; H, 2.53; N, 11.72. Found: C, 42.71; H, 2.53; N, 11.51(%). IR data (cm^{-1}): 1574 m, 1447 s, 1384 m, 723 m, 625 s. ^{1}HNMR(400 MHz, d^6-DMSO $CDCl_3$)δ 9.85(m, 2H), 9.34(*s*, 2H), 9.06(*d*, 2H), 9.01(*d*, 2H). UV λmax nm (log ε): 304.7(4.50), 254.7(4.85), 220.7(4.92).

RESULTS AND DISCUSSION

Voltammetric studies

There are a couple of redox peaks corresponding to $[Co(phen)_2TATP]^{3+}$ and $[Co(bipy)_2TATP]^{3+}$, respectively. The E_{pc} and E_{pa} are 0.196 V and 0.121 V for $[Co(phen)_2TATP]^{3+}$, and 0.055 V and 0.128 V for $[Co(bipy)_2TATP]^{3+}$. The half-wave potentials $E_{1/2}$, taken as $(E_{pc} + E_{pa})/2$, are 0.159 V and 0.092 V for above two complexes, respectively. The separations of the anodic and cathodic peak potentials (ΔE_p) are 75 mV and 73 mV. In the range of 20 ~ 200 mv/s, all the peak potentials are independent of scan rates (v) and the i_{pc} and i_{pa} are proportional to symbol $v^{1/2}$. It indicates that this process may be a quasi-reversible, 1-electron redox reaction.

Electronic absorption spectra

In the UV region, the intense absorption bands observed in the Co(III) complexes are attributable to internal π to π* transition of the coordinated groups. The absorption spectra of the complexes in the

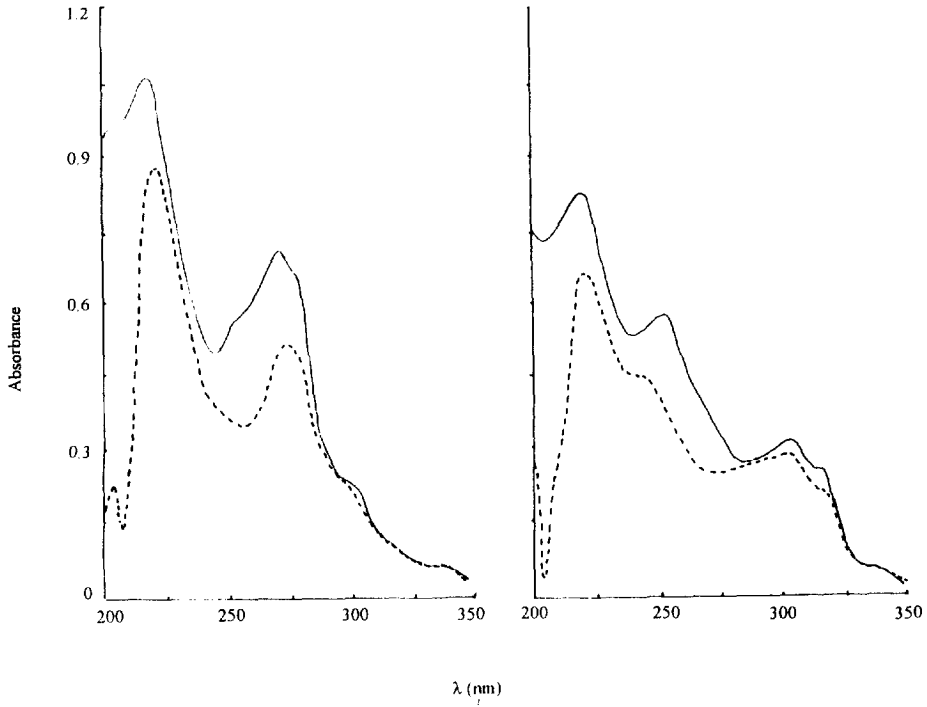

Fig. 2. Electronic absorption spectra of $[Co(phen)_2TATP]^{3+}$ (left) and $[Co(bipy)_2TATP]^{3+}$ (right) with no DNA (———) and [DNA]:[Co] = 40:1(- - -) with subtraction of the DNA absorbance.[Co] = 10 μM.

absence and the presence of calf thymus DNA (with subtraction of the DNA absorbance for the latter) are illustrated in Fig. 2. According to the data in Table 1, $[Co(phen)_2TATP]^{3+}$ and $[Co(bipy)_2TATP]^{3+}$ show the largest changes in absorption in the presence of DNA, hence, these two complexes appear to bind strongly to DNA, whereas $[Co(phen)_3]^{3+}$ and $[Co(bipy)_3]^{3+}$ bind more weakly and give smaller hypochromic effects. This is just the expected result on the basis that TATP possesses a greater planar area and hence higher hydrophobicity than that of phen and bipy, which would lead to TATP intercalating more deeply into the DNA base pairs [16, 17]. For $[Co(phen)_2TATP]^{3+}$, $[Co(bipy)_2TATP]^{3+}$ and $[Co(phen)_3]^{3+}$, a spectral shift to lower energy is found, which supports an electronic stacking interaction of the TATP and phen ligands with the base pairs of the helix.$[Co(bipy)_3]^{3+}$ shows weak hypochromism and no spectral red shift, because it only electrostatically binds with DNA [18].

Flourescence spectroscopic studies

Binding of Co(III) complexes to the DNA helix was found to quench the DNA flourescence very strongly.

Table 1. Absorption spectroscopic properties of the Co(III) complexes on binding to DNA

Complex[a]	Absorption λ_{max}(nm) free	bound	$\Delta\lambda$	Hypocromicity(%)
$[Co(phen)_2TATP]^{3+}$	218	222	4	17
	273	275	2	26
$[Co(phen)_3]^{3+}$	219	223	4	9
	274	276	2	15
$[Co(bipy)_2TATP]^{3+}$	221	222	1	20
	305	305	0	8
$[Co(bipy)_3]^{3+}$	222	222	0	5
	306	306	0	0

a.[Co] = 10 μM at [DNA]/[Co] = 40

For Co(III) complexes, no detectable emission is observed in aqueous solution. Fig. 3 reveals that the fluorescence intensity of DNA decreases rapidly with increasing concentration of Co(III) complexes with excitation at 320 nm. These quenching processes occur by electron and energy transfer. The data in Table 2 show that $[Co(phen)_2TATP]^{3+}$ exhibits higher quenching efficiency to DNA than that of $[Co(phen)_3]^{3+}$ and $[Co(bipy)_2TATP]^{3+}$ exhibits higher quenching efficiency than that of $[Co(bipy)_3]^{3+}$, which is consistent with the stronger binding ability of these two new Co(III) complexes with DNA. Besides, $[Co(bipy)_2TATP]^{3+}$ possesses the highest quenching efficiency to DNA because for non-intercalated coligands, steric interaction will influence the intercalating degree between the TATP and DNA base pairs; the reduced size of non-intercalated co-ligand bipy may increase the binding affinity of complexes with DNA [19].

Viscosity studies

The effect of Co(III) complexes on the viscosity of DNA is shown in Fig. 4. Hydrodynamic data provide perhaps the most critical test for intercalative binding in the absence of X-ray crystallographic or NMR structural data [20]. For complexes $[Co(phen)_2TATP]^{3+}$ and $[Co(bipy)_2TATP]^{3+}$, the viscosity of DNA increases with the increase of the concentration of the complexes, which is similar to that of proven DNA intercalator, $[Ru(phen)_2DPPZ]^{2+}$ [21]. Both complexes increase the relative viscosity of DNA in a manner consistent with binding by classical intercalation. This result parallels with the pronounced hypochromism and a large spectral red shift of the two new complexes.$[Co(phen)_3]^{3+}$ and $[Co(bipy)_3]^{3+}$ have no effect on the viscosity of DNA. Weak hypochromism, no spectral red shift and viscosity measurement support that $[Co(bipy)_3]^{3+}$ binds to DNA only by electrostatic force. Although Barton et al. proposed that $[Co(phen)_3]^{3+}$ intercalated into double-strandad DNA [18], but this viscosity experiment shows that $[Co(phen)_3]^{3+}$ may be a 'nonclassical' DNA intercalating agent.

Photoactivated cleavage of pBR322 DNA by Co(III) complexes

Figure 5 shows the gel electrophoretic separations of plasmid pBR322 DNA after incubation with Co(III) complexes and irradiation at 302 nm. DNA cleavage is followed by monitoring the conversion of supercoiled (form I) closed circular plasmid DNA to

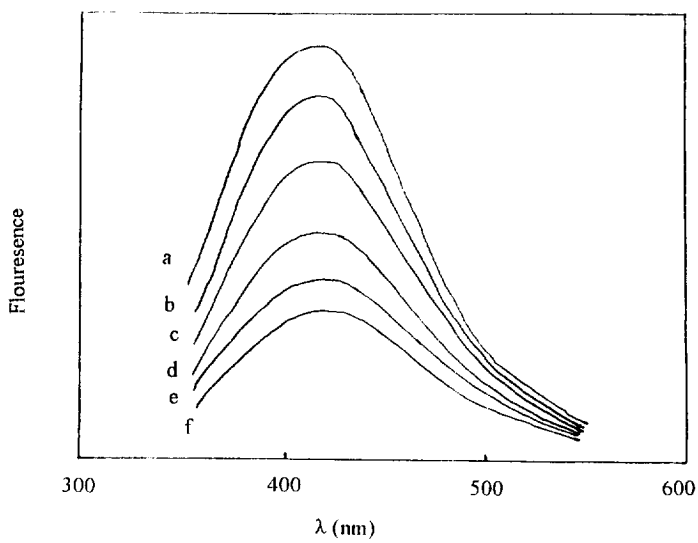

Fig. 3. Fluoresence quenching of DNA (2 mM) by increasing concentration of $[Co(phen)_2TATP]^{3+}$ [Co] = 0, 20, 40, 60, 80, 100 μM for a ~ f, respectively.

Table 2. The data for DNA fluoresence quenching by Co(III) complexes

Complex[a]	$[Co(phen)_2TATP]^{3+}$	$[Co(phen)_3]^{3+}$	$[Co(bipy)_2TATP]^{3+}$	$[Co(bipy)_3]^{3+}$
I_0/I	1.86	1.07	4.12	2.86

a.[DNA] = 2 mM, [Co] = 60 μM, Emission was monitored at 416 nm with excitation at 320 nm.

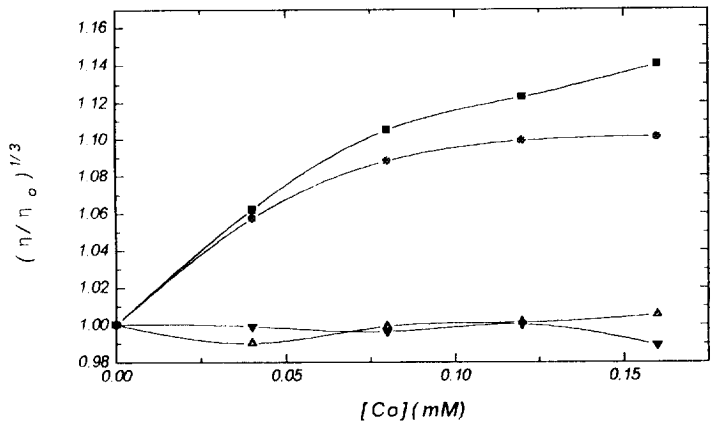

Fig. 4. Effect of increasing amounts of Co(III) complexes on the related viscosity of calf thymus DNA. (■), $[Co(phen)_2TATP]^{3+}$; (●), $[Co(bipy)_2TATP]^{3+}$; (▲), $[Co(phen)_3]^{3+}$; (▼), $[Co(bipy)_3]^{3+}$.

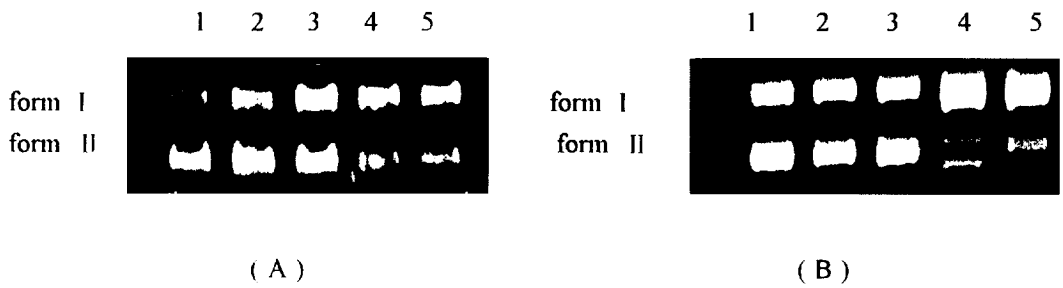

(A) (B)

Fig. 5. (A) Cleavage of pBR322 DNA in the presence of $[Co(phen)_2TATP]^{3+}$ and light. The 0.8% agarose gel shows the distribution of DNA forms initially without coblt (lane 1) and after irradiation at 302 nm in the presence of $[Co(phen)_2TATP]^{3+}$ for 0, 10, 20, and 30 min(lane 2 ~ 5, left to right). (B) Photoactivated cleavage of pBR322 DNA after 40 min irradiation at 302 nm with 1 = no complexes, 2 = $[Co(bipy)_3]^{3+}$, 3 = $[Co(phen)_3]^{3+}$, 4 = $[Co(bipy)_2TATP]^{3+}$, 5 = $[Co(phen)_2TATP]^{3+}$

the nicked circular (form II) species. Fig. 5A reveals the almost complete conversion of form I to II after 30 min irradiation in the presence of $[Co(phen)_2TATP]^{3+}$. Neither irradiation of the DNA at these low intensities without Co(III) nor incubation with Co(III) without light yielded significant strand scission. Fig. 5B examines the different binding mode of Co(III) complexes to the helix.$[Co(phen)_2TATP]^{3+}$ and $[Co(bipy)_2TATP]^{3+}$ cleave DNA to a much larger extent than $[Co(phen)_3]^{3+}$ and $[Co(bipy)_3]^{3+}$, which is consistent with their stronger intercalating ability to DNA base pairs. While $[Co(phen)_2TATP]^{3+}$ induced single-strand scissions in supercoiled DNA, $[Co(bipy)_2TATP]^{3+}$ induced the double-strand scissions. The higher strand scission efficiency of $[Co(bipy)_2TATP]^{3+}$ is related to the more intense absorption at 302 nm and the stronger quenching ability to DNA. The photoreduction of Co(III) complexes with concomitant hydroxide oxidation may be the important step in the DNA cleavage reaction [22]. Further study is necessary to clarify the reaction mechanism.

Acknowledgements This work was supported by the National Natural Science Foundation of China (29571033) and Doctoral Program Foundation of Institution of High Education (9555806). We thank Prof. Hui-Ying Yang, Dr Xiong Ya for many helpful discussions and Miss Li Hong for assistance in voltammetric experiment.

REFERENCES

1. Jenkins, Y., Friedman, A. E., Turro, N. J. and Barton, J. K., *Biochemistry*, 1992, **31**, 10809.
2. Margan, R. J., Chatterjee, S. and Baker, A. D., *Inorg. Chem.*, 1991, **30**, 2678.
3. Wu, J.-Z., Li, L., Zeng, T.-X., Ji, L.-N., Zhou, J.-Y. and Luo, T., Li, R.-H., *Polyhedron*, 1997, **16**, 103.
4. Yang, G., Wu, J.-Z., Wang, L. and Ji, L.-N., Tian, X., *J. Inorg. Biochem.*, 1997, **66**, 141.
5. Rehmann, J. P. and Barton, J. K., *Biochemistry*, 1990, **29**, 1701.
6. Barton, J. K. and Raphael, A. L., *Proc. Natl. Acad. U. S. A.*, 1985, **82**, 6460.

7. Barton, J. K. and Paranawithana, S. R., *Biochemistry*, 1986, **25,** 2205.
8. Barton, J. K. and Raphael, L. A., *J. Am. Chem. Soc.*, 1984, **106,** 2466.
9. Zwelling, C. A., Michaels, S., Schwarts, H., Dobson, P. P. and Kohn, K. W., *Cancer Res.*, 1981, **41,** 640.
10. Ablov, A. V., *Russ. J. Inorg. Chem.*, 1961, **6,** 157 (English ed).
11. Vlcek, A. A., *Inorg. Chem.*1967, **6**(7), 1425.
12. Strazza, G. and Sinibold, M., *Inorg. Chim. Acta*, 1980, **44,** L295.
13. Marmur, J., *J. Mol. Biol.*, 1961, **3,** 208.
14. Barton, J. K., Goldberg, J. M., Kumar, C. V. and Turro, N. J., *J. Am. Chem. Soc.*, 1986, **108,** 2081.
15. Satyanaryana, S., Daborwiak, J. C. and Chaires, J. B., *Biochemistry*, 1993, **32,** 2573.
16. Wu, J.-Z., Ye, B.-H., Wang, L., Ji, L.-N., Zhou, J.-Y., Li, R.-H. and Zhou, Z.-Y., *J. Chem. Soc., Dalton Trans.*, 1997, **8,** 1395.
17. Tysoe, S. A., Morgan, R. J., Baker, A. D. and Strekas, T. C., *J. Phys. Chem.*, 1993, **97,** 1707.
18. Fleisher, M. B., Waterman, K. C., Turro, N. J. and Barton, J. K., *Inorg. Chem.*1986, **25**(20), 3549.
19. Wang, L., Wu, J.-Z., Yang, G., Zeng, T.-X. and Ji, L.-N., *Transition Met. Chem.*, 1996, **21,** 487.
20. Satyanarayana, S., Dabrowiak, J. C. and Chaires, J. B., *Biochemistry*1992, **31**(39), 9319.
21. Haq, I., Lincoln, P., Suh, D., Norden, B., Chowdhry, B. Z. and Chaires, J. B., *J. Am. Chem. Soc.*, 1995, **117,** 4788.
22. Subramanian, R. and Meares, C. F., *J. Am. Chem. Soc.*, 1986, **108,** 6427.

Pergamon

PII: S0277-5387(98)00088-6

Polyhedron Vol. 17, No. 18, pp. 3167–3174, 1998
© 1998 Elsevier Science Ltd
All rights reserved. Printed in Great Britain
0277-5387/98 $19.00+0.00

Syntheses and X-ray crystal structure of $(dq)_2[M(CN)_8]\cdot 5H_2O$ (M = Mo, W; dq = diquat)

Beata Nowicka[a], Alina Samotus[a,*], Janusz Szklarzewicz[a], John Burgess[b], John Fawcett[b] and David R. Russell[b]

[a] Faculty of Chemistry, Jagiellonian University, Ingardena 3, 30-060 Kraków, Poland

[b] Department of Chemistry, University of Leicester, Leicester LE1 7RH, U.K.

(Received 8 December 1997; accepted 26 February 1998)

Abstract—Reaction between diquat (dq = 6,7-dihydrodipyrido-[1,2-a:2′,1′-c]pyrazinediium) and $[M(CN)_8]^{4-}$ (M = Mo or W) led to the isolation of $(dq)_2[M(CN)_8]\cdot 5H_2O$ salts. Both salts were found to be isomorphic. The $[M(CN)_8]^{4-}$ anion has an approximately dodecahedral D_{2d} configuration. The structure consists of a three dimensional hydrogen bonded network. The intensely coloured solids (hydrated and anhydrous) show ion-pair charge-transfer (IPCT) interaction which is discussed in terms of their structure. © 1998 Elsevier Science Ltd. All rights reserved

Keywords: octacyanomolybdate (IV); octacyanotungstate (IV); diquat; ion pair charge transfer; crystal structure; IR spectra.

The structure of octacyanometallates depends strongly on the nature of cation and other species, such as water of crystallization, capable of formation of hydrogen bonds. Considering cation-anion interaction several salts were synthesized and structurally characterized [1, 2]. Previously we have studied salts with bipyridinium cations of the following formulae: $(bpyH)_3(H_3O)[M(CN)_8]\cdot 2H_2O$ (bpy = 2,2′-bipyridyl) [3] and $(4,4'\text{-bpyH}_2)_2[M(CN)_8]\cdot 4.5H_2O$ (4,4′-bpy = 4,4′-bipyridyl) [4]. All these salts show the ion-pair charge-transfer (IPCT) phenomenon due to electron shift from anion to cation.

The structural data available for the 4,4′-bipyridinium salt show that there are several possibilities of charge dissipation through different types of hydrogen bonds in which the nitrogen end of cyano ligands, water molecules and the nitrogen atoms of pyridine rings participate [4]. It was also found that the electron can be transferred through the π stack systems of pyridine rings. To gain more information about the nature of electron transfer we extended our study to cover cases in which a direct hydrogen bond between anion and pyridine nitrogens cannot be formed. In this paper we present the synthesis and structure of octacyanometallates with the N,N′-alkylated derivative of 2,2′-bipyridinium, diquat (dq = 6,7-dihydrodipyrido-[1,2-a:2′,1′-c]pyrazinediium), as cation.

EXPERIMENTAL

Materials

The initial molybdenum (IV) and tungsten (IV) complexes $K_4[M(CN)_8]\cdot 2H_2O$ were prepared by methods described in the literature [5, 6]. The aqueous solutions of acids, $H_4[M(CN)_8]$, were obtained from potassium salts using ion exchange techniques (IR 120 ion exchange resin in H^+ form) [7]. $dqBr_2$ was purchased as a crude product-'Reglone' (Imperial Chemical Industries, ab. 20% $dqBr_2$ content) and refined by column chromatography in reverse-phase system on modified silica gel (RP 18) with methanol as a solvent, and then recrystallized twice from hot methanol. The purity of the product was checked by

* Correspondence to: fax: (48 12) 6340515, e-mail: samotus@ trurl.ch.uj.edu.pl.

measuring the UV spectrum and melting point ($\lambda_{max} = 308$ nm, mp. 320 C) [8]. Other reagents and solvents of analytical grade (POCh, Poland) were used as supplied.

Syntheses

Bis(6,7 - *dihydrodipyrido*[1,2 - *a*:2′,1′ - *c*]*pyrazi* - *nediium*) *octacyanomolybdate* (*IV*) *pentahydrate*, $(dq)_2[Mo(CN)_8]\cdot 5H_2O$ (**1**). 2.35 mmol (0.851 g) of $dqBr_2\cdot H_2O$ was dissolved in 100 ml of the aqueous solution containing 1.28 mmol (0.394 g) of $H_4[Mo(CN)_8]$ and then 300 ml of acetone was carefully added to form a separate top layer. The mixture was allowed to stand for 3 days at room temperature. The resulting precipitate was filtered off, washed with 1:2 water-acetone mixture and dried in air *via* suction. Yield: 0.89 g (91.0%). Found: C, 50.47; H, 4.49; N, 22.04; H_2O, 13.8%. Calc. for $C_{32}H_{34}N_{12}O_5Mo$: C, 50.40; H, 4.49; N, 22.04; H_2O, 13.8%.

Bis(6,7-*dihydrodipyrido*[1,2-*a*:2′,1′-*c*]*pyrazinediium*) *octacyanotungstate* (*IV*) *pentahydrate*, $(dq)_2[W(CN)_8]\cdot 5H_2O$ (**2**). The salt was obtained in a similar way to (**1**), except that 1.28 mmol (0.521 g) of $H_4[W(CN)_8]$ was used instead of the molybdenum compound. Yield: 0.89 g (81.5%). Found: C, 45.28; H, 3.78; N, 19.66; H_2O, 10.4%. Calc. for $C_{32}H_{34}N_{12}O_5W$: C, 45.19; H, 4.03; N, 19.76; H_2O, 10.6%.

The anhydrous salts $(dq)_2[Mo(CN)_8]$ (**3**) and $(dq)_2[W(CN)_8]$ (**4**) were obtained from (**1**) and (**2**) respectively by thermal dehydration at 90 C for about two hours (till the weight was constant).

Analytical methods and physical measurements

Carbon, nitrogen and hydrogen were determined by organic microanalysis. The content of water was determined by thermogravimetric analyses (t.g.). These analyses as well as differential thermal analyses (d.t.a.) were performed under argon within the temperature range 25–400 C, with a heating rate of 2.5 C/min on a MOM-Q 1500 thermoanalyser (Hungary). Uv-vis absorption and reflectance spectra (Shimadzu 2101 PC spectrometer with ISR-260 device) and e.s.r. spectra (Se/X-25, Poland) were recorded in the normal manner at room temperature. Infrared spectra were measured in KBr pellets (hydrated salts) and as nujol mulls (anhydrous salts) on a Brüker IFS 48 spectrometer. Raman spectra in water solution were recorded on a Cary 82 spectrometer (Varian USA).

Structures

Crystal structure analysis of $(dq)_2[Mo(CN)_8]\cdot 5H_2O$ (**1**), M = 762.65, orthorhombic, space group Pbca, a = 13.209(2), b = 14.639(4), c = 35.325(4) Å, $\alpha = \beta = \gamma = 90$ °, U = 6831(2) Å^3, $D_c = 1.483$ g cm^{-3}, Z = 8, $\lambda = 0.71073$ Å, T = 293 K, $\mu = 0.444$ mm^{-1}, dark purple blocks, crystal dimensions $0.51 \times 0.44 \times 0.27$ mm.

Data were collected with a Siemens P4 four-circle diffractometer using omega scans. Maximum 2θ was 50 with scan range ±1.2 around the $K_{\alpha 1} - K_{\alpha 2}$ angles, scan speed 3–30 min^{-1}, depending on the intensity of a 2-s pre-scan. Three standard reflections were monitored every 100 reflections, showing only slight changes during data collection. Unit-cell dimensions and standard deviations were obtained by least-squares fit to 33 reflections ($4.6 < \theta < 12.5$ °). The intensities of 5151 unique reflections were collected; 3484 were considered observed [$I/\sigma(I) > 2.0$). Reflections were corrected for Lorentz, polarization and absorption effects, the last by psi scans: maximum and minimum transmission factors were 0.8767 and 0.6907. Systematic absences were consistent with the space group Pbca, which was confirmed by successful refinement. Heavy atoms were located by the Patterson interpretation section of SHELXTL ver. 5.0 and the light atoms then found on successive Fourier syntheses, including H_2O. Anisotropic thermal parameters were used for all non-H atoms. Hydrogen atoms for the water molecules were located from difference Fourier maps then allowed to ride on the bonded oxygen atom; all other hydrogen atoms were included in calculated positions and not refined. Hydrogen atoms were given fixed isotropic thermal parameters, U = 0.08 Å^2. Final refinement was on F by least-squares methods with 458 parameters. Largest positive and negative peaks on a final difference Fourier synthesis were of height +0.409 and −0.364 eÅ^3. A weighting scheme of the form $w = 1/[\sigma^2(F_o^2) + (0.0384P)^2 + 6.18P]$ was used and shown to be satisfactory by weight analysis. Final R1 = 0.0445, ωR2 = 0.112 for all data. Maximum shift/error in final cycle 0.07. Computing was with SHELXTL ver. 5.0 [9]. Scattering factors in the analytical form and anomalous dispersion factors were taken from ref. [9].

Crystal structure analysis of $(dq)_2[W(CN)_8]\cdot 5H_2O$ (**2**), M = 850.52. The structure was determined in a similar manner. The tungsten salt (**2**) was found to be isomorphous with the molybdenum compound (**1**): orthorhombic, space group Pbca, a = 13.208(2), b = 14.642(3), c = 35.325(3) Å, $\alpha = \beta = \gamma = 90$ °, U = 6832(2) Å^3, $D_c = 1.646$ g/cm^3, Z = 8, dark green blocks, crystal dimensions $0.62 \times 0.38 \times 0.16$ mm.

Selected bond lengths and angles are given in Tables 1 and 2.

Additional materials available from the Cambridge Crystallographic Data Centre comprise atomic co-ordinates and equivalent isotropic displacement parameters, H-atom co-ordinates, displacement parameters, and the remaining bond lengths and angles.

Table 1. Selected bond lengths [Å] for $(dq)_2[Mo(CN)_8]\cdot 5H_2O$ (**1**) and $(dq)_2[W(CN)_8]\cdot 5H_2O$ (**2**) with estimated standard deviations (e.s.d.s.) in parentheses

Mo(1)–C(2)	2.178 (5)	C(2)–N(2)	1.140 (6)
Mo(1)–C(4)	2.180 (6)	C(4)–N(4)	1.140 (6)
Mo(1)–C(5)	2.173 (5)	C(5)–N(5)	1.149 (6)
Mo(1)–C(8)	2.174 (5)	C(8)–N(8)	1.151 (6)
Mo(1)–C(1)	2.156 (5)	C(1)–N(1)	1.135 (6)
Mo(1)–C(3)	2.158 (5)	C(3)–N(3)	1.141 (6)
Mo(1)–C(6)	2.161 (6)	C(6)–N(6)	1.151 (6)
Mo(1)–C(7)	2.154 (5)	C(7)–N(7)	1.155 (6)
W(1)–C(2)	2.175 (9)	C(2)–N(2)	1.161 (11)
W(1)–C(4)	2.178 (9)	C(4)–N(4)	1.143 (10)
W(1)–C(5)	2.178 (9)	C(5)–N(5)	1.147 (10)
W(1)–C(8)	2.164 (8)	C(8)–N(8)	1.162 (10)
W(1)–C(1)	2.155 (9)	C(1)–N(1)	1.144 (11)
W(1)–C(3)	2.162 (8)	C(3)–N(3)	1.134 (10)
W(1)–C(6)	2.172 (8)	C(6)–N(6)	1.135 (10)
W(1)–C(7)	2.160 (9)	C(7)–N(7)	1.143 (10)

Table 2. Selected bond angles (°) for $(dq)_2[Mo(CN)_8]\cdot 5H_2O$ (**1**) with e.s.d.s. in parentheses

C(1)–Mo(1)–C(2)	71.3 (2)	C(1)–Mo(1)–C(3)	86.5 (2)
C(1)–Mo(1)–C(4)	76.8 (2)	C(6)–Mo(1)–C(7)	89.5 (2)
C(1)–Mo(1)–C(8)	75.8 (2)	C(1)–Mo(1)–C(6)	101.6 (2)
C(2)–Mo(1)–C(3)	78.0 (2)	C(3)–Mo(1)–C(7)	102.2 (2)
C(2)–Mo(1)–C(5)	73.0 (2)	C(2)–Mo(1)–C(8)	124.9 (2)
C(2)–Mo(1)–C(6)	73.8 (2)	C(4)–Mo(1)–C(5)	125.1 (2)
C(3)–Mo(1)–C(4)	70.5 (2)	C(2)–Mo(1)–C(4)	136.0 (2)
C(3)–Mo(1)–C(5)	75.8 (2)	C(5)–Mo(1)–C(8)	135.9 (2)
C(4)–Mo(1)–C(7)	75.3 (2)	C(1)–Mo(1)–C(5)	142.7 (2)
C(4)–Mo(1)–C(8)	73.1 (2)	C(1)–Mo(1)–C(7)	145.9 (2)
C(5)–Mo(1)–C(6)	78.3 (2)	C(2)–Mo(1)–C(7)	142.7 (2)
C(5)–Mo(1)–C(7)	71.0 (2)	C(3)–Mo(1)–C(6)	146.1 (2)
C(6)–Mo(1)–C(8)	71.1 (2)	C(3)–Mo(1)–C(8)	142.2 (2)
C(7)–Mo(1)–C(8)	77.6 (2)	C(4)–Mo(1)–C(6)	143.4 (2)
N(2)–C(2)–Mo(1)	178.6 (4)	N(1)–C(1)–Mo(1)	179.6 (4)
N(4)–C(4)–Mo(1)	177.8 (4)	N(3)–C(3)–Mo(1)	178.3 (4)
N(5)–C(5)–Mo(1)	179.1 (4)	N(6)–C(6)–Mo(1)	178.2 (5)
N(8)–C(8)–Mo(1)	178.4 (4)	N(7)–C(7)–Mo(1)	179.4 (3)

RESULTS AND DISCUSSION

Characterization of the complexes

When the diquat dibromide is added to an aqueous solution of $H_4[M(CN)_8]$, the originally yellow colour changes to brownish-red (Mo) or green (W). (**1**) and (**2**) crystallize in the form of intensely coloured purple (**1**) or green (**2**) needles. They are soluble in water and insoluble in common organic solvents. Both salts are photosensitive as solids and in solution, but in diffused light they remain unaltered for a long period.

The thermograms show that dehydration takes place in two steps. The weight loss measurements indicate that in the first step at *ca.* $t_{max} = 90$ °C (**1**) or 70 °C (**2**) four water molecules are released. The remaining strongly bonded water molecule leaves at $t_{max} = 120$ °C (**1**) or 115 °C (**2**). The anhydrous salts are stable up to about 250 °C (**3**) and 280 °C (**4**), at which temperatures endothermal decomposition processes occur without separated steps.

The anhydrous salts (**3**) and (**4**) can be obtained by thermal dehydration of (**1**) and (**2**) at 100 °C for about two hours. They differ in colour from their hydrated analogues: (**3**) is green and (**4**) is brown. Exposed to humid air they gather moisture and return to their original colour and composition. This suggests that the water of crystallization fills structural cavities and becomes zeolitic in nature.

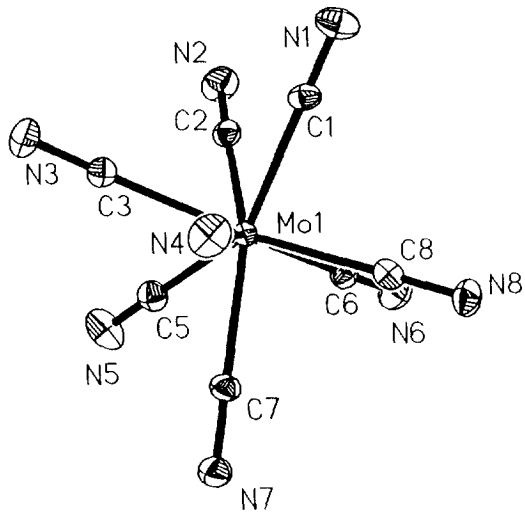

Fig. 1. The structure of $[Mo(CN)_8]^{4-}$ anion.

Structure

The crystal structure determination of (**1**) and (**2**) show that both salts are isomorphic. The metal atom is bonded to eight CN^- ligands (Figure 1) with coordination geometry close to dodecahedral (D_{2d} symmetry). An ideal dodecahedron is characterized by a set of shape parameters (Figure 2). There are two models proposed for the dodecahedral symmetry: the purely geometrical hard sphere model (HSM with parameters: $\theta_A = 36.9$, $\theta_B = 69.5$, a = m = g = 1.20, b = 1.50) and the so-called most favourable polyhedron (MFP: $\theta A = 35.2$, $\theta_B = 73.5$, a = m = 1.17, g = 1.24, b = 1.49), which includes the ligand-to-ligand repulsion energy minimalization [10]. The second approach results in two interpenetrating bispheroids and two symmetry-equivalent sets of metal-ligand bonds: longer M-L_A ('elongated' tetrahedron) and shorter M–L_B ('flattened' tetrahedron). The two groups of ligands with different bond lengths can be identified in the structure of (**1**) and (**2**), with the average metal-nitrogen distances: Mo–N_A = 3.322 Å, W–N_A = 3.327 Å (N2, N4, N5, N8) and Mo–N_B = 3.303 Å, W–N_B = 3.301 Å (N1, N3, N6, N7) Table 1. Such two sets of bonds were found for the anion of approximated D_{2d} symmetry in $(C_6H_6NO_2)_4[Mo(CN)_8]$ [11], $Rb_4[Mo(CN)_8]\cdot 3H_2O$ [12] and $K_5[Nb(CN)_8]$ [13], but no significant differences in bond lengths were observed for $(n\text{-}Bu_4N)_3[M(CN)_8]$ [14] and $K_4[M(CN)_8]\cdot 2H_2O$ [15] (M = Mo or W) (also approximated to D_{2d}). The values of shape parameters for (**2**) ($\theta_A = 36.4°$, $\theta_B = 73.3°$, a = 1.19, m = 1.16, g = 1.24, b = 1.47) are in good agreement with those calculated for the most favourable polyhedron model. Thus the $(dq)_2[M(CN)_8]\cdot 5H_2O$ structure belongs to the group of the best dodecahedrons known for molybdenum and tungsten octacyano complexes. (**1**) and (**2**) are also the first $[M(CN)_8]^{4-}$ salts with a high content of water of crystallization which exhibit D_{2d} symmetry of anion [1].

The M–C≡N chain is nearly linear, with bond angle differing from 180° by no more than 3°.

The diquat cations (Figure 3) are in preferred cis conformation with the angle between the pyridine rings equal to 22.9°. The bond lengths and bond angles Table 2 are almost the same as in the dibromide salt [16].

The $[M(CN)_8]^{4-}$ anions and the dq^{2+} cations form a three-dimensional net connected by hydrogen bonds (Figure 4). There are two non-equivalent locations of diquat in that net. A set of cations in positions parallel

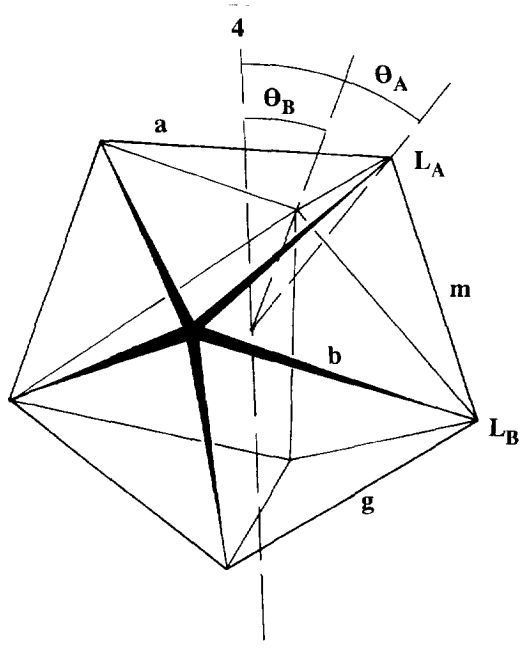

Fig. 2. Ideal dodecahedron with shape parameters.

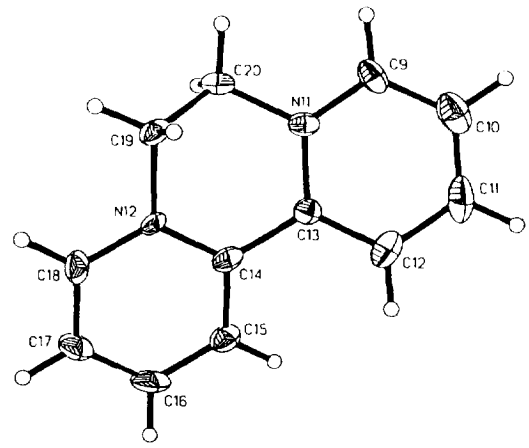

Fig. 3. The structure of diquat cation.

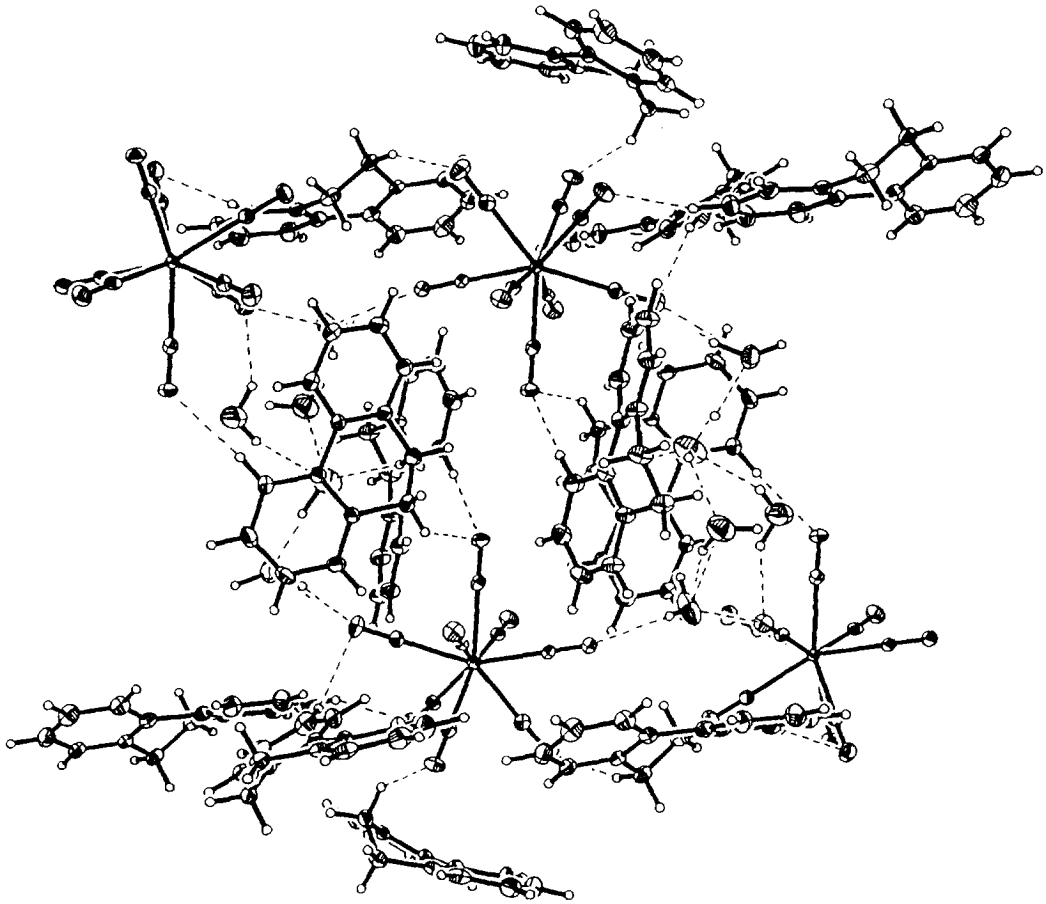

Fig. 4. The structure of $(dq)_2[Mo(CN)_8]\cdot 5H_2O$ (**1**).

to the z axis (central part of Fig. 4) separates layers containing cations perpendicular to the z axis (top and bottom part of Fig. 4).

The net is stabilized by strong hydrogen bonds (Figure 5) between cyanide nitrogens and water molecules (e.g. N1-O1 = 2.83 Å, N4-O1 = 2.88 Å) and water molecules (O1-O2 = 2.79 Å). In contrast to other similar species, there are also weak hydrogen bonds including cyanide nitrogen and cation aromatic carbon (e.g. N3-C21 = 2.97 Å), cyanide nitrogen and cation ethylene carbon (N5-C31 = 3.25 Å), and cation ethylene carbon and water molecule (C19-O5 = 3.26 Å).

The water molecules are close to each other linked through hydrogen bonds and form a column that fills a tunnel along the x axis (Figure 6). The distances between water oxygens and the bond angles are very close to those in ice, indicating weak interaction with ions. This is consistent with the zeolitic character of the water of crystallization shown by reversible dehydration at relatively low temperature. The differences in water molecule environments account for the two-step dehydration: the strongest bonded water molecule O1, linked *via* hydrogen bonds to two anions and to two other water molecules can be identified as the one released at higher temperature.

Spectra

In comparison to analogous potassium salts the visible spectra of (**1**) and (**2**) in aqueous solution show new absorption band in the 500–650 nm region (Figure 7) assigned to optical charge transfer (IPCT) from complex anion to diquat cation. Similarly to other polypyridinium octacyanometallates [3, 4] the tungsten compound absorbs light of lower energy than its molybdenum analogue ($\lambda_{max} = 545$ (Mo) and 625 nm (W)), due to the lower reduction potential of tungsten in the $[M(CN)_8]^{3-}/[M(CN)_8]^{4-}$ couple (0.78 V (Mo), 0.51 V (W) in water solution). In diluted solution, where ion-pairing is incomplete, the IPCT bands have low intensity. In the solid state they become stronger than $[M(CN)_8]^{4-}$ d-d transitions and shift to longer wavelength (592 for (**1**) and 710 nm for (**2**)). This bathochromic shift is justified by the Marcus-Hush theory [17, 18], according to which the energy of

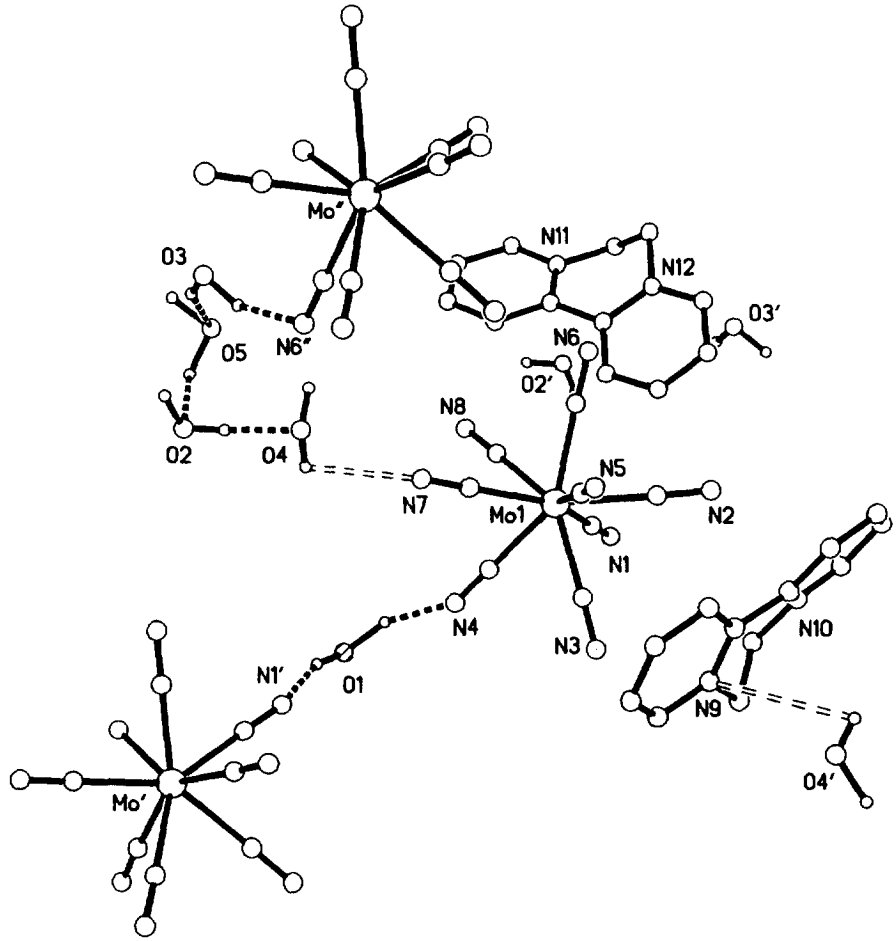

Fig. 5. Hydrogen bonds (broken filled line) and weak interactions of hydrogen-bond type (broken empty line) in the structure of (**1**).

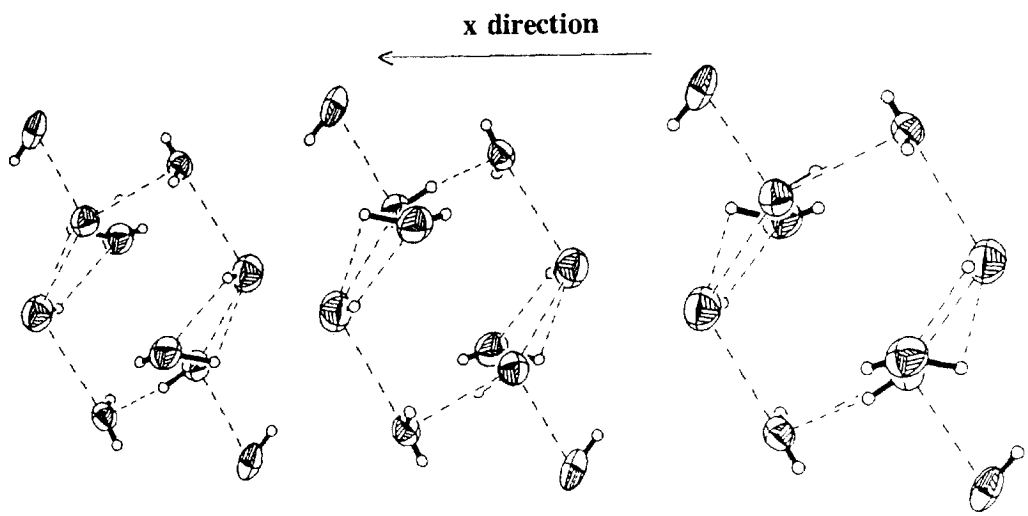

Fig. 6. The arrangement of water molecules in (**1**).

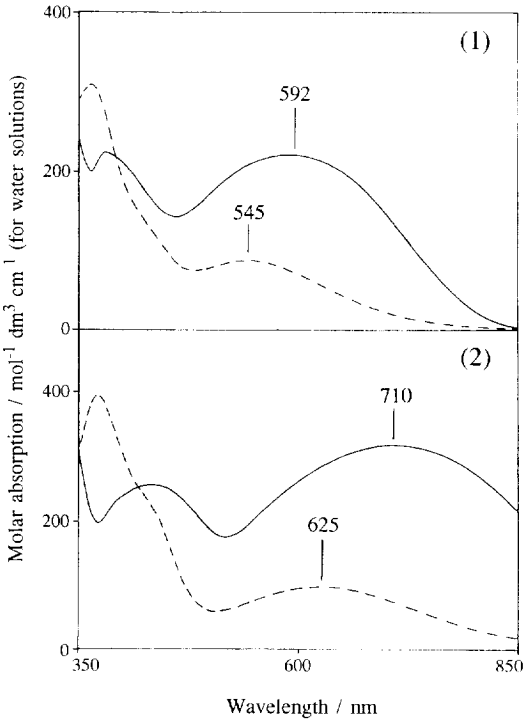

Fig. 7. Electronic absorption spectra in water solutions (broken line) and reflectance spectra (solid line) of $(dq)_2[Mo(CN)_8]\cdot 5H_2O$ (**1**) and $(dq)_2[W(CN)_8]\cdot 5H_2O$ (**2**).

optical electron transfer decreases as the distance between reacting moieties becomes shorter. The values of the shift, equal to 1500 (Mo) and 1900 cm^{-1} (W), fall between those observed for other bipyridinium octacyanomolybdates and tungstates [3, 4], so it seems that neither the extremely short distance between ions nor direct hydrogen bonding of the anion to cation carbons affect the process of optical electron transfer.

In the case of tungsten salts (**2**) and (**4**) the presence of the IPCT band in the electronic spectra is accompanied by 'real' electron transfer from anion to cation. The metal configuration changes from diamagnetic d^2 to paramagnetic d^1, so that an ESR signal due to this transition can be observed. The amount of paramagnetic (d^1) M(V) centres in (**2**) and (**4**) (0.67% and 2.19%) are of the same order of magnitude as for other salts [3, 4]. The increased paramagnetism observed for the anhydrous salt is connected with the shorter distance between ions. Molybdenum compounds (**1**) and (**3**) remain diamagnetic, which corresponds to the lower oxidation potential of molybdenum (IV) octacyanide.

The IR spectra of (**1**), (**2**), (**3**) and (**4**) (Table 3) are dominated by the bands of cation origin which change their position and intensity slightly in comparison to $dqBr_2\cdot H_2O$. This can be explained by the hydrogen bonding to anion. The differences are easily recognizable in the C–H stretching mode region (2950–3100 cm^{-1}).

The strong absorption near 2100 cm^{-1} is associated with C≡N stretching. This region is considered indicative of $[M(CN)_8]^{4-}$ local symmetry. Group theory predicts 2 IR and 3 Raman vibrational modes for D_{4d} and 4 IR and 6 Raman for D_{2d} symmetry [19, 20]. The number of absorption bands alone cannot be used to estimate geometry, because real structures are hardly ever ideal polyhedra. However the shape of the band (Figure 8) is a very characteristic feature, and provides enough information for rough symmetry estimation to be made.

Table 3. Selected IR absorption bands (cm^{-1})*

$dqBr_2$	**1**	**2**	**3**	**4**	assignment
773 w	771 s	771 s	771 s	771 s	γ (C–H)
793 vs	781 s	781 s			
1286 s	1288 s	1288 s	1286 m	1286 m	
1464 m	1469 m	1469 m			ring stretching
1496 vs	1501 vs	1501 vs	1498 s	1498 s	
1579 m	1584 s	1584 m	1581 m	1581 m	
1613 s	1615 vs	1615 vs	1613 s	1613 vs	
	2061 w	2057 w	2079 s	2072 vs	
	2099 vs	2095 vs	2086 vs	2082 vs	ν (C≡N)
	2114 vs	2117 vs	2095 s	2091 vs	
			2106 s	2104 s	
2866 vw		2854 vw			ν (C–H) aliphatic
2916 vw		2926 vw			
2951 w	2997 w	2996 w			
3000 w	3016 vw	3014 vw			ν (C–H) aromatic
3043 w	3077 v	3061 vw			
3062 w	3096 w	3096 w			

*$dqBr_2$, (**1**) and (**2**) spectra were measured in KBr pellets, (**3**) and (**4**) as nujol mulls.

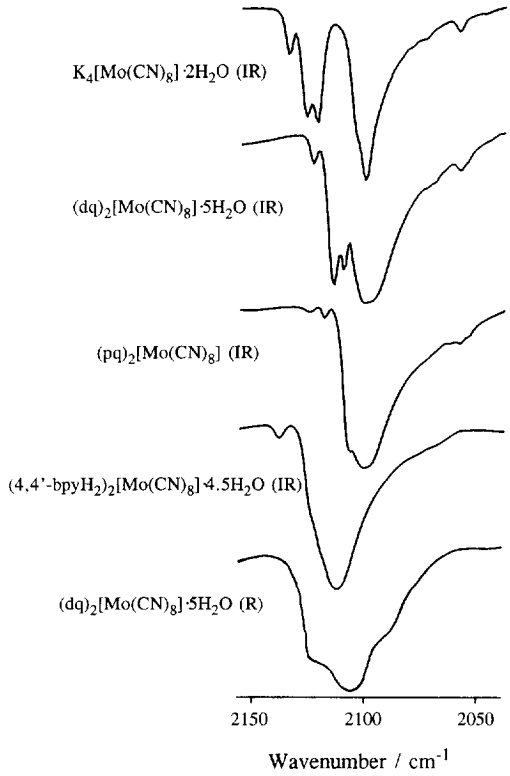

Fig. 8. IR (solid state) and Raman (solution) spectra of selected $[Mo(CN)_8]^{4-}$ salts in CN stretching region.

CONCLUSIONS

It was found that i) isomorphic salts (**1**) and (**2**) have anions of approximately D_{2d} symmetry, providing one of the best dodecahedrons known for molybdenum and tungsten octacyanides; ii) cation and anion are directly linked *via* hydrogen-bonds between cyanide nitrogens and diquat carbons; iii) the water of crystallization fills linear cavities in the structure and has a zeolitic character shown by reversible dehydration; iv) the electronic spectra in both solids and solutions show new band characteristic for outer-sphere charge-transfer within the ion pair; v) there is no significant connection between direct hydrogen bonding between ions and the character of optical and thermal electron transfer; this problem needs further investigation.

Acknowledgements—This work was supported in part by the Polish Grant Committee, KBN No. 141/T09/95/09.

REFERENCES

1. Samotus, A. and Szklarzewicz, J., *Coord. Chem. Rev*, 1993, **125,** 62 and references therein.
2. Leipoldt, J. G., Basson, S. S. and Roodt, A. in *Advances in Inorganic Chemistry*, vol. 40, (ed. A. G. Sykes), and references therein, (1993).
3. Szklarzewicz, J., Samotus, A. and Kanas, A., *Polyhedron*, 1986, **5,** 1733.
4. Alcock, N. W., Samotus, A. and Szklarzewicz, J., *J. Chem. Soc. Dalton Trans.*, 1993, 885.
5. Leipoldt, J. G., Bok, L. C. D. and Cilliers, P.J., *Z. Anorg. Allg. Chem*, 1974, **409,** 343.
6. Leipoldt, J. G., Bok, L. D. C. and Cilliers, P. J., *Z. Anorg. Allg. Chem*, 1974, **407,** 350.
7. Samotus, A., Kosowicz-Czajkowska, B., *Roczniki Chem*, 1971, **45,** 1623.
8. *Merck Index* 3370, ninth edition, 1976, p. 449.
9. Sheldrick, G. M., SHELXTL, ver. 5.0, 1996.
10. Hoard, J. L. and Silverton, J. V., *Inorg. Chem*, 1963, **2,** 235.
11. Basson, S. S., Leipoldt, J. G. and van Wyk, A. J., *Acta Crystallogr*, 1980. **B36,** 2025.
12. Semenishyn, D. I., Glowiak, T. and Myskiv, M. G., *Koord. Khim. (Russ)*, 1985, **11,** 122.
13. Hursthouse, M. B., Galas, A. M., Soares, A. M. and Griffith, W. P., *J. Chem. Soc. Chem. Commun.*, 1980, 1167.
14. Corden, B. J., Cunningham, J. A. and Eisenberg, R., *Inorg. Chem*, 1970, **9,** 356.
15. Hoard, J. L., Hamor, T. A. and Glick, M. D., *J. Am. Chem. Soc*, 1968, **90,** 3177.
16. Sullivan, P. D. and Williams, M. L., *J. Am. Chem. Soc*, 1976, **98,** 1711.
17. Kisch, H., Dümler, W., Nüßlein, F., Zenn, I., Chiorboli, C., Scandola, F., Albrecht, W. and Meier, H., *Z. Phys. Chem*, 1991, **170,** 117 and references therein.
18. Billing, R., Rehorek, D. and Hennig, H., *Topics in Current Chemistry*, 1990, **158,** 151.
19. Long II, T. V. and Vernon, G. A., *J. Am. Chem. Soc*, 1971, **93,** 1919.
20. König, E., *Z. Naturforsch*, 1968, **23,** 853.

Pergamon

PII: S0277-5387(98)00087-4

Polyhedron Vol. 17, No. 18, pp. 3175–3180, 1998
© 1998 Elsevier Science Ltd
All rights reserved. Printed in Great Britain
0277-5387/98 $19.00+0.00

Synthesis and characterization of cyanohydroisocyanoborates. Reactivity of the isocyano group towards nucleophiles

Béla Győri*, Zoltán Berente and István Lázár

Department of Inorganic and Analytical Chemistry, Lajos Kossuth University, P.O. Box 21., H-4010, Debrecen, Hungary.

(Received 27 January 1998; accepted 26 February 1998)

Abstract—$AgCNBH_2CN$ and $AgCNBH(CN)_2$ were synthesized with AgCN in Me_2S from $Me_2S{\cdot}BH_2CN$ and 4-cyanopyridine·$BH(CN)_2$, respectively. These silver complexes were transformed into $Na[BH_2(CN)NC]$ and $Na[BH(CN)_2NC]$ salts. In these hydrolytically very stable borates the isocyano group proved to be the most reactive site. This observation was demonstrated by reactions with nucleophiles, namely H_2S, NH_4N_3 and NH_4SCN. In the first two cases isocyano group underwent transformation into $-N(H)-C(H)=S$ and -1-(5H)tetrazolyl groups, respectively, which remarkably increase the stability of hydroborates towards acidic hydrolysis. Unlike alkyl- or arylisocyanides, isocyano groups here do not form ring in reaction with NH_4SCN, but most probably transform into $-N=C(H)-NCS$ groups. All compounds, including the *E*- and *Z*-isomers (where appropriate), were characterized by IR, ^1H, ^{11}B and ^{13}C NMR spectroscopy. © 1998 Elsevier Science Ltd. All rights reserved

Keywords: cyanohydroisocyanoborates; cyanohydrothioformamidoborates; cyanohydrotetrazolylborates; *E,Z*-isomerism; multinuclear NMR.

A large number of cyanoboron compounds, containing B-CN units, have become known so far and sodium cyanoborohydride play a distinguished role in organic and organometallic syntheses. However, the number of isocyanoboron compounds, with B-NC units, prepared in the last two decades is quite limited. Several amine-isocyanoboranes ($A{\cdot}BH_2NC$) have been synthesized from the corresponding iodoborane complexes with transition metal cyanides or cyano complexes [1–4]. Moreover, their silver [1, 2], manganese [1] and nickel [4] complexes have also been reported. Chemical properties of amine-isocyanoboranes have not been extensively studied yet, however, in comparison with alkyl isocyanides $Me_3N{\cdot}BH_2NC$ appeared similar [5] but somewhat stronger in basicity [3].

Likewise, only a few representatives of isocyanoborates have been reported so far. The formation of $Na[BH_3NC]$ [6] was disproved based on our detailed investigations [7]. Nevertheless, silver complexes and sodium salts of bis- and tris-isocyanohydroborates could be obtained in pure form and proved rather stable towards both isomerisation and acidic hydrolysis [8]. Furthermore, borate ions with composition $[BX_2(NC)_2]$ (X=F,Br,Ph) are known also, but exclusively as ligands in cyclopentadienyl-carbonyl-μ-(bisisocyano-dihydroborate) complexes [9].

Hydrolytic stabilities of $Na[BH_2(NC)_2]$ and $Na[BH(NC)_3]$ are markedly lower than those of corresponding cyanohydroborates [8]. In reactions with HCl, amine hydrochlorides or bromine, the desired borane $BH(NC)_2$ or its amine complexes could not be obtained, apart from pyridine·$BH(NC)_2$, which was synthesized in low yield [8]. Studying the possibilities of chemical transformations to be made on the isocyano group (with H_2S, NH_4N_3 or NH_4SCN), we found that reactions generally led to decomposition, accompanied by extensive isomerization into cyanohydroborates, particularly in the case of $Na[BH_2(NC)_2]$. In order to obtain more stable isocyanoborates, we attempted to synthesize

* Corresponding Author. Tel.: +36-52-316666/2002, Fax: +36-52-489667, E-mail: bgyori@tigris.klte.hu.

compounds, which, besides isocyano group, contain strong electron-withdrawing cyano group(s) attached to boron. Here we report the preparation of two cyanohydroisocyanoborates and some reactions they are involved in.

EXPERIMENTAL

General comments

All reactions, except those involving water or noted otherwise, were performed under an oxygen and water free N_2 atmosphere using the general Schlenk techniques in flamed or oven dried glassware with absolutized solvents freshly distilled prior to use.

Me_2S was dried with sodium, then fractionally distilled. MeCN was dried over CaH_2, then distilled from P_2O_5. Ether and dioxane were distilled from Na–benzophenone. Acetone was distilled from a 1.5 m Raschig packed column. Pentane was fractionally distilled.

$(BH_2CN)_n/Me_2S$ [8, 10], 4-CN-py·$BH(CN)_2$ [8] and NH_4N_3 [11] were prepared by known methods. AgCN, NH_4Cl (Reanal), $Na_2S·9H_2O$, H_2S and NaN_3 (Merck) were used as received.

NMR spectra were recorded on a Bruker AM 360 instrument in 5 mm o.d. tubes. ^1H spectra were referred to DSS in D_2O and TMS in acetone. ^{13}C (90.5 MHz) spectra were referred to deuterated solvent signals in acetone-d_6 (29.9 ppm) and DSS in D_2O (0.00 ppm) as external reference. The measurements were run with quite concentrated solutions (≈ 1 M) and relatively long relaxation delays (usally 12 s) to approach quantitativity. Where assigning the spectra necessitated, homonuclear decoupling and *J*-modulated experiments were carried out. ^{11}B (115.5 MHz) spectra were referred to $Et_2O·BF_3$ in a capillary inserted into the tube. The coupling constants, unless otherwise noted, were measured between adjacent nuclei.

IR spectra were recorded on a Perkin Elmer Paragon PC 1000 FT-IR spectrometer.

The boron content of the samples was determined with acid-base titration in the presence of mannitol after fusion with NaOH and KOH.

Syntheses

$AgCNBH_2(CN)$ (*1*). A methyl sulfide solution of cyanodihydroborane (50.0 ml 1.876 M, 93.8 mmol) was added dropwise to the stirred methyl sulfide solution (30 ml) of silver cyanide (12.56 g, 93.81 mmol). At the beginning the solution turned black, due to the appearance of a small amount of silver, and later some precipitate fell out. This mixture was kept stirred at r.t. for 20 h, then filtered, and the filtrate was evaporated *in vacuo* to obtain a mixture of a solid and an oil. Acetonitrile (5 ml) was added to this residue, which completely solidified upon thorough evaporation *in vacuo*. The solid was redissolved in acetonitrile (40 ml), the insoluble parts were filtered off. The filtrate was evaporated to dryness *in vacuo*, the solid residue was suspended in ether (30 ml) and the suspension was filtered. The product was washed with ether (3 × 10 ml) and dried in a N_2-stream to give a light brown powder. Yield: 13.52 g (83%). Anal. Calcd for $C_2H_2AgBN_2$: B, 6.26. Found: B, 6.09%. IR (KBr, cm^{-1}): ν(B-H) 2422, 2405; ν(C≡N) 2223, 2198. ^{11}B NMR (CH_3CN):δ −27.2 (t, $J_{BH} = 98$ Hz).

$AgCNBH(CN)_2·CH_3CN$, $AgCNBH(CN)_2$ (*2*). Silver cyanide (16.07 g, 120 mmol) was added to the methyl sulphide suspension (80 ml) of 4-cyanopyridine-dicyanoborane (10.09 g, 60.07 mmol), and the mixture was refluxed for 48 h. The insoluble parts were filtered off and evaporation of the filtrate *in vacuo* gave a solid of constant weight. This solid was placed on a filter and 4-cyanopyridine was removed by extraction with acetone (50 ml) 25 times. The residue was dried with a N_2-stream and extracted with acetonitrile (60 ml) five times to separate the product from excess silver cyanide. The extract was evaporated *in vacuo* to leave a few mls of acetonitrile besides the solid residue. Ether (25 ml) was added to the residue, the product was filtered, washed with ether (3 × 10 ml) and dried in a N_2 stream to obtain 10.66 g (74%) $AgCNBH(CN)_2·CH_3CN$. This was in turn suspended in water (60 ml), the slurry was vigorously stirred for 2 h, filtered, the solid residue was washed with water (3 × 10 ml) and dried in a N_2 stream. Yield: 8.77 g (74%). Anal. Calcd for: B, 5.47. Found: B, 5.32%. IR (KBr, cm^{-1}): ν(B-H) 2453, ν(C≡N) 2212. ^{11}B NMR (CH_3CN):δ −27.9 (d, $J_{BH} = 108$ Hz).

$Na[BH_2(CN)NC]$ (*3*). To a stirred aqueous suspension of $AgCNBH_2(CN)$ (10.12 g, 58.59 mmol in 10 ml) was added an aqueous solution of $Na_2S·9H_2O$ (6.85 g, 28.5 mmol in 10 ml) in 5 min. Na_2S solution (0.300 M) was then added in small (0.1 − 0.2 ml) portions until a sample of the supernatant caused browning of approx. the same extent with Na_2S and lead(II) acetate solutions on a filter paper. Silver sulfide was separated on a filter and washed with water (3 × 15 ml). The washings were combined with the filtrate and evaporated *in vacuo* under r.t. to obtain a viscous resin. (In the final period of the evaporation blackening and precipitation of a gelly solid may occur.) The residue was dissolved in ether (40 ml), evaporated *in vacuo*, redissolved in ether and evaporated again. The residue was mixed with ether (40 ml) to give a two-phase system, and in case it was not clear, it was filtered. The filtrate was evaporated and the residue was kept under vacuum for 2 h. Pentane (25 ml) was added, the product was collected on a filter, washed with pentane (10 ml) and dried in a N_2 stream. Yield: 4.53 g, 88%. Anal. Calcd for $C_2H_2BN_2Na$: B, 12.31. Found: B, 12.14. IR (KBr, cm^{-1}): ν(B-H) 2406; ν(C≡N) 2204; ν(N≡C) 2157. ^1H NMR (D_2O):δ 1.75 (br q, BH). ^{11}B NMR (D_2O):δ −29.9 (t, $J_{BH} = 102$ Hz). ^{13}C $\{^1H\}$ NMR (D_2O):δ

162.86 (s, 1C, BNC), 139.49 (q, 1C, BCN, $J_{BC}=56$ Hz).

Na[BH(CN)$_2$NC] (**4**). To a stirred aqueous suspension of AgCNBH(CN)$_2$·CH$_3$CN (5.10 g, 21.4 mmol in 5 ml) was added Na_2S solution (34.50 ml, 0.300 M, 10.4 mmol) in 5–10 min. The addition of this solution was continued by 0.1 ml portions until the supernatant over silver sulfide became clear, and then administered by 50 μl portions until addition of a new portion caused no opalescence at the spot of instillation. After 0.5 h stirring silver sulfide was filtered off, washed with water (3 × 5 ml) and the filtrate combined with the washings was evaporated *in vacuo* under 40 C to yield a viscous resin. The residue was triturated with ether (20 ml), which was in turn removed with a N_2 stream and the residue was kept under vacuum for 1 h. The remaining solid was suspended in ether (20 ml), collected on a filter, washed with ether (2 × 5 ml) and dried in a N_2 stream. Yield: 2.37 g, 98%. Anal. Calcd for C_3HBN_3Na: B, 9.58. Found: B, 9.40%. IR (KBr, cm^{-1}): ν(B-H) 2445; ν(C≡N) 2224; ν(N≡C) 2167. ^{1}H NMR (D_2O):δ 2.3 (br q, BH). ^{11}B NMR (D_2O):δ −30.3 (d, $J_{BH}=108$ Hz). ^{13}C $\{^1H\}$ NMR (D_2O):δ 167.13 (s, 1C, BNC), 132.6 (br q, 2C, BCN, $J_{BC}=64$ Hz).

Na[BH$_2$(CN)(N(H)C(H)=S)] (**5**). To an aqueous suspension of AgCNBH$_2$(CN) (1.55 g, 8.97 mmol in 3 ml) was added Na_2S solution (14.55 ml 0.300 M, 4.37 mmol) in 3–5 min. The addition of Na_2S solution was continued dropwise until a sample of the supernatant caused browning of approx. the same extent with Na_2S and lead(II) acetate solutions on a filter paper. Hydrogen sulfide was bubbled through the vigorously stirred solution for 30 min. Silver sulfide was filtered off, the filtrate was evaporated and acetonitrile (5 ml) was added to the residue. It was then evaporated, the residue was redissolved in acetonitrile (8 ml), the insoluble parts were filtered off, the filtrate was evaporated *in vacuo* until the solidification was complete. Ether (10 ml) was added to the product, it was then collected on a filter, and dried in a N_2 stream.

Yield: 0.93 g (85%). Anal. Calcd for $C_2H_4BN_2NaS$: B, 8.87. Found: B, 8.97%. IR (KBr, cm^{-1}): ν(N-H) 3348(*Z*), 3330(*E*); ν(B-H) 2381(*Z*), 2383(*E*); ν(C≡N) 2191(*Z*), 2196(*E*); (thioamide B) 1507, 1463(*Z*), 1539(E); ν(CS) 794(*Z*), 821(*E*). ^{1}H NMR (D_2O):δ 9.22 (s, 1H, (*Z*)-C(=S)H), 8.85 (s, 1H, (*E*)-C(=S)H); 2.05 (br q, (*Z*)-BH), 2.0 (br q, (*E*)-BH). ^{11}B NMR (D_2O):δ −26.8 (t, (*Z*), $J_{BH}=96$ Hz), −23.1 (t, (*E*), $J_{BH}=98$ Hz). ^{13}C $\{^1H\}$ NMR (D_2O):δ 191.76 ((*Z*)-C=S), 193.77 ((*E*)-C=S); 138.5 (br q, (*ZE*)-BCN).

Na[BH(CN)$_2$(N(H)C(H)=S)]·C$_4$H$_8$O (**6**). To a stirred aqueous suspension of AgCNBH(CN)$_2$·CH$_3$CN (1.202 g, 5.03 mmol in 1 ml) was added Na_2S solution (8.00 ml, 0.300 M, 2.40 mmol) in 5–10 min. The addition of this solution was continued by 50 μl portions until the supernatant over silver sulfide became clear, and then administered by 25 μl portions until addition of a new portion caused no opalescence at the spot of instillation. Hydrogen sulfide was bubbled through the vigorously stirred solution for 80 min. Silver sulfide was filtered off, the filtrate was evaporated and the yellowish resinous residue was dissolved in acetonitrile (6 ml). The insoluble parts were filtered off, and the filtrate was evaporated *in vacuo*. Ether (5 ml) and then dioxane (0.7 ml) were added to the resinous residue, which solidified upon trituration in minutes. The product was collected on a filter, washed with an ether-dioxane (10:1) mixture (2 × 3 ml), then with ether (1 × 3 ml) and dried in a N_2 stream. Yield: 1.13 g (96%). Anal. Calcd for $C_7H_{11}BN_3NaO_2S$: B, 4.60. Found: B, 4.49%. IR (KBr, cm^{-1}): ν(N-H) 3229(*ZE*); ν(B-H) 2403 (*Z*), 2436 (*E*); ν(C≡N) 2232 (*Z*), 2216 (*E*); (thioamide B) 1502, 1456 (*Z*), 1534 (*E*); ν(CS) 727(*Z*), 754(*E*). ^{1}H NMR (D_2O):δ 9.37 (s, 1H, (*Z*)-C(=S)H), 9.05 (s, 1H, (*E*)-C(=S)H); 3.74 (s, 8H, DO); 2.6 (br q, 1H, (*Z*)-BH), 2.5 (br q, 1H, (*E*)-BH). ^{11}B NMR (D_2O):δ −27.7 (d, (*Z*), $J_{BH}=103$ Hz), −24.5 (d, (*E*), $J_{BH}=103$ Hz). ^{13}C $\{^1H\}$ NMR (D_2O):δ 196.42 (*Z*)-(C=S), 198.05 (*E*)-(C=S); 134.4 (br q, (*ZE*)-BCN, $J_{BC}\approx 60$ Hz); 69.42 (DO).

Na[BH$_2$(CN)(1-(5H)-tetrazole)] (**7**). Na[BH$_2$(CN)NC] (0.460 g, 5.24 mmol), sodium azide (0.341 g, 5.24 mmol) and ammonium chloride (0.280 g, 5.24 mmol) were suspended in acetonitrile (5 ml). The mixture was refluxed for 3 h, then cooled to r.t.. Sodium chloride was filtered off, washed with acetonitrile (3 ml) and the filtrate combined with the washings was evaporated *in vacuo*. Ether (15 ml) was added to the extremely vigorously stirred residual oil, the solid product was collected on a filter, extracted with the filtrate twenty times and dried with a N_2 stream. Yield: 0.38 g (55%). Anal. Calcd for $C_2H_3BN_5Na$: B, 8.26. Found: B, 8.21%. IR (KBr, cm^{-1}): ν(C-H) 3150; ν(B-H) 2424, 2377; ν(C≡N) 2216. ^{1}H NMR (D_2O):δ 8.81 (s, 1H, CH), 2.7 (br q, 2H, BH). ^{11}B NMR (D_2O):δ −24.1 (t, $J_{BH}=103$ Hz). ^{13}C $\{^1H\}$ NMR (D_2O):δ 150.72 (s, 1C, CH), 139.6 (br, 1C, BCN).

Na[BH(CN)$_2$(1-(5H)-tetrazole)] (**8**). To an aqueous solution of Na[BH(CN)$_3$NC] (0.480 g, 4.25 mmol in 5 ml) ammonium azide (0.511 g, 8.50 mmol) was added. The reaction mixture was kept at 85 C for 1.5 h, then evaporated to dryness *in vacuo* in a 75–80 C bath. Ether (10 ml) was added to the residue, the suspension was filtered, and the product was extracted with the filtrate five times, then dried in a N_2 stream. Yield: 0.58 g, 88%. Anal. Calcd for $C_3H_2BN_6Na$: B, 6.94. Found: B, 7.08%. IR (KBr, cm^{-1}): ν(C-H) 3155; ν(B-H) 2460; ν(C≡N) 2231. ^{1}H NMR (D_2O):δ 8.99 (s, 1H, CH), 3.15 (br q, 1H, BH). ^{11}B NMR (D_2O):δ −25.1 (d, $J_{BH}=108$). ^{13}C $\{^1H\}$ NMR (D_2O):δ 150.59 (s, 1C, CH), 132.2 (br q, 2C, BCN).

RESULTS AND DISCUSSION

Synthesis of cyanohydroisocyanoborates (**1–4**)

In the methyl sulfide solution of BH_2CN, which is an equilibrium mixture of $Me_2S·BH_2CN$ and $(BH_2CN)_n$

(n = 5,6) [8], AgCN slowly expels Me_2S to form $AgCNBH_2CN$, according to eq. (1). Similarly, 4-cyanopyridine, a weak base, can be displaced from its complex with dicyanoborane in a similar but even slower reaction, using excess AgCN in methyl sulfide solution, as described in eq. (2).

$$Me_2S{\cdot}BH_2CN + AgCN \xrightarrow[\text{r.t., 20h}]{Me_2S} \underset{\mathbf{1}}{AgCNBH_2CN} \quad (1)$$

$$4\text{-CN-py}{\cdot}BH(CN)_2 + AgCN \xrightarrow[\text{reflux 48h}]{Me_2S} \underset{\mathbf{2}}{AgCNBH(CN)_2} + 4\text{-CN-py} \quad (2)$$

Reaction (1) is accompanied by the reduction of a small amount of Ag(I) into finely divided elementary silver. The extent of this side reaction became considerable at higher temperatures or in not satisfactorily absolutized solvents. Reaction (2) was carried out using 100% excess of AgCN and the product could be separated from the remaining AgCN with acetonitrile in the form of an adduct $AgCNBH_2CN{\cdot}CH_3CN$. Acetonitrile could be removed by stirring in aqueous suspension.

1 and **2** could be transformed into their sodium salts with sodium metal in THF in the presence of 10 mol% benzophenone, or with Na_2S in water.

$$AgCNBH_n(CN)_{3-n} \xrightarrow[\text{(i) Na, } Ph_2CO/THF\quad \text{(ii) } Na_2S/H_2O]{\text{(i) or (ii)}} \underset{\substack{\mathbf{3}\ (n=2)\\ \mathbf{4}\ (n=1)}}{Na[BH_n(CN)_{3-n}(NC)]} \quad (3)$$

In reactions with Na-benzophenone silver occasionally fell out in colloid form and the isomerization of B-NC group can also take place to a small extent. Transformation of **2** with Na_2S could be carried out with no problem, while after the transformation of **1**, **3** could be obtained with small amount of silver as impurity. Transformation was attempted using NaI in both water and acetone, but no pure material could be obtained this way, because of formation of silver isocyano-iodo mixed complexes.

The presence and number of hydrogens attached to boron was confirmed by ^{11}B NMR spectra. Accordingly, **1** gave a triplet and **2** showed a doublet in acetonitrile solution. Binding mode of CN groups could not be determined from IR spectra, since in solid phase both B-CN and B-NC groups can coordinate to silver, resulting two nearby $\nu(C\equiv N)$ bands in the case of **1** and one broad $\nu(C\equiv N)$ band for **2** in the 2198–2223 cm^{-1} region. This is in agreement with the fact, that B-CN and B-NC groups give rise to similar $\nu(C\equiv N)$ frequencies (2190–2218 cm^{-1}) in the silver complexes of $[BH_n(NC)_{4-n}]^-$ and $[BH_n(CN)_{4-n}]^-$ ions (n = 1,2) [8]. The presence of cyano and isocyano groups in **3** and **4**, obtained from the silver complexes as described in (3, ii), was confirmed by their IR and ^{13}C NMR spectra. Both compounds show IR resonances in the regions characteristic to both cyanoborates (2200–2230 cm^{-1}) and isocyanoborates (2150–2170 cm^{-1}) [8]. ^{13}C NMR spectroscopy is an excellent tool for the determination of the binding mode of CN groups, since carbons directly attached to boron give broad quartets, due to the nuclear spin of 3/2 and the quadrupolar moment of ^{11}B nuclei, while carbons in B-NC groups show sharp singlets 22–24 ppm downfield from B-CN signals.

Hydrolytic stabilities of **3** and **4** are similar to those of cyanotrihydroborate [12] and dicyanodihydroborate [8], respectively. ^{11}B NMR monitoring of their 1 M aqueous solutions showed 18% hydrolysis into H_3BO_3 in the case of **3** after 48 h at 50 °C, while **4** showed no detectable decomposition of this kind. Simultaneously, 39% of **3** underwent isomerization into dicyanodihydroborate, while the similar conversion of **4** did not reach 1 mol%. The remarkable difference between the rates of isomerization is in accordance with our earlier experience, namely the rate increases as the number of hydrogens attached to boron increases [7, 8].

Isocyano group is described quite reactive, however, undergoes electrophilic rather than nucleophilic attack [13]. Nevertheless, we found that isocyano groups in these compounds readily react with certain nucleophiles, namely H_2S, NH_4N_3 and NH_4SCN (Scheme 1), under mild conditions.

*Reactions of **3** and **4** with hydrogen sulfide*

Cyanohydroisocyanoborates do not react with H_2S neither in Me_2S, nor in MeCN, even at 1–5 bar. On the other hand, the addition of H_2S to isocyano group took place with ease in water at ambient conditions, leading to the formation of a thioformyl group on the nitrogen, analogously to isocyano groups attached to carbon [13]. The products **5** and **6** were obtained in high yields, **6** as a dioxane adduct.

Like secondary thioformamides, **5** and **6** appeared in the reactions as a mixture of *E*- and *Z*-isomers in *Z*/*E* proportions of 15.4 for **5** and 1.59 for **6**. The isomers could be distinguished by either their ^1H, ^{11}B or ^{13}C NMR signals and identified by the coupling constants ($^3J_{HH}$) between NH and CH protons [14]. This constant could not be observed in D_2O, as NH protons are in a fast exchange equilibrium with the solvent, but in acetone-d_6 they appeared 16 Hz for *E*- and undetectably small for *Z*-isomers, due to the significant line width of these signals at room temperature. From both mixtures pure *E*-forms could be obtained after isomerization in acetone at 55 °C for 10 h (**5**) and 1 h (**6**). The isomerization could not be completed in water, where a *Z*/*E* proportion of 0.63

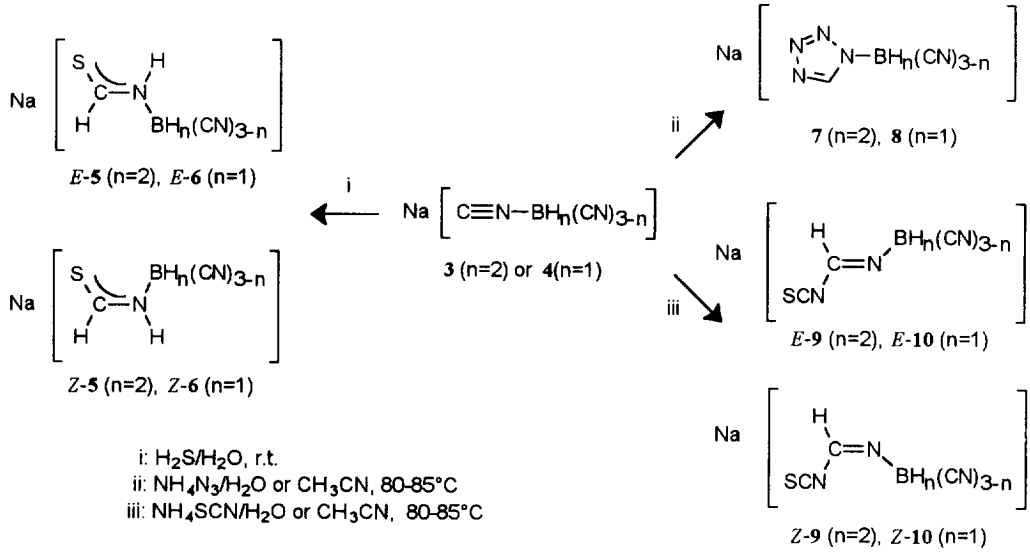

Scheme 1.

appeared to be equilibrial for **6** both at 50°C and 85°C. *Z*- and *E*-isomers show differences in their IR spectra as well, particularly the ν(N-H), thioformamide B (ν(CN) + NHR bending) and ν(CS) bands.

Both compounds are very stable towards acidic hydrolysis. Decomposition of **5**, accompanied by the simultaneous evolution of H_2 and H_2S, reached a considerable extent only in concentrated HCl. Decomposition of **6** was slow even in cc. HCl at boiling temperature, and the evolving gas could be identified as H_2S only. Of these experiences the former is more informative concerning the electronic effect of *N*-thioformamido group, since cyanotrihydroborate ion decomposes very quickly in 1 M HCl [12], while dicyanodihydroborate could be demolished only in cc. sulfuric acid at 100–120°C [8]. Thus, *N*-thioformamido group has a considerable electron-attracting effect which decreases the hydridic character of the hydrogen on the boron.

It should be noted, that the reaction of $Na[BH_2(NC)_2]$ with H_2S in water resulted in vigorous H_2 evolution and the formation of a red resin, which solidified upon treatment with ether. This product did not contain B-H group, but significant amount of NaSCN, identified by its intensive IR band at 2080 cm^{-1}.

Reactions of 3 and 4 with ammonium azide

Reactions between isocyanides and HN_3, producing 1-substituted tetrazoles, are rather slow in the absence of catalysts [15]. Azide ion could be added to isocyano groups in cyanohydroisocyanoborates also, to form 1-(5H)-tetrazolyl groups (Scheme 1) in relatively fast reactions.

Transformations of **3** could be accomplished with HN_3 in ether/THF, with NH_4N_3 (or NaN_3 and NH_4Cl) in acetonitrile or in water, or with NaN_3 in water in the presence of HCl. Yields, depending on the conditions, fall in a narrow range (46–65%). These reactions were accompanied by more or less isomerization of the isocyano groups, particularly in acidic aqueous medium, but the byproduct ($Na[BH_2CN)_2]$) could be separated from tetrazolylborate.

4 underwent an analogous reaction with NH_4N_3 either in acetonitrile or in water at 50–80°C. The transformation proceeded through intermediate of composition $[BH(CN)_2\text{-}N{=}C(H)\text{-}N_3]^-$ the *E*- and *Z*-isomers of which gave distinct signals both in ^1H and ^{11}B NMR spectra [*E*: δ(^1H, D_2O): 7.51 (s, CH), δ(^{11}B, D_2O): around −25.0 (d), under the signal of the endproduct; *Z*: δ(^1H, D_2O): 7.70 (s, CH), δ(^{11}B, D_2O): −28.8 (d)]. This intermediate accumulated to a remarkable extent (20–35 mol% depending on the conditions) in acetonitrile. In water the reaction was considerably faster, and the amount of the intermediate remained under 3–5% during the whole course of the reaction. Consequently, the ring closure, the second step of the reaction, seems to be favoured in water in comparison with acetonitrile.

Both tetrazolylborates are extremely stable towards acidic hydrolysis. Evolution of H_2 could be observed in cc. HCl solution of **7** only upon heating above 40–50°C. Decomposition of **8** is very slow in cc. HCl even at boiling temperature.

Contrary to **3** and **4**, in the reaction between $Na[BH_2(NC)_2]$ and HN_3 in ether/THF the presence of only a small amount of $[BH_2(CHN_4)_2]^-$ could be rendered likely by the appearence of IR bands at 3142

and 3136 cm^{-1} and a singlet at 8.98 ppm (D_2O) in ^1H NMR spectrum, but it could not be obtained in pure form.

Reactions of **3** *and* **4** *with ammonium thiocyanate*

Alkyl- and arylisocyanides react with two molar equivalents of HSCN to form 1-alkyl- or 1-aryl-2,4-dithioxo-1,2,3,4-tetrahydro-1,3,5-triazole rings [16]. In contrast, both **3** and **4** in both water and acetonitrile react with one molar equivalent of NH_4SCN exclusively. The reactions, monitored by means of ^{11}B NMR spectoscopy, were found considerably slower than those with NH_4N_3 and accompanied by decomposition into H_3BO_3 and isomerization of the isocyano group, particularly in the case of **3**. ^1H, ^{11}B and ^{13}C NMR spectra of the reaction mixtures strongly suggest that the main products of the reactions were most probably the mixtures of *E*- and *Z*-isomers of **9** [δ(^1H, D_2O): 7.61 s, (*Z*)-CH; 7.37 s, (*E*)-CH; δ(^{11}B, D_2O): -28.4 t, $J_{BH}=100$ Hz, (*Z*); -23.8 t, $J_{BH}=101$ Hz, (*E*)] and **10** [δ(^1H, D_2O): 7.69 s, (*Z*)-CH; 7.50 s, (*E*)-CH; δ(^{11}B, D_2O): -28.8 d, $J_{BH}=105$ Hz, (*Z*); -25.0 d, $J_{BH}=96$ Hz, (*E*)]. This assumption is based on the similarity to spectral patterns shown by **5**, **6** and the open-chain intermediates in the reactions between **3**, **4** and NH_4N_3. ^{13}C NMR spectra [δ(NCS) in D_2O: around 136 ppm] clearly confirmed that the products in question are isothiocyanates and not thiocyanates [17]. Despite our meticulous efforts, neither isothiocyanate derivative could be prepared in pure form.

CONCLUSION

Facile reactivity of isocyano group in cyanohydroisocyanoborates towards H_2S, NH_4N_3 and NH_4SCN implies the possibility of further versatile transformations. Anions in **3** and **4**, which possess exceptional hydrolyitic stability, can be regarded as potential ligands for transition metals, having three different possible coordinative sites. Indeed, platinum complexes of $[BH_2(CN)NC]^-$ ion have been recently reported formed in a reaction of coordinated cyanide [18]. With respect to the analogy between tetrazolyl and carboxyl groups [19], biological studies of **7** and **8** seems promising, in the light of the biological and pharmacological activities of carboxyboron compounds [20]. **5** and **7** are hydrolytically much more stable than **3**, consequently, *N*-thioformamido- and 1-(5H)-tetrazolyl groups appear to efficiently decrease the hydridic character of hydrogen in boron hydrides.

Acknowledgements This work was supported by the Hungarian Scientific Research Fund (OTKA T014985/1995).

REFERENCES

1. Vidal, J. L. and Ryschkewitsch, G. E., *J. Chem. Soc., Chem. Comm.*, 1976, 192.
2. Vidal, J. L. and Ryschkewitsch, G. E., *Inorg. Chem.*, 1977, **16,** 1898.
3. Miller, N. E., *Inorg. Chem.*, 1991, **30,** 2228.
4. Harris, G.L., Ryschkewitsch, G.E., *Proc.-NOBCChE*, 1995, **22**, 145; (*Chem. Abstr.*, 1996, **124**, 218656u).
5. Vidal, J. L. and Ryschkewitsch, G. E., *Inorg. Chem.*, 1977, **16,** 1673.
6. Wade, R. C., Sullivan, E. A., Berschied, R. J. Jr. and Purcell, K. F., *Inorg. Chem.*, 1970, **9,** 2146.
7. Emri, J. and Győri, B., *Polyhedron*, 1994, **13,** 2353.
8. Győri, B. and Emri, J., Fehér, I., *J. Organomet. Chem.*, 1983, **255,** 17 and refs therein.
9. Emri, J., Győri, B. and Bakos, A., Czira, G., *J. Organomet. Chem.*, 1976, **112,** 325.
10. Győri, B., Kovács, Z., Emri, J. and Lázár, I., *Inorg. Chim. Acta.*, 1994, **218,** 21.
11. Frost, W. S., Cothran, J. C. and Browne, A. W., *J. Am. Chem. Soc.*, 1933, **55,** 3516.
12. Kreevoy, M. M. and Hutchins, J. E. C., *J. Am. Chem. Soc.*, 1969, **91,** 4329.
13. Tennant, G., in *Comprehensive Organic Chemistry*, Ed. D. Barton and W. D. Ollis, Vol. 2., Pergamon, Oxford, 1979, p. 568.
14. Walter, W. and Voss, J., in *The chemistry of amides*, Ed. J. Zabicky, Interscience, London, 1970, p. 383.
15. Zimmermann, D. M. and Olofson, R. A., *Tetrahedron Lett.*, 1969, 5081.
16. Ugi, I. and Rosendahl, F. K., *Liebigs Ann. Chem.*, 1963, **670,** 80.
17. Ben-Efraim, D. A., in *The chemistry of cyanates and their derivatives*, Ed. S. Patai, Wiley, Chichester, 1977, p. 191.
18. Khan, M. N. I., King, C., Wang, J.-C., Wang, S., Fackler, J. P. Jr., *Inorg. Chem.*, 1989, **28,** 4656.
19. Singh, H., Chawla, A. S., Kapoor, V. K., Paul, D. and Malhotra, R. K., in *Progress in Medicinal Chemistry*, Ed. G. P. Ellis and G. B. West, Vol. 17., Elsevier/North-Holland Biomedical Press, Amsterdam, 1980, p. 151.
20. Spielvogel, B. F., *Phosphorus Sulfur*, 1994, **87,** 267 and refs therein.

Pergamon

PII: S0277-5387(98)00094-1

Polyhedron Vol. 17, No. 18, pp. 3181–3192, 1998
© 1998 Elsevier Science Ltd
All rights reserved. Printed in Great Britain
0277 5387/98 $19.00+0.00

Synthesis, structure, spectra and magnetic properties of the unsymmetrical oxo-bridged complex $[Fe_2O(OAsPh_3)_4Cl_3]_2[Fe_2OCl_6].2CH_3CN$

Iveta Ondrejkovičová,[a,*] Tadeus Lis,[b] Jerzy Mroziński,[b] Vlasta Vančová[a] and Milan Melník[a]

[a]Department of Inorganic Chemistry, Slovak Technical University, 812 37 Bratislava, Slovakia

[b]Faculty of Chemistry, Wrocław University, 50-383 Wrocław, Poland

(Received 20 October 1997; accepted 26 February 1998)

Abstract—A new unsymmetrical (μ-oxo)diiron(III) complex $[Fe_2O(OAsPh_3)_4Cl_3]_2[Fe_2OCl_6].2CH_3CN$ (I), where $OAsPh_3$ is triphenylarsine oxide, has been prepared by several ways and characterized by X-ray structural analysis, elemental analysis, spectral and magnetic methods. The complex (I) is formed simultaneously with another two complexes of the composition $[Fe_2O(OAsPh_3)_4Cl_3][FeCl_4].CH_3CN$ (II) and $[Fe(OAsPh_3)_4Cl_2][FeCl_4]$ (III). In compound (I) the complex cation has one Fe atom coordinated by four $OAsPh_3$ which form a plane, and the oxo-bridged ligand occupies an apex and form a square pyramid configuration about the second iron atom. In the complex anion each Fe atom is tetrahedrally coordinated by three chlorine atoms and the oxo bridge. The magnetic properties have been investigated in the 4.2–300 K temperature range and these data correspond to the EPR spectra. © 1998 Elsevier Science Ltd. All rights reserved

Keywords: iron(III) complexes; unsymmetrical oxo-bridged complexes; triphenylarsine oxide; magnetism; spectroscopic data; structure.

We are interested in the formation of iron complexes with triphenylphosphine oxide ($OPPh_3$) by autocatalytic oxidation of PPh_3 by dioxygen to $OPPh_3$ in the presence of some iron salts and corresponding anions [1–5]. In spite of the simplicity of the PPh_3-system we have explored the $AsPh_3$-system, too. How-

* Author to whom correspondence should be addressed.

Abbreviations: acac: acetylacetonate; acacen: N,N′-ethylenebis(acetylacetonylideneiminate); bpy: 2,2′-bipyridine; Bz: benzyl; cbpN: 2-hydroxy-5-chlorobenzophenone with 1,5,9- triazanonane; $C_6H_{15}N_3$: 1,4,7-triazacyclononane; Cl-dipic: 4-chloro-2,6-pyridinedicarboxylate; dbat: 7, 16-dihydro-6, 8, 16, 17-tetramethyldibenzo[b,i][1,4,8,11] tetraazacyclotetradecinate; dmso: dimethylsulfoxide; dsit: S-methyl-N^1,N^4-di(salicyliden)isothiosemikarbazidate-S,N^1,N^4; $Fe(cp)_2$: ferrocenium; $hbpz_3$: hydrotris-1-pyrazolylborate; hfacac: hexafluoroacetylacetonate; hp: hemiporphyrazinate; Me: methyl; 2-Mequin: 2-methyl-8-hydroxyquinolinate; mim: 1-methylimidazole; n5: N-(hydroxyethyl)-N,N′,N′-tris(2-benzimi-dazolylmethyl)-1,2-diaminoethane; n6: N,N,N′,N′-tetrakis((2-benzimidazolyl)methyl)ethanediamine: N-n-propyl-sal: N-n-propylsalicylideneiminate; N-p-Cl-Ph-sal: N-p-chlorophenylsalicylaldiminate; nta: nitrilotriacetate; odm: 5,15-dimethyl-2,3,7,8,12,13,17,18-octaethylporphinate; o-xy: o-xylene; pc: phthalocyaninate; phen: 1,10-phenanthroline; py: pyridine; salen: 1,2-bis(salicylideneaminato)ethane(2-); taab: tetrabenzo[b,f,j,n][1,5,9,13] tetraazacyclohexadecane; 3-tBusaltmen: 2,3-dimethyl-2,3-bis(3-tert-butylsalicylideneamino)butane(2-); tetren: tetraethylenepentaamine; tpa: tris(2-pyridylmethyl)amine; tmpyp: tetrakis(1-methylpyridinium-4-yl) porphyrinate(2-); tpc: 7,8-dihydroxo-5,10,15,20-tetraphenylporphyrinate; tpp: 5,10,15, 20-tetraphenylporphyrinate(2-); $tpp(F_5)$: 5,10,15,20-tetrakis-pentafluorophenylporphinate(2-).

ever, in the later case we have found that besides the monomeric Fe(III) complex there are also formed the diiron(III) complexes. The monomeric $[Fe(OAsPh_3)_4Cl_2][FeCl_4]$ salt is known which was prepared by direct reaction of $FeCl_3$ with $OAsPh_3$ in ethanol [6] or toluene under anaerobic conditions [7]. Two oxo-bridged diiron salts: $[Fe_2O(OAsPh_3)_4Cl_3]_2[Fe_2OCl_6].2CH_3CN$ (I) and $[Fe_2O(OAsPh_3)_4Cl_3][FeCl_4].CH_3CN$ (II) have different anions. The $[(OAsPh_3)_4FeOFeCl_3]^+$ cation is the first nonbiological unsymmetrical oxo-bridged Fe(III) complex ion with penta- and tetracoordinated iron atoms. However, until to-date, in all the known oxo-bridged Fe(III) complexes both Fe(III) atoms are tetracoordinated [8–20], pentacoordinated [21–37], hexacoordinated [38–48] or even heptacoordinated [49]. There are examples [50–53], in which two non-equivalent Fe(III) atoms, (viz. hexa- and tetra- coordinated) are bridged by a single O atom. It is known [54] that unsymmetrical Fe–O–Fe bridge angle is present in a class of dinuclear iron proteins. The (μ-oxo)-diiron(III) complexes have been prepared by several ways and are characterized by spectral and magnetic methods as well as by X-ray analysis. (The compound (II) has been characterized by us previously [55]).

EXPERIMENTAL

Preparations of the compounds

Complexes of the composition, $[Fe_2O(OAsPh_3)_4Cl_3]_2[Fe_2OCl_6].2CH_3CN$ (I) $[Fe_2O(OAsPh_3)_4Cl_3][FeCl_4].CH_3CN$ (II) and $[Fe(OAsPh_3)_4Cl_3][FeCl_4]$ (III) are formed simultaneously and amounts of the individual complexes are dependent on the reaction conditions. These complexes were prepared by several ways:

Method 1

Solution of $OAsPh_3$ (2.575 g, 8.0 mmol) in ethanol (ca. 70 ml) or toluene (ca. 100 ml) was added to $FeCl_3$ (0.648 g, 4.0 mmol) at room temperature and the resulting mixture stirred for 2 h. The yellow product which precipitated was filtered out and recrystallized from acetonitrile. The individual complexes were separated by fractional crystallization using acetonitrile, yielding the following three products:

1. $[Fe_2O(OAsPh_3)_4Cl_3]_2[Fe_2OCl_6].2CH_3CN$ (I) as the least soluble complex (dark yellow sticks). Found: C, 51.56; H, 3.60; Cl, 12.90; Fe, 9.65. Calcd. for $C_{148}H_{126}As_8Cl_{12}Fe_6N_2O_{11}$: C, 51.3; H, 3.7; Cl, 12.3; Fe, 9.7%.
2. $[Fe_2O(OAsPh_3)_4Cl_3][FeCl_4].CH_3CN$ (II) as more soluble complex (yellow needles). Found: C, 50.76; H, 3.59; N, 0.83; Cl, 14.22; Fe, 9.46. Calcd. for $C_{74}H_{63}As_4Cl_7Fe_3NO_5$: C, 50.45; H, 3.60; N, 0.80; Cl, 14.09; Fe, 9.51%.
3. $[Fe(OAsPh_3)_4Cl_2][FeCl_4]$ (III) as the most soluble complex (light yellow plates). Found: C, 53.58; H, 3.78; Cl, 13.41; Fe, 6.67. Calc. for $C_{72}H_{60}O_4As_4Cl_6Fe_2$: C, 53.60; H, 3.75; Cl, 13.18; Fe, 6.92%.

When the reaction mixture is kept under argon, the complex (III) is a major fraction. However, when the raw product is slowly recrystallized from hot CH_3CN in the presence of O_2, both dimeric complexes (I + II) are formed in larger amounts.

Method 2

Solutions of acetonitrile (ca. 30 ml) and 0.70 ml of a 36% solution (by weight) of aqueous HCl (8.0 mmol) ($T = 333$ K) containing excess iron powder (0.33 g, 5.9 mmol) and $AsPh_3$ (1.23 g, 4.0 mmol) were stirred for about 2 days under a dioxygen atmosphere. The completion of the oxidation of $AsPh_3$ to $OAsPh_3$ was ascertained by comparing the electronic absorption spectrum of the reaction solution with the spectrum of pure $OAsPh_3$ which exhibits four absorption bands with the maxima at 252, 259, 262 and 270 nm. The resulting mixture was filtered (mainly from Fe_2O_3) and separated by fractional crystallization using CH_3CN by the same procedure of *Method* 1. In this case complex (III) was a minor fraction. Both dimeric complexes were obtained in equally amounts.

Method 3

$AsPh_3$ (0.61 g, 2.0 mmol) dissolved in ca. 40 ml CH_3CN was transfered to $FeCl_3$ (0.17 g, 1.0 mmol) in the reaction vessel. The contents were stirred and heated to a temperature of ~ 333 K under a O_2 atmosphere for ca. 2 days. Monitoring of the reaction course and fractional crystallization were done in the manner as mentioned above. In this case the dimers were obtained in larger amounts than complex (III) and were suitable for X-ray analyses.

Method 4

$Fe_2(SO_4)_3.7H_2O$ (1.10 g, 2.1 mmol) and KCl (0.60 g, 8.0 mmol) were placed into a thermostated vessel, the acetonitrile solution (ca. 30 ml) of $AsPh_3$ (1.23 g, 4.0 mmol) was added and the mixture was stirred under O_2 for about 2 days. The course on this reaction was monitored according to the manner mentioned above. After the oxidation, the K_2SO_4 as a by-product was filtered out. The crude product was separated by fractional crystallization, too. The complex (II) was the major product.

Method 5

The acetonitrile solution (30 ml) of complex (III) (0.41 g, 0.25 mmol) was stirred for about 10 h under

O_2 in a thermostated vessel ($T = 323$ K). The dark-yellow solution containing all the complexes was separated by fractional crystallization (see *Method* 1). The amount of (II) was larger than that of (I).

Elemental analyses confirm the composition of the separated complexes (*Method* 2 to 5). Elemental analyses were carried out using a Carlo-Erba C,H,N,S-O (EA 1108) analyser.

Spectroscopic studies

Infrared spectra were recorded using Philips Analytical PU 9800 FTIR spectrometer in Nujol mulls on KBr plates over 4000–200 cm^{-1} range. Electronic spectra were recorded on Specord M 40 spectrophotometer by Carl Zeiss. Resonance Raman spectra were recorded on a Bruker ER 200 E-SRC spectrometer. Electron paramagnetic resonance (EPR) spectrum was measured with X-band Radiopan SE/X spectrometer for powder. Solid sample of Mn(II) in MgO was used as the reference and the magnetic field was calibrated with a nuclear magnetometer MJ 110R.

Magnetic measurements

Magnetic susceptibility of the polycrystalline samples of the compounds were measured by the Faraday method in the temperature range 4.2–293 K, using a sensitive Sartorius M-25D electrobalance. Susceptometer was equipped with Oxford Instruments CF-1200 continuous-flow cryostat and an electromagnet operating at 6.25 kG. The calibrant employed was $HgCo(NCS)_4$ [56], for which the magnetic susceptibility taken as 16.44×10^{-6} $cm^3 g^{-1}$. The correction for diamagnetism of the constituent atoms was calculated using Pascal's constants [57] and found to be -928×10^{-6} cm^3 mol^{-1} and -1820×10^{-6} cm^3 mol^{-1} per molecule of complexes I and II, respectively. The value $N\alpha = 0$ ($cm^3 mol^{-1}$) was used for the temperature independent paramagnetism of the compounds. The effective magnetic moment was calculated from the equation, $\mu_{eff} = 2.83 \times (\chi_M \times T)^{1/2}$ (B.M.). The value of the exchange parameters were determined by least-square procedure, and the minimization of the function:

$$R = \sum_{i=1}^{n} (\chi_i^{exp\,tl} - \chi_i^{calcd})^2 / (\chi_i^{exp\,tl})^2$$

was the criterion used to determine the best fit.

X-ray structure determination

$[Fe_2O(OAsPh_3)^4Cl_3]_2[Fe_2OCl_6].2CH_3CN$ (I) A well-formed dark yellow crystal was affixed to the end of glass fiber using silicone grease and transferred to the goniostat where it was cooled to 120 K for data collection ($4^\circ < 2\Theta < 44^\circ$) (Table 1). Standard inert atmosphere techniques were used. A systematic search of a limited hemisphere of reciprocal space located no symmetry or systematic absences indicating a triclinic space group. Subsequent solution and refinement of the structure confirmed the proper space group to be $P\bar{1}$. The structure was solved by direct methods and refined by SHELXL-93 program [58]. The phenyl ring H-atoms were included in geometrically calculated positions and the acetonitrile H-atoms were not determined from final difference map. No absorption correction was applied. A final difference map was essentially featureless, the largest peaks being in the vicinity of the As atoms. The high values of anisotropic temperature factors for acetonitrile molecules may suggest partially disorder of these molecules. Bond lengths and angles, atomic coordinates, displacement parameters and lists of structure factors for (I) are deposited.

Table 1. Crystal and structure refinement data for $[(Ph_3AsO)_4FeOFeCl_3]_2[Fe_2OCl6].2CH_3CN$ (I)

Formula	$C_{148}H_{126}As_8Cl_{12}Fe_6N_2O_{11}$
M_r	3468.4
Crystallographic system	triclinic
a (Å)	13.523(11)
b (Å)	13.618(12)
c (Å)	24.009(15)
α ( )	76.17(7)
β ( )	87.93(7)
γ ( )	59.53(9)
V (Å^3)	3681(7)
F(000)	1740
Space group	$P\bar{1}$
Z	1
T (K)	120(2)
λ (Å)	0.71069
$\rho_{calcd.}$ (g cm^{-3})	1.565(4)
$\rho_{meas.}$ (g cm^{-3})	1.469
μ (cm^{-1})	26.4
No. of reflcns collcd.	9014
No. of obsd. reflcns	6690($I > 3\sigma$)
$R (= \Sigma \|\|F_o\| - \|F_c\|\| / \Sigma \|F_o\|$	0.0371
wR^2	0.0985
w	$1/[(\sigma^2(F_o^2) + 0.067P)^2 + 10.4P$

RESULTS AND DISCUSSION

Anhydrous $FeCl_3$ and $OAsPh_3$ interact rapidly in several solvents (e.g. ethanol [6], toluene [7], acetonitrile) to afford yellow solutions. When the interaction is carried out under anaerobic conditions, the complex (III) is formed as a major product. However, in the presence of oxygen the I and II complexes are also formed, (*Method* 1). A similar mixture of these 3 complexes were also obtained when the following reactants were used as the starting compounds:

$Fe–HCl–AsPh_3–O_2$	(*Method* 2)
$FeCl_3–AsPh_3–O_2$	(*Method* 3)
$Fe_2(SO_4)_3.7H_2O–KCl–AsPh_3–O_2$	(*Method* 4)
$[Fe(OAsPh_3)_4Cl_2][FeCl_4]–O_2$	(*Method* 5)

Autocatalytic oxidation of $AsPh_3$ to $OAsPh_3$ by O_2, which has taken place in the Methods 2, 3 and 4, were used for the preparation of mainly diiron complexes. During oxidation of $AsPh_3$ mentioned reaction systems consumed O_2, what was demonstrated by measurements of dioxygen uptake on the apparatus described previously [1].

Both the complexes (I) and (II) are built with identical cationic forms (Fig. 1), different anions ($FeCl_4^-$ [55] and $Fe_2OCl_6^{2-}$ (Fig. 2)) and acetonitrile solvate molecules. Selected bond distances and angles of the complex (I) are given in Tables 2 and 3, respectively. The complex cations of (I) and (II) have similar structures. They contain two unsymmetrical iron(III) μ-oxo species (Fig. 1). The Fe(1) atom is coordinated by four $OAsPh_3$ ligands which form a distorted square pyramide configuration about the Fe(1). The Fe(2) is tetrahedrally coordinated by three chlorine atoms and the oxo bridge. They differ significantly with Fe–O–Fe bond angle of 161.0(3) in (II) and of 170.3(3) in (I). The Fe(2)–O(5) bonds of 1.759(4) Å in (II) and 1.776(4) Å in (I) are slightly shorter than the Fe(1)–O(5) bonds (1.784(4) Å in (II) and 1.779(4) Å in (I)), as expected. Both lengths, as well as the Fe–O–Fe angle, fall in the range of values observed for the diiron(III) μ-oxo analogues (Table 5). The bond lengths for Fe(2)–Cl in (II) (average 2.204(3) Å) are identical with those observed in the $[(n5)FeOFeCl_3]^-$ cation (average 2.203(3) Å) [52] and they are the slightly shorter than Fe(2)–Cl bond lengths in (I) (average 2.218(4) Å). To our knowledge, the Fe–

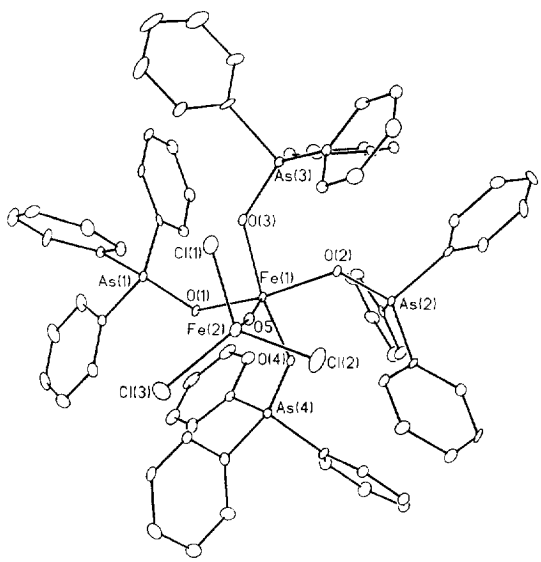

Fig. 1. The overall view of $[(OAsPh_3)_4FeOFeCl_3]^+$ cation in (I).

Table 2. Selected bond lengths (Å), bond angles ( ) and torsion angles ( ) for $[(Ph_3AsO)_4FeOFeCl_3]^+$ in (I).

Fe(1)...Fe(2)	3.543(3)
Fe(1)–O(1)	1.972(4)
Fe(1)–O(2)	1.974(4)
Fe(1)–O(3)	1.993(5)
Fe(1)–O(4)	2.002(5)
Fe(1)–O(5)	1.779(4)
Fe(2)–O(5)	1.776(4)
Fe(2)–Cl(1)	2.223(4)
Fe(2)–Cl(2)	2.213(2)
Fe(2)–Cl(3)	2.219(3)
As(1)–O(1)	1.682(4)
As(2)–O(2)	1.691(4)
As(3)–O(3)	1.680(4)
As(4)–O(4)	1.675(4)
As(1)–O(1)–Fe(1)	136.6(3)
As(2)–O(2)–Fe(1)	129.7(3)
As(3)–O(3)–Fe(1)	133.6(3)
As(4)–O(4)–Fe(1)	138.2(3)
O(1)–Fe(1)–O(5)	105.1(2)
O(2)–Fe(1)–O(5)	106.5(2)
O(3)–Fe(1)–O(5)	103.4(2)
O(4)–Fe(1)–O(5)	105.2(2)
O(1)–Fe(1)–O(2)	148.4(2)
O(1)–Fe(1)–O(3)	87.9(2)
O(1)–Fe(1)–O(4)	87.0(2)
O(2)–Fe(1)–O(3)	84.8(2)
O(2)–Fe(1)–O(4)	84.9(2)
O(3)–Fe(1)–O(4)	151.4(2)
Fe(1)–O(5)–Fe(2)	170.3(3)
O(5)–Fe(2)–Cl(1)	110.6(2)
O(5)–Fe(2)–Cl(2)	111.2(2)
O(5)–Fe(2)–Cl(3)	112.2(2)
Cl(1)–Fe(2)–Cl(2)	105.4(2)
Cl(1)–Fe(2)–Cl(3)	106.3(2)
Cl(2)–Fe(2)–Cl(3)	110.9(2)
Cl(1)–Fe(2)–O(5)–Fe(1)	15.8(15)
Cl(2)–Fe(2)–O(5)–Fe(1)	–100.9(15)
Cl(3)–Fe(2)–O(5)–Fe(1)	134.3(15)
Fe(2)–O(5)–Fe(1)–O(1)	–110.8(15)
Fe(2)–O(5)–Fe(1)–O(2)	69.1(15)
Fe(2)–O(5)–Fe(1)–O(3)	–19.5(15)
Fe(2)–O(5)–Fe(1)–O(4)	158.2(15)
O(5)–Fe(1)–O(1)–As(1)	94.6(4)
O(5)–Fe(1)–O(2)–As(3)	102.6(4)
O(5)–Fe(1)–O(3)–As(3)	104.6(4)
O(5)–Fe(1)–O(4)–As(4)	82.4(4)

$(OAsPh_3)$ fragment has not been characterized previously.

In (II) the Fe(3) atom in the $[FeCl_4]^-$ anion is tetrahedrally coordinated by four chlorine atoms (Fe–Cl range from 2.158(4) Å to 2.180(3) Å and Cl–Fe–Cl angles from 108.0 to 111.6(2) what is typically for these anions [59].

The iron atoms in the oxo-bridged dinuclear $[Cl_3Fe–O–FeCl_3]^{2-}$ anion in (I) each possess a slightly

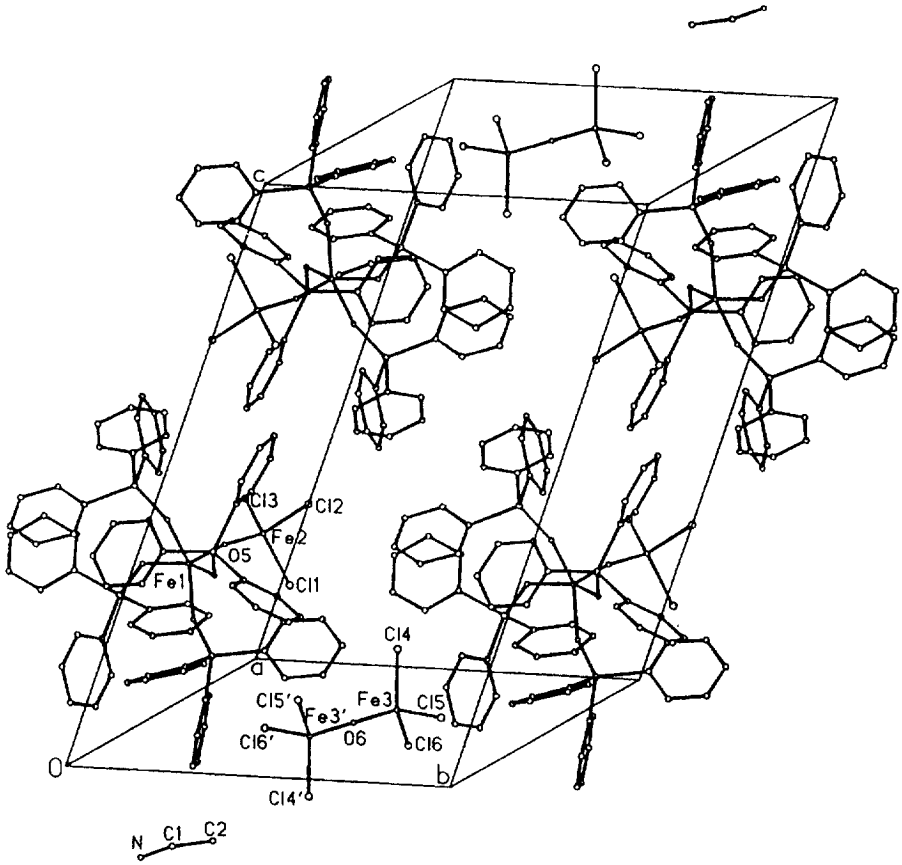

Fig. 2. The packing in the (I) crystal (approximately along the Fe...Fe axis).

Table 3. Selected bond lengths (Å), bond angles (°) and torsion angles (°) for $Fe_2OCl_6^{2-}$ in (I)

Fe(3)...Fe(3')	3.512(3)
Fe(3)–Cl(4)	2.232(3)
Fe(3)–Cl(5)	2.208(3)
Fe(3)–Cl(6)	2.218(4)
Fe(3)–O(6)	1.756(2)
Cl(4)–Fe(3)–Cl(5)	108.5(2)
Cl(4)–Fe(3)–Cl(6)	106.2(2)
Cl(4)–Fe(3)–O(6)	112.5(2)
Cl(5)–Fe(3)–Cl(6)	111.2(2)
Cl(5)–Fe(3)–O(6)	109.2(2)
Cl(6)–Fe(3)–O(6)	109.3(2)

Symmetry code: (I) $1-x, 1-y, -z$.

distorted tetrahedral ligand environment. The bond distances of the anion agree with those of the compounds investigated so far. The Fe–O–Fe angle is relatively large (Table 5).

Table 4 summarized infrared spectroscopic data of three Fe(III)–$OAsPh_3$ complexes. In the IR spectra of these complexes showed that ν(As–O) bands are shifted to lower energies compared with the free $OAsPh_3$, as the result of $OAsPh_3$ coordination. The dimeric complexes I and II have a strong new absorption at 849 cm^{-1} and 841 cm^{-1}, respectively. It is attributed to the asymmetric Fe–O–Fe stretching vibration (ν_{as}). Intense absorption in the region 800–860 cm^{-1} is commonly used as diagnostic criterion for identification of the oxo-monobridged Fe(III) complexes [8, 52]. The bands assigned to the symmetric Fe–O–Fe stretching vibration (ν_s) observed at 415 (I) and at 411 cm^{-1} (II) are within the range expected for these monobridged structures [60]. The Fe–O–Fe vibrations of I and II correlate with bond angles: the Fe–O–Fe angles can be predicted within 10° from knowledge of ν_s and ν_{as} [60]. In the infrared spectrum the Fe–O–Fe frequencies are nearly identical with those observed in the Raman spectrum. Whereas ν_{as}(Fe–O–Fe) are stronger and ν_s(Fe–O–Fe) are weaker in the IR spectra of I and II, in the Raman spetra the stretching vibration intensities are opposite. Infrared bands at

Table 4. Characteristic IR data (cm^{-1}) for the Fe(III)–$OAsPh_3$ complexes

Compound	ν(As–O)	ν(FeOFe)		ν($FeCl_4^-$)	ν($FeCl_3$)	
		ν_{as}	ν_s		ν_{as}	ν_s
III	869s 828s	—	—	380s		
II	860s 828s	841s	411m	382s	369m	307m
I	881s 830vs	849vs	415m	—	363vs	314m

363 (I) and 369 cm^{-1} (II) are assigned to the respective Fe–Cl_3 asymmetric stretch by comparison with $[Fe_2OCl_6]^{2-}$ and bands at 314 (I) and 307 cm^{-1} (II) are assigned similarly to the symmetric $FeCl_3$ mode in agreement with literature data [51]. IR spectra of II and III show a characteristic strong band at 383 and 380 cm^{-1} (ν_3) of $FeCl_4^-$, respectively [8].

In Table 5 are summarized selected structural data for μ-oxo-bridged dimeric Fe(III) compounds. As can be seen, the mean Fe–O(bridge) bond distance increases with increasing coordination number in the sequence: 1.754 Å (tetra coordinated) < 1.771 Å (penta coordinated) < 1.786 Å (hexa coordinated), as expected. The Fe–O–Fe bridge angles in the series of tetra-, penta- and hexa-coordinated species are well comparable, i.e. they are in the range of 147.7 to 180°, of 142.7 to 180° and of 146.6 to 180°, respectively. There are relationships between the Fe–O–Fe bridge angle and Fe–Fe distances. When the former closses the latter is shortened.

The anion $FeCl_4^-$ is a strong paramagnet with $S=5/2$ spin, but the $Fe_2OCl_6^{2-}$ ion is a molecular antiferromagnet. Using the theoretical equation [61]

$$\chi_M = \left(\frac{N_g^2\mu_B^2}{kT}\right) \times \left(\frac{2e^{2x}+10e^{6x}+28e^{12x}+60e^{20x}+110e^{30x}}{1+3e^{2x}+5e^{6x}+7e^{12x}+9e^{20x}+11e^{30x}}\right)$$

(where χ_M was corrected for diamagnetism, and $TIP=0$ and $\chi=J/kT$) and X-ray data (this work) for $Fe_2OCl_6^{2-}$ in the crystal lattice of the complex (I), the relation $\chi_{Fe_2OCl_6^{2-}} = f(T)$ was prepared (Fig. 3). The magnetic interaction in a dimer is expressed by the Heisenberg–Dirac-van Vleck Hamiltonian. $H_{HDVV} = -2J_{S_aS_b}$, where $\hat{S}_a$ and $\hat{S}_b$ are the spins of the magnetically interacting iron(III) ions ($\hat{S}_a = \hat{S}_b = 5/2$).

The cationic forms observed in both the complexes indicate lack of any symmetry and a difference in the bridging angle Fe–O–Fe, 170.3° and 161.0° for the complexes I and II, respectively.

In the crystal lattice of the complex II two magnetically isolated paramagnetic forms exist, which confirms the absence of the maximum on the experimental curve $\chi_M = f(T)$ up to 4.2 K. A weak anomaly observed in the region 4.2–20 K and the value $\Theta \sim -2.5$ K may suggest weak antiferromagnetic superexchange interaction. The relation between

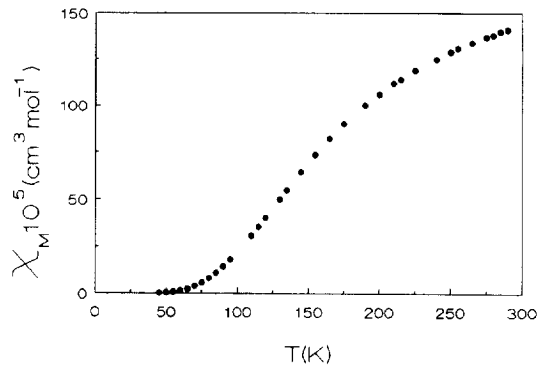

Fig. 3. Plots of the magnetic susceptibility versus T for $Fe_2OCl_6^{2-}$ anions calculated for $g=2$, $J=-170$ cm^{-1}, diamagnetic correction $= -188.10^{-6}$ cm^3 mol^{-1}.

molar magnetic susceptibility and the magnetic moment for both the complexes as a function of temperature enables us to compare their properties (Fig. 4; magnetic data are given for whole molecular system.). Both the complexes indicate a relation typical for a paramagnet, although the magnetic effect for the complex (II) is stronger (Table 6).

In the EPR spectrum of the complex (II) only one

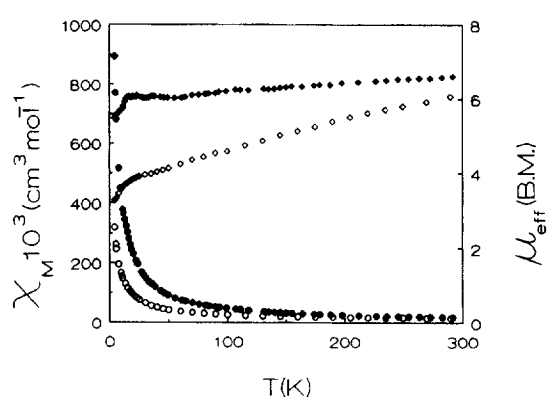

Fig. 4. Experimental magnetic susceptibility and magnetic moment vs. temperature for $[(OAsPh_3)_4FeOFeCl_3][FeCl_4]$ (●, ◆) and $[(OAsPh_3)_4FeOFeCl_3]_2[Fe_2OCl_6]$ (o, ◇), respectively.

Table 5. Selected structural data for μ-oxo-bridged dimeric Fe(III) compounds[a]

Complex	Chromophore		Fe–L (Å)	Fe–Fe (Å) Fe–O–Fe ( )		L–Fe–L ( )	Ref.
$(Ph_4P)_2[Fe_2OCl_6]$	$FeCl_5O$	μO	1.744 (4,0)	not given	Cl, Cl[b]	108.4 (2,1.5)	[8]
		Cl[b]	2.210 (2,6)	170.4 (4)	μO, Cl	110.5 (2,1.5)	
$(Ph_4P)_2[Fe_2OCl_6]\cdot 2CH_2Cl_2$	$FeCl_5O$	μO	1.740 (1)	3.480	Cl, Cl	108.1 (1,8)	[9]
		Cl	2.211 (2,11)	180.0	μO, Cl	110.8 (1,2.6)	
$(BzPh_3P)_2[Fe_2OCl_6]$	$FeCl_5O$	μO	1.760 (3,3)	3.467(2)	Cl, Cl	108.7 (1,2.5)	[8],[10]
		Cl	2.216 (2,21)	160.2 (5)	μO, Cl	110.3 (2,2.2)	
$(BzPhMe_2N)_2[Fe_2OCl_6]$	$FeCl_5O$	μO	1.766 (5,9)	3.393(1)	Cl, Cl	109.5 (1,1.8)	[11]
		Cl	2.210 (2,14)	147.7(3)	μO, Cl	109.4 (2,1.5)	
$(Hpy)_2[Fe_2OCl_6]\cdot py$	$FeCl_5O$	μO	1.755 (3,0)	3.428(3)		not given	[8],[10],[12]
		Cl	2.214	155.6 (7)			
$(Ph_4As)_2[Fe_2OCl_6]$	$FeCl_5O$	μO	1.74 (3)	3.469[d]		not given	[8],[13]
		Cl	2.207	170.8 (5)			
$[(Ph_3P)_2CSe]_2[Fe_2OCl_6]\cdot 4CH_2Cl_2$	$FeCl_5O$	μO	1.752(2)	3.504		not given	[14]
		Cl	not given	180.0			
$(BzEt_3N)_2[Fe_2OCl_6]$	$FeCl_5O$	μO	1.755 (5,3)	not given		not given	[8]
		Cl	2.219	155.3 (3)			
$[FeCl(dmso)_5][Fe_2OCl_6]$	$FeCl_5O$	μO	1.760 (8,6)	not given	Cl, Cl	109.0 (2,1.5)	[15]
		Cl	2.203 (4,11)	150.3 (4)	μO, Cl	109.8(3, 2.9)	
$[FeCl(dmso)_5][Fe_2OCl_6]$ (at 103 K)	$FeCl_5O$	μO	1.776 (5,2)	3.401[d]	Cl, Cl	109.3 (1,1.5)	[15]
		Cl	2.223 (2,9)	146.5 (2)	μO, Cl	109.5 (1,2.0)	
$[FeCl(dmso)_5][Fe_2OCl_6]$ (at 223 K)	$FeCl_5O$	μO	1.763 (7,0)	not given	Cl, Cl	109.2 (1,1.4)	[15]
		Cl	2.216(4,14)	149.7(4)	μO, Cl	109.7 (2,1.9)	
$[FeCl(dmso)_5][Fe_2OCl_6]$ (at 343 K)	$FeCl_5O$	μO	1.737(7,6)	3.374[d]	Cl, Cl	108.8 (2,2.8)	[15]
		Cl	2.190(3,9)	152.7(4)	μO, Cl	110.0(3,2.8)	
$[Fe(phen)_3][Fe_2OCl_6]\cdot dmf$	$FeCl_5O$	μO	1.75 (2.1)	3.455(7)	Cl, Cl	109.1 (2,2.0)	[16]
		Cl	2.22 (2.2)	161.6 (9)	μO, Cl	109.9 (5,3.3)	
$[Fe(bpy)_3][Fe_2OCl_6]$	$FeCl_5O$	μO	1.752(11.12)	3.374[d]		not given	[17]
		Cl	2.209(6,16)	148.9(7)			
$[Fe(bpy)_3][Fe_2OCl_6]$ (at 223 K)	$FeCl_5O$	μO	1.765(3,1)	3.394[d]	Cl, Cl	108.69(5,1.92)	[18]
		Cl	2.222(1,1.6)	148.1(2)	μO, Cl	110.2(10,1.0)	
$[Fe(cp)_2]_2[Fe_2OCl_6]$	$FeCl_5O$	μO	1.749(4,0)	3.455(5)	Cl, Cl	108.4(2.1.3)	[19]
		Cl	2.197(5.7)	162.1(5)	μO, Cl	110.5(4.5)	
$[Fe_2O(OAsPh_3)_4Cl_3]_2-$ $[Fe_2OCl_6]\cdot 2MeCN$ (at 120 K)	$FeCl_5O$ (anion)	μO	1.756(2,0)	3.512(3)	Cl, Cl	108.6(2.2.6)	this work
		Cl	2.219(4,13)	180.00	μO, Cl	110.3(2,2.2)	
$[Fe(cp)_2]_2[Fe_2OBr_6]$	$FeBr_5O$	μO	1.752(2,0)	not given	Br, Br	108.8(1,2.4)	[20]
		Br	2.347(4,7)	159.8(4)	μO, Br	110.2(4,1.3)	
$[Fe_2O(2\text{-Mequin})_4]\cdot CHCl_3$	FeO_3N_2	O	1.925(14,15)	3.451[d]	O, O	123.4(6)	[21]
		μO	1.781(11,21)	151.6(7)	μO, O	118.3(5,5)	
		N	2.184(14,4)		N, N	160.9(5)	
					O, N	79.3(5,1.3)	
					μO, N	91.8(5,2.1)	
						99.4(5,1)	
$[Fe_2O(N\text{-p-ClPh-sal})_4]$	FeO_3N_2	O	1.89(2,3)	3.53	O, O	127.1(7,2.6)	[22]
		μO	1.77(1,1)	175(1)	μO, O	116.4(7,3.0)	
		N	2.16(2,5)		N, N	168.6(7,1.1)	
					O, N	87.7(7,3.5)	
					μO, N	95.7(7,2.3)	
$[Fe_2O(N\text{-n-propyl-sal})_4]$	FeO_3N_2	O	1.93(2,1)	not given	μO, O	114(2,3)	[23]
		μO	1.77(1,1)	164(5)	O, N	86(1,1)	
		N	2.14(2,1)		μO, N	98(2,4)	
$[Fe_2O(acacen)_2]\cdot CH_2Cl_2$[c]	FeO_3N_2	O	1.962(8,7)	not given	O, O	87.6(3,2)	[24]
		μO	1.783(7,14)	154.6(4)	μO, O	108.6(4,2.6)	
		N	2.077(9,29)		N, N	79.1(4,1.2)	
					O, N	87.0(4,8)	
					μO, N	145.7(4,5.6)	
						105.2(4,3.0)	

continued

Table 5—*continued.*

Complex	Chromophore		Fe–L (Å)	Fe–Fe (Å) Fe O Fe ( )		L–Fe–L ( )	Ref.
$[Fe_2O(acacen)_2]\cdot CH_2Cl_2$[c]	FeO_3N_2	O	1.955(8,5)	not given	O, O	88.5(3,8)	[24]
		μO	1.780(7,5)	155.6(5)	μO, O	109.3(4,3.8)	
		N	2.080(9,18)		N, N	79.1(4,6)	
					O, N	86.5(4,6)	
					μO, N	145.4(4,5.8)	
						104.6(4,2.9)	
$[Fe_2O(salen)_2]\cdot 2py$	FeO_3N_2	O	1.92(1,2)	3.391	μO, O	109.6(5,2.3)	[25]
		μO	1.78(1,0)	144.6(6)	O, N	85.4(5,3)	
		N	2.12(2,1)		μO, N	145.4(5.4.7)	
						103.3(5.3.0)	
$[Fe_2O(salen)_2]\cdot CH_2Cl_2$	FeO_3N_2	O	1.94(3,0)	not given	O, O	95(4)	[26]
		μO	1.80(5,0)	144(2)	N, N	76(4)	
		N	2.12(3,1)		O, N	86(4,1)	
$[Fe_2O(3\text{-}tBusaltmen)_2]$	FeO_3N_2	O	1.923(4,8)	3.551	O, O	92.49(19,15)	[27]
		μO	1.779(4,5)	173.45(27)	N, N	75.80(22,2)	
		N	2.124(5.19)		O, N	85.10(19.78)	
						136.02(18,1.80)	
						149.02(19,1.08)	
$[Fe_2O(dsit)_2]\cdot 2H_2O$	FeO_3N_2	O	1.912(4,10)	3.481(4)	O, O	93.3(2,4)	[28]
		μO	1.769(3,0)	156.4(2)	N, N	72.6(2,2)	
		N	2.104(5,3)		O, N	86.2(2,1.7)	
$[Fe_2O(dbat)_2]\cdot MeCN$	FeN_4O	μO	1.792(1,1)	3.397[d]	N, N	83.32(7,5.36)	[29]
		N	2.053(2,11)	142.75(9)	μO, N	140.19(7,1.01)	
						109.91(7,1.51)	
$[Fe_2O(tpp)_2]$	FeN_4O	μO	1.763 (1)	not given	N, N	86.8 (3.4)	[30]
		N	2.087 (6.11)	174.5(1)	N, N	152.5 (2,1.4)	
					μO, N	103.7 (2,4.0)	
$[Fe_2O(tpp)_2]$ (at 122 K)	FeN_4O	μO	1.759(1,0)	3.516[d]	N, N	86.9(4,0)	[31]
		N	2.081(3,0)	176.1(2)		153(2.0)	
$[Fe_2O(NCH_3tpp)(tpp)]$-ClO_4 (at 133 K)	FeN_4O	μO	1.767(4)	not given	N, N	87.4 (2,9)	[32]
		N	2.067(6,12)	165.4(3)	μO, N	155.4(2,1.4)	
	FeN_4O	μO	1.740(4)		N, N	102.3(2,2.6)	
		MeN	2.257(5)		μO, N	86.1(2,2.4)	
		N	2.058(6,8)			149.7(2.4)	
						105.0(2.5.5)	
$[Fe_2O(tpc)_2]\ 4CHCl_3$ (at 143 K)	FeN_4O	μO	1.755(5,8)	3.510(8)	N, N	86.8(2,3)	[33]
		N	2.084(5,18)	180	μO, N	152.5(3.3.5)	
						103.7(1,1.8)	
$[Fe_2O(odm)_2]$	FeN_4O	μO	1.752(1)	3.504[d]	N, N	86.5(2,2.8)	[34]
		N	2.065(4,12)	178.5(6)	μO. N	104.4(2,1.6)	
$[Fe_2O(tmpyp)_2]$-$(ClO_4)_8\cdot 4H_2O$ (at 118 K)	FeN_4O	μO	1.750(2)	not given	N, N	87.2(4,4)	[35]
		N	2.081(9,15)	175.1(7)	μO, N	154.2(4,2)	
						102.2(4,1.2)	
$[Fe_2O(tpp(F_5))_2]$ (at 173 K)	FeN_4O	μO	1.775(1,0)	3.550	μO, N	105.1(3,1.6)	[36]
		N	2.088(7,16)	178.4(5)			
$[Fe_2O(taab)_2(MeO)_4]$	FeN_4O	μO	1.777(4,6)	3.552(1)	N, N	88.7(2,3.3)	[37]
		N	2.064(5,68)	176.3(3)	μO, N	93.2(2,2.5)	
						115.6(2,4.4)	
$[Fe_2O(Cl\text{-}dipic)_2(H_2O)_4]$ $\cdot 4H_2O$	FeO_5N	O	2.075(3,22)	3.545(1)	O, O	89.3(1.6)	[38]
		μO	1.773(3,1)	180	μO, O	149.1(1,3)	
		N	2.105(3,3)		O, N	175.1(1,2)	
					μO, N	98.9(1,6.6)	
						81.1(1,6.6)	
						180	
$Ba[Fe_2O(nta)_2(H_2O)_2]$ $\cdot 4H_2O$	FeO_5N	O	2.05(1,14)	not given	μO, O	103.5(5)	[39]
		μO	1.82(1,1)	153.2(6)	O, N	78.1(4)	
		N	2.23(1,0)				

continued

Table 5—*continued.*

Complex	Chromophore		Fe–L (Å)	Fe–Fe (Å) Fe–O–Fe (°)		L–Fe–L (°)	Ref.
$[Fe_2O(phen)_2(H_2O)_6]$– $(NO_3)_4 \cdot 4H_2O$	FeO_4N_2	O μO N	2.068(5,86) 1.775(4,10) 2.155(6,12)	3.506(2) 162.0(3)	O, O μO, O	86.9(2,9.7) 94.6(2,1.9) 175.7(2,1.2)	[40]
					N, N	76.8(2,4)	
					O, N	89.3(2,4.6) 164.8(2,2.1)	
					μO, N	97.4(2,2.6)	
$[Fe_2O(MeC(CH_2NCMe–$ $CH_2C(CF_3)_2))_2(CH_2NH_2)_2]$	FeO_3N_3	O μO N	1.972(2,20) 1.811(1) 2.231(3,82)	3.468(1) 146.6(2)	O, O μO, O N, N	99.7(1.5.0) 99.9(1) 81.2(1.7.4)	[41]
					O, N	85.7(1.3.9) 162.8(1,2.2)	
					μO, N	94.4(1,4.5) 166.0(1)	
$[Fe_2O(cbpN)_2] \cdot 3o\text{-}xy$	FeO_3N_3	μO O N	1.806(3,2) not given	3.440[d] 144.5(2)		not given	[42]
$[Fe_2O(C_6H_{15}N_3)_2)(acac)_2]$– $(ClO_4)_2$	FeO_3N_3O	μO N	2.007(5,11) 1.787(5,5) 2.178(7,51)	3.512(2) 158.6(3)	O, O μO, O N, N	89.1(2,2) 98.9(2,1.2) 78.0(3,1.7)	[43]
					O, N	90.5(3,6.7) 163.7(3,2.3)	
					μO, N	96.2(3,4.1) 170.5(2,8)	
$[Fe_2O(hbpz_3)(hfacac)_2]$	FeO_3N_3	O μO N	2.071(7,12) 1.776(7,2) 2.127(9,82)	3.537(2) 169.4(4)		not given	[44]
$[Fe_2O(tetren)_2]I_4$	FeN_5O	μO N	1.77(1.0) 2.25(5.13)	3.531[d] 172	N,N	73(1,1) 81(1,1) 91(4,2) 100(4,2) 160(2,9)	[45]
					μO, N	155(2) 103(5,6) 88(1)	
$[Fe_2O(pc)_2)(mim)_2]$– $[Fe(pc)(mim)_2] \cdot 3Me_2CO$	FeN_5O	μO $_{pc}$N $_{im}$N	1.749(1.0) 1.922(8,27) 2.039(7.0)	not given 175.1	N,N μO, N	89.6(4,2.0) 178.3(4.1.0) 90.8(3,1.2) 178.9(4)	[46]
$[Fe_2O(phen)_4(H_2O)_2]$– $(NO_3)_4 \cdot 5H_2O$	FeN_4O_2	μO O N	1.785(5,2) 2.024(9,3) 2.175(9,88)	3.49 155.1(4)	N,N μO, O O,N	82.5(3,8.4) 158.2(3,9) 96.4(3.5) 91.0(3,7.6) 164.1(2,1.7)	[47]
					μO, N	98.5(3,4.2) 172.5(3,1.0)	
$[Fe_2O(tpa)_2Cl_2](ClO_4)_2$	FeN_4OCl	μO N Cl	1.785(1,0) 2.192(7,54) 2.298(2)	3.565(2) 174.7(5)	N,N μO, N	79.8(3,8.1) 151.9(3) 93.4(3,1.2) 170.6(2)	[48]
					N,Cl	98.7(2,8.8) 165.2(2)	
					μO, Cl	99.3(1)	
$[Fe_2O(NO_3)_4(bpy)_2]$ (at 201 K)	FeO_5N_2	O μO N	2.191(2,70) 1.7755(4) 2.159(2,19)	3.5510(7) 180	O, O μO, O N,N O,N μO, N	58.49(7,52) 75.09(7) 94.91(6,3.76) 75.02(8) 83.38(8,3.54) 95.31(6) 169.19(6)	[49]

continued

Table 5—*continued.*

Complex	Chromophore		Fe–L (Å)	Fe–Fe (Å) Fe–O–Fe ( )	L–Fe–L ( )		Ref.
$[Fe_2O(OAsPh_3)_4Cl_3]$– $[FeCl_4]\cdot MeCN$	$FeCl_3O$	Cl	2.204(3,14)	3.494(3)	Cl, Cl	108.4(2,2.4)	[55]
		μO	1.759(4)	161.0(3)	μO, Cl	110.5(2,9)	
	FeO_5	O	1.976(4,21)		O, O	86.2(2,9)	
		μO	1.784(4)		μO, O	150.1(3,3.5)	
						105.0(2,2.4)	
$[Fe_2O(OAsPh_3)_4Cl_3]_2$ $[Fe_2OCl_6]\cdot 2MeCN$ (at 120 K)	$FeCl_3O$	Cl	2.218(4.5)	3.543(3)	Cl, Cl	107.5(2.3.4)	this work
		μO	1.776(4)	170.3(3)	μO, Cl	111.3(2.9)	
	FeO_5	O	1.985(5,17)		O, O	86.2(2,1.7)	
	(cation)	μO	1.779(4)			149.9(2,1.5)	
					μO, O	105.1(2,1.7)	
$[Fe_2O(n6)Cl_3]Cl\cdot 0.5$– $HCl\cdot 3H_2O\cdot 2EtOH$	$FeCl_3O$	Cl	2.201(4.13)	3.440(2)	Cl, Cl	109.0(2,6)	[50]
		μO	1.745(7)	153.2(4)	μO, Cl	109.9(3,1.3)	
	FeN_5O	aN	2.32(1,4)		aN,aN	77.9(3)	
		iN	2.08(1,3)		iN, iN	93.5(4.3.8)	
		μO	1.791(7)			162.4(3)	
					aN, iN	83.0(3.5.7)	
						152.7(3)	
					iN, μO	99.5(3.5.2)	
					aN, μO	101.3(3)	
						172.7(3)	
$[Fe_2O(n5)Cl_3]Cl\cdot 2EtOH$	$FeCl_3O$	Cl	2.203(3,5)	3.411(1)	Cl, Cl	110.1(1,2.5)	[51] [52]
		μO	1.751(4)	149.5(3)	μO, Cl	108.8(2,2.4)	
	FeN_5O	aN	2.320(5,37)		aN, aN	78.0(2)	
		iN	2.095(6,19)		iN, iN	91.9(2,2.5)	
		μO	1.784(4)			162.0(2)	
					aN, iN	81.2(2,8.7)	
						149.5(2)	
					iN, μO	101.4(2,7.5)	
					aN, μO	100.6(2)	
						172.6(2)	
$[Fe_2O(n5)Br_3]Br\cdot 2EtOH$	$FeBr_3O$	Br	2.348(3,19)	3.408(3)	Br, Br	109.8(1,2.0)	[52]
		μO	1.726(9)	150.6(4)	μO, Br	109.1(3,3.2)	
	FeN_5O	aN	2.31(1,3)		aN, aN	78.2(4)	
		iN	2.09(1,2)		iN, iN	92.0(4.2.3)	
		μO	1.797(9)			162.1(4)	
					aN, iN	81.2(4.7.7)	
						150.1(4)	
					iN, μO	101.3(4,7.3)	
					aN, μO	100.6(4)	
						172.7(3)	
$[Fe_2O(hp)_2(H_2O)]$	FeN_4O	N	1.986(10.5)	3.52	N, N	87.9(3,4)	[53]
			2.193(11,13)	180		148.6(4)	
		μO	1.739(6)			164.6(4)	
					μO, N	101.7(3,4.0)	
	FeN_4O_2	N	2.098(11,108)		N, N	89.8(4,1)	
		O	2.212(6)			171.9(4,1.5)	
		μO	1.782(6)		O, N	94.1(3,7)	
					μO, N	85.9(3,7)	

[a] Where more than one chemically equivalent distance or angle present, the mean value is tabulated. The first number in parenthesis is e.s.d., the second is maximum deviation from the mean value.

[b] The chemical identity of coordinated atom/ligand is specified in these columns.

[c] There are two crystallographically independent molecules.

[d] It indicates that the distance was calculated trigonometrically [60].

Table 6. Magnetic data

Compound	Temperature $T(K)$	Magnetic susceptibility $\chi_M \times 10^6$ ($cm^3\ mol^{-1}$)	Magnetic moment μ_{eff} (B.M.)
$[Fe_2O(OAsPh_3)_4Cl_3][FeCl_4].CH_3CN$	4.2 292	894000 18700	5.48 6.62
$[Fe_2O(OAsPh_3)_4Cl_3]_2[Fe_2OCl_6].2CH_3CN$	4.2 290	319000 25800	3.28 6.06

single line is present, with $g = 2.04$ (room temperature and 77 K).

The EPR spectrum of the cation of complex (I) presents one single line with $g = 2.06$ and two additional weak lines with $g = 4.34$ and 6.08 at room temperature. It suggests a doublet ground state $< \pm 1/2$ I with admixture of $< \pm 3/2$ I and $< \pm 5/2$ I states.

The magnetic data for the $[(Ph_3AsO)_4FeOFeCl_3]^+$ cation, indicated only one unpaired electron per every Fe(III) centre, in a core of Fe(III) [D_{4h} deformed]–O–Fe(III) [T_d deformed]).

Further, the magnetic data at temperatures lower than 20 K are identical with the expected magnetism exclusively for the cation and indicate a singlet ground state and upper triplet state.

However, for complex II calculation of the magnetic moment of the cation was found to be impossible because we have not any possibility to estimate magnetism of the isolated $FeCl_4^-$ anion. It was imposible, too, to compare magnetic properties of $[(Ph_3AsO)_4FeOFeCl_3]^+$ cations from crystal lattice of the complexes I and II.

We also prepared another unsymmetrical oxo-bridged diiron(III) complexes with $[(Ph_3AsO)_4FeOFeBr_3]^+$ cation and study of their properties is in progress.

Atomic coordinates, displacement factor coefficients, full list of bond length and angles and lists of F_o/F_c values have been deposited as supplementary data with the Editor, from whom copies are available on request. Atomic coordinates have also been deposited with the Cambridge Crystallographic Data Centre.

Acknowledgements—The work was financial supported by the State Committee for Scientific Research (Warsaw, Poland) and the Ministry of Education of the Slovak Republic for financial support.

REFERENCES

1. Vančová, V., Ondrejkovičová, I. and Ondrejovič, G., *Chem. Zvesti.*, 1984, **36,** 363.
2. Ondrejkovičová, I., Vančová, V. and Ondrejovič, G., *Chem. Papers*, 1991, **45,** 35.
3. Ondrejkovičová, I., Vančová, V. and Ondrejovič, G., *Studies in Surface Science and Catalysis*, 1991, **66,** 649.
4. Ondrejkovičová, I., Melnik, M., Smolander, K. and Ahlgrén, M., *Acta Chem. Scandinavica*, 1995, **49,** 475.
5. Olejnik, Z., Lis, T. and Ondrejkovičová, I., *Acta Cryst.*, 1995, **C51,** 2246.
6. Cotton, S. A. and Gibson, J. F., *J. Chem. Soc., A.*, 1971, 859.
7. Beagley, B., Kelly, D. G., Mac Rory, P. P., McAuliffe, C. A. and Pritchard, R. G., *J. Chem. Soc., Dalton Trans.*, 1990, 2657.
8. Haselhorst, G., Wieghardt, K., Keller, S. and Schrader, B., *Inorg. Chem.*, 1993, **32,** 520.
9. Dehnicke, K., Prinz, H., Massa, W., Pebler, J. and Schmidt, R., *Z. Anorg. Allg. Chem.*, 1983, **499,** 20.
10. Petridis, D. and Terzis, A., *Inorg. Chim. Acta*, 1986, **118,** 129.
11. Neuse, E. W., Khan, F. B. D., Berhalter, K. and Thewalt, U. J., *Crystallogr. Spectr. Res.*, 1986, **16,** 483.
12. Drew, M. G. B., McKee, B. and Nelson, S. M., *J. Chem. Soc., Dalton Trans.*, 1978, 80.
13. Vasilevski, I., Stenkamp, R. E., Lingafelter, E. C. and Rose, N. J., *J. Coord. Chem.*, 1988, **19,** 171.
14. Schmidbaur, H., Zybill, C. E. and Neugebauer, D., *Angew. Chem., Int. Ed. Engl.*, 1983, **22,** 156.
15. Ponomarev, V. I., Arutyunyan, L. D. and Atovmyan, L. O., *Kristallografiya*, 1984, **29,** 910.
16. Reiff, W. M., Witten, E. H., Mottle, K., Brennan, T. F. and Garafalo, A. R., *Inorg. Chim. Acta*, 1983, **77,** L83.
17. Healy, P. C., Skelton, B. W. and White, A. H., *Aust. J. Chem.*, 1983, **36,** 2057.
18. Weiss, H. and Strähle, J., *Z. Naturforsch*, 1984, **39b,** 1453.
19. Carty, P., Clare, K. C., Creighton, J. R., Metcalfe, E. and Raper, E. S., *Inorg. Chim. Acta*, 1986, **112,** 113.
20. Evans, P. J. M., Fritzsimmons, B. W., Marshall, W. G., Golder, A. J., Larkworthy, L. F., Povey, D. C. and Smith, G. W., *J. Chem. Soc., Dalton Trans.*, 1992, 1065.
21. Mabbs, F. E., McLachlan, V. N., McFadden, D. and McPhail, A. T., *J. Chem. Soc., Dalton Trans.*, 1973, 2016.
22. Davies, J. E. and Gatehouse, B. M., *Acta Cryst.*, 1973, **B29,** 2651.
23. Davies, J. E. and Gatehouse, B. M., *Cryst. Struct. Comm.*, 1972, **1,** 115.

24. Wang, X., Pennington, W. T., Ankers, D. L. and Fanning, J. C., *Polyhedron*, 1992, **11,** 2253.
25. Davies, J. E. and Gatehouse, B. M., *Acta Cryst.*, 1973, **B29,** 1934.
26. Atovmyan, L. O., Dyaczenko, A. O. and Soboleva, S. V., *Zh. Strukt. Khim.*, 1970, **11,** 557.
27. Mukherjee, R. N., Stack, T. D. P. and Holm, R. H., *J. Am. Chem. Soc.*, 1988, **110,** 850.
28. Yampolskaja, M. A., Shova, S. G., Gerbeleu, N. V., Simonov, J. A., Belskij, V. K. and Dvorkin, A. A., *Zh. Neorgan. Khim.*, 1983, **28**, 1744; *J. Coord. Chem.*, 1983, **28**, 984.
29. Weiss, M. C. and Goedken, V. L., *Inorg. Chem.*, 1979, **18,** 819.
30. Hoffman, A. B., Collins, D. M., Day, V. W., Fleischer, E. B., Srivastava, T. S. and Hoard, J. L., *J. Am. Chem. Soc.*, 1972, **94,** 3620.
31. Swepston, P. N. and Ibers, J. A., *Acta Cryst.*, 1985, **C41,** 671.
32. Bartczak, T. J., Latos-Grażynski, L., Wysłouch, A., *Inorg. Chim. Acta*, 1990, **171,** 205.
33. Strauss, S. H., Pawlik, M. J., Skowyra, J., Kennedy, J. R., Anderson, O. P., Spartalian, K. and Dye, J. L., *Inorg. Chem.*, 1987, **26,** 724.
34. Kiong-Lam, Lay, Buchler, J. W., Kenny, J. E. and Scheidt, W. R., *Inorg. Chim. Acta*, 1986, **123,** 91.
35. Ivanca, M. A., Lappin, A. G. and Scheidt, W. R., *Inorg. Chem.*, 1991, **30,** 711.
36. Gold, A., Jayaraj, K., Doppelt, P., Fischer, J. and Weiss, R., *Inorg. Chim. Acta*, 1988, **150,** 177.
37. Kamenar, B. and Kaitner, B., *Cryst. Struct. Comm.*, 1982, **11,** 2043.
38. Chia Chih, Ou., Wollmann, R. G., Hendrickson, D. N., Potenza, J. A. and Schugar, H. J., *J. Am. Chem. Soc.*, 1978, **100,** 4717.
39. Heath, S. L., Powell, A. K., Utting, H. L. and Helliwell, M., *J. Chem. Soc., Dalton Trans.*, 1992, 305.
40. Healy, P. C., Patrick, J. M. and White, A. H., *Aust. J. Chem.*, 1984, **37,** 1405.
41. Konefal, E., Loeb, S. J., Willis, C. J. and Stephan, D. W., *Inorg. Chim. Acta*, 1986, **115,** 147.
42. Wieghardt, K., Pohl, K., Bossek, U., Nuber, B. and Weiss, J., *Z. Naturforsch*, 1988, **43b,** 1184.
43. Mockler, G. M., de Jersey, J., Zerner, B., O'Connor, C. J. and Sinn, E., *J. Am. Chem. Soc.*, 1983, **105,** 1891.
44. Kitajima, N., Ito, M., Fukui, H. and Moro-oka, Y., *J. Chem. Soc., Chem. Commun.*, 1991, 102.
45. Coda, A., Kamenar, B., Prout, K., Carruthers, J. R. and Rollett, J. S., *Acta Cryst.*, 1975, **B31,** 1438.
46. Ercolani, C., Monacelli, F., Dzugan, S., Goedken, V. L., Pennesi, G. and Rossi, G., *J. Chem. Soc., Dalton Trans.*, 1991, 1309.
47. Plowman, J. E., Loehr, T. M., Schauer, C. K. and Anderson, O. P., *Inorg. Chem.*, 1984, **23,** 3553.
48. Hazell, A., Jensen, K. B., McKenzie, C. J. and Toftlund, H., *Inorg. Chem.*, 1994, **33,** 3127.
49. Taft, K. L., Masschelein, A., Liu, S., Lippard, S. J., Garfinkel-Shweky, D. and Bino, A., *Inorg. Chim. Acta*, 1992, **198-200,** 627.
50. Gomez-Romero, P., DeFotis, G. C. and Jameson, G. B., *J. Am. Chem. Soc.*, 1986, **108,** 851.
51. Gomez-Romero, P., Witten, E. H., Reiff, W. M., Backes, G., Sanders-Loehr, J. and Jameson, G. B., *J. Am. Chem. Soc.*, 1989, **111,** 9039.
52. Gomez-Romero, P., Witten, E. H., Reiff, W. M. and Jameson, G. B., *Inorg. Chem.*, 1990, **29,** 5211.
53. Collamati, I., Dessy, G. and Fares, V., *Inorg. Chim. Acta*, 1986, **111,** 149.
54. Lippard, S. J., *Angew. Chem., Int. Ed. Engl.*, 1988, **27,** 344.
55. Ondrejkovičová, I., Lis, T., Mroziński, J., Vančová, V. and Melník, M., *Inorg. Chim. Acta*, in press.
56. Figgis, B. N. and Nyholm, R. S., *J. Chem. Soc.*, 1958, 4190.
57. König, E., Magnetic Properties of Coordination and Organometallic Transition Metal Compounds, Springer–Verlag, Berlin, 1966.
58. Sheldrick G. M., SHELXL 93. Program for Crystal Structure Refinement. University of Göttingen, Germany, 1993.
59. Melník, M., Ondrejkovičová, I., Vančová, V. and Holoway, C. E., *Rev. Inorg. Chem.*, 1997, **17,** 55.
60. Kurtz, D. M. Jr., *Chem. Rev.*, 1990, **90,** 585.
61. Hart, J. R., Rappe, A. K., Gorun, S. M. and Upton, T. H., *Inorg. Chem.*, 1992, **31,** 5254.

Pergamon

PII: S0277-5387(98)00086-2

Polyhedron Vol. 17, No. 18, pp. 3193–3199, 1998
© 1998 Elsevier Science Ltd
All rights reserved. Printed in Great Britain
0277-5387/98 $19.00+0.00

Synthesis, structure and magnetic properties of a quasi-one-dimensional copper(II) compound. An unusual oxalato-bridged copper dimer

Hui-Zhong Kou[a], Dai-Zheng Liao[a,*], Guang-Ming Yang[a], Peng Cheng[a], Zong-Hui Jiang[a], Shi-Ping Yan[a], Geng-Lin Wang[a], Xin-Kan Yao[b] and Hong-Gen Wang[b]

[a]Department of Chemistry, Nankai University, Tianjin 300071, P. R. China

[b]Central Laboratory, Nankai University, Tianjin 300071, P. R. China

(Received 18 December 1997; accepted 27 February 1998)

Abstract—A new compound $[Cu(Him)_2(ox)]_2[Cu(Him)_2(H_2O)]_2$ (Him = imidazole, ox = dianion of oxalic acid) has been prepared and structurally determined. The structure consists of quasi-one-dimensional chains built from two different neutral $[Cu(Him)_2(ox)]_2$ and $[Cu(Him)_2(H_2O)(ox)]_2$ units linked by hydrogen bonds. Two centrosymmetrically related copper ions in the former unit are five-coordinated by two nitrogen atoms from the imidazole ligands and two oxygen atoms from the oxalate anion occupying the basal plane and the oxygen atom of another chelating oxalate situated at the apical position with a weak contact of 2.837(2) Å. The coordination environment of the other two copper ions connected by O–H · · · O hydrogen bonds in the other unit can be described as a distorted square pyramid, with two oxygen atoms of the oxalate ion and two nitrogen atoms from the imidazole ligands in the basal plane and one oxygen atom of the coordinated water molecule in the apical position. The (Him)N–H · · · O(ox) hydrogen bonds connect the adjacent units to give rise to a quasi-one-dimensional structure. The room-temperature ESR study gives a $g_\perp$ value of 2.07 and a $g_\parallel$ value of 2.23. From magnetic susceptibility measurements the compound was found to exhibit a weak antiferromagnetic interaction ($J = -2.64\,cm^{-1}$) between the copper(II) ions through the Cu–O–Cu pathways. © 1998 Elsevier Science Ltd. All rights reserved. © 1998 Elsevier Science Ltd. All rights reserved

Keywords: crystal structure; copper(II) complex; hydrogen bonding; magnetic behaviour; oxalate bridges; tetranuclear complex.

The oxalate has been proven to be a bridging ligand to propagate magnetic interactions and the exchange interaction between the copper ions through this bridge was found to vary from $J = -340\,cm^{-1}$ to $-0.5\,cm^{-1}$ [1–6]. To date, two different bridging modes (Scheme 1a and 1b [7]) have been observed for the oxalato group, of which the former mode is commonly seen.

In the present paper, we describe a new copper(II) compound $[Cu(Him)_2(C_2O_4)]_2[Cu(Him)_2(C_2O_4)(H_2O)]_2$ which has an unusual oxalate-bridged copper pair and a hydrogen-bonded copper pair (Him = midazole). Its dimeric arrangement and the presence of novel oxalate bridges (Scheme 1c) make this compound of considerable interest.

EXPERIMENTAL

Copper nitrate trihydrate, sodium oxalate and Him were of analytical grade. $K_3[Cr(ox)_3] \cdot 3H_2O$ (ox^{2-} = dianion of oxalic acid) were prepared by the literature method [8].

Synthesis

The compound $[Cu(Him)_2(C_2O_4)]_2[Cu(Him)_2(C_2O_4)(H_2O)]_2$ was prepared by two different procedures.

Method 1: To $Cu(NO_3)_2 \cdot 3H_2O$ (241.6 mg, 1 mmol)

*Author to whom correspondence should be addressed.

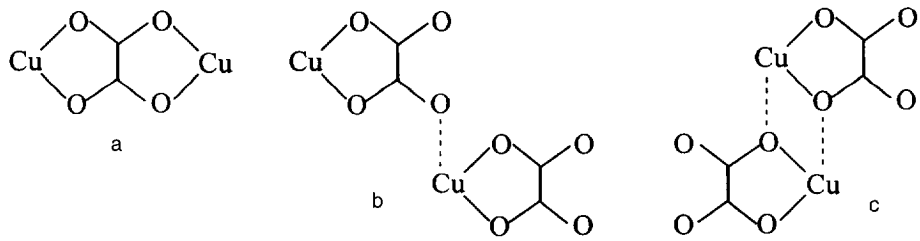

Scheme 1. Different bridging modes for oxalate ligands.

and Him (136.2 mg, 2 mmol) in an aqueous solution (10 cm^3) was added Na_2ox (134 mg, 1 mmol) in water (5 cm^3). Blue microcrystals were obtained from the resulting solution upon standing for several hours. Yield: 50%. Found: C, 32.5; H, 3.1; N, 18.8. Calcd. for $C_{16}H_{18}Cu_2N_8O_9$: C, 32.4; H, 3.0; N, 18.9%. Method 2: To $Cu(NO_3)_2 \cdot 3H_2O$ (241.6 mg, 1 mmol) in 10 cm^3 of water was added an aqueous solution of $K_3[Cr(ox)_3] \cdot 3H_2O$ (487.4 mg, 1 mmol) in 10 cm^3 of H_2O. Then, to the resulting mixture was added Him (136.2 mg, 2 mmol) and the dark blue solution was stirred for 10 min and then filtered. The filtrate was left to stand at ambient temperature. After 3 d, prismatic blue crystals were obtained in 40% yield. Found: C, 32.5; H, 3.2; N, 19.3. Calcd. for $C_{16}H_{18}Cu_2N_8O_9$: C, 32.4; H, 3.0; N, 18.9%.

Physical measurements

Elemental analyses of carbon, hydrogen and nitrogen were carried out with a Perkin–Elmer analyzer model 240. The electronic spectrum was measured with a Perkin Elmer Hitachi-240 spectrophotometer. The powder ESR spectrum was recorded on a JES-FE1XG ESR spectrometer using an X-band and Mn^{2+} (MgO) reference. IR spectra on KBr pellets were performed on a Shimadzu IR-408 infrared spectrophotometer in the 4000–600 cm^{-1} region. Magnetic susceptibility measurement of a crystalline sample was carried out in the temperature range 2–290 K on a vibrating sample magnetometer, model CF-1. The experimental susceptibilities were corrected for the diamagnetism of the constituent atoms (Pascal' Tables).

Crystallographic data collection and structure determination

Data were measured at 299(1) K with a CAD-4 diffractometer using the ω-2θ scan technique with ω-scan width = $(0.65 + 0.35 \tan\theta)^\circ$, scan speed = 0.92–5.49° min^{-1}, graphite-monochromated M-Kα radiation; 2978 independent reflections $2 < \theta < 23^\circ$; hkl, h = −8–8, k = −8–8, l = 0–20, giving 2792 observed reflections ($I > 3\sigma(I)$). Intensity data were corrected for Lorentz-polarization factors and empirical absorption correction was made during processing.

The structure was solved by direct method (MULTAN 82). All non-hydrogen atoms were refined anisotropically by full-matrix least squares method. Atomic scattering factors were taken from ref.[9]. The weighting scheme w = 1 for all of observed reflections gave satisfactory agreement analyses. Calculations were performed with the SPD-PLUS program system [10] on a PDP11/44 computer.

RESULTS AND DISCUSSION

Preparation of $[Cu(Him)_2C_2O_4][Cu(Him)_2(C_2O_4)(H_2O)]_2$

The oxalate as a multidentate anionic ligand has been proven to have the tendency to bridge two transition metal centres to give rise to dinuclear complexes. We initially investigated the reaction of equimolar amounts of $Cu(Him)_2^{2+}$ and Na_2ox in an aqueous solution and found that no crystals but microcrystals were obtained. The electrophilic attack of the CuL^{2+} complexes on the coordinated oxalate ligands in $Cr(ox)_3^{3-}$ ion has commonly been used to synthesize oxalate-bridged copper complexes [3–6]. In order to obtain the single crystals of the present compound suitable for X-ray structure analysis, we adopted the same way by employing the reaction between $Cu(Him)_2^{2+}$ and $Cr(ox)_3^{3-}$ in a 1:1 molar ratio. The result shows that an oxalate-bridged copper(II) compound is obtained. It may be accounted for if the following reaction (Scheme 2) is assumed. In addition, it follows that the preparation method 2 possesses a slower reaction so as to afford larger crystals with respect to the method 1.

Crystal structure of $[Cu(Him)_2(C_2O_4)]_2$ $[Cu(Him)_2(C_2O_4)(H_2O)]_2$

Crystal data, selected interatomic bond distances and bond angles and the intermolecular contacts are given in Tables 1, 2 and 3, respectively. The molecular structure and the view of the cell are shown in Figs 1 and 2, respectively.

The structure consists of quasi-one-dimensional chains built from two different binuclear units $[Cu(Him)_2(ox)]_2$ and $[Cu(Him)_2(H_2O)(ox)]_2$ linked by hydrogen bonds (Fig. 2). The Cu(1) and Cu(1a) (a:

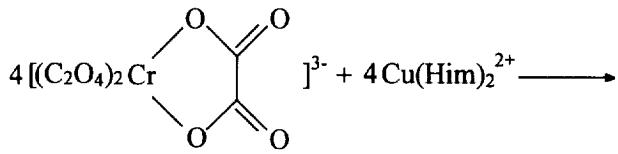

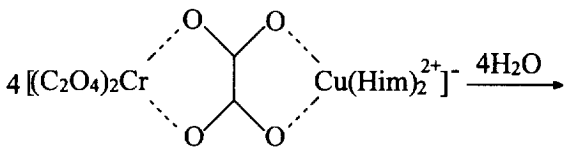

$$[Cu(Him)_2(C_2O_4)]_2[Cu(Him)_2(C_2O_4)(H_2O)]_2 + 4\ Cr(C_2O_4)_2(H_2O)_2^-$$

Scheme 2. The representation of the mechanism of the electrophilic attack of $Cu(Him)_2^{2+}$ on $Cr(C_2O_4)_3^{3-}$.

Table 1. Crystallographic data and data-collection parameters for the compound

Formula	$C_{32}H_{36}Cu_4N_{16}O_{18}$
M	1186.9
Crystal system	Triclinic
Space group	$P\bar{1}$
a/Å	8.033(1)
b/Å	8.136(1)
c/Å	18.454(3)
α/°	100.05(1)
β/°	94.13(1)
γ/°	108.60(1)
U/Å^3	1114.9(6)
Z	1
D_c/Mg m^{-3}	1.768
Crystal dimensions/mm	0.25 × 0.3 × 0.4
μ/mm-1	1.9759
F(000)	600
Transmission factors: minimum, maximum	0.934, 1.102
Agreement factor(on I)	0.017
No. variables	316
Largest shift/e.s.d. in final cycle	0.01
R^a	0.036
R'^b	0.042
Goodness of fit^c	1.378

[a] $\Sigma||F_0|-|F_c||/\Sigma|F_0|$.
[b] $[\Sigma(w|F_0|-|F_c|)^2/\Sigma w|F_0|^2]^{1/2}; w = 1$.
[c] $[\Sigma w(|F_0-F_c|)^2/(N_{obs}-N_{para})]^{1/2}$

$1+x$, $1+y$, $2+z$) ions of the centrosymmetrically related $[Cu(Him)_2(ox)]_2$ unit are five-co-ordinated (Fig. 1a) by two nitrogen atoms from the imidazole ligands and two oxygen atoms from the oxalate anion forming the basal plane and the square pyramidal is completed by the apical oxygen atom of another oxalate ligand at a distance of 2.837(2) Å from the copper ion, which is comparable with the Cu–O distances found previously in other copper(II) compounds [7, 11, 12, 13]. The bond angles of O(1a)–Cu(1)–O(3) and O(1a)–Cu(1)–O(1) are 106.8° and 76.4° which deviate remarkably from 90°. This apparently suggests some interaction between the O(1a) atom and Cu(1) atom. The largest deviations from the least-squares plane for Cu(1) defined by N(11), N(21), O(1) and O(3) are 0.1862 Å at O(1) and −0.1848 Å at O(3) and Cu(1) lies 0.0948 Å out of this plane toward O(1a). The Cu(1)···Cu(1a) separation is 5.879(5) Å.

Table 2. Selected interatomic bond distances (Å) and angles (°)

Cu(1)–O(1)	1.941(3)	Cu(1)–O(3)	1.962(3)
Cu(1)–N(11)	1.961(3)	Cu(1)–N(21)	1.948(3)
Cu(1)–O(1a)	2.837(2)	Cu(2)–O(5)	1.982(3)
Cu(2)–O(7)	1.938(3)	Cu(2)–N(31)	1.953(3)
Cu(2)–O(9)	2.447(3)	Cu(2)–N(41)	1.981(3)
C(1)–O(1)	1.278(5)	C(4)–O(8)	1.222(5)
C(1)–O(2)	1.217(5)	C(2)–O(3)	1.260(6)
C(2)–O(4)	1.244(5)	C(3)–O(5)	1.278(5)
C(3)–O(6)	1.217(5)	C(4)–O(7)	1.267(6)
O(1)–Cu(1)–O(3)	84.1(1)	O(1)–Cu(1)–N(11)	91.7(1)
O(1)–Cu(1)–N(21)	173.4(1)	O(3)–Cu(1)–N(11)	163.2(1)
O(3)–Cu(1)–N(21)	92.4(1)	N(11)–Cu(1)–N(21)	93.2(1)
Cu(1)–O(1)–Cu(1a)	103.6(1)	C(1)–O(1)–Cu(1a)	110.7(1)
O(1a)–Cu(1)–N(11)	87.8(1)	O(1a)–Cu(1)–N(21)	99.5(1)
O(1a)–Cu(1)–O(3)	106.8(1)	O(1a)–Cu(1)–O(1)	76.4(1)
O(5)–Cu(2)–O(7)	82.8(1)	O(5)–Cu(2)–N(31)	92.6(1)
O(5)–Cu(2)–N(41)	166.6(1)	O(5)–Cu(2)–O(9)	101.1(1)
O(7)–Cu(2)–N(31)	175.3(1)	O(7)–Cu(2)–N(41)	90.5(1)
O(7)–Cu(2)–O(9)	91.2(1)	N(31)–Cu(2)–N(41)	94.2(1)
N(31)–Cu(2)–O(9)	89.1(1)	N(41)–Cu(2)–O(9)	90.6(1)

Symmetry operation: a $1+x$, $1+y$, $2+z$

Table 3. Intermolecular contacts

O(4d)···N(44)	2.879 Å	O(9)···O(5b)	2.904 Å
C(45)–N(44)···O(4d)	139.1	C(2)–O(4d)···N(44)	115.1
C(43)–N(44)···O(4d)	112.5	Cu(2)–O(9)···O(5b)	115.5

Symmetry operations: d x, y, $1+z$; b x, $1+y$, $1+z$

The co-ordination environment of Cu(2) can be described as a distorted square pyramid, with two oxygen atoms of one oxalate ion and two nitrogen atoms from the imidazole ligands in the equatorial plane and one oxygen atom of the coordinated water molecule in the apical position. The oxygen and nitrogen atoms are alternatively below and above the plane with the deviations being N(41) 0.0967 Å, N(31) −0.0944 Å, O(5) 0.1052 Å and O(7) −0.1075 Å. The Cu(2) atom lies out of this plane by −0.0976 Å toward the coordinated O(9) atom. The centrosymetric copper groups are linked by the O(9)–H···O(5b) hydrogen bonds with the O(9)···O(5b) distance of 2.906(5) Å to give rise to another binuclear unit (Fig. 1b).

The Cu–N(Him) bond distances of both entities are similar, ranging from 1.948(3) to 1.981(3) Å, which are approximately equal and similar to corresponding lengths found in other imidazole copper complexes [14, 15]. Each imidazole ring is almost planar with deviations from the least-squares planes less than 0.0087 Å. The two imidazole planes in each neutral moiety are not coplanar with the dihedral angles of 108.5° and 100.5°, respectively.

As usual, the chelating oxalate possesses two pairs of C–O bonds with different bond lengths [7, 13, 16]: the coordinated oxygen atoms invariably possess longer C–O bonds which can be considered as single with respect to the short terminal C–O bonds. The difference observed is 0.055 Å (average value) excluding that between C(2)–O(3) and C(2)–O(4) of 0.016 Å, which is due to the existence of O(4d)···N(44) hydrogen bonding (d = x, y, $1+z$) undermining the C(2)–O(4) bond strength.

The O(4d)···N(44) hydrogen bonds of 2.879(6) Å (d = x, y, $1+z$) connect the adjacent units to give rise to a quasi-one-dimensional structure (Fig. 2).

Spectroscopic and magnetic properties

The infrared spectra display features characteristic of the chelating modes of oxalate and coordinated imidazole. The band at 3110 cm^{-1} can be attributed to the N-H vibration of Him. the broad band at 2900 cm^{-1} indicates the presence of hydrogen bond in the present complex. In the 1720–1630 cm^{-1} range the strong bands are characteristic of C–O stretch of the

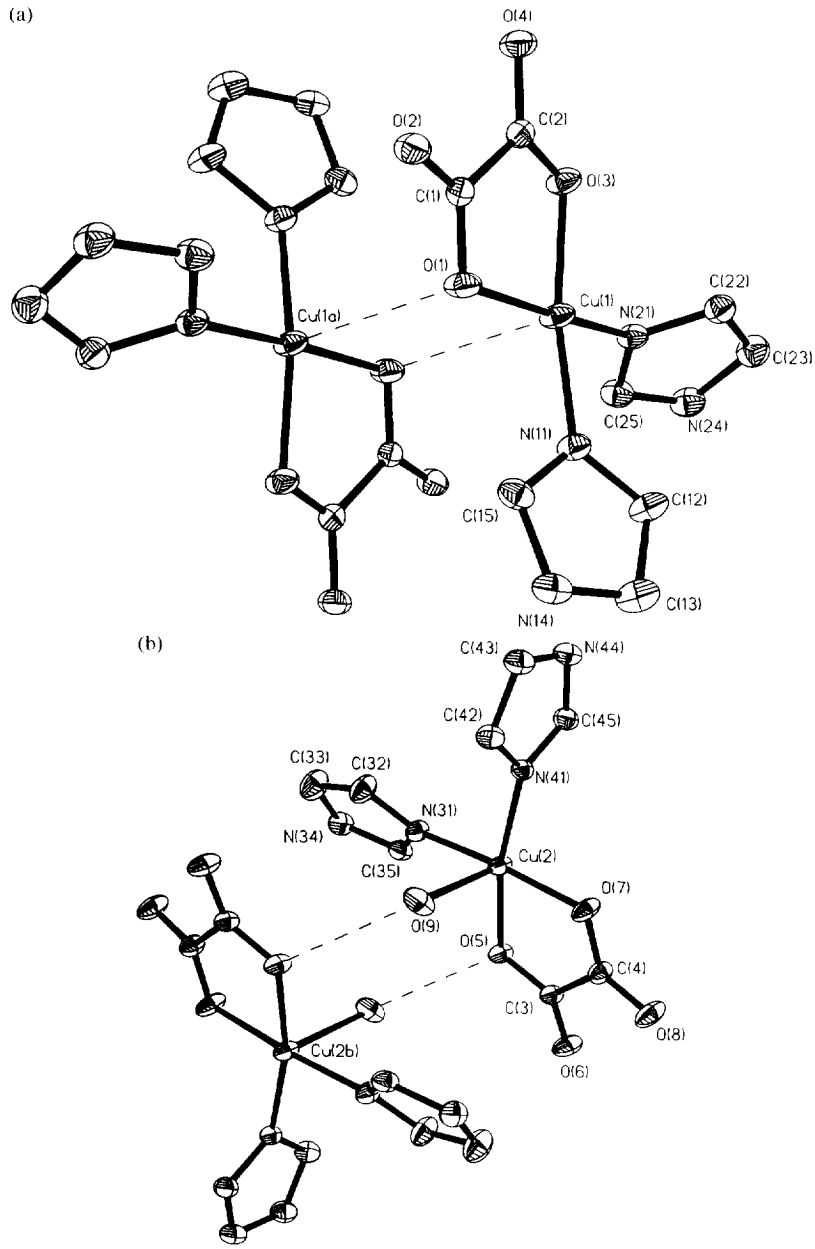

Fig. 1. The ORTEP [18] drawing of $[Cu(Him)_2(C_2O_4)]_2[Cu(Him)_2(C_2O_4)(H_2O)]_2$, showing thermal ellipsoids drawn at the 30% probability level: (a) $[Cu(Him)_2(C_2O_4)]_2$; (b) $[Cu(Him)_2(C_2O_4)(H_2O)]_2$.

oxalate ligand. Four bands at 1710, 1695 and 1670 cm^{-1} are observed which is in good agreement with the presence of chelating oxalate ligands [17] determined by the crystal structure analysis.

The solid-state reflectance electronic spectrum shows a broad band at 640 nm of medium-intensity which is assigned to d-d transition of copper ions in square pyramidal surroundings.

The powder X-band ESR spectrum at room temperature is anisotropic having a $g_\perp$ parameter value of 2.07 and a g value of 2.23. No half-field transition was observed.

Magnetic susceptibility data were collected on a crystalline sample in the temperature range 2–290 K. The variations of X_m and μ_{eff} is represented in Fig. 3 from 150 to 2 K. From 290 to 150 K, μ_{eff} remains practically constant and equal to 3.8 μ_B, which is the value expected for four isolated copper(II) ions with a g value of 2.17. Upon further lowering the temperature, μ_{eff} decreases, reaching a value of 2.6 μ_B at 2 K, which indicates the presence of an antiferromagnetic interaction between the copper(II) ions at low temperature.

The quasi-one-dimensional chain, formed by alter-

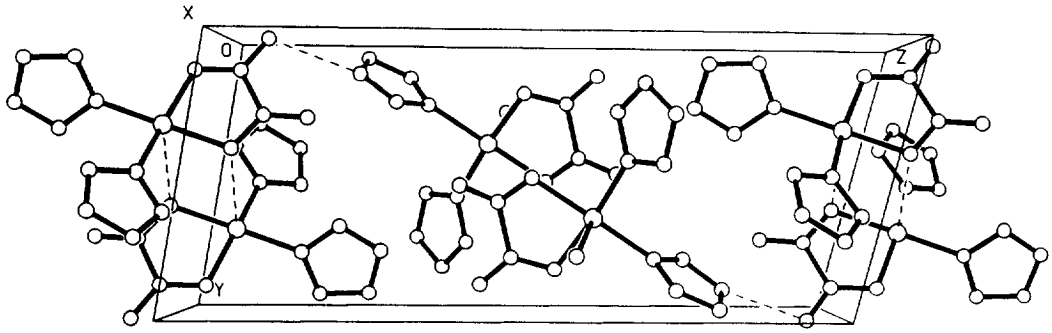

Fig. 2. View of the crystal cell of the compound showing the hydrogen bonds connecting the binuclear units.

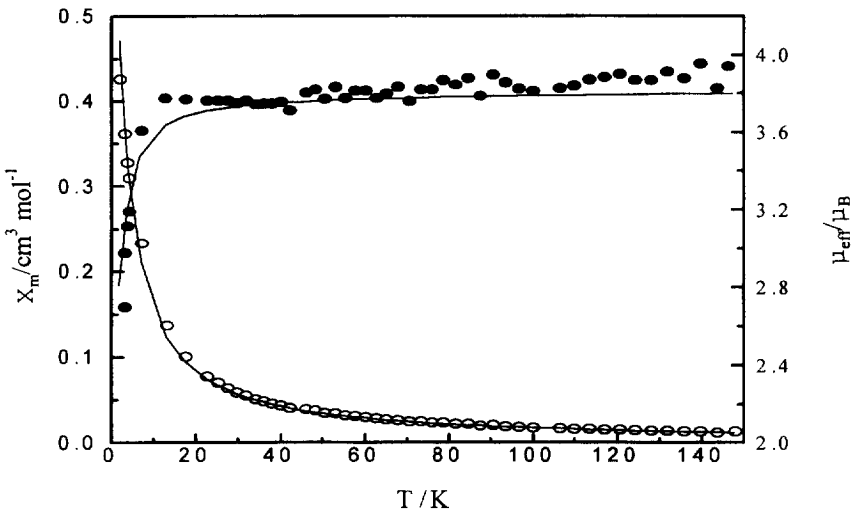

Fig. 3. Plots of μ_{eff} and X_m vs temperature for $[Cu(Him)_2(C_2O_4)]_2[Cu(Him)_2(C_2O_4)(H_2O)]_2$. The solid lines represent the theoretical values.

nation of (Cu_1–Cu_1) and (Cu_2–Cu_2) binuclear units through hydrogen bonds, can be schemtized as hereunder:

$$\cdots Cu_1 \overset{J}{\text{——}} Cu_1 \cdots Cu_2 \text{——} Cu_2$$

$$\cdots Cu_1 \overset{J}{\text{——}} Cu_1 \cdots Cu_2 \text{——} Cu_2 \cdots$$

Upon neglecting the very weak interactions through all of the hydrogen bonds, the magnetic susceptibility of the present compound can be generated by eqn (1) considering Cu_1–Cu_1 as a binuclear unit and Cu_2–Cu_2 as two temperature-independent copper ions.

$$X_m = \frac{2N\beta^2g^2}{KT}[3 + \exp(-2J/KT]^{-1} + 2 \times \frac{N\beta^2g^2}{4KT} + N\alpha \quad (10)$$

where X_m is the mole susceptibility per Cu_4 unit, J the exchange integral between the Cu_1 ions ($\hat{H} = -2J\hat{S}_1\hat{S}_2$) and the other symbols have their usual meanings. As shown in Fig. 3, a good least-square fit with the experimental data was attained with eqn (1), giving magnetic parameters $g = 2.17$, $J = -2.64\,cm^{-1}$, and the agreement factor defined as $R = \Sigma(X_{obs}\text{-}X_{calc})^2/\Sigma(X_{obs})^2$ equal to 8.8×10^{-4}. The small negative J value suggests that the Cu1a–O–Cu1 pathway within the present compound is unfavourable to achieve an effective overlap between magnetic orbitals of the copper ions. On the basis of the molecular structure of the compound, we see that the unpaired electron of the copper ion with a square pyramidal configuration can be described by a magnetic orbital built from the $d_{x^2-y^2}$ orbital with little contribution from the d_{z^2} orbital, and localized basically in the basal plane. Hence, two parallel magnetic orbitals unfavour the magnetic exchange and the weak coupling must be due to the slight delocalization of the magnetic orbitals towards the apical position occupied by the bridging oxygen atoms [19].

Acknowledgements—This work was supported by the National Natural Science Foundation of China (No. 59772020 and No. 29631040) and the State Key Laboratory of Structural Chemistry of China.

REFERENCES

1. Shi, J., Yang, G.-M., Cheng, P., Liao, D.-Z., Jiang, Z.-H. and Wang, G.-L., *Polyhedron*, 1997, **16,** 531.
2. Julve, M., Verdaguer, M., Kahn, O., Gleizes, A., Philoche-Levisalles, M., *Inorg. Chem.*, 1983, **22,** 258.
3. Bencini, A., Benelli, C., Gatteschi, D., Zanchini, C. and Fabretti, A. C., *Inorg. Chim. Acta.*, 1984, **86,** 169.
4. Goswami, L., Sarker, S. and Banerjea, D., *Z. Anorg. Allg. Chem.*, 1977, **435,** 301.
5. Basak, A. K. and Chatterjee, C., *Bull. Chem. Soc. Jpn.*, 1983, **56,** 318.
6. Felthouse, T. R., Laskowski, E. J. and Hendrickson, D. N., *Inorg. Chem.*, 1977, **16,** 1077.
7. Viswamitra, M. A., *J. Chem. Phys.*, 1962, **37,** 1408.
8. Bushra, E. and Johnson, C. H., *J. Chem. Soc.*, 1939, **142,** 1937.
9. International Tables for X-Ray Crystallography, the Kynoch Press, Birmingham. England, 1974, Vol. 4.
10. SPD-PLUS, Enraf-Nonius, Delft, 1985.
11. Friebel, C., Plesch, G., Kettmann, V., Krätsmar-Šmogrovic, J. and Švajlenovc, O., *Inorg. Chim. Acta*, 1997, **254,** 273.
12. Kovbasyuk, L. A., Fritsky, I. O., Kokozay, V. N. and Iskenderov, T. S., *Polyhedron*, 1997, **16,** 1723.
13. Stephens, F. S., *J. Chem. Soc.*, 1969, **A,** 2493.
14. Koh, L. L., Ranford, J. O., Robinson, W. T., Svensson, J. O., Tan, A. L. C. and Wu, D., *Inorg. Chem.*, 1996, **35,** 6466.
15. Casanovo, J., Alzuet, G., Borras, J. and Carugo, O., *J. Chem. Soc., Dalton Trans.*, 1996, 2239.
16. Fabretti, A. C., Franchini, G., Zannini, P. and Divaira, M., *Inorg. Chim. Acta*, 1985, **105,** 187.
17. Nakamoto, K., *Infrared and Raman Spectra of Inorganic and Coordination Compounds*, 4th edition., Wiley & Sons, New York, 1986.
18. Johnson, C. K., ORTEP, Report ORNL-5138, Oak Ridge National Laboratory, Oak Ridge, TN, 1976.
19. Escrivà, E., Server-Carrio, J., Lezama, L., Folgado, J.-V., Pizarro, J. L., Baallesteros, R. and Abarca, B., *J. Chem. Soc., Dalton Trans.*, 1997, 2033 and references therein.

Pergamon

PII: S0277-5387(98)00092-8

Polyhedron Vol. 17, No. 18, pp. 3201–3210, 1998
© 1998 Elsevier Science Ltd
All rights reserved. Printed in Great Britain
0277-5387/98 $19.00+0.00

Silver(I) and gold(I) complexes of hydrotris(3,5-dimethylpyrazol-1-yl)borate: synthesis, spectroscopic and structural characterization, and reactivity toward C-, N- and S-donor ligands.

C. Santini[a], C. Pettinari[a,*] G. Gioia Lobbia[a], D. Leonesi[a], G. Valle[b] and S. Calogero[c]

[a]Dipartimento di Scienze Chimiche, Università di Camerino, via S. Agostino 1, I-62032 Camerino, Italy

[b]Centro di Ricerca sui Biopolimeri del CNR-Padova, I-35100 Padova, Italy

[c]Dipartimento di Chimica Fisica, Università di Venezia, Calle Larga S. Marta 2137, I-30123, Venezia, Italy

(Received 7 January 1998)

Abstract—Reaction of $Ag(NO_3)$ with 1 equiv of $K[HB(3,5\text{-}Me_2pz)_3]$ (pzH = pyrazole) and 1 equiv of PR_3 (R=OPh or C_6F_5) in methanol provides two new air stable derivatives $\{[HB(3,5\text{-}Me_2pz)_3]Ag(PR_3)\}$. When the interaction between $Ag(O_3SCF_3)$, CNR (R=Bu^t or cyclohexyl), and $K[HB(3,5\text{-}Me_2pz)_3]$ was carried out in CH_2Cl_2 at 0°C the air stable neutral compounds $\{[HB(3,5\text{-}Me_2pz)_3]Ag(CNR)\}$ were obtained. The borderline monodentate imidazole (ImH) reacts with the dinuclear $\{[HB(3,5\text{-}Me_2pz)_3]Ag\}_2$ yielding the mixed-ligand complex $\{[HB(3,5\text{-}Me_2pz)_3]Ag(ImH)\}$. On the other hand when the soft donor 1-methyl-2-mercaptoimidazole (Hmimt) was employed, no stable compound was obtained. We also synthesized $[Phen_2Ag](O_3SCF_3)$ (Phen = 1,10-phenanthroline) and its reaction with $K[HB(3,5\text{-}Me_2pz)_3]$ yielded the complex $\{Phen[HB(3,5\text{-}Me_2pz)_3]Ag\}$, which is not fluxional in solution. Instead only unmanageable material was obtained from the reaction between $(Hmimt)_2Ag(O_3SCF_3)$ and $K[HB(3,5\text{-}Me_2pz)_3]$. Finally, the gold(I) complex $[HB(3,5\text{-}Me_2pz)_3]Au(PPh_3)_2$ was obtained when the reaction between PPh_3AuCl and $[HB(3,5\text{-}Me_2pz)_3]$ was carried out in presence of 1 equiv of PPh_3. The solid state structures of $\{[HB(3,5\text{-}Me_2pz)_3]Ag(PPh_2Me)\}$ and $\{[HB(3,5\text{-}Me_2pz)_3]Ag(P\text{-}o\text{-}tolyl_3)\}$, show that the silver(I) atoms are in a strongly distorted tetrahedral environment, with the $[HB(3,5\text{-}Me_2pz)_3]^-$ donor acting in the tridentate form. The Ag–P and Ag–N bond distances in $\{[HB(3,5\text{-}Me_2pz)_3]Ag(PPh_2Me)\}$ are 2.336(2) Å and 2.316(6), 2.336(5) and 2.329(6) Å, respectively; they are shorter than in the more sterically hindered $\{[HB(3,5\text{-}Me_2pz)_3]Ag(P\text{-}o\text{-}tolyl_3)\}$ (Ag–P: 2.375(2) Å; Ag–N: 2.361(4) Å). The ligand bite N–Ag–N ranges from 82.1(2)° to 84.8(2)°, whereas the N–Ag–P angle ranges from 125.1(1) to 134.1(1)°. © 1998 Elsevier Science Ltd. All rights reserved

Keywords: hydrotris dimethylpyrazol borate; spectroscopic; structural characterization; donor ligands.

The chemistry of poly(pyrazol-1-yl)borate complexes containing group 12 metals has recently attracted much interest [1–4]. In the case of copper(I) stable carbonyl complexes, such as $Cu(CO)[HB(pz)_3]$ [5], and triorganophosphine derivatives, such as $Cu(PR_3)[HB(pz)_n]$ (R = aryl or cyclohexyl; $n = 2$, 3 or 4) [6–8], have been obtained and characterized with analytical, spectral and X-ray data. The solid state and solution properties of the dinuclear $Cu_2[HB(pz)_3]_2$ and $Cu_2[HB(3,5\text{-}Me_2pz)_3]_2$ have also been described [9]. These two compounds show significative differences ascribed to steric influence of the methyl groups in the latter complex.

More recently, silver(I)poly(pyrazol-1-yl)borate derivatives have received great interest [10]. This is likely due to the fact that complex formation of silver(I) cations by ammonia, amines and other N-donor

*Author to whom correspondence should be addressed.

ligands has been well established in analytical and chemical technology of silver(I) for more than a century [11, 12], and it has been shown that this kind of compounds can have potential application in photography [13] or silver plating by electrochemical processes [14].

However to date the majority of these studies involves the use of polyfluorinated tris(pyrazol-1-yl)borate ligand [10]. These compounds can be used as new silver precursors: they possess a good combination of thermal stability and volatility and so promise to be excellent precursors for CVD of silver.

We have previously reported the synthesis, structural and spectroscopic characterization of several new silver{poly(pyrazol-1-yl)}borates(triorganophosphine) complexes [15, 16], and have indicated some relevant molecular and spectroscopic features. For example, it has been shown that the behavior in solution of $[Ag(PR_3)(HB(pz)_3]$ species is very different from that in solid state: the stability in solution is strongly dependent on the Tolman cone angle and pK_a of PR_3 [17], whereas in the solid state the bonding of $HB(pz)_3$ to $Ag(PR_3)$ is similar, despite the steric and electronic features of the N- and P-donor ligand.

In order to fully understand the coordination chemistry of poly(pyrazolyl)borates towards silver(I) acceptors, we now report the synthesis and reactivity of six new complexes containing the N_3-donor tris(3,5-dimethylpyrazol-1-yl)borato. Comparison was made with the results previously obtained and also with the new [gold(I){triphenylphosphine}tris(3,5-dimethylpyrazol-1-yl)borato] complex. The reactivity of silver(I)tris(3,5-dimethylpyrazolyl)borate derivatives towards N- and S- donor was also investigated.

We also report the crystal and molecular structure of tris(3,5-dimethylpyrazol-1-yl)boratosilver(I){tri-*o*-tolylphosphine} and tris(3,5-dimethylpyrazol-1-yl)boratosilver(I){methyldiphenylphosphine}, two compounds previously synthesized by us [15]. The present structural study was performed in order to support some of the hypotheses previously indicated.

EXPERIMENTAL

General comments.

All reactions were carried out under an atmosphere of dry, oxygen-free dinitrogen using standard Schlenk techniques. Solvents were freshly distilled over an appropriate drying agent and further degassed before use where necessary. In some cases the reactions were protected from light by covering reaction vessels with aluminium foil. Concentration was always carried out *in vacuo* (water aspirator). The samples for microanalysis were dried *in vacuo* to constant weight (20°C, *ca* 0.1 Torr). Elemental analyses (C,H,N) were performed in-house with a Carlo–Erba model 1106 instrument. IR spectra were recorded from 4000 to 100 cm^{-1} with a Perkin–Elmer System 2000 FT-IR instrument. ^1H, ^{13}C and ^{31}P NMR spectra were recorded on a VXR-300 Varian spectrometer operating at room temperature (300 MHz for ^1H, 75 MHz for ^{13}C and 121.4 MHz for ^{31}P). The electrical resistance of acetone solutions was measured with a Crison CDTM 522 conductimeter at room temperature.

Syntheses

The donor $K[HB(3,5\text{-}Me_2pz)_3]$ was prepared in accordance with the procedure reported in literature [18]. KBH_4, P-(*o*-tolyl)$_3$, $PMePh_2$, $P(C_6F_5)_3$, $P(OPh)_3$, 3,5-Me_2pzH, Hmimt, RNC (R=Bu^t or cyclohexyl), $Ag(O_3SCF_3)$, 1,10-phenanthroline, $(PPh_3)AuCl$ were purchased (Aldrich) and used as received.

Synthesis of $\{[HB(3,5\text{-}Me_2pz)_3]Ag\}_2$ (**1**). A mixture of $K[HB(3,5\text{-}Me_2pz)_3]$ (0.34 g, 1 mmol) in CH_3OH (30 ml) was added to $AgNO_3$ (0.17 g, 1 mmol) in CH_3OH (20 ml) at room temperature. A pale rose precipitate was immediately formed which was stirred ca. 30 min and then filtered off. The precipitate (**1**) was washed with CH_3OH and diethyl ether (0.283 g, yield 70%). Mp: 210°C dec. ^1H NMR($CDCl_3$), δ: 1.91 (s, 9H, 3 or 5-CH_3), 2.31 (s, 9H, 3 or 5-CH_3), 4.0 (br, 1H, B-*H*), 5.77 (s, 3H, 4-C*H*). $^{13}C\{^1H\}$ NMR ($CDCl_3$), δ: 13.9 (s, CH_3), 14.8 (s, CH_3), 105.3 (s, 4-*C*H), 146.8 s, 150.0 s (5-*C*-CH_3 and 3-*C*-CH_3). IR, cm^{-1}: 3119 w (CH) 2508 m (BH), 1538 s (ring). Anal. Calcd for $C_{15}H_{22}BN_6Ag$; C, 44.5; H, 5.5; N, 20.7. Found: C, 44.2; H, 5.6; N, 20.6%.

Synthesis of $[HB(3,5\text{-}Me_2pz)_3]Ag\{CNBu^t\}$ (**2**). A CH_2Cl_2 (10 ml) suspension of $Ag(O_3SCF_3)$ (0.26 g, 1.0 mmol) was treated with a CH_2Cl_2 solution of $K[HB(3,5\text{-}Me_2pz)_3]$ (0.34 g, 1.0 mmol) by slow cannula transfer. The solution became homogeneous and was stirred 1 h in the dark before addition of Bu*t*NC (8.3 ml of a 0.01 g/ml hexane solution, 1.0 mmol). The reaction mixture was stirred overnight. The volatile materials were removed under reduced pressure and the residue was extracted into benzene. Filtration through Celite followed by the removal of benzene from the filtrate gave **2**, which was purified from benzene/ethyl acetate (1:1) (0.391 g, yield 80%). Mp: 148°C dec. ^1H NMR($CDCl_3$), δ: 1.59 (s, 9H C_4H_9), 2.21 (s, 9H, CH_3), 2.35 (s, 9H, CH_3), 3.8 (br, 1H, B*H*), 5.66 (s, 3H, 4-C*H*); $^{13}C\{^1H\}$ NMR ($CDCl_3$), δ: 13.4 (s, CH_3), 14.8 (s, CH_3), 30.8 (s, C_4H_9), 104.2 (s, 4-*C*H), 116.6 (*C*N), 144.3 s, 147.5 s (5-*C*-CH_3 and 3-*C*-CH_3). IR, cm^{-1}: 3113 w (CH), 2506 m (BH), 2178 s (CN), 1536 m (ring). Anal. Calcd for $C_{20}H_{31}BN_7Ag$; C, 49.2; H; 6.4. N, 20.1. Found: C, 48.8; H, 6.5; N, 19.8%.

Synthesis of $[HB(3,5\text{-}Me_2pz)_3Ag\{CNCy\}$ (**3**). Compound **3** was prepared similarly to compound **2** by using $K[HB(3,5\text{-}Me_2pz)_3]$ (0.34 g, 1 mmol), CyNC (0.11 g, 1 mmol) and $Ag(O_3SCF_3)$ (0.26 g, 1 mmol) in CH_2Cl_2 (50 ml) at room temperature. Compound **3** was purified from acetonitrile/diethyl ether (1:1) (0.334 g, yield 65%). Mp: 218°C dec. ^1H NMR($CDCl_3$), δ: 2.21 (s, 9H, CH_3), 2.34 (s, 9H, CH_3),

1.49–1.60, 1.70–2.10 (m br, 11H C_6H_{11}), 3.9 (br, 1H, B*H*), 5.65 (s, 3H, 4-C*H*); $^{13}C\{^1H\}$ NMR ($CDCl_3$), δ: 12.9 (s, CH_3), 14.3 (s, CH_3), 22.6 s, 24.8 s, 32.2 s, 53.3 s (C_6H_{11}), 116.1 (*C*N), 103.7 (s, 4-*C*H), 143.8 s, 147.0 s (5-*C*-CH_3 and 3-*C*-CH_3). IR, cm^{-1}: 3111 w (CH), 2503 m (BH), 2191 m (CN), 1537 s (ring). Anal. Calcd for $C_{22}H_{33}BN_7Ag$; C, 51.4; H; 6.5, N, 19.1. Found: C, 51.3; H, 6.5; N, 18.7%.

Synthesis of [$HB(3,5\text{-}Me_2pz)_3$]Ag{$P(OPh)_3$} (**4**). A mixture of K[$HB(3,5\text{-}Me_2pz)_3$] (0.34 g, 1.0 mmol) in CH_3OH (30 ml) and $P(OPh)_3$ (0.310 g, 1.0 mmol) was added to $Ag(O_3SCF_3)$ (0.26 g, 1 mmol) in CH_3OH (20 ml). After the addition the solution was stirred 2 h at room temperature. The volatile materials were removed under reduced pressure, and the residue was extracted into CH_2Cl_2. Filtration through Celite, followed by the removal of CH_2Cl_2 from the filtrate gave **4** (0.572 g, yield 80%). Mp: 184 C dec. ^1H NMR($CDCl_3$), δ: 1.82 (s, 9H, CH_3), 2.35 (s, 9H, CH_3), 4.0 (br, 1H, B*H*), 5.62 (s, 3H, 4-C*H*), 7.10–7.40 (m br, 15H C_6H_5); ^{31}P NMR ($CDCl_3$, 293 C), δ: −38.5 dd ($J^{107}Ag\text{–}^{31}P = 845.9$ Hz, $J^{109}Ag\text{–}^{31}P = 977.6$ Hz); ($CDCl_3$, 223 C), δ: −36.1 dd ($J^{107}Ag\text{–}^{31}P = 847.7$ Hz, $J^{109}Ag\text{–}^{31}P = 978.2$ Hz). IR, cm $^{-1}$: 3100 w (CH), 2518 br (BH), 1587 s, 1540 s (ring). Anal. Calcd for $C_{33}H_{37}BN_6O_3PAg$; C, 55.5; H; 5.2, N, 11.8. Found: C, 55.3; H, 5.4; N, 11.6%.

Synthesis of [$HB(3,5\text{-}Me_2pz)_3$]Ag{$P(C_6F_5)_3$} (**5**). Compound **5** was prepared similarly to compound **4** by using K[$HB(3,5\text{-}Me_2pz)_3$] (0.34 g, 1.0 mmol), $P(C_6F_5)_3$ (0.532 g, 1.0 mmol) and $Ag(O_3SCF_3)$ (0.26 g, 1 mmol) in CH_3OH at room temperature. Compound **5** was purified from acetonitrile/benzene 1/1 (0.843 g, yield 90%). Mp: 210 C dec. ^1H NMR($CDCl_3$): δ 1.92 (s, 9H, CH_3), 2.31 (s, 9H, CH_3), 4.1 (br, 1H, B*H*), 5.77 (s, 3H, 4-C*H*); ^{31}P NMR ($CDCl_3$, 293 C), δ: −73.8 m ($J^{19}F\text{–}^{31}P = 35.4$ Hz); ($CDCl_3$, 223 C), δ: −74.0 m, −63.1 dd of multiplet ($J^{107}Ag\text{–}^{31}P = 572.4$ Hz, $J^{109}Ag\text{–}^{31}P = 658.5$ Hz, $J^{19}F\text{–}^{31}P = 31.1$ Hz). ^{19}F NMR ($CDCl_3$, 303 C) δ: −158.9 m [relative intensity ratio: 20], −156.8 m [1], −147.0 [20], −143.3 [1], −129.9 [20], 128.5 [1]. ^{19}F NMR ($CDCl_3$, 223 C) δ: −156.8 m, −143.3, 128.5. IR, cm^{-1}: 3118 w (CH), 2507 m (BH), 1643 m, 1537 s, 1518 s (ring). Anal. Calcd for $C_{33}H_{22}BF_{15}N_6PAg$; C, 42.3; H; 2.4, N, 9.0. Found: C, 42.5; H, 2.5; N, 9.1%.

Synthesis of [bis(1,10-phenanthroline)Ag]O_3SCF_3 (**6**). Compound **6** was prepared by adding a methanol solution (25 ml) of 1,10-phenanthroline (0.36 g, 2.0 mmol) to a stirred methanol solution of $Ag(O_3SCF_3)$ (0.26 g, 1.0 mmol). A colorless precipitate formed immediately. The reaction mixture was stirred 2 h. This material was then collected on a filter, washed with methanol and dried under vacuum to give **6** (0.376 g, yield 61%). Mp: 375 C dec. ^1H NMR(DMSO-d_6): δ 8.0 (pq, 4H, Phen), 8.2 (s, 4H, Phen), 8.8 (d, 4H, Phen), 9.2 (d, 4H, Phen). IR, cm^{-1}: 3120 w, 3060 w (CH), 1619 w, 1605 w, 1589 w, 1572 w, 1512 m (ring). Anal. Calcd for $C_{25}H_{16}F_3N_4O_3SAg$; C, 48.6; H, 2.6; N, 9.1; S, 5.2. Found: C, 48.2; H, 2.6; N, 9.0; S, 5.1%.

Synthesis of [$HB(3,5\text{-}Me_2pz)_3$]Ag(1,10-phenanthroline) (**7**). To a methanol solution of compound **6** (0.308 g, 0.5 mmol) K[$HB(3,5\text{-}Me_2pz)_3$] (0.17 g, 0.5 mmol) was added. After 2 days, the suspension was filtered and the precipitate washed with *n*-hexane and diethyl ether and shown to be compound **7** (0.438 g, yield 75%). Mp: 92–93 C. ^1H NMR($CDCl_3$): δ 2.0(s br, 9H, CH_3), 2.21 (s, 3H, CH_3), 2.23 (s, 3H, CH_3), 2.35 (s, 3H, CH_3), 5.29 (s, 1H, 4-C*H*), 5.60 (s, 1H, 4-C*H*), 5.68 (s, 1H, 4-C*H*), 7.65 (dd, 2H, Phen), 7.81 (s, 2H, Phen), 8.28 (d, 2H, Phen), 9.16 (d, 2H, Phen). $^{13}C\{^1H\}$ NMR ($CDCl_3$): δ 12.1 (s, CH_3), 13.2 (s, CH_3), 13.9 (s, CH_3), 15.1 (s, CH_3), 104.5 (s, 4-*C*H), 105.2 (s, 4-*C*H), 144.5 s, 144.8 s, 146.6 s, 148.3 s (5-*C*-CH_3 and 3-*C*-CH_3), 123.6 s, 127.0 s, 129.1 s, 136.6 s, 144.8 s, 150.9 s (C_{Phen}). IR, cm^{-1}: 2519 (BH), 1616 w, 1586 w, 1559 w, 1538 m, 1505 s (ring). Anal. Calcd for $C_{27}H_{30}BN_8Ag$; C, 55.4; H, 5.2; N, 19.1 Found: C, 55.3; H, 5.4; N, 19.3%.

Synthesis of [$HB(3,5\text{-}Me_2pz)_3$]Ag(imidazole) (**8**). A solution of imidazole (0.068 g, 1.0 mmol) in CH_2Cl_2 (20 ml) was added to a solution of {[$HB(3,5\text{-}Me_2pz)_3$]Ag}$_2$ (0.40 g) in CH_2Cl_2 (20 l) at room temperature. After the addition the solution was stirred 2 h. The volatile materials were removed under reduced pressure and the residue was washed with diethyl ether (0.374 g, yield 75%). Mp: 124 C dec. ^1H NMR ($CDCl_3$, 293 C): δ 1.92 (s br, 9H, CH_3), 2.30 (s br, 3H, CH_3), 4.00 (br, 1H, B*H*), 5.76 (s, 3H, 4-C*H*), 7.10 (s, 2H, 4- and 5-C*H*), 7.67 (s, 1H, 2-C*H*); ($CDCl_3$, 193 C): δ 1.85 (s, 3H, CH_3), 2.08 (br, 6H, CH_3), 2.29 (s, 9H, CH_3), 4.7 (br, 1H, B*H*), 5.65 (s, 1H, 4-C*H*), 5.71 (s, 2H, 4-C*H*), 6.97 (s, 2H, 4- and 5-C*H*), 7.53 (s, 1H, 2-C*H*), 13.0 (br, 1H, N*H*). $^{13}C\{^1H\}$ NMR ($CDCl_3$): δ 13.0 (s, CH_3), 13.3 (s, CH_3), 14.2 (s, CH_3), 104.7 (s, 4-*C*H), 121.7, 122.1 (s, 4- and 5-*C*H), 135.4 (s, 2-*C*H) 1146.1, 149.3 br (5-*C*-CH_3 and 3-*C*-CH_3). IR, cm^{-1}: 3118 w, 3060 w (CH), 2507 m (BH), 1534 s (ring) Anal. Calcd for $C_{18}H_{26}BN_8Ag$; C, 45.7; H, 5.5; N, 23.7 Found: C, 45.6; H, 5.5; N, 23.5%.

Synthesis of [bis(1-methyl-2-mercaptoimidazole)Ag]O_3SCF_3 (**9**). Compound **9** was prepared by adding an ethanol solution of $Ag(O_3SCF_3)$ (0.26 g, 1.0 mmol) to a stirred ethanol solution of 1-methyl-2-mercaptoimidazole (0.230 g, 2.0 mmol). A pale rose precipitate was formed immediately. The reaction mixture was stirred 2 h. This material was then collected on a filter, washed with ethanol and diethyl ether and dried to vacuum to give **9** (0.291 g, yield 60%). Mp: 182–183 C dec. ^1H NMR (DMSO-d_6, 293 C): δ, 3.6 (s, 6H, CH_3), 7.2 (d, 2H, 4- or 5-C*H*), 7.3 (d, 2H, 4- or 5-C*H*), 12.9 (s br, 2H, N*H*). IR cm^{-1}: 3200 br (NH), 3136 w (CH), 1574 m (ring). Anal. Calcd for $C_9H_{12}F_3N_4O_3S_3Ag$; C, 22.3; H, 2.5; N, 11.5; S, 19.8. Found: C, 22.3; H, 2.5; N, 11.4; S, 19.8%.

Synthesis of [$HB(3,5\text{-}Me_2pz)_3$]Au{PPh_3}$_2$ (**10**). A CH_2Cl_2 solution of K[$HB(3,5\text{-}Me_2pz)_3$] (0.71 g, 1.0 mmol) was added to a stirred solution of

PPh_3AuCl (0.49 g, 1.0 mmol) and PPh_3 (0.26 g, 1.0 mmol) in CH_2Cl_2. The mixture was stirred for ca. 3 h. Filtration through Celite followed by the removal of CH_2Cl_2 from the filtrate gave **10** as a pure colorless solid, which was washed and purified with diethyl ether and n-heptane (0.865 g, yield 85%) M.p. 128°C dec. ^{1}H NMR ($CDCl_3$, 293°C): δ 1.82 (s, 9H, CH_3), 2.33 (s, 9H, CH_3), 4.6 (br, 1H, BH), 5.66 (s, 3H, 4-CH), 7.37 (m br, 20H C_6H_5), 7.51 (m br, 10H C_6H_5); ($CDCl_3$, 193°C): δ 1.82 (s, 6H, CH_3), 2.29 (s, 3H, CH_3), 2.35 (s, 9H, CH_3), 4.6 (br, 1H, BH), 5.68 (s, 2H, 4-CH), 5.78 (s, 1H, 4-CH), 7.40–8.10 (m br, 30H C_6H_5); ^{31}P NMR ($CDCl_3$, 298°C): 0.7 br, 31.5 br; ($CDCl_3$, 193°C): 31.9 s, 32.4 s, 37.0 br, 39.0 br. IR, cm^{-1}: 3070 w, 3052 (CH), 2503 br (BH), 1538 s (ring). Anal. Calcd for $C_{51}H_{52}BN_6P_2Au$; C, 60.2; H, 5.2; N, 8.2. Found: C, 60.1; H, 5.4; N, 8.3%.

Synthesis of [hydrotris(3,5-dimethylpyrazol-1-yl)borate]Ag(PMePh$_2$) (**11**) *and [hydrotris(3,5-dimethylpyrazol-1-yl)borate]Ag(P-o-tolyl$_3$)* (**12**). Compounds **11** and **12** were prepared according to literature [15], and were recrystallized from acetonitrile/ethyl acetate.

X-ray data collection and solution and refinement of structures

Crystal data and a summary of data collection parameters for compounds **[Hydrotris(3,5-dimethylpyrazol-1-yl)borate]Ag(PMePh$_2$) (11)** and **[Hydrotris(3,5-dimethylpyrazol-1-yl)borate]Ag(P-o-tolyl$_3$) (12)** are summarized in Table 1. Data were collected on a Philips PW 1100 diffractometer by using Mo–Kα radiation in the range $4.1° < 2\theta < 56.0°$ and $4.5° < 2\theta < 56.0°$. Data were corrected for the Lorentz and polarization effects. The structures were solved by SHELXS 86 or SHELXL-93 direct methods [19]. Full-matrix least-squares refinement on F was computed and the function $\Sigma w[|F_o| - |F_c|]^2$ minimized. The non-hydrogen atoms were refined anisotropically. The position of the hydrogen atoms in **11** was calculated and in **12** was partially calculated, but all were refined. Selected bond lengths and bond angles for **11** and **12** are listed in Tables 2 and 3, respectively. The ORTEP plots of **11**, and **12** together with the numbering scheme are displayed in Figs 1 and 2, respectively.

RESULTS AND DISCUSSION

Synthesis

From the interaction between silver(I) nitrate and the potassium salts of tris(3,5-dimethylpyrazol-1-yl)borate $[HB(3,5\text{-}Me_2pz)_3]^-$ (pzH = pyrazole) in methanol at room temperature, complex **1** is obtained in accordance with the following general equations **1**:

$$2AgNO_3 + 2K[HB(3,5-Me_2pz)_3] \xrightarrow{CH_3OH,\,r.t.} [HB(3,5-Me_2pz)_3]Ag_2 + 2KNO_3 \quad (1)$$

1

The analytical and spectral data of **1** are in accordance with those reported in literature [20]. For this

Table 1. Crystal data and summary of data collection and refinement for compounds 11 and 12

Compound	[HB(3,5-Me$_2$pz)$_3$]Ag(PMePh$_2$) (11)	[HB(3,5-Me$_2$pz)$_3$]Ag(P-*o*-tolyl$_3$) (12)
Formula	$C_{28}H_{25}BN_6PAg$	$C_{36}H_{37}BN_6PAg$
M	595.2	703.4
Crystal system	orthorombic	trigonal
Space group	Pbca (No. 69)	R 3 (No. 148)
Crystal size/mm	0.1 × 0.3 × 0.4	0.2 × 0.2 × 0.1
a (Å)	18.299(2)	13.670(2)
b (Å)	22.283(2)	13.670(2)
c (Å)	14.784(2)	37.725(3)
V (Å^3)	6028(1)	6105(1)
Z	8	6
D_c (g/cm^{-3})	1.33	1.29
μ(Mo–Kα) (cm^{-1})	6.69	7.14
Data collection range (°)	$4.5 < 2\theta < 56.0$	$4.1 < 2\theta < 56.0$
No. of collectd reflns.	3734	3247
No. of obsd reflns.	2015	2006
IT (K)	293	293
λ (Å)	0.71070	0.71070
F(000)	2416	2172
R[a]	0.040	0.054
R_w[b]	0.044	0.063

[a] $R = (\Sigma||F_o| - k|F_c||)/\Sigma|F_o|$. [b] $R_w = [\Sigma w(|F_o| - k|F_c|)^2/\Sigma w|F_o|^2]^{1/2}$.

Table 2. Selected bond lengths (Å) for compounds **11** and **12**

[HB(3,5-Me_2pz)$_3$]Ag(PMePh_2) (**11**)		[HB(3,5-Me_2pz)$_3$]Ag(P-*o*-tolyl$_3$) (**12**)	
Ag–P	2.336(2)	Ag–P	2.375(2)
Ag–N(1)	2.336(5)	Ag–N(1)	2.361(4)
Ag–N(3)	2.329(6)		
Ag–N(5)	2.316(6)		
P–C(22)	1.824(6)	P–C(6)	1.837(4)
P–C(16)	1.822(5)		
P–C(28)	1.820(9)		
B–N(2)	1.57(1)	B(1)–N(2)	1.539(5)
B–N(4)	1.539(9)		
B–N(6)	1.559(8)		
N(1)–N(2)	1.36(1)	N(1)–N(2)	1.367(5)
N(3)–N(4)	1.383(7)		
N(5)–N(6)	1.362(7)		
N(1)–C(1)	1.32(1)	N(1)–C(1)	1.315(6)
N(3)–C(6)	1.314(8)		
N(5)–C(11)	1.341(8)		
N(2)–C(3)	1.387(9)	N(2)–C(3)	1.361(6)
N(4)–C(8)	1.345(9)		
N(6)–C(13)	1.374(9)		
C(1)–C(2)	1.39(1)	C(1)–C(2)	1.387(7)
C(6)–C(7)	1.36(1)		
C(11)–C(12)	1.37(1)		
C(2)–C(3)	1.38(2)	C(2)–C(3)	1.369(8)
C(7)–C(8)	1.35(1)		
C(12)–C(13)	1.370(9)		

Table 3. Selected bond angles (Å) for compounds **11** and **12**

[HB(3,5-Me_2pz)$_3$]Ag(PMePh_2) (**11**)		[HB(3,5-Me_2pz)$_3$]Ag(P-*o*-tolyl$_3$) (**12**)	
N(1)–Ag–N(3)	82.1(2)	N(1)–Ag–N(1)	83.9(9)
N(1)–Ag–N(5)	84.8(2)		
N(3)–Ag–N(5)	83.0(2)		
P–Ag–N(1)	130.4(2)	P–Ag–N(1)	130.0(9)
P–Ag–N(3)	124.1(1)		
P–Ag–N(5)	125.1(1)		
Ag–P–C(16)	113.7(2)	Ag–P–C(6)	114.69(9)
Ag–P–C(22)	111.5(2)		
Ag–P–C(28)	116.3(2)		
C(16)–P–C(22)	104.9(2)	C(6)–P–C(6)	103.8(2)
C(22)–P–C(28)	106.6(3)		
C(16)–P–C(28)	102.9(3)		
Ag–N(1)–C(1)	136.2(5)	Ag–N(1)–C(1)	133.7(3)
Ag–N(3)–C(6)	138.6(4)		
Ag–N(5)–C(11)	136.8(4)		
Ag–N(1)–N(2)	116.0(4)	Ag–N(1)–N(2)	113.7(3)
Ag–N(3)–N(4)	115.6(3)		
Ag–N(5)–N(6)	117.2(3)		

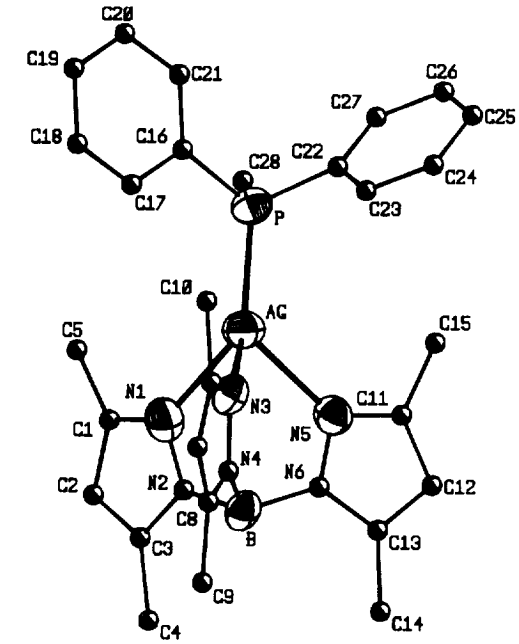

Fig. 1. ORTEP drawing of the molecular structure of **11**, with H atoms omitted.

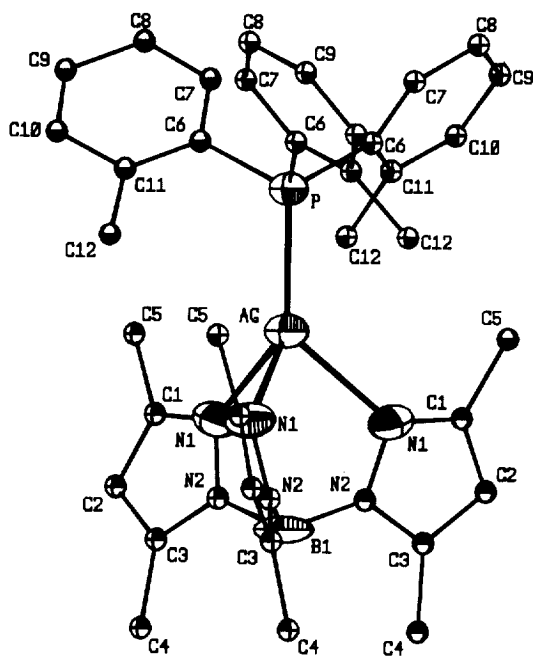

Fig. 2. ORTEP drawing of the molecular structure of **12**, with H atoms omitted.

compound a dinuclear structure such as in Fig. 3, has been previously hypothesized on the basis of vaporimetric molecular weight measurements and also on the basis of the similarity with the analogous copper complex [9].

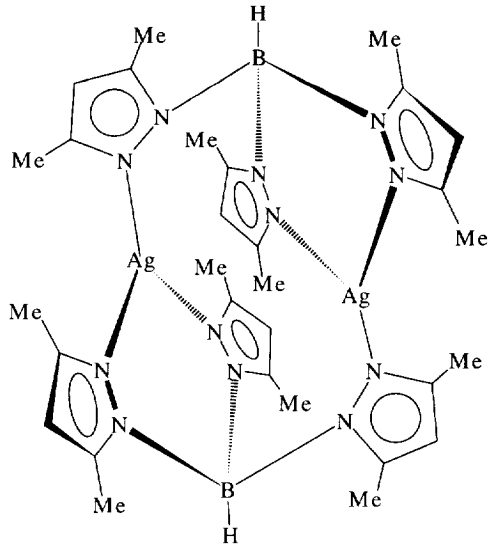

Fig. 3. Dinuclear structure proposed for derivative **1**.

The stable four-coordinate complexes [HB(3,5-$Me_2pz)_3$]Ag(CNBu*t*) (**2**) and [HB(3,5-$Me_2pz)_3$]Ag(CNCy) (**3**) were prepared upon addition of 1 molar equiv of *tert*-butyl- and cyclohexyl-isocyanide to a CH_2Cl_2 suspension of K[HB(3,5-$Me_2pz)_3$] and $Ag(O_3SCF_3)$ (equation **2**).

$$CNR + Ag(O_3SCF_3) + K[HB(3,5-Me_2pz)_3] \xrightarrow{CH_2Cl_2} [HB(3,5-Me_2pz)_3](RNC)Ag + KCF_3SO_3 \quad (2)$$

2: R=Bu^t
3: R=Cy

P(OPh)$_3$ and $P(C_6F_5)_3$ react with $AgNO_3$ and K[HB(3,5-$Me_2pz)_3$] in methanol at room temperature yielding the 1:1 adduct {[HB(3,5-$Me_2pz)_3$]Ag(P(OPh)$_3$)} (**4**) and {[HB(3,5-$Me_2pz)_3$]Ag(P(C_6F_5)$_3$)} (**5**).

From the reaction between 1,10-phenanthroline (Phen) and $Ag(O_3SCF_3)$ the 2:1 complex [(Phen)$_2$Ag]O_3SCF_3 (**6**) was obtained. Compound **6** reacts with K[HB(3,5-$Me_2pz)_3$] yielding, upon displacement of one of the Phen ligands, the neutral derivative {[HB(3,5-$Me_2pz)_3$](Phen)Ag} (**7**) (Fig. 4) in accordance with eqn (3):

$$[(Phen)_2Ag](O_3SCF_3) + nK[HB(3,5-Me_2pz)_3] \longrightarrow \underset{7}{\{[HB(3,5-Me_2pz)_3](Phen)Ag\}} + Phen + KCF_3SO_3 \quad (3)$$

Instead, the derivative {[HB(3,5-$Me_2pz)_3$]Ag(ImH)} (**8**) was obtained when complex **1** reacted with the neutral imidazole (ImH) in CH_2Cl_2 solutions.

The 1-methyl-2-mercapto-imidazole (Hmimt) is able to coordinate the Ag(I)O_3SCF_3 salts, yielding the derivative [(Hmimt)$_2$Ag]O_3SCF_3 (**9**). As expected, a ligand-to-metal ratio greater than 2-to-1 could not be obtained by addition of strong excess of Hmimt: the

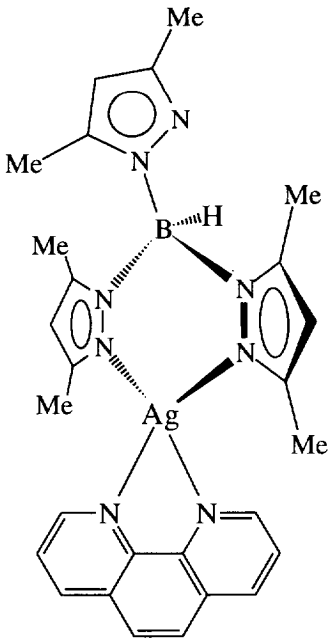

Fig. 4. Structure proposed for derivatives **7**.

steric hindrance of the methyl substituent at the 1 position of the ring blocks the formation of this ligand's product. From the reaction of complex **9** with $K[HB(3,5\text{-}Me_2pz)_3]$ only unmanageable material was obtained.

Finally, the gold(I) complex $\{[HB(3,5\text{-}Me_2pz)_3]Au(PPh_3)_2\}$ (**10**) was synthesized only when $K[HB(3,5\text{-}Me_2pz)_3]$ reacted with PPh_3AuCl in presence of 1 equiv. of PPh_3. It was not possible to obtain the 1:1 $\{[HB(3,5\text{-}Me_2pz)_3]Au(PPh_3)\}$ when the reaction was carried out in the same conditions in absence of PPh_3, the starting materials being always recovered.

With the exception of **6** and **9**, the electrical conductivity values show that none of the compounds are electrolyte both in acetone and dichloromethane. Derivatives **6** and **9** are soluble only in DMSO, in which they show conductance values typical of 1:1 electrolytes. All the complexes **1**–**10** are air stable yet decompose slowly when exposed to light.

In the IR spectra (see experimental section) of compounds **1**–**5**, **7**, **8**, and **10**, we always found the absorptions required by the presence of the tris(pyrazolyl)borate donor: amongst these, there are weak vibrations at ca. 3100 cm^{-1}, typical of ν(C–H) and other more intense absorption between 1550 and 1500 cm^{-1}, characteristic of the breathing of the heterocyclic ring, which may be taken as diagnostic of this type of ligand [21]. In addition, in these derivatives, the ν(B–H) generally appears as a single peak at ca. 2500 cm^{-1}. This absorption seems not to be dependent on the nature and basicity of the P-, N- and C-donor linked to silver(I).

In the IR spectra of **2** and **3** the ν(CN) stretching vibration of the isonitrile ligand falls at ca. 2190 cm^{-1}. This value is higher than that in the free CNBu^t (2138 cm^{-1}) [22] and CNCy (2137 cm^{-1}) [23] and suggests that also in these complexes the bonding is dominated by σ-donation [24]. There is no significant difference between the ν(CN) stretching frequency in the $[HB(3,5\text{-}Me_2pz)_3]$ derivatives with respect to $[HB(3,5\text{-}Ph_2pz)_3]$ and $[HB(3,5\text{-}(CF_3)_2pz)_3]$ ones. This fact also seems to indicate that bonding to RCN is similar despite the difference in the tris(pyrazol-1-yl)borate ligand.

In the spectra of derivatives **3**, **4** and **10**, it is impossible to assign the ν(Ag–P) and ν(Au–P) since these complexes exhibit a number of ligand vibrations in the low frequency region, whereas in the spectra of all the compounds **1**–**5** and **7** there are some bands between 350 and 240 cm^{-1}, absent in the spectrum of the potassium salt of $[HB(3,5\text{-}Me_2pz)_3]$ and of all the other donors, which can be tentatively assigned to ν(Ag–N) stretching vibration [25].

The IR spectra of derivatives **6** and **9** are characteristic for free uncoordinating O_3SCF_3 [26]; in fact, in the stretching regions $\nu[SO_3(E)]$ and $\nu[SO_3(A_1)]$ were assigned at ca. 1280 and 1030 cm^{-1}, respectively, with $\nu[CF_3(A_1)]$ and $\nu[CF_3(E)]$ at 1230 and 1160 cm^{-1}, respectively. The absence of absorptions due to Ag–O and Ag–S stretching vibrations confirm the cationic structure proposed for these complexes also on the basis of conductivity data.

The ^1H NMR spectra of **1**–**5**, **7**, **8**, and **10** were obtained using chloroform as solvent, whereas in the case of the slightly soluble derivatives **6** and **9**, the spectra were obtained in DMSO-d_6.

In most cases, the boron-hydrogen resonance is a broad signal due to interaction with the ^{11}B quadrupole.

The magnitude of Δ (=difference between the chemical shift related to the same type of proton in the silver(I) derivatives with respect to potassium salt of [hydrotris(3,5-dimethylpyrazolyl)borate]) suggests the existence of the complexes **2**, **3**, **4**, **8**, and **10** in weak donor solvent such as chloroform.

If a dinuclear structure such as that proposed in Fig. 3 is assumed for complex **1**, in the ^1H NMR spectrum at least two different sets of signals should be found for each equivalent group of protons; however, at room temperature the ^1H NMR spectrum of **1** exhibits only three sharp singlets at ca. 1.91, 2.31, and 5.77 ppm, suggesting equivalence of the three 3-Me, 5-Me, and 4-CH resonances. These results indicate that compound **1** is fluxional in solution, likely with a complete dissociation and reassociation of the pyrazolyl nitrogen occurring rapidly at 293 K. The fluxional behavior of **1** is also operative at low temperature. No change was observed on cooling the sample until 223 K.

In $CDCl_3$ at 293 K, the ^1H NMR spectrum of compound **5** is similar to that of derivative **1**. At the same temperature, the ^{31}P coordination chemical shift of **5** ($\delta(^{31}P)$ of $P(C_6F_5)_3$: −73.8 ppm) is ca. 0.01 ppm, in

accordance with the extensive dissociation (4) in chloroform:

$$2[HB(3,5-Me_2pz)_3]AgP(C_6F_5)_3 \longrightarrow \underset{\mathbf{5}}{} \underset{\mathbf{1}}{\{[HB(3,5-Me_2pz)_3]Ag\}_2} + 2P(C_6F_5)_3 \quad (4)$$

At 223 C, the spectrum of **5** is constituted by two different resonances, a sharp multiplet due to the free phosphorous donor and a double doublet of multiplet due to the silver(I)tris(pyrazolyl)borate complex, in which the separate coupling of ^{31}P to the ^{107}Ag, ^{109}Ag and ^{19}F nuclei are resolved. Also at this temperature, the coordination chemical shift is the smallest with respect to those previously observed [10, 15, 16]; however, the value of the silver–phosphorous coupling constants is typical of tetracoordinate silver(I) derivatives [27].

The ^{19}F resonances due to $P(C_6F_5)_3$ also shifted downfield upon coordination. At room temperature, three different multiplets due to ortho-, meta-, and para-F substituents in the complex were respectively observed, together with analogous resonances due to the free P-donor. The relative intensity ratio of complex/free donor is *ca.* 1/20. At *ca.* 203 K, the resonances due to the free P-donor disappear.

In the ^1H NMR spectra of **8** and **10**, two different sets of signals for each equivalent group of protons were also found at room temperature. On the basis of previous reports in literature [15] and of the well-known preference of analogous silver(I) [28] and gold(I) systems [29] for tetracoordination, we suggest that the donor $[HB(3,5\text{-}Me_2pz)_3]$ coordinates in this case in the bidentate form.

The ^{31}P NMR data of compounds **4** and **10** show several interesting features. The ^{31}P NMR spectrum of **4** at room temperature appears as a double doublet, owing to coupling with ^{107}Ag and ^{109}Ag nuclei, centered at -38.5 ppm. The signal is downfield shifted by ca 90 ppm with respect to the signal of the free P-donor $P(OPh)_3$. The coordination chemical shift (Δ) is the greatest with respect to those recorded to date for tris(pyrazolyl)borate-silver(I) complexes [10, 15, 16]. $P(OPh)_3$, in fact, is a stronger π-acceptor ligand than those investigated to date: in this case, an important π-contribution to bonding cannot be excluded. The magnitude of the $^{109}/^{107}Ag$–^{31}P coupling constants indicates that exchange processes and/or equilibria of dissociation of the phosphorous donor are not operative in these conditions. This fact is also confirmed by the negligible shift of the ^{31}P resonance on going from 313 K to 203 K.

The ^{31}P NMR spectrum of the gold(I) complex **10** is typical of a tetracoordinate species containing two triorganophosphine ligands [30]. The Δ is greater than those reported for similar complexes of rhodium(I) [31] and silver(I) acceptors [10, 15, 16], but is in the range reported for gold(I) derivatives [32, 33].

Description of the molecular structure of {[*hydrotris*(3,5-*dimethylpyrazol*-1-*yl*)*borate*]*Ag*(*PPh*$_2$Me)} (**11**)

The cell content consists of eight discrete molecules of {[hydrotris(3,5-dimethylpyrazol-1-yl)borate]Ag(PPh_2Me)} (**11**). Selected bond lengths and angles are listed in Tables 2 and 3 respectively. For clarity, only one molecule is displayed in the ORTEP plot of Fig. 1.

The molecules do not have significant intermolecular interaction within 3.5 Å.

The silver(I) atom adopts a strongly distorted tetrahedral coordination owing to the steric hindrance of both P- and N_3-donors.

The Ag–P and Ag–N bond distances are 2.336(2) and 2.316(6), and 2.336(5), and 2.329(6) Å, respectively. These values are similar to those found in the derivative {[hydrotris(3,5-dimethylpyrazol-1-yl)borate]Ag(P-*p*-tolyl$_3$)} [15] and slightly shorter than those found in {[hydrotris(pyrazol-1-yl)borate]Ag(PBenzyl$_3$)} [15] and {[hydrotris(pyrazol-1-yl)borate]Ag(P-*o*-tolyl$_3$)} [15], which contain a more hindered P-donor, and also than those in {[hydrotris(3,5-diphenylpyrazol-1-yl)borate]Ag(PPh_3)} [16] which contains a more sterically hindered N_3-donor.

The three P–Ag–N bond angles are markedly different from each other. This feature was not observed in the parent derivative {[hydrotris(3,5-dimethylpyrazol-1-yl)borate]Ag(P-*p*-tolyl$_3$)}. The N–Ag–N bond angles are of the same order of magnitude as those found in the silver(I)phosphinotris(pyrazolyl)borate complexes structurally characterized [10, 15, 16], and smaller than those found in analogous copper poly(pyrazolyl)borate complexes [6–8].

There is another interesting difference with respect to silver(I) poly(pyrazolyl)borates described in literature [10, 15, 16]. In complex **11** one of the three pyrazolyl ring shows a reliable distortion upon coordination: the N–N bond distance is significantly longer than those found in the other two azole rings, whereas the N–C and C–C ones are shorter. Analogously in the former ring the C–N–N bond angle corresponding to larger Ag–P–N bond angle is smaller than those in the latter ring, whereas that corresponding to smaller Ag–P–N is the largest.

Description of the molecular structure of {[*hydrotris*(3,5-*dimethylpyrazol*-1-*yl*)*borate*]*Ag*(*P-o*-tolyl$_3$)} (**12**)

The cell content consists of six discrete molecules of {[hydrotris(3,5-dimethylpyrazol-1-yl)borate]Ag(P-*o*-tolyl$_3$)} (**12**). Selected bond lengths and angles are listed in Tables 2 and 3 respectively. For clarity only one molecule is displayed in the ORTEP plot of Fig. 2.

The molecules do not have significant intermolecular interaction within 3.5 Å.

Also in complex **12**, the silver(I) atom adopts a strongly distorted tetrahedral environment: the Ag–N (2.361(4) Å and Ag–P (2.375(2) Å) bond lengths are longer than those found in other silver(I)phosphino derivatives containing the same donor. This is due to greater steric hindrance of P-*o*-tolyl$_3$ (cone angle = 194°) with respect to PPh_2Me and P-*p*-tolyl$_3$ (cone angle of 136 and 145°, respectively). This is also evident in the lengthening of the P–C bonds, which in **12** are longer with respect to P–C distances in analogous complexes. No remarkable effects were produced on the N–Ag–N and N–Ag–P angles by the coordination of the hindered P-*o*-tolyl$_3$. Instead the Ag–P–C and C–P–C are smaller with respect to those previously reported.

The weighted least-squares pyrazolate plane (N1–N2–C1–C2–C3) and the phenyl plane (C6–C11) do not deviate significantly from planarity and their dihedral angle is 119.1(1)°.

CONCLUSIONS

We prepared and characterized a series of new silver(I)phosphino complexes of the anionic donor tris(3,5-dimethylpyrazolyl-1-yl)borate, and used X-ray crystallography and NMR spectroscopy to examine how the silver(I) complexes properties are dependent on the electronic and steric properties of the azolate donor and/or of the neutral supporting P-, N or S-donor. We found that the behavior in solution can be very different from that in solid state: for example, comparison between the Ag–N and Ag–P bond lengths in the structures here solved and those in analogous complexes previously described suggests that bonding of [HB(pz)$_3$] to the AgPR$^t_3$ fragment is similar despite the steric and electronic differences of the P-donor ligands. On the other hand, the magnitude of the Ag–^{31}P coupling constant and ^{31}P chemical shift indicates that the structure and stability of complexes in solution are strongly dependent on the Tolman cone angle and pK_a of PR_3.

It has been noted that mixed ligand complexes can be synthesized starting from the dinuclear {[HB(3,5-Me$_2$pz)$_3$]Ag}$_2$ or [(Phen)$_2$Ag]O$_3$SCF$_3$, but it is not possible to displace the P-donor, for example from compound **4**, with a neutral N-donor mono or bidentate ligand such as imidazole or ortho-phenanthroline, even if it is more basic. On the other hand, the donor [HB(3,5-Me$_2$pz)$_3$] is not able to displace Hmimt or to substitute the O$_3$SCF$_3$ group in [(Hmimt)$_2$Ag]O$_3$SCF$_3$ (**9**).

It has been observed that 1:1 triorganophosphine complexes of gold(I) containing tris(pyrazolyl)borate cannot be synthesized, but that it is possible to obtain stable tris(pyrazolyl)borate compounds only if a 2:1 PR_3/gold ratio was used. However, more structural and spectroscopic studies, including bis- and tetrakis-(pyrazolyl)borates, bidentate diphosphine and different anionic and neutral donors, will be required to see whether these results are general and to develop the coordination chemistry of poly(azol-1-yl)borato donors with respect to Ag^I and Au^I metal centers.

Supporting information available

Tables listing anisotropic displacement parameters of non-hydrogen atoms, derived hydrogen coordinates and isotropic displacement parameters, and bond lengths and angles are available on request from one of the authors.

Acknowledgements—We thank the MURST, CNR—Rome and the Universities of Camerino and Venice for financial help.

REFERENCES

1. Dias, H. V. R. and Jin, W., *J. Am. Chem. Soc.*, 1995, **117,** 11381.
2. Carrier, S. M., Ruggiero, C. E., Houser, R. P. and Tolman, W. B., *Inorg. Chem.*, 1993, **32,** 4889.
3. Dias, H. V. R. and Jin, W., *Inorg. Chem.*, 1995, **34,** 5380.
4. Amoroso, A. J., Jeffery, J. C., Jones, P. L., McCleverty, J. A., Psillakis, E. and Ward, M. D., *J. Chem. Soc., Chem. Commun.*, 1995, 1175.
5. Bruce, M. I., Ostazewski, A. P. P., *J. Chem. Soc. Dalton Trans.*, 1973, 2433.
6. Cecchi, P., Bovio, B., Gioia Lobbia, G., Pettinari, C. and Leonesi, D., *Polyhedron*, 1995, **14,** 2441.
7. Gioia Lobbia, G., Pettinari, C., Marchetti, F., Bovio, B. and Cecchi, P., *Polyhedron*, 1996, **15,** 881.
8. Gioia Lobbia, G., Pettinari, C., Santini, C., Colapietro, M. and Cecchi, P., *Polyhedron*, 1997, **16,** 207.
9. Mealli, C., Arcus, C. S., Wilkinson, J. L., Marks, T. J. and Ibers, J. A., *J. Am. Chem. Soc.*, 1976, **98,** 711.
10. Dias, H. V. R., Jin, W., Kim, H.-J. and Lu, H.-L., *Inorg. Chem.*, 1996, **35,** 2317.
11. Smith, W. V., Brown, U. L. J. and Pitzer, K. S., *J. Am. Chem. Soc.*, 1937, **57,** 1213.
12. Maeda, M., Nakagawa, G. and Biedermann, G., *J. Phys. Chem.*, 1983, **87,** 121.
13. Nittel, F., Ohlschlager, H. and Schranz K.-W., (Agfa-Gevaert A.-G.), *Fr. Demande*, 1970, 2014345; *Chem. Abstr.*, 1971, **74,** 81772f).
14. Lockhardt, H. B. Jr., in *Kirk-Othmer Encyclopedia of Chemical Technology*, 3rd edn., Vol. 21, eds. M. Grayson and D. Eckroth. Wiley, New York, 1983, p. 16.
15. Santini, C., Gioia Lobbia, G., Pettinari, C., Pellei, M., Valle, G. and Calogero, S., *Inorg. Chem.*, 1998, 37, 890.
16. Santini, C., Gioia Lobbia, G., Pellei, M., Pettinari, C., Valle, G. and Calogero, S., *Inorg. Chim. Acta*, (in press).
17. Tolman, C. A., *Chem. Rev.*, 1977, **77,** 313.
18. Trofimenko, S., *J. Am. Chem. Soc.*, 1967, **89,** 3170.
19. Sheldrich, G. M., *SHELXS*-86 *and SHELXL*-93.

Programs for the automatic solution of crystal structure. Göttingen, 1990 and 1993.
20. Bruce, M. I. and Walsh, J. D., *Aust. J. Chem.*, 1979, **32,** 2753.
21. Nieuwpoort, G., Vos, J. G. and Groeneveld, W. L., *Inorg. Chim. Acta*, 1978, **29,** 117.
22. Reger, D. L., Collins, J. E., Rheingold, A. L., Liable-Sands, L. M. and Yap, G. P. A., *Organometallics*, 1997, **16,** 349.
23. Ugi, I., Betz, W., Fetzer, U. and Offermann, K., *Chem. Ber.*, 1986, **94,** 2814.
24. Malatesta, L. and Bonati, F., *Isocyanide Complexes of Metals*. Wiley–Interscience publications, John Wiley & Sons, Ltd, London.
25. Nakamoto, K., *Infrared and Raman Spectra of Inorganic and Coordination Compounds*, 4th edn. Wiley Interscience, New York, 1986, pp. 201–220.
26. Lawrance, G. A., *Chem. Rev.*, 1986, **86,** 17.
27. Muetterties, E. L. and Alegranti, C. W., *J. Am. Chem. Soc.*, 1972, **94,** 6386.
28. Lancashire, R. J., "Silver". in *Comprehensive Coordination Chemistry*, Vol. 5, eds. Sir. G. Wilkinson, R. D. Gillard, and J. A. McCleverty. Pergamon Press, Oxford, 1987, p. 775–860.
29. Gimeno, M. C. and Laguna, A., *Chem. Rev.*, 1997, **97,** 511.
30. Bowmaker, G. A., Dyason, J. C., Healy, P. C., Engelhardt, L. M., Pakawatchai, C. and White, A. H., *J. Chem. Soc. Dalton Trans*, 1987, 1089.
31. Bonati, F., Oro, L. A. and Pinillos, M. T., *Polyhedron*, 1985, **4,** 357.
32. Attar, S. and Malito, J., *Polyhedron*, 1992, **11,** 2409.
33. Berners-Price, S. J. and Sadler, P. J., *Inorg. Chem.*, 1986, **25,** 3822.

Pergamon

PII: S0277-5387(98)00093-X

Polyhedron Vol. 17, No. 18, pp. 3211–3220, 1998
© 1998 Elsevier Science Ltd
All rights reserved. Printed in Great Britain
0277-5387/98 $19.00+0.00

Nickel(II), palladium(II), and platinum(II) complexes containing cis- or trans-1,2-bis(diphenylphosphino)ethene: isomorphous crystal structures in the cyanide case

Werner Oberhauser[a], Christian Bachmann[a], Thomas Stampfl[a], Rainer Haid[a], Christoph Langes[a], Alexander Rieder[b] and Peter Brüggeller[a]*

[a]Institut für Allgemeine, Anorganische und Theoretische Chemie, Universität Innsbruck, Innrain 52a, 6020 Innsbruck, Austria

[b]Institut für Organische Chemie, Universität Innsbruck, Innsbruck, Innrain 52a, 6020 Austria

(Received 8 December 1997; accepted 27 February 1998)

Abstract—Mono- and binuclear Ni^{II}, Pd^{II}, and Pt^{II} complexes of cis- or trans-1,2-bis(diphenylphosphino)ethene (cis- or trans-dppen) have been prepared and characterized by X-ray diffraction methods, ^{195}Pt ^{1}H and ^{31}P ^{1}H NMR spectroscopy, FAB mass spectrometry, IR spectroscopy, elemental analyses and melting points. The X-ray structures of some rare examples of cis-dicyanide complexes of the type $[M(CN)_2(cis\text{-}dppen)]$ (M=Ni (**1**), M=Pd (**2**), M=Pt (**3**)) are given for the first time. All three crystal lattices are isomorphous and allow comparison of the radii of Ni, Pd, and Pt atoms. In **1**–**3** the coordination is square planar. In all cases the ethene bridges are nearly coplanar with the coordination planes, which can be explained by π-bonding interactions. Due to the isomorphous crystal lattices, **1**–**3** show analogous shortest intermolecular repulsive C–H···M contact approaches leading to small deviations from coplanarity.

The removal of one coordinated chloride in $[NiCl_2(cis\text{-}dppen)]$ by $AgBF_4$ followed by subsequent treatment with bis(diphenylphosphino)amine, $NH(PPh_2)_2$ (dppam), leads to the novel complex $[NiCl(cis\text{-}dppen)(dppam)](BF_4)$ (**4**). However, the analogous abstraction of both chlorides in $[MCl_2(cis\text{-}dppen)]$ (M=Pd, Pt) and reaction with dppam produces $[M(cis\text{-}dppen)(dppam)](BF_4)_2$ (M=Pd (**5**), M=Pt (**6**)). In the case of trans-dppen, the reaction with $Pd(CN)_2$ leads to another novel cis-dicyanide complex of the type $[Pd_2(CN)_4(\mu\text{-}trans\text{-}dppen)_2]$ (**7**). Substitution of chloride in $[Pt_2Cl_4(\mu\text{-}trans\text{-}dppen)_2]$ by cyanide leads to the analogous Pt^{II} compound $[Pt_2(CN)_4(\mu\text{-}trans\text{-}dppen)_2]$ (**8**). It is believed, that the unsaturated nature of cis- or trans-dppen leading to π-bonding interactions with the metal-ligand bonds, is responsible for the unusual stability of cis-dicyanide complexes. For dppam the presence of electronic delocalization is well-known. These effects are discussed in view of the X-ray structures of **1**–**3** and related compounds. © 1998 Elsevier Science Ltd. All rights reserved

Keywords: crystal structures; nickel complexes; palladium complexes; platinum complexes; cyanide complexes; diphosphine complexes.

Though cyanide complexes of the d^8 metals Ni^{II}, Pd^{II}, and Pt^{II} are well-known [1], no X-ray structure analyses of the rare square planar cis-dicyanides containing phosphines have been reported. The given crystal structures include square planar trans-dicyanides [2], five-coordinate dicyanides [3] and dinuclear complexes containing square planar trans-dicyanide units [4]. In this work the first X-ray structures of the cis-dicyanide compounds $[M(CN)_2(cis\text{-}dppen)]$ (M=Ni (**1**), M=Pd (**2**), M=Pt (**3**), structure type (A) in Scheme 1, where cis-dppen is cis-1,2-bis(diphenylphosphino)ethene, are presented. These three structures fulfil the criteria of the same ligands, the same coordination number and geometry, isomorphous crystal lattices and equal experimental conditions, and therefore allow comparison of the radii of Ni, Pd, and Pt atoms [5]. Ni shows the smallest radius, but Pt is

* Author for correspondence.

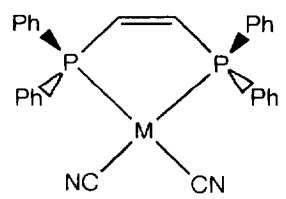

M=Ni,Pd,Pt

A

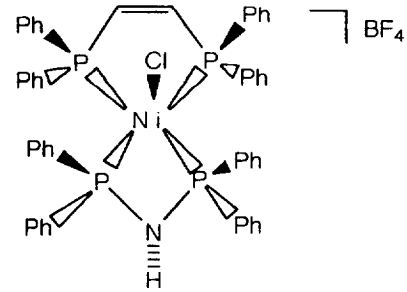

B

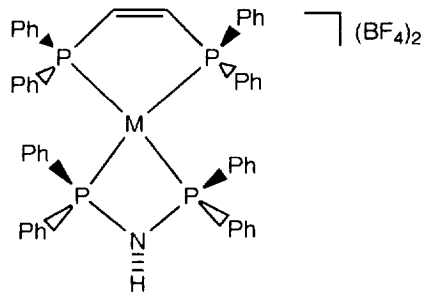

M=Pd,Pt

C

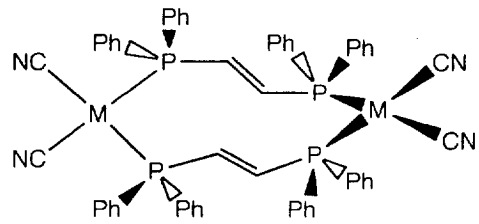

M=Pd,Pt

D

Scheme 1. Structure types observed in the compounds **1**–**8**. The P-M-P (M = Ni, Pd, Pt) angles of chelating cis-dppen or dppam are constrained to values below 90°. Structure (A) occurs in $[M(CN)_2(\text{cis-dppen})]$ (M = Ni (**1**), M = Pd (**2**), M = Pt (**3**)), structure (B) in $[NiCl(\text{cis-dppen})(\text{dppam})](BF_4)$ (**4**), structure (C) in $[M(\text{cis-dppen})(\text{dppam})](BF_4)_2$ (M = Pd (**5**), M = Pt (**6**)) and structure (D) in $[M_2(CN)_4(\mu\text{-trans-dppen})_2]$ (M = Pd (**7**), M = Pt (**8**)).

smaller than Pd. Furthermore, in **1**–**3** the ethene bridges are nearly coplanar with the coordination planes due to π-bonding interactions. This effect has been observed earlier in several related compounds [1](b),[1](c),[6]. Interestingly, all three structures show analogous repulsive intermolecular C–H···M(d^8) contact approaches, where the presence of these structural anomalies has been emphasized only recently [7].

Furthermore, several novel d^8 metal complexes containing both cis-dppen and bis(diphenylphosphino)amine, $NH(PPh_2)_2$ (dppam), are presented. The transition metal chemistry of dppam, which is isoelectronic with bis(diphenylphosphino)methane, $CH_2(PPh_2)_2$ (dppm), has received widespread attention [8]. These complexes are of interest because of their potential as catalysts for the oligomerization and polymerisation of alkenes [9]. $[NiCl(\text{cis-dppen})(\text{dppam})](BF_4)$ (**4**, structure type (B) in Scheme 1), shows five-coordinate square pyramidal coordination, whereas the compounds $[M(\text{cis-dppen})(\text{dppam})](BF_4)_2$ (M=Pd (**5**), M=Pt (**6**), structure type (C) in Scheme 1) are square planar. The stability of halide-associated species containing dppam is well-known [10]. The replacement of $(BF_4)^-$ in **6** by Cl^- leads to the typical shift of ν(N–H) towards lower energies due to Cl ···H-N< hydrogen-bridging [11]. Furthermore, it is of great interest to combine the observed electronic delocalization in complexes of neutral or deprotonated dppam [12] with similar effects in compounds of cis-dppen.

$[Pd_2(CN)_4(\mu\text{-trans-dppen})_2]$ (**7**), where trans-dppen is trans-1,2-bis(diphenylphosphino)ethene, is a novel rare example of a trans-dppen-bridged dimer containing cis-dicyanide groups (structure type (D) in Scheme 1). The analogous Pt^{II} complex $[Pt_2(CN)_4(\mu\text{-trans-dppen})_2]$ (**8**) shows the same structure. A comparable trans-dppen-bridged dimer of the type rac-$[Pt_2Cl_2(\mu\text{-Cl})(\mu\text{-trans-dppen})P4]Cl$, where P4 is 1,1,4,7,10,10-hexaphenyl-1,4,7,10-tetraphosphadecane (tetraphos-1, P4), has already been reported [13].

There is continuing interest in ligands like cis-or trans-dppen, since they are heteroatom compounds that are isolobal with unsaturated hydrocarbon fragments [14].

EXPERIMENTAL

Reagents and chemicals

Reagent-grade chemicals were used as received unless stated otherwise. cis-1,2-Bis(diphenylphosphino)ethene (cis-dppen) and trans-1,2-bis(diphenylphosphino)ethene (trans-dppen) were purchased from Aldrich. Bis(diphenylphosphino)amine (dppam) was obtained from Strem. All other reagents and solvents were obtained from Fluka. Solvents used for NMR measurements and crystallization purposes were of purissimum grade quality. $NiCl_2 \cdot 6H_2O$, $PdCl_2$, $Na_2PtCl_4 \cdot 4H_2O$, $Pd(CN)_2$, and $Pt(CN)_2$ were also received from Fluka.

Instrumentation

Fourier-mode ^{195}Pt ^1H and ^{31}P ^1H NMR spectra were obtained by use of a Bruker AC-200 spectrometer (internal deuterium lock) and were recorded at 43.02 and 80.96 MHz, respectively. Positive chemical shifts are downfield from the standards, where 1.0 M Na_2PtCl_6 and 85% H_3PO_4 were used as standards, respectively.

Synthesis of Ni^{II}, Pd^{II}, and Pt^{II} complexes

A Schlenk apparatus and oxygen-free, dry Ar were used in the synthesis of all complexes. Solvents were degassed by several freeze-pump-thaw cycles prior to use. All reactions were carried out at room temperature unless stated otherwise.

[Ni(CN)$_2$(cis-dppen)] (1) and [Pd(CN)$_2$(cis-dppen)] (2)

Compounds **1** and **2** were prepared as described earlier [1](b),[1](c). Samples for X-ray diffraction studies were crystallized from CH_3NO_2/DMF (v/v = 1:1).

[Pt(CN)$_2$(cis-dppen)] (3)

$Pt(CN)_2$ (0.20 mmol, 0.049 g) was suspended in DMF (7 cm^3). Then cis-dppen (0.20 mmol, 0.079 g) was added with stirring. The reaction mixture was stirred at 75 C until a clear, colourless solution was obtained. The volume of the solvent was reduced and Et_2O was added. A white precipitate was filtered off, washed with Et_2O and dried in vacuo. A white powder was recrystallized from CH_3NO_2/DMF (v/v = 1:1): yield 0.103 g (80%); m.pt > 310 C. IR (KBr, cm^{-1}) CN: 2142 ν. Found: C, 52.1; H, 3.5; N, 4.3. Calc. for $C_{28}H_{22}N_2P_2Pt$: C, 52.3; H, 3.4; N, 4.4%. A sample for X-ray diffraction study was crystallized from CH_3NO_2/DMF (v/v = 1:1).

[NiCl(cis-dppen)(dppam)](BF$_4$) (4)

[$NiCl_2$(cis-dppen)] (0.15 mmol, 0.079 g) was dissolved in CH_2Cl_2/DMF (v/v = 5:1, 5 cm^3). Then $AgBF_4$ (0.15 mmol, 0.029 g) was added with stirring. The reaction mixture was stirred for 30 min, the formed AgCl was filtered off and a greenish solution was obtained. To this solution, dppam (0.15 mmol, 0.058 g) dissolved in CH_2Cl_2 was added slowly with vigorous stirring. After 2 h an orange-yellow solution formed. The volume of the solvent was reduced, EtOH was added and a yellow precipitate immediately formed. The precipitate was filtered off and dried in vacuo. A yellow powder was recrystallized from DMF: yield 0.056 g (39%); m.pt = 222–224 C. IR (KBr, cm^{-1}) N–H: 3239 ν, 2510 2δ. FAB mass spectrum: m/z 875.9 [NiCl(cis-dppen)(dppam)]$^+$, 840.45 [Ni(cis-dppen)(dppam)]$^+$. Found: C, 62.2; H, 4.6; N, 1.7. Calc. for $C_{50}H_{43}BClF_4NP_4Ni$: C, 62.4; H, 4.5; N, 1.5%.

[Pd(cis-dppen)(dppam)](BF$_4$)$_2$ (5)

[$PdCl_2$(cis-dppen)] (0.18 mmol, 0.103 g) was dissolved in CH_2Cl_2/DMF (v/v = 5:1, 6 cm^3). Then $AgBF_4$ (0.36 mmol, 0.070 g) was added with stirring. The reaction mixture was stirred for 2 h, the formed AgCl was filtered off and the solvent completely removed. The residue was dissolved in CH_2Cl_2 and dppam (0.18 mmol, 0.069 g) was added slowly with vigorous stirring. After 3 h a white precipitate was filtered off, washed with CH_2Cl_2 and dried in vacuo. A white powder was recrystallized from DMF: yield 0.172 g (90%); m.pt = 272–274 C dec. IR (KBr, cm^{-1}) N–H: 3237 ν, 2524 2δ. FAB mass spectrum: m/z 888.2 [Pd(cis-dppen)(dppam)]$^+$, 502.8 [Pd(cis-dppen)]$^+$. Found: C, 56.5; H, 4.3; N, 1.4. Calc. for $C_{50}H_{43}B_2F_8NP_4Pd$: C, 56.6; H, 4.1; N, 1.3%.

[Pt(cis-dppen)(dppam)](BF$_4$)$_2$ (6)

Compound **6** was prepared in an analogous manner to **5**, where after addition of dppam the reaction mixture was stirred for 20 h. A white powder was recrystallized from DMF/EtOH: yield 0.166 g (80%); m.pt = 291–293 C. IR (KBr, cm^{-1}) N–H: 3243 ν, 2520 2δ. FAB mass spectrum: m/z 976.9 [Pt(cis-dppen)(dppam)]$^+$, 899.8 [Pt(cis-dppen)(dppam)-Phenyl]$^+$. Found: C, 52.0; H, 3.9; N, 1.1. Calc. for $C_{50}H_{43}B_2F_8NP_4Pt$: C, 52.2; H, 3,8; N, 1.2%.

[Pd$_2$(CN)$_4$(μ-trans-dppen)$_2$] (7)

$Pd(CN)_2$ (0.20 mmol, 0.032 g) was suspended in DMF (7 cm^3). Then trans-dppen (0.20 mmol, 0.079 g)

was added with stirring and prevention of light. The reaction mixture was stirred at 45 C for 48 h and a white precipitate formed. The solvent was completely removed, the white residue was filtered off in CH_2Cl_2, washed with CH_2Cl_2 and dried in vacuo. A white powder was recrystallized from DMF: yield 0.077 g (69.5%); m.pt > 310 C. IR (KBr, cm^{-1}) CN: 2130 *v*. Found: C, 60.4; H, 4.1; N, 5.2. Calc. for $C_{56}H_{44}N_4P_4Pd_2$: C, 60.6; H, 4.0; N, 5.0%.

$[Pt_2(CN)_4(\mu\text{-}trans\text{-}dppen)_2]$ (**8**)

$[Pt_2Cl_4(\mu\text{-trans-dppen})_2]$ (0.080 mmol, 0.106 g) was dissolved in DMF. To this solution, NaCN (0.32 mmol, 0.016 g) was added with vigorous stirring and prevention of light. The reaction mixture was stirred for 4 h and then the solvent was completely removed. The residue was filtered off in H_2O, washed with H_2O and dried in vacuo. A white powder was recrystallized from CH_2Cl_2: yield 0.093 g (90%); m.pt > 310 C. IR (KBr, cm^{-1}) CN: 2130 *v*. Found: C, 52.1; H, 3.6; N, 4.4. Calc. for $C_{56}H_{44}N_4P_4Pt_2$: C, 52.3; H, 3.4; N, 4.4%.

X-ray crystallography

Crystal data. $C_{28}H_{22}N_2P_2Ni$ (**1**), M = 507.14, yellow crystal (prismatic; 1.0 × 0.5 × 0.4 mm), monoclinic, a = 8.463(2), b = 14.267(3), c = 19.994(4) Å, β = 90.89(3)°, V = 2413.82 Å^3, Z = 4, space group $P2_1/n$, D_c = 1.395 Mg m^{-3}, F(000) = 1048, μ(Mo-K$_\alpha$) = 0.955 mm^{-1}; $C_{28}H_{22}N_2P_2Pd$ (**2**), M = 554.84, colourless crystal (prismatic; 0.6 × 0.4 × 0.2 mm), monoclinic, a = 8.654(2), b = 14.222(3), c = 20.206(4) Å, β = 90.35(3)°, V = 2486.85 Å^3, Z = 4, space group $P2_1/n$, D_c = 1.482 Mg m^{-3}, F(000) = 1120, μ(Mo-K$_\alpha$) = 0.893 mm^{-1}; $C_{28}H_{22}N_2P_2Pt$ (**3**), M = 643.53, colourless crystal (prismatic; 1.0 × 0.6 × 0.4 mm), monoclinic, a = 8.665(2), b = 14.273(3), c = 20.063(4) Å, β = 90.79(3)°, V = 2481.07 Å^3, Z = 4, space group $P2_1/n$, D_c = 1.723 Mg m^{-3}, F(000) = 1248, μ(Mo-K$_\alpha$) = 5.803 mm^{-1}.

Data collection. Unit-cell dimensions and intensity data were obtained at 213 K using a Siemens P4 diffractometer and graphite monochromated Mo-K$_\alpha$ radiation. 2θ range = 4.0–55.0°, scan type = ω, scan speed = variable (2.0–29.3 min^{-1} in ω). Index ranges = $-1 \leqslant h \leqslant 10$, $-1 \leqslant k \leqslant 18$, $-25 \leqslant l \leqslant 25$ (**1**); $-1 \leqslant h \leqslant 11$, $-1 \leqslant k \leqslant 18$, $-26 \leqslant l \leqslant 26$ (**2**, **3**). No decay in the intensities of three standard reflections was observed during the course of each data collection. The data were corrected for Lorentz and polarization effects. In each case the empirical absorption correction was based on ψ-scans of nine reflections [range of transmission factors: 0.825–1.00 (**1**), 0.830–1.00 (**2**), 0.447–1.00 (**3**)] [15]. A total of 6995 (**1**), 7304 (**2**), and 7242 (**3**) reflections were measured, of which 5454 (**1**, R_{int} = 0.026), 5670 (**2**, R_{int} = 0.035), and 5629 (**3**, R_{int} = 0.036) were unique and 3973 (**1**), 3557 (**2**), and 4199 (**3**) satisfied the condition $I > 3\sigma(I)$.

Structure solution. All structure determination calculations were carried out on 80486- and Pentium-PCs using the PC-version of SHELXTL PLUS and SHELXL93 [16]. The positions of the nickel, palladium and platinum atoms were found by the Patterson method. Other atom positions were located from successive difference-Fourier maps.

In all three cases the non-hydrogen atoms have been refined with anisotropic thermal parameters. In **1** the hydrogen atoms were isotropically refined with fixed isotropic U. In **2** and **3** the hydrogen atoms were included using a riding model with isotropic U values depending on U_{eq} of the adjacent carbon atoms. The final R values of 0.030 (R′ = 0.030) (**1**), 0.032 (R′ = 0.032) (**2**), and 0.027 (R′ = 0.027) (**3**) were computed for 364 (**1**) and 298 (**2**,**3**) parameters, respectively. The largest features on the final difference maps were 0.39 eÅ^{-3} (**1**) [GOF = 1.05, largest Δ/σ = −0.005, weighting scheme: $w^{-1} = \sigma^2(F^2) + (0.0445P)^2 + 0.12P$], 0.38 eÅ^{-3} (**2**) [GOF = 0.99, largest Δ/σ = 0.001, weighting scheme: $w^{-1} = \sigma^2(F^2) + (0.0237P)^2$], and 0.83 eÅ^{-3} (**3**) [GOF = 1.02, largest Δ/σ = −0.001, weighting scheme: $w^{-1} = \sigma^2(F^2) + (0.0312P)^2 + 0.75P$].

Final atomic fractional coordinates and other relevant data have been deposited.

RESULTS

The X-ray structures of $[M(CN)_2(cis\text{-dppen})]$ (M=Ni (**1**), M=Pd (**2**), M=Pt (**3**)) show several interesting common features: π-bonding interactions leading to nearly coplanar coordination planes and ethene bridges, intermolecular repulsive C–H···M contact approaches, and isomorphous crystal lattices allowing comparison of the radii of Ni, Pd, and Pt atoms. All three structures show one discrete $[M(CN)_2(cis\text{-dppen})]$ molecule per asymmetric unit. Views of **1**, **2**, and **3** demonstrating the identical conformations including the orientations of the phenyl rings are given in Fig. 1; Table 1 contains selected bond distances and bond angles.

Figure 2 reveals the nearly coplanar arrangements of the coordination planes and the ethene bridges in **1**, **2**, and **3**. **1** shows the largest mean deviation of 0.036 Å from a least-squares plane through the metal, the phosphorus and the cyanide carbon atoms, which has to be compared with the corresponding values of 0.024 and 0.023 Å in **2** and **3**, respectively. In all three cases these deviations stem from very slight tetrahedral distortions of the coordination planes. Furthermore, also the five-rings are nearly planar, where the mean deviations from least-squares planes through the metal, the phosphorus and the carbon atoms of the ethene bridges are 0.017 (**1**), 0.016 (**2**), and 0.015 Å (**3**), respectively. These planar five-rings

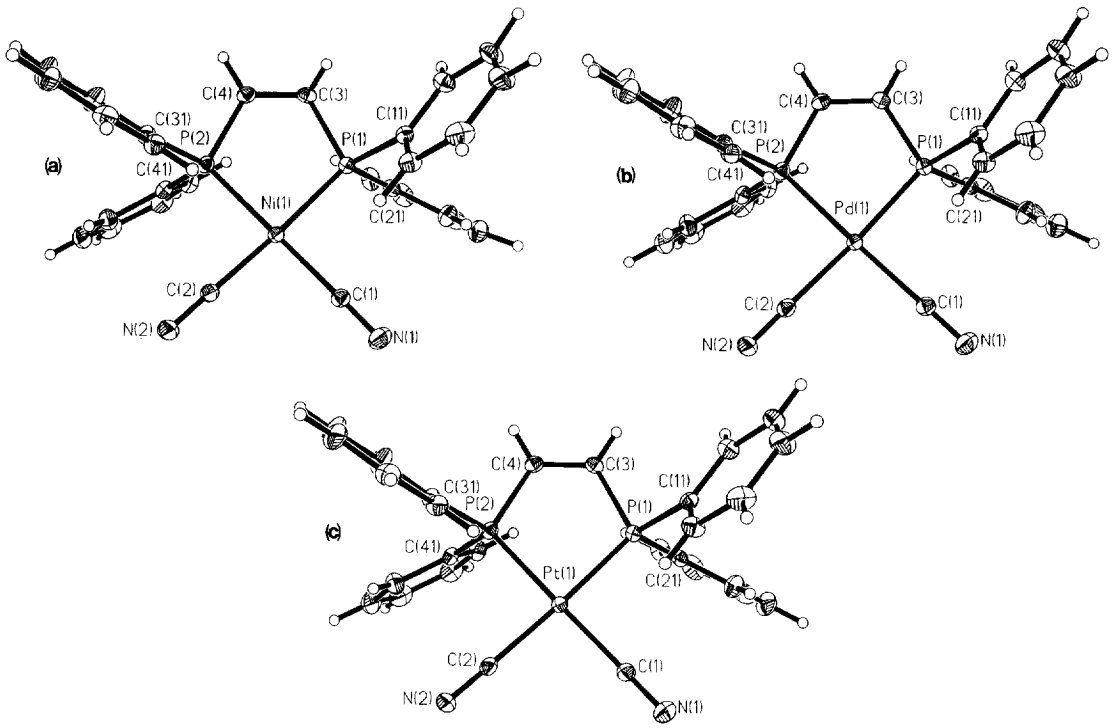

Fig. 1. Views of $[M(CN)_2(cis\text{-}dppen)]$ with the coordination planes through the metal atoms, the P atoms and the cyanide carbon atoms in the projection planes and showing the atom labelling scheme. (a) M=Ni (**1**); (b) M=Pd (**2**); (c) M=Pt (**3**). The coordination geometries including the orientations of the phenyl groups are identical.

have now been observed in several square planar d^8 metal complexes containing cis-dppen [1](b), [1](c), [6](a), [7](b) and are due to an enhancement of M-to-P π-bonding as a consequence of the unsaturated nature of cis-dppen. However, Fig. 2 also shows, that the most significant deviations from a coplanar arrangement of the coordination planes and the ethene bridges in **1**, **2**, and **3** are caused by a bowing of the C(2)N(2) cyanide groups away from these planes. A careful analysis of all three crystal structures indicates, that the only relevant intermolecular contact approaches are phenyl group C–H $\cdots$ M interactions of 2.850 (**1**), 2.781 (**2**), and 2.807 Å (**3**), as depicted in Fig. 2. These approaches cause the following deviations from least-squares planes through the phosphorus atoms, the carbon atoms of the ethene bridges, and the C(1)N(1) cyanide groups: Ni(1): −0.069, C(2): −0.189, N(2): −0.255 Å (**1**); Pd(1): −0.056, C(2): −0.120, N(2): −0.136 Å (**2**); Pt(1): −0.053, C(2): −0.122, N(2): −0.133 Å (**3**). Therefore, these C–H $\cdots$ M interactions are clearly repulsive (Fig. 2). The presence of these C–H $\cdots$ $M(d^8)$ contacts with H $\cdots$ M distances of 2.65–3.5 Å has been found only recently [7](a), where the nature of these interactions remained unclear. However, the X-ray structures of the two crystal modifications of $[PtCl_2(cis\text{-}dppen)]$ [7](b) also confirm, that these C–H $\cdots$ $M(d^8)$ interactions are repulsive: in one modification the coordination plane and the ethene bridge are strictly coplanar, whereas in the second the coordination plane of one molecule is tilted away from the incoming C–H group of a second molecule (C–H $\cdots$ Pt = 2.833 Å) leading to deviations from complete coplanarity.

Fig. 1 and Fig. 2 clearly show, that the three X-ray structures allow comparison of the radii of Ni, Pd, and Pt atoms [5]. There are three common trends, which indicate the same order of atomic radii: the mean M–P bond lengths of 2.1652(6) Å (**1**) < 2.2688(9) Å (**3**) < 2.2759(7) Å (**2**); the mean M–C bond lengths of 1.879(1) Å (**1**) < 2.010(4) Å (**3**) < 2.029(2) Å (**2**); the five-ring chelate angles of 87.57(3)° (**1**) > 86.06(4)° (**3**) > 85.82(3)° (**2**). All parameters significantly show the smallest radius for Ni. For Pd and Pt the differences of the mean M–C bond lengths and the five-ring chelate angles are at the margin of statistical significance, the values indicating that the platinum radius is slightly smaller than that for palladium. However, the mean M–P bond length is significantly smaller for Pt than for Pd. Assuming a covalent radius of tetra-coordinate phosphorus as $r(P)_{cov} = 1.11$ Å [17], the covalent radii of square planar d^8 Ni, Pd, and Pt are estimated as 1.06, 1.17, and 1.16 Å, respectively. The results presented here are in full agreement with the recently given smaller covalent radius for Au than for Ag, a phenomenon

Table 1. Selected bond lengths (Å) and angles (°) for $[Ni(CN)_2(cis\text{-}dppen)]$ (**1**), $[Pd(CN)_2(cis\text{-}dppen)]$ (**2**), and $[Pt(CN)_2(cis\text{-}dppen)]$ (**3**)

Ni(1)–P(1)	2.1653(8)
Ni(1)–P(2)	2.1650(8)
Ni(1)–C(1)	1.883(2)
Ni(1)–C(2)	1.875(2)
P(1)–C(3)	1.814(2)
P(1)–C(11)	1.807(2)
P(1)–C(21)	1.811(2)
P(2)–C(4)	1.809(2)
P(2)–C(31)	1.812(2)
P(2)–C(41)	1.812(2)
C(1)–N(1)	1.141(3)
C(2)–N(2)	1.139(3)
C(3)–C(4)	1.312(3)
Pd(1)–P(1)	2.2741(10)
Pd(1)–P(2)	2.2777(10)
Pd(1)–C(1)	2.028(3)
Pd(1)–C(2)	2.030(3)
P(1)–C(3)	1.808(3)
P(1)–C(11)	1.814(3)
P(1)–C(21)	1.816(3)
P(2)–C(4)	1.810(3)
P(2)–C(31)	1.811(3)
P(2)–C(41)	1.813(4)
C(1)–N(1)	1.145(4)
C(2)–N(2)	1.141(4)
C(3)–C(4)	1.330(4)
Pt(1)–P(1)	2.2655(13)
Pt(1)–P(2)	2.2721(13)
Pt(1)–C(1)	2.018(5)
Pt(1)–C(2)	2.002(5)
P(1)–C(3)	1.810(4)
P(1)–C(11)	1.801(5)
P(1)–C(21)	1.819(4)
P(2)–C(4)	1.805(5)
P(2)–C(31)	1.811(4)
P(2)–C(41)	1.805(5)
C(1)–N(1)	1.142(6)
C(2)–N(2)	1.151(6)
C(3)–C(4)	1.326(6)
P(1)–Ni(1)–P(2)	87.57(3)
C(1)–Ni(1)–P(1)	91.08(6)
C(2)–Ni(1)–P(1)	176.51(6)
C(1)–Ni(1)–P(2)	176.46(6)
C(2)–Ni(1)–P(2)	89.56(6)
C(1)–Ni(1)–C(2)	91.90(9)
C(11)–P(1)–C(21)	105.24(9)
C(11)–P(1)–C(3)	103.52(9)
C(21)–P(1)–C(3)	105.40(9)
C(11)–P(1)–Ni(1)	115.90(6)
C(21)–P(1)–Ni(1)	117.08(7)
C(3)–P(1)–Ni(1)	108.40(7)
C(4)–P(2)–C(31)	104.43(9)
C(4)–P(2)–C(41)	104.59(9)
C(31)–P(2)–C(41)	106.88(9)
C(4)–P(2)–Ni(1)	108.53(7)
C(31)–P(2)–Ni(1)	117.77(7)
C(41)–P(2)–Ni(1)	113.48(6)
N(1)–C(1)–Ni(1)	178.8(2)
N(2)–C(2)–Ni(1)	179.3(2)
C(4)–C(3)–P(1)	117.7(2)

Table 1 –*continued.*

C(3)–C(4)–P(2)	117.7(2)
P(1)–Pd(1)–P(2)	85.82(3)
C(1)–Pd(1)–P(1)	91.57(10)
C(2)–Pd(1)–P(1)	176.21(9)
C(1)–Pd(1)–P(2)	176.45(10)
C(2)–Pd(1)–P(2)	90.41(9)
C(1)–Pd(1)–C(2)	92.21(13)
C(3)–P(1)–C(11)	103.8(2)
C(3)–P(1)–C(21)	105.3(2)
C(11)–P(1)–C(21)	105.63(14)
C(3)–P(1)–Pd(1)	107.96(11)
C(11)–P(1)–Pd(1)	115.81(11)
C(21)–P(1)–Pd(1)	117.05(11)
C(4)–P(2)–C(31)	104.5(2)
C(4)–P(2)–C(41)	104.6(2)
C(31)–P(2)–C(41)	107.8(2)
C(4)–P(2)–Pd(1)	107.57(11)
C(31)–P(2)–Pd(1)	117.07(12)
C(41)–P(2)–Pd(1)	114.14(11)
N(1)–C(1)–Pd(1)	178.7(4)
N(2)–C(2)–Pd(1)	179.0(4)
C(4)–C(3)–P(1)	119.0(3)
C(3)–C(4)–P(2)	119.5(3)
P(1)–Pt(1)–P(2)	86.06(4)
C(1)–Pt(1)–P(1)	92.11(14)
C(2)–Pt(1)–P(1)	177.41(12)
C(1)–Pt(1)–P(2)	177.1(2)
C(2)–Pt(1)–P(2)	91.43(13)
C(1)–Pt(1)–C(2)	90.4(2)
C(11)–P(1)–C(3)	103.5(2)
C(11)–P(1)–C(21)	105.2(2)
C(3)–P(1)–C(21)	105.7(2)
C(11)–P(1)–Pt(1)	116.6(2)
C(3)–P(1)–Pt(1)	107.9(2)
C(21)–P(1)–Pt(1)	116.8(2)
C(4)–P(2)–C(41)	105.4(2)
C(4)–P(2)–C(31)	105.1(2)
C(41)–P(2)–C(31)	107.3(2)
C(4)–P(2)–Pt(1)	107.4(2)
C(41)–P(2)–Pt(1)	113.49(14)
C(31)–P(2)–Pt(1)	117.3(2)
N(1)–C(1)–Pt(1)	178.0(5)
N(2)–C(2)–Pt(1)	178.0(5)
C(4)–C(3)–P(1)	118.8(3)
C(3)–C(4)–P(2)	119.9(3)

which is generally referred to as the 'relativistic or Lanthanide contraction' [5](a).

Due to the presence of π-bonding interactions throughout the coordination planes and the ethene bridges of **1**–**3**, the aliphatic double-bond lengths of 1.312(3) Å (**1**), 1.330(4) Å (**2**), and 1.326(6) Å (**3**) are shortened compared with the ideal value of a simple double bond of 1.337(6) Å [18]. Interestingly, also the double-bond lengths of **1**–**3** reflect the above trend of covalent radii of Ni < Pt < Pd, since a smaller covalent radius facilitates the overlap of orbitals necessary for π-bonding interactions between the metal and the phosphorus atoms, which after some degree of rehy-

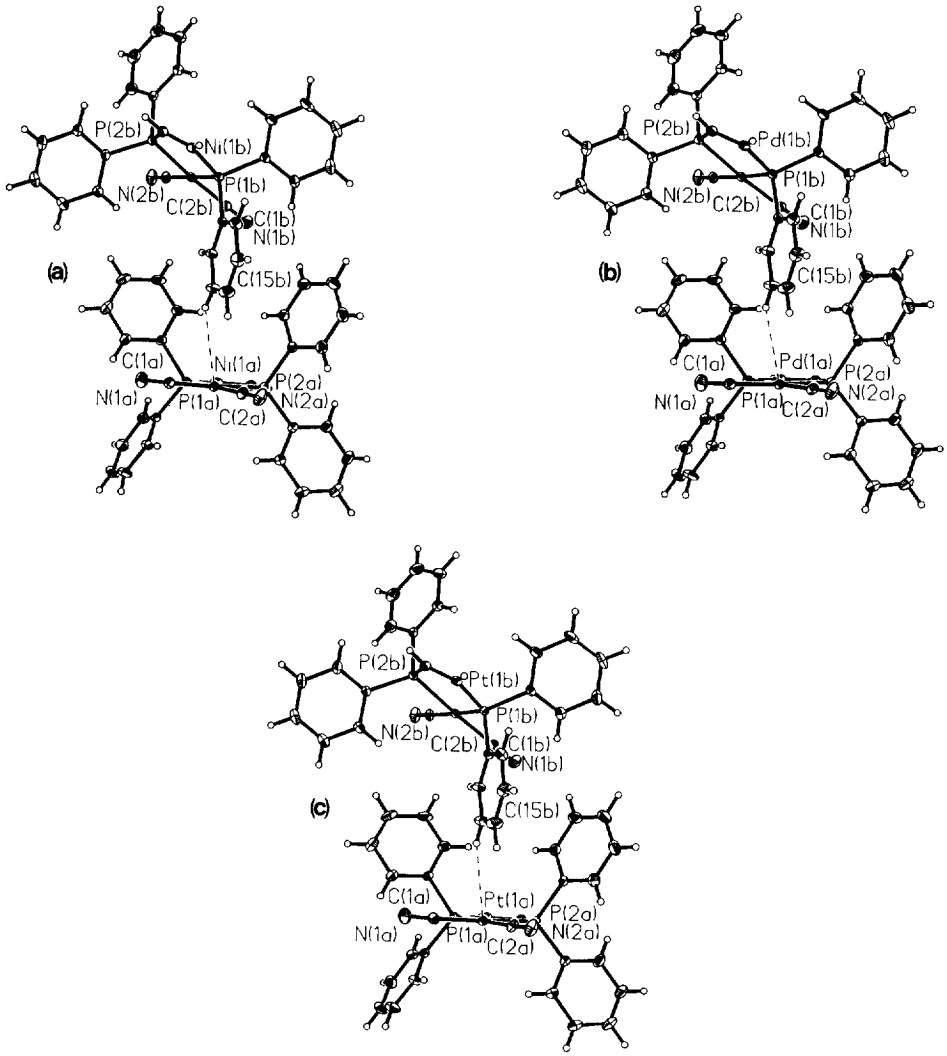

Fig. 2. Packing plots of $[M(CN)_2(cis\text{-}dppen)]$ showing the repulsive contact approaches between the hydrogen atoms attached to C(15b) and the metal atoms. (a) M=Ni (**1**); (b) M=Pd (**2**); (c) M=Pt (**3**). The largest deviations from coplanarity of the coordination planes and the ethene bridges occur in the case of (a).

bridization are responsible for the reduction of the double-bond lengths [1](c),[19]. Smaller than normal double-bond lengths have now been observed in several comparable d^8 complexes containing cis-dppen [1](b),[1](c),[7](b). The mean values of the CN bond lengths of 1.140(2) Å (**1**), 1.143(3) Å (**2**), and 1.147(4) Å (**3**) are within the usual range of 1.11–1.16 Å [2](a),[2](b),[3](a),[3](c),[4](c),[4](d).

In the syntheses of the complexes **4** and **5** the removal of chloride from $[MCl_2(cis\text{-}dppen)]$ (M=Ni, Pd) by precipitating AgCl with a silver salt leading to cationic intermediates was necessary for the completion of the reactions. However, in $[NiCl_2(cis\text{-}dppen)]$, also in the case of an excess of $AgBF_4$, only one chloride can be abstracted. It seems likely, that a chloride-bridged dimer of the composition $[Ni_2(\mu_2\text{-}Cl)_2(cis\text{-}dppen)_2](BF_4)_2$ is formed, since it has been found, that these species play an important role for chloride abstractions [20]. In the case of Pd both chlorides are removed and $[Pd(cis\text{-}dppen)(DMF)_2](BF_4)_2$ is produced [1](c). For Pt and compound **6** the same is true and an analogous intermediate occurs [1](c). However, it is also possible to treat $[PtCl_2(cis\text{-}dppen)]$ with dppam without chloride abstraction and $[Pt(cis\text{-}dppen)(dppam)]Cl_2$ is formed as indicated by its ^{31}P ^{1}H NMR parameters which are nearly identical with **6**.

The ^{195}Pt ^{1}H and ^{31}P ^{1}H NMR data for the complexes **3**–**8** are summarized in Table 2. δP of 52.6 in $[Pt(CN)_2(cis\text{-}dppen)]$ (**3**) shows the typical downfield five-ring contribution of chelating cis-dppen [21], which has also been observed in $[M(CN)_2(cis\text{-}dppen)]$ (M=Ni (**1**), Pd (**2**)) [1](b),[1](c). The $^{1}J(Pt,P)$ value of 2450 Hz indicates the strong trans influence of cyanide

Table 2. ^{195}Pt ^{1}H and ^{31}P ^{1}H NMR data for **3**–**8**[a]

Compound	δP	^{1}J(Pt,P)	^{2}J(P,P)$_{trans}$	^{2}J(P,P)$_{cis}$ + ^{4}J(P,P)
3	52.6	2450		
4	72.7d		162	
	43.7d		162	
5	70.7dt		361	34
	27.2dt		361	34
6[b]	61.6d	2359	317	
	18.3d	2095	317	
7	16.8			
8	17.4	1577		

[a] *J* values in Hz. d = doublet, dt = doublet of triplets. Spectra were run at 298 K. The following solvents were used: DMF (**3**–**7**) and CH_2Cl_2 (**8**). [b] $\delta Pt = -4912$tt (tt = triplet of triplets).

[1](d),[22], in full agreement with the X-ray structure of **3** given above. The stronger trans influence of cyanide versus chloride can be directly observed in the elongated M–P bond lengths in **1** and **3** compared with [$NiCl_2$(cis-dppen)] [1](b) and [$PtCl_2$(cis-dppen)] [1](c),[7](b).

The ^{31}P ^{1}H NMR spectra of compounds **4**–**6** are of the AA′XX′ type, where A,A′ represent the dppam phosphorus nuclei and X,X′ the cis-dppen chelate. In [NiCl(cis-dppen)(dppam)](BF_4) (**4**) δP of 72.7 also stems from a downfield five-ring effect, which is only possible for cis-dppen (see structure (B) in Scheme 1). Therefore, the signal at 43.7 is attributed to dppam showing no upfield four-ring contribution [21], since δP for free dppam is 42.2 [11](b). Together with the small ^{2}J(P,P)$_{trans}$ value of only 162 Hz [22], this is consistent with the distorted square pyramidal coordination shown in structure (B) of Scheme 1, where the central Ni atom deviates from the basal plane. The m/z value of the molecular ion peak in the FAB mass spectrum is also in agreement with the five-coordinate species [NiCl(cis-dppen)(dppam)]$^{+}$. Comparable five-coordinate complexes containing bis(diphenylphosphino)methylamine have already been reported [10].

In [Pd(cis-dppen)(dppam)](BF_4)$_2$ (**5**) δP of 70.7 indicates the typical five-ring contribution of bidentate cis-dppen, whereas the signal at 27.2 shows a four-ring upfield effect and is therefore attributed to chelating dppam in a square planar coordination [21]. Together with the ^{2}J(P,P)$_{trans}$ value of 361 Hz in the usual range [22] this is consistent with structure (C) of Scheme 1. The presence of ^{2}J(P,P)cis + ^{4}J(P,P) of 34 Hz leads to virtually coupled triplets further split by ^{2}J(P,P)$_{trans}$. Comparable virtual couplings have been observed in complexes with dppm which is isoelectronic with dppam [1](a). In contrast to **4** the m/z value of the molecular ion peak in the FAB mass spectrum of **5** shows no chloride-associated species and is in agreement with [Pd(cis-dppen)(dppam)]$^{+}$. In a similar square planar Pd^{II} complex containing chelating dppam, [$Pd(C_6F_5)_2$(dppam)] [11](c), the presence of an upfield shift for δP of 28.73 is also indicative of a pure square planar coordination.

For [Pt(cis-dppen)(dppam)](BF_4)$_2$ (**6**) δPt of −4912 is in line with the corresponding value of −4765 in [Pt(dppe)(dppam)]Cl_2 (**9**) [9], where dppe is 1,2-bis(diphenylphosphino)ethane. In **6** the δP parameters of 61.6 for cis-dppen and 18.3 for dppam again show the downfield five-ring and upfield four-ring contributions, respectively. Also the ^{1}J(Pt,P) values of 2359 and 2095 Hz, which are typical for the relative strong trans influence of phosphorus [23], and the usual magnitude of ^{2}J(P,P)$_{trans}$ of 317 Hz [22] are in agreement with structure (C) of Scheme 1. In both **6** and **9** [9] the ^{1}J(Pt,P) parameters for the five-rings exceed ^{1}J(Pt,P) for the four-rings by about 250 Hz. The reduction in ^{1}J(Pt,P) for the phosphorus atoms of the dppam chelates stems from an increase in the proportion of p character in the Pt–P bond at the expense of s character. Also in **6** like in **5** the m/z value of the molecular ion peak in the FAB mass spectrum is consistent with [Pt(cis-dppen)(dppam)]$^{+}$, showing no chloride-association.

The ν(N–H) bands in the IR spectra of **4**–**6** at 3239, 3237, and 3243 cm^{-1}, respectively, are slightly shifted toward higher energies relative to that for the free ligand at 3230 cm^{-1} [11](c). This effect has been observed earlier and attributed to weak N–H···N- or N–H···P-bridges in the solid state of free dppam [11](b). However, no hydrogen bridges have been observed in the X-ray structure of free dppam [24]. Therefore it seems likely, that metal-phosphorus dπ-dπ back bonding in the case of coordinated dppam leads to an enhanced electron density at the nitrogen atom thus strengthening the N–H bond. A comparable effect is present in complexes of 1,2-bis(diphenylphosphino)acetylene (dppa) [6](b). It has generally been observed for complexes containing dppam, that there is significant reduction in ν(N–H) in the case of hydrogen bridging interactions of the NH group [9],[11](a),[11](c),[12](a). The replacement

of the $(BF_4)^-$ anions in **6** by chlorides leads to a shift of ν(N–H) to 2817 cm^{-1} certainly due to a N–H $\cdots$ Cl^- bridge. Comparable to this, ν(N–H) of $[Pt(dppe)(dppam)]Cl_2$ (**9**) occurs at 2801 cm^{-1}. The lack of this shift of ν(N–H) toward lower energies in $[NiCl(cis\text{-}dppen)(dppam)](BF_4)$ (**4**) (see above), clearly confirms the presence of coordinated chloride.

The compounds $[M_2(CN)_4(\mu\text{-}trans\text{-}dppen)_2]$ (M=Pd (**7**), M=Pt (**8**)) are two further rare examples of d^8 metal cis-dicyanide complexes. The δP values of 16.8 (**7**) and 17.4 (**8**) clearly indicate a normal coordination shift without any ring contribution, since it is impossible for trans-dppen to chelate. Together with the single $^{31}P\{^1H\}$ NMR resonances in both cases, this is in agreement with the symmetrical binuclear structure type (D) in Scheme 1 containing two trans-dppen bridges. Furthermore, the cis-dicyanide structure is clearly confirmed by the ^1J(Pt,P) value of 1577 Hz in **8** indicating the strong trans influence of cyanide [1](d),[22]. Analogous binuclear complexes with dppa have been described only recently [6](b).

DISCUSSION

It seems likely, that the easy formation of the otherwise rare d^8 metal cis-dicyanide complexes in **1**–**3**, **7**, and **8** is a consequence of the unsaturated nature of the diphosphines cis- and trans-dppen. In the case of d^8 metal complexes containing both the electron rich anions of β-diketones and cis-dppen, the above described π-bonding between the metals and cis-dppen stabilizes these compounds by decreasing the electron density at the metal atoms [25]. Furthermore, it has been shown by numerous X-ray structures that the linkage isomerism in $[Pd(SCN)_2(cis\text{-}dppen)]$ and [Pd(SCN)(NCS)(cis-dppen)] cannot be explained by a strictly steric model and also concurrent electronic effects have to be considered [26]. In **1**–**3** containing the also electron rich cyanides, the coordination planes and the ethene bridges are nearly coplanar clearly showing this π-bonding interaction. In **7** and **8** π-bonding between the coordination units and the trans-dppen bridges should also be present, since several X-ray structures of the analogous binuclear complexes with dppa clearly indicate π-bonding [6](b),[27]. Therefore, the lack of the π-bonding stabilization of cis-dicyanides leads to the preference of square planar trans-dicyanides [2], five-coordinate dicyanides [3] or binuclear complexes with square planar trans-dicyanide units [4]. Comparable to the cis-dicyanides a cooperative stabilization effect could be present in the compounds **4**–**6**, since it has been shown, that like cis-dppen also dppam is able to accept π-electron density from a metal centre producing a reduced P–N bond length [12](a).

The slight distortions in the X-ray structures of **1**–**3** as a consequence of the repulsive C–H $\cdots$ M contact approaches are in agreement with the flexibility of complexes in crystals [28]. With respect to the unclear nature of these C–H $\cdots$ M(d^8) interactions [7](a), an attractive weak hydrogen bond can now be ruled out [7](b),[29]. The distortions could be a result of the general trend in molecular crystals to produce closest packings [30] and a repulsive Coulomb interaction between the positive partial charges on the d^8 metals and the aryl protons.

The above given trend of 1.06, 1.17, and 1.16 Å for the covalent radii of square planar d^8 Ni, Pd, and Pt, respectively, is in agreement with the trend of the corresponding ionic radii in crystals for the square planar d^8 metals Ni of 0.44, Pd of 0.64, and Pt of 0.60 Å [31]. A similar tendency for the same d^8 metals has been found only recently in the X-ray structures of another isomorphous series of complexes comparable to **1**–**3** [5](b). Together with a reduction in radius of as much as 6% from Ag to Au [5](a), this could be a general result of the 'relativistic contraction' [32] from 4d to 5d metals. Further work on this is in progress.

Acknowledgements—We thank the Fonds zur Förderung der wissenschaftlichen Forschung, Austria, for financial support. T. S., R. H. and Ch. L. thank the Co. Swarovski and the Austrian Society of Industrialists for support.

REFERENCES

1. (a) Hassan, F. S. M., Markham, D. P., Pringle, P. G. and Shaw, B. L., *J. Chem. Soc., Dalton Trans.*, 1985, 279; (b) Oberhauser, W., Bachmann, Ch., Stampfl, T., Haid, R. and Brüggeller, P., *Polyhedron*, 1997, **16**, 2827; (c) Oberhauser, W., Bachmann, Ch. and Brüggeller, P., *Inorg. Chim. Acta*, 1995, **238**, 35; (d) Brüggeller, P., *Z. Naturforsch., Teil B*, 1986, **41**, 1561.
2. (a) Corain, B., Basato, M., Favero, G., Rosano, P. and Valle, G., *Inorg. Chim. Acta*, 1984, **85**, L27; (b) Bendiksen, B., Riley, W. C., Babich, M. W., Nelson, J. H. and Jacobson, R. A., *Inorg. Chim. Acta*, 1982, **57**, 29.
3. (a) Hope, H., Olmstead, M. M., Power, P. P. and Viggiano, M., *Inorg. Chem.*, 1984, **23**, 326; (b) Powell, H. M., Watkin, D. J. and Wilford, J. B., *J. Chem. Soc. (A)*, 1971, 1803; (c) Stalick, J. K. and Ibers, J. A., *Inorg. Chem.*, 1969, **8**, 1084.
4. (a) Balch, A. L., Davis, B. J., Fung, E. Y. and Olmstead, M. M., *Inorg. Chim. Acta*, 1993, **212**, 149; (b) Balch, A. L. and Catalano, V. J., *Inorg. Chem.*, 1992, **31**, 3934; (c) Yip, H.-K., Lai, T.-F. and Che, C.-M., *J. Chem. Soc., Dalton Trans.*, 1991, 1639; (d) Che, C.-M., Yam, V. W.-W., Wong, W.-T. and Lai, T.-F., *Inorg. Chem.*, 1989, **28**, 2908.
5. (a) Bayler, A., Schier, A., Bowmaker, G. A. and Schmidbaur, H., *J. Am. Chem. Soc.*, 1996, **118**, 7006; (b) Papadimitriou, Ch., Veltsistas, P., Novosad, J., Cea-Olivares, R., Toscano, A., Garcia y Garcia, P., Lopez-Cardosa, M., Slawin, A. M. Z. and Woollins, J. D., *Polyhedron*, 1997, **16**, 2727.
6. (a) Calligaris, M., Carturan, G., Nardin, G., Scri-

vanti, A. and Wojcicki, A., *Organometallics*, 1983, **2**, 865; (b) Oberhauser, W., Bachmann, Ch., Stampfl, T. and Brüggeller, P., *Inorg. Chim. Acta*, 1997, **256**, 223.
7. (a) Yao, W., Eisenstein, O. and Crabtree, R. H., *Inorg. Chim. Acta*, 1997, **254**, 105; (b) Oberhauser, W., Bachmann, Ch., Stampfl, T., Haid, R., Langes, Ch., Rieder, A. and Brüggeller, P., *Inorg. Chim. Acta*, to be published.
8. Bhattacharyya, P., Slawin, A. M. Z., Smith, M. B. and Woollins, J. D., *Inorg. Chem.*, 1996, **35**, 3675.
9. Bhattacharyya, P., Sheppard, R. N., Slawin, A. M. Z., Williams, D. J. and Woollins, J. D., *J. Chem. Soc., Dalton Trans.*, 1993, 2393.
10. Browning, C. S. and Farrar, D. H., *J. Chem. Soc., Dalton Trans.*, 1995, 2005.
11. (a) Liehr, G., Szucsányi, G. and Ellermann, J., *J. Organomet. Chem.*, 1984, **265**, 95; (b) Ellermann, J. and Mader, L., *Z. Naturforsch., Teil B*, 1980, **35**, 307; (c) Usón, R., Fornies, J., Navarro, R. and Cebollada, J. I., *J. Organomet. Chem.*, 1986, **304**, 381.
12. (a) Pohl, D., Ellermann, J., Knoch, F. A. and Moll, M., *J. Organomet. Chem.*, 1995, **495**, C6; (b) Gómez, M., Muller, G., Sales, J. and Solans, X., *J. Chem. Soc., Dalton Trans.*, 1993, 221; (c) Schmidbaur, H., Lauteschläger, S. and Milewski-Mahrla, B., *J. Organomet. Chem.*, 1983, **254**, 59.
13. Oberhauser, W., Bachmann, Ch. and Brüggeller, P., *Polyhedron*, 1995, **14**, 787.
14. (a) Alcock, N. W., Wilson, W. L. and Nelson, J. H., *Inorg. Chem.*, 1993, **32**, 3193; (b) Bechthold, H.-Ch. and Rehder, D., *J. Organomet. Chem.*, 1979, **172**, 331.
15. North, A. C. T., Phillips, D. C. and Mathews, F. S., *Acta Cryst.*, 1968, **A24**, 351.
16. Sheldrick, G. M., SHELXS86, Crystallographic Computing 3, in *SHELXL93, Program for Crystal Structure Determination*, eds. G. M. Sheldrick, C. Krüger and R. Goddard. Oxford University Press, London, 1985, p. 175. Sheldrick, G. M., Universität of Göttingen, Göttingen, Germany, 1993.
17. Corbridge, D. E. C., *Phosphorus. An Outline of its Chemistry, Biochemistry, and Technology*. Elsevier, Amsterdam, 1978, p. 440.
18. *Handbook of Chemistry and Physics*, 55th edn. CRC, Cleveland, OH, U.S.A., 1974–1975, p. F-200.
19. Cotton, F. A. and Wilkinson, G., *Advanced Inorganic Chemistry*, 5th edn. Wiley, New York, 1988, p. 65.
20. Mattson, B. C. and Graham, W. A. G., *Inorg. Chem.*, 1981, **20**, 3186.
21. Garrou, P. E., *Chem. Rev.*, 1981, **81**, 229.
22. Pregosin, P. S. and Kunz, R. W., in *NMR Basic Principles and Progress*, Vol. 16, eds. P. Diehl, E. Fluck and R. Kosfeld. Springer-Verlag, Berlin, 1979, p. 16.
23. Tau, K. D. and Meek, D. W., *Inorg. Chem.*, 1979, **18**, 3574.
24. Nöth, H. and Fluck, E., *Z. Naturforsch., Teil B*, 1984, **39**, 744.
25. Okeya, S., Nakamura, Y. and Kawaguchi, S., *Bull. Chem. Soc. Jpn.*, 1981, **54**, 3396.
26. Paviglianiti, A. J., Minn, D. J., Fultz, W. C. and Burmeister, J. L., *Inorg. Chim. Acta*, 1989, **159**, 65.
27. Hogarth, G. and Norman, T., *Polyhedron*, 1996, **15**, 2859.
28. Martin, A. and Orpen, A. G., *J. Am. Chem. Soc.*, 1996, **118**, 1464.
29. Albinati, A., Pregosin, P. S. and Wombacher, F., *Inorg. Chem.*, 1990, **29**, 1812.
30. Kitaigorodski, A. I., *Molecular Crystals and Molecules*, Academic Press, 1973.
31. Shannon, R. D., *Acta Cryst.*, 1974, **A32**, 751.
32. Schwerdtfeger, P., Dolg, M., Schwarz, W. H. E., Bowmaker, G. A. and Boyd, P. D. W., *J. Chem. Phys.*, 1989, **91**, 1762.

Pergamon

PII: S0277-5387(98)00095-3

Polyhedron Vol. 17, No. 18, pp. 3221–3226, 1998
© 1998 Elsevier Science Ltd
All rights reserved. Printed in Great Britain
0277-5387/98 $19.00+0.00

Preparation and X-ray crystal structure study of a polypyridyl ruthenium(II) complex containing a dehydrodithizone ligand

Jerry L. Walsh,[a]* Randy McCracken[a] and Andrew T. McPhail[b]

[a]Department of Chemistry, University of North Carolina at Greensboro, Greensboro, North Carolina 27412, U.S.A.

[b]Department of Chemistry, Paul M. Gross Chemical Laboratory, Duke University, Durham, North Carolina 27708, U.S.A.

(Received 15 December 1997)

Abstract—Coordination of 2,3-diphenyltetrazolium-5-thiolate (tet) to an Ru(trpy)(bpy)$(OH_2)^{2+}$ (trpy = 2,2′:6′,2″-terpyridine; bpy = 2,2′-bipyridine) centre resulted in the formation of [Ru(trpy)(bpy)(tet)]$(ClO_4)_2$. Single-crystal X-ray analysis revealed that the tet ligand is bound through the sulfur atom to a somewhat distorted-octahedral ruthenium centre. The Ru–S bond distance is 2.393(2) Å, and the Ru–S–C bond angle is 115.1(2)°; the tet N–N bonded distances [1.306(10) Å–1.316(9) Å] are essentially equal. These data, as well as spectroscopic and electrochemical evidence, suggest that the tetrazolium ring exhibits delocalized, mesoionic character with some thiolate character on the sulfur atom. © 1998 Elsevier Science Ltd. All rights reserved

Keywords: ruthenium; tetrazolium-5-thiolate; terpyridine; bipyridine; synthesis; structure.

In spite of uncertainty about its composition and stability [1], dithizone has been used for years as a ligand in colourimetric determination of metals such as lead, mercury, copper, and silver [2]. Our interest in potential sulfur-nitrogen bidentate ligands for polypyridyl ruthenium complexes has led to the preparation of polypyridyl ruthenium complexes containing dithizone [3], dtz (I), and to the consideration of redox products of dithizone as ligands. In particular, 2,3-diphenyltetrazolium-5-thiolate, tet (II), is readily prepared by oxidation of dithizone and can be reduced back to dithizone [4].

In considering that there may be interesting relationships between the coordination of dithizone and tet to metal centres, we have prepared complexes of each using polypyridyl ruthenium moieties as the coordination centres. Dithizone often acts as a bidentate ligand, binding through the sulfur and a nitrogen atom to form a five-membered ring. NMR studies [3] indicate that this is the case also with $Ru(bpy)_2(dtz)^+$ (bpy-2,2′-bipyridine). Tet has not, however, been extensively studied as a ligand, and thus its coordination characteristics are poorly defined. In general, tetrazoles can coordinate to metal centres through either the 1 or 4 nitrogen [5–12], through the 2 or 3 nitrogen [13–18], or through two nitrogens as a bridging ligand [19, 20]. The tin complex, $Sn(CH_3)_2(phen)L_2$ (phen = 1,10-phenanthroline; L = 1-phenyl-5-thione-1,2,3,4-tetrazolate), contains one tetrazolate unit bound through nitrogen and another bound through sulfur [21]. In $[HgCl_2(tet)]$, the tet sulfur atom acts as a bridging ligand in a polymeric structure [22]. Because of the limited reports of characterization of tet complexes, especially structural characterization of classical transition metal complexes involving this ligand, we have performed a single crystal X-ray analysis of the tet complex reported here.

EXPERIMENTAL

The complex [Ru(trpy)(bpy)Cl]Cl [23] and tet [1] were prepared according to literature procedures. Other substances were of reagent grade quality and

* Address for correspondence.

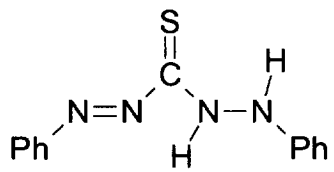

(I)

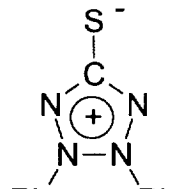

(II)

were used as received. Spectrophotometric measurements were made with a Varian DMS-100 spectrophotometer. Electrochemical measurements were made with a Bioanalytical Systems Model CS-1087 Electrochemical Analyzer.

Synthesis

Preparation of $[Ru(trpy)(bpy)(tet)](ClO_4)_2$. A mixture of 0.300 g (0.535 mmol) of $[Ru(trpy)(bpy)Cl]Cl$ and 0.241 g (1.07 mmol) of $AgClO_4.H_2O$ was placed in a 100 cm^3 flask and 40 cm^3 of 75/25 acetone/water was added. The solution was flushed with nitrogen and refluxed for 1.5 h and then cooled. After filtration, 0.200 g (0.79 mmol) of tet was added to the filtrate. The solution was flushed with nitrogen and refluxed for 6 h. After cooling, the solution volume was reduced to 10 cm^3 by rotary evaporation. After cooling overnight, the solution was filtered to collect a brown precipitate. The precipitate was chromatographed on an alumina column using dichloromethane/acetone as eluent. Reprecipitation of the red-brown band gave 0.164 g (0.174 mmol) of product (33% yield). Anal. Calcd for $RuC_{38}H_{29}Cl_2N_9O_8S$: C, 48.36; H, 3.10; N, 13.36. Found: C, 46.77; H, 3.08; N, 12.88.

Crystal structure determination

Crystals of $[Ru(trpy)(bpy)(tet)](ClO_4)_2 \cdot H_2O$ were grown by slow evaporation of solvent from a 2:1:1 acetone:ethanol:water solution of $[Ru(trpy)(bpy)(tet)](ClO_4)_2$.

A crystal of dimensions *ca.* $0.06 \times 0.06 \times 0.60$ mm was mounted on the end of a thin glass fibre. Oscillation and Weissenberg photographs yielded preliminary unit-cell parameters and space group information. An Enraf–Nonius CAD-4 diffractometer (Cu-$K\alpha$ radiation, graphite monochromator) was used for all other measurements. Refined unit-cell parameters were derived from the diffractometer setting angles for 25 reflections ($36 < \theta < 40$) widely separated in reciprocal space. Intensity data were corrected for the usual Lorentz and polarization effects; an empirical absorption correction [T_{max}:T_{min}(rel.) = 1.00:0.93], based on the ϕ-dependency of the intensities of several reflections with χ *ca.* 90°, was also applied. Laue symmetry indicated that the crystals belonged to the trigonal system. The systematic absences ($00l$ when $l \neq 3n$) were consistent with the space group $P3_1$ and its enantiomorph $P3_2$.

The crystal structure was solved by direct methods (MULTAN11/82) [24] assuming at the outset that the space group was $P3_1$. Approximate non-hydrogen atom coordinates were derived in part from an *E*-map and from a series of weighted F_o and difference Fourier syntheses phased successively by an increasing number of atoms. One of the perchlorate ions and the water molecule are disordered over two sites, with the alternative location of the latter being masked by a perchlorate ion; moreover, the perchlorate ion at one of these sites is further disordered over two orientations. Non-hydrogen atom positional and temperature factor parameters (first isotropic and then anisotropic), with hydrogen atoms incorporated at their calculated positions in the later cycles, were adjusted by means of several rounds of full-matrix least-squares calculations. An extinction correction was included as a variable during the later iterations. The parameter refinement converged at $R = 0.0495$ ($R_w = 0.0637$). The chirality of the crystal used for data collection was established at this stage by introducing the imaginary contributions to the anomalous dispersion corrections into the structure-factor calculations. For parameters in space group $P3_1$, R was 0.0522 while R_w was 0.0692, whereas when those for the enantiomer were used in space group $P3_2$, the values were $R' = 0.0578$ and $R_w = 0.0782$. These differences are significant at the 0.005 level [25] when R'_w/R_w (0.0782/0.0692 = 1.130) equals to or exceeds 1.0012 and indicated that $P3_1$ was the correct choice. Continuation of the least-squares parameter refinement led to convergence at $R = 0.048$ ($R_w = 0.062$). A final difference Fourier synthesis contained no unusal features.

Crystallographic calculations were performed on PDP11/44 and MicroVAX computers by use of the Enraf–Nonius Structure Determination Package (SDP 3.0) [26]. For all structure-factor calculations, neutral atom scattering factors and their anomalous dispersion corrections were taken from ref. [27]. Further information concerning data collection and refinement are provided in Table 1. Atomic coordinates, thermal parameters, least-squares planes, and a listing of observed and calculated structure ampli-

Table 1. Crystallographic data and data collection parameters for $[Ru(tryp)(bpy)(tet)](ClO_4)_2 \cdot H_2O$

Molecular formula	$[C_{38}H_{29}N_9RuS][ClO_4]_2 \cdot H_2O$
Formula weight	961.77
Crystal system	trigonal
Space group	$P3_1(C_3^2)$-No.144
a(Å)	13.185(1)
b(Å)	13.185(1)
c(Å)	21.288(2)
α( )	90.0( )
β( )	90.0( )
γ( )	120.0( )
V(Å^3)	3205.0(8)
Z	3
$D_{calcd.}$(g cm^{-3})	1.495
Radiation (λ, Å)	Cu-$K\alpha$ (1.5418)
Absorption coefficient, μ(cm^{-1})	51.9
Temp.(C)	25
Scan type	ω–2θ
Scanwidth ( )	$0.90+0.14\tan\theta$
θ_{max}.( )	75
Intensity control refls.;	2 1 4, 2 1 3, 4 −5 2, 4 −2 1;
Variation; repeat time (hr)	<1.0%; 2
Total no. of refls. ($+h, \pm k, +l$) recorded	7050
No. of non-equiv. refls. recorded	4958
R_{merge} (on I)	0.025
No. of refls. retained [$I > 3.0\sigma(I)$]	4050
No. of parameters refined	557
Extinction correction	$6.2(5) \times 10^{-7}$
R (R_w)[a]	0.048 (0.062)
Goodness-of-fit[b]	1.37
Max. shift:esd in final least-squares cycle	0.03
Final $\Delta\rho$(e Å^{-3})max.; min.	0.80; −1.19

[a] $R = \Sigma||F_o|-|F_c||/\Sigma|F_o|$; $R_w = [\Sigma w(|F_o|-|F_c|)^2/\Sigma w|F_o|^2]^{1/2}$; $\Sigma w\Delta^2[w = 1/\sigma^2(|F_o|)$, $\Delta = (|F_o| - |F_c|)]$ was minimized.

[b] Goodness-of-fit $= [\Sigma w\Delta^2/(N_{observations}-N_{parameters})]^{1/2}$.

tudes have been deposited with the Editor as supplementary material.

RESULTS AND DISCUSSION

The complex $[Ru(trpy)(bpy)(tet)](ClO_4)_2$ was prepared by direct reaction of tet with $Ru(trpy)(bpy)Cl^+$ in aqueous ethanol solution. The intensely red-coloured complex exhibits properties consistent with the tet binding as a monodentate ligand through the sulfur atom. An MLCT absorption band at 480 nm ($\epsilon = 7200\ M^{-1}cm^{-1}$) is similar to those of Ru(trpy)(bpy)X^+ (X = anion) complexes [28]. The cyclic voltammogram of $Ru(trpy)(bpy)(tet)^{2+}$ in acetonitrile exhibits a pseudoreversible wave at 0.86 V vs. SSCE ($\Delta Ep = 80$ mV), consistent with $Ru^{III\,II}$ potentials for Ru(trpy)(bpy)X^+ complexes. However, bulk oxidation at a potential just above 0.86 V leads to complete loss of the wave. The foregoing evidence suggests that tet binds through the sulfur atom which possesses significant thiolate character, consistent with the mesoionic character of the free ligand. Thioether or thione ligands [29, 30] exhibit higher energy MLCT bands and higher $Ru^{III\,II}$ redox couples.

Single-crystal X-ray analysis of $[Ru(trpy)(bpy)(tet)](ClO_4)_2 \cdot H_2O$, Fig. 1 [31], confirms that the six-coordinate ruthenium centre binds to the sulfur atom of the tetrazolium ligand. Important bond distances and angles are listed in Table 2. Distortions from an octahedral arrangement around the ruthenium centre may be ascribed to constraints imposed by the bite angles of the bpy and trpy ligands, and are probably little influenced by the tet ligand. Distances and angles within the trpy ligands are close to the average values in related species [32–37] such as $Ru(bpy)_3^{2+}$ and $Ru(trpy)L_3^{2+}$ complexes. The Ru–N distances and angles are also in accord with expected values. The short Ru–N(7) distance [1.957(6) Å] and the N(1)–Ru–N(13) angle of only 158.5(2) are the result of the restricted bite angle of the trpy. Likewise, the bpy bite angle is only 78.4(2) .

Comparison of the structure of the bound tet to that of the free ligand [38, 39] reveals very little difference. In particular, the C(41)–S(46) and N(43)–N(44)

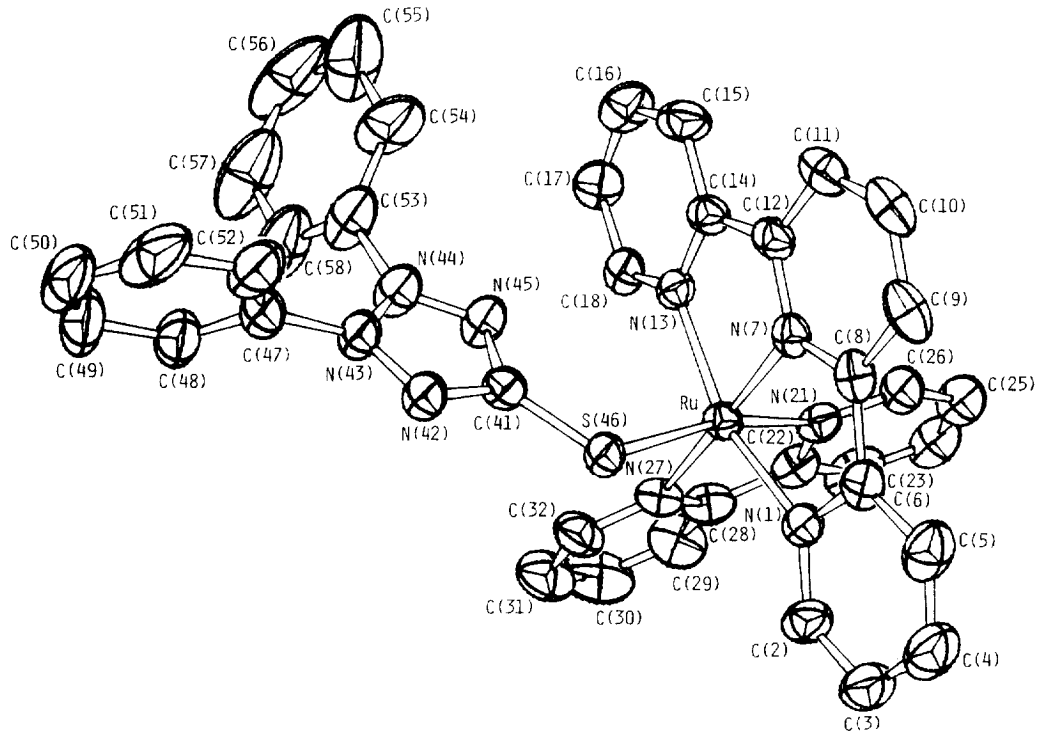

Fig. 1. ORTEP diagram (30% probability ellipsoids) showing the crystallographic atom numbering scheme and solid-state conformation of the $[C_{35}H_{29}N_9RuS]^{2+}$ ion; hydrogen atoms have been omitted.

bond lengths in the coordinated tet [1.686(8) Å and 1.316(9) Å, respectively] do not differ significantly from those in the free ligand {1.692(4) Å and 1.328(4) Å [38], and 1.687(5) Å and 1.313(4) Å [39], respectively, from two independent determinations}. The tetrazolium ring is essentially planar and its

Table 2. Selected interatomic distances (Å) and angles (°) in $[Ru(trpy)(bpy)(tet)^{2+}]$, with estimated standard deviations in parentheses

(a) Bond Lengths			
Ru–N(1)	2.087(6)	Ru–N(21)	2.075(6)
Ru–N(7)	1.957(6)	Ru–N(27)	2.088(6)
Ru–N(13)	2.077(6)	Ru–S(46)	2.393(2)
C(41)–N(42)	1.362(10)	N(43)–N(44)	1.316(9)
C(41)–C(45)	1.375(9)	N(43)–C(47)	1.443(11)
C(41)–S(46)	1.686(8)	N(44)–N(45)	1.306(10)
N(42)–N(43)	1.313(10)	N(44)–C(53)	1.473(13)
(b) Bond Angles			
N(1)–Ru–N(7)	79.2(3)	N(7)–Ru–S(46)	90.1(2)
N(1)–Ru–N(13)	158.5(2)	N(13)–Ru–N(21)	92.1(3)
N(1)–Ru–N(21)	88.5(2)	N(13)–Ru–N(27)	97.1(2)
N(1)–Ru–N(27)	104.0(3)	N(13)–Ru–S(46)	98.5(2)
N(1)–Ru–S(46)	83.6(2)	N(21)–Ru–N(27)	78.4(2)
N(7)–Ru–N(13)	79.4(2)	N(21)–Ru–S(46)	168.2(2)
N(7)–Ru–N(21)	97.0(2)	N(27)–Ru–S(46)	95.1(2)
N(7)–Ru–N(27)	174.2(2)	Ru–S(46)–C(41)–S(46)–C(41)	115.1(2)

Table 3 Bond Lengths (Å) in Tetrazoles*, with estimated standard deviations in parentheses

Species	$C-N_1$, $C-N_4$	N_1-N_2, N_3-N_4	N_2-N_3	Reference
Tet and related species				
tet[a]	1.360(4)	1.318(3)	1.313(4)	[38]
	1.368(3)	1.316(3)	1.328(4)	[30]
$Ru(trpy)(bpy)(tet)^{2+}$	1.362(10),1.375(9)	1.313(10), 1.306(10)	1.316(9)	This work
$(tetHgCl_2)_2$	1.38(2),1.31(3)	1.31(3),1.33(3)	1.25(3)	[22]
2,3-diphenyltetrazolium-5-olate	1.377(4),1.379(4)	1.312(4),1.310(4)	1.326(4)	[41]
Other tetrazoles				
1,3-diphenyltetrazolium-5-thiolate	1.348(3),1.390(4)	1.333(3),1.331(3)	1.293(3)	[41]
Bis(1-phenyl-5-thiotetrazole)dibutyltin	1.34(2),1.29(2)	1.35(2),1.37(2)	1.28(2)	[42]
(5-methyltetrazolate)(OEP)indium(III)[b]	1.28(2),1.33(2)	1.35(1),1.34(1)	1.29(1)	[15]
(5-methyltetrazolate)(OEP)iron(III)[b]	1.31(2),1.34(2)	1.39(3),1.38(3)	1.32(2)	[15]
$Co(PBu_3)(DH)_2$(5-trifluoromethyl-tetrazole)[c]	1.320(9),1.34(1)	1.321(9),1.320(10)	1.321(9)	[18]

[a] Molecule lies on a crystallographic two-fold axis.
[b] OEP = 2,3,7,8,12,13,17,18-octaethylporphinate.
[c] DH = monoanion of dimethylglyoxime

* 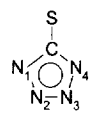

directly bonded substitutents lie close to the ring plane [Δ(Å): S(46) 0.008, C(47) 0.110, C(53) 0.035] as does the Ru atom [Δ 0.062 Å; N(45)–C(41)–S(46)–Ru torsion angle = 2(1)°]. Dihedral angles between the tetrazolium and phenyl ring planes are 63.1° and 70.8°, while that between the latter is 85.7° [torsion angles: N(44)–N(43)–C(47)–C(48) = 70(1)°, N(43)–N(44)–C(53)–C(58) = −72(2)°]. The bent geometry at the sulfur atom [C(41)–S(46)–Ru = 115.1(2)°] and the Ru–S distance [2.393(2) Å] are comparable to those observed in species like $Ru(CO)_2(pyridine)_2$(mercaptobenzothiazole)$_2$ [40] where the corresponding values are 109.0(1)° and 2.406(4) Å.

Table 3 lists bond distances in a number of tetrazoles. Distances in the coordinated and free tet are consistent with a mesoionic tetrazole structure. Thus, very similar N–N bond lengths are observed for tet [22, 38, 39] and related species [41]. Other tetrazoles [6–18, 41–43] typically exhibit longer N_1-N_2/N_3-N_4 than N_2-N_3 bond lengths indicative of greater double bond localization in the N_2-N_3 bond. These observations are consistent with considerable electron delocalization within the tetrazole ring of tet [44].

Even though considerable anionic character is anticipated for the sulfur atom of tet (and spectral and electrochemical properties are consistent with that character), the C–S bond length at 1.686(8) Å in the coordinated tet is significantly shorter than that usually observed for thiolato C–S species. For example, thiolato ligands in ruthenium complexes have C–S bond lengths ranging from 1.769(3) Å in *cct*-RuH$(SC_6H_4p\text{-}Me)(CO)_2(PPh_3)_2$ [45], 1.778(8), 1.788(7) Å in *cct*-$Ru(SC_6H_4p\text{-}Me)_2(CO)_2(PPh_3)_2$ [45], 1.77(2)–1.83(2) Å in (η^6-arene)$Ru(SAr)_2$ complexes [46], 1.77(1), 1.79(1) Å in *trans*-Ru-(2,6-$C_6H_3Me_2S)_2$$(CN^tBu)_4$ [46], to 1.848(5), 1.852(5) Å in Cp*Ru(NO)$(SCMe_3)_2$ [47]. The C–S bond length found here is also shorter than that at 1.711(8) Å in [Ru(4-methylpyrimidine-2-thionate)$(bipy)_2]^{2+}$ [48], but it is slightly longer than that of 1.632(5) Å in the coordinated thione [Cp(dppe)RuSCHC$_6$H$_4$OMe$)^+$] [49].

Acknowledgements– Financial support from the Research Council of the University of North Carolina at Greensboro is gratefully acknowledged.

REFERENCES

1. Irving, H. M. N. H., Kiwan, A. M., Rupainwar, D. C. and Sahota, S. S., *Anal. Chim. Acta*, 1971, **56**, 205.
2. Sandell, E. B., *Colorimetric Determination of Traces of Metals*, 3rd Ed., Wiley, New York, 1959.
3. Walsh, J. L., Morgan, C. L., and Hunt, A., work in progress.
4. Tomscanyi, L., *Anal. Chim. Acta*, 1977, **88**, 371.
5. Tomscanyi, L., *Anal. Chim. Acta*, 1974, **70**, 411.
6. Peyronel, G. and Fabretti, A. C., *J. Coord. Chem.*, 1977, **7**, 119.
7. Blunden, S. J., Mahon, M. F., Molloy, K. C. and Waterfield, P. C., *J. Chem. Soc., Dalton Trans.*, 1994, **00**, 2135.
8. Lambert, C., Hampel, F., von Rague Schleyer, P., *J. Organomet. Chem.*, 1993, **455**, 29.
9. Rigby, W., Bailey, P. M., McCleverty, J. A. and Maitlis, P. M., *J. Chem. Soc., Dalton Trans.*, 1979, **00**, 371.
10. Guilard, R., Jagerovic, N., Tabard, A., Richard, P., Courthaudon, L., Louati, A., Lecomte, C. and Kadish, K. M., *Inorg. Chem.*, 1991, **30**, 16.

11. Guilard, R., Perrot, I., Tabard, A., Richard, P., Lecomte, C., Liu, Y. H. and Kadish, K. M., *Inorg. Chem.*, 1991, **30,** 27.
12. Graeber, E. J. and Morosin, B., *Acta Crystallogr. Sect. C: Crystal Structure Commun.*, 1983, **C39,** 567.
13. Oro, L. A., Pinillos, M. T., Tejel, C., Apreda, M. C., Foces-Foces, C. and Cano, F. H., *J. Chem. Soc., Dalton Trans.*, 1988, **00,** 1927.
14. Alvanipour, A., Buttrus, N. H., Eaborn, C., Hitchcock, P. B., Monsour, A. I. and Saxena, A. K., *J. Organomet. Chem.*, 1988, **349,** 29.
15. Guilard, R., Gerges, S. S., Tabard, A., Richard, P., El Borai, M. A. and Lecomte, C., *J. Am. Chem. Soc.*, 1987, **109,** 7228.
16. Das, R., Paul, P., Nag, K. and Venkatsubramanian, K., *Inorg. Chim. Acta*, 1991, **185,** 221.
17. Gaughan, A. P., Bowman, K. S. and Dori, Z., *Inorg. Chem.*, 1972, **11,** 601.
18. Takach, N. E., Holt, E. M., Alcock, N. W., Henry, R. A. and Nelson, J. H., *J. Am. Chem. Soc.*, 1980, **102,** 2968.
19. John, E. O., Willett, R. D., Scott, B., Kirchmeier, R. L. and Shreeve, J. M., *Inorg. Chem.*, 1989, **28,** 893.
20. Oro, L. A., Pinillos, M. T., Tejel, C., Apreda, M. C., Foces-Foces, C. and Cano, F. H., *J. Chem. Soc., Dalton Trans.*, 1988, **00,** 1927.
21. Bravo, J., Cordero, M. B., Casas, J. S., Castaño, M. V., Sánchez, A. and Sordo, J., *J. Organomet. Chem.*, 1996, **513,** 63.
22. Kozarek, W. J. and Fernando, Q., *J. Chem. Soc., Chem. Commun.*, 1972, **00,** 604.
23. Takeuchi, K. J., Thompson, M. S., Pipes, D. W. and Meyer, T. J., *Inorg. Chem.*, 1984, **23,** 1845.
24. "MULTAN11/82", Main, P., Fiske, S. J., Hull, S. E., Lessinger, L., Germain, G., DeClerq, J. P. and Woolfson, M. M., Universities of York, England, and Louvain, Belgium, 1982.
25. Hamilton, W. C., *Acta Crystallogr.*, 1965, **18,** 502.
26. Frenz, B. A. and Associates, Inc., SDP 3.0: Structure Determination Package, College Station, Texas, U.S.A., and Enraf-Nonius, Delft, The Netherlands, 1985.
27. *International Tables for X-Ray Crystallography*, vol. IV, Kynoch, Birmingham, U.K., 1974.
28. Juris, A., Balzani, V., Barigelletti, F., Campagna, S., Belser, P. and von Zelewsky, A., *Coord. Chem. Rev.*, 1988, **84,** 85.
29. Kroener, R., Heeg, M. J. and Deutsch, E., *Inorg. Chem.*, 1988, **27,** 558.
30. Root, M. J., Sullivan, B. P., Meyer, T. J. and Deutsch, E., *Inorg. Chem.*, 1985, **24,** 2731.
31. C. K. Johnson, "ORTEPII: Report ORNL-5138", Oak Ridge National Laboratory, Oak Ridge, Tennessee, U.S.A., 1976.
32. Rillema, D. P., Jones, D. S. and Woods, C., Levy, H., *A. Inorg. Chem.*, 1992, **31,** 2935.
33. Krausz, E., Riesen, H. and Rae, A. D., *Aust. J. Chem.*, 1995, **48,** 929.
34. Sutter, J.-P., James, S. L., Steenwinkel, P., Karlen, T., Grove, D. M., Veldman, N., Smeets, W. J. J., Spek, A. L. and van Koten, G., *Organometallics*, 1996, **15,** 941.
35. Grover, N., Gupta, N., Singh, P. and Thorp, H. H., *Inorg. Chem.*, 1992, **31,** 2014.
36. Leising, R. A., Kubow, S. A., Churchill, M. R., Buttrey, L. A., Ziller, J. W. and Takeuchi, K. J., *Inorg. Chem.*, 1990, **29,** 1306.
37. Gulyas, P. T., Hambley, T. W. and Lay, P. A., *Aust. J. Chem.*, 1996, **49,** 527.
38. Kushi, Y. and Fernando, Q., *J. Am. Chem. Soc.*, 1970, **92,** 1965.
39. Liu, S. and Zubieta, J., *Polyhedron*, 1989, **8,** 677.
40. Jeannin, S., Jeannin, Y. and Lavigne, G., *Transition Met. Chem. (Weinhein Ger.)*, 1976, **1,** 192.
41. King, T. J., Preston, P. N., Suffolk, J. S. and Turnbull, K., *J. Chem. Soc., Perkin Trans.*, 1979, **2,** 1751.
42. Deeth, R. J., Molloy, K. C., Mahon, M. F. and Whittaker, S., *J.Organomet. Chem.*, 1992, **430,** 25.
43. Bravo, J., Cordero, M. B., Casas, J. S., Sánchez, A., Sordo, J., Castellano, E. E., Zuckerman-Scheptor, J., *J. Organomet. Chem.*, 1994, **482,** 147.
44. Ogilvie, J. W. and Corwin, A. H., *J. Am. Chem. Soc.*, 1961, **83,** 5023.
45. Jessop, P. G., Rettig, S. J., Lee, C.-L. and James, B. R., *Inorg. Chem.*, 1991, **30,** 4617.
46. Mashima, K., Kaneyoshi, H., Kaneko, S., Mikami, A., Tani, K. and Nakamura, A., *Organometallics*, 1997, **16,** 1016.
47. Tagge, C. D. and Bergman, R. G., *J. Am. Chem. Soc.*, 1996, **118,** 6908.
48. Yamanari, K., Nozaki, T., Fuyuhiro, A., Kushi, Y. and Kaizaki, S., *J. Chem. Soc., Dalton Trans.*, 1996, **00,** 2851.
49. Schenk, W. A., Stur, T. and Dombrowski, E., *J. Organomet. Chem.*, 1994, **472,** 257.

Pergamon

PII: S0277-5387(98)00097-7

Polyhedron Vol. 17, No. 18, pp. 3227–3234, 1998
© 1998 Elsevier Science Ltd
All rights reserved. Printed in Great Britain
0277-5387/98 $19.00+0.00

Synthesis and properties of a tetraaza macrocyclic ligand containing 2-pyridylmethyl pendant arms and its copper(II) and nickel(II) complexes: crystal structure of the copper(II) complex

Shin-Geol Kang,[a,*] Seong-Jin Kim[a] and Jong Hwa Jeong[b]

[a]Department of Chemistry, Taegu University, Kyungsan 712-714, S. Korea

[b]Department of Chemistry, Kyungpook National University, Taegu 702-701, S. Korea

(Received 18 November 1997; accepted 12 March 1998)

Abstract—A new functionalized macrocyclic ligand 2,13-bis(2′-pyridylmethyl)-5,16-dimethyl-2,6,13,17-tetraazatricyclo[16.4.0.^{1,18}O^{7,12}]docosane (L^2) containing two 2-pyridylmethyl pendant arms has been prepared by the one-step reaction of 3,4-dimethyl-2,6,13,17-tetraazatricyclo[16.4.0.^{1,18}O^{7,12}]docosane (L^1) with 2-(chloromethyl) pyridine. The octahedral complexes $[NiL^2](ClO_4)_2$ and $[CuL^2](ClO_4)_2$, in which two pyridyl groups are coordinated to the metal ion, have been prepared and characterized. The crystal structure of $[CuL^2](ClO_4)_2$ shows that the complex is centrosymmetric and the metal center has a tetragonally distorted octahedral geometry. In concentrated $HClO_4$ solutions, the coordinated pyridyl groups of $[CuL^2]^{2+}$ are protonated and are removed from the coordination sphere. However, those of $[NiL^2]^{2+}$ are not protonated but are coordinated to the metal ion even in 3.0 *M* $HClO_4$. The macrocycle L^2 reacts more slowly with copper(II) ion than does L^1. © 1998 Elsevier Science Ltd. All rights reserved

Keywords: tetraaza macrocycle; functionalized macrocycle; nickel(II) complex; copper(II) complex; crystal structure.

The synthesis of polyaza macrocyclic ligands and their metal complexes containing additional functional pendant arms is of growing importance to various fields of coordination chemistry, since the introduction of functional groups into a polyaza macrocyclic compound causes a considerable change in chemical properties and structures [1–14]. The structures and chemical properties of such compounds are also influenced by various factors, such as the type and number of the functional groups. For example, the fully N-hydroxyethylated macrocycle L^6 forms 1:1 metal–ligand complexes [6]. However, the macrocycle L^5, containing four N-pyridylmethyl pendant arms, generally acts as a binucleating ligand [7, 8]. Recently, we reported the preparation of di-N-hydroxyethylated macrocycle L^3 from the reaction of L^1 with an excess of 2-bromoethanol [9]. Interestingly, L^3 reacts with the Cu^{2+} ion more slowly than the unsubstituted macrocycle L^1, indicating that the reaction is retarded by the N-hydroxyethyl groups of L^3. This result contradicts those for various N-functionalized macrocycles, such as L^6, L^7, and L^8; the complexation reaction of L^6, L^7, and L^8 with Cu^{2+} ion is much faster than that for L^4 or the fully N-methylated derivative of L^4 [6, 10]. It has been also observed that, although the hydroxyl groups of $[CuL^3]^{2+}$ are not involved in coordination, those of $[NiL^3]^{2+}$ and $[CuL^6]^{2+}$ are coordinated to the metal ion [7, 9]. However, the origins of the differences are not thoroughly understood. To further investigate the effects of the nature of functional pendant arms on the coordination behaviors, we have been interested in the synthesis of new polyaza macrocycles containing various types of functional pendant arms.

In this work, we have prepared a new macrocyclic

* Author to whom correspondence should be addressed.

ligand L^2, containing two 2-pyridylmethyl pendant arms, from the one-step reaction of L^1 with an excess amount of 2-(chloromethyl)pyridine. This paper reports the synthesis and chemical properties of L^2 and its copper(II) and nickel(II) complexes. Crystal structure of $[CuL^2](ClO_4)_2$ is also determined. A number of studies have reported on the properties of tetraaza macrocyclic compounds containing 2-pyridylmethyl pendant arms [7, 8, 11, 12]. However, to our knowledge, examples of saturated 14-membered tetraaza macrocyclic compounds containing two N-(2-pyridylmethyl) pendant arms are not reported to date.

1. EXPERIMENTAL

1.1. *Materials and Measurements*

All chemicals used in syntheses were of reagent grade and were used without further purification. The macrocyclic ligand L^1 was prepared as described previously [15].

Electronic spectra were obtained using a Shimadzu UV-160 spectrophotometer. IR spectra were recorded as either Nujol mulls or KBr pellets on a Shimadzu IR-440 spectrophotometer, conductance measurements with a Metrohm Herisau Conductometer E518, and NMR spectra with a Bruker WP 300 FT NMR spectrometer. Mass spectra and elemental analyses were performed at the Korea Basic Science Institute, Seoul, Korea. Magnetic moments were calculated from magnetic susceptibility data obtained using a Johnson Matthey MK-1 magnetic susceptibility balance. Cyclic voltammograms were recorded using a Yanaco Voltammetric Analyzer p-1000 equipped with a FG-121B function generator and a Watanabe X–Y recorder. The electrochemical measurements were conducted in oxygen free 0.1 *M* $(n\text{-Bu})_4NClO_4$ acetonitrile solutions at 20 C.

Kinetic measurements of the formation of the copper(II) complexes of L^1 and L^2 were carried out in acetate buffer solutions (pH 5.4) of methanol–water (1:1) mixture at 20 C. The initial concentrations of the ligands and the metal ion in the reaction mixtures are 1.0×10^{-3} and 2.0×10^{-2} *M*, respectively. The reaction was monitored using the absorbance increase at 520 (L^1) or 553 nm (L^2).

1.2. *Synthesis of the Compounds*

1.2.1. L^2. A toluene (50 mL) suspension of L^1 (2.0 g, 6.0 mmol), 2-(chloromethyl)pyridine hydrochloride (3.0 g, 18 mmol), and KOH (4.0 g, 71 mmol) was heated to reflux over 30 h. The reaction mixture was filtered, and the filtrate was evaporated to dryness. The residue was dissolved in a minimum volume of chloroform. The chloroform solution was filtered and then the filtrate was re-evaporated to dryness. After methanol (20 mL) had been added to the resulting residue, the mixture was allowed to stand overnight. The white solid formed was filtered, washed with methanol and dried in air. Yield: >60%. Mass (*m/z*): 519 (M^+). Found: C, 73.94; H, 9.74; N, 16.30. Calc. for $C_{32}H_{50}N_6$: C, 74.09; H, 9.71; N, 16.20%. IR: 3260 (νN–H), 1600 (νC=N), and 1580 cm^{-1} (νC=C). ^{13}C-NMR ($CDCl_3$): 20.5 (Me), 22.0, 25.5, 26.5, 31.2, 33.8, 46.6, 50.5, 53.8, 55.9, 61.1, 121.9 (Py), 136.5 (Py), 136.8 (Py), 148.6 (Py), and 162.8 (Py) ppm.

1.2.2. $[NiL^2](ClO_4)_2$. A methanol suspension (30 cm^3) of $Ni(OAc)_2\cdot4H_2O$ (2.0 g, 8 mmol) and L^2 (2.0 g, 5 mmol) was heated to reflux for 30 min and then cooled at room temperature. After adding an excess of $HClO_4$, the mixture was stored in a refrigerator until the purple precipitates formed. The product was filtered and recrystallized from a hot water–acetonitrile (1:1) mixture. Yield: ~90%. Found: C, 49.34; H, 6.38; N, 10.75. Calc. for $C_{32}H_{50}N_6NiCl_2O_8$: C, 49.51; H, 6.49; N, 10.82%. IR: 3240 (νN–H), 1620 (νC=N), and 1580 cm^{-1} (νC=C). Magnetic moment (μ_{eff}): 2.88 μB.

1.2.3. $[CuL^2](ClO_4)_2$. The blue–purple complex was prepared by a method similar to that for the nickel(II) complex $[NiL^2](ClO_4)_2$, except that $Cu(OAc)_2.H_2O$ (2.0 g, 8 mmol) was reacted instead of $Ni(OAc)_2\cdot4H_2O$. Yield: ~90%. Found: C, 48.96; H, 6.42; N, 10.69. $C_{32}H_{50}N_6CuCl_2O_8$: C, 49.20; H, 6.45; N, 10.76%. IR: 3240 (νN–H), 1620 (νC=N), and 1580 cm^{-1} (νC=C).

1.3. *Crystallographic analysis of* $[CuL^2](ClO_4)_2$

A well-shaped crystal was mounted in a thin-walled glass capillary on an Enraf–Nonius CAD-4 diffractometer with graphite-monochromated Mo–Kα radiation ($\lambda=0.71073$ Å) at room temperature. Unit cell parameters were obtained by least-squares analysis of 25 well centered reflections ($10<\theta<13$). Reflection data were collected using $\omega/2\theta$ scan mode in θ range of 1.92–24.98 and monitored every 1 h using two standard reflections ($h, k, l = -4, 6, 0; 3, 7, -3$). The data were corrected for Lorentz-polarization effects and decay (less than 0.03% variation). Empirical absorption correction with 3ψ scans was carried out in the correction range of 0.80–1.00. The structure in C2/c was determined with Patterson method as well as difference Fourier techniques and refined on F^2 by using a full-matrix least-squares method with SHELXS-97 and SHELXL-97 [16]. All non-hydrogen atoms were refined by using anisotropic thermal factors and all hydrogen atoms were located geometrically by means of a riding model with 1.2 times isotropic thermal factors of the attached non-hydrogen atoms. Oxygen atoms on one of two ClO_4 anions were refined with half occupancies due to the disorder. The final cycle of the refinement gave the error indices, $R=0.040$ and $R_w=0.095$. The mean value of shift/esd. is 0.01 and the remaining largest peak is 0.39 e/Å^3 at 0.89 Å from Cl atom. Crystal data, details of the data

collection and refinement of the structure are listed in Table 1.

2. RESULTS AND DISCUSSION

2.1. *Synthesis*

The di-N-functionalized macrocycle L^2, in which two 2-pyridylmethyl groups are attached to the less sterically hindered nitrogen atoms, can be readily prepared by the direct reaction (*see* Experimental) of L^1 with an excess of 2-(chloromethyl)pyridine in the presence of KOH. It has been reported that the reaction of L^4 with 2-(chloromethyl)pyridine in a 1:4 molar ratio produces the fully N-pyridylmethylated macrocycle L^5 in high yield [7]. However, all efforts to introduce the pyridylmethyl groups into the secondary nitrogen atoms of L^2 were unsuccessful in the similar experimental conditions; the only compound isolated was the di-N-substituted macrocycle L^2 even after prolonged (6 days) heating of the mixture of L^1 or L^2 and 2-(chloromethyl)pyridine in a 1:8 molar ratio. It has also been reported that the reaction of L^1 with an excess of 2-bromoethanol produces only the di-N-substituted macrocycle L^3 as a main product [9]. However, the present result is different from the reported result that all secondary amino groups of L^1 are readily alkylated by the reaction of the macrocycle with an excess amount of bromoethane or 1-bromopropane [17]. No further substitution of the secondary amino groups of L^2 or L^3 may be attributed to the interactions between the amino groups and the pyridyl or hydroxyl groups, such as hydrogen bonding, which prevent the reaction, in addition to the steric hindrance caused by the C-substituents.

The new macrocycle L^2 readily dissolves in chloroform but slightly dissolves in methanol at room temperature. The mass spectrum of L^2 gives a m/z of 518, which is in accordance with the molecular weight of the macrocycle containing two 2-pyridylmethyl pendant arms. In the infrared spectrum of the macrocycle, νC=N and νC=C of the pendant pyridylmethyl groups are observed at *ca.* 1640 and 1580 cm^{-1}. One peak at 3260 cm^{-1}, corresponding to νN–H of the secondary amino groups, was also observed. The ^{13}C NMR spectrum of L^2 shows 16 peaks (see Section 1, Experimental), indicating that the macrocycle is a single isomer with a symmetrical arrangement of the carbon atoms. The above spectral data, together with the elemental analyses, are consistent with the structure of L^2; the structure was confirmed by the crystal structure of its copper(II) complex (see below).

The octahedral complexes, $[NiL^2](ClO_4)_2$ and $[CuL^2](ClO_4)_2$, in which two 2-pyridylmethyl groups are coordinated to the metal ion, are prepared by the reaction of each metal ion with L^2, followed by addition of an excess amount of perchloric acid or sodium perchlorate.

Table 1. Crystal data and structure refinement for $[CuL^2](ClO_4)_2$

Empirical formula	$C_{32}H_{50}N_6CuCl_2O_8$
Formula weight	781.22
Crystal system, space group	Monoclic. C2/c (No. 15)
a (Å)	14.002(4)
b (Å)	16.653(3)
c (Å)	15.096(3)
β, deg	100.0(2)
V (Å^3)	3467(2)
Z	4
D_{calc} (g/cm^3)	1.497
μ (cm^{-1})	8.44
$F(000)$	1644
Crystal size	0.45 × 0.40 × 0.40 mm
T (°C)	20(2)
λ (Å)	0.71073
θ range (deg)	1.92 to 24.98
Reflections collected[a]	6584
Refinement method	Full-matrix least-squares on F^2
Data/restraints/parameters	2175/0/247
Goodness-of-fit on F^2	1.071
Final R indices [$I>2\sigma(I)$][b]	$R=0.0398$, $R_w=0.0954$
R indices (all data)[b]	$R=0.0433$, $R_w=0.0962$
Largest diff. peak and hole (e/Å^3)	0.389 and −0.354

[a] Number 6584 includes lattice C-centering absences.

[b] $R=\Sigma||F_o|-|F_c||/\Sigma|F_o|$. $R_w=[\Sigma w(F_o^2-F_c^2)^2/\Sigma w(F_o^2)^2]^{1/2}$, where $w=1/[\sigma^2(F_o^2)+0.0431P]^2+8.11P]$; $P=[\max(F_o^2,0)+2F_c^2]/3$.

2.2. *Crystal structure of* $[CuL^2](ClO_4)_2$

The ORTEP drawing (Fig. 1) of the complex cation $[CuL^2]^{2+}$ shows that the two 2-pyridylmethyl groups are attached to the less sterically hindered nitrogen atoms of the macrocyclic ligand. The nitrogen atoms of the pendant pyridyl groups are coordinated to the metal ion and the ligand serves as a hexadentate ligand. The complex has a tetragonally distorted octahedral coordination geometry, with an inversion center at the copper(II) ion; the metal atom and the four nitrogen atoms (N(1), N(2), N(1)′, N(2)′) are exactly in a plane. The macrocyclic ligand adopts the *trans*-III sterochemistry.

Selected bond distances and angles of the complex are summarized in Table 2. The Cu–N(1) and Cu–N(2) bond distances are in the normal range for Cu–N (amine) distances of six-coordinate copper(II) complexes with 14-membered tetraaza macrocyclic ligands [18, 19]. As expected from the Jahn–Teller effect, the apical Cu–N(3) (pyridine) distance (2.565(3) Å) is *ca.* 0.5 Å longer than the Cu–N(1) and Cu–N(2) distances. Somewhat interestingly, the Cu–N(3) distance is longer than the apical Cu–O (carboxylate group) distances (2.20–2.35 Å) of $[CuL^9]$ or various related macrocyclic copper(II) complexes containing coordinated acetate groups [18, 19]. The long Cu–N(3) distance is due to the steric hindrance between the N(3) atom and the methyl group at the six-membered chelate ring; the N(3)—C(10)′ distance was found to be 3.400(6) Å, which is shorter than the summation of Van der Waals radii of the nitrogen atom (1.55 Å) and methyl group (2.00 Å) [20]. The N(3)–Cu–N(3)′ angle is 180°, indicating that the three atoms are in a line. The Cu–N(3) bond is not perpendicular to the NiN_4 (N(1), N(2), N(1)′, N(2)′) plane with N(1)–Cu–N(3) and N(2)–Cu–N(3) angles of 77.3(2) and 80.2(2), respectively. The angle of Cu–N(3)–C(12) (103.1(2)°) is much smaller than that of Cu–N(3)–C(16) (133.3(2)°). The distorted angles about the coordinated N(3) atom may be due to the rigid structure of the pendant pyridylmethyl group and/or to the steric hindrance of the methyl group and the pyridyl group.

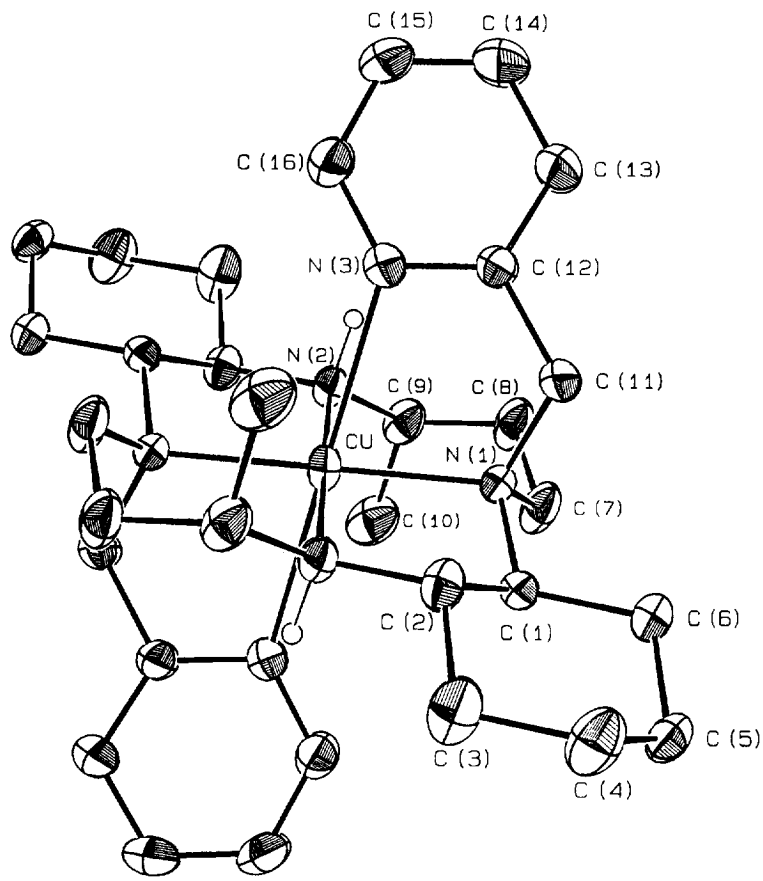

Fig. 1. Structure of $[CuL^2]^{2+}$ cation with atomic numbering scheme. Hydrogen atoms, except those attached to nitrogen atoms, are omitted for clarity.

Table 2. Selected bond distances (Å) and angles (deg) for $[CuL^2](ClO_4)_2$.[a]

Cu–N(1)	2.076(3)	Cu–N(2)	2.047(3)
Cu–N(3)	2.565(3)	N(1)–C(7)	1.494(5)
N(3)–C(12)	1.330(4)	C(12)–C(13)	1.373(5)
N(1)–Cu–N(2)	94.9(2)	N(1)–Cu–N(2)′	85.1(2)
N(1)–Cu–N(3)	77.3(2)	N(1)–Cu–N(3)′	102.7(2)
N(1)–Cu–N(1)′	180.0	N(3)–Cu–N(3)′	180.0
Cu–N(1)–C(1)	103.9(2)	Cu–N(1)–C(7)	110.4(2)
Cu–N(1)–C(11)	114.1(2)	Cu–N(2)–C(9)	119.8(2)
Cu–N(2)–C(2)′	110.3(2)	Cu–N(3)–C(12)	103.1(2)
Cu–N(3)–C(16)	133.3(2)	N(1)–C(11)–C(12)	117.6(3)

[a] Primed atom: $-x+1/2, -y+1/2, -Z$.

2.3. *Characterization of the nickel(II) and copper(II) complexes*

The complexes $[NiL^2](ClO_4)_2$ and $[CuL^2](ClO_4)_2$ are soluble in acetonitrile and nitromethane, but are nearly insoluble in water at room temperature. They are extremely stable in the solid state and in the solutions. The infrared spectra of the complexes are similar to that of the free ligand L^2, except that $\nu(ClO_4)$ of the counter anions is observed at *ca.* 1100 cm^{-1}. The molar conductance values of the complexes measured in acetonitrile (*ca.* 270 $\Omega^{-1}mol^{-1}cm^2$) and nitromethane (*ca.* 180 $\Omega^{-1}mol^{-1}cm^2$) indicate that the complexes are 1:2 electrolytes.

The magnetic moment (2.88 μ_B at 20° C) of $[NiL^2](ClO_4)_2$ in the solid state is consistent with a d^8 electronic configuration in octahedral geometry. Visible absorption spectra (Table 3) of the nickel(II) complex in various solvents show d–d bands at *ca.* 530 nm. The wavelength and molar absorption coefficient of the band are comparable with those reported for the octahedral complex $[NiL^3]^{2+}$, in which two oxygen atoms of the pendant arms are coordinated to the metal ion [9]. The visible spectra and the magnetic moment clearly show that the metal ion of the nickel(II) complex is in an octahedral environment; the nitrogen atoms of the pendant pyridyl groups are coordinated to the metal ion. The visible spectrum of $[CuL^2]^{2+}$ measured in nitromethane shows a d–d band at 554 nm ($\epsilon = 111\ M^{-1}cm^{-1}$). The spectra measured in coordinating solvents, such as acetonitrile, are quite similar to that measured in nitromethane, indicating that the solvent molecules are not involved in coordination in the solvents. The wavelength of the band for $[CuL^2]^{2+}$ is *ca.* 30 nm longer than those for the square-planar complex $[CuL^3]^{2+}$ in which the oxygen atoms of the hydroxyethyl groups are not involved in coordination [9]. This is attributed to the coordination of the pendant pyridyl groups to the metal ion.

Cyclic voltammetric data of the complexes of L^2 are listed in Table 4. The redox potentials for $[ML^2]^{2+}$ ($M=Ni^{2+}$ or Cu^{2+}) are more positive than those for $[ML^1]^{2+}$. This agrees with the widely observed trend that substitution of coordinated secondary amino groups by tertiary ones in a polyaza macrocyclic nickel(II) or copper(II) complex makes the oxidation more difficult and the reduction easier [9, 17, 21, 22]. As expected from the electronic spectra, the potentials for $[NiL^2]^{2+}$ are comparable with those for $[NiL^3]^{2+}$ in which the hydroxyl groups are coordinated to the

Table 3. Electronic spectral Data[a]

Complex	λ_{max}, nm ($\epsilon = M^{-1}cm^{-1}$)	
$[NiL^1]^{2+}$ *b*	463(73)	465(66)[c]
$[NiL^2]^{2+}$	530(6.0)	527(6.4)[c]
$[NiL^3]^{2+}$ *d*		520(6.8)[c]
$[CuL^1]^{2+}$ *b*	487(113)	508(150)[c]
$[CuL^2]^{2+}$	554(111)	553(109)[c]
$[CuL^3]^{2+}$ *d*	522(98)	523(98)[c]

[a] In nitromethane at 20° C unless otherwise specified.
[b] Ref.[15].
[c] In acetonitrile.
[d] Ref.[9].

Table 4. Cyclic voltammetric data for the nickel(II) and copper(II) complexes[a]

Complex	*E*/*V vs.* SCE	
	M(II)–M(III)	M(II)–M(I)
$[NiL^1]^{2+}$ *b*	+1.08	−1.28
$[NiL^2]^{2+}$	+1.15	−1.15(i)[c]
$[NiL^3]^{2+}$ *d*	+1.14	−1.13(i)
$[CuL^1]^{2+}$ *b*	+1.41	−0.92(i)
$[CuL^2]^{2+}$	+1.50(i)	−0.87(i)
$[CuL^3]^{2+}$ *d*	+1.68(i)	−0.73(i)

[a] Measured in 0.1 *M* $(n\text{-}Bu)_4NClO_4$ acetonitrile solution at 20° C.
[b] Ref.[15].
[c] i = irreversible.
[d] Ref.[9].

metal ion. However, in the case of the copper(II) complex $[CuL^2]^{2+}$, the redox potentials are distinctly less positive than those for $[CuL^3]^{2+}$. This is attributed to the coordination of the pyridyl groups; coordination of the pendant arms of a macrocyclic M(II) complex makes the oxidation to M(III) state easier and the reduction to M(I) more difficult [9, 13, 22]. The above results, together with the crystal structure, clearly show that the pendant pyridyl groups of $[CuL^2]^{2+}$ are coordinated to the metal.

2.4. *Kinetic and solution behaviors*

In order to investigate the effects of the pyridylmethyl groups of L^2 on the complex formation reaction, pseudo-first order rate constants (k) for the reaction of Cu^{2+} with L^1 and L^2 were determined in sodium acetate buffer solutions (pH 5.7) at 25 °C. The approximate k value for L^2 was found to be $1.6 \times 10^{-3}\,sec^{-1}$, which is lower than that for L^1 (*ca.* $1.7 \times 10^{-1}\,sec^{-1}$) under the same conditions, indicating that the introduction of 2-pyridylmethyl groups into L^1 to give L^2 reduces the rate. We could observe that the present result is similar to those reported for L^3 [9] and L^9 [19], in which two functional pendant arms are attached to diagonally related nitrogen atoms (not neighboring nitrogen atoms); the complexation reaction is retarded by the presence of the functional groups. However, this trend contradicts those reported for L^7 and L^8, in which two hydroxyethyl groups are attached to adjacent nitrogen atoms; in the cases of L^7 and L^8, the pendant hydroxyl groups enhance the rate of metal ion entry into the macrocycle by binding the metal ion outside the ring [10]. The present results and the above discussion strongly support the belief that the roles of functional pendant arms of a macrocyclic compound are strongly affected by the position of the pendant arms [10, 14]. It is likely that the diagonally substituted pyridylmethyl groups of L^2 cannot effectively bind the metal ion outside the macrocyclic ring and is insufficient to cause rate enhancement; the promoting effect of the functional pendant arms may be more than counterbalanced by their steric effect.

The complexes $[NiL^2](ClO_4)_2$ and $[CuL^2](ClO_4)_2$ are decomposed very slowly even in concentrated acid solutions, in analogy with the complexes of L^1 and L^3 [9, 15]. Visible spectra of the complexes ($1.0 \times 10^{-3}\,M$) in 0.5 M $HClO_4$ acetonitrile–water (1:1) indicated that only less than 3% of the complexes are decomposed in 20 h at 25 °C. The visible spectra of $[NiL^2]^{2+}$ measured in 0.1–3.0 M HCl CH_3CN–H_2O (1:1) solutions were found to be essentially the same as those observed in neutral and 0.1–2.0 M NaOH solutions. This result indicates that, somewhat unexpectedly, the pyridyl groups of the nickel(II) complex are not protonated even in concentrated acid solutions and that the hydroxide ion is not involved in coordination even in 2.0 M NaOH solution. In the case of the copper(II) complex $[CuL^2]^{2+}$, the spectra measured in 0.1–2.0 M NaOH solutions were quite similar to that in pure solvent. The spectrum of $[CuL^2]^{2+}$ measured in 0.1 M $HClO_4$ solution is also essentially the same as that obtained in pure solvent. However, further addition of the acid to the resulting solution increases the absorption at *ca.* 550 nm (Fig. 2), in contrast to the

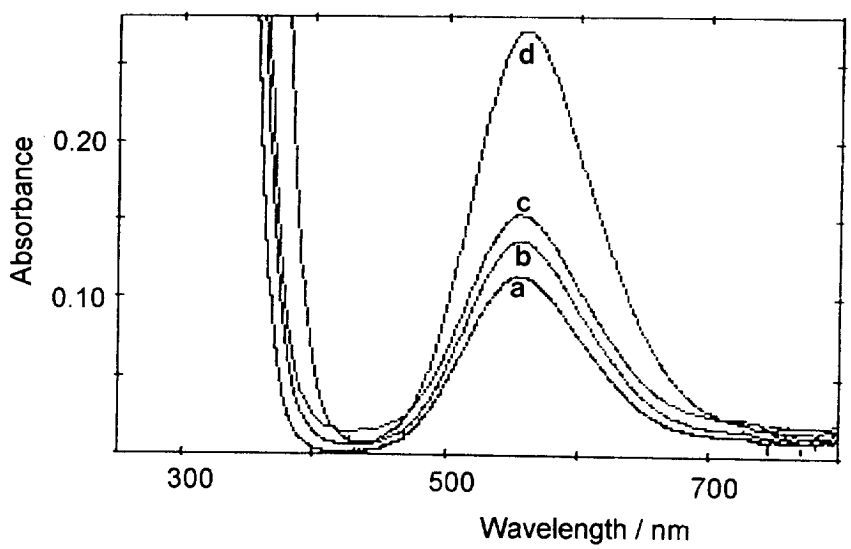

Fig. 2. Visible absorption spectra of $[CuL^2](ClO_4)_2$ ($1.0 \times 10^{-3}\,M$) in $HClO_4$ acetonitrile–water solution.$[HClO_4] = 0.0$ (a), 0.5 (b), 1.0 (c), and 2.0 M (d). The spectrum measured in 0.1 M $HClO_4$ solution is overlapped with curve (a). No apparent spectral change was observed in 2.0–4.0 M $HClO_4$ solutions.

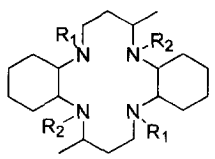

L^1: $R_1 = R_2 = H$
L^2: $R_1 = X$; $R_2 = H$
L^3: $R_1 = (CH_2)_2OH$; $R_2 = H$

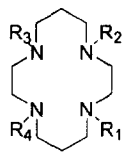

L^4: $R_1 = R_2 = R_3 = R_4 = H$
L^5: $R_1 = R_2 = R_3 = R_4 = X$
L^6: $R_1 = R_2 = R_3 = R_4 = (CH_2)_2OH$
L^7: $R_1 = R_2 = (CH_2)_2OH$; $R_3 = R_4 = Me$
L^8: $R_1 = R_4 = (CH_2)_2OH$; $R_2 = R_3 = Me$

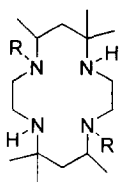

HL^9: $R = CH_2COOH$

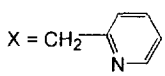

Scheme 1.

corresponding nickel(II) complex; the molar absorption coefficient ($270\ M^{-1}cm^{-1}$) of the band measured in 2.0 *M* $HClO_4$ is more than twice that in pure solvent. Such a marked spectral change indicates that the addition of the acid changes the coordination geometry and/or the degree of the solvation of the copper(II) complex. It is likely that, in the presence of the acid (>0.1 *M*), the pyridyl groups of the copper(II) complex are protonated and removed from the coordination sphere and then solvent molecules are coordinated to the metal ion. The easy protonation of $[CuL^2]^{2+}$, compared to that of $[NiL^2]^{2+}$, can be attributed to the weaker apical Cu–N interactions caused by the Jahn–Teller distortion.

3. CONCLUSION

The di-N-functionalized macrocycle L^2 is prepared in high yield by the direct reaction of L^1 and an excess of (2-chloromethyl)pyridine. The macrocycle L^2 reacts with nickel(II) and copper(II) ions to form stable octahedral complexes $[NiL^2]^{2+}$ and $[CuL^2]^{2+}$, respectively, in which the pyridyl groups are axially coordinated to the metal ions. The pyridyl groups of $[CuL^2]^{2+}$ are protonated in concentrated $HClO_4$ solutions, whereas those of $[NiL^2]^{2+}$ are not, even in 3.0 *M* $HClO_4$ solution. This work strongly suggests that two functional groups, attached to diagonally related nitrogen atoms of a 14-membered tetraaza macrocyclic ligand, reduce the formation of the copper(II) complex, in contrast to those attached to neighboring nitrogen atoms.

Acknowledgements—This work was supported by the Basic Science Research Institute Program (97-3403), the Ministry of Education of the Republic of Korea.

REFERENCES

1. Cooper, S. R., *Crown Compounds: Toward Future Applications*, VCH Publishers, Inc., New York, USA, 1992; Lindoy, L. F., *The Chemistry of Macrocyclic Ligands Complexes*, Cambridge University Press, Cambridge, U.K., 1989 and refs therein.
2. Costa, J., Delgado, R., Figueira, M. do C., Henriques, R. T., and Teixeira, M., *J. Chem. Soc., Dalton trans.*, 1997, **65**, and refs therein.
3. Hay, R. W., Hassan, M. M., *Polyhedron*, 1997, **16**, 2205; Turonek, M. L., Duckworth, P. A., Laurence, G. S., Lincoln, S. F. and Wainwright, K. P., *Inorg. Chim. Acta*, 1995, **230**, 51; Davies, P. J., Taylor, M. R., Wainwright, K. P., Harriott, P. and Duckworth, P. A., *Inorg. Chim. Acta*, 1996, **246**, 1; Iitata, Y., Koike, T. and Kimura, E., *Inorg. Chem.*, 1986, **25**, 402; Pallavicini, P. S., Perotti, I., Poggi, A., Seghi, B. and Fabbrizzi, L., *J. Am. Chem. Soc.*, **109**, 1987, 5139.
4. Josceanu, A. M., Moore, P., Rawle, S. C., Sheldon, P., Smith, S.M., *Inorg. Chim. Acta*, 1995, **240**, 159 and refs therein; Murase, I., Ueda, I., Marubayashi, N., Kida, S., Matsumoto, N., Kudo, M., Toyohara, M. and Hiate, K., *J. Chem. Soc., Dalton Trans.*, 1990, 2763; Bu, X. H., Zhang, Z. H., An, D. L., Chen, Y. T., Shionoya, M. and Kimura, E., *Inorg. Chim. Acta.*, **249**, 996, 25.
5. Kimura, E., Wada, S., Shionoya, M., Okazaki, Y., *Inorg. Chem.*, 1994, **33**, 770; Barefield, E. K., Foster, K. A., Freeman, G. M. and Hodges, K. D., *Inorg. Chem.*, **25**, 1986, 4663.
6. Hay, R. W., Pujari, M. P., Moodie, W. T., Craig, S., Richens, D. T., Perotti, A., Ungaretti, L., *J. Chem. Soc., Dalton Trans.*, 1987, 2605; Madeyski, C. M., Michael, J. P. and Hancock, R. D., *Inorg. Chem.*, 1984, **23**, 1487; Dey, B., Coates, J. H., Duckworth, P. A., Lincoln, S. P. and Wainwright, K. P., *Inorg. Chim. Acta*, **214**, 1993, 77.
7. Alcock, N. W., Balakrishnan, K. P. and Moore, P., *J. Chem. Soc., Dalton Trans.*, 1986, 1743.
8. *Asato, E., Hashimoto, S., Matsumoto, N., Kida, S., J. Chem. Soc., Dalton Trans.*, 1990, 1741; Vuckovic, G., Asto, E., Matsumoto, N. and Kida, S., *Inorg. Chim. Acta*, **171**, 1990, 45.
9. Kang, S.-G., Kim, M.-S., Choi, J.-S. and Whang, D., Kim, K., *J. Chem. Soc., Dalton Trans.*, 1995, 363.
10. *Boeyens, J. C. A., Cook, L., Duckworth, P. A., Rahardjo, S. B., Taylor, M. R. and Wainwright, K. P., Inorg. Chim. Acta*, 1996, **246**, 321.
11. Alcock, N. W., Clarke, A. J., Errington, W., Josceanu, A. M., Moore, P., Rawle, S. C., Sheldon, P., Smith, S. M. and Turonek, M. L., *Supramol. Chem.*, 1996, **6**, 281; Grant, S. J., Moore, P., Omar, H. A. A. and Alcock, N. W., *J. Chem. Soc., Dalton Trans.*, 1994, 485; Balakrishnan, K. P., Omar, H. A. A., Moore, P., Alcock, N. W. and Pike, G. A., *J. Chem. Soc., Dalton Trans*, 1990, 2965; Tamburini, S., Vigato, P. A., Casellato, U. and Graziani, R., *J. Chem. Soc., Dalton*

Trans, 1989, 1993; Fabbrizzi, L., Pallavicini, P., Parodi, L., Perotti, A. and Taglietti, A., *J. Chem. Soc., Chem. Commun.*, 1995, 2439.
12. Kimura, E., Kotake, Y., Koike, T., Shionoya, M. and Shiro, M., *Inorg. Chem.*, 1990, **29,** 4991.
13. Kang, S.-G., Kim, M.-S. and Kim, S.-J., Ryu, K., *Polyhedron*, 1996, **15,** 1835.
14. Rahardjo, S. B. and Wainwright, K. P., *Inorg. Chim. Acta*, 1997, **255,** 29.
15. Kang, S.-G., Kweon, J. K. and Jung, S.-K., *Bull. Korean Chem. Soc.*, 1991, **12,** 483.
16. Sheldrick, G. M., *Program for the solution of crystal structures*, Univ. of Göttingen, Germany, 1997; Sheldrick, G. M., *Program for crystal structure refinements*, Univ. of Göttingen, Germany, 1997.
17. Kang, S.-G., Kim, M.-S., Choi, J. S. and Cho, M. H., *Polyhedron*, 1995, **14,** 781.
18. Chapman, J., Ferguson. G., Gallagher, J. F., Jennings, M. C. and Parker, D., *J. Chem. Soc., Dalton Trans.*, 1992, 345; Chen, L., Thompson, L. K., Bridson, J. N., Xu, J., Ni, S. and Guo, R., *Can. J. Chem.*, **71**, 1993, 1805.
19. Belsky, V. L., Streltsova, N. R., Kuzmina, E. N. and Nazarenko, A. Y., *Polyhedron*, 1993, **12,** 831.
20. Huheey, J. E., Keiter, E. A. and Keiter, R. L., *Inorganic Chemistry: Principles of Structure and Reactivity*, Harper Collins College Publishers, New York, USA, 1993, p. 292.
21. Barefield, E. K., Freeman, G. M., Derveer, D. G. V., *Inorg. Chem.*, 1986; *J. Chem. Soc., Dalton Trans.*, 552; Kang, S.-G. and Kweon, J. K., *Bull. Korean Chem. Soc.*, 1992, **13**, 256.
22. Pallavicini, P. S., Perotti, A., Poggi, A., Seghi, B. and Fabbrizzi, L., *J. Am. Chem. Soc.*, 1987, **109,** 5139.

Pergamon

PII: S0277-5387(98)00228-9

Polyhedron Vol. 17, No. 18, pp. 3235–3241, 1998
© 1998 Elsevier Science Ltd
All rights reserved. Printed in Great Britain
0277-5387/98 $19.00+0.00

The reaction of $P_3N_3Cl_5NH_2$ with $SOCl_2$: the crystal structures of $P_3N_3Cl_5NSO$ and $Cl_5N_3P_3OP_3N_3Cl_5$

Josef Břínek, Milan Alberti, Jaromír Marek, Zdirad Žák and Jiří Toužín†

Department of Inorganic Chemistry, Masaryk University, 611 37 Brno, Czech Republic

Received 3 April 1998; accepted 2 June 1998

Abstract—Depending on reaction conditions, the reaction of $P_3N_3Cl_5NH_2$ with $SOCl_2$ gives four compounds: $P_3N_3Cl_5NSO$, $P_3N_3Cl_5NSNP_3N_3Cl_5$, $P_3N_3Cl_5NSCl_2$ and $P_3N_3Cl_5OP_3N_3Cl_5$. The reaction course and the composition of the reaction mixture can be easily monitored by ^{31}P NMR spectroscopy. $P_3N_3Cl_5NSO$ and $P_3N_3Cl_5OP_3N_3Cl_5$ were isolated in the form of single crystals and their structures have been determined by X-ray structure analysis. The vibrational spectra of $P_3N_3Cl_5NSO$, $P_3N_3Cl_5NSNP_3N_3Cl_5$ and $P_3N_3Cl_5NSCl_2$ are also briefly discussed. © 1998 Elsevier Science Ltd. All rights reserved

Keywords: Cyclotriphosphazene; thionylchloride; X-ray structural analysis; NMR spectra; vibrational spectra.

INTRODUCTION

The reactivity of NH_2- and NSO-group in partly substituted halogeno-*cyclo*-triphosphazenes was studied mainly on pentafluoroderivatives. $P_3N_3F_5NH_2$ reacts with $SOCl_2$ to give $P_3N_3F_5NSO$ (yield >80%) and $P_3N_3F_5NSNP_3N_3F_5$ (yield <5%). For the preparation of pure $P_3N_3F_5NSNP_3N_3F_5$ the thermal condensation of $P_3N_3F_5NSO$ in the presence of pyridine as an acceptor of SO_2 is recommended [1]. Reaction of $P_3N_3F_5NH_2$ with SF_4 yields $P_3N_3F_5NSF_2$ contaminated by small amounts of $P_3N_3F_5NSNP_3N_3F_5$ [1]. $P_3N_3F_5NPCl_3$ is available by the reaction of $P_3N_3F_5NH_2$ with PCl_5 [2].

$P_3N_3F_5NCO$ can be prepared either by the reaction of $P_3N_3F_5NH_2$ with $ClSO_2NCO$ [3] or $P_3N_3F_5NSO$ with $(COCl)_2$ [4]. $P_3N_3F_5NCS$ was obtained by the reaction of $P_3N_3F_5Cl$ with AgSCN. Under UV-light excitation it reacts with Cl_2 giving $P_3N_3F_5NCCl_2$ [3]. $P_3N_3F_5NCO$ or $P_3N_3F_5NCS$ reacts with dimethylamine yielding N-substituted derivative of urea or thiourea $P_3N_3F_5NHCON(CH_3)_2$ and $P_3N_3F_5NHCSN(CH_3)_2$, respectively [3]. Substituted amides $P_3N_3F_5NHCOR$ were obtained by the reaction of $P_3N_3F_5NSO$ with carbonic acids [4]. Reactions of $P_3N_3F_5NH_2$ with $(COCl)_2$ [5] and BCl_3 [6] lead to $(P_3N_3F_5NHCO)_2$ and $(P_3N_3F_5NH)_3B$, respectively. $P_3N_3F_5NSCl_2$ in high yield and purity arises from the reaction of $P_3N_3F_5NSO$ and PCl_5 [1]. However, the formation of -$NPCl_3$ derivative, which was observed in the reaction of C_6H_5NSO with PCl_5 [7], was not detected.

Surprisingly, from all possible reactions of $P_3N_3Cl_5NH_2$ with halides of non-metals only that with PCl_5 leading to $P_3N_3Cl_5(NPCl_3)$ was studied [8]. This contribution comprises the results of our study of the reaction of monoaminopentachloro-*cyclo*-triphosphazene, $P_3N_3Cl_5NH_2$ (**1**), with $SOCl_2$ which yields, besides expected $P_3N_3Cl_5NSO$ (**2**) and $P_3N_3Cl_5NSNP_3N_3Cl_5$ (**3**), two other compounds $P_3N_3Cl_5NSCl_2$ (**4**) and $P_3N_3Cl_5OP_3N_3Cl_5$ (**5**).

EXPERIMENTAL

All manipulations were carried out by using standard Schlenk techniques under dry air atmosphere. The solvents were purified and dried by common methods. $P_3N_3Cl_5NH_2$ was prepared by reaction of $P_3N_3Cl_4(NH_2)_2$ with gaseous HCl in acetonitrile [9]. $P_3N_3Cl_4(NH_2)_2$ was prepared according to the method [10] modified in [11]. $SOCl_2$ was received from Aldrich and purified by distillation before use. For reactions

†Author to whom correspondence should be addressed.

the fraction with the boiling point 76 C was used. IR spectra were measured with Bruker IFS 28 spectrometer in nujol mulls between KBr or AgCl discs. Raman spectra were recorded at Spex Ramalog 3 spectrometer. The samples were measured in sealed glass capillary tubes, the spectra were excited by the 488 nm line of a Spectra Physics Model 165-03 argon laser (100–200 mW). Emission lines of the Ar^+ plasma were employed for the spectral calibration. MS spectra were obtained on HP 5970 MSD spectrometer (70 eV, EI) connected with gas chromatograph GC 5890 HP. ^{31}P NMR spectra were recorded in thionylchloride solution on a Bruker 500 DRX spectrometer at 202.5 MHz with respect to 85% H_3PO_4 as an external standard for ^{31}P measurement and without solvent at 50.7 MHz with respect to liquid NH_3 as an external standard for ^{15}N measurement of liquid (**3**). The samples were sealed in Simax tubes and inserted in original Wilmad tubes (diameter 5 mm) filled with D_2O as an external lock.

X-ray structure analysis[1]

The intensity data were collected on a KUMA KM4 four-circle κ-axis diffractometer [12] equipped with a modified Nonius low-temperature device with ω–2ϑ scan ($2\vartheta_{max} = 50^\circ$) and a variable scan speed using graphite-monochromatized MoK_α ($\lambda = 0.70930$ Å) radiation. The stability of the crystal was checked by remeasuring of three reference reflections after every 60 measurements, no significant decrease in their intensities was observed. An empirical absorption correction based on psi-scan was applied for (**2**) during the data reduction process. Because the shape of crystals of (**5**) can be described as thin plate, empirical absorption correction (DIFABS [13]) was applied. T_{max} and T_{min} are 1.000 and 0.473 and 1.000 and 0.276 for (**2**) and (**5**), respectively. The structures were solved by direct methods and refined anisotropically by a full-matrix least-squares procedure on F^2. Details of the data collection and structure refinement both structures are presented in the Table 1. The lists of the structure factors can be obtained upon request from the authors Z. Ž (**2**) or J. M. (**5**). The structures were solved by SHELXS-86 [14] and refined by SHELXL-93 [15].

Preparation of $P_3N_3Cl_5NSO$ (2)

1.0 g (3.0 mmol) of $P_3N_3Cl_5NH_2$ was dissolved in 10 ml of $SOCl_2$ at laboratory temperature and the reaction mixture was heated under reflux for 3.5 h at atmospheric pressure. After the reaction mixture was cooled to laboratory temperature and the excess of thionylchloride was removed *in vacuo*, a white crystalline compound was obtained.

Yield: 1.1 g (2.94 mmol) 96.4%. M.p.: 71.5°C (in sealed capillary). MS: $m/z = 374$ ($P_3N_3Cl_5NSO^+$, 65.8%), 339 ($P_3N_3Cl_4NSO^+$, 100%), 337 ($P_3N_3Cl_4NSO^+$, 65.8%), 326 ($P_3N_3Cl_5N^+$, 7.9%), 312 ($P_3N_3Cl^+_5$, 60.5%), 258 ($P_3N_3Cl_3O^+$, 15.8%), 242 ($P_3N_3Cl^+_3$, 13.2%). RA: 215 s, 227 m, 237 sh, 266 vw, 293 vw, 339 sh, 345 s, 373 vs, 404 vs, 420 sh, 520 bvw, 579 w, 659 m, 687 w, 764 w, 787 w, 872 vw, 970 vw, 1146 s, 1165 bvw, 1264 w. IR: 542 sh, 528 m, 585 w, 602 m, 649 w, 687 vw, 865 vw, 875 sh, 975 vw, 1148 sh, 1160 m, 1207 vs, 1216 sh, 1272 m, 1342 w.

Preparation of $P_3N_3Cl_5NSNCl_5N_3P_3$ (3)

(a) 1.0 g (3.0 mmol) of $P_3N_3Cl_5NH_2$ was dissolved in 10 ml of $SOCl_2$ at laboratory temperature and was heated in a sealed Schlenk tube at 120°C for 24 h. The reaction mixture was then cooled to laboratory temperature and an excess of $SOCl_2$ and released gases were removed *in vacuo* and a yellow clear oil was obtained. Yield: 0.93 g (1.36 mmol); 89%.

(b) 1.0 g (2.67 mmol) of $P_3N_3Cl_5NSO$ was dissolved in 15 ml of dichloromethane and 0.56 g (2.67 mmol) of PCl_5 was added. The reaction mixture was shaken at laboratory temperature until complete dissolution of PCl_5. After removal of the solvent and volatile reaction products ($POCl_3$ and $SOCl_2$), a yellow clear oil was obtained.

Yield: 0.87 g (1.45 mmol); 94.8%. Analysis: $P_3N_3Cl_5NSNCl_5N_3P_3$ (684.490): P 26.17 (calc. 27.15), S 5.60 (4.68), C 51.30 (51.80)%. RA: 128 s, 150 vs, 169 vs, 197 vs, 205 sh, 221 s, 254 w, 300 vw, 313 sh, 321 w, 337 w, 355 sh, 369 s, 385 m, 415 s, 433 m, 465 sh, 497 vw, 526 vw, 569 bvw, 603 vw, 657 w, 697 w, 748 sh, 756 vw, 797 w, 812 vw, 822 vw, 1139vw, 1170 w, 1202 vw, 1271 bvw. IR: 417 w, 436 w, 472 vw, 528 vs, 539 sh, 563 s, 592 vs, 598 vs, 651 s, 692 w, 741 bvw, 794 vw, 878 w, 973 bvw, 1179 vs, 1263 s, 1342 sh.

Preparation of $P_3N_3Cl_5NSCl_2$ (4)

1.0 g (2.67 mmol) of $P_3N_3Cl_5NSO$ was dissolved in 15 ml of dichloromethane and 0.6 g (2.88 mmol) of PCl_5 was added. The reaction mixture was shaken at laboratory temperature until complete dissolution of PCl_5. By removing the solvent and evasive reaction products ($POCl_3$ a $SOCl_2$) a yellow oil was obtained from which microcrystalline product precipitated within 48 h at laboratory temperature. The crude product was washed twice with pentane and dried *in vacuo* yielding white microcrystals.

Yield: 0.11 g (0.26 mmol); 9.6%. M.p.: 154.5–155°C (in sealed capillary). MS: $m/z = 429$ ($P_3N_3Cl_5NSCl^+_2$, 36.4%), 393 ($P_3N_3Cl_5NSCl^+$, 72.7%), 358 ($P_3N_3Cl_5NS^+$, 18.2%), 312 ($P_3N_3Cl^+_5$, 77.3%), 254

[1] Further details of the crystal structure determination can be ordered from Fachinformationzentrum Karlsruhe, 76344 Eggenstein-Leopoldshafen (e-mail: crysdata@fiz-karlsruhe.de) under the depository numbers CSD-408585 (**2**) and CSD-408584 (**5**).

Table 1. Crystal data and structure refinement for (**2**) and (**5**)

Empirical formula	$Cl_5N_4OP_3S$ (**2**)	$Cl_{10}N_6OP_6$ (**5**)
Formula weight	374.26	640.38
Temperature (K)	120(2)	148(2)
Wavelength (Å)	0.71073	0.71073
Crystal system	orthorhombic	monoclinic
Space group	Pnma	$P2_1/c$
Unit cell dimensions	$a = 16.935(7)$ Å, $b = 8.865(4)$ Å, $c = 7.829(3)$ Å, $\alpha = 90°$, $\beta = 90°$, $\gamma = 90°$	$a = 11.037(4)$ Å, $b = 9.044(3)$ Å, $c = 21.337(6)$ Å, $\alpha = 90°$, $\beta = 104.88(6)°$, $\gamma = 90°$
Volume (Å^3)	1175.4(8)	2058.4(12)
Z	4	4
Density (calculated) (Mg/m^3)	2.115	2.066
Absorption coefficient (mm^{-1})	1.791	1.825
$F(000)$	728	1240
Crystal size (mm)	$0.40 \times 0.30 \times 0.20$	$0.80 \times 0.40 \times 0.10$
ϑ range for data collection (°)	2.41 to 30.01	1.91 to 25.03
Index ranges	$0 \leqslant h \leqslant 23$, $-12 \leqslant k \leqslant 0$, $-11 \leqslant l \leqslant 11$	$-13 \leqslant h \leqslant 0$, $-1 \leqslant k \leqslant 9$, $-24 \leqslant l \leqslant 25$
Reflections collected	2182	3296
Independent reflection	Full-matrix least-squares on F^2	
Data/restraints/parameters	1815/0/73	3296/0/208
Goodness-of-fit on F^2	1.097	0.994
Final R indices [$I > 2\sigma(I)$]	$R_1 = 0.0681$, $wR_2 = 0.2005$	$R_1 = 0.0372$, $wR_2 = 0.0989$
R indices (all data)	$R_1 = 0.1110$, wR2 = 0.2257	$R_1 = 0.0487$, $wR_2 = 0.1066$
Weight scheme	$a = 0.1407$, $b = 1.1646$	$a = 0.06$, $b = 10.0$
Largest diff. peak and hole (e Å^{-3})	1.271 and −1.637	0.676 and −0.578

($P_3N_3Cl_3N^+$, 54.5%), 221 ($P_3N_3Cl_2N^+$, 40.9%), 203 ($P_3N_3Cl^+_2$, 100%), 176 ($P_2N_3Cl^+_2$, 31.8%). IR: 408 m, 416 m, 426 m, 493 m, 528 s, 570 s, 601 s, 626 sh, 655 m, 689 vw, 746 vw, 752 m, 784 sh, 810 w, 864 w, 875 w, 1137 s, 1170 s, 1220 vs. RA: 125 vs, 149 vs, 166 m, 187 s, 209 m, 251 w, 337 sh, 352 s, 371 w, 389 w, 407 w, 430 w, 494 w, 526 bvw, 569 vw, 605 vw, 663 w, 700 bvw, 747 vw, 785 w, 808 vw, 873 vw, 1127 w, 1169 vs, 1226 vw, 1237 sh.

RESULTS AND DISCUSSION

In analogy with $P_3N_3F_5NH_2$, (**1**) reacts with $SOCl_2$ yielding $P_3N_3Cl_5NSO$ (**2**). ^{31}P NMR spectroscopy showed that in boiling $SOCl_2$ at atmospheric pressure the conversion is quantitative in 3.5 h. Single crystals of (**2**) suitable for X-ray analysis can be obtained directly from the reaction mixture after partial removal of thionylchloride *in vacuo* at laboratory temperature.

If the reaction was performed in a sealed system at 80–120°C, compounds (**3**) and (**4**) were also detected by ^{31}P NMR spectroscopy. Heating of the reaction mixture to 120°C for 24 h leads practically to pure (**3**) formed probably by the condensation reaction of (**1**) with (**2**) and/or (**2**) with (**4**). The alternative way to preparation of (**3**) is the reaction of (**2**) with PCl_5 in dichlormethane which is finished at laboratory temperature in a few minutes. If an excess of PCl_5 is used, a small amount of (**4**) as an intermediate product of reaction can be detected and isolated. Thermal condensation, used for the preparation of $P_3F_5N_3P_3NSNP_3N_3F_5$ from liquid $P_3N_3F_5NSO$, is not applicable for solid (**2**) and has not been observed in its boiling dichlormethane solution yet.

Up to now, (**5**) was always detected as one of the products of controlled hydrolysis of $P_3N_3Cl_6$ [16, 17]. We isolated (**5**) during the attempts to separate (**4**) from the reaction mixture containing also (**1**), (**2**) and (**3**) after removal of $SOCl_2$ by extraction with pentane. Apparently, the formation of (**3**) is connected with condensation of (**1**) with (**2**) under the release of water, which can react further with some of the phosphazene derivatives presented in the reaction mixture to give (**5**). The formation of (**5**) is not possible in the reaction mixture containing $SOCl_2$, which gives SO_2 and HCl with water.

NMR spectroscopic data

^{31}P NMR data for compounds (**1**)–(**4**) together with the data for $P_3N_3Cl_4(NH_2)_2$ [8] and $P_3N_3Cl_4NH_2NCO$ [18] are presented in Table 2. Only ^{19}F NMR data are available for $P_3N_3F_5NSO$, $P_3N_3F_5NSCl_2$ and $P_3N_3F_5NSNP_3N_3F_5$. The ^{31}P NMR spectra of (**2**), (**3**) and (**4**) have always the character of simple AB_2 systems and consist of a doublet of the PCl_2 group in the range between 22.77 and 22.11 ppm and a triplet for PClX (X = NSO, $NSCl_2$ and $NSNP_3N_3Cl_5$) with

Table 2. ^{31}P NMR spectroscopic data for (**1**)–(**4**) and related compounds

Compound		^{31}P chem. shift (ppm)	$^{2}J(^{31}PN^{31}P)$ (Hz)
$P_3N_3Cl_5NH_2$ (**1**)	PCl_2	22.11 (d)	
	$PClNH_2$	20.23 (t)	49.62
$P_3N_3Cl_5NSO$ (**2**)	PCl_2	22.77 (d)	
	PClNSO	0.84 (t)	53.35
$P_3N_3Cl_5NSNP_3N_3Cl_5$ (**3**)	PCl_2	22.11 (d)	
	PClNSN	8.06 (t)	53.97
$P_3N_3Cl_5NSCl_2$ (**4**)	PCl_2	22.55 (d)	
	$PClNSCl_2$	7.08 (t)	51.48
$P_3N_3Cl_4(NH_2)_2$ [8]	PCl_2	18.3 (d)	
	$P(NH_2)_2$	9.03 (t)	48.45
$P_3N_3Cl_4NH_2NCO$ [18]	PCl_2	21.50 (d)	
	PNH_2NCO	−3.20 (t)	59.00

chemical shifts from 8.06 to 0.84 ppm and coupling constants slightly over 51 Hz. Substitution of the amino group of (**1**) by -NSO or -$NSCl_2$ group in (**2**) or (**3**) and -$NSNP_3N_3Cl_5$ fragment in (**4**) results in a down-field shift of substituted phosphorus atom. Similar dependence was already reported [18].

The molecular structure of (**3**) has been confirmed

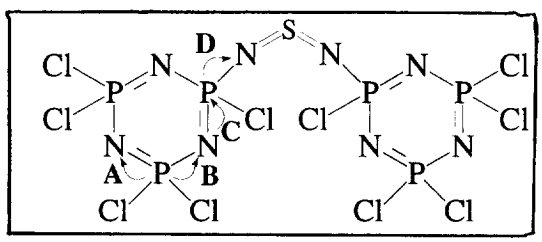

by 2D HETCOR ^{31}P–^{15}N NMR study. The obtained data suggests the presence of three NMR spectroscopic non-equivalent nitrogen atoms in the molecule, two of them making phosphazene cycle only. The ^{15}N NMR spectrum of (**3**) consists of a multiplet with chemical shift 112.0 ppm belonging to the $^{15}N_{endo}PClN_{exo}$ group, the multiplet at 123.0 ppm of $^{15}N(PCl_2)_2$ group and the multiplet at 185.5 ppm corresponding to the exocyclic ^{15}N atom. Observed ^{31}P–^{15}N coupling constants are $J(A) = 33$ Hz, $J(B) = 18$ Hz, $J(C) = 22$ Hz and $J(D) = 17$ Hz, respectively. Used experimental conditions are detailed in Ref. [19].

Available ^{31}P NMR data of (**5**) are summarized in Table 3. From the presence of the doublet for the PCl_2 group at 22.51 ppm and the triplet for the PClO group at 8.11 ppm a simple AB_2 spin system can be inferred from our ^{31}P NMR spectrum of (**5**). A simple character of this spectrum is in accordance with that reported in Ref. [16], although the published value of δ(PClO) seem to be somewhat high. On the other hand, the value of the chemical shift for the PClO group obtained in our study is in better agreement with results reported for (**5**) or similar P–O–P bridged phosphazene compounds (δ(PClO) in the range from 10 to −2.5 ppm) in Refs. [17, 20, 21]. However, second order spin systems were postulated in this papers. The relatively high value of J_{PNP} (58.93 Hz) suggests [21], in agreement with X-ray analysis, that (**5**) is a neutral molecule.

Vibrational spectra

The stretching vibrations of multiple bonds in -NSO, -$NSCl_2$ and -NSN-groups together with the antisymmetric stretching vibration of the phosphazene P_3N_3 cycle appear [1, 22–24] in the region 1100–1300 cm^{-1}. In Raman spectra the intensity of

Table 3. ^{31}P NMR spectroscopic data for (**5**)

Type	^{31}P chem. shift PCl_2 (ppm)	^{31}P chem. shift PClO (ppm)	$^{2}J(^{31}PN^{31}P)$ (Hz)	Refs.
AB_2	22.51 (d)	8.11 (t)	58.93	this work
AB_2	22.7 (d)	15.0 (t)	62.3	[16]
$AA'B_2B_2'$	21.8 (t)	2.9 (t), 2.3 (t)	not reported	[17]
	21.2 (t)	1.7 (t)		

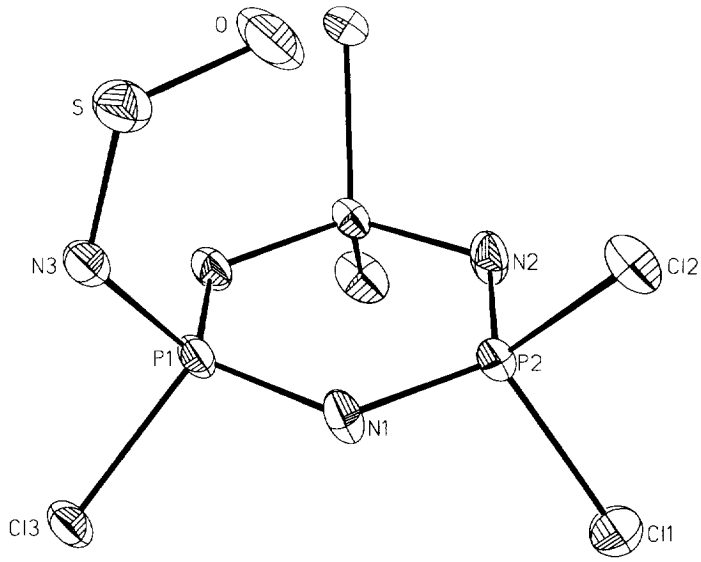

Fig. 1. View of the molecule of $P_3N_3Cl_5NSO$. The atoms are drawn as thermal ellipsoids at 50% probability level.

bands attached to ν (S=N) and ν (S=O) stretching vibrations are high, whereas in IR spectra these bands are weak. The ratio of intensities becomes reverse with bands of antisymmetric stretching vibrations of P_3N_3 cycle.

More bands than were expected for fundamental vibrations only were observed in the discussed region of all spectra. It can be explained for solid samples (**2**) and (**4**) as a consequence of crystal lattice arrangement. For example, in the Raman spectrum of (**4**) we observed the splitting of bands of ν N=S (1127 and 1169 cm^{-1}) and ν_{as} P_3N_3 (1226 and 1237 cm^{-1}), respectively. On the other hand, in the spectra of liquid sample (**3**) similar splitting was detected. Therefore the presence of bands of overtones or combination vibrations in the discussed region must be admitted [for example weak band at 1139 cm^{-1} in Raman spectrum of (**3**)].

Comparison of the vibrational spectra of (**1**)–(**4**) shows that stretching vibrations ν (P–N_{exo}) in (**2**) and (**4**) correspond to the bands with wavenumbers close to 870 cm^{-1}. In the case of (**3**) with two such bonds the corresponding pair of bands was observed at 794 and 878 cm^{-1}. In the Raman spectra of (**4**) the bands with wavenumbers 430 and 494 cm^{-1} can be assigned to the stretching vibrations ν_s and ν_{as} SCl_2, in agreement [1] with the results for $P_3N_3F_5NSCl_2$.

Description of the structures

The ORTEP [25] drawing of (**2**) is in Fig. 1 and bond lengths and angles are listed in Table 4. The

Table 4. Bond lengths (Å) and angles (°) for (**2**)

P(1)–N(1)	1.592(5)	P(2)–Cl(2)	1.990(2)
P(1)–N(3)	1.681(7)	P(2)–Cl(1)	2.000(2)
P(2)–N(2)	1.584(3)	P(1)–Cl(3)	1.990(2)
P(2)–N(1)	1.588(4)	N(3)–S	1.506(6)
		S–O	1.441(7)
N(1)–P(1)–N(1)#1	118.4(3)	N(1)–P(2)–Cl(2)	109.5(2)
N(1)–P(1)–N(3)	110.2(2)	N(2)–P(2)–Cl(1)	108.7(3)
P(2)–N(1)–P(1)	120.8(3)	N(1)–P(2)–Cl(1)	108.3(2)
N(1)–P(1)–Cl(3)	108.2(2)	Cl(2)–P(2)–Cl(1)	101.28(9)
N(3)–P(1)–Cl(3)	100.2(2)	P(2)–N(2)–P(2)#1	121.2(4)
N(2)–P(2)–N(1)	118.9(3)	S–N(3)–P(1)	126.9(4)
N(2)–P(2)–Cl(2)	108.7(3)	O–S–N(3)	117.9(4)

Symmetry transformations used to generate equivalent atoms: #1 x, $-y-(1/2)$, z.

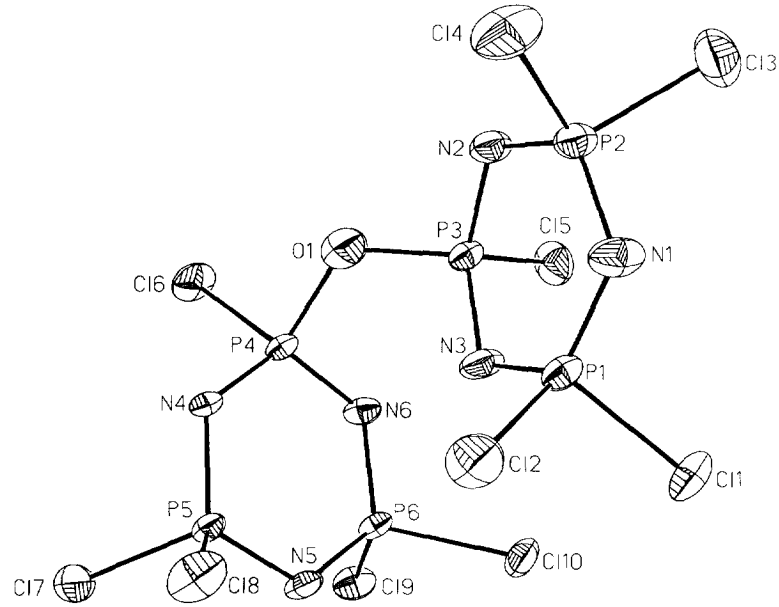

Fig. 2. View of the molecule of $P_3N_3Cl_5OP_3N_3Cl_5$. The atoms are drawn as thermal ellipsoids at 50% probability level.

Table 5. Bond lengths (Å) and angles (°) for (**5**)

Cl(1)–P(1)	1.983(2)	P(2)–N(2)	1.577(4)
Cl(2)–P(1)	1.985(2)	P(2)–N(1)	1.582(4)
Cl(3)–P(2)	1.990(2)	P(3)–N(2)	1.581(4)
Cl(4)–P(2)	1.987(2)	P(3)–N(3)	1.595(4)
Cl(5)–P(3)	2.007(2)	P(3)–O(1)	1.650(4)
Cl(6)–P(4)	1.992(2)	P(4)–N(6)	1.577(4)
Cl(7)–P(5)	1.988(2)	P(4)–N(4)	1.598(4)
Cl(8)–P(5)	1.979(2)	P(4)–O(1)	1.663(4)
Cl(9)–P(6)	1.995(2)	P(5)–N(5)	1.575(4)
Cl(10)–P(6)	1.981(2)	P(5)–N(4)	1.590(3)
P(1)–N(3)	1.568(4)	P(6)–N(6)	1.582(3)
P(1)–N(1)	1.591(4)	P(6)–N(5)	1.587(4)
N(3)–P(1)–N(1)	118.1(2)	N(6)–P(4)–Cl(6)	110.9(2)
N(3)–P(1)–Cl(1)	109.5(2)	N(4)–P(4)–Cl(6)	106.65(14)
N(1)–P(1)–Cl(1)	108.3(2)	O(1)–P(4)–Cl(6)	101.19(14)
N(3)–P(1)–Cl(2)	108.4(2)	N(5)–P(5)–N(4)	118.5(2)
N(1)–P(1)–Cl(2)	109.5(2)	N(5)–P(5)–Cl(8)	108.4(2)
Cl(1)–P(1)–Cl(2)	101.75(8)	N(4)–P(5)–Cl(8)	108.8(2)
N(2)–P(2)–N(1)	118.7(2)	N(5)–P(5)–Cl(7)	108.8(2)
N(2)–P(2)–Cl(4)	108.5(2)	N(4)–P(5)–Cl(7)	109.2(2)
N(1)–P(2)–Cl(4)	109.5(2)	Cl(8)–P(5)–Cl(7)	101.81(8)
N(2)–P(2)–Cl(3)	110.1(2)	N(6)–P(6)–N(5)	118.6(2)
N(1)–P(2)–Cl(3)	107.4(2)	N(6)–P(6)–Cl(10)	109.3(2)
Cl(4)–P(2)–Cl(3)	101.30(9)	N(5)–P(6)–Cl(10)	108.9(2)
N(2)–P(3)–N(3)	117.8(2)	N(6)–P(6)–Cl(9)	108.3(2)
N(2)–P(3)–O(1)	106.9(2)	N(5)–P(6)–Cl(9)	108.4(2)
N(3)–P(3)–O(1)	110.0(2)	Cl(10)–P(6)–Cl(9)	102.08(7)
N(2)–P(3)–Cl(5)	109.0(2)	P(3)–O(1)–P(4)	122.9(2)
N(3)–P(3)–Cl(5)	108.2(2)	P(2)–N(1)–P(1)	121.3(3)
O(1)–P(3)–Cl(5)	104.1(2)	P(2)–N(2)–P(3)	119.6(2)
N(6)–P(4)–N(4)	117.2(2)	P(1)–N(3)–P(3)	120.3(3)
N(6)–P(4)–O(1)	108.5(2)	P(5)–N(4)–P(4)	121.4(2)
N(4)–P(4)–O(1)	111.3(2)	P(5)–N(5)–P(6)	120.5(2)
P(4)–N(6)–P(6)	122.5(2)		

comparison of crystal data of (**1**) [9] and (**2**) shows that the substitution of -NH_2 by an -NSO group causes slight extension of the exocyclic P–N bond and contraction of endocyclic P–N bonds at the substituted phosphorus atom. A decrease in the value of the angle $N_{exo}PCl$ [100.2(2)° in (**2**) compared to 108.20(14)° in (**1**)] can be explained by the steric effect of the -NSO group. The six-membered ring P_3N_3 of (**2**) is deviated more significantly from planarity as in (**1**), the deviations of the P_1, N_1, P_2, N_2, P_{2A} and N_{1A} atoms from the least-squares plane fitted to P_3N_3 ring are −0.0695, 0.0113, 0.0114, −0.0390, 0.0113 and 0.0114 Å, respectively, which suggests a boat conformation of the P_3N_3 ring. The plane of the sulfinyl group is perpendicular to the plane formed by P and N atoms of the ring and thus the molecular symmetry of (**2**) is C_s. Bond lengths in the -NSO fragment of (**2**) agree very well with those found in organic -NSO derivatives [26–28] and their values [1.506(6) Å for S–N and 1.441(7) Å for S–O] suggest an important π-bond part (for single S–N and S–O bonds the lengths 1.76 and 1.69 Å were assigned [29]). The value of the angle [117.9(4)°] in the -NSO group of (**2**) is somewhat lower in comparison with those established in the compounds mentioned above.

Figure 2 shows the ORTEP [25] drawing of (**5**), bond lengths and angles are listed in Table 5. The crystal structure of the other crystal modification of (**5**) has already been published [17]. Both structures are monoclinic with the same space group ($P2_1/c$ and $P2_1/a$, respectively), but with different lattice parameters and Z: $a = 11.037$ Å, $b = 9.044$ Å, $c = 21.337$ Å, $\alpha = \gamma = 90°$, $\beta = 104.88°$, $Z = 4$ (our structure) and $a = 15.563$ Å, $b = 12.771$ Å, $c = 21.302$ Å, $\alpha = \gamma = 90°$, $\beta = 107.64°$, $Z = 8$ [17]. Comparison of both structures shows that values of bond lengths and angles in phosphazene rings are close. Significant differences were found for values of angles and bond lengths in the POP fragment when the POP angle [122.9(2)°] is smaller than those reported in Ref. [17] (128.8° and 135.6°). On the other hand, distances between bridged oxygen atom and adjacent phosphorus atoms are substantially longer, 1.663(4) and 1.650(4) Å, respectively (mean value reported in Ref. [17] is 1.594 Å).

Acknowledgements—The authors wish to express their gratitude to the Grant Agency of the Czech Republic for the grants No. 203/97/0955 and 203/98/0676.

REFERENCES

1. Niecke, E., Glemser, O. and Thamm, H., *Chem. Ber.*, 1970, **103,** 2864.
2. Roesky, H. W. and Niecke, E., *Inorg. Nucl. Chem. Lett.*, 1969, **4,** 463.
3. Roesky, H. W. and Janssen, E., *Z. Naturforsch.*, 1974, **29B,** 174.
4. Roesky, H. W. and Janssen, E., *Z. Naturforsch.*, 1971, **26B,** 679.
5. Thamm, H., Lin, T. P., Glemser, O. and Niecke, E., *Z. Naturforsch.*, 1972, **27B,** 1431.
6. Roesky, H. W., *Chem. Ber.*, 1972, **105,** 1726.
7. Halasz, S. P., Dissertation, University Göttingen, 1969 (cited from *Chem. Ber.*, 1970, **103,** 2864).
8. Feistel, G. R. and Moeller, T., *J. Inorg. Nucl. Chem.*, 1967, **29,** 2731.
9. Alberti, M., Břínek, J., Marek, J. and Toužín, J., *Z. Anorg. Allg. Chem.*, 1997, **623,** 637.
10. de Ficquelmont, A. M., *Ann. Chim.*, 1939, **12,** 169.
11. Alberti, M., Mareček, A., Žák, Z. and Pastera, P., *Z. Anorg. Allg. Chem.*, 1995, **621,** 1771.
12. KUMA Diffraction, Al.Akacjowa 15b, 53-122 Wroclaw, Poland.
13. Walker, N. and Stuart, D., *Acta Cryst. A*, 1983, **39,** 158.
14. Sheldrick, G. M., *Acta Cryst. A*, 1990, **46,** 467.
15. Sheldrick, G. M., *J. Appl. Cryst.* (in preparation).
16. Gabler, D. G. and Haw, J. F., *Inorg. Chem.*, 1990, **29,** 4018.
17. Brandt, K., Van de Grampel, J. C., Meetsma, A. and Jekel, A. P., *Rec. Trav. Chim. Pays-Bas*, 1991, **110,** 27.
18. van der Huizen, A. A., Buwalda, P. L., Wilting, T., Pol, H., Jekel, A. P., Meetsma, A. and van de Grampel, J. C., *J. Chem. Soc. Dalton Trans.*, 1994, 577.
19. Marek, R., Humpa, O. and Sklenář, V., *Coll. Czech. Chem. Comm.* (in press).
20. Murray, M., Rillie, I. M. and Woodward, G., *Phosphorus Sulfur Silicon*, 1992, **65,** 83.
21. Murray, M., Penkett, C. J., Rillie, I. M. and Singh, G., *Phosphorus Sulfur Silicon*, 1994, **93–94,** 313.
22. Richert, H., *Z. Anorg. Allg. Chem.*, 1961, **309,** 171.
23. Eysel, H. H., *J. Mol. Struct.*, 1970, **5,** 275.
24. Armitage, D. A. and Brand, J. C., *J. Chem. Soc. Chem. Commun.*, 1979, 1078.
25. Johnson, C. K., *ORTEP II.* Report ORNL-5138. Oak Ridge National Laboratory, Tennessee, U.S.A., 1976.
26. Cerioni, G., Piras, P., Marongiu, G., Macciantelli, D. and Lunazzi, L., *J. Chem. Soc. Perkin Trans.*, 1981, **2,** 1449.
27. Cannas, M. and Marongiu, G., *Cryst. Struct. Commun.*, 1982, **11,** 1115.
28. Butler, R. N., Duffy, J. P., McArdle, P., Cunningham, D. and O'Halloran, G. A., *J. Chem. Soc. Chem. Comm.*, 1989, 1210.
29. Cruickshank, D. W. J., *J. Chem. Soc.*, 1961, 5486.

Pergamon

Polyhedron Vol. 17, No. 18, p. 3243, 1998
© 1998 Elsevier Science Ltd
All rights reserved. Printed in Great Britain
0277-5387/98 $19.00+0.00

ERRATUM

Foreword: Recent advances in metal alkoxide and amide chemistry. Malcolm H. Chisholm, *Polyhedron*, 1998, **17,** 623.

The publisher regrets that the following references were omitted from the above paper:

REFERENCES

1. Edelman, M., *Ann. 1846*, **56,** 269.
2. Frankland, J., *J. Chem. Soc. 1857*, 419.
3. Bradley, D. C., *Nature* (London), 1958, **182,** 1211.
4. Bradley, D. C., *Coord. Chem. Rev.*, 1967, **2,** 299.
5. Bradley, D. C. and Chisholm, M. H., *J. Chem. Soc.*, Section A, 1971, 2741; Chisholm, M. H., Cotton, F. A. and Extine, M. W., *Inorg. Chem.*, 1978, **17,** 1329.
6. Alyea, E. C., Basi, J. S., Bradley, D. C. and Chisholm, M. H., *J. Chem. Soc.*, Section A, 1971, 772.
7. (a) Bradley, D. C. and Chisholm, M. H., *Acc. Chem. Res.*, 1976, **9,** 273; (b) Bradley, D. C., *Chemistry in Britain*, 1975, **11,** 393.
8. (a) Chisholm, M. H., *Chem. Tracts-Inorg.* 1992, **4,** 273; (b) Caulton, K. G., *New J. Chem.*, 1994, **18,** 25; (c) Gibson, V. C., *Angew. Chem. Int. Edit. Engl.*, 1994, **33,** 1565; (d) Wolczanski, P. T., *Polyhedron*, 1995, **14,** 3335; (e) Rothwell, I. P., *Chem. Comm.*, 1997, 1331.
9. Bradley, D. C., *New Scientist*, 1988, 3841; *Appl. Surf. Sci.*, 1990, **46,** 1; *Polyhedron*, 1994, **13,** 1111 and references therein.
10. (a) Cummins, C. C., Laplaza, C. E. and Davis, W. M., *Angew. Chem. Int. Edit. Engl.*, 1995, **34,** 2042; (b) Laplaza, C. E., Johnson, M. J. A., Peters, J. C., Odom, A. L., Kim, E., Cummins, C. C., George, G. N. and Pickering, I. J., *J. Am. Chem. Soc.*, 1996, **118,** 8623; (c) Johnson-Carr, J. A., Zanetti, N. C., Schrock, R. R. and Hopkins, M. D., *J. Am. Chem. Soc.*, 1996, **118,** 11305; (d) Scheer, M., Muller, J. and Haser, M., *Angew. Chem. Int. Edit. Engl.*, 1996, **35,** 2492; (e) Peters, J. C., Odom, A. L and Cummins, C. C., *J. Chem. Soc. Chem. Comm.*, 1997, 1995.

Pergamon

PII: S0277-5387(98)00151-X

Polyhedron Vol. 17, No. 18, p. 3245, 1998
© 1998 Elsevier Science Ltd
All rights reserved. Printed in Great Britain
0277-5387/98 $19.00+0.00

BOOK REVIEW

Comprehensive Organometallic Chemistry Edition Pergamon, 1997. 14 Volumes.

It is hard to know where to start when reviewing superlative compendia like COMC. This set of 14 volumes covering the literature from 1982–1994 was edited by Abel, Stone and Wilkinson and is a great testament to their (and many authors') diligence and effort. Volumes covering all of the elements compile an excellent source of primary information. Furthermore, vol. 10 (M–M bonds), vol. 11 (main group organometallics in synthesis) and vol. 12 (transition metal organometallics in synthesis) provide excellent outlines of the usefulness of organometallic reagents. Volume 13 is a compendium of organometallic structures and vol. 14 provides a good culumative index.

It would be unfair to cite individual chapters for special mention. Dipping into individual volumes always provides some interesting chemistry which will doubtless spark new ideas. This is a super achievement and should be in every chemistry library. Individuals may find the price just a little bit taxing, though.

J. D. Woolins

Pergamon

PII : S0277–5387(98)00071–0

Polyhedron Vol. 17, No. 19, pp. 3247–3253, 1998
© 1998 Elsevier Science Ltd
All rights reserved. Printed in Great Britain
0277–5387/98 $19.00 + 0.00

Preparation and spectral study of mixed-ligand nickel(II) chelates containing *N*- or *N*,*N*′-methylated ethylenediamines and tropolonate or hinokitiolate ligands

Y. Ihara,[a]* K. Teranishi,[a] N. Hirose,[a] and K. Sone[b]

[a] Laboratory of Chemistry, Faculty of Education, Kanazawa University, Kakumamachi, Kanazawa 920-1192, Japan

[b] Department of Chemistry, Faculty of Science, Josai University, Keyakidai 1-1, Sakado, Saitama 350-0290, Japan

(Received 14 October 1997 : accepted 13 February 1998)

Abstract—Eleven mixed-ligand chelates of Ni(II) containing a molecule of *N*,*N*-di-, *N*,*N*,*N*′-tri-, or *N*,*N*,*N*′,*N*′-tetramethylethylenediamine, and a tropolonate (trop) or hinokitiolate (hino) ligand, were prepared, and their electronic spectra in solid state and in various organic solvents were studied. Most systems studied were green, containing octahedral chelate species $[Ni(trop/hino)(diamine)(H_2O/Solvent)_2]^+$ or $[Ni(NO_3)(trop/hino)(diamine)]$, but some were red, containing square planar $[Ni(trop/hino)(diamine)]^+$, and an equilibrium between the octahedral and square planar species was sometimes observed in solutions. Strong spectral resemblances with the corresponding diamine-β-diketonate chelates of Ni(II) could be pointed out. © 1998 Elsevier Science Ltd. All rights reserved

Keywords: nickel(II) chelates; tropolonate; hinokitiolate; solvatochromism.

It is known that β-diketonates (β-dike) and *N*- or *N*,*N*′-alkylated ethylenediamines ($R_n$en) react with Ni(II) or Cu(II) to produce the mixed-ligand chelates, [M(β-dike)($R_n$en)]X (X is a univalent anion such as ClO_4^-), which are soluble both in polar and non-polar solvents exhibiting pronounced solvatochromic behaviors [1–3]. Such chelates may serve as visual indicators to estimate the polarities of organic solvents, with which their electronic spectra regularly vary [3].

We have recently reported on the solvatochromic properties of the mixed-ligand chelates of Cu(II) with *N*,*N*-/*N*,*N*′-di-, *N*,*N*,*N*′-tri-, or *N*,*N*,*N*′,*N*′-tetramethylethylenediamine and a tropolonate (trop) or hinokitiolate (hino; 4-isopropyltropolonate) ligand [4]. In continuation of the study, we tried to prepare similar chelates of Ni(II) and investigate their spectral behaviors. As was the case with the Cu(II) chelates, a close resemblance was found between the chelates obtained in this study and the corresponding diamine-β-diketonate chelates, in particular with respect to their solvatochromic behaviors, which will now be reported in this paper.

EXPERIMENTAL

Preparation of the chelates

All the reagents, including the solvent molecules, used for preparing the mixed nickel(II) chelates were commercial reagent grade chemicals and used without further purification. Tropolone and hinokitiol were supplied by Tokyo Chem. Ind. Co.

(i) $[Ni(trop)(tetmen)(H_2O)_2]ClO_4$ (**a**): Nickel(II) perchlorate hexahydrate (2 mmol, 0.73 g) was dissolved in a small amount of water, and an ethanolic solution (5 cm^3) containing equimolar amounts of *N*,*N*,*N*′,*N*′-tetramethylethylenediamine (tetmen, 0.23 g) and tropolone (trop, 0.25 g) was added to it with

* Author to whom correspondence should be addressed.

stirring. After sodium carbonate (1 mmol, 0.11 g) was added to neutralize the solution, it was gently heated for 1 h and filtered. The filtrate was kept in a refrigerator for several days, and the green crystals precipitated were recrystallized from nitromethane. Yield : 0.56 g, 65%.

(ii) [Ni(trop)(tetmen)]$B(C_6H_5)_4$(**b**) : An excess amount of sodium tetraphenylborate (1.5 mmol, 0.51 g) was added to the suspension of **a** (1 mmol, 0.43 g) in 1,2-dichloroethane (10 cm^3) with stirring and gentle heating. After the insoluble residue was removed, the solution was kept in a refrigerator for several days to precipitate the red crystals. Yield : 0.26 g, 43%.

(iii) [$Ni(NO_3)$(trop)(tetmen)] (**c**) : Nickel(II) nitrate hexahydrate (2 mmol, 0.58 g) was dissolved in ethanol (5 cm^3), and a chloroform solution (15 cm^3) containing equimolar amounts of trop and tetmen was added to it with stirring. After an aqueous solution (0.5 cm^3) of sodium carbonate (1 mmol) was added to the solution, it was gently heated for an hour and filtered. The resulting solution was kept in a refrigerator for a week to precipitate the deep green crystals. Yield : 0.51 g, 71%.

(iv) [Ni(trop)(trimen)$(H_2O)_2$]ClO_4 (**d**) : Nickel(II) perchlorate hexahydrate (2 mmol), trop (2 mmol) and *N*,*N*,*N*′-trimethylethylenediamine (trimen, 3 mmol, 0.31 g) were mixed successively in acetone (5 cm^3). The resulting solution was evaporated to dryness on a hot plate and the residue was suspended in diethyl ether. The green powder obtained from the suspension was further treated with 1,2-dichloroethane (10 cm^3). After the insoluble residue was filtered off, the deep green crystals separated out immediately from the filtrate. Yield : 0.29 g, 35%.

(v) [Ni(trop)(trimen)]$B(C_6H_5)_4 \cdot H_2O$ (**e**) : This complex was prepared from **d** by the same method as that used for **b** ; 1.5 mmol of sodium tetraphenylborate was added to the suspension of **d** (1 mmol, 0.42 g) in 10 cm^3 of 1,2-dichloroethane. Yield : 0.15 g, 24%.

(vi) [$Ni(NO_3)$(trop)(trimen)] (**f**) : Nickel(II) nitrate hexahydrate (2 mmol) was mixed with trop (2 mmol) and trimen (3 mmol) in acetone (5 cm^3), and the solution was evaporated to dryness. The green powder obtained was extracted with 1,2-dichloroethane (5 cm^3), and the insoluble residue was removed. The resulting solution was evaporated to dryness again. The crude gummy product was suspended in diethyl ether (20 cm^3), and the green crystalline powder obtained was washed with diethyl ether thoroughly. Yield : 0.51 g, 74%.

(vii) [Ni(trop)(*NN*-dmen)$(H_2O)_2$]NO_3 (**g**) : An acetone solution containing the reaction mixture of nickel(II) nitrate hexahydrate (2 mmol), trop (2 mmol) and *N*,*N*-dimethylethylenediamine (*NN*-dmen, 3 mmol, 0.26 g) was evaporated to dryness. The green powder obtained was extracted with 1,2-dichloroethane (10 cm^3), and the oily residue was filtered off. The resulting solution was concentrated slowly at room temperature to precipitate the green crystals after a few days. Yield : 0.37 g, 51%.

(viii) [Ni(hino)(tetmen)$(H_2O)_2$]ClO_4 (**h**) : Hinokitiol (hino, 1.5 mmol, 0.25 g) and tetmen (1.5 mmol, 0.17 g) were added to a methanolic solution (10 cm^3) of nickel(II) perchlorate hexahydrate (1.5 mmol, 0.55 g), successively. The resulting suspension became a deep green solution by adding sodium carbonate (0.8 mmol, 0.08 g) with gentle heating. The solution was evaporated to dryness, and the green powder obtained was dissolved in 1,2-dichloroethane (10 cm^3) and filtered. The filtrate was kept in a refrigerator for several days. The green crystals which separated out were recrystallized from 1,2-dichloroethane. Yield : 0.42 g, 59%.

(ix) [Ni(hino)(tetmen)]$B(C_6H_5)_4 \cdot H_2O$ (**i**) : This complex was prepared from **h** by the same method as that used for **b** ; 1.5 mmol of sodium tetraphenylborate was added to the suspension of **h** (1 mmol, 0.47 g) in 10 cm^3 of 1,2-dichloroethane. Yield : 0.22 g, 32%.

(x) [$Ni(NO_3)$(hino)(tetmen)] (**j**) : Nickel(II) nitrate hexahydrate (1.5 mmol, 0.44 g) was mixed with hino (1.5 mmol) and tetmen (2.3 mmol, 0.27 g) in acetone (5 cm^3), and the solution was gently heated to dryness. The resulting solid was dissolved in 1,2-dichloroethane (10 cm^3) and then the insoluble residue was filtered off. After the filtrate was evaporated to dryness again, the green powder was extracted with three 10 cm^3 portions of diethyl ether. The combined ether solution was let stand for a day at room temperature to precipitate the deep green crystals which were recrystallized from diethyl ether. Yield : 0.24 g, 40%.

(xi) [Ni(hino)(*NN*-dmen)$(H_2O)_2$]NO_3 (**k**) : Nickel(II) nitrate hexahydrate (1.5 mmol) dissolved in methanol (5 cm^3), and a methanolic solution (5 cm^3) containing hino (1.5 mmol) and *NN*-dmen (1.5 mmol, 0.13 g) were mixed together, and sodium carbonate (0.8 mmol) was added to it with stirring and gentle heating. The solution was concentrated on a hot plate, and the oily product obtained was suspended in 1,2-dichloroethane (10 cm^3). The pale green powder isolated from the suspension was recrystallized from 1,2-dichloroethane. Yield : 0.51 g, 83%.

Attempts to prepare the mixed chelates containing hino and trimen in a pure form always failed in spite of many efforts.

Measurements

The visible and near-UV spectra of the chelates were recorded with a JASCO V-570 spectrophotometer at room temperature (ca 20°C). Solvents used for the spectral studies were GR or Spectro Grade products and were stored over molecular sieves (5 Å). The IR spectra were measured with a HORIBA FT-210 infrared spectrophotometer by the KBr disk and Nujol mull methods. The effective magnetic moments were evaluated from the susceptibilities measured by a Sherwood magnetic balance MSB-MKI. Thermogravimetry was carried out with a Seiko SSC/580

TG/DTA-30 apparatus. Each run was performed under a constant flow of nitrogen (0.2 $dm^3\ min^{-1}$) at a heating rate of 2°C min^{-1}; about 20 mg of sample was used.

RESULTS AND DISCUSSION

Structures of the chelates in solid state

Table 1 summarizes the solid-state properties and analytical data of the eleven mixed nickel(II) chelates obtained, and Fig. 1 shows the solid-phase (powder reflection) electronic spectra of some trop chelates. It can be seen that there are two types of chelates: the red diamagnetic ones with square planar geometry, which show a strong *d–d* band at ca 21×10^3 cm^{-1}, and the green paramagnetic ones with octahedral geometry, which show two weaker bands at ca 9×10^3 cm^{-1} (Band I) and 16×10^3 cm^{-1} (Band II), respectively [1,3,5,6]. All the tetraphenylborates belong to the former, while all the hydrated perchlorates, hydrated nitrates, and anhydrous nitrates (or nitrato chelates; cf. below) belong to the latter.

Among the chelates containing an NO_3^- ion, the spectrum of an anhydrous chelate is characteristically different from that of a hydrated chelate: (1) the Band II is notably stronger than the Band I in the former spectrum, while both are of comparable strength in the latter; (2) the Band I in the former is much broader than that in the latter, and is apparently split, indicating a stronger deformation of its geometry from octahedral symmetry. The case of **c** and **g** is compared in Fig. 1.

In this connection, it is also noted that hydrated nitrates (**g** and **k**) show a single IR band (a weak combination band of NO_3^-) at ca 1760 cm^{-1}, while anhydrous nitrates (**c, f** and **j**) show two such bands with a large separation (ca 50 cm^{-1}). These data imply that the nitrate ion in the hydrated nitrates is outside of the coordination sphere, while that in the anhydrous nitrates is a chelating nitrate ligand [7], which forms a 4-membered chelate ring with an anomalously small O—Ni—O angle [8].

The presence of two water molecules in chelates **a, d, g, h** and **k,** and one water molecule in **e** and **i** was also confirmed thermogravimetrically. Among the anhydrous chelates obtained by thermal dehydration, those from **a, d** and **h** are red, so that they should be formulated as square planar [Ni(trop/hino)(diamine)]ClO_4-type chelates. The anhydrous chelates from **g** and **k** are green, on the other hand, and their IR spectra show two bands around 1750 cm^{-1} with a large separation (42 and 33 cm^{-1}, respectively), implying that they are nitrato chelates [$Ni(NO_3)$(trop/hino)(*NN*-dmen)] like **c, f** and **j**.

All these considerations lead to the formulations of the obtained chelates given in Table 1.

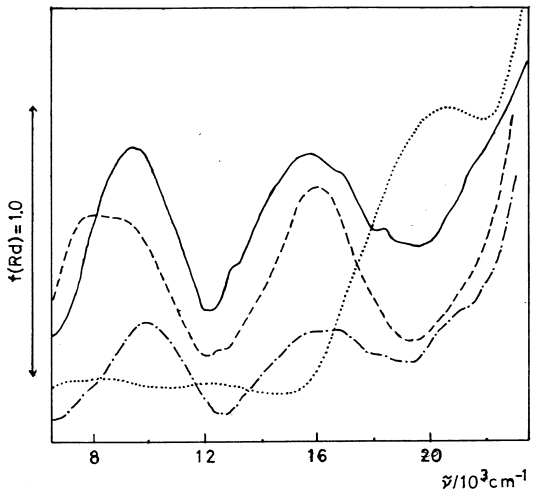

Fig. 1. Reflectance spectra of [Ni(trop)(tetmen)$(H_2O)_2$]ClO_4 (—), [Ni(trop)(tetmen)]$B(C_6H_5)_4$ (···), [$Ni(NO_3)$(trop)(tetmen)] (– –) and [Ni(trop)(*NN*-dmen)$_2(H_2O)_2$]NO_3 (— · —).

Structures of the chelates in solutions

The chelates obtained are, in most cases, slightly soluble in water, but they are fairly soluble in most organic solvents. Typical data of the electronic spectra of trop and hino chelates in various solvents are summarized in Tables 2 and 3, respectively. It can be seen that the red square planar species predominate in some solutions, but the green octahedral species (of the hydrated-chelate type spectra; *vide supra*) predominate in most others, and equilibrium mixtures of the two species occur in certain cases.

Figures 2 and 3 show the spectra of **a** and **b** in 1,2-dichloroethane (DCE), nitromethane (NM), THF and DMSO, respectively. In strongly polar and coordinating solvents like DMF, DMSO, and pyridine, the spectra of the two chelates are nearly identical, showing that the same octahedral species, most probably [Ni(trop)(tetmen)(Solvent)$_2$]$^+$, predominate in every case. In weakly polar and poorly coordinating solvents like DCE and NM, on the other hand, their spectra are that of the square planar species [Ni(trop)(tetmen)]$^+$ (so the chelate cation in **a** is readily dehydrated in such a solvent), whereas the very weak absorption in the red-to-IR region indicates that small amounts of octahedral species coexist in equilibrium with it. In solvents of intermediate coordinating power, such as alcohols, acetone and THF, the solutions are green, and their spectra are similar to those in strongly coordinating solvents; however, on heating they become yellowish to orange (thermochromism), and their absorption band around 21×10^3 cm^{-1} sensibly increases, forming a shoulder or hump at the skirt of the strong band of trop which appears at the blue end of the visible spectrum (this hump is most

Table 1. Solid-state properties and analytical data of the chelates

Chelate	Color	μ_{eff}/B.M.	$\tilde{\nu}_{max}/10^3$ cm^{-1} (refl.[a])		$\tilde{\nu}_{NO_3}$/cm^{-1} (IR[b])		Dehydration[c] Temp/°C	Mass loss/%[d]	Analytical data[d] C(%)	H(%)	N(%)
a [Ni(trop)(tetmen)$(H_2O)_2$]ClO_4	green	3.06	9.5	15.8			65–110	8.3(8.3)	35.91(36.19)	5.77(5.84)	6.40(6.49)
b [Ni(trop)(tetmen)]$B(C_6H_5)_4$	red	diamag.	20.9					0	72.37(72.23)	6.74(6.72)	4.69(4.55)
c [Ni(NO_3)(trop)(tetmen)]	deep green	2.91	8.6	16.1	1722	1770		0	43.24(43.61)	5.83(5.91)	11.87(11.74)
d [Ni(trop)(trimen)$(H_2O)_2$]ClO_4	green	2.93	9.6	15.7			60–155[e]	8.5(8.6)	34.33(34.52)	5.53(5.55)	6.58(6.71)
e [Ni(trop)(trimen)]$B(C_6H_5)_4 \cdot H_2O$	red	diamag.	21.0				50–95	2.6(2.9)	69.41(69.83)	6.54(6.67)	4.89(4.52)
f [Ni(NO_3)(trop)(trimen)]	green	3.01	9.1	16.6	1716	1766		0	42.38(41.90)	5.69(5.57)	11.95(12.22)
g [Ni(trop)(*NN*-dmen)$(H_2O)_2$]NO_3	pale green	2.90	10.0	16.1	1763		85–110	9.7(9.8)	35.95(36.16)	5.80(5.74)	11.74(11.48)
h [Ni(hino)(tetmen)$(H_2O)_2$]ClO_4	green	3.20	9.2	15.7			45–90	7.2(7.6)	40.03(40.58)	6.25(6.60)	5.97(5.92)
i [Ni(hino)(tetmen)]$B(C_6H_5)_4 \cdot H_2O$	red	diamag.	20.8				40–70	2.6(2.7)	71.10(71.14)	7.05(7.31)	4.12(4.15)
j [Ni(NO_3)(hino)(tetmen)]	deep green	3.17	8.3	15.9	1722	1770		0	47.84(48.03)	6.77(6.80)	10.29(10.50)
k [Ni(hino)(*NN*-dmen)$(H_2O)_2$]NO_3	pale green	3.10	9.8	15.9	1757		70–145	8.5(8.8)	40.76(41.21)	6.58(6.67)	10.25(10.30)

[a] Wave numbers of the *d-d* bands in reflectance spectrum.
[b] Characteristic combination band of NO_3^- ; see text.
[c] Thermogravimetric data.
[d] Calculated values are in parentheses.
[e] Dehydration takes place in two steps.

Table 2. Values of $\tilde{\nu}_{max}/10^3$ cm^{-1} and ε_{max} of the trop chelates in various solvents

Chelate	Solvent DCE	NM	MeCN	Me_2CO	THF	MeOH	EtOH	DMF	DMSO	Py
a	20.6(198)	20.5(157)	9.9(10)	9.4(11)	9.1(10)	9.4(9)	9.4(9)	9.5(12)	9.4(10)	10.0(7)
			16.8(18)	15.7(13)	15.6(11)	15.6(11)	15.4(11)	15.7(14)	15.4(12)	16.7(18)
b	20.7(272)	20.6(189)	10.0(12)	9.5(12)	9.0(7)	9.4(10)	9.3(11)	9.5(12)	9.4(11)	10.2(8)
			16.7(21)	15.7(14)	15.6(8)	15.6(11)	15.4(13)	15.7(14)	15.4(13)	16.7(21)
					20.8(71)					
c	9.4(13)	9.5(12)	9.6(12)	9.4(12)	9.4(12)	9.4(10)	9.3(12)	9.6(12)	9.4(11)	10.1(8)
	16.0(27)	16.0(27)	16.1(24)	16.0(26)	16.1(25)	15.8(14)	16.0(20)	15.8(16)	15.4(13)	16.7(21)
d	20.8(147)	20.7(121)	10.2(13)	9.7(13)	9.4(12)	9.7(10)	9.6(11)	9.8(13)	9.7(11)	10.0(9)
			16.8(21)	16.6(14)	16.6(15)	16.0(11)	16.7(15)	16.6(18)	15.7(14)	16.7(21)
									16.6(13)	
e	20.8(170)	20.9(106)	10.1(13)	9.6(14)	9.4(11)	9.6(11)	9.8(12)	9.9(13)	9.6(12)	10.0(9)
			16.7(23)	16.6(18)	16.7(16)	16.7(14)	16.6(23)	16.6(19)	15.9(16)	16.7(23)
									16.6(16)	
f	9.6(13)	9.6(13)	9.9(13)	9.5(13)	9.6(13)	9.7(10)	9.7(9)	9.8(13)	9.6(11)	10.0(9)
	16.6(28)	16.6(29)	16.7(24)	16.6(25)	16.6(27)	16.7(14)	16.6(17)	16.6(18)	16.6(14)	16.7(21)
g	9.5(13)	9.6(13)	9.9(13)	9.2(13)	9.4(12)	9.7(9)	9.6(12)	9.8(13)	9.5(11)	9.9(11)
	16.6(27)	16.3(28)	16.7(23)	15.9(23)	16.6(26)	16.7(12)	16.7(20)	16.6(17)	16.6(13)	16.7(21)

Table 3. Values of $\tilde{\nu}_{max}/10^3$ cm^{-1} and ε_{max} of the hino chelates in various solvents

Chelate	Solvent DCE	NM	MeCN	Me_2CO	THF	MeOH	EtOH	DMF	DMSO	Py
h	20.7(197)	20.6(178)	9.9(10)	9.4(13)	9.1(12)	9.4(10)	9.3(11)	9.6(12)	9.4(11)	10.1(9)
			16.8(16)	15.7(15)	15.7(20)	15.6(13)	15.6(13)	15.8(16)	15.4(14)	16.9(21)
i	20.7(215)	20.6(191)	9.8(13)	9.4(12)	8.9(9)	9.2(10)	9.5(14)	9.5(12)	9.4(10)	10.0(10)
			16.8(21)	15.7(14)	15.6(12)	15.9(16)	16.0(25)	15.7(17)	15.3(12)	16.8(21)
					21.6(59)					
j	9.4(14)	9.5(13)	9.5(13)	9.4(13)	9.4(13)	9.4(10)	9.4(13)	9.5(11)	9.3(11)	10.1(9)
	16.1(28)	16.0(29)	16.1(25)	16.0(26)	16.1(27)	15.7(14)	15.9(24)	15.8(16)	15.3(14)	16.9(20)
k	Insol.	9.6(13)	9.9(13)	9.3(14)	9.4(13)	9.7(10)	9.6(9)	9.7(13)	9.6(11)	9.9(10)
		16.2(28)	16.7(24)	16.0(25)	16.5(26)	16.1(12)	16.1(15)	16.6(17)	15.7(13)	16.8(20)

clearly seen in THF even at room temperature; cf. Fig. 3). The equilibrium

$$[Ni(trop)(tetmen)]^+ + 2Solvent \rightleftharpoons [Ni(trop)(tetmen)(Solvent)_2]^+ \quad (1)$$

which is predominant in these solutions is thus shifted to the left hand side with the rise of temperature.

All these spectral behaviors are quite similar to those observed in the corresponding chelates with a β-diketonate ligand, in particular in those with an acetylacetonate (acac) ligand [1,3,7] of which trop is a vinylog [9], even with respect to the numerical values of $\tilde{\nu}_{max}$ of the individual case. A closer spectral comparison of **a** with that of its acac analogue [Ni(acac)(tetmen)$(H_2O)_2$]ClO_4 indicates however that, in solvents (ethanol, butanol, acetone and THF) where the equilibrium (1) is established, the relative concentration of the red species seems to be considerably lower in the case of **a,** although its reliable estimate is hindered by the strong blue band of trop which overlaps with its band too severely [10].

Figure 4 shows the spectra of **c** in the same solvents as those in Fig. 2. Here the predominating species is always green and octahedral, but there are evidently two kinds of them. The species formed in a strongly coordinating solvent (e.g. pyridine, DMF, DMSO, and now alcohols) shows nearly the same spectrum as that of **a** and **b** in the same solvent, i.e. [Ni(trop)(tetmen)$(Solvent)_2]^+$. The species formed in a less coordinating solvent shows a different spectrum, where the ε_{max} of the Band II is notably higher than that of the Band I, which is very broad with a somewhat split appearance. This latter species is most probably the undissociated nitrato chelate [Ni(NO_3)(trop)(tetmen)], in view of its spectral analogy with the solid chelates and, here again, with the corresponding β-diketonate chelates [1,3,6,8]. The pre-

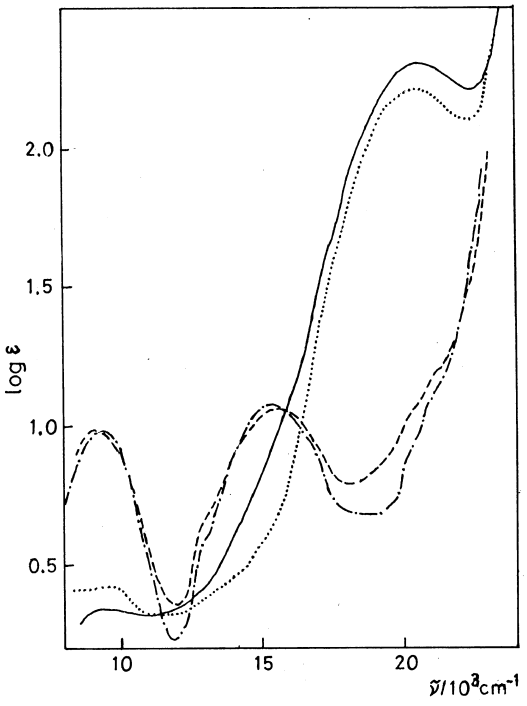

Fig. 2. Electronic spectra of $[Ni(trop)(tetmen)(H_2O)_2]ClO_4$ in DCE (—), NM(···), THF (– –) and DMSO (— · —).

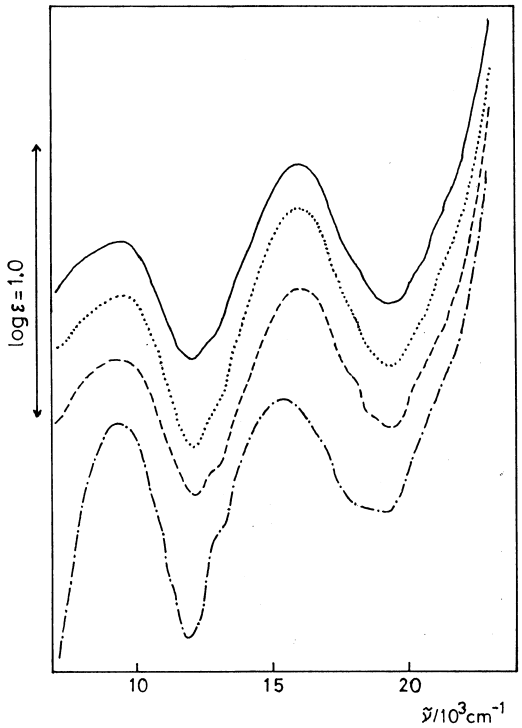

Fig. 4. Electronic spectra of $[Ni(NO_3)(trop)(tetmen)]$ in DCE (—), NM (···), THF (– –) and DMSO (— · —).

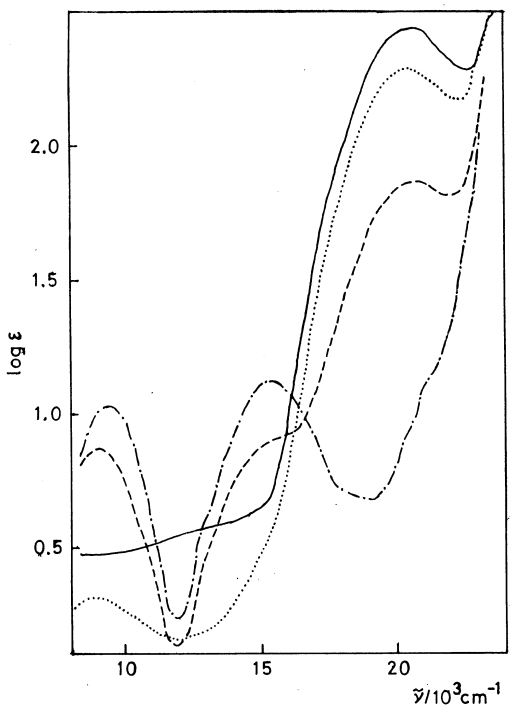

Fig. 3. Electronic spectra of $[Ni(trop)(tetmen)]B(C_6H_5)_4$ in DCE (—), NM (···), THF (– –) and DMSO (— · —).

dominating equilibrium in these solutions is, therefore, that of the dissociation/solvation of nitrato chelate, i.e.

$$[Ni(NO_3)(trop)(tetmen)] + 2Solvent \rightleftharpoons [Ni(trop)(tetmen)(Solvent)_2]^+ + NO_3^- \quad (2)$$

The spectra of the tetmen chelates of hino (**h, i** and **j**) are quite similar to those of the corresponding trop chelates (**a, b** and **c**). In addition, the solvatochromic behaviors of the trimen chelates of trop (**d, e** and **f**) can be understood similarly; even the change from tetmen to trimen does not alter the apparent solvatochromic changes of the chelates seriously, unlike the case of the Cu(II) chelates where the extent of solvatochromism depends sensitively on the structures of the diamine ligands [4]. On the other hand, the spectra of the hydrated nitrates with *NN*-dmen, **g** and **k,** which are probably formed as the result of decreased hydrophobicity of *NN*-dmen, show that they are readily dehydrated and dissolved as $[Ni(NO_3)$-(trop/hino)(*NN*-dmen)] in most solvents (even in DCE or NM, unlike the hydrated perchlorates **a, d** and **h** which are merely dehydrated into [Ni(trop/hino)(diamine)]$^+$ in them), and are converted into $[Ni(trop/hino)(NN\text{-dmen})(Solvent)_2]^+$ only in strongly coordinating solvents [11], as in the case of **c** and **j**.

A problem which still remains unsolved is whether the $[Ni(trop/hino)(diamine)(H_2O/Solvent)_2]^+$-type

chelate cations are *cis* or *trans*. Recent X-ray crystal structural studies of the corresponding acac-diamine chelates [12–14] proved that they are always *cis*, suggesting that the trop/hino-diamine chelates are also *cis*; there is still no direct evidence for it, however, and the reason why this structure is favored among these chelates is by no means clear. Further structural studies are now going on along these directions.

Acknowledgements—This work was partially supported by Grant-in-Aid for Scientific Research (C) (No. 07640741) from Ministry of Education, Science, Sports and Culture.

REFERENCES

1. Fukuda, Y. and Sone, K., *J. Inorg. Nucl. Chem.*, 1972, **34,** 2315.
2. Tsiamis, C., Alkam, H. H. and Hadjikostas, C. C., *Inorg. Chim. Acta*, 1994, **221,** 17.
3. Sone, K. and Fukuda, Y., *Inorganic Thermochromism*, Springer, Heidelberg, 1987.
4. Ihara, Y., Yoshizakiya, M., Yoshiyama, R. and Sone, K., *Polyhedron*, 1996, **15,** 3643.
5. Cf., e.g., Cotton, F. A. and Wilkinson, G., *Advanced Inorganic Chemistry*, 5th edn, Wiley, New York, 1988.
6. Fukuda, Y. and Sone, K., *J. Inorg. Nucl. Chem.*, 1975, **37,** 455.
7. Lever, A. B. P., Mantovani, E. and Ramaswamy, B. S., *Can. J. Chem.*, 1971, **49,** 1957.
8. Fukuda, Y., Fujita, C., Miyamae, H., Nakagawa, H. and Sone, K., *Bull. Chem. Soc. Jpn.*, 1989, **62,** 745.
9. Yamada, S. and Tsuchida, R., *Bull. Chem. Soc. Jpn.*, 1956, **29,** 694.
10. As to the relative stabilities of trop and acac chelates, cf. Bryant, B. E. *et al.*, *J. Am. Chem. Soc.*, 1953, **75,** 3784.
11. Cf. also Nga, N. T., Fukuda, Y. and Sone, K., *Bull. Chem. Soc. Jpn.*, 1977, **50,** 154.
12. Yamada, K., Thesis (M.Sc.), Ochanomizu University, 1992, and Yamada, K., Hori, K. and Fukuda, Y., *Acta Cryst.*, 1993, **C49,** 445: [Ni(acac)(tetmen)(MeOH)(H_2O)]ClO_4, [Ni(acac)(tetmen)(MeOH)(H_2O)]BPh_4 · [$Ni_2(acac)_2(CO_3)$(tetmen)$_2$].
13. Ogino, T., unpublished data at Josai University, 1996: [Ni(acac)(tetmen)(H_2O)$_2$]ClO_4.
14. Mafune, K., Thesis (M.Sc.), Ochanomizu University, 1989: [(tetmen)Ni(taet)Ni(tetmen)(H_2O)$_2$](ClO_4)$_2$ · H_2O (taet = tetraacetylethanate). Cf. also Sone, K. and Fukuda, Y., *Rev. Inorg. Chem.*, 1991, **11,** 123.

Pergamon

PII: S0277–5387(98)00098–9

Polyhedron Vol. 17, No. 19, pp. 3255–3261, 1998
© 1998 Elsevier Science Ltd
All rights reserved. Printed in Great Britain
0277–5387/98 $19.00+0.00

Structural characterization by ESR of copper complexes with unsymmetrical S,O or S,N bidentate thiourea derivative ligands

Emmanuel Guillon, Isabelle Déchamps-Olivier and Jean-Pierre Barbier*

G.R.E.C.I., Université de Reims Champagne-Ardenne, BP1039, 51687 Reims, Cédex 2, France

(Received 22 September 1997; accepted 12 March 1998)

Abstract—ESR spectra show the simultaneous presence of a planar *trans* and a nearly planar *cis* isomers in the 1:2 ratio for all "S,O" compounds $Cu(R_1R_2N\text{-}CS\text{-}N\text{-}COR)_2$ whereas an only isomer is present with the analogous "S,N" compounds. A strong tetrahedral distortion is observed when a bulky substituent is present on the nitrogen donor atom. © 1998 Elsevier Science Ltd. All rights reserved

Keywords: thiocarbamide copper complexes; benzamidine copper complexes; ESR copper complexes.

In preceding papers [1–3], we have reported on the coordination of copper, nickel and cobalt with unsymmetrical bidentate ligands as:

"S,O substituted" ligand
with R = H, Cl, Br, OCH_3 or NO_2
in *ortho, meta* or *para* position

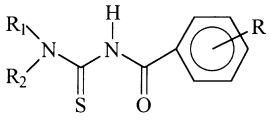

$R_1 = R_2 = Et$ or $R_1,R_2N =$

Et_2R btu H morphR btu H

"S,O ethoxy" ligand

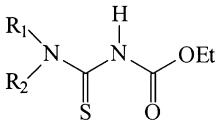

$R_1,R_2N =$ or

morph OEttu H or pyrro OEttu H

"S,NH_2" or "S,NHPh" ligand
if R_3 = H or Ph
with R = H or Cl

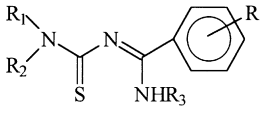

$R_1 = R_2 = Et$ or $R_1,R_2 =$

Et_2 tcR b H or { morph tcR b H ; morph tcPhR b H }

Whereas the configuration of diamagnetic cobalt complexes has been determined by ^1H and ^{13}C NMR spectroscopy, the geometry of the other complexes has not. The bis (*N*,*N*-diethyl,*N'*-benzoylthioureato) copper (II) has been investigated by Beyer *et al.* [4,5]: this compound can crystallize in three monoclinic forms. The crystal structure of one of these forms indicates that the S and O atoms are arranged in *cis* position in a slightly tetrahedrally distorted square geometry [4]. A single-crystal ESR study of this compound diluted in the corresponding *cis* nickel (II) chelate is in good agreement with this structure [5].

* Author to whom correspondence should be addressed.

Moreover, an X-ray structure analysis on the isosteric bis (*N*,*N*-diethyl-2-benzoylthioacetamidato) copper (II) has shown a simultaneous presence of two *cis* and one *trans* molecules in the unit cell [6]. In this paper, we report on the ESR study of the copper complexes in order to determine the influence of all substituents on their configuration.

EXPERIMENTAL

The "S,O" ligands were prepared as before by condensation of the morpholine or diethylamine with the benzoyl chloride or ethylformiate substituted by the ammonium thiocyanate [1, 2]. The "S,N" ligands were obtained from the nickel complexes with "S,O" ligands by substitution of the oxygen donor atom by chloride and then by ammoniac or a primary amine [3].

All the complexes were synthesized as described before, using copper (II) acetate or tetraethylammonium tetrachlorocuprate [1–3]. The ESR spectra of these complexes solutions (5×10^{-3} mol dm^{-3}) in chloroform-ethanol mixture (80–20) were obtained in the X-band at 77 K and at room temperature with a Varian E 109 spectrophotometer. The g values were measured relative to DPPH.

RESULTS AND DISCUSSION

The room-temperature solution ESR spectra show the typical four-lines patterns expected for coupling of the electron to the spin 3/2 copper (II) nucleus. ESR spectra of frozen solutions at 77 K are characterized by axial g and A tensors with $g_\parallel$ values $> g_\perp$ values. Three of the four parallel hyperfine features are well resolved while the fourth one at high field is overlapped in the broad $g_\perp$ signal. The g_0, $|A_0|$, $g_\parallel$ and $|A_\parallel|$ values could be readily determinated from spectra. As chloroform is a non coordinating solvent, dg_0/dT may be presumed negligible over the range 77–300 K, the $g_\perp$ and $|A_\perp|$ values could be calculated via the relationships $g_0=(g_\parallel+2\ g_\perp)/3$ and $|A_0|=(|A_\parallel|+2|A_\perp|)/3$ [7]. However, a possible small temperature dependence of $|A_0|$ renders approximate the values of $|A_\perp|$ derived from the room temperature $|A_0|$ values.

ESR spectra are similar for all the *N*,*N*-disubstituted, *N'*-benzoyl thioureas copper (II) complexes. At 77 K and at room temperature they show the presence of two four-line patterns. The two systems observed at room temperature involve the presence of two species and exclude the fact that the two four-lines systems arise from the isotopes ^{63}Cu and ^{65}Cu. Although the highest field $g_\parallel$ copper lines for the two isomers are superimposed on the $g_\perp$ copper lines, the partially resolved low field lines permit the determination of ESR parameters (Figure 1). The ESR parameters obtained from a single crystal of the *cis* $Cu(Et_2N\text{-}CS\text{-}N\text{-}CO\text{-}Ph)_2$ complex [5] are very close to our values for one system. By analogy with the isosteric $Cu(Et_2N\text{-}CS\text{-}CH\text{-}CO\text{-}Ph)_2$ complex, which present two *cis* and one *trans* molecules in the unit cell, the other system can be assigned to the *trans* isomer. All the EPR parameters are given in the Table 1. The $g_\parallel$ and $|A_\parallel|$ values indicate a square planar coordination geometry for the CuS_2O_2 moiety. All the spectra are almost superimposable. Whatever the electron-withdrawing or donor power and the *ortho*, *meta* or *para* position of the substituent on the aromatic ring, the consonant variation observed in $g_\parallel$ value is only of the same magnitude as the experimental error. In fact, the ESR parameters which relate to electron density in CuS_2O_2 plan are relatively insensitive to the substitution in these ligands aryl groups. Moreover the ratio $g_\parallel/|A_\parallel|$ is an indication of the stereochemistry of the copper (II) complexes. Addison has suggested that this ratio may be an empirical indication of the tetrahedral distortion of a square-planar geometry [8]. The values lower than 135 cm are observed for square-planar structures and those higher than 150 cm for tetrahedrally distorted complexes.

The lowest values of the ratio $g_\parallel/|A_\parallel|$ for the *trans* species are indicative of a planar *trans* arrangement whereas the slightly higher values of the ratio $g_\parallel/|A_\parallel|$ for the *cis* compounds indicate only a nearly planar *cis* arrangement as it is shown for the isosteric $Cu(Et_2N\text{-}CS\text{-}CH\text{-}COPh)_2$ compounds. It is noteworthy that the substitution of the aryl group by an ethoxy generates a small distortion around the metallic ion. These spectra were simulated with the following parameters $|A_0|=88\times10^{-4}$ cm^{-1}, $g_0=2.088$ for *cis* compounds and $|A_0|=76\times10^{-4}$ cm^{-1}, $g_0=2.097$ for *trans* compounds, with a line width equal to 10G. The sum of simulated spectra in the ratio *cis* 66% and *trans* 33% is in good agreement with the experimental spectra.

On the other hand, the ESR spectra of "$Cu(S,NH)_2$" compounds have only shown a nearly planar species in solution. The two bands at high field are well resolved and show five $(2nI_N+1)$ superhyperfine lines due to the interaction of the two nitrogen donor atoms ($I_N=1$) (Figure 2). Moreover, the spectra at 77 K which present, at high field, nine lines (eight and a shoulder), indicate unambigously a superhyperfine structure characteristic of an interaction with the two nitrogen donor atoms (Figure 3). The four supplementary lines can arise either from the two other non coordinated nitrogen atom or from the $g_\perp$ signal. All data are given in Table 2. The presence of a bulky substituent as phenyl on the nitrogen donor atom involves a tetrahedral geometry, the ratio $g_\parallel/|A_\parallel|$ being neighbouring 150 cm, with an important reduction of $|A_0|$ values.

The plot of $|A_\parallel|$ *vs* $g_\parallel$ (Figure 4) shows a linear relationship between $g_\parallel$ and $|A_\parallel|$ for each chro-

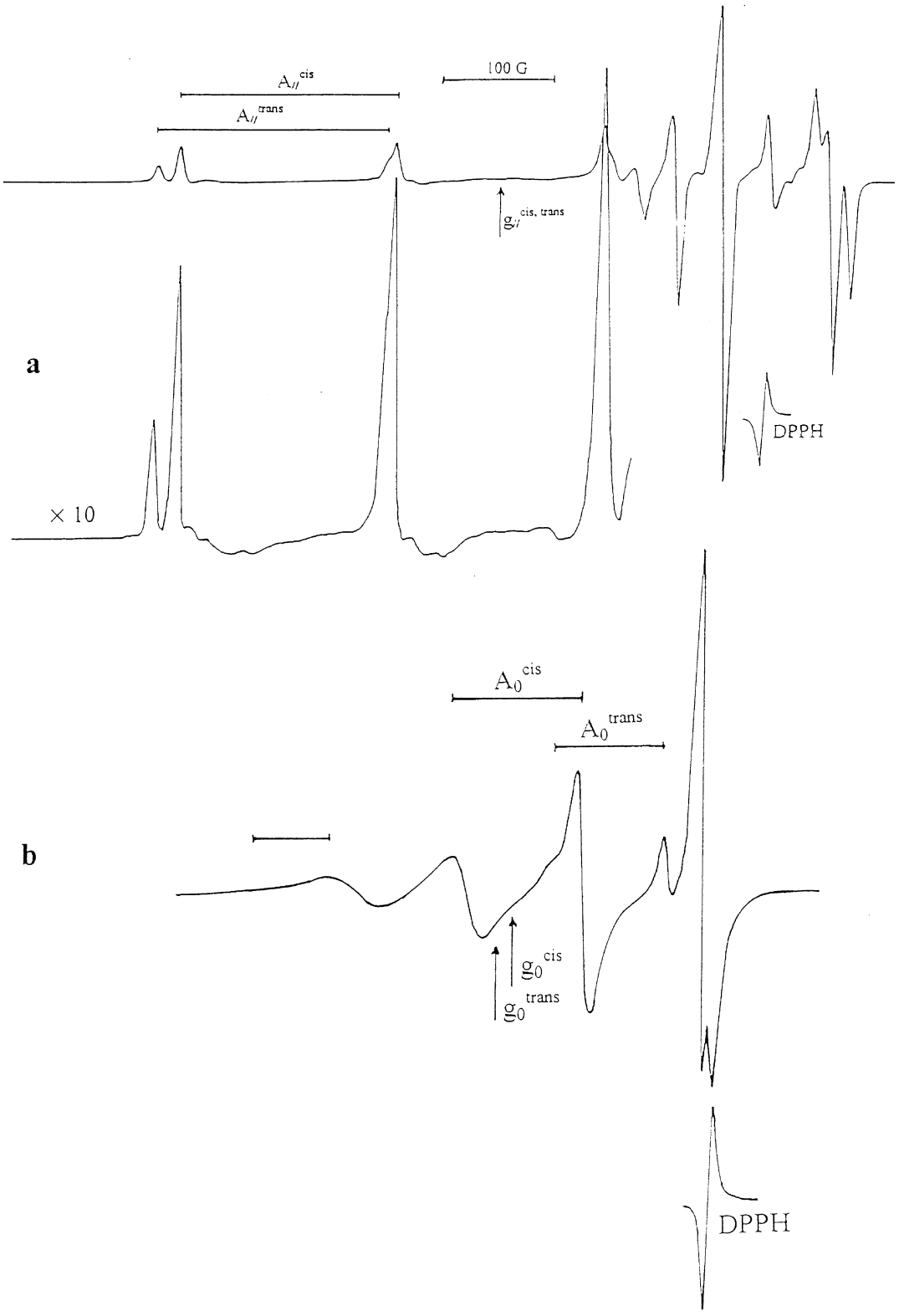

Fig. 1. ESR spectra of Cu(morph *m*-Br btu)$_2$ in $CHCl_3$–Ethanol solution, (a) at liquid nitrogen temperature, (b) at room temperature.

Table 1. ESR data for Cu(S,O substituted)$_2$ and Cu(S,O ethoxy)$_2$ complexes

	$\lvert A_0\rvert \times 10^4\,cm^{-1}$		g_0		$\lvert A_\parallel\rvert \times 10^4\,cm^{-1}$		$g_\parallel$		$\lvert A_\perp\rvert \times 10^4\,cm^{-1}$		$g_\perp$		$g_\parallel/\lvert A_\parallel\rvert$ cm	
Compounds	*cis*	*trans*	*cis*	*trans*	*cis*	*trans*	*cis*	*trans*	*cis*	*trans*	*cis*	*trans*	*cis*	*trans*
Cu(morph btu)$_2$	86	79	2.086	2.092	189	202	2.160	2.159	34	17	2.049	2.059	114	107
Cu(Et$_2$ btu)$_2$	88	76	2.089	2.095	191	199	2.162	2.165	36	14	2.052	2.060	113	109
Cu(morph *o*Cl btu)$_2$	88	76	2.088	2.097	187	199	2.167	2.167	39	15	2.048	2.062	116	109
Cu(morph *m*Cl btu)$_2$	83	80	2.087	2.101	189	200	2.160	2.160	30	20	2.050	2.071	114	108
Cu(Et$_2$ *o*Cl btu)$_2$	83	76	2.086	2.095	184	200	2.162	2.161	32	15	2.048	2.062	118	108
Cu(Et$_2$ *m*Cl btu)$_2$	83	74	2.086	2.092	184	199	2.164	2.166	32	16	2.047	2.055	118	109
Cu(Et$_2$ *p*Cl btu)$_2$	85	73	2.087	2.095	189	206	2.161	2.160	33	8	2.050	2.055	114	105
Cu(morph *o*Br btu)$_2$	83	72	2.081	2.086	190	198	2.165	2.173	30	10	2.039	2.043	114	110
Cu(morph *m*Br btu)$_2$	86	78	2.091	2.098	190	204	2.159	2.159	34	16	2.057	2.067	114	106
Cu(Et$_2$ *m*Br btu)$_2$	85	78	2.091	2.097	188	202	2.165	2.165	33	17	2.054	2.063	115	107
Cu(Et$_2$ *p*Br btu)$_2$	83	76	2.086	2.094	184	200	2.163	2.165	32	15	2.047	2.058	118	108
Cu(morph *m*OMe btu)$_2$	85	75	2.090	2.095	192	204	2.165	2.165	31	11	2.052	2.060	113	106
Cu(morph *p*OMe btu)$_2$	84	77	2.091	2.096	187	204	2.162	2.160	32	14	2.055	2.064	116	106
Cu(Et$_2$ *o*OMe btu)$_2$	83	75	2.091	2.092	182	199	2.174	2.171	33	14	2.050	2.052	120	109
Cu(Et$_2$ *m*OMe btu)$_2$	86	78	2.087	2.095	187	205	2.165	2.161	35	15	2.048	2.062	116	105
Cu(Et$_2$ *p*OMe btu)$_2$	85	77	2.089	2.095	192	207	2.158	2.157	31	13	2.054	2.064	113	104
Cu(morph *o*NO$_2$ btu)$_2$	83	75	2.087	2.094	183	204	2.164	2.154	33	11	2.048	2.064	118	105
Cu(Et$_2$ *o*NO$_2$ btu)$_2$	83	72	2.092	2.098	189	201	2.163	2.161	30	11	2.056	2.066	114	108
Cu(Et$_2$ *m*NO$_2$ btu)$_2$	85	73	2.088	2.092	182	198	2.167	2.168	36	12	2.048	2.058	119	110
Cu(Et$_2$ *p*NO$_2$ btu)$_2$	83	73	2.088	2.095	186	204	2.165	2.159	31	8	2.049	2.063	117	106
Cu(morph OEttu)$_2$	85	66	2.094	2.103	170	185	2.206	2.204	46	7	2.038	2.052	130	119
Cu(pyrro OEttu)$_2$	88	64	2.083	2.094	177	188	2.204	2.202	44	2	2.022	2.040	125	117

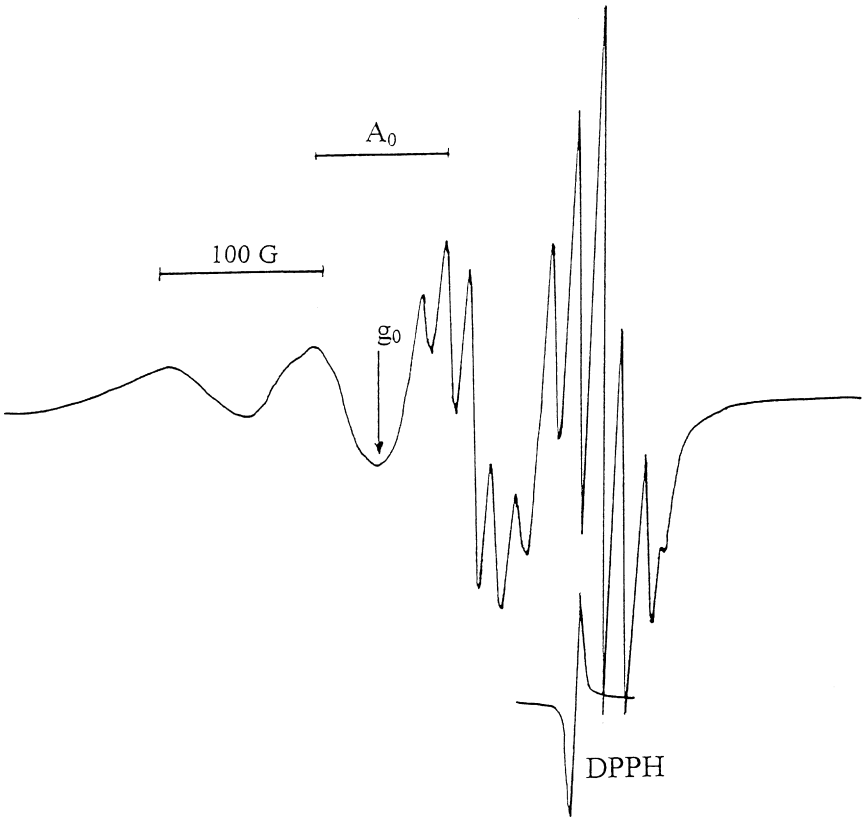

Fig. 2. ESR spectra of Cu(morph tc *m*-Cl b)$_2$ in $CHCl_3$-Ethanol solution at room temperature.

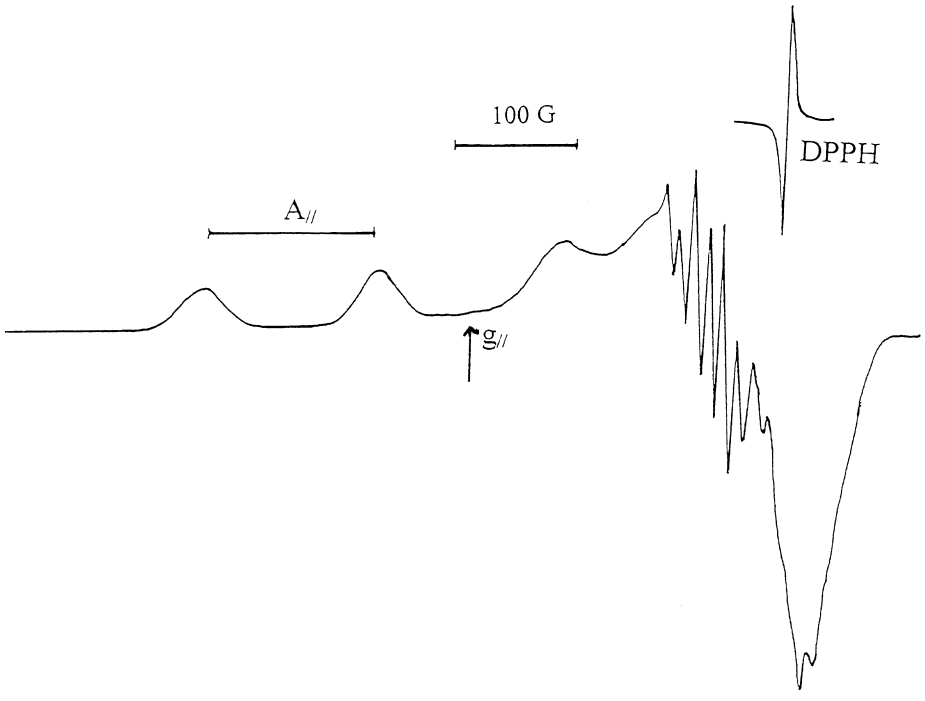

Fig. 3. ESR spectra of Cu(Et_2 tcPhb)$_2$ in $CHCl_3$-Ethanol solution at liquid-nitrogen temperature.

Table 2. ESR data for $Cu(S,NH)_2$ and $Cu(S,NHPh)_2$ complexes

Compounds	$\|A_0\| \times 10^4\,cm^{-1}$	g_0	$\|A_\parallel\| \times 10^4\ cm^{-1}$	$g_\parallel$	$\|A_\perp\| \times 10^4\,cm^{-1}$	$g_\perp$	$g_\parallel/\|A_\parallel\|$ cm
$Cu(morph\ tcb)_2$	80	2.069	186	2.136	27	2.035	115
$Cu(morph\ tc\ p\text{-}Clb)_2$	82	2.067	190	2.137	28	2.032	112
$Cu(morph\ tc\ m\text{-}Clb)_2$	82	2.069	190	2.141	28	2.033	113
$Cu(morph\ tcPhb)_2$	67	2.083	140	2.173	31	2.038	155
$Cu(morph\ tcPh\ p\text{-}Clb)_2$	68	2.080	147	2.174	29	2.033	148
$Cu(morph\ tcPh\ m\text{-}Clb)_2$	68	2.082	149	2.173	28	2.036	146
$Cu(Et_2\ tcPhb)_2$	63	2.082	149	2.169	20	2.038	146

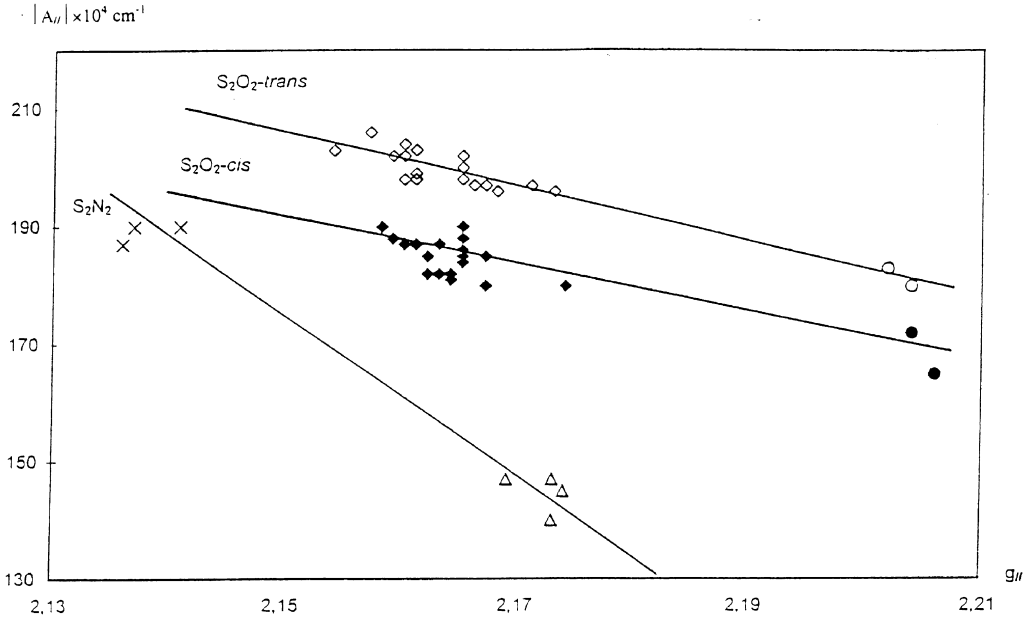

Fig. 4. Plot of $|A_\parallel|$ *vs* $g_\parallel$ with, ◇: *trans* $Cu(S,O\text{-substituted})_2$, ◆: *cis* $Cu(S,O\text{-substituted})_2$, ○: *trans* $Cu(S,O\text{-ethoxy})_2$, ●: *cis* $Cu(S,O\text{-ethoxy})_2$, ×: $Cu(S,NH)_2$, Δ: $Cu(S,NPh)_2$.

mophore. The $|A_\parallel|$ and $g_\parallel$ values are relatively insensitive to the inductive effect of the phenyl ring substituents and chiefly depend on the stereochemical factors as the redox properties. The $g_\parallel$ values are weaker in the "S,N" compounds in agreement with the more electron donating character of the nitrogen atom.

This study has shown the simultaneous presence of *cis* and *trans* isomers in the ratio 2:1 for all the "S,O" compounds as in the isosteric $Cu(Et_2N\text{-}CS\text{-}CH\text{-}CO\text{-}Ph)_2$ compound, whereas an only configuration seems present in the "S,N" complexes. The ratio $g_\parallel/|A_\parallel|$ is an empirical index of the tetrahedral distortion and the studied compounds can be arranged in the order square planar *trans* $Cu(S,O\ substituted)_2 \approx Cu(S,NH)_2 <$ *cis* $Cu(S,O\ substituted)_2 \approx$ *trans* $Cu(S,O\ ethoxy)_2 <$ *cis* $Cu(S,O\ ethoxy)_2 <$ strong tetrahedrally distorted $Cu(S,NPh)_2$.

REFERENCES

1. Mohamadou, A., Dechamps-Olivier, I. and Barbier, J. P., *Polyhedron*, 1994, **13,** 3277.
2. Guillon, E., Mohamadou, A., Dechamps-Olivier, I. and Barbier, J. P., *Polyhedron*, 1996, **15,** 947.
3. Guillon, E., Dechamps-Olivier, I., Mohamadou, A. and Barbier, J. P., *Inorg. Chim. Acta*, 1998, **268,** 13.
4. Richter, R., Beyer, L. and Kaiser, J., *Z. Anorg. Allg. Chem.*, 1980, **461,** 67.

5. Kirmse, R., Beyer, L. and Hoyer, E., *Chem. Phys. Lett*., 1976, **44,** 173.
6. Richter, R., Sieler, J., Ludwig, E., Uhlemann, E. and Golic, L., *Z. Anorg. Allg. Chem*., 1984, **513,** 114.
7. Yokoi, H. and Addison, A. W., *Inorg. Chem*., 1977, **16,** 1341.
8. Sagakuchi, U. and Addison, A. W., *J. Chem. Soc. Dalton Trans*., 1979, 600.

Pergamon

PII: S0277–5387(98)00102–8

Polyhedron Vol. 17, No. 19, pp. 3263–3268, 1998
© 1998 Elsevier Science Ltd
All rights reserved. Printed in Great Britain
0277–5387/98 $19.00+0.00

Syntheses and crystal structures of two isomers of $CuL_2(NO_3)_2 \cdot 2H_2O$ (L = N^1-isopropyl-2-methyl-1,2-propanediamine) and their thermochromism in the solid state

Chandi Pariya,[a] Ashutosh Ghosh,[b] Mohan M. Bhadbhade,[c] Beena Narayanan[c] and Nirmalendu Ray Chaudhuri[a,]†

[a]Department of Inorganic Chemistry, Indian Association for the Cultivation of Science, Calcutta 700 032, India

[b]Department of Chemistry, Calcutta University, 92, A.P.C. Road, Calcutta 700 009, India

[c]Sophisticated Analytical Instruments Laboratory, Central Salt and Marine Chemicals Research Institute, Gijubhai Badheka Marg, Bhavnagar 364 002, India

(Received 21 October 1997; accepted 3 March 1998)

Abstract—Two isomeric complexes, $[CuL_2](NO_3)_2 \cdot 2H_2O$, (**1**, red) and $[CuL_2](H_2O)](NO_3)_2 \cdot H_2O$, (**2**, blue) (L = N^1-isopropyl-2-methyl-1,2-propanediamine) have been synthesised and their X-ray crystal structures have been determined. Both the isomers possess the same space group, $P2_1/n$. However, **1** is square planar and **2** is square pyramid having N_4 and N_4O chromophore, respectively around copper(II). The red isomer (**1**) upon heating loses water molecules yielding a violet dehydrated species, **1a** which on further heating undergoes an exothermic phase transition accompanied by thermochromism, violet (**1a**) to blue-violet (**1b**) in the solid state. (**1a**) and (**1b**) are probably conformational isomers and they revert to **1** in humid atmosphere. The blue isomer (**2**) upon heating transforms to blue-violet species on dehydration, which reverts immediately after cooling in open atmosphere. © 1998 Elsevier Science Ltd. All rights reserved

Keywords: copper(II) nitrate; N^1-isopropyl-2-methyl-1,2-propanediamine; thermochromism; single crystal structure; isomer.

Thermochromism phenomena in nickel(II) and copper(II) complexes with N,N-diethyl-1,2-ethanediamine having counter anion as ClO_4^- and BF_4^- were studied extensively [1–5]. It was established that the sudden colour change in these compounds is due to the onset of dynamic disorder of diamine chelate rings. Later, a similar kind of thermochromism has been observed with other diamines (C-substituted [6, 7] and N-substituted [8]) with NO_3^- as counter anion which is coordinated in both the phases. In those studies it was found that the nature of substitution and the counter anion are very crucial for the thermochromic phase transition. Recently, we reported novel thermochromic phenomenon of nickel(II) salts using N^1-isopropyl-2-methyl-1,2-propanediamine [9, 10]. In these studies it was observed that slight variation of the experimental condition yielded different species. In the present paper we report the syntheses of two isomers of N^1-isopropyl-2-methyl-1,2-propanediamine copper(II) nitrate, their crystal structures and thermochromism in the solid state.

EXPERIMENTAL

General details

All the chemicals used were of A.R. grade. High-purity N^1-isopropyl-2-methyl-1,2-propanediamine

Non-SI unit employed: $\mu_B \approx 9.27402 \times 10^{-24}\,JT^{-1}$.

† Corresponding author.

(Aldrich) and $Cu(NO_3)_2 3H_2O$ (Merck) were available commercially. Analyses (C, H and N) were made by a 2400 (Series II) Perkin-Elmer elemental analyser. IR (in KBr and in nujol) and electronic spectra (in nujol) were recorded on a Perkin-Elmer IR (model 783) and Hitachi UV-VIS-NIR (model U-3410) spectrophotometer, respectively. The effective magnetic moments were evaluated from magnetic susceptibility measurements with an EG and G PAR 155 vibrating magnetometer. The thermal analyses (TG–DTA) were carried out on a Shimadzu DT-30 thermal analyser in dynamic atmosphere of dinitrogen (flow rate: 30 $cm^3 min^{-1}$). The sample (particle size within 150–200 mesh) was heated in a platinum crucible at a rate of 10°C min^{-1} with inert alumina as reference. The enthalpy changes of phase transformations were calculated using a Perkin-Elmer (model DSC-7) differential scanning calorimeter with indium metal as a calibrant (rate of heating 10°C min^{-1}).

Preparation of $[CuL_2](NO_3)_2 \cdot 2H_2O$ (**1**)

This was prepared by adding N^1-isopropyl-2-methyl-1,2-propanediamine (2 mmol) dropwise to copper(II) nitrate trihydrate (1 mmol, 241.6 mg) dissolved in ethanol-water (9:1) (10 cm^3) on stirring. The resulting violet solution on slow evaporation in a desiccator yielded the desired red crystalline complex. The crystals were separated, washed with ethanol and dried in a desiccator. Found: C, 34.8; H, 8.4; N, 17.3; Cu, 13.2. Calc. for $C_{14}H_{40}N_6O_8Cu$: C, 34.7; H, 8.3; N, 17.4; Cu, 13.1% μ_{eff} 1.64 μ_B, λ_{max} (nujol) 481 nm. Single crystals suitable for X-ray single crystal analysis were obtained by the diffusion technique from methanol and diethylether layer.

Preparation of $[CuL_2(H_2O)](NO_3)_2 \cdot H_2O$ (**2**)

N^1-isopropyl-2-methyl-1,2-propanediamine (3 mmol) was added dropwise to copper(II) nitrate trihydrate (1 mmol, 241.6 mg) dissolved in methanol on stirring. The resulting violet solution on slow evaporation in a desiccator yielded the desired blue crystalline complex. The crystals were separated, washed with methanol and dried in a desiccator. (Found: C, 34.7; H, 8.3; N, 17.4; Cu, 13.1. Calc. for $C_{14}H_{40}N_6O_8Cu$: C, 34.7; H, 8.3; N, 17.4; Cu, 13.1%) μ_{eff} 1.72 μ_B, λ_{max} (nujol) 652 and 580 nm. Recrystallisation from methanol yielded a mixture of blue and red crystals. The blue crystals were separated carefully and used for X-ray analysis.

X-ray data collection and structure refinement

Crystallographic data for complexes **1** and **2** are summarised in Table 1. Both the structures were solved by the heavy-atom method and refined by the full-matrix least-squares procedures. The H-atom positions were mostly found from the difference Fourier maps, the remaining were fixed at appropriate geometries. The refinement parameters are given in Table 1. All computations were carried out on a PDP-II/73 computer using Structure Determination Package (SDP) available from Enraf Nonius [11]. The selected bond distances and angles of complexes **1** and **2** are listed in Table 2. Recognised strong hydrogen bonds are given in Table 3. Table 4–13 containing the final positional parameters of non-hydrogen atoms, along with their isotropic equivalent temperature factors, complete bond distances and bond angles, anisotropic thermal parameters, H-atom coordinates, and list of observed and calculated structure factors for **1** and **2** are parts of supplementary materials.

RESULTS AND DISCUSSION

The red species, $CuL_2(NO_3)_2 \cdot 2H_2O$ (**1**) is generated on mixing copper(II) nitrate trihydrate and diamine in exactly 1:2 ratio in ethanol-water (9:1). Addition of excess ligand to the Cu-salt (*ca.* 3:1 ratio) in the same solvent yields a mixture of red and blue isomers. The pure blue species (**2**) is produced in presence of excess diamine when methanol is used as solvent. However, on recrystallisation either from methanol and ethanol-water, the blue species yields a mixture of red and blue isomers. The water molecules in complex **2** which is synthesised from methanol, comes from the hydrated Cu-salt as there is no other apparent source.

Structures of (**1**) *and* (**2**)

ORTEP [12] view of the complex molecules **1** and **2** with the two NO_3^- ions and water molecules are shown in Figs 1 and 2. Both the isomers (**1** and **2**) possess space group $P2_1/n$ but they differ in geometry. In structure **1** four nitrogen atoms from the two diamine molecules provide the tetra coordination which has a bias towards tetrahedral distortion, the deviation of N(1), N(2), N(3) and N(4) from the best plane through them is ± 0.08 Å. An additional long axial coordination from O(1w) (Cu(1)...O(1w) = 2.205(5) Å) makes the Cu(II) environment as square-pyramidal in **2**, the base of the pyramid is much more distorted tetrahedral than in **1**, the deviations of N(1), N(2), N(3) and N(4) are ± 0.11 Å from the least square plane and the displacement of Cu atom is 0.31 Å towards O(1w) from this plane. Average of Cu–N(primary amine) distances Cu(1)–N(2) and Cu(1)–N(3) is 1.987(3) Å for **1** and 2.003(3) Å for **2**, whereas average of Cu to secondary amine bonds Cu(1)–N(1) and Cu(1)–N(4) is more, 2.028(3) Å and 2.129(3) Å for **1** and **2**, respectively. The tendency of metal-nitrogen (primary) lengths shorter than the metal-nitrogen (secondary) lengths is noticed in N-substituted amines [13], and particularly reported for copper complexes of this ligand, with different anions [13, 14]. Bite angles N–Cu–N vary from the ideal value of 90°, which are

Table 1. Crystallographic data for complexes **1** and **2**

	1	**2**
Molecular formula	$C_{14}H_{40}N_6O_8Cu$	$C_{14}H_{40}N_6O_8Cu$
Molecular weight	484.05	484.05
Space group	Monoclinic, $P2_1/n$	Monoclinic, $P2_1/n$
a (Å)	8.624(4)	10.283(3)
b (Å)	19.361(8)	13.364(5)
c (Å)	14.599(5)	17.208(4)
β (°)	90.02(2)	101.51(2)
Z	4	4
V (Å^3)	2437.6(2)	2317.2(2)
Radiation used, λ (Å)	Mo–Kα, 0.7107	Cu–Kα, 1.5418
D_c (g cm^{-3})	1.319	1.387
Absorption coeff, μ(cm^{-1})	9.41	17.23
Temperature (K)	295	295
Colour and description	red plates	blue plates
Crystal dimensions (mm)	$0.40 \times 0.14 \times 0.04$	$0.28 \times 0.20 \times 0.08$
Diffractometer	Enraf-Nonius CAD-4	Enraf-Nonius CAD-4
Scan mode	$\omega/2\theta$	$\omega/2\theta$
Absorption correction	empirical	empirical
Transmission min, max	0.931, 0.999	0.755, 0.999
Measured reflections	2507	3882
Observed reflection $I > 3\sigma(I)$	2421	2938
θ_{max}	24	38
h_{min}, h_{max}	0, 9	0, 12
k_{min}, k_{max}	0, 22	0, 15
l_{min}, l_{max}	−16, 16	−20, 19
Refinement on	$\|F\|$	$\|F\|$
Final R	0.041	0.072
Weighted R	0.053	0.091
Reflections used	2421	2938
No. of parameters in least-squares	262	262
Hydrogen atom positions	not refined	not refined
$(\Delta/\sigma)_{max}$	0.02	0.02
Weighting scheme	$1/\sigma^2(F)$	$1/\sigma^2(F)$
$\Delta\rho_{max}$ (eÅ^{-3})	0.51	0.69
$\Delta\rho_{min}$ (eÅ^{-3})	−0.37	−0.73
Extinction correction	not applied	not applied

$R = \Sigma \| F_0 | - | F_c \| / \Sigma | F_o |$, $wR = [\Sigma w(F_0^2 - F_c^2) / \Sigma w(F_0^2)^2]^{1/2}$, $w = 1/[\sigma^2(F_0) + p(F_o)^2]$

slightly larger in **1** (average 84.8(1)°) than in **2** (average 83.5(2)°) (Table 3). Bond lengths and bond angles in the ligand moiety of **1** and **2** are similar except for the presence of a rather long bond C(3)–C(11) = 1.567(8) Å in **1**, which is also reported in the structure of Ni, Cu, Zn and Cd complexes of the same ligand [10, 14, 15, 16]. Conformations of N^1-isopropyl-2-methyl-1,2-propanediamine chelate ring are envelopes in both the structures (Figs 1 and 2); the deviations of the flap atoms C(2) and C(3) are 0.51 Å and 0.71 Å, respectively in **1** and 0.60 Å and 0.63 Å, respectively in **2**. The isopropyl groups in **2** are rotated about the N(1)–C(7) and N(4)–C(12) bonds in such a way that positions of C(8) and C(13) are essentially same as in **1** but the C(9) and C(14) are rotated away from the incoming water O(1w) to avoid the steric hindrance. This is clearly reflected in the torsion angles C(1)–N(1)–C(7)–C(8) and C(1)–N(1)–C(7)–C(9) are 52.6(1)° and −72.6(1)°, respectively in **1**, whereas these values are 57.6(1)° and 179.7(1)°, respectively in **2**. Similarly torsion angles C(4)–N(4)–C(12)–C(13) and C(4)–N(4)–C(12)–C(14) are 54.2(1)° and −72.5(1)°, respectively in **1** but 55.8(1)° and 178.0(1)°, respectively in **2**.

Intermolecular interaction

In both the structures, NO_3^- anions present in the crystal lattice take part only in the hydrogen bonding interactions with the amine nitrogens of the ligand, but do not coordinate to the metal ion directly. However, the role of anions is very significant in governing the intermolecular interactions that influence the thermochromic behaviour in solid state. It may be mentioned here that the ClO_4 [13] and NO_3 [14] salts

Table 2. Selected bond distances (Å) and angles (°) for complexes **1** and **2** with e.s.d.'s in parentheses

A–B	**1**	**2**
Cu(1)–O(1 w)		2.205(4)
Cu(1)–N(1)	2.028(4)	2.114(4)
Cu(1)–N(2)	1.991(4)	1.998(3)
Cu(1)–N(3)	1.982(4)	2.008(3)
Cu(1)–N(4)	2.029(4)	2.145(5)
N(1)–C(1)	1.482(6)	1.489(6)
N(1)–C(7)	1.521(5)	1.501(7)
N(2)–C(2)	1.501(7)	1.488(7)
N(3)–C(3)	1.487(6)	1.504(7)
N(4)–C(4)	1.493(6)	1.497(6)
N(4)–C(12)	1.510(6)	1.505(7)
O(1W)–Cu(1)–N(1)		96.9(1)
O(1W)–Cu(1)–N(2)		100.0(2)
O(1W)–Cu(1)–N(3)		104.1(2)
O(1W)–Cu(1)–N(4)		94.1(2)
N(1)–Cu(1)–N(2)	84.8(2)	83.3(2)
N(1)–Cu(1)–N(3)	95.4(1)	94.3(2)
N(1)–Cu(1)–N(4)	179.3(2)	168.9(2)
N(2)–Cu(1)–N(4)	95.1(2)	94.1(2)
N(2)–Cu(1)–N(3)	171.6(2)	155.9(2)
N(3)–Cu(1)–N(4)	84.8(2)	83.7(2)
Cu(1)–N(1)–C(1)	107.8(3)	106.2(3)
Cu(1)–N(2)–C(2)	109.3(3)	109.8(3)
Cu(1)–N(3)–C(3)	106.7(2)	108.9(3)
Cu(1)–N(4)–C(4)	109.7(3)	105.4(3)
N(1)–C(1)–C(2)	110.3(4)	111.2(4)
N(2)–C(2)–C(1)	104.2(4)	103.9(4)
N(3)–C(3)–C(4)	105.8(3)	105.3(4)
N(4)–C(4)–C(3)	108.3(4)	112.1(4)

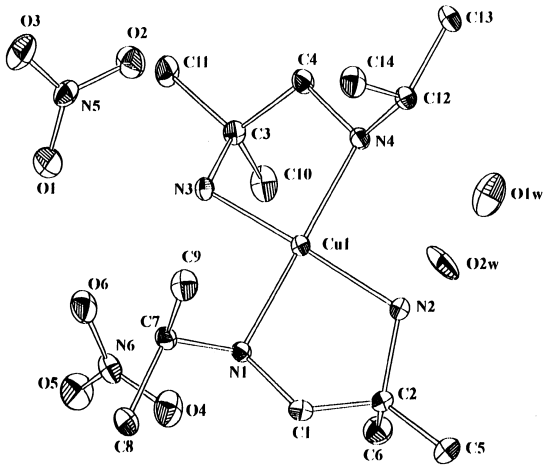

Fig. 1. ORTEP view of $[CuL_2](NO_3)_2 \cdot 2H_2O$ **1**.

of Cu-complexes with the ligand under investigation are nonthermochromic. There are extensive hydrogen bonding network between the oxygens of the nitrates, water molecules and the N–H groups of the ligand (Table 3). Remarkably, the two nitrate groups have their H-bond attachments with the ligand conserved in both the structures a strong H-bond N(3)–H(2)N(3)...O(1) (from the nitrate group N(5), O(1), O(2), O(3)) and N(3)–H(1)N(3)...O(5) (from the nitrate group N(6), O(4), O(5), O(6)) are retained in the two isomers (Table 3). The hydrogen bonding interactions of the two water molecules are in a sense

Table 3. Hydrogen bonding parameters for complexes **1** and **2** (e.s.d.'s of X...Y in the range 0.005–0.008 Å)

Atom X–H...Y/symm 1/	Atom	Atom	Dist (Å) X–H	Dist (Å) H...Y	Dist (Å) X...Y	Angle (°) (X–H...Y)	Symm 1
$[CuL_2](NO_3)_2 \cdot 2H_2O$ **1**							
N1	H1	O4	1.01	2.01	3.005	166.3	X,Y,Z
N2	H2	O6	1.01	2.30	3.224	152.1	1+X,Y,Z
N2	H3	O1W	1.01	1.94	2.915	161.8	X,Y,Z
N3	H4	O6	1.01	1.97	2.969	169.9	X,Y,Z
N3	H5	O1	1.01	2.52	3.264	130.3	−1+X,Y,Z
N4	H6	O2W	1.01	1.89	2.902	169.6	X,Y,Z
O1W	H1W	O1	1.09	1.74	2.839	179.9	X,Y,Z
O1W	H2W	O3	1.09	1.72	2.811	179.6	2−X,1−Y,−Z
O2W	H3W	O2	1.10	1.77	2.880	179.7	X,Y,Z
O2W	H4W	O5	1.10	1.96	3.064	179.4	1+X,Y,Z
$[CuL_2(H_2O)](NO_3)_2 \cdot H_2O$ **2**							
N2	H3	O2	1.01	2.14	3.114	160.5	1−X,−Y,1−Z
N3	H5	O5	1.01	2.28	3.240	158.7	X,−1+Y,Z
O1W	H1W	O3	1.10	1.62	2.721	179.0	X,Y,Z
O1W	H2W	O4	1.10	1.69	2.793	179.8	X,Y,Z
O2W	H3W	O5	1.10	1.88	2.981	179.5	X,Y,Z
O2W	H4W	O6	1.10	1.74	2.838	179.6	X,Y,Z

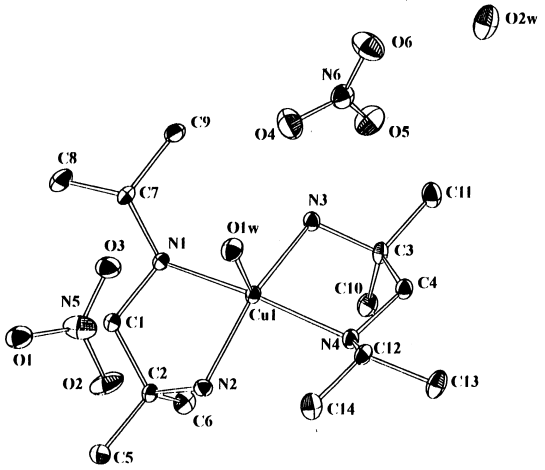

Fig. 2. ORTEP view of $[CuL_2(H_2O)](NO_3)_2 \cdot H_2O$ **2**.

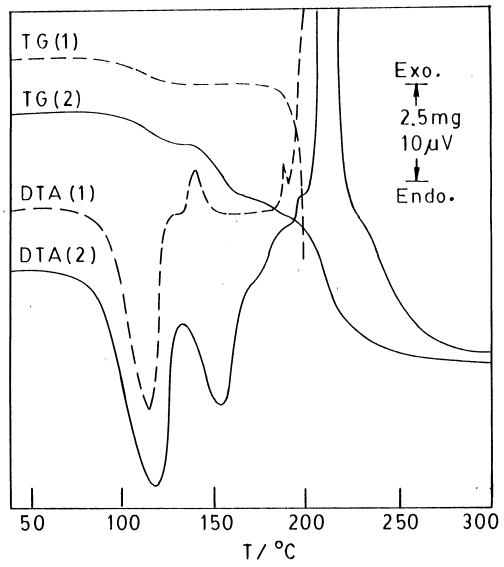

Fig. 3. TG and DTA curves of $[CuL_2](NO_3)_2 \cdot 2H_2O$ **1** (weight taken = 8.32 mg - - -) and $[CuL_2(H_2O)](NO_3)_2 \cdot H_2O$ **2** (weight taken = 10.14 mg ———).

complementary in the two structures, O(1w) makes H-bonding interactions with N(2), O(4) and O(2w) makes only single interactions with N(4) in **1**; O(1w) upon coordination to the Cu(II) ion in **2** retains only the interactions with O(4), the H-bond lost with N(2) and O(6) are provided by the water molecule O(2w). It is worth noting that the thermal anisotropies of the water molecules O(1w) and O(2w) are higher in **1** compared to **2.** It is tempting to surmise that free water molecules and anions upon heating would enhance their thermal vibrations furthermore, creating a dynamic situation for the thermochromic phase transition to take place.

Thermal analysis and thermochromism

The simultaneous thermogravimetric analyses and differential thermal analysis (TG–DTA) of complexes of **1** and **2** are shown in Fig. 3. The weight loss observed in the TG curves in the temperature regions (80–120°C and 80–130°C, for **1** and **2**, respectively) corresponds to the liberation of two molecules of water. In complex **1** (red), the dehydration proceeds endothermally resulting in a violet species (**1a**). **1a** on further heating undergoes an exothermic phase transformation (138–160°C; $\Delta H = -6.4\,kJ\,mol^{-1}$) and transforms to **1b** associated with a colour change, violet to blue-violet. The species, **1b** is metastable and transforms to **1** on keeping in a humid atmosphere for a few h. In a P_4O_{10}-desiccator, however, it slowly reverts to **1a** and the reversion completes in several days. The dehydrated species of complex **2** is extremely hygroscopic and transforms to **2** immediately on exposure to open atmosphere. Moreover, complex **2** starts to decompose (140°C) immediately after dehydration. Therefore, isolation and characterisation of the dehydrated species of **2** in pure form is difficult.

Electronic spectra and magnetic moments

The electronic spectrum (Fig. 4) of the red species **1** shows a broad band at 481 nm and that of the blue species shows a broad band at 580 nm and a shoulder at 653 nm consistent with the square planar geometry in the former and the axial interaction of the water molecule in the later [4]. The band position of higher

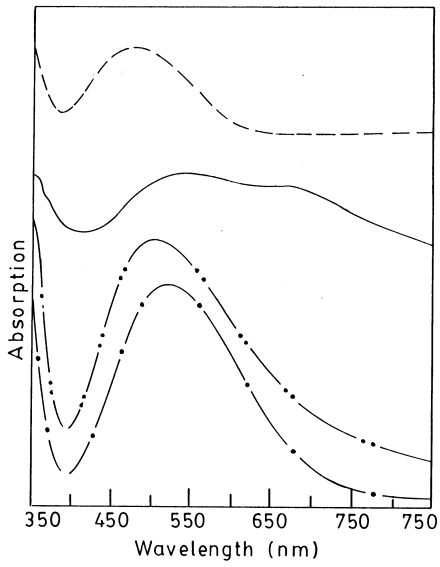

Fig. 4. Electronic spectra (nujol) of $[CuL_2](NO_3)_2 \cdot 2H_2O$ **1** (—-), $[CuL_2](NO_3)_2$ **1a** (—— ——), $[CuL_2](NO_3)_2$ **1b** (- -) and $[CuL_2(H_2O)](NO_3)_2 \cdot H_2O$ **2** (———).

energy of the red complex is also compatible with the increased involvement of the copper orbitals with the in-plane ligands due to electronic or steric reasons. The electronic spectra of **1a** and **1b** are very similar to that of **1** consisting of a broad structureless band in the visible region suggesting retention of square planar geometry in both of them. The only difference is that the band positions are shifted towards lower energy.

The magnetic moments of all the complexes are around 1.7 μ_B, indicating the presence of one unpaired electron in all of them.

Infrared spectra

IR spectroscopy in the region 1700–1800 cm^{-1} where a weak combination band of the ν_1 symmetric stretching and the doubly degenerate in-plane bending mode of NO_3^- ion in a metallic complex appear was used by several groups of researchers to determine the coordination mode of the NO_3^- ion [17–20]. It is believed that an ionic nitrate group gives rise to one relatively strong and very sharp peak at *ca.* 1750 cm^{-1} while coordinated nitrate groups give two peaks with the bidentate coordination mode giving a wider separation (20–66 cm^{-1}) of these two peaks than the unidentate coordination mode (5–26 cm^{-1}). X-ray single crystals analyses of **1** and **2** show that the NO_3^- ions are free in both of them. Therefore, a single relatively strong peak is expected at *ca.* 1750 cm^{-1}. The IR spectra in nujol mull however, show two additional peaks in this region. It is very difficult to assign whether those peaks correspond to i) the splitting of the combination band or ii) to the appearance of some other combination bands or iii) to the intermolecular or intramolecular correlation coupling of the nitrate groups. However, considering the uncoordinated mode of the NO_3^- ion only the peak near 1730 cm^{-1} is considered here as the combination band. The IR spectra of **1a** and **1b** in this region are very similar to complex **2**; thus the NO_3^- ions in both of them are considered as uncoordinated. The IR spectra of **1a** and **1b** differ appreciably in the regions of 3300–3100, 3000–2800, 1400–1350, 1330–1100 and 1000–430 cm^{-1} where the vibrations of $\nu(NH_2)$, $\nu(CH_2)$, $\rho w(CH_2)$, $\tau(NH_2)$ + $\rho w(NH_2)$ + $\tau(CH_2)$, and $\rho w(NH_2)$ + ν(M–N) appear. In our earlier studies it was observed that the isomers which differ only in the conformations of the diamine chelate rings usually show such differences [21, 22].

Conclusion

The single crystal X-ray analysis, IR and electronic spectra of the complexes reveal that the red complex (**1**) retains its square planar geometry on deaquation. The deaquated species on further heating undergoes thermochromic phase transition due to conformational isomerism. The blue isomer (**2**), on the other hand, is square pyramidal, having an additional coordination from one of the water molecules. It starts to decompose immediately after deaquation. Thus the characterisation and thermal studies of the deaquated species (from **2**) was not possible.

Acknowledgements—The authors thank the Council of Scientific and Industrial Research, New Delhi (grant to NRC and Senior Research Fellowship to BN) and Department of Science and Technology, Govt. of India (grant to MMB) for providing financial support. They are also grateful to The Director, CSMCRI for providing a single crystal diffractometer.

REFERENCES

1. Hatfield, W. E., Piper, T. S. and Klabunde, U., *Inorg. Chem.*, 1963, **2,** 629.
2. Pylkki, R. J., Willett, R. D. and Dodgen, H. W., *Inorg. Chem.*, 1984, **23,** 594.
3. Yokoi, H. and Sai, M., Isobe, T., *Bull. Chem. Soc. Jpn.*, 1969, **42,** 2232.
4. Lever, A. B. P., Mantovani, E. and Donini, J. C., *Inorg. Chem.*, 1971, **10,** 2424.
5. Bloomquist, D. R. and Willett, R. D., *Coord. Chem. Rev.*, 1982, **47,** 125.
6. Menabue, L., Pellacani, G. C., Battaglia, L. P., Corradi, A. B., Sandrolini, F., Motori, A., Pylkki, R. J. and Willett, R. D., *J. Chem. Soc., Dalton Trans.*, 1984, 2187.
7. Koner, S., Ghosh, A., Pariya, C., Das, D., Kikuchi, H., Okamoto, K. and Ikeda, R., *J. Mol. Struct.*, 1995, **345,** 265.
8. Koner, S., Ghosh, A., Ray Chaudhuri, N., Mukherjee, A. K., Mukherjee, M. and Ikeda, R., *Polyhedron*, 1993, **12,** 1311.
9. Pariya, C., Ghosh, A. and Ray Chaudhuri, N., *J. Chem. Res.* (*S*), 1994, 136.
10. Pariya, C., Ghosh, S., Ghosh, A., Mukherjee, M., Mukherjee, A. K. and Ray Chaudhuri, N., *J. Chem. Soc., Dalton Trans.*, 1995, 337.
11. B. A. Frenz and Associates, *SDP Structures Determinations Package*. College Station, Taxas and Enraf-Nonius, Deltt, The Netherlands, 1985.
12. Johnson, C. K., *ORTEP II Report ORNL*-3794. Oak Ridge National Laboratory, Tennessee, 1976.
13. Kansikas, J., *Acta Chem. Scand.*, 1987, **A41,** 533.
14. Pajunen, A. and Pajunen, S., *Acta Cryst.*, 1979, **B35,** 3058.
15. Pariya, C., Ray Chaudhuri, N. and Das, A., Seth, S., *Acta Chem. Scand.*, 1995, **49,** 859.
16. Pariya, C., Ray Chaudhuri, N. and Seth, S., Das, A., *Acta Cryst*, 1996, **52C,** 358.
17. Curtis, N. F. and Curtis, Y. M., *Inorg Chem.*, 1965, **4,** 804.
18. Lever, A. B. P., Mantovani, E. and Ramaswamy, B. S., *Can. J. Chem.*, 1971, **49,** 1957.
19. Ihara, Y. and Fukuda, Y., Sone, K., *Inorg Chem.*, 1987, **26,** 3745.
20. Koner, S., Ghosh, A. and Ray Chaudhuri, N., *J. Chem. Soc., Dalton Trans.*, 1990, 1563.
21. De, G., Biswas, P. K. and Ray Chaudhuri, N., *J. Chem Soc., Dalton Trans.*, 1984, 2591.
22. Mukherjee, A. K., Mukherjee, M., Welch, A. J., Ghosh, A., De, G. and Ray Chaudhuri, N., *J. Chem Soc., Dalton Trans.*, 1987, 997.

Pergamon

PII: S0277–5387(98)00105–3

Polyhedron Vol. 17, No. 19, pp. 3269–3274, 1998
© 1998 Elsevier Science Ltd
All rights reserved. Printed in Great Britain
0277–5387/98 $19.00+0.00

X-ray characterization of an unusual product obtained from [VO(Sal–Phe)(H_2O)] in H_2O/pyridine solutions

A. Bernalte,[a] F. J. G. Barros,[a] I. Cavaco,[b] J. Costa Pessoa,[b,*] R. D. Gillard,[c*] F. J. Higes[a*] and I. Tomaz[b]

[a]Departamento Química Inorgánica, Universidad de Extremadura, 06071, Badajoz, España.

[b]Centro Química Estrutural, Instituto Superior Técnico, Av. Rovisco Pais, 1096, Lisboa, Portugal.

[c]Department of Chemistry, University of Wales, P.O. Box 912, CF1 3TB, Cardiff, U.K.

(Received 10 December 1997; accepted 3 March 1998)

Abstract—A vanadium(V) dimer [{$VO_2(py)_2$}$_2$(μ–C_2O_4)] **1**, has been isolated from a solution of [VO(sal–Phe)(H_2O)] **2** (sal–Phe = N–salicylidene–L–phenylalaninate) in H_2O/pyridine. Its crystal and molecular structure has been determined by X-ray diffraction analysis, the oxalate acting as a symmetrical bis(chelating) bridge. Possible mechanisms for the formation of oxalate are briefly discussed. © 1998 Elsevier Science Ltd. All rights reserved

Complexes of metal ions with N–salicylideneamino acids serve as model systems for pyridoxal-potentiated enzymes [1] and several studies [2–9] have focused on vanadium in this context.

Several unusual reactions have been recently reported involving such systems. One case involves the reaction of VO^{2+} with salicylaldehyde, D, L-asparagine (D,L-Asn) and pyridine, first forming [VO(sal–D,L–Asn)(py)(H_2O)]; ageing with di-oxygen produced coumarine–3–carboxamide [10]. Other coumarine–3–carboxamides are produced starting with salicylaldehyde derivatives [11]. These reactions cannot be simply explained by mechanisms described for pyridoxal model systems [12]. Another interesting reaction occurred from solutions of [VO(sal–L–Trp)(H_2O)] (L–Trp = L–tryptophan) in H_2O/pyridine. Brown crystals of $(Hpy^+)_4(L^+)_2[V_{10}O_{28}{}^{6-}]$ (py = pyridine, $L^+ = C_{14}H_{13}N_2$, product of the condensation of the tryptophan side group with pyridine), have been isolated after 4 weeks and characterized by X-ray crystallography [13]. The formation of L^+ can be explained assuming a mechanism similar to that for model systems of pyridoxal-potentiated enzymes [12], which involves the release of the side group of the amino acid [13].

The present paper describes the synthesis and characterization (by X-ray crystallography and IR) of the vanadium(V) dimer [{$VO_2(py)_2$}$_2$(μ–C_2O_4)] **1** containing a bridging bis(chelating) oxalato ligand. Part of this work has been communicated [14]. Rather similar dinuclear complexes are known with crystal and molecular structures determined by X-ray diffraction, *e.g.*[$Ni(NO_2)(py)_3$–μ–(ox)–$Ni(NO_2)(py)_3$].2py [15] **3** (py = pyridine, ox = oxalate), [$Ru(NO_2)(py)_4$–μ–(ox)–$Ru(py)_4$].(BF_4) [16] **4**, [{Cu(terpy)(H_2O)}$_2$(ox)].[{Cu(terpy)}$_2$(ox)].(ClO_4).2H_2O] [17] (terpy = 2,2′:6′,2″–terpyridine), [Cu(bipy)(H_2O)–μ–(ox)–Cu(bipy)(H_2O)]$^{2+}$.[Cu(bipy)(ox)](NO_3^-)$_2$ [18]. (bipy = 2,2′–bipyridyl). Many other dinuclear complexes with the oxalate ion functioning as a bridging bis(chelating) ligand were characterized by X-ray diffraction [19–30]; most are dimeric compounds of Ni(II) or Cu(II) with interesting magnetic properties. A similar bis-bidentate bridging oxalate has been proposed for several other complexes mainly by consideration of the infrared spectra (*e.g.* [31–33]). These include the dinuclear vanadium(IV) complexes (Ct)$_2$[$V_2O_2Cl_4$(ox)(H_2O)$_2$].2H_2O (Ct = $(CH_3)_4N$), $(C_2H_5)_4N$) [33]. There are, of course, several vanadium complexes [34] with

*Author to whom correspondence should be addressed.

the oxalate acting as a bidentate ligand, including several compounds characterized by single crystal X-ray diffraction [21, 35, 36, 37]. All these, from **3** onwards, required oxalate ion for their synthesis, in contrast to **1**, which involves the unexpected formation of oxalate.

EXPERIMENTAL

Reagents and apparatus

[VO(sal–Phe)(H_2O)] **2** (sal–Phe = N–salicylidene–L–phenylalaninate) was prepared as described earlier [6, 38]. This (0.25 g, 0.71 mmol) was dissolved in the minimum amount of pyridine ($\approx$1.5 ml), and $\approx$0.2 ml of water were added. The mixture was kept at $\approx$4°C in a small tube with a polyethylene stopper. After a week the brown solution became yellow and after $\approx$3 months yellow crystals of **1** were separated. No recrystallization was needed. The compound is slightly sensitive to moisture, but can be kept in its mother liquor for several months. The FTIR spectrum of **1** was recorded with the solid dispersed in KBr disk using a Perkin-Elmer 1720 spectrometer.

The reaction was repeated twice and is reproducible; in these two distinct batches **1** was isolated and characterized by FTIR and/or determination of cell constants.

X-ray crystal structure determination of complex **1**

Crystal data. $V_2O_4(C_2O_4)(C_5H_4N)_2$, $M_r = 285.1$, monoclinic, space group $P2_1/c$, $a = 6.267(1)$, $b = 19.432(3)$, $c = 10.626(1)$ Å, $\beta = 103.13(1)°$, $V = 1260.2(3)$ Å^3, $Z = 4$, $F(000) = 580$, $D_c = 1.50$ g cm^{-3}, μ(Mo–K_α) = 7.94 cm^{-1}. Crystal dimensions 0.37 × 0.20 × 0.18 mm.

Data collection. X-ray measurements were made at room temperature with a Siemens P4 diffractometer and graphite monochromatized Mo–K_α radiation ($\lambda = 0.71073$ Å). Cell dimensions were determined from the measured θ-values for 40 intense reflections with $8.9 < \theta < 24.8°$. 4475 reflections were scanned in the range $1 < \theta < 30°$ by the ω–2θ scan mode, and of these 3635 were independent ($R_{int} = 0.025$). Examination of three standard reflections, monitored after 97 scans, showed no sign of crystal deterioration. Data were corrected for Lorentz and polarization effects, and also for absorption effects using an empirical method based on azimuthal scan data.

Structure determination and refinement. The structure was solved by direct methods and subsequent Fourier differences and refined by full-matrix least-squares using anisotropic thermal parameters for non-hydrogen atoms. The hydrogen atoms were located from a differential Fourier synthesis and placed in idealised positions (C–H = 0.96 Å) riding on their respective bonded atoms. The final refinement was carried out with a weighting scheme of $w = [1/\sigma^2(F_0) + 0.0004F^2_0]$ and converged to $R(F) = 0.043$ and $R_w(F) = 0.043$ for 2274 reflections with $F_0 > 4\sigma(F_0)$ and 163 refined parameters. The largest negative and positive peaks in the final difference map were 0.31 and -0.27 e Å^{-3} and were located near the vanadium atoms. All calculations were performed on an Silicon Graphics Iris Indigo XS24 computer using the SHELXTL-IRIS program package [39].

Additional material is available from the Cambridge Crystallographic Centre: it comprises hydrogen atom co-ordinates, atomic thermal motion parameters, remaining bond lengths and angles and a list of observed and calculated structure factors.

RESULTS AND DISCUSSION

The solid dimer **1** was isolated from H_2O/pyridine solutions. Although pyridine and bipyridyl may stabilise oxovanadium(IV) complexes [4, 6, 9, 34, 40], the formation of a vanadium(V) compound may be explained by the slow diffusion of atmospheric dioxygen into the solution, and its reaction with oxovanadium(IV). Several examples of similar oxidations have been reported (*e.g.*[5, 6, 41]).

A molecular diagram presenting the numbering scheme is shown in Fig. 1; selected bond distances and bond angles are listed in Table 1. The crystal contains two centrosymmetrical binuclear molecules per unit cell, with the vanadium(V) ions separated by 5.787(1) Å and bridged by a bis-bidentate oxalate group. The co-ordination geometry around each vanadium atom is distorted octahedral; the equatorial positions are occupied by two vanadyl oxygen atoms [O(1) and O(2)] and two oxalate oxygen atoms [O(3)

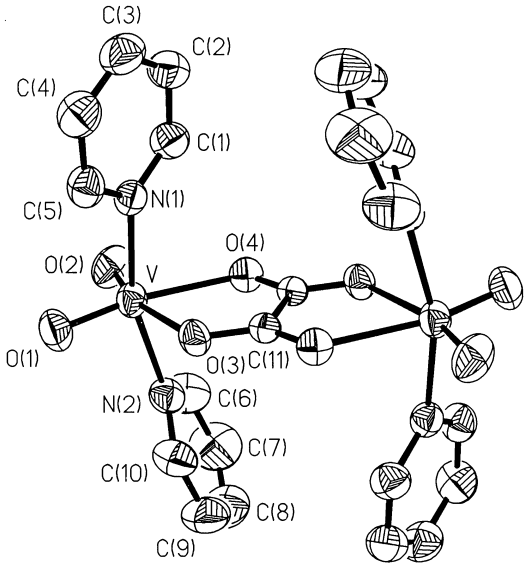

Fig. 1. Molecular structure of [{$VO_2(py)_2$}$_2$(μ–C_2O_4)] **1** showing the atomic numbering scheme. The thermal ellipsoids are drawn at the 50% level.

Table 1. Selected bond lengths (Å) and angles (°) for [{$VO_2(py)_2$}$_2$(μ–C_2O_4)] **1**.

V–O(1)	1.618(2)	V–O(2)	1.616(2)
V–O(3)	2.205(2)	V–O(4)	2.219(2)
V–N(1)	2.133(2)	V–N(2)	2.141(2)
O(3)–C(11)	1.249(3)	O(4)–C(11A)	1.247(3)
C(11)–C(11A)	1.539(5)	N(1)–C(1)	1.341(4)
N(1)–C(5)	1.336(4)	C(1)–C(2)	1.374(4)
C(2)–C(3)	1.381(5)	C(3)–C(4)	1.361(5)
C(4)–C(5)	1.380(4)	N(2)–C(6)	1.328(4)
N(2)–C(10)	1.343(4)	C(6)–C(7)	1.379(5)
C(7)–C(8)	1.362(7)	C(8)–C(9)	1.369(6)
C(9)–C(10)	1.375(5)		
O(1)–V–O(2)	105.8(1)	O(1)–V–O(3)	90.1(1)
O(1)–V–N(1)	95.2(1)	O(1)–V–N(2)	96.9(1)
O(2)–V–O(4)	90.7(1)	O(2)–V–N(1)	95.8(1)
O(2)–V–N(2)	93.8(1)	O(3)–V–O(4)	73.4(1)
O(3)–V–N(1)	82.0(1)	O(3)–V–N(2)	84.5(1)
O(4)–V–N(1)	84.5(1)	O(4)–V–N(2)	80.1(1)
O(1)–V–O(4)	163.4(1)	O(2)–V–O(3)	164.0(1)
N(1)–V–N(2)	161.9(1)	V–O(3)–C(11)	117.5(2)
V–O(4)–C(11A)	116.7(2)	V–N(1)–C(1)	122.4(2)
V–N(1)–C(5)	120.0(2)	V–N(2)–C(6)	119.1(2)
V–N(2)–C(10)	123.0(2)	O(3)–C(11)–O(4A)	127.5(2)
O(3)–C(11)–C(11A)	115.9(2)	O(4A)–C(11)–C(11A)	116.5(2)

Atoms labelled with letter A are related to respective atoms by symmetry operation 1–x, 1–y, 1–z.

and O(4)] from the two different carboxylate groups, whereas the apical positions are occupied by two nitrogen atoms [N(1) and N(2)] of two pyridine ligands. The bond distances between the central atom and the vanadyl oxygen atoms are practically identical [V–O(1), 1.618(2); V–O(2), 1.616(2) Å] and are in the expected range for this type of bond. The bond lengths [V–O(3), 2.205(2); V–O(4), 2.219(2) Å] of the vanadium atom to the oxalate O-atoms, *trans* to the vanadyl bonds, are relatively long, as expected [34], and are comparable to the bond lengths to oxalato O-atoms co-ordinated *trans* to V=O bonds reported [21] for $(NH_4)_3[V^VO_2(ox)_2].2H_2O$ [2.185(2); 2.235(2) Å]. Finally, the apical bonds V–N(1) [2.133(2) Å] and V–N(2) [2.141(2) Å] are similar to the corresponding distances in $[Ni(NO_2)(py)_3$–μ–C_2O_4–$Ni(NO_2)(py)_3]$[15] **3** [2.139(5), 2.152(5)], [VO(sal–D,L–Asn)(py)(H_2O)] [2.151(4)] and [VO(sal–gly)$(py)_2$] [equatorial py: 2.144(7)] [4], slightly longer than the corresponding distances in $[Ru(NO_2)(py)_4$–μ–C_2O_4–$Ru(py)_4]$ [16] **4** [2.089(7), 2.095(7)], and somewhat shorter than V–N(bipyridine) bonds reported for $[V_4O_8(CH_3O)_4\}_2(bipy)_2]$ [2.189(1), 2.168(1) Å][41].

The oxalate ligand here has a bite of only 73.4(1)°. Normally, the dimensions of the oxalate ion are relatively insensitive to co-ordination and hence the angle subtended at a metal by a bidentate oxalate group is largely determined by the M–O distances [22]. Thus, M–O distances larger than 2.1 Å are normally accompanied by O–M–O angles smaller than 80° [22, 42, 43]. As a consequence of the value for the O(3)–V–O(4) angle, the other bond angles between adjacent equatorial positions are greater than 90° (Table 1). The angle between the two apical V–N bonds is 161.9(1)°, smaller than for **3** (177.9(2)°) where a NO_2^- and a pyridine are co-ordinated to Ni(II) in positions equivalent to the two oxo-atoms O(1) and O(2) of vanadyl. The corresponding angle in **4** is 177.8(8)°.

The bond lengths and angles of the oxalate ligand are not significantly different from those reported previously for the free oxalate ion [43] and other compounds in which such an ion acts as a bis(chelating) ligand [15, 16, 17, 22]. This anion is planar with maximum mean-plane deviation for C(11) (0.003 Å). In addition, the oxalate ion, the vanadium atoms and the vanadyl O-atoms are all in a plane, with maximum deviation for O(1) (0.027 Å).

Bond angles and distances in the pyridine moieties are normal. All are planar. The largest deviation from the plane occurs for C(1) (0.005 Å) and N(2) (0.014 Å). Pyridine rings A [N(1)–C(1)–C(2)–C(3)–C(4)–C(5)] and B [N(2)–C(6)–C(7)–C(8)–C(9)–C(10)] are at 40.7° to each other with their normals forming angles with the V–V axis of the dimer of 160.8 and 157.1°, respectively. In the molecule, there is no significant interaction between pyridine rings A and B co-ordinated to different vanadium ions, since the distance between them is 4.599 Å.

Table 2. Frequencies and band assignments for the FTIR spectrum of $[\{VO_2(py)_2\}_2(\mu\text{–}C_2O_4)]$ **1**.

Frequencies/cm^{-1}	Assignment	Assignment [43]
3069 m	aromatic CH stretch	
1707 vs	ν_{as}(CO)	ν_7
1685 vs, 1638(sh)	ν_{as}(CO)	ν_1
1620(sh)	pyridine ring	
1537 m	pyridine ring	
1487 m	pyridine ring	
1407m – s	ν_s(CO) + ν(CC)	ν_2
1273 w, 1255 w	ν_s(CO) + δ(OCO)	ν_8
1200 w	δ(CH)	
1166 w	δ(CH)	
1057 w	δ(CH)	
975 s	ν(V=O)	
905 w	ν_s(CO) + δ(OCO) or ν(CC) [36]	ν_3
807 vs	ν(VO) + δ(OCO)	ν_9
752 vs	out–of–plane H(py) wag	
681 vs	ring bending [45]	
609 m	ν_s(OVO) (?)	
527m–s	ν(VO) + ν(CC)	ν_4
478 m	ring deform. + δ(OCO)	ν_{10}

Infrared spectra.

The present bis-bidentate μ-oxalato ligand is symmetrical (within experimental error), and due to the *trans* effect of the vanadyl O-atoms the bonds O(ox)–V are relatively weak. This is probably why the IR spectra has features of both bi- and bis-bidentate oxalate. Table 2 summarizes the assignment of bands based on previous assignments for several complexes containing oxalate ligands and pyridine [15, 17, 30–32, 35, 36, 44, 45].

The formation of **1** from [VO(sal–Phe)(H_2O)] is quite surprising. It is not straightforward to explain the formation of oxalate from any known amino acid reaction activated by pyridoxal model systems. The formation of CO_2 could be explained as resulting from the decarboxylation of the amino acid [12]

It is known that with strong reducing agents reactions such as (1) may proceed:

$$2Na\ (\text{liquid}\ NH_3) + 2CO_2 \rightarrow Na_2C_2O_4 \qquad (1)$$

It is further known that for L_xCu^I the reductive formation of bridging $C_2O_4^{-2}$ may occur [46]:

where L_x is a terdentate ligand co-ordinating by three N-atoms.

These reactions occur in reductive medium. In the present case vanadium(V) is present in the final product, perhaps suggesting that mechanisms involving steps equivalent to those corresponding to eqns (1) or (2) are not likely to explain our results. However, the initial oxidation state of vanadium is IV, so a reaction akin to (1) cannot be ruled out.

Instead of oxalate arising from reductive coupling of CO_2 formed in the decarboxylation of the amino acid, it could have formed by a mechanism involving first the oxidation of salicylaldehyde to salicylate (salct) (*e.g.* by V(V)), followed by oxidative degradation of salicylate yielding oxalate. This type of reaction has been described [47, 48] for $(-)-[Co(en)_2(salct)]^+$, which on oxidation by acid $KMnO_4$ produced $[Co(en)_2(C_2O_4)]^+$ in 100% yield (eqn (3)).

In reaction (3) there is retention of optical configuration and purity: ^{14}C-labelling at C-7 of **5** is entirely lost in the product [47, 48], while the retention of C-2 in the contraction of the 6-membered ring in **5**

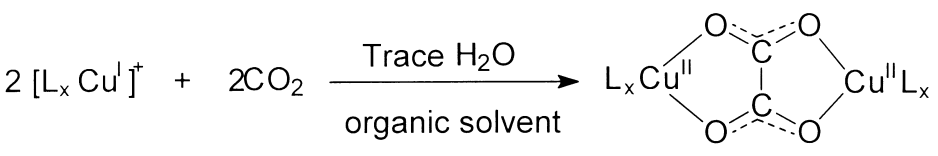

(2)

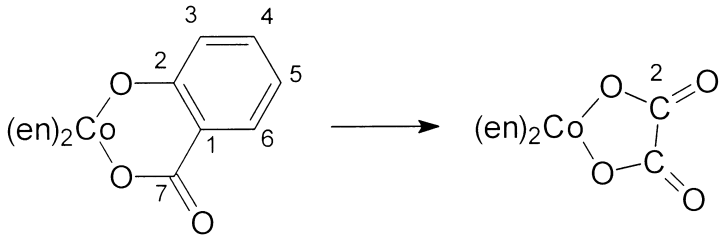

5 **6** (3)

to 5-membered in **6** was ≈83% [48]. In the absence of acid the salicylato-complex reacted only very slowly [47, 48]. The reaction of **6** with acid permanganate is negligible under the conditions used for the degradation of **5**; this is in marked contrast with the behaviour of free oxalate, which very readily undergoes oxidation.

Whether the present reaction involves the formation of a [VO_2(salct)($X)_n$] complex is not clear. However oxalate is normally readily oxidised by V(V), while **1** may be kept in its mother liquor for many months without decomposition. This behaviour parallels that in eqn (3). Loss of C-7 early in the reaction and attack by an oxidising agent (O_2, V(V) or other) to produce intermediates of the type proposed by Gillard and coworkers [47, 48] could in fact explain the formation of **1** in the present system.

Acknowledgements—We thank Fundo Europeu para o Desenvolvimento Regional, Junta Nacional de Investigação Científica e Tecnológica, and program PRAXIS XXI: project PRAXIS/2/2.1/QUI/151/94.

REFERENCES

1. Houghton, R. P., *Metal Complexes in Organic Chemistry*, Cambridge University Press, 1979, 101.
2. Bergel, F., Harrap, K. R. and Scott, A. M., *J. Chem. Soc.*, 1962, 1101.
3. Murakami, Y., Kondo, H. and Martell, A. E., *J. Am. Chem. Soc.*, 1973, **95,** 7138.
4. Cavaco, I., Costa Pessoa, J., Costa, D., Duarte, M. T. L., Matias, P. M. and Gillard, R. D., *J. Chem. Soc. Dalton Trans.*, 1994, 149.
5. Cavaco, I., Costa Pessoa, J., Luz, S., Duarte, M. T. L., Matias, P. M., Henriques, R. T. and Gillard, R. D., *Polyhedron*, 1995, **14,** 429.
6. Cavaco, I., Costa Pessoa, J., Costa, D., Duarte, M. T. L., Henriques, R. T., Matias, P. M. and Gillard, R. D., *J. Chem. Soc. Dalton Trans.*, 1996, 1989.
7. Cavaco, I., Costa Pessoa, J., Costa, D., Duarte, M. T. L., Gillard, R. D. and Matias, P. M., *Inorg. J. Biochem.*, 1993, **51,** 157.
8. Dutta, S., Mondal, S. and Chakravorty, A., *Polyhedron*, 1995, **14,** 1163.
9. Dutta, S., Mondal, S. and Chakravorty, A., *J. Chem. Soc. Dalton Trans.*, 1995, 1115.
10. Cavaco, I., Costa Pessoa, J., Duarte, M. T. L., Gillard, R. D. and Matias, P. M., *J. Chem. Soc. Chem. Commun.*, 1996, 1365.
11. Cavaco, I. and Costa Pessoa, J. to be published.
12. Metzler, D. E., Ikawa, M. and Snell, E. E., *J. Am. Chem. Soc*, 1954, **76,** 648.
13. Costa Pessoa, J., Duarte, M. T. L., Fraústo da Silva, J. J. R., Gillard, R. D., Madeira, C., Matias, P. M. and Tomaz, I., *J. Inorg. Biochem.*, 1997, **67,** 389.
14. Bernalte, A., Cavaco, I., Costa Pessoa, J., Barros, F. J. G., Gillard, R. D. and Higes, F. J., 'Unusual Product Obtained from [VO(Sal-Phe)(H_2O)] in H_2O/pyridine Solutions', poster at the 32nd International Conference on Coordination Chemistry, Santiago, Chile, 1997.
15. Kopf, J., Behrens, U., Kastner, M. and Klar, G., *J. Inorg. Nucl. Chem.*, 1977, **39,** 889.
16. Cheng, P. T., Loescher, B. R. and Nyburg, S. C., *Inorg. Chem.*, 1971, **10,** 1275.
17. Castro, I., Faus, J., Julve, M., Gleizes, A., *J. Chem. Soc., Dalton Trans.* 1991, 1937, and refs. therein.
18. Julve, M., Faus, J., Verdaguer, M. and Gleizes, A., *J. Am. Chem. Soc.*, 1984, **106,** 8306.
19. Garaj, J., *J. Chem. Soc., Chem. Commun.*, 1968, 904.
20. Drew, M. G. B., Fowles, G. W. A. and Lewis, D. F., *J. Chem. Soc., Chem. Commun.*, 1969, 876.
21. Scheidt, W. R., Tsai, C. and Hoard, J. L., *J. Am. Chem. Soc.*, 1971, **93,** 3867.
22. Curtis, N. F., Ross, I., McCormick, N. and Waters, T. N., *J. Chem. Soc., Dalton Trans.*, 1973, 1537.
23. Felthouse, T. R., Laskowski, E. J. and Hendrickson, D. N., *Inorg. Chem.*, 1977, **16,** 1077.
24. Bottomley, F., Lin, I. J. B. and White, P. S., *J. Organom. Chem.*, 1981, **212,** 341.
25. Fitzgerald, W., Foley, J., McSweeney, D., Ray, N., Sheahan, D., Tyagi, S., Hathaway, B. and

O'Brien, P., *J. Chem. Soc., Dalton Trans.*, 1982, 1117.
26. Sletten, J., *Acta Chem. Scand., Ser.A*, 1983, **37,** 569.
27. Julve, M., Verdaguer, M., Gleizes, A., Philoche-Levisalles, M. and Kahn, O., *Inorg. Chem.*, 1984, **23,** 3808.
28. Alcock, N. W., Moore, P. and Omar, H. A. A., *Acta Crystallogr., Sect. C*, 1987, **43,** 2074.
29. Bencini, A., Fabretti, A. C., Zanchini, C. and Zannini, P., *Inorg. Chem.*, 1987, **26,** 1445.
30. Ribas, J., Monfort, M. and Diaz, C., Solans, X., *An. Chím.*, 1988, **B84,** 186.
31. Curtis, N. F., *J. Chem Soc.*, 1963, 4109.
32. Curtis, N. F., *J. Chem Soc. A*, 1968, 1584.
33. Floch, F. L., Sala-Pala, J. and Guerchais, J. E., *Bull. Soc. Chim. Fr.*, 1975, 120.
34. Vilas Boas, L.F., Costa Pessoa, J., in *Comprehensive Coordination Chemistry*, eds. G. Wilkinson, R.D. Gillard and J.A. McCleverty, Pergamon, Oxford **3**, 1987, 453-583 and refs. therein.
35. Edwards, A. J., Slim, D. R., Sala-Pala, J. and Guerchais, J. E., *Bull. Soc. Chim. Fr.*, 1975, 2015.
36. Rieskamp, H., Gietz, P. and Mattes, R., *Chem. Ber.*, 1976, **109,** 2090.
37. Oughtred, R. E., Raper, E. S. and Shearer, H. M. M., *Acta Crystallogr., Sect. B*, 1976, **32,** 82.
38. Theriot, L. J., Carlisle, G. O. and Hu, H. J., *J. Inorg. Nucl. Chem.*, 1969, **31,** 3303.
39. Sheldrick, G.M., SHELXTL-IRIS. Release 4.2. Siemens Analytical X-ray Instruments Inc., Madison, Wisconsin, U.S.A. 1991.
40. Fraústo da Silva, J. J. R., Wootton, R. and Gillard, R. D., *J. Chem. Soc. A*, 1970, 3369.
41. Cavaco, I., Costa Pessoa, J., Duarte, M. T., Matias, P. M. and Henriques, R. T., *Polyhedron*, 1993, **12,** 1231.
42. Glen, G. L., Silverton, J. V. and Hoard, J. L., *Inorg. Chem.*, 1963, **2,** 250.
43. Hodgson, D. J. and Ibers, J. A., *Acta Cryst. Sect. B*, 1969, **25,** 469.
44. Nakamoto, K., *Infrared and Raman Spectra of Inorganic and Coordination Compounds*, 3rd ed., John Wiley & Sons, New York, 1978, 234.
45. Colthup, N.B., Daly, L.H., Wiberley, S.E., *Introduction to Infrared and Raman Spectroscopy*, Academic Press, New York, 1964, 227.
46. Personal communication from Professor R.D. Peacock (Univ. of Glasgow) to R.D. Gillard, 1996.
47. Beaumont, A. G. and Gillard, R. D., *J. Chem. Soc.* (*A*), 1970, 1757.
48. Beaumont, A. G., Gillard, R. D. and Lyons, J. R., *J. Chem. Soc.* (*A*), 1971, 1971.

Pergamon

PII: SS027–7538(79)80010–65

Polyhedron Vol. 17, No. 19, pp. 3275–3280, 1998
© 1998 Elsevier Science Ltd
All rights reserved. Printed in Great Britain
0277–5387/98 $19.00+0.00

Synthesis and structure of bis(thiomethyl)magnesium compounds $[Mg(CH_2SR)_2(thf)_3]$ (R = Me, Ph) - the first dimethylmagnesium compounds functionalized by a Lewis-basic heteroatom

Dirk Steinborn,* Tobias Rüffer, Clemens Bruhn and Frank W. Heinemann

Institut für Anorganische Chemie der Martin-Luther-Universität Halle–Wittenberg, Kurt-Mothes-Str. 2, D-06120 Halle (Saale), Germany

(Received 26 November 1997; accepted 6 March 1998)

Abstract—$Hg(CH_2SR)_2$, (R = Me (**1**), R = Ph (**2**)), prepared by reaction of $HgCl_2$ with $[Li_2(CH_2SR)_2(tmeda)_2]$, reacts with magnesium activated by mercury in boiling THF to give $[Mg(CH_2SR)_2(thf)_3]$ (R = Me (**3**), R = Ph (**4**)). **3** readily splitts off THF in vacuo to give the solvate free complex $[Mg(CH_2SMe)_2]$ (**3′**). The complexes **3′** and **4** are fully characterized by microanalysis and NMR spectroscopy (^1H, ^{13}C).

The X-ray structure analyses of **3** and **4** reveal mononuclear compounds with two symmetry independent molecules in the unit cell of **3**. In both complexes the coordination of Mg is trigonal–bipyramidal. The two apical positions are occupied by THF and the three equatorial positions by one THF and the two thiomethyl ligands. The C–Mg–C angles are slightly greater (123.9(1)–131.0(2)°) than the ideal angle for equatorial atoms in a trigonal–bipyramidal coordination. In neither case, the sulfur atoms are involved in the coordination of Mg. © 1998 Elsevier Science Ltd. All rights reserved.

Keywords: thiomethyl magnesium compounds; functionalized methyl magnesium compounds; mercury-magnesium transmetallation; crystal structures.

INTRODUCTION

The very low thermal stability ($T_{dec.} < -100°C$) and the carbenoid reactivity of Köbrich's (halogeno)-methyl lithium compounds [1] had exhibited, that a Lewis-basic heteroatom may strongly influence the reactivity and stability of functionalized methyl lithium compounds. Since then, the influence of Lewis-basic heteroatoms Y on structure, reactivity and stability of organolithium complexes of the type $LiCH_2YR_n$ (**A**) (YR_n = NR_2, PR_2, OR, SR, Cl, ...) has been investigated thoroughly [2, 3]. X-ray structure investigations reveal a wide variety of solid state structures exhibiting a coordination Y → Li in most cases [4]. The THF adducts, $[Li(CH_2YR_n)(thf)_x]$ are polymeric (YR_n = SMe [5], PPh_2 [6]), tetrameric (YR_n = NC_5H_{10} [7], NMe_2 [8]) or dimeric with a four-membered Li_2C_2 ring (YR_n = SPh [5], NPh_2 [7]). Monomeric compounds are not known at all.

Compared to the numerous lithium compounds **A**, there are far fewer examples of functionalized methyl Grignard compounds $Mg(CH_2YR_n)X$ (**B**) with Lewis-basic heteroatoms Y (YR_n = OR, SR, X) [2, 9, 10]. To date, there have been no reports of functionalized dimethyl magnesium compounds $Mg(CH_2YR_n)_2$ (**C**). Although a lot of structures of organomagnesium compounds had been described [11], those of type **B** and **C** are not known at all.

We report here the synthesis of thiomethyl magnesium compounds $[Mg(CH_2SR)_2(thf)_3]$ (R = Me (**3**), R = Ph (**4**)) and their solid state structures being the first compounds of type **C**.

RESULTS AND DISCUSSION

The thiomethyl mercury complexes $Hg(CH_2SR)_2$ (R = Me (**1**), R = Ph (**2**)) were prepared by the reac-

* Author to whom correspondence should be addressed.

tion of $HgCl_2$ with $[Li_2(CH_2SR)_2(tmeda)_2]$ in THF, cf. Equation (1). The identities of **1** and **2** were confirmed by microanalysis and NMR spectroscopy (^1H and ^{13}C). In the case of the complex **2** these values agree with the data given in the literature [12].

The organomercury compounds **1** and **2** undergo with magnesium in boiling THF a transmetallation reaction yielding the bis(thiomethyl)magnesium complexes $[Mg(CH_2SR)_2(thf)_3]$ (R = Me (**3**), R = Ph (**4**)) that precipitate from the concentrated solutions at $-40°C$ as well shaped colorless crystals, eq. (1).

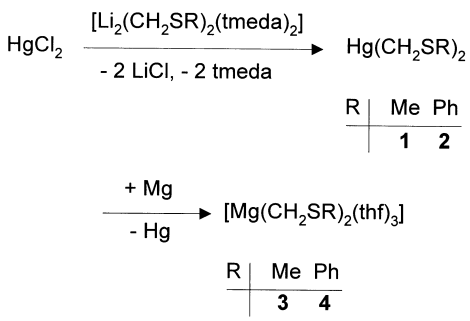

(1)

There is an induction period of several hours. Activating the magnesium with one drop of mercury, the reactions take not more than three hours (degree of conversion >90%). The transmetallation of **2** with magnesium was proved to proceed also in boiling toluene and xylene with mercury activated magnesium (degree of conversion >80%). Within eight hours no reaction was observed in boiling ether, not even with magnesium activated by mercury.

For Hg–Mg transmetallation reactions, a wide range of reactivity was described in the literature: Me_2Hg was found to react with magnesium immediately in a strong exothermic reaction [13]. On the other hand, transmetallation reactions of aryl mercury compounds take up to two weeks in THF at room temperature [14]. An activation of the Hg–Mg transmetallation with $HgCl_2$ was observed [15], but the isolation of R_2Mg in a pure state might be difficult due to the Schlenk equilibrium.

The thiomethyl magnesium complexes **3** and **4** are very sensitive against air and moisture. The (methylthio)methyl complex **3** loses the coordinated THF very easily in vacuo to give the solvate free complex $[Mg(CH_2SMe)_2]$ (**3′**). **3** and **4** are well soluble in THF and ether and insoluble in aromatic and aliphatic hydrocarbons. The identities of **3′** and **4** were confirmed by microanalysis and NMR spectroscopy (^1H and ^{13}C).

Table 1 shows the resonances of the methylene group in **3**, **4** and in related lithium complexes. Compared with their lithium analogues, the ^1H resonances of **3** and **4** are shifted downfield because of the magnesium is less electropositive. The difference $\Delta\delta(^1H) = 0.20$ ppm between **3** and **4** should be caused by the electronic effect of the phenyl substituent. As in the (phenylthio)methyl lithium compounds, there is an unusual high field shift of the methylene carbon in **4**. The coupling constants $^1J(^{13}C,^1H)$ for the CH_2 groups of all compounds in Table 1 are in the expected range exhibiting no unusual bonding relationships.

Structures of $[Mg(CH_2SMe)_2(thf)_3]$ (*3*) *and* $[Mg(CH_2SPh)_2(thf)_3]$ (*4*)

The molecular structures of complexes **3** and **4** along with the atom numbering schemes are shown in Figs 1 and 2. Selected bond lengths and angles are listed in Table 2.

The two structures consist of monomeric molecules without any unusal intermolecular interactions. The unit cell of complex **3** contains two symmetry independent molecules (**3** and **3a**); one of them (**3a**) exhibits a crystallographically imposed C_2 symmetry. Related bond lengths of **3** and **3a** differ less than 1% while related bond angles show noteable differences (up to 5–6%).

Both in **3** and in **4**, the magnesium displays a distorted trigonal–bipyramidal coordination. As usual for trigonal–bipyramidal structures [18], the more electronegative ligands (THF) occupy the apical positions. These Mg–O bonds are longer than that to the

Table 1. ^1H and ^{13}C NMR resonances (in ppm) and $^1J(^{13}C, ^1H)$ coupling constants (in Hz) of the methylene group in thiomethyl magnesium and lithium complexes

Compound[a]	$\delta(^1H)$	$\delta(^{13}C)$	$^1J(^{13}C, ^1H)$	Ref.
$[Mg(CH_2SMe)_2(thf)_3]$ (**3**)	0.66	12.9	121.3	[b]
$[Mg(CH_2SPh)_2(thf)_3]$ (**4**)	0.86	4.9	121.7	[b]
$[Li_2(CH_2SMe)_2(tmeda)_2]$	0.38	15.3	116.4	[c]
$[Li_2(CH_2SPh)_2(tmeda)_2]$	0.36	4.1	121.0	[c]
$[\{Li(CH_2SMe)(thf)\}_\infty]$	0.36	14.8	116.0	[5]
$[Li_2(CH_2SPh)_2(thf)_4]$	0.31	3.8	121.0	[5]

[a] Formulae refer to aggregation in solid state.
[b] This work.
[c] Own measurements, prepared according to the literature [16, 17].

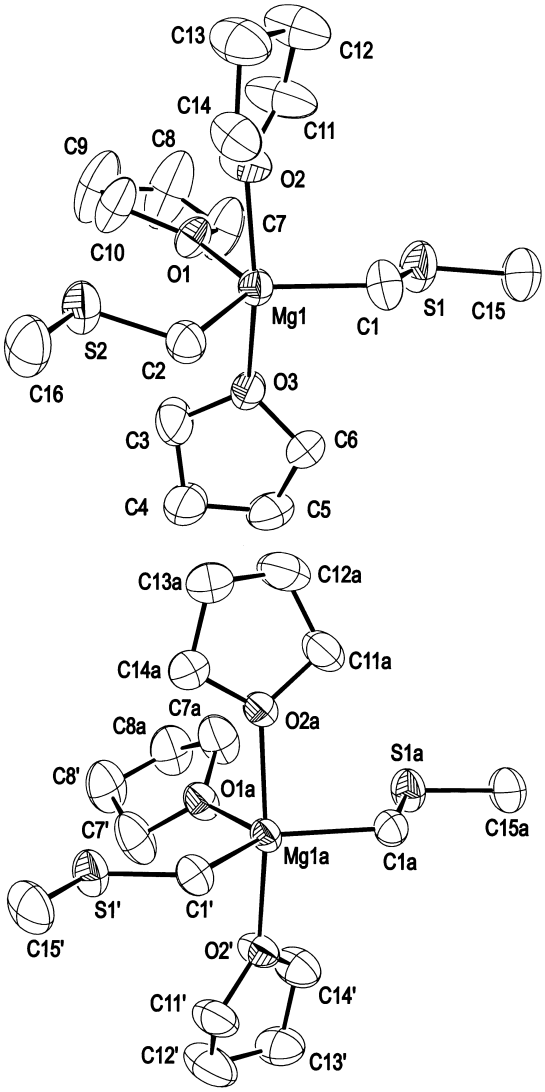

Fig. 1. Molecular structure and numbering scheme of the two crystallographically independent molecules **3** (above) and **3a** (below). To make the correspondence between them clear, the atoms are numbered in the same way, but 'a' was added to independent atoms of **3a**; ' ' ' refers to symmetry related atoms of **3a**. Ellipsoids are drawn at 50% probability. Hydrogen atoms are omitted for clarity.

Table 2. Selected bond lengths (in Å) and angles (in °) for $[Mg(CH_2SR)_2(thf)_3]$

	3 (R = Me)	**3a** (R = Me)[a]	**4** (R = Ph)
Mg1–C1	2.178(3)	2.196(3)	2.168(6)
Mg1–C2	2.191(3)		2.195(6)
C1–S1	1.757(3)	1.775(3)	1.777(6)
C2–S2	1.770(3)		1.767(6)
S1–C15	1.803(4)	1.811(3)	1.766(5)
S2–C16	1.811(4)		1.773(6)
Mg1–O1	2.095(2)	2.107(2)	2.087(4)
Mg1–O2	2.178(2)	2.189(2)	2.236(4)
Mg1–O3	2.185(2)		2.140(4)
C1–Mg1–C2	123.9(1)	131.0(2)[b]	128.4(3)
C1–Mg1–O1	118.1(1)	114.49(7)	110.8(2)
C2–Mg1–O1	118.0(1)		120.4(2)
C1–Mg1–O2	94.7(1)	91.62(9)	90.6(2)
C2–Mg1–O3	95.1(1)		93.9(2)
C1–Mg1–O3	92.3(1)	92.69(9)[c]	97.2(2)
C2–Mg1–O2	93.5(1)		91.1(2)
O1–Mg1–O2	81.59(7)	84.79(6)	81.4(2)
O1–Mg1–O3	81.83(7)		84.2(2)
O2–Mg1–O3	163.40(8)	169.6(1)[d]	165.2(2)
Mg1–C1–S1	115.1(2)	111.7(1)	113.9(3)
Mg1–C2–S2	112.0(1)		114.6(3)
C1–S1–C15	106.4(2)	107.0(2)	108.4(3)
C2–S2–C16	107.7(2)		108.9(3)

[a]Symmetry transformations used to generate equivalent atoms: ': $-x, y, -z+1/2$.
[b]C1a–Mg1a–C1′.
[c]C1a–Mg1a–O2′.
[d]O2a–Mg1a–O2′.

equatorially bonded THF molecule (d(Mg–O_{ap}) = 2.140(4)–2.236(4) Å vs. d(Mg–O_{eq}) = 2.087(4)–2.107(2) Å).

The distortions of the coordination polyhedron around Mg are relatively small: The angles O_{ap}–Mg–O_{ap} are between 163.40(8)° and 169.6(1)° and the sum of angles in the equatorial planes is between 359.6(4)° and 360.0(2)°. The less electronegative organo ligands are more space-demanding as can be seen at the widening of the C–Mg–C angles (123.9(1)–131.0(2)°) and at the lowering of the O_{ap}–Mg–O_{eq} angles (81.4(2)–84.79(6)°).

The Mg–C bond lengths in **3** and **4** (d(Mg–C) = 2.168(6)–2.196(3) Å) are in the range for Mg–C bond lengths of other monomeric five-coordinate dialkylmagnesium compounds such as $[MgR_2(pmdta)]$ [19] (R = Me, Et; pmdta = *N*,*N*,*N*′,*N*″,*N*″-pentamethyldiethylenetriamine) (d(Mg–C) = 2.158(5)–2.223(9) Å).

The CH_2–S distances (d(C–S) = 1.757(3)–1.777(6) Å) are substantially shorter than the S–CH_3 distances in **3** (d(C–S) = 1.803(4)–1.811(4) Å). They are in the same range as the S–C_{Ph} distances in **4** (d(C–S) = 1.766(5) and 1.773(6) Å) in spite of the smaller covalent radii of sp^2 hybridized carbons in comparison with sp^3 hybridized ones [18]. This indicates a stabilizing influence on the carbanionoid centre of sulfur by polarization.

The complexes **3** and **4** are the first functionalized dimethylmagnesium complexes $Mg(CH_2YR_n)_2$ with a Lewis-basic heteroatomic centre Y. Unexpectedly, the sulfur is not involved in the coordination sphere of magnesium. Furthermore, for the first time a trigonal–bipyramidal coordination around magnesium was found with monodentate coligands L ($[MgR_2L_3]$). To date, monomeric five-coordinate diorganomagnesium compounds were observed only with tridentate co-

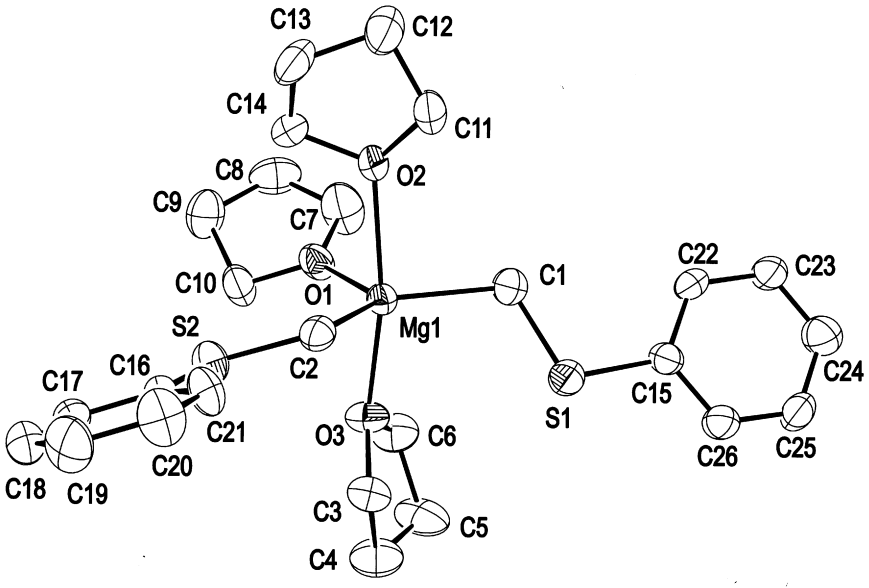

Fig. 2. Molecular structure and numbering scheme of complex **4**. Ellipsoids are drawn at 50% probability. Hydrogen atoms are omitted for clarity.

ligands ([MgR_2L_3]; R = alkyl, aryl; L_3 = pmdta, diglyme, tetraglyme) [19, 20]. With mono- and oligodentate coligands, tetrahedral complexes [MgR_2L_2] (R = alkyl, aryl; L = THF, quinuclidine; L_2 = TMEDA) [19, 21–26] and octahedral complexes [MgR_2L_4] (R = alkyl, alkynyl; L_2 = TMEDA, L_4 = crown ether) [20, 27–29] are formed.

EXPERIMENTAL

General comments

All reactions and manipulations were carried out under purified argon using standard Schlenk techniques. *n*-Hexane, *n*-pentane, TMEDA and THF-d_8 were dried with $LiAlH_4$. Toluene, xylene, THF and diethyl ether were distilled from sodium benzophenone ketyl. NMR spectra were recorded on Varian Unity 500 spectrometer using the protio impurities and ^{13}C resonances of the deuterated solvents as references for ^1H and ^{13}C NMR spectroscopy, respectively. Microanalyses (C, H, S) were obtained from the microanalytical laboratory of the Department of Chemistry. A CP9000 (Chrompack) was used for gas-chromatographic analyses. [$Li_2(CH_2SR)_2(tmeda)_2$] (R = Me, Ph) was prepared according to the literature [16, 17].

Synthesis of $Hg(CH_2SR)_2$ (*R = Me* (*1*), *R = Ph* (*2*))

To a solution of $HgCl_2$ (6.5 g, 24 mmol) in THF (50 ml), [$Li_2(CH_2SR)_2(tmeda)_2$] (R = Me, Ph) (48 mmol) in THF (50 ml) was added dropwise at −78°C. After stirring for 1 h and warming up to r.t. water (100 ml) was added. The half of the solvent was removed in vacuo and the colorless precipitate formed was filtered off, washed with water and cold methanol and dried in vacuo. Yields: **1** (5.6 g, 75%); **2** (9.7 g, 90%).

Anal. Calcd for **1**: C, 14.88; H, 3.12; S, 19.86. Found: C, 15.24; H, 3.20; S, 18.74. ^1H NMR (500 MHz, THF-d_8): δ 2.27 (s, 4H, $^2J(^{199}Hg, ^1H)$ = 104.0 Hz, CH_2), 2.15 (s, 6H, CH_3). ^{13}C NMR (125 MHz, THF-d_8): δ 43.1 (s+d, $^1J(^{199}Hg, ^{13}C)$ = 820.1 Hz, CH_2), 22.8 (s+d, $^3J(^{199}Hg, ^{13}C)$ = 137.0 Hz, CH_3).

Anal. Calcd for **2**: C, 37.62; H, 3.16; S, 14.35. Found: C, 38.13; H, 3.22; S, 14.08. ^1H NMR (500 MHz, THF-d_8): δ 2.60 (s, 4H, $^2J(^{199}Hg, ^1H)$ = 107.3 Hz, CH_2), 7.06–7.46 (m, 10H, *Ph*). ^{13}C NMR (125 MHz, THF-d_8): δ 39.2 (s+d, $^1J(^{199}Hg, ^{13}C)$ = 855.4 Hz, CH_2), 124.9 (*p*-C), 125.9 (*o*-C), 128.3 (*m*-C), 142.0 (*i*-C).

Synthesis of [$Mg(CH_2SR)_2(thf)_3$] (*R = Me* (*3*), *R = Ph* (*4*))

A mixture of $Hg(CH_2SR)_2$ (R = Me (**1**), R = Ph (**2**)) (3.4 mmol), powdered magnesium (0.75 g, 31 mmol) and mercury (about 0.1 g, 0.5 mmol) in THF (10 ml) was refluxed under vigorous stirring for about 3 h. The amalgam formed was filtered off and the solution was concentrated in vacuo up to about 5 ml. At −40°C, **3** and **4** precipitated in well shaped crystals which were filtered off, washed with hexane and dried in vacuo. Yield: **3′** (0.3 g, 60%); **4** (1.1 g, 65%). To

Table 3. Crystal data and structure refinement for **3** and **4**

	3	**4**
Empirical formula	$C_{16}H_{34}MgO_3S_2$	$C_{26}H_{38}MgO_3S_2$
fw	362.88	487.02
Crystal system/space group	orthorhombic/P b c n	triclinic/$P\bar{1}$
a, b, c (Å)	10.387(2), 17.213(3), 35.355(8)	9.563(2), 12.344(3), 12.800(4)
α, β, γ (deg)	90, 90, 90	115.08(2), 98.38(4), 91.36(3)
V (Å^3)	6321(2)	1347.7(6)
Z	12	2
D_{calcd} (g cm^{-3})	1.144	1.200
μ(MoKα) (mm^{-1})	0.291	0.245
F(000)	2376	524
Scan range (deg)	$2.27 < \theta < 24.06$	$1.78 < \theta < 22.50$
Index ranges	$-11 \leqslant h \leqslant 11$, $-18 \leqslant k \leqslant 19$, $-40 \leqslant l \leqslant 40$	$-10 \leqslant h \leqslant 10$, $-13 \leqslant k \leqslant 13$, $-13 \leqslant l \leqslant 13$
Reflections collected	25569	5990
Independent reflections	4895 ($R_{int} = 0.1044$)	3526 ($R_{int} = 0.1156$)
Observed reflections [$I > 2\sigma(I)$]	3837	1725
Parameters refined	479	441
Goodness-of-fit on F^2	1.088	1.014
Final R indices [$I > 2\sigma(I)$]	$R1 = 0.0512$, $wR2 = 0.1210$[a]	$R1 = 0.0583$, $wR2 = 0.0748$[b]
R indices (all data)	$R1 = 0.0669$, $wR2 = 0.1300$[a]	$R1 = 0.1639$, $wR2 = 0.0998$[b]
Largest diff. peak and hole (e Å^{-3})	0.325 and -0.168	0.303 and -0.281

[a] $w = 1/[(\sigma^2/F_o^2) + (0.0723P)^2 + 1.9927P]$; $P = (F_o^2 + 2F_c^2)/3$.
[b] $w = 1/[(\sigma^2/F_o^2)$.

determine the degree of conversion, in separate experiments MeOH/THF (1/4; 0.5 ml) was added dropwise at -78°C to the reaction mixture. The yield of MeSR was determined by gaschromatography using naphthalene as internal standard. Degree of conversion: **3** (THF, 93%), **4** (THF, 97%; toluene, 83%; xylene, 93%).

Anal. Calcd for **3′**: C, 32.78; H, 6.88. Found: C, 33.20; H, 6,82. ^{1}H NMR (500 MHz, THF-d$_8$): δ 0.66 (s, 4H, CH_2), 1.89 (s, 6H, CH_3). ^{13}C NMR (125 MHz, THF-d$_8$): δ 12.9 (*C*H$_2$), 27.2 (*C*H$_3$).

Anal. Calcd for **4**: C, 64.12; H, 7.86. Found: C, 63.38; H, 7.02. ^{1}H NMR (500 MHz, THF-d$_8$): δ 0.86 (s, 4H, CH_2), 6.79–6.91 (m, 2H, *p*-H), 7.05–7.08 (m, 4H, *m*-H), 7.22–7.24 (m, 4H, *o*-H). ^{13}C NMR (125 MHz, THF-d$_8$): δ 4.9 (*C*H$_2$), 122.4 (*p*-C), 128.3 (*m*-C), 124.1 (*o*-C), 151.8 (*i*-C). (Due to partial hydrolysis a small amount ot MeSPh was detected in the spectra.)

*X-ray structure determinations of **3** and **4***

Suitable single crystals of **3** ($0.4 \times 0.3 \times 0.3$ mm) and **4** ($0.8 \times 0.2 \times 0.1$ mm) were obtained from pentane/THF solution at -40°C. X-ray measurements were performed on a Stoe IPDS (**3**) and on a Stoe STADI 4 diffractometer (**4**), respectively, with $Mo_{K\alpha}$ radiation ($\lambda = 0.71073$ Å). The structures were solved by direct methods (SHELXS86 [30]) and refined using full-matrix least-squares procedures on F^2 (SHELXL93 [31]). Non-hydrogen atoms were refined with anisotropic displacement parameters. The hydrogen atoms were found in the Fourier list and refined isotropically, except of some in **3**, which were placed in calculated positions. Crystal data, details of data collections, structure solutions and refinements are summarized in Table 3. Complete tables of the atomic coordinates, H-atom parameters, bond distances, bond angles and anisotropic displacement parameters atoms have been deposited with the Editor as supplementary material.

Acknowledgements—T. R. thanks the Land Sachsen-Anhalt for a scholarship. We gratefully acknowledge support by Deutsche Forschungsgemeinschaft and Fonds der Chemischen Industrie as well as the company Merck (Darmstadt) for gifts of chemicals.

REFERENCES

1. Köbrich, G., *Angew. Chem.*, 1972, **84,** 557.
2. Peterson, D. J., *Organomet. Chem. Rev. A.*, 1972, **7,** 295.
3. Krief A., *Tetrahedron*, 1980, **36,** 2531.
4. Setzer, W. N. and v. Ragué Schleyer, P., *Adv. Organomet. Chem.*, 1985, **24,** 353.
5. Becke, F., Heinemann, F. W. and Steinborn, D., *Organometallics*, 1997, **16,** 2736.
6. Steinborn, D., Neumann, O., Weichmann, H., Heinemann, F. W. and Wagner, J-P., *Polyhedron*, 1998, **17,** 351.
7. Becke, F., Heinemann, F. W., Rüffer, T.,

Wiegeleben. P., Boese, R., Bläser, D. and Steinborn, D., *J. Organomet. Chem.*, 1997, **548,** 205.
8. Bruhn, C., Becke, F. and Steinborn, D., *Organometallics*, 1998, **17,** 2124.
9. Villiéras, J., *Organomet. Chem. Rev. A.*, 1971, **7,** 81.
10. Lindsell, W. E., *Comprehensive Organometallic Chemistry II*, ed. E. W. Abel, F. G. A. Stone, G. Wilkinson, Pergamon, Oxford, 1995, Vol. 1, p. 57.
11. Markies, P. R., Akkerman, O. S., Bickelhaupt, F., Smeets, W. J. J. and Spek, A. L., *Adv. Organomet. Chem.*, 1991, **32,** 147.
12. Taube, R., Steinborn, D. and Adler, B., *J. Organomet. Chem.*, 1984, **275,** 1.
13. Ashby, E. C. and Arnott, R. C., *J. Organomet. Chem.*, 1968, **14,** 1.
14. Markies, P. R., Altink, R. M., Villena, A., Akkerman, O. S., Bickelhaupt, T., Smeets, W. J. J. and Spek, A. L., *J. Organomet. Chem.*, 1991, **402**, 289.
15. Gilman, H. and Schulze, F., *J. Am. Chem. Soc.*, 1927, **49,** 2328.
16. Peterson, D. J., *J. Org. Chem.*, 1967, **32,** 1717.
17. Amstutz, R., Laube, T., Schweizer, W. B., Seebach, D. and Dunitz, J. D., *Helvet. Chim. Acta.*, 1984, **67,** 224.
18. Huheey, J. E., Keiter, E. A. and Keiter, R. L., *Inorganic Chemistry*, *Principles of Structure and Reactivity*, 4th edition, Harper Collins College Publ., New York, 1993.
19. Viebrock, H. and Weiss, E., *J. Organomet. Chem.*, 1994, **464,** 121.
20. Markies, P. R., Akkerman, O. S., Bickelhaupt, F., Smeets, W. J. J. and Spek, A. L., *Organometallics* 1994, **13,** 2616.
21. Toney, J. and Stucky, G. D., *J. Organomet. Chem.*, 1970, **22,** 241.
22. Waggoner, K. M. and Power, P. P., *Organometallics*, 1992, **11,** 3209.
23. Thoennes, D. and Weiss, E., *Chem. Ber.*, 1978, **111,** 3381.
24. Greiser, T., Kopf, J., Thoennes, D. and Weiss, E., *J. Organomet. Chem.*, 1980, **191,** 1.
25. Yasuda, H., Yamauchi, M., Nakamura, A., Sei, T., Kai, Y., Yasuoka, N. and Kasai, N., *Bull. Chem. Soc. Jpn.*, 1980, **53,** 1089.
26 Markies, P. R., Schat, G., Akkerman, O. S., Bickelhaupt, F., Smeets, W. J. J., v.d. Sluis, P. and Spek, A. L., *J. Organomet. Chem.*, 1990, **393,** 315.
27. Geissler, M., Kopf, J. and Weiss, E., *Chem. Ber.*, 1989, **122,** 1395.
28. Schubert, B., Behrens, U. and Weiss, E., *Chem. Ber.*, 1981, **114,** 2640.
29. Markies, P. R., Nomoto, T., Akkerman, O. S., Bickelhaupt, F., Smeets, W. J. J. and Spek, A. L., *J. Am. Chem. Soc.*, 1988, **110,** 4845.
30. Sheldrick, G. M., SHELXS-86, *Program for the Solution of Crystal Structures*, University of Göttingen, Germany, 1986; Sheldrick, G. M., *Acta Cryst.*, 1990, **A46,** 467.
31. Sheldrick, G. M., SHELXL-93, *Program for the Refinement of Crystal Structures*, University of Göttingen, Germany, 1993.

Pergamon

PII: S0277–5387(98)00107–7

Polyhedron Vol. 17, No. 0, pp. 3281–0000, 1998
© 1998 Elsevier Science Ltd
All rights reserved. Printed in Great Britain
0277–5387/98 $19.00+0.00

Convergent metal-directed and divergent approaches to multiply cyclometallated complexes

Edwin C. Constable[a,*] and David G.F. Rees[b]

[a]Institut für Anorganische Chemie, Spitalstrasse 51, CH-4056 Basel, Switzerland

[b]University Chemical Laboratory, Lensfield Road, Cambridge CB2 1EW, U.K.

(Received 16 February 1998; accepted 7 March 1998)

Abstract—Alternative routes to bis(cyclometallated) complexes have been explored. Divergent approaches involving a final multiple cyclometallation step and convergent approaches in which cyclometallated complexes of multinucleating ligands are prepared *in situ* from mononuclear cyclometallated complexes are exemplified. © 1998 Elsevier Science Ltd. All rights reserved. © 1998 Elsevier Science Ltd. All rights reserved

Keywords: Cyclometallates; ruthenium complexes; metallosupramolecular chemistry; oligopyridines

We are interested in the synthesis and utilisation of metallodendrimers [1] and related species [2] and are currently probing ways of controlling the redox and photochemical properties of multinuclear species. One approach that seemed to be worth pursuing involved the replacement of oligopyridine-metal substructures by cyclometallated motifs involving 2-phenylpyridine (Hppy) or 6-phenyl-2,2′-bipyridine (Hpbpy) [3].

Although the fundamental chemistry of such potentially cyclometallating ligands is well-developed [3], there are remarkably few examples of complexes containing two or more such cyclometallated sites [4–13]. Two strategies for the synthesis of such compounds appear feasible: (i) preparation of a ligand with two or more of the desired metal-binding domains with subsequent multiple metallation and (ii) preparation of suitable mononuclear cyclometallated complexes bearing functionality which will allow a subsequent coupling reaction. The former approach is, formally, divergent whilst the latter is convergent. The divergent approach is a conventional one, but in view of the subtlety involved in the selective addressing of either *NN* or *CNN* bonding domains in 6-phenyl-2,2′-bipyridines [13, 14] we anticipated considerable problems in controlling a large number of parallel or consecutive cyclometallation reactions. The convergent approach is attractive in that only a single cyclometallation reaction is required, although the stability of cyclometallates under the coupling conditions was a cause for concern. However, recent reports [4, 9, 15, 16] describing coupling reactions of metal complexes encouraged us to pursue this approach. In this paper we compare the two approaches in the synthesis of a bis(cyclometallated) complex.

* Corresponding author. Tel.: +41 61 267 1001; FAX: +41 61 267 1015; Email: constable@ubaclu.unibas.ch

EXPERIMENTAL

Infrared spectra were recorded on a Mattson Genesis Fourier-transform spectrophotometers with samples in compressed KBr discs. Proton NMR spectra were recorded on Brüker WM250, AM400 or Varian Gemini 300 MHz spectrometers. All coupling constants within the aromatic systems are typical and are not explicitly reported. Time of flight (MALDI) spectra were recorded using a PerSeptive Biosystems Voyager-RP Biospectrometry Workstation. Electrochemical measurements were performed with an Eco Chemie Autolab PGSTAT 20 system using platinum bead or glassy carbon working and auxiliary electrodes with an Ag/AgCl electrode as reference. The experiments were conducted using purified acetonitrile as solvent and freshly recrystallised 0.1 M [Bu^n_4N, BF_4] or [Bu^n_4N, PF_6] as supporting electrolyte; ferrocene was added at the end of each experiment as an internal reference. 2-Oxo-2-pyridylethylpyridinium iodide [17], [$NiCl_2(PPh_3)_2$] [18] and [Ru(tpy)Cl_3] [19]

were prepared by the literature methods. Hydrated ruthenium trichloride was purchased from Oxchem.

[4-*Bromo*(3-*ammonio*-1-*oxopropyl*)*benzene*]*chloride*, **3**

N,*N*-Dimethylammonium chloride (1.20 g, 0.015 mol), paraformaldehyde (3.52 g, 0.059 mol) and 4-bromoacetophenone (2.78 g, 0.014 mol) were heated to reflux in dry ethanol (40 cm^3) containing three drops of concentrated hydrochloric acid for 4 h. After this period an additional quantity of paraformaldehyde (0.71 g, 0.012 mol) was added and the heating continued for a further 4 h. The clear yellow solution so obtained was concentrated *in vacuo* to 10 cm^3 volume and treated with acetone (120 cm^3) to give a suspension of a white solid. This suspension was cooled to −18°C for 12 h and the salt **3** collected by filtration. Yield: 2.79 g (68%). (Found: C, 45.3; H, 5.1; N, 4.8%. $C_{11}H_{15}NBrOCl$ requires: C, 45.15; H, 5.2; N, 4.8%). Mass spectrum (+ve FAB): *m*/*z*: 291/293/295 (M). IR (KBr): 2957 m, 2938 m, 2910 m, 1681 vs, 1601 s, 1476 m, 1464 m, 1411 m, 1383 m, 1297 m, 1019 m, 951 m, 823 m, 782 m cm^{-1}.

6-(4-*Bromophenyl*)-2,2′-*bipyridine*, *H***1**

A mixture of ammonium acetate (4.20 g, 55 mmol) and-2-oxo-2-(2-pyridyl)ethylpyridinium iodide (1.41 g, 4.32 mmol) were heated to reflux for 10 min. in dry ethanol (10 cm^3) under an atmosphere of dinitrogen. After this period, **3** (1.26 g, 4.32 mmol) was added and the mixture heated to reflux for a further 4.5 h. The reaction mixture was then cooled and the beige precipitate collected by filtration. Recrystallisation from ethanol gave **H1** as an off-white solid. Yield: 0.47 g (92%); m.p. 89.2°C. (Found: C, 61.9; H, 4.2; N, 8.8%. $C_{16}H_{12}N_2Br$ requires: C, 61.6; H, 3.9; N, 9.0%). Mass spectrum (+ve FAB): *m*/*z*: 310/312 (M). IR (KBr): 1582 m, 1560 m, 1430 m, 1008 m, 771 s, 745 m, 510 m cm^{-1}. ^{1}H NMR ($CDCl_3$): δ 8.70 (H, d, $H^{6'}$), 8.58 (H, d, H^3), 8.39 (H, d, $H^{3'}$), 8.02 (2H, d, H^{ortho}), 7.85 (2H dd, $H^{4'}$, H^4), 7.70 (1H, d, H^5), 7.62 (2H, d, H^{meta}), 7.32 (H, ddd, H^{5A}). ^{13}C NMR ($CDCl_3$): δ 156.1(C^6), 155.8(C^2), 155.2($C^{2'}$), 149.1 ($C^{6'}$), 138.2(C^4), 137.8 (C^{ipso}, 136.8 ($C^{4'}$), 131.8 (C^{meta}), 128.4 (C^{ortho}), 123.8 ($C^{3'}$), 123.4(C^{para}), 121.2 ($C^{5'}$), 119.9 ($C^{5/3}$), 119.6 ($C^{3/5}$).

4,4′-*Diacetylbiphenyl*, **4**

[$NiCl_2(PPh_3)_2$] (2.29 g, 3.51 mmol), zinc dust (3.44 g, 52.6 mmol) and tetraethylammonium iodide (0.90 g, 3.51 mmol) were placed in a flask fitted with a condenser. The apparatus was then purged with dinitrogen and freshly dried THF (70 cm^3) added. The reaction mixture was stirred at room temperature until the initial blue-green colour had changed to reddish-brown, after which a solution of 4-bromoacetophenone (6.9 g, 35.1 mmol) in degassed THF (30 cm^3) was rapidly added to the stirring solution. The resulting mixture was heated to 60°C for 48 h. After completion of the reaction, the mixture was filtered and the solid residues washed with dichloromethane. The filtrate and the washings were evaporated *in vacuo* and the residue purified by flash column chromatography (silica gel/CH_2Cl_2). Yield: 3.26 g (77%); M.p.: 192–193.4°C (lit. 192–193°C [20], 193.5–194°C [21]). (Found: C, 80.4; H, 6.0%. $C_{16}H_{14}O_2$ requires; C, 80.6; H, 5.9%). Mass spectrum (EI): *m*/*z*:238 (M), 223 (M-CH_3). ^{1}H NMR ($CDCl_3$): δ 7.91 (2H, d, *J* 7.8 Hz, H^3), 7.29 (2H, d, *J* 7.81 Hz, H^2), 2.60 (3H, s, CH_3). IR (KBr): 1680 s, 1606 m, 1395 m, 1363 m, 1275 s, 961 m, 819 m, 513 s cm^{-1}.

4,4′-*Bis*[3-(*N*,*N*-*dimethylammonio*)-1-*oxopropyl*]*biphenyl dichloride*, **5**

4,4′-Diacetylbiphenyl (**1**) (3.1 g, 12.9 mmol), paraformaldehyde (4.6 g, 158 mmol) and rigorously dried *N*,*N*-dimethylammonium chloride (2.3 g, 28.2 mmol) were placed in a reflux apparatus under a dinitrogen atmosphere. Freshly dried absolute ethanol (50 cm^3) and 3 drops of concentrated hydrochloric acid were added and the mixture heated at reflux for 4 h. The initially milky-white suspension changed to a straw-coloured solution over this period. An additional portion of paraformaldehyde (1.2 g, 41 mmol) was added and the mixture heated at reflux for a further two hours. Precipitation of the Mannich salt was effected after cooling of the reactant mixture (3°C) by the addition of cold (−18°C) acetone. The formation of an oil can be suppressed by a short period in an ultrasonic cleaning tank. The Mannich salt was precipitated as a white powder after standing for 12 h at −18°C. Yield (2.3 g, 42%). Mass spectrum (EI): *m*/*z*: 354 (M-2Cl). IR (KBr): 2682 m, 2464 m, 1680 s, 1604 m, 1471 m, 1395 m, 1357 m, 1230 s, 977 m, 823 m, 790 m cm^{-1}.

4,4′-*Bis*(2,2′-*bipyridin*-6-*yl*)*biphenyl*, H_2**2**

Method 1: A mixture of ammonium acetate (2.00 g, 2.6 mmol) and 2-oxo-2-(2-pyridyl)ethylpyridinium iodide (0.76 g, 2.33 mmol) was heated to reflux for 10 min. in ethanoic acid (8 cm^3) under dinitrogen. After this period, **5** (0.50 g, 1.14 mmol) was added and the mixture heated to reflux for a further 4.5 h. After this period, the suspension was cooled, and the beige precipitate collected by filtration. Recrystallisation from EtOH gave H_2**2** as an off-white solid. Yield: 0.47 g (85%); m.p. 204–205°C. (Found: C, 83.3; H 4.7; N, 12.0%. $C_{32}H_{22}N_4$ requires: C, 83.1; H, 4.8; N, 12.1%). Mass spectrum (MALDI-TOF, 1,8,9-trihydroxyanthracene matrix): *m*/*z*: 462 (M). ^{1}H NMR ($CDCl_3$): δ 8.69 (2H, d, *J* 4.53 Hz, H^{6A}), 8.63 (2H, d, *J* 7.95 Hz, H^{3B}), 8.36 (2H, d, *J* 7.74 Hz, H^{3A}), 8.10 (4H, d, *J* 8.28 Hz, H^{3C}), 7.83 (6H, m, $H^{4A,4B,5B}$), 7.38 (4H,

d, J 8.25 Hz, H^{2C}), 7.31 (2H, m, H^{5A}). IR. (KBr): 1582 m, 1561 m, 1454 m, 1427 s, 815 m, 776 s cm^{-1}.

Method 2: H**1** (0.20 g, 0.65 mmol) and the nickel reagent prepared as above from $[NiCl_2(PPh_3)_2]$ (1.51 g, 2.64 mmol), zinc dust (0.17 g, 2.64 mmol) and tetraethylammonium iodide (0.32 g) in THF under a dinitrogen atmosphere were treated as described for the preparation of **4**. After demetallation in a mixture of aqueous KCN and MeCN and filtration, extraction of the aqueous phase into dichloromethane and subsequent purification by column chromatography (silica gel, CH_2Cl_2), H_2**2** was isolated as an off-white solid in 65% yield (0.098 g). Mass spectrum: (TOF, 1,8,9-trihydroxyanthracene matrix) m/z: 462 (M). All spectroscopic and analytical data as above.

[*Ru*(*tpy*)(*CNN*-**1**), PF_6]

A mixture of [Ru(tpy)Cl_3 (0.13 g, 0.30 mmol), H**1** (0.095 g, 0.31 mmol) and *N*-ethylmorpholine (0.5 mL) was heated to reflux in water:methanol (5:1) (30 cm^3) for 2 hours. After this time the product distribution was checked by thin layer chromatography using an eluent of MeCN:KNO_3(saturated aqueous solution):H_2O, 14:2:1. After two hours, three products were detected: orange $[Ru(tpy)_2]^{2+}$ (Rf: 0.3), purple [Ru(tpy)(*CNN*-**1**), PF_6] (Rf: 0.85) and crimson [Ru(tpy)(*NN*-H**1**)Cl, PF_6] (Rf: 0.81). The crude purple mixture was treated with methanolic [NH_4, PF_6] and purified by column chromatography (silica gel with a MeCN:saturated aqueous KNO_3:H_2O; 14:2:1 mobile phase). The cyclometallated product was collected as a fast-running purple band and the complex [Ru(tpy)(*CNN*-**1**), PF_6] was isolated as a dark purple-black microcrystalline solid after the addition of [NH_4, PF_6]. Yield 0.18 g (75%). (Found: C, 47.0; H, 2.9; N, 8.8%. $RuC_{31}N_5H_{21}BrPF_6$ requires: C, 47.2; H, 2.7; N, 8.9%). Mass spectrum (FAB): m/z: 644/646 (M-PF_6); (MALDI-TOF): m/z 644/646 (M-PF_6). ^{1}H NMR (CD_3CN): δ 8.61 (2H, d, H^{3E}), 8.42 (4H, 2d, $H^{3A,3B,3D}$), 8.23 (1H, d, H^{5B}), 8.08 (2H, t, $H^{4B,4E}$), 7.85 (1H, d, H^{4A}), 7.77 (2H, t, H^{4D}), 7.72 (1H, d, H^{3C}), 7.43 (1H, d, H^{6A}), 7.39 (2H, d, H^{6D}), 7.06 (3H, t, $H^{5A,5D}$), 6.91 (1H, dd, H^{4C}), 5.81 (1H, d, H^{6C}). IR (KBr): 1135 m, 1063 m, 841 vs, 765 m cm^{-1}. UV-VIS (MeCN): λ_{max} (ϵ) 274 (36,000), 318 (46,500), 511 nm (12,300) nm.

[(*tpy*)*Ru*(μ-κ^3*CNN*:κ^3*CNN*-**2**)Ru(tpy), PF_6]$_2$

Method 1: A mixture of [Ru(tpy)Cl_3] (0.072 g, 0.16 mmol) and H_2**2** (0.039 g, 0.085 mmol) was heated to reflux in methanol:water (5:1, 15 cm^3) for 16 hours. The resulting deep purple solution was quenched with water, treated with a methanolic solution of [NH_4, PF_6] and cooled to -18°C. The deep purple cyclometallated complex which precipitated was collected by filtration and purified by preparative thin layer chromatography (silica on glass, 0.5 mm thickness, MeCN:saturated aqueous KNO_3:H_2O; 14:2:1 mobile phase). The fastest running purple band (Rf: 0.68) was the collected and isolated as the hexafluorophosphate salt [(tpy)Ru(μ-κ^3*CNN*:κ^3*CNN*-**2**)Ru(tpy), PF_6]$_2$ (75%). (Found C, 50.6; H, 3.0; N, 9.5%. $Ru_2C_{62}H_{42}N_{10}P_2F_{12}.2H_2O$ requires: C, 50.1; H, 2.99; N, 9.4%). Mass spectrum (MALDI-TOF, 1,8,9-trihydroxyanthracene matrix): 1275 (M-PF_6), 1130 (M-2PF_6). ^{1}H NMR (CD_3CN) δ: 8.59 (2H, d, $H^{3,5E}$), 8.41 (1H, d, H^{3A}), 8.37 (3H, d, $H^{3B,3D}$), 8.13 (1H, d, H^{5B}), 8.07 (1H, dd, H^{4B}), 8.01 (1H, d, H^{4E}), 7.83 (1H, m, H^{4A}), 7.73 (2H, m, H^{4D}), 7.32 (3H, 2d, $H^{6A,6D}$), 7.09 (1H, br s, H^{3C}), 7.03 (3H, m, $H^{5A,5D}$), 6.35 (1H, d, H^{4C}), 5.19 (1H, s, H^{6C}). UV-VIS (MeCN): λ_{max} (ϵ) 274 (52,000), 318 (46,500) 519 (14,800) nm.

Method 2: [$Ni(PPh_3)_2Cl_2$] (151 mg, 0.26 mmol) and PPh_3 (0.14 g, 0.53 mmol) were added to a dry, degassed stirred sample of DMF (40 cm^3). After 30 minutes, the deep blue solution was treated with zinc dust (0.017 g, 0.26 mmol) and stirring continued until a brick-red suspension had been obtained. To this suspension was added a solution of [(tpy)Ru(*CNN*-**1**), PF_6] (0.042 g, 0.054 mmol) in the minimum quantity of dry, degassed DMF. The system was then heated to reflux for 24 h, after which time, TLC analysis showed the formation of a new purple species with RF 0.68. The purple compound [(tpy)Ru(μ-κ^3*CNN*:κ^3*CNN*-**2**)Ru(tpy), PF_6]$_2$ was isolated in the same way as in Method 1. Yield: 0.026 g (71%). The compound was identical in all respects to that above.

RESULTS AND DISCUSSION

6-*Phenyl*-2,2′-*bipyridine complexes*

The ligand Hpbpy gives rise to two series of complexes: in the first series, the ligand behaves as a conventional didentate 2,2′-bipyridine and acts as an *NN* donor, whilst in the second the *ortho*-position of the phenyl ring is deprotonated to give an anionic terdentate *CNN* donor ligand (Fig. 1). We [4, 14, 22–25] and others [26–28] have studied the factors which control the adoption of a particular bonding motif and have shown that protic solvents favour the formation of the cyclometallated species [13, 14].

Although a number of ligands incorporating two

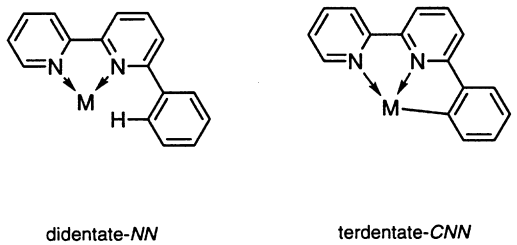

Fig. 1. Cyclometallated and non-metallated bonding modes for Hpbpy.

or more Hpbpy metal-binding domains have been described, their structures have not been such to allow a facile comparison of the various strategies for the formation of multiply cyclometallated complexes. Accordingly, we decided to investigate a system which would be amenable to both convergent and divergent syntheses.

Ligand synthesis

We initially prepared a functionalised Hpbpy ligand which had a reactive group which would allow dimerisation in both free and coordinated forms. We decided to adopt the nickel(0) coupling of haloarenes for the dimerisation step, a method which we [29–36] and others [37–45] have successfully used for the synthesis of oligopyridines. Accordingly, our initial step was the synthesis of a suitable 6-(4-halophenyl)-2,2′-bipyridine.

The initial target was 6-(4-bromophenyl)-2,2′-bipyridine H**1** which was prepared using the Kröhnke method [17] as shown in Scheme 1. Commercially available 4-bromoacetophenone was converted in 68% yield to the Mannich salt **3** by reaction with *N*,*N*-dimethylammonium chloride and paraformaldehyde in dry ethanol to give the salt as a white solid with a typical carbonyl absorption in its IR spectrum at 1681 cm^{-1}. Compound **3** was then reacted with the enolate precursor 2-(2-pyridyl)-2-oxoethylpyridinium iodide in the presence of ammonium acetate in ethanol to give the desired ligand in 92% yield as a cream-coloured solid. Spectroscopic and analytical data for the new ligand H**1** fully support the proposed formulation. The mass spectrum exhibited parent ions at *m*/*z* 310 and 312 with the 1:1 isotopic distribution expected of a monobromo compound and the ^{1}H NMR spectrum of a $CDCl_3$ solution of H**1** (Fig. 2a) showed nine aromatic proton environments. The ^{13}C NMR spectrum of a $CDCl_3$ solution of H**1** displayed the expected 14 resonances.

The potentially dinucleating ligand H_2**2** is formally a dimer of Hpbpy and could exhibit a range of coordination modes including mononuclear didentate *NN*, mononuclear terdentate *CNN*, dinucleating κk^2-*NN*:κ^2-*NN*, dinucleating κ^2-*NN*:κ^3-*CNN* and dinucleating κ^3-*CNN*:κ^3-*CNN* (Fig. 3). For the synthesis of H_2**2** we considered two routes. In both cases, the B ring was to be prepared in a Kröhnke synthesis, but in the first route the biphenyl unit was constructed as the first step, whilst in the second it was assembled as the last reaction step. Once again, 4-bromoacetophenone was the starting point and was converted to 4,4′-diacetylbiphenyl **4** in 77% yield using the Iyoda [40] nickel-coupling reaction. This method is more convenient than the Friedel-Crafts acetylation of biphenyl [46] or the use of $[Ni(COD)_2]$ as a reagent [21]. The conversion of **4** to the bis(Mannich) salt **5** was achieved in 42% yield by reaction with *N*,*N*-dimethylammonium chloride and paraformaldehyde in dry ethanol. Finally, H_2**2** was obtained as a pale

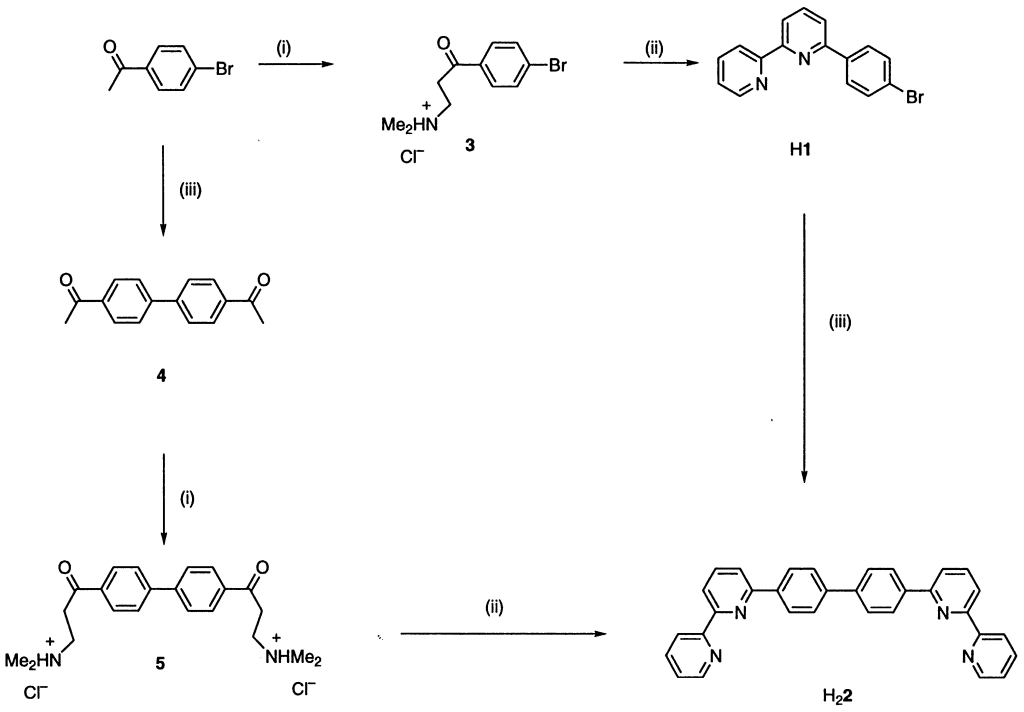

Scheme 1. (i) $[Me_2NH]Cl$, CH_2O, EtOH (ii) 2-oxo-2-pyridylethylpyridinium iodide, $[NH_4]OAc$ (iii) '$[Ni(PPh_3)_n]$'.

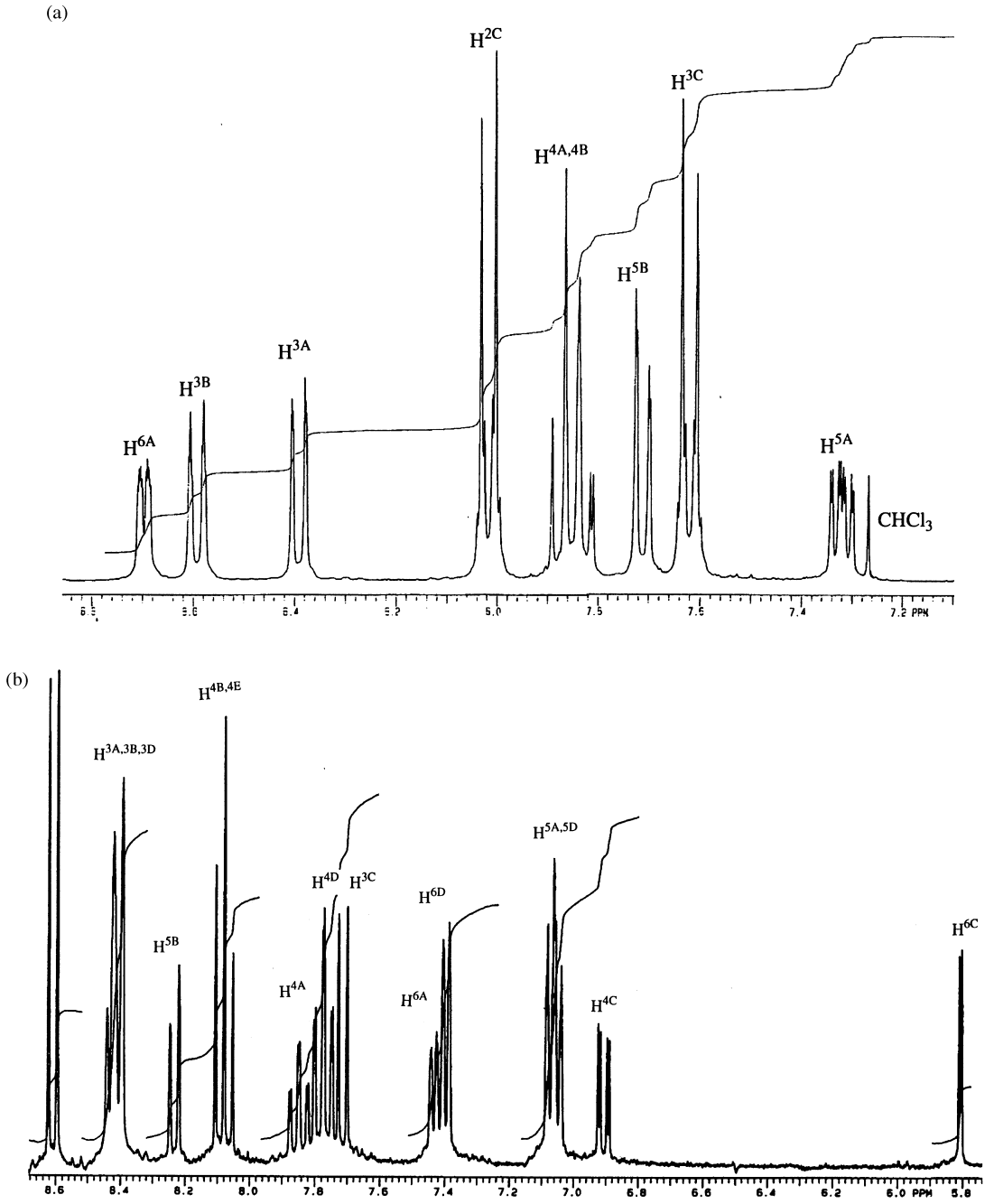

Fig. 2. 300 MHz ^{1}H NMR spectra of (a) a $CDCl_3$ solution of H**1** and (b) a CD_3CN solution of [Ru(tpy)(*CNN*-**1**), PF_6] showing the assignments.

beige solid in 85% yield after recrystallisation from EtOH, from the reaction of **5** with 2-(2-pyridyl)-2-oxoethylpyridinium iodide and ammonium acetate in acetic acid under an atmosphere of dinitrogen for 4.5 h. The mass spectrum displayed a parent ion at m/z 462 and no carbonyl absorptions were observed in the IR spectrum. The ^{1}H NMR spectrum of a $CDCl_3$ solution exhibited the expected 9 resonances in the aromatic region and was generally similar to the spectra of H**1** and Hpbpy.

The second approach to H_2**2** involved the coupling of H**1**under Iyoda conditions. The ligand H_2**2** was obtained in 65% yield and was in all respects identical to that obtained above. Comparing the efficiency of the two routes with respect to 4-bromoacetophenone, H_2**2** was obtained in 25% yield when the dimerisation

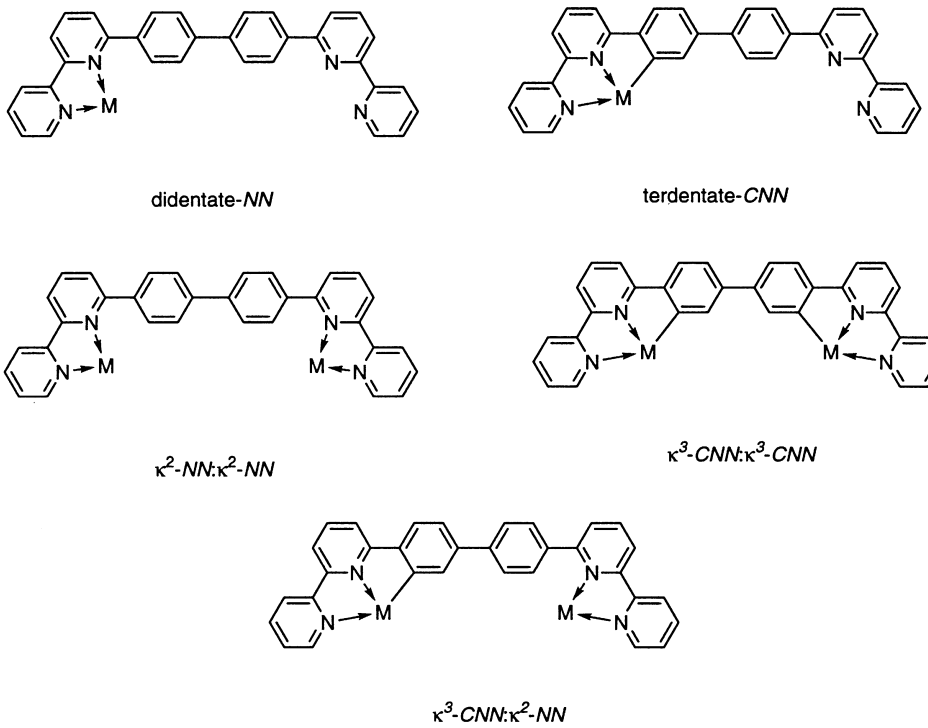

Fig. 3. Cyclometallated and non-metallated bonding modes for H_2**2**.

was made early in the synthesis and in 41% yield when the dimerisation was used as the final step. This suggests that the convergent approach will prove to be of more general utility for ligands incorporating additional metal-binding domains *and* that a convergent approach to the metal complexes might also be effective.

*Cyclometallation reactions of H***1** *and* H_2**2**

The mononucleating ligand H**1** can exhibit *NN* or *CNN* bonding modes. Thus, reaction with [Ru(tpy)Cl_3] in which three of the coordination sites at the metal are occupied by a non-labile chelating tpy ligand, under reductive conditions leading to ruthenium(II) compounds could give the cyclometallated species [Ru(tpy)(*CNN*-**1**)]$^+$ or the non-metallated complex cation [Ru(tpy)(*NN*-H**1**)Cl]$^+$ in which the remaining coordination site is occupied by a chloride ligand. We have shown that the formation of the cyclometallated complex is favoured by reaction under mildly basic, aqueous conditions [13, 14]. The cyclometallated complex [Ru(tpy)**1**, PF_6] was prepared from the reaction of H**1** with [Ru(tpy)Cl_3] in aqueous methanol:water containing *N*-ethylmorpholine. As the reaction progressed, the reactants dissolved to give a deep purple solution. Chromatographic purification of this dark solution followed by precipitation with ammonium hexafluorophosphate yielded [Ru(tpy)(*CNN*-**1**), PF_6] as a dark purple-black micro-crystalline solid. Small amounts of crimson [Ru(tpy)(*NN*-H**1**)Cl, PF_6] were also isolated (Scheme 2).

The time-of-flight mass spectrum of [Ru(tpy)(*CNN*-**1**), PF_6] exhibited base peaks at m/z 644 and 646 (M-PF_6). The cyclic voltammogram of an acetonitrile solution of the complex exhibits a single reversible ruthenium(II)/ruthenium(III) wave at $+0.27$ V *versus* Fc/Fc$^+$. This value is relatively high compared to that of the analogous complex [Ru(tpy)(*CNN*-pbpy), PF_6] which is observed at $+0.12$ V [14] an effect which may be ascribed to the electron-withdrawing bromine substituent destabilising the ruthenium(III) state. The electronic spectrum of the complex exhibits absorption maxima at 274, 316 and 514 nm which correlate well with those in [Ru(tpy)(*CNN*-pbpy), PF_6] (274, 317 and 512 nm).

The ^{1}H NMR spectrum of a CD_3CN solution of [Ru(tpy)(*CNN*-**1**), PF_6] is shown in Fig. 2(b). The most noticeable feature of the spectrum is the upfield-shifted doublet at δ 5.81 which is characteristic [14] of the proton adjacent to the site of cyclometallation, H^{6C}. The equivalent proton in the ^{1}H NMR spectrum of [Ru(tpy)(*CNN*-pbpy), PF_6] is observed at δ 5.69 and the down-field shift correlates well with that of δ-0.13 predicted on the basis of a *meta* bromo substituent [47].

The reaction of H_2**2** with two equivalents of [Ru(tpy)Cl_3] was investigated under a wide range of experimental conditions. In most cases, dark purple-

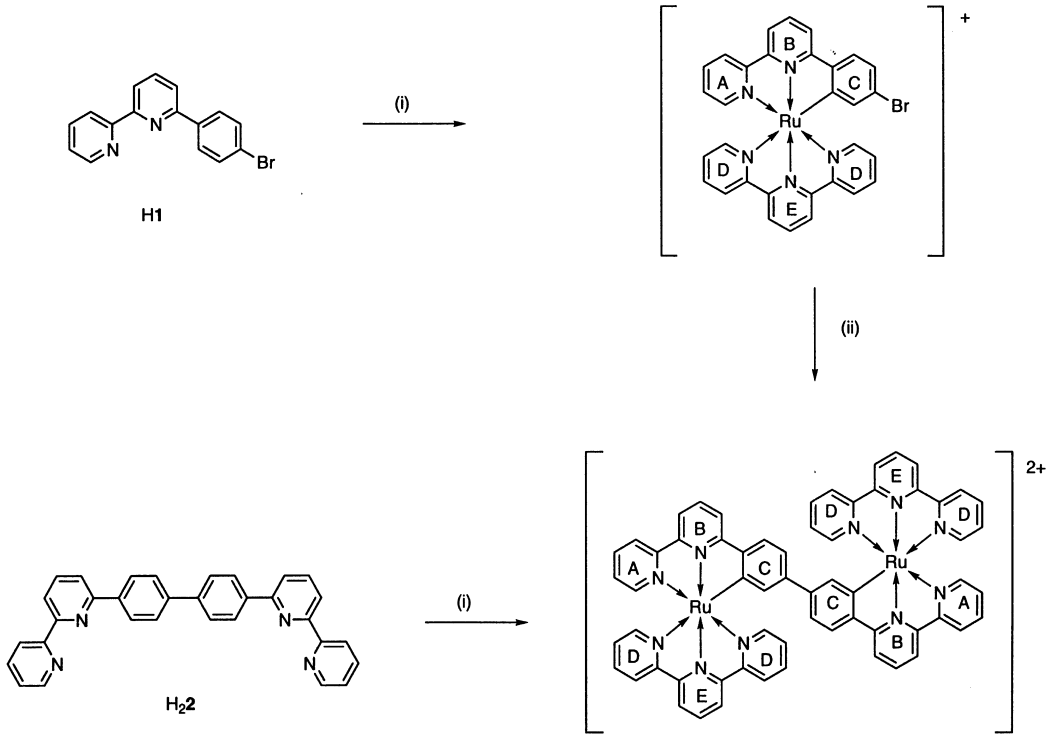

Scheme 2. (i) [Ru(tpy)Cl_3], *N*-ethylmorpholine, H_2O-MeOH (ii) '[$Ni(PPh_3)_n$]'.

coloured solutions were formed but chromatographic analysis indicated the formation of a large number of species. The addition of ammonium hexafluorophosphate to these solutions precipitated mixtures of salts which were shown by ^{1}H NMR spectroscopy to contain the various species indicated in Fig. 3. However, we eventually found a procedure that maximised the formation of [(tpy)Ru(μ-κ^3*CNN*:κ^3*CNN*-**2**)Ru(tpy), PF_6]$_2$. The most convenient experimental procedure is to add water to a solution of H_2**2** in methanol until the ligand begins to precipitate (about 5:1 MeOH:H_2O) and then to heat this solution with two equivalents of [Ru(tpy)Cl_3]. Chromatographic purification of the dark coloured solution yielded [(tpy)Ru(μ-κ^3*CNN*:κ^3*CNN*-**2**)Ru(tpy), PF_6]$_2$ as a purple-black solid in 75% yield. The mass spectrum of this compound exhibited intense peaks at *m*/*z* 1276 (M-PF_6) and 1130 (M-2PF_6) and the cyclic voltammogram of an acetonitrile solution exhibited a single reversible (E_a-E_c = 60 mV) ruthenium(II)/ruthenium(III) process at +0.18 V, typical of a ruthenium centre in an N_5C environment (*c.f.* +0.12 V for [Ru(tpy)(*CNN*-pbpy), PF_6]). The observation of a single process is somewhat disappointing and indicates that with the biphenylene spacer, no significant metal-metal interaction is occurring. We note that the most efficient interactions between metal centres appear to occur when the cyclometallated sites are linearly connected-*i.e.* when the cyclometallated ring replaces the central ring of the tpy to give a *CNN* donor [5, 8]. The electronic spectrum of the complex is also characteristic and exhibits absorptions at 274, 318 and 513 nm in full accord with [Ru(tpy)(*CNN*-pbpy), PF_6] (see above). The ^{1}H NMR spectrum of a CD_3CN solution of [(tpy)Ru(μ-κ^3*CNN*:κ^3*CNN*-**2**)Ru(tpy), PF_6]$_2$ is presented in the experimental section and exhibits the expected upfield shifted resonance for H^{6C} which is observed at δ 5.19.

Finally, we investigated the nickel-mediated coupling of [(tpy)Ru(*CNN*-**1**), PF_6], which may be regarded as a bromoarene which also bears a ruthenium-containing substituent. This allows us to prepare the complex [(tpy)Ru(μ-κ^3*CNN*:κ^3*CNN*-**2**)Ru(tpy), PF_6]$_2$ by an *in situ* ligand synthesis. In view of the use of soft iodide ions in the Iyoda reaction, we used an alternative procedure which has proved successful for us in the past. The nickel(0) reagent was prepared *in situ* as a red solid by the reduction of [$Ni(PPh_3)_2Cl_2$] by zinc dust in the presence of excess triphenylphosphine in dmf solution. Subsequent reaction with [(tpy-)Ru(*CNN*-**1**), PF_6] resulted in the formation of [(tpy)Ru(μ-κ^3*CNN*:κ^3*CNN*-**2**)Ru(tpy), PF_6]$_2$ in 71% yield and in all respects identical to the material obtained directly from H_2**2**.

Although the direct cyclometallation of H_2**2** gives a slightly higher yield than the coupling of [(tpy-)Ru(*CNN*-**1**), PF_6], it is instructive to consider the overall yields from 4-bromoacetophenone. The direct

cyclometallation route involves 4 steps and gives [(tpy)Ru(μ-κ^3*CNN*:κ^3*CNN*-**2**)Ru(tpy), PF_6]$_2$ in 31% overall yield, whilst the coupling of the metal complex [(tpy)Ru(*CNN*-**1**), PF_6] also involves four steps but give the bis(cyclometallate) in 33% yield. Clearly in the case of only two metal-binding domains there is no clear choice between the approaches in terms of yields. However, in species with more than two metal-binding domains, the convergent approach involving the coupling of metal complexes is expected to prove superior.

CONCLUSIONS

We have investigated a series of strategies for the synthesis of multiply cyclometallating ligands and their metal complexes. The synthesis of the free ligands is best achieved using a convergent approach in which pre-formed metal-binding domains are combined late in the reaction sequence. Bis(cyclometallates) may be obtained directly by reaction of a ligand bearing two *CNN*-metal-binding domains with a metal source or by the nickel-mediated dimerisation of a haloarene functionalised cyclometallate. Although yields in the direct bis(cyclometallation) reaction are marginally higher under optimised conditions, considerable investment of time is required to establish these optimal experimental conditions. In conclusion, we have shown that cyclometallated complexes may be coupled in nickel-mediated reactions to give multiply cyclometallated species.

Acknowledgements—We should like to thank the Schweizerischer Nationalfonds zur Förderung der wissenschaftlichen Forschung and the University of Basel for support.

REFERENCES

1. Constable, E. C., *Chem. Commun.*, 1997, **0,** 1073.
2. Constable, E. C., *Makromol. Symp.*, 1995, **98,** 503.
3. Constable, E. C., *Polyhedron*, 1984, **3,** 1037.
4. Constable, E. C., Cargill Thompson, A. M. W. and Greulich, S., *J. Chem. Soc., Chem. Commun.*, 1993, **0,** 1444.
5. Barigelletti, F., Flamigni, L., Guardigli, M., Juris, A., Beley, M., Chodorowski-Kimmes, S., Collin, J. P. and Sauvage, J. P., *Inorg. Chem.*, 1996, **35,** 136.
6. Sutter, J. P., Beley, M., Collin, J.-P., Veldman, N., Spek, A. L., Sauvage, J.-P. and Van Koten, G., *Mol. Cryst. Liq. Cryst. Sci. Tec. A*, 1994, **252,** 507.
7. Beley, M., Collin, J.-P. and Sauvage, J.-P., *Inorg. Chem.*, 1993, **32,** 4539.
8. Beley, M., Chodorowski, S., Collin, J. P., Sauvage, J.-P., Flamigni, L. and Barigelletti, F., *Inorg. Chem.*, 1994, **33,** 2543.
9. Sutter, J. P., Grove, D. M., Beley, M., Collin, J.-P., Veldman, N., Spek, A. L., Sauvage, J.-P. and Van Koten, G., *Angew. Chem. Int. Ed. Engl.*, 1994, **33,** 1282.
10. Beley, M., Chodorowski-Kimmes, S., Collin, J.-P., Laine, P., Launay, J.-P. and Sauvage, J.-P., *Angew. Chem. Int. Ed. Engl.*, 1994, **33,** 1775.
11. Beley, M., Chodorowski, S., Collin, J.-P. and Sauvage, J.-P., *Tetrahedron Lett.*, 1993, **34,** 2932.
12. Beley, M., Collin, J.-P., Louis, R., Metz, B. and Sauvage, J.-P., *J. Am. Chem. Soc.*, 1991, **113,** 8521.
13. Constable, E. C. and Rees, D. G. F., *New J Chem*, 1997, **21,** 369.
14. Constable, E. C. and Hannon, M. J., *Inorg. Chim. Acta*, 1993, **211,** 101.
15. Chodorowski-Kimmes, S., Beley, M., Collin, J.-P. and Sauvage, J.-P., *Tetrahedron Lett.*, 1996, **37,** 2963.
16. Tzalis, D. and Tor, Y., *Chem Commun*, 1996, **0,** 1043.
17. Krohnke, F., *Synthesis*, 1976, **0,** 1.
18. Cotton, F. A., Faut, O. D. and Goodgame, D. M. L., *J. Am. Chem. Soc.*, 1961, **83,** 344.
19. Constable, E. C., Thompson, A. M. W. C., Tocher, D. A. and Daniels, M. A. M., *New J Chem*, 1992, **16,** 855.
20. Sloan, G. J. and Vaughan, W. R., *J. Org. Chem.*, 1957, **22,** 750.
21. Semmelhack, M. F., Helquist, P. M. and Jones, L. D., *J. Am. Chem. Soc.*, 1971, **93,** 5908.
22. Constable, E. C., Henney, R. P. G., Leese, T. A. and Tocher, D. A., *J. Chem. Soc., Dalton Trans.*, 1990, **0,** 443.
23. Constable, E. C., Henney, R. P. G., Leese, T. A. and Tocher, D. A., *J. Chem. Soc., Chem. Commun.*, 1990, **0,** 513.
24. Constable, E. C., Cargill Thompson, A. M. W., *Supramol. Chem.*, 1994, **4,** 95.
25. Constable, E. C., Cargill Thompson, A. M. W., *New. J. Chem.*, 1996, **20,** 65.
26. Collin, J. P., Kayhanian, R., Sauvage, J. P., Calogero, G., Barigelletti, F., DeCian, A. and Fischer, J., *Chem Commun*, 1997, **0,** 775.
27. Liu, H. Q., Cheung, T. C., Peng, S. M. and Che, C.M., *J. Chem. Soc., Chem. Commun.*, 1995, **0,** 1787.
28. Collin, J.-P., Beley, M., Sauvage, J.-P. and Barigelletti, F., *Inorg. Chim. Acta*, 1991, **186,** 91.
29. Constable, E. C. and Ward, M. D., *J. Chem. Soc., Dalton Trans.*, 1990, **0,** 1405.
30. Constable, E. C., Elder, S. M., Healy, J. A. and Tocher, D. A., *J. Chem. Soc., Dalton Trans.*, 1990, **0,** 1669.
31. Constable, E. C., Elder, S. M., Hannon, M. J., Martin, A., Raithby, P. R. and Tocher, D. A., *J. Chem. Soc., Dalton Trans.*, 1996, **0,** 2423.
32. Constable, E. C., Ward, M. D. and Tocher, D.A., *J. Chem. Soc., Dalton Trans.*, 1991, **0,** 1675.
33. Constable, E. C., Edwards, A. J., Martínez-Máñez, R. and Raithby, P. R., *J. Chem. Soc., Dalton Trans.*, 1995, **0,** 3253.
34. Chotalia, R., Constable, E. C., Neuburger, M., Smith, D. R. and Zehnder, M., *J. Chem. Soc., Dalton Trans.*, 1996, **0,** 4207.
35. Constable, E. C., Hannon, M. J., Edwards, A. J. and Raithby, P. R., *J. Chem. Soc., Dalton Trans.*, 1994, **0,** 2669.

36. Constable, E. C., Morris, D. J. and Carr, S., *New J. Chem*., 1998, **22,** 287.
37. Tiecco, M., Testaferri, L., Tingoli, M., Chianelli, D. and Montanucci, M., *Synthesis*, 1984, **0,** 736.
38. Van Deresse, R., Lourak, M., Fort, Y. and Caubere, P., *Tetrahedron Lett*., 1986, **27,** 5483.
39. Tiecco, M., Tingoli, M., Testaferri, L., Bartoli, D. and Chianelli, D., *Tetrahedron*, 1989, **45,** 2857.
40. Iyoda, M., Otsuka, H., Sato, K. and Nisato, N., Oda, M., *Bull. Chem. Soc. Jpn*., 1990, **63,** 80.
41. Baxter, P., Lehn, J.-M., De Cian, A. and Fischer, J., *Angew. Chem. Int. Ed. Engl*., 1993, **32,** 69.
42. Torii, S., Tanaka, H. and Morisaki, K., *Tetrahedron Lett*., 1985, **0,** 1655.
43. Moran, D. B., Morton, G. O. and Albright, J. D., *J. Heterocycl. Chem*., 1986, **0,** 1071.
44. Yamamoto, Y. and Azuma, Y., Mitoh, H., *Synthesis*, 1986, **0,** 564.
45. Fort, Y., Becker, S. and Caubère, P., *Tetrahedron*, 1994, **0,** 11893.
46. Tani, H., Toda, F. and Matsumiya, K., *Bull. Chem. Soc. Jpn*., 1963, **36,** 391.
47. Günther, H., *NMR Spectroscopy. An introduction*, Wiley, Chichester, 1980.

Pergamon

PII: S0277–5387(98)00108–9

Polyhedron Vol. 17, No. 19, pp. 3291–3303, 1998
© 1998 Elsevier Science Ltd
All rights reserved. Printed in Great Britain
0277–5387/98 $19.00 + 0.00

Coordination studies of the ligand series $RNH{\cdot}C\O{\cdot}(CH_2)_n{\cdot}C\O{\cdot}NHR$ where R = alkyl, aryl; Ø = O, S and $n = 0,1,2$. Part 6. Crystal structures and bonding considerations of the ligands $MeNH{\cdot}CO{\cdot}CH_2{\cdot}CO{\cdot}NHMe$ (L^1), $MeNH{\cdot}CO{\cdot}CH_2{\cdot}CH_2{\cdot}CO{\cdot}NHMe$ (L^4), $MeNH{\cdot}CS{\cdot}CH_2{\cdot}CS{\cdot}NHMe$($L^5$) and the Sn^{IV} complexes $SnBr_4L^1{\cdot}L^1$, $SnBr_4L^2{\cdot}2THF$ and $SnBr_4L^3{\cdot}MeCN$ where $L^2 = {}^iC_3H_7NH{\cdot}CO{\cdot}CH_2{\cdot}CO{\cdot}NH{}^iC_3H_7$ and $L^3 = {}^iC_3H_7NH{\cdot}CS{\cdot}CH_2{\cdot}CS{\cdot}NH{}^iC_3H_7$

Gerald R. Willey[a]*, Robert J. Baker[a], John V. Haslop[a], Marcus P. Spry[a], Michael G. B. Drew[b]

[a]Department of Chemistry, University of Warwick, Coventry, CV4 7AL, U.K.

[b]Department of Chemistry, University of Reading, Whiteknights, Reading, RG6 2AD, U.K.

(Received 8 January 1998; accepted 6 March 1998)

Abstract—Crystal structures of the ligands $MeNH{\cdot}CO{\cdot}CH_2{\cdot}CO{\cdot}NHMe$, $MeNH{\cdot}CO{\cdot}CH_2{\cdot}CH_2{\cdot}CO{\cdot}NHMe$ and $MeNH{\cdot}CS{\cdot}CH_2{\cdot}CS{\cdot}NHMe$ have been determined by X-ray diffraction studies. The framework C–C, C–N, and C=O/C=S bond distances and the associated interbond angles are all closely similar and the packing of these molecules is dominated by intermolecular hydrogen bonding of the type N–H···O=C and, to a lesser extent, N–H···S=C. For means of comparison the bond parameters of all the structurally characterised related ligands belonging to the N,N′-disubstituted series $RNH{\cdot}C\O{\cdot}(CH_2)_n{\cdot}C\O{\cdot}NHR$ where R = alkyl; Ø=O, S and n = O, 1, 2 are listed and a general overview of the characteristics of such ligands including conformational variations is provided. Structural characterisation (X-ray diffraction) of $SnBr_4$ ($MeNH{\cdot}CO{\cdot}CH_2{\cdot}CO{\cdot}NHMe$)·$MeNH{\cdot}CO{\cdot}CH_2{\cdot}CO{\cdot}NHMe$, $SnBr_4({}^iPrNH{\cdot}CO{\cdot}CH_2{\cdot}CO{\cdot}NH{}^iPr){\cdot}2THF$ and $SnBr_4({}^iPrNH{\cdot}CS{\cdot}CH_2{\cdot}CS{\cdot}NH{}^iPr){\cdot}MeCN$ reveals bidentate chelate ligand attachment for these six coordinate mononuclear *cis*-octahedral Sn(IV) complexes. In all three structures, the NH groups are involved in intermolecular hydrogen bonding being linked either to C=O/C=S groups of adjacent molecules, or solvent molecule(s) entrapped in the lattice and/or halogen atom(s) of a neighbouring $SnBr_4$ moiety. The general range of Sn-Br distances is 2.504(3)-2.565(12) Å excluding those halogen atoms directly involved in N-H···Br-Sn interactions. These several types of intermolecular hydrogen bonding are viewed as a direct cause of ring puckering in the chelated rings approximating to a chair conformation. © 1998 Elsevier Science Ltd. All rights reserved

Keywords: X-ray structures; octahedral Sn(IV) complexes; oxalamides; malonamides; succinamides; oxa/thia derivatives.

*Author to whom correspondence should be addressed.

The generic series RHN·CØ·$(CH_2)_n$·CØ·NHR [H_2L] comprising oxa (Ø═O) and thia (Ø═S) derivatives of oxalamides ($n=0$), malonamides ($n=1$) and succinamides ($n=2$) has been used extensively in metal complexation both for analytical purposes and in the development of novel p-and d-block metal compounds [1]. With both 'hard' (N, Ø═O) and 'soft' (Ø═S) donor centres available this is clearly a versatile family of ligands in terms of metal selectivity. In view of the structural diversity of these ligands e.g., the co-ordination mode(s) adopted for specific metal ion(s) and the conformational rearrangements consequent with complexation, we have undertaken a crystallographic investigation of representative members of the series. Recent studies from these laboratories have been focused on the structural classification of **neutral** H_2L-*p*-block metal complexes involving the halides of Groups 14/15 as reference Lewis acids [2]. Perhaps the main point that has emerged from our work relates to the ligand binding; of the potential donor sites, it is always the oxygen (sulphur) atoms that are involved in bonding to the metal. The trigonal (sp^2) geometry around the nitrogen atoms indicates that the formal lone pair of electrons is incorporated in 'internal' p_π-p_π bonding within the thia (oxa)-amide moiety.

Related studies by other research groups have been directed towards the coordination behaviour of these ligands, often in the anionic form and sometimes involving nitrogen coordination, with transition metal ions [3]. De-protonation of the nitrogen centres provides the amide forms HL^- and L^{2-} and typical examples of the former include: [$Pd(C_6H_{11}NH{\cdot}CS{\cdot}CS{\cdot}NC_6H_{11})_2$] [4] featuring square planar Pd^{II} with S_4 coordination and [$Pd(C_5H_9NH{\cdot}CS{\cdot}CS{\cdot}NC_5H_9)_2$] [5] with a similar metal environment. One other variation of proton-loss leading to HL^- has been noted: This is specific to malonamide ligands and features loss of a proton from the methyne backbone to provide six-membered ring formation of the type

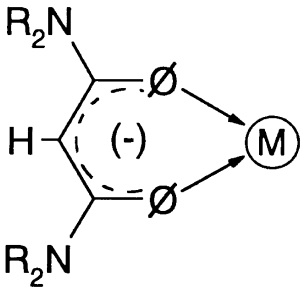

with accompanying delocalised π-character similar to M(acac) complexation. The compound Ni(dpdtma)$_2$·2DMF [6] where dpdtma-,N,N′-diphenyldithiomalonamide mono-anion provides a typical example. Examples of L^{2-} include $Na_2[Ni(etox)_2]{\cdot}H_2O$ (H_2etox = $H_2N{\cdot}CO{\cdot}CO{\cdot}NH(CH_2)_2OH$) [7] where each ligand is bonded to the central Ni^{2+} ion through both of its deprotonated nitrogen atoms and the Cu(II) complexes $\{Cu_2[S_2C_2(NCH_2CH_2OH)_2](H_2O)_2\}SO_4$ and $[\{Cu_2[S_2C_2(NCH_2CH_2OH)_2](H_2O)(SO_4)\}(H_2O)_2$ [8] where the deprotonated amine centres of each ligand bind to separate metal ions resulting in zig-zag chain structures.

In this report we describe the crystal and molecular structures of the ligands, MeNH·CO·CH_2·CO·NHMe (L^1), MeNH·CO·CH_2·CH_2·CO·NHMe (L^4), MeNH·CS·CH_2·CS·NHMe (L^5) and the Sn(IV) derivatives $SnBr_4L^1{\cdot}L^1$ (I), $SnBr_4L^2{\cdot}2THF$ (2) and $SnBr_4L^3{\cdot}MeCN$ (3) where $L^2 = {}^iC_3H_7NH{\cdot}CO{\cdot}CH_2{\cdot}CO{\cdot}NH{}^iC_3H_7$ and $L^3 = {}^iC_3H_7NH{\cdot}CS{\cdot}CH_2{\cdot}CS{\cdot}NH{}^iC_3H_7$.

EXPERIMENTAL

Manipulations of materials were carried out using standard Schlenk techniques in conjunction with a dinitrogen-filled 'dry-box'. Solvents were stored over CaH_2-P_4O_{10} and distilled under a dinitrogen atmosphere immediately prior to use. Infrared spectra (4000-200) cm^{-1} were recorded on a Perkin Elmer 580B instrument with samples as Nujol mulls between CsI plates. The ^1H (400 MHz) nmr spectra were recorded on a Bruker ACP 400 spectrometer using CD_3CN solutions. Microanalytical data were obtained using a Leeman Labs Inc., PS 1000 sequential inductively coupled plasma (ICP) spectrometer and a CE440 elemental (C,H,N) analyser.

REAGENTS

$SnBr_4$ was obtained commercially and used directly. The oxa ligands were prepared from the corresponding acid esters via direct aminolysis with the appropriate primary amine as previously described [2]. Conversion of these oxa ligands to their corresponding thia derivatives can be carried out by direct thiation using Lawesson's reagent i.e., 2,4-bis(p-methoxyphenyl) - 2,4 - dithioxo - 1,3,2,4 - dithiaphosphetane [9, 10].

Typically for L^3: N,N′-di-isopropyl malonamide (20.0 g, 107.4 mmol) dissolved in toluene (25 cm^3) was added to a solution of Lawesson's Reagent (43.4 g, 107.4 mmol) in toluene (80 cm^3) and the mixture was heated at reflux for 3 hrs. The resulting yellow solution was cooled, and the solvent removed *in vacuo* to give a yellow solid, which was purified by column chromatography (Silica gel, 50:50 ether/acetone as elutant). Recrystallisation from acetonitrile provided yellow needle crystals of the product (14.5 g, 62%). Anal. Calcd. for $C_9H_{18}N_2S_2$:C, 49.5; H, 8.3; N, 12.8. Found: C, 49.2; H, 8.2; N, 12.7%. IR, $\bar{\nu}/cm^{-1}$ (Nujol) 3187 s (NH); 1538 m (CN), 904 m (CS); $\delta_H(CDCl_3)$ 8.83 (s, 2H, NH), 4.55–4.44 (m, 2H, CH), 4.05 (s, 2H, CH_2), 1.24, 1.21 (d, 12H, CH_3).

PREPARATION OF THE METAL COMPLEXES

(*a*) *$SnBr_4L^1{\cdot}L^1$*(1)

$SnBr_4$ (1.0 g, 2.3 mmol) in acetonitrile (20 cm^3) was added to a solution of N,N′-dimethylmalonamide (0.3 g, 2.3 mmol) and the mixture was stirred for 6 hrs at 50°C under an inert atmosphere of dinitrogen. Removal of solvent *in vacuo* provided a white powder which was washed with n-hexane (3×10 cm^3). Recrystallisation from THF/CH_2Cl_2 (50:50) provided colourless rhomboid crystals suitable for X-ray diffraction. Yield (1.09 g, 68%). Anal. Calcd. for $C_{10}H_{20}N_4O_4SnBr_4$. C, 17.2; H, 2.9; N, 8.0. Found: C, 17.4; H, 2.8; N, 8.1%. IR $\bar{\nu}/cm^{-1}$ (Nujol) 3235 m(NH), 1624 s (CO), 320 m, 280 vs (SnBr). δ_H ($CDCl_3$) 8.41 (s, 2H, NH), 3.87 (s, 2H, CH_2) 2.90 (2, 6H, CH_3).

(*b*) *$SnBr_4L^2{\cdot}2THF$* (2)

To a solution of N,N′-di-isopropylmalonamide (0.4 g, 2.2 mmol) in THF (25 cm^3) was added a solution of $SnBr_4$ (0.94 g, 2.15 mmol) in THF (25 cm^3). The mixture was maintained at 50°C and stirred under an atmosphere of argon for 6 hrs. Removal of the

Table 1. Crystal data and structure refinement for 1,2,3,4 and 5[1]

Identification code	$SnBr4L^1$,L^1	$SnBr4L^2$,2thf	$SnBr_4L^3$,MeCN	L^4	L^5
Empirical formula	C10H20Br4N4O4Sn	C17H34Br4N2O4Sn	C11H21Br4N3S2Sn	C5H1202N2	C5H10N2S2
Formula weight	698.63	768.79	697.76	144.2	162.27
Temperature K	293 (2)	293 (2)	293 (2)	293 (2)	293 (2)
Wavelength Å	0.71073	0.71073	0.71073	0.71073	0.71073
Crystal system	monoclinic	monoclinic	monoclinic	monoclinic	tetragonal
Space group	$P2_1/n$	$P2_1/n$	$P2_1$	$P2_1/c$	$P4_32_22$
Unit cell dimensions (Å, °) a	11.227 (8)	10.818 (11)	8.167 (9)	8.660 (7)	6.523 (9)
b	11.694 (9)	14.645 (14)	14.093 (14)	4.908 (5)	=a
c	17.667 (12)	17.738 (18)	10.179 (10)	9.767 (11)	19.90 (2)
β	108.67 (1)	94.87 (1)	107.95 (1)	100.0 (1)	(90)
Volume/A^3	2197	2800	1115	409	847
Z,	4	4	2	2	4
Calculated density Mgm^{-3}	2.112	1.824	2.079	1.172	1.273
Absorption coefficient (mm − 1)	8.455	6.642	8.501	0.085	0.551
F (000)	1320	1488	660	156	344
Crystal size mm	0.25*0.30*0.35	0.25*0.15*0.10	0.25*0.20*0.20	0.30*0.40*0.20	0.15*0.20*0.25
θ range for data collection	2.58 to 24.08	2.35 to 26.06	2.55 to 26.08	3.0 to 25.0	3.29 to 26.15
Index ranges	0 < =h< =12, −13 < =k< =13, −20 < =1< =19	−13 < =h< =0 −17 < =k< =17 −21 < =1< =21	0 < =h< =10 −17 < =k< =17 −12 < =1< =11	0 < =h< =10 0 < =k< =5 −11 < =1< =11	0 < =h< =9 −7 < =k< =8 −23 < =1< =23
Reflections collected	6048	9231	3531	850	2854
Unique [R (int)]	3422 [0.0373]	5235 (0.0373)	3531	850	1578 (0.0722)
Weighting Scheme (a,b)[a]	0.078, 6.397	0.167, 0.000	0.099, 6.390	n/a[b]	0.183, 0.147
Data/restraints/ parameters	3422/0/213	5235/0/235	3531/0/196	288	1578/0/44
Final R indices R1 [I > 2σ(I)]	0.0534,	0.0783	0.0577	0.0820[c]	0.0791
wR2	0.1383	0.1292	0.0724	n/a	0.0971
R indices (all data) R1	0.0741,	0.2296	0.1581	n/a	0.2561
wR2	0.1515	0.2296	0.1689	n/a	0.2833
Largest diff. peak hole eÅ-3	0.704, −0.986	2.078, −1.020	0.922, −0.919	0.23, −0.18	0.486, −0.439

[a]Weighting scheme $w = 1/(\sigma^2(F_o^2) + (aP)^2 + bP)$, where $P = (F_o^2 + 2F_c^2)/3$. [b]Weighting scheme $w = 1/[\sigma^2(F) + 0.003F^2]$. [c]$I > 3\sigma(I)$.

solvent *in vacuo* gave a white powder which was washed with n-hexane ($3 \times 10\,cm^3$). Recrystallisation from THF provided colourless rod crystals of X-ray quality. Yield (1.15 g, 62%). Anal. Calcd. for $C_{17}H_{34}N_2O_4SnBr_4$. C, 26.6; H, 4.5; N, 3.6. Found. C, 26.4; H, 4.4; N. 3.6%. IR $\bar{\nu}/cm^{-1}$ (Nujol) 3235 m (NH), 1624 m (CO), 330 m, 260 vs (SnBr). $\delta_H(CD_3CN)$ 8.36 (s, 2H, NH), 4.22–4.16 (m, 2H, CH), 3.74 (s, 2H, CH_2), 1.36–1.33 (d, 12H, CH_3).

(*c*) *$SnBr_4L^3{\cdot}MeCN$* (3)

$SnBr_4$ (1.0 g, 2.28 mmol) in acetonitrile ($20\,cm^3$) was added to a stirred solution of N,N′-di-isopropyldithio malonamide (0.50 g, 2.28 mmol) in acetonitrile. After stirring the mixture at 50°C under an atmosphere of argon for 6 hrs, the solvent was removed *in vacuo* to give a yellow/orange powder which was washed with n-hexane ($3 \times 10\,cm^3$). Recrystallisation from $MeCN/CH_2Cl_2$ (50:50) gave yellow block crystals of X-ray quality.

Yield (1.28 g, 80%). Anal. Calcd. for $C_{11}H_{21}N_3S_2SnBr_4$, C 18.9; H, 3.3; N, 6.0; Found, C, 19.1; H, 3.2; N, 5.8; IR $\bar{\nu}/cm^{-1}$ (Nujol), 3226 s, (NH), 1573 m, (CN), 908 m, (CS), 326 m, 266 vs (SnBr). $\delta_H(CD_3CN)$, 8.90 (s, 2H, NH), 4.52–4.64 (m, 2H, CH), 4.15 (s, 2H, CH_2), 1.25, 1.20 (d, 12H, CH_3).

X-RAY CRYSTALLOGRAPHY

Crystal Data for the 5 compounds are given in Table 1, together with refinement details. Data for (1), (2), (3) and L^5 were collected with MoKα radiation using the MARresearch Image Plate System. The crystals were positioned at 70 or 75 mm from the Image Plate. 95 frames were measured at 2° intervals with a counting time of 2 mins. Data analysis was carried out with the XDS program [11]. Data for L^4 were collected on a Stoe Stadi2 diffractometer via variable ω scan. All structures were solved using direct methods with the Shelx86 program [12].

The non-hydrogen atoms were refined with anisotropic thermal parameters. The hydrogen atoms were included in geometric positions. Empirical absorption corrections were carried out on (1), (2) and (3) using DIFABS [13]. Structures (1), (2), (3) and L^5 were refined on F^2 using Shelxl [14]. Structure L^4 was refined on F^2 using Shelx76 [15].

RESULTS AND DISCUSSION

As a convenient summary the bonding modes of neutral $RNH{\cdot}C\phi{\cdot}(CH_2)_n{\cdot}C\phi{\cdot}NHR$ (H_2L) that are feasible for metal complexation are depicted in Fig. 1.

Types **A** and **B** have the ligand in a 'trans-bridging' arrangement with either **one** (type A) or **both** (Type B) of the lone pairs on ϕ (O,S) involved in bonding to a metal. In contrast types **C** and **D** feature a 'cis-chelating' arrangement whereby one (type C) or both (type D) of the lone pairs associated with ϕ are involved in ϕ: $\rightarrow$M bond formation. Further interactions involving the hydrogen atoms of the NHR groups with either (a) the residual lone pair(s) on ϕ of an adjacent molecule(s) (b) entrapped lattice solvent molecules or (c) halogen atoms of an adjacent molecule (Lewis acid) are possible and have been observed; these hydrogen bonding interactions are denoted by the dotted lines. Previous structures of metal complexes incorporating the neutral $RNH{\cdot}C\phi{\cdot}(CH_2)_n{\cdot}C\phi{\cdot}NHR$ ligands confirm bonding types A, B and C but there is a conspicuous absence of type D. As noted later, all the oxamide and thiaoxamide ligands ($n=0$) adopt the *trans-*ϕ geometry in the free form. In metal complexation of types A/B this arrangement is retained unchanged but in the case of type C internal rotation about the C–C bond must occur in order for the ligand to achieve the required *cis-*ϕ configuration. Using Fenske-Hall molecular orbital calculations, Busch et al [1] and Stufkens et al [3] show that this conformational change for dithiooxamide brings no detrimental change to the bonding/electronic structure of the ligand [the valence group orbitals LUMO/HOMO of the two forms are closely similar in energy and composition] which can function as an effective bidentate chelate σ-donor. Clearly there are no structural/conformational restrictions present in the malonamide and succinamide derivatives where the skeletonal CH_2 unit(s) allow free rotation about C–C bonds. As a general point bidentate binding (whether bridging or chelation) is the hallmark of ligand attachment to a metal centre throughout the series. However, there is one example of monodentate binding i.e., the neutral complex $CuCl(PPh_3)_2(H_2N{\cdot}CS{\cdot}CS{\cdot}NH_2)$ [16] where the dithiaoxamide ligand retains its *trans*-configuration but is bound to the tetrahedral Cu(I) via only **one** of the two available S donor atoms leaving the other in a non-coordinating role.

STRUCTURAL CHARACTERISATION OF THE LIGANDS

Structures of the three ligands L^1, L^4 and L^5 are shown in Fig. 2, Fig. 3 and Fig. 4 respectively together with the atomic notation. The structures of L^4 and L^5 both have crystallographic symmetry with L^4 containing a centre of symmetry and L^5 a two-fold axis. The structure of L^1 was obtained from the adduct $SnBr_4L^1{\cdot}L^1$ (1) and this presumably could affect its conformation. We can describe the conformation by the O═C···C═O torsion angle: in the free ligand, the angle for L^1 is $-83.2°$ compared to a value of 0.5° in the complexed molecule present in the structure of (1). The two carbonyl groups in L^1 are both hydrogen bonded to N–H groups in a chelating ligand. For L^5 the analogous S═C··· C═S angle is $-112.4°$. whereas the equivalent torsion angle in L^4 is perforce 180°.

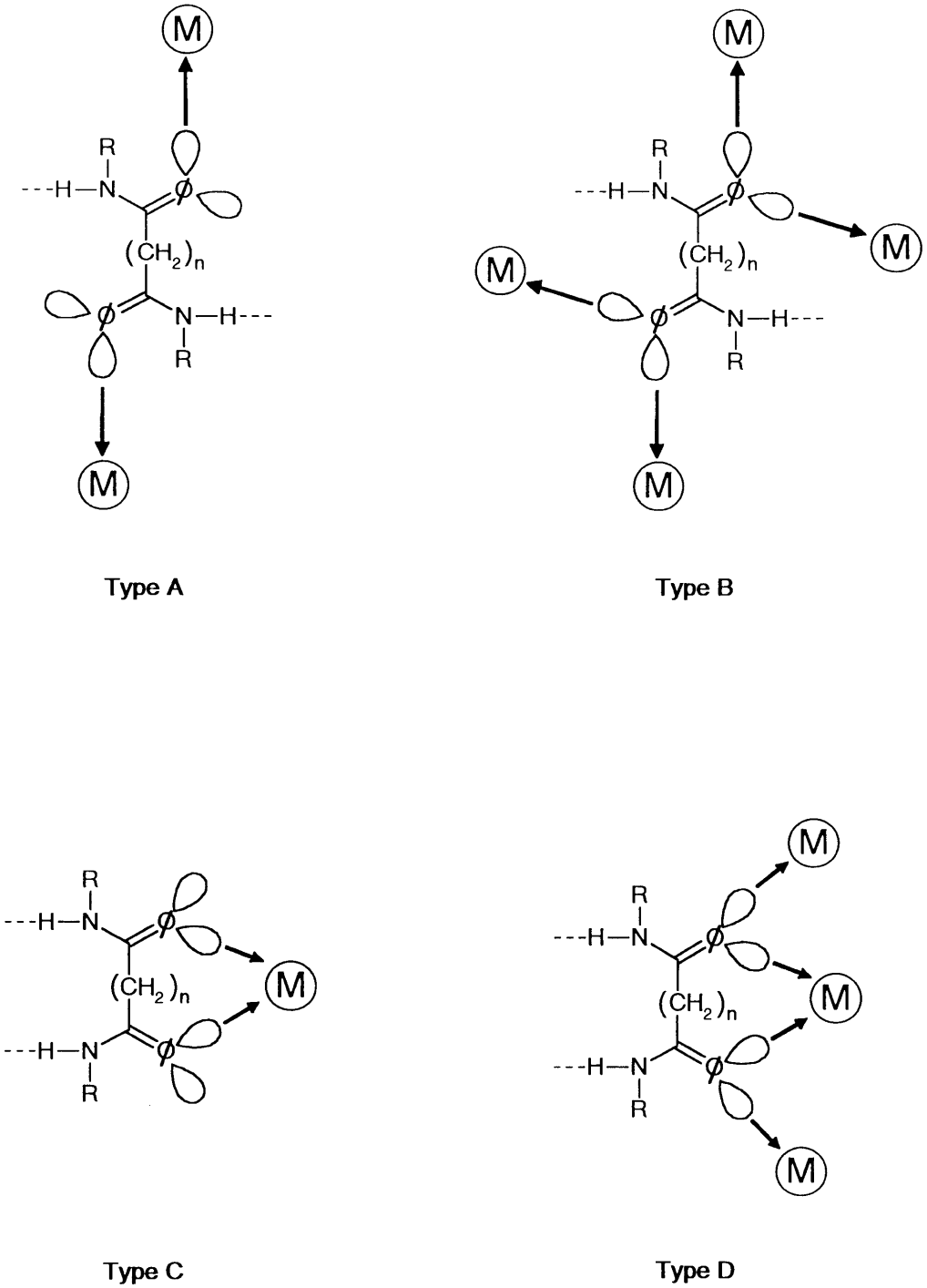

Fig. 1. Bonding modes of neutral (RNH·CØ·$(CH_2)_n$·CØ·NHR ligands.

Several features emerge for these ligands that are consistent throughout and can be summarised as follows: the angles at the central carbon atom(s) are tetrahedral; the bond arrangements and angles at each of the terminal nitrogen atoms indicate a trigonal planar (120°) disposition; the NHR groups, R=Me(L^1, L^4, L^5) are clearly rotated about the linkage C–N bonds and lie outside the O–C–N (L^1, L^4) and S–C–N (L^5) planes; the framework C–C, C–N and C–Ø bond distances and the associated interbond angles are all closely similar and can be favourably compared with those observed previously for other

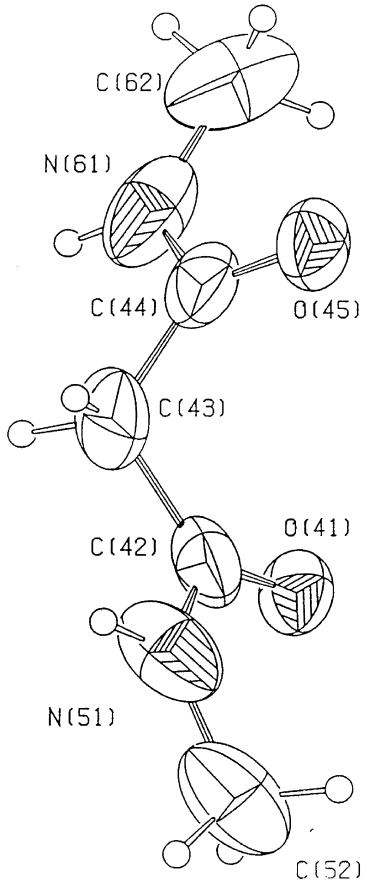

Fig. 2. The structure of L^1 as found in the structure of $SnBr_4L^1 \cdot L^1$ (1). Ellipsoids shown at 30% probability.

members of the series. For convenience a listing of the related LH_2 ligands that have been structurally characterised is included in Table 2 along with their pertinent bond dimensions.

It is clear that the $n=0$ compounds invariably have the trans conformation as do the $n=2$ compounds though there is much less evidence for this. However the $n=1$ compounds have much greater flexibility. The torsion angles in L^1 and L^5 are -83.2°, -112.4° respectively and this can be compared with values of 90.8° and -144.6° found in the analogous diamines. A recent study of the structures of disubstituted malonamides [1(d)] has established a wide range of low energy conformations. With R^1 = methyl, R^2 = phenyl, the four lowest energy conformations have O═C···C═O torsion angles of -70.4, 132.7, -158.0, 174.4 while for R^1 = methyl, R^2 = cyclohexyl, the corresponding values are 161.2, 164.4, 168.5, -71.0°. The conformational analyses are all consistent with facile reorientation of the ligand to form chelates with metal atoms.

The packing of the molecules L^4 and L^5 is dominated by intramolecular hydrogen bonding and details are listed for all structures in Table 3. L^4 forms hydrogen bonds between amide N-H and amide carbonyls on adjacent molecules N(21)···O(11) 2.84 Å. In L^5 similar bonding is found between adjacent N–H and S atoms N(21)···S(11) 3.35 Å.

STRUCTURES OF Sn(IV) COMPLEXES

Previous examples of metal complexation involving a Sn(IV) halide as reference Lewis acid include $SnBr_4(^tC_4H_9NH \cdot CO \cdot CO \cdot NH^tC_4H_9) \cdot THF$ [2(f)], (X), $SnBr_4(^nC_4H_9NH \cdot CS \cdot CS \cdot NH^n \cdot C_4H_9)$ [2(c)] (Y) and $SnBr_4$ (MeNH·CO·CH_2·CH_2·CO·NHMe). THF [2(f)] (Z). All feature type C bonding. In this present study we show that the ligand types $n=1$, Ø═0 and $n=1$, Ø═S also provide bidentate chelation with Sn(IV).

The three metal complex structures are shown in Fig. 5, Fig. 6 and Fig. 7 and include the atom notation used. The principal bond lengths and angles are listed in Table 4. In all cases the metal atom is octahedral being bonded to four bromine atoms and a bidentate ligand. It is remarkable that in all three structures the metal complex co-crystallises with other molecules [in (1) this is L^1 and in (2) and (3) these are solvent molecules] so that both amide nitrogen atoms can form intramolecular hydrogen bonds. Thus in (1),

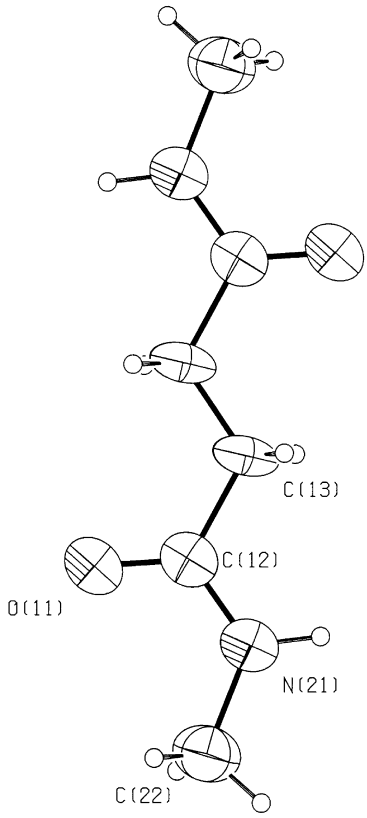

Fig. 3. The structure of L^4. Ellipsoids shown at 30% probability.

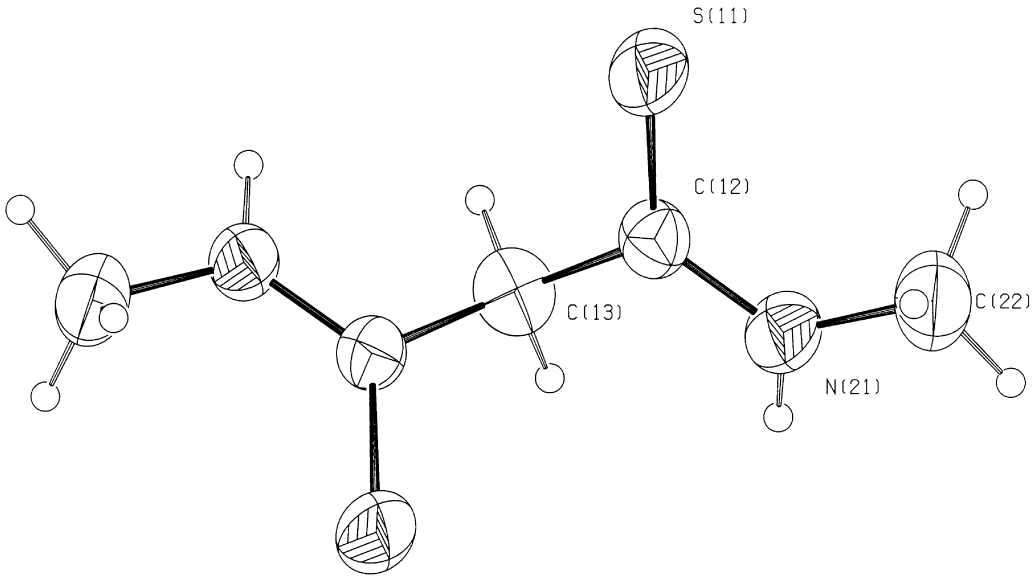

Fig. 4. The structure of L^5. Ellipsoids shown at 30% probability.

Table 2. Dimensions of uncomplexed RNH·CØ·$(CH_2)_n$·CØ·RNH ligands

n	R	ϕ	Configuration	C═ϕ (Å)	C–N (Å)	C–C (Å)	ϕCC (°)	NCC (°)	ϕCN (°)	Ref
O	H	O	trans	1.243(4)	1.315(4)	1.542(6)	119.5(3)	114.8(3)	125.7(3)	(a)
				1.2359(4)	1.3211(5)	1.5340(5)	120.26(4)	114.47(4)	125.28(4)	(b)
				1.25	1.31	1.49				(c)
							[No structure available]			(d)
O	Me	O	trans	1.227(2)	1.323(2)	1.544(3)	121.4(2)	113.3(2)	125.4(1)	(e)
O	$–CH_2–C(NO_2)_3$	O	trans	1.206(2)	1.341(3)	1.539(3)	121.5(2)	112.5(2)	126.0(2)	(f)
O	$–(CH_2)_2COOH$	O	trans	1.231	1.321	1.531	121.3	113.9	124.7	(g)
O	C_6F_5	O	trans	1.211(2)	1.342(2)	1.533(4)	121.5(2)	112.9(2)	125.5(1)	(h)
O	$–(CH_2)_3ONO_2$	O	trans	1.226	1.323	1.538	121.1	113.4	125.5	(i)
O	H	S	trans	(a) 1.665(5)	1.336(7)	1.536(14)	119.6(3)	115.0(4)	125.4(4)	(j)
				(b) 1.633(5)	1.311(7)	1.538(14)	120.5(4)	114.8(4)	124.6(4)	
				where (a) and	(b) are two	independent	molecules			
							[No structure available]			(k)
O	Et	S	trans	1.664(4)	1.305(6)	1.542(6)	121.4(3)	114.0(4)	–	(l)
O	iso-prop	S	trans	1.660(2)	1.314(2)	1.547(3)	121.3(2)	113.2(2)	125.5(1)	(e)
				1.680(7)	1.308(8)	1.508(14)	121.3(5)	115.0(6)	124.0(5)	(m)
O	$SiMe_3$	S	trans	1.659(4)	1.324(5)	1.535(7)	119.8	115.9	124.4	(n)
O	p-C_6H_5Cl	S	trans	1.659(5)	1.336(7)	1.537(10)	121.3(4)	111.1(4)	127.6(4)	(o)
				1.654(5)	1.321(7)	1.541(10)	120.4(4)	112.5(4)	127.1(4)	
				values for two	independent	centro-	symmetric	molecules		
O	CH_2CH_2OH	S	trans	1.660	1.321	1.535	121.837	113.357	124.799	(p)
1	H	O	O═C···C═O 90.8	1.253(4)	1.334(4)	1.507(4)	119.8	117.4	122.8	(q)
1	H	S	S═C···C═S −144.6	1.675	1.310	1.528	121.0	115.3	123.6	(r)
1	Me	O	O═C···C═O −83.2	1.199 (15), 1.208 (14)	1.36(2), 1.277(18)	1.52(2), 1.50(2)	119.4(18), 122.5(16)	113.5(14), 118.1(16)	123.7(15) 122.4(16)	this work
1	Me	S	S═C···C═S −112.4	1.662(5)	1.307(7)	1.508(6)	122.2(3)	115.6(4)	122.1(4)	this work
2	Me	O	O═C···C═O 180°	1.234(9)	1.330(11)	1.493(11) 1.432(13)	122.9(8)	114.8(7)	122.2(8)	this work
2	H	O	0═C···C═O 180°	1.238	1.333	1.501 1.512	122.4	115.6	122.0	(s)

(a) Ayerst, E. M. and Duke, J. R. C., *Acta Crystallogr*., 1954, **7**, 588. (b) de With, G. and Harkema, S., *Acta Crystallogr*., *Sect*. *B*, 1977, **33**, 2367. (c) Romers, C., *Acta Crystallogr*., 1953, **6**, 429. (d) Swaminathan, K. S. and Craven, B. M., *Am*. *Cryst*. *Assoc*., *Ser*. 2, 1982, **10**, 13. (e) Klaska, K-H., Jarchow, O., Scham, W., Widjaja, H., Voss, J. and Schmalle, H. W., *J*. *Chem*. *Research* (*S*), 1980, 104; *J*. *Chem*. *Research* (*M*), 1980, 1643. (f) Bhattacharjee, S. K. and Ammon, H. L., *Acta Crystallogr*., *Sect*. *B*, 1982, **38**, 2503. (g) Shkol'nikova, L. M., Gasparyan, A. V., Poznyak, A. L., Bel'skii, V. K. and Dyatlova, N. M., *Koord Khim*., 1990, **16**, 50. (h) Yamaguchi, K., Matsumura, G., Haga, N. and Shudo, K., *Acta Crystallogr*., *Sect*. *C*, 1992, **48**, 558. (i) Chen, R., Rheingold, A. L. and Brill, T. B., *J*. *Cryst*., *Spectrosc*., 1991, **21**, 173. (j) Wheatley, P. J., *J*. *Chem*. *Soc*., 1965, 396; preliminary account: Long, B., Markey, P. and Wheatley, P. J., *Acta Crystallogr*., 1954, **7**, 140. (k) Mo, F. and Thorkildsen, G., *Acta Crystallogr*., *Sect*. *A* (*Fnd*. *Cryst*), 1984, **40**, C-160. (l) Drew, M. G. B., Kisenyi, J. M. and Willey, G. R., *J*. *Chem*. *Soc*., *Dalton Trans*., 1982, 1729. (m) Drew, M. G. B., Kisenyi, J. M., Willey, G. R. and Wandiga, S. O., *J*. *Chem*. *Soc*., *Dalton Trans*., 1984, 1717. (n) Rinne, D. and Thewalt, U., *Z*. *Anorg*. *allg*. *Chem*., 1978, **443**, 185. (o) Shimanouchi, H. and Sasada, Y., *Acta Crystallogr*., *Sect*. *B*, 1979, **35**, 1928. (p) Geboes, P., Hofmans, H., Desseyn, H. O., Dommisse, R., Lenstra, A. T. H., Sanni, S. B., Smits, J. M. M. and Beurskens, P. T., *Spectrochim*, *Acta*, *Part A*, 1987, **43**, 35. (q) Chieh, P. C., Subramian, E. and Trotter, J., *J*. *Chem*. *Soc* (*A*), 1970, 179. (r) Hlawatschek, H., Kiel, G. and Gattow, G. F., *Z*. *Naturforsch*, *Teil B*, 1981, **36**, 1386. (s) Davies, D. R. and Pasternak, R. A., *Acta Crystallogr*., 1956, **9**, 334.

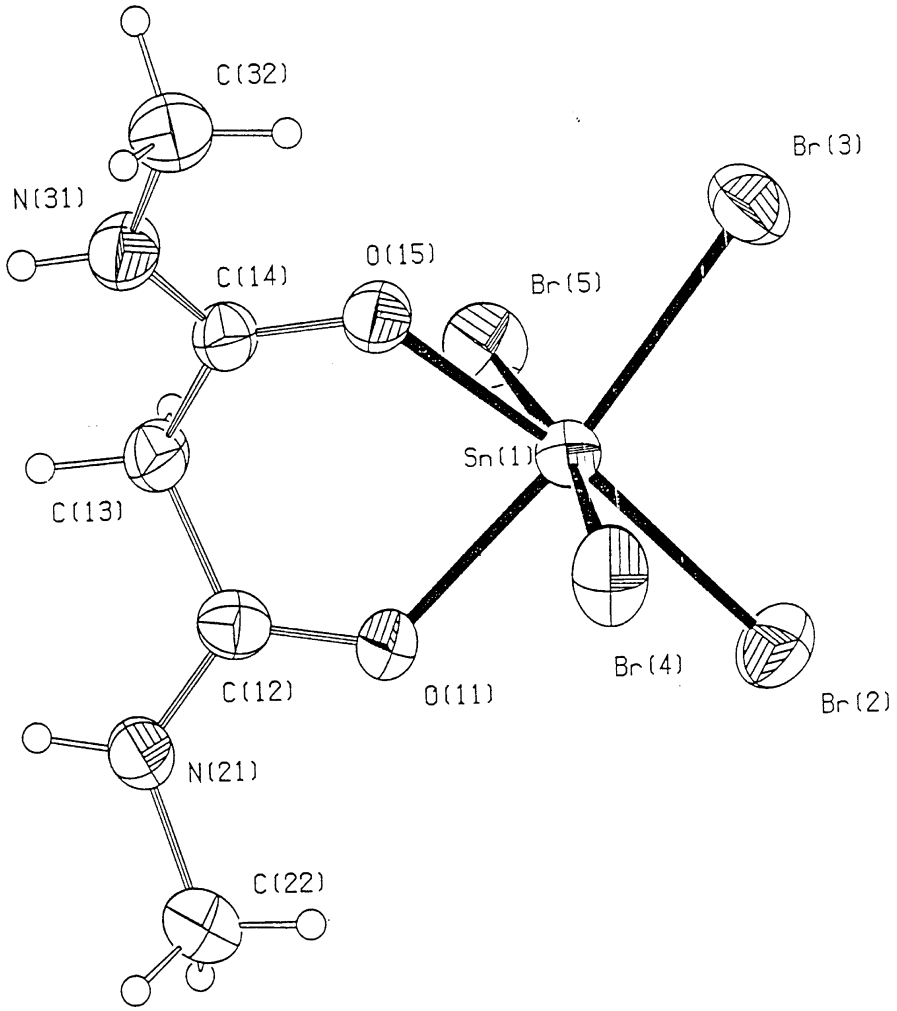

Fig. 5. The structure of $SnBr_4L^1$. Ellipsoids shown at 30% probability.

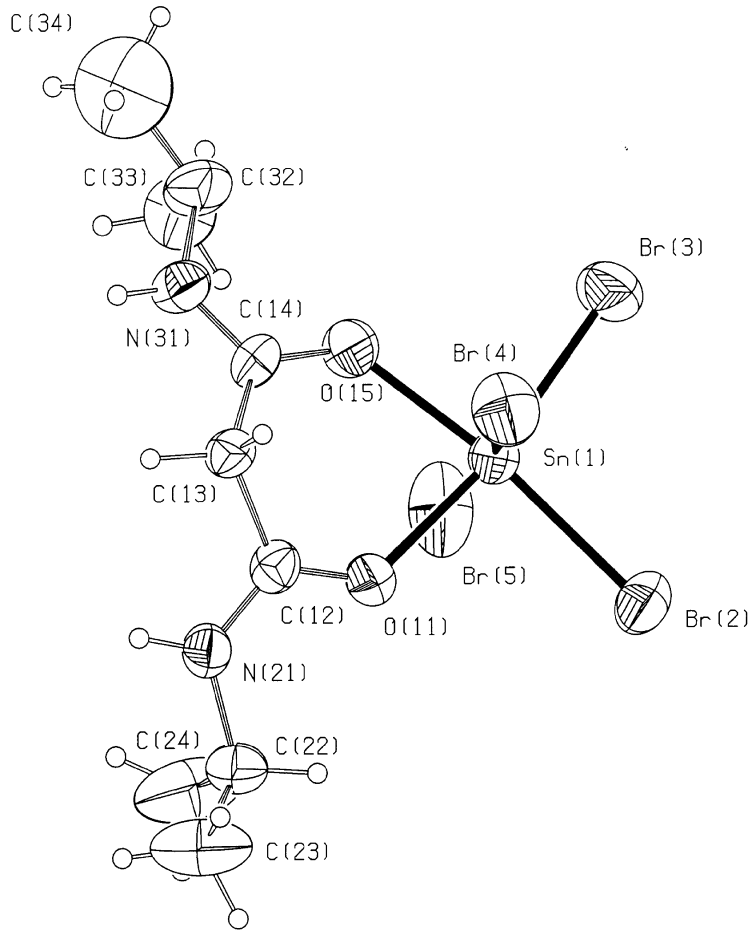

Fig. 6. The structure of $SnBr_4L^2$. Ellipsoids shown at 30% probability.

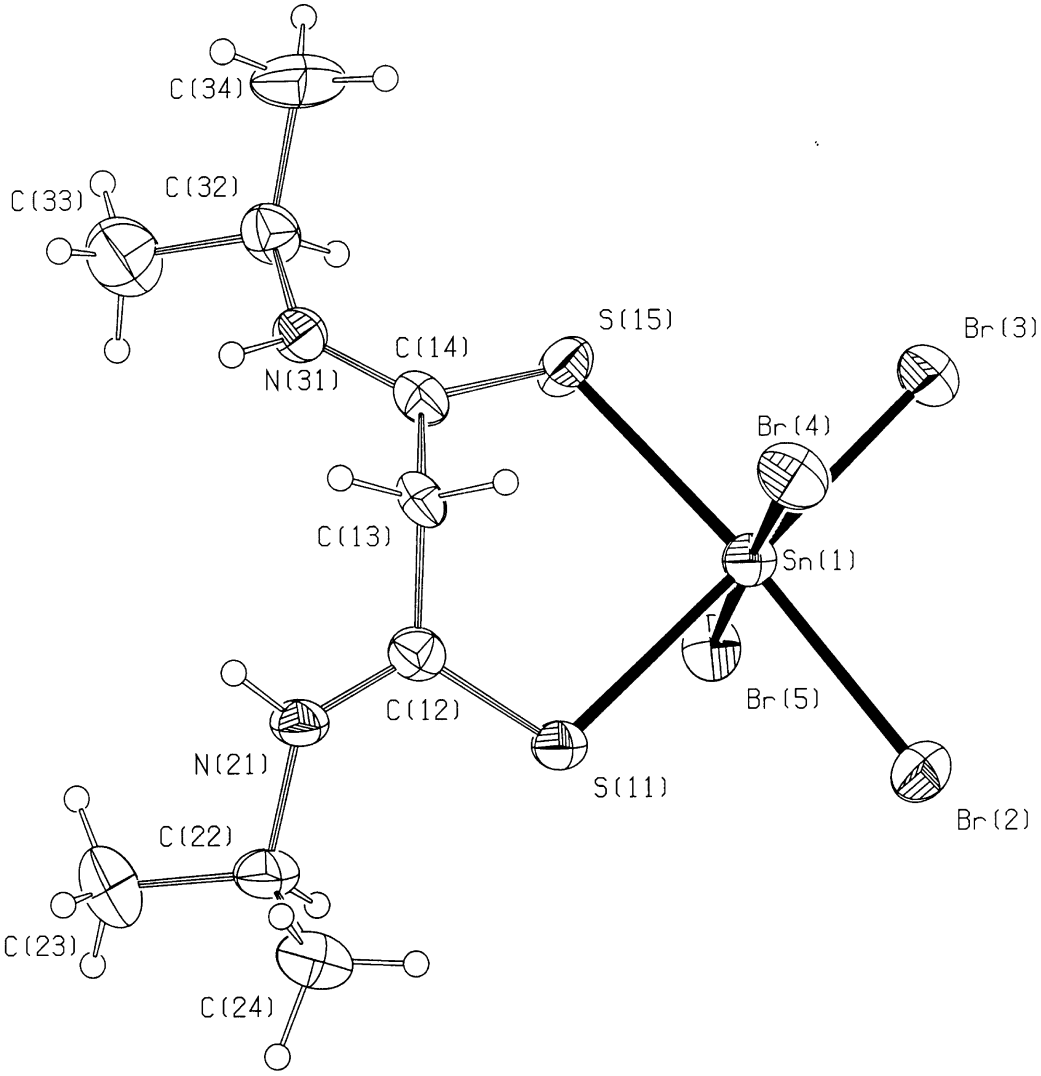

Fig. 7. The structure of $SnBr_4L^3$. Ellipsoids shown at 30% probability.

Table 3. Hydrogen Bond Distances (Å)

In (1)	
Br(2)... N(21) $1	3.52
Br(2)... N(31) $1	3.74
Br(5)... N(51) $2	3.75
N(21)... O(41) $1	2.85
N(31)... O(45) $1	2.75
N(61)... O(41) $2	3.06
Symmetry operators	$1 .5-x,.5+y,.5-z $2 1-x, 1-y,-z
In (2)	
N(21)... O(41$1)	2.85
N(31)... O(51$2)	2.90
Symmetry operators	$1 .5-x, y-.5,.5-z $2 1-x, -y, -z
In (3)	
N(21)... N(100)$2	3.19
N(21)... Br(2) $1	3.57
N(31)... N(100) $2	3.23
N(31)... Br(5) $1	3.52
Symmetry Operators	$1 x-1, y, z $2 -x, y-1/2, -z+2
In (4)	
N(13)... O(1) $1	2.84
Symmetry Operator	$1 1-x, 1-y, 1-z
In (5)	
N(21)... S(11) $1	3.35
Symmetry operator	$1 y, 1-x,. 25+z

each nitrogen on the chelating ligand forms strong hydrogen bonds to the free ligand N(21)···O(31) 2.85, N(31)···O(41) 2.75 Å. In (2) these bonds are to THF solvent molecules N(21)···O(41) 2.85, N(31)···O(51) 2.90 Å and in (3) to a solvent acetonitrile N(21)···N(100) 3.19 Å, N(21)···N(100) 3.23 Å. In addition there are short contacts with the bromine atoms that could represent hydrogen bond interactions. These are also listed in Table 3. By way of comparison the oxalamide derivative compound (X) features a highly symmetrical N–H···$O_{solvent}$ hydrogen bonding interaction whereby the **two** N–H groups of the chelated ligand are linked directly to the oxygen atom of the single solvate (THF) molecule with dimensions O·····H–N 178°, O·····H 1.90, O·····N 2.85 (3) Å. In the particular case of compound (Z) whereas one of the NH centres is involved in N–H·····$O_{solvent}$ hydrogen bonding (N–H·····O 176°, H·····O 1.75, N·····O 2.69 Å) the other is linked to a bromine atom of an adjacent molecule with dimensions Br·····H–N 172°, Br·····H 2.67 Å, Br·····N 3.56 Å. It is interesting that in all three of the present structures (1)-(3) the chelate ring around the metal is not planar and indeed takes up a chair conformation. Thus taking the plane of O(11), C(12), C(14) and O(15), the distances of Sn and C(13) from the plane are 0.48, 0.54 Å in (1), 0.38, 0.53 Å in (2) and 0.87, 0.75 Å in (3). Clearly the presence of the donating sulphur atoms in (3) has had a significant effect on the ring conformation compared to the oxygen atoms in (1) and (2). This is also demonstrated by the Sn-Br bond lengths which are perceptibly longer in (3) by *ca*. 0.07 Å than those in (1) or (2).

Table 4. Bond lengths [A] and angles [deg] in the metal coordinations spheres

Dimensions in 1.	
Sn(1)-O(15)	2.133(6)
Sn(1)-O(11)	2.151(6)
Sn(1)-Br(3)	2.531(2)
Sn(1)-Br(2)	2.532(2)
Sn(1)-Br(4)	2.541(2)
Sn(1)-Br(5)	2.553(2)
O(15)-Sn(1)-Br(3)	88.10(16)
O(11)-Sn(1)-Br(3)	171.72(15)
O(15)-Sn(1)-Br(2)	173.74(17)
O(11)-Sn(1)-Br(2)	90.39(15)
Br(3)-Sn(1)-Br(2)	97.88(5)
O(15)-Sn(1)-Br(4)	85.67(19)
O(11)-Sn(1)-Br(4)	85.27(17)
Br(3)-Sn(1)-Br(4)	94.13(5)
Br(2)-Sn(1)-Br(4)	92.06(6)
O(15)-Sn(1)-Br(5)	89.55(19)
O(11)-Sn(1)-Br(5)	87.97(17)
Br(3)-Sn(1)-Br(5)	91.98(4)
Br(5)-Sn(1)-Br(2)	92.04(6)
Br(4)-Sn(1)-Br(5)	172.11(4)
Dimensions in (2)	
Sn(1)-O(11)	2.158(7)
Sn(1)-O(15)	2.164(8)
Sn(1)-Br(5)	2.511(2)
Sn(1)-Br(2)	2.511(2)
Sn(1)-Br(3)	2.518(2)
Sn(1)-Br(4)	2.554(2)
O(11)-Sn(1)-O(15)	82.5(3)
O(11)-Sn(1)-Br(5)	84.6(2)
O(15)-Sn(1)-Br(5)	84.2(3)
O(11)-Sn(1)-Br(2)	90.6(2)
O(15)-Sn(1)-Br(2)	173.1(2)
Br(5)-Sn(1)-Br(2)	94.28(7)
O(11)-Sn(1)-Br(3)	170.4(2)
O(15)-Sn(1)-Br(3)	87.9(2)
Br(5)-Sn(1)-Br(3)	94.76(8)
Br(2)-Sn(1)-Br(3)	98.94(5)
O(11)-Sn(1)-Br(4)	86.0(2)
O(15)-Sn(1)-Br(4)	87.5(2)
Br(5)-Sn(1)-Br(4)	168.27(7)
Br(2)-Sn(1)-Br(4)	92.89(6)
Br(3)-Sn(1)-Br(4)	93.28(7)
Dimensions in (3)	
Sn(1)-S(15)	2.568(4)
Sn(1)-Br(2)	2.569(2)
Sn(1)-Br(3)	2.574(2)
Sn(1)-S(11)	2.576(4)
Sn(1)-Br(5)	2.582(3)
Sn(1)-Br(4)	2.663(2)
S(15)-Sn(1)-Br(2)	173.37(12)
S(15)-Sn(1)-Br(3)	94.99(13)
Br(2)-Sn(1)-Br(3)	91.15(10)
S(15)-Sn(1)-S(11)	92.64(13)
Br(2)-Sn(1)-S(11)	84.34(10)
Br(3)-Sn(1)-S(11)	94.72(11)
S(15)-Sn(1)-Br(5)	84.51(11)
Br(2)-Sn(1)-Br(5)	97.89(8)
Br(3)-Sn(1)-Br(5)	91.21(9)
S(11)-Sn(1)-Br(5)	173.63(11)
S(15)-Sn(1)-Br(4)	85.99(13)
Br(2)-Sn(1)-Br(4)	87.92(9)
Br(3)-Sn(1)-Br(4)	178.66(7)
S(11)-Sn(1)-Br(4)	86.15(11)
Br(5)-Sn(1)-Br(4)	87.97(8)

The general range of Sn-Br bond distances observed for the six structures (1)-(3) and (X)-(Z) is 2.504(3)-2.565(12) Å excluding those halogen atoms involved in hydrogen bonding. For the latter type a discernible lengthening is noted *e.g.*, 2.625(13) Å in compound (Y). For oxa ligand complexes, the Sn–O bond distances remain fairly constant *viz.*, (1) 2.131(6), 2.152(6), (2) 2.158(7), 2.164(8), (X) 2.180(14), (Z) 2.124(18), 2.148(20) Å; similarly the Sn-S bond distances do not vary overmuch for the thia ligand complexes *viz.*, (3) 2.568(4), 2.576(4), (Y), 2.565(28), 2.551(25) Å. The bite of the bidentate ligands, as gauged by the angle Ø-Sn-Ø, follows the series: Ø═0: $n=0$, 73.3(5)°(X); $n=1$, 83.6(2)°(1); $n=1$, 82.5(3)°(2); $n=2$, 84.0(7)°(Z) and Ø=S: $n=0$, 83.6(7)°(Y); $n=1$, 92.64(12)°(3) *e.g.*, as the size of the ligand increases there is an **increase** in bite angle with the change from $n=0\rightarrow n=1$ showing a dramatic increase of *ca.* 10° in both systems. At the same time the Br–Sn–Br angle subtended by the Br atoms positioned *trans* to the Ø atoms follows the opposite trend: Ø═0: $n=0$, 106.2(1)° (X); $n=1$, 97.89(5)° (1); $n=1$, 98.94(5)° (2); $n=2$, 99.18(14)° (Z) and Ø=S: $n=0$, 101.8(4)° (Y); $n=1$, 97.89(6)° (3).

Supplementary material

Tables of hydrogen coordinates, anisotropic displacement parameters, complete bond distances and angles and F_o/F_c listings are available from the authors upon request.

Acknowledgements—Financial support by the EPSRC and the University of Reading for the image plate system is gratefully acknowledged. We thank Mr A W Johans for technical assistance with X-ray crystallographic studies.

REFERENCES

1. (a) Green, M. R., Jubran, N., Bursten, B. E. and Busch, D. H., *Inorg. Chem.*, 1987, **26**, 2326. (b) Harris, H. A., Kanis, D. R. and Dahl, L. F., *J. Amer. Chem. Soc.*, 1991, **113**, 8602. (c) Aversa, M. C., Bonaccorsi, P., Bruce, D. W., Caruso, F., Giannetto, P., Lanza, S. and Morrone, S., *Inorg. Chim. Acta*, 1997, **256**, 235. (d) Chan, G. Y. S., Drew, M. G. B., Hudson, M. J., Iveson, P. B., Liljenzin, J-O., Skalberg, M., Spjuth, L. and Madic, C., *J. Chem. Soc., Dalton Trans.*, 1997, 649.
2. (a) Drew, M. G. B., Kisenyi, J. M. and Willey, G. R., *J. Chem. Soc., Dalton Trans.*, 1982, 1729. (b) Drew, M. G. B., Kisenyi, J. M., Wandiga, S. O. and Willey, G. R., *J. Chem. Soc., Dalton Trans.*, 1984, 1717. (c) Drew, M. G. B., Kisenyi, J. M. and Willey, G. R., *J. Chem. Soc., Dalton Trans.*, 1984, 1723. (d) Drew, M. G. B., Kisenyi, J. M. and Willey, G. R., *J. Chem. Soc., Dalton Trans.*, 1985, 1073. (e) Claire, P. P. K., Willey, G. R. and Drew, M. G. B., *J. Chem. Soc., Dalton Trans.*, 1987, 263. (f) Claire, P. P. K., Willey, G. R. and Drew, M. G. B., *Inorg. Chim. Acta*, 1987, **128**, 147.
3. (a) Servaas, P. C., Stufkens, D. J., Oskram, A., Vernooijs, P., Baerends, E. J., De Ridder, D. J. A. and Stam, C. H., *Inorg. Chem.*, 1989, **28**, 4104. (b) Baggio, R., Garland, M. T. and Perec, M., *J. Chem. Soc., Dalton Trans.*, 1995, 987. (c) Ye, Q-Y., Nakano, Y., Frauenhoff, G. R., Whitcomb, D. R., Takusagawa, F. and Busch, D. H., *Inorg. Chem.*, 1991, **30**, 1503. (d) Battaglia, L. P., Corradi, A. B., Marzotto, A., Menabue, L. and Pellacani, G. C., *J. Chem. Soc., Dalton Trans.*, 1988, 1713. (e) Lloret, F., Julve, M., Real, J. A., Faus, J., Ruiz, R., Mollar, M., Castro, I. and Bois, C., *Inorg. Chem.*, 1992, **31**, 2956. (f) Hereygers, M. L. B. F., Desseyn, H. O., Verhulst, K. A. F., Henstra, A. T. H. and Perlepes, S. P., *Polyhedron*, 1996, **15**, 3437.
4. Antolini, L., Fabretti, A. C., Franchini, G., Menabue, L., Pellacani, G. C., Desseyn, H. O., Dommisse, R. and Hofmans, H. C., *J. Chem. Soc., Dalton Trans.*, 1987, 1921.
5. Hofmans, H. C., Desseyn, H. O., Dommisse, R. A., Van Nuffel, P. and Lenstra, A. T. H., *Transition Met. Chem.*, 1984, **9,** 213.
6. Battaglia, L. P., Corradi, A. B., Marzotto, A., Menabue, L. and Pellacani, G. C., *J. Crystallogr., Spectrosc. Res.*, 1988, **18,** 101.
7. Van Riel, W., Desseyn, H. O., Vande Mieroop, W. and Lenstra, A. T. H., *Transition Met. Chem.*, 1980, **5,** 330.
8. Girerd, J. J., Jeannin, S., Jeannin, Y., Kahn, O., *Inorg. Chem.*, 1978, **17**, 3034; Chauvel, C., Girerd, J. J., Jeannin, Y., Kahn, O. and Lavigne, G., *Inorg. Chem.*, 1979, **18**, 3015.
9. Scheibye, S., Pedersen, B. S. and Lawesson, J. O., *Bull. Soc. Chim. Belge*, 1978, **87,** 229.
10. Bret, J-M., Castan, P. and Laurent, J-P., *J. Chem. Soc., Dalton Trans.*, 1984, 1975.
11. Kabsch, W., *J. Appl. Cryst.*, 1988, **21,** 916.
12. Shelx86, Sheldrick, G. M., *Acta Crystallogr., Sect. A*, 1990, **46**, 467.
13. Walker, N. and Stuart, D., *Acta Crystallogr., Sect. A*, 1983, **39,** 158.
14. Shelxl, Sheldrick, G. M., program for crystal structure refinement, University of Gottingen, 1993.
15. Shelx76, Sheldrick, G. M., Program for structure solution and refinement, Cambridge, 1976.
16. Ferrari, M. B., Fava, G. G., Pelizza, C. and Tarasconi, P., *Inorg. Chim. Acta*, 1985, **98,** L49.

Pergamon

PII: S0277–5387(98)00109–0

Polyhedron Vol. 17, No. 19, pp. 3305–3314, 1998
© 1998 Elsevier Science Ltd
All rights reserved. Printed in Great Britain
0277–5387/98 $19.00+0.00

1D polymeric copper(II) complexes containing bridging tridentate pyrazinato and terminal chloro or azido anions. Synthesis, spectral, structural and thermal study of $[CuCl(pyrazinato)(H_2O)]_n$ and $[Cu(N_3)(pyrazinato)(H_2O)]_n$ complexes

Mohamed A. S. Goher[a]*, Morsy A. M. Abu-Youssef[b] and Franz A. Mautner[c]

[a]Department of Chemistry, Faculty of Science, Kuwait University, P.O. Box 5969 Safat, 13060 Kuwait

[b]Department of Chemistry, Faculty of Science, Alexandria University, Alexandria 21321, Egypt

[c]Institut fur Physikalische und Theoretische Chemie, Technische Universitat Graz, A-8010 Graz, Austria

(Received 26 November 1997; accepted 7 March 1998)

Abstract—The polymeric complexes $[CuCl(pyrazinato)(H_2O)]_n$ (1) and $[Cu(N_3)(pyrazinato)(H_2O)]_n$ (2) have been synthesized and characterized by spectroscopic methods and X-ray crystallography. The overall spectral results indicate that these complexes contain tridentate pyrazinato ligands, terminal chloride or azide groups and aqua molecules. In the structure of complex (1), each copper atom, which is chelated by O(1) and N(1) atoms of the pyrazinato anions, links Cl(1) atom, O(3) atom from an aqua molecule and the second nitrogen, N(2) from a pyrazinato group of a neighbouring unit giving rise to a 1D polymeric structure. The structure of complex (2), which is very similar to 1 features five coordinate copper(II) atom, *N*, *N*,*O*-tridentate pyrazinato ligand, terminal azido ligand, aqua molecule and 1D polymeric structure. There are different types of hydrogen bonds in both complexes. The thermal decomposition of complexes (1) and (2) was investigated thermogravimetrically in nitrogen atmosphere. © 1998 Elsevier Science Ltd. All rights reserved

Keywords: copper(II) chloride; copper(II) azide; pyrazinato complexes; crystal structure; spectra; thermal analysis.

It is now well estalished that the picolinate anion, also known as pyridine-2-carboxylate, acts as a chelating bidentate ligand [1–4], as a N,O,O′-tridentate chelating bridging ligand as found in the structure of $[Cu(picolinato)_2 \cdot 2H_2O$ [5], as a N,O,O-tridentate ligand as in $[Mn(picolinato)(N_3)(H_2O)]_n$ [6] and as a N,O,O,O′-tetradentate ligand as in the structure of $[Cu(picolinato)Cl]_n$ [7] or $[Cd(picolinato)X]_n$ (X = N_3 or NCS) [8]. Both coordinative interactions to transition metal centers and ionic interaction to alkali metals, have been observed in the crystal structures of $[NaCu(picolinato)_2(N_3)(H_2O)_2]_n$ [9] and $[MCu(picolinato)(N_3)_2]_n$ [M = Na or K] [10]. Thus, the picolinato anion is a versatile ligand that can bind metal ions in a variety of bonding modes.

Pyrazine and pyrazinic acid, also called pyrazine-2-carboxylic acid (hereafter abbreviated as H-pyz) combine the coordinating properties of the pyridine-2-carboxylic acid with the fact that the pyrazine moiety may act as a bridge and thus aid the formation of polymeric structures [11, 12]. Pyrazinic acid is therefore expected to be at least as versatile as the picolinic acid. Recently we established that pyrazinic acid serves as a N,O-chelating bidentate ligand as found in the structures of $[NaMn(pyrazinato)(X)_2(H_2O)_2]_n$ (X = N_3 or NCO) [13, 14], and as a monodentate ligand in $[Cu_2(pyrazinic\ acid)_2I_2] \cdot 3H_2O$ [15]. In the

* Author to whom correspondence should be addressed.

later complex, the two pyrazinic acid molecules in the asymmetric unit behave differently; one acid molecule acts as a neutral ligand whereas the other molecule functions as a zwitterion. We also established that the structure of KCu_2(pyrazinato)$(N_3)_4$ complex consists of a dinuclear complex anion $[Cu_2(N_3)_6]^{2-}$, potassium cations and neutral polymeric complex [Cu(pyrazinato)(N_3)] [16]. Further studies led to the isolation of dark green complexes of the general formula Cu(pyrazinato)X(H_2O), for X = Cl or N_3, the first to have been reported. The structure characterizations of these two new hydrated complexes as elucidated by spectroscopic and crystallographic methods are the subject of the present paper.

EXPERIMENTAL

Pyrazinic acid was obtained from Aldrich and other chemicals are of analytical grade quality.

Preparation of [Cu(pyrazinato)Cl$(H_2O)]_n$ *complex* (1)

Mixing of the components in aq/ethanol media yields a mixture of pale green powder and blue microcrystalline powder.

Crystals of this complex suitable for X-ray diffraction were prepared by mixing $CuCl_2 \cdot 2H_2O$ (0.68 g, 4 mmol) and pyrazinic acid (0.37 g, 3 mmol) in boiled 2:1 ethanol/water (30 cm^3) and several drops of 0.1 M sodium azide. This mixture was allowed to stand in the open air for several days to growth a small amount of green crystals along with a blue microcrystalline powder. The yield is 15%.

Anal. Found. C, 24.5; *H*, 2.2; *N*, 11.7; *Cl*, 15.1; *Cu*, 26.9. **Calcd. for $C_5H_5ClCuN_2O_3$**: *C*, 25.0; *H*, 2.1; *N*, 11.7; *Cl*, 14.9; *Cu*, 26.4 (%).

Preparation of [Cu(pyrazinato)$(N_3)(H_2O)]_n$ *complex* (2)

This complex was prepared by adding ethyl pyrazinate (0.43 g, 3 mmol) in 20 cm^3 ethanol to 10 cm^3 ethanol solution of $Cu(NO_3)_2 \cdot 3H_2O$ (0.68 g, 4 mmol) followed by dropwise addition of an aqueous solution (5 cm^3) NaN_3 (0.19 g, 3 mmol), The mixture was shaken after each addition, and then allowed to stand over several days until dark green crystals of the complex deposited together with a blue microcrystalline powder. The yield is 28%.

Anal. Found C, 24.2; *H*, 2.1; *N*, 28.0; *Cu*, 25.2. **Calcd. for $C_5H_5CuN_5O_3$:** *C*, 24.3; *H*, 2.0; *N*, 28.4; *Cu*, 25.7 (%).

Physical measurements

The procedure and instruments used for other physical measurements were as described previously [14, 16].

X-ray crystal structure analysis

A modified STOE four circle diffractometer was used for single crystal X-ray measurements. Orientation matrix and lattice parameters were obtained by least-squares refinement of the diffraction data from 45 (compound 1) and 59 (compound 2) reflections in the 2θ range 7–33°. Data were collected at 298(2) K using graphite crystal-monochromatized Mo–K_α radiation ($\lambda = 0.71069$ Å) and the ω-scan technique. The intensities were corrected for Lorentz-polarisation effects and for absorption. Crystallographic data are given in Table 1.

The structure was solved by direct methods and subsequent Fourier analysis. Anisotropic displacement parameters were applied to non-hydrogen atoms in full-matrix least-squares refinements based on F^2. The hydrogen atoms were assigned with common isotropic displacement factors and included in the final refinement cycles by use of geometrical restraints. Analytical expressions of neutral-atom scattering factors were employed, and anomalous dispersion corrections were incorporated. The program DIFABS [17], and SHELXTL/PC [18] program package were used for computations. Selected bond distances and bond angles are given in Tables 2 and 3. Additional material, consisting of fractional atomic coordinates, displacement parameters, observed and calculated structure factors and complete lists of bond distances and bond angles, has been deposited with the editor.

RESULTS AND DISCUSSION

Mixing of $CuCl_2 \cdot 2H_2O$ and pyrazinic acid (1:1 molar ratio) in aq./EtOH medium afforded a pale green powder of the chloride complex, whereas addition of pyrazinic acid to $Cu(NO_3)_2 \cdot 3H_2O$ in ethanol followed by an aq. solution of NaN_3 (1:1:1 molar ratio) afforded an olive green powder of the azide complex. In both cases, however, a blue crystalline powder is co-precipitated, the amount of which can be reduced by decreasing the amount of pyrazinic acid to be less than 1:1 to copper. Single crystals of the chloride complex were prepared by mixing the components in ethanol followed by addition of several drops of 0.1 M NaN_3 aq. solution. Dark green crystals of the azide complex were isolated by mixing ethyl pyrazinate and copper(II) nitrate in ethanol followed by sodium azide, which suggests that the ethyl ester is easily hydrolyzed. Both complexes are insoluble in many non-polar solvents, e.g. benzene, CCl_4, etc., as well as polar solvents, e.g. alcohols, acetone, chloroform, etc., but they are soluble in DMSO and DMF giving non-conducting solutions.

Structures

The principle structural features of complex (1) are illustrated in Fig. 1. The pyrazinato anion chelates the

Table 1. Cystallograpic data and processing parameters[1]

Compound	1	2
Molecular formula	$C_5H_5ClCuN_2O_3$	$C_5H_5CuN_5O_3$
Molecular Weight	240.10	246.68
Color	green	green
System	Monoclinic	Monoclinic
Space group	$P2_1/n$ (no. 14)	12/a (no. 15)
a (Å)	5.645 (3)	13.472 (4)
b (Å)	12.775 (5)	6.659 (2)
c (Å)	11.054 (6)	18.247 (6)
β (°)	102.07 (4)	97.14 (2)
V (A^3)	779.5 (7)	1633.0 (9)
Z	4	8
μ (Mo–Kα) (mm^{-1})	3.107	2.663
Normal transmission factors	1.000–0.124	1.000–0.176
D_{calc}/D_{obs} (Mg/m^3)	2.046/2.03 (4)	2.007/1.97 (6)
Approx. crystal size (mm)	$0.55 \times 0.30 \times 0.15$	$0.20 \times 0.20 \times 0.12$
θ range of data collection (°)	3.19–27.49	3.05–29.86
Reflections collected	1807	2253
Independ. Refl./R_{int}	1457/0.0378	1826/0.0693
Parameters	117	134
Goodness-of-Fit on F_0^2	1.099	1.078
R_1/wR_2 [$I > 2\sigma(I)$]	0.0368/0.0897	0.0908/0.1623
Weighting factors*: a/b	0.0390/1.2578	0.0727/0.0000
Largest Peak/hole (eA^{-3})	0.560/−0.482	1.235/−0.935

*$w^{-1} = [\sigma^2(F_0^2) + (aP)^2 + bP]$ and $P = (F_0^2 + 2F_c^2)/3$

Table 2. Selected bond distances (Å) and angles (°) of complex (1)

Cu(1)–O(1)	1.975(3)	Cu(1)–N(2)	2.009(3)
Cu(1)–N(1)	2.013(3)	Cu(1)–O(3)	2.213(3)
Cu(1)–Cl(1)	2.241(1)	N(1)–C(4)	1.331(5)
N(1)–C(1)	1.343(5)	C(1)–C(2a)	1.375(5)
C(1)–C(5)	1.509(5)	C(2)–N(2)	1.351(5)
N(2)–C(3)	1.331(5)	C(3)–C(4b)	1.384(5)
C(5)–O(2)	1.223(5)	C(5)–O(1)	1.267(4)
O(3)...O(2c)	2.697(4)	O(3)...Cl(1d)	3.181(3)
O(1)–Cu(1)–N(2)	89.37(12)	O(1)–Cu(1)–N(1)	81.87(12)
N(2)–Cu(1)–N(1)	170.46(13)	O(1)–Cu(1)–O(3)	100.12(13)
N(2)–Cu(1)–O(3)	95.81(13)	N(1)–Cu(1)–O(3)	89.48(13)
O(1)–Cu(1)–Cl(1)	156.40((11)	N(2)–Cu(1)–Cl(1)	91.90(10)
N(1)–Cu(1)–Cl(1)	94.62(10)	O(3)–Cu(1)–Cl(1)	103.19(10)
O(2)–C(5)–O(1)	126.1(4)	O(2c)–O(3)–Cl(1d)	117.85(12)
Hydrogen bonding systems			
O(3)...O(2c)	2.697(4)	O(3)...Cl(1d)	3.181(3)
O(3)–H(4)	0.83(2)	O(3)–H(5)	0.83(2)
H(4)...O(2c)	1.88(2)	H(5)...Cl(1d)	2.37(2)
H(4)–O(3)–H(5)	108(3)	O(2c)–O(3)...Cl(1d)	117.9(1)
O(3)–H(4)...O(2c)	170(4)	O(3)–H(5)...Cl(1d)	166(5)

Symmetry codes: (a) $x-1/2, -y+1/2, z+1/2$; (b) $x+1/2, -y+1/2, z-1/2$; (c) $-x-1/2, y-1/2, -z+1/2$; (d) $x-1, y, z$.

Table 3. Selected bond distances (Å) and angles (°) of complex (2)

Cu(1)–N(11)	1.942(7)	Cu(1)–O(1)	1.973(4)
Cu(1)–N(1)	2.009(4)	Cu(1)–N(2)	2.024(4)
Cu(1)–O(3)	2.244(6)	N(11)–N(12)	1.144(8)
N(12)–N(13)	1.139(8)	N(1)–C(4)	1.327(7)
N(1)–C(1)	1.337(7)	C(1)–C(2a)	1.392(7)
C(1)–C(5)	1.524(8)	C(2)–N(2)	1.329(7)
N(2)–C(3)	1.334(7)	C(3)–C(4b)	1.387(7)
C(5)–O(2)	1.219(7)	C(5)–O(1)	1.276(6)
O(3)...O(1c)	2.848(7)	O(3)...O(2d)	2.858(7)
Cu(1)...Cu(1e)	4.156(2)	Cu(1)...N(11e)	3.146(8)
N(11)–Cu(1)–O(1)	156.6(3)	N(11)–Cu(1)–N(1)	92.8(2)
O(1)–Cu(1)–N(1)	81.7(2)	N(11)–Cu(1)–N(2)	93.2(2)
O(1)–Cu(1)–N(2)	91.7(2)	N(1)–Cu(1)–N(2)	173.4(2)
N(11)–Cu(1)–O(3)	102.7(3)	O(1)–Cu(1)–O(3)	99.9(2)
N(1)–Cu(1)–O(3)	88.4(2)	N(2)–Cu(1)–O(3)	93.0(2)
N(12)–N(11)–Cu(1)	124.3(6)	N(13)–N(12)–N(11)	176.3(8)
O(2)–C(5)–O(1)	127.3(5)	O(1c)–O(3)–O(2d)	114.6(2)
Cu(1)–N(11)–Cu(1e)	107.2(3)	O(3)–Cu(1)–N(11e)	175.5(2)
Hydrogen bonding systems			
O(3)...O(1c)	2.848(7)	O(3)...O(2d)	2.858(7)
O(3)–H(4)	0.82(7)	O(3)–H(5)	0.83(8)
H(4)–O(2d)	2.05(7)	H(5)...O(1c)	2.03(8)
H(4)–O(3)–H(5)	112(7)	O(1c)...O(3)...O(2d)	114.6(2)
O(3)–H(4)...O(2d)	169(7)	O(3)–H(5)...O(1c)	170(7)

Symmetry codes: (a) $x+1/2, -y, z$; (b) $x-1/2, -y, z$; (c) $-x, y+1/2, -z+1/2$; (d) $x, y+1, z$; (e) $-x, -y, -z$.

copper(II) atom via its ring nitrogen atom, N(1), and a carboxylato oxygen, O(1), to form a five membered chelate ring. The chelating ring deviates only 0.030(3) Å from planarity and the N(1)–O(1) distance is 2.613(4) Å. Each copper center is further coordinated by a chloride atom, Cl(1), and an oxygen atom, O(3), from an aqua molecule and a nitrogen atom, N(2) from a pyrazinato ligand of a neighbouring unit giving rise to a 1D chain along the *c*-axis (Fig. 2). The coordination environment of each five-coordinate copper atom is best described as a square pyramid with the oxygen atom, O(3) of the aqua molecule at its apex.

The structure determination has established the title

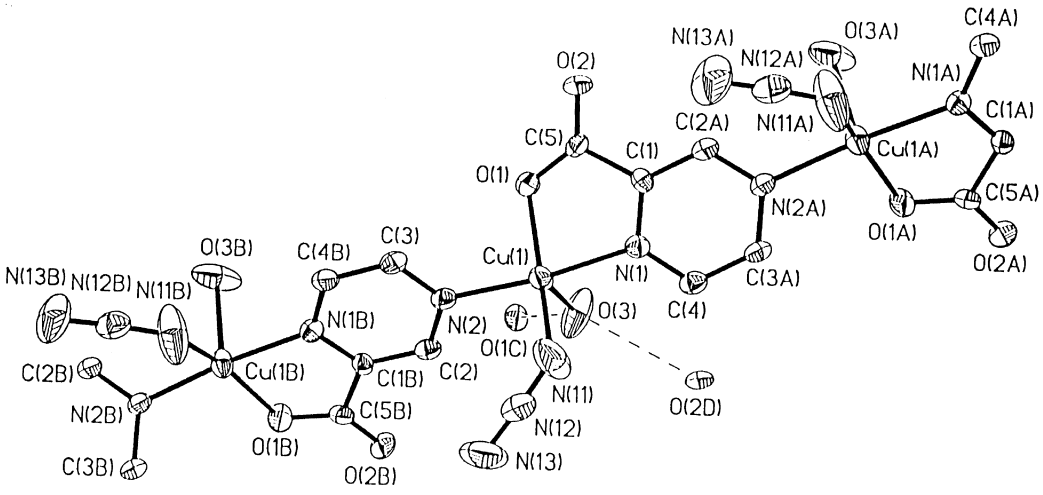

Fig. 1. Molecular geometry and atom labelling scheme of $[CuCl(pyz)(H_2O)]_n$, 1. Hydrogen atoms are omitted.

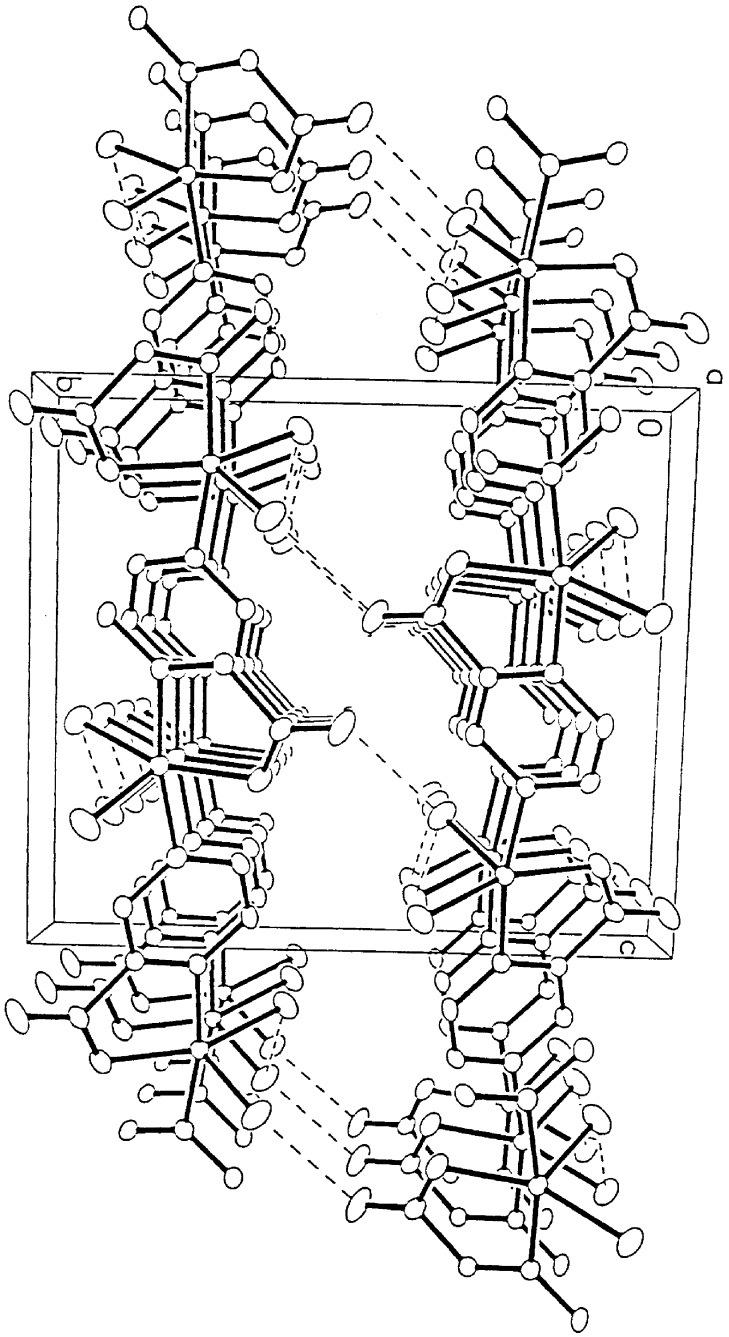

Fig. 2. Packing plot of $[CuCl(pyz)(H_2O)]_n$, 1. Viewed along the *a*-axis of the unit cell.

complex (2) as $[Cu(N_3)(pyrazinato)(H_2O)]_n$, for which Fig. 3 illustrates the principle structural features. The structure of complex (2) is very close to that of complex (1) except that a terminal azide replaces the chloride atom. The deviation of the chelating ring from planarity of 0.036(4) Å, and the N(1)–O(1) distance of 2.605(6) Å found in 2, are slightly greater, whereas the Cu–N(1) and Cu–O(1) distances of 2.009(4) and 2.605(6) Å, respectively are very close to corresponding values in (1). As in the structure of complex (1), the geometry around each copper atom in 2 attains a distorted square pyramid with O(3) at its apex forming 1D chain along the *a*-axis.

The structures 1 and 2 differ from that of the polymeric complex $[Cu(pyrazinato)(N_3)]_n$ (3) found in the structure of $KCu_2(pyrazinato)(N_3)_4$ [20]. In the later complex, also contains *O*,*N*,*N*′-tridentate chelating bridging pyrazinato anion, each copper atom is four

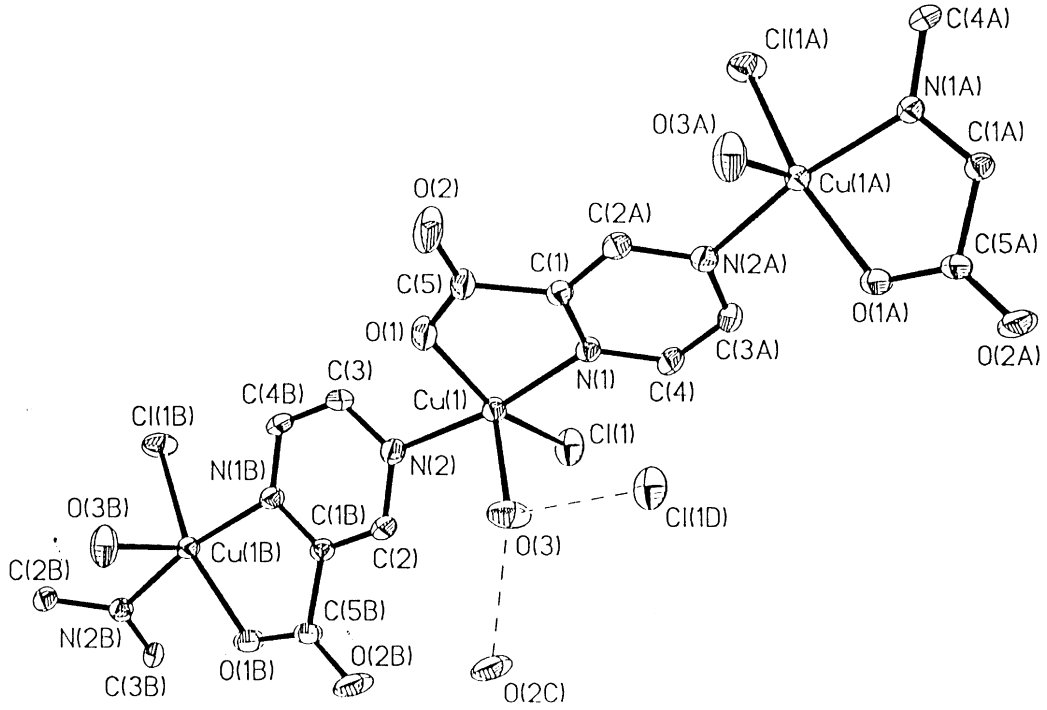

Fig. 3. Molecular geometry and atom labelling scheme of $[Cu(N_3)(pyz)(H_2O)]_n$, 2. Hydrogen atoms are omitted.

coordinated with the fourth position occupied by a nitrogen atom of a terminal azide. The Cu–N(11) distance of 1.942(7) Å in 2 is very similar to corresponding value of 1.943(5) Å found in 3. The Cu–N(1) and Cu–N(2) bond lengths are very close, whereas the Cu–O(1) distances in complexes (1) and (2) are little longer than corresponding values of 2.010(4), 2.022(4) and 1.944(5) Å, respectively, found in complex (3). The structures of both complexs 1 and 2 also differ from the structures of the monomer $[Cu(pyrazinato)_2(H_2O)_2]$, polymer $[Cu(pyrazinato)_2]_n$ and dimer $[Cu(pyrazinic\ acid)Cl_2]_2$ complexes [19, 20], where the pyrazinate ligand acts as chelating *N-O*-bidentate in the monomer and dimer complexes and as a chelating bridging *N-O-O′*-tridentate in the polymer. In accordance with the infrared spectra (see later), different kinds of hydrogen bonds exist in both structures. In 1 the interaction between chains of polyhedra occurs by hydrogen bonds only Fig. 2, whereas in 2 hydrogen bonds cause the formation of double sheets of polyhedra chains oriented parallel to the *ab*-plane, followed by stacking interaction of these double layers (Fig. 4). Details of the hydrogen-bonding geometry are given in Tables 2 and 3.

IR spectra

The IR spectra (Table 4) of complexes 1 and 2 exhibit a strong broad band around 34000 cm^{-1} due to H-bonds of the type O–H...O between H_2O molecule and oxygen atoms of the carboxylato groups. The H-bonds of the types N–H...O and O–H...N or O–H...O in free pyrazinic acid are replaced by O–H...O bonds since both nitrogen atoms of the pyrazinato ligand are involved in coordination to copper. Both complexes show a substantial decrease of the $\nu_{as}(COO^-)$ to about 1660 cm^{-1}, compared to that of free ligand (1720 cm^{-1}), and an increase of the $\nu_s(COO^-)$ to 1365 and 1343 cm^{-1} for 1 and 2, respectively. This large separation between the ν(COO) indicates the unidentate coordination of the carboxylato group to the metal atom as found for many metal complexes of carboxylic acids [21–23]. Vibrations related to the pyrazine moiety are substantially shifted to higher wave numbers when compared with those of the free ligand. Such shifts are much greater than in other complexes containing N,O-bidentate pyrazinato ligand [13]. Thus the coordination of the pyrazinato group via its two nitrogens manifests itself in a greater shift of the pyrazine vibrations as compared with those when it coordinates via one nitrogen atom only.

The IR specrum of the azide complex, 2 shows a very strong band at 2051 cm^{-1} due to $\nu_{as}(N_3)$. This value is very similar to those reported for metal azide complexes containing symmetrical azide groups [24, 25]. In support, the $\nu_s(N_3)$mode which appears as a weak band at 1295 cm^{-1}, suggests a slightly asymmetric azide. In the far IR region a medium band appeared at 392 cm^{-1}, in 2, assigned to the νCu–$N(N_3)$, and a band at 325 cm^{-1} in 1, assigned as the

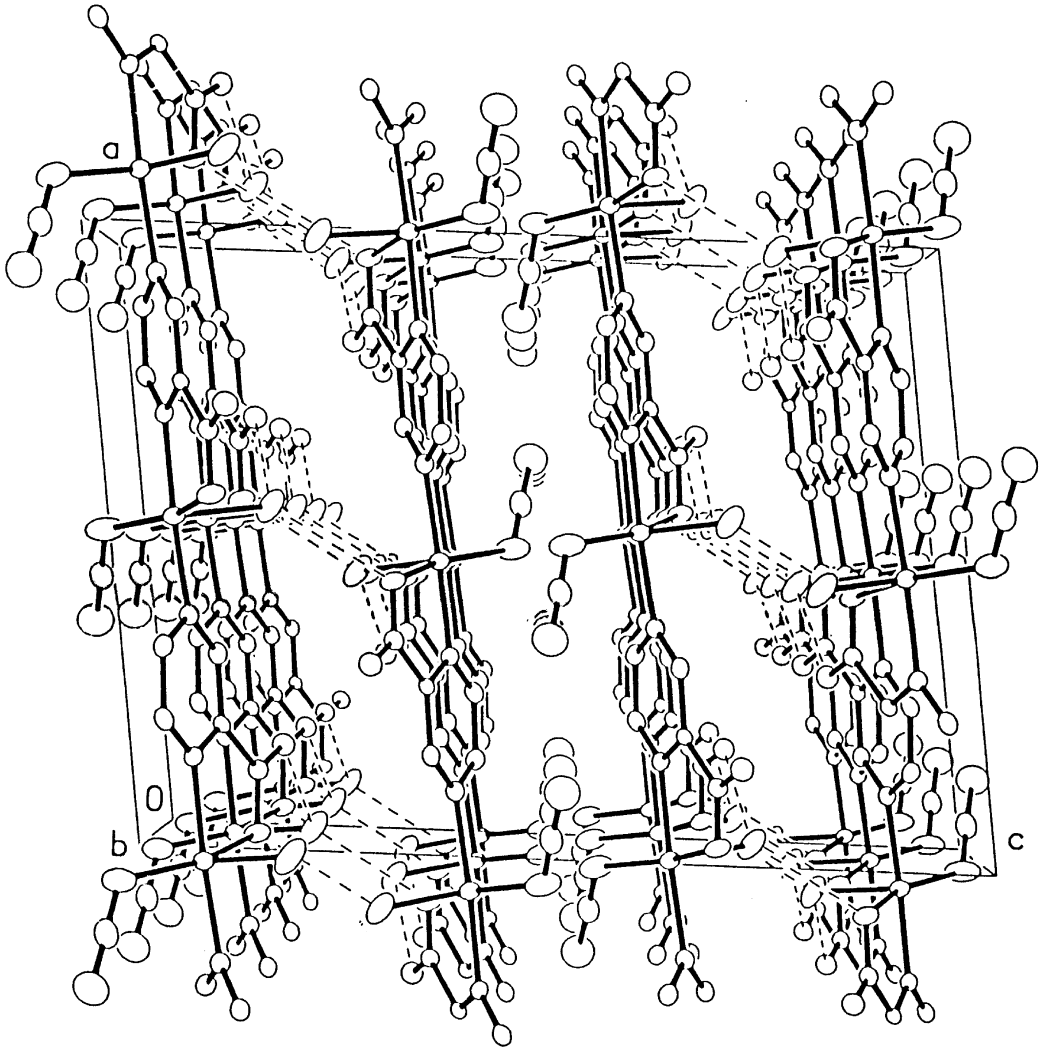

Fig. 4. Packing plot of $[Cu(N_3)(pyz)(H_2O)]_n$, 2. Viewed along the *b*-axis of the unit cell.

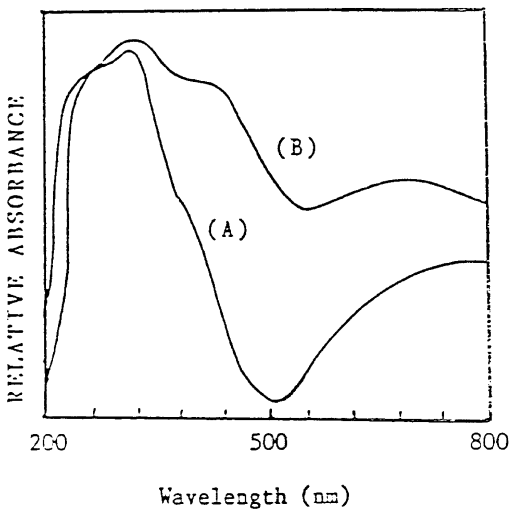

Fig. 5. Electronic spectra of solid complexes: (a) [CuCl (pyrazinato)$(H_2O)]_n$, 1, (b) $[Cu(N_3)$(pyrazinato)$(H_2O)]_n$, 2.

terminal *ν*Cu–Cl vibration, since only one band appeared in each case.

Electronic spectra

The electronic spectra (Fig. 5) of both solid complexes as mulled in Nujol exhibit the *d-d* transitions as a very broad band centered at *ca* 12680 cm^{-1}, and a broad band with a maximum around 14570 cm^{-1} for 1 and 2, respectively. The position of these bands suggests that the copper atoms are five-coordinated in both complexes [26]. In DMSO solution, the spectra show these bands at 12500 and 14265 cm^{-1}, for 1 and 2 respectively. Thus, both complexes retain their five-coordination in this solvent. Additionally, the solid state electronic spectrum of 1 shows a pronounced shoulder around 25000 cm^{-1}, whereas that of the azide complex, 2 exhibits a strong band centered around 22730 cm^{-1}. These bands are due to LMCT tran-

Table 4. IR spectral data[4]

H-pyz	$[CuCl(pyz)(H_2O)]_n$ (1)	$[Cu(N3))pyz)(H2O)]_n$ (2)	Assignments
2450 vs, br	3398 ms, br	3421 ms, br	*v*O–H...O+
1800 s, br			*v*N–H...O
		2951 vs	$v_{as}(N_3)$
1720 s, br	1660 vs	1654 vs	$v(C{=}O)/v_{as}(COO^-)$
1580 wm	1608 m	1605 m	Pyrazine ring
	1500 wm	1505 w	Pyrazine
1440 wm	1466 wm	1470 w	Pyrazine
1395 s	1424 m	1422 m	Pyrazine
1317 s	1365 s	1343 s	
		1295 wm	$v_s(N_3)$
1170 ms	1168 m	1177 ms	Pyrazine
1154 s	1145 sh	1159 ms	Pyrazine
1045 vs	1063 m	1069 m	Ring breathing
1019 vs	1040 sh	1040 wm	Ring breathing
883 ms	870 m	864 m	
777 s	793 m	790 m	
710 s	739 m	745 wm	
		610 w	δ(N3)
	566 wm	560 w	Pyrazine
487 wm	492 m	495 ms	Pyrazine
438 m	461 wm	452 wm	
		392 m	v[Cu–N(N_3)]
	325 m		*v*[Cu–Cl]
	305 m	315 m	*v*[Cu–O(pyz)]
	265 ms	272 ms	*v*[Cu–N(pyz)]
	235 ms	240 ms	*v*[Cu–N(pyz)]

s = strong, m = medium, w = weak, v = very, br = broad, sh = shoulder, pyz = pyrazineato.

sitions from the chloride or azide to copper. The position of these bands indicate the influence of the azide group on the charge transfer as compared to the chloride ion. In DMSO, The N_3^-–Cu^{II} CT band is shifted to higher energy and appeared at 25125 cm^{-1}, whereas the chloride complex shows a less pronounced shoulder at the same position. Previous studies [27, 28] have shown that the electronic spectra of solid copper(II) azide complexes containing cyclic $Cu_2N_2(N_3)$ units usually exhibit a distinct absorption band in the vicinity of 17000–20000 cm^{-1}. This band was considered as due to LMCT transition bridging azides of the type $\mu-1,1$ to copper(II) [28]. The disappearance of any absorption in the range 17000–20000 cm^{-1} from the spectrum of complex 2 having only one terminal azide, confirms our previous conclusion that the existence of such a band should be taken as strong evidence of the existence of binuclear cyclic Cu_2N_2 units, and hence at least two $\mu-1,1$ azides.

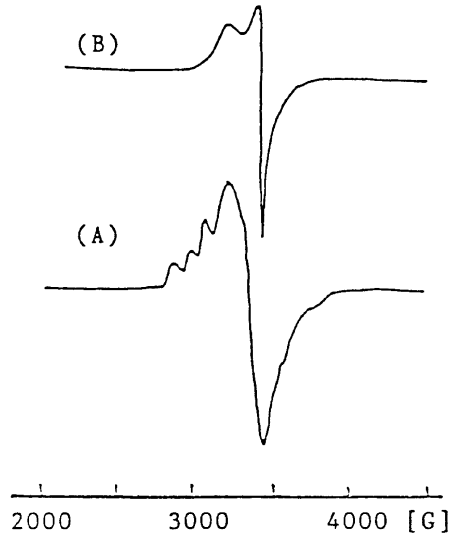

Fig. 6. EPR spectra of solid complexes: (a) [CuCl (pyrazinato)$(H_2O)]_n$, 1, (b) $[Cu(N_3)$(pyrazinato)$(H_2O)]_n$, 2.

EPR spectra

The room temperature EPR spectra of polycrystalline samples of complexes 1 and 2 are given in Fig. 6. The spectrum of the chloride complex 1, shows hyperfine coupling with the copper nucleus of the g parallel, the hyperfine constant $A_\parallel$ (average) is 102 G, and $g_\perp = 2.044$. The spectrum of the azide complex, 2, however, is a well defined typical spectrum of cop-

per(II) system of axial type with $g_{\parallel} = 2.21$ and $g_{\perp} = 2.07$. The value of G, calculated as the ratio of $(g_{\parallel}-2)/(g_{\perp}-2)$ is below 4 suggesting exchange coupling [29] between bridged copper(II) centers in complex 2. Such exchange coupling is expected because pyrazine is an excellent ligand providing exchange pathways when paramagnetic metals are involved [30, 31]. Both complexes, 1 and 2 dissolve in DMF and their spectra in this solvent display four hyperfine lines of uncoupled copper(II) ($I = 3/2$) with $A_o(Cu) = 73$ and 51 G (average), respectively.

Thermal properties

The results of the thermal decomposition of complexes 1 and 2 are represented in Fig. 7. In case of the chloride complex, (1) the residue of the decomposition was followed by measuring its IR spectrum at 200, 250, 275, 300 and 380°C. The first step of the thermal decomposition of complex 1 consists of a dehydration around 160–210°C [loss of weight (%); experimental 7.5 and theortical 7.5]. The DTA curve shows two successive endothermic peaks with maxima at 171.9 and 280°C, corresponding to a loss of weight of 5.4 and 2.13%, respectively. The IR spectrum at 200°C shows that there is some amount of water. This indicates that the dehydration process occurs at two successive stages. In the second step which starts around 275°C, the dehydrated complex starts to lose the pyrazinate and a loss of weight of 43.2% is completed around 310°C. The DTA curve shows this step as a sharp endotherm with a maximum at 304.4°C. This loss of weight does not correspond to all the pyrazinate in the complex. The IR spectrum at 300°C, shows that the residue contains about 10% of the pyrazinato ligand. This step is followed by a gradual loss of weight until *ca* 700°C, at which it reaches 75%, corresponding to a complete loss of pyr and Cl giving rise to a residue of copper metal.

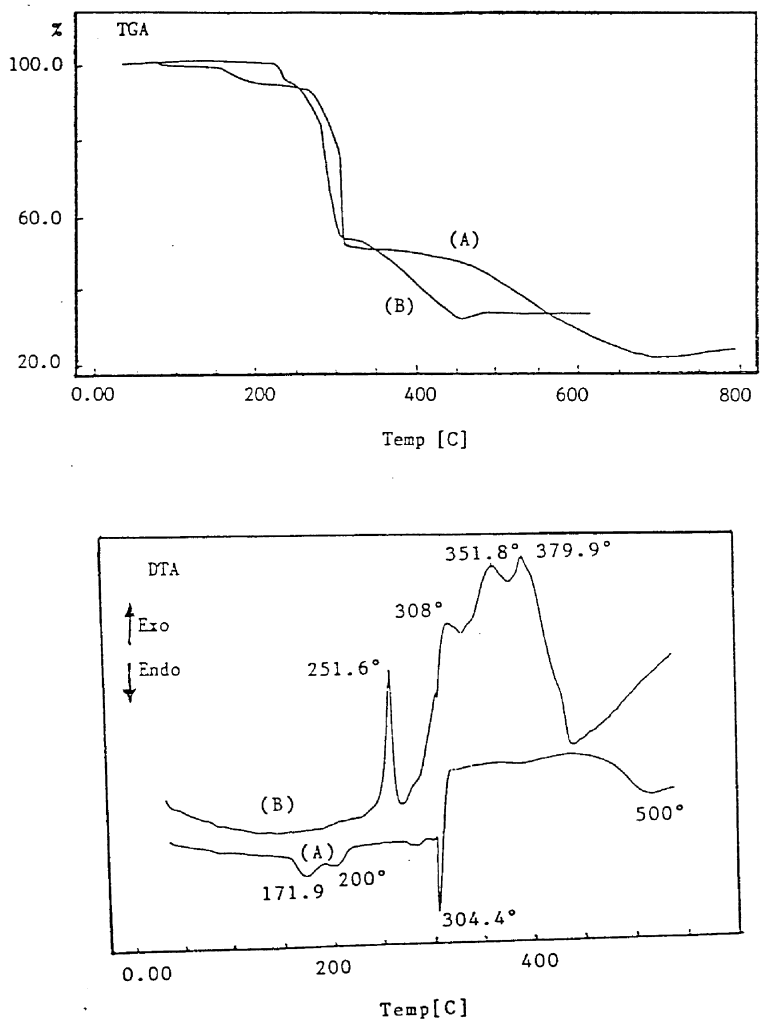

Fig. 7. Thermal decomposition of: (a) $[CuCl(pyrazinato)(H_2O)]_n$, 1, (b) $[Cu(N_3)(pyrazinato)(H_2O)]_n$, 2.

The DTA curve of the azide complex, 2 is similar to that of complex, 1, except the narrow range of temperature upon which the different decomposition steps take place. Thus the thermal decomposition which starts around 210°C is completed around 470°C. As seen from Fig. 7. complex 2 is stable until 210°C, at which the dehydration process takes place. This step is completed around 260°C with an experimental loss of weight of 6.9% (theoretical 7.2%). The DTA curve of this complex, however, does not show the endotherms which observed in case of 1, instead a smooth slight curvature is continued and ended with an exothermic peak with $T_{max} = 251.6$°C. This may suggest a smooth phase transition of the complex. The ΔH corresponds to this exotherm is 85.2 kJ/mol. The following step for the dehydrated compound does not reflect a simple one-stage process and the DTA curve shows a very broad exotherm with three peaks ($T_{max} = 308$, 351.8 and 379.9°C, respectively). The ΔH for this exotherm is 1462.2 kJ/mol. The loss of weight in the range 260–290°C is 46.1%, which represents 92% of the pyrazinate. Unfortunately we could not measure the IR spectrum of the residue in this case at different temperatures, therefore it is not clear if the pyrazinate is the only eliminated radical despite the similarity between the TG curves of 1 and 2. This stage is followed by a gradual decomposition until about 450°C, with a total weight loss of 69.9% which corresponds to a complete loss of pyz, N_2 and H_2O (theoretical = 68.8%).

Acknowledgements—The authors thank Prof. Kratky and Dr Belaj (Univ. Graz) for use of the STOE diffractometer. M.A.S.G. thanks the Department of Chemistry (KU) General Facility Projects (Analab) for the thermal analysis measurements.

REFERENCES

1. Anagnostopolus, A., Matthews, R. A. and Walton, R. A., *Can. J. Chem.*, 1972, **50,** 1307.
2. Fowles, D. W. A., Matthews, R. A. and Wallton, R. A., *J. Chem. Soc.* (*A*), 1968, 1108.
3. Kleinstein, A. and Webb, G. A., *J. Inorg. Nucl. Chem.*, 1971, **33,** 405.
4. Chang, S. C., Ma, J. K. H., Wang, J. S. and Li, N. C., *J. Coord. Chem.*, 1972, **2,** 31.
5. Takenak, A., Utsumi, N., Yamamoto, T. and Nita, I., *Nippon Kagaku Zsashi*, 1970, **91,** 928.
6. Goher, M. A. S., Abu-Youssef, M. A. M., Mautner, F. A. and Popitsch, A., *Polyhedron*, 1992, **11,** 2137.
7. Goher, M. A. S., Hafez, A. K., Abu-Youssef, M. A. M., Popitsch, A., Fritzer, H. P. and Mautner, F. A., *Monatsh. Chem.*, 1994, **125,** 833.
8. Mautner, F. A., Abu-Youssef, M. A. M. and Goher, M. A. S., *Polyhedron*, 1997, **16,** 235.
9. Goher, M. A. S. and Mautner, F. A., *Polyhedron*, 1994, **13,** 2194.
10. Goher, M. A. S. and Mautner, F. A., *Polyhedron*, 1995, **14,** 1439.
11. Matthews, R. W. and Wallton, R. A., *Inorg. Chem.*, 1971, **7**, 1433; Beatti, J. K., Hush, N. S., Taylor, P. R., Raston, C. L. and White, A. H., *J. Chem. Soc., Dalton Trans.*, 1977, 1121; Baker, E. C. and Raymond, K. N., *Inorg. Chem.*, 1977, **16**, 2710.
12. Newkom, G. R., Kohli, D. K. and Fronczek, F. R., *J. Am. Chem. Soc.*, 1982, **104**, 994; Otieno, T., Rettig, S. J., Thompson, R. C. and Trotter, J., *Inorg. Chem.*, 1993, **32**, 1607.
13. Goher, M. A. S., Mautner, F. A. and Popitsch, A., *Polyhedron*, 1993, **12,** 2557.
14. Goher, M. A. S., Al-Salem, N. A. and Mautner, F. A., *Polyhedron*, 1996, **15,** 3575.
15. Goher, M. A. S. and Mak, T. C. W., *Polyhedron*, 1995, **14,** 2587.
16. Goher, M. A. S., Al-Salem, N. A., Mautner, F. A. and Klepp, K. O., *Polyhedron*, 1997, **16,** 825.
17. Walker, N. and Stuart, D., *Acta Cryst.*, 1983, **A39,** 158.
18. SHELXTL/PC v. 5.03, *Analytical Instrumentation*. Siemens Industrial Automation Inc., Madison, WI, 1995.
19. Klein, C. L., Majeste, R. J., Trifonas, L. M. and O'Conner, C. J., *Inog. Chem.*, 1982, **21,** 1891.
20. Klein, C. L., Trefonas, L. M., O'Conner, C. J. and Majeste, R. J., *Cryst. Struct. Commun.*, 1981, **10,** 891.
21. Magri, A. L., Magri, A. D., Balestrieri, F., Cardarelli, E., D'Ascenzo, G. and Chiacchierini, E., *Thermochim. Acta*, 1980, **38,** 225.
22. Allan, J. R., Paton, A. D., Turvey, K., Bowley, H. J. and Gerrad, D. L., *Inorg. Chim. Acta*, 1987, **132,** 41.
23. O'Conner, J. C. and Sinn, E. K. K., *Inorg. Chem.*, 1981, **20,** 454.
24. Agrell, I., *Acta Chem. Scand.*, 1971, **25**, 2965; Dori, Z. and Ziolo, R. F., *Chem. Rev.*, 1973, **73**, 247.
25. Goher, M. A. S., *Acta Chim. Hung.*, 1990, **127,** 213.
26. Sacconi, L. and Bertini, L., *Inorg. Chem.*, 1966, **5**, 1520; Mangia, A., Nardilli, M., Pelizzi, C. and Pelizzi, G., *J. Chem. Soc., Dalton Trans.*, 1972, 2483.
27. Goher, M. A. S. and Mak, T. C. W., *Inorg. Chim. Acta*, 1984, **85**, 117; 1984, **89**, 119.
28. Goher, M. A. S., *Acta Chim. Hung.*, 1988, **125**, 877; Mautner, F. A., Goher, M. A. S. and Abdou, A. E. H., *Polyhedron*, 1993, **12**, 2815; Mautner, F. A. and Goher, M. A. S., *Polyhedron*, 1994, **13**, 2141; Goher, M. A. S. and Mautner, F. A., *Polyhedron*, 1996, **15**, 5.
29. Bew, M. J., Hathway, B. J. and Feredy, R. J., *J. Chem. Soc., Dalton Trans.*, 1972, 1229.
30. Creutz, C. and Taube, H. J., *J. Am. Chem. Soc.*, 1969, **91**, 3988; 1973, **95**, 1086; Meyer, T. J., Powers, M. J., Salmon, D. J. and Callahan, R. W., *J. Am. Chem. Soc.*, 1977, **99**, 1064; Baumann, J. A., Salmon, D. J., Wilson, S. T. and Meyer, T. J., *Inorg. Chem.*, 1979, **18**, 2472.
31. Inoue, M. and Kubo, M., *Coord. Chem. Rev.*, 1976, **21**, 1; Blake, A. B. and Hatfield, W. E., *J. Chem. Soc., Dalton. Trans.*, 1978, 863; Haddad, M. S., Hendrickson, D. N., Cannady, J. P., Drago, R. S. and Bieckza, D. S., *J. Am. Chem. Soc.*, 1979, **101**, 898.

Pergamon

PII: S0277–5387(98)00110–7

Polyhedron Vol. 17, No. 19, pp. 3315–3320, 1998
© 1998 Elsevier Science Ltd
All rights reserved. Printed in Great Britain
0277–5387/98 $19.00+0.00

Equilibria of the H^+-MoO_4^{2-}-$CH_3PO_3^{2-}$ system in aqueous 1.0 M Na(Cl) medium

A. Kobayashi and A. Yagasaki*

Department of Chemistry, School of Science, Kwansei Gakuin University, 1-155 Uegahara-Ichibancho, 662-8501 Nishinomiya, Japan

(Received 8 January 1998; accepted 7 March 1998)

Abstract—The equilibria $pH^+ + qMoO_4^{2-} + rCH_3PO_3^{2-} \rightleftarrows (H^+)_p(MoO_4^{2-})_q(CH_3PO_3^{2-})_r$ have been investigated at 25.0°C in 1.000 M Na(Cl) by the combined emf-NMR method. Quantitative analysis of the emf and ^{31}P NMR data confirmed the existence of the following ternary species, denoted by (p, q, r) according to the general equilibria above: (10, 5, 2), (11, 5, 2), (11, 7, 1), (12, 7, 1), and (12, 6, 1). Least-squares calculation gave $\log \beta_{10,5,2} = 69.51 \pm 0.01$, $\log \beta_{11,5,2} = 71.07 \pm 0.08$, $\log \beta_{11,7,1} = 72.69 \pm 0.04$, $\log \beta_{12,7,1} = 76.23 \pm 0.05$, and $\log \beta_{12,6,1} = 70.31 \pm 0.05$. The formation constants of the (p, 5, 2) species of the current system and the molybdoselenite system correlate with the pK_a of the heteroatom source. © 1998 Elsevier Science Ltd. All rights reserved

Keywords: molybdophosphonate; heteromolybdate; solution equilibria; ^{31}P NMR; methylphosphonate; formation constants.

Molybdate is known to condense in acidic aqueous solution to form polynuclear oxometalates [1]. If other ions such as AsO_4^{3-} coexists in solution, molybdate condenses together with those ions and forms various heteropolymolybdates, incorporating those ions in their metal-oxygen framework. The nature of those ions should affect the stability or formation constants of heteropolymolybdates formed. However, our knowledge on this matter is still very limited.

Some time ago we found that the formation constants of molybdoarsenates and molybdoarsonates correlate with the pK_a's of arsenate and its organic derivatives [2]. An arsonate that has greater pK_a forms more stable heteropolymolybdates. Is this correlation between pK_a's and formation constants a phenomenon observed just for a series of organic derivatives of a certain hetero-atom group? Or, is it rather a "general rule" that is applicable to different heteroatom groups?

To answer this question, we need to know the formation constants of different heteromolybdates that have the same basic structure but contain different heteroatoms. The X_2Mo_5 species is suitable for this purpose. It forms for X = P [3], As [4], S [5], and Se [6]. The formation constants of the P [7], As [8], and Se [9] species have been determined. Unfortunately, however, they were all determined in different media. The formation constants of the P species were determined in either 0.6 M Na(Cl) or 3.0 M Na(ClO_4) medium. For the Se species, 1.0 M Na(Cl) was used as a medium. The 1.0 M Na(Cl) medium was also used for the As system, but the solvent there was D_2O.

Methylphosphonoate is expected to form relatively strong P_2Mo_5 complex [3b, 10]. In addition, the equilibria of the molybdomethylphosphonate system are expected to be much simpler than that of the parent molybdophosphate system. Thus we have carried out a complete equilibrium analysis of the molybdomethylphosphonate system in aqueous 1.0 M Na(Cl) medium, and compared the formation constant of the P_2Mo_5 species with that of Se_2Mo_5.

EXPERIMENTAL

Reagents and general procedures

$Na_2MoO_4 \cdot 2H_2O$ (Wako, S) was used as received. $CH_3PO_3H_2$ (Aldrich) was recrystallized from acetone.

* Author to whom correspondence should be addressed.

NaCl (Manack, JIS Primary Standard) was dried at 300°C for 30 min before use. The Na^+ concentrations of all sample solutions were kept constant at 1.000 M by adding appropriate amounts of NaCl. The least-squares calculations were performed by using the program LAKE [7b, 11].

Emf measurements

The same apparatus as in our previous report was employed [2]. The temperature was kept constant at 25.0 ± 0.1°C throughout the experiment. Six series of titrations were performed and 452 data points were collected. The data covered the ranges $1.53 < -\log h < 7.04$, $0.00 < B/\text{mM} \leq 100$, $10.4 < C/\text{mM} \leq 19.4$, and $0.00 < B/C \leq 9.61$, where h is the concentration of the free hydrogen ion in solution. B stands for the total concentration of molybdate and C that of phosphonate.

NMR measurements

$^{31}P\{^1H\}$ NMR spectra were recorded on a Varian UNITY-plus 300 spectrometer operating at 121.46 MHz and referenced externally to 85% H_3PO_4. An inner concentric tube ($o.d. = 2.5$ mm) that contains D_2O was inserted to a sample tube ($o.d. = 5$ mm) to provide the lock signal. The spin-lattice relaxation time (T_1) of 0.1 M aqueous solution of $CH_3PO_3H_2$ was determined to be 7.9 s, and a recycle time of 52.4 s was used for all spectra recording. In total 64 spectra were recorded in the ranges $1.19 < -\log h < 7.04$, $0.00 < B/\text{mM} \leq 100$, $10.4 < C/\text{mM} \leq 19.4$, and $0.00 < B/C \leq 9.61$.

Binary systems

Since there was no former report on the binary H^+-$CH_3PO_4^{2-}$ equilibria in 1.000 M Na(Cl), several separate emf and NMR titrations were performed to determine the formation constants of this system. They covered the ranges $1.60 < -\log h < 11.00$ and $2.00 \leq C/\text{mM} \leq 20.80$. Both emf and ^{31}P NMR data did not show any sign of concentration dependence, meaning that only monomeric species existed in the ranges investigated. The system was well explained by $CH_3PO_3^{2-}$, $CH_3PO_3H^-$, and $CH_3PO_3H_2$ [(0, 0, 1), (1, 0, 1), and (2, 0, 1), respectively, in the (p, q, r) notation] with the formation constants $\log \beta_{1,0,1} = 7.18(4)$ and $\log \beta_{2,0,1} = 9.26(5)$ [12]. Least-squares calculations on the δ *vs* $-\log h$ curve gave the ^{31}P NMR chemical shifts of (0, 0, 1), (1, 0, 1), and (2, 0, 1) as 23.6(1) ppm, 27.42(2) ppm, and 33.54(9) ppm, respectively [12].

For the $H^+ - MoO_4^{2-}$ equilibria the constants reported elsewhere were used [13].

RESULTS AND DISCUSSION

The equilibria of the current system can be written in the general form

$$pH^+ + qMoO_4^{2-} + rCH_3PO_3^{2-} \leftrightarrows (H^+)_p(MoO_4^{2-})_q(CH_3PO_3^{2-})_r$$

The complex on the right-hand side will simply be referred as (p, q, r) and its formation constant $\beta_{p,q,r}$.

In Fig. 1 chemical shifts of different peaks are plotted against $-\log h$. Peak A is assigned unambiguously to the free phosphonate in solution, because it appears in the spectra even if the solution contains no molybdate.

When $B/C \leq 2.5$, both emf and NMR data clearly showed the existence of only one ternary species over a wide $-\log h$ range. Only one ternary NMR peak (peak B) was observed under such conditions irrespective of $-\log h$. Its chemical shift remained unchanged when $-\log h$ was larger than 2.4. The potentiometric $Z_{B,C}$ vs $-\log h$ curves at low B/C ratios showed plateaus over a relatively wide range of $-\log h$ [14].

Figure 2 shows the result of a series of NMR measurements in which B/C was varied and $-\log h$ was kept around 2.0. The figure implies that the q/r ratio for the ternary species that gives rise to peak B is 2.5. Although this experiment does not tell us much about the p value of this species, potentiometric data gives us a good estimate of that. The potentiometric titration curve at $B/C = 2.5$ showed a plateau at $Z_{B,C}$ somewhat higher than 1.4, indicating this species is $(H^+)_{10}(MoO_4^{2-})_5(CH_3PO_3^{2-})_2$ $(10/(5+2) = 1.43)$. In fact, the *pqr* search performed on the emf data of $B/C \leq 2.5$ and $-\log h > 2$ confirmed this speciation. All the other species tested gave unacceptably high residuals in the least-squares calculation.

However, the residuals in the least-squares analysis of the emf data showed some systematic trend in the very acidic region when we tried to explain these low-ratio data only by (10, 5, 2). This systematic deviation disappeared after the introduction of (11, 5, 2) to the system. Slight changes in chemical shift of peak B in the low -log h region also indicates protonation of (10, 5, 2) (see Fig. 1).

Figure 2 also tells us that one more ternary species of considerably higher q/r ratio forms when B/C is increased. Since peak B is now assigned unambiguously to the $(p, 5, 2)$ species, we can calculate the amount of molybdate left available for the formation of the species responsible for peak C from the NMR intensity data. Such calculations revealed that the q/r ratio of this species should be less than 8. In addition, chemical shift dependence of peak C on $-\log h$ indicated that (at least) two different species were involved, either a protonation series or a fast exchange between species that have different q and/or r. Thus we tried different pairs that have q/r ratio smaller than 8 on the NMR data. The least-squares calculations

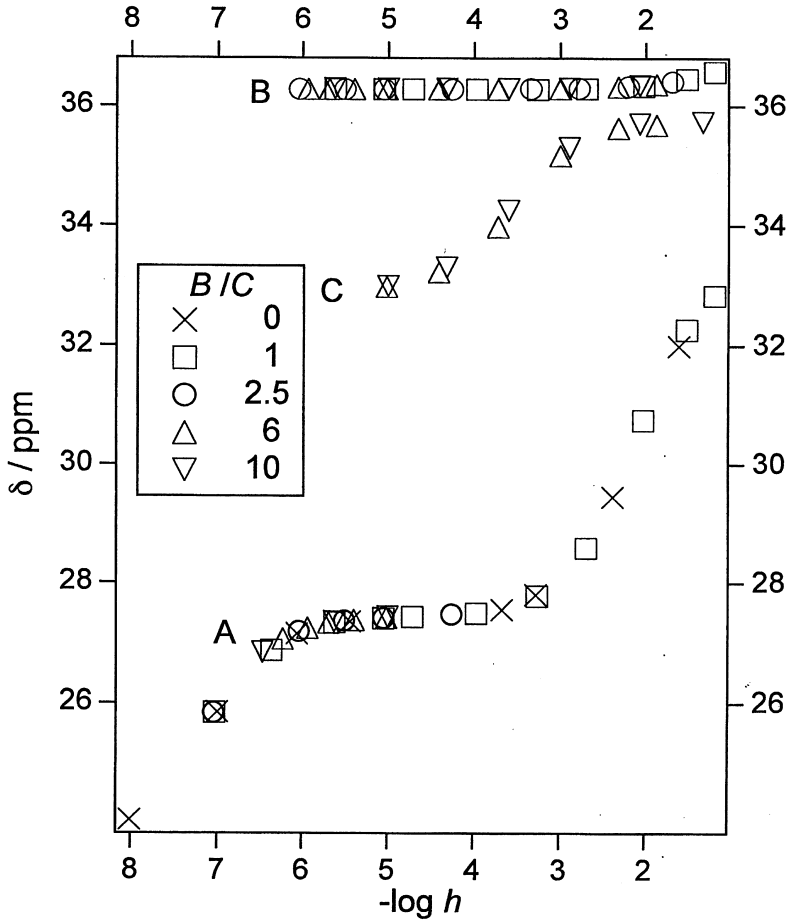

Fig. 1. ^{31}P chemical shifts, δ, as a function of $-\log h$.

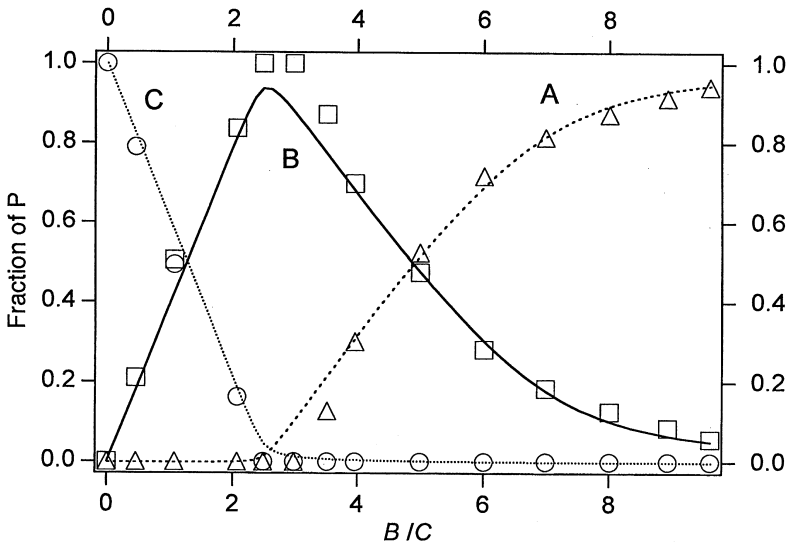

Fig. 2. Relative intensities of different peaks as a function of the B/C ratio at $-\log h \approx 2$. C was kept constant at 10.41 mM. Solid and dotted lines have been calculated by using the determined formation constants.

gave us two pairs, (10, 6, 1)/(11, 6, 1) and (11, 6, 1)/(11,7, 1), as possible candidates.

When we tried these pairs on the emf data, however, both gave unsatisfactory results. They consumed less protons than observed in very acidic region and the fit between the calculated and observed titration curves got worse in a systematic manner in the range $-\log h < 2.5$. This means species that consume more protons exist in solution. We performed several more least-squares calculations including species of greater p values into the candidates mentioned above. The combination of (11, 6, 1), (12, 6, 1), and (11, 7, 1) gave the lowest residual on the NMR intensity data. However, this model did not improve the fit on the emf data. The pK_a value calculated for (12, 6, 1) (~ 1.4) was not consistent with the observed δ vs $-\log h$ curve, either. The NMR intensity residual for the combination of (12, 6, 1), (11, 7, 1), and (12, 7, 1) was slightly larger, but the calculated pK_a of (12, 7, 1) (~ 3.5) was consistent with the δ vs $-\log h$ curve. This model also explained the emf data satisfactorily.

The results of the least-squares calculations are summarized in Table 1. The species found in the current system are the same as those found in the closely related $H^+ - MoO_4^{2-}$-$C_6H_5PO_3^{2-}$ system [7b]. Figure 3 illustrates the distribution of molybdenum and phosphorus among different species. Formation of the ternary species starts at $-\log h \approx 6$, which is a common feature of heteropolymolybdate systems that have tetrahedral heteroatoms [7–9, 11]. The diagram also tells us that (p, 7, 1) of the current system are weak, just like their phenyl analog in the $H^+ - MoO_4^{2-}$-$C_6H_5PO_3^{2-}$ system. Notable amounts of isopolymolybdates form even at such a low B/C ratio as 5.6.

The composition of (10, 5, 2) coincides with that of

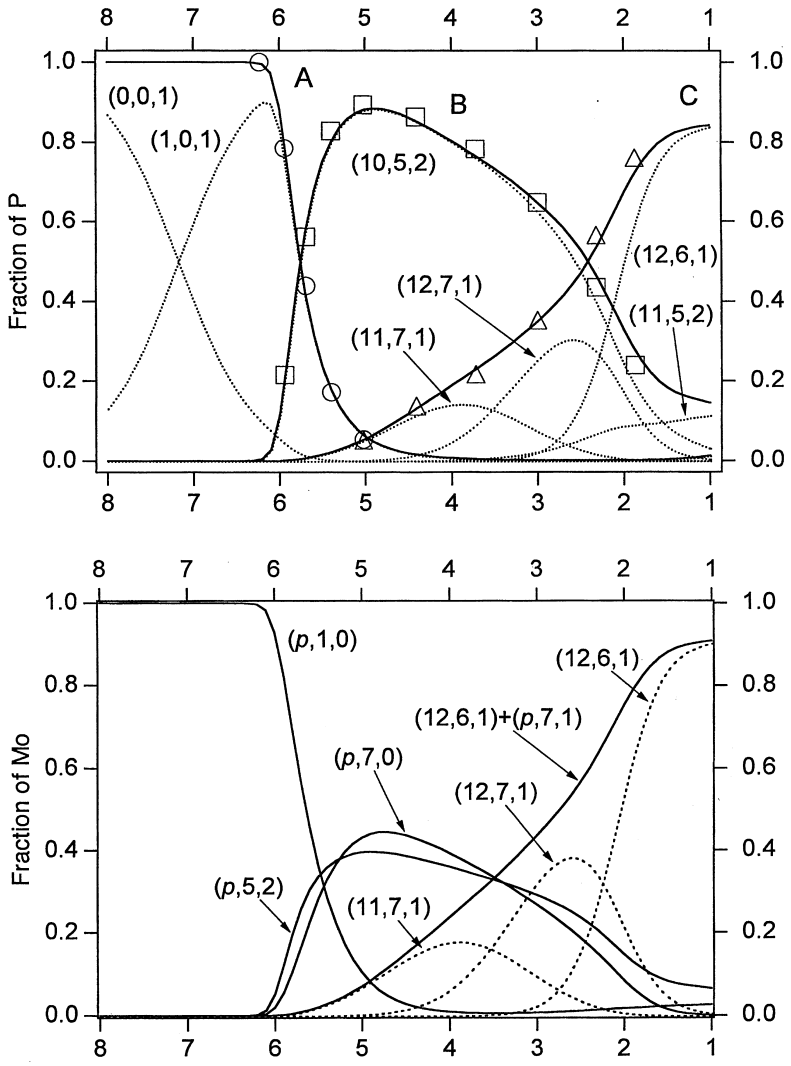

Fig. 3. Calculated distribution of molybdenum (2) and phosphorus (1) among different species at $B = 60.00$ M and $C = 10.76$ M. Observed data points are plotted together with the calculated curves for phosphorus.

Table 1. Summary of the Results

(p, q, r)	$\log \beta_{p,q,r}$*	pK_a	Peak	δ/ppm*	Proposed formula
(0, 0, 1)			A	23.6(1)	$CH_3PO_3^{2-}$
(1, 0, 1)	7.18(4)	7.18		27.42(2)	$CH_3PO_2(OH)^-$
(2, 0, 1)	9.26(5)	2.08		33.54(9)	$CH_3PO(OH)_2$
(10, 5, 2)	69.51(1)		B	36.28(1)	$[(CH_3P)_2Mo_5O_{21}]^{4-}$
(11, 5, 2)	71.07(8)	1.56		36.65(3)	$[(CH_3P)_2Mo_5O_{20}(OH)]^{3-}$
(11, 7, 1)	72.69(4)		C	32.89(1)	$[CH_3PMo_7O_{25}(OH)]^{5-}$
(12, 7, 1)	76.23(5)	3.54		35.61(2)	$[CH_3PMo_7O_{25}(OH_2)]^{4-}$
(12, 6, 1)	70.31(5)			35.73(1)	$[CH_3PMo_6O_{21}(OH_2)_6]^{2-}$

* See [12].

$[(CH_3P)_2Mo_5O_{21}]^{4-}$, whose structure is depicted in Fig. 4 [3b]. We assume this structure is maintained in solution. Single ^{31}P NMR peak observed for (10, 5, 2) is also consistent with this structure. Possible protonation sites are indicated by asterisks in the figure. Bond order calculation [15] showed that the oxygen atoms doubly shared by one Mo atom and one P atom are slightly more basic than others. Protonation of either of these sites would yield (11, 5, 2).

The observed pK_a's of the (11, 5, 2) species and the bond orders of $[(CH_3P)_2Mo_5O_{21}]^{4-}$ and $[Se_2Mo_5O_{21}]^{4-}$ are consistent with the argument above. Both anions have the same basic structure [3b], [6]. Replacing CH_3P groups in Fig. 4 with Se atoms would yield $[Se_2Mo_5O_{21}]^{4-}$. The average bond order sum of the oxygen atoms marked with asterisks is 1.7 in the $[(CH_3P)_2(Mo_5O_{21})]^{4-}$ structure. The bond order sum for the same type of oxygen atom in $[Se_2Mo_5O_{21}]^{4-}$ is 1.8. This implies that the former anion is more basic than the latter. The pK_a's of (11, 5, 2) in the current system and the $H^+ - MoO_4^{2-}$-SeO_3^{2-} system [9] are 1.56 and 1.41, respectively, and agree with the bond order difference of $[(CH_3P)_2(Mo_5O_{21})]^{4-}$ and $[Se_2Mo_5O_{21}]^{4-}$.

When we compare the formation constants of (p, 5, 2) species of the current system and those of the $H^+ - MoO_4^{2-}$-SeO_3^{2-} system, we notice another interesting thing. The formation constants for the current system is somewhat smaller than those for the latter ($\log \beta_{10,5,2} = 71.32(2)$ and $\log \beta_{11,5,2} = 72.73(4)$ for the $H^+ - MoO_4^{2-}$-SeO_3^{2-} system). Selenite ($pK_1 = 2.36$, $pK_2 = 8.28$ in aqueous 1.0 M Na(Cl) medium [9]) is more basic than methylphosphonate. Here we see the same kind of correlation that was observed for molybdoarsenates and its organic derivatives: hetero atom source that has greater p*Ka* forms more stable heteropolymolybdates.

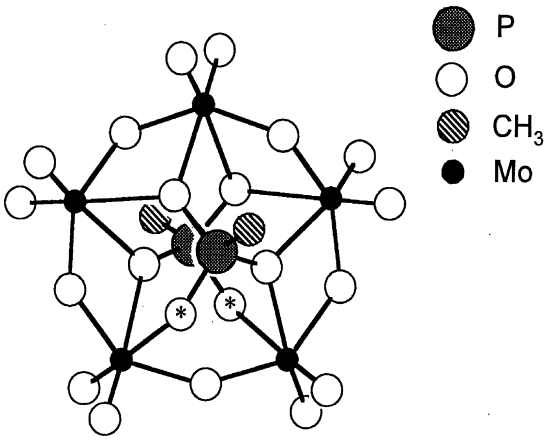

Fig. 4. Perspective view of the $[(CH_3P)_2Mo_5O_{21}]^{4-}$ structure. Possible protonation cites are indicated by *.

Acknowledgements—This work was supported in part by a Grant-in-Aid for Scientific Research No. 09218256 from Monbusho (Ministry of Education, Science, and Culture of Japan).

REFERENCES

1. See for example: Wells, A. F. *Structural Inorganic Chemistry*, 5th edn., pp. 514–530.
2. Yagasaki, A., Takahama, H. and Sasaki, Y., *Bull. Chem. Soc. Jpn.*, 1987, **60,** 3925.
3. (a) Strandberg, R., (1973) *Acta. Chem. Scand.*, **27**, 1004. (b) J. Stalick K. and Quicksall, C. O. (1976) *Inorg. Chem.*, **15**, 1577. (c) Lyxell, D.-G., Strandberg, R., Boström, D. and Pettersson, L. (1991) *Acta. Chem. Scand.*, **45**, 681. (d) Lyxell D.-G. and Strandberg, R. (1988) *Acta Cryst.*, **C44**, 1535. (e) Lowe, M. P., Lockhart, J. C., Clegg, W. and Fraser, K. A.(1994) *Angew. Chem. Int. Ed. Engl.*, **33**, 451. (f) Lowe, M. P., Lockhart, J. C., Forsyth, G. A., Clegg, W. and Fraser, K. A. (1995) *J. Chem. Soc. Dalton Trans.*, 145.
4. (a) Liu, B., Ku, Y., Wang, M. and Zheng, P. (1988) *Inorg. Chem.*, **27**, 3868. (b) Wang, M., Zeng, P., Liu, B. and Gu, Y. (1988) *Acta Cryst.*, **C44**, 1503. (c) Liu, B., Ku, Y. and Wang, X. (1989) *Inorg. Chim. Acta*, **161**, 233.
5. (a) Hori, T., Himeno, S. and Tamada, O. (1992)

J. Chem. Soc., Dalton Trans., 275. (b) Matsumoto, K. Y., Kato, M. and Sasaki, Y. (1976) *Bull. Chem. Soc. Jpn.*, **49**, 106.
6. Ichida, H., Fukushima, H. and Sasaki, Y. (1986) *Nippon Kagaku Kaishi*, 1521.
7. (a) Pettersson, L., Andersson, I. and Öhman, L.-O. (1986) *Inorg. Chem.*, **25**, 4726. (b) Yagasaki, A., Andersson, I. and Pettersson, L., *Inorg. Chem.*, 1987, **26**, 3926.
8. Kobayashi, A. and Yagasaki, A., *Inorg. Chem.*, 1997, **36,** 126.
9. Ozeki, T., Yagasaki, A., Ichida, H. and Sasaki, Y., *Polyhedron*, 1988, **12,** 1131.
10. Kwak, W., Pope, M. T. and Scully, T. F., *J. Am. Chem. Soc.*, 1975, **97,** 5736.
11. Ingri, N., Andersson, I., Pettersson, L., Yagasaki, A., Andersson, L. and Holmström, K., *Acta Chem. Scand.*, 1996, **50,** 717.
12. The figures in parentheses are three times estimated standard deviations for the least significant digits.
13. Yagasaki, A. and Sasaki, Y., *Bull. Chem. Soc. Jpn.*, 1987, **60,** 763.
14. Average H^+ consumption factor, $Z_{B,C}$, is defined as $Z_{B,C}=(H\text{-}h)/(B+C)$, where H is the total hydrogen concentration over the chosen zero level (H_2O, MoO_4^{2-}, and $CH_3PO_3^{2-}$) [7b].
15. Brown, I. D. and Altermatt, D., *Acta Cryst.*, 1985, **B41,** 244.

Pergamon

PII: S0277–5387(98)00111–9

Polyhedron Vol. 17, No. 19, pp. 3321–3325, 1998
© 1998 Elsevier Science Ltd
All rights reserved. Printed in Great Britain
0277–5387/98 $19.00+0.00

New dinuclear thiobenzoato complexes of molybdenum(V) containing $Mo_2O_2S_2$ core. X-ray crystal structures of $[Mo_2O_2S_2(OSCC_6H_5)_2(py)_2]$ and $[Mo_2O_2S_2(OSCC_6H_5)_2(\gamma\text{-pic})_2]\cdot 2H_2O$

Marina Cindrić, Višnja Vrdoljak, Biserka Prugovečki and Boris Kamenar*

Laboratory of General and Inorganic Chemistry, Chemistry Department, Faculty of Science, University of Zagreb, Ulica kralja Zvonimira 8, POB 153, 10001 Zagreb, Croatia

(Received 17 December 1997; accepted 9 March 1998)

Abstract—The $[Mo_2O_2S_2(OSCC_6H_5)_2]$ (**1**) has been prepared either by the reaction of $[Mo_2O_3(C_5H_7O_2)_4]$ or of $[Mo_4Cl_2O_6(O_2CCH_3)_6]\cdot(CH_3CO)_2O$ with thiobenzoic acid. The product was then used to prepare two complexes of the general formula $[Mo_2O_2S_2(OSCC_6H_5)_2L_2]$ (where L = pyridine (**2**) or γ-picoline (**3**)). All complexes were characterized by elemental analyses, IR spectra and magnetic measurements. The structures of (**2**) and (**3**) were proved by X-ray structure analysis. Both complexes are dinuclear containing $Mo_2O_2S_2$ core with two Mo atoms linked by a Mo–Mo single bond. The Mo atoms are octahedrally coordinated by oxo-oxygen, two bridging sulfido-sulfurs, one pyridine (or γ-picoline)-nitrogen and thiobenzoato-sulfur and thiobenzoato-oxygen atoms.
© 1998 Elsevier Science Ltd. All rights reserved

Keywords: crystal structure; molybdenum(V) complexes; thiobenzoato complexes; dimeric structure.

Relevance of molybdenum(V) complexes containing Mo–S bonding to the molybdoenzymes is well known and extensively studied [1–4]. This is particularly true due to the suggestion that the molybdoenzymes in the oxidized forms such as xanthine oxidase and sulfite oxidase contain oxo-molybdenum cores with the molybdenum atom coordinated by two or more sulfur ligands. The usual octahedral surroundings about molybdenum atoms in such systems are commonly completed by the additional nitrogen donor ligands [5]. In addition, interest in Mo–S chemistry has also grown due to the implication of this metal in the catalytic hydrodesulfurization processes [6, 7].

In this paper we describe the synthesis and structural characterization of three new complexes containig MoS_2Mo bridging core with thiobenzoato ligands as simultaneous oxygen and sulfur donors. Two of them with additional pyridine and γ-picoline as nitrogen donor ligands. Similar dinuclear di-μ-oxo and μ-oxo-μ-sulfido molybdenum(V) complexes of the formulae $[Mo_2O_3X(OSCC_6H_5)_2]_n$ and $[Mo_2O_3X(OSCC_6H_5)_2(py)_2]$ (X = O or S) have been prepared by M. Rakowski DuBois in 1978 but their structures have never been determined by X-ray diffraction method [8]. They were prepared using molybdenum(VI) compounds, MoO_2Cl_2 and Na_2MoO_4.

* Author to whom correspondence should be addressed.

EXPERIMENTAL

The starting acetylacetonato $[Mo_2O_3(acac)_4]$ [9] and acetato $[Mo_4Cl_2O_6(O_2CCH_3)_6]\cdot(CH_3CO)_2O$ [10] complexes were prepared as described earlier. Reagent grade solvents and all other chemicals were used without further purification.

The IR spectra of KBr pellets were recorded on a FTIR 1600 Fourier-transform spectrometer in the 4500–450 cm^{-1} region. Magnetic measurements were carried out at room temperature using Gouy method.

Preparation of $[Mo_2O_2S_2(OSCC_6H_5)_2]$ (1)

Procedure (*i*). A mixture of $[Mo_2O_3(acac)_4]$ (1 g, 1.57 mmol) and thiobenzoic acid (1.8 g, 13.03 mmol) in dichloromethane (10 cm^3) was heated for 2 hours.

The resulting red-brown precipitate was filtered and washed with dichloromethane and methanol. Yield: 0.5 g, 57%.

Procedure (*ii*). The same product was prepared by warming a mixture of $[Mo_4Cl_2O_6(O_2CCH_3)_6]\cdot(CH_3CO)_2O$ (0.25 g, 0.25 mmol) with thiobenzoic acid (0.35 g, 2.53 mmol) in dichloromethane (10 cm^3) for 45 min. After 2 days at room temperature red-brown product was isolated. Yield: 0.25 g, 86%. Found: C, 29.97; H, 1.58; Mo, 34.18; S, 22.16. Calc. for $C_{14}H_{10}Mo_2O_4S_4$: C, 29.90; H, 1.79; Mo, 34.12; S, 22.81%. IR (cm^{-1}): 3061w, 1592m, 1455s, 1421s, 1310m, 1230s, 1175s, 974s, 937s, 839s, 678s, 475m.

Preparation of $[Mo_2O_2S_2(OSCC_6H_5)_2(py)_2]$ (**2**)

Pyridine (1.5 cm^3) was added to a suspension of $[Mo_2O_2S_2(OSCC_6H_5)_2]$ (0.15 g, 0.27 mmol) in dichloromethane (15 cm^3) and the reaction mixture warmed up for 15 min. After three days an orange-red crystalline product was isolated. Yield: 0.05 g, 26%. Found: C, 40.12; H, 2.75; Mo, 27.06; N, 3.36; S, 17.93. Calc. for $C_{24}H_{20}Mo_2N_2O_4S_4$: C, 40.0; H, 2.80; Mo, 26.63; N, 3.89; S, 17.80%. IR (cm^{-1}): 3065m, 1595m, 1460s, 1446s, 1435s, 1309m, 1248s, 1220s, 1012m, 978s, 940s, 469m.

Preparation of $[Mo_2O_2S_2(OSCC_6H_5)_2(\gamma\text{-pic})_2]\cdot 2H_2O$ (**3**)

Analogously as above, to a suspension of $[Mo_2O_2S_2(OSCC_6H_5)_2]$ (0.15 g, 0.27 mmol) in dichloromethane (10 cm^3) γ-picoline was added and the reaction mixture warmed up for 15 min. From the resulting solution after three days an orange crystalline product was isolated. Yield: 0.05 g, 25%. Found: C, 39.29; H, 3.79; Mo, 24.67; N, 3.91; S, 16.01. Calc. for $C_{26}H_{28}Mo_2N_2O_6S_4$: C, 39.80; H, 3.60; Mo,

Table 1. Crystal data for $[Mo_2O_2S_2(OSCC_6H_5)_2(py)_2]$ (**2**) and $[Mo_2O_2S_2(OSCC_6H_5)_2(\gamma\text{-pic})_2]\cdot 2H_2O$ (**3**)

	2	**3**
Formula	$C_{24}H_{20}Mo_2N_2O_4S_4$	$C_{26}H_{28}Mo_2N_2O_6S_4$
Mol. wt	720.54	784.62
Crystal size (mm)	$0.25\times0.20\times0.35$	$0.20\times0.10\times0.55$
Colour	red	orange-red
a (Å)	14.453(3)	13.917(2)
b (Å)	10.256(2)	9.822(1)
c (Å)	18.547(3)	24.781(6)
α (°)	90	90
β (°)	97.32(3)	102.36(2)
γ (°)	90	90
V (Å^3)	2726.8(9)	3308.9(10)
Crystal system	monoclinic	monoclinic
Z	4	4
$d_{calc.}$ (gcm^{-3})	1.755	1.575
Space group	$C2/c$	$P2_1/c$
Temp. (°C)	23	23
Scan method	Θ–2Θ	ω
2Θ range (°)	4–60	4–60
hkl range	$\pm20, +14, +26$	$\pm19, +13, +34$
Max time/rfln(h)	1.5	2
μ(Mo–K_α) (cm^{-1})	12.59	10.49
Data measured	4320	9965
Unique data	3993	9395
Observed data [$I>2\sigma(I)$]	1600	2575
Number of variables	163	361
Max/min $\Delta\rho$ (e^3/Å^3)	0.663/−0.802	1.337/−1.274
$R1$[a] for rfln. with $I>2\sigma(I)$	0.062	0.094
$wR2$[b](F_o^2)	0.148	0.243
GooF[c]	0.918	0.916

[a] $R1=\Sigma||F_c|-|F_c||/\Sigma|F_o|$.

[b] $wR2=[\Sigma w(F_o\text{-}F_c)^2/\Sigma\ wF_o^2]^{1/2}$, $w=1/[\sigma^2(F_o^2)+(aP)^2+bP]$, $a=0.0587$ for **2**, $a=0.0934$ for **3**, $b=0.00$ for **2** and **3**, $P=(\max(F_o^2\text{ or }0)+2\ F_c^2)/3$.

[c] $GooF=S=[\Sigma w(F_o^2\text{-}F_c^2)^2/(n\text{-}p)]^{1/2}$.

24.45; N, 3.57; S, 16.34%. IR (cm^{-1}): 3067m, 1618s, 1595m, 1462s, 1435s, 1307m, 1235s,1025m, 978s, 944s, 465m.

X-ray crystallography

Intensity data were collected at 293 K by using graphite-monochromated Mo-K_α radiation ($\lambda =$ 0.7107 Å) on a STOE updated Philips PW1100 diffractometer. Three standard reflections were monitored periodically. Intensity variations of 8.9% (**2**) and 9.9% (**3**) were observed and consequently corrected for in the data reduction. The intensities were reduced to *F*o by applying corrections for Lorentz and polarization effects. Absorption corrections were not applied.

The structures of both compounds were solved by using direct methods implemented in SIR92 programs [11] and succesive Fourier syntheses. The refinements were performed by full matrix least squares method assuming anisotropic temperature factors for all non-H atoms using SHELXL96 [12] program. All hydrogen atoms, except those belonging to the water molecules, were calculated on the geometrical ground and treated with the constrained lengths in the refinement. Hydrogen atoms of water molecules were not located. Crystal parameters, data collection details for both compounds and the results of the refinements are summarized in Table 1. Selected bond lengths and angles are listed in Table 2. Crystals of **3** were extremely fragile thus causing difficulties to manipulate with them. They cracked very easily. This is most probably the reason for relatively high reliability index for the structure of **3**. The distances and angles were calculated by SHELXL96 and PARST [13] program, the molecular and crystal structures by ORTEP-3 [14]. All calculations were performed on an IBM PC/AT compatible microcomputer (processor 80486/ 66 MHz).

Tables with complete interatomic distances and angles, positional and anisotropic thermal parameters, and observed and calculated structure factors for the two structures have been deposited with the Editor, from whom copies are available on request.

RESULTS AND DISCUSSION

The complex **1** was prepared by two alternative ways, either by the reaction of $[Mo_2O_3(C_5H_7O_2)_4]$ or of $[Mo_4Cl_2O_6(O_2CCH_3)_6]\cdot(CH_3CO)_2O$ with thiobenzoic acid. The product was stable and insoluble in all common solvents suggesting its polynuclear nature $[Mo_2O_2S_2(OSCC_6H_5)_2]_n$ rather with six than five-coordinated molybdenum atom. The complex containing five-coordinated molybdenum would be unsaturated and therefore more reactive. Its IR spectrum supports such structure: strong broad band at 839 cm^{-1} is indicative for an intermolecular metal... oxygen interaction (Mo=O···Mo=O···) the same as it has been observed for $[Mo_2O_4(OSCC_6H_5)_2]_n$ at 830 cm^{-1} [8]. Due to its insolubility we were not able to prepare

Table 2. Selected bond lengths (Å) and angles (°) for $[Mo_2O_2S_2(OSCC_6H_5)_2(py)_2]$ (**2**) and $[Mo_2O_2S_2(OSCC_6H_5)_2(\gamma\text{-pic})_2]\cdot 2H_2O$ (**3**)

2		**3**			
Mo1–O1	1.685(5)	Mo11–O11	1.679(8)	Mo21–O21	1.684(8)
Mo1–O2	2.257(4)	Mo11–O12	2.263(8)	Mo21–O22	2.270(7)
Mo1–N1	2.305(5)	Mo11–N11	2.279(8)	Mo21–N21	2.272(8)
Mo1–S1	2.310(2)	Mo11–S11	2.316(3)	Mo21–S11	2.321(3)
Mo1–S1′	2.322(2)	Mo11–S12	2.314(3)	Mo21–S21	2.318(3)
Mo1–S2	2.580(2)	Mo11–S12	2.567(3)	Mo21–S22	2.579(3)
Mo1–Mo1′	2.822(1)	Mo11–Mo21	2.831(1)		
O1–Mo1–N1	86.9(2)	O11–Mo11–N11	87.2(3)	O21–Mo21–N21	88.2(3)
O2–Mo1–N1	76.1(2)	O12–Mo11–N11	74.4(3)	O22–Mo21–N21	75.7(3)
O1–Mo1–S1	107.8(2)	O11–Mo11–S11	108.6(3)	O21–Mo21–S21	107.4(3)
O2–Mo1–S1	88.37(12)	O12–Mo11–S11	89.7(2)	O22–Mo21–S21	91.8(2)
N1–Mo1–S1	84.3(2)	N11–Mo11–S11	85.1(2)	N21–Mo21–S21	84.4(2)
O1–Mo1–S1′	103.4(2)	O11–Mo11–S21	104.4(3)	O21–Mo21–S11	104.2(3)
O2–Mo1–S1′	90.63(11)	O12–Mo11 –S21	90.4(2)	O22–Mo21 –S11	88.8(2)
S1–Mo1–S1′	102.31(7)	S21–Mo11–S11	101.96(11)	S21–Mo21–S11	101.68(10)
O1–Mo1–S2	97.4(2)	O11–Mo11–S12	95.3(3)	O21–Mo21–S22	95.1(3)
O2–Mo1–S2	62.90(11)	O12–Mo11–S12	62.9(2)	O22–Mo21–S22	62.5(2)
N1–Mo1–S2	81.76(14)	N11–Mo11–S12	81.0(2)	N21–Mo21–S22	81.9(2)
S1–Mo1–S2	150.33(7)	S11–Mo11–S12	151.72(11)	S21–Mo21–S22	153.14(12)
S1′–Mo1–S2	86.20(7)	S21–Mo11–S12	86.00(11)	S11–Mo21–S22	86.25(10)
Mo1–S1–Mo1′	75.08(6)	Mo11–S11–Mo21	75.25(9)	Mo11–S21–Mo21	75.34(10)

suitable crystals to prove this structure also by the X-ray diffraction method. The formation of the MoS_2Mo bridge may be explained by the apperance of H_2S produced *in situ* from the molybdenum catalyzed hydrolysis of thiobenzoic acid. The analogous observations have been made also in preparing some other molybdenum(V) complexes with thio-ligands [15–18]. The strong donor ligands such as pyridine or γ-picoline stabilized the dinuclear structures producing complexes **2** and **3**.

The structures of $[Mo_2O_2S_2(OSCC_6H_5)_2(py)_2]$ (**2**) and $[Mo_2O_2S_2(OSCC_6H_5)_2(\gamma\text{-pic})_2]\cdot 2H_2O$ (**3**) are built up of dinuclear complex molecules as shown in Fig. 1. However, while the molecular structure of the **2** has crystallographically imposed two-fold symmetry axis the structure **3** exhibits a pseudo two-fold symmetry. The octahedral coordination about each molybdenum atom within a dimer is considerably distorted with the angles ranging from 76.1(2) to 107.8(2)° in **2** and from 74.4(3) to 108.6(3)° in **3**. The distances between two Mo atoms of 2.822(1) in **2**, and 2.831(1) Å in **3** are indicative of a single Mo–Mo bond [19, 20]. The observed diamagnetism of these complexes suggests a strong metal-metal interactions. In both compounds the two molybdenum atoms are bridged *via* two sulfur atoms with average values for the $Mo–S_{br}$ bond lengths

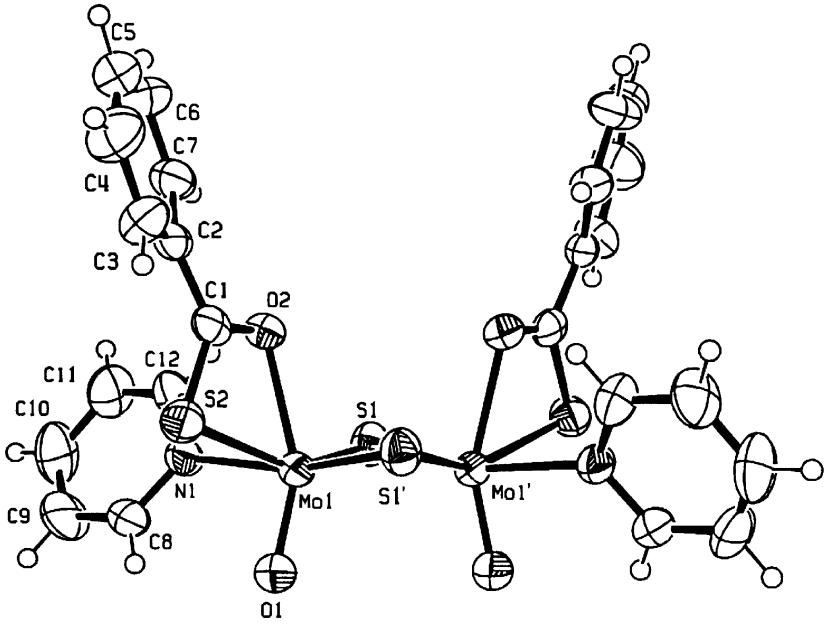

(a)

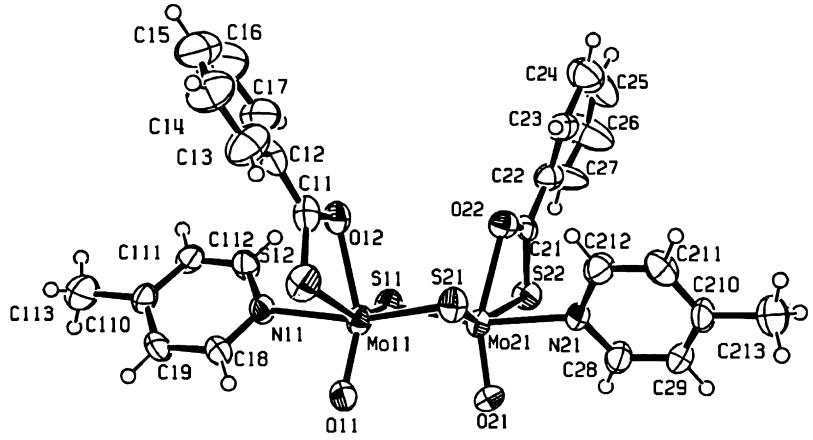

(b)

Fig. 1. ORTEP-3 illustration of the structures of (a) $[Mo_2O_2S_2(OSCC_6H_5)_2(py)_2]$ (**2**) and (b) $[Mo_2O_2S_2(OSCC_6H_5)_2(\gamma\text{-pic})_2]\cdot 2H_2O$ (**3**) showing the atom numbering schemes and thermal ellipsoids (50%) for the atoms. The H atoms are unlabelled.

of 2.316(2) Å in **2** and of 2.315(3) Å in **3**, respectively [17, 21]. The four-membered rings of the Mo_2S_2 bridging core are not planar but folded along the lines connecting two bridging sulfur atoms: the dihedral angles between two SMoS planes are 158.35(0) and 157.2(2)° in **2** and **3**, respectively. The Mo═O bond lengths of 1.685(5), and 1.679(8) and 1.684(8) Å for **2** and **3**, respectively are normal values for such bond to the terminal oxo-oxygen atoms [22]. The Mo–S bond lengths [2.580(2) in (**2**), 2.567(3) and 2.579(3) Å in **3**] as well as the Mo–O bond lengths [2.257(4) in **2**, 2.263(8) and 2.270(7) Å in **3**] from the thiobenzoato ligands are in good agreement with the values found for such bonds in similar molybdenum(V) structures [23–25]. The molybdenum-to-thiobenzoato-oxygen bond lengths are lengthened due to the *trans* influence of the terminal oxo-oxygen atoms. The same applies to the molybdenum-to-thiobenzoato sulfur and molybdenum-to-nitrogen bonds [2.305(5) in **2**, 2.279(9) and 2.272(8) Å in **3**] owing to their *trans* positions to the bridging sulfido-sulfur atoms [26, 27]. Bond lengths and angles within thiobenzoato ligands, pyridine and γ-picoline are within expected values.

Two water molecules in **3** are hydrogen-bonded to each other having O1w...O2w distance amounting to 2.76(1) Å. Otherwise there are no any other than van der Waals interactions between the complex and water molecules.

The IR spectra of all three complexes confirm the presence of C–S group at 937 (complex **1**), 940 (**2**) and 944 cm^{-1}(**3**), as well as of the C–O group at 1445 (complex **1**), 1460 (**2**) and 1462 cm^{-1} (**3**), respectively. The strong apsorption maxima at 974 and 475 (complex **1**), 978 and 469 (**2**), 978 and 465 cm^{-1} (**3**), belong to the Mo–O (terminal) and Mo–S (bridging) stretching frequencies, respectively [8, 17, 28].

Acknowledgements—This research was supported by the Ministry of Science and Technology of the Republic of Croatia (Grant No. 119407).

REFERENCES

1. Stiefel, E. I., *Progr. Inorg. Chem.*, 1977, **22,** 1.
2. Swedo, K. B. and Enemark, J. H., *J. Chem. Educ.*, 1979, **56,** 70.
3. Stiefel, E. I. *et al.*, in *Molybdenum Chemistry of Biological Significance*, ed. W. E. Newton and S. Otsuka, Plenum Press, New York, 1980, p. 279.
4. Stiefel, E. I., in *Molybdenum and Molybdenum-Containing Enzymes*, ed. M. P. Coughlan, Pergamon Press, New York, 1980, p. 41.
5. Hahn, R., Kusthardt, U. and Scherer, W., *Inorg. Chim. Acta.*, 1993, **210,** 177.
6. Massoth, F. E., *Adv. Catal.*, 1978, **87,** 265.
7. Enemark, J. H., in *Nitrogen Fixation*, *The Chemical-Biochemical-Genetic Interface*, ed. A. Müller and W. E. Newton, Plenum Press, New York, 1983, p. 329.
8. Rakowski DuBois, M., *Inorg. Chem.*, 1978, **17,** 2405.
9. Moore, F. W. and Rice, R. E., *Inorg. Chem.*, 1968, **7,** 2510.
10. Kamenar, B., Korpar-Čolig, B. and Penavić, M., *J. Chem. Soc., Dalton Trans.*, 1981, 311.
11. Altomare, A., Burla, M. C., Camalli, M., Cascarano, G., Giacovazzo, C., Guagliardi, A. and Polidori, G., *SIR*92, 1994.
12. Sheldrick, G. M., SHELXL96, *Program for the Solution of Crystal Structure*. University of Gottingen, Germany (1996).
13. Nardelli, M., *Comput. Chem.*, 1983, **7,** 1995.
14. Farrugia, L. J., *ORTEP*-3, Version 1.02β. University of Glasgow, U.K., 1997.
15. Ott, V. R., Swieter, D. S. and Schultz, F. A., *Inorg. Chem.*, 1977, **16,** 2538.
16. Kamenar, B., Korpar-Čolig, B., Cindrić, M., Penavić, M. and Strukan, N., *J. Chem. Soc., Dalton Trans.*, 1992, 2093.
17. Bhattacharyya, R., Chakrabarty, P. K., Ghosh, P. N., Mukherjee, A. K., Podder, D. and Mukherjee, M., *Inorg. Chem.*, 1991, **30,** 3948.
18. Howlader, N. C., Haight, G. P. Jr., Hambley, T. W., Snow, M. R. and Lawrance, G. A., *Inorg. Chem.*, 1984, **23,** 1811.
19. Dulebohn, J. I., Stomatakos, T. C., Ward, D. L. and Nocera, D. C., *Polyhedron*, 1991, **10,** 2813.
20. Mizutani, J. and Imoto, H., Saito, T., *Acta Crystallogr., Sect. C*, 1997, **53,** 47.
21. Schröder, F. A., *Z. Naturforsch.*, 1975, **30b,** 638.
22. Schröder, F. A., *Acta Cryst.*, 1975, **B31,** 2294.
23. Kamenar, B., Korpar-Čolig, B., Penavić, M. and Cindrić, M., *J. Cryst. Spectr. Res.*, 1992, **22,** 391.
24. Alyea, E. C., Ferguson, G., Parvez, M. and Somogyvari, A., *Polyhedron*, 1985, **4,** 783.
25. Coucouvanis, D., Hadjikyriacou, A., Toupadakis, A., Koo, S.-M., Ileperuma, O., Draganjac, M. and Salifoglou, A., *Inorg. Chem.*, 1991, **30,** 754.
26. Kamenar, B., Kaitner, B. and Strukan, N., *Croat. Chem. Acta.*, 1991, **64,** 329.
27. Kamenar, B., Kaitner, B. and Strukan, N., *Vestn. Slov. Kem. Drus.*, 1992, **39,** 357.
28. Holste, G., *Z. Anorg. Allg. Chem.*, 1976, **425,** 57.

Pergamon

PII: S0277–5387(98)00112–0

Polyhedron Vol. 17, No. 19, pp. 3327–3330, 1998
© 1998 Elsevier Science Ltd
All rights reserved. Printed in Great Britain
0277–5387/98 $19.00+0.00

Tungsten(VI) *p–tert–*butylcalix[4]arene diolato complexes. Crystal structure and reactions of [W(*t–*butylcalix)(eg)]

Ari Lehtonen* and Reijo Sillanpää

Department of Chemistry, University of Turku, FIN-20014, Turku, Finland

(Received 23 January 1998; accepted 12 March 1998)

Abstract—Air- and moisture stable tungsten(VI) calixarene complex was prepared from $[W(eg)_3]$ (H_2eg = 1,2–ethanediol) and H_4tbcalix (*p–tert–*butylcalix[4]arene) by a ligand exchange reaction. X-ray structure of [W(tbcalix)(eg)] reveals that tungsten ion is octahedrally surrounded by six oxygen atoms. The reaction of the obtained complex with thionyl chloride or water leads to known dichloro and oxo complexes. © 1998 Elsevier Science Ltd. All rights reserved

INTRODUCTION

Calix[*n*]arenes [1] can provide a polyphenolic binding surface that resembles the surface of inorganic oxide carriers. Metalation of these compounds facilitates to study the chemistry of metal sites bonded on a polyoxo surface and calix[*n*]arenes can be treated as potential organic supports for reactive metal fragments of catalytic utility [2, 3]. Several oxo and chloro tungsten(VI) complexes with calix[4]arenes have been prepared. In the syntheses the starting chemicals are normally $WOCl_4$ or WCl_6 [4]. We have earlier used $[W(eg)_3]$ (**1**) (eg = 1,2–ethanediolato dianion) in the preparation of silica supported tungsten catalysts and also as starting material for new tungsten(VI) complexes [5, 6]. In continuation of this work, we have studied the reaction of **1** with organic polyfunctional OH-donor. The present paper describes synthesis and crystal structure of a new W(VI) calixarene complex [W(tbcalix)(eg)] (**2**) and its conversions to complexes [WO(tbcalix)] (**3**) and $[W(tbcalix)Cl_2]$ (**4**) (tbcalix = tetravalent anion of *p–tert–*butylcalix[4]arene). Complex **4** is known to be suitable starting material to the calixarene supported organotungsten complexes [3].

* Author to whom correspondence should be addressed. Tel: 358-2-3336733; Fax: 358-2-3336700; E-mail: Ari.Lehtonen@utu.fi.

RESULTS AND DISCUSSION

Syntheses

The treatment of the ethanediolato complex **1** with one equivalent of H_4tbcalix in boiling toluene produces complex **2** leads to the formation of intense red coloured solution (Scheme 1). The reaction can be run into an end by distilling out liberated H_2eg, as a toluene azeotrope. Evaporation of the volatiles and crystallisation of the orange–red residue from hexane–CH_2Cl_2 mixture gives crystalline, air-stable complex **2** as a dichloromethane solvate in high yield. Crystallisation from acetonitrile produces an acetonitrile solvate. Complex **2** is stable in moist air and does not react further with other diols to exchange the last eg ligand with a diol. The exchange of the eg ligand in $[W(diol)_2(eg)]$ can be done easily [6].

As the diolato group (eg) in **2** is not very reactive, we tried to remove it in order to get more labile complexes. Several deprotection reactions for alkoxide moiety were tested. To produce the oxo functionality complex **2** was treated with wet ethanol, which is known to hydrolyse comparable trisdiolato complexes, e.g. $[W(eg)(pin)_2]$ (pin = pinacolate dianion) [7].

Complex **2** resist hydrolysis in neutral conditions, but it can be converted to tungstenyl compound by using an acidic solution (Scheme 2). Thus reaction of **2** with aqueous hydrochloride in acetonitrile solution

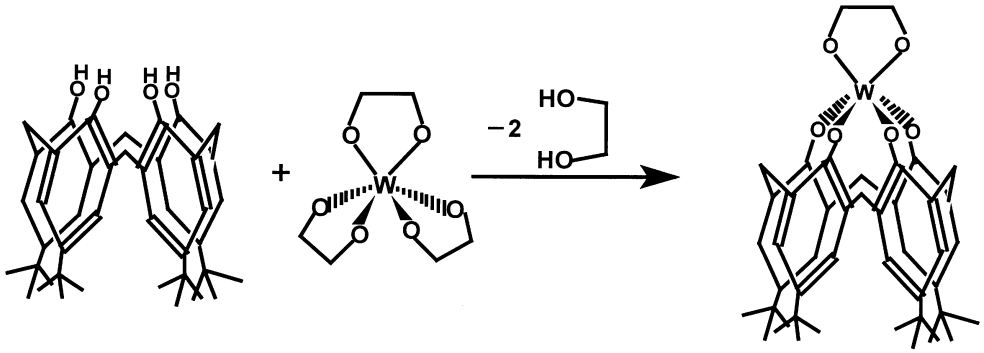

Scheme 1.

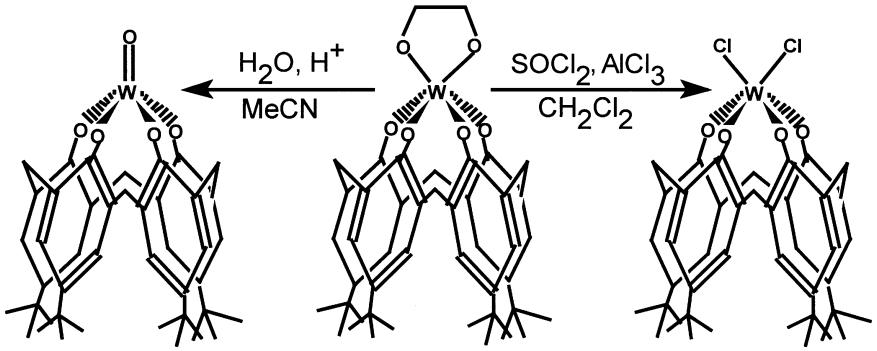

Scheme 2.

leads to the formation of yellow [WO(tbcalix)] **3** in 58% yield.

Complex **2** does not react with typical halide-for-alkoxide substitution reagents ($AlCl_3$, MeCOCl), as reported for comparable cyclohexanediolato complex [8]. It also resists reaction with $SOCl_2$, although ethanediolato ligand in $[W(eg)(pin)_2]$ is easily replaced by this method [9]. However, treatment of **2** (Scheme 2) with excess of thionylchloride in the presence of $AlCl_3$ leads to the displacement of eg ligand and formation of [W(calix[4]arene)Cl_2] **4**. Vigorous reaction indicates that also some decomposition of **2** could happen, but in spite of that complex **4** was isolated in relative high yield (63%).

Crystal structure of ***2***

Complex **2** crystallises as monomeric distorted octahedral tungsten(VI) species with one dichloromethane molecule in the asymmetric unit. The refinements of the data suggest that there is one dichloromethane in the asymmetric unit, but the elemental analysis of the bulk material gives the value 1/2. The dichloromethane molecules are not inside the calixarene cavities but in the empty spaces of the unit cell. The complex unit is described in Fig. 101. The eg ligands are randomly distributed in a 1:1 ratio over W(VI) atoms of the complex **2** in the unit cell, and display two conformations with the torsion angles of 33(3) and $-29(4)^\circ$, respectively. Also two *t*–butyl groups of the calixarene ligand and the dichloromethane molecule have two orientations (a and b). In one *t*–butyl group and CH_2Cl_2 molecule the ratio for the disordered groups is 1:1, but in the other *t*–butyl group the ratios for different rotamers are 58% and 42%.

The tungsten(VI) ion is surrounded by four phenolato oxygen atoms of the calixarene ligand and by two oxygen atoms of chelating diolato ligand. Selected bond parameters are presented in Table 1. The W–O distances vary from 1.860(6) to(W–O(4)) to 1.933(5) (W–O(5)) and are typical for alcoholato and arylato tungsten(VI) complexes. Differences between aliphatic and aromatic W–OR bond distances are quite small. The W–O–C_{aryl} angles vary from 123.6(4) to 179.0(5). The largest angle is associated with the shortest W–O bond distance and *vice versa* as expected [10]. Angular variation of W–O–C_{aryl} angles is most probably caused by W(VI) ion as it modifies the calixarene conformation in order to get a less strained six coordination. This W–O–C_{aryl} angular arrangement indicates for the calixarene a conformation in which

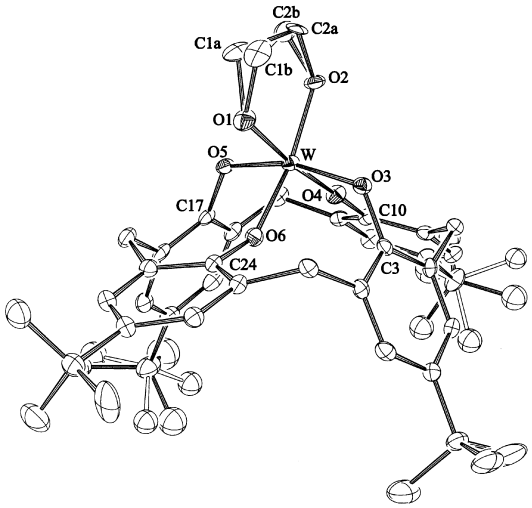

Fig. 1. ORTEP drawing of [W(tbcalix)(eg)]. Thermal ellipsoids are drawn at 20% probability. Hydrogen atoms are omitted for clarity.

Table 1. Selected bond lengths [A] and angles [deg] for 2

W–O(1)	1.884(5)
W–O(2)	1.886(5)
W–O(3)	1.932(5)
W–O(4)	1.860(5)
W–O(5)	1.933(5)
W–O(6)	1.888(5)
O(1)–C(1a)	1.461(13)
O(1)–C(1b)	1.452(13)
O(2)–C(2a)	1.453(14)
O(2)–C(2b)	1.452(14)
O(3)–C(3)	1.378(7)
O(4)–C(10)	1.357(8)
O(5)–C(17)	1.376(8)
O(6)–C(24)	1.350(8)
C(1a)–C(2a)	1.51(2)
C(1b)–C(2b)	1.51(2)
O(1)–W–O(2)	79.8(2)
O(1)–W–O(3)	96.5(2)
O(1)–W–O(4)	173.4(2)
O(1)–W–O(5)	96.0(2)
O(1)–W–O(6)	86.1(2)
O(2)–W–O(3)	97.1(2)
O(2)–W–O(4)	93.6(2)
O(2)–W–O(5)	96.9(2)
O(2)–W–O(6)	165.9(2)
O(3)–W–O(4)	84.3(2)
O(3)–W–O(5)	162.69(17)
O(3)–W–O(6)	84.46(19)
O(4)–W–O(5)	84.6(2)
O(4)–W–O(6)	100.4(2)
O(5)–W–O(6)	84.5(2)
C(1a)–O(1)–W	116.8(11)
C(1b)–O(1)–W	122.4(10)
C(2a)–O(2)–W	121.8(11)
C(2b)–O(2)–W	117.4(12)
C(3)–O(3)–W	123.6(4)
C(10)–O(4)–W	179.0(5)
C(17)–O(5)–W	124.4(4)
C(24)–O(6)–W	145.7(5)

the cavity adopts a half-ellipsoid shape. In this conformation the dihedral angles of the opposite phenyl groups show the values of 52.1(2) and 132.2(2)°.

CONCLUSION

Tungsten(VI) *p–tert*–butylcalix[4]arene complex [W(eg)(tbcalix)] can be prepared by the reaction of $[W(eg)_3]$ with the calixarene ligand. This new complex crystallises as monomeric species, in which the tungsten(VI) ion is surrounded by four phenolato oxygen atoms of calixarene and two alkoxide oxygen atoms of diolato ligand. The reaction of the obtained compound with $SOCl_2$–$AlCl_3$ or water leads to comparable dichloro and oxo complexes.

EXPERIMENTAL

Solvents and reagents were commercial products and used as received. Complex **1** was prepared as described earlier [6]. ^{1}H NMR spectra were measured on a JEOL GSX-400 spectrometer in $CDCl_3$. Elemental analysis were performed by a Perkin-Elmer series II analyser.

Preparation of (**2**)

p–tert–butylcalix[4]arene (320 mg, 0.50 mmol) and $[W(eg)_3]$ (180 mg, 0.50 mmol) were suspended in 50 ml of toluene. The reaction mixture was allowed to reflux overnight, upon which period the colour of the solution turned intense red. The formed H_2eg was removed by azeotropic distillation with toluene. After evaporation of the solvent *in vacuo*, the red residue was dissolved by warming in hexane–CH_2Cl_2 mixture (15 ml + 3 ml) and filtered as hot. The solution was allowed to cool and then kept at −18°C for a week. Red needles (355 mg, 80%) were separated and washed with hexane. The formula of the crystalline material was $[W(tbcalix)(eg)]\cdot 1/2CH_2Cl_2$ as was indicated by X-ray and elemental analysis. (Found: C, 60.20; H, 6.15. $C_{46}H_{56}O_6W\cdot 1/2CH_2Cl_2$ requires C, 59.97 H, 6.17%). NMR (Solvent $CDCl_3$, standard $SiMe_4$): δ_H 7.14 (s, 4 H, ArH), 6.97 (s, 4H, ArH), 5.66 (s, 8 H, CH_2O), 4.55 (d, 4 H, CH_2Ar), 3.28 (d, 4 H, CH_2Ar), 1.28 (s, 18 H, CH_3), 1.12 (s, 18 H, CH_3).

Reaction of (**2**) *with water*

Concentrated, aqueous HCl (1.0 ml) was added to the solution of complex **2** (100 mg, 0.11 mmol) in acetonitrile (20 ml). The colour of the solution changed from dark red to yellow while it was stirred for an

hour. The volatiles were evaporated and the yellow residue was extracted with 20 ml of hot toluene. Cooling the solution yielded complex **3** as yellow microcrystals containing a toluene molecule of crystallisation. The yield was 60 mg, 58%. (Found: C, 65.30; H, 6.55. $C_{51}H_{60}O_5W$ requires C, 65.40 H, 6.45%). NMR (Solvent $CDCl_3$, standard $SiMe_4$): δ_H 7.15 (m, ArH and toluene), 4.55 (d, $ArCH_2$), 3.32 (d, $ArCH_2$), 2.32 (s, CH_3 (toluene)), 1.20 (m, CH_3). The spectrum is identical to that given in reference 4.

Reaction of (**2**) *with* $SOCl_2$ *and* $AlCl_3$

Compound **2** (200 mg, 0.22 mmol) and $AlCl_3$ (30 mg, 0.22 mmol) were dissolved in dichloromethane (10 ml), then $SOCl_2$ (0.10 ml, 1.4 mmol) was quickly added to the solution. The reaction mixture was stirred about 15 min and the colour of the solution changed from orange–red to purple. After volatiles had been removed, the residue was extracted with hot hexane–CH_2Cl_2–mixture (10 + 3 ml) yielding complex **4** as red crystalline solid (125 mg, 63%). (Found: C, 58.65; H, 5.90. $C_{44}H_{52}O_4Cl_2W$ requires C, 58.75 H, 5.85%). NMR (Solvent $CDCl_3$, standard $SiMe_4$): δ_H 7.12 (m, ArH), 4.50 (d, $ArCH_2$), 3.30 (d, $ArCH_2$), 1.20 (m, CH_3). The spectrum is identical to that given in reference 4.

X-ray studies

Single-crystal data collections for **2** were performed at ambient temperature on a Rigaku AFC5S diffractometer using graphite monochromatized Mo K_α radiation ($\lambda = 0.71069$ Å). The unit cell parameters were determined by least-squares refinement of 25 carefully centered reflections. The data (8941 reflections) were collected by ω–2θ technique to a maximum 2θ value of 50°. The data were corrected for Lorentz and polarization effects, decay (−5%) and for absorption (PSI scans, $T_{min} = 0.559$ and $T_{max} = 0.718$). Data reduction and subsequent calculations were performed with *teXsan for Windows* [11].

The structures were solved by direct methods by using the *SIR*92 program [12]. Full-matrix least-squares refinements on F^2 were performed using the *SHELXL*-97 program [13]. Non-hydrogen atoms except the atoms of disordered t–butyl groups and dichloromethane group were refined with anisotropic displacement parameters and the hydrogen atoms were included in the calculations at the fixed distances from their host atoms (riding model). The hydrogen atoms of the dichloromethane molecule were not included. The refinement cycle with 67 restraints and 511 parameters gave a $R1$[a] value 0.048 for 5463 reflections ($F_o > 4\sigma(F_o)$) and a $wR2$[b] value 0.118 for all reflections (8541). The figure is plotted with *ORTEP-3 for Windows* [14].

$$^{a}R1 = \Sigma||F_o| - |F_c||/\Sigma|F_o|,$$

$$^{b}wR2 = \{\Sigma[w(F_o^2 - F_c^2)]/\Sigma[W(F_o^2)^2]\}^{1/2}$$

Crystal Data for $C_{46}H_{56}O_6W \cdot CH_2Cl_2$: $M_r = 973.68$, red needles, crystal size $0.14 \times 0.24 \times 0.26$ mm, monoclinic, space group $P2_1/c$, $a = 12.830(3)$, $b = 24.215(7)$, $c = 16.638(4)$ Å, $\beta = 109.93(2)°$, $V = 4860(2)$ Å^3, $Z = 4$, $\mu(MoK_\alpha) = 2.53$ mm^{-1}.

REFERENCES

1. Gutsche, C.D., *Calixarenes*, Royal Society of Chemistry, Cambridge, 1989.
2. Giannini, L., Solari, E., Zanotti-Gerosa, A., Floriani, C., Chiesi-Villa, A. and Rizzoli, C., *Angew. Chem., Int. Ed. Engl.*, 1996, **35,** 85.
3. Giannini, L., Solari, E., Zanotti-Gerosa, A., Floriani, C., Chiesi-Villa, A. and Rizzoli, C., *Angew. Chem., Int. Ed. Engl.*, 1996, **35,** 2825.
4. Corazza, F., Floriani, C., Chiesi-Villa, A. and Rizzoli, C., *Inorg. Chem.*, 1991, **30,** 4464.
5. Lehtonen, A. and Sillanpää, R., *J. Catal.*, 1996, **161,** 867.
6. Lehtonen, A. and Sillanpää, R., *Polyhedron*, 1994, **13,** 2519.
7. Lehtonen, A. and Sillanpää, R., *J. Chem. Soc., Dalton Trans.*, 1994, 2119.
8. Xu, B., Carroll, P. J. and Swager, T. M., *Angew. Chem., Int. Ed. Engl.*, 1996, **35,** 2094.
9. Lehtonen, A. and Sillanpää, R., *Polyhedron*, 1995, **14,** 455.
10. Kanehisa, N., Kai, Y., Kasai, N., Yasuda, H., Nakayama, Y. and Nakamura, A., *Bull. Chem. Soc. Jpn.*, 1992, **65,** 1197.
11. teXsan for Windows, Structure Analysis Software, Molecular Structure Corporation, Texas 77381, USA, 1997.
12. Altomare, A., Cascarano, G., Giacovazzo, C., Gualiardi, A., Burla, M. C., Polidori, G. and Camalli, M., *J. App. Cryst.*, 1994, **27,** 435.
13. Sheldrick, G. M., SHELXL-97, Program for Crystal Structure Refinement. University of Göttingen, Germany, 1997.
14. Farrugia, L. J., *J. App. Cryst.*, 1997, **30,** 565.

Pergamon

PII: S0277–5387(98)00113–2

Polyhedron Vol. 17, No. 19, pp. 3331–3342, 1998
© 1998 Elsevier Science Ltd
All rights reserved. Printed in Great Britain
0277–5387/98 $19.00+0.00

Equilibrium studies on copper(II)- and iron(III)-monohydroxamates

Etelka Farkas,[a] Emese Kozma,[a] Menyhért Pethő,[b] Kara M. Herlihy[c] and Giovanni Micera[d]

[a]Department of Inorganic and Analytical Chemistry, Lajos Kossuth University, Debrecen, Hungary

[b]Agricultural University, Debrecen, Hungary

[c]Department of Chemistry, University College Dublin, Dublin, Ireland

[d]Dipartimento di Chimica, Universita di Sassari, Sassari, Italy

(Received 19 January 1998; accepted 15 March 1998)

Abstract—Chelating properties exhibited by a series of monohydroxamic acids toward copper(II) and iron(III) ions were studied by pH-metric, spectrophotometric and EPR methods. The ligands can be divided into three groups: **(i)** ligands with alkyl substituents either on the hydroxamate carbon atom (acetohydroxamic acid, Aha; propanohydroxamic acid, Pha; and hexanohydroxamic acid, Hha) or on both the carbon and nitrogen atoms (N-methyl-acetohydroxamic acid, MAha; N-isopropyl-acetohydroxamic acid, iPAha) **(ii)** ligands with aryl substituents (benzohydroxamic acid, Bha; N-phenyl-acetohydroxamic acid, PhAha; and N-phenyl-benzohydroxamic acid, PhBha); **(iii)** cyclic derivatives (the natural 2,4-dihydroxy-2H-1,4-benzoxazin-3-(4H)-on-glucoside, DIBOA-gl; and 2-hydroxypyridine-N-oxide,PYRha).

In addition to the complexes with the well-known hydroxamate type chelate(s), 1:2 species containing one or both of the coordinated ligands in hydroximato (R_C-$CONO^{2-}$) form, have been found in the copper(II)-Aha and copper(II)-Bha systems. Complex formation with iron(III) starts at a very acidic pH and in the most systems, if the ligand excess is high enough, the 1:3 species solely exists in the pH range ca. 4–8. Hydroxo complexes are generally formed above pH 8–8.5. However, in the cases of iron(III)-iPAha or -Hha, where the ligands have quite large bulky groups, the hydrolysis starts at somewhat lower pH if the metal to ligand ratios are below 1:5 and precipitation starts to form in iron(III)-DIBOA-gl system at ca. pH 5–5.5. In all systems, the stability constants were determined only for the complexes formed below hydrolytic regions. Evaluation of calculated stability constants show that they are determined by a combination of different substituent effects (electronic, resonance and steric effects). The most significant effects are due to substituents on the nitrogen atom in the hydroxamate moieties. The phenyl ring on carbon atom results in somewhat higher stabilities of the complexes. © 1998 Elsevier Science Ltd. All rights reserved

Keywords: Cu(II)complexes; Fe(III)complexes; hydroxamic acids; EPR; pH-metry; spectrophotometry.

The hydroxamic acid group is generally present in natural compounds and for example often is the specific iron(III) chelating moiety in microbial siderophores [1–3]. Special cyclic monohydroxamic acids are synthesized by several types of plants [4, 5] first of all to inhibit plant pathogens [4], but also for metal ion uptake from soil as recently suggested [5]. Moreover, hydroxamic acids have a wide spectrum of activities in all types of biological systems [1, 6]. The relationship between the biological effects and the strong chelating ability of hydroxamic acids is in no doubt. In spite of this, equilibrium results for metal complexes formed with natural cyclic monohydroxamic acids are extremely rare [7, 8]. The main problem is the decomposition of these types of compounds in solution and precipitation occurring in presence of metal ions e.g. copper(II) [8].

Some synthetic monohydroxamic acids (first of all acetohydroxamic acid), have already been studied [9–16], as useful analytical reagents for a range of metal ions [9] and primarily as models of iron(III) binding siderophores. Stability constants determined for 1:1

iron(III)-monohydroxamate complexes showed systematic, parallel changes with the electron donor or acceptor ability of R_C and especially R_N substituents [10, 11]. The R_N and R_C substituents can also modify the cis/trans (Z/E) ratio as was found for a series of monohydroxamic acids [17, 18]. As the required conformation for the formation of a normal (O,O) chelate is cis(Z), correlation between the Z/E ratio and the stability of the chelate (both thermodynamic and kinetic) can be expected.

Very few stability constants have been published for iron(III)-monohydroxamato 1:2, 1:3 species [13, 19–21].

Due to the poor solubility of many copper(II)-monohydroxamate complexes, the equilibrium data in these cases are even fewer [16, 17].

We have performed equilibrium studies on a number of iron(III)- and a couple of copper(II)-monohydroxamate systems using pH-metric. UV-VIS spectrophotometric and EPR techniques.

EXPERIMENTAL

Chemicals

Acetohydroxamic acid (Aha), benzohydroxamic acid (Bha), 2-hydroxypyridine-*N*-oxide (PYRha) and *N*-phenyl-benzohydroxamic acid (PhBha) were pure commercially available chemicals (Aldrich or Sigma). The propanohydroxamic acid (Pha), hexanohydroxamic acid (Hha), *N*-phenyl-acetohydroxamic acid (PhAha), *N*-methyl-acetohydroxamic acid (MAha) and *N*-isopropyl-acetohydroxamic acid (iPAha) were prepared by standard procedures from the corresponding carboxylic esters and hydroxylamine [22]. The isolation of 2,4-dihydroxy-2H-1,4-benzoxazin-3-(4H)-on-glucoside (DIBOA-gl) was carried out as described previously [5]. The glucoside derivative was found to be stable in solution. The purity of the ligands and the concentrations of the ligand stock solutions were determined by Gran's method [23].

The metal ion stock solutions were prepared from $CuCl_2 \cdot 2H_2O$ and $FeCl_3 \cdot 6H_2O$ (Reanal). To prevent hydrolysis of the metal ion, the iron(III) stock solution contained HCl in known concentration ($\sim 0.1\,mol/dm^3$). Concentrations of the metal ion stock solutions were determined gravimetrically via precipitation of the quinolin-8-olate. $CuSO_4 \cdot 5H_2O$ was used to prepare $Cu(Bha)_2$ and $Cu(PhBha)_2$.

Potentiometric and spectroscopic studies

The pH-metric and spectrophotometric measurements were carried out at an ionic strength of $0.2\,mol/dm^3$ (KCl). Carbonate-free KOH solutions of known concentrations (ca. $0.2\,mol/dm^3$) were used as titrant.

The pH-metric titrations were performed throughout the approximate pH range 2.0–10.0, or below precipitation, on samples of 5.00 or $10.00\,cm^3$. The ligand concentration was varied in the range $6 \cdot 10^{-3} - 3 \cdot 10^{-3}\,mol/dm^3$. The metal-ligand ratios were 1:1–1:10. Measurements were made with samples at four or five different ratios. As a result of the very poor solubility of the $Cu(Bha)_2$ complex in water, the stability constants for copper(II)-Bha complexes were determined in mixed solvents: (water-methanol, water-DMSO 50–50%(m/m)). For comparison, the copper(II)-Aha was also studied in these mixed solvents. The analytical concentrations and ratios were the same as for the other systems in aqueous solutions. The pH-metric measurements were carried out with a Radiometer pHM 84 instrument equipped with CMAWL/5 Russel combined electrode. The titrant was added from an ABU 13 autoburette. The electrode system was calibrated by the method of Irving et al [24]. so that the pH-meter readings could be converted into hydrogen ion concentration. The calibration and measurements in mixed solvents were performed by a known method [25].

The UV-visible measurements for the iron(III)-monohydroxamate systems were carried out in two sets. Individual samples were prepared in the first series, in which the $0.2\,mol/dm^3$ KCl was replaced by HCl in some part or completely. The pH values, varying in the range 0.7–1.3, were calculated from HCl contents. In the second set, titrations were made with samples containing the iron(III) ion in $5 \cdot 10^{-4}\,mol/dm^3$. The metal ion to ligand ratios were 1:5 and 1:10, the pH was varied in the range 1.7–8.5 (-9.0) and spectra were recorded at 10–15 different pH values. A HP 8453 spectrophotometer was used to record the spectra in the region 300–600 nm. The spectra for the copper(II)-DIBOA-gl system were collected in the region 200–600 nm at a $5 \cdot 10^{-4}\,mol/dm^3$ copper(II)-concentration and a metal to ligand ratio of 1:4.

Both the pH-metric and spectrophotometric results were used to find the stoichiometry of the species and to calculate the stability constants. Calculations were not performed for the pH-regions where the experimental findings showed the possibility of hydrolysis (continuous decrease of the pH or formation of precipitate). The calculations were made with the PSEQUAD computer program [26] using literature data for the iron(III) hydroxo complexes [27]. Volumes of titrant were fitted in the case of pH-metric data and absorbance values of spectrophotometric titration curves. Accepted fittings were below 1.10^{-2} in the former cases and below ca. 2.10^{-2} in the latter ones.

X-band EPR spectra (9.15 GHz) were recorded at 140 K with varying pH and ligand to metal molar ratios, using a Varian E-9 spectrometer. As usual, a few drops of DMSO was used to ensure good glass formation in frozen solutions. DPPH was used as a standard field marker.

Syntheses of Cu(Bha)$_2$ and Cu(PhBha)$_2$ for EPR measurements

The Cu(II) complexes of Bha and PhBha acids were prepared by adding $1 \cdot 10^{-3}$ moles of ligand to 25 cm^3 of an aqueous solution containing $5 \cdot 10^{-4}$ mole of $CuSO_4 \cdot 5H_2O$ and adjusting the pH to 5–6. Precipitates were immediately obtained which, after filtration, washing with water and then with EtOH and drying under a nitrogen stream, exhibited analytical data consistent with the formula $Cu(A)_2$, where A is the monoanionic form of the ligand. *Anal.*[Cu(Bha)$_2$]: Calcd.: for $CuC_{14}H_{12}N_2O_4$: C, 50.07; H, 3.60; N, 8.34; Found: C, 50.4; H, 3.7; N, 8.2%; Residue from TG analysis (CuO): Calcd.: 23.69; Found: 23.5% [Cu(PhBha)$_2$]: Calcd.: for $CuC_{26}H_{20}N_2O_4$ C, 63.99; H, 4.13; N, 5.74; Found: C, 64.0; H, 4.3; N, 5.7%. Residue from TG analysis (CuO): Calcd.: 16.29; Found: 16.0%. Microanalyses (C, H, and N) were performed using a Perkin-Elmer 240B elemental analyser. Thermogravimetric data were obtained with a Perkin-Elmer TGS-2 apparatus in a nitrogen atmosphere.

RESULTS AND DISCUSSION

Acidity of the ligands

These ligands (formulas shown in Scheme 1) can each release one proton in the measurable pH-range. The pK_{HA} values measured by pH-metry are listed in Table 1. Due to the measurable decomposition of PhBha in solution during the pH-metric titration period, Table 1 does not contain a value for this ligand. The values in Table 1 are consistent with hydroxamic acid acidity in general and they are also in good agreement with the related literature data [10, 11, 13–16, 20]. Evaluation of the effects of C- and N-substituents on the acidity of the hydroxamic acid group leads to the conclusion that the pK_{HA} increases slightly in the series Aha < Pha < HhA and is significantly lower for Bha. This is probably due to the increased electron donating effect of alkyl chain in the above series and electron withdrawing effect of the phenyl moiety in Bha. The differences in the electronic effects result in more definite changes in the acidity of secondary hydroxamic acids. As expected, there is a significant increase in the acidity of the hydroxamic acid moiety if the C–N bond is involved in a delocalised ring-system [12, 13]. The OH in the 'hydroxamic acid like' PYRha is the most acidic.

The pK_{HA} values determined in 50–50% (m/m) methanol-water or DMSO-water solvent mixtures for Bha and Aha are 9.32(1), 9.64(1) as well as 9.93(1), 10.57(1), respectively. The study of solvent effects was beyond the scope of this work.

Copper(II) complexes

Precipitation which occurs quite frequently in copper(II)-hydroxamic acid systems was found in some of our systems too. It occurs at pH ca. 2.5 in the aqueous solution of copper(II)-Bha. The precipitate, known as Cu(Bha)$_2$ both from former work [9] and from the synthetic results of this work, starts to dissolve at ca. pH 9 consuming two equivalents of base up to pH ~ 11. The precipitate is also formed in mixed solvents, at pH ca. 4–5 and 6–7 in MeOH-H_2O and DMSO-H_2O, respectively. We could not calculate any stability constant in aqueous solution but values could be calculated for $[CuA]^+$ and $[CuA_2]$ in mixed solvents, as can be seen in Table 2. Due to the slow decomposition of PhBha in solution (see former section) stability constants for copper(II)-PhBha have not been calculated. In the case of Aha, if the copper(II):Aha ratio is at least 1:4, precipitation occurs at ca. or above pH 9. The model involving $[CuA]^+$, $[CuA_2]$ and $[CuA_2H_{-1}]^-$ yields the best fit of the experimental results. The calculated data are in good agreement with those formerly published for $[CuA]^+$ and $[CuA_2]$ [20]. Representative concentration distribution curves are shown in Fig. 1. As model data, the stability constants for copper(II)-Aha complexes formed in mixed solvents were also determined. Precipitation occured at pH 5–5.5 in the copper(II)-DIBOA-gl system even at the highest ligand excess. Below this pH, the formation of $[CuA]^+$ and $[CuAH_{-1}]$ was found. The calculated stability constants for these species and also for $[CuA]^+$ and $[CuA_2]$ complexes formed in copper(II)-PYRha system are also shown in Table 2.

For copper(II) complexes, EPR measurements were also carried out to obtain information about the complexes formed with Aha, Bha or with models without NH proton (PYRha and PhBha). In the case of Bha the complexes formed following dissolution of the precipitate, Cu(Bha)$_2$ were studied. As representative example, X-band EPR spectra recorded for copper(II)-Aha system at different pH values, at 140 K are shown in Fig. 2. The parameters calculated from the EPR spectra are summarized in Table 3.

Based on the pH-metric and EPR results the following conclusions can be done: Varying pH and metal-to-ligand molar ratios, a number of species were detected in the copper(II)-Aha system. Their distinctive EPR parameters as well as their formation ranges provide information on the complexation behaviour in this system. Based on the sequence of EPR spectra (see Fig. 2) mononuclear species taking part in the complex formation equilibria can be identified. Complexation starts at pH somewhat below 3, with the formation of the mono-chelated complex ($[CuA]^+$) containing the ligand in the monoanionic form. This species is in equilibrium with aqua ion up to pH ca. 4–5, depending on molar ratios. The increase of ligand excess allows the detection of the corresponding bis-chelated species, $[CuA_2]$. (The relating EPR parameters are in good agreement with those for other bis-hydroxamato species [28]). This species is a single component in the system from pH 5 to 9.5 if the ligand-to-metal molar ratio is 10:1 (see Fig. 2). Concentration distribution curves in Fig. 1 show the

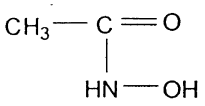

Aha

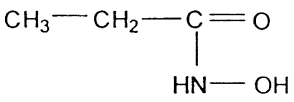

Pha

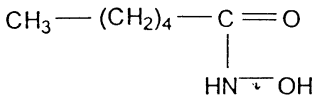

Hha

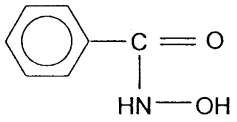

Bha

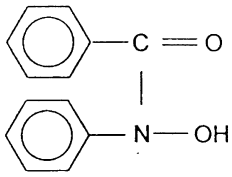

PhBha

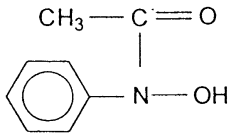

PhAha

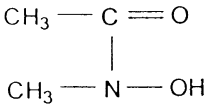

MAha

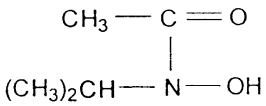

iPAha

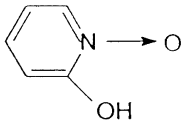

PYRha

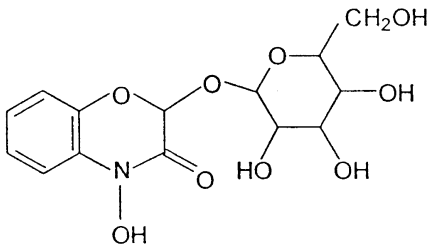

DIBOA-gl

Scheme 1.

Table 1. Acid dissociation constants (pK_{HA}) for the different monohydroxamic acids $t = 25°C$; $I = 0.2\,mol/dm^3$ (KCl)

Ligand	Aha	Pha	Hha	MAha	iPAha	PhAha	Bha	PYRha	DIBOA
pK_{HA}	9.27(1)	9.33(1)	9.36(1)	8.70(1)	9.26(1)	8.47(1)	8.69(1)	5.79(1)	6.85(1)

Table 2. Logarithmic stability constants for the Cu^{2+} complexes of some monohydroxamic acids $\beta_{pqr} = \frac{[Cu_pA_qH_r]}{[Cu]^p[A]^q[H]^r}$; $I = 0.2$ M (KCl); $t = 25°C$

A	Species	Solvent		
		H_2O	H_2O–CH_3OH50–50%(m/m)	H_2O–DMSO50–50%(m/m)
Aha	$[CuA]^+$	7.89(1)	9.00(2)	9.19(2)
	$[CuA_2]$	14.06(1)	15.89(7)	16.48(3)
	$[CuA_2H_{-1}]^-$	4.44(3)		
Bha	$[CuA]^+$	–	8.62(1)	8.55(1)
	$[CuA_2]$	–	15.33(3)	15.22(2)
PYRha	$[CuA]^+$	6.84(5)		
	$[CuA_2]$	12.46(3)		
DIBOA-gl	$[CuA]^+$	4.95(5)		
	$[CuAH_{-1}]$	−0.01(4)		

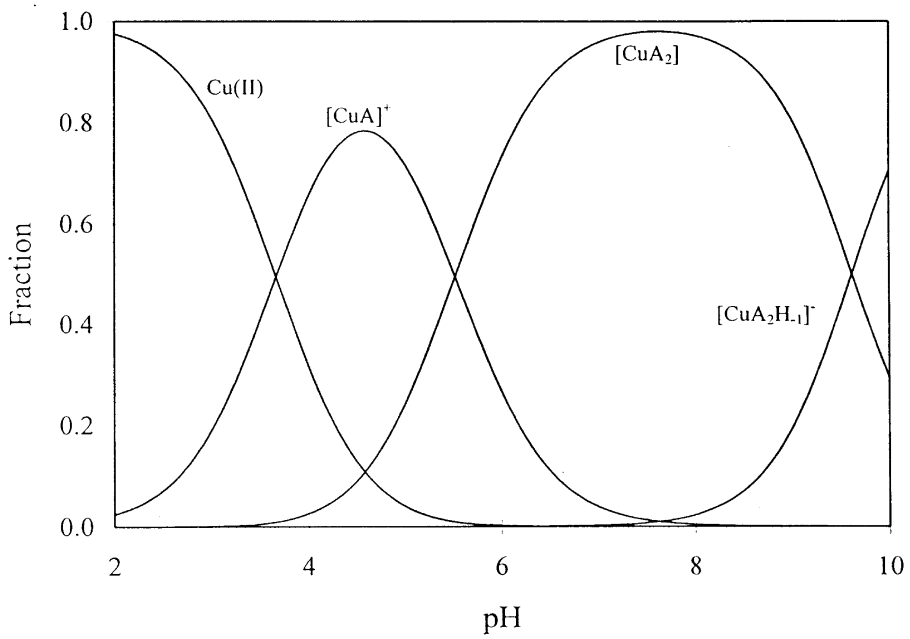

Fig. 1. Concentration distribution curves for the complexes formed in Cu(II)-Aha system; $C_{Cu(II)} = 1.5 \cdot 10^{-3}$ mol/dm^3; $C_{Aha} = 6 \cdot 10^{-3}$ mol/dm^3.

dominance of the $[CuA_2]$ also at lower ligand-to-metal molar ratio (4:1). Additional complexes were detected in copper(II)-Aha system by EPR at high pH. In two of these species, the change in the $g_\parallel$ and $A_\parallel$ parameters suggests the stronger coordination of the ligands (see *f* and *g* spectra in Fig. 2). It is in accord with further stepwise deprotonation processes of the ligand molecules. As a consequence, the bis-hydroxamato(1-) complex, $[CuA_2]$ is transformed into the bis-hydroximato(-2) species, $[CuA_2H_{-2}]^{2-}$ yielding $[CuA_2H_{-1}]^-$ as the intermediate species with mixed hydroximato-hydroxamato coordination (the most probable bonding modes are shown in Scheme 2). Hydrolysis starts at higher pH values to yield mixed hydroxo species (the change in $g_\parallel$ and $A_\parallel$ values support this), presumably a monohydroxo derivative, where only one ligand molecule, in the hydroximate(2-) form, is bound to the metal species (spectrum *h* in Fig. 2). In this pH region the decrease in linewidth of EPR signals was found what is also supportive of a diminished number of nitrogen atoms in metal coordination. As it is known, pH-metry can not differentiate between deprotonated and mixed hydroxo species. Taking into account the quite low ligand

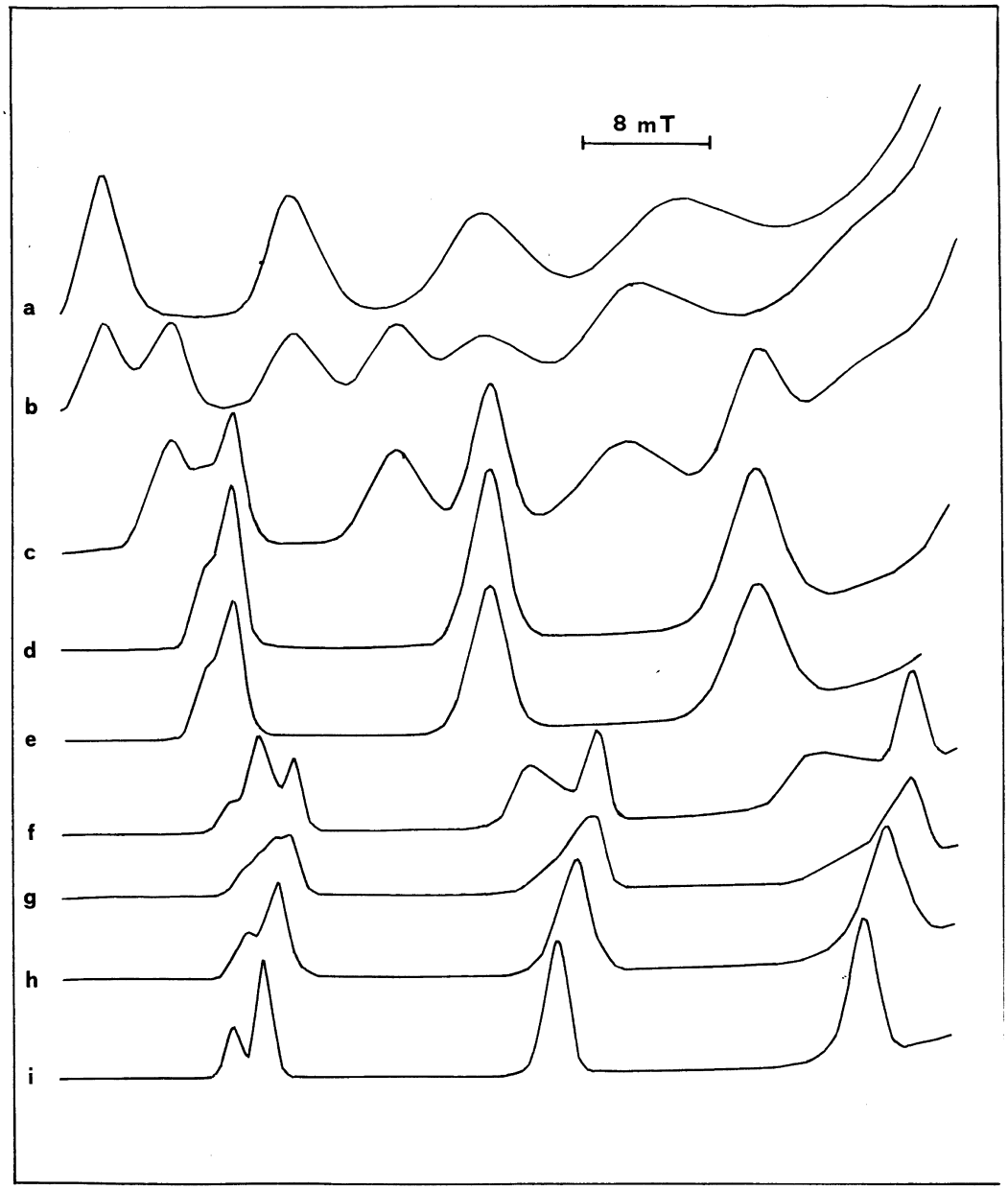

Fig. 2. X-band EPR spectra recorded at 140 K on aqueous solutions of copper(II)-Aha at a ligand-to-metal molar ratio of 10:1 with varying pH: (a) 2.70; (b) 3.35; (c) 4.55; (d) 6.80; (e) 9.55; (f) 11.10; (g) 12.30; (h) 13.35; $C_{Cu} = 5 \cdot 10^{-3}$ mol/dm^3.

excess, the $[CuA_2H_{-1}]^-$ in Fig. 1 represents in that case most probably a mixture of deprotonated and mixed hydroxo species.

The interaction between Cu(II) and Bha in aqueous solution leads to the precipitation of an insoluble complex at pH values as low as 2.5. The compound, after the purification procedure described in the experimental section, satisfactorily analysed as $[Cu(Bha)_2]$, as found previously with the VO^{2+} ion [29], indicating the presence of two benzohydroxamate(1-) anions bound to the metal. A complex with analogous composition was obtained in a former paper [9]. The solid compound completely redissolves in aqueous solution at pH values as high as 11. (As it was stated above, exactly two equivalents of base was necessary to do this.) The redissolution allows the identification of a single species which has EPR parameters quite comparable with those of $[CuA_2H_{-2}]^{2-}$ formed with Aha. However, in case of Aha this species is formed at somewhat higher pH. This result, may supports the suggestion that the second deprotonation process for the Bha is more favoured than in the case of the Aha. The same trend was previously found with the VO(IV) ion [29]. A further indication of the rather high stab-

Table 3. Anisotropic EPR Data for the Complexes

Ligand	Solvent	Complex	$g_{\parallel}$	$A_{\parallel}$
Aha	water	$[CuA]^{+}$	2.340	170
	water	$[CuA_2]$	2.282	182
	water	$[CuA_2H_{-1}]^{-}$	2.258	192
	water	$[CuA_2H_{-2}]^{2-}$	2.219	207
	water	mixed hydroxo species	2.230	204
Bha	water	$[CuA_2H_{-2}]^{2-}$	2.218	207
PYRha	water	$[CuA]^{+}$	2.328	163
	water	$[CuA_2]$	2.288	182
	water	mixed hydroxo species	2.272	186
	dioxane	$[CuA_2]$	2.290	188
	MeOH	$[CuA_2]$	2.285	180
PhBha	dioxane	$[CuA]^{+}$	2.323	169
	dioxane	$[CuA_2]$	2.267	190
	MeOH	$[CuA_2]$	2.271	184

$A_{\parallel}$ values are given in 10^{-4} units.

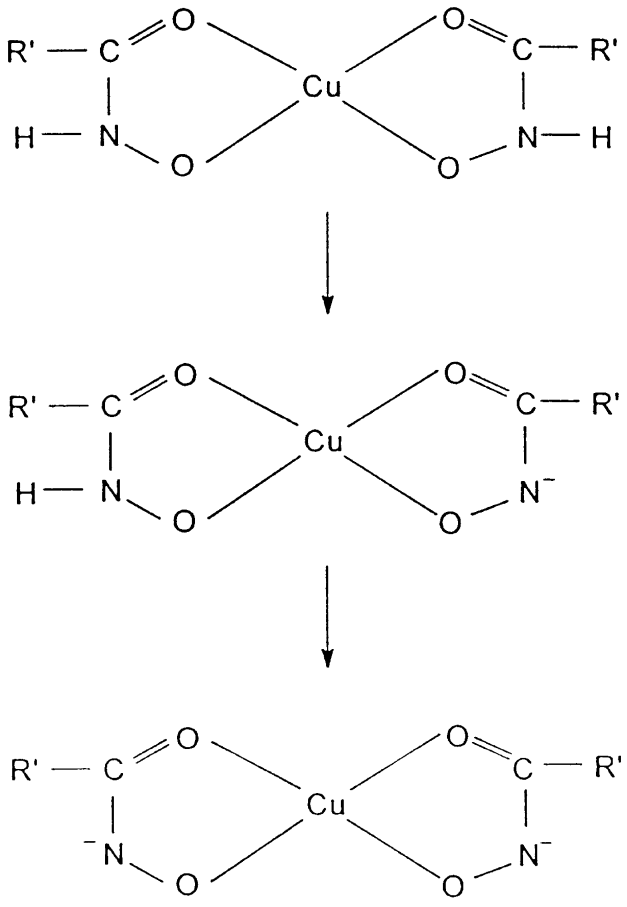

Scheme 2.

ility of the complex $[CuA_2H_{-2}]^{2-}$ formed by Bha is the absence of any hydrolytic processes, at least up to pH 13.

As the EPR results show, the behaviour of PYRha and PhBha, which do not contain dissociable protons on their nitrogen atoms, is remarkably different from that of simple hydroxamic acid molecules. With the hydroxamic-like ligand PYRha, the complexation starts with formation of a species analogous to [CuA], which is favoured to a larger extent if the ligand excess is lowered to 1:1. As for Aha and Bha, the complexation process is associated with a single proton dissociation. The bis-chelated complex, $[CuA_2]$ is formed with increasing ligand to metal ratio, with maximum formation being detected over the pH range 7–10. A solid compound also separates from solution in this case. It can not be satisfactorily characterized by analytical data, most likely because of some ligand decomposition reaction which occurs during the purification procedure. However, its redissolution, with increasing amount of base, yields EPR spectra characteristic only for a mixed hydroxo species and then the tetrahydroxocuprate(II) ion, demonstrating that no more acidic protons are available on the ligand. The different chelating mode of the PYRha, as compared to Aha and Bha, is reflected also by different parameters relating to the mixed hydroxo species formed with Aha or Bha and PYRha.

The solid compound may also be dissolved in MeOH or 1,4-dioxane, where spectral parameters similar to those measured for $[CuA_2]$ in aqueous solution are observed. Also, some effects due to solvent coordination are evident in these systems. Actually, the higher $A_{\parallel}$ value measured in dioxane suggests a more pronounced tetragonal elongation at the metal site, as a consequence of weaker axial binding of solvent molecules.

The ligand PhBha is sparingly soluble in water. However, a solid complex with formula $[Cu(PhBha)_2]$ may be obtained on stirring aqueous Cu^{2+} solutions in the presence of the undissolved ligand at pH ca. 5. The solid compound may be dissolved in MeOH or 1,4-dioxane. In the latter solvent, an equilibrium mixture of $[CuA]^+$ and $[CuA_2]$ can be observed by EPR. Complete transformation of $[CuA]^+$ into $[CuA_2]$ is achieved by adding an excess of ligand indicating their nature of mono- and bis-chelated species respectively. Again, the comparison of the EPR parameters measured for $[CuA_2]$ in MeOH indicates that a stronger axial interaction occurs with this solvent.

Iron(III) complexes

It is general that hydroxamic acids, compared to their pK_{HA} values, form very stable iron(III) complexes. Consequently, the determination of the formation constants is impossible only by pH-metry. Fortunately, the iron(III)hydroxamate interaction is characterized by a charge transfer absorption band. Each added hydroxamate group results in a characteristic change both in λ_{max} and the absorption intensities [13]. The 1:1 complexes have spectra with λ_{max} of ca. 510 nm ($E^{\circ} \sim 1000\ mol^{-1}cm^{-1}$), the 1:2 ones display λ_{max} of ca. 470 nm ($E^{\circ} \sim 1800\ mol^{-1}cm^{-1}$) and the 1:3 complexes show λ_{max} of 420–430 nm ($E^{\circ} \sim 2500$–$2700\ mol^{-1}cm^{-1}$).

Based on this possibility, pH-metric studies were complemented with uv-visible spectrophotometric measurements. The pH-metric titrations were performed above pH 2. Precipitation occurred with Pyrha at already pH 2 and with DIBOA-glucoside at pH ca. 5. In the former case the iron(III)-PYRha complex(es) can be assumed to precipitate whereas most probably, hydrolysis of the metal ion occurs in the latter case.

In the case of spectrophotometry two sets of measurements were made. In the first set, the iron(III)-ligand ratio was maintained at the same value in the different samples and the pH was changed by replacing the KCl electrolyte by HCl partly or completely. From the spectra, those recorded for iron(III)-Hha are shown, as representative examples, in Fig. 3. As can be seen in Fig. 3a, only one type of iron(III)-Hha complex exists in measurable concentration in the pH-range 0.7–1.3. Its amount increases with increasing pH. The λ_{max} value (ca. 510 nm) is characteristic of the 1:1 species. (A minimal shift in λ_{max} at pH ~ 1.3 towards a lower wavelength stars in the case of iron(III)-iPAha indicating the appearance of some 1:2 species already under these conditions.)

In the second set of spectrophotometric measurements, titrations were performed. Figures 3b shows some of the spectra recorded at different pH values for iron(III)-Hha system. The Figure shows significant shifts in λ_{max} values and increase in absorbances as well as two well-defined isosbestic points each; at λ_{max} ca. 530 nm at lower pH and at λ_{max} ca. 470 nm at higher pH. This supports the formation of three species in the pH-ranges shown in Figure 3b.

Using all the spectrophotometric and pH-metric experimental results we calculated the formation constants for the different species formed in the systems below hydrolytic regions (in the most systems up to ca. pH 8.5). The results are summarized in Table 4. Representative concentration distribution curves for complexes formed in iron(III)-iPAha system in the pH range 1–7 are shown on Fig. 4.

Taking into account the differences in conditions, the stability constants formerly determined for iron(III)-Aha, -MAha, -Bha and -PhAha (in the cases of latter two ligands only for 1:1 species) are in good agreement with our data [10, 13, 16, 20, 21]. The ligands involved in these studies differ in many respects. Some of them are primary hydroxamic acids containing alkyl or aryl R_C substituents, others also have R_N substituents and there are cyclic derivatives too. The above differences sometimes result in significant differnces of pK_{HA} values (Table 1). The correlation between the basicity of hydroxamate moieties and the stability of their metal complexes can be evalu-

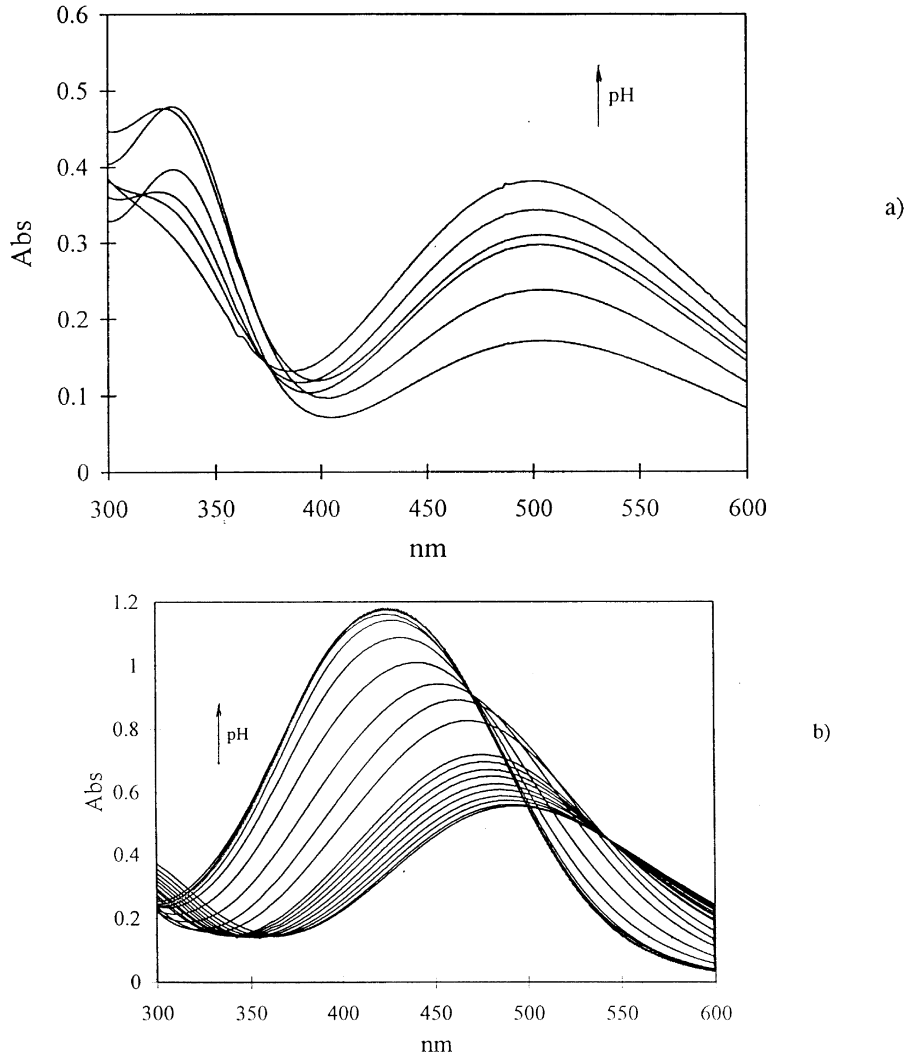

Fig. 3. (a) UV-Vis spectra recorded for Fe(III)-Hha samples at pH = (1)0.70, (2)0.70, (3)0.82, (4)0.82, (5)1.00 and (6)1.30 from the smallest to the largest absorbance at 430 nm. $C_{Fe} = 5 \cdot 10^{-4}$ mol/dm^3; $C_{Hha} = 1 \cdot 10^{-3}$ mol/dm^3 in the cases of (1), (3), (5), (6) and $2 \cdot 10^{-3}$ mol/dm^3 in the (2), (4). (b) UV-Vis spectra recorded for Fe(III)-Hha samples at pH = 1.62, 1.70, 1.80, 1.90, 2.00, 2.10, 2.21, 2.30, 2.41, 2.50, 2.99, 3.52, 4.02, 4.50, 4.99, 5.51, 6.22, 6.83, 7.22, 7.60, 8.01 and 8.51 from the smallest to the largest absorbance at 430 nm. $C_{Fe} = 5 \cdot 10^{-4}$ mol/dm^3; $C_{Hha} = 3 \cdot 10^{-3}$ mol/dm^3.

Table 4. Logarithmic stability constants for the Fe(III) complexes of monohydroxamic acids $\beta_{pqr} = \dfrac{[Fe_pA_qH_r]}{[Fe]^p[A]^q[H]^r}$; $I = 0.2$ M (KCl); $t = 25°C$

A	$[FeA]^{2+}$	$[FeA_2]^+$	$[FeA_3]$
Aha	11.09(1)	20.69(2)	28.80(5)
Pha	11.16(1)	20.74(1)	28.44(8)
Hha	11.18(1)	20.65(3)	28.40(1)
Bha	11.08(2)	21.20(8)	28.80(1)
PhAha	10.92(5)	20.12(4)	28.87(3)
MAha	11.85(1)	21.58(1)	29.36(2)
iPAha	12.04(1)	21.94(1)	29.64(1)
DIBOA-gl	7.41(6)	13.52(5)	$[FeA_2H_{-1}]$: 8.80(5)

ated e.g. by the adequate competition reactions. From these, the values relating to the reaction $M + HA \rightleftharpoons MA + H$ are shown in Table 5. Table 5 also contains the data for the copper(II) complexes. (The higher value for the above equilibrium, means more favoured complex formation.) From the data in Table 5, it can be concluded that the superposition of many substituent effects can modify the stability of chelates formed with copper(II) and iron(III). As the data in Table 5 shows, the position of the substituent in the molecule seems to be one of the main effects, as was found formerly also by Crumbliss [10–13]. This dominance originates from the more significant effect of R_N on delocalisation of the lone electron pair of N into the C–N bond (see below). As is evident, delocalisation of the N atom lone pair inreases the electron density on the carbonyl oxygen thus increasing the

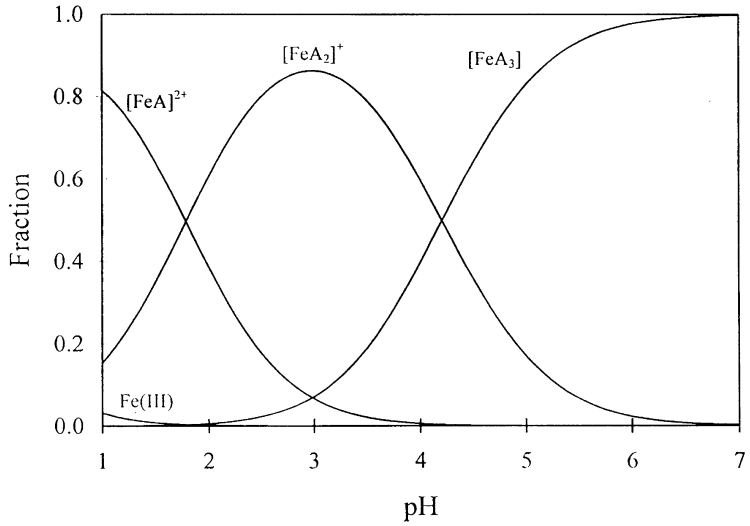

Fig. 4. Concentration distribution curves for the complexes formed in Fe(III)-iPAha system $C_{Fe(III)} = 1.5 \cdot 10^{-3}$ mol/dm^3; $C_{iPAha} = 6 \cdot 10^{-3}$ mol/dm^3.

Table 5. Logarithmic equilibrium constants for the process $M + AH \rightleftharpoons MA + H$ in the different systems

M	A	Solvent		
		H_2O	H_2O-CH_3OH50–50%(m/m)	H_2O-DMSO50–50%(m/m)
Cu^{2+}	Aha	−1.38	−0.93	−1.38
	Bha	–	−0.70	−1.09
	PYRha	1.05	–	–
	DIBOA-gl	−1.90		
Fe^{3+}	Aha	1.82		
	Pha	1.83		
	Hha	1.82		
	Bha	2.39		
	PhAha	2.45		
	MAha	3.15		
	iPAha	2.78		
	DIBOA-gl	0.56		

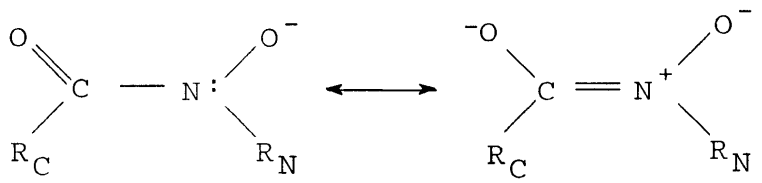

stability of the metal chelate. The correlation of the data is very good in the case of iron(III) 1:1 complexes formed with Aha, Pha, Hha. However, if we try to calculate the adequate constants for their 1:2 and 1:3 species ($MA + HA \rightleftharpoons MA_2 + H$ and $MA_2 + HA \rightleftharpoons MA_3 + H$ reactions) we do not find such a good correlation what is most probably due to steric effects. This assumption is supported by the experimental finding that the quite bulky R_C substituent in the Hha caused precipitation in the iron(III)-Hha system at

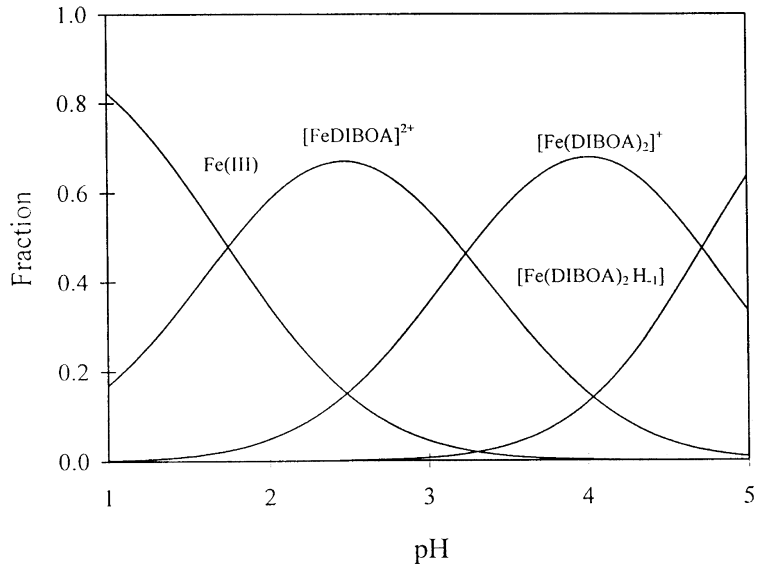

Fig. 5.

around neutral pH if the ligand excess was not larger than 1:5. The steric hindrance of the iso-propyl substituent may exceed its electron donating effect resulting in the lower stability of the iron(III) 1:1 complex formed with iPAha compared to that with MAha.

Superposition of different effects cause that electron withdrawing effect of the phenyl ring (being in the R_C position) doesn't appear in the stability of the complexes. (E.g. it can be assumed that the presence of π-electrons results in the more favoured charge distribution in the chelates)

When proton dependent equilibria involving HA are expessed (Table 5) the data show that the pyridine-oxide derivative forms the most stable Cu(II) complex, while less stable complexes are formed with the natural monohydroxamate DIBOA-gl. However, even in this latter case, the formation of iron(III) DIBOA-gl complex starts below pH 1 as can be seen in Fig. 5. The fact that the iron(III)-DIBOA-gl complex(es) can be formed under acidic conditions (pH ca. 2) existing in the rhizosphere (root-soil surface), supports the recent findings, that DIBOA (together with some other monohydroxamic acids synthesized by grasses) can play a role in iron(III) uptake from the soil [5].

Acknowlegements—E. F. and E. K. would like to thank for support OTKA T 023612.

REFERENCES

1. *Chemistry and Biology of Hydroxamic Acids*, ed. H. Kehl. Karger, New York, 1982.
2. Raymond, K. N., Mülle, G. and Matzanke, B. F., *Top. Curr. Chem.*, 1984, **123,** 51.
3. Weinberg, E. D., *Quart. Rev. Biol.*, 1989, **64,** 261.
4. Corcuera, L. J., Woodward, M. D., Helgeson, J. P., Kelman, A. and Upper, C. D., *Plant Physiol*, 1978, **61,** 791.
5. Pethö, M., *Acta Agron. Hung.*, 1992, **41**, 167, and 1993, **42**, 203.
6. Miller, M. J., *Chem. Rev.*, 1989, **89**, 1563, and references therein.
7. Tipton, C. L. and Buell, E. L., *Phytochem.*, 1970, **9,** 1215.
8. Hiriart, M. V., Corcurea, L. J., Audrade, C. and Crivelli, I., *Phytochem.*, 1985, **24,** 1919.
9. Brown, D. A., McKeith, D. and Glass, W. K., *Inorg. Chim. Acta*, 1979, **35,** 5.
10. Monzyk, B. and Crumbliss, A. L., *J. Amer. Chem. Soc.*, 1979, **101,** 6203.
11. Brink, C. P. and Crumbliss, A. L., *Inorg. Chem.*, 1984, **23,** 4708.
12. Crumbliss, A. L., in *CRC Handbook in Microbal Iron Chelates*, ch. 7, ed. G. Winkelmann. CRC Press, New York, 1991.
13. Candle, M. T. and Crumbliss, A. L., *Inorg. Chem.*, 1994, **33,** 4077.
14. Monzyk, B. and Crumbliss, A. L., *J. Org. Chem.*, 1980, **45,** 4670.
15. Brink, C. P. and Crumbliss, A. L., *J. Org. Chem.*, 1982, **47,** 1171.
16. Brink, C. P., Fish, L. L. and Crumbliss, A. L., *J. Org. Chem.*, 1985, **50,** 2277.
17. Brown, D. A., Glass, W. K., Mageswaran, R. and Mohamed, S. A., *Magn. Res. Chem.*, 1991, **29,** 40.
18. Brown, D. A., Coogan, R. A., Fitzpatrick, N. J., Glass, W. K., Abuksima, D. E., Shiels, L., Ahlgrén, M., Smolander, K., Pakhanen, T. T., Pakhanen, T. A. and Peräkylä, M., *J. Chem. Soc. Perkin* 2, 1996, 2673.
19. Kurzak, B., Kozlowski, H. and Farkas, E., *Coord. Chem. Rev.*, 1992, **114,** 169.
20. Schwarzenbach, G. and Schwarzenbach, K., *Helv. Chim. Acta*, 1963, **46,** 1390.
21. Birus, M., Bradic, Z., Kujundzic, N., Pribanic,

M., Wilkins, P. C. and Wilkins, R. G., *Inorg. Chem.*, 1985, **24,** 3980.
22. Blatt, A. H., *Organic Syntheses*, Wiley, New York, 1963.
23. Gran, G., *Acta Chem. Scand.*, 1950, **4,** 599.
24. Irving, H., Miles, M. G. and Pettit, L. D., *Anal. Chem. Acta*, 1967, **38,** 475.
25. Mussini, T., Covington, A. K., Longhi, P. and Rondinini, S., *Pure and Appl. Chem.*, 1985, **57,** 865.
26. Zékány, L. and Nagypál, I., in *Computational Methods for the Determination of Stability Constants*, ed. D. Legett. Plenum Press, New York, 1985.
27. Khoe, G. H., Brown, P. L. and Sylva, R. N., *J. Chem. Soc. Dalton Trans.*, 1986, 1901.
28. Farkas, E., Csóka, H., Micera, G. and Dessi, A., *J. Inorg. Biochem.*, 1997, **65,** 281.
29. Dessi, A., Micera, G., Sanna, D. and Strinna, L., *J. Inorg. Biochem.*, 1992, **48,** 279.

Pergamon

PII: S0277–5387(98)00114–4

Polyhedron Vol. 17, No. 19, pp. 3343–3350, 1998
© 1998 Elsevier Science Ltd
All rights reserved. Printed in Great Britain
0277–5387/98 $19.00+0.00

Pd(II) and Pt(II) D-penicillamine complexes. Crystal structure of a tridentate D-penicillamine cluster of Pd(II)

G. Cervantes[a], V. Moreno[a]*, E. Molins[b] and M. Quirós[c]

[a] Departament de Química Inorgànica, Universitat de Barcelona, Avgda Diagonal, 647. 08028 Barcelona, Spain

[b] Institut de Ciència de Materials de Barcelona, CSIC, Bellaterra, 08193 Cerdanyola, Spain

[c] Departamento de Química Inorgánica, Universidad de Granada, Campus de Fuentenueva, 18071 Granada, Spain

(Received 13 January 1998; accepted 15 March 1998)

Abstract—Complexes of formula $[M_2(D\text{-}Pen^-)_2Cl_2]$, where M = Pd or Pt and D-Pen$^-$ = D-penicillaminate were synthesized and characterized by the usual spectroscopic methods. Red crystals suitable for X-ray study were obtained, after several days, from the mixture of K_2PdCl_4/D-Penicillamine solutions. The crystals were identified as $[Pd_3(Pen^{2-})_3].7/8KCl.19/8H_2O$. The structure shows four chemically but not crystallographically equivalent trinuclear clusters in the cell. Three D-penicillamine molecules act as divalent anions in tridentate fashion between three palladium atoms forming neutral units. Each S atom bridges two palladium atoms inside the molecular units. Potassium and chloride ions are curiously distributed along the crystallographic units contributing, together with the water molecules, to the stability of the crystal. The capacity of the penicillamine to act as tridentate ligand can be related to the capacity to capture toxic metals. © 1998 Elsevier Science Ltd. All rights reserved

Keywords: Pd trinuclear clusters; D-penicillamine complexes; tridentate D-penicillamine complex; crystal structure Pd cluster; S bridging pencillamine ligands.

INTRODUCTION

Penicillamine is an active molecule related to natural amino acids that has been used in the treatment of Wilson's disease and other cases of metal toxicity [1, 2]. In contrast to the protein-forming amino acids which are present in the L form, the natural form is D-penicillamine, the L and DL forms being both toxic and non-active. Due to the presence of a sulfur atom in the thiolate group, penicillamine is also a good ligand to coordinate soft metals such as Pb, Hg, Pd or Pt. This possibility of binding led to the administration of D-penicillamine together with platinum antitumor drugs, to reduce their nephrotoxicity [3]. However, the interest of D-penicillamine as a ligand can be extended to its several possibilities of coordination. The molecule of penicillamine, together with its zwitterionic form, with the three functional groups ($-NH_2$, $-S^-$ and COO^-), is shown in Scheme 1. This molecule usually forms bidentate complexes by coordination of N and S atoms [4, 5] but the formation of monodentate (S) [6, 7], tridentate (N,O,S) or tetradentate (N,O,O,S) complexes [8, 9] cannot be ruled out. The sulfur, nitrogen or oxygen atoms can also act as a bridge between two or more metallic atoms.

The complex $[Pd(DL\text{-}Pen)Cl]_2$ was synthesized and characterized by IR spectroscopy by McAuliffe [10]. Later Srinivasan et al. [11] synthesized the complex $[Pt(DL\text{-}Pen)Cl]_2$ and studied both Pd(II) and Pt(II) dimer complexes using other techniques such as XPS. A dimer structure with two chlorides acting as bridges and bidentate coordination (N,S) for the DL-penicillamine was assigned in both cases. No crystal structure has been described for Pd(II) or Pt(II) penicillamine derivatives. Although several complexes

* Author to whom correspondence should be addressed.

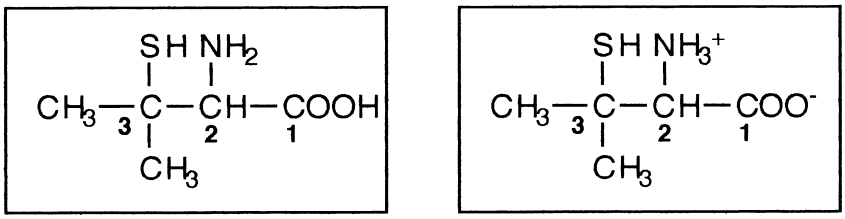

Scheme 1

of other metals such as Co, Pb, Cd and Cr showing anionic penicillamine tridentate coordinated (N,S,O) [8, 12, 13] have been characterized, no complexes of Pd(II) and Pt(II) with the tricoordinated ligand are known. We have synthesized and characterized compounds of Pd(II) and Pt(II) with D-penicillamine of formula $[M(D\text{-}Pen)Cl]_2$ and a tripalladium cluster with composition $Pd_3(D\text{-}Pen)_3.(KCl)_{7/8}.(H_2O)_{19/8}$, the crystal structure of which was solved. This is the first Pd(II) compound described in which the trimer unit shows the double anionic tridentate D-penicillamine acting as bridge between two Pd atoms via the S atom and via NH_2 and COO^- groups simultaneously.

MATERIALS AND METHODS

The complexes were prepared using $K_2[PdCl_4]$ and $K_2[PtCl_4]$ from Johnson Matthey and D-penicillamine from Fluka.

Elemental analyses were carried out on a Carlo Erba 1500 microanalyzer at the Serveis Científico-Tècnics at the University of Barcelona. Monocrystal chlorine and potassium analysis were carried out by ESCA. The infrared spectra were recorded in solid state (KBr pellets) on an FT-IR Nicolet 5DZ spectrometer in the 4000–400 cm^{-1} range and on an FT-IR Bomem DA-3 spectrometer in the 400–150 cm^{-1} range. $^1H\{^{13}C\}$ and $^{13}C\{^1H\}$ NMR spectra were obtained on a Bruker 250 spectrometer using DMSO as solvent. Chemical shifts were measured relative to TMS.

Suitable crystals for X-ray diffraction experiments were mounted on an Enraf-Nonius CAD4 four-circle diffractometer. Unit cell parameters were determined from 25 reflections and refined by least-squares method. Intensity data were collected using graphite monochromated MoK_α radiation. The unit cell was checked trying to find (unsuccessfully) higher metric symmetry by means of the facility included in the program package [14]. The chirality of penicillamine left P1 as the only possible choice for the space group.

Palladium and sulfur atoms were located by direct methods; other atoms were identified in successive different syntheses. Interstitial peaks were assigned to chloride and potassium ions or water molecules according to their intensity and their environment, some of them with partial occupancy and were used to define the formula $[Pd_3(Pen^{2-})_3].7/8KCl.19/8H_2O$. The formula was also checked by chemical analysis.

The structure was refined by full-matrix least-squares on F^2. Palladium and sulfur atoms were refined anisotropically, as were full occupancy chlorine and potassium atoms; all others were refined isotropically. Distances and angles within the penicillaminate anion (except those involving the sulfur atom) were constrained to be equal for the twelve units applying the SAME instruction of the program SHELX-93 [15]. Hydrogen atoms were introduced at ideal positions with an isotropic thermal parameter 1.2 times that of their parent atoms.

The program package SHELXTL Plus [14] was used for the structure solution and for the drawings. The program SHELX-93 [15] was used for structure refinement. A summary of crystal data and data collection is given in Table 1.

Syntheses of the complexes

(*a*) $[Pd_2(D\text{-}Pen^-)_2Cl_2]$ (***1***). A solution of 1 mmol of $K_2[PdCl_4]$ in 10 mL of water was mixed with another solution of 1 mmol of D-penicillamine in 10 mL of water at room temperature. An orange solid was immediately obtained from the final solution. The pH of this solution was then 1.1. The solution was stirred for 1 h at 40°C and the pH rose to 5.1. The orange solid was filtered from a red solution, washed in distilled water and dried overnight over silica gel. Found: C, 20.82; N, 4.81; H, 3.76; S, 10.89; Cl, 12.17. $Pd_2C_{10}H_{20}N_2S_2Cl_2O_4$ requires: C, 20.70; N, 4.83; H, 3.47; S, 11.05; Cl, 12.22. Red crystals suitable for X-ray diffraction were obtained from the solution, pH = 5.1. The crystals correspond to $[Pd_3(Pen^{2-})_3].7/8KCl.19/8H_2O$ (**2**). Found: C, 20.51; N, 4.66; H, 3.92; S, 10.94; Cl, 3.47; K, 3.91; $Pd_3C_{15}H_{31.75}N_3S_3Cl_{0.88}K_{0.88}O_{8.38}$ requires: C, 20.72; N, 4.83; H, 3.65; S, 11.05; Cl, 3.60; K, 3.96. The same crystals were repeatedly collected from the red solution, pH = 5.07, in further syntheses.

(*b*) $[Pt_2(D\text{-}Pen^-)_2Cl_2]$ (***3***). A solution of 1 mmol of $K_2[PtCl_4]$ in 10 mL of water was mixed with another solution of 1 mmol of D-penicillamine in 10 mL of water at room temperature. The solution was stirred for 2 h at 40°C and for 24 h at room temperature and

Table 1. Crystal Data and Structure Refinement for $Pd_3(C_5H_9NO_2S)_3.(KCl)_{7/8}.(H_2O)_{19/8}$

Empirical formula	$C_{15}N_3H_{31.75}S_3O_{8.38}Cl_{0.88}K_{0.88}Pd_3$
Crystal system	Triclinic
Space group	P_1
a (Å)	11.076(1)
b (Å)	11.045(1)
c (Å)	24.728(1)
α (°)	91.19(1)
β (°)	94.50(1)
γ (°)	108.67(1)
V (Å^3)	2853.7(6)
Z	4
Mol.wt.	868.0
Temperature	293(2) K
F(000)	1709
D_c(g cm^{-3})	2.022
Absorption coefficient (mm^{-1})	2.342
Crystal size (mm)	$0.42 \times 0.20 \times 0.06$
Radiation	MoK_α($\lambda = 0.71073$ Å)
Scan method	ω-2θ
θ range for data collection	2.39–30.35°
Range of hkl	$-15<h<14$, $0<k<15$, $-32<l<33$
Reflections collected	18078
Independent reflections	16314
Reflections observed	11542
Refinement method	Full-matrix least-squares on F^2
Data/restraints/parameters	16309/1056/702
Goodness-of-fit on F^2	1.022
Final R indices [$I>2\sigma(I)$]	R1 = 0.0583, wR2 = 0.1439
R indices (all data)	R1 = 0.1265, wR2 = 0.1765
Absolute structure parameter	0.01(5)
Largest diff. peak and hole (eÅ^{-3})	1.878 and −1.650

Table 2. Significant IR frequencies (cm^{-1}) for D-penicillamine and complexes (**1**), (**2**) and (**3**)

Assignment	D-Pen	[Pd(D-Pen)Cl]$_2$	[Pt(D-Pen)Cl]$_2$	[Pd$_3$(Pen^{2-})$_3$].7/8KCl.19/8H$_2$O
		(1)	(3)	(2)
ν(OH)				3428 m,br
$\nu_{as}(NH_2)$		3213 s, 3121 s	3211 s, 3115 s	3179 m, 3126 m, 3047 m
$\nu_{as}(NH_3^+)$	3174 m, 2967 s			
ν(S–H)	2609 m, 2513 m	d	d	d
ν(C═O,COOH)		1718 s	1721 vs	
$\nu_{as}(C{=}O)_{coord}$				1632 s,sh
$\delta_d(NH_3^+)$	1618 vs, sh			
$\delta(NH_2)$		1598 vs	1603 s	1594 vs
$\nu_{as}(COO^-)$	1595 vs			
$\delta_{sym}(NH_3^+)$	1526 vs			
ν(Pd–O)				500 w
ν(Pd–N)				443 w
ν(M–S)		395 m	385 m	397 m
ν(M–Cl)		303 m, 295 m	312 m, 300 m	

d: disappears, s: strong, vs: very strong, sh: shoulder m: medium, w: weak, br: broad

a reddish orange solution with a yellow precipitate was obtained. The solid was filtered, washed in distilled water and dried overnight over silica gel. Found: C, 14.84; N, 3.45; H, 2.97; S, 7.83; Cl, 7.95. $Pt_2C_{10}H_{20}N_2S_2Cl_2O_4$ requires: C, 14.80; N, 3.45; H, 3.24; S, 7.90; Cl, 8.74. All efforts to obtain crystals suitable for study by X-ray were unsuccessful. Only twinned needles were isolated.

RESULTS AND DISCUSSION

IR Spectra

The FT-IR data of the D-penicillamine and the Pd(II) and Pt(II) compounds are shown in Table 2. The most important bands in the spectrum of the D-penicillamine are assigned to $\nu_{st}(NH_3^+)$ at 3174–2967 cm^{-1}, $\nu_{as}(COO^-)$ at 1595 cm^{-1} corresponding to the zwitterionic form of amino acids. Consequently, the ν(C═O) at 1700 cm^{-1} of the protonated carboxylic group is absent. The frequencies corresponding to $\delta_d(NH_3^+)$ (aa-I) and $\delta_{sym}(NH_3^+)$ (aa-II) appear, respectively, at 1618 cm^{-1} and 1526 cm^{-1}. The bands at 2609 and 2513 cm^{-1} assigned to ν(S–H) in the D-penicillamine disappear in the spectra of the three compounds, indicating the coordination of the S atom to the metal. The shift of $\nu_{as}(NH_3^+)$ toward higher frequencies in the spectra of the complexes, typical for coordination of NH_2 [10], and the changes in the bands related with $\delta(NH_3^+)$ confirm the coordination through the nitrogen atom [16].

The presence in the spectra of (**1**) and (**3**) of bands at frequencies higher than 1700 cm^{-1}, assigned to the free carboxylic group, indicates no coordination by the oxygen atom [5]. The spectrum of (**2**) is quite different. No band corresponding to free carboxylic group was observed, while a wide band between 1632 and 1594 cm^{-1} includes ν(C═O) from the coordinated carboxylic group and $\delta(NH_2)$. The new bands at 395 cm^{-1} for the $[Pd_2(D\text{-}Pen)_2Cl_2]$ (**1**), at 385 cm^{-1} for the $[Pt_2(D\text{-}Pen)_2Cl_2]$ (**3**), and at 397 cm^{-1} for the cluster of palladium (**2**) were assigned to ν(M–S) [17]. The bands observed in the zone about 300 cm^{-1} for both (**1**) and (**3**) were assigned to bridge ν(M–Cl). These bands are split and shifted to lower values, as corresponds to *cis* bridged chlorine atoms [10, 18]. Only in the spectrum of (**2**) was a band at 500 cm^{-1} assigned to ν(Pd–O). In this spectrum ν(Pd–N) also appear at 443 cm^{-1}. These findings are consistent with the tridentate coordination through N, S and O atoms shown by the penicillamine in (**2**). In this case, the penicillamine has lost two protons, while in complexes (**1**) and (**3**) the coordination is only bidentate through N and S atoms, acting as a mononegative anion.

^1H and ^{13}C NMR study

The complex $[Pt_2(D\text{-}Pen)_2Cl_2]$ (**3**) presents low solubility in DMSO and other solvents and it was impossible to register its ^1H, ^{13}C and ^{195}Pt NMR spectra. The palladium complex $[Pd_2(D\text{-}Pen)_2Cl_2]$ (**1**), is quite soluble in DMSO but several species were formed in solution, probably due to the coordination of DMSO to palladium atom which replaces the penicillamine molecule and breaks the dimer to give monomer complexes. The ^1H and ^{13}C NMR spectra are very complicated and it is difficult to assign the signals corresponding to several species co-existing in equilibrium. Attempts to isolate and identify the differents species chromatographically using solvents such as chloroform or DMF were unsuccessful, because a mixture of several species was always obtained. Both orange crystals and yellow crystals were isolated from an eluted fraction, but unfortunately, they were not suitable for X-ray study.

In Table 3, the chemical shifts (ppm) corresponding to the ^1H and ^{13}C NMR spectra of D-penicillamine and the compound $[Pd_3(Pen^{2-})_3]$ (**2**) are shown. The

Table 3. ^1H and ^{13}C NMR shifts (ppm) of D-penicillamine and $[Pd_3(Pen^{2-})_3]$*

^1H NMR Compound	NH_2	CH(2)	CH_3
D-penicillamine	6.52	3.27	1.47, 1.39
$[Pd_3(Pen^{2-})_3]$	6.21	3.21	1.55, 1.53
	4.87		1.38, 1.35

^{13}C NMR Compound	COOH(1)	CH(2)	C(3)	CH_3
D-penicillamine	167.85	64.27	44.97	30.02
				28.56
$[Pd_3(Pen^{2-})_3]$	170.82	70.98	55.09	31.01
				25.74

*in DMSO

shift observed for the methyl groups in the complex is consistent with the coordination by the S atom. Likewise, the signal assigned to NH_2 proton in free penicillamine shifts upfield due to the coordination of the NH_2 group to the palladium atom. In the spectrum of the complex, two signals appear for each type of proton. It is possible that new species are formed in solution due to the opening of the ring in the cluster as observed for other penicillamine compounds [19].

In the ^{13}C spectrum of $[Pd_3(Pen^{2-})_3]$ (**2**), a significant shift in the signal assigned to C═O can be observed. It is consistent with the coordination of Pd(II) by O atoms. Changes in C(3) signals are also due to the coordination of the metal atom to S. The signal assigned to CH(2) also shifts downfield as a consequence of the coordination of palladium to the NH_2 group.

X-ray study

Crystal parameters for the complex (**2**), $[Pd_3(Pen^{2-})_3].7/8KCl.19/8H_2O$ and a summary of the data-collection and refinement process are given in Table 1. Tables 4 and 5 contain a selection of bond distances and angles with their e.s.d.'s. The complete list of bond distances and angles and final atomic coordinates as well as anisotropic thermal parameters and the listing of observed and calculated structure factors are included as supplementary material.

The structure is built of trimeric [Pd_3(penicillaminate)$_3$] units plus potassium ions, chloride ions and water molecules in interstitial positions. There are four crystallographically independent but chemically equivalent trimeric clusters in the unit cell. In Fig. 1 one of the units is represented. The other three are included as supplementary material.

The palladium atoms in each trimer define an isosceles triangle (Table 6). Each pair of metal atoms in the trimer is bridged by a penicillaminate anion, which is linked via its amino group to one palladium atom, via its carboxylate group to the other and via the sulfur atom to both. Two chelate rings, one five-membered and the other six-membered are defined in this way.

Table 4. Selected Bond Lengths (Å) for A, B, C and D Clusters

Cluster A		Cluster B	
Pd(1A)–N(3A)	2.090 (12)	Pd(1B)–O(12B)	2.088 (11)
Pd(1A)–O(12A)	2.094 (11)	Pd(1B)–N(3B)	2.070 (12)
Pd(1A)–S(2A)	2.278 (4)	Pd(1B)–S(3B)	2.259 (4)
Pd(1A)–S(3A)	2.257 (4)	Pd(1B)–S(2B)	2.273 (4)
Pd(1A)–Pd(2A)	3.0206 (14)	Pd(1B)–Pd(2B)	3.017 (2)
Pd(1A)–Pd(3A)	3.219 (2)	Pd(1B)–Pd(3B)	3.2259 (13)
Pd(2A)–O(13A)	2.068 (10)	Pd(2B)–O(13B)	2.070 (10)
Pd(2A)–N(1A)	2.091 (12)	Pd(2B)–N(1B)	2.092 (12)
Pd(2A)–S(1A)	2.258 (4)	Pd(2B)–S(1B)	2.258 (3)
Pd(2A)–S(3A)	2.290 (4)	Pd(2B)–S(3B)	2.289 (4)
Pd(2A)–Pd(3A)	3.2088 (14)	Pd(2B)–Pd(3B)	3.2137 (14)
Pd(3A)–N(2A)	2.092 (11)	Pd(3B)–N(2B)	2.053 (12)
Pd(3A)–O(11A)	2.067 (10)	Pd(3B)–O(11B)	2.058 (10)
Pd(3A)–S(2A)	2.253 (4)	Pd(3B)–S(2B)	2.249 (4)
Pd(3A)–S(1A)	2.276 (4)	Pd(3B)–S(1B)	2.277 (4)
Cluster C		Cluster D	
Pd(1C)–N(3C)	2.058 (13)	Pd(1D)–O(12D)	2.039 (12)
Pd(1C)–O(12C)	2.055 (13)	Pd(1D)–N(3D)	2.106 (13)
Pd(1C)–S(3C)	2.244 (4)	Pd(1D)–S(3D)	2.240 (4)
Pd(1C)–S(2C)	2.270 (5)	Pd(1D)–S(2D)	2.269 (4)
Pd(1C)Pd(2C)	3.037 (2)	Pd(1D)–Pd(2D)	3.057 (2)
Pd(1C)–Pd(3C)	3.139 (2)	Pd(1D)–Pd(3D)	3.171 (2)
Pd(2C)–N(1C)	2.058 (14)	Pd(2D)–N(1D)	2.089 (13)
Pd(2C)–O(13C)	2.046 (12)	Pd(2D)–O(13D)	2.073 (12)
Pd(2C)–S(1C)	2.252 (4)	Pd(2D)–S(3D)	2.278 (4)
Pd(2C)–S(3C)	2.275 (4)	Pd(2D)–S(1D)	2.252 (4)
Pd(2C)–Pd(3C)	3.208 (2)	Pd(2D)–Pd(3D)	3.202 (2)
Pd(3C)–O(11C)	2.059 (13)	Pd(3D)–O(11D)	2.065 (12)
Pd(3C)–N(2C)	2.10 (2)	Pd(3D)–N(2D)	2.06 (2)
Pd(3C)–S(2C)	2.265 (5)	Pd(3D)–S(2D)	2.272 (4)
Pd(3C)–S(1C)	2.281 (4)	Pd(3D)–S(1D)	2.283 (4)

Table 5. Selected Bond Angles (°) for Cluster A

N(3A)–Pd(1A)–O(12A)	87.1 (4)
N(3A)–Pd(1A)–S(2A)	175.6 (4)
O(12A)–Pd(1A)–S(2A)	96.7 (3)
N(3A)–Pd(1A)–S(3A)	85.8 (3)
O(12A)–Pd(1A)–S(3A)	169.5 (3)
S(3A)–Pd(1A)–S(2A)	90.62 (13)
O(13A)–Pd(2A)–N(1A)	87.8 (4)
O(13A)–Pd(2A)–S(1A)	172.7 (3)
N(1A)–Pd(2A)–S(1A)	85.3 (3)
O(13A)–Pd(2A)–S(3A)	97.2 (3)
N(1A)–Pd(2A)–S(3A)	169.1 (3)
S(1A)–Pd(2A)–S(3A)	90.03 (13)
N(2A)–Pd(3A)–O(11A)	86.5 (4)
N(2A)–Pd(3A)–S(2A)	87.1 (3)
O(11A)–Pd(3A)–S(2A)	173.5 (3)
N(2A)–Pd(3A)–S(1A)	176.4 (3)
O(11A)–Pd(3A)–S(1A)	96.5 (3)
S(2A)–Pd(3A)–S(1A)	89.95 (13)
C(11A)–O(11A)–Pd(3A)	130.2 (8)
Pd(1A)–S(3A)–Pd(2A)	83.26 (13)
C(21A)–N(1A)–Pd(2A)	117.1 (8)
C(31A)–S(1A)–Pd(2A)	96.4 (4)
C(31A)–S(1A)–Pd(3A)	105.5 (4)
Pd(2A)–S(1A)–Pd(3A)	90.08 (14)
C(12A)–O(12A)–Pd(1A)	130.5 (9)
C(22A)–N(2A)–Pd(3A)	114.9 (8)
C(32A)–S(2A)–Pd(1A)	103.8 (4)
C(32A)–S(2A)–Pd(3A)	99.0 (4)
Pd(1A)–S(2A)–Pd(3A)	90.53 (13)
C(13A)–O(13A)–Pd(2A)	129.6 (8)
C(23A)–N(3A)–Pd(1A)	115.8 (8)
C(33A)–S(3A)–Pd(1A)	99.9 (4)
C(33A)–S(3A)–Pd(2A)	105.8 (4)

The environment of the metal atoms deviates appreciably from ideal square planar (Table 7), especially the angle inside the six-membered chelate ring (O–Pd–S(O)). The twelve Pd–N and the twelve Pd–O distances are similar, whereas Pd–S distances are slightly shorter (in average) for the O-chelated sulphur than for the N-chelated.

In all cases, the metal atom slightly (below 0.1 Å) deviated from the average NOS_2 plane away from the centre of the triangle. Only two other structures with Pd_3S_3 triangles have been published [20, 21], but the molecule bearing the sulfur atoms in these cases does not doubly chelate the palladium atoms, so the Pd-Pd distances are considerably longer.

The conformation of the bonds in the organic ligand is severely constrained by the formation of the chelate rings. In all cases, O1 is gauche respect to C3 and the nitrogen atoms (the ranges for the corresponding torsion angles are: O1–C1–C2–N, 59,9···83,3° and O1–C1–C2–C3, −42,0···−66,7°). The sulfur atom is gauche respect to the nitrogen atom and Cl (torsional angle ranges: C1–C2–C3–S, 75,4···81,0° and N–C2–C3–S, −41,8···−49,2°).

Crystal packing, showing the distribution of potassium and chloride ions between the cluster units, is depicted in Fig. 2.

Although several complexes containing tridentate penicillamine have been reported, this is the first palladium compound in which the penicillamine bridges three atoms in a cluster. Appleton, on the basis of NMR studies, proposed a tridentate coordination for a penicillamine molecule acting as bridge between two

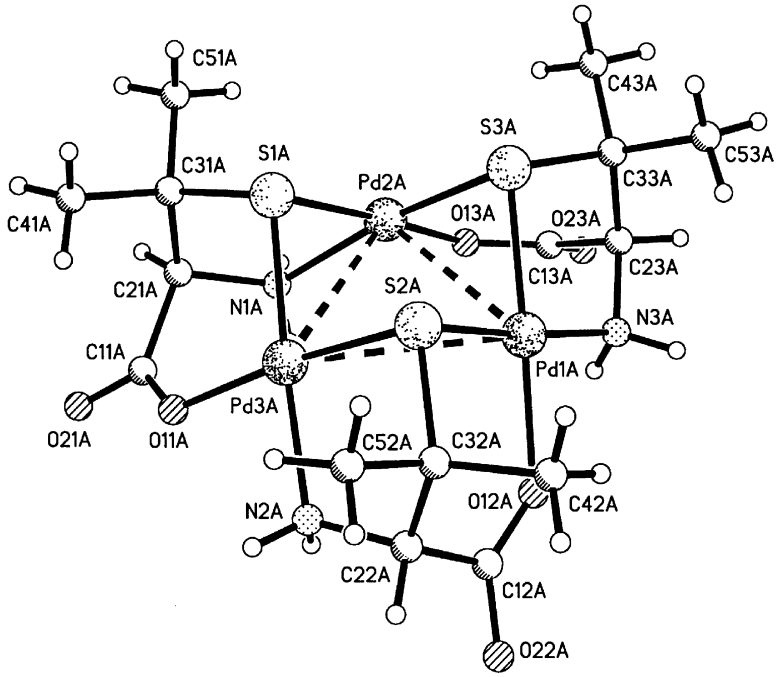

Fig. 1. Molecular structure of one (A) of the four crystallographically independent clusters $[Pd_3(Pen^{2-})_3]$.

Table 6. Geometry of the Pd_3 triangles

Distances (Å)		Angles (°)	
Pd(1A)–Pd(2A)	3.021(1)	Pd(2A)–Pd(1A)–Pd(3A)	61.80(3)
Pd(1A)–Pd(3A)	3.219(2)	Pd(1A)–Pd(2A)–Pd(3A)	62.14(3)
Pd(2A)–Pd(3A)	3.209(1)	Pd(1A)–Pd(3A)–Pd(2A)	56.06(3)
Pd(1B)–Pd(2B)	3.017(2)	Pd(2B)–Pd(1B)–Pd(3B)	61.86(3)
Pd(1B)–Pd(3B)	3.226(1)	Pd(1B)–Pd(2B)–Pd(3B)	62.27(3)
Pd(2B)–Pd(3B)	3.214(1)	Pd(1B)–Pd(3B)–Pd(2B)	55.87(3)
Pd(1C)–Pd(2C)	3.037(2)	Pd(2C)–Pd(1C)–Pd(3C)	62.57(4)
Pd(1C)–Pd(3C)	3.139(2)	Pd(1C)–Pd(2C)–Pd(3C)	60.27(4)
Pd(2C)–Pd(3C)	3.208(2)	Pd(1C)–Pd(3C)–Pd(2C)	57.16(4)
Pd(1D)–Pd(2D)	3.057(2)	Pd(2D)–Pd(1D)–Pd(3D)	61.84(4)
Pd(1D)–Pd(3D)	3.171(2)	Pd(1D)–Pd(2D)–Pd(3D)	60.84(4)
Pd(2D)–Pd(3D)	3.202(2)	Pd(1D)–Pd(3D)–Pd(2D)	57.32(3)

Table 7. Average distances (Å) and angles (°).The maximum and minimum values are indicated in parentheses except for parameters that have been constrained to be equal for all units. S(N) and S(O) represent the chelate ring including nitrogen and oxygen respectively

Distances (Å)		Angles (°)	
Pd–N	2.08 (2.05–2.11)	N–Pd–O	87.7 (86.4–90.8)
Pd–O	2.07 (2.04–2.09)	N–Pd–S(N)	85.9 (84.4–87.1)
Pd–S(N)	2.255 (2.240–2.272)	N–Pd–S(O)	174.0 (169.1–176.8)
Pd–S(O)	2.278 (2.269–2.290)	O–Pd–S(N)	173.1 (169.5–176.2)
		O–Pd–S(O)	96.5 (94.4–97.3)
		S(N)–Pd–S(O)	90.0 (89.0–90.9)
C(1)–O(1)	1.25	O(1)–C(1)–C(2)	121.7
C(1)–O(2)	1.25	O(1)–C(2)–C(1)	121.6
C(1)–C(2)	1.54	O(2)–C(1)–C(2)	116.5
C(2)–N	1.50	C(1)–C(2)–C(3)	115.2
C(2)–C(3)	1.52	C(1)–C(2)–N	109.0
C(3)–C(4)	1.52	C(3)–C(2)–N	111.1
C(4)–C(5)	1.52	C(2)–C(3)–C(4)	111.5
C(3)–S	1.85 (1.83–1.88)	C(2)–C(3)–C(5)	111.5
		C(4)–C(3)–C(5)	109.8
		C(2)–C(3)–S	109.0 (107.6–110.8)
		C(4)–C(3)–S	107.4 (103.1–111.0)
		C(5)–C(3)–S	107.4 (103.1–111.0)

platinum atoms [19]. The type of coordination proposed for the penicillamine was identical to that found in $[Pd_3(Pen^{2-})_3]$ (**2**) but the complex was a dimer in which each Pt coordination was completed with two amine ligands. In other metal complexes reported [22–24], the penicillamine does not act as a tridentate ligand but the S atom bridges two or three metallic atoms other than Pd or Pt. The methionine molecule has also shown its capacity to act as a tridentate ligand and to bridge metallic atoms, but through the N atom [25]. Finally, structures have been reported in which cysteine acts as a tridentate ligand but to date there is no report of this forming part of a cluster [26].

The synthesis of a tridentate penicillamine complex of a heavy metal offers interesting possibilities. The capacity of penicillamine to act as a tridentate ligand can be related to its capacity to capture toxic metals. Müller et al. [9]. have studied the decrease of toxicity of Cr(VI) in animals when penicillamine was administered. In this case the Cr(VI) was reduced to Cr(III) and a tridentate Cr(III)-penicillamine complex was formed.

Acknowledgements—We are grateful to Johnson Matthey for supplying K_2PdCl_4 and K_2PtCl_4 and to DGICYT, project PB94-0922-C02, for financial support.

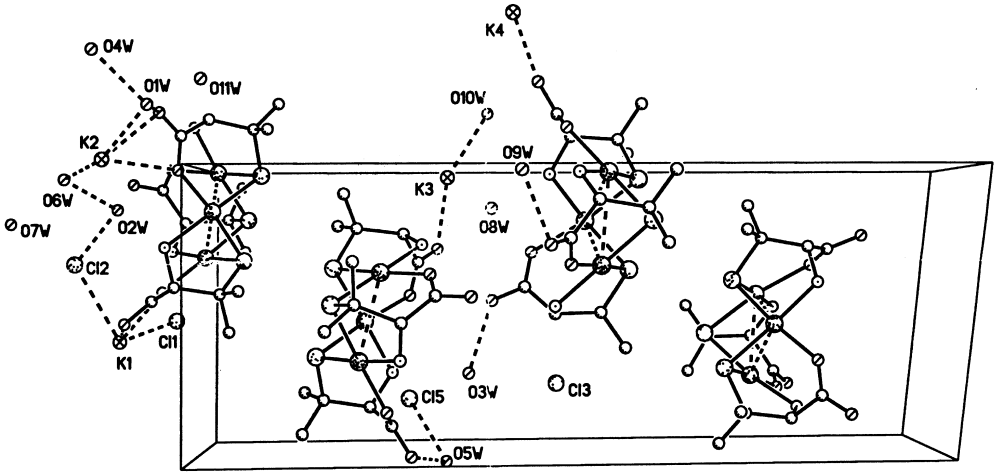

Fig. 2. View of the unit cell of $[Pd_3(Pen^{2-})_3].7/8KCl.19/8H_2O$.

REFERENCES

1. Lippard, S. J., in *Bioinorganic Chemistry*, eds I. Bertini, H. B. Gray, S. J. Lippard and J. S. Valentine. University Science Books, Mill Valley, California, 1994, p. 505.
2. Gergely, A. and Sovago, I., in *Metal Ions in Biological Systems*, ed. H. Sigel, Vol. 9. Marcel Deker, New York, 1980.
3. Slater, T. F., Ahmed, M. and Ibrahim, S. A., *J. Clin. Hemat. Oncol.*, 1977, **7,** 534.
4. Birker, P. J., Reedijk, J. and Verschoor, G. C., *Inorg. Chem.*, 1981, **20,** 2087.
5. Baidya, N., Olmstead, M. M. and Mascharak, P. K., *Inorg. Chem.*, 1991, **30,** 3967.
6. Carty, A. J. and Taylor, J., *J. Chem. Soc. Chem. Comm.*, 1976, 214.
7. Wong, Y. S., Chieh, P. C. and Carty, A. J., *Can. J. Chem.*, 1973, **51,** 2597.
8. Freeman, H. C., Huq, F. and Stevens, G. N., *J. Chem. Soc. Chem. Comm.*, 1976, 90.
9. Müller, A., Johannes, K. U., Straube, M., Krickemeyer, E. and Bögge, H., *Z. anorg. allg. Chem.*, 1993, **619,** 1037.
10. Chow, S. T., McAuliffe, C. A. and Sayle, B. J., *J. Inorg. Nucl. Chem.*, 1973, **35,** 4349.
11. Srinivasan, V., Stiefel, E. I., Elsberry, A. and Walton, R. A., *J. Am. Chem. Soc.*, 1979, **101,** 2611.
12. De Meester, P. and Hodgson, D. J., *J. Am. Chem. Soc.*, 1977, **99,** 101.
13. Freeman, H. C., Stevens, G. N. and Taylor, I. F., *J. Chem. Soc. Chem. Comm.*, 1974, 366.
14. Sheldrick, G. M., SHELXTL-Plus. Release 3.4 for Nicolet R3 m/V crystallographic system. Nicolet Instrument Corporation, Madison, Wisconsin, USA, 1987.
15. Sheldrick, G. M., SHELX-93, A program for crystal structure refinement, University of Göttingen, Germany, 1993.
16. Hojo, Y., Sugiura, Y. and Tanaka, H., *J. Inorg. Nucl. Chem.*, 1976, **38,** 641.
17. Iakovidis, A. and Hadjiliadis, N., *Coord. Chem. Rev.*, 1994, **135,** 17.
18. Nakamoto, K., Infrared and Raman Spectra of Inorganic and Coordination Compounds, 4th ed. Wiley Interscience, Chichester, 1986.
19. Appleton, T. G., Connor, J. W., Hall, J. R. and Prenzler, P. D., *Inorg. Chem.*, 1989, **28,** 2030.
20. Fackler, J. P. and Zegarski, W. J., *J. Am. Chem. Soc.*, 1973, **95,** 8566.
21. McPartlin, E. M. and Stephenson, N. C., *Acta Cryst.*, 1969, **B20,** 1659.
22. Baami, M., Doctoral Thesis, Universitat Autònoma, Barcelona, 1996.
23. Birker, P. J. and Freeman, H. C., *J. Am. Chem. Soc.*, 1977, **99,** 6890.
24. Birker, P. J. and Verschoor, G. C., *Inorg. Chem.*, 1982, **21,** 990.
25. Davidson, Y., Chang, S. and Norman, R., *J. Chem. Soc. Dalton*, 1995, 77.
26. Kay, A. and Mitchell, P. C., *J. Chem. Soc* (*A*), 1970, 2421.

Pergamon

PII: S0277–5387(98)00115–6

Polyhedron Vol. 17, No. 19, pp. 3351–3360, 1998
© 1998 Elsevier Science Ltd
All rights reserved. Printed in Great Britain
0277–5387/98 $19.00+0.00

A hydroxo-and phenoxo-bridged dinuclear Nickel(II) Complex: structure and characterization

Yilma Gultneh,* A. Raza Khan, Bijan Ahvazi and Ray J. Butcher

Contribution from the Department of Chemistry, Howard University, 525 College St. NW, Washington, DC 20059, U.S.A.

(Received 25 August 1997; accepted 16 March 1998)

Abstract—The structure and properties of the dinuclear complex $[Ni(II)_2(\mu\text{-LO})(\mu\text{-OH})](ClO_4)_2 \cdot 2CH_3CN$(**1**) (LOH = 2,6-bis((bis (2-(2-pyridyl)ethyl)amino)methyl)phenol is reported. The structure of the cation $[Ni(II)_2(\mu\text{-LO})(\mu\text{-OH})]^{2+}$ shows two doubly bridged, square pyramidal Ni(II) ions. The electronic absorption spectrum showed maxima at 204, 264, 300, 362, 607 and 820 nm. Cyclic voltammetry in dry acetonitrile showed irreversible reduction peaks at −1.25 V and −1.45 V (vs. Ag/AgCl) assigned to the stepwise reduction to the Ni(II)Ni(I) and the $Ni(I)_2$ state and also irreversible oxidation waves at +0.13 V and +0.87 V (vs. Ag/AgCl) assigned to the stepwise oxidation to the Ni(II)Ni(III) and the $Ni(III)_2$ state. The room temperature magnetic moment, corrected for diamagnetism, is 2.67 BM indicating an antiferromagnetic coupling of the two Ni(II) ions. © 1998 Elsevier Science Ltd. All rights reserved

The interest in the structures and reactions of transition metal complexes is, in part, as small molecule models for the active sites of metalloenzymes. Nickel is found at the catalytic active sites of several redox [1, 2] and hydryoltic [3] enzymes. In synthetic nickel complex catalysts [4] for redox reactions of organic substrates [5], nickel oxidation states range from +1 to +4, while in the redox enzymes nickel ions are cycled between the formal oxidation states of +3 and +1 [6, 7]. Bacterial and plant urease contain two nickel ions per catalytic subunit [8]. However, it has not been settled whether the Ni(II) ions are magnetically coupled [9, 10] since a recent magnetic saturation study of jack bean and *Klebsiella aerogenes* urease by Day *et al* [11] has been interpreted as showing no evidence for magnetic coupling. The mechanism of the catalysis of hydrolysis of urea by urease is thought to involve a two-Ni(II) center wherein urea coordinates to one Ni(II) ion inducing greater susceptibility to nucleophilic attack by the OH^- that is coordinated to the other Ni(II) ion in the binuclear active site [12]. This is similar to the widely accepted mechanism for catalysis by dinuclear Zn(II) hydrolytic enzymes [13]. Recently, Yamaguchi *et al* [14]. have reported a carboxylate (or bicarbonate)-bridged dinuclear Ni(II) model complex that catalyzes the ethanolysis of urea to ethyl carbamate.

X-ray absorption spectroscopy [15] of urease shows 5 or 6-coordinate tetragonal Ni(II) [16] with histidyl-imidazole donors and the UV-visible absorption spectrum is similar to those of some octahedral dinuclear Ni(II)model complexes [17]. EXAFS data indicate Ni–N and Ni–O distances of about 2.03 Å and a Ni–Ni distance of about 3.3 Å [18].

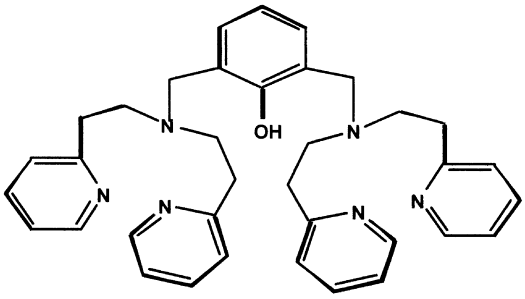

LOH

Dinuclear Ni(II) complexes with phenol and polyimidazole ligand donor sets have been reported [19] as

*Author to whom correspondence should be addressed.

models for the active site of urease. The dinucleating ligand, LOH has been used in the syntheses of phenoxo bridged dinuclear complexes of Mn(II) [20], Fe(II) [21] and Cu(II) [22] with exogenous bridging by acetate, methoxide, halide or azide groups.

Here we are reporting the synthesis, structure, electrochemistry, spectral, and magnetic properties of the dinuclear Ni(II) complex of LO^-.

EXPERIMENTAL

Reagents and solvent purification

Reagent grade dry solvents were used without further purification for synthetic and purification procedures. Dimethylsulfoxide was refluxed over and distilled from P_4O_{10} and redistilled from anhydrous $CaCl_2$. Diethyl ether was refluxed and distilled under nitrogen from Na/benzophenone. Acetonitrile was refluxed and distilled from P_4O_{10}. Commercial anhydrous $(n\text{-}Bu)_4NClO_4$ was recrystallized from ethyl acetate/hexane (1:2, v/v).

Synthesis of the ligand LOH

The ligand, LOH, was made and purified according to the literature method [22].

Synthesis of the complex $[Ni(II)_2(\mu\text{-LO})(\mu\text{-OH})](Clo_4)_2.\ 2CH_3CN$ (1) [23]

To a stirred methanol solution (50 mL) of $Ni(ClO_4)_2.6H_2O$ (3.66 g, 10 mmole) and 5 mL dimethoxypropane was added, dropwise, a methanol solution (30 mL) of the ligand (2.78 g, 5 mmole) and triethylamine (0.55 g, 5.5 mmole). The green solution formed was refluxed slowly overnight. A green powdery precipitate was formed which was filtered, washed with ether and dried in air (yield 2.73 g, 55%). Crystals suitable for crystallography were obtained by recrystallization from an acetonitrile solution layered with dry ether. Green crystals formed over three days, which were isolated, washed with ether, and dried in air. Elemental analysis: Calculated for $C_{40}H_{46}\ Cl_2N_8\ Ni_2\ O_{10}$ C: 47.20%, H: 4.42%; N: 9.28%; Found: C: 46.45%; H: 4.52%; N 9.80%.

pH-metric titrations

Potentiometric titrations of the ligand and **1** were done using Fisher accumet model 50 pH/ion conductivity meter and Fisher combination glass electrodes. Typically, 0.18 mmole of the complex (or ligand) was dissolved in 25 mL of water/DMF (3:5, v/v) mixture that had been purged of dissolved CO_2 by bubbling with nitrogen gas. A standard aqueous solution of $HClO_4$ (5.1 mL of 0.10 M) was added and stirred for about 10 minutes under a nitrogen atmosphere and followed by potentiometric back-titration against a standard aqueous solution of NaOH (0.10 M).

Cyclic voltammetry

Cyclic voltammetry was carried out with a BAS CV-27 voltammograph at 25°C. The sample solution was 1.0 mM in **1** and 0.10 M in the supporting electrolyte, $(n\text{-}Bu)_4NClO_4$. (degassed by bubbling dry N_2 gas for 10 min). Glassy carbon working electrode, Ag/AgCl reference, and Pt auxiliary electrodes supplied by Bioanalytical Systems Inc. were used in the electrochemical measurements. Experiments were run at 100 mV/s scan rate.

Magnetism

Room temperature magnetic susceptibility measurements were done on powdered samples of **1** with a Johnson-Matthey magnetic susceptibility balance and calculations included correction for diamagnetic effects of the ligand.

Rates of catalysis of the hydrolysis of bis(p-nitrophenyl)phosphate (BNPP)

In a typical experiment, 3.0 mL of 0.1 M buffer solution of THAM, adjusted to the desired pH by adding $HClO_4$ solution and made to be 0.1 M $NaClO_4$, was transferred to a quartz cuvette and the solution was thermostated at 75°C. To this was added 0.15 mL of 50.0 mM solution of the substrate BNPP and 0.15 mL of 4.81 mM solution of 1, both in 1:1 DMF/water mixture. UV-Visible absorption scans were taken every 5 minutes for 3 hours.

X-ray structure determination and refinement

A bright green crystal of the title compound having approximate dimensions of $0.43 \times 0.33 \times 0.25$ mm was mounted on a glass fiber using quick setting epoxy cement. All measurements were made on a Siemens P4S diffactometer with graphite monochromated Mo Kα radiation. Cell constants and an orientation matrix for data collection were obtained by standard methods [24] and corresponded to a monoclinic cell. Systematic absences intensity statistics based on the collected data set indicated the space group P2/n. Crystal data and structure refinement data are summarized in Table 1. Data were collected by standard techniques [25]. Of the 3745 reflections collected, 3400 were unique. The structure was solved by direct methods [26] and refined by full matrix least-swuares methods (based on F^2) as implemented in the SHELXTL system [27] of computer programs. Hydrogen atoms were included in structure factor calculations in their idealized positions and considered to ride on the atoms to which

Table 1. Crystal data and structure refinement for 1

Identification code	nidimer
Empirical formula	$C_{40}H_{51}Cl_2N_6Ni_2O_{12}$
Formula weight	996.19
Temperature	293(2) K
Wavelength	0.71073 Å
Crystal system	Monoclinic
Space group	P2/n
Unit cell dimensions	$a = 11.6401(12)$ Å $\alpha = 90^\circ$ $b = 10.9950(1)$ Å $\beta = 108.638\ (7)^\circ$ $c = 18.029(2)$ Å $\gamma = 90^\circ$
Volume	2186.4(4) Å^3
Z	2
Density (calculated)	1.513 Mg/m^3
Absorption coefficient	1.052 mm^{-1}
F(000)	1038
Crystal size	$0.33 \times 1. \times 0.4$ mm
θ range for data collection	3.02 to 27.32°
Index ranges	$0 \sim h \sim 13,\ -12 \sim k \sim 0,\ -20 \sim l \sim 22$
Reflections collected	3745
Independent reflections	3400 ($R_{int} = 0.0284$)
Absorption correction	None
Refinement method	Full-matrix least-squares on F^2
Data/restraints/parameters	3400/0/299
Goodness-of-fit on f^2	1.054
Final R indices [$I > 2\sigma(I)$]	R1 = 0.0680, wR2 = 0.1554
R indices (all data)	R1 = 0.1112, wR2 = 0.1820
Largest diff. peak and hole	0.748 and −0.295 eÅ^{-3}

they were attached. In the lattice, there are two disordered CH_3CN molecules. The occupancy factors of these carbon atoms were constrained to sum to 1.0. The refinement converged with R_1 [28] = 6.80% for the 2242 reflections for which $I > 2\sigma(I)$.

RESULTS AND DISCUSSION

Dinucleating ligands, with the general structure of LOH presenting a potentially bridging phenoxy oxygen and two N_3 chelating donor sets per molecule with imidazolyl, pyrazolyl, pyridyl, phenolate, and benzimidazolyl donor groups (or their ring substituted derivatives), have been widely utilized in the syntheses of dinuclear complexes of copper [29], manganese [30], cobalt [31], iron [32], and zinc [31]. The donor properties of pyridyl groups approximate those of histidylimidazole in urease and in several Zn(II) hydrolytic enzymes [33, 34].

Structure of the complex $[Ni(II)_2(\mu\text{-LO})(\mu\text{-OH})](ClO_4)_2.2CH_3CN$ (1)

Tables 1 and Table 2 show the crystal data and atomic coordinates of **1** respectively. Table 3 summarizes selected bond lengths and angles. The ORTEP drawing of the cation $[Ni_2(\mu\text{-LO})(\mu\text{-OH})]^{2+}$ is shown in Fig. 1.

The structure of the cation of **1** consists of a discrete dinuclear complex in which two Ni(II) ions are each coordinated in a nearly square pyramidal geometry, to two pyridyl and an amine nitrogen, and to the bridging phenoxide oxygen of the chelating ligand and a bridging exogenous hydroxide. The apical positions taken by pyridyl groups are on opposite faces of the two square bases. There is a crystallographic C_2 axis passing through the phenoxy and hydroxide oxygens of the planar Ni_2O_2 unit. The $Ni–N_{amine}$ bond lengths are about 0.1 Å longer than the $Ni–N_{pyridyl}$ lengths attributable to the π-bonding potential of the pyridyl group. The intramolecular $Ni\cdots Ni$ distance, 3.174(1) Å, is significantly shorter than those in doubly acetate-bridged complexes (3.40 to 3.62 Å) [14, 19, 35] attributed to the larger bite of carboxylate bridges but longer than those in diphenoxy- and acetate triply bridged complex of a macrocyclic ligand (3.043 Å) [36]. It is in the range (3.10–3.20 Å) observed in the doubly phenoxy-bridged Ni(II) complexes [37]. Each nickel ion is displaced towards the apical pyridyl nitrogen, by 0.313(5) Å also evidenced by the greater than 90° N_{apical}–Ni–N and N_{apical}–Ni–O angles. The analogous hydroxide-[22] and methoxide-bridged [38] Cu(II) complexes of LOH also show a planar Cu_2O_2 geometry with the Cu (II) ion similarly displaced toward the apical N. The basal and apical $Ni–N_{pyridyl}$ bond lengths are similar, whereas in the Cu(II) analog, Jahn-Teller lengthening of the $N–N_{apical}$ bond is observed [22].

Table 2. Atomic coordinates [$\times 10^4$] and equivalent isotropic displacement parameters [$Å^2 \times 10^3$] for 1. U(eq) is defined as one third of the trace of the orthogonalized U_{ij} tensor

	x	y	z	U(eq)
Ni	6086(1)	−7831(1)	2297(1)	49(1)
Cl	3711(2)	−2014(2)	4305(1)	75(1)
O(1)	7500	−8932(5)	2500	56(2)
O(2)	7500	−6763(9)	2500	84(3)
O(11)	3338(11)	−3132(7)	4452(5)	185(4)
O(12)	4934(8)	−2144(11)	4472(6)	194(5)
O(13)	3477(8)	−1164(6)	4815(4)	135(3)
O(14)	3252(9)	−1654(7)	3535(4)	156(3)
O(1ME)	2931(14)	−4749(13)	5137(11)	274(7)
N	5090(5)	−9133(5)	2695(3)	57(1)
N(1A)	5311(5)	−8176(5)	1141(3)	52(1)
N(1B)	5000(5)	−6411(5)	2369(3)	65(2)
C(1MA)	2368(20)	−5129(18)	6111(14)	229(8)
C(2MA)	2070(28)	−5374(26)	5454(16)	132(6)
C(2MB)	916(25)	− 5227(10)	2500	82(3)
C(1)	7500	−12635(10)	2500	82(3)
C(2)	6723(7)	−12012(7)	2793(5)	78(2)
C(3)	6714(6)	−10749(6)	2814(4)	59(2)
C(4)	7500	−10136(8)	2500	55(2)
C(5)	5949(6)	−10039(6)	3206(4)	63(2)
C(6A)	4186(6)	−9794(7)	2040(4)	64(2)
C(7A)	3494(6)	−8977(7)	1373(4)	64(2)
C(8A)	4183(6)	−8626(6)	824(4)	57(2)
C(9A)	3683(7)	−8783(7)	20(4)	70(2)
C10A)	4335(8)	−8465(7)	−457(4)	76(2)
C(11A)	5493(7)	−8039(7)	−134(4)	72(2)
C(12A)	5938(6)	−7904(6)	659(4)	61(2)
C(6B)	4436(7)	−8514(8)	3182(4)	75(2)
C(7B)	4987(7)	−7341(8)	3568(4)	77(2)
C(8B)	4719(6)	−6279(7)	3031(4)	67(2)
C(9B)	4218(8)	−5198(9)	3179(6)	92(3)
C(10B)	4007(8)	−4258(9)	2643(7)	99(3)
C(11B)	4271(8)	−4393(9)	1976(6)	94(3)
C(12B)	4783(7)	−5481(7)	1860(5)	76(2)

Table 3. Selected bond lengths [Å] and angles [°] for 1

Ni–O(2)	1.959(6)	Ni–O(1)	1.980(4)
Ni–N(1A)	2.024(5)	Ni–N(1B)	2.039(6)
Ni–N	2.107(5)	O(1)–C(4)	1.323(10)
O(2)–Ni–O(1)	74.5(3)	O(2)–Ni–N(1A)	112.1(2)
O(1)–Ni–N(1A)	98.4(2)	O(2)–Ni–N(1B)	91.7(3)
O(1)–Ni–N(1B)	162.1(2)	N(1A)–Ni–N(1B)	97.3(2)
O(2)–Ni–N	149.9(2)	O(1)–Ni–N	92.1(2)
N(1A)–Ni–N	96.3(2)	N(1B)–Ni–N	94.5(2)
C(4)–O(1)=Ni#1	127.67(14)	C(4)–O(1)–Ni	127.67(14)
Ni#1–O(1)–Ni	104.7(3)	Ni–O(2)Ni#1	106.3(5)

Symmetry transformations used to generate equivalent atoms:
#1 -x+3/2, y,-z+1/2

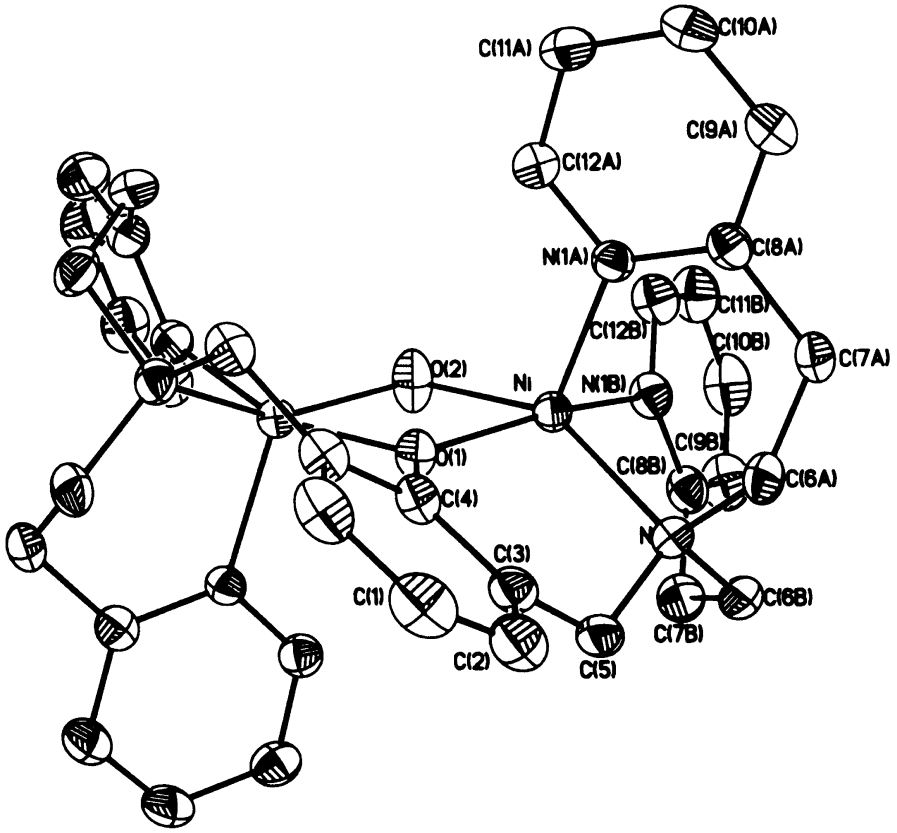

Fig. 1. ORTEP drawing of the cation $[Ni_2(\mu\text{-OH})(\mu\text{-LO}]^{2+}$ of complex **1**.

Electronic absorption spectrum

The electronic absorption spectrum of **1** in acetonitrile solution in the region 300 to 1100 nm shows maxima at (λ_{max}, nm (ϵ, $M^{-1}-cm^{-1}$)) 306 (3.78×10^3), 362 (1.21×10^3), 607 (128.9) and 820 (29.0). Four absorption bands (with a fifth band in the near IR region) have been observed for square pyramid, high spin Ni(II) complexes [24, 36] whereas octahedral Ni(II) complexes of ligands analogous to LOH [22, 35] show three weak absorption peaks expected for octahedral d^8 Ni(II) ions [39]. The native jack bean urease exhibits three week d-d bands at 407, 645 and 1060 nm consistent with an octahedral coordination [40] but also additional peaks at 630, 820 and 910 nm [17].

Nanda *et al* [36]. have reported the conversion of octahedral complexes to square pyramidal Ni(II) complexes which then show absorption peaks at 600 and 630 nm. This is in agreement with the observation of the broad absorption peak at 607 nm in the spectrum of 1. Addition of one equivalent aqueous $HClO_4$ to an acetonitrile solution of **1**, decreases the absorbances at 364 and 607 nm to very low values, while subsequent neutralization with aqueous NaOH reverses the reaction and restores the absorption. This process is observed for several such cycles. The addition of acid protonates the bridging hydroxide with subsequent coordination of water molecules to give an octahedral complex with far lower absorbances (Fig. 2).

$$[Ni_2LO(\mu-OH)]^{2+}+2H_2O\underset{OH^-}{\overset{H_3O^+}{\rightleftharpoons}}[Ni_2(LO)(OH_2)_4]^{3+}$$

Equilibrium shifts between square planar and octahedral coordinations on adding strong acid and strong base are known [41] in Ni(II) complexes of cyclic amines.

pH-metric titrations

Fig. 3 shows the superimposed pH-metric titration curves of acidified DMF/H_2O (5/3, v/v) solutions of the ligand and that of the ligand plus $Ni(ClO_4)_2.6H_2O$ (in 1:2 mole ratio). Three equivalents of aqueous $HClO_4$ were added each to, (a) a solution of the ligand and, (b) a solution of the ligand plus 2× mmoles of $Ni(ClO_4)_2.6H_2O$. On back-titration of each solution with standard aqueous NaOH, the titration of the solution of the ligand plus metal ion required one more equivalent of the base and showed one more end

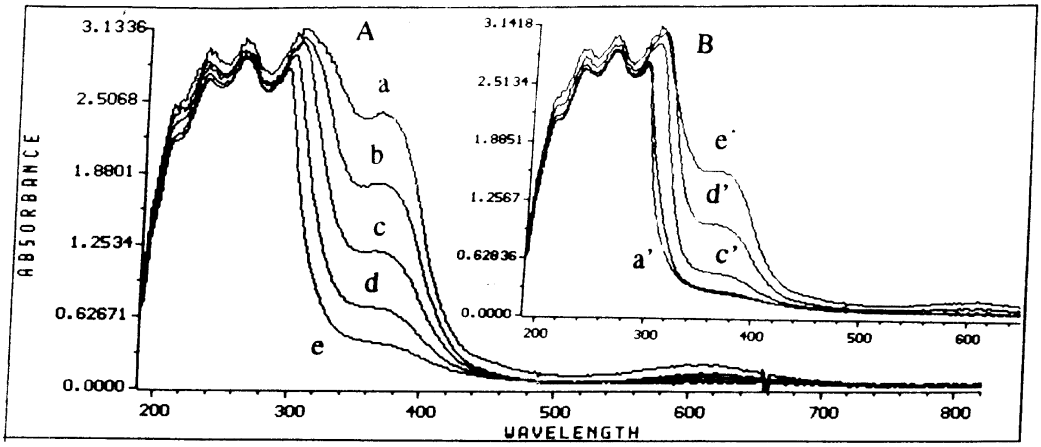

Fig. 2. A. Changes in the UV- Visible absorption spectrum, in the 190–650 nm region, of a 2.34 M acetonitrile solution of complex **1**, on stepwise addition of aqueous $HClO_4$ solution (0.1 M). Number of equivalents of acid added: **a**. 0.; **b**. 1; **c**.2; **d**. 3; **e**. 4. **B**. Reversal of the changes in the spectra in **A** on addition of aqueous NaOH solution (0.1 M) on the acidified solution in A. Number of equivalents of base added: **a′**. 0; **b′**. 1; **c′**.2; **d′**.3; **e′**.4. (Note: the absorbances of the starting solution (spectrum '**a**') and that of the final solution (spectrum '**e′**') are the same when dilution effects are factored).

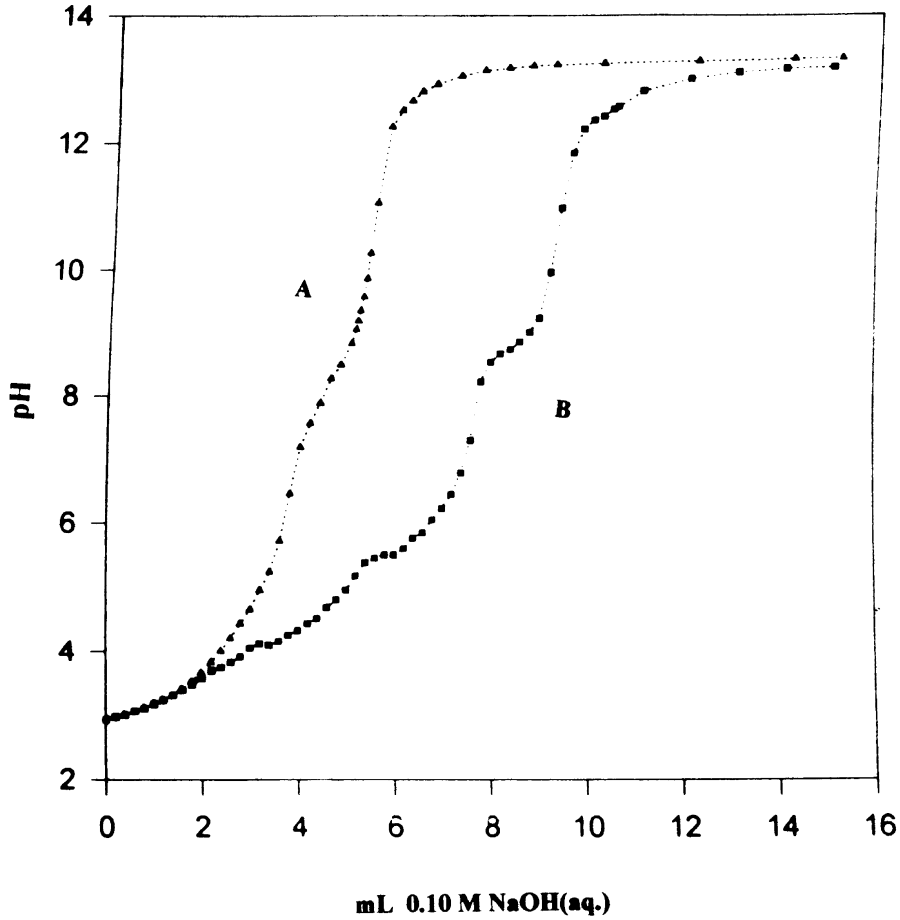

Fig. 3. Potentiometric titration curve for the back titration, vs. a 0.10 M aqueous NaOH solution, of 0.18 mmole of the ligand (**A**) and 0.18 mmole of the ligand plus 2X moles of $Ni(ClO_4)_2$ (B) each dissolved in 25 mL DMF/water (5:3, v/v) mixture that has been acidified by addition of 0.51 mmole (5.1 mL of a 0.10 M) aqueous $HClO_4$.

point (curve b) than the titration of the solution of the ligand alone (curve a). This additional end point is due to the titration of one Ni-coordinated water molecule (pKa $\approx$8.5) forming the bridging OH. This is also confirmed by the increase, during the titration, of the absorbances at 362 nm and 607 nm when the titration is followed spectrophotometrically.

Catalysis of hydrolysis

We studied the rate of the catalysis of the hydrolysis of a diester, bis(p-nitrophenyl)-phosphate (BNPP) in water/DMF (1:1, v/v) solution in buffers with pH ranging from 6 to 10. A plot of the rate constant (Kobs.) vs pH (Fig. 4) showed a sigmoid curve with an inflection point at a pH close to the pK_a of the Ni-coordinated water($\approx$8.5) consistent with the accepted mechanism that the metal-coordinated hydroxide is the effective nucleophile.

Magnetism

The room temperature magnetic moment of **1**, corrected for diamagnetic effects of the ligands and anions, is 2.67 BM per Ni(II) ion. For high spin square pyramidal Ni(II) complexes [42], this value indicates antiferromagnetic coupling between the bridged Ni(II) ions. This value is close to the value reported (2.68 BM) [24] for a doubly phenoxy bridged Ni(II) complexes similar to **1** in bridging angles and Ni $\cdots$ Ni distance.

The size of the Ni(II) magnetic exchange coupling constants (-J) of doubly oxy-bridged Cu(II) and Ni(II) tetragonal macrocyclic complexes show a linear correlation with the size of the bridging M-μ-O-M angle and the M $\cdots$ M distance (M = Cu(II) or Ni(II)) [43]. Antiferromagnetic interactions decrease with decreasing M-μ-O-M angle and crossover at 97.5° to ferromagnetic interactions [44]. The observed magnetic moment and antiferromagnetic interactions in **1** (average Ni-μ-O-Ni angle = 105.5°) are consistent with this correlation.

Cyclic voltammetry

The cyclic voltammetry of **1** in dimethylsulfoxide solution is shown in Fig. 5. Four distinct irreversible

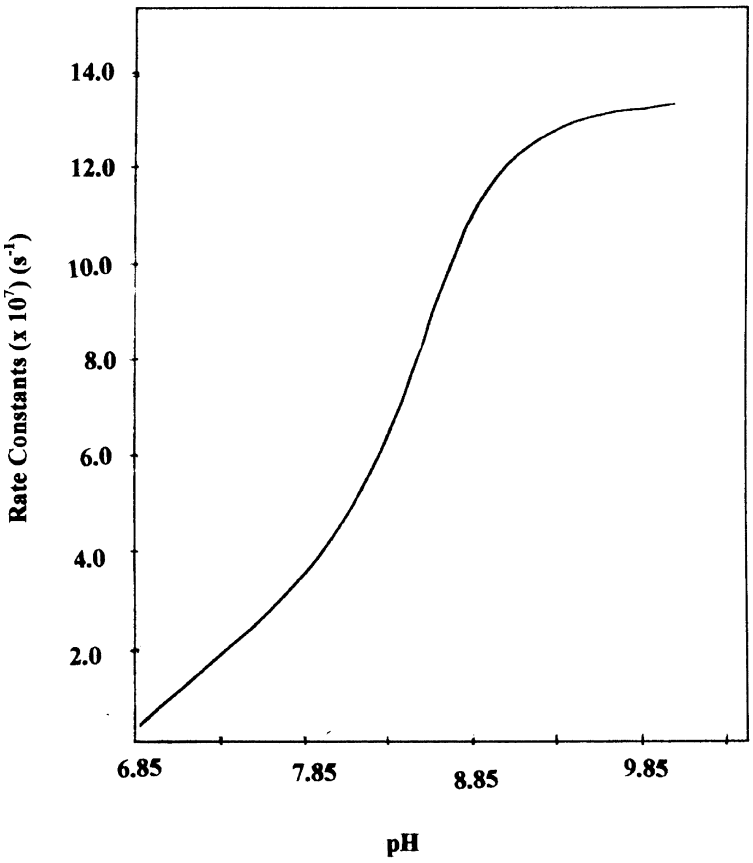

Fig. 4. K_{obs} vs. pH in the hydrolysis of BNPP (0.15 mL of 50 mM solution) in the presence of complex **1** (0.15 mL of 4.81 mM solution) in 3.0 mL of 0.1 solution of tris(hydroxymethyl)aminomethane buffer that was also made 0.01 M in $NaClO_4$ to maintain constant ionic strength.

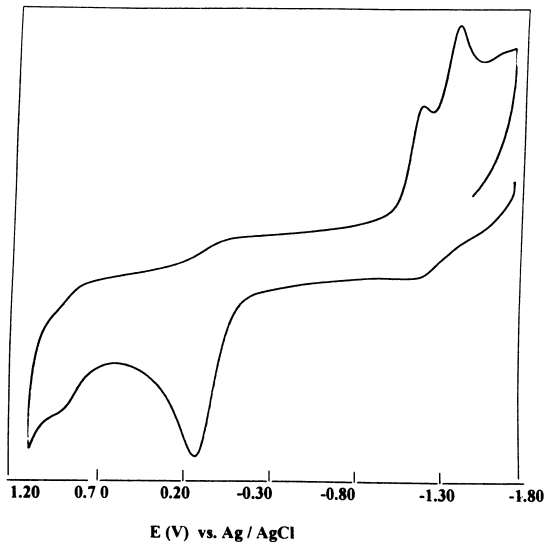

Fig. 5. Cyclic voltammogram of a 1.0 mM solution of complex **1** in dry DMSO using glassy carbon working electrode, Ag/AgCl reference electrode and Pt. auxillary electrode with $(t\text{-}Bu)_4NaClO_4$ (0.1 M) as a supporting electrolyte (scan rate = 100 mV/s.

peaks, two cathodic and two anodic, are observable. The cathodic waves at $E_p = -1.25$ V and -0001.45 V (vs Ag/AgCl) are assigned to the stepwise one-electron reductions of $Ni(II)_2$ to Ni(II),Ni(I), and to Ni(I),Ni(I) states respectively while the two anodic peaks at $E_p = +0.15$ V and $+0.87$ V (vs. Ag/AgCl) are assigned to the irreversible stepwise one-electron oxidations of **1** to Ni(II),Ni(III) and to $Ni(III)_2$ states respectively. By comparison, in the reported cyclic voltammetry (in dimethylsulfoxide) of the dinuclear square pyramidal Ni(II) complex of a tetraaminodiphenol macrocyclic ligand with aliphatic amine nitrogens and phenolate oxygen bridging, successive reversible one-electron processes are observed with potential peaks (vs SCE) of -1.32 V and -01.65 V (reductions) [45] and $+0.98$ and $+1.08$ V (oxidations). Both the reduction oxidation potentials of the corresponding processes are lower in **1** showing the easier accessibility of the various oxidation states. This result could be attributed to the greater flexibility of the ligand. Coordination geometry rearrangement, which often accompanies oxidation state changes in metal complexes, may be more difficult in the constrained cyclic ligand compared with the open chain structure of the ligand LOH. Other dinuclear octahedral Ni(II) complexes of macrocyclic ligands containing unsaturated and saturated amine and phenolic oxygen donor sets show reduction potentials in the range of -1.6 to -1.9 V (vs. SCE) [28]. The lower reduction potentials exhibited by **1** are also expected since the soft base pyridyl nitrogen donor, with its π -bonding ability, stabilizes the lower oxidation states better.

CONCLUSION

We have reported a new phenoxy and hydroxy doubly-bridged dinuclear Ni(II) complex in which each nickel is square pyramidally coordinated. The cyclic voltammetric studies in dimethylsulfoxide demonstrate that the complex can be reduced electrochemically to the Ni(II),Ni(I) state, the $Ni(I)_2$ state and oxidized to the Ni(II),Ni(III) and the $Ni(III)_2$ states at more moderate potentials than is observed for other Ni(II) dinuclear complexes of macrocylic ligands. The observed room temperature magnetic moment indicates antiferromagnetic coupling between the Ni(II) ions, which is consistent with the known correlation between the Ni-μ-O-Ni bridging angle and the sign of the magnetic coupling constant J in Ni(II) (and Cu(II) dinuclear) complexes. The electronic absorption spectral features are similar to those observed in other five coordinate square pyramidal Ni(II) complexes.

Supplementary material available

Bond lengths and angles (Table S1), anisotropic displacement parameters (Table S2), hydrogen coordinates and isotropic displacement parameters (Table S3) and observed and calculated structure factors (Table S4) (total 11 pages). Ordering information is given on any current masthead page.[??]List of Supplementary Material.Table S1: Bond Lengths (Å) and Angles (°) for 1.Table S2: Anisotropic Displacement Parameters [$Å^2 \times 10^3$] for **1**.Table S3: Hydrogen Coordinates ($\times 10^3$) and Isotropic Displacement Parameters ($Å^2 \times 10^3$) for Complex **1**Table S4: Observed and Calculated Structure Factors for Complex 1.

Acknowledgements—We would like to acknowledge the NIH-MBRS program of the Graduate School of Arts and Sciences of Howard University (YG) for the support of this work. RJB wishes to acknowledge DoD-ONR Grant N00014-93-1-1376 for funds to upgrade the existing Siemens P3 diffractometer to a P4 diffractometer.

REFERENCES

1. Kolodziej, A. F., In *Progress in Inorganic Chemistry*, K. D. Karlin, Ed., Wiley, N.Y. 494, 1994.
2. (a). Kovac, J. A., In *Advances in Inorganic Biochemistry*; Eichorn, G. L. and Marzilli, L. G. Eds. Prentice Hall, Englewood Cliffs, N. H. **9**, 1993. (b) Commack, R., Hall, D. O. and Rao, K. K., In *Microbial Gas Metabolism Mechanistic, Metabolic and Biotechnological Aspects*, 1985. Poole, R. K., Dow, C. S. Eds. Academic Press, London, 209. (c). Kubas, G., *Acc. Chem. Res.*, 1988, **21**, 120.
3. Andrews, R. K., Blakely, R. I. and Zerner, B., In *The Bioinorganic Chemistry of Nickel*, Lancaster, J. F. Ed., VCH, New York, 141–166, 1988.
4. Lappin, A. G. and McAuley, A., in *Advances in Inorg. Chem.* **32**, Sykes, A. G. Ed. Academic

Press, Inc. N.Y. 241–295 and references therein, 1988.
5. (a). Kinneary, J. F., Albert, J. S. and Burrows, C. J., *J. Am. Chem. Soc.*, 1988, **110**, 6124. (b). Yoon, H., Wagler, T. R., O'Connor, K. J. and Burrows, C. J., *J. Am.Chem. Soc.*, 1990, **112**, 4568. (c). Burrows, C. J., Muller, J. G., Poulter, G. T. and Rokita, S. E., *Acta Chim. Scand.*, 1996, **50**, 337.
6. Van der Zwaan, J. W., Coremans, J. M., Bouwens, E. C. and Albracht, S. P. J., Biochim. Biophys, *Acta*, 1990, **1041,** 101.
7. (a). Wolfe, R. S., *Trends in Biochem. Sci.*, 1985, **16**, 306. (b). Commack, R., *Nickel in Metalloproteins*, In *Advances in Inorganic Chemistry*, **32**, Sykes, A. G. Ed. Acad. Press, 1988, 297–333. (c). Commack, R., Fernandez, V. M. and Schneider, K. In *Bioinorganic Chemistry of Nickel*; Lancaster, J. R., Jr. Ed. VCH Publ. Deerfield Beach, Florida, 1988.
8. (a). Blakely, R. L. and Zerner, B., *J. Mol. Catal.*, 1984, **23**, 263. (b). Dixon, N.E., Gazzola, C., Blakely, R. L., Zerner, B., *J. Am. Chem. Soc.*, 1975, **97**, 4131. (c). Todd, M. J. and Hausinger, R. P., *J. Biol. Chem.*, 1989, **264**, 15835.
9. Johnson, M. K., In *Metal Clusters in Proteins*; Que, L. Ed. *ACS Symposium Series* 372, American Chemical Society, Washington, D.C., 1988, 326–342.
10. Perutz, M. F., Hasnain, S. S., Duke, P. J., Sessler, J. L. and Hain, J., *Nature*, 1982, 295.
11. Day, E. P., Peterson, J., Sendova, M. S., Todd, M. J. and Hausinger, R. P., *Inorg. Chem.*, 1993, **32,** 6634.
12. (a). Dixon, N. E., Riddles, P. W., Gazzola, C., Blakely, R. L. and Zerner, B., *Can. J. Biochem.*, 1980, **58**, 1335. (b). Jabri, E., Carr, M. B., Hausinger, R. P., Karplus, P. A., *Science*, 1995, **268**, **998** and references therein.
13. (a). Kim, H. and Lipscomb, W. N., *Biochemistry*, 1990, **29**, 5546. (b). Christianson, D. W., Lipscomb, W. N., *Acc. Chem. Res.*, 1989, **22**, 62.
14. Yamaguchi, K., Koshino, S., Akagi, F., Suzuki, M., Uehara, A. and Suzuki, S., *J. Am. Chem. Soc.*, 1997, **119,** 5752.
15. Clark, P. A., Wilcox, D. E. and Scott, R. A., *Inorg. Chem.*, 1990, **29,** 579.
16. Colpas, G. J., Maroney, M. J., Bgyinka, C., Kuman, M., Willis, W. S., Suib, S. L., Baidya, N. and Mascharak, P. K., *Inorg. Chem.*, 1991, **30,** 920.
17. Blakely, R. L., Dixon, N. E. and Zerner, B., *Biochim. Biophys Acta*, 1983, **744,** 219.
18. Wang, S., Lee, M. H., Hausinger, R. P. and Clark, P. A., *Inorg. Chem.*, 1993, **33,** 1589.
19. Buchanan, R. M., Mashuta, M. S., Oberhausen, K .J., Richardson, J. F., Li, Q. L. and Hendrickson, D. N., *J. Am. Chem. Soc.*, 1989, **111,** 4497.
20. Gultneh, Y., Farooq, A., Liu, S., Karlin, K. D. and Zubieta, J., *Inorg. Chem.*, 1992, **31,** 3607.
21. Mashuta, M. S., Webb, R. J., Oberhausen, K. J., Richardson, J. F., Buchanan, R. M. and Hendrickson, D. M., *J. Am. Chem. Soc.*, 1989, **111,** 2745.
22. Karlin, K. D., Gultneh, Y., Hayes, J. C., Cruse, R. W., McKown, J. W., Hutchinson, J. P. and Zubieta, J., *J. Am. Chem. Soc.*, 1984, **106,** 2121.
23. **Caution**: Although perchlorate salts are moderately stable, they are potential hazards and should therefore be handled with care and in small amounts.
24. (a). Storm, C. B., Freeman, C. M., Butcher, R. J., Turner, A. H., Rowan, N. S., Johnson, F. O. and Sinn, E., *Inorg. Chem.*, 1983, **22**, 678. (b). Spencer, J.T., Pourian, M. R., Butcher, R. J., Sinn, E. and Grimes, R. N., *Organometallics*, 1987, **6**, 335.
25. Mohan, M., Holmes, S. M., Butcher, R. J., Jasinski, J. P. and Carrano, C. J., *Inorg. Chem.*, 1992, **31,** 2029.
26. Karle, J. and Karle, I. L., *Acta Cryst.*, 1966, **21,** 849.
27. G. M. Sheldrick, SHELXTL, Siemens Analytical Instruments, Madison, WI.
28. Definitions of terms used in table 1 are as follows:

$$R(int) = \sum|F^2_o - F^2_o(mean)|/\sum[F^2_o]$$

$$R(sigma) = \sum[\sum(F_o)^2]/\sum[F^2_o]$$

$$R1 = \sum||F_o| - F_c||/\sum|F_o|$$

$$wR2 = [\sum[w(F^2_o - F^2_c)^2]/\sum[w(F)o^2)^2]]^{1/2}$$

$$Goof = S = [\sum[w(F^2_o - F^2_c)^2]/(n-p)]^{1/2},$$

where n is the number of reflections and p is the total number of parameters refined.
29. (a). Karlin, K. D., Cruse, R. W., Gultneh, Y., Hayes, J. C. and Zubieta, J., *J. Am. Chem. Soc.*, 1984, **106**, 3372. (b). Sorrel, T. N. and Garrity, M. L., *Inorg. Chem.*, 1991, **30**, 210.
30. Diril, H., Chang, H.-R., Zhang, X., Larasen, S. K., Potenza, J. A., Pierpont, C. G., Schugar, H. J., Isied, S. S. and Hendrickson, D. N., *J. Am. Chem. Soc.*, 1987, **109,** 6207.
31. (a). Suzuki, M., Kanatomi, H. and Murase, I., *Chem. Lett.*, 1981, 1745. (b). Suzuki, M., Ueda, I., Kanatomi, H. and Murase, I., *Chem. Lett.*, 1983, 185.
32. (a). Nie, H., Aubin, S. M. J., Mashuta, M. S., Wu, C., Richardson, J. F., Hendrickson, D. N. and Buchanan, R. M., *Inorg. Chem.*, 1995, **34**, 2382. (b). Uhlenbrock, S. and Krebs, B., *Angew. Chem. Int. Ed. Engl.*, 1992, **31**, 1647.
33. Kim, E. E. and Wykoff, H .W., *J. Mol. Biol.*, 1991, **218,** 449.
34. Vallee, B. L., Galdes, A., Auld, D. S. and Riordan, J. In *Zinc Enzymes* Spiro, T. G. Ed. Wiley, N.Y. 1983, 25–76.
35. Chaudhuri, P., Kuppers, H.-J., Wieghardt, K., Gehring, S., Haase, W., Nuber, B. and Weiss, J. *J. Chem. Soc. Dalton Trans.*, 1988, 1367.
36. Nanda, K., Das, R., Thompson, L. K., Krishnan, V. and Nag, K., *Inorg. Chem.*, 1994, **33,** 5934.
37. Nanda, K., Das, R., Venkatsubramanian, K., Paul, P. and Nag, K., *J. Chem. Soc. Dalton Trans.*, 1993, 2515. (b). Nanda, K. K., Das, R., Newlands, M. J., Hynes, R., Gabe, E. J. and Nag, K., *J. Chem. Soc. Dalton Trans.*, 1992, 897.
38. Karlin, K. D., Dahlstrom, P. L., Cozzette, A. N., Scensny, P. M. and Subieta, J., *J. Dalton Trans.*, 1993, 2515., (b) Nanda, K. K., Das, R., Newlands,

M. J., Hynes, R., Gabe, E. H. and Nag, K., *J. Chem Soc. Dalton Trans*., 1992, 897.[??]Karlin, K. D., Dahlstrom, P. L., Cozzette, A. N., Scensny, P. M. and Zubieta, J., *J. Chem. Soc. Chem. Commun*., 1981, 881.

39. Duggan, D. M. and Hendrickson, D. N., *Inorg. Chem*., 1984, **13,** 2956.
40. Blakely, R. L. and Zerner, G., *J. Mol. Catal*., 1984, **23,** 263.
41. Hay, R. W., Darby, A., Lightfoot, P. and Lampeka, Y. D., *Polyhedron*, 1997, **16,** 2777.
42. The range of magnetic moments typically observed among isolated Ni(II) complexes vary with coordination geometry: octahedral: 2.9–3.2 μ_B; square pyramidal and trigonal bipyramid: 3.2–3.4 μ_B; tetrahedral: near 4.0 and distorted tetrahedral: 3.5–3.9 μ_B while square planar Ni(II) are diamagnetic. See Clark, P. A. and Wilcox, D. E. *Inorg. Chem*. 1989, 28, 1326.
43. (a). Nanada, K. K., Thompson, L. K., Bridson, J. N. and Nag, K., *J. Chem. Soc. Chem. Commun*., 1994, 1337. (b). Nanda, K. K., Das, R., Thompson, L. K., Venkatsubramanian, K. and Nag, K., *Inorg. Chem*., 1994, **33**, 5934. (c). Estes, E. D., Hatfield, W. E., Hodgson, D. J., *Inorg. Chem*., 1974, **13**, 1645. (d). Lewis, D. L., McGregor, K. T., Hatfield, W. E. and Hodgson, D. J., *Inorg. Chem*., 1974, **13**, 1013.
44. (a). Aratake, Y., Ohba, M., Sakiyama, H., Tadokoro, M., Matsumoto, N. and Okawa, H., *Inorg. Chim. Acta*, 1993, **212**, 183–190. (b). Hodgson, D. J. Prog. *Inorg. Chem*. 1975, **19**, 174.
45. Das, R. and Nag, K., *Inorg. Chem*., 1991, **30,** 2831.

Pergamon

PII: S0277–5387(98)00117–X

Polyhedron Vol. 17, No. 19, pp. 3361–3370, 1998
© 1998 Elsevier Science Ltd
All rights reserved. Printed in Great Britain
0277–5387/98 $19.00+0.00

Comparison of divalent dimethoxyethane-solvated thulium and samarium diiodides in hexamethylphosphoramide and pyridine: Isolation of the cations $\{[TmI_2(HMPA)_4][I](pyridine)_5\}$ and $\{[TmI(HMPA)_4(pyridine)][I]_2\}$ and a single crystal containing both linear and bent dimethoxyethane-solvated SmI_2

William J. Evans*, Randy N. R. Broomhall-Dillard and Joseph W. Ziller

Department of Chemistry, University of California, Irvine, Irvine, California, 92697-2025, U.S.A.

(Received 8 December 1997; accepted 16 March 1998)

Abstract—The highly reducing nature of $TmI_2(DME)_3$ is shown by comparison with SmI_2 in its reactions in hexamethylphosphoramide (HMPA) and pyridine. Addition of 4 equiv. of HMPA to green $TmI_2(DME)_3$ in dimethoxyethane (DME) forms pale yellow solids which dissolve in pyridine and can be isolated as $TmI_3(HMPA)_4$, **1**. Recrystallization of **1** from pyridine yields $\{[TmI_2(HMPA)_4][I](pyridine)_5\}$, **2**, or $\{[TmI(HMPA)_4(pyridine)][I]_2\}$, **3**, depending upon conditions. Both **2** and **3** crystallize with distorted octahedral geometries around thulium. Addition of HMPA to TmI_3 in DME also forms **1**. $TmI_2(DME)_2$, formed by the loss of DME from $TmI_2(DME)_3$ under vacuum, reacts with pyridine to form intensely colored materials, which have magnetic moments consistent with the presence of Tm(III). In comparison, $SmI_2(THF)_2$ dissolves in a mixture of pyridine and DME and can be recrystallized as divalent $SmI_2(DME)_3$, **4**. **4** crystallizes with both linear and bent I-Sm-I arrangements in the same crystal. In the former case a hexagonal bipyramidal coordination geometry is present and in the latter a dodecahedral geometry is observed. © 1998 Elsevier Science Ltd. All rights reserved

Keywords: thulium; samarium; iodide; divalent; trivalent.

Divalent lanthanide chemistry traditionally has been limited to the three elements, Eu, Yb, and Sm, which have the most accessible +2 oxidation states [1]. Samarium is the most strongly reducing of these metals and $SmI_2(THF)_x$ is widely used in organic chemistry as a one-electron reducing agent [2]. However, recently the synthesis and X-ray crystal structure of the first molecular complex of Tm(II), $TmI_2(DME)_3$ (DME=$MeOCH_2CH_2OMe$) was reported [3]. The Tm(III)/Tm(II) reduction potential, cited in the literature as −2.3 V vs. NHE [4], suggests that $TmI_2(DME)_3$ should be highly reactive. We report here some comparisons of the behavior of thulium diiodide and samarium diiodide in strongly coordinating polar solvents commonly used with the samarium reagent. The isolation of two different forms of cationic solvated trivalent thulium iodide complexes is reported as well as a single crystal of $SmI_2(DME)_3$ containing both linear and bent I-Sm-I units.

EXPERIMENTAL

General procedures

The chemistry described below was performed under nitrogen with rigorous exclusion of air and

* Author to whom correspondence should be addressed..

water using standard Schlenk, vacuum line and glove box techniques. $TmI_2(DME)_2$ was prepared from TmI_3 and Tm metal following the procedure for the preparation of $TmI_2(DME)_3$ [5]. Removal of solvent from the initially obtained solution of $TmI_2(DME)_3$ without subsequent recrystallization gives $TmI_2(DME)_2$. (Anal. Calcd. for $C_8H_{20}O_4I_2Tm$: C, 15.8; H, 3.3; O, 11.6, I, 41.6, Tm, 27.7. Found: C, 15.00; H, 3.21; I, 39.75; Tm, 26.85.) $SmI_2(THF)_2$ was prepared as described previously [5]. Dimethoxyethane (Acros) was pre-dried over molecular sieves and distilled from NaK before use. Pyridine and hexamethylphosphoramide (Acros) were dried over molecular sieves, distilled, and degassed before use. NMR spectrometry and magnetic susceptibility measurements were recorded on either General Electric GN500 or QE300 or Bruker DRX400 spectrometers following the Evans' method [6]. Infrared spectra were obtained on a Perkin Elmer 1600 FTIR. Elemental analyses were done by Analytische Laboratorien, D-51779 Lindlar, Germany, or by complexometric titration [7].

Synthesis and spectroscopic characterization

Reactions of $TmI_2(DME)_2$ with HMPA. In a glove box, addition of HMPA (0.95 g, 5.31 mmol) to a green DME solution of $TmI_2(DME)_2$ (0.80 g, 1.33 mmol) caused immediate formation of a deep brown solution. Within 2 h, the color faded to pale yellow with the formation of a pale yellow precipitate which was separated by centrifugation. The pale yellow precipitate was dissolved in pyridine to form a clear, pale yellow solution. Evaporation of the solvent by rotary evaporation gave pale yellow $TmI_3(HMPA)_4$, **1** (1.073 g, 60% based on $TmI_2(DME)_2$). IR (KBr): 2916s, 2815s, 1752w, 1484s, 1451s, 1307s, 1191s, 1124s, 1067s, 990s, 797w, 756s, 711w, 649w, 478s cm^{-1}. Anal. Calcd for $C_{24}H_{72}I_3N_{12}O_4P_4Tm$: C, 22.76; H, 5.73; I, 30.06; N, 13.27; P, 9.78; Tm, 13.34. Found: C, 23.01; H, 5.70; I, 30.30; N, 13.25; P, 9.64; Tm, 13.60. Magnetic susceptibility (293 K, pyridine) $\chi_M = 2.42 \times 10^{-2}$; $\mu_{eff} = 7.5\ \mu_B$. Recrystallization of **1** in pyridine at $-38^\circ C$ yielded pale yellow crystals of $\{[TmI_2(HMPA)_4][I](pyridine)_5\}$, **2**.

The reaction of $TmI_2(DME)_2$ (0.200 g, 0.332 mmol) with a smaller amount of HMPA (0.119 g, 0.664 mmol) in DME immediately formed a brown solution whose color faded slowly over 12 hours to green with the formation of a pale yellow precipitate. The pale yellow precipitate was separated by centrifugation, dissolved in pyridine, and dried by rotary evaporation to pale yellow **1** (0.175 g, 0.138 mmol, 40%). Recrystallization at $-38^\circ C$ of these pale yellow solids in pyridine yielded crystals of $\{[TmI(HMPA)_4(pyridine)][I]_2\}$, **3**, in one case, and crystals of **2** when the procedure was repeated several times.

The reaction of $TmI_2(DME)_2$ (0.150 g, 0.249 mmol) with HMPA (0.268 g, 1.49 mmol) in DME and the reaction of $TmI_2(DME)_2$ (0.150 g, 0.249 mmol) with neat HMPA (5 mL) also gave pale yellow solids which dissolved in pyridine and could be recrystallized as $\{[TmI_2(HMPA)_4][I](pyridine)_5\}$, **2**.

Reactions of TmI_3 with HMPA In a glovebox, HMPA (0.098 g, 0.546 mmol; 0.196 g, 1.09 mmol; and 0.293 g, 1.64 mmol in three separate reactions) was added to grey TmI_3 (0.150 g, 0.273 mmol for each reaction) in DME and the mixture was stirred for 5 h. The pale yellow solution was separated by centrifugation from the precipitate and was dried by rotary evaporation to a yellow/brown oil containing excess HMPA (0.064 g, 0.102 g, or 0.164 g, respectively). The pale yellow precipitate was dissolved in pyridine to form a clear, pale yellow solution which was dried by rotary evaporation to a pale yellow solid, **1**, (0.134 g, 0.106 mmol, 40%; 0.230 g, 0.182 mmol, 65%; or 0.250 g, 0.197 mmol, 70% respectively). Recrystallization of **1** in each case yielded $\{[TmI_2(HMPA)_4][I](pyridine)_5\}$, **2**, by unit cell determination.

Reactions of $TmI_2(DME)_2$ with pyridine. In a glovebox, pyridine (0.197 g, 2.488 mmol) was added to a green solution of $TmI_2(DME)_2$ (0.300 g, 0.498 mmol) in DME (10 mL) at ambient temperature producing a deep green brown solution instantly. After stirring for 4–5 hours, a red/purple precipitate and a pale orange solution were present. The precipitate was separated from the solution by centrifugation. The pale orange solution was dried on a rotary evaporator to an oily dark orange solid (0.141 g), which darkened overnight to a deep blue color. IR (KBr): 3025m, 2919s, 1631w, 1596s, 1525w, 1484w, 1437s, 1261w, 1214w, 1091m, 1038s, 1002w, 854w, 802m, 750m, 697s, 626m cm^{-1}. Metal content: Tm, 23.9%. Magnetic susceptibility (293 K, pyridine) $\chi_M = 2.29 \times 10^{-2}$; $\mu_{eff} = 7.3\ \mu_B$. The red/purple precipitate was dried on a rotary evaporator (0.164 g). IR (KBr): 3031w, 2938m, 1547m, 1577w, 1458m, 1370w, 1280m, 1213w, 1190w, 1086m, 1028s, 975w, 860s, 747m, 631w cm^{-1}. Metal content: Tm, 24.5%. Magnetic susceptibility (293 K, pyridine) $\chi_M = 2.07 \times 10^{-2}$; $\mu_{eff} = 7.0\ \mu_B$.

$TmI_2(DME)_2$ (0.300 g, 0.498 mmol) was dissolved in pyridine (approximately 10 mL) instantly producing a very dark blue solution. The intense blue solution was stirred overnight and dried on a rotary evaporator yielding a thick oily, black solid (0.345 g). IR (KBr): 3049m, 2928s, 1601s, 1488m, 1441s, 1220m, 1149w, 1098w, 1067m, 1039s, 1006s, 963s, 808w, 755m, 700s, 624m cm^{-1}. Metal content: Tm, 22.7%. Magnetic susceptibility (293 K, pyridine) $\chi_M = 2.12 \times 10^{-2}$; $\mu_{eff} = 7.1\ \mu_B$.

Reactions of $SmI_2(THF)_2$ with pyridine. In a glovebox, pyridine (0.144 g, 1.823 mmol) was added to a mixture of deep blue $SmI_2(THF)_2$ (0.200 g, 0.365 mmol) in DME (approximately 10 mL) at ambient temperature. The solution immediately turned black and was stirred for 4–5 hours. The dark purple solids remaining after this time were separated from the solution by centrifugation and were extracted

three times with 10 mL of DME. The combined DME solutions were dried on a rotary evaporator yielding deep purple/black solids (0.212 g). ^{1}H NMR (THF-d_8): 7.90 (br. s, 2H), 6.96 (t, 1H), 6.54 (d, 2H), 3.42 (s, 10H), 3.25 (s, 14H) d. IR (KBr): 2931s, 1640w, 1461s, 1367w, 1284w, 1261w, 1190w, 1120m, 1091m, 1026s, 850s, 803m, 756w, 697w cm^{-1}. Metal Content: Sm, 21.3%. Magnetic susceptibility (293 K, THF) $\chi_M = 3.64 \times 10^{-3}$; $\mu_{eff} = 2.9\,\mu_B$. Recrystallization of the purple/black solids in DME at -38°C yielded red/purple crystals of $SmI_2(DME)_3$, **4**.

X-ray structure determinations

$\{[TmI_2(HMPA)_4][I](pyridine)_5\}$, ***2***. A pale yellow crystal of approximate dimensions $0.13 \times 0.16 \times 0.24$ mm was immersed in Paratone-D oil under nitrogen and then manipulated in air onto a glass fiber and transferred to the nitrogen stream of a Syntex P4 diffractometer. The determination of Laue symmetry, crystal class, unit cell parameters and the crystal's orientation matrix were carried out according to standard procedures [8]. Intensity data were collected at 163 K using a $2\theta/\omega$ scan technique with Mo Kα radiation.

The raw data were processed with a local version of CARESS [9] which employs a modified version of the Lehman-Larsen algorithm to obtain intensities and standard deviations from the measured 96-step peak profiles. Subsequent calculations were carried out using the SHELXTL program [10]. All 1745 data were corrected for absorption and for Lorentz and polarization effects and were placed on an approximately absolute scale. The diffraction symmetry was 4/m with the systematic extinction *hkl* for $h+k+l=2n+1$. It was later determined that the noncentrosymmetric tetragonal space group $I\bar{4}[S_4^2;\text{No.82}]$ was correct.

The structure was solved by direct methods and refined on F^2 by full-matrix least-squares techniques. The analytical scattering factors for neutral atoms were used throughout the analysis [11]. The molecule is located on a site of $\bar{4}$ symmetry. There are five molecules of pyridine present per formula unit. One pyridine molecule is in a general position and one is located on a $\bar{4}$ site. The pyridine located on the $\bar{4}$ site is disordered. Three atoms defined as carbon with SOF = 0.51388 were included to account for the disorder. Hydrogen atoms (except those on the disordered pyridine) were included using a riding model. At convergence, w$R2 = 0.0590$ and GOF = 1.058 for 175 variables refined against all 1736 unique data ($R1 = 0.0276$ for those 1539 data with $F > 4.0\sigma(F)$). The absolute structure was determined by refinement of the Flack parameter [12].

$\{[TmI(HMPA)_4(pyridine)][I]_2\}$, ***3***. A pale yellow crystal of approximate dimensions $0.10 \times 0.21 \times 0.23$ mm was handled at 158 K on a Syntex P4 diffractometer solved and as described for **2**. All 7030 data were corrected for absorption and for Lorentz and polarization effects and were placed on an approximately absolute scale. The diffraction symmetry was 2/m with the systematic extinction *hkl* for $h+k=2n+1$ and *h0l* for $l=2n+1$. The two possible monoclinic space groups are Cc and C2/c. It was later determined that the centrosymmetric space group C2/c was correct.

The structure was solved and refined as described for **2**. Atoms N(4), N(5), N(6), C(7), C(9), C(10, C(11), and C(12) are disordered. Each of these atoms was included with two components which were assigned site-occupancy-factors of 0.5. There appears to be a pyridine solvent molecule present which is disordered. It was not possible to model the disordered solvent and it was not included in the refinement or in the calculation of density, absorption coefficient, etc. Hydrogen atoms were not included in the refinement. At convergence, w$R2 = 0.1772$ and GOF = 1.115 for 190 variables refined against all 6757 unique data. (As a comparison for refinement on *F*, $R1 = 0.0572$ for those 5298 data with $F > 4.0\sigma(F)$)

$SmI_2(DME)_3$, ***4***. A red/purple crystal of approximate dimensions $0.10 \times 0.20 \times 0.23$ mm was handled at 163 K on a Siemens P4 rotating-anode diffractometer, solved, and refined as described for **2**. All 5059 data were corrected for absorption and for Lorentz and polarization effects and were placed on an approximately absolute scale. The diffraction symmetry was 2/m with systematic absences *hkl* for $h+k=2n+1$ and *h0l* for $l=2n+1$. The two possible monoclinic space groups are Cc and C2/c. It was determined that the centrosymmetric space group C2/c was correct.

There are two independent molecules of the formula unit present. One molecule is located on a two-fold rotation axis while the other is located on an inversion center ($Z=8$). Molecule 1 has a SmI_2 unit which is bent (I-Sm-I = 157.65(2)$^\circ$), while the SmI_2 unit in molecule 2 is linear due to the crystallographic inversion center. There is no indication that the SmI_2 unit in molecule 2 is disordered which might result in the observed linear arrangement. The dimethoxyethane ligands on molecule 2 are disordered. All twelve carbon atoms associated with this molecule were included with site-occupancy-factors = 0.50. The three unique oxygen atoms were assigned occupancy factors of 1.0. Hydrogen atoms were included using a riding model. At convergence, w$R2 = 0.0698$ and GOF = 1.055 for 246 variables refined against all 4950 unique data. (As a comparison for refinement on *F*, $R1 = 0.0309$ for those 3915 data with $F > 4.0\sigma(F)$.)

Further evidence for this linear SmI_2 arrangement is that the same pattern is observed when the structure is refined in the noncentrosymmetric space group Cc. In the space group Cc there are three independent molecules ($Z=8$). Two of the molecules are located on two-fold rotation axes while the third is in a general position. The I-Sm-I angles of the molecules on the two-fold axes are 157.50(12)$^\circ$ and 157.82(13)$^\circ$. The I-

Sm-I angle for the molecule in the general position is 179.86(8)°. There is no disorder observed, however, the light atoms could not be refined anisotropically. It is concluded that the SmI_2 units adopt different (bent and linear) arrangements and that refinement of the structure in the centrosymmetric space group C2/c is preferred.

RESULTS

Hexamethylphosphoramide (HMPA) reactions

HMPA is a strongly coordinating ligand which displaces THF from blue $SmI_2(THF)_x$ to form divalent black-purple $SmI_2(HMPA)_4$ and displaces the iodide ligands in yellow $YbI_2(THF)_x$ to form dark yellow $[Yb(HMPA)_4(THF)_2]I_2$ [13]. Similar behavior was investigated with $TmI_2(DME)_3$ and its bis(dimethoxyethane) derivative $TmI_2(DME)_2$, which is isolated when solutions of $TmI_2(DME)_3$ are dried on a rotary evaporator.

The intense green color of $TmI_2(DME)_3$ in DME immediately changes to brown upon addition of HMPA. This color fades within 2 to 12 hours to a pale yellow color characteristic of Tm(III) and the precipitation of pale yellow $TmI_3(HMPA)_4$, **1**, is observed. Complex **1** can also be obtained from the reaction of TmI_3 with HMPA in DME. Although insoluble in DME and HMPA, **1** dissolves in pyridine to form a pale yellow solution from which crystals of $\{[TmI_2(HMPA)_4][I](pyridine)_5\}$, **2** (Figure 1), or $\{[TmI(HMPA)_4(pyridine)][I]_2\}$, **3** (Figure 2), can be obtained. Even though crystals of **2** and **3** readily desolvate, structural data were obtainable on each. **2** can also be obtained from the reaction of TmI_3 with HMPA in pyridine.

The isolation of the two different forms of solvated thulium iodides **2** and **3** is consistent with previously studied HMPA/lanthanide chemistry. For example, both $YbCl_3(HMPA)_4$ and $\{[Yb(H_2O)_5(HMPA)_2]Cl_3(H_2O)(HMPA)\}$ can be isolated from reactions of $YbCl_3$ with HMPA in THF depending on crystallization conditions [13]. As a strongly solvating ligand, it is also not uncommon for HMPA to displace anionic ligands from the coordination sphere of the metal. Examples include $[Yb(HMPA)_4(THF)_2][I]_2$ [14], $[\{Yb(HMPA)_3\}_2(\mu\text{-}SPh)_3][SPh]$ [15], and $\{[Yb(H_2O)_5(HMPA)_2]Cl_3(H_2O)(HMPA)\}$ [13].

In both **2** and **3**, the geometry around thulium is distorted octahedral. In **2**, the two iodide ligands are trans and in **3**, the iodide is trans to pyridine. The Tm-I distances in **2** and **3** are 3.0452(6) and 3.0057(14) Å, and, as expected, are shorter than the Tm-I average distances (3.16(2) Å) in divalent $TmI_2(DME)_3$ [3]. The difference is consistent with the difference in effective ionic radii of six coordinate Tm(III) (0.88 Å) and seven coordinate Tm(II) (1.09 Å) [17]. The Tm-I distances in **2** and **3** are also consistent with other trivalent lanthanide iodide and thulium chloride distances in the literature after the appropriate differences in radii are considered [17–19]. Hence, no significant elongation of the Tm-I bonds is observed in

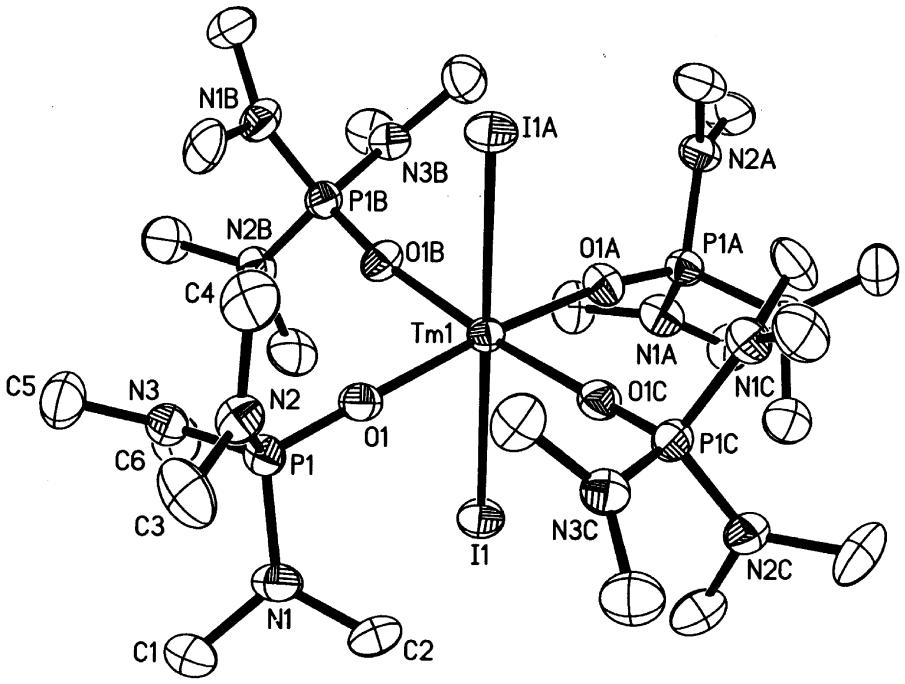

Fig. 1. Thermal ellipsoid plot of $\{[TmI_2(HMPA)_4][I](pyridine)_5\}$, **2**, drawn at the 50% probability level with pyridine omitted for clarity.

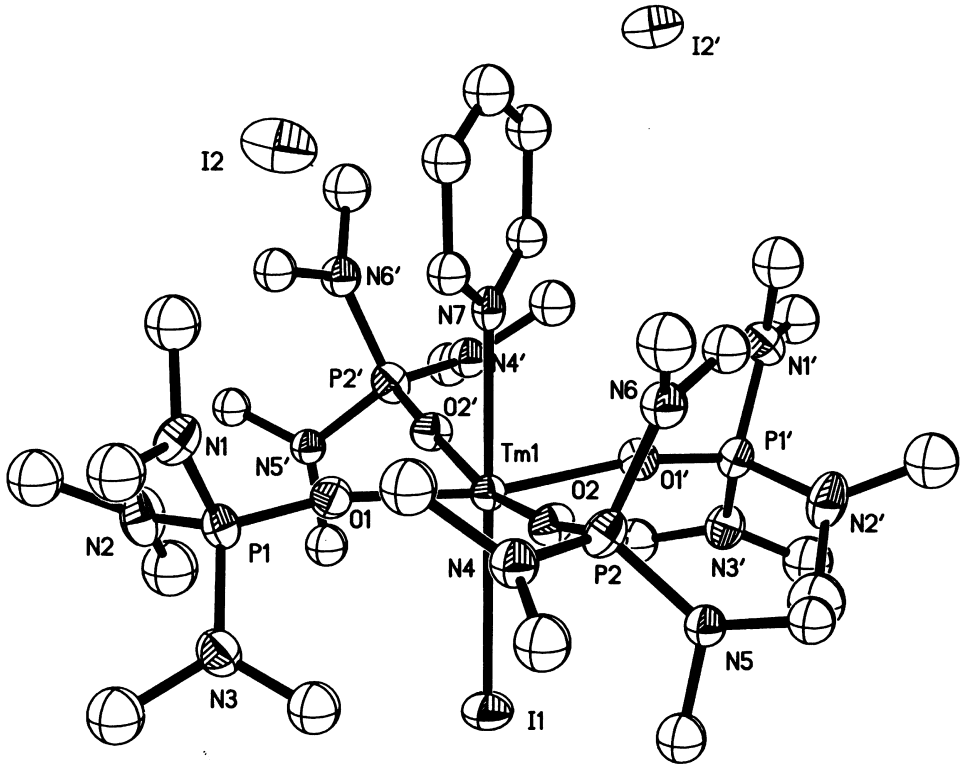

Fig. 2. Thermal ellipsoid plot of $\{[TmI(HMPA)_4(pyridine)][I]_2\}$, **3**, drawn at the 50% probability level.

the presence of the strongly coordinating HMPA [13, 14], as was observed in divalent $SmI_2(HMPA)_4$ [13].

The Tm(III)-O(HMPA) distances vary between 2.189(4) Å and 2.208(5) Å in **2** and **3**. These are significantly shorter than the 2.353(3) and 2.315(3) Å Tm(III)-O(THF) distances of in trivalent $(C_8H_8)Tm[PhC(NSiMe_3)_2](THF)$ [20] and $Tm[P(SiMe_3)_2]_3(THF)_2$ [21] respectively. The short Tm(III)-O(HMPA) distances are consistent with the analogous distances in $DyCl_3(HMPA)_3$ [22].

Pyridine reactions

The addition of pyridine to DME solutions of $TmI_2(DME)_3$ produces intensely colored compounds: a red/purple precipitate and a solution which yielded a deep blue oil. Addition of $TmI_2(DME)_2$ to pure pyridine generated a black oil. Although these intense colors are often characteristic of divalent lanthanides, in this case magnetic moments of these materials were found to be 7.0–7.1 μ_B and are consistent with the presence of Tm(III) [23].

In contrast, addition of pyridine to $SmI_2(THF)_2$ in DME gives divalent products. Deep blue/purple solids can be isolated which have a magnetic moment of 2.9 μ_B consistent with Sm(II) [23]. Recrystallization of this material in DME yields red/purple crystals of $SmI_2(DME)_3$, **4**, which have not incorporated any of the pyridine.

Complex **4** crystallizes with two different eight coordinate molecular geometries (Figs 3 and 4) and two very different I-Sm-I angles within the same unit cell. In each of the independent molecules in the unit cell, the samarium center is surrounded by two iodide and three chelating DME ligands, but the arrangements of the ligands differ. In the asymmetric molecule **4A**, the I-Sm-I angle is bent, 157.65(2)°, and the eight ligands form a distorted dodecahedron, Fig. 5. In the symmetric molecule **4B**, the I-Sm-I angle is linear at 180°, and a distorted hexagonal bipyramidal coordination environment surrounds samarium, Fig. 6. Although, in previously characterized SmI_2 complexes an extensive range of I-Sm-I angles have been observed, in no case have both bent and linear I-Sm-I units been found in the same crystal. Previously reported I-Sm-I angles include: 87.75(1)–173.04(2)° for $[SmI_2(NCCMe_3)_2]_n$ [24], 92.0(1)° for cis-$SmI_2[(O(CH_2CH_2OMe)_2]_2$ [25], 84.0(1)–175.7(1)° for $[Sm(\mu\text{-}I)(N\text{-}MeIm)_3]_2$ [26], 178.1(1)° for $SmI_2(DME)_2(THF)$ [27] and $SmI_2(DME)(THF)_3$ [27], and 180.0° for the complexes trans-$SmI_2[(O(CH_2CH_2OMe)_2]_2$ [24] and $[SmI_2(OPMePh_2)_4]I$ [28].

The Sm-I distances in **4** are similar: 3.2897(4) Å for the linear I-Sm-I molecule and 3.3091(5) Å for the bent compound. These distances are also similar to the analogous lengths in eight coordinate cis- and trans-$SmI_2[(O(CH_2CH_2OMe)_2]_2$, 3.333(1) [25] and 3.265(1) Å [24], respectively, except that the difference

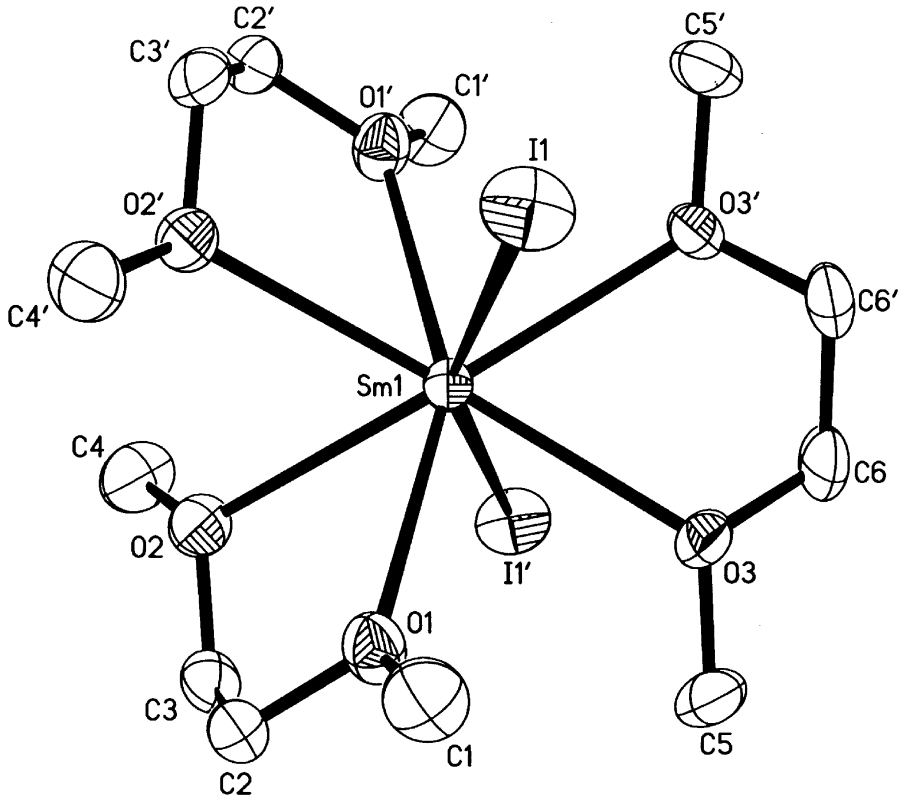

Fig. 3. Thermal ellipsoid plot of the bent I-Sm-I molecule of $SmI_2(DME)_3$, **4A**, drawn at the 50% probability level.

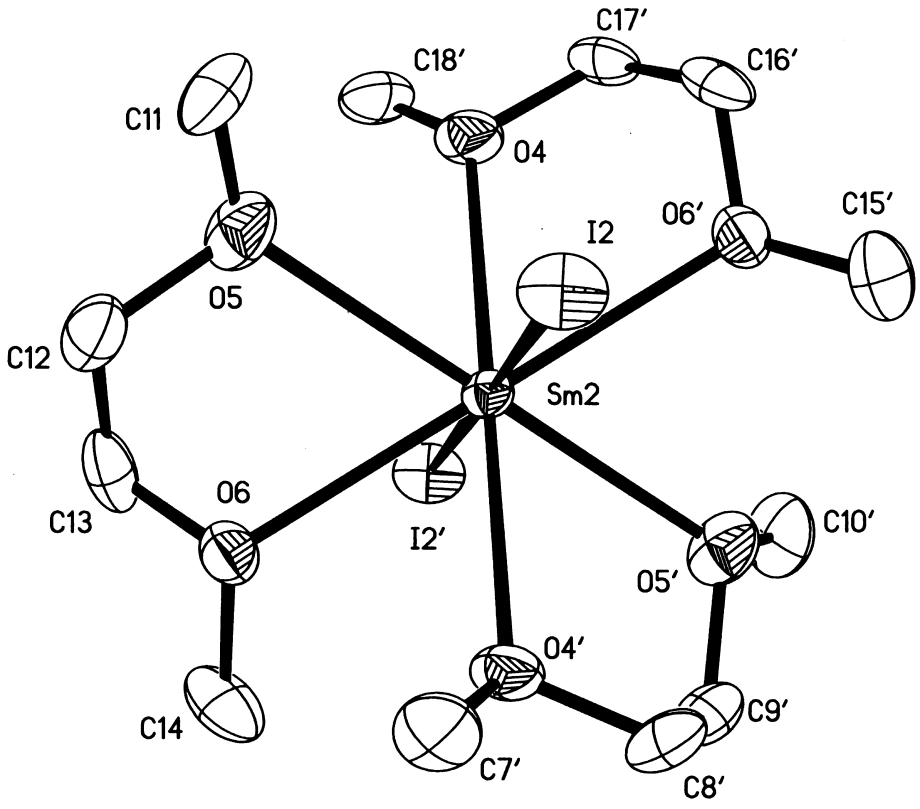

Fig. 4. Thermal ellipsoid plot of the linear I-Sm-I molecule of $SmI_2(DME)_3$, **4B**, drawn at the 50% probability level.

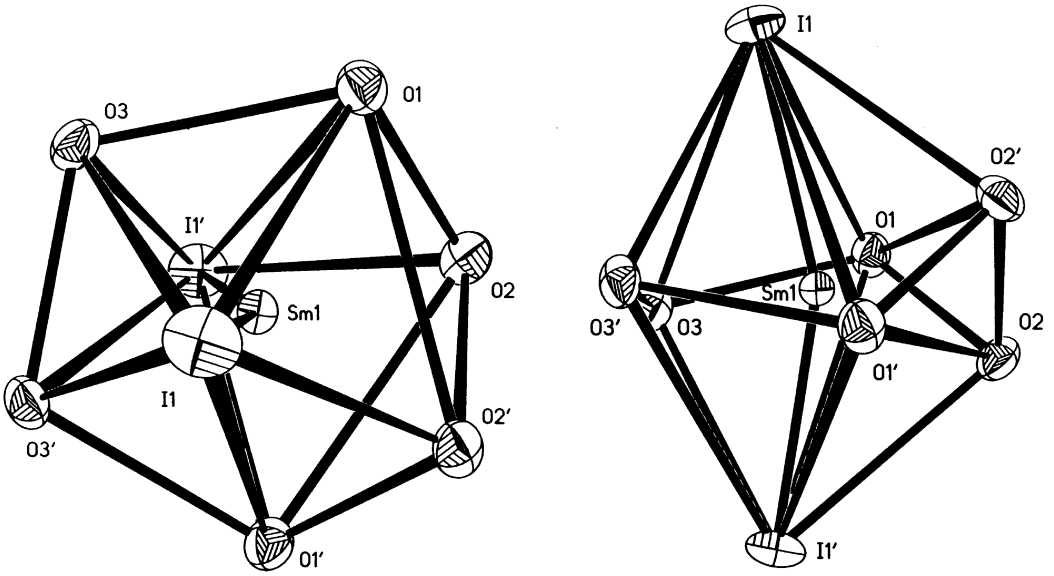

Fig. 5. Top and side views of the distorted dodecahedron of donor atoms surrounding samarium in the bent I-Sm-I form of $SmI_2(DME)_3$, **4A**.

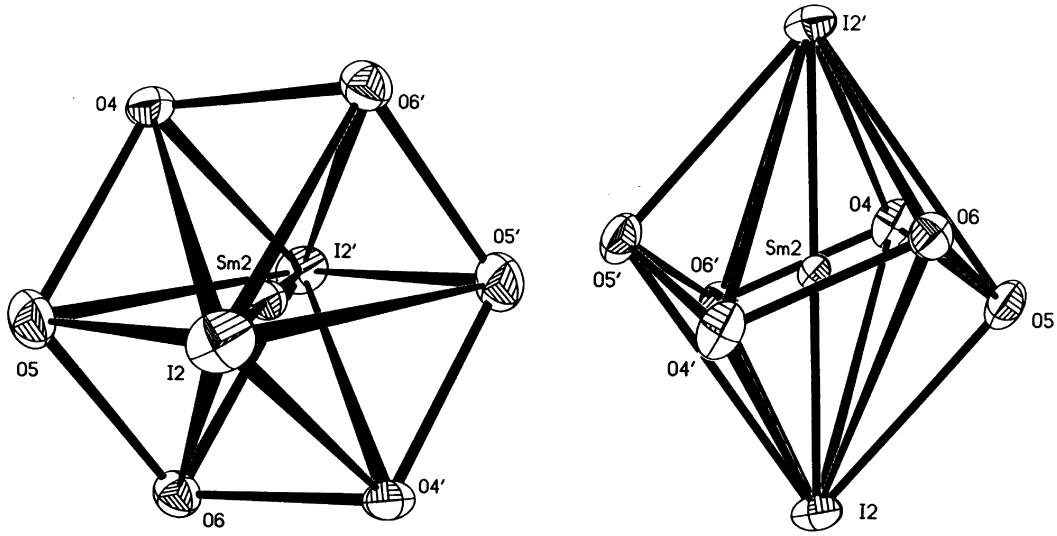

Fig. 6. Top and side views of the distorted hexagonal bipyramid of donor atoms surrounding samarium in the linear I-Sm-I form of $SmI_2(DME)_3$, **4B**.

between cis and trans is smaller in **4**. The Sm-I distances of **4** are longer than the distances found in the seven coordinate complexes $SmI_2(DME)_2(THF)$ [27] (3.246(1) Å) and $SmI_2(DME)(THF)_3$ [27] (3.231(1) and 3.235(1) Å) as expected for a higher coordinate structure. However, the six coordinate $SmI_2(HMPA)_4$ [13] complex has longer Sm-I bonds of length 3.390(2) Å.

The average Sm-O distance of 2.68(3) Å in **4** is not significantly longer than the average Sm-O(DME) distances of 2.62(2) and 2.641(5) Å in the seven coordinate complexes $SmI_2(DME)_2(THF)$ [27] and $SmI_2(DME)(THF)_3$ [27] respectively. Nor does this value differ from the Sm-O(diglyme) distances of 2.68(2) and 2.70(2) Å in the eight coordinate complexes cis- and trans-$SmI_2[(O(CH_2CH_2OMe)_2]_2$ [24, 25], respectively.

DISCUSSION

The strong reduction potential of Tm(II) is evident when thulium diiodide is placed in HMPA and compared to samarium diiodide. The strongly solvating

Table 1. Experimental Data for the X-ray Diffraction Studies of $\{[TmI_2(HMPA)_4][I](pyridine)_5\}$, **2** and $\{[TmI(HMPA)_4(pyridine)][I]_2\}$, **3**, and $SmI_2(DME)_3$, **4**

Compound	2	3	4
Formula	$C_{49}H_{97}I_3N_{17}O_4P_4Tm$	$C_{29}H_{77}I_3N_{17}O_4P_4Tm$	$C_{12}H_{30}I_2O_6Sm$
FW	1661.95	1345.55	674.51
Temp (K)	163	158	163
Crystal System	Tetragonal	Monoclinic	Monoclinic
Space Group	$I\bar{4}$	C2/c	C2/c
a (Å)	15.9110(6)	14.052(9)	25.0594(12)
b (Å)	15.9110(6)	16.203(5)	13.0995(8)
c (Å)	13.8885(11)	25.930(10)	14.5743(12)
α (deg)	90	90	90
β (deg)	90	92.61(3)	115.843(5)
γ (deg)	90	90	90
Volume (Å^3)	3516.0(3)	5898(5)	4305.8(5)
Z	2	4	8
D_{calcd} (Mg/m^3)	1.570	1.515	2.081
Limiting Indices	$0 \leqslant h \leqslant 18$, $0 \leqslant k \leqslant 18$, $0 \leqslant l \leqslant 16$	$0 \leqslant h \leqslant 18$, $0 \leqslant k \leqslant 21$, $-33 \leqslant l \leqslant 33$	$-22 \leqslant h \leqslant 32$, $-16 \leqslant k \leqslant 17$, $-18 \leqslant l \leqslant 17$
Scan Width, in ω (deg)	1.2° plus α_1, α_2 separation	1.2° plus α_1, α_2 separation	1.1° plus α_1, α_2 separation
Scan Speed, in ω (deg min^{-1})	3.0	5.0	4.0
θ Range (deg)	2.56 to 25.00	2.05 to 27.50	2.10 to 27.50
Absorption Correction, μ (mm^{-1})	2.720	3.221	5.613
F(000)	1660	2648	2544
Reflections Collected	1745	7030	5059
Independent Reflections	1736 (R_{int} = 0.0179)	6757 (R_{int} = 0.0221)	4950 (R_{int} = 0.0129)
Observed Reflections [I > 2σ(I)]	1539	5298	3915
Data/Restraints/Parameters	1736/0/175	6757/0/190	4950/0/246
Refinement [I > 2σ(I)]	R1, 2.76%; wR2, 5.53%	R1, 5.72%, wR2, 16.40%	R1, 3.09%, wR2, 6.32%
Refinement (all data)	R1, 3.61%; wR2, 5.90%	R1, 7.74%, wR2, 17.72%	R1, 4.79%, wR2, 6.98%
Goodness of Fit	1.058	1.115	1.055
Max. and Min. Transmission	0.5178 and 0.4679	0.4437 and 0.3911	0.7263 and 0.4931
Diffractometer: Siemens P4;	Monochromator: highly oriented graphite		
Radiation: Mo Kα (λ = 0.71073 Å);	Intensity Measurement Method: 2θ/ω		
Refinement Method: Full-matrix least-squares on F^2;			
Absorption Correction: Semi-empirical from psi-scans			
$R1 = R_F = [\Sigma\|\|F_o\| - \|F_c\|\|/\Sigma\|F_o\|]$; w$R2 = [\Sigma[w(F_o^2 - F_c^2)^2/\Sigma[w(F_o^2)^2]]^{1/2}$			

Table 2. Selected Bond Distances (Å) and Angles (°) for $\{[TmI_2(HMPA)_4][I](pyridine)_5\}$, **2**

Tm(1)–O(1)	2.189(4)	Tm(1)–I(1)	3.0452(6)
P(1)–O(1)	1.497(5)	P(1)–N(1)	1.622(7)
P(1)–N(2)	1.626(7)	P(1)–N(3)	1.631(6)
O(1)–Tm(1)–O(1A)	174.3(3)	O(1)–Tm(1)–O(1B)	90.14(2)
O(1)–Tm(1)–I(1)	87.1(2)	O(1A)–Tm(1)–I(1)	92.9(2)
P(1)–O(1)–Tm(1)	171.3(4)		

HMPA can be added to SmI_2 to increase the reduction potential of this reagent and make the divalent samarium ion a more potent reducing agent for added substrates [29]. In contrast, the intense green color characteristic of $TmI_2(DME)_3$ is immediately discharged upon the addition of HMPA and Tm(III) products form without an added substrate. Isolation of the trivalent complex $TmI_3(HMPA)_4$, **1**, indicates that ligand redistribution occurs in addition to the redox chemistry. These results are consistent with the large reduction potential expected for Tm(II) and indicate that the coordination environment of this ion

Table 3. Selected Bond Distances (Å) and Angles (°) for $\{[TmI(HMPA)_4(pyridine)][I]_2\}$, **3**

Tm(1)–O(1)	2.189(6)	Tm(1)–I(1)	3.0057(14)	Tm(1)–O(2)	2.208(5)
Tm(1)–N(7)	2.442(10)	P(1)–O(1)	1.517(6)	P(1)–N(1)	1.649(8)
P(1)–N(2)	1.638(8)	P(1)–N(3)	1.637(8)	P(2)–O(2)	1.512(6)
P(2)–N(4)	1.64(2)	P(2)–N(5)	1.619(13)	P(2)–N(6)	1.69(2)
N(7)–C(13)	1.347(10)	C(13)–C(14)	1.415(12)	C(14)–C(15)	1.362(11)
O(1)–Tm(1)–O(1′)		169.5(3)	O(1)–Tm(1)–O(2)		87.8(2)
O(1)–Tm(1)–O(2′)		91.1(2)	O(2)–Tm(1)–O(2′)		168.0(3)
O(1)–Tm(1)–N(7)		84.8(2)	O(2)–Tm(1)–N(7)		84.0(2)
O(1)–Tm(1)–I(1)		95.2(2)	O(2)–Tm(1)–I(1)		96.0(2)
N(7)–Tm(1)–I(1)		180.0	P(1)–O(1)–Tm(1)		167.9(4)
P(2)–O(2)–Tm(1)		173.0(4)			

Table 4. Selected Bond Distances (Å) and Angles (°) for both molecules of $SmI_2(DME)_3$, **4**

Sm(1)–O(1)	2.646(4)	Sm(2)–O(4)	2.644(4)
Sm(1)–O(2)	2.673(4)	Sm(2)–O(5)	2.685(4)
Sm(1)–O(3)	2.671(4)	Sm(2)–O(6)	2.735(4)
Sm(1)–I(1)	3.3091(5)	Sm(2)–I(2)	3.2897(4)

O(1)–Sm(1)–O(1′)[a]	152.5(2)	O(4′)[b]–Sm(2)–O(4)	180.0
O(1)–Sm(1)–O(3)	73.22(12)	O(4)–Sm(2)–O(5)	63.61(12)
O(1)–Sm(1)–O(2)	60.28(12)	O(4′)[b]–Sm(2)–O(6)	63.89(12)
O(3′)[a]–Sm(1)–O(2)	160.36(12)	O(5)–Sm(2)–O(6)	63.89(12)
O(2)–Sm(1)–O(2′)[a]	62.5(2)	O(6)–Sm(2)–O(6′)[b]	180.0
O(2)–Sm(1)–I(1′)[a]	77.45(8)	O(4)–Sm(2)–I(2′)[b]	78.87(9)
O(3′)[a]–Sm(1)–I(1)	74.86(8)	O(6)–Sm(2)–I(2′)[b]	77.58(8)
O(2)–Sm(1)–I(1)	123.27(8)	O(5)–Sm(2)–I(2)	79.40(9)
O(1)–Sm(1)–O(3′)[a]	133.86(12)	O(4′)[b]–Sm(2)–O(5)	116.39(12)
O(3′)[a]–Sm(1)–O(3)	63.6(2)	O(5)–Sm(2)–O(5′)[b]	180.0
O(1′)[a]–Sm(1)–O(2)	95.11(12)	O(4)–Sm(2)–O(6)	116.11(12)
O(3)–Sm(1)–O(2)	120.77(11)	O(5′)[b]–Sm(2)–O(6)	116.11(12)
O(1)–Sm(1)–I(1′)[a]	98.09(8)	O(5)–Sm(2)–I(2′)[b]	100.60(9)
O(1)–Sm(1)–I(1)	87.22(8)	O(4)–Sm(2)–I(2)	101.13(9)
O(3)–Sm(1)–I(1)	86.08(8)	O(6)–Sm(2)–I(2)	102.42(8)
I(1′)[a]–Sm(1)–I(1)	157.65(2)	I(2′)[b]–Sm(2)–I(2)	180.0

Symmetry transformations used to generate equivalent atoms: a) $-x,y,-z+1/2$; b) $-x-1/2,-y+1/2,-z$

needs to be adjusted to *lower* its reduction potential if it is to be a viable one electron reagent.

Addition of pyridine to divalent $TmI_2(DME)_3$ also demonstrates the strong reducing power of Tm(II) when compared to samarium. Trivalent thulium products are produced upon the addition of pyridine to $TmI_2(DME)_3$, whereas divalent Sm(II) can be recovered from solutions of $SmI_2(THF)_x$ and pyridine in DME. Remarkably in the case of samarium, the crystalline form isolated from DME is pyridine free: $SmI_2(DME)_3$, **4**. Complex **4** has another interesting feature: both cis and trans arrangements of the I-Sm-I unit are observed in the same crystal. Although SmI_2 has previously been found to form cis- and trans-isomers of eight coordinate $SmI_2[(O(CH_2CH_2OMe)_2]_2$ [24, 25], these were obtained from different systems of crystallization. The isolation of two different structures in the same crystal under the same conditions shows that the two structural types are very close in energy. Previously, this phenomenon had been observed in $[Cr(NH_2CH_2CH_2NH_2)_3][Ni(CN)_5]$ $(1.5H_2O)$, which contains both trigonal bipyramidal and square pyramidal geometries in the same crystal [30]. The formation of two different eight coordinate geometries in the same crystal is consistent with the similarity of the energies of eight coordinate geometries [31]. However, it has not been established that linear and bent ligand-lanthanide-ligand geometries are so similar in energy. This is an area of considerable theoretical interest [32–36].

CONCLUSION

The formation of Tm(III) products directly upon addition of HMPA or pyridine to $TmI_2(DME)_3$ emphasizes how much more reducing thulium diiodide is compared to $SmI_2(THF)_2$ which remains divalent in the presence of these strong donor ligands. These results show that the strong reduction potential of Tm(II) needs to be moderated with donor ligands to allow substrate reductions to be carried out.

Acknowledgements—For support of this research, we thank the National Science Foundation.

Supplementary Material—Figures and tables of crystal data, atomic coordinates, bond distances and angles, anisotropic displacement parameters, models showing the disorder in **3** and **4B**, and structure factors for compounds **2**–**4** (77 pages). Ordering information is given on any current masthead page.

REFERENCES

1. (a) Marks, T. J. and Ernst, R. D., In *Comprehensive Organometallic Chemistry*, eds. G. Wilkinson, F. G. A. Stone and E. W. Abel, Chap. 21. Pergamon Press, Oxford, 1982. (b) Edelmann, F. T., In *Comprehensive Organometallic Chemistry II*, eds. G. Wilkinson, F. G. A. Stone and E. W. Abel, Vol. 4, Chap. 2. Pergamon Press, Oxford, 1995. (c) Evans, W. J., *Polyhedron* 1987, **6**, 803.
2. (a) Kagan, H. B. and Namy, J. L., In *Handbook on the Physics and Chemistry of Rare Earths*, eds. K. A. Gschneider Jr. and L. Eyring, Vol. 6, Chapter 50. Elsevier, Amsterdam, 1984. (b) Kagan, H. B. and Namy, J. L., *Tetrahedron* 1986, **42**, 6573. (c) Kagan, H. B., *New. J. Chem.* 1990, **14**, 453. (d) Molander, G. A., *Chem. Rev.* 1992, **92**, 29.
3. Bochkarev, M. N., Fedushkin, I. L., Fagin, A. A., Petrovskaya, T. V., Ziller, J. W., Broomhall-Dillard, R. N. R. and Evans, W. J., *Angew. Chem. Int. Ed. Engl.*, 1997, **36,** 133.
4. Mikheev, N. B., *Russ. J. Inorg. Chem.*, 1984, **29,** 258.
5. Girard, P., Namy, J. L. and Kagan, H. B., *J. Am. Chem. Soc.*, 1980, **102,** 2693.
6. (a) Evans, D. F., *J. Chem. Soc.* 1959, 2003. (b) Becconsall, J. K., *Mol. Phys.* 1968, **15**, 129.
7. Atwood, J. L., Hunter, W. E., Wayda, A. L. and Evans, W. J., *Inorg. Chem.*, 1981, **20,** 4115.
8. *XSCANS Software Users Guide*, Version 2.1. Siemens Industrial Automation, Inc., Madison, WI, 1994.
9. Broach, R. W., Argonne National Laboratory, Illinois, 1978.
10. Sheldrick, G. M., Siemens Analytical X-Ray Instruments, Inc., Madison, WI, 1994.
11. *International Tables for X-Ray Crystallography*, Vol. C. Kluwer Academic Publishers, Dordecht, 1992.
12. Flack, H. D., *Acta Cryst.*, 1983, **A39,** 876.
13. Hou, Z., Kobayahi, K. and Yamazaki, H., *Chem. Lett.*, 1991, 265.
14. Hou, Z. and Wakatsuki, Y., *J. Chem. Soc., Chem. Commun.*, 1994, 1205.
15. Mashima, K., Nakayama, Y., Shibahara, T., Fukumoto, H. and Nakumura, A. A., *Inorg. Chem.*, 1996, **35,** 93.
16. Shannon, R. D., *Acta Cryst.*, 1976, **A32,** 751.
17. When compared to the complexes $LnI_3(HO^iPr)_4$ (Ln=La, Ce). Barnhart, D. M., Frankcom, T. M., Gordon, P. L., Sauer, N. N., Thompson, J. A. and Watkin, J. G., *Inorg. Chem.* 1995, **34**, 4862.
18. Also the complex, $[TmCl(terpy)(OH_2)_4]Cl_2(H_2O)_3$. Kepert, C. J., Lu, W., Skelton, B. W. and White, A. H., *Aust. J. Chem.* 1994, **47**, 365.
19. And the complex, $[TmCl_2(OH_2)_2$(12-crown-4)$]Cl$. Rogers, R. D., Rollins, A. N. and Benning, M. M., *Inorg. Chem.* 1988, **27**, 3826.
20. Schumann, H., Winterfeld, J., Hemling, H., Hahn, F. E., Reich, P., Brzezinka, K.-W., Edelmann, F. T., Kilimann, U., Schafer, M. and Herbst-Irmer, R., *Chem. Ber.*, 1995, **128,** 395.
21. Rabe, G. W., Riede, J. and Schier, A., *J. Chem. Soc., Chem. Comm.*, 1995, 577.
22. Xing-Wang, Z., Xing-Fu, L., Benetollo, F. and Bombieri, G. G., *Inorg. Chim. Acta*, 1987, **139,** 103.
23. Evans, W. J. and Hozbor, M. A., *J. Organometallic Chem.*, 1987, **326,** 299.
24. Chebolu, V., Whittle, R. R. and Sen, A., *Inorg. Chem.*, 1985, **24,** 3082.
25. Sen, A., Chebolu, V. and Rheingold, A. L., *Inorg. Chem.*, 1987, **26,** 1821.
26. Evans, W. J., Rabe, G. W. and Ziller, J. W., *Inorg. Chem.*, 1994, **33,** 3072.
27. Evans, W. J., Gummersheimer, T. S. and Ziller, J. W., *J. Am. Chem. Soc.*, 1995, **117,** 8999.
28. Sen, A., Chebolu, V. and Holt, E. M., *Inorg. Chim. Acta*, 1986, **118,** 87.
29. See reference 14 and the references therein.
30. Raymond, K. N., Corfield, P. W. R. and Ibers, J. A., *Inorg. Chem.*, 1968, **7,** 1362.
31. Muetterties, E. L. and Wright, C. M., *Quart. Rev., Chem. Soc.* 1967, **21**, 109. Keppert, D. L., *Prog. Inorg. Chem.* 1978, **24**, 179.
32. Ortiz, J. V. and Hoffmann, R., *Inorg. Chem.*, 1985, **24,** 2095.
33. Hollis, T. K., Burdett, J. K. and Bosnich, B., *Organometallics*, 1993, **12,** 3385.
34. Boudreaux, E. A. and Baxter, E., *Int. J. Quantum Chem.: Quantum Chem. Symp.*, 1994, **28,** 565.
35. Timofeeva, T. V., Lii, J.-H. and Allinger, N. L., *J. Am. Chem. Soc.*, 1995, **117,** 7452.
36. (a) Kaupp, M., Schleyer, P. v. R., Stoll, H. and Preuss, H., *J. Am. Chem. Soc.* 1991, **113**, 6012. (b) Kaupp, M. and Schleyer, P. v. R., *J. Am. Chem. Soc.* 1992, **114**, 491.

Pergamon

PII: S0277–5387(98)00119–3

Polyhedron Vol. 17, No. 19, pp. 3371–3378, 1998
© 1998 Elsevier Science Ltd
All rights reserved. Printed in Great Britain
0277–5387/98 $19.00+0.00

Interaction of divalent metal ions with D-aldonic acids in the solid phase-II. Structural information[1]

Alejandro A. Frutos,[a] Sandra Signorella,[a] Luis F. Sala,[a]* Graciela M. Escandar,[b] Juan M. Salas Peregrin[c] and Virtudes Moreno[d]

[a]Departamento de Química Fisica, Facultad de Ciencias Bioquímicas y Farmacéuticas, Universidad Nacional de Rosario, Suipacha 531 (2000) Rosario, Argentina

[b]Departamento de Química Analítica, Facultad de Ciencias Bioquímicas y Farmacéuticas, Universidad Nacional de Rosario, Suipacha 531 (2000) Rosario, Argentina

[c]Departamento de Química Inorgánica, Facultad de Ciencias, Universidad de Granada, 18071 Granada España

[d]Departament de Química Inorgánica, Universitat de Barcelona, E-08028 Barcelona, España

(Received 3 November 1997; accepted 16 March 1998)

Abstract—Complexes formed between D-glucoheptonate, D-galactonate, D-gulonate and D-ribonate, and several metal ions were obtained in the solid state. Specifically: D-glucoheptonates, $Be(C_7H_{13}O_8)_2 \cdot 1/2H_2O$, $Mn(C_7H_{13}O_8)_2 \cdot 2H_2O$, $Co(C_7H_{13}O_8)_2 \cdot 2H_2O$, $Ni(C_7H_{13}O_8)_2 \cdot 2H_2O$, $Cu(C_7H_{13}O_8)_2 \cdot 2H_2O$, $Pb(C_7H_{13}O_8)_2$; D-galactonates, $Mn(C_6H_{11}O_7)_2 \cdot 2H_2O$, $Co(C_6H_{11}O_7)_2 \cdot 3H_2O$, $Ni(C_6H_{11}O_7)_2 \cdot 3H_2O$, $Cu(C_6H_{11}O_7)_2$, $Pb(C_6H_{11}O_7)_2$; D-gulonates, $Co(C_6H_{11}O_7)_2 \cdot H_2O$, $Ni(C_6H_{11}O_7)_2 \cdot 2H_2O$, $Cu(C_6H_{11}O_7)_2 \cdot 2H_2O$; D-ribonates, $Mn(C_5H_9O_6)_2$, $Co(C_5H_9O_6)_2 \cdot 2H_2O$, $Ni(C_5H_9O_6)_2 \cdot 2H_2O$, $Cu(C_5H_9O_6)_2.2H_2O$ and $Pb(C_5H_9O_6)_2$ have been isolated. These metal sugar salts were characterized by elemental analysis, thermogravimetric analysis, magnetic susceptibility measurements, FT–IR, diffuse reflectance and EPR spectroscopies. © 1998 Elsevier Science Ltd. All rights reserved

Keywords: D-aldonic acids; metal sugar complexes; divalent metal ions.

INTRODUCTION

Solid complexes formed between the metal ions beryllium (II), manganese (II), cobalt (II), nickel (II), copper (II) and lead (II), and ligands of biological interest, such as D-glucoheptonic acid (I), D-galactonic acid (II), D-gulonic acid (III) and D-ribonic acid (IV) (Fig. 1), were isolated. This work is part of our program on the coordination chemistry of sugar acids [1–8]. In previous papers, studies were carried out on equilibrium reactions in aqueous solution and in the solid state for metal complexes of both D-gluconolactone and D-lactobionic acid [1, 2]. The importance of studying the interaction between carbohydrates and transition metal ions is related to the use of this type of ligands as sequestering agents for metal ions present in biological media [9, 10]. The present work complements previous information afforded with metal ions cobalt (II), nickel (II) and copper (II), and the ligands I, II, III and IV in solution studies [2, 4, 8]. Interactions of the above-mentioned D-aldonic acids with beryllium (II), manganese (II) and lead (II) are given as additional information.

The studies in the solid state were performed by elemental, thermogravimetric and susceptibility analyses, and by FT–IR, diffuse reflectance and EPR spectroscopies.

These studies represent a contribution to future crystallographic analyses, which are complicated by the difficulties in obtaining X-ray quality crystals of complexes containing carbohydrates with non-blocked hydroxyl groups.

[1] Presented at the X Physicochemical Argentine Meeting, April 21 to 25, 1997, Tucumán, Argentina.

* Author to whom correspondence should be addressed. Fax: 54-41-350214; E-mail: inquibir@satlink.com.

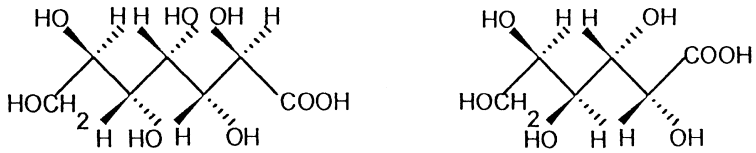

D-glucoheptonic acid
(I)

D-galactonic acid
(II)

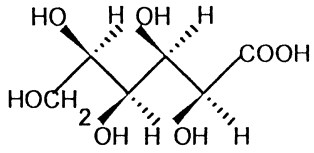

D-gulonic acid
(III)

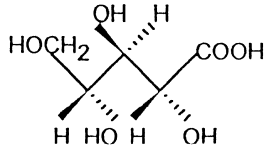

D-ribonic acid
(IV)

Fig. 1. Ligands.

EXPERIMENTAL

Reagents

D-glucoheptono-γ-lactone, D-galactono-γ-lactone, D-gulono-γ-lactone and D-ribono-γ-lactone were purchased from Sigma. Their purities were checked by elemental analysis, chromatography and potentiometric titrations. The metal carbonates or oxides used were: $Co(CO_3)\cdot xH_2O$ (Aldrich), $2NiCO_3\cdot 3Ni(OH)_2\cdot 4H_2O$ (Aldrich), $CuCO_3\cdot Cu(OH)_2$ (Aldrich), $MnCO_3$ (BDH), $BeCO_3\cdot 5H_2O$ (BDH) and $PbCO_3$ (Aldrich).

Synthesis of complexes in the solid state

The complexes were prepared following the procedures described previously [11]. Briefly, the metal ion was added to a previously refluxed (1 h) solution of the lactone, in order to promote the opening of the sugar ring affording the aldonic acid. This mixture was boiled for 2 hrs. The metal–lactone ratio was 1:2. Ethanol was added to the clear solution and a solid phase was obtained. The precipitate was separated by filtration and recrystallized four times from a mixture of ethanol–water (4:1). Finally, the product was washed with ethanol, dried under vacuum over phosphorus pentoxide at room temperature and again dried for 2 hrs. at 80°C under vacuum over phosphorus pentoxide.

The purity of the obtained complexes was checked by elemental analysis.

Analysis of the solid complexes

Microanalyses of C and H were performed using a Fisons 1108 CHNS microanalyser. The nickel (II) percentages in its complexes was determined by complexometric titration with EDTA and zinc nitrate solutions employing eriochrome black T as an indicator [12]. The content of beryllium was calculated from the thermogravimetrical residue. The metal percentage in the other complexes were determined by atomic absorption using a Metrolab 250 AA atomic absorption spectrophotometer. Thermogravimetric curves were obtained in an atmosphere of pure air using a Shimadzu TGA-50 H, with a heating speed of $20^{\circ}C\,min^{-1}$, equipped with a Nicolet model 550 IR gas analyzer and Fisons model Thermolab mass detector. DSC data were obtained on a Shimadzu DSC-50 differential scanning calorimeter, using a heating speed of $10^{\circ}C\,min^{-1}$. The diffuse reflectance spectra were obtained with a Cary-5E refractometer provided with a praying mantis module. IR spectra were performed on a FT–IR Nicolet 20 SX8 spectrophotometer. Susceptibility magnetic measurements were carried out on Manics DSM-8 instrument in the 80–290 K temperature range. X-band ($\sim$9.2 GHz) EPR spectra were recorded as the first derivative of absorption at 77 and 298 K, on a Bruker ESP 300E EPR spectrometer with 100 kHz field modulation. The microwave frequency was generated with a Bruker 04 ER and measured with a Racal–Dana frequencymeter. The magnetic field was measured with a Bruker NMR-probe gaussmeter.

RESULTS AND DISCUSSION

Elemental Analysis

The analytical results for the synthesized complexes are reported in Table 1. All the complexes present a 1:2 metal–ligand ratio and were obtained either in

Table 1. Analytical data and colors for D-aldonic complexes

Complexes	colors	%C		%H		%M	
		Calc.	Exp.	Calc.	Exp.	Calc.	Exp.
D-glucoheptonates:							
$Be(C_7H_{13}O_8)_2 \cdot 1/2H_2O$	white	35.90	35.62	5.81	5.83	1.92	1.94
$Mn(C_7H_{13}O_8)_2 \cdot 2H_2O$	light pink	31.06	30.78	5.59	5.75	10.32	10.42
$Co(C_7H_{13}O_8)_2 \cdot 2H_2O$	pink	30.84	30.46	5.54	5.78	10.81	10.50
$Ni(C_7H_{13}O_8)_2 \cdot 2H_2O$	green	30.85	30.84	5.37	5.88	10.77	10.29
$Cu(C_7H_{13}O_8)_2 \cdot 2H_2O$	blue	30.58	29.45	5.50	5.25	11.56	11.80
$Pb(C_7H_{13}O_8)_2$	white	25.57	25.22	3.99	4.03	31.51	31.10
D-galactonates:							
$Mn(C_6H_{11}O_7)_2 \cdot 2H_2O$	white	29.95	29.69	5.44	5.36	11.41	11.20
$Co(C_6H_{11}O_7)_2 \cdot 3H_2O$	pink	28.64	28.79	5.61	5.70	11.71	12.01
$Ni(C_6H_{11}O_7)_2 \cdot 3H_2O$	green	28.65	28.43	5.61	5.87	11.68	11.17
$Cu(C_6H_{11}O_7)_2$	blue	31.76	31.88	4.89	5.16	14.00	13.65
$Pb(C_6H_{11}O_7)_2$	white	24.12	24.07	3.71	3.59	34.68	34.68
D-gulonates:							
$Co(C_6H_{11}O_7)_2 \cdot H_2O$	pink	30.85	31.28	5.18	5.27	12.61	12.40
$Ni(C_6H_{11}O_7)_2 \cdot 2H_2O$	green	29.71	29.69	5.40	5.40	12.10	11.90
$Cu(C_6H_{11}O_7)_2 \cdot 2H_2O$	blue	29.42	29.69	5.35	4.81	12.97	12.65
D-ribonates:							
$Mn(C_5H_9O_6)_2$	light pink	31.18	30.84	4.71	4.70	14.26	14.40
$Co(C_5H_9O_6)_2 \cdot 2H_2O$	pink	28.25	28.75	5.21	5.23	13.86	13.60
$Ni(C_5H_9O_6)_2 \cdot 2H_2O$	green	28.27	28.51	5.22	5.46	13.81	13.28
$Cu(C_5H_9O_6)_2 \cdot 2H_2O$	blue	27.95	27.71	5.16	4.67	14.79	14.52
$Pb(C_5H_9O_6)_2$	white	22.35	22.29	3.38	3.41	38.55	38.73

anhydrous or solvated form. It was not possible to prepare pure Be(II) D-ribonate because it was contaminated with the starting material ($BeCO_3$). This fact would be due to low acidity of the ribonic acid which makes it less reactive towards the carbonate.

Thermogravimetric curves

As was already reported [1, 2, 6], the thermogravimetric curves of this type of complexes present two steps: dehydration (between 100–200°C) and pyrolytic processes (above 200°C). Figure 2 shows two typical thermal decompositions for both hydrated and anhydrous complexes, respectively. Thermoanalytical data are in good agreement with the elemental analysis. The temperature of water loss and the sharp peak on the DSC diagram may indicate that these molecules are coordinated to the metal. The pyrolitic process took place in two, three or four steps. The pyrolitic products identified by IR spectra were: water, carbon monoxide and carbon dioxide. The pyrolitic residues at 400–800°C were determined to be oxides or mixture of carbonates and oxides of the corresponding metal ion. Thermoanalytical data are given in supplementary material.

Reflectance spectra

As an example, Fig. 3 shows reflectance spectra for different complexes of cobalt (II), copper (II) and nickel (II). The bands of the recorded spectra are shown in Table 2 (A and B). In this table both the calculated and experimental frequency ratios according to the DQ/B values are presented [14]. The band of the spectra of cobalt (II) complexes were these expected for the electronic transition of a d^7 metal ion in an octahedral arrangement [15](a)[16](b). The spectra of the nickel (II) complexes also show three absorption bands and the relationship between the first two bands (1.7) suggests octahedral geometries for these complexes [15](b)[16](a). In all cases, the second bands were found to split into two signals. This fact can be attributed either to interactions with the nearest electronic level ^1Eg or to spin–orbit coupling. The copper (II) complexes showed spectra with a single wide band with maxima in the range 799–

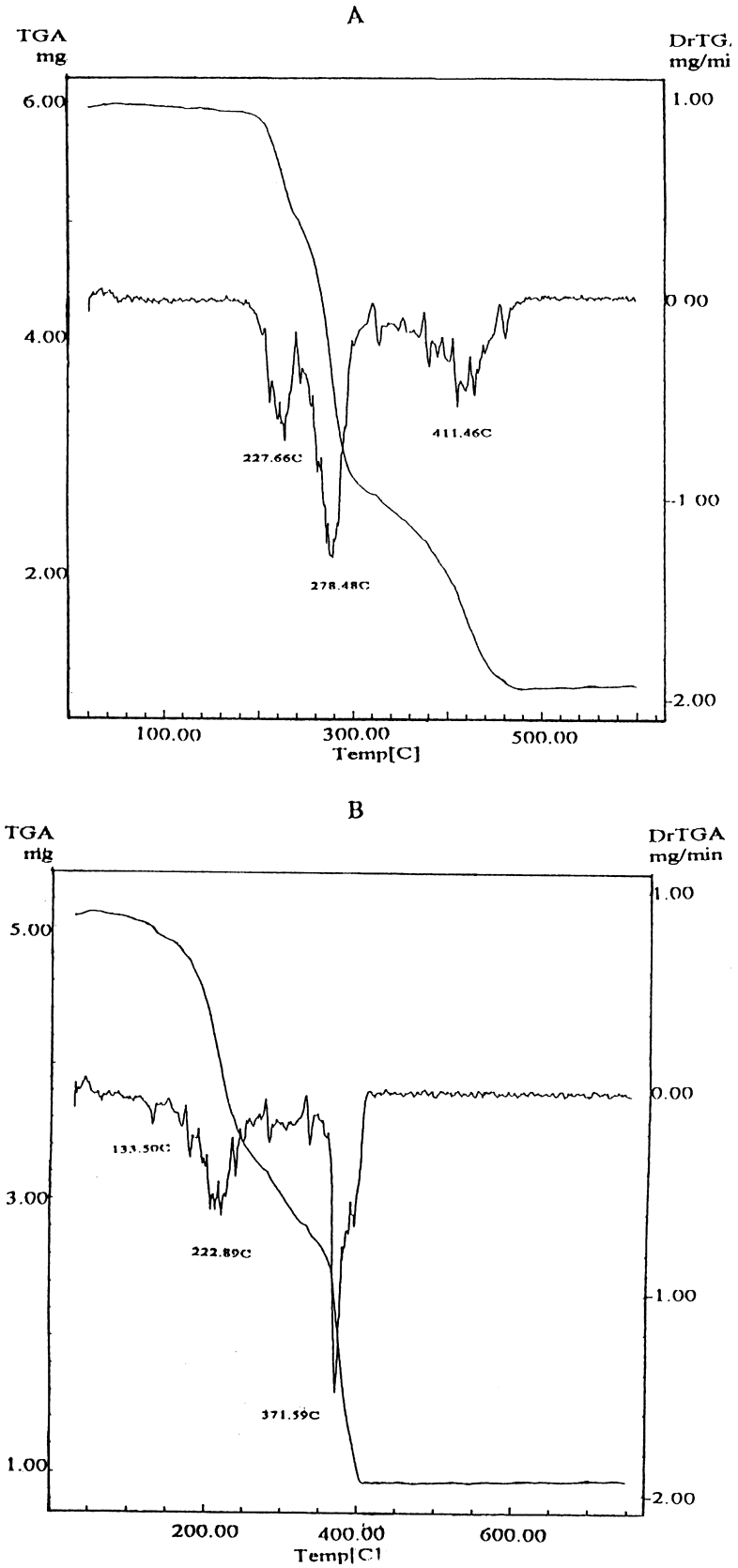

Fig. 2. Thermogravimetric curves for (a) Cu (II) D-galactonate (initial mass: 5.973 mg); (b) Co (II) D-gulonate (initial mass: 5.093 mg).

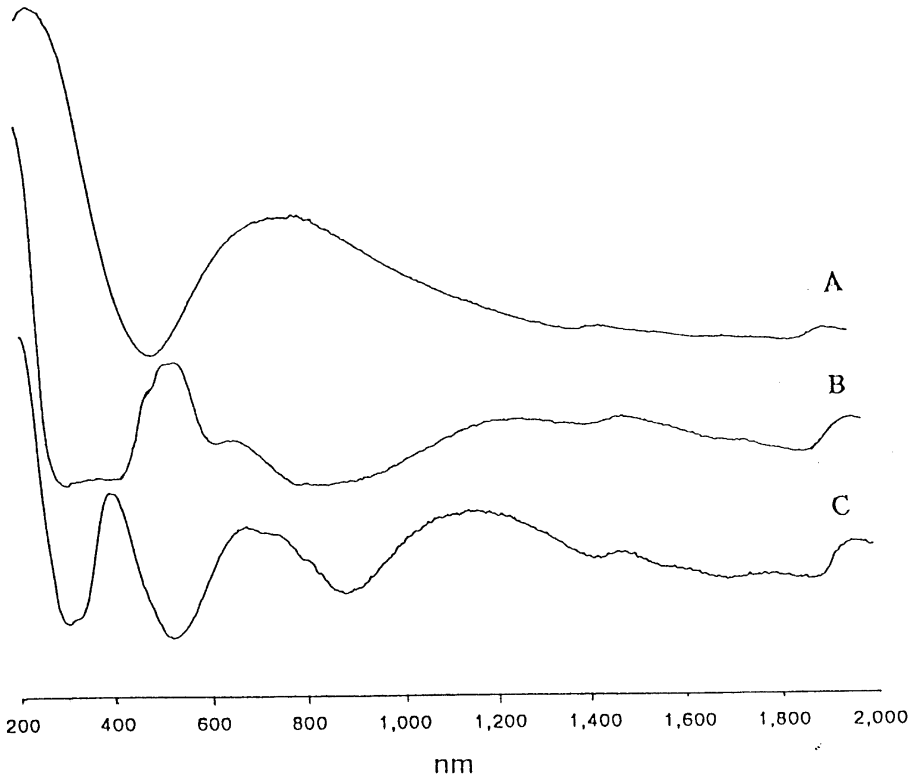

Fig. 3. Reflectance spectra for (a) Cu (II) D-gulonate; (b) Co (II) D-galactonate; (c) Ni (II) D-glucoheptonate.

814 nm. The frequencies of these maxima are coincident with the value of the crystal field splitting and correspond to the electronic transitions $^2T_2g \leftarrow ^2Eg$. According to these results tetragonal distortion of octahedral arrangements was proposed for these complexes [15](c)[16](c).

IR spectra

The IR spectra of the solid complexes were carried out between 4000–400 cm^{-1} and the interpretation was based on a comparison with both the corresponding sugar acids and structurally related compounds.

The wide bands at 3500–3100 cm^{-1} in the spectra of the free ligands were assigned to strongly hydrogen-bonded OH groups. The interaction between the hydroxyl groups of the aldonolactones and the metals produces broadening, but not shifting, of the sugar OH stretching vibrations. The carbonyl stretching bond in the spectra of the studied lactones appeared at 1700–1800 cm^{-1}. In the spectra of the complexes, this band disappeared and two new bands were detected at about 1600 and 1400 cm^{-1}. The latter were assigned to the antisymmetric and symmetric frequencies of stretching carboxyl groups, respectively [17]. The difference in frequency between these two bands allowed us to infer the coordination mode of the metal center towards the carboxylate groups. Most of the complexes under study showed values which were equal to, or higher than, 200 cm^{-1}, always related to a monodentate coordination [18]. Lead (II) D-glucoheptonate and cobalt (II), nickel (II) and copper (II) D-galactonate presented values in the range 160–200 cm^{-1}, which were in agreement with an additional hydrogen-bonded coordination between the carbonyl oxygen and protons of the carbonate chain [18]. Lead (II) D-ribonate complex spectrum showed a splitting of the signals corresponding to symmetric and antisymmetric stretching, suggesting that the metal ion is not located in a symmetric environment. In the spectral region of 1400–1100 cm^{-1}, shifting and broadening for the CH_2, OH and COH bending modes were observed in the presence of the metal ions, and were attributed to the metal–OH interaction in the complexation. Both the sugar C–O stretching vibrations (1100–940 cm^{-1}) and the deformation modes of the lactone ring skeletal (900–500 cm^{-1}) showed major changes upon metal ion chelation. Selected infrared absorption frequencies for complexes and aldonolactones are given in supplementary material.

Table 2. Electronic absorption spectral data in the solid phase

(**A**)

Complex	ν_1	ν_2	ν_3	Δ_o (cm^{-1})	B^* (cm^{-1})
Co(II) D-glucoheptonate	$^4T_{2g}\leftarrow{}^4T_{1g}$ (8123 cm^{-1})	$^4A_{2g}\leftarrow{}^4T_{1g}$ (15699 cm^{-1})	$^4T_{1g}(P)\leftarrow{}^4T_{1g}$ (18762 cm^{-1})	7576	673
Ni(II) D-glucoheptonate	$^3T_{2g}\leftarrow{}^3A_{2g}$ (8772 cm^{-1})	$^3T_{1g}\leftarrow{}^3A_{2g}$ (14881 cm^{-1})	$^3T_{1g}(P)\leftarrow{}^3A_{2g}$ (25381 cm^{-1})	8772	904
Cu(II) D-glucoheptonate	$^2T_{2g}\leftarrow{}^2E_g$ (12285 cm^{-1})	—	—	12285	—
Co(II) D-galactonate	$^4T_{2g}\leftarrow{}^4T_{1g}$ (7949 cm^{-1})	$^4A_{2g}\leftarrow{}^4T_{1g}$ (15798 cm^{-1})	$^4T_{1g}(P)\leftarrow{}^4T_{1g}$ (18349 cm^{-1})	7849	687
Ni(II) D-galactonate	$^3T_{2g}\leftarrow{}^3A_{2g}$ (8734 cm^{-1})	$^3T_{1g}\leftarrow{}^3A_{2g}$ (15106 cm^{-1})	$^3T_{1g}(P)\leftarrow{}^3A_{2g}$ (24752 cm^{-1})	8734	890
Cu(II) D-galactonate	$^2T_{2g}\leftarrow{}^2E_g$ (12438 cm^{-1})	—	—	12438	—
Co(II) D-gulonate	$^4T_{2g}\leftarrow{}^4T_{1g}$ (8052 cm^{-1})	$^4A_{2g}\leftarrow{}^4T_{1g}$ (15337 cm^{-1})	$^4T_{1g}(P)\leftarrow{}^4T_{1g}$ (18939 cm^{-1})	7285	675
Ni(II) D-gulonate	$^3T_{2g}\leftarrow{}^3A_{2g}$ (8873 cm^{-1})	$^3T_{1g}\leftarrow{}^3A_{2g}$ (14925 cm^{-1})	$^3T_{1g}(P)\leftarrow{}^3A_{2g}$ (25445 cm^{-1})	8873	894
Cu(II) D-gulonate	$^2T_{2g}\leftarrow{}^2E_g$ (12516 cm^{-1})	—	—	12516	—
Co(II) D-ribonate	$^4T_{2g}\leftarrow{}^4T_{1g}$ (8071 cm^{-1})	$^4A_{2g}\leftarrow{}^4T_{1g}$ (15384 cm^{-1})	$^4T_{1g}(P)\leftarrow{}^4T_{1g}$ (18692 cm^{-1})	7313	658
Ni(II) D-ribonate	$^3T_{2g}\leftarrow{}^3A_{2g}$ (8636 cm^{-1})	$^3T_{1g}\leftarrow{}^3A_{2g}$ (14925 cm^{-1})	$^3T_{1g}(P)\leftarrow{}^3A_{2g}$ (25445 cm^{-1})	8636	925
Cu(II) D-ribonate	$^2T_{2g}\leftarrow{}^2E_g$ (12346 cm^{-1})	—	—	12346	—

*Calculated according to Ref. [13].

(**B**)

Complex	Dq/B	ν_1/ν_2	ν_3/ν_1	ν_3/ν_2
Co(II) D-glucoheptonate	1.1	1.933 (2.138)	2.310 (2.414)	1.195 (1.129)
Ni(II) D-glucoheptonate	1.0	1.696 (1.648)	2.893 (2.852)	1.706 (1.731)
Co(II) D-galactonate	1.1	1.987 (2.138)	2.308 (2.414)	1.161 (1.129)
Ni(II) D-galactonate	1.0	1.730 (1.648)	2.834 (2.852)	1.639 (1.731)
Co(II) D-gulonate	1.1	1.905 (2.138)	2.352 (2.414)	1.235 (1.129)
Ni(II) D-gulonate	1.0	1.682 (1.648)	2.868 (2.852)	1.705 (1.731)
Co(II) D-ribonate	1.1	1.906 (2.138)	2.316 (2.414)	1.215 (1.129)
Ni(II) D-ribonate	0.9	1.728 (1.667)	2.946 (3.000)	1.705 (1.800)

( )According to Ref. [14].

Magnetic susceptibility measurements

Table 3 shows the magnetic data for the studied complexes. In all cases the Curie–Weiss law was verified: $\chi_M = C/(T-\theta)$, where χ_M is the corrected molar susceptibility, C is the Curie Constant, T is the absolute temperature and θ is the Weiss Constant. Copper (II) and nickel (II) D-galactonates, and manganese (II) D-glucoheptonate showed ferromagnetic interactions while the rest of the isolated compounds displayed an antiferromagnetic coupling. The values of the effective magnetic moment (μ_{eff}) for all the complexes studied suggest that the metal ions are in an octahedral high spin environment. The plots of χ_M *vs.* T (not shown) for both cobalt (II) and copper (II) D-ribonates present a significant deviation of the linearity at values lower than 170 and 150 K respectively.

EPR measurements

Cu(II) D-aldonic acids complexes. The polycrystalline samples exhibit rhombic EPR spectra with EPR parameters (g factors and hyperfine splitting constants A) summarized in Table 4. The spectra recorded at 77 K are very similar to those at room temperature, indicating no significant change in the coordination geometry (Fig. 4).

Table 3. Magnetic moments for complexes

Complex	Temperature (K)	θ (K)	μ_{eff} (BM)
Mn (II) D-glucoheptonate	93–290	0.85	6.08
Co (II) D-glucoheptonate	119–290	−8.95	4.96
Ni (II) D-glucoheptonate	79–290	−2.57	3.24
Cu (II) D-glucoheptonate	85–290	−18.4	1.99
Mn (II) D-galactonate	140–290	−8.48	5.60
Co (II) D-galactonate	100–290	−10.31	5.14
Ni (II) D-galactonate	81–280	0.47	3.27
Cu (II) D-galactonate	90–290	2.18	1.75
Co (II) D-gulonate	99–290	−12.25	4.92
Ni (II) D-gulonate	90–290	−9.83	3.37
Cu (II) D-gulonate	130–290	−14.0	2.04
Mn (II) D-ribonate	101–290	−0.33	5.81
Co (II) D-ribonate	170–290	−11.9	5.22
Ni (II) D-ribonate	122–290	−4.98	3.34
Cu (II) D-ribonate	150–290	−24.58	1.95

Table 4. Room temperature (or 77 K) EPR parameters for copper (II) complexes

Compound	gz ($g_\parallel$)	$A_\parallel$ (G)	gx, gy ($g_\perp$)
Cu (II) D-gluconate	2.36	135	2.05, 2.02
Cu (II) D-lactobionate	2.34	143	2.05
Cu (II) D-gulonate	2.34	143	2.05
Cu (II) D-glucoheptonate	2.34	143	2.05

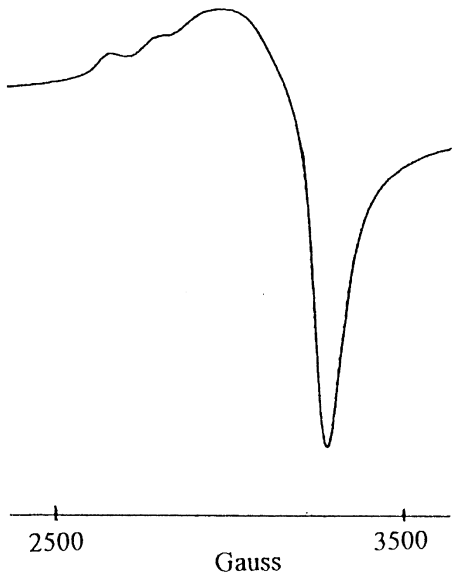

Fig. 4. EPR spectra for Cu (II)-D-gulonate (77 K).

The EPR spectral patterns and parameters observed for the Cu(II) D-gluconate, Cu(II) D-lactobionate [1], Cu(II) D-gulonate and Cu(II) D-glucoheptonate were typical for molecules of pseudo-axial symmetry, having $gz > gx \approx gy > 2$; generally showing a hyperfine structure due to the nuclear spin ($I = 3/2$) at the $g_\parallel$ region and were indicative for a predominantly dx^2–dy^2 ground state with small mixing of a dz^2 contribution [19, 20]. The rhombic signal was probably a consequence of the bulkiness of the carbohydrate moiety as well as its tendency to form intermolecular hydrogen bonds [21]. For Cu(II) D-galactonate a rhombic signal centered at $\approx$3135 G was observed. In this case the coordination sphere of the copper center was less distorted than for the other complexes and the different anisotropic components of g were not resolved.

CONCLUSION

All isolated complexes presented a 1:2 metal–ligand stoichiometry, with different hydration degrees. Both the presence or absence of water in the compounds was confirmed by thermogravimetric analyses. The water molecules would be coordinated to the metal center. The infrared spectra suggest that the carboxylic groups of sugars are involved in the chelation. The structural data obtained from magnetic measurements would indicate that the metal ions in manganese (II), cobalt (II), nickel (II) and copper (II) complexes are in an octahedral environment. For cobalt (II), nickel (II) and copper (II) complexes was confirmed an octahedral geometry by diffuse reflectance spectra. In the case of the copper (II) complexes, the EPR measurements confirm also octahedral environment. The molecular flexibility of the studied sugar acids would enable on octahedral coordination mode.

Acknowledgements—We are grateful for financial support from the Universidad Nacional de Rosario (UNR), Argentine and from the Agreement between Consejo Nacional de Investigaciones Científicas y Tecnicas (CONICET, Argentine) and the Universidad de Granada, Spain.

REFERENCES

1. Frutos, A. A., Escandar, G. M., Salas Peregrín, J. M., Gonzalez Sierra, M. and Sala, L. F., *Can. J. Chem.*, 1997, **75,** 405.
2. Escandar, G. M., Salas Peregrin, J. M., Gonzalez Sierra, M., Martino, D., Santoro, M. I., Frutos, A. A., García, S. I., Labadié, G. and Sala, L. F., *Polyhedron*, 1996, **15,** 2251.
3. Escandar, G. M., Gandolfo, F. H. and Sala, L. F., *Anal. Asoc. Quím. Argent.*, 1990, **78,** 37.
4. Escandar, G. M. and Sala, L. F., *Can. J. Chem.*, 1992, **70,** 2053.
5. Escandar, G. M., Olivieri, A. C., Gonzalez Sierra, M. and Sala, L. F., *J. Chem. Soc. Dalton Trans.*, 1994, 1189.
6. Escandar, G. M., Gonzalez Sierra, M., Salas Per-

egrin, J. M., Labadié, G., Santoro, M., Frutos, A. and Sala, L. F., *Polyhedron*, 1994, **13,** 909.
7. Escandar, G. M., Olivieri, A. C., Gonzalez Sierra, M., Frutos, A. A. and Sala, L. F., *J. Chem. Soc. Dalton Trans*., 1995, 799.
8. Escandar, G. M., Gonzalez Sierra, M. and Sala, L. F., *Polyhedron*, 1994, **13,** 143.
9. Whitfield, D. M., Stojkooski, S. and Sarkas, B., *Coord. Chem. Rev*., 1993, **122,** 171.
10. Bandwar, R. P., Rao, C. P., Giralt, H., Hidalgo, J. and Kulckarni, G. U., *J. Inorg. Biochem*., 1997, **66,** 37.
11. Melson, G. A., Pickering, *Aust. J. Chem*., 1969, **21,** 2889.
12. Schwarzenbach, G., *Complexometric Titrations*. Interscience, New York, 1960, pp. 79–82.
13. Dou, Yu-sheng, *J. Chem. Ed*., 1994, **67,** 134.
14. Lever, A. B. P., *J. Chem. Ed*., 1968, **45,** 711.
15. Lever, A. B. P., *Inorganic Electronic Spectroscopy*, 2nd edn., Elsevier, New York, 1984, a: pp. 480–490, b: pp. 507–511 and p. 742, c: pp. 560–567.
16. Sutton, D., *Espectros Electrónicos de los Complejos de los Metales de Transición*. Reverté, Barcelona, 1975, a: pp. 119–122, b: p. 139, c: p. 141.
17. Nakamoto, K., *Infrared Spectra of Inorganic and Coordination Compounds*. John Wiley & Sons, 1967, pp. 231–233.
18. Deacon, G. B. and Phillips, R. J., *Coord. Chem. Rev*., 1980, **33,** 227.
19. Addison, A. W. In *Copper coordination chemistry*: *Biochemical and Inorganic perspectives*, eds. K. D. Varlin and J. A. Zubieta, Adenine Press, Guiderland, New York, 1983.
20. Hathaway, B. H. and Billing, D. E., *Coord. Chem. Rev*., 1970, **5,** 143.
21. Diaz, A., García, I., Cao, R., Beraldo, H., Salberg, M., West, D., Gonzalez, L. and Ochoa, E., *Polyhedron*, 1997, **16,** 3549.

Pergamon

PII: S0277–5387(98)00120–X

Polyhedron Vol. 17, No. 19, pp. 3379–3390, 1998
© 1998 Elsevier Science Ltd
All rights reserved. Printed in Great Britain
0277–5387/98 $19.00+0.00

Oxidative dehydrogenation of the ligand coordinated to the *fac*-tris(2-aminomethylpyridine)cobalt(III) complex

Neyde Yukie Murakami Iha[a,*], Maria Amelia de Almeida Azzelini[a] and Shunji Utsuno[b]

[a] Instituto de Química, Universidade de São Paulo, Caixa Postal 26077, CEP 05599-970, São Paulo, SP Brazil

[b] Shizuoka University, 836 Ohya, Shizuoka-shi, 422, Japan

(Received 20 October 1997; accepted 12 March 1998)

Abstract—Kinetics of the oxidative dehydrogenation of the tris(2-aminomethylpyridine)cobalt(III) complex, $[Co(pic)_3]^{3+}$, have been studied following spectrophotometrically the appearance of blue species under nitrogen atmosphere. The mechanism involves a deprotonation step, in a pre-equilibrium, generating an intermediate which is susceptible to an oxidation by either the complex itself or the perchlorate ion. The equilibrium constant ($K_{OH} = 27.2 \pm 0.2\ M^{-1}$) and the rate constant ($k_{el} = 0.41 \pm 0.001\ M^{-1}s^{-1}$) were obtained by two distinct and independent treatments as well as different sets of experiments. © 1998 Elsevier Science Ltd. All rights reserved

Keywords: oxidative dehydrogenation; cobalt(II)/(III); 2-aminomethylpyridine; kinetics; ligand reactivity; catalysis.

INTRODUCTION

Several reactions involving the oxidative dehydrogenation of coordinated amines to imines have been reported for macrocyclic amines [1, 3], diamines [4–10], aminopyridines [11–15] and primary amines [16, 17]. These reactions exemplify a determining role of transition metal ions in the reactivity of organic substrates which present also an important catalytic and biological interest.

The process has been investigated in a variety of ruthenium, iron and nickel complexes containing amine ligands that undergo oxidative dehydrogenations, yielding the corresponding imine complexes. Little has been focused for cobalt complexes, except for the α-amino acidato ones in the studies of the oxidative deamination process [18–22]. α-imino-acids are postulated as the intermediate of the reaction, since the first step of the process is the dehydrogenation of the amino group. The blue color of basic anaerobic Co(II) solutions with 2-aminomethylpyridine (pic) and 2-dipicolylamine (dpa) has once been attributed to a deprotonation of the ligand [23], although Huchital and Debesis referred to the formation of a triply-bridged binuclear species in which the two metal centers were linked by one μ-hydroxo and two μ-amido bridges [24].

Martell and coworkers [25, 26] have also reported a ligand-centered oxidative dehydrogenation in some cobalt-macrocyclic aminopyridine complexes that meet a certain steric requirement and a stabilization of the C=N bond by conjugation with an aromatic ring, although the irreversible metal-centered autooxidation is the most common decomposition reaction of cobalt dioxygen complexes. The mechanism, as well as the identity of the blue species, are therefore still controversial and not completely understood.

To have a better understanding of these systems, we carried out a detailed kinetic study of the metal-activated dehydrogenation reaction on the $[Co(pic)_3]^{3+}$ complex in basic aqueous solutions.

* Author to whom correspondence should be addressed. Fax: +55(11)815 5579; E-mail: neydeiha@usp.br

EXPERIMENTAL

The *fac*-$[Co(pic)_3]Cl_3.3H_2O$ complex was synthesized from *trans*-$[CoCl(py)_4]Cl.6H_2O$ and 2-aminomethylpyridine (Aldrich) following the method previously described [27]. Anal. calcd. for *fac*-$[Co(pic)_3]Cl_3.3H_2O$; C, 39.8, N, 15.5, H, 5.6, Co, 10.8. Found: C, 39.7, N, 15.4, H, 5.5, Co, 10.8.

Lithium perchlorate was prepared and purified as described previously [28].

All other chemicals were reagent grade and used as supplied.

The electronic spectra in the visible and near-UV region were recorded on a Cary 14 or a model 8451-A Hewlett–Packard diode-array spectrophotometer at 293.0 K.

Reaction rate measurements

Spectra or optical densities at the maximum absorptivity wavelength of the blue species were recorded at appropriate time intervals after the rapid mixing of deaerated aqueous solutions of *fac*-$[Co(pic)_3]^{3+}$ and OH^-.

All the kinetic experiments were carried out at 293.0 ± 0.2 K under continuous N_2 bubbling, in triplicate, under pseudo nth order conditions in the presence of a high excess of the reactants over the cobalt complex. The ionic strength was maintained at 0.10 M (NaCl). The observed rate constants, k_{obs}, were obtained from linear regression of the dependence of $\ln(A_\infty - A_t)$ or $1/(A_\infty - A_t)$ versus time.

RESULTS AND DISCUSSION

Solutions of the *fac*-$[Co(pic)_3]^{3+}$ complex are stable in neutral or slightly acidic medium and present a pale yellow color with absorption bands at 464 ($\epsilon = 119\ M^{-1}\,cm^{-1}$) and 341 nm ($\epsilon = 128\ M^{-1}\,cm^{-1}$) ascribed to the $^1A_1 \rightarrow {}^1T_1$ and $^1A_1 \rightarrow {}^1T_2$ ligand field transitions, respectively.

In basic solutions, a deep blue color (formal molar absorbance ca. $6.0 \times 10^3\ M^{-1}\,cm^{-1}$) appears gradually with a maximum at 590 nm, as can be seen in Fig. 1(a). The same color change has also been reported for *mer*-$[Co(pic)_3]^{3+}$ or $[Co(XX)(pic)_2]^{3+}$ (XX = CO_3^{2-}, $C_2O_4^{2-}$, en or bpy) yielding a remarkable similar spectra with approximately the same molar absorbance [29, 30]. Traces of oxygen, as well as the interruption of N_2 bubbling during kinetic determinations, result in the appearance of a shoulder at 654 nm (Figure 1b). The blue species decays rapidly in the atmosphere with oxygen, resulting in a brown yellow solution.

In anaerobic basic solutions, the kinetics of the blue species formation exhibited a second order behavior for at least two half-lives, as can be seen in Fig. 2(a). The plots of the reciprocal of $(A_\infty - A_t)$ versus $[OH^-]$ are linear and the k_{obs} values are obtained from the angular coefficients, Fig. 2b and 2c. The dependence of the observed rate constants on the OH^- ion concentrations, both from NaOH solutions or Na_3PO_4/Na_2HPO_4 buffers is presented in Fig. 3.

Using ClO_4^- ion as an oxidant, or even keeping the ionic strength with a $LiClO_4$ solution, the reaction is typically pseudo first order for at least three half lives as follows:

$$dP/(P_\infty - P_t) = k_{obs}.dt$$

Figure 4(a) presents the plots of $\ln(A_\infty - A_t)$ versus time at different OH^- ion concentrations at a constant ClO_4^- ion concentration in a high excess, and Fig. 4(b) shows similar plots at several ClO_4^- concentrations keeping a high excess of OH^- ion concentration as well. Table 1 displays the k_{obs} values obtained from these plots.

The kinetic behavior is characteristic of an induced electron transfer process, where the perchlorate ion or the complex itself is acting as the oxidizing agent, assisted by OH^- ions [14], leading to an oxidative dehydrogenation of the ligand coordinated to the complex, as represented in Scheme 1.

Similar to the oxidative dehydrogenation process

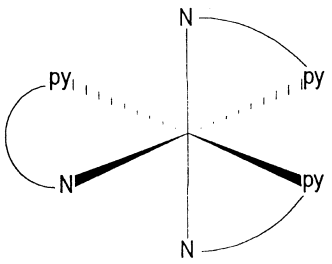

mer

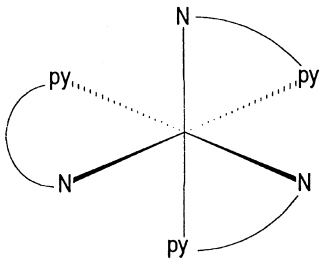

fac

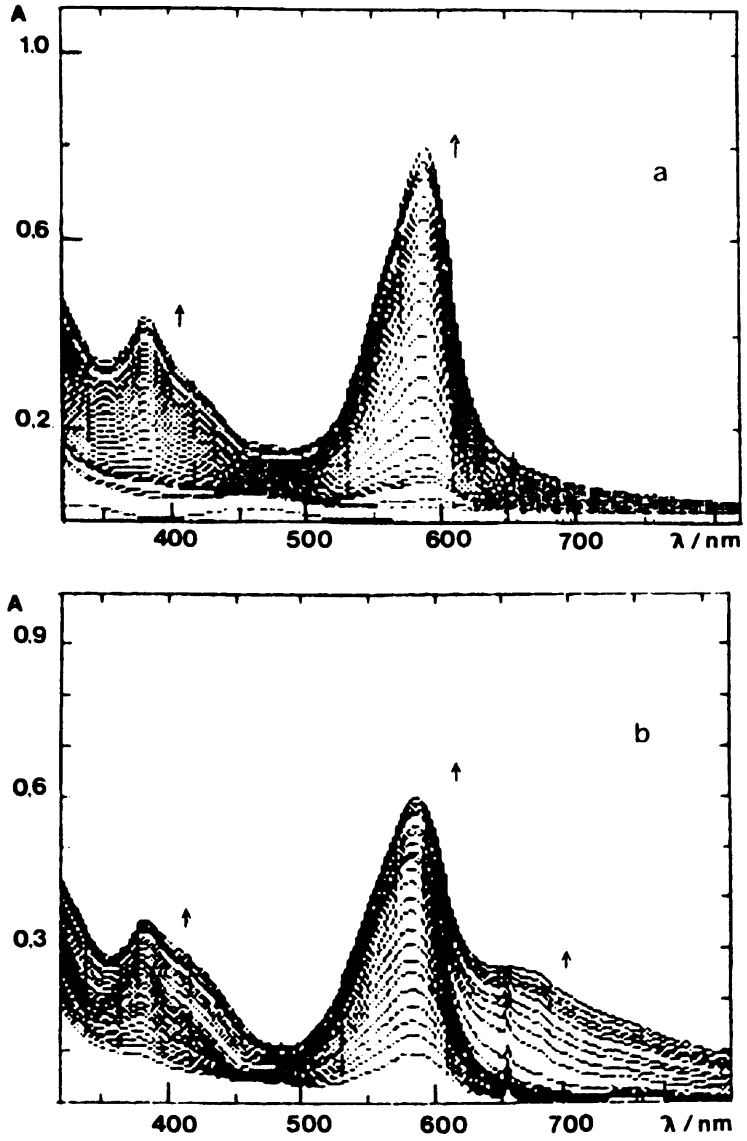

fig. 1. Spectral variation after the mixture of the $[Co(pic)_3]^{3+}$ 2.01×10^{-4} M solution and the OH^- 4.86×10^{-3} M solution at 293.0 K and $I=0.10$ M ($LiClO_4$). (a) under continuous N_2 bubbling. (b) without continuous N_2 bubbling.

of the 2-aminomethylpyridine ligand coordinated to a cyanoferrate compound [31], the first step involved is a rapid reversible deprotonation of the coordinated ligand followed to the oxidation by ClO_4^- or $[Co(pic)_3]^{3+}$. This process does not need a previous electron transfer step, as in the Fe(II) system, since the cobalt already presents the high oxidation state as Co(III) species.

According to the mechanism,

$$k_{obs}=\frac{k_{el}K_{OH}[OH^-][Ox]}{1+K_{OH}[OH^-]} \qquad (1)$$

The k_{el} and K_{OH} values were obtained independently, using two distinct treatments from independent sets of experiments at different conditions as described as follow.

For experiments carried out with a high excess of OH^- and ClO_4^-, in which the latter acts as an oxidant, two sets of measurements are made.

In the first one, keeping the OH^- concentration constant, the expression (1) can be rewritten as a function of reciprocal of the ClO_4^- concentration.

$$\frac{1}{k_{obs}}=\left[\frac{1}{k_{el}}+\frac{1}{k_{el}K_{OH}[OH^-]}\right]\cdot\frac{1}{[Ox]} \qquad (2)$$

Figure 5 presents the plots of $1/k_{obs}$ versus $1/[ClO_4^-]$, which are straight lines that intercept the origin. From the angular coefficient of each plot, called $\mathbf{b_1}$ from now

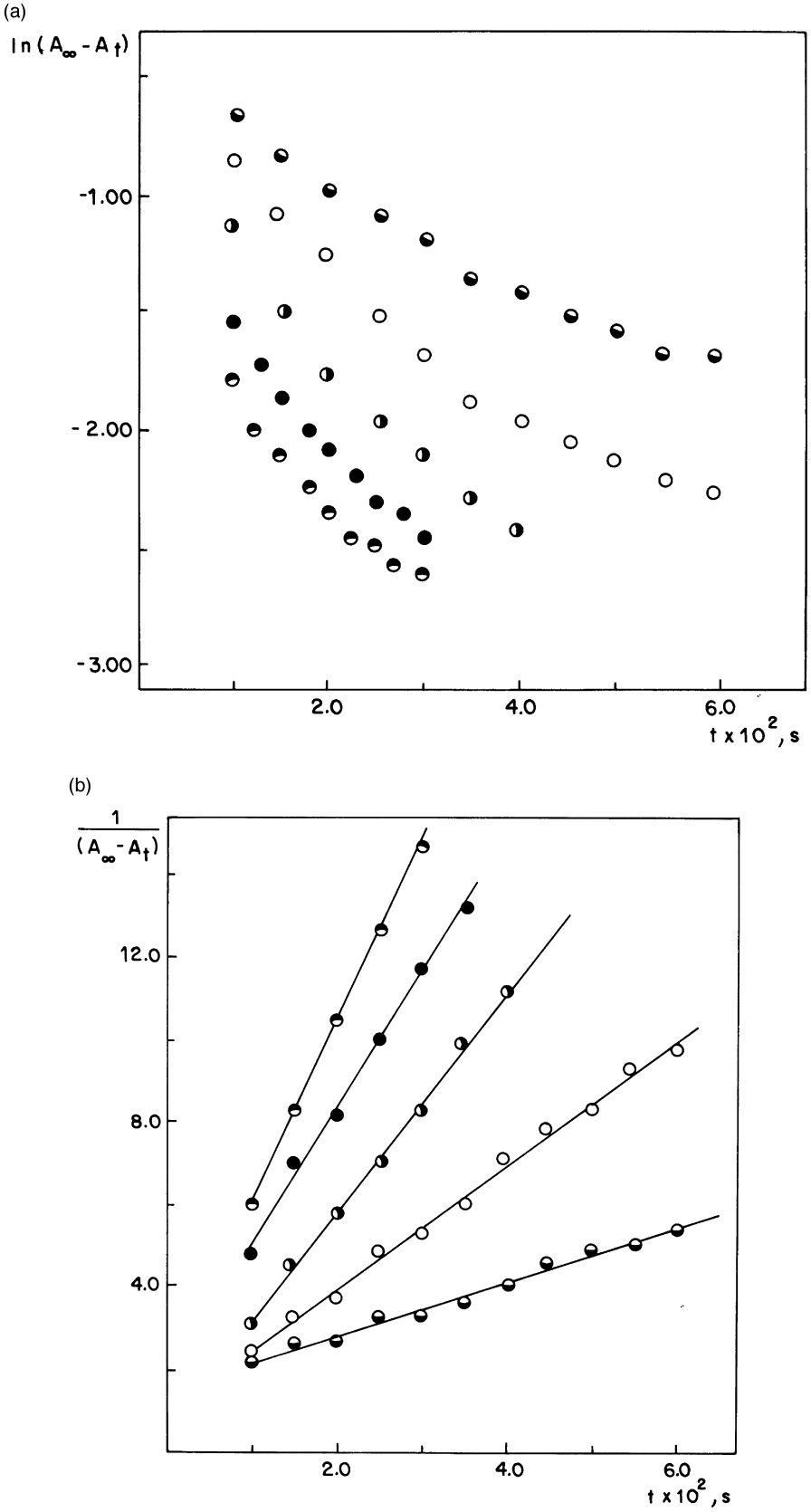

Fig. 2. (a) $\ln(A_\infty - A)$ versus time $[OH^-] = 2.43 \times 10^{-3}$ M, ◒; 3.65×10^{-3} M, ○; 4.86×10^{-3} M, ◑; 6.08×10^{-3} M, ●; 7.29×10^{-3} M, ◓; $[[Co(pic)_3]^{3+}] = 2.01 \times 10^{-4}$ M, $I = 0.10$ (NaCl), $T = 293.0$ K, $[OH^-]$ from NaOH solutions. (b) $1/(A_\infty - A)$ versus time $[OH^-] = 2.43 \times 10^{-3}$ M, ◒; 3.65×10^{-3} M, ○; 4.86×10^{-3} M, ◑; 6.08×10^{-3} M, ●; 7.29×10^{-3} M, ◓; $[[Co(pic)_3]^{3+}] = 2.01 \times 10^{-4}$ M, $I = 0.10$ (NaCl), $T = 293.0$ K, $[OH^-]$ from NaOH solutions.(c) $1/(A_\infty - A)$ versus time $[OH^-] = 2.34 \times 10^{-3}$ M, ○; 4.29×10^{-3} M, ◑; 5.36×10^{-3} M, ●; 7.03×10^{-3} M, ◓; $[[Co(pic)_3]^{3+}] = 2.01 \times 10^{-4}$ M, $I = 0.10$ (NaCl), $T = 293.0$ K, $[OH^-]$ from Na_3PO_4/Na_2HPO_4 solutions.

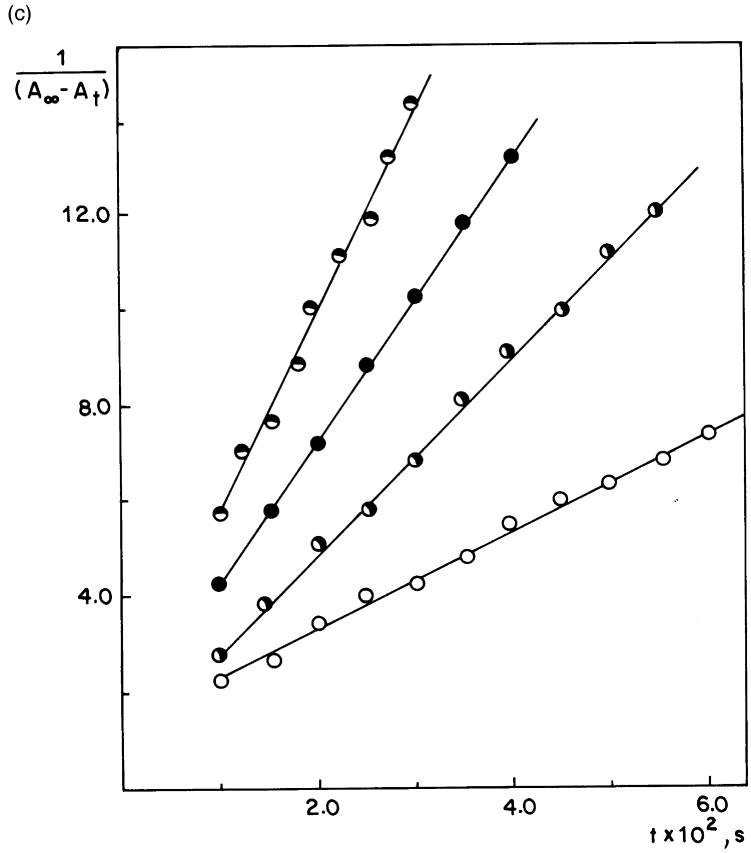

Fig. 2 (continued).

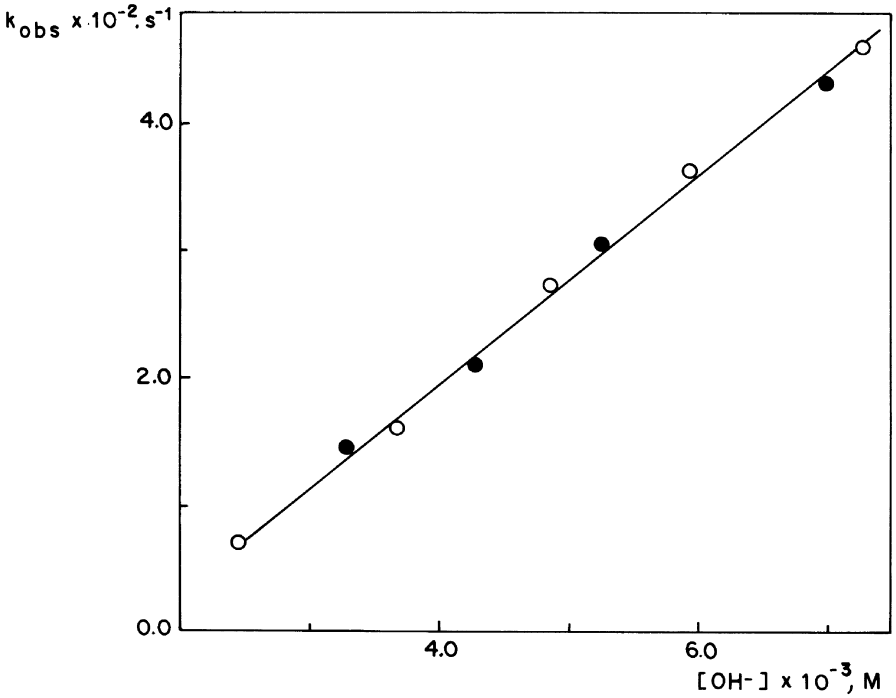

Fig. 3. Plot of k_{obs} versus $[OH^-][[Co(pic)_3]^{3+}] = 2.01 \times 10^{-4}$ M, $I = 0.10$ (NaCl), $T = 293.0$ K ○ $[OH^-]$ from NaOH solutions ● $[OH^-]$ from Na_3PO_4/Na_2HPO_4 solutions.

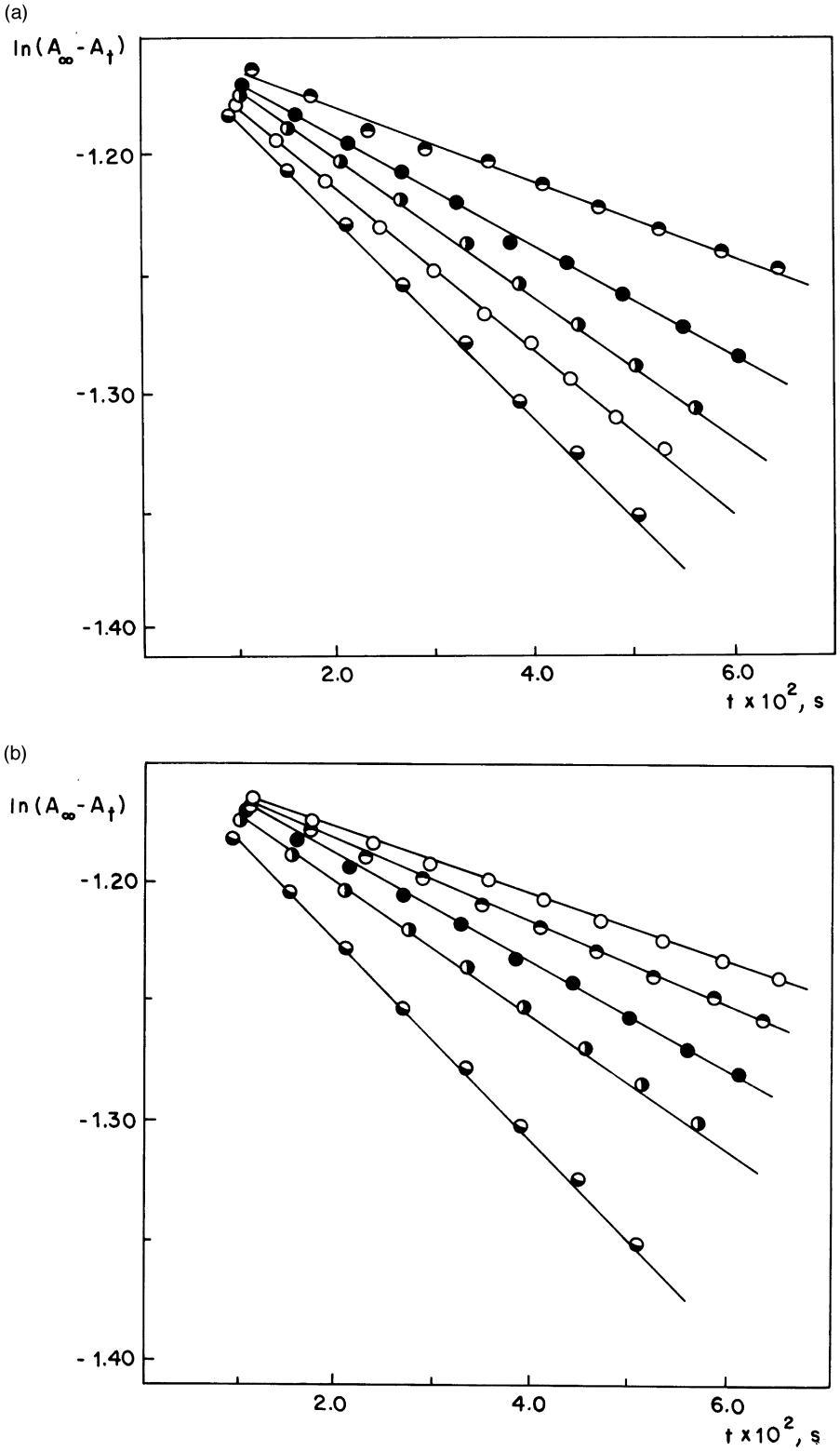

Fig. 4. (a) $\ln(A_\infty - A)$ versus time $[OH^-] = 2.43 \times 10^{-3}$ M, ◓; 3.65×10^{-3} M, ●; 4.86×10^{-3} M, ◑; 6.08×10^{-3} M, ○; 7.29×10^{-3} M, ◒; $[[Co(pic)_3]^{3+}] = 2.01 \times 10^{-4}$ M, $I = 0.10$ (NaCl), $[ClO_4^-] = 6.03 \times 10^{-3}$ M, $T = 293.0$ K. (b) $\ln(A_\infty - A)$ versus time $[ClO_4^-] = 2.01 \times 10^{-3}$ M, ○; 2.38×10^{-3} M, ◓; 2.94×10^{-3} M, ●; 4.02×10^{-3} M, ◑; 6.03×10^{-3} M, ◒; $[[Co(pic)_3]^{3+}] = 2.01 \times 10^{-4}$ M, $I = 0.10$ (NaCl), $[OH^-] = 7.29 \times 10^{-3}$ M, $T = 293.0$ K.

Table 1. k_{obs} values obtained for different OH^- and ClO_4^- concentrations[1]

$[OH^-] \times 10^{-3}$func /M	$[ClO_4^-] \times 10^3$/M	$k_{obs} \times 10^4/s^{-1}$
2.43	2.01	0.50
	2.38	0.59
	2.94	0.73
	4.02	1.00
	6.03	1.49
3.65	2.01	0.74
	2.38	0.86
	2.94	1.06
	4.02	1.46
	6.03	2.17
4.86	2.01	0.94
	2.38	1.12
	2.94	1.38
	4.02	1.89
	6.03	2.82
6.08	2.01	1.15
	2.38	1.36
	2.94	1.68
	4.02	2.31
	6.03	3.44
7.29	2.01	1.34
	2.38	1.59
	2.94	1.96
	4.02	2.70
	6.03	4.01

$[[Co(pic)_3]^{3+}] = 2.01 \times 10^{-4}$ M, $I = 0.10$ (NaCl), $T = 293.0$ K

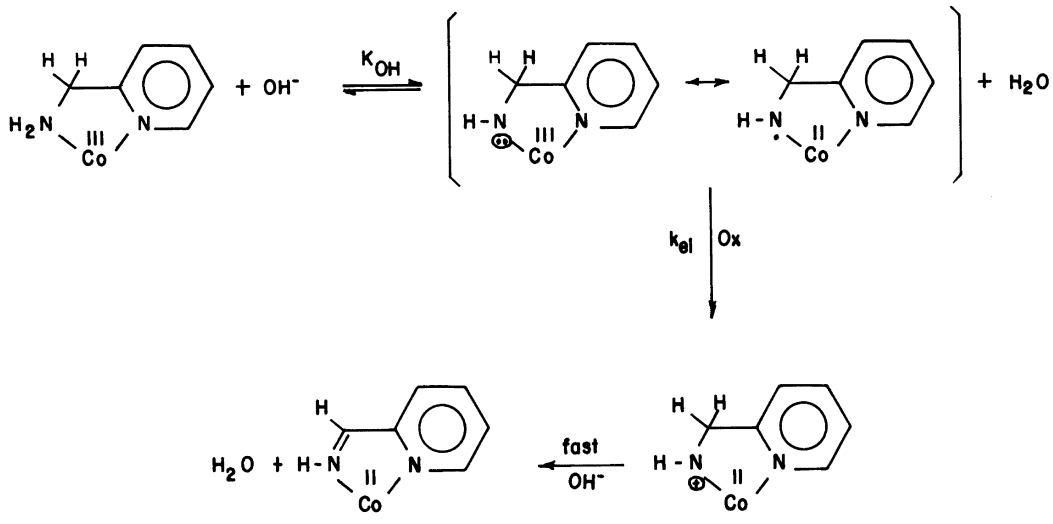

Scheme 1

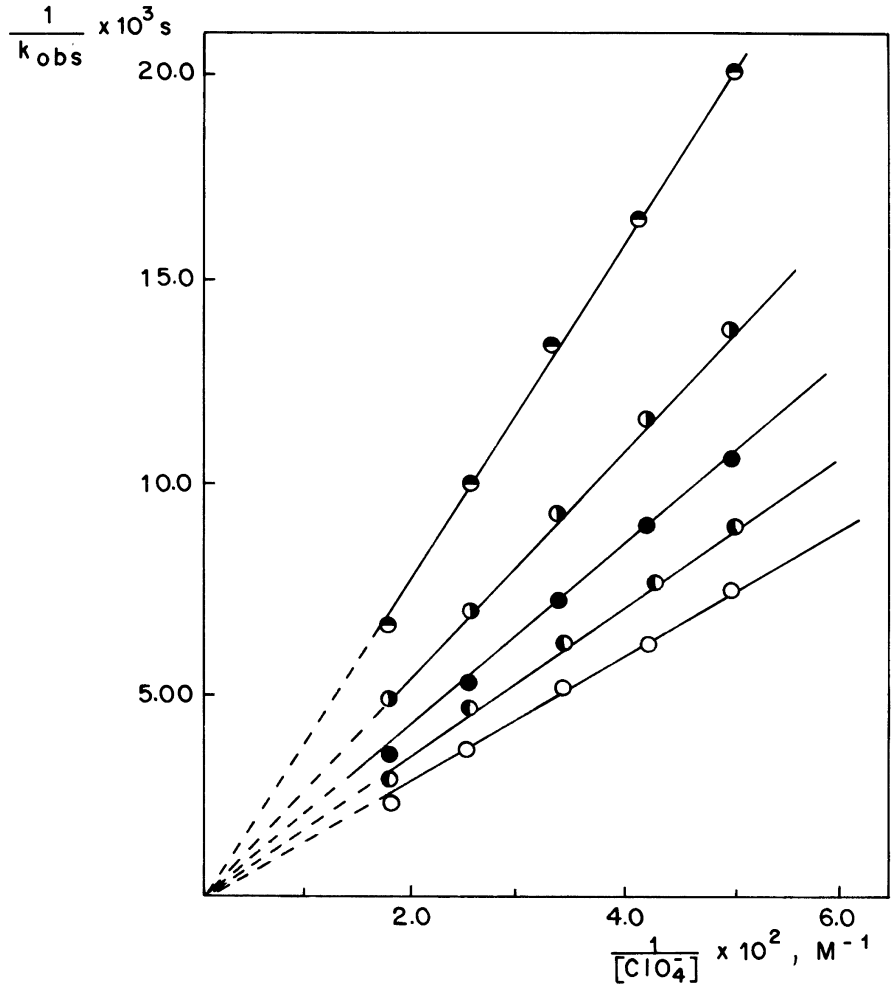

Fig. 5. Plots of $1/k_{obs}$ versus $1/[ClO_4^-][OH^-] = 2.43 \times 10^{-3}$ M, ○; 3.65×10^{-3} M, ◐; 4.86×10^{-3} M, ●; 6.08×10^{-3} M, ◑; 7.29×10^{-3} M, ◓; $[[Co(pic)_3]^{3+}] = 2.01 \times 10^{-4}$ M, $I = 0.10$ (NaCl), $[ClO_4^-] = 6.03 \times 10^{-3}$ M, $T = 293.0$ K.

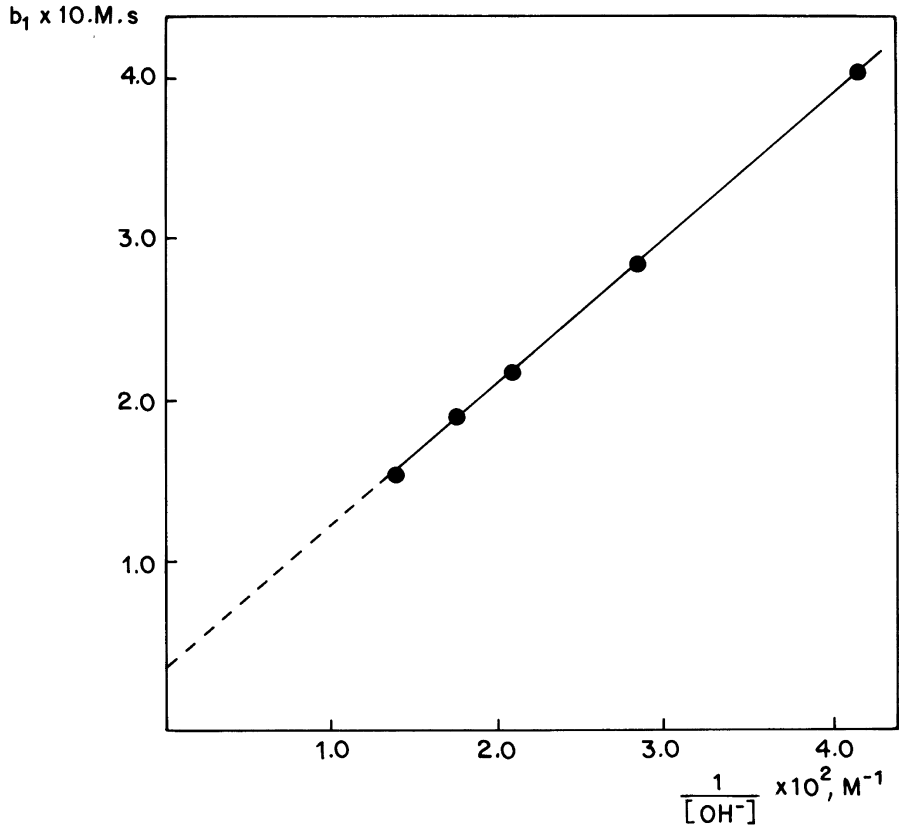

Fig. 6. Plots of $\mathbf{b_1}$ versus $1/[OH^-][[Co(pic)_3]^{3+}] = 2.01 \times 10^{-4}$ M, $I = 0.10$ (NaCl), $[ClO_4^-] = 6.03 \times 10^{-3}$ M, $T = 293.0$ K.

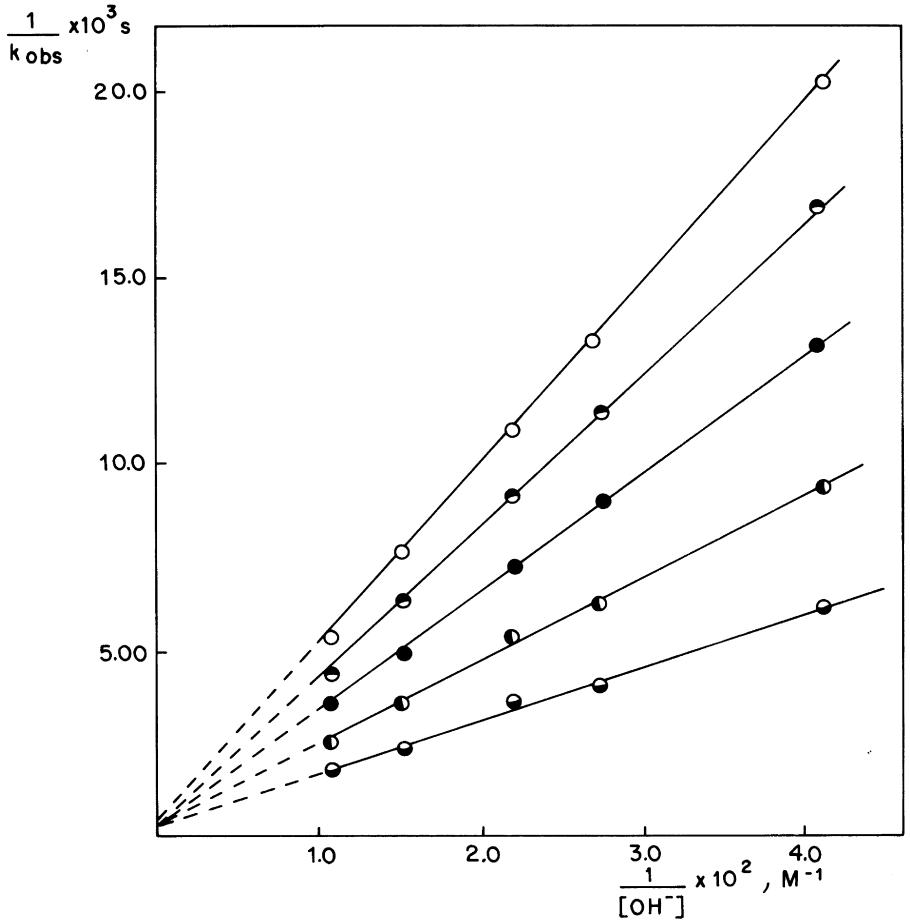

Fig. 7. Plots of $1/k_{obs}$ versus $1/[OH^-]$, ◒; $=2.01\times10^{-3}$ M, ◐; 2.38×10^{-3} M, ●; 2.94×10^{-3} M, ◓; 4.02×10^{-3} M, ○; 6.03×10^{-3} M $[[Co(pic)_3]^{3+}]=2.01\times10^{-4}$ M, $I=0.10$ (NaCl), $T=293.0$ K.

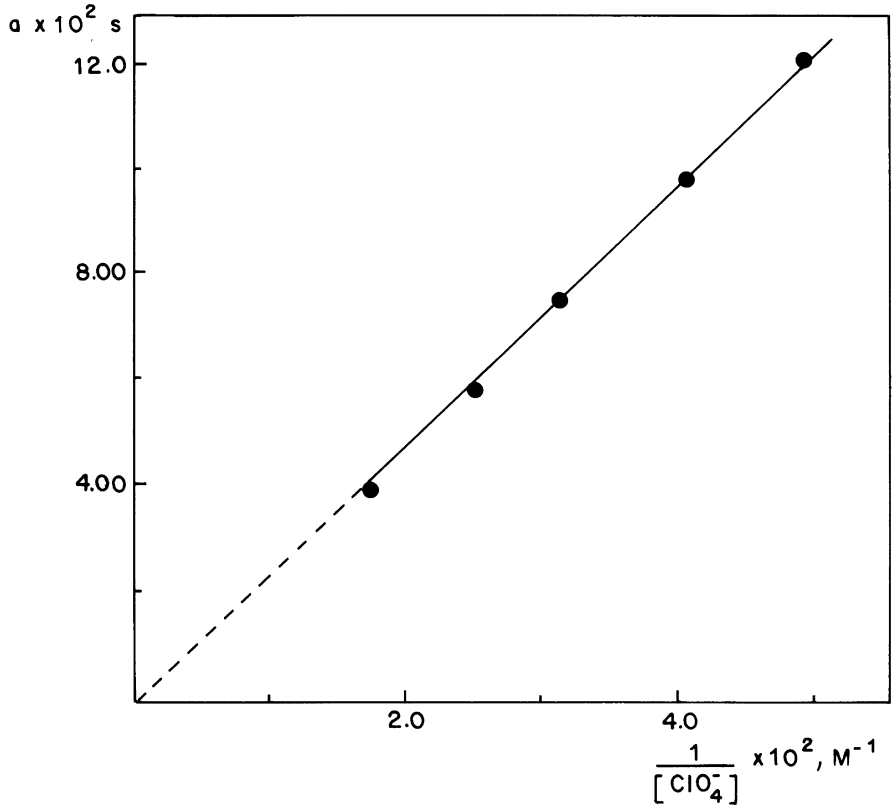

Fig. 8. Plots of **a** versus $1/[ClO_4^-][[Co(pic)_3]^{3+}] = 2.01 \times 10^{-4}$ M, $I = 0.10$ (NaCl), $T = 293.0$ K.

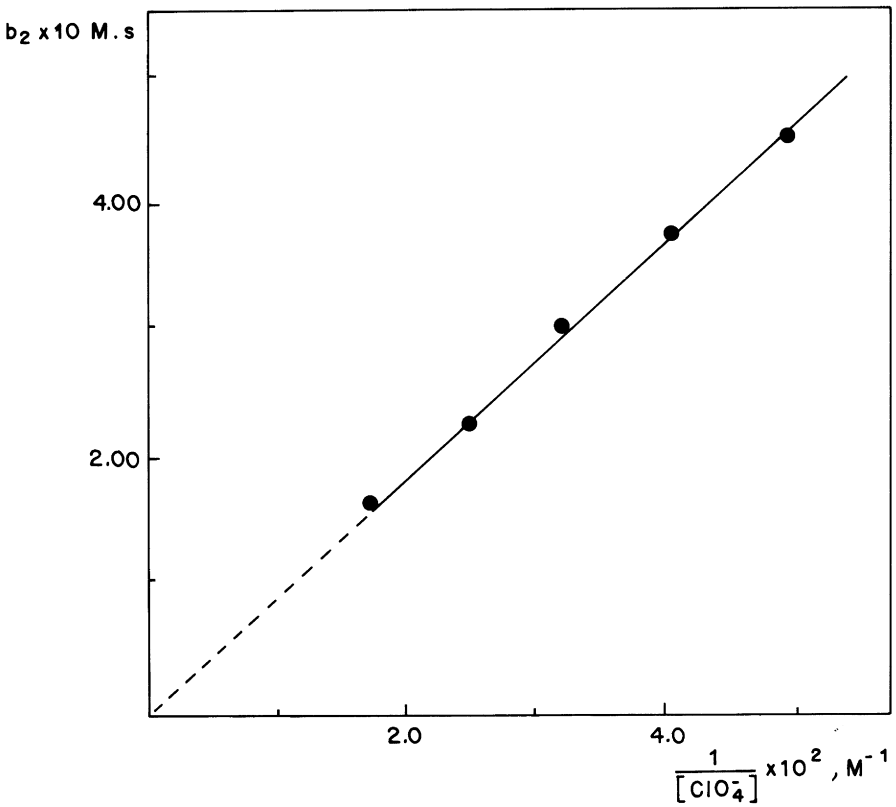

Fig. 9. Plots of $\mathbf{b_2}$ versus $1/[ClO_4^-][[Co(pic)_3]^{3+}] = 2.01 \times 10^{-4}$M, $I = 0.10$ (NaCl), $T = 293.0$ K.

on, versus the reciprocal of the $[OH^-]$ concentration, Fig. 6, the k_{el} and K_{OH} values of $0.40\,M^{-1}s^{-1}$ and $27.4\,M^{-1}$, respectively, are obtained.

In the second one, keeping the ClO_4^- concentration constant, the expression (1) can be rewritten as follows:

$$\frac{1}{k_{obs}}=\frac{1}{k_{el}[OH^-]}+\left[\frac{1}{k_{el}K_{OH}[Ox]}\right].\frac{1}{[OH^-]} \qquad (3)$$

The dependence is plotted in Fig. 7 and each plots of $1/k_{obs}$ versus $1/[OH^-]$ leads to a corresponding linear coefficient, represented as **a**, and an angular coefficient, $\mathbf{b_2}$. The plots of **a** and $\mathbf{b_2}$ versus the reciprocal of the oxidant concentration, respectively Figs 8 and 9, give the k_{el} and K_{OH} values of $0.41\,M^{-1}s^{-1}$ and $27.0\,M^{-1}$, respectively. The consistency of the mechanism and rate law are proved by k_{el} and K_{OH} values independently obtained from the two distinct treatments. They are also in complete agreement with those values obtained from an independent set of experiments, using $LiClO_4$ to control the ionic strength. In this case, the approach is the same of the above described condition and the k_{el} and K_{OH} values, obtained from expression (3), are $0.44\,M^{-1}s^{-1}$ and $24.5\,M^{-1}$.

In the absence of the perchlorate ion, as described initially, Fig. 2(a–c), the $[Co(pic)_3]^{3+}$ complex itself acts as an oxidant, and the blue species formation process follows the pseudo second order kinetic.

$$dP/(P_\infty - P)^2 = k_{obs}.dt$$

where k_{obs} is:

$$k_{obs}=\frac{k_{el}K_{OH}[OH^-]}{(1+K_{OH}[OH^-])^2} \qquad (4)$$

The plot of k_{obs} versus $[OH^-]$, from Fig. 3, is a straight line and its angular coefficients, $10.1\,M^{-2}s^{-1}$, is in accord with the $k_{el}K_{OH}$ product obtained from the treatments previously described. This treatment considered, at first rough approximation, the $K_{OH}[OH^-]$ term negligible and much lower than 1.

The autoconsistency of the results and the reproducibility of the independent constant values evaluated from different treatments, mainly from the first two sets which do not require any approximation, led to the validity of the mechanism proposed in Scheme 1, which is able to account quantitatively for the rate determining steps involved in the overall reaction.

Acknowledgements—The supports of the Fundação de Amparo à Pesquisa do Estado de São Paulo (FAPESP) and of the Conselho Nacional de Desenvolvimento Científico e Tecnológico (CNPq) are gratefully acknowledged.

REFERENCES

1. Curtis, N. F., *Coord. Chem. Rev*, 1968, **3,** 3.
2. Dabrowiak, J. C., Lovecchio, F. V., Goedken, V. L. and Busch, D. H., *J. Am. Chem. Soc*, 1972, **94,** 5502.
3. Goedken, V. L. and Busch, D. H., *J. Am. Chem. Soc*, 1972, **94,** 7355.
4. Elsbernd, H. and Beattie, J. K., *J. Chem. Soc., A*, 1970, 2598.
5. Lane, B. C., Lester, J. E. and Basolo, F., *J. Chem. Soc., Chem. Commun*, 1971, 618.
6. Mahoney, D. F. and Beattie, J. K., *Inorg. Chem*, 1973, **12,** 2561.
7. Goedken, V. L., *J. Chem. Soc., Chem. Commun*, 1972, 207.
8. Brown, G. M., Weaver, T. R., Keene, F. R. and Meyer, T. J., *Inorg. Chem*, 1976, **15,** 190.
9. Ferreira, A. M. C. and Toma, H. E., *J. Chem. Soc. Dalton Trans*, 1983, 2051.
10. Kuroda, Y., Tanaka, N. and Goto, M., Sakai, T., *Inorg. Chem*, 1989, **28,** 2163.
11. Alvarez, V., Allen, R. J., Matsubara, T. and Ford, P. C., *J. Am. Chem. Soc*, 1974, **96,** 7686.
12. Keene, F. R., Ridd, M. J. and Snow, E., *J. Am. Chem. Soc*, 1983, **105,** 7075.
13. Goto, M., Takeshita, M., Kanda, N., Sakai, T. and Goedken, V. L., *Inorg. Chem*, 1985, **24,** 582.
14. Toma, H. E., Ferreira, A. M. C. and Murakami Iha, N. Y., *Nouv. J. Chim*, 1985, **9,** 473.
15. Toma, H. E. and Tsurumaki, M., *J. Braz. Chem. Soc*, 1990, **1,** 17.
16. Diamond, S. E., Tom, G. M. and Taube, H., *J. Am. Chem. Soc*, 1975, **97,** 2661.
17. Keene, F. R., Salmon, D. J. and Meyer, T. J., *J. Am. Chem. Soc*, 1976, **98,** 1884.
18. Yamaguchi, M., Saburi, M. and Yoshikawa, S., *J. Am. Chem. Soc*, 1984, **106,** 8293.
19. Hammarshoi, A., Hartshorn, R. M. and Sargeson, A. M., *J. Chem. Soc., Chem. Commun*, 1988, 1226.
20. Hammarshoi, A., Hartshorn, R. M. and Sargeson, A. M., *Inorg. Chem*, 1990, **29,** 4525.
21. Drok, K. J., Harrowfield, J. M., McNiven, S. J., Sargeson, A. M., Skelton, B. W. and White, A. H., *Aust. J. Chem*, 1993, **46,** 1557.
22. Yamaguchi, M., Saburi, M., Yoshikawa, S. and Yamagishi, T., *Bull. Chem. Soc. Jpn*, 1994, **67,** 1341.
23. Walker, J. K. and Nakon, R., *J. Am. Chem. Soc*, 1977, **99,** 8359.
24. Huchital, D. H. and Debesis, E., *Inorg. Chim. Acta*, 1985, **98,** 79.
25. Raleigh, C. and Martell, A. E., *Inorg. Chem*, 1985, **24,** 142.
26. Basollote, M. G., Chen, D. and Martell, A. E., *Inorg. Chem*, 1989, **28,** 3494.
27. Azzellini, M. A. A., Oliveira, M. F. P., Murakami Iha, N. Y. and Osorio, V. K. L., *Pohyhedron*, 1996, **15,** 4579.
28. Murakami Iha, N. Y. and Toma, H. E., *Inorg. Chim. Acta*, 1984, **71,** 181.
29. Michelsen, K., *Acta Chem. Scand*, 1974, **A28,** 428.
30. Utsuno, S. and Sekizaki, M., *Inorg. Nucl. Chem. Let*, 1979, **15,** 259.

Pergamon

PII: S0277–5387(98)00121–1

Polyhedron Vol. 17, No. 19, pp. 3391–3407, 1998
© 1998 Elsevier Science Ltd
All rights reserved. Printed in Great Britain
0277–5387/98 $19.00+0.00

Synthesis and characterization of a protected amino alcohol containing *ortho*-carborane

Ye Wu,[a] Patrick J. Carroll[b] and William Quintana[a,*]

[a] Department of Chemistry and Biochemistry, New Mexico State University, Box 30001, Dept. 3C, Las Cruces, NM 88003-8001, U.S.A.

[b] Department of Chemistry and Laboratory for Research on the Structure of Matter, University of Pennsylvania, Philadelphia, Pennsylvania, 19104-6323, U.S.A.

(Received 12 December 1997; accepted 16 March 1998)

Abstract—The reaction between the alkyne, N-(5-Benzyloxy-2-pentynyl)phthalimide and decaborane (14) in the presence of dimethyl sulfide resulted in the isolation of 1-$C_6H_4(CO)_2NCH_2$-2-$C_6H_5CH_2OCH_2CH_2$-1, 2-$C_2B_{10}H_{10}$ **(5)**, 1-methylphthalimido-2-ethylbenzyl ether-*o*-carborane, in moderate yield. Compound **5** was characterized by single crystal X-ray diffraction study. Compound **5** crystallizes in the $P\bar{1}$ space group, a = 10.5328 (5) Å, b = 11.9209 (6) Å, c = 10.3451 (3) Å, $\alpha = 110.492$ (3)°, $\beta = 102.868$ (3)°, $\gamma = 87.279$ (2)°, Z = 2, $D_{calc} = 1.226$ g/cm^3, $R = 0.0491$ for 3521 reflections with $F > 4.0\sigma$. Deprotection of the ether linkage of **5** results in the formation of 1-$C_6H_4(CO)_2NCH_2$-2-$HOCH_2CH_2$-1, 2-$C_2B_{10}H_{10}$ **(6)**, 1-methylphthalimido-2-ethylalcohol-*o*-carborane. The transformation is accomplished by hydrogenation of **(5)** over a Pd/C catalyst and resulted in the efficient conversion of **(5)** into **(6)** (83% yield). Experimental details and analytical data leading to the identification of the reported compounds is provided. © 1998 Elsevier Science Ltd. All rights reserved

Keywords: carborane; synthesis; amino; alcohol; reactivity; crystallography.

INTRODUCTION

The recent report by Hawthorne and coworkers and that of Kahl and Kasar regarding the high-yield synthesis of polyhedral carborane amino acids are significant steps in the field of boron neutron capture therapy [1–3]. There is definitely a need for the synthesis and characterization of a wide variety of these compounds if progress is to be made in this field. Our approach relies in the introduction of a protected amine and a protected alcohol into the carborane cage, using the well established synthetic route for the preparation of substituted *ortho*-carboranes, relying on the reaction of an alkyne with decaborane (14) [4–10].

The scope of the presented work is the synthesis of compounds that might be suitable for use in boron neutron capture therapy (BNCT). Although in recent years there is an apparent acceptance of this technique as a viable option for the treatment of certain tumors, specifically malignant melanoma and glioblastoma multiforme, there are too few compounds that are sufficiently selective to perform this task. The two compounds currently under clinical trials, $Na_2B_{12}H_{11}SH$ (BSH) and boronophenylalanine (BPA) exhibit a tumor to normal brain ratio of 1.69:1 and 3:1 respectively [11, 12]. Another problem is the low solubility of these compounds at physiological pH, this is especially true for BPA. Therefore, synthetic methodology for the synthesis of bifunctional carboranes is highly desirable.

The introduction of bifunctional alkynes into the decaborane (14) framework to produce heterobifunctional *o*-carboranes is not unprecedented in the literature [4–10, 13, 14]. This methodology is simple and efficient. The main obstacle is choosing the appropriate bifunctional alkyne needed to perform the reaction. Our objective was to find the appropriate alkyne containing a protected amine and a protected alcohol precursor that could be reacted with decaborane (14). Given the fact that this type of compound is not commercially available, one of the tasks for this study

* Author to whom correspondence should be addressed. Fax: 001 505 646 2649.

was the synthesis of such a compound. We chose $C_6H_4(CO)_2NCH_2C{\equiv}CCH_2CH_2OC_6H_5$ as our precursor, since it contained a protected amine and a protected alcohol. In this communication we describe the synthesis of this alkyne from its precursors and its subsequent transformation to the heterobifunctional *ortho*-carborane. The synthesis of this carborane could open the door for the preparation of other bifunctional carboranes needed for BNCT. The key to successful BNCT is the delivery of ^{10}B-containing compounds to the malignant tumor cell selectively. The necessary tumor/normal tissue and tumor/blood ratios must be at least two [15, 16].

Common strategies used to achieve the above indicated objective include the attachment of boron containing residues to existing compounds known to accumulate in tumor tissues [17] and to a variety of recognition elements, such as amino acids [18, 19], peptides [15], antibodies [20], nucleosides [21–24], liposomes [25] and other regulatory biomolecules [26]. The most commonly used boron containing residues are carborane clusters, such as *ortho*-carborane and derivatives. These clusters have the advantage over monoboronated compounds, since they contain up to ten boron atoms and naturally abundant ^{10}B may be used [27]. Also these clusters are stable at physiological pH. The main task is the design and combination of the boron clusters with the recognition elements or derivative thereof. This communication intends to address this strategy.

EXPERIMENTAL

All manipulations were carried out using standard high vacuum or inert atmosphere techniques, when warranted, as described by Shriver [28].

Materials

3-butynyl-1-ol, benzyl bromide, sodium hydride, tetrahydrofuran, dimethylformamide, paraformaldehyde, n-butyllithium (2.0 M in cyclohexane), magnesium sulfate, chloroform, acetonitrile, methanol, ethanol, potassium phthalimide, hexanes, silica gel, acetone-d_6, CD_3CN and $CDCl_3$ were purchased form Aldrich. All solvents were dried prior to use. Decaborane (14) was obtained from Strem Chemicals.

Physical measurements

The 128.4 MHz boron-11 and 400.0 MHz proton spectra were obtained on a Varian Unity-400 Fourier transform spectrometer. All boron-11 chemical shifts were referenced to $BF_3{\cdot}O(C_2H_5)_2 = 0.0$ ppm with a negative sign indicating an upfield shift. Proton NMR at 200 MHz and carbon-13 NMR at 50.0 MHz were obtained on Varian Gemini-200 Fourier transform spectrometer. Proton chemical shifts and carbon-13 chemical shifts were referenced to TMS = 0.00 ppm with positive values indicating downfield shifts. Infrared spectra were recorded on a Perkin-Elmer 337 grating infrared spectrophotometer and on Perkin Elmer 1720 Fourier transform spectrophotometer. Low resolution mass spectrometry data was obtained in a HP GC/MS system, model 5995.

X-ray crystallography

X-ray intensity data were collected on a Rigaku R-AXIS IIc area detector employing graphite-monochromated Mo-Kα radiation ($\lambda = 0.71069$ Å) at a temperature of 223 K for compound **5**. Indexing was performed from a series of 1° oscillations with exposures of 8 minutes per frame. A hemisphere of data was collected using 6° oscillations with exposures of 4 minutes per frame. The crystal to detector distance was 82 mm. Oscillation images were processed using bioteX [29], producing a listing of unaveraged F^2 and $\sigma(F^2)$ values which were then passed to the teXsan [30] program package for further processing and structure solution on a Silicon Graphics Indigo R4000 computer. A total of 9100 reflections were measured over the ranges: $5.18 \leqslant 2\theta \leqslant 50.70°$, $-12 \leqslant h \leqslant 12$, $-14 \leqslant k \leqslant 12$, $-12 \leqslant l \leqslant 12$, yielding 3949 unique reflections ($R_{int} = 0.0176$). Other relevant crystallographic data are given in Table 1. The intensity data were corrected for Lorentz and polarization effects but not for absorption.

The structure was solved by direct methods (SIR92) [31]. The refinement was full-matrix least squares based on F^2 using SHELXL-93 [32]. All reflections were used during refinement (F^2's that were experimentally negative were replaced by $F^2 = 0$). The weighting scheme was $w = 1/[\sigma^2(F_o^2) + 0.0586P^2 + 0.3395P]$ where $P = (F_o^2 + 2F_c^2)/3$.

Non-hydrogen atoms were refined anisotropically; cage hydrogens were refined isotropically; all other hydrogen atoms were refined using a 'riding' model which the positions of the hydrogen atoms were re-idealized before each least squares cycle by applying the coordinate shifts of the atom to which each hydrogen atom is attached. Refinement converged to $R_1 = 0.0491$ and $wR_2 = 0.1215$ for 3521 reflections for which $F > 4\sigma(F)$ and $R_1 = 0.0556$, $wR_2 = 0.1270$ and GOF = 1.070 for all 3949 unique, non-zero reflections and 348 variables. The maximum Δ/σ in the final cycle of least squares was 0.000 and the two most prominent peaks in the final Fourier were +0.191 and −0.176 e/Å^3.

Selected bond distances and angles are given in Table 2 and Table 3 respectively. Final atomic positions for non Hydrogen atoms and their isotropic parameters, Hydrogen atom coordinates and displacement parameters, non-hydrogen atom thermal parameters, full listing of interatomic distances and bond angles are available as supplementary material.

Table 1. Summary of Structure Determination of 1-$C_6H_4(CO)_2NCH_2$-2-$C_6H_5CH_2OCH_2CH_2$-1, 2-$C_2B_{10}H_{10}$ (5)

Formula:	$C_{20}B_{10}H_{27}NO_3$
Formula weight:	437.54
Crystal class:	triclinic
Space group:	$P\bar{1}$ (#2)
Z	2
Cell constants:	
a	10.5328(5) Å
b	11.9209(6) Å
c	10.3451(3) Å
α	110.492(3)°
β	102.868(3)°
γ	87.279(2)°
V	1185.52(9) Å^3
μ	0.72 cm^{-1}
crystal size, mm	$0.50 \times 0.35 \times 0.22$
D_{calc}	1.226 g/cm^3
$F(000)$	456
Radiation:	Mo-K_α ($\lambda = 0.71069$ Å)
2θ range	5.18–50.70°
hkl collected:	$-12 \leqslant h \leqslant 12$; $-14 \leqslant k \leqslant 12$; $-12 \leqslant l \leqslant 12$
No. reflections measured:	9100
No. unique reflections:	3949 ($R_{int} = 0.0176$)
No. observed reflections	3521 ($F > 4\sigma$)
No. reflections used in refinement	3949
No. parameters	348
R indices ($F > 4\sigma$)	$R_1 = 0.0491$, w$R_2 = 0.1215$
R indices (all data)	$R_1 = 0.0556$, w$R_2 = 0.1270$
GOF:	1.070
Final Difference Peaks, e/Å^3	+0.191, −0.176

Table 2. Selected Bond Distances in 1-$C_6H_4(CO)_2NCH_2$-2-$C_6H_5CH_2OCH_2CH_2$-1, 2-$C_2B_{10}H_{10}$ (5), Å

Bond		Bond		Bond	
O23–C15	1.209(2)	O24–C22	1.211(2)	O27–C28	1.413(3)
O27–C26	1.421(2)	N14–C22	1.395(2)	N14–C15	1.399(2)
N14–C13	1.452(2)	C1–C13	1.528(2)	C1–C2	1.684(2)
C1–B5	1.707(3)	C1–B9	1.709(3)	C1–B6	1.722(2)
C1–B8	1.727(2)	C2–C25	1.527(3)	C2–B3	1.706(3)
C2–B7	1.711(3)	C2–B8	1.722(3)	C2–B6	1.732(2)
C15–C16	1.484(2)	C16–C17	1.383(3)	C16–C21	1.387(2)
C17–C18	1.383(3)	C18–C19	1.378(4)	C19–C20	1.389(3)
C20–C21	1.382(2)	C21–C22	1.486(2)	C25–C26	1.505(3)
C29–C30	1.364(3)	C29–C34	1.369(3)	C30–C31	1.378(5)
C31–C32	1.367(6)	C32–C33	1.341(6)	C33–C34	1.345(4)
B3–B7	1.772(3)	B3–B11	1.773(3)	B3–B4	1.774(3)
B3–B6	1.779(3)	B4–B6	1.767(3)	B4–B5	1.775(3)
B4–B11	1.779(3)	B4–B10	1.782(3)	B5–B10	1.766(3)
B5–B9	1.772(3)	B5–B6	1.776(3)	B7–B11	1.765(3)
B7–B12	1.766(4)	B7–B8	1.772(3)	B8–B12	1.770(3)
B8–B9	1.777(3)	B9–B12	1.773(3)	B9–B10	1.779(3)
B10–B11	1.776(3)	B10–B12	1.784(4)	B11–B12	1.787(3)

Table 3. Selected Bond Angles in 1-$C_6H_4(CO)_2NCH_2$-2-$C_6H_5CH_2OCH_2CH_2$-1, 2-$C_2B_{10}H_{10}$ (5), °

Bond	Angle	Bond	Angle
C28–O27–C26	111.4(2)	C22–N14–C15	111.79(13)
C22–N14–C13	123.88(14)	C15–N14–C13	123.54(13)
C13–C1–C2	118.74(14)	C13–C1–B5	118.69(13)
C2–C1–B5	110.58(13)	C13–C1–B9	123.16(14)
C2–C1–B9	110.43(13)	B5–C1–B9	62.51(12)
C13–C1–B6	113.72(13)	C2–C1–B6	61.14(10)
B5–C1–B6	62.40(11)	B9–C1–B6	113.89(14)
C13–C1–B8	121.11(14)	C2–C1–B8	60.64(11)
B5–C1–B8	113.54(14)	B9–C1–B8	62.32(13)
B6–C1–B8	113.17(13)	C25–C2–C1	120.75(14)
C25–C2–B3	121.1(2)	C1–C2–B3	110.17(13)
C25–C2–B7	118.5(2)	C1–C2–B7	110.00(14)
B3–C2–B7	62.46(12)	C25–C2–B8	115.7(2)
C1–C2–B8	60.92(10)	B3–C2–B8	113.7(2)
B7–C2–B8	62.16(12)	C25–C2–B6	120.6(2)
C1–C2–B6	60.51(10)	B3–C2–B6	62.31(11)
B7–C2–B6	113.3(2)	B8–C2–B6	112.87(14)
N14–C13–C1	114.40(13)	O23–C15–N14	124.7(2)
O23–C15–C16	129.4(2)	N14–C15–C16	105.89(14)
C17–C16–C21	121.4(2)	C17–C16–C15	130.4(2)
C21–C16–C15	108.2(2)	C18–C17–C16	117.2(2)
C19–C18–C17	121.6(2)	C18–C19–C20	121.2(2)
C21–C20–C19	117.3(2)	C20–C21–C16	121.2(2)
C20–C21–C22	130.6(2)	C16–C21–C22	108.2(2)
O24–C22–N14	124.7(2)	O24–C22–C21	129.4(2)
N14–C22–C21	105.89(14)	C26–C25–C2	117.2(2)
O27–C26–C25	108.9(2)	O27–C28–C29	109.9(2)
C30–C29–C34	118.6(2)	C30–C29–C28	120.7(3)
C34–C29–C28	120.7(3)	C29–C30–C31	119.8(3)
C32–C31–C30	119.6(3)	C33–C32–C31	120.4(3)
C32–C33–C34	120.0(3)	C33–C34–C29	121.6(3)
C2–B3–B7	58.91(11)	C2–B3–B11	105.4(2)
B7–B3–B11	59.72(13)	C2–B3–B4	105.76(14)
B7–B3–B4	107.9(2)	B11–B3–B4	60.20(13)
C2–B3–B6	59.57(11)	B7–B3–B6	108.17(14)
B11–B3–B6	107.9(2)	B4–B3–B6	59.65(12)
B6–B4–B3	60.32(11)	B6–B4–B5	60.19(11)
B3–B4–B5	108.0(2)	B6–B4–B11	108.2(2)
B3–B4–B11	59.89(13)	B5–B4–B11	107.5(2)
B6–B4–B10	107.93(14)	B3–B4–B10	107.7(2)
B5–B4–B10	59.53(12)	B11–B4–B10	59.83(13)
C1–B5–B10	105.6(2)	C1–B5–B9	58.79(11)
B10–B5–B9	60.38(12)	C1–B5–B4	105.43(14)
B10–B5–B4	60.43(12)	B9–B5–B4	108.6(2)
C1–B5–B6	59.20(11)	B10–B5–B6	108.2(2)
B9–B5–B6	108.2(2)	B4–B5–B6	59.67(12)
C1–B6–C2	58.34(10)	C1–B6–B4	105.18(14)
C2–B6–B4	104.92(14)	C1–B6–B5	58.39(10)
C2–B6–B5	105.20(14)	B4–B6–B5	60.14(12)
C1–B6–B3	105.11(13)	C2–B6–B3	58.12(11)
B4–B6–B3	60.03(12)	B5–B6–B3	107.8(2)
C2–B7–B11	105.6(2)	C2–B7–B12	105.9(2)
B11–B7–B12	60.81(14)	C2–B7–B3	58.63(12)
B11–B7–B3	60.19(13)	B12–B7–B3	108.8(2)
C2–B7–B8	59.23(11)	B11–B7–B8	108.7(2)
B12–B7–B8	60.04(13)	B3–B7–B8	108.14(14)
C2–B8–C1	58.44(10)	C2–B8–B12	105.2(2)
C1–B8–B12	104.9(2)	C2–B8–B7	58.61(12)
C1–B8–B7	105.25(14)	B12–B8–B7	59.81(13)
C2–B8–B9	105.52(14)	C1–B8–B9	58.35(11)
B12–B8–B9	59.98(13)	B7–B8–B9	107.6(2)

(*continued on next page*)

Table 3 (continued)

Bond	Angle	Bond	Angle
C1–B9–B5	58.70(11)	C1–B9–B12	105.6(2)
B5–B9–B12	108.0(2)	C1–B9–B8	59.34(11)
B5–B9–B8	108.0(2)	B12–B9–B8	59.81(13)
C1–B9–B10	105.0(2)	B5–B9–B10	59.64(12)
B12–B9–B10	60.28(13)	B8–B9–B10	107.9(2)
B5–B10–B11	108.1(2)	B5–B10–B9	59.98(12)
B11–B10–B9	108.0(2)	B5–B10–B4	60.04(12)
B11–B10–B4	59.99(13)	B9–B10–B4	108.0(2)
B5–B10–B12	107.8(2)	B11–B10–B12	60.26(14)
B9–B10–B12	59.70(13)	B4–B10–B12	108.1(2)
B7–B11–B3	60.09(13)	B7–B11–B10	107.8(2)
B3–B11–B10	108.0(2)	B7–B11–B4	108.0(2)
B3–B11–B4	59.91(12)	B10–B11–B4	60.18(13)
B7–B11–B12	59.63(14)	B3–B11–B12	107.8(2)
B10–B11–B12	60.08(14)	B4–B11–B12	108.1(2)
B7–B12–B8	60.15(13)	B7–B12–B9	108.1(2)
B8–B12–B9	60.22(12)	B7–B12–B10	107.4(2)
B8–B12–B10	108.0(2)	B9–B12–B10	60.03(13)
B7–B12–B11	59.57(14)	B8–B12–B11	107.8(2)
B9–B12–B11	107.8(2)	B10–B12–B11	59.66(13)

Synthesis of $HC{\equiv}CCH_2CH_2OCH_2C_6H_5$ (**1**)

In a 250 cm^3 round bottom flask were placed 7.0 g (0.10 mol) of 3-butyn-1-ol and 100 cm^3 of anhydrous THF. To the resulting suspension, 2.8 g (0.11 mol) of sodium hydride were added slowly. After gas evolution had ceased, 19.0 g (0.11 mol) of benzyl bromide were added to the solution and stirred at room temperature overnight. After 12 hrs, a voluminous precipitate had formed. The precipitate was filtered and the solvent removed by rotary evaporation. The resulting residue was distilled under reduced pressure, resulting in the isolation of a colorless oil which was identified as benzyl-3-butynyl ether (12.3 g, 0.077 mol, 77% yield, bp 66–68°C/0.6 mm Hg). ^{1}H NMR: ($CDCl_3$), 1.98 (1H, t, $J=2.64$ Hz), 2.47 (2H, d of t, $J_{AB}=2.64$ Hz, $J_{AX}=6.96$ Hz), 3.58 (2H, t, $J=6.96$ Hz), 4.54 (2H, s), 7.32 (5H, m), ^{13}C NMR: ($CDCl_3$), 19.66 (CH_2), 67.90 (CH_2O), 69.21 (OCH_2), 72.71 (≡C), 81.04 (HC≡), 127.47 (C_6H_5), 128.19 (C_6H_5), 137.82 (C_6H_5), IR (cm^{-1}): 3296 (s), 3028 (m), 2868 (s), 2220 (w), 1720 (m), 1496 (m), 1456 (m), 1364 (m), 1275 (w), 1204 (w), 1100 (s), 1028 (m), 795 (w), 740 (m), 700 (m), 648 (m). MS (EI): *m*/*z* relative intensity 159 (M^+-H, 100), 107 (M^+-$HC{\equiv}CCH_2CH_2$, 9.1), 83 (M^+-C_6H_5, 22.7).

Synthesis of $HOCH_2C{\equiv}CCH_2CH_2OCH_2C_6H_5$ (**2**)

To a solution containing 9.6 g (0.060 mol) of benzyl-3-butynyl ether in 90 cm^3 of dry THF kept at −20°C, 31 cm^3 (0.061 mol) of a 2.0 M solution n-BuLi in cyclohexane were added slowly. The mixture was allowed to warm to room temperature and stirred for one hour. To this solution, 2.0 g (0.066 mol) of paraformaldehyde were added and stirring of the resulting solution was continued for an additional 2 hrs. The THF was removed by rotary evaporation and to the resulting residue, 25 cm^3 of distilled water were added. This solution was extracted with three 20 cm^3 of anhydrous ether. The ethereal solution was dried over $MgSO_4$. The ether was then removed by rotary evaporation. The resulting oil was distilled and a colorless oil (8.2 g, 0.043 mol, 72% yield, bp 130–132°C/0.5 mm Hg) was obtained and identified as 5-benzylox-2-pentyn-1-ol. ^{1}H NMR: ($CDCl_3$), 2.31 (1H, t, $J=5.94$ Hz), 2.52 (2H, m), 3.57 (2H, t, $J=6.88$ Hz), 4.20 (2H, m), 4.54 (2H, s), 7.33 (5H, m). ^{13}C NMR: ($CDCl_3$), 19.84 (CH_2), 50.86 ($HOCH_2$), 67.90 (CH_2O), 72.69 (OCH_2), 79.34 (C≡), 82.61 (C≡), 127.27 (C_6H_5), 128.20 (C_6H_5), 137.66 (C_6H_5). IR (cm^{-1}): 3444 (s, br), 2872 (s), 2240 (m), 1716 (m), 1680 (sh), 1480 (w), 1456 (m), 1310 (m), 1272 (m), 1096 (m), 975 (m), 750 (m), 700 (m). MS (EI): *m*/*z* relative intensity 189 (M^+-H, 3.6), 159 (M^+-$HOCH_2$, 3.6), 121 (M^+-$HOCH_2C{\equiv}CCH_2$, 92.6), 113 (M^+-C_6H_5, 7.1), 107 (M^+-$HOCH_2C{\equiv}CCH_2CH_2$, 3.6), 83 (M^+-$OCH_2C_6H_5$, 3.6).

Synthesis of $BrCH_2C{\equiv}CCH_2CH_2OCH_2C_6H_5$ (**3**)

In a 250 cm^3 round bottom flask were placed 7.0 g (0.037 mol) of $HOCH_2C{\equiv}CCH_2CH_2OCH_2C_6H_5$ and 10.0 g (0.046 mol) of $(CH_3)_2NCHBr_2$, which was prepared according to the literature procedure [33]. To this mixture, 100 cm^3 of dry acetonitrile was added

and the resulting solution was heated to reflux for 2 hrs. The acetonitrile was removed *in vacuo* and the resulting residue extracted with ether. After evaporation of the ether from the solution, the extract was separated on a silica gel column chromatography using a 2:1 mixture of hexanes/methylene chloride. The resulting oil obtained was identified as benzyl-5-bromo-2-pentynyl ether. (8.0 g, 0.031 mol, 85% yield). ^{1}H NMR ($CDCl_3$), 2.56 (2H, m), 3.58 (2H, t, $J=6.88$ HZ), 3.91 (2H, t, $J=2.24$ Hz), 4.55 (2H, s), 7.34 (5H, m). ^{13}C NMR ($CDCl_3$), 15.03 ($BrCH_2$), 20.13 (CH_2), 67.61 (CH_2O), 72.71 (OCH_2), 77.37 (C≡), 84.49 (C≡), 127.43 (C_6H_5), 128.16 (C_6H_5), 137.68 (C_6H_5). IR (cm^{-1}): 3028 (m), 2868 (s), 2236 (m), 1720, 1648 (w), 1496 (w), 1456 (s), 1364 (s), 1212 (s), 1100 (s), 740 (s), 700 (s), 608 (s). MS (EI, ^{81}Br) m/z relative intensity 255 ($M^+ + H$, 5.3), 254 (M^+, 4.1), 252 (M-2^+, 1.2), 173 (M^+-Br, 35.8), 159 (M^+-$BrCH_2$, 2.6), 147 (M^+-$BrCH_2C$, 3.0), 143 (M-2^+-$HOCH_2C_6H_5$, 100), 121 (M^+-$BrCH_2C{\equiv}CCH_2$, 4.7), 108 (M^+-$BrCH_2C{\equiv}CCH_2CH_2$, 2.1), 77 (M^+-$BrCH_2C{\equiv}CCH_2CH_2O$, 15.9).

Synthesis of $C_6H_4(CO)_2NCH_2C{\equiv}CCH_2CH_2OCH_2C_6H_5$ (**4**).

A solution consisting of 2.53 g (0.010 mol) of $BrCH_2C{\equiv}CCH_2CH_2OCH_2C_6H_5$ dissolved in 15 cm^3 of DMF was added to 2.04 g (0.011 mol) of potassium phthalimide and stirred at room temperature overnight. After that time, 50 cm^3 of distilled water was added to the solution and the mixture extracted with three 20 cm^3 portions of chloroform. This solution was dried over $MgSO_4$ and the chloroform stripped off *in vacuo*. The residue was dissolved in a minimal amount of methylene chloride and separated via silica gel column chromatography. This resulted in the isolation of a viscous oil which was identified as N-(5-benzyloxy-2-pentynyl)phthalimide (3.05 g, 0.0096 mol, 96% yield). ^{1}H NMR: ($CD_3C(O)CD_3$), 2.45 (2H, m), 3.53 (2H, t, $J=7.12$ Hz), 4.41 (2H, t, $J=2.24$ Hz), 4.50 (2H, s), 7.30 (5H, m), 7.86 (4H, m). ^{13}C NMR: ($CD_3C(O)CD_3$), 20.08 (CH_2), 27.36 (CH_2), 68.50 (CH_2O), 72.67 (OCH_2), 75.44 (C≡), 80.54 (C≡), 123.65 (C_6H_5), 127.86 (C_6H_5), 128.67 (C_6H_5), 132.57 (C_6H_5), 134.86 (C_6H_5), 139.23 (C_6H_5), 167.22 (C═O). IR (cm^{-1}): 3020 (m), 2872 (m), 2245 (w), 1772 (s), 1716 (s), 1650 (m), 1550 (w), 1520 (w), 1420 (m), 1392 (m), 1320 (m), 1116 (s), 944 (m), 724 (s), 628 (m), 532 (m). MS (EI), m/z relative intensity 320 ($M^+ + H$, 5.9), 212 (M^+-$OCH_2C_6H_5$, 3.0), 198 (M^+-$CH_2OCH_2C_6H_5$, 5.3), 173 (M^+-$C_6H_4(CO)_2N$, 8.3), 172 (M^+-$CH_2CH_2OCH_2C_6H_5$, 21.6), 160 (M^+-$C{\equiv}CCH_2CH_2OCH_2C_6H_5$, 42.4), 159 ($M^+$-$C_6H_4(CO)_2NCH_2$, 83.2), 131 ($M^+$-CO and $HC{\equiv}CCH_2CH_2OCH_2C_6H_5$, 3.5), 104 ($M^+$-CO and $NCH_2C{\equiv}CCH_2CH_2OCH_2C_6H_5$, 15.1), ($M^+$-91($M^+$-$C_6H_4(CO)_2NCH_2C{\equiv}CCH_2CH_2$, 100), 77 ($M^+$-$C_6H_4(CO)_2NCH_2C{\equiv}CCH_2CH_2OCH_2$, 12.8).

Synthesis of 1-$C_6H_4(CO)_2NCH_2$-2-$C_6H_5CH_2OCH_2CH_2$-1, 2-$C_2B_{10}H_{10}$ (**5**)

In a 100 cm^3 round bottom flask, 0.400 g (0.0033 mol) of decaborane (14) and 0.60 cm^3 (0.008 mol) of dimethyl sulfide were dissolved in 35.0 cm^3 of dry benzene. The solution was stirred to reflux for 4 hrs. After allowing the solution to cool to room temperature, 1.03 g (0.0033 mol) of N-(5-benzyloxy-2-pentynyl)phthalimide were added quickly and stirred at room temperature for 10 min., to ensure complete dissolution of the alkyne. The resulting solution was then heated to reflux for 10 hrs. The benzene was removed *in vacuo* and to the resulting solid, 2.5 cm^3 of methanol were added and stirred at room temperature for 4 hrs. The suspension was filtered, resulting in a white solid which was washed with three portions of 5.0 cm^3 of cold ethanol. The white solid was dissolved in a 1:1 mixture of CH_3CN/CH_2Cl_2 and recrystallized from this solution, resulting in the isolation of 1-methylphthalimido-2-ethylbenzyl ether-*o*-carborane (0.70 g, 50% yield, mp 1175–177°C). The identity of this compound was confirmed by a single crystal X-ray diffraction study. ^{1}H NMR: ($CD_3C(O)CD_3$), 3.04 (2H, t, $J=5.86$ Hz), 3.77 (2H, t, $J=5.86$ Hz), 4.56 (2H, s), 4.57 (2H, s), 7.35 (5H, m), 7.89 (4H, m). ^{13}C NMR ($CD_3C(O)CD_3$), 35.68 (CH_2), 40.49 (CH_2), 68.79 (CH_2O), 73.26 (OCH_2), 78.16 (carborane C), 80.89 (carborane C), 124.20 (C_6H_5), 128.16 (C_6H_5), 128.76 (C_6H_5), 131.95 (C_6H_5), 135.30 (C_6H_5), 138.36 (C_6H_5), 167.36 (C═O). ^{11}B NMR: ($CD_3C(O)CD_3$), −0.48 (2B), −5.49 (8B). The coupling constants for this compound could not be reliably determined due to coincidental overlap of signals. IR (cm^{-1}): 2996 (m), 2888 (m), 2580 (s), 1776 (s), 1724 (s), 1612 (w), 1484 (m), 1468 (w), 1456 (w), 1420 (m), 1400 (s), 1364 (s), 1288 (m), 1136 (m), 1104 (s), 1080 (s), 1036 (m), 960 (m), 864 (w), 848 (w), 824 (w), 792 (w), 752 (m), 716 (s), 700 (m), 646 (w), 608 (w), 528 (m). MS (EI), m/z relative intensity 439 (M^+, 6.5), 348 (M^+-$CH_2C_6H_5$, 7.6), 332 (M^+-$OCH_2C_6H_5$, 42.7), 303 (M^+-H and $CH_2CH_2OCH_2C_6H_5$, 7.8), 160 (M^+-$C_2B_{10}H_{10}CH_2CH_2OC_6H_5$, 14.4), 107 ($M^+$-$C_6H_4(CO)_2NCH_2C_2B_{10}H_{10}CH_2CH_2$, 39.7), 91 ($M^+$-$C_6H_4(CO)_2NCH_2C_2B_{10}H_{10}CH_2CH_2O$, 100), 77 ($M^+$-$C_6H_4(CO)_2NCH_2C_2B_{10}H_{10}CH_2CH_2OCH_2$, 15.9).

Synthesis of 1-$C_6H_4(CO)_2NCH_2$-2-$HOCH_2CH_2$-1, 2-$C_2B_{10}H_{10}$ (**6**)

In a 5.0 cm^3 round bottom flask, 0.045 g (0.10 mmol) of 1-methylphthalimido-2-ethylbenzyl ether-*o*-carborane were placed and 0.50 cm^3 of $CHCl_3$ added. To the resulting solution, 0.50 cm^3 of ethanol and 30 mg of Pd/C were added. The flask was then attached to a three-way vacuum stopcock, the contents frozen and degassed. A balloon filled with H_2 gas was then attached to the three-way vacuum stopcock and opened to fill the flask with an atmosphere

of hydrogen. The solution was then stirred at room temperature overnight. The solution was then filtered to remove the catalyst and the solvent was removed *in vacuo*. The resulting residue was dissolved in CH_2Cl_2 and purified via column chromatography (packed with silica gel). The elutant used was a 2% CH_3OH mixture in CH_2Cl_2. This resulted in the isolation of 29 mg of a white solid, which was identified as 1-methylphthalimido-2-ethylalcohol-*o*-carborane (0.029 g, 0.083 mmol, 83% yield, mp 137–139°C). ^{1}H NMR: (CD_3CN), 2.83 (2H, t, $J = 6.50$ Hz), 3.10 (1H, t, $J = 5.20$ Hz), 3.75 (2H, m, $J_{AB} = 6.50$ Hz, $J_{AX} = 5.20$ Hz), 4.47 (2H, s), 7.86 (4H, m). ^{13}C NMR: (CD_3CN), 38.24 (CH_2), 41.18 (CH_2), 61.15 (CH_2O), 78.89 (carborane C), 81.53 (carborane C), 124.65 (C_6H_5), 132.52 (C_6H_5), 135.90 (C_6H_5), 168.55 (C═O). ^{11}B NMR: (CD_3CN), 0.89 (1B, $J_{BH} = 129$ Hz), −0.89 (1B, $J_{BH} = 129$ Hz), −4.76 (4B, the coupling constant for this peak could not be reliably be calculated due to coincidental overlap of signals), −5.44 (4B, $J_{BH} = 128$ Hz). IR (cm^{-1}): 3536 (s), 3444 (br), 2956 (w) 2596 (s), 1776 (m), 1716 (s), 1488 (m), 1420 (m), 1400 (s), 1360 (m), 1140 (w), 1088 (w), 1054 (w), 960 (w), 716 (m), 532 (w). MS (EI), *m*/*z* relative intensity, 349 (M^+, 87.8), 348 (M^+-H, 41.1), 331 (M^+-H_2O, 87.6), 130 (M^+-$HOCH_2CH_2C_2B_{10}H_{10}$, H_2 and CO, 100).

RESULTS AND DISCUSSION

In order to prepare the desired precursor, it was necessary to first synthesize the corresponding alkyne needed for the reaction with decaborane (14). This procedure was a multistep synthesis starting from 3-butyn-1-ol, which is the commercially available alkyne needed for the synthesis of the desired alkyne. The synthesis of **1** was accomplished by adapting the reported literature procedure [33]. The isolation of benzyl-3-butynyl ether in significant yield (77%) allowed for the continuation of the proposed synthetic scheme, shown in Fig. 1. The identity of this compound was determined by ^{1}H and ^{13}C NMR, mass spectrometry, as well as IR spectroscopy. The nature of **1**, an air stable colorless oil, allowed for the easy handling of this compound. The ^{1}H NMR data shows an interesting pattern of resonances. The proton assigned to the terminal hydrogen of the alkyne appears at δ 1.98 ppm, as a triplet. Obviously there is coupling between this proton and the CH_2 group next to the β-carbon of the alkyne, even though they are separated by four bonds. This is confirmed by the splitting of resonances arising from the CH_2 group of protons bonded directly to the alkylinic carbon, these protons show a resonance at δ 2.47 ppm, as a doublet of triplets. The coupling constant of the doublets is 2.64 Hz, which corresponds to the coupling constant obtained for the triplet at δ 1.98 ppm. Furthermore, the downfield triplet at δ 3.58 ppm, assigned to the CH_2 group bonded to that CH_2 group and to the $OCH_2C_6H_5$ group, exhibits a coupling constant of 6.96 Hz, matching that of the triplets of the resonance at δ 2.47 ppm. The benzylic hydrogens appear as a singlet at 4.54 ppm, typical of benzylic protons. The IR spectra also shows the typical peaks, especially the C≡C triple bond stretch, which is found at 2220 cm^{-1}, also typical for this class of compounds. The ^{13}C NMR consists of eight resonances, at the typical shifts for the type of functional groups present in compound **1**.

The next step in the synthesis of the alkyne precursor is the preparation of the amino end of the molecule. Care had to be taken in choosing an appropriate procedure that would carry the protected alcoholic part of the alkyne intact. For this reason, the reaction of **1** with n-BuLi, followed by the addition of paraformaldehyde was chosen. The method is simple and does not result in deprotection of the benzylic group to form the corresponding alcohol. Compound **2** was isolated in reasonable yield (72%), as a colorless air stable oil. The identification of this compound was not as straightforward as that of **1**. The presence of multiplets at δ 2.52 ppm and δ 4.20 ppm, each due to two set of protons, prevents an analysis based on coupling constants as that performed for **1**. Nonetheless, the peak as δ 2.31 ppm, is due to the OH group and the resonance at δ 3.57 ppm is due to the CH_2O group. The other two resonances, δ 2.52 and δ 4.20 ppm respectively are assigned to the CH_2 groups bonded to the C≡C bond. The downfield resonance is that of the CH_2 group bonded to the OH and the other one corresponds to the other CH_2 group. The fact that the obtained coupling constants are similar in value, resulted in the observed multiplets for these resonances. The benzylic protons were assigned to the resonance at δ 4.54 ppm, again typical for these type of protons. The ^{13}C NMR showed nine resonances, which is the expected number of resonances for compound **2**. The IR spectra was more informative, the presence of a broad peak at 3440 cm^{-1}, typical of a OH group, coupled with a resonance at 2240 cm^{-1} assignable to the C≡C triple bond, indicated the formation of **2**. Based on this information, the fact that the benzylic group was left intact, as indicated by the ^{1}H and ^{13}C NMR data, the task of continuing toward the formation of the alkyne precursor could be continued.

Compound **3** was prepared by the reaction of **2** with $(CH_3)_2NCHBr_2$. This procedure resulted in the bromination of the CH_2 group carrying the alcohol, while keeping the protected alcohol on the other side of the alkyne unaffected. The isolated yield (85%) of the colorless oil, which was purified by column chromatography was high enough to allow the continuation of the synthetic strategy proposed. The ^{1}H and ^{13}C NMR data agrees with the formulation of compound **3**. The IR spectra also showed the presence of the C≡C triple bond, which is of paramount importance for the synthesis of the sought carborane. The mildness of the bromination method and the ease of synthesis of **3** in high yield is an attractive feature of

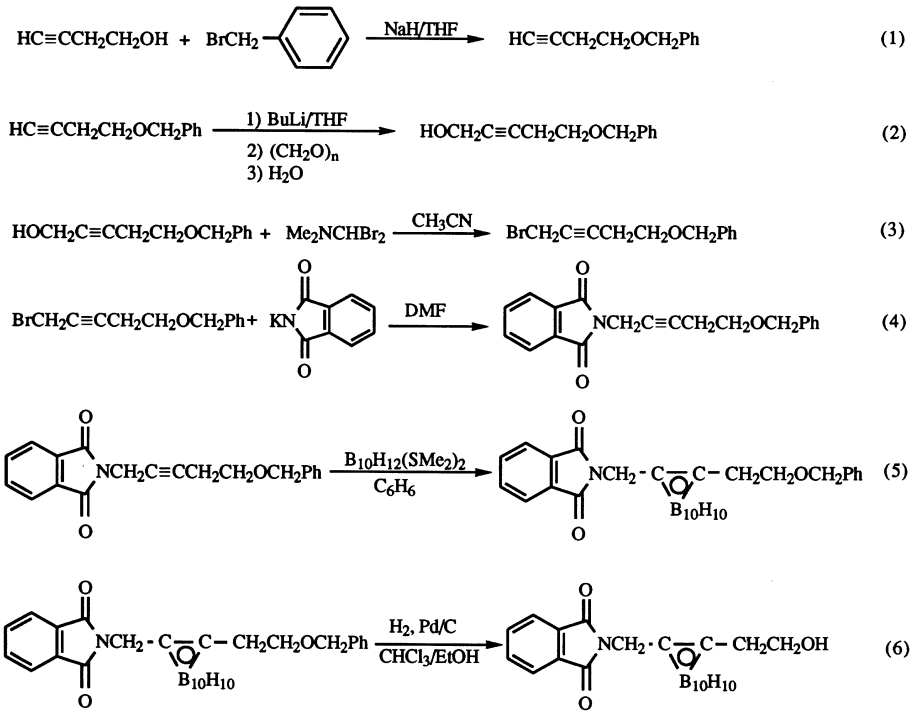

Fig. 1. Reaction sequence leading to the synthesis of heterodisubstituted *ortho*-carboranes.

this synthetic strategy. Compound **3** is the immediate precursor to the protected amino alcohol alkyne sought for the preparation of carborane **5**.

The preparation of compound **4** was accomplished by using Gabriel's reagent, potassium phthalimide, this allowed for the convenient preparation of the protected amine in high yield (96%). Compound **4** was isolated as a viscous oil. The ^{1}H NMR showed a multiplet at δ 2.45 ppm, assignable to CH_2 protons bonded to the β-carbon of the alkyne, a triplet at δ 3.53 ppm, corresponding to the NCH_2 group, a triplet at δ 4.41 ppm, due to the CH_2O group, a singlet at δ 4.50 ppm, for the benzylic protons of the protected alcohol, an two different sets of aromatic multiplets at δ 7.30 and δ 7.84 ppm, respectively, due to the $OCH_2C_6H_5$ and $C_6H_4(CO)_2N$ groups. The ^{13}C NMR of **4** should consist of thirteen peaks, which were observed. The C=O resonance was found at δ 167.22 ppm, typical for an amide group. The IR spectra of **4** also indicated its identity. The weak resonance at 2245 cm^{-1} coupled with the strong carbonyl stretch at 1716 cm^{-1} clearly indicated that compound **4** was formed. The high yield of this reaction indicates that this is a convenient method to prepare the desired precursor. The next step is simply the reaction of decaborane (14) in the presence of dimethyl sulfide with **4**, in order to produce the sought compound.

The identities of compounds **1** through **4** were further confirmed by mass spectrometric experiments and the synthesis and characterization of compound **5**. The single crystal X-ray structure determination of **5** is ample evidence of the identity of every intermediate leading to its formation.

The identity of **5** is supported by the ^{1}H, ^{11}B, and ^{13}C NMR data, as well as the IR spectra, mass spectrometry and the single crystal X-ray diffraction study of this compound. An ORTEP diagram for this compound is shown in Fig. 2.

The ^{1}H NMR data shows the expected peaks for a compound of this type. The triplet at δ 3.04 ppm is due to the CH_2 group of the ethylene unit in the carborane, which is coupled to the CH_2 group of the ether moiety and the CH_2 group of the phthalimide unit. The triplet at δ 3.77 ppm is due to the other CH_2 of the ethylene group in this carborane. The coupling constants were found to be identical for these protons, indicating that they are neighbors. The singlets at δ 4.56 and δ 4.57 ppm respectively are the result of the protons in the CH_2 group linked to the oxygen atom of the ether unit and the CH_2 group in the phthalimide unit. The expected multiplets, consisting of 4 protons and 5 protons respectively, are due to the benzene groups present in this molecule. The ^{13}C NMR data shows the expected thirteen peaks. The presence of the carbonyl resonance at δ 167.36 ppm clearly indicates that the alkyne incorporated into the cage. This fact coupled to the resonances are δ 78.16 and δ 80.89 ppm, assignable to the carborane carbons showed that the expected product was indeed synthesized.

The IR data for **5** further supports the identity of this compound. Peaks at 2558 cm^{-1}, typical of B–H

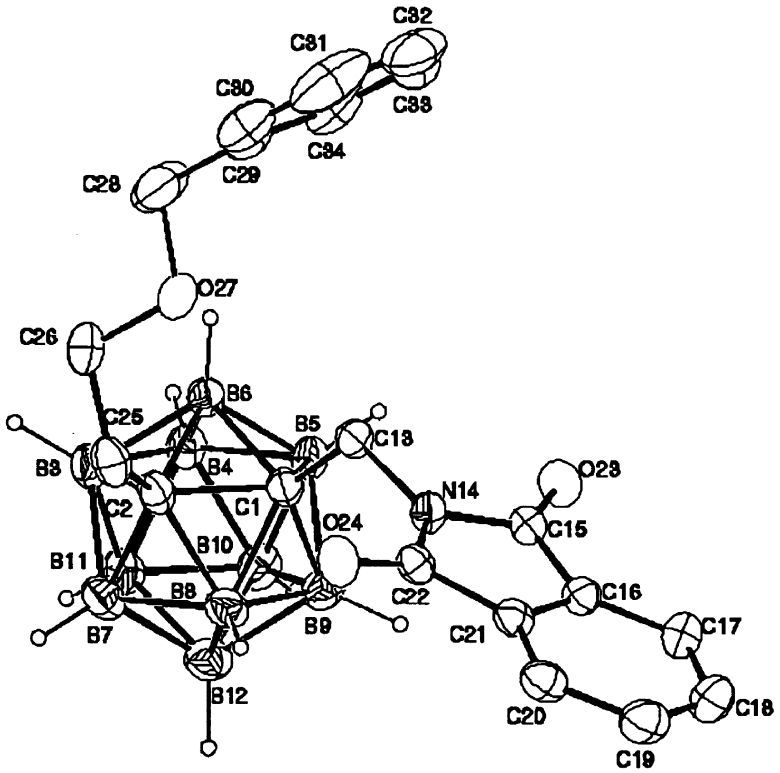

Fig. 2. ORTEP drawing of 1-$C_6H_4(CO)_2NCH_2$-2-$C_6H_5CH_2OCH_2CH_2$-1, 2-$C_2B_{10}H_{10}$ (5) with 30% probability thermal ellipsoids.

stretches, coupled with peaks at 1776 and 1724 cm^{-1} respectively, due to the carbonyl groups of the phthalimide unit are indicative of the incorporation of the alkyne into the decaborane (14) framework.

The single X-ray data shows the expected bond distances for a compound of this type. The boron-boron distances are within the expected range, 1.765 to 1.787 Å, typical of these type of compounds. The carbon-carbon in the cage and the boron-carbon distances are also typical, 1.684 to 1.732 Å. This clearly indicates that the steric effects imposed by the substituent groups are minimal, since in systems like 1-diphenylphosphino-2-methyl-1, 2-dicarba-*closo*-dodecaborane (12) [34], 1-diphenylphosphino-2-phenyl-1, 2-dicarba-*closo*-dodecaborane (12) [35], 1-phenyl-2-(*tert*-butyldimethylsilyl)-1, 2-dicarba-*closo*-dodecaborane (12) [36], 1-phenyl-2-trimethylsilyl-1, 2-dicarba-*closo*-dodecaborane (12) [37], 1-diisopropylphosphino-2-methyl-1, 2-dicarba-*closo*-dodecaborane (12) [38], 1, 2-Bis(diisopropylphosphino)-1, 2-dicarba-*closo*-dodecaborane (12) [38], 2-bromo-1-phenyl-1, 2-dicarba-*closo*-dodecaborane (12) [39], 1-diisopropylphosphino-2-phenyl-1, 2-dicarba-*closo*-dodecaborane (12) [40], and 1-phenyl-2-methyl-1, 2-dicarba-*closo*-dodecaborane (12) [41] the carbon-carbon bond length is significantly lengthened due to the steric constraints placed by the exopolyhedral groups in the cage. The values obtained in these compounds for the carbon-carbon bond length range from a minimum of 1.692 (8) Å for 2-bromo-1-phenyl-1, 2-dicarba-*closo*-dodecaborane (12) [39], which could be argued to be the less sterically demanding of these compounds and therefore closer in electronic structure to that of **5** to a maximum of 1.769 (4) Å in 1-diisopropylphosphino-2-phenyl-1, 2-dicarba-*closo*-dodecaborane (12) [40], which would be more sterically demanding and dissimilar to the electronic structure of **5**. The argument used for the lengthening of the carbon-carbon bond in these compounds is the partial overlap of tangentially oriented p orbitals of the cluster carbon with orbitals having the appropriate symmetry in the exopolyhedral group. When the overlap is between a sp^3 hybridized carbon and the cluster carbon, no significant effect should be observed, as is the case in compound **5**.

The relative importance of the characterization of **5** lies in the fact that a viable precursor to an amino acid containing carborane has been isolated. The exploration of its chemistry could potentially lead to the synthesis of such a compound, which could prove useful in BNCT.

The identity of compound **6** is based on the ^1H, ^{11}B, ^{13}C NMR, IR spectral and mass spectrometric data obtained. The ^1H NMR consists of two triplets at δ 2.83 and δ 3.10 ppm of relative intensities two and one respectively. The first triplet is due to the CH_2 group

bonded directly to the cluster carbon. Its coupling constant of 6.50 Hz, which corresponds to one of the coupling constants found in the resonance at δ 3.75 ppm, allows for the identification of these protons, as well as those at δ 3.75 ppm, which is a triplet of doublets. The coupling constant of the doublets is 5.20 Hz, which corresponds to the coupling constant found for the resonance at δ 3.10 ppm, assigned to the alcoholic proton. The singlet at δ 4.47 ppm is due to the CH_2 group in the phthalimide unit. The downfield multiplet of area four is due to the phenyl group in the compound. The ^{13}C NMR shows a total of nine peaks, which the number of resonances expected for compound **6**.

The IR spectral data shows the expected OH stretch at 3444 cm^{-1}, as well as the expected BH and C=O stretches in the normal regions.

The ^{11}B NMR data, as mentioned earlier consists of four peaks, of relative intensities 1:1:4:4. The signals observed are not the expected pattern of signals for a compound of this type, but similarly heterodisubstituted compounds had shown the same type of pattern in the ^{11}B NMR spectra [42, 43]. The coincidental overlap of resonances in the ^{11}B NMR time scale is not unprecedented, a relevant example for the observation of this type of pattern in the ^{11}B NMR spectrum is 1-phenyl-2-methyl-1, 2-dicarba-*closo*-dodecaborane (12) [41], which is also a bifunctionally substituted *ortho*-carborane.

With the isolation of compound **6**, the goal of preparing an amino acid *ortho*-carborane derivative is in principle possible. Unfortunately, all attempts to isolate this compound have proven unsuccessful at this time. Although there is some evidence that upon deprotection of the phthalimide group and oxidation of the alcohol, a compound that could possibly be the amino acid carborane is formed, its isolation has not been possible. The conditions upon which the deprotection is being carried out might be too harsh and unwanted side reactions could be taking place. We are continuing to investigate alternate routes for the preparation of the amino acid carborane and the results from this effort will be reported in the future.

Supporting information available—Tables of bond lengths and angles, atomic coordinates and thermal parameters (10 pages) are available. Order information is available on any current masthead page.

Acknowledgements—The authors wish to thank the National Science Foundation (Grant # CHE-9502406) for support of this research. We also thank Mr. Monte Mauldin for his help in the collection of ^{1}H and ^{11}B and ^{13}C NMR data.

REFERENCES

1. Sjoeberg, S., Hawthorne, M. F., Wilmouth, S. and Lindstroem, P., *Angew. Chem., Int. Ed. Engl.*, 1995, **34,** 430–435.
2. Vardarajan, A. and Hawthorne, M. F., *Bioconjugate Chem.*, 1991, **2,** 242–253.
3. Kahl, S. B. and Kasar, R. A., *J. Am. Chem. Soc.*, 1996, **118,** 1223–1224.
4. Heying, T. L., Ager, J. W. Jr., Clark, S. L., Mangold, D. L., Goldstein, H. L., Hillman, M., Pollack, R. J. and Szymanski, J. W., *Inorg. Chem.*, 1963, **2,** 1089–1092.
5. Fein, M. M., Bobinski, J., Mayes, N., Schwartz, N. and Cohen, M. S., *Inorg. Chem.*, 1963, **2,** 1111–1115.
6. Fein, M. M., Grafstein, D., Paustian, J. E., Bobinski, J., Liechstein, B. M., Mayes, M., Schwartz, N. N. and Cohen, M. S., *Inorg. Chem.*, 1963, **2,** 1115–1119.
7. Dupont, J. A. and Hawthorne, M. F., *J. Am. Chem. Soc.*, 1964, **86,** 1643.
8. Zakharkin, L. I., Stanko, V. I., Brattsev, V. A., Chapovskii, Yu. A., Klimova, A. I., Oxlobystin, O. Yu. and Ponomarenko, A. A., *Dokl Akad. Nauk SSSR*, 1964, **155,** 1119–1122.
9. Kutal, C. R., Owen, D. A. and Todd, L., *J. Inorg. Synth.*, 1968, **11,** 19–23.
10. Paxson, T. E., Callahan, K. P. and Hawthorne, M. F., *Inorg. Chem.*, 1973, **12,** 708–709.
11. Fukuda, H., Hiratsuka, J. and Honda, C., *Radiat. Res.*, 1994, **138,** 435–442.
12. Mallesch, J. L., Moore, D. E., Allen, B. J., McCarthy, W. H., Jones, R. and Stenning, W. A., *Int. J. Radiat. Oncol. Biol. Phys.*, 1994, **28,** 1183–1188.
13. Wilson, G. J., Anisuzzaman, A. K. M., Alam, F. and Soloway, A. H., *Inorg. Chem.*, 1992, **31,** 1955.
14. Heying, T. L., Ager, J. W. Jr., Clark, S. L., Alexander, R. P., Papetti, S., Reid, J. A. and Trotz, S. I., *Inorg. Chem.*, 1963, **2,** 1097–1105.
15. Hawthorne, M. F., *Angew. Chem. Int. Ed. Engl.*, 1993, **32,** 950.
16. Fairchild, R. G. and Bond, V. P., *Int. J. Radiat. Oncol. Biol. Phys.*, 1985, **11,** 831.
17. Shelly, K., Hawthorne, M. F. and Knobler, C. B., in *Advances in Neutron Capture Therapy*, eds. A. H. Soloway et al. Plenum Press, New York, NY, 1993, pp. 325.
18. Wyzlic, I. M. and Soloway, A. H., *Tetrahedron Lett.*, 1992, **33,** 7489.
19. Sjoberg, S., Hawthorne, M. F., Lindstrom, P., Malmquist, J., Carlsson, J., Andersson, A. and Petterson, O., in *Advances in Neutron Capture Therapy*, eds. A. H. Soloway et al. Plenum Press, New York, NY, 1993, pp. 269.
20. Barth, R., Soloway, A. H., Adams, D. M. and Alam, F. in *Progress in Neutron Capture Therapy for Cancer*, eds. B. J. Allen et al. Plenum Press, New York, NY, 1992, pp. 243.
21. Anisuzzaman, A. K. M., Alam, F. and Soloway, A. H., *Polyhedron*, 1990, **9,** 891.
22. Tjarks, W., Anisuzzaman, A. K. M. and Soloway, A. H., *Nucleosides and Nucleotides*, 1992, **11,** 1765.
23. Yamamoto, Y., *Pure Appl. Chem.*, 1991, **63,** 423.
24. Schinazi, R. F., Goudgoan, N. M., Lesnikowski, Z., Fulcand, G., El Kattan, Y., Ullas, G., Moravek, J. and Liotta, D. C., *Int. J. Radiat. Oncol. Biol. Phys.*, 1994, **28,** 1113.
25. Shelly, K., Feakes, D. A., Hawthorne, M. F.,

Schmidt, P. G., Krisch, T. A. and Bauer, W. F., *Proc. Natl. Acad. Sci.*, 1992, **89,** 9039.
26. Miura, M., Gabel, D., Oenbrink, G. and Fairchild, R. G., *Tetrahedron Lett.*, 1990, **50,** 325.
27. Barth, R. F. and Soloway, A. H., *Cancer*, 1992, **70,** 2995.
28. Shriver, D. F. and Dredzdon, M. A., *Manipulation of Air Sensitive Compounds*, 2nd edn. Wiley, New York, 1986.
29. *biotex*: A suite of Programs for the Collection, Reduction and Interpretation of Imaging Plate Data, Molecular Structure Corporation, 1995.
30. *teXsan*: Crystal Structure Analysis Package, Molecular Structure Corporation, 1985 & 1992.
31. *SIR*92: Altomare, A., Burla, M. C., Camalli, M., Cascarano, M., Giacovazzo, C., Guagliardi, A. and Polidoro, G., *J. Appl. Cryst.* 1994, **27**, 435.
32. *SHELXL*-93: Program for the Refinement of Crystal Structures, Sheldrick, G. M., University of Göttingen, Germany, 1993.
33. a) Larock, R., *Comprehensive Organic Transformations*: *A Guide to Functional Group Preparations*, VCH Publishers, Inc., New York, 1989. b) Hijfte, L. V., Little, R. D., Petersen, J. L. and Moeller, K. D. *J. Org. Chem.*, 1987, **52**, 4647–4660. c) Hart, D. J., Hong, W.-P. and Hsu, L.-Y. *J. Org. Chem.*, 1987, **52**, 4665–4673.
34. Kivekäs, R., Sillanpää, R., Teixidor, F. and Viñas, C., Nuñez, R., *Acta Cryst.*, 1994, **C50,** 2027–2030.
35. McWhannel, M. A., Rosair, G. M., Welch, A. J., Teixidor, F. and Viñas, C., *Acta Cryst.*, 1996, **C52,** 3135–3138.
36. McGrath, T. D. and Welch, A. J., *Acta Cryst.*, 1995, **C51,** 654–657.
37. McGrath, T. D. and Welch, A. J., *Acta Cryst.*, 1995, **C51,** 651–654.
38. Kivekäs, R., Sillanpää, R., Teixidor, F., Viñas, C. and Nuñez, R., Abad, M., *Acta Cryst.*, 1995, **C51,** 1864–1868.
39. McGrath, T. D. and Welch, A. J., *Acta Cryst.*, 1995, **C51,** 649–651.
40. Sillanpää, R., Kivekäs, R., Teixidor, F., Viñas, C. and Nuñez, R., *Acta Cryst.*, 1996, **C52,** 2223–2225.
41. McGrath, T. D. and Welch, A. J., *Acta Cryst.*, 1995, **C51,** 646–649.
42. Todd, L. J. and Siedle, A. R., *Prog. in NMR Spectrosc.*, 1979, **13,** 87–176.
43. Siedle, A. R., *Ann. Rep. on NMR Spectrosc.*, Vol. 20, 1988, pp. 205–314.

Table 4. Refined Positional Parameters for 1-$C_6H_4(CO)_2NCH_2$-2- $C_6H_5CH_2OCH_2CH_2$-1, 2-$C_2B_{10}H_{10}$ (5)[1]

Atom	*x*	*y*	*z*	U_{eq}, Å^2
O23	0.36158(13)	−0.07683(11)	0.06008(13)	0.0528(3)
O24	0.42218(14)	0.23720(11)	0.47923(13)	0.0583(4)
O27	0.65719(12)	0.38849(11)	0.3092(2)	0.0555(4)
N14	0.39435(13)	0.10015(12)	0.25185(14)	0.0394(3)
C1	0.3464(2)	0.23644(14)	0.1108(2)	0.0406(4)
C2	0.3500(2)	0.3873(2)	0.1699(2)	0.0449(4)
C13	0.4481(2)	0.1728(2)	0.1885(2)	0.0421(4)
C15	0.3599(2)	−0.02155(14)	0.1824(2)	0.0407(4)
C16	0.3257(2)	−0.0639(2)	0.2896(2)	0.0435(4)
C17	0.2832(2)	−0.1758(2)	0.2778(2)	0.0604(5)
C18	0.2616(2)	−0.1891(2)	0.3988(3)	0.0729(7)
C19	0.2809(2)	−0.0949(2)	0.5260(3)	0.0688(6)
C20	0.3237(2)	0.0175(2)	0.5379(2)	0.0556(5)
C21	0.3453(2)	0.0311(2)	0.4172(2)	0.0426(4)
C22	0.3912(2)	0.1375(2)	0.3948(2)	0.0424(4)
C25	0.4419(2)	0.4594(2)	0.3086(2)	0.0545(5)
C26	0.5777(2)	0.4867(2)	0.3015(2)	0.0581(5)
C28	0.7846(2)	0.4066(3)	0.2958(4)	0.1147(13)
C29	0.8716(2)	0.3150(2)	0.3325(2)	0.0584(5)
C30	0.9459(2)	0.3394(2)	0.4658(3)	0.0773(7)
C31	1.0250(3)	0.2530(5)	0.4981(4)	0.121(2)
C32	1.0273(3)	0.1432(5)	0.3962(7)	0.135(2)
C33	0.9547(4)	0.1197(3)	0.2649(5)	0.1106(12)
C34	0.8785(3)	0.2044(2)	0.2332(3)	0.0789(7)
B3	0.3131(2)	0.4374(2)	0.0309(2)	0.0493(5)
B4	0.2825(2)	0.3071(2)	−0.1234(2)	0.0487(5)
B5	0.3059(2)	0.1801(2)	−0.0697(2)	0.0447(5)
B6	0.4100(2)	0.3096(2)	0.0214(2)	0.0422(4)
B7	0.1965(2)	0.4377(2)	0.1307(3)	0.0557(6)
B8	0.2221(2)	0.3120(2)	0.1861(3)	0.0509(5)
B9	0.1907(2)	0.1811(2)	0.0320(2)	0.0513(5)
B10	0.1464(2)	0.2271(2)	−0.1176(3)	0.0557(5)
B11	0.1504(2)	0.3862(2)	−0.0557(3)	0.0565(6)
B12	0.0938(2)	0.3083(2)	0.0411(3)	0.0598(6)

$U_{eq} = {}^1/_3[U_{11}(aa^*)^2 + U_{22}(bb^*)^2 + U_{33}(cc^*)^2 + 2U_{12}aa^*bb^*\cos\gamma + 2U_{13}aa^*cc^*\cos\beta + 2U_{23}bb^*cc^*\cos\alpha]$

Table 5. Refined Positional Parameters of Hydrogen Atoms for 1-$C_6H_4(CO)_2NCH_2$-2-$C_6H_5CH_2OCH_2CH_2$-1, 2-$C_2B_{10}H_{10}$ (5)[2]

Atom	*x*	*y*	*z*	U_{eq}, Å^2
H13a	0.4972(2)	0.1219(2)	0.1224(2)	0.056
H13b	0.5084(2)	0.2326(2)	0.2623(2)	0.056
H17	0.2696(2)	−0.2395(2)	0.1921(2)	0.080
H18	0.2333(2)	−0.2633(2)	0.3944(3)	0.097
H19	0.2650(2)	−0.1068(2)	0.6052(3)	0.091
H20	0.3371(2)	0.0811(2)	0.6237(2)	0.074
H25a	0.4020(2)	0.5349(2)	0.3491(2)	0.073
H25b	0.4487(2)	0.4162(2)	0.3735(2)	0.073
H26a	0.5760(2)	0.4997(2)	0.2137(2)	0.077
H26b	0.6131(2)	0.5589(2)	0.3795(2)	0.077
H28a	0.8177(2)	0.4861(3)	0.3584(4)	0.153
H28b	0.7828(2)	0.4007(3)	0.1995(4)	0.153
H30	0.9433(2)	0.4141(2)	0.5348(3)	0.103
H31	1.0764(3)	0.2694(5)	0.5886(4)	0.160
H32	1.0796(3)	0.0843(5)	0.4180(7)	0.179
H33	0.9571(4)	0.0450(3)	0.1959(5)	0.147
H34	0.8292(3)	0.1874(2)	0.1416(3)	0.105
H3	0.363(2)	0.522(2)	0.043(2)	0.057(5)
H4	0.306(2)	0.306(2)	−0.221(2)	0.055(5)
H5	0.351(2)	0.096(2)	−0.119(2)	0.047(5)
H6	0.514(2)	0.307(2)	0.032(2)	0.041(4)
H7	0.173(2)	0.521(2)	0.210(2)	0.066(6)
H8	0.221(2)	0.314(2)	0.291(2)	0.061(6)
H9	0.162(2)	0.097(2)	0.044(2)	0.062(6)
H10	0.076(2)	0.173(2)	−0.215(2)	0.066(6)
H11	0.087(2)	0.439(2)	−0.107(2)	0.066(6)
H12	−0.008(2)	0.310(2)	0.054(2)	0.069(6)

$$U_{eq} = {}^1/_3[U_{11}(aa^*)^2 + U_{22}(bb^*)^2 + U_{33}(cc^*)^2 + 2U_{12}aa^*bb^*\cos\gamma + 2U_{13}aa^*cc^*\cos\beta + 2U_{23}bb^*cc^*\cos\alpha]$$

Table 6. Refined Thermal Parameters (U's) for 1-$C_6H_4(CO)_2NCH_2$-2- $C_6H_5CH_2OCH_2CH_2$-1, 2-$C_2B_{10}H_{10}$ (5)[3]

Atom	U_{11}	U_{22}	U_{33}	U_{23}	U_{13}	U_{12}
O23	0.0638(8)	0.0492(7)	0.0402(7)	0.0077(6)	0.0141(6)	0.0030(6)
O24	0.0807(9)	0.0450(7)	0.0428(8)	0.0074(6)	0.0142(6)	0.0039(6)
O27	0.0525(7)	0.0483(7)	0.0680(9)	0.0258(6)	0.0070(6)	−0.0068(6)
N14	0.0492(8)	0.0366(7)	0.0339(8)	0.0127(6)	0.0114(6)	0.0019(6)
C1	0.0454(9)	0.0401(9)	0.0398(10)	0.0155(7)	0.0143(7)	0.0045(7)
C2	0.0547(10)	0.0401(9)	0.0429(10)	0.0152(7)	0.0170(8)	0.0093(7)
C13	0.0467(9)	0.0438(9)	0.0417(10)	0.0201(7)	0.0135(7)	0.0050(7)
C15	0.0403(9)	0.0394(9)	0.0406(10)	0.0123(7)	0.0090(7)	0.0046(7)
C16	0.0418(9)	0.0441(9)	0.0484(11)	0.0198(8)	0.0125(7)	0.0054(7)
C17	0.0646(12)	0.0474(11)	0.075(2)	0.0232(10)	0.0221(10)	−0.0007(9)
C18	0.0752(14)	0.0664(14)	0.101(2)	0.0480(14)	0.0369(13)	0.0058(11)
C19	0.0687(13)	0.086(2)	0.084(2)	0.0578(14)	0.0376(12)	0.0203(11)
C20	0.0570(11)	0.0705(13)	0.0519(12)	0.0323(10)	0.0225(9)	0.0183(9)
C21	0.0425(9)	0.0495(10)	0.0423(10)	0.0225(8)	0.0139(7)	0.0114(7)
C22	0.0473(9)	0.0419(9)	0.0368(9)	0.0124(7)	0.0104(7)	0.0075(7)
C25	0.0709(12)	0.0427(10)	0.0432(11)	0.0069(8)	0.0136(9)	0.0087(9)
C26	0.0716(13)	0.0380(10)	0.0583(13)	0.0131(8)	0.0061(10)	−0.0050(9)
C28	0.0550(14)	0.123(2)	0.214(4)	0.121(3)	0.024(2)	−0.0007(14)
C29	0.0440(10)	0.0672(13)	0.0706(14)	0.0353(11)	0.0034(9)	−0.0154(9)
C30	0.078(2)	0.093(2)	0.0580(14)	0.0230(12)	0.0064(12)	−0.0368(14)
C31	0.072(2)	0.205(4)	0.109(3)	0.112(3)	−0.038(2)	−0.063(2)
C32	0.045(2)	0.163(4)	0.259(6)	0.151(4)	0.034(2)	0.014(2)
C33	0.108(3)	0.077(2)	0.172(4)	0.042(2)	0.083(3)	0.007(2)
C34	0.088(2)	0.090(2)	0.0568(14)	0.0226(13)	0.0057(12)	−0.042(2)
B3	0.0609(12)	0.0422(11)	0.0500(13)	0.0207(9)	0.0164(10)	0.0075(9)
B4	0.0609(12)	0.0478(11)	0.0418(12)	0.0215(9)	0.0111(9)	0.0036(9)
B5	0.0545(11)	0.0421(11)	0.0386(11)	0.0161(8)	0.0087(8)	0.0005(9)
B6	0.0518(11)	0.0385(10)	0.0393(11)	0.0146(8)	0.0148(8)	0.0033(8)
B7	0.0591(13)	0.0570(13)	0.0588(14)	0.0268(11)	0.0214(11)	0.0197(10)
B8	0.0521(12)	0.0582(13)	0.0534(14)	0.0277(10)	0.0225(10)	0.0139(10)
B9	0.0469(11)	0.0569(13)	0.0562(14)	0.0287(10)	0.0081(9)	−0.0004(9)
B10	0.0568(13)	0.0588(13)	0.0547(14)	0.0290(11)	0.0031(10)	−0.0017(10)
B11	0.0577(13)	0.0588(13)	0.061(2)	0.0330(11)	0.0123(11)	0.0117(10)
B12	0.0474(12)	0.074(2)	0.071(2)	0.0415(13)	0.0162(11)	0.0123(11)

The form of the anisotropic displacement parameter is: $\exp[-2p^2(a^{*2}U_{11}h^2+b^{*2}U_{22}k^2+c^{*2}U_{33}l^2+2b^*c^*U_{23}kl+2a^*c^*U_{13}hl+2a^*b^*U_{12}hk)]$.

Table 7. Bond Distances in Compound 1-$C_6H_4(CO)_2NCH_2$-2-$C_6H_5CH_2OCH_2CH_2$-1, 2-$C_2B_{10}H_{10}$ (5), Å

O23–C15	1.209(2)	O24–C22	1.211(2)	O27–C28	1.413(3)
O27–C26	1.421(2)	N14–C22	1.395(2)	N14–C15	1.399(2)
N14–C13	1.452(2)	C1–C13	1.528(2)	C1–C2	1.684(2)
C1–B5	1.707(3)	C1–B9	1.709(3)	C1–B6	1.722(2)
C1–B8	1.727(2)	C2–C25	1.527(3)	C2–B3	1.706(3)
C2–B7	1.711(3)	C2–B8	1.722(3)	C2–B6	1.732(2)
C13–H13a	0.97	C13–H13b	0.97	C15–C16	1.484(2)
C16–C17	1.383(3)	C16–C21	1.387(2)	C17–C18	1.383(3)
C17–H17	0.93	C18–C19	1.378(4)	C18–H18	0.93
C19–C20	1.389(3)	C19–H19	0.93	C20–C21	1.382(2)
C20–H20	0.93	C21–C22	1.486(2)	C25–C26	1.505(3)
C25–H25a	0.97	C25–H25b	0.97	C26–H26a	0.97
C26–H26b	0.97	C28–C29	1.488(3)	C28–H28a	0.97
C28–H28b	0.97	C29–C30	1.364(3)	C29–C34	1.369(3)
C30–C31	1.378(5)	C30–H30	0.93	C31–C32	1.367(6)
C31–H31	0.93	C32–C33	1.341(6)	C32–H32	0.93
C33–C34	1.345(4)	C33–H33	0.93	C34–H34	0.93
B3–B7	1.772(3)	B3–B11	1.773(3)	B3–B4	1.774(3)
B3–B6	1.779(3)	B3–H3	1.11(2)	B4–B6	1.767(3)
B4–B5	1.775(3)	B4–B11	1.779(3)	B4–B10	1.782(3)
B4–H4	1.09(2)	B5–B10	1.766(3)	B5–B9	1.772(3)
B5–B6	1.776(3)	B5–H5	1.10(2)	B6–H6	1.08(2)
B7–B11	1.765(3)	B7–B12	1.766(4)	B7–B8	1.772(3)
B7–H7	1.10(2)	B8–B12	1.770(3)	B8–B9	1.777(3)
B8–H8	1.08(2)	B9–B12	1.773(3)	B9–B10	1.779(3)
B9–H9	1.11(2)	B10–B11	1.776(3)	B10–B12	1.784(4)
B10–H10	1.11(2)	B11–B12	1.787(3)	B11–H11	1.08(2)
B12–H12	1.11(2)				

Table 8. Bond Angles in 1-$C_6H_4(CO)_2NCH_2$-2-$C_6H_5CH_2OCH_2CH_2$-1, 2-$C_2B_{10}H_{10}$ (5), Å

C28–O27–C26	111.4(2)	C22–N14–C15	111.79(13)	C22–N14–C13	123.88(14)
C15–N14–C13	123.54(13)	C13–C1–C2	118.74(14)	C13–C1–B5	118.69(13)
C2–C1–B5	110.58(13)	C13–C1–B9	123.16(14)	C2–C1–B9	110.43(13)
B5–C1–B9	62.51(12)	C13–C1–B6	113.72(13)	C2–C1–B6	61.14(10)
B5–C1–B6	62.40(11)	B9–C1–B6	113.89(14)	C13–C1–B8	121.11(14)
C2–C1–B8	60.64(11)	B5–C1–B8	113.54(14)	B9–C1–B8	62.32(13)
B6–C1–B8	113.17(13)	C25–C2–C1	120.75(14)	C25–C2–B3	121.1(2)
C1–C2–B3	110.17(13)	C25–C2–B7	118.5(2)	C1–C2–B7	110.00(14)
B3–C2–B7	62.46(12)	C25–C2–B8	115.7(2)	C1–C2–B8	60.92(10)
B3–C2–B8	113.7(2)	B7–C2–B8	62.16(12)	C25–C2–B6	120.6(2)
C1–C2–B6	60.51(10)	B3–C2–B6	62.31(11)	B7–C2–B6	113.3(2)
B8–C2–B6	112.87(14)	N14–C13–C1	114.40(13)	N14–C13–H13a	108.66(8)
C1–C13–H13a	108.66(8)	N14–C13–H13b	108.66(9)	C1–C13–H13b	108.66(9)
H13a–C13–H13b	107.6	O23–C15–N14	124.7(2)	O23–C15–C16	129.4(2)
N14–C15–C16	105.89(14)	C17–C16–C21	121.4(2)	C17–C16–C15	130.4(2)
C21–C16–C15	108.2(2)	C18–C17–C16	117.2(2)	C18–C17–H17	121.41(14)
C16–C17–H17	121.41(12)	C19–C18–C17	121.6(2)	C19–C18–H18	119.18(12)
C17–C18–H18	119.18(14)	C18–C19–C20	121.2(2)	C18–C19–H19	119.39(12)
C20–C19–H19	119.39(13)	C21–C20–C19	117.3(2)	C21–C20–H20	121.35(12)
C19–C20–H20	121.35(13)	C20–C21–C16	121.2(2)	C20–C21–C22	130.6(2)
C16–C21–C22	108.2(2)	O24–C22–N14	124.7(2)	O24–C22–C21	129.4(2)
N14–C22–C21	105.89(14)	C26–C25–C2	117.2(2)	C26–C25–H25a	107.99(10)
C2–C25–H25a	107.99(9)	C26–C25–H25b	107.99(11)	C2–C25–H25b	107.99(10)
H25a–C25–H25b	107.2	O27–C26–C25	108.9(2)	O27–C26–H26a	109.90(10)
C25–C26–H26a	109.90(11)	O27–C26–H26b	109.90(10)	C25–C26–H26b	109.90(10)
H26a–C26–H26b	108.3	O27–C28–C29	109.9(2)	O27–C28–H28a	109.7(2)
C29–C28–H28a	109.7(2)	O27–C28–H28b	109.7(2)	C29–C28–H28b	109.7(2)
H28a–C28–H28a	108.2	C30–C29–C34	118.6(2)	C30–C29–C28	120.7(3)
C34–C29–C28	120.7(3)	C29–C30–C31	119.8(3)	C29–C30–H30	120.1(2)
C31–C30–H30	120.1(2)	C32–C31–C30	119.6(3)	C32–C31–H31	120.2(3)
C30–C31–H31	120.2(2)	C33–C32–C31	120.4(3)	C33–C32–H32	119.8(3)
C31–C32–H32	119.8(3)	C32–C33–C34	120.0(3)	C32–C33–H33	120.0(3)
C34–C33–H33	120.0(2)	C33–C34–C29	121.6(3)	C33–C34–H34	119.2(2)
C29–C34–H34	119.2(2)	C2–B3–B7	58.91(11)	C2–B3–B11	105.4(2)
B7–B3–B11	59.72(13)	C2–B3–B4	105.76(14)	B7–B3–B4	107.9(2)
B11–B3–B4	60.20(13)	C2–B3–B6	59.57(11)	B7–B3–B6	108.17(14)
B11–B3–B6	107.9(2)	B4–B3–B6	59.65(12)	C2–B3–H3	117.4(10)
B7–B3–H3	121.5(10)	B11–B3–H3	128.7(10)	B4–B3–H3	125.8(10)
B6–B3–H3	117.2(10)	B6–B4–B3	60.32(11)	B6–B4–B5	60.19(11)
B3–B4–B5	108.0(2)	B6–B4–B11	108.2(2)	B3–B4–B11	59.89(13)
B5–B4–B11	107.5(2)	B6–B4–B10	107.93(14)	B3–B4–B10	107.7(2)
B5–B4–B10	59.53(12)	B11–B4–B10	59.83(13)	B6–B4–H4	119.4(10)
B3–B4–H4	120.9(10)	B5–B4–H4	121.5(10)	B11–B4–H4	123.4(10)
B10–B4–H4	123.7(10)	C1–B5–B10	105.6(2)	C1–B5–B9	58.79(11)
B10–B5–B9	60.38(12)	C1–B5–B4	105.43(14)	B10–B5–B4	60.43(12)
B9–B5–B4	108.6(2)	C1–B5–B6	59.20(11)	B10–B5–B6	108.2(2)
B9–B5–B6	108.2(2)	B4–B5–B6	59.67(12)	C1–B5–H5	115.5(9)
B10–B5–H5	129.4(9)	B9–B5–H5	119.3(9)	B4–B5–H5	128.1(9)
B6–B5–H5	117.4(9)	C1–B6–C2	58.34(10)	C1–B6–B4	105.18(14)
C2–B6–B4	104.92(14)	C1–B6–B5	58.39(10)	C2–B6–B5	105.20(14)
B4–B6–B5	60.14(12)	C1–B6–B3	105.11(13)	C2–B6–B3	58.12(11)
B4–B6–B3	60.03(12)	B5–B6–B3	107.8(2)	C1–B6–H6	116.0(9)
C2–B6–H6	118.1(9)	B4–B6–H6	131.3(9)	B5–B6–H6	122.6(9)
B3–B6–H6	126.2(9)	C2–B7–B11	105.6(2)	C2–B7–B12	105.9(2)
B11–B7–B12	60.81(14)	C2–B7–B3	58.63(12)	B11–B7–B3	60.19(13)
B12–B7–B3	108.8(2)	C2–B7–B8	59.23(11)	B11–B7–B8	108.7(2)
B12–B7–B8	60.04(13)	B3–B7–B8	108.14(14)	C2–B7–H7	115.8(11)
B11–B7–H7	130.2(11)	B12–B7–H7	126.2(11)	B3–B7–H7	121.2(11)
B8–B7–H7	115.7(11)	C2–B8–C1	58.44(10)	C2–B8–B12	105.2(2)
C1–B8–B12	104.9(2)	C2–B8–B7	58.61(12)	C1–B8–B7	105.25(14)
B12–B8–B7	59.81(13)	C2–B8–B9	105.52(14)	C1–B8–B9	58.35(11)
B12–B8–B9	59.98(13)	B7–B8–B9	107.6(2)	C2–B8–H8	116.9(11)
C1–B8–H8	117.0(10)	B12–B8–H8	131.3(10)	B7–B8–H8	124.7(10)

(*continued on next page*)

Table 8 (continued)

B9–B8–H8	124.1(10)	C1–B9–B5	58.70(11)	C1–B9–B12	105.6(2)
B5–B9–B12	108.0(2)	C1–B9–B8	59.34(11)	B5–B9–B8	108.0(2)
B12–B9–B8	59.81(13)	C1–B9–B10	105.0(2)	B5–B9–B10	59.64(12)
B12–B9–B10	60.28(13)	B8–B9–B10	107.9(2)	C1–B9–H9	117.1(11)
B5–B9–H9	120.9(10)	B12–B9–H9	126.5(10)	B8–B9–H9	117.3(11)
B10–B9–H9	129.1(11)	B5–B10–B11	108.1(2)	B5–B10–B9	59.98(12)
B11–B10–B9	108.0(2)	B5–B10–B4	60.04(12)	B11–B10–B4	59.99(13)
B9–B10–B4	108.0(2)	B5–B10–B12	107.8(2)	B11–B10–B12	60.26(14)
B9–B10–B12	59.70(13)	B4–B10–B12	108.1(2)	B5–B10–H10	121.9(11)
B11–B10–H10	121.8(11)	B9–B10–H10	121.4(11)	B4–B10–H10	122.2(11)
B12–B10–H10	121.3(11)	B7–B11–B3	60.09(13)	B7–B11–B10	107.8(2)
B3–B11–B10	108.0(2)	B7–B11–B4	108.0(2)	B3–B11–B4	59.91(12)
B10–B11–B4	60.18(13)	B7–B11–B12	59.63(14)	B3–B11–B12	107.8(2)
B10–B11–B12	60.08(14)	B4–B11–B12	108.1(2)	B7–B11–H11	119.4(11)
B3–B11–H11	119.6(11)	B10–B11–H11	124.5(11)	B4–B11–H11	122.7(11)
B12–B11–H11	122.4(11)	B7–B12–B8	60.15(13)	B7–B12–B9	108.1(2)
B8–B12–B9	60.22(12)	B7–B12–B10	107.4(2)	B8–B12–B10	108.0(2)
B9–B12–B10	60.03(13)	B7–B12–B11	59.57(14)	B8–B12–B11	107.8(2)
B9–B12–B11	107.8(2)	B10–B12–B11	59.66(13)	B7–B12–H12	119.7(11)
B8–B12–H12	118.7(11)	B9–B12–H12	121.9(11)	B10–B12–H12	125.1(11)
B11–B12–H12	123.6(11)				

Pergamon

PII: S0277–5387(98)00122–3

Polyhedron Vol. 17, No. 19, pp. 3409–3418, 1998
© 1998 Elsevier Science Ltd
All rights reserved. Printed in Great Britain
0277–5387/98 $19.00+0.00

Synthesis and structural studies on 1:1 metal complexes with 1,3–dimethyllumazine and 1,3,6,7–tetramethyllumazine. Crystal structure of two dichloro copper(II) and mercury(II) compounds and a polymeric chloro–nitrato bridged–mercury(II) complex

Francisco Hueso-Ureña,[a] Sonia B. Jiménez-Pulido,[a] Miguel N. Moreno-Carretero,[a,*] Miguel Quirós-Olozábal[b] and Juan M. Salas-Peregrín[b]

[a] Departamento de Química Inorgánica y Orgánica, Universidad de Jaén, 23071, Jaén, España

[b] Departamento de Química Inorgánica, Universidad de Granada, 18071, Granada, España

(Received 30 January 1998; accepted 23 March 1998)

Abstract—In absolute methanol medium, eight new 1:1 metal complexes of general formula $M^{II}X_2L{\cdot}nH_2O$ have been isolated (L = 1,3–dimethyllumazine (DLM) or 1,3,6,7–tetramethyllumazine (DLMD); M = Cu, Cd, Hg, Pd and Pt; X = Cl^- or NO_3^-). The experimental techniques used for their structural characterization were thermal (TG and DSC) and spectral methods (IR, ^{13}C and ^1H–NMR and EPR) and magnetic measurements (77–290 K). Single-crystal X-ray diffraction studies have been performed on the complexes $[CuCl_2(DLMD)(H_2O)]{\cdot}H_2O$ (**1**), $[HgCl_2(DLMD)]$ (**2**) and $[HgCl(NO_3)(DLMD)]$ (**3**). In all the complexes, the lumazine-derived ligands seem to be coordinated in bidentate form through the N5 and O4 atoms. The complex **1** shows a monomeric five-coordinated structure in which the coordination polyhedron can be best described as a trigonal bipyramid. The equatorial plane is occupied by two chlorine atoms (Cu–Cl 2.268 and 2.261 Å) and an oxygen O(4) from the organic ligand (Cu–O(4) 2.294 Å), whereas the apical positions were designed by a coordinated water molecule and the N(5) atom of the bidentate pteridine ligand (Cu–O(1W) 1.950 Å and Cu–N(5) 2.038 Å). The crystal structure is conformed by an extense hydrogen bonds scheme in which the non-coordinated water molecule plays an important role. In the compound **2**, the pteridine ligand interacts only weakly with the Hg(II) ion (Hg–O(4) 2.772 Å and Hg–N(5) 2.675 Å); the structure must be described as an adduct between the $HgCl_2$ and the organic ligand in which the molecules of metallic salt retain their identity (Hg–Cl 2.284 and 2.288 Å). These units are weakly paired through long interactions of each metal centre with chloride ions of a neighbour molecule (Hg···Cl 3.664 Å). The mixed complex **3** displays a polymeric structure in which the nitrate groups act as bridging bifurcate ligands between two Hg(II) ions through only one of their three oxygen atoms. The coordination polyhedron around the Hg(II) ion must be described as a trigonal bipyramid in which the metal is surrounded by the O(4), O(1N) and O(1N′) atoms in the equatorial plane at distances of 2.551, 2.563 and 2.618 Å, respectively. In the axial positions, a terminal chloride ligand (Hg–Cl(1) 2.307 Å) and the N(5) atom of pteridine ligand (Hg–N(5) 2.208 Å) can be found.
© 1998 Elsevier Science Ltd. All rights reserved

Keywords: crystal structure; complexes; pteridine; lumazine.

* Author for correspondence (fax 34 53 212186; e-mail mmoreno@ujaen.es).

The biological importance of lumazines and pterines has been extensively pointed out. Their capability to undergo electron-transfer reactions through their potentially metal-chelating α–carbonylpyrazine moiety [1, 2] have promoted their use as model to determine the reactivity metal sites in several enzymes [3–13]. Also, they have been used as a basic skeleton to construct extended hydrogen bonded systems to explain the cooperative interaction between electron transfer and proton transfer in hydrogen-bonded charge-transfer systems [14–16].

There are a few structurally characterized compounds in which these organic compounds act as ligand [17–27]. In this way, and following our research program focused to the structural characterization of metal complexes with lumazine (pteridin–(1*H*,3*H*)–2,4–dione) methylated derivatives, we have already published the molecular and crystal structure of several complexes $[ML_2(H_2O)_2]X_2{\cdot}nH_2O$ [28–31] (X = nitrate or perchlorate) containing both 1,3–dimethyllumazine and 1,3,6,7–tetramethyllumazine, hereafter denoted as DLM and DLMD. In this paper, we now report the study of eight new $MLX_2{\cdot}nH_2O$ complexes, where M = Cu(II), Cd(II), Hg(II), Pd(II) and Pt(II), L = DLM and DLMD, and X = chloride or nitrate.

EXPERIMENTAL SECTION

Synthesis

The pteridine-derived ligands were prepared from glyoxal (for DLM) or dimethylglyoxal (for DLMD) and 5,6–diamino–1,3–dimethyluracil, as described elsewhere [28].

The synthesis of the complexes was carried out as follows:

$Cu(NO_3)_2(DLM){\cdot}3H_2O$ and $CuCl_2(DLMD){\cdot}2H_2O$. 1 mmol of pteridine ligand dissolved in hot MeOH (*ca.* 50 ml and 50°C) was reacted, slowly with stirring, with 1 mmol of the corresponding copper salt dissolved in the minimum amount of methanol. The resulting solution was allowed to stand at room temperature. By evaporation over several days, the crystalline green solids were isolated.

$Cd(NO_3)_2(DLM){\cdot}2H_2O$. To a hot aqueous solution of DML (*ca.* 50 ml, 50°C and 0.5 mmol), 1 mmol of cadmium nitrate was added under continuous stirring. On evaporating the resulting solution at room temperature, a yellow solid complex was isolated.

$HgCl_2(DLM)$ and $HgCl_2(DLMD)$. On heating at 40–50°C, 1 mmol of pteridine ligand was dissolved in MeOH. This solution was mixed and stirred with another containing 1 mmol of mercury(II) chloride in the minimum amount of MeOH. After standing a few days, the solid complexes were isolated.

$HgCl(NO_3)(DLMD)$. A hot solution (50°C, 50 ml, MeOH/H_2O 1:1) containing 1 mmol of DLMD ligand was treated with 1 mmol of mercury(II) nitrate dissolved in the minimum volume of water. On adding the metallic salt, the solution, initially orange and clear, became opaque and yellow. To remove the turbidity, 5 ml of concentrated hydrochloric acid (25%) was added drop by drop until the solution was clear. On cooling to room temperature, orange crystals of the complex were obtained.

$PdCl_2(DLM)$ and $PtCl_2(DLM)$. 1 mmol of DLM ligand dissolved in hot MeOH (*ca.* 50 ml and 50°C) was reacted, slowly with stirring, with 1 mmol of either Na_2PdCl_4 or K_2PtCl_4 dissolved in the minimum amount of methanol. In both cases, the resulting solution was allowed to stand at room temperature and after a few minutes, a brown solid appeared.

All the solids were filtered off, washed with ethanol and diethylether and air dried. The analytical data, color, conductivity values ($mho{\cdot}cm^2{\cdot}mol^{-1}$) were as follows: $Cu(NO_3)_2(DLM){\cdot}3H_2O$ (green, 105), found 22.6%C, 3.5%H, 20.0%N, 13.2%H_2O, calcd. 22.2%C, 3.3%H, 19.4%N, 12.5%H_2O; $CuCl_2(DLMD){\cdot}2H_2O$ (green, 43), found 30.5%C, 4.2%H, 14.2%N, 9.8%H_2O, calcd. 30.7%C, 4.1%H, 14.3%N, 9.2%H_2O; $Cd(NO_3)_2(DLM){\cdot}2H_2O$ (yellow, 86), found 20.5%C, 2.5%H, 18.0%N, 7.8%H_2O, calcd. 20.7%C, 2.6%H, 18.1%N, 7.7%H_2O; $HgCl_2(DLM)$ (orange, 14), found 20.7%C, 1.8%H, 12.3%N, calcd. 20.7%C, 1.7%H, 12.1%N; $HgCl_2(DLMD)$ (yellow, 11), found 24.2%C, 2.4%H, 11.3%N, calcd. 24.2%C, 2.5%H, 11.4%N; $HgCl(NO_3)(DLMD)$ (orange, 85), found 22.9%C, 2.4%H, 13.7%N, calcd. 23.2%C, 2.3%H, 13.5%N; $PdCl_2(DLM)$ (brown, 58), found 26.6%C, 2.2%H, 15.2%N, calcd. 26.0%C, 2.2%H, 15.2%N; $PtCl_2(DLM)$ (brown, 13), found 21.2%C, 1.9%H, 12.4%N, calcd. 21.0%C, 1.8%H, 12.2%N.

Crystallographic studies

The structures were solved using a Siemens P4 diffractometer with MoKα radiation ($\lambda = 0.71073$ Å). Data were semiempirically corrected by absorption (ψ scans). Other crystal data and structure refinement details are given in Table 1. Non-H atoms were located in successive ΔF maps and refined anisotropically by full-matrix least-squares on F^2; hydrogens from the ligand were idealized whereas those of water molecules were refined with fixed O–H (0.86 Å) and H–H (1.40 Å) distances. The isotropic displacement coefficient for H-atoms was taken as 1.2 times the isotropic displacement parameter of the parent atom.

All calculations and drawings have been performed using the Siemens SHELXTL PLUS system.

Apparatus

Microanalyses of C, H and N were performed in a Fisons EA1108 apparatus; the water content of the complexes were determined from the TG plot. Conductivity measurements have been carried out using 10^{-3} M freshly prepared dimethylformamide solu-

Table 1. Crystal data and structure refinement.[1]

Compound	$[CuCl_2(DLMD)(H_2O)]\cdot H_2O$	$[HgCl_2(DLMD)]$	$[HgCl(NO_3)(DLMD)]$
Empirical formula	$C_{10}H_{16}Cl_2CuN_4O_4$	$C_{10}H_{12}Cl_2HgN_4O_2$	$C_{10}H_{12}ClHgN_5O_5$
Formula weight	390.71	491.73	518.29
Temperature (K)	293	291	293
Crystal system	Orthorhombic	Triclinic	Monoclinic
Space group	Pbca	$P\bar{1}$	$P2_1/n$
Unit cell dimensions a (Å)	14.045(1)	8.0064(6)	13.315(2)
b (Å)	11.7490(7)	9.3736(6)	8.539(2)
c (Å)	19.701(2)	10.6279(5)	13.932(2)
α (°)	90	71.414(7)	90
β (°)	90	81.536(6)	108.728(9)
δ (°)	90	70.904(8)	90
Volume (Å^3)	3251.0(4)	713.59(8)	1500.2(5)
Z	8	2	4
Density (calc. Mg·m^{-3})	1.597	2.289	2.295
Absorption coeff. (mm^{-1})	1.690	11.161	10.469
F(000)	1592	460	976
Crystal size (mm^3)	$0.70\times0.40\times0.10$	$0.50\times0.425\times0.35$	$0.50\times0.42\times0.35$
θ range for	2.07 to 25.00	2.02 to 29.99	1.84 to 30.03
Index ranges	$0\leqslant h\leqslant16$	$-10\leqslant h\leqslant11$	$-18\leqslant h\leqslant17$
	$-13\leqslant k\leqslant13$	$-12\leqslant k\leqslant13$	$0\leqslant k\leqslant12$
	$-23\leqslant l\leqslant0$	$0\leqslant l\leqslant14$	$0\leqslant l\leqslant19$
Reflections collected, independent	10912, 2855	8302, 4151	8730, 4365
R_{int}	0.0464	0.0049	0.0059
Max. and min. transmission	0.6218, 0.3608	0.0617, 0.0226	0.0626, 0.0134
Weighting scheme:			
$w^{-1}=\sigma^2(F_0^2)+(yP)^2+xP$*	y = 0.05, x = 5.0	y = 0.07, x = 3.0	y = 0.09, x = 5.0
Data/restraints/parameters	2853/6/206	4150/0/177	4363/0/203
Goodness-of-fit on F^2	1.070	1.063	1.111
Δ/σ last cycle	<0.001	0.015	<0.001
Final R indices [$I>2\sigma(I)$] R, wR^2	0.0415, 0.0967	0.0436, 0.1182	0.0583, 0.1418
R indices (all data) R, wR^2	0.0658, 0.1168	0.0520, 0.1266	0.0772, 0.1589
Largest diff. peak and hole (e·Å^{-3})	0.409, −0.349	2.242, −1.578	1.915, −2.490

(*) $P-1/3(F_0^2+2F_c^2)$

tions on a Hanna HI8820 instrument. TG and DSC studies were carried out under pure air on a Mettler TA-3000 system (TG-50 thermobalance and DSC-20 differential scanning calorimeter), using *ca.* 5 mg of sample and a 10°C·min^{-1} heating rate. Infrared spectra were measured on a Perkin-Elmer FT-IR 1760-X (KBr pellets, 4000–400 cm^{-1}) and Perkin-Elmer 983-G spectrophotometer (polyethylene pellets, 600–180 cm^{-1}). The electron paramagnetic resonance spectra were obtained in the X-band at room temperature on a Bruker ESP 300E apparatus, with a microwave frequency of 9.79 GHz and a modulation frequency of 100 kHz. Magnetic measurements were carried out on a Manics DSM-8 system between 77 and 290 K.

RESULTS AND DISCUSSION

Crystallographic studies

The molecular structure of the complex $[CuCl_2(DLMD)(H_2O)]\cdot H_2O$ is shown in Fig. 1. The metal ion is surrounded by a pteridine ligand, in bidentate form through N(5) and O(4) atoms, two chloride and a water molecule, the other water molecule being linked to the first by hydrogen bonding.

Bond distances and angles around the metal ion are listed in Table 2. A detailed analysis indicates that the N(5)–O(4) edge substended by the bidentate pteridine ligand is perpendicular (89.9°) to the Cl(1)–Cl(2) edge, which shows that the coordination polyhedron may be described as a distorted trigonal bipyramid [32], whose equatorial plane is formed by the atoms O(4), Cl(1) and Cl(2), the N(5) and O(1W) being in the apical positions. The ratio between apical and equatorial bond lengths is 0.88, which indicates that the TBP is flattened. This fact does not satisfy the electron pair repulsion model since, following this theory, the ligands in equatorial positions must be less repelled than those in apical positions, resulting in an elongation of the coordination polyhedron. The explanation may be found if we consider that the molecules which fit the VSEPR model usually contain relatively simple M–L bonds and ligands with low π-bonding capability (type α) [32]. Therefore, in the

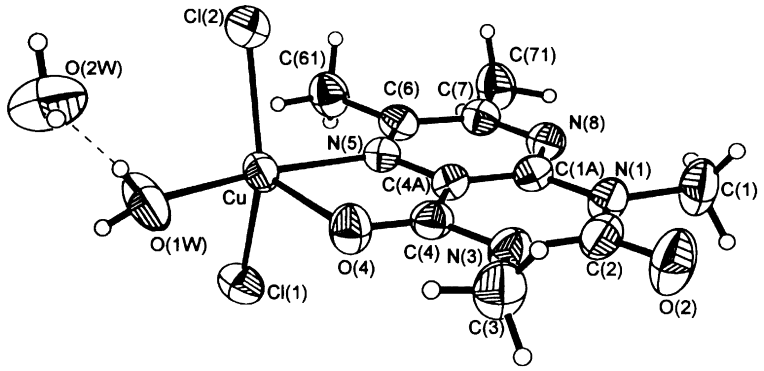

Fig. 1. Molecular drawing and numbering scheme for the monomeric unit of $[CuCl_2(DLMD)(H_2O)]\cdot H_2O$ (ellipsoids at 50% probability).

Table 2. Bond lengths (Å) and angles (°) around the metal ion in the crystal structures of $[CuCl_2(DLMD)(H_2O)]\cdot H_2O$, $[HgCl_2(DLMD)]$ and $[HgCl(NO_3)(DLMD)]$

$[CuCl_2(DLMD)(H_2O)]\cdot H_2O$			
Cu–O(4)	2.294(3)	N(5)–Cu–O(1W)	170.0(2)
Cu–N(5)	2.038(3)	N(5)–Cu–Cl(1)	90.4(1)
Cu–O(1W)	1.950(3)	N(5)–Cu–Cl(2)	91.8(1)
Cu–Cl(1)	2.268(1)	O(1W)–Cu–Cl(1)	90.1(1)
Cu–Cl(2)	2.261(1)	O(1W)–Cu–Cl(2)	92.6(1)
O(4)–Cu–N(5)	78.5(1)	Cl(1)–Cu–Cl(2)	150.76(5)
O(4)–Cu–O(1W)	91.6(2)	Cu–O(4)–C(4)	107.1(3)
O(4)–Cu–Cl(1)	103.8(1)	Cu–N(5)–C(4A)	114.0(3)
O(4)–Cu–Cl(2)	105.2(1)	Cu–N(5)–C(6)	127.0(3)
$[HgCl_2(DLMD)]$			
Hg–Cl(1)	2.284(2)	Cl(1)–Hg–O(4)	88.4(2)
Hg–Cl(2)	2.288(2)	Cl(2)–Hg–O(4)	100.7(2)
Hg–N(5)	2.675(6)	N(5)–Hg–O(4)	61.4(2)
Hg–O(4)	2.772(6)	Hg–O(4)–C(4)	111.7(5)
Cl(1)–Hg–Cl(2)	166.66(9)	Hg–N(5)–C(6)	121.1(5)
Cl(1)–Hg–N(5)	88.7(2)	Hg–N(5)–C(4A)	113.4(5)
Cl(2)–Hg–N(5)	104.2(2)		
$[HgCl(NO_3)(DLMD)]$			
Hg–O(4)	2.551(6)	N(5)–Hg–O(1N)[a]	77.9(2)
Hg–N(5)	2.208(7)	Cl–Hg–O(1N)[a]	100.4(2)
Hg–Cl	2.307(3)	O(4)–Hg–O(1N)[a]	103.3(2)
Hg–O(1N)	2.563(8)	O(1N)–Hg–O(1N)[a]	118.87(8)
Hg–O(1N)[a]	2.618(7)	Hg–O(4)–C(4)	107.9(5)
N(5)–Hg–Cl	168.8(2)	Hg–N(5)–C(6)	124.1(6)
N(5)–Hg–O(4)	72.3(2)	Hg–N(5)–C(4A)	115.0(5)
Cl–Hg–O(4)	97.6(2)	Hg–O(1N)–N(1N)	106.0(6)
N(5)–Hg–O(1N)	101.9(3)	Hg[b]–O(1N)–N(1N)	104.2(6)
Cl–Hg–O(1N)	88.7(2)	Hg–O(1N)–Hg[b]	148.9(3)
O(4)–Hg–O(1N)	135.5(2)		

Equivalent positions: (a) 1/2−x,y+1/2,1/2−z; (b) 1/2−x,y−1/2,1/2−z

present complex, the presence of a more complicated type of metal–ligand bonding may be suspected (type β complexes), this assumption being in according with the π–bonding capability through the N5 atom found in the methylated derivatives of lumazine by means of semiempirical methods [33]. Also, the geometry of the coordination polyhedron has been quantified in terms of trigonal bipyramid (TBP) and tetragonal pyramid (TP)limits as indicated by Galy, the dihedral angles of the polyhedron being defined following Muetterties

and Guggenberger [34, 35]. The results point out that the polyhedron can be best described as a trigonal bipyramid because it only displays 15% TP (85% TBP). The three equatorial donor atoms and the metal ion are virtually coplanar, the latter being 0.042 Å displaced from this plane. The mean values of the three angles over Cu atom towards O(1W) and towards N(5) atoms are 91(1)° and 87(6)°, respectively; the O(1W)–Cu–N(5) angle is 170.0°.

The metallic atom and the DLMD ligand are practically coplanar (deviation 0.005 Å). The organic ligand is also planar, the atoms more deviated from the mean plane being C(2) (endo 0.043 Å) and C(1) (exo 0.102 Å). The chelate and pteridine mean planes are angled by 179.0°. The metal–ligand distances are in the range cited in the bibliography for analogous compounds [17–31].

The values of bond lengths and angles in the DLMD ligand for the three compounds are very similar showing, as also reported elsewhere [14, 26, 28–31], a great electronic delocalization. The C4═O4 bond (*ca.* 1.23 Å) is a little longer than the C2═O2 (*ca.* 1.20 Å) as consequence of the O4-coordination.

In Fig. 2, a view of the unit cell of the copper compound together with some geometrical features of the hydrogen bonds are shown. There is a hydrogen bond O(1W)–H···O(2W) (x,y,z) which links the non-coordinated water molecule with the complex moiety. The coordinated water molecule also establishes an intermolecular hydrogen bond with a neighbour chlorine atom O(1W)–H···Cl(2) (1/2−x,y−1/2,z). The crystallization water also acts as donor in other two intermolecular hydrogen bonds, with the atoms O(2) (x,1/2−y,z−1/2) and Cl(1) (x−1/2,y,−z−1/2). The hydrogen bonding pattern can be described as a tridimensional network in which each molecule is attached to three other ones, the non-coordinated water molecule playing a fundamental role.

The structure of two-paired molecules of [$HgCl_2$(DLMD)] is shown in Fig. 3. In this compound, the interactions between the organic ligands and metal ions take place in the usual way for the lumazine-derived ligands, this is through N(5) and O(4) atoms, but these interactions (Hg–N(5) 2.675 Å, Hg–O(4) 2.772 Å) are weaker (see Table 2) if compared with the Hg–Cl distances (2.284 and 2.288 Å). These Hg–Cl lengths are slightly longer than those found in the solid $HgCl_2$ (2.25 Å) [36]. The Cl(1)–Hg–Cl(2) angle, 166.66°, is near to exact lineality (180°) found in $HgCl_2$. Therefore, this compound could be an addition compound between DLMD and mercury(II) chloride, in which practically none of them have lost their identity. The structural features of this compound are very similar to those reported for the dichloro–(octachloro– 1,10–phenantroline–N,N′) mercury(II), in which there also are very long Hg–N bonds (2.269(3) and 2.586(3) Å), and *quasi*-linear $HgCl_2$ moieties (∠ Cl–Hg–Cl 162.19(6)°) [37].

The metal is distanced 1.193 Å from the pteridine plane; the direction Cl(1)–Cl(2) defines an angle with

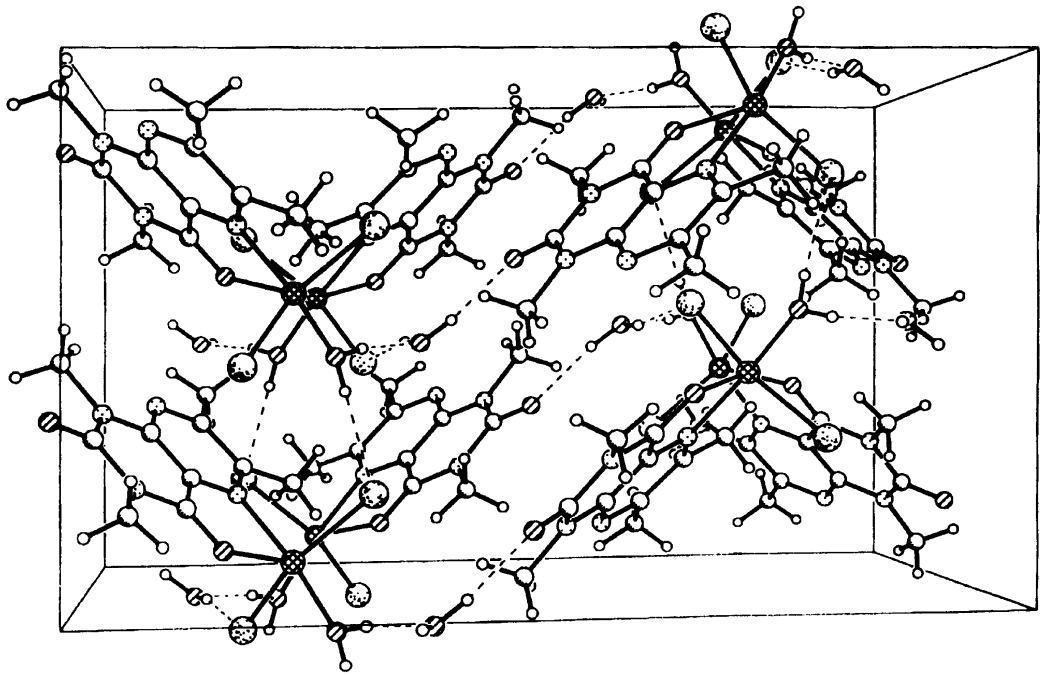

Fig. 2. A view along the *a* axis of the unit cell of [$CuCl_2$(DLMD)(H_2O)]·H_2O. Hydrogen bonds are as follow (A···B: d(A···B),Å, ∠(A–H···B),°): O(1W)···O(2W): 2.648(5), 171; O(1W)···Cl(2)(1/2−x,y−1/2,z): 3.175(4), 164; O(2W)···O(2)(x,1/2−y,z−1/2): 2.844(5), 172; O(2W)···Cl(1)(x−1/2,y,−z−1/2): 3.198(4), 167.

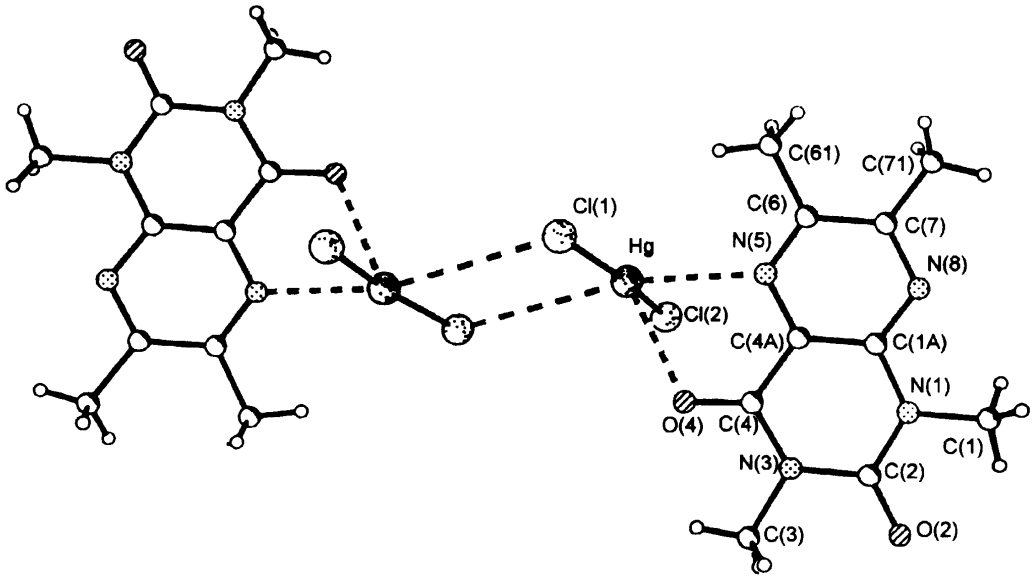

Fig. 3. A view of two-paired molecules of $[HgCl_2(DLMD)]$, showing the atom numbering.

this plane of 37.9°. As in previous copper complex, the pteridine ligand is planar, the atoms more deviated being O(2) (exo 0.129 Å) and C(2) (endo 0.052 Å).

In addition to the above-described bonds, the molecular units are paired (see Fig. 3) through very long-distance interactions Hg···Cl(2) (2 − x, − y,1 − z; 3.664 Å). The planes defined by two $HgCl_2$ units are roughly perpendicular to the *b* axis. The mean plane of the pteridine is parallel to [0 3 1] direction and the Cl(1)–Cl(2) segment of each unit is practically aligned (12.3°) with the *c* axis.

The molecular unit of $[HgCl(NO_3)(DLMD)]$ is shown in Fig. 4 and the bond distances and angles around the metal ion are given in Table 2. Although apparently it seems to be closely related with the above described mercury complex, it is really very distinct from the structural point of view. In this compound, there are Hg–O(4) (2.551 Å) and Hg–N(5) (2.208 Å)

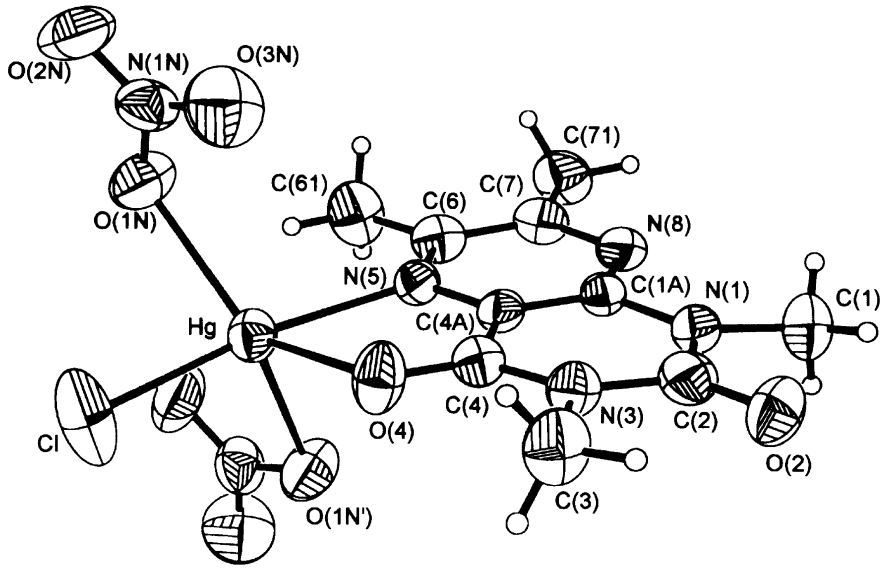

Fig. 4. Molecular structure of the monomeric unit of $[HgCl(NO_3)(DLMD)]$ with the numbering scheme (ellipsoids at 50% probability).

bonds significantly shorter and stronger than those found in the previous mercury complex. In addition, there are a terminal Hg–Cl bond (2.307 Å) and two Hg–O bonds with nitrate-bridging groups (Hg–O(1N) 2.563 Å, Hg–O(1N′) 2.618 Å). The metal ion is five-coordinated and the coordination polyhedron can be described as a distorted trigonal bipyramid, but in this case the geometry is a little nearer to TBP than in the above-described copper complex because it has 87% TBP [34]. The equatorial plane is designed by O(4), O(1N) and O(1N′) atoms and the axial positions are occupied by Cl and N(5) atoms. In this polyhedron, the angle defined by N(5)–O(4) and O(1N)–O(1N′) is 93.4°. The mean angles over the Hg towards Cl and towards N(5) — this is over and under the equatorial plane — are 96 and 84°, respectively, the metal being 0.221 Å over the equatorial plane. The axial Cl–Hg–N(5) angle is 168.8°. As in the previous described copper complex, the trigonal bipyramid is also flattened, the axial bonds being *ca.* 12% shorter than those in equatorial positions. The coordination mode of the nitrate is similar to the one found in the chloro–pyridyl–mercury(II) nitrate, but in this compound the interaction between O–nitrate bifurcate bridges and Hg atoms is significantly weaker (Hg–O 2.9 Å) [38].

The DLMD skeleton is practically planar, the greatest deviated atoms being N(3) (endo 0.056 Å) and C(1) (exo 0.229 Å). The metal ion is distanced by 0.359 Å from this mean plane.

In the Fig. 5, a portion of the polymeric chain is shown. The nitrate anion acts as bridging ligand between two metal centres but only through one of their oxygen atoms, thus making a zig-zag chain which follows the *b* direction with the pteridine planes parallel to the [5 0 4] direction. The polymeric chains are linked to each others through Van der Waals' interactions.

Conductivity and thermal studies

Conductivity values of complexes $CuCl_2(DLMD)\cdot 2H_2O$, $HgCl_2(DLM)$, $HgCl_2(DLMD)$ and $PtCl_2(DLM)$, obtained in DMF solutions, clearly indicate their non-electrolyte character. The other Pd(II), Cd(II) and Hg(II) compounds show conductivity values corresponding to 1:1 electrolytes, but, it is possible that some degree of solvolisis exists, since, as it has been shown from X-ray diffraction and far-infrared spectra, in all cases, the anions are coordinated to the metal ion. Otherwise, the $Cu(NO_3)_2(DLM)\cdot 3H_2O$ has 1:2 electrolyte molar conductivity, corroborating the presence of free nitrate groups [39].

The main features of thermal studies (TG and DSC) were as follows. In $Cu(NO_3)_2(DLM)\cdot 3H_2O$ and $CuCl_2(DLMD)\cdot 2H_2O$, DSC curves show two different endothermic effects assignable to the loss of both crystallization and coordination water molecules. The DSC peak temperatures were 95 and 120°C for the first one and 75 and 149°C, for the second one. These endothermic effects were followed by a third at around 180°C, without weight loss, assignable to the melting of the anhidrous compounds. For the $Cd(NO_3)_2(DLM)\cdot 2H_2O$, the presence of only one endothermic peak for the loss of the water may suggest that both molecules are structurally equivalent.

Infrared and NMR spectra

The infrared spectra of these complexes are very similar, which indicates that the coordination of pteridine ligands takes place in the same way. Also, the spectral data are very similar to those reported elsewhere for other complexes with DLM and DLMD ligands [28–31]. Two bands, one slightly over

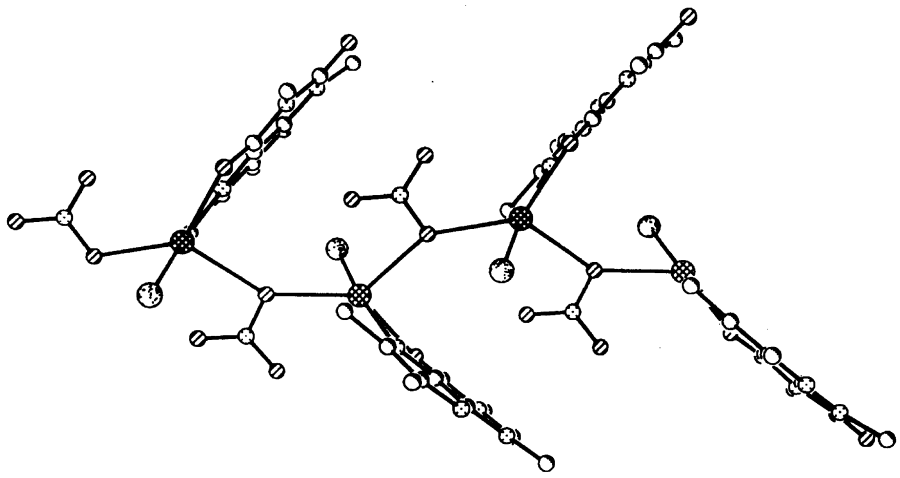

Fig. 5. View, along [5 0 4] direction, of the zig-zag polymeric structure of $[HgCl(NO_3)(DLMD)]$.

1700 cm^{-1} (1705–1728) and another from 1635 to 1660 cm^{-1} may be assigned to a combination of the stretching vibrations of both exocyclic carbonyl groups, the first, weaker, being mainly due to ν(C2═O) whereas the second must be assigned to ν(C4═O). In all cases, these bands appear shifted to lower wavenumber with respect to their position in the IR spectrum of free ligands (*ca.* 1725 and 1685 cm^{-1}, respectively), but, as it may be expected due to the involvement of O4 atom in the coordination, this displacement is stronger in the second band than in the first one. Other vibration modes related to potential donor atoms may be assigned as follows: ν(C═N) (1558–1596 cm^{-1}), ν(C═C)+ν(C–N) (two bands at 1445–1475 and 1270–1305 cm^{-1}). These bands also appear shifted to higher wavelengths with respect to their position in the IR spectrum of the free ligands [28–31]. In the IR spectra of the nitrate-containing complexes, a band corresponding to ν(N–O) of the nitrate group [40] appears at 1385 cm^{-1}; however, in the $Cu(NO_3)_2(DLM)\cdot 3H_2O$ spectrum, this band is very strong and sharp, which may indicate the presence of free nitrate, whereas in the Cd(II) and Hg(II) complexes, this band is broadened due to the behavior of the nitrate anion as ligand [40]. In the far-infrared region, chloro-complexes display bands assignable to ν(M–Cl) mode at the following wavenumbers (cm^{-1}): $CuCl_2(DLMD)\cdot 2H_2O$, 300; $HgCl_2(DLM)$, 343; $HgCl_2(DLMD)$, 367; $HgCl(NO_3)(DLMD)$, 355; $PdCl_2(DLM)$, 348 and 366; $PtCl_2(DLM)$, 321. In all cases, this bands must be attributed to terminal M–Cl bonds and, in the two latter compounds, both M–Cl bonds must be in *cis* position [41].

Within experimental error, ^1H and ^{13}C–NMR spectra of Cd(II), Hg(II), Pd(II), and Pt(II) complexes (DMSO–d_6 solution) display signals at the same values of chemical shift than the free ligands [30]. This fact may be justified taking into account that, on coordinating to the metal, the π electronic density in the ligand remains practically unaffected, although an alternative explanation based on the existence of solvolysis processes in both DMF and DMSO solutions, as suggested by conductivity values, cannot be rejected.

EPR spectra and magnetic measurements

The complex $Cu(NO_3)_2(DLM)\cdot 3H_2O$ displays an axial EPR powder spectrum (Figure 6a) with $g_\perp = 2.04$ and $g_\parallel = 2.40$ and is in accordance with the existence around the Cu(II) ion of a square-plane based geometry with the tetragonal axes aligned [42, 43]. The values of magnetic susceptibility have been fitted to the Curie–Weiss' law ($1/\chi_M = (T-\theta)/C$) (Figure 7a) with the following parameters: r = 0.9929, C = 0.220(6) cgsu·K·mol^{-1} and $\theta = -86(9)$ K. The high value of the latter parameter and the positive slope of the χT *versus* T plot may be indicative of the existence of a strong antiferromagnetic coupling between metallic centres, which could justify the low value found for the effective magnetic moment (1.2 ± 0.1 BM) if compared with the one expected in mononuclear magnetically diluted Cu(II) compounds (1.7–2.2 BM) [44]. This permits us to suggest the existence of any interaction between metal centres, although, in order to corroborate this fact, both the knowledge of structure and the magnetic behaviour up to 4 K would be needed. The value of the effective magnetic moment (1.98 ± 0.01 BM) and the fit of the magnetic susceptibility values of the $[CuCl_2(DLMD)(H_2O)]\cdot H_2O$ at different temperatures (Fig-

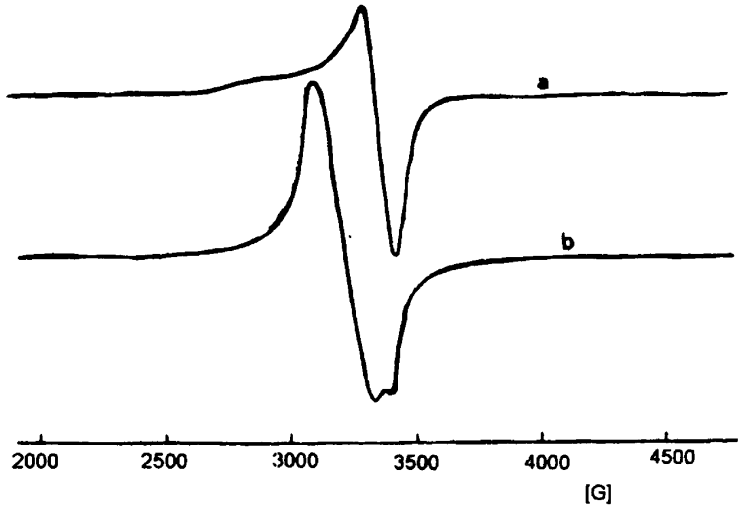

Fig. 6. EPR powder spectra of (a) $Cu(NO_3)_2(DLM)\cdot 3H_2O$ and (b) $[CuCl_2(DLMD)(H_2O)]\cdot H_2O$.

ure 7b) to the Curie–Weiss' law ($C = 0.425(5)$ cgsu·K·mol^{-1}, $\theta = 12(3)$ K, $r = 0.9987$) clearly corroborate the existence of monomeric magnetically diluted units [44], as it has been shown from X-ray diffraction studies. Also, the EPR spectrum (Figure 6b) — axial, $g_{\perp} = 2.05$ and $g_{\parallel}$ not observed — may be explained on the basis of the existence of a trigonal bipyramid [43].

CONCLUSIONS

About the structure of the complexes which have not been studied by X-ray diffraction, the following suggestions could be made. The spectral and thermal data of $Cu(NO_3)_2(DLM)\cdot 3H_2O$ complex allow us to propose a structure based in roughly square-planar $[Cu(DLM)(H_2O)_2]^{2+}$ cations, free nitrate anions and

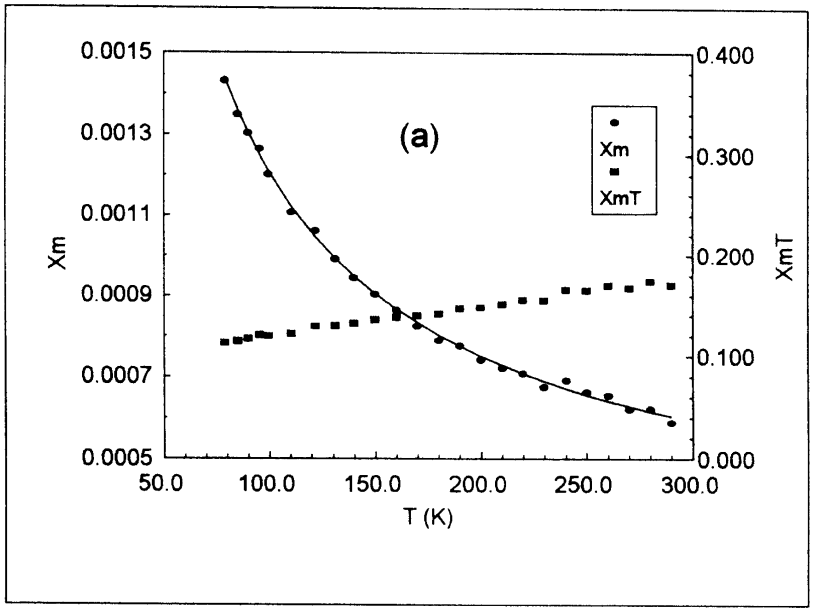

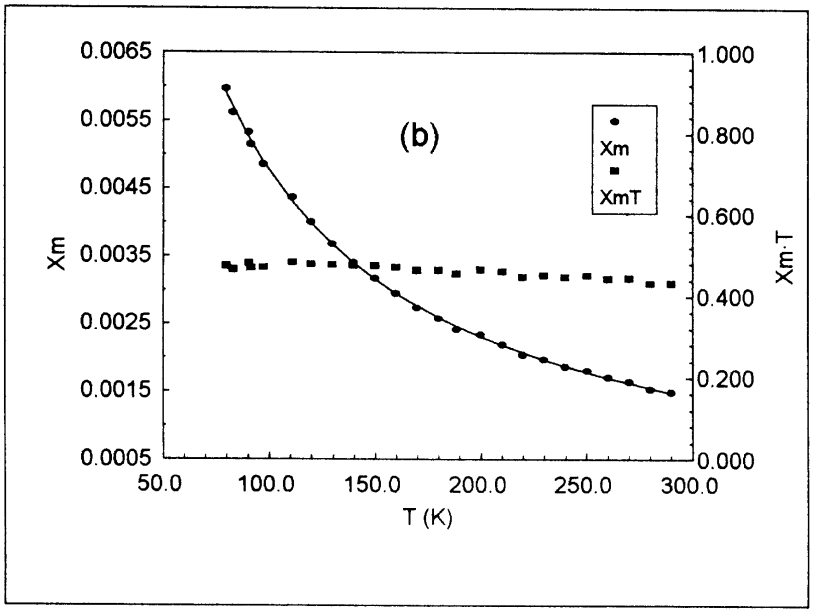

Fig. 7. Magnetic susceptibility values at different temperatures of (a) $Cu(NO_3)_2(DLM)\cdot 3H_2O$ and (b) $[CuCl_2(DLMD)(H_2O)]\cdot H_2O$.

one water molecule only linked by hydrogen bonds, which justifies the existence of two types of water molecules and the possibility of antiferromagnetic interactions between the square-planar Cu(II) units. For the $Cd(NO_3)_2(DLM)\cdot 2H_2O$ complex, an eight-coordinate structure designed by bidentate O,O′–nitrate and N5,O4–DLM ligands and two water molecules may be proposed; this structure is very related with the one reported for the $[Cd(NO_3)_2(DLMD)_2]$ complex [30]. The structure of the $HgCl_2(DLM)$ may be very similar to that found for its analogous DLMD compound. Finally, the two Pd(II) and Pt(II) studied complexes seem to be a *cis*–MCl_2(N5,O4–DLM) structure.

Supplementary material—For each reported structure, a list of structure factors and tables with atomic coordinates and isotropic thermal parameters for non-H atoms, bond, lengths and angles, anisotropic temperature factors for non-H atoms, hydrogen atom coordinates, equations of planes and dihedral angles (40 pages) are available.

REFERENCES

1. Bessenbacher, C. and Vogler, C., Kaim, W., *Inorg. Chem.*, 1989, **28,** 4645.
2. Bessenbacher, C. and Kaim, W., *Z. Anorg. Allg. Chem.*, 1989, **577,** 39.
3. Burgmayer, S. J. N., Baruch, A. and Kerr, K., Yoon, K., *J. Am. Chem. Soc.*, 1989, **111,** 4982.
4. Clarke, M. J., Dowling, M. G., Garafalo, A. R. and Brennan, T. F., *J. Am. Chem. Soc.*, 1979, **101,** 223.
5. Clarke, M. J., Dowling, M. G., Garafalo, A. R. and Brennan, T. F., *J. Biol. Chem.*, 1980, **255,** 3472.
6. Yu, M. W., Fritchie, C. J. Jr., *J. Biol. Chem.*, 1975, **250,** 946.
7. Benno, R. H., Fritchie, C. J. Jr., *Acta Cryst.*, 1973, **B29,** 2493.
8. Garland, W. T. Jr., Fritchie, C. J. Jr., *J. Biol. Chem.*, 1974, **249,** 2228.
9. Kierkegaard, P., Leijonmarck, M. and Werner, P. E., *Acta Chem. Scand.*, 1972, **26,** 2980.
10. Fischer, B., Schmalle, H., Dubler, E., Schafer, A. and Viscontini, M., *Inorg. Chem.*, 1995, **34,** 5726.
11. Hornung, F. M. and Kaim, W., *J. Chem. Soc. Faraday Trans.*, 1994, **90,** 2909.
12. Schwederski, B. and Kaim, W., *Inorg. Chim. Acta*, 1992, **195,** 123.
13. Fischer, B., Strahle, J. and Viscontini, M., *Helv. Chim. Acta*, 1991, **74,** 1544.
14. Mitsumi, M., Toyoda, J. and Nakasuji, K., *Inorg. Chem.*, 1995, **34,** 3367.
15. Nakasuji, K., Sugiura, K., Kitagawa, T., Toyoda, J., Okamoto, H., Okamura, K., Yamamoto, H., Murara, I., Kawamoto, A. and Tanaka, J., *J. Am. Chem. Soc.*, 1991, **113,** 1862.
16. Mirani, T., Saito, G. and Uruyama, H., *Phys. Rev. Lett.*, 1988, **60,** 2299.
17. Burgmayer, J. N. and Stiefel, E. I., *J. Am. Chem. Soc.*, 1986, **108,** 8310.
18. Burgmayer, J. N. and Stiefel, E. I., *Inorg. Chem.*, 1988, **27,** 4059.
19. Perkinson, J., Brodie, S., Keum, Y., Mosny, K., Carroll, P. J., Morgan, T. V. and Burgmayer, S. J. N., *Inorg. Chem.*, 1991, **30,** 719.
20. Odani, A., Masuda, H., Inukai, K. and Yamauchi, O., *J. Am. Chem. Soc.*, 1992, **114,** 6294.
21. Kohzuma, T., Masuda, H. and Yamauchi, O., *J. Am. Chem. Soc.*, 1989, **111,** 3431.
22. Heilmann, O., Hausen, H. D. and Kaim, W., *Z. Naturforsch.*, 1994, **49B,** 1554.
23. Nasir, M. S., Karlin, K. D., Chen, Q. and Zubieta, J., *J. Am. Chem. Soc.*, 1992, **114,** 2264.
24. Abelleira, A., Galang, R. D. and Clarke, M. J., *Inorg. Chem.*, 1990, **29,** 633.
25. Black, K. J., Huang, H., High, S., Starks, L., Olson, M. and Mcguire, M. E., *Inorg. Chem.*, 1993, **32,** 5591.
26. Mitsumi, M., Toyoda, J., Nakasuji, K., Kanehisa, N. and Kai, Y., *Mol. Cryst. Liq. Cryst.*, 1996, **276,** 229.
27. Heilmann, O., Hornung, F. M., Kaim, W. and Fiedler, J., *J. Chem. Soc. Faraday Trans.*, 1996, **92,** 4233.
28. Hueso-Ureña, F., Jiménez-Pulido, S. B., Moreno-Carretero, M. N., Quirós-Olozábal, M., Salas-Peregrín, J. M., *Polyhedron*, 1997, **16,** 607.
29. Hueso-Ureña, F., Jiménez-Pulido, S. B., Moreno-Carretero, M. N., Quirós-Olozábal, M., Salas-Peregrín, J. M., *Inorg. Chim. Acta*, 1998, **268,** 77.
30. Hueso-Ureña, F., Jiménez-Pulido, S. B., Moreno-Carretero, M. N., Quirós-Olozábal, M. and Salas-Peregrín, J. M., *Inorg. Chim. Acta*, 1998, **277,** 103.
31. Hueso-Ureña, F., Jiménez-Pulido, S. B., Moreno-Carretero, M. N., Quirós-Olozábal, M. and Salas-Peregrín, J. M., submitted.
32. Kepert, D. L., *Inorganic Stereochemistry*, Springer-Verlag, Berlin, 1982.
33. Hueso-Ureña, F., Jiménez-Pulido, S. B., and Moreno-Carretero, M. N., unpublished results.
34. Galy, J., Bonnet, J. and Andersson, S., *Acta Chem. Scand.*, 1979, **A33,** 383.
35. Muetterties, E. L. and Guggenberger, L. J., *J. Am. Chem. Soc.*, 1974, **96,** 1748.
36. Wells, A. F., *Structural Inorganic Chemistry*, 5th ed., Oxford University Press, Oxford 1984.
37. Titze, C. and Kaim, W., Zalis, S., *Inorg. Chem.*, 1997, **36,** 2505.
38. Baker, L. J., Bowmaker, G. A., Hendrickson, N. J., Skelton, B. W. and White, A. H., *J. Chem. Soc. Dalton Trans.*, 1992, p. 2601.
39. Geary, W. J., *Coord. Chem. Rev.*, 1971, **7,** 81.
40. Nakamoto, K., *Infrared and Raman Spectra of Inorganic and Coordination Compounds*, 4th ed., Wiley & Sons, New York, 1986.
41. Ferraro, J. R., *Low-Frequency Vibrations of Inorganic and Coordination Compounds*, Plenum Press, New York, 1971.
42. Pilbrow, J. R., *Transition Ion Electron Paramagnetic Resonance*, Oxford Science Publications, Oxford, 1990.
43. Hathaway, B. J. and Billing, D. E., *Coord. Chem. Rev.*, 1970, **5,** 143.
44. Carlin, R. L., *Magnetochemistry*, Springer-Verlag, Berlin, 1986.

Pergamon

PII: S0277–5387(98)00123–5

Polyhedron Vol. 17, No. 19, pp. 3419–3426, 1998
© 1998 Elsevier Science Ltd
All rights reserved. Printed in Great Britain
0277–5387/98 $19.00 + 0.00

Spectroscopic properties, structure and reactivity of $[WCl(SnCl_3)(CO)_3(NCMe)_2]$

Teresa Szymańska-Buzar* and Tadeusz Głowiak

Faculty of Chemistry, University of Wrocław, 14 F.Joliot-Curie, 50-383 Wrocław, Poland

(Received 13 February 1998; accepted 25 March 1998)

Abstract—A series of seven-coordinate tungsten(II) nitrile complexes of the type $[WCl(SnCl_3)(CO)_3(NCR)_2]$(**1**–**4**), R=Me, Et, *n*-Bu, Ph, has been synthesized. These new complexes have been characterized by IR, NMR and UV-vis spectroscopy. In addition single-crystal X-ray diffraction was used to structurally characterize $[WCl(SnCl_3)(CO)_3(NCMe)_2]$(**1**). The most prominent feature of complex **1** is the facility by which acetonitrile and carbonyl ligands can be replaced by other ligands. Complexes were isolated in which CO and acetonitrile ligands were substituted by alkyne ligands. The alkyne tungsten(II) complexes **5**–**8** formed were structurally characterized by IR and NMR spectroscopy. The complex **1** has been found to be an active catalyst for the polymerization of phenylacetylene. The structures and mechanisms of the formation of various new types of complexes and their role in the catalytic process are discussed. © 1998 Elsevier Science Ltd. All rights reserved

Keywords: tungsten; tin; crystal structure; nitrile complexes; alkyne complexes; polymerization of phenylacetylene.

A number of seven-coordinated compounds with a tungsten-tin or a molybdenum-tin bond have been prepared by reaction of tungsten- and molybdenum-substituted carbonyls, $[M(CO)_4L_2]$ (2L = 2,2′-bipyridyl, 2,5-dithiahexane, 1,2-bis(diphenylphosphino)ethane, RN=CHCH=NR, R = *i*-Pr, *n*-Bu or Cy, two molecules of acetonitrile) and tin tetrahalides or organometallic halides, R_nSnCl_{4-n}, R=Me, Bu, Ph [1–10]. Among them acetonitrile compounds are especially interesting as useful starting materials in which the labile acetonitrile groups can be easily replaced by other ligands [10–17]. This can be the basis for synthetic procedures, including the preparation of alkene and alkyne derivatives as well as a model of a catalytic centre. In the reaction of $[WCl(SnCl_3)(CO)_3(NCMe)_2]$(**1**) with norbornadiene two acetonitrile ligands are replaced by one molecule of norbornadiene and $[WCl(SnCl_3)(CO)_3(\eta^4\text{-NBD})]$ is formed [17]. In this paper we present results concerning the reactivity of complex **1** towards alkynes. Complexes were isolated in which CO and acetonitrile ligands were replaced by alkyne ligands. The complex **1** has been found to be an active catalyst for the polymerization of phenylacetylene.

The unknown coordination geometry of acetonitrile compound **1** together with the fact that compounds of this class have been used for synthetic purpose on several occasions [10–17], make it an interesting problem for X-ray structure analysis.

EXPERIMENTAL

All operations were carried out in an inert atmosphere using standard Schlenk techniques. All solvents and liquid reagents were dried and distilled over CaH_2. IR spectra (KBr pellets) were recorded on an FT-IR Model-400 Nicolet instrument and Far-IR spectra (500–50 cm^{-1}) were recorded with a Brücker IFSv instrument in Nujol mull on a polyethylene film. ^1H and $^{13}C\{^1H\}$ NMR spectra were run using a Bruker AMX-300 spectrometer. UV-visible absorption spectra were recorded on a Hewlett–Packard 8452A spectrophotometer. The analysis of the catalytic reaction products was performed on a Hewlett–Packard GC-MS system and by ^1H NMR spectroscopy.

Synthesis of $[WCl(SnCl_3)(CO)_3(NCMe)_2]$(**1**)

To $[W(CO)_4(NCMe)_2]$ [18] (1.8 g, 4.7 mmol) dissolved in CH_2Cl_2 (50 cm^3) with continuous stirring

* Author to whom correspondence should be addressed.

under a stream of nitrogen, was added a stoichiometric amount of $SnCl_4$ (0.56 cm^3, 4.7 mmol) by means of a syringe. The mixture was stirred for 6 hours, during which time the yellow solution gradually changed to an orange colour, while the ν(CO) frequency of $[W(CO)_4(NCMe)_2]$ disappeared. After the completion of the reaction, the solution was separated from some insoluble blue powder by filtration and evaporated to dryness. The crystallization from CH_2Cl_2/heptane produced the analytically pure dark orange crystalline complex **1** (Table 1).

Preparation of $[WCl(SnCl_3)(CO)_3(NCR)_2]$, **2** (R=$C_2H_5$); **3** (R=$C_3H_7$); **4** (R=$C_6H_5$).

1 was dissolved in an appropriate nitrile and the solution was stirred for 60 min. Filtration, followed by removal of the solvent *in vacuo*, gave a residue coloured from orange **2** to red **4**, which was recrystallized from CH_2Cl_2-heptane giving a pure crystalline bis(nitrile) complex **2**-**4** (Table 1).

Reaction of **1** *with PhC≡CPh*

To a solution of **1** (0.2 g, 0.33 mmol) in 15 cm^3 of CH_2Cl_2 was added PhC≡CPh (0.12 g, 0.66 mmol) in 5 cm^3 of CH_2Cl_2. The mixture was stirred for two hours, after which time the full conversion of **1** was observed by IR. Evaporation of the solvent followed by washing with heptane produced a mixture of compounds identified by IR and NMR studies as $[WCl_2(CO)(NCMe)(PhC{\equiv}CPh)_2]$ **5**, and $[WCl_2(NCMe)_2(PhC{\equiv}CPh)_2]$ **6** (Table 2). Crystallization of the above greenish-yellow solid from CH_2Cl_2/heptane always produced mixture of the compounds **5** and **6**, but with different molar ratios depending on reaction time. Beside **5** and **6**, a side products were formed. One was identified by IR: ν(CO) 2069 (vw), 1939 (vs) and ^{13}C NMR: δ 202.47 (1 CO), 196.54 (4 CO) ppm as $[W(CO)_5SnCl_2]$ and other was separated by filtration as white, insoluble in CH_2Cl_2 solid of $SnCl_2$.

Reaction of **1** *with phenylacetylene* (*PA*)

A slight excess of PA (0.125 cm^3, 1.18 mmol) was syringed into a stirred CH_2Cl_2 solution (15 cm^3) of **1** (0.2 g, 0.33 mmol) at room temperature. Immediately the solution became dark orange. Stirring for 2 hours followed by the evaporation of the solvent under low pressure gave an orange solid, which was washed out with a small portion of heptane and dried *in vacuo* to give a greenish yellow mixture of compounds containing mainly $[WCl_2(CO)(NCMe)(PhC{\equiv}CH)_2]$ **7** and $[WCl_2(NCMe)_2(PhC{\equiv}CH)_2]$ **8** as was shown by ^1H and $^{13}C\{^1H\}$ NMR spectra (Table 2). The heptane extract contained organic products: 1,2,4-triphenylbenzene (41%), 1,3,5-triphenylbenzene (39%), different isomers of diphenylbutadienes (19%), and a dimer of PA detected by MS as 1*H*-indene-1-(phenylmethylene) (1%).

Procedures for testing catalytic activity and characterization of organic products

Polymerization experiments were carried out in a reaction mixture composed of toluene or CH_2Cl_2 as solvent, *ortho*-xylene (the internal chromatographic standard), phenylacetylene (PA)(1 mol dm^{-3}), and complex **1**(PA/W 100). The reaction mixture was stirred by a magnetic stirrer at room temperature in a 50 cm^3 glass reactor provided with a septum through which liquid reactants were introduced and removed by a syringe. The gas-samples were removed with a syringe and injected into the PORA PLOT-Q 15 m column of the chromatograph fitted with a flame ionization detector. The conversion of PA, monitored by chromatography, was not higher than 10% after 24 h reaction. For the analysis of PA reaction products, reactions were continued for 24 h and then methanol was added. The polymer (PPA) was collected, washed with methanol, dried and weighed. The polymerization yield (%) is defined by comparing the polymer weight to the weight of the PA used and 24 h reaction catalyzed by **1** was about 7%. The polymer was analysed by ^1H NMR, IR spectroscopy and gel-permeation chromatography. Molecular weights of the PPA were measured using $CHCl_3$ solutions, a refractive index monitor and a Plgel 10 m MIXED-B column. The value recorded ($M_w = 5 \times 10^3$) is the weight of polystyrene that would exhibit the chromatogram observed.

The filtrate obtained after the precipitation of the polymers was evaporated to dryness and the CH_2Cl_2 solution of the residue was investigated by GC-MS (HP5 25 m column). Analysis showed 1,2,4-triphenylbenzene (45%), 1,3,5-triphenylbenzene (34%), different isomers of diphenylbutadienes (16%), and a dimer of PA detected by MS as 1*H*-indene-1-(phenylmethylene) (5%).

^1H NMR spectra of the polymers were recorded in a $CDCl_3$ solution at 300 MHz. The microstructural details of the polymers were deduced from the ^1H NMR integrals [19] as mainly *trans*.

Crystallography

Crystal data for **1**. $C_7H_6Cl_4N_2O_3SnW$, $M = 610.48$, monoclinic, space group $P2_1/m$, $a = 6.803(1)$, $b = 13.669(3)$, $c = 8.640(2)$ Å, $\beta = 102.68(3)^\circ$, $U = 783.9(3)$ $Å^3$, $Z = 2$, $D_c = 2.586$ g cm^{-3}, $F(000) = 556$, μ(Mo-Kα) = 96.04 cm^{-1}. The dark orange crystals of **1** were grown from a CH_2Cl_2/toluene/heptane solution. The crystals were stable enough when handled in an inert atmosphere or coated with a light hydrocarbon oil to protect them from the atmosphere. Crystallographic data were

Table 1. Spectroscopic data for the seven-coordinate nitrile complexes [WCl(SnCl$_3$)(CO)$_3$(NCR)$_2$] **1**–**4**; R=CH$_3$ (**1**), C$_2$H$_5$ (**2**), C$_3$H$_7$ (**3**), C$_6$H$_5$ (**4**)

Complex	IR(ν, cm^{-1})			^{1}H NMR	^{13}C{^{1}H} NMR	UV-vis, λ, nm
	ν(CO)[a]	ν(CN)[a]	ν(SnCl)[b]	(δ, ppm; J, Hz)	(δ, ppm; J, Hz)	(ϵ, dm^3 mol^{-1} cm^{-1}
1	2030 (vs) 1935 (s,sh) 1903 (vs)	2327 (w) 2299 (w)	344 (w) 325 (w)	2.53 (s, 2 CH_3CN)[c]	211.93 (s, 3 CO), 126.80 (s, 2 CH$_3$*C*N), 4.54 (s, 2 CH_3CN)[c]	250 (9386), 290 (4225), 398 (464)[d]
2	2022 (vs) 1936 (s,sh) 1907 (vs)	2293 (m)		2.82 (q, J_{HH}=7.5, 2 CH$_3$CH_2CN) 1.46 (t, J_{HH}=7.5, 2 CH_3CH$_2$CN)[e]	211.01 (s, 3 CO), 129.47 (s, 2 CH$_3$CH$_2$*C*N), 12.75 (s, 2 CH$_3$*C*H$_2$CN), 9.45 (s, 2 *C*H$_3$CH$_2$CN)[e]	
3	2021 (s) 1940 (s,sh) 1915 (vs)	2292 (m)		2.80 (t, J_{HH}=7.0, 2 CH$_3$CH$_2$CH_2CN) 1.89 (q, J_{HH}=7.5, 2 CH$_3$CH_2CH$_2$CN) 1.14 (t, J_{HH}=7.5, 2 CH_3CH$_2$CH$_2$CN)[e]	211.27 (s, 3 CO, J_{WC}=125, $^2J_{117Sn-13C}$=261, $^2J_{119Sn-13C}$=277) 128.94 (s, 2 CH$_3$CH$_2$*C*H$_2$CN), 20.49 (s, 2 CH$_3$CH$_2$*C*H$_2$CN), 18.60 (s, 2 CH$_3$*C*H$_2$CH$_2$CN), 13.48 (s, 2 CH_3CH$_2$CH$_2$CN)[e]	
4	2026 (s) 1945 (s) 1912 (s)	2263 (m)		7.86 (d, *o*-Ph, J=7.3) 7.78 (t, *p*-Ph, J=7.7) 7.59 (t, *m*-Ph, J=7.8)[e]	211.09 (s, 3 CO, $^1J_{WC}$=127, $^2J_{117Sn-13C}$=267, $^2J_{119Sn-13C}$=280) 135.98 (s, C$_p$–Ph) 133.61 (s, C$_o$–Ph) 129.84 (s, C$_m$–Ph) 129.05 (s, C$_i$–Ph) 126.93 (s, 2 Ph*C*N),[e]	

[a] Spectra recorded in KBr plates. [b] Spectra recorded in Nujol mull on a polyethylene film. [c] Spectra recorded in CD_2Cl_2 at 293 K. [d] Spectra recorded in CH_2Cl_2. [e] Spectra recorded w $CDCl_3$ at 293 K.

Table 2. Selected IR and NMR data for tungsten (II) alkyne complexes **5**–**8**

Complex	IR(ν, cm^{-1})[a]		^{1}H NMR[b]	^{13}C{^{1}H} NMR[b]
	ν(CO)	ν(CN)	(δ, ppm; J, Hz)	(δ, ppm; J, Hz)
[WCl$_2$(CO)(NCMe)(PhC≡CPh)$_2$] (**5**)	2088 (s)	2329 (w) 2298 (vw)	2.42 (s, CH_3CN)	200.73 (s, 1 CO), 176.18 (s, 2 Ph*C*≡CPh), 167.22 (s, 2 PhC≡*C*Ph), 140.44 (s, 2 C$_i$–Ph), 139.48 (s, 2 C$_i$–Ph), 126.96 (s, 1 CH$_3$*C*N), 5.17 (s, 1 *C*H$_3$CN)
[WCl$_2$(NCMe)$_2$(PhC≡CPh)$_2$] (**6**)	—	2327 (w) 2299 (vw)	2.39 (s, 2 CH_3CN)	195.96 (s, 2 Ph*C*≡CPh), 189.26 (s, 2 PhC≡*C*Ph), 138.63 (s, 2 C$_i$–Ph), 137.85, (s, 2 C$_i$–Ph), 127.63 (s, 2 CH$_3$*C*N), 5.56 (s, 2 *C*H$_3$CN)
[WCl$_2$(CO)(NCMe)(PhC≡CH)$_2$] (**7**)	2089 (s)	2329 (w) 2292 (vw)	2.55 (s, 1 CH_3CN) 11.90, (s, 2 PhC≡C*H*)	196.24 (s, 1 CO), 183.63 (s, 2 PhC≡*C*H), 176.73 (s, 2 Ph*C*≡CH), 137.04 (s, 2 C$_i$–Ph), 4.82 (s, 1 *C*H$_3$CN)
[WCl$_2$(NCMe)$_2$(PhC≡CH)$_2$] (**8**)	—	2326 (w) 2300 (vw)	2.42 (s, 2 CH_3CN) 11.61,11.55 (s, 2 PhC≡C*H*)	196.64 (s, 2 PhC≡*C*H), 188.50 (s, 2 Ph*C*≡CH), 136.44 (s, 2 C$_i$–Ph), 5.22 (s, 2 *C*H$_3$CN)

[a] Spectra recorded in KBr disc. [b] Spectra recorded w $CDCl_3$ at 293 K.

obtained for a crystal approximately $0.10 \times 0.10 \times 0.15$ mm using a KM4 κ-axis computer-controlled [20] four-circle diffractometer operating in the ω-2θ scan mode. All measurements were made using graphite-monochromated Mo Kα radiation ($\lambda = 0.71069$ Å) at 293 (3) K. The accurate cell dimensions and the crystal orientation matrix were determined by a least-squares refinement of the setting angles of 30 carefully centred reflections in the range $20.6^\circ < 2\theta < 37.3^\circ$. A total of 2114 unique reflections were measured, of which 1995 (137 variables) with $I \geq 4\sigma(I)$ in the range 5 to 70° were used to solve and refine the structure in the monoclinic space group $P2_1/m$. A surprisingly high R value ($R_1 = 0.0791$, $wR_2 = 0.1981$) was obtained after first refinement. A difference synthesis at this stage revealed two regions of significant electron density (11.2, 8.0, e/Å^3) located at approximately 0.5 Å from both sides of W(1), Sn(1) and Cl(1) atoms. During refinement the molecule was found to be disordered between three adjacent positions with occupancy factor 0.76, 0.12 and 0.12 for W(1), Sn(1), Cl(1). Further refinement of this three site model gave a final R_1 value of 0.0560 ($wR_2 = 0.1546$). The largest peak in the final difference map was 2.86 e/Å^3. Goodness-of-fit was 1.130. The structure was given a weighting scheme in the form $w = 1/[\sigma^2(F_0^2) + (0.0278P)^2 + 0.0000P]$, where $P = (F_0^2 + 2F_c^2)/3$.

The structure was solved by the heavy-atom method with the SHELXS-86 program [21] and refined by a full-matrix least-squares method, using the SHELXL-93 program [22]. Neutral atomic scattering factors were taken from the SHELXL-93 program [22]. The positions of C-bonded H atoms were calculated assuming typical stereochemistry and three atoms were refined with fixed positions at 0.96 Å from the C atoms to which they were bonded.

The remaining dimensions, positional parameters and equivalent isotropic thermal parameters and anisotropic thermal parameters are deposited in supplementary material.

RESULTS AND DISCUSSION

In 1995 we reported [23] that a photochemical reaction of $W(CO)_6$ with $SnCl_4$ led to the formation of an orange crystalline air-sensitive complex. This was structurally identified by single-crystal X-ray crystallography as the first example of a dinuclear halogenocarbonyl complex of tungsten(II) with a W–Sn bond. When this product is dissolved in toluene and acetonitrile added, an equimolecular mixture of $[WCl(SnCl_3)(CO)_3(NCMe)_2]$(**1**) and $[WCl_2(CO)_3(NCMe)_2]$ is formed immediately [24]. Recrystallization of the mixture from CH_2Cl_2/toluene/heptane produces quite stable orange crystals of **1** while considerable less stable $[WCl_2(CO)_3(NCMe)_2]$ decomposes with loss of carbon monoxide and formation of deep blue, insoluble solid in methylene chloride, most probably the chloro-bridged dimer.

Another method which proved useful in obtaining the compound **1** was the oxidative-addition reaction of $[W(CO)_4(NCMe_2]$ with $SnCl_4$ in dichloromethane. Baker and Bury briefly mentioned the formation of mixture of compounds containing **1** by reaction of $[W(CO)_3(NCMe)_3]$ with $SnCl_4$ in acetonitrile, but without synthetic and spectroscopic details for **1** [10].

The compounds **2**–**4** containing nitriles with a longer carbon chain, were prepared in the reaction of **1** with an appropriate nitrile at room temperature. The compounds **1**–**4** are very soluble in nitriles and in acetone, less soluble in chlorinated solvents (CH_2Cl_2, $CHCl_3$) but insoluble in hydrocarbon solvents. They are air-sensitive in solution but in the solid state it can be stored under nitrogen for a month without decomposition.

Structure of **1**

The molecule $[WCl(SnCl_3)(CO)_3(NCMe)_2]$(**1**), is shown in Fig. 1 together with the atomic numering scheme Selected interatomic bond distances and angles are presented in Table 3.

The environment of the tungsten atom is an almost ideal capped octahedron with the tin atom occupying the unique capping position above an octahedral face defined by the bridging chlorine and two crystallographically equivalent carbonyl groups. The octahedral face that is capped by the $SnCl_3$ group is distorted to allow a close approach of the tin atom. The angles subtended at the tungsten atom by the three atoms determining the capped face are in the range 107.7(8)–108.2(4)°; compared with the opposite face, determined by C(2), N(1) and N(1)^i, where the angles are in the range 80.0(7)–93.3(5)°. Thus, there is a distortion of octahedral symmetry in order to accommodate the tin atom.

In addition one may notice that the molecule of **1** is remarkable in its symmetry. The crystallographic plane of symmetry extends through W, Sn, Cl(1) and

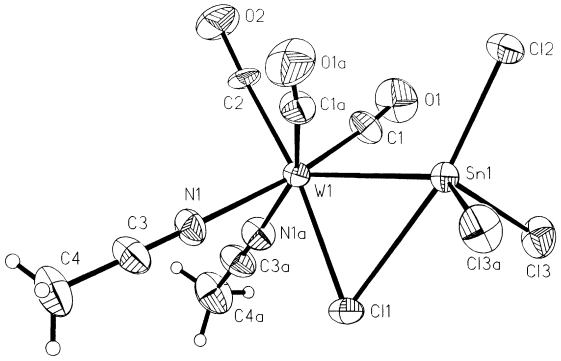

Fig. 1. Molecular geometry of $[WCl(SnCl_3)(CO)_3(NCMe)_2]$(**1**).

Table 3. Selected bond lengths (Å) and angles (°) with e.s.d.s in parentheses for **1**

W(1)–Sn(1)	2.710(1)	W(1)–C(1)	1.997(13)
W(1)–Cl(1)	2.511(5)	Sn(1)–Cl(1)	2.840(5)
W(1)–N(1)	2.18(1)	Sn(1)–Cl(2)	2.333(4)
W(1)–C(2)	2.00(2)	Sn(1)–Cl(3)	2.344(5)
C(1)–W(1)–C(2)	76.6(6)	Sn(1)–W(1)–C(2)	123.1(6)
C(2)–W(1)–N(1)	93.3(5)	Sn(1)–W(1)–C(1)	70.8(4)
C(2)–W(1)–Cl(1)	171.1(6)	Cl(3)–Sn(1)–Cl(3)^{i}	101.3(3)
C(1)–W(1)–C(1)^{i}	107.7(8)	Cl(3)–Sn(1)–Cl(2)	97.9(1)
Cl(1)–W(1)–C(1)	108.2(4)	Cl(1)–Sn(1)–Cl(3)	89.5(1)
Cl(1)–W(1)–N(1)	80.0(3)	Cl(1)–Sn(1)–Cl(2)	168.4(2)
N(1)–W(1)–N(1)^{i}	80.0(7)	Cl(1)–Sn(1)–W(1)	53.7(1)
N(1)–W(1)–C(1)	161.2(5)	W(1)–Sn(1)–Cl(2)	114.6(2)
N(1)i–W(1)–C(1)	84.8(5)	W(1)–Sn(1)–Cl(3)	120.4(1)
Sn(1)–W(1)–Cl(1)	65.8(1)	W(1)–Cl(1)–Sn(1)	60.5(1)
Sn(1)–W(1)–N(1)	127.5(3)		

Symmetry elements represented by i: x, 0.5-y, z.

Cl(2). In such an arrangement two acetonitrile ligands are crystallographically equivalent and effectively *cis* with N(1)–W–N(1)^{i} angle 80.0(7)° and the W–N distances identical (2.18(1) Å). Two CO groups in the capped face are mutually *cis* with C(1)–W–C(1)^{i} angle 107.7(8)° and the same W–C distance 2.00(1) Å. The angles between carbonyl groups in the capped and uncapped face are smaller with 76.6(6)° for C(2)–W–C(1) angle.

The W–N–C angle is 178(1)° to evidence that the nitrile ligand is coordinated in an almost linear manner. The C–N lengths of 1.13(2) Å are not significant but are shorter than C–N distance of 1.155 Å observed in free CH_3CN [25]. Comparison of bond length for **1** and tungsten(0) complex, reveals that the W–N distance is shorter in **1**, being 2.18(1) Å *vs.* 2.21 Å(av) in $[W(CO)_3(NCMe)_3]$ [26], while the tungsten-carbonyls distances in **1** are about 0.07 Å longer, being 2.00 Å (av) *vs.* 1.93 Å (av) in tungsten(0) complex. This correlates qualitatively with the expected lower electron density and π-donor ability of the tungsten in the higher oxidation state.

The tungsten atom is seven-coordinate and tin atom is five-coordinate, with one chlorine atom occupying a bridging position between the two metal atoms. The tungsten-tin bond is short at 2.710(1) Å compared to the sum of the relevant covalent radii of 2.97 Å [27, 28]. The W–Sn distances of 2.759(3) [4], 2.731(1) [18], 2.711(1) [29] and 2.737(1) [29] Å have been observed previously. In view of the established π-acceptor properties of the $[SnCl_3]^-$ group it seems probable that the bond does possess some double-bond character [30]. The tin to bridging chlorine distance is 2.840(5) Å, being considerably longer than the other tin-chlorine distances, which are average 2.34 Å, indicates that this bond is much weaker than a tin-chlorine single bond. The tungsten to bridging chlorine distance is 2.511(5) Å and indicates that the bridging chlorine forms a stronger bond with the tungsten while the Sn–Cl bond is weakened. The angle of 60.5(1)° subtended at the chlorine by the tungsten-tin bond agrees with the value 59.9(2)° for bridging chlorine in $[WCl(MeSnCl_2)(CO)_3(C_4H_{10}S_2)]$ [4], 60.5(1)° in $[MoCl(SnCl_3)(CO)_3(C_4H_{10}S_2)](CH_2Cl_2)$ [6] and 61.6(1)° in $[MoCl(MeSnCl_2)(CO)_3(C_{10}H_8N_2)]$ [3]. The form of the tungsten atom coordination in **1** is indeed very similar to the monocapped octahedral geometries observed earlier in W–Sn or Mo–Sn compounds [3, 4, 6]. A common feature of those structures is the presence of a tin atom in the unique capping position and a chlorine atom bridging the W–Sn or Mo–Sn bond.

The tin atom in **1** is five-coordinate with a geometry that is best described as trigonal bipyramidal with the two chlorine atoms occupying the axial sites. The $WSnCl_2$ unit is nearly planar with the tin atom only 0.605(3) Å out of the W–Cl(1)–Cl(2) plane. The Cl(1)–Sn–Cl(3) and Cl(1)–Sn–Cl(3)^{i} angles are identical (89.5(1)°) as are the W–Sn–Cl(3) and W–Sn–Cl(3)^{i} angles (120.4(1)°). However, the Cl(1)–Sn–Cl(2) angle is 168.4(2)°, and the Cl(1)–Sn–W angle is much smaller than 90°, at 53.7(1)°; so the trigonal bipyramid is significantly distorted.

Similar capped octahedral geometry with two crystallographically equivalent nitrile and carbonyl groups seen in **1** has been detected for $[WI_2(CO)_3(NCR)_2]$, R=Me, Et [31]. However, those complexes contain a carbonyl ligand in the unique capping position and two mutually *trans* iodine ligands.

The molecular structure of the recently investigated $[WCl(SnCl_3)(CO)_3(\eta^4\text{-NBD})]$ [17] is best described as a capped trigonal prism with the tin atom lying above a square face formed by the chlorine atom and three carbonyl groups. Unlike the situation in other W–Sn compounds in $[WCl(SnCl_3)(CO)_3(\eta^4\text{-NBD})]$ the chlorine attached to the tungsten does not bridge the W–

Sn bond. The W–Cl bond length is much shorter at 2.454(2) Å and W–Sn distance longer at 2.764(1) Å than in other W–Sn or Mo–Sn compounds [3, 4, 6].

Spectroscopic studies of nitrile compounds **1**–**4**

The carbonyl region of the infrared spectra of the compounds **1**–**4** in KBr are almost identical in showing three carbonyl bands (Table 1). The infrared spectrum of compound **1** shows three carbonyl bands at ν(CO) 2030vs, 1935s(sh) and 1903vs cm^{-1} and is similar to that for the analogous molybdenum-tin complex obtained first time by Baker and Bury, (ν(CO) 2026s, 1939s and 1912vs cm^{-1} [10]) but qualitatively different from that reported by Baker and Bury for the tungsten compound (ν(CO) 2017, 1978 and 1934 cm^{-1} [10]). As noted by Baker and Bury their tungsten complex was extremely unstable to exposure to air and could not be isolated in a pure state. This is marked contrast to the quite good stability of the complex obtained by us. However, IR spectra of **1** in a dichloromethane solution shows more than three bands in the carbonyl stretching region: 2040 (s), 2020 (s), 1970 (m) and 1930 (vs) cm^{-1}. The spectral differences correspond to different coordination geometries, and in a dichloromethane solution distinct isomers of **1** may co-exist, as was proposed previously by Kummer and Graham [1]. In the ν(C≡N) region of the IR spectra for **1** two bands are observed. One is the ν(C≡N) band and the other a combination band resulting from the symmetrical CH_3 deformation and the C–C stretch which borrows its intensity from the ν(C≡N) [25]. For the compound **1** those bands are at 2320 and 2292 cm^{-1}, these are at higher frequencies than the ν(C≡N) band in the free acetonitrile observed at 2268 cm^{-1} [25]. The intensity ratio of the ν(C≡N) band to that of the combination band was found to differ greatly between *cis* and *trans* isomers [25]. Two sharp bands of comparable intensities in the ν(C≡N) region of **1** are consistent with *cis* acetonitrile ligands [25]. The ν(C≡N) frequencies of coordinated propionitrile and butyronitrile in **2** and **3** were observed as one band at 2292 cm^{-1}. The lower frequency region of the infrared spectrum is dominated by the principal absorptions at 344, 325 cm^{-1}, which can be regarded as ν_s and ν_{as} (Sn–Cl) vibration. This is in good agreement with increased frequencies of these bands upon coordination to metal or other ligand. Tin-halide frequencies of $[SnCl_3]^-$ ion were observed in, for example, $^1Et_4N[SnCl_3]$ at 295 (A_1) and 253 cm^{-1} (E) [32].

The similarity of the IR spectra in a solid state of the series of nitrile compounds obtained by us, shows that the most probable solid state structure for those compounds is the same as that of **1** (Fig. 1).

The ^1H and ^{13}C NMR spectra of the nitrile compounds **1**–**4** are very similar and are consistent with the solid-state structure of **1** (Fig. 1). The spectrum shows one carbonyl resonance from three equivalent CO groups and a single signal from each carbon of the two nitriles (Table 1).

The electronic spectrum of **1** is quite similar to those of the starting tungsten (II) compound [23] and shows one strong band at 250 nm with a shoulder at 290 nm which, because of its high intensity and its position is assigned to CT transition π^*(CO)←dπ(W). There is also another band at 398 nm. Because of its relatively low intensity it is assigned to a ligand-field transition.

Reaction of **1** *with alkynes*

When the reaction of **1** with two molecular equivalents of PhC≡CPh at room temperature in CH_2Cl_2 was monitored by IR, the substitution of the CO ligands by an alkyne can be observed. The ν(CO) bands for **1** decrease, while this of the alkyne complex at 2101 (s) appears. The ^1H, ^{13}C NMR and IR spectral data for the reaction product indicate that it is a mixture of two alkyne compounds (Table 2). One compound, with acetonitrile *trans* to CO ligand, two *cis* PhC≡CPh ligands and two *cis* anionic ligands (Cl^-) in the coordination sphere, can be formulated as $[WCl_2(CO)(NCMe)(PhC{\equiv}CPh)_2]$ **5**, which probably has a structure similar to that observed by Baker *et al.* for $[WI_2(CO)(MeCN)(MeC{\equiv}CMe)_2]$ [33]. The other alkyne compound does not contain CO in coordination sphere and can be formulated as $[WCl_2(NCMe)_2(PhC{\equiv}CPh)_2]$ **6**. Both compounds dimerize in solution, first with a loss of carbon monoxide and second with a loss of acetonitrile molecule to give probably the chloride-bridged dimer $[W(\mu\text{-}Cl)Cl(NCMe)(PhC{\equiv}CPh)_2]_2$. The dimeric compound is less soluble than monomeric and could not be characterized by ^{13}C NMR spectroscopy in solution. A similar dimerization process was observed by Baker *et al.* in their molybdenum(II) and tungsten(II) diiodide alkyne complexes [33, 34]. In ^{13}C NMR spectra of the reaction products two sets of carbon signals of coordinated PhC≡CPh for **5** and **6** are observed. However, after prolonged reaction time (24 h) ν(CO) band characteristic of alkyne complex **5** disappears and in the residue obtained after evaporation of solvent only compound **6** was identified by NMR. ^{13}C NMR spectra of **5** and **6** revealed acetylenic carbon resonances in the range from 196–167 ppm, as is typical for three-electron-donor alkynes. The white precipitate which appeared as the side product during the reaction of **1** with alkynes was identified as $SnCl_2$, what suggests that the $SnCl_3^-$ ligand undergoes hydrolysis to $SnCl_2$ and Cl^- in the presence of an alkyne.

In the reaction of **1** with two molecular equivalents of phenylacetylene, a mixture of alkyne complexes is formed. The monomeric compound $[WCl_2(CO)(MeCN)(PhC{\equiv}CH)_2]$ **7**, with a solitary CO ligand was identified as the main product by IR and NMR spectroscopy. The other alkyne complex does not contain CO and most probably can be formulated as

$[WCl_2(NCMe)_2(PhC{\equiv}CH)_2]$ **8** (Table 2). However, complexes **7** and **8** are not the only reaction products because several other proton signals of coordinated PA in the region 11–14 ppm appeared in the reaction of PA with **1**. Also several lower intensity carbon signals of coordinated PA were observed in ^{13}C NMR spectra.

Catalytic activity of **1**. The starting point of the present investigation was to examine the scope of our earlier finding [35, 36, 37] that the formation of tungsten(II) might be an important event in the creation by Lewis acids (Group 14 tetrachlorides) of the catalytic activity of tungsten(0) compounds. To be precise, polymerization of PA occurs at room temperature in CH_2Cl_2 containing tungsten(II) compound **1**. Treatment of the resultant deep-red solution with a large amount of methanol produced, quantitatively, poly(phenylacetylene) (PPA) as a fine dark-orange powder with a number-average molecular weight (M_w) of 5×10^3, determined by GPC. The polymers produced were soluble in CH_2Cl_2, $CHCl_3$ and toluene. IR and ^1H NMR spectroscopy was used to establish the stereochemistry in PPA as mainly *trans* [19].

However, the catalytic coupling of alkynes in the presence of **1** yields at least two types of product, namely polymers with conjugated polyenic structures and cyclic oligomers, especially the aromatic cyclotrimers 1,2,4- and 1,3,5-triphenylbenzene. Minor amounts of other oligomers arise, mainly linear diphenylbutadienes, which contain, for example, hydrogen derived from the solvent and also a dimer of PA detected by MS as 1*H*-indene-1-(phenylmethylene).

The intermediates formed in mechanisms most frequently suggested for the catalytic polymerization and cyclotrimerization of alkynes are alkylidene complexes [38] and metallacyclic species [39]. The catalytically active species are, as yet, rather poorly characterized. Our results provide direct information only as regards to the first step and strongly suggest that the loss of three labile two-electron-donor ligands (CO or CH_3CN), and coordination of two alkyne molecules as three-electron-donor ligands, is common to all the reactions studied. In the reactions of **1** with alkynes that we investigated, the tungsten complexes that could be isolated contained a *cis* arrangement of the two alkyne ligands. We were unable to isolate any intermediates beyond the first bis(alkyne) complexes and their decomposition product: 1*H*-indene-1-(phenylmethylene). The formation of dimers, cyclotrimers and linear conjugated polyenic polymers involves oxidative coupling and formation of a series of metalacyclic species [39]. The metallacycle formed with four molecules of alkyne can then rearrange to an alkylidene ligand, as was observed by Yeh *et al.*[40]. The mechanism of PA polymerization induced by tungsten(II) complex is therefore seen to involve a series of stepwise *cis* insertions of coordinated PA into a C–W bond giving a metallacycloheptatriene complex. A further PA *cis* insertion then occurs to give an alkylidene complex initiating the increase of the polymer chain.

Acknowledgements—Authors thank KBN (Grant No 3T09A 094 10) for financial support of this work.

REFERENCES

1. Kummer, R. and Graham, W. A. G., *Inorg. Chem.*, 1968, **7,** 310.
2. Edgar, K., Jonson, B. F. G., Lewis, J. and Wild, S. B., *J. Chem. Soc., A*, 1968, **11,** 2851.
3. Elder, M. and Hall, D., *Inorg. Chem.*, 1969, **8,** 1268.
4. Elder, M. and Hall, D., *Inorg. Chem.*, 1969, **8,** 1273.
5. Einstein, F. W. B. and Field, J. S., *J. Chem. Soc. Dalton*, 1975, **16/17,** 1628.
6. Anderson, R. A. and Einstein, F. W. B., *Acta Cryst.*, 1976, **B32,** 966.
7. Panizo, M. and Cano, M., *J. Organomet. Chem.*, 1985, **287,** 221.
8. Bell, A. and Walton, R. A., *J. Organomet. Chem.*, 1985, **290,** 341.
9. Iglesias, M., Lorente, A. L., Del Pino, C. and Santos, A., *J. Organomet. Chem.*, 1983, **256,** 73.
10. Baker, P. K. and Bury, A., *J. Organomet. Chem.*, 1989, **359,** 189.
11. Baker, P. K. and Bury, A., *Polyhedron*, 1989, **8,** 917.
12. Baker, P. K. and Quinlan, A. J., *Inorg. Chim. Acta*, 1989, **162,** 179.
13. Miguel, D., Pérez-Martinez, J. A., Riera, V. and Garcia-Granda, S., *Polyhedron*, 1991, **10,** 1717.
14. Miguel, D., Pérez-Martinez, J. A., Riera, V. and Garcia-Granda, S., *J. Organomet. Chem.*, 1993, **455,** 121.
15. Barrado, G., Miguel, D., Pérez-Martinez, J. A., Riera, V. and Garcia-Granda, S., *J. Organomet. Chem.*, 1993, **463,** 127.
16. Cano, M., Panizo, M., Campo, J. A., Tornero, J. and Menéndez, N., *J. Organomet. Chem.*, 1993, **463,** 121.
17. Szymańska-Buzar, T., Głowiak, T., *Polyhedron*, 1997, **16,** 1599.
18. Dobson, G. R., Amr El Syed, M. F., Stolz, I. W. and Sheline, R. K., *Inorg. Chem.*, 1961, **1,** 526.
19. Simionescu, C. I., Percec, V. and Dumitrescu, S., *J. Polym. Sci. Polym. Chem.*, 1977, **15,** 2497.
20. G. R., *KUMA KM4 Software*, *User's Guide*, *Version* 3.1, KUMA DIFFRACTION, Wrocław, Poland, 1989.
21. Sheldrick, G. M., *Acta Crystallogr., A.*, 1990, **46,** 467.
22. Sheldrick, G. M., *SHELXL*93, Program for the Refinement of Crystal Structure, University of Göttingen, Germany.
23. Szymańska-Buzar, T., Głowiak, T., *J. Organomet. Chem.*, 1995, **489,** 207.
24. Szymańska-Buzar, T., *J. Organomet. Chem.*, 1995, **492,** 241.
25. Storhoff, B. N. and Lewis, Jr., H. C., *Coord. Chem. Rev.*, 1977, **23,** 1.
26. Hamilton, E. J., Smith, D. E. and Welch, A. J., *Acta Crystallogr., C*, 1987, **43,** 1214.

27. Siemion, V. A., Chapovskii, Y. A., Struchkov, Yu. T. and Nesmeyanov, A. N., *Chem. Commun.*, 1968, 666.
28. O'Connor, J. E. and Corey, E. R., *J. Am. Chem. Soc.*, 1967, **89,** 3930.
29. Balch, A. L. and Oram, D. E., *Organometallics*, 1988, **7,** 155.
30. Petz, W., *Chem. Rev.*, 1986, **86,** 1019.
31. Drew, M. G. B., Baker, P. K., Amstrong, E. M., Fraser, S. G., Muldoon, D. J., Lavery, A. J. and Shawcross, A., *Polyhedron*, 1995, **14,** 617.
32. Clark, R. J. H., Maresca, L. and Smith, P. J., *J. Chem. Soc., A.*, 1970, **16,** 2687.
33. Armstrong, E. M., Baker, P. K. and Drew, M. G. B., *J. Organomet. Chem.*, 1987, **336,** 377.
34. Armstrong, E. M., Baker, P. K. and Drew, M. G. B., *Organometallics*, 1988, **7,** 319.
35. Szymańska-Buzar, T., *J. Mol. Catal.*, 1991, **68,** 177.
36. Szymańska-Buzar, T., *J. Mol. Catal.*, 1994, **93,** 137.
37. Szymańska-Buzar, T., *J. Mol. Catal., A: Chemical*, 1997, **123,** 113.
38. Schrock, R. R., *J. Organomet. Chem.*, 1986, **300,** 249 and references therein.
39. Vollhardt, K. P. C., *Angew. Chem. Int. Ed. Engl.*, 1984, **23,** 539.
40. Yeh, W.-Y., Pengband, S.-M. and Lee, G.-H., *J. Chem. Soc. Chem. Comm.*, 1993, **13,** 1056.

Pergamon

PII: S0277–5387(98)00124–7

Polyhedron Vol. 17, No. 19, pp. 3427–3432, 1998
© 1998 Published by Elsevier Science Ltd
All rights reserved. Printed in Great Britain
0277–5387/98 $19.00+0.00

Synthesis of a new binucleating ligand and its binuclear Cu(II) complex: X-ray crystal structure, spectral and electrochemical properties

T. M. Rajendiran,[a]* R. Venkatesan,[a] P. Sambasiva Rao[a] and M. Kandaswamy[b]

[a]Department of Chemistry, Pondicherry University, R. V. Nagar, Kalapet, Pondicherry 605014, India

[b]Department of Chemistry, University of Madras, Guindy Campus, Madras 600 025, India

(Received 6 January 1998; accepted 25 March 1998)

Abstract—The preparation of a pentadentate binucleating ligand 2,6-bis[(N-methyl piperazin-1-yl)methyl]-4-cyano phenol (HL) is described together with the corresponding acetato bridged Cu(II) complex $[Cu_2L(CH_3COO)_2]ClO_4$. Both the ligand and the complex were characterized by elemental analysis and spectral studies. The electro-chemical behavior of the complex is discussed in detail. A Crystal structure analysis shows that the ligand is pentadentate donating two nitrogens as well as a bridging oxygen to each copper. Two acetates bridge the coppers through axial and apical positions to yield square-pyramidal coppers with a distorted square base. Perchlorates occupy interstitial positions. The structure is held in three-dimensional space by electrostatic attractions and Vander Waals forces. © 1998 Published by Elsevier Science Ltd. All rights reserved

Keywords: binucleating ligand; copper complex; crystal structure; electrochemical.

INTRODUCTION

As a part of a wide study of structure, magnetism and redox relation of binuclear Cu(II) complexes [1–5], we have synthesized a binucleating ligand HL by the Mannish reaction of a para substituted phenol, formaldehyde and N-methyl piperazine [6, 7]. Molecular models showed that simultaneous coordination of the phenol oxygen and the four piperazine nitrogen atoms to the two copper(II) ions in the presence of exogenous bridging ligands would be difficult in view of the sterically controlled ligand conformation. In attempting to insert exogenous X groups, particularly those having two or more coordinating atoms, we have come across an unusual and unexpected product. In the case of X = acetate, a triply bridged (μ-phenoxo) bis (μ-acetato) complex $[Cu_2(CH_3COO)_2]ClO_4$ was obtained. This observation is in contrast with similar studies with other binucleating ligands in which mono (μ-acetato) copper (II) derivatives are obtained. Interestingly, similar bis(μ-acetato) bridged complexes of Cu(II) [8], Fe(III) [9] and Mn(III) [10] have been reported with other ligands; the bridging unit found in these structures have been proposed by Anderson *et al* [11]. to be a thermodynamically favored core structure. In this paper, we describe the synthesis, structure, spectral and electrochemical properties of bis(μ-acetato) and (μ-phenoxo) bridged binuclear copper complex $[Cu_2(CH_3COO)_2]\ ClO_4$.

EXPERIMENTAL

Synthesis of the ligand

The ligand 2,6-bis[(N-methyl piperazin-1-yl)methyl]-4-cyano phenol (HL) was prepared by a slight modification of the reported procedure [7].

4-cyanophenol (0.05 mol) in ethanol (75 ml) was mixed with excess (0.12 mol) N-methyl piperazine and stirred on with slow addition of 35% formaldehyde (12.5 ml, 0.125 mol). The solution was refluxed for 24

*Author to whom correspondence should be addressed.

hours with further addition of 2.5 ml formaldehyde at intervals of 8 hrs. The alcohol was evaporated under vacuum and the resulting oil, washed with saturated aqueous solution of sodium carbonate, was extracted with benzene. After evaporation of benzene, brown crystals were obtained which were recrystallised from light petroleum.

^{1}H NMR: $CDCl_3$ δppm 7.1 (m) aromatic H, 3.5 (s) benzylic CH_2, 2.6 (s) N-CH_2, 2.25 (s) N-CH_3; IR: νCH_2, 2800–3000 cm^{-1}, νOH, 3400 (b) cm^{-1}, ν-aromatic CH_2 1600 cm^{-1}, νCN 2220 cm^{-1}. Found C, 66.4; H, 8.2; N, 20.1. $C_{19}H_{29}N_5O$ requires C, 66.4; H, 8.5; N, 20.4.

Synthesis of the complex

Copper(II) acetate monohydrate (0.99 g, 0.005 mol) was dissolved in warm aqueous ethanol (100 ml). Addition of the ethanolic solution of the ligand HL(0.88, 0.0025 mol) and of sodium perchlorate (1.756 g, 0.0125 mol) to the above solution led to the formation of a dark green solution, which on slow evaporation gave blue diamond-shaped crystals in 75% yield. Anal. Calculated for $C_{23}H_{28}N_5O_9ClCu_2$: C, 40.2; H, 4.9; N, 10.1; Found C, 39.5; H, 4.8; N, 9.5.

Physical measurements

IR spectrum was recorded on a Perkin Elmer IR 598 instrument (KBr pellet) in the 4000–200 cm^{-1} spectral range. Proton NMR spectrum was recorded using $CDCl_3$ on a JEOL FX-400 FT-NMR spectrometer. The electronic spectrum of the complex was recorded with a Hitachi-320 UV-Visible double beam spectrophotometer. C, H and N were analyzed with Hetueuas C-H-N rapid analyser. Electrochemical measurements were carried out with a PAR model 175 Universal programmer.

X-ray structure determination

Blue diamond-shaped crystals, suitable for X-ray diffraction were obtained by slow evaporation of an alcoholic solution. A crystal of dimensions $0.18 \times 0.24 \times 0.32$ mm was used for data collection using an Enraf-Nonius CAD-4 diffractometer with graphite-monochromatised Mo-Kα radiation in the 2θ range 2°–47°. Two sets of three control reflections were measured at specified intervals to monitor orientation and decay. The data were corrected for Lorentz polarization factors. Absorption corrections were applied using the psi-scan method [12].

The structure was solved by direct methods using Multan 82 [13] with magic integers. Hydrogen positions were generated using stereochemical constrains and were given isotropic thermal parameters based on the heavy atom to which they are connected. A mixed-mode block-diagonal refinement, in which the non-hydrogens were refined anisotropically, keeping hydrogens fixed resulted in convergence at an R of 0.040 (Rw = 0.042) for 3203 observed reflections. A weighting scheme with Dunitz Seiler [14] factor was used in the refinement. The scattering factors for copper, chlorine, oxygen, nitrogen and carbon were from Volume IV of the international Tables for Crystallography [15] while the scattering factors for hydrogen were from Stewart *et al.*[16]. All the computations were carried out using the SDP package available for the PDP-11/73 system [17]. The relevant crystallographic data are given in Table 1.

RESULT AND DISCUSSIONS

The complex $[Cu_2L(CH_3COO)_2]ClO_4$ was obtained by the reaction of copper(II) acetate and the ligand in a 2:1 molecular ratio with subsequent addition of sodium perchlorate in ethanol. The I.R. spectrum of the complex exhibits a symmetrical band at 1095 cm^{-1} indicating the presence of uncoordinated perchlorate ion; strong bands at 1606 cm^{-1} and 1420 cm^{-1} are due to ν(-COO). The expected absorbance for νCu-N and νCu-O are found at 480 and 280 cm^{-1} respectively [18]. The band at 2220 cm^{-1} is indicative of the presence of the -CN group. The electronic spectrum of the complex shows two bands at 635 nm ($\epsilon = 260$) and 420 nm ($\epsilon = 657$) which are assigned to the d-d transitions and to the phenolato to Cu(II) charge-transfer band respectively [19]. The third band at 346 nm ($\epsilon = 878$) is assigned to acetate LMCT [20].

The redox behviour of the binucleating complex is given in Fig. 1; the large ΔEp value shows that the complex is not a truly reversible system. The value of cathodic current is larger than the value of the anodic current, indicating that the complex undergoes a chemical change after reduction. In addition to the oxidation peak at 0.62 V, we observed another small oxidation peak at -0.04 V. After the first cycle, the shape of the reduction peak is altered and a small reduction peak is observed at -0.52 V, apart from the main reduction peak at -1.25 V. Thus after the first complete cycle, the system shows two redox couples, the reduction at -1.25 V corresponding to the oxidation wave at -0.62 V and the reduction at -0.52 V corresponding to the oxidation peak at -0.04 V. The second redox couple may be due to a new species generated after the reduction of the original complex. As can be seen from the figure, the shape of the cyclicvoltammogram during the continuous scan shows that the peak current of the original complex decreases with increase in the peak current of the generated species.

A number of important observations follow from our cyclicvoltametric studies. The coulometric analysis of reduction process indicates that two electron per mole are transferred suggesting the formation of two Cu(II) ions and it occurs in a single step electron transfer process. The huge difference between Epc and

Table 1. Cryatallographic Data

Molecular Formula	:$Cu_2ClO_9C_{23}N_5H_{28}$
Molecular Weight	:677.5
System	:Monoclinic
Space group	:$P2_1/c$
a (Å)	:13.404(1)
b (Å)	:10.345(1)
c (Å)	:20.623(1)
β (°)	:96.18(1)
V (Å^3)	:2843.2(6)
D_{calec} (g cm^{-3})	:1.608
μ(for Mo-Kα)	:20.725 cm^{-1}
Transmission factors	:80.051(mim), 99.90(max), 92.38(ave)
2θ range	$=2°$–47°
Data zone	:+h, +k, ±1
Total no. of reflections measured	:4188
Total no of reflections observed($I>3\sigma I$)	:2487
$\Delta/\sigma=0.03$	
$\Delta\zeta$ (max) = 1.12 Å^{-3}	
R = 0.048	
$R_w=0.053$	

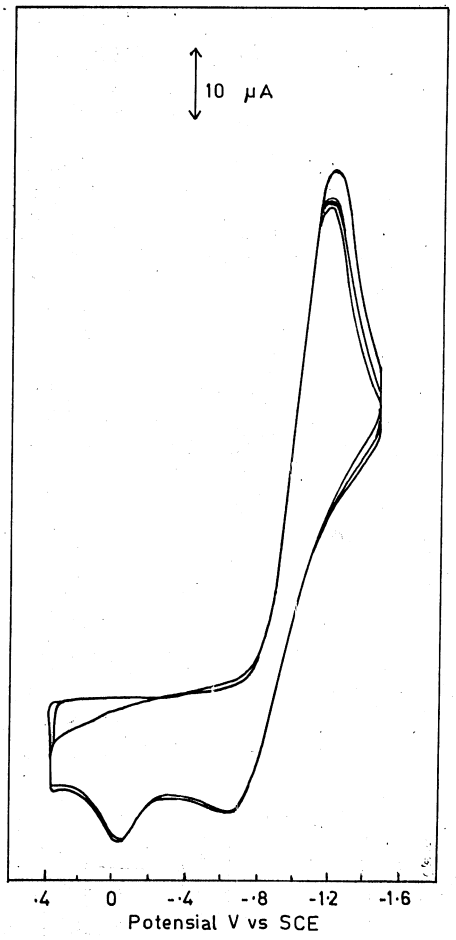

Fig. 1. Cyclic voltammogram of the copper complex.

Epa suggests that the system is quasireversible and a chemical change is occurring with electron transfer resulting most probably from a structural reorganization of the copper coordination sphere. The presence of the new redox couple can be attributed to the formation of a new complex, which may contain only endogenous bridging unit, by the first reduction of the original complex. Our results are in confirmity with the earlier reports of stereochemical changes [21] and the observation of the ligand loss [22–24] induced by the electron transfer in related complexes. We speculate that the reduction of the complex can be described by Scheme 1.

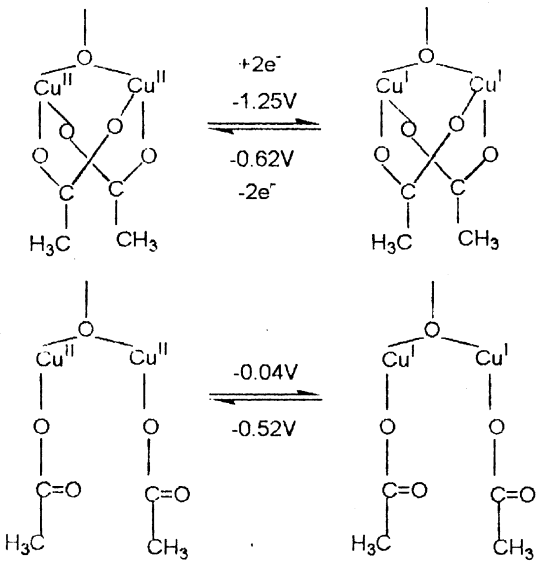

Crystal and molecular structure of the complex

Bond lengths and bond angles, along with estimated standard deviations are shown in Table 2. The quoted deviations are underestimates because of the use of block-diagonal least-squares methods.

Figure 2 shows the ORTEP [25] view of the molecule, along with the numbering scheme. The triply bridged cationic complex and perchlorate anions occur as DL-diasteromeric pairs, related by the centre of inversion of the space group by $P2_1/c$. The pentadentate ligand connects both the coppers through the phenoxy bridge and donates three coordination sites to each of the copper atoms. Two acetates bridge both

Table 2. Selected Bond Lengths (A°) of $[Cu_2L(CH_3COO)_2]ClO_4$. (numbers in parenthesis are estimated standard deviation in the least significant digits)

Atom 1	Atom 2	Distance	Atom 1	Atom 2	Distance
Cu1	O1	1.990(5)	Cu1	O2	1.914(6)
Cu1	O4	2.184(6)	Cu1	N1	2.091(6)
Cu1	N2	1.993(6)	Cu2	O1	1.974(5)
Cu2	O3	2.160(7)	Cu2	O5	1.912(7)
Cu2	N3	2.074(8)	Cu2	N4	2.005(7)
Cl1	O6	1.385(9)	Cl1	O7	1.33(1)
Cl1	O8	1.30(2)	Cl1	O9	1.37(1)
O1	C7	1.33(1)	O2	C20	1.27(1)
O3	C20	1.23(1)	O4	C22	1.24(1)
O5	C22	1.28(2)	N1	C2	1.49(1)
N1	C4	1.48(1)	N1	C18	1.48(1)
N2	C1	1.48(2)	N2	C3	1.49(1)
N2	C5	1.48(2)	N3	C15	1.48(1)
N3	C17	1.47(1)	N3	C19	1.50(2)
N4	C13	1.47(1)	N4	C14	1.50(1)
N4	C16	1.48(1)	N5	C12	1.14(1)
C1	C2	1.56(1)	C3	C4	1.54(1)
C5	C6	1.51(1)	C6	C7	1.41(1)
C6	C11	1.37(1)	C7	C8	1.40(1)
C8	C9	1.40(1)	C8	C13	1.50(1)
C9	C10	1.38(1)	C10	C11	1.40(1)
C10	C12	1.44(1)	C14	C15	1.52(2)
C16	C17	1.51(2)	C20	C21	1.51(1)
C22	C23	1.50(1)			

Selected Bond Angles (degrees) of $[Cu_2L(CH_3COO)_2]ClO_4$ (numbers in parenthesis are estimated standard deviation in the least significant digits)

Atom 1	Atom 2	Atom 3	Angle	Atom 1	Atom 2	Atom 3	Angle
O1	Cu1	O2	98.8(2)	O1	Cu1	O4	92.4(3)
O1	Cu1	N1	157.3(2)	O1	Cu1	N2	92.1(2)
O2	Cu1	O4	101.7(3)	O2	Cu1	N1	91.9(3)
O2	Cu1	N2	163.2(3)	O4	Cu1	N1	105.1(2)
O4	Cu1	N2	90.5(3)	N1	Cu1	N2	73.6(3)
O1	Cu2	O3	94.8(2)	O1	Cu2	N3	161.0(3)
O1	Cu2	O5	98.3(2)	O3	Cu2	O5	104.1(3)
O1	Cu2	N4	91.5(3)	O3	Cu2	N4	99.5(3)
O3	Cu2	N3	99.4(3)	O5	Cu2	N4	153.6(3)
O5	Cu2	N3	90.5(4)	Cu1	O1	Cu2	111.1(3)
N3	Cu2	N4	73.8(3)	Cu2	O1	C7	122.7(4)
Cu2	O1	C7	122.7(4)	Cu2	O3	C20	126.4(1)
Cu1	O2	C20	135.9(5)	Cu2	O5	C22	133.8(7)
Cu1	O4	C22	128.1(6)	Cu1	N1	C4	100.9(4)
Cu1	N1	C2	101.6(5)	Cu1	N2	C1	105.2(5)
Cu1	N1	C18	121.8(5)	Cu1	N2	C5	115.5(5)
Cu1	N2	C3	103.2(5)	Cu2	N3	C17	103.2(6)
Cu2	N3	C15	99.0(6)	Cu2	N4	C13	117.0(5)
Cu2	N3	C19	119.4(7)	Cu2	N4	C16	105.6(6)
Cu2	N4	C14	100.4(6)				

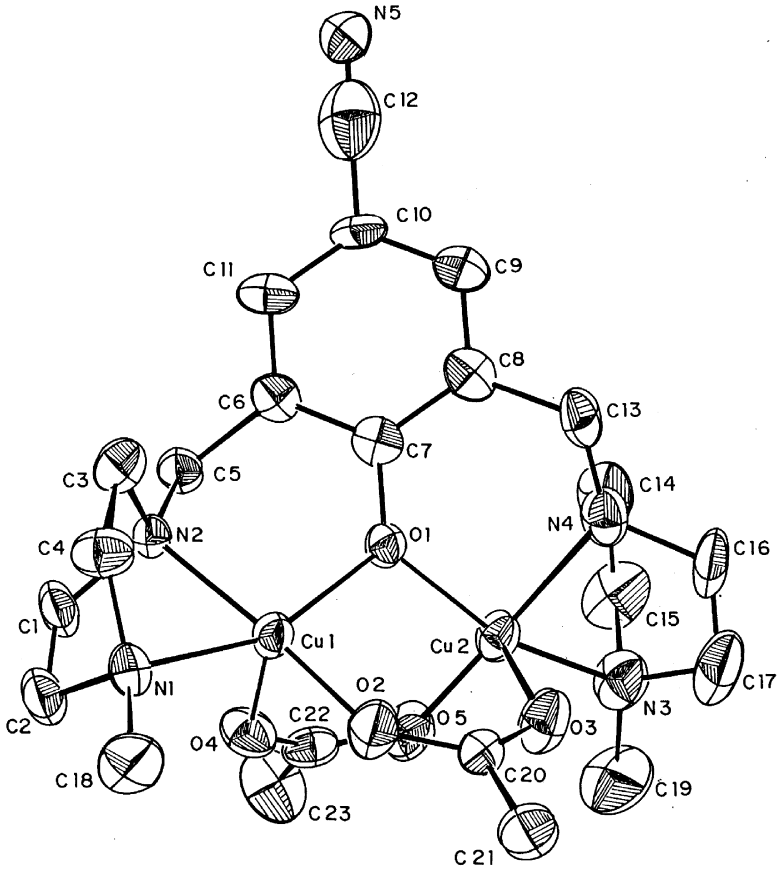

Fig. 2. ORTEP view of $[Cu_2L(CH_3COO)_2]ClO_4$ complex.

the coppers, through -O-C-O- bridge, and provide coordination sites to the square base and apexes. The resulting square pyramidal geometry around Cu1 and Cu2 exhibits angular distortions caused by the ring constraints. The distances Cu-O [1.990(5) Å, 1.914(6) Å and 1.974(5) Å and 1.912(7) Å in Cu1 and Cu2 polyhedra respectively] and distances Cu-N [2.091 (6) Å, 1.993(6) Å in Cu1 and 2.074(8) and 2.005(7) Å in Cu2 polyhedra] lie in the range reported for such values in other Cu(II) square-pyramidal complexes [26–34]. The distribution of Cu-O values follows the expected pattern, and shows that the oxygens of the acetates bind more strongly. Within experimental errors, Cu1-O1 and Cu2-O1 distances are equal, which is in line with a number of observations reported before [35]. The bonds Cu–N trans to Cu–O1 are elongated. The differences between Cu–O(av) to Cu–N(av) is 0.094 Å; part of this difference obviously arises due to differences in the atomic radii of oxygen and nitrogen ($\sim$0.05 Å), while the remainder can be attributed to steric constraints. The distortion in the basal squares are reflected in the trans angles, which are 157.3(2)° and 163.3(2)° for Cu(1) polyhedron and 153.6 (3)° and 161.0(3)° for Cu(2) polyhedron; the cis angles have a span of 25.2° [73.6(3)° to 98.8(2)°] and 24.5 [73.8(3)° to 98.3(2)° in Cu(1) and Cu(2) polyhedra respectively] showing that tetrahedral like deviations from planarity result from steric interferences. The pendants offer constraining five-membered rings that result in a contraction of the N–Cu–N angles i.e. 73.6(3)° and 73.8(3)° in Cu(1) and Cu(2) polyhedra. As a result, angles O1–Cu1–O2 and O1–Cu2–O5 open up to 98.8(2) and 98.3(2) respectively. The apical O4–Cu1 and O3–Cu2 distances are 2.184(6) Å and 2.160 (7) Å and lie in the short range, showing that the metal-oxygen (apical) interactions are strong in this complex. Literature values range from 2.114(6) Å [32] to 2.414(6) Å [31]. Longer distances than this denote weak interactions.

Atoms Cu1 and Cu2 are displaced by 0.259(1) Å and $-0.325(1)$ Å from the planes O1N1O2N2(A) [maximum deviation of any of the constituent atom, m = 0.082(7) Å] and O1N3N4O5(B) [m = 0.072(7) Å] towards the apical oxygens O(4) and O(3); O(4) lies 2.419(6) Å above plane A and O(3) lies 2.480(6)Å below plane B respectively. The five membered rings in the structure have envelope conformation. Atom Cu(1) is displaced by 1.373(1) Å and 1.401(1) Å from the planes defined by N1N2C1C2 (C) [m = 0.013(9) Å] and N1N2C3C4(D) [m = 0.009(9) Å] respectively. Similarly, atom Cu2 is displaced by $-1.441(1)$ and $-1.330(1)$ Å from planes defined by N3N4C14C15(E)

[m = 0.008(12) Å] and N3N4C16C17(F) [m = 0.001(12) Å] respectively. The six membered rings connected through the phenolic oxygen O1, N2C6C7Cu1C5O1 and N4C7C8Cu2C13O1 occur as boats flattened at one end. Atoms C(5) and O(1) deviate by 0.523(8) Å and 0.340(5) Å from the plane Cu1N2C6C7(G) [m = 0.024(7) Å, while atoms C13 and O1 deviate by −0.583(9) Å and −0.450(5) Å from the plane Cu2N4C7C8(H) [m = 0.009(8) Å]. Two more six-membered rings formed by the triple-bridge occur as envelopes. O1 displaced by −0.897(5) Å and 0.967(5) Å.

REFERENCES

1. Murray, K. S. (1986) In biological and Inorganic Copper Chemistry, K. D. Karlin and J. Zubieta, Eds; Adenine, New York, **2**, 161.
2. Mazurek, W., Berry, K. J., Murray, K. S., O'Connor, M. J., Snow, M. R. and Wedd, A. G., *Inorg. Chem.*, 1982, **21,** 3071.
3. Mazurek, W., Kennedy, B. J., Murray, K. S., O'Connor, M. J., Rodgers, J. R., Snow, M. R., Wedd, A. G. and Zwack, P. R., *Inorg. Chem.*, 1985, **24,** 3258.
4. Mazurek, W., Bond, A. M., Murray, K. S., O'Connor, M. J. and Wedd, A. G., *Inorg. Chem.*, 1985, **24,** 2484.
5. Hiopoulos, P., Fallon, G. D. and Murray, K. S., *J.Chem. Soc., Dalton Trans.*, 1986, 437.
6. Fallon, G. D., Murray, K. S., Spethmann, B., Yandell, J. K., Hodgkin, J. H. and Loft, B. C., *J. Chem. Soc., Chem Commun.*, 1984, **37,** 1561.
7. Hodgkin, J. H., *Aust. J. Chem.*, 1984, **37,** 2371.
8. Bertoncello, K., Fallon, G. D., Hodgkin, J. H. and Murray, K. S., *Inorg. Chem.*, 1988, **27,** 4750.
9. Murch, B. P., Bradley, F. C., Que, I. jr, *J. Am. Chem. Soc.*, 1986, **108,** 5027.
10. (a) Drill, H., Chang, H. R., Zhang, X., Larson, S. K., Potenza, J. P., Piperpont, C. G., Schugar, H. J., Isied, S. S., Hendrickson, D. N., *J. Am. Chem. Soc.*, 1987, **109**, 6207. (b) Buchanan, R. M., Oberhausen, K. J., Richardson, J. F., *Inorg. Chem.*, 1987, **27**, 971.
11. Anderson, A. S., Que, I. Jr., Papaefthymiou, V., Munck, E., Taylor, L. F. and Anderson, O.P., *J. Am. Chem. Soc.*, 1988, **110,** 1986.
12. North, A. C. T., Philips, D. C. and Mathews, F. S., *Acta. Cryst.*, 1968, **A24,** 351.
13. Main, P., Fiske, S. F., Hull, S. E., Lessinger, L., Germain, G., Declerq J. P., Woolfson M. M., (1982) Multon 11/82. A system of computer programs for the automatic solution of crystal structures from X-ray diffraction data, University of York, England and University of Louvain, Belgium.
14. Dunitz, J. D. and Seiler, P., *Acta. Cryst.*, 1973, **B29,** 586.
15. International tables for crystallography, Vol. IV, D. Reidel Publishing Co., Dordrecht, Holland, 1983.
16. Stewart, R. F., Davidson, E. R. and Simpson, W. T., *J. Chem. Phys.*, 1965, **42,** 3175.
17. SDP structure detemination package, Enrof. Nonius, Delft, Holland (1986).
18. Kwik, W. L. and Tay, Alice W. W., *Polyhedron*, 1990, **9,** 1293.
19. Oberhausen, K. J., Richardson, J. F., Buchanan, R. M., McCusker, James K., Hendrickson, D. N. and Latour, Jean-Marc., *Inorg. Chem.*, 1991, **30,** 1357.
20. Lever, A. B. P., (1984) *Inorganic Electronic Spectroscopy*, 2nd Ed., Elsvier, Amsterdam, **356**, 553–572, 626–638, 1, 23.
21. Ammer, F. and Saveant, J., *J. Electro analytical. Chem. Interfacial Electrochem.*, 1973, **47,** 115.
22. Mandal, S. K. and Nag, K., *J. Chem. Soc., Dalton. Trans.*, 1984, 2141.
23. Flanagan, J. B., Margel, S., Bard, A. J. and Anson, F. C., *J. Am. Chem. Soc.*, 1978, **180,** 4248.
24. Gane, R. R., Kreh, R. P. and Dodge, J. A., *J. Am. Chem. Soc.*, 1979, **101,** 6917.
25. Johnson, C. K., ORTEP-II Oak Ridge Thermal Ollipsoid plotting program, Oak Ridge National Laboratories, Tennessee, 1976.
26. Lu, T. and Lu, Y. and Chung, C., *Acta. Cryst.*, 1992, **C48,** 267.
27. Abuhijileh, A. L., Woods, C. and Ahmed, I. Y., *Inorg. Chim. Acta.*, 1991, **11,** 190.
28. Lloret, F., Sletten, J., Ruiz, R., Julve, M., Fans, J. and Verdeguer, M., *Inorg. Chem.*, 1992, **31,** 778.
29. Bakalbassis, E., Beregerat, P., Kahn, O., Jeannin, S., Jeannin, Y., Dromzee, Y. and Guillot, M., *Inorg. Chem.*, 1992, **31,** 625.
30. Speier, G., Tirza, S., Rockenbauer, A., Boone, S. R. and Pierpoint, C. G., *Inorg. Chem.*, 1992, **31,** 1017.
31. Wu, L., Keniry, M. and Hathaway, B., *Acta. Cryst.*, 1992, **C48,** 35.
32. Hundal, M. S., Sandhu, S. S., Sood, G., McKie, V. and Tandon, S. S., *Acta. Cryst.*, 1991, **C47,** 1160.
33. Mergehenn, R., Merz, L. and Hasse, W. J., *J. Chem. Soc., Dalton Trans.*, 1980, 1703.
34. Gulacio, E., Dominguez-Vera, J., Costes, J., Kikevas, R., Laurant, J., Ruiz, R. and Sundberg, M., *Inorg. Chem.*, 1992, **31,** 774.
35. Doedens, R. J., *Prog. Inorg. Chem.*, 1976, **21,** 209.

Pergamon

PII: S0277–5387(98)00126–0

Polyhedron Vol. 17, No. 19, pp. 3433–3438, 1998
© 1998 Published by Elsevier Science Ltd
All rights reserved. Printed in Great Britain
0277–5387/98 $19.00+0.00

Synthesis and X-ray crystal structure of $[Ru_3(CO)_7(\mu\text{-}H)(\mu\text{-}PCy_2)_3]$: reaction with carbon monoxide to the electron-rich cluster $[Ru_3(CO)_9(\mu\text{-}H)(\mu\text{-}PCy_2)_3]$[1]

Hans-Christian Böttcher*, Marion Graf, Kurt Merzweiler and Clemens Bruhn

Department of Chemistry, Martin Luther University, Halle–Wittenberg, Kurt-Mothes-Str. 2, D-06120 Halle/Saale, Germany

(Received 13 February 1998; accepted 25 March 1998)

Abstract—The reaction of $[Ru_3(CO)_{12}]$ with dicyclohexylphosphine (Cy_2PH) in refluxing toluene leads to the metal clusters $[Ru_3(CO)_7(\mu\text{-}H)(\mu\text{-}PCy_2)_3]$ (**1**) and $[Ru_3(CO)_6(\mu\text{-}H)(\mu\text{-}PCy_2)_3(Cy_2PH)]$ (**2**). Complexes **1** and **2** react with carbon monoxide under elevated pressure to give the novel 52-electron cluster $[Ru_3(CO)_9(\mu\text{-}H)(\mu\text{-}PCy_2)_3]$ (**3**), which could be isolated as a solid and characterized spectroscopically. The molecular structure of **1** has been determined by means of a single-crystal X-ray structure analysis. © 1998 Published by Elsevier Science Ltd. All rights reserved

Keywords: ruthenium; carbonyl; phosphido-bridged; electron-rich clusters; crystal structure.

A rich and fascinating chemistry of phosphido-bridged metal complexes and clusters has been developed over the past two decades [1]. The class of electron-rich clusters, i.e., molecules having similar structural features, like electron-precise compounds, but possessing more electrons and expanded metal frameworks, has now received more attention [2]. As part of a study of the chemistry of transition metal complexes containing bulky phosphido groups, we recently described the synthesis and X-ray crystal structure of the electron-rich cluster $[Ru_3(CO)_6(\mu\text{-}Cl)_3(\mu\text{-}PBu^t_2)(Bu^t_2PH)]$ (50 cluster valence electrons, c.v.e.) [3]. Herein, we report the reaction of $[Ru_3(CO)_{12}]$ with the secondary phosphine Cy_2PH (Cy = cyclohexyl) leading to the complexes $[Ru_3(CO)_7(\mu\text{-}H)(\mu\text{-}PCy_2)_3]$ (**1**) and $[Ru_3(CO)_6(\mu\text{-}H)(\mu\text{-}PCy_2)_3(Cy_2PH)]$ (**2**). The crystal and molecular structure of compound **1** is presented and the reactions of **1** and **2** with carbon monoxide have been investigated, affording the 52-electron cluster $[Ru_3(CO)_9(\mu\text{-}H)(\mu\text{-}PCy_2)_3]$ (**3**). A preliminary X-ray crystal structure investigation of **3** gives a satisfactory explanation to describe **3** in the solid as an electron-rich cluster containing three expanded metal–metal bonds.

RESULTS AND DISCUSSION

Treatment of $[Ru_3(CO)_{12}]$ with the phosphine Cy_2PH in refluxing toluene for 2 h resulted in a reaction with a colour change from orange to brown. Cooling to room temperature, removal of the solvent and recrystallization from dichloromethane/hexane afforded orange microcrystals in good yield which could be identified by elemental analysis and spectroscopic means as the metal cluster $[Ru_3(CO)_7(\mu\text{-}H)(\mu\text{-}PCy_2)_3]$ (**1**). A second fraction of orange crystals could be obtained by fractional crystallization and identified as a substitution product of **1**, namely $[Ru_3(CO)_6(\mu\text{-}H)(\mu\text{-}PCy_2)_3(Cy_2PH)]$ (**2**) (Scheme 1). The molecular structure of complex **1** has been established by X-ray crystallography (*vide infra*). This compound was recently prepared by two other groups and characterized spectroscopically [4, 5].

The infrared spectrum of **1** contains ν(CO) absorption bands in the region characteristic of terminal carbonyl ligands. The ^{1}H NMR spectrum of this compound (C_6D_6) shows, besides signals corresponding to

[1] Dedicated to Dr. Bernhard Walther on the occasion of his 60th birthday.

* Author to whom correspondence should be addressed.

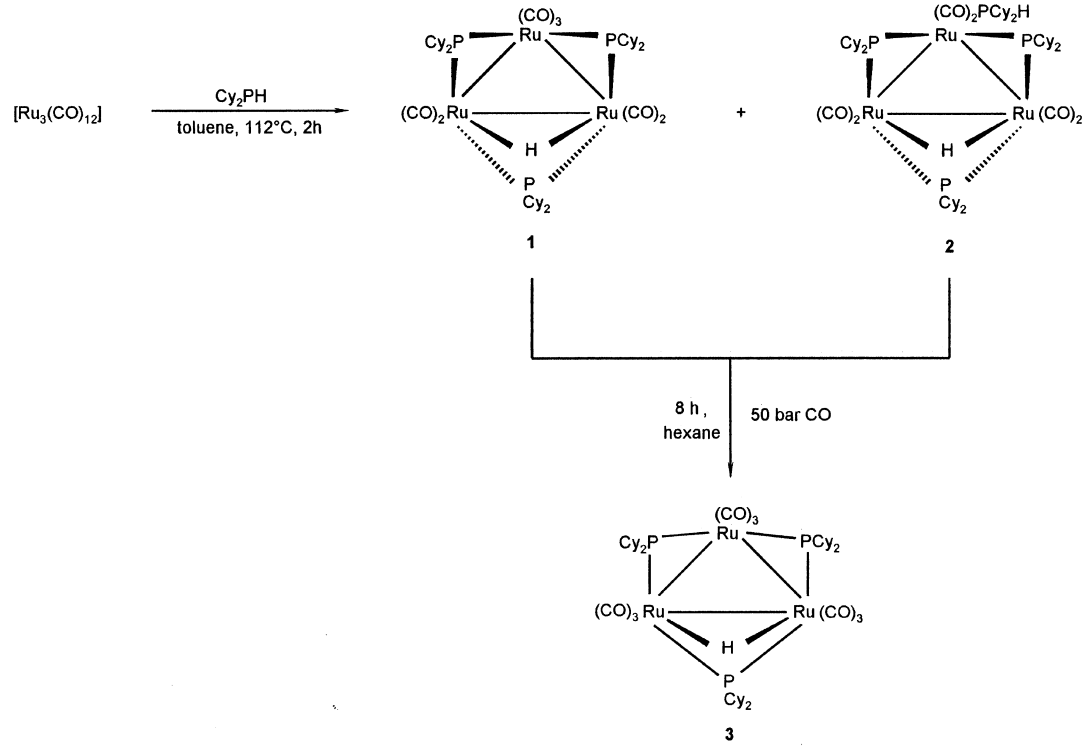

Scheme 1

the protons of the cyclohexyl groups, a resonance in the metal hydride region at δ −17.97 (dt, $^2J_{PH}$ = 19.4 Hz, $^2J_{PH}$ = 14.6 Hz). The splitting pattern is indicative of two chemically equivalent phosphorus nuclei and a third phosphorus, which couple with one hydride ligand. This is additionally confirmed by the $^{31}P\{^1H\}$ NMR spectrum, which exhibits signals corresponding to a typical AB_2 spin system at δ 207.06 (ν_A) and 203.69 (ν_B) with $^2J_{AB}$ = 80.6 Hz. These observations are in disagreement with the NMR data found for the homologue $[Os_3(CO)_7(\mu\text{-H})(\mu\text{-PCy}_2)_3]$ (**4**) [6]. For the latter, the $^{31}P\{^1H\}$ NMR spectrum at room temperature shows only a singlet at δ 112.75 (C_6D_6), indicating that the three phosphido ligands are equivalent in solution. Additionally, this fact is affirmed by the proton NMR spectrum, which shows only a simple quartet for the hydride indicating that this ligand is fluxional and is equivalent to all three phosphido groups. On the contrary, the molecular structure of **4** in the solid differs from that in solution [6]. Unfortunately, variable-temperature $^{31}P\{^1H\}$NMR studies of complex **1** (toluene-d_8, −80 to +80°C) revealed no significant changes in the spectra, therefore there is no indication of a fluxional behaviour of the molecular structure of the latter in solution in the examined temperature range.

The infrared spectrum of **2** exhibits ν(CO) absorption bands in the region characteristic of terminal CO groups. The proton NMR spectrum of complex **2** contains, besides signals corresponding to cyclohexyl protons, a complex multiplet centered at δ −17.32 which can be assigned to a hydride ligand in a similar chemical environment like the hydride in compound **1**. The $^{31}P\{^1H\}$ NMR spectrum of **2**, recorded at room temperature, is of higher order. It contains two sets of peaks centered at δ 204.88 and 181.52, respectively, corresponding to the phosphido bridges across metal–metal bonds. Furthermore, a set of peaks at δ 11.92 can be assigned to a terminal bound Cy_2PH ligand (calculated coupling constants see Section 2, Experimental).

*Reactions of **1** and **2** with carbon monoxide*

Inspired by the investigations of Haines and coworkers, including the reactions of $[Ru_3(CO)_7(\mu_3\text{-PPh})(\mu\text{-PPh}_2)_2]$ with carbon monoxide [7], we became interested in similar reactions of compounds **1** and **2**. Bubbling a stream of carbon monoxide through a solution of the corresponding complex resulted in a slight colour change from orange to yellow. Monitoring by means of $^{31}P\{^1H\}$ NMR spectroscopy showed that the reaction seemed not to be complete under these conditions. The reaction can be completed by using a pressure of 50 bar CO in an autoclave for 5 h. Evaporation of the solvent and crystallization from dichloromethane/hexane afforded an orange

crystalline product which could be identified by elemental analysis and spectroscopic means as a compound with the formula $[Ru_3(CO)_9(\mu\text{-}H)(\mu\text{-}PCy_2)_3]$ (**3**) (Scheme 1). Both species (**1** as well as **2**) gave complex **3** in the same manner, therefore, we assume that **2** reacts with CO in a first step to afford **1**, which then yields compound **3** by additional treatment with carbon monoxide.

The infrared spectrum of **3** shows ν(CO) absorption bands in the region characteristic of terminal carbonyl ligands. The ^{1}H NMR spectrum of this compound (C_6D_6) exhibits, besides the signals corresponding to the cyclohexyl protons, a hydride resonance centered at δ −10.24 (t, $^2J_{PH}$ = 21.0 Hz). Only one coupling to the phosphorus nuclei could be found, the second is assumed to be very small. The $^{31}P\{^1H\}$ NMR data of compound **3** are in accordance with the structural formulation shown in Scheme 1. The spectrum recorded in C_6D_6 at room temperature contains two signals centered at δ 90.66 (d) and 48.88 (t) with a coupling $^2J_{PP}$ = 54.3 Hz. Normally, such chemical shift values indicate phosphido bridges across two metal centers without a metal–metal bond [8]. Therefore, these ambiguous NMR data complicate the description of **3** as an 'opened' framework with only one metal–metal interaction. A preliminary crystal structure investigation of **3** (*vide infra*) confirms that three elongated metal–metal bonds are involved in the structure and supports the formulation of **3** as an electron-rich species containing 52 cluster valence electrons. Moreover, recent investigations on phosphido-bridged 50-electron derivatives with expanded metal–metal bonds generally showed considerable shifts of the ^{31}P resonances of the phosphido ligands towards lower frequencies [2, 9]. The same tendency is observed during the transformation of **1** into **3**.

The molecular structure of $[Ru_3(CO)_7(\mu\text{-}H)(\mu\text{-}PCy_2)_3]$ (***1***)

Compound **1** crystallizes from dichloromethane in the triclinic space group $P\bar{1}$ with two molecules in the unit cell. The molecular structure of **1** is shown in Fig. 1, selected bond lengths and angles are summarized in Table 1.

Compound **1** consists of a triangular metal core, while each Ru–Ru edge is supported by a μ-PCy_2 group. Additionally, the Ru(1)–Ru(2) bond is bridged by a hydride ligand, therefore a shortening of this bond is observed, caused by the doubly-bridged nature [Ru(1)–Ru(3), 3.013(1); Ru(2)–Ru(3), 3.034(1) vs. Ru(1)–Ru(2), 2.808(1) Å]. The hydride ligand in **1** has been found during the refinement by difference fourier analysis [Ru(1)–H, 1.78; Ru(2)–H, 1.71 Å; angle Ru(1)–H–Ru(2), 107.3°]. The metal–metal distances agree well with those found in the closely related $[Ru_3(CO)_7(\mu\text{-}H)(\mu\text{-}PPh_2)_3]$ [10, 11] and the mixed bridging species $[Ru_3(CO)_7(\mu-H)(\mu-PBu^t_2)(\mu-PCy_2)_2]$ [12]. Moreover, the same bonding characteristics were observed in the osmium analogue $[Os_3(CO)_7(\mu\text{-}H)(\mu\text{-}PCy_2)_3]$ (**4**) with Os(1)–Os(3), 3.022(1); Os(2)–Os(3), 3.059(1) vs. Os(1)–Os(2), 2.817(1) Å [6]. However, in the light of the found NMR data at room temperature for the latter (*vide supra*), the structure of **4** in the solid seems to differ from that in solution. The found NMR data in solution of **1** agree better with the structure in the solid, i.e., there is no indication of a fluxional behaviour of the hydride under these conditions.

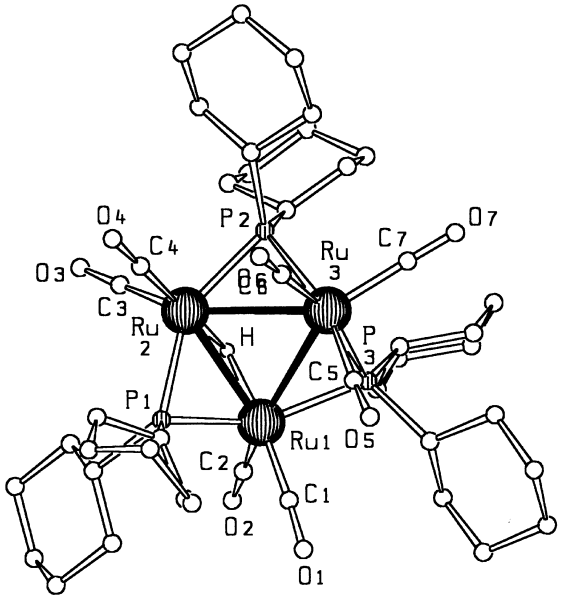

Fig. 1. The molecular structure of $[Ru_3(CO)_7(\mu\text{-}H)(\mu\text{-}PCy_2)_3]$ (**1**).

As in **4**, one of the phosphido bridges [P(1)] in **1** is bent below the plane of the three ruthenium atoms, while the other two μ-PCy_2 ligands are situated above the triangular plane. Neglecting the metal–metal bonds, each ruthenium in **1** has a roughly square–pyramidal coordination sphere. The average of the Ru–P distances falls within normal limits [av. d(Ru–P) = 2.377(1) Å] and are comparable to those found in other phosphido-bridged ruthenium clusters.

Preliminary X-ray investigations of ***2*** *and* ***3***

Despite intense efforts, only a very small crystal size of compounds **2** and **3** could be obtained, therefore, merely preliminary crystal structure data can be discussed here. The compound **2** crystallizes from dichloromethane/hexane in the monoclinic space group $P2_1/n$ (a = 10.396, b = 26.223, c = 22.371 Å; β = 91.9°; V = 6095 Å^3) with four molecules in the unit cell. The structural arrangement of **2** is closely related to that of the parent cluster **1** with a carbonyl from the ruthenium atom unbridged by the hydride ligand, having been replaced by the Cy_2PH. As in **1**, two longer Ru–Ru distances have been determined

Table 1. Selected bond lengths (Å) and bond angles (°) for **1**.

Ru(1)–Ru(2)	2.808(1)	Ru(1)–H	1.78
Ru(2)–Ru(3)	3.034(1)	Ru(2)–H	1.71
Ru(1)–Ru(3)	3.013(1)	Ru(1)–C(1)	1.881(3)
Ru(1)–P(1)	2.347(1)	Ru(1)–C(2)	1.859(3)
Ru(2)–P(2)	2.329(1)	Ru(2)–C(3)	1.851(4)
Ru(1)–P(3)	2.335(1)	Ru(2)–C(4)	1.875(4)
Ru(3)–P(3)	2.438(1)	Ru(3)–C(5)	1.934(3)
Ru(2)–P(1)	2.370(1)	Ru(3)–C(6)	1.927(3)
Ru(3)–P(2)	2.445(1)	Ru(3)–C(7)	1.901(4)

Ru(1)–Ru(2)–Ru(3)	61.9(1)	P(3)–Ru(1)–C(1)	95.7(1)
Ru(2)–Ru(3)–Ru(1)	55.4(1)	P(3)–Ru(1)–C(2)	104.1(1)
Ru(2)–Ru(1)–Ru(3)	62.7(1)	P(1)–Ru(2)–H	81.8(11)
Ru(2)–P(1)–Ru(2)	73.1(1)	P(1)–Ru(2)–C(3)	107.7(1)
Ru(2)–P(2)–Ru(3)	78.9(1)	P(1)–Ru(2)–C(4)	96.8(1)
Ru(3)–P(3)–Ru(1)	78.3(1)	P(2)–Ru(2)–H	82.0(11)
Ru(1)–H–Ru(2)	107.3	P(2)–Ru(2)–C(3)	101.1(1)
P(1)–Ru(1)–P(3)	149.6(1)	P(2)–Ru(2)–C(4)	96.8(1)
P(1)–Ru(2)–P(2)	147.5(1)	P(2)–Ru(3)–C(5)	164.7(1)
P(2)–Ru(3)–P(3)	99,8(1)	P(2)–Ru(3)–C(6)	85.5(1)
P(1)–Ru(1)–C(1)	93.5(1)	P(2)–Ru(3)–C(7)	95.5(1)
P(1)–Ru(1)–C(2)	105.0(1)	P(3)–Ru(3)–C(5)	85.9(1)
P(1)–Ru(1)–H	81.1(10)	P(3)–Ru(3)–C(6)	164.9(1)
P(3)–Ru(1)–H	89.5(11)	P(3)–Ru(3)–C(7)	92.2(1)

[Ru(1)–Ru(2), 3.00; Ru(1)–Ru(3), 2.98 Å], while the third was found to be shorter [Ru(2)–Ru(3), 2.82 Å]. The presence of a hydride in **2** is clearly indicated by the proton NMR spectrum (*vide supra*) and, in analogy to **1**, we assume for this ligand a bridging position across the shortest Ru–Ru bond [Ru(2)–Ru(3)].

Moreover, the composition of **2** is closely related to that of $[Ru_3(CO)_6(\mu\text{-H})(\mu\text{-PPh}_2)_3(Ph_2PH)]$ (**5**) [11]. In the molecular structure of the latter, no hydride ligand has been found during the X-ray study and its position is assumed to be bridging the shortest Ru–Ru edge [2.793(1) Å]. The most remarkable difference is that in **2** the secondary phosphine is bonded to the ruthenium atom, which is unbridged by the hydride ligand, while in **5** the phosphine is bonded to one ruthenium bridged by the hydride. We assume that the position of the phosphine in **2** is favoured by sterical reasons, since the two phosphido ligands unbridged by the hydride lie below the triruthenium plane, whereas the phosphine is situated above the triangle.

Crystals of **3** suitable for X-ray diffraction studies were grown from a dichloromethane/hexane mixture. The compound crystallizes in the monoclinic space group $P2_1/n$ ($a = 12.080$, $b = 17.215$, $c = 23.388$ Å; $\beta = 90.4°$; $V = 4864$ Å^3) with four molecules in the unit cell. The preliminary crystal structure analysis confirms the trinuclear structure of **3**. In the light of the discussion of **3** either as an 'opened' trimetal core or an electron-rich 52-electron cluster with three metal–metal bonds, the Ru–Ru distances are of interest. On the basis of the 18-electron rule, the trimetal cluster **3** (52 c.v.e.) would be expected to exhibit a triangle with only one direct Ru–Ru bond. However, in **3** the metal–metal distances are roughly equivalent and a global expansion is found [Ru(1)–Ru(3), 3.18; Ru(1)–Ru(2), 3.19; Ru(2)–Ru(3), 3.16 Å]. These values are in accordance with 'elongated' metal–metal interactions and a description of **3** as an electron-rich cluster seems to be reasonable. The three very similar Ru–Ru bond lengths refer to a hydride ligand in a μ_3-coordination. However, this would be in disagreement with the found NMR data for **3** in solution (*vide supra*). Therefore, a better structure refinement would be desirable. In comparison with the molecular structure of **1**, the most remarkable feature of **3** is that the three phosphorus atoms lie essentially in the triruthenium plane. This fact is rarely found for complexes containing three bridging phosphido ligands, for instance for the 50-electron clusters $[Ru_3(CO)_6(\mu_3\text{-}\eta^2\text{-PPhpy})(\mu\text{-PPh}_2)_3]$ [1] and $[Ru_3(CO)_6(\mu_3\text{-H})\{\mu_3\text{-}\eta^2\text{-P(Ph)C}_6H_4\}]$ [13]. It seems that it could be a characteristic for such electron-rich triruthenium species only.

EXPERIMENTAL

General considerations

All manipulations were performed under oxygen-free argon, using conventional Schlenk techniques. Solvents were dried over molecular sieves or sodium/benzophenone ketyl and were distilled under argon

prior to use. Starting materials were either commercially available or were prepared according to literature procedures. IR spectra were obtained using a Mattson 5000 instrument. ^1H NMR and $^{31}P\{^1H\}$ NMR spectra were recorded on the spectrometer Gemini 200 (^1H at 199.975 MHz, referenced to Me_4Si; ^{31}P NMR at 80.950 MHz, referenced to 85% H_3PO_4 aq). The mass spectra were obtained on a Hitachi Perkin Elmer RMU 6, Nermag R30-10 instrument. The elemental analyses were performed by the Analytisches Laboratorium des Pharmazeutischen Institutes der Martin-Luther-Universität Halle–Wittenberg.

Synthesis of $[Ru_3(CO)_7(\mu\text{-}H)(\mu\text{-}PCy_2)_3]$ (***1***) *and* $[Ru_3(CO)_6(\mu\text{-}H)(\mu\text{-}PCy_2)_3(Cy_2PH)]$ (***2***)

A mixture of $[Ru_3(CO)_{12}]$ (300 mg, 0.47 mmol) and Cy_2PH (372 mg, 1.88 mmol) was heated in toluene (40 cm^3) under reflux for 2 h. After cooling to room temperature and removal of the solvent, the residue was dissolved in a minimum of dichloromethane and hexane (10 cm^3) was added. After standing at $-30°C$ for two days, compound **1** crystallized as orange microcrystals. Yield: 319 mg **1** (62%). Filtration and further standing for two days at $-30°C$ afforded compound **2** as orange crystals. Yield: 82 mg (15%), based on $[Ru_3(CO)_{12}]$.

*Analytical data for **1***. Found: C, 47.0, H, 5.9, P, 8.8; Calc. for $C_{43}H_{67}O_7P_3Ru_3$; C, 47.2, H, 6.2, P, 8.5%. IR (KBr pellet, cm^{-1}): ν(CO): 2042(m), 1996(vs), 1975(m), 1940(s). ^1H NMR (C_6D_6): δ 2.57–1.08 (m, 66H, C_6H_{11}), −17.97 (dt, 1H, $^2J_{PH} = 19.4$ Hz, $^2J_{PH} = 14.6$ Hz, μ-H).

$^{31}P\{^1H\}$ NMR (C_6D_6): AB_2 pattern, δ 207.06 (m, P_A), 203.69 (m, P_B), $^2J_{PP} = 80.6$ Hz. Mass spectrum: $m/z = 1094$ $[M]^+$.

*Analytical data for **2***. Found: C, 50.9, H, 6.8, P, 9.8; Calc. for $C_{54}H_{90}O_6P_4Ru_3$; C, 51.4, H, 7.2, P, 9.8%. IR (KBr pellet, cm^{-1}): ν(CO): 2040(m), 1992(s), 1972(vs), 1944(vs), 1906(s), 1876(sh). ^1H NMR (C_6D_6): δ (dt, br, $J_{PH} = 329.4$ Hz), δ 2.59–0.80 (m, 88H, C_6H_{11}), −17.32 (m, 1H, μ-H). $^{31}P\{^1H\}$ NMR (C_6D_6): δ 204.88 (m, $^2J_{P3P2/P4} = 26.3$ Hz, $^3J_{P1P3} = 2.2$ Hz, μ-P3), 181.52 (m, $^2J_{P3P2/P4} = 26.3$ Hz, $^2J_{P1P2/P4} = 101.3$ Hz, μ-P2/P4), 11.92 (m, $^2J_{P1P2/P4} = 101.3$ Hz, $^3J_{P1P3} = 2.2$ Hz, Cy_2PH).

*Reaction of **1** with carbon monoxide*

Compound **1** (110 mg, 0.10 mmol) was dissolved in a mixture of dichloromethane (5 cm^3) and hexane (30 cm^3) and the solution transferred into a glass tube containing a magnetic stir bar and placed into a 200 ml steel autoclave. The solution was pressurized with 50 bar CO and stirred at room temperature for 5 h. After venting, the resulting yellow solution was evaporated to dryness. The residue was crystallized from dichloromethane/hexane at $-30°C$ to give **3** as orange microcrystals. Yield: 115 mg (nearly quantitative).

The reaction of **2** with carbon monoxide under pressure was carried out in the same manner as described before with similar results.

*Analytical data for **3***. Found: C, 47.1, H, 5.8, P, 7.7; Calc. for $C_{45}H_{67}O_9P_3Ru_3$; C, 46.9, H, 5.9, P, 8.1%. IR (KBr pellet, cm^{-1}): ν(CO):2042(s), 2007(vs), 1990(s), 1972(vs), 1936(s), 1885(sh). ^1H NMR (C_6D_6): δ 2.67–0.82 (m, 66H, C_6H_{11}), −10.24 (dt, 1H, μ-H). $^{31}P\{^1H\}$ NMR (C_6D_6): δ 90.66 (d, $^2J_{PP} = 54.3$ Hz, μ-PCy_2), 48.88 (t, $^2J_{PP} = 56.0$ Hz). Mass spectrum: m/z: 1150 $[M]^+$.

*X-ray crystal structure determination of **1***

Crystal data, data collection and refinement parameters are summarized in Table 2. Crystals of **1** suitable for X-ray diffraction studies were grown by crystallization from dichloromethane/hexane. For

Table 2. Crystal data and details of the X-ray analysis for complex **1**.

Complex	**1**
Empirical formula	$C_{43}H_{67}O_7P_3Ru_3$
Formula weight	1092.09
Temperature (K)	220
Wavelength (Å)	0.71073
Crystal system	triclinic
Space group	*P*-1
Unit cell dimensions	a = 13.026(4)
	b = 13.455(4)
	c = 13.823(4)
	$\alpha = 100.00(3)°$
	$\beta = 99.66(3)(2)°$
	$\gamma = 93.50(3)°$
V (Å^3)	2342 (12)
Z	2
Density (calculated) (g/cm^3)	1.549
Absorption coefficient (mm^{-1})	1.103
$F(000)$	1116
θ range for data collection (°)	2.44–26.96
Index ranges	$-16 \leqslant h \leqslant 16$
	$-17 \leqslant k \leqslant 17$
	$-17 \leqslant l \leqslant 17$
Reflections collected	24463
Independent reflections	9361
Refinement method	Full-matrix least-squares on F^2
Data/restraints/parameters	9361/0/505
Goodness-of-fit on F^2	0.972
Final R indices [$I > 2\sigma(I)$]	$R1 = 0.0293$
	$wR2 = 0.0742$
R indices (all data)	$R1 = 0.0414$
	$wR2 = 0.0781$
Largest diff. peak and hole (Å^{-3})	0.832/−0.660

data collection the diffractometer Stoe–IPDS was used. The structure was solved by direct methods and refined on F^2 (program systems: SHELXS-86, SHELXL-93 [14]). It should be mentioned, that one cyclohexyl ring on P(1) is disordered. Full details of the structure determination of **1** has been deposited at the Fachinformationszentrum Karlsruhe, Gesellschaft für wissenschaftlich-technische Information mbH, D-76344 Eggenstein–Leopoldshafen, Germany, from where this material may be ordered on quoting the full literature citation and the reference number CSD 408426 (**1**).

CONCLUSION

The complexes $[Ru_3(CO)_7(\mu\text{-H})(\mu\text{-PCy}_2)_3]$ (**1**) and $[Ru_3(CO)_6(\mu\text{-H})(\mu\text{-PCy}_2)_3(Cy_2PH)]$ (**2**) were prepared and the X-ray crystal structure of **1** has been determined. Both compounds react in solution with carbon monoxide to yield the novel triruthenium cluster $[Ru_3(CO)_9(\mu\text{-H})(\mu\text{-PCy}_2)_3]$ (**3**). Because of unsufficient crystal qualities, only preliminary X-ray crystal structure data of compounds **2** and **3** could be obtained. These investigations showed that the three intermetallic distances in **3** are short enough to be considered as metal–metal bonds. Therefore, complex **3** exhibits, at present, the first electron-rich trimetal cluster containing 52 cluster valence electrons.

Acknowledgements—We thank the Fonds der Chemischen Industrie for financial support and the Degussa AG for a generous loan of $RuCl_3xH_2O$.

REFERENCES

1. Lugan, N., Fabre, P.-L., de Montauzon, D., Lavigne, G., Bonnet, J.-J., Saillard, J.-Y. and Halet, J. F., *Inorg. Chem.*, 1993, **32,** 1363 (and references cited therein).
2. Corrigan, J. F., Dinardo, M., Doherty, S., Hogarth, G., Sun, Y., Taylor, N. J. and Carty, A. J., *Organometallics*, 1994, **13,** 3572 (and references cited therein).
3. Böttcher, H.-C., Graf, M., Merzweiler, K. and Bruhn, C., *Polyhedron*, 1997, **16,** 3253.
4. Béguin, A., Rheinwald, G., Stoeckli-Evans, H. and Süss-Fink, G., *Helv. Chim. Acta*, 1994, **77,** 525.
5. Safarowic, F. J., Bierdeman, D. J. and Keister, J. B., *J. Am. Chem. Soc.*, 1996, **118,** 11805.
6. Arif, A. M., Bright, T. A., Heaton, D. E., Jones, R. A. and Nunn, C. M., *Polyhedron*, 1990, **9,** 1573.
7. Field, J. S., Haines, R. J. and Mulla, F., *J. Organomet. Chem.*, 1992, **439,** C56.
8. Carty, A. J., MacLaughlin, S. A. and Nucciarone, D., in *Phosphorus*-31 *NMR Spectroscopy in Stereochemical Analysis*, ed. J. G. Verkade and L. D. Quinn. VCH, New York, 1987, Chap. 16, p. 559.
9. Cabeza, J. A., del Río, I., Riera, V., Santiago, G.-G. and Sanni, S. B., *Organometallics*, 1997, **16,** 1743 (and references cited therein).
10. Rosen, R. P., Geoffroy, G. L., Bueno, C., Churchill, M. R. and Ortega, R. B., *J. Organomet. Chem.*, 1983, **254,** 89.
11. Bullock, L. M., Field, J. S., Haines, R. J., Minshall, E., Moore, M. H., Mulla, F., Smit, D. N. and Steer, L. M., *J. Organomet. Chem.*, 1990, **381,** 429.
12. Graf, M., Merzweiler, K., Bruhn, C. and Böttcher, H.-C., *J. Organomet. Chem.*, 1998, **553,** 371.
13. Corrigan, J. F., Doherty, S., Taylor, N. J., Carty, A. J., Boroni, E. and Tiripicchio, A., *J. Organomet. Chem.*, 1993, **462,** C24.
14. Sheldrick, G. M., *SHELXS*-86, *SHELXL*-93, Programs for Crystal Structure Determination. University of Göttingen.

Pergamon

PII: S0277–5387(98)00127–2

Polyhedron Vol. 17, No. 19, pp. 3439–3444, 1998
© 1998 Elsevier Science Ltd
All rights reserved. Printed in Great Britain
0277–5387/98 $19.00+0.00

Complexes of hexadentate NSO donor ligands-III. Nickel(II) complexes of 1,3-di(*o*-salicylaldiminophenylthio)propane and 1,2-di(*o*-salicylaldiminophenylthio)xylene

Shefali Pal,[a] Saktiprosad Ghosh,[a]* Gurucharan Mukherjee[b] and Asok Kumar Nandi[c]

[a]Department of Inorganic Chemistry, Indian Association for the Cultivation of Science, Jadavpur, Calcutta, 700 032, India

[b]Department of Chemistry, Presidency College, Calcutta, 700 073, India

[c]Central Glass and Ceramic Research Institute, Calcutta, 700 032, India

(Received 8 October 1997; accepted 27 March 1998)

Abstract—Nickel(II) complexes of the hexadentate $N_2S_2O_2$ donor ligands, 1,3-di(*o*-salicylaldiminophenylthio)propane (H_2DSALPTP) and 1,2-di(*o*-salicylaldiminophenylthio)xylene (H_2DSALPTX) have been synthesised and characterised. H_2DSALPTP reacted with $NiCl_2.6H_2O$ or $Ni(ClO_4)_2.6H_2O$ in presence of ammonia to give the complex [Ni(DSALPTP)] (**1**). H_2DSALPTX reacted smoothly with $Ni(ClO_4)_2$ to yield the corresponding complex [Ni(DSALPTX)] (**2**). The ligand did not react with $NiCl_2$ in the absence of ammonia but in its presence produced the complex (**2**). The molecular and crystal structure of [Ni(DSAL PTX)] exhibits a very unusual deployment of the six donor sites of the ligand. It crystallises in the orthorhombic system with space group $P2_12_12_1$. In dichloromethane solution both the complexes are found to exhibit Ni(II)/Ni(III) redox couples in their cyclic voltammograms at room temperature with $E_{1/2}$ values 0.87 and 0.78 V (vs. Ag/AgCl).
© 1998 Elsevier Science Ltd. All rights reserved

Keywords: hexadentate NSO-donors; Ni(II) complexes; X-ray and molecular structure; electrochemical studies.

Hexacoordinating flexidentate ligands with ONS donor sites in strategic positions of the donor framework are not commonly encountered in coordination chemistry and our group has explored some of them previously [1, 2]. Disclosure of the fact that nickel is an essential constituent of several hydrogenases [3] and that nickel sites are believed to have a distorted octahedral arrangement consisting of 2 or 3 sulphur atoms and the rest nitrogen and/or oxygen atoms [4, 5] prompted us to undertake the study of nickel complexes of the ligands which have $N_2S_2O_2$ donor sites. Nickel bound to sulphur and nitrogen/oxygen is also present in carbon monoxide dehydrogenases [6]. The catalytic properties of hydrogenase arise from the remarkably low oxidation potential for the nickel(II)/nickel(III) redox couple [3b,7]. In this paper we report the synthesis, characterisation and cyclic voltammetric studies of the nickel(II) complexes of two $N_2S_2O_2$ donor ligands. The molecular structure of [Ni(DSALPTX)] is also reported and it reveals a very large distortion of the coordination environment around the nickel(II) acceptor centre from the perfect octahedron.

EXPERIMENTAL

Synthesis of the ligands

They were prepared by methods described earlier [1].

* Author to whom correspondence should be addressed.

Synthesis of the complexes

[Ni(DSALPTP)](**1**): A solution of $NiCl_2.6H_2O$ (0.24 g, 1 mmol) or $Ni(ClO_4)_2.6H_2O$ (0.33 g, 1 mmol) in methanol (20 cm^3) was added to a stirring solution of the ligand (0.49 g, 1 mmol) in chloroform (20 cm^3) and the mixture was stirred for 1 h. A few drops of 6(N) NH_3 was then added to the mixture. The mixture was further stirred for 48 h. Red precipitate separated out which was recrystallised from methanol (yields: 75%).

[Ni(DSALPTX)] (**2**): This complex was prepared by the same procedure as above by taking $NiCl_2.6H_2O$ (0.24 g, 1 mmol) as the starting metal salt and H_2DSALPTX (0.56 g, 1 mmol) as the ligand, with a few drops of 6(N) NH_3. The complex was recrystallised from methanol with an yield of about 70%. $Ni(ClO_4)_2.6H_2O$ readily reacts with the ligand in the same ratio in absence of NH_3 to give the same orange-red product. It was recrystallised from methanol (yield 75%).

Physical measurements

Physical measurements were done as reported in our earlier communications [1, 2]. Electrochemical data were collected with a BAS CV-27 and a BAS model X-Y recorder at 298 K. The electrodes used were flat platinum disc working electrode, Pt wire auxiliary electrode and a Ag/AgCl reference electrode.

Crystal structure determination of [*Ni*(*DSALPTX*)] (***2***)

X-ray data were collected in Enraf-Nonius-CAD-4 diffractometer for a crystal mounted on top of a glass fibre. The unit cell parameters were determined from a least-square refinement of 17 high angle reflections. The three intensity controlled reflections (-3 1-2, 3-1-2, -4-3-4) checked every hour, showed no significant variations ($\pm 0.5\%$). The intensities were corrected for Lorentz-polarisation effects and an empirical absorption correction was also made [8]. A total of 3250 unique reflections measured contained 3118 with $F_o \geqslant 4\sigma(F_o)$. The structure was solved by direct methods using the program, SHELXS-86 [9] which revealed the positions of all the non-hydrogen atoms. The program SHELXL-93 [10] was used to refine the structure. Refinement on F using anisotropic displacement parameters for all non-hydrogen atoms was performed. Positions of 11 hydrogen atoms were located from the difference Fourier map. The other 14 residual hydrogen atoms were placed in their calculated positions with a temperature factor 1.2 times the U_{eq}. of the parent atom to which it is attached. Coordinates of the 11 hydrogen atoms and their isotropic temperature factors were refined. Figure 1 shows thermal ellipsoid of the molecule, excluding the hydrogen atoms for the clarity of the figure. The final full matrix least-square refinement coverged at R to 0.053. Crystallographic data and additional details regarding data collected and refinement are given in Table 1.

Structure description

The compound [Ni(DSALPTX)] crystallises in the $P2_12_12_1$ space group with four molecules in general position. The ligand binds the Ni(II) acceptor centre in a distorted octahedral pattern. The square base of the octahedron is defined by the O(A), S(B), S(A) and O(B) atoms with two nitrogen N(A) and N(B) in the two apical positions. Selected bond lengths and bond angles are given in Table 2 and a few selected torsion angles are listed in Table 3. The two phenolate oxygen and thioether sulphur donors occupy cis-positions of the distorted square plane defined by O(A)–O(B)–S(A) and S(B) with the Ni(II) ion centrally placed on it with a mean deviation of −0.012(2)A. The bite

Table 1. Crystal data and structure refinement for [Ni(DSALPTX)] (**2**)

Identification code	(**2**)
Empirical formula	$C_{34}H_{26}N_2NiO_2S_2$
Formula weight	617.40
Temperature	293(2) K
Wavelength	1.54187 A
Crystal system	Orthorhombic
Space group	P_{212121}
Unit cell dimensions	$a = 13.0850(10)$ Å $\alpha = 90^\circ$ $b = 14.1150(10)$ Å $\beta = 90^\circ$ $c = 15.252(3)$ Å $\gamma = 90^\circ$
Volume	2817.0(6) $Å^3$
Z	4
Density (calculated)	1.456 gm/cm^3
Absorption coefficient	2.659 mm^{-1}
$F(000)$	1280
Crystal size	$0.20 \times 0.20 \times 0.25$ mm
Theta range for data collection	4.27 to 74.91°
Index ranges	$0 \leqslant h \leqslant 16$, $0 \leqslant k \leqslant 17$, $0 \leqslant l \leqslant 19$
Reflections collected	3250
Unique reflections	3250
$F_o \geqslant 4\sigma(F_o)$	3118
Refinement method	Full-matrix least-squares on F
Data/restraints/parameters	3250/0/415
Goodness-of-fit on F_o	0.292
Final R indices $[F_o > 2\sigma(F_o)]$	$R = 0.0527$
R indices (all data)	$R = 0.0543$
Extinction coefficient	0.0018(3)
Largest diff. peak and hole	1.023 and −0.699 e. $Å^{-3}$

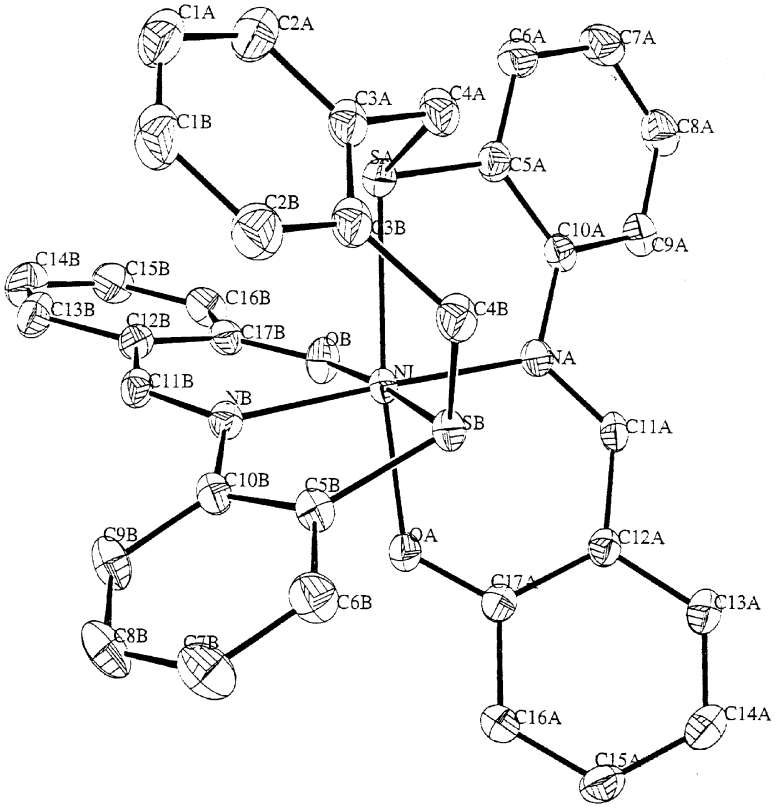

Fig. 1. The thermal ellipsoid of [Ni(DSALPTX)] excluding the hydrogen atoms.

angles involving the two sulphur atoms S(A) and S(B) generates highly distorted seven membered ring Ni–S(B)–C(4B)–C(3B)–C(3A)–C(4A)–S(A). Each bite angle corresponding to a pair of nitrogen and oxygen donors attached to the Ni(II) centre is found to form two six membered rings (Ni–O–C(17)–C(12)–C(11)–N) and the N–S donor pairs to create two five membered chelate rings (Ni–S–C(5)–C(10)–N). The bite angle corresponding to the pair S(A)–Ni–S(B), O(A)–Ni–O(B) are 96.99(5)° and 96.7(2)° respectively and for the other other pair O(A)–Ni–S(B) and O(B)–Ni–S(A) are 81.97(13)° and 84.90(14)° respectively. The severe distortion of the coordination octahedron being clearly manifested in the values of the angles at the metal centre generated by the six donor points. The observed bond distances (vide Table 2) fall well within the range found in most of the distorted octahedral Ni(II) complexes accommodating thioether sulphur coordination [11]. The large distortion of the coordination octahedron is probably arising due to the unusual orientation of the donor sites of the ligand which is very difficult to anticipate and is a clear indication of the flexidentate nature of the ligand.

No hydrogen bonding or any intermolecular short contacts are observed in the lattice. The molecules are packed in the lattice by intermolecular van der Waals forces. Each five-membered and six-membered chelate ring formed with the Ni(II) ion is also attached with a benzene ring and the dihedral angles of each chelate ring with its corresponding benzene ring lie in the range of 6–16°.

RESULTS AND DISCUSSION

The complexes synthesised and characterised during the present investigation are [Ni(DSALPTP)] (**1**) and [Ni(DSALPTX)] (**2**) in which both the ligands function as dibasic hexadentate donors. The ligand H_2DSALPTP did not react at all with either $NiCl_2$ or $Ni(ClO_4)_2$ in the absence of ammonia, but H_2DSALPTX is found to react with $Ni(ClO_4)_2$ in absence of NH_3 to produce a yellowish-green compound. On recrystallisation from methanol it yielded the orange-red compound (**2**). However, H_2DSALPTX does not react with $NiCl_2$ without the presence of ammonia. When, however, the ligand is reacted with $Ni(ClO_4)_2$ in presence of ammonia, a different compound separated out which was identified as $[Ni(DAPTX)(NH_3)](ClO_4)_2$, H_2DAPTX being the diamine dithioether ligand 1,2-di(*o*-aminophenylthio)xylene whose Pd(II), Ni(II) and Cu(II) compounds were reported earlier [12, 13]. It is quite probable that base hydrolysis of the Schiff base generated the ligand *in situ* which then coordinated to the Ni(II) ion. Single crystals for X-ray diffraction

Table 2. Selected bond lengths [Å] and angles [°] for [Ni(DSALPTX)]

Bond lengths (Å) and angles (°) involving Ni atom			
Ni–O(B)	1.988(4)	Ni–N(A)	2.045(5)
Ni–O(A)	1.995(4)	Ni–S(A)	2.448(2)
Ni–N(B)	2.032(4)	Ni–S(B)	2.476(2)
O(B)–Ni–O(A)	96.7(2)	N(B)–Ni–S(A)	98.24(14)
O(B)–Ni–N(B)	91.4(2)	N(A)–Ni–S(A)	83.57(13)
O(A)–Ni–N(B)	88.2(2)	O(B)–Ni–S(B)	174.51(12)
O(B)–Ni–N(A)	90.3(2)	O(A)–Ni–S(B)	81.97(13)
O(A)–Ni–N(A)	90.0(2)	N(B)–Ni–S(B)	83.24(13)
N(B)–Ni–N(A)	177.7(2)	N(A)–Ni–S(B)	95.08(13)
O(B)–Ni–S(A)	84.90(14)	S(A)–Ni–S(B)	96.99(5)
O(A)–Ni–S(A)	173.35(12)		
Bond lengths and angles in the five-membered ring			
S(A)–C(5A)	1.766(6)	S(B)–C(5B)	1.762(5)
C(5A)–C(10A)	1.413(8)	C(5B)–C(10B)	1.398(7)
N(A)–C(10A)	1.408(7)	N(B)–C(10B)	1.428(7)
C(7B)–C(8B)–C(9B)	121.8(6)	C(7A)–C(8A)–C(9A)	120.6(6)
C(5B)–C(10B)–N(B)	118.3(5)	C(5A)–C(10A)–N(A)	118.6(5)
C(10B)–N(B)–Ni	117.4(3)	C(10A)–N(A)–Ni	118.1(4)
C(5B)–S(B)–Ni	93.0(2)	C(5A)–S(A)–Ni	94.6(2)
Bond lengths and angles in the six-membered ring			
N(A)–C(11A)	1.297(7)	N(B)–C(11B)	1.292(7)
C(11A)–C(12A)	1.435(8)	C(11B)–C(12B)	1.434(8)
C(12A)–C(17A)	1.430(8)	C(12B)–C(17B)	1.410(8)
O(A)–C(17A)	1.284(6)	O(B)–C(17B)	1.292(7)
C(11A)–N(A)–Ni	122.0(4)	C(11B)–N(B)–Ni	122.4(4)
N(A)–C(11A)–C(12A)	126.7(5)	N(B)–C(11B)–C(12B)	127.4(5)
C(11A)–C(12A)–C(17A)	123.2(5)	C(17B)–C(12B)–C(11B)	123.2(5)
O(A)–C(17A)–C(12A)	124.4(5)	O(B)–C(17B)–C(12B)	125.7(5)
C(17A)–O(A)–Ni	124.3(3)	C(17B)–OB–Ni	125.5(4)
C(4A)–S(A)–Ni	113.7(2)		
Bond lengths and angles in the seven-membered ring			
S(A)–C(4A)	1.837(6)	C(4B)–S(B)–Ni	125.4(2)
C(3A)–C(3B)	1.400(10)	C(3B)–C(4B)–S(B)	116.1(4)
C(3A)–C(4A)	1.505(9)	C(3A)–C(3B)–C(4B)	122.3(6)
S(B)–C(4B)	1.827(6)	C(3B)–C(3A)–C(4A)	121.8(6)
C(3B)–C(4B)	1.513(8)	C(3A)–C(4A)–S(A)	108.8(4)

Table 3. Lists of selected torsion angles for [Ni(DSALPTX)]

Atoms defining the torsion angles	Angle (°)	Atoms defining the torsion angles	Angle (°)
N(B)–Ni–O(A)–C(17A)	−145.9(4)	N(B)–Ni–S(A)–C(5A)	−166.7(2)
N(A)–Ni–O(A)–C(17A)	32.7(4)	N(A)–Ni–S(A)–C(5A)	14.9(2)
O(B)–Ni–S(A)–C(5A)	−75.9(2)	O(B)–Ni–O(A)–C(17A)	122.9(4)
S(B)–Ni–S(A)–C(5A)	109.2(2)	S(B)–Ni–O(A)–C(17A)	−62.5(4)
O(A)–Ni–S(A)–C(5A)	28.7(2)		

were grown from methanol-ether solution. Two compounds were identified in the crop of crystals. One was the complex (2) and the other one was the Ni(II)-salicylaldehyde complex. This indicates that partial hydrolysis of the imine moiety occurred leading to the rupture of the Schiff base ligand to produce salicylaldehyde, which led to the formation of the Ni(II) salicylaldehyde complex.

Table 4. Analytical data[a], electrical conductivity[b], magnetic moments, infrared and electronic spectral[c] data for the complexes

Complex	C	H	N	Ni	Λ_M (ohm^{-1} cm^2 mol^{-1})	μ_{eff} (B.M.)	ν(C=N)/ ν(Ni–S) (cm^{-1})		λ_{max}, cm^{-1} (ϵ, dm^3 mol^{-1} cm^{-1})
	(%)								
[Ni(DSALPTP)] (**1**)	62.5 (62.7)	4.1 (4.3)	4.9 (5.05)	10.9 (10.6)	3.4	2.95	1605	305	17241(sh), 22727 (17,429), 34482 (24,645)
[Ni(DSAL PTX)] (**2**)	66.4 (66.2)	4.1 (4.2)	4.3 (4.5)	9.9 (9.5)	6.9	3.25	1590	360	17857(sh) 22988(1,794), 31250(38,277) 38461(14,738)

[a]Calculated values in parentheses.
[b]Measured in nitromethane.
[c]Measured in dichloromethane.

Infrared, electronic spectra, magnetic moment and conductance

In the IR spectra of the complex [Ni(DSALPTP)](**1**) and [Ni(DSALPTX)](**2**) the ν(O–H) band of the corresponding ligands observed at 3500 and 3400 cm^{-1} respectively are absent due to the coordination of the deprotonated phenolic –OH to the Ni(II) acceptor centre. The ν(C=N) bands of the ligands observed at 1610 and 1600 cm^{-1} respectively are red shifted by 5–10 cm^{-1} in the spectra of the complexes (**1**) and (**2**) pointing to the involvement of the azomethine nitrogen in coordination. In the complexes (**1**) and (**2**), bonding from the thioether sulphur is indicated by the 50–35 cm^{-1} red shift of the ν(–S–CH_2) mode of the ligands observed as split bands at 700 and 650 cm^{-1} for H_2DSALPTP and at 660 and 640 cm^{-1} for H_2DSALPTX. Bands observed below 400 cm^{-1} (Table 4) (which are absent in the spectra of the ligand) are attributed to Ni–S linkage. These observations are in complete agreement with X-ray crystallographic data. The electronic spectral data supports the octahedral stereochemistry of the complexes (vide Table 4). [Ni(DSAL PTP)] and [Ni(DSAL PTX)] both exhibit bands in the 17,000 cm^{-1} region. The expected lower energy band could not be detected as it is out of the range of the scanning instrument. The third *d-d* band expected in the higher energy region could not be identified due to the presence of intense charge-transfer bands in the UV region. Both the complexes exhibit normal room temperature magnetic moment values of 2.95–3.25 B.M. and both behave as non electrolytes in nitromethane solution. The findings corroborate that both the phenolic-OH are deprotonated during complexation, the ligands coordinating as their dianions DSALPTP^{-2} and DSAL PTX^{-2}.

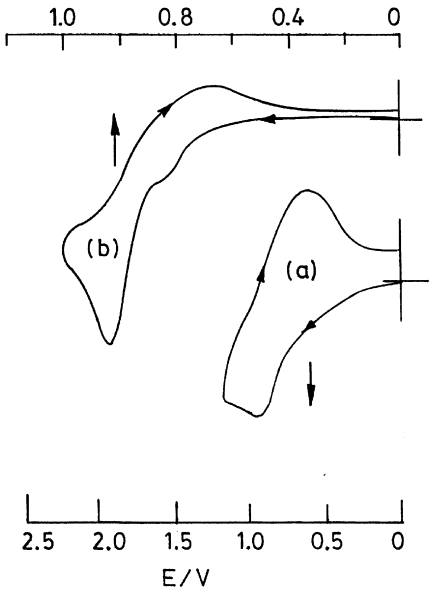

Fig. 2. Cyclic voltammograms of solutions of (a) [Ni(DSALPTP)] (scan rate 200 mvs^{-1}) and (b) [Ni(DSALPTX)](scan rate 50 mvs^{-1}) in dichloromethane using platinum electrode and NEt_4ClO_4 as supporting electrolyte.

Electrochemical studies

Cyclic voltammograms of [Ni(DSALPTP)] and [Ni(DSALPTX)] are shown in Fig. 2 with peak potentials listed in Table 5. Ni(II)-Ni(III) oxidation potential data in the case of thioether complexes generally lie in the range, 0.3–0.8 V [14]. The redox behaviour of the complexes have been examined in dichloromethane solution. The cyclic voltammogram of [Ni(DSALPTP)] exhibits a quasi-reversible Ni(II)/Ni(III) redox couple centered at 0.87 V vs. Ag/AgCl and that of [Ni(DSALPTX)] displays a reversible couple at 0.78 V. Therefore the $E_{1/2}$ values of these complexes lie at the higher end of the thioether contaning Ni(II) species indicating that Ni(II) is fairly stabilised in both the complexes. The ligand

Table 5. Electrochemical data[a]

Complex	$E_{1/2}$ (V)	ΔE_p (mV)[c]
[Ni(DSAL PTP)] (**1**)	0.87	300
[Ni(DSAL PTX)] (**2**)	0.78	120

[a] In CH_2Cl_2 (0.1 M TEAP) at a platinum electrode with an Ag/AgCl reference electrode.
[b] From cyclic voltammetry at a scan rate of 200 mVs^{-1}.
[c] Peak-to-peak separation.

H_2DSALPTP offers comparatively better stabilisation of the Ni(II) state towards oxidation. No cathodic responses was observed for both the complexes up to −1.5 V.

CONCLUSION

This work illustrates the coordination behaviour of two interesting hexadentate NSO donor ligands towards Ni(II). Structure of [Ni(DSALPTX)] exhibits the very unusual deployment of the six donor points of the ligand H_2DSALPTX while coordinating to the Ni(II) acceptor centre. Only single crystal X-ray diffraction study could establish such unusual orientation of the donor sites.

Acknowledgements—We are thankful to the National Diffractometer Facility (DST), Department of Biophysics, All India Institute of Medical Science, New Delhi for X-ray diffraction data collection. S. P. is grateful to C.S.I.R. for financial support in the form of a Research Associateship.

REFERENCES

1. Pal, S., Poddar, S. N. and Mukherjee, G., *Polyhedron*, 1993, **12,** 2465.
2. Pal, S., Poddar, S. N., Ghosh, S. and Mukherjee, G., *Polyhedron*, 1995, **14,** 3023.
3. (a) Thompson, A. J., *Nature*, 1982, **298**, 602; (b) Cammack, R., Lancaster, Jr., J. R. (ed.), *The Bioinorganic Chemistry of nickel*, VCH, New York, (1988), Chapter 8.
4. (a) Lindahl, P. A., Kojima, N., Hausinger, R. P., Fox, J. A., Teo, B. K., Walsh, C. T.and Orme-Johnson, W. H., *J. Am. Chem. Soc*., 1984, **106**, 3062. (b) Scott, R. A., Wallis, S. A., Czechowski, M., Vartannian, D. V. De, Gall, J Le, Peck, Jr., H. D. and Moura, I., *J. Am. Chem. Soc*., 1984, **106**, 3864.
5. (a) Teixeira, M., Moura, I., Xavier, A. V., Huynh, B. H., Vartannian, D. V. De, Peck, Jr., H. D., Gall, J. Le and Moura, J. J., *J. Biol Chem*., 1985, **260**, 8942. (b) Cammack, R., Patil, D., Hatchikian, E. C. and Fernandez, V. M., *Biochem. Biophys. Acta*, 1987, **912**, 98. (c) Teixeira, M., Moura, I., Xavier, A. V., Moura, J. J. G., Gall, J. Le, Vartannian, D. V. De, Peck, Jr., H. D. and Huynh, B. H., *J. Biol. Chem*., 1989, **264**, 16435.
6. Shukla, R., Mondal, S. and Bharadwaj, P. K., *Polyhedron*, 1993, **12,** 83 and references cited therein.
7. Cammack, R., *Adv. Inorg. Chem*., 1988, **32,** 297.
8. North, A. C., Philips, D. C. and Mathews, F. S., *Acta Crystallography*, 1968, **A24,** 351.
9. Sheldrick, G. M., *SHELXS* 86, A program for the solution of crystal structure. University of Gottingen, Germany, (1986).
10. Sheldrick, G. M., *SHELXL* 93, A program for the refinement of crystal structure. University of Gottingen, Germany, (1986).
11. Cooper, S. R., Rawle, S. C., Hartman, J. A. R., Hintsa, E. J. and Admans, G. A., *Inorg. Chem*., 1988, **27,** 1209.
12. Pal, S., Mukherjee, G. and Poddar, S. N., *Trans. Met. Chem*., 1994, **19,** 99.
13. Pal, S., Poddar, S. N. and Mukherjee, G., *Trans. Met. Chem*., 1994, **19,** 449.
14. Karmakar, S., Bhanjachoudhury, S., Ray, D. and Chakraborty, A., *Polyhedron*, 1993, **12,** 291.

Pergamon

PII: S0277–5387(98)00131–4

Polyhedron Vol. 17, No. 19, pp. 3445–3453, 1998
© 1998 Elsevier Science Ltd
All rights reserved. Printed in Great Britain
0277–5387/98 $19.00+0.00

Synthesis, characterisation, electrochemical studies and catecholase activity of a new series of binuclear copper(II) complexes

S. Parimala, K. N. Gita and M. Kandaswamy*

Department of Inorganic Chemistry, University of Madras, Guindy campus, Madras, 600 025, India

(Received 17 February 1998; accepted 13 April 1998)

Abstract—New binucleating ligands L (L-, N′-R-bis(methyl-N-(2-pyridinyl)ketoacetamide) where R = ethylene, 1,3-propylene, o-phenylene were prepared by the condensation of 2 equivalents of methyl-N-(2-pyridinyl) ketoacetamide with the diamines. The binuclear copper(II) complexes of the type $[Cu_2L]X_4$ where

$$X = ClO_4^-$$

and $[Cu_2LX_2]X_2$ where $X = Cl^-$ and Br^- were synthesised by refluxing the ligand with 2 equivalents of Cu(II) salts. Conductivity studies showed a 1:4 electrolyte for perchlorate complexes and a 1:2 electrolyte for chloro and bromo complexes. Room temperature magnetic studies gave moment for the complexes in the range 1.08 to 1.45 B.M which are less than 1.73 B.M for d^9 system. This shows that there is antiferromagnetic coupling between the two copper centers. ESR spectra of the complexes show a broad band which is centered at 3300G and the g values obtained were in the range 2.09–2.14. Electrochemical studies show a quasireversible two electron reduction occuring at the negative potential in the range −0.25 to −0.70 V. The initial rate constant for the oxidation of catechol to o-quinone by the complexes are in the range 1.504×10^{-1} to 3.83×10^{-1} min^{-1}.
© 1998 Elsevier Science Ltd. All rights reserved

Keywords: binucleating ligands; Binuclear Cu(II) complexes; Electrochemical studies; Catecholase activity.

Binuclear copper(II) complexes have attracted immense attention with the onset of the studies of metalloproteins [1–8]. Proteins and enzymes have binuclear metallocites in which the metals are essential for the biological activity [9, 10]. The enzymes like hemocyanin [11], tyrosinase [12] etc, have binuclear copper centers in their active sites. Though these proteins have binuclear copper centers, the functions of the centers vary. For example hemocyanin acts as oxygen carriers, tyrosinase acts as phenolic oxidases. Therefore the properties of the binuclear centers are defined by the geometry, the coordination sites, the bridging ligands between the centers, etc. With the aim of understanding the properties of the metalloproteins, many binucleating ligands and their copper(II) complexes have been synthesised and studied [13, 14].

With the continuation of our studies [15, 16], in this paper, we report the synthesis, characterisation, magnetic and electrochemical studies of new series of binuclear copper(II) complexes. The ability of the complexes to oxidise catechol to o-quinone is also studied.

EXPERIMENTAL

All the reagents and solvents used in this study were commercially obtained. o-phenylenediamine and 2-aminopyridine were used as received. Ethylacetoacetate, ethylenediamine and 1,3-propylenediamine were distilled once before use. Catechol was used after recrystallisation. Copper(II)perchlorate hexahydrate

* Author to whom correspondence should be addressed. Fax: 2352494; E-mail-mkands@unimad.ernet.in

was prepared by treating copper(II)carbonate with an excess of concentrated perchloric acid. All the samples were thoroughly dried prior to elemental analysis, which were performed by Regional Sophisticated Instrumentation Centre, Indian Institute of Technology, Madras.

UV-Visible spectra were recorded using Hitachi 320 model double beam spectrophotometer. Proton NMR spectra were obtained using a Varian XL 300 spectrometer. IR spectra were recorded on a Shimadzu IR 408 spectrometer. Room temperature solid state magnetic susceptibility data were obtained from Guoy balance using $Hg[Co(SCN)_4]$ as the calibrant. Diamagnetic corrections were obtained using Pascal's constants [17]. Conductivity measurements were made using Elico digital conductivity bridge model CM-88 using freshly prepared solutions of the complexes in acetonitrile. Electrochemical measurements were performed at room temperature in DMF using PAR model 173 potentiostat/galvanostat, 175 universal programmer, 176 current follower and 179 coulometer. The cyclic voltammogram were recorded using Perkin Elmer Hitachi model 057 X-Y recorder. A three electrode cell assembly was used in which the working electrode, as well as the counter electrode were platinum and a saturated calomel electrode (SCE) was the reference. Tetrabutylammoniumperchlorate (0.1 M) was used as supporting electrolyte. The concentration of the complexes were 10^{-3}–10^{-4} M. The solutions were deoxygenated by purging nitrogen. Kinetic studies were conducted using Hitachi model 320 double beam spectrophotometer. The catalytic oxidation of catechol to o-quinone by the complexes were studied in a 10^{-4} M DMF solutions. The reaction was followed spectrophotometrically by choosing the strongest absorption band of o-quinone at 390 nm and monitoring the increase in the absorbance at this wavelength as a function of time. A plot of $\log(A_\infty/A_\infty - A_t)$ (where A = Absorbance) Vs time was made for each complex and the rate constant for the catalytic oxidation were calculated.

Ligand synthesis

Methyl-N-(2-pyridinyl)ketoacetamide [18] (*PC*). The compound was prepared by boiling 0.11 mol, 15 ml of ethylacetoacetate with 0.1 mol, 9.4 g of 2-aminopyridine for two minutes. The above mixture was cooled to 0°C, filtered and recrystallised from warm 95% ethanol (Yield:85%). M.p:112°C (lit. 113–114°C).

N,N′-R-bis(methyl-N-(2-pyridinyl)ketoacetamide) (R = ethylene,1,3-propylene, o-phenylene)

The compounds N,N′-R-bis(methyl-N-(2-pyridinyl)ketoacetamide) R = ethylene, 1,3-propylene, o-phenylene) were prepared by dissolving 0.02 mol, 3.56 g of (PC) in minimum amount of ethanol and adding 0.01 mol of the corresponding diamines (ethylenediamine, 1,3-propylenediamine, o-phenylenediamine) and refluxed for one hour. The above solution was cooled and the product obtained was filtered and dried.

N,N′-ethylenebis(methyl-N-(2-pyridinyl) ketoacetamide) (L^1)

Yellow coloured compound (Yield: 95%); M.p:214°C; ^{1}H NMR (DMSO,δ) 1.8 (s, $-CH_3$), 2.7 (s, $-CH_2$ between two imine groups), 4.2 (s, $-CH_2$ between ketone and imine groups), 6.5–8.5 (m, aromatic), 9.1 (s, NH). Mass spectrum, major mass (m/e (relative intensity)): 380 (3.2)P, 287 (2), 259 (3), 204 (4), 176 (4), 162 (12), 97 (34), 83 (28), 78 (7), 68 (12), 57 (100), 42 (10).

N,N′-1,3-propylenebis(methyl-N-(2-pyridinyl) ketoacetamide) (L^2)

Yellow coloured compound (Yield: 80%); M.p: 213°C;^{1}H NMR (DMSO, δ): 1.8 (s, $-CH_3$), 3.1 (s, $-CH_2$ between two imine groups), 4.5 (s, $-CH_2$ between ketone and imine groups), 6.5–7.9 (m, aromatic), 9.1 (s, NH). Mass spectrum, major mass (m/e (relative intensity)): 394 (2)P, 379 (3.2), 261 (2), 218 (3), 162 (8), 121 (10), 97 (40), 83 (40), 68 (8), 57 (100), 42 (9).

N,N′-o-phenylenebis(methyl-N-(2-pyridinyl) ketoacetamide) (L^3)

Yellow coloured compound (Yield: 82%); M.p: 123°C; ^{1}H NMR (DMSO, δ): 1.3 (s, $-CH_3$), 3.6 (s, $-CH_2$ between ketone and imine groups), 8.2–7.4 (m, aromatic). Mass spectrum, major mass (m/e (relative intensity)): 413 (0.05)P, 336 (0.09), 294 (0.14), 176 (2), 162 (2), 135 (3), 121 (6), 93 (2), 253 (1).

Synthesis of metal complexes

Copper(II)perchlorate complexes. $[Cu_2(L)](ClO_4)_4$ were prepared by adding 0.002 mol, 0.74 g of $Cu(ClO_4)_4.6H_2O$ to a hot ethanolic suspension of the ligands (0.001 mol) and refluxing the solution for two hours. The above solution was filtered, the filtrate was cooled and the green coloured crystals obtained were filtered and dried in vacuum.

$[Cu_2(L^1)](ClO_4)_4{\cdot}4H_2O$

Elemental analysis: Calculated for $C_{20}H_{24}O_{18}N_6Cu_2Cl_4$:Theor: C, 26.54; H, 2.65; N, 8.66; Cu, 13.12. Found: C, 26.23; H, 2.45; N, 8.42; Cu, 13.07.

$[Cu_2(L^2)](ClO_4)_4{\cdot}4H_2O$

Elemental analysis: Calculated for $C_{21}H_{26}O_{18}N_6Cu_2Cl_4$: Theor:C, 27.45; H, 2.83; N, 8.55; Cu, 12.93. Found: C, 27.18; H, 2.54; N, 8.49; Cu, 11.89.

$[Cu_2(L^3)](ClO_4)_4{\cdot}4H_2O$

Elemental analysis: Calculated for $C_{24}H_{24}O_{18}N_6Cu_2Cl_4$: Theor: C, 30.17; H, 2.72; N, 8.25; Cu, 12.48. Found: C, 30.08; H, 2.57; N, 8.19; Cu, 12.35.

Copper(II)chloride complexes

$[Cu_2(L)Cl_2]Cl_2$ were prepared by adding 0.002 mol, 0.35 g of $CuCl_2$ to a hot ethanolic suspension of 0.001 mol of the ligand and refluxing for two hours. The resulting solution was filtered and the filtrate was cooled to obtain a brown coloured complex, filtered and dried in vacuum.

$[Cu_2(L^1)Cl_2]Cl_2{\cdot}2H_2O$

Elemental Analysis: Calculated for $C_{20}H_{24}O_2N_6Cu_2Cl_4$: Theor:C, 38.50; H, 4.05; N, 12.45; Cu, 18.50. Found: C, 37.80; H, 4.10; N, 12.40; Cu, 18.35.

$[Cu_2(L^2)Cl_2]Cl_2{\cdot}2H_2O$

Elemental analysis: Calculated for $C_{21}H_{26}O_2N_6Cu_2Cl_4$: Theor:C, 42.50; H, 4.39; N, 12.03; Cu, 18.20. Found: C, 42.35; H, 4.19; N, 12.13; Cu, 18.12.

$[Cu_2(L^3)Cl_2]Cl_2{\cdot}2H_2O$

Elemental analysis: Calculated for $C_{24}H_{24}O_2N_6Cu_2Cl_4$: Theor:C, 45.30; H, 4.30; N, 11.85; Cu, 18.03. Found: C, 45.15; H, 4.28; N, 11.81; Cu, 18.01.

Copper(II)bromide complexes

$[Cu_2(L)Br_2]Br_2$ complexes was prepared by refluxing an ethanolic suspension of the ligand (0.001 mol) with 0.002 mol, 0.442 g of $CuBr_2.2H_2O$ for two hours. The resulting solution was filtered, the filtrate was cooled and the brown coloured complex obtained was filtered and dried in vacuum.

$[Cu_2(L^3)Br_2]Br_2{\cdot}2H_2O$

Elemental analysis: Calculated for $C_{24}H_{24}O_2N_6Cu_2Br_4$: Theor:C, 40.18; H, 3.62; N, 9.58; Cu, 11.5. Found: C, 40.05; H, 3.46; N. 9.69; Cu, 11.43.

RESULTS AND DISCUSSION

The ligand Methyl-N-(2-pyridinyl) ketoacetamide was prepared by the condensation of ethylacetoacetate and 2-aminopyridine [18]. The IR spectrum of the compound showed υ(N–H) at 3250 cm^{-1} and υ(C═O) frequencies at 1725 cm^{-1} corresponding to the keto group and 1670 cm^{-1} corresponding to the amido carbonyl group [18, 19]. The binucleating ligands were prepared by the condensation of one mole of diamine and two moles of methyl-N-(2-pyridinyl)ketoacetamide.

IR spectra of the ligands showed a peak in the range 3245–3255 cm^{-1} which corresponds to υ(N–H) vibrations, a peak at 1660–1680 cm^{-1} which corresponds to υ(amido carbonyl group) and a peak at 1620–1640 cm^{-1} which corresponds to υ(C═N). The precursor compound and the ligand have common peaks at 3200 and 1670 cm^{-1}. This is due to υ(N–H) and amido carbonyl vibrations. The 1725 cm^{-1} peak present in the precursor compound, which corresponds to the keto group, is not present in the ligands. In the ligands there is an additional peak at 1620 cm^{-1} corresponding to the C═N frequency. This indicates that a complete Schiff base condensation has taken place in the reaction.

Synthesis of copper complexes are shown in scheme 1. The copper complexes showed υ(C═O) in the range 1640–1660 cm^{-1}, υ(N–H) in the range 3250–3350 cm^{-1}, υ(C═N) in the range 1620–1630 cm^{-1}, $\upsilon(ClO_4)$ in the range 1100–1110 cm^{-1} and $\upsilon(H_2O)$ in the range 3480–3550 cm^{-1}. The IR spectral data of the ligands and the complexes are given in Table 1.

Electronic spectra

The data of electronic spectra of the complexes are given in Table 2. These complexes show peaks in the visible as well as in the UV region. A broad band was observed for all the complexes in the visible region of 800–500 nm which are assigned to the d–d transitions of the metal ions. A ligand to metal charge transfer band was observed in the range 310–380 nm. The chloro and bromo complexes show d–d band at longer wavelengths than the perchlorate complexes. This

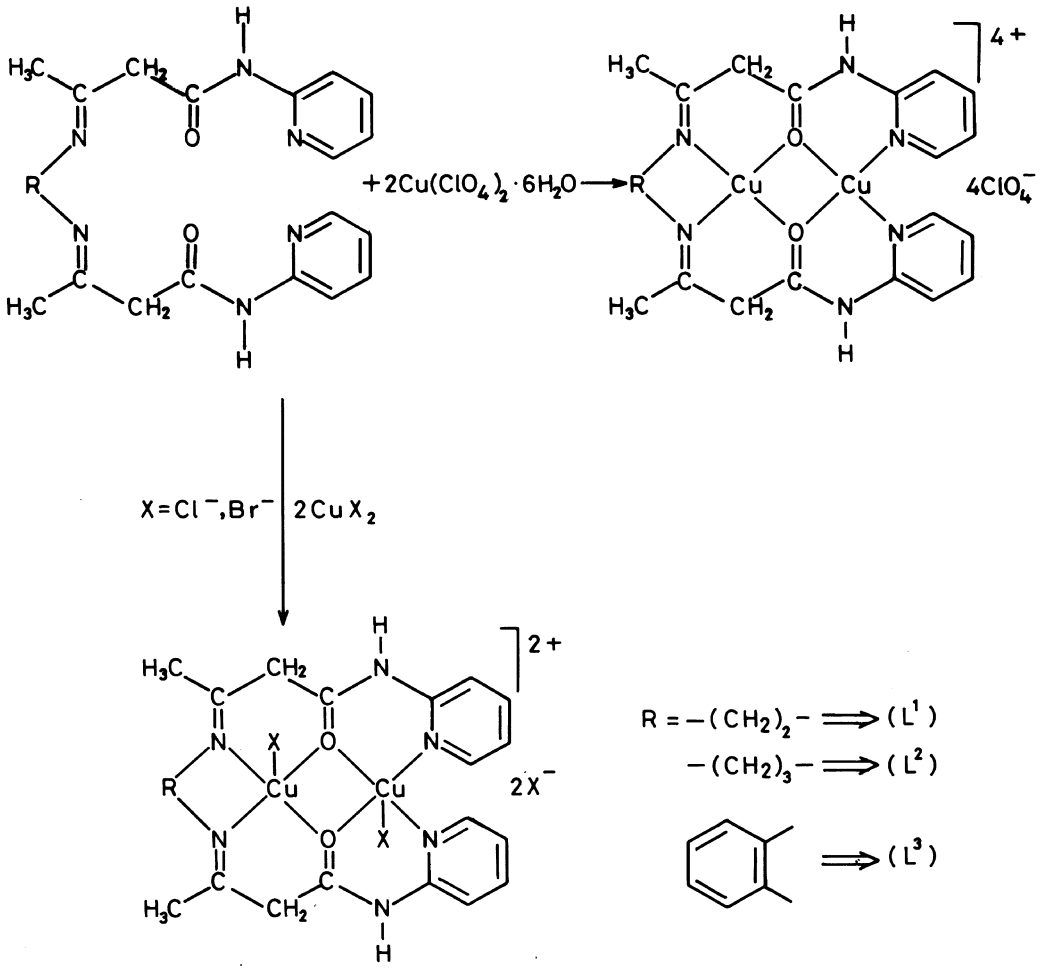

Scheme 1.

may be due to the distortion of geometry upon coordination of chloride or bromide to copper ions.

Conductance measurements

The equivalent conductance of the perchlorate complexes were carried out in acetonitrile and the values were found to be in the range 391–481 ohm $^{-1}$ cm^2 mol^{-1} suggesting that the complexes belong to 1:4 electrolytes [20]. This indicates that the perchlorate is not coordinated to the metal in solution. Equivalent conductance of chloride complexes carried out in acetonitrile were found in the range 180–209.1 ohm $^{-1}$ cm^2 mol^{-1} suggesting that the chloride complexes belong to 1:2 electrolytes. Two chloride ions are outside the coordination sphere and the other two chloride ions are in the axial positions of the Cu(II) centers. The same effect was observed for bromo complex with the equivalent conductance 170.1 ohm$^-$ cm^2 mo1^{-1}. The equivalent conductance data are listed in Table 2.

Magnetic studies

The magnetic susceptibility studies measured at room temperature (298 K) are substantially lower than the spin only value of 1.73 B.M, which may be due to the presence of antiferromagnetic coupling. Room temperature susceptibilities gave μ_{eff} values in the range 1.02–1.13 B.M for the complexes $[Cu_2(L^1)](ClO_4)_4$ and $[Cu_2(L^1)Cl_2]Cl_2$. The reason for such an observation is due to the quenching of the

Table 1. Important Infrared spectral data of the ligands and the complexes

Ligand and Complex	υ N–H cm^{-1}	υ C═O cm^{-1}	υ C═N cm^{-1}	υClO_4^- cm^{-1}
(L^1)	3250	1670	1620	
(L^2)	3245	1675	1625	
(L^3)	3255	1680	1630	
$[Cu_2(L^1)](ClO_4)_4$	3300	1660	1620	1110
$[Cu_2(L^2)](ClO_4)_4$	3280	1655	1625	1110
$[Cu_2(L^3)](ClO_4)_4$	3290	1660	1625	1110
$[Cu_2(L^1)Cl_2]Cl_2$	3250	1660	1630	
$[Cu_2(L^2)Cl_2]Cl_2$	3300	1655	1625	
$[Cu_2(L^3)Cl_2]Cl_2$	3350	1650	1620	
$[Cu_2(L^3)Br_2]Br_2$	3300	1640	1620	

Table 2. Electronic spectral data and equivalent conductance of the complexes

Complex	λ_{max}/nm (ϵ dm^3 mol^{-1} cm^{-1})		Equivalent conductance ohm^{-1} cm^2 mol^{-1}	Type of electrolyte
	Charge transfer band	d-d band		
$[Cu_2(L^1)](ClO_4)_4$ [a]	370 (35000)	680 (520)	392	1:4
$[Cu_2(L^2)](ClO_4)_4$ [a]	320 (24000)	640 (740)	403	1:4
$[Cu_2(L^3)](ClO_4)_4$ [a]	310 (20000)	680 (470)	482	1:4
$[Cu_2(L^1)Cl_2]Cl_2$ [b]	360 (38000)	700 (270)	209	1:2
$[Cu_2(L^2)Cl_2]Cl_2$ [b]	320 (22000)	660 (190)	187	1:2
$[Cu_2(L^3)Cl_2]Cl_2$ [b]	320 (20000)	720 (250)	181	1:2
$[Cu_2(L^3)Br_2]Br_2$ [b]	320 (22000)	750 (220)	170	1:2

a = Acetonitrile b = DMF.

unpaired spin of the metal ion by the unpaired spin on the adjacent Cu(II) ion, coupled by superexchange interaction (Cu–O–Cu). Similar results were observed for the $[Cu_2(L^2)](ClO_4)_4$ and $[Cu_2(L^2)Cl_2]Cl_2$ in the range 1.02–1.15 B.M and for $[Cu_2(L^3)Br_2]Br_2$ with $\mu_{eff} = 1.04$ B.M. The magnetic moment are listed in Table 3.

Table 3. ESR spectral data and Magnetic moment values

Complex	g	μ_{eff} B.M
$[Cu_2(L^1)](ClO_4)_4$	2.09	1.13
$[Cu_2(L^2)](ClO_4)_4$	2.09	1.15
$[Cu_2(L^3)](ClO_4)_4$	2.10	1.03
$[Cu_2(L^1)Cl_2]Cl_2$	2.14	1.02
$[Cu_2(L^2)Cl_2]Cl_2$	2.11	1.03
$[Cu_2(L^3)Br_2]Br_2$	2.13	1.04

ESR spectra

The ESR spectra of the complexes (at 298 K) were obtained in the X band region. The absorption signal for the complexes consist of a broad band centered at 3300 G with a width of 1000 G. The g values were calculated using the equation $h\upsilon = g\beta H$. The hyperfine splitting of copper nucleus was not observed due to the broad signal. The g values are listed in Table 3 and the ESR spectra are shown in Fig. 1.

Electrochemical measurements

The redox behaviour of the complexes have been studied in the negative potential region. The electrochemical data are summarised in the Table 4 and the cyclic voltammogram of some of the complexes are reproduced in the Fig. 2. The cyclic voltammogram exhibit a quasireversible redox wave at negative potential. The quasireversibility is confirmed by the shift in

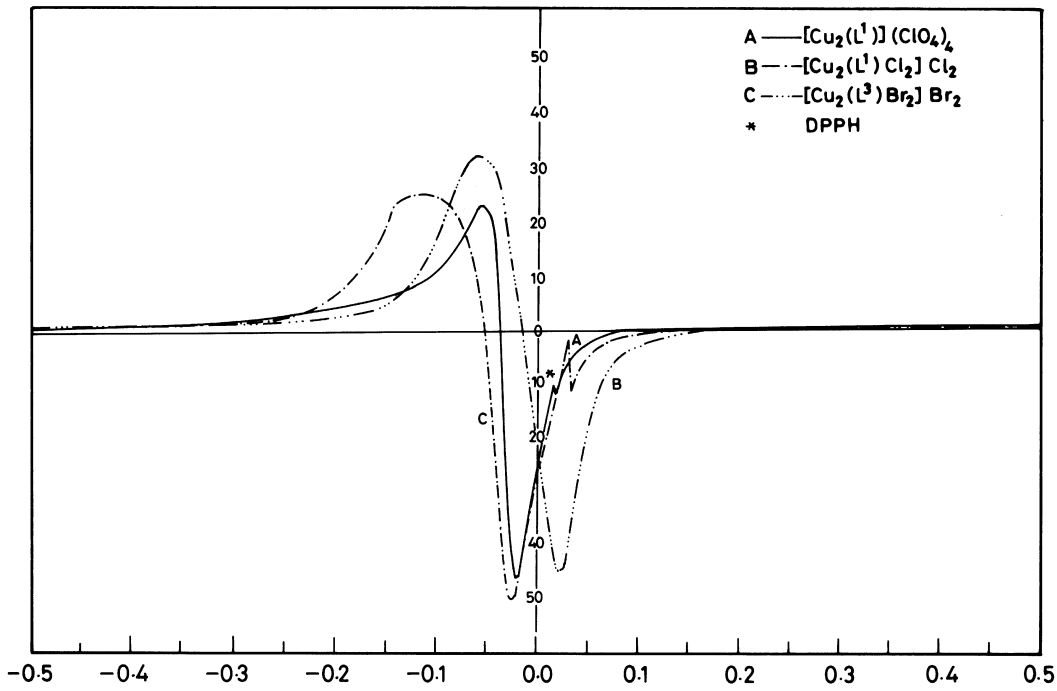

Fig. 1. ESR Spectrum of Dicopper(II) complexes.

Table 4. Cyclic voltammetric data of the complexes

Complex	Scan rates mV/sec	Ep_cV	Ep_aV	ΔEp mV	$E_{1/2}V$
$[Cu_2(L^1)](ClO_4)_4$	20	−0.28	−0.20	80	−0.24
	50	−0.30	−0.20	100	
	100	−0.32	−0.20	120	
	200	−0.34	−0.20	140	
$[Cu_2(L^2)](ClO_4)_4$	20	−0.63	−0.36	270	−0.50
	50	−0.72	−0.36	360	
	100	−0.76	−0.36	400	
	200	−0.78	−0.36	420	
$[Cu_2(L^3)](ClO_4)_4$	20	−0.86	−0.54	320	−0.70
	50	−0.90	−0.50	400	
	100	−0.96	−0.56	400	
	200	−1.04	−0.44	600	

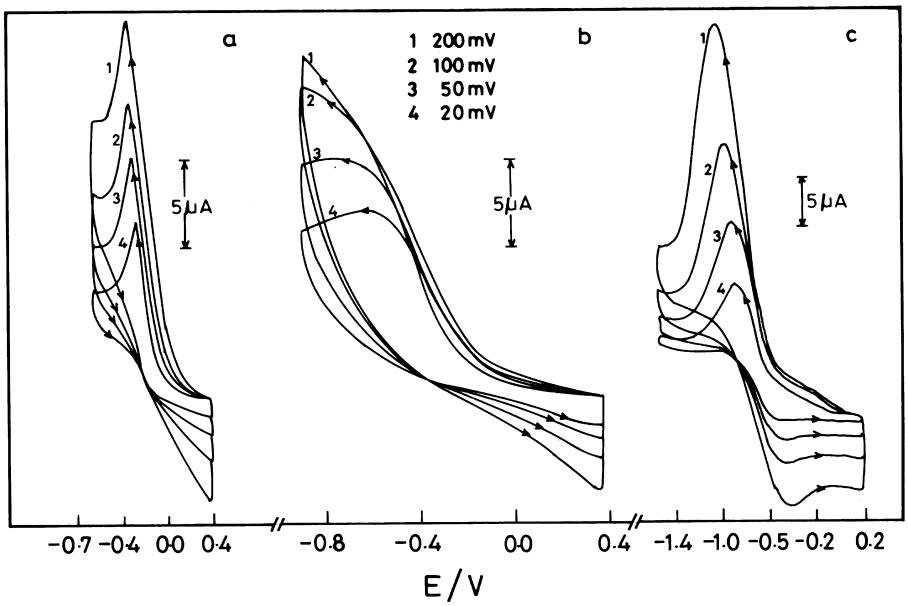

Fig. 2. Cyclic voltammogram of the complexes. a. $[Cu_2(L^1)](ClO_4)_4$; b. $[Cu_2(L^2)](ClO_4)_4$; c. $[Cu_2(L^3)](ClO_4)_4$.

the Ep values and an increase in the ΔEp value with increasing scan rate. The coulometric experiments confirm that the redox couple is associated with two electron transfer process. The electron transfer process of the complexes can be explained by the following scheme.

$$[Cu(II)Cu(II)L]^{n+} + e^- \rightleftharpoons [Cu_2L]^{(n-1)+} + e^- \rightleftharpoons [Cu_2L]^{(n-2)+}$$

This type of reduction process is in agreement with the earlier reports made by Lintvedt [21] *et al.* and E. L. Urbach [22, 23] *et al.* The reduction potentials of the metal centers are influenced by the chelate ring size. The $E_{1/2}$ value for the six membered chelate ring i.e propylenediamine complex is −0.50 V. The $E_{1/2}$ value for the five membered chelate ring i.e. ethylenediamine complex is −0.25 V. The decrease in the $E_{1/2}$ value for the complex $[Cu_2(L^1)](ClO_4)_4$ is due to the distortion in the geometry of the complex as a result of decrease in the chelate ring size [24]. Increased distortion in the coordination geometry around the metal center favours easy electrochemical reduction. The $E_{1/2}$ value for the complex $[Cu_2(L^3)](ClO_4)_4$ is −0.70 V which is higher than the complexes $[Cu_2(L^1)](ClO_4)_4$ and $[Cu_2(L^2)](ClO_4)_4$. This may be due to the presence of o-phenylene moiety, which makes the complex more planar.

Kinetic studies of oxidation of catechol

The Kinetics of oxidation of catechol were determined by the method of initial rates by monitoring the growth of the 390 nm band of the product o-quinone. A linear relationship for initial rate and the complex concentration is obtained for complexes, meaning a first order dependence on the catalytic concentration for the systems. The plot of $\log(A_\infty/A_\infty - A_t)$ Vs time for the catecholase activity of the complexes are shown in Fig. 3 and the rate constant values are reported in Table 5. The perchlorato and the chloro complexes have lower activities than the bromo complexes. This may be attributed to the bromide ligand to be more susceptible for catechol substitution than the chloro or aquo (perchlorato counter ion complexes) ligands. The rate constant for the oxidation of catechol to o-quinone by the complex of ligand L^1 and ligand L^3 are nearly equal and are lower than the complex of ligand L^2. The high value for the complex $[Cu_2(L^2)Br_2]Br_2$ is due to the fact that the complex of ligand L^2 is more planar than the other two ligand (L^1 and L^3) complexes and a planar structure favours easy oxidation [25]. The planarity enhances coordination of one molecule of catechol to two copper ions which increases the rate of oxidation of catechol. It is also observed that the rate constant of the catecholase activity of the binuclear Cu(II) complexes

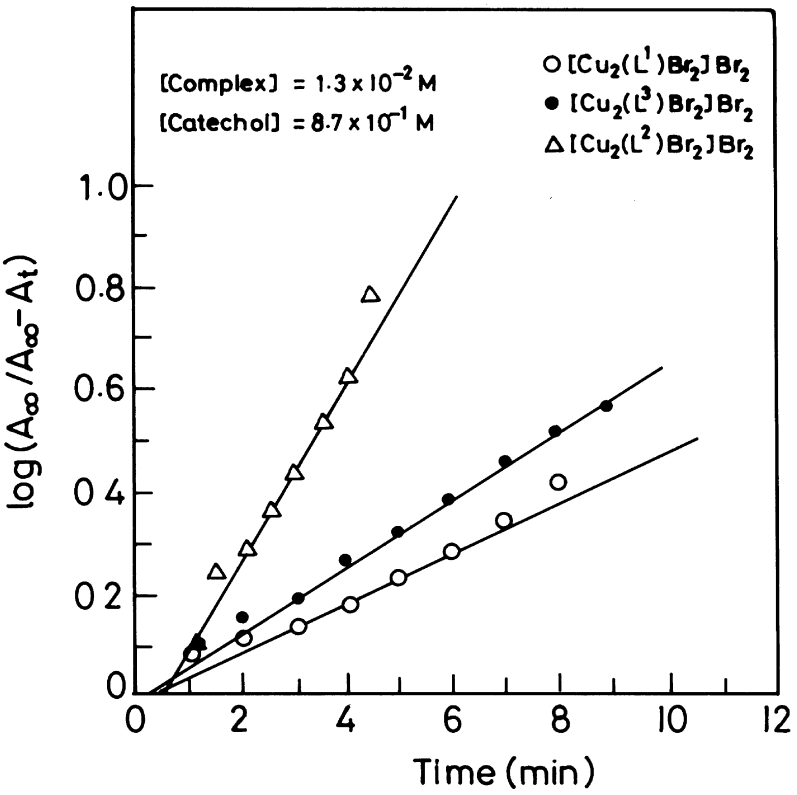

Fig. 3. Oxidation of catechol by Dicopper(II) complexes.

Table 5. Rate constant values for the oxidation of catechol by the complexes

Complexes	Rate constant hr^{-1}
$[Cu_2(L^1)Br_2]Br_2$	9.00
$[Cu_2(L^2)Br_2]Br_2$	23.04
$[Cu_2(L^3)Br_2]Br_2$	11.04
$[Cu_2(L^2)(ClO_4)_4$	8.40
$[Cu_2(L^2)Cl_2]Cl_2$	15.18

is higher than the mononuclear Cu(II) complexes [26, 27].

REFERENCES

1. Vigato, P. A., Tamburini, S. and Fenton, D. E., *Coord. Chem. Rev.*, 1990, **106,** 25.
2. Toman, W. B., Bino, A. and Lippard, S. J., *J. Am. Chem. Soc.*, 1989, **111,** 8522.
3. Wilkins, R. G., *Chem. Soc. Rev.*, 1992, 171.
4. Stassinopoules, A. and Caradonna, J., *J. Am. Chem. Soc.*, 1990, **112,** 7071.
5. Stephan, D. W., *Coord. Chem. Rev.*, 1989, **95,** 41.
6. Doyle, M. P., *Chem. Rev.*, 1986, **86,** 919.
7. Wei, L., Bell, A., Ahn, K. H., Holl, M. M., Warner, S., Williams, I. and Lippard, J., *Inorg. Chem.*, 1990, **29,** 825.
8. Schenk, T., Milne, C. R. C., Sawyer, J. F. and Bosnich, B., *Inorg. Chem.*, 1985, **24,** 2338.
9. Earl Frieden, in *Advances in Experimental medicine and biology in Metal-Protein Interactions*, Vol. 48, p. 11, Plenum Press, New York (1974).
10. Urbach, F. L. *Metal ions in biological systems*, Vol. 13, p. 73 Dekker, New York and Basel (1981).
11. Alben, J. O., Yen, L. and Farrier, N. J., *J. Am. Chem. Soc.*, 1970, **92,** 4475.
12. Moore, K. and Vigee, G. S., *Inorg. Chim. Acta.*, 1982, **66,** 125.
13. Atkins, A. J., Black, D., Blake, A. J., Marin Bacera, A., Parsons, S., Ruiz-Ramirez, L. and Schröder, M., *Chem. Commun.*, 1996, 457.
14. Rybak-Akimova, E. V., Busch, D. H., Kahol, P. K., Pinto, N., Alcock, N. W. and Clase, H. J., *Inorg. Chem.*, 1997, **36,** 510.
15. Karunakaran, S. and Kandaswamy, M., *J. Chem. Soc., Dalton Trans.*, 1994, 1595.
16. Karunakaran, S. and Kandaswamy, M., *J. Chem. Soc., Dalton Trans.*, 1995, 1851.
17. Porterfield, A., (Ed) in Inorganic chemistry, Addison–Wesley p. 456.
18. Iliopoules, P., Fallon, G. D. and Murray, K. S., *J. Chem. Soc., Dalton Trans.*, 1986, 437.
19. Nakamato, K. in *Infrared and Raman Spectra of*

Inorganic and coordination compounds, 3rd Edition., Wiley, New York (1978).
20. Geary, W. J., *Coord. Chem. Rev*., 1971, **7,** 81.
21. Fenton, D. E., Schroeder, R. R. and Iintvedt, R. L., *J. AM. Chem. Soc*., 1978, **100,** 1931.
22. Gagne, R. R., Freh, R. P. and Dodge, J. A., *J. Am. Chem. Soc*., 1979, **101,** 6917.
23. Latour, J. M., Lamonsin, D. and Tandon, S. S., *Inorg. Chim. Acta*., 1985, **107,** L1.
24. Lever, A. B., Pickens, S. R., Ramaswamy, B. S. and Thomson, L. K., *Inorg. Chim. Acta*., 1980, **46,** L59.
25. Fraser, C. and Bosnich, B., *Inorg. Chem*., 1984, **33,** 338.
26. Moore, K. and Vigee, G. S., *Inorg. Chim. Acta*., 1982, **66,** 125.
27. Vigee, G. S. and Eduok, E. E., *J. Inorg. Nucl. Chem*., 1981, **43,** 2171.

Pergamon

PII: S0277–5387(98)00132–6

Polyhedron Vol. 17, No. 19, pp. 3455–3466, 1998
© 1998 Elsevier Science Ltd
All rights reserved. Printed in Great Britain
0277–5387/98 $19.00+0.00

Halocarbonyl alkyne complexes of molybdenum(II): crystal structures of $[MoI_2(CO)(NCMe)(\eta^2\text{-}RC_2R)_2]$ (R = Me and Ph) and $[MoI_2(CO)(5,6\text{-}Me_2\text{-}1,10\text{-}phen)(\eta^2\text{-}PhC_2Ph)]$

Nicholas G. Aimeloglou,[a] Paul K. Baker,[a,*] Margaret M. Meehan[a] and Michael G. B. Drew[b]

[a] Department of Chemistry, University of Wales, Bangor, Gwynedd, LL57 2UW, U.K.

[b] Department of Chemistry, University of Reading, Whiteknights, Reading, RG6 6AD, U.K.

(Received 16 January 1998; accepted 13 April 1998)

Abstract—Reaction of $[MoXX'(CO)_3(NCMe)_2]$ with RC_2R' in CH_2Cl_2 at room temperature gave the bis (alkyne) complexes $[MoXX'(CO)(NCMe)(\eta^2\text{-}RC_2R')_2]$ (X = X′ = I, R = R′ = Me; X = X′ = Br, R = R′ = Me, Ph; X′ = I, X = Cl, Br, R = R′ = Me, Ph) (**1**→**7**) in high yield. The molecular structures of $[MoI_2(CO)(NCMe)(\eta^2\text{-}RC_2R)_2]$ (R = Me, Ph) have been determined by X-ray crystallography. The two structures are very similar, with the two alkyne ligands *cis*- and parallel to each other and *trans*- to the two iodo ligands. The carbon monoxide and acetonitrile ligands occupy the two axial sites. Treatment of $[MoI_2(CO)(NCMe)(\eta^2\text{-}RC_2Ph)_2]$ with an equimolar amount of L⌒L {for R = Ph, L⌒L = 5,6-Me_2-1,10-phen, $Ph_2P(CH_2)_2PPh_2$; for R = Me, L⌒L = 2,2′-bipy, $Ph_2P(CH_2)_nPPh_2$, $n = 1, 3, 4$} yielded the mono(alkyne) complexes $[MoI_2(CO)(L⌒L)(\eta^2\text{-}RC_2Ph)]$ (**8**→**13**), which for L⌒L = 5,6-Me_2-1,10-phen, R = Ph (**8**) was crystallogaphically characterised. The geometry around the molybdenum centre is essentially octahedral, with the phenanthroline ligand *trans*- to a carbonyl and an iodide ligand, with the alkyne and other iodide group in the axial sites. Reaction of $[MoI_2(CO)(NCMe)(\eta^2\text{-}MeC_2Ph)_2]$ with two equivalents of NaS_2CNMe_2 in CH_2Cl_2 gave $[Mo(CO)(S_2CNMe_2)_2(\eta^2\text{-}MeC_2Ph)]$ (**14**). © 1998 Elsevier Science Ltd. All rights reserved

Keywords: halocarbonyl alkyne complex; molybdenum(II); crystal structures.

Alkyne ligands have orthogonal p_π-orbitals which enables them to have variable electron-donor interactions to a transition-metal centre. This can range from two to four electrons depending upon which complex is being considered [1]. Both experimental studies [2,3] and theoretical calculations [4–7] support this variable electron donor ability of alkynes. A wide range of alkyne complexes of molybdenum(II) and tungsten(II) have been reported [8,9], and the majority of these have alkyne ligands which donate four electrons to the metal.

In 1988 [10], we described the reactions of $[MI_2(CO)_3(NCMe)_2]$ (M = Mo or W) with two equivalents of RC_2R' to yield $[MI_2(CO)(NCMe)(\eta^2\text{-}RC_2R')_2]$ (M = Mo, W, R = R′ = Ph, R = Me, R′ = Ph; M = W, R = R′ = Me, CH_2Cl, *p*-tol, R = Ph, R′ = CH_2OH) and the dimeric molybdenum complex $[\{Mo(\mu\text{-}I)I(CO)(\eta^2\text{-}MeC_2Me)_2\}_2]$. The molecular structures of $[WI_2(CO)(NCMe)(\eta^2\text{-}RC_2R)_2]$ (R = Me and Ph) were crystallographically determined [10]. At the time we considered the molybdenum complexes were much less stable than their tungsten analogues; in particular it was found difficult to isolate [10] the bis(but-2-yne) complex $[MoI_2(CO)(NCMe)(\eta^2\text{-}MeC_2Me)_2]$, which dimerised to give $[\{Mo(\mu\text{-}I)I(CO)(\eta^2\text{-}MeC_2Me)_2\}_2]$. One example of the different reactivity pattern of the two metals has also been previously observed [11], namely the reaction of $[MI_2(CO)(NCMe)(\eta^2\text{-}PhC_2Ph)_2]$ with one equivalent

* Author to whom correspondence should be addressed.

of PPh_3 which gave $[MoI_2(CO)(PPh_3)(\eta^2\text{-}PhC_2Ph)_2]$ or a mixture of products for M = W, namely $[WI_2(CO)(NCMe)(\eta^2\text{-}PhC_2Ph)_2]$, $[WI_2(CO)(PPh_3)(\eta^2\text{-}PhC_2Ph)_2]$ and $[WI_2(CO)(PPh_3)_2(\eta^2\text{-}PhC_2Ph)]$.

We have reinvestigated the reactions of $[MoXX'(CO)_3(NCMe)_2]$ with alkynes to give $[MoXX'(CO)(NCMe)(\eta^2\text{-}RC_2R')_2]$, and in this paper describe their reactivity with both neutral and anionic donor ligands. The molecular structures of the complexes $[MoI_2(CO)(NCMe)(\eta^2\text{-}RC_2R)_2]$ (R = Me and Ph) and $[MoI_2(CO)(5,6\text{-}Me_2\text{-}1,10\text{-phen})(\eta^2\text{-}PhC_2Ph)]$ are also described.

EXPERIMENTAL

All reactions described in this paper were carried out under a dry dinitrogen atmosphere using vacuum/Schlenk line techniques. The starting materials, $[MoXX'(CO)_3(NCMe)_2]$ (X = X′ = I [12], Br [13]; X = Cl, X′ = I [14]; X = Br, X′ = I [15]) and $[MoI_2(CO)(NCMe)(\eta^2\text{-}RC_2Ph)_2]$ (R = Me, Ph) [10] were prepared by the published methods. The solvents diethyl ether and dichloromethane were dried and distilled before use. All chemicals used in this research were purchased from commercial sources.

Elemental analyses (C, H and N) were determined using a Carlo Erba Elemental Analyser MOD 1108 (using helium as a carrier gas). Infrared spectra were recorded as thin $CHCl_3$ films between NaCl plates on a Perkin-Elmer 1600 series FTIR spectrophotometer. ^1H and ^{13}C (referenced to $SiMe_4$) and ^{31}P (referenced to 85% H_3PO_4) NMR spectra were recorded on a Bruker AC 250 NMR spectrometer.

Preparations

$[MoI_2(CO)(NCMe)(\eta^2\text{-}MeC_2Me)_2].\frac{1}{2}CH_2Cl_2$ **1**

To a solution of $[MoI_2(CO)_3(NCMe)_2]$ (1.0 g, 1.9 mmol) dissolved in CH_2Cl_2 (30 cm^3) in a foil covered Schlenk tube at room temperature was added but-2-yne (0.6 g, 7.8 mmol) and the reaction was stirred for 1 hr. The resulting red solution was filtered, and the solvent removed *in vacuo* giving a red crystalline solid of $[MoI_2(CO)(NCMe)(\eta^2\text{-}MeC_2Me)_2].\frac{1}{2}CH_2Cl_2$ **1**. This was recrystallised by cooling a CH_2Cl_2 solution of the complex to −17°C to yield single crystals suitable for X-ray crystallography of **1** as a $\frac{1}{2}$MeOH solvate, which must have arisen as a result of a small amount of MeOH remaining in the degassing unit before degassing the CH_2Cl_2 used in this reaction. Yield 0.9 g, 90%.

Similar reactions of $[MoXX'(CO)_3(NCMe)_2]$ (X = X′ = Br, I, X = Br, Cl, X′ = I) with two equivalents of diphenylacetylene or 4 equivalents of but-2-yne in CH_2Cl_2 gave the products $[MoXX'(CO)(NCMe)(\eta^2\text{-}RC_2R)_2]$ (X = X′ = Br, I; X = Br, Cl, X′ = I; R = Me, Ph) **2**→**7**.

$[MoI_2(CO)(5,6\text{-}Me_2\text{-}1,10\text{-}phen)(\eta^2\text{-}PhC_2Ph)]$ **8**

To a solution of $[MoI_2(CO)(NCMe)(\eta^2\text{-}PhC_2Ph)_2]$ (0.2 g, 0.258 mmol) dissolved in CH_2Cl_2 (20 cm^3) with continuous stirring at room temperature was added, 5,6-Me_2-1,10-phen (0.054 g, 0.258 mmol) and the reaction mixture stirred for 24 hrs. The product was then washed with hexane (20 cm^3) and diethyl ether (30 cm^3) to give the dark orange complex $[MoI_2(CO)(5,6\text{-}Me_2\text{-phen})(\eta^2\text{-}PhC_2Ph)]$ (**8**) (yield = 0.17 g, 93%). Suitable crystals as their $CDCl_3$ solvate for X-ray analysis were grown from $CDCl_3$ at 298 K in an NMR tube over 7 days.

In a similar reaction of $[MoI_2(CO)(NCMe)(\eta^2\text{-}PhC_2Ph)_2]$ with an equimolar amount of $Ph_2P(CH_2)_2PPh_2$ gave $[MoI_2(CO)\{Ph_2P(CH_2)_2PPh_2\}(\eta^2\text{-}PhC_2Ph)]$ (**9**).

$[MoI_2(CO)\{Ph_2P(CH_2)PPh_2\}(\eta^2\text{-}MeC_2Ph)]$ **11**

To a solution of $[MoI_2(CO)(NCMe)(\eta^2\text{-}MeC_2Ph)_2]$ (0.3 g, 0.461 mmol), dissolved in degassed CH_2Cl_2 (20 cm^3), with continuous stirring under a stream of dry dinitrogen, was added $Ph_2P(CH_2)PPh_2$ (0.177 g, 0.461 mmol), and the mixture stirred for 24 hrs. Filtration over Celite and removal of the solvent *in vacuo* gave the dark red crystalline complex $[MoI_2(CO)\{Ph_2P(CH_2)PPh_2\}(\eta^2\text{-}MeC_2Ph)]$ (**11**) (Yield = 0.37 g, 91%), which was then washed with hexane (30 cm^3) and diethylether (20 cm^3).

In a similar fashion, reactions of $[MoI_2(CO)(NCMe)(\eta^2\text{-}MeC_2Ph)_2]$ with an equimolar amount 2,2′-bipy or $Ph_2P(CH_2)_nPPh_2$ ($n = 3, 4$) in CH_2Cl_2 gave the complexes $[MoI_2(CO)(2,2'\text{-bipy})(\eta^2\text{-}MeC_2Ph)]$ (**10**) and $[MoI_2(CO)\{Ph_2P(CH_2)_nPPh_2\}(\eta^2\text{-}MeC_2Ph)]$ (**12**) ($n = 3$) and (**13**) ($n = 4$).

$[Mo(CO)(S_2CNMe_2)_2(\eta^2\text{-}MeC_2Ph)]$ **14**

To a solution of $[MoI_2(CO)(NCMe)(\eta^2\text{-}MeC_2Ph)_2]$ (0.2 g, 0.31 mmol) dissolved in CH_2Cl_2 (20 cm^3) at room temperature was added $Na[S_2CNMe_2]$ (0.08 g, 0.61 mmol) and the reaction mixture stirred for 24 hrs. The resulting solution was filtered, and the solvent removed *in vacuo* giving a purple powder, which was washed with hexane (30 cm^3) and diethyl ether (20 cm^3) to give $[Mo(CO)(S_2CNMe_2)_2(\eta^2\text{-}MeC_2Ph)]$ (**14**). Yield = 0.10 g, 83%.

X-ray crystallography

Crystals of complexes, **1**, $[MoI_2(CO)(NCMe)(\eta^2\text{-}PhC_2Ph)_2]$, and **8** were grown as described in the experimental section. Crystal data for the three structures are given in Table 1, together with refinement details. Bond lengths and angles for the metal coordination spheres of **1**, $[MoI_2(CO)(NCMe)(\eta^2\text{-}PhC_2Ph)_2]$ and **8** are given in Table 2. Data were collected with MoKα

Table 1. Crystal data and structure refinement for 1, $[MoI_2(CO)(NCMe)(\eta^2\text{-}PhC_2Ph)_2]$ and 8.

	(1)	$[MoI_2(CO)(NCMe)(\eta^2\text{-}PhC_2Ph)_2]$	(8)
Empirical formula	C11.5 H17 I_2 Mo N O1.5	C31.25 H23.5 Cl0.5 I2 Mo N O	C29.5 H24.5 Cl1.5 I2 Mo N2
Formula weight	559.02	796.47	825.93
Temperature (K)	293 (2)	293 (2)	293 (2)
Wavelength (Å)	0.71073	0.71073	0.71073
Crystal system	triclinic	monoclinic	monoclinic
Space group	P-1	C2/c	$P2_1/n$
Unit cell dimensions a(Å)	7.662(9)	34.51(3)	14.074(12)
b(Å)	8.024 (9)	10.673(10)	16.496(14)
c(Å)	15.615(14)	19.69(2)	14.862(12)
α(deg)	79.01(1)	(90)	(90)
β(deg)	77.52(1)	115.29(1)	106.23(1)
τ(deg)	88.91(1)	(90)	(90)
Volume ($Å^3$)	920(2)	6558(11)	3315(5)
Z	2	8	4
Density (calculated) (Mg/m^3)	1.960	1.612	1.656
Absorption coefficient (mm^{-1})	4.060	2.345	2.403
F(000)	524	3056	1588
Crystal size (mm)	$0.15 \times 0.20 \times 0.20$	$0.25 \times 0.25 \times 0.35$	$0.3 \times 0.25 \times 0.25$
θ range for data collection (deg)	2.72 to 24.98	2.02 to 25.30	2.47 to 25.15
Index ranges	$0<=h<=9$, $-8<=k<=9$, $-17<=l<=18$	$0<=h<=41$ $-11<=k<=11$ $-23<=l<=21$	$0<=h<=16$ $-19<=k<=19$ $-17<=l<=16$
Reflections collected	2439	7232	6658
Independent reflections (Rint)	2439	4353 (0.0789)	4719 (0.0784)
Data/restraints/parameters	2439/0/171	4353/0/339	4719/0/355
Weighting Scheme (a,b)*	0.093, 5.142	0.251, 0.000	0.209, 0.000
Goodness-of-fit on F^2	1.053	1.002	0.978
Final R indices [$I>2\sigma(I)$] R1	0.0486,	0.1039	0.0894
wR2	0.1385	0.2912	0.2335
R indices (all data) R1	0.0538,	0.1575	0.1442
wR2	0.1453	0.3579	0.2777
Largest diff. peak and hole e.A–-3	1.014, −1.024	1.561, −0.846	2.370, −1.369

* Weighting scheme $w=1/(\sigma^2(F_o^2)+(aP)^2+bP)$, where $P=(F_o^2+2F_c^2)/3$

radiation using the MAR Research Image Plate System. The crystals were positioned at 75 mm from the Image Plate. 95 frames were measured at 2° intervals with a counting time of 2 mins. Data analysis was carried out with the XDS program [16]. All three structures were solved using direct methods with the Shelx86 program [17]. The non-hydrogen atoms were refined with anisotropic thermal parameters. The hydrogen atoms were included in geometric positions and given thermal parameters equivalent to 1.2 times those of the atom to which they were attached. In all three structures, disordered solvent molecules were located. In (**1**), a solvent methanol was given 50% occupancy, in $[MoI_2(CO)(NCMe)(\eta^2\text{-}PhC_2Ph)_2]$ a solvent dichloromethane was given 25% occupancy and in (**8**) a solvent trichloromethane was given 50% occupancy. Empirical absorption corrections were applied [18]. The structures were then refined using Shelxl [19]. All calculations were carried out on a Silicon Graphics R4000 Workstation at the University of Reading.

RESULTS AND DISCUSSION

$[MXX'(CO)(NCMe)(\eta^2\text{-}RC_2R')_2]$ complexes

The starting materials for this research, namely $[MoXX'(CO)_3(NCMe)_2]$ (X=X′=I [12], Br [13]; X=Cl, X′=I [14]; X=Br, X′=I [15]) were prepared as described previously [12–15] by reacting the zero-valent complex *fac*-$[Mo(CO)_3(NCMe)_3]$ (prepared *in situ*) with an equimolar amount of XX′. Reaction of $[MoXX'(CO)_3(NCMe)_2]$ with two equivalents of RC_2R' in CH_2Cl_2 at room temperature gives the bis(alkyne) complexes $[MoXX'(CO)(NCMe)(\eta^2\text{-}RC_2R')_2]$ (X=X′=I, R=R′=Me; X=X′=Br, R=R′=Me, Ph; X=Br, X′=I, R=R′=Me, Ph; X=Cl, X′=I,

Table 2. Bond lengths [A] and angles [deg] for the metal coordination spheres of 1, $[MoI_2(CO)(NCMe)(\eta\text{-}PhC_2Ph)_2]$ and 8.

in (1)	
Mo(1)–C(11)	2.028(10)
Mo(1)–C(51)	2.098(9)
Mo(1)–C(21)	2.104(9)
Mo(1)–C(41)	2.144(10)
Mo(1)–C(31)	2.154(8)
Mo(1)–N(12)	2.206(8)
Mo(1)–I(2)	2.905(2)
Mo(1)–I(1)	2.924(2)
C(11)–Mo(1)–C(51)	109.8(4)
C(11)–Mo(1)–C(21)	109.6(4)
C(51)–Mo(1)–C(21)	96.3(4)
C(11)–Mo(1)–C(41)	74.8(4)
C(51)–Mo(1)–C(41)	35.1(4)
C(21)–Mo(1)–C(41)	105.4(4)
C(11)–Mo(1)–C(31)	74.8(4)
C(51)–Mo(1)–C(31)	105.4(4)
C(21)–Mo(1)–C(31)	34.9(4)
C(41)–Mo(1)–C(31)	93.5(4)
C(11)–Mo(1)–N(12)	163.8(4)
C(51)–Mo(1)–N(12)	80.8(3)
C(21)–Mo(1)–N(12)	80.5(3)
C(41)–Mo(1)–N(12)	115.6(3)
C(31)–Mo(1)–N(12)	115.1(3)
C(11)–Mo(1)–I(2)	83.7(3)
C(51)–Mo(1)–I(2)	163.1(3)
C(21)–Mo(1)–I(2)	88.4(3)
C(41)–Mo(1)–I(2)	157.3(3)
C(31)–Mo(1)–I(2)	87.8(2)
N(12)–Mo(1)–I(2)	84.0(2)
C(11)–Mo(1)–I(1)	83.4(3)
C(51)–Mo(1)–I(1)	87.8(3)
C(21)–Mo(1)–I(1)	163.9(2)
C(41)–Mo(1)–I(1)	86.9(3)
C(31)–Mo(1)–I(1)	157.3(3)
N(12)–Mo(1)–I(1)	84.8(2)
I(1)–Mo(1)–I(2)	83.47(8)
In $[MoI_2(CO)(NCMe)(\eta^2\text{-}PhC_2Ph)_2]$	
Mo(1)–C(11)	2.08(2)
Mo(1)–C(51)	2.09(2)
Mo(1)–C(21)	2.10(2)
Mo(1)–C(31)	2.11(2)
Mo(1)–N(12)	2.17(2)
Mo(1)–C(41)	2.19(2)
Mo(1)–I(2)	2.914(3)
Mo(1)–I(1)	2.946(3)
C(11)–Mo(1)–C(51)	111.1(6)
C(11)–Mo(1)–C(31)	115.0(7)
C(51)–Mo(1)–C(31)	96.5(7)
C(11)–Mo(1)–C(21)	80.1(7)
C(51)–Mo(1)–C(21)	104.1(6)
C(31)–Mo(1)–C(21)	35.5(6)
C(11)–Mo(1)–N(12)	159.0(7)
C(51)–Mo(1)–N(12)	79.4(6)
C(31)–Mo(1)–N(12)	80.4(6)
C(21)–Mo(1)–N(12)	115.9(6)
C(11)–Mo(1)–C(41)	75.6(7)
C(51)–Mo(1)–C(41)	36.1(6)
C(31)–Mo(1)–C(41)	106.3(6)

(*continued on next page*)

Table 2 (continued)

C(21)–Mo(1)–C(41)	92.0(6)
N(12)–Mo(1)–I(2)	115.2(6)
C(11)–Mo(1)–I(2)	81.8(5)
C(51)–Mo(1)–I(2)	162.0(4)
C(31)–Mo(1)–I(2)	88.6(4)
C(21)–Mo(1)–I(2)	90.0(4)
N(12)–Mo(1)–I(2)	84.5(4)
C(41)–Mo(1)–I(2)	156.7(4)
C(11)–Mo(1)–I(1)	76.2(6)
C(51)–Mo(1)–I(1)	86.9(5)
C(31)–Mo(1)–I(1)	165.7(5)
C(21)–Mo(1)–I(1)	156.1(5)
N(12)–Mo(1)–I(1)	86.6(4)
C(41)–Mo(1)–I(1)	84.7(4)
I(2)–Mo(1)–I(1)	84.16(8)
in (8)	
Mo(1)–C(51)	2.033(13)
Mo(1)–C(41)	2.042(11)
Mo(1)–C(11)	2.00(2)
Mo(1)–N(22)	2.202(10)
Mo(1)–N(11)	2.260(10)
Mo(1)–I(2)	2.834(2)
Mo(1)–I(1)	2.868(2)
C(51)–Mo(1)–C(41)	37.3(5)
C(51)–Mo(1)–C(11)	111.9(5)
C(41)–Mo(1)–C(11)	74.6(5)
C(51)–Mo(1)–N(22)	88.0(4)
C(41)–Mo(1)–N(22)	91.5(4)
C(11)–Mo(1)–N(22)	95.5(4)
C(51)–Mo(1)–N(11)	83.8(4)
C(41)–Mo(1)–N(11)	120.3(4)
C(11)–Mo(1)–N(11)	161.0(5)
N(22)–Mo(1)–N(11)	73.6(4)
C(51)–Mo(1)–I(2)	96.2(3)
C(41)–Mo(1)–I(2)	98.6(4)
C(11)–Mo(1)–I(2)	93.3(4)
N(22)–Mo(1)–I(2)	168.1(2)
N(11)–Mo(1)–I(2)	95.7(3)
C(51)–Mo(1)–I(1)	162.7(3)
C(41)–Mo(1)–I(1)	157.0(4)
C(11)–Mo(1)–I(1)	83.8(4)
N(22)–Mo(1)–I(1)	82.9(3)
N(11)–Mo(1)–I(1)	79.5(2)
I(2)–Mo(1)–I(1)	90.1(1)

R = Me, Ph) (**1**→**7**) in good yield. Complexes **1**→**7** have been characterised by elemental analysis (C, H and N) (Table 3), IR (Table 4) and ^{1}H NMR spectroscopy (Table 5). Repeated elemental analysis results and ^{1}H NMR spectroscopy confirmed complexes **1**, **2**, **6** and **7** contained various amounts of CH_2Cl_2 as a solvate in the crystal lattice. Complexes **1**→**7**, although less stable than related tungsten complexes [10, 20, 21], can be stored in the solid state under dinitrogen for several days in the absence of light. Complexes **1**→**7** are soluble in polar chlorinated solvents such as CH_2Cl_2, $CHCl_3$, but very much less soluble in diethyl ether and hydrocarbon solvents.

The IR spectra for complexes **1**→**7**, all show single carbonyl bands which are as expected at lower wavenumber for the but-2-yne complexes compared to the diphenylacetylene analogues. All the complexes **1**→**7** have alkyne stretching bands at considerably lower wavenumber compared to the uncoordinated alkyne.

The complex $[MoI_2(CO)(NCMe)(\eta^2\text{-}PhC_2Ph)_2]$ was prepared as previously described [10]. Single crystals suitable for X-ray analysis of

Table 3. Physical and Analytical Data[a] for the halocarbonyl alkyne complexes of molybdenum(II)

	Complex	Colour	Yield (%)	Analysis (%) C	H	N
1	$[MoI_2(CO)(NCMe)(\eta^2\text{-}MeC_2Me)_2].\frac{1}{2}CH_2Cl_2$	Red	90	23.8 (24.1)	2.9 (2.8)	2.7 (2.6)
2	$[MoBr_2(CO)(NCMe)(\eta^2\text{-}MeC_2Me)_2].2CH_2Cl_2$	Orange	68	26.1 (26.0)	3.2 (3.2)	3.4 (2.6)
3	$[MoBr_2(CO)(NCMe)(\eta^2\text{-}PhC_2Ph)_2]$	Orange	77	54.3 (54.6)	3.4 (3.4)	2.1 (2.0)
4	$[MoBrI(CO)(NCMe)(\eta^2\text{-}MeC_2Me)_2]$	Dark red	81	26.5 (27.5)	3.2 (3.1)	2.4 (2.9)
5	$[MoBrI(CO)(NCMe)(\eta^2\text{-}PhC_2Ph)_2]$	Dark red	81	50.5 (51.0)	3.4 (3.2)	1.6 (1.9)
6	$[MoClI(CO)(NCMe)(\eta^2\text{-}MeC_2Me)_2].CH_2Cl_2$	Orange/Red	89	27.1 (26.5)	2.2 (3.0)	3.0 (2.7)
7	$[MoClI(CO)(NCMe)(\eta^2\text{-}PhC_2Ph)_2].CH_2Cl_2$	Red/Brown	90	49.8 (49.2)	3.5 (3.1)	2.0 (1.8)
8	$[MoI_2(CO)(5,6\text{-}Me_2\text{-}1,10\text{-phen})(\eta^2\text{-}PhC_2Ph)]$	Dark Orange	93	45.4 (45.5)	3.6 (2.9)	3.3 (3.7)
9	$[MoI_2(CO)\{Ph_2P(CH_2)_2PPh_2\}(\eta^2\text{-}PhC_2Ph)]$	Orange	97	52.2 (51.6)	3.1 (3.5)	–
10	$[MoI_2(CO)(2,2'\text{-bipy})(\eta^2\text{-}MeC_2Ph)]$	Dark Green	66	35.0 (34.5)	2.4 (2.3)	4.0 (4.5)
11	$[MoI_2(CO)\{Ph_2P(CH_2)PPh_2\}(\eta^2\text{-}MeC_2Ph)]$	Dark red	91	47.9 (47.9)	3.7 (3.4)	–
12	$[MoI_2(CO)\{Ph_2P(CH_2)_3PPh_2\}(\eta^2\text{-}MeC_2Ph)]$	Brown	80	49.3 (49.0)	4.2 (3.8)	–
13	$[MoI_2(CO)\{Ph_2P(CH_2)_4PPh_2\}(\eta^2\text{-}MeC_2Ph)]$	Purple	67	50.0 (49.6)	4.8 (4.0)	–
14	$[Mo(CO)(S_2CNMe_2)_2(\eta^2\text{-}MeC_2Ph)]$	Dark purple	83	46.9 (46.2)	5.3 (4.9)	6.5 (6.7)

[a] Calculated values in parenthesis.

Table 4. Infrared spectral[a] data for the halocarbonyl alkyne complexes of molybdenum(II)

Complex	$\nu(N\equiv C)/cm^{-1}$	$\nu(C\equiv O)/cm^{-1}$	$\nu(C\equiv C)/cm^{-1}$
1	2307(*w*), 2291(*w*)	2061(*s*)	1612(*w*)
2	2281(*w*), 2254(*w*)	2067(*s*)	1602(*w*)
3	2320(*w*), 2294(*w*)	2095(*s*)	1604(*w*)
4	2319(*w*), 2291(*w*)	2062(*s*)	1598(*w*)
5	2320(*w*), 2282(*w*)	2090(*s*)	1617(*w*)
6	2219(*w*), 2299(*w*)	2062(*s*)	1608(*w*)
7	2323(*w*), 2293(*w*)	2087(*s*)	1601(*w*)
8	–	1958(*s*)	1599(*w*)
9	–	1977(*s*)	1601(*w*)
10	–	1947(*s*)	1600(*w*)
11	–	1953(*s*)	1588(*w*)
12	–	1951(*s*)	1589(*w*)
13	–	1948(*s*)	1590(*w*)
14	–	1963(*m*)	1956(*w*)

[a] Spectra were recorded in $CHCl_3$ as thin films between NaCl plates.
s = strong, *m* = medium, *w* = weak.

$[MoI_2(CO)(NCMe)(\eta^2\text{-}RC_2R)_2]$ (R = Me, Ph) were grown by cooling a CH_2Cl_2 solution of the complexes to $-17^\circ C$ for 24 hrs. The single crystal chosen for X-ray analysis of complex **1** contained a $\frac{1}{2}$MeOH solvate in the crystal lattice which probably arose from small quantities of MeOH in the degassing unit containing CH_2Cl_2. This is surprising, but complex **1** has been prepared a number of times and from elemental analysis results and ^1H NMR spectroscopy is always confirmed as a $\frac{1}{2}CH_2Cl_2$ solvate. It must be that the suitable single crystal of **1** chosen for X-ray analysis as a $\frac{1}{2}$MeOH solvate is not representative of the bulk sample of complex **1**. The structures of **1** and $[MoI_2(CO)(NCMe)(\eta^2\text{-}PhC_2Ph)_2]$ are shown in Figs 1 and 2 together with the atomic numbering schemes. The geometry of the coordination spheres for both complexes are listed in Table 2. Both structures are isomorphous with their tungsten analogues [10] and contain equivalent coordination spheres with the molybdenum atoms bonded to two iodide atoms, one carbonyl group, one acetonitrile group and two alkyne ligands. The geometry of the coordination spheres can best be considered as six-coordinate with the alkyne ligands each occupying one coordination site. The two

Table 5. Proton NMR data (δ)* for the halocarbonyl alkyne complexes of molybdenum(II)

Complex	δ (ppm)
1	5.3 (*s*, 1 H, $C\underline{H}_2Cl_2$); 2.9 (*s*, 6 H, C_2Me); 2.8 (*s*, 6 H, MeC_2); 2.3 (*s*, 3 H, NC*Me*)
2	5.3 (*s*, 4 H, $C\underline{H}_2Cl_2$); 3.0 (*s*, 6 H, C_2Me); 2.8 (*s*, 6 H, MeC_2); 2.2 (*s*, 3 H, NC*Me*)
3	7.9→7.5 (*m*, 20 H, *Ph*); 2.2 (*s*, 3 H, NC*Me*)
4	2.9 (*s*, 6 H, MeC_2); 2.7 (*s*, 6 H, MeC_2); 2.3 (*s*, 3 H, NC*Me*)
5	7.8→7.4 (*m*, 20 H, *Ph*); 2.3 (*s*, 3 H, NC*Me*)
6	5.3 (*s*, 2 H, $C\underline{H}_2Cl_2$); 3.0 (*s*, 6 H, C_2Me); 2.9 (*s*, 6 H, C_2Me); 2.2 (*s*, 3 H, NC*Me*)
7	7.8→7.6 (*m*, 20 H, Ph); 5.3 (*s*, 2 H, $C\underline{H}_2Cl_2$); 2.2 (*s*, 3 H, NC*Me*)
8	9.7→9.6 (*br m*, 2 H, phen); 8.9→8.6 (*br m*, 2 H, phen); 8.0→7.6 (*br m*, 2 H, phen); 7.6–7.3 (*br m*, 10 H, Ph); 2.9→2.7 (*br m*, 6 H, Me)
9	8.0→6.5 (*br m*, 30 H, Ph); 3.4→3.2 (*br m*, 2 H, PCH_2); 2.9→2.7 (*br m*, 2 H, PCH_2)
10	8.5→8.4 (*d*, 2 H, bipy); 8.3→8.0 (*br m*, 2 H, bipy); 7.8→7.7 (*br m*, 2 H, bipy); 7.5→7.4 (*br m*, 2 H, bipy); 7.3→7.2 (*br s*, 5 H, C_2Ph); 2.8 (*s*, 3 H, C_2Me)
11	8.0→6.9 (*br m*, 25 H, Ph); 4.8→4.7 (*br m*, 2 H, PCH_2); 2.6 (*s*, 3 H, C_2Me)
12	7.5→6.6 (*br m*, 25 H, Ph); 2.9→2.7 (*br m*, 4 H, PCH_2); 2.6 (*s*, 3 H, C_2Me); 2.5→2.3 (*br m*, 2 H, PCH_2CH_2)
13	7.9→6.6 (*br m*, 25 H, Ph); 2.9→2.7 (*br m*, 4 H, PCH_2); 2.6 (*s*, 3 H, C_2Me); 2.5→2.3 (*br m*, 4 H, PCH_2CH_2)
14	7.5→7.0 (*br m*, 5 H, Ph); 3.1 (*s*, 12 H, S_2CNMe_2); 2.7 (*s*, 3 H, C_2Me)

* Spectra recorded in $CDCl_3$ (+25°C) and referenced to $SiMe_4$: *s* = singlet, *br* = broad, *d* = doublet, *m* = multiplet.

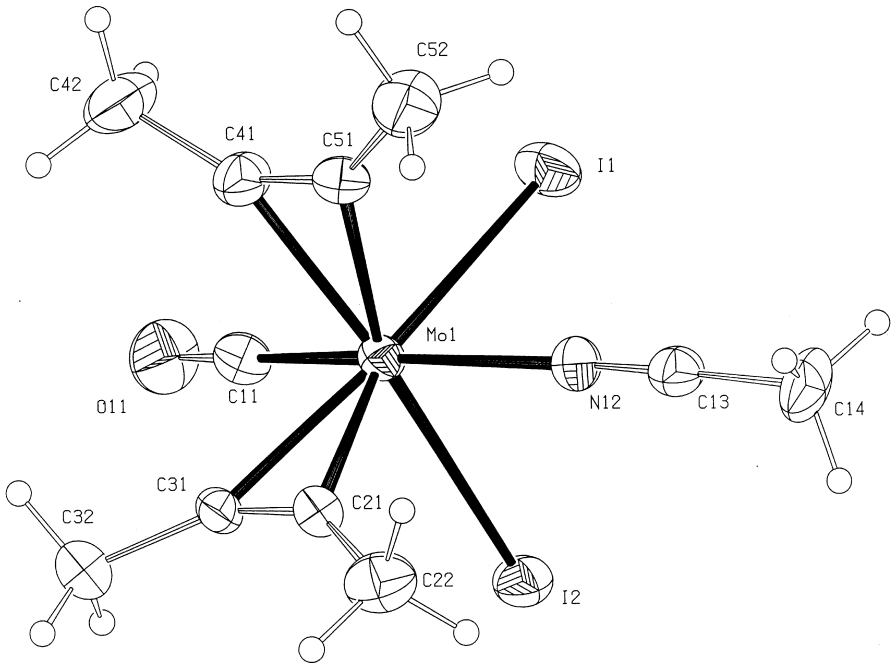

Fig. 1. Crystal structure of $[MoI_2(CO)(NCMe)(\eta^2\text{-}MeC_2Me)_2]$ (**1**) showing the atom numbering scheme. Ellipsoids shown at 30% probability.

iodine atoms are mutually *cis* and each is *trans* to an alkyne group. The carbonyl group is *trans* to the acetonitrile group.

There is some small difference in geometry between these two molybdenum complexes and their tungsten analogues reflecting the larger size of the molybdenum atom. Thus the Mo–I bond lengths are 2.905 (2), 2.924 (2) in (**1**) and 2.914 (3), 2.946 (3) Å in $[MoI_2(CO)(NCMe)(\eta^2\text{-}PhC_2Ph)_2]$ compared to W–I distances of 2.843–2.862 Å in the tungsten analogues. Similar differences are found in the Mo–N distances and to a lesser extent in the Mo–C distances.

The ^{1}H NMR spectra of complexes **1**→**7** conforms with the structures shown in Figs 1 and 2. The ^{13}C

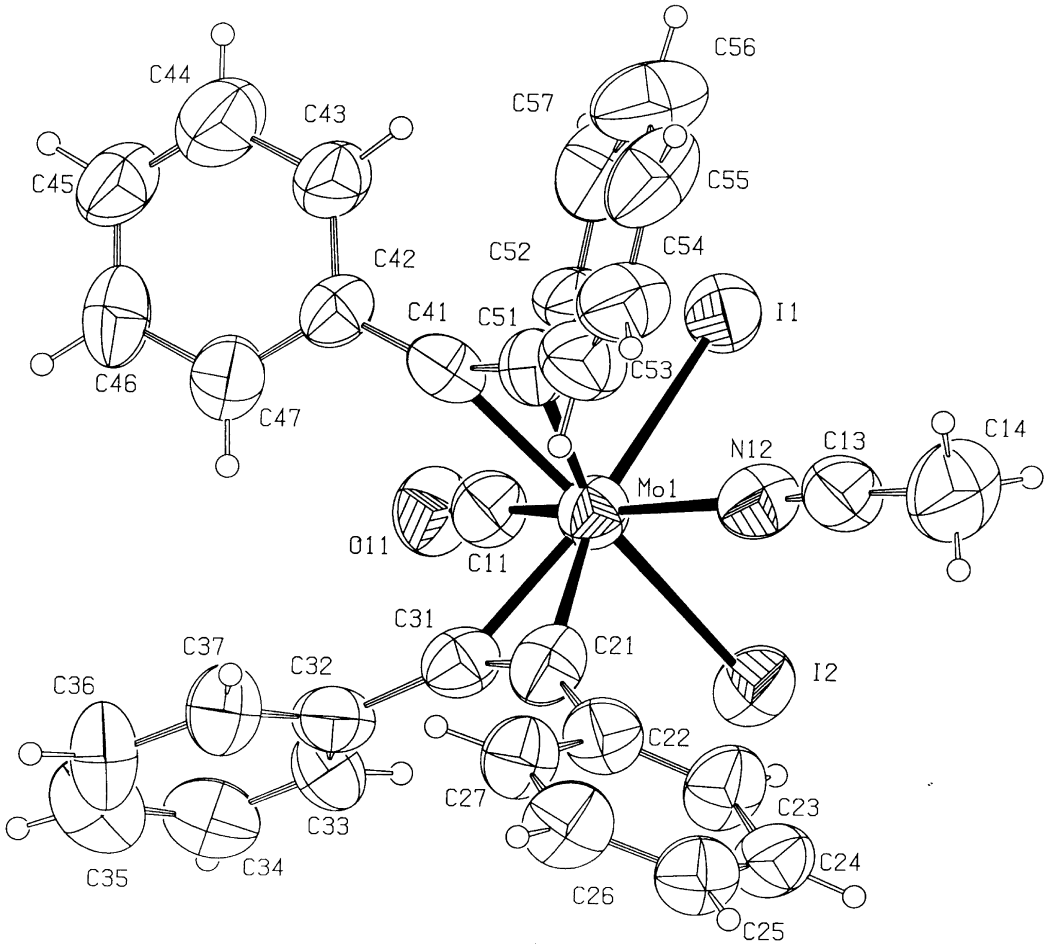

Fig. 2. Crystal structure of $[MoI_2(CO)(NCMe)(\eta^2\text{-}PhC_2Ph)_2]$, showing the atom numbering scheme. Ellipsoids shown at 50% probability.

NMR spectrum of complex **1** has alkyne contact carbon resonances at $\delta = 168.0$ and 159.0 ppm, which conforms with the two alkyne ligands donating a total of six-electrons to the molybdenum [1], which enables the complex to obey the effective atomic number rule.

It should be noted that we reported the mono(acetonitrile) complex $[MoI_2(CO)(NCMe)(\eta^2\text{-}MeC_2Me)_2]$ (**1**) 'could not be isolated in a pure state' [10]. When reinvestigating this reaction we found that reaction of $[MoI_2(CO)_3(NCMe)_2]$ with excess but-2-yne gave high yields of pure complex **1**. As we have previously observed complex **1** reacts in CH_2Cl_2 at room temperature (17 hrs) to afford the dimeric complex $[\{Mo(\mu\text{-}I)I(CO)(\eta^2\text{-}MeC_2Me)_2\}_2]$. The ease of dimerisation of complexes **1** and **2** was investigated by IR spectroscopy. The room temperature reactions of $[MoX_2(CO)_3(NCMe)_2]$ (X = I, Br) with four equivalents of but-2-yne in $CHCl_3$ were followed by IR spectroscopy. Complete dimerisation of the initially formed bis(alkyne) complexes $[MoX_2(CO)(NCMe)(\eta^2\text{-}MeC_2Me)_2]$ to $[\{Mo(\mu\text{-}X)X(CO)(\eta^2\text{-}MeC_2Me)_2\}_2]$ {for X = I, $\upsilon(CO) = 2020$ and 1966 cm^{-1}; for X = Br, $\upsilon(CO) = 2023$ and 1987 cm^{-1}} were observed after 2 hrs (for **1**) and 1 hr (for **2**) respectively. This might be explained by the smaller size of the bromide ligands enabling more rapid formation of the dimeric complex. It should be noted that Davidson and Vasapollo [22] described the reactions of RC_2R (R = Me, Et, Ph) with $[\{W(\mu\text{-}Br)Br(CO)_4\}_2]$ to give the bromide-bridged dimers $[\{W(\mu\text{-}Br)Br(CO)(\eta^2\text{-}RC_2R)_2\}_2]$, which were fully characterised, and are analogous to the dimers, $[\{Mo(\mu\text{-}X)X(CO)(\eta^2\text{-}MeC_2Me)_2\}_2]$ (X = Br, I) described in this paper. The spectroscopic properties of the $[\{Mo(\mu\text{-}X)X(CO)(\eta^2\text{-}MeC_2Me)_2\}_2]$ (X = Br, I) and $[\{W(\mu\text{-}Br)Br(CO)(\eta^2\text{-}RC_2R)_2\}_2]$ (R = Me, Et, Ph) [22] complexes are very similar.

$[MoI_2(CO)(L^{\frown}L)(\eta^2\text{-}RC_2Ph)]$ *complexes*

The reactions of $[MoI_2(CO)(NCMe)(\eta^2\text{-}RC_2Ph)_2]$ with neutral and anionic ligands described in this

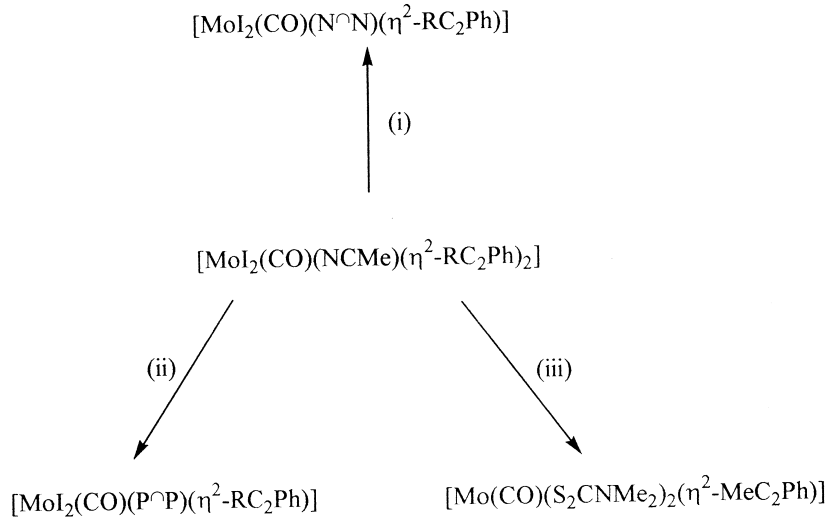

Scheme 1

All reactions were carried out in CH_2Cl_2.

(i) R = Ph, N⌒N = 5,6-Me_2-1,10-phen; R = Me, N⌒N = 2,2′-bipy;
(ii) R = Ph, P⌒P = $Ph_2P(CH_2)_2PPh_2$; R = Me, P⌒P = $Ph_2P(CH_2)_nPPh_2$, n = 1, 3, 4;
(iii) R = Me; 2Na[S_2CNMe_2].

paper are given in Scheme 1. Equimolar quantities of $[MoI_2(CO)(NCMe)(\eta^2\text{-}RC_2Ph)_2]$ and L⌒L in CH_2Cl_2 react at room temperature to give the neutral mono (alkyne) complexes $[MoI_2(CO)(L⌒L)(\eta^2\text{-}RC_2Ph)]$ {R = Ph, L⌒L = 5,6-Me_2-1,10-phen; $Ph_2P(CH_2)_2PPh_2$, R = Me, L⌒L = 2,2′-bipy, $Ph_2P(CH_2)_nPPh_2$ (n = 1, 3, 4)} (**8**→**13**) in high yield. All complexes **8**→**13** have been characterised as shown in Tables 3→5. Complexes **8**→**13** are generally more stable, but less soluble that their bis(alkyne) precursors **1**→**7**.

It is interesting to note [23] that reaction of the analogous tungsten complexes $[WI_2(CO)(NCMe)(\eta^2\text{-}RC_2R)_2]$ (R = Me, Ph) react with an equimolar amount of N⌒N (N⌒N = 2,2′-bipy, 1,10-phen) to afford the cationic bis(alkyne) complexes [WI(CO)(N⌒N)(η^2-$RC_2R)_2$]I, which was crystallographically characterised for N⌒N = 2,2′-bipy, R = Me, as its $[BPh_4]^-$ salt. It is well known that low valent molybdenum organometallic complexes are much more labile than their analogous tungsten compounds. This probably accounts for the greater lability of the alkyne ligand bonded to molybdenum. However, reaction of $[WI_2(CO)(NCMe)(\eta^2\text{-}RC_2R)_2]$ (R = Me, Ph) with an equimolar quantity of $Ph_2P(CH_2)_nPPh_2$ (n = 1→6) in CH_2Cl_2 at room temperature yields the mono(alkyne) complexes $[WI_2(CO)\{Ph_2P(CH_2)_nPPh_2\}(\eta^2\text{-}RC_2R)]$ [11], ie. analogous to the molybdenum reactions. The infra red spectra of **8**→**13** all show a single carbonyl band between 1947 and 1977 cm^{-1}. Alkyne stretching bands are also observed at considerably lower wavenumber compared to the free alkyne.

Single crystals of $[MoI_2(CO)$(5,6-Me_2-1,10-phen)(η^2-$PhC_2Ph)]$ (**8**) have been grown from a concentrated $CDCl_3$ solution of **8** in an NMR tube for one week. The molecular structure of $[MoI_2(CO)$(5,6-Me_2-1,10-phen)(η^2-$PhC_2Ph)]$ (**8**) is shown in Fig. 3 together with the atomic numbering scheme and can also best be described as a distorted octahedron in which the PhC_2Ph ligand occupies one site which is *trans*- to an iodide. The second iodide is *trans*- to a nitrogen atom of the phenanthroline ligand, while the carbonyl group is *trans* to the other nitrogen atom. There is half a molecule of $CDCl_3$ per unit formula of **8** in the crystal lattice since suitable single crystals for X-ray analysis were grown from $CDCl_3$. Complex **8**, prepared in CH_2Cl_2 does not have a molecule of solvent as shown by elemental analysis (C, H and N) Table 3 and ^{1}H NMR spectroscopy Table 5. It is interesting that the two Mo–I bond lengths are considerably shorter than in **1** and $[MoI_2(CO)(NCMe)(\eta^2\text{-}PhC_2Ph)_2]$[2.834 (2), 2.868 (2) Å] but presumably this is due to a decrease in strain as the angle subtended at the metal by the two iodides is 90.1° compared to 83.5 (1), 84.2 (1)° in (**1**) and $[MoI_2(CO)(NCMe)(\eta^2PhC_2Ph)_2]$ respectively.

The ^{1}H NMR data (Table 5) for complexes **8**→**13** comply with the formulation of the complexes. Since we have previously described [11] the synthesis and structure of the but-2-yne complex $[WI_2(CO)\{Ph_2P(CH_2)PPh_2\}(\eta^2\text{-}MeC_2Me)]$, we tried to grow single crystals of complexes **9**, **12** and **13**. Suitable single crystals of $[MoI_2(CO)\{Ph_2P(CH_2)_2PPh_2\}(\eta^2$-$PhC_2Ph)]$ (**9**) were grown and subjected to X-ray analysis. The data collected were poor, however the

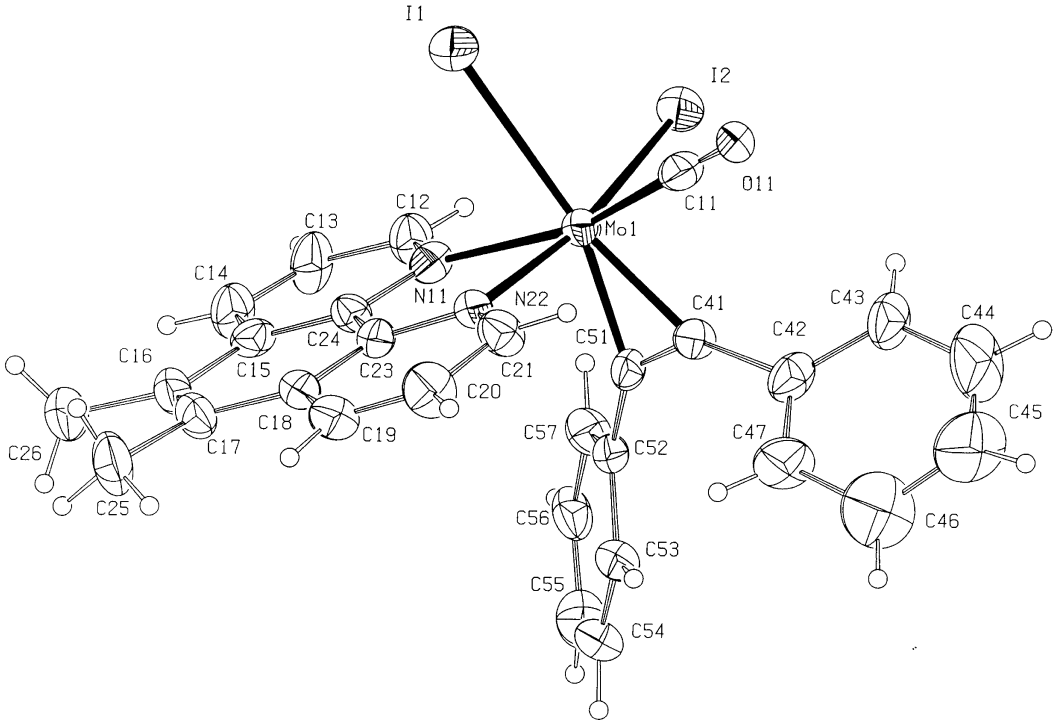

Fig. 3. Crystal structure of $[MoI_2(CO)(5,6\text{-}Me_2\text{-}1,10\text{-phen})(\eta^2\text{-}PhC_2Ph)]$ (**8**), showing the atom numbering scheme. Ellipsoids shown at 30% probability.

basic coordination geometry for the structure is shown in Fig. 4 and is discussed in a footnote[1].

$[Mo(CO)(S_2CNMe_2)_2(\eta^2\text{-}MeC_2Ph)]$ (14) *complex*

Treatment of $[MoI_2(CO)(NCMe)(\eta^2\text{-}MeC_2Ph)_2]$ with two equivalents of NaS_2CNMe_2 in CH_2Cl_2 at room temperature gives the mono(alkyne) complex $[Mo(CO)(S_2CNMe)_2(\eta^2\text{-}MeC_2Ph)]$ (**14**). Complex **14** has been fully characterised in the normal manner (see Tables 3→5). The bis(dithiocarbamate) complex $[Mo(CO)(S_2CNMe_2)_2(\eta^2\text{-}MeC_2Ph)]$ is closely related to the previously reported complexes $[Mo(CO)(S_2CNEt_2)_2(\eta^2\text{-}RC_2R')]$ (R = R′ = H, Ph of CO_2Me; R = H, R′ = Me or Ph; R = Me, R′ = Ph) [24,25], $[Mo(CO)(S_2P^iPr_2)_2(\eta^2\text{-}HC_2H)]$ [26,27] $[W(CO)(S_2CNEt_2)_2(\eta^2\text{-}RC_2R')]$ (R = R′ = H, Me, Et or Ph; R = H, P′ = Ph) [28,29] $[Mo(CO))(S_2CNR_2)(\eta^2\text{-}C_8H_{12})]$ (M = Mo W; R = Me or Ph) [30] and $[W(CO)(L^{\frown}L')_2(\eta^2\text{-}RC_2R')]$ (R = R′ = Me, $L^{\frown}L' = S_2CNMe_2$ or $2\text{-}SC_5H_4N$; R = Ph, R′ = Me, $L^{\frown}L' = S_2CNMe_2$ or S_2PMe_2; R = R′ = Ph, $L^{\frown}L' = S_2PMe_2$) [31]. Since the spectral properties of **14** are similar to the crystallographically characterised complex $[W(CO)(S_2CNEt_2)_2(\eta^2\text{-}HC_2H)]$ [28], the structure of **14** is likely to be similar as shown in Fig. 5.

[1]Data for (**9**), $[MoI_2(CO)\{Ph_2P(CH_2)_2PPh_2\}(\eta^2\text{-}PhC_2Ph)]$, $C_{41}H_{38}I_2MoP_2$, $M = 958.4$, $a = 11.333$ (9), $b = 23.70$ (2), $C = 14.990$ (12) Å, $\beta = 107.50$ (1), $U = 3839$ Å^3, monoclinic, spacegroup $P2_1/c$, $Z = 4$. The crystals gave a highly disordered diffraction pattern, and while the structure was determined, it is of insufficient quality to be reported here in detail. The molybdenum atom occupies an octahedral environment being bonded to two phosphorus atoms *trans* to iodide and the carbonyl group, and a diphenylalkyne *trans* to the second iodide group. The arrangement of ligands is thus different from that observed in $[WI_2(CO)\{Ph_2P(CH_2)PPh_2\}(\eta^2\text{-}MeC_2Me)]$ [11] where the alkyne is *trans* to one of the phosphorus atoms and the iodide groups are *trans* to the remaining phosphorus atom and the carbonyl group.

CONCLUSIONS

Although the bis(alkyne) complexes of molybdenum(II) $[MoXX'(CO)(NCMe)(\eta^2\text{-}RC_2R')_2]$ are less stable than their tungsten analogues, they can be isolated and their chemistry studied. Many of the reactions of the molybdenum and tungsten bis(alkyne) complexes $[MXX'(CO)(NCMe)(\eta^2\text{-}RC_2R')_2]$ are very similar, however their reactions with bidentate nitrogen donors are quite different. For example, the reaction of $[MI_2(CO)(NCMe)(\eta^2\text{-}MeC_2Ph)_2]$ with 2,2′-bipy gives the cationic bis(alkyne) tungsten complex $[WI(CO)(2,2'\text{-bipy})(\eta^2\text{-}MeC_2Ph)_2]I$ [23] and the

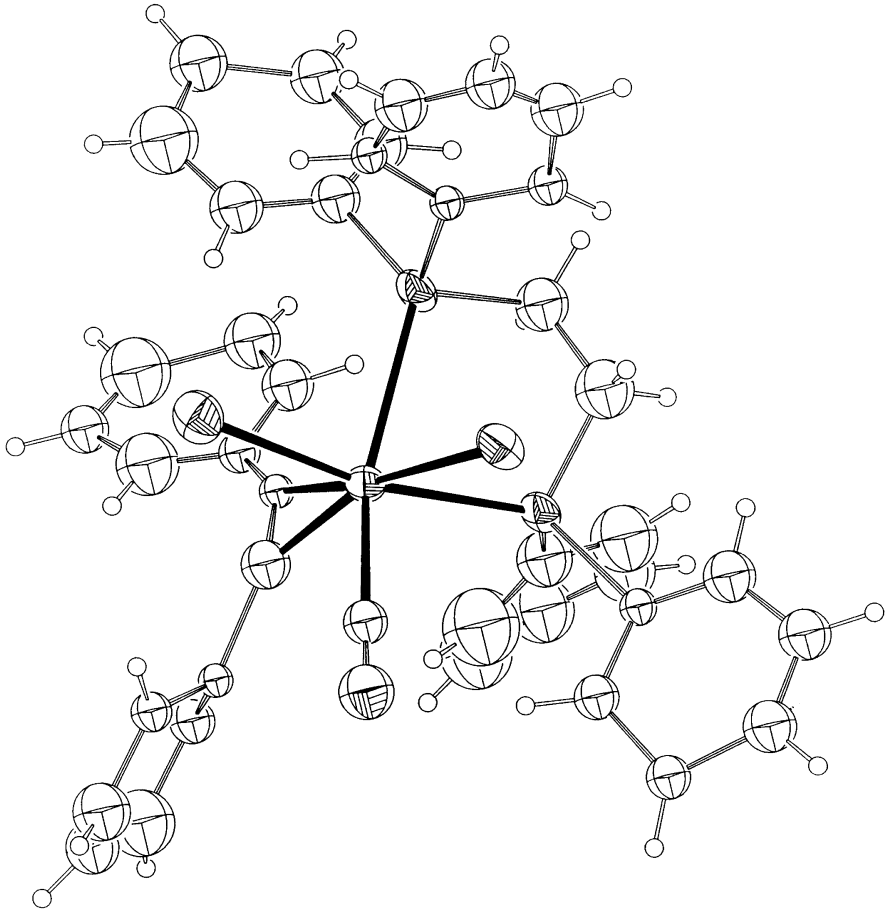

Fig. 4. Ortep picture of $[MoI_2(CO)\{Ph_2P(CH_2)_2PPh_2\}(\eta^2\text{-}PhC_2Ph)]$ (**9**). Ellipsoids shown at 30% probability.

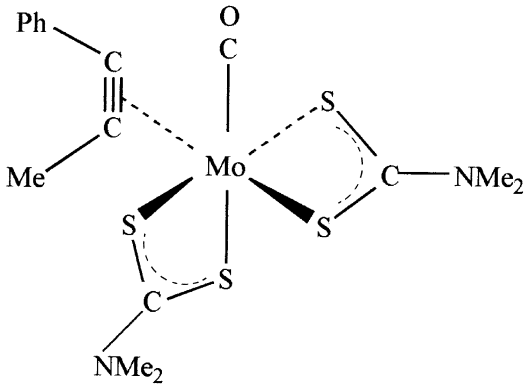

Fig. 5. Proposed structure for $[Mo(CO)(S_2CNMe_2)_2(\eta^2\text{-}MeC_2Ph)]$ (**14**)

neutral mono(alkyne) molybdenum complex $[MoI_2(CO)(2,2'\text{-bipy})(\eta^2\text{-}MeC_2Ph)]$ respectively.

Acknowledgements—M.M.M. thanks the EPSRC for a studentship and N.G.A. thanks the Training for Work scheme for support. We also thank A.W. Johans for his assistance with the crystallographic investigations and the EPSRC and the University of Reading for funds for the Image Plate System.

REFERENCES

1. Templeton, J. L. and Ward, B. C., *J. Am. Chem. Soc.*, 1980, **102,** 3288.
2. Mead, K. A., Morgan, H. and Woodward, P., *J. Chem. Soc., Dalton Trans.*, 1983, 271.
3. Davidson, J. L., *J. Chem. Soc., Dalton Trans.*, 1983, 1667.
4. King, R. B., *Inorg. Chem.*, 1968, **7,** 1044.
5. Braterman, P. S., Davidson, J. L. and Sharp, D. W. A., *J. Chem. Soc., Dalton Trans.*, 1976, 241.
6. Tatsumi, K., Hoffmann, R. and Templeton, J. L., *Inorg. Chem.*, 1982, **21,** 466.
7. Kamata, M., Hirotsu, K., Higuchi, T., Kido, M., Tatsumi, K., Yoshida, T. and Otsuka, S., *Inorg. Chem.*, 1983, **22,** 2416.
8. Templeton, J. L., *Adv. Organomet. Chem.*, 1989, **29,** 1.
9. Baker, P. K., *Adv. Organomet. Chem.*, 1996, **40,** 45.

10. Armstrong, E. M., Baker, P. K. and Drew, M. G. B., *Organometallics*, 1988, **7,** 319.
11. Armstrong, E. M., Baker, P. K., Harman, M. E. and Hursthouse, M. B., *J. Chem. Soc., Dalton Trans.*, 1989, 295.
12. Baker, P. K., Fraser, S. G. and Keys, E. M., *J. Organomet. Chem.*, 1986, **309,** 319.
13. Baker, P. K., Hursthouse, M. B., Karaulov, A. I., Lavery, A. J., Malik, K. M. A., Muldoon, D. J. and Shawcross, A., *J. Chem. Soc., Dalton Trans.*, 1994, 3493.
14. Baker, P. K., Birkbeck, T., Bräse, S., Bury, A. and Naylor, H. M., *Transition-Met. Chem.*, 1992, **17,** 401.
15. Baker, P. K., Flower, K. R., Naylor, H. M. and Voigt, K., *Polyhedron*, 1993, **12,** 357.
16. Kabsch, W., *J. Appl. Cryst.*, 1988, **21,** 916.
17. Shelx86, Sheldrick, G. M., *Acta. Cryst.*, 1990, **A46**, 467.
18. Walker, N. and Stuart, D., *Acta. Cryst.*, 1983, **A39,** 158.
19. Shelxl, Sheldrick, G. M., program for crystal structure refinement, University of Göttingen, 1993.
20. Baker, P. K., Muldoon, D. J., Lavery, A. J. and Shawcross, A., *Polyhedron*, 1994, **13,** 2915.
21. Baker, P. K., Bury, A. and Flower, K. R., *Polyhedron*, 1989, **8,** 2587.
22. Davidson, J. L. and Vasapollo, G., *J. Chem. Soc., Dalton Trans.*, 1985, 2239.
23. Baker, P. K., Armstrong, E. M. and Drew, M. G. B., *Inorg. Chem.*, 1988, **27,** 2287.
24. McDonald, J. W., Newton, W. E., Creedy, C. T. C. and Corbin, J. L., *J. Organomet. Chem.*, 1975, **92,** C25.
25. Templeton, J. L., Herrick, R. S. and Morrow, J. R., *Organometallics*, 1984, **3,** 535.
26. McDonald, J. W., Corbin, J. L. and Newton, W. E., *J. Am. Chem. Soc.*, 1975, **97,** 1970.
27. Newton, W. E., Corbin, J. L. and McDonald, J. W., *Inorg. Synth.*, 1978, **18,** 53.
28. Ricard, L., Weiss, R., Newton, W. E., Chen, G. J.-J. and McDonald, J. W., *J. Am. Chem. Soc.*, 1978, **100,** 1318.
29. Ward, B. C. and Templeton, J. L., *J. Am. Chem. Soc.*, 1980, **102,** 1532.
30. Bennett, M. A. and Boyd, I. W., *J. Organomet. Chem.*, 1985, **290,** 165.
31. Carlton, L. and Davidson, J. L., *J. Chem. Soc., Dalton Trans.*, 1988, 2071.

Pergamon

PII: S0277–5387(98)00133–8

Polyhedron Vol. 17, No. 19, pp. 3467–3475, 1998
© 1998 Elsevier Science Ltd
All rights reserved. Printed in Great Britain
0277–5387/98 $19.00+0.00

Photoassisted reduction of thionyl chloride by neodymium, europium, thulium and lutetium diphthalocyanines

Ngudiankama Nensala and Tebello Nyokong*

Department of Chemistry, Rhodes University, Grahamstown, 6140, South Africa

(Received 11 February 1998; accepted 7 April 1998)

Abstract—Diphthalocyanine complexes of Nd^{III}, Eu^{III}, Tm^{III} and Lu^{III} ($[Pc(-2)Nd^{III}Pc(-2)]^-$, $[Pc(-2)Eu^{III}Pc(-2)]^-$, $[Pc(-2)Tm^{III}Pc(-2)]^-$ and $[Pc(-2)Lu^{III}Pc(-2)]^-$, respectively), undergo one or two-electron oxidation in the presence of thionyl chloride. The oxidation products depend on the concentration of the thionyl chloride. At low concentrations of $SOCl_2$ ($<10^{-4}$ mol dm^{-3}) one-electron oxidation occurs only upon photolysis, giving the neutral lanthanide diphthalocyanine, $Pc(-2)LnPc(-1)$, complexes. The $Pc(-2)LnPc(-1)$ species undergo one-electron photooxidation to the $[Pc(-1)LnPc(-1)]^+$ in dichloromethane and in the presence of $SOCl_2$. At large concentrations of $SOCl_2$ ($>10^{-2}$ mol dm^{-3}), two electron oxidation of the $[Pc(-2)LnPc(-2)]^-$ species directly to $[Pc(-1)LnPc(-1)]^+$ occurs. © 1998 Elsevier Science Ltd. All rights reserved

Keywords: thionyl chloride; diphthalocyanine; photolysis; lanthanide.

Batteries based on lithium–thionyl chloride (Li–$SOCl_2$) chemistry are receiving increasing attention due to their high current density. Research into the reduction mechanism of $SOCl_2$ is thus of current interest [1–3]. It is generally accepted that the cell reaction involves the formation of sulphur, sulphur dioxide and lithium chloride by eq. (1).

$$SOCl_2 + 4LI \rightarrow S + SO_2 + LiCl \quad (1)$$

The formation of sulphur and sulphur dioxide as final products has been confirmed by electrochemical and spectroscopic methods [2]. Intermediate species such as SO and S_2O have been reported [2, 3]. The $SOCl_2$ reduction mechanism is sometimes complicated by the reaction between $SOCl_2$ and the electrolytes [4]. Possible aggregation of $SOCl_2$ may also further complicate the mechanism for its reduction.

The Li/$SOCl_2$ battery can, however, be explosive. Explosions during storage or exposure to the environment of a partly discharged cell have been attributed to unstable intermediates from the $SOCl_2$ reduction [5]. Another disadvantage of the Li/$SOCl_2$ battery is the polarization of the Li anode associated with the prolonged storage of the batteries. It has been suggested that this polarization is caused by a passive film of LiCl formed on the lithium anode. The LiCl film also adds to the complication of the reduction mechanism of $SOCl_2$.

It has been shown that the modification of the carbon cathode of the Li/$SOCl_2$ battery with metallophthalocyanines (MPc(−2), Pc(−2) = phthalocyanine dianion) complexes improves the cell voltage and the lifetime of the battery [6]. The MPc complexes also prevent passivation of the electrode by LiCl. Studies have shown that CoPc and FePc complexes show catalytic activity towards the reduction of $SOCl_2$ [6]. Lanthanide diphthalocyanine (Pc_2Ln) complexes have been extensively studied for their possible applications in visual display devices [7–10]. There has not been much attention paid to the possible use of Pc_2Ln complexes as electrocatalysts. Studies on the photochemical properties of the Pc_2Ln complexes and on the use of these complexes as photocatalysts are limited [11, 12]. We report in this work on the photocatalytic behaviour of the neodymium^{III}, europium^{III}, thulium^{III} and lutetium^{III} diphthalocyanine complexes (**1**) towards the reduction of $SOCl_2$. Redox processes are centred at the phthalocyanine rings in Pc_2Ln complexes. The cationic and

* Email: CHTN@warthog.ru.ac.za.

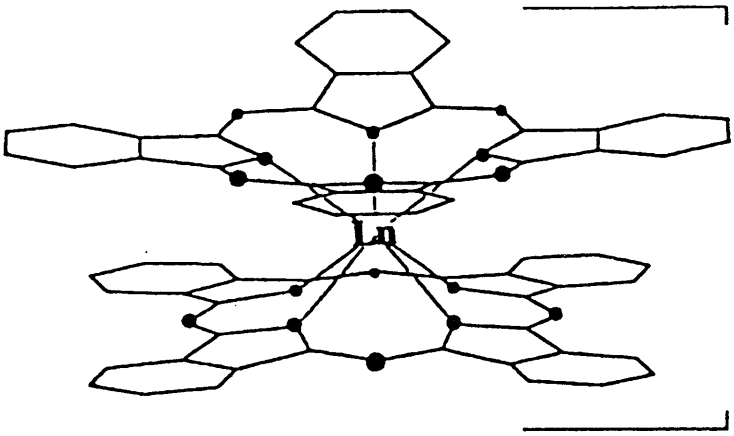

1

anionic species of Pc_2Ln complexes are generally described in terms of their colour. The electronic spectra of the blue, $[Pc(-2)LnPc(-2)]^-$; the green, $Pc(-2)LnPc(-1)$; and the orange/red, $[Pc(-1)LnPc(-1)]^+$complexes have been reported [8, 11, 13–15]. Electronic spectra thus provide a reliable method for assessing the redox state changes following interaction between lanthanide diphthalocyanine complexes and $SOCl_2$. It is expected that photolysis of the Pc_2Ln species in the visible region populates the $^3\pi\pi^*$ states as was observed for the tin(IV) diphthalocyanine species [16]. Our studies on the catalytic reactions of the Pc_2Ln complexes towards the reduction of SO_2 and pentachlorophenol have shown that following photoexcitation, the $[Pc(-2)LnPc(-2)]^-$ species transfers one electron to the species being catalysed, with the reversible formation of its one-electron oxidation product, the $Pc(-2)LnPc(-1)$ species. So far, attempts to photochemically induce one-electron oxidation of $Pc(-2)LnPc(-1)$ to the $[Pc(-1)LnPc(-1)]^+$ species have been unsuccessful. We show in this work that the $[Pc(-1)LnPc(-1)]^+$ species is formed in the presence of $SOCl_2$.

EXPERIMENTAL

Materials

The blue forms of neodymium, europium, thulium and lutetium diphthalocyanines ($[Pc(-2)Nd^{III}Pc(-2)]^-$, $[Pc(-2)Eu^{III}Pc(-2)]^-$, $[Pc(-2)Tm^{III}Pc(-2)]^-$ and $[Pc(-2)Lu^{III}Pc(-2)]^-$) were synthesized by reported procedures [8, 17], by mixing 1 mole the appropriate lanthanide acetate with 9 moles of 1,2 dicyanobenzene and heating the mixture in a crucible (with a lid) at 200°C for 3 hours. The $[Pc(-2)Ln^{III}Pc(-2)]^-$ complexes were purified as described before [8], by extraction of the complex with dimethylformamide (DMF), followed by chromatography on a silica column. Only fractions with a ratio of Soret to Q bands of less than 1.4 were retained. The samples gave satisfactory IR (KBr discs, Perkin Elmer Spectrum 2000 IR Spectrophotometer) and UV/vis spectra (Cary 1E Spectrophotometer). The cyclic voltammograms (Bio Analytical Services CV-50W Voltammetric Analyser) obtained for the $[Pc(-2)Ln^{III}Pc(-2)]^-$ complexes were similar to those reported in the literature [18]. The green forms of the lanthanide diphthalocyanine complexes, $(Pc(-2)Ln^{III}Pc(-1))$ were obtained on dissolving the blue forms in neat dichloromethane. These complexes gave reported electronic absorption spectra and cyclic voltammetry [14]. Extinction coefficients [11, 19, 20] for $Pc(-2)Lu^{III}Pc(-1)$, $Pc(-2)Nd^{III}Pc(-1)$, $Pc(-2)Tm^{III}Pc(-1)$ and $Pc(-2)Eu^{III}Pc(-1)$ of $\epsilon = 2\times10^5$, 2×10^5, 1.9×10^5 and 1.8×10^5 $1\,mol^{-1}\,cm^{-1}$, respectively, were used in estimating the concentration of these species in solution. All solvents were freshly distilled before use.

Photochemical methods

Solutions to be photolysed were contained in a 1 cm pathlength UV/vis cell fitted with a stopper. Solutions of the blue, $[Pc(-2)Ln^{III}Pc(-2)]^-$, complex dissolved in acetonitrile or a mixture of acetonitrile and dimethylformamide (DMF) were degassed, then known amounts of thionyl chloride in the same solvent (or solvent mixture) were added to the cell and the solution deoxygenated. The electronic absorption spectra were recorded (Cary 1E spectrophotometer) before photolysis and periodically during the photolysis with a 50 W tungsten lamp. For some experiments photolysis was carried in the visible region, and this was achieved by using a 590 nm filter to exclude the UV radiation. The reported quantum yields were determined using unfiltered radiation. The

$Pc(-2)Ln^{III}Pc(-1)$ species were photolysed in the presence of $SOCl_2$ as described for the blue $[Pc(-2)Ln^{III}Pc(-2)]^-$ species. Concentrations of the lanthanide diphthalocyanine complexes were in the range 1×10^{-6} to 1×10^{-5} mol dm^{-3}, whereas concentrations of thionyl chloride were varied from 1×10^{-6} to 0.1 mol dm^{-3}, depending on the type of experiment. The light intensity was determined at 545 nm, using Reinecke's salt actinometry [21], to be 1.1×10^{-8} einstein sec^{-1}.

RESULTS AND DISCUSSION

Interaction of $[Pc(-2)LnPc(-2)]^-$ species with $SOCl_2$

The interaction of the lanthanide diphthalocyanine complexes with $SOCl_2$ was concentration dependent. At concentrations of $SOCl_2$ less than 10^{-4} mol dm^{-3} for lanthanide diphthalocyanine concentrations of the order of 10^{-6} mol dm^{-3}, no noticeable reaction between $SOCl_2$ and the $[Pc(-2)LnPc(-2)]^-$ was observed. At these low concentrations, photolysis of the solution containing $[Pc(-2)LnPc(-2)]^-$ and $SOCl_2$ resulted in significant spectral changes. When solutions containing 4×10^{-5} mol dm^{-3} of $SOCl_2$ and 1×10^{-6} mol dm^{-3} $[Pc(-2)EuPc(-2)]^-$ in acetonitrile were photolysed with unfiltered radiation from the a tungsten lamp, spectral changes shown in Fig. 1 were observed. These spectral changes were also observed when DMF or a mixture of DMF and acetonitrile were employed as solvents. Spectral changes shown in Fig. 1 were also observed for $[Pc(-2)NdPc(-2)]^-$, $[Pc(-2)TmPc(-2)]^-$ and $[Pc(-2)LuPc(-2)]^-$. Figure 1(a) shows the spectra of $[Pc(-2)EuPc(-2)]^-$ before the addition of $SOCl_2$. This spectra is typical of the blue $[Pc(-2)LnPc(-2)]^-$ species and shows a relatively intense absorption band at 623 nm and a weaker band at 667 nm. The spectra observed on addition of $SOCl_2$, prior to photolysis, was similar to the spectra shown in Fig. 1(a). There was no shift in the Q band spectra. Shifting in the spectra of the MPc complexes on addition of $SOCl_2$ has been attributed to the formation of an adduct between $SOCl_2$ and the MPc species [3]. When the solution containing $SOCl_2$ and the $[Pc(-2)EuPc(-2)]^-$ was photolysed, the 623 nm band decreased in intensity and the low energy band increased in intensity, Fig. 1. The new spectra was formed with a clear isosbestic point at 593 nm showing that only two species are involved. The colour of the solution changed from blue to green. The spectra at the end of photolysis, Fig. 1(b), is typical of the spectra of the $Pc(-2)LnPc(-1)$ species [21], with a charac-

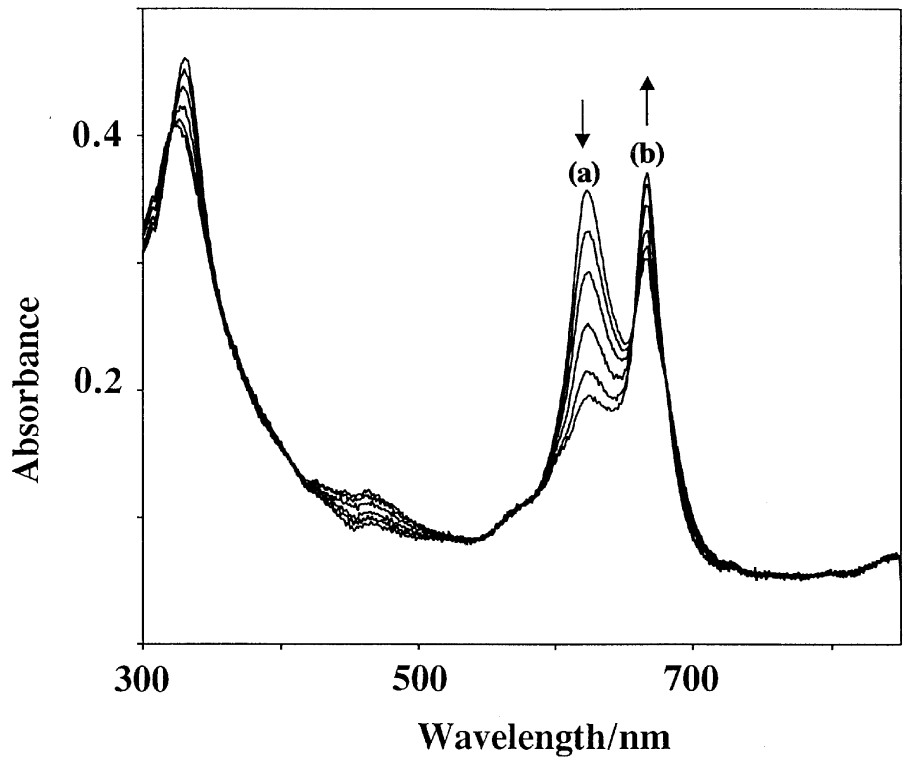

Fig. 1. Absorption spectral changes observed during the photolysis of acetonitrile solutions of 1×10^{-6} mol dm^{-3} of $[Pc(-2)EuPc(-2)]^-$ in the presence of 4×10^{-5} mol dm^{-3} $SOCl_2$, using unfiltered radiation from the tungsten lamp. a) spectra of $[Pc(-2)EuPc(-2)]^-$ before addition of $SOCl_2$ and b) spectra after 20 minutes of photolysis.

teristic weak band near 460 nm associated with electronic transition into the semi−occupied molecular orbital (SOMO) of the phthalocyanine ring. Similarly, photolysis of the $[Pc(-2)NdPc(-2)]^-$, $[Pc(-2)TmPc(-2)]^-$ and $[Pc(-2)LuPc(-2)]^-$ species in the presence of $SOCl_2$ gave spectra due to the corresponding green $[Pc(-2)NdPc(-1)$, $Pc(-2)TmPc(-1)$ and $Pc(-2)LuPc(-1)$, respectively. The $[Pc(-2)NdPc(-2)]^-$, $[Pc(-2)TmPc(-2)]^-$ and $[Pc(-2)LuPc(-2)]^-$ species were found to have low solubility in acetonitrile, thus the photochemical reactions of these complexes were carried out in DMF or a mixture of DMF and acetonitrile. The oxidation of the $[Pc(-2)LnPc(-2)]^-$ species was reversible since the green species could be reduced back to the starting blue complexes by chemical reductants such as sodium borohydride. Spectral changes shown in Fig. 1 were observed even when the UV light was excluded by using a 590 nm filter. Without photolysis, no changes in the spectra were observed at these low concentrations of $SOCl_2$.

We examined the possibility of the photodecomposition of $SOCl_2$ under our conditions. At low concentrations of $SOCl_2$ ($<3\times10^{-4}$ mol dm^{-3}), the spectra consists of a single absorption band near 220 nm in acetonitrile. The observation of a single absorption band at 220 nm confirmed that $SOCl_2$ was not aggregated at these low concentrations. Since concentrations lower than 1×10^{-4} mol dm^{-3} were employed for the photolysis studies Fig. 1 we assume that $SOCl_2$ is not aggregated under our conditions. Photolysis of 4×10^{-5} mol dm^{-3} of $SOCl_2$, in the absence of the lanthanide diphthalocyanine complexes, and using unfiltered radiation resulted in no changes in the absorption spectra of $SOCl_2$, hence suggesting that $SOCl_2$ does not photodecompose under these conditions. Also, we observed no spectral changes when we photolysed the $[Pc(-2)LnPc(-2)]^-$ species in acetonitrile, in the absence of $SOCl_2$. No noticeable spectral changes were observed, without photolysis, for the solutions containing $SOCl_2$ and $[Pc(-2)LnPc(-2)]^-$ at the concentrations used in Fig. 1.

It has been shown before that $SOCl_2$ rapidly (within seconds) oxidizes cobalt^{I} tetraneopentoxyphthalocyanine ($[Co^{I}TnPc(-2)]^-$) by a two-electron transfer process to form the $[Co^{III}TnPc(-2)]^+$ species [3]. Whereas the two-electron oxidation of $Co^{II}TnPc(-2)$ by $SOCl_2$ occurred relatively, more slowly with the formation of a $[Co^{III}TnPc(-1)]^{2+}$ species [3]. One-electron oxidation of the $[Co^{III}TnPc(-2)]^+$ to $[Co^{III}TnPc(-1)]^{2+}$ by $SOCl_2$ occurred very slowly. As mentioned above, oxidation of the $[Pc(-2)LnPc(-2)]^-$ species by $SOCl_2$ was concentration dependent. When concentrations of $SOCl_2$ greater than 1×10^{-4} mol dm^{-3} were employed for $[Pc(-2)LnPc(-2)]^-$ concentrations in the range 1×10^{-6} to 1×10^{-5} mol dm^{-3}, oxidation of the later occurred immediately without photolysis. As the concentration of the $SOCl_2$ decreased, the extent of the oxidation of the $[Pc(-2)LnPc(-2)]^-$ decreased and at very low concentrations of $SOCl_2$ ($<1\times10^{-4}$ mol dm^{-3}), no noticeable oxidation of $[Pc(-2)LnPc(-2)]^-$ was observed spectroscopically, without photolysis of the solution. The actual concentration of $SOCl_2$ needed for oxidation of the $[Pc(-2)LnPc(-2)]^-$ species without need for photolysis depended on the central lanthanide metal ion. The ease of oxidation of lanthanide diphthalocyanine species increase across the series [18]. Thus, $[Pc(-2)LuPc(-2)]^-$ is more readily oxidized, followed by $[Pc(-2)TmPc(-2)]^-$, then $[Pc(-2)EuPc(-2)]^-$, with $[Pc(-2)NdPc(-2)]^-$ being the least readily oxidized. Considering the same concentrations of the lanthanide diphthalocyanine species, the $[Pc(-2)LuPc(-2)]^-$ species requires lower concentration of the $SOCl_2$ species to initiate one-electron oxidation (without photolysis) to the green, $Pc(-2)LnPc(-1)$, complex than the rest of the blue $[Pc(-2)LnPc(-2)]^-$ species.

As shown by equation. 1, SO_2 and S are the expected final products for the four electron reduction of $SOCl_2$. Since only one electron was transferred to $SOCl_2$ from the $[Pc(-2)LnPc(-2)]^-$ species, it is unlikely that S or SO_2 are formed during the photolysis reactions shown in Fig. 1. Spectra due to the $SOCl_2$ species is located in the ultraviolet region and hence it is masked by the Soret band absorption of the $[Pc(-2)LnPc(-2)]^-$ species, hence it was not possible to monitor changes in the spectra of $SOCl_2$ during photolysis. The species formed by the one-electron transfer reaction occurring between $SOCl_2$ and the $[Pc(-2)LnPc(-2)]^-$ species is most likely the reactive intermediate, SOCl, eq. (2):

$$SOCl_2 + e^- \rightarrow SOCl^{\cdot} + Cl^- \qquad (2)$$

The $SOCl^{\cdot}$ radical is not good for the safe operation of the $Li/SOCl_2$ battery since the radical is known to dimerize and decompose into hazardous intermediates [22]. In the presence of metallophthalocyanine complexes, the $SOCl^{\cdot}$ radical can undergo a further one-electron reduction, leading to safer reduction products. Attempts to photoinduce the transfer of the second electron from the green, $Pc(-2)LnPc(-1)$ species formed following the photolysis of solutions containing $SOCl_2$ and $[Pc(-2)LnPc(-2)]^-$ in acetonitrile or DMF, at low concentrations of $SOCl_2$, were unsuccessful. There was no spectroscopic evidence for the formation of the red, $[Pc(-1)LnPc(-1)]^+$, species expected to be formed by one-electron oxidation of $Pc(-2)LnPc(-1)$. As will be discussed below, one-electron oxidation of the green $Pc(-2)LnPc(-1)$ species to the red $[Pc(-1)LnPc(-1)]^+$ occurred in dichloromethane on photolysis in the presence of low concentrations of $SOCl_2$.

Kinetic data for the photolysis of $[Pc(-2)LnPc(-2)]^-$ species in the presence of $SOCl_2$ were collected by keeping the concentration of the former constant at 1×10^{-6} mol dm^{-3} and varying the con-

centration of the latter, then photolysing the solution. Since concentrations of the $SOCl_2$ were larger than those of the lanthanide diphthalocyanines by a factor of at least 20, pseudo first order conditions were assumed. The formation of the Pc(−2)LnPc(−1) species was followed by monitoring the absorption spectra at 667 nm. Plots of $\ln(A_\infty - A_t)$ versus time were linear for at least 80% completion, confirming a first order dependence of the photocatalytic reaction on the lanthanide diphthalocyanine complexes. A_t and A_∞, represent the absorbances at time t and infinity, respectively. The slopes of the plots of $\ln(A_\infty - A_t)$ ver-

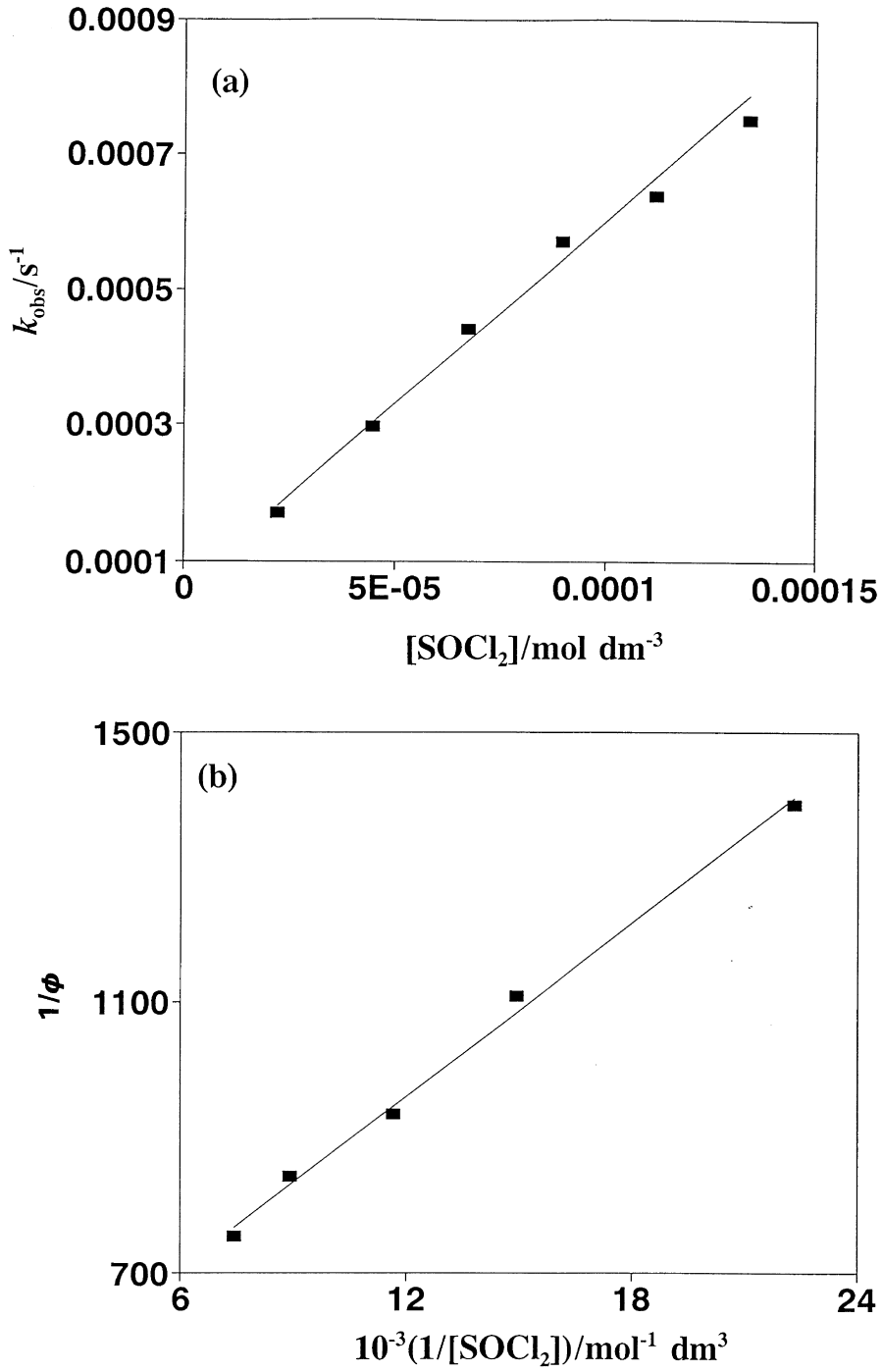

Fig. 2. a) Plots of k_{obs} (s^{-1}) versus $[SOCl_2]$ and b) plots of $1/\phi$ versus $1/[SOCl_2]$ for the photooxidation of 1×10^{-6} mol dm^{-3} $[Pc(-2)EuPc(-2)]^-$ in the presence $SOCl_2$.

sus time gave the observed rate constant, k_{obs}, and plots of k_{obs} versus the concentration of $SOCl_2$ were linear as shown if Fig. 2(a) for the $[Pc(-2)EuPc(-2)]^-$ species, confirming a first order dependence of the reaction on $SOCl_2$. As has been discussed before[11] and in comparison with Pc_2Sn^{IV} [16], it is expected that the triplet states of the lanthanide diphthalocyanine species are populated by photolysis of these complexes in the visible region. The $^3\pi\pi^*$ states may then be quenched by the reaction with $SOCl_2$, eqs. (3–4):

$$[Pc(-2)\,Ln\,Pc(-2)]^- \xrightarrow{h\nu} *[Pc(-2)LnPc(-2)]^- \quad (3)$$

$$*[Pc(-2)LnPc(-2)]^- + SOCl_2 \rightarrow SOCl^{\cdot} + Cl^- + Pc(-1)LnPc(-2) \quad (4)$$

The inverse of the quantum yields for the reaction between $SOCl_2$ and the $*[Pc(-2)LnPc(-2)]^-$ species were plotted versus the inverse of $SOCl_2$ concentration, Fig. 2(b) for $[Pc(-2)EuPc(-2)]^-$, giving linear Stern–Volmer plots and hence showing that $SOCl_2$ is a quencher for the photoexcited $*[Pc(-2)LnPc(-2)]^-$ species. The quantum yields were of the order of 10^{-4} to 10^{-3}. The relative quantum yields for the quenching of $*[Pc(-2)LnPc(-2)]^-$ with $SOCl_2$ are of the same order of magnitude as the quantum yields reported for the quenching of these species by pentachlorophenol and SO_2 [11].

Interaction of the Pc(−2)LnPc(−1) species with $SOCl_2$

When $[Pc(-2)LnPc(-2)]^-$ was dissolved in dichloromethane, the $Pc(-2)LnPc(-1)$ species was formed instantly. Electron transfer from the photoexcited $Pc(-2)LnPc(-2)H$ to CH_2Cl_2 has been observed before [12]. It was thus important to determine the role of the solvent in the photolysis studies involving the $Pc(-2)LnPc(-1)$ species. When solutions of $Pc(-2)LnPc(-1)$ in CH_2Cl_2 were photolysed in the absence of $SOCl_2$, no significant spectral changes were observed, hence showing that CH_2Cl_2 does not act as a quencher of the photoexcited $*[Pc(-2)LnPc(-1)]$ species. The interaction between $Pc(-2)LnPc(-1)$ and $SOCl_2$ was also concentration dependent, with no significant spectral changes observed without photolysis for concentrations of $SOCl_2$ of the order of $10^{-5}\,mol\,dm^{-3}$, for

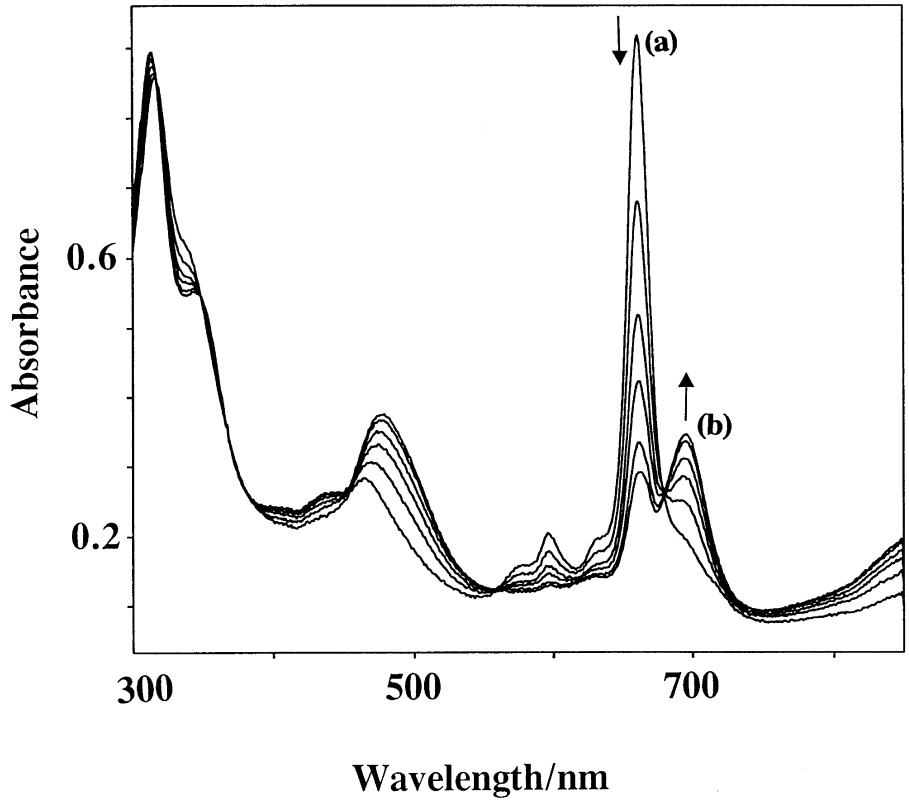

Fig. 3. Absorption spectral changes observed during the photolysis of CH_2Cl_2 solutions of $Pc(-2)TmPc(-1)$ in the presence of $2\times10^{-5}\,mol\,dm^{-3}$ $SOCl_2$, using unfiltered radiation from the tungsten lamp. a) spectra of $Pc(-2)TmPc(-1)$ before addition of $SOCl_2$ and b) spectra after 30 minutes of photolysis.

Pc(−2)LnPc(−1) concentrations ranging from 1×10^{-6} to 1×10^{-5} mol dm^{-3}.

Photolysis of a solution containing Pc(−2)LnPc(−1) and 2×10^{-5} mol dm^{-3} $SOCl_2$ in CH_2Cl_2 resulted in the spectral changes shown in Fig. 3. There was a decrease in the intensity of the Q band at 622 nm and a formation of a new weaker band at lower energies, 696 nm. The band near 464 nm due to the transition into the SOMO shifted to 475 nm. The new spectra was formed with clear isosbestic points at 346, 375, 557 and 681 nm. The solution turned from green to red. The spectral changes and the corresponding colour changes are typical of the formation of the $[Pc(-1)LnPc(-1)]^+$ species [8, 23].

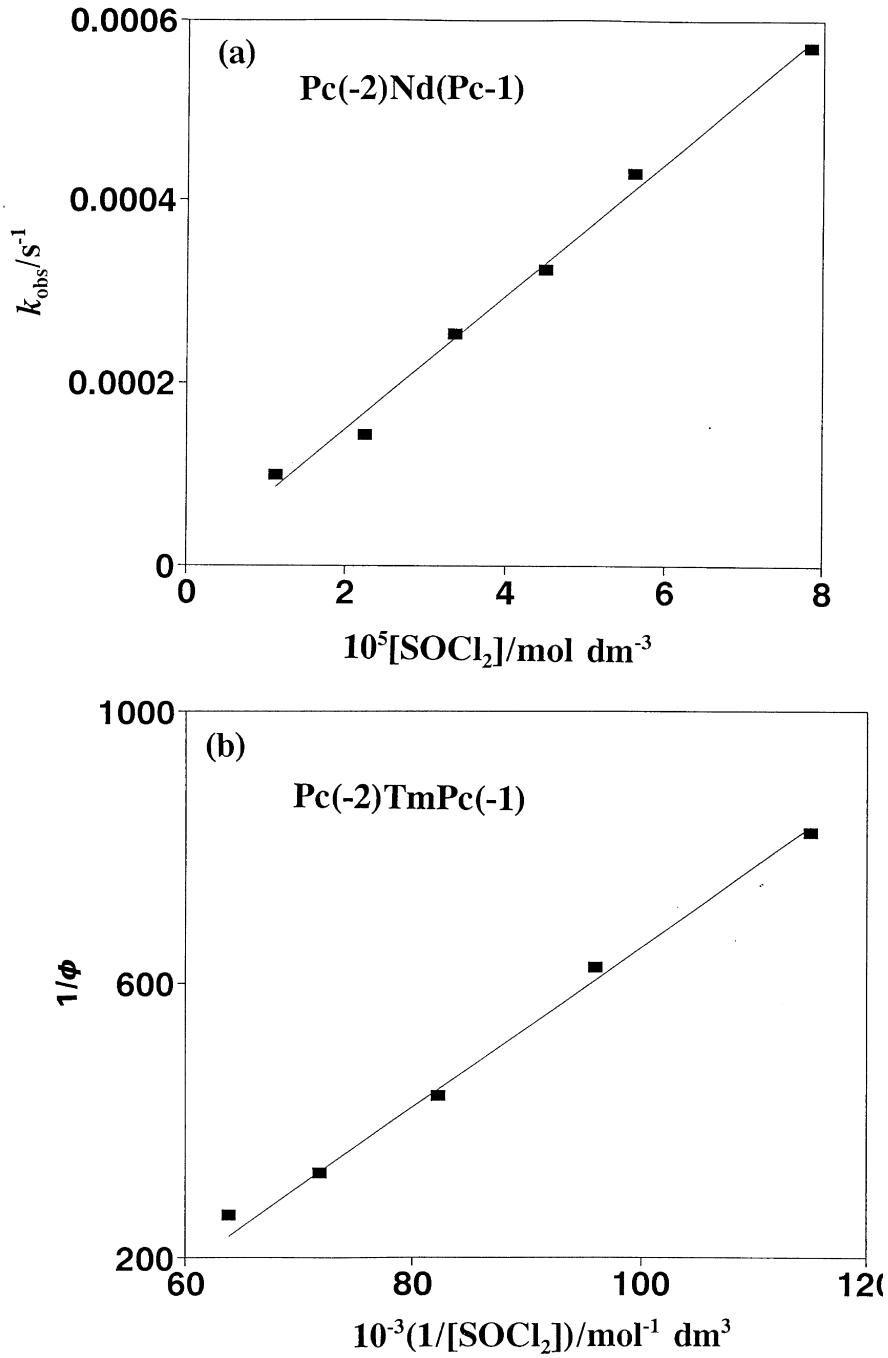

Fig. 4. a) Plots of k_{obs} (s^{-1}) versus $[SOCl_2]$ and b) plots of $1/\phi$ versus $1/[SOCl_2]$ for the photooxidation of [Pc(−2)NdPc(−1)] (a) and Pc(−2)TmPc(−1) (b) in the presence $SOCl_2$.

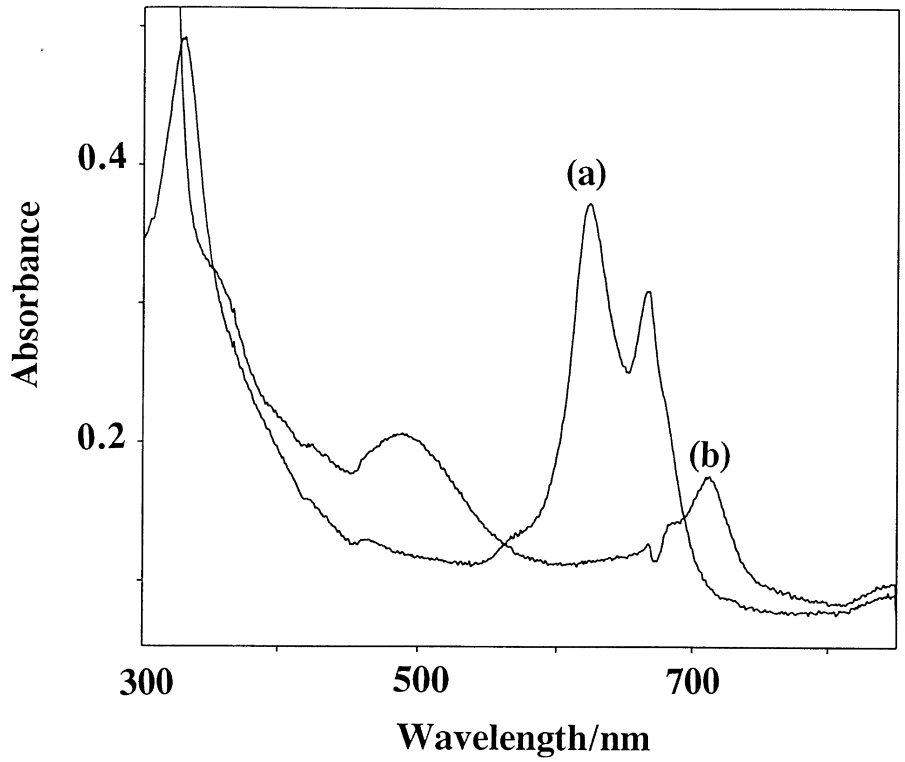

Fig. 5. Absorption spectral changes observed when a large concentration ($\sim 10^{-2}$ mol dm^{-3}) of $SOCl_2$ was added to the acetonitrile solution of 1×10^{-6} mol dm^{-3} of $[Pc(-2)EuPc(-2)]^{-3}$. a) spectra of $[Pc(-2)EuPc(-2)]^{-}$ before addition of $SOCl_2$ and b) spectra after addition of $SOCl_2$.

The formation of the $[Pc(-1)LnPc(-1)]^{+}$ species was reversible. At concentrations larger than 10^{-4} mol dm^{-3}, oxidation of the $Pc(-2)LnPc(-1)$ species to $[Pc(-2)LnPc(-2)]^{+}$ occurred by $SOCl_2$ without the need for photolysis.

The one-electron oxidation of $Pc(-2)LnPc(-1)$ suggests that the reduction of $SOCl_2$ under these circumstances again involves the formation of the same species (SOCl) as was formed by the photolysis of $[Pc(-2)LnPc(-2)]^{-}$ in the presence of thionyl chloride. We thus suggest that eqs. (5–6) are applicable for the photolysis of $Pc(-2)LnPc(-1)$ in the presence of $SOCl_2$.

$$Pc(-1)\,LnPc(-2) \xrightarrow{h\nu} *[Pc(-1)LnPc(-2)] \quad (5)$$

$$*[Pc(-1)\,LnPc(-2)] + SOCl_2 \quad (6)$$

$$\rightarrow SOCl^{\cdot}Cl^{-} + [Pc(-1)LnPc(-1)]^{+}$$

We collected the kinetic data for the photolysis of $Pc(-2)LnPc(-1)$ in the presence of $SOCl_2$ as described above for $[Pc(-2)LnPc(-2)]^{-}$. The disappearance of the $Pc(-2)LnPc(-1)$ species was followed by monitoring its Q band absorption spectra. Plots of the logarithm of absorbance versus time were linear confirming a first order dependence of the photocatalytic reaction on the $Pc(-2)LnPc(-1)$ complexes. Plots of k_{obs} versus the concentration of $SOCl_2$ were linear as shown in Fig. 4(a) for the $Pc(-2)NdPc(-1)$ species, confirming a first order dependence of the reaction on $SOCl_2$. Plots of the inverse of the quantum yields versus the inverse of the concentration of $SOCl_2$ for the reaction between $SOCl_2$ and the $*[Pc(-2)LnPc(-1)]$ species gave linear Stern–Volmer plots, Fig. 4(b) for the $Pc(-2)TmPc(-1)$, again showing that $SOCl_2$ is a quencher for this reaction. Quantum yield values were of the order of 10^{-3} for the Lu^{III} and Tm^{III} complexes and of the order of 10^{-4} for the Nd^{III} and Eu^{III} complexes.

A direct two-electron reduction of $SOCl_2$ in the presence of lanthanide diphthalocyanine complexes was observed when large concentrations ($>10^{-2}$ mol dm^{-3}) of $SOCl_2$ were added to solutions of the blue $[Pc(-2)LnPc(-2)]^{-}$ species. There was no need for photolysis. The solution went directly from blue to red, hence confirming the formation of the $[Pc(-2)LnPc(-1)]^{+}$, species, Fig. 5. The two electron reduction was reversible in that the red species could be reduced in a stepwise manner to the green, $Pc(-2)LnPc(-1)$, and finally to the blue, $[Pc(-2)LnPc(-1)]^{-}$; in the presence of chemical reductants. The most likely product formed by the two electron reduction of $SOCl_2$ is the SO species [3].

In conclusion we have shown in this work that photolysis enhances oxidation of the Pc(−2)LnPc(−1) or $[Pc(-2)LnPc(-2)]^-$ species by $SOCl_2$. At low concentrations of $SOCl_2$, oxidation occurs by one-electron transfer only, probably generating the reactive $SOCl^{\cdot}$ intermediate in the presence of light. At high concentrations of $SOCl_2$, it is possible for one or two-electron reductions of this species to occur, most likely producing $SOCl^-$ or SO, respectively, without photolysis. The one-electron reduction of $SOCl_2$ in the presence of the photoexcited lanthanide diphthalocyanine species, may be useful in the elucidation of the mechanism for reduction of $SOCl_2$ by MPc complexes.

Acknowledgements—This work was supported by Rhodes University and by the Foundation of Research Development in South Africa. NN wishes to thank Deutscher Akademischer Austauschdienst (DAAD) for a graduate scholarship.

REFERENCES

1. Kim, B.-S. and Park, S.-M., *J. Phys. Chem.*, 1995, **99,** 9918.
2. Kim, B.-S. and Park, S.-M., *J. Electrochem. Soc.*, 1995, **142,** 34.
3. Bernstein, P. A. and Lever, A. B. P., *Inorg. Chem.*, 1990, **29,** 608.
4. Kovač, M., Milićev, S., Kovač, A. and Pejovnik, S., *J. Electrochem. Soc.*, 1995, **142,** 1390.
5. Bowdeb, W. L. and Dey, A. N., *J. Electrochem. Soc.*, 1980, **127,** 1419.
6. Zagal, J. H., *Coord. Chem. Rev.*, 1992, **119,** 89.
7. Nicholson, M. M., in *Phthalocyanines, Properties and Applications*, Eds. A. B. P. Lever and C. C. Leznoff, Vol. 3, Ch. 2. VCH Publishers, New York, 1993.
8. Daniels, R. B., Payne, G. L. and Peterson, J., *J. Coord. Chem.*, 1993, **28,** 23.
9. Collins, G. C. S. and Schiffrin, D. J., *J. Electrochem. Chem.*, 1982, **139,** 335.
10. Corker, G. A., Grant, B. and Clecak, N. J., *J. Electrochem. Soc.*, 1979, **126,** 1339.
11. Nensala, N. and Nyokong, T., *Polyhedron*, 1997, **16,** 2971.
12. Kasuga, K., Morimoto, H. and Ando, M., *Inorg. Chem.*, 1986, **25,** 2478.
13. Castaneda, F., Piechocki, C., Plichon, V., Simon, J. and Vaxiviere, J., *Electrochim. Acta*, 1986, **31,** 131.
14. L'her, M., Cozien, Y. and Courtot-Coupez, J., *J. Anal. Chem.*, 1983, **157,** 183.
15. Gugon, F., Pondaven, A., Guenot, P. and L'Her, M., *Inorg. Chem.*, 1994, **33,** 4787.
16. Ferraudi, G., in *Phthalocyanines, Properties and Applications*, Eds. A. B. P. Lever and C. C. Leznoff, Vol. 1, Ch.4. VCH Publishers, New York, 1989.
17. Chang, A. T. and Marchon, J.-C., *Inorg. Chim. Acta*, 1981, **53,** L241.
18. Konami, H., Hatano, M., Kobayashi, N. and Osa, T., *Chem. Phys. Lett.*, 1990, **165,** 397.
19. Markovitsi, D., Tran-Thi, T.-H. and Even, R., Simon, J., *J. Chem. Phys. Lett.*, 1987, **137,** 107.
20. M'Sadak, M., Roncali, J. and Garnier, F., *J. Electroanal. Chem.*, 1985, **189,** 99.
21. Wegner, E. E. and Adamson, A. W., *J. Am. Chem. Soc.*, 1966, **88,** 394.
22. Vasudevan, P., Phougat, N. and Shukla, A. K., *Appl. Organomet. Chem.*, 1996, **10,** 591.
23. Stillman, M. J., in *Phthalocyanines, Properties and Applications*, Eds. A. B. P. Lever and C. C. Leznoff, Vol. 3, Ch.5, VCH Publishers, New York, 1993.

Pergamon

PII: S0277–5387(98)00118–1

Polyhedron Vol. 17, No. 20, pp. 3477–3484, 1998
© 1998 Elsevier Science Ltd
All rights reserved. Printed in Great Britain
0277–5387/98 $19.00+0.00

Reaction of the iodo-bridged tungsten(IV) dimer $[(PhN)W(CO)_2I_2]_2$ with $LiOCH_3$

Yingxia He, Khalil A. Abboud and Lisa McElwee-White*

Department of Chemistry, University of Florida, Gainesville, Florida, 32611-7200 U.S.A.

(Received 23 January 1998; accepted 16 March 1998)

Abstract—Reaction of the iodo-bridged tungsten dimer $[(PhN)W(CO)_2I_2]_2$ with 2 equiv of $LiOCH_3$ produced new dimers of the type $[(PhN)W(CO)_2I(OCH_3)]_2$. The intermediate iodo-bridged dimer $[(PhN)W(CO)_2(\mu\text{-}I)(OCH_3)]_2$ (**5**) reacted with PMe_3, $P(OMe)_3$ or $NH_2C_6H_2Me_3$ to yield mononuclear derivatives of the type $(PhN)W(CO)I(OCH_3)L_2$ [for **10**: L = PMe_3, for **11**: $P(OMe)_3$] or $(PhN)W(CO)_2I(OCH_3)(NH_2C_6H_2Me_3)$ (**9**). In solution, **5** slowly isomerized to $[(PhN)W(CO)_2I(\mu\text{-}OCH_3)]_2$ (**6**), for which an X-ray crystal structure confirmed the presence of bridging methoxide ligands. Further reaction of **6** with excess $LiOCH_3$ resulted in substitution of methoxide for the remaining iodides of **6** to produce $[(PhN)W(CO)_2(OCH_3)_2]_2$ (**7**) in low yield. © 1998 Elsevier Science Ltd. All rights reserved

Keywords: metal imido; iodo-bridged dimer; ligand substitution; metal-metal interaction; binuclear complex.

INTRODUCTION

Despite the high level of interest in transition metal imido complexes [1], examples containing π-acceptor ligands such as CO, alkenes, alkynes and isocyanides still remain relatively rare. The conflicting requirements of an electrophilic metal center that can accept electrons from the strongly donating NR^{2-} ligand and high lying filled metal *d* orbitals for back donation into the π^* levels of the acceptor ligands restrict such complexes to a d^2 electron configuration. Because competition for the available *d* electrons limits the strength of the backbonding interaction, imido complexes can generally support only a single π-acid ligand [2–6], although a few examples contain two [7].

We recently reported the preparation of the tungsten imido dimer $[(PhN)W(CO)_2I_2]_2$ (**1**) by oxidation of the zwitterion $(CO)_5WNPhNPhC(OMe)Ph$ with one equiv of I_2 [8]. The iodide bridges of **1** can be readily replaced by two-electron donor ligands to yield the series of mononuclear complexes $(PhN)W(CO)_2I_2L$ [L = CH_3CN, THF, NEt_3 or C_5H_5N; for **2**: $C_6H_2(CH_3)_3NH_2$] [9]. When **1** is treated with the more strongly nucleophilic PMe_3 or $P(OMe)_3$, a second equivalent of L replaces one of the carbonyls to produce $(PhN)W(CO)I_2L_2$ [for **3**: L = PMe_3; for **4**: $P(OMe)_3$] [8b]. Although the iodide bridges are broken in the reactions, no further displacement of iodide occurs.

We now report the reactions of dimer **1** with the harder nucleophile CH_3O^-. In contrast to the previously reported chemistry with neutral two-electron donors, methoxide displaces iodide to yield new dimeric complexes in which the alkoxide ligands occupy terminal or bridging positions. These complexes contain strongly donating imido and alkoxide ligands at the same metal center as π-acid carbonyls. The interplay of these ligands can be seen in the structure and bonding of the alkoxide-bridged dimer $[(PhN)W(CO)_2I(\mu\text{-}OCH_3)]_2$ (**6**).

RESULTS AND DISCUSSION

Reaction of $[(PhN)W(CO)_2I_2]_2$ (**1**) *with* $LiOCH_3$ *and* $NaOCH_3$

Treatment of dimer **1** with 2 equiv $LiOCH_3$ in CH_2Cl_2 resulted in the substitution of methoxide for two of the iodide ligands over the course of 4 hr (Scheme 1). The initial major product could not be isolated but was assigned as iodo-bridged dimer **5** on the basis of its spectral data and the products of subsequent reactions. Most significant is the single $-OCH_3$ signal at 3.53 ppm in the ^1H NMR spectrum of **5**, indicative

* Author to whom correspondence should be addressed.

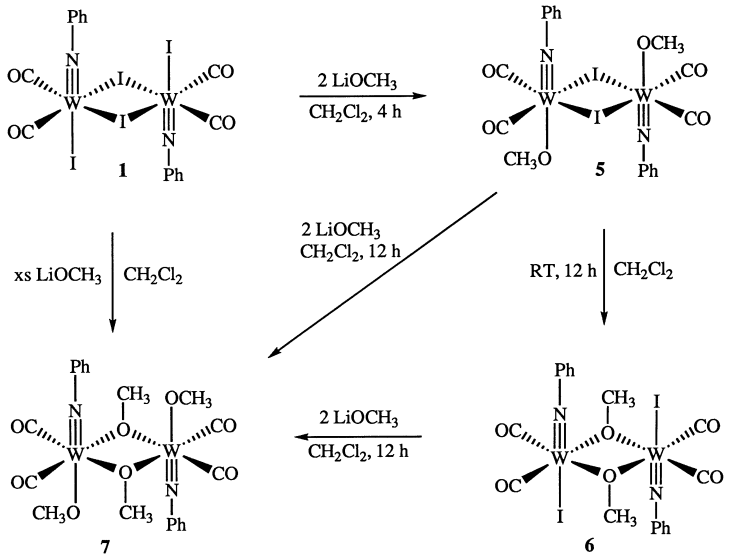

Scheme 1.

of equivalent methoxy ligands. Comparison of the chemical shift of the methoxy groups in **5** with the lower field signals in the isomeric dimer **6** (*vide infra*) allowed the assignment of terminal $-OCH_3$ groups in **5** [10, 11].

After the reaction mixtures had stirred for 6 hr, the characteristic IR bands for the carbonyl ligands of dimer **1** at 2069 and 2009 cm^{-1} had completely given way to new signals at 2055 and 1984 cm^{-1}. The ^1H NMR spectra showed the reaction mixtures to contain small amounts of **5** and a new major product whose only $-OCH_3$ signal at 4.71 ppm indicated the presence of equivalent bridging methoxy groups [11]. Conversion of dimer **5** to the new product was complete within 12 hr. Identification of the new product as dimer **6** was confirmed by X-ray crystallography (*vide infra*).

Dimer **1** was also treated with 4–10 equiv of $LiOCH_3$ in CH_2Cl_2, in attempt to induce further substitutions of iodide by methoxide. Increasing the amount of $LiOCH_3$ led to mixtures of **6** and a new dimeric complex which has been identified as **7** (Scheme 1). Dimer **7** could also be obtained by treating isolated **6** with 2 equiv of $LiOCH_3$ in CH_2Cl_2. Although addition of 2 equiv of $LiOCH_3$ to **5** also generates **7**, the time scale of the reaction is consistent with initial rearrangement of **5** to **6**, followed by formation of **7**. Complete conversion of all four original iodide ligands of **1** to methoxide ligands was indicated by the ^1H NMR spectrum of **7**, in which signals of equal intensity at 3.46 and 4.60 ppm established the presence of both terminal and bridging methoxy groups.

The sequence of reactions in Scheme 1 suggests that the facile substitution reactions in this system are conversions of the terminal iodide ligands to terminal methoxy groups. This process converts complex **1** to **5**. Cleavage of the iodo bridges in **5** then produces mononuclear complexes that can either revert to **5** or recombine through bridging methoxy groups to yield **6**. Although complexes with one iodide and one methoxide bridge could also be generated in this process, they have not been unambiguously identified in the reaction mixtures. Once the conversion of **5** to **6** regenerates terminal iodide ligands, excess $LiOCH_3$ can convert **6** to **7** via substitution. The isomerization of **5** to **6** and the reluctance of **6** and **7** to undergo bridge cleavage reactions (*vide infra*) are indicative of greater stability of methoxide bridges in this system as compared with bridging iodide ligands.

In an attempt to increase the selectivity in substitution reactions of dimer **1**, the source of methoxide was changed to $NaOCH_3$. Although NaOR/ROH systems have been used for substitution of halide ligands by OR groups [12], reaction of **1** with $NaOCH_3$ in CH_3OH did not yield the expected products. Instead, as the reaction of **1** with 2 eq $NaOCH_3$ in CH_3OH was monitored by IR spectroscopy, the CO bands for dimer **1** disappeared within 4 h, and the only new CO band at 1929 cm^{-1} belonged to a species that could not be identified. Following removal of the solvent under vacuum, no identifiable products could be isolated. Similarly disappointing results were obtained in CH_2Cl_2 and C_6H_6. These reaction mixtures exhibited a new IR stretch at 1742 cm^{-1}, suggesting the presence of a bridging CO ligand and a new bridging OCH_3 signal (4.17 ppm) in the ^1H NMR spectrum but the complexity of the reaction mixtures and the lability of the species involved prevented characterization of the products.

Crystal structure of dimer **6**

A crystal structure of compound **6** was obtained as described in the Experimental Section. The crystal

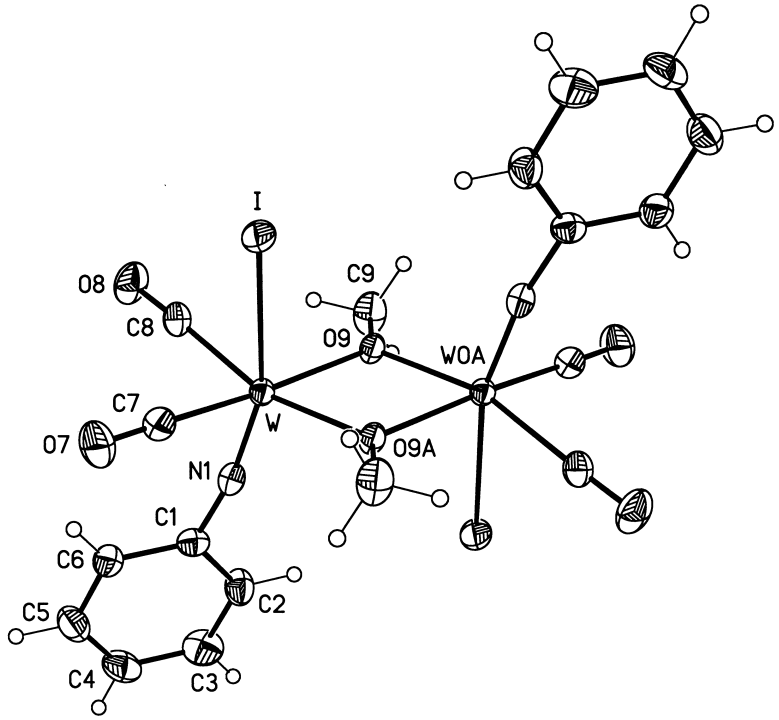

Fig. 1. Thermal ellipsoids diagram of $[(PhN)W(CO)_2(I)(\mu\text{-}OCH_3)]_2$ (**6**) showing the crystallographic numbering scheme. Ellipsoids are drawn at the 40% probability level.

structure of **6** confirmed the presence of bridging methoxide ligands as assigned from spectroscopic data. A thermal ellipsoids diagram appears in Fig. 1 and selected structural data are collected in Table 1. The $(CO)_2W(NPh)$ moiety of **6** bears a strong resemblance to the analogous fragment in the iodo-bridged dimer **1** [8b], in that the three ligands maintain nearly 90° bond angles to one another. In both complexes the terminal iodide ligands are distorted toward the carbonyls [for **6**: C7–W–I = 79.0(2)°; for **1** the analogous angle is 81.4(4)]. The more strongly donating nature of the bridging $-OCH_3$ groups in **6** can be seen in the more strongly bent imido ligand [for **6**: C1–N1–W = 168.7(4)°; for **1** the analogous angle is 177.0(8)]. The W–CO bond lengths are also slightly shorter in **6**, consistent with stronger backbonding to the carbonyl ligands. This analysis is supported by the lowered CO stretching frequencies in the IR spectrum of **6** as compared to **1** [**6**: 2055, 1984 cm^{-1} vs. **1**: 2069, 2009 cm^{-1}].

Table 1. Selected distances [Å] and angles [°] for $[(PhN)W(CO)_2I(\mu\text{-}OCH_3)]_2$ (**6**)

W–N1	1.764(4)
W–C8	2.039(5)
W–C7	2.042(5)
W–O9	2.093(3)
W–I	2.8308(4)
O7–C7	1.133(7)
C8–O8	1.131(6)
O9–C9	1.423(6)
W–W	3.393(1)
N1–W–C8	88.7(2)
N1–W–C7	87.8(2)
N1–W–O9	103.9(2)
O9A–W–O9	71.7(1)
C7–W–I	79.0(2)
C9–O9–W	123.8(3)
C1–N1–W	168.7(4)
W–O9–WOA	108.3(2)

The structure of the center W_2O_2 core of **6** provides an interesting contrast to the analogous fragment in $W_2Cl_4(OCH_3)_4(CH_3OH)_2$ (**8**), which also contains W(IV) centers bridged by methoxy groups [11a]. The W–N multiple bonding in the linear imido ligands of **6** provides electron density at the metal that obviates the need for metal-metal bonding. In the case of **8**, the W–W distance of 2.481(1) Å is indicative of a metal-metal double bond. However, the W–W distance of 3.393(1) Å in **6** is a nonbonding metal-metal distance [13]. This difference in the metal-metal interaction is reflected in the remainder of the W_2O_2 core. In W=W doubly-bonded **8**, the short metal-metal distance forces the W–O–W bond angles to narrow to 75.2(2)°. In contrast, because there is no metal-metal bond in **6**, the W_2O_2 ring distorts to relieve repulsion between the metal centers [14]. The W–O–W bond angles in **6** have

expanded to 108.3(2)° (instead of 90°) while the O–W–O angles are compressed to 71.7(1)°. In fact, the bond angles in **6** closely resemble those in the Nb(V)–Nb(V) alkoxide-bridged dimer $Nb_2(OMe)_{10}$ [O–Nb–O = 70.1(3)°; Nb–O–Nb = 109.9(3)] [15], for which no metal-metal bonding is possible.

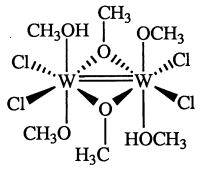

8

Electronic structure calculations on dimer **6**

The differences in metal-metal interaction between the two W(IV)–W(IV) methoxy-bridged dimers **6** and **8** led us to perform Extended Hückel calculations [16] on **6** for comparison to published calculations on **8** [11a]. The atomic coordinates of **6** were taken from the crystal structure described above and the HOMO is depicted in Fig. 2. The HOMO and the occupied orbital immediately below (HOMO-1) are similar in character, both being primarily devoted to back-bonding from metal *d* orbitals to the carbonyl ligands. The availability of these high lying filled metal *d* orbitals for backbonding is a consequence of the strong π-donation from the imido ligands. Although the *d* orbitals are in phase in the HOMO, the overlap between them is minimal as both are distorted toward the carbonyl carbons. This lack of interaction is reflected in the structure of **6**, where the W(IV) centers maintain a nonbonding distance. This situation can be contrasted to the metal-metal interaction in **8** [11a], where the HOMO ($11b_u$) is primarily comprised of the π-bonding combination of d_{xz} orbitals and the HOMO-1 ($10a_g$) contains a major contribution from the σ-bonding combination of the d_{z2} orbitals. Thus, in **8**, the two highest occupied orbitals form the metal-metal double bond. The difference is attributable to the fact that **6** bears the strongly donating imido ligands as well as four π-acid carbonyls.

Reactions of dimers **5** and **6** *with* $NH_2C_6H_2Me_3$, PMe_3 *and* $P(OMe)_3$

Mixtures of methoxide-substituted dimers **5** and **6** were generated by the reaction of dimer **1** with 2 equiv of $LiOCH_3$. After 3–4 h, when the concentration of terminal methoxide **5** was at its maximum, mesityl amine ($NH_2C_6H_2Me_3$) was added to the reaction mixtures. Dimer **5** was converted to the monomeric amine complex $(PhN)W(CO)_2I(OCH_3)(NH_2C_6H_2Me_3)$ (**9**)

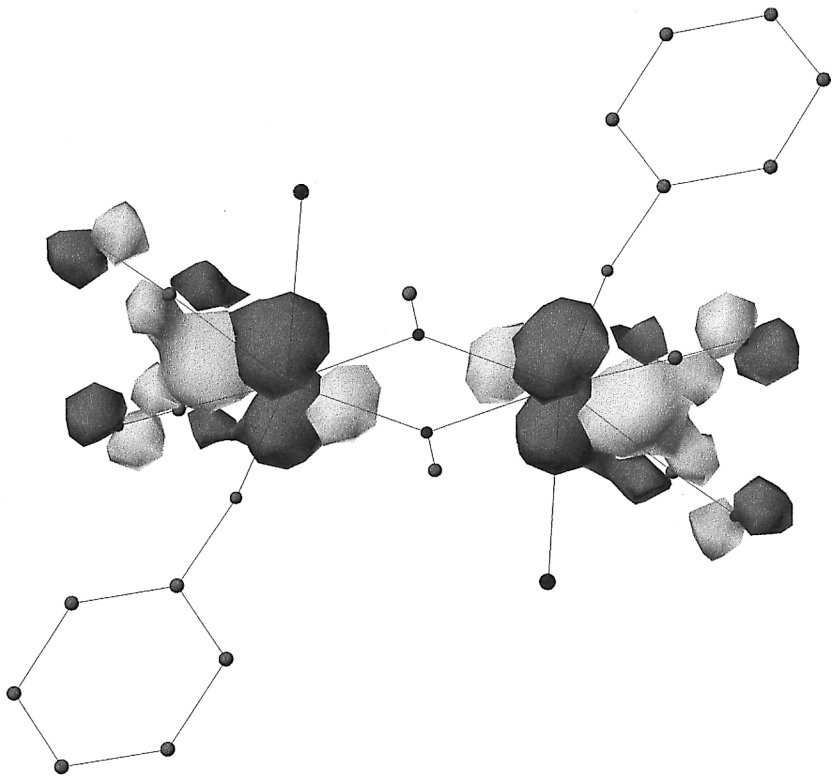

Fig. 2. HOMO of **6**. Orbital surfaces are taken from EHT calculations as described in text and plotted with an isosurface value of 0.055. The orientation of the molecule is as in Figure 1 but the hydrogens are omitted for clarity.

while **6** remained untouched (Scheme 2). The lack of reactivity between **6** and mesityl amine was confirmed in a control experiment in which pure **6** was treated with 4 equiv of $NH_2C_6H_2Me_3$ in CH_2Cl_2 overnight. Complex **9** was also independently synthesized by reacting the known amine complex $(PhN)W(CO)_2I_2(NH_2C_6H_2Me_3)$ (**2**) [8a] with 1 equiv of $NaOCH_3$ in CH_2Cl_2 overnight.

Mixtures of **5** and **6** were generated as described above for reaction with PMe_3. When the concentration of **5** had reached its maximum, 4 equiv of PMe_3 were added to the solution to yield $(PhN)W(CO)I(OCH_3)(PMe_3)_2$ (**10**) (Scheme 3). In contrast to the reaction with mesityl amine, both isomeric dimers **5** and **6** reacted with the more nucleophilic PMe_3. This observation was corroborated by treatment of pure **6** with excess PMe_3, resulting in the formation of **10**. Although the initial product of cleavage of the ligand bridges was most likely the unobserved monophosphine complex $(PhN)W(CO)_2I(OCH_3)(PMe_3)$, the final product **10** was the result of a second substitution in which a carbonyl was replaced by PMe_3. Similar chemistry was observed in the reaction of dimer **1** with PMe_3, in which two equivalents of phosphine were incorporated into the final monomeric product $(PhN)W(CO)I_2(PMe_3)_2$ (**3**) [8b]. Although mesityl amine derivative **9** could be prepared from the corresponding diiodide **2**, efforts to synthesize **10** independently from **3** and $NaOCH_3$ were not successful.

The products of dimers **5** and **6** with other potential ligands were highly dependent on the nucleophilicity

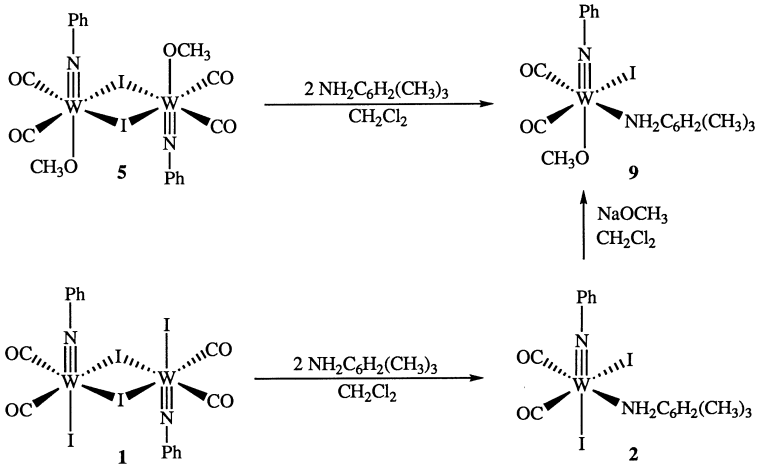

Scheme 2.

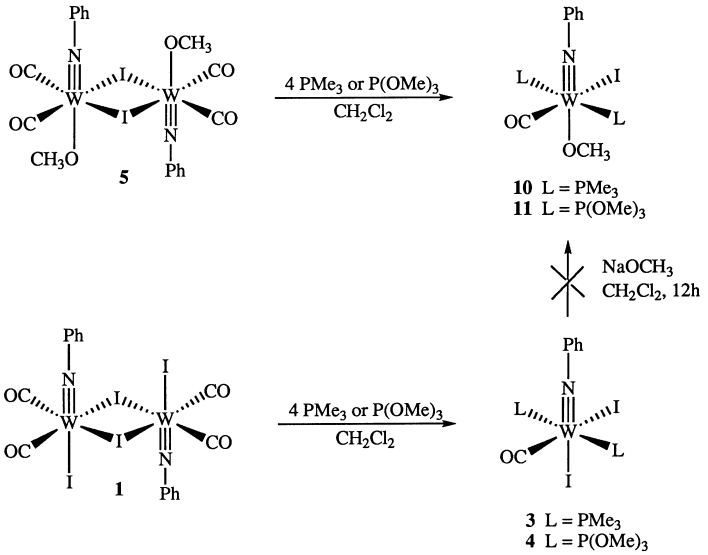

Scheme 3.

and base strength of the reacting species. As shown in Scheme 3, reaction of dimer **5** with $P(OMe)_3$ gave a similar result to the PMe_3 reaction. The isolated product, $(PhN)W(CO)I(OCH_3)[P(OMe)_3]_2$ (**11**), also bore a single carbonyl due to a second substitution involving $P(OMe)_3$. As was the case with PMe_3, dimer **6** also reacts with $P(OMe)_3$ to yield **11**. Reactions of similar mixtures of **5** and **6** with CH_3CN, $C_5H_{10}NH_2$, NEt_3 and *p*-$TolNMe_2$ were also attempted. In the cases of CH_3CN and *p*-$TolNMe_2$, complex **5** decomposed to unidentifiable material while **6** remained in the mixture as unreacted starting material. When $C_5H_{10}NH_2$ and NEt_3 served as nucleophiles, no inorganic products could be identified but the amine salts $[C_5H_{10}NH_3]I$, and $[HNEt_3]I$ could be isolated from the reaction mixtures.

CONCLUSION

Reaction of dimer **1** with $LiOCH_3$ demonstrates that substitution for the terminal iodide ligands is a facile process. The resulting iodo-bridged dimer **5** can then undergo further reactions with PMe_3, $P(OMe)_3$ or $NH_2C_6H_2Me_3$ to yield mononuclear derivatives. Rearrangement of iodo-bridged **5** to its methoxide-bridged isomer **6** produces a binuclear complex that is less prone to bridge-cleavage reactions, although the phosphorus nucleophiles PMe_3 and $P(OMe)_3$ do react with **6** to yield mononuclear complexes. X-ray crystallography of **6** confirms its structural assignment and establishes the lack of a metal-metal bonding interaction. Although related alkoxide-bridged binuclear W(IV) complexes are metal-metal doubly bonded, the strongly π-donating nature of the imido ligands and the backbonding to the carbonyl ligands of **6** prevent strong metal-metal interaction.

EXPERIMENTAL

General considerations

Standard inert atmosphere techniques were used throughout. Hexane and methylene chloride were distilled from CaH_2. Diethyl ether and THF were distilled from Na/Ph_2CO. NMR solvents were degassed by three freeze-pump-thaw cycles and stored over 3 Å molecular sieves in a dry box. All reagents were purchased in reagent grade and used without further purification. ^1H, ^{13}C and ^{31}P NMR spectra were recorded on Gemini-300 or VXR-300 NMR spectrometers. IR spectra were recorded on a Perkin-Elmer 1600 spectrometer. High resolution mass spectrometry was performed by the University of Florida analytical service. Elemental analyses were performed by Robertson Microlit Laboratories, Madison, NJ. Column chromatography was performed at 20°C on neutral alumina (Brockmann Activity 1). Dimer **1** was synthesized as previously reported [8].

$[(PhN)W(CO)_2(\mu\text{-}I)(OCH_3)]_2$ (**5**)

Dimer **1** (165 mg, 0.141 mmol) and $LiOCH_3$ (10.7 mg, 0.282 mmol) were dissolved in 10 mL of CH_2Cl_2 and stirred at room temperature for 3 h, during which a white solid formed. After the IR spectrum of the solution showed disappearance of the CO bands from dimer **1** and appearance of the CO bands for dimer **5**, the solid was filtered out, and the solvent was removed under vacuum. The ^1H NMR of this crude product showed a mixture of dimers **5** and **6**, which converted to **6** upon standing at room temperature in $CDCl_3$. The lability of **5** precluded its purification. IR (CH_2Cl_2): ν_{CO} 2048, 1983 cm^{-1}. ^1H NMR ($CDCl_3$): δ 7.36, 7.24 (m, 10H, Ph), 3.53 (s, 6H, OCH_3).

$[(PhN)W(CO)_2I(\mu\text{-}OCH_3)]_2$ (**6**)

Dimer **1** (75.0 mg, 0.064 mmol) and $LiOCH_3$ (4.86 mg, 0.128 mmol) were loaded into a Schlenk flask in the dry box. CH_2Cl_2 (5 mL) was added to dissolve the mixture and then the solution was stirred at room temperature in the dry box for 14 h. During this time, white solid formed in the red solution. The solvent was removed under vacuum. The residue was then dissolved in a very small amount of CH_2Cl_2 and transferred to a neutral alumina column. Elution with ether yielded complex **6** (48.0 mg, 76.6%). IR (CH_2Cl_2): ν_{CO} 2055, 1984 cm^{-1}. ^1H NMR ($CDCl_3$): δ 7.48 (d, $J=7$ Hz, 4H, Ph), 7.33 (m, 6H, Ph), 4.71 (s, 6H, μ-OCH_3). ^{13}C NMR ($CDCl_3$): δ 215.2 (W–CO), 153.1, 129.1, 128.6, 127.1 (Ph), 75.4 (μ-OCH_3). HRMS (FAB): calcd 949.8168 $(M–CO)^+$, found 949.8175.

$[(PhN)W(CO)_2(OCH_3)_2]_2$ (**7**)

A Schlenk flask was charged with dimer **6** (32 mg, 0.033 mmol) and $LiOCH_3$ (5 mg, 0.132 mmol). CH_2Cl_2 (5 mL) was then added to dissolve the mixture. The solution was stirred 3 h while the color of the solution changed to orange red and white solid precipitated out. The solid was removed by filtration through Celite and the solvent was removed under vacuum. The residue was recrystallized in CH_2Cl_2/hexane to yield dimer **7** (16 mg, 61.7%). IR (CH_2Cl_2): ν_{CO} 2052, 1964 cm^{-1}. ^1H NMR ($CDCl_3$): δ 7.14 (t, $J=8$ Hz, 4H, Ph), 6.75 (t, $J=7$ Hz, 2H, Ph), 6.68 (d, $J=7$ Hz, 4H, Ph), 4.60 (s, 6H, μ-OCH_3), 3.46 (s, 6H, OCH_3). ^{13}C NMR ($CDCl_3$): δ 218.2 (W–CO), 154.1, 128.8, 128.5, 127.6 (Ph), 75.4 (W-μ-OCH_3), 50.7 (W–OCH_3). The lability of the complex precluded obtaining an elemental analysis.

$(PhN)WI(CO)_2(NH_2C_6H_2Me_3)(OCH_3)$ (**9**)

Dimer **1** (63 mg, 0.054 mmol) and $LiOCH_3$ (4.08 mg, 0.108 mmol) were dissolved in 8 mL of CH_2Cl_2. The solution was stirred 3 h, during which white solid pre-

cipitated and the CO stretches in the IR spectrum of **1** were replaced by new CO bands at 2050 and 1984 cm^{-1}. The solution was filtered through Celite, 15.1 μL (0.108 mmol) of $NH_2C_6H_2Me_3$ was added, and the solution was stirred for another 4 h. The solvent was removed under vacuum and the residue was washed with hexane to yield a red powder. The ^1H NMR spectrum showed the product to be a mixture of complexes **9** and **6** (ratio of **9:6** = 9:1, based on ^1H NMR integration). The isolated yield of the mixture was 34 mg or 44.5% yield of **9**. IR (CH_2Cl_2): ν_{CO} 2072, 1986 cm^{-1}. ^1H NMR ($CDCl_3$): δ 7.50, 7.41 (m, 3H, Ph), 7.31 (t, 2H, Ph), 6.82 (s, 2H, C_6H_2), 6.47, 5.63 (d, 2H, NH_2), 2.46 (s, 6H, $C_6H_2Me_3$), 2.29 (s, 3H, $C_6H_2Me_3$), 2.17 (s, 3H, OCH_3). ^{13}C NMR ($CDCl_3$): δ 209.0, 207.1 (W–CO), 152.7, 139.3, 135.4, 129.7, 129.2, 129.1, 127.1 124.9 (Ph, C_6H_2), 20.5, 18.9, 18.1. HRMS (FAB): calcd 624.0107, found 624.0110.

(PhN)WI(CO)(PMe$_3$)$_2$(OCH$_3$) (**10**)

Dimer **1** (92.0 mg, 0.079 mmol) and $LiOCH_3$ (5.96 mg, 0.158 mmol) were loaded into a Schlenk flask in a dry box and 6 mL of CH_2Cl_2 was added to dissolve the mixture. The solution was stirred for 3 h during which white solid (LiI) precipitated out. Hexane (3 mL) was added to the solution and the solid was filtered out. A 1.0 M solution of PMe_3 in THF (0.316 mL, 0.316 mmol) was added and the solution was stirred 1 h while the color changed to dark red. The solvent was removed under vacuum and the residue was recrystallized with hexane/CH_2Cl_2 to yield pure **10** as a red solid (34.0 mg, 35.1%). IR (CH_2Cl_2): ν_{CO} 1951 cm^{-1}. ^1H NMR ($CDCl_3$): δ 7.40, 7.30, 7.23 (m, 5H, Ph), 3.86 (s, 3H, OCH_3), 1.97 (d, 18H, PMe_3). ^{13}C NMR ($CDCl_3$): δ 233.6 (W–CO), 154.3, 129.2, 127.0, 123.6 (Ph), 68.1 (OCH_3), 18.4 [d, $P(CH_3)_3$]. ^{31}P NMR ($CDCl_3$): δ −39.0 (J_{WP} = 281.6 Hz). Anal. Calcd for $C_{14}H_{26}O_2NIP_2W$: C, 27.43; H, 4.28; N, 2.29. Found: C, 27.32; H, 4.30; N, 2.20.

(PhN)WI(CO)[P(OMe)$_3$]$_2$(OCH$_3$) (**11**)

Dimer **1** (65 mg, 0.056 mmol) and $LiOCH_3$ (4.2 mg, 0.111 mmol) were dissolved in 8 mL of CH_2Cl_2 and the solution was stirred 3 h while a white solid precipitated out and the IR stretches of **1** were replaced by CO bands at 2058 and 1984 cm^{-1}. The solution was filtered through Celite and $P(OMe)_3$ (13.2 μL, 0.111 mmol) was added. After stirring at room temperature for 15 h, the solution had become dark red. The solvent was removed under vacuum and the residue was recrystallized with CH_2Cl_2/hexane to yield **11** as a red solid (28.0 mg, 38.8%). IR (CH_2Cl_2): ν_{CO} 1974 cm^{-1}. ^1H NMR ($CDCl_3$): δ 7.37, 7.29, 7.16 (m, 5H, Ph), 3.80 [dd, 18H, $P(OCH_3)_3$], 3.70 (s, 3H, OMe). ^{13}C NMR (CD_2Cl_2): δ 234.4 (W–CO), 154.5, 129.0, 127.7, 124.5 (Ph), 55.1 (W–OCH_3), 54.2 ($P\{OCH_3\}_3$). ^{31}P NMR ($CDCl_3$): δ 109.7. Anal. Calcd for $C_{14}H_{26}O_4NIP_2W$: C, 26.07; H, 4.06; N, 2.17. Found: C, 25.85; H, 4.16; N, 2.47.

X-ray structure determination for [(PhN)W(CO)$_2$I(μ-OCH$_3$)]$_2$ (**6**)

Data were collected at 173 K on a Siemens SMART PLATFORM equipped with a CCD area detector and a graphite monochromator utilizing MoKα radiation (λ = 0.71073 Å). Cell parameters were refined using 3901 reflections. A hemisphere of data (1381 frames) was collected using the ω-scan method (0.3° frame width). The first 50 frames were remeasured at the end of data collection to monitor instrument and crystal stability (maximum correction on I was <1%). Empirical (psi scan) absorption corrections were applied based on the entire data set.

Crystal data

$C_{18}H_{16}I_2N_2O_6W_2$, M = 977.83, triclinic, space group $P\bar{1}$, a = 6.6853(5), b = 9.5201(6), c = 10.3551(7) Å, α = 97.960(1), β = 107.413(1), γ = 92.328(1)°, V = 620.44(7) Å^3 at 173(2) K, Z = 1, D_c = 2.617 Mg/m^3, μ = 11.784 mm^{-1}, $F(000)$ = 440.

Data collection and processing

Crystal size 0.19 × 0.17 × 0.11 mm, θ range 2.09–27.48°, index ranges $-9 \leqslant h \leqslant 7$, $-12 \leqslant k \leqslant 12$, $-14 \leqslant l \leqslant 13$, transmission 0.219–0.405, 4290 measured reflections, 2731 unique data, R(int) = 0.0199.

The structure was solved by the direct methods in *SHELXTL5* [17], and refined using full-matrix least squares. Each dimer is located on a center of inversion, thus the asymmetric unit contains a half dimer. The non-H atoms were treated anisotropically, whereas the hydrogen atoms were calculated in ideal positions and were riding on their respective carbon atoms. A total of 137 parameters were refined in the final cycle of refinement using 2584 reflections with $I > 2\sigma(I)$ to yield $R_1 = \Sigma(\|F_o| - |F_c\|)/\Sigma|F_o\| = 2.76\%$ and $wR_2 = [\Sigma[w(F_o^2 - F_c^2)^2]/\Sigma[w(F_o^2)^2]]^{1/2} = 7.27\%$, respectively. Refinement was done using F^2. Extinction coefficient 0.0087(6), final difference map between 1.752 and −1.278 e•Å^{-3}, goodness-of-fit = 1.047 on F^2.

Atomic coordinates, complete bond lengths and angles, and displacement parameters have been deposited as supplementary material at the Cambridge Crystallographic Data Center.

Acknowledgments—Funding for this research was provided by the Office of Naval Research. K.A.A. wishes to acknowledge the National Science Foundation and the University of Florida for funding the purchase of the X-ray equipment.

REFERENCES

1. (a) Wigley, D. E., *Prog. Inorg. Chem.*, 1994, **42**, 239; (b) Nugent, W. A. and Mayer, J. M., *Metal-Ligand Multiple Bonds*. Wiley-Interscience, New York, (1988); (c) Nugent, W. A. and Haymore, B. L., *Coord. Chem. Rev.*, 1980, **31**, 123.
2. (a) Hall, K. A. and Mayer, J. M., *J. Am. Chem. Soc.*, 1992, **114**, 10402; (b) Atagi, L. M., Over, D. E., McAlister, D. R. and Mayer, J. M., *J. Am. Chem. Soc.*, 1991, **113**, 870; (c) Su, F.-M., Bryan, J. C., Jang, S. and Mayer, J. M., *Polyhedron*, 1989, **8**, 1261; (d) Bryan, J. C., Geib, S. J., Rheingold, A. L. and Mayer, J. M., *J. Am. Chem. Soc.*, 1987, **109**, 2826.
3. (a) Clark, G. R., Nielson, A. J., Rickard, C. E. F. and Ware, D. C., *J. Chem. Soc., Dalton Trans.*, 1990, 1173; (b) Nielson, A. J. and Ware, D. C., *Polyhedron*, 1990, **9**, 603; (c) Clark, G. R., Nielson, A. J. and Rickard, C. E. F., *J. Chem. Soc., Chem. Commun.*, 1989, 1157; (d) Clark, G. R., Nielson, A. J., Rickard, C. E. F. and Ware, D. C., *J. Chem. Soc., Chem. Commun.*, 1989, 343.
4. (a) Green, J. C., Green, M. L. H., James, J. T., Konidaris, P. C., Maunder, G. H. and Mountford, P., *J. Chem. Soc., Chem. Commun.*, 1992, 1361; (b) Green, M. L. H., Konidaris, P. C., Mountford, P. and Simpson, S. J., *J. Chem. Soc., Chem. Commun.*, 1992, 256; (c) Dyer, P. W., Gibson, V. C., Howard, J. A. K., Whittle, B. and Wilson, C., *J. Chem. Soc., Chem. Commun.*, 1992, 1666; (d) Poole, A. D., Gibson, V. C. and Clegg, W., *J. Chem. Soc., Chem. Commun.*, 1992, 237; (e) Siemeling, U. and Gibson, V. C., *J. Organomet. Chem.*, 1992, **426**, C25; (f) Chao, Y-W., Wexler, P. A. and Wigley, D. E., *Inorg. Chem.*, 1989, **28**, 3860.
5. (a) Williams, D. S., Schofield, M. H. and Schrock, R.R., *Organometallics*, 1993, **12**, 4560; (b) Williams, D. S. and Schrock, R. R., *Organometallics*, 1993, **12**, 1148; (c) Robbins, J., Bazan, G. C., Murdzek, J. S., O'Regan, M.B. and Schrock, R. R., *Organometallics*, 1991, **10**, 2902; (d) Weinstock, I. A., Schrock, R. R., Williams, D. S. and Crowe, W. E., *Organometallics*, 1991, **10**, 1; (e) Williams, D. S., Schofield, M. H., Anhaus, J. T. and Schrock, R. R., *J. Am. Chem. Soc.*, 1990, **112**, 6728; (f) Rocklage, S. M. and Schrock, R. R., *J. Am. Chem. Soc.*, 1982, **104**, 3077; (g) Rocklage, S. M. and Schrock, R. R., *J. Am. Chem. Soc.*, 1980, **102**, 7809.
6. Hillhouse, G. L. and Haymore, B. L., *J. Organomet. Chem.*, 1978, **162,** C23.
7. (a) Francisco, L. W., White, P. S. and Templeton, J. L., *Organometallics*, 1997, **16**, 2547; (b) Feng, S. G., White, P. S. and Templeton, J. L., *Organometallics*, 1995, **14**, 5184; (c) Pérez, P. J., White, P. S., Brookhart, M. and Templeton, J. L., *Inorg. Chem.*, 1994, **33**, 6050; (d) Powell, K. R., Pérez, P. J., Luan, L., Feng, S. G., White, P. S., Brookhart, M. and Templeton, J. L., *Organometallics*, 1994, **13**, 1851; (e) Feng, S. G., White, P. S. and Templeton, J. L., *J. Am. Chem. Soc.*, 1994, **116**, 8613; (f) Luan, L., Brookhart, M. and Templeton, J. L., *Organometallics*, 1992, **11**, 1433; (g) Pérez, P. J., Luan, L., White, P. S., Brookhart, M. and Templeton, J. L., *J. Am. Chem. Soc.*, 1992, **114**, 7928; (h) Luan, L., White, P. S., Brookhart, M. and Templeton, J. L., *J. Am. Chem. Soc.*, 1990, **112**, 8190.
8. (a) Barnett, N. D. R., Massey, S. T., McGowan, P. C., Wild, J. J., Abboud, K. A. and McElwee-White, L., *Organometallics*, 1996, **15**, 424; (b) McGowan, P. C., Massey, S. T., Abboud, K. A. and McElwee-White, L., *J. Am. Chem. Soc.*, 1994, **116**, 7419.
9. For related substitution reactions of iodo-bridged tungsten dimers, see: (a) Baker, P. K. and Flower, K. R., *Polyhedron*, 1990, **9**, 2135; (b) Baker, P. K. and Keys, E. M., *Polyhedron*, 1986, **5**, 1233; (c) Umland, P. and Vahrenkamp, H., *Chem. Ber.*, 1982, **115**, 3565; (d) Schmid, G. and Boese, R., *Chem. Ber.*, 1976, **109**, 2148; (e) Colton, R. and Rix, C. J., *Aust. J. Chem.*, 1969, **22**, 305.
10. (a) Ren, J.-G., Tomita, H., Minato, M., Ito, T., Osakada, K. and Yamasaki, M., *Organometallics*, 1996, **15**, 852; (b) Minato, M., Sakai, H., Weng, Z.-G., Zhou, D.-Y., Kurishima, S., Ito, T., Yamasaki, M., Shiro, M., Tanaka, M. and Osakada, K., *Organometallics*, 1996, **15**, 4863.
11. (a) Anderson, L. B., Cotton, F. A., DeMarco, D., Fang, A., Ilsley, W. H., Kolthammer, B. W. S. and Walton, R. A., *J. Am. Chem. Soc.*, 1981, **103**, 5078; (b) Seifert, H. J., Petersen, F. and Wöhrmann, H., *J. Inorg. Nucl. Chem.*, 1973, **35**, 2735; (c) Reagan, W. J. and Brubaker, C. H., *Inorg. Chem.*, 1970, **9**, 827; (d) Clark, P. W. and Wentworth, R. A. D., *Inorg. Chem.*, 1969, **8**, 1223.
12. (a) Bergman, R. G., *Polyhedron*, 1995, **14**, 3227; (b) Bryndza, H. E., Calabrese, J. C., Marsi, M., Roe, D. C., Tam, W. and Bercaw, J. E., *J. Am. Chem. Soc.*, 1986, **108**, 4805–4813; (c) Michelin, R., Napoli, M. and Ros, R., *J. Organomet. Chem.*, 1979, **175**, 239.
13. Chisholm, M. H., Kirkpatrick, C. C. and Huffman, J. C., *Inorg. Chem.*, 1981, **20,** 871.
14. Cotton, F. A., DeMarco, D., Kolthammer, B. W. S. and Walton, R. A., *Inorg. Chem.*, 1981, **20,** 3048.
15. Pinkerton, A. A., Schwartzenbach, D., Hubert-Pfalzgraf, L. G. and Riess, J. G., *Inorg. Chem.*, 1976, **15,** 1196.
16. *CAChe WorkSystem*, Release 3.8. CAChe Scientific, Beaverton, OR.
17. Sheldrick, G. M., *SHELXTL*5. Siemens Analytical Instrumentation, Madison, WI, (1995).

Pergamon

PII: S0277–5387(98)00135–1

Polyhedron Vol. 17, No. 20, pp. 3485–3494, 1998
© 1998 Elsevier Science Ltd
All rights reserved. Printed in Great Britain
0277–5387/98 $19.00+0.00

Three coordinate copper(I) complexes. Synthesis, spectral, and structural study of copper(I) complexes of 4-benzoylpyridine and X-ray crystal structure of the dimer [CuCl(4-benzoylpyridine)]$_2$

Mohamed A. S. Goher[a,*] and Thomas C. W. Mak[b]

[a] Department of Chemistry, Faculty of Science, Kuwait University, P.O. Box 5969 Safat, 13060 Kuwait

[b] Department of Chemistry, the Chinese University of Hong Kong, Shatin, New Territories, Hong Kong

(Received 19 January 1998; accepted 18 March 1998)

Abstract—Yellow to red–brown copper(I) complexes of the type CuXL for X = Cl, Br,I, CN, SCN and N_3 and $CuXL_2$ for X − NO_3 and ClO_4, where L = 4-benzoylpyridine, have been synthesized and characterized. All complexes exhibit MLCT bands in the visible region and the neutral complexes gave non-conducting solutions in DMF. The IR and Raman spectral data suggest monodentate 4-Bzpy, bridging halides or pseudohalides, *bidentate* nitrate and perchlorate in the respective complexes in the solid state. The structure of the 1:1 chloride complex, as determined by X-ray crystallography, features a discrete centrosymmetric [CuCl(4-benzoylpyidine)]$_2$ molecule with a Cu···Cu distance of 2.953 Å. Each copper atom in the dimeric molecule is trigonally planar coordinated by two μ-chlorine atoms and the nitrogen atom of 4-benzoylpyridine. All the isolated complexes display emission spectra in the solid state at room temperature. The neutral halide or pseudohalide complexes show one emission band with λ_{max}^{em} in the range 586–642 nm which is independent of the excitation wavelength and is related to MLCT or XLCT excited state. The 1:2 nitrate and perchlorate complexes exhibit their λ_{max}^{em} around 468–504 nm. © 1998 Elsevier Science Ltd. All rights reserved

Keywords: copper(I) complexes; 4-benzoylpyridine; crystal structure; vibration spectra; luminescence spectra.

Copper(I) usually forms four-coordinate tetrahedral complexes [1], compounds with lower coordination numbers are known but are less common [2]. Structural evidence has been reported for some trigonal planner three-coordinate copper(I) complexes, e.g., $[Cu(C_6H_7N)_3]^+$ [3], $[Cu(CN)_3]^-$ [4] and $[Cu(CN)_2]^-$ [5]. On the other hand, copper(I) halides form complexes with unidentate nitrogen donor ligands which display a variety of stoichiometries, structures [6] and emission characteristics [7] in the solid state. In some instances, CuX–ligand clusters of the same stoichiometry (1:1:1) exist in more than one crystaline format.

For example, $[CuI(py)]_4$ is a cube, whereas $[CuI(py)]_n$ is a pleated sheet polymer [8]. Similarly, $[CuI(CH_3CN)]_n$, a pleated sheet and $[CuI(CH_3CN)]_4$-dibenzo-18-crown-6, a distorted cubic structure with second sphere interactions between crown ether and acetonitrile methyl hydrogens, are both of stoichiometry Cu:I:CH_3CN of 1:1:1 [9]. These families of structures are of particular interest because the emission behaviour of the solid state material varies with structure. Thus, $[CuI(py)]_n$ displays broad band emission at room temperature and shows no shift of λ_{max} at cooling, whereas $[CuI(py)]_4$ displays two emission maxima corresponding to differing excitation maxima [10].

Recently, we isolated and characterized two types of copper(I) complexes of 2-benzoylpyridine; red to dark brown CuXL type complexes, for X = Cl, Br, I, CN, SCN and N_3, and orange yellow $(CuX)_2L$ complexes for X = Cl and Br and structurally characterized those of the first type for X = Br, I and CN [11]. In all

* Author to whom correspondence should be addressed.

complexes of the first type, 2-benzoylpyridine behaves as a bidentate ligand and all of them display no emission when excited in the UV region at room temperature. Both complexes of the second type contain *monodentate* 2-benzoylpyridine ligand, as inferred from their IR spectra and display visible emission when excited in the UV region at room temperature. Further work led to the isolation of copper(I) complexes of 4-benzoylpyridine (hereafter abbreviated as 4-Bzpy). These complexes exhibit solid state emission at room temperature. We have now performed an X-ray structure determination of the title complex for which suitable crystals are available.

EXPERIMENTAL

4-Benzoylpyridine was obtained from Aldrich company and the other chemicals were of analytical grade quality.

Preparation of the complexes:

1. CuCl(4-Bzpy) and $CuX(4\text{-Bzpy})_2$ complexes, X = NO_3 and ClO_4. These complexes were prepared by mixing the corresponding copper(II) salt (4 mmol) dissolved in water with an ethanolic solution of 4-Bzpy ligand (10 mmol) and the subsequent addition of excess L(+)-ascorbic acid. The mixture was boiled for several minutes and allowed to stand over several hours to produce the complexes.
2. CuX(Bzpy), X = Br, I, CN, SCN and N_3. These complexes were prepared by one of the following general procedures.

(i) An aqueous solution of $Cu(NO_3)_2.3H_{22}O$ (4 mmol) was mixed with KX or NaX, followed by the addition of L(+)-ascorbic acid. An ethanolic solution of the benzoylpyridine ligand (10 mmol) was then added and the mixture stirred for ca. 15 minutes. The final mixture was allowed to stand over several houres or days until a crystalline product separated.

(ii) A boiled ethanolic solution of benzoylpyridine (10 mmol) was mixed with $Cu(NO_3)_2{\cdot}3H_2O$ (4 mmol) in ethanol and the subsequent addition of L(+)-ascorbic acid resulted in a clear yellow to orange solution. To this solution, an aqueous solution of KX was added dropwise, the mixture was boiled for several minutes and allowed to stand over several hours to produce the complex.

Crystals of the yellow copper(I) chloride complex suitable for X-ray structure analysis were prepared by the procedure given under (i), except that ethanol was used as the medium and a very slow evaporation of the solvent was used.

Elemental analysis results of the isolated complexes are given in Table 1.

Physical measurements

The IR absorption spectra of solid samples were measured as KBr pellets using a Bruker IFS-25 model FT–IR spectrophotometer. Raman spectra were obtained using a Perkin–Elmer System 2000 NIR FT–

Table 1. Analytical data for the copper(I) complexes

Complex	Color	M.P. °C	Analysis; Found (calc)				
			C	H	N	X	Cu
Cu(4–Bzpy)Cl	yellow fine crystals	171–3 dec.	51.2 (51.1)	3.0 (3.2)	4.9 (5.0)	12.4 (12.6)	22.3 (22.5)
Cu(4–Bzpy)Br	yellow fine needles	190–5 dec.	44.2 (44.1)	2.7 (2.8)	4.5 (4.3)	24.3 (24.5)	19.3 (19.5)
Cu(4–Bzpy)I	orange microcryst. powder	216–8 dec.	38.7 (38.6)	2.3 (2.4)	3.6 (3.7)	33.4 (34.0)	16.8 (17.0)
Cu(4–Bzpy)CN	yellow microcrryst powder	176 dec.	57.2 (57.3)	3.3 (3.3)	10.2 (10.3)		23.5 (23.3)
Cu(4–Bzpy)SCN	orange red powder	217 dec.	50.9 (51.2)	3.1 (3.0)	9.0 (9.2)		21.0 (20.8)
$Cu(4\text{–Bzpy})N_3$	red brown	158 dec.	49.7 (49.9)	3.2 (3.1)	18.8 (19.4)		22.3 (22.0)
$Cu(4\text{–Bzpy})_2NO_3$	can yellow needles	(58.6)	58.0 (3.7)	3.6 (8.5)	8.7	(12.9)	12.5
$Cu(4\text{–Bzpy})_2ClO_4$	can. Yellow needles	208 dec.	54.0 (54.5)	3.2 (3.4)	5.6 (5.3)		11.7 (12.0)

Raman spectrometer. The laser power was ca. 200 mW. Electronic spectra of complexes were measured as solids mulled in Nujol using a varian cary-5 double beam spectrophotometer. The experimental procedures and instruments used for other measurements are as described previously [12].

X-ray structure analysis of dimeric CuCl(4-benzoylpyridine) complex (1)

Intensity data were collected at 294 K on a MSC/Rigaku RAXIS IIc imaging plate system, with a rotating-anode X-ray source (Mo–Kα radiation, $\lambda = 0.71073$ Å) [13] and corrected for absorption using the ABSCOR program [14]. Information concerning crystallographic data and structure refinement are summarized in Table 4.

The structure was solved by Patterson superposition and Fourier methods. All non-hydrogen atoms were subjected to anisotropic refinement. The aromatic hydrogen atoms were generated geometrically (C–H fixed at 0.96 Å), allowed to ride on their respective carbon atoms and included in structure-factor calculations with assigned isotropic thermal parameters.

All computations were performed on a DEC Micro VAX-II computer with the SHELXTL-PLUS system [15, 16]. Analytical expressions of neutral atom scattering factors, incorporating the real and imaginary components of anomalous dispersion, were employed [17]. Least-squares refinement converged to the *R* indices and other parameters, as listed in Table 4. Selected bond distances and angles are listed in Table 5. Positional parameters, anisotropic thermal parameters, hydrogen atom coordinates, a full list of bond lengths and angles and observed and calculated structure factors have been deposited with the editor as supplementary material; copies are available on request.

RESULTS AND DISCUSSION

The reaction between copper(I) salts and 4-Bzpy afforded the complexes given in Table 1. 4-Benzoylpyridine, therefore behaves differently from ethyl isonicotinate which affords copper(I) halide complexes of the type CuL_nX, where $n = 1$ and 2, and complexes of the type $[CuL_n]X$, where $n = 2$, 3 and 4 for $X = NO_3$ and ClO_4 [18]. All the isolated complexes are colored and sufficiently stable against air-oxidation when well-dried. In acetone and DMF, the neutral complexes gave non-conducting solutions, whereas the nitrate and perchlorate complexes behave as 1:1 electrolytes [19] with molar conductivities in the range 125–140 $\Omega^{-1}\,cm^{-2}\,mol^{-1}$ in acetone. Thus, the last two complexes may be formulated as $[CuL_2]X$, possessing ionic structures in acetone.

IR and Raman spectra

The IR and Raman spectra (Table 2) of free 4-Bzpy and its copper(I) complexes are similar except the systematic shifts of the vibration bands related to the pyridine moiety as expected for N-ligating pyridine ligands [20]. The carbonyl stretching vibrations appear almost at the same positions in complexes as well as in free 4-Bzpy. In the far IR region, 200–400 cm^{-1}, no bands could be attributable to terminal νCu–Cl or νCu–Br, suggesting bridging halide atoms whose copper–halogen absorption bands are expected below 200 cm^{-1} [21]. For 1:1:1 Cu: bridging halide: monodentate ligand, there are several possible structures including dimer, cubane, stepped cubane, stair and split stair [7].

As seen from Table 3, the ν_2 vibration mode of the perchlorate group in $Cu(4\text{-Bzpy})_2ClO_4$ is split into three peaks at 1148, 1110, 1048 cm^{-1} (IR) and 1160, 1049, 1025 cm^{-1} (Raman). For the ν_3 mode, at least two peaks are observed in the IR spectrum, but only one peak in the Raman. These results are consistent with a *bidentate* perchlorate group [21]. The spectral results of the nitrate 1:2 complex are consistent with a *bidentate* nitrato group [21]. A distorted tetrahedral structure is therefore assigned for the monomeric perchlorato and nitrato complexes.

The 1:1 azide complex shows a very strong band at 2030 cm^{-1} (IR) and a weak line at 2070 cm^{-1} (Raman) associated with the $\nu_{as}(N_3)$mode. In the 1350–1250 cm^{-1} region, we would not assign any absorption band related to the $\nu_s(N_3)$mode due to the absorption bands of the ligand and, therefore, the IR spectra could not tell us whether the azide group is symmetric or asymmetric in this complex. For symmetric azide groups, the $\nu_s(N_3)$mode is expected to be IR inactive but Raman active. The Raman spectrum of the azide complex shows a medium to strong band at 1336 cm^{-1}, suggesting symmetric azide. As symmetric azide groups of the type μ-1,3 bridging in the complex $[Cu(Ph_3P)_2(N_3)]_2$ exhibit a $\nu_{as}N_3$ band at 2053 cm^{-1} [22], we may assign bridging azides of the type μ-1,1,3 in this complex since azido ligands of this type usually absorb around 2040–2020 cm^{-1} [23, 24]. For the 1:1 thiocyanato complex, a single νCN band is observed above 2100 cm^{-1}, a result which is suggestive of bridging thiocyanato groups [25]. The anionic complex, $[Cu(SCN)_2]^-$, which contains two independent thiocyanato groups; a terminal and a μ-N,S,S shows two νCN bands at 2105 and 2085 cm^{-1}. The later band is related to the terminal N-thiocyanate, whereas the former is due to the second group [12]. We may assign μ-N,S,S bridging thiocyanate in the 1:1 complex. The results given for the 1:1 cyano complex with such higher νCN bands compared with those for terminal cyanides [2075–2095 cm^{-1}.] [26], or the bridging –CN– group [2100–2105 cm^{-1}.] [27], suggest a structure similar to that of $CuCN{\cdot}NH_3$ [28], in which the cyano group acts as a *tridentate* ligand.

Table 2. Infrared and Raman spectra (cm^{-1}) of 4-benzoylpyridine and copper(I) complexes

4-Bzpy		Cu(4-Bzpy)Cl		Cu(4-Bzpy)I		
IR	Raman	IR	Raman	IR	Raman	Assignments
	222 ms		232 w		229 wm	*ν*Cu–N(L)
	222 ms		242 w		253 w	
	289 ms		311 vw		314 w	
			370 vw		376 w	
	383 wm		386 w		390 w	
	407 w	426 w	430 w	423 w	425 w	ring, pyridine/phenyl
472 m	425* vw	451 w	465 vw	454 w	460 w	
568 w	571 wm	580 wm	582 w	583 w	584 w	
	618 wm	615 vw	619 w	616 w	614 w	ring
638 vs	640 w	645 s	648 w	646 m	646 wm	ring
	663 wm		668 w	693 m	660 w	
695 vs		694 vs		693 m		ring
	722 ms	720 w	729 wm	720 w	720 wm	ring
745 s	748 m	745 wm	750 m	745 w	750* wm	
782 ms	787 wm	790 m		792 wm		
847 ms		845 m	842 vw	849 w	850 w	407 + 425
	865 w	860 ms		860 w	870 w	ring
899 w		903 vw	895 vw			
943 ms		942 ms	950 w	942 wm	945 w	
	995 vs	996 w	1001 s	997 ms	1001 ms	
996 wm	1001 vs	1019 vw	1018 vs		1017 vs	ring breathing
1027 wm	1028 m	1072 wm	1065 ms	1060 wm	1051 vs	ring breathing
1074 m	1064 m	1152 m	1152 s	1153 wm	1151 s	ring
1149 m	1154 vs	1180 m	1185 ms	1178 w	1172 wm	ring
1177 wm	1178 m	1217 w	1212 m	1218 w	1220 m	ring
1230 m	1215 m	1278 vs	1280 w	1279 ms	1280 w	ring
1280 vs	1284 wm	1300 s	1310 w	1310 wm		
1400 m		1404 ms	1405 w			
1433 m	1415 vw	1439 m	1442 w	1437 m	1440 w	ring
	1500	1532 wm		1535 wm		
1534 m	1574 w	1570 m	1585 m	1584 m	1585 wm	ring
1584 ms		1583 ms	1598 vs		1597 vs	ring
	1594 vs		1606 vs	1609 w	1605 s	
1642 vs	1655 vs	1650 vs	1658 vs	1649 vs	1659 vs	*ν*C═O

w weak, m medium, s strong, v very.

Table 3. Vibrational frequencies (cm^{-1}) of the perchlorate, nitrate, cyanide and thiocyanate anions

	CO_4 or NO_3						*ν*CN or $\nu_{as}(N_3)$		*ν*CS or $\nu_s(N_3)$	
	ν_1		ν_2		ν_3					
Compound	IR	Raman	IR	Raman	IR	Raman	IR	Raman	IR	Raman
$Cu(4\text{-Bzpy})_2ClO_4$	934 sh	932 ms	1148 vs	1160 s	638 s	662 wm				
		1110 vs	1049 s	625 s						
		1084 vs	1025 s							
$Cu(4\text{-Bzpy})_2NO_3$			1370 s	1370 vs						
Cu(4-Bzpy)CN							2164 ms	2166 vs		
						2130 vs	2132 vs			
Cu(4-Bzpy)SCN							2105 vs	2119 w	745	790 m
$Cu(4\text{-Bzpy})N_3$							2030 vs	2070 w	—	1336 m

Table 4. Data collection and processing parameters

Empirical formula	$C_{12}H_9ClCuNO$
color, habit	yellow plate
Crystal size	$0.04 \times 0.20 \times 0.20$
Crystal system	Triclinic
Space group	$P\bar{1}$
a (Å)	3.58(1)
b (Å)	8.565(1)
c (Å)	16.276(2)
α (°)	95.02(1)
β (°)	92.12(1)
γ (°)	101.10(1)
volume (Å^3)	524.9(3)
Z	2
Formula weight	282.2
Density (calc)	1.785 Mg/m^{-3}
Absorption coefficient	2.306 mm^{-1}
F(000)	284
Diffractometer	Rigaku RAXIS IIc
Radiation	Mo–K_α ($\lambda = 0.71073$) Å
Temperature (K)	294
Collection range	$-4 \leqslant h \leqslant 4,\ -10 \leqslant k \leqslant 10$
	$20 \leqslant 1 \leqslant 0$
2θ range	3.0 to 55.0°
Independent reflections	1768 ($R_{int} = 2.69\%$)
Observed reflections	1593 ($F > 4.0\sigma(F)$)
Extinction correction	$\aleph = 0.0025(12)$, where $F^* = F[1 + 0.002\ \aleph F^2/\sin(2\theta)]^{-1/4}$
Weighting scheme	$w^{-1} = \sigma^2(F) + 0.0003F^2$
Number of parameters, p	146
Final R indices (obs. data)	$R = 6.01\%$, $wR = 6.59\%$
R indices (all data)	$R = 7.10\%$, $wR = 33.93\%$
Goodness-of-fit, S	1.94
Largest and mean Δ/σ	0.002, 0.000
Residual extrema	0.69 to -0.88 eÅ^{-3}

Structure of the 1:1 *copper(I) chloride complex*

The structure determination has shown the title complex as $[CuCl(4\text{-benzoylpyridine})]_2$ (Figures 1 and 2), another example of a metal–halide monodentate ligand with hetero atoms of the stoichiometry CuClL, to be structurally characterized. This dinuclear complex is disposed about a crystallographic inversion center with a planar Cu_2Cl_2 rhombohedral core of alternating copper and chlorine atoms. The Cu–Cl distance of 2.291(2) and 2.323(2) Å are shorter than those usually observed for $[CuClL]_n$ polymeric pleated sheets where each copper has three chlorine neighbours [av. 2.410 Å] [29–31]. The Cu–N bond length is a little shorter than that found (2.035(4) Å) in $[CuI(2\text{-benzoylpyridine})]_2$ [11], but very close to the corresponding value of 1.995(7) Å found in [CuClL], where L is isonicotinic acid [32].

The structure of the title complex with a trigonal planar geometry about each copper atom is one of the rare examples of copper(I) chloride complexes of nitrogen donor ligands of such stoichiometry having three coordinate copper atoms. Three coordinate copper(I) complexes are known for $[CuL_3]^+$, L is 2-picoline [3], $[CuXL_2]$, for X = Cl or I [33] and $[CuIL]_2$ for L = 2,6-dimethylpyridine [31], in all of these examples, the steric hinderance of the methyl group(s) in the pyridine ring is the reason for such coordination number 3 and not the usual tetrahedral geometry. In case of complex (1), however, there is no such steric hindrance. The existence of a bulk group, such as a benzoyl in position 4 in the pyridine ring is responsible for the formation of a dimer complex with three coordinate copper, rather than polymeric pleated structure with four coordinate copper atoms. This explains why we could not isolate copper(I) halide complexes of this ligand with ligand content higher than 1:1:1. The Cu···Cu separation of 2.953 Å in the present structure is comparable with the corresponding value found (2.995(3) Å) in the structure of $[CuCl(2,4\text{-dimethylpyridine})_2]_2$ [34], but shorter than that found (3.145(3) Å) in the structure of $[CuCl(2\text{-Picoline})_2]$ [34].

Table 5. Bond lengths (A°) and bond angles(°) for [CuCl(4-benzoylpyridine)]$_2$ complex

Cu(1)–Cl(1)	2.291(2)	Cu(1)–N(1)	1.992(4)
Cu(1)–Cl(1A)	2.323(2)	N(1)–C(5)	1.343(6)
N(1)–C(1)	1.330(6)	C(1)–C(2)	1.369(7)
O(1)–C(6)	1.207(5)	C(3)–C(4)	1.381(7)
C(2)–C(3)	1.394(6)	C(4)–C(5)	1.371(7)
C(3)–C(6)	1.494(7)	C(7)–C(8)	1.393(6)
C(6)–C(7)	1.479(6)	C(8)–C(9)	1.380(6)
C(7)–C(12)	1.388(7)	C(10)–C(11)	1.373(7)
C(9)–C(10)	1.366(9)	C(11)–C(12)	1.375(7)
Cu(1)–Cu(1A)	2.953		

Cl(1)–Cu(1)–N(1)	120.4(1)	Cl(1)–Cu(1)–Cl(1A)	113.5(1)
N(1)–Cu(1)–Cl(1A)	117.3(1)	Cu(1)–N(1)–C(1)	120.2(3)
Cu(1)–Cl(1)–Cu(1A)	113.5(1)	C(1)–N(1)–C(5)	117.0(4)
Cu(1)–N(!)–C(5)	122.7(3)	C(1)–C(2)–C(3)	119.2(4)
N(1)–C(1)–C(2)	123.7(4)	C(2)–C(3)–C(6)	118.2(4)
C(2)–C(3)–C(4)	117.3(4)	C(3)–C(4)–C(5)	119.8(4)
C(4)–C(3)–C(6)	124.1(4)	O(1)–C(6)–C(3)	118.6(4)
N(1)–C(5)–C(4)	123.0(5)	C(3)–C(6)–C(7)	120.6(4)
O(1)–C(6)–C(7)	120.8(4)	C(6)–C(7)–C(12)	119.1(4)
C(6)–C(7)–C(8)	121.5(4)	C(7)–C(8)–C(9)	119.1(5)
C(8)–C(9)–C(10)	121.0(5)	C(9)–C(10)–C(11)	120.4(5)
C(8)–C(7)–C(12)	119.3(4)	C(7)–C(12)–C(11)	120.6(4)
C(10)–C(11)–C(12)	119.6(5)		

* Symmetry transformation: a $(-x,-y,-z)$.

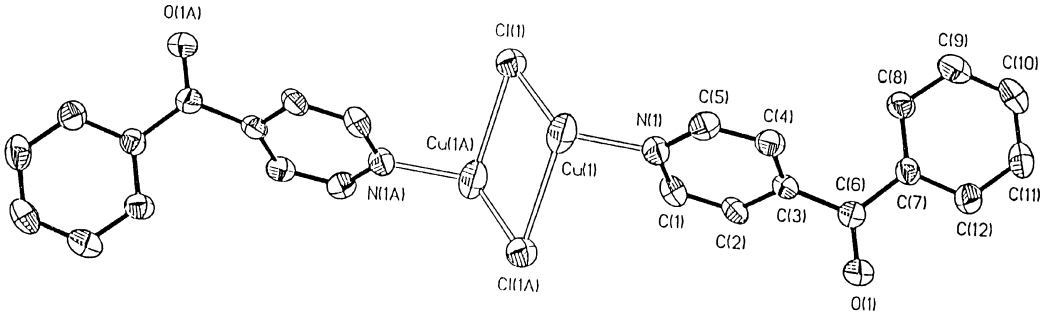

Fig. 1. Perspective view of the structure of the [CuCl(4-benzoylpyridine)]$_2$ *dimer with atom labeling scheme*.

Electronic absorbtion spectra

The electronic absorption spectra of the solid complexes mulled in Nujol (Table 6 and Fig. 3) exhibit a strong absorption band in the visible region due to charge transfer transitions from Cu (I) d^{10} to the empty π^* orbital on the pyridine ligand. The MLCT bands is dependent on the nature of the counter ion, as found for other copper(I) complexes [35]. That the position of the MLCT bands appear at lower energies in the case of the red–brown 1:1 azide and thiocyanate complexes reflects the influence of these anions on the MLCT. These ligands enhance the MLCT transitions, particularly the azide one.

Emission spectra

Table 6 and Figs 4–6 summarize the results of the emission and excitation spectra of the isolated copper(I) complexes in the solid state at room temperature. The following points are observed. (1) The emission spectra of the 1:1 halide and pseudohalide complexes exhibit a single slightly asymmetric band in the range 586–642 nm, whereas the 1:2 nitrate and perchlorate complexes show their emission bands in the range 468–504 nm with more than one maxima. (2) The emissions, as well as the excitation spectra of the nitrate and perchlorate complexes, could not be distinguished from each other. (3) The luminescence

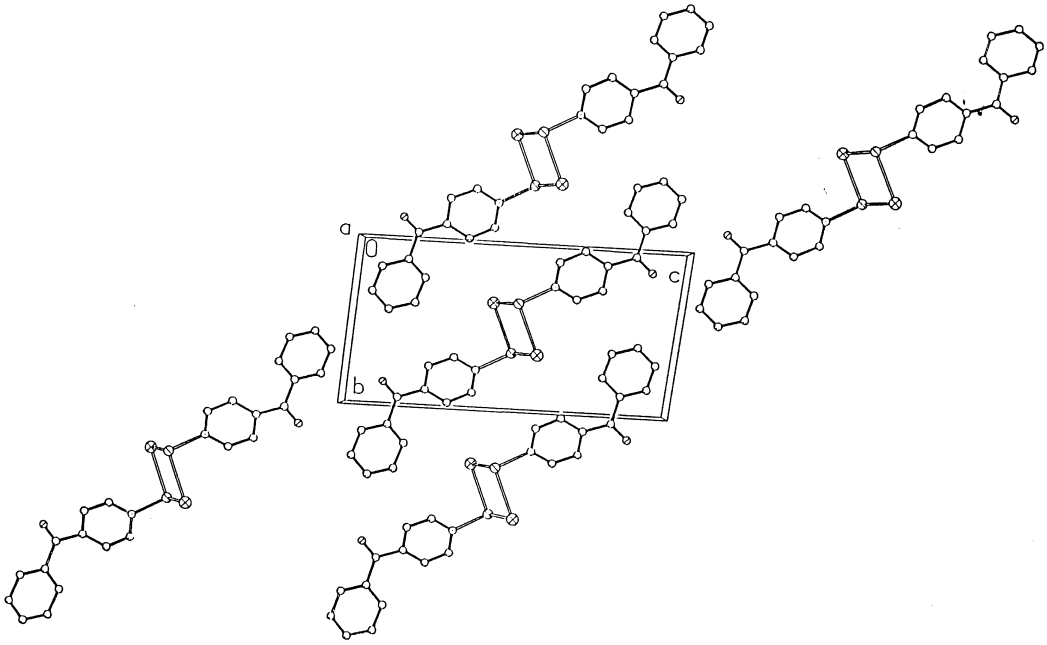

Fig. 2. Paking in the unit cell of $[CuCl(4\text{-benzoylpyridine})]_2$ dimer.

Table 6. Electronic, excitation and emission spectra of solid complexes at room temperature

Complex	λ_{max}^{abs} (a) (nm)	λ_{max}^{em} (b) (nm)	λ_{max}^{ex} (c) (nm)
Cu(4-Bzpy)Cl	370–450	642	359, 397, 468
Cu(4-Bzpy)Br	350–450	600	358, 397
Cu(4-Bzpy)I	400	631	359, 398, 468
Cu(4-Bzpy)CN	420	586	350, 405,469
Cu(4-Bzpy)SCN	400–550	460	357, 397, 468
$Cu(4\text{-Bzpy})N_3$	400–550		
$Cu(4\text{-Bzpy})_2NO_3$	375	469, 483, 504	334, 359, 402
$Cu(4\text{-Bzpy})_2ClO_4$	375	469, 483, 502	334, 359, 402[3]

(a) Solid samples are measured as Nujol mulls.
(b) Emission maxima (excitation wavelength at λ_{max}^{ex}).
(c) Excitation maxima (monetored at λ_{max}^{em}).

spectra of these solid complexes proved independent of the excitation wavelength at room temperature. (4) It is also observed that the λ_{max}^{em} changes from 642 for the chloride to 631 nm for the iodide complex, i.e., the emission maxima is shifted to a lower energy on going from the iodide complex to the chloride. (5) The 1:1 bromide complex shows its λ_{max}^{em} at 600 nm and its excitation spectrum differs a little from the other halide complexes.

Extensive studies of the emission spectra of a series of $[CuI(py\text{–}X)]_4$ complexes, both in solid state and in solutions at room temperature and at 77 K, have been undertaken [36–38]. These complexes display two emission maxima; a low energy (LE) band (620–698 nm) and a high energy (HE) band (430–540 nm). The LE band was observed for complexes with Cu–Cu distances less than the summed Cu(I) Van der Waals radii (2.8 Å) and considered as a property of the Cu_4X_4 core and involves extensive interactions between the copper(I) centers owing to the σ bonding nature of the LUMO for these clusters with short metal–metal distances [39]. The HE band, which was

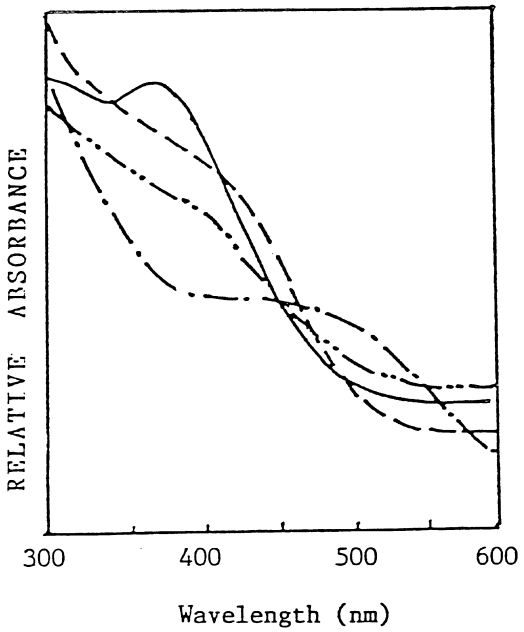

Fig. 3. Electronic absorption spectra of (————) Cu(4-Bzpy)$_2$ClO$_4$; (— — —) Cu(4-Bzpy)Cl; (——··——) Cu(4-Bzpy)I; (——·——) Cu(4-Bzpy)SCN.

also observed for $[CuXpy]_n$, was attributed to metal-to-ligand charge transfer (MLCT) or halide-to-ligand charge transfer (XLCT) [40]. In order to assign the emission spectra of the present complexes, the following points have to be considered. (1) The structure of the chloride complex, as shown by crystal structure analysis is a dimer and not a cubic tetramer. (2) The Cu–Cu distance of 2.953 Å in the chloride complex exceed the 2.8 Å value required for emission due to the Cu–Cu interactions as observed in complexes having the Cu_4X_4 core. (3) Point 4, given above, is consistent with what has been observed previously [41] that the emission bands for the chloride clusters occur at lower energy than the HE bands of the respective iodide clusters. Thus, the emitting state in the present copper(I) halides or pseudohalide complexes of 4-benzoylpyridine would be triplet MLCT or XLCT excited states. That the position of the emission λ_{max} for the present complexes appear at lower energies (586–642 nm) compared with those of $[CuI(py)]_n$ or the HE bands of $[CuI(py)]_4$ is due to the fact that the HE band energies are quite sensitive to substituents on the pyridine: electron withdrawing substituents shift these to lower values [41, 42]. X-ray powder diffraction has shown the bromide complex to be different from the chloride or iodide, this may explain the difference in their emission and excitation spectra.

The 1:2 nitrate and perchlorate complexes display their emission spectra in the range 468–504 nm with more than one emission maxima, which differs from the range where the halide complexes emit. This may support the assignments of the emission of the halide complexes as arising from MLCT and XLCT excited states. In the case of the 1:2 complexes, the emission may arise from the MLCT states, There is, however, another possibility for their emission. It was found that when aromatic ligands are packed in parallel planes separated by 3.225–3.279 Å, it results in emission spectra of the ligand alone [42]. As a solution of 4-benzoylpyridine in ethanol displays emission spectra at room temperature with λ_{max}^{em} at 453 nm and a pronounced shoulder around 492 nm, the emission spectra of the nitrate and perchloratye complexes may arise from ligand interactions alone and from MLCT interactions between Cu(I) and 4-benzoylpyridine.

Acknowledgements—M.A.S.G. thanks the Kuwait University Adminstration Project (SC 084) for support of this work, and the Department of Chemistry General Facility Projects (Analab).

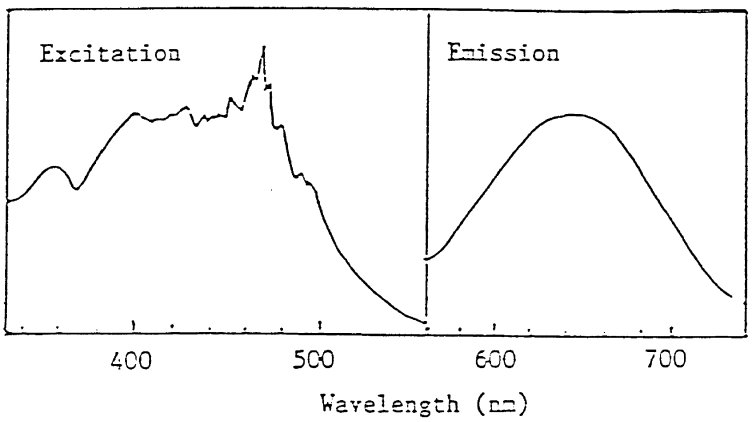

Fig. 4. Excitation and emission spectra of solid $[CuCl(4\text{-Bzpy})]_2$ complex at room temperature.

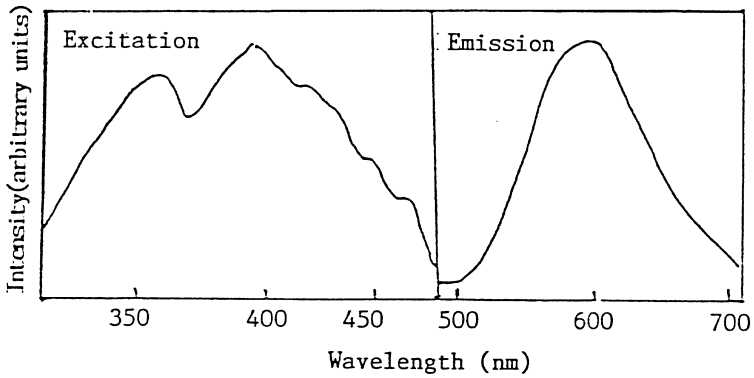

Fig. 5. Excitation and emission spectra of solid CuBr(4-Bzpy) complex at room temperature.

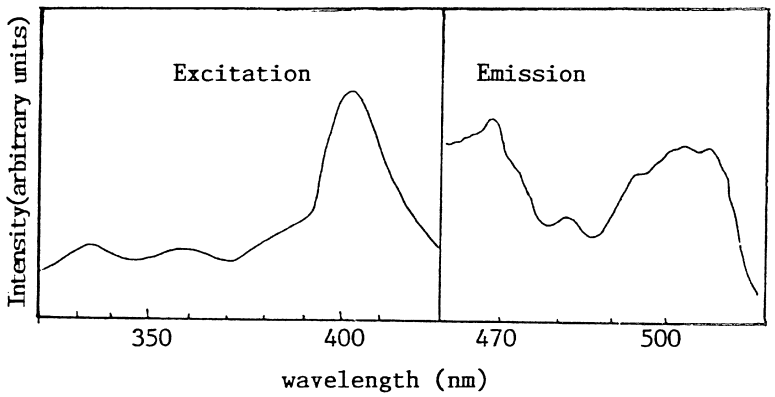

Fig. 6. Excitation and emission spectra of solid $Cu(NO_3)(4\text{-Bzpy})_2$ complex at room temperature.

REFERENCES

1. (a) Jardine, F. H., *Adv. Inorg. Chem. Radiochem.*, 1975, **17**, 115; (b) Greenwood, N. N. and Earnshaw, A., *Chemistry of the Elements*. Pergamon, Oxford, 1984, pp. 1386–1390.
2. (a) Eller, P. G., Bradley, D. C., Hursthouse, M. B. and Meek, D. W., *Coord, Chem. Rev.*, 1977, **24**, 1; (b) Sorrell, T. N. and Jameson, D. L., *J. Am. Chem. Soc.*, 1983, **105**, 6013.
3. Lewin, A. H., Michl, R. J., Ganis, P. and Lepore, U., *J. Chem. Soc., Chem. Commun.*, 1972, **00,** 1140.
4. Kappenstein, C. and Hugel, R. P., *Inorg. Chem.*, 1978, **17,** 1945.
5. Cromer, D. T., *J. Chem. Phys.*, 1957, **61,** 1388.
6. (a) Dyason, J. C., Healy, P. C., Engelharddt, L. M., Pakawatchai, C., Patrick, V. A., Raston, C. L. and White, A. H., *J. Chem. Soc. Dalton Trans.*, 1981, 831; (b) Healy, P. C., Pakawatchai, C., Raston, C. L., Skelton, B. W. and White, A. H., *J. Chem. Soc. Dalton. Trans.*, 1983, 1905.
7. Hardt, H. D., *Naturwissen*, 1974, **61,** 107.
8. (a) Eitel, E., Oelkurg, D., Hiller, W. and Strahle, J., *Naturforsch.*, Teil B., 1980, **35**, 1247; (b) Raston, C. L. and White, A. H., *J. Chem. Soc., Dalton Trans.*, 1976, 2153.
9. Jasinski, J. P., Rath, N. P. and Holt, E. M., *Inorg. Chim. Acta*, 1985, **97,** 91.
10. Hardt, H. D. and DeAhna, H. D., *Naturwissen.*, 1970, **57**, 244; *Z. Anorg. Allg. Chem.*, 1972, **387**, 61.
11. (a) Goher, M. A. S., Abdou, A. E. H., Yip, W. H. and Mak, T. C. W., *Polyhedron*, 1993, **12**, 2981; *J. Coord. Chem.*, 1995, **36**, 71.
12. Goher, M. A. S., Wang, R. J. and Mak, T. C. W., *J. Coord, Chem.*, 1996, **38,** 151.
13. (a) Tanner, J. and Krause, K., *The Regaku Journal*, 1994, **11**, 4 and 1990, **7**, 28; (b) Krause, K. L. and Phillips, G. N. Jr., *J. Appl. Cryst.*, 1992, **25**, 146; (c) Sato, M., Yammamoto, M., Imada, K., Katsube, Y., Tanaka, N. and Higashi, T., *J. Appl. Cryst.*, 1992, **25**, 348.
14. Higashi, T., *ABSCOR*, An Emperical Absorption Correction Based on Fourier Coefficient Fitting. Rigaku Corporation, Tokyo, 1995.
15. (a) Sheldrick, G. M., *SHELXL PC Manual*. Siemens Analytical X-Ray Instruments Incorporation, Madison, Wisconsin, 1990; (b) Sheldrick, G. M., *Computation Crystallography*, ed. D. Sayra. Oxford University Press, New York, 1982, p. 506.
16. Sheldrick, G. M., In *Crystallographic computing* 3: *Data Collection Structure Determination, Pro-*

teins and Data Bases, eds. G. M. Sheldrick, C. Kruger and R. Goddard. Oxford University Press, New York, 1985, p. 175.
17. Ibers, J. A. and Hamilton, W. C., *International Tables for X-Ray Crystallography*, Vols. 3 and 4. Kynoch Press, Brimingham, 1974, pp. 55, 99, 149.
18. Goher, M. A. S., Dratovsky, M. , *J. Inorg. Nucl. Chem.*, 1976, **38,** 1269.
19. (a) Ainscough, E. W. and Plowman, R. A., *Austral, J. Chem.*, 1970, **23**, 131; (b) Fergusson, J. E. and Hickford, J., *J. Austral. J. Chem.*, 1970, **23**, 453.
20. Gill, N. S., Nuttall, R. H., Scaife, D. E. and Sharp, R. W., *J. Inorg. Nucl. Chem.*, 1961, **18,** 79.
21. Nakamoto, K., *Infrared Spectra of Inorganic and coordination compounds*, 2nd. edn. London, 1970 (and references therein).
22. Dori, Z. and Ziolo, R. F., *Chem. Rev.*, 1973, **73,** 247 and references therein.
23. Goher, M. A. S., Wang, R. J. and Mak, T. C. W., *J. Mol. Struct.*, 1991, **243,** 179.
24. (a) Agrell, I., *Acta Chem. Scand.*, 1967, **21**, 2647; (b) Agrell, I. and Lamnevik, S., *Acta Chem Scand*, 1968, **22**, 450; (c) Soderquist, R., *Acta Cryst.*, 1968, **24B**, 2038.
25. (a) Gaughan, A. P., Ziolo, R. F. and Dori, Z., *Inorg. Chim. Acta* 1970, **4**, 640; (b) Goher, M. A. S., *Coll Czech. Chem. Commun.*, 1977, **42**, 1478.
26. Jones, L. H., *J. Chem. Phys.*, 1958, **29,** 463.
27. Copper, D. and Plane, R. A., *Inorg. Chem.*, 1966, **5,** 2209.
28. Walter, M. L., *Z. Chem.*, 1968, **8,** 389.
29. (a) Massaux, M., Bernard, M. J. and Le Bihan, M. T., *Bull. Soc. Fr. Mineral. Crystallogr.*, 1972, **2**, 23; (b) Massaux, M., Bernard, M. J. and Le Bihan, M. T., *Acta Cryst. Sect. B.*, 1971, **27**, 2419.
30. (a) Massaux, M. and Le Bihan, M. T., *Axta Cryst. Sec. B*, 1976, **32**, 1586; Brown, I. D. and Dunitz, J. D., *Acta Cryst.*, 1960, **13**, 28.
31. Campbell, J. A., Raston, C. L. and White, A. H., *Aust. J. Chem.*, 1977, **30,** 1937.
32. Goher, M. A. S. and Mak, T. C. W., *Inorg Chim Acta*, 1985, **101,** L27.
33. Healy, P. C., Pakawatchai, C. and White, A. H., *J. Chem. Soc., Dalton Trans.*, 1983, **00,** 1917 and references therein.
34. (a) Dyason, J. C., Engelhardt, L. M., Healy, P. C., Pakawatchai, C. and White, A. H., *Inorg. Chem.*, 1985, **24**, 1950; (b) Dyason. J. C., Healy, P. C., Pakawatchai, C., Patrick, V. A. and White, A. H., *Inorg Chem.*, 1985, **24**, 1957.
35. Mak, T. C. W., Goher, M. A. S. and Hafez, A. K., *Inorg. Chim. Acta*, 1988, **146,** 103.
36. (a) Voglar, A. and Kunkely, H., *J. Am. Chem Soc.*, 1986, **108**, 7211; (b) Kyle, K. R., DiBenedetto, J. and Ford, P. C., *J. Chem Soc., Chem. Commun.*, 1989, 714.
37. (a) Kyle, K. R. and Ford, P. C., *J. Am. Chem. Soc.*, 1989, **111**, 5005; (b) Kyle, K. R., Palke, W. E. and Fond, P. C., *Coord. Chem. Rev.*, 1990, **97** 35.
38. (a) Kyle, K. R., Ryu, C. K. and Ford, P. C., *J. Am Chem., Soc.*, 1991, **113**, 2954; (b) Hardt, H. D. and Pierre, A., *Inorg. Chim. Acta*, 1977, **25**, L59.
39. Rath, N. P., Holt, E. M. and Tanimura, K., *Inorg. Chem.*, 1985, **24,** 3934.
40. Vitale, M., Palke, W. E. and Ford, P. C., *J. Phys. Chem.*, 1992, **96,** 3329.
41. Ryu, C. K., Kyle, K. R. and Ford, P. C., *Inorg. Chem.*, 1991, **30,** 3982.
42. (a) Ryu, C. K., Vitale, M. and Ford, P. C., *Inorg. Chem.*, 1993, **32**, 869; (b) Rath, N. P. and Holt, R., *J. Chem. Soc. Dalton Trans.*, 1986, 2303; (c) Kyle, R. K., Ryu, C. K., DiBenedetto, J. A. and Ford, P. C., *J. Am. Chem. Soc.*, 1991, **113**, 2954.

Pergamon

PII: S0277–5387(98)00137–5

Polyhedron Vol. 17, No. 20, pp. 3495–3500, 1998
© 1998 Elsevier Science Ltd
All rights reserved. Printed in Great Britain
0277–5387/98 $19.00+0.00

Preparative and spectroscopic studies of $[PtCl_3(4\text{-}XC_6H_4NO)]^- K^+$ complexes

Brian G. Gowenlock,[a] Keith G. Orrell,[a] Vladimir Šik[b] and Giuseppe Vasapollo[a]

[a]Department of Chemistry, University of Exeter, Exeter, EX4 4QD, Devon, U.K.

[b]Department of Materials Science, University of Lecce, Via Arnesano, 73100, Lecce, Italy

(Received 26 November 1997; accepted 18 March 1998)

Abstract—σ_N-Coordinated compounds $[PtCl_3(4\text{-}X\text{-}C_6H_4NO)]^- K^+$ have been prepared and studied by ^{13}C NMR spectroscopy and by variable temperature ^1H NMR spectroscopy. It is shown that the anomalous behaviour of the NO group on the ^{13}C chemical shifts is modified by coordination but where X = $N(CH_3)_2$ or OCH_3 the free energy barriers to rotation of the NO group determined by ^1H NMR studies are closely similar to those of the free ligands. Restricted rotation of the $N(CH_3)_2$ group was also studied in $[PtCl_3(2\text{-}CH_3\text{-}4\text{-}N(CH_3)_2\text{-}C_6H_3NO)]^- K^+$. © 1998 Elsevier Science Ltd. All rights reserved

Keywords: nitrobenzenes; Pt complexes; restricted N=O rotation; $^1H/^{13}C$ NMR shifts.

Some years ago [1] we demonstrated from ^{13}C NMR studies that the nitroso group in *para*-substituted nitrosobenzenes behaves in a manner different from all other functional groups (twenty eight in number at that time and now thirty four) in that the chemical shift for *C*-NO was *always* found to be upfield of that in the unsubstituted nitrosobenzene. Such behaviour is, of course, found for all *para*-π-electron donor groups in conjunction with any functional group Z in the 1-position, but when the *para*-substituent is a π-electron acceptor group the shift of the Cl carbon rises above the value for the unsubstituted reference compound C_6H_5Z. Following upon a suggestion made by Topsom [2], we tentatively ascribed this behaviour to the very strong π-electron accepting character of the nitroso group the effect of which is to produce the extreme conditions under which *para*-π-electron acceptor groups such as NO_2 and CN act as π-electron donors. In collaboration with Topsom [3], molecular orbital calculations were carried out both by the semi-empirical CNDO/2 method and at the STO-3G level. These showed that the observed, unexpected, upfield chemical shifts of *C*–NO in substituted nitrosobenzenes are not a function of unusual electron distribution in these molecules in so far as this can be measured using these theoretical tools. In view of the wide variety of coordination compounds that can be formed by substituted nitrosobenzenes [4] it was of interest to see whether this anomalous property of the NO group persists on coordination to metals. We have recently demonstrated [5] that the anomalous effect is modified but not completely removed on σ_N coordination of *para*-substituted nitrosobenzenes to palladium dichloride in contrast to the complete removal of the effect when *para*-substituted nitrosobenzenes are π-coordinated to molybdenum [6].

We had previously observed that $[PtCl_3(C_6H_5NO)]^- K^+$ displays a downfield shift [7] of the *C*–NO signal compared with free ligand in contrast to all other known examples of nitrosobenzene coordination compounds where an upfield shift is observed.

Our earlier studies [8] of the energy barrier to free rotation of the nitroso group in $4\text{-}X\text{-}C_6H_4NO$, where X = NRR′, suggested their extension to the corresponding $PtCl_3$-complexes in order to investigate whether σ_N coordination to the metal has any effect on the energy barrier to rotation of the nitroso group with respect to the aromatic ring.

EXPERIMENTAL

Measurements of the natural abundance, broad band proton-decoupled ^{13}C NMR spectra were made using a Bruker DRX 400 spectrometer equipped with a standard B-VT-1000 variable-temperature unit for

^{13}C and ^{1}H NMR measurements, the solvent being $(CD_3)_2CO$.

IR measurements were made for the platinum complexes on a Nicolet Magna FT-IR spectrometer equipped with a CsI beamsplitter operating in the range 4000–200 cm^{-1} using CsI discs.

Preparation of nitroso compounds

(a) 4-*Substituted nitrosobenzenes*. With the exception of the nitrosoanilines these were prepared from the corresponding aniline by catalytic oxidation using Porta's method [9]. The nitrosoanilines were prepared by direct nitrosation of the corresponding aniline [5].

(b) *Complexes of substituted nitrosobenzenes with* $PtCl_3^-$. The method of Mansuy [10] as previously used by us [7] was adapted in the following manner. K_2PtCl_4 (1 g, 2.4 mmol) was dissolved in 20 cm^3 water. To this solution was added a solution of the nitrosoarene (2.4 mmol) in 10 cm^3 acetone. The mixture was stirred at room temperature for 30 h, the acetone removed by rotary film evaporation, the remaining solution filtered and the filtrate evaporated to dryness. The residue was then dissolved in acetone; after concentration of the solution addition of ether resulted in precipitation of the complex. This was then recrystallized from acetone/ether. In every case the complex did not melt below 260°C. Microanalytical data are given in Table 1, ^{13}C NMR data in Table 2 and ^{1}H NMR data in Table 3. In addition to the complexes $[PtCl_3(4\text{-}X\text{-}C_6H_4NO)]^-K^+$, the complex $[PtCl_3$ $(2\text{-}CH_3\text{-}4\text{-}N(CH_3)_2\text{-}C_6H_3NO)]^-$ K^+ was also prepared.

Variable temperature NMR studies

^{1}H NMR spectra of hexadeuteroacetone solutions of the complexes $[PtCl_3(4\text{-}X\text{-}C_6H_4NO)]^-$ K^+, [X = $(CH_3)_2N$ and OCH_3] were recorded in the temperature ranges −20°C to 50°C and −90°C to 30°C respectively in order to determine whether hindering of the rotation of the coordinated NO group was occurring. In addition to this the complex of 2-methyl-4-dimethylaminonitrosobenzene with $PtCl_3^-$ was investigated over the temperature range −90°C to 30°C.

DISCUSSION OF RESULTS

Our interpretation of the ^{13}C NMR data follows that given by Lynch [11] whose relationship is

$$S(\underline{C}-NO) = a + bSCS_{para}(PhX)$$

where S(*C*-NO) is the chemical shift of the carbon attached to the NO group and $SCS_{para}(PhX)$ is the substituent chemical shift in the *para* position of the monosubstituted phenyl compound [12]. Our earlier studies showed that for *para*-substituted nitrosobenzenes b is approx. 0.25 for π-electron donor substituents X and approx. −0.5 for π-electron acceptor substituents X.

The data given in Table 2, are used together with other published data [1, 5, 12] to obtain values for the Lynch parameter b for the coordination compounds $[PtCl_3(4\text{-}X\text{-}C_6H_4NO)]^-$ K^+. The C–1 chemical shift occurs downfield of X = H for three of the four π-electron acceptor groups X, whereas when X is a π-electron donor group the C–1 shifts occur upfield. This is parallelled [5] in the case of the σ_N-coordinated compounds $[PdCl_2$ $(4\text{-}X\text{-}C_6H_4NO)_2]$, where we concluded that there is some modification of the high electron demand of the NO group following σ_N coordination. In these two cases of σ_N coordination, as for $4\text{-}X\text{-}C_6H_4\text{-}NO$, the standard plot is bilinear and the effect upon the b values is far more marked than that noted for $4\text{-}X\text{-}C_6H_4\text{-}NO_2$ (see Table 4) which Bromilow *et al.* [13] found to be the most marked case of such behaviour in *para*-disubstituted benzene derivatives. We therefore conclude that the electron demand exerted by the σ_N coordinated NO group is much greater than that for the nitro group though less than that for the free NO group. This is in marked contrast to the results obtained when substituted nitrosobenzenes are π-bonded to molybdenum(VI) [6] for which the plot is linear [5] with a slope b = 0.70. The

Table 1. Calculated and required analytical data for the complexes $[PtCl_3(4\text{-}X\text{-}C_6H_4NO)]^-$ K^+

	Requires				Found			
X	C	H	N	Cl	C	H	N	Cl
H	16.10	1.15	3.15	23.80	16.20	1.30	3.20	24.00
MeO	17.60	1.50	2.95	22.25	17.29	1.45	2.90	22.80
Me	18.20	1.55	3.05	23.05	18.40	1.50	2.90	22.50
NO_2	14.65	0.80	5.70	21.60	14.25	0.85	5.50	21.00
CN	17.80	0.85	5.95	22.50	17.66	0.85	5.80	21.90
Me_2N	19.60	2.05	5.70	21.65	19.70	2.10	5.80	21.00
MeCO	19.60	1.45	2.85	21.70	20.00	1.50	2.75	22.00
$MeCO_2$	19.00	1.40	2.75	21.05	19.10	1.50	2.60	21.30

Table 2. ^{13}C NMR data[a] for $[PtCl_3(4\text{-}X\text{-}C_6H_4NO)]^- K^+$ in acetone-d_6

	Values in ppm				
X	C–1	C–2,6	C–3,5	C–4	Other
H	171.4	126.9	129.3	135.7	
$(CH_3)_2N$	161.3	b	111.4	156.3	40.3
CH_3O	166.6	130.8	114.5	166.3	56.3
CH_3	170.0	127.3	129.8	148.4	21.2
NO_2	171.9	124.5	127.0	150.3	
CN	171.2	126.5	133.3	117.5	117.5
CO_2CH_3	172.2	126.4	130.1	135.0	165.3 52.3
$COCH_3$	172.0	126.6	128.7	140.7	197.0 26.5

[a] δ values relative to Me_4Si ($\delta = 0$) [b] Undetectably broad.

Table 3. ^1H NMR shift data[a] for $[PtCl_3(4\text{-}XC_6H_4NO)]^- K^+$ complexes in acetone-d_6

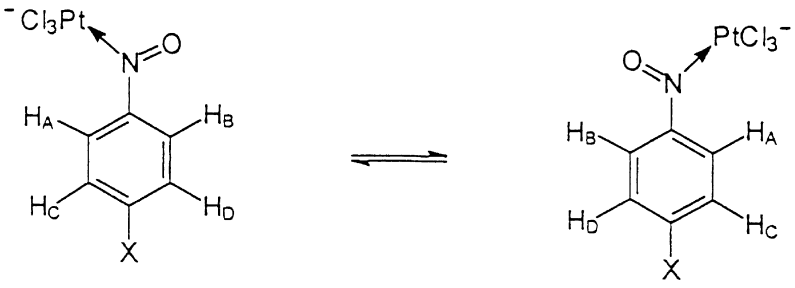

X	T/K	δ_A	δ_B	δ_C	δ_D	δ_X
H	303	8.64	8.64	7.66	7.66	7.96
NMe_2	303	b	b	6.88	6.88	3.29
NMe_2	213	9.96	7.24	6.98	6.71	3.24
OMe	303	8.77	8.77	7.15	7.15	4.05
OMe	183	10.17	7.47	7.38	7.00	4.04
Me	303	8.57	8.57	7.45	7.45	2.38
NO_2	303	8.75	8.75	8.49	8.49	—
CN	303	8.70	8.70	8.09	8.09	—
CO_2Me	303	8.66	8.66	8.22	8.22	3.98
COMe	303	8.67	8.67	8.19	8.19	2.73

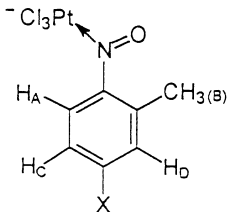

X	T/K	δ_A	δ_B	δ_C	δ_D	δ_X
NMe_2	303	10.36	2.21	6.94	6.44	3.23
NMe_2	213	10.44	2.14	7.01	6.50	3.262 3.222

[a] Relative to Me_4Si ($\delta = 0$) b Undetectably broad.

Table 4. Comparison of the Lynch slope values, b, for C-nitrosobenzenes and related compounds

Series	X		Reference
	π-Donor group	π-Acceptor group	
X-C_6H_4NO	0.25	−0.50	1
$PdCl_2$(X-NOB)$_2$	0.55 ± 0.1	0.05	5
$PtCl_3$(X-NOB)$^-K^+$	0.85 ± 0.05	0.08	a
X-$C_6H_4NO_2$	0.92	0.46	15
X-C_6H_4CHO	0.85	0.6	15

a = this work.

structural changes in the NO group are much greater when π-coordination occurs as evidenced by the extension of the NO bond to lengths approaching those of a single bond in contrast to the examples of σ_N coordination where the NO bond length increases by very small amounts [14]. Further preparative and ^{13}C NMR studies of both σ_N and π-coordinated compounds of 4-X-C_6H_4–NO are required in order to substantiate these suggestions.

We conclude that the NO group reduces the sensitivity at *C*-NO to electron density changes in *para*-substituted nitrosobenzenes to a much greater extent than is operative for any other functional group, in particular the isoelectronic pairs –CH═CH_2, –CH═O and the pairs –N═N–R and –CH═N–R (analogous to the isoelectronic pairs –N═NH and –CH═NH) and the –NO_2 group which is a strong π-electron acceptor.

The variable temperature proton NMR studies were initiated in order to discover whether the large barriers to free rotation in 4-nitrosoanilines [10, 15–17] and in nitrosoanisole [18] were significantly altered on σ_N coordination. There appears to have been only one previous example of evidence for the hindering of rotation of the NO about the CN bond in a coordinated compound of 4-dimethylamino-nitrosobenzene [19] and in this case no calculation of the free energy barrier to rotation was made.

^1H NMR spectra of the complex where X = $N(CH_3)_2$ were recorded in the temperature range 50 to −30°C. At the lowest temperature the spectrum indicated that the –N═O rotation was arrested as four aromatic hydrogen shifts were detected (Table 3). The pairs of *ortho*- and *meta*-hydrogen signals broadened and coalesced on warming as a result of the increasing rate of –N═O rotation. From the coalescences of the *ortho* signals (at 303 K) and the *meta* signals (at 278 K), rate constants for the rotation process were calculated to be 2422 s^{-1} and 240 s^{-1} respectively. These values gave activation free energies $\Delta G^{\ddagger}$ (303 K) = 54.6 kJ mol^{-1} and $\Delta G^{\ddagger}$ (278 K) = 55.3 kJ mol^{-1} (Table 5) which are of similar magnitude to that of the nitrosoligand itself [8].

Table 5. Free energies of activation for C–NO rotation in 4-X-nitrosobenzene and in coordination to $PtCl_3^-$

X	Free ligand	Coordination compound
	$\Delta G^{\ddagger}$/kJ mol^{-1}	$\Delta G^{\ddagger}$/kJ mol^{-1}
$(CH_3)_2N$	53.6 (298 K)[16]	54.6(303 K)(H 2,6)
		55.3(278 K)(H 3,5)
CH_3O	41.0 (298 K)[16]	39.7(223 K)(H 2,6)
		41.3(213 K)(H 3,5)

^1H NMR spectra of the complex X = OCH_3 showed similar changes to the 4-$N(CH_3)_2$ complex but these occurred in a much lower temperature range, 30 to −90°C. The –N═O rotation process became slow on the NMR timescale at temperatures below −70°C and clear distinction between the four ring hydrogen environments was obtained at −90°C (Table 3). The spectral changes in the range −80 to 20°C are depicted in Fig. 1. Rate data for the –N═O rotation process were derived from the band coalescences of the *ortho* hydrogen signals (223 K) and *meta* hydrogen signals (213 K). These data provided activation free energies, $\Delta G^{\ddagger}$, of 39.7 kJ mol^{-1} (223 K) and 41.3 kJ mol^{-1} (213 K). The former magnitude is considered somewhat more reliable. Both values are very similar to the value of $\Delta G^{\ddagger}$ (298 K) for the free ligand of 41.0 ± 0.3 kJ mol^{-1} [18].

$[PtCl_3(2\text{-}CH_3\text{-}4\text{-}N(CH_3)_2\text{-}C_6H_3NO)]^-\ K^+$

^1H NMR spectra of this complex recorded in the range −90 to 50°C showed no significant changes in the aromatic region, only the $N(CH_3)_2$ signal changing from a doublet (at temperatures ⩽ −40°C) to a singlet (at temperatures ⩾ −30°C) with coalescence at −35°C (238 K). The spectra indicate the existence in solution of a single rotameric species. The low δ value (2.14) of the 2-methyl group is characteristic of the group lying in the strong shielding zone of the aniso-

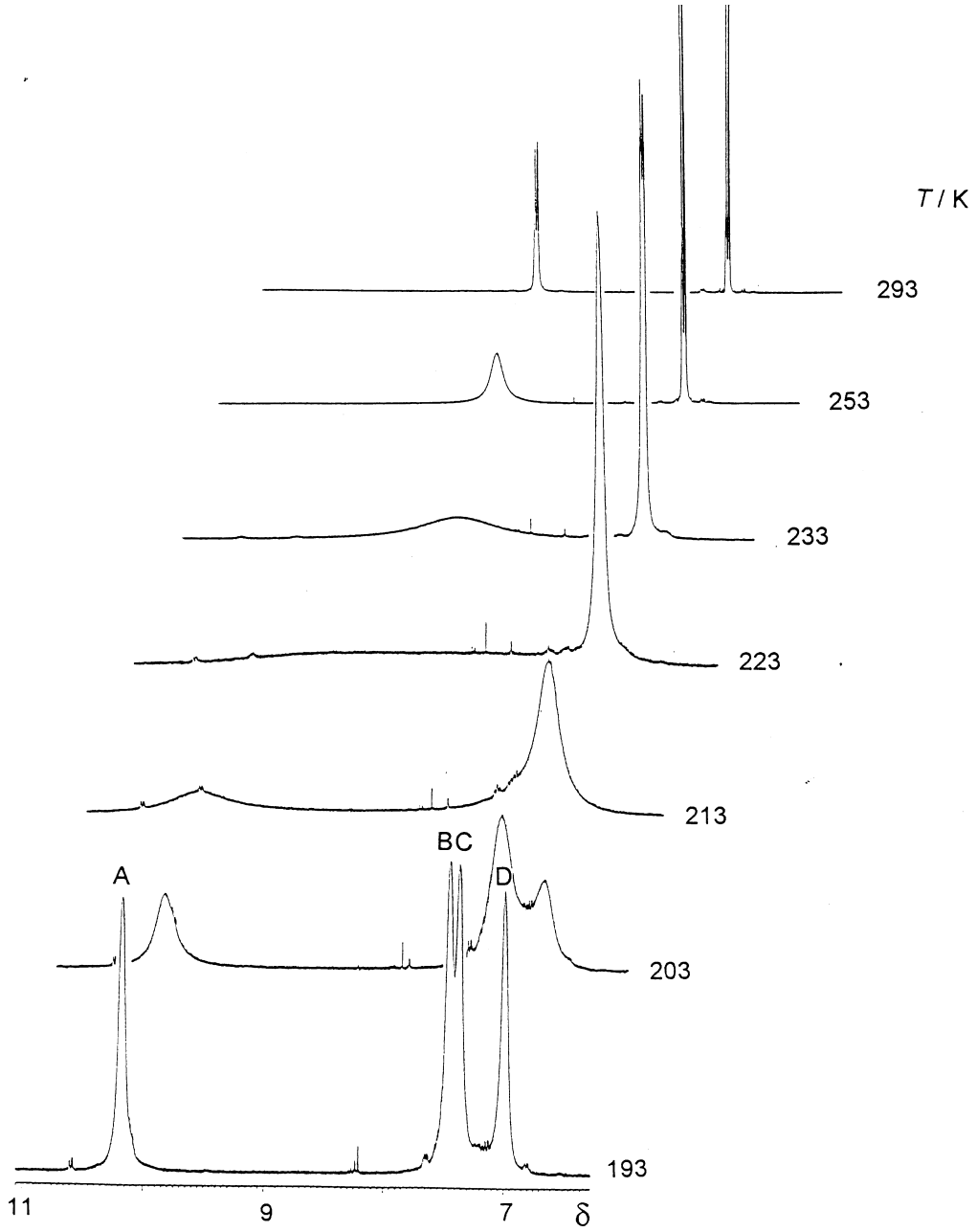

Fig. 1. Variable temperature ^1H NMR spectra of $[PtCl_3\ (4\text{-}CH_3OC_6H_4NO)]^-\ K^+$ in deuteroacetone showing the effects of the restricted rotation (see Table 3 for signal labelling).

tropic –N=O group, namely *cis* to this group [8, 18]. The structure of the complex is thus as indicated in Table 3. The NMR spectra are therefore insensitive to the –N=O rotation process, and the changes of the dimethylamino signal are attributed to restricted rotation of this group relative to the aromatic ring. Measurements of the dimethylamino bandshapes both at coalescence (238 K) and slightly above coalescence (243 K) and use of the appropriate analytical expressions [20] for the rate constants at these two temperatures gave energy data ($\Delta G^{\ddagger}$ of 50.8 and 50.9 kJ mol^{-1} respectively. These values are slightly lower than those obtained [8] for methylamino rotation in *p*-nitroso-N-methylaniline where $\Delta G^{\ddagger}$ (298 K) = 57.4 kJ mol^{-1} (major → minor rotamer). The relatively large activation free energies reflect the considerable contribution of the quinonoid forms to the overall structures of these free and coordinated ligand species with strong π-electron donors in the 4-position.

Table 6. Comparison of ν_{NO} for the free ligand 4-X-C_6H_4NO and for the complex $[PtCl_3(4\text{-X-}C_6H_4NO)]^- K^+$

X	$\tilde{\nu}_{NO}/cm^{-1}$ Free ligand	$\tilde{\nu}_{NO}/cm^{-1}$ Complex[a]	$\Delta\tilde{\nu}/cm^{-1}$
H	1506[21]	1495	11
CH_3O	1508[22]	1501	7
CH_3	1508[21]	1499	9
NO_2	1513[21]	1490	23
CN	1499[a]	1491	8
$(CH_3)_2N$	1363[23]	1351	12
$COOCH_3$	1524[a]	1503	21

[a]This work.

The close correspondence of the $\Delta G^{\ddagger}$ values for the coordination compound and the free ligand is shown in Table 5. We conclude that the values can be regarded as equal within experimental error. Applying the same treatment for deriving $\Delta G^{\ddagger}$ to the rhodium complex [19] RhCl[cod][4-$(CH_3)_2N$–C_6H_4–NO] yields a value of 53 kJ mol^{-1}. The data suggest that σ_N coordination of C-nitroso groups to transition metals has virtually no effect on the barriers to rotation of the –N═O group relative to the aromatic ring. More precisely, any change in electronic nature of the C–N bond attaching the nitroso group to the ring must affect the near co-planar ground state and orthogonal transition state structures of the complexes equally. This is a somewhat surprising result as the electronic effects of coordination are considerable, viz the paramagnetic shielding, $\Delta\delta$, of the 6-position hydrogen, H_A, is 0.8 to 1.0 for $X = N(CH_3)_2$ or OCH_3.

The effects of σ_O and π_{NO} coordination of nitroso groups [4] might be expected to affect the rotational characteristics of the group more extensively, but this has yet to be explored.

In Table 6 the values of the wave numbers of the NO stretching mode in the complexes are compared with those of the corresponding ligand. The value of ν_{NO} falls on coordination within the range 7–23 cm^{-1}. This is characteristic of σ_N coordination and is associated with a small lengthening of the NO bond when coordination occurs [14].

CONCLUSIONS

Our results imply that the structural and electronic properties of the NO group are only slightly changed on σ_N coordination to metals implying that the π-electrons of the –N═O bond must be only slightly influenced by this coordination. Any significant reduction in π-character would have led to an appreciable lowering of the energy barrier by virtue of the smaller contribution of the quinonoid form of structure. A recent paper by Witanowski *et al.* [24] has demonstrated the remarkable deficit of electronic charge in the rings of nitrosoaromatic compounds due to the strong electron withdrawing effect of the nitroso group. This supports our case for the nitroso group being uniquely strong in its electron withdrawing power and for its anomalous effects on 4-substituents as evidenced by the C-1 substituent chemical shifts.

Acknowledgements—We thank Drs M. Cameron and A. S. F. Boyd for some early studies. B.G.G. thanks the Leverhulme Trust for the award of an Emeritus Fellowship.

REFERENCES

1. Al-Tahou, B. M. and Gowenlock, B. G., *Recl. Trav. Chim. Pays-Bas*, 1986, **105**, 253.
2. Topsom, R. D., *Acc. Chem. Res.*, 1983, **16**, 292.
3. Butt, G., Topsom, R. D., Gowenlock, B. G. and Hunter, J. A., *J. Mol. Struct.* (*Theochem*), 1988, **164**, 399.
4. Cameron, M., Gowenlock, B. G. and Vasapollo, G., *Chem. Soc. Rev.*, 1990, **19**, 355.
5. Cameron, M., Gowenlock, B. G. and Vasapollo, G., *Polyhedron*, 1995, **14**, 2087.
6. Møller, E. R. and Jørgensen, K. A., *J. Am. Chem. Soc.*, 1993, **115**, 11814.
7. Boyd, A. S. F., Browne, G., Gowenlock, B. G. and McKenna, P., *J. Organomet. Chem.*, 1988, **345**, 217.
8. Fletcher, D. A., Gowenlock, B. G., Orrell, K. G. and Šik, V., *Magn. Reson. Chem.*, 1995, **33**, 561.
9. Porta, F., *J. Chem. Soc. Chem. Commun.*, 1993, 1510.
10. Mansuy, D., Drême, D., Chottard, J. C. and Guilhem, J., *J. Organomet. Chem.*, 1978, **161**, 207.
11. Lynch, B. M., *Can. J. Chem.*, 1977, **55**, 541.
12. Ewing, D. F., *Org. Magn. Reson.*, 1979, **12**, 499.
13. Bromilow, J., Brownlee, R. T. C., Craik, D. J., Sadek, M. and Taft, R. W., *J. Org. Chem.*, 1980, **45**, 2429.
14. Cameron, M., Gowenlock, B. G. and Vasapollo, G., *J. Organomet. Chem.*, 1991, **403**, 325.
15. MacNicol, D. D., Wallace, R. and Brand, J. C. D., *Trans. Faraday Soc.*, 1965, **61**, 1.
16. Korver, P. K., van der Haak, P. J. and de Boer, Th. J., *Tetrahedron*, 1966, **22**, 3157.
17. Furness, A. R., Buckley, P. D. and Jolley, K. W., *Aust. J. Chem.*, 1975, **28**, 2303.
18. Fletcher, D. A., Ph.D. Thesis, University of Exeter (1996).
19. Matsubayashi, G. and Tanaka, T., *J. Chem. Soc., Dalton Trans.*, 1990, 437.
20. Sandstrom, J., Dynamic NMR Spectroscopy, Chapter 6, Academic Press, London 1982.
21. Lüttke, W., *Z. Elektrochem.*, 1957, **61**, 302.
22. Talberg, H. J., *Acta Chem. Scand. A*, 1979, **33**, 289.
23. Knieriem, B., Ph.D. Thesis, University of Göttingen (1972).
24. Witanowski, M., Biedrzycka, Z., Sicinska, W. and Webb, G. A., *Magn. Reson. Chem.*, 1997, **35**, 262.

Pergamon

PII: S0277-5387(98)00134-X

Polyhedron Vol. 17, No. 20, pp. 3501–3505, 1998
© 1998 Elsevier Science Ltd
All rights reserved. Printed in Great Britain
0277–5387/98 $19.00+0.00

An EPR and electronic spectral study of some interactions of bis(diethyl–diselenocarabamato)copper(II) complexes in solution

N. D. Yordanov,[a]* M. Y. Mihaylov[a] and P. O'Brien[b]

[a]Institute of Catalysis, Bulgarian Academy of Sciences, 1113 Sofia, Bulgaria

[b]Department of Chemistry, Imperial College of Science, Technology and Medicine, South Kensington, London SW7 2AY, U.K.

(Received 14 October 1997; accepted 30 March 1998)

Abstract—Interactions of the complex bis(diethyl–diselenocarbamato)copper(II), ($Cu(dsc)_2$) with some copper(II) salts in solution have been studied by EPR and electronic spectroscopy. The complex interacts with copper salts (CuX_2, X = Cl, Br, NO_3) to produce EPR silent dimers of the type [(dsc)CuX_2Cu(dsc)] which are formed in equilibrium with mixed-ligand Cu(dsc)X complexes. The same dimers are found to be formed in the course of the exchange reaction between the zinc diselenocarbamate and copper chloride. The electronic spectrum of the bis-chelate has a characteristic absorption band at 20,200 cm^{-1} (ϵ = 11,800 m^{-1} dm^3 cm^{-1}) whereas the dimers are characterized by a band at 22,600 cm^{-1} (ϵ = 23,800 m^{-1} dm^3 cm^{-1}). This property of complex could be used in analytical practice for increasing sensitivity of photometric estimations. © 1998 Elsevier Science Ltd. All rights reserved

Keywords: EPR; UV-vis; bis(diselenocarbamato)copper(II); mixed-ligand complexes; dimeric structure.

INTRODUCTION

In the last decades complexes of dialkyl–diselenocarbamates have been shown to be useful in several different areas of science and technology. They, for example, are used as: analytical reagents [1–4], photo stabilizer [5], antioxidant additives to hydrocarbons like polymers [5, 6] or motor oil [7], metal deactivators [8], pesticides and fungicides [9, 10], floatation agents [11], precursors e.g. in preparation of solar cell materials [12–22]. In some applications they exhibit better properties than the corresponding sulfur-containing complexes, e.g. the dialkyl–dithiocarbamates or dithiophosphates. However, the inherent problems in the synthesis of the ligands makes them a less popular choice of reagent unless there is a major advantage or the element selenium must be used for some technological reason. The literature on their properties and reactivity is generally quite limited but their use as precursor for selenium containing materials had led to an increased interest in recent years [14–22].

In this paper we describe some of our results obtained by EPR and electronic spectral studies on the interaction of bis(diethyl–diselenocarbamato) copper(II) ($Cu(dsc)_2$) with CuX_2 (X = Cl, Br, NO_3). In the previous work from our laboratory interesting intermolecular interactions were observed for the related bis(dithiocarbamato)copper(II) complex ($Cu(dtc)_2$) [23–28] and the possibility of such effects for the selenium analogue has been investigated in the present work.

EXPERIMENTAL

Starting materials

The complex [$Zn(Et_2$–$dsc)_2$] was obtained by the reaction of $Et_2NH + CSe_2$ in the presence of zinc sulfate as previously described [29]. All other chemicals

* Author to whom correspondence should be addressed. E-mail: ndyepr@bgearn.acad.bg.

and solvents were of reagent grade and used as obtained.

The copper complex [$Cu(Et_2–dsc)_2$] was obtained by exchanging the zinc ion of $Zn(Et_2–dsc)_2$ with Cu^{2+} as previously described [30]. [$Zn(dsc)_2$] (0.2 g) dissolved in 10 ml $CHCl_3$ was shaken with $CuSO_4 \cdot 5H_2O$ (4 g) in water (40 ml). The chloroform layer was separated, evaporated and the black product was recrystallized from acetone/chloroform. The purity of the product obtained was checked by its electronic spectrum ($\epsilon = 11{,}800\,m^{-1}\,dm^3\,cm^{-1}$ at $\lambda = 20{,}200\,cm^{-1}$) [30–32] as well as by its elemental analysis: For $C_{10} \cdot H_{20} \cdot N_2Se_4$ calculated (found) Cu calc. 11.6 (11.4); C 21.9 (22.1); H 3.6 (2.4), N 5.1 (5.3). The same product was not obtained when $CuCl_2$ was used instead of $CuSO_4$ (*vide infra*).

The EPR spectra were taken at 315 K on an X-band, portable, model PS100.X, spectrometer produced by ADANI (Minsk), using 100 kHz magnetic field modulation. A full description of this spectrometer has been given in an earlier publication [33]. The electronic spectra were recorded on a SPECORD UV-Vis (Carl Zeiss, Jena) spectrophotometer.

RESULTS AND DISCUSSIONS

Peculiarities noted in synthesis of Cu(dsc)$_2$

In the course of attempting the synthesis of $Cu(dsc)_2$ using the exchanged reaction eq. (1)

$$Zn(dsc)_2 + Cu^{2+} \rightarrow Cu(dsc)_2 + Zn^{2+} \qquad (1)$$

significant differences were found in the product obtained by the use of $CuSO_4$ [30] from that with $CuCl_2$. The sulphate salt gave a 100% yield of Cu $(Et_2–dsc)_2$ characterized by an absorption maximum at 20,200 cm^{-1} (Fig. 1(a)) and a strong EPR spectrum (Fig. 2) stable with the time. The material obtained when $CuCl_2$ was used instead of $CuSO_4$ showed an absorption maximum at 22,600 cm^{-1} with a shoulder at 20,200 cm^{-1} (Fig. 1(b)). In addition the EPR spectrum was very weak as compared to those recorded with the same quantity of the substance produced in the first case. The crystals were slightly soluble in benzene and this solution gave an intensive EPR signal and an absorption maximum at 20,200 cm^{-1}. The remaining main portion was $CHCl_3$ soluble with an absorption band at 22,600 cm^{-1}, but the solution was EPR silent. Two possibilities were considered that the insoluble material was the product of a redox reaction or a dimeric complex of the type (dsc)$CuCl_2$Cu(dsc) with strongly antiferromagnetically coupled copper ions. The former assumption was rejected because the EPR spectrum of $Cu(dsc)_2$ did not change over the period of study (5 months). Therefore, assuming the formation of a dimeric form, we have observed by gradual addition to its $CHCl_3$ solution of known amounts of $Zn(dsc)_2CHCl_3$ solution a stoichiometric formation of the same product as obtained by the use of $CuSO_4$. This fact we consider as evidence for the formation of dimeric (dsc)$CuCl_2$Cu(dsc) complex. A similar chloride bridged dimeric mixed-ligand complex of copper(II) dithiocarbamate (dtc)$CuCl_2$Cu(dtc) was recently observed as a product of $Cu(dtc)_2$ photolysis in $CHCl_3$ [34].

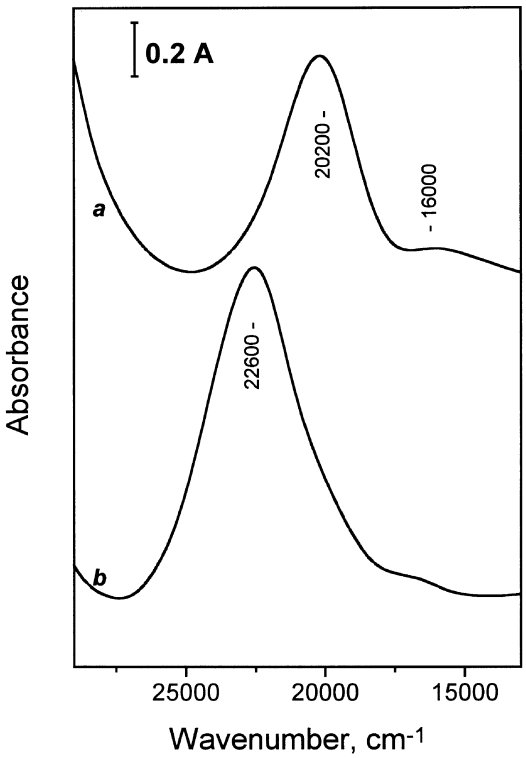

Fig. 1. (a) Electronic spectrum recorded of the sample obtained when $Zn(dsc)_2$ is exchanged with $CuSO_4$. This is the spectrum typical for $Cu(dsc)_2$ complex; (b) Electronic spectrum recorded of the sample obtained when $Zn(dsc)_2$ is exchanged with $CuCl_2$. This is the spectrum typical for the dimer (dsc)CuZ_2Cu(dsc).

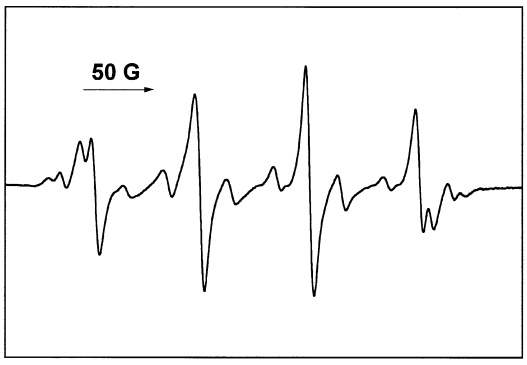

Fig. 2. Typical room temperature EPR spectrum of $Cu(dsc)_2$ complex dissolved in organic solvents.

EPR spectra of Cu(dsc)$_2$ complex

The structure of the isotropic EPR spectrum of Cu(dsc)$_2$ (Fig. 1) dissolved in solvent in which specific interactions are not expected (e.g. in benzene, toluene, $CHCl_3$, acetone, DMFA) was as has been described in the literature [35–38]. The spectrum (Fig. 2) consists of four hyperfine lines due to the interaction of the unpaired electron with ^{63,65}Cu (nuclear spin $I = 3/2$). Furthermore, since the natural abundance of ^{77}Se ($I = 1/2$) is 7.5%, approximately 30% of the Cu(dsc)$_2$ molecules will contain one ^{77}Se atom from which shf splitting is expected. The remaining 70% of Cu(dsc)$_2$ will not exhibit ^{77}Se shf splitting. Therefore, the EPR spectrum, Fig. 2, is a superimposition of the two spectra from the two different molecules — one consisting of only four Cu hf lines and other in which each of the Cu hf lines is split into two superhypefine lines because the nuclear spin of ^{77}Se. The EPR parameters typical of Cu(dsc)$_2$ in benzene, toluene, $CHCl_3$, acetone or DMFA are given in Table 1. It is worthy of note that the value of $g_o = 2.02 \pm 0.002$ is the lowest known to date and suggests an extremely covalent character for the Cu–Se bonds. In pyridine solution Cu(dsc)$_2$ forms an adduct with axial coordination of pyridine molecules(s) along the z-axis of the complex. The EPR parameters of this adduct (obtained at 324 K by Cu(dsc)$_2$ dissolved in pure pyridine) are also given in Table 1. These results are in excellent agreement with our previous studies and show that upon axial adduct formation g_o increases while A_o decreases [28, 39]. This fact was attributed to the decreased covalent character of the Cu–Se bonds and a rhombic deformation in the chromophore $CuSe_4$ result of the axial adduct formation [28, 39].

Interaction of Cu(dsc)$_2$ with some copper(II) salts

EPR studies. In Fig. 3 are shown several EPR spectra obtained upon mixing DMFA solutions of Cu(dsc)$_2$ and Cu(NO$_3$)$_2$. As seen from this figure increasing of the molar ratio Cu(dsc)$_2$/Cu(NO$_3$)$_2$ is accompanied by the appearance of new EPR spectrum due to mixed-ligand complex [Cu(dsc)$^+$·Solv...NO$_3$]. For this mixed-ligand complex shfs from the NO_3 anion can not be expected because ^{16}O has a nuclear spin $I = 0$ the ion is unlikely to interact directly with copper and to lie in the second coordination sphere [24, 25]. The EPR parameters of this spectrum are given in Table 1.

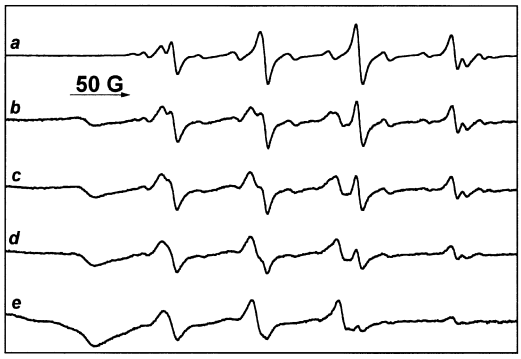

Fig. 3. Several room temperature EPR spectra taken after mixing of Cu(dsc)$_2$ with Cu(NO$_3$)$_2$. The ratio Cu(dsc)$_2$/Cu(NO$_3$)$_2$ is: (a) 1:0; (b) 3:2; (c) 1:1; (d) 3:4; (e) 1:2. Solution DMFA.

On mixing Cu(dsc)$_2$ (dissolved in $CHCl_3$ or in acetone) with CuX_2 (X = Cl, Br, dissolved in EtOH or i-PrOH or acetone) EPR spectra of the Cu(dsc)Cl mixed-ligand complex are recorded (Fig. 4). These complexes may be identified unambiguously by the shfs due to ^{35,37}Cl nuclear spin ($I = 3/2$) and therefore four shf lines should be recorded. The EPR parameters of this mixed-ligand spectra are given in Table 1. In pyridine however EPR spectrum of only Cu (dsc)Cl complex is observed. When $CuBr_2$ was used it

Table 1. EPR parameters of the parent and mixed-ligand complexes obtained by the interactions of Cu(dsc)$_2$ with Cu(II) salts

Complex	Solvent	$g_o \pm 0.002$	$^{Cu}A_o \pm 1$ G	$^{Se}A_o \pm 1$ G	$^{Cl}A_o \pm 0.5$ G
Cu(dsc)$_2$	$CHCl_3$, DMFA	2.022	80	46	–
	C_6H_6, acetone	2.030	72	48	–
	pyridine				
Cu(dsc)Cl	pyridine	2.074	66	–	8
	DMFA	2.066	75	–	8
	$CHCl_3$/EtOH (1:1)	2.064	76	–	8
	acetone	2.063	78	–	8
	$CHCl_3$/i-PrOH (1:1)	2.062	78	–	9
Cu(dsc)$^+ \cdots Cl^-$	DMFA	2.076	73	a	–
Cu(dsc)+...NO$_3$	DMFA	2.073	73	50	–
	EtOH	2.067	80	40	–

[a]Can not be estimated due to overlapping of the lines.

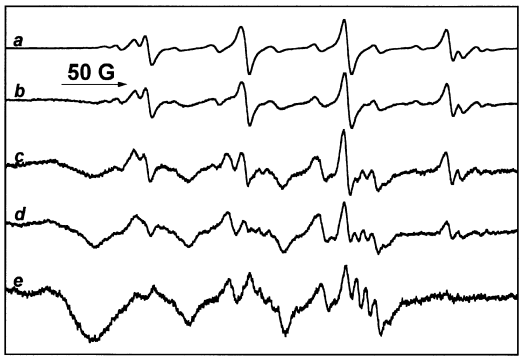

Fig. 4. Several room temperature EPR spectra taken after mixing of $Cu(dsc)_2$ with $CuCl_2$. The ratio $Cu(dsc)_2/CuCl_2$ is: (a) 1:0; (b) 3:1; (c) 1:1; (d) 2:3; (e). 1:2. Solution DMFA.

was impossible to record any EPR spectrum of mixed-ligand complexes. Only a progressive gradual decrease of the intensity of $Cu(dsc)_2$ was observed.

When DMFA is used as a solvent EPR spectra of two mixed-ligand complexes are recorded (Fig. 4)—that of Cu(dsc)Cl characterized by its shf splitting form one $^{35,37}Cl$ nucleus and another with EPR parameters fully consistent with those of $Cu(dsc)^+ \cdot Solv_2$. In order to record the mixed-ligand CuCl(dsc) complexes the instrument amplification was increased 100 fold times.

The general conclusion is that when a solution of $Cu(dsc)_2$ in an organic solvents ($CHCl_3$, DMFA, acetone or pyridine) reacts with solutions of CuX_2 (X = Cl, Br, NO_3, dissolved in C_2H_5OH, i-C_3H_7OH, DMFA), and pyridine mixed-ligand complexes are obtained. The above qualitative observations however show that the equilibrium position for the reaction leads to a predominance of the dimer.

$$Cu(dsc)_2 + CuX_2 \Leftrightarrow (dsc)CuX_2Cu(dsc) \overset{Solv}{\Leftrightarrow}$$

$$2Cu(dsc)_2 \cdot X \cdot solv \overset{Solv}{\Leftrightarrow} 2[Cu(dsc) \cdot Solv_2]^+ ... X^-.$$

$$(X = Cl, Br, NO_3) \qquad (2)$$

The extent of reaction is affected by the anions in the order $NO_3^- < Cl^- < Br^-$ and the EPR silent dimeric (dsc)$CuBr_2$Cu(dsc) complex is formed in contrast with $Cu(dtc)_2$ complexes where at room temperature the equilibrium eq. (2) is shifted to the right [24–28] hence the above result is specific for $Cu(dsc)_2$.

Inspecting the EPR parameters of the mixed-ligand complexes given in Table 1 it is clear that g_o increases whereas A_o decreases with the increasing of the donor properties of the solvents; which follows the order: i-PrOH < acetone < EtOH < pyridine [24, 25, 39]. On the other hand the Se shf splitting, which is due to only 15% of the mixed-ligand copper(II) complexes (*vide supra*) is 40 G when EtOH is used and increases to 50 G in the case of DMFA. This effect may be explained by considering the coordinating properties of the solvents and *trans*-effects of NO_3 group. In the presence of DMFA the Cu complex is solvated by two molecules of the solvent and NO_3^- group is in the second coordination sphere [24, 25, 27]. Thus dsc ligand may be shifted into more close contact with copper and Se shf splitting will increase. In contrast to this observation when EtOH is used as a solvent NO_3 group is in the first coordination sphere and from electrostatic point of view it may be expected that repulsion between the ligands which take place will increase the distance Cu–Se and it will reflect to decrease of the Se shf splitting.

Electronic spectral studies. When to solutions of $Cu(dsc)_2$ in different organic solvents ($CHCl_3$, DMFA, acetone, pyridine) CuX_2 (X = Cl, Br, NO_3) dissolved in C_2H_5OH, i–C_3H_7OH, DMFA or pyridine was added hypsochromic and hyperchromic shift was observed (Fig. 5). The new band at 22,600 cm^{-1} is the same as those reported above for the dimeric (dsc)CuX_2Cu(dsc) (X = Cl, Br) complexes. On the other hand it is clear from Fig. 5 that the doubling (ε = 23,800) of the intensity of the band at 22,600 cm^{-1} takes place compared to that at 20,200 cm^{-1}. The isosbestic point at 21,000 cm^{-1} clearly supports the reaction scheme as is proposed in

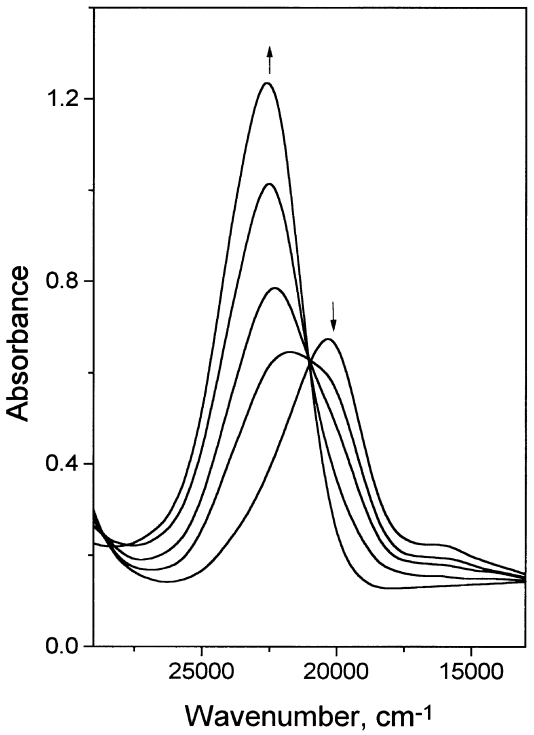

Fig. 5. Several electronic spectra taken after mixing of $Cu(dsc)_2$ (in $CHCl_3$) with $CuCl_2$ (in EtOH). The gradual hypsochromic and hyperchromic shift of the initial absorption maxima of 5.5×10^{-5} M/l $Cu(dsc)_2$ at 20,200 cm^{-1} to 22,600 cm^{-1} with isosbestic point at 21,000 cm^{-1} is observed when the ratio $Cu(dsc)_2/CuCl_2$ is changed from 1:0 to 2:1.

eq. (2). This property of the dimer may be used in the analytical work for increasing sensitivity of photometric estimations of the $Cu(dsc)_2$ complex.

Acknowledgements—The financial support from the National Foundation "Scientific Research" (Project X-419) is gratefully acknowledged. POB thanks the EPSRC for grants supporting work on selenium compounds at both QMW and ICTMS. POB is the Sumitomo/STS Professor of Materials Chemistry and The Royal Society Amersham International Research Fellow (1997/98). We thank Dr M. A. Malik of ICTMS for the synthesis of the original sample of the zinc diselenenocarbamate used in this study.

REFERENCES

1. Busev, A. I. and Kirspuu, H., *Taru Riikliki Ulikooli Toim*, 1968, **219,** 215.
2. Busev, A. I., Kirspuu, H. and Kook, H., Tulp, A., *Taru Riikliki Ulikooli Toim*, 1971, **289,** 25.
3. Ladogorski, P. and Terpilpwski, J., *Farm. Pol.*, 1975, **31,** 393.
4. Kirspuu, H. and Busev, A. I., *Zh. Anal. Khim.*, 1968, **23,** 354.
5. Oslawa, Z. and Nakano, K., *J. Polym. Sci.*, 1977, **57,** 267.
6. Brit. Patent 821872.
7. U.S. Patent 3,976,439.
8. Japan Patent 7, 404, 820.
9. Takeo, S. and Yosiyuki, I., *Nippon Makuzai Gakkaishi*, 1961, **8,** 108.
10. Takeo, S. and Yosiyuki, I., *Nippon Makuzai Gakkaishi*, 1960, **6,** 182 (CA 54, 25482y).
11. Trindade, T. and O'Brien, P., *Chemistry of Materials*, 1997, **9,** 523.
12. Japan Patent 01, 298, 009 (89, 298, 009).
13. Japan Patent 01, 298, 0010 (89, 298, 010).
14. Hursthouse, M. B., Malik, M. A., Motevalli, M. and O'Brien, P., *Journal of Materials Chemistry*, 1992, **2,** 949.
15. Malik, M. A., Motevalli, M., O'Brien, P. and Walsh, J. R., *Organometallics*, 1992, **11,** 3136.
16. Nomura, R. and O'Brien, P., *J. Mater. Chem.*, 1995, **5,** 1761.
17. Trindade, T. and O'Brien, P., *Advanced Materials*, 1996, **8,** 160.
18. O'Brien, P., Walsh, J. R., Watson, I. M., Motevalli, M. and Henriksen, L., *J. Chem. Soc., Dalton Trans*, 1996, 2491.
19. Trindade, T. and O'Brien, P., *J. Mater. Chem.*, 1996, **6,** 343.
20. O'Brien, P., Malik, M. A., Chunggaze, M., Trindade, T., Walsh, J. R. and Jones, A. C., *J. Crystal Growth*, 1997, **170,** 23.
21. Malik, M. A. and O'Brien, P., *Polyhedron*, 1997, **16,** 3593.
22. O'Brien, P., Otway, D. J. and Walsh, J. R., *Advanced Materials, CVD*, 1997, **3,** 227.
23. Yordanov, N. D., *Theoret. Eksp. Khim.*, 1973, **9,** 706.
24. Yordanov, N. D., Terziev, V. and Shopov, D., *Compt. Rend. Acad. Sci. Bulg.*, 1974, **27,** 1529.
25. Yordanov, N. D. and Shopov, D., *J. Inorg. Nucl. Chem.*, 1976, **38,** 137.
26. Iliev, V. I., Yordanov, N. D. and Shopov, D., *Polyhedron*, 1984, **3,** 297.
27. Yordanov, N. D., *J. Mol. Stuct.*, 1976, **47,** 107.
28. Yordanov, N. D., in *Advances in Solution Chemistry*, eds, I. Bertini, L. Lunazzi and A. Dei. Plenum Press, NY, 1980, p. 81.
29. Malik, M. A. and O'Brien, P., *Materials Chemistry*, 1991, **3,** 999.
30. Barnard, D. and Woodbridge, D. T., *J. Chem. Soc.*, 1961, 2922.
31. Furlani, C., Cervone, E. and Diomedi Camassei, F., *Inorg. Chem.*, 1968, **7,** 265.
32. Jansen, K. A. and Krishnan, V., *Acta Chem. Scand.*, 1970, **24,** 743.
33. Linev, V. N., in *Electron Magnetic Resonance of Disordered Systems*, ed., N. D. Yordanov. World Scientific Publishers, Singapore, 1991, p. 53.
34. Jeliazkova, B. G. and Sarova, G., *J. Photochem. Photobiol. A*, 1996, **97,** 5.
35. Larin, G. M., Solozenkin, P. M., Dyatkina, M. E. and Kopitsja, N. I., *Izv. Akad. Nauk USSR* (*ser. Chem.*), 1968, 968.
36. Kirmse, R., *Chem. Phys. Lett.*, 1969, **4,** 565.
37. Buluggiu, E. and Vera, A., *J. Chem. Phys.*, 1973, **59,** 2886.
38. Keizers, C. P., Ph.D. Thesis, Nijmegen University, 1974.
39. Yordanov, N. D. and Shopov, D., *J. Chem. Soc. Dalton Trans.*, 1976, 883.
40. Rosenbaum, A., *Freiberger Forschungs A*, 1964, **328,** 59.

Pergamon

PII: S0277–5387(98)00138–7

Polyhedron Vol. 17, No. 20, pp. 3507–3514, 1998
© 1998 Elsevier Science Ltd
All rights reserved. Printed in Great Britain
0277–5387/98 $19.00+0.00

Structure of Fe_3O complexes with long alkyl chain fatty acid, $[Fe_3O(O_2CC_nH_{2n+1})_6L_3]NO_3$ ($L=H_2O$, $n=11$, 13, 15, 17; $L=py$, $n=13$, 15, 17); crystal structure of $[Fe_3O(O_2CC_{13}H_{27})_6(py)_3]NO_3$

Tadahiro Nakamoto,[a]* Motomi Katada,[b] Kazutoyo Endo[c] and Hirotoshi Sano[d]

[a]Advanced Science Research Center, Japan Atomic Energy Research Institute, Tokai, Ibaraki 319-1195, Japan

[b]Radioisotope Research Center, Tokyo Metropolitan University, Minamiohsawa, Hachioji, Tokyo 192-0397, Japan

[c]Showa College of Pharmaceutical Sciences, Higashi-tamagawagakuen, Machida, Tokyo 194-8543, Japan

[d]Department of Environmental Science, School of Social Information Studies, Otsuma Women's University, Karakida, Tama, Tokyo 206-8540, Japan

(Received 15 December 1997; accepted 31 March 1998)

Abstract—Two series of trinuclear iron(III) carboxylate complexes with long alkyl chains, $[Fe_3O(O_2CR)_6L_3]NO_3$ where $L=H_2O$ or py (pyridine), were prepared. Powder X-ray diffraction patterns of each series suggested that the aqua series has a double-layer structure and the pyridine series has a single-layer structure. The single crystal X-ray structure determination of $[Fe_3O(O_2CC_{13}H_{27})_6(py)_3]NO_3$ revealed that the compound forms a single-layer structure with the interlamellar orientation of alkyl chains being arranged alternately to those of adjacent layers. © 1998 Elsevier Science Ltd. All rights reserved

Keywords: trinuclear iron complex; long alkyl chain carboxylate complex.

INTRODUCTION

Complexes with long-alkyl chains prefer to construct layer structures, in which the metallic lamellae are layered apart from each interposing alkyl-chain layer, showing a long interlayer distance. The distance can easily be controlled by changing the carbon number of the alkyl chain in the starting materials. Such characteristics of the long-alkyl chain complexes are useful to investigate how the structure can modulate the intermolecular interactions.

In a previous study, we reported the preparation and the mixed-valence states of a series of mixed-valence Fe_3O complexes with long alkyl chain fatty acid, $[Fe_3O(O_2CC_nH_{2n+1})_6(py)_3]$ ($n=13$, 15, 17) [1]. In their ^{57}Fe Mössbauer spectra, a temperature-dependent mixed-valence state was observed for each complex; two quadrupole-split doublets ascribed to a high-spin Fe^{II} and a high-spin Fe^{III} were observed with an area ratio of $\sim$1:2 at low temperature, whereas only one quadrupole-split doublet ascribed to an intermediate valence state between Fe^{II} and Fe^{III} was observed at room temperature. The result was interpreted in terms of the rate of intramolecular electron transfer in the Fe_3O system, *i.e.*, the rate is slower than the time-scale of ^{57}Fe Mössbauer spectroscopy at lower temperature, while it goes quicker and

* Author to whom correspondence should be addressed.

exceeds the ^{57}Fe Mössbauer time scale at room temperature. This result has indicated that the valence-detrapping process in the Fe_3O type complexes is not always related to the dynamics of the solvate molecules of the crystal [1], although a close relation between the valence-detrapping and the dynamics of solvate molecules has been found for an acetate series, $[Fe_3O(O_2CCH_3)_6L_3]S$ (S is the solvate molecule) [2].

In the recent studies of mixed-valence Fe_3O complexes, the structural studies have become more important for studying the mixed-valence properties [3, 4]. However, no crystal structure analysis of the mixed-valence complexes with long alkyl chains has been done because of the difficulties of preparation of a single crystal suitable for structure determination. The available structural information is only that these complexes have a single-layer structure because the reflection lines of their powder X-ray diffraction patterns appeared with an equal interval in the small 2θ angle region and with a monotonously decreasing intensity [1].

In the previous studies, some fully oxidized Fe_3O–aqua complexes with long alkyl chains, $[Fe_3O(O_2CC_nH_{2n+1})_6(H_2O)_3]NO_3$ ($n=14$, 15, 17), were prepared and their IR and electronic spectra were reported [5]. However, the crystal structure of the Fe_3O-type complexes with long alkyl chains is, so far, still unknown regardless of whether they are mixed-valent or fully oxidized. Therefore, the crystal structure determination of the Fe_3O-type complexes with long alkyl chains will be very important for adding new information to the crystallographic data base. The crystal structure of the fully oxidized Fe_3O complex is expected to give some insight into the crystal structure of the mixed-valence Fe_3O complexes. In the present paper, the layer-structure of two series of fully-oxidized Fe_3O complexes, $[Fe_3O(O_2CC_nH_{2n+1})_6L_3]NO_3$ ($L=H_2O$, $n=11$, 13, 15, 17; L = py, $n=13$, 15, 17) and the crystal structure of the myristate–pyridine complex, $[Fe_3O(O_2CC_{13}H_{27})_6(py)_3]NO_3$, will be reported.

EXPERIMENTAL

Preparation of $[Fe_3O(O_2CC_nH_{2n+1})_6(H_2O)_3]NO_3$ (n = 11, 13, 15, 17)

Palmitate ($n=15$) and stearate ($n=17$) complexes were prepared according to the previously reported method [5](a), and laurate ($n=11$) and myristate ($n=13$) complexes were prepared according to the method for palmitate and stearate complexes by using lauric acid or myristic acid instead of stearic acid and palmitic acid. One portion of finely powdered $Fe(NO_3)_3{\cdot}9H_2O$ was added to the diethyl ether solution of triple the molar quantity of the corresponding acid by stirring, the mixture then being refluxed in a flask fitted with a reflux condenser. Pale orange precipitates, insoluble in diethyl ether, were filtered off. They were washed with diethyl ether, then dried in air. Found: C, 58.45; H, 9.99; N, 0.81. Calc. for $n=11$, $C_{72}H_{144}NO_{19}Fe_3$: C, 57.83; H, 9.71; N, 0.94%. Found: C, 61.49; H, 10.64; N, 0.70. Calc. for $n=13$, $C_{84}H_{168}NO_{19}Fe_3$: C, 60.64; H, 10.18; N, 0.84%. Found: C, 63.17; H, 11.02; N, 0.75. Calc. for $n=15$, $C_{96}H_{192}NO_{19}Fe_3$: C, 62.94; H, 10.56; N, 0.76%. Found: C, 64.98; H, 11.12; N, 0.70. Calc. for $n=17$, $C_{108}H_{216}NO_{19}Fe_3$: C, 64.85; H, 10.88; N, 0.70%.

Preparation of $[Fe_3O(O_2CC_nH_{2n+1})_6(py)_3]NO_3$ (n = 13, 15, 17)

The pyridine complexes were prepared by recrystallizing the aqua complexes from a pyridine–ethanol (1:1) mixture. The stearate and palmitate complexes were obtained as yellow–green powder, while the myristate complex was obtained as dark-green well-grown rectangular crystals suitable for X-ray crystal structure analysis when the solution was cooled. The laurate complex ($n=11$) was not obtained by this method. Found: C, 64.18; H, 10.01; N, 2.87. Calc. for $n=13$, $C_{99}H_{177}N_4O_{16}Fe_3$: C, 64.38; H, 9.66; N, 3.03%. Found: C, 66.29; H, 10.32; N, 2.54. Calc. for $n=15$, $C_{111}H_{201}N_4O_{16}Fe_3$: C, 66.15; H, 10.05; N, 2.78%. Found: C, 67.68; H, 10.63; N, 2.39. Calc. for $n=17$, $C_{123}H_{225}N_4O_{16}Fe_3$: C, 67.65; H, 10.38; N, 2.57%.

Powder X-ray diffraction measurement

Powder X-ray diffraction patterns were measured by using Cu–$K\alpha$ (40 kV, 20 mA) radiation on a Rigaku RAD-C system.

X-Ray structure determination

The data were collected on an Enraf Nonius CAD-4 diffractometer by using graphite-monochromated Mo–$K\alpha$ (0.71069 Å) radiation at 296 K. The structures were solved by using a direct method SIR88 [6] and refined by full-matrix least-squares. All calculations were carried out with MolEN computer software [7] on a Micro VAX 3400.

A crystal of $[Fe_3O(O_2CC_{13}H_{27})_6(py)_3]NO_3$ with dimensions $0.3\times0.3\times0.3\,mm^3$ cut out from one of the large crystals was mounted on a glass fiber in random orientation by using epoxy cement. Cell parameters and an orientation matrix for data collection were obtained from least-squares refinement by using the setting angles of 14 reflections in the range $9^\circ\leqslant\theta\leqslant11^\circ$. Three reflections (1,8,9;$\bar{6}$,3,11; $\bar{6}$,0,$1\bar{4}$) were remeasured every 120 minutes to monitor instrument and crystal stability and showed 3.1% variation in intensity. The intensities were corrected for Lorentz-polarization effects, and empirical absorption correction based on a series of ψ scans was applied. The minimum and maximum correction factors were 0.982 and 0.999, respectively. The structure was

refined with anisotropic thermal parameters for all atoms in the cation. Four intense peaks found in the difference Fourier map were regarded as the nitrate anion and refined isotropically with nonfixed positional parameters and thermal parameters. No hydrogen atoms were found in the final differential Fourier map. Crystal data for $[Fe_3O(O_2CC_{13}H_{27})_6(py)_3]NO_3$ are summarized in Table 1. The selected bond distances (Å) and bond angles (deg) are summarized in Table 2 and Table 3, respectively.

Table 1. Summary of crystallographic data

T (K)	296
empirical formula	$C_{99}Fe_3H_{177}N_4O_{16}$
f.w.	1847.05
crystal system	orthorhombic
space group	*Pbcn* (No. 60)
a (Å)	14.337(2)
b (Å)	17.183(2)
c (Å)	44.598(3)
V (Å^3)	10987(2)
Z	4
F(000)	4020
d_{calc} (g/cm^3)	1.12
radiation (Å)	Mo–$K\alpha$, 0.71073
μ (cm^{-1})	4.5
scan type	$\omega-2\theta$
2θ range (deg)	5–55
no. of unique reflections	12589
reflections used, $F_o^2 \geq 3\sigma(F_o^2)$	3018
R[a]	0.0711
R_w[b]	0.0819
S (godness of fit)	2.39
largest shift/esd	0.00
highest peak in final diff. map	0.40(8) e/Å^3
lowest peak in final diff. map	−0.23(8) e/Å^3
no. of parameters refined	550

[a] $R=(\Sigma\|\|F_o|-|F_c\|\|)/(\Sigma|F_o|)$.
[b] $R_w=[\Sigma w(F_o|-|F_c|)^2)/(\Sigma w|F_o|2)]^{1/2}$.

Table 2. Selected bond lengths (Å) with esd's in parentheses

Fe1–O	1.908(7)	O1–C1	1.29(1)
Fe1–O1	2.020(5)	O2–C1	1.23(1)
Fe1–O5	1.987(6)	O3–C15	1.24(1)
Fe1–N1	2.23(1)	O4–C15	1.26(1)
Fe2–O	1.898(4)	O5–C29	1.25(1)
Fe2–O2	1.995(6)	O6–C29	1.25(1)
Fe2–O3	1.999(6)	N1–C51	1.36(1)
Fe2–O4	2.006(5)	N2–C54	1.36(1)
Fe2–O6	1.988(6)	N2–C58	1.37(1)
Fe2–N2	2.189(7)	Fe1···Fe2	3.303(2)
		Fe2···Fe2′[a]	3.275(2)

[a] Symmetry code: (′) $1-x$, y, $3/2-z$.

RESULTS AND DISCUSSION

X-Ray diffraction patterns of $[Fe_3O(O_2CC_nH_{2n+1})_6(H_2O)_3]NO_3$ ($n=11$, 13, 15, 17) and $[Fe_3O(O_2CC_nH_{2n+1})_6(py)_3]NO_3$ ($n=13$, 15, 17) are shown in Fig. 1 and Fig. 2, respectively. One of the most remarkable features of them is that the reflection lines appear with an equal interval in the small 2θ angle region, suggesting a layer structure for both series. But their intensity variation is different from each other; in the aqua complexes the intensity of reflections decreases alternately whereas, in the pyridine complexes, it decreases monotonously with increasing 2θ. The second reflection of the myristate–pyridine complex at $\sim 8^\circ$ shows an irregularly high intensity because a weak reflection, which is observed separately for the cases of palmitate and stearate complexes, may be superimposed. The estimated interlayer distances are plotted in Fig. 3, together with the interlayer distances of the mixed-valence series [1]. The interlayer distance of each series increases linearly with increase of the number of carbon atoms in the alkyl chain, suggesting that each series has the same structure in which the only difference is the length of the alkyl chains, respectively. The pyridine series of the fully-oxidized complexes has a slightly longer interlayer distances than the mixed-valence pyridine series and the slope of the straight lines of both series are very close to each other. The differences of the interlayer distance between $n=11$ and $n=13$, $n=13$ and $n=15$, and $n=15$ and $n=17$ are 3.79, 4.15, and 3.71 Å, respectively, for the aqua complexes. These values are more than the length of two methylene groups $-(CH_2)_2-$, ca. 2.5 Å and less than twice the length of $-(CH_2)_2-$, ca 5.0 Å. This indicates that the aqua complexes have a double-layer structure with an interlamellar orientation of alkyl chains being of a head-to-head configuration, as shown in Fig. 4(a). On the other hand, the differences in the interlayer distance between $n=13$ and $n=15$, and $n=15$ and $n=17$ are 2.40, and 2.51 Å, respectively, which are almost equal to the length of two methylene groups. This indicates that the pyridine complexes have a single-layer structure with an interlamellar orientation of mutually inserted alkyl chains, as shown in Fig. 4(b). The monotonous decrease of the reflection intensity also supports this structure.

An ORTEP [8] drawing of the central part of $[Fe_3O(O_2CC_{13}H_{27})_6(py)_3]^+$ cation is shown in Fig. 5. The Fe_3O cations are located on sites of C_2 symmetry. The two-fold axis passes through O–Fe1–N1–C53 atoms, thus two iron atoms are related by the imposed symmetry and the Fe_3O triangle is planar. The nitrate anion located near the Fe_3O core should be disordered at least in two positions related to the C_2 axis. The position of the nitrate anion could not be precisely determined, probably because of further disordering. The Fe–(μ_3-O) distances of 1.908(7) Å and 1.898(4) Å are consistent with the typical value for Fe(III) [9] in $[Fe_3O(O_2CR)_6L_3]^+$ [10]. Two of the three coordinated

Table 3. Selected bond angles (deg) with esd's in parentheses

O–Fe1–O1	94.4(2)	Fe2–O–Fe2′ [a]	119.2(4)
O–Fe1–O5	93.2(2)	Fe1–O1–C1	126.6(5)
O–Fe1–N1	180	Fe2–O2–C1	134.1(5)
O1–Fe1–O1′ [a]	171.3(2)	Fe2–O3–C15	130.6(5)
O1–Fe1–O5	92.7(2)	Fe2–O4–C15	132.8(5)
O1–Fe1–O5′ [a]	86.8(2)	Fe1–O5–C29	135.4(6)
O1–Fe1–N1	85.6(2)	Fe2–O6–C29	128.6(5)
O5–Fe1–O5′ [a]	173.6(3)	Fe1–N1–C51	119.5(6)
O5–Fe1–N1	86.8(2)	C51–N1–C51′ [a]	121.0(9)
O–Fe2–O2	94.6(2)	Fe2–N2–C54	117.1(5)
O–Fe2–O3	93.8(2)	Fe2–N2–C58	119.1(6)
O–Fe2–O4	95.8(2)	C54–N2–C58	123.8(8)
O–Fe2–O6	95.2(2)	O1–C1–O2	125.6(7)
O–Fe2–N2	176.7(2)	O1–C1–C2	115.3(7)
O2–Fe2–O3	88.3(2)	O2–C1–C2	119.0(7)
O2–Fe2–O4	169.6(2)	O3–C15–O4	124.8(8)
O2–Fe2–O6	90.3(2)	O3–C15–C16	120.5(7)
O2–Fe2–N2	83.4(2)	O4–C15–C16	114.6(8)
O3–Fe2–O4	92.5(2)	O5–C29–O6	124.6(8)
O3–Fe2–O6	170.9(2)	O5–C29–C30	113.0(8)
O3–Fe2–N2	83.6(2)	N1–C51–C52	121(1)
O4–Fe2–O6	87.3(2)	N2–C54–C55	120.2(8)
O4–Fe2–N2	86.4(2)	N2–C58–C57	116(1)
O6–Fe2–N2	87.3(2)	Fe2–Fe1–Fe2′ [a]	59.45(4)
Fe1–O–Fe2	120.4(2)	Fe1–Fe2–Fe2′ [a]	60.27(4)

[a] Symmetry code: (′) $1-x$, y, $3/2-z$.

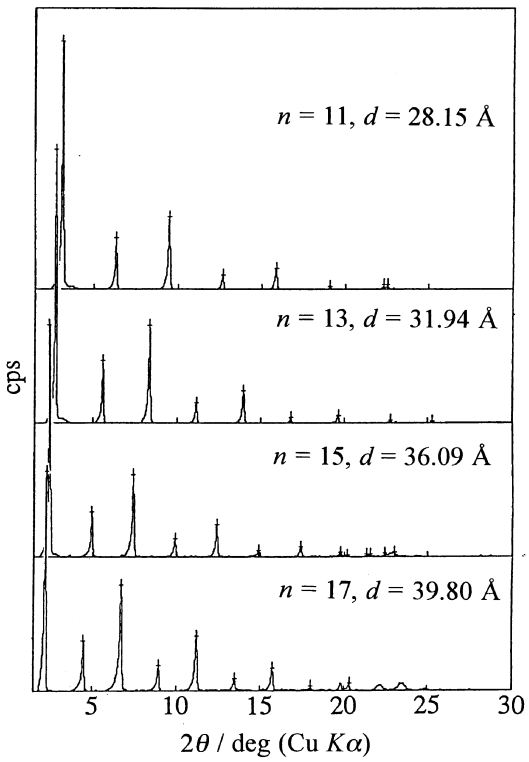

Fig. 1. Powder X-ray diffraction patterns of $[Fe_3O(O_2CC_nH_{2n+1})_6(H_2O)_3]NO_3$ ($n=11$, 13, 15, 17).

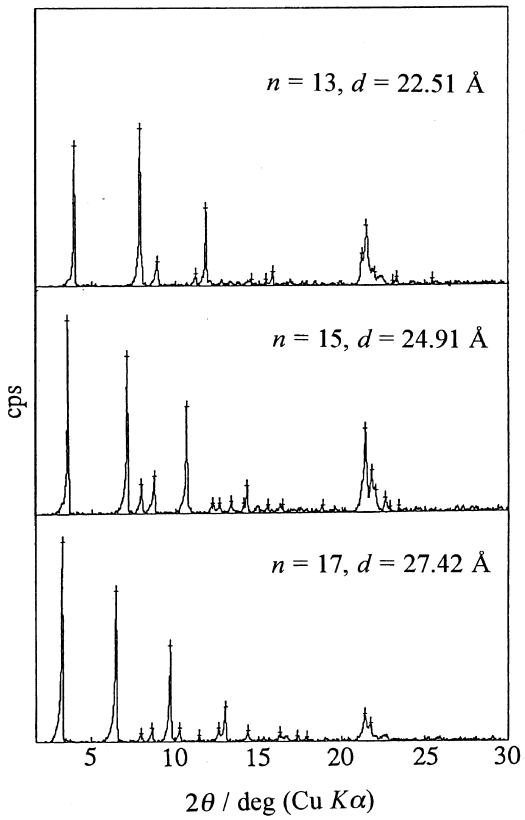

Fig. 2. Powder X-ray diffraction patterns of $[Fe_3O(O_2CC_nH_{2n+1})_6(py)_3]NO_3$ ($n=13$, 15, 17).

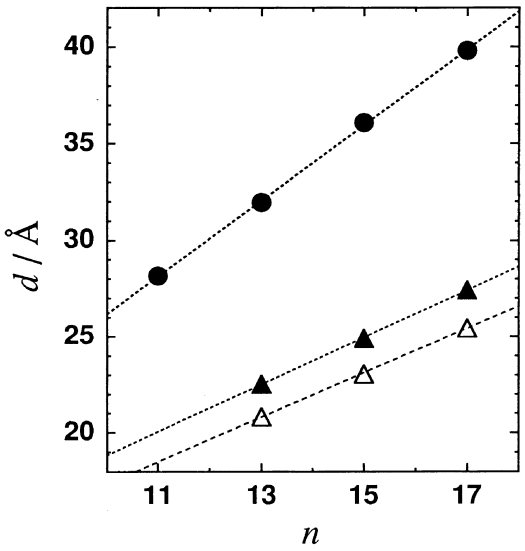

Fig. 3. Plot of interlayer distances for $[Fe_3O(O_2CC_nH_{2n+1})_6(H_2O)_3]NO_3$ (●), $[Fe_3O(O_2CC_nH_{2n+1})_6(py)_3]NO_3$ (▲), and $[Fe_3O(O_2CC_nH_{2n+1})_6(py)_3]$ (△). The straight lines are least-squares fitting.

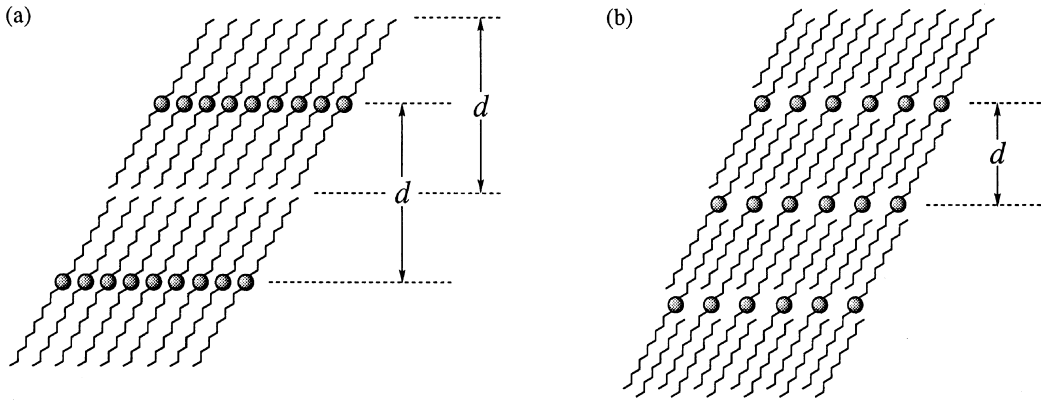

Fig. 4. Schematic representation of layer structures; (a) double-layer structure, (b) single-layer structure.

pyridine rings (N2, C54–C58) related to the C_2 axis are approximately parallel to the Fe_3 plane, whereas one pyridine ring (N1, C51–C53) is tilted by 51.3(2)° with respect to the Fe_3O plane. The Fe_3O plane is also tilted by 25.43(3)° with respect to the *ab* plane.

In Fig. 6, an ORTEP drawing of the whole cation structure is presented. The structure shows the presence of three inequivalent alkyl chains named A chain (C2–C14), B chain (C16–C28), and C chain (C31–C42). The directions of the three chains lying on the same side of the Fe_3O plane are approximately parallel to one another. As listed in Table 4, the A and B chains are regarded to have all-*trans* configuration within the torsion angle of 5°. However, a *gauche* conformation is seen at the bond between α and β carbon atoms of the C chain with the torsion angle of −63.56°. The bond between β and γ carbon is also significantly deformed from a *trans* conformation with the torsion angle of −164.82°. This indicates that the C chain must introduce a *gauche* conformation and a slightly deformed *trans* conformation to be accommodated in the same direction as the A, B chains.

A stereo view of the unit cell is shown in Fig. 7. As frequently seen in a number of long alkyl chain compounds, the myristate complex was found to form a single layer structure with interlamellar orientation of mutually inserted alkyl chains. The interlayer distance is found to be $c/2 = 22.30$ Å, which agrees with the estimated value, according to the Bragg condition, of 22.51 Å. Since the directions of the alkyl chains lying on the opposite side of the Fe_3O plane are different from each other, the inclination of the alkyl chains varies alternately as the alkyl chains are oriented in a zigzag along the *c*

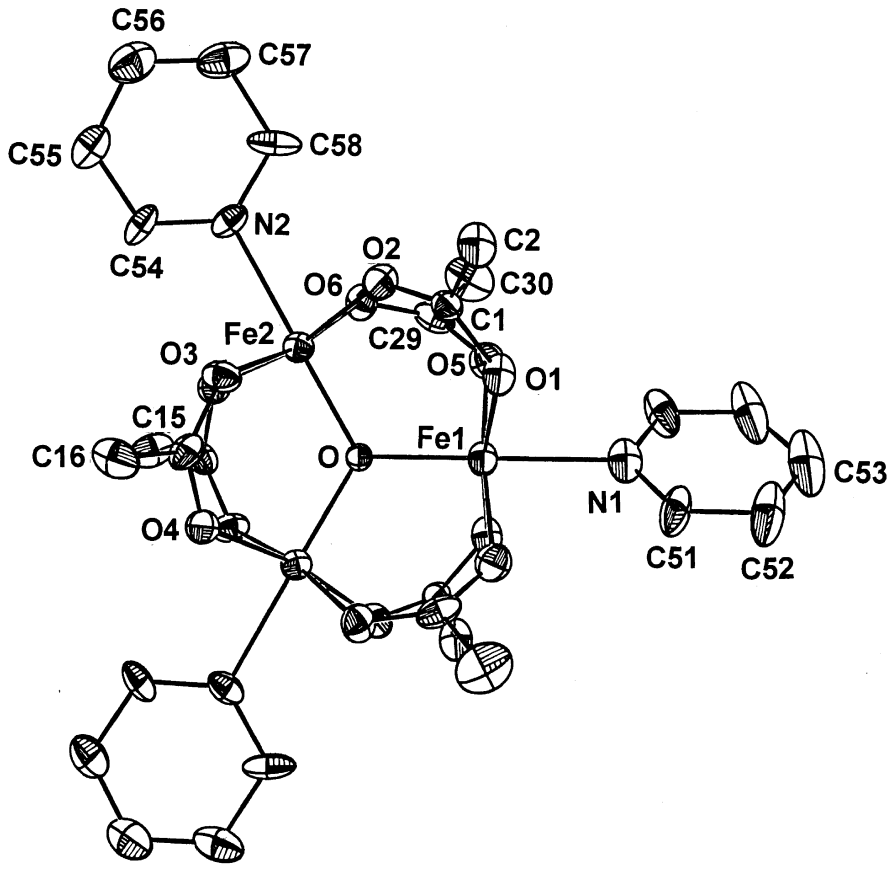

Fig. 5. ORTEP drawing of central part of the cation $[Fe_3O(O_2CC_{13}H_{27})_6(py)_3]^+$. The long alkyl chains are omitted. The thermal ellipsoids are drawn at the 20% probability level.

Table 4. Torsion angles (deg) of alkyl chains

Chain A		Chain B		Chain C	
C1–C2–C3–C4	−175.2(8)	C15–C16–C17–C18	−179.4(8)	C29–C30–C31–C32	−64(1)
C2–C3–C4–C5	−178.7(8)	C16–C17–C18–C19	177.0(9)	C30–C31–C32–C33	−165(1)
C3–C4–C5–C6	−178.2(8)	C17–C18–C19–C20	−177.5(9)	C31–C32–C33–C34	178(1)
C4–C5–C6–C7	−176.4(8)	C18–C19–C20–C21	−176.1(9)	C32–C33–C34–C35	−178(1)
C5–C6–C7–C8	−175.6(9)	C19–C20–C21–C22	−179.4(9)	C33–C34–C35–C36	−176(1)
C6–C7–C8–C9	−177.5(9)	C20–C21–C22–C23	180.0(9)	C34–C35–C36–C37	−175(1)
C7–C8–C9–C10	−178.0(9)	C21–C22–C23–C24	178(1)	C35–C36–C37–C38	−178(1)
C8–C9–C10–C11	−178.6(9)	C22–C23–C24–C25	179(1)	C36–C37–C38–C39	178(1)
C9–C10–C11–C12	−177.7(9)	C23–C24–C25–C26	−179(1)	C37–C38–C39–C40	179(1)
C10–C11–C12–C13	−176.8(9)	C24–C25–C26–C27	179(1)	C38–C39–C40–C41	179(1)
C11–C12–C13–C14	−177(1)	C25–C26–C27–C28	180(1)	C39–C40–C41–C42	179(1)

axis. They are tilted by $\sim 20^\circ$ with respect to the *c* axis. The fundamental structure of the palmitate and the stearate complexes is probably the same as that of the myristate complex. On the other hand, it is difficult to conclude whether the crystal structure of the mixed-valence pyridine series is similar to that of the fully-oxidized pyridine series or not, because the *intra*lamellar packing arrangement and the conformation of the alkyl chains are unknown in the mixed-valence series, although their powder X-ray diffraction patterns are very similar to those of the fully-oxidized pyridine series.

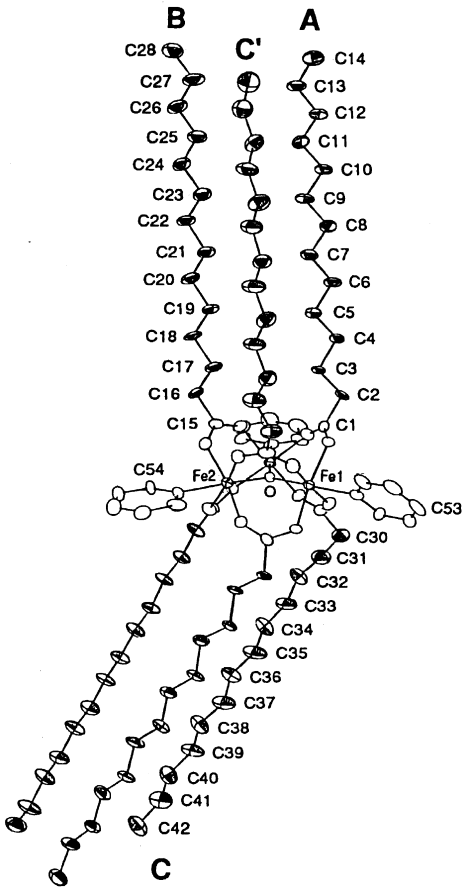

Fig. 6. ORTEP drawing of the cation $[Fe_3O(O_2CC_{13}H_{27})_6(py)_3]^+$. The thermal ellipsoids are drawn at the 20% probability level.

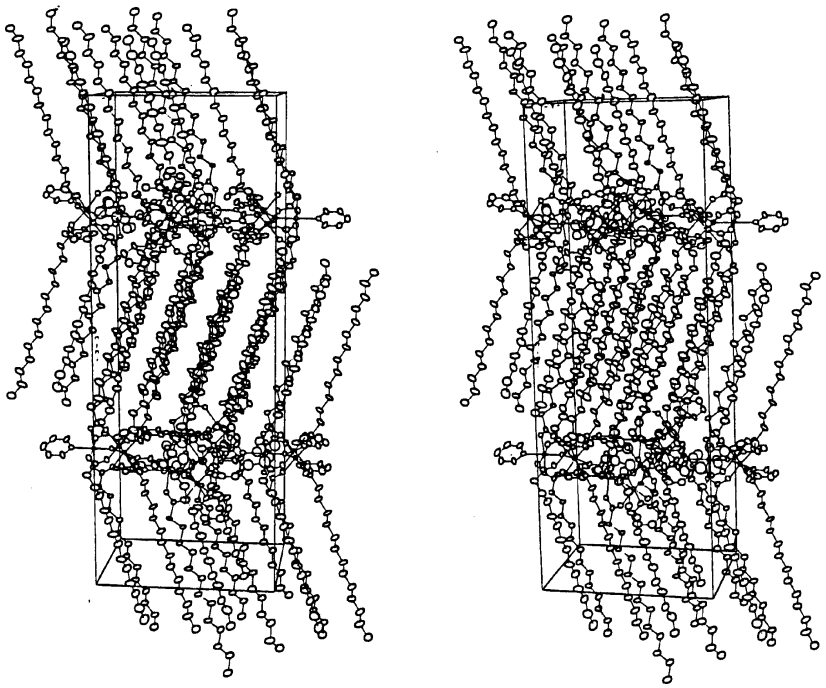

Fig. 7. Stereo view of the unit cell of $[Fe_3O(O_2CC_{13}H_{27})_6(py)_3]NO_3$. The thermal ellipsoids are drawn at the 20% probability level.

REFERENCES

1. Nakamoto, T., Katada, M. and Sano, H., *Chem. Lett*., 1990, 225; 1991, 1323.
2. Jang, H. G., Wittebort, R. J., Sorai, M., Kaneko, Y., Nakano, M. and Hendrickson, D. N., *Inorg. Chem*., 1992, **31**, 2265 and references cited therein.
3. Nakamoto, T., Hanaya, M., Katada, M., Endo, K., Kitagawa, S. and Sano, H., *Inorg. Chem*., 1997, **36**, 4347.
4. Wu, C.-C., Hunt, S. A., Gantzel, P. K., Gütlich, P. and Hendrickson, D. N., *Inorg. Chem*., 1997, **36**, 4717.
5. (a) Mansurov, M. M., Semenova, G. L., Yakubov, Kh. M. and Zhemchuzhnikova, T. A., *Zh. Neorg. Khim*., 1983, **28**, 1460; *Russ. J. Inorg. Chem*., 1983, **28**, 823; (b) Mansurov, M. M., Semenova, G. L. and Yakubov, Kh. M., *Zh. Neorg. Khim*., 1985, **30**, 368; *Russ. J. Inorg. Chem*., 1985, **30**, 206; (c) Semenova, G. L., Sarukhanov, M. A., Mansurov, M. M. and Yakubov, Kh. M., *Zh. Neorg. Khim*., 1987, **32**, 1377; *Russ. J. Inorg. Chem*., 1987, **32**, 829.
6. Burla, M. C., Camalli, M., Cascarano, G., Giacovazzo, C., Polidori, G., Spagna, R. and Viterbo, D., *J. Appl. Cryst*., 1989, **22**, 389.
7. Enraf–Nonius, *MolEN*, An Interactive Structure Solution Procedure. Enraf–Nonius, Delft, The Netherlands, 1990.
8. Johnson, C. K., *ORTEP*, Report ORNL-3794. Oak Ridge National Laboratory, Tennessee, U.S.A., 1965.
9. ^{57}Fe Mössbauer parameters: $\Delta E_Q = 0.612(8)$ mm/s, $\delta = 0.416(4)$ mm/s at 298 K. $\Delta E_Q = 0.673(2)$ mm/s, $\delta = 0.5140(9)$ mm/s at 82 K.
10. Cannon, R. D. and White, R. P., *Prog. Inorg. Chem*., 1988, **36**, 195.

Pergamon

PII: S0277–5387(98)00140–5

Polyhedron Vol. 17, No. 20, pp. 3515–3518, 1998
© 1998 Elsevier Science Ltd
All rights reserved. Printed in Great Britain
0277–5387/98 $19.00+0.00

1,2,3,5-*Tetrakis*(diphenylthiophosphino) benzene: n.m.r. and x-ray diffraction studies of a markedly distorted aromatic molecule

William Clegg, Andrew J. Edwards, H. Christina E. McFarlane and William McFarlane*

Department of Chemistry, University of Newcastle upon Tyne, Newcastle upon Tyne, NE1 7RU, U.K.

(Received 30 January 1998; accepted 30 March 1998)

Abstract—The presence of three adjacent bulky groups in 1,2,3,5-*tetrakis*(diphenyl-thiophosphino)benzene leads to structural distortion and hindered rotation about P–C bonds with concomitant inequivalence of P_1 and P_3 in the solution-state ^{31}P n.m.r. spectrum at low temperatures. The crystal structure shows that in the solid there are substantial deviations [up to 71 pm] from planarity of the central C_6P_4 skeleton, although the aromaticity appears to be retained. © 1998 Elsevier Science Ltd. All rights reserved

Keywords: poly-*tertiary*-phosphinesulfide; hindered rotation; ^{31}P n.m.r.; X-ray diffraction; aromaticity; molecular distortion.

In earlier preparative and n.m.r. spectroscopic studies [1, 2] of the *polykis*(diphenylphosphino)benzenes, $(Ph_2P)_nC_6H_{6-n}$($n=1$ to 4), we have attributed the patterns of their ^{31}P chemical shifts and vicinal ^{31}P–^{31}P coupling constants to steric interference of adjacent diphenylphosphino groups which leads to specific phosphorus electron lone-pair orientations, although in no case was rotation about any bond between the phosphorus and carbon atoms of the central skeleton found to be slow on an n.m.r. time-scale.

In connection with studies of derivatives of these species in which there is even greater potential for internal steric hindrance we now report that the low temperature proton-decoupled ^{31}P n.m.r. spectrum at 202 MHz of 1,2,3,5-*tetrakis*-(diphenylthio-phosphino)benzene, 1,2,3,5-$\{Ph_2P(S)\}_4C_6H_2$, **1**, shows P_1 and P_3 to be inequivalent with a chemical shift separation of 3.5 ppm at 198 K [Fig. 1]. At higher temperatures the resonances of P_1 and P_3 exhibited characteristic coalescence behaviour, and above 270 K a normal A_2MX spectrum [i.e. P_1 equivalent to P_3] was obtained [Fig. 1] with $^3J(P_1–P_2)=10.9$ Hz, $^4J(P_1–P_5)<1$ Hz and $^5J(P_2–P_5)=4.9$ Hz. Spectra at intermediate temperatures showed that the P_5 signal remained sharp [$v_{1/2}<3$ Hz] throughout, and from the coalescence of the P_1/P_3 resonances [$\Delta v=716$ Hz] a value of 39 kJmol^{-1} for the free energy of activation at 214 K was obtained. At the lowest attainable temperatures the P_1, P_2, and P_3 resonances still had widths in excess of 100 Hz, presumably owing to slow internal molecular motions, and therefore only the high temperature averaged values could be obtained for $^3J(P_1–P_2)$, $^3J(P_2–P_3)$ and $^4J(P_1–P_5)$, $^4J(P_3–P_5)$. In view of the large line widths at the lower temperatures no attempt was made to calculate an entropy of activation.

Consideration of a physical molecular model of **1** indicates that it is likely that this free energy of activation refers to concerted ["geared"] rotations about the phosphorus-carbon bonds linking P_1, P_2, and P_3 to the central C_6 skeleton. In principle, the observed inequivalence of P_1 and P_3 could be due to restricted rotation about any one of these bonds, and since the middle diphenylthiophosphino moiety will be the most sterically crowded its preferential adoption of any conformation with the sulfur atom at different distances from P_1 and P_3 could lead to the observed effect. The model shows that in practice the crowding is likely to be so great that the motions of all three adjacent diphenylthiophosphino moieties will be correlated and that the conformations adopted by P_1 and P_3 should be different, thus potentially enhancing their inequivalence. It is striking that between 296 and 198 K $\delta(^{31}P)$ for P_2, the most hindered phosphorus

* Author to whom correspondence should be addressed.

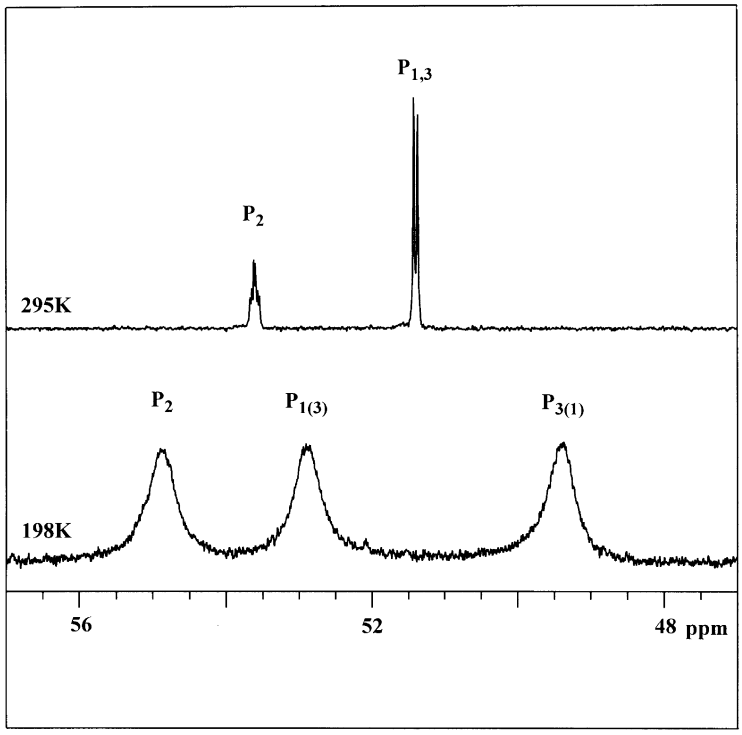

Fig. 1. Part of the proton-decoupled ^{31}P n.m.r. spectra at 202.4 MHz of 1,2,3,5-*tetrakis*-. (diphenylthiophosphino)benzene at 295 and 198 K.

atom, increases by 1.4 ppm, whereas that for P_5 is essentially unchanged and the mean chemical shift for P_1, P_3 decreases by only 0.25 ppm.

The above conclusions regarding steric compression were confirmed by a single crystal X-ray diffraction study which gave the solid state molecular structure of **1** represented in Fig. 2. Selected bond lengths and interbond angles are in Table 1. The unit cell contains four molecules of the tetrathiophosphine and a total of approximately three molecules of disordered dichloromethane. There are no significant intermolecular contacts and so the overall conformation adopted must be dominated by intramolecular constraints. Fig. 3 summarises the key features of the central C_6P_4 skeleton in which there are considerable distortions from an idealised geometry. The substituted benzene ring is not exactly planar with the largest deviations [6 pm] from the mean C_6 plane of individual carbon atoms substantially exceeding those found in hexaiodobenzene [3] but being less than those [up to 11 pm] in *hexakis*(trimethylsilyl)benzene [4]. The steric compression near C_2 leads to the C_1–C_2 and C_2–C_3 bonds of the ring being some 3–4 pm longer than those in benzene [5], triphenylphosphinesulfide [6], and indeed the phenyl groups of **1** itself, and this is compensated by a slight shortening of the C_4–C_5 and C_5–C_6 bonds. The C_1–P_1, C_2–P_2, and C_3–P_3 bonds are also elongated compared with C_5–P_5 in **1** and the P–C bond in triphenylphosphinesulfide [6].

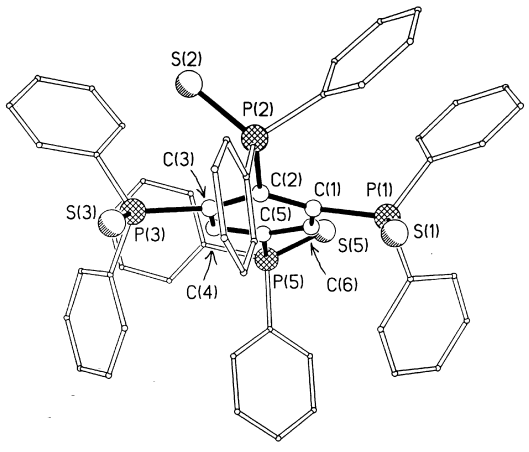

Fig. 2. Molecular structure of 1,2,3,5-*tetrakis* (diphenylthiophosphino)benzene determined by single crystal X-ray diffraction and viewed from somewhat below the central C_6 mean plane.

In this structure P_1 and P_3 are forced away from P_2, the $P_1C_1C_2$ and $P_3C_3C_2$ interbond angles being enlarged to 129°, and the $P_1C_1C_6$ and $P_3C_3C_4$ interbond angles correspondingly reduced to 111°. Most strikingly, P_1 and P_3 are on the opposite side to P_2 of the mean C_6 plane with deviations of up to 71 pm, so that the P_1-C_1-C_2-P_2 dihedral angle exceeds 36°.

Table 1. Selected bond lengths (pm) and angles (°) for 1

C(1)–C(2)	143.2(6)	C(2)–C(3)	141.8(5)
C(3)–C(4)	139.2(5)	C(4)–C(5)	137.6(6)
C(5)–C(6)	137.1(6)	C(6)–C(1)	138.9(6)
P(1)–C(1)	185.8(9)	P(2)–C(2)	185.9(4)
P(3)–C(3)	186.8(4)	P(5)–C(5)	182.1(4)
P(1)–S(1)	193.46(16)	P(2)–S(2)	195.16(16)
P(3)–S(3)	193.63(15)	P(5)–S(5)	194.16(16)
C(6)–C(1)–C(2)	119.4(3)	C(6)–C(1)–P(1)	111.4(3)
C(2)–C(1)–P(1)	128.5(3)	C(3)–C(2)–C(1)	117.2(3)
C(3)–C(2)–P(2)	117.7(3)	C(1)–C(2)–P(2)	123.4(3)
C(4)–C(3)–C(2)	119.7(4)	C(4)–C(3)–P(3)	110.9(3)
C(2)–C(3)–P(3)	129.2(3)	C(5)–C(4)–C(3)	122.0(4)
C(6)–C(5)–C(4)	118.5(4)	C(6)–C(5)–P(5)	118.9(3)
C(4)–C(5)–P(5)	122.0(3)	C(5)–C(6)–C(1)	122.2(4)
C(1)–P(1)–S(1)	116.17(14)	C(2)–P(2)–S(2)	108.89(13)
C(3)–P(3)–S(3)	119.83(13)	C(5)–P(5)–S(5)	111.68(15)

Although this amount of distortion is exceeded in *hexakis*(trimethylsilyl)benzene [4] in which all six substituents are very large, and in other highly hindered substituted benzenes such as *hexakis*(trimethylgermyl)benzene [7] and the 1,3,5-*tris*-(dialkylamino)-2,4,6-trinitrobenzenes [8], we are unaware of any other example in which the presence of only three adjacent bulky substituents on a benzene or other aromatic ring leads to so great an effect. In hexaiodobenzene [3] no iodine atom deviates by more than 5 pm from the carbon plane and all I-C-C-I dihedral angles are less than 5°, while in *hexakis*(trimethylsilyl)benzene [4] the corresponding Si-C-C-Si dihedral angles have an average value of 61°.

It is not clear to what extent the distortion from planarity of the benzene ring in *hexakis*(trimethylsilyl)benzene [4] perturbs its aromaticity, but the chemistry is unusual [4]. In the proton n.m.r. spectrum of **1** H_4 and H_6 were found to resonate at δ 7.6 [high temperature average] which is in the range expected for protons attached to an aromatic carbon ring, implying that the electronic ring current is intact. It was not possible to identify the corresponding resonances in the ^{13}C spectrum which extended from 125 to 155 p.p.m.; however, it should be noted that carbon shieldings are generally less satisfactory as criteria of aromaticity. The pattern of C–C bond lengths in the central carbon ring of **1** indicates that the π-electron density is somewhat greater near C_5 than C_2. Our results therefore suggest that approximate planarity of the ring itself, even when the extra-cyclic bonds are seriously displaced from ideal positions, is sufficient for the retention of aromaticity in carbocyclic molecules. It is likely that the synthesis of **1** was possible only because the diphenylphosphino substituents were attached to the central carbon ring prior to their

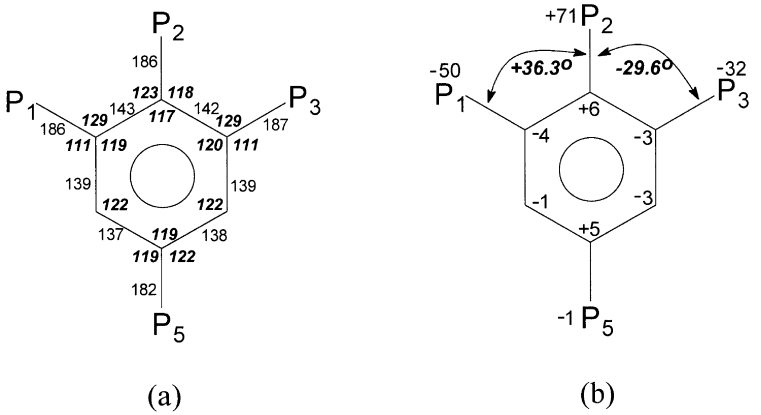

Fig. 3. Geometry of the central C_6P_4 skeleton of 1,2,3,5-*tetrakis*(diphenylthio-phosphino)benzene. (a) Bond lengths in pm in normal type, interbond angles in degrees in **bold italic** type. (b) Atomic deviations in pm above (+) or below (−) the mean central C_6 plane in normal type, dihedral angles in degrees in **bold italic** type.

steric demands being increased by the reaction with elemental sulfur. There is a clear parallel here with the synthesis of *hexakis*(trimethylsilyl)benzene from *hexakis*(dimethylsilyl)benzene by the conversion of Me_2SiH into the more bulky Me_3Si groups [4]. Prolonged reaction of elemental selenium with 1,2,3,5-*tetrakis*(diphenylphosphino)benzene did not progress beyond the formation of 1,3,5-*tris*(diphenylselenophosphino)-2-diphenylphosphinobenzene, presumably because the greater size of selenium compared with sulfur prevented its addition to the more crowded P_2.

EXPERIMENTAL

Preparation

1,2,3,5-*tetrakis*(diphenylthiophosphino)benzene, **1**, was made by the reaction between 1,2,3,5-*tetrakis*(diphenylphosphino)benzene and four equivalents of elemental sulfur in dichloromethane at room temperature for three weeks. It was recrystallized from a 1:1 mixture of dichloromethane and diethylether as yellow crystals suitable for X-ray diffraction. These lost solvent of crystallization under vacuum at 160° to give a pale yellow powder m.p. 267–270°. Found C 68.8, H 4.49, P13.1%; $C_{54}H_{42}P_4S_4$ requires C68.6, H4.47, P 12.9%.

N.m.r. Spectroscopy

^1H, $^{13}C\{^1H\}$, and $^{31}P\{^1H\}$ n.m.r spectra were measured at 500.15, 125.7 and 200.2 MHz respectively on a JEOL Lambda 500 spectrometer on solutions of **1** in CD_2Cl_2. Chemical shifts are to high frequency of Me_4Si, Me_4Si, and external 85% H_3PO_4 respectively. Spectral assignments were confirmed by 2D proton COSY, ROESY [9] and $^1H\{^{31}P\}$ decoupling experiments.

X-ray diffraction

Crystal data for **1**. $0.75(CH_2Cl_2)$: $C_{54}H_{42}P_4S_4 \cdot 0.75(CH_2Cl_2)$, M = 1006.7, monoclinic, space group $P2_1/n$, $a = 1235.6(3)$, $b = 1.885.1(4)$, $c = 2315.3(6)$ pm, $\beta = 103.57(4)°$, $V = 5.242(2)$ nm^3, $Z = 4$, $D_c = 1.276$ g cm^{-3}, $\mu = 0.415$ mm^{-1} (Mo–Kα radiation $\lambda = 71.073$ pm), $F(000) = 2086$, $T = 160$ K, crystal size $0.53 \times 0.42 \times 0.34$ mm. Measurements were made on a Stoe-Siemens four-circle diffractometer. Cell parameters were refined from 2θ values (20–24°) of 20 reflections measured at $\pm\omega$; intensities were measured with ω/θ scans and on-line profile-fitting [10]. Absorption corrections were based on azimuthal scan measurements for selected sets of symmetry-equivalent reflections [11]. 9286 reflections were collected ($2\theta_{max} = 50°$, maximum indices 14, 22, 27), giving 9250 unique data ($R_{int} = 0.0776$ for a few high-angle reflections only).

The structure was solved by direct methods and refined [11] by full-matrix least-squares on F^2 values, with weighting $w^{-1} = \sigma^2(F_o^2) + (0.092P)^2 + 9.8265P$, where $P = (F_o^2 + 2F_c^2)/3$.. Anisotropic displacement parameters were refined; isotropic hydrogen atoms were constrained with a riding model. Extinction effects were negligible. The structure was found to contain disordered solvent. Satisfactory refinement was achieved with one molecule of CH_2Cl_2 disordered over three orientations on one general position, and half a molecule of CH_2Cl_2 distributed equally over two sites around an inversion centre, giving a total of three molecules per unit cell; only Cl atoms were anisotropic, H atoms were not included, and geometrical restraints were applied.

At convergence, $wR = \{\Sigma[w(F_o^2 - F_c^2)^2]/\Sigma[w(F_o^2)^2]\}^{1/2} = 0.1810$ for all data, conventional $R = 0.0608$ on F values of 7140 reflections having $F_o^2 > 2\sigma(F_o^2)$, goodness of fit = 1.044 for all F^2 values and 617 refined parameters. A final difference synthesis showed a few peaks of height up to 1464 e nm^{-3} in the disordered solvent regions, but no other significant features.

Supplementary material

Additional material submitted comprises a complete list of fractional coordinates, H-atom coordinates, displacement parameters, bond lengths, interbond angles, and structure factors.

Acknowledgements—We thank the EPSRC for equipment grants and the Leverhulme Trust for financial support.

REFERENCES

1. McFarlane, H. C. E. and McFarlane, W., *Polyhedron*, 1983, **2,** 303.
2. McFarlane, H. C. E. and McFarlane, W., *Polyhedron*, 1988, **7,** 1875.
3. Steer, R. J., Walkins, S. F. and Woodward, P., *J. Chem. Soc. C*, 1970, 403.
4. Sakurai, H., Ebata, K., Kabuto, C. and Sekiguchi, A., *J. Am. Chem. Soc.*, 1990, **112,** 1799.
5. Cox, E. G., Cruikshank, D. W. J. and Smith, J. A. S., *Proc. Roy. Soc. London, Ser. A.*, 1958, **247,** 1.
6. Codding, P. W. and Kerr, K. A., *Acta Crystallogr., Sect. B.*, 1978, **34,** 3785.
7. Weissensteiner, W., Schuster, I. I., Blount, J. F. and Mislow, K. J., *J. Am. Chem. Soc.*, 1986, **108,** 6664.
8. Chance, J. M., Kahr, B., Buda, A. B. and Siegel, J. S., *J. Am. Chem. Soc.*, 1989, **111,** 5940.
9. Bax, A. and Lewis, D. G., *J. Magn. Reson.*, 1985, **63,** 207.
10. Clegg, W., *Acta Crystallogr., Sect. A*, 1981, **37,** 22.
11. Sheldrick, G. M., SHELXTL version 5, Bruker AXS, Madison, Wi, U.S.A., 1994.

Pergamon

PII: S0277–5387(98)00141–7

Polyhedron Vol. 17, No. 20, pp. 3519–3530, 1998
© 1998 Elsevier Science Ltd
All rights reserved. Printed in Great Britain
0277–5387/98 $19.00 + 0.00

Synthesis, characterization and X-ray crystal structure of $[Ag(Htsa)(PPh_3)_3]$ ($H_2tsa = o\text{-}HS(C_6H_4)CO_2H$). Comparison with $[Au(Htsa)(PPh_3)]$

Kenji Nomiya,*, Noriko Chikaraishi Kasuga, Izumi Takamori and Kazuhiro Tsuda

Department of Materials Science, Faculty of Science, Kanagawa University, Hiratsuka, Kanagawa 259-1293, Japan

(Received 2 February 1998; accepted 6 April 1998)

Abstract—A novel, monomeric triphenylphosphine silver(I) complex $[Ag(Htsa)(PPh_3)_3]$ ($H_2tsa = o\text{-}HS(C_6H_4)CO_2H$) was synthesized from three different ligand-exchange reactions, as **3** without any solvate or as **3a** with CH_2Cl_2 solvate, in good yield. The complex **3** can be interconverted with the previously obtained, two antimicrobially-active silver(I) thiosalicylates; one was the oligomeric, water-soluble complex $\{Na[Ag(tsa)] \cdot H_2O\}_n$, **1** ($n = 21$–$27$) and the other the polymeric, water-insoluble complex $[Ag(Htsa)]_n$, **2**. The analogous gold(I) complex $[Au(Htsa)(PPh_3)]$, **4**, was also isolated. The complexes **3**, **3a** and **4** were characterized with complete elemental analyses, TG/DTA, FT-IR and multinuclear NMR (^1H, ^{13}C, ^{31}P and ^{109}Ag) spectroscopies. The crystal structures of **3** and **4** were determined with single-crystal X-ray diffraction. The monomeric structure for **3** and the dimeric structure via hydrogen bonds of the carboxylic acid for **4** in the solid state were found.
© 1998 Elsevier Science Ltd. All rights reserved

Keywords: thiosalicylate; triphenylphosphine; silver(I) complex; gold(I) complex; X-ray crystal structure; NMR.

1. INTRODUCTION

In the medicinally or pharmaceutically active compounds of silver(I) and gold(I), most of the complexes formed with thiol and nitrogen-containing heterocyclic ligands are harder to crystallize and are believed to be polymeric [1–43]. In general, tertiary phosphine ligands have been usually employed in order to obtain crystalline compounds [23–35, 41, 42], although several crystalline thiolatogold(I) complexes without tertiary phosphines such as $[Au(SR)_2]^{n-}$ (HSR = mercapto-group compound) have been recently found [17–22, 39]. Probably, a recent development of monomeric Au^I compounds composed of both thiol and tertiary phosphine ligands stems from a discovery of auranofin ((2,3,4,6-tetra-*O*-acetyl-β-1-thio-D-glucopyranosato-*S*)(triethylphosphine)gold(I)) [6–10, 14–16], which has been used in chemotherapy as an effective antiarthritic agent and also as a realized medicine of oral-administration, although its mechanism or mode of action is unclarified as yet [6–10]. On the other hand, for non-crystalline, polymeric metal–thiolate and metal–imidazolate compounds, only a few structural studies have been performed by synchrotron X-ray studies containing EXAFS, XANES, WAXS and DAS [11, 12] and by Rietveld analysis using powder X-ray diffraction data [44, 45].

Very recently, we have prepared a monomeric imidazolatotris(triphenylphosphine) silver(I) complex $[Ag(imd)(PPh_3)_3]$ (Himd = imidazole) [41] by a reaction of PPh_3 ligands in CH_2Cl_2 with a polymeric complex $[Ag(imd)]_n$ which has shown wide spectra of excellent antibacterial and antifungal activities [42]. This monomeric complex was neither obtained from reactions of precursors $[AgCl(PPh_3)_3]$ and $[AgCl(PPh_3)_2]_2$ with a free Himd ligand in the presence of NaOH nor of $[AgCl(PPh_3)_2]_2$ with sodium salt of

*Author to whom correspondence should be addressed. Tel.: +81-463-594111; Fax: +81-463-589684; E-mail: nomiya@info.kanagawa-u.ac.jp

imidazolate. On the contrary, the corresponding Au^{I} complex [Au(imd)(PPh_3)] was obtained from a reaction of the precursor [AuCl(PPh_3)] with the Himd ligand in the presence of NaOH.

Also, two types of thiosalicylatosilver(I) complexes have been recently found [38]; one was an oligomeric, water-soluble and yellow complex $\{Na[Ag(tsa)]\cdot H_2O\}_n$, **1** ($n = 21$–$27$; $H_2tsa = o$-$HS(C_6H_4)CO_2H$) and the other a polymeric, water-insoluble and orange complex $[Ag(Htsa)]_n$, **2**, both of which have displayed effective antimicrobial activities against selected bacteria, yeast and molds. The present work has been aimed at (i) preparing a monomeric form of the thiosalicylatosilver(I) complex, e.g. [Ag(Htsa)(PPh_3)$_3$], **3**, through ligand-exchange reactions of polymeric complex **2** or of some precursor silver(I) complexes such as [AgCl(PPh_3)$_3$] and [AgCl(PPh_3)$_2$]$_2$, (ii) applying the same concept to gold(I) chemistry to obtain the thiosalicylatogold(I) complex, e.g. [Au(Htsa)(PPh_3)], **4**, (iii) providing X-ray crystal structures of **3** and **4** in the solid state and (iv) clarifying the behavior in solution of **3** and **4**. The X-ray crystal structures of several (arenethiolato)metal complexes have been determined such as [Au(Htsa)(PCy_3)] (PCy_3 = tricyclohexylphosphine) [26], [Cu($SC_6H_4NMe_2$-2)]$_3$, [Cu(S-1-$C_{10}H_6NMe_2$-8)]$_9$, [Cu$_3$(S-1-$C_{10}H_6NMe_2$-8)$_2$(C≡C^{t}Bu)]$_2$ [46], [Cu$_8${$SC_6H_3(CH_2NMe_2)_2$-2,6}$_3$Br$_5$] [47], [Mg{S(C_6H_4-2-CH_2NMe_2)}$_2$]$_2$ [48] and [Li{SC_6H_4((R)-CH(Me)NMe_2)-2}]$_6$ and [Li{$SC_6H_3(CH_2NMe_2)_2$-2,6}]$_6$ [49].

Herein we report the full details of the synthesis and characterization of the complexes [Ag(Htsa)(PPh_3)$_3$], **3**, in 37% yield and [Ag(Htsa)(PPh_3)$_3$]·CH_2Cl_2, **3a**, in 52% yield both as colorless needle crystals, and [Au(Htsa)(PPh_3)], **4**, in 72% yield as pale yellow prism crystals. The X-ray crystal structures of **3** and **4** were determined by single-crystal X-ray diffraction. Also reported are the compositional characterization of **3**, **3a** and **4** by full elemental analyses, FT-IR, thermoglavimetric and differential thermal analyses (TG/DTA) and their structural characterization in solution by ^{1}H, ^{13}C and ^{31}P NMR spectroscopies, and additionally by solution ^{109}Ag NMR spectroscopy for **3**.

2. EXPERIMENTAL

2.1. *Materials*

All chemicals were reagent grade and were used as received: thiosalicylic acid (H_2tsa; *o*-mercaptobenzoic acid), $AgNO_3$, Na[$AuCl_4$]·$2H_2O$, $(C_6H_5)_3P$, NaOH, ethanol, acetone, diethyl ether, dichloromethane (all from Wako); $CDCl_3$, DMSO-d_6 (Aldrich); CD_2Cl_2 (Isotec). Several precursor complexes such as [AgCl(PPh_3)$_3$] [50], [AgCl(PPh_3)$_2$]$_2$ [51] and [AuCl(PPh_3)] [52–54] were prepared according to the literature, respectively. Polymeric, water-insoluble and orange complex $[Ag(Htsa)]_n$, **2**, was prepared as previously described [38].

2.2. *Instrumentation/analytical procedures*

Elemental analyses on samples dried overnight at room temperature under 10^{-3}–10^{-4} Torr were carried out by Mikroanalytisches Labor Pascher (Remagen, Germany). Infrared spectra were obtained on a JASCO FT-IR 300 spectrometer as KBr disks at room temperature. Thermogravimetric (TG) and differential thermal analyses (DTA) were acquired using a Rigaku TG 8101D and TAS 300 data-processing system. TG/DTA measurements were run under air with a temperature ramp of 1°C/min between 20 and 500°C.

^{1}H NMR (399.65 MHz), ^{13}C NMR (100.4 MHz) and ^{31}P NMR (161.70 MHz) spectra were recorded at 22°C in 5 mm o.d. tubes on a JEOL JNM-EX 400 FT-NMR spectrometer with a JEOL EX-400 NMR data-processing system. ^{1}H and ^{13}C{^{1}H} NMR spectra of the complexes were measured in $CDCl_3$ with reference to an internal standard of tetramethylsilane (TMS). Chemical shifts are reported on the δ scale and resonances downfield of TMS (δ 0) are recorded as positive. ^{31}P{^{1}H} NMR spectra of the complexes were measured in $CDCl_3$ with reference to an external standard of 25% H_3PO_4 in H_2O in a sealed capillary. Chemical shifts are reported as negative for resonances upfield of H_3PO_4 (δ 0). The ^{31}P{^{1}H} NMR spectra at −90°C were measured in CD_2Cl_2 with an external standard of 25% H_3PO_4 by a substitution method.

The two-dimensional ^{1}H–^{13}C COSY NMR spectra and both two-dimensional NMR spectra of ^{1}H–^{13}C HMBC (heteronuclear multiple bond correlation) method by a correlation $^3J_{C-H}$ between ^{1}H and ^{13}C atoms separated by three bonds and ^{1}H–^{13}C HMQC (heteronuclear multiple quantum coherence) by a correlation between ^{1}H and ^{13}C which are directly spin–spin coupled, were measured in $CDCl_3$ solution, all spectra referenced to an internal TMS in 5 mm o.d. tubes using a JEOL JNM-EX 400 NMR spectrometer and JEOL EX-400 NMR data-processing system or using a VARIAN UNITY 500 FT-NMR spectrometer. Pulse sequences and spectral parameters for the HMBC and HMQC methods are reported elsewhere [55].

^{109}Ag NMR (18.45 MHz) spectra were recorded at 22°C in 10 mm o.d. tubes on a JEOL JNM-EX 400 FT-NMR spectrometer equipped with a JEOL NM-40T10L low-frequency tunable probe. The ^{109}Ag NMR spectra of the complexes were measured in $CDCl_3$ with reference to an external standard of saturated $AgNO_3$–D_2O solution by a substitution method. Chemical shifts are reported on the δ scale with resonances downfield of $AgNO_3$ (δ 0) as positive. Spectral parameters for ^{109}Ag NMR include: pulse width of

13.2 μs, acquisition time of 0.39 s, recycle time of 1.39 s and sweep width of 21,008 Hz.

2.3. *Preparation of the complexes*

[Ag(Htsa)(PPh_3)$_3$], **3**: From a reaction of [AgCl(PPh_3)$_2$]$_2$ with H_2tsa in the presence of NaOH. To 0.600 g (0.449 mmol) [AgCl(PPh_3)$_2$]$_2$ dissolved in 40 ml dichloromethane was added a clear yellow solution of 0.140 g (0.908 mmol) of H_2tsa and 0.036 g (0.900 mmol) of NaOH in 50 ml ethanol. The yellow–white suspension obtained was stirred for 30 min and filtered through a folded filter paper (Whatman No. 5). The clear filtrate was concentrated at 60°C to a volume of *ca*. 70 ml by rotary evaporation, followed by standing for a few days in a refrigerator at 5°C. Colorless needle crystals formed were collected on a membrane filter (JG 0.2 μm), washed with water (100 ml × 2), then with ethanol (100 ml × 2) and finally with 100 ml diethyl ether, and dried *in vacuo* for 2 h. Yield: 0.35 g (37.4%) of light- and thermally-stable, colorless needle crystals, which were soluble in chloroform and dichloromethane, sparingly soluble in DMSO, acetone and acetonitrile, but insoluble in water, ethanol and diethyl ether.

Found: H, 4.81; C, 70.00. Calc. for $H_{50}C_{61}O_2P_3SAg$ or [Ag(Htsa)(PPh_3)$_3$]: H, 4.81; C, 69.92. TG/DTA: no weight loss observed below 150°C; decomposition started around 150°C with an endothermic peak at 170°C. IR (KBr disk): *v* 1701vs, 1583m, 1479s, 1433vs, 1327m, 1309m, 1271m, 1217m, 1184w, 1157m, 1093m, 1026m, 997m, 742vs, 694vs, 515s, cm^{-1}. ^{1}H and ^{13}C NMR in $CDCl_3$ are shown in Table 3.

[Ag(Htsa)(PPh_3)$_3$]·CH_2Cl_2, **3a**: From a reaction of [AgCl(PPh_3)$_3$] with H_2tsa in the presence of NaOH. To 2.79 g (3.00 mmol) [AgCl(PPh_3)$_3$] dissolved in 60 ml dichloromethane was added a clear yellow solution of 0.463 g (3.00 mmol) of H_2tsa and 0.120 g (3.00 mmol) of NaOH in 180 ml ethanol. The yellow–white suspension obtained was stirred for 30 min and filtered through a folded filter paper (Whatman No. 5). The clear filtrate was concentrated at 60°C to a volume of *ca*. 200 ml by rotary evaporation, followed by standing for a few days in a refrigerator at 5°C. Colorless needle crystals formed were collected on a membrane filter (JG 0.2 μm), washed with water (100 ml × 2), then with ethanol (100 ml × 2) and finally with 100 ml diethyl ether and dried *in vacuo* for 2 h. Yield: 1.75 g (51.5%) of colorless needle crystals, which were soluble in chloroform and dichloromethane, sparingly soluble in DMSO, acetone and acetonitrile, but insoluble in water, ethanol and diethyl ether.

Found: H, 4.74; C, 65.91; O, 2.66; P, 8.10; S, 2.63; Cl, 5.75; Ag, 9.68; total 99.47%. Calc. for $H_{52}C_{62}O_2P_3SCl_2Ag$ or [Ag(Htsa)(PPh_3)$_3$]·CH_2Cl_2: H, 4.63; C, 65.74; O, 2.82; P, 8.20; S, 2.83; Cl, 6.26; Ag, 9.52. TG/DTA: weight loss of 6.82% observed below 117°C with an endothermic point at 110°C. Calc. for [Ag(Htsa)(PPh_3)$_3$]·$x$$CH_2Cl_2$, 7.50% ($x$ = 1); decomposition gradually started around 150°C. IR (KBr disk): *v* 1703vs, 1583m, 1479s, 1433vs, 1327m, 1309m, 1273m, 1221w, 1182w, 1157w, 1092s, 1026m, 999m, 742vs, 694vs, 513vs cm^{-1}. ^{1}H and ^{13}C NMR in $CDCl_3$ are shown in Table 3. ^{31}P NMR ($CDCl_3$): δ 4.55 (PPh_3). ^{109}Ag NMR ($CDCl_3$): δ 1196.

3a: From a reaction of polymer [Ag(Htsa)]$_n$ with PPh_3. To a yellow suspension of 0.522 g (2.00 mmol) of powder-solid [Ag(Htsa)]$_n$ in 40 ml ethanol was added a clear colorless solution of 1.57 g (6.00 mmol) of triphenylphosphine in 120 ml dichloromethane. Stirring continued for 3 h. During the initial 15 min-stirring, the solution became clear yellow. The clear filtrate obtained by passing through a folded filter paper (Whatman No. 2) was slowly evaporated at room temperature. A crude compound of pale yellow plate crystals formed within a few days was collected on a membrane filter (JG 0.2 μm), washed with ethanol (100 ml × 2) and then with diethyl ether (100 ml × 2) and dried *in vacuo* for 2 h. The yield of this crude product was 1.64 g.

To the crude product redissolved in 40 ml dichloromethane was added 40 ml ethanol, followed by filtering through a filter paper (Whatman No. 2) and the filtrate was slowly evaporated by standing for a few days at room temperature. Colorless needle crystals formed here were collected on a membrane filter (JG 0.2 μm), washed twice each with 100 ml ethanol and 100 ml diethyl ether and dried *in vacuo* for 2 h. Yield: 0.95 g (42.1%).

Found: H, 4.59; C, 65.94. Calc. for $H_{52}C_{62}O_2P_3SCl_2Ag$ or [Ag(Htsa)(PPh_3)$_3$]·CH_2Cl_2: H, 4.63; C, 65.74. TG/DTA: weight loss of 7.24% observed below 125°C with an endothermic peak at 104°C; Calc. for [Ag(Htsa)(PPh_3)$_3$]·$x$$CH_2Cl_2$, 7.50% ($x$ = 1); decomposition started around 150°C with an endothermic peak at 170°C. IR (KBr disk): *v* 1704vs, 1584m, 1478s, 1433vs, 1327w, 1308w, 1272m, 1222w, 1182w, 1157m, 1092s, 1027m, 998m, 742vs, 694vs, 512vs, cm^{-1}. ^{1}H and ^{13}C NMR in $CDCl_3$ are shown in Table 3. ^{31}P NMR ($CDCl_3$): δ 4.57 (PPh_3).

[Au(Htsa)(PPh_3)], **4**: This compound was prepared by a modification of the literature method [26], using 0.247 g (0.500 mmol) of [AuCl(PPh_3)], 0.077 g (0.500 mmol) of H_2tsa in 50 ml ethanol and 1 ml (0.500 mmol) of 0.5 M NaOH aqueous solution. Yield: 0.22 g (72.0%) of pale yellow cubic crystals with melting point 154–156°C, which were soluble in acetone, chloroform and benzene, sparingly soluble in ethanol, but insoluble in water and diethyl ether. This compound was light- and thermally-stable.

Found: H, 3.31; C, 48.92; O, 5.47; P, 5.19; S, 5.09; Au, 31.40; total 99.38%. Calc. for $H_{20}C_{25}O_2PSAu$ or [Au(Htsa)(PPh_3)]: H, 3.29; C, 49.03; O, 5.22; P, 5.06; S, 5.23; Au, 32.16. TG/DTA: negligible weight loss (0.3%) observed below 150°C with an endothermic peak at 163°C; decomposition began at 270°C. IR (KBr disk): *v* 1682vs, 1585m, 1477m, 1464m, 1433s, 1406m, 1309s, 1265m, 1248m, 1099s, 1053m, 1036m, 997w, 958w, 754s, 694s, 538s, 507s, 496s cm^{-1}. ^{1}H and

^{13}C NMR in $CDCl_3$ are shown in Table 3. ^{31}P NMR ($CDCl_3$) δ 37.56 (PPh_3).

2.4. *X-ray structural analysis*

Crystals of complex **3** were obtained as colorless needles from a solution of the solvent mixture, dichloromethane–ethanol, and those of **4** as pale yellow cubes from a solution of dichloromethane–acetone. During a few days' standing at room temperature, crystals of sufficient quality suitable for single-crystal X-ray diffraction studies were grown.

Each single-crystal of **3** and **4** was mounted on glass fiber and transferred to a Rigaku AFC5S diffractometer. Cell contents and orientation matrix of **3** and **4** were obtained from the least-squares refinement of 25 and 23 reflections, respectively. The reflection data were collected using ω–2θ scan with graphite-monochromated Mo–Kα radiation at room temperature. The intensities of three standard reflections which were measured after every 150 reflections remained constant throughout the data collection. The data were corrected for Lorentz and polarization effects and empirical absorption corrections based on PSI scan were applied to the data. For the overall averaged transmission curve, the transmission factors of **3** and **4** were in the range of 0.93–1.00 and 0.23–1.00, respectively. The structures were solved by direct methods followed by subsequent difference Fourier calculation and refined by a full-matrix least-squares procedure using TEXSAN package [56]. For **3**, all atoms except hydrogen and carbon were refined anisotropically. Carbon and hydrogen atoms were refined isotropically. For **4**, all atoms except hydrogen were refined anisotropically and hydrogen atoms isotropically.

Crystal data, data collection and refinement for **3** and **4** are summarized in Table 1.

3. RESULTS AND DISCUSSION

3.1. *Molecular formula and compositional characterization*

The composition and molecular formula of **3** which consists of one silver(I) atom, one coordinating $Htsa^-$ ligand and three PPh_3 ligands without any solvated molecules, those of **3a** with one solvated CH_2Cl_2 molecule and those of **4** composed of one gold(I) atom, one $Htsa^-$ ligand and one PPh_3 ligand without any solvated molecules are based on elemental analyses (in particular for **3a** and **4**, all elements including oxygen, 99.47 and 99.38% totals are observed; see Section 2), TG/DTA and single-crystal X-ray analyses described later.

As to the solvation by one CH_2Cl_2 molecule in **3a**, in the absence of any other sources of chlorine, the Cl analysis (calc. 6.26, found 5.75%) reflects the presence of solvated CH_2Cl_2. The additional evidence for the presence of solvated CH_2Cl_2 is provided by a proton signal at 5.27 ppm observed in ^1H NMR spectra and by a carbon signal at 53.42 ppm in ^{13}C NMR spectra. TG/DTA analyses of two independent samples prepared from different starting materials also confirm the presence of one solvated CH_2Cl_2 as the observed weight loss 6.82 and 7.24% (calc. 7.50%) with an endothermic peak at 110 and 104°C, respectively.

The solid FT-IR spectra (Fig. 1) of complexes **3** and **4** show a disappearance of the S–H stretching band around 2560 cm^{-1} due to the SH group in the free H_2tsa ligand, suggesting the metal–S bond formation. Also shown is that the carbonyl stretching bands around 1700 cm^{-1} are unchanged after complexation, compared with that of the free H_2tsa ligand, suggesting that the carboxyl group remains protonated and does not coordinate to the central metal ions. Many small bands observed in 3000–2500 cm^{-1} region are also attributed to the presence of a protonated carboxylic group as usually observed. Thus, the IR spectra of all complexes **3**, **3a** and **4** show that the coordination by the $Htsa^-$ ligand to metal centers is only through the sulfur atom in the mercapto group.

No coordination of the carboxyl oxygen atoms to the metal is also supported by the X-ray analysis described later. It has been also clarified by ESCA measurements of the two thiosalicylatosilver(I) complexes **1** and **2** that even the deprotonated carboxyl group does not participate in the coordination to the silver(I) atom [38].

3.2. *Synthetic reactions and ligand replacement*

The conceptually straightforward, synthetic reactions of thiosalicylatotris(triphenylphosphine)silver(I), which has been herein isolated as **3** without any solvate and/or as **3a** with CH_2Cl_2 solvate, are outlined in equations (1)–(3) (Scheme 1). On the other hand, the synthesis of thiosalicylato(triphenylphosphine)gold(I) obtained as **4** is shown in equation (6).

The reactions in equations (2) and (6) exhibit a simple ligand replacement of the coordinated Cl^- ligand with free H_2tsa without change in the coordination number of the starting silver(I) and gold(I) atoms. In the reaction shown in equation (1), the dimeric silver(I) structure with bridged Cl^- ligands is transformed to the monomeric structure by their ligand exchange with free H_2tsa, where the coordination number of silver(I) remains unchanged. In the reaction in equation (3), the polymeric structure with bridged sulfur atoms is changed to the monomeric structure accompanied with a change in the coordination number of the silver(I) atom from 2 to 4.

From the synthetic reactions in equations (1)–(3), the ease of ligand replacement, i.e. the relative ordering of ligand replacement, is suggested for the formation of the silver(I) complexes $[AgL(PPh_3)_n]_m$ from the starting complexes $[AgL]_x$ (L = N, S donor atoms) and $[AgCl(PPh_3)_n]_m$ to be: Ag–P $\gg$ Ag–S > Ag–Cl

Table 1. Summary of X-ray diffraction data

	3 [Ag(Htsa)(PPh_3)$_3$]	**4** [Au(Htsa)(PPh_3)]
Formula	$C_{61}H_{50}O_2P_3AgS$	$C_{25}H_{20}O_2PAuS$
MW	1047.91	612.43
Crystal system	monoclinic	triclinic
Space group	$P2_1/n$ (#14)	$P\bar{1}$ (#2)
a (Å)	10.74(1)	11.542(3)
b (Å)	24.993(3)	12.091(4)
c (Å)	19.846(3)	8.750(3)
α (°)	90	97.85(3)
β (°)	105.30(4)	107.79(3)
γ (°)	90	102.44(3)
V (Å^3)	5136(6)	1108.2(7)
F(000)	2160	592.00
Z	4	2
$d_{calc.}$ (g · cm^{-1})	1.355	1.904
Crystal size (mm)	0.2 × 0.2 × 0.2	0.2 × 0.3 × 0.2
No. of reflections used for	25	23
Unit cell dimension (2θ range)	(30.1–33.0)	(30.2–34.5)
Radiation	Mo–Kα (λ = 0.71069 Å)	Mo–Kα (λ = 0.71069 Å)
Scan mode	2θ–ω	2θ–ω
Scan width	0.84 + 0.30 tan θ	1.63 + 0.30 tan θ
Scan speed (min^{-1})	16	32
2θ range	6–50	6–55
μ (cm^{-1})	5.69	68.16
Total reflections	7912	5351
Reflections unique	7392	5099
Reflections observed	2143 [$I > 2\sigma(I)$]	3223 [$I > 3\sigma(I)$]
R, R_w	0.086, 0.055	0.055, 0.041
GOF	1.58	1.89

$R = \Sigma[|F_o| - |F_c|]/\Sigma|F_o|$, $R_w = [\Sigma(\omega\,[|F_o| - |F_c|]^2/\Sigma\omega(|F_o|)^2]^{1/2}$, with $\omega = 4F_o^2/[\sigma^2(F_o^2)]$.

and, from equation (6), that for the gold(I) complexes is also suggested to be: Au–P ≫ Au–S > Au–Cl. On the other hand, the synthetic reactions of the recently found, metal(I) complexes containing nitrogen-containing heterocycles such as imidazole and triazoles have indicated that the relative ordering for silver(I) follows Ag–P ≫ Ag–Cl > Ag–N ≫ Ag–O, while that for gold(I) follows: Au–P ≫ Au–N > Au–Cl ≫ Au–O [41–43]. Thus, we can deduce the relative ligand replacement for the silver(I) complexes as Ag–P ≫ Ag–S > Ag–Cl > Ag–N ≫ Ag–O, while that for the gold(I) complexes, i.e, as Au–P ≫ Au–S > Au–N > Au–Cl ≫ Au–O. This information allows us to know if target molecules by medicinally or pharmaceutically active compounds of silver(I) and gold(I) are proteins containing enzymes as N,O,S-donors or nucleic acids as N,O-donors of biological ligands. In fact, the wide spectra of excellent antibacterial and antifungal activities found in the [Ag(imd)]$_n$ (Him-d = imidazole) has been attributed to proteins containing a sulfur donor atom as the potential target molecule for inhibition of growth of the test organisms, but not to nucleic acids without a sulfur donor [41, 42].

The proton attached to the carboxyl group in the present complexes **3** and **4** could not be exchanged with an alkali metal ion such as sodium ion; i.e. neither "Na[Ag(tsa)(PPh_3)$_3$]" nor "Na[Au(tsa)(PPh_3)]" can be derived by the reactions of aqueous NaOH with **3**, **3a** or **4**, respectively. We found, or rather, that the reactions of **3** and **3a** with aqueous NaOH resulted in reproducing the water-soluble, oligomeric species, {Na[Ag(tsa)]}$_n$ **1** by a loss of the PPh_3 ligands. Since the polymeric compound **2** can be converted to the oligomer **1** by its reaction with aqueous NaOH and **1** can also be transformed to **2** by its reaction with aqueous HCl [38], there exists an interconversion relationship between **3** and **2** via the oligomer **1** as a mediator as shown in equations (3)–(5) (Scheme 1).

3.3. *Molecular and crystal structures of* **3** *and* **4**

The molecular structures of **3** and **4** were determined with single-crystal X-ray diffraction analysis and are shown in Figs 2 and 3, respectively. Their selected distances and angles are listed in Table 2.

The silver atom of **3** is coordinated with three phosphorus atoms of the PPh_3 ligands and the sulfur atom of the Htsa$^-$ ligand to form a tetrahedral geometry.

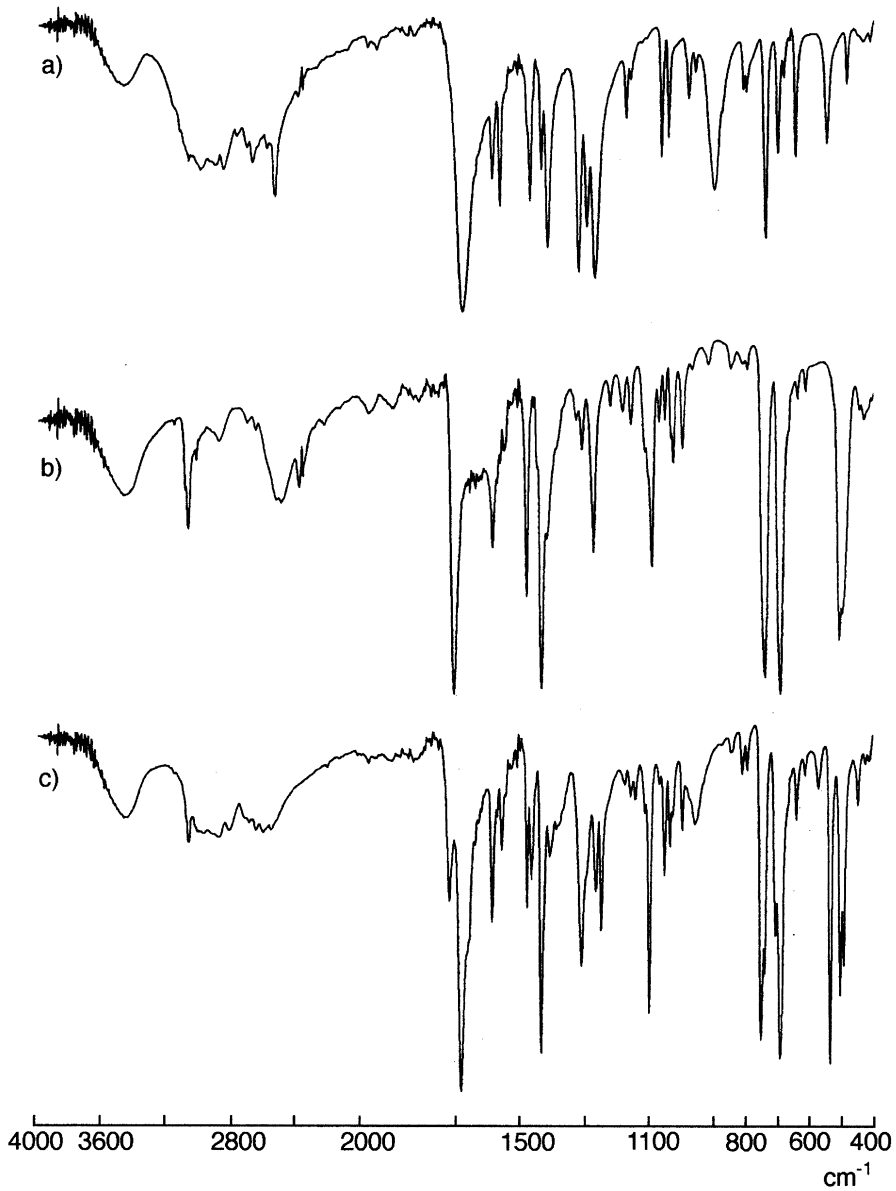

Fig. 1. Solid FT-IR spectra measured in KBr disks in the 4000–400 cm^{-1} region of (a) free H_2tsa ligand, of (b) [Ag(Htsa)$(PPh_3)_3$], **3**, and of (c) [Au(Htsa)(PPh_3)], **4**.

As found in Table 2, the angles around the silver atom deviate from the ideal value of 109.5°. One S–Ag–P angle is smaller and two of them are greater than 109.5°. All P–Ag–P angles are greater than 109.5°. The geometries around the silver atoms of the starting materials [$AgCl(PPh_3)_3$] and [$AgCl(PPh_3)_2]_2$ are also tetrahedral [50, 51]. Three structures of the silver(I) complexes can be compared with each other. The distances and angles of **3** are similar to those of [$AgCl(PPh_3)_3$], except longer Ag–S bond vs Ag–Cl bond, rather than those of [$AgCl(PPh_3)_2]_2$. The dihedral angle between the planes of the carboxyl group (A; O1, O2, C61) and the $Htsa^-$ (B; S1, C55, C56, C57, C58, C59, C60) is 176°, showing the $SC_6H_4CO_2H$ moiety of **3** planar. The dihedral angles between the plane C (Ag–S–C56) and the A or the B are 139° and 43°, respectively. The distances between the silver and oxygen atoms are 6.70 (Ag–O1), 6.84 (Ag–O1′) and 5.10 (Ag–O2) Å. These angles and distances indicate that the carboxyl group is directed away from the silver atom. From the intermolecular oxygen distances, no intermolecular hydrogen bond between the carboxyl groups of the $Htsa^-$ is observed for **3**. Thus, the complex **3** is monomeric.

The gold atom in **4** is placed in the linear geometry defined by the phosphorus atom of the PPh_3 ligand and the sulfur atom of the $Htsa^-$. The P–Au–S angle of **4** is smaller (173.0(1)°) than that of the recently

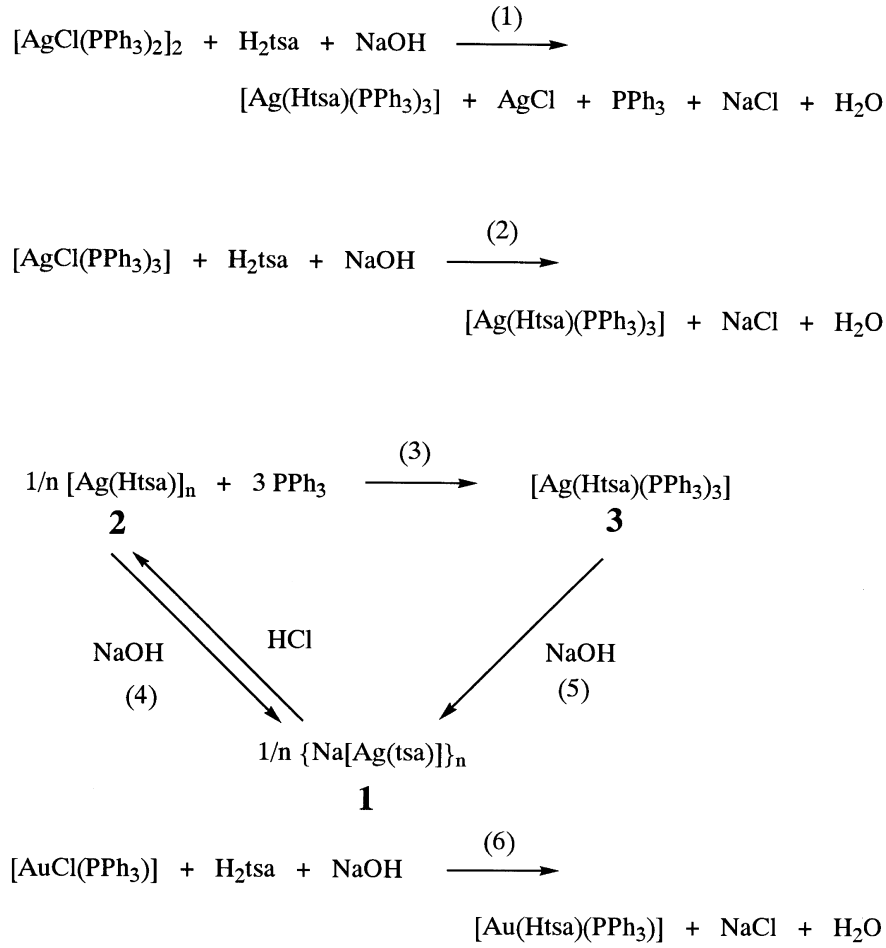

Scheme 1. Reaction schemes.

reported, related complex [Au(Htsa)(PCy_3)] (PCy_3 = tricylcohexylphosphine) (176.8°) [26]. The Au–S and the Au–P distances of 4 ((2.292(4), 2.260(3) Å) are slightly shorter than those of [Au(Htsa)(PCy_3)] (2.313(1), 2.271(1) Å) and they are equal within experimental errors to the distances of other gold(I) complexes with a PPh_3 ligand, [Au(2-tu)(PPh_3)] (2-Htu = 2-thiouracil) (Au–S 2.296(2) A; Au–P 2.300(2) Å) [30]. This picture may be attributed to the difference in cone-angles of the phosphine ligands. The dihedral angles of the carboxyl group (D; O2, O3, C4) and the $Htsa^-$ (E; S1, C5, C6, C7, C8, C9, C10) is 142°, indicating some delocalization of π-electron density occurs between the SC_6H_4 and CO_2H moieties. The dihedral angles of the planes of F (Au–S1–C10) and the D or the E are 48° and 138°, respectively. The Au–O3 distance of **4** is 3.21 Å, which is much shorter than that of [Au(Htsa)(PCy_3)] [26]. These angles and distances show that the carboxyl group is not directed away from the gold atom as seen in [Au(Htsa)(PCy_3)] (5.10 and 6.35 Å). The distance of O2–$O3^i$ of the $Htsa^-$ is 2.56(1) Å (a symmetry operation i; $-x$, $1-y$, $-z$), revealing that an intermolecular hydrogen bond is formed in **4**. This is contrasted with the structure of **3**. In **4**, two [Au(Htsa)(PPh_3)] units are centrosymmetrically associated via the carboxylic moieties to form a dimeric unit. This picture has also been shown in [Au(Htsa)(PCy_3)] [26].

3.4. *Solution NMR* (^{1}H, ^{13}C, ^{31}P *and* ^{109}Ag) *characterization*

The ^{31}P NMR spectra measured in $CDCl_3$ at 22°C show a single peak due to the coordinating PPh_3 ligands at 4.79 ppm for **3** [Fig. 4(a)], at 4.55–4.57 ppm for **3a** and at 37.56 ppm for **4** [Fig. 4(c)], while at −5.33 ppm for the free PPh_3 ligand. It is obvious that the coordination of the phosphorus donor atom to the metal center significantly influences the phosphorus resonance and the ^{31}P chemical shift also reflects a difference between silver(I) and gold(I) as the metal center.

On the other hand, the ^{31}P NMR [Fig. 4(b)] at

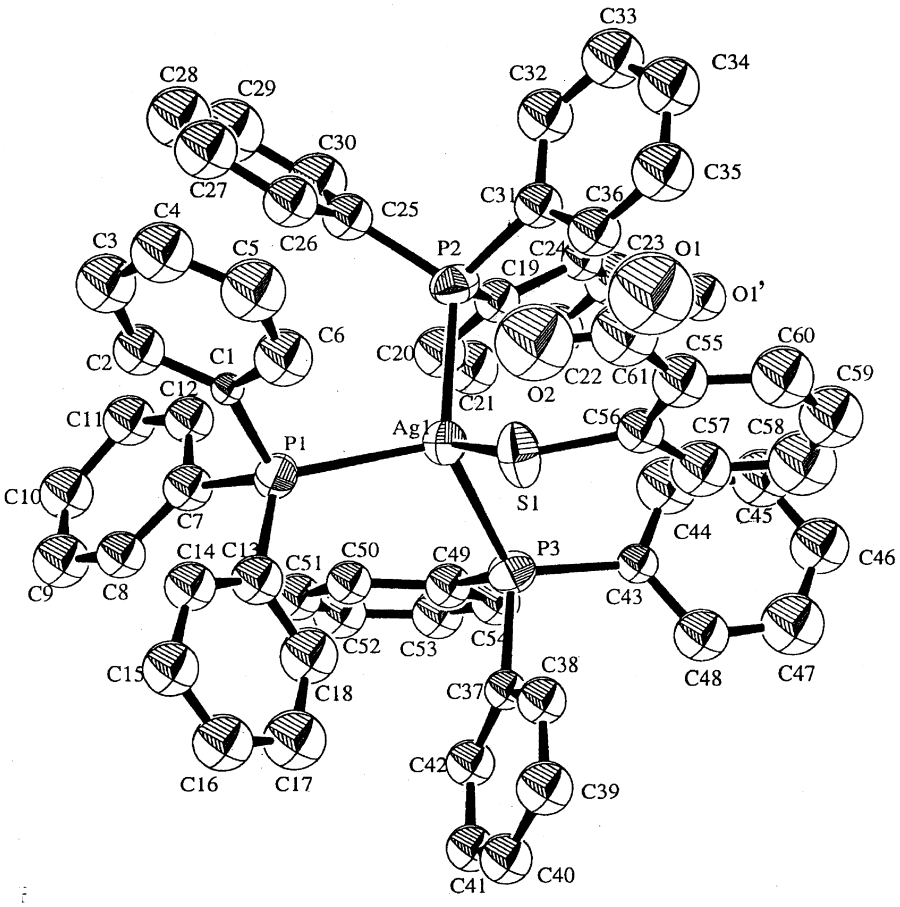

Fig. 2. Molecular structure of $[Ag(Htsa)(PPh_3)_3]$, **3**, with 50% probability ellipsoids.

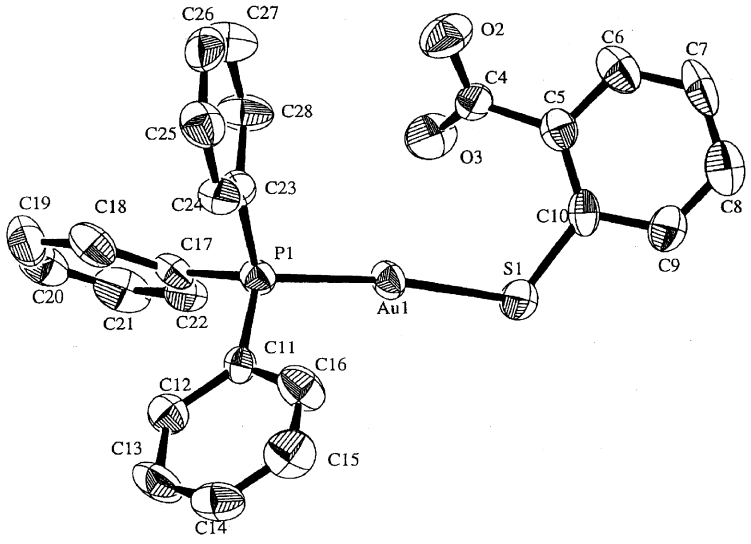

Fig. 3. Molecular structure of $[Au(Htsa)(PPh_3)]$, **4**, with 50% probability ellipsoids.

Table 2. Selected bond distances (Å) and angles (°) for the complexes

	3 [Ag(Htsa)(PPh_3)$_3$]				**4** [Au(Htsa)(PPh_3)]
Ag–S	2.608(7)	Ag–P2	2.577(6)	Au–S1	2.292(4)
Ag–P1	2.574(7)	Ag–P3	2.611(6)	Au–P1	2.260(3)
P1–C1	1.82(2)	P2–C19	1.83(2)	P1–C11	1.79(1)
P1–C7	1.84(2)	P2–C25	1.81(2)	P1–C17	1.79(1)
P1–C13	1.82(2)	P2–C31	1.81(2)	P1–C23	1.84(1)
S1–C56	1.76(2)	P3–C37	1.84(2)	S1–C10	1.77(1)
C55–C61	1.47(3)	P3–C43	1.85(2)	C5–C4	1.47(2)
C61–O1	1.17(4)	P3–C49	1.81(2)	C4–O2	1.30(1)
C61–O1′	1.40(6)			C4–O3	1.25(1)
C61–O2	1.28(3)				
(O1–O1′	0.75(6))				
S–Ag–P1	92.8(2)	S–Ag–P2	116.7(2)	S1–Au–P1	173.0(1)
Ag–P1–C1	114.2(6)	S–Ag–P3	108.7(2)	Au–P1–C11	111.3(4)
Ag–P1–C7	112.5(7)	P1–Ag–P2	112.0(2)	Au–P1–C17	113.7(4)
Ag–P1–C13	118.2(8)	P1–Ag–P3	112.9(2)	Au–P1–C23	114.0(4)
Ag–S–C56	117.4(7)	P2–Ag–P3	112.3(2)	Au–S1–C10	110.7(4)
S–C56–C55	123(1)	Ag–P2–C19	109.2(7)	S1–C10–C5	126.5(9)
C56–C55–C61	124(2)	Ag–P2–C25	119.1(7)	C10–C5–C4	125(1)
C55–C61–O1	129(3)	Ag–P2–C31	115.6(7)	C5–C4–O2	116(1)
C55–C61–O2	120(2)	Ag–P3–C37	116.7(7)	C5–C4–O3	122(1)
O1–C61–O2	110(3)	Ag–P3–C43	117.4(6)	O2–C4–O3	120(1)
		Ag–P3–C49	112.6(7)		

−90°C measured in CD_2Cl_2 of **3** showed two signals with equal intensity at 4.90 and 3.26 ppm, each with splittings, which are attributed to a coupling of ^{31}P with ^{109}Ag ($I = 1/2$) or ^{107}Ag ($I = 1/2$) nucleus as previously observed in [Ag(imd)(PPh_3)$_3$] [42], [AgCl(PPh_3)$_3$] [57], [Ag(dppe)$_2$]NO_3 (dppe = 1,2-bis(diphenylphosphino)ethane) [58], [Ag(pz)(PPh_3)$_3$] (Hpz = pyrazole) [59] and [Ag(triz)(PPh_3)$_2$]$_n$ (Htriz = 1,2,3- or 1,2,4-triazole) [43]. The coupling constants $^1J(^{109}Ag–^{31}P)$ and $^1J(^{107}Ag–^{31}P)$ were estimated as 285 and 266 Hz, respectively, and the chemical shift was as δ (^{31}P) = 4.08 ppm. These data are consistent with those of four-coordinate, tetrahedral complexes included in the above related complexes in solution [57–60].

The ^{31}P NMR spectrum of **3** at −90°C consisting of only two major peaks is in contrast to those of the related silver(I)–N bonding complexes such as [Ag(imd)(PPh_3)$_3$] [42], [Ag(pz)(PPh_3)$_3$] [59] and [Ag(triz)(PPh_3)$_2$]$_n$ [43], all of which have furthermore exhibited additional several signals due to various degrees of association in addition to dissociation of PPh_3 and perhaps also of the nitrogen-donor ligands, i.e. due to the dynamic exchange very rapidly in the NMR timescale. These results reveal that the four-coordinate geometry of **3** is kept in solution and the complex **3** is also present only as a monomeric species in solution. Thus, we conclude that the behavior of **3** in solution is unusually static.

^{109}Ag NMR spectra in $CDCl_3$ measured at 22°C exhibit only one resonance at 1196 ppm for **3a**, also suggesting that only a single species is present in solution, because of the monomeric structure of **3** kept in solution. The chemical shift is assignable to a four-coordinate silver(I) complex with sulfur and phosphorus donor atoms. This resonance is compared with those of the two-coordinate silver(I) complexes formed only by the bridged sulfur atom, previously measured at room temperature in D_2O; at 855.6 ppm for **1** [38] and at 868.7 ppm for {Na[Ag(Htma)] · 0.5H_2O)}$_n$ [36] (H_3tma = thiomalic acid; $HO_2CCH(SH)CH_2CO_2H$). Also, this chemical shift is compared with those of the averaged single peak due to the rapid, dynamic exchange among unequivalent ^{109}Ag species present in $CDCl_3$ solution at room temperature; at 1186 ppm for [Ag(imd)(PPh_3)$_3$] [42] and at 994 ppm for [Ag(1,2,3-triz)(PPh_3)$_2$]$_n$ and at 925 ppm for [Ag(1,2,4-triz)(PPh_3)$_2$]$_n$ [43].

In ^{1}H and ^{13}C NMR spectra measured in $CDCl_3$ at 22°C of the complexes **3**, **3a** and **4**, four proton and seven carbon resonances of the coordinating Htsa$^-$ ligand were completely assigned using several two-dimensional NMR (^{1}H–^{13}C COSY, ^{1}H–^{13}C HMBC and ^{1}H–^{13}C HMQC) methods and their chemical shifts are shown in Table 3.

4. CONCLUSIONS

In conclusion, the novel complex [Ag(Htsa)(PPh_3)$_3$], **3**, as a monomeric form of the oligomeric or polymeric silver(I) thiosalicylates **1** or **2** showing effective antimicrobial activities, has been isolated in good yield and also as its CH_2Cl_2 solvate, **3a**. These

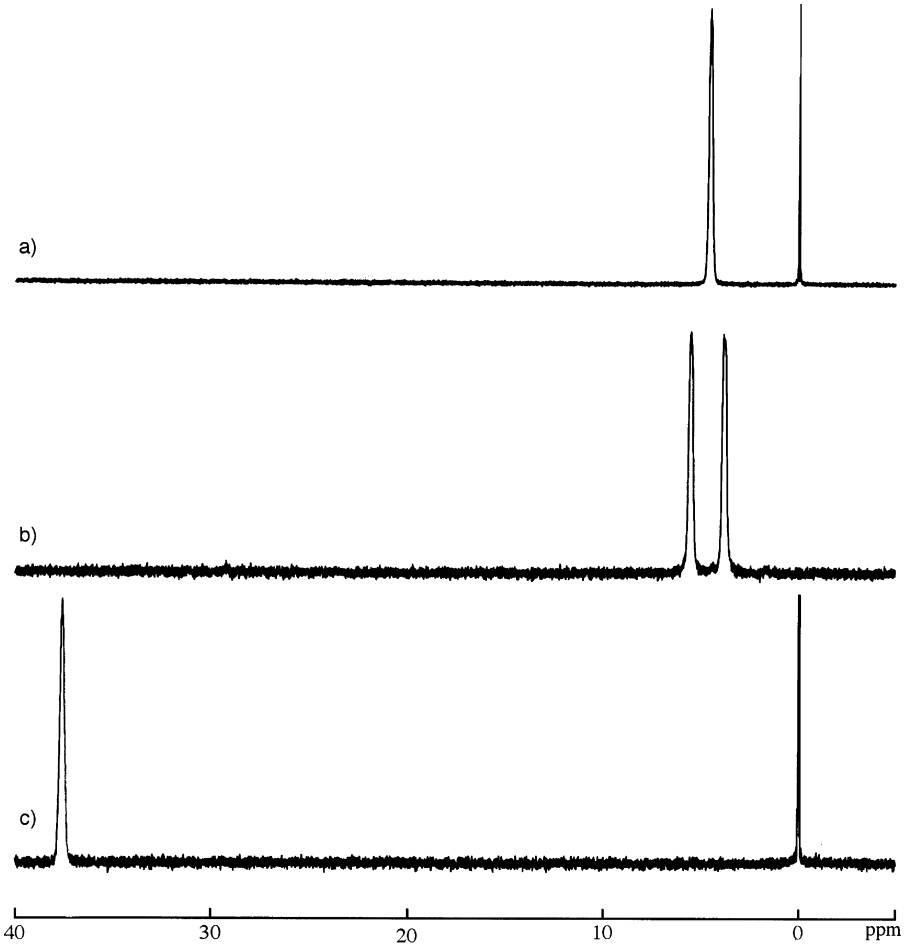

Fig. 4. $^{31}P\{^{1}H\}$ NMR spectra measured with reference to an external 25% H_3PO_4 of $[Ag(Htsa)(PPh_3)_3]$, **3**, measured (a) in $CDCl_3$ at 22°C and (b) in CD_2Cl_2 at −90°C and of (c) $[Au(Htsa)(PPh_3)]$, **4,** measured in $CDCl_3$ at 22°C.

Table 3. Assignment of ^{1}H and ^{13}C NMR signals of thiosalicylatometal(I) complexes[a]

^{1}H NMR								
		Ha			Hd	Hc	Hb	
$[Ag(Htsa)(PPh_3)_3]$	**3**	8.14			7.23[b]	6.62	6.82	
$[Ag(Htsa)(PPh_3)_3]\cdot CH_2Cl_2$	**3a**	8.15			7.19[b]	6.56	6.80	
$[Au(Htsa)(PPh_3)]$	**4**	8.33			7.73	7.30	7.21	
H_2tsa		8.04			7.63	7.35	7.57	
^{13}C NMR								
		C1	C2	C3	C4	C5	C6	C7
$[Ag(Htsa)(PPh_3)_3]$	**3**	132.44	130.10	149.19	136.85	130.58	122.20	170.01
$[Ag(Htsa)(PPh_3)_3]\cdot CH_2Cl_2$	**3a**	132.53	130.17	148.81	136.87	130.65	122.46	169.77
$[Au(Htsa)(PPh_3)]$	**4**	133.17	131.31	138.73	137.56	131.51	125.75	167.98
H_2tsa		128.11	138.93	133.23	125.00	131.54	125.97	167.59

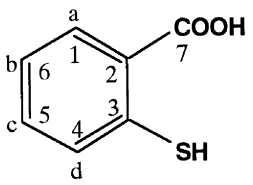

H_2tsa : thiosalicylic acid

[a]Both ^{1}H and ^{13}C NMR spectra of **3**, **3a** and **4** were measured in $CDCl_3$ at 22°C with reference to an internal TMS and those of free ligand H_2tsa measured in DMSO-d_6. The assignment of the chemical shifts was based on the 2D-NMR (COSY, HMBC and HMQC) methods.

[b]These signals were overlapped with the PPh_3 multiplet signals.

complexes, **3** and **3a**, have been derived from three different ligand-exchange reactions. The interconversion relationship among three thiosalicylatosilver(I) complexes, **1**, **2** and **3** was clarified. The corresponding gold(I) analog, [Au(Htsa)(PPh_3)], **4**, was also isolated. From a synthetic viewpoint, the relative ordering of ligand replacement in the silver(I) complexes was found to be: Ag–P ≫ Ag–S > Ag–Cl > Ag–N, while that in the gold(I) complexes followed Au–P ≫ Au–S > Au–N > Au–Cl. The crystal structures of **3** and **4** were determined with single-crystal X-ray diffraction, suggesting the monomeric structure of **3** and the dimeric structure of **4** in the solid state. All complexes obtained have been fully characterized with complete elemental analyses, TG/DTA, FT-IR and multinuclear (^{1}H, ^{13}C, ^{31}P and ^{109}Ag) NMR spectroscopies. In particular, it was found that the monomeric, 4-coordinate geometry of **3** was kept in solution.

Acknowledgements—Financial support from Meiji Cell Technology Center, Meiji Milk Products Co. is gratefully acknowledged.

REFERENCES

1. Abrams, M. J. and Murrer, B. A., *Science*, 1993, **261,** 725.
2. Kaim, W. and Schwederski, B., *Bioinorganic Chemistry*: *Inorganic Elements in the Chemistry of Life*, John Wiley and Sons, New York, 1994, p. 373.
3. Sadler, P. J., *Struct. Bonding* (*Berlin*), 1976, **29,** 171.
4. Shaw, C. F., *Inorg. Perspect. Biol. Med.*, 1978, **2,** 287.
5. Brown, D. H. and Smith, W. E., *Chem. Soc. Rev.*, 1980, **3,** 217.
6. Corey, E. J., Mehrotra, M. and Khan, A. U., *Science*, 1987, **236,** 68.
7. Bryan, D. L. B., Mikuriya, Y., Hempel, J. C., Mellinger, D., Hashim, M. and Pasternack, R. F., *Inorg. Chem.*, 1987, **26,** 4180.
8. Sutton, B. M., McGusty, E., Walz, D. T. and DiMartino, M. J., *J. Med. Chem.*, 1972, **15,** 1095.
9. Chan, M. K. and Minta, J. O., *Immunopharmacology*, 1985, **10,** 61.
10. Razi, M. T., Sadler, P. J., Hill, D. T. and Sutton, B. M., *J. Chem. Soc. Dalton Trans.*, 1983, 1331.
11. Elder, R. C. and Eidness, M. K., *Chem. Rev.*, 1987, **87,** 1027.
12. Mazid, M. A., Razi, M. T., Sadler, P. J., Greaves, G. N., Gurman, S. J., Koch, M. H. J. and Phillips, J. C., *J. Chem. Soc. Chem. Commun.*, 1980, 1261.
13. Rhodes, M. D., Sadler, P. J., Scawen, M. D. and Silver, S., *J. Inorg. Biochem.*, 1992, **46,** 129.
14. Hill, D. T., Sutton, B. M., Isab, A. A., Razi, T., Sadler, P. J., Trooster, J. M. and Calis, G. H. M., *Inorg. Chem.*, 1983, **22,** 2936.
15. Mirabelli, C. K., Johnson, R. K., Hill, D. T., Faucette, L. F., Girard, G. R., Kuo, G. Y., Sung, C. M. and Crooke, S. T., *J. Med. Chem.*, 1986, **29,** 218.
16. Hill, D. T. and Sutton, B. M., *Cryst. Struct. Commun.*, 1980, **9,** 679.
17. Vicente, J., Chicote, M.-T., Gonzalez-Herrero, P. and Jones, P. G., *J. Chem. Soc. Dalton Trans.*, 1994, 3183.
18. Bowmaker, G. A. and Dobson, B. C., *J. Chem. Soc. Dalton Trans.*, 1981, 267.
19. Bates, P. A. and Waters, J. M., *Acta Crsytallogr. C*, 1985, **41,** 862.
20. Beck, W., Stetter, K. H., Tadros, S. and Schwarzhans, K. E., *Chem. Ber.*, 1967, **100,** 3944.
21. Vicente, J., Chicote, M.-T., Saura-Llamas, I. and Lagunas, M. C., *J. Chem. Soc. Chem. Commun.*, 1992, 915.
22. Schroter, I. and Strahle, J., *Chem. Ber.*, 1991, **124,** 2161.
23. Cookson, P. D. and Tiekink, E. R. T., *J. Chem. Soc. Dalton Trans.*, 1993, 259.
24. Cookson, P. D. and Tiekink, E. R. T., *J. Crystallogr. Spectrosc. Res.*, 1993, **23,** 231.
25. Isab, A. A., Hormann, A. L., Hill, D. T., Griswold, D. G., DiMarino, M. J. and Shaw, C. F., *Inorg. Chem.*, 1989, **28,** 1321.
26. Cookson, P. D. and Tiekink, E. R. T., *J. Coord. Chem.*, 1992, **26,** 313.
27. Harker, C. S. W., Tiekink, E. R. T. and Whitehouse, M. W., *Inorg. Chim. Acta*, 1991, **181,** 23.
28. Tiekink, E. R. T., Cookson, P. D., Linahan, B. M. and Webster, L. K., *Metal Based Drugs*, 1994, **1,** 299.
29. Girard, G. R., Hill, D. T. and DiMartino, M. J., *Inorg. Chim. Acta*, 1989, **166,** 141.
30. Hoskins, B. F., Zhenrong, L. and Tiekink, E. R. T., *Inorg. Chim. Acta*, 1989, **158,** 7.
31. Clement, J. L. and Jarrett, P. S., *J. Inorg. Biochem.*, 1993, **51,** 105.
32. Felici, M., Pietroni, B. R. and Burini, A., *Gazz. Chim. Ital.*, 1982, **112,** 5.
33. Bonati, F., Burini, A., Pietroni, B. R. and Giorgini, E., *Inorg. Chim. Acta*, 1987, **137,** 81.
34. Amagi, T., Miyamoto, T. K., Ichida, H. and Sasaki, Y., *Bull. Chem. Soc. Jpn.*, 1989, **62,** 1078.
35. Bonati, F., Burini, A., Pietroni, B. R., Giorgini, E. and Bovio, B., *J. Organometal. Chem.*, 1988, **344,** 119.
36. Nomiya, K., Onoue, K., Kondoh, Y., Kasuga, N. C., Nagano, H., Oda, M. and Sakuma, S., *Polyhedron*, 1995, **14,** 1359.
37. Nomiya, K., Kondoh, Y., Nagano, H. and Oda, M., *J. Chem. Soc. Chem. Commun.*, 1995, 1679.
38. Nomiya, K., Kondoh, Y., Onoue, K., Kasuga, N. C., Nagano, H., Oda, M., Sudoh, T. and Sakuma, S., *J. Inorg. Biochem.*, 1995, **58,** 255.
39. Nomiya, K., Yokoyama, H., Nagano, H., Oda, M. and Sakuma, S., *J. Inorg. Biochem.*, 1995, **60,** 289.
40. Nomiya, K., Yokoyama, H., Nagano, H., Oda, M. and Sakuma, S., *Bull. Chem. Soc. Jpn.*, 1995, **68,** 2875.
41. Nomiya, K., Tsuda, K., Sudoh, T. and Oda, M., *J. Inorg. Biochem.*, 1997, **68,** 39.
42. Nomiya, K., Tsuda, K., Tanabe, Y. and Nagano, H., *J. Inorg. Biochem.*, 1998, **69,** 9.
43. Nomiya, K., Tsuda, K. and Kasuga, N. C., *J. Chem. Soc. Dalton Trans.*, 1998, 1653.
44. Masciocchi, N., Moret, M., Cairati, P., Sironi,

A., Ardizzoia, G. A. and LaMonica, G., *J. Chem. Soc. Dalton Trans.*, 1995, 1671.
45. Baumgartner, M., Schmalle, H. and Baerlocher, C., *J. Solid State Chem.*, 1993, **107,** 63.
46. Janssen, M. D., Donkervoort, J. G., van Berlekom, S. B., Spek, A. L., Grove, D. M. and van Koten, G., *Inorg. Chem.*, 1996, **35,** 4752.
47. Janssen, M. D., Spek, A. L., Grove, D. M. and van Koten, G., *Inorg. Chem.*, 1996, **35,** 4078.
48. Janssen, M. D., van der Rijst, R., Spek, A. L., Grove, D. M. and van Koten, G., *Inorg. Chem.*, 1996, **35,** 3436.
49. Janssen, M. D., Rijnberg, E., de Wolf, C. A., Hogerheide, M. P., Kruis, D., Kooijman, H., Spek, A. L., Grove, D. M. and van Koten, G., *Inorg. Chem.*, 1996, **35,** 6735.
50. Cassel, A., *Acta Crystallogr. B*, 1981, **37,** 229.
51. Cassel, A., *Acta Crystallogr. B*, 1979, **35,** 174.
52. Bruce, M. I., Nicolson, B. K. and Shawkataly, O. B., *Inorg. Synth.*, 1989, **26,** 324.
53. Goodgame, D. M. L., O'Mahoney, C. A., Plank, S. D. and Williams, D. J., *Polyhedron*, 1993, **12,** 2705.
54. Baenziger, N. C., Bennett, W. E. and Soboroff, D. M., *Acta Crystallogr. B*, 1976, **32,** 962.
55. Summers, M. F., Marzilli, L. G. and Bax, A., *J. Am. Chem. Soc.*, 1986, **108,** 4285.
56. *TEXSAN*: *Crystal Structure Analysis Package*. Molecular Structure Corporation, 1985 and 1992.
57. Sanghani, D. V., Smith, P. J., Allen, D. W. and Taylor, B., *Inorg. Chim. Acta*, 1982, **59,** 203.
58. Berners-Price, S. J., Brevard, C., Pagelot, A. and Sadler, P. J., *Inorg. Chem.*, 1985, **24,** 4278.
59. Ardizzoia, G. A., La Monica, G., Maspero, A., Moret, M. and Masciocchi, N., *Inorg. Chem.*, 1997, **36,** 2321.
60. Brevard, C., van Stein, G. C. and van Koten, G., *J. Am. Chem. Soc.*, 1981, **103,** 6746.

Pergamon

PII: S0277-5387(98)00142-9

Polyhedron Vol. 17, No. 20, pp. 3531–3540, 1998
© 1998 Elsevier Science Ltd
All rights reserved. Printed in Great Britain
0277–5387/98 $19.00+0.00

Amidinato- and triazenido-bridged binuclear complexes of palladium and platinum

Anshu Singhal[a], Vimal K. Jain[a]*, Munirathinam Nethaji[b], Ashoka G. Samuelson[b], D. Jayaprakash[b] and Ray J. Butcher[c]

[a]Chemistry Division, Bhabha Atomic Research Centre, Mumbai, 400 085, India

[b]Department of Inorganic and Physical Chemistry Indian Institute of Science, Bangalore, 560012, India

[c]Department of Chemistry, Howard University, Washington, DC 20059, U.S.A

(Received 2 December 1997; accepted 6 April 1998)

Abstract—The reaction of $[M_2Cl_2(\mu\text{-}Cl)_2(PR_3)_2]$ (M = Pd or Pt; $PR_3 = PEt_3$, PBu_3, PMe_2Ph, $PMePh_2$) with lithium amidinate or sodium triazenide gave binuclear complexes containing amidinato- or triazenido-bridges, $[M_2Cl_2(\mu\text{-}ArNENAr)_2(PR_3)_2]$ (E = CH, CMe or N). These complexes were characterized by elemental analysis and NMR (^1H, ^{31}P or ^{195}Pt) data. The structures of two complexes, $[Pd_2Cl_2\{\mu\text{-}PhNC(Me)NPh\}_2(PMe_2Ph)_2]$ (**10**) and $[Pt_2Cl_2(\mu\text{-}PhNNNPh)_2(PEt_3)_2]$ (**11**) were established by single crystal X-ray structural analyses. The ^{195}Pt NMR data show coupling between two metal centers in the *cis* triazenido-bridged complex. The corresponding amidinate bridged complex does not show coupling. The role of the bridging ligand in mediating interaction between the metal centers is probed through Extended Huckel Theory (EHT) calculations. It is suggested that M–M interactions are primarily affected by the bridging ligands. © 1998 Elsevier Science Ltd. All rights reserved.

Keywords: palladium; platinum; amidine; triazene; X-ray structure; Extended Huckel Theory

INTRODUCTION

Recently we have synthesised and characterised a series of binuclear palladium and platinum complexes [1–5] of the type $[M_2X_2(\mu\text{-}Y)_2L_2)]$ (I and II). In particular, molecules with anionic bidentate three-atom bridging ligands showed unusual properties. For example, complexes containing bridging carboxylate [2] and triazenido [3] groups exhibited unusually strong M–M interactions with a formal bond order of zero, whereas such interactions were vanishingly small for the corresponding acetamidinato [4]- and 2- hydroxypyridinato [5]-bridged complexes. This has motivated us to initiate a systematic study on palladium and platinum complexes with anionic three-atom ligands. Amidines are one of the members of this class of ligands. They are known to stabilize metal-metal bonds [6]. Amidines coordinate either in the neutral form (via amine-N or imine-N atom) or as the amidinate ion [7, 8]. Electronic and steric properties of an amidine ligand can be modified by varying the organic substituents on the nitrogen atoms and the central carbon atom. For example, formamidinate ligands are known to favour unusual structural features in metal complexes [9, 10].

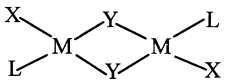

trans
I

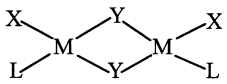

cis
II

(where M = Pd or Pt; X = halide, alkyl or aryl groups, Y = anionic one-atom bridging ligand such as halide, SR etc., two-atom bridging ligand such as pyrazolate ion or three-atom bridging ligands such as AcO, $RNNNR^-$, $RNCR'NR^-$, etc.)

Herein we report, as part of our ongoing investigation, synthesis and characterisation of palladium

* Author to whom correspondence should be addressed. Fax: 91-022-556-0750; Tel: 91-022-551-1576.

and platinum complexes with amidinate ligands. For comparison, X-ray structure and ^{195}Pt NMR data for a triazenido-bridged platinum complex, $[Pt_2Cl_2(\mu\text{-}PhNNNPh)_2(PEt_3)_2]$ (**11**) are also included.

RESULTS AND DISCUSSION

Amidinato-bridged binuclear palladium and platinum complexes, $[M_2Cl_2(\mu\text{-}ArN{=}CH{-}NAr)_2\ (PR_3)_2]$ (M = Pd or Pt; Ar = tol, $MeOC_6H_4$) can readily be obtained by the reaction of $[M_2Cl_2(\mu\text{-}Cl)_2(PR_3)_2]$ (M = Pd or Pt; $PR_3 = PEt_3$, PBu_3, PMe_2Ph or $PMePh_2$) with the lithium salt of formamidine in 1:2 molar ratio. The treatment of $[M_2Cl_2(\mu\text{-}Cl)_2(PR_3)_2]$ with formamidines affords mononuclear complexes containing neutral formamidine. These complexes are yellow to orange coloured crystalline solids, soluble in common organic solvents.

The $^{31}P\{^1H\}$ NMR spectra (Table 1) of these complexes exhibited a single resonance for tertiary phosphines indicating the formation of only one isomeric form exclusively. The magnitude of ^1J(Pt–P) for the $[Pt_2Cl_2\{\mu\text{-}tolNCHNtol\}_2(PMe_2Ph)_2]$ is comparable to the corresponding acetamidinato- and triazenido-bridged [3, 4] platinum complexes. The ^{1}H NMR spectra of these complexes showed two singlets of equal integration each for methyl and methoxy protons of aryl groups attached to the nitrogen atoms. One can be assigned to the NAr group *trans* to the phosphine and other *trans* to the terminal chloride. The sym *trans* configuration is further substantiated by the presence of one NCHN resonance for the formamidinate group, however in the platinum complex two closely spaced singlets were observed. The complexes containing PMe_2Ph ligands displayed two doublets due to $J(^{31}P\text{–}^1H)$ couplings for methyl protons indicating non-equivalence of the methyl groups. The ^{195}Pt NMR spectrum of $[Pt_2Cl_2\{\mu\text{-}tolNC(H)Ntol\})_2(PMe_2Ph)_2)]$ exhibited a doublet at δ-3245 ppm with $^1J(^{195}Pt\text{–}^{31}P)$ 3555 Hz. The ^{195}Pt NMR spectrum of $[Pt_2Cl_2(\mu\text{-}PhNNNPh)_2(PEt_3)_2]$ (11) showed a doublet at δ-3194 ppm with $^1J(^{195}Pt\text{–}^{31}P)$ 3542 Hz (Fig. 1). Unlike the amidinato bridged complex **10**, the spectrum of **11** also showed ^nJ(Pt–Pt) coupling of 1535 Hz in the ^{195}Pt

Table 1. ^{1}H and $^{31}P\{^1H\}$ NMR data for the palladium and platinum complexes with amidimes

Complex	δ^{31}P	^{1}H NMR data
$[PtCl_2(dtfH)(PBu_3)]$ (1)	−7.0[a]	0.96(t, 7.2 Hz, PCCCMe); 1.46–1.65 (m, PCH_2CH_2–);1.87 (m, PCH_2); 2.32 (s, tol-Me, 6 H); 6.95(d, 8.4 Hz, 2 H); 7.14(d, 7.6 Hz, 4 H); 7.42(d, 8.3 Hz, 2 H) [C_6H_4];8.18(d,d, 10.7 Hz, NC*H*N); 8.97 (d, 12 Hz, NH-)
$[Pt_2Cl_2(\mu\text{-}dtf)_2(PMe_2Ph)_2]$ (2)	−26.2[b]	1.73, 1.95 (each d, 11.6 Hz, PMe_2); 2.13 (s), 2.26 (s) (each 6 H, tol-Me); 6.60(d) 6.74 (d), 6.97 (d), 7.15 (d) (each 6.2 Hz, C_6H_4); 7.31-7.41 (m), 7.70-7.76 (m) [Ph]; 7.57, 7.61 (each s, NC*H*N)
$[Pd_2Cl_2(\mu\text{-}dtf)_2(PEt_3)_2]$ (3)	21.8	1.03 (d,t, 7.7 Hz (t), 16 Hz(d), PCH_2*Me*); 1.62 (m), 1.86(m) (PCH_2−); 2.18(s), 2.34(s) (tol-Me); 6.71 (s)*; 7.07 (d), 7.37 (d) (each 8.2 Hz, C_6H_4); 7.34 (s, NC*H*N)
$[Pd_2Cl_2(\mu\text{-}bpmpf)_2(PEt_3)_2]$ (4)	22.0	1.06 (d,t, 7.7 Hz(t), 16 Hz(d), PCH_2*Me*); 1.56–1.61 (m), 1.80–1.89 (m) (PCH_2−); 3.69(s); 3.80(s) (OMe); 6.48(d), 6.73(d), 6.83(d), 7.41 (d) (each 8.8 Hz, C_6H_4); 7.28 (s), 7.34 (s) (NC*H*N)
$[Pd_2Cl_2(\mu\text{-}dtf)_2(PBu_3)_2]$ (5)	15.7	0.90 (t, 7.2 Hz, PCCC*Me*); 1.32 (m, $PCCH_2CH_2$); 1.46–1.86 (m, PCH_2−); 2.18 (s), 2.34 (s) (tol-Me); 6.68 (d,)**; 7.06(d), 7.40 (d) (each 8.2 Hz, C_6H_4); 7.35(s, NC*H*N)
$[Pd_2Cl_2(\mu\text{-}bpmpf)_2(PBu_3)_2]$ (6)	15.8	0.91(t, 7.2 Hz, PCCC*Me*); 1.24–1.46 (m, $PCCH_2CH_2$−); 1.87 (m, PCH_2−); 3.68(s), 3.81 (s) (OMe); 6.47 (d), 6.69 (d), 6.83(d), 7.44 (d) (each 8.8 Hz, C_6H_4); 7.29 (s), 7.33 (s); 7.35 (s) (NC*H*N)
$[Pd_2Cl_2(\mu\text{-}dtf)_2(PMe_2Ph)_2]$ (7)	1.0	1.72 (d), 1.95 (d) (each 12.2 Hz, PMe_2); 2.11 (s), 2.26 (s) (tol-Me); 6.51 (d), 6.60(d), 6.98 (d) (each 8.2 Hz, C_6H_4, 6 H); 7.21-7.40 (m), 7.60-7.65 (m, Ph + C_6H_4 (2 H) + NC*H*N)
$[Pd_2Cl_2(\mu\text{-}bpmpf)_2(PMe_2Ph)_2]$ (8)	1.1	1.72 (d), 1.92 (d) (each 12.2 Hz, PMe_2); 3.62 (s), 3.75 (s) (OMe); 6.24 (d) 6.58 (d), 6.74 (d) (each 8.8 Hz, C_6H_4, 6 H); 7.24-7.58 (m, Ph + C_6H_4 (2 H) + NC*H*N)
$[Pd_2Cl_2(\mu\text{-}dtf)_2(PMePh_2)_2]$ (9)	13.8	2.25 (d, 12.0 Hz, PMe); 2.05 (s), 2.33 (s) (tol-Me); 6.35 (d), 6.42 (d) (C_6H_4, 4 H); 7.05 (m), 7.44 (m), 8.03 (m) (Ph + C_6H_4 + NC*H*N)
$[Pd_2Cl_2(\mu\text{-}dpa)_2(PMe_2Ph)_2]$ (10)	2.9	1.78 (s, C*Me*); 1.84 (d) 2.08 (d) (each 12.4 Hz PMe_2); 6.17–7.18 (m), 8.06 (m) [Ph]
$[Pt_2Cl_2(\mu\text{-}dpt)_2(PEt_3)_2]$ (11)	−12.2[c]	1.06 (m, 18 H, PC*Me*); 1.69 (m, 6 H), 1.91(m, 6 H) (PCH_2−); 6.99 (m) 7.60 (t, 7.3 Hz), 7.32 (t, 7.8 Hz) 7.60 (d, 7.9 Hz) [20 H, Ph]

dtfH = tolN=C(H)NHtol; dtf = $[tolNC(H)Ntol]^-$; bpmpf = $[MeOC_6H_4NC(H)NC_6H_4OMe]^-$ dpa = $[PhNC(Me)NPh]^-$ dpt = $[PhNNNPh]^-$ (a)^{1}J(Pt–P) = 3351 Hz (b)^{1}J(Pt–P) = 3570 Hz (c)^{1}J(Pt–P) = 3496 Hz * integrated to 4 H protons **AB quartet, integrated to 4 H protons.

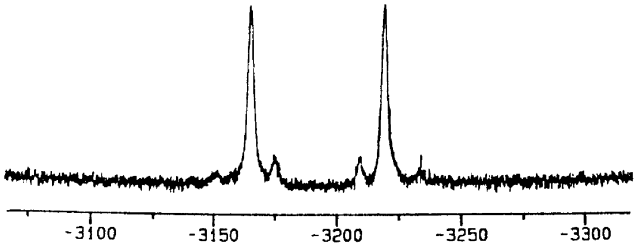

Fig. 1. $^{195}Pt\{^{1}H\}$NMR spectrum of $[Pt_2Cl_2(\mu\text{-PhNNNPh})_2(PEt_3)_2]$ in $CDC1_3$.

NMR spectrum indicating significant platinum platinum interaction as reported earlier by us [3].

A few reactions of formamidinato-bridged palladium complexes were also investigated. The complex $[Pd_2Cl_2\{\mu\text{-tolNCHNtol}\}_2(PBu_3)_2]$ on treatment with an ethereal solution of HCl afforded a mononuclear complex, $[PdCl_2(tolN{=}CH{-}NHtol)(PBu_3)]$ (δ ^{31}P 26.1 ppm) formed by protonation of the bridging ligand eq. (1). A similar species (δ ^{31}P 26.1 ppm) was formed when $[Pd_2Cl_2(\mu\text{-Cl})_2(PBu_3)_2]$ was treated with di-p-tolylformamidine. It is interesting to note that the triazenido-bridged complexes react reversibly with HCl [3]. Addition of triphenylphosphine to a $CDCl_3$ solution of $[Pd_2Cl_2\{\mu\text{-tolNCHNtol}\}_2(PBu_3)_2]$ has no effect on its ^{31}P NMR spectra indicating non-lability of the formamidinato-bridges with neutral donor ligands.

$$[Pd_2Cl_2\{\mu-tolNC(H)Ntol\}_2(PBu_3)_2]+2HCl \rightarrow 2[PdCl_2\{tolNHC(H)Ntol\}(PBu_3)]\ldots. \quad (1)$$

The molecular structures of acetamidinato- and triazenido-bridged complexes, $[Pd_2Cl_2\{\mu\text{-PhNC(Me)NPh}\}_2(PMe_2Ph)_2]$ (**10**) and $[Pt_2Cl_2(\mu\text{-PhNNNPh})_2(PEt_3)_2]$ (**11**) were established by X-ray diffraction. The structures of **10** and **11** comprise of four molecules per unit cell separated by normal van der Waals distances. Molecular structures together with the crystallographic numbering scheme are shown in ORTEP drawings (Figs 2 and 3). Each molecule consists of two distorted square planar metal (Pd or Pt) atoms bridged together by [PhNC(Me)NPh]$^-$ or $[PhNNNPh]^-$ groups. The bridging ligands in both molecules are *cis* with respect to each other, whereas the ancillary ligands Cl and PR_3 are *trans* related.

In **10** the C–N bond distances [N(1A)–C(11A), N(1B)–C(11A), N(1C)–C(11B), N(1D)–C(11B) [av. 1.326 Å] are intermediate between the typical C–N (1.48 Å) and C=N (1.24 Å) covalent bond distances, indicating π-electron delocalozation in the NCN skeleton. This is further substantiated by the sum of inter bond angles around carbon (359.9°) and nitrogen (av. 359.7(5)°) atoms of the NCN skeleton. The NCN bite angles [121.7(6), 122.6(6)°] and bite distances [(N(1A)–N(1B) 2.321 Å and N(1C)–N(1D) 2.324 Å] are of the same magnitude as reported for other bridging amidinato-bridged complexes [11–13]. There are distinctly two types of Pd–N distances (Table 2). One with chloride *trans* to nitrogen is shorter than the other one where phosphine is *trans* to nitrogen, owing to the stronger *trans* influence of the phosphine. The two Pd–N distances lie in the range 1.86 and 2.15 Å reported in several palladium complexes [6, 11, 14–16]. The two Pd–P and Pd–Cl distances are essentially identical and compare well with the reported values [17, 18]. The Pd–Pd separation [2.914(2) Å] is shorter than the $[Pd_2(\mu\text{-NHCPhNH})_2(\eta^3\text{-}C_3H_5)_2]$ [3.218(1) Å], however it is comparable to $[Pt_2(\mu\text{-PhNCHNPh})_2(\eta^2\text{-PhNCHNPh})_2]$(2.918(9) Å) [13]. The two palladium atoms lie within the distances reported for binuclear complexes containing anionic three-atom bridging ligands (Table 3) [19–25].

The complex **11** has two platinum atoms at a separation of 2.9302(8) Å (Table 4). This distance is comparable with other binuclear complexes containing anionic three atom bridging ligands (Table 3). The two N–N bonds are nearly equivalent and the N–N–N angle is 116.6(6)° indicating pronounced π-electron deloclization [20]. The Pt–N bond distance *trans* to the phosphine ligand is longer than the Pt–N bond *trans* to the chloride. The bridging PhNNNPh ligands are *cis* with respect to each other. Unlike complex **10**, complex **11** has a crystallographically imposed C_2 symmetry.

The face to face juxtaposition of two square planar d^8 metal centres is expected to result in antibonding interactions between the metal centres on the basis of qualitative molecular orbital theory. However, the frequent occurrence of short contacts in such units has caused much debate [26] regarding the possible ways by which these metal–metal interactions could become favorable. Recent work in this area has suggested several factors which make the metal–metal interaction in these systems less antibonding [27]. In the present work, it was possible to observe Pt–Pt coupling in the ^{195}Pt NMR spectra of the triazenido-bridged complexes, whereas in the corresponding acetamidinato-bridged platinum derivatives no coupling between the metal centres could be observed. The metal–metal distance in the complex **10** should be comparable to that of complex **11** since M–M distances are primarily controlled by the ligand [28]. It is

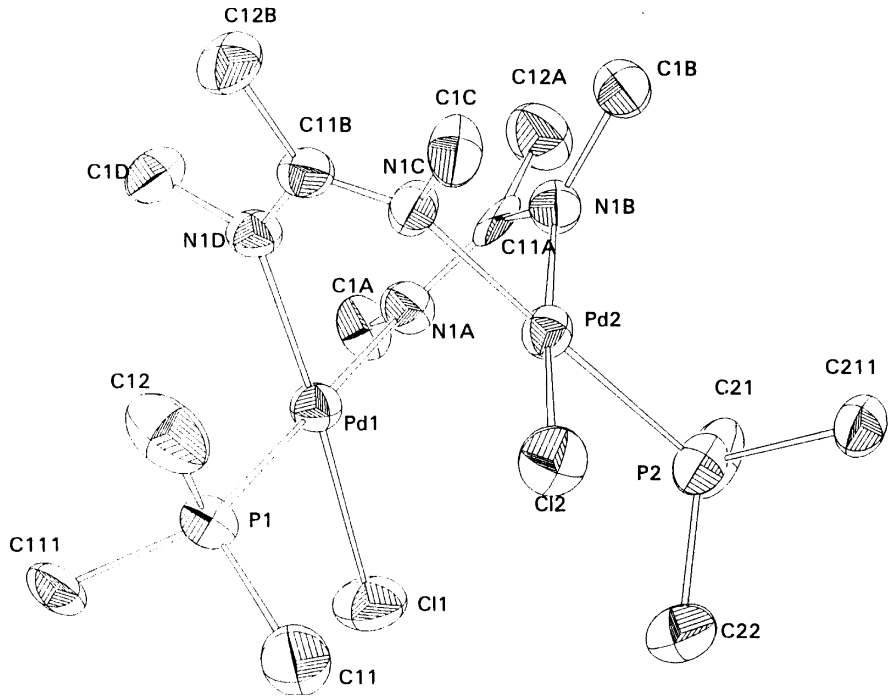

Fig. 2. Molecular structure with crystallographic numbering scheme for $[Pd_2Cl_2\{\mu\text{-PhNC(Me)NPh}\}_2(PMe_2Ph)_2]$ (**10**) (phenyl groups are omitted for clarity).

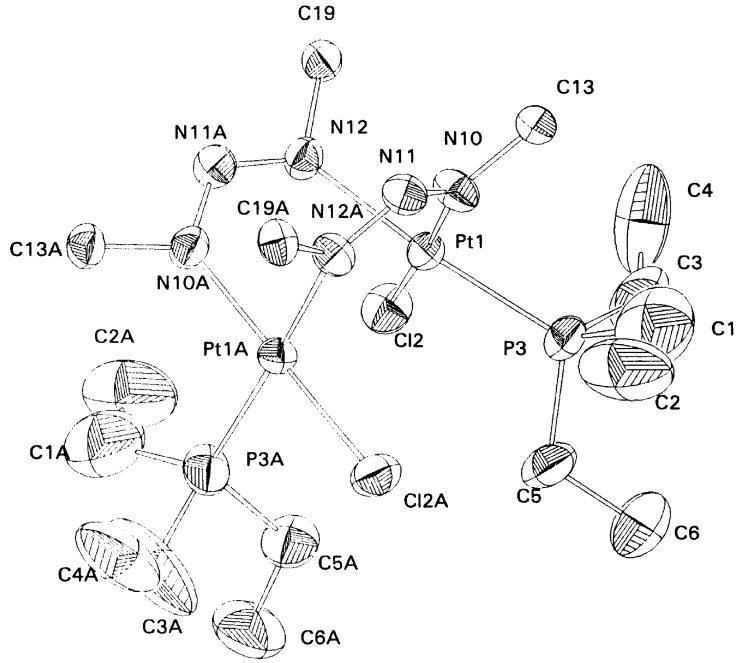

Fig. 3. ORTEP view with crystallographic numbering scheme for $[Pt_2Cl_2(\mu\text{-PhNNNPh})_2(PEt_3)_2]$ (**11**) (phenyl groups are omitted for clarity).

Table 2.Selected bond lengths (Å) and angles (°) for $[Pd_2Cl_2\{\mu\text{-PhNC(Me)NPh}\}_2(PMe_2Ph)_2]$ (10)

Pd(1)–N(1A)	2.097(5)	Pd(2)–N(1C)	2.112(5)
Pd(1)–N(1D)	2.059(5)	Pd(2)–N(1B)	2.062(5)
Pd(1)–P(1)	2.262(2)	Pd(2)–P(2)	2.262(2)
Pd(1)–Cl(1)	2.311(2)	Pd(2)–Cl(2)	2.314(2)
P(1)–C(11)	1.817(7)	P(2)–C(21)	1.810(7)
P(1)–C(12)	1.799(7)	P(2)–C(22)	1.806(7)
P(1)–C(111)	1.831(8)	P(2)–C(211)	1.809(8)
N(1A)–C(1A)	1.440(8)	N(1C)–C(1C)	1.431(9)
N(1A)–C(11A)	1.321(8)	N(1C)–C(11B)	1.297(9)
N(1B)–C(1B)	1.438(8)	N(1D)–C(1D)	1.422(8)
N(1B)–C(11A)	1.332(8)	N(1D)–C(11B)	1.354(8)
Pd(1)–Pd(2)	2.914(2)		
N(1D)–Pd(1)–N(1A)	88.5(2)	N(1B)–Pd(2)–N–(1C)	89.0(2)
N(1A)–Pd(1)–P(1)	176.5(2)	N(1C)–Pd(2)–P(2)	176.2(2)
N(1A)–Pd(1)–Cl(1)	91.1(2)	N(1C)–Pd(2)–Cl(2)	90.4(2)
N(1D)–Pd(1)–P(1)	93.2(2)	N(1B)–Pd(2)–P(2)	93.0(2)
N(1D)–Pd(1)–Cl(1)	175.2(2)	N(1B)–Pd(2)–Cl(2)	174.5(2)
P(1)–Pd(1)–Cl(1)	86.92(8)	P(2)–Pd(2)–Cl(2)	87.31(8)
C(11A)–N(1A)–Pd(1)	124.0(5)	C(11A)–N(1B)–Pd(2)	126.6(5)
C(11B)–N(1D)–Pd(1)	124.7(5)	C(11B)–N(1C)–Pd(2)	124.5(5)
N(1A)–C(11A)–N(1B)	121.7(6)	N(1C)–C(11B)–N(1D)	122.6(6)
N(1A)–C(11A)–C(12A)	118.8(6)	N(1C)–C(11B)–C(12B)	118.7(7)
N(1B)–C(11A)–C(12A)	119.4(6)	N(1D)–C(11B)–C(12B)	118.6(6)

Table 3. Pd–Pd distance in some binuclear palladium complexes

Complex	Pd–Pd distance (Å)	Reference
$[Pd_2\{\mu\text{-MeNNNMe}\}_2(\eta^3\text{-}C_4H_7)_2]$	2.97	19
$[Pd_2\{\mu\text{-tolNNNtol}\}_2(\eta^3\text{-}C_4H_7)_2]$	2.86	20
$[Pd_2(\mu\text{-OAc})_2(\eta^3\text{-}C_3H_5)_2]$	2.94	21
$[Pd_2(\mu\text{-NHCPhNH})_2(\eta^3\text{-}C_3H_5)_2]$	3.128(1)	11
$[Pd_2(\mu\text{-Cl})_2(\eta^3\text{-}C_3H_5)_2]$	3.460	22
$[Pd_2Cl_2(\mu\text{-OAc})_2(PMe_2Ph)_2]$	2.946(2)	23
$[Pd_2Cl_2(\mu\text{-Spy})_2(PMe_3)_2]$	2.942(2)	24
$[Pd_2Cl_2(\mu\text{-Spy})_2(PMe_2Ph)_2]$	2.921(2)	25
$[Pd_2Cl_2(\mu\text{-Spy})_2(PMePh_2)_2]$	2.982(3)	25

Spy = SC_5H_4N (2-mercaptopyridinate ion).

possible that the ligand controls, not only the distance but the interaction between the two metal centres in a significant fashion. In order to probe the role of the ligand in mediating metal–metal interactions, we have carried out Extended Huckel Theory (EHT) calculations on model systems. Our results suggest that in addition to the factors identified earlier, the nature of bridging ligands and their relative disposition (Scheme 1) in the metal complex could play a significant role in determining the metal–metal interactions.

Calculations were carried out using the program CACAO [29], on model complexes constructed using the crystallographic coordinates for the heavy atoms wherever available. In other cases, models were constructed based on observed metal-ligand geometries of related d^8 complexes. The reduced overlap population (ROP) computed by EHT, gives a measure of the relative interaction between the metal centres in various complexes studied. Being fully aware of the limitations of EHT to reliably quantify interaction energies, we merely interpret trends in the computed ROP as done by Aullon and Alvarez [30]. The computed ROPs along with the M–M distances and the nature of the bridge are given in Table 5 together with the ROP computed in the absence of the bridging ligand. In general the bridging ligand has greater influence on metal–metal interactions in these systems compared to the ancillary ligands Cl and PH_3. While

Table 4. Selected bond lengths (Å) and angles (°) for $[Pt_2CI_2(\mu\text{-PhNNNPh})_2\ (PEt_3)_2]$ (11)

Pt(1A)–Pt(1)	2.9302(8)	P(1)–C(3)	1.73(2)
Pt(1)–CI(1)	2.323(2)	P(1)–C(5)	1.809(9)
Pt(1)–P(1)	2.257(2)	N(1A)–N(1B)	1.319(9)
Pt(1)–N(1A)	2.014(6)	N(1B)–N(1C)	1.296(8)
Pt(1A)–N(1C)	2.110(6)	N(1C)–C(1B)	1.460(9)
P(1)–C(1)	1.79(2)	N(1A)–C(1A)	1.453(8)
P(1)–Pt(1)–N(1A)	93.9(2)	Pt(1)–N(1A)–C(1A)	122.5(5)
C1(1)–Pt(1)–P(1)	89.12(7)	N(1A)–N(1B)–N(1CA)	116.6(6)
C1(1)–Pt(1)–N(1A)	175.4(2)	N(1BA)–N(1C)–C(1B)	109.6(6)
Pt(1)–N(1A)–N(1B)	127.6(4)	N(1B)–N(1A)–C(1A)	109.4(6)
Pt(1A)–N(1CA)–N(1B)	115.8(4)	Pt(1)–P(1)–C(1)	124.1(6)
Pt(1A)–N(1CA)–C(1BA)	134.4(5)	Pt(1)–P(1)–C(3)	113.7(7)
		Pt(1)–P(1)–C(5)	113.6(3)

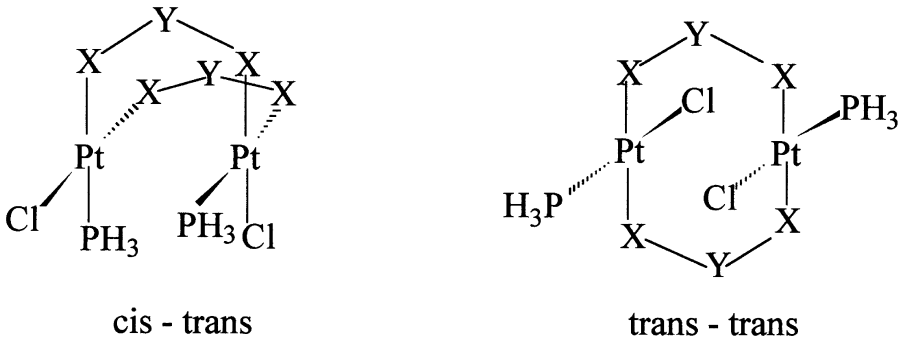

X-Y-X = O=C(Me)-O or HN=N-NH or HN=C(H)-NH

Scheme 1. X-Y-X = O═C(Me)–O or HN═N–NH or HN═C(H)–NH

Table 5. Reduced Overlap Populations computed by EHT

	Geometry		Pt–Pt				
					ROP ($\times 10^3$)		
Complex	Bridge	Cl and PH_3	Distance (Å)	Coupling constant (Hz)	With bridge	Without bridge	Ref.
$[Pt_2(NNN)_2Cl_2(PH_3)_2]$	*cis*	*trans*	2.930	1587	59	54	3
	trans	*trans*			50		
	cis	*cis*			59	53	
	trans	*cis*			46		
$[Pt_2(OAc)_2Cl_2(PH_3)_2]$	*cis*	*trans*	2.943	1148	42	52	2
	trans	*trans*			26		
	cis	*cis*			41	50	
	trans	*cis*			26		
$[Pt_2(NCN)_2C1_2(PH_3)_2]$	*cis*	*trans*	2.912		36	56	13
	trans	*trans*		Not observed	25		4
	cis	*cis*			34	57	
	trans	*cis*			25		

Bridging ligands: NNN═HNNNH; OAc = $OC(CH_3)O$; NCN═HNC(H)NH.

the σ donor and $\pi-$ acceptor capabilities of the ligand, PH_3 (with no d orbitals on the P) would be different from that of PPh_3, we expect the trends would be similar even if PPh_3 were to be used in the calculations. The bridging ligand reduces the observed ROP except in the case of triazenide ligand where the ROP is increased marginally. It is also important to note that the relative orientation of the supporting ligands Cl and PH_3, do not change the ROP to a significant degree. However, the *cis* or *trans* nature of the bridging ligand changes the ROP between the metal centres by approximately 0.01 units which is 20% of the computed ROP. This suggests that the metal–metal interaction is significantly affected by the nature and relative orientation of the bridging ligand.

The ROP in these three cases are not very different. However, it is important to note the relative changes the ligands bring about in the computed ROP. For the amidinato complex and the acetato complex, the ROP is decreased by 36% and 19% respectively on adding the bridging ligands. In the case of amidinato complex, the reduction in the ROP is even greater (55%) when the bridging ligands are *trans*. A significant change is observed in the case of the triazenido complex where a small increase (1%) in the computed ROP is observed. To understand how the amidinato complex enhances the antibonding interaction between the metal centres, and the triazenido ligand decreases the antibonding interaction, a fragment molecular orbital analysis was carried out. The results of this analysis suggest that the bridging ligand primarily interacts through its non bonding σ donor orbitals and the empty π^* orbitals. Apart from donation of electrons to the empty metal orbitals, the σ orbitals interact with the metal–metal σ (*cis* or *trans* geometry) and π (*trans* geometry only) orbitals. The empty π^* orbitals on the other hand have the appropriate symmetry to interact with the metal–metal δ type orbitals. The former interaction results in the interaction of the filled shells and reduces the ROP and the latter is responsible for a marginal increase in ROP. In the trans geometry, there is a greater reduction in the M–M ROP due to destabilisation of the π type M–M bonding orbitals. The metal–metal interaction is significantly decreased on adding the amidinato bridging ligands, because of the larger overlap of the the nonbonding electrons in the ligand with the filled metal–metal σ orbital. In addition, the amidinato ligand is a poor π acceptor because the π^* levels lie much higher in energy and have smaller contributions on the interacting atoms compared to the π acceptor orbitals of the triazenido ligand. On the other hand the triazenido ligand has suitable π^* orbitals of low energy which stabilize the M–M δ bond. As a result the triazenido ligand increases the M–M ROP, albeit, to a small extent.

Our results are in complete agreement with a recent study carried out on the interaction between d^8 metal centres stacked in a face to face fashion by Aullon and Alvarez [28]. While the nature of bridging ligands has not been addressed, the effect of π acidic ligands in modulating the ROP of the interacting metal centres has been studied. They have noted an increase in the ROP with increase in the number of π acid-ligands surrounding the metal atom. Where structures are available, the corresponding M–M distances observed in such complexes are also smaller. The X-ray crystallographic database analysis done by them demonstrates the generality of the phenomenon. Similarly, π donor ligands were shown to increase the antibonding effect between the metal atoms.

On the basis of the results obtained above, it is clear how the nature and relative disposition of the bridge determines whether one observes Pt–Pt coupling in the ^{195}Pt NMR. There are two three-atom bridged complexes for which Pt–Pt coupling have been observed and one, the amidinato-bridged complex where there is no Pt–Pt coupling. In the case of the amidinato complex some of us had studied earlier [4], the geometry of the bridging ligands are *trans* and no Pt–Pt coupling was observed. This is readily explained by the large reduction in ROP (55%) with amidinato ligands in the *trans* geometry. In cases where the bridging ligands are *cis* to each other, the reduction in ROP is less, especially in the case of triazenido- and acetato-bridged complexes. Hence it is possible to observe the Pt–Pt coupling in the ^{195}Pt NMR spectra of the latter systems.

EXPERIMENTAL

Formamidines (ArN=CH–NHAr); Ar = 4-MeC_6H_4 (tol), 4-$MeOC_6H_4$) [31] and $[M_2Cl_2(\mu\text{-}Cl)_2(PR_3)_2]$ (M = Pd or Pt) [32] and $[Pt_2Cl_2(\mu\text{-}PhNNNPh)_2(PEt_3)_2]$[3] were prepared according to the literature methods. All the reactions were carried out in dried and distilled analytical grade solvents under a nitrogen atmosphere. The ^{1}H, $^{31}P\{^1H\}$ and $^{195}Pt\ \{^1H\}$ NMR spectra were recorded on a Bruker DPX-300 spectrometer in freshly prepared $CDCl_3$ solutions. Chemical shifts are referred to internal chloroform peak (δ $CHCl_3$ 7.26 ppm) for ^{1}H, external 85% H_3PO_4 for ^{31}P and external Na_2PtCl_6 solution in D_2O for ^{195}Pt. Elemental analyses were carried out by the Analytical Chemistry Division of this research centre.

Preparation of $[PtCl_2\{tolNCH\text{-}NHtol\}(PBu_3)]$

To a dichloromethane (10 cm^3) solution of $[Pt_2Cl_2(\mu\text{-}Cl)_2(PBu_3)_2]$ (119 mg, 0.127 mmol) was added a dichloromethane (5 cm^3) solution of N,N′-di-p-tolylformamidine (64 mg, 0.284 mmol) and the reaction mixture was stirred for 1 h at room temperature. The solvent was stripped off in vacuo and the residue was recrystallised from hexane as a pale yellow colored solid (70 mg, 40% yield).

Table 6.Physical and analytical data for palladium and platinum complexes with amidine ligands

Complex	Recry.solvent (% yield)	melting point (°C)	% analyses found (calcd.) C	H	N
$[PtCl_2(dtfH)(PBu_3)]$ (1)	hexane (40)	124–126	47.2 (46.8)	6.2 (6.3)	3.9 (4.0)
$[Pt_2Cl_2\{\mu\text{-dtf}\}_2(PMe_2Ph)_2]$ (2)	benzene-hexane (60)	250–255 (d)	47.2 (46.7)	4.1 (4.4)	4.7 (4.7)
$[Pd_2Cl_2\{\mu\text{-dtf}\}_2(PEt_3)_2]$ (3)	benzene-hexane (48)	195–199 (d)	49.6 (52.2)	6.4 (6.3)	5.6 (5.8)
$[Pd_2Cl_2\{\mu\text{-bpmpf})_2)(PEt_3)_2]$ (4)	benzene-hexane (62)	194–199 (d)	48.0 (48.9)	5.3 (5.8)	5.3 (5.4)
$[Pd_2Cl_2\{\mu\text{-dtf})_2(PBu_3)_2]$ (5)	hexane (62)	170–172	55.6 (57.1)	7.1 (7.5)	4.6 (4.9)
$[Pd_2Cl_2\{\mu\text{-bpmpf})_2(PBu_3)_2]$ (6)	benzene-hexane (62)	180–182	53.5 (54.1)	6.7 (7.0)	4.8 (4.7)
$[Pd_2Cl_2\{\mu\text{-dtf}\}_2(PMe_2Ph)_2]$ (7)	benzene-hexane (58)	198–203 (d)	54.6 (54.9)	5.6 (5.2)	5.5 (5.6)
$[Pd_2Cl_2\{\mu\text{-bpmpf}\}_2(PMe_2Ph)_2]$ (8)	benzene-hexane (59)	192–196 (d)	51.7(51.6)	4.0 (4.9)	5.5 (5.2)
$[Pd_2Cl_2\{\mu\text{-dtf}\}_2(PMePh)_2)_2]$ (9)	benzene-hexane (59)	206–210 (d)	58.7 (59.5)	4.9 (5.0)	4.9 (4.9)
$[Pd_2Cl_2\{\mu\text{-dpa})_2(PMe_2Ph)_2]$ (10)	benzene-hexane (59)	186–190 (d)	53.3 (54.0)	5.1 (4.9)	5.8 (5.7)
$[Pt_2Cl_2\{\mu\text{-dpt})_2(PEt_3)_2]$ (11)	CH_2C1_2-benzene-hexane (65)	174–178 (d)	39.7 (39.5)	4.5 (4.6)	7.5 (7.7)

dtfH = tolN = CH–NHtol; dtf = $[tolNC(H)Ntol]^-$; bpmpf = $[MeOC_6H_4NC(H)NC_6H_4OMe]^-$ dpa = $[PhNC(Me)NPh]^-$; dpt = $[PhNNNPh]^-$.

Preparation of $[Pd_2Cl_2\{\mu\text{-}tolNC(H)Ntol\}_2(PMe_2Ph)_2]$

To a lithioformamidinate suspension, prepared by neutralizing a THF solution of N,N′-di-p-tolylformamidine (98 mg, 0.436 mmol) with a hexane solution of n-butyllithium (0.45 N, 1 cm^3, 0.45 mmol), solid $[Pd_2Cl_2(\mu\text{-Cl})_2(PMe_2Ph)_2]$ (128 mg, 0.203 mmol) was added. The resulting solution was stirred for two days at room temperature under a nitrogen atmosphere. The solvents were removed in vacuo and the residue was extracted with benzene ($3 \times 3\ cm^3$) and filtered. The filterate was concentrated *in vacuo* and the residue was recrystallised from benzene-hexane mixture in 58% (119 mg) yield as an orange crystalline solid. Similarly all other complexes were prepared. Pertinent data are given in Table 6.

Reaction between $[Pd_2Cl_2\{\mu\text{-}tolNC(H)Ntol\}_2(PBu_3)_2]$ *and* PPh_3

To a $CDCl_3$ solution of $[Pd_2Cl_2\{\mu\text{-tolNC(H)Ntol}\}_2(PBu_3)_2]$ (24.5 mg, 0.022 mmol) in a 5 mm NMR tube was added solid triphenylphosphine (11.5 mg, 0.044 mmol). The resulting solution was studied by ^{31}P NMR spectroscopy.

Reaction between $[Pd_2Cl_2\{\mu\text{-}tolNC(H)Ntol\}_2(PBu_3)_2]$ *and HCl*

To a dichloromethane (5 cm^3) solution of $[Pd_2Cl_2\{\mu\text{-tolNC(H)Ntol}\}_2(PBu_3)_2]$ (26.7 mg, 0.024 mmol) was added an ethereal solution of HCl (0.02 cm^3, 2.44 N, 0.048 mmol). After stirring for 30 min, the solvent was stripped off and the residue was dissolved in $CDCl_3$. The resulting solution was studied by ^{31}P NMR spectroscopy.

Crystallography

All measurements for $[Pd_2Cl_2\{\mu\text{-PhNC(Me)NPh}\}_2(PMe_2Ph)_2]$ (**10**) were made at $20 \pm 2°C$ on a Rigaku AFC 6S diffractometer using graphite monochromated Mo–Kα radiation ($\lambda = 0.71073$ Å). The crystallographic data together with data collection and structure refinement details are given in Table 7. The numbering scheme employed is shown in Fig. 2 drawn with the ORTEP program [33]. All the data were corrected for Lorentz and polarization effects. The structure was solved by a combination of the Patterson method and direct methods [34] and refined by full-matrix least-squares on F^2. Neutral atom scattering factors were taken from Cromer and Waber [35]. Anamolous dispersion effects were included in F_{calc} [36]. The values of $\Delta f'$ and $\Delta f''$ were those of Cromer [37]. All calculations were performed using the TEXSAN [38] crystallographic software package of the Molecular Structure Corporation.

The crystal data for the complex $[Pt_2Cl_2\{\mu\text{-PhNNNPh}\}_2(PEt_3)_2]$ (**11**) were collected on an Enraf Nonius CAD-4 with monochromated MoKα. Three check reflections were measured for every 100 reflections; these showed no decay in intensity during the period of data collection. The structure was solved by Patterson and full matrix least squares refinement on F_o using SHELX -76 [39]. The refinement was carried out first with isotropic thermal parameters and subsequently with anisotropic thermal parameters for all non-hydrogen atoms. The scattering factors for Pt were taken from International tables for X-ray crystallography [35] and the absorption corrections were made using Psi data [40].

Acknowledgements—We thank Drs. J.P. Mittal and C. Gopinathan for encouragement of this work. We are grateful to

Table 7. Crystal data and structure refinement details for $[Pd_2Cl_2\{\mu\text{-PhNC(Me)NPh}\}_2(PMe_2Ph)_2]$ (10) and $[Pt_2Cl_2\{\mu\text{-PhNNNPh}\}_2(PEt_3)_2]$ (11)

	10	11
Empirical Formula	$C_{44}H_{48}Cl_2N_4P_2Pd_2$	$C_{36}H_{50}Cl_2N_6P_2Pt_2$
Formula Weight	978.50	1089.87
Temperature	293(2) K	293 K
Wavelength	0.71073 Å	0.7107 Å
Crystal System	Monoclinic	Monoclinic
Space group	$P2_1/c$	C2/c
Unit cell dimensions	a = 12.158(6) Å b = 19.490(7) Å c = 19.290(8) Å β = 90.49(2)°	a = 23.028(1) Å b = 9.834(3) Å c = 19.066(1) Å β = 109.32(3)°
Volume	4571(3) Å^3	4074(1) Å^3
Z	4	4
Density	1.422 Mg/m^3	1.7767 g/cm^3
Absorption coefficient	1.007 mm^{-1}	71.73 cm^{-1}
F(000)	1984	2112
Crystal Size	0.47 × 0.32 × 0.17 mm	0.4 × 0.3 × 0.25 mm
θ range for data collection	2.09 to 27.50^0	$2 \leqslant 2\theta \leqslant 50°$
Index ranges	$0 \leqslant h \leqslant 15$, $0 \leqslant k \leqslant 25, -25 \leqslant l \leqslant 25$	$0 \leqslant h \leqslant 24$, $0 \leqslant k \leqslant 10$, $-20 \leqslant l \leqslant 20$
Reflections collected	10912	4125
Independent reflections	10427 (R_{int} = 0.0337)	3582 (R_{int} = 0.042)
Absorption correction	SHELXA	Empirical
Max. and min. transmission	0.927 and 0.383	1.277 and 0.899
Refinement method	Full-matrix least-squares on F^2	Full-matrix least squares on $\|F_0\|$
Data/restraints/parameters	10419/0/494	2999/0/163
Goodness-of-fit on F^2	1.018	1.2102
Final R indices [$I > 2\sigma(I)$]	R1 = 0.0652, wR2 = 0.0756	R1 = 0.0346, wR2 = 0.0399
R indices (all data)	R1 = 0.1644, wR2 = 0.2996	—
Extinction coefficient	0.00019(5)	—
Largest diff. peak and hole	0.664 and −0.656 eÅ^{-3}	1.2 and −1.1 eÅ^{-3}

the Head of the Analytical Chemistry Division BARC, for providing microanalyses for the complexes.

REFERENCES

1. Jain, V. K., Patel, R. P. and Venkatasubramanian, K., *Polyhedron*, 1991, **10**, 265; Jain, V. K. and Kannan, S., *J. Organomet. Chem.*, 1991, **418**, 349; Jain, V. K. and Kannan, S., *Polyhedron*, 1992, **11**, 27; Jain, V. K., Kannan, S. and Bohra, R., *Polyhedron*, 1992, **11**, 1551; Jain, V. K. and Kannan, S., *J. Organomet. Chem.*, 1992, **439**, 231; Jain, V. K., Kannan, S., Butcher, R. J. and Jasinski, J. P., *J. Chem. Soc. Dalton Trans.*, 1993, 1509; Singhal, A. and Jain, V. K., *J. Chem. Soc., Dalton Trans.*, 1993, 1515; Singhal, A. and Jain, V. K., *J. Organomet. Chem.*, 1995, **494**, 74.
2. Kannan, S. and Jain, V. K., *Mag, Res. Chem.*, 1990, **28,** 1007.
3. Singhal, A. and Jain, V. K., *Polyhedron*, 1995, **14,** 285.
4. Singhal, A. and Jain, V. K., *Can. J. Chem.*, 1996, **74,** 2018.
5. Jain, V. K., *Trans. Met. Chem.*, 1996, **21,** 494.
6. Cotton, F. A., Matusz, M. and Poli, R., Feng, X., *J. Am. Chem. Soc.*, 1988, **110,** 1144.
7. Patai, S. (Editor) *The Chemistry of Amidines and Imidates*, 1991, Vol. 2, Wiley, New York.
8. Barker, J. and Kilner, M., *Coord. Chem. Rev.*, 1994, **133,** 219.
9. Berno, P., Hao, S., Minhas, R. and Gambarotta, S., *J. Am. Chem. Soc.*, 1994, **116,** 7417.
10. Zhuo, Y. and Richeson, D. S., *Organometallics*, 1995, **14,** 3558.
11. Edelmann, F. T., Ziegler, W. and Behrens, U., *J. Organomet. Chem.*, 1992, **426,** 261.
12. Boyad, D. C., Connelly, N. G., Herbosa, G. G., Hill, M. G., Kann, K. R., Mealli, C., Orpen, A. G., Richardson, K. E. and Rieger, P. H., *Inorg. Chem.*, 1994, **33,** 960.

13. Cotton, F. A., Matonic, J. H. and Murillo, C. A., *Inorg. Chem.*, 1996, **35,** 498.
14. Frusson, E., Panattoni, C. and Sacconi, L., *Acta. Crystallogr.*, 1964, **17,** 85.
15. Clark, G. R., Palenik, L. L. and Meek, D. W., *J. Am. Chem. Soc.*, 1970, **92,** 1077.
16. Barker, J., Kilner, M. and Gould, R. O., *J. Chem. Soc., Dalton Trans.*, 1987, 2687.
17. Jain, V. K., Patel, R. P., Muralidharan, K. V. and Bohra, R., *Polyhedron*, 1989, **8,** 2151.
18. Jain, V. K., Kannan, S. and Tiekink, E. R. T., *J. Chem. Soc., Dalton Trans.*, 1992, 2231.
19. Hendriks, P., Olie, K. and Vrieze, K., *Cryst. Structure. Commun.*, 1975, **4**, 611; *Chem. Abst.*, 1976, **84**, 52479.
20. DeSanctis, S. C., Pavel, N. V. and Toniolo, L., *J. Organomet. Chem.*, 1976, **108,** 409.
21. Churchill, M. R., *Nature* (*London*), 1964, **204,** 777.
22. Oberhansli, W. E. and Dahl, L. F., *J. Organomet. Chem.*, 1965, **3,** 43.
23. Ng, W. W., Cheng, P. T., Kocman, V., Luth, L. and Nyburg, S. C., *Inorg. Chem.*, 1979, **18,** 2620.
24. Yamamoto, J. H., Yoshida, W. and Jensen, C. M., *Inorg. Chem.*, 1991, **30,** 1353.
25. Gupta, M., Cramer, R. E., Ho, K., Pettersen, C., Mishina, S., Belli, J. and Jensen, C. M., *Inorg. Chem.*, 1995, **34,** 60.
26. Novoa, J. J., Aullon, G., Alemany, P. and Alvarez, S., *J. Am. Chem. Soc.*, 1995, **117,** 7169.
27. Aullon, G., Alemany, P. and Alvarez, S., *Inorg. Chem.*, 1996, **35,** 5061.
28. Aullon, G. and Alvarez, S., *Chem. Eur. J.*, 1997, **3,** 655.
29. Meali, C. and Prosperio, D. M., *J. Chem. Educ.*, 1990, **67,** 399.
30. Aullon, G. and Alvarez, S., *Inorg. Chem.*, 1996, **35,** 3137.
31. Taylor, E. C. and Ehrhart, W. A., *J. Org. Chem.*, 1963, **28,** 1108.
32. Hartley, F. R., *The Chemistry of platinum and palladium*, Applied Science Publishers Ltd. London, (1973).
33. Johnson, C. K., ORTEP II, Report ORNL-5138 Oak Ridge National Laboratory, Oak Ridge, TN, (1976).
34. Calabrese, J. C. Ph.D., Thesis, University of Wisconsin, Madison (1972); Beueskens, P. T. (1984/1) Technical Report Crystallography Laboratory, Toernooiveld 6525 Ed, Nijimegien, The Netherlands.
35. Cromer, D. T. and Waber, J. T., International Tables for X-ray Crystallography, Vol 4, Table 2.2. A. Kynoch Press, Bermingham, (1974).
36. Ibers, J. A. and Hamilton, W. C., *Acta. Cryst.*, 1964, **17,** 781.
37. Cromer, D. T., International Tables for X-ray Crystallography, Vol. 4, Table 2.3.1, Kynoch Press, Bermingham, (1974).
38. TEXSAN, Structure Analysis Package, Molecular Structure Corporation, 1985.
39. Sheldrick, G. M., SHELX-76 Program for crystal structure determinations, University of Cambridge, 1976.
40. North, A. C. T., Philips, D. C. and Mathews, F. S., *Acta. Cryst A*, 1968, **24,** 351.

Pergamon

PII: S0277-5387(98)00145-4

Polyhedron Vol. 17, No. 20, pp. 3541–3550, 1998
© 1998 Elsevier Science Ltd
All rights reserved. Printed in Great Britain
0277–5387/98 $19.00+0.00

Structures, electrochemical and spectroscopic properties of ternary ruthenium(II)-polypyridyl complexes with additional carboxylate, biguanide or sulfonamide donors

Samantha M. Couchman, José M. Dominguez-Vera, John C. Jeffery, Colin A. McKee, Simon Nevitt, Matthias Pohlman, Claire M. White and Michael D. Ward*

School of Chemistry, University of Bristol, Cantock's Close; Bristol, BS8 1TS, U.K.

(Received 16 February 1998; accepted 17 April 1998)

Abstract—The following complexes have been prepared: $[Ru(bipy)_2(pic)][PF_6]$ (bipy = 2,2′-bipyridine; Hpic = picolinic acid); [Ru(terpy)(dipic)] (terpy = 2,2′:6′,2″-terpyridine; H_2dipic = dipicolinic acid); $[Ru(bipy)_2(Hbig)][PF_6]_2$ (Hbig = biguanide); and $[Ru(bipy)_2(apps)][PF_6]$ [where Happs is the *p*-tolylsulfonamide of 2-(2-aminophenyl)-pyridine]. The latter three have been characterised by X-ray crystallography and are all mononuclear pseudo-octachedral complexes. Electrochemical studies reveal the relationship between the potential of the metal-based Ru(II)/Ru(III) couple, with the potential values being clearly related to the σ-donor or π-acceptor capabilities of the ligands. The energies of the lowest-energy m.l.c.t. maxima in the electronic spectra also correlate with ligand properties. $[Ru(bipy)_2(Hbig)][PF_6]_2$, which has a dissociable proton on the biguanide ligand, undergoes deprotonation in strongly basic conditions ($pK_a = 12.3 \pm 0.2$), which results in a red-shift of the m.l.c.t. transition consistent with weakening of the ligand field due to the increased π-donor capability of the deprotonated ligand. © 1998 Elsevier Science Ltd. All rights reserved

Keywords: ruthenium complexes; electrochemistry; crystal structures.

INTRODUCTION

We [1–3] and others [4, 5] have been interested in studying the properties of ruthenium complexes with a variety of ligand donor sets. One impetus for this is the particularly clear correlations which can be observed between electrochemical properties and ligand donor set [1, 4]. Another is the widespread use of redox-active ruthenium fragments as components of polynuclear complexes linked by conjugated bridging ligands, in which inter-valence charge transfer is studied as a model for electron transport in molecular wires [6]. The kinetic stability of ruthenium in several different oxidation states (particularly +2 and +3), the often reversible nature of the +2/+3 couple, and the relative ease with which mixed-ligand complexes can be prepared by controllable stepwise methods, all make ruthenium complexes particularly attractive targets of study.

We describe here the syntheses and the electrochemical and electronic spectroscopic properties of four mononuclear complexes of ruthenium(II) with mixed donor sets. These complexes are $[Ru(bipy)_2(pic)][PF_6]$ (bipy = 2,2′-bipyridine; Hpic = pyridine-2-carboxylic acid, also known as picolinic acid); [Ru(terpy)(dipic)] (terpy = 2,2′:6′,2″-terpyridine; H_2dipic = pyridine-2,6-dicarboxylic acid, also known as dipicolinic acid); $[Ru(bipy)_2(Hbig)][PF_6]_2$ (Hbig = biguanide); and $[Ru(bipy)_2(apps)][PF_6]$ [where Happs is the *p*-tolylsulfonamide of 2-(2-aminophenyl) pyridine]. The ligands are shown below; the latter three complexes have been crystallographically characterised. The complexes $[Ru(bipy)_2(pic)][PF_6]$ [7, 8] and [Ru(terpy)(dipic)] [9] were both reported very recently while this work was in progress but have not been directly compared.

* Author to whom correspondence should be addressed.

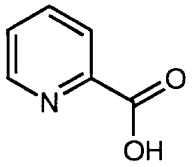

Hpic

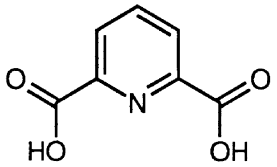

H_2dipic

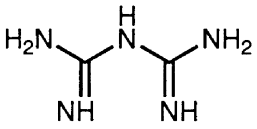

Hbig

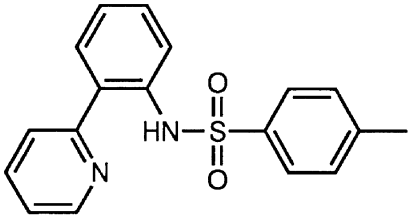

Happs

EXPERIMENTAL

General details

$[Ru(bipy)_2Cl_2]\cdot 2H_2O$ [10], $[Ru(terpy)Cl_3]$ [11], biguanide [12], Happs [13] and $[Ru(bipy)_2(pic)][PF_6]$ [7, 8] were prepared according to the published procedures. Dipicolinic acid was obtained from Aldrich and used as received. Instrumentation used for routine spectroscopic and electrochemical analyses has been described in earlier papers [1, 2].

Preparations

[*Ru*(*terpy*)(*dipic*)]. A mixture of dipicolinic acid (15.2 mg, 0.09 mmol) and Na_2CO_3 (20 mg, 0.18 mmol) was dissolved in water and heated to reflux. [Ru(terpy)Cl_3] (40 mg, 0.09 mmol) was then added and the mixture heated to reflux for a further 5 hours, during which time a purple solid precipitated and the supernatant solution became green. The solid was filtered off, washed with water, and air-dried to give [Ru(terpy)(dipic)] in 65% yield. X-ray quality crystals were grown by diffusion of diethyl ether vapour into a saturated solution of the complex in dmf. Found: C, 49.0; H, 3.5; N, 10.4%. Required for $C_{22}H_{14}N_4O_4Ru\cdot H_2O$: C, 49.3; H, 3.4; N, 10.5%. The complex is not sufficiently volatile to give a good mass spectrum.

$[Ru(bipy)_2(Hbig)][PF_6]_2$. A mixture of $[Ru(bipy)_2Cl_2]\cdot 2H_2O$ (0.130 g, 0.25 mmol) and Hbig (0.029 g, 0.29 mml) in dry ethanol (15 cm^3) was heated to reflux under N_2 for 4 hours to give a purple solution. After cooling, aqueous KPF_6 was added and the mixture was concentrated *in vacuo* until a purple precipitate appeared. This was collected by filtration and dried to give $[Ru(bipy)_2(Hbig)][PF_6]_2$ in 80% yield. Recystallisation from MeCN/ether afforded X-ray quality crystals. Found: C, 33.8; H, 3.0; N, 16.5%. Required for $C_{22}H_{23}F_{12}N_9P_2Ru\cdot MeCN$: C, 34.1; H, 3.1; N, 16.6%. Electrospray MS: *m*/*z* 513 [50%, $\{Ru(bipy)_2(big)\}^+$]. ^{1}H NMR (300 MHz, CD_3CN): δ 8.92 (2 H, d, *J* 5.5), 8.43 (2 H, d, *J* 7.9), 8.34 (2 H, d, *J* 7.9), 8.08 (2 H, td, *J* 7.9, 1.5), 7.83 (2 H, td, *J* 7.9, 1.5), 7.66 (4 H, m), 7.17 (2 H, ddd, *J* 7.5, 5.7, 1.3 Hz), 5.64 (*ca.* 1 H, br s, NH), 5.02 (*ca.* 2 H, br s, NH).

$[Ru(bipy)_2(apps)][PF_6]$. A solution of $[Ru(bipy)_2(H_2O)_2]^{2+}$ (0.16 mmol) was generated by reaction of $[Ru(bipy)_2Cl_2]\cdot 2H_2O$ (84 mg, 0.16 mmol) with $AgNO_3$ (2 equiv.) in $EtOH/H_2O$ (1:1, 30 cm^3) at reflux for 1 hour, followed by removal of the AgCl by filtration. To this was added Happs (50 mg, 0.16 mmol) and the mixture was refluxed with stirring for a further 1 h. Addition of aqueous KPF_6 precipitated a solid which was collected by filtration and dried. The crude product was purified by chromatography on silica with $MeCN/H_2O$/saturated aqueous KNO_3 (14:2:1) as eluent. The main deep red/purple band was collected, the solution concentrated *in vacuo*, and the product precipitated by addition of aqueous KPF_6. Filtration and drying *in vacuo* afforded pure $[Ru(bipy)_2(apps)][PF_6]$ in 70% yield. Recrystallisation from CH_2CI_2/hexane afforded X-ray quality crystals. Found: C, 49.0; H, 3.4; N, 8.3%. Required for $C_{38}H_{31}F_6N_6O_2PRuS\cdot CH_2Cl_2$: C, 48.5; H, 3.4; N, 8.7%. FAB MS: *m*/*z* 737 [80%, $\{Ru(bipy)_2(apps)\}^+$].

X-ray crystallography

Suitable crystals were quickly transferred from the mother liquor to a stream of cold N_2 at -100°C on a Siemens SMART diffractometer fitted with a CCD-type area detector. In all cases data were collected at -100°C to a 2θ limit of 55° using graphite-monochromatised Mo–Kα radiation. A detailed experi-

mental description of the methods used for data collection and integration using the SMART system has been published [14]. Table 1 contains a summary of the crystal parameters, data collection and refinement. Empirical absorption corrections were applied to the datasets using SADABS [15]. The structures were solved by conventional heavy-atom or direct methods and refined by the full-matrix least-squares method on all F^2 data using the SHELXTL 5.03 package on a Silicon Graphics Indy computer [16]. Non-hydrogen atoms were refined with anisotropic thermal parameters; hydrogen atoms were included in calculated positions and refined with isotropic thermal parameters riding on those of the parent atom. The structural determinations of $[Ru(bipy)_2(Hbig)][PF_6]_2 \cdot MeCN$ and $[Ru(bipy)_2(apps)][PF_6] \cdot CH_2Cl_2$ were straightforward and presented no particular problems; the only point to note is that in $[Ru(bipy)_2(Hbig)][PF_6]_2 \cdot MeCN$ the asymmetric unit contains two crystallographically independent molecules of the complex and two molecules of MeCN.

Crystals of $[Ru(terpy)(dipic)] \cdot H_2O \cdot Et_2O$ were very thin plates (those used had a thickness of 0.02 mm) and therefore diffracted rather weakly. Only data to a 2θ limit of 50° was used in the final refinement, as no significant diffracted intensity was observed between 50° and 55°, and inclusion of the higher-angle data only increased the R indices with no concomitant improvement in the precision of the structure. The molecule lies on a C_2 axis which passes through C(24), N(21), Ru(1), N(31) and C(34); there are therefore 16 complete molecules in the *F*ddd unit cell which has 32 general positions. Each asymmetric unit contained one half of the complex molecule, one half of a water molecule (the oxygen atom also being on a special position), and a badly disordered solvent molecule around the intersection of two C_2 axes. This could only be modelled by putting carbon atoms at the sites of maximum electron density and allowing the site occupancies to refine. The result was approximately 2.5 atoms, which we assume corresponds to half a disordered ether molecule in the asymmetric unit *per* half complex molecule and half solvent molecule, i.e. $[Ru(terpy)(dipic)] \cdot H_2O \cdot Et_2O$. Hydrogen atoms were not included in the refinement for the disordered solvent molecule.

RESULTS AND DISCUSSION

Synthesis of and crystal structure of [*Ru*(*terpy*)(*dipic*)]

Preparation and purification of this complex was straightforward and it was isolated cleanly in good yield. It is only very sparingly soluble in dmf and dmso, and insoluble in other solvents, so a good mass spectrum could not be obtained. Attempts to obtain NMR spectra were likewise unsuccessful, due to a

Table 1. Crystallographic data for the new complexes

Compound	$[Ru(terpy)(dipic)] \cdot H_2O \cdot Et_2O$	$[Ru(bipy)_2(Hbig)][PF_6]_2 \cdot MeCN$	$[Ru(bipy)_2(apps)][PF_6] \cdot CH_2Cl_2$
Formula	$C_{26}H_{26}N_4O_6Ru$	$C_{24}H_{26}F_{12}N_{10}P_2Ru$	$C_{39}H_{33}Cl_2F_6N_6O_2PRuS$
M	591.58	845.56	966.71
System, space group	Orthorhombic, *F*ddd	Triclinic, $P\bar{1}$	Monoclinic, $P2_1/c$
$a/Å$	8.746(2)	11.4390(13)	8.8815(9)
$b/Å$	19.897(4)	14.548(2)	19.903(2)
$c/Å$	53.914(12)	19.712(2)	22.857(5)
$\alpha/°$	90	80.698(9)	90
$\beta/°$	90	76.701(7)	94.27(2)
$\gamma/°$	90	88.174(8)	90
$U/Å^3$	9382(4)	3150.3(6)	4029.3(10)
Z	16	4	4
$D_c g\ cm^{-3}$	1.675	1.783	1.594
μ/mm^{-1}	0.721	0.707	0.685
$F(000)$	4832	1688	1952
Crystal size/mm	$0.50 \times 0.50 \times 0.02$	$0.4 \times 0.3 \times 0.1$	$0.5 \times 0.2 \times 0.1$
Reflections collected: total, independent, R_{int}	18750, 2076, 0.0810	32358, 14196, 0.0278	25509, 9224, 0.0446
2θ limits for data,°	3–50	3–55	3–55
Data, restraints, parameters	2071, 0, 184	14196, 0, 885	9224, 0, 534
Final R_1, wR_2[a,b]	0.0548, 0.1475	0.0342, 0.0907	0.0407, 0.1001
Weighting factors (a,b)[b]	0.0886, 2.0184	0.0497, 0	0.0459, 0.9476
Largest peak, hole /e $Å^{-3}$	+1.572, −1.181	+1.117, −0.687	+0.700, −0.863

[a]Structure was refined on F_0^2 using all data; the value of R_1 is given for comparison with older refinements based on F_o with a typical threshold of $F \geq 4\sigma(F)$.

[b] $wR_2 = [\Sigma[w(F_0^2 - F_c^2)^2]/\Sigma w(F_0^2)^2]^{1/2}$ where $w^{-1} = [\sigma^2(F_0^2) + (aP)^2 + bP]$ and $P = [\max(F_0^2, 0) + 2F_c^2]/3$.

combination of poor solubility and the ease with which it oxidises in solution to the paramagnetic Ru(III) state (see below). However the elemental analysis and crystal structure (below) provide unambiguous characterisation.

[Ru(terpy)(dipic)] (Fig. 1, Table 2) has the expected pseudo-octahedral structure, with a *trans*-N_4O_2 donor set. The terpy ligand shows the usual pattern of Ru–N bond lengths, with a short bond to the central atom [Ru(1)–N(21), 1.964(5) Å] and longer ones to the terminal two atoms [Ru(1)–N(11)/N(11A), 2.060(5) Å], which arise from the steric limitations of the terpyridyl ligand [17]. The dipicolinate ligand behaves similarly for the same steric reasons, with the two Ru–O bonds being significantly longer than the four Ru–N bonds, and the localisation of single and double C–O bond character being apparent in the two carboxylate fragments [7, 8]. The presence of two anionic σ-donor ligands on the same axis *trans* to one another has not resulted in any significant lengthening of the Ru–O bonds compared to those complexes with N_5O donor sets where a carboxylate donor is *trans* to a pyridyl ring, as in $[Ru(bipy)_2(pic)][PF_6]$ [8] and $[Ru(bpy\text{-}CO_2)_2]$ (where bpy-CO_2H is 2,2′-bipyridine-6-carboxylic acid) [7]. The non-coordinated oxygen atom O(36) is hydrogen-bonded to the lattice water molecule, with the non-bonded O(36)···O(water) separation being 2.91 Å, typical of O–H···O hydrogen-bonding.

Synthesis and crystal structure of $[Ru(bipy)_2(Hbig)][PF_6]_2$

Although complexes of first-row transition metal ions with biguanide have been known for a long time [18–24], there are no reports of any complexes with ruthenium. As a bidentate ligand with two unsaturated (formally sp^2-hybridised) N-donors there is an obvious similarity with other diimines such as 2,2′-bipyridine (bipy). A notable property of biguanide is that it can coordinate in either the neutral form (Hbig) or in the deprotonated form $[big]^-$ with a delocalised structure reminiscent of the acetylacetonate anion [18], and crystal structures of both types of complex are known.

Reaction of $[Ru(bipy)_2Cl_2]$ with Hbig in refluxing ethanol, followed by precipitation of the complex as its hexafluorophosphate salt and recrystallisation, afforded in high yield a material whose elemental analysis was consistent with the formulation $[Ru(bipy)_2(Hbig)][PF_6]_2$. This implies that the biguanide ligand is neutral, rather than coordinating in the anionic deprotonated form which would have given $[Ru(bipy)_2(big)][PF_6]$ with only one hexafluorophosphate anion and a substantially different elemental analysis. The ES mass spectrum confirmed the presence of the expected complex cation, and the structure was finally confirmed by X-ray crystallography (Figure 2, Table 2).

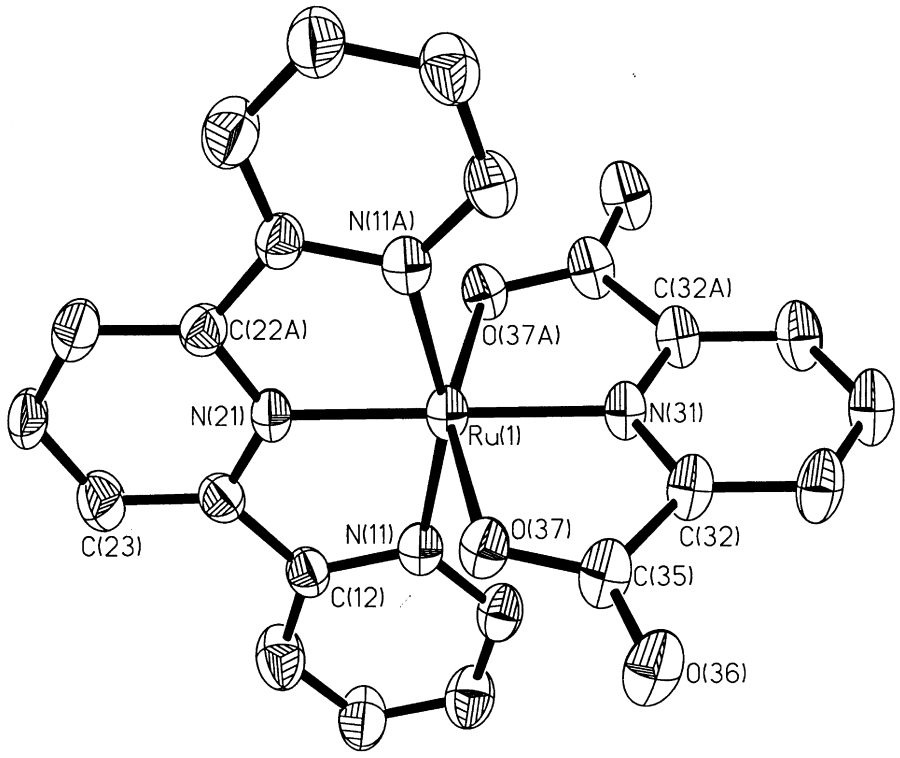

Fig. 1. Crystal structure of [Ru(terpy)(dipic)].

Table 2. Selected bond lengths (Å) and angles (°) for the three crystal structures

[Ru(terpy)(dipic)]·H_2O·0.5Et_2O		[Ru(bipy)$_2$(Hbig)[PF_6]$_2$·MeCN		[Ru(bipy)$_2$(apps)[PF_6]·CH_2Cl_2	
Ru–N(21)	1.964(5)	Ru–N(111)	2.046(2)	Ru–N(21)	2.058(3)
Ru–N(31)	1.979(6)	Ru–N(141)	2.046(2)	Ru–N(31)	2.060(2)
Ru–N(11A)	2.060(5)	Ru–N(121)	2.050(2)	Ru–N(11)	2.061(3)
Ru–N(11)	2.060(5)	Ru–N(131)	2.063(2)	Ru–N(41)	2.063(2)
Ru–O(37A)	2.111(3)	Ru–N(156)	2.067(2)	Ru–N(51)	2.099(3)
Ru–O(37)	2.111(3)	Ru–N(151)	2.070(2)	Ru–N(60)	2.141(3)
N(21)–Ru–N(31)	180.0	N(111)–Ru–N(141)	90.62(8)	N(21)–Ru–N(31)	82.44(10)
N(21)–Ru–N(11A)	79.61(12)	N(111)–Ru–N(121)	78.94(9)	N(21)–Ru–N(11)	78.86(10)
N(31)–Ru–N(11A)	100.39(12)	N(141)–Ru–N(121)	96.58(9)	N(31)–Ru–N(11)	100.10(10)
N(21)–Ru–N(11)	79.60(12)	N(111)–Ru–N(131)	96.27(8)	N(21)–Ru–N(41)	94.63(10)
N(31)–Ru–N(11)	100.40(12)	N(141)–Ru–N(131)	78.84(9)	N(31)–Ru–N(41)	78.57(10)
N(11A)–Ru–N(11)	159.2(2)	N(121)–Ru–N(131)	173.41(9)	N(11)–Ru–N(41)	173.48(10)
N(21)–Ru–O(37A)	101.29(9)	N(111)–Ru–N(156)	173.56(9)	N(21)–Ru–N(51)	100.26(10)
N(31)–Ru–O(37A)	78.71(9)	N(141)–Ru–N(156)	92.48(8)	N(31)–Ru–N(51)	175.02(10)
N(11A)–Ru–O(37A)	88.7(2)	N(121)–Ru–N(156)	95.09(8)	N(11)–Ru–N(51)	84.58(10)
N(11)–Ru–O(37A)	95.4(2)	N(131)–Ru–N(156)	89.87(8)	N(41)–Ru–N(51)	96.97(10)
N(21)–Ru–O(37)	101.29(9)	N(111)–Ru–N(151)	91.40(8)	N(21)–Ru–N(60)	172.49(9)
N(31)–Ru–O(37)	78.71(9)	N(141)–Ru–N(151)	174.09(9)	N(31)–Ru–N(60)	93.96(9)
N(11A)–Ru–O(37)	95.4(2)	N(121)–Ru–N(151)	89.26(9)	N(11)–Ru–N(60)	95.37(10)
N(11)–Ru–O(37)	88.7(2)	N(131)–Ru–N(151)	95.42(9)	N(41)–Ru–N(60)	91.09(9)
O(37A)–Ru–O(37)	157.4(2)	N(156)–Ru–N(151)	86.07(9)	N(51)–Ru–N(60)	83.83(10)

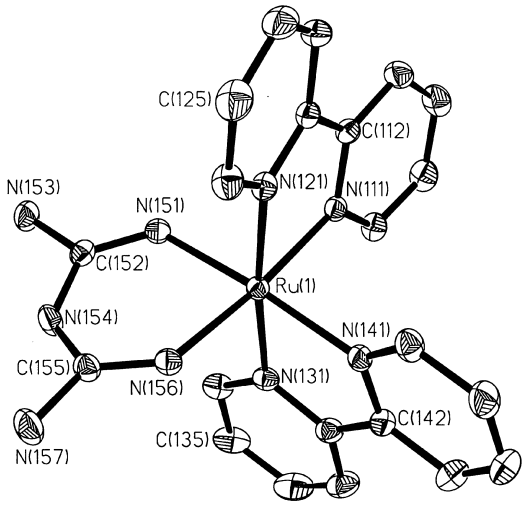

Fig. 2. Crystal structure of the cation of [Ru(bipy)$_2$(Hbig)][PF_6]$_2$.

The asymmetric unit contains two independent [Ru(bipy)$_2$(Hbig)][PF_6]$_2$·MeCN groups. Figure 2 shows one of the independent complex cations; the structure of the alternate one is very similar. It has the expected octahedral structure with unremarkable bond lengths and angles in the coordination sphere. There is no sign of any significant *trans* effect, as the Ru–N(pyridyl) bonds *trans* to the biguanide donor atoms are very similar to the other two. The Ru–N(biguanide) distances are consistent with the N atoms being sp^2-hybridised. Two geometric features of the coordinated biguanide ligands are worth a comment. Firstly, the angle at the central N atom, C(155)–N(154)–C(152), is 129.0(2)° [129.1(3)° at N(254) in the independent complex dication]. This is consistent with the ligand being in the neutral Hbig form, with steric repulsion between the two bulky arms attached to the central N atom resulting in the C–N–C angles being considerably "opened out"; [20, 21] when the ligand is deprotonated, the increased delocalisation throughout the chelate ring results in these C–N–C angles being much closer to the ideal 120° [20, 22, 24]. Secondly, the Ru atom is not quite in the same plane as the (near-planar) biguanide ligand; the angle between the mean plane of the five ligand atoms in the chelate ring [N(151), C(152), N(154), C(155), N(156)] and the RuN_2 coordination plane [Ru(1), N(151), N(156)] is 6.9° in the cation depicted (9.2° for the independent complex dication). This is again a common, but not consistent, feature of biguanide complexes [20, 21].

The solution ^{1}H NMR spectrum showed the presence of the expected 8 aromatic proton environments (relative intensity 2 H each) for the bipyridyl ligands, which are equivalent but within which the two pyridyl rings are inequivalent. Two broad singlets at 5.02 and 5.65 ppm we assign to NH protons, but the integrals are rather low, presumably due to exchange with pro-

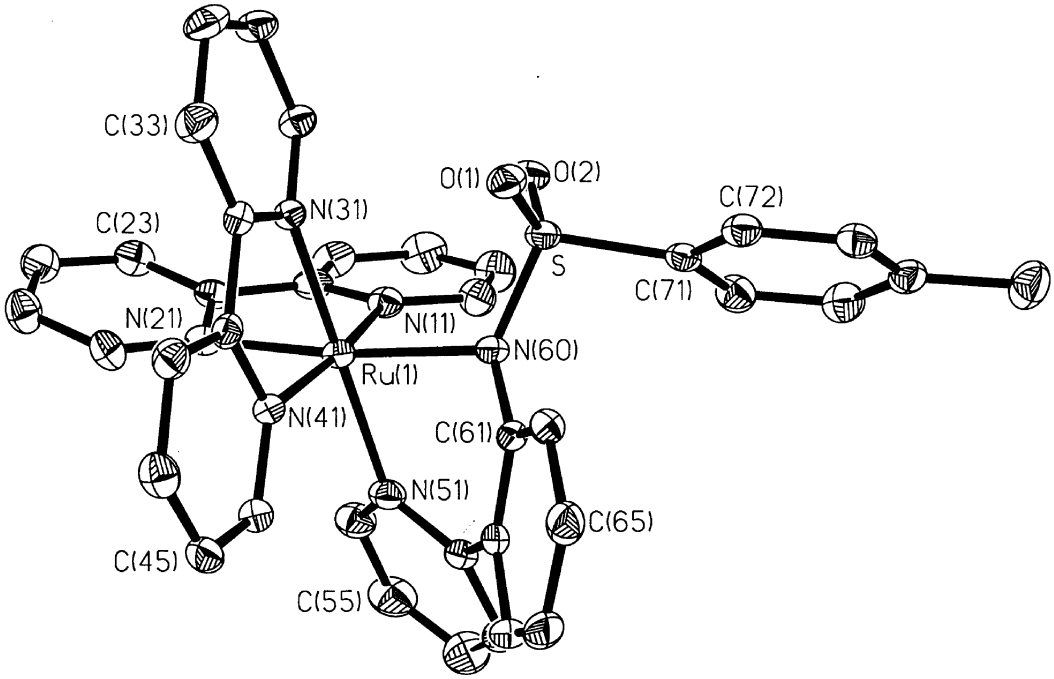

Fig. 3. Crystal structure of the cation of $[Ru(bipy)_2(apps)][PF_6]$.

tons in the moisture that is present in the solvent. We would expect three different NH proton environments on the basis of the crystal structure, so we assume that the most acidic proton (the central NH) is in fast exchange with the H_2O protons and the signal for this is therefore invisible.

Synthesis and crystal structure of $[Ru(bipy)_2(apps)][PF_6]$.

We recently reported the synthesis of Happs, a bidenatate chelating ligand with one pyridyl and one sulfonamide donor, and the crystal structures of some of its complexes [13]. The new complex $[Ru(bipy)_2(apps)][PF_6]$, with five pyridyl ligands and one anionic sulfonamide ligand, was simply prepared by reaction of Happs with the labile complex $[Ru(bipy)_2(H_2O)]^{2+}$; we found that this gave a cleaner product than that obtained from the reaction of Happs directly with $[Ru(bipy)_2Cl_2]$. The elemental analysis and FAB mass spectrum confirmed the formulation of the complex. The ^1H NMR spectrum in MeCN gave the correct ratio of integrals for the aromatic and aliphatic (methyl) protons, but the 28 inequivalent aromatic protons occurred in an overlapping mass between 6.5 amd 8.5 ppm which could not be individually assigned.

The crystal structure (Figure 3, Table 2) shows that the usual octahedral structure has been adopted despite the bulky and sterically hindering nature of the *p*-tolyl-sulfonamide fragment. There is an interaction between O(1) of the sulfonamide group and one of the pyridyl rings, with a distance of 3.11 Å between O(1) and the mean plane of this pyridyl ring. This appears to lengthen the Ru–N bonds to the apps ligand, as Ru–N(51) is the longest of the Ru–N(pyridyl) bonds at 2.099(3) Å, and the Ru–N(sulfonamide) distance [2.141(3) Å] is even longer. This contrasts with the four-coordinate, relatively unhindered, complexes of the same ligand with Cu(II), Co(II) and Pd(II) in which the metal-N(sulfonamide) bonds were shorter than, or about the same length as, the metal-N (pyridyl) bonds [13].

Electrochemical properties of $[Ru(bipy)_2(pic)][PF_6]$ *and* $[Ru(terpy)(dipic)]$

Cyclic voltammetry in dmf showed that $[Ru(bipy)_2(pic)][PF_6]$ has a reversible one-electron wave at $+0.40$ V *vs.* the ferrocene/ferrocenium couple (Fc/Fc^+), corresponding to a metal-centred Ru(II)/Ru(III) couple, and two reversible one-electron waves at -1.87 and -2.12 V *vs.* Fc/Fc^+, corresponding to ligand-centred processes (electrochemical data are collected in Table 3). By "reversible" is meant that the waves were symmetric (equal cathodic and anodic peak currents), with peak-peak separations in the

Table 3. Electronic spectral and electrochemical data for the complexes. The maxima of the lowest-energy m.l.c.t. transitions are in bold type

Complex	λ_{max} (nm) [$10^{-3}\epsilon$ ($dm^3\ mol^{-1}\ cm^{-1}$)]	Cyclic voltammetric data [$E_{1/2}$ V *vs.* Fc/Fc^+]	
$[Ru(bipy)_2(pic)][PF_6]$	**495** (**14**), 455 (sh), 369 (13), 295 (78)[a]	+0.40	−1.87, −2.12[a]
[Ru(terpy)(dipic)]	660 (sh), 595 (sh), **532** (**8.3**), 393 (10.6), 323 (27), 279 (24)[a]	+0.12	−2.01[a]
$[Ru(bipy)_2(Hbig)][PF_6]_2$	**504** (**4.9**), 360 (6.0), 340 (6.0), 292 (40), 244 (25)[b]	+0.21[c]	
$[Ru(bipy)_2(apps)][PF_6]$	560 (sh), **494** (**3.5**), 333 (6.6), 297 (28)[a]	+0.20	−1.91[c]

[a]In dmf; [b]in H_2O; [c]in MeCN.

region of 60–100 mV, at a range of scan rates. These results agree well with recently reported values of +0.88, −1.43 and −1.68 V *vs.* SCE in acetonitrile [7].

The Ru(II)/Ru(III) couple of $[Ru(bipy)_3][PF_6]_2$ under the same conditions is +0.89 V *vs.* Fc/Fc^+, so replacement of a neutral pyridyl ligand by an anionic carboxylate therefore stabilises the Ru(III) state by 490 mV. This may be compared with the 860 mV stabilisation of the Ru(III) state which occurs on replacing a pyridyl residue of $[Ru(bipy)_3]^{2+}$ with a phenolate group in $[Ru(bipy)_2(no)][PF_6]$ [Hno is 2-(2-hydroxyphenyl)pyridine], which also has a N_5O donor set containing one anionic oxygen donor [1]. The comparison of $[Ru(bipy)_2(pic)]^+$ with $[Ru(bipy)_2(no)]^+$ allows us to cancel out the electrostatic part of the stabilisation of the Ru(III) state which arises just as a consequence of reducing the overall charge on the complex from +2 to +1, which will be common to both complexes. The fact that a phenolate donor results in a cathodic shift of the Ru(II)/Ru(III) couple which is 370 mV larger than that caused by the carboxylate donor is an indication of the different σ-donor/π-acceptor properties of the two groups. Clearly carboxylate is a poorer net electron donor than phenolate, because of the partial delocalisation of the negative charge within the carboxylate group onto the non-coordinated oxygen atom. The potentials of the two one-electron bipy-based reductions may be compared with $[Ru(bipy)_3]^{2+}$, whose first two reductions occur at −1.72 and −1.92 V *vs.* Fc/Fc^+. The more negative potentials required to reduce the bipy ligands of $[Ru(bipy)_2(pic)]^+$ reflect the smaller positive charge on the complex.

Cyclic voltammetry of [Ru(terpy)(dipic)] in dmf revealed reversible one-electron waves centred at +0.12 V and −2.01 V *vs.* Fc/Fc^+. The first of these corresponds to the Ru(II)/Ru(III) couple, which has undergone an additional cathodic shift of 280 mV compared to $[Ru(bipy)_2(pic)][PF_6]$ (which in turn was cathodically shifted by 490 mV from $[Ru(bipy)_3]^{2+}$). The couple at −2.01 V *vs.* Fc/Fc^+ we assign to reduction of the terpy ligand; a reduction of the doubly negatively-charged dipicolinate ligand was not observed.

The relationship between Ru(II)/Ru(III) redox potential and donor set in the series $[Ru(bipy)_3]^{2+}$, $[Ru(bipy)_2(pic)]^+$ and [Ru(terpy)(dipic)] (with N_6, N_5O and *trans*-N_4O_2 donor sets respectively) is clearly not linear: the second substitution of pyridyl by carboxylate has a much smaller effect than the first substitution. In [Ru(terpy)(dipic)] the two carboxylates are *trans* to one another, and each will repel the other electrostatically, reducing their ability to donate electron density to the metal centre compared to the carboxylate donor of $[Ru(bipy)_2(pic)]^+$ which is *trans* to an electron-withdrawing pyridyl group (although this is not really detectable in the crystal structures, as described above). Further support for this comes from the observation that in $[Ru(bpy\text{-}CO_2)_2]$, with a *cis*-N_4O_2 donor set, the shift in the potential of the Ru(II)/Ru(III) couple is almost exactly double that found for $[Ru(bipy)_2(pic)][PF_6]$, since in this case both carboxylate donors are *trans* to pyridyl groups [7].

Electrochemical properties of $[Ru(bipy)_2(hbig)][PF_6]$ *and* $[Ru(bipy)_2(apps)][PF_6]$

Cyclic voltammetry of $[Ru(bipy)_2(Hbig)][PF_6]_2$ in MeCN using a glassy carbon working electrode gave a single reversible wave at +0.21 V *vs.* Fc/Fc^+. We ascribe this to the Ru(II)/Ru(III) couple. Replacing one bipy ligand by Hbig therefore results in stabilisation of the Ru(III) state by 680 mV, indicating that the metal centre of $[Ru(bipy)_2(Hbig)][PF_6]_2$ is much more electron rich than that of $[Ru(bipy)_3]^{2+}$ because of the poorer π-acceptor capability of Hbig compared to the highly delocalised bipy. At high negative potentials only poorly-defined irreversible processes could be observed which were not examined further. Use of a Pt working electrode instead of glassy carbon resulted in a very asymmetric wave for the Ru(II)/Ru(III) couple because of absorption of the oxidised species onto the electrode surface.

Cyclic voltammetry of $[Ru(bipy)_2(apps)][PF_6]$ at a

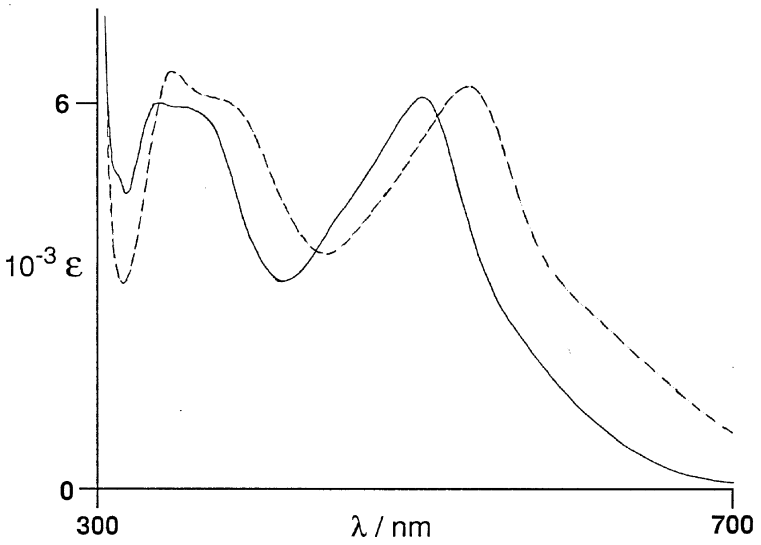

Fig. 4. Electronic spectra of $[Ru(bipy)_2(Hbig)]^{2+}$ in water at pH 7 (solid line), and $[Ru(bipy)_2(big)]^{+}$ in water at pH 13 (dotted line).

Pt-bead electrode in MeCN gave reversible waves centred at +0.20 V and −1.91 V *vs.* Fc/Fc^+, assignable to Ru(II)/Ru(III) and bipy-centred couples respectively. The stabilisation of the Ru(III) state by 690 mV compared to $[Ru(bipy)_3]^{2+}$ arises because apps is both a better σ-donor than bipy because of its negative charge, and a poorer electron-acceptor because it contains only one pyridyl ring. Interestingly, the Ru(II)/Ru(III) couple of $[Ru(bipy)_2(apps)][PF_6]$ is 200 mV more cathodic than that of $[Ru(bipy)_2(pic)][PF_6]$, indicating that the anionic sulfonamide group is a better net electron donor to ruthenium than the anionic carboxylate group, possibly because nitrogen is less electronegative than oxygen and therefore more polarisable.

Electronic spectra of the complexes and pH titration of $[Ru(bipy)_2(Hbig)][PF_6]_2$

The electronic spectra of the complexes are summarised in Table 3. In all cases the lowest-energy feature, in the visible region, may be ascribed to the $Ru[d(\pi)]\rightarrow L(\pi^*)$ m.l.c.t. process, where L = bipy or terpy as appropriate. The red-shift of these compared to the same transition in $[Ru(bipy)_3][PF_6]_2$ (*ca.* 450 nm) [25] arises because of the weakening of the ligand field by replacement of a strong-field pyridyl donors by weaker-field carboxylate, sulfonamide or biguanide ligands, which raises the $d(\pi)$ levels. The incremental weakening of the ligand field on addition of one and then two carboxylates to the donor set is apparent in the shift of the m.l.c.t. maximum from 450 to 495 and then 534 nm in the series $[Ru(bipy)_3][PF_6]_2$, $[Ru(bipy)_2(pic)][PF_6]$ and [Ru(terpy)(dipic)]. All of the complexes have one or two near-UV transitions in the 300–400 nm range, and the usual intense ligand-centred transitions in the higher-energy UV region.

A pH titration of the electronic spectrum of $[Ru(bipy)_2(Hbig)][PF_6]_2$ was effected by dissolving it in aqueous 0.1 M KCI acidified to pH 1, and slowly raising the pH to 13 by addition of very small portions of solid KOH. In the pH range 1 to 11 the spectrum was invariant, but in the pH range 11–13 the spectrum changes significantly, which we ascribe to deprotonation of the central NH group of the coordinated Hbig ligand to give $[Ru^{II}(bipy)_2(big)]^+$, since $[Ru(bipy)_3]^{2+}$ undergoes no such pH-induced spectral change. The pair of transitions at 340 and 360 nm become red-shifted to 348 and 384 nm, and the lowest-energy MLCT band at 504 nm is likewise red-shifted to 533 nm (Figure 4). A graph of λ_{max}(MLCT) *vs.* pH (Figure 5) indicates that the pK value is 12.3 (±0.2), and the same pK value could be obtained from plotting other spectral parameters (*e.g.* absorbance at 400 nm) as a function of pH. The red-shift of the m.l.c.t. transitions indicates that on deprotonation the metal $d(\pi)$ orbitals are raised, *i.e.* $[big]^-$ is a weaker-field ligand than Hbig; that the bipy-based orbitals are not significantly perturbed is shown by the fact that the two intense UV transitions are hardly affected by deprotonation of the complex. Deprotonation of Hbig to $[big]^-$ results in formation of a negatively-charged, delocalised "acac-like" ligand [19] which is expected to be a better π-donor than neutral Hbig, consistent with the above observation.

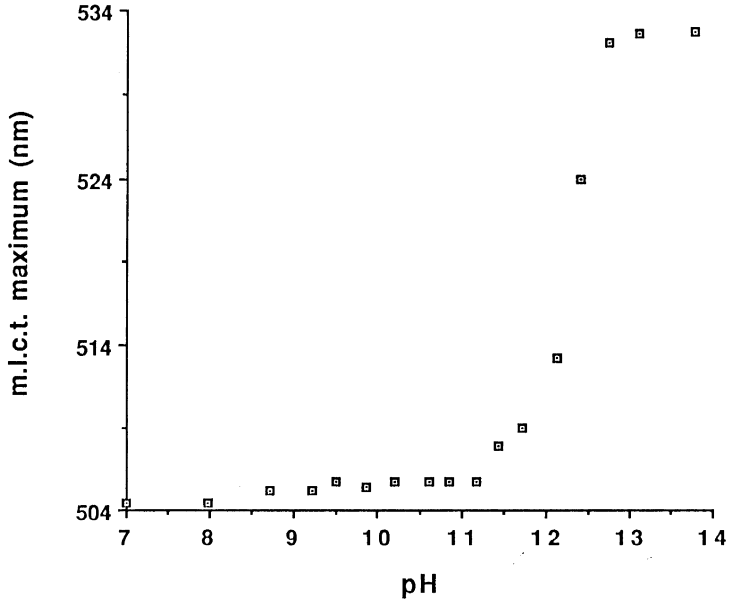

Fig. 5. Wavelength of the m.l.c.t. maximum of $[Ru(bipy)_2(Hbig)]^{2+}$ as a function of pH.

Acknowledgements—We thank the EPSRC for financial support.

REFERENCES

1. Mononuclear complexes with N,O-donor sets: (a) Bardwell, D. A., Black, D., Jeffery, J. C., Schatz, E. and Ward, M. D., *J. Chem. Soc., Dalton Trans.*, 1993, 2321; (b) Holligan, B. M., Jeffery, J. C., Norgett, M. K., Schatz, E. and Ward, M. D., *J. Chem. Soc., Dalton Trans.*, 1992, 3345.
2. Mononuclear complexes with other donor sets: (a) Bardwell, D. A., Jeffery, J. C., Schatz, E., Tilley, E. E. M. and Ward, M. D., *J. Chem. Soc., Dalton Trans.*, 1995, 825; (b) Cargill Thompson, A. M. W., Bardwell, D. A., Jeffery, J. C., Rees, L. H. and Ward, M. D., *J. Chem. Soc., Dalton Trans.*, 1997, 721; (b) Cargill Thompson, A. M. W., Batten, S. R., Jeffery, J. C., Rees, L. H. and Ward, M. D., *Aust. J. Chem.*, 1997, **50**, 109.
3. Dinuclear complexes: (a) Joulié, L. F., Schatz, E., Ward, M. D., Weber, F. and Yellowlees, L. J., *J. Chem. Soc., Dalton Trans.*, 1994, 799; (b) Cargill Thompson, A. M. W., Jeffery, J. C., Liard, D. J. and Ward, M. D., *J. Chem. Soc., Dalton Trans.*, 1996, 879; (c) Ward, M. D., *Inorg. Chem.*, 1996, **35**, 1712; (d) Bardwell, D. A., Horsburgh, L., Jeffery, J. C., Joulié, L. F., Ward, M. D., Webster, I. and Yellowlees, L. J., *J. Chem. Soc., Dalton Trans.*, 1996, 2527; (e) Jeffery, J. C., Liard, D. J. and Ward, M. D., *Inorg. Chim. Acta*, 1996, **251**, 9.
4. Duff, C. M. and Heath, G. A., *Inorg. Chem.*, 1991, **30,** 2528 and refs. therein.
5. (a) Shirin, Z. and Mukherjee, K., *Polyhedron*, 1992, **11**, 2625; (b) Lahiri, G. K., Bhattacharya, S., Ghosh, B. K. and Chakravorty, A., *Inorg. Chem.*, 1987, **26**, 4323; (c) Constable, E. C. and Hannon, M. J., *Inorg. Chim. Acta.*, 1993, **211**, 101; (d) Pramanik, R. and Bhattacharya, S., *Polyhedron*, 1997, **16**, 3047; (e) Sinha, P. K., Chakravarty, J. and Bhattacharya, S., *Polyhedron*, 1997, **16**, 81.
6. Ward, M. D., *Chem. Soc. Rev.*, 1995, **24**, 121.
7. Norrby, T., Börje, A., Åkermark, B., Hammarström, L., Alsins, J., Lashgari, K., Norrestam, R., Martennson, J. and Stenhagen, G., *Inorg. Chem.*, 1997, **36,** 5850.
8. Canty, A. J., Traill, P. R., Skelton, B. W. and White, A. H., *Inorg. Chim. Acta.*, 1997, **255,** 117.
9. Nishiyama, H., Shimada, T., Itoh, H., Sugiyama, H. and Motoyama, Y., *Chem. Commun.*, 1997, 1863.
10. Sullivan, B. P., Salmon, D. J. and Meyer, T. J., *Inorg. Chem., Inorg. Chem.*, 1978, **17,** 3334.
11. Sullivan, B. P., Calvert, J. M. and Meyer, T. J., *Inorg. Chem.*, 1980, **19,** 1404.
12. (a) Karipides, D. and Fernelius, W. C., *Inorg. Synth.*, 1963, **7**, 56; (b) Holter, S. N. and Karipides, D., *Inorg. Synth.*, 1963, **7**, 58.
13. Otter, C. A., Couchman, S. M., Jeffery, J. C., Mann, K. L. V., Psillakis, E. and Ward, M. D. *Inorg. Chim. Acta.*, in press.
14. Jones, P. L., Amoroso, A. J., Jeffery, J. C., McCleverty, J. A., Psillakis, E., Rees, L. H. and Ward, M. D., *Inorg. Chem.*, 1997, **36,** 10.
15. SADABS (a program for absorption correction using the Siemens Area Detector system), Sheldrick, G. M. University of Göttingen (1996).
16. SHELXTL 5.03 program system, Siemens Analytical X-Ray Instruments, Madison, WI, USA (1995).

17. Constable, E. C., *Adv. Inorg. Chem. Radiochem.*, 1986, **30,** 69.
18. Ray, P., *Chem. Rev.*, 1961, **61,** 313.
19. Kennard, C. H. L., Smith, G. and O'Reilly, E. J., *Inorg. Chim. Acta.*, 1983, **77,** L113.
20. Moucharafieh, N. C., Eller, P. G., Bertrand, J. A. and Royer, D. J., *Inorg. Chem.*, 1978, **17,** 1220.
21. Tada, T., Kushi, Y. and Yoneda, H., *Bull. Chem. Soc. Japan*, 1982, **55,** 1063.
22. Coghi, L., Nardelli, M. and Pelizzi, G., *Acta Cryst.*, 1976, **B32,** 842.
23. Brubaker, G. R. and Webb, L. E., *J. Am. Chem. Soc.*, 1969, **91,** 7199.
24. Hart, R. O. C., Bott, S. G., Atwood, J. L. and Cooper, S. R., *J. Chem. Soc., Chem. Commun.*, 1992, 894.
25. Juris, A., Balzani, V., Barigeletti, F., Campagna, S., Belser, P. and von Zelewsky, A., *Coord. Chem. Rev.*, 1988, **84,** 85.

Pergamon

PII: S0277–5387(98)00148–X

Polyhedron Vol. 17, No. 20, pp. 3551–3556, 1998
© 1998 Elsevier Science Ltd
All rights reserved. Printed in Great Britain
0277–5387/98 $19.00+0.00

Spontaneous and base-catalyzed nitrito to nitro linkage isomerization of *trans*-$[Co(NH_3)_4(NH_2CH_3)ONO]^{2+}$ complex

Fernando Bozoglián, Marcelo Queirolo and Beatriz Sienra*

Química Inorgánica, Facultad de Quimica, C.C. 1157, Montevideo, Uruguay

(Received 8 November 1997; accepted 8 April 1998)

Abstract—The nitrito ion *trans*-$[Co(NH_3)_4(NH_2CH_3)ONO]^{2+}$ rearranges to its nitro form *trans*-$[Co(NH_3)_4(NH_2CH_3)NO_2]^{2+}$ in aqueous base according to the rate law $k_{obs}=k_s+k_{bc}[OH^-]$. At $\mu=1.0$ M, 25°C $k_s=1.01\times10^{-4}$ s^{-1}; $\Delta H_s^*=98$ kJ mol^{-1}; $\Delta S_s^*=7$ JK^{-1}; $k_{bc}=3.3\times10^{-2}$ $M^{-1}s^{-1}$; $\Delta H_{bc}^*=121$ kJ mol^{-1}; $\Delta S_{bc}^*=132$ JK^{-1} mol^{-1}. The base-catalyzed isomerization proceeds enterely *via* an intramolecular conjugate-base mechanism. The reaction is fully retentive and *trans*-$[Co(NH_3)_4(NH_2CH_3)NO_2]^{2+}$ is the only species that could be detected by ^{1}H nmr after the reaction was completed. The results are discussed in the light of the reaction mechanisms proposed so far and in relation to the normal substitution chemistry of pentaamminecobalt(III) complexes. © 1998 Elsevier Science Ltd. All rights reserved

Keywords: nitrito ion; nitro linkage isomerization; pentaamminecobalt(III) complexes.

The nitrito ligand shows an ambident character [1]: coordination to a metal center can be achieved by either its O or N atoms in Co(III) complexes. The O-bound nitrito complexes isomerize spontaneously and stereoretentively [2] to the more stable N-bound nitro complexes, both in the solid state [3, 4] and in solution [5–10]. This reaction [11] is confirmed to be an intramolecular process [3, 6] for which a seven-coordinated [1, 3, 7] or a six-coordinated π bonded species [8] has been proposed as reaction intermediate. Despite the extensive investigations in this field, little attention has been paid to the kinetics aspects of this reaction in basic solution. In fact, the existence of a base-catalyzed path (eqn (1)) for the rearrangement has been recognized some years ago [12–14], but only one nitrito complex of Co(III) has been subjected to kinetic measurements: $[Co(NH_3)_5ONO]^{2+}$.

$$[Co(NH_3)_5ONO]^{2+} \xrightarrow{OH^-} [Co(NH_3)_5NO_2]^{2+} \quad (1)$$

We have been studying the base hydrolysis of *trans*-$[Co(NH_3)_4(NH_2CH_3)X]^{(3-n)+}$ in the presence of excess of NO_2^-, which lead to the production of some $[Co(NH_3)_4(NH_2CH_3)ONO]^{2+}$ and $[Co(NH_3)_4(NH_2CH_3)NO_2]^{2+}$ along with $[Co(NH_3)_4(NH_2CH_3)OH_2]^{3+}$ and so, became interested in the nitrito-to-nitro linkage isomerization reaction. In the present study, the spontaneous and base-catalyzed isomerization for the *trans*-$[Co(NH_3)_4(NH_2CH_3)ONO]^{2+}$ ion was followed, in order to determine the influence of methylation on the isomerization rate. Furthermore, the availability of a nitrito complex of *trans* configuration makes it possible to determine the stereochemical course of the isomerization reaction. Since the present linkage isomerization is an intramolecular process in which no Co(III)-ligand bonds are ruptured, it is likely that configuration is retained during the process.

EXPERIMENTAL

Spectrophotometric measurements were made on a Spectronic 3000 diode array spectrophotometer. Cation exchange experiments were performed with a Dowex 50 W × 2 (Na^+ form, 200–400 mesh) resin. A Varian XL-100 spectrometer was used for the ^{1}H nmr spectra.

Materials

trans-$[Co(NH_3)_4(NH_2CH_3)ONO]^{2+}$ and *trans*-$[Co(NH_3)_4(NH_2CH_3)NO_2]^{2+}$ were prepared as

* Author to whom correspondence should be addressed.

described in the literature [15], and their authenticy were checked by their UV-VIS (in aqueous solution) and ^{1}H nmr (in deuterated dimethylsulfoxide *vs* tetramethylsilane as internal reference) spectra. Ion-exchange chromatography and ^{1}H nmr spectroscopy were used to establish the absence of trace impurities, particularly *trans*-$[Co(NH_3)_4(NH_2CH_3)OH_2]^{3+}$ [15]. The isomeric purity of the complexes was confirmed by this last technique [15]. Freshly prepared (or stored at $-18°C$ for less than a week) nitrito complex was used for the experiments, since it isomerizes even in the solid state.

All other reagents and solvents used were of analytical grade.

Reaction stoichiometry and product analyses

The absorption spectrum of *trans*-$[Co(NH_3)_4(NH_2CH_3)ONO]^{2+}$ in water and in aqueous NaOH changed with time and displayed isosbestic points at 295,6 (ϵ 469) and 367 nm (ϵ 284). These agree with those expected for *trans*-$[Co(NH_3)_4(NH_2CH_3)NO_2]^{2+}$ as the only product. Furthermore, the final (10 $t_{1/2}$) absorption spectra were identical with that of the authentic nitro complex (Fig. 1). The absence of any significant base hydrolysis of *trans*-$[Co(NH_3)_4(NH_2CH_3)ONO]^{2+}$ to give $[Co(NH_3)_4(NH_2CH_3)OH_2]^{3+}$was confirmed as follows. A sample of the nitrito complex (0.5 g) was dissolved in 0.10 M NaOH ($\mu = 1.0$, $NaClO_4$) and allowed to react for 10 $t_{1/2}$ (35 min). The reaction was quenched to pH 2 with $HClO_4$ and the solution was sorbed on and eluted from Dowex resin with 0.2 M $NaClO_4$. No $[Co(NH_3)_4(NH_2CH_3)OH_2]^{3+}$ complex was detected. The absence of *trans-cis* rearrangement during the isomerization reaction of *trans*-$[Co(NH_3)_4(NH_2CH_3)ONO]^{2+}$ ion was confirmed by ^{1}H nmr. The chloride salt (0.15 mg) was dissolved in a D_2O/NaOD (0.5 ml, 0.01M) solution, and its spectrum recorded. After the reaction was completed, the final spectrum was recorded. Tetramethylsilane (tms) was used as internal reference.

Kinetic studies

The reactions were followed spectrophotometrically, with the reaction cell thermostated ($\pm 0.1°C$) by a thermoelectric cuvette holder (Peltier effect). After preliminary spectral searching experiments to characterize the reaction and identify the most suitable wavelength, the progress of the isomerization was monitored at 327 nm. Solutions containing NaOH and $NaClO_4$ were brought to the reaction temperature in the thermostated cell com-

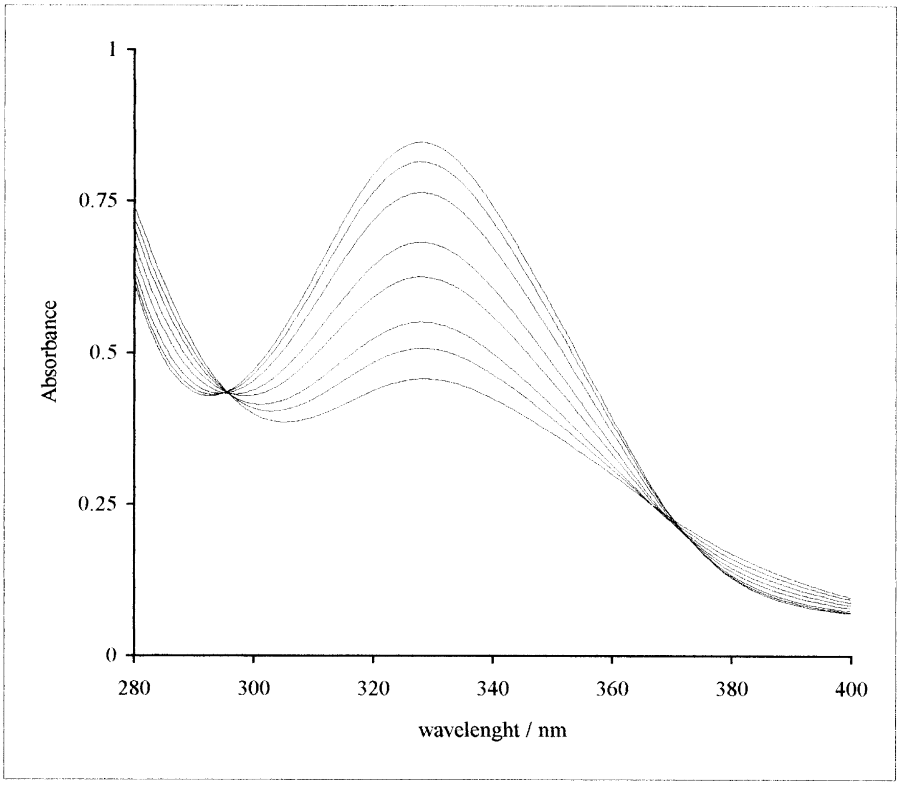

Fig. 1. Change in the absorption spectrum of *trans*-$[Co(NH_3)_4(NH_2CH_3)ONO]^{2+}$ in aqueous NaOH solution, accompanied by its isomerization to the nitro complex.

partment and the reaction was iniciated by adding 40 μL of a solution (2.5×10^{-2} M) of the complex which was rapidly mixed with the cuvette stirrers. Base concentrations between 0.0025 and 0.1 M were employed, at unit ionic strength adjusted with sodium perchlorate. Plots of $\ln(A_t\text{-}A_\infty)$ *vs.* time were linear to completion of reaction. Rate constants for the base-catalyzed isomerization were determined by the usual least-squares analysis of absorbance data. Activation entalphy and entropy were determined from plots of ln(k/T) *vs.* 1/T. The spontaneous isomerization of *trans*-$[Co(NH_3)_4(NH_2CH_3)ONO]^{2+}$ complex was studied in aqueous solution at unit ionic strength adjusted with sodium perchlorate. The same procedure outlined above was followed.

RESULTS AND DISCUSSION

The observed rate constants, k_{obs}, for the base-catalyzed isomerization of *trans*-$[Co(NH_3)_4(NH_2CH_3)ONO]^{2+}$ ion studied at base strengths between 0.0025 and 0.1 M, at 25°C obey (Fig. 2) the relationship

$$k_{obs} = k_{s3} + k_{bc}[OH^-] \quad (2)$$

and least-square analysis yielded the two independent rate constants k_s(spontaneous) $= 1.01 \times 10^{-4}\,s^{-1}$ and k_{bc}(base-catalyzed) $= 3.3 \times 10^{-2}\ M^{-1}s^{-1}$. The temperature dependence of k_{bc} is shown in Table 1.

The linkage isomerization reaction was also followed in aqueous solution at ionic strength 1M($NaClO_4$). The isomerization rate, k_s, at 25°C, obtained

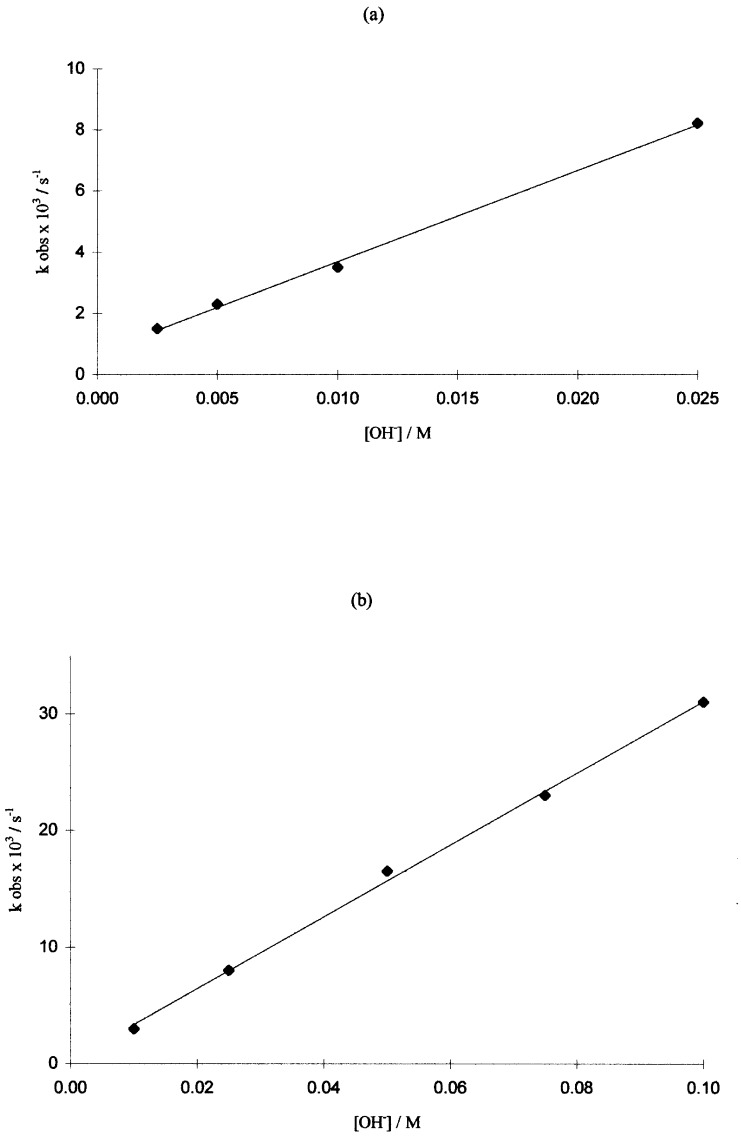

Fig. 2. Base-dependence of the linkage isomerization rate of $[Co(NH_3)_4(NH_2CH_3)ONO]Cl_2$ in (a) 0.0025–0.01M NaOH, $\mu = 1.0$ ($NaClO_4$); (b) 0.01–0.1 M NaOH, $\mu = 1.0$ ($NaClO_4$), at 25°C.

Table 1. Temperature dependence of the rate constant for the base-catalyzed linkage isomerization of *trans*-$[Co(NH_3)_4(NH_2CH_3)ONO]^{2+}$ ion[a]

T(°C)	10.0	16.8	25.0	30.3	40.0
$k_{bc}(s^{-1}\,M^{-1})$	1.5×10^{-3}	6.7×10^{-3}	3.3×10^{-2}	6.3×10^{-2}	2.4×10^{-1}

[a] Complex concentration 5×10^{-4} M, base concentration 0.05M and ionic strength 1.0 M ($NaClO_4$).

in this independent way agrees, within experimental error, with the value obtained from the application of eqn (2) to the data in basic solution. Table 2 shows the temperature dependence of k_s.

Rate constants and activation parameters for the spontaneous and base-catalyzed isomerization of *trans*-$[Co(NH_3)_4(NH_2CH_3)ONO]^{2+}$ ion are collected in Table 3 together with the corresponding data for the $[Co(NH_3)_5ONO]^{2+}$ ion. Literature data for the acid and base-catalyzed hydrolysis of some acidoamminecobalt(III) complexes are also included for comparison.

For both the spontaneous and base-catalyzed paths, the rates of isomerization of *trans*-$[Co(NH_3)_4(NH_2CH_3)ONO]^{2+}$ complex are greater than the corresponding rates for the $[Co(NH_3)_5ONO]^{2+}$ ion. In the substitution chemistry of pentaamminecobalt(III) complexes, there is also a modest rate enhancement of both, aquation and base hydrolysis, when one NH_3 is substituted by a NH_2CH_3 ligand (*trans* position), as shown in Table 3 [16–19]. This acceleration has been attributed to inductive effect of the methyl substituent [19]. The same interpretation holds for the reaction under study since it is conceivable that the methyl

Table 2. Temperature dependence of the rate constant for the spontaneous linkage isomerization of *trans*-$[Co(NH_3)_4(NH_2CH_3)ONO]^{2+}$ ion[a]

T(°C)	24.8	30.6	40.8	50.7
k_s (s^{-1})	8.83×10^{-5}	2.48×10^{-4}	8.50×10^{-4}	2.57×10^{-3}

[a] complex concentration: 5×10^{-4} M, ionic strength 1.0 M ($NaClO_4$).

Table 3. Rate constants at 25°C and activation parameters for the reactions of acidoamminecobalt(III) complexes

	Spontaneous			Base-catalyzed		
Complex	$10^6\,k_s$[a]	ΔH_s^{*}[a]	ΔS_s^{*}[a]	k_{bc}[b]	ΔH_{bc}^{*}[b]	ΔS_{bc}^{*}[b]
$[Co(NH_3)_5ONO]^{2+}$	69	95(±4)	4(±1)	0.59×10^{-2}	110(±1)	82(±4)
trans-$[Co(NH_3)_4(NH_2CH_3)ONO]^{2+}$	101	98(±1)	7(±4)	3.3×10^{-2}	121(±1)	132(±4)
	$10^6\,k_{aq}$[c]	Δ_{aq}^{*}[c]	ΔS_{aq}^{*}[c]	k_{OH}[d]	Δ_{OH}^{*}[d]	ΔS_{OH}^{*}[d]
$[Co(NH_3)_5NO_3]^{2+}$	24.1	100.3	3.3	9.2	118	180
trans-$[Co(NH_3)_4(NH_2CH_3)NO_3]^{2+}$	134	99	13	59	91.2	95
$[Co(NH_3)_5Br]^{2+}$	5.97	97	−19.6	3.3	124	187
trans-$[Co(NH_3)_4(NH_2CH_3)Br]^{2+}$	31.7	97	−5	14	105	129
$[Co(NH_3)_5Cl]^{2+}$	1.77	94.2	−39	0.6	120	154
trans-$[Co(NH_3)_4(NH_2CH_3)Cl]^{2+}$	8.89	97	−15	4.8	105	121

[a] This work. k_s (s^{-1}), ΔH_s^{*} (kJ mol^{-1}) and ΔS_s^{*} (J mol^{-1} K^{-1}): rate constants and activation parameters for spontaneous isomerization.

[b] This work. k_{bc} ($M^{-1}\,s^{-1}$), ΔH_{bc}^{*} (kJ mol^{-1}) and ΔS_{bc}^{*} (J mol^{-1} K^{-1}): rate constants and activation parameters for base-catalyzed isomerization.

[c] Ref. [19]. k_{aq} (s^{-1}), ΔH_{aq}^{*} (kJ mol^{-1}) and ΔS_{aq}^{*} (J mol^{-1} K^{-1}): rate constants and activation parameters for acid hydrolysis.

[d] Ref. [19]. k_{OH} ($M^{-1}\,s^{-1}$), ΔH_{OH}^{*} (kJ mol^{-1}) and ΔS_{OH}^{*} (J mol^{-1} K^{-1}): rate constants and activation parameters for base-catalyzed hydrolysis.

group influences the stretching of the Co–O bond, donating negative charge to the cobalt. The present results are therefore compatible with the assumption that the isomerization is an intramolecular process which is facilitated in the *trans*-$[Co(NH_3)_4(NH_2CH_3)ONO]^{2+}$ complex when compared with the $[Co(NH_3)_5ONO]^{2+}$ ion.

The ratios k_{OH}/k_{aq} are $5.4\times10^5\,M^{-1}$, $4.4\times10^5\,M^{-1}$ for *trans*-$[Co(NH_3)_4(NH_2CH_3)X]^{2+}$ ions, where $X=Cl^-$, Br^- and NO_3^- respectively and comparable ratios are observed for the corresponding pentaammines complexes ($3.8\times10^5\,M^{-1}$, $5.5\times10^5\,M^{-1}$ and $3.8\times10^5\,M^{-1}$) [19]. The isomerization reaction does not follow this pattern; the ratio k_{bc}/k_s is $3.3\times10^2\,M^{-1}$ for *trans*-$[Co(NH_3)_4(NH_2CH_3)ONO]^{2+}$ ion and $0.86\times10^2\,M^{-1}$ for $[Co(NH_3)_5ONO]^{2+}$ complex, *i.e.*, it differs significantly.

Moreover, the greater reactivity towards base hydrolysis of *trans*-$[Co(NH_3)_4(NH_2CH_3)X]^{2+}$ ions when compared with the parent pentaammines lies in the lower ΔH^* values, while the faster base-catalyzed isomerization reaction of *trans*-$[Co(NH_3)_4(NH_2CH_3)ONO]^{2+}$ ion compared with that of $[Co(NH_3)_5ONO]^{2+}$ complex is originated in a greater ΔS^* for the former. For example ΔH^*_{OH} of the $[Co(NH_3)_5ONO_2]^{2+}$ complex is 27 kJ mol^{-1} higher than for the *trans*-$[Co(NH_3)_4(NH_2CH_3)ONO_2]^{2+}$ ion whereas ΔH^*_{bc} for the pentammine complex is 11 kJ mol^{-1} lower. Similar observations can be made for the variations in ΔS^*_{OH} and ΔS^*_{bc}.

Differences to normal substitution chemistry are also apparent in the stereochemistry of the linkage isomerization reaction. The hydrolysis of $[CoA_5L]^{n+}$ complexes, which yield $[CoA_5OH_2]^{m+}$, often proceeds with stereochemical change. This is particularly true of base-catalyzed hydrolysis. For example, the base hydrolysis of *trans*-$[Co(NH_3)_4(NH_2CH_3)X]^{2+}$ ions yield 11, 13 and 17% of *cis*-$[Co(NH_3)_4(NH_2CH_3)OH_2]^{3+}$ complex, where $X=Cl^-$, Br^- and NO_3^- respectively [19]. This is not the situation with the reaction under study. The ^1H nmr spectrum of *trans*-$[Co(NH_3)_4(NH_2CH_3)ONO]Cl_2$ in D_2O/NaOD solution only showed the methyl ^1H resonance, due to complete exchange of amine protons [16] (chemical shift = 2.04 ppm relative to tms). After the reaction was completed the spectrum showed the methyl ^1H signal at 2.2 ppm. The presence of only one methyl resonance proves that the reaction proceeds under complete (>98%) stereochemical retention of configuration [15]. This result is consistent with synchronous bond breaking (Co–O) and bond making (Co–N) and with nitrito ion remaining bonded to cobalt throughout the rearrangement.

However, inspection of Table 3 also shows that for the spontaneous reactions ΔH^* values are essentially the same, whether or not the reactions are aquations or isomerizations. Furthermore the ΔS^* values for the nitrate complexes aquations are very similar to those for the isomerization reaction. This behaviour may be originated in the fact that for the nitrato and the nirito complexes the reactions, aquations or isomerizations respectively, involve Co–O bonds.

The activation parameters for the k_s and k_{bc} pathways differ substantially, indicating obvious mechanistic differences. For the base-catalyzed path, a conjugate base (CB) deprotonation preequilibrium has been proposed [12]. Support for this mechanism derives from the large positive ΔV^* [12] and ΔS^* values found for the isomerization reaction of $[Co(NH_3)_5ONO]^{2+}$ ion.

$$[Co(NH_3)_5ONO]^{2+} + OH^- \xrightleftharpoons{K} [Co(NH_3)_4(NH_2)ONO]^+ + H_2O,\ \Delta S^o_{CB}$$

$$[Co(NH_3)_4(NH_2)ONO]^+ \xrightarrow{k_2} [Co(NH_3)_4(NH_2)NO_2]^+,\ \Delta S^*_2$$

$$[Co(NH_3)_4(NH_2)NO_2]^+ + H_2O \xrightarrow{fast} [Co(NH_3)_5NO_2]^{2+} + OH^-$$

Since k_{bc} is a composite quantity ($=K\,k_2$) the corresponding activation parameters listed in Table 3 can not be readily rationalized. However a positive value of ΔS^*_{bc} ($=\Delta S^o_{CB}+\Delta S^*_2$) is predicted for this mechanism, the first step of which is closely similar to known "neutralization" reactions in the literature [20], because of the considerable charge neutralization. The second step is expected to have a ΔS^*_2 near zero, as the one found for the spontaneous pathway. The conclusion is that k_s and k_{bc} isomerization processes are mechanistically similar after account is taken of the base preequilibrium step.

Acknowledgements—The authors are grateful for financial assistance from CONICYT, Uruguay.

REFERENCES

1. Basolo, F. and Pearson, R. G. in *Mechanisms of Inorganic Reactions*, p. 291, Wiley, New York (1967).
2. Murmann, R. K., *J. Am. Chem. Soc.*, 1955, **77,** 5190.
3. Grenthe, I. and Nordin, E., *Inorg. Chem.*, 1979, **18,** 1109.
4. Zanella, A. W. and Fucaloro, A. F., *Inorg. Nucl. Chem. Lett.*, 1980, **16,** 515.
5. Pearson, R. G., Henry, P. M., Bergmann, J. G. and Basolo, F., *J. Am. Chem. Soc.*, 1954, **76,** 5920.
6. Murmann, R. K. and Taube, H., *J. Am. Chem. Soc.*, 1956, **78,** 4886.
7. Mares, M., Palmer, D. A. and Kelm, H., *Inorg. Chim. Acta*, 1978, **27,** 153.
8. Jackson, W. G., Lawrence, G. A., Lay, P. A. and Sargeson, A. M., *J. Chem. Soc. Chem. Commun.*, 1982, **00,** 270.
9. Miyoshi, K., Katoda, N. and Yoneda, H., *Inorg. Chem.*, 1983, **22,** 1839.
10. Jackson, W. G., *Inorg. Chem.*, 1987, **26,** 3857.
11. For reviews, see: Balahura, R. J. and Lewis, N.

A., *Coord. Chem. Rev.*, 1976, **20**, 109; Burmeister, J. L., *ibid.*, 1990, **105**, 77.
12. Jackson, W. G., Lawrence, G. A., Lay, P. A. and Sargeson, A. M., *Inorg. Chem.*, 1980, **19,** 904.
13. Balt, S., Kuipers, H. J. A. M. and Renkema, W. E., *J. Chem. Soc. Dalton Trans.*, 1983, **00,** 1739.
14. Balt, S., Renkema, W. E. and Ronde, H., *Inorg. Chim. Acta*, 1984, **86,** 87.
15. Massaferro, A., Queirolo, M. and Sienra, B., *An Quim.*, 1992, **88,** 230.
16. Balt, S., Gamelkoorn, H. J., Piriz Mac-Coll, C. R. and Renkema, W. E., *Transition Met. Chem.*, 1984, **9,** 224.
17. Buckingham, D. A., Foxman, B. M. and Sargeson, A. M., *Inorg. Chem.*, 1970, **9,** 1790.
18. Lawrence, G. A., Shneider, K. and van Eldik, R., *Inorg. Chem.*, 1984, **23,** 3922.
19. Benzo, F., Capparelli, A. L., Mártire, D. O., Massaferro, A., Queirolo, M. and Sienra, B., *Polyhedron*, 1996, **15,** 1915.
20. Edwards, J. O., Monacelli, F. and Ortaggi, G., *Inorg. Chim. Acta*, 1974, **11,** 47.
21. Tobe, M. L. in *Advances in Inorganic and Bioinorganic Mechanisms*, (ed A. G. Sykes), **2**, Academic Press, London (1983).
22. Swaddle, T. W., *Can J. Chem.*, 1977, **55,** 3166.

Pergamon

PII: S0277–5387(98)00149–1

Polyhedron Vol. 17, No. 20, pp. 3557–3564, 1998
© 1998 Elsevier Science Ltd
All rights reserved. Printed in Great Britain
0277–5387/98 $19.00+0.00

Ruthenium substituted Keggin type polyoxomolybdates: synthesis, characterization and use as bifunctional catalysts for the epoxidation of alkenes by molecular oxygen

Ronny Neumann* and Mazal Dahan

Casali Institute of Applied Chemistry, Graduate School of Applied Science, The Hebrew University of Jerusalem, Jerusalem, Israel, 91904

(Received 24 February 1998; accepted 14 April 1998)

Abstract—The ruthenium substituted polyoxomolybdate of the Keggin structure, $Q_4PRu^{III}(H_2O)Mo_{11}O_{39}$ ($Q = n\text{-}Bu_4N$), has been synthesized and characterized. The IR spectra show that this compound is isostructural with the known manganese and cobalt analogs. The cyclic voltammogram showed similar redox potentials and the UV–vis spectra showed similar energies for the *d–d* transitions compared to the corresponding tungstate, $Q_4PRu^{III}(H_2O)W_{11}O_{39}$. The catalytic activity of the molybdate *versus* tungstate in reactions with molecular oxygen was, however, significantly different. IR and ^{31}P NMR evidence indicated that treatment of $Q_4PRu^{III}(H_2O)Mo_{11}O_{39}$ with oxygen showed no structural changes whereas, for $Q_4PRu^{III}(H_2O)W_{11}O39$, a clear change was observed. This finding probably explains the lack of catalytic activity for the latter in the co-oxidation of cumene and 1-octene to cumyl alcohol and 1-octene oxide. For the molybdenum compound, this reaction took place by a kinetic balance of ruthenium metal-catalyzed autooxidation of cumene to cumene hydroperoxide and the molybdenum catalyzed oxygen transfer from cumene hydroperoxide to 1-octene to yield the products. High catalyst loading led to reaction inhibition whereas low loading and excess cumene led to increased autooxidation. © 1998 Elsevier Science Ltd. All rights reserved

Keywords: polyoxomolybdates; bifunctional catalysts; alkenes; molecular oxygen.

INTRODUCTION

Transition metal substituted polyoxometalates have, over the last decade, attracted considerable interest as oxidatively stable catalysts for oxidation of hydrocarbons [1]. Transition metal substituted polyoxometalates can be defined as having a transition metal octahedrally or tetragonally coordinated by a lacunary polyoxometalate. The lacunary polyoxometalate may also be viewed as integrating 'hard' donor oxide ions with adjacent d^0 addenda atoms (Mo^{VI} and/or W^{VI}) providing acceptor orbitals. The interaction of a substituted transition metal with the addenda should be a function of the reduction potential of the heteropolyoxometalate, especially for a second-row transition metal such as ruthenium which has extended *d*-orbitals. Despite the known difference in the redox properties of polyoxotungstates *versus* polyoxomolybdates, the transition metal polyoxomolybdates and their catalytic properties have been only scarcely investigated. A typical transition metal substituted Keggin structure with the transition metal in a polyhedral representation is presented in Fig. 1. Numerable oxidation reactions for these structures and some others have been reported for polyoxotungstates containing chromium [2], manganese [3], iron [4], cobalt [5], nickel [6], niobium [7], rhodium [8] and ruthenium [9] active centers, using a variety of oxidants such as iodosobenzene, *t*-butylhydroperoxide, periodate, amine-oxides, hydrogen peroxide and oxygen. One current interest of our research group is the utilization of oxygen in catalytic transformations involving ruthenium substituted polyoxometalates [9]. In this context, we describe in this paper the synthesis and characterization of ruthenium substituted polyoxomolybdates of the Keggin structure and their use as bifunctional catalysts for the aerobic

*Author to whom correspondence should be addressed.

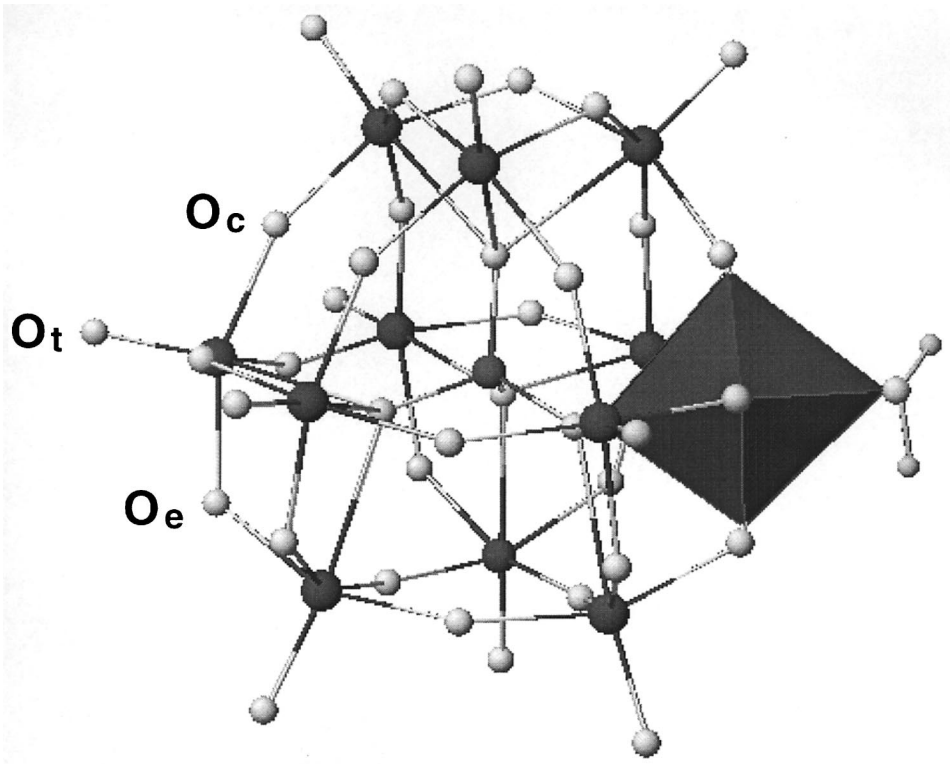

Fig. 1. Representation of the Keggin transition metal substituted polyoxometalate.

epoxidation of alkenes using alkanes as the source of electron donors [10]. In the past, there have been several reports on the combined use of two metals for such reactions in the intramolecular (cyclohexene) [11] and intermolecular mode [12]. The scheme for epoxidation is summarized in Scheme 1. First, there is an autooxidation of alkanes, for example, cumene presumably catalyzed at the ruthenium site to intermediate hydroperoxides. Instead of the usual metal catalyzed decomposition of the hydroperoxide, there occurs heterolytic oxygen transfer (epoxidation) from the intermediate hydroperoxide catalyzed at a molybdenum site to the alkene yielding epoxide and alcohol as co-product.

RESULTS AND DISCUSSION

Synthesis and characterization

As has been pointed out in the past, the relative instability of Keggin type lacunary polyoxomolybdates prevents the preparation of such transition metal substituted polyoxomolybdates in water [13]. Instead however, they may be prepared in non-aqueous solvents such as acetonitrile using quaternary ammonium cations, as has been described for $Q_4HPMMo_{11}O_{39}$ where $M = Co^{II}$, Mn^{II} and Cu^{II} and $Q = (n\text{-}Bu_4N)$ [13]. We have now adapted the non-aqueous procedure for the preparation of $Q_4PRu^{III}(L)Mo_{11}O_{39}$ for $L = H_2O$ and $(CH_3)_2SO$. The synthesis and purification of the lacunary species, $Q_4H_3PMo_{11}O_{39}$, was carried out as published [13]. The lacunary species was then reacted both with an equivalent amount of solid $RuCl_3 \times H_2O$ or $Ru^{II}(DMSO)_4Cl_2$ to yield $Q_4PRu^{III}(H_2O)Mo_{11}O_{39}$, **1**, and $Q_4PRu^{III}(DMSO)Mo_{11}O_{39}$ [14], **2**, respectively, which were purified by recrystallization. The labile ligand on the ruthenium atom in **1** is rather arbitrarily given as being water although it could well be acetonitrile or a mixture of both (see analysis of IR spectrum below). The IR spectra of the two ruthenium substituted polyoxomolybdates are shown in Fig. 2, along with the spectrum of $Q_4PRu^{III}(H_2O)W_{11}O_{39}$, **3** [15], for com-

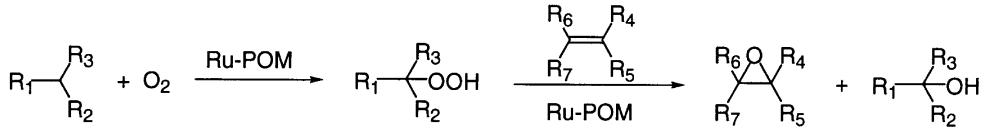

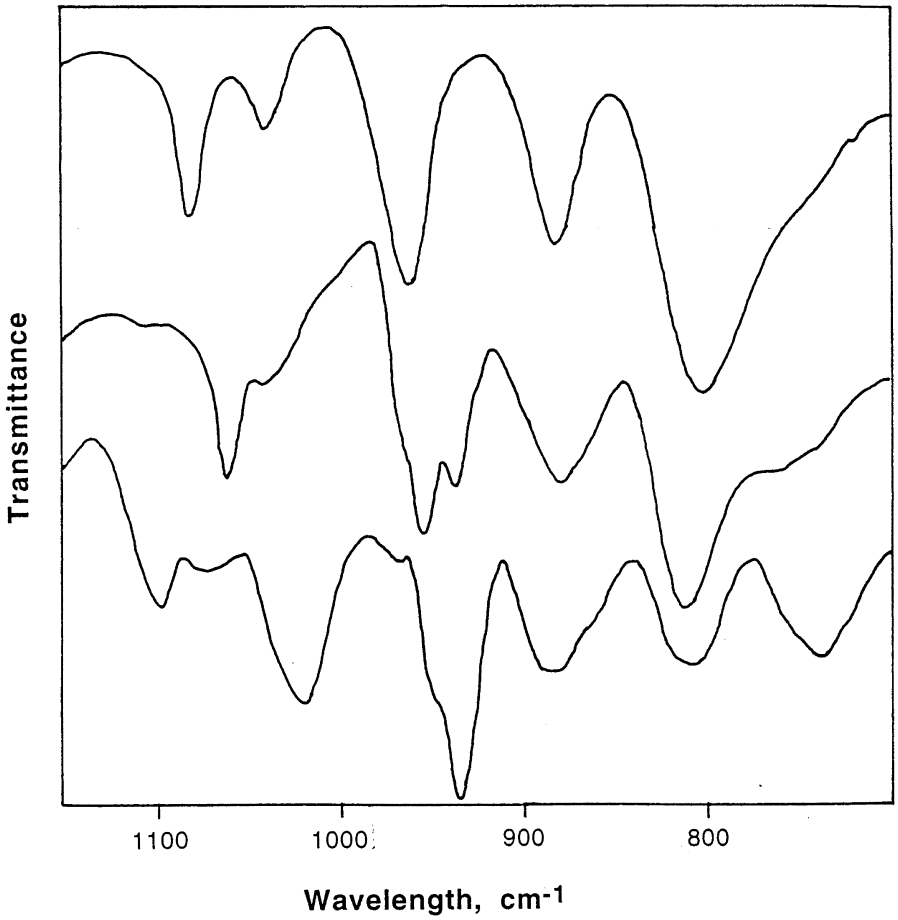

Fig. 2. IR spectra of ruthenium substituted polyoxometalates. Top: $Q_4PRu^{III}(H_2O)W_{11}O_{39}$ 1080, 1036 cm^{-1} P–O; 961 cm^{-1} W–O_t; 881 cm^{-1} W–O_c–W; 802 cm^{-1} W–O_e–W. Middle: $Q_4PRu^{III}(H_2O)Mo_{11}O_{39}$ 1061, 1038 cm^{-1} P–O; 952, 936 cm^{-1} Mo–O_t; 878 cm^{-1} Mo–O_c–Mo; 813 cm^{-1} Mo–O_e–Mo. Bottom: $Q_4PRu^{III}(DMSO)Mo_{11}O_{39}$ 1098, 1021 cm^{-1} P–O; 933 cm^{-1} Mo–O_t; 884 cm^{-1} Mo–O_c–Mo; 806 cm^{-1} Mo–O_e–Mo; 737 cm^{-1}.

parison. The spectra (not shown) measured for $Q_4HPMMo_{11}O_{39}$ (M = Co^{II} and Mn^{II})[13] were practically identical to that of $Q_4PRu^{III}(H_2O)Mo_{11}O_{39}$. The IR peaks attributable to stretching vibrations at corner shared bridges, M–O_c–M, and edge shared bridges, M–O_e–M, were similar for all three compounds. The peaks attributable to P–O vibrations were all split due to the reduction in symmetry from T_d in the parent Keggin structure to a C_s symmetry found in the transition metal substituted analog [16]. The large split observed in $Q_4PRu^{III}(L)Mo_{11}O_{39}$ with DMSO as ligand indicates a large displacement of the ruthenium cation from the heteroatom with the strongly coordinating DMSO. For the less coordinating water or acetonitrile ligands, a much smaller split is observed. Thus, there is a smaller displacement and a more compact structure is postulated [16]. For compounds **2** and **3**, there were single peaks attributable to the terminal M–O_t moiety. However, for $Q_4PM(H_2O)Mo_{11}O_{39}$ (M = Co, Mn and Ru) two peaks at 952 and 936 cm^{-1} were observed. We have no certain explanation for this phenomenon but hypothesize that it may be connected to the labile ligand at the ruthenium atom with compounds with different ligands yielding different peaks [17].

$Q_4PRu^{III}(DMSO)Mo_{11}O_{39}$ proved to be catalytically inactive due to the non-lability of the DMSO ligand [15]. Thus, further characterization was limited to the catalytically active $Q_4PRu^{III}(H_2O)Mo_{11}O_{39}$. The ^{31}P NMR spectrum in acetonitrile showed a single very broad peak at -105 ppm ($\Delta\nu_{1/2} = 1200$ Hz) which indicated a pure paramagnetic compound. The UV–vis spectrum [Fig. 3(a)] shows the expected charge transfer peak at $\lambda = 240$ nm, $\epsilon = 7 \times 10^4$ M^{-1} cm^{-1} with relatively intense *d–d* transitions at 410 and 576 nm ($\epsilon = 10000$ and 3000 M^{-1} cm^{-1} respectively). These *d–d* absorptions are slightly shifted (10–25 nm) relative to the reported spectrum of the tungsten analog [15]. The cyclic voltammetry measurement in CH_3CN (Fig. 4) showed two reversible waves assigned by literature precedence of other ruthenium subtituted polyoxometalates [15] to Ru(III)/Ru(II) at -0.11 V and

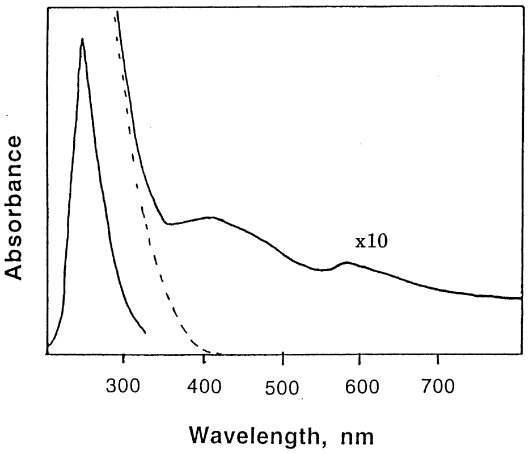

Fig. 3. UV–vis spectrum of $Q_4PRu^{III}(H_2O)Mo_{11}O_{39}$ in acetonitrile. (a) ——— without treatment. (b) - - - after bubbling O_2 for 12 h.

Ru(IV)/Ru(III) at 0.08 V. These reduction potentials are only marginally lower compared to those reported for the tungsten compound at neutral pH. No Ru(V)/Ru(IV) transition was observed due to solvent interference. In the past [15] it had been concluded that the low spin configuration of the ruthenium atom allows partial π-delocalization into vacant $p\pi^*$ orbitals of oxygen atoms bridging ruthenium and the addenda atoms. Inasmuch as it is well known that polyoxomolybdates, *e.g.*, $PMo_{12}O_{40}^{3-}$, are significantly stronger oxidants than their analogous polyoxotungstates *e.g.*, $PW_{12}O_{40}^{3-}$ and show significant bathochromic shifts [18], a more significant effect on both the ruthenium redox chemistry and electronic spectrum was expected [15], however, only slight differences were observed. It would appear that there is little π-delocalization between the ruthenium cation and the neighboring addenda atoms, which has little effect on the properties at the ruthenium center. Despite these observations, the $Q_4PRu^{III}(H_2O)Mo_{11}O_{39}$ compound showed different (a) reactivity to molecular oxygen and (b) catalytic activity and selectivity compared to the $Q_4PRu^{III}(H_2O)W_{11}O_{39}$ analog, as will be shown below.

Reaction of $Q_4PRu^{III}(H_2O)M_{11}O_{39}$ *with molecular oxygen*

Since we were interested in the catalytic co-oxidation of two substrates with molecular oxygen as presented in Scheme 1, the reaction of $Q_4PRu^{III}(H_2O)M_{11}O_{39}$ with molecular oxygen was examined by FTIR, UV–vis and ^{31}P NMR. Reaction of the molybdenum compound, 0.01 M $Q_4PRu^{III}(H_2O)Mo_{11}O_{39}$ in acetonitrile with 1 atm molecular oxygen for 8 h at 60°C yielded only the disappearance of the peak at 936 cm^{-1} in the IR spectrum (Fig. 5) and *no* formation

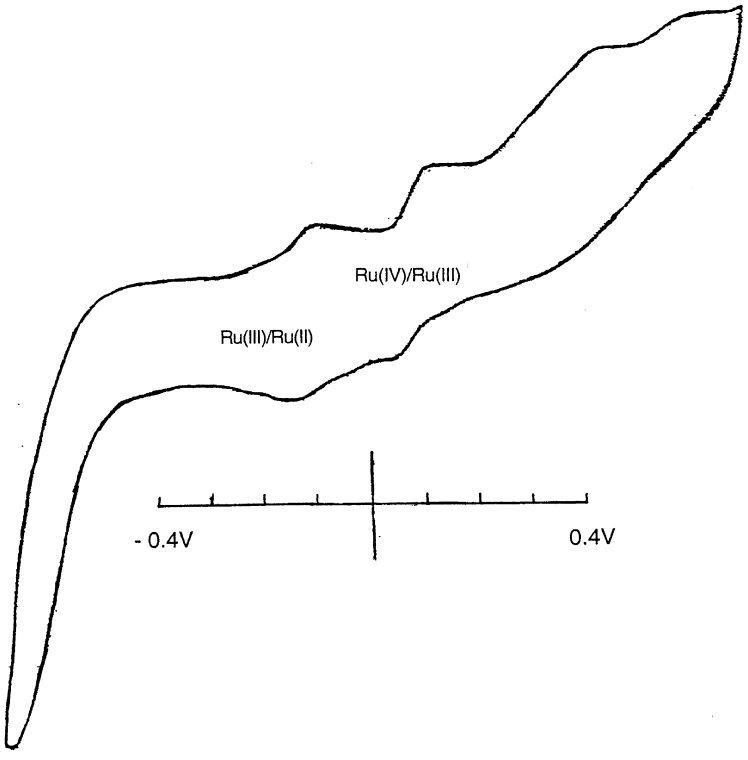

Fig. 4. Cyclic voltammogram of $Q_4PRu^{III}(H_2O)Mo_{11}O_{39}$.

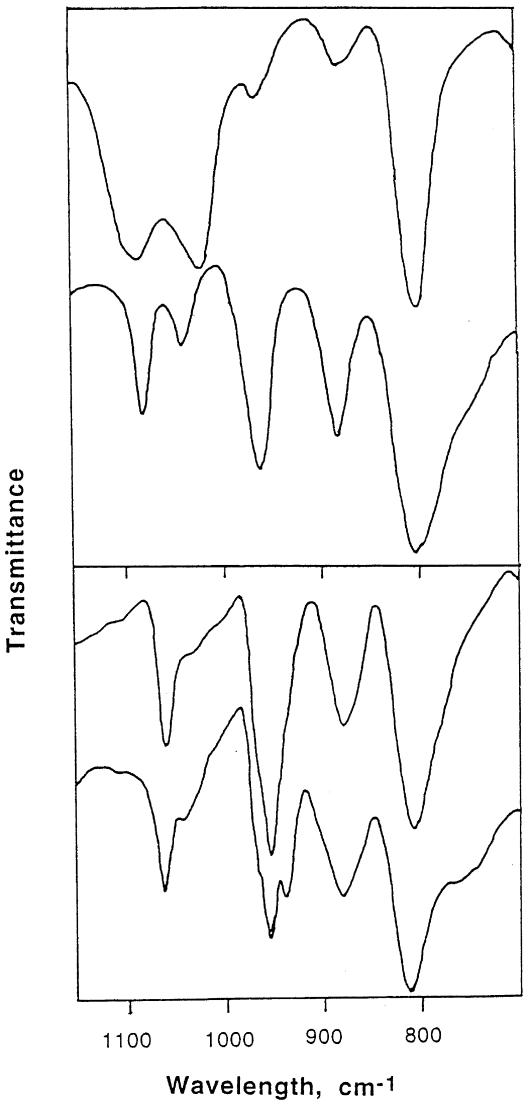

Fig. 5. IR spectrum of $Q_4PRu^{III}M_{11}O_{39}$ before and after treatment with O_2. Upper box: $Q_4PRu^{III}W_{11}O_{39}$ (top: before treatment with O_2, bottom: after treatment with O_2). Lower box: $Q_4PRu^{III}Mo_{11}O_{39}$ (top: before treatment with O_2, bottom: after treatment with O_2).

of a new absorption peak. An identical experiment replacing dioxygen with dinitrogen yielded the same change in the IR spectrum. A further UV–vis experiment (0.1 mM in acetonitrile, 1 atm O_2, 8 h, 60°C) with both the molybdenum and tungsten compounds showed the disappearance of the peaks in the visible region [Fig. 3(b)]. Our explanation of these results is that the bubbling of dioxygen or dinitrogen through a solution of $Q_4PRu^{III}(H_2O)Mo_{11}O_{39}$ in an apolar solvent only leads to the removal of the labile ligand [19]. This removal of the labile ligand manifests itself in the absence of peaks in the visible spectrum as has been reported also for the $ZnWRu(ZnW_9O_{34})_2^{12-}$ compound [9]. For the $Q_4PRu^{III}(H_2O)Mo_{11}O_{39}$ compound, there was also a change in the IR *i.e.*, the disappearance of the peak at 936 cm^{-1}. As stated above, we have postulated that the split peaks at 952 and 936 cm^{-2} were due to the presence of a labile ligand at the ruthenium atom. Removal of the ligand leads due a single peak indicative of only Mo–O_t stretching vibrations; importantly the Keggin structure is retained. Another indication of the absence of a significant structural change was obtained by ^{31}P NMR. The original broad peak at −105 ppm was unchanged after treatment with oxygen.

By contrast, in the case of the tungsten compound, $Q_4PRu^{III}(H_2O)W_{11}O_{39}$, after treatment with oxygen, there appeared in the IR spectrum a new distinct peak at 1019 cm^{-1} whilst the other peaks remained unchanged (Fig. 5). However, in this case, application of dinitrogen instead of dioxygen yielded only the original spectrum. The change in the IR spectrum of the tungsten analog, $Q_4PRu^{III}(H_2O)W_{11}O_{39}$, would seem to indicate some structural change in the polyoxometalate. There was also a clear change in the ^{31}P NMR spectrum. The original compound has a very broad peak at −70 ppm [15] whereas, after treatment, a new, narrower peak at 268 ppm ($\Delta\nu_{1/2}$ = 120 Hz) is formed. In addition, to the change in the IR and ^{31}P NMR spectra, heating of $Q_4PRu^{III}(H_2O)W_{11}O_{39}$ was also coupled with the formation of a black precipitate which was insoluble in a wide range of polar and apolar solvents. We have no certain explanation of which change has occurred, but the formation of a dimeric μ-oxo bridged species followed by precipitation of RuO_2 is a very distinct possibility [20]. Unfortunately, our hypothesis concerning the identity of the new ruthenium tungstate could not be verified due to our inability to obtain single crystals of sufficient quality. This speculation is also supported by the catalytic inertness of the tungsten compound *versus* the active molybdate (see below) [10]. Another puzzling point to explain concerns the reasoning behind the different reactivity of the molybdate and tungstate with molecular oxygen. The IR spectra of the original compounds (see above) indicate that the ruthenium is more tightly bound in the molybdate *versus* tungstate, as borne out by the smaller split in the vibrations atttributed to the P–O stretch. In the one case where a dimeric compound with a Ru^{IV}–O–Ru^{IV} bridge has been isolated [20], the bridge is placed over rather than in the lacunary position. It is possible but of course not certain that the more labile structure *vis a vis* the ruthenium position in the tungsten *versus* molybdenum compound may lead to a more facile formation of the bridged compound and ruthenium removal from the lacunary site of the tungstate.

Catalytic oxidation

In our previous communication, we reported that in a reaction according to Scheme 1 (1 M cumene, 1 M 1-octene, 1 mM $Q_4PRu^{III}(H_2O)M_{11}O_{39}$ (M = Mo, W)

in CH_3CN 1 atm O_2, 80°C, 24 h), the tungstate showed essentially no reactivity, whereas the molybdate, ~100 turnovers, gave ~1:1 ratio of 1-octene oxide/cumyl alcohol and only traces of acetophenone [10]. For the tungstate compound, the formation of an inert compound is postulated as mentioned and discussed above. For the molybdenum compound, there was a clear balance in the rate of formation of the intermediate cumene hydroperoxide and the oxygen transfer reaction from the intermediate to the alkene. An induction period of three to four hours was typically observed for these reactions. The ratio of cumene/1-octene (Fig. 6) was a critical parameter for determining the activity and selectivity in the $Q_4PRu^{III}(H_2O)Mo_{11}O_{39}$ catalyzed reaction. As the amount of cumene was increased, the turnover frequency to cumene hydroperoxide decomposition products (acetophenone and cumyl alcohol in excess of the amount of 1-octene oxide formed) increased significantly, whereas the amount of 1-octene oxide formed, (~100 turnovers) remained more or less constant. This shows that increased amounts of cumene had no positive effect on the rate of epoxide formation in the oxygen transfer reaction but, rather simply, was 'wasted' in the formation of decomposition products. The effect of $Q_4PRu^{III}(H_2O)Mo_{11}O_{39}$/substrate ratio on the conversions and selectivities is presented in Fig. 7 (ratio cumene/1-octene = 1). Here, one may observe that high catalyst loading *inhibited* the reaction. At $Q_4PRu^{III}(H_2O)Mo_{11}O_{39}$/substrate ratios up to 1/1500, there was an excellent selectivity to 1-octene oxide. As the solution became more dilute in catalyst and the $Q_4PRu^{III}(H_2O)Mo_{11}O_{39}$/substrate ratios decreased, there was a loss of activity in parallel with loss of selectivity for formation of the epoxide.

The results of the catalytic reaction are most easily explained via a combination of the classical [21] low valent metal (Ru^{III}) catalyzed autooxidation mechanism together with the heterolytic oxygen transfer mechanism at the high valent metal (Mo^{VI}), see

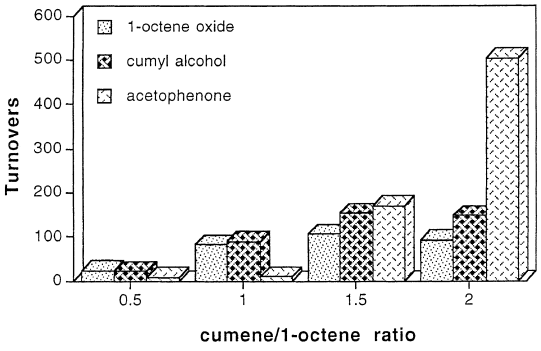

Fig. 6. Catalytic activity of $Q_4PRu^{III}(H_2O)Mo_{11}O_{39}$ as a function of the amount of cumene and 1-octene. Reaction conditions: 0.5–2.0 mmol cumene, 1 mmol 1-octene, 1 μmol $Q_4PRu^{III}(H_2O)Mo_{11}O_{39}$, 1 mL acetonitrile, 1 atm O_2, 80°C, 24 h.

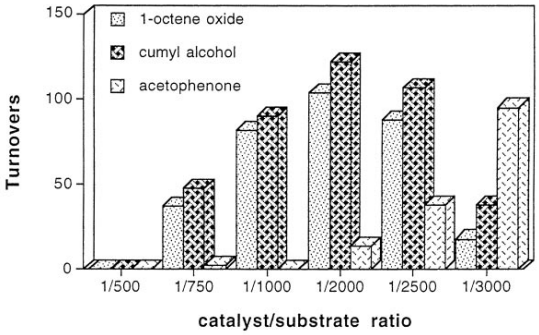

Fig. 7. The effect of the amount of $Q_4PRu^{III}(H_2O)Mo_{11}O_{39}$ on activity and selectivity. Reaction conditions: 1 mmol cumene, 1 mmol 1-octene, 0.33–2 μmol $Q_4PRu^{III}(H_2O)Mo_{11}O_{39}$, 1 mL acetonitrile, 1 atm O_2, 80°C, 24 h.

Scheme 2 [22]. First, the catalyst (Ru) initiates a chain reaction for the formation of cumene hydroperoxide. The intermediate alkyl hydroperoxo or peroxo species react with the molybdenum based polyoxometalate ligand to form an active Mo–O–O-alkyl species which transfers oxygen to the alkene to form epoxide and alcohol. When the catalyst loading is high the intermediate cumene peroxide is shunted by the catalyst from the propagation (autooxidation) reaction, leading to low turnover numbers and apparent reaction inhibition. Such phenomena have been observed in the past for transition metal substituted polyoxometalate catalyzed reactions [23]. When the amount of cumene is too high or the amount of catalyst is too low, the propagation of the cumene peroxide and hydroperoxide, independent of the catalyst, becomes the major reaction pathway. This then leads to excess autoxidation products, especially acetophenone via decomposition of the cumyl oxo radical [24].

CONCLUSION

A ruthenium substituted polyoxomolybdate, $Q_4PRu^{III}(H_2O)Mo_{11}O_{39}$, of the Keggin structure has been prepared and characterized. The compound is an effective bifunctional catalyst for the co-oxidation of cumene and 1-octene, in contrast to the analogous tungsten compound which undergoes, in the presence of molecular oxygen, an apparent structural change to an inert form.

EXPERIMENTAL PART

Materials and polyoxometalate synthesis

Organic substrates of highest available purity (Aldrich and Fluka) were purified prior to use by passing the compound over a neutral alumina column. The known polyoxometalates, $n-(C_4H_9)_4N]_4PRu^{III}(H_2O)W_{11}O_{39}^{15}$ and $[n\text{-}(C_4H_9)_4N]_4HPM(H_2O)Mo_{11}O_{39}$,

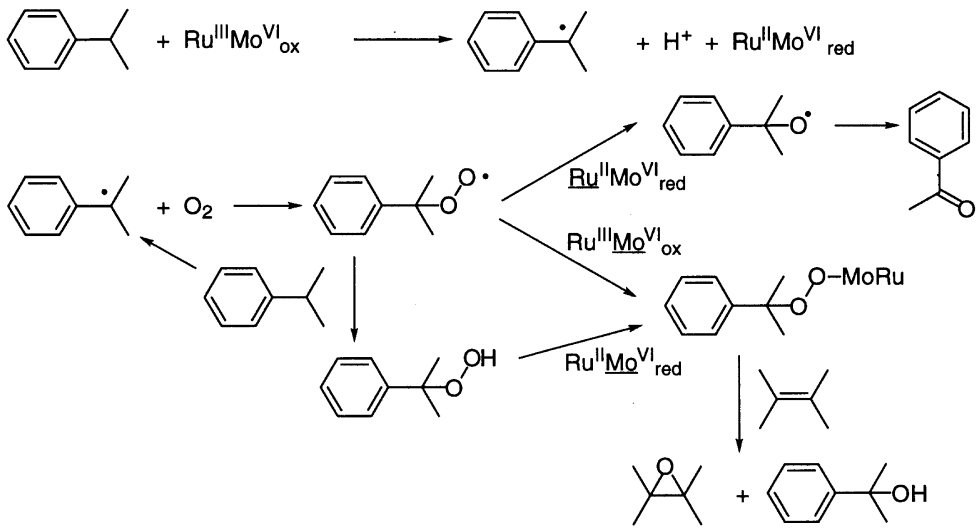

M = Mn (II), and Co(II) were prepared by the published literature procedures. Similarly, $[n\text{-}(C_4H_9)_4N]_4PRu^{III}(H_2O)Mo_{11}O_{39}$ was prepared by dissolving 0.30 mmol (800 mg) $[n-(C_4H_9)_4N]_4H_3PMo_{11}O_{39}$ [13] in 15 mL acetonitrile to form a light green solution followed by addition of 0.31 mmol (65 mg) solid $RuCl_3 \times H_2O$. After stirring for two hours under argon at room temperature, a few drops of water were added, air was passed through the solution for one hour and the solvent was evaporated. It may be noted that the insertion reaction failed when an aqueous solution of $RuCl_3 \times H_2O$ was used. The dark green ruthenium substituted polyoxomolybdate, $[n\text{-}(C_4H_9)_4N]_4PRu^{III}(H_2O)Mo_{11}O_{39}$ was recrystallized from 3 mL acetonitrile, yield 78%. Carbon, hydrogen, nitrogen and phosphorous were determined by microanalysis, ruthenium as RuO_2 and molybdenum as the 8-hydroxy quinolate were determined gravimetrically after decomposition with 1 M NaOH. Analysis: found (calculated) C 28.12 (27.46); H 5.57 (5.26); N 2.35 (2.00); P 1.00 (1.11); Ru 3.3 (3.61); Mo 36.93 (37.70). ^{31}P NMR -105 ppm ($\Delta\nu_{1/2} = 1500$ Hz). IR 1061, 1038, 952, 936, 878, 813 cm^{-1}

In an analogous procedure, $[n\text{-}(C_4H_9)_4N]_4PRu^{III}(DMSO)Mo_{11}O_{39}$ was prepared by reacting 0.30 mmol (800 mg) $[n\text{-}(C_4H_9)_4N]_4H_3PMo_{11}O_{39}$ in 15 mL with 0.31 mmol (130 mg) solid $Ru^{II}(DMSO)_4Cl_2$ [25]. After removal of the solvent overnight under vacuum, the product was recrystallized from 3 mL acetonitrile, yield 48%. Analysis: found (calculated) C 28.58 (27.72); H 5.65 (5.29); N 2.55 (1.96); P 1.00 (1.08); Ru 3.3 (3.53); Mo 38.45 (36.91). IR 1098, 1021, 933, 884, 806, 737 cm^{-1}.

Instruments and polyoxometalate characterization

UV–vis spectra were measured using a diode array spectrometer (HP 8452) using 1 cm quartz cuvettes. Solutions, 20 μM, were prepared by dissolving $Q_4PRu^{III}(L)Mo_{11}O_{39}$ ($Q = n\text{-}(C_4H_9)_4N$, $L = H_2O$, DMSO) in acetonitrile. IR spectra were measured on a Nicolet 510 M FTIR instrument. Spectra were measured neat by placing a few drops of the polyoxometalate dissolved in acetonitrile on a KBr plate. The acetonitrile was evaporated off and the spectra were measured. ^{31}P NMR spectra were measured using a Bruker DRX-400 instrument at 161.976 MHz with 85% D_3PO_4 as external standard. Approximately 10 mM solutions were prepared in 80% CH_3CN, 20% $CDCl_3$. A cyclic voltammogram of 5 mM $Q_4PRu^{III}(H_20)Mo_{11}O_{39}$ was measured using a BAS-1 instrument in a 0.1 M solution of $n\text{-}(C_4H_9)_4NBF_4$ in acetonitrile using a glassy-carbon working electrode, an $Ag/AgNO_3$ reference electrode and a platinum auxiliary electrode; scan rate 300 mV/sec. Potentials were referenced to the ferrocene/ferrocenium couple (-0.22 V).

Epoxidation of alkenes

The epoxidation of alkenes were carried out in $\sim$13 mL pressure tubes (Ace Glass). In a typical procedure, 1.0 mmol 1-octene, 1.0 mmol cumene and 1.0 μmol $[n\text{-}(C_4H_9)_4N]_4PRu^{III}(H_2O)Mo_{11}O_{39}$, dissolved in 1 mL acetonitrile, were placed in the glass tube with a teflon stirrer. Dioxygen, >99% purity, was introduced to the reaction at 80°C and 1 atm dioxygen after a series of three pump–thaw operations. The tubes were immersed in a temperature controlled oil bath equipped with a magnetic stirrer. Samples of the reaction mixture were taken at the desired time intervals and directly injected into a gas chromatograph (HP 5890, FID detector, He carrier gas) fitted with a capillary methyl silicone bonded phase column (RTX 1, length 15 m, ID 0.32 mm, coating thickness 0.25 μm).

Acknowledgements—This research was supported by the Israel Science Foundation founded by the Israel Academy of Science and Humanities. Professor Michael T. Pope of Georgetown University is kindly thanked for his sample of $Q_4PRu^{III}(H_2O)W_{11}O_{39}$.

REFERENCES

1. (a) Hill, C. L. and Prosser-McCartha, C. M., *Coord. Chem. Rev*., 1995, **143**, 407; (b) Okuhara, T., Mizuno, N. and Misono, M., *Adv. Catal*., 1996, **41**, 113; (c) Neumann, R., *Prog. Inorg. Chem*., 1998, **47**, 317.
2. Khenkin, A. M. and Hill, C. L., *J. Am. Chem. Soc*., 1993, **115,** 8178.
3. (a) Hill, C. L. and Brown, R. B., *J. Am. Chem. Soc*., 1986, **108**, 536; (b) Faraj, M. and Hill, C. L., *J. Chem. Soc*., *Chem. Commun*., 1987, 1487; (c) Katsoulis, D. E. and Pope, M. T., *J. Chem. Soc*., *Dalton Trans*., 1989, 1483; (d) Mansuy, D., Bartoli, J.-F., Battioni, P., Lyon, D. K. and Finke, R. G., *J. Am. Chem. Soc*., 1991, **113**, 7222; (e) Neumann, R. and Gara, M., *J. Am. Chem. Soc*., 1994, **116**, 5509; (f) Neumann, R. and Gara, M., *J. Am. Chem. Soc*., 1995, **117**, 5066; (g) Neumann, R. and Juwiler, D., *Tetrahedron*, 1996, **47**, 8781; (h) Pope, M. T. and Zhang, X.-Y., *J. Mol. Catal. A*, 1996, **114**, 201; (i) Neumann, R., Khenkin, A. M., Juwiler, D., Miller, H. and Gara, M., *J. Mol. Catal. A*, 1997, **117**, 169.
4. (a) Khenkin, A. M. and Hill, C. L., *Mendeleev Commun*., 1993, 140; (b) Zhang, X., Chen, Q., Duncan, D. C., Campana, C. F. and Hill, C. L., *Inorg. Chem*., 1996, **36**, 4208; (c) Zhang, X., Chen, Q., Duncan, D. C., Lachicotte, R. J. and Hill, C. L., *Inorg. Chem*., 1996, **36**, 4381.
5. (a) Mizuno, N., Tateishi, M., Hirose, T. and Iwamoto, M., *Chem. Lett*., 1993, 1985; (b) Mizuno, N., Hirose, T., Tateishi, M. and Iwamoto, M., *Chem. Lett*., 1993, 1839, (c) Zhang, X., Sasaki, K. and Hill, C. L., *J. Am. Chem. Soc*., 1996, **118**, 4809.
6. (a) Mizuno, N., Tateishi, M., Hirose, T. and Iwamoto, M., *Chem. Lett*., 1993, 2137; (b) Mizuno, N., Hirose, T., Tateishi, M. and Iwamoto, M., *J. Mol. Catal*., 1993, **88**, 125.
7. Droege, M. W. and Finke, R. G., *J. Mol. Catal*., 1991, **69,** 323.
8. Neumann, R. and Khenkin, A. M., *J. Mol. Catal*., 1996, **114,** 169.
9. (a) Neumann, R. and Abu-Gnim, C., *J. Chem. Soc*., *Chem. Commun*., 1989, 1324; (b) Neumann, R. and Abu-Gnim, C., *J. Am. Chem. Soc*., 1990, **112**, 6025; (c) Steckhan, E. and Kandzia, C., *Synlett*, 1992, 139; (d) Neumann, R., Khenkin, A. M. and Dahan, M., *Angew. Chem*., *Int. Eng. Ed*., 1995, **34**, 1587; (e) Neumann, R. and Khenkin, A. M., *Inorg. Chem*., 1995, **34**, 5753; (f) Neumann, R. and Dahan, M., *Nature*, 1997, **388**, 353.
10. Neumann, R. and Dahan, M., *J. Chem. Soc*., *Chem. Commun*., 1995, **00,** 171.
11. (a) Chang, C. J., Labinger, J. A. and Gray, H. B., *Inorg. Chem*., 1997, **36**, 5927; (b) Arzoumanian, H., Blanc, A., Hartig, U. and Metzger, J., *Tetrahedron Lett*., 1974, 1011; (c) Ciborowski, S., *Pol. J. Appl. Chem*., 1994, **38**, 525.
12. Arzoumanian, H., Bitar, H. and Metzger, J., *J. Mol. Catal*., 1980, **7,** 373.
13. Combs-Walker, L. A. and Hill, C. L., *Inorg. Chem*., 1991, **30,** 4016.
14. There is a possiblity that after insertion with $Ru^{II}(DMSO)_4Cl_2$, the product obtained is a ruthenium(II) species, $Q_4HPRu^{II}(DMSO)Mo_{11}O_{39}$, despite the oxidizing workup conditions.
15. Rong, C. and Pope, M. T., *J. Am. Chem. Soc*., 1992, **114,** 2932.
16. Rocchiccioli-Deltcheff, C. and Touvenot, R., *J. Chem. Res*. (*M*), 1977, **00,** 546.
17. From Ref. 13, it would appear that the position of the peak at these wavenumbers is strongly a function of the acetonitrile/aquo ligand.
18. Pope, M. T., *Heteropoly and Isopoly Oxometalates*. Springer, New York (1983).
19. Katsoulis, D. E. and Pope, M. T., *J. Am. Chem. Soc*., 1984, **106,** 2737.
20. Randall, W. J., Weakley, T. J. R. and Finke, R. G., *Inorg. Chem*., 1993, **32,** 1068.
21. Sheldon, R. A. and Kochi, J. K., *Metal Catalyzed Oxidations of Organic Compounds*. Acadenic Press, New York (1981).
22. The reduced Ru–POM species is represented where the electron is localized at the ruthenium atom. This is not necessarily so, although the degree of delocalization onto the molybdenum addenda is unknown.
23. Kholdeeva, O. A., Grigoriev, V. A., Maksimov, G. M., Fedotov, M. A., Golovin, A. V. and Zamaraev, K. I., *J. Mol. Catal*., 1996, **114**, 123.
24. Neumann, R. and Khenkin, A. M., *Chem. Commun*., 1996, **00,** 2643.
25. Evans, I. P., Spencer, A. and Wilkinson, G., *J. Chem. Soc*., *Dalton Trans*., 1973, **00,** 204.

Pergamon

PII: S0277-5387(98)00150-8

Polyhedron Vol. 17, No. 20, pp. 3565–3573, 1998
© 1998 Elsevier Science Ltd
All rights reserved. Printed in Great Britain
0277–5387/98 $19.00+0.00

Synthesis, crystal structure and magnetic properties of bis(1,1,1,5,5,5-hexafluoropentane-2,4-dionato) manganese(II) complexes with diazine ligands

Dang-Ming Hong[a], Ho-Hsiang Wei[b]*, Kuo-Hui Chang[b], Gene-Hsiang Lee[c] and Yu Wang[c]

[a]Tzu-Chi Junior College of Nursing, Hualien, Taiwan

[b]Department of Chemistry, Tamakng University, Tamsui, Taiwan

[b]Instrumental Center of College of Science, National Taiwan University, Taipei, Taiwan

(Received 8 December 1997; accepted 14 April 1998)

Abstract—One dinuclear $[Mn_2(hfac)_4(\mu\text{-pyz})(H_2O)_2]2H_2O$ (**1**) and three mononuclear complexes $[Mn(hfac)_2(pym)(H_2O)]$ (2), $[Mn(hfac)_2(pydz)_2]$ (3), and $[Mn(hfac)_2(mpydz)_2]$ (**4**) (Hhfac = 1,1,1,5,5,5-hexafluoropentane-2,4-dione, pyz = pyrazine, pym = pyrimidine, pydz = pyridazine, and mpydz = 3-methylpyridazine) have been synthesized and their crystal structures and cryomagnetic properties have been investigated. Complex **1** has a centrosymmetric dinuclear structure with two adjacent manganese atoms linked by a pyz ligand. The geometry about each manganese atom is distorted octahedral with NO_5 coordination sphere. The structure of complex **2** is a mononuclear manganese complex with a distorted octahedral geometry of NO_5 coordination sphere. The crystal structures of complexes **3** and **4** consist of mononuclear manganese complex with the *cis*-N_2O_4 six-coordination sphere. The temperature dependence of magnetic data for **1** revealed a dinuclear spin ($S_1 = S_2 = 5/2$) weak antiferromagnetic exchange interaction with $J = -0.47\,cm^{-1}$. Complexes **2**–**4** play a cryomagnetic behaviour followed the Curie–Weiss law. © 1998 Elsevier Science Ltd. All rights reserved

Keywords: crystal structure; magnetic properties; manganese complexes; binuclear complexes; diazine complexes.

INTRODUCTION

The coordination chemistry of manganese has achieved remarkable progress in the past decade due to the increased recognition of this metal's role in the biological system involved in the oxygen-evolving complexes of photosystem II of green plants [1, 2] and catalases [1, 3, 4].

A number of manganese-containing, non-haem catalases have, in recent years, been isolated and characterized [3, 4]. This important class of metalloprotein catalyses the disproportionation of hydrogen peroxide to dioxygen and water very efficiently. Recently, some studies have been achieved in the preparation of a number of functional, non-haem catalase mimics of the model manganese complexes [5, 6].

As part of our continuing studies into the magneto-structural correlation of manganese(II) complexes with 2,2′-dipyrimidine (bpym) [7], very recently, we have prepared three complexes of bis(2,4-pentanedionate)manganese(II) with diazine ligands and these complexes exhibited high catalytic activity for H_2O_2 disproportionation [8]. Heterocyclic diazines, such as pyrazine, pyrimidine and pyridazine, are known to be an excellent bidentate ligand when coordinated to metal ions [9]. In our laboratory, we have continually prepared four new bis(1,1,1,5,5,5-hexafluoropentane-2,4-dionate)manganese(II) complexes with diazines: $[Mn_2(hfac)_4(\mu\text{-pyz})(H_2O)_2]2H_2O$ (**1**), $[Mn(hfac)_2(pym)(H_2O)]$ (**2**), $[Mn(hfac)_2(pydz)_2]$ (**3**) and $[Mn(hfac)_2(mpydz)_2]$ (**4**) (pyz = pyrazine, pym =

* Author to whom correspondence should be addressed.

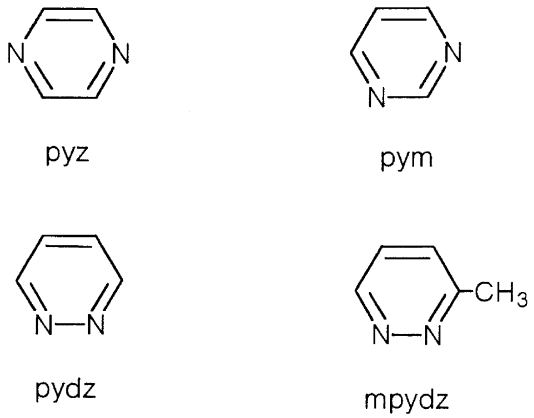

Scheme 1.

pyrimidine, pydz = pyridazine, and mpydz = 3-methylpyridazine) (Scheme 1). Here, we reported on the synthesis, X-ray crystal structure and cryomagnetic properties.

EXPERIMENTAL

2.1. *Preparation of compounds*

Bis(1,1,1,5,5,5-hexafluoropentane-2,4-dionate)manganese(II) dihydrate, $Mn(hfac)_2 \cdot 2H_2O$, was prepared from the metal acetate by the literature procedures [10]. Pyrazine (pyz), pyrimidine (pym), pyridazine (pydz) and 3-methylpyridazine (mpydz) were purchased from a commercial source (Aldrich Chemical Co.) and used without further purification.

$[Mn_2(hfac)_4(\mu\text{-pyz})(H_2O)_2]2H_2O$ (**1**), $[Mn(hfac)_2(pym)(H_2O)]$ (**2**), $[Mn(hfac)_2(pydz)_2]$ (**3**) and $[Mn(hfac)_2(mpydz)_2]$ (**4**) were synthesized by mixing the absolute ethanol solutions of an equimolar quantity of the complex $Mn(hfac)_2 2H_2O$ and the diazines. The solutions were allowed to stand for a few days, orange–yellow crystals of **1** (75% yield), light-yellow crystals of **2** (85% yield), **3** (75% yield) and **4** (80% yield) were filtered off, air dried and characterized initially by elemental analysis and then by single-crystal X-ray diffractional analysis. (Found: C, 26.5; H, 1.4; N, 2.7. Calc. for $C_{24}H_{16}F_{24}N_2Mn_2O_{12}$ (**1**): C, 2.64; H, 1.5; N, 2.6%. IR (KBr disc): 1650 vs, 1572 m, 1530 m, 1502 s, 1250 vs, 1200 s, 1152 vs, 801 m, 670 s, 600 m cm^{-1} Found: C,29.5; H, 1.4; N, 4.9. Calc. for $C_{14}H_8F_{12}N_2MnO_5$ (**2**): C, 29.6; H, 1.4, N, 4.9%. IR (KBr disc): 1648 vs, 1594 m, 1561 m, 1535 s, 1491 s, 1254 vs, 1209 vs, 1147 vs, 1079 m, 804 s, 715 m, 666 s, 587 m cm^{-1}. Found: C, 34.2; H, 1.7; N, 8.9. Calc. for $C_{18}H_{10}F_{12}N_4MnO_4$ (**3**): C, 34.3; H, 1.6; N, 8.9%. IR (KBr disc): 1652 vs, 1589 m, 1529 m, 1502 vs, 1450 m, 1423 m, 1259 vs, 1224 vs, 1199 vs, 1143 vs, 1090 m, 1068 m, 972 s, 796 s, 765 m, 605 vs, 586 m cm^{-1}. Found: C, 36.3; H, 2.2; N, 8.5. Calc. for $C_{20}H_{14}F_{12}N_4MnO_4$ (**4**): C, 36.5; H, 2.1; N, 8.5%. IR (KBr disc): 1648 vs, 1591 m, 1555 s, 1526 s, 1459 vs, 1449 s, 1253 vs, 1216 s, 1197 s, 1147 vs, 1095 m, 821 m, 794 s, 663 s, 581 m cm^{-1}.

Physical measurements

IR spectra were recorded on a Bio-Rad FTS40-FTIR spectrophotometer as KBr pellets in the 4000–400 cm^{-1} region. X-band EPR spectra at 25°C for the complexes in powder were recorded on a Bruker ESC-106 spectrometer. Temperature dependence of magnetic susceptibilities of the polycrystalline samples were measured between 4 and 300 K at field 1 T, using a Quantum Design Model MPMS computer-controlled SQUID magnetometer. Corrections for the diamagnetism of the complexes were estimated from Pascal's constants [11].

Crystal structure determination

Crystallographic data for complexes **1**–**4** were collected on an Enraf–Nonius CAD-4 diffractometer with graphite-monochromatized Mo–K_α radiation ($\lambda = 0.7107$ Å) at 25°C. Crystallographic parameters and pertinent refinement results are summarized in Tables 1 and 2. The structures were solved by the heavy-atom method using a Patterson map and refined by a full-matrix least-squares method based on *F*, using the NRCVAX software package [12]; the function minimized was $\Sigma w(|F_o| - |F_c|)^2$ with $w = 1/\sigma^2(F_o)$ and unit weights were used. All non-hydrogen atoms were readily located and refined with anisotropic thermal parameters.

RESULTS AND DISCUSSION

3.1. *Crystal structures of complexes **1**–**4***

Perspective views with the atomic numbering of complexes **1, 2, 3**, and **4** are shown in Figs 1–4, respectively. The selected bond distances and angles relevant to manganese coordination spheres are given in Tables 3–6.

Complex **1** has a centrosymmetric dinuclear structure and two adjacent manganese atoms, 5.968(4) Å apart, are linked by a pyz bridging ligand. This intermetallic separation is expected for a weak intramolecular antiferromagnetic exchange interaction between two Mn(II) atoms. The geometry about each manganese atom is distorted octahedral with NO_5 coordination sphere. The axial positions are filled with the nitrogen atom of the bridging pyz ligand and the oxygen atom [O(5)] of the water molecule, while the four equatorial positions are occupied by four oxygens [O(4),O(2),O(3),O(4)] from the bidentate hfac ligands. It is notable that F(10), F(11) and F(12) of the CF_3 group of the hfac ligand are rotationally disordered about the C(11)–C(12) bond.

Table 1. Crystallographic data for complexes **1**–**2**

	1	**2**
Formula	$C_{24}H_{16}F_{24}N_2Mn_2O_{12}$	$C_{14}H_8F_{12}N_2Mn_2O_5$
Formula weight	1090.22	567.14
Space group	Monoclinic, $P2_1/c$	Triclinic, $P\bar{1}$
a (Å)	11.4342(19)	8.8790(14)
b (Å)	24.937 (6)	10.8927(22)
c (Å)	7.007(3)	11.759(3)
α (Å)		110.737(17)
β (Å)	104.17(3)	90.351(15)
γ (Å)		103.066(15)
V (Å^3)	1937.1(11)	1031.4(3)
Z	2	2
D_{calc} (g cm^{-3})	1.869	1.826
$F(000)$	1072	558
Unit-cell detectionl 2θ range	25; (14.70–24.10)	25, (15.52–24.66)
Scan type	$\theta/2\theta$	$\theta/2\theta$
2θ scan width (°)	$2(0.80+0.35\tan\theta)$	$2(0.60+0.35\tan\theta)$
2θ range (°)	45.0	50
μ(Mo–K$_\alpha$) (cm^{-1})	4.026	7.562
Crystal size (mm)	$0.05\times0.05\times0.50$	$0.40\times0.40\times0.5$
Temperature (K)	298	298
No. of uniqueness reflections	2524	3638
No. of observed reflections [$I>2\sigma(I)$]	1198	2945
R, R_w [a]	0.057; 0.051	0.050; 0.051
GoF	1.77	1.58
$(\Delta/\sigma)_{max}$	0.0241	0.0018
$(\Delta\rho)_{min,max}$ (e Å^{-3})	−0.380; 0.450	−0.430; 0.510

[a] $R=[\Sigma|F_o-F_c|/F_o]$, $R_w=\Sigma w[|F_o-F_c|^2/\Sigma w(|F_o|^2)]^{1/2}$.

Table 2. Crystallographic data for complexes **3**–**4**

	3	**4**
Formula	$C_{18}H_{14}F_{12}N_4MnO_4$	$C_{20}H_{14}F_{12}N_4MnO_4$
Formula weight	633.253	657.27
Space group	Monoclinic, $P2_1/c$	Monoclinic, $P2_1/n$
a (Å)	13.333(3)	14.993(7)
b (Å)	11.0580(13)	8.575(3)
c (Å)	17.510(3)	21.101(4)
β (Å)	111.882(16)	92.89(3)
V (Å^3)	2395.7(7)	2709.4(17)
Z	4	4
D_{calc} (g cm^{-3})	1.745	1.611
$F(000)$	1260	1308
Unit-cell detection; 2θ range	25, (18.64–30.00)	25; (14.96–22.32)
Scan type	$\theta/2\theta$	$\theta/2\theta$
2θ scan width(°)	$2(0.70+0.35\tan\theta)$	$2(0.80+0.35\tan\theta)$
2θ range (°)	50	45
μ(Mo–K$_\alpha$) (cm^{-1})	6.486	5.794
Crystal size (mm)	$0.20\times0.30\times0.50$	$0.20\times0.20\times0.20$
Temperature (K)	298	298
No. of uniqueness reflections	4214	3739
No. of observed reflections [$I>2\sigma(I)$]	2717	1812
R, R_w [a]	0.064; 0.060	0.065; 0.065
GoF	1.33	2.37
$(\Delta/\sigma)_{max}$	0.0714	0.0107
$(\Delta\rho)_{min,max}$ (e Å^{-3})	−0.590; 0.690	−0.390; 0.460

[a] $R=[\Sigma|F_o-F_c|/F_o]$, $R_w=\Sigma w[|F_o-F_c|^2/\Sigma w(|F_o|^2)]^{1/2}$.

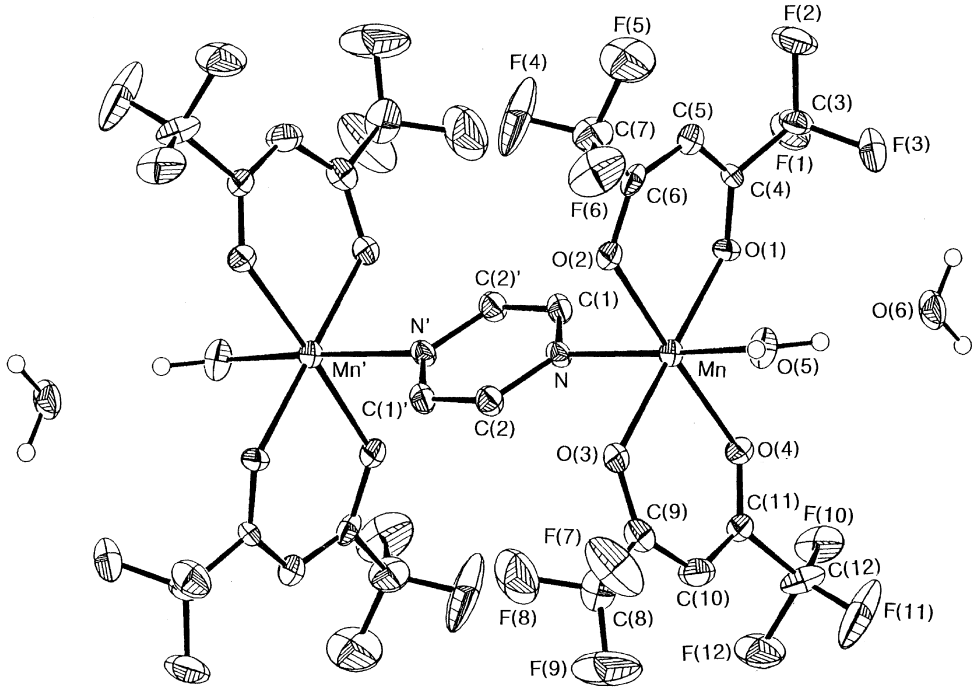

Fig. 1. Molecular structure of $[Mn_2(hfac)_4(pyz)(H_2O)_2 2H_2O$ **1** with the atomic numbering scheme (30% probability thermal ellipsoids).

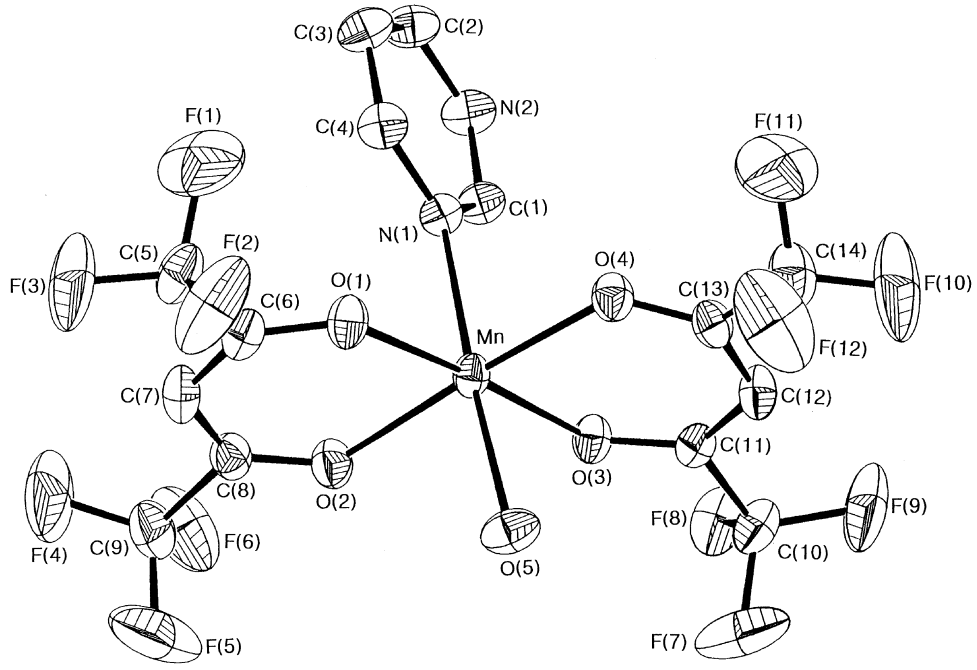

Fig. 2. Molecular structure of $[Mn(hfac)_2(pym)(H_2O)]$ **2** with the atomic numbering scheme (30% probability thermal ellipsoids).

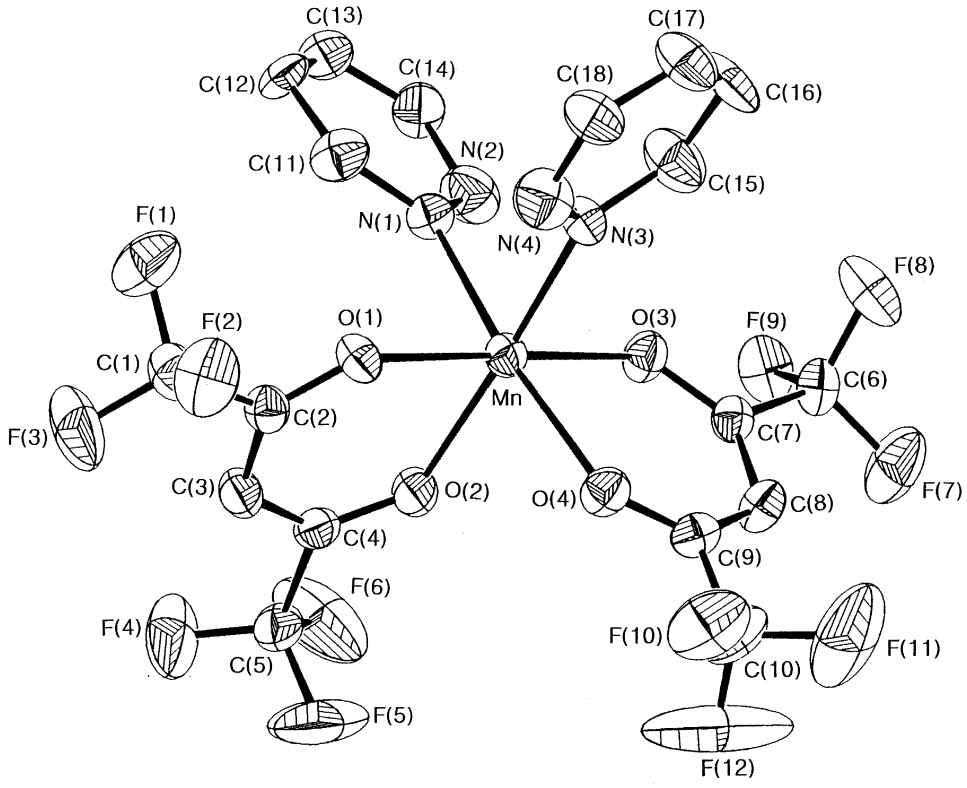

Fig. 3. Molecular structure of $[Mn(hfac)_2(pydz)_2]$ **3** with the atomic numbering scheme (30% probability thermal ellipsoids).

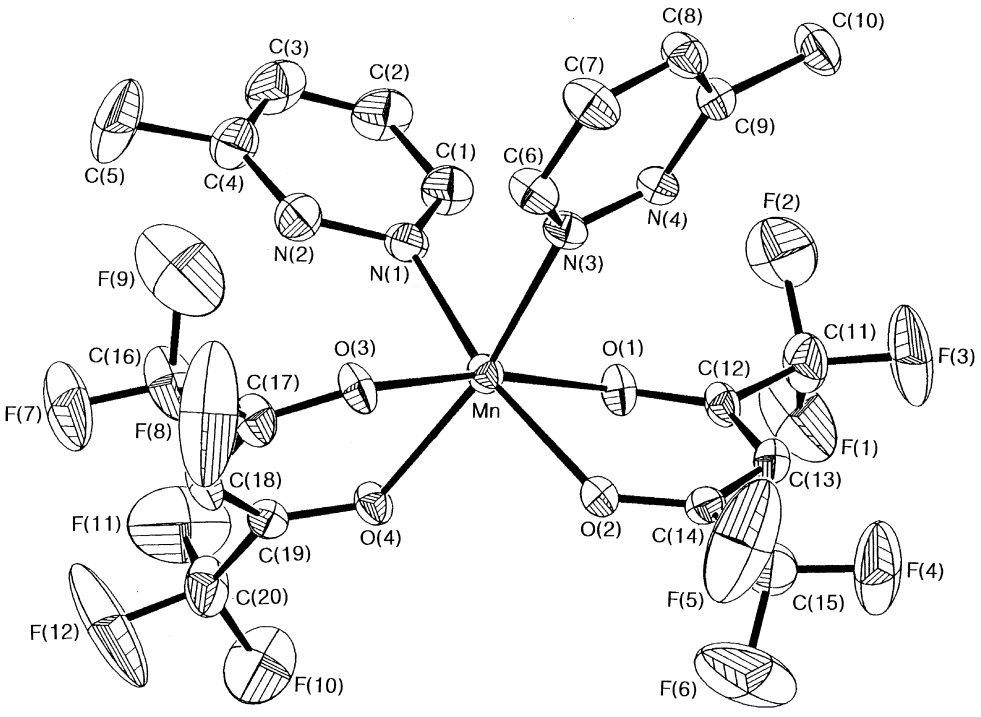

Fig. 4. Molecular structure of $[Mn(hfac)_2(mpydz)_2]$ **4** with the atomic numbering scheme (30% probability thermal ellipsoids).

Table 3. Selected bond distances (Å) and angles (°) for **1**

Mn–N	2.332(18)	Mn–O(1)	2.120(6)
Mn–O(2)	2.163(6)	Mn–O(3)	2.140(6)
Mn–O(4)	2.136(6)	Mn–O(5)	2.172(7)
Mn···Mn	5.968(4)		
N–Mn–O(5)	172.6(3)	O(1)–Mn–O(3)	178.7(3)
O(2)–Mn–O(4)	175.1(3)	O(1)–Mn–O(2)	84.24(24)
O(3)–Mn–O(4)	84.46(25)	O(2)–Mn–O(3)	95.2(3)
O(1)–Mn–O(4)	95.94(24)	O(2)–Mn–N	89.63(25)
O(3)–Mn–N	89.71(25)	C(1)–N–C(2)	115.9(8)
Mn–N–C(2)	122.5(6)		

Table 4. Selected bond distances (Å) and angles (°) for **2**

Mn–N(1)	2.285(3)	Mn–O(1)	2.132(3)
Mn–O(2)	2.154(3)	Mn–O(3)	2.132(3)
Mn–O(4)	2.139(3)	Mn–O(5)	2.214(3)
N(1)–Mn–O(5)	176.90(13)	O(1)–Mn–O(3)	176.62(12)
O(2)–Mn–O(4)	176.67(12)	O(1)–Mn–O(2)	83.84(12)
O(3)–Mn–O(4)	84.91(11)	O(1)–Mn–N(1)	90.48(12)
O(2)–Mn–O(5)	89.80(13)	O(3)–Mn–O(5)	85.16(12)
O(4)–Mn–N(1)	90.98(12)	O(1)–Mn–O(4)	96.81(12)
O(2)–Mn–O(3)	94.28(11)	Mn–N(1)–C(4)	122.2(3)
Mn–N(1)–C(1)	122.0(3)		

Table 5. Selected bond distances (Å) and angles(°) for **3**

Mn–N(1)	2.270(5)	Mn–N(3)	2.258(5)
Mn–O(1)	2.130(4)	Mn–O(2)	2.188(4)
Mn–O(3)	2.118(4)	Mn–O(4)	2.195(4)
N(1)–Mn–O(4)	168.74(17)	N(3)–Mn–O(2)	171.78(17)
O(1)–Mn–O(3)	175.1(17)	O(1)–Mn–O(2)	24.36(15)
O(3)–Mn–O(4)	82.28(15)	O(1)–Mn–N(1)	91.73(17)
O(2)–Mn–O(4)	87.40(17)	O(4)–Mn–N(3)	91.04(13)
N(1)–Mn–N(3)	90.72(19)	O(3)–Mn–N(3)	94.06(18)
Mn–N(1)–C(11)	122.1(4)	Mn–N(1)–N(2)	121.8(4)
Mn–N(3)–N(4)	122.0(4)	Mn–N(3)–C(15)	122.5(4)

The average Mn–O [2.115 Å] bond distances of Mn–O(1), Mn–O(2), Mn–O(3) and Mn–O(4) are somewhat shorter than those of Mn–O(5) [2.172(7) Å] and Mn–N [2.332(8) Å] Table 2. The bond angles of N–Mn–O(1) [91.46(25)°] and N–Mn–O(4) [95.2(3)°] are larger than those of N–Mn–O(2) [89.63(25)°] and N–Mn–O(3) [89.71(25)°]. Furthermore, the resultant bond angle of the axial N–Mn–O(5) [172.6(3)°] deviated from 180°.

The structure of **2** is a mononuclear manganese(II) complex with a distorted octahedral geometry of NO_5 coordination sphere. The manganese coordination sphere consists of two chelating hfac ligands, one monodentate pym ligand and one water molecule. The axial positions are occupied by nitrogen [N(1)] of the pym and oxygen [O(5)] of the water molecule, and the four equatorial positions are occupied by oxygen atoms from the bidentate hfac ligands that form a tetragonal plane. The in-plane equatorial average Mn–O bond distances of 2.139 Å are somewhat shorter than the axial Mn–O(5) [2.214(3) Å] and Mn–N(5) [2.285(3) Å] bond distances.

The crystal structure of **3** consists of the neutral $[Mn(hfac)_2(pydz)_2]$ units. The complex has an approxi-

Table 6. Selected bond distances (Å) and angles (°) for **4**

Mn–N(1)	2.233(7)	Mn–N(3)	2.247(7)
Mn–O(1)	2.145(3)	Mn–O(2)	2.177(6)
Mn–O(3)	2.137(5)	Mn–O(4)	2.174(5)
N(1)–Mn–O(2)	166.33(24)	N(3)–Mn–O(4)	167.14(23)
O(1)–Mn–O(3)	170.38(52)	O(1)–Mn–O(2)	80.97(21)
O(3)–Mn–O(4)	81.58(21)	N(1)–Mn–O(3)	102.3(3)
N(3)–Mn–O(1)	98.60(25)	N(1)–Mn–O(4)	86.04(24)
N(3)–Mn–N(1)	87.13(24)	N(3)–Mn–O(3)	86.77(24)
O(1)–Mn–O(1)	85.90(25)	N(1)–Mn–N(3)	91.1(3)
Mn–N(1)–N(2)	109.4(5)	Mn–N(1)–C(1)	130.9(6)
Mn–N(3)–N(4)	110.4(5)	Mn–N(3)–C(6)	128.9(6)

mate C_2 axis of symmetry. The coordination geometry of Mn belongs to the six-coordination type by virtue of two bidentate hfac and two pydz ligands, in which two pydz ligands are of *cis* arrangement. The three oxygens [O(2),O(3),O(4)] from the hfac and one nitrogen [N(1)] from the pydz ligand are approximately coplanar and the atoms of nitrogen [N(3)] of pydz and oxygen [O(2)] lie on an axial perpendicular to this plane. The bond distances of Mn–O(2) [2.188(4) Å] and Mn–O(4) [2.195(4) Å] show longer lengths than those of Mn–O(1) [2.130(4) Å] and Mn–O(3) [2.118(4) Å]. Both of the Mn–O(2) and Mn–O(4) bonds are *trans* to the two pydz basic ligands, are lengthened compared with the others of Mn–O(1) and Mn–O(3) bonds due to a *trans* effect of the pydz ligands. The bond angles of O(1)–Mn–O(3) [175.65(17)°] are somewhat larger than those of O(2)–Mn–N(3) [171.78(17)°] and O(4)–Mn–N(1) [168.74(17)°]. Furthermore, The bond angles of Mn–N(1)–N(2) [121.8(4)°], Mn–N(1)–C(11) [122.1(4)°], Mn–N(3)–N(4) [122.0(4)°] and Mn–N(3)–C(15) [122.5(4)°] are similar and normal [13].

The crystal structure of **4** is also a mononuclear manganese(II) complex. The coordination geometry of Mn also belongs to the N_2O_4 distorted octahedral type, being similar to that of Mn in complex **3**. The two pydz molecules are coordinated by the less hindered 1-nitrogen atoms [N(1) and N(3)]. Mn–O(2) [2.177(6) Å] and Mn–O(4) [2.174(5) Å] bonds show longer lengths than Mn–O(4) [2.145(5) Å] and Mn–O(3) [2.137(5) Å] as well as in complex **3**, these elongations are also due to a *trans* effect of the mpydz ligands. The bond angles of Mn–N(1)–N(2) [109.4(5)°] and Mn–N(3)–N(4) [110.4(5)°] are smaller than those of Mn–N(1)–C(1) [130.9(6)°] and Mn–N(3)–C(6) [128.9(6)°]. These different angles are probably due to the substantial steric interactions between the methyl groups of mpydz and the trifluoromethyl groups of hfac ligands. The resultant bond angles of O(2)–Mn–N(1) and O(4)–Mn–N(3) are 166.33(24)° and 167.14(23)°, respectively. Comparison of the Mn–N(1) and Mn–N(3) bond distances for **4** and **3** give 2.233(7) *vs.* 2.270(7) Å and 2.247(7) *vs.* 2.258(5) Å. This may result from the rather higher basicity of the mpydz than the pydz ligand.

EPR spectra and cryomagnetic properties

The powder X-band EPR spectra (9.80 GHz) at 300 K of complexes **1** and **2** display *ca* 0.062 and 0.095 T, respectively, symmetric broad resonance absorptions with the same g value of 2.02. Whereas, at 300 K, the EPR spectra, without discernible hyperfine structure of ^{55}Mn, for **3** and **4** are observed with resonances at g: 5.4 (w), 3.18 (w), 2.03 (s) and 1.42 (w) for **3**; 6.7 (w), 2.70 (w), 1.96 (s) and 1.47 (w) for **4**. These data thus indicate that, in complexes **3** and **4**, and even in complexes **1** and **2**, there exist weak magnetic interactions or zero-field splitting interactions (D). Although the low temperature EPR spectrum for the present complexes has not been determined, in our case however, for octahedral high-spin Mn(II), due to its smaller Jahn–Teller effect, in general, the values of D for the present species are of the order of $10^{-2}\,cm^{-1}$ [14, 15].

The cryomagnetic behavior of complex **1** represented by the plots of molar magnetic susceptibility, χ_m and $\chi_m T$ *vs.* T is depicted in Fig. 5. At 300 K, $\chi_m T = 8.15\,cm^3\,K mol^{-1}$, a value somewhat smaller than expected for two uncoupled manganese(II) ions; $\chi_m T$ slowly decreases upon cooling and reaches a value of $7.34\,cm^3\,K mol^{-1}$ at 4 K. Such a behavior is characteristic of a weak antiferromagnetic interaction between two high-spin manganese(II) ions. We have attempted to reproduce theoretically the experimental magnetic data of dinuclear complex **1** by use of the temperature-dependent magnetic susceptibility expression eq. (1) [16],

$$\chi_m = (2Ng^2\mu_B/kT)(A/B), \qquad (1)$$

based on the isotropic Heisenberg model ($H = -2JS_1S_2$), without intermolecular interaction and the Mn(II) single-ion zero-field considerations, coupling for $S_1 = S_2 = 5/2$, where $A = x^{28} + 5x^{24} + 14x^{18} + 30x^{10} + 55$, $B = x^{30} + 3x^{28} + 5x^{24} + 7x^{18} + 9x^{10} +$

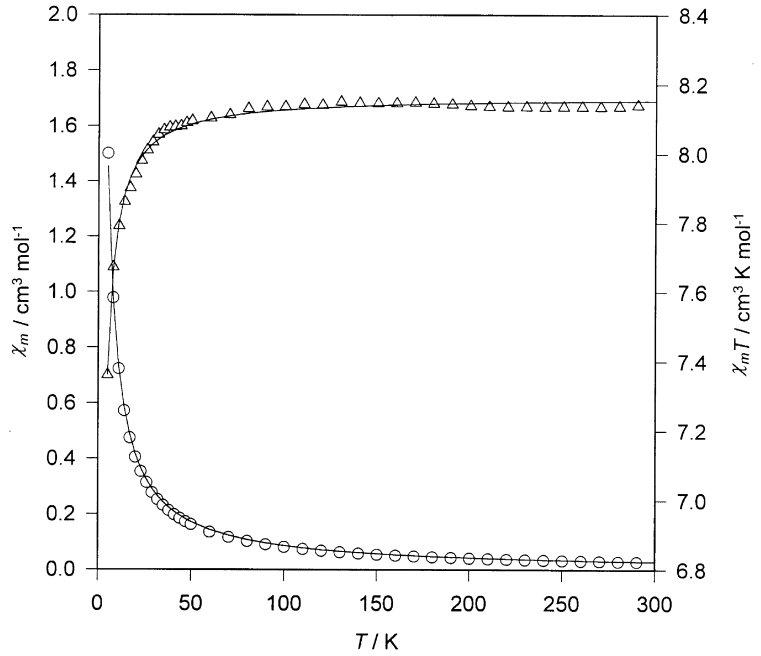

Fig. 5. Plots of χ_m (○) and $\chi_m T$ (△) *vs.* T for $[Mn_2(hfac)_4(pyz)(H_2O)_2]2H_2O$ **1**. The solid line is the fit provided by equation (1) (see text).

11 and $x = \exp(-J/kT)$; the other symbols have their usual meanings. The temperature-independent paramagnetics for Mn(II) are assumed to be zero. Values of $-0.47\,cm^{-1}$ and 2.02 were obtained for J and g, respectively. The best data fits, as shown in Fig. 5 (the solid lines), display that a satisfactory match to the experimental data is achieved. Consequently, the weak antiferromagnetic coupling J for **1** most likely accounts for the longer metal–metal separation (5.97 Å) through the bridged pyrazine ligand.

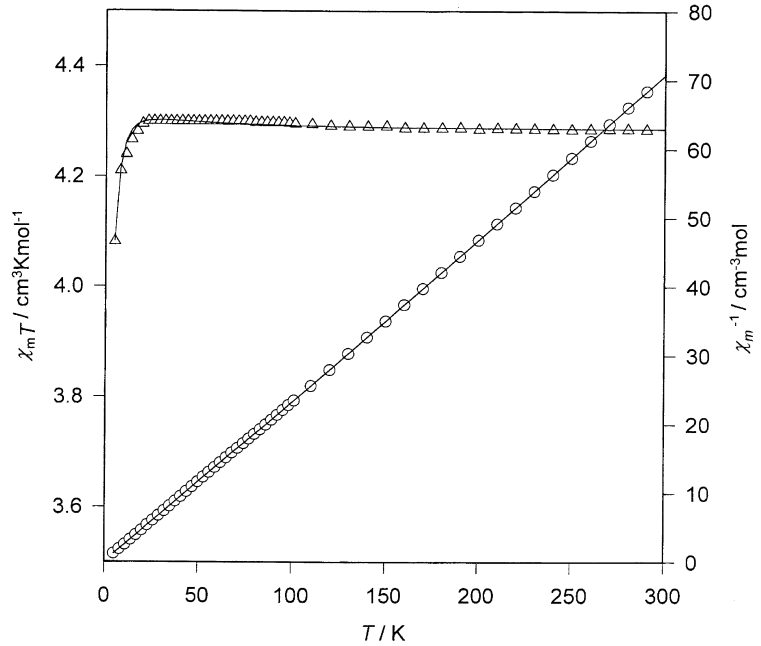

Fig. 6. Plots of χ_m^{-1} (○) and $\chi_m T$ (△) *vs.* T for $[Mn(hfac)_2(pydz)_2]$ **3**. The solid line is the fit provided by equation (2) (see text).

Magnetic susceptibility measurements for mononuclear complexes **2**–**4** were made on powder samples in the temperature range 4–300 K. The values of $\chi_m T$ at 300 K are in the range 4.30–4.38 $cm^3 Kmol^{-1}$ and are close to the spin-only value (4.377 $cm^3 Kmol^{-1}$) of the high-spin Mn(II) ion. The χ_m^{-1} and $\chi_m T$ *vs.* T plots for **2**–**4** show a typical behavior for the paramagnetic species which obey the Curie–Weiss law. The presentative plots of χ_m^{-1} and $\chi_m T$ *vs.* T for complex **3**, as shown in Fig. 6 and the $\chi_m T$ values decrease as the temperature below *ca* 15 K. The drop in $\chi_m T$ below 15 K may be the result of an intermolecular antiferromagnetic interaction or zero-field splitting (D) of the spin multiples [14–16]. Since the inverse susceptibility plots are linear as a function of temperature for complexes **2**–**4**, the Curie–Weiss law eq. (2), without zero-field splitting consideration, was used in the preliminary fits of the data.

$$\chi_m = Ng^2\mu_B S(S+1)/3k(T-\theta) \qquad (2)$$

The solid lines in Fig. 6 for complex **3** are the fit of the data to the susceptibility eq. (2), using the parameters $g=2.01$, and $\theta=-1.05$ K. Similarly, the cryomagnetic properties of **2** and **4** are also well reproduced by eq. (2). The best-fitting magnetic parameters are $g=2.0$ with $\theta=-1.25$ K for **2** and $g=2.02$ with $\theta=-1.45$ K for **4**. The molecular field exchange constant, J', may be calculated from $\theta=zJ'S(S+1)/3k$ [17] and z is the number of the nearest neighbours. The values obtained for zJ' in this manner are -0.25, -0.30 and $-0.34\,cm^{-1}$ for **2**, **3** and **4**, respectively. These zJ' values indicate the existence of very weak intermolecular antiferromagnetic interactions in complexes **2**–**4**.

Acknowledgements—This work was supported by the National Science Council of Taiwan through Grant No. NSC87-2113-M-032-002.

REFERENCES

1. (a) Pecoraro, V. L. (ed.), *Managnese Redox Enzymes*. VCH, New York, 1992, p. 29–45; (b) Dismukes, G. C., *Chem. Rev.*, 1996, **96**, 2909–2926.
2. Dismukes, G. C., *Photochem. Photobiol.*, 1986, **42,** 187.
3. Barynin, V. V., Vagin, A. A., Melik-Adamyan, V. R., Grebenko, A. I., Khangulov, S. V., Popov, A. N., Andrianova, M. E. and Vainstein, B. K., *Dolk. Akad. Nauk. S.S.S.R.*, 1986, **228,** 877.
4. George, G., Prione, R. C. and Cramer, S. P., *Science*, 1989, **243,** 789.
5. (a) Laeson, E. J. and Pecoraro, V. L., *J. Am. Chem. Soc.*, 1991, **113**, 7809; (b) Laeson, E. J., Riggs, P. J., Penner-Hahn, J. E. and Pecoraro, V. L., *J. Chem. Soc., Chem. Commun.*, 1992, 102; (c) Nagata, T., Ikawa, Y. and Maruyama, K., *J. Chem. Soc., Chem. Commun.*, 1994, 471; (d) Naruta, N. and Sasayama, M., *J. Chem. Soc., Chem. Commun.*, 1994, 2667; (e) Casey, M. T., McCann, M., Dervereux, M., Curran, M., Cardin, C., Convery, M., Quillet, V. and Harding, C., *J. Chem. Soc., Chem. Commun.*, 1994, 2643; (f) Pessiki, P. J. and Dismukes, G. C., *J. Am. Chem. Soc.*, 1994, **116**, 898; (g) Devereux, M., Mccann, M., Casey, M. T., Curran, M., Ferguson, G., Cardin, C., Convery, M. and Quillet, V., *J. Chem. Soc., Dalton Trans.*, 1995, 771.
6. (a) Higuchi, C., Sakiyama, H., Okawa, H. and Fenton, D. E., *J. Chem. Soc., Dalton Trans.*, 1995, 5015; (b) Sakiyama, H., Okawa, H. and Isobe, R., *J. Chem. Soc., Chem. Commun.*, 1993, 882; (c) Higuchi, C., Sakiyama, H., Okawa, H., Isobe, R. and Fenton, D. E., *J. Chem. Soc., Dalton Trans.*, 1994, 1097; (d) Aono, T., Wada, H., Yonemura, M., Ohba, M., Okawa, H. and Fenton, D. E., *J. Chem. Soc., Dalton Trans.*, 1997, 1527.
7. Hong, D. M., Wei, H. H., Gan, L. L., Lee, G. H. and Wang, Y., *Polyhedron*, 1996, **15,** 2335.
8. Hong, D. M., Wei, H. H. and Chang, K. H., *J. Chin. Chem. Soc.*, (Taipei) In press.
9. (a) Thompson, L. K., Tandon, S. S. and Manuel, M. E., *Inorg. Chem.*, 1995, **34**, 2356; (b) Otieno, T., Rettig, S. J., Thompson, R. C. and Trotter, J., *Inorg. Chem.*, 1995, **34**, 1718; (c) Carlussi, L., Ciani, G., Moret, M. and Sironi, A., *J. Chem. Soc., Dalton Trans.*, 1994, 2397; (d) Masciocchi, N., Cairati, P., Carlucci, L., Ciani, G., Mezza, G. and Sironi, A., *J. Chem. Soc., Dalton Trans.*, 1996, 2117.
10. Charles, R. G., *Inorg. Syn.*, 1960, **6,** 164.
11. Carlin, R. L., *Magnetochemistry*. Springer Verlag, Berlin Heidelberg, 1986, p. 3.
12. Gate, E. J., Le Page, Y., Cherland, J. P., Lee, F. L. and White, P. S., *J. Appl. Crystallogr.*, 1989, **22,** 384.
13. Kogane, T., Kobayashi, K., Ishii, M., Hirota, R. and Nakahara, A. A., *J. Chem. Soc., Dalton Trans.*, 1994, 13.
14. (a) Ménage, S., Vitols, S. E., Bergerat, P., Codjovi, E., Kahn, O., Girerd, J. J., Guillot, M., Solans, X. and Calvet, T., *Inorg. Chem.*, 1991, **30**, 2666; (b) Mabad, B., Cassoux, P., Tuchgues, J. P. and Hendrickson, D. N., *Inorg. Chem.*, 1986, **25**, 1420.
15. (a) Mathur, P., Crowder, M. and Dismukes, G. C., *J. Am. Chem. Soc.*, 1989, **109**, 5227; (b) Pessik, P. J., Khangulov, S. V., Ho, D. M. and Dismukes, G. C., *J. Am. Chem. Soc.*, 1994, **116**, 891.
16. (a) Ginsberg, P. and Lines, M. E., *Inorg. Chem.*, 1972, **11**, 2289; (b) O'Connor, C. J., *Prog. Inorg. Chem.*, 1982, **29**, 203.
17. Kahn, O., *Molecular Magnetism*. VCH, New York, 1993, p. 26.

Pergamon

PII: S0277-5387(98)00152-1

Polyhedron Vol. 17, No. 20, pp. 3575–3581, 1998
© 1998 Elsevier Science Ltd
All rights reserved. Printed in Great Britain
0277–5387/98 $19.00+0.00

Copper(II) and zinc(II) complexes of N,N-bis(benzimidazole-2-ylmethyl)-amine. Synthesis, formation constants and the crystal structure of $[ZnLCl]_2$]. MeOH. Catalytic activity of the complexes in the hydrolysis of the phosphotriester 2,4-dinitrophenyl diethyl phosphate

Robert W. Hay,* Thomas Clifford and Philip Lightfoot

School of Chemistry, University of St Andrews, St Andrews, KY16 9ST, U.K.

(Received 24 February 1998; accepted 17 April 1998)

Abstract—The copper(II) and zinc(II) complexes of N,N-bis(benzimidazole-2-ylmethyl)amine (L) have been prepared and the crystal structure of $[ZnLCl_2]$. MeOH determined. The complex is five-coordinate with a distorted square pyramidal geometry on zinc. Two pyridine nitrogen donors from the imidazole groups, the secondary amino group and one chloride act as in-plane donors with the axial site occupied by chloride. The zinc(II) lies some 0.65 Å above the basal plane. The stepwise protonation constants of the ligand have been obtained, $\log K_{11} = 5.638(3)$ and $\log K_{12} = 10.12(1)$ and the stability constants ($\log \beta_{1mh}$) for the copper(II) and zinc(II) complexes determined using 50% MeOH–H_2O as solvent. The hydroxoaqua complexes $[ML(OH)(OH_2)]^+$ show only slight catalytic activity in the hydrolysis of the phosphotriester 2,4-dinitrophenyl diethyl phosphate. © 1998 Elsevier Science Ltd. All rights reserved

Keywords: benzimidazole ligand; crystal structure; copper(II); zinc(II); catalytic activity; phosphotriester.

Currently there is considerable interest in the use of benzimidazole complexes to model the active site of a variety of metalloenzymes such as carbonic anhydrase and carboxypeptidase. Ligands incorporating benzimidazole are useful in the preparation of model complexes as they relate to the biologically important imidazole group found in histidine [1]. Fenton and coworkers [1–3] have previously described the complexing properties of the two ligands bis(benzimidazole-2ylmethyl)amine ($1 = L$) and bis(benzimidazole-y2ylmethyl)methylamine ($2 = L'$) towards the first row transition metals Mn(II) and Fe(III).

The benzimidazole complex (3) has been found to be active in the transesterification of 2-hydroxypropyl-4-nitrophenyl phosphate ($hpnp = 4$) [4] which has been used as a model for RNA [5]. The complex (3) was shown to be much more active towards phosphodiesters than the catalysts (5) and (6) which form inactive dihydroxo-bridged dimers as the concentration is increased. It has been suggested that the steric bulk of the benzene rings in (3) prevents the formation of the dihydroxo-bridged dimer but allows the formation of the monohydroxo-bridged complex (7) which is catalytically active.

In the present paper we describe the characterisation of the copper(II) and zinc(II) complexes of ($1 = L$) and the crystal structure of $[ZnLCl_2]$MeOH. Formation constants for the copper(II) and zinc(II) complexes have been determined and their potential as catalysts for the hydrolysis of the phosphotriester 2,4-dinitrophenyl diethyl phosphate (8) assessed.

* Author to whom correspondence should be addressed.

EXPERIMENTAL

Synthesis

N,N-bis(benzimidazole-2-ylmethyl)amine.3HCl (*L.3HCl*). The ligand was prepared essentially as described by Berend and Stephen [6]. Iminodiacetic acid (108.1 g, 1 mol) and *o*-phenylenediamine (108 g, 1.2 mol) were refluxed in 6 mol dm^{-3} hydrochloric acid for 72 hours. On cooling a blue powder formed which was filtered off, washed with acetone and recrystallised from 40–60 (v/v) water-acetone (yield 62 g, 16%).

N,N-bis(benzimidazole-2-ylmethyl)amine hydrate (*L.H_2O*). The hydrochloride salt prepared above (5.72 g, 14.8 mmol) was dissolved in water (100 cm^3) and sodium hydrogen carbonate (3.73 g, 44.5 mmol) added in portions to give a pale lilac precipitate. The precipitate was filtered off then refluxed with methanol containing active charcoal for 2 hr and filtered hot. Pale mauve needles crystallised on standing and were filtered off and dried (yield 3.95 g, 81%). Found: C, 65.0; H, 6.05; N, 23.8. Calc. for $C_{16}H_{17}N_5O$: C, 65.1; H, 5.8; N, 23.7%. IR 3433 (*v* OH), 3224, 3206 (*v* imidNH), 3052 (*sec* NH). ^{13}C NMR 157, 141.3, 126, 118, 50 ppm.

N,N-bis(benzimidazole-2-ylmethyl)amine dihydrochloride (*L.2HCl*). The amine (2.71 g, 9.2 mmol) was dissolved in hot methanol (50 cm^3) and conc. HCl added dropwise. The white precipitate which formed was immediately filtered off, washed with ethanol then ether and dried in *vacuo* (yield 2.51 g, 78%). Found: C, 54.9; H, 4.8; N, 20.0. Calc. for $C_{16}H_{17}N_5Cl_2$: C, 54.9; H, 4.9; N, 20.0%. Titration studies confirmed

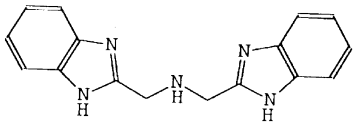

(1) = L

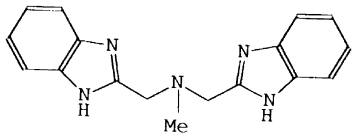

(2) = L'

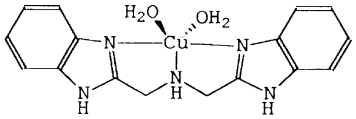

(3)

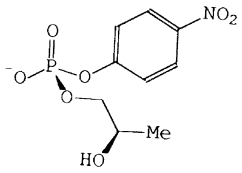

(4)

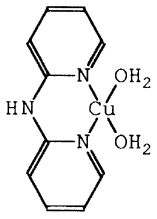

(5)

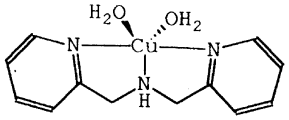

(6)

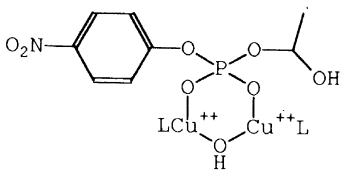

(7)

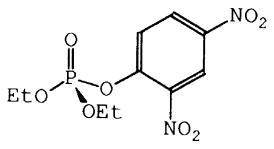

DNPDEP

(8)

that the halide salt is diprotonated and not triprotonated. The dihydrobromide salt was prepared in a similar manner using conc. HBr. Found: C, 43.8; H, 4.3; N, 15.9. Calc. for $C_{16}H_{17}N_5Br_2$: C, 43.9; H, 3.9; N, 15.95%.

[*CuLCl*$_2$].*MeOH*. The ligand (0.5 g, 1.8 mmol) in methanol (50 cm^3) was added to a hot solution of copper(II) chloride dihydrate (0.5 g, 1.8 mmol) in methanol (20 cm^3) to give a blue-green solution. On standing the blue complex crystallised and was filtered off, washed with ethanol and dried in *vacuo*. Found: C, 46.1; H, 4.2; N, 16.3. Calc. for $C_{17}H_{19}N_5OCuCl_2$: C, 46.4; H, 4.9; N, 15.7%. IR ν OH 3373(br) cm^{-1}. The complex has λ_{max} 684 nm in water ($\epsilon = 97$) with $\Lambda_M = 221$ S cm^2 mol^{-1} in aqueous solution.

[*ZnLCl*$_2$].*EtOH*. The ligand (2.5 g, 8.5 mmol) in ethanol (50 cm^3) was added rapidly to a hot solution of zinc(II) chloride (1.23 g, 4.2 mmol) in ethanol (20 cm^3). On standing colourless plates formed which were filtered off, washed with ethanol and dried in *vacuo*. Found: C, 47.0; H, 4.4; N, 15.2. Calc. for $C_{18}H_{22}N_5OZnCl_2$: C, 47.0; H, 4.6; N, 15.2%. IR ν OH 3370 cm^{-1}. The complex has $\Lambda_M = 213$ S cm^2 mol^{-1} in aqueous solution. Colourless crystals suitable for X-ray diffraction were grown by vapour diffusion of diethyl ether into a solution of the complex in methanol-water.

Crystal data

$C_{17}H_{19}N_5ZnCl_2O$, $M = 445.66$, primitive orthorhombic $a = 14.642(1)$, $b = 18.357(2)$, $c = 13.962(4)$ Å, $U = 3752.8(9)$ Å^3 (by least square refinement on diffractometer angles for 25 automatically centred reflections in the range $32.17 < 2\theta < 34.77^\circ$, $\lambda = 0.71069$ Å, space group Pbca (No. 61), $Z = 8$, $D_c = 1.577$ g cm^{-3}, $F(000) = 1824$. Pale block crystal approximate crystal dimensions $0.50 \times 0.40 \times 0.30$ mm, μ(Mo–K$_\alpha$) = 16.10 cm^{-1}.

Data collection and processing

Rigaku AFC7S diffractometer, ω-2θ scan type with ω scan width $= (1.47 + 0.35\tan\theta)^\circ$, ω scan width 16.00° min^{-1} (up to 4 scans), graphite monochromated MoK$_\alpha$ radiation, 3724 reflections measured (max $2\theta = 50^\circ$), 3718 unique ($R_{int} = 0.74$). No decay correction or absorption correction was required. Corrections were made for Lorentz and polarisation effects.

Structure analysis and refinement

Direct methods were employed [7] and expanded using Fourier techniques [8]. Non-hydrogen atoms were refined anisotropically, hydrogens were included but not refined. The final cycle of full matrix least squares refinement was based on 2245 observed reflections ($I > 3.00\sigma(I)$) and 235 variable parameters and converged with agreement factors of $R = 0.036$ and $R_w = 0.034$. The goodness-of-fit was 2.17. The maximum and minimum peaks on the final difference Fourier map correspond to 0.45 and -0.41 e$^-$ Å^{-3} respectively. The secondary nitrogen atom N1 was initially refined anisotropically, but after finding large anisotropy perpendicular to the plane of the complex at this position, the model was replaced by one with the nitrogen occupying two positions (designated N1 and N6). All calculations were carried out using the TEXSAN [9] crystallographic software package of the Molecular Structure Corporation.

Potentiometric titrations

Potentiometric measurements and the computation of the protonation and stability constants were carried out by procedures which have been described in detail [10]. Solutions were made up with 50 weight percent aqueous methanol and the ionic strength was adjusted to 0.1 mol dm^{-3} with KNO_3. The concentrations of the components in the titrations are summarised in Table 1. The potentiometric results were processed using SUPERQUAD [11] and the stability constants are expressed in the form β_{1mh}. The glass electrode was calibrated and checked for linearity with borax and potassium hydrogen phthalate buffers in aqueous solution. Checks for the presence of carbonate were made using a Gran plot and the determination of K_w for the solvent system. Although a correction was not made to compensate for the methanol-water liquid junction potential a correction of 0.1236 pH units can be substracted from the measured pH readings as suggested by Bates *et al*. [12] to enable a comparison to be made with measurements in aqueous solution.

Table 1. Summary of experimental parameters for the system Cu(II)–L and Zn(II)–L (L-,N-bis(benzimidazole-2-ylmethyl)amine

Solution composition	
$[T_L]$ range/mol dm^{-3}	3.6×10^{-3}–1.5×10^{-4}
$[T_M]$ range/mol dm^{-3}	Cu^{2+} 4×10^{-4}–1.2×10^{-3}
	Zn^{2+} 8×10^{-4}–1×10^{-4}
I/mol dm^{-3}, electrolyte	0.1, KNO_3
pH Range	Cu 3–10.5
	Zn 3–7
Experimental method	pH Titration, calibrated by standard buffers
T/°C	25 ± 0.1
Total number of data points	
Protonation	205 (5 curves)
Copper complexation	351 25 curves)
Zinc complexation	204 (4 curves)
Method of calculation	SUPERQUAD

Kinetic studies

Hydrolysis of the phosphotriester 2,4-dinitrophenyl diethyl phosphate in the presence of the metal complexes was monitored using the absorption increase at 360 nm due to the release of the 2,4-dinitrophenolate ion. Measurements were made at 25°C using a Perkin Elmer Lambda 14 spectrophotometer. Solutions were buffered at the required pH using MES (pH 5.0–6.0), HEPES (6.5–7.5) and TAPS (8.0–9.0) buffers (0.05 mol dm^{-3}). The ionic strength was adjusted to 0.1 mol dm^{-3} with KNO_3. To prevent the formation of insoluble copper hydroxo complexes the ligand was present in a three fold excess over the metal ion.

RESULTS AND DISCUSSION

The crystal structure of $[ZnLCl_2].MeOH$

An ORTEP view of the complex is shown in Fig. 1 with the atomic numbering scheme. Selected bond lengths and angles are summarised in Table 2. The coordination sphere around the zinc is made up of the two pyridine nitrogens of the imidazole rings, the secondary amino group and two chlorides which form a distorted square pyramid with a chloride in the axial site. The benzimidazole nitrogen-zinc bond distances are 2.079(3) and 2.078(3) Å. Average zinc-imidazole bond distances are 2.02–2.08 Å in six coordination [13]. The zinc–N(1) bond distance to the secondary nitrogen donor is 2.300(5) Å which compares well with the average value of 2.27 Å observed for *sec*-NH donors in five-coordinate zinc(II) complexes [13]. The benzimidazole donors and one chloride form the base of the pyramid and the zinc atom lies approximately 0.65 Å above this plane. Five coordinate zinc complexes are frequently found with tetradentate nitrogen macrocycles. In these complexes the basal plane is occupied by the four nitrogen donors with the apical position occupied by pyridine or chloride [13]. The displacement of the zinc atom from the basal plane ranges from 0.31 to 0.71 Å. The mean Zn–L apical distance increases with the covalent radius of the ligand atom in the sequence 2.082 Å (oxygen donor) < 2.158 Å (nitrogen donor) < 2.31 Å (chloride). The zinc-apical chlorine bond distance in the present complex is 2.316 Å. The structure also contains one molecule of methanol which is hydrogen bonded to an imidazole nitrogen (N–5). It was found that there were two conformations at the secondary amino nitrogen (N–1). Two positions were refined, N(1) and N(6)

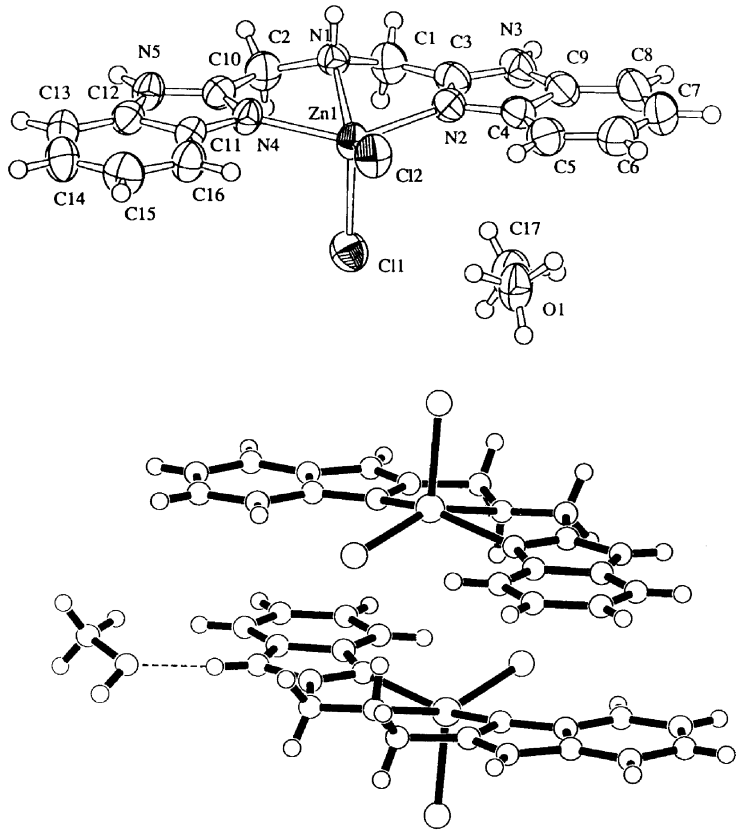

Fig. 1. ORTEP diagram and atomic numbering scheme for the complex $[ZnLCl_2]$.MeOH. The packing diagram is also shown.

Table 2. Selected bond lengths (Å) and bond angles (°) for $[ZnLCl_2].MeOH$

Zn(1)–N(1)	2.300(5)	N(1)–Zn(1)–N(2)	72.6(2)
Zn(1)–N(2)	2.079(3)	N(1)–Zn(1)–N(4)	73.1(2)
Zn(1)–N(4)	2.078(3)	N(4)–Zn(1)–N(2)	143.5(1)
Zn(1)–Cl(1)	2.316(1)	N(1)–Zn(1)–Cl(2)	144.1(2)
Zn(1)–Cl(2)	2.304(7)	N(1)–Zn(1)–Cl(1)	109.4(2)
O(1)–N(5)	2.827(4)	Cl(1)–Zn(1)–Cl(2)	106.51(5)

with a total occupancy equal to one. Refined occupancies were 0.68 and 0.32 corresponding to *trans* and *cis* configurations with respect to the axial chloride. The imidazole ligand is remarkably planar. A plane described by the two benzene rings indicates a deviation of only 0.02 Å with the zinc atom sitting approximately 0.4 Å above the plane. The structure of $[ZnLCl_2]$ is analogous to that of $[CuLCl_2]$ which has recently been described [4].

Potentiometry

The titration curve for the ligand dihydrobromide is shown in Fig. 2. A sharp inflection point occurs after addition of two equivalents of base. The ratio B/L is the number of moles of base added per mole of the ligand. The log β values obtained are summarised in Table 3 and give a pK of 4.48(1) for loss of the first proton and 5.638(2) for the second. The low pK values indicate that the protonation sites are the imidazole nitrogens rather than the secondary amino group. A secondary amine would be expected to have a much higher pK. For example, the pK for the dibenzylamine cation is 8.08 in 50% ethanol [14]. Protonation of the pyridine nitrogen of imidazole is probably favoured as this minimises electrostatic repulsion in the dication LH_2^{2+}.

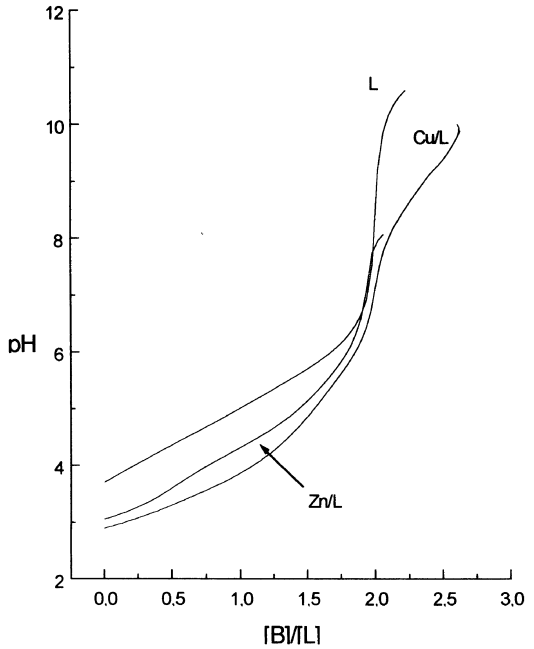

Fig. 2. Titration curves for the ligand alone and in the presence of copper(II) and zinc(II). The experimental conditions are listed in Table 1.

The titrations in the presence of copper(II) show an inflection point after addition of two equivalents of base indicating the formation of mono complexes. The potentiometric results obtained at a three to one ligand to metal ratio can be rationalised in terms of the equilibria summarised in Table 3. At high pH the important complexes are the hydroxo complexes (11–1 and 11–2). Using the β values listed the following pK values can be calculated for the equilibria:

$$[CuL(OH_2)_2]^{2+} \rightleftarrows [CuL(OH)(OH_2)]^{+} + H^{+}\,;\, pK = 7.31(7)$$

$$[CuL(OH)(OH_2)]^{+} \rightleftarrows [CuL(OH)_2] + H^{+}\,;\, pK = 9.10(5)$$

The speciation curve, Fig. 3 indicates that the species CuL^{2+} disappears prior to the formation of $[CuL(OH)]^{+}$, and that the major species in solution is the bis-complex $[CuL_2]^{2+}$. As a result it seems probable that the monohydroxo complex is formed by hydroxide ion displacement of a benzimidazole ligand rather than by deprotonation of a coordinated water molecule.

Titration curves in the presence of zinc(II) were rather similar to those observed with copper(II) except that precipitates formed above pH 7. The stability constants obtained are summarised in Table 3. The monohydroxo complex forms in the pH range where precipitation begins and as a result the stability constant for the 11–1 species and the calculated pK of the zinc bound water (8.29 ± 0.06) can only be regarded as estimates.

Kinetic studies

A number of hydroxoaqua complexes such as $[Cu(dpa)(OH)(OH_2)]^{+}$ (dpa = 2,2′-dipyridylamine) have been found to be very effective catalysts for the hydrolysis of phosphotriesters [15]. For this reason we studied the effect of the copper(II) and zinc(II) complexes on the hydrolysis of 2,4-dinitrophenyl

Table 3. Protonation constants and stability constants for the copper(II) and zinc(II) complexes of N,N-bis(benzimidazole-2ylmethyl)amine

Protonation constants (ligand = L, errors as σ)		
$\log \beta_{HL}$	$H^+ + L = HL^+$	5.638 ± 0.003
$\log \beta_{H2L}$	$2H^+ + L = H_2L^{2+}$	10.12 ± 0.01
Copper(II) stability constants		
$\log \beta_{Cu2L}$	$Cu^{2+} + 2L = CuL_2^{2+}$	10.64 ± 0.03
$\log \beta_{CuL}$	$Cu^{2+} + L = CuL^{2+}$	6.34 ± 0.02
$\log \beta_{Cu(OH)L}$	$Cu^{2+} + OH^- + L = Cu(OH)L^+$	-0.97 ± 0.07
$\log \beta_{Cu(OH)2L}$	$Cu^{2+} + 2OH^- + L = Cu(OH)_2L$	-10.07 ± 0.06
$\log \beta_{CuHL2}$	$Cu^{2+} + 2L + H^+ = L_2CuH^{3+}$	15.05 ± 0.05
Zinc(II) stability constants		
$\log \beta_{ZnL}$	$Zn^{2+} + L = ZnL^{2+}$	5.96 ± 0.02
$\log \beta_{ZnL2}$	$Zn^{2+} + 2L = ZnL_2^{2+}$	8.97 ± 0.08
$\log \beta_{ZnLOH}$	$Zn^{2+} + OH^- + L = ZnL(OH)^+$	-2.33 ± 0.06

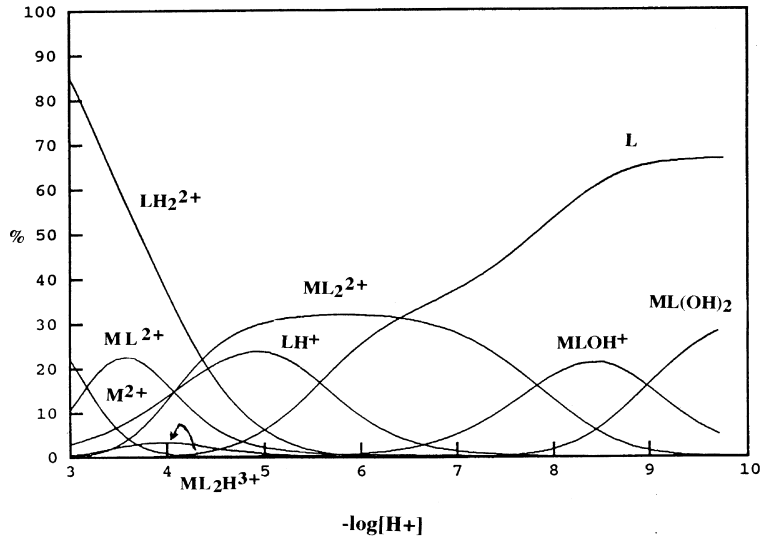

Fig. 3. Speciation curves for the copper(II) complexes.

diethyl phosphate. Hydrolysis of this ester to give diethyl phosphate can be readily monitored spectrophotometrically at 360 nm due to the release of 2,4-dinitrophenoxide. The complexes exhibit only small catalytic effects. The pH dependence of the catalysis with the copper(II) complex was consistent with the monohydroxo complex being the active catalytic species. Studies with zinc were limited due to the insolubility of the monohydroxo zinc complex. These complexes do not act as effective catalysts for the hydrolysis of phosphotriesters.

REFERENCES

1. Crane, J. D. and Fenton, D. E., *Polyhedron*, 1991, **10,** 187.
2. Adams, H., Bailey, N. A., Crane, J. D., Fenton, D. E., Latour, J. M. and Williams, J. M., *J. Chem. Soc. Dalton Trans.*, 1990, **00,** 1727.
3. Crane, J. D. and Fenton, D. E., *J. Chem. Soc. Dalton Trans.*, 1990, **00,** 3647.
4. Wahnon, D., Hynes, R. C. and Chin, J., *J. Chem. Soc. Chem. Commun.*, 1994, **00,** 1441.
5. Jubian, V., Dixon, R. P. and Hamilton, A., *J. Am. Chem. Soc.*, 1992, **114**, 3686; Morrow, J. R., Buttrey, L. A., Skelton, V. M. and Berback, K. A., *J. Am. Chem. Soc.*, 1992, **114**, 1903; Breslow, R., Berger, D. and Huang, D. L., *J. Am. Chem. Soc.*, 1990, **112**, 3686.
6. Berends, H. P. and Stephan, D. W., *Inorg. Chim. Acta*, 1984, **93,** 173.
7. Altomare, A., Burla, M. C., Camalli, M., Cascarano, M., Giacovazzo, C., Gugliardi, A., Polidori, G., SIR 92, *J. Appl. Crystallogr.*, 1993, **26,** 343.
8. Beurskens, P. T., Admiraal, G., Beurskens, G., Bosman, W. P., de Gelder, R., Israel, R. and

Smits, J. M. M., The DIRDIF-94 Program System, Technical Report of the Crystallography Laboratory, University of Nijmegan, The Netherlands.
9. TEXSAN, Crystal Structure Analysis Package, Molecular Structure Corporation, Houston, TX, 1985 and 1992.
10. Martell, A. E. and Motekaitis, R. J., Determination and Use Of Stability Constants, VCH, Weinheim, 1988.
11. Gans, P., Sabatini, A. and Vacca, A., *J. Chem. Soc. Dalton Trans.*, 1985, **00,** 1195.
12. Bates, R. G., Paabo, M. and Robinson, R. A., *J. Phys. Chem.*, 1963, **67,** 1833.
13. Melnick, M., Gyoryova, K., Skorsepa, J. and Holloway, C. E., *Coord. Chem. Rev.*, 1995, **35,** 179.
14. Sillen, L. G. and Martell, A. E., Stability Constants, Special Publication No. 17, The Chemical Society, London, 1964.
15. Chin, J., *Acc. Chem. Res.*, 1991, **24,** 145; Hay, R. W., Govan, N., Parchment, K. E., Kiss, E. and Clifford, T., *Inorg. React. Mech.* (in press).

Pergamon

PII: S0277–5387(98)00153–3

Polyhedron Vol. 17, No. 20, pp. 3583–3593, 1998
© 1998 Elsevier Science Ltd
All rights reserved. Printed in Great Britain
0277–5387/98 $19.00+0.00

Consecutive crystallisation of $[Cu(MeppdCl)_2]BF_4$ and $[Cu(MeppdCl)_2Cl]BF_4 \cdot 0.5(C_2H_5)_2O$ from dichloromethane

Alexander J. Blake,[a] David E. Hibbs,[b] Peter Hubberstey[a,*] and Claire E. Russell[a]

[a]Department of Chemistry, Nottingham University, Nottingham NG7 2RD, UK

[b]Department of Chemistry, University of Wales, Cardiff CF1 3TB, Wales

(Received 2 February 1998; accepted 7 April 1998)

Abstract—Treatment of copper(I) with 3-chloro-6-(3,5-dimethylpyrazol-l-yl)pyridazine (MeppdCl) in dichloromethane yields firstly red crystals of $[Cu(MeppdCl)_2]BF_4$ and secondly blue crystals of $[Cu(MeppdCl)_2Cl]BF_4 \cdot 0.5(C_2H_5)_2O$. The provenance of the chloride anion is uncertain; it may be attributed to either copper(I) activation of dichloromethane or minor impurities arising during MeppdCl synthesis. In the copper(I) cation, two MeppdCl molecules, which are N-donor bidentate chelating ligands, generate a squashed tetrahedral coordination geometry [Cu...N = 2.000(3)-2.052(3) Å] with an open side [N–Cu–N = 140.1(1)°]—effectively a trigonal bipyramid with a missing equatorial ligand. In the copper(II) cation, a trigonal biypramidal arrangement is formed by two MeppdCl ligands, which straddle equatorial [Cu...N = 2.066(4), 2.151(4) Å] and axial [Cu...N = 1.976(4), 1.979(4) Å] sites and an equatorially located chlorine atom [Cu...Cl = 2.292(1) Å]. Viewing the two coordination geometries as trigonal bipyramidal, the orientation of the MeppdCl molecules reverses on oxidation, the pyrazole nitrogens moving from equatorial to axial sites [N–Cu–N increases from 98.9(1)° to 168.5(2)°] and the pyridazine nitrogens vice versa [N–Cu–N decreases from 140.1(1)° to 110.8(2)°].

The copper(I) complex is the most severely distorted, structurally characterised, $[Cu(diimine)_2]^+$ complex. A novel method of parameterising the stereochemistry of $[Cu(diimine)_2]^+$ complexes is proposed; four readily calculated parameters are used to assess the extent of distortion of the molecule from D_{2d} symmetry. © 1998 Elsevier Science Ltd. All rights reserved

Keywords: copper(I); copper(II); chelating diimines; stereochemistry; chloride abstraction.

Although the coordination chemistry of symmetrical chelating diimines [e.g., 2,2-bipyridine (bipy), 1,10-phenanthroline (phen) and 2,9-dimethyl-l,10-phenanthroline (dmp)] with copper(I) and copper(II) has been extensively studied [1–10], there are few data on complexes with unsymmetrical diimines [11]. 3-Chloro-6-(pyrazol-l-yl)pyridazine (ppdCl) and 3-chloro-6-(3,5-dimethylpyrazol-l-yl)pyridazine (MeppdCl) provide examples of such ligands (Scheme 1) [12]. Following our work in which we compared the coordination chemistry of the mixed ligand complexes copper(II)-ppdCl or MeppdCl-cnge and copper(II)-bipy-cnge (cnge = 2-cyanoguanidine) [12, 13], we have initiated a study of copper(I)-ppdCl or MeppdCl complexes. In this paper, we described the synthesis, isolation and structural characterisation of $[Cu(MeppdCl)_2Cl]BF_4$, **1**, and its oxidation product, $[Cu(MeppdCl)_2Cl]BF_4 \cdot 0.5(C_2H_5)_2O$ (**2**).

Complex **1** adopts the tetrahedral structure typical of $[Cu(diimine)_2]^+$ cations [1–7] and complex **2** the trigonal bipyramidal structure typical of $[Cu(diimine)_2Cl]^+$ cations [8, 9, 10]. The former is, however, the most severely distorted $[Cu(diimine)_2]^+$ coordination geometry determined thus far. Although stereochemical descriptions for these cations already exist [1, 2], we propose an alternative approach in which readily calculated parameters are used to

* Author to whom correspondence should be addressed.

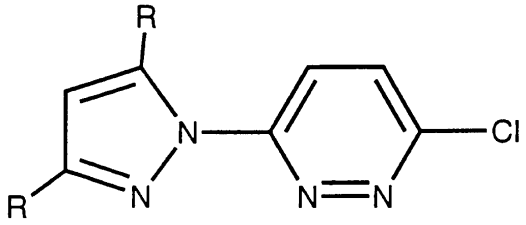

Scheme 1. Pyrazolylpyridazines. R = H; 3-chloro-6-(pyrazol-1-yl)pyridazine (ppdCl), R = Me; 3-chloro-6-(3,5-dimethyl-pyrazol-1-yl)pyridazine (MeppdCl).

assess the relative orientation of the two diimine ligands.

The process by which complex **2** is generated is uncertain; it may be attributed to either activation of the solvent, CH_2Cl_2, by the copper(I) complex or to adventitious oxidation in the presence of chloride impurity. Dichloromethane activation is well established, particularly with conversion of square planar d^8 to octahedral d^6 metal centres (e.g., $Ir^I \rightarrow Ir^{III}$ [14] and $Rh^I \rightarrow Rh^{III}$ [15]). More recently [16], it has been observed for the conversion of the tetrahedral d^{10} Ni^O centre in $[Ni(dmp)_2]$ (dmp = 2,9-dimethyl-1,10-phenanthroline), an isoelectronic analogue of $[Cu(MeppdCl)_2]^+$, to the square pyramidal d^8 metal centre in $[\{Ni(dmp)Cl\}_2(\mu\text{–}Cl)_2]$.

EXPERIMENTAL

Preparation of 3-*chloro*-6-(3,5-*dimethylpyrazol-l-yl*) *pyridazine* (*MeppdCl*)

3,5-Dimethylpyrazole (Aldrich Chemical Co., 4.005 g, 0.0417 mol) was dissolved in dry tetrahydrofuran (100 cm^3) and small pieces of clean potassium metal (1.629 g, 0.0417 mol) added with stirring under nitrogen to yield a white precipitate. An exit needle was fitted to the reaction vessel to permit hydrogen release. Upon complete reaction (12 hours), a solution of 3,6-dichloropyridazine (Aldrich Chemical Co., 9.289 g, 0.0624 mol) in dry tetrahydrofuran (50 cm^3) was added with stirring to yield a red/brown solution which was refluxed for 4 hours. After cooling, the resulting red/brown suspension was added to ice-cold deionised water (250 cm^3) to yield a white precipitate which was filtered under suction, washed with ice-cold deionised water and dried under vacuum over P_4O_{10} to give MeppdCl as a white powder. Yield, 6.00 g (69%), m.p. 104–106°C. Analysis: found (calculated for $C_9H_9ClN_4$) {RMM = 208.7}; C 52.00 (51.80), H 4.40 (4.35), N 26.75 (26.85). ^{1}H NMR ($CDCl_3$) (δ(ppm), J (Hz)); 8.16 (*d*, J 9.30, 1 H), 7.56 (*d*, J 9.21, 1 H), 6.06 (*s*, 1 H), 2.72 (*s*, 3 H), 2.29 (*s*, 3H). IR (KBr disc) (ν/cm^{-1}) 3054 m, 1576s, 1543 m, 1425s, 1364 m, 1270 w, 1141 m, 1066 m, 1008 w, 972 m, 854 m, 792 m, 744 m, 591 w, 529 w, 511 m. EI mass spectrum (*m*/*e*, relative intensity): 208 $\{[M]^+, [(C_5H_7N_2)(C_4H_2ClN_2)]^+$, 100%}, 191 $\{[(C_4H_4N_2)(C_4H_2ClN_2)]^+$, 31%}, 180 $\{[(C_5H_7N_2)(C_4H_2Cl)]^+$, 18%}, 173 $\{[(C_5H_7N_2)(C_4H_2N_2)]^+$, 20%}, 95 $\{[(C_5H_7N_2)]^+$, 68%}. Although the elemental analytical data are consistent with a pure sample and there is no evidence for impurities in the ^{1}H-nmr and mass spectra, the synthetic route could give KCl or hydrochloride impurity which could lead.to small quantities of **2** following adventitious oxidation of **1**. Such impurities are invisible to ^{1}H-nmr and E.I.-M.S. methods and chloride analysis was unsuccessful. An attempt to identify KCl by X-ray powder diffraction methods also failed; the experiment, a relatively insensitive technique which needs >2 mole % for detection, neither confirmed nor refuted the presence of KCl.

Preparation of $[Cu(MeppdCl)_2]BF_4$ (**1**) *and* $[Cu(MeppdCl)_2Cl]BF_4 \cdot 0.5(C_2H_5)_2O$ (**2**)

Dichloromethane (50 cm^3) was added under nitrogen to a mixture of tetrakis(acetonitrile)copper(I) tetrafluoroborate (0.151 g, 0.48 mmol) and MeppdCl (0.10 g, 0.48 mmol). After stirring for 16 hours a pale red and solid was recovered from a red solution by canula filtration. The product (0.104 g, 0.18 mmol; 75%) was identified as $[Cu(MeppdCl)_2]BF_4$ from elemental analytical data obtained in the University of Nottingham Chemistry Department by Mr. T. J. Spencer. Analysis: found (calc. for $C_{18}H_{18}BCl_2CuF_4N_8$): C, 37.85 (38.10); H, 3.35 (3.20); N, 19.30 (19.75). Infrared spectra {ν/cm^{-1}; 3050 w, 1580 s, 1535 w, 1428 s, 1375 m, 1085–1035 s br, 831 m, 799 m, 740 w}, obtained on a Perkin Elmer PE983G spectrometer as KBr pressed pellets, confirmed the presence of MeppdCl ligand and BF_4^- anion.

Tiny red crystals of **1** were obtained by vapour phase diffusion of Et_2O into the mother liquor. Although too small for data collection using a four circle diffractometer, they diffracted sufficiently well for study with an area detector. On prolonged standing, a limited number of small blue crystals appeared. X-ray diffraction experiments with an area detector showed them to be the copper(II) complex, $[Cu(MeppdCl)_2Cl]BF_4 \cdot 0.5(C_2H_5)_2O$ (**2**).

X-ray crystallography

Selected crystals of **1** were mounted in Lindemann glass capillary tubes for preliminary study. Oscillation and Weissenberg photographs revealed approximate cell dimensions (a = 10.10, b = 20.50, c = 11.05 Å, β = 100°) and space group $P2_1/n$. Diffraction data for **1** and **2** were collected for more than one hemisphere at 150 K using an Enraf Nonius FAST TV area detector situated at the window of a rotating anode generator with a molybdenum anode [17]. The data sets for both compounds were extremely weak owing to the small size of the crystals. They were corrected for Lorentz

Table 1. Crystallographic data for $[Cu(MeppdCl)_2]BF_4$ (**1**) and $[Cu(MeppdCl)_2Cl]BF_4 \cdot 0.5(C_2H_5)_2O$ (**2**)[a]

Complex	**1**	**2**
Formula	$C_{18}H_{18}BCl_2CuF_4N_8$	$C_{18}H_{18}BCl_3CuF_4N_8.0.5(C_4H_{10}O)$
M	567.65	640.17
Crystal System	monoclinic	monoclinic
Space group	$P2_1/n$ (#14)	$P2_1/c$ (#14)
a/Å	10.199(3)	12.836(5)
b/Å	20.403(3)	25.393(20)
c/Å	10.988(4)	8.857(30)
β/°	100.39(2)	109.26(17)
Z	4	4
U/Å^3	2249.0(8)	2725(3)
μ_{calc}/mm^{-1}	1.27	1.15
D_c/g cm^{-3}	1.676	1.560
D_m/g cm^{-3} (bromoform/hexanes)	1.68	–
$F(000)$	1144	1296
Crystal dimensions/mm^3	$0.15 \times 0.12 \times 0.05$	$0.18 \times 0.10 \times 0.06$
2θ range for data collection/°	3.76–50.06	3.72–49.92
Index ranges	$-11 \le h \le 11$	$-15 \le h \le 12$
	$-21 \le k \le 22$	$-29 \le k \le 28$
	$-12 \le l \le 13$	$-10 \le l \le 9$
Reflections collected	10038	9591
Independent reflections	5859 ($R_{int} = 0.106$)	6717 ($R_{int} = 0.095$)
Observed reflections [$I \ge 2\sigma(I)$]	2095	2399
DIFABS correction; min,max	0.798, 1.084	0.761, 1.095
Data/restraints/parameters	5401/0/367	6717/7/406
ρmin, ρmax/eÅ^{-3}	−1.26, 1.59	−1.55, 2.55
$(\Delta/\sigma)_{max}$	0.2	0.05
R, R_w (all data)	0.0978, 0.0692	0.1203, 0.1147
R, R_w (data with $I \ge 2\sigma(I)$)	0.0450, 0.0419	0.0574, 0.0716

[a] Mo–Kα radiation ($\lambda = 0.71073$ Å); $T = 150$ K; refinement method: full-matrix least squares on F^2.

and polarisation effects as well as absorption (DIFABS) [18]. Crystal data, together with details of both diffraction experiments, are listed in Table 1.

The structures were solved by direct methods (SIR92) [19]. The majority of the hydrogen atoms were located from difference Fourier syntheses (CRYSTALS) [20] Those which could not be found were placed (d(C...H) = 1.00 Å; $U_{iso} = 0.05$ Å^2) except for the ether hydrogens in **2** which were omitted. In **2**, both the anions and solvent molecules exhibit disorder. The anion was modelled by two full occupancy and four half occupancy fluorines based on a common boron. The solvent molecule was modelled by half occupancy atoms (equivalent to one Et_2O molecule per two cations) lying in channels at $\pm 1/4, \pm 1/4$, 0. Both structures were refined by full-matrix least squares method on F^2 using all positive data, with anisotropic displacement parameters for non-hydrogen atoms, except those of the ether molecules in **2** which, together with the located hydrogen atoms, were allocated isotropic displacement parameters (CRYSTALS) [20]. The final cycle of refinement, with two-parameter Chebychev weighting schemes [parameters 93.8, 96.4, for **1**; parameters 15.2, 14.3 for **2**] gave conventional R indices of 0.0450 and 0.0574 for **1** and **2**, respectively. Full details of the structure solutions are given in Table 1. Selected interatomic distances and angles are collected in Table 2 and structure diagrams, generated using the CAMERON suite of programs [21], are shown in Figs. 1–3. The numbering sequences for the two MeppdCl ligands differ solely in starting at 101 and 201; in the text, they are designated by the notation 1xx and 2xx, respectively.

RESULTS AND DISCUSSION

Crystal and molecular structure of $[Cu(MeppdCl)_2]BF_4$ (**1**)

The structure of **1** comprises $[Cu(MeppdCl)_2]^+$ cations and BF_4^- anions. Although the tetrahedral copper(I) coordination sphere of the cation is structurally similar to those in other $[Cu(diimine)_2]^+$ (diimine = phen, dmp, 2,2′-bipy, 3,3′-dimethyl-2,2′-bipyridine and 3,3′5,5′-tetramethyl-2,2′-bipyridine) cations [1–7], it is much more severely distorted (Fig. 1). The bidentate ligands are not orthogonal as their normals subtend a dihedral angle of 52.8°. Furthermore, they are not planar but have internal dihedral angles of

Table 2. Interatomic distances and angles in the copper coordination spheres of $[Cu(MeppdCl)_2]BF_4$ (**1**), and $[Cu(MeppdCl)_2Cl]BF_4 \cdot 0.5(C_2H_5)_2O$ (**2**)

1		**2**	
Distances/Å			
Cu–N(101)	2.009(3)	Cu–N(101)	2.151(4)
Cu–N(162)	2.052(3)	Cu–N(162)	1.979(4)
Cu–N(201)	2.000(3)	Cu–N(201)	2.066(4)
Cu–N(262)	2.049(3)	Cu–N(262)	1.976(4)
		Cu–Cl(2)	2.292(1)
Angles/°			
N(101)–Cu–N(162)	79.0(1)	N(101)–Cu–N(162)	76.3(2)
N(101)–Cu–N(201)	140.1(1)	N(101)–Cu–N(201)	110.8(2)
N(101)–Cu–N(262)	130.9(1)	N(101)–Cu–N(262)	98.8(2)
N(162)–Cu–N(201)	128.1(1)	N(162)–Cu–N(201)	93.6(2)
N(162)–Cu–N(262)	98.9(1)	N(162)–Cu–N(262)	168.5(2)
N(201)–Cu–N(262)	78.8(1)	N(201)–Cu–N(262)	78.3(2)
		N(101)–Cu–Cl(2)	118.6(1)
		N(162)–Cu–Cl(2)	95.2(1)
		N(201)–Cu–Cl(2)	130.5(1)
		N(262)–Cu–Cl(2)	96.3(1)

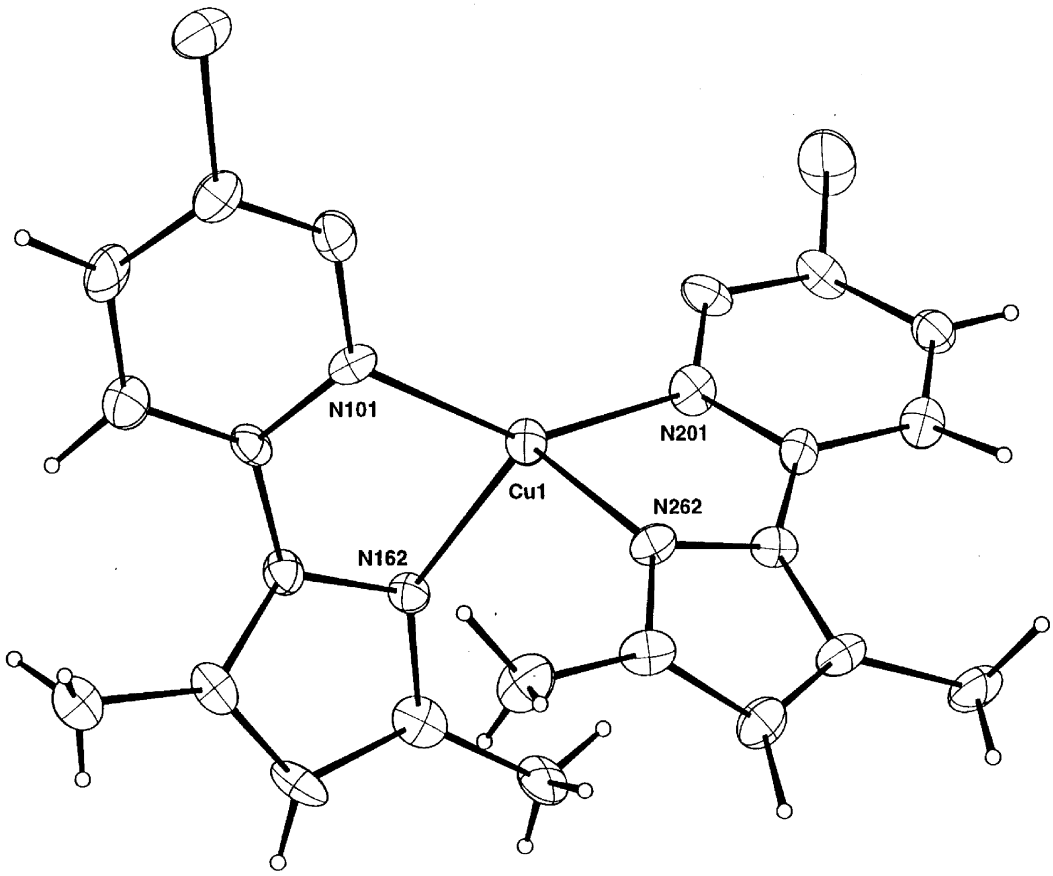

Fig. 1. Molecular structure and numbering scheme for $[Cu(MeppdCl)_2]^+$

14.6° (ligand 1xx; Fig. 1) and 20.8° (ligand 2xx; Fig. 1) between their pyridazine and pyrazole rings. These distortions result in a 'squashed tetrahedral' geometry, reminiscent of the entatic state of type 1 copper proteins [22]. The small bite angles of the ligands dictate one large (~140°), two medium (~130°) and one small (~100°) interligand angle (Table 2). The two bidentate ligands are arranged such that the pyridazine nitrogens are marginally closer to the copper atom than the pyrazole nitrogens (Table 2). The BF_4^- anion exhibits no disorder.

Crystal and molecular structure of $[Cu(MeppdCl)_2Cl]BF_4 \cdot 0.5(C_2H_5)_2O$ (**2**)

The structure of **2** comprises $[Cu(MeppdCl)_2Cl]^+$ cations, BF_4^- anions and ether solvent molecules. The five co-ordinate copper(II) coordination sphere in **2** is shown in Fig. 2. The bidentate MeppdCl ligands straddle equatorial and axial sites. The third equatorial site is occupied by a relatively weakly bound chlorine atom [Cu...Cl 2.292(1) Å]. Although the normals to the least squares through the two diimines subtend a dihedral angle of 70.7°, they are both effectively perpendicular to the copper(II) equatorial plane (dihedral angles, 90.0, 88.2°). The stronger binding of the axial sites is confirmed by the axially located pyrazole nitrogens being much closer to the copper atom than the equatorially located pyridazine nitrogens (Table 2). The bidentate ligands are somewhat more planar than in **1**, with dihedral angles of only 11.3° (ligand 1xx; Fig. 2) and 11.5° (ligand 2xx; Fig. 2) between their pyridazine and pyrazole rings.

The BF_4^- anion is disordered over two equally occupied sites. Two fluorines (F11, F12) are common, the other four (F131, F132, F141, F142), which are coplanar and orthogonal to F11 and F12, form two pairs related by a rotation of ~45°. The boron atom has an elongated thermal ellipsoid to accommodate this disorder. Somewhat disordered solvent molecules (equivalent to one Et_2O molecule per two cations) lie in channels, centered at $\pm 1/4$, $\pm 1/4$, 0, which run parallel to the *c* axis (Fig. 3).

The molecular geometry of $Cu(MeppdCl)_2]^+$ is typical of those of [Cu(diimine)X]$^+$ (diimine = 2,2′-bipyridine or phenanthroline, X = Cl^-, I^-, CN^-, N_3^-, NCS^-, $NCSe^-$, $CH_3CO_2^-$, HCO_2^-) cations [8, 9, 10], for which the structural pathways of $[Cu(phen)_2Cl]^+$ [8] and $[Cu(bipy)_2Cl]^+$ [9] have been discussed in detail. Using the notation of Addison *et al.*[23], the copper(II) co-ordination geometry is best described as square based pyramidal distorted trigonal bipyramidal [τ = (168.5–130.8)/60} = 0.63].

Comparison of the structures of the two cations

A significant relationship exists between the two cations. The copper(I) cation can be considered to be based on a trigonal bipyramidal arrangement with a missing equatorial ligand; the pyridazine nitrogens [Cu...N = 2.000(3), 2.009(3) Å] occupy the pseudo-axial positions [angle NCuN = 140.1 (1)°] and the more remote pyrazole nitrogens [Cu...N = 2.049(3), 2.052(3) Å] the pseudo-equatorial positions [angle NCuN = 98.9(1)°] (Fig. 1). Other than the presence of the equatorial chlorine atom in the copper(II) cation, the only difference is the inversion of the ligands, the pyrazole nitrogens [Cu...N = 1.976(4), 1.979(4) Å]

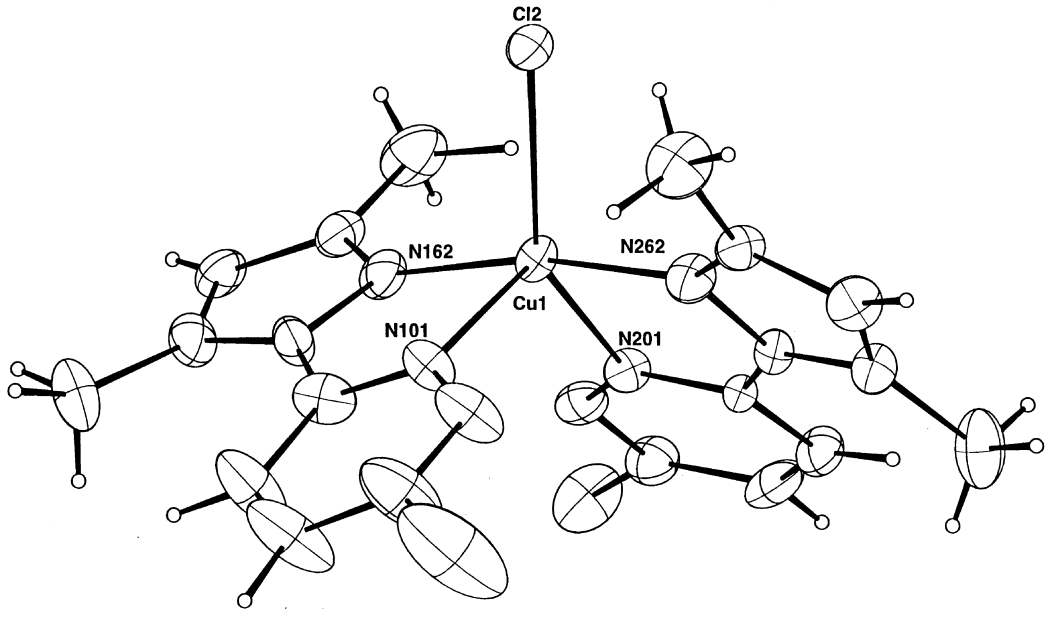

Fig. 2. Molecular structure and numbering scheme for $[Cu(MeppdCl)_2Cl]^+$

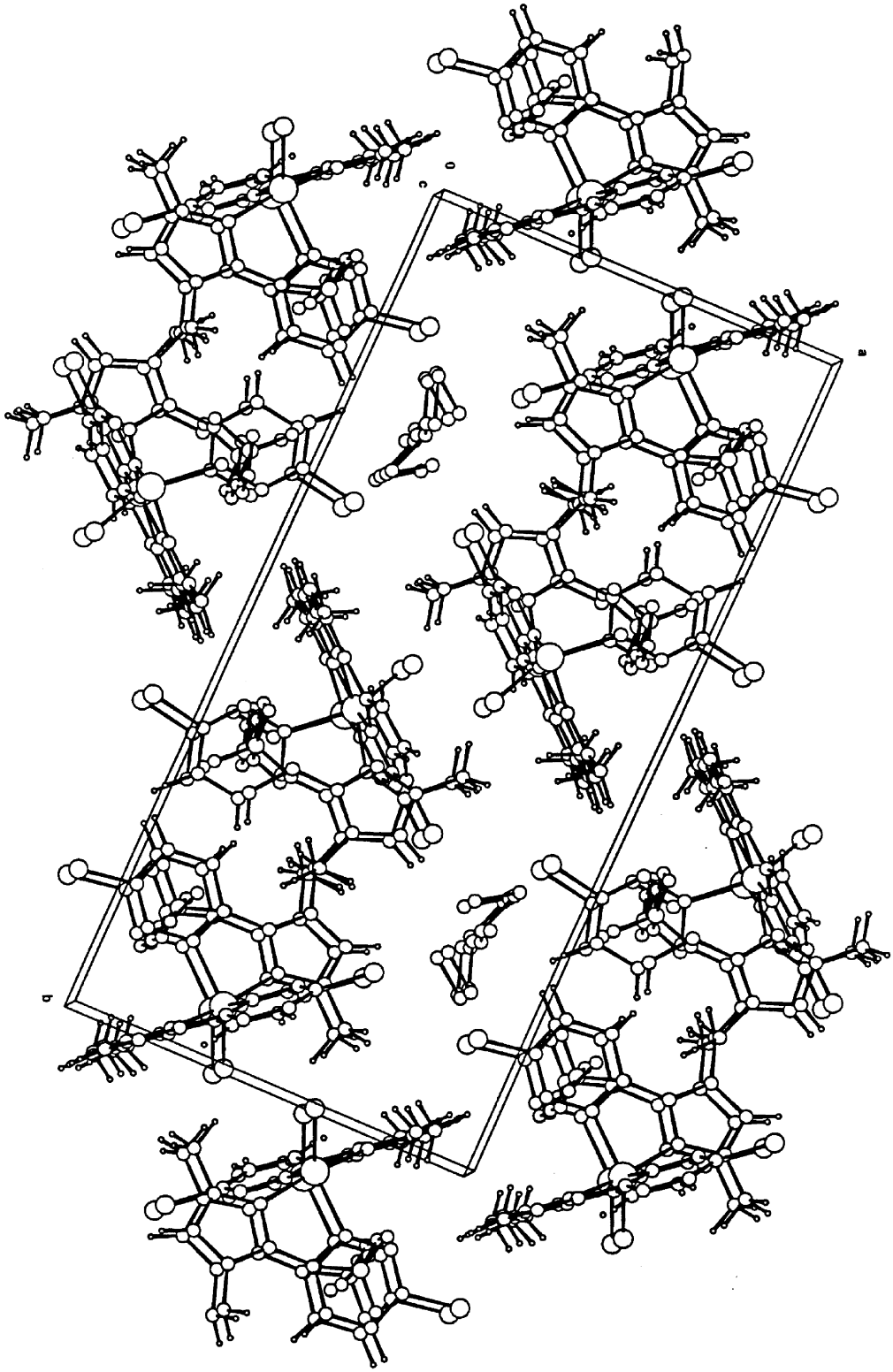

Fig. 3. Packing diagram for $[Cu(MeppdCl)_2Cl]BF_4 \cdot 0.5(C_2H_5)_2O$ showing the channels, centred on ($\pm 1/4$. $\pm 1/4$, 0), containing the ether solvent molecules.

occupying the axial positions [NCuN = 168.5(2)°] and the more remote pyridazine nitrogens [Cu...N = 2.066(4), 2.151(4) Å] the equatorial positions [NCuN = 110.8(2)°] (Fig. 2). The copper(II) cation is analogous to the only other structurally characterised bis(MeppdCl) copper(II) cation, $[Cu(MeppdCl)_2(cnge)]^{2+}$ (cnge = 2-cyanoguanidine) [13], in which the diimine ligands adopt an identical arrangement, the pyrazole nitrogens [Cu...N = 1.965(5), 1.965(5) Å] occupying the axial positions [angle NCuN = 169.5(2)°] and the more remote pyridazine nitrogens [Cu...N = 2.052(5), 2.070(5) Å] the equatorial positions [angle NCuN = 119.2(2)°].

The geometry of the copper(I) cation has an open face giving ready access to the metal centre. This may responsible for the activation of the dichloromethane molecule and the chlorine abstraction process which would result in the generation of **2**.

Stereochemistry of bis(diimine)copper(I) complexes

Bis(diimine)copper(I) complexes adopt diverse stereochemistries. The majority exhibit little symmetry containing two crystallographically independent diimines. A small number, $[Cu(bipy)_2]ClO_4$ [1], $[Cu(phen)_2]CuBr_2$ [3], $[Cu(dmp)_2]NO_3$ [4] and $[Cu(dmp)_2]BF_4$ toluene [5], are, however, located on 2-fold axes of symmetry which pass through the copper ion thus crystallographically relating the two diimines. Finally, in one example, $[Cu(phen)_2]ClO_4$ [3], the cation is located on a 2-fold axis, which not only passes through the copper ion but also bisects both of the crystallographically independent diimines.

Several authors have devised models to describe the stereochemistry of these cations. They range from the consideration of the dihedral angle between the two ligands [1] to the application of complex vector algebra techniques to the determination of the three angles, θ_x, θ_y and θ_z, which refer to the orientation of the N, Cu, N, triangle in ligand A relative to that of the corresponding triangle in ligand B (Scheme 2) [2]. We wish to propose an alternative method of describing the stereochemistry of $[Cu(diimine)_2]^+$ cations, which is more realistic than the simple consideration of the dihedral angle but which is more readily assessed quantitatively than by the application of complex vector algebra techniques.

The orientation of the plane of diimine ligand B with respect to that of diimine ligand A is described by three angles, named, by analogy with spacecraft manoeuvres, the pitch, roll and yaw angles. These three angles, Φ, Ω and Ψ are shown and defined in Scheme 3. They are comparable with θ_x, θ_z and θ_y, as defined by Dobson et al. (Scheme 2) [2]. Difficult to calculate precisely, they can be assessed semi-quantitatively in terms of four readily calculated parameters:

1. τ-the twist parameter-the sum of the perpendicular distances of the nitrogen atoms of ligand B from the plane of ligand A [(Na + Nc): observed range 2.69–2.04 Å],
2. η-the tilt parameter–the ratio of the perpendicular distance of point P [the mid-point of the intraligand N...N vector (Scheme 3)] of ligand A from the plane containing ligand B to the sum of the perpendicular distances of the nitrogen atoms of ligand A from the plane containing ligand B [Pb/(Na + Nc): observed range 0.00–0.23].
3. δ-the bisector parameter–the angle between the lines bisecting the two N–Cu–N angles (ie the lines which radiate from the copper atom and pass through points P) [observed range 180–155°],
4. ε-the dihedral parameter–the angle at the intersection of the perpendiculars to the planes of the two diimine ligands [observed range 90–50°].

The twist parameter, τ, is a measure of the roll angle, Ω, and the tilt parameter, η, is a measure of the pitch angle, Φ. The effect of roll on Φ is allowed for by calculating the ratio, Pb/(Na + Nc), rather than the absolute length, Pb. The bisector parameter δ is a combination of the pitch and yaw angles, Φ and Ψ,

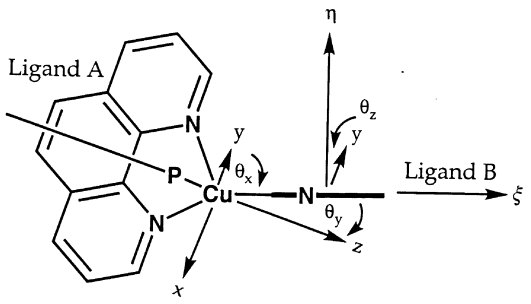

Scheme 2. Definition of the three angles, θ_x, θ_y, and θ_z, which refer to the orientation of the N, Cu, N triangle in ligand A relative to that of the corresponding N, Cu, N triangle in Ligand B [2]. x, y and z are orthonormal vectors chosen such that ligand A is in the xz plane with z as the bisector of the NCuN angle; ξ and η are unit vectors defined to lie along the bisector of the NCuN angle of ligand B and perpendicular to ligand B, respectively. θ_x is the angle between ξ and y, θ_y between ξ and x, θ_z between η and y.

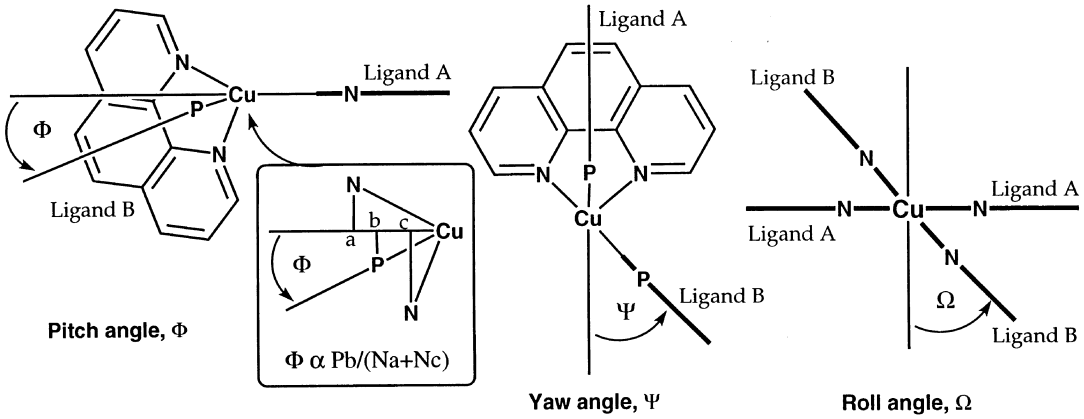

Scheme 3. Definition of the pitch, yaw and roll angles relating the orientation of ligand B with respect to ligand A.

and the dihedral parameter, ϵ, although affected by pitch, yaw and roll, is primarily a measure of the roll angle, Φ.

For $[Cu(diimine)_2]^+$ cations with D_{2d} symmetry (Cu...N = 2.05 Å, NCuN = 82°) the parameters would be $\tau = 2.69$ Å, $\eta = 0.00$, $\delta = 180°$ and $\epsilon = 90°$. For symmetrical diimines (diimine = 2,2′-bipy, phen or their substituted derivatives), maximum observed distortion values are $\tau = 2.05$ Å $[Cu(phen)_2]ClO_4$ [3], $\eta = 0.19$ $[Cu(phen)_2]CuBr_2$ [3], $\delta = 160.4°$ $[Cu(dmp)_2]BF_4 \cdot CH_2Cl_2$ [5] and $\epsilon = 49.7°$ $[Cu(phen)_2]ClO_4$ [3]. Even greater distortion is observed, however, for the unsymmetrical diimine (MeppdCl) in $[Cu(MeppdCl)_2]BF_4$ with $\tau = 2.04$ Å, $\eta = 0.23$, $\delta = 155.8°$ and $\epsilon = 52.8°$. Full details for a representative selection of $[Cu(diimine)_2]^+$ cations are given in Table 3.

The cation with symmetry closest to D_{2d}, $[Cu(dmp)_2]BF_4$ toluene [5] [Fig. 4(a); Table 3], is located on a 2-fold axis. Surprisingly, the other complexes located on 2-fold axes are less symmetrical. In fact, that for which the 2-fold axis also bisects the diimine ligands, $[Cu(phen)_2]ClO_4$ [3], has a very large twist distortion [Fig. 4(b)] as indicated by the small dihedral angle (Table 3).

Trends in the parameters collated in Table 3 can be discerned by comparison with data calculated for molecules with distortions restricted to one of the three angles, pitch, roll and yaw. The bisector parameter is dependent on both pitch and yaw angles. To ascertain the relative significance of these two angles on bisector parameter, tilt parameters are plotted as a function of bisector parameters in Fig. 5 together with the calculated variation of the tilt parameter assuming increasing pitch angle only (AB, Fig. 5). Increasing the yaw angle has no effect on the tilt parameter (AC, Fig. 5). For the majority of the complexes, the variation in bisector parameter can be attributed to a change in the pitch angle, as exemplified by $[Cu(dmp)_2]Br \cdot H_2O$ [Fig. 4(c)] [2]. The exception is $[Cu(dmp)_2]BF_4 \cdot CH_2Cl_2$ [5] which exhibits a

Table 3. Stereochemical parameters for $[Cu(diimine)_2]^+$ cations

Complex	τ/Å	η	δ/°	ϵ/°
$[Cu(phen)_2]ClO_4$[a,3]	2.05	0.000	180.0	49.7
$[Cu(dmp)_2]BF_4 \cdot$ toluene[a,5]	2.62	0.031	178.1	83.7
$[Cu(Me_4bipy)_2]ClO_4$[a,6]	2.40	0.009	176.1	67.9
$[Cu(dmp)_2]NO_3$[a,4]	2.50	0.069	173.1	67.9
$[Cu(bipy)_2]ClO_4$[a,1]	2.49	0.108	170.1	76.6
$[Cu(Me_4bipy)_2]Cl \cdot 2H_2O$[2]	2.54	0.072	175.5	75.8
$[Cu(Me_2bipy)_2]BF_4$[7]	2.61	0.031	174.6	76.9
$[Cu(dmp)_2]NO_3 \cdot 2H_2O$[2]	2.66	0.046	173.9	85.2
$[Cu(dmp)_2]Br \cdot H_2O$[2]	2.56	0.119	171.6	77.9
$[Cu(phen)_2]CuBr_2$[3]	2.62	0.183	162.3	78.2
$[Cu(dmp)_2]BF_4 \cdot CH_2Cl_2$[5]	2.50	0.002	160.4	79.1
$[Cu(MeppdCl)_2]BF_4$[b]	2.04	0.230	155.8	52.8

[a] Located on a 2-fold axis of symmetry.
[b] This work.

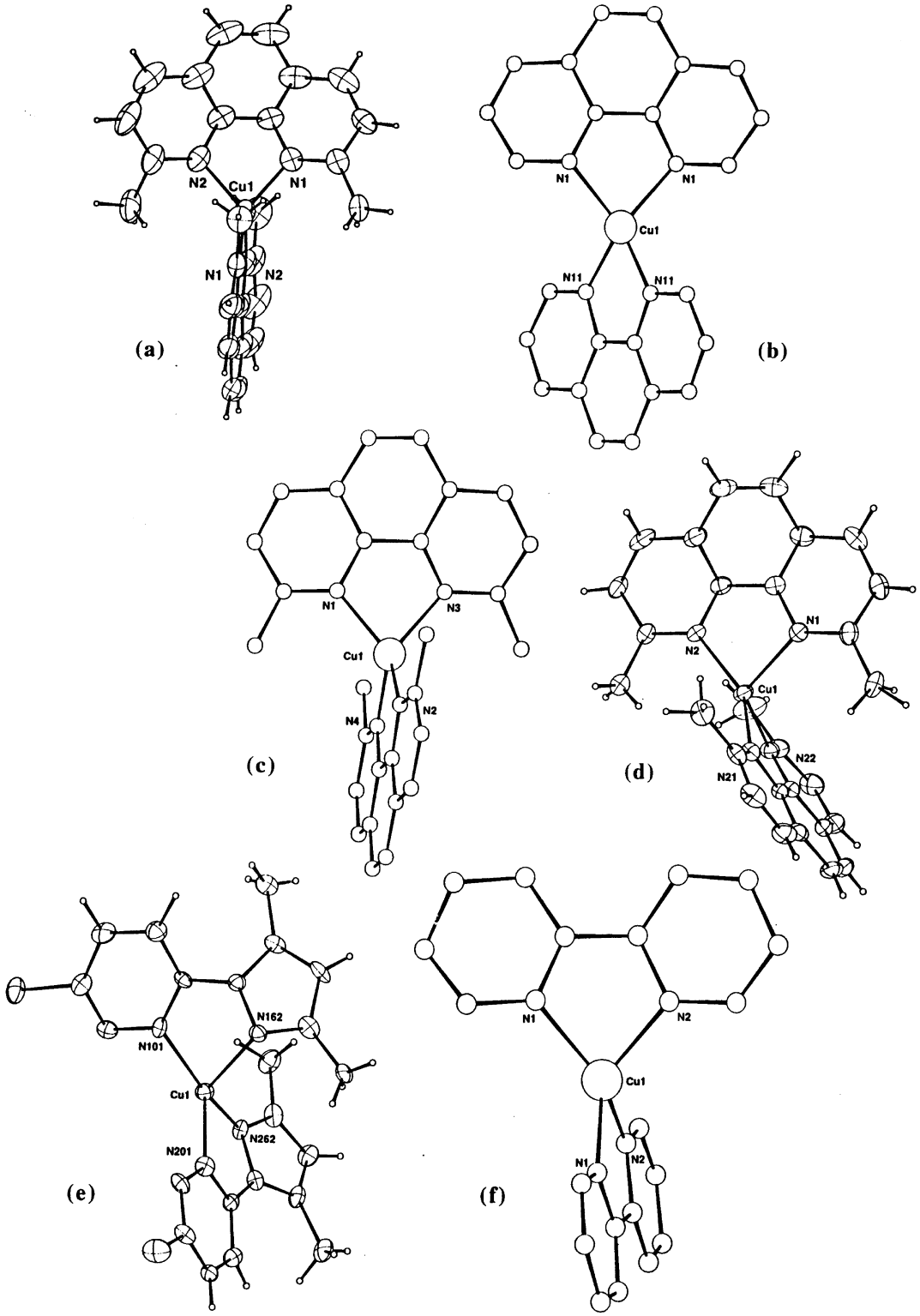

Fig. 4. Molecular structures of the $[Cu(diimine)_2]^+$ cations in (a) $[Cu(dmp)_2]BF_4 \cdot$ toluene, (b) $[Cu(phen)_2]ClO_4$, (c) $[Cu(dmp)_2]Br \cdot H_2O$, (d) $[Cu(dmp)_2]BF_4 \cdot 0.5CH_2Cl_2$, (e) $[Cu(MeppdCl)_2]BF_4$, (f) $[Cu(bipy)_2]ClO_4$ showing the diverse types of pitch, yaw and roll distortions. Each cation is shown such that the plane of the upper ligand is parallel to the plane of the paper.

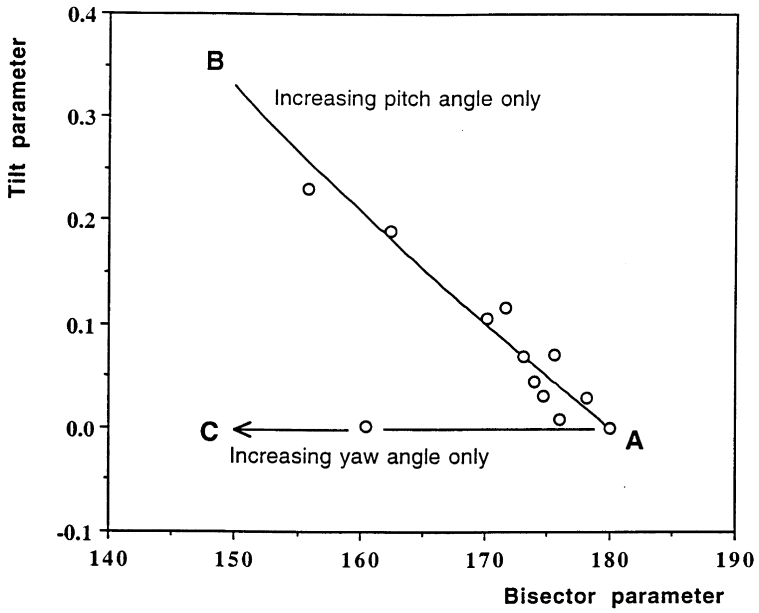

Fig. 5. Variation of tilt parameters with bisector parameters.

large yaw angle, but virtually no pitch distortion [Fig. 4(d)].

The dihedral parameter is dependent on all three angles. To ascertain their relative significance, dihedral parameters are plotted as a function of twist parameters in Fig. 6 together with the calculated variation of the dihedral parameter assuming increasing roll angle only (DE, Fig. 6). Increasing either yaw and/or pitch angle only has no effect on the dihedral parameter (DF, Fig. 6). All complexes exhibit some degree of roll. For the majority, the variation in dihedral parameter reflects solely a change in the roll angle, Ω, the maximum being observed for $[Cu(phen)_2]ClO_4$ [Fig. 4(b)] [3] and $[Cu(MeppdCl)_2]BF_4$ [Fig. 4(e)]. Of the cations which deviate significantly from curve DE (Fig. 6), $[Cu(dmp)_2]BF_4 \cdot CH_2Cl_2$ [5] [Fig. 4(d)] and

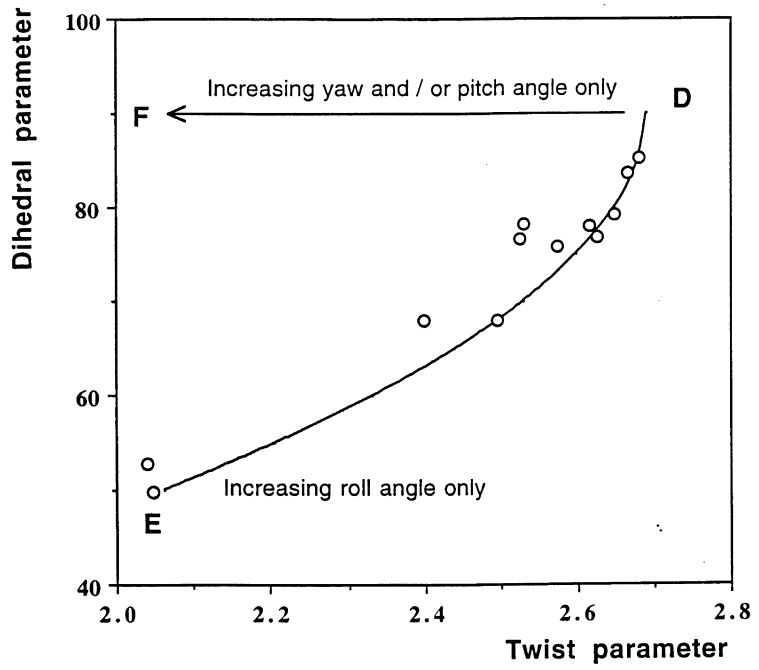

Fig. 6. Variation of dihedral parameters with twist parameters.

$[Cu(bipy)_2]ClO_4$ [1] [Fig. 4(f)] exhibit yaw and pitch distortions, respectively.

In summary, distortion of the pitch and roll angles, Φ and Ω, is dominant. Few complexes exhibit distortion of yaw angle, Ψ. The relative significance of yaw and pitch angle increase can be extricated from a consideration of tilt and bisector parameters (Fig. 5) while the significance of increasing roll angle relative to yaw and/or pitch angle increase can be assessed from a consideration of dihedral and twist parameters (Fig. 6).

CONCLUSION

Unsymmetrical diimines form $[Cu(diimine)_2]^+$ and $[Cu(diimine)_2X]^+$ cationic complexes structurally similar to their symmetrical analogues. For the copper(I) complex, however, the extent of distortion from the predicted tetrahedral geometry is much greater for the unsymmetrical diimine. The distortion, the relative orientations of the planes of the two diimine ligands, can be described, by analogy with spacecraft manoeuvres, the pitch, roll and yaw angles. The majority of structurally characterised $[Cu(diimine)_2]^+$ cations exhibit either pitch or roll distortion or some combination of both. Those few complexes which do exhibit yaw distortion do so without pitch or roll distortion. $[Cu(MeppdCl)_2]^+$ exhibits severe pitch, yaw and roll distortion.

Acknowledgements—We thank Professor M.B. Hursthouse and the EPSRC Crystallography Service at the University of Wales, Cardiff for X-ray data collection and the EPSRC for PDRA support.

REFERENCES

1. Munakata, M., Kitagawa, S., Asahara, A. and Masuda, H., *Bull. Chem. Soc. Japan*, 1987, **60,** 1927.
2. Dobson, J. F., Green, B. E., Healy, P. C., Kennard, C. H. L., Pakawatchai, C. and White, A. H., *Aust. J Chem.*, 1984, **37,** 649.
3. Healy, P. C., Engelhardt, L. M., Patrick, V. A. and White, A. H., *J. Chem. Soc., Dalton Trans.*, 1985, 2541.
4. Hämäläinen, R., Ahlgren, M., Turpeinen, U. and Raikas, T., *Cryst. Struct. Commun.*, 1979, **8,** 75.
5. Blake, A. J., Hill, S. J., Hubberstey, P. and Li, W.-S. *J. Chem. Soc., Dalton Trans.*, 1998, 909.
6. Burke, P. J., Henrick, K. and McMillin, D. R., *Inorg. Chem.*, 1982, **21,** 1881.
7. Burke, P. J., McMillin, D. R. and Robinson, W. R., *Inorg. Chem.*, 1980, **19,** 1211.
8. Murphy, G., Nagle, P., Murphy, B. and Hathaway, B. J., *J. Chem. Soc., Dalton Trans.*, 1997, 2645.
9. Harrison, W. D., Kennedy, D. M., Power, M., Sheahan, R. and Hathaway, B., *J. Chem. Soc., Dalton Trans.*, 1981, 1556; Nagle, P., O'Sullivan, E. Hathaway, B. J. and Muller, E., *J. Chem. Soc., Dalton Trans.*, 1990, 3399.
10. Boys, D., *Acta Crystallogr. Sect C*, 1988, **44**, 1539; Boys, D., Escobar, C. and Martinez-Carrera, S., *Acta Crystallogr. Sect C*, 1981, **44**, 351; Nagle, P. and Hathaway, B. J., *Acta Crystallogr. Sect C*, 1991, **47**, 1386; Potocnak, I., Dunaj-Jurco, M., Miklos, D. and Jager, L., *Acta Crystallogr. Sect C*, 1996, **52**, 1653; Potocnak, I., Dunaj-Jurco, M., Miklos, D. and Jager, L., *Acta Crystallogr. Sect C*, 1996, **52**, 48; Dunaj-Jurco, M., Potocnak, I., Cibik, J., Kabesova, M., Kettmann, V. and Miklos, D., *Acta Crystallogr. Sect C*, 1993, **49**, 1479; Parker, O. J., Manson, J. L. and Breneman, G. L., *Acta Crystallogr. Sect C*, 1994, **50**, 1201; Potocnak, I., Dunaj-Jurco, M., Miklos, D. and Jager, L., *Acta Crystallogr. Sect C*, 1996, **52**, 532; Potocnak, I., Dunaj-Jurco, M., Miklos, D., Kabesova, M. and Jager, L., *Acta Crystallogr. Sect C*, 1995, **51**, 1291; Bkouchewaksman, I., Kvick, A., Boillot, M. L. and Kahn, O., *J. Cryst. Spectroscopic Research*, 1991, **21**, 595; Sedov, A., Kabesova, M., Dunaj-Jurco, M., Gazo, J. and Garaj, J., *Chemicke Zvesti*, 1983, **37**, 43; Fitzgerald, W., Hathaway, B. J. and Simmons, C. J., *J. Chem. Soc., Dalton Trans.*, 1985, 141; Escobar, C. and Wittke, O., *Acta Crystallogr. Sect C*, 1983, **39**, 1643; Morehouse, S. M., *Inorg. Chim. Acta*, 1996, **243**, 327.
11. Halcrow, M. A., Cromhout, N. L. and Raithby, P. R., *Polyhedron*, 1997, **24**, 4257; Bardwell, D. A., Cargill-Thompson, A. M. W., Jeffrey, J. C., Tilley, E. E. M. and Ward, M. D., *J. Chem. Soc., Dalton Trans.*, 1995, 835.
12. Blake, A. J., Hubberstey, P., Li, W.-S., Russell, C. E., Smith, B. J. and Wraith, W. D., *J. Chem. Soc., Dalton Trans.*, 1998, 647.
13. Batsanov, A. S., Hubberstey, P., Russell, C. E. and Walton, P. H., *J. Chem. Soc., Dalton Trans.*, 1997, 2667.
14. Werner, H., Schulz, M. and Windmuller, B., *Organometallics*, 1995, **14,** 3659.
15. Marder, T. B., Fultz, W. C., Calabrese, J. C., Harlow, R. L. and Milstein, D., *J. Chem. Soc., Chem. Commun.*, 1987, 1543.
16. Pallenberg, A. J., Marschner, T. M. and Barnhardt, D. M., *Polyhedron*, 1997, **16,** 2711.
17. Darr, J. A., Drake, S. R., Hursthouse, M. B. and Malik, K. M. A., *Inorg. Chem.*, 1993, **32,** 5704.
18. Walker, N. and Stuart, D., *Acta Crystallogr., Sect. A.*, 1983, **39,** 158.
19. Altomare, A., Cascarano, G., Giacovazzo, G., Guagliardi, A., Burla, M. C., Polidori, G. and Camalli, M., *J. Appl. Crystallogr.*, 1994, **27,** 435.
20. Watkin, D. J., Prout, C. K., Carruthers, R. J. and Betheridge, P., CRYSTALS Issue 10. Chemical Crystallography Laboratory, University of Oxford, 1996.
21. Watkin, D. J., Prout, C. K. and Pearce, L. J., CAMERON, Chemical Crystallography Laboratory, University of Oxford, 1996.
22. Williams, R. J. P., *Inorg. Chim. Acta Rev.*, 1971, **5,** 137.
23. Addison, A. W., Nageswara Rao, T., Reedijk, J., van Rijn, J. and Verschoor, *J. Chem. Soc., Dalton Trans.*, 1984, 1349.

Pergamon

PII: S0277–5387(98)00154–5

Polyhedron Vol. 17, No. 20, pp. 3595–3606, 1998
© 1998 Elsevier Science Ltd
All rights reserved. Printed in Great Britain
0277–5387/98 $19.00 + 0.00

Syntheses and characterization of four novel monooxovanadium(v) hydrazone complexes with hydroxamate or alkoxide ligand

Shan Gao, Zhi-Qiang Weng and Shi-Xiong Liu*

Dept. of Chem., Fuzhou University, Fuzhou 350002, P. R. China

(Received 3 December 1997; accepted 6 April 1998)

Abstract—Four novel monooxovanadium(V) hydrazone complexes, $[VOL^1(Hshi)]$ (**1**), $[VOL^1(bz)]$ (**2**), $[VOL^2(bz)]\cdot CH_2Cl_2$ (**3**), and $[VOL^2(OCH_3)(CH_3OH)]\cdot CH_3OH$ (**4**) (H_2L^1 = salicylaldehyde benzoylhydrazone, H_2L^2 = o-vanillin benzoylhydrazone, H_2shi = salicylhydroxamic acid, Hbz = benzohydroxamic acid), were prepared and characterized by IR, Raman, UV, ^{1}H NMR spectra, cyclic voltammetry measurements and X-ray diffraction. The geometry around the vanadium atoms is a distorted VO(ONO)(OO) octahedron in complexes **1**, **2** and **3**, while the geometry is a distorted VO(ONO)(O)(O) octahedron in **4**. The V═O bond distance is 1.574(4), 1.593(5), 1.594(4) and 1.577(4) Å for complexes **1**, **2**, **3** and **4**, respectively. In complexes **1**, **2** and **3**, the O, N, O atoms of a tridentate hydrazone ligand and one oxime oxygen atom of a bidentate hydroxamate ligand are coordinated to the vanadium(V) atom, forming an equatorial plane. In complexes **1**, **2** and **3**, the axial position *trans* to the oxo group is occupied by the carbonyl oxygen atom of the hydroxamate ligand, but not by the oxime oxygen atom. The bond distances in the equatorial plane in the title complexes follow the order: alkoxide oxygen < phenoxide oxygen, oxime oxygen < enolic oxygen < imine nitrogen. The complexes **1**, **2** and **3** represent the first structural examples of vanadium complexes containing both hydrazone and hydroxamate ligands. © 1998 Elsevier Science Ltd. All rights reserved

Keywords: monoxovanadium(V) complexes; hydrazone complexes; hydroxamate complexes; crystal structures; spectroscopic properties.

Knowledge of the biological role of vanadium as a trace element has considerably increased over the past decade [1, 2]. A vanadium enzyme has been described which exhibits histidine-nitrogen coordination to vanadium [3]. The active sites of some biological enzymes include the hydroxamic acids [4]. Many small biomolecules such as hydroxy- or mercaptocarboxylates, amino acids, hydroxamates, hydrazones, phosphates, phosphonates, catechol derivatives, etc. are able to bind this element rather strongly in both the +4 and +5 oxidation states [5–15].

However, only a few structures of the simplest vanadium complexes with hydroxamate ligands have been studied [5, 16–18]. Up to now, only a few oxovanadium hydrazone complexes have been reported. These hydrazone complexes are only limited to dioxovanadium(V) complexes with VO_2(ONO) coordination [8, 19–21], and to monooxovanadium(V) complexes with square pyramidal VO(ONO)(O) coordination [10, 22–27] and octahedral (VO(ONO)(O)(O) [28] or VO(ONO)(ON) [9, 15] coordination.

The relationships between structure, spectroscopy, and reactivity must be elucidated in order to understand fully the role of vanadium in biological systems. We have undertaken the syntheses and characterization of some vanadium compounds containing tridentate ligand with VO(ONO)(ON) or VO(ONO)(OO) coordination [15, 29]. Herein we report four monooxovanadium(V) hydrazone complexes with the hydroxamate or alkoxide ligand, $[VOL^1(Hshi)]$ (**1**), $[VOL^1(bz)]$ (**2**), $[VOL^2(bz)]\cdot CH_2Cl_2$ (**3**), and $[VOL^2(OCH_3)(CH_3OH)]\cdot CH_3OH$ (**4**) (H_2L^1 = salicylaldehyde benzoylhydrazone, H_2L^2 = o-vanillin benzoylhydrazone, H_2shi = salicylhydroxamic acid, Hbz = benzohydroxamic acid). To the best of our knowledge, the complexes **1**, **2**, and **3** are the first examples of vanadium hydrazone complexes with VO(ONO)(OO) coordination.

* Author to whom correspondence should be addressed.

EXPERIMENTAL

Materials

The materials $VO(acac)_2$ (acac = acetylacetonate), Hbz and H_2shi, were synthesized according to references [30, 31], respectively. The ligand H_2L^1 was prepared by condensing salicylaldehyde with equimolor benzoylhydrazine in ethanol. The ligand H_2L^2 was synthesized by condensing o-vanillin with equimolor benzoylhydrazine in ethanol. Analytically pure dichloromethane was distilled over calcium hydride before use. All other analytical grade chemicals and solvents were purchased commercially and used without further purification.

Synthesis of $[VOL^1$ *(Hshi)]* (*1*)

$[VO(acac)_2]$ (0.263 g, 1.00 mmol) dissolved in 10 cm^3 methanol was added dropwise to a methanol solution containing 0.240 g (1.00 mmol) of H_2L^1 with stirring, and then the mixture was heated at reflux with stirring for 1 h and cooled to room temperature. 10 cm^3 of mixed solution of methanol and salicylhydroxamic acid (1 mmol) was slowly added to the above red-black solution. The reaction mixture was stirred for 30 min. and filtered. Then deep red solid was dissolved in the dichloromethane and filtered. The deep red crystals of the complex **1** were obtained by slow diffusion of hexane into the filtrate for several days and collected under vacuum over P_4O_{10}.

Synthesis of $[VOL^1(bz)]$ (*2*)

The synthesis of complex $[VOL^1(bz)]$ (**2**) was analogous to that of complex **1**, only except that salicylhydroxamic acid was replaced by benzohydroxamic acid. The deep red crystals of the complex **2** were formed upon slow evaporation of the filtrate for several days and collected under vacuum over P_4O_{10}.

Synthesis of $[VO(L^2)(bz)]\cdot CH_2Cl_2$ (*3*)

A 15 cm^3 CH_3OH solution of $VO(acac)_2$ (0.263 g, 1.00 mmol) was added dropwise to a 15 cm^3 CH_3OH solution of H_2L^2 (1.00 mmol). The mixture was refluxed with stirring for 1.5 h, cooled to room temperature. A 10 cm^3 solution of benzohydroxamic acid (1.00 mmol) in CH_3OH was added to the above dark red solution. The mixture was stirred for 30 min. and filtered. The red brown solid was dried under vacuum over P_4O_{10} for 2 days, dissolved in the dichloromethane and filtered. The deep red crystals of the complex **3** were isolated by slow diffusion of hexane into the above filtrate for several days and collected under vacuum over P_4O_{10}.

Synthesis of $[VO(L^2)(OCH_3)(CH_3OH)]\cdot CH_3OH$ (*4*)

To H_2L^2 (1.00 mmol) dissolved in 15 cm^3 CH_3OH was added $VO(acac)_2$ (0.263 g, 1.00 mmol) in 15 cm^3 CH_3OH. The mixture was refluxed with stirring for 1 h, cooled to room temperature and filtered. The deep red crystals of the complex **4** were obtained by slow evaporation of the deep red filtrate at room temperature in a few days, and then collected under vacuum over P_4O_{10}.

Physical measurements

IR spectra and Raman spectra were measured on a Nicolet Magna 750 Fourier transform IR spectrometer and a Nicolet Raman 910 Fourier transform laser-Raman spectrometer, respectively. UV-vis spectra were obtained on a Perkin-Elmer lambda 9 UV/vis/near-IR spectrometer in CH_2Cl_2 solution and in the 300–1000 mm range. ^{1}H NMR spectra were collected on a Varian FT-80A spectrometer in $CDCl_3$, using TMS as internal standard. Electrochemical measurements were undertaken on a BAS 100 A electrochemical analyzer on CH_2Cl_2 solution (1 mM complex, 0.1 M $(Et_4N)ClO_4$). A three-electrode system was composed of a platinum working electrode, a platinum wire auxiliary electrode, and a Ag/AgCl reference electrode.

X-ray structure determination

X-ray diffraction data were recorded on a Rigaku AFC5R diffractometer with graphite-monochromated Mo–K_α radiation ($\lambda = 0.71069$ Å), the scan mode being ω-2θ. Cell dimensions were refined using 25 reflections in the ranges $20 < 2\theta < 30^\circ$. The diffraction data were corrected for Lorentz effect and polarization effect for the title complexes. The crystallographic data are given in Table 1.

The structures were solved by direct methods and refined by a full-matrix least-squares procedure. All non-hydrogen atoms were refined with anisotropic thermal parameters. All hydrogen atoms were located by difference Fourier map or HYDROGEN program and added to the structure factor calculation, but their positions were not refined.

RESULT AND DISCUSSION

Spectroscopic studies

Table 2 summarizes the IR and Raman spectra data of the free ligands and the title complexes. A strong and broad band near 3138 ~ 3057 cm^{-1} is observed in IR spectra of the free ligands and assigned to the ν(OH) absorption with hydrogen bond [32, 33], but disappeared in the four title complexes. The bands at 3234 cm^{-1} in **1** and at 3158 cm^{-1} in **4** are due to the

Table 1. Crystallographic data

Complex	**1**	**2**	**3**	**4**
Formula	$C_{21}H_{16}N_3O_6V$	$C_{21}H_{16}N_3O_5V$	$C_{23}H_{20}Cl_2N_3O_6V$	$C_{18}H_{23}N_2O_7V$
M_r	457.32	441.32	556.27	430.33
Crystal system	Monoclinic	Monoclinic	Monoclinic	Monoclinic
Space group	$P2_1/n$	$P2_1/a$	$P2_1/n$	$P2_1/a$
a (Å)	12.858(3)	12.299(5)	10.772(3)	13.400(4)
b (Å)	10.1404(9)	8.877(3)	20.458(3)	7.413(2)
c (Å)	15.600(4)	18.871(5)	11.938(3)	20.592(6)
β (°)	94.17(2)	107.71(3)	110.15(2)	97.73(2)
V (Å^3)	2029(1)	1963(1)	2470(1)	2027.0(9)
Z	4	4	4	4
$F(000)$	936	904	1136	896
$D_{calc.}$ (g·cm^{-3})	1.50	1.49	1.50	1.41
μ Mo K_α (mm^{-1})	0.514	0.525	0.648	0.511
Temperature (K)	298	298	296	296
Shape	Prism	Rhombus	Rhombus	Prism
Colour	Deep red	Deep red	Deep red	Deep red
Crystal dimensions (mm)	$0.30\times0.35\times0.25$	$0.45\times0.45\times0.20$	$0.30\times0.30\times0.20$	$0.35\times0.25\times0.45$
$2\theta_{max.}$(°)	50.2	50.2	50.0	50.1
Collected data	4001	3917	4747	4071
Unique data	3822	3733	4497	3896
Observed data ($I>3\sigma(I_0)$)	2173	2033	2495	2263
No. variables	281	271	316	254
R	0.051	0.062	0.060	0.053
R_w	0.063	0.085	0.077	0.068
Largest diff. peak/hole(e/Å^3)	0.38/−0.42	0.52/−0.39	0.35/−0.34	0.39/−0.45
Max. shift	0.01	0.01	0.01	0.01

Ar–OH absorption in **1** and the coordinated CH_3–OH absorption in **4**, respectively. The medium strong bands at 966–980 cm^{-1} (IR) and at 960–979 cm^{-1} (Raman) in these title complexes are attributed to the typical V═O stretching frequencies, falling within the range of 950–990 cm^{-1} reported for six-coordinated oxovanadium(V) complexes [9, 15–17, 29]. The very strong stretching vibrations of ν (C═N) and ν(C═O) are displaced to lower frequency [27, 33], and the strong ν(C–O) (phenolato oxygen) and the middle ν(N–H) absorption bands in the title complexes display a shift to higher frequency with respect to the free ligands [15, 27, 33]. The new medium bands at 1255–1279 cm^{-1} (IR) and at 1251–1278 cm^{-1} (Raman) may be due to the enolic ν(C–O) absorption [25, 29]. It shows that the hydrazone ligands in the title complexes are in a dianionic form of the type ($^-$O∼N∼O$^-$) and the two hydroxamate ligands are in a monoanionic form of the type (O∼O$^-$). The stretching vibrations of the V–O bond and the V–N bond have been observed at 499–355 cm^{-1} (far-IR), and 500–356 cm^{-1} (Raman) [25].

The ^{1}H NMR spectra data of the free ligands and the title complexes are also shown in Table 2. As expected, O–H and N–H resonances of the free hydrazone ligand are absent in the title complexes. Broad NH–OH resonances (δ 8.77 and 8.90 ppm) of free salicylhydroxamic acid and benzohydroxamic acid change into a singlet (δ = 8.98, 8.96 and 8.93 ppm in **1**, **2** and **3**, respectively) [33], indicating the coordination through their deprotonation of the hydroxyl group in the hydroxamate ligand. In complex **1**, the peak at δ 10.86 ppm is assigned to O–H resonance bonding to aromatic ring of the salicylhydroximate ligand. In complex **3**, the peak at 5.30 ppm is assigned to CH_2 resonance to a dichlormethane molecule. In complex **4**, the peaks at 5.31 ppm and 3.44–3.94 ppm are assigned to H and –CH_3 resonances of the bonded methanol molecule. These are agreement with the results of their single crystal analysis.

The LMCT transition (λ = 454, 448, 537 and 492 nm for **1**, **2**, **3** and **4**, respectively) is considered as a charge transfer from a p-orbital on the lone-pair of phenolato or oximate oxygen to the empty d-orbital of vanadium atom. In contrast to other oxovanadium(V) hydrazone complexes with 8-quinolinol co-ligand [29, 34], the absorption peaks of the visible region in the title complexes are obviously moved to the UV region. The other strong bands (λ = 338, 335, 352 and 365 nm in **1**, **2**, **3** and **4**, respectively) are generally attributed to the intraligand absorption peaks [34]. The other LMCT band observed in the UV region (365 nm in **4**, 352 nm in **3**) is due to alkoxo/enolic oxygen bound to vanadium(V) [34].

As illustrated in Fig. 1, there is a quasi-reversible redox behavior corresponding to V^V/V^{IV} couple in

Table 2. IR (Raman*) and ^{1}H NMR spectral data

IR (Raman*) (cm^{-1}) Compound	ν(NH)	ν(OH)	ν(C═O)	ν(C═N)	ν(C–O)$_{phenolic}$	ν(C–O)$_{enolic}$	ν(N–O)	ν(V═O)	ν(V–O),ν(V–N)
Hbz	3290	3060	1644				890		
H_2Shi	3280	3138	1657						
H_2L^1	3265	3057	1673	1645	1279				
H_2L^2	3267	3097	1670	1643	1279				
Complex 1	3331	3234	~1590	1608	1352	1255		968	461,355
			(~1546)	(1596)	(1334)	(1253)		(960)	(451,356)
Complex 2	3446		~1597	1608	1342	1279		980	457,362
			(~1557)	(1598)	(1330)	(1278)		(979)	(445,362)
Complex 3	3446		~1560	1604	1286	1259	914	966	498,457,428
			(~1582)	(1596)	(1312)	(1251)	(905)	(971)	(500,456,428)
Complex 4		3158		1608	1346	1259		975	482,428
				(1596)	(1334)	(1262)		(978)	(470,410)

^{1}H NMR (δ ppm)	Ar–OH	N–H	NH–OH	Phenyl	–OH(CH_3OH)	Ar–OCH_3	–CH═N–	CH_2Cl_2	–CH_3(CH_3OH)
Hbz			8.77	7.26~7.76					
H_2Shi	10.48		8.90	6.92~7.93					
H_2L^1	11.03	9.82		6.92~8.05			8.53		
H_2L^2	9.93	9.12		6.88~7.85		3.93	8.65		
Complex 1	10.86		8.98	6.94~8.07			8.46		
Complex 2			8.96	6.98~8.06			8.48		
Complex 3			8.93	6.98~8.01		3.83	8.04	5.30	
Complex 4				7.06~8.16	5.31	3.96	8.52		3.44~3.94

*The bands at Raman spectra are given in parentheses.

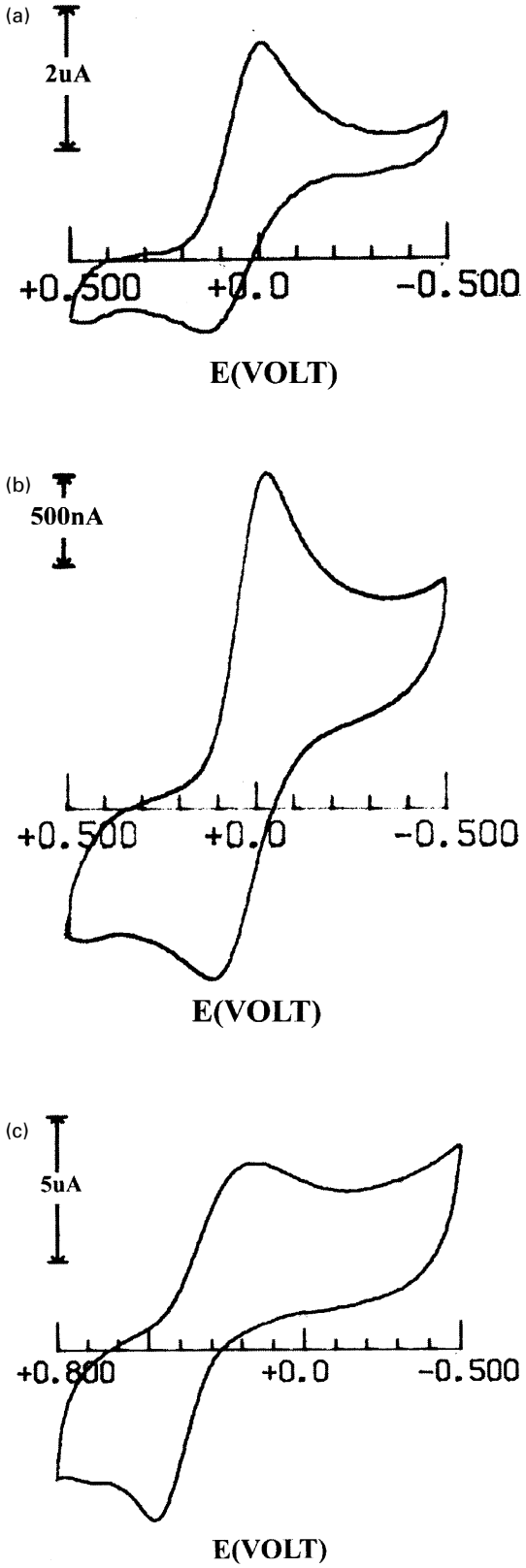

Fig. 1. Cyclic voltammogram of the title complexes **2**, **3** and **4** in dichloromethane (a) complex **2** (b) complex **3** (c) complex **4**

dichloromethane solution in the title complexes. Their redox potentials in complexes **1**, **2**, **3** and **4** are at $E_{1/2}=0.131$ V, 0.060 V, 0.030 V and 0.338 V with respect to Ag/AgCl, respectively. The peak-to-peak separations ($\triangle E_p$ of coupled peaks D/E) are 94 mV (**1**) and 90 mV (**2**) at a rate of 200 mV s^{-1}. The $E_{1/2}$ value of the complex **1** is smaller of 71 mV than that of the complex **2** due to the difference between the bidentate hydroximate ligands. It is noteworthy that the potentials of the VO^{3+}-VO^{2+} couple in the complexes **3** and **4** are significantly more positive than those observed for some VO^{3+} complexes [34], indicating that the complexes **3** and **4** are relatively unstable.

Description of the structures of complexes $[VOL^1(Hshi)]$ (*1*), $[VOL^1(bz)]$ (*2*) *and* $[VOL^2(bz)]\cdot CH_2Cl_2$ (*3*)

The selected bond lengths and angles in complexes **1**, **2** and **3** are listed in Table 3, Table 4 and Table 5, respectively. The molecular structures of complexes **1**, **2** and **3** are shown in Fig. 2, Fig. 3 and Fig. 4.

There are seven common structural features in the complexes **1**, **2** and **3**.

(a) The coordination sphere around the vanadium atoms is a distorted octahedral configuration with $[V^VO(ONO)(OO)]$ type. However, most of vanadium atoms in the known vanadium hydrazone complexes have a square pyramidal $[V^VO(ONO)(O)]$ coordination [10, 22–27], only one complex has octahedral $[V^VO(ONO)(O)(O)]$ coordination [28] and two complexes have $[V^VO(ONO)(ON)]$ coordination [9, 15]. The title complexes **1**, **2** and **3** represent the first structural characterization of any vanadium hydrazone complex with VO(ONO)(OO) coordination.

(b) The equatorial plane is formed by the O, N, O atoms of the fully deprotonated tridentate hydrazone ligand (L) and an oxime oxygen atom of the hydroxamate ligand. The vanadium atom is 0.271 Å, 0.279 Å and 0.271 Å out the equatorial plane and toward the oxo oxygen atom in the complexes **1**, **2** and **3**, respectively.

(c) The atom lying *trans* to the oxo oxygen atom (O_o) is the carbonyl oxygen atom (O_c.) of the hydroximate ligand, but not the oxime oxygen of the same ligand. It may be related to the structural *trans* effect and the delocalized conjugated system between the V=O unit and the related group in hydroxamic acids. The *trans* angle O_o–V–O_c. is 171.4(2)°, 172.8(2)° and 170.5(2)° in complexes **1**, **2** and **3**, respectively. The vanadyl bond of V=O is 1.574(4), 1.593(5) and 1.594(4) Å in complexes **1 2** and **3**, respectively. The vanadyl bond length in complex **1** is at the shortest limit of normal V=O bond lengths, although it is within the range (1.57–1.61 Å) found in VO^{3+} complexes [15–18, 22–28]. In complex **2**, the V=O bond length and V–O(3)(carbonyl) are 1.593(5) and 2.201(5) Å,

Table 3. Selected bond distances (Å) and angles (°) for complex [VOL^1(Hshi)] (**1**)

V(1)–O(6)	1.574(4)	O(3)–C(15)	1.258(5)
V(1)–O(1)	1.842(3)	O(4)–N(3)	1.372(5)
V(1)–O(4)	1.860(3)	O(5)–C(17)	1.337(6)
V(1)–O(2)	1.946(3)	N(1)–C(7)	1.286(6)
V(1)–N(1)	2.090(4)	N(1)–N(2)	1.404(5)
V(1)–O(3)	2.159(3)	N(2)–C(8)	1.286(6)
O(1)–C(1)	1.328(6)	N(3)–C(15)	1.308(6)
O(2)–C(8)	1.302(5)	C(15)–C(16)	1.470(6)
O(5) ... N(2a)	2.724(5)	O(6) ... N(3b)	2.903(5)
O(6)–V(1)–O(1)	98.8(2)	O(4)–V(1)–N(1)	155.8(1)
O(6)–V(1)–O(4)	94.8(2)	O(4)–V(1)–O(3)	76.9(1)
O(6)–V(1)–O(2)	92.7(2)	O(2)–V(1)–N(1)	74.5(1)
O(6)–V(1)–N(1)	107.9(2)	O(2)–V(1)–O(3)	86.0(1)
O(6)–V(1)–O(3)	171.4(2)	N(1)–V(1)–O(3)	80.0(1)
O(1)–V(1)–O(4)	101.0(1)	N(2)–C(8)–O(2)	122.7(5)
O(1)–V(1)–O(2)	158.0(1)	C(15)–O(3)–V(1)	111.4(3)
O(1)–V(1)–N(1)	84.1(1)	N(3)–O(4)–V(1)	117.1(2)
O(1)–V(1)–O(3)	85.2(1)	C(15)–N(3)–O(4)	117.4(4)
O(4)–V(1)–O(2)	96.7(1)	O(3)–C(15)–N(3)	116.8(4)
O(5)–H (22) ... N(2a)	171.2	O(6) ... H(23b)–N(3b)	152.8

Symmetry code: a, x, 1 + y, z; b, 0.5-x, −0.5 + y, 1.5-z.

Table 4. Selected bond distances (Å) and angles (°) for complex [VOL^1(bz)] (**2**)

V(1)–O(5)	1.593(5)	O(2)–C(8)	1.308(7)
V(1)–O(1)	1.847(5)	O(3)–C(15)	1.242(7)
V(1)–O(4)	1.855(4)	O(4)–N(3)	1.352(6)
V(1)–O(2)	1.931(5)	N(1)–C(7)	1.285(8)
V(1)–N(1)	2.056(5)	N(1)–N(2)	1.405(7)
V(1)–O(3)	2.201(5)	N(2)–C(8)	1.288(8)
O(1)–C(1)	1.325(7)	N(3)–C(15)	1.316(8)
O(5)–V(1)–O(1)	100.8(2)	O(4)–V(1)–N(1)	164.1(2)
O(5)–V(1)–O(4)	97.7(2)	O(4)–V(1)–O(3)	75.8(2)
O(5)–V(1)–O(2)	97.9(2)	O(2)–V(1)–N(1)	75.4(2)
O(5)–V(1)–N(1)	97.0(2)	O(2)–V(1)–O(3)	79.9(2)
O(5)–V(1)–O(3)	172.8(2)	N(1)–V(1)–O(3)	89.2(2)
O(1)–V(1)–O(4)	99.3(2)	O(2)–C(8)–N(2)	121.9(6)
O(1)–V(1)–O(2)	153.5(2)	C(15)–O(3)–V(1)	110.7(4)
O(1)–V(1)–N(1)	83.8(2)	N(3)–O(4)–V(1)	118.9(3)
O(1)–V(1)–O(3)	83.5(2)	C(15)–N(3)–O(4)	117.0(5)
O(4)–V(1)–O(2)	96.6(2)	O(3)–C(15)–N(3)	117.5(6)

which are longer than the corresponding bond distances of the complex **1**. It may be related to the difference between hydroxamate ligands in these two complexes.

(d) The four V–O or V–N bond distances in the equatorial plane follow the order: alkoxide oxygen < phenoxide oxygen, oxime oxygen < enolic oxygen < imine nitrogen. The bond length of V(1)–O(2) (enolic oxygen) in complex **1** is ~0.1 Å longer than that of the V(1)–O(1) (phenolate) and V(1)–O(4) (oxime) in the equatorial plane. It can been explained that the phenolate and oxime oxygen atoms have a high basicity and ensure significant back bonding of their O→V bond as revealed by the bond length data.

(e) The V–N bond distance is 2.090(4), 2.056(5) and 2.073(5) Å in complexes **1**, **2** and **3**, respectively, which lie in the range (2.05–2.12 Å) reported in the VO^{3+} hydrazone complexes [9, 10, 15, 22–28]. The V–N bond length (2.090(4) Å) in complex **1** is slightly shorter than the corresponding one (2.119(6) Å) in complex [VOL^1(OCH$_3$)(CH$_3$OH)]

Table 5. Selected bond distances (Å) and angles (°) for complex [VOL^2(bz)] CH_2Cl_2 (**3**)

V(1)–O(6)	1.594(4)	O(5)–N(3)	1.345(6)
V(1)–O(5)	1.874(4)	N(1)–C(7)	1.294(7)
V(1)–O(1)	1.887(4)	C(6)–C(7)	1.435(8)
V(1)–O(2)	1.950(4)	C(9)–C(10)	1.480(8)
V(1)–N(1)	2.073(5)	N(1)–N(2)	1.379(6)
V(1)–O(4)	2.202(4)	N(2)–C(9)	1.312(7)
O(1)–C(1)	1.332(6)	N(3)–C(16)	1.329(7)
O(2)–C(9)	1.302(6)	C(16)–C(17)	1.495(8)
O(3)–C(2)	1.378(7)	Cl(1)–C(23)	1.720(8)
O(3)–C(8)	1.414(8)	Cl(2)–C(23)	1.734(8)
O(4)–C(16)	1.246(6)	N(3) ... O(3a)	2.818(6)
O(6)–V(1)–O(5)	94.8(2)	O(1)–C(1)–C(2)	119.1(5)
O(6)–V(1)–O(1)	99.8(2)	C(3)–C(2)–O(3)	124.9(6)
O(6)–V(1)–O(2)	98.8(2)	O(3)–C(2)–C(1)	113.9(5)
O(6)–V(1)–N(1)	99.4(2)	C(5)–C(6)–C(7)	119.8(6)
O(6)–V(1)–O(4)	170.5(2)	C(1)–C(6)–C(7)	120.3(5)
O(5)–V(1)–O(1)	101.2(2)	N(1)–C(7)–C(6)	125.0(5)
O(5)–V(1)–O(2)	95.2(2)	O(2)–C(9)–N(2)	121.9(6)
O(5)–V(1)–N(1)	163.9(2)	O(2)–C(9)–C(10)	118.9(5)
O(5)–V(1)–O(4)	75.8(2)	N(2)–C(9)–C(10)	119.2(5)
O(1)–V(1)–O(2)	154.0(2)	C(15)–C(10)–C(9)	121.4(6)
O(1)–V(1)–N(1)	84.0(2)	C(11)–C(10)–C(9)	120.0(6)
O(1)–V(1)–O(4)	83.4(2)	O(4)–C(16)–N(3)	118.5(5)
O(2)–V(1)–N(1)	75.1(2)	O(4)–C(16)–C(17)	122.1(6)
O(2)–V(1)–O(4)	81.2(2)	N(3)–C(16)–C(17)	119.2(5)
N(1)–V(1)–O(4)	89.8(2)	C(7)–N(1)–V(1)	128.3(4)
N(2)–N(1)–V(1)	116.6(4)	C(9)–O(2)–V(1)	117.5(4)
C(9)–N(2)–N(1)	108.9(5)	C(2)–O(3)–C(8)	118.2(5)
C(16)–N(3)–O(5)	115.9(4)	C(16)–O (4)–V(1)	110.2(4)
O(1)–C(1)–C(6)	122.8(5)	N(3)–O(5)–V(1)	119.3(3)
C(22)–C(17)–C(16)	118.1(5)	C(7)–N(1)–N(2)	115.0(5)
C(18)–C(17)–C(16)	122.0(6)	Cl(1)–C(23)–Cl(2)	112.4(4)
C(1)–O(1)–V(1)	133.6(3)	N(3)–H(24) ... O(3a)	151.9

Symmetry code: a, -x, -y, -z.

[28]. It means that the presence of hydroxamate ligand in complex **1** results in the difference of V–N bond lengths between these two complexes.

(f) The hydrazone ligand in all four title complexes, except the methanol group in complexes **3** and **4**, constitute a good plane with mean derivation of 0.032, 0.019, 0.010 and 0.073 Å in complexes **1**, **2**, **3** and **4**, owing to the existence of delocalized π bond in hydrazone ligand.

(g) The N–N bond distance in salicylhydroxamate or benzohydroxamate ligand is 1.404(5), 1.405(7), 1.379(6) and 1.388(5) Å in complexes **1**, **2**, **3** and **4**, respectively, which agree well with the N–N bond distances (1.38–1.41 Å) observed in the known VO^{3+} hydrazone complexes [9, 10, 15, 22–28].

The first four common structural features mentioned above have also been observed in the two vanadium hydroxamate complexes reported by our group [29].

For the first time the salicylhydroxamate ligand $(Hshi)^{-1}$ is coordinated to oxovanadium(V) in a monoanion form of the type (O ~ O^-) in complex **1**. In all known VO^{3+} salicylhydroxamate complexes, the salicylhydroxamate ligand is a dianion [5] or trianion [17]. It is interesting to note that there is no intramolecular hydrogen bond between the oxygen atom of the pendant phenol and the hydroxamate nitrogen in complex **1**, although this kind of the hydrogen bond has been found in complex [VO(HSHED)(shi)] [5]. In complex **1**, there are two kinds of intermolecular hydrogen bonds between the pendant O(5)–H group in the hydroxamate ligand and the nitrogen atom N(2a) in the hydrazone ligand of a neighbouring molecule and between vanadyl oxygen atom O(6) and N(3b)–H group in the hydroxamate ligand of another neighbouring molecule, as given in Table 3.

In complex **2**, the bond length of V(1)–O(4) is 1.855(4) Å, somewhat shorter than the average observed in the complex $VOCl(bz)_2$ (1.902 Å) [16].

In complex **1**, the five-membered chelate ring of O(2), C(8), N(2), N(1), V(1) and the six-membered chelate ring of O(1), C(1), C(6), C(7), N(1), V(1) for-

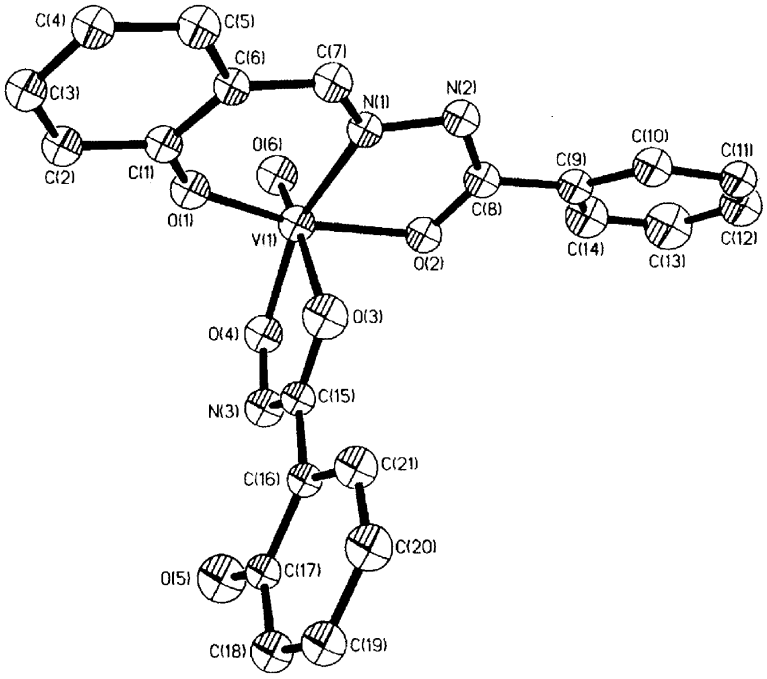

Fig. 2. Molecular structure of complex **1** showing the atom numbering and 30% probability displacement ellipsoids

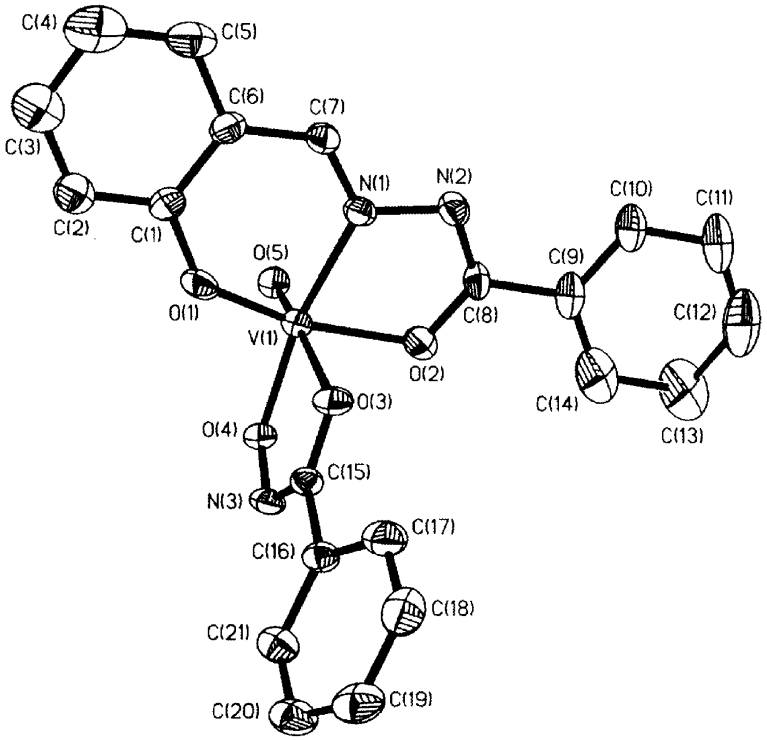

Fig. 3. Molecular structure of complex **2** showing the atom numbering and 30% probability displacement ellipsoids

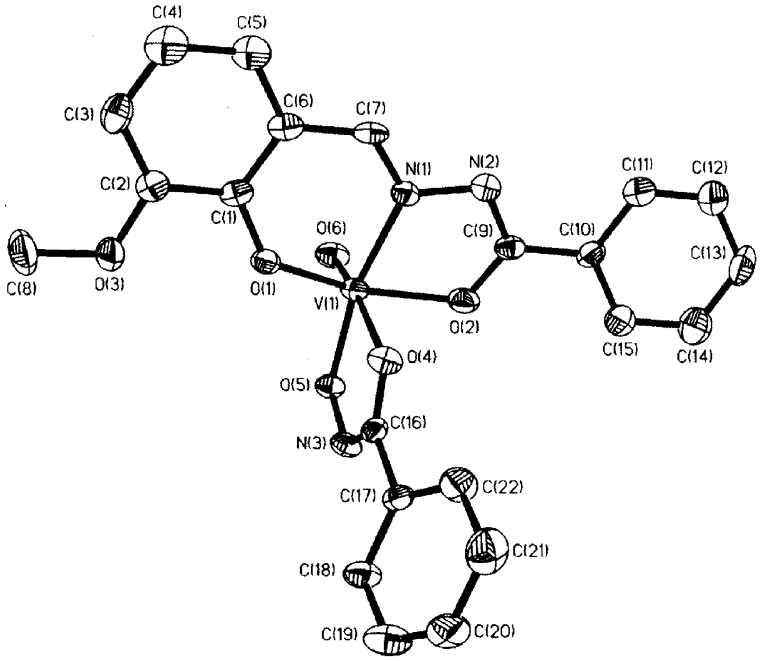

Fig. 4. Molecular structure of complex **3** showing the atom numbering and 30% probability displacement ellipsoids

med by the tridendate hydrazone ligand are planar with mean deviations of 0.040 Å and 0.057 Å, respectively. However, in complex **2** the five-membered chelate ring is a good plane with a mean deviation of 0.006 Å, but the six-membered chelate ring is not planar. The dihedral angle of two benzene rings of the hydrazone ligand is 21.2° in **1** and 9.2° in **2**. The dihedral angle between the hydroxamate ligand and the tridentate hydrazone ligand is 85.4° in **1** and 82.4° in **2**. In complex **3**, the atoms V(1), N(1), N(2), C(9), O(2) constitute an excellent plane with a mean deviation of 0.005 Å and the atoms V(1), O(4), C(16), N(3), O(5) also constitute a good plane with a mean deviation of 0.028 Å.

As illustrated in Table 5 and Fig. 5, two [VO(L)(bz)] units related by a center of symmetry in complex **3** are joined by the two intermolecular hydrogen bonds N(3)–H(24) ... O(3a) and N(3a)–H(24a) ... O(3) (symmetry code: a, -x, -y, -z).

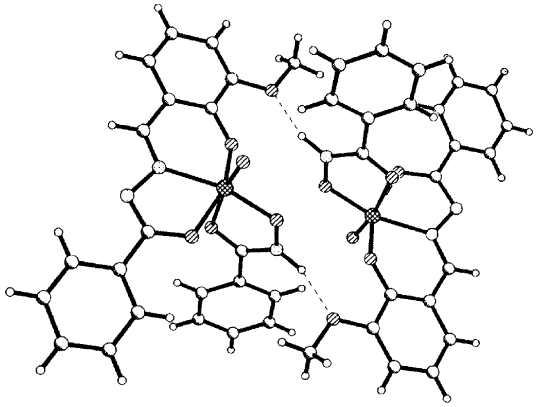

Fig. 5. Packing diagram of complex **3** showing H-bonding as broken lines

Description of the structure of complex [VOL^2 (OCH_3)(CH_3OH)] CH_3OH (4)

The selected bond lengths and angles for complex **4** are listed in Table 6. As shown in Fig. 6, the complex **4**, $VOL^2(OCH_3)(CH_3OH)]CH_3OH$, has a distorted octahedral VO^{3+} species with VO(ONO)(O)(O) type. The atoms O(1), O(2), N(1) from the dinegative tridentate hydrazone ligand and atom O(4) from a methoxide ion define a basal plane with small mean deviation (0.019 Å). The vanadium atom deviates by 0.324 Å from the equatorial plane towards the oxo oxygen atom. The oxo oxygen atom O(6) and the oxygen atom O(5) of the methanol molecule occupy the apical positions with a *trans* angle of 173.89(1)°, the bond distances of the vanadyl V═O(6) and the V(1)–O(5) (methanol) are 1.577(4) Å and 2.346(4) Å, respectively, due to the structural *trans* effect. The structural *trans* effect in the complexes with VO(ONO)(O)(O) type, such as in complex 4 and VO(sal-L-ala) (OCH_3)(CH_3OH) [35], is stronger than that in the ones with VO(ONO)(OO) type.

The vanadyl V═O distance (1.577(4) Å) in complex [$VOL^2(OCH_3)(CH_3OH)$] CH_3OH is shorter than that in complex [VOL^2(bz)]·CH_2Cl_2, but is in the accept-

Table 6. Selected bond distances (Å) and angles (°) for complex $[VOL^2(OCH_3)(CH_3OH)]CH_3OH$ (**4**)

V(1)–O(6)	1.577(4)	O(3)–C(8)	1.432(5)
V(1)–O(4)	1.769(3)	O(4)–C(16)	1.400(6)
V(1)–O(1)	1.840(3)	O(5)–C(17)	1.390(7)
V(1)–O(2)	1.966(3)	O(7)–C(18)	1.399(7)
V(1)–N(1)	2.109(4)	N(1)–C(7)	1.282(5)
V(1)–O(5)	2.346(3)	N(1)–N(2)	1.388(5)
O(1)–C(1)	1.336(5)	N(2)–C(9)	1.308(6)
O(2)–C(9)	1.286(5)	O(7)... N(2)	2.794(5)
O(3)–C(2)	1.360(5)	O(5)... O(7a)	2.670(5)
O(6)–V(1)–O(4)	104.2(2)	O(3)–C(2)–C(3)	124.4(4)
O(6)–V(1)–O(1)	101.0(2)	O(3)–C(2)–C(1)	115.5(4)
O(6)–V(1)–O(2)	96.5(2)	N(1)–C(7)–C(6)	124.0(4)
O(6)–V(1)–N(1)	96.1(2)	O(2)–C(9)–C(10)	118.0(4)
O(4)–V(1)–O(1)	103.2(1)	C(2)–O(3)–C(8)	116.9(4)
O(4)–V(1)–O(2)	91.7(1)	N(2)–C(9)–C(10)	118.8(4)
O(4)–V(1)–N(1)	156.6(2)	C(7)–N(1)–N(2)	116.2(3)
O(1)–V(1)–O(2)	153.4(1)	C(9)–N(2)–N(1)	108.4(3)
O(1)–V(1)–N(1)	84.0(1)	O(1)–C(1)–C(2)	119.3(4)
O(2)–V(1)–N(1)	74.2(1)	O(1)–C(1)–C(6)	121.4(4)
O(5)–V(1)–O(6)	173.9(1)	O(2)–C(9)–N(2)	123.2(4)
O(5)–V(1)–N(1)	78.7(1)	C(17)–O(5)–V(1)	132.9(3)
O(5)–V(1)–O(1)	81.7(1)	O(7)–H(20) ... N(2)	160.6
O(5)–V(1)–O(4)	80.4(1)	O(5)–H(19) ... O(7a)	177.1
O(5)–V(1)–O(2)	79.2(1)		

Symmetry code: a, 0.5+x, −0.5-y, z.

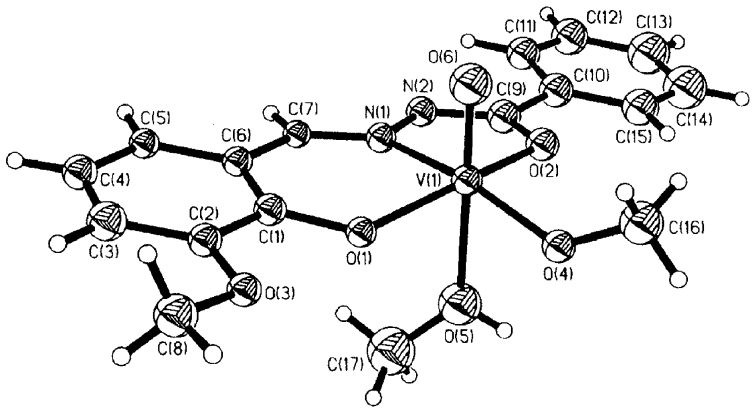

Fig. 6. Molecular structure of complex **4** showing the atom numbering and 30% probability displacement ellipsoids

able range of 1.55–1.60 Å observed for VO^{3+} complexes. The V–O(carbonyl) bond lying *trans* to V═O in complex **4** has a distance 2.346(3) Å, which is longer than the corresponding bond (2.202(4) Å) in complex **3**.

In complex **4**, there are intramolecular hydrogen bonds between the OH group of the uncoordinated CH_3OH and the nitrogen atom of the hydrazone ligand and intermolecular hydrogen bonds between the OH group of the coordinated CH_3OH and the oxygen atom of the uncoordinated CH_3OH in the neighbouring molecule, shown in Fig. 7 and Table 6.

Supplementary material

The atomic coordinates for non-hydrogen atoms and hydrogen atoms, anisotropic thermal parameters,

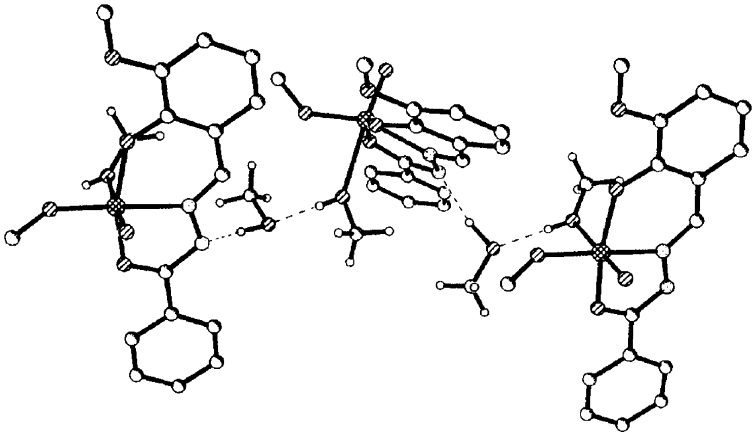

Fig. 7. Packing diagram of complex **4** showing H-bonding as broken lines

and full bond distances and angles have been deposited at the Cambridge Crystallographic Data Centre (CCDC). Any request to the CCDC for this material should quote the reference numbers 101322, 101323, 101324 and 101325 for the title complexes **1**, **2**, **3** and **4**.

Acknowledgements—The authors thank the financial support of the Natural Science Foundation of Fujian Province of China. The authors thank associated professor Yu Zheng for the IR and Raman measurements and her valuable discussion.

REFERENCES

1. Rehder, D., *Angew. Chem. Int. Ed. Engl.*, 1991, **30,** 148.
2. Butler, A. and Walker, J. V., *Chem. Rev.*, 1993, **93,** 1937.
3. Messerschmidt, A. and Wever, R., *Proc. Natl. Acad. Sci., USA*, 1996, **93,** 392.
4. Kehl, H. Ed., *Chemistry & Biology of Hydroxamic Acids*, S. Karger: New York, 1982.
5. Cornman, C. R., Colpas, G. J., Hoeschele, J. D., Kampf, J. and Pecoraro, V. L., *J. Am. Chem. Soc.*, 1992, **114,** 9925.
6. Kiss, T., Buglyò, P., Micera, G., Dessì, A. and Sanna, D., *J. Chem. Soc., Dalton Trans.*, 1993, 1849.
7. Khan, M. I., Lee, Y.-S., O'connor, C. J., Haushalter, R. C. and Zubieta, J., *Inorg. Chem.*, 1994, **33,** 3855.
8. Wang, X., Zhang, X.-M. and Liu, H.-X., *Inorg. Chim. Acta*, 1994, **223,** 193.
9. Chakravarty, J., Dutta, S., Dey, A. and Chakravorty, A., *J. Chem. Soc., Dalton Trans.*, 1994, 557.
10. Ludwig, E., Hefele, H., Friedrich, A., Kallies, B., Schilde, U., Uhlemann, E. and Hahn, E., *Z. Anorg. Allg. Chem.*, 1995, **621,** 488.
11. Fulwood, R., Schmidt, H. and Rehder, D., *J. Chem. Soc., Chem. Commun.*, 1995, 1443.
12. Cavaco, I., Pessoa, J. C., Duarte, M. T., Henriques, R. T., Matias P. M. and Gillard, R. D., *J. Chem. Soc., Dalton Trans.*, 1996, 1989.
13. Hamstra, B. J., Houseman, A. L. P., Colpas, G. J., Kampf, J. W., LoBrutto, R., Frasch, W. D. and Pecoraro, V. L., *Inorg. Chem.*, 1997, **36,** 4866.
14. Plass, W., *Z. Anorg. Allg. Chem.*, 1997, **623,** 461.
15. Liu, S.-X. and Gao, S., *Polyhedron*, 1998, **17,** 81.
16. Fisher, D. C., Barclay-Peet, S. J., Balfe, C. A. and Raymond, K. N., *Inorg. Chem.*, 1989, **28,** 4399.
17. Pecoraro, V. L., *Inorg. Chim. Acta*, 1989, **155,** 171.
18. Gibney, B. R., Stemmler, A. J., Pilotek, S., Kampf, J. W. and Pecoraro, V. L., *Inorg. Chem.*, 1993, **32,** 6008.
19. Petrovic, A. F., Ribar, B., Petrovic, D. M., Leovac, V. M. and Gerbeleu, N. V., *J. Coord. Chem.*, 1982, **11,** 239.
20. Leovac, V. M. and Petrovic, A. F., *Transition Met. Chem.*, 1983, **8,** 337.
21. Zhang, X.-M., You, X.-Z. and Wang, X., *Polyhedron*, 1996, **15,** 1793.
22. Diamantis, A. A., Frederiksen, J. M., Salam, M. A., Snow, M. R. and Tiekink, E. R. T., *Aust. J. Chem.*, 1986, **39,** 1081.
23. Yan, S.-P., Wang, G.-L., Wang, H.-G. and Yao, X.-K., *Chinese J. Struct. Chem.*, 1992, **11,** 47.
24. Wang, W., Wang, X., Liu, H.-X. and Tan, M.-Y., *J. Coord. Chem.*, 1995, **36,** 49.
25. Wang, W., Zeng, F.-L., Wang, X. and Tan, M.-Y., *Polyhedron*, 1996, **15,** 1699.
26. Hefele, H., Ludwig, E., Schilde, U. and Uhlemann, E., *Z. Kristallogr.*, 1996, **211,** 655.
27. Palacios, M. S., Rocio, M. J., Dominguez, S., Gili, P., Ruiz-Perez, C., Rodriguez-Romero, F. V. and Dance, J.-M., *Polyhedron*, 1997, **16,** 1143.
28. Bansse, W., Ludwig, E., Uhlemann, E., Weller, F., Dehnicke, K. and Herrmann, W., *Z. Anorg. Allg. Chem.*, 1992, **613,** 36.
29. Liu, S.-X. and Gao, S., to be published in *Inorg. Chim. Acta*.
30. Rowe, R. and Jones, M. M., *Inorg. Synth.*, 1957, **5,** 113.
31. Gale, G. R., *J. Med. Chem.*, 1968, **11,** 191.

32. Nakamota, K., Infrared and Raman Spectra of Inorganic and Coordination Compounds, 4th edn., John Willy & Sons, New York, 1986.
33. Yang, P. and Li, Q.-S., *Chinese J. Struct. Chem.*, 1996, **15,** 163.
34. Asgedom, G., Sreedhara, A. and Rao, C. P., *Polyhedron*, 1995, **14,** 1873.
35. Nakajima, K., Kojima, M., Toriumi, K., Saito, K. and Fujita, J., *Bull. Chem. Soc. Jpn.*, 1989, **62,** 760.

Pergamon

PII: S0277–5387(98)00156–9

Polyhedron Vol. 17, No. 20, pp. 3607–3612, 1998
© 1998 Elsevier Science Ltd
All rights reserved. Printed in Great Britain
0277–5387/98 $19.00+0.00

Synthesis, spectroscopic and structural characterization of the pentacoordinate high-spin Fe(III) isothiocyanate "picket fence" porphyrin complex

Habib Nasri[a,*] and Mongi Debbabi[b]

[a] Faculté des Sciences de Monastir, 5000 Monastir, Tunisia

[b] Ecole Nationale d'Ingénieurs de Monastir (E.N.I.M.), 5000 Monastir, Tunisia

(Received 11 February 1998; accepted 2 April 1998)

Abstract—The preparation and the characterization of the (isothiocyanato)(α,α,α,α-tetrakis(*o*-pivalamidophenyl)porphinato)iron(III) complex is described. The synthesis procedure utilizes the crown ether 18-C-6 to solubilize potassium thiocyanate. ^{1}H NMR and EPR data of the isolated product are in accordance with a high-spin ($S=5/2$) ferric porphyrin species. The X-ray molecular structure confirms the above deductions. The iron atom is pentacoordinated by the four nitrogen atoms of the pyrrole rings of the porphyrin and the nitrogen atom of the NCS^- group. It lies at 0.504 Å out of the porphinato plane and 0.462 Å out of the four nitrogen plane. The Fe–N(NCS) bond length is 1.956(5) Å and the Fe–N–C(NCS) bond angle is 176.1(5)°. © 1998 Elsevier Science Ltd. All rights reserved

Keywords: porphyrin; iron(III) complex; isothiocyanate complex; high-spin Fe(III); molecular structure.

INTRODUCTION

The interest in iron porphyrins stems not only from the diverse biological roles of the iron porphyrin moiety found in proteins, cytochromes, peroxidases, etc. but also from the array of physical properties observed for the coordinated Fe(II) and Fe(III).

In most cases, when weak crystal field ligands such as halides or pseudohalides are bound to an iron(III) of a metalloporphyrin or a hemoprotein, the resulting porphyrinate is high spin and five coordinate. Nevertheless, many examples of six coordinate high-spin heme-like species exist, i.e. (2-MeHIm)[Fe(F)$_2$(TPP)] [1]. In some special circumstances the ferric ion may be in the spin "crossover" region and show thermal spin-equilibrium. Thus, in the case of the azide ligand, Scheidt *et al.* [2], confirmed the high spin ($S=5/2$)⇔low spin ($S=1/2$) equilibrium of the bisazide Fe(III) porphyrin species; [Fe(N$_3$)$_2$(TpivPP)]$^-$. Korszun and Moffat [3] have determined the structure of the isothiocyanato-liganded hemoglobin which shows a spin equilibrium between the high-spin NCS^- pentacoordinate heme and the "(NCS)MetHb proximal histidine" low spin six coordinate methemoglobine.

The isothiocyanate ferric porphyrinate was mentioned in the literature for decades [4] as a high-spin ($S=5/2$) pentacoordinate derivative. However, a complete characterization of such species has not been previously reported.

It is the aim of this work to synthesize and spectroscopically and structurally characterize the isothiocyanate Fe(III) picket fence porphyrin complex.

We also report in this paper the use of crown ethers to solubilize the inorganic potassium thiocyanate salt in organic solvents typically used with iron porphyrinates.

The use of the picket fence porphyrin for the characterization of this ferric porphyrinate was directly related to the fact that ionic not very bulky ligands as it is shown by X-ray molecular structures [5], are in

* Author to whom correspondence should be addressed.

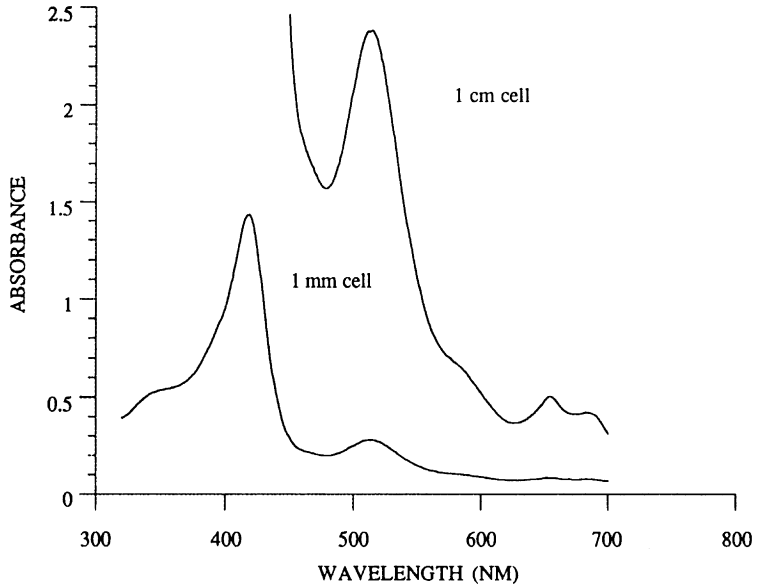

Fig. 1. Visible spectrum of [Fe(NCS)(TpivPP)] in chlorobenzene solution (room temperature).

all cases bound to the iron by the pocket side of the protected porphyrin. Consequently, these complexes are remarkably stable.

RESULTS AND DISCUSSION

The reported synthesis for halide and pseudohalide Fe(III) porphyrin species make use of organic-soluble iron porphyrinates and typically water-soluble inorganic salts [6] (KCl, KBr, NaN_3, etc.) or aqueous acids (CH_3COOH [7], HNO_3 [8], etc.). In our case, the (isothiocyanato)(α,α,α,α-tetrakis(*o*-pivalamidophenyl)porphinato)iron(III) complex has been prepared by using only one organic phase. The 18-C-6 crown ether was used to solubilize the potassium thiocyanate in chlorobenzene solution[1]. Our synthetic strategy has the advantage of avoiding the use of a mixture of an organic and an aqueous solution and obtaining the anionic reagent in high concentration.

Figure 1 represents the electronic spectrum of the [Fe(NCS)(TpivPP)] species recorded in chlorobenzene. The spectrum belongs to the hyper class [9]. The Soret and the β bands values (respectively, 417 and 513 nm) are quite identical to those of other pentacoordinate Fe(III) high-spin *meso*-porphyrin species [10].

The EPR spectra carried out at 77 K show similar features in solution and in solid state. Both spectra are axially symmetric; $g\perp = 5.8$ and $g_{\parallel} = 1.98$ for the frozen chlorobenzene solution and $g\perp = 5.7$ for the powder (crushed single crystals). These results provide unequivocal evidence that either in solid state or in solution the [Fe(NCS)(TpivPP)] complex is high-spin ($S = 5/2$).

A proton NMR spectrum of [Fe(NCS)(TpivPP)] in $CDCl_3$, recorded at room temperature, supports the latter conclusion. Thus, the pyrrole proton resonance at 75.7 ppm (line with ≈ 365 Hz) is in the range 100–70 ppm, a downfield region characteristic of high-spin iron(III) tetraarylporphyrin complexes [11]. The *ortho*-phenyl protons of the macrocycle are not observed. Strong dipolar interactions should be the cause of the important broadening. *Meta*-phenyl protons are highly anisotropic giving rise to two singlets at 11.5 and 14.4 ppm.

The IR spectrum of [Fe(NCS)(TpivPP)] shows that the value of the stretching frequency ν(CN) which is 2015 cm^{-1}, is a clear evidence that NCS^- is N-bonded to the iron (an isothiocyanate) [12].

The molecular structure of the [Fe(NCS)(TpivPP)] complex is illustrated in Fig. 2. The NCS^- ligand lies, as expected, in the axial position inside the cavity formed by the pivalamide arms of the picket fence porphyrin. The iron atom is five coordinated and the resulting polyhedron is a slightly deformed square pyramid with the nitrogen atom of the NCS^- group in the axial position. Selected bond distances and angles for this complex are given in Table 1. Other distances and angles, fractional coordinates and thermal parameters have been deposited as supplementary data with the editor.

The bond parameters for the coordination environment of the Fe(III) in this compound and for a selec-

[1] The Kryptofix 222 can also be used.

[2] The process is based on an adoption of the DIFABS [19] logic to area detector geometry [18].

[3] R-factors based on F^2 (wR_2) are statistically about twice as large as those based on *F*.

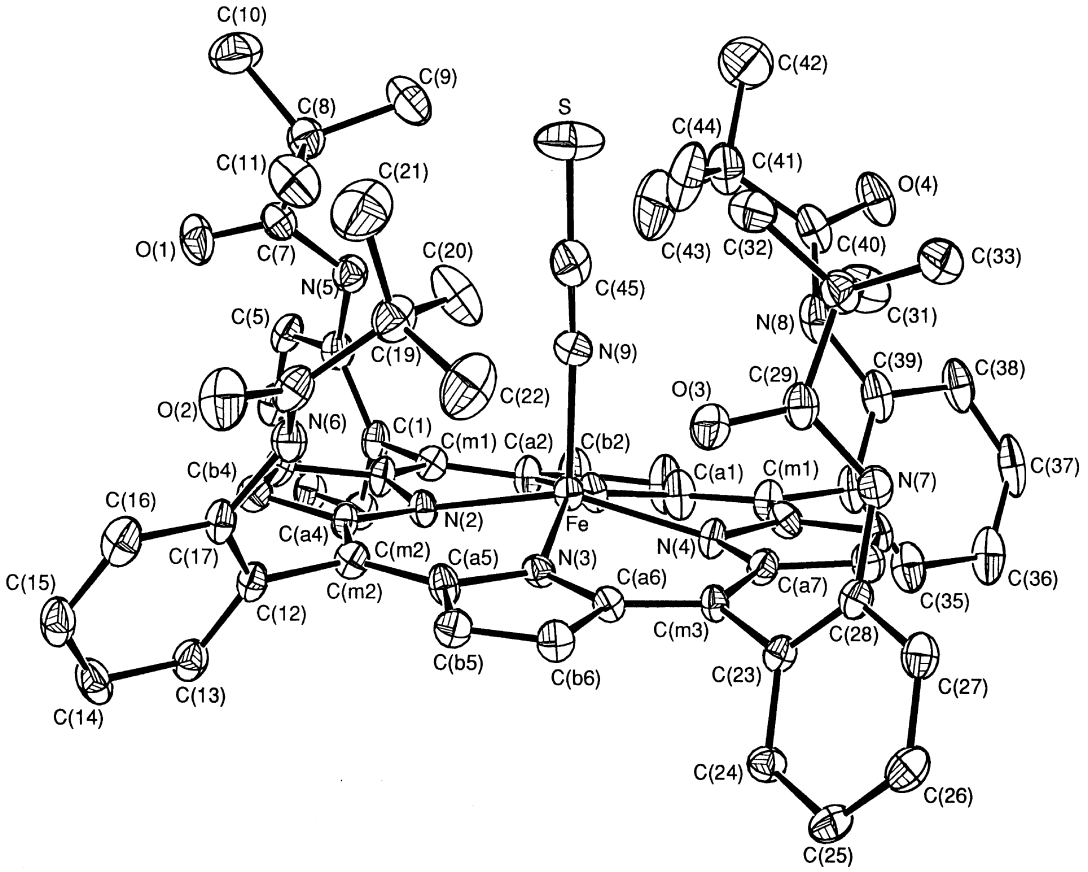

Fig. 2. ORTEP diagram of the [Fe(NCS)(TpivPP)] molecule displaying the atom-labeling scheme used throughout the paper. Ellipsoids are drawn at the 30% probability level.

Table 1. Selected bond distances (Å) and angles (°) for [Fe(NCS)(TpivPP)][a]

Iron coordination polyhedron			
Fe–N(9)	1.956(5)	N(1)–Fe–N(9)	104.2(2)
Fe–N(1)	2.057(4)	N(2)–Fe–N(9)	100.6(2)
Fe–N(2)	2.054(4)	N(3)–Fe–N(9)	104.5(2)
Fe–N(3)	2.056(4)	N(4)–Fe–N(9)	102.8(2)
Fe–N(4)	2.054(4)		
		Thiocyanate ligand	
N(1)–Fe–N(2)	86.7(2)	N(9)–N(45)	1.149(8)
N(1)–Fe–N(3)	151.3(2)	C(45)–S	1.602(7)
N(1)–Fe–N(4)	87.5(2)		
N(2)–Fe–N(3)	87.3(2)	Fe–N(9)–C(45)	176.1(5)
N(2)–Fe–N(4)	156.6(2)	S–C(45)–N(9)	178.6(6)

[a]The numbers in parentheses are the estimated standard deviations.

tion of some other Fe(III) metalloporphyrins are given in Table 2. A brief description of the molecular structure of the otherwise analogous [Fe(NCS)(TPP)] complex was mentioned by Bloom and Hoard [13]. The values of the Fe–Np distances of the TpivPP and TPP derivatives are, respectively, 2.055(2) and 2.065 Å. These values are a clear indication that these species are high-spin [14]. In order to accommodate the high-spin iron(III) atom, the porphinato cores undergo a significant radial expansion. This is very well illustrated by the long Fe–P_C and Fe–P_N distances shown by [Fe(NCS)(TpivPP)] and [Fe(NCS)(TPP)].

Table 2. Porphinato core parameters (Å) for selected Fe(III) porphyrin complexes

Complex	Fe–Np	Fe–X_L	Fe–P_C	Fe–P_N	δ[a]	Spin (S)	Refs.
[Fe(NCS)(PivPP)]	2.055 (2)	Fe–N_L[b]: 1.956 (5)	0.504	0.462	0.042	5/2	this work
[Fe(NCS)(TPP)]	2.065	Fe–N_L[b]: 1.957	0.550	0.485	0.065	5/2	[13]
[Fe(NCS)(Py)(OEP)]	2.048 (4)	Fe–N_L[b]: 2.031 (2)	0.240[c]	0.180[c]	—	5/2	[15]
[Fe(NCS)(Py)(TPP)]	1.988 (9)	Fe–N_L[b]: 1.942 (4)	0.050[c]	0.050[c]	—	1/2	[15]

[a]δ = the doming.
[b]Fe–N_L = Fe–N(NCS) distance.
[c]Displacement toward the isothiocyanate ligand.

The corresponding values are, respectively, 0.504 and 0.462 Å for the former complex and 0.55 and 0.485 Å for the latter. For both [Fe(NCS)(Porph)] derivatives, the Fe–N(NCS) distances have the same values; 1.956(5) Å for the picket fence porphyrin product and 1.957 Å for the tetraphenylporphyrin moiety.

As expected for an N-bonded thiocyanate to an iron atom, the Fe–NCS group, is found to be essentially linear for all NCS^- derivatives shown in Table 2 (except the ambiguous [Fe(NCS)(Py)(TPP)] [15] case). Both isothiocyanate TpivPP and OEP derivatives exhibit rather identical values for the Fe–N–C(NCS) angle [respectively, 176.1 (5)° and 176.0 (2)°]. These two derivatives present very close N–C–S angle values with 178.6° (6) for the picket fence complex and 179.6° (2) for the OEP six coordinate species.

The porphyrinato core in [Fe(NCS)(TpivPP) is decidedly non-planar as can be seen from an inspection of Fig. 3. The pattern of the atom displacements in the porphinato core correspond closely to those

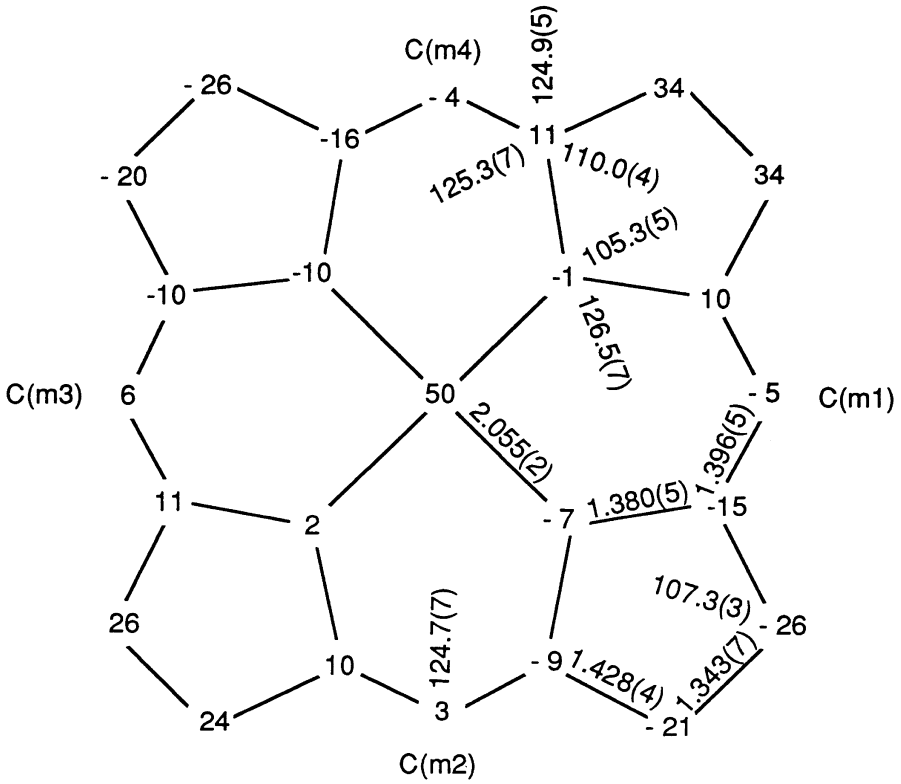

Fig. 3. Formal diagram of the porphinato core in the [Fe(NCS)(TpivPP)] molecule displaying the displacement, in units of 0.01 Å, from mean plane of the porphinato core. Also displayed on the diagram is the average value of each type of bond distance and angle in the porphinato core.

required by exact D_{2d} symmetry, often simply called S_4-ruffling. Least squares planes calculations indicate a small doming of the porphyrin (0.042 Å).

EXPERIMENTAL

The complex [Fe(SO_3CF_3)(H_2O)(TpivPP)] was prepared as described previously [16]. The 18-C-6 crown ether was recrystallized in toluene, dried under vacuum overnight and stored under argon. Toluene and hexanes were distilled from their sodium–benzophenone solution under a nitrogen atmosphere. Chlorobenzene was purified by washing with sulfuric acid and then distilled over P_2O_5.

UV-VIS spectra were recorded on a Perkin-Elmer Lambda 19 spectrometer, Fourier-transform IR data on a Bio-Rad FT S4000 spectrometer and EPR spectra were obtained at 77 K on a Varian E-line spectrometer operating at X-band frequency.

^{1}H NMR data were obtained on a Nicolet NT300 spectrometer operating at 300.063 MHz.

Preparation of the [Fe(NCS)(TpivPP)] compound

The (isothiocyanato)(α,α,α,α-tetrakis(*o*-pivalamidophenyl)porphinato)iron(III) complex was prepared by reacting [Fe(SO_3CF_3)(H_2O)(TpivPP)] (0.016 mmol) with KSCN (0.32 mmol) and 18-crown-6 (0.16 mmol) in 20 ml of C_6H_5Cl. The resulting red brownish solution was then filtered and an X-ray quality crystals were prepared by slow diffusion of hexanes into C_6H_5Cl. The crystalline material was washed with several portions of water and then with hexanes.

UV-VIS [C_6H_5Cl, λ_{max} in nm, ($\log\varepsilon$)]: 417 (4.99); 513 (4.21); 586 sh (3.63); 655 (3.54) IR (KBr, cm^{-1}): ν(CN): 2015. EPR (C_6H_5Cl, 77 K): $g\perp = 5.8$; $g_\parallel = 1.98$. ^{1}H NMR (300 MHz, $CDCl_3$): H(pyrr): 75.7 ppm; H(*meta*-Ph): 11.5, 14.4; H(*para*-Ph): 8.0 ppm.

Determination of crystal and molecular structure

Crystal data. $C_{65}H_{64}N_9O_4SFe$, $M = 1123.2$, monoclinic, space group $P2_1/n$, $a = 13.237(3)$ Å, $b = 18.272(4)$ Å, $c = 23.678$ Å, $\beta = 94.910(10)^\circ$, $V = 5706.0$ Å^3, $D_c = 1.31$ g·cm^{-3}, $Z = 4$, $F(000) = 2724$, $\lambda = 0.71073$ Å, μ(Mo–Kα) = 35.3 cm^{-1}.

Data collection and processing. A dark single crystal of approximate size $0.6 \times 0.3 \times 0.3$ mm^3 was examined on an Enraf-Nonius FAST area detector diffractometer at 127 K. All measurements were performed with graphite-monochromated Mo–Kα radiation. Data collection and reduction were defined as before [17]. Intensity data were corrected for absorption effects using a modified version of the absorption correction program DIFABS[2].

A total of 10020 unique reflections was collected and 6791 having $I > 2\sigma(I)$ [merging R(int) = 0.132].

Structure analysis and refinement. The structure was solved in the centrosymmetric space group $P2_1/n$ using the direct methods program SHELXS-86 [20]. All non-hydrogen atoms were refined anisotropically and all hydrogen atoms were idealized with the standard SHELXL-93 [21] idealization method. The final cycles of refinement based on F^2 of 733 variables converged to the final $R_1 = 0.079$ and $wR_2 = 0.167$[3] for reflections with $I > 2\sigma(I)$. The final difference Fourier map had the largest peak at 0.76 eÅ^{-3}.

Acknowledgements—We gratefully acknowledge professor W. R. Scheidt of the University of Notre Dame (Indiana, U.S.A.) for the use of the Enraf Nonius area detector FAST diffractometer. We also acknowledge M. K. Ellison from the University of Notre Dame (Indiana, U.S.A.) for her kind help in recording the EPR spectra.

REFERENCES

1. Scheidt, W. R., Lee, Y. J., Tamai, S. and Hatano, K., *J. Am. Chem. Soc.*, 1983, **105,** 778.
2. Ellison, M. K., Nasri, H., Xia, Y.-M., Marchan, J. C., Schultz, C. E., Debrunner, P. G. and Scheidt, W. R., *Inorg. Chem.*, 1997, **36,** 4804.
3. Korszun, Z. R. and Moffat, K., *J. Mol. Biol.*, 1981, **145,** 815.
4. S. Mitra, *Iron Porphyrins*, Part II, eds. A. B. P. Lever and H. B. Gray. Addison-Wesley Publishing Company, Massachusetts, 1983, Chap 1.
5. M. Schappacher, Ph.D. Thesis, Université Louis Pasteur, Strasbourg, France, 1982.
6. J. W. Buchler, *Porphyrins and Metalloporphyrins*, ed. K. M. Smith. Elsener Scientific Publishing Company, Amsterdam, 1975, Chap. 5.
7. Oumous, H., Lecomte, C., Protas, J., Cocolios, P. and Guillard, R., *Polyhedron*, 1984, **3,** 651.
8. Phillipi, M. A., Shimomura, E. T. and Goff, H. M., *Inorg. Chem.*, 1981, **20,** 3904.
9. M. Gouterman, *The Porphyrins*, Vol. III, ed. D. Dolphin. Academic Press, New York, 1978, Chap. I.
10. H. Nasri, Ph.D. Thesis, Université Louis Pasteur, Strasbourg, France, 1987.
11. G. N. La Mar and F. A. Walker, *The Porphyrins*, Vol. IV, ed. D. Dolphin. Academic Press, New-York, 1978.
12. K. Nakamoto, *Infrared and Raman Spectra of Inorganic and Coordination Complexes*, 4th edn. J. Wiley and Sons, New York, 1986.
13. A. Bloom and J. L. Hoard, unpublished results.
14. Scheidt, W. R. and Reed, C., *Chem. Rev.*, 1981, **81,** 543.
15. Scheidt, W. R., Lee, Y. J., Geiger, D. K., Taylor, K. and Hatano, K., *J. Am. Chem. Soc.*, 1982, **104,** 3367.
16. Gismelseed, A., Bominaar, E. L., Bill, E., Trautwein, A. X., Nasri, H., Doppelt, P., Mandon, D., Fischer, J. and Weiss, R., *Inorg. Chem.*, 1990, **29,** 2741.

17. Scheidt, W. R. and Tyrk, I. T., *Inorg. Chem.*, 1994, **33,** 1314.
18. Karaulov, A. I., School of Chemistry and Applied Chemistry, University of Wales, College of Cardiff, Cardiff CF1 3TB, U.K., personal communication.
19. Walker, N. P. and Stuart, D., *Acta Crystallogr. A*, 1983, **39,** 158.
20. Scheldrick, G. M., *Acta Crystallogr. A*, 1990, **46,** 467.
21. G. M. Scheldrick, *J. Appl. Crystallogr.* (in preparation).

Pergamon

PII: S0277–5387(98)00157–0

Polyhedron Vol. 17, No. 20, pp. 3613–3623, 1998
© 1998 Elsevier Science Ltd
All rights reserved. Printed in Great Britain
0277–5387/98 $19.00+0.00

Anion-dependence of the polymeric structures of manganese(II) complexes of N,N′-butylenebis(imidazole)

Loreto Ballester,[a] Ian Baxter,[b] Patrick C. M. Duncan,[b] David M. L. Goodgame,*[b] David A. Grachvogel[b] and David J. Williams*[b]

[a]Departamento de Quimica Inorgánica I, Facultad de Ciencias Químicas, Universidad Complutense, E-28040 Madrid, Spain

[b]Chemistry Department, Imperial College of Science, Technology and Medicine, London, SW7 2AY, U.K.

(Received 11 February 1998; accepted 2 April 1998)

Abstract—The preparations and X-band EPR spectra are reported of a series of manganese(II) complexes with N,N′-butylenebis(imidazole) (=BBI) of the types $Mn(BBI)_2X_2$ (X = Cl, Br, NO_3, NCS) and $[Mn(BBI)_3]X_2$ (X = ClO_4, I). An X-ray crystallographic study on $Mn(BBI)_2Cl_2$ (**1**) shows that each Mn atom is coordinated to four imidazole nitrogen atoms and two chloride ions in a *trans*-octahedral arrangement and that the BBI ligands link the Mn centres into sheets of contiguous 44-membered rings. X-Ray studies on $[Mn(BBI)_3](ClO_4)_2$, and on analogous compounds containing combinations of ClO_4^-/PF_6^- or ClO_4^-/AsF_6^- as counter anions, reveal the formation of a family of interpenetrating network structures with anion-dependent cavity sizes. © 1998 Elsevier Science Ltd. All rights reserved

Keywords: X-ray structures; polymeric complexes; manganese complexes; bis(imidazole).

There is appreciable interest in the development of new zeolites, and related materials (zeotypes), with redox active metals incorporated into their frameworks [1]. As recently summarised by Janiak [2], a promising line of development in this field is the formation of zeotypes based on polymers comprising metal-organic ligand coordination arrays. Providing one can overcome the potential problem of matrix instability under the operating conditions required for effective catalysis or separation process activity, such materials offer a number of advantages. These include, *inter alia*: (a) a wide variation in the incorporated metal ions and their consequent redox activity and (b) an enhanced potential for alteration in the sizes, shapes and natures of the cavities and channels, by selective changes in the design of the organic ligands and the coordination geometries available to the metal ions which link them.

Various approaches based on the self-assembly principle, using extended reach ligands, have been adopted for the formation of discrete molecular "boxes" [3] or polymeric networks containing cavities and/or channels [4]. In practice, the aim of creating materials genuinely capable of taking up guest molecules in a controllable and useful fashion can be vitiated by a number of factors. Energy minimisation of the crystal lattice frequently results in arrays in which any "cavities" are essentially self-filled by the surrounding matrix. The cavities may also be occupied by counter ions and/or solvent molecules, though solvent inclusion may not preclude zeotype utility if the matrix is sufficiently robust to permit solvent removal followed by its replacement by other substrates without major structural reorganisation.

Another serious obstacle to the formation of "box" arrays containing cavities of useful size is the formation of interpenetrating lattices either by interweaving of adjacent sheets (polycatenances and polyrotaxanes) [5] or multiple interpenetrating 3-D lattices [6]. Elucidation of the factors leading to avoidance of such interweaving or interpenetration, and

*Authors to whom correspondence should be addressed.

consequent formation of new materials combining metal centres potentially capable of redox action and also genuinely useful large cavities, is an intriguing challenge.

To exemplify this problem, one may compare the structures of three recently reported arrays of contiguous rhomboidal "boxes" based on octahedrally coordinated metal centres. In $[Mn(BBI)_3](BF_4)_2$ (**2**), where BBI = N,N′-butylenebis(imidazole) **I**, rhomboid lattice interpenetration occurs [7], but in [Mn(N,N′-*p*-phenylenedimethylenebis(4-methylpyridin-2-one)$_3$]$(ClO_4)_2$, formed by **II** [8], and in [Ni(N,N′-1,2-ethylenebis(pyridin-2-thione)$_3$]$(ClO_4)_2$, formed by **III** [9], there is no such interpenetration. We are currently attempting to investigate the factors influencing the onset of lattice penetration in compounds of this type and we report here the results of a study of the anion dependence of the structures of the manganese(II) complexes formed by **I**.

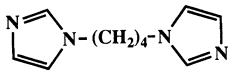

I

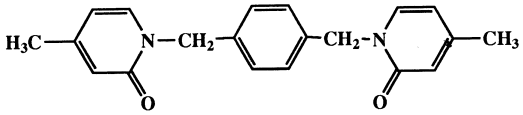

II

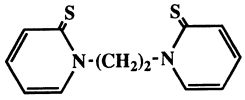

III

EXPERIMENTAL

Preparation of compounds

N,N′-butylenebis(imidazole). This was prepared as described previously [10].

Metal complexes of N,N′-butylenebis(imidazole)

Elemental analyses were by the Microanalytical Laboratory, Imperial College.

$[Mn(BBI)_2Cl_2 \cdot H_2O$.

Dropwise addition of $MnCl_2 \cdot 4H_2O$ (0.05 mmol) in methanol (4 cm^3) to a solution of BBI (0.1 mmol) in a mixture of acetonitrile (4 cm^3) and methanol (1 cm^3) gave a colourless microcrystalline solid which was collected by filtration, washed with acetonitrile and methanol and dried over P_2O_5. Yield 62%. Found: C, 45.8; H, 5.3; N, 20.6; Calc. for $C_{20}H_{28}N_8Cl_2Mn \cdot H_2O$: C, 45.8; H, 5.8; N, 21.4%. The same compound was obtained (in 76% yield) when $MnCl_2 \cdot 4H_2O$ and BBI were reacted in 1:4 mole ratio in methanol.

Single crystals for the X-ray studies were obtained by slow diffusion (15 days in the refrigerator) of a methanolic solution of $MnCl_2 \cdot 4H_2O$ (0.05 mmol in 8 cm^3) into a DMF solution of BBI (0.1 mmol in 10 cm^3).

$Mn(BBI)_2Br_2 \cdot MeOH$.

A solution of $MnBr_2 \cdot 4H_2O$ (0.2 mmol) in methanol (3 cm^3) was added to a methanolic solution of BBI (0.8 mmol in 3 cm^3). Upon standing, an off-white microcrystalline powder separated in 72% yield. Found: C, 39.8; H, 5.1; N, 17.7; Calc. for $C_{20}H_{28}N_8Br_2Mn \cdot MeOH$: C, 40.2; H, 5.1; N, 17.9%.

$Mn(BBI)_2(NO_3)_2$.

A solution of $Mn(NO_3)_2 \cdot 6H_2O$ (0.05 mmol) in a mixture of methanol (1 cm^3) and acetonitrile (3 cm^3) was slowly added to a solution of BBI (0.1 mmol) also dissolved in methanol (1 cm^3) and acetonitrile (4 cm^3). Upon standing overnight, a pale tan microcrystalline powder separated in 68% yield. Found: C, 42.8; H, 4.9; N, 24.5; Calc. for $C_{20}H_{28}N_{10}MnO_6$: C, 42.9; H, 5.0; N, 25.0%. The same compound was obtained (but in 48% yield) when $Mn(NO_3)_2 \cdot 6H_2O$ and BBI were reacted in 1:4 mole ratio in methanol.

$Mn(BBI)_2(NCS)_2.0.5EtOH$.

This white complex precipitated immediately on mixing ethanol solutions of BBI (0.72 mmol in 1 cm^3) and manganese(II) thiocyanate (0.36 mmol in 5 cm^3). Yield 67%. Found: C, 47.6; H, 4.7; N, 24.1; Calc. for $C_{22}H_{28}N_{10}MnS_2 \cdot 0.5EtOH$: C, 48.1; H, 5.4; N, 24.4%. IR: ν(CN) 2053 cm^{-1}.

$Mn(BBI)_3(ClO_4)_2$, (**3**).

A solution of $Mn(ClO_4)_2 \cdot 6H_2O$ (0.033 mmol) in acetonitrile (3 cm^3) was added to a solution of BBI (0.1 mmol) also dissolved in methanol (1 cm^3) and acetonitrile (4 cm^3). Colourless crystals formed overnight. Yield 50%. Found: C, 43.9; H, 5.0; N, 20.1; Calc. for $C_{30}H_{42}N_{12}Cl_2MnO_8$: C, 43.7; H, 5.1; N, 20.4%.

$Mn(BBI)_3I_2 \cdot 2H_2O$.

This off-white complex precipitated immediately on mixing ethanolic solutions of MnI_2 (0.2 mmol in 2.5 cm^3) and BBI (0.8 mmol in 3 cm^3). Yield 61%. Found: C, 39.6; H, 5.0; N, 18.6; Calc. for $C_{30}H_{42}N_{12}I_2Mn \cdot 2H_2O$: C, 39.4; H, 5.1; N, 18.4%.

Reactions of BBI with mixtures of MnX_2 (X = ClO_4, PF_6, AsF_6)

The general procedure was to mix a solution of $Mn(ClO_4)_2 \cdot 6H_2O$ (0.033 mmol) in acetonitrile (4 cm^3) with one of either NH_4PF_6 (0.133 mmol) or $KAsF_6$ (0.066 mmol) respectively in methanol (2 cm^3) and then to add the resulting solution to one of BBI (0.1 mmol) in a mixture of acetonitrile (3 cm^3) and methanol (1 cm^3). The colourless crystals which formed overnight were characterised by X-ray diffraction methods.

Spectroscopy

EPR spectra were measured at room temperature on a Varian E12 X-band (*ca.* 9.5 Ghz) spectrometer using powdered samples.

Crystallography

Data for $Mn(BBI)_2Cl_2$ (**1**), $Mn(BBI)_3(ClO_4)_2$ (**3**) and the compounds $Mn(BBI)_3XY$ containing the anion combinations ClO_4^-/PF_6^- or ClO_4^-/AsF_6^- **4–6**, were collected on a Siemens P4 diffractometer using either Cu–Kα or Mo–Kα radiation and ω-scans. The data were corrected for Lorentz and polarisation effects and, for compounds **1** and **3**, for absorption by ψ scans. All five structures were solved by direct methods and the major occupancy non-hydrogen atoms were refined anisotropically on F^2, using the SHELXTL suite of programs [11]. The absolute structure was determined for compounds **3–6** by refinement of the Flack parameter. In the case of **3** the Flack parameter indicated a racemic twinned crystal. A summary of the crystal data, structure solution and refinement parameters is given in Table 1.

Compounds **3–6** comprise a framework containing two distinct sites for counter anions. In compound **3** both sites are occupied by perchlorate ions but the anion in one of the sites is crystallographically disordered within that site. Compounds **4–6** contain mixed counter ion systems, the constituents of which were found from the difference maps, and their relative occupancies were refined. Compound **4** contains one fully occupied ClO_4^- ion on one site and the other site refined as $0.5ClO_4^-/0.5PF_6^-$; **5** contains $0.7ClO_4^-/0.3AsF_6^-$ on one site and $0.8ClO_4^-/0.2AsF_6^-$ on the other; **6** contains one fully-occupied PF_6^- ion on one site and $0.7ClO_4^-/0.3PF_6^-$ on the other.

Selected bond lengths and angles for compounds **1** are given in Table 2 and those for **3–6** are listed in Table 3.

RESULTS AND DISCUSSION

The stoichiometries of the products formed from the reaction of **I** with the salts of manganese(II), MnX_2, depend on the anion X. For X = Cl, Br, NO_3, or NCS the complexes are of the type $Mn(BBI)_2X_2$, even when an excess of BBI was used in the reaction mixture. On the other hand, with iodide or with non- or poorly-coordinating anions such as BF_4^- [7] or ClO_4^- complexes with a 3:1 BBI:Mn stoichiometry are formed.

The effect changing the anion has on the metal ion coordination geometry is clearly seen from the X-band EPR spectra of the solid compounds. The spectra of the complexes of type $Mn(BBI)_3X_2$ (X = BF_4, ClO_4 or I) are virtually identical and comprise a single sharp band at $g_{eff} = 2.00$, indicating a symmetry very close to O_h about the metal ion. In contrast, the spectra of the 2:1 complexes, $Mn(BBI)_2X_2$, are typical of Mn(II) in a *trans*-MnL_4X_2 coordination environment, where L represents a heterocyclic nitrogen-donor ligand [12] (Fig. 1).

The chloride, bromide, and nitrate all show the characteristic complex spectra, with bands well away from the $g_{eff} = 2.00$ region (*ca.* 0.34 Tesla for the operating frequency employed), arising from the zero-field splitting terms in the spin Hamiltonian for high-spin d^5 in ligand fields of lower than cubic symmetry [12]. The spectra show that the axial asymmetry increases markedly in the order X = NO_3 < Cl < Br. The zero-field splitting for $Mn(BBI)_2(NCS)_2$ is, however, much less as the main band is still at $g_{eff} = 2.00$ but this has additional, weaker components at lower field, as in e.g. Mn(4-methylpyridine)$_4$(NCS)$_2$ [12], pointing to a much smaller distortion of the ligand field at the Mn centre. This is in accord with the observation of ν(CN) at 2053 cm^{-1}, indicating coordination of the anion via nitrogen and the consequent presence of a slightly distorted MnN_6 coordination geometry.

Although these observations provide good evidence for the main coordination geometry about the metal centres in these compounds, it is the long-range structure that is of particular interest in the present context. As we were able to obtain crystals of the chloride, **1**, we have determined its structure by X-ray methods.

Structure of $Mn(BBI)_2Cl_2$ (**1**)

The X-ray results show that in the structure of **1** each Mn centre is coordinated to four nitrogen atoms, one from each of four different BBI ligands, and two chloride ions in a *trans*-octahedral arrangement (Fig. 2). Distortions from octahedral geometry are small, with *cis*-angles ranging from 88.9(1) to 91.1(1)°. The *trans*-angles are all 180° as the Mn atom is positioned on a crystallographic inversion centre. The Mn–N bonds, 2.249(3) and 2.270(3) Å, are the same as those observed in $[Mn(BBI)_3](BF_4)_2$, **2**, [7] and the Mn–Cl distance of 2.579(1) Å is unexceptional. The planes of the pairs of coordinated imidazole rings are steeply inclined, by 59 and 85° respectively, to the equatorial coordination plane.

The BBI ligand has an extended geometry with a near planar, all *anti*, N–$(CH_2)_4$–N backbone, the planes of the imidazole rings both being steeply inclined (58 and 71°) to that of the backbone. The rotations of each imidazole ring are in opposite senses so that, unlike the co-planar conformation observed for these rings in **2**, here they are inclined by *ca.* 60° to each other.

Each BBI ligand links adjacent, symmetry equivalent Mn centres in the crystal to form a contiguous two-dimensional network (Fig. 3). Each macrocyclic component of this network has a pseudo-rhombic shape with opposite arms having either a concave or convex relationship to each other—this is a con-

Table 1. Crystallographic data for 1–6[a]

Compound number	**1**	**2**[7]	**3**	**4**	**5**	**6**
Formula	$C_{20}H_{28}N_8Cl_2Mn$	$C_{30}H_{42}N_{12}Mn$	$C_{30}H_{42}N_{12}Mn$	$C_{30}H_{42}N_{12}Mn$	$C_{30}H_{42}N_{12}Mn$	$C_{30}H_{42}N_{12}Mn$
Counter-ions	—	$\cdot 2BF_4$	$\cdot 2ClO_4$	$\cdot 1.5ClO_4 \cdot 0.5PF_6$	$\cdot 1.5ClO_4 \cdot 0.5AsF_6$	$\cdot 1.3PF_6 \cdot 0.7ClO_4$
M	506.34	799.3	824.60	847.36	869.33	883.77
Colour, habit	colourless prism	colourless prism	colourless prism	colourless prism	colourless prism	colourless prism
Crystal size (mm)	$0.40 \times 0.17 \times 0.12$	$0.23 \times 0.15 \times 0.15$	$0.23 \times 0.10 \times 0.10$	$0.23 \times 0.20 \times 0.10$	$0.37 \times 0.27 \times 0.23$	$0.27 \times 0.27 \times 0.13$
Crystal system	monoclinic	rhombohedral	rhombohedral	rhombohedral	rhombohedral	rhombohedral
Space group (No.)	$P2_1/n$ (14)	$R\bar{3}$ (148)	$R3$ (146)	$R3$ (146)	$R3$ (146)	$R3$ (146)
T (K)	203(2)	293	293(2)	293(2)	293(2)	293(2)
a (Å)	7.562(1)	13.783(1)	13.918(1)	13.983(1)	14.010(3)	14.060(1)
b(Å)	18.543(1)	—	—	—	—	—
c(Å)	8.625(1)	17.777(2)	17.733(2)	17.715(2)	17.711(2)	17.681(1)
β (°)	112.12(1)	—	—	—	—	—
V (Å^3)	1120.6(1)	2924.7(4)	2974.9(4)	2999.8(5)	3010.7(8)	3026.9(4)
Z	2	3	3	3	3	3
D_c (g cm^{-3})	1.501	1.361	1.381	1.407	1.438	1.455
Radiation	Cu–K_α[b]	Mo–K_a	Cu–K_a	Mo–K_a	Mo–K_a	Mo–K_a
μ (mm^{-1})	7.189	0.416	4.469	0.520	0.907	0.508
F(000)	526	1239	1287	1317	1344	1365
2θ range (°)	0–126	0–50	0–127	0–50	0–60	0–50
Independent reflections	1806	689	1185	1192	1990	1202
(R_{int})	(0.031)	(0.023)	(0.052)	(0.029)	(0.036)	(0.024)
Observed reflections [$F_o > 4\sigma(\lvert F_o \rvert)$]	1540	634	1111	944	1156	936
Absorption Correction	ψ-scan	None	ψ-scan	None	None	None
Max., min. transmission	0.333, 0.181	—	0.469, 0.406	—	—	—
Number of parameters	143	81	175	181	202	187
a, b in weighting scheme[c]	0.067, 0.679	0.0838, 2.4474	0.1132, 0	0.047, 0.645	0.053, 0	0.061, 2.425
Final $R1$ ($wR2$)[d]	0.045 (0.109)	0.056 (0.148)	0.054 (0.147)	0.034 (0.083)	0.057 (0.120)	0.043 (0.103)
Largest, mean Δ/σ	0.000, 0.000	0.000, 0.004	0.000, 0.001	0.000, −0.001	0.003, 0.046	0.001, 0.006
Data/parameter ratio	10.8:1	7.8:1	6.3:1	5.2:1	5.7:1	5.0:1
Largest difference peak, hole (e Å^{-3})	0.366, −0.663	0.276, −0.199	0.563, −0.291	0.167, −0.173	0.225, −0.241	0.225, −0.345

[a]Details in common: Siemens P4/PC diffractometer, graphite monochromated radiation, refinement based on F^2.
[b]Rotating Anode.
[c]$w^{-1} = \sigma^2(F_o^2) + (aP)^2 + bP$.
[d]$wR2 = \sqrt{\{\Sigma[w(F_o^2 - F_c^2)^2]/\Sigma[w(F_o^2)^2]\}}$.

Table 2. Selected bond lengths (Å) and angles (°) for 1

Mn–N(1)	2.270(3)	Mn–N(12)	2.249(3)
Mn–Cl	2.5785(7)		
N(1)–Mn–N(12B)	89.97(11)	N(1)–Mn–N(12C)	90.03(11)
N(1)–Mn–Cl	90.28(8)	N(1)–Mn–Cl(A)	89.72(8)
N(12B)–Mn–Cl	88.90(7)	N(12C)–Mn–Cl	91.10(7)

Table 3. Selected bond lengths (Å) and angles (°) for 3–6

	3	4	5	6
Mn–N(1)	2.29(1)	2.27(1)	2.24(1)	2.28(3)
Mn–N(12C)	2.26(1)	2.30(1)	2.32(1)	2.30(3)
N(1)–Mn–N(1A)	88.8(5)	90.7(3)	91.0(3)	90.1(11)
N(1)–Mn–N(12C)	177.1(6)	178.7(5)	177.8(6)	179.0(20)
N(1)–Mn–N(12D)	88.3(5)	88.7(3)	88.0(4)	89.9(11)
N(1)–Mn–N(12E)	90.8(5)	90.5(3)	91.0(4)	88.7(11)
N(12C)–Mn–N(12D)	92.0(4)	90.1(3)	90.1(3)	91.3(10)

sequence of the non-coplanarity of the two imidazole ring systems within each bridge. The edges of the rhomb (Mn ... Mn) are 14.02 Å, with inter-edge angles of 82.8 and 97.2°. The trans-annular separations between the centres of opposite aliphatic linkages are 12.1 and 16.4 Å, reflecting a very open ring conformation.

In network structures comprising open-ring systems the sheets are sometimes aligned in register, thus creating "nanotubes" which are filled either by counter ions or by solvent molecules [13]. Alternatively the sheets can interweave and become self-filling via polycatenation [5, 14]. In **1** the voids are filled via partial interpenetration of successive (ABCABC) stacked, slightly corrugated sheets—shown schematically in Fig. 4. This packing is remarkably efficient, the separation between adjacent planes of Mn atoms being only 2.88 Å. Indeed, one of the imidazole rings [that containing N(12)] of each BBI ligand within one sheet interpenetrates and π-stacks with its C_i related neighbour in the next (mean interplanar separation 3.27 Å, centroid-centroid distance 3.67 Å). There is also evidence for secondary edge-to-face C–H ... π interactions between the C(4) hydrogen atom of the imidazole rings in one sheet and the N(12) imidazole rings in the next (C ... π 3.01 Å, C–H ... π angle 163°).

Structures of $Mn(BBI)_3X_2$

The next logical step in the progression from the above two-dimensional array to a three-dimensional network is the replacement of the two chloride atoms by the imidazole rings of an additional pair of BBI ligands. As we have shown in a preliminary communication for **2** [7], the resulting charged species not only formed a contiguous three-dimensional network but also, because of the size of the voids created, satisfied the "self-filling" preference via interlinked interpenetration. The two BF_4^- anions were located in the cusp of two interpenetrating rhombohedra.

We speculated that such a system would have the potential to adjust its dimensions so as to accommodate different anions of varying size and/or shape. The number of variable parameters to achieve this is limited, namely the effective ligand length and the distortions from octahedral geometry at the metal centres. To this end we have investigated the structural changes induced by replacement of the BF_4^- anions by perchlorate ions and also by varying proportions of ClO_4^-/PF_6^- or ClO_4^-/AsF_6^- combinations. The products for which we were successful in obtaining crystalline samples of appropriate quality for X-ray studies are listed in Table 1.

A notable feature of all of these new products is that, although they crystallise in the rhombohedral system with unit cell dimensions similar to, but larger than, those for $[Mn(BBI)_3](BF_4)_2$, **2**, they no longer possess inversion symmetry, all being polar.

Analyses of their structures show them to be virtually identical to that of **2** (Fig. 5), the interpenetrating three-dimensional $\{Mn(BBI)_3\}_n$ network being retained with the new anions trapped within the cusp formed between the interpenetrating rhomboids (Fig. 6). On progressing from the tetrafluoroborate to the somewhat larger [15] perchlorate ion as counter ion the structure changes from being centrosymmetric to polar, thereby destroying the inversion symmetry of the BBI ligand [16]. Overall, the gross structure is unchanged.

Anion competition experiments with the combinations ClO_4^-/PF_6^- and ClO_4^-/AsF_6^- resulted in the formation of polar, mixed anion, inclusion materials each of which retains the same basic structure (Fig. 7).

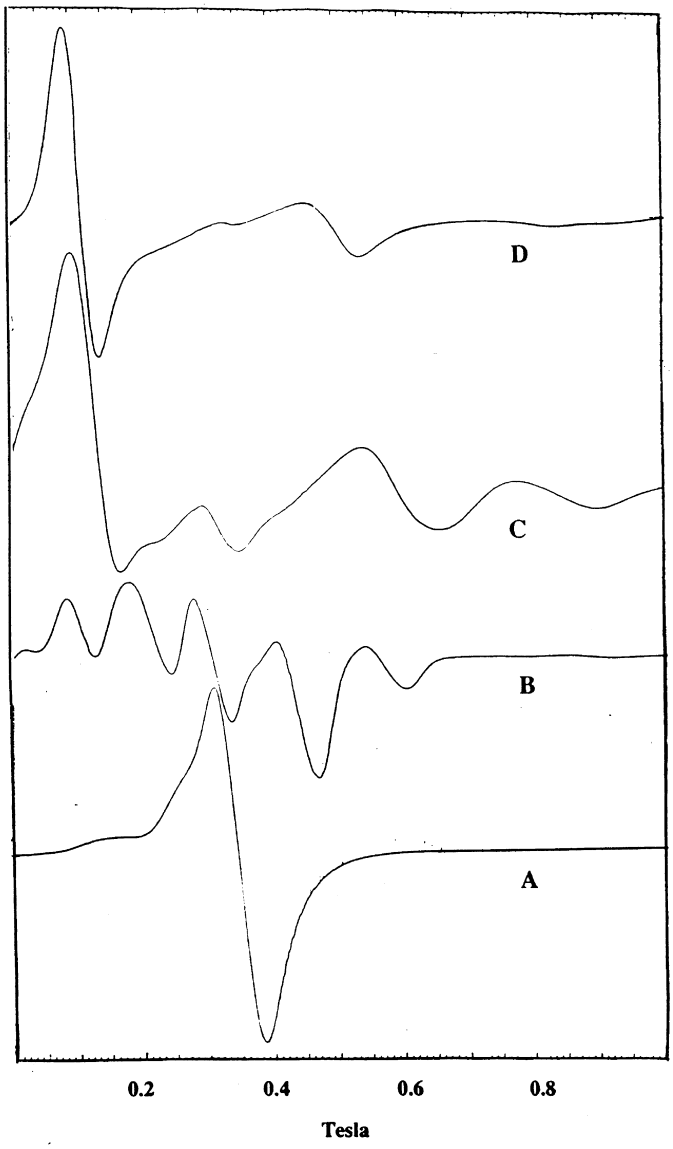

Fig. 1. X-Band EPR spectra of powdered samples of $Mn(BBI)_2X_2$: A, X = NCS; B, X = NO_3; C, X = Cl; D, X = Br.

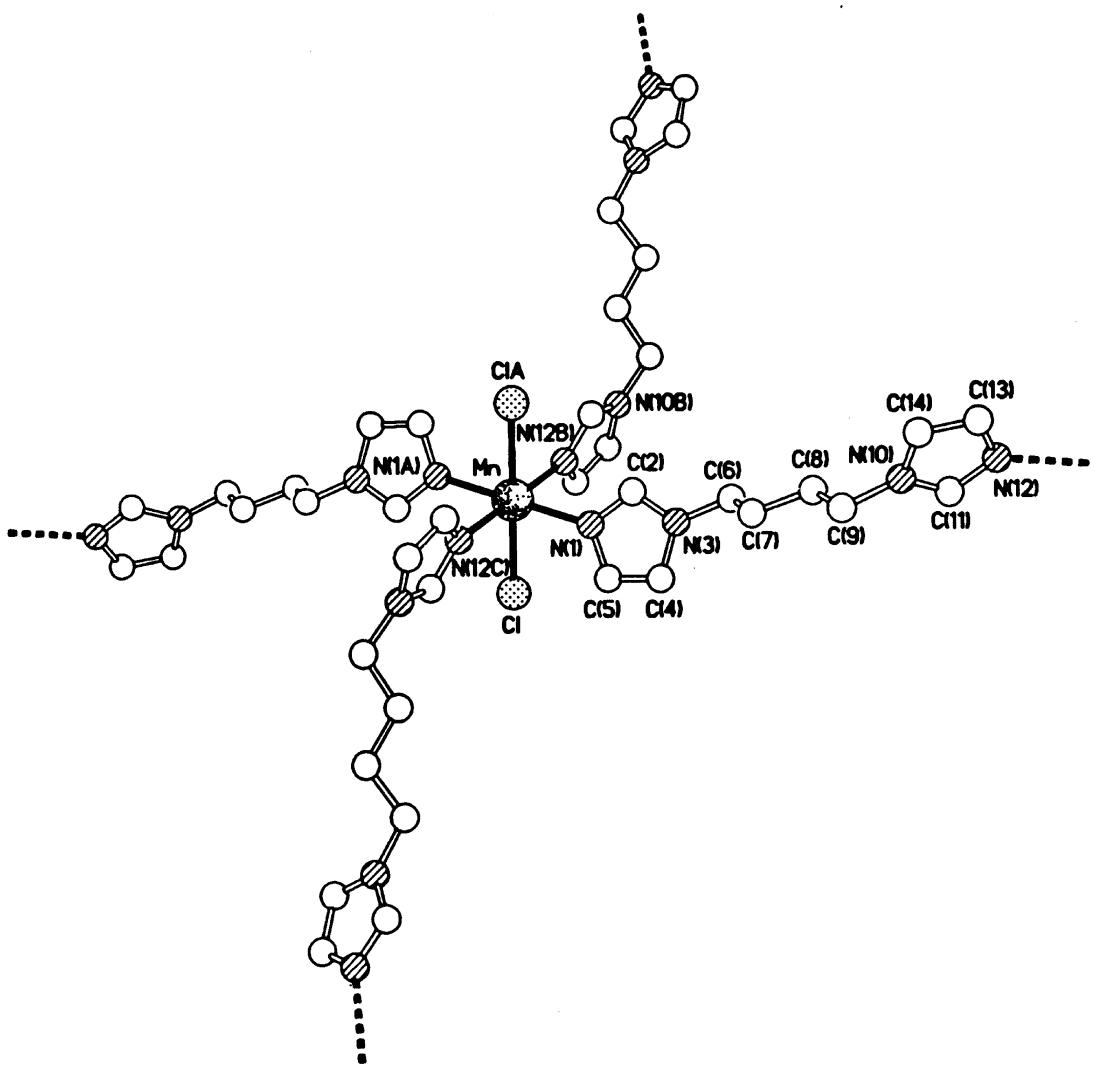

Fig. 2. The Mn coordination environment in the structure of **1**.

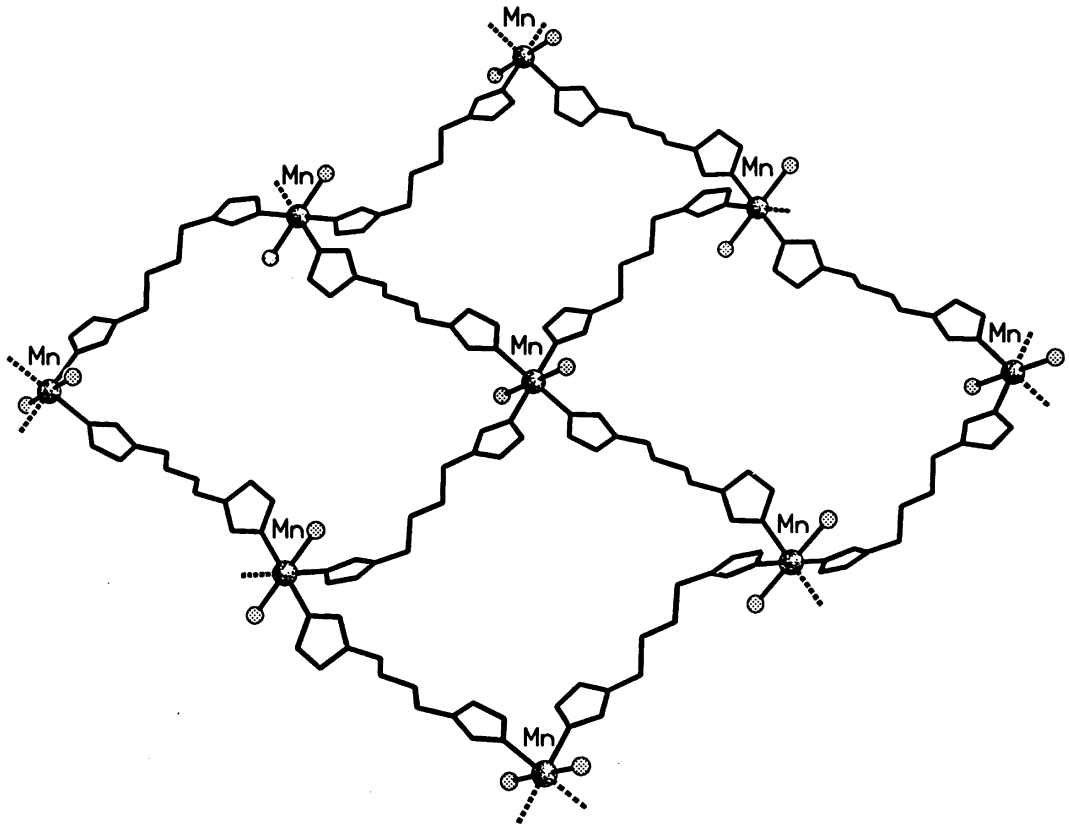

Fig. 3. Part of one of the two-dimensional polymer sheets formed by **1** in the solid state.

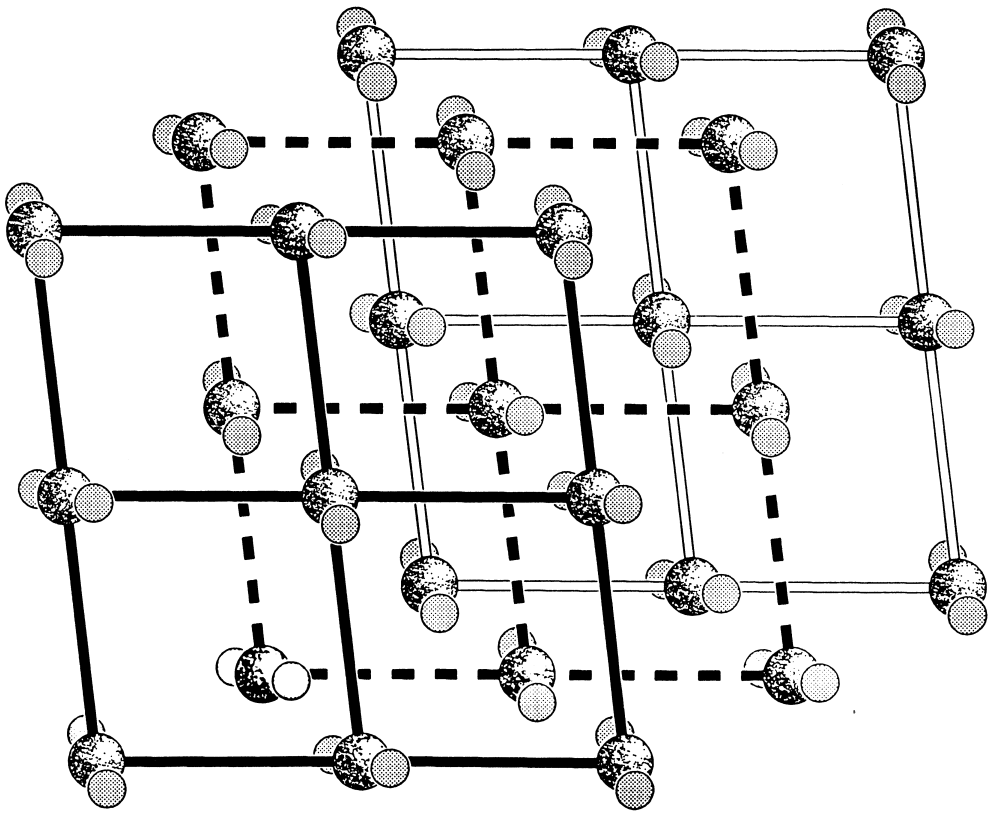

Fig. 4. Schematic representation of the stacking of polymeric sheets in the structure of **1**.

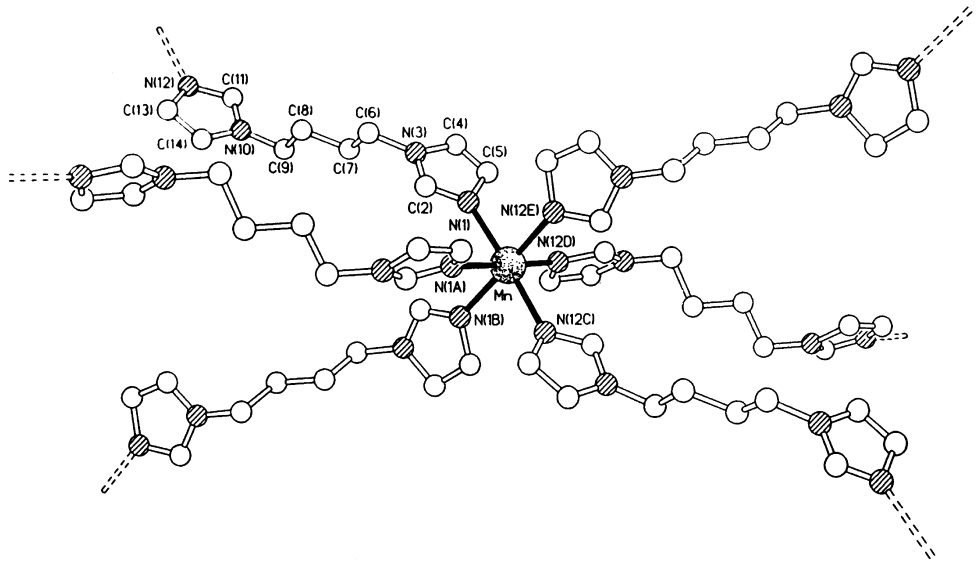

Fig. 5. The Mn coordination environment in the structures of **3**–**6**.

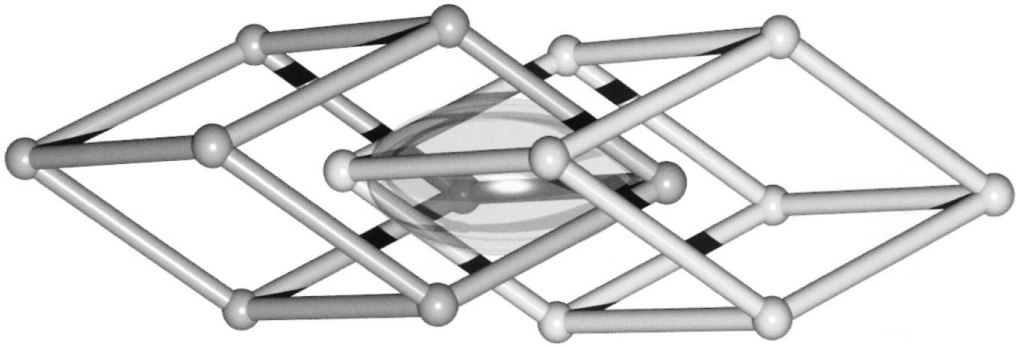

Fig. 6. The domain between the intersecting cuboids where the anions are located in **3**–**6**.

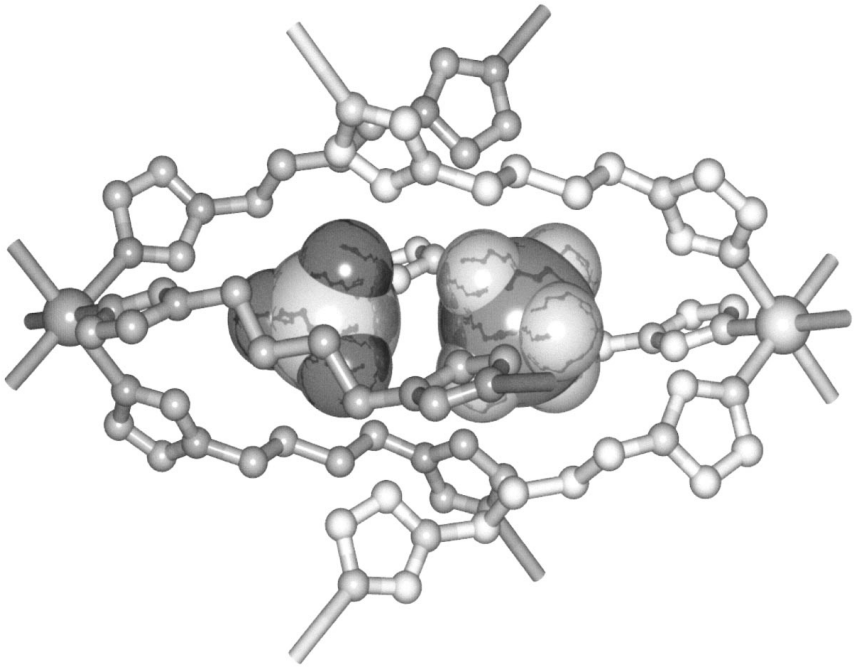

Fig. 7. The location of the ClO^-_4/PF^-_6 anions in the structure of **4**.

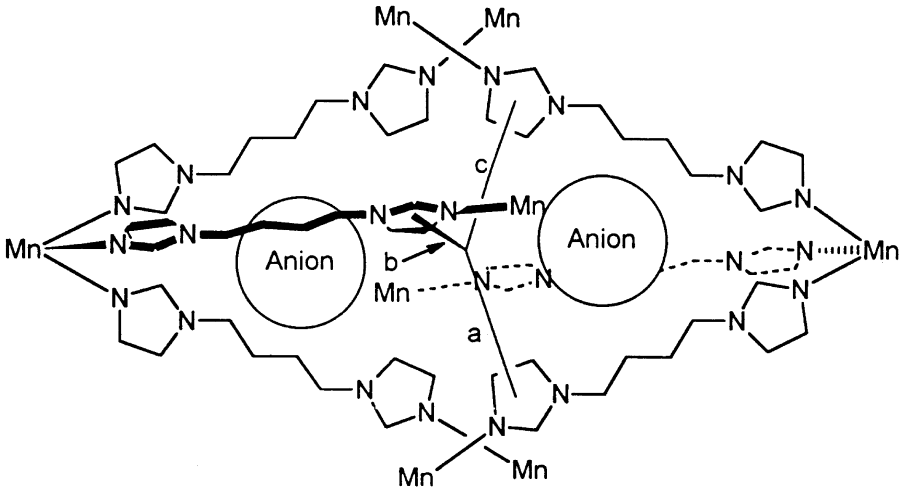

Fig. 8. Schematic representation of Figure 7 indicating the equatorial radii of the ellipsoidal cavity.

On increasing the mean encapsulated anion volume requirements, the internuclear Mn ... Mn separation within the cage decreases from 17.78 Å for **2** to 17.68 Å for **6**, whilst the maximum radii, taken from the centre of the Mn–Mn vector to the centroids of the imidazole rings about the "equator" of the cage (b in the schematic view shown in Fig. 8), increase from 5.33 to 5.45 Å. Thus with these essentially spherical anions there is a measure of "spare" capacity along the longest dimension (Mn ... Mn) of the cage which is relaxed to accommodate the change in anion. The other notable feature of this series of anion encapsulating structures is an increase in the unit cell volume, and hence those of the associated rhomboids, from 2925 $Å^3$ in **2** to 3027 $Å^3$ in **6**. There is therefore a slight expansion of the same basic lattice to accommodate the change in anions.

Acknowledgements—We thank the EPSRC for a Research Studentship (to D.A.G.), a Postdoctoral Fellowship (to I.B.) and for equipment, and also the Nuffield Foundation for an Undergraduate Research Bursary (to P.C.M.D.). L.B. thanks the Complutense University for sabbatical leave and DGES (Project PB 94/0240) for financial support.

REFERENCES

1. For a recent review see Arends, I. W. C. E., Sheldon, R. A., Wallau, M. and Schuchardt, U., *Angew. Chem., Int. Ed. Eng.*, 1997, **36,** 1144.
2. Janiak, C., *Angew. Chem., Int. Ed. Eng.*, 1997, **36,** 1431; and references therein.
3. See e.g. Hunter, C. A., *Angew. Chem. Int. Ed. Eng.*, 1995, **34,** 1079; and references therein.
4. Recent examples of some of the approaches employed include: Abrahams, B. F., Batten, S. R., Hamit, H., Hoskins, B. F. and Robson, R., *Angew. Chem., Int. Ed. Eng.*, 1996, **35**, 1690; Bertelli, M., Carlucci, L., Ciani, G., Proserpio, D. M. and Sironi, A., *J. Mater. Chem.*, 1997, **7**, 1271; Goodgame, D. M. L., Menzer, S., Smith, A. M. and Williams, D. J., *Chem. Commun.*, 1997, 339; Blake, A. J., Champness, N. R., Chung, S. S. M., Li, W. S. and Schröder, M., *Chem. Commun.*, 1997, 1675; Yaghi, O. M., Jernigan, R., Li, H., David, C.E. and Groy, T. L., *J. Chem. Soc., Dalton Trans.*, 1997, 2383; Vaid, T. P., Lobkovsky, E. B. and Wolczanski, P. T., *J. Amer. Chem. Soc.*, 1997, **119**, 8742; Henniger, T. L., MacQuarrie, D. C., Losier, P., Rogers, R. D. and Zaworotko, M. J., *Angew. Chem., Int. Ed. Eng.*, 1997, **36**, 972.
5. Hoskins, B. F., Robson, R. and Slizys, D. A., *J. Amer. Chem. Soc.*, 1997, **119,** 2952; and references therein.
6. Zaworotko, M. J., *Chem. Soc. Rev.*, 1994, 283; Hoskins, B. F., Robson, R. and Scarlett, N. V. Y., *J. Chem. Soc., Chem. Commun.*, 1994, 2025; Robinson, F. and Zaworotko, M. J., *J. Chem. Soc., Chem. Commun.*, 1995, 2413; Kuroda-Sowa, T., Yamamoto, M., Munakata, M., Seto, M. and Maekawa, M., *Chem. Letters*, 1996, 349; Carlucci, L., Ciani, G., Proserpio, D. M., Sironi, A. and Blake, A. J., *Chem. Commun.*, 1996, 1393; Champness, N. R., Khlobystov, A. N., Lemonovskii, D. A., Li, W. S. and Schröder, M., *Chem. Commun.*, 1997, 1339; and references therein.
7. Duncan, P. C. M., Goodgame, D. M. L., Menzer, S. and Williams, D. J., *Chem. Commun.*, 1996, 2127.
8. Goodgame, D. M. L., Menzer, S., Smith, A. M. and Williams, D. J., *J. Chem. Soc., Dalton Trans.*, 1997, 3213.
9. Atherton, Z., Goodgame, D. M. L., Katahira, D. A., Menzer, S., White, A. J. P. and Williams, D. J., *Polyhedron*, 1998, **17,** 2257.
10. Schutze, V. W. and Schubert, H., *J. Prakt. Chem.*, 1959, **8,** 307.
11. Sheldrick, G. M., SHELXTL, version 5.03, University of Göttingen (1995).
12. Dowsing, R. D., Gibson, J. F., Goodgame, M. and Hayward, P. J., *J. Chem. Soc.* (*A*), 1969, 187.

13. Doyle, G. A., Goodgame, D. M. L., Hill, S. P. W. and Williams, D. J., *J. Chem. Soc., Chem. Commun.*, 1993, 207.
14. Stumpf, H. O., Ouahab, L., Pei, Y., Bergerat, P. and Kahn, O., *J. Amer. Chem. Soc.*, 1994, **116**, 3866; Goodgame, D. M. L., Menzer, S., Smith, A. M. and Williams, D. J., *Angew. Chem. Int. Ed. Eng.*, 1995, **34**, 574; Champness, N. R., Khlobystov, A., Lemonovskii, D. A., Li, W. S. and Schröder, M., *Chem. Commun.*, 1997, 2713; and references therein.
15. Mingos, D. M. P. and Rohl, A. L., *J. Chem. Soc., Dalton Trans.*, 1991, 3419.
16. Initial attempts at solving the structure as being isomorphous with **2** resulted in poor convergence and a high residual *R* of *ca.* 0.15, which, on changing to the non-centrosymmetric space group immediately dropped to 0.054.

Pergamon

PII: S0277–5387(98)00158–2

Polyhedron Vol. 17, No. 20, pp. 3625–3631, 1998
© 1998 Elsevier Science Ltd
All rights reserved. Printed in Great Britain
0277–5387/98 $19.00 + 0.00

A thermal study of several lanthanide triflates

Naohisa Yanagihara,* Shin Nakamura and Masayoshi Nakayama

Department of Materials Science and Engineering, Teikyo University, 1-1 Toyosatodai, Utsunomiya, 320, Japan

(Received 6 March 1998; accepted 8 April 1998)

Abstract—Five lanthanide triflates, $Ln(TfO)_3 \cdot nH_2O$, where $TfO^- = CF_3SO_3^-$, $Ln = La^{3+}$, Nd^{3+}, Sm^{3+}, Gd^{3+} and Yb^{3+}, and $n = 9$ and 13, have been prepared and the thermal decomposition processes of these triflates up to 600°C were characterized by means of TG, DTA, XRD. The thermal studies have shown almost all the lanthanide triflates prepared in this study to exist as a stable nonahydrate. During the stepwise dehydration processes, it was found that mono-, di-, tri-, penta-, and heptahydrates were formed. Decompositions were found to be exothermic, and calcinations of these triflates at 600°C resulted in the formation of the corresponding LnF_3. Crystal systems of the trifluorides thus obtained were hexagonal for La, Nd and Sm trifluorides, whereas those of Gd and Yb were found to be orthorhombic. The volatile decomposition products at 600°C were identified by MS, and it was revealed that the over all reaction scheme for the thermal decomposition proceeds as follows: $Ln(OTf)_3 \rightarrow LnF_3 + 3SO_2 + CO_2 + CF_3OCF_3$. © 1998 Elsevier Science Ltd. All rights reserved

Keywords: lanthanide triflates; thermal process; stable nonahydrate.

INTRODUCTION

Trifluoromethanesulfonic acid, commonly known as triflic acid (TfOH), was first reported in 1954 by Haszeldine and Kidd [1]. Since then, there has been a rapid growth in the chemistry of triflate and its derivatives, and a great variety of metal complexes containing the coordinated trifluoromethanesulfonate (triflate) have been synthesized [2–4]. Interest in these compounds as a potential use in both inorganic and organic synthons stems from specific properties of the triflate anion, e.g., the low basicity and the poor coordinating ability [5]. A recent striking example in this area is the use of lanthanide triflates as Lewis acid catalysts in organic synthesis [7]. Until now, however, it appears that most of the interest in the derivatives has centered on the chemistry involving transition metals, and that little attention has been paid to the lanthanide triflates. Moreover, a survey of the literature revealed only a few studies [7–10] on the thermal decomposition of lanthanide compounds.

Recently, we reported a study on the thermal decomposition of lanthanum triflate [11]. In our continuing investigations, we report, here, the results obtained in studies of the thermal decomposition of several other lanthanide triflates.

EXPERIMENT

Preparation of lanthanide triflates

Trifluoromethanesulfonic acid (TfOH) was used as received. Lanthanide oxides were of 99.5% pure (Wako Pure Chemical, Japan). Prior to use the oxides were freshly ignited at 800°C in quartz crucibles. On the basis of reports in the literature [12, 13], an excess of the corresponding sesquioxide was added to a 50% aqueous solution of TfOH, and the mixture was boiled and filtered to remove the unreacted oxide. The water was then removed from the filtrate under reduced pressure until the hydrate was formed. The hydrates were dried in a rotary vacuum evaporator at 80°C for 1 h. The drying was not prolonged in order to maintain the same dehydration conditions, and the triflates thus obtained were used for the thermal analysis studies. The IR spectra of the hydrated triflates that were used initially were prepared as KBr disks and recorded with the aid of a Shimadzu FTIR 4300.

The lanthanide content and the water content of the each starting triflates were determined by titration

* Author to whom correspondence should be addressed.

with a standard EDTA solution and TGA experiments, respectively. Found: La, 18.5. Calc for $[(LaC_3F_9S_3O_9)\cdot 9H_2O]$: La, 18.6%. Found: Nd, 19.1. Calc for $[(NdC_3F_9S_3O_9)\cdot 9H_2O]$: Nd, 19.0%. Found: Sm, 19.9. Calc for $[(SmC_3F_9S_3O_9)\cdot 9H_2O]$: Sm, 19.8%. Found: Gd, 20.8. Calc for $[(GdC_3F_9S_3O_9)\cdot 9H_2O]$: Gd, 20.5%. Found: Yb, 20.5. Calc for $[(YbC_3F_9S_3O_9)\cdot 13H_2O]$: Yb, 20.3%.

Thermal analysis

TG and DTA curves were obtained on heating up to 600°C, using a Shimadzu DT-40. The heating rate was 5°C min^{-1} in a static atmosphere of air. A small portion (*ca.* 15–20 mg) of sample was used for the TG, and the highly sintered α-Al_2O_3 was the thermally inert reference material used for the DTA.

Using copper(II) sulfate pentahydrate as an external standard, a computational integration of the endothermic area on the DTA curves of each Ln triflate was applied to estimate roughly an enthalpy change for the process encountered throughout the dehydrations.

Analysis of solid and gaseous products obtained by the calcination

The calcined solid was fused with NaOH, and dissolved in a minimum of 6 m HCl, diluted, and the lanthanide content was determined by titration with a standard EDTA solution [14]. The oxygen content in the calcined product was not determined. Found: La, 71.0. Calc for LaF_3: La, 70.9%. Found: Nd, 71.4. Calc for NdF_3: Nd, 71.7%. Found: Sm, 72.1. Calc for SmF_3: Sm, 72.5%. Found: Gd, 73.0. Calc for GdF_3: Gd, 73.4%. Found: Yb, 74.8. Calc for YbF_3: Yb, 75.2%.

Powder diffractograms of the calcination products were obtained by means of a Shimadzu XD-610 with a source of Cu Kα radiation. For identification purposes, diffraction patterns [(I/I_0) vs d spacing (Å)] of the products were matched with the relevant data on JCPDS cards.

Mass spectra (MS) of a gas phase decomposition products were obtained with a JEOL A V505W in the electron impact positive ion mode.

RESULTS AND DISCUSSION

Dehydration and decomposition processes

While Fig. 1 shows the simultaneous DTA and TG curves for La triflate as a typical example of the thermal analysis of lanthanide triflates, DTA curves for all the triflates studied are shown in Fig. 2. For convenience, each weight loss (WL) steps monitored on the TG curve is designated in Roman Numerals, and the corresponding peak temperature on the DTA curve is denoted as T_{1max}, T_{2max}, and so on. In addition, the superscript s in the peak temperature means that the peak is poor or a shoulder. The reaction temperatures along with the WL obtained from both TG and DTA curves are summarized in Table 1.

TG studies revealed that the decomposition of triflates occurred in two main stages. The first stage involved a stepwise dehydration to the anhydrous state, followed by the decomposition of the triflates to stable final products. As shown in Table 1, the observed WL values that were found in both dehydration and decomposition processes are in good agreement with the calculated values. In conjunction with the TG curves, it is obvious that the multiplicity of the endothermic peaks corresponds to each dehydration step, and the exothermic peaks correspond to the decomposition (see Fig. 2). Rather complex peaks observed in the decomposition temperature region may be explained by the postulate that the decomposition process also occurs step by step.

The triflates began to lose water of hydration from 42–64°C giving two or three clearly defined steps prior to reaching the anhydrous state. The corresponding to the anhydrous state, beginning around 190–220°C were not quite horizontal, and suggests that a slow decomposition occurs. Finally, more rapid decompositions at 360–410°C resulted in a sharp weight loss to a continuous horizontal plateau. After the complete decompositions, however, some of the TG curves tend to increase and the weight increases, which suggests a probable slow oxidation of the final product. These oxidations are anticipated from reexaminations, in which when the same experiments were carried out in a dynamic atmosphere of N_2, the resulting final plateaus on the TG curves remained quite horizontal until a temperature reached 600°C.

As shown in Table 1, the number of hydrated water molecules in almost all starting triflates were found to be 9, except for Yb triflates. These stoichiometries of the hydrated water molecules are consistent with the results of X-ray structural studies of the hydrates of lanthanide triflates, $[Ln(H_2O)_9][TOf]_3$; (Ln = La, Nd, Gd, Ho and Lu) [15, 16] and with those analogous compounds such as $Tb(H_2O)_9(BrO_3)_3$ [17] and non-aquasamarium(III) bromide-1,4-dioxane adduct, e.g., $Sm(H_2O)_9\cdot Br_3(C_4H_8O_2)_2$ [18]. In the present study, although the number of hydration molecules varies in each triflate, it is of interest to note that all the triflates lose the 6 hydrated water molecules at the first dehydration step, which corresponds to the strongest endothermic peak in the DTA curves. On the basis of the IR measurements of the starting hydrated Ln triflates, it was suggested [9] that there exist two types of distinct water molecules in the triflates. The IR bands, attributed to the OH stretching frequency, which appeared around 3690 and 3650 cm^{-1} may be due to very weakly held water while the broad OH band around 3450 cm^{-1} may be due to more strongly hydrogen-bonded water in the complexes. Therefore, it is reasonable to conclude that the aforementioned 6

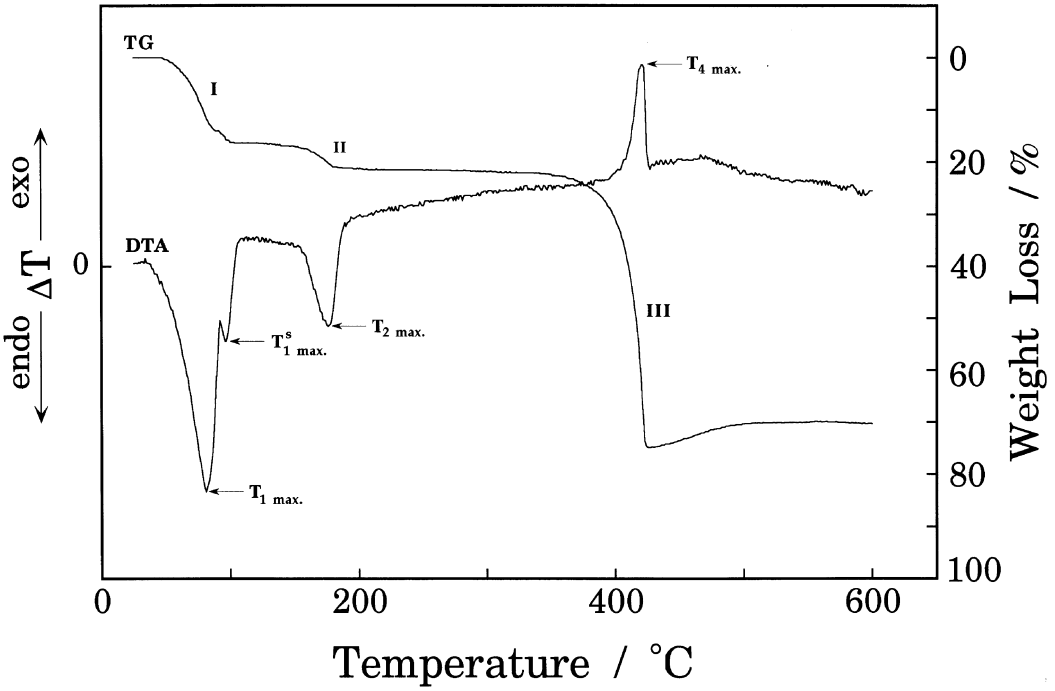

Fig. 1. TG and DTA curves for lanthanum triflate.

water molecules which were liberated at relatively low temperature regions are those that are not strongly bonded to the salts.

In the subsequent series of the stepwise dehydration processes, a variety of hydrated intermediates were formed (see Table 1). However, the most stable hydrate formed as an intermediate was the dihydrated species for the La, Pr, Nd, and Sm triflates. Mono and trihydrates were found to be stable for Gd and Yb triflates, respectively. The observations of the series of intermediates also confirm that there exist different types bonded water molecules in the lanthanide triflate, and they play a special role in the coordination of the ligands with the lanthanide metal. Similar findings were reported by Rillings *et al.* [9], during the thermal study of the lanthanide salts. They reported that Pr, Sm and Er trifluoroacetates show mono-, sesqui- and dihydrate intermediates while the corresponding pentafluoropropionates show sesqui- and dihydrate intermediates during their dehydrations.

In addition, the roughly estimated enthalpy values [$\Delta H_{\text{dehyd.}}$ (kJ mol^{-1})] for the total dehydration process of each Ln triflate are: 123 (La); 125 (Nd); 131 (Sm); 135 (Gd) and 125 (Yb). These values are within the range characteristic of dehydration processes [10].

In Table 1, it is also worth noting that the initial temperature of the dehydration process increases as the atomic number of the lanthanide increases thus reflecting the lanthanide contraction and decreasing base strength of the elements. In contrast to this tendency, however, the decomposition behavior of the triflates is somewhat more complicated. It appears that the initial decomposition temperature tends to decrease gradually with an increase in atomic number of the lanthanide.

Solid decomposition products

In an effort to confirm the products remaining after decomposition at 600°C in a static atmosphere of air, the products were subjected to an XRD study. In order to identify the solid products, the relevant JCPDS cards were employed. The JCPDS cards used for the verification were 32–483, 9–416, 12–792, 12–788 and 34–102 for the trifluorides of La, Nd, Sm, Gd and Yb, respectively. In a typical result, the XRD data of the La and Yb samples are compared with the reference data of LaF_3 and YbF_3, respectively, in Table 2. As shown in Table 2, it is clear that both the XRD data match very well, and this is the case for the rest of the triflates. Furthermore, since no peaks corresponding to lanthanide oxyfluorides were found on the XRD profiles, it is reasonably safe to conclude that all the lanthanide triflates prepared in this study are converted almost completely to the corresponding trifluorides at 600°C. This conclusion is also substantiated by the quantitative analysis of the each trifluoride (see Experimental section).

When the calcinations of the triflates were carried out at higher than 700°C, almost all of them decomposed gradually to a mixture of oxyfluoride and oxide, and finally at 1000°C, they were all converted into the Ln_2O_3. These observations are consistent with the

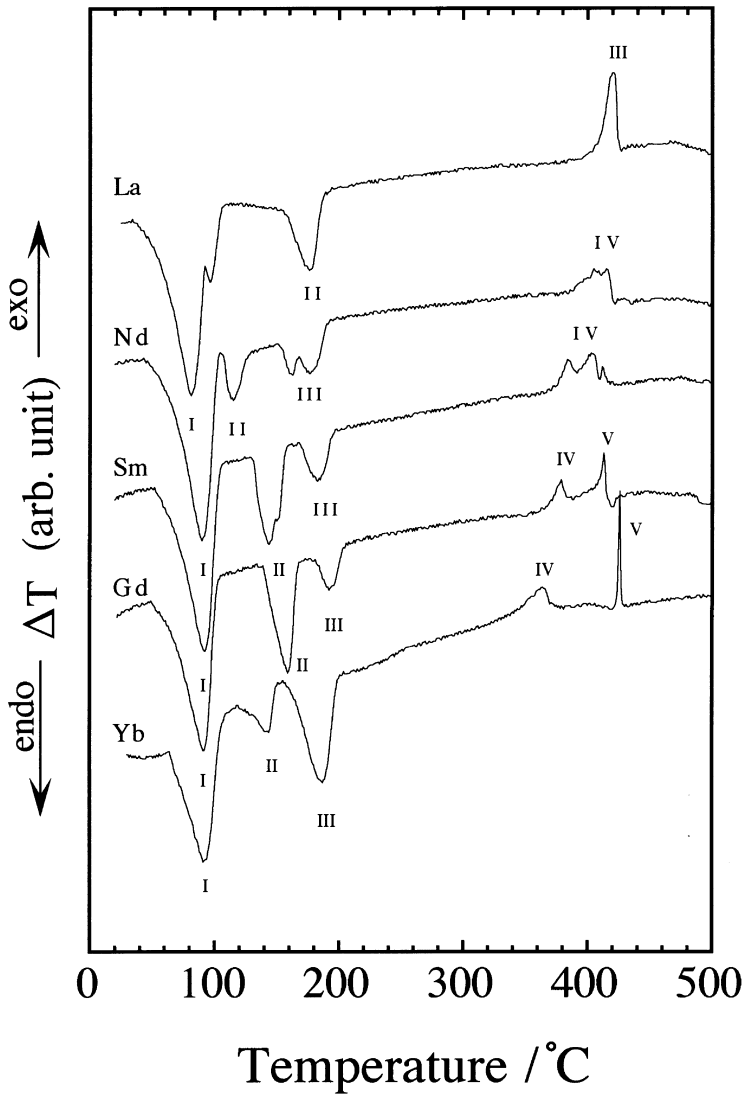

Fig. 2. DTA curves for lanthanide triflates (see text for roman numerals).

results reported by Rillings *et al.* [9]. During a study of the thermal decomposition of several lanthanide perfluoroacetates, they found that LnF_3 and LnOF (Ln = Pr, Sm and Er) are formed around 450°C and 700°C upon the decomposition of the corresponding trifluoroacetates and pentafluoroacetates. In addition, they reported that the decomposition of the fluoride to oxyfluoride is a hydrolysis reaction. Thus, there is a little chance of the formation of LnOF under the experimental conditions of this study.

On the other hand, based on the JCPDS cards, the trifluorides of La, Nd and Sm are hexagonal, whereas GdF_3 and YbF_3 are found to be orthorhombic and isostructural with YF_3. It was reported [19–21] that the trifluorides of the rare earths of La to Nd and those of Sm to Lu are thought to occur in the hexagonal form and the orthorhombic form, as stable forms at atmospheric temperature, respectively. These results are consistent with our observations, except for the crystal system of the SmF_3. It is known [19, 22] that samarium trifluoride is dimorphic occurring as a high-temperature phase (β-SmF_3, hexagonal) and low-temperature phase (α-SmF_3, orthorhombic), and the latter is substantially more stable than the former. Thus, it is noteworthy that the β-SmF_3 can be easily obtained upon the thermal decomposition of the corresponding Sm triflate.

Volatile decomposition products and overall reaction

When the triflates were pyrolyzed at a slightly higher temperature at the end of the decomposition, it was found that volatile products are evolved. The

Table 1. Thermal analysis data for lanthanide triflates

						Weight loss (%)			
		Temperature (°C)		Num. of dehydration		dehydration		decomposition	
Ln	Stage Num.	range	peak	in each stage	total	obsd.	calcd.	obsd.	calcd.[a]
La	I	42 ~ 105	$T_{1max} = 80$	6		14.6	14.4		
			$T_{1max}{}^{1s} = 95$	1	9	16.7	16.8		
	II	156 ~ 188	$T_{2max} = 175$	2		21.5	21.7		
	III	400 ~ 427	$T_{3max} = 421$					75.2	73.8
Nd	I	48 ~ 104	$T_{1max} = 90$	6		14.7	14.3		
	II	106 ~ 129	$T_{2max} = 114$	1	9	17.3	16.7		
	III	151 ~ 190	$T_{3max}{}^{1s} = 162$	2		21.7	21.5		
			$T_{3max}{}^{2s} = 177$						
	IV	386 ~ 422	$T_{4max}{}^{1s} = 405$						
			$T_{4max}{}^{2s} = 416$					73.4	73.3
Sm	I	52 ~ 103	$T_{1max} = 93$	6		13.7	14.2		
	II	131 ~ 156	$T_{2max} = 144$	1	9	18.6	16.6		
	III	168 ~ 197	$T_{3max} = 183$	2		21.3	21.3		
	IV	374 ~ 418	$T_{4max}{}^{1s} = 384$						
			$T_{4max}{}^{2s} = 403$						
			$T_{4max}{}^{3s} = 412$					72.1	72.7
Gd	I	51 ~ 103	$T_{1max} = 92$	6		13.8	14.1		
	II	139 ~ 168	$T_{2max} = 160$	2	9	18.6	18.8		
	III	180 ~ 203	$T_{3max} = 194$	1		20.8	21.1		
	IV	363 ~ 385	$T_{4max} = 379$						
	V	405 ~ 420	$T_{5max} = 413$					71.6	72.1
Yb	I	64 ~ 108	$T_{1max} = 94$	6		13.8	12.6		
	II	119 ~ 149	$T_{2max} = 143$	4	13	21.7	21.1		
	III	156 ~ 299	$T_{3max} = 188$	3		27.5	27.4		
	IV	347 ~ 375	$T_{4max} = 363$						
	V	420 ~ 430	$T_{5max} = 426$					74.3	73.1[1]

[a]Calculated as LnF_3.

MS analysis of the gases showed that three peaks at m/z 44, 64 and 85 with relatively high intensity are present in the spectra (see Fig. 3). The first two peaks are easily assigned to be molecular ion peaks of CO_2 and SO_2, respectively, and each of them has isotopic peaks at m/z 45 and 66. The peak at m/z 85 can be considered as a fragment ion peak that was generated as a result of the cleavage from the molecular ion, $[CF_3OCF_3]^{\bullet +}$, which is probably unstable and easily decomposes during the ionization process in the MS analyzer. And the $[CF_3]^+$ peak at m/z 69 arises subsequently from the $[CF_3O]^+$. Thus, the probable pathway of the fragmentation can be rationalized as:

$$[CF_3OCF_3]^{\bullet +} \xrightarrow{-CF_3^{\bullet}}$$

$$[CF_3O]^+ (m/z\,85) \xrightarrow{-O^{\bullet}} [CF_3]^+ (m/z\,69)$$

Consequently, the present studies revealed that the general thermal decomposition reaction for the lanthanide triflates proceed according to an overall reaction scheme as follows:

$$Ln(CF_3SO_3)_3 \rightarrow LnF_3 + 3SO_2 + CO_2 + CF_3OCF_3$$

This reaction mechanism is different from those that have been proposed by Rillings *et al.* [9] and others [7, 23]. They studied the thermal decomposition of Pr and Sm trifluoroacetates in the temperature range from 275 to 300°C. In this study, on the basis of IR analysis, they suggested that trifluoroacetic anhydride exists as an intermediate during the decomposition in the first stage, in the next stage the anhydride decomposes to trifluoroacetyl fluoride, carbonyl difluoride and carbon monoxide. Accordingly, they reported the pyrolysis of the trifluoroacetates to proceed as:

$$2Ln(CF_3CO_2)_3 \rightarrow 2LnF_3 + 3CF_3COF + 3CO_2 + 3CO$$

The main difference in the thermal decomposition of the trifluoroacetacs and triflates can be found in the gaseous products; i.e., CF_3COF and CF_3OCF_3. Although it is difficult to compare both mechanisms since the gases formed during pyrolysis are usually very complicated, the difference between the mechanisms and the major gaseous products might be attributable to the counter anion in these compounds, and also to the temperatures at which decomposition occurs.

Table 2. A comparison of X-ray powder diffraction data of (A) LaF_3 and (B) YbF_3

	Reference[a,c]		Observed		
h k l	*d* (Å)	I/I_0	*d* (Å)	I/I_0	Δd/Å[b]
			(a) LaF_3		
0 0 2	3.678	50	3.687	46	0.009
1 1 0	3.596	40	3.603	31	0.007
1 1 1	3.231	100	3.237	100	0.006
1 1 2	2.570	15	2.574	9	0.004
3 0 0	2.074	55	2.078	52	0.004
1 1 3	2.024	65	2.026	59	0.002
3 0 2	1.807	40	1.808	31	0.001
2 2 1	1.745	25	1.747	20	0.002
2 2 3	1.449	18	1.450	15	0.001
3 0 4	1.376	16	1.376	11	0
1 1 5	1.389	12	1.361	7	−0.028
			(b) YbF_3		
0 0 1	3.712	19	3.720	17	0.008
1 0 1	3.610	60	3.615	64	0.005
0 2 0	3.394	62	3.398	58	0.004
1 1 1	3.187	100	3.191	100	0.004
2 1 0	2.826	66	2.827	61	0.001
1 2 1	2.472	27	2.474	25	0.002
0 0 2	2.216	12	2.219	10	0.003
2 2 1	2.036	15	2.036	15	0
1 1 2	1.996	20	1.998	17	0.002
1 3 1	1.916	40	1.918	36	0.002
3 0 1	1.877	26	1.877	25	0
0 2 2	1.855	15	1.858	12	0.003
2 3 0	1.829	32	1.829	27	0
3 1 1	1.809	18	1.809	15	0
1 2 2	1.778	14	1.779	11	0.001
2 1 2	1.744	23	1.745	22	0.001
0 4 0	1.696	12	1.697	10	0.003
3 2 1	1.642	17	1.642	17	0
1 4 1	1.535	12	1.535	10	0
3 3 1	1.444	12	1.444	11	0
2 3 2	1.411	16	1.412	16	0.001

[a]JCPDS 32-483.
[b]$\Delta d = d_{\text{obsd.}} - d_{\text{ref.}}$.
[c]JCPDS 34-102.

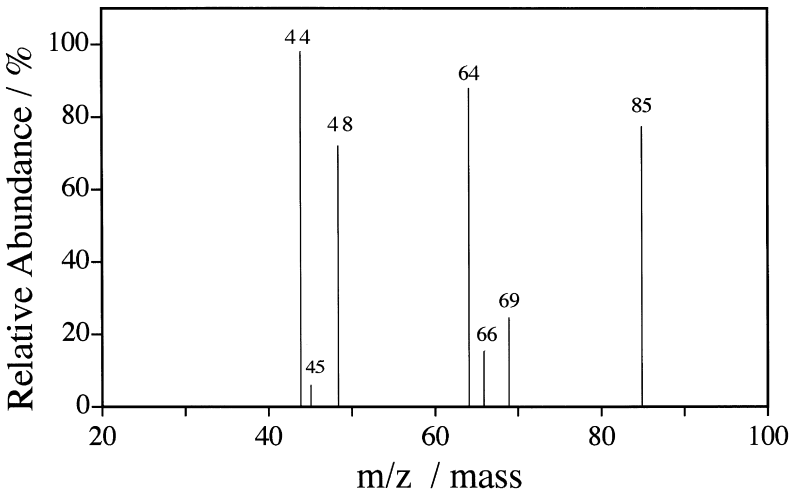

Fig. 3. Mass spectra of the volatile products obtained by the pyrolysis of lanthanum triflate.

Acknowledgements—N. Y. would like to express his grateful thanks to *Eno Science Foundation* for the financial support.

REFERENCES

1. Haszeldine, R. N. and Kidd, J. M., *J. Chem. Soc.* 1954, 4228.
2. Senning, A., *Chem. Rev.*, 1965, **65,** 385.
3. Howells, R. D. and McCown, J. D., *Chem. Rev.*, 1977, **77,** 69.
4. Lawrance, G. A., *Chem. Rev.*, 1986, **86,** 17.
5. Stang, P. J. and White, M. R., *Aldrichimica Acta*, 1983, **16,** 15.
6. Kawada, A., Mitamura, S. and Kobayashi, S., *J. Chem. Soc., Chem. Commun.*, 1993, 1157.
7. Roberts, J. E., *J. Am. Chem. Soc.*, 1961, **83,** 1087.
8. Paul, R. C., Bains, M. S. and Ghotra, J. S., *Indian J. Chem.*, 1964, **7,** 514.
9. Rillings, K. W. and Roberts, J. E., *Thermochimica Acta*, 1974, **10,** 285.
10. Hussen, G. A.-H. and Ismail, H. M., *Bull. Chem. Soc. Jpn.*, 1994, **67,** 285.
11. Yanagihara, N., Nakamura, S. and Nakayama, M., *Chem. Lett.*, 1995, 555.
12. Solomon, R. G. and Kochi, J. K., *J. Chem. Soc., Chem. Commum.*, 1979, 552.
13. Fosberg, J. H., Spaziano, V. T., Balasubramanian, T. M., Liu, G. K., Kinsley, S. A., Duckworth, C. A., Poteruca, J. J., Brown, P. S. and Miller, J. L., *J. Org. Chem.*, 1987, **52,** 1017.
14. Catalano, E., Bedford, R. G. and Silveria, V. G., *J. Phys. Chem. Solids*, 1969, **30,** 1613.
15. Harrowfield, J. M., Keper, D. L., Patrick, J. M. and White, A. H., *Aust. J. Chem.*, 1983, **36,** 483.
16. Santos, C. O. P. and Castellano, E. E., *Inorganica Chimica Acta*, 1985, **110,** 83.
17. Gallucci, J. C., Gerkin, R. E. and Reppart, W. J., *Cryst. Struct. Chem.*, 1982, **11,** 1141.
18. Barries, J. C. and Nicoll, G. Y. R., *Inorganica Chimica Acta*, 1985, **110,** 47.
19. Zalkin, A. and Templeton, D. H., *J. Am. Chem. Soc.*, 1953, **75,** 2453.
20. Thoma, R. E. and Brunton, G. D., *Inorg. Chem.*, 1966, **5,** 1937.
21. Weigel, F. and Scherrer, V., *Radiochem. Acta*, 1967, **7,** 40.
22. Oftedal, I., *Z. Phys. Chem. B*, 1929, **5,** 271.
23. Corbett, P. J. and Whittle, E., *J. Chem. Soc.*, 1963, 3247.

Pergamon

PII: S0277–5387(98)00159–4

Polyhedron Vol. 17, No. 20, pp. 3633–3642, 1998
© 1998 Elsevier Science Ltd
All rights reserved. Printed in Great Britain
0277–5387/98 $19.00 + 0.00

Constitutional isomers and stereoisomers of lanthanum(III) complexes of the dimethyl-substituted six-nitrogen-donor ligand $C_{24}H_{30}N_6$ and crystal structure of $[La(C_{24}H_{30}N_6)(NCS)_3(H_2O)]\cdot 0.5H_2O$

F. Benetollo,[a] G. Bombieri,[b] W. A. Gootee,[c] K. K. Fonda,[c] K. M. Samaria[c] and L. M. Vallarino[c]*

[a]I.C.T.M.A., C.N.R., Corso Stati Uniti 4, Padova, 35127, Italy

[b]Istituto di Chimica Farmaceutica, Università di Milano, Milano, Italy

[c]Department of Chemistry, Virginia Commonwealth University, Richmond, VA 23284, U.S.A.

(Received 21 November 1997; accepted 2 April 1998)

Abstract—Complexes of La(III) with the macrocyclic ligand $C_{24}H_{30}N_6$, in which each di-imine side chain carries a $-CH_3$ substituent, were synthesized by the metal-templated cyclic Schiff-base condensation of 2,6-diacetylpyridine with (R)-, (S)- and (R,S)-1,2-diaminopropane. The complexes were obtained as mixtures of constitutional isomers and stereoisomers, which were identified by ^1H NMR spectra and separated by fractional crystallization. The molecular structure of the 10-coordinate complex $[La(C_{24}H_{30}N_6)(NCS)_3(H_2O)]\cdot 0.5H_2O$ was established by X-ray crystallography. © 1998 Elsevier Science Ltd. All rights reserved

Keywords: lanthanum(III); complexes; diaminopropane; diacetylpyridine.

Complexes containing a lanthanide(III) ion bound into the six-nitrogen-donor macrocyclic cavity schematically illustrated in Fig. 1 have potential bio-medical applications. Specifically, the luminescent complexes of europium(III) can serve as markers in cell analysis and immmunology, provided they contain functional groups for covalent linking to bio-substrates [1–5]. The complexes of gadolinium(III), which have high relaxivity [6], could be useful as contrast enhancers for *in vivo* magnetic resonance imaging, if their tolerance were enhanced by appropriate functional groups incorporated into the macrocyclic ligand. Thus, functionalization of the macrocycle is a prerequisite for these bio-medical applications, and lanthanide(III) complexes with two peripheral hydroxo or primary amino groups have been synthesized by the metal-templated cyclic Schiff-base condensation of 2,6-diacetylpyridine with carbon-substituted 1,2-diaminoethanes [2–5]. In these functionalized complexes, the lanthanide-macrocycle entities retained the chemical and spectroscopic properties characteristic of the non-functionalized analogues and the peripheral functional groups retained their typical reactivities. For example, the Eu(III) complex of a diamino-macrocycle reacted with thiophosgene to give the corresponding di-isothiocyanate, and this in turn reacted with the primary amino groups (lysine residues) of avidin to produce a highly luminescent conjugate which exhibited the usual avidin-biotin affinity [2, 5].

The preceding considerations focus attention on this class of disubstituted macrocyclic complexes and their isomeric forms. For each complex, two constitutional isomers are possible, with the substituents attached to the 5,14 or 5,15 positions of the macrocycle cavity (see Fig. 1 for numbering scheme). In addition, the carbon atom to which the substituent

* Author to whom correspondence should be addressed.

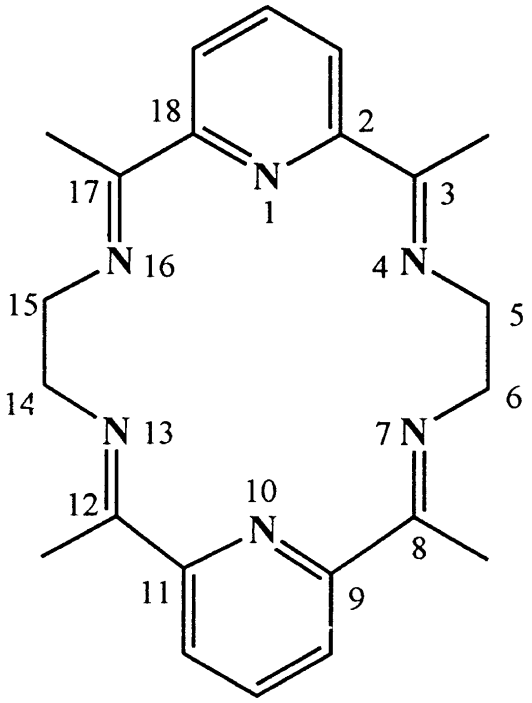

Fig. 1. Schematic formula of the six-nitrogen-donor macrocycle cavity with conventional numbering scheme.

is attached is a stereocenter and each constitutional isomer can exist as stereoisomers, the (R,R) and (S,S) enantiomer pair and the (R,S) *meso* form [7, 8]. Three questions then arise: (1) Are constitutional isomers formed in the Ln(III)-templated macrocycle synthesis and, if so, are they distinguishable? (2) Can synthetic conditions provide some degree of isomer selectivity? (3) Can isomers be separated and identified structurally? In an effort to answer these questions, a study was carried out using as model the simplest member of this series—the macrocyclic complex with two $-CH_3$ substituents on the di-imine side chains, $=N-CH_2-CH(CH_3)-N=$. Lanthanum(III) was selected as the metal center to permit the use of nuclear magnetic resonance spectrometry as a diagnostic tool without the complication of internal paramagnetic shifts; La(III) acetate was used as template in the syntheses because preliminary screening had shown it to produce high yields of complexes with desirable solubilities.

EXPERIMENTAL

Materials and procedures

Lanthanum(III) acetate hydrate, 2,6-diacetylpyridine, (R)- and (S)-1,2-diaminopropane dihydrochloride, 1,3-diphenyl-propane-1,3-dione (dibenzoylmethane, HDBM), and deuterated solvents (all from Aldrich) were used as received. (R,S)-1,2-Diaminopropane (Aldrich) was dried over solid KOH, distilled, and stored over 3A Molecular Sieves. The sodium salt of HDBM was prepared by reaction of the diketone with sodium ethoxide (1:1 mole ratio) in anhydrous ethanol at 0°C, followed by precipitation with diethyl ether and recrystallization from ethanol/diethyl ether. Micronalyses (C, H, N) were performed by Atlantic Microlabs, Atlanta, GA; all compounds had correct analyses corresponding to the given formulas.

NMR spectra were obtained with a GE QE-300 spectrometer at ambient temperature (24–26°C). Chemical shifts (as δ for ^{1}H spectra) are reported in ppm; coupling constants, *J*, are given in Hz. Proton spectra were referenced to TMS (0.00 ppm) or to the residual proton signal of the solvent ($CDCl_3$ 7.26 ppm; deuterated dimethylsulfoxide, DMSO-d_6 2.49); carbon spectra were referenced to the solvent signal ($CDCl_3$ 77.00 ppm; DMSO-d_6 39.50 ppm).

Infrared spectra were obtained on a Perkin-Elmer Model 1600 FT instrument (4000–500 cm^{-1}). Samples were examined as KBr pellets as well as mulls in hexachloro-butadiene/NaCl disks (4000–1800 and 1500–1300 cm^{-1}) and Nujol/KBr disks (1800–1500 and 1300–400 cm^{-1}); no difference was observed between the two sets of spectra. Absorption frequencies are reported in cm^{-1}; abbreviations: s = strong, m = medium, w = weak, br = broad, v = very; an asterisk indicates an absorption only partly resolved from an adjacent stronger peak.

Thermograms were obtained with a Perkin-Elmer TGS4 system, with helium flow of 40 cm^3/min.

La(III) complexes of the dimethyl-macrocyclic ligand $L = 2C_{24}H_{30}N_6$

Only general procedures are given here. Reactions were carried out on a scale of one-to-two millimoles for reagents, and 150–200 cm^3 for solvents. Details are available from L. M. Vallarino upon request.

Complexes from metal-templated Schiff-base condensation

{LaL} triacetate from (R,S)-1,2-diaminopropane. La(III) acetate hexahydrate, 2,6-diacetylpyridine and (R,S)-1,2-diaminopropane (1:2:2 mole ratio) were dissolved in methanol at room temperature. The subsequent procedure varied as follows. The mixture was: (1) refluxed for 6 h in methanol (65°C) or ethanol (78°C), (2) kept at 40°C for 3 days, (3) kept at room temperature (24–26°C) for 5 days, (4) kept at 4°C for 10 days. (Optimum reaction times were determined in pilot experiments by withdrawing aliquots of the reaction mixture at regular intervals, isolating the product, and measuring yields.) At the end of each reaction period, the solution was taken to dryness under reduced pressure without heating and the resulting yellow-brown gummy solid was bulk-purified by

washing it with diethyl ether, dissolving it in chloroform, stirring with charcoal, filtering, and diluting the filtered solution with diethyl ether at 0°C.

The purified bulk product, {LaL}$(CH_3COO)_3 \cdot nH_2O$ with $n = 4.0$–6.5, was obtained as small colourless crystals, very soluble in water and polar organic solvents, insoluble in diethyl ether and hydrocarbons. Thermogravimetric analyses showed a gradual loss of water in the 35–105°C range; dried samples rapidly rehydrated when exposed to moist air. The complexes decomposed above 170°C. *IR absorptions* (cm^{-1}) and selected assignments: 3400 vs, br, ν(OH), water; 3093 vw, 2977 w, 2932 w, 1640 s, ν(C═N), imine; 1588 s, ν(C═N), pyridine; 1540 vs, $\nu_{asym.}$(COO); 1429 vs, $\nu_{sym.}$(COO); 1380 m*, 1278 vvw, 1251 s, 1198 s, 1153–1150 m, 1002 m, 966 vw, 928 w, 817 m, 745 m-w, 667 m-s, δ(COO); 619 w, 568 w. The latter four peaks were overlaid on the broad absorption centered at *ca* 600 cm^{-1} (librational mode of lattice water). The ^1H *NMR spectra* of the bulk products in $CDCl_3$ showed three distinct set of signals, diagnostic of the macrocycle structure and assigned to three isomers provisionally designated as A, B, and C (for structural assignment, see Discussion). Total yields and isomer ratios (calculated from the intensities of the $-CH_3$ side-chain signals and reproducible within *ca*. 5%): (1) 78 or 65°C, 6 hr: 80% (A:B:C = 55:25:20); (2) 40°C, 3 days: 50% (A:B:C = 20:10:70); (3) 24–26°C, 5 days: 45% (A:B:C = 15:5:80); (4) 4°C, 10 days: no product.

{*LaL*} *acetate-chlorides from* (*R*)- *and* (*S*)-1,2-*diaminopropane*. The diamine precursors were obtained from their dihydrochlorides by reaction with KOH (1:1 mole ratio) in methanol at 0°C. The solutions were dried over 3A Molecular Sieves, filtered, and used directly for the macrocycle syntheses. Two sets of reactions were carried out, following the procedure outlined in Section 1.1 for the (R,S)- analog: (1) 65°C, 6 hr and (2) 24–26°C, 5 days. The products, {LaL}-$(CH_3COO)_{3-x}Cl_x \cdot nH_2O$, with $x = 0.2$–1.0 and $n = 3.0$–6.5, were very similar to those from the R,S-diamine in their general properties, including IR spectra. The NMR spectra of products obtained at the same temperature from the (R)- and (S)-diamine were indistinguishable and showed the presence of two isomers, identical to those designated as A and B in the products from the R,S-diamine. Total yields and isomer ratios: (1) 65°C, 6 hr: A:B = 55:45; (2) 24–26°C, 5 days: A:B = 75:25.

Separation of the isomers. Fractional crystallization of the bulk products from methanol/diethyl ether gave the following yield of single isomers relative to bulk product: C, 15–25%: A, 5–10%; B from (S)-diamine, $< 5\%$. The B isomer from the (R)-diamine was not obtained pure. The ^1H *NMR spectra* and ^{13}C *spectra* of the isomers are given in Tables 1 and 2.

Complexes from anion metathesis

The precursors were {LaL} triacetate or diacetate chloride complexes of known isomer composition. From these, the acetate diperchlorate and the tri-isothiocyanate were obtained by treatment with an excess of $NaClO_4$ and NaNCS, respectively, in methanol solution. The trichloride was obtained by treatment with an excess of hydrogen chloride in methanol-diethyl ether at °C. The (DBM) hydroxide chloride was obtained by treatment with NaDBM (1:1 mole ratio) in chloroform. For all these complexes, fractional crystallization of isomer mixtures failed to yield single isomers.

$\{LaL\}Cl_3 \cdot 4H_2O$. Colourless microcrystals, less soluble in polar solvents than the corresponding triacetate and diacetate chloride. *IR absorptions* (cm^{-1}) and selected assignments: 3400 vs, br, ν(OH), water; 3072 vw, 2970 w, 2928 w, 2919 w, 1637 s, ν(C═N), imine; 1587 s, ν(C═N), pyridine; 1442 m, 1372 s, 1278 vvw, 1247 m-s, 1196 s, 1147 m, 997 m, 966 vw, 928 w, 806 m, 745 m, 620 w, 568 w (the latter four peaks overlaid on the broad H_2O absorption at *ca*. 600 cm^{-1}).

$\{LaL\}(CH_3COO)(ClO_4)_2 \cdot 3.5H_2O$. Colorless microcrystals, with solubility similar to the diacetate chloride. The *IR spectrum* was similar to that of the diacetate chloride, except for the lower relative intensity of the carboxylate absorptions in the 1500–1380 cm^{-1} region and the additional presence of the absorptions of ionic perchlorate (ν_3 1109 vs, br; ν_4 625 s).

$\{LaL\}(DBM)(OH)Cl \cdot 5H_2O$. Almond-colored crystals, with solubility similar to that of the triacetate. *IR absorptions* (cm^{-1}) and selected assignments: 3400 vs, br, ν(OH), water; 3040 vw, 2966 vw, 2931 vw, 1637 m-s, ν(C═N), imine; 1599 vs, ν(C═N), pyridine; 1550 vs, 1519 s, 1478 m, 1455 m, 1384 vs, ν(C–C), ν(C–O) of DBM; 1308 vw, 1249 m, 1196 m-w, 1155 vw, 1067 vw, 997 w, 814 w, 750 m, 727 m, 700–500 numerous weak and poorly resolved absorptions. ^1H *NMR spectrum* ($CDCl_3/CD_3OD$, v/v = 90/10; ppm vs. TMS) of the A-DBM isomer from the S-diamine: CH_3 side-chain: 1.01 d (6H) d, J 6.9, coupling to CH of macrocycle; CH_3 macrocycle: 2.54 s (6H), 2.68 s (6H); CH_2: AB spin pattern (total 4H), J 15.0, νH_A 3.94 and νH_B 4.16 (both components of H_B signal showed ill-resolved splitting, J *ca*. 2, coupling to CH of macrocycle); CH of macrocycle: 4.41–4.47 m (2H); CH of DBM: 6.68 s (1H); phenyl: 7.10–7.40 m (10H); pyridine: AMX spin pattern (total 6H), νH_A 8.14, νH_M 8.25, νH_X 8.34; $J_{AX} = J_{MX}$ 7.8, J_{AM} *ca*. 0.6.

$\{LaL\}(NCS)_3 \cdot nH_2O$ (n = 0–2.0). Colourless prisms or needles, moderately soluble in DMSO and dimethylformamide, very sparingly soluble in methanol, insoluble in other common solvents and water. When the precursors were the single-isomers C or B from (S)-diamine, crystals suitable for X-ray analysis were obtained. *IR absorptions* of [{LaL}$(NCS)_3(H_2O)] \cdot 0.5H_2O$, B isomer from (S)-diamine: 3400 m-w, br, ν(OH), water; 3085 vw, 2970 w, 2928 w, 2826 vvw, 2060–2031 vvs, ν(C≡N), coordinated NCS^-; 1641–1626 vs, ν(C═N), imine; 1588 vs, ν(C═N), pyridine; 1449 m, 1371 s, 1328 vvw, 1312 w, 1278 vvw, 1249 s, 1194 s, 1154 m-w, 1128 m, 1068

Table 1. Proton NMR spectra[a] of lanthanum(III) complexes of di-methyl-substituted six-nitrogen-donor macrocyclic ligands

	Isomer						
Group	(R,R)/(S,S)-5,14 diacetate chloride[b]	(R,R)/(S,S)-5,14 triacetate[b]	(R,R)/(S,S)-5,15 diacetate chloride[b]	(R,S)-5,15 triacetate[b]	(S,S)-5,14 tri-(NCS)[c]	(S,S)-5,15 tri-(NCS)[c]	(R,S)-5,15 tri-(NCS)[c]
CH_3 side-chain	1.24 d J 6.9[d]	1.25 d J 6.9[d]	1.34 d J 6.9[d]	1.33 d J 6.9[d]	1.18 d J 6.9[d]	1.22 d J 6.9[d]	1.20 d J 6.6[d]
CH_3 acetate	1.61 s	1.73 s	1.62 s	1.64 s	—	—	—
CH_3 macrocycle	2.63 s[e]	2.63 s[f]	2.62 s, 2.67 s	2.57 d J = 0.6–1.0[g]	2.68 s[f]	2.66 s, 2.70 s	2.65 s
CH_2 macrocycle	H_A 4.08[h] H_B 4.21[h,i] J_{AB} 12.6[h]	H_A 4.05[h] H_B 4.24[h,i] J_{AB}12.6[h]	4.04 s	H_A 3.93[h,j] H_B 4.10[h,k] J_{AB} 14.7[h]	H_A 3.94[h,l] H_B 4.09[h] J_{AB} 13.5[h]	H_A 3.87[h,l] H_B 4.05[h] J_{AB} 13.5[h]	H_A 4.02[h,i] H_B 4.17[h,m] J 13.2[h]
CH	4.42–4.52 m, br	4.40–4.52 m, br	4.49 m, br	4.52 m[n]	4.52–4.60 br	4.5 m, br	4.47–4.90 m, br
pyridine	β-H 8.18 γ-H 8.31 J 8.0[o]	β-H 8.17 d β-H′ 8.18 d γ-H 8.32 dd[p] J 7.9 J' 8.1	β-H 8.17 γ-H 8.30 J 8.1[o] β-H′ 8.22 γ-H′ 8.33 J' 7.9[o]	β-H 8.06 γ-H 8.26 J 8.1[o] β-H′ 8.08 γ-H′ 8.28 J' 8.1[o]	β-H 8.45 γ-H 8.52 J 8.3[o]	7.3–7.5 m[q]	β-H 8.37 γ-H 8.46 J 8.1[o] β-H′ 8.39 γ-H′ 8.46 J' 8.0[o1]

[a]Chemical shifts in ppm vs. TMS; coupling constants in Hz; small variations in chemical shifts were observed for samples with different concentrations and/or different water contents. All signal integrations were consistent with assignments. Spectra of the (R,R)/(S,S)-5,15 complexes were obtained from enriched isomer mixtures. Abbreviations: s = singlet, d = doublet, dd = doublet of doublets, t = triplet, m = multiplet, br = broad.

[b]In $CDCl_3$.

[c]In DMSO-d_6.

[d]Coupling to vicinal CH.

[e]In some samples, the signal is a doublet (J = 0.6–1.5, long-range coupling to H_B of CH_2).

[f]Some samples show two equal intensity, closely spaced signals (12H total), with the signal at higher field split into a doublet (J = 0.6–1.0, long-range coupling to H_B of CH_2 group).

[g]Long-range coupling to H_B of CH_2.

[h]Chemical shifts and coupling constant calculated from AB spin pattern.

[i]Broad signals with ill-resolved splittings.

[j]Each component of the H_A signal is further split into a doublet (J = 2.1, coupling to vicinal CH).

[k]Both components of the H_B signal are broad and show splitting consistent to coupling to the vicinal CH (J = *ca.* 3.8) and to the higher-field CH_3 of macrocycle (J = 0.9–1.3).

[l]Both components of the H_A signal are broad, with ill-defined splittings.

[m]Each component of the H_A signal is further split into a doublet (J = 2.1, coupling to vicinal CH).

[n]Pattern consistent with a quartet of doublets of doublets (J = 6.8, 3.8, 2.1, coupling to vicinal CH, and to H_A and H_B of CH_2,, respectively).

[o]Chemical shifts and coupling constants calculated from A_2B pattern where A = β-H and B = γ-H of pyridine moiety.

[p]Central peaks merged to give an apparent triplet.

[q]Pattern could not be identified.

Table 2. Carbon-13 NMR spectra[a] of lanthanum(III) complexes of di-methyl-substituted six-nitrogen-donor macrocyclic ligands

Isomer Group	(S,S)-5,14 diacetate chloride[b]	(S,S)- 5,15 diacetate chloride[b]	(R,S) 5,15 tri-acetate[b]	(S,S) 5,14 tri-(NCS)[c]	(S,S) 5,15 tri-(NCS)[c]	(R,S) 5,15 tri-(NCS)[c]
CH_3 macrocycle	16.99	17,04	16.82	16.86	16.88	16.86
		17.24		17.05	16.85	
CH_3 side chain	17.41	17.36	17.44	17.61	17.69	18.25
CH_3 acetate	24.25	24.28	24.47	—	—	—
CH	57.38	57.84	57.43	56.68[d]	56.77[d]	56.61[d]
CH_2	58.10	58.13	58.01	56.68[d]	56.77[d]	56.61[d]
C ß-py	126.47	126.42	125.74	127.47	127.50	126.82
	126.70	126.88	125.81	127.75	129.95	126.90
C γ-py	141.16	141.11	141.07	142.04	141.30	141.40
		141.27	141.24		142.00	141.87
C α-py	154.56	154.45	155.29	153.79	153.70	153.51
		154.75	155.59	154.18	154.00	154.62
–C═N–	168.76	169.06	167.16	169.95	170.61	168.65
	170.85	170.76	170.38	173.68	172.96	171.67
–C═O acetate	186.02	186.17	(e)	—	—	—[2]

[a]Chemical shifts in ppm; small variations were observed for samples with different water contents. Assignments were confirmed by attached proton test (ATP) and heteronuclear correlation (HETCOR) experiments.
[b]In $CDCl_3$.
[c]In DMSO-d_6.
[d]Signals of CH and CH_2 groups were coincident.
[e]Not observed.

vvw, 1021 vvw, 1002 m-s, 964 m-w, 859 vvw, 810 m-s, 788 w, 743 m-w, 682 vvw, 634 m-w, 562 w, 492 m-w. The other isomers had identical spectra, except for the absence of water absorptions in some samples. ^1H *NMR spectra* and ^{13}C *spectra*: Tables 1 and 2.

Attempted {LaL}-Eu(III) transmetallation

{LaL} triacetate and Eu(III) acetate hexa-hydrate (1:1 mole ratio) were heated at reflux in methanol for 6 hr. Work up of the mixture gave only unreacted starting materials.

X-ray measurements and structure determination

Crystal data for $[La(C_{24}H_{30}N_6)(NCS)_3(H_2O)]\cdot 0.5H_2O$, Mr = 742.7 triclinic, space group $P\bar{1}$, a = 8.666(3), b = 11.980(3), c = 16.889(4) Å, α = 78.36(3), β = 95.98(4), γ = 110.13(2); V = 1611.3(8) Å^3, Z = 2, Dx = 1.54 Mg m^{-3}, λ = (Mo-Kα) = 0.71069 Å, μ(Mo-Kα) = 15.6 cm^{-1}, $F(000)$ = 750, T = 293 K.

A prismatic white trasparent crystal of dimensions 0.20 × 0.22 × 0.38 mm was centered on a four-circle Philips PW1100 (Febo System) [9] diffractometer operating in $\theta/2\theta$ scan mode with graphite-monochromated (Mo-Kα) radiation λ = 0.71069 Å), following standard procedures. There were no significant fluctuations of intensities other than those expected from Poisson statistics. The intensity data were corrected for Lorentz-Polarization effects and for absorption, as described by North *et al* [10]. No correction was made for extinction.

The structure was solved by heavy atoms methods [11]. Refinement was carried out by full-matrix least-squares; the function minimized was $\Sigma w(Fo^2\text{-}Fc^2)^2$, with weighting scheme $w = 1/[\sigma^2(Fo^2) + (0.0475P)^2 + 5.26P]$, where $P = \max(Fo^2 + 2Fc^2)/3$. All non-hydrogen atoms were refined with anisotropic thermal parameters, except for the clathrated water molecule that was refined isotropically. The H-atoms were located from difference Fourier maps and refined isotropically, except for those belonging to the methyl groups which were placed in calculated positions with fixed, isotropic thermal parameters (1.2 $\mathbf{U}_{equiv}$ of the parent carbon atom). For a total of 416 parameters, $wR' = [\Sigma w(Fo^2\text{-}Fc^2)^2/\Sigma w(Fo^2)^2]^{1/2} = 12.45$, $S = 1.098$, and conventional $R = 0.047$, based on the F values of 4937 reflections having $Fo^2 \geq 3\sigma(Fo^2)$. Structure refinement and final geometrical calculations were carried out with SHELXL-93 [12] and PARST [13] programs, drawings were produced using *ORTEP II* [14]. Selected geometric parameters are reported in Table 3.

Lists of structure factors, H-atom coordinates and anisotropic thermal parameters have been deposited

Table 3. Selected bond lengths (Å) and angles (°) for $[La(C_{24}H_{30}N_6)(NCS)_3(H_2O)\cdot 0.5H_2O$

La–N(1)	2.639(7)	La–N(2)	2.645(7)
La–N(3)	2.557(6)	La–N(4)	2.819(6)
La–N(5)	2.742(5)	La–N(6)	2.851(5)
La–N(7)	2.787(4)	La–N(8)	2.788(5)
La–N(9)	2.730(5)	La–O(1)	2.536(6)
S(1)–C(1)	1.632(7)	S(2)–C(2)	1.64(1)
S(3)–C(3)	1.65(1)	C(1)–N(1)	1.161(9)
C(2)–N(2)	1.14(1)	C(3)–N(3)	1.23(1)
N(4)–C(4)	1.340(7)	N(4)–C(8)	1.345(8)
N(5)–C(9)	1.276(9)	N(5)–C(11)	1.468(9)
N(6)–C(12)	1.467(8)	N(6)–C(14)	1.265(8)
N(7)–C(16)	1.345(7)	N(7)–C(20)	1.337(7)
N(8)–C(21)	1.278(8)	N(8)–C(23)	1.478(8)
N(9)–C(25)	1.478(8)	N(9)–C(26)	1.27(1)
C(4)–C(26)	1.477(9)	C(8)–C(9)	1.478(9)
C(9)–C(10)	1.51(1)	C(11)–C(12)	1.52(1)
C(12)–C(13)	1.51(1)	C(14)–C(15)	1.503(9)
C(14)–C(16)	1.489(8)	C(20)–C(21)	1.496(8)
C(21)–C(22)	1.510(9)	C(23)–C(24)	1.53(1)
C(23)–C(25)	1.50(1)	C(26)–C(27)	1.51(1)
N(4)–La–N(5)	58.0(2)	N(4)–La–N(9)	57.7(1)
N(4)–La–O(1)	72.3(2)	N(5)–La–N(6)	60.7(2)
N(6)–La–N(7)	56.8(1)	N(7)–La–N(8)	58.6(1)
N(8)–La–N(9)	61.3(2)	N(5)–La–O(1)	82.4(2)
N(6)–La–O(1)	74.6(2)	N(7)–La–O(1)	77.8(1)
N(8)–La–O(1)	73.1(2)	N(9)–La–O(1)	82.7(2)
N(1)–La–N(3)	70.5(2)	N(1)–La–N(2)	68.0(2)
N(2)–La–N(3)	72.7(2)	S(1)–C(1)–N(1)	178.8(6)
S(2)–C(2)–N(2)	177.7(8)	S(3)–C(3)–N(3)	173(1)
La–N(1)–C(1)	165.6(6)	La–N(2)–C(2)	176.6(6)
La–N(3)–C(3)	146.5(7)	N(1)–La–O(1)	137.4(2)
N(2)–La–O(1)	139.3(2)	N(3)–La–O(1)	137.9(2)

with the Cambridge Crystallographic Data Centre (deposit@ccdc.cam.ac.uk), deposition number 102418.

RESULTS AND DISCUSSION

Synthesis and characterization of the complexes

Complexes of La(III) acetate containing the macrocyclic ligand $L = C_{24}H_{30}N_6$, in which a methyl group is attached to each of the di-imine side chains, $=N–CH(CH_3)–CH_2–N=$, were synthesized using (R,S)- as well as (R)- and (S)-diaminopropane as precursors. The complex obtained from the (R,S)-diamine had formula $\{LaL\}(CH_3COO)_3\cdot nH_2O$. with $n = 3.0–6.5$, whereas the products obtained from the R- and S-diamines (formed *in situ* by neutralization of the respective hydrochlorides) were isolated as hydrated species with non-integer acetate/chloride ratios, e.g. $\{LaL\}(CH_3COO)_{2.5}Cl_{0.5}.\ 4H_2O$, from which the corresponding triacetates and diacetate-chlorides were isolated by fractional crystallization. All complexes were colourless, crystalline solids, very soluble in water and polar organic solvents, insoluble in diethyl ether and hydrocarbons. The hydrated solids lost water completely when heated between 45 and 110°C, but dry samples rehydrated rapidly when exposed to the atmosphere; the complexes began to decompose at 170°C. In this thermal behavior, as in their other general properties, the La(III) complexes of the dimethyl-substituted macrocycles resembled very closely those of the corresponding non-substituted analogues [15–19]. In particular, the La-macrocycle moieties were resistant to decomposition by hydrogen chloride; they did not undergo metal release in the presence of competing ligands such as β-diketonates or metal exchange in the presence of competing metal ions such as Eu(III). The acetate counter-ion ligands, however, were labile; complexes of formula $\{LaL\}Cl_3\cdot nH_2O$ with $n = 4–6$, $\{LaL\}(CH_3COO)_2(ClO_4)\cdot 3.5H_2O$, and $\{LaL\}(NCS)_3\cdot nH_2O$, where $n = 0–2$, were obtained from the triacetate or acetate chlorides by anion metathesis.

The infrared spectra of all complexes showed identical patterns for the $\{LaL\}$ moieties, with the charac-

teristic absorptions arising from the C=N stretching modes of the imine and pyridine at 1640–1637 and 1588–1584 cm^{-1}, respectively. The absorptions of the counterion-ligands appeared in their usual ranges and were structurally informative. The tri-isothiocyanates had very strong, slighly split absorptions at 2060–2030 cm^{-1}, consistent with the presence of N-coordinated SCN^- ligands in slightly different environments. The triacetate and acetate chloride complexes had two strong carboxylate absorptions at *ca.* 1540 and 1430 cm^{-1}. For each complex, these absorptions were identical to those of the non-substituted europium(III) analogues, $[Eu(CH_3COO)_2(C_{22}H_{26}N_6)](CH_3COO)\cdot 9H_2O$ [17] and $[Eu(CH_3COO)_2(C_{22}H_{26}N_6)]Cl\cdot 4H_2O$ [16], suggesting similar structures with two acetates acting as bidentate chelating ligands on opposite sides of the La-macrocycle moiety, and either an ionic acetate or an ionic chloride balancing the residual +1 charge of the coordination entity. A somewhat similar structure can be assigned to the acetate diperchlorate complex, which in addition to the carboxylate absorptions showed the absorptions characteristic of ionic ClO_4^- at 1109 cm^{-1} and 625 cm^{-1}. In all these complexes, the frequency separation between the absorptions of the antisymmetric and symmetric carboxylate stretching modes, $\Delta\nu = ca.$ 110 cm^{-1}, was consistent with the suggested formulation [20, 21].

The proton and carbon-13 nuclear magnetic resonance spectra of the bulk products obtained from the (R)-, (S)- and (R,S)-diamines clearly showed the presence of non-interconvertible isomers: two (provisionally designated as A and B) in the products from the (R)- and (S)-diamines and three (A and B, plus a new species designated as C) in the product from the (R,S)-diamine. A very minor quantity of a fourth isomer (less than 3% of the total) was present in some samples of the bulk-product from the (R,S)-diamine. Repeated fractional crystallization of the bulk products from methanol/diethyl ether, using ^1H NMR spectra to monitor the composition of each fraction, gave minute quantities of pure A, B, and C. Their ^1H NMR spectra, discussed in a following section, suggested the following isomer identifications: A = (R,R)/(S,S)-5,14, B = (R,R)/(S,S)-5,15 and C = (R,S)-5,15, where the numbers identify the carbon atoms of the di-imine side chains to which the CH_3 substituents are attached (Fig. 1). When single-isomer triacetates or acetate chlorides were used to prepare the tri-isothiocyanates by anion metathesis, well formed crystals of $[La(NCS)_3$(S,S-5,15-dimethyl-macrocycle)] and $[La(NCS)_3(H_2O)$(R,S-5,15-dimethyl-macrocycle)] were obtained. The crystal structure of the former has been reported [8], that of the latter is discussed in the following section; both confirmed the formulation suggested by ^1H NMR spectra.

Crystal structure of $[La(C_{24}H_{30}N_6)(NCS)_3(H_2O)]\cdot 0.5H_2O$. An ORTEP view of the molecule with the atom numbering scheme is shown in Fig. 2. The complex is identified as the *meso* (R,S)-5,15 (S-5, R-15 or R-5, S-15) isomer. The La(III) ion is 10-coordinate, being linked to the six N atoms of the macrocyclic ligand, to the N atoms of three isothiocyanates on one side of the macrocycle, and to a water molecule on the opposite side. This uncommon mode of coordination for the three NCS^- ions, which in other complexes of this type are usually located two on one side of the macrocycle and one on the opposite side (see for example the (S,S)-5,15-[LaL$(NCS)_3$] [8] and the two forms of the non-substituted analog $[Eu(NCS)_3(C_{22}H_{26}N_6)]$) [22], is favored by the conformation of the {LaL} moiety. In the (R,S)-5,15 complex the torsion angles of the di-imine side chains, =N–CH_2–CH(CH_3)–N=, are very different from those of the previously reported (S,S)-5,15 isomer: N(5)–C(11)–C(12)–N(6) is -59.9(7)° v.s. 59(2)° and N(8)–C(23)–C(25)–N(9) is 57.7(7)° v.s. -72(2)°. These torsion angles determine a rather flat structure for the {LaL} moiety, with the two -CH_3 substituents at the 5 and 15 positions in the same hemisphere and with nearly parallel orientations, thus allowing sufficient space for the coordination of one molecule of water in the same hemisphere and of the three NCS^- ions in the other. The structure of the (R,S)-5,15 {LaL} moiety shows a total puckering amplitude of 0.493(6) Å for the six N atoms of the macrocycle and an interplanar angle of 14.4(1)° between the two pyridine-containing sections. In contrast, the six-nitrogen ring of the (S,S)-5,15 isomer has an approximate 'chair' conformation, with a total puckering amplitude of 0.84(1) Å and an interplanar angle of 38.3(3)° between the two pyridine-containing sections. A side view of the complex is shown in Fig. 3, together with that of the 9-coordinate (S,S)-5,15 isomer for comparison [8].

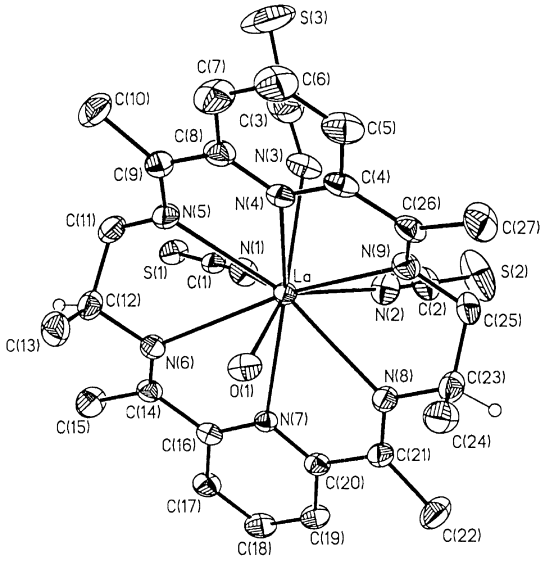

Fig. 2. ORTEP drawing of the $[La(C_{24}H_{30}N_6)(NCS)_3(H_2O)]$ molecule containing the (R,S)-5,15-dimethyl-substituted macrocyclic ligand.

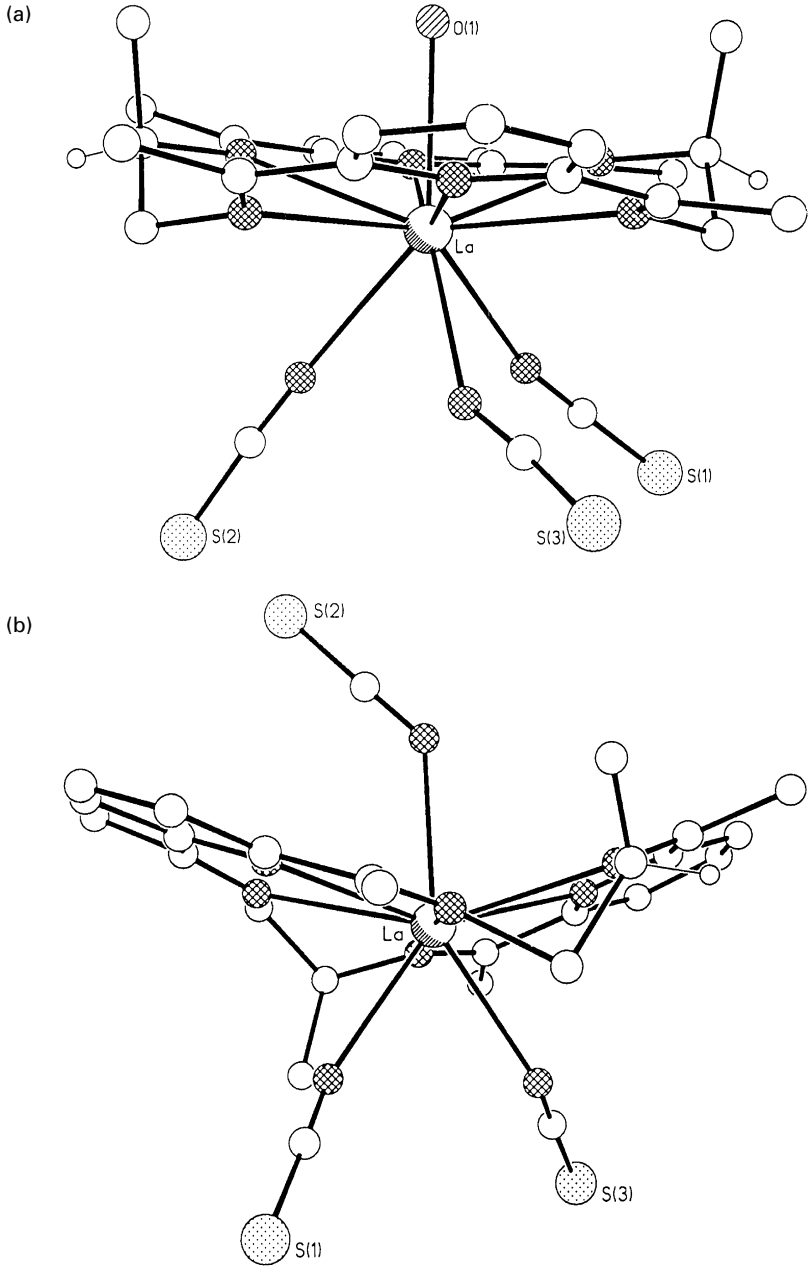

Fig. 3. Side view of the two isomeric complexes: (a) [La{(R,S)-5,15-($C_{24}H_{30}N_6$)}$(NCS)_3(H_2O)$] and (b) [La{(S,S)-5,15-($C_{24}H_{30}N_6$)}$(NCS)_3$].

In the (R,S)-5,15 isomer, the non-bonded interatomic distances C(13)···O(1)*w* 3.725(8) Å and C(24)····O(1)*w* 3.641(8) Å between the coordinated water molecule and the $-CH_3$ substituents show a rather symmetric arrangement promoted by the particular conformation of the ligand. The La-N(pyridine) bond distances are greater than in the (S,S)-5,15 isomer: 2.787(4) vs. 2.72(1) Å and 2.819(6) vs. 2.75(1); also the La-N(imine) bond distances cover a broader range, 2.730(5)–2.851(5), v.s. 2.67(1)–2.74(1) Å in the (S,S)-5,15 isomer. The La-(NCS) bond distances, which vary from 2.557(6) to 2.645(7) Å, are again greater than those observed for the (S,S)-5,15 isomer (2.55(2) to 2.58(2) Å). The longer bond lengths for the coordinated N-ligands are consistent with the increase in coordination number from 9 in the (S,S)-5,15 isomer to 10 in the (R,S)-5,15 analog, and could also be indicative of a weaking of the La-ligand bonds.

NMR spectra. Representative proton and carbon-13 NMR spectra of the isomeric complexes are reported in Tabs. 1–2. A summary discussion of the proton spectra follows.

CH_3 side-chain. In each isomer the CH_3 groups attached the $=N–CH_2–CH(CH_3)–N=$ side chains gave rise to a single signal in the 1.1–1.3 ppm region (doublet, $J = 6.6$–6.9 Hz, coupling to vicinal CH group). The signals of the isomers were well separated, and their integrated intensities were used to determine the isomer ratios of mixtures.

CH_3 acetate. In the triacetates and acetate chlorides, the acetate CH_3 gave a single sharp signal at 1.6–1.7 ppm, showing the coordinated and ionic acetates present in the triacetates to be in fast equilibrium on the NMR time-scale. The integrated intensity of the acetate signal, relative to the signals of the macrocycle, was in agreement with the stoichiometry of the sample as determined by microanalysis.

CH_3 macrocycle. The signals of the CH_3 groups originally belonging to the diacetylpyridine precursor occurred in the 2.4–2.7 ppm region. The spectra of the (R,R)/(S,S)-5,14 enantiomer pair showed either a single signal or two closely spaced, equal intensity signals, with that at lower-field split by long range coupling ($J = 1.2$–1.5 Hz) to the lower-field proton (H_B) of the neighboring CH_2 group. The (R,R)/(S,S)-5-15 enantiomers showed two well separated, equal intensity signals, and the (R,S)-5,15 isomer had two closely spaced equal intensity signals, with that at higher field slightly broadened and sometimes split into a doublet ($J = ca.$ 1 Hz) by long-range coupling to H_B of the CH_2 group.

CH. In the spectra of the (R,S)-5,15 isomer and of the (R,R)/(S,S)-5,14 enantiomer pair, the proton of the CH group appeared as a multiplet centered at about 4.5 ppm. For the (R,S)-5,15 isomer, the multiplet pattern was well defined and consistent with coupling to the vicinal CH_3 'side-chain' ($J = 6.8$ Hz) and to the two non-equivalent protons of the vicinal CH_2 group ($J = 3.8$ Hz to H_B and 2.1 Hz to H_A). In the (R,R)/(S,S)-5,15 enantiomers, the CH proton appeared as a doublet ($J = 6.9$ Hz, coupling to CH_3 side-chain).

CH_2. In the spectra of the (R,S)-5,15 isomer and of the (R,R)/(S,S)-5,14 enantiomers, the non equivalent protons of the CH_2 group gave rise to an AB spin pattern in the 3.9–4.2 ppm region, with geminal coupling $J = 12$–14 Hz. For the (R,S)-5,15 triacetate, each component of the lower-field B subspectrum was further split by coupling to the vicinal CH ($J = 3.8$ Hz), whereas each component of the A subspectrum was severely broadened with ill-defined splitting. The spectra of the (R,R)/(S,S)-5,15 diacetate chlorides showed instead a single sharp signal at 4.04 ppm.

Pyridine. The protons of the pyridine moieties gave signals in the 8.0–8.5 ppm region. For the (R,R)/(S-S)-5,14 enantiomers, in which the two pyridine moieties are identical and non-symmetrical, the diacetate chloride produced a single A_2B spin pattern, whereas the triacetate gave two well separated doublets for the two β-H and a partly overlapping doublet of doublets for the γ-H. In contrast, both the (R,R)/(S-S)-5,15 enantiomers and the (R,S)-5,15 isomer, in which the pyridine moieties are symmetrical and different from one another, produced two equal intensity A_2B patterns. The pyridine sections of the spectra, which were well resolved for the acetates and acetate chlorides in chloroform solutions, correlated univocally with the isomer structure established by X-ray crystallography.

CONCLUSIONS

The results of this work, taken in conjunction with the previously reported structure of the (S,S)-5,15 $[LaL(NCS)_3]$ complex [8], answer some of the questions raised in the introduction. First, when La(III) acetate was used as template in the synthesis of dimethyl-substituted macrocycles, constitutional isomers were indeed formed and could be distinguished on the basis of their different ^{1}H NMR spectra. The (R,R)/(S,S) enantiomers of the same constitutional isomer, however, had identical NMR spectra. Second, the temperature at which the synthesis was carried out provided a remarkable degree of isomer selectivity: at room temperature, products obtained from the (R)- or (S)-diamine were greatly enriched in the respective 5,14 isomers, whereas products obtained from the (R,S)-diamine consisted primarily of the (R,S)-5,15 *meso* isomer. A rather surprising aspect of this selectivity is the virtually complete absence of a (R,S)-5,14 isomer in products obtained from the (R,S)-diamine at any temperature. It can be noted that in each of the more abundant isomers the side-chain $-CH_3$ groups are in the same hemisphere relative to the macrocycle, but no rationalization for this preference can be suggested at this time. Third, constitutional isomers with somewhat different solubilities could be separated, although in minimal yields, by NMR-monitored fractional crystallization. The molecular structures of two single-isomers, the 9-coordinate $[La(NCS)_3\{$(S,S)-5,15-dimethyl-macrocycle$\}]$ [8] and the 10-coordinate $[La(NCS)_3(H_2O)\{$(R,S-5,15-dimethyl-macrocycle$\}]$ (this work), were established by X-ray crystallography and the La-macrocycle moieties were found to have different conformations in the two complexes. In the (R,S)-5,15 isomer, with the $–CH_3$ substituents in the same hemisphere, the La-macrocycle is nearly flat, whereas in the (S,S)-5,15 isomer, with the two $–CH_3$ substituents in opposite hemispheres, the La-macrocycle is puckered and appreciably folded at the flexible $–CH–CH_2–$ side chains. These conformational changes also account for the different coordination numbers of the two isomers. Finally, this work has shown that there is an unambiguous correlation between isomer structure and certain features of the proton NMR spectra; this correlation may prove very useful in the identification of similar disubstituted macrocyclic systems for which crystallographic evidence can not be obtained.

REFERENCES

1. Leif, R. C. and Vallarino, L. M., ACS Symposium

Series 464, in *Cell Separation Science and Technology*, (Eds D. S. Kompala and P. W. Todd), 41. American Chemical Society (1991).
2. Leif, R. C., Harlow, P. M., Vallarino, L. M., in *Proc. of Advances in Fluorescence-Sensing Technology*, J. R. Lakovicz and R.B. Thompson (Eds.), Vol. 1885, 376, A. Katzir Progress in Biomedical Optics, SPIE Proc. Series (1993).
3. Vallarino, L. M. and Leif, R. C., 1994, US Patent 5 373 093.
4. Leif, R. C., Vallarino, L. M., Harlow, P. M., in Progress in Biomedical Optics, *SPIE Proc. Series*, R. F. Bonner, G. E., Cohn, T. M. Laue, and A. V. Priezzhex (Eds.), Vol. 2136, 255 (1993).
5. Vallarino, L. M., *J. Alloys and Compounds*, 1997, **249,** 69.
6. Smith, P. H., Brainard, J. R., Morris, D. R., Jarvinen, G. D. and Ryan, R. R., *J. Am. Chem. Soc*., 1989, **111,** 7437.
7. Gootee, W. A., *Doctoral Dissertation*, Virginia Commonwealth University, Richmond, VA, 1989.
8. Benetollo, F., Bombieri, G., Samaria, K. M. and Vallarino, L. M., *J. Chem. Crystall*., 1996, **26,** 9.
9. Belletti, D., "*FEBO*". *A New Hardware and Software System for Controlling a Philips PW*1100 *Single Crystal Diffractometer*. Internal Report 1/93. Centro di Studio per la Strutturistica Diffrattometrica del CNR, Parma.
10. North, A. C. T., Philips, D. C. and Mathews, F. S., *Acta Cryst*., 1968, **87,** 902.
11. Sheldrick, G. M., in SHELX-86 *Crystallographic Computing* 3, G. M. Sheldrick, C. Kruger and R. Goddard (Eds.), Oxford University Press, England (1985).
12. a) Sheldrick, G. M., *Acta Crystallogr*., *Sect. A*, 1990, **46**, 467; b) Sheldrick, G. M., Dauter, Z., Wilson, K. S., Hope, H. and Sieker, L. C., *Acta Crystallogr. Sect. D*, 1993, **49**, 18.
13. Nardelli, M., *Computing Chem*., 1983, **7,** 95.
14. Johnson, C. K., "*ORTEP II*" report ORNL-5138, Oak Ridge National Laboratory, Tennessee.
15. De Cola, L., Smailes, D. L. and Vallarino, L. M., *Inorg. Chem*., 1986, **25,** 1729.
16. Benetollo, F., Polo, A., Bombieri, G., Fonda, K. K. and Vallarino, L., *M*., *Polyhedron*, 1990, **9,** 1411.
17. Fonda, K. K., Smailes, D. L., Vallarino, L. M., Bombieri, G., Benetollo, F., Polo, A. and De Cola, L., *Polyhedron*, 1993, **11,** 549.
18. Benetollo, F., Polo, A., Bombieri, G., Fonda, K. K. and Vallarino, L. M., *Polyhedron*, 1991, **10,** 1385.
19. Benetollo, F., Bombieri, G., Fonda, K. K. and Vallarino, L. M., *Polyhedron*, 1997, **16,** 1907.
20. Nakamoto, K., "*Infrared and Raman Spectra of Inorganic and Coordination Compounds*", John Wiley, New York, 1986, 231.
21. Benetollo, F., Polo, A., De Cola, L., Hawkins, W. T., Bombieri, G. and Vallarino, L. M., *Polyhedron*, 1989, **8,** 2157.
22. Benetollo, F., Bombieri, G. and Vallarino, L. M., *Acta Cryst*., 1996, **C52,** 1190.

Pergamon

PII: S0277–5387(98)00160–0

Polyhedron Vol. 17, No. 20, pp. 3643–3648, 1998
© 1998 Elsevier Science Ltd
All rights reserved. Printed in Great Britain
0277–5387/98 $19.00+0.00

Hydrolysis of spirophosphoranes with a saturated 1,3,2-dioxaphosphorinane ring: X-ray Structure of the intermolecularly H-bonded phosphate ester ($OCH_2CMe_2CH_2O$) P(O) (2,2′-O–C_6H_4–C_6H_4OH)

K. C. Kumara Swamy,[a]* Musa A. Said,[a] Sudha Kumaraswamy,[a]
R. Herbst-Irmer[b] and Melanie Pülm[b]

[a]School of Chemistry, University of Hyderabad, Hyderabad-500046, India

[b]Institut für Anorganische Chemie der Universität Göttingen, Tammannstr. 4, D-37077 Göttingen, Germany

(Received 8 January 1998; accepted 7 April 1998)

Abstract—Hydrolysis of (6,5), (6,7) and (6,8)-spirophosphoranes containing the six-membered ring P($OCH_2CMe_2CH_2O$) has been studied; in all the cases the six-membered phosphorinane ring is retained during the first stage of hydrolysis. The X-ray structure of one such product, ($OCH_2CMe_2CH_2O$) P(O)(2,2′–O–C_6H_4–C_6H_4OH) which exhibits intermolecular H-bonding, has been determined. © 1998 Elsevier Science Ltd. All rights reserved. © 1998 Elsevier Science Ltd. All rights reserved

Keywords: spirophosphorane; phosphorinane; hydrolysis; hydrogen bonding; X-ray structure.

While investigating the acid hydrolysis of the cyclic (5,6)-spirophosphorane **I**, McGall and McClelland have noted the formation of several products (**II**–**IV**) [1]. The cyclic ester **IV** with the five membered ring

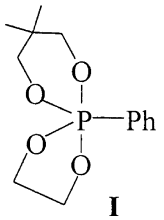

I

was observed under mild acidic conditions whereas the phosphorinane **V** was not detectable at all. In a somewhat contrasting way, Gallucci and Holmes isolated the phosphorinane **1** in an attempted synthesis of the cyclic (5,6)-spirophosphorane **VI** [2, 3].

In our efforts to obtain penta- and hexa-coordinated cyclic phosphoranes with six and higher membered rings, in addition to the expected products, we encountered hydrolysis products—the phosphate esters on several occasions [4–6]. In particular, during the synthesis of hexacoordinated spirophosphoranes with an oxinate substituent, quite often we ended up

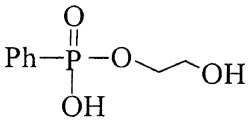

II

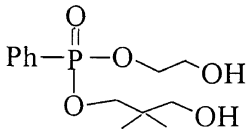

III

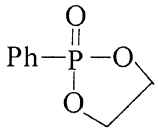

IV

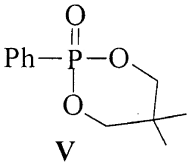

V

*Author to whom correspondence should be addressed: E-mail: kckssc@uohyd.ernet.in.

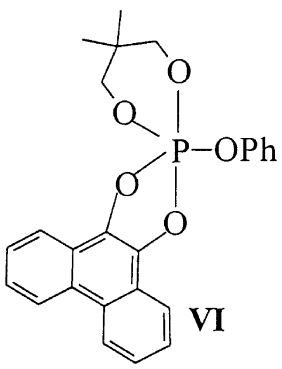

VI

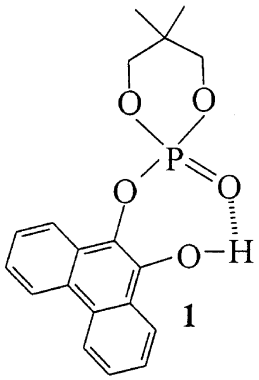

1

isolating the hydrolyzed products. We believe that a knowledge of these reactions is useful in ascertaining the hydrolytic stability of phosphoranes of different ring sizes; besides, the residual -OH functionalities in these phosphates can be connected to other reactive substrates. In this paper we report the directed synthesis of **1**–**5**; the X-ray structure of **3** featuring intermolecular H-bonding is also described.

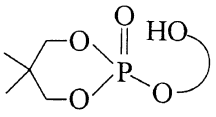

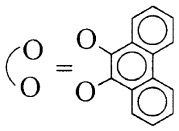

(**1**), 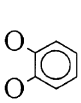

(**2**), 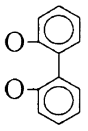

(**3**),

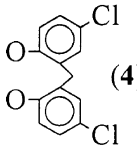

(**4**), 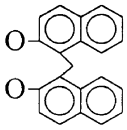

(**5**)

EXPERIMENTAL

Chemicals were procured from Aldrich or from local manufacturers; they were purified when required. Solvents were purified according to standard procedures [7]. NMR spectra were recorded on a Bruker 200 MHz spectrometer. Chemical shifts ($CDCl_3$, ppm) are measured against tetramethylsilane (^1H, ^{13}C) or ext. 85% H_3PO_4. IR spectra were recorded on a Perkin-Elmer 1310 spectrophotometer. Elemental analysis was performed on a Perkin-Elmer 240C CHN analyzer.

The compound $(OCH_2CMe_2CH_2O)(PhO)P(9,10–O_2C_{14}H_8)$ (**VI**) was prepared according to the procedure of Ramirez *et al.*[3]; synthesis/ identification of compounds $(OCH_2CMe_2CH_2O)P(9,10–O_2C_{14}H_8)(OC_9H_6N)$ (**6**), $(OCH_2CMe_2CH_2O)P(1,2–O_2C_6H_4)(OC_9H_6N)$ (**7**), $(OCH_2CMe_2CH_2O)P(2,2'–OC_6H_4–C_6H_4O)(OC_9H_6N)$ (**8**), $(OCH_2CMe_2CH_2O)P[(OC_6H_3–4–Cl)_2CH_2]$ (OC_9H_6N) (**9**), $(OCH_2CMe_2CH_2O)P(2,2'–OC_{10}H_6–C_{10}H_6O)(OC_9H_6N)$ (**10**) has been described in detail elsewhere [5].

(*a*) *Preparation of the phosphate esters* $(OCH_2CMe_2CH_2O)P(O)(9,10–OC_{14}H_8OH)$ (**1**) *and* $[(HOCH_2CMe_2CH_2O)P(O)(9,10–OC_{14}H_8OH)(O)]^-[HOC_9H_6NH]^+ 1/2H_2O$ (**11**)

Compound **VI** (1.00 g, 2.3 mmol) was dissolved in a mixture of chloroform (1 cm^3) and ether (3 cm^3) and kept in open air till all the solvent evaporated. The residue was crystallized from dichloromethane-*n*-heptane to obtain **1**. Yield: 0.55 g (67%). M.p. 162°C [lit. m.p. 162–164°C] [2]. IR: 3185 cm^{-1} (ν(OH)). ^1H NMR: δ 1.00 (*s*, 3H, CH_3), 1.35 (*s*, 3H, CH_3), 4.05 (*dd*, $J \approx 14$, 25 Hz, OCH_2(A)), 4.50 (*d*, $J \approx 140$ Hz, 2H, OCH_2(X)), 7.50–8.70 (*m*, 8H, *H*(Ar)), 9–50 (*br*, 1H, O*H*). ^{31}P NMR: −10.2.

The same compound (**1**) was observed [^1H, ^{31}P] when **6** (1.0 g) was dissolved in chloroform (5 cm^3) and kept aside for 2 days in open air. Although the product was pure by ^{31}P NMR, it could not be obtained free of 8-hydroxy quinoline. Upon washing this product with hot water, the doubly hydrolyzed product **11** (which could be recrystallized from CH_2Cl_2-*n*-heptane (1:1)) was obtained. Yield of **11**: 0.4 g. M.p. 162°C. ^1H NMR: δ 0.74 (*s*, 6H, CH_3), 3.23 (*s*, 2H, $HOCH_2$), 3.80 (*d*, $^3J = 20.0$ Hz, 2H, P–O–CH_2), 4.45 (*br*, variable, OH_2?)). 7.30–8.80 (*m*, 14H, *H*(Ar)). ^{31}P NMR: −0.6. Anal. calcd. for $C_{28}H_{28}NO_7P$. $1/2H_2O$: C, 63.39; H, 5.47; N, 2.64. Found: C, 63.47; H, 5.45; N, 2.85.

(*b*) *Preparation of the phosphate ester* $(OCH_2CMe_2CH_2O)P(OC_6H_4OH)$ (**2**)

(i) To a mixture of the cyclic phosphite $(OCH_2CMe_2CH_2O)P(OC_9H_6N)$ (**12**) [5] (1.33 g, 4.79 mmol), and catechol (0.53 g, 4.79 mmol) in dry ether (40 cm^3) maintained at −60°C was added $ClN(i\text{-}Pr)_2$ (0.65 g, 4.79 mmol), in ether (30 cm^3) over a period of 15 min with continuous stirring. The mixture was gradually brought to 30°C, stirred overnight and filtered. The precipitate was given a quick water wash (2×5 cm^3) and dried *in vacuo*. The product was crystallized from dichloromethane-*n*-heptane (2:1) to afford **2**. Yield 0.7 g (57%). M.p. 142°C. IR (KBr): 3202 cm^{-1}(ν(OH)). ^1H NMR: δ 0.96 (*s*, 3H, CH_3), 1.35 (*s*, 3H, CH_3), 4.04 (*dd*, 2H, OCH_2(A)), 4.36 (*d*, 2H, OCH_2(X)), 6.80–7.20 (*m*, 4H, *H*(Ar)), 7.79 (*s*, 1H, O*H*). ^{13}C NMR: 20.16, 21.69 (2 CH_3), 32.28 (*d*, ^3J(P–C) = 6.2 Hz), 78.84 (*d*, ^2J(P–C) = 6.8 Hz), 119.35, 120.65, 120.88 (^3J(P–C) = 3.9 Hz), 126.61, 138.16 (^2J(P–C) = 8.5 Hz), 147.59. ^{31}P NMR: −11.93. Anal. calcd. for $C_{11}H_{15}O_5P$: C, 51.17; H, 5.86. Found: C, 51.74; H, 6.17.

(ii) When the reaction of $(1,2\text{-}C_6H_4O_2)P(OC_9H_6N)$ [5] (1.17 g, 4.12 mmol) with 2,2-dimethyl-1,3-propanediol (0.43 g, 4.12 mmol) and $ClN(i\text{-}Pr)_2$ (0.52 g,

4.12 mmol) was conducted, the same product **2** [^{1}H, ^{31}P] was observed.

(iii) Reaction of 5.34 mmol each of ($OCH_2CMe_2CH_2O$)P(O)Cl, catechol and triethylamine in toluene at room temperature, and washing the obtained solid with water, afforded **2** (0.88 g, 64%) which was recrystallized from CH_2Cl_2-toluene [m.p.; ^{1}H NMR].

(*c*) *Preparation of the phosphate ester* ($OCH_2CMe_2CH_2O$)P(2,2′–OC_6H_4–C_6H_4OH) (**3**)

Following the same procedure as in *b*(*i*), the precipitate obtained by treating **12** (2.33 g, 8.42 mmol), 2,2′-biphenol (1.57 g, 8.42 mmol) and ClN(*i*-pr)$_2$ (1.14 g, 8.42 mmol) was washed quickly with water and dried *in vacuo*. The residue was crystallized from CH_2Cl_2-n-heptane (3:1). Yield 1.1 g (39%), M.p. 182°C. IR: 3292 cm^{-1}(*v*(OH)). ^{1}H NMR: δ 0.40 (*s*, 3H, C*H*$_3$), 1.10 (*s*, 3H, C*H*$_3$), 3.35–3.62 (*m*, 4H, OC*H*$_2$), 5.4 (*br*, 1H, O*H*), 6.81–7.65 (*m*, 8H, *H*(Ar)). ^{31}P NMR: −15.1. Anal. calcd. for $C_{17}H_{19}O_5P$: C, 61.08; H, 5.69. Found: C, 61.00; H, 5.55.

(*d*) *Preparation of the phosphate ester* ($OCH_2CMe_2CH_2O$) P(OC_6H_3(Cl)–CH_2–OC_6H_3(Cl)–OH) (**4**)

(i) Following the same procedure as in **b**(i), the precipitate obtained using 3.73 mmol each of **12**, 2,2′-methylene-bis-(4-chlorophenol) and ClN(*i*-pr)$_2$ was dissolved in dichloromethane and left in open air to obtain **4**. Yield: 0.3 g (19%). M.p. 175°C. IR: 3350, 3295 cm^{-1} (*v*(OH)). ^{1}H NMR (DMSO + $CDCl_3$): δ 0.52 (*s*, 3H, C*H*$_3$), 1.03 (*s*, 3H, C*H*$_3$), 3.50–3.80 (*m*, 4H, OC*H*$_2$), 4.35 (*s*, 2H, C*H*$_2$Ar), 6.56–7.28 (*m*, 6H, *H*(Ar)). ^{31}P NMR: −14.4. Anal. calcd. for $C_{18}H_{19}Cl_2O_5P$:C, 51.81; H, 4.56. Found: C, 51.80; H,4.81.

(ii) When compound **8** (0.5 g, 1.28 mmol) was dissolved in acetone (3 cm^3) and left in open air a solid was obtained which was washed with ether to remove 8-hydroxyquinoline. The residue was pure **3** [M.p. IR]. Yield: 0.2 g (47%).

(*e*) *Preparation of the phosphate ester* ($OCH_2CMe_2CH_2O$) P(O){$OC_{10}H_6$–CH_2–$C_{10}H_6$OH} (**5**)

The procedure was essentially the same as in **b**(i) using toluene as the solvent and 2.95 mmol each of **12** and bis-(2-hydroxy-1-naphthyl) methane. The reaction mixture showed peaks at −124.5, −69.8 −14.7 and −14.2 ppm in the ^{31}P NMR spectrum. The product was recrystallized from toluene to afford pure **5**. Yield: 0.31 g, 23%. M.p. 128–134°C. IR: 3287 cm^{-1}(*v*(OH)). ^{1}H NMR: δ 0.73, 1.26 (2s, 6H, C*H*$_3$), 2.38, 3.80–4.20 (*m*, 4H, OC*H*$_2$), 4.94 (*s*, 2H, Ar-C*H*$_2$-Ar), 6.95 (*s*, 1H, O*H*), 7.0–8.2 (*m*, 12H, *H*(Ar)). An unassigned peak at 2.38 ppm was also observed. ^{13}C NMR: 20.05, 21.64 (2s, *C*H$_3$), 23.58 (*C*H$_2$), 32.09 (*C*H$_2$, ^3J (P–C) = 5.5 Hz), 78.42 (O*C*H$_2$, ^2J (P–C) = 5.5 Hz), 117.73–152.20 (many lines, *C* (Ar)). ^{31}P NMR: −14.0 ppm. Anal. calcd. for $C_{26}H_{25}O_5P$: C, 69.99; H, 5.88. Found: C, 69.64; H, 5.62.

(*f*) *Reaction of* **12** *with pinacol*/ClN(*i*-Pr)$_2$

Using the same procedure as in *b*(*i*), the residue upon evaporating the filtrate (^{31}P NMR: -57.45, −55.46, −42.50, −13.76, −5.58, 11.85; the intensities of the peaks varied with time as well as the batch) and keeping in air over a prolonged period of time ($\approx$10 days) exhibited ^{1}H NMR signals at 1.00 (CH_2-C*Me*$_2$), and 4.00 (d, ^3J = 12 Hz, OC*H*$_2$P) ppm in addition to the signals for 8-hydroxyquinoline and pinacol. Peaks corresponding to ≡P($OCH_2CMe_2CH_2OH$) were not observed and ^{31}P NMR showed peaks at −5.6 (90%) and 11.85 (10%) ppm.

X-ray Structure Determination of **3**

Data were collected at −120°C on a Stoe-Siemens-AED-diffractometer with monochromated MoKα radiation (λ = 0.71073 Å). Data were collected from a oil-coated rapidly cooled crystal [8] with a profile-fitted method [9]. The structure was solved by direct methods [10]. All non-hydrogen atoms were refined anisotropically [11]. For the hydrogen atoms bonded to carbon the riding model was used. The hydrogen atom bonded to oxygen was localized in a difference electron density map and refined freely. An extinction correction was applied. The structure was refined against F^2 with a weighting scheme of $w^{-1} = \sigma^2(F_o^2) + (0.0323P)^2 + 0.8659P$ with $P = (F_o^2 + 2F_c^2)/3$. The R values are defined as $R1 = S\|F_o| - |F_c\|/\Sigma|F_o|$ and $wR2 = [\Sigma w(F_o^2 - F_c^2)^2/\Sigma wF_o^4]^{0.5}$. Crystal data for **3**: $C_{17}H_{19}O_5P$, M_r = 334.29, monoclinic, space group Cc, a = 15.372(1), b = 9.725(1), c = 10.678(1) Å, β = 97.23(1)°, V = 1583.6(2) Å^3, Z = 4, ρ(calcd) = 1.402 Mg/m^3, μ = 0.197 mm^{-1}, F(000) = 704, crystal size (mm) 0.3 × 0.3 × 0.4, 2810 reflections in the range of $8° < 2\theta < 50°$ collected, 2805 unique reflections (R_{int} = 0.003), 2803 reflections and 2 restraints used for the refinement of 215 parameter, S = 1.028, R1 = 0.028 for $I > 2\sigma(I)$, wR2 = 0.068 for all data, absolute structure parameter −0.01(8) [12], extinction coeffient 0.0039(5), maximum/minimum residual density 0.172/–0.183 eÅ^{-3}.

Further details on the crystal structure analysis are available on request from the Director of the Cambridge Crystallographic Data Centre, 12 Union Road, Cambridge CB2 1EZ, U. K. by quoting the full journal citation.

RESULTS AND DISCUSSION

Synthesis and Spectroscopy

Compound **1** (δ_p −10.02) is readily isolated in a pure state by the hydrolysis of Ramirez's compound

Scheme 1

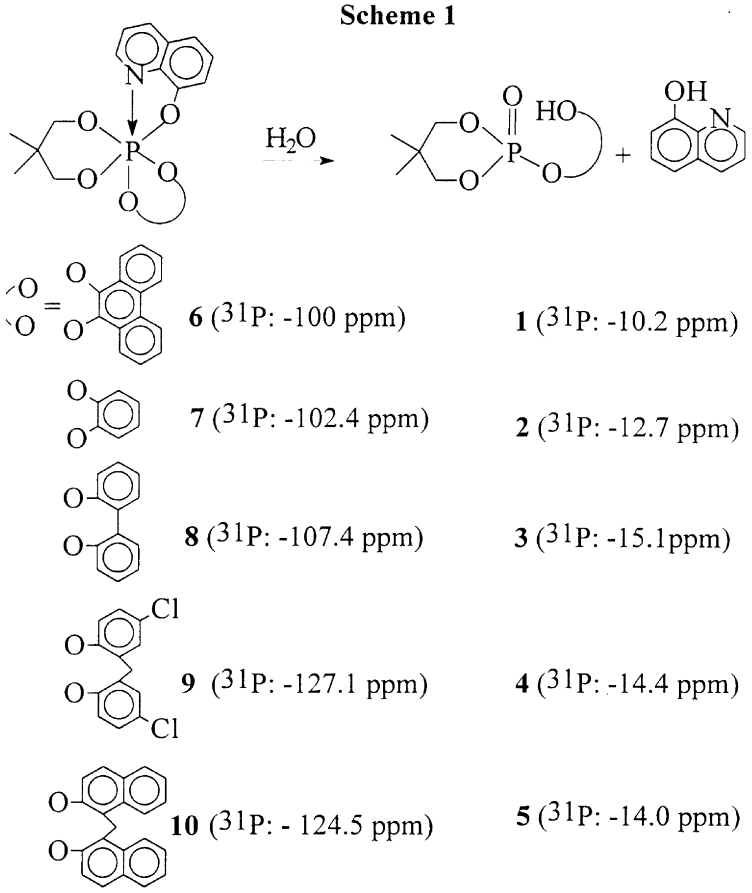

VI [3] in open air. It is also the only phosphorus product observed in the hydrolysis of our hexacoordinated phosphorane **7** (see Scheme 1 for structure) [5]; however compound **1** could not be obtained free of the 8-hydroxy quinoline this way. The synthetic route leading to **1**–**5** *via* the oxinate compounds is illustrated in Scheme 1; the hexacoordinated compounds themselves have been prepared by the oxidative addition of a quinone or diol/N-chlorodiisopropylamine to a cyclic phosphite as described earlier [5]. The intermediates **6** and **8** have been structurally characterized by us previously [5]; others (**7**, **9** & **10**) have been identified by ^{31}P NMR spectroscopy.

That compounds **1** and **3** result from the hydrolysis of the hexacoordinated phosphoranes is shown by isolation followed by hydrolysis of **6** (or **VI**) and **8**. Compound **2** has also been independently synthesized by treating $(OCH_2CMe_2CH_2O)P(O)Cl$ with equimolar quantities of catechol and triethylamine.

The δ(P) values for **1**–**5** are in the range expected for tetracoordinated phosphate esters; in the ^{1}H NMR the OCH_2 protons show an AX (**1** and **2**) or AB (**3**–**5**) pattern with coupling to phosphorus [^{3}J(P–O–C–H)] and two separate signals for the CH_3 protons of the neopentyl glycolate residue, thus clearly showing that the six-membered phosphorinane ring is retained in these compounds. The similarity in the spectra of **1** and **2** suggests that **2** also has intramolecular H-bonding (structure **VII**) analogous to that observed by Gallucci and Holmes for **1** [2]; on a similar note it may be expected that compounds **3** and **5** exhibit intermolecular H-bonding similar to that in **4** (see below) [13].

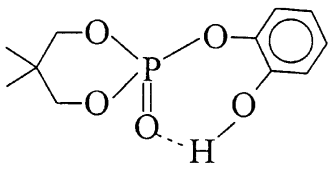

VII

In the hydrolysis of **6**, when the initial product mixture was washed with hot water to remove 8-hydroxy quinoline, further hydrolysis leading to the cleavage of the six-membered ring occurred to give a crystalline product (Scheme 2). On the basis of ^{1}H and ^{31}P NMR as well as elemental analysis, structure **11** is assigned to this compound. It can be noted that in

Scheme 2

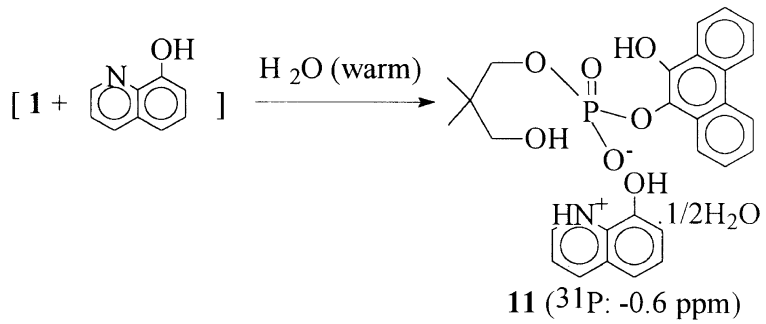

11 (^{31}P: -0.6 ppm)

this compound both the five and six-membered rings are cleaved (*cf* structure **III**). We have also tried to analyze the hydrolysis products from the reaction of $(OCH_2CMe_2CH_2O)P(OC_9H_6N)$ (**12**) with an aliphatic diol like pinacol. Although there are several hydrolysis products in the reaction mixture as shown by ^{31}P NMR, there is at least one of these in which the six-membered ring is retained (see experimental). Thus this result is different from the acid hydrolysis of **I** studied by McGall and McClelland [1].

In summary, the first stage of the hydrolysis of spirophosphoranes containing a 1,3,2-dioxaphosphorinane ring occurs by retaining this six-membered ring. Such a feature contrasts with the acid hydrolysis of the (5,6)-spirophosphorane **I** in which a product with the phosphorinane ring intact was not observed.

X-ray Structure of **3**

Compound **3** crystallizes in the space group *Cc*. The molecular structure of **3** along with atom labeling scheme is depicted in Fig. 1. The phosphorus atom is coordinated tetrahedrally with the O=P–O angles larger and the O–P–O angles smaller than the ideal tetrahedral angle as expected. All bond lengths are in typical ranges. The 1,3,2-dioxaphosphorinane ring adopts a chair conformation, which is quite typical for six membered rings perpendicular to oxo groups [2]. The most important feature in the structure is perhaps the presence of *intermolecular* hydrogen bonding involving the OH group of the 2,2′-biphenoxy group [O(5)–H(5O), 0.86(4) Å; O(5) . . . O(1A), 2.702(2) Å; H(5O) . . . O(1A), 1.85(4) Å; O(5)–

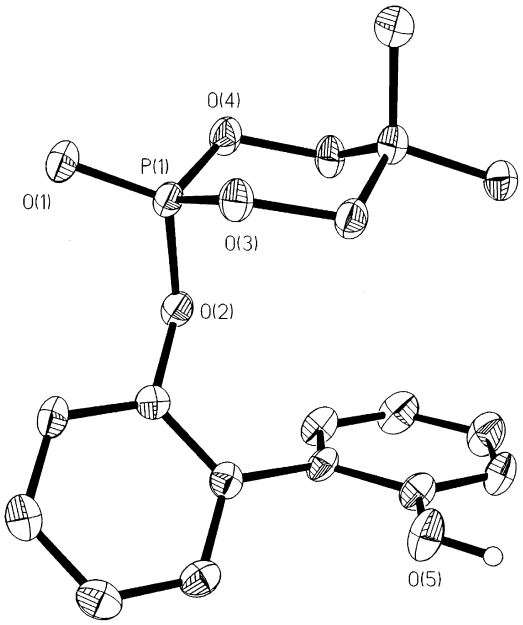

Fig. 1. Crystal structure of **3**, selected bond lengths [Å] and angles [°]: P(1)–O(1) 1.459(2), P(1)–O(3) 1.556(2), P(1)–O(4) 1.559(2), P(1)–O(2) 1.583(2), O(1)–P(1)–O(3) 111.97(9), O(1)–P(1)–O(4) 113.45(9), O(3)–P(1)–O(4) 107.15(8), O(1)–P(1)–O(2) 115.18(8), O(3)–P(1)–O(2) 106.92(8), O(4)–P(1)–O(2) 101.32(8).

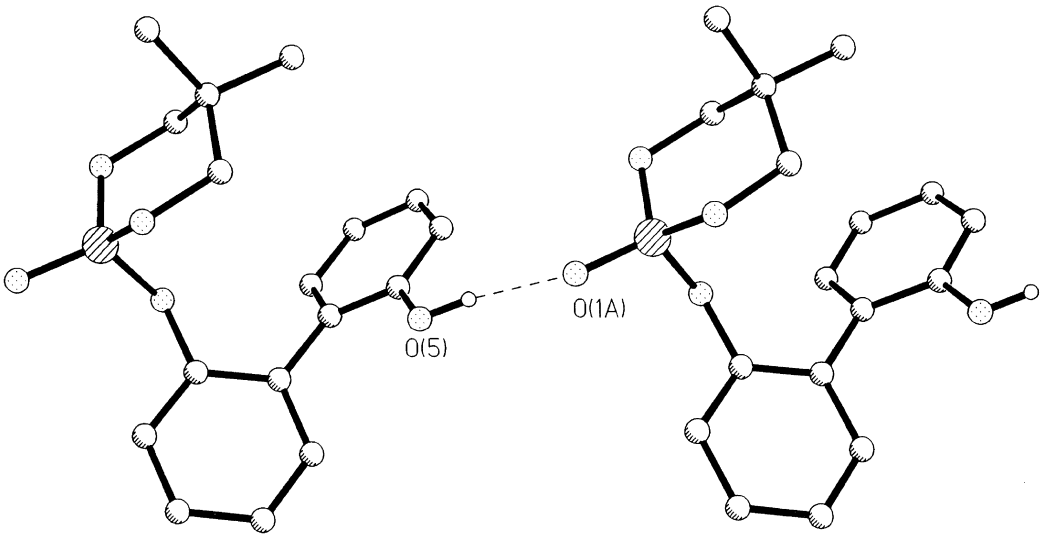

Fig. 2. Hydrogen bonding pattern in **3**: O(5)–H(5O), 0.86(4) Å; O(5) . . . O(1A), 2.702(2) Å; H(5O) . . . O(1A), 1.85(4) Å; O(5)–H(5O) . . . . O(1A), 169(3)°.

H(5O) . . . O(1A), 169(3)°] leading to chains in the crystal (Fig. 2). This pattern is different from the *intramolecular* hydrogen bonding observed in Holmes' compound **1** [2, 14]. Such a difference arises because in **3** the –OH group is too far from the P=O in the molecule.

Acknowledgements—Financial support by Council of Scientific and Industrial Research (New Delhi) is gratefully acknowledged. Thanks are also due to UGC, India (COSIST and Special Assistance Programme) as well as AvH Foundation (Germany) for instrumental facilities. We are thankful to Prof. Dr. G. M. Sheldrick for his interest in this work.

REFERENCES

1. McGall, G. H. and McClelland, R. A., *Can. J. Chem.*, 1991, **69,** 2064.
2. Gallucci, J. C. and Holmes, R. R., *Inorg. Chem.*, 1980, **19,** 3540.
3. Ramirez, F., Nagabhushanam, M. and Smith, C. P., *Tetrahedron*, 1968, **24,** 1785.
4. Said, M. A., Kumara Swamy, K. C., Chandra Mohan, K. and Venkata Lakshmi, N., *Tetrahedron*, 1994, **50,** 6989.
5. Said, M. A., Pülm, M., Herbst-Irmer, R. and Kumara Swamy, K. C., *J. Am. Chem. Soc.*, 1996, **118,** 9841.
6. Said, M. A., Pülm, M., Herbst-Irmer, R. and Kumara Swamy, K. C., *Inorg. Chem.*, 1997, **36,** 2044.
7. Perrin, D. D., Armarego, W. L. F. and Perrin, D. R., *Purification of Laboratory Chemicals*. Pergamon, Oxford, 1986.
8. Kottke, T. and Stalke, D., *J. Appl. Crystallogr.*, 1993, **26,** 615.
9. Clegg, W., *Acta Crystallogr.*, 1981, **A37,** 22.
10. Sheldrick, G. M., SHELXS-90, *Acta Crystallogr.*, 1990, **A46,** 467.
11. Sheldrick, G. M., *SHELXL*-93. University of Göttingen, 1993.
12. Flack, H. D., *Acta Crystallogr.*, 1983, **A39,** 876.
13. Since **1**–**5** are insoluble in nonpolar solvents (e.g. CCl_4) we could not investigate this point further by IR spectroscopy.
14. Malinovskii, S. T., Simonov, Yu. A., Kudrya, T. N., Chaikovskaya, A. A. and Malinovskii, T. I., *Zh. Strukt. Khim.*, 1984, **25,** 130; a phosphorus macrocycle with an intramolecular P=S· ·H—C interaction has been reported in this paper.

Pergamon

PII: S0277-5387(98)00162-4

Polyhedron Vol. 17, No. 20, pp. 3649–3656, 1998
© 1998 Elsevier Science Ltd
All rights reserved. Printed in Great Britain
0277–5387/98 $19.00+0.00

Solvent extraction of alkaline-earth ions by dicarboxylated calix[4]arenes

N. Barakat[a], M. Burgard[a]*, Z. Asfari[a], J. Vicens[a], G. Montavon[b] and G. Duplâtre[b]

[a]Laboratoire de Chimie Minérale et Analytique (U.M.R. 7512 du C.N.R.S.), Ecole Européenne de Chimie Polymères et Matériaux (E.C.P.M.), 1, rue Blaise Pascal, B.P. 296, 67008 Strasbourg Cedex, France

[b]Laboratoire de Chimie Nucléaire, Centre de Recherches Nucléaires, IN2P3/ C.N.R.S. B.P. 28, 67037 Strasbourg Cedex 2, France

(Received 10 December 1997; accepted 7 April 1998)

Abstract—The extraction of the alkaline-earth metal ions by 25,27-dicarboxymethyl-26,28-dimethoxy-5,11,17,23-tetra-*tert*-butylcalix[4]arene (L^IH_2) and 25,27-dicarboxymethyl-26,28-dimethoxyethoxy-5,11,17,23-tetra-*tert*-butylcalix[4]arene ($L^{II}H_2$) in 1,2-dichloroethane is shown to be pH dependent. The analysis of the extraction equilibrium results indicates that the extraction process takes place via the formation of $ML_2^IH_2$ ($M^{2+} = Ca^{2+}$, Sr^{2+} and Ba^{2+}), $ML_2^{II}H_2$ ($M^{2+} = Ca^{2+}$ and Sr^{2+}) and ML^{II} ($M^{2+} = Ba^{2+}$) complexes. Both ligands show a high selectivity for calcium. The existence of the ML_2H_2 complexes is supported by ^{1}H-NMR and FAB^+ experiments on the corresponding Ca^{2+} complexes. ^{1}H-NMR investigations show that the calcium ion is located outside the calixarene cavity. Competitive extraction of Mg, Ca, Sr and Ba suggests the formation of mixed complexes. © 1998 Elsevier Science Ltd. All rights reserved

Keywords: calix[4]arene-dicarboxylic; liquid–liquid extraction; alkaline-earth; complex; selectivity.

INTRODUCTION

In previous studies [1] on the extraction properties of the dicarboxycalix[4]arene derivatives (L^IH_2 and $L^{II}H_2$) (Fig. 1) we have shown that the extraction of the alkali ions occurs in a relatively acidic pH range with a high selectivity for sodium.

It was shown that mono and dinuclear complexes of formula MLH and M_2L can be formed. The location of an alkali ion in the calix[4]arene moiety was confirmed by ^{1}H-NMR spectrometry [2].

Rare earth extractions [3] were also investigated with a dicarboxymethyl–dimethoxycalix[4]arene (L^IH_2). It was shown in particular that the extraction takes place via the formation of mixed alkali-rare earth complexes.

In this paper we present some results on the extraction of alkaline-earth by dicarboxymethyl–dimethoxycalix[4]arene (L^IH_2) and the more rigid dicarboxymethyl–dimethoxyethoxycalix[4]arene ($L^{II}H_2$) in the cone conformation. Alkaline-earth dicarboxylic systems are of particular interest because of the equality of ion charge (+2) and the number of acidic protons in the extractant molecule.

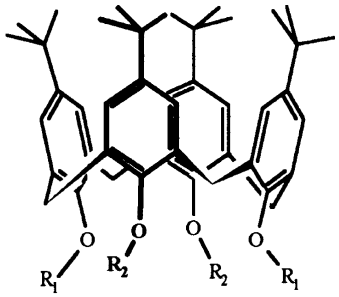

Fig. 1. The studied calixarenes in this work: (I) $R_1 = CH_3$, $R_2 = CH_2COOH$: 25,27-dicarboxymethyl-26,28-dimethoxy-5,11,17,23-tetra-*tert*-butylcalix[4]arene (L^IH_2). (II) $R_1 = CH_2CH_2OCH_3$, $R_2 = CH_2COOH$: 25,27-dicarboxymethyl-26,28-dimethoxyethoxy-5,11,17,23-tetra-*tert*-butylcalix[4]arene ($L^{II}H_2$).

*Author to whom correspondence should be addressed.

MATERIALS AND EXPERIMENTAL

Materials

The dicarboxylated compounds 25,27-dicarboxymethyl-26,28-dimethoxy-5,11,17,23-tetra-*tert*-butylcalix[4]arene ($L^{I}H_2$), and 25,27-dicarboxymethyl-26,28-dimethoxyethoxy-5,11,17,23-tetra-*tert*-butylcalix[4]arene ($L^{II}H_2$) were prepared according to the literature [4–6].

1,2-Dichloroethane (SDS) was washed by pre-equilibration with water in order to remove the stabilizer. The organic solutions were freshly prepared by dissolving a weighted amount of the ligand in the 1,2-dichloroethane. Commercially available $MgCl_2 \cdot 6H_2O$ (Prolabo), $CaCl_2 \cdot 6H_2O$, $SrCl_2 \cdot 6H_2O$ and $BaCl_2 \cdot 2H_2O$ (Merck) were used as received and stock solutions were prepared by dissolving the salts in deionized water.

Extraction procedure

Liquid–liquid extraction experiments were carried out by stirring equal volumes of aqueous and organic phases (90 mL) for 20 min. This time was found to be sufficient to reach equilibrium. The temperature was kept at $25.0 \pm 0.1^{\circ}C$ during the experiments. The pH was adjusted by adding small volumes of the cesium hydroxide (0.2 M). The cesium hydroxide was chosen, because this metal is not extracted by the ligands [7]. The metal organic concentrations were determined by sampling the organic phase (2 mL) which were then stripped with 0.1 M hydrochloric acid (10 mL). In this way quantitative transfers of the alkaline-earth ions from the organic to the acidic water phase were obtained. The aqueous phase was analyzed by using a Perkin-Elmer (2380) Atomic Absorption instrument with an air-acetylene flame or by Varian-Liberty 220 ICP/AES.

FAB^+ and ^1H-NMR experiments

FAB^+ spectra were obtained on a VG-Analytical ZAB HF apparatus. ^1H-NMR spectra were recorded on a Bruker SY200 spectrometer (200 MHz, $CDCl_3$).

Free ligand $L^{II}H_2$. 7.17 and 6.57 ppm (2s, 8H, Ar*H*); 4.75 ppm (s, 4H, OCH_2COOH); 4.42 ppm (d, 4H, $J_{H-H} = 13$ Hz, $ArCH_AH_BAr$); 3.97 ppm (m, 4H, $ArOCH_2CH_2OCH_3$); 3.75 ppm (m, 4H, $ArOCH_2CH_2OCH_3$); 3.46 ppm (s, 6H, OCH_3); 3.24 ppm (d, 4H, $J_{H-H} = 13$ Hz, $ArCH_AH_BAr$); 1.34 ppm (s, 18H, C_4H_9); 0.83 ppm (s, 18H, C_4H_9).

$CaL_2^{II}H_2$ complex. 7.17 ppm (s, 4H, Ar*H*); 7.13 and 7.11 ppm (2s, 8H, Ar*H*); 6.57 ppm (s, 4H, Ar*H*); 4.74 ppm (s, 4H, OCH_2COOH); 4.42 ppm (d, 4H, $J_{H-H} = 13$ Hz, $ArCH_{A1}H_{B1}Ar$); 4.36 ppm (d, 4H, $J_{H-H} = 13$ Hz, $ArCH_{A2}H_{B2}Ar$); 4.33 ppm (m, 4H, $ArOCH_2CH_2OCH_2$); 3.96 ppm (m, 8H, $ArOCH_2CH_2OCH_3$); 3.81 ppm (s, 6H, OCH_3); 3.75 ppm (m, 4H, $ArOCH_2CH_2OCH_3$); 3.45 ppm (s, 6H, OCH_3); 3.41 ppm (d, 4H, $J_{H-H} = 13$ Hz, $ArCH_{A2}H_{B2}Ar$); 3.24 ppm (d, 4H, $J_{H-H} = 13$ Hz, $ArCH_{A1}H_{B1}Ar$); 1.34 ppm (s, 18H, C_4H_9); 1.15 ppm (s, 18H, C_4H_9); 1.13 ppm (s, 18H, C_4H_9); 0.83 ppm (s, 18H, C_4H_9).

RESULTS AND DISCUSSION

Single metal extractions

The extraction of an alkaline-earth ion by a calixarene dicarboxylic derivative ($L^{I}H_2$ or $L^{II}H_2$) is analyzed by plotting experimentally $r_M = [M]_{org}/L_o$ as a function of pH for three different concentrations (L_o) of extractant (Fig. 2).

The aqueous metal ion concentration $[M^{2+}]_{aq}$ is considered as constant and equal to the initial metal concentration (0.16 M) within the experimental conditions.

The experimental results confirm that the extraction takes place via an ion exchange process. In some cases the r_M plots exhibit a plateau value $r_{M\,max}$ which is independent of L_o, suggesting that the $r_{M\,max}$ value corresponds to the metal ion/ligand stoichiometry of the extracted species. The plateau for $r_M = 0.5$ observed in the $Ca/L^{I}H_2$ and $Ba/L^{I}H_2$, systems suggests the formation of a 1:2 ion/ligand complex. The $Sr/L^{I}H_2$ system appears to be more complicated because of the occurrence of a solubility limit which induces a decrease of the plateau value with increase of the extractant concentration. It was observed that magnesium is not extracted. $L^{I}H_2$ extracts preferentially calcium according to the selectivity order:

$$Ca \gg Sr > Ba >>> Mg$$

The extraction of alkaline-earth by $L^{II}H_2$ is generally accompanied by the occurrence of a precipitation which hides the observation of a plateau. The experimental $r_M = f(pH)$ plots with $L^{II}H_2$ show that the extraction takes place at a higher pH range than for $L^{I}H_2$. Moreover, in contrast with $L^{I}H_2$ the $r_{Ba} = f(pH)$ plots suggest the existence of a complex 1:1 metal/ligand stoichiometry.

A quantitative analysis of the $r_M = f(pH)$ curves was made on the basis of the following assumptions:

—a single equilibrium is involved in the extraction process,
—a single metal ion is involved in the extracted species.

If a complex with 1:2 metal/ligand stoichiometry is formed, the corresponding equilibrium can be written:

$$M_{aq}^{2+} + 2/m(LH_2)_{m\,org} \rightleftharpoons ML_2H_{2org} + 2H_{aq}^{+}$$

(equilibrium 1)

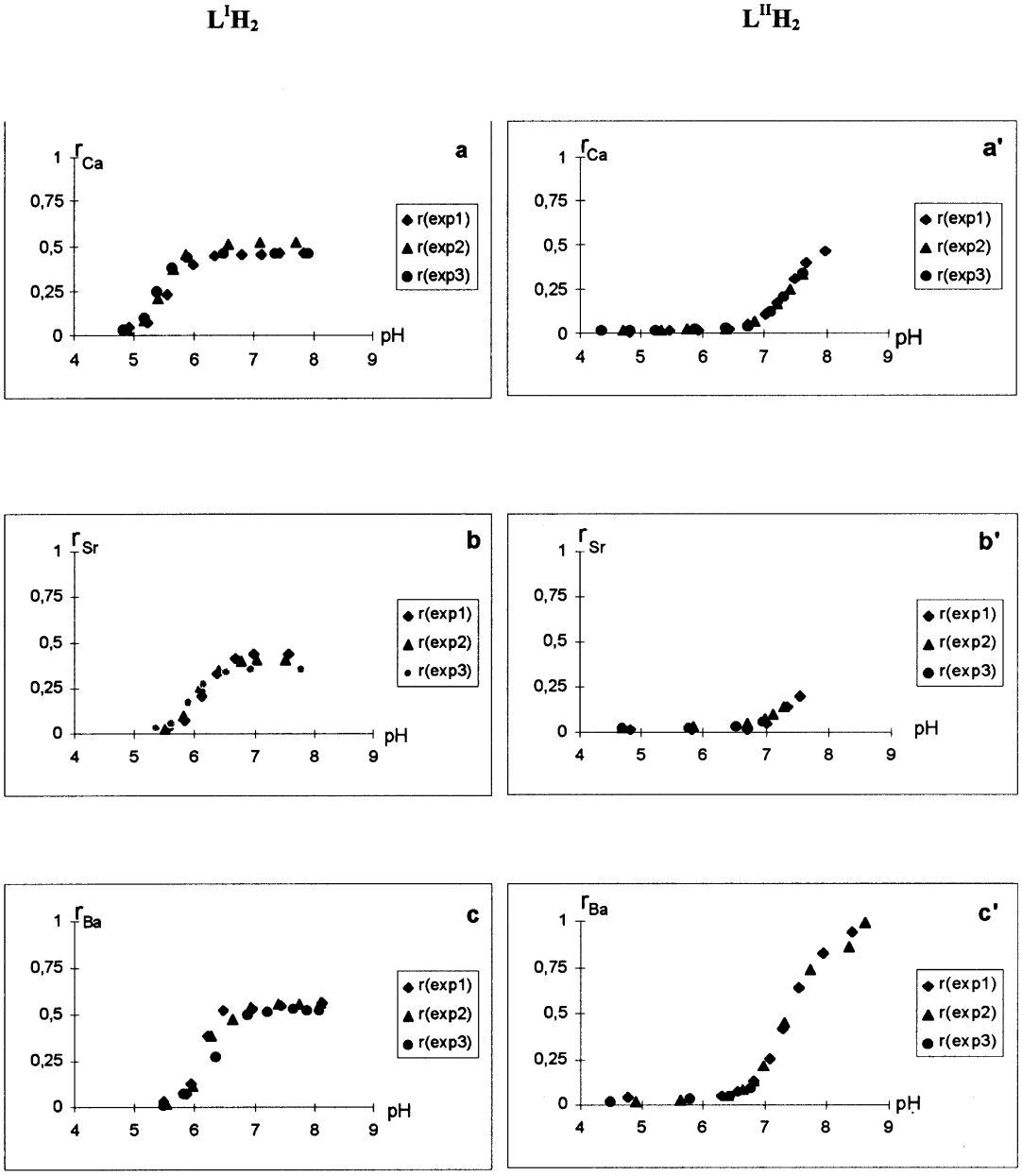

Fig. 2. Extraction of alkaline-earth by $L^{I}H_2$ (a, b, c) and $L^{II}H_2$ (a′, b′ c′) in 1,2-dichloroethane at 298 K, $r_M = f(pH)$ plots. Experimental conditions: aqueous initial concentration 0.16 M; ligand concentration: L_o: ◆ 5×10^{-4} M: r(exp1); ▲ 1×10^{-3} M: r(exp2); ● 2×10^{-3} M: r(exp3) a, a′: Ca; b, b′: Sr; and c, c′: Ba.

where m is the degree of association of the free ligand.

The conditional equilibrium constant is defined as:

$$K_{12m} = \frac{[ML_2H_2]_{org}[H^+]^2_{aq}}{[LH_2]^{2/m}_{m\,org}[M^{2+}]_{aq}} \quad (1)$$

where $[ML_2H_2]_{org} = [M]_{org}$.

Hence the $r_M = f(pH)$ curve can be drawn by introducing an equilibrium constant defined as

$$K'_{12m} = K_{12m}[M^{2+}]_{aq} = \frac{[M]_{org}[H^+]^2_{aq}}{[LH_2]^{2/m}_{m\,org}} = \frac{[M]_{org}[H^+]^2_{aq}}{1/m[L_o - 2M_{org}]^{2/m}}$$

Using the same general assumptions (single equilibrium, monometallic complex) the formation of a 1:1 metal–ligand complex is described by the equilibrium:

$$M^{2+}_{aq} + 1/m(LH_2)_{m\,org} \rightleftharpoons ML_{org} + 2H^{+}_{aq}$$

(equilibrium 2)

$$K_{11m} = \frac{[ML]_{org}[H^+]^2_{aq}}{[LH_2]^{1/m}_{m\,org}[M^{2+}]_{aq}} \qquad (2)$$

with $[ML]_{org} = [M]_{org}$.

The quantity

$$K'_{11m} = K_{11m}[M^{2+}]_{aq} = \{[M]_{org}[H^+]_{aq}{}^2\}/\{(1/m)[L_o - M_{org}]^{1/m}\}$$

can be considered as an equilibrium constant.

By setting the appropriate mass balance equations, the computed $r_M = f(pH)$ functions were drawn with arbitrary values of K' and for $m = 1$ (monomer) and $m = 2$ (dimer) (Fig. 3). It is shown that the approach should be able in principle to show whether the ligand is monomeric or dimeric.

The model is tested with $m = 1$ and $m = 2$ by introducing appropriate K values and fitting the calculated curves and the experimental plots [Fig. 4(a, b)]. It is confirmed [Fig. 4(a)] that the extraction of alkaline earth by L^IH_2 takes place via the formation of complexes of formula $ML_2{}^IH_2$ according to equilibrium 1. The formation of BaL^{II} complex according to equilibrium 2 is also confirmed [Fig. 4(b)].

In addition, it was shown that the 1:2 ion/ligand stoichiometry is highly probable for the extracted species formed in the $M/L^{II}H_2$ systems (M = Ca, Sr) [Fig. 4(b)].

So it is seen that the experimental data provide information on the number of ligand molecules involved in the extraction of a given alkaline-earth. However the data do not provide a confirmation on the monomeric or dimeric nature of the free extractant.

^{1}H-NMR and FAB$^+$ investigations

To confirm the $ML_2{}^{II}H_2$ species with $M = Ca^{2+}$, we run an extraction from water to 1,2-dichloroethane at pH 7.4.

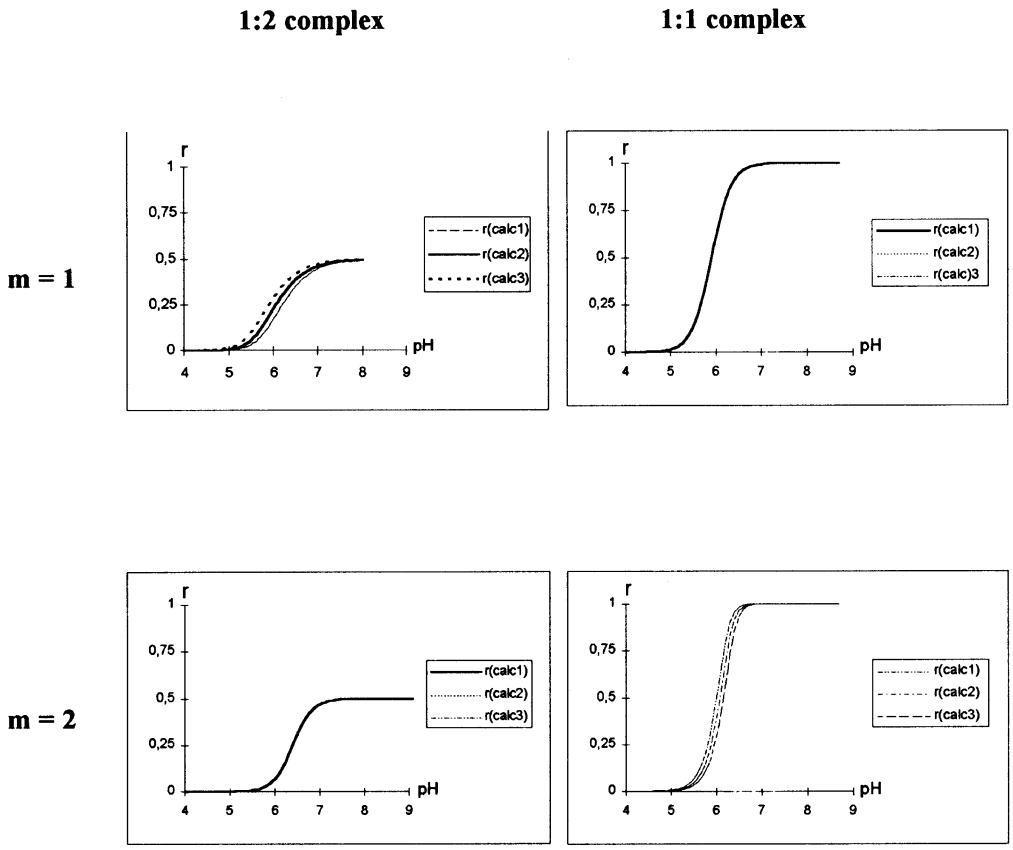

Fig. 3. Calculated curves $r_M = f(pH)$, using the experimental conditions given in the caption of Fig. 2: L_o: 5×10^{-4} M: r(calc1); 1×10^{-3} M: r(calc2); 2×10^{-3} M: r(calc3). The following arbitrary values for the equilibrium constants are used: $m = 1$, $K_{12} = (5.00 \pm 0.03) \times 10^{-9}$ and $K_{11} = (1.00 \pm 0.02) \times 10^{-11}$. $m = 2$, $K_{12} = (1.05 \pm 0.05) \times 10^{-12}$ and $K_{11} = (1.00 \pm 0.02) \times 10^{-13}$.

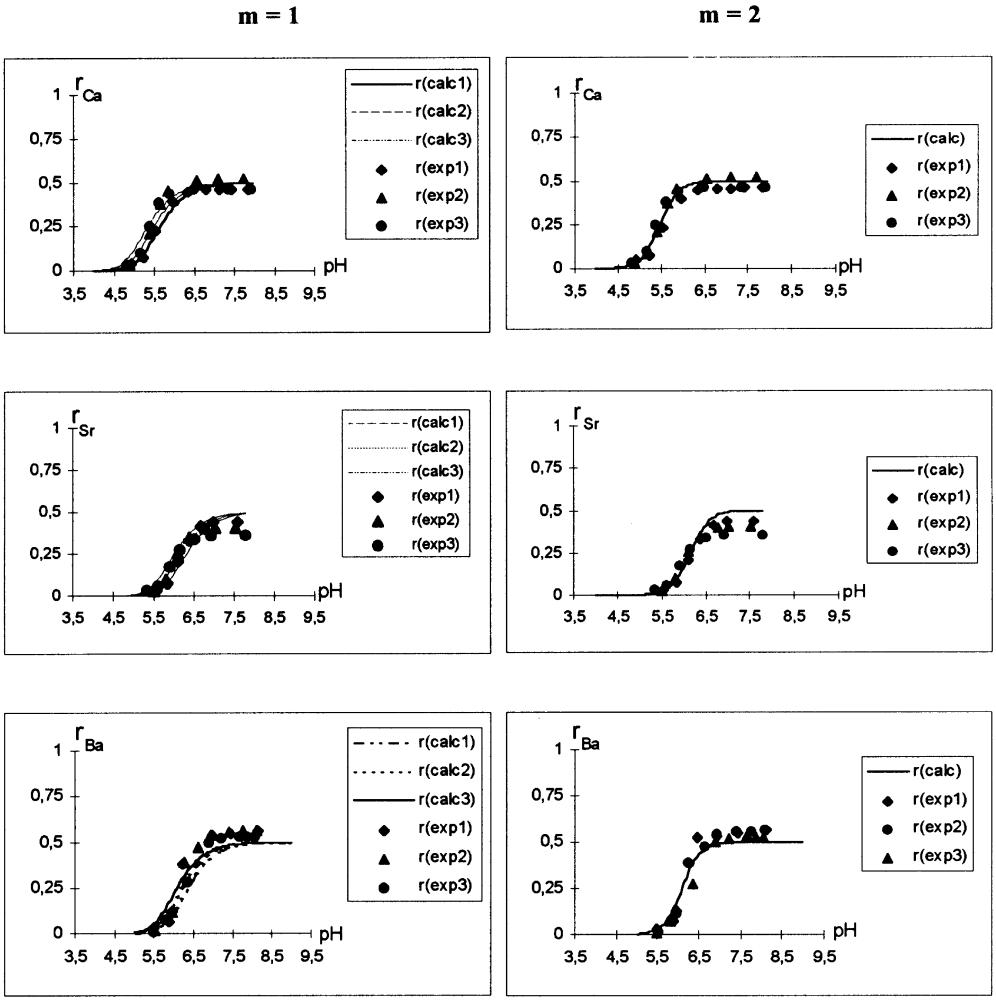

Fig. 4. Fitting of the $r_M = f(\text{pH})$ data according to equilibrium 1 and 2 (see caption of Figs. 2–3 for the definition of $r(\text{expi})$ and $r(\text{calci})$ $(i = 1, 2, 3)$). (a): $L^{I}H_2$. $m = 1$, $K_{12}(\text{Ca}) = (6.5 \pm 0.03) \times 10^{-8}$, $K_{12}(\text{Sr}) = (3.00 \pm 0.30) \times 10^{-9}$ and $K_{12}(\text{Ba}) = (2.20 \pm 0.07) \times 10^{-9}$. $m = 2$, $K_{12}(\text{Ca}) = (7.00 \pm 0.80) \times 10^{-11}$, $K_{12}(\text{Sr}) = (3.15 \pm 0.35) \times 10^{-12}$ and $K_{12}(\text{Ba}) = (4.00 \pm 0.70) \times 10^{-12}$.

Then the solvent was evaporated to dryness and the solid was investigated with FAB^+ and ^{1}H-NMR techniques. Figure 5 shows the FAB^+ spectrum of the solid giving a m/z peak at 1838.36 (calculated for $(C_{54}H_{72}O_{10})_2Ca^{2+}K^+$-$2H^+$ 1838.02, K^+ is coming from the matrix). The solid was dissolved in $CDCl_3$ and the ^{1}H-NMR spectrum is shown in Fig. 6 with the spectrum of the free ligand. The spectrum [Fig. 6(b)] was interpreted considering the formation of a 1:2 (metal/ligand) complex, the spectrum of the free ligand [Fig. 6(a)] being recovered by the formation of an *exo*-complex. Similar 1:2 (metal/ligand) *exo*-complexes had already been observed with alkali metal cations and related calixcrown compounds [8].

Competitive extraction

Competitive extractions involving the four alkaline-earth and one of the two LH_2 extractants were investigated.

With the $L^{II}H_2$ extractant it was observed that the extraction is accompanied by a precipitation for pH > 7. A simultaneous extraction of Mg, Ca, Sr and Ba by $L^{I}H_2$ takes place according to the order:

$$\text{Ca} > \text{Ba} > \text{Sr} >> \text{Mg}$$

(Mg was not detected in the organic phase).

In addition, plateau values for r_M were observed for Ca (r_{Ca} # 0.5), Sr (r_{Sr} # 0.07) and Ba (r_{Ba} # 0.19) (Fig. 7). Such a behavior cannot be explained by assuming the existence of extracted species formed in the single ion metal systems.

The experimental plots $r_M = f(\text{pH})$ for Ca^{2+}, Sr^{2+} and Ba^{2+} suggest the existence of coupled extractions via the formation of mixed extracted species.

This can be understood if one considers that the charge of a given alkaline-earth cation cannot be neutralized by two carboxylate functions which belong to the same calixarene molecule. This observations is

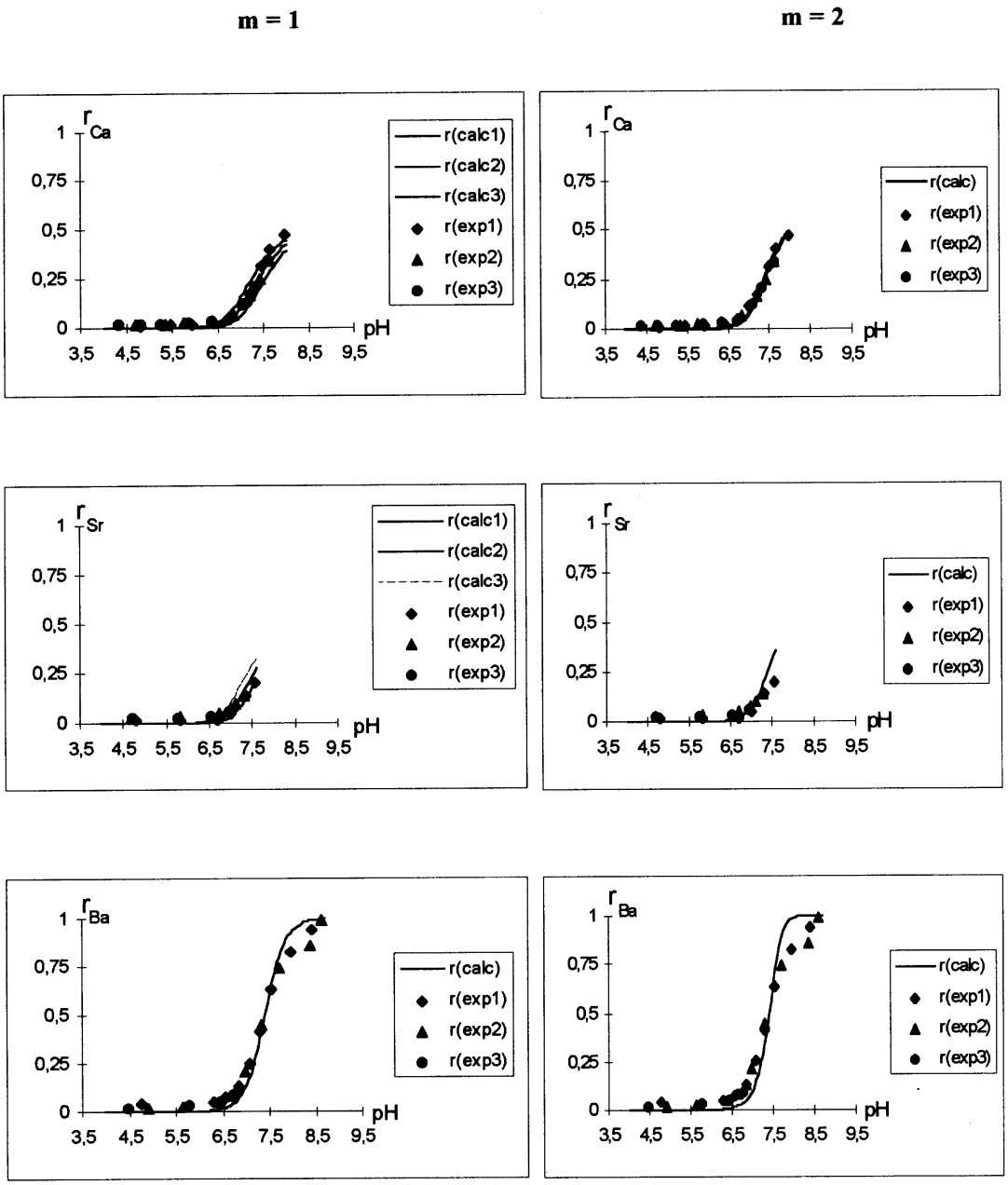

Fig. 4(b): $L^{II}H_2$. $m = 1$, $K_{12}(Ca) = (1.00 \pm 0.03) \times 10^{-11}$, $K_{12}(Sr) = (5.45 \pm 0.30) \times 10^{-12}$ and $K_{11}(Ba) = (2.20 \pm 0.07) \times 10^{-14}$ mol l^{-1}. $m = 2$, $K_{12}(Ca) = (1.05 \pm 0.02) \times 10^{-14}$, $K_{12}(Sr) = (1.00 \pm 0.08) \times 10^{-14}$ and $K_{11}(Ba) = (1.50 \pm 0.20) \times 10^{-16}$ mol l^{-1}.

also valid for the $ML_2{}^{II}H_2$ species which exist in the single metal systems.

CONCLUSION

The liquid–liquid extraction of calcium, strontium and barium by dicarboxylic calix[4]arene derivatives takes place via a proton–cation exchange process and is accompanied by the formation of metallic complexes having the 1:2 ion–ligand stoichiometry in most cases.

It was shown by ^{1}H-NMR that these complexes have an "*exo*" structure. It was also shown that the competitive extraction of calcium, strontium and barium cannot be considered as the superimposition of individual extractions. The experimental feature is

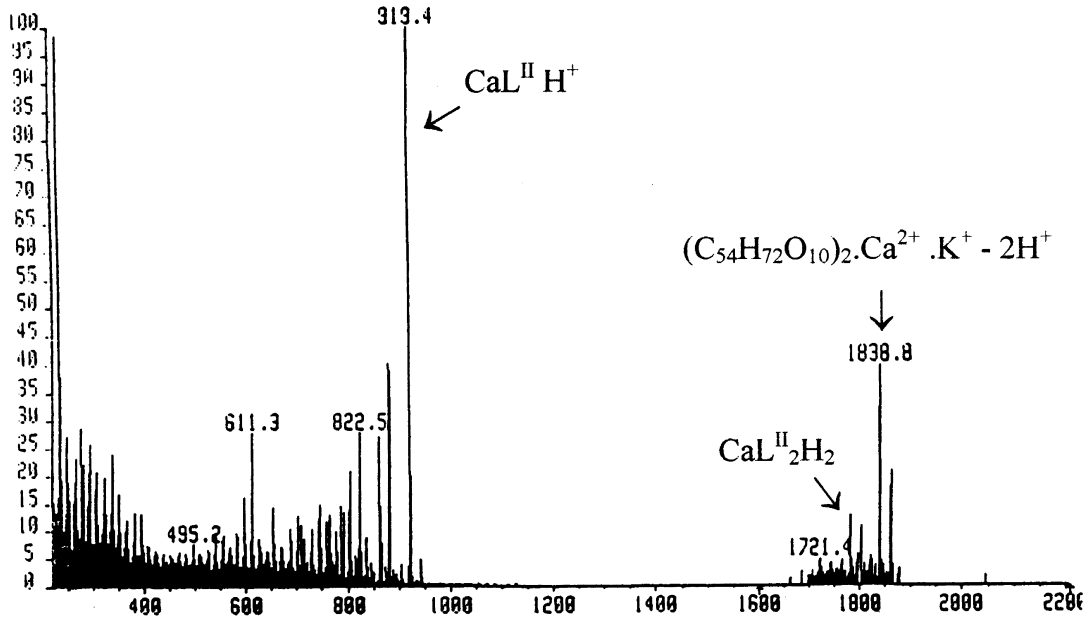

Fig. 5. FAB^+ mass spectrum of an evaporated organic solution in the extraction of calcium by $L^{II}H_2$ (corresponding pH = 7.4).

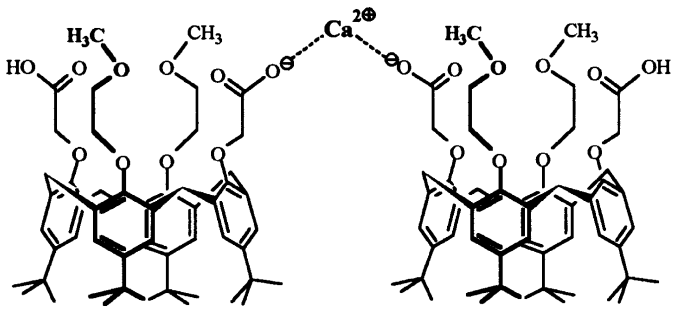

b

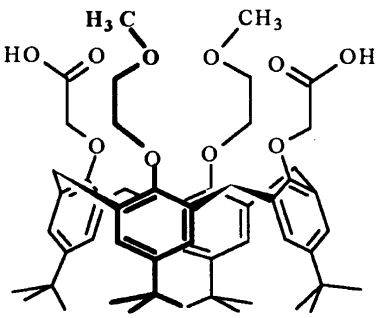

a

Fig. 6. ^{1}H-NMR spectra (200 MHz) in $CDCl_3$ at 298 K of the (a) free ligand $L^{II}H_2$ and (b) $CaL_2{}^{II}H_2$ (pH = 7.4).

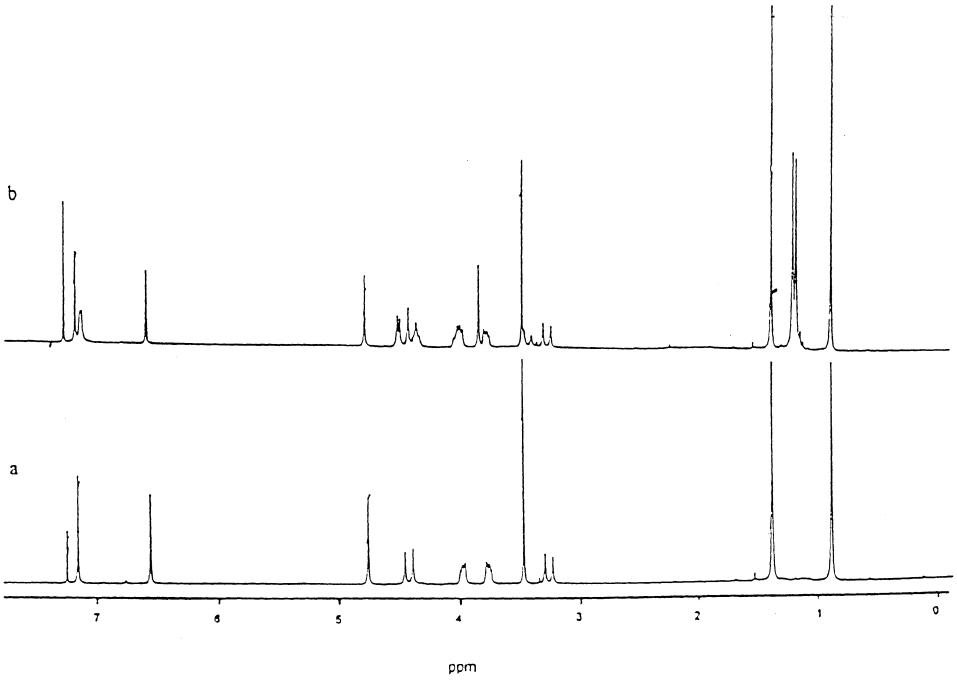

Fig. 6. *Continued.*

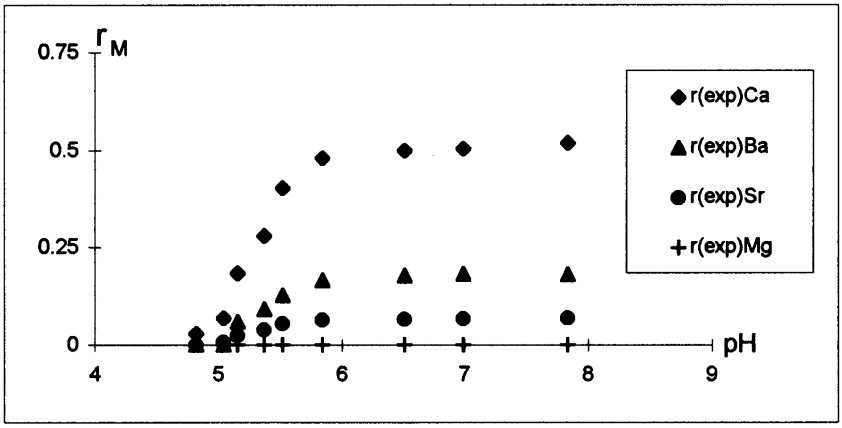

Fig. 7. Competitive extraction of Mg^{2+}, Ca^{2+}, Sr^{2+} and Ba^{2+} by $L^{I}H_2$ (1×10^{-3} M) in 1,2-dichloroethane, (initial aqueous concentration for each ion 0.04 M). The extraction of Mg^{2+} was not detected.

explained by assuming the existence of binary metallic complex including calcium and strontium or barium.

REFERENCES

1. Soedarsono, J., Burgard, M., Asfari, Z. and Vicens, J., *Solv. Extr. Ion Exch.*, 1995, **13,** 755.
2. Montavon, G., Duplâtre, G., Barakat, N., Burgard, M., Asfari, Z. and Vicens, J., *J. Incl. Phenom.*, 1997, **27,** 155.
3. Soedarsono, J., Hagège, A., Burgard, M., Asfari, Z. and Vicens, J., *Ber. Bunsenges. Phys. Chem.*, 1996, **100,** 477.
4. Gutsche, C. D., in *Calixarenes*, *Monographs in Supramolecular Chemistry*, ed. J. F. Stoddart. Royal Society of Chemistry, Cambridge, 1989.
5. Vicens, J. and Böhmer, V., eds., *Calixarenes*: *A Versatile Class of Macrocylic Compounds*. Kluwer Academic Publishers, Dordrecht, 1991.
6. Guelzim, A., Khrifi, S., Baert, F., Asfari, Z. and Vicens, J., *Acta Crystallogr.*, 1993, **C49,** 2121.
7. Barakat, N., Burgard, M., Asfari, Z. and Vicens, J., unpublished results, 1997.
8. Abidi, R., Asfari, Z., Harrowfield, J. M., Naumann, C., Sobolev, A. N. and Vicens, J., *Anal. Quimica Int. Ed.*, 1996, **92,** 51.

Pergamon

Polyhedron Vol. 17, No. 20, pp. 3657–3663, 1998
© 1998 Elsevier Science Ltd
All rights reserved. Printed in Great Britain
0277–5387/98 $19.00+0.00

PII: S0277–5387(98)00163–6

Synthesis and crystal structure of dinuclear and tetranuclear palladium dppm complexes. $[Pd_2(\mu\text{-dppm})_2(vpy)Cl]$ and $[Pd_4(\mu\text{-dppm})_4(\mu\text{-X})_2](ClO_4)_2$ (X = Cl, Br and I)

Masahiko Maekawa,[a]* Megumu Munakata,[b] Takayoshi Kuroda-Sowa[b] and Yusaku Suenaga[b]

[a]Research Institute for Science and Technology, Kinki University, 3-4-1 Kowakae, Higashi-Osaka, Osaka, 577-8502, Japan

[b]Department of Chemistry, Kinki University, 3-4-1 Kowakae, Higashi-Osaka, Osaka, 577-8502, Japan

(Received 8 January 1998; accepted 7 April 1998)

Abstract—Reaction of the intermediate $[Pd_2(\mu\text{-dppm})_2]^{2+}$ which was prepared from $[Pd_2(\mu\text{-dppm})_2X_2]$ (X = Cl, Br and I) and $AgClO_4$ in ethanol with 2-vinylpyridine (vpy) afforded dinuclear Pd(I) dppm complex $[Pd_2(\mu\text{-dppm})_2(vpy)Cl]$ (**1**). When the intermediate $[Pd_2(\mu\text{-dppm})_2]^{2+}$ was allowed to stand for a few days, tetranuclear Pd dppm complex $[Pd_4(\mu\text{-dppm})_4(\mu\text{-X})_2](ClO_4)_2$ (X = Cl (**2**), Br (**3**) and I (**4**)) was systematically formed. The structure for **1** and **2** were crystallographically determined. On complex **1** two Pd atoms are doubly bridged by two dppm ligands to form an eight-membered $Pd_2P_4C_2$ framework in a twist-chair conformation. Each Pd atoms is also coordinated by the Cl atom and the N atom of vpy in unsymmetrical side-by-side mode. The Pd–Pd distance is 2.597(2) Å and the torsion angle between two Pd_2P_2 plane is 43.2°. On the other hand four Pd atoms on **2** are bridged by four dppm ligands to form a rectangular Pd_4 core, which is composed of the shorter Pd–Pd separations (2.590(1) Å) and the close Pd···Pd separations (3.818(2) Å). The later Pd···Pd separation is also bridged by the Cl atom. The Pd–P distance (2.351(1) Å) bridging the close Pd···Pd separation is rather longer than that (2.238(2) Å) bridging the shorter Pd–Pd separation. © 1998 Elsevier Science Ltd. All rights reserved. © 1998 Elsevier Science Ltd. All rights reserved

Keywords: palladium complexes; dinuclear complexes; tetranuclear complexes; crystal structures; bidentate phosphine ligands; nitrogen donor ligands.

Bidentate phosphine ligands such as bis(diphenylphosphino)methane (dppm) and 2-(diphenylphosphino)pyridine (Ph_2Ppy) are useful bridging ligands to form homo- and heteronuclear Pd(I) complexes with a close metal-metal distance. There has been considerable interests in synthesis, structure and reaction of dinuclear Pt(I) and Pd(I) complexes [1–3], since these dinuclear complexes can provide unique properties for an unusual coordination mode of small molecules, their activation and catalytic transformation. Three typical coordination modes of (a) $[Pd_2(\mu\text{-dppm})_2L_2]$ (side-by-side) [4–9], (b) $[Pd_2(\mu\text{-X})(\mu\text{-dppm})_2L_2]$ (A-frame) [10–18] and (c) $[Pd_2(\mu\text{-dppm})_2L_4]$ (face-to-face) [19, 20] have been known in dinuclear Pd(I) complexes. It has been reported that dinuclear Pd(I) dppm complexes in a side-by-side mode react with small molecules such as CO, SO_2, RCN, $CR{=}{=}CR_2$ to afford those in A-frame mode via a insertion reaction into a Pd–Pd bond [14, 17, 21, 22]. Although crystal structures of several trinuclear [23–26] and tetranuclear Pd complexes [27–30] bridged by dppm ligands has been investigated, investigations to polynuclear Pd dppm complexes are relatively few and their structure, property and reactivity are not fully researched [2].

We have so far interested in the reactivity of the intermediate $[Pd_2(\mu\text{-dppm})_2]^{2+}$ which was prepared from $[Pd_2(\mu\text{-dppm})_2X_2]$ and $AgClO_4$ in alcohol (Scheme) [31, 32]. It has been reported that reaction of

*Author to whom correspondence should be addressed.

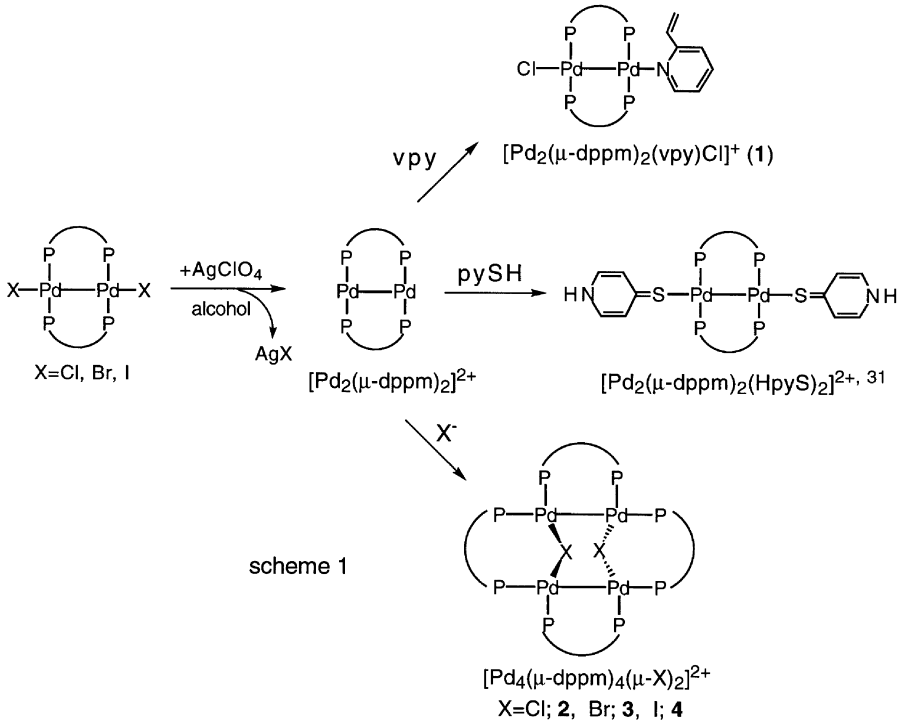

scheme 1

Scheme 1.

the intermediate $[Pd_2(\mu\text{-dppm})_2]^{2+}$ with 4-mercaptopyridine (pySH) as a S-donor ligand afforded the dinuclear Pd(I) complex $[Pd_2(\mu\text{-dppm})_2(HpyS)_2](ClO_4)_2$ [31]. In this study, the reaction of the intermediate $[Pd_2(\mu\text{-dppm})_2]^{2+}$ with 2-vinylpyridine (vpy) as a N donor ligand was furthermore attempted and dinuclear Pd(I) complex $[Pd_2(\mu\text{-dppm})_2(vpy)Cl]$ (1) was obtained. It was found that tetranuclear Pd complex $[Pd_4(\mu\text{-dppm})_4(\mu\text{-X})_2](ClO_4)_2$ (X = Cl(**2**), Br(**3**) and I(**4**)) were systematically constructed by the standing of the intermediate $[Pd_2(\mu\text{-dppm})_2]^{2+}$ in ethanol. The structure for **1** and **2** were determined by a single crystal X-ray structure analysis.

EXPERIMENTAL

General

Dinuclear Pd(I) dppm complex $[Pd_2(\mu\text{-dppm})_2X_2]$ (X = Cl, Br and I) were prepared according to the literature [22]. Bis(diphenylphosphino)methane (dppm), 2-vinyl-pyridine (vpy) and $AgClO_4$ were purchased from Aldrich and used without further purification. All organic solvents were dried by general procedures and distilled before use. All operations were carried out using standard Schlenk techniques under Ar. IR spectra were measured with a JASCO 8000 FT IR spectrometer, using a CsI pellet. ^{1}H NMR and ^{31}P NMR spectra were obtained with a JEOL GSX 270 FT NMR spectrometer at 23°C. Deuterium solvents were available from Merck and were dried by molecular sieves before use. Tetramethylsilane and 85% H_3PO_4 in D_2O were used as a reference, respectively.

Synthesis of $[Pd_2(\mu\text{-dppm})_2(vpy)Cl]ClO_4$ (**1**)

$[Pd_2(\mu\text{-dppm})_2Cl_2]$ (21.0 mg, 0.02 mmol) and $AgClO_4$ (9.0 mg, 0.04 mmol) were mixed in ethanol (10 ml) for 3 hours. The reddish brown suspension was filtered. The vpy ligand (1.0 ml) was then added to the filtrate. After stirring for 2 hours, the orange suspension was filtered and the filtrate was sealed in a 5 mm diameter glass tube. The orange solution was allowed to stand for 1 week at an ambient temperature and the yellow crystals were collected. Yield. 17 mg (32%). Found: C, 55.83; H, 3.99; N, 1.09. Calc. for $Pd_2P_4C_{57}NCl_2O_4H_{51}$: C, 56.04 H, 4.21; N, 1.15. IR (CsI, cm^{-1}): 1435(ν_{P-C}). ^{1}H NMR ($CDCl_3$): δ {7.92 and 7.40} (40 H, *br m*, Ph) and 4.39 (4 H, *br s*, CH_2) for dppm, 8.69 (1 H, *br s*, 2-H), 7.71 (1 H, *br s*, 4-H), 7.10 (1 H, *br s*, 5-H), 6.87 (1 H, *br s*, 3-H), 6.73 (1 H, *br s*, CH=), 6.40 (1 H, *br d*, $=CH_2$) and 5.80 (1 H, *br d*, $-CH_2$) for vpy. ^{31}P NMR (ethanol): −1.28. UV-VIS (nm ($\epsilon(M^{-1}cm^{-1})$), ethanol): 332 (1.7×10^4), 395 (7×10^3).

Synthesis of $[Pd_4(\mu\text{-dppm})_4(\mu\text{-Cl})_2](ClO_4)_2$ (**2**)

$[Pd_2(\mu-dppm)_2Cl_2]$ (21.0 mg, 0.02 mmol) and $AgClO_4$ (9.0 mg, 0.04 mmol) were mixed in ethanol

(10 ml) for 3 hours. The reddish brown suspension was filtered and the filtrate was sealed in a 5 mm diameter glass tube. The reddish brown solution was allowed to stand at an ambient temperature for 3 days and the red prism crystals were collected. Yields. 15 mg (69%). Found: C, 53.21; H, 3.65. Calc. for $Pd_4Cl_4P_8O_8C_{100}H_{88}$: C, 53.79; H, 3.97. IR (CsI, cm^{-1}): 1437 (ν_{P-C}), 1098 (ν_{ClO4}). ^1H NMR ($CDCl_3$): δ {7.98, 7.51 and 7.45} (80 H, m, Ph), 4.41 (8 H, tt, CH_2). ^{31}P NMR (ethanol): -4.91. UV-VIS (nm ($\epsilon(M^{-1}cm^{-1})$), THF): 358 (1.0×10^4), 431 (8.7×10^3), 512 (8.7×10^3). XPS (eV): 342.9 ($3d_{3/2}$), 337.5 ($3d_{5/2}$).

Synthesis of $[Pd_4(\mu\text{-dppm})_4(\mu\text{-X})_2](ClO_4)_2$ (X = Br(**3**) *and* I(**4**))

In a similar manner as **2**, red brick crystals of **3** or red needle crystals of **4** were obtained using $[Pd_2(\mu\text{-dppm})_2Br_2]$ (45.6 mg, 4.0×10^{-5} mol) or $[Pd_2(\mu\text{-dppm})_2I_2]$ (49.5 mg, 0.04 mmol) and $AgClO_4$ (18.0 mg, 0.08 mmol) in ethanol (10 ml). **3**: Yields. 17 mg (40%). Found: C, 51.25; H, 3.58. Calc. for $Pd_4Br_2P_8C_{100}H_{88}Cl_2O_8$: C, 51.73; H, 3.82. IR (CsI, cm^{-1}): 1437 (ν_{P-C}), 1096 (ν_{ClO4}). ^1H NMR ($CDCl_3$): δ {7.97, 7.52 and 7.46} (80 H, *m*, Ph), 4.28 (8 H, *t*, CH_2). ^{31}P NMR (ethanol): -4.96. UV-VIS (nm ($\epsilon(M^{-1}cm^{-1})$), THF): 356 (8.3×10^3), 435 (7.8×10^3), 515(7.5×10^3). **4**: Yields. 11 mg (37%). Found: C, 49.37; H, 3.49. Calc. for $Pd_4I_2P_8C_{100}H_{88}Cl_2O_8$: C, 49.71; H, 3.67. IR (CsI, cm^{-1}): 1435 (ν_{P-C}), 1096 (ν_{ClO4}). ^1H NMR ($CDCl_3$): δ {7.97, 7.48 and 7.46} (80 H, *m*, Ph), 4.39 (8 H, *br s*, CH_2). ^{31}P NMR (ethanol, 23°C): -4.91. UV-VIS (nm ($\epsilon(M^{-1}cm^{-1})$), THF): 342 (1.3×10^4), 444 (9.9×10^3), 512 (7.6×10^3).

Data collection, structure solution and refinements for **1** and **2**

A suitable crystal for **1** or **2** was attached to the end of a glass fiber and were mounted on a Rigaku AFC-5R diffractometer with a graphite mono-chromated Mo Kα radiation ($\lambda = 0.71069$ Å). The detailed measurement conditions and crystal data are summarized in Table 1. The intensity data were collected at 23°C using the ω scan technique for **1** and ω-2θ scan technique for **2**. The reflection data of 5721 and 11222 reflections were collected. On **1** the intensities of three representative reflections which were measured after every 150 reflections remained constant through data collection, indicative of crystal and electronic stability. No decay correction was applied. On the other hand the intensities of three representative reflections on **2** which were measured after every 150 reflections declined by 8.1%. A linear correction factor was applied to the data to account for this phenomena. The linear absorption coefficient for Mo

Table 1. Crystal data and measurement conditions for **1** and **2**

Complex	**1**	**2**
Formula	$Pd_2P_4C_{57}NCl_2O_4H_{51}$	$Pd_4Cl_4P_8O_8C_{100}H_{88}$
M	1221.64	2233.0
Crystal system	Orthorhombic	Triclinic
Space group	$P2_12_12_1$	$P\bar{1}$
a (Å)	11.882(5)	14.256(6)
b (Å)	11.909(7)	15.348(9)
c (Å)	38.676(5)	13.366(5)
α (°)	90.0	114.65(3)
β (°)	90.0	105.90(3)
γ (°)	90.0	62.74(3)
U (Å^3)	5473(3)	2350(4)
Z	4	1
D_{calc} (gcm^{-3})	1.482	1.577
λ(Mo Kα) (Å)	0.71069	0.71069
μ(Mo Kα) (cm^{-1})	9.06	10.47
Scan type	ω	ω-2θ
Scan rate (°/min)	2.0	8.0
Scan width (°)	$0.76+0.30\tan\theta$	$1.30+0.30\tan\theta$
$2\theta_{max}$ (°)	55.0	55.0
No. of reflections measured	5721	11222
No. of observations	2579 ($I > 2\sigma(I_0)$)	7704 ($I > 3\sigma(I_0)$)
F(000)	2472	1124
R^a	0.048	0.035
$R_w{}^b$	0.046	0.041

[a] $R = \|\|F_0|-F_c\|/|F_0|$.
[b] $R_w = [(w(|F_0|-|F_c|)^2/w|F_0|^2)]^{1/2}$, $w = 4F_0^2/\sigma^2(F_0)^2$.

Kα is 9.1 and 10.5 cm^{-1} for **1** and **2**, respectively. Azimuthal scans of several reflections indicated no need for an absorption correction. The data were corrected for Lorentz and polarization effects.

The structures were solved by a direct method (MITHRIL) [33]. The non-hydrogen atoms were refined anisotropically. Hydrogen atoms were included but not refined. The final cycle of the full-matrix least squares refinement was based on 2579 and 7704 observed reflections ($I > 3\sigma(I)$), and 618 and 559 variable parameters for **1** and **2**, respectively. Reliability factors are defined as $R = \Sigma(|F_o| - |F_c|)/\Sigma|F_o|$ and $R_w = [\Sigma w \ (|F_o| - |F_c|)^2/\Sigma w|F_o|^2]^{1/2}$, where $w = 4F_o^2/\sigma(F_o^2)$. The final R and R_w values were 0.048 and 0.046 for **1**, and 0.035 and 0.041 for **2**, respectively. The maximum and minimum peaks on the final difference Fourier map corresponded to 0.50 and $-0.50\,e\text{Å}^{-3}$ for **1**, and 1.01 and $-0.45\,e\text{Å}^{-3}$ for **2**, respectively. Atomic scattering factors and anomalous dispersion terms were taken from the International Tables for X-ray Crystallography, Vol. IV [34]. All calculations were performed using the program TEXSAN crystallographic software package [35].

RESULTS AND DISCUSSION

Crystal structure of $[Pd_2(\mu\text{-dppm})_2(vpy)Cl]ClO_4$ (**1**)

According to the Scheme, reaction of the intermediate $[Pd_2(\mu\text{-dppm})_2]^{2+}$ with 2-vinylpyridine (vpy) gave the dinuclear Pd(I) complex $[Pd_2(\mu\text{-dppm})_2(vpy)Cl](ClO_4)$ (**1**). Crystal structure of **1** is shown in Fig. 1, together with the atomic labeling scheme. Selected bond distances and bond angles are listed in Table 2. The two Pd atoms are doubly bridged by two dppm ligands to form an eight-membered $Pd_2P_4C_2$ ring framework in a twist-chair conformation: The P(1)–Pd(1)–P(4) and P(2)–Pd(2)–P(3) angles are 176.2(2) and 171.6(2)°, respectively. Each Pd atoms is furthermore coordinated by the Cl atom and the N atom of the vpy ligand, providing an unsymmetrical side-by-side mode. The Cl(1)–Pd(1)–Pd(2)–N(1) axis is almost linear. The Pd(2)–Pd(1)–Cl(1) and Pd(1)–Pd(2)–N(1) angle are 176.9(1) and 179.4(4)°, respectively, which are slightly larger than those (169.1(3), 173(1)°) of other dinuclear Pd(I) dppm complexes [4, 8].

The average Pd–P distance of 2.291(3) Å is within those (2.274(2)–2.302(2) Å) of other dinuclear Pd(I) dppm complexes in a side-by-side mode [4–9, 36], whereas the distance is rather shorter than those (2.307(2)–2.358(4) Å) in a A-frame mode [10–18]. The Pd(1)–Cl(1) distance of 2.381(5) Å is similar to those in other dinuclear Pd(I) dppm complexes [7, 8].

The Pd(1)–Pd(2) distance of 2.597(2) Å is rather shorter than that (2.75Å) in Pd metal and those (2.594(2)–2.699(5) Å) of other dinuclear Pd(I) dppm complexes with Pd–Pd bond [4–9], indicative of a direct Pd–Pd bond. It has been theoretically reported on dinuclear Pd(I) dppm complexes that the twist

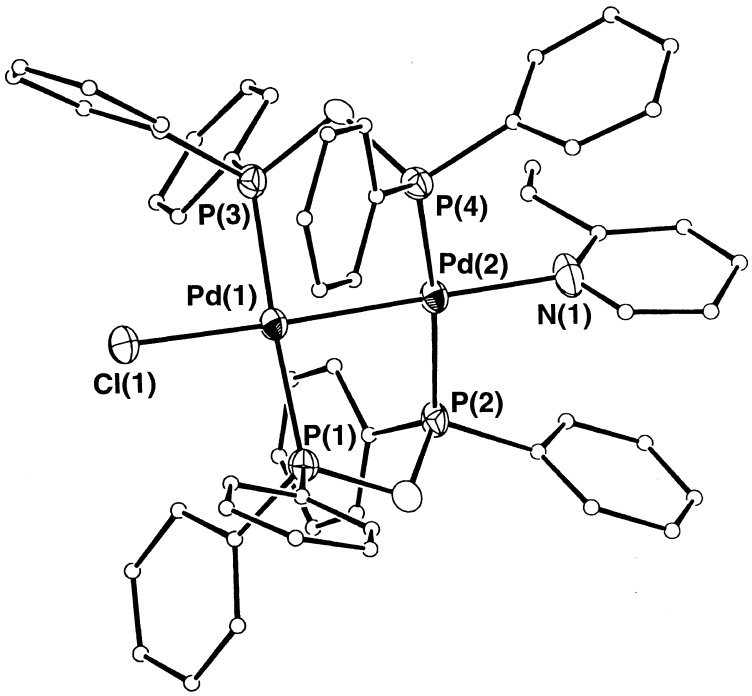

Fig. 1. Molecular structure of $[Pd(\mu\text{-dppm})_2(vpy)Cl]^+$ (**1**) and the atomic labeling scheme. Only Pd(1), Pd(2), P(1), P(2), P(3), Pd(4), Cl(1) and N(1) in the coordination sphere are labeled.

Table 2. Selected bond distance (Å) and bond angles (°) of **1**

Pd(1)–Pd(2)	2.597(2)	Pd(1)–Cl(1)	2.381(5)
Pd(1)–P(1)	2.309(5)	Pd(1)–P(3)	2.308(5)
Pd(2)–P(2)	2.312(5)	Pd(2)–P(4)	2.285(5)
Pd(2)–N(1)	2.16(1)		
Pd(2)–Pd(1)–Cl(1)	176.9(1)	Pd(2)–Pd(1)–P(1)	88.8(1)
Pd(2)–Pd(1)–P(3)	87.7(1)	P(1)–Pd(1)–Cl(1)	93.2(2)
P(3)–Pd(1)–Cl(1)	90.2(2)	P(1)–Pd(1)–P(3)	176.2(2)
Pd(1)–Pd(2)–P(2)	87.5(1)	Pd(1)–Pd(2)–P(4)	85.1(1)
Pd(1)–Pd(2)–N(1)	179.4(4)	P(2)–Pd(2)–P(4)	171.6(2)
P(2)–Pd(2)–N(1)	91.9(4)	P(4)–Pd(2)–N(1)	95.5(4)
P(1)–C(1)–P(2)	107(1)	P(3)–C(2)–P(4)	104.8(8)

along the Pd–Pd axis is due to anti-bonding interactions of filled metal *d* orbitals which are minimized when the torsion angle equals 45° [4, 5]. The twisted conformation allows the ligands to span a shorter metal-metal bond. The crystallographic data for **1** reveal that the torsion angle between the plane defined by {P(1), Pd(1), P(3) and Pd(2)} and {P(2), Pd(2), P(4) and Pd(2)} is 43.2° and the Pd–Pd distance is 2.597(2) Å. The torsion angle is more close to 45° and the Pd–Pd distance is correspondingly more short, compared with other dinuclear Pd(I) dppm complexes {[Pd_2(μ-dppm)$_2$$Br_2$] (39°, 2.699(5) Å) [9], [Pd_2(μ-dppm)$_2$($SnCl_3$)Cl] (41.3°, 2.644(2) Å) [6], [Pd_2(μ-dppm)$_2$($OCOF_3$)$_2$] (44.5°, 2.594(2) Å) [4], [Pd_2(μ-dppm)$_2$(C_6Cl_5)$_2$] (44.98°, 2.6704(21) Å) [8], [Pd_2(μ-dmpm)$_2$$Br_2$] (50.5°, 2.603(1) Å)[5]}. This facts illustrate that the smaller deviation from 45° leads to the shortening of Pd–Pd distance.

Crystal structure of [Pd_4(μ-dppm)$_4$(μ-Cl)$_2$](ClO_4)$_2$

When the intermediate [Pd_2(μ-dppm)$_2$]$^{2+}$ was allowed to stand in ethanol according to the Scheme, tetranuclear Pd complex [Pd_4(μ-dppm)$_4$(μ-X)$_2$](ClO_4)$_2$ (X = Cl(**2**), Br(**3**) and I(**4**)) was systematically formed. This facts indicate that if no other suitable ligands (or higher affinity solvents and counter anion) were present in solution, tetranuclear Pd complex [Pd_4(μ-dppm)$_4$(μ-X)$_2$](ClO_4)$_2$ was constructed from [Pd_2(μ-dppm)$_2$]$^{2+}$ and dissolving halogen anions. It has been reported that the similar complex [Pd_4(μ-dppm)$_4$(μ-Cl)$_2$]Y_2 (Y = BF_4 and PF_6) was obtained from reaction of [Pd_2(μ-dppm)$_2$$Cl_2$] with copper or gold complexes [27]. Crystal structure of **2** was shown in Fig. 2, together with the atomic labeling scheme. Selected bond distances and bond angles are listed in Table 3. Complex **2** has the center of inversion at the midpoint of Pd(1)···P(1′). Four Pd atoms are bridged by four dppm ligands to form the rectangular Pd_4 core, which consists of the shorter Pd–Pd separations and the close Pd···Pd separations. The close Pd···Pd separations are moreover bridged by the Cl atom, which is situated 1.45 Å from the mean Pd_4 plane. All the Pd atoms are coplanar. The similar Pd_4 core has been known in [Pd_4(μ-dppm)$_4$(μ-Cl)$_2$](BF_4)$_2$• (CH_3)$_2$CO [27, 28] and [Pd_4(μ-dppm)$_4$(μ-Cl)$_2$](ClO_4)$_2$•bpe [29].

The shorter Pd(1)–Pd(2) distance of 2.590(1) Å is rather shorter than that (2.75 Å) in Pd metal and those (2.53–2.77 Å) of other dinuclear Pd(I) complexes [2,

Table 3. Selected bond distances and bond angles for **2**

Pd(1)–Pd(2)	2.590(1)	Pd(1)···Pd(2′)	3.818(2)
Pd(1)–Cl(1)	2.427(2)	Pd(2)–Cl(1)	2.414(2)
Pd(1)–P(1)	2.237(2)	Pd(1)–P(3)	2.331(1)
Pd(2)–P(2)	2.240(2)	Pd(2)–P(4)	2.372(2)
P(1)–C(49)	1.814(4)	P(2)–C(49)	1.848(4)
P(3)–C(50)	1.828(4)	P(4)–C(50)	1.833(4)
P(1)–Pd(1)–P(3)	100.14(6)	P(3)–Pd(1)–Cl(1)	91.33(5)
Pd(2)–Pd(1)–Cl(1)	88.70(5)	Pd(2)–Pd(1)–P(1)	82.23(5)
P(2)–Pd(2)–P(4)	110.64(6)	P(4)–Pd(2)–Cl(1′)	90.77(6)
Pd(1)–Pd(2)–Cl(1′)	76.16(5)	Pd(1)–Pd(2)–P(2)	82.44(5)
Pd(1)–Cl(1)–Pd(2′)	104.14(6)	P(1)–C(49)–P(2)	105.2(2)
P(3)–C(50)–P(4′)	121.6(2)		

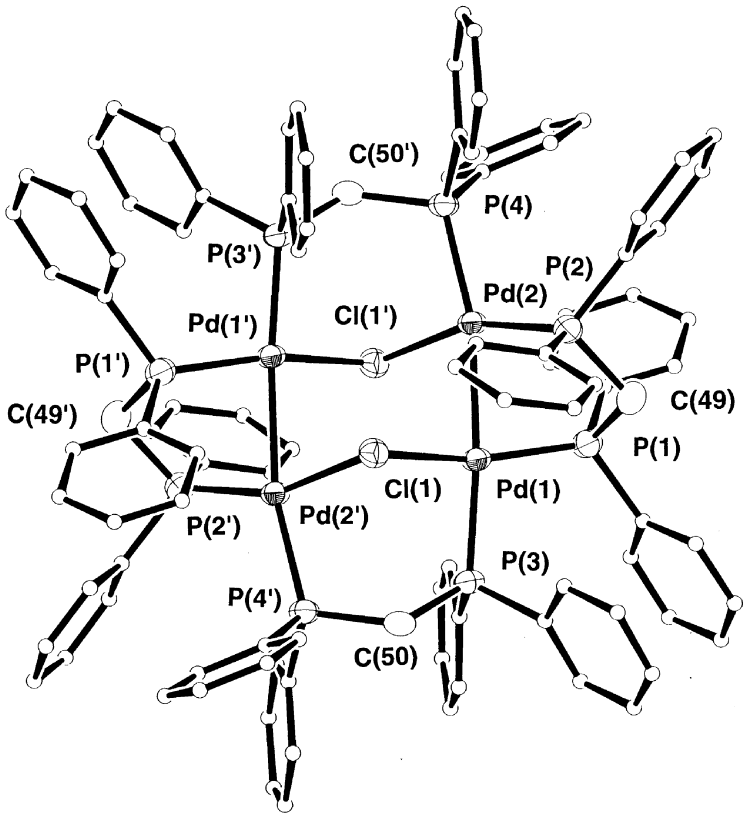

Fig. 2. Molecular structure of $[Pd_4(\mu\text{-dppm})_4(\mu\text{-Cl})_2]^{2+}$ (**2**) and the atomic labeling scheme. Only Pd(1), Pd(2), P(1), P(2), P(3), Pd(4), Cl(1), C(49), C(50), Pd(1′), Pd(2′), P(1′), P(2′), P(3′), P(4′), Cl(1′), C(49′) and C(50′) in the coordination sphere are labeled.

4, 5, 37], indicative of a direct Pd–Pd bond. On the other hand the close Pd(1)···Pd(2′) separation of 3.818(2) Å are longer than that in Pd metal, no indicative of a direct Pd–Pd bond. The shorter Pd–Pd distance is shorter than those (2.594(2)–3.332(1) Å) of other tetranuclear Pd complexes with the rectangular Pd_4 core [27–43]. The close Pd···Pd separation is longer than those (2.831(1)–3.742(2) Å) [27–43]. Consequently the Pd_4 core is rather rectangular.

The average Pd–P distance of 2.295(2) Å is within those (2.220(5)–2.353(7) Å) of dinuclear [4, 5, 37], trinuclear [24–26] and tetranuclear Pd complexes [27–30] bridged by dppm ligands. It is interesting that the Pd–P distance of 2.351(1) Å bridging the close Pd···Pd separation is very longer than that (2.238(2) Å) bridging the shorter Pd–Pd bond. The difference is considered due to both steric and electronic factors arising from the *trans* influence of the Pd–Pd bond and the bulk of the phenyl substituents. The average Pd–Cl of 2.420(2) Å is close to those (2.406(5)–2.430(1) Å) in other tetranuclear Pd complexes [27, 30, 39]. The Pd(1)–Cl(1)–Pd(2′) of 104.14(6)° is rather larger than those (78.1(1)° [30] and 93.15(3)° [39]) in other tetranuclear Pd complexes.

SUPPLEMENTARY MATERIALS

Complete listings of the atomic coordinates, bond distances, bond angles, hydrogen atomic coordinates, anisotropic thermal parameters, and a listing of observed and calculated structure factors for **1** and **2** are available from the Cambridge Crystallographic Data Centre and the author.

Acknowledgements—We thank Mr. Tamotsu Goto, Mr. Yasuhiro Tsujita and Mr. Hisaaki Ohnishi for their assistances. This work was partially supported by a Grant-in-Aid for Science Research from the Ministry of Education, Science and Culture in Japan.

REFERENCES

1. Puddephatt, R. J., *Chem. Soc. Rev.*, 1983, **12,** 99.
2. Barnard, C. F. J., Russell, M. J. H., In G. Wilkinson, Ed, Pergamon Press, Oxford, (1987) Vol, 5(51), Comprehensive Coordination Chemistry, pp. 1099–1130.
3. Balch, A. L., *Reactivity of Metal-Metal Bonds*, In M. H. Chisholm, ACS Symposium Series, (1981), Chap. 8, pp. 167–185.

4. Krafft, T. E., Hejna, C. I. and Smith, J. S., *Inorg. Chem.*, 1990, **29,** 2682.
5. Kullberg, M. L., Lemke, F. R., Powell, D. R. and Kubiak, C. P., *Inorg. Chem.*, 1985, **24,** 3589.
6. Olmstead, M. M., Benner, L. S., Hope, H. and Balch, A. L., *Inorg. Chim. Acta*, 1979, **32,** 193.
7. Brown, M. P., Puddephatt, R. J., Rashidi, M., Manojlovic-Muir, L., Muir, K. W., Solomuin, T. and Seddon, K. R., *Inorg. Chim. Acta*, 1977, **23,** L33.
8. Espinet, P., Fornies, J., Fortuno, C., Hidalgo, G., Martinez, F., Tomas, M. and Welch, A. T., *J. Organomet. Chem.*, 1986, **317,** 105.
9. Holloway, R. G., Penfold, B. R., Colton, R. and McCormick, M. J., *J. Chem. Soc., Chem. Comm.*, 1976, **0,** 485.
10. Olmstead, M. M., Farr, J. P. and Balch, A. L., *Inorg. Chim. Acta*, 1981, **52,** 47.
11. Young, S. J., Kellenberger, B., Reibenspies, J. H., Himmel, S. E., Manning, M., Anderson, O. P. and Stille, J. K., *J. Am. Chem. Soc.*, 1988, **110,** 5744.
12. Kullberg, M. L. and Kubiak, C. P., *Organometallics*, 1984, **3,** 632.
13. Hanson, A. W., McAlees, A. J. and Taylor, A., *J. Chem. Soc., Perkin Trans. Part I*, 1985, **0,** 441.
14. Olmstead, M. M., Hope, H., Benner, L. S. and Balch, A. L., *J. Am. Chem. Soc.*, 1977, **99,** 5502.
15. Olmstead, M. M., Benner, L. S. and Balch, A. L., *J. Chem. Soc., Chem. Comm.*, 1977, **0,** 823.
16. Davies, J. A., Pinkerton, A. A. and Syed, R., Vilmer, M., *J. Chem. Soc., Chem. Comm.*, 1988, **0,** 47.
17. Balch, A. L., Lee, C. L., Lindsay, C. H. and Olmstead, M. M., *J. Organomet. Chem.*, 1979, **177,** C22.
18. Besenyei, G., Lee, C., Gulinski, J., Rettig, S. J., James, B. R., Nelson, D. A. and Lilga, M. A., *Inorg. Chem.*, 1987, **26,** 3622.
19. Hunt, C. T. and Balch, A. L., *Inorg. Chem.*, 1981, **20,** 2267.
20. ref 5 and references therein.
21. Benner, L. S., Olmstead, M. M., Hope, H. and Balch, A. L., *J. Organomet. Chem.*, 1978, **153,** C31.
22. Benner, L. S. and Balch, A. L., *J. Am. Chem. Soc.*, 1978, **100,** 6099.
23. Puddephatt, R. J., Manojlovic-Muir, L. and Muir, K. W., *Polyhedron*, 1990, **9,** 2767.
24. Manojlovic-Muir, L., Muir, K. W., Lloyd, B. R. and Puddephatt, R. J., *J. Chem. Soc., Chem. Comm.*, 1983, **0,** 1336.
25. Manojlovic-Muir, L., Muir, K. W., Lloyd, B. R. and Puddephatt, R. J., *J. Chem. Soc., Chem. Comm.*, 1985, **0,** 536.
26. Lloyd, B. R., Manojlovic-Muir, L., Muir, K. W. and Puddephatt, R. J., *Organometallics*, 1993, **12,** 1231.
27. Braunstein, P., Luke, M. A., Tiripicchio, A., Camellini, M. T., *Angew. Chem., Int. Ed. Engl.*, 1987, **26**, 768; Braunstein, P., Luke, M. A., Tiripicchio, A. and Camellini, M. T., *New. J. Chem.*, 1988, **12**, 429.
28. Maekawa, M., Munakata, M., Kuroda-Sowa, T. and Goto, T., *Inorg. Chim. Acta*, 1995, **239,** 159.
29. Maekawa, M., Munakata, M., Kuroda-Sowa, T. and Suenaga, Y., *Anal. Sci.*, 1998, **14,** 451.
30. Kluwe, C. and Davies, J., *Organometallics*, 1995, **14,** 4257.
31. Maekawa, M., Munakata, M., Kuroda-Sowa, T. and Suenaga, Y., *Inorg. Chim. Acta*, in press.
32. Maekawa, M., Munakata, M., Kuroda-Sowa, T. and Suenaga, Y., *Anal. Sci.*, 1998, **14,** 447.
33. Gilmore, C. J., *MITHRIL*, an intergated direct methods computer program, *J. Appl. Crystallogr.*, 1984, **17,** 42. University of Glasgow, Scotland, UK.
34. International Tables for X-ray Crystallography, Kynoch, Birmingham, UK, (1974), Vol. IV.
35. TEXSAN-*TEXARAY*, structure analysis package, Molecular Structure Corporation, The Woodlands, TX, USA, 1985.
36. Braunstein, P., Jud, J., Dusausoy, Y. and Fischer, J., *Organometallics*, 1983, **2,** 180.
37. Holloway, R. G. and Penfold, B. R., *J. Chem. Soc., Chem. Comm.*, 1976, **0,** 485.
38. Mednikov, E. G., Eremenko, N. K., Gubin, S. P., Slovokhotov, Y. L. and Struchkov, Y. T., *J. Organomet. Chem.*, 1982, **239,** 401.
39. King, C., Roundhill, D. M. and Fronczek, F. R., *Inorg. Chem.*, 1987, **26,** 4288.
40. Moiseev, I. I., Stromnova, T. A., Vargafting, M. N., Mazo, G. J., Kuz'mina, L. G. and Struchkov, Y. T., *J. Chem. Soc., Chem. Comm.*, 1978, **0,** 27.
41. Mimoun, H., Charpentier, R., Mitschler, A., Fischer, J. and Weiss, R., *J. Am. Chem. Soc.*, 1980, **102,** 1047.
42. Tanase, T., Nomura, T., Fukushima, T. and Yamamoto, Y., *Inorg. Chem.*, 1993, **32,** 4578.
43. Kuz'mina, L. G. and Struchkov, Y. T., *Koord. Khim.*, 1979, **5,** 1558.

Pergamon

PII: S0277–5387(98)00116–8

Polyhedron Vol. 17, No. 21, pp. 3665–3669, 1998
© 1998 Elsevier Science Ltd
All rights reserved. Printed in Great Britain
0277–5387/98 $19.00+0.00

Self-assembled one-dimensional zigzag structure of mercury(II) complex with sulphur rich ligand 4,5-ethylenedithio-1,3-dithiole-2-thione

Qing-Hua Wang, De-Liang Long and Jin-Shun Huang*

State Key Laboratory of Structural Chemistry, Fujian Institute of Research on the Structure of Matter, Chinese Academy of Sciences, Fuzhou, Fujian, 350002, P. R. China

(Received 28 January 1998; accepted 20 March 1998)

Abstract—Mercury(II) complex of 4,5-ethylenedithio-1,3-dithiole-2-thione ($C_5H_4S_5$), $[Hg_2(C_5H_4S_5)_2Cl_4]_n$, was synthesized and characterized crystallographically. It possesses the one-dimensional polymeric structure composed of centrosymmetric quasi-isolated binuclear subunits. The mercury atoms in zigzag arrangement achieve five-coordination in a distorted trigonal bipyramidal geometry by bonding to two bridging Cl, a terminal Cl, a thione S and a thioether S atom of $C_5H_4S_5$. The S ... S contacts of 3.568(3) Å between two nearby chains generate a two-dimensional network. Through S ... S interactions of 3.583(3) Å between the two-dimensional layers, a three-dimensional supramolecular network is formed. © 1998 Elsevier Science Ltd. All rights reserved

Keywords: crystal structure; mercury; supramolecule; S ... S contact

INTRODUCTION

Supramolecular chemistry has developed rapidly in the past ten years. Intermolecular interactions such as hydrogen bonding [1], S ... S contacts [2, 3] and π-π stackings [4] are efficient organizing forces in supramolecular architecture and the design of new solid state materials for a number of applications [5]. Molecular conductors derived from organic donor molecules such as tetrathiafulvalene (TTF), bis(ethylenedithio)tetrathiafulvalene (BEDT-TTF), and 4,5-dimercapto-1,3-dithio-2-thione (dmit) are of these kinds of solid state materials. These ligands contain plentiful sulphur atoms and when they are combined with suitable metal ions to form certain structure, molecular metals and superconductors may be produced via intermolecular S ... S interaction [3, 6, 7].

The sulphur rich compound 4,5-ethylenedithio-1,3-dithiole-2-thione ($C_5H_4S_5$) is a derivative of dmit. It is well known as an electron donor and has available sites to coordinate to metal ions. The particular affinity of sulphur for mercury has been known for a long time. Recently, we used $C_5H_4S_5$ and $HgCl_2$ as starting materials and obtained a new compound, $[Hg_2(C_5H_4S_5)_2Cl_4]_n$. It has a unique polymeric chain structure and through S ... S contacts it forms a three-dimensional network.

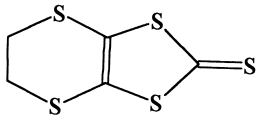

$C_5H_4S_5$

EXPERIMENTAL

Synthesis

The reagent $C_5H_4S_5$ was prepared according to literature [8]. A solution of $C_5H_4S_5$ (0.12 g, 0.5 mmol) in 3 ml CH_2Cl_2 was added to the solution of $HgCl_2$

* Author to whom correspondence should be addressed. e-mail: hjs@ms.fjirsm.ac.cn

(0.14 g, 0.5 mmol) in 20 ml acetonitrile with stirring at room temperature. A red precipitate was formed immediately. Then the mixture was heated with stirring until the precipitate was redissolved. The solution was rapidly filtered and cooled slowly in air. After two hours, fine red plate crystals of $[Hg_2(C_5H_4S_5)_2Cl_4]_n$ **1** were formed. Yield 0.11 g. Chemical analyses are consistent with the formula. IR (KBr pellet): ν/cm^{-1} 1508m, 1443s, 1400m, 1383w, 1238w, 1011s, 968m, 918m, 878m, 814w, 733w, 696w, 459m.

X-RAY CRYSTALLOGRAPHY

Crystal data for **1**: $C_5H_4Cl_2HgS_5$, $F_w = 495.90$, triclinic, space group $P\bar{1}$, $a = 8.373(3)$, $b = 8.509(3)$, $c = 9.800(7)$ Å, $\alpha = 102.71(4)$, $\beta = 100.67(4)$, $\gamma = 118.07(3)^\circ$, $v = 566.2(6)$ Å3, $z = 2$, μ(Mo-$K\alpha$) = 14.91 cm^{-1}. A single crystal with approximate dimensions $0.25 \times 0.12 \times 0.12$ mm^3 was mounted on a glass fibber in a random orientation. The determination of unit cell and the data collection were performed with Mo-$K\alpha$ radiation ($\lambda = 0.71073$ Å) on an Enraf-Nonius CAD4 diffractometer equipped with a graphite monochromator. A total of 2470 independent reflections were collected in the range of $2 < 2\theta < 54.0$ ($0 < h < 10$, $-10 < k < 10$, $-12 < l < 12$) by using an ω-2θ scan mode at room temperature, of which 1918 reflections with $I > 3.0\sigma(I)$ were used in the succeeding structure solution and refinement. Intensities were corrected for *L*p factors and empirical absorption based on Ψ scan technique with transmittance in the range from 0.440 to 0.999. The structure was solved using direct method. Hg, two Cl and a S atoms were located from the *E*-map. Other non-hydrogen atoms were derived from the successive difference Fourier syntheses. The hydrogen atoms were located theoretically and refined on riding mode ($d_{C\text{-}H} = 0.95$ Å). The final full-matrix least-squares refinement converged with unweighted and weighted agreement factors $R = \Sigma(|F_o| - |F_c|)/\Sigma|F_o| = 0.030$ and $Rw = [\Sigma w(|F_o| - |F_c|)^2/\Sigma w|F_o|^2]^{1/2} = 0.036$, $w = 1/[\sigma^2(F_o) + (0.020\,F_o)^2 + 1.0]$. $S = 1.19$, $(\Delta/\sigma)_{max} = 0.000$. The highest peak on the final difference Fourier map has a height of 1.33 $e \cdot Å^{-3}$, which is located at a position 1.0 Å away from Hg atom. All calculations were performed on a COMPAQ PC 486 computer using MOLEN program package [9].

RESULTS AND DISCUSSION

The selected bond distances and bond angles are shown in Table 1. The ORTEP drawing and labelling scheme of the complex are shown in Fig. 1. The mercury achieves effective five-coordination in a trigonal bipyramidal geometry which is composed of Cl(1), Cl(2) and S(1) on the equatorial plane and Cl(1^i), S(4^{ii}) on axis (symmetry code i: $-x, -y, -z$; ii: $-x, -y, 1-z$). The bond angles around Hg atoms, S(1)–Hg–Cl(2), S(1)–Hg–Cl(1) and Cl(1)–Hg–Cl(2) sum to 355.13° indicating that the mercury atom is quasi coplanar with the equatorial plane. In fact the mercury atom is displaced by 0.3 Å from the equatorial plane toward Cl(1^i). The bond angle S(4^{ii})–Hg–Cl(1^i) is 169.80(7)° showing some distortion from ideal trigonal bipyramidal geometry. Similar five-coordination geometry of mercury is also found in the structure of $Hg(L)Cl_2$ (L = Tetrahydrothiophen [10], Dehydrodithizone [11] and Etheyl N,N-dimethylthiocarbamate [12]). Each mercury is bonded to two types of sulphur atoms: one is the thiocarbonyl sulphur S(1), the other is the thioether sulphur S(4^{ii}). The Hg–S(1) bond distance of 2.454(2) Å is within the expected Hg–S bond distances, whereas the Hg–S(4^{ii}) separation of 3.271(2) Å can be taken as a weak coordination. These data demonstrate that the thiocarbonyl sulphur atom (C=S) more strongly coordinates to the metal ion than the ether type sulphur atom (–S–) [13]. All of the atoms of $C_5H_4S_5$ in the complex except for C(4) are in a conjugated plane with a deviation less than 0.04 Å. The C(4) is deviated from the conjugated plane by 0.75 Å.

Two $HgCl_2$ units are bounded together through two chlorine bridges and form a centrosymmetric Hg(μ–Cl)$_2$Hg ring. The Hg–Hg^i distance of 3.936(1) Å is much longer than the sum of 2.94 Å of the covalent radii of the two Hg atoms indicating that there exists no Hg–Hg bond. The distance between Hg and the two bridge chlorine atom is not equal. The bond lengths Hg–Cl(1), Hg–Cl(1^i) are 2.564(2) and 2.791(2) Å, respectively. The distance between Hg and the terminal chlorine Cl(2) is 2.381(1) Å and it is much shorter than Hg–Cl(1). This proves that the connection of bridging chlorine Cl(1) to Hg is weaker than terminal chlorine Cl(2) to Hg. A survey of the literature indicate that most Hg–Cl bond distances are in the range 2.28–2.33 Å, irrespective of the coordination number at mercury, and that larger Hg–Cl bond distance are always found in compounds where the chlorine atoms are bridging, or hydrogen bonded, or weakly bonded in polymeric structures [12].

As shown in Fig. 1, the subunits $Hg_2(C_5H_4S_5)_2Cl_4$ through weak coordination of Hg–S(4) form a one-dimensional infinite chain, $[Hg_2(C_5H_4S_5)_2Cl_4]_n$. A zigzag arrangement of metal atoms could be considered if the whole polymer is viewed. The molecular packing diagram viewed down the *c* axis is shown in Fig. 2. The S ... S contacts of 3.568(3) Å between two nearby chains along *c* axis is shorter than the sum of 3.70 Å of the van der Waals radii of the two S atoms and result in the formation of two-dimensional layers. The shortest S ... S distance between two nearby two-dimensional layers is 3.583(3) Å and also fall in the range of van der Waals interaction. Thus, this complex come forth a supramolecule with a three-dimensional structure assembled by S ... S contacts. Since the average S ... S contact distance of highly conductive compound of TTF, BEDT-TTF and their derivatives are

Table 1. Selected bond distances and angles for **1**

Hg–Cl(1)	2.564(2)	S(5)–C(3)	1.729(8)
Hg–Cl(1^{i})	2.791(2)	S(5)–C(5)	1.830(8)
Hg–Cl(2)	2.381(1)	S(2)–C(2)	1.716(8)
Hg–S(4^{ii})	3.271(2)	S(2)–C(1)	1.696(7)
Hg–S(1)	2.454(2)	S(3)–C(3)	1.741(6)
S(4)–S(4^{iii})	3.583(3)	S(3)–C(1)	1.684(9)
S(4)–C(2)	1.743(7)	S(1)–C(1)	1.690(8)
S(4)–C(4)	1.80(1)	C(3)–C(2)	1.36(1)
S(5)–S(1^{iv})	3.568(3)	C(4)–C(5)	1.47(1)
Cl(1)–Hg–Cl(1^{i})	85.47(7)	Cl(2)–Hg–S(1)	129.66(7)
Cl(1)–Hg–Cl(2)	111.97(6)	S(4^{ii})–Hg–S(1)	85.46(6)
Cl(1)–Hg–S(4^{ii})	85.08(6)	Hg–Cl(1)–Hg^{i}	94.53(7)
Cl(1)–Hg–S(1)	113.50(7)	C(2)–S(4)–C(4)	99.4(4)
Cl(1^{i})–Hg–Cl(2)	102.10(6)	C(3)–S(5)–C(5)	102.3(4)
Cl(1^{i})–Hg–S(4^{ii})	169.80(7)	C(2)–S(2)–C(1)	97.2(4)
Cl(1^{i})–Hg–S(1)	101.86(6)	C(3)–S(3)–C(1)	97.3(4)
Cl(2)–Hg–S(4)	77.98(6)	Hg–S(1)–C(1)	107.2(3)

Symmetry code i $-x, -y, -z$; ii $-x, -y, 1-z$; iii $1-x, 1-y, 2-z$; iv $x, 1+y, z$

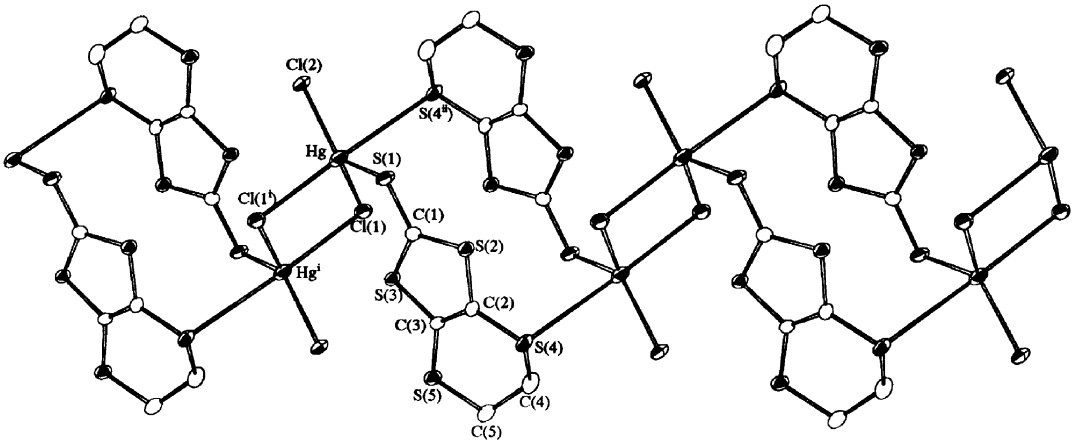

Fig. 1. Molecular structure and labelling scheme of $[Hg_2(C_5H_4S_5)_2Cl_4]_n$. Displacement ellipsoids are shown at the 30% probability level. Hydrogen atoms have been omitted for clarity.

about 3.50 Å, [3, 13] the distance of 3.568(3) Å and 3.583(3) Å here is an example of strong S ... S contact. In $Hg(SC_6H_{11})_2$ [14], which also has a polymeric chain structure, the inter-chain S ... S distances are all larger than 8 Å, so it is a pure one-dimensional chain structure. $[Ag(C_5H_4S_5)NO_3]_\infty$ [13] with the inter-chain S ... S distance of 3.41 Å is a supramolecule of two-dimensional structure. However, the shortest S ... S distance of 3.84 Å between the two-dimensional layers of this complex shows no inter-layer S ... S contacts.

The 'side-by-side' or 'up-down' arrangement of $C_5H_4S_5$ with short S ... S distances indicates an efficient intermolecular π-π orbital interaction, which forms a broadened energy band over the whole lattice [3]. The S ... S contact is one of the most important factors by which the sulphur-rich compound exhibit high con-

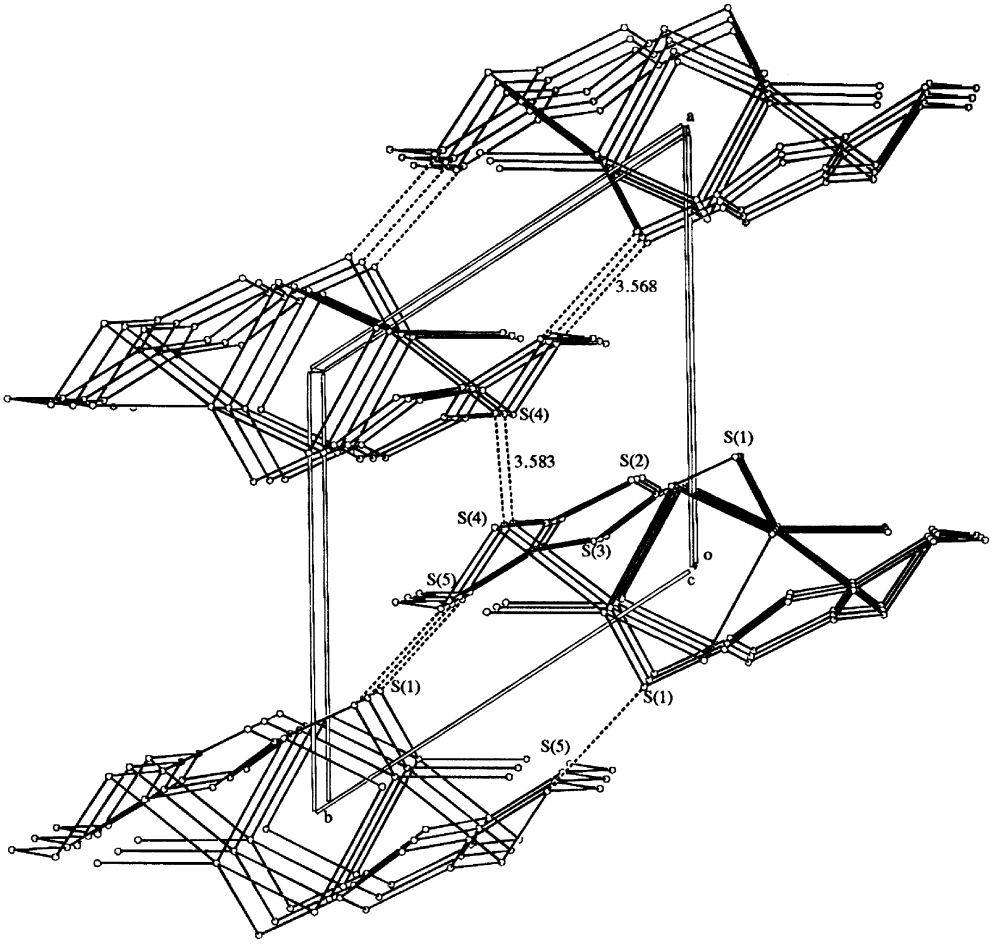

Fig. 2. Packing diagram viewed down the *c*-axis indicating the interchain S ... S interaction of S(4) ... S(4) as well as S(1) ... S(5).

ductivity. It is known that the stronger the S ... S contact, the more effective the increase in the conductivity. When the temperature is decreased or the pressure increased, the S ... S distance is shorter than in ambient conditions and accordingly the conductivity is increased [15]. A conductivity measurement is still undertaken with the title compound.

REFERENCES

1. Aakeroy, C. B. and Seddon, K. R., *Chem. Soc. Rev.*, 1993, **22,** 397.
2. Munakata, M., Kuroda-Sowa, T., Maekawa, M., Hirota, A. and Kitagawa, S., *Inorg. Chem.*, 1995, **34,** 2705.
3. (a) Cassoux, P., Valade, L., Kobayashi, H., Kobayachi, A., Clark, R. A. and Underhill, A. E., *Coord. Chem. Rev.*, 1991, **110**, 115; (b) Olk, R. M., Olk, B., Dietzsch, W., Kirmse, R. and Hoyer, E., *Coord. Chem. Rev.*, 1992, **117**, 99.
4. Kato, M., Sasano, K., Kosuge, C., Yamazaki, M., Yano, S. and Kimura, M., *Inorg. Chem.*, 1996, **35,** 116.
5. Dai, J., Kuroda-Sowa, T., Munakata, M., Maekawa, M., Suenaga, Y. and Ohno, Y., *J. Chem. Soc., Dalton Trans.*, 1997, pp. 2363.
6. (a) Williams, J. M., Wang, H. H., Emge, T. J., Geiser, U., Beno, M. A., Leung, P. C. W., Carlson, K. D., Thorn, R. J., Schultz, A. J. and Whangbo, M., *Prog. Inorg. Chem.*, 1987, **35**, 1; (b) Bryce, M. R., *Chem. Soc.Rev.*, 1991, **20**, 355.
7. Williams, J. M., Schultz, A. J., Geiser, U., Carlson, K. D., Kini, A. M., Wang, H. H., Kwok, W. K., Whanbo, M. H. and Schirber, J. E., *Science*, 1991, **252,** 1501.
8. Hartke, K., Kissel, Th., Quante, J. and Matusch, R., *Chem. Ber.*, 1980, **113,** 1898.
9. Fair, C. K., *MolEN*. An interactive intelligent system for crystal structure analysis. Enraf-Nonius, Delft, The Netherland, (1990).
10. Branden, C. I., *Ark. Kemi*, 1964, **22,** 495.
11. Kozarek, W. J. and Fernando, Q., *Inorg. Chem.*, 1973, **12,** 2129.
12. Faraglia, G., Graziani, R., Sindellari, L., Forsel-

lini, E. and Casellato, U., *Inorg. Chim. Acta*, 1982, **58,** 167.
13. Dai, J., Munakata, M., Kuroda-Sowa, T., Suenaga, Y., Wu, L. P. and Yamamoto, M., *Inorg. Chim. Acta*, 1997, **255,** 163.
14. Alsina, T., Clegg, W., Fraser, K. A. and Sola, J., *J. Chem. Soc. Dalton Trans.*, 1992, pp. 1393.
15. Mori, H., Tanaka, S., Oshima, M., Saito, G., Mori, T., Maruyama, Y. and Inokuchi, H., *Bull. Chem. Soc. Jpn.*, 1990, **63,** 2183.

Pergamon

PII: S0277–5387(98)00128–4

Polyhedron Vol. 17, No. 21, pp. 3671–3679, 1998
© 1998 Elsevier Science Ltd
All rights reserved. Printed in Great Britain
0277–5387/98 $19.00+0.00

Solid-state chemistry of $[Ni(AA)_3][PdCl_4] \cdot nH_2O$ complexes (AA = bipy, phen) and crystal structures of *cis*-diaqua-bis(phenanthroline)nickel(II) tetrachlorozincate and *cis*-dichloro-bis(bipyridine)nickel(II)

Marilena Ferbinteanu,[a] Fanica Cimpoesu,[a] Marius Andruh[a]* and Fernande D. Rochon[1b]

[a] University of Bucharest, Faculty of Chemistry, Inorganic Chemistry Laboratory, Str. Dumbrava Rosie nr. 23, 70254 Bucharest, Romania

[b] Chemistry Departement, Université du Québec à Montréal, C.P. 8888, Montréal, Que., Canada H3C 3P8

(Received 9 January 1998; accepted 27 March 1998)

Abstract—The thermal analysis of the complexes $[Ni(phen)_3][PdCl_4]\cdot 3H_2O$ and $[Ni(bipy)_3][PdCl_4]\cdot 2\frac{1}{2}H_2O$ revealed, after the elimination of the molecules of water, the reciprocal migration of the ligands between the coordination spheres of the two metal ions. This solid-state reaction leads to mixtures of two neutral complexes: $Ni(AA)_2Cl_2$ and $Pd(AA)Cl_2$ (AA = phenanthroline or bipyridine). In both cases, the migration was found to be exothermic. The bis-chelated nickel complexes, $Ni(AA)_2Cl_2$, were extracted in ethanol and separated from $Pd(AA)Cl_2$. Subsequent addition of an hydrochloric acid solution of $ZnCl_2$ to the ethanol solution containing $Ni(phen)_2Cl_2$ led to the formation of $[Ni(phen)_2(H_2O)_2][ZnCl_4]\cdot H_2O$ which was studied by X-ray diffraction methods. The Ni–N bond distances vary from 2.078(3) to 2.089(4) Å, while the *cis* Ni–O distances are 2.057(3) and 2.073(3) Å. The crystal structure of $Ni(bipy)_2Cl_2\cdot 2H_2O\cdot\frac{1}{2}CH_3CN$ was also determined. The compound is the *cis* isomer, with the Ni atom located on a 2-fold axis. The Ni–N bonds distances are 2.084(3) and 2.094(2) Å, while the Ni–Cl bonds distances are 2.428(1) Å. The compound crystallizes with two water molecules situated in the lattice and $\frac{1}{2}$ molecule of acetonitrile located on a 2-fold axis. The two crystals are stabilized by hydrogen bonds involving the water molecules. © 1998 Elsevier Science Ltd. All rights reserved

Keywords: nickel complexes; palladium complexes; 2,2′-bipyridine; 1,10-phenanthroline; irreversible thermochromism

INTRODUCTION

In a series of papers we have reported on the thermochromic behavior of some ionic coordination compounds, where the cation is a tris-chelate complex with aromatic diamine ligands, while the anion is a tetrahalocomplex [1–4]. The general formula is $[M(AA)_3][M'X_4]$, with M(II) = Co(II), Ni(II), M′ = Cu(II), Zn(II), Pd(II), AA = 2,2′-bipyridine, 1,10-phenanthroline, 4,7-diphenyl-1,10-phenanthroline, $X^- = Cl^-$, Br^-. The irreversible thermochromism [5] in these complexes is due to the reciprocal migration, in the solid-state, of one molecule of the aromatic neutral ligand from the tris-chelated cationic sphere towards the anionic one, accompanied by a transfer of a pair of X^- ligands in the reverse direction:

$$[M(AA)_3][M'X_4](s) \rightarrow M(AA)_2X_2(s) + M'(AA)X_2(s)$$

Similar migrational processes have been studied especially when M = M′ (Pt(II), Pd(II) and Ni(II)) [6–8]. These reactions can be considered as isomerization

* Author to whom correspondence should be addressed.
[1] Alternative corresponding author.

reactions and have important preparative significance, e.g.:

$$[Pd(en)_2][PdCl_4](s) \rightarrow 2Pd(en)Cl_2(s)$$

The migration of ligands between the coordination spheres of the two metallic centers is clearly indicated by thermal effects (DTA or DSC analyses) without any mass loss, or by electronic spectroscopy, which allows the characterization of the different chromophores. The latter technique is particularly useful for complexes of Co(II or III), Ni(II) and Cu(II), since their *d–d* spectra are very sensitive towards modifications of the coordination sphere. For the complexes $[M(AA)_3][M'X_4]$ mentioned above [1–4], the transition temperatures were in the range 200–315°C. In one case, the process was found to be reversible [4]. The final products can usually be separated, because of their different solubilities in adequate solvents.

Such solid state rearrangements can be useful for the synthesis of complexes possessing interesting magnetic properties. For example, the spin-crossover complex $Fe(phen)_2(NCS)_2$ has been obtained by heating the parent compound $[Fe(phen)_3]_2[Fe(NCS)_4](NCS)_2$ [9].

New examples of solid-state reaction involving ligand migration between different coordination spheres are presented in this paper. This work is focused on the $[Ni(bipy)_3][PdCl_4]\cdot 2\frac{1}{2}H_2O$ system. The crystal structures of two complexes, $[Ni(phen)_2(H_2O)_2][ZnCl_4]\cdot H_2O$ and $[Ni(bipy)_2Cl_2]\cdot 2H_2O\cdot \frac{1}{2}CH_3CN$ were determined. These compounds were obtained through solid-state migration from the parent compounds $[Ni(phen)_3][PdCl_4]\cdot 3H_2O$ and $[Ni(bipy)_3][PdCl_4]\cdot 2\frac{1}{2}H_2O$, respectively.

EXPERIMENTAL

Synthesis

The chemicals were purchased from Aldrich and all manipulations were performed using materials as received. $[Ni(phen)_3][PdCl_4]\cdot 3H_2O$ (**1**) was synthesized as already reported [2].

$[Ni(phen)_2(H_2O)_2][ZnCl_4]\cdot H_2O$ (**2**): By heating **1** (1 mmol) at 230°C, the color changed from pink–beige to green, and a mixture containing $Ni(phen)_2Cl_2$ and $Pd(phen)Cl_2$ was obtained. The nickel compound, $Ni(phen)_2Cl_2$, was extracted from the mixture with 25 mL ethanol and filtered from the insoluble palladium complex. A 3 mL solution of concentrated hydrochloric acid (12 M) containing 1 mmol of $ZnCl_2$ was added to the green ethanolic solution of $Ni(phen)_2Cl_2$. Lilac crystals of $[Ni(phen)_2(H_2O)_2][ZnCl_4]\cdot H_2O$, adequate for crystal structure determination, appeared within a few days. Yield: 63%. IR data (KBr, cm^{-1}): 3420br, 1630m, 1590m, 1520s 1430vs, 1345w, 1230w, 1145m, 1110m, 1050w, 870m, 850s, 725vs, 645w, 600w, 500w, 430w.

$[Ni(bipy)_3][PdCl_4]\cdot 2\frac{1}{2}H_2O$ (**3**) was prepared as follows: An ethanolic solution (10 mL) containing 1 mmol of $[Ni(bipy)_3]Cl_2$ (prepared as already reported [10]) was mixed with 10 mL aqueous solution containing 1 mmol $PdCl_2$ and 4 mL HCl 12 M (HCl was added in order to achieve the formation of $[PdCl_4]^{2-}$ anions). The reaction was carried out at 0°C. The resulting precipitate was filtered off, washed with cold ethanol and dried in a desiccator. Yield: 87%. $[Ni(bipy)_3][PdCl_4]\cdot 2\frac{1}{2}H_2O$: pink–beige; IR data (KBr, cm^{-1}): 3497m, 3101m, 3055m, 1630w, 1598s, 1569w, 1491m, 1470m, 1449vs, 1312m, 1246w, 1156m, 1103w, 1061w, 1043w, 1019m, 902w, 811w, 766vs, 735m, 651w, 632w, 417w. Analysis: calc.: 43.91% C, 3.56% H, 10.24% N; found: 44.1% C, 3.3% H, 10.6% N.

Compound **3** was heated to 200°C and the resulting mixture was treated as described above. $Ni(bipy)_2Cl_2$ was obtained by separation from the palladium complex, $Pd(bipy)Cl_2$, as for the phenanthroline complex. The evaporation of the corresponding ethanolic solutions gave blue–green microcrystals. Yield: 72%. Crystals suitable for crystallographic studies were obtained by recrystallization from acetonitrile: $Ni(bipy)_2Cl_2\cdot 2H_2O\cdot \frac{1}{2}CH_3CN$ (**4**): IR data (KBr, cm^{-1}): 3160br, 2105m 1610s, 1600s, 1580m, 1570m, 1495m, 1475s, 1445vs, 1315s, 1250m, 1225w, 1170w, 1150s, 1105m, 1060w, 1040w, 1020s, 815w, 770vs, 730s, 650m, 630m, 420w.

The two palladium compounds were identified by elemental analysis, after separation from the nickel complexes as described above. Analysis: $Pd(phen)Cl_2$: calc.: 40.31% C, 2.26% H, 7.83% N; found: 40.2% C, 2.3% H, 7.2% N. $Pd(bipy)Cl_2$: calc.: 36.01% C, 2.42% H, 8.40% N; found: 35.9% C, 2.3% H, 8.6% N.

The final degradation products of compound **3** obtained at a temperature greater than 520°C was a mixture of Pd and NiO which were identified from their powder diffraction patterns [11].

Physical measurements

The IR spectra (KBr pellets) were measured on a BIO-RAD FTS 135 spectrometer. UV-VIS spectra (diffuse reflectance technique) were recorded with a VSU2 spectrophotometer. The thermal analysis (TG, DTG and DTA) were performed in air with a Q-1500D (MOM Budapest) instrument and the DSC curves were obtained on a DuPont 2000 instrument. The heating rate was 10°/min. X-Ray powder diffraction data were measured on a Philips PW 1140 diffractometer, using Ni filtered CuKα radiation.

Crystal structure determinations

The crystals were selected after examination under a polarizing microscope for homogeneity. The unit cell parameters were obtained by least-squares refinement of the angles 2θ (14–25°C), ω and χ for 26 and 44 well-centered reflections. The data collections were made at room temperature on a Siemens P4

diffractometer with graphite-monochromatized MoKα radiation using the XSCANS program. The $\omega-2\theta$ scan technique was used and three standard reflections were measured after every 97 reflections. The coordinates of the heavy atoms were determined from direct methods and the positions of all the other non-hydrogen atoms were found by the usual Fourier methods. The refinement of the structures was done by full-matrix least-squares analysis. The H atoms of the phenanthroline and the dipyridyl ligands were fixed at their calculated positions (riding model) with $U_{iso}=0.08$ Å^2. Those of the aqua ligands and of the lattice molecules of water were located on the Fourier difference map and were refined isotropically. Crystal **4** was found to contain molecules of CH_3CN located on the two-fold axis. The N and methyl C atoms were found to be disordered. Therefore the C–C and C–N distances are not precise. The best results were obtained assuming a site occupancy of CH_3CN of 0.5. The TG curve confirmed this result. The H atoms of CH_3CN were neglected because of the disorder. For crystal **4**, the largest residual peaks were found around the CH_3CN molecule. The calculations were done on a SHELXTL system [12]. The crystallographic data and other pertinent information are summarized in Table 1.

RESULTS AND DISCUSSION

The solid-state migration of the ligands between the coordination spheres of two different metal ions, $[M(AA)_3]^{2+}$ and $[M'X_4]^{2-}$, seems to be general, at least for systems where the anion is a tetrahalocomplex. New examples of such solid-state migrational processes are reported in this work. The molecular and crystal structures of the two compounds, $[Ni(phen)_2(H_2O)_2][ZnCl_4]\cdot H_2O$ and $Ni(bipy)_2Cl_2\cdot 2H_2O\cdot \frac{1}{2}CH_3CN$, obtained through the interchange of the ligands between the coordination spheres of the two different metallic centers, were determined. This solid-state reaction could be an alternative method for the synthesis of some bis-chelated complexes. This rearrangement is particularly important, since such complexes are relatively unstable in aqueous solutions, where they usually disproportionate to the more stable tris-chelated species and, probably, the hexaaqua metal(II) complexes [13].

The solid-state reaction of the complex $[Ni(phen)_3][PdCl_4]\cdot 3H_2O$ (**1**) will first be discussed. When the pink–beige compound **1** was heated to about 230°C, a green mixture of $Ni(phen)_2Cl_2$ and $Pd(phen)Cl_2$ was formed. One phenanthroline molecule from the cation $[Ni(phen)_3]^{2+}$ was caught in the solid state by the palladium complexed ion. The greater stability of the Pd(II) chelate is probably an important factor in this reaction. The two compounds $Ni(phen)_2Cl_2$ and $Pd(phen)Cl_2$ were separated by dissolving the mixture in ethanol.

The insoluble complex $Pd(phen)Cl_2$ was filtered out and identified by elemental analysis. An aqueous solution of $[ZnCl_4]^{2-}$ was added to the $Ni(phen)_2Cl_2$ ethanol solution. The resulting product $[Ni(phen)_2(H_2O)_2][ZnCl_4]\cdot H_2O$ (**2**) was characterized by crystallographic methods.

Table 1. Summary of crystallographic data

Crystal	**2**	**4**
Chemical formula	$C_{24}H_{22}Cl_4N_4NiO_3Zn$	$C_{21}H_{21.5}Cl_2N_{4.5}NiO_2$
M_w	680.3	498.5
Crystalline system	Monoclinic	Monoclinic
Space group	$P2_1/n$	C2/c
a (Å)	14.604(3)	18.379(2)
b (Å)	10.111(2)	13.2360(10)
c (Å)	19.082(5)	10.9890(10)
β (°)	91.70(2)	120.300(10)
Volume (Å^3)	2816.6(11)	2308.0(4)
Z	4	4
$F(000)$	1376	1028
ρ_{calcd} (Mg m^{-3})	1.604	1.435
λ(MoKα) (Å)	0.71073	0.71073
μ(MoKα) (mm^{-1})	1.933	1.098
2θ max (°)	55	55
No. of ind. reflections (R_{int})	6468 (0.0285)	3348 (0.0293)
No. of obs. reflections	3484 [$F>5\sigma(F)$]	2346 [$F>5\sigma(F)$]
$R=\Sigma\|F_o-F_c\|/\Sigma\|F_o\|$	0.0406	0.0440
$Rw=[\Sigma w(\|F_o\|-\|F_c\|)^2/\Sigma w\|F_o\|2]^{1/2}$	0.0392	0.0455
Largest difference peak eÅ^{-1}	0.39	0.63
Goodness-of-fit	1.14	1.32

The thermal analysis of the pink–beige compound (**1**) has shown that the endothermic elimination of the three lattice molecules of water takes place in the region 70–106°C. No other mass change is observed on the TG curve up to 357°C, where the loss of the phenanthroline molecules starts. The migration of the phenanthroline molecule and of the two chloride ions takes place in the range 195–230°C, during an exothermic process. The heat of the transformation ΔH is -67 kJ/mol. The green color of the resulting mixture is due to the superposition of the spectra of two chromophores, $Ni(phen)_2Cl_2$ (blue–green) and $Pd(phen)Cl_2$ (yellow) [2].

The crystal structure of $[Ni(phen)_2(H_2O)_2][ZnCl_4]\cdot H_2O$ (**2**) consists of discrete *cis*-$[Ni(phen)_2(H_2O)_2]^{2+}$ cations, tetrahedral $[ZnCl_4]^{2-}$ anions and lattice molecules of water. A labeled diagram is shown in Fig. 1. The selected bond distances and angles are listed in Table 2. The coordination sphere of the nickel atom is a distorted octahedron, the aqua ligands being disposed in *cis* positions to each other. The Ni–N distances [ave. 2.083(4) Å] are identical to the average value found in the tris-chelated cation, $[Ni(phen)_3]^{2+}$ [2.090(5) Å [14] and 2.091(8) Å [15]]. As expected, the N–Ni–N chelate angles [80.2(1) and 80.6(1)°] are significantly smaller than the other *cis* angles which vary between 88.1(1) and 96.3(1)°. The *trans* angles are in the range 171.5(1)–174.1(1)°. The Ni–O (H_2O) bonds are 2.057(3) and 2.073(3) Å. The external angles with the phenanthroline ligands, Ni–N–C [ave. 129.5(3)°] are much larger than the Ni–N–C chelate angles [ave. 112.3(3)°].

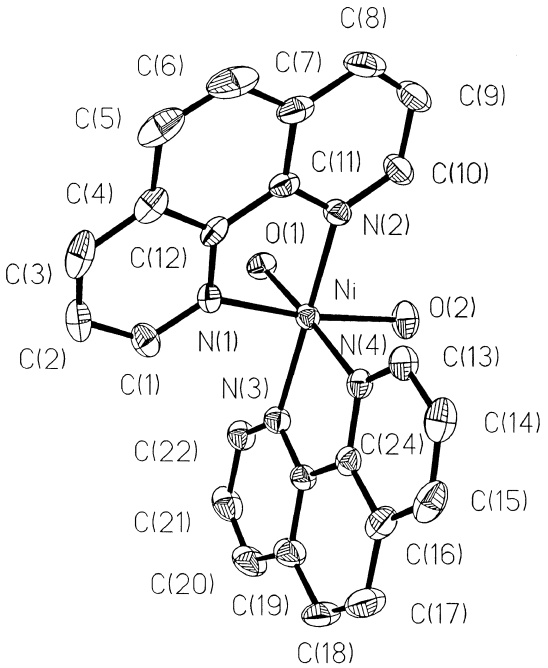

Fig. 1. Labeled diagram of the cation $[Ni(phen)_2(H_2O)_2]^{2+}$ in **2**.

The $[ZnCl_4]^{2-}$ anions exhibit the characteristic features already reported in the literature [16]. The Zn–Cl bond distances vary between 2.242(2) and 2.293(1) Å and the angles are close to the tetrahedral value [105.1(1)–112.2(1)°].

The complex salt crystallizes with a molecule of water. The complexed ions and the lattice water molecules are held together by an extensive three-dimensional hydrogen-bond network. The aqua ligands are hydrogen-bonded to the lattice water molecules with distances of O(1)···O(3) = 2.713 Å and the angle Ni–O(1)···O(3) is 121.6°. The aqua ligands are also hydrogen-bonded to the chloride ligands with distances O(1)···Cl(1) = 3.102 Å [angle Ni–O(1)···Cl(1) = 105.7°] and O(2)···Cl(2) = 3.163 Å [angle Ni–O(2)···Cl(2) = 124.0°]. The distance O(2)···Cl(1) is also short (3.174 Å) but the angle is not favorable [Ni–O(2)···Cl(1) = 165.8°]. Furthermore, the lattice molecule of water is hydrogen-bonded to two different Cl(3) atoms with distances O(3)···Cl(3) = 3.178 and 3.192 Å, and angle Cl(3)···O(3)···Cl(3′) = 122.3°. Face-to-face stacking interactions between the phenanthroline aromatic rings of the cationic entities (Figure 2) play also an important stabilization role in the packing energy of the crystal.

The diffuse reflectance spectrum of **2**, measured in the range 380–1100 nm, exhibits the characteristic features of a pseudo-octahedral $[Ni(II)N_4O_2]$ chromophore. Two of the three expected *d–d* bands are observed at 920 and 580 nm, and are assigned to the transitions $^3A_2 \rightarrow {}^3T_2$ and $^3A_2 \rightarrow {}^3T_1(F)$, respectively (assuming the *O* point group for the Ni(II) chromophore). The electronic spectrum of the nickel chromophore of the solid mixture obtained after the migration process is identical to the one reported for $Ni(phen)_2Cl_2$ [13].

The solid state rearrangement of the tris-bipyridine complex $[Ni(bipy)_3][PdCl_4]\cdot 2\frac{1}{2}H_2O$ (**3**) is quite similar to the phenanthroline complex. The TG, DTG and DTA curves are shown in Fig. 3. The DSC curve of the compound was also measured. A first decomposition step due to the loss of the water molecules was observed below 120°C. Between 120 and about 220°C, the TG curve showed no weight loss, while the DTA curve exhibited an exothermal peak centered around 190°C, assigned to the migration of the ligands:

$$[Ni(bipy)_3][PdCl_4](s) \xrightarrow{190^\circ C} Ni(bipy)_2Cl_2(s) + Pd(bipy)Cl_2(s)$$

The migration of the bipyridine molecule and of the two chloride ions occurred in the range 160–220°C, during an exothermic process, the total heat of the transformation being $\Delta H = -35$ kJ/mol. This value is significantly lower than the one observed for the phenanthroline compound discussed above (-67 kJ/mol). It is noteworthy to point out that in the case of the tetrachlorozincate complexes,

Table 2. Selected distances (Å) and angles (°)

$[Ni(phen)_2(H_2O)_2][ZnCl_4]\cdot H_2O$ (**2**)			
Ni–O(1)	2.057(3)	Ni–O(2)	2.073(3)
Ni–N(1)	2.085(3)	Ni–N(2)	2.083(4)
Ni–N(3)	2.089(4)	Ni–N(4)	2.078(3)
Zn–Cl(1)	2.294(1)	Zn–Cl(2)	2.285(2)
Zn–Cl(3)	2.272(2)	Zn–Cl(4)	2.242(2)
O(1)-Ni-O(2)	88.9(1)	O(1)-Ni-N(1)	91.6(1)
O(2)–Ni–N(1)	171.5(1)	O(1)–Ni–N(2)	91.1(1)
O(2)–Ni–N(2)	91.4(1)	N(1)–Ni–N(2)	80.1(1)
O(1)–Ni–N(3)	93.6(1)	O(2)–Ni–N(3)	92.2(1)
N(1)–Ni–N(3)	96.3(1)	N(2)–Ni–N(3)	174.1(1)
O(1)–Ni–N(4)	173.4(1)	O(2)–Ni–N(4)	88.1(1)
N(1)–Ni–N(4)	92.3(1)	N(2)–Ni–N(4)	94.8(1)
N(3)–Ni–N(4)	80.6(1)	Cl(1)–Zn–Cl(2)	105.1(1)
Ni–N(1)–C(12)	111.8(3)	Ni–N(2)–C(10)	129.3(3)
Ni–N(2)–C(11)	112.6(3)	Ni–N(3)–C(22)	129.9(3)
Ni–N(3)–C(23)	112.0(3)	Ni–N(4)–C(13)	129.1(3)
Ni–N(4)–C(24)	112.7(3)	Cl(1)–Zn–Cl(2)	105.1(1)
Cl(1)–Zn–Cl(3)	105.7(1)	Cl(2)–Zn–Cl(3)	112.0(1)
Cl(1)–Zn–Cl(4)	109.3(1)	Cl(2)–Zn–Cl(4)	112.2(1)
Cl(3)–Zn–Cl(4)	112.0(1)		
$Ni(bipy)_2Cl_2\cdot 2H_2O\cdot\frac{1}{2}CH_3CN$ (**4**)			
Ni–Cl	2.428(1)	Ni–N(1)	2.084(3)
Ni–N(2)	2.049(2)	N–C (ave)	1.345(4)
C–C (ave)	1.380(5)	C(5)–C(6)	1.476(4)
Cl–Ni–N(1)	90.8(1)	Cl–Ni–N(2)	89.6(1)
N(1)–Ni–N(2)	78.5(1)	Cl–Ni–ClA	91.7(1)
N(1)–Ni–ClA	94.7(1)	N(2)–Ni–ClA	173.1(1)
N(1)–Ni–N(1A)	172.1(1)	N(2)–Ni–N(1A)	95.9(1)
N(2)–Ni–N(2A)	89.9(1)	Ni–N(1)–C(1)	126.2(2)
Ni–N(1)–C(5)	115.2(2)	Ni–N(2)–C(6)	115.2(2)
Ni–N(2)–C(10)	126.7(2)		

$[Ni(AA)_3][ZnCl_4]$, the migration of the ligands was found to be endothermic [17].

Heating $[Ni(bipy)_3][PdCl_4]\cdot 2{\cdot}5H_2O$ (**3**) close to 200°C caused an irreversible thermochromic change from the initial pink–beige to a green color. The green mixture was treated with ethanol in order to separate the two compounds. $Ni(bipy)_2Cl_2$ is soluble, while $Pd(bipy)Cl_2$ is very insoluble in this solvent, and the latter was characterized by elemental chemical analysis.

The green color is due to the superposition of the electronic spectra of two chromophores (as seen in Fig. 4): $Ni(bipy)_2Cl_2$ (blue–green) and $Pd(bipy)Cl_2$ (yellow). The color changes accompanying the ligand interchanges merely reflect the modifications of the coordination spheres of the metal ions, that is, the nature of the chromophores. The visible spectra recorded before and after the migration reflect the features of the two nickel(II) chromophores, $[NiN_6]$ and $[NiN_4Cl_2]$. The electronic spectrum of the pure nickel compound obtained after the migration process exhibits the characteristic bands [13] at 1010 and 610 nm, which are assigned to the transitions $^3A_2\rightarrow{}^3T_2$ and $^3A_2\rightarrow{}^3T_1(F)$, respectively (assuming again the *O* point group). It is identical to the one reported for $Ni(bipy)_2Cl_2$ [13].

The nickel compound was recrystallized in acetonitrile and its crystal structure was determined by X-ray diffraction methods. A labeled diagram of $Ni(bipy)_2Cl_2\cdot 2H_2O\cdot\frac{1}{2}CH_3CN$ (**4**) is shown in Fig. 5. The coordination sphere around Ni atoms is octahedral with the two chloro ligands located in *cis* positions to each other. The metal atom is situated in special position on a two-fold axis. The bond distances and angles are listed in Table 2. The Ni–Cl bond distances are 2.428(1) Å, and the Ni–N bonds are 2.084(3) and 2.094(2) Å. The latter values compare well with those [2.088(2) Å] observed in a $[Ni(bipy)_3]^{2+}$ complex [18]. The N–Ni–N chelated angles are smaller [78.5(1)°] than the *cis* angles [89.6(1)–95.9(1)°] around the Ni atom, as expected. The *trans* angles are 172.1(1) and 173.1(1)°. The external angles with the bipyridine ligands, Ni–N–C [ave. 126.5(2)°] are larger than the Ni–N–C chelate angles [ave. 115.2(2)°], but the differ-

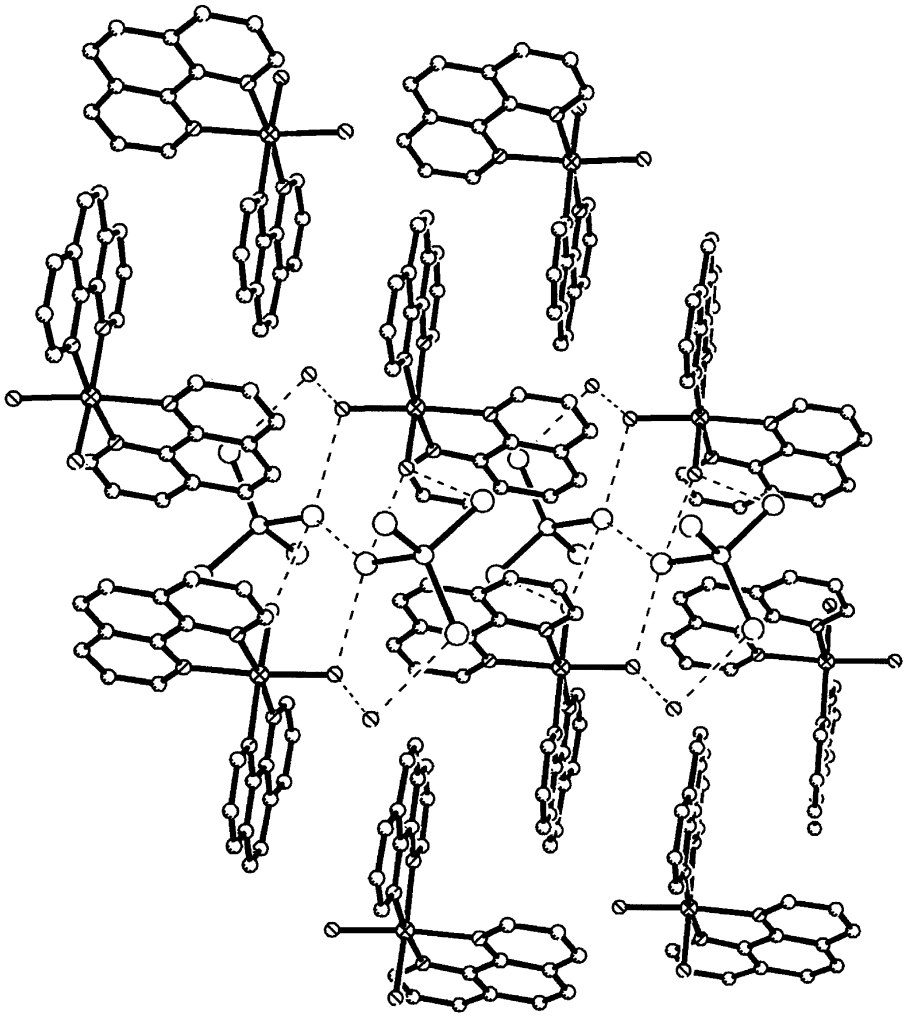

Fig. 2. Packing diagram of the molecules in the crystal $[Ni(phen)_2(H_2O)_2][ZnCl_4]\cdot H_2O$ (**2**).

ence is smaller than the one observed in the phenanthroline compound **2** described above. The average N–C distance is 1.345(4) Å, while the aromatic C–C bonds have an average value of 1.380(5) Å. The C(5)–C(6) bond is 1.476(4) Å. The *ortho* aromatic internal angles around C(1), C(5), C(6) and C(10) are slightly larger [ave. 122.0(3)°] than the other internal aromatic angles [ave. 119.1(4)°]. The internal angles around the C atoms in the chelate rings are 115.4(2) and 115.6(3)°, while the external angles C(4)–C(5)–C(6) and C(5)–C(6)–C(7) are 123.0(2) and 123.1(3)°, respectively.

The compound crystallized with two molecules of water (general position) and $\frac{1}{2}$ molecule of CH_3CN, located on a two-fold axis. The methyl group and the N atom of the CH_3CN molecules are disordered on the two sides of the central C atom. Therefore the distances in the CH_3CN molecules are not precise.

The molecules are held together by hydrogen bonding around the lattice molecules of water. Each water molecule is hydrogen bonded to two chloro ligands, with Ow···Cl distances of 3.235 and 3.238 Å and an angle Cl···Ow···Cl = 120.0°. The acetonitrile molecules are not involved in the hydrogen bonding system, but contribute to the packing energy. Stacking interactions between the dipyridyl aromatic rings play also an important stabilization role in the packing energy of the crystal.

The IR spectrum of the green mixture obtained after the ligand interchange is simply the sum of the corresponding spectra of $Ni(bipy)_2Cl_2$ and $Pd(bipy)Cl_2$. For comparison, the solvent free compound $Ni(bipy)_2Cl_2$ was obtained by heating **4** at 160°C (according to its thermal analysis) and by the controlled thermal decomposition of $[Ni(bipy)_3]Cl_2\cdot 7H_2O$ [19]. The two corresponding spectra were identical. Furthermore, all the characteristic frequencies of $Ni(bipy)_2Cl_2$ were identified in the IR spectrum of the green mixture.

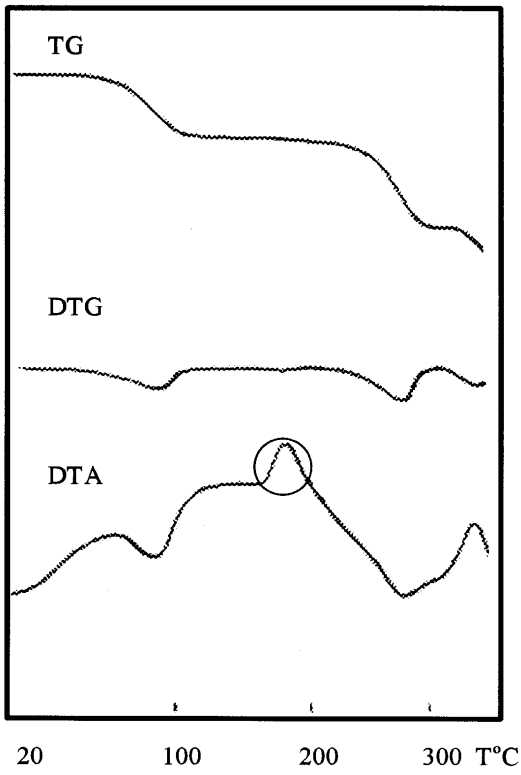

Fig. 3. Thermal analysis curves (TG, DTG, DTA) for $[Ni(bipy)_3][PdCl_4]\cdot 2\frac{1}{2}H_2O$ (**3**).

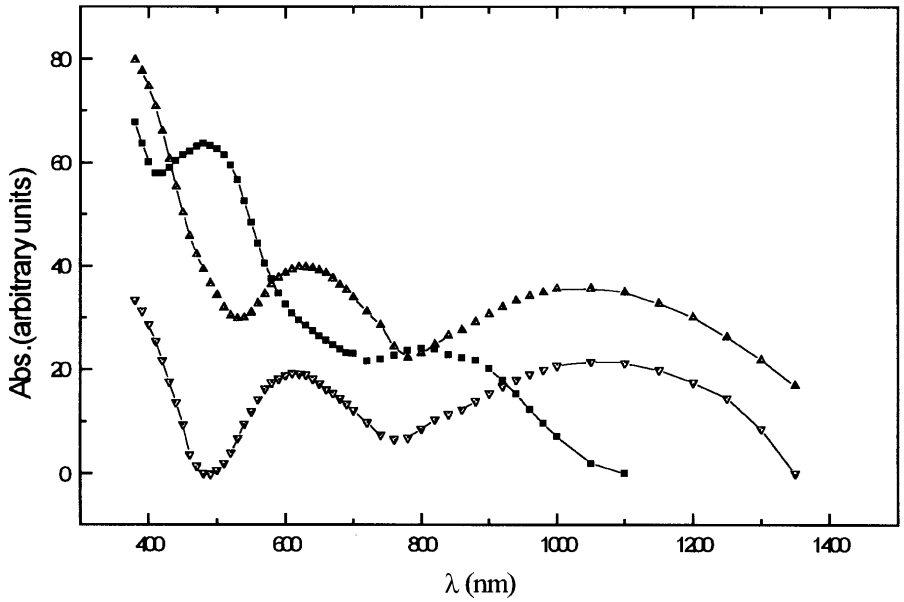

Fig. 4. Diffuse reflectance spectra for: $[Ni(bipy)_3][PdCl_4]\cdot 2\frac{1}{2}H_2O$ (■), $[Ni(bipy)_2Cl_2]+[Pd(bipy)Cl_2]$ (▲) and $[Ni(bipy)_2Cl_2]$ (▼) (after the elimination of the molecules of solvent).

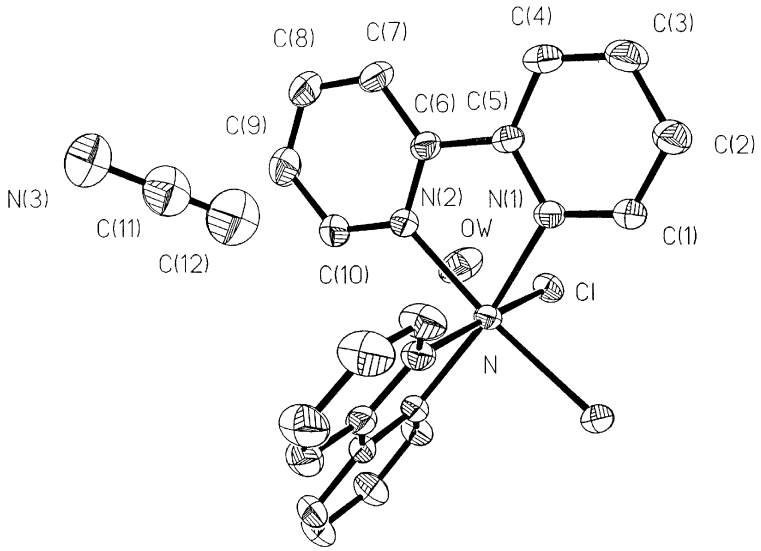

Fig. 5. Labeled diagram of $Ni(bipy)_2Cl_2{\cdot}2H_2O{\cdot}\frac{1}{2}CH_3CN$ (**4**).

According to the TG curve of the compound $[Ni(bipy)_3][PdCl_4]{\cdot}2\frac{1}{2}H_2O$ (**3**), the loss of the organic ligands starts at 220°C:

$$Ni(bipy)_2Cl_2(s) + Pd(bipy)Cl_2(s) \xrightarrow{220\text{–}280^\circ C} \{Ni(bipy)_{2.56}PdCl_4\} \times (s) + 0.44bipy(g)$$

$$\{Ni(bipy)_{2.56}PdCl_4\}(s) \xrightarrow{280\text{–}370^\circ C} \{Ni(bipy)_{2.34}PdCl_4\}(s) + 0.22bipy(g)$$

$$\{Ni(bipy)_{2.34}PdCl_4\}(s) \xrightarrow{370\text{–}520^\circ C} \{Ni(bipy)PdCl_4\}(s) + 1.34bipy(g)$$

$$\{Ni(bipy)PdCl_4\}(s) \xrightarrow{520\text{–}840^\circ C} NiO(s) + Pd(s) + bipy(g) + 2Cl_2(g)$$

The final products of the complete oxidative degradation of compound **3** are Pd and NiO. They were identified from their powder X-ray patterns [11].

The loss of bipyridine in the compound $Ni(bipy)_2Cl_2{\cdot}2H_2O{\cdot}\frac{1}{2}CH_3CN$ (**4**) starts around 160°C. Its thermal decomposition is as follows:

$$[Ni(bipy)_2Cl_2]{\cdot}2H_2O{\cdot}\tfrac{1}{2}CH_3CN(s) \xrightarrow{20\text{–}160^\circ C} Ni(bipy)_2Cl_2(s) + 2H_2O + \tfrac{1}{2}CH_3CN$$

$$Ni(bipy)_2Cl_2(s) \xrightarrow{160\text{–}320^\circ C} Ni(bipy)_{1.33}Cl_2(s) + 0.67bipy(g)$$

The degradation process seems to follow the decomposition pathway of the reported compound $[Ni(bipy)_3]Cl_2{\cdot}7H_2O$ [19] (after the loss of the first bipy molecule), namely:

$$[Ni(bipy)_3]Cl_2{\cdot}7H_2O(s) \xrightarrow{20\text{–}120^\circ C} [Ni(bipy)_3]Cl_2(s) + 7H_2O(g)$$

$$[Ni(bipy)_3]Cl_2(s) \xrightarrow{120\text{–}250^\circ C} Ni(bipy)_2Cl_2(s) + bipy(g)$$

$$Ni(bipy)_2Cl_2(s) \xrightarrow{250\text{–}325^\circ C} Ni(bipy)_{1.33}Cl_2(s) + 0.67bipy(g)$$

The temperatures are slightly different, probably caused by different heating rates. The following stages of the decomposition are identical for both compounds and consist in a multistep oxidation process, leading finally to NiO at about 700°C.

The examples presented in this work fall in the category of irreversible thermochromism [5], the color changes being caused by major structural modifications.

Acknowledgements—We gratefully acknowledge financial support from Romanian Academy (Grant No. 525/1997) and the Natural Sciences and Engineering Research Council of Canada.

Supplementary material: lists of the coordinates with equivalent isotropic temperature factors, anisotropic temperature factors, bond distances and angles, hydrogen coordinates and observed and calculated structure ampli-

tudes have been deposited at the Cambridge Crystallographic Data Centre.

REFERENCES

1. Andruh, M., Brezeanu, M., Cimpoesu, M., Dragoe, N., Segal, E. and Cimpoesu, F., *Roum. Chem. Quart. Rev.*, 1994, **2,** 83 and references therein.
2. Andruh, M., *Rev. Roumaine Chim.*, 1991, **36,** 101.
3. Cimpoesu, F., Andruh, M. and Segal, E., *Thermochim. Acta*, 1990, **177,** 93.
4. Dragoe, N., Andruh, M. and Segal, E., *Thermochim. Acta*, 1993, **220,** 185.
5. Sone, K. and Fukuda, Y., *Inorganic Thermochromism*. Springer, Berlin, 1987.
6. Wendlandt, W. W. and Smith, J. P., *The Thermal Properties of Transition Metal Ammine Complexes*. Elsevier, Amsterdam, 1967.
7. LeMay, H. E., Jr., in *Comprehensive Coordination Chemistry*, Vol. 1, ed. G. Wilkinson, R. D. Gillard and J. A. McCleverty, Pergamon, Oxford, 1987, p. 463.
8. Kukushkin, I. N., Panina, N. S. and Yakolev, V. N., *Koord. Khim.*, 1990, **11,** 539 and references therein.
9. Savage, S., Jia-Long, Z. and Maddok, A. G., *J. Chem. Soc., Dalton Trans*. 1985, 991.
10. Morgan, G. T. and Burstall, F. H., *J. Chem. Soc.*, 1931, 2213.
11. Joint Comitee on Powder Diffraction Standards, ed., *Inorganic Index to the Powder Diffraction File* 1971, Pennsylvania, U.S.A. Files: Pd, 5-0681; NiO, 4-0835.
12. SHELXTL PLUS (PC version, 1990–1993). Siemens Analytical Instruments Inc. Madison, WI, U.S.A.
13. Harris, C. M. and McKenzie, E. D., *J. Inorg. Nucl. Chem.*, 1967, **29,** 1047.
14. Frenz, B. A. and Ibers, J. A., *Inorg. Chem.*, 1972, **11,** 1109.
15. Decurtins, S., Schmalle, H. W., Pellaux, R., Schneuwly, P. and Hauser, A., *Inorg. Chem.*, 1996, **35,** 1451.
16. Kent Murmann, R., Schlemper, E. O., Barnes, C. and Vassian, E. G., *Inorg. Chim. Acta*, 1995, **240,** 191.
17. Andruh, M., Brezeanu, M., Paraschivoiu, I. and Segal, E., *Thermochim. Acta*, 1990, **161,** 247.
18. Decurtins, S., Schmalle, H. W., Schneuwly, P., Ensling, J. and Gütlich, P., *J. Am. Chem. Soc.*, 1994, **116,** 9521.
19. Lee, R. H., Griswood, E. and Kleinberg, J., *Inorg. Chem.*, 1964, **3,** 1278.

Pergamon

PII: S0277–5387(98)00129–6

Polyhedron Vol. 17, No. 21, pp. 3681–3688, 1998
© 1998 Elsevier Science Ltd
All rights reserved. Printed in Great Britain
0277–5387/98 $19.00+0.00

Synthesis and crystallographic characterisation of silver complexes with the ligand diferrocenylphenylphosphine

M. Concepción Gimeno,[a] Peter G. Jones,[b] Antonio Laguna[a]* and Cristina Sarroca[a]

[a]Departamento de Química Inorgánica, I.C.M.A. Universidad de Zaragoza-CSIC E-50009 Zaragoza, Spain

[b]Institut für Anorganische und Analytische Chemie der Technischen Universität, Postfach 3329, D-38023 Braunschweig, Germany

(Received 11 February 1998; accepted 27 March 1998)

Abstract—Diferrocenylphosphine (PFc_2Ph) reacts with Ag(TfO) or $[Ag(TfO)(PR_3)]$ (TfO = trifluoromethanesulfonate) to afford the three-coordinate complexes $[Ag(TfO)(PFc_2Ph)_2]$ or $[Ag(TfO)(PFc_2Ph)(PR_3)]$ ($PR_3 = PPh_2Me$, PPh_3), respectively. The complex $[Ag(TfO)(PFc_2Ph)_2]$ further reacts with bidentate ligands, such as bis(diphenylthiophosphoryl)methane (dptpm) or $S_2CNEt_2^-$ leading to the cationic, $[Ag(PFc_2Ph)_2(dptpm)]TfO$, or neutral, $[Ag(S_2CNEt_2)(PFc_2Ph)_2]$, four-coordinate complexes. The reaction with 1,10-phenanthroline (phen) gives to the four-coordinate $[Ag(TfO)(PFc_2Ph)(phen)]$. © 1998 Elsevier Science Ltd. All rights reserved. © 1998 Elsevier Science Ltd. All rights reserved

Keywords: Silver; Ferrocene; Diferrocenylphenylphosphine

The study of the coordination chemistry of ferrocenylphosphines, such as the diphosphine 1,1′-bis(diphenylphosphino)ferrocene, has attracted a great deal of interest because the resultant complexes often find applications in homogeneous catalysis, in organic synthesis, manipulation of materials and production of fine chemicals [1, 2]. However, diferrocenylphenylphosphine (PFc_2Ph), although synthesised more than three decades ago, by interaction of ferrocene with dichlorophenylphosphine in the presence of anhydrous aluminium chloride [3], has scarcely been studied. Only very few complexes, such as $[M(CO)_5(PFc_2Ph)]$ (M = Mo or W), $[CoMe(DH)_2(PFc_2Ph)]$ (DH = dimethylglioximate), $[Ni(acac)_2(PFc_2Ph)]$ [4] or the gold derivative $[AuCl(PFc_2Ph)]$ [5], have been reported, but no silver derivative has been described so far.

Here we report on the synthesis of mononuclear three- or four coordinate silver(I) complexes that contain one or two diferrocenylphenylphosphine ligands.

* Author to whom correspondence should be addressed. Fax: +34 976 761187; E-mail: alaguna@posta.unizar.es

RESULTS AND DISCUSSION

The reaction of Ag(TfO) (TfO = trifluoromethanesulfonate) with diferrocenylphenylphosphine (PFc_2Ph) in diethyl ether, in a 1:2 molar ratio, gives a suspension from which $[Ag(TfO)(PFc_2Ph)_2]$ **1** can be isolated (Scheme 1). Other mononuclear complexes with two different phosphines, $[Ag(TfO)(PFc_2Ph)(PR_3)]$ ($PR_3 = PPh_2Me$ **2**, PPh_3 **3**), can be prepared by reaction of $[Ag(TfO)(PR_3)]$ with the ferrocenylphosphine in dichloromethane. Complexes **1**–**3** are yellow solids, air- and moisture stable. They behave as 1:1 electrolytes in acetone solution, which confirms an ionic nature, $[Ag(PFc_2Ph)(PR_3)]TfO$, in solution. In the IR spectra, the trifluoromethanesulfonate group gives rise to strong absorptions at 1625 (br) [$\nu(SO_3)$], 1225 [$\nu_{sym}(CF_3)$] and 1559 [$\nu_{as}(CF_3)$] cm^{-1}.

In the positive-ion liquid secondary ion mass spectra (LSIMS) the cation peaks $[Ag(PFc_2Ph)(PR_3)]^+$ appear at m/z 1063 (**1**, 50) and 847 (**3**, 57%). Additionally, other fragments in the spectrum of **3** correspond to $[Ag(PPh_3)_2]^+$ (633, 85) and $[Ag(PFc_2Ph)_2]^+$ (1063, 25%).

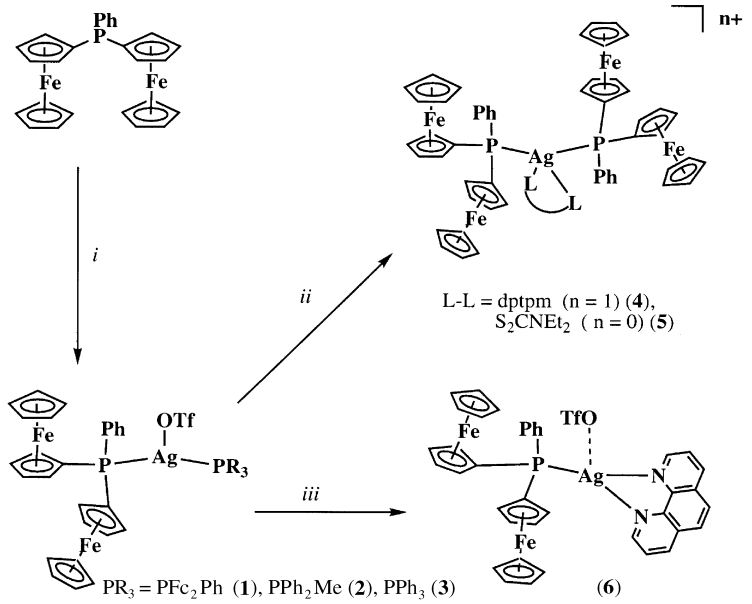

Scheme 1. (i) 1/2 Ag(TfO) or [Ag(TfO)(PR_3)], (ii) **1** + P(S)$Ph_2CH_2PPh_2$(S) or NaS_2CNEt_2, (iii) **1** + phen.

The ^{1}H NMR spectra of complexes **1**–**3** show the four different protons of the P(C_5H_4) rings as four multiplets or as a broad multiplet and the equivalent protons of the C_5H_5 rings as a singlet (see Table 1). In the spectrum of complex **3** the resonances due to complex **1** are also present. In the $^{31}P\{^1H\}$ NMR spectrum of **1**, $CDCl_3$ at -55°C, two doublets are observed as a consequence of chemically equivalent phosphorus atoms coupled to ^{107}Ag and ^{109}Ag nuclei. Complexes **2** and **3** present an AB system, both coupled to the two silver nuclei (Table 1). In the spectrum of **3** the resonances due to complex **1** and $[Ag(PPh_3)_2]^+$ [two doublets at δ -3.2, J(AgP) 604.3, 524.0 Hz] are also observed, indicating the existence of a ligand exchange equilibrium of **3** and the corresponding homoleptic species, although complex **3** is predominant. In complex **2** only signals of very low intensity at δ -2 ($[Ag(PFc_2Ph)_2]^+$) and -4 ($[Ag(PPh_2Me)_2]^+$) are present.

The structure of complex **1** was confirmed by X-ray diffraction analysis. The molecule is shown in Fig. 1, with selected bond lengths and angles in Table 2. The trifluoromethanesulfonate is coordinated by one oxygen to the silver atom. The silver presents a somewhat distorted trigonal-planar coordination, probably due to the steric requirements of the phosphines, with angles P(2)–Ag–P(1) of 135.20(6), O(1)–Ag–P(1) of 104.6(2) and O(1)–Ag–P(2) of 120.2(2)°. The silver atom lies only 0.01 Å out of the plane of the two phosphorus and oxygen atoms. The Ag–P distances [2.450(2) and 2.445(2) Å] are similar to those found in other tri-coordinate silver complexes $[Ag(dppf)(PPh_3)]ClO_4$ [dppf = 1,1′-bis(diphenylphosphino)ferrocene] [6] which range from 2.424(1) to 2.480(1) Å and slightly longer than those found in $[Ag_2(PPh_3)_2(SPPh_2CHPPh_2CHCO_2Me)]ClO_4$, 2.372(3) and 2.404(3) Å [7]. The Ag–O bond length of 2.345(7) Å is smaller than in the preceding dinuclear compound, 2.488(7) Å [7], but longer than in $[Ag(NO_3)(4\text{-}NO_2C_5H_4NO)_2]$, 2.364(3) and 2.318(3) Å [8]. The cyclopentadienyl rings are as expected parallel and planar. The rings are staggered by 13, 18 and 13° for Fe(2), Fe(3) and Fe(4), respectively, but by 29° for Fe(1), around the Cp · · · Cp axis (Cp = centre of cyclopentadienyl ring) defined by the torsion angles C–Cp–Cp–C. The Fe–Cp distances are in the range 1.639(3)–1.650(3) Å.

We have studied the reactivity of complex **1** with bidentate ligands such as bis(diphenylthiophosphoryl)methane (dptpm), $S_2CNEt_2^-$ (from NaS_2CNEt_2) or 1,10-phenanthroline (phen). Treatment of equimolecular amounts of **1** with the first two ligands affords the four-coordinate cationic or neutral complexes, $[Ag(PFc_2Ph)_2(dptpm)]TfO$ (**4**) and $[Ag(S_2CNEt_2)(PFc_2Ph)_2]$ (**5**). They are air- and moisture stable yellow solids. The IR spectrum of **4** shows bands at 1258 (s, br), 1224 (s) and 1157 (s) cm^{-1}, from the TfO anion, and the ν(P=S) vibration appears at 557 (m) cm^{-1}. A band at 1515 (m) cm^{-1} in the IR spectrum of **5** is attributable to ν(C=N) of the dithiocarbamate ligand. In the LSIMS spectra the molecular peak does not appear, but the peaks assigned to the fragments $[Ag(PFc_2Ph)(L\text{-}L)]^+$ at m/z 1035 (**1**, 50) and 847 (**3**, 57%) are present. Complex **4** is an 1:1 electrolyte in acetone solution, but **5** behaves as nonconductor in solution.

The ^{1}H NMR spectra of complexes **4** and **5** show the expected four resonances for the P(C_5H_4) protons

Table 1. ^{1}H and ^{31}P-$\{^{1}H\}$ NMR data for complexes **1**–**6**

	^{1}H			^{31}P	
Complex	$P(C_5H_4)$	(C_5H_5)	L	PFc_2Ph	L
1 $[Ag(TfO)(PFc_2Ph)_2]$	4.27(m) 4.46(m) 4.52(m) 4.67(m)	4.07(m)		−2(dd)[a] *J*(AgP) 577.0, 501.1	
2 $[Ag(TfO)(PFc_2Ph)(PPh_2Me)]$	4.17(m) 4.28(m) 4.34(m) 4.37(m)	3.90(m)	2.26(s) 7–8(m)	−2[a] *J*(AB) 35.8 *J*(AgP) 603.3, 519.8	−3.8 *J*(AgP) 566.0, 470.2
3 $[Ag(TfO)(PFc_2Ph)(PPh_3)]$	4–5(m)	4.04(m)	7–8(m)	11.05[a] *J*(AB) 35.8 *J*(AgP) 604.3, 444.6	11.8 *J*(AgP) 582.9, 422.2
4 $[Ag(PFc_2Ph)_2(dptpm)]TfO$	4.09(m) 4.29(m) 4.36(m) 4.40(m)	4.04(m)	4.57(t) *J*(PH) 14.3	4.5(dd)[b] *J*(AgP) 640.9, 555.7	45.8(s)
5 $[Ag(S_2CNEt_2)(PFc_2Ph)_2]$	4.08(m) 4.30(m) 4.31(m) 4.34(m)	4.10(m)	1.37(t) 4.07(q) *J*(HH) 6.96	7.1 (dd)[b] *J*(AgP) 598.1, 517.8	
6 $[Ag(TfO)(PFc_2Ph)(phen)]$	4.18(m) 4.22(m) 4.40(m) 4.43(m)	4.05(m)	7.44(m) 7.94(d) 8.56(d) 9.32(m)	−5.4(d, br)[a] $J_{aver.}$ 442	

[a] Recorded in $CDCl_3$ at −55°C, [b] Recorded in $(CD_3)_2CO$ at −85°C, coupling constant in Hz; s = singlet, d = doublet, dd = two doublets, t = triplet, m = multiplet, br = broad.

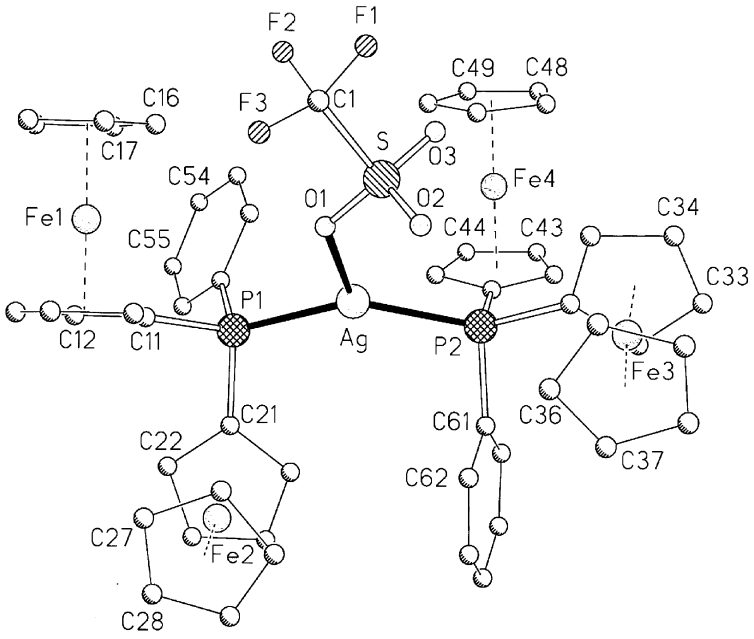

Fig. 1. The molecule of complex **1** in the crystal showing the atom-numbering scheme, radii are arbitrary. H atoms are omitted for clarity.

Table 2. Selected bond lengths [Å] and angles [°] for complex **1**.

Ag–O(1)	2.345(7)	Ag–P(2)	2.445(2)
Ag–P(1)	2.450(2)	P(1)–C(11)	1.805(7)
P(1)–C(21)	1.812(6)	P(1)–C(51)	1.829(6)
P(2)–C(31)	1.803(6)	P(2)–C(41)	1.812(6)
P(2)–C(61)	1.824(6)	S–O(1)	1.399(7)
O(1)–Ag–P(2)	120.2(2)	O(1)–Ag–P(1)	104.6(2)
P(2)–Ag–P(1)	135.20(6)	C(11)–P(1)–C(21)	102.9(3)
C(11)–P(1)–C(51)	103.2(3)	C(21)–P(1)–C(51)	105.2(3)
C(11)–P(1)–Ag	120.9(2)	C(21)–P(1)–Ag	110.6(2)
C(51)–P(1)–Ag	112.5(2)	C(31)–P(2)–C(41)	101.5(3)
C(31)–P(2)–C(61)	103.5(3)	C(41)–P(2)–C(61)	103.4(3)
C(31)–P(2)–Ag	130.0(2)	C(41)–P(2)–Ag	109.8(2)
C(61)–P(2)–Ag	105.7(2)	S–O(1)–Ag	125.0(4)

and a singlet for the C_5H_5 rings (Table 1). The CH_2 groups of **4** appears as a triplet at 4.57 ppm [*J*(PH), 14.3 Hz] and ethyl groups of **5** are present as a quartet (CH_2, 4.07 ppm, *J*(HH) 6.96 Hz) and a triplet (CH_3, 1.37 ppm). The $^{31}P\{^1H\}$ NMR spectrum of **4**, $(CD_3)_2CO$ at $-85°C$, shows a singlet for the two phosphorus of the diphosphine and two doublets for the phosphorus of the ferrocenylphosphine coupled with the ^{107}Ag and ^{109}Ag nuclei. In complex **5** only the resonance due to the phosphorus coupled to the silver nuclei (two doublets) is observed.

The crystal structure of complex **5** has been established by X-ray diffraction. The compound crystallises as a chloroform solvate. The molecule is shown in Fig. 2, with selected bond lengths and angles in Table 3. The silver atom is coordinated to two phosphines and one chelating dithiocarbamate ligand and has a distorted tetrahedral geometry. The distortion arises from the restricted bite of the dithiocarbamate, S(1)–Ag–S(2) 67.40(6)°, whereas the other angles are wider than ideal, P(2)–Ag–S(2) 131.73(7) or P(1)–Ag–S(1) 126.87(7)°. The dihedral angle between the planes Ag–P(1)–P(2) and Ag–S(1)–S(2) is 66°. The cyclopentadienyl rings of Fe(1), Fe(2), Fe(3) and Fe(4) are staggered by 10, 2, 19 and 15°, respectively, around the Cp · · · Cp axis. The Ag–P distances are 2.500(2) and 2.528(2) Å, similar to those in $[Ag\{(PPh_2)_2C_2B_{10}H_{10}\}(dptpm)]ClO_4$, 2.526(2) and 2.532(2) Å [9], or in other four-coordinate complexes, such as $[Ag(dppe)_2]^+$ [10]. However the two different Ag–S distances, 2.605(2) and 2.739(2) Å, are longer than in $[Ag\{(PPh_2)_2C_2B_{10}H_{10}\}(dptpm)]ClO_4$, 2.540(2) and 2.588(2) Å [9].

Complex **1** reacts with equimolecular amounts of 1,10-phenanthroline in a different way; substitution of one ferrocenylphosphine is now observed to give [Ag(TfO)(PFc_2Ph)(phen)] (**6**). Complex **6** is an air- and moisture stable light orange solid. It behaves as an 1:1 electrolyte in acetone solution, which indicates the dissociation of the trifluoromethanesulfonate ligand to give the ions $[Ag(PFc_2Ph)(phen)]^+$ TfO^-. In the LSIMS spectrum the cation peak $[Ag(PFc_2Ph)(phen)]^+$ appears at *m*/*z* 765 as the most intense one.

The ^1H NMR spectrum of **6** shows the expected resonances of the ferrocenylphosphine (Table 1) and four multiplets at 7.44, 7.94, 8.56 and 9.32 ppm due to the eight protons of the phenanthroline. The phosphorus atom appears as a broad doublet ($CDCl_3$, $-55°C$), due to the coupling with the silver nuclei, in the $^{31}P\{^1H\}$ NMR spectrum.

The molecule of complex **6** is shown in Fig. 3 with selected bond lengths and angles in Table 4. The silver atom presents a distorted tetrahedral geometry, lying 0.39 Å out of the plane formed by the two nitrogen and phosphorus atoms in the direction of the triflate oxygen O(1), with Ag–O(1) 2.626(3) Å. The interplanar angle between AgN(1)N(2) and AgPO(1) is 88°. The restricted "bite" of the phenanthroline, N(1)–Ag–N(2) 72.12(10)°, represents one major deviation from ideal geometry. The Ag–P bond, 2.3445(12) Å, is shorter than in complex **1** or in other three-coordinate derivatives, such as $[Ag(dppf)(PPh_3)]ClO_4$, 2.424(1) to 2.480(1) Å [6], or $[Ag\{(PPh_2)_2C_2B_9H_{10}\}(PPh_3)]$, 2.3974(10) to 2.4942(10) Å [11], reflecting the correspondingly weak Ag coordination to N and O atoms in **6**. The phenanthroline is asymmetrically coordinated through two different Ag–N bonds of 2.289(3) and 2.351(3) Å which are of the same order as those found in other phenanthroline complexes, such as $[Ag\{(PPh_2)_2C_2B_{10}H_{10}\}(phen)]ClO_4$ [9] or [Ag(dppf)(phen)]ClO_4 [6]. The shorter Ag–N distance is associated with the widest angle, P–Ag–N(1) 142.11(7)°. The ferrocene systems display twists of 7 and 17° for Fe(1) and Fe(2), respectively.

EXPERIMENTAL

General

Infrared spectra were recorded in the range 4000–200 cm^{-1} on a Perkin-Elmer 883 spectrophotometer

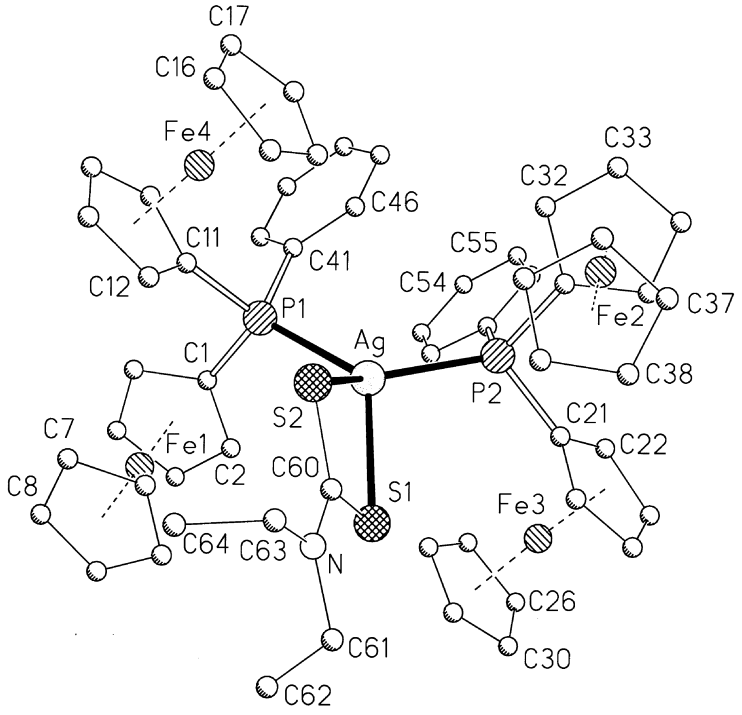

Fig. 2. Molecular structure of complex **5** in the crystal. H atoms are omitted for clarity.

Table 3. Selected bond lengths [Å] and angles [°] for complex **5**.

Ag–P(1)	2.500(2)	Ag–P(2)	2.528(2)
Ag–S(1)	2.605(2)	Ag–S(2)	2.739(2)
P(1)–C(1)	1.799(7)	P(1)–C(11)	1.811(7)
P(1)–C(41)	1.853(7)	P(2)–C(21)	1.807(7)
P(2)–C(31)	1.823(7)	P(2)–C(51)	1.835(7)
S(1)–C(60)	1.733(8)	S(2)–C(60)	1.721(8)
N–C(60)	1.340(9)	N–C(63)	1.450(10)
N–C(61)	1.482(9)		
P(1)–Ag–P(2)	115.95(7)	P(1)–Ag–S(1)	126.86(7)
P(2)–Ag–S(1)	105.70(7)	P(1)–Ag–S(2)	103.06(7)
P(2)–Ag–S(2)	131.73(7)	S(1)–Ag–S(2)	67.40(6)
C(1)–P(1)–Ag	116.5(2)	C(11)–P(1)–Ag	118.9(2)
C(41)–P(1)–Ag	112.7(2)	C(21)–P(2)–Ag	117.9(2)
C(31)–P(2)–Ag	120.0(3)	C(51)–P(2)–Ag	112.1(2)
C(60)–S(1)–Ag	89.1(3)	C(60)–S(2)–Ag	85.0(3)
C(60)–N–C(63)	122.5(7)	C(60)–N–C(61)	120.9(7)
C(63)–N–C(61)	116.6(6)	N–C(60)–S(2)	121.4(6)
N–C(60)–S(1)	120.1(6)	S(2)–C(60)–S(1)	118.4(4)
N–C(61)–C(62)	114.9(7)	N–C(63)–C(64)	112.3(7)

using Nujol mulls between polyethylene sheets. Conductivities were measured in *ca.* 5×10^{-4} mol dm^{-3} solutions with a Philips 9509 conductimeter. C and H analyses were carried out with a Perkin-Elmer 2400 microanalyser. Mass spectra were recorded on a VG autospec, with the LSIMS technique, using nitrobenzyl alcohol as matrix. NMR spectra were recorded on a Varian Unity 300 spectrometer and a Bruker ARX 300 spectrometer in $CDCl_3$ or $(CD_3)_2CO$. Chemical shifts are cited relative to $SiMe_4$ (^{1}H, external) and 85% H_3PO_4 (^{31}P, external). The starting complexes [Ag(TfO)(PR_3)] ($PR_3 = PPh_2Me$, PPh_3) where prepared by reaction of equimolar amounts of Ag(TfO) and the ligand PR_3 in dichloromethane.

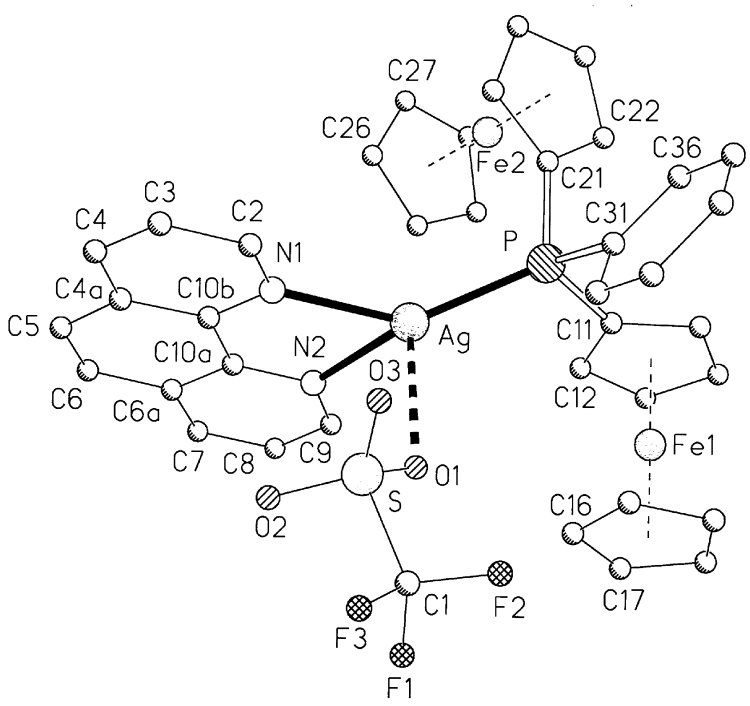

Fig. 3. The molecule of complex **6** in the crystal. H atoms are omitted for clarity.

Table 4. Selected bond lengths [Å] and angles [°] for complex **6**.

Ag–N(1)	2.289(3)	Ag–P	2.3445(21)
Ag–N(2)	2.351(3)	Ag–O(1)	2.626(3)
P–C(21)	1.800(3)	P–C(11)	1.800(3)
P–C(31)	1.820(3)	N(1)–C(2)	1.316(4)
N(1)–C(10B)	1.362(4)	N(2)–C(9)	1.326(4)
N(2)–C(10A)	1.355(5)	C(2)–C(3)	1.394(5)
C(3)–C(4)	1.359(6)	C(4)–C(4A)	1.395(6)
C(4A)–C(10B)	1.410(5)	C(4A)–C(5)	1.433(5)
C(5)–C(6)	1.342(6)	C(6)–C(6A)	1.421(6)
C(6A)–C(7)	1.402(6)	C(6A)–C(10A)	1.417(5)
C(7)–C(8)	1.363(6)	C(8)–C(9)	1.394(5)
C(10A)–C(10B)	1.435(5)		
N(1)–Ag–P	1.42.11(7)	N(1)–Ag–N(2)	72.12(10)
P–Ag–N(2)	135.01(7)	N(1)–Ag–O(1)	90.28(9)
P–Ag–O(1)	110.19(7)	N(2)–Ag–O(1)	92.63(10)
C(21)–P–C(11)	101.2(2)	C(21)–P–C(31)	102.0(2)
C(11)–P–C(31)	105.05(14)	C(21)–P–Ag	115.73(11)
C(11)–P–Ag	115.54(11)	C(31)–P–Ag	115.37(12)
C(2)–N(1)–C(10B)	118.3(3)	C(2)–N(1)–Ag	125.4(2)
C(10B)–N(1)–Ag	116.3(2)	C(9)–N(2)–C(10A)	118.1(3)
C(9)–N(2)–Ag	127.5(3)	C(10A)–N(2)–Ag	114.2(2)
N(1)–C(2)–C(3)	123.5(4)	C(4)–C(3)–C(2)	118.8(4)
C(3)–C(4)–C(4A)	119.9(4)	C(4)–C(4A)–C(10B)	117.8(3)
C(4)–C(4A)–C(5)	123.5(4)	C(10B)–C(4A)–C(5)	118.7(4)
C(6)–C(5)–C(4A)	121.2(4)	C(5)–C(6)–C(6A)	121.7(4)
C(7)–C(6A)–C(10A)	117.3(4)	C(7)–C(6A)–C(6)	123.5(4)
C(10A)–C(6A)–C(6)	119.2(4)	C(8)–C(7)–C(6A)	120.2(4)
C(7)–C(8)–C(9)	118.6(4)	N(2)–C(9)–C(8)	123.7(4)
N(2)–C(10A)–C(6A)	122.2(3)	N(2)–C(10A)–C(10B)	118.7(3)
C(6A)–C(10A)–C(10B)	119.1(3)	N(1)–C(10B)–C(4A)	121.6(3)
N(1)–C(10B)–C(10A)	118.3(3)	C(4A)–C(10B)–C(10A)	120.1(3)

Table 5. Details of data collection and structure refinement for the complexes **1**, **5** and **6**.

Compound	**1**	**5** · $CHCl_3$	**6**
Chemical Formula	$C_{53}H_{46}AgF_3Fe_4O_3P_2S$	$C_{58}H_{57}AgCl_3Fe_4NP_2S_2$	$C_{39}H_{31}AgF_3Fe_2N_2O_3PS$
Crystal habit	yellow prism	yellow plate	yellow plate
Crystal size/mm	$0.70\times0.50\times0.20$	$0.40\times0.40\times0.10$	$0.40\times0.30\times0.15$
Crystal system	Triclinic	Triclinic	Triclinic
Space group	$P\bar{1}$	$P\bar{1}$	$P\bar{1}$
a/Å	11.719(4)	11.395(2)	11.152(4)
b/Å	13.595(4)	12.154(2)	11.720(4)
c/Å	15.698(4)	20.030(3)	14.024(5)
α/°	73.56(3)	77.771(14)	77.95(3)
β/°	76.58(3)	79.167(10)	89.26(3)
γ/°	89.58(3)	77.981(14)	80.37(3)
U/Å^3	2328.7(12)	2621.6(7)	1768.8(11)
Z	2	2	2
D_c/g cm^{-3}	1.730	1.687	1.720
M	1213.17	1331.73	915.26
F(000)	1224	1352	920
T/°C	−100	−100	−130
$2\theta_{max}$/°	50	50	55
μ(Mo-$K\alpha$)/cm^{-1}	18.0	17.82	15.21
Transmission	0.75–0.93	—	0.748–0.886
No. of reflections measured	8614	9410	8406
No. of unique reflections	8177	8964	8134
R_{int}	0.034	0.068	0.127
R^a ($F>4\sigma(F)$)	0.054	0.054	0.038
wR^b (F^2, all refl.)	0.145	0.123	0.089
No. of reflections used	8177	8925	8101
No. of parameters	604	642	469
No. of restraints	452	478	0
S^c	1.016	0.951	1.096
Max. $\Delta\rho$/eÅ^{-3}	1.263	0.8	0.441

[a] $R(F)=\Sigma\|\|F_o|-|F_c\|/\Sigma|F_o|$,

[b] $wR(F^2)=[\Sigma\{w(F_o^2-F_c^2)2\}/\Sigma\{w(F_o^2)^2\}]^{0.5}$; $w^{-1}=\sigma^2(F_o^2)+(aP)^2+bP$, where $P=[F_o^2+2F_c^2]/3$ and a and b are constants adjusted by the program

[c] $S=[\Sigma\{w(F_o^2-F_c^2)^2\}/(n-p)]^{0.5}$, where n is the number of data and p the number of parameters.

$[Ag(TfO)(PFc_2Ph)_2]$ (**1**)

To a suspension of PFc_2Ph [3] (0.096 g, 0.2 mmol) in diethyl ether (20 cm^3) was added Ag(TfO) (0.021 g, 0.1 mmol). The mixture was stirred for 1 h and then filtered. The product was dissolved in dichloromethane (20 cm^3) and the solution was concentrated to *ca.* 5 cm^3. Addition of diethyl ether (15 cm^3) gave complex **1** as a yellow solid. Yield 79%, Λ_M 121 Ω^{-1} cm^2 mol^{-1} (Found: C, 52.05; H, 3.5; S, 3.0. Calc. for $C_{53}H_{46}AgF_3Fe_4O_3P_2S$: C, 52.5; H, 3.7; S, 2.6%).

$[Ag(TfO)(PFc_2Ph)(PR_3)]$ ($PR_3=PPh_2Me$ (**2**), PPh_3 (**3**))

To a solution of PFc_2Ph (0.048 g, 0.1 mmol) in dichloromethane (25 cm^3) was added $[Ag(TfO)(PR_3)]$ (0.046 g, $PR_3=PPh_2Me$; 0.052, $PR_3=PPh_3$; 0.1 mmol) and the mixture was stirred for 1 h. The solution was concentrated to *ca.* 5 cm^3 and addition of hexane (15 cm^3) gave complex **2** and **3** as a yellow solids. Complex **2**: Yield 65%, Λ_M 106 Ω^{-1} cm^2 mol^{-1} (Found: C, 52.05; H, 3.95; S, 3.4. Calc. for $C_{40}H_{36}AgF_3Fe_2O_3P_2S$: C, 52.35; H, 3.85; S, 3.4%). Complex **3**: Yield 86%, Λ_M 111 Ω^{-1} cm^2 mol^{-1} (Found: C, 54.1; H, 3.85; S, 3.05. Calc. for $C_{45}H_{38}AgF_3Fe_2O_3P_2S$: C, 54.25; H, 3.85; S, 3.2%).

$[Ag(PFc_2Ph)_2(dptpm)]TfO$ (**4**)

To a solution of complex **1** (0.121 g, 0.1 mmol) in dichloromethane (20 cm^3) was added $P(S)Ph_2CH_2PPh_2(S)$ [12] (0.045 g, 0.1 mmol) and the mixture was stirred for 1 h. The solution was concentrated to *ca.* 5 cm^3 and addition of diethyl ether (15 cm^3) gave complex **4** as a yellow solid. Yield 60%, Λ_M 140 Ω^{-1} cm^2 mol^{-1} (Found: C, 56.25; H, 4.15; S, 6.3. Calc. for $C_{78}H_{68}AgF_3Fe_4O_3P_4S_3$: C, 56.35; H, 4.1; S, 5.8%).

$[Ag(S_2CNEt_2)(PFc_2Ph)_2]$ (**5**)

To a dichloromethane solution (20 cm^3) of complex **1** (0.121 g, 0.1 mmol) was added NaS_2CNEt_2 (0.023 g,

0.1 mmol). The mixture was stirred for 4 h and then filtered off to remove the sodium trifluoromethanesulfonate. The solvent was evaporated under vacuum to *ca.* 5 cm^3; addition of diethyl ether (15 cm^3) afforded complexes **5** as a yellow solid. Yield 68% (Found: C, 55.9; H, 4.3; N, 1.15; S, 5.1. Calc. for $C_{57}H_{56}AgFe_4NP_2S_2$: C, 56.45; H, 4.65; N, 1.15; S, 5.2%).

[*Ag*(*TfO*)(*PFc*$_2$Ph)(phen)] (**6**)

To a dichloromethane solution (20 cm^3) of complex **1** (0.121 g, 0.1 mmol) was added 1,10-phenanthroline (0.018 g, 0.1 mmol). The mixture was stirred for 1 h and then the solution was concentrated under vacuum to *ca.* 5 cm^3; addition of diethyl ether (15 cm^3) afforded complexes **6** as a light orange solid. Yield 75%, Λ_M 140 $\Omega^{-1}\,cm^2\,mol^{-1}$ (Found: C, 51.9; H, 3.45; N, 3.05; S, 3.75. Calc. for $C_{39}H_{31}AgF_3Fe_2N_2O_3PS$: C, 52.6; H, 3.4; N, 3.05; S, 3.5%).

Crystal Structure Determinations

The crystals were mounted in inert oil on glass fibres and transferred to the cold gas stream of a Siemens R3 (**1**) or P4 (**5**) or a STOE Stadi4 (**6**) diffractometers equipped with an LT-2 low temperature attachment. Data were collected using monochromated MoKα radiation ($\lambda = 0.71073$ Å). Scan type ω (**1**,**5**) or ω/θ (**6**). Cell constants were refined from setting angles (**1**,**5**) or $\pm\omega$ angles of *ca.* 60 reflections in the range 2θ 10–25°. Absorption corrections were applied on the basis of Ψ-scans (**1**,**6**). Structures were solved by the heavy-atom method and refined on F^2 using the program SHELXL-93 [13]. All non-hydrogen atoms were refined anisotropically. Hydrogen atoms were included using a riding model. A system of restraints to light-atom displacement-factor components was used. Special refinement details for **1**: The high displacement parameters of O(1) may indicate some disorder (flexibility of coordination geometry at silver). Crystal data are given in Table 5.

Acknowledgements—We thank the Dirección General de Investigación Científica y Técnica (No. PB97-1010-C02-01) and the Fonds der Chemischen Industrie for financial support.

REFERENCES

1. Togni, A. and Hayashi, T., Ed., *Ferrocenes. Homogeneus Catalysis*, *Organic Synthesis and Materials Science*, VCH, Weinheim, Germany, 1995 (and references cited therein).
2. See for example (a) Cullen, W. R. and Woollins, J. D., *Coord. Chem. Rev.*, 1982, **39**, 1; (b) Hayashi, T. and Kumada, M., *Acc. Chem. Res.*, 1982, **15**, 395.
3. Sollot, G. P., Mertwoy, H. E., Portnoy, S. and Snead, J. L., *J. Org. Chem.*, 1963, **28,** 1090.
4. Kotz, J. C. and Nivert, C. L., *J. Organomet. Chem.*, 1973, **52,** 387.
5. Jones, P. G., Erdbrügger, C. F., Hohbein, R. and Schwarzmann, E., *Acta Cryst.*, 1988, **C44,** 1302.
6. Gimeno, M. C., Jones, P. G., Laguna, A. and Sarroca, C., *J. Chem. Soc., Dalton Trans.*, 1995, 1473.
7. Gimeno, M. C., Jones, P. G., Laguna, A. and Villacampa, M. D., *J. Chem. Soc., Dalton Trans.*, 1995, 805.
8. Aoyama, T., Yamamaka, M. and Ohba, S., Saito, V., *Acta Cryst.*, 1990, **C46,** 762.
9. Bembenek, E., Crespo, O., Gimeno, M. C., Jones, P. G. and Laguna, A., *Chem. Ber.*, 1994, **127,** 835.
10. Harker, C. S. W. and Tiekink, E. R. T., *J. Coord. Chem.*, 1990, **21,** 287.
11. Crespo, O., Gimeno, M. C., Jones, P. G. and Laguna, A., *J. Chem. Soc., Dalton Trans.*, 1996, 4583.
12. Davison, A. and Reger, D. L., *Inorg. Chem.*, 1971, **10,** 1967.
13. Sheldrick, G.M., *SHELXL*-93. *A program for Crystal Structure Refinement*, University of Göttingen, Germany, 1993.

Pergamon

PII: S0277–5387(98)00164–8

Polyhedron Vol. 17, No. 21, pp. 3689–3700, 1998
© 1998 Elsevier Science Ltd
All rights reserved. Printed in Great Britain
0277–5387/98 $19.00+0.00

Cyclopentadienylmolybdenum(II) and -(III) complexes containing diene and allyl ligands. Part 4. Reactivity studies of the bisallyl complex CpMo(*supine*-η-C_3H_5)$_2$ and the allyl-butadiene complex [CpMo(*supine*-η-C_3H_5)(*supine*-η-C_4H_6)][PF_6] [1].

Rinaldo Poli,[a]* and Li-Sheng Wang[b]

[a]Laboratoire de Synthèse et d'Electrosynthèse Organométalliques, Faculté des Sciences "Gabriel", Université de Bourgogne, 6 Boulevard Gabriel, 21100 Dijon, France

[b]Department of Chemistry and Biochemistry, University of Maryland, College Park, Maryland 20742, U.S.A.

(Received 26 February 1998; accepted 7 April 1998)

Abstract—Compound CpMo(η^3-C_3H_5)$_2$, **3**, has been synthesized from $CpMoCl_4$ and four equivalents of allylmagnesium bromide. While the compound is stable in donor solvents at room temperature, warming in refluxing MeCN induces the formation of 1,5-hexadiene by a metal-mediated allyl-allyl coupling process. Treatment of **3** with Bu^{t}NC at room temperature affords CpMo(η^3-C_3H_5)(Bu^{t}NC)$_2$, **4**. A similar reduction with presumed allyl radical loss occurs for [CpMo(η^3-C_3H_5)(η^4-C_4H_6)]$^+$, [**1c**]$^+$, to afford [CpMo(η^4-C_4H_6)(Bu^{t}NC)$_2$]$^+$, **5**. Treatment of [**1c**]$^+$ with methyllithium affords two products, the major one (**1c**) corresponding to the one-electron reduction pathway and the minor one (CpMo(η^3-C_3H_5)(η^3-C_3H_4-1-Et), **6**, ca. 4%) corresponding to nucleophilic addition. Protonation of the **1c**:**6** mixture affords a 2:1 mixture of *cis* and *trans* 2-pentene, in addition to propene. The room temperature $Cp_2Fe^+PF_6^-$ oxidation of **3** in MeCN induces the immediate release of 1,5-hexadiene. The oxidation of **3** in Bu^{t}NC gives complexes [CpMo(CNBu^t)$_3$(η^2−CH_2═$CHCH_2CH_2CH$═CH_2)]$^+PF_6^-$ (**7**, major) and [CpMo(CNBu^t)$_4$]$^+PF_6^-$ (**8**, minor). Finally, the oxidation of **3** in the presence of butadiene, followed by treatment with CD_3CN, affords a mixture of [CpMo(η^3:η^3−$C_3H_4CH_2CH_2C_3H_4$)(CD_3CN)]$^+PF_6^-$, **9**, and [CpMo(η^4−C_4H_6)(CD_3CN)$_2$]$^+PF_6^-$, **10**. Thermal decomposition of this mixture affords butadiene and 1,5-cyclooctadiene. © 1998 Elsevier Science Ltd. All rights reserved

INTRODUCTION

We have recently reported the preparation and properties of a molybdenum complex that contains a cyclopentadienyl, a butadiene, and an allyl ligand in four different isomeric forms and in two redox-related oxidation states, namely [CpMo(η-C_3H_5)(η-C_4H_6)]n+ (n=0, **1a**–**c**; 1, [**1a**–**d**]$^+$), see Scheme 1 [2]. In these isomers, the allyl ligand can adopt either a *prone* (**a** or **d**) or a *supine* (**b** or **c**) configuration, while the butadiene ligand adopts either a *supine* (*s-cis*) (**a** or **b**) or an *s-trans* (**c** or **d**) configuration. While the isomerization rates are slow in the Mo(II) manifold, allowing the isolation of each of the three isomers, they are rapid in the Mo(III) manifold, thus only the most stable isomer [**1b**]$^+$ has been isolated in crystalline form as a PF_6^- salt.

We have subsequently reported on the reactivity of the coordinated ligands in the isomers **1a**–**c** and in the

*Author to whom correspondence should be addressed: Tel +33-03.80.39.68.81; fax +33-03.80.39.60.98; E-mail poli@u-bourgogne.fr.

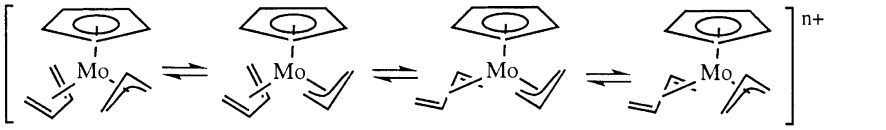

1a **1b** **1c** (n = 0)

$[\mathbf{1a}]^+$ $[\mathbf{1b}]^+$ $[\mathbf{1c}]^+$ $[\mathbf{1d}]^+$ (n = 1)

Scheme 1.

bis(diene) derivative $[CpMo(\eta\text{-}supine\text{-}C_4H_6)(\eta\text{-}s\text{-}trans\text{-}C_4H_6)]^+$, **2**, which is obtained by protonation of **1a** in the presence of butadiene. While the *s-cis*-coordinated butadiene ligand is resistant to any kind of attack, the *s-trans*-coordinated butadiene can be attacked by either electrophilic or nucleophilic reagents depending on the electron richness of the system: electrophilic attack by protons has been observed for the neutral compound **1c** [3], while nucleophilic attack occurs for the cationic complex **2** [4]. The allyl ligand has only been found to engage in electrophilic addition for any of the three isomers of **1** [3].

The reactivity of organic ligands coordinated to Mo(III) has not been the subject of extensive investigations. Compounds with either diene of allyl ligands on Mo(III) are known, e.g. $CpMoCl_2(\eta\text{-}C_4H_6)$ [5] and $CpMo(\eta\text{-}C_3H_5)_2$ [6, 7], in addition to the complexes $[\mathbf{1a}\text{–}\mathbf{d}]^+$ recently reported by us. However, there is apparently no report on the reactivity of the coordinated π ligands in these or other related compounds. In fact, compound $CpMo(\eta\text{-}C_3H_5)_2$, **3**, has been described as "depressively unreactive" [8]. A study of the reactivity of the allyl and diene ligands on Mo(III) is of interest for several reasons. First, it is interesting to examine the effect of the metal oxidation state on the reactivity of the ligands. Second, it is conceivable that a stoichiometric or electron-transfer-catalytic (ETC) [9, 10] oxidation of the more accessible Mo(II) precursors could allow the development of new stoichiometric or catalytic transformations that involve the coordinated ligands. In this report, we describe our exploratory investigations of the reactivity of the isoelectronic Mo(III) compounds **3** and $[\mathbf{1b}]^+$ under a variety of conditions. We show that these complexes, under suitable conditions, are attacked by nucleophiles and electrophiles, undergo Mo–C bond breaking and C–C bond forming reactions, and engage in oxidative and reductive redox processes. A new and improved synthesis of compound **3** is also presented.

RESULTS

(*a*) *New synthesis of* $CpMo(C_3H_4)_2$

The reaction of $CpMoCl_4$ with 4 equivalents of allylmagnesium bromide involves chloride/allyl metathesis and metal reduction, to provide a single-step synthesis of $CpMo(\eta\text{-}C_3H_5)_2$ (see eq. (1). The unoptimized yield is moderate (44%). Nevertheless, considering that $CpMoCl_4$ can be easily prepared in a single, nearly quantitative step from commercially available $[CpMo(CO)_3]_2$ [11], this procedure represents an improvement over the previously reported 3-step synthesis from $MoCl_4(THF)_2$ via $Mo(\eta^3\text{-}C_3H_4)_4$ and $MoCl(\eta^3\text{-}C_3H_4)_3$ [6, 7]. The precursor $MoCl_4(THF)_2$ must also be prepared in two steps from commercially available $MoCl_5$ [12].

$$CpMoCl_4 + 4CH_2{=}CHCH_2MgBr \rightarrow \underset{\mathbf{3}}{CpMo(\eta\text{-}C_3H_5)_2} \quad (1)$$

Compound **3** has previously been characterized by X-ray crystallography, magnetic susceptibility, and cryoscopic molecular weight determination [6]. An EPR spectrum was not reported. We have recently observed that allyldiene complexes such as $[\mathbf{1}]^+$, isoelectronic with **3**, exhibit sharp EPR absorptions with observable coupling to the diene and allyl protons [2]. Comparative studies have shown that the *supine* allyl ligand in $[\mathbf{1b}]^+$ gives measurable coupling to the *syn* H atoms but not to the *anti* H atoms or to the central H atom, whereas no coupling can be observed with either type of H atom for the *prone* allyl ligand in $[\mathbf{1a}]^+$ [2, 4]. The spectrum of compound **3**, shown in Fig. 1, consists of a pentet of pentets, indicating coupling with all the H atoms of the terminal allyl positions. This suggests that the configuration of **3** in solution is identical with that previously determined in the solid state, with both allyl ligands adopting a *supine* configuration. By comparison with our previous EPR studies, the stronger coupling of 6.6 G is assigned to the *syn* H atoms and the weaker one of 3.3 G to the *anti* H atoms.

(*b*) *Reaction of* $CpMo(\eta\text{-}C_3H_5)_2$ *with nucleophiles*

Compound **3** is stable in donor solvents, including MeCN at room temperature. Warming a MeCN solution to the reflux temperature caused the complete decomposition of the complex and the formation of 1,5-hexadiene and propene in a ca: 2:1 ratio as the major products (>80% by ^{1}H NMR integration).

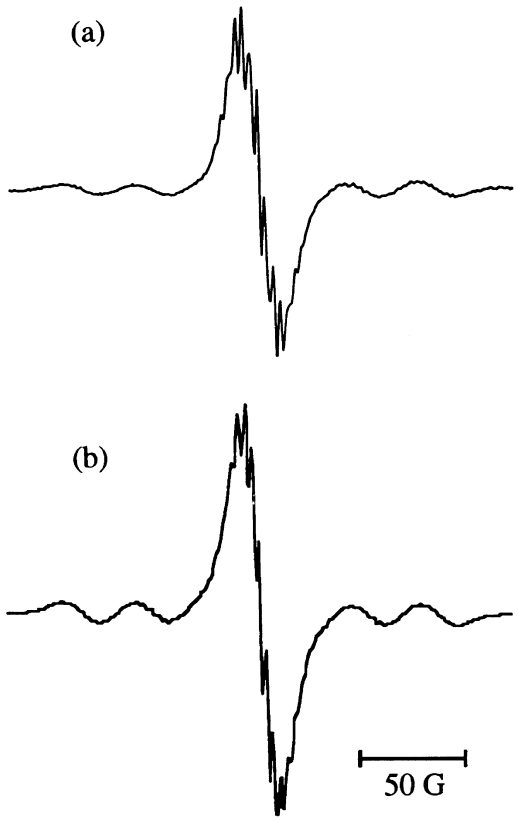

Fig. 1. Experimental (top) and simulated (bottom) EPR spectrum for compound **1** (solvent = THF, T = −100°C).

Neither does **3** react with a large excess of butadiene at room temperature. However, treatment in neat Bu^tNC leads to the smooth formation of the diamagnetic compound $CpMo(\eta\text{-}C_3H_5)(CNBu^t)_2$, **4**, see eq. (2).

$$CpMo(\eta-C_3H_5)_2 + Bu^tNC(\text{excess}) \rightarrow \underset{\mathbf{4}}{CpMo(\eta-C_3H_5)(CNBu^t)_2} \quad (2)$$

The reaction is relatively slow, starting material being still present after several hours at room temperature. NMR spectroscopy shows the initial selective formation of **4**. Prolonged exposure to the Bu^tNC solvent, however, results in the formation of a new diamagnetic material that shows only resonances for the Cp ligand and for the *tert*-Bu group, thus indicating decomposition of **4** with loss of the residual allyl ligand. This by-product is different from $[CpMo(CNBu^t)_4]^+$ (*vide infra*) and was not further characterized. Its formation did not permit the isolation of compound **4** in an analytically pure form. The identity of **4**, however, is established by ^1H NMR. The allyl proton chemical shifts and coupling pattern are consistent with a *supine* coordination mode. In particular, the indiscernible geminal coupling between *syn* and *anti* protons is a clear indication of the *supine* conformation of the allyl ligand [2, 13–15].

(*c*) *Reaction of* $[CpMo(\eta\text{-}C_3H_5)(\eta\text{-}C_4H_6)]^+$ *with nucleophiles*

The reaction between complex $[\mathbf{1b}]^+$ and Bu^tNC follows the same path observed for compound **3**, namely reduction with formal expulsion of an allyl radical, see eq. (3). Compound **5** has previously been obtained by HBF_4 protonation of **1a** in the presence of Bu^tNC and fully characterized [3]. As established above for compound **3**, no reaction is observed between $[\mathbf{1b}]^+$ and MeCN or butadiene under mild conditions.

$$[CpMo(\eta-C_3H_5)(\eta-C_4H_6)]^+ + Bu^tNC(\text{excess}) \rightarrow \underset{\mathbf{5}}{[CpMo(\eta-C_4H_6)(CNBu^t)_2]^+} \quad (3)$$

The existence of bisallyl Mo(III) complexes such as **3**, and the established nucleophilic attack by carbanions on Mo(II)-coordinated diene ligands to afford allyl complexes, made us wonder whether the same reactivity could be observed for the Mo(III)-coordinated diene ligand. Indeed, reaction of $[\mathbf{1b}]^+$ with methyllithium in THF generates a new EPR-active complex which is formulated as $CpMo(\eta\text{-}C_3H_5)(\eta\text{-}C_3H_4Et)$, **6**. This nucleophilic addition process, however, corresponds to a minor reaction pathway (4% according to the intensity of the double-integrated EPR signal). The main product of the reaction, compound **1** [2], derives from a single electron transfer process (see eq. (4)). As expected from the previously reported investigation of the reduction of $[\mathbf{1b}]^+$ [2], the kinetically controlled reduction product is $CpMo(\textit{supine}\text{-}\eta\text{-}C_3H_5)(\textit{supine}\text{-}\eta\text{-}C_4H_6)$, **1b**, followed by the slow isomerization to the thermodynamically favored $CpMo(\textit{prone}\text{-}\eta\text{-}C_3H_5)(\textit{supine}\text{-}\eta\text{-}C_4H_6)$, **1a**.

$$[CpMo(\eta-C_3H_5)(\eta-C_4H_6)]^+ + MeLi \rightarrow \underset{\mathbf{1}}{CpMo(\eta-C_3H_5)(\eta-C_4H_6)} + \underset{\mathbf{6}}{CpMo(\eta-C_3H_5)(\eta-C_3H_4Et)} \quad (4)$$

The nature of the paramagnetic product as **6** is supported by the results of a protonation study of the **1**/**6** mixture in C_6D_6 with HBF_4Et_2O. The ^1H-NMR of the organic phase shows the formation of *cis*- and *trans*-2-pentene in a relative 2:1 ratio, in addition to propene, see eq. (5). There is no observable formation of 1-pentene from this reaction. The formation of propene by protonation of **1** has previously been studied in detail [3].

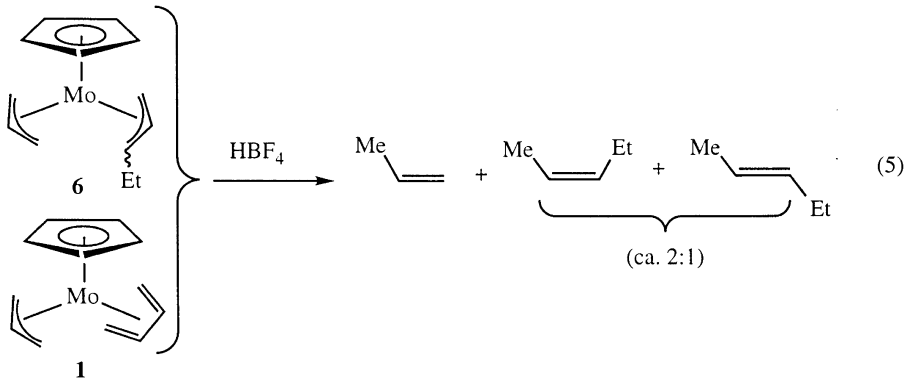

(5)

(*d*) *Oxidation of* $CpMo(\eta\text{-}C_3H_5)_2$

While compound **3** is stable in acetone and MeCN at room temperature, oxidation with Cp_2Fe^+ in either solvent induces an immediate allyl-allyl coupling and release of free 1,5-hexadiene (see eq. (6). The fate of the [$CpMo^+$] fragment is unknown but probably leads to paramagnetic products, since no resonances attributable to the Cp ligand are observed in the ^1H NMR spectrum.

$$CpMo(\eta-C_3H_5)_2 + Cp_2Fe^+PF_6^- \rightarrow CH_2{=}CHCH_2CH_2CH{=}CH_2 \quad (6)$$

When the oxidation reaction is carried out in the presence of Bu^tNC as a trapping agent, two products are observed in a ca. 2:1 ratio (eq. (7). The predominant product is $[CpMo(CNBu^t)_3(\eta^2-CH_2{=}CHCH_2CH_2CH{=}CH_2)]^+PF_6^-$, **7**. This compound could not be obtained as a pure crystalline material because the minor product, compound $[CpMo(CNBu^t)_4]^+PF_6^-$, **8**, crystallizes preferentially. The latter compound has previously been obtained by a different synthetic method [16]. The NMR properties show the equivalence of the four Bu^tNC ligands as expected for the ubiquitous four-legged piano stool geometry, while the three IR bands observed in the CN stretching region are consistent with the expected C_{4v} local symmetry (A_1+B_1+E).

$$CpMo(\eta-C_3H_5)_2 + Cp_2Fe^+PF_6^- + Bu^tNC(\text{excess}) \rightarrow [CpMo(CNBu^t)_3(\eta^2-CH_2{=}CHCH_2CH_2CH{=}CH_2)]^+PF_6^- \quad \mathbf{7}$$

$$+ [CpMo(CNBu^t)_4]^+PF_6^- \quad \mathbf{8} \quad (7)$$

The identification of compound **7** rests on the ^1H and ^{13}C NMR properties. Unlike **8**, which has four equivalent *tert*-butyl isocyanide ligands, complex **7** has three inequivalent isocyanide ligands because of the low symmetry. All 10 protons of the coordinated 1,5-hexadiene ligand are visible in the ^1H NMR spectrum. The proton nomenclature is as shown in **I**. All assignments have been confirmed by selective homonuclear decoupling experiments, which also assisted in the determination of the coupling constants. The proton resonances of the dangling vinyl group show typical chemical shifts and coupling pattern. The coordinated vinyl group, on the other hand, exhibits resonances at higher field. The methylene protons adjacent to the coordinated vinyl group (H_d and H_e) show distinct resonances, while the other methylene protons (H_f) are chemically equivalent (2.30 ppm). Echoing the proton NMR data, the ^{13}C NMR spectrum also shows the inequivalence of the three isocyanide ligands. While the coordinated carbon resonances are significantly different, both the methyl and the tertiary carbon atoms of the three *tert*-butyl groups give common resonances, indicating the insensitivity of these nuclei to the immediate chemical environment of the metal center.

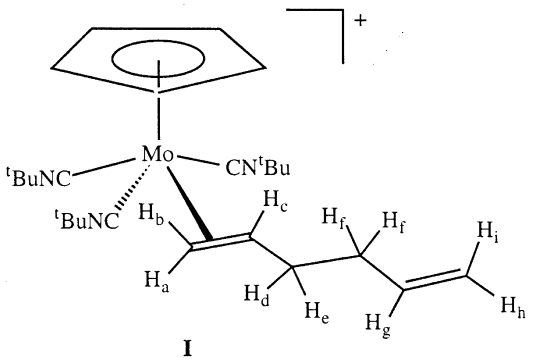

I

The oxidation of **1** has also been carried out in the presence of butadiene. In this case, a 2.5:1 mixture of the bisallyl Mo(IV) complex $[CpMo(\eta^3{:}\eta^3\text{-}C_3H_4CH_2CH_2C_3H_4)(CD_3CN)]^+PF_6^-]$, **9**, and the butadiene Mo(II) complex $[CpMo(\textit{supine-}\eta\text{-}C_4H_6)(CD_3CN)_2]^+PF_6^-]$, **10**, forms after treating the reaction residue in CD_3CN, see eq. (8). Both complexes have previously been obtained by protonation of **1c** in the presence of butadiene [3]. As reported previously, compound **9** is indefinitely stable in CD_3CN at room temperature. A thermal study at 100°C in CD_3CN in a sealed NMR tube, however, revealed its decomposition to yield

cyclooctadiene in 70% spectroscopic yield. Free butadiene is also observed, presumably deriving from the thermal decomposition of **10**.

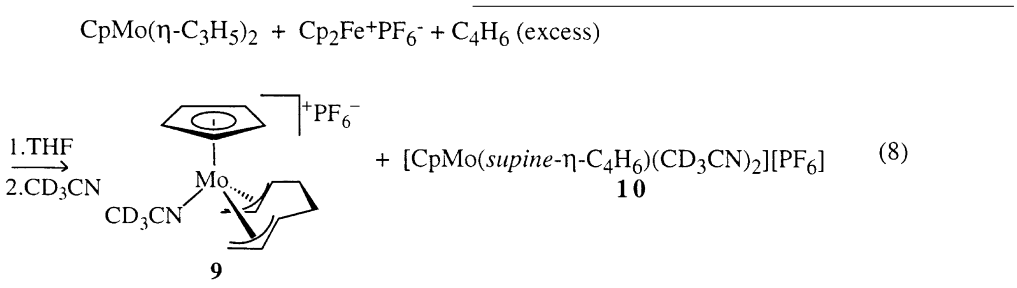

DISCUSSION

(*a*) *Nucleophilic attack to* Mo(III) *vs.* Mo(II)

From our previous studies, we have established that the neutral Mo(II) system $CpMo(\eta\text{-}C_3H_4)(\eta\text{-}C_4H_6)$, in either of its three stable isomeric forms (**1a**–**c**), is not susceptible to nucleophilic attack [3]. However, the cationic Mo(II) complex $[CpMo(supine\text{-}\eta\text{-}C_4H_6)(s\text{-}trans\text{-}\eta\text{-}C_4H_6)]^+$, **2**, can be attacked by nucleophiles either at the metal (with substitution of the *s-trans*-butadiene ligand) or at the *s-trans*-butadiene *endo* terminal carbon atom (with formation of an allyl derivative) [4]. For these reasons, we reasoned that a nucleophilic attack to either the metal, the butadiene ligand or the allyl ligand in the Mo(III) complexes **3** and $[\mathbf{1b}]^+$ might occur under the influence of the higher formal oxidation state, especially for the cationic system. As mentioned in the Introduction, no studies of the reactivity of Mo(III)-coordinated allyl and butadiene ligands appear to have been reported.

The results obtained show that the dominant pathway is metal reduction. The tendency of the metal to reach an 18-electron configuration, especially in the presence of π-acidic ligands, is sufficiently high to force the elimination of allyl radicals. This pathway is observed for both **3** and $[\mathbf{1b}]^+$ in their reaction with Bu^tNC. It is remarkable that, for complex $[\mathbf{1b}]^+$, the observed reaction pathway is more favorable than either substitution of the neutral diene ligand or insertion of the diene into the Mo(III)-allyl bond. Weaker neutral 2-electron donor such as MeCN do not react. The reaction of the cationic substrate with methyllithium does indeed lead to the addition product **6** (eq. (4)), but the main product is the neutral derivative **1b** obtained from the single electron transfer pathway. This result, nevertheless, indicates an increased reactivity of the coordinated ligands on going from Mo(II) to Mo(III). For the Mo(II) complexes of the types investigated by us, a nucleophilic attack takes place (only in the cationic systems) at the *s-trans* butadiene ligand but never at the *s-cis* butadiene or at the allyl ligands. For the Mo(III) cationic complex reported here, we have seen for the first time a nucleophilic addition to the *s-cis* butadiene ligand.

The nature of the products obtained by protonating **6** (see section (c) below) indicate that this compound is a mixture of isomers with *syn* and *anti* ethylallyl ligand (2:1 in favor of the *anti* isomer). This mixture is probably formed by direct nucleophilic addition to the *s-cis* butadiene ligand to afford the *anti* allyl product, followed by partial isomerization. An alternative pathway to the *syn* product involving an initial isomerization to $[\mathbf{1c}]^+$, followed by nucleophilic attack at the *s-trans* diene ligand can be excluded because, according to our previous studies [2], the thermodynamics and kinetics for the isomer interconversion reaction would not allow the formation of a significant amount of the *s-trans* isomer during the short time scale of the methylation process.

(*b*) *Allyl-allyl coupling in* Mo(III) *and* Mo(IV)

Processes of allyl-allyl coupling in transition metal complexes are relevant as elementary steps of catalytic dimerization and oligometization of diene ligands [17]. The metal-assisted coupling of allyl ligands to afford 1,5-hexadiene products is a widely known reaction [17–19]. Previous reports for molybdenum complexes include the interaction of a "violet solution", presumably containing $(\eta^6\text{-}C_6H_6)Mo(\eta^3\text{-}C_3H_5)(\mu\text{-}Cl)_2AlClEt$, with propene to ultimately afford a 2,4-hexadiene complex via formation of an intermediate containing coordinated 1,5-hexadiene [20]. The proposed bis(allyl) Mo(IV) intermediate, i.e.$[(\eta^6\text{-}C_6H_6)Mo(\eta^3\text{-}C_3H_5)_2(C_3H_7)]^+$, however, was not directly observed. More recently, the reaction of the metal-metal bonded $Mo_2(\mu\text{-}\eta\text{-}C_3H_5)_2(\eta\text{-}C_3H_5)_2$ complex with CO was shown to produce $Mo(CO)_6$ and 1,5-hexadiene, via an isolable $Mo(CO)_4(\eta^4\text{-}1,5\text{-hexadiene})$ intermediate [21]. The corresponding reaction of $Mo(\eta^3\text{-}C_3H_5)_2(PMe_3)_3$ with CO yields $Mo(CO)_2(PMe_3)_4$ and 1,5-hexadiene [22].

No allyl-allyl coupling process has been described for Mo(III) complexes. A spontaneous coupling has

been reported to occur upon ligand addition to the Cr(III) complex $CpCr(\eta^3\text{-}C_3H_5)_2$ [23], while the corresponding Mo complex **3** does not undergo a similar process under mild conditions [6–8], in accord with the expected greater stability of the heavier metal in the higher oxidation state. In fact, while σ-donor ligands do not react with **3**, π acidic ligands induce a reductive process with loss of an allyl radical, rather than an allyl-allyl coupling, as discussed in the previous section. When compound **3** is heated in the σ-donor solvent MeCN, however, the allyl-allyl coupling becomes possible, paralleling the reactivity of the chromium analogue.

It may be questioned whether the formation of 1,5-hexadiene during the thermal decomposition of **3** in MeCN derives from a truly metal-assisted allyl-allyl coupling or from the coupling of free allyl radicals in solution after elimination of the latter from the coordination sphere. We have not been able to find previous studies of the allyl radical reactivity in the presence of MeCN. We note, however, that the H-allyl bond is stronger than the $H\text{–}CH_2CN$ bond (89 ± 1 and 82.3 kcal/mol, respectively) [24]. This suggests that the allyl radical should preferentially abstract a H atom from the large excess of MeCN and generate propene. The ^1H NMR monitoring of the decomposition reaction shows the predominant formation of the coupling product (1,5-hexadiene:propene = ca. 2:1), in agreement with the proposed direct allyl-allyl coupling. A thermal allyl radical elimination, however, may be competing and be responsible for the formation of propene.

Even more rapid (instantaneous at room temperature) is the elimination of 1,5-hexadiene upon oxidation of **3**. No formation of propene is observed under these conditions. A hypothetical $[CpMo(\eta\text{-}C_3H_5)_2(S)]^+$ intermediate probably forms first, but its lifetime must be very short because it was not spectroscopically observed neither in acetone nor in MeCN. It is interesting to compare this rapid C–C coupling process with our previous findings in bisallyl Mo(IV) chemistry (Scheme 2). Complex $[CpMo(\eta\text{-}C_3H_5)(\eta\text{-}C_3H_4Me)(MeCN)]^+$, which is generated by HBF_4 protonation of **1c** in MeCN, is sufficiently stable to be observed in solution at room temperature but slowly decomposes by the same C–C coupling process in a regioselective manner to afford 3-methyl-1,5-hexadiene [3]. Complex **9**, on the other hand, is perfectly stable in MeCN at room temperature, whereas it eliminates cyclooctadiene upon warming to 100°C. This elimination is also regioselective: no significant amount of the possible alternative coupling products (1,2-divinylcyclobutane and 4-vinylcyclohexene) is spectroscopically observed.

It is to be emphasized that we have no detailed information on the structure of the Mo(IV) bis-allyl materials, thus the mechanism of regiocontrol is open to speculation. Mo(IV) half-sandwich derivatives adopt pseudo-octahedral geometries with one (axial) ligand trans to the Cp and four (pseudo-equatorial)

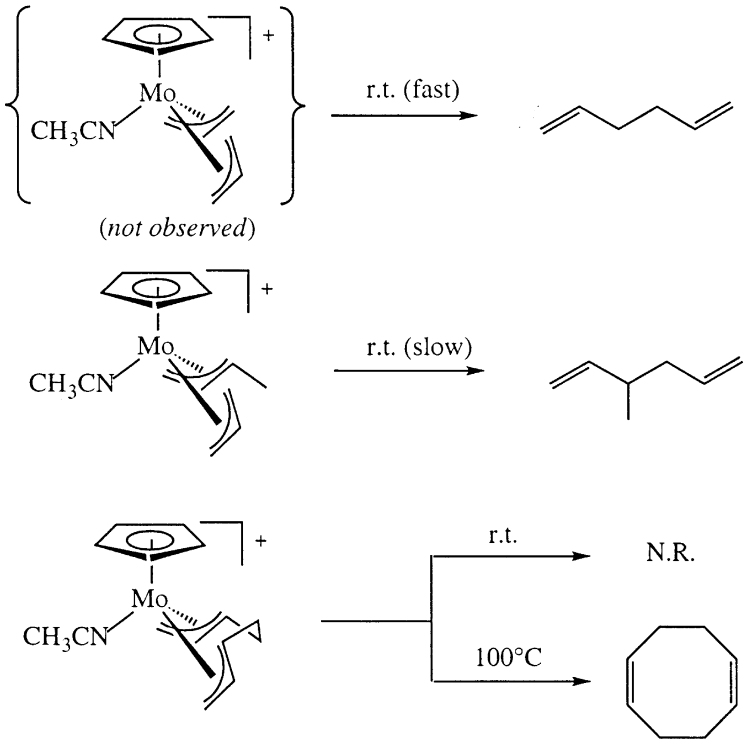

Scheme 2.

ligands slightly deviating from the perpendicular plane away from the bulkier Cp ligand [25–29]. The X-ray structure of an isoelectronic $CpMo(CO)Br_2(\eta^3$-C_3H_4-2-Me) has pseudo-equatorial Br and CO ligands, whereas the allyl ligand formally occupies one pseudo-equatorial and the pseudo-axial positions [30]. On the basis of the above information, we presume that the structures of the bisally Mo(IV) derivatives are as drawn in Scheme 2.

A product of allyl-allyl coupling containing a coordinated 1,5-hexadiene is sufficiently stable and can be observed spectroscopically when the oxidation of **3** is carried out in Bu^tNC (compound **7**). Interestingly, the 1,5-hexadiene ligand remains coordinated in a η^2 (monodentate) fashion to the metal center, rather than as a η^2:η^2 (chelating) ligand or being eliminated from the coordination sphere under the large excess of Bu^tNC which is present. No spectroscopic evidence was obtained for the intermediacy of a chelating hexadiene complex, which is presumed to form as shown in Scheme 3. The coordination mode is probably dictated by the electronic requirements of the metal and the balance between σ-donation and π back-donation, a situation which is commonplace in the chemistry of carbonyl complexes. Strain in the chelated intermediate may also be responsible for the observed outcome of the reaction.

When the oxidation of **3** is carried out in the presence of excess butadiene, a similar coupling mechanism presumably takes place (Scheme 4), leading to the formation of a mixture of **9** and **10** after treatment with CD_3CN. The formation of these two products can be understood on the basis of our previous studies: coordination of two butadiene ligands in the *s-trans* mode leads to C–C coupling; coordination of one *s-trans* and one *s-cis* ligands leads to the stable **2**; finally, coordination of two *s-cis* ligands does not occur [3]. Complex **2** is known to exchange the *s-trans* butadiene ligand upon dissolution in acetonitrile [3].

(*c*) *Electrophilic reactivity of* Mo(III)-*bonded allyl ligands*

The protonation of the allyl ligands in compound **6** to generate 2-pentene isomers (eq. (5)) demonstrates that Mo(III)-coordinated allyl ligands are sufficiently electron-rich to be subjected to electrophilic attack by protons. The absence of any 1-pentene among the reaction products shows that the proton attacks regioselectively the unsubstituted terminal allyl position, in agreement with the electron-releasing effect of the alkyl substituent. This result is identical to what we have observed for the protonation of *syn*-1-ethylallyl in the Mo(II) complex $CpMo(\eta^4$-$C_4H_6)(\eta^3$-*syn*-C_3H_4-1-Et) [4]. In that case, only *trans*-2-pentene was obtained from the *syn*-ethylallyl ligand. Therefore, the results of the protonation of **6** indicates that this is a mixture of *syn*- and *anti*-ethylallyl isomers, with a prevalence for the *anti* isomer. This, in turn, indicates that the alkylation of the *s-cis-supine* butadiene ligand is followed by partial (either for thermodynamic or kinetic reasons) isomerization of the resulting *anti*-allyl ligand to the *syn* isomer (see Scheme 5).

CONCLUSIONS

The reactivity of allyl and diene ligands coordinated to paramagnetic Mo(III) centers has been explored for the first time. A variety of transformations have been established, including electrophilic addition to the allyl ligand, nucleophilic addition to the butadiene ligand, allyl-allyl coupling, metal reduction by single-electron transfer or via allyl radical elimination, and metal oxidation. A few pathways have been compared with those in analogous complexes of Cr(III), Mo(II) and Mo(IV). The observed patterns can be summarized as follows:

1. While allyl-allyl coupling occurs spontaneously at room temperature in $CpCr(\eta^3$-$C_3H_5)_2$ [23], it takes place only at higher temperatures for the Mo(III) compound **3**.
2. The σ-donor/π-acceptor Bu^tNC ligand induces reduction of both **3** and $[\mathbf{1b}]^+$ at room temperature, with loss of an allyl radical and formation of 18-electron Mo(II) products.
3. The stronger σ-donor ligand LiMe induces a one-electron reduction process on $[\mathbf{1b}]^+$, to produce the parent complex **1b**.
4. While nucleophilic addition of Me^- to a *s-cis*-coordinated butadiene ligand is not observed for the Mo(II) complexes **1a**, **1b** and **2**, it does occur for the Mo(III) complex $[\mathbf{1b}]^+$, although it does not compete effectively with the preferred reduction pathway.

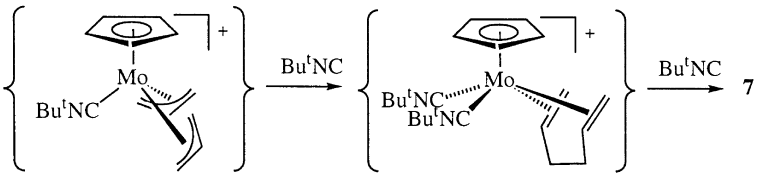

Scheme 3.

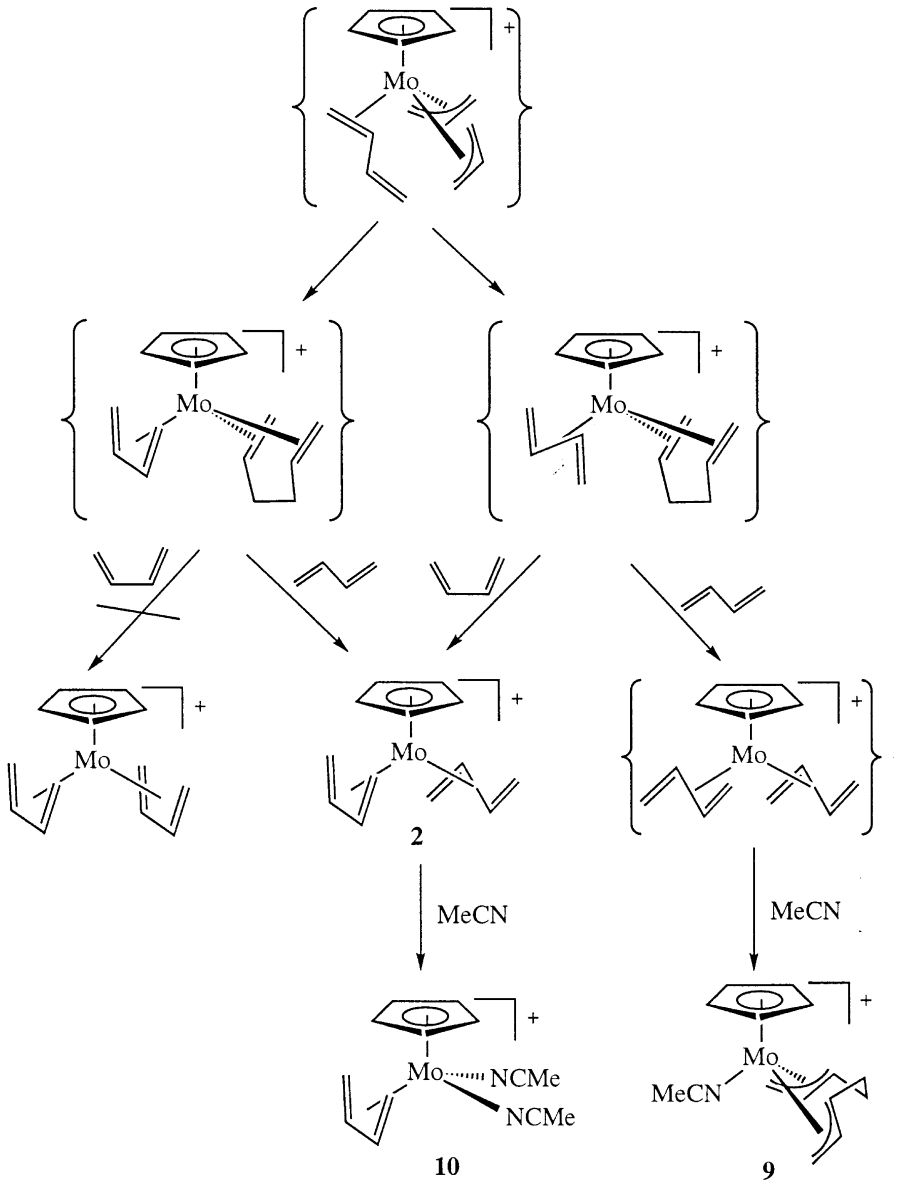

Scheme 4.

5. Protonation of the Mo(III)-bonded allyl ligands in **6** by strong acids parallels the protonation of allylmolybdenum(II) complexes, with the generation of olefins. The protonation of 1-ethylallyl occurs regioselectively to generate 2-pentenes.
6. The allyl-allyl coupling reaction is greatly accelerated by oxidation to Mo(IV). The rate of this coupling process is greatly affected by the substitution at the allyl carbons. Regioselectivity is observed for substituted allyl ligands, with the η^3:η^3-1,1′-$C_3H_4CH_2CH_2C_3H_4$ ligand giving rise to cyclooctadiene as the sole coupling product.

EXPERIMENTAL PROCEDURE

General Procedures

All operations were carried out by standard Schlenk-line techniques under a dinitrogen atmosphere. Solvents were dried by conventional methods (THF and Et_2O on Na/benzophenone, toluene and heptane on Na, CH_2Cl_2 on P_4O_{10}) and distilled directly from the drying agent under dinitrogen. All routine NMR experiments were carried out on a Bruker AM400 or WF 200 spectrometers. The ^1H and ^{13}C NMR data of

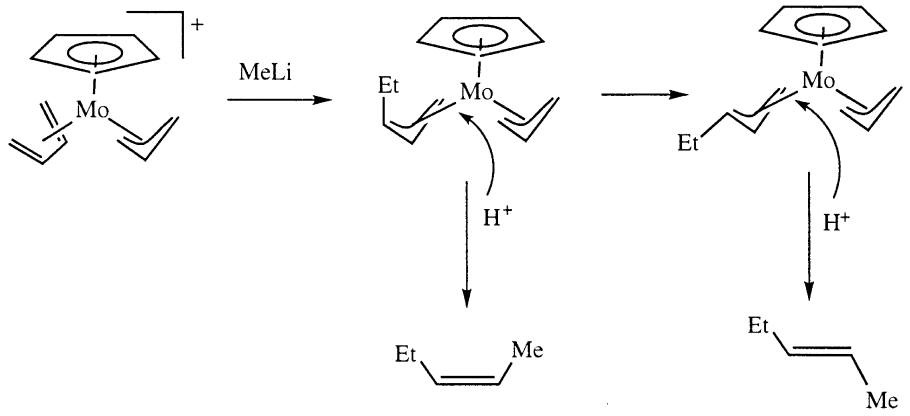

Scheme 5.

all compounds are given in Table 1. Other spectrometers used were as follows: EPR, Bruker ER200; IR, Perkin-Elmer FTIR 1600; MS, VG 7070E. Elemental analyses were performed by Atlantic Microlab, Inc. or the analytical service at the LSEO, Dijon. Compounds $CpMoCl_4$ [11] and [**1b**][PF_6] [2] were prepared according to the literature.

Preparation of $CpMo(\eta\text{-}C_3H_5)_2$, **3**

To a diethyl ether solution of allylmagnesium chloride (66 mL, 1 M, 66 mmol) was added 60 mL of THF at $-78^{\circ}C$. Solid $CpMoCl_4$ (4.5 g, 14.9 mmol) was added to the solution over 15 min, causing the precipitation of a yellow solid. The suspension was stirred for 1 h at $-78^{\circ}C$ and then an additional hour at $0^{\circ}C$. All solvent was evacuated and the solid was dried overnight under vacuum. The product was extracted with heptane (2×100 mL), each washing being stirred for 1 h to ensure maximum extraction. The combined filtered extracts were evaporated to dryness under reduced pressure. The residue was redissolved in 150 mL of heptane, leaving a small amount of undissolved grey solid which was filtered off. The solvent was removed again by evaporation and the residue

Table 1. ^{1}H-NMR data

Compd	^{1}H-NMR (δ)	^{13}C-NMR (δ)
$CpMo(supine\text{-}\eta\text{-}C_3H_5)(CNBu^t)_2$ (**4**)[a]	4.95 (5H, Cp, s); 3.61 ($1H_d$, tt, $^3J_{HHe} = 5$Hz, $^3J_{HHf} = 7$Hz); 2.37 ($2H_e$, d, $^3J_{HHd} = 5$Hz); 1.57 ($1H_f$, d, $^3J_{HHd} = 7$Hz); 1.13 (18H, $2CNBu^t$)	
[$CpMo(\eta^2\text{-}CH_2{=}CHCH_2{-}CH_2CH{=}CH_2)(CNBu^t)_3$][$PF_6$] (**7**)[b]	5.89 ($1H_g$, ddt, $^3J_{HHi} = 16$Hz, $^3J_{HHh} = 9$Hz, $^3J_{HHf} = {}^3J_{HHf} = 13$Hz), 5.00 ($1H_i$, ddt, $^3J_{HHg} = 16$Hz, $^2J_{HHh} = 2$Hz, $^4J_{HHf} = 1.5$Hz), 4.94 (5H, s, Cp), 4.93 ($1H_h$, ddt, $^3J_{HHg} = 9$Hz, $^2J_{HHi} = 2$Hz, $^4J_{HHf} = 1$Hz), 2.92 ($1H_c$, dddd, $^3J_{HHb} = 9$Hz, $^3J_{HHa} = 12$Hz, $^3J_{HHd} = 10$Hz, $^3J_{HHe} = 4$Hz), 2.30 ($2H_f$, m), 1.99 ($1H_b$, dd, $^3J_{HHc} = 9$Hz, $^3J_{HHa} = 3$Hz), 1.99 (1Hd, m) 1.73 ($1H_a$, dd, $^3J_{HHc} = 12$Hz, $^3J_{HHb} = 3$Hz), 1.50 (9H, $CNBu^t$), ~1.4 (1He, overlapping with $CNBu^t$), 1.40 (9H, $CNBu^t$), 1.37 (9H, $CNBu^t$)	168.1 (1C, s, $\underline{C}NC(CH_3)_3$), 164.3 (1C, s, $\underline{C}NC(CH_3)_3$), 162.4 (1C, s, $\underline{C}NC(CH_3)_3$), 140.0 ($1C_g$, d, $^1J_{CH} = 155$ Hz), 114.6 ($1C_{hi}$, t, $^1J_{CH} = 155$ Hz), 88.9 (5C, d, $^1J_{CH} = 181$ Hz), 68.8 ($1C_c$, d, $^1J_{CH} = 176$ Hz), 59.2 (3C, b, $CN\underline{C}(CH_3)_3$), 41.4 ($1C_{ff}$ or $1C_{de}$, t, $^1J_{CH} = 120$ Hz), 40.4 ($1C_{de}$ or $1C_{ff}$, t, $^1J_{CH} = 120$ Hz), 30.4 (9C, quartet, $^1J_{CH} = 128$ Hz, $CNC(\underline{C}H_3)_3$), ~30 ($1C_{ab}$, overlapping with $CNC(\underline{C}H_3)_3$)
[$CpMo(CNBu^t)_4$][PF_6] (**8**)[b]	5.10 (5H, s, Cp), 1.46 (36H, s, $CNC(CH_3)_3$)	174.0 (4C, s, $\underline{C}NC(CH_3)_3$), 90.1 (5C, d, $^1J = 177$ Hz, Cp), 59.3 (4C, s, $CN\underline{C}(CH_3)_3$), 31.1 (12C, quartet, $^1J = 128$ Hz, $CNC(\underline{C}H_3)_3$)

(a) C_6D_6; (b) acetonitrile-d_3.

was recrystallized from heptane at $-80^{\circ}C$, yielding a violet microcrystalline solid which was dried under vacuum for 2 h (yield 1.6 g, 44%). Anal. Calcd for $C_{11}H_{15}Mo$: C, 54.32; H, 6.17. Found: C, 54.05; H, 6.04. The solid has a dichroic behavior. Powder and small crystals appear violet to reflected light but orange to transmitted light. Larger crystals are orange as previously reported [6]. The solid is extremely air sensitive, turning immediately black upon exposure to the laboratory atmosphere. EPR (THF, $-100^{\circ}C$): $g = 2.032$, $a_{Mo} = 33$ G, $a_{4H} = 6.6$ G, $a_{4H} = 3.3$ G. EPR (THF or benzene, room temperature): broad singlet at $g = 2.028$ with Mo satellites, $a_{Mo} = 33$ G.

Reaction of 3 *with* tert-*butyl isocyanide. Formation of* CpMo(*supine*-η-C_3H_5)($CNBu^t$)$_2$, **4**

Compound **1** (10 mg, 41 μmol) was placed in a NMR tube together with 250 μL of Bu^tNC. Standing at room temperature overnight yielded a maroon solution. The excess of *tert*-butyl isocyanide was removed under reduced pressure and 0.5 mL of C_6D_6 was added. The ^1H NMR spectrum showed the formation of compound **4**, while the EPR spectrum indicated the presence of the unreacted starting complex **3**. The separation of these two complexes was not successful. When the experiment was repeated with longer standing in Bu^tNC, decomposition of **4** occurred to generate another species with the Cp resonance at δ 5.36 in C_6D_6 and another resonance at δ 1.30, assigned to Bu^t groups. No allyl resonances are observed for this species.

Reaction of [1b][PF_6] *with* tert-*butyl isocyanide. Formation of* [CpMo(*supine*-η-C_4H_6)($CNBu^t$)$_2$][PF_6], **5**

Compound [**1b**][PF_6] (10 mg, 25 μmol) was mixed with Bu^tNC (100 μL, 0.885 mmol) in a NMR tube. Upon heating to $60^{\circ}C$ for 10 min, a yellow solution was formed, accompanied by a black precipitate. The solution was centrifuged and the supernatant was transferred into another NMR tube via cannula. After removal of excess tert-butylisocyanide under reduced pressure, a yellow oil was obtained. A ^1H NMR spectrum in $CDCl_3$ showed resonances at δ 5.56 (*m*, 2H), 5.10 (*s*, 5H), 2.32 (*d*, 2H), 1.45 (*s*, 18H), 1.00 (*d*, 2H), which are attributed to the cation of **5** by comparison with the literature [3], in addition to two unidentified species with the Cp resonances at δ 5.03 and 4.96. Integration showed a 61:16:23 ratio of the three products. No EPR active species were detected.

Reaction of [1b][PF_6] *with MeLi. Formation of* CpMo(η-C_3H_5)(η-C_4H_6), **1**, and CpMo(η-C_3H_5)(η-C_3H_4Et), **6**

Compound [**1b**][PF_6] (60 mg, 0.15 mmol) was suspended in 20 mL of THF. MeLi (107 μL, 1.4 M in Et_2O, 0.15 mmol) was added by syringe, causing the formation of a red solution. After stirring at room temperature for 1 h, all solvent was removed by evaporation under reduced pressure and the residue was extracted with 20 mL of heptane. After filtration, the solution was evaporated to dryness under reduced pressure, giving a red solid (yield 25 mg). The ^1H NMR spectrum in C_6D_6 showed resonances of Cp at δ 4.10 and 4.27 in a ca. 4:1 ratio, which are attributed to CpMo(*supine*-η-C_3H_5)(*supine*-η-C_4H_6) (**1b**) and CpMo(*prone*-η-C_3H_5)(*supine*-η-C_4H_6) (**1a**), respectively, by comparison with the literature [2]. Continued monitoring of this solution showed the slow conversion of **1b** to **1a** according to the previous report [2]. An EPR study of the C_6D_6 solution showed an unresolved multiplet resonance at $g = 2.033$, $a_{Mo} = 33$ G, which is assigned to compound **6**. Double integration of the EPR resonance against that of the starting material gives a 4% yield of the paramagnetic species.

Protonation of the mixture of CpMo(η-C_3H_5)(η-C_4H_6) (**1a** and **1b**) *and* CpMo(η-C_3H_5)(η-C_3H_4Et), **6**

The mixture of complex **1** and **6** obtained by the procedure described in the previous section (10 mg) was dissolved in 0.5 mL of C_6D_6 in an NMR tube. $HBF_4 \cdot Et_2O$ (10 μL, excess) was added, causing the immediate formation of a grey precipitate. The supernatant was transferred into another NMR tube by vacuum condensation. The ^1H NMR spectrum showed the formation of both *cis*-2-pentene and *trans*-2-pentene with a ratio of ca. 2:1, in addition to the signals of propene. The products were identified by analysis of the olefinic proton resonances, in comparison with those reported in the literature [31]. The other aliphatic resonances overlap extensively. ^1H NMR of *cis*-2-pentene (δ, C_6D_6): 5.37 (m), 1.95 (m), 1.55 (m), 1.08 (overlap with large Et_2O resonance). ^1H NMR of *trans*-2-pentene (δ, C_6D_6): 5.47 (*m*, 2H), 1.95 (*m*), 1.55 (*m*), 1.08 (overlap with large Et_2O resonance). ^1H NMR of propene (δ, C_6D_6): 5.70 (*m*, 1H), 4.99 (*dm*, 1H), 4.93 (*dm*, 1H), 1.53 (overlap). No other resonances that could be attributed to a vinyl group (e.g. of 1-pentene) could be observed.

Reactions of **3** *with ferrocenium hexafluorophosphate*

1. In acetone-d^6. Compound **3** (10 mg; 42 μmol) and $Cp_2Fe^+PF^-{}_6$ (14 mg; 42 μmol) were mixed in an NMR tube, to which 0.5 mL of CD_3COCD_3 was added. The formation of 1,5-hexadiene (δ 5.79, *m*, 2H; 4.95, *m*, 4H; 2.07, *m*, 4H) and ferrocene (δ 4.15, s) were detected by ^1H NMR. No significant amount of other species was found by ^1H NMR.
2. In acetonitrile-d^3. CpMo(*supine*-η-C_3H_5)$_2$ (5 mg, 21 μmol) and $Cp_2Fe^+PF_6^-$ (7 mg, 21 μmol) were placed in an NMR tube, to which 0.5 mL of CD_3CN was added. The ^1H NMR spectrum of the

resulting solution showed the formation of 1,5-hexadiene (δ 5.83, *m*, 2H; 4.97, *m*, 4H; 2.13, *m*, 4H) and ferrocene (δ 4.15, s) in a ca. 1:1 ratio. No significant amount of other species was detected by ^{1}H NMR, while the EPR spectrum showed several resonances with no discernible coupling pattern.

Reaction of **3** *with ferrocenium hexafluorophosphate in* tert-*butyl isocyanide. Formation of* [CpMo(CNBu^t)$_3$(η^2-CH$_2$=CHCH$_2$CH$_2$CH=CH$_2$)][PF$_6$], **7**, *and* [CpMo(CNBu^t)$_4$][PF$_6$], **8**

1. NMR tube reaction. Compound **3** (12 mg; 49 μmol) and $Cp_2Fe^+PF_6^-$ (17 mg; 51 μmol) were placed in an NMR tube, to which 100 μL of Bu^{t}NC was added by syringe. The mixture was vigorously shaken for 15 min. C_6D_6 (0.5 mL) was then added, yielding a yellow solution. Two species with Cp signals at δ 4.85 (complex **7**) and 5.03 (complex **8**) in a ca. 2:1 ratio were observed by ^{1}H NMR.
2. Isolation of compound **8**. Compound **3** (200 mg; 0.82 mmol) and $Cp_2Fe^+PF_6^-$ (272 mg; 0.82 mmol) were mixed in a Schlenk tube, to which 2 mL of Bu^{t}NC was added. The mixture was stirred at room temperature for 0.5 h, giving a yellow suspension. The excess Bu^{t}NC was completely removed by evaporation under reduced. Benzene (10 mL) was added to the yellow residue, and the resulting suspension was stirred for 1 h. The supernatant was decanted and the yellow solid was recrystallized from THF (5 mL) at -80°C, to yield a bright yellow crystalline solid which was recovered by filtration and dried under vacuum for 0.5 h (yield 85 mg, 15%). *Anal.* Calcd for $C_{25}H_{41}N_4MoPF_6 \cdot 0.75C_4H_8O$: C, 48.56; H, 6.84. Found: C, 48.31; H, 6.80. The THF of solvation was observed in the ^{1}H NMR spectrum in the correct integrated intensity. IR (Nujol, cm^{-1}): 2162 m, 2096 s, 2050 s, 841 s (PF6). Low resolution mass spectrum (FAB$^+$): m/z 495 [CpMo(CNBu^t)$_4$]$^+$, 100%.

Reaction of **3** *with ferrocenium hexafluorophosphate in THF/butadiene. Formation of* [CpMo(η^3:η^3-C$_3$H$_4$CH$_2$CH$_2$C$_3$H$_4$)(CD$_3$CN)PF$_6$], **9** *and* [CpMo(*supine*-η-C$_4$H$_6$)(CD$_3$CN)$_2$][PF$_6$], **10**

Complex **3** (ca. 10 mg) and 14 mg of $Cp_2Fe^+PF_6^-$ were placed in a Schlenk flask. Butadiene (ca. 5 mL) was condensed at -196°C. After stirring for 0.5 h at -78°C, THF (5 mL) was added and the mixture was stirred at room temperature for an additional 0.5 h. All volatiles were removed under reduced pressure and heptane (10 mL) was added to the residue. An orange-red extract containing ferrocene, as shown by ^{1}H NMR, was filtered off. The residue was dried under vacuum and then redissolved in 0.5 mL of CD$_3$CN. A ^{1}H NMR spectrum showed the formation of two major products in a 2.5:1 ratio. These have been identified as the cations of **9** and **10**, respectively, by comparison with the NMR spectra reported in the literature [3]. These two main products are accompanied by several additional Cp containing by-products, whose overall integrated intensity is $<30\%$ of the total.

Thermal treatment of compound **9** *in* CD$_3$CN

The NMR tube containing the CD$_3$CN solution of **9** and **10** obtained as described in the previous section was flame-sealed. The solution was heated to 100°C for 1 h and monitored by ^{1}H NMR spectroscopy. The formation of octa-1,5-diene [δ 5.53 (*br*, 4H), 2.33 (*br*, 8H)] was observed in 75% spectroscopic yield relative to the initial amount of **9**. Resonances attributable to free butadiene were also observed. No resonances attributable to Cp containing Mo products were observed.

Thermal treatment of complex **3** *in* CD$_3$CN

Complex **3** (15 mg) was placed in an NMR tube with 0.5 mL of CD$_3$CN. The tube was flame-sealed and heated to 100°C in an oil bath for 1 h. A ^{1}H NMR spectrum showed the formation of hexa-1,5-diene (CH$_2$=CH–C*H*$_2$C*H*$_2$–CH=CH$_2$ resonance at δ 2.14) and propene (CH$_2$=CH–C*H*$_3$ resonance at δ 1.70, doublet with $J = 6.1$ Hz) in a ca. 2:1 ratio, plus small amounts ($<20\%$) of other unidentified species, the major component of which shows a C*H*$_3$ resonance at δ 1.46 (*d*, $J = 5.1$ Hz).

Acknowledgements—We are grateful to the National Science Foundation (CHE-9508521) for support of this work.

REFERENCES

1. For Part 3, see ref. 4.
2. Wang, L.-S., Fettinger, J. C. and Poli, R., *J. Am. Chem. Soc.*, 1997, **119,** 4453–4464.
3. Poli, R. and Wang, L.-S., *J. Am. Chem. Soc.*, 1988, **120,** 2831–2842.
4. Wang, L.-S., Fettinger, J. C., Poli, R. and Meunier-Prest, R., *Organometallics*, in press.
5. Davidson, J. L., Davidson, K. and Lindsell, W. E., *J. Chem. Soc., Chem. Commun.*, 1983, 452–453.
6. Jolly, P. W., Krüger, C., Romão, C. C. and Romão, M. J., *Organometallics*, 1984, **3,** 936–937.
7. Andell, O., Goddard, R., Holle, S., Jolly, P. W., Krüger, C. and Tsay, Y. H., *Polyhedron*, 1989, **8,** 203–209.
8. Jolly, P. W., *Acc. Chem. Res.*, 1996, **29,** 544–551.
9. Astruc, D., *Angew. Chem, Int. Ed. Engl.*, 1988, **27,** 643–660.
10. Trogler, W. C. (Ed), *Organometallic radical processes*, Elsevier, Amsterdam, 1990.
11. Gordon, J. C. and Poli, R., in *Synthetic Methods of Organometallic and Inorganic Chemistry*,

(*Herrmann/Brauer*), W. A. Herrmann, ed., Vol 8, Georg Thieme Verlag, Stuttgart, 1997, p. 97–98.
12. Dilworth, J. R. and Richards, R. L., *Inorg. Synth.*, 1990, **28,** 33–37.
13. Faller, J. W., Chen, C.-C., Mattina, M. J. and Jakubowski, A., *J. Organomet. Chem.*, 1973, **52,** 361–386.
14. Faller, J. W., Johnson, B. V. and Dryja, T. P., *J. Organomet. Chem.*, 1974, **65,** 395–400.
15. Gibson, D. H., Hsu, W.-L., Steinmetz, A. L. and Johnson, B. V., *J. Organomet. Chem.*, 1981, **208,** 89–102.
16. Filippou, A. C. and Grünleitner, W., *J. Organomet. Chem.*, 1989, **378,** 387–399.
17. Wilke, G., *J. Organomet. Chem.*, 1980, **200,** 349–364.
18. Baker, R., *Chem. Rev.*, 1973, **73,** 487–530.
19. Tsuji, J., *Adv. Organomet. Chem.*, 1979, **17,** 141–193.
20. Green, M. L. H. and Knight, J., *J. Chem. Soc., Dalton Trans.*, 1974, 311–319.
21. Blau, R. J. and Siriwardane, U., *Organometallics*, 1991, **10,** 1627 < last-page > 1630.
22. Borgmann, C., Limberg, C. and Driess, A., *J. Organometal. Chem.*, 1997, **541,** 367–375.
23. Betz, P., Döhring, A., Emrich, R., Goddard, R., Jolly, P. W., Krüger, C., Romão, C. C., Schönfelder, K. U. and Tsay, Y.-H., *Polyhedron*, 1993, **12,** 2651–2662.
24. Weast, R. C., *CRC Handbook of Chemistry and Physics*, CRC Press, Cleveland, Ohio, 1976.
25. Stärker, K. and Curtis, M. D., *Inorg. Chem.*, 1985, **24,** 3006–3010.
26. Owens, B. E. and Poli, R., *Inorg. Chim. Acta*, 1991, **179,** 229–237.
27. Feng, Q., Ferrer, M., Green, M. L. H., Mountford, P. and Mtetwa, V. S. B., *J. Chem. Soc., Dalton Trans.*, 1992, 1205–1215.
28. Abugideiri, F., Gordon, J. C., Poli, R., Owens-Waltermire, B. E. and Rheingold, A. L., *Organometallics*, 1993, **12,** 1575–1582.
29. Blackburn, H., Kraatz, H.-B., Poli, R. and Torralba, R. C., *Polyhedron*, 1995, **14,** 2225–2230.
30. Faller, J. W. and Ma, Y., *Organometallics*, 1986, **5,** 1949–1952.
31. Pouchert, C. J. and Behnke, J., *The Aldrich Library of* ^{13}C and ^{1}H FT NMR Spectra, 1993.

Pergamon

PII: S0277–5387(98)00165–X

Polyhedron Vol. 17, No. 21, pp. 3701–3709, 1998
© 1998 Elsevier Science Ltd
All rights reserved. Printed in Great Britain
0277–5387/98 $19.00+0.00

Synthesis of [2-(pyridin-2′-yl)phenyl]-mercury(II) arylthiosemicarbazonates: An unusual coordination mode of a deprotonated 2-formyl-(2-hydroxy-benzene)-thiosemicarbazone

T. S. Lobana,*† A. Sánchez, J. S. Casas,† A. Castiñeiras, J. Sordo and M. S. García-Tasende

Departamento de Química Inorgánica, Facultad de Farmacia, Universidad de Santiago, 15706 Santiago de Compostela, Galicia, Spain

(Received 16 February 1998; accepted 8 April 1998)

Abstract—The reactions of [2-(pyridin-2′-yl)phenyl]mercury(II) acetate with 2-formyl-benzene-(Hbtsc), 2-formyl-(2-hydroxybenzene)-(H_2stsc) and 2-formyl-(4-methoxybenzene)-(Hmbtsc) thiosemicarbazones in ethanol in 1:1 ratio at room temperature formed [Hg($C_6H_4C_5H_4N$)L] (L = btsc, **1**; Hstsc, **2**; mbtsc, **3**). The derivative [Hg($C_6H_4C_5H_4N$)L] **2** crystallises in the triclinic space group P/1 (n. 2), $Z=2$, $R=0.0353$ and $V=906.8(3)$Å^3. Mercury is bonded strongly only to sulphur atom of thiosemicarbazonate anion [Hg–S, 2,357(2)Å] and Hg...N(3) distance of 3.126(6)Å, slightly less than the sum of the van der Waal's radii (3.28 Å) shows a weak interaction. The pyridyl nitrogen binds strongly to Hg [Hg–N(4), 2.575(6)Å] with a short C(9)HgN(4) bite angle of 74.6(2)°, but Hg retains near linearity in C_{Ph}HgS bond angle [177.8(2)°]. ^{1}H and ^{199}Hg NMR spectra in $CDCl_3$ solution reveal two isomers (A and B) for each of **1–3** and probably also a third isomer (C) for **2**. The similarity of ^{1}H and ^{199}Hg data of B isomers (minor for **1** and **3**; major for **2**) clearly support that thiosemicarbazones are unidentate S-donors as established for crystallized B isomer of **2** (major) by X-ray study, with pyridyl nitrogen of 2-pyridylphenyl coordinating to Hg. The A isomers (major for **1** and **3**; minor for **2**) have presumably N^3,S-coordinated thiosemicarbazonates with weak Hg–N(pyridyl) interaction and the Hg atom formally tetracoordinated. © 1998 Elsevier Science Ltd. All rights reserved

Keywords: Mercury Complexes; Arylmercury Complexes; Thiosemicarbazone Complexes; Crystal Structure.

The cleavage of one or more C–M bonds (M=Al, Ga, In, Tl, Pb or Sn) using acids such as dithiophosphorus acids [$X_2P(S)SH$, X = R, OR, R = Et, Ph, etc.] or trifluoroacetic acid leads to the protodemetallation reactions forming the corresponding dithiophosphinates, dithiophosphates or trifluoroacetates and the hydrocarbons [1–6]. Such cleavage reactions have recently generated acute interest in the activation of C–Hg bonds and their subsequent cleavage to generate parent hydrocarbons and inorganic mercury(II) [7–9] on the pattern of protodemercuriation of organomercury(II) substrates by organomercury lyase enzymes which are believed to form enzyme-substrate intermediates (via cysteine SH groups) [10, 11].

The coordination chemistry of particularly, transition metals with heterocyclic thiones or thiosemicarbazones containing active –N(H)–C(S)– chromophore has been widely explored [12, 13], the corresponding interaction of such organic substrates with organomercury(II) salts, a potential area of interest, has been scarcely investigated [12, 14–16]. As a part of our interest to study the cleavage of C–M bonds (protodemetallation reactions [6, 11]) and activation of such bonds by coordination with organic substrates containing –N(H)–C(S)– chromophores, recently deprotonation reactions of 2-thiouracil with

* Visiting Professor from the Guru Nanak Dev University, Department of Chemistry, Amritsar 143005, India (February 1996–April 1997).

† Authors to whom correspondence should be addressed.

phenylmercury(II) and pyridinephenyl-mercury(II) [15, 16] and of cyclopentanonethiosemicarbazone with methylmercury(II) [14] have been described.

In this paper, we report the results of deprotonation reactions of 2-formyl-benzene- (hereafter Hbtsc), 2-formyl-(2-hydroxybenzene)-(hereafter H_2stsc) and 2-formyl-(4-methoxybenzene)-(hereafter Hmbtsc) thiosemicarbazones (Scheme 1) with [2-(pyridin-2′-yl)phenyl]mercury(II) acetate in ethanol.

EXPERIMENTAL

General materials and instrumentation

Thiosemicarbazide (Merck, Muchen), benzaldehyde (Probus, Barcelona), salicylaldehyde (Merck, Munchen) and p-methoxybenzaldehyde (Ega-Chemie, Steinheim) were used as received.[2-(pyridin-2′-yl)phenyl]mercury(II) acetate was prepared by mercuration of 2-pyridylbenzene using mercury(II) acetate by a reported method [17]. The ligands were prepared by the literature methods [18].

The elemental analyses for C, H and N were obtained with a Carlo Erba 1108 microanalyser. The melting points were determined with a Gallenkamp electrically heated apparatus. The infrared spectra were recorded in KBr pellets (4000–400 cm^{-1}) or nujol mull in polythene sheets (500–100 cm^{-1}) on a Bruker IFS 66V spectrometer. The NMR spectra were recorded in $CDCl_3$ or $(CD_3)_2SO$ using a Bruker AMX 300 spectrometer at 300.14 MHz frequency (^1H) with TMS as the internal reference or a Bruker AMX 500 spectrometer at 89.51 MHz probe frequency (^{199}Hg) with neat Me_2Hg as external reference.

Syntheses

$$[Hg(C_6H_4C_5H_4N)(btsc)] \quad \textbf{(1)}$$

To a stirred solution of the ligand, Hbtsc (0.130 g, 0.73 mmol) in ethanol (25 ml) was added the solution of [2-(pyridin-2′-yl)phenyl]mercury(II) acetate (0.300 g, 0.73 mmol) in the same solvent (40 ml). The contents were stirred for 4 h and the light green solid was filtered, washed with EtOH and dried *in vacuo*; m.p. 138–42 (d) °C, yield, 52% (found, C, 42.39, H, 2.61, N, 10.03; required for $C_{19}H_{16}N_4SHg$, C, 42.78, H, 3.00, N, 10.51). It is partially soluble in $CHCl_3$, CH_2Cl_2, soluble in DMSO, DMF, and poorly soluble in EtOH and MeOH. It decomposes slowly in $CHCl_3$, and rapidly in DMSO or DMF.

$$[Hg(C_6H_4C_5H_4N)(Hstsc)] \quad \textbf{(2)}$$

To a solution of the ligand, H_2stsc (0.142 g, 0.73 mmol) in 30 ml of ethanol was added the solution of [2-(pyridin-2′-yl)phenyl]mercury(II) acetate (0.300 g, 0.73 mmol) in 20 ml of ethanol and the contents were stirred for 20 h. The light yellow solid was filtered, washed with ethanol and dried *in vacuo*; m.p. 165–70 (d) °C, yield, 73% (found, C, 41.04, H, 3.04, N, 10.15; required for $C_{19}H_{16}HgN_4OS$, C, 41.53, H, 2.91, N, 10.20).

It is partially soluble in $CHCl_3$, CH_2Cl_2, ethanol, methanol but soluble in DMSO and DMF. The decomposition behaviour in solution is similar to that of **1**.

$$[Hg(C_6H_4C_5H_4N)(mbtsc)] \quad \textbf{(3)}$$

To a stirred solution of the ligand, Hmbtsc (0.252 g, 1.20 mmol) in ethanol (20 ml) was added the solution of [2-(pyridin-2′-yl)phenyl]mercury(II) acetate (0.500 g, 1.20 mmol) in ethanol (20 ml). The contents were stirred for 30 h and the light green solid was filtered, washed with ethanol and dried *in vacuo*; m.p. 130–35°C (d), yield, 65% (found, C, 41.01, H, 3.13, N, 9.56; required for $C_{20}H_{18}N_4OSHg$, C, 42.63, H, 3.20, N, 9.95). It is partially soluble in $CHCl_3$, CH_2Cl_2, poorly soluble in ethanol and methanol and soluble in DMSO, where decomposes rapidly and more slowly in $CHCl_3$.

Crystallography

The light yellow crystals of **2** were grown from a mixture of $CH_2Cl_2/CHCl_3/CH_3OH$ and its ^1H NMR spectrum was identical with that of the major isomer labelled B (vide infra). A prismatic crystal of dimensions 0.1 × 0.30 × 0.40 mm was mounted in an ENRAF-NONIUS MACH3 automatic diffractometer [19]. Unit cell dimensions along with other crystal, data collection and refinement data are listed in Table 1. Data were collected at 293 K using a ω scan technique. Intensities of reflections were corrected for

$$R = N^3 - N^2(H) - C^1(S) - N^1H_2.$$

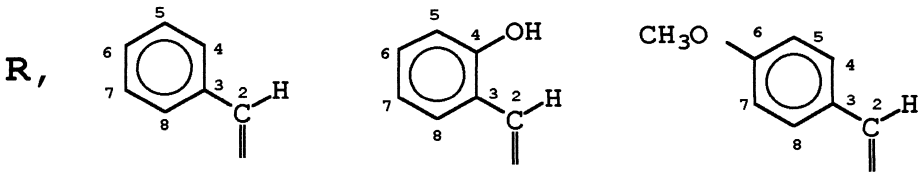

Scheme 1.

Table 1. Crystal data and details of intensity, data collection and structure refinement.

Compound	$C_{19}H_{16}HgN_4OS$
Formula weight	549.01
Crystal system	triclinic
Space group	P/1 (n. 2)
Cell constants	
a, Å	7.579(2)
b, Å	9.998(2)
c, Å	13.181(2)
α, deg	111.237(11)
β, deg	92.97(2)
γ, deg	100.74(2)
Cell volume, Å^3	906.8(3)
Formula units/unit cell	2
D_{calc}, g cm^{-3}	2.011
μ_{calc}, mm^{-1}	8.617
Radiation	MoKα ($\lambda = 0.71073$ Å)
Monochromator	graphite
Reflections measured	3843
θ range, deg	2.76–26.28
Range of h, k, l	$-9 \leq h \leq 9, -11 \leq k \leq 2, -16 \leq l \leq 0$
Number of all reflections	3843
Number of independent reflections	3677
Reflections observed ($I > 2\sigma(I)$)	2813
Number of parameters	235
Weights	$w = 1/[\sigma^2(F_o^2) + (0.0273P)^2 + 0.5628P]$, $P = (F_o^2 + 2F_c^2)/3$
$S = [\sum[w(F_o^2 - F_c^2)^2/(n-p)]^{1/2}$	1.053
$R_1 = \sum \|\|F_o\| - \|F_c\|\| / \sum \|F_o\|$	0.0353
$WR_2 = [\sum[w(F_o^2 - F_c^2)^2 / \sum(F_o^2)^2]]^{1/2}$	0.0667

Lorentz and polarization effects [20]. Empirical absorption corrections were applied as reported [21].

The structure was solved using direct methods [22] which revealed the positions of all non-hydrogen atoms and refined on F^2 by full matrix least-squares procedure using anisotropic parameters for all non-hydrogen atoms [23]. The hydrogen atoms were included in the model on geometrically calculated positions (C–H = 0.93–0.96 Å).

Atomic scattering factors were taken from International Tables for X-ray Crystallography [24], while molecular graphics were done using ZORTEP and SCHAKAL [25].

RESULTS AND DISCUSSION

The aryl thiosemicarbazones (Scheme 1) deprotonate the most acidic hydrazinic (–NH–) proton on reaction with [2-(pyridin-2′-yl)phenyl]mercury(II) acetate in ethanol at room temperature forming [2-(pyridin-2′-yl)phenyl]mercury(II) thiosemicarbazonates, [Hg(PyPh)L] **(1–3)** where L represents deprotonated thiosemicarbazone and these are characterised with the help of analytical data, infrared and NMR spectroscopy and compound **2** using single crystal X-ray crystallography. The compounds are light green (**1** and **3**) and light yellow (**2**), stable in solid phase, have partial solubility in general organic solvents and finally decomposes rapidily in DMSO or DMF, but slowly in other solvents.

The crystal and molecular structure of [*Hg*($C_6H_4C_5H_4N$)(Hstsc]

Figure 1 shows the SCHAKAL drawing of [Hg($C_6H_4C_5H_4N$)(Hstsc] (**2**) and the atom numbering scheme used; selected bond distances and angles are listed in Table 2.

The crystal structure consists of discrete molecular units of **2** and there are no close intermolecular contacts in the lattice (Fig. 2). The geometry about Hg center is distorted T-shaped with thiosemicarbazonate anion, Hstsc$^-$, coordinating essentially via S atom leading to a nearly linear C(9)–Hg–S bond angle [C(9)–Hg–S, 177.7(2)°] and Hg–N(Py) bond [bite C(9)–Hg–N(4) = 74.6(2)°] is distorted from being at expected 90° angle for undistorted T-shaped molecule [26]. The C(9)HgS angle in **2** is higher than in methyl-(cyclopentanonethiosemicarbazonate)mercury(II) [**4**, C–Hg–S, 167,7°] [14] and the difference is attributed to N^3,S-chelation in **4** [Hg–N(3), 2.537(8), Hg–S = 2.380(3) Å] [14] and unidentate S-bonding [Hg–S, 2.357(2) Å] in **2** with very weak Hg...N(3) interaction

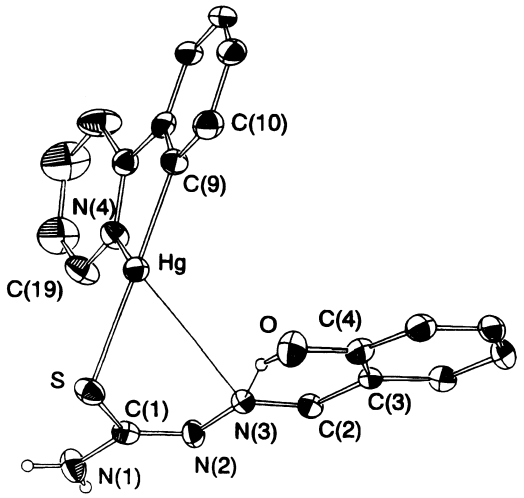

Fig. 1. ORTEP drawing showing the crystal structure of $[Hg(C_6H_5C_5H_4N)(Hstsc)]$ **2** with the numbering scheme used.

Table 2. Selected bond lengths [Å] and angles [°] for $[Hg(C_6H_4C_5H_4N)(Hstsc)]$ (**2**).

Hg–C(9)	2.083(7)
Hg–S	2.357(2)
Hg–N(4)	2.576(6)
Hg–N(3)	3.126(6)
Hg–O	3.519(6)
S–C(1)	1.782(7)
N(4)–C(19)	1.327(9)
N(4)–C(15)	1.341(9)
N(3)–C(2)	1.274(9)
N(3)–N(2)	1.387(7)
N(3)–O	2.647(7)
N(2)–C(1)	1.288(9)
O–(4)	1.366(9)
C(2)–C(3)	1.456(9)
C(3)–C(4)	1.400(10)
N(1)–C(1)	1.352(8)
C(9)–C(14)	1.394(10)
C(14)–C(15)	1.499(10)
C(9)–Hg–S	177.7(2)
C(9)–Hg–N(4)	74.6(2)
S–Hg–N(4)	106.74(14)
C(9)–Hg–N(3)	118.5(2)
S–Hg–N(3)	63.45(12)
N(4)–Hg–N(3)	92.7(2)
C(1)–S–Hg	98.8(2)
C(19)–N(4)–C(15)	119.0(6)
C(15)–N(4)–Hg	106.2(4)
C(2)–N(3)–N(2)	114.7(6)
C(2)–N(3)–Hg	134.4(5)
N(2)–N(3)–Hg	93.8(4)
C(1)–N(2)–N(3)	114.0(6)
N(3)–C(2)–C(3)	122.5(6)
C(4)–C(3)–C(2)	122.5(7)
N(2)–C(1)–N(1)	118.0(6)
N(2)–C(1)–S	128.1(5)
N(1)–C(1)–S	113.9(6)
C(14)–C(9)–Hg	118.6(5)
C(9)–C(14)–C(15)	121.3(6)
N(4)–C(15)–C(14)	117.3(6)

[Hg–N(3), 3.126(6) Å], only sligtly less than the sum of the van der Waals radii (3.28 Å) [27]. Hg–S distances are comparable in two cases, though as anticipated it is shorter in **2** than in **4**.

Table 3 shows the angles between various planes and it can be seen that the plane III of thiosemicarbazonate moiety (except N(1)) is at an angle of 76.3° with plane II containing pyridylphenyl moiety chelated to Hg. Further, phenyl and pyridyl rings are not coplanar (13.4°) as nearly are plane II and the coordination plane I (5.9°). Non-planarity of pyridyl and phenyl rings has been observed in related compounds $[\{Hg(C_6H_4C_5H_4N)_2\}_2(tuc)]$ (H_2tuc = 2-thiouracil) [16], $[Hg(C_6H_4C_5H_4N)_2]$ [17], $[Hg(C_6H_4C_5H_4N)(OAc)]$ [28] and $[Hg(C_6H_4C_5H_4N)(Cl)]$ [29].

The unidentate S-bonding by $Hstsc^-$ anion is probably influenced by Hg–N(Py) intramolecular coordination and this bond length [Hg–N(4), 2.576(6) Å] is indeed comparable with Hg–N(3) distance in N^3,S-chelation in **4**. The lack of similar N(3)–Hg coordination in **2** could be the effect of strong intramolecuar O–H...N(3) hydrogen bonding [O...N(3), 2.647(7) Å; the sum of van der Waals radii, 3.05 Å [30]; N(3)...H(O) = 1.867 Å, O–H, 0.78 Å], which weakens Hg–N(3) interaction considerably [Hg...N(3), 3.126(6) Å]. This hydrogen bond is of the same order as in the free H_2stsc ligand [N(3)...O = 2.664(3) Å, N(3)...H(O) = 1.96(3) Å [31]]. Further, the conformational change of $Hstsc^-$ moiety from E configuration (free H_2stsc) to Z-configuration (Scheme 2) as in complex **2** is necessitated by both weak Hg...N(3) interaction and relatively strong O...N(3) interaction.

The deprotonation of N(2) proton of H_2stsc and subsequent coordination to Hg via essentially S atom, affects significantly the bond distances: C(1)–S = 1.782(7), C(1)–N(1) = 1.352(8); C(1)–N(2) = 1.288(9) Å [free H_2stsc, C(1)–S = 1.689(4), C(1)–N(1) = 1.317(4), C(1)–N(2) = 1.346(4) Å] [31]. The lengthening of C(1)–S is higher in **2** than in $R_2Sn(stsc)$ [C(1)–S, 1.724–1.733 Å, R = Me, Ph, stsc is a dianion coordinating via O, N(3) and S donor atoms] [32] in agreement with strong Hg–S interaction.

The deprotonated thiosemicarbazones coordinate to a metal in the usual N^3,S-coordination mode [13, 14, 33], though one example of N(2), S-mode is also known [34]. The thiosemicarbazones with R groups containing 2-hydroxy benzene, pyridyl or similar other groups may coordinate also via additional donor atoms [13, 32, 35]. The unidentante S bonding by deprotonated $Hstsc^-$ in **2** represents an unusual coordination mode for main group and transition metals thiosemicarbazonate complexes, the only other

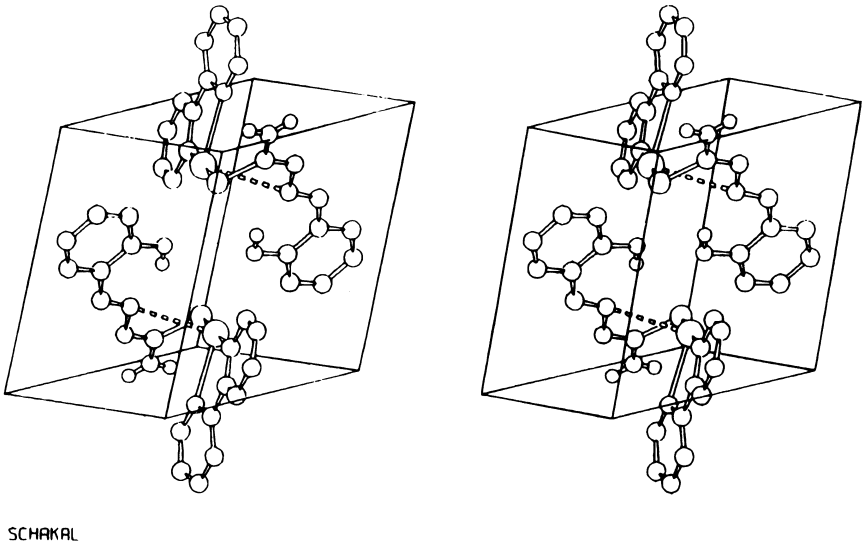

Fig. 2. Stereoview of $[Hg(C_6H_5C_5H_4N)(Hstsc)]$ **2**.

Table 3. The angles between planes of $[Hg(C_6H_4C_5H_4N)(Hstsc)]$ (**2**)

Plane	Rms*	Atoms defining a plane	Angle (°) between planes
I	0.080	Hg, C^9, C^{14}, C^{15}, N^4, S	
II	0.128	C^9, C^{10}, C^{11}, C^{12}, C^{13}, C^{14}, C^{15}, C^{16}, C^{17}, C^{18}, C^{19}, N^4, Hg	5.9(0.2) (I and II)
III	0.060	S, C^1, N^2, N^3, C^2, C^3, C^4, C^5, C^6, C^7, C^8, O	76.3(0.1) (II and (III)
IV	0.005	C^9, C^{10}, C^{11}, C^{12}, C^{13}, C^{14}	72.5(0.2) (III and IV)
V	0.014	N^4, C^{15}, C^{16}, C^{17}, C^{18}, C^{19}	13.4(0.3) (IV and V)

* Rms deviation of fitted atoms

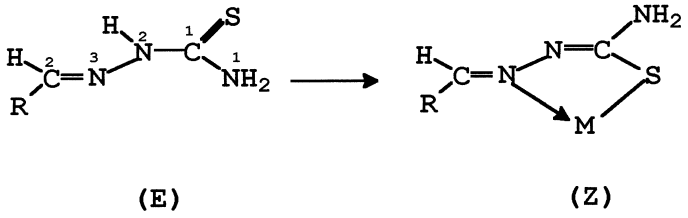

Scheme 2.

example being S-coordination in Ph_3SnL by a related deprotonated 2-acetyl-(2-hydroxybenzene) thiosemicarbazonate $[(2\text{-}HOC_6H_4)\text{–}C(CH_3)=N^3\text{–}N^2=C(NH_2)S^-]$ where steric bulk of Ph_3Sn moiety prevents N^3,S-coordination and the ligand retains E-configuration in the complex [36].

Table 4 gives a comparative data for some important bond lengths/angles of Hg-bonded 2-pyridylphenyl moiety. It is significant to observe that more electronegative donor atoms positioned trans to $Hg\text{–}C_{Ph}$ bond seems to shorten it (and probable deactivates the breaking of this bond) and *vice versa*. Thus, order of Hg–C bond activation appears to be: C > S > Cl > O (**5** > **6**, **2** > **7** > **8**) and consequently the study of Hg–S interactions gain significance. Hg–N(pyridyl) intramolecular coordination varies in more complicated manner. Despite the steric bulkiness of $Hstsc^-$ moiety, **2** shows the strongest Hg–N bond and this is attributed to more positional flexibility of $Hstsc^-$ with the result that the plane III makes an angle of 76.3° with plane II as discussed earlier. The CHgN bite angles are similar in **2**, **6**, and **7**, shortest in **5** and largest in **8**. The $C_{Ph}HgD$ bond angles (D=C, O, Cl, S) are similar in **2**, **7** and **8**, but shortest in **6**, imposed

Table 4. Selected bond lengths (Å) and bond angles (°) of related Hg-2-pyridylphenyl derivatives

Compound	Hg–C	Hg–N(py)	C–Hg–N (bite)	C_{Ph}–Hg–D (D=C, O, Cl, S)	Ref.
$[Hg(C_6H_5C_5H_4N)(Hstsc)]$ **(2)**	2.083(7)	2.58(1)	74.6(2)	177.2 (D=S)	This work
$[Hg(C_6H_5C_5H_4N)_2]$ **(5)**	2.10(1)	2.80(1)	70.7(3)	180.0 (D=C)	17
$[\{Hg(C_6H_5C_5H_4N)\}_2(tuc)]$ **(6)**	2.07(1)	2.61(2)	74.5(6)	174.8(6)(D=N)	16
	2.10(2)	2.69(2)	73.0(6)	173.3(5)(D=S)	
	2.085(1.5)(*av.*)	2.65(2)(*av.*)	73.8(6) (*av.*)		
$[Hg(C_6H_5C_5H_4N)Cl]$ **(7)**	2.07(1)	2.65(1)	73.1(5)	178.1(4)(D=Cl)	29
$[Hg(C_6H_5C_5H_4N)(OAc)]$ **(8)**	1.99(1)	2.73(1)	76.2(3)	176.1(4)(D=O)	28

probably by bridging requirements of 2-thiouracilate dianion (tuc^{2-}).

IR studies

The three complexes show IR bands due to the $Hg(C_6H_4C_5H_4N)$ fragment in practically the same position showing that in all the three the N atom of the pyridine ring is coordinated to the Hg as the X-ray study indicates it to be in **2**. Bands of this fragment around 1600 cm^{-1} difficult the analysis of the N(3)-coordination in **1** and **3**. As in other systems [32, 34] the S-coordination shifts to lower wavenumbers or induces an intensity decrease in ν(C=S) bands compared with the free ligand.

The slight shift to 3445, 3280 in **2** of the $\nu(NH_2)$ bands of the free ligand (3446, 3321 cm^{-1}) is common to the other complexes showing that the NH_2 group is not coordinated to Hg.

NMR studies

Transformation of the spectrum for the ligands under complexation is as usually: i) Spectrum of compounds **1–3** do not contain the signals due to the hydrazinic -N^2H- proton due to the deprotonation of arylthiosemicarbazones, ii) thioamidic protons [-$C(S)N^1H_2$] of the free thiosemicarbazones which show two signals at low-field (6.29–8.12 ppm) shift to the high (5.07–5.94 ppm) and merge to only one signal probably due to the reduction in the double bond character in C^1-N^1 after deprotonation of -N^2H- group (Scheme 3) and to disappearance of $N^3...H_2N^1$ hydrogen bonding when free thiosemicarbazones transform to Z-configuration in their complexes (Scheme 2). The aryl rings protons all show high-field shift and the resolution of most multiplets into clear signals is apparent.

A most interesting feature of these compounds is the existence of isomers labelled A and B. For **1** and **3**, isomers A are in major proportion (*ca* 70%, B, 30%), while for **2**, B isomer is major (*ca*. 90%; A, *ca*. 10%) (proportions were calculated from the integrals of $C^{11}H$, N^1H_2 or OH protons). Separated signals were identified for all except A isomer of **2**, for which only N^1H_2, C^2H and OH signals could be identified and others obscured by the major isomer B; however, for **1** and **3**, signals for A and B were clearly visible. Based on X-ray analysis of isomer B of **2** [being in higher proportion (90%), crystallised preferentially and for isomers **1** and **3** repeated efforts failed to give crystals] as well as similarity of ^{1}H and ^{199}Hg NMR (*vide infra*) data, similar structure for isomers of **1** and **3** is proposed. For A isomers of **1–3** ^{199}Hg NMR reveals clearly a different chemical enviroment about Hg center and N^3,S-chelation by thiosemciarbazonates is proposed as increasing coordination number in Hg generally decreases Hg chemical shift [37] (*vide infra*).

The ^{199}Hg NMR data of the compounds **1–3** is given in Table 5 and Fig. 3. Each compound showed two peaks differing in percentage, and for **2** second peak could be seen only when massive scans were taken. All the three compounds have one common isomer (B) at *ca.* $\delta -868$ ppm and it shows the similar chemical enviroment about Hg atom in these isomers. Since, the X-ray structure of **2** has established S-bonded thiosemicarbazonate ($Hstsc^-$), it can be argued that all the three compounds have one common S-bonded isomer, in addition to Hg–N(Py) and Hg–C_{Ph} bonds.

The major isomers (A) of **1** and **3** show δHg values at -715 and -709 ppm respectively indicating chemical enviroments about Hg in these isomers different from those in the isomers described above. It is known in case of Hg NMR spectroscopy that the increasing coordination number generally lowers the chemical shift [37] and that it is suggested that Hg in these isomers (A) have higher coordination number and thiosemicarbazonates are probably chelating via N^3,S-donor atoms, a usual mode of bonding of deprotonated thiosemicarbazones [13, 14]. The N^3,S-chelation by thiosemicarbazonates might affect Hg...N(Py) interaction by weakening it and it is confirmed by upfield shift in diagnostic $C^{11}H$ proton of 2-pyridylphenyl moiety of these major isomers (A) of **1** and **3**.

Minor isomer of 2 appears at -783 ppm, a different position from A isomers of **1** and **3**. Anomalous position for the signal of 2 may be due to $Hstsc^-$ which exhibits additional chelating possibilities respect to

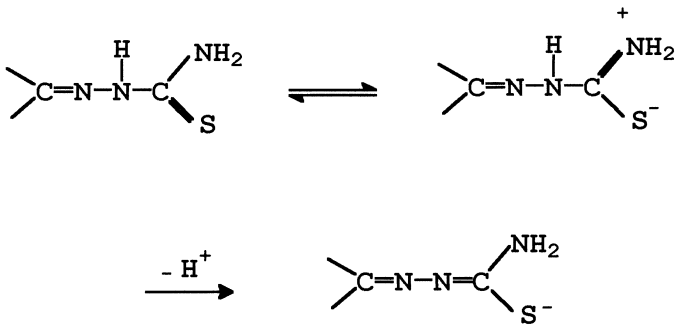

Scheme 3.

Table 5. The ^{1}H and ^{199}Hg NMR data (ppm)[a]

Compound	Thiosemicarbazone signals			Pyridylphenyl signals		^{199}Hg ($^{3}J_{Hg-H}$)
	NH_2	C^2H	Aryl ring	Pyridyl ring	Phenyl ring	
1(A)[b]	5.12*s*	8.33*s*	6.80*t*($C^{5,7}H$)	8.49*d*($C^{11}H$)	7.87*d*($C^{5}H$)	−715*d*
			7.31–7.37*m*($C^{4,6,8}H$)	7.80*t*($C^{8}H$)	7.66*t*($C^{2}H$)	(179.0)
				7.62*td*($C^{9}H$)	7.53*dd*($C^{3}H$)	
				7.22*t*($C^{10}H$)	7.39*t*($C^{4}H$)	
(B)[c]	5.33*s*	7.77*s*	7.05*t*($C^{5,7}H$)	8.65*d*($C^{11}H$)	8.06*d*($C^{5}H$)	−868*sb*
	5.94*sb*		7.31–7.37*m*($C^{4,6,8}H$)	8.02*d*($C^{8}H$)	7.72*t*($C^{2}H$)	
				7.91*t*($C^{9}H$)	7.64*d*($C^{3}H$)	
				7.26*t*($C^{10}H$)	7.45*t*($C^{4}H$)	
2(A)[c,d]	5.07*s*	8.24*s*	*e*	*e*	*e*	−783*sb*
(B)[b]	5.54*sb*	7.77*s*	7.22*m*($C^{6}H$)	8.58*d*($C^{11}H$)	8.00*d*($C^{5}H$)	−868*d*
			7.01*dd*($C^{5}H$)	7.91*d*($C^{8}H$)	7.65*s*($C^{2}H$)	(159.1)
			6.93*d*($C^{8}H$)	7.75*td*($C^{9}H$)	7.47*t*($C^{3}H$)	
			6.83*td*($C^{7}H$)	7.22*m*($C^{10}H$)	7.41*t*($C^{4}H$)	
3(A)[b]	5.06*s*	8.23*s*	7.23*d*($C^{5,7}H$)	8.43*d*($C^{11}H$)	7.83*d*($C^{5}H$)	−709*d*
			6.26*d*($C^{4,8}H$)	7.60*sb*($C^{8}H$)	7.67*t*($C^{2}H$)	(166.5)
			3.62*s*(CH_3O)	7.49*t*($C^{9}H$)	7.49*t*($C^{3}H$)	
				7.17*sb*($C^{10}H$)	7.34*t*($C^{4}H$)	
(B)[c]	5.25*s*	7.69*s*	7.60*sb*($C^{5,7}H$)	8.58*sb*($C^{11}H$)	7.99*t*($C^{5}H$)	−868*sb*
	5.84*sb*		6.84*d*($C^{4,8}H$)	7.92*d*($C^{8}H$)	7.72*t*($C^{2}H$)	
			3.80*s*(CH_3O)	7.89*t*($C^{9}H$)	7.49*t*($C^{3}H$)	
				7.28*t*($C^{10}H$)	7.39*t*($C^{4}H$)	
	NH_2	C^2H	Aryl ring	N^2H		
Hbtsc[f]	7.27*sb*	9.26*s*	7.69*m*($C^{4,8}H$)	10.22*sb*		
	6.60*sb*		7.43*m*($C^{5,6,7}H$)			
H_2stsc[g]	8.12*sb*	8.36*s*	7.91*sb*($C^{5}H$)	11.38*sb*		
	7.89*sb*		7.19*m*($C^{6}H$)	9.87*sb*(OH)		
			6.86*m*($C^{7,8}H$)			
Hmbtsc[f]	7.18*sb*	7.78*s*	7.61*d*($C^{5,7}H$)	9.31*sb*		
	6.29*sb*		6.94*d*($C^{4,8}H$)			
			3.86*s*(CH_3O)			

[a] *s*-singlet, *d*-doublet, *t*-triplet, *b*-broad, *m*-multiplet.
[b] Major isomer.
[c] Minor isomer.
[d] $\delta OH = 11.26s$ ppm for B isomer and 12.00 ppm for A isomer.
[e] Assignement was not possible due to the very low percentage of this isomer together with the overlaping with the signals for the major isomer.
[f] $CDCl_3$ solvent.
[g] $(CD_3)_2SO$ solvent.

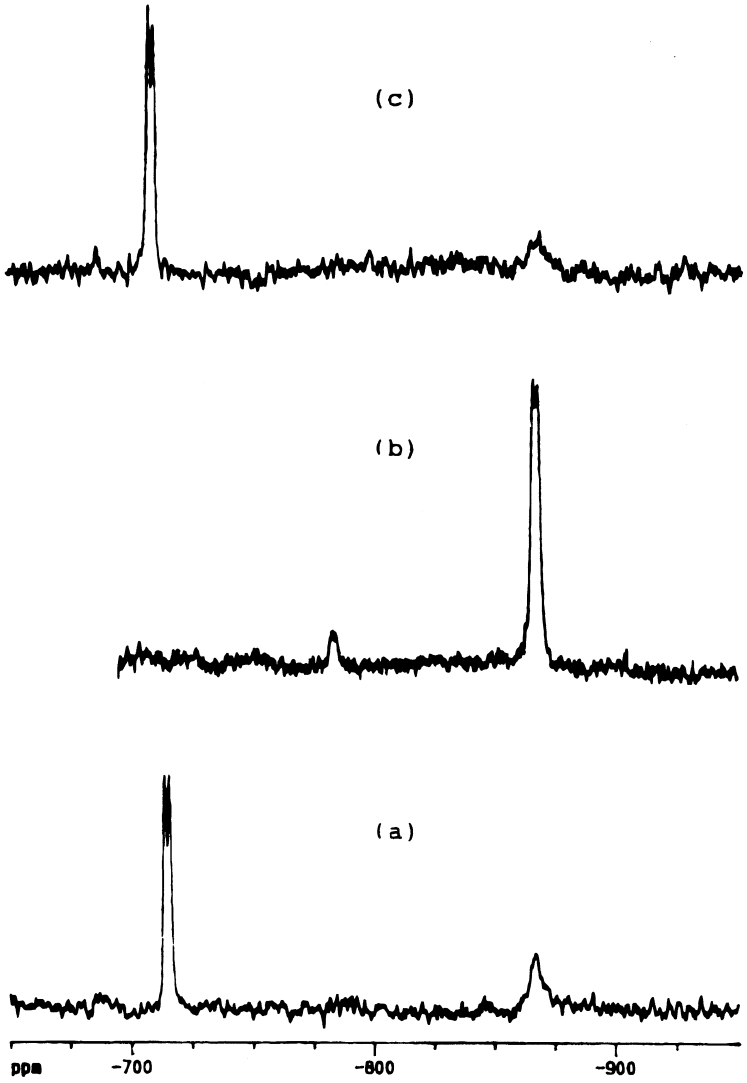

Fig. 3. The ^{199}Hg NMR spectra of (*a*) [Hg($C_6H_5C_5H_4N$)(btsc)] **1**, (*b*) [Hg($C_6H_5C_5H_4N$)(Hstsc)] **2** and (*c*) [Hg($C_6H_5C_5H_4N$)(mbtsc)] **3**.

btsc$^-$ and mbtsc$^-$ through phenolic O atom. This could originate a third isomer (C) with Hg coordinated to C^9, N^4, N^3 and O (previous proton transference, for example, from the OH group to N^2) and minor isomers (A) and (C) in a fast interchange are conceivable. Although the (C) isomer of 2 must be expected to have less importance than (A) (if both the mercury-sulphur affinity and the relationship between the chelating ring size and the stability are considered), its presence introduces an oxygen atom in the coordiantion sphere of the metal increasing the shielding [37].

Among the B isomers of compounds **1–3**, the $^3J_{Hg\text{-}H}$ coupling was observed in **2** only and that too after massive scans and the value is lower than $^3J_{Hg\text{-}H}$ value show by the major isomers (A) of **1** and **3**. It shows that the electron density on phenyl bonded to Hg is higher in the latter cases as compared to that in the former case. It can occur by both weakening of Hg...N(Py) interaction and/or by chelation of thiosemicarbazonates.

Acknowledgements—Professor T.S. Lobana thanks Dirección General de Enseñanza Superior del Ministerio de Educación y Cultura (SAB95–0185), Spain for financial support as Visiting Professor and the Guru Nanak Dev University, Amritsar, Punjab, India for sanctioning leave.

REFERENCES

1. Pudovik, A. N., Cherkasov, R. A. and Shergina, I. V., *J. Gen. Chem. USSR*, 1971, **41,** 1477.
2. Pudovik, A. N., Cherkasov, R. A., Bykova, I. V.,

Evstaf'ev, G. I., Zemskaya, Z. I. and Nazypov, M. N., *J. Gen. Chem. USSR*,, 1972, **42,** 76.
3. Elkhaldy, A. A. S., Mehrotra, R. K. and Srivastiva, G., *Synth. React. Inorg. Met-Org. Chem.*, 1992, **22,** 997.
4. Coates, G. E., and Mukherjee, R. N., *J. Chem. Soc.* 1964, 1295.
5. Gurikin, I. F., Idelevich, A. I. and Butin, K. P., *Organomet. Chem. USSR*, 1990, **3,** 304.
6. Casas, J. S., Castellano, E. E., Castiñeiras, A., Sánchez, A., Sordo, J., Vázquez-López, E. M. and Zukerman-Schpector, J., *J. Chem. Soc. Dalton Trans.*, 1995, 1403.
7. Barbaro, P., Cecconi, F., Ghilardi, C. A., Midolini, S., Orlandini, A. and Vacca, A., *Inorg. Chem.*, 1994, **33,** 6163.
8. Garoufis, A., Perlepes, S. P., Schreiber, A., Bau, R. and Hadjiliadis, N., *Polyhedron*, 1996, **15,** 177.
9. Moore, M. J., Distefano, M. D., Zydowsky, L. D., Cummings, R. T. and Walsh, C. T., *Acc. Chem. Res.*, 1990, **23,** 301.
10. Gopinath, E. and Bruice, T. C., *J. Am. Chem. Soc.*, 1987, **109,** 7903.
11. Casas, J. S., García-Tasende, M. S., Sánchez, A., Sordo, J., Vázquez-López, E. M., *Inorg. Chim. Acta*, 1997, **256,** 211.
12. (a) Raper, E. S., *Coord. Chem. Rev.*, 1985, **61**, 115; (b) Raper, E. S., *Coord. Chem. Rev.* 1994, **129**, 91; (c) Raper, E. S., *Coord. Chem. Rev.* 1996, **153**, 199.
13. (a) Campbell, M. J. M., *Coord. Chem. Rev.*, 1975, **15**, 279; (b) Padhye, S., and Kauffman, G. B. *Coord. Chem. Rev.*, 1985, **63**, 127; (c) West, D. X., Padhye, S. B., and Sonawane, P. B., *Structure and Bonding*, 1991, **76**, 4; (d) West, D. X., Liberta, A. E., Padhye, S. B., Chilate, R. C., Sonwane, P. B., Kumbhar, A. S., and Yerande, R. G., *Coord. Chem. Rev.*, 1993, **123**, 49.
14. Zukerman-Schpector, J., Rodríguez-Argüelles, M. C., Suarez, M. I., Sánchez, A., Casas, J. S. and Sordo, J., *J. Coord. Chem.*, 1991, **24,** 177.
15. García-Tasende, M. S., Suarez-Gimeno, M. I., Sánchez, A., Casas, J. S., Sordo, J. and Castellano, E. E., *J. Organomet. Chem.*, 1990, **384,** 19.
16. Casas, J. S., Castellano, E. E., García-Tasende, M. S., Sánchez, A., Sordo, J., Vázquez-López, E. M. and Zukerman-Schpector, J., *J. Chem. Soc. Dalton Trans.*, 1996, 1973.
17. Black, D.St.C., Deacon, G. B., Edwards, G. L. and Gatehouse, B. M., *Aust. J. Chem.*, 1993, **46,** 1323.
18. (a) Andersen, F. E., Duca, C .J., and Scudi, J. V., *J. Amer. Chem. Soc.* 1951, **73**, 4967; (b) Tobias, R. S., Ogrins, I., and Nervett, B. A., *Inorg. Chem.* 1962, **1**, 638; (c) Mukkanti, K., Pandeya, K. B., and Singh, R. P., *Indian J. Chem. Sect. A*, 1982, **21**, 641.
19. ENRAF-NONIUS, CAD4-Express Sofware. Version 5.1. Enraf-Nonius, Delft, The Netherlands, 1995.
20. Spek, A. L., HELENA, A Program for data reduction of CAD4 data, University of Utrecht, The Netherlands, 1993.
21. Walker, N. and Stuart, D., *Acta Cryst.*, 1983, **A39,** 158.
22. Sheldrick, G. M., *Acta Cryst.*, 1990, **A46,** 467.
23. Sheldrick, G.M., SHELXL93, A Program for the Refinement of Crystal Structures, University of Göttingen, Germany, 1993.
24. International Tables for X-ray Crystallography, Vol. C, Kluwer Academic Publishers: Dordrecht, The Netherlands, 1995.
25. (a) Zsolnai, L., ZORTEP, A Program for the Presentation of Thermal Ellipsoids, University of Heidelberg, Germany, 1994; (b) Keller, E., SCHAKAL, Program for Plotting Molecular and Crystal Structures, University of Freiburg, Germany, 1988.
26. Lobana, T. S., *Coord. Chem. Rev.*, 1985, **63,** 161.
27. a) Bondi, A., *J. Phys. Chem.*, 1964, **68**, 441; (b) Carty, A. J., and Deacon, G. B., *Inorg. Chim. Acta*, 1980, **49**, L225.
28. Casas, J. S., Castellano, E. E., García-Tasende, M. S., Sánchez, A., Sordo, J., Vázquez-López, E. M., Zukerman-Schpector, J., *J. Chem. Crystallog.*, 1996, **26,** 123.
29. Constable, E. C., Leese, T. A., and Tocher, D. A., *Chem. Commun.*, 1989, 570.
30. Huheey, J. E., Keiter, E. A., and Keiter, R. L., Inorganic Chemistry: Principles of Structure and Reactivity, 4th Edn, Harper Collins College Publishers, New York, 1993.
31. Chattopadhyay, D., Mazumdar, S. K., Banerjee, T., Ghosh, S. and Mak, T. C. W., *Acta Cryst.*, 1988, **C44,** 1025.
32. Casas, J. S., Sánchez, A., Sordo, J., Vázquez-López, A., Castellano, E. E., Zukerman- Schpector, J., Rodríguez-Argüelles, M. C. and Russo, U., *Inorg. Chim. Acta.*, 1994, **216,** 169.
33. Macias, A., Rodríguez-Argüelles, M. C., Suárez, M. I., Sánchez, A., Casas, J. S., and Sordo, J., *J. Chem. Soc. Dalton Trans.* 1989, 1787.
34. Casas, J. S., Castellano, E. E., Macias, A., Rodríguez-Argüelles, M. C., Sánchez, A. and Sordo, J., *J. Chem. Soc. Dalton Trans.*, 1993, 353.
35. Casas, J. S., Castiñeiras, A., Sánchez, A., Sordo, J., Vázquez-López, A., Rodríguez-Argüelles, M. C. and Russo, U., *Inorg. Chim. Acta.*, 1994, **221,** 61.
36. Ng, S. W., Das, V. G. K., Skelton, B. W. and White, A. H., *J. Organomet. Chem.*, 1989, **377,** 211.
37. (a) Wrackmeyer, B., and Contreras, R., *Ann. Reports NMR Spectra*, 1992, **24**, 267; (b) Goodfelow, R. J., in *Multinuclear NMR* (edited by Joan Mason), Plenum Press, New York, 1987, p. 563.

Pergamon

PII: S0277–5387(98)00169–7

Polyhedron Vol. 17, No. 21, pp. 3711–3720, 1998
© 1998 Elsevier Science Ltd
All rights reserved. Printed in Great Britain
0277–5387/98 $19.00+0.00

A mixed-ligand P,S,N-*cis*-dioxorhenium(V) complex by ligand exchange reactions on *trans*-monooxo-trichlorobis(triphenylphosphine)rhenium(V): formation and structural studies

Matthias Friebe,[a]* Ruediger Jankowsky,[a] Hartmut Spies,[a] Wilhelm Seichter,[b] Minas Papadopoulos,[c] Efstratios Chiotellis[c] and Bernd Johannsen[a]

[a] Forschungszentrum Rossendorf, Institut für Bioanorganische und Radiopharmazeutische Chemie, Postfach 510119, 01314 Dresden, Germany

[b] Institut für Organische Chemie, TU-Bergakademie Freiberg, Leipziger Straße 29, 09596 Freiberg, Germany

[c] Institutes of Radioisotopes-Radiodiodiagnostic Products and Material Science, NCSR "Demokritos", P.O. Box 60228, 15310 Ag. Paraskevi, Athens, Greece

(Received 11 February 1998; accepted 20 April 1998)

Abstract—In the course of our efforts to synthesize rhenium(V) complexes for potential use in nuclear medicine, tridentate dithiolate ligands were combined with (dialkylamine) ethylene thiols [HS–$(CH_2)_2$–NR'_2] (R′ = alkyl, alkoxy) to form amine group bearing mixed-ligand complexes [ReO(SNS)(S)]. The reaction of HS–CH_2–CH_2–N–(CH_2–CH_2–N(C_2H_5)$_2$)CH_2–CH_2–SH (*N*,*N*-bis(2-mercaptoethyl)-*N*′,*N*′-diethylethylenediamine, **2**, as a tris-chelating ligand and 1,4-dioxa-8-azaspiro-*N*-2-mercaptoethylene-[4,5]-decane, **3**, with the neutral Re(V) complex [$ReOCl_3(PPh_3)_2$], **1**, yields, in addition to the expected square-pyramidal "**3**+**1**" compound (1,4-dioxa-8-azaspiro-*N*-2-thiolatoethylene-[4,5]-decane)*N*,*N*-bis(2-mercaptoethyl)(*N*′,*N*′-di-ethyl-ethylenediamine) oxorhenium(V), **4**, the new five-coordinated complex [1,4-dioxa-8-azaspiro-*N*-2-mercaptoethylene-[4,5]-decane(triphenylphosphinato)dioxorhenium(V)], **5**. Being the only product in the absence of the tridentate component, **5** has a trigonal–bipyramidal structure, where the coordination sphere is formed by two oxo groups in an uncommon *cis*-arrangement, S and N from the aminothiolate and by the phosphorus atom from the phosphine group originating from the precursor molecule. The structure was verified by mass, ^{1}H NMR, IR spectroscopy as well as by XRD. In addition, extended x-ray absorption spectroscopy (EXAFS) was applied to both the precursor and the resulting compound **5** to compare the complex structures in the solid and the soluted state. Experiments with ^{18}O labelled water added to the reaction mixture led to ^{18}O in the dioxo core, showing that water is the origin of the additional oxo group. © 1998 Elsevier Science Ltd. All rights reserved.
© 1998 Elsevier Science Ltd. All rights reserved

Keywords: rhenium(V) mixed ligand complexes; *cis*-dioxo; trigonal–bipyramidal; X-ray structure; XANES; EXAFS

INTRODUCTION

There is great interest in the chemistry of technetium and rhenium [1] because of the high significance that the radioactive nuclides ^{99m}Tc and ^{186}Re/^{188}Re have in nuclear medicine. Our special attention is focused on the so-called "3+1" mixed-ligand complexes, a class of compounds useful for the design of new radiotracer molecules [2, 3], where the MO^{3+} core is coordinated by both a tridentate and a monodentate ligand.

We were particularly interested in "3+1" com-

* Author to whom correspondence should be addressed. Fax: +49-351-260-3232; E-mail: friebe@fz-rossendorf.de.

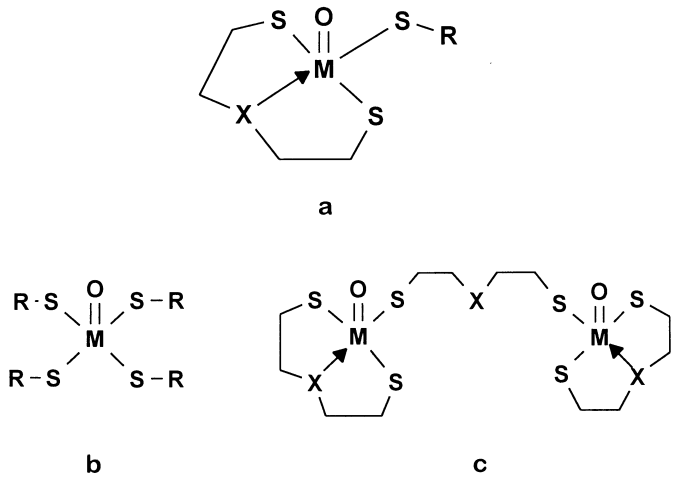

Fig. 1. A selection of known oxometal(V) complexes as the results of ligand exchange reactions on oxometal(V) precursors.

plexes in which dialkylaminothiolates are the monodentate ligands, since some of the "3+1" complexes are of interest with respect to brain imaging agents [4, 5] and play an important role in the search for neuroreceptor–affine complexes.

The involvement of two competing ligands in the formation of the mixed-ligand complexes gives rise to various species (Figure 1). Depending on the stoichiometric ratios of the ligands, not only the desired "3+1" compound (a) but also complexes of only the monodentate ligands having a formal S_4 coordination (b) [6] and dinuclear complexes (c) containing only the tridentate ligand may be formed [7, 8].

In order to optimize the reaction conditions for the preparation of such a complex **4** (Figure 2) by ligand exchange reactions, we studied the reaction of $[ReOCl_3(PPh_3)_2]$ (**1**) with the tridentate ligand [HS–$(CH_2)_2$–N(CH_2–CH_2NEt_2)–$(CH_2)_2$–SH] (**2**) [9, 10] and dialkylaminothiolates such as **3** Fig. 2. When the tridentate ligand was used as the minor compound versus one to one ratios of the dialkylaminothiolate and the metal precursor in reaction mixtures in order to avoid the formation of dinuclear bridged complex products, two compounds were obtained. One consists of the expected "3+1"-product **4** while the other is a hitherto unknown type of a *cis*-dioxorhenium(V) complex, **5**.

Here we describe the formation and structural characterization of these new compounds. Structure investigations in solution using EXAFS were performed in addition.

RESULTS AND DISCUSSION

Starting from *trans*-monooxotrichlorobis-(triphenylphosphine)rhenium(V) $[ReOCl_3(PPh_3)_2]$ (**1**) as a rhenium(V) precursor [11] with a mixture of **2** [SNS] and **3** [S(N)], the reactants **1**, **2** and **3** were used in various stoichiometric amounts (1:1:2, 1:0.5:1 or 1:1:1). In all cases the expected "3+1" mixed-ligand complex **4** was formed and a second neutral rhenium(V) complex **5** was observed with an excess of **3** over **1** and **2** or with the tridentate ligand as a minor compound Fig. 2. **5** became the major product and could be isolated as a dark red, stable, crystalline solid in a 49 percent yield (Figure 2, route b) when **2** was omitted in the reaction mixture. A base such as sodium acetate or triethyl amine in the reaction mixture seems to be essential for the formation of **4** and **5**. No formation of **5** and less yields for **4** are observed after refluxing in methanol for one hour [12] without addition of the described bases. **5** was also formed in oxygen free solvents such as dichloromethane or acetonitrile (Figure 3).

Complexes **4** and **5** are readily soluble in organic solvents. Elemental analysis shows that **4**, as expected, contains both the tridentate ligand **2** and the monodentate ligand **3,** while complex **5** contains ligand **3** and one triphenylphosphane.

^{1}H *NMR spectroscopy*

^{1}H NMR studies of **4** show signals with chemical shifts identical to those found for the O-methylene-bound protons of ligand **3** as well as the typical signal pattern of the two ethyl groups bound to the ethylene diamine fragment. All this verifies the presence of the tris chelating ligand **2** in the complex. In order to identify the other protons of the coordinated ligand **2**, NOESY spectra of a similar compound [9] bearing **2** were used for comparison.

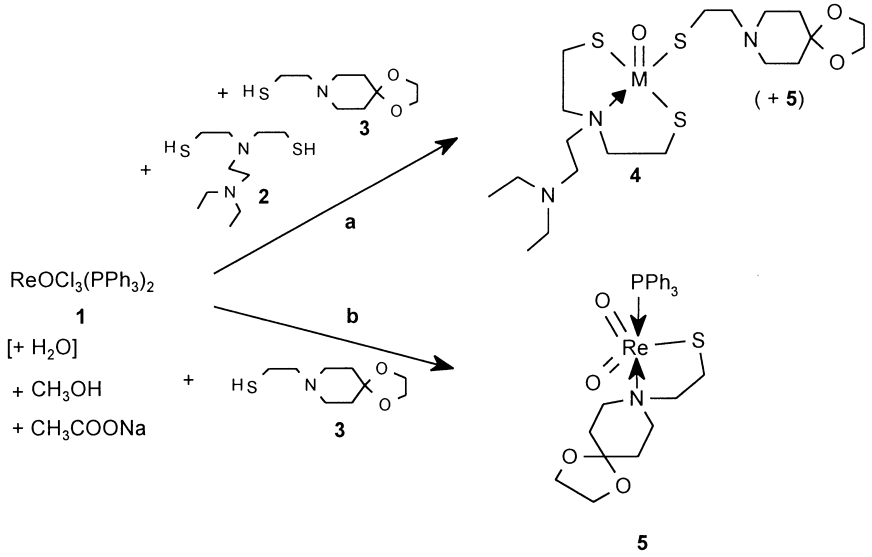

Fig. 2. Reaction scheme of the formation of the mono-oxo rhenium(V) complex **4** and the *cis*-dioxo rhenium(V) complex **5**.

^{1}HNMR investigations of **5** confirm the formulation, showing a signal pattern typical of phosphorus bound to arylic protons and a defined multiplet signal of four O-methylene bound protons in the expected range. Due to the bound nitrogen of the ring system of **3** in case of **5**, the symmetry of the O-methylene protons is disturbed and shows the splitting of the signal pattern as expected. The measured intensities of the arylic/aliphatic signals yield a 1:1 ratio corresponding to **3**/PPh_3.

IR spectroscopy

The IR spectrum of **5** did not show the intensive signal at $\nu = 945\,cm^{-1}$ for Re═O as observed for **4**. Two intense bands shifted to shorter wave numbers at $\nu = 836$ and $907\,cm^{-1}$ were detected. These values are typical of the *cis*-O═Re═O group as recorded for postulated [13] or established [14] *cis*-dioxorhenium(V) coordinated complexes.

Unlike **4**, **5** needs the attack of an oxygen donor on **1** for its formation. We assume that traces of water are the source of the second oxygen in the *cis*-dioxo arrangement of **5**. To prove this assumption, [^{18}O] water was added to the reaction mixture. As described in literature [15] the increased mass of the (^{18}O)-oxygen in the molecule should effect a noticeable shift of the obtained O═Re═O signals to shorter wave numbers. The resulting **5** shows a modified IR spectrum [Fig. 4(a)], where the oxo-rhenium stretches were shifted to $\eta = 798\,cm^{-1}$ and $\eta = 856\,cm^{-1}$ and the exactly identical fingerprint range clearly revealed the formation of an [^{18}O]-containing compound **5**. The found shifts are in a comparable range to IR data of (^{18}O)–CO vs (^{16}O)–CO [15] studies.

X-ray crystal structure

Crystals of **5** suitable for X-ray diffraction studies were obtained by recrystallization from ether/*n*-heptane. The structure determination clearly reveals the formation of a trigonal bipyramid. As already anticipated from IR data, the O-donors are arranged in a *cis* configuration and form a plane with the S-atom. The phosphorus and nitrogen donors compose the apices of the trigonal P–Re–N bipyramid. The small distortion of the ideal 180° P–Re–N angle is caused by the S-donor in the trigonal plane. In contrast to a *trans*-dioxo configuration, the O–Re–O angle is decreased to 135°. Due to the O_x–Re–S angles of about 112° and to P,N donors being perpendicular to the trigonal plane, a distorted trigonal bipyramid is formed. The parameter τ, introduced to classify five coordinated complexes to square–pyramidal ($\tau = 0$) or trigonal–bipyramidal geometry ($\tau = 1$) [16], was determined as 0.64. Discrepancies concerning the ideal trigonal bipyramid can be explained by the O_3–Re–O_4 angle of oxygen coordination in the equatorial plane. In accordance with theory, the bond length found for the dioxo core increases to 1.73 Å, compared with 1.65 Å for the mono-oxo core (Re═O, **4**) [10]. The bond lengths of the other donors show no significant differences between structures [10] such as **4** and **5** (Table 1).

The occurrence of a dioxo core shows a remarkable parallel to *trans*-dioxorhenium(V) compounds containing [P, N, Cl] or [P, I] chelating systems [14, 17]. We assume that this phenomenon results from the tendency of the metal core to become neutral. The *cis*-dioxo configuration of **5** is obviously influenced by the steric effects of the ligand **3**. The C_2 distance of

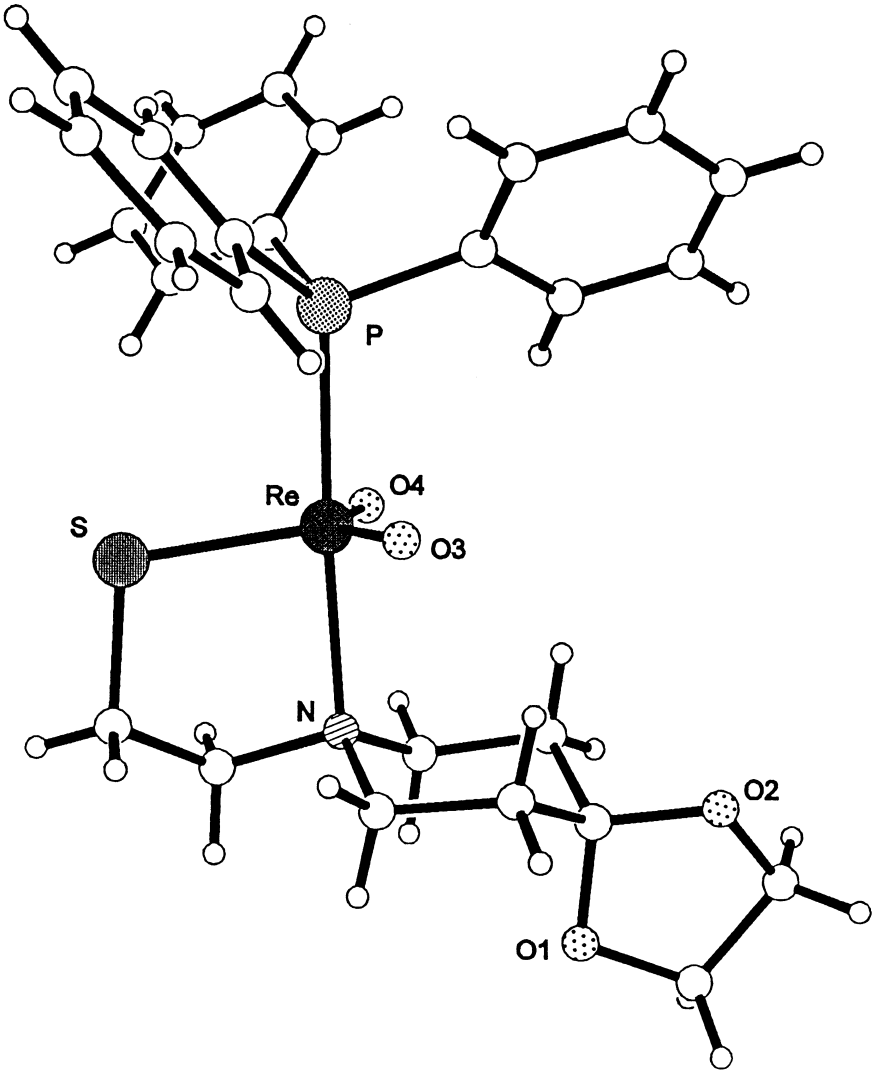

Fig. 3. X-ray crystallographic structure of **5**.

both the nitrogen and sulphur donors affects the arrangement out of the trigonal equatorial plane. This is caused by the intramolecular tension in **5** in opposition to the coordination mode in the base plane of a square pyramidal complex such as **4**. That fact excludes the *trans*-configuration of the dioxo core.

XANES/EXAFS measurements

To better understand the changes in the atomic environment of the central atom associated with the formation of the *cis*-dioxo compound, investigations of the rhenium coordination sphere at the precursor state and the final *cis*-dioxo complex state appeared to be helpful. Therefore, EXAFS measurements were applied to deliver atomic radial distributions of the ligand atoms around the rhenium central atom. EXAFS investigations made it possible to trace the structural relationships in the reaction mixture by considering the neighbourhood closest to rhenium in the solid (suspended) precursor state as well as in the soluted *cis*-dioxo compound state, which are both present in the reaction mixture. A comparison of the clarified crystal structure of **5** with its rhenium coordination sphere in a non-crystalline state was of special interest from a nuclear medical point of view.

XANES data

A strong white line as typical of measurements at the rhenium L_{III} absorption edge [16] was observed for both complexes under investigation. The absorption edge position of complex **1** was determined to be 10533 eV, that of complex **5** was 10535 eV. The differ-

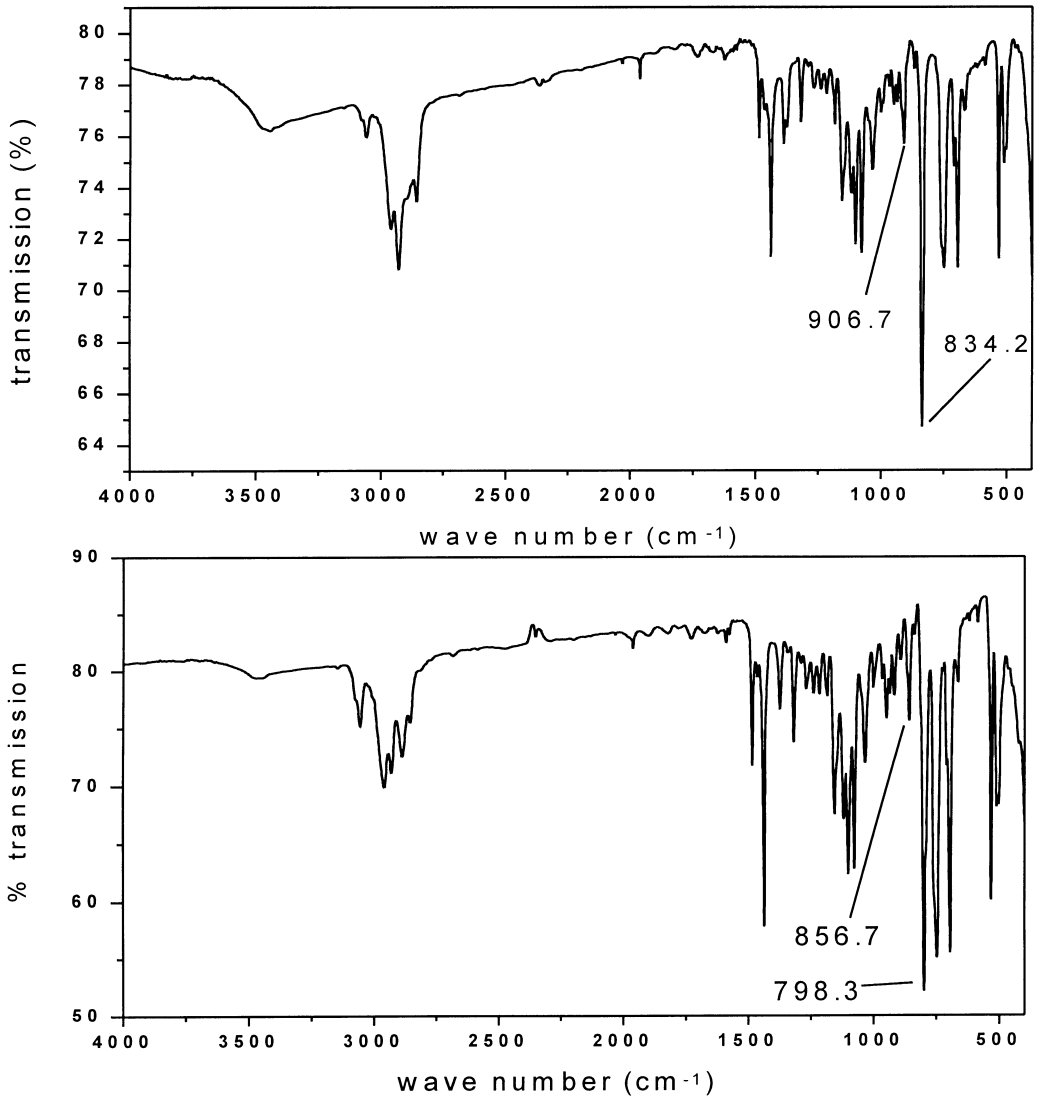

Fig. 4. IR spectrum of **5** obtained by the reaction without addition of water (measured in $CHCl_3$). (a) IR spectrum of **5** obtained by addition of [^{18}O] water to the reaction mixture (measured in $CHCl_3$).

Table 1. Selected bond distances (Å) and angles (°) of **5**

Atoms	Bond length (Å) and angles (°)	Atoms	Bond length (Å) and angles (°)
Re–O(3)	1.736(5)	O(3)–Re–N	87.6(3)
Re–O(4)	1.735(5)	O(4)–Re–N	93.0(2)
Re–S	2.269(2)	S(1)–Re–N	85.5(2)
Re–N	2.280(6)	O(3)–Re–P	86.5(2)
Re–P	2.403(2)	O(4)–Re–P	90.7(2)
O(3)–Re–O(4)	135.9(3)	S(1)–Re–P	97.43(8)
O(3)–Re–S	111.1(2)	N(1)–Re–P	174.0(2)
O(4)–Re–S	113.0(2)		

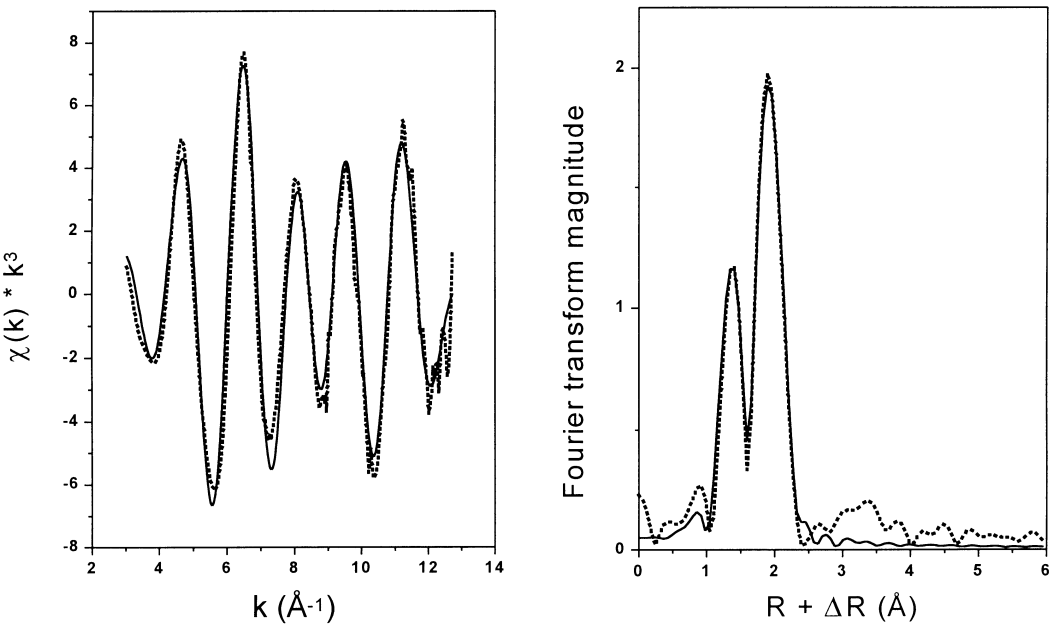

Fig. 5. (a) EXAFS data of complex **1**. Dotted lines, experimental data; solid lines, fit data. (b) Fourier transform corresponding to (a).

Table 2. EXAFS fit results for complex **1**

Shell	N	R^a (Å)	σ^2 (Å^2)
O	1.1(1)	1.70(1)	0.001(1)
P/Cl	5.2(4)	2.41(1)	0.005(1)

N is the number of coordinating atoms. R: distance to rhenium central atom. σ^2: Debye–Weller factor. Fit mode: Marquardt algorithm using least squares method. Calculated resolution in distance: 0.16 Å. The theoretical resolution in distance is given by the formula $\Delta R = 2\pi/k_{max}$ [19] ΔE_0: −8 eV.

a Distance to the rhenium central atom.

ence in the absorption edge position suggests different electron densities at both complex central atoms.

EXAFS data of ***1***

The Fourier transform of the complex **1** EXAFS data consists of two coordination shells which are well resolved. Figure 5(a) and (b) show the EXAFS data, their Fourier transforms and the corresponding fit data of complex **1**.

The peak at 1.4 Å in the Fourier transform (not corrected for scattering phase-shift) is thought to represent the short-bound oxygen atom, the large peak at 1.9 Å is probably generated by the mixed chlorine/phosphorus coordination shell. Taking this model as a default to fit the data, the EXAFS fit data shown in Table 2 were obtained.

A short-bound oxygen atom is detected at a distance of 1.70 Å as is typical of a rhenium central atom with a formal oxidation state of +5. The second coordination shell was fitted with a backscattering function of the atomic number 16 as the mean number of phosphorus (atomic number 15) and chlorine (atomic number 17), since EXAFS functions for the latter are not expected to be resolvable. As the fit result for this shell, five P/Cl atoms at a mean distance of 2.41 Å were found. The Debye–Weller factor of 0.005 Å^2 suggests a distribution of the backscattering atoms over a distance range within the coordination shell. On the one hand, this may be due to the difference in distance between the chlorine and the phosphorus atoms, on the other, the relatively high coordination number of five may also lead to increased Debye–Weller terms. As described elsewhere [20], the precursor complex **1** may occur in various forms of the general constitution $ReOCl_3(PPh_3)_2$. These conformation isomers are mainly characterized by differences in the PPh_3 ligand conformation and crystal packing patterns (monoclinic and triclinic), which lead to changes in the rhenium–ligand distances. The rhenium–oxygen bond distances as elucidated by XRD analysis are 1.66 Å for one monoclinic (A) and one triclinic isomer (B) and 1.73 Å for the other triclinic monomer (C). EXAFS analysis of the precursor showed a rhenium–oxygen distance of 1.70 Å, which is regarded as a mean value of various isomers, including the triclinic isomer C and one or both other isomers. The EXAFS value of the bond distance of the P/Cl coordination shell also seems to represent a mean value of various isomers, since the mean value of this shell as shown

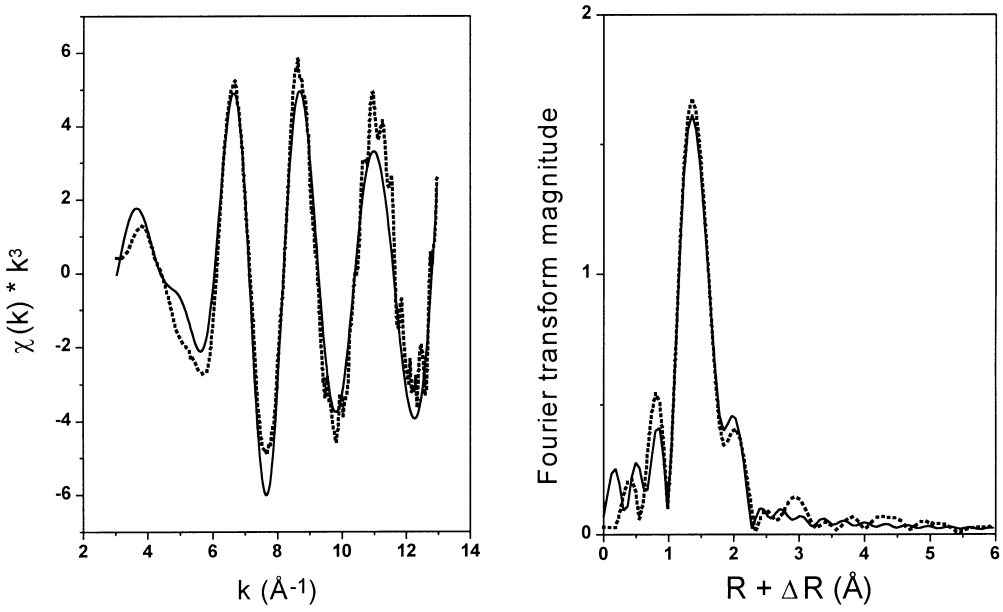

6. (a) EXAFS data of complex **5**. (b) Fourier transform corresponding to (a).

by XRD analysis was 2.45, 2.40 and 2.44 Å for isomers A, B and C. Hence, an unambiguous assignment of the analyzed isomers is not possible, although the existence of the triclinic isomer C can be assumed. However, the constitutional identity of the precursor could be proven by EXAFS.

EXAFS data of ***5***

Complex **5** exhibits a significantly different radial distribution function around the rhenium central atom. Figure 6(a) and (b) show the EXAFS data and their Fourier transform of complex **5**. Dotted lines represent the experimental data, solid lines the best fit.

A strong Fourier transform amplitude is detected at 1.3 Å (not corrected for scattering phase-shift) suggesting a remarkably changed first coordination shell with respect to the rhenium precursor. A second peak occurs at 2.1 Å, obviously caused by the second coordination shell. Taking the complex structure as elucidated by XRD analysis as a default to fit the data, the results presented in Table 3 were obtained.

A substantial increase in the coordination number of the oxygen shell as well as an increase in its mean bond distance to rhenium were observed. This strongly suggests the existence of a dioxo rhenium core. The bond distance is in excellent agreement with the value determined by XRD analysis of the crystalline complex. Considering the second coordination shell, two sulphur backscatterers were used to fit the data and gave results of two backscattering atoms with a mean distance of 2.33 Å. It is noteworthy that the Debye–Weller factor of this coordination shell is increased, probably caused by two distant backscatterers which were fitted within one coordination shell. These two atoms are thought to be a sulphur atom at a distance of around 2.27 Å and a phosphorus backscatterer located at around 2.40 Å. The detected bond length seems likely to represent the mean distance between these two atoms. The results obtained are in good agreement with the values determined by XRD analysis of the complex. However, there is a discrepancy in view of the comparison of the crystal and the solution structure. The nitrogen atom located at 2.28 Å as determined in crystal is not detectable. Attempts to include it in the EXAFS fit gave unreasonable results and thus failed. This problem is obviously caused by the strong dominance of the phosphorus/sulphur shell contribution in the complex EXAFS. The relatively weak backscattering contribution of the amine nitrogen atom at the expected

Table 3. EXAFS fit results for complex **5**

Shell	N	R^a (Å)	σ^2 (Å^2)
O	2.2(4)	1.74(1)	0.001(1)
P/S	1.8(3)	2.33(1)	0.006(1)

N is the number of coordinating atoms. R: distance to rhenium central atom. σ^2: Debye–Weller factor. Fit mode: Marquardt algorithm using least squares method. Calculated resolution in distance: 0.16 Å. The theoretical resolution in distance is given by the formula $\Delta R = 2\pi/k_{max}$ [19].ΔE_0: -9 eV.

a Distance to the rhenium central atom.

distance of 2.28 Å is therefore not believed to be resolvable. Similar phenomena were observed on other systems [21, 22]. However, it can be stated that the unexpected complex as determined in XRD analysis is also existent in solution and seems therefore to represent a relatively stable coordination.

CONCLUSIONS

The described ligand exchange reaction procedure resulted in **4** and the new complex species **5** with the remarkable configuration of the O-donor atoms and an unexpected bidentate coordination of one mercaptoethylene amine derivative. ^{1}H NMR, FAB/CI mass spectroscopy investigations and the elemental analysis suggest a 1:1:1 ratio of **3**, a triphenylphosphane and a dioxo metal core. The *cis*-arrangement of the dioxo core could be proved by IR investigations. The completely trigonal–bipyramidal structure was elucidated by XRD measurements. The origin of the second short-bound oxygen proved to be water present in the reaction mixture, as shown by ^{18}O labelling studies. Even at 1:1 to 1:3 ratios of the reactants **1**/**3** no formation of further compounds analogous to that shown in Fig. 1 was observed.

Five-fold coordinated compounds of trigonal–bipyramidal O-coordination [23], S, or bis-alkyl coordination [24] and *cis*-configuration of the oxo groups have previously been described mainly for rhenium(VII) compounds. For the oxidation state of +5, however, only the *trans*-configuration has been published, with the exceptions of one P,P,I *cis*-dioxo complex characterized [14] by XRD, as well as two complexes containing bipyridyl compounds and a *cis*-dioxo structure characterized by IR data [13].

XRD and EXAFS studies of **5** showed that the coordination of the *cis*-dioxo compound is nearly identical in the solid and in the soluted state.

The formation of the *cis*-dioxo complex is not specific to the applied amine thiol **3**. Products containing other amino alkyl thiols which were obtained further show almost the same UV-spectra and was characterized by XRD in one special case (part of a further publication).

Regarding the "3+1" approach it has to be remarked the reactants should be used strictly in a 1:1:1 ratio in cases of such potentially bidentate ligands. A compensation of the higher reactivity of the tris chelating unit by the use of an excess of the "monodentate" co-ligand **3** is impossible.

EXPERIMENTAL SECTION

Materials and instrumentation

Elemental analyses were performed on a LECO CHNS-932 elemental analyser. Infrared spectra (KBr pellets, in $CHCl_3$) were measured on a Specord M80 or on a Perkin Elmer FT-IR Spectrum 2000. Proton NMR investigations were carried out on a Varian Inova-400 device (solvent $CDCl_3$). Mass spectrometry was done using a Finnigan MAT 95 mass spectrometer. Column chromatography was done using Silica gel 60 (0.04–0.063 mm) from Merck.

Preparation of ligands and the precursor

The *trans*-mono-oxotrichlorobis(triphenylphosphine)rhenium(V) was prepared starting from perrhenate as described in the literature [11].

To prepare the ligands *N*,*N*-bis(2-mercaptoethyl)-*N*′,*N*′-diethylethylenediamine **2** and 1,4-dioxa-8-aza-spiro-*N*-2-mercaptoethylene-[**4**,**5**]-decane **3**, a published procedure was applied [25].

*Preparation of compounds **4** and **5***

The precursor **1** (166.0 mg, 0.2 mmol) was suspended in 20 ml of methanolic sodium acetate solution (0.15 N) by gentle stirring. The ligand **2** (17.9 mg, 0.1 mmol) and the co-ligand **3** (40.7 mg, 0.2 mmol) were dissolved in dichloromethane/methanol and added as a mixture. The resulting suspension was heated at 70°C for 30 min and a change of colour from yellowish green to greenish brown was observed. The reaction mixture was diluted with 10 ml of dichloromethane, washed twice with 10 ml of water and the organic phase was extracted with 10 ml of 0.1 N hydrochloric acid. A dark red organic phase (**5**) and a dark green aqueous phase ("3+1" product **4**) were obtained. The organic portion was dried over sodium sulphate, filtered, reduced in volume by evaporation and purified by chromatography over silica gel 60 with trichloromethane as the liquid phase. The eluate was evaporated to dryness and the precipitate dissolved in diethyl ether. After adding a mixture of ether/n-heptane (1:1), dark red, analytically pure crystals were obtained by slow evaporation of the solvents. Yield: 67 mg (*ca.* 49%, referred to **1**); m.p. 172–174°C. - IR(KBr): $\nu = 836$; 907 cm^{-1} (O═Re═O). Mass spectrum: (FAB pos.) *m*/*z* 681(32)/683(78) $[M]^+$; 682(62)/684(100) $[M+H]^+$; ^{1}H NMR($CDCl_3$): δ 3.943 [m, 4H, O–CH_2–CH_2–O (3)], δ 3.366 [m, 2H, N–CH_2–CH_2–S (3)], δ 2.700 [m, 2H, S–CH_2–CH_2 (3)], δ 2.660; 2.345 [2m, 4H, N–CH_2–CH_2 (3)], δ 1.696; 1.528 [2m, 4H, C–CH_2–CH_2 (3)].

A quantity of dichloromethane was added to the dark green aqueous phase and the pH was increased to 10 by adding a small volume of sodium hydroxide in order to re-extract compound **4**. The organic portion was dried over sodium sulphate, filtered and reduced in volume by evaporation. Compound **4** was purified by chromatography as described above and eluted by using a mixture of dichloromethane/methanol (19:1). The solvent mixture was removed by allowing to stand overnight and crude green crystals were obtained. Yield: 40 mg (*ca.* 62%, referred to **2**); m.p. 134–136°C. IR(KBr): $\nu = 945$ cm^{-1}

(Re═O). Mass spectrum: (CI neg.) m/z 637(58)/639(100) $[M]^+$. ^1H NMR ($CDCl_3$): δ 3.953 [s, 4H, O–CH_2–CH_2–O (**3**)], δ 2.721 [m, 4H, N–CH_2–CH_2 (*3*)], δ 1.805 [t, 4H, N–CH_2–CH_2–C (**3**)], δ 3.872 [t, 2H, N–CH_2–CH_2–NEt_2 (**2**)], δ 3.626; 3.584; 3.292; 2.971 [m, 8H, N–CH_2–CH_2–S (**2**)], δ 2.860 [t, 2H, N–CH_2–CH_2–NEt_2 (**2**)], δ 2.602 [m, 2H, S–CH_2–CH_2–N (**2**)], δ 2.566 [q, 4H, N–CH_2–CH_3 (**2**)], δ 1.061 [t, 6H, N–CH_2–CH_3 (**2**)].

Preparation of the [^{18}O]*-bearing complex* ***5***

The precursor **1** (166.0 mg, 0.20 mmol) was suspended in a mixture of 1 ml of [^{18}O] water and 5 ml dried methanol which contained water-free sodium acetate (0.15 N). After addition of **3** (47.8 mg, 0.24 mmol) dissolved in 0.5 ml of dried methanol the reaction mixture was stirred and refluxed for 30 min. The dark reddish solution obtained was reduced in volume by evaporation to give a final volume of approximately 2 ml. The solution was applied to a silica gel column and purified by eluting with chloroform. The dark reddish chloroformic solution obtained was used for IR measurements.

X-ray crystal structure analysis of ***5***

The structure was determined using a single crystal, obtained by slow evaporation of an ether/*n*-heptane solution of **5**. $C_{27}H_{31}N_1O_4P_1S_1Re_1$ ($M = 682.79$). The intensity data for compound **5** were collected on a ENRAF-NONIUS CAD4 diffractometer. The reflections were performed by the ω–2θ scan method, using graphite monochromated CuK_α radiation ($\lambda = 1.5418$ Å) at $T = 296(2)$ K. Triclinic space group P-1 (No. 2), $a = 9.323(3)$ Å, $b = 15.438(3)$ Å, $c = 20.671(3)$ Å, $\alpha = 103.18(3)^\circ$, $\beta = 100.39(3)^\circ$, $\gamma = 105.39(3)^\circ$, $V = 2699.6(11)$ Å^3, $Z = 4$, $D_c = 1.677$ g cm^{-3}, $\mu = 10.355$ mm^{-1}. The number of totally measured reflections was 11077, of which 9947 were considered to be significant and were used for the structure determination. The refinement procedure was carried out by full-matrix least-squares, where the minimized function was $\omega(|F_0| - |F_c|)^2$. Refinement converged at $R = 0.0514$ and $R_w = 0.1521$.

Crystallographic data (excluding structure factors) for the structure reported in this paper have been deposited at the Cambridge Crystallographic Data Center. Copies of the data can be obtained free of charge on application to The Director, CCDC, 12 Union Road, Cambridge CB2 1EZ, U.K. (fax: +44-1223-336-033; e-mail: teched@chemcrys.cam.ac.uk) (CCDC-No. 100471).

EXAFS measurements of ***1*** *and* ***5***

Rhenium L_{III} edge data were collected in transmission mode using ionization chambers at beamline X1.1 of the HASYLAB synchrotron, Hamburg, Germany. To monochromatize the synchrotron beam, a monochromator system consisting of a Si(211) double-crystal monochromator was used. The DORIS III storage ring was operated at 3 GeV at ring currents between 40 and 70 mA during measurements. Higher harmonics were rejected by detuning the monochromator crystals to 50% of the incident beam intensity. A rhenium(V) complex served as a reference for energy calibration of the monochromator. Three scans were used per sample on average. A check for anomalies was carried out after each scan. Data were energy-calibrated using the first derivative method, where the first inflected point in the reference derivative was set to 10535 eV. Sample absorption edge positions were determined by derivatizing the sample spectra and detecting the first inflected points. Data processing and analysis were performed using the program package EXAFSPAK [26]. The experimental data were analyzed by being fitted with theoretical EXAFS functions generated by the FEFF6.01a program [27]. Since phosphorus, sulphur and chlorine produce very similar backscattering functions, mixed-atom coordination shells consisting of these atoms were fitted with EXAFS functions for sulphur backscatterers. To fit the data, coordination numbers were at first kept constant. When constant values for DE_0 and distances were obtained, coordination numbers were allowed to float.

Acknowledgements—We are grateful to S. Machill of the Technische Universität Dresden for measuring the FAB/CI mass spectra.

REFERENCES

1. Yoshihara, K., Baldas, J., Johannsen, B., Spies, H., Volkert, W., Jurisson, S., Alberto, R., Kryutchkov, S., Omori, T. and Hashimoto, K., *Topics in Current Chemistry*. Springer-Verlag, Berlin/Heidelberg/New York, 1996.
2. Pietzsch, H.-J., Spies, H., Hoffmann, S. and Stach, J., *Inorg. Chim. Acta*, 1989, **161,** 15.
3. Spies, H., Syhre, R. and Pietzsch, H.-J., *Plzen Lek. Sb.*, 1990, **62,** 85.
4. Johannsen, B., Scheunemann, M., Spies, H., Brust, P., Wober, J., Syhre, R. and Pietzsch, H.-J., *Nucl. Med. Biol.*, 1996, **23,** 429–438.
5. Meegalla, S., Plössl, K., Kung, M.-P., Chumpradit, S., Stevenson, C., Frederick, D. and Kung, H. F., *Bioconj. Chem.*, 1996, **7,** 421–429.
6. Mc Donell, A. C. *et al.*, *Aust. J. Chem.*, 1983, **36,** 253.
7. Pietzsch, H.-J., Spies, H. and Hoffmann, S., *Inorg. Chim. Acta*, 1989, **165,** 163.
8. Papadopoulos, M. *et al.*, Private communication (submitted).
9. Spyriounis, D. M., Pelecanou, M., Stassinopoulou, C. I., Raptopoulou, C. P., Terzis, A.

and Chiotellis, E., *Inorg. Chem.*, 1995, **34,** 1077–1082.
10. Papadopoulos, M. S., Pirmettis, I. C., Pelecanou, M., Raptopoulou, C. P., Terzis, A., Stassinopoulou, C. I. and Chiotellis, E., *Inorg. Chem.*, 1996, **25,** 7377–7383.
11. Johnson, N. P., Lock, C. J. and Wilkinson, G., *J. Chem. Soc.* 1964, 1064.
12. Gerber, T. I., Perils, J., Du Perez, J. G. and Bandoli, G., *Acta Cryst. C*, 1997, **53,** 217–219.
13. Ram, M. S. and Hupp, J. T., *Inorg. Chem.*1991, **30**(1), 130–133.
14. Ciani, G. F., D'Alfonso, G., Romiti, G. F., Sironi, A. and Freni, M., *Inorg. Chim. Acta*, 1983, **72,** 29–37.
15. Brodsky, A. E., *Isotopenchemie*. Akademie-Verlag, Berlin, 1961, pp. 291–299.
16. Addison, A. W., Rao, T. N., Reedijk, J., van Run, J. and Verschoor, G. C., *J. Chem. Soc. Dalton Trans.*, 1984, 1349.
17. Bolzati, C., Tisato, F., Refosco, F., Bandoli, G. and Dolmella, A., *Inorg. Chem.*, 1996, **35,** 6221–6229.
18. Fröba, M. and Lochte, K., Metz, W., *J. Phys. Chem. Solids*, 1996, **57,** 635–641.
19. Koningsberger, D. C. and Prins, R. (eds.), *X-ray Absorption Spectroscopy. Principles, Applications, Techniques of EXAFS, SEXAFS and XANES*. John Wiley and Sons, New York, 1988.
20. Lebuis, A.-M. and Beauchamp, A. L., *Can. J. Chem.*, 1993, **71,** 441–449.
21. Chance, M. R., Sagi, I., Wirt, M. D., Frisbie, S. M., Scheuring, E., Chen, E., Bess, J. W., Henderson, L. E., Louis, E. and Arthur, L. O., *Proc. Natl. Acad. Sci. U.S.A.*, 1992, **89,** 10041–10045.
22. Summers, M. F., Henderson, L. E., Chance, M. R., Bess, J. W., Julian, W., South, T. L., Blake, P. R. and Sagi, I., *Protein Sci.*, 1992, **1,** 563–574.
23. Herrmann, W. A., Wojtczak, W. A., Artus, G. R., Kühn, F. E. and Mattner, M. R., *Inorg. Chem.*, 1997, **36,** 465–471.
24. Shiang, Cai, Hoffmann, D. M. and Wierda, D. A., *Inorg. Chem.*, 1989, **28,** 3784–3786.
25. Marabella, C., Enemark, J., Miller, A., Bruce, A., Parayadath, N., Corbin, J. and Stiefel, E., *Inorg. Chem.*, 1983, **22,** 3456.
26. George, G. G. and Pickering, I. J., *EXAFSPAK, A Suite of Computer Programs for Analysis of X-ray Absorption Spectra*. Stanford Synchrotron Radiation Laboratory, Stanford, U.S.A., 1995.
27. Zabinsky, S., Rehr, J., Ankudinov, A., Albers, R. C. and Eller, M. J., *Phys. Rev. B*, 1995, **52,** 2995–3009.

Pergamon

PII: S0277-5387(98)00170-3

Polyhedron Vol. 17, No. 21, pp. 3721–3725, 1998
© 1998 Elsevier Science Ltd
All rights reserved. Printed in Great Britain
0277–5387/98 $19.00+0.00

A novel hydroxo-bridged ferric bisubstituted Keggin heteropolytungstate dimer: synthesis and crystal structure of $(Me_4N)_{10}[Fe_4(OH)_4(PW_{10}O_{37})_2]\cdot 15H_2O$

Ming-Xing Li,[a] Song-Lin Jin,[a]* Hui-Zhang Liu,[a] Gao-Yang Xie,[a] Ming-Qin Chen,[b] Zheng Xu[c] and Xiao-Zeng You[c]

[a]Department of Chemistry, Fudan University, Shanghai, 200433 P. R. China.

[b]Research Center of Analysis and Measurement, Fudan University, Shanghai, 200433 P. R. China.

[c]The State Key Laboratory of Coordination Chemistry, Nanjing University, Nanjing, 210093 P. R. China.

(Received 19 January 1998; accepted 20 April 1998)

Abstract—The previously unknown heteropolytungstate $(Me_4N)_{10}[Fe_4(OH)_4(PW_{10}O_{37})_2]\cdot 15H_2O$ has been prepared by the reaction of Δ–$Na_8HPW_9O_{34}$ and $FeCl_3$ in aqueous solution, and characterized by elemental analysis, infrared spectrum as well as X-ray single crystal structure determination. Four bridging hydroxo groups link with four Fe^{III} ions, forming an eight-member ring; and this $Fe_4(OH)_4$ aggregation is sandwiched by two bi-vacant Keggin type heteropolyanion fragments. The bridging hydroxo groups are divided into two classes: one is the hydroxo groups linking two $PW_{10}Fe_2$ half moieties, the other is the hydroxo group linking two FeO_6 octahedra in each half moiety. The location of the bridging hydroxo groups is identified by the bond valence sum (BVS) calculations for various oxygen atoms. © 1998 Elsevier Science Ltd. All rights reserved.
© 1998 Elsevier Science Ltd. All rights reserved

Keywords: heteropolytungstate; synthesis; crystal structure; bridging hydroxo group; ferric compound; Keggin heteropolyanion dimer

In recent years there has been a growing interest in the heteropolymetalates, especially in the transition metal di- and tri-substituted Keggin or Dawson type heteropolytungstates. These substituted series can serve as ideal model compounds in the domains of magnetic chemistry study, and are also regarded as a class of potential magnetic materials [1, 2]. Finke *et al.* reported the rational syntheses and characterization of a series of di-valence transition metal trisubstituted Keggin and Dawson type heteropolytungstate dimers in 1987 [3]. These substituted heteropolytungstates contain an oxo-bridged tetranuclear transition metal cluster sandwiched by two trivacant heteropolyanion fragments. In the view of magnetic chemistry, the large and robust framework of heteropolyanions may block intermolecular magnetic interaction, therefore they are favourable models to understand the magneto-structural correlation for encapsulated magnetic clusters. During the past decade, the syntheses of this series of heteropolytungstates have been successively reported, and their magnetic investigations show ferro- or antiferro-magnetic interactions in the oxo-bridged magnetic clusters [4, 5].

In order to expand this study from di-valence transition metals to tri-valence transition metals, we attempt to synthesize an Fe^{III} or Cr^{III} tri-substituted Keggin type heteropolyanion dimer using a similar method described by Finke *et al.* Many efforts failed, however we have separated some light brown single crystals from the resultant mixtures. The X-ray structure determination reveals that this crystalline heteropolytungstate has an unexpected hydroxo-bridged dimeric structure. There are two sets of Fe^{III} ions, related by a central symmetry, which are symetrically

* Author to whom correspondence should be addressed.

placed in two Keggin type $PW_{10}Fe_2$ half moieties. Two kinds of bridge hydroxo groups that linked two Fe^{III} ions are found: one is the bridge hydroxo group in each $PW_{10}Fe_2$ half moiety, the other is the bridge hydroxo group in two $PW_{10}FE_2$ half moieties. To our knowledge, the bridging hydroxo group within the framework of heteropolyanion has not been previously reported. Here we report the synthesis, infrared spectrum and X-ray crystal structure of the title compound.

EXPERIMENTAL

Materials

Analytical grade $Na_2WO_4{\cdot}2H_2O$, $FeCl_3{\cdot}6H_2O$, Me_4NBr, H_3PO_4 (85%) and glacial acetic acid were used without further purification. The tri-vacant tungstophosphate, Δ–$Na_8HPW_9O_{34}{\cdot}19H_2O$ was prepared according to the procedure described by Finke *et al.* and identified by infrared spectrum [3].

Analytical methods and apparatus

The elemental analysis for C, H and N were performed on a Perkin-Elmer 240C Analyzer. The amounts of other elements were obtained on a Jarrell-Ash Division Atomscan 2000 ICP analyzer. Infrared spectrum was recorded on a Nicolet 5DX FTIR spectrophotometer using KBr pellet. The number of H_2O was identified by a LCT-2 Thermogravimetric Analyzer.

Synthesis

The title heteropolytungstate was synthesized by addition of (5.5 g 2.0 mmol) tri-vacant tungstophosphate Δ–$Na_8HPW_9O_{34}$ to a 10 ml aqueous solution of $FeCl_3{\cdot}6H_2O$ (1.1 g, 4.0 mmol) with vigorous stirring, yielding a homogeneous orange–red solution. The solution was stirred for 12 h, and then a 10 ml Me_4NBr (1.0 g, 6.5 mmol) aqueous solution was added carefully and kept stratified with the solution. As Me_4NBr diffused slowly into the orange–red solution, a mixture containing small light brown crystals and unknown pale yellow powdery compounds was precipitated out after two weeks, the yield being 20%. The crystals were selected for elemental analysis, infrared spectrum analysis and X-ray crystal structure determination. Elemental analysis for $(Me_4N)_{10}[Fe_4(OH)_4(PW_{10}O_{37})_2]{\cdot}5H_2O$ calculated (found): C, 7.72% (7.61); H, 2.49% (2.33); N, 2.25% (2.20); Fe, 3.59% (3.63); P, 0.99% (1.01); W, 59.05% (58.87); H_2O, 4.34% (4.41). IR (ν/cm^{-1}): 3476sb, 3033m, 2959w, 1634m, 1488s, 1450w, 1419w, 1059s, 956s, 881s, 775sb, 516m.

Crystal structure determination

A single crystal ($0.30 \times 0.15 \times 0.15$ mm) of title compound was sealed in a Lindeman glass capillary and aligned on an Enraf-Nonius CAD-4 diffractometer equipped with graphite-monochromotatic Mo–Kα radiation ($\lambda = 0.71073$ Å). Unit cell parameters were determined on the basis of 25 reflections in the range $12 < \theta < 16^\circ$. The intensity data were collected by ω–2θ scan technique in the 2θ range 0–46°. During data collection, the intensities of three standard reflections were monitored every hour and showed no significant variation. The intensity data were corrected for Lorentz-polarization effects and empirical absorption. Details of the crystal data, intensity collection and refinement are listed in Table 1.

The crystal structure was solved by direct methods and refined by full-matrix least squares techniques using anisotropic temperature factors for non-hydrogen atoms. Hydrogen atoms were placed on the related atoms and refined in the riding mode with fixed thermal parameters. 7032 reflections with $I > 3\sigma(I)$ were used in the refinement of 601 parameters, and the refinement converged at

Table 1. Summary of crystal and intensity collection data

Empirical formula	$C_{40}H_{154}Fe_4N_{10}O_{93}P_2W_{20}$
Formula weight	6225.75
Crystal system	Monoclinic
Space group	$P2_1/C$
a(Å)	13.228(5)
b(Å)	35.634(3)
c(Å)	15.226(2)
β(°)	94.20(0)
V(Å^3)	7157.6
Z	2
D_c (g/cm^3)	2.888
F(000)	5576
Radiation	Mo–K_α ($\lambda = 0.71073$ Å)
μ(cm^{-1})	168.534
Temperature (K)	293
Scan width	$0.5 + 0.350 \tan\theta$
$(h,k,l)_{min}$, $(h,k,l)_{max}$	(−14,0,0), (14,39,16)
Number of reflections collected	10597
Number of unique reflections	9954
Observed reflections, $I > 3\sigma(I)$	7032
Function minimized	$\Sigma W(\|F_o\| - \|F_c\|)^2$
Variable refined	601
R	0.036
R_w	0.049
Maximum shift in final cycle	0.03
Largest peak in final difference map (e/Å^3)	1.95

$R = 0.036$ and $R_w = 0.049$. All calculations were performed on a Micro VAX II computer using SDP/VAX PLUS programs.

RESULTS AND DISCUSSION

Finke *et al.* found that the thermolyzed $Na_8HPW_9O_{34}$ (Δ–PW_9O_{34}) was predominantly a B type tri-vacant heteropolyanion, and also was the key structural requirement for the formation of di-substituted, dimeric heteropolytungstates. These compounds such as $[M_4(H_2O)_2\ (PW_9O_{34})_2]^{10-}$ ($M = M_n^{2+}$, Co^{2+}, Ni^{2+}, Cu^{2+}, Zn^{2+}) could be separated as K^+ salts precipitation from reacting solution with good yields [3, 4]. We therefore reacted Δ–PW_9O_{34} with $FeCl_3$ in 1:2 molar rate, under the same conditions as Finke *et al.* described previously. No expected K^+ salt or Li^+, Na^+, Ca^{2+}, Mg^{2+} salts of $[Fe_4(H_2O)_2(PW_9O_{34})_2]^{6-}$ heteropolyanion was precipated from the orange–red reactive solution; however an orange amorphous material, which was difficult to purify further, precipated immediately from the aqueous solution after adding of Me_4NBr. Only when Me_4NBr was diffused very slowly, did small crystals of title compound appear, together with pale yellow powdery unknown complexes.

The infrared spectrum of the title compound strongly suggested that the framework of this heteropolyanion was structurally similar to the Keggin anion. Four strong absorption bands near 1059, 956, 881 and 775 cm^{-1} are assigned to P–O, W=O, W–O–W (corner-sharing and edge-sharing) vibratory absorptions respectively. Comparing to the Keggin type $[PW_{12}O_{40}]^{3-}$ heteropolyanion, the corresponding four characteristic bands appeared at 1080, 985, 887 and 807 cm^{-1} [6]. A single band appeared at P–O position indicating that the central PO_4 group has a high tetrahedral symmetry. Bands near 3033, 1488 cm^{-1} were ascribed to C–H and C–N stretching vibrations of countercations Me_4N^+. Finally, the broad bands near 3476 cm^{-1} and middle strong band at 1634 cm^{-1} were attributed to the vibratory absorptions of lattice water molecules and bridging hydroxo groups.

The X-ray crystal structure determination revealed that the title compound consisted of one heteropolyanion, ten countercations Me_4N^+ and about nineteen lattice water molecules. The structure of heteropolyanion was shown in Fig. 1, and selected bond distances as well as bond angles were listed in Table 2. The heteropolyanion was centrosymmetric with only half of the molecule crystallographically independent, and thus could be viewed as a dimer of ferric disubstituted Keggin type heteropolyanion. On the basis of charge balance, four protons were associated with each heteropolyanion; furthermore, these protons were confidently located on four bridging oxygen atoms O32, O33, O32A and O33A according to the result of bond valence sum (BVS) calculations. The BVS equation was shown: $BVS = \Sigma BV_i = \Sigma\exp[(r_0 - r_i)/B]$, where $r_0 = 1.917$ Å for $W^{6+}-O^2$; $r_0 = 1.759$ Å for $Fe^{3+}-O_2$; $B = 0.37$ [7, 8].

The bond valence sums of oxygens in heteropolyanion were given in Table 3. For the terminal

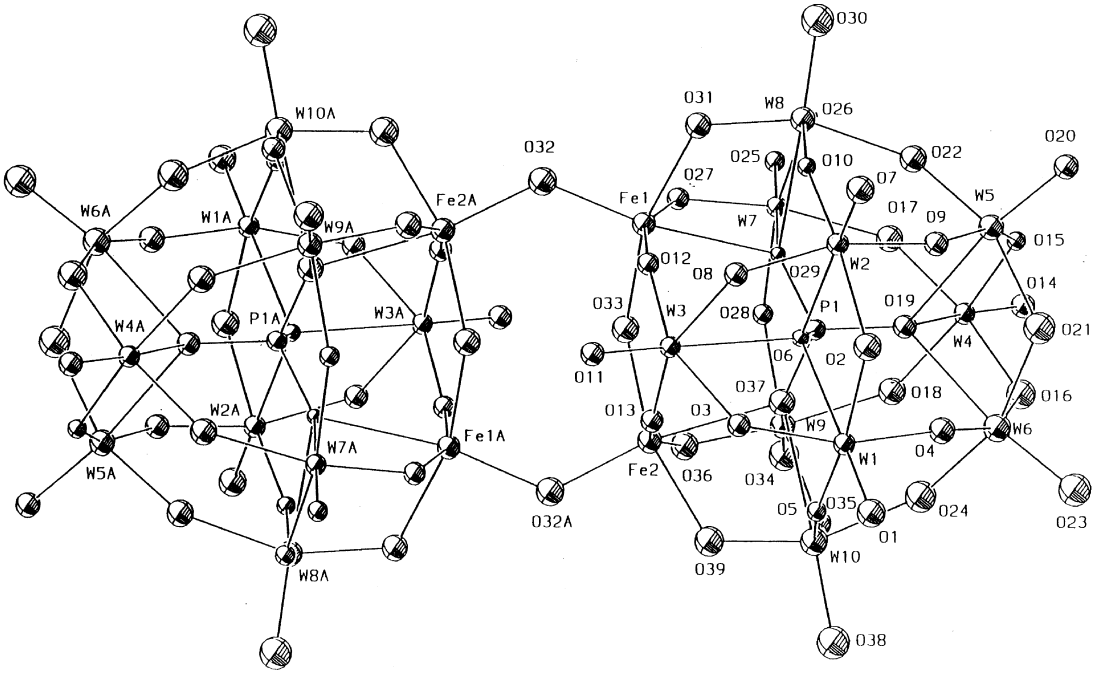

Fig. 1. The structure of $[Fe_4(OH)_4(PW_{10}O_{37})_2]^{10-}$ anion.

Table 2. Selected bond distances (Å) and angles (°)

W(1)–O(1)	1.72(2)	W(3)–O(11)	1.73(1)
W(1)–O(2)	1.91(1)	W(3)–O(8)	2.02(1)
W(1)–O(3)	1.89(1)	W(3)–O(3)	2.00(1)
W(1)–O(4)	1.94(1)	W(3)–O(12)	1.81(1)
W(1)–O(5)	1.89(1)	W(3)–O(13)	1.82(1)
W(1)–O(6)	2.43(1)	W(3)–O(6)	2.47(1)
Fe(1)–O(12)	1.92(1)	P(1)–O(6)	1.54(1)
Fe(1)–O(27)	1.99(1)	P(1)–O(19)	1.54(1)
Fe(1)–O(29)	2.40(1)	P(1)–O(29)	1.52(1)
Fe(1)–O(31)	1.99(1)	P(1)–O(37)	1.54(1)
Fe(1)–O(32)	1.90(1)	Fe(2)–O(32A)	1.93(1)
Fe(1)–O(33)	1.95(1)	Fe(2)–O(33)	1.99(2)
O(32)–Fe(1)–O(12)	99.2(6)	O(11)–W(3)–O(3)	98.2(7)
O(32)–Fe(1)–O(27)	101.7(6)	O(11)–W(3)–O(6)	164.7(6)
O(32)–Fe(1)–O(29)	169.6(5)	O(11)–W(3)–O(8)	97.8(7)
O(32)–Fe(1)–O(31)	96.5(6)	O(11)–W(3)–O(12)	104.6(7)
O(32)–Fe(1)–O(33)	101.7(6)	O(11)–W(3)–O(13)	104.8(7)
O(6)–P(1)–O(19)	107.8(7)	O(19)–P(1)–O(29)	110.2(8)
O(6)–P(1)–O(29)	109.3(7)	O(19)–P(1)–O(37)	109.5(8)
O(6)–P(1)–O(37)	108.7(8)	Fe(1)–O(33)–Fe(2)	139.2(7)

Table 3. Bond Valence Sums (BVS) for some oxygen atoms in $(Me_4N)_{10}[Fe_4(OH)_4(PW_{10}O_{37})_2]\cdot 15H_2O$

	Oxygen	BVS	Oxygen	BVS
Terminal	W(1)–O(1)	1.70	W(2)–O(7)	1.70
	W(3)–O(11)	1.66	W(4)–O(14)	1.66
	W(5)–O(20)	1.70	W(6)–O(23)	1.75
	W(7)–O(25)	1.75	W(8)–O(30)	1.75
	W(9)–O(34)	1.70	W(10)–O(38)	1.70
Bridge	Fe(1)–O(32)–Fe(2A)	1.31	Fe(1)–O(33)–Fe(2)	1.13
	Fe(1)–O(31)–W(8)	1.80	Fe(1)–O(27)–W(7)	1.87
	Fe(1)–O(12)–W(3)	1.98	Fe(2)–O(36)–W(9)	1.87
	Fe(2)–O(13)–W(3)	1.91	Fe(2)–O(39)–W(10)	1.85
	W(8)–O(22)–W(5)	2.03	W(6)–O(24)–W(10)	2.00
	W(2)–O(8)–W(3)	1.92	W(1)–O(3)–W(3)	1.86

oxygen atoms, their BVS values were within the range 1.66–1.75; whereas for the bridging oxygen atoms, their values fall within the range 1.80–2.03 except for O32 and O33. We note that the BVS values were rather high for the bridging oxygen atoms in Fe–O–W and W–O–W bonds, and they were therefore ascribed to the oxo groups. The bridging atoms, O32 and O33, had much lower BVS values (1.31 and 1.13); were presumed to be hydroxo groups [9]. Similar situations were encountered in the manganese di-substituted γ–$[SiW_{10}O_{36}Mn_2(OH)_2(OH_2)_2]^{4-}$ and chromium di-substituted γ–$[SiW_{10}O_{36}Cr_2(OH)(OH_2)_2(OOCCH_3)_2]^{5-}$ heteropolyanions [9, 10]. Moreover, a hydrogen bond was observed between O32 and O40 with O32–O40 distance 2.764 Å, the oxygen O40 belonged to a crystal water molecule.

There were two kinds of bridging hydroxo group in this dimeric structure: one is the bridge hydroxo group (O33 or O33A) in each Fe_2PW_{10} half moiety; the other was the bridge hydroxo group (O32 or O32A) linking two Fe_2PW_{10} half moieties. To our knowledge, a bridging hydroxo group within the framework of an heteropolyanion has not been reported previously. The former bridging hydroxo groups were shared by two FeO_6 octahedra in the same Fe_2PW_{10} half moiety with a Fe–O–Fe angle of 139.2°; while the latter bridging hydroxo groups were shared by two FeO_6 octahedra belonging to different Fe_2PW_{10} half moieties with a Fe–O–Fe angle of 131.4°. The Fe–O bond lengths for the former bridging hydroxo groups were 1.95 Å and 1.99 Å, whereas they were only 1.90 Å and 1.93 Å for the latter bridging hydroxo groups.

Comparing the structure details of $[Fe_4(OH)_4(PW_{10}O_{37})_2]^{10-}$ to that of the Keggin type

$[PW_{12}O_{40}]^{3-}$ [11], the W–O and P–O bond lengths and angles are not substantially affected by the substitution of two Fe^{III} ions. Only slightly shorter W–O bond lengths appeared at oxygen atoms linking to FeO_6 octhedra. The FeO_6 octahedra were obviously distorted with Fe–O bond 2.40 Å linking to the central PO_4 tetrahedron and 1.90(1) 1.99(1) Å to the bridging oxygen atoms linking with WO_6 octahedra.

The hydroxo- or oxo-bridges dimers for the Fe^{III} mono-substituted heteropolyanions have been reported by Tourne *et al*. in 1982, and a series of these compounds including $K_nO[FeXW_{11}O_{39}]_2$ (X = Si, Ge, B) and $K_mO[FEX_2W_{17}O_{61}]_2$ (X = P, As) were prepared [12]. However, these dimer species were only characterized by limited means, such as elemental analysis and UV-vis spectrum; no other unambiguous evidence was provided to confirm their dimeric structure. Our work provided not only a direct view of the of the hydroxo-bridged dimeric structure, but also an ideal model for the future magnetic exchange interaction study in hydroxo-bridged compounds.

Acknowledgements—are grateful to the National Nature Science Foundation and the State Key Laboratory of Coordination Chemistry for financial support.

REFERENCES

1. Pope, M. T., (1983) *Heteropoly and Isopoly Oxometalates*. Springer-Verlag, New York.
2. Pope, M. T. and Muller, A., *Angew. Chem. Int. Ed. Engl*., 1991, **30,** 34.
3. Finke, R. G., Droege, M. W. and Domaille, P. J., *Inorg. Chem*., 1987, **26,** 3886.
4. Gomez-Garcia, C. J., Borras-Almenar, J. J., Coronado, E. and Ouahab, L., *Inorg. Chem*., 1994, **33,** 4016.
5. Clemente, J. M., Andres, H., Aebersold, M., Borras-Almenar, J. J., Coronado, E., Gudel, H. U., Buttner, H. and Kearly, G., *Inorg. Chem*., 1997, **36,** 2244.
6. Rocchiccioli-Deltcheff, C., Thouvenot, R. and Franck, R., *Spectrochim. Acta*, 1976, **32a,** 587.
7. Brown, I. D. and Altermatt, D., *Acta cryst*., 1985, **B41,** 244.
8. Thorp, H. H., *Inorg. Chem*., 1992, **31,** 1585.
9. Wassermann, K., Lunk, H. J., Palm, R., Fuchs, J., Steinfeldt, N., Stosser, R. and Pope, M. T., *Inorg. Chem*., 1996, **35,** 3273.
10. Zang, X.-Y., O'Connor, C. J., Jameson, G. B. and Pope, M. T., *Inorg. Chem*., 1996, **35,** 30.
11. Brown, G. M., Noe-Spirlet, M. R., Busing, W. R. and Levy, H. A., *Acta. Cryst*., 1977, **B33,** 1038.
12. Zonnevijlle, F., Tourne, C. M. and Tourne, G. F., *Inorg. Chem*., 1982, **21,** 2751.

Pergamon

Polyhedron Vol. 17, No. 21, pp. 3727–03734, 1998
© 1998 Elsevier Science Ltd
All rights reserved. Printed in Great Britain
0277–5387/98 $19.00+0.00

PII: S0277–5387(98)00171–5

Synthesis, reactivity, and X-ray structures of face-sharing Ti(III) complexes; the new trinuclear ion, $[Ti_3Cl_{12}]^{3-}$

Linfeng Chen and F. Albert Cotton*

Department of Chemistry and Laboratory for Molecular Structure and Bonding, Texas A&M University, College Station, Texas 77843, U.S.A.

(Received 3 December 1997; accepted 18 April 1998)

Abstract—Reduction of $TiCl_4$ with $HSnBu_3$ followed by treatment of the brown solid with a chloride salt produced a precursor (**B**) for synthesis of face-sharing Ti(III) complexes. The precursor, **B**, can be converted into dinuclear complexes, $[Ti_2Cl_7(PEt_3)_2]^-$ (**1′**) and $[Ti_2Cl_9]^3$3-(**3′**) when treated with one equivalent of PEt_3 or Cl^-. When only half an equivalent of Cl^- was used, a trinuclear complex $[Ti_3Cl_{12}]^{3-}$ (**2′**) was isolated. **2′** can be further converted into **3′** by treating with Cl^-. Substitution of the phosphine ligands in **1′** with Cl^- converted **1′** into **3′**. There is no reaction between **3′** and Cl^-. Reaction of **1′** or **3′** with py resulted in the formation of a mononuclear species, [*trans*-$Ti(py)_2Cl_4]^-$ (**4′**). In complexes **1′**, **2′**, and **3′**, the Ti atoms are bridged by three Cl atoms. © 1998 Elsevier Science Ltd. All rights reserved

Keywords: titanium(III); face-sharing complex; chloride; pyridine; crystal structure.

Titanium chlorides tend to form polynuclear complexes with bridging chloride ligands [1]. Two types of structure are dominant in these complexes: a structure with two octahedra fused together by sharing a common edge (**I**), and a face-sharing structure (**II**). In a previous study [2], reduction of $TiCl_4$ with $HSnBu_3$ yielded a brown solid (**A**). When this brown solid was treated with PMe_3, an edge-sharing dinuclear complex, $[(PMe_3)_2Cl_2Ti(\mu\text{–}Cl)_2TiCl_2(PMe_3)_2]$, was formed (Scheme 1). When bidentate formamidinates were used, similar complexes, also with two Cl atoms bridging two Ti atoms, were isolated. Interestingly, when **A** was treated with 0.5 equivalent of Cl^-, the brown solid was converted into a green solid, **B**, a precursor of face-sharing complexes [3]. Reaction of **B** with phosphines resulted in the formation of dinuclear face-sharing complexes, $[(PR_3)Cl_2Ti(\mu\text{–}Cl)_3TiCl_2(PR_3)]^-$ [3]. From magnetic susceptibility measurement and *ab initio* calculations with configuration interaction it was concluded that there is essentially no metal-metal bonding between the two Ti atoms, and the Ti(III)–Ti(III) interaction in these face-sharing complexes can be best described as strong antiferromagnetic coupling that leads to a singlet ground state and a thermally accessible triplet first excited state [3]. When a trace of water was present, reaction of **B** with Cl^- yielded a heptanuclear complex, $[Ti_7Cl_{19}O_3]^{3-}$, which contains both edge-sharing and face-sharing components [4].

More face-sharing complexes have now been synthesized from the green solid (**B**) (Scheme 2). These include both dinuclear and trinuclear complexes. The syntheses and reactivity of these compounds as well as their structures are reported here.

EXPERIMENTAL

All manipulations were conducted under an argon atmosphere by using standard vacuum line and Schlenk techniques. Glassware was oven dried at 150°C for 24 hr prior to use. Solvents were predried over molecular sieves and freshly distilled under nitrogen from appropriate drying reagents. $TiCl_4$, $HSnBu_3$, and $[PPh_4]Cl$ were purchased from Aldrich. $TiCl_4$ and $HSnBu_3$ were used as received.$[PPh_4]Cl$ was dried at 150°C under vacuum for 24 hr.$[PPh_4$, $(PEt_3)Cl_2Ti(\mu\text{–}Cl)_3TiCl_2(PEt_3)] \cdot 2CH_2Cl_2$ (**1** · $2CH_2Cl_2$) was prepared according to the previously reported method [3]. The magnetic susceptibility measurements were conducted

* Author to whom correspondence should be addressed.

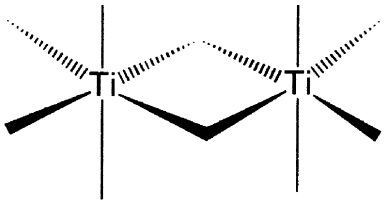

I

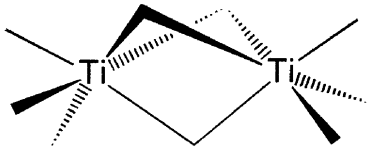

II

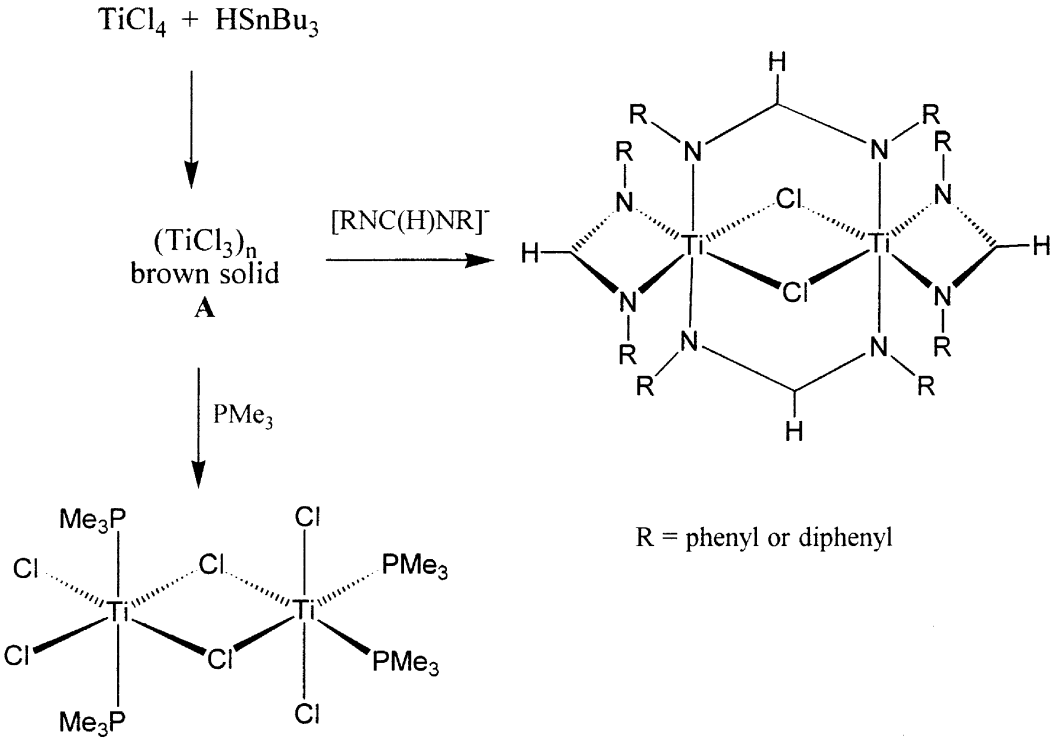

Scheme 1.

at room temperature on a Johnson–Matthey, model MSB-1, balance.

Reduction of $TiCl_4$

$TiCl_4$ was reduced with one equivalent of $HSnBu_3$ in the previously described way [2, 3]. $TiCl_4$ (0.22 mL, 2.0 mmol) was dissolved in toluene (20 mL). The yellow solution was stirred while $HSnBu_3$ (0.53 mL, 2.0 mmol) was added dropwise by syringe. A brown precipitate formed immediately and the reaction mixture was stirred for 4 hr. The precipitate was separated by decantation, washed with two portions of toluene (20 mL), and then dried in vacuum to give a brown solid (**A**, *ca.* 300 mg).

Reaction of **A** *with* $[PPh_4]Cl$

To the above brown solid (**A**) was added dropwise a solution of $[PPh_4]Cl$ (375 mg, 1.0 mmol) in CH_2Cl_2 (15 mL) with stirring. The brown solid (**A**) became a dark green solid (**B**) immediately.

Synthesis of $[PPh_4]_3[Cl_3Ti(\mu\text{–}Cl)_3Ti(\mu\text{–}Cl)_3TiCl_3]$ (**2**)

A solution of $[PPh_4]Cl$ (375 mg, 1.0 mmol) in CH_2Cl_2 (15 mL) was added slowly to the suspension of green solid (**B**) in CH_2Cl_2 prepared above and placed in a dry ice-acetone bath (*ca.* −78°C). The reaction mixture was warmed up slowly to room temperature by removing the cold bath and stirred at

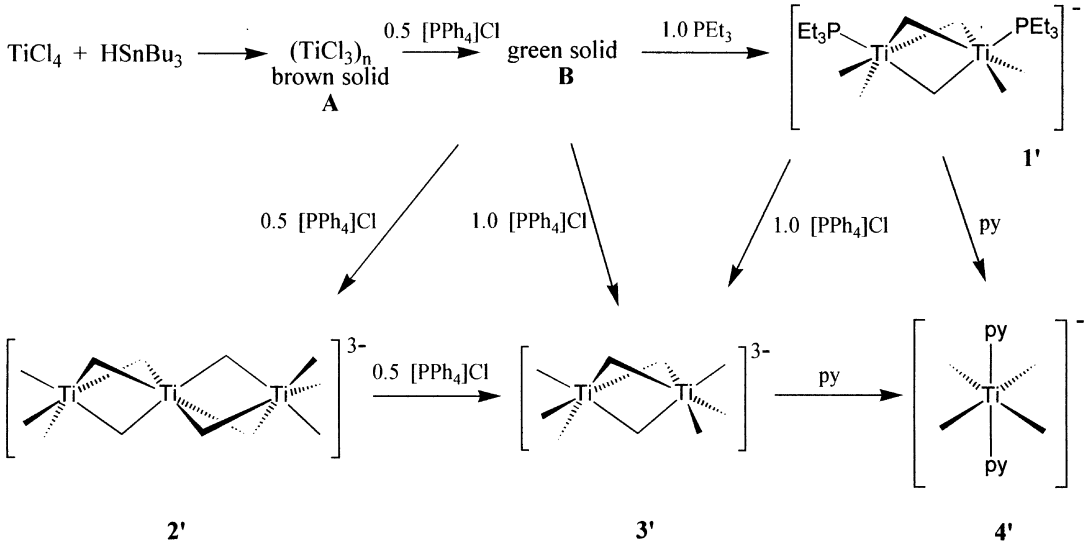

Scheme 2.

room temperature for 3 hr. A green solution was obtained. It was evaporated under vacuum to *ca.* 20 mL in volume and then layered with hexane (40 mL). After one week, block-shaped green crystals of $\mathbf{2}\cdot 2CH_2Cl_2$ were isolated in 74% yield (865 mg). Magnetic susceptibility of $\mathbf{2}\cdot 2CH_2Cl_2$: $X = 1.79\times10^{-3}$ emu at 298 K after diamagnetic correction; $\mu_{eff} = 2.07$ BM per trinuclear complex anion.

Synthesis of $[PPh_4]_3[Cl_3Ti(\mu\text{–}Cl)_3TiCl_3]$ (**3**)

(1) *From green solid* **b** To the suspension of **B** in CH_2Cl_2 obtained as explained above was added slowly a solution of $[PPh_4]Cl$ (2.0 mmol, 750 mg) in CH_2Cl_2 (30 mL). The resulting greenish-brown solution was layered with toluene. After the diffusion was complete (about two weeks later) large plate-shaped greenish brown crystals of $\mathbf{3}\cdot 4CH_2Cl_2\cdot 0.5C_6H_5CH_3$ were obtained in 85% yield (1550 mg). Magnetic susceptibility of $\mathbf{3}\cdot 4CH_2Cl_2\cdot 0.5C_6H_5CH_3$: $X = 1.21\times10^{-3}$ emu at 298 K after diamagnetic correction; $\mu_{eff} = 1.70$ BM per dinuclear complex anion.

(2) *From* $[PPh_4]_3[Cl_3Ti(\mu\text{–}Cl)_3Ti(\mu\text{–}Cl)_3TiCl_3]$ (**2**) Compound $\mathbf{2}\cdot 2CH_2Cl_2$ (300 mg, 0.171 mmol) was dissolved in CH_2Cl_2 (20 mL). To this green solution was added slowly a solution of $[PPh_4]Cl$ (96 mg, 0.256 mmol) in CH_2Cl_2 (15 mL). The solution turned greenish-brown gradually. After stirring at room temperature for 3 hr, the solution was reduced to *ca.* 15 mL in volume under vacuum and then layered with toluene (30 mL). Crystals of $\mathbf{3}\cdot 4CH_2Cl_2\cdot 0.5C_6H_5CH_3$ were obtained in 95% yield (440 mg).

(3) *From* $[PPh_4][(PEt_3)Cl_2Ti(\mu\text{–}Cl)_3TiCl_2(PEt_3)]$ (**1**) A solution of $[PPh_4]Cl$ (206 mg, 0.550 mmol) in CH_2Cl_2 (10 mL) was added slowly to a green solution of compound $\mathbf{1}\cdot 2CH_2Cl_2$ (300 mg, 0.275 mmol) in CH_2Cl_2 (15 mL). The resulting greenish-brown solution was layered with toluene (40 mL). After two weeks, crystals of $\mathbf{3}\cdot 4CH_2Cl_2\cdot 0.5C_6H_5CH_3$ were harvested in 87% yield (436 mg).

Treatment of **3** *with* $[PPh_4]Cl$

Compound $\mathbf{3}\cdot 4CH_2Cl_2\cdot 0.5C_6H_5CH_3$ (200 mg, 0.110 mmol) was dissolved in CH_2Cl_2 (15 mL) to give a greenish-brown solution. To this solution was added a solution of $[PPh_4]Cl$ (0.330 mmol, 124 mg) in CH_2Cl_2 (10 mL). There was no change in the color and the solution was then layered with toluene (35 mL). Two weeks later, compound $\mathbf{3}\cdot 4CH_2Cl_2\cdot 0.5C_6H_5CH_3$ was recovered in 93% yield (186 mg). No reaction was observed between compound **3** and $[PPh_4]Cl$ even when ten equivalents of $[PPh_4]Cl$ was used.

Synthesis of $[PPh_4][trans\text{-}Ti(py)_2Cl_4]$ (**4**) *and* $[PPh_4]_2[trans\text{-}Ti(py)_2Cl_4]Cl$ (**4a**)

(1) *From* $[PPh_4]_3[Cl_3Ti(\mu\text{–}Cl)_3TiCl_3]$ (**3**) Compound $\mathbf{3}\cdot 4CH_2Cl_2\cdot 0.5C_6H_5CH_3$ (200 mg, 0.110 mmol) was dissolved in py (20 mL) to give a brown solution. The solution was layered with hexane (40 mL). After 10 days, two products were isolated: prismatic greenish-brown crystals of **4** (47%, 71 mg) and thin plate-shaped, olive-green crystals of **4a** (45%, 105 mg). Magnetic susceptibility for **4**: $X = 1.23\times10^{-3}$ emu at 298 K after diamagnetic correction; $\mu_{eff} = 1.71$ BM per complex anion; for **4a**: $\Omega = 1.25\times10^{-3}$ emu at 298 K after diamagnetic correction; $\mu_{eff} = 1.73$ BM per complex anion.

(2) *From* $[PPh_4][(PEt_3)Cl_2Ti(\mu\text{–}Cl)_3TiCl_2(PEt_3)]$ (**1**)

The reaction was carried out as in (1) above to give products **4** and **4a** in 44% and 46% yield, respectively.

X-ray crystallography

Crystals of $\mathbf{2}\cdot 2CH_2Cl_2$, $\mathbf{3}\cdot 4CH_2Cl_2\cdot 0.5C_6H_5CH_3$, and **4a** were measured on an Enraf FAST diffractometer with an area detector by placing each crystal on the tip of a quartz fiber under a cold stream of nitrogen at -60°C. The crystal of **4** was measured on an Enraf CAD4 automated diffractometer at 20°C with the crystal sealed in a thin-walled glass capillary. Graphite-monochromated Mo Kα radiation (0.70930 Å) was used for both diffractometers. For the crystal on the CAD4 diffractometer, the unit cell was determined by using search, center, index, and least-squares routines. The Laue class and lattice dimensions were verified by axial oscillation photography. The intensity data were corrected for Lorentz and polarization effects and for anisotropic decay. An empirical absorption correction based on psi scans was also applied. For the crystals on the FAST diffractometer, a preliminary data collection was carried out to establish all parameters and to obtain an orientation matrix. Fifty reflections were used in indexing and about 250 reflections in cell refinement. Axial images were taken to determine the Laue groups and cell dimensions. Neither a decay correction nor an absorption correction was applied [5].

Each structure was solved by a combination of direct methods using the SHELXS-86 program [6] and difference Fourier analyses using the SHELXL-93 program [6]. Crystallographic data and results are listed in Table 1.

Compound $\mathbf{2}\cdot 2CH_2Cl_2$ crystallized in the triclinic crystal system. Space group $P\bar{1}$ (No. 2) was first tried, but the solution gave a chemically unreasonable structure. Space group $P1$ (No. 1) was then chosen and confirmed by the successful solution and refinement of the structure. In the unit cell, there are one $[Ti_3Cl_{12}]^{3-}$ anion, three $[PPh_4]^+$ cations, and two CH_2Cl_2 solvate molecules. One of the two CH_2Cl_2 molecules was disordered over two positions with occupancies of 52% and 48%. All non-hydrogen atoms were refined with anisotropic thermal parameters. Hydrogen atoms were calculated by assuming idealized geometry and refined with fixed thermal parameters set at 1.2 B_{eq} of the corresponding carbon atoms. Being mindful of the somewhat uncommon occurrence of space group $P1$, an attempt was made to see if $P\bar{1}$ might not, after all, be possible, but it was unequivocally found not to be.

Compound $\mathbf{3}\cdot 4CH_2Cl_2\cdot 0.5C_6H_5CH_3$ also crystallized in the triclinic system. Space group $P\bar{1}$ (No. 2) was assumed and confirmed by the successful solution and refinement of the structure. In the unit cell, there are two $[Ti_2Cl_9]^{3-}$ anions, six $[PPh_4]^+$ cations, eight CH_2Cl_2 and one $C_6H_5CH_3$ solvate molecules. The toluene molecule is disordered on an inversion center. The non-hydrogen atoms were refined anisotropically, and the hydrogen atoms were treated as mentioned above for compound **2**.

Compound **4** crystallized in the monoclinic crystal system. The absences in the data indicated that the space group is either Cc or C2/c. The centrosymmetric space group C2/c (No. 15) was chosen and confirmed by successful solution of the structure. In the asymmetric unit, there are one $[Ti(py)_2Cl_4]^-$ anion and one $[PPh_4]^+$ cation. All non-hydrogen atoms were refined with anisotropic thermal parameters. Hydrogen atoms were located and refined with isotropic thermal parameters.

Compound **4a** crystallized in the triclinic system. The space group $P\bar{1}$ (No. 2) was determined as in compound $\mathbf{3}\cdot 4CH_2Cl_2\cdot 0.5C_6H_5CH_3$ and the structure was solved similarly. In the asymmetric unit, there are one $[Ti(py)_2Cl_4]^-$ and one Cl^- anion, as well as two $[PPh_4]^+$ cations.

RESULTS AND DISCUSSION

Treatment of the brown solid (**A**) (from reduction of $TiCl_4$ with $HSnBu_3$) with 0.5 equivalent of $[PPh_4]Cl$ converts **A** into a green solid (**B**), probably a material containing face-sharing units (**II**). A dinuclear face-sharing complex, $[(PEt_3)Cl_2Ti(\mu\text{–}Cl)_3TiCl_2(PEt_3)]^-$ (**1′**), was formed from reaction of the green solid (**B**) with one equivalent of PEt_3 [3]. When **B** was treated with 0.5 equivalent of Cl^-, the reaction resulted in the formation of $[Cl_3Ti(\mu\text{–}Cl)_3Ti(\mu\text{–}Cl)_3TiCl_3]^{3-}$ (**2′**) where two face-sharing units are fused to give a linear Ti_3 trimer. In this complex, all three Ti atoms are in the oxidation state 3+, each with one unpaired electron.

Compound $\mathbf{2}\cdot 2CH_2Cl_2$ was characterized by single crystal x-ray diffraction study. The structure of the $[Cl_3Ti(\mu\text{–}Cl)_3Ti(\mu\text{–}Cl)_3TiCl_3]^{3-}$(**2′**) ion in $\mathbf{2}\cdot 2CH_2Cl_2$ is shown in Fig. 1. Selected bond distances and angles are listed in Table 2. The structure of **2′** is similar to those of $[Cr_3Cl_{12}]^{3-}$ [7], $[Ni_3(acac)_6]$ (acac = acetylacetonato) [8], and $[Ru_3Cl_{12}]^{4-}$ as well as its phosphine derivatives [9], all of which contain three atoms bridging two metal atoms. The distances between the central Ti atom and the other two Ti atoms are 3.185(1) and 3.098(4) Å, respectively. These distances are longer than those found in the $[(PR_3)Cl_2Ti(\mu\text{–}Cl)_3TiCl_2(PR_3)]^-$ ions (3.031(2) Å for $PR_3 = PEt_3$ (**1′**); 2.942(1) Å for $PR_3 = PMe_2Ph$) [3]. From the study of variable temperature magnetic susceptibility and *ab initio* CI calculation, it was concluded that the bonding between the two Ti atoms in **1′** is negligible. Accordingly, we expect that there is no strong bonding between the Ti atoms in **2′**. There are two types of bond lengths between a Ti atom and a bridging chlorine atom Cl_b: the one involving the central Ti atom (Ti(2)–Cl_b) is significantly shorter than the one involving a terminal Ti atom (Ti_t–Cl_b), 2.406(4) *vs.* 2.548(4) Å on average, probably due to the different kinds of Cl atoms at the *trans* positions.

Table 1. Crystal Data for compounds **2** · $2CH_2Cl_2$, **3** · $4CH_2Cl_2$ · $0.5C_6H_5CH_3$, **4**, and **4a**.

Compound	**2** · $2CH_2Cl_2$	**3a** · $4CH_2Cl_2$ · $0.5C_6H_5CH_3$	**4**	**4a**
formula	$C_{74}H_{64}Cl_{16}P_3Ti_3$	$C_{79.5}H_{74}Cl_{17}P_3Ti_2$	$C_{34}H_{30}Cl_4N_2PTi$	$C_{58}H_{50}Cl_5N_2P_2Ti$
formula weight	1757.06	1820.75	687.27	1062.09
crystal system	triclinic	triclinic	monoclinic	triclinic
space group	P1 (No. 1)	P (No. 2)	C2/c (No. 15)	P (No. 2)
a, Å	11.408(4)	14.265(6)	23.169(7)	9.2398(4)
b, Å	11.622(5)	14.542(6)	7.879(2)	9.4804(7)
c, Å	16.494(2)	23.200(8)	17.741(5)	15.574(2)
α, (°)	73.206(9)	81.66(3)	90	70.90(1)
β, (°)	70.413(9)	85.99(3)	90.89(2)	73.98(2)
δ, (°)	82.3(2)	62.36(1)	90	84.38(1)
V, Å^3	1971(1)	4218(3)	3238(2)	1276.2(2)
Z	1	2	4	1
$d_{calc.}$, g/cm^3	1.480	1.433	1.410	1.382
μ, cm^{-1}	9.41	8.27	6.71	5.33
data collection instrument	FAST	FAST	CAD4	FAST
temperature, °C	−60	−60	20	−60
$2\theta_{max}$ (°)	50	42	46	50
no. of observns(I > 2s(I))	11603	8319	2251	4262
no. of variables	893	919	252	305
residuals: *R*1[a], *wR*2[b]	0.049, 0.106	0.076, 0.145	0.030, 0.075	0.058, 0.118
quality-of-fit indicator[c]	1.046	1.143	1.062	1.021
max shift in final cycle	0.002	0.003	0.001	0
largest peak, e/Å^3	0.88(8)	0.63(9)	0.25(5)	0.36(8)
absorption correction	none	none	empirical	none

[a] $R1 = \sum||F_o| - |F_c||/\sum|F_o|$ (based on reflections with $F_o^2 > 2\sigma F_o^2$).
[b] $wR2 = [\sum[w(F_o^2 - F_c^2)^2]/\sum[w(F_o^2)^2]]^{1/2}$; $w = 1/[\sigma^2(F_o^2) + (0.095*P)^2]$; $P = [Max(F_o^2,0) + 2*F_c^2]/3$ (also with $F_o^2 > 2\sigma F_o^2$).
[c] Quality-of-fit (on F^2) = $[\sum[w(F_o^2 - F_c^2)^2]/(N_{observns} - N_{params})]^{1/2}$.

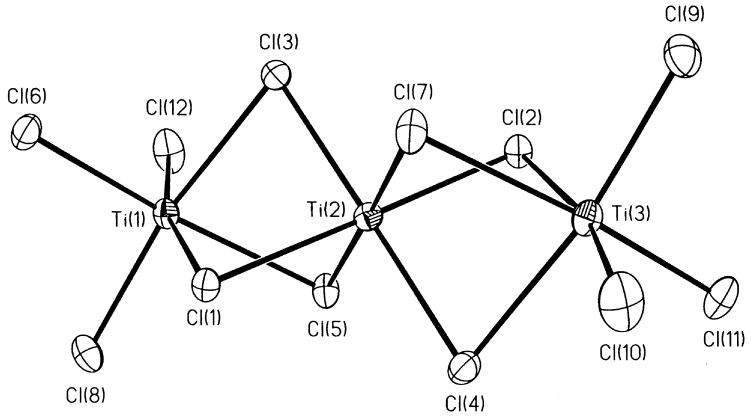

Fig. 1. X-ray structure of the $[Ti_3Cl_{12}]^{3-}$ anion (**2′**) in **2** · $2CH_2Cl_2$ showing 30% probability thermal ellipsoids of Ti and Cl atoms.

They are both longer than the bond length between a Ti atom and a terminal chlorine atom, Ti–Cl_t = 2.329(4) Å. The two terminal Ti atoms are both in a distorted octahedral coordination geometry with Cl_b–Ti_t–Cl_b = 81.1(2)° and Cl_t–Ti_t–Cl_t = 96.7(2)°. The central Ti atom is also in a slightly distorted octahedral geometry with Cl_b(A)–Ti(2)–Cl_b(B) = 87.0(2)° (Cl_b(A) = Cl(1), Cl(3), or Cl(5); Cl_b(B) = Cl(2), Cl(4), or Cl(7)). The average Ti–Cl_b–Ti angle is 78.6(2)°, obviously larger than that in an idealized face-sharing unit (70.53°) [10], indicating there is a repulsion between the Ti(III) atoms.

From the room-temperature magnetic susceptibility of **2**, a magnetic moment of 2.07 BM was calculated. Since this is far less than would be expected for three independent unpaired electrons, while the structure shows that no direct Ti–Ti bonding occurs, it must be concluded that there is strong antiferromagnetic

Table 2. Selected bond lengths (Å) and angles (°) for $\mathbf{2}\cdot 2CH_2Cl_2$.

Ti(1)···Ti(2)	3.185(4)	Ti(2)–Cl(1)	2.420(4)
Ti(2)···Ti(3)	3.098(4)	Ti(2)–Cl(5)	2.425(4)
Ti(1)–Cl(1)	2.550(2)	Ti(1)–Cl(12)	2.322(3)
Ti(1)–Cl(3)	2.551(5)	Ti(1)–Cl(6)	2.323(4)
Ti(1)–Cl(5)	2.559(4)	Ti(1)–Cl(8)	2.349(4)
Ti(3)–Cl(2)	2.540(2)	Ti(3)–Cl(10)	2.313(3)
Ti(3)–Cl(7)	2.540(4)	Ti(3)–Cl(9)	2.332(4)
Ti(3)–Cl(4)	2.551(5)	Ti(3)–Cl(11)	2.338(4)
Ti(2)–Cl(7)	2.390(4)	Ti(2)–Cl_b(av)	2.406(4)
Ti(2)–Cl(4)	2.394(2)	Ti_t–Cl_b (av)	2.548(4)
Ti(2)–Cl(3)	2.402(2)	Ti–Cl_t (av)	2.329(4)
Ti(2)–Cl(2)	2.405(4)		
Cl(12)–Ti(1)–Cl(6)	98.5(1)	Cl(3)–Ti(2)–Cl(1)	86.65(7)
Cl(12)–Ti(1)–Cl(8)	96.8(1)	Cl(3)–Ti(2)–Cl(5)	86.88(8)
Cl(6)–Ti(1)–Cl(8)	95.4(1)	Cl(1)–Ti(2)–Cl(5)	84.9(2)
Cl(10)–Ti(3)–Cl(9)	97.3(2)	Ti(2)–Cl(1)–Ti(1)	79.7(2)
Cl(10)–Ti(3)–Cl(11)	98.2(2)	Ti(2)–Cl(2)–Ti(3)	77.5(2)
Cl(9)–Ti(3)–Cl(11)	94.3(1)	Ti(2)–Cl(3)–Ti(1)	79.98(7)
Cl(1)–Ti(1)–Cl(3)	80.9(2)	Ti(2)–Cl(4)–Ti(3)	77.53(7)
Cl(1)–Ti(1)–Cl(5)	79.6(1)	Ti(2)–Cl(5)–Ti(1)	79.4(1)
Cl(3)–Ti(1)–Cl(5)	81.01(8)	Ti(2)–Cl(7)–Ti(3)	77.8(1)
Cl(2)–Ti(3)–Cl(7)	81.4(1)	Ti(3)–Ti(2)–Ti(1)	179.44(7)
Cl(2)–Ti(3)–Cl(4)	81.6(1)	Cl_b–Ti_t–Cl_b (av)	81.1(2)
Cl(7)–Ti(3)–Cl(4)	82.19(8)	Cl_b(A)–Ti(2)–Cl_b(B) (av)	87.0(2)
Cl(7)–Ti(2)–Cl(4)	88.79(8)	Ti–Cl_b–Ti (av)	78.6(2)
Cl(7)–Ti(2)–Cl(2)	87.3(2)	Cl_t–Ti_t–Cl_t (av)	96.7(2)
Cl(4)–Ti(2)–Cl(2)	87.78(8)		

Numbers in parentheses are estimated standard deviations in the least significant digits.

coupling among the electrons. The value of 2.07 BM could be explained if there is a ground state with $S=1/2$ and a thermally accessible excited state with $S=3/2$.

Reaction of **2′** with 0.5 equivalent of $[PPh_4]Cl$ yielded a dinuclear face-sharing complex, $[Cl_3Ti(\mu\text{–}Cl)_3TiCl_3]^{3-}$ (**3′**). The reaction is:

$$2[Ti_3Cl_{12}]^{3-} + 3Cl^- = 3[Ti_2Cl_9]^{3-}$$

Under the conditions used, the reaction was almost quantitative (95% yield). Complex **2′** can also be synthesized directly from the reaction of the green solid **B** with one equivalent of $[PPh_4]Cl$. Substitution of the phosphine ligands in **1′** also led to the formation of **3′**. Although $[Ti_2Cl_9]^{3-}$ has been extensively studied for its magnetic and spectroscopic properties [11], its full structural characterization was only recently reported [12] for the compound $[NEt_4]_3[Ti_2Cl_9]$. The present results are almost identical; in particular, exactly the same Ti···Ti separation, 3.216 Å, was found in both cases.

The structure of **3′** in $\mathbf{3}\cdot 4CH_2Cl_2\cdot 0.5C_6H_5CH_3$ is shown in Fig. 2. Selected bond lengths and angles are listed in Table 3. The important structural parameters in **3′** are comparable with those quoted for $Cs_3Ti_2Cl_9$ [11b], Ti···Ti = 3.216(3) *vs.* 3.191, Ti–Cl_b = 2.501(3) *vs.* 2.503, Ti–Cl_t = 2.365(4) *vs.* 2.328 Å, Cl_b–Ti–Cl_b = 83.0(1) *vs.* 83.7, Cl_t–Ti–Cl_t = 95.2(2) *vs.* 95.2°. The distance between two Ti atoms in **3′** is longer than the two in **2′** (3.185(4) and 3.098(4) Å. The Ti–Cl_b–Ti angle is also larger, 80.0(1) *vs.* 78.6(2)°. The Ti–Cl_b bond length is between the values of two sets of such bond lengths in **2′**, 2.501(3) *vs.* 2.406(4) and 2.548(4) Å, while the Ti–Cl_t bond length is just slightly

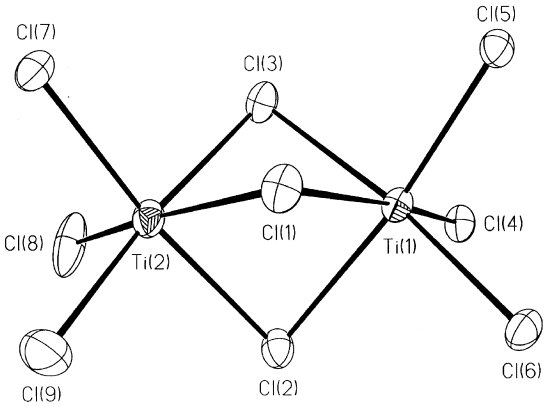

Fig. 2. X-ray structure of the $[Ti_2Cl_9]^{3-}$ anion (**3′**) in $\mathbf{3}\cdot 4CH_2Cl_2\cdot 0.5C_6H_5CH_3$ showing 30% probability thermal ellipsoids of Ti and Cl atoms.

Table 3. Selected bond lengths (Å) and angles (°) for $\mathbf{3}\cdot 4CH_2Cl_2\cdot 0.5C_6H_5CH_3$.

Ti(1)···Ti(2)	3.216(3)	Ti(1)–Cl(5)	2.362(3)
Ti(1)–Cl(1)	2.492(3)	Ti(1)–Cl(6)	2.383(3)
Ti(1)–Cl(3)	2.496(3)	Ti(2)–Cl(9)	2.353(4)
Ti(1)–Cl(2)	2.521(3)	Ti(2)–Cl(8)	2.360(4)
Ti(2)–Cl(2)	2.494(3)	Ti(2)–Cl(7)	2.373(3)
Ti(2)–Cl(3)	2.498(3)	Ti–Cl_b (av)	2.501(3)
Ti(2)–Cl(1)	2.505(3)	Ti–Cl_t (av)	2.365(4)
Ti(1)–Cl(4)	2.358(3)		
Cl(4)–Ti(1)–Cl(5)	96.3(1)	Cl(2)–Ti(2)–Cl(3)	84.1(1)
Cl(4)–Ti(1)–Cl(6)	96.4(1)	Cl(2)–Ti(2)–Cl(1)	82.2(1)
Cl(5)–Ti(1)–Cl(6)	94.1(1)	Cl(3)–Ti(2)–Cl(1)	83.2(1)
Cl(9)–Ti(2)–Cl(8)	96.4(2)	Ti(1)–Cl(1)–Ti(2)	80.1(1)
Cl(9)–Ti(2)–Cl(7)	92.1(1)	Ti(2)–Cl(2)–Ti(1)	79.8(1)
Cl(8)–Ti(2)–Cl(7)	96.1(1)	Ti(1)–Cl(3)–Ti(2)	80.2(1)
Cl(1)–Ti(1)–Cl(3)	83.6(1)	Clb–Ti–Cl_b (av)	83.0(1)
Cl(1)–Ti(1)–Cl(2)	81.9(1)	Clt–Ti–Cl_t (av)	95.2(2)
Cl(3)–Ti(1)–Cl(2)	83.6(1)		

Numbers in parentheses are estimated standard deviations in the least significant digits.

longer, 2.365(3) *vs.* 2.329(4) Å. For the same reason mentioned above, there should be no metal-metal bond between the two Ti atoms in **3′**.

In complex **3′**, each Ti atom is in the oxidation state of 3+ and has one unpaired electron. However, the effective magnetic moment for compound **3** is appreciably lower than the idealized value for a compound with two unpaired electrons, 1.70 *vs.* 2.83 BM. Actually, the magnetic moment is very close to that for compound **1**, 1.72 BM, probably also due to the strong antiferromagnetic coupling between the electrons as in **1**. More extensive magnetic data were reported and discussed in Ref [12].

Even though it is rather easy to break one of the two face-sharing units in **2′** to form **3′**, it is impossible to convert the dinuclear complex **3′** into a mononuclear complex by using $[PPh_4]Cl$. This might be due to the fact that the Ti–Cl_b bond (2.501(3) Å) in **3′** is shorter than the Ti_t–Cl_b bond (2.548(4) Å) in **2′**, indicating a stronger Ti–Cl_b bonding. As a result, the reaction between the green solid **B** and excess of $[PPh_4]Cl$ always ends up with the product **3**.

It appears that in order to break the face-sharing unit in **3′**, stronger ligands are needed. When compound **3** was dissolved in pyridine, it was converted into a mononuclear complex, $[trans\text{-}Ti(py)_2Cl_4]^-$ (**4′**). It is possible that the reaction resulted in the formation of **4′** and $[Ti(py)Cl_5]^{2-}$ in which one Cl atom was then substituted by a pyridine ligand to form **4′**. The Cl^- anion was isolated as $[PPh_4]_2[trans\text{-}Ti(py)_2Cl_4]Cl$ (**4a**). Complex **4′** has been reported before as a pyridinium salt from reaction of $TiCl_2$, py, and CH_2Cl_2 [13].

Both of compounds **4** and **4a** were charaterized crystallographically. The structures of **4′** in **4** and **4a** are similar and they are displayed in Fig. 3 and Fig. 4, respectively. The structure of **4′** in **4** is almost ident-

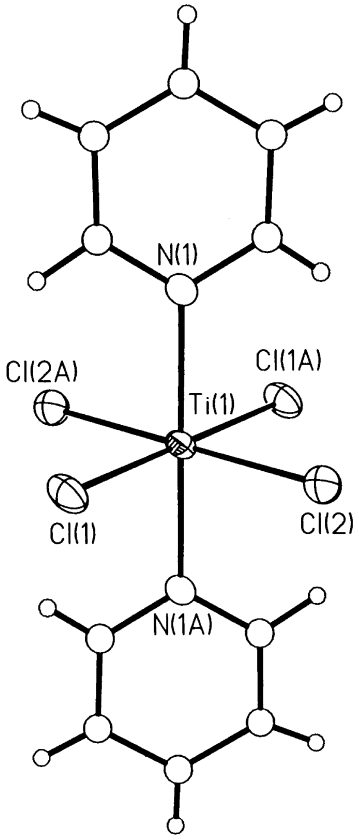

Fig. 3. X-ray structure of the $[Ti(py)_2Cl_4]^-$ anion (**4′**) in **4** showing 30% probability thermal ellipsoids of Ti, Cl, and N atoms. Carbon and hydrogen atoms are represented with arbitrarily small circles for clarity.

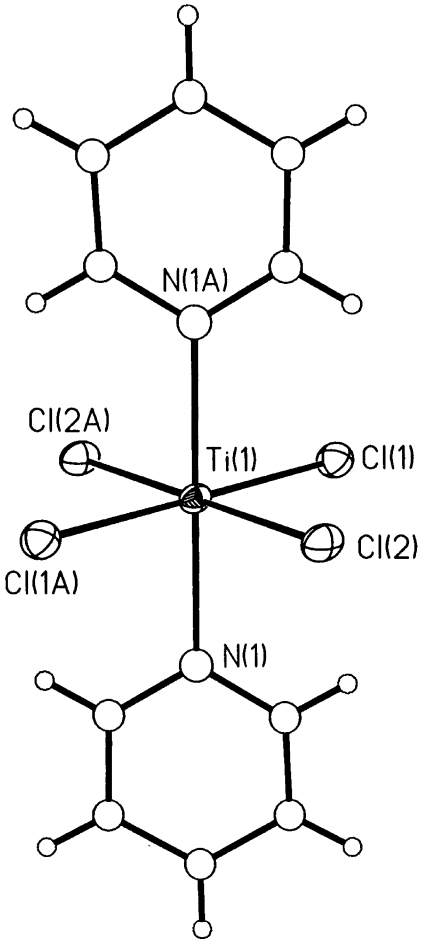

Fig. 4. X-ray structure of the $[Ti(py)_2Cl_4]^-$ anion (**4′**) in **4a** showing 30% probability thermal ellipsoids of Ti, Cl, and N atoms. Carbon and hydrogen atoms are represented with arbitrarily small circles for clarity.

ical to that in $(pyH)[Ti(py)_2Cl_4] \cdot CH_2Cl_2$ [13] with Ti–N = 2.208(2) *vs.* 2.21(1), Ti–Cl = 2.4001(9) *vs.* 2.405(3) Å. However, the corresponding bond lengths of **4′** in **4a** are obviously different. The Ti–N bond is longer, 2.235(4) Å. And there are two sets of Ti–Cl bonds in **4a**, Ti–Cl(1) = 2.365(1) and Ti–Cl(2) = 2.447(1) Å. This might be caused by the presence of the Cl^- anion in the crystal. The distance between the Cl^- anion, Cl(11), and Cl(2) is much shorter than that between Cl(11) and Cl(1), 5.61 *vs.* 7.46 Å. Cl(11) is located between Cl(2) and Cl(2)′ in another [*trans*-$Ti(py)_2Cl_4]^-$ anion. The results from magnetic susceptibility measurements indicated that both compounds, **4** and **4a**, contain one unpaired electron with $\mu_{eff} = 1.71$ and 1.73 BM, respectively.

Acknowledgements—We thank the Robert A. Welch Foundation for support under Grant No. A494.

REFERENCES

1. Bottrill, M., Gavens, P. D. and McMeeking J., Low Valent Complexes of Titanium in *Comprehensive Organometallic Chemistry*. Wilkinson, G., Stone, F. G. A. and Abel, E. W., Eds., Vol. 3, Chapter 22.2, Pergamon Press, 1982. (b) McAuliffe, C. A. and Barrat D. S., Titanium in *Comprehensive Coordination Chemistry*. Wilkinson, G., Gillard, R. D. and McCleverty, J. A., Eds., Vol. 3, Chapter 31, Pergamon Press, 1987.
2. Cotton, F. A. and Wojtczak, W. A., *Gazz. Chim. Ital.*, 1993, **123,** 499.
3. Chen, L., Cotton, F. A., Dunbar, K. R., Feng, X., Heintz, R. A. and Uzelmeir, C., *Inorg. Chem.*, 1996, **35,** 7358.
4. Chen, L. and Cotton, F. A., *Inorg. Chim. Acta*, 1997, **257,** 1351.
5. For more details concerning use of the area-detector, see: Scheidt, W. R. and Turowska-Tyrk, I., *Inorg. Chem.*, 1994, **33**, 1314.
6. (a) Sheldrick, G. M., *SHELXS*-86, *Program for Crystal Structure Determination*, University of Cambridge, UK, 1986. (b) Sheldrick, G. M., *SHELXL*-93, *Program for Crystal Structure Refinement*, University of Göttingen, Göttingen, Germany, 1993.
7. Babar, M. A., Ladd, M. F. C., Larkworthy, L. F., Povey, D. C., Proctor, K. J. and Summers, L. J., *J. Chem. Soc., Chem. Commun.*, 1981, 1046.
8. (a) Charles, R. G. and Pawlikowski, M. A., *J. Phys. Chem.*, 1958, **62**, 440. (b) Ginsberg, A. P., Martin, R. L. and Sherwood, R. C., *Inorg. Chem.*, 1968, **7**, 932.
9. (a) Bino, A. and Cotton, F. A., *J. Am. Chem. Soc.*, 1980, **102**, 608. (b) Cotton, F. A., Matusz, M. and Torralba, R. C., *Inorg. Chem.*, 1989, **28**, 1516. (c) Cotton, F. A. and Torralba, R. C., *Inorg. Chem.*, 1991, **30**, 3293.
10. Cotton, F. A. and Walton, R. A., *Multiple Bonds Between Metal Atoms*, 2nd edn., Oxford University Press, 1993.
11. (a) Crouch, P. C., Fowles, G. W. A. and Walton, W. A., *J. Chem. Soc.* (A), 1969, 972. (b) Briat, B., Kahn, O., Morgenstern-Badarau, I. and Rivoal, J. C., *Inorg. Chem.*, 1981, **20**, 4193. (c) Leuenberger, B., Gudel, H. U. and Furrer, A., *Chem. Phys. Lett*, 1986, **126**, 255. (d) Drillon, M. and Georges, R., *Phys. Rev. B*, **1982**, 26, 3882. (e) Kahn, O., *Molecular Magnetism*, VCH, New York, 1993; and references therein.
12. Castro, S. L., Streib, W. E., Huffman, J. C. and Christou, G., *Chem. Comm.*, 1996, 2177.
13. Troyanov, S. I., Mazo, G. N., Rybakov, V. B. and Budkina, K. V., *Koord. Khim.*, 1990, **16,** 246 (English).

Pergamon

PII: S0277-5387(98)00172-7

Polyhedron Vol. 17, No. 21, pp. 3735–3738, 1998
© 1998 Elsevier Science Ltd
All rights reserved. Printed in Great Britain
0277–5387/98 $19.00+0.00

Preparation and crystal structure of new one-dimensional Ta selenide: $[Ta(Se_2)_2]_2TaBr_6$

Maxim Sokolov,[ab] Hideo Imoto,[b] Taro Saito[b,*] and Vladimir Fedorov[a]

[a]Institute of Inorganic Chemistry of the Russian Academy of Sciences, pr. Lavrentyeva 3, 630090 Novosibirsk, Russia

[b]Department of Chemistry, School of Science, The University of Tokyo, Hongo, Bunkyo-ku, Tokyo 113-0033, Japan

(Received 16 January 1998; accepted 22 April 1998)

Abstract—Compound $[Ta(Se_2)_2]_2TaBr_6$ was prepared from elements by high temperature (450°C) stoichiometric reaction in high yield. The structure has been determined by single crystal X-ray diffraction. It contains infinite positively charged chains $Ta(Se_2)_2\ldots$ separated by octahedral $TaBr_6^-$ anions. The slightly alternating Ta–Ta distances within the chains [3.182(2)–3.234(2) Å] show a considerable degree of metal–metal interaction along the chain. © 1998 Elsevier Science Ltd. All rights reserved

Keywords: crystal structure; tantalum complexes; selenium complexes; bromides; one-dimensional materials.

INTRODUCTION

Chemistry and solid state physics of low-dimensional materials is a well established field of research activity [1, 2]. Chalcogenides and chalcohalides of Group 5 transition elements have so far furnished dozens of one-dimensional materials, the prominent examples being $TaSe_3$ [3] and a remarkable family of "intercalated" selenides $(NbSe_4)_yI$ ($y = 2$–4) [4]. The polymeric NbS_2Cl_2 has a $Nb_2(S_2)_2^{4+}$ core and was one of the first well-characterized transition metal chalcohalides [5]. It has recently been shown to be a convenient lead-in compound into the still largely unexplored area of molecular niobium chalcogen complexes [10, 11]. The corresponding Ta chemistry is far less developed. Well characterized products are $Ta(Te_2)_2I$ [6], $[Ta(Te_2)_2]_4I_2(TaI_6)$ [7], $[Ta(Se_2]_2]_2I$ [12] and $[Ta(Te_2)_2]_6I_4(TaI_6)$ [9]. Here we report synthesis and crystal structure of a novel one-dimensional Ta selenide bromide, $[Ta(Se_2)_2]_2TaBr_6$ (**1**) as a result of our investigations in Ta/Se/X_2 (X = Cl, Br) systems.

[1] Further details of the crystal structure can be ordered from Fachinformationszentrum Karlsruhe, 76344 Eggenstein-Leopoldshafen (e-mail: crysdata@fiz-karlsruhe.de) under the depository number CSD-408596.

* Author to whom correspondence should be addressed. Fax: +81-3-3814-2627; E-mail: imoto@chem.s.u-tokyo.ac.jp.

EXPERIMENTAL

A mixture of Ta powder (1.00 g, 5.53 mmol), gray Se (1.16 g, 14.69 mmol) and Br_2 (0.28 ml, 5.43 mmol) was placed in a quartz tube which then was sealed under vacuum and heated at 450°C for 1 week. A temperature gradient was maintained. The tube was cooled at 20°C h^{-1} rate to promote crystal growth. After cooling down, almost complete transport into the cooler end of the tube was observed. The compound crystallizes in the form of long (up to 1 cm), thin black needles. The yield was 90%. The elemental analysis agreed with the formula $Ta_3Se_8Br_6$ (**1**). The compound can be handled in air for a limited period but must be stored under nitrogen to avoid degradation which releases HBr and H_2Se in moist air.

Small amounts of bronze-colored $TaSe_2$ and red $TaBr_5$ (less than 5%) also form as byproducts but can be easily separated manually from the main product.

The electrical conductivity of crystals of **1** at room temperature was measured by a two-point contact method; $\sigma = 10^{-4}\,\Omega^{-1}\,cm^{-1}$.

Crystal structure determination of 1

The structure was determined by the single crystal X-ray crystallography. X-ray data were measured at 295 K on a Rigaku AFC-5R diffractometer with

graphite-monochromated MoK_α radiation ($\lambda =$ 0.71069 Å) with the ω–2θ scan mode. The DIFABS program was used for absorption correction. A slight decay (5.42% in intensity) was detected during the data collection and the data were corrected accordingly. The structure was solved by direct methods (SHELX-86) [18]. The full-matrix refinements were performed with the teXsan programs [19]. Crystal data and refinement results are given in Table 1. Selected interatomic distances are given in Table 2.

RESULTS AND DISCUSSION

Figure 1 shows the ORTEP drawing of the structure of **1**. The Ta atoms form linear chains running along the *c*-axis with slightly alternating Ta–Ta distances 3.198(2), 3.234(2) and 3.182(2) Å. The sequence is Ta(1)–Ta(1)–Ta(2)–Ta(2)–Ta(1)–Ta(1)..., Ta(1)–Ta(2) being the largest distance. Se(1) and Se(2) are bridging Ta(1) atoms, two Ta(2) atoms are bridged by Se(3) and Se(4) whereas four non-equivalent Se atoms [Se(5), Se(6), Se(7) and Se(5)] connect Ta(1) with Ta(2). The closest analog to **1** is $[Ta(Se_2)_2]_2I$, where all the distances are equal at 3.206(1) Å [12]. Each Ta atom is coordinated to eight Se atoms of four diselenide bridges. The Se–Se distances in the Se_2 ligands vary between 2.35–2.38 Å which can be compared with 2.40 Å in $[Ta(Se_2)_2]_2I$ [12]. It has already been pointed that Se_2 groups are rather flexible and use their π-antibonding orbitals to serve as an electronic pool for adjacent metal chains [1]. The significantly shorter Se–Se distance in **1** than in closely related $[Te(Se_2)_2]_2I$ can thus be explained by stronger electronic demand of metal chains in the bromine compound. The four Se atoms of each bridging pair of the Se_2 ligands lie approximately in planes perpendicular to the chains of Ta atoms, thus forming a

Table 2. Bond lengths (Å) and some characteristic angles (°)

Ta(1)–Ta(1)	3.198(2)	Ta(1)–Se(5)	2.713(3)
Ta(1)–Ta(2)	3.234(2)	Ta(1)–Se(2)	2.626(2)
Ta(1)–Se(1)	2.653(3)	Ta(1)–Se(6)	2.593(3)
Ta(1)–Se(7)	2.690(3)	Ta(1)–Se(8)	2.593(2)
Ta(2)–Ta(2)	3.182(2)	Ta(2)–Se(3)	2.625(2)
Ta(2)–Se(4)	2.654(3)	Ta(2)–Se(7)	2.595(3)
Ta(2)–Se(5)	2.602(3)	Ta(3)–Br(1)	2.518(3)
Ta(2)–Se(8)	2.698(2)	Ta(3)–Br(2)	2.520(3)
Ta(2)–Se(6)	2.731(3)	Ta(3)–Br(5)	2.490(3)
Ta(3)–Br(3)	2.466(3)	Ta(3)–Br(6)	2.498(3)
Ta(3)–Br(4)	2.516(3)	Se(5)–Se(8)	2.364(4)
Se(1)–Se(2)	2.345(4)	Se(6)–Se(7)	2.375(4)
Se(3)–Se(4)	2.353(4)		

Ta(1)–Ta(1)–Ta(2)	179.35(6)
Ta(1)–Ta(2)–Ta(2)	179.36(6)
Ta–Se–Ta	61.21(8)–75.44(7)
Se(7)–Ta(2)–Se(6)	52.89(8)
Se(7)–Ta(2)–Se(8)	81.03(8)
Se(5)–Ta(2)–Se(7)	107.71(8)
Se(2)–Ta(1)–Se(5)	165.25(9) and 78.88(8)
Se(1)–Ta(1)–Se(8)	93.30(8) and 130.67(9)
Br–Ta–Br (*cis*)	87.9(1)–93.0(1)
Br–Ta–Br (*trans*)	175.3(1)–178.1(1)

Table 1. Crystal data and refinement results for **1**

Formula	$Ta_3Se_8Br_6$
a (Å)	11.239 (2)
b (Å)	12.847 (2)
c (Å)	7.201 (1)
α (°)	102.51 (1)
β (°)	98.04 (1)
γ (°)	70.49 (1)
V (Å^3)	954.2 (3)
Z	2
Formula weight	1653.95
Space group	$P\bar{1}$ (No. 2)
F_{000}	1402.00
Calculated density (g cm^{-3})	5.756
μ (cm^{-1})	411.52
Reflections collected	5823
Unique	5561
Observed [$I > 2.00\sigma(I)$]	3970
Reflections/parameters ratio	25.78
R[a]	0.063
R_w[b]	0.058

[a] $R = \Sigma|F_o - F_c|/\Sigma F_o$.
[b] $R_w = [\Sigma w(F_o - F_c)^2/\Sigma w F_o^2]^{1/2}$.

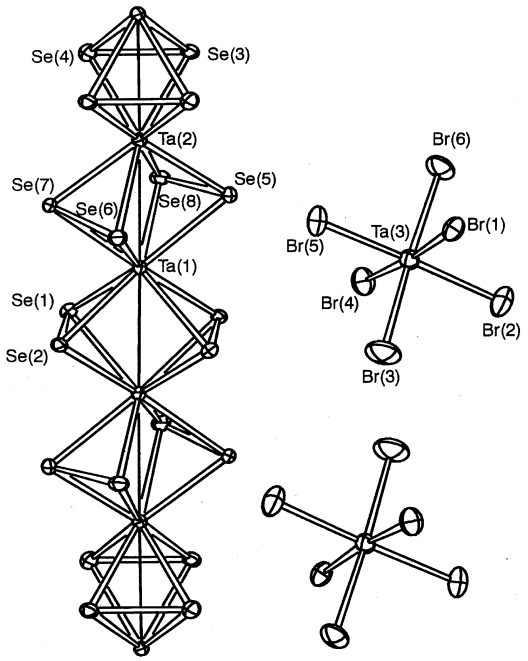

Fig. 1. ORTEP drawing of two repeating units of **1**. Thermal ellipsoids are drawn at the 50% probability level.

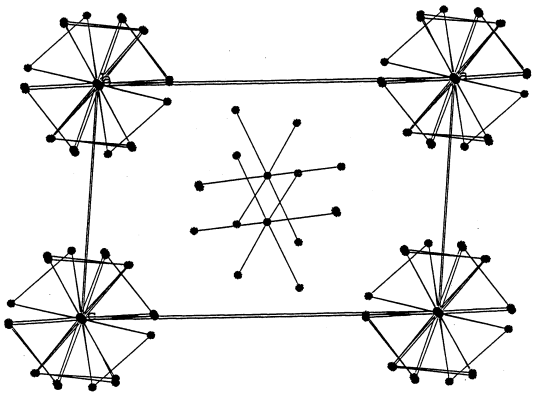

Fig. 2. Structure projection on the *xyO* plane.

rectangle with two short and two long sides. The dihedral angles between each pair of adjacent Se_4 units are close to 45° to minimize repulsion between Se atoms and to increase the overlap with 5d orbitals of Ta [6]. These restrictions still leave enough room for different modes of stacking of the Se_4 rectangles in the chain [6]. In **1** (Fig. 2) the stacking pattern is the same as found in the structure of $[Nb(Te_2)_2]I$ [6] but differs from those observed for other $Ta(Se_2)_2$ and $Ta(Te_2)_2$ chains [6, 12]. The chains are separated by slightly distorted $TaBr_6^-$ anions (the Ta–Br distances are in the range 2.47–2.52 Å). In a relevant complex $[TaBr_4(diars)_2][TaBr_6]$, this anion forms almost perfect octahedron (Ta–Br 2.49 Å) [14]. The distortions may be due to additional Se...Br contacts (the shortest one, between Se(5) and Br(5), is 3.162(4) Å), which may also favor the observed stacking pattern for the Se_4 rectangles. The contacts of this kind fall well shorter than the corresponding sum of van-der Waals radii and are a well established feature in the chemistry of heavier chalcogens [15].

Since the bond distances in the anion show the oxidation state of the Ta atom in the $TaBr_6^-$ unit to be five, a positive charge +1 should he assigned to the $[Ta(Se_2)_2]_2$ unit. It means that the Ta atoms have the oxidation state +4.5 which leaves 0.5 e per one Ta–Ta bond (if we consider the diselenium bridges as Se_2^{2-}). If we take into account the donation of an extra electron density from the bridging ligands it will give us less negative charge on the Se_2 unit and correspondingly stronger bonding interaction between tantalum atoms. This is in keeping with the observed distances of about 3.20 Å for **1** and $[Ta(Se_2)_2]_2I$ with the same formal oxidation state. It is thus considerably shorter than that in $[Ta(Te_2)_2]I$ (3.33–3.35 Å) where the oxidation state is +5 which implies zero bonding order. Accordingly, preliminary resistivity measurements on the single crystals of **1** gave value which may indicate semiconductive behavior.

The prepared material thus belongs to the by now extensive family of one-dimensional structures, hav-

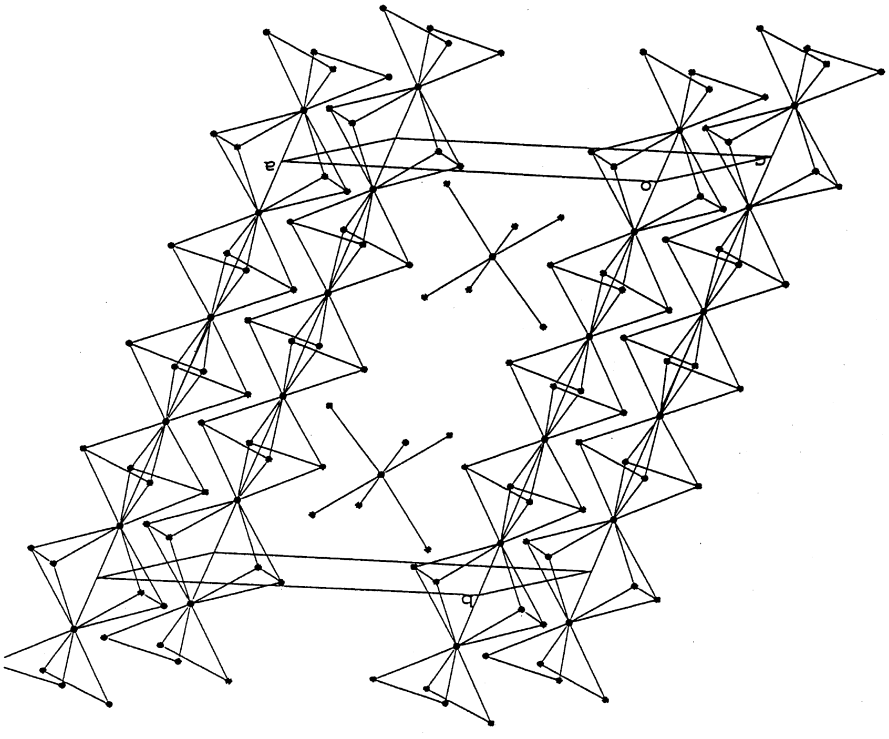

Fig. 3. Unit cell drawing of **1**.

ing positively charged metal–dichalcogen chains separated by counteranions (Fig. 3). As for the latter, both simple small anions (like I^-) and large complex ones (PtI_6^{2-} [8], TaI_6^- [7, 9], $TaBr_6^-$) are effective in the stabilization of this type of structure. It seems possible that other anions of various shape and size may be good candidates as well.

In conclusion it may be mentioned that the synthesis of **1** is one of the rare cases when Nb and Ta do not behave in a similar way. Thus, in the reaction conditions similar to those used in the present study, Nb forms $NbSe_2Br_2$, a coordination polymer where $Nb_2(Se_2)_2$ cluster units are linked by bromine atoms similar to NbS_2Cl_2 [13]. On the other hand it was not possible to prepare the Ta analog of NbS_2Cl_2, only TaS_3 and $TaCl_5$ could be detected [13]. One of the reasons may be the greater reluctance of Ta to form low oxidation states, in keeping with the overall trend in the periodic table.

Acknowledgements—We thank the Japan Society for the Promotion of Science for a research fellowship to M. S. Financial support by the Russian Foundation for Basic Research (grant RFBR-9603-32954) is also acknowledged.

REFERENCES

1. Rouxel, J., *Acc. Chem. Res.*, 1992, **25,** 328.
2a. Rouxel, J. (ed.), *Crystal Chemistry and Properties ofMaterials with Quasi-One Dimensional Structures*. D. Reidel Publishing Company, Dordrecht, 1986, pp. 205–279.
2b. Fedorov, V. E., *Refractory Metals Chalcogenides. Quasi One-Dimensional Compounds*. Nauka, Novosibirsk, 1988.
3. Bjerkelund, E. and Kjekshus, A., *Acta Chem. Scand.*, 1965, **19,** 701.
4. Gressier, P., Meerchaut, A., Guemas, L., Rouxel, L. and Monceau, P., *J. Solid State Chem.*, 1984, **51,** 141.
5. von Schnering, H.-G. and Beckmann, W., *Z. Anorg. Allg. Chem.*, 1966, **347,** 231.
6. Tremel, W., *Chem. Ber.*, 1992, **125,** 2165.
7. Liu, S.-X., Huang, D.-P., Huang, C.-C. and Huang, J.-L., *Polyhedron*, 1996, **15,** 2295.
8. Tremel, W. and Stork, K.-L., *Z. Naturforsch.*, 1993, **48b,** 1155.
9. Huang, J.-L., Liu, S.-X., Huang, D.-P., Huang, C.-C., *Jiegou Huaxue*, 1995, **14,** 342.
10. Sokolov, M., Virovets, A., Nadolinnyi, V., Hegetschweiler, K., Fedin, V., Podberezskaya, N. and Fedorov, V., *Inorg. Chem.*, 1994, **33,** 3503.
11. Sokolov, M., Hernandez-Molina, R., Elsegood, M. R. J., Heath, S. L., Clegg, W. and Sykes, A. G., *J. Chem. Soc. Dalton Trans.*, 1997, 2059.
12. Gressier, P., Guemas, L. and Meerchaut, A., *Acta Cryst. B*, 1982, **38,** 2877.
13. von Schnering, H.-G. and Beckmann, W., *Z. Anorg. Allg. Chem.*, 1966, **347,** 225.
14. Drew, M. G. B., Walters, A. P. and Wilkins, J. D., *Acta Cryst.*, 1975, **31b,** 324.
15. Krebs, B. and Ahlers, F.-P., in *Advances in Inorganic Chemistry*, Vol. 35, ed. A. G. Sykes. Academic Press, 1990, p. 235.
16. Grenouilleau, J. P., Meerchaut, A., Guemas, L. and Rouxel, J., *J. Solid State Chem.*, 1987, **66,** 293.
17. Gressier, P., Meerchaut, A., Guemas, L., Rouxel, J. and Monceau, P., *J. Solid State Chem.*, 1984, **51,** 141.
18. Sheldrick, G. M., in *Crystallographic Computing*, Vol. 3, eds. G. M. Sheldrick, C. Kruger and R. Goddard. Oxford University Press, 1985, pp. 175–189.
19. *teXsan*: *Crystal Structure Analysis Package*. Molecular Structure Corporation, 1985 and 1992.

Pergamon

PII: S0277–5387(98)00175–2

Polyhedron Vol. 17, No. 21, pp. 3739–3745, 1998
© 1998 Elsevier Science Ltd
All rights reserved. Printed in Great Britain
0277–5387/98 $19.00+0.00

Palladium(II) complexes of 2-acetyl- and 2-formylpyridine 3-hexamethyleneiminyl-thiosemicarbazones; a synthetic, spectral and structural study

Dimitra Kovala-Demertzi,[a]*Mavroudis A. Demertzis,[a] Alfonso Castiñeiras[b] and Douglas X. West[c]

[a]Department of Chemistry, University of Ioannina, 45110Ioannina, Greece.

[b]Departamento de Quimica Inorganica, Universidad de Santiago de Compostela, E-15706, Santiago de Compostela, Spain.

[c]Department of Chemistry, Illinois State University, Normal, Illinois, 61761, U.S.A.

(Received 15 January 1998; accepted 15 April 1998)

Abstract—Reaction of Li_2PdCl_4 with 2-acetyl- and 2-formylpyridine 3-hexamethyleneiminyl-thiosemicarbazones, HFohexim and HAchexim, respectively, affords the complexes [Pd(Achexim)Cl] and [Pd(Fohexim)Cl]. [Pd(Fohexim)Cl] crystallizes in the triclinic space group $P\bar{1}$ with $a=7.9447(17)$ Å, $b=9.6402(13)$ Å, $c=10.3739(18)$ Å, $\alpha=79.128(12)^\circ$, $\beta=75.104(15)^\circ$ and $\gamma=75.558(14)^\circ$. Crystals of [Pd(Achexim)Cl] are monoclinic, space group $P2(1)/n$, with four formula units in a unit cell of dimensions $a=7.2243(7)$ Å, $b=9.6402(13)$ Å, $c=24.937(3)$ Å, and $\beta=104.048(9)^\circ$. Anions of HFohexim and HAchexim coordinate in a planar conformation to a central palladium(II) via the pyridyl nitrogen, azomethine nitrogen and thiolato sulfur atoms. The complexes have been characterized by spectroscopic techniques (IR and ^{1}H NMR). The protonation constants of HFohexim, $K_{a1}=11.83\pm0.01$ and $K_{a2}=3.70\pm0.02$, were determined spectrophotometrically. © 1998 Elsevier Science Ltd. All rights reserved

Keywords: thiosemicarbazone; hexamethyleneimine; palladium; crystal structure.

INTRODUCTION

Heterocyclic thiosemicarbazones (TSCs) are important because of their possible beneficial biological activity [1]. The 3-hexamethyleneiminyl-thiosemicarbazones of 2-acetyl- and 2-formylpyridine, HAchexim [2] and HFohexim [2, 3], have been screened against HSV-1, HSV-2 and leukemia P388 because of their potential for medicinal use. We have initiated an investigation on complexes of palladium(II) in an effort to correlate structure with biological activity [4–9]. This report includes the crystal structures of the newly prepared [Pd(Fohexim)Cl], and [Pd(Achexim)Cl], which was included in a previous spectral and biological study [9]. This work is an extension of previously studied palladium(II) complexes of 2-acetylpyridine TSC with potentially interesting biological activity [4–9], as well as copper(II) complexes of these TSCs [10].

EXPERIMENTAL

Solvents were purified and dried according to standard procedures. The complexes were analyzed for C, H, and N at the European Environmental Research Institute (Ioannina). The methods of measurement and instrumentation used were as reported previously [4].

*Author to whom correspondence should be addressed.

Preparations

HAchexim and HFohexim were prepared according to the method described by Scovill [11]. The 2-acetyl- and 2-formylpyridine (Aldrich) were mixed with a 3:1 molar excess of hexamethyleneimine (Aldrich) in ethanol with warming. N(4)-methyl-N(4)-phenylthiosemicarbazide, prepared as described [11], was added in small portions to the warmed solution over a period of 1 h after which the mixtures were refluxed for 2 hours. The preparation of [Pd(Achexim)Cl] was described previously [9], and the light yellow crystals were grown by slow evaporation of a DMSO solution. [Pd(Fohexim)Cl] was prepared by mixing 1.5 mmol of Li_2PdCl_4 prepared *in situ* from $PdCl_2$ and LiCl in methanol (15 mL) and 1.3 mmol of HFohexim in methanol (15 mL) and stirred for 24 h. Crystals of the yellow-orange powder of [Pd(Fohexim)Cl] were grown by slow evaporation from a mixture of CH_3CN:DMF (2:1). For [Pd(Fohexim)Cl]: %Found: C = 38.6; H = 4.0; N = 14.0; S = 7.6. %Calcd: C = 38.7; H = 4.2; N = 13.9; S = 7.9.

X-ray data collection and reduction

A yellow prismatic crystal of [Pd(Achexim)Cl] and an orange pyramidal crystal of [Pd(Fohexim)Cl] were mounted on glass fibers and used for data collection. Cell constants and an orientation matrix for data collection were obtained by least-squares refinement of the diffraction data from 25 reflections in the range of $8.895^\circ < \theta < 18.142^\circ$ for [Pd(Fohexim)Cl] and $8.822^\circ < \theta < 18.076^\circ$ for [Pd(Achexim)Cl] with an ENRAF-NONIUS MACH3 automatic diffractometer [12]. Data were collected at 291(2) K using MoKα radiation ($\lambda = 0.71073$ Å) and the ω scan technique; the data were corrected for Lorentz and polarization effects [13]. A semi-empirical absorption correction was made [14].

Structure solution and refinement

The structure was solved by direct-methods [15] which revealed the position of all non-hydrogen atoms, and refined on F^2 by a full-matrix least-squares procedure using anisotropic displacement parameters [16]. The majority of the hydrogen atoms in both structures were located from difference Fourier maps and refined isotropically. The exceptions are the hydrogens attached to C9, C10 and C11 of [Pd(Achexim)Cl], which were located in their calculated positions (C–H 0.97 Å) and refined using a riding model. Atomic scattering factors were taken from the *International Tables for X-ray Crystallography* [17]. Molecular graphics are from *PLATON* [14]. A summary of the crystal data, experimental details and refinement results are listed in Table 1.

Protonation constants

All solutions were prepared using distilled water obtained from a borosilicate autostill (Jencons Ltd.). A 1×10^{-4} M stock solution of HFohexim was prepared by suspending the appropriate amount of purified, ground thiosemicarbazone in warmed distilled water for some hours until dissolution was achieved, cooling to room temperature, filling the flask to the required volume with distilled water and mixing throughly. Working thiosemicarbazone solutions (1×10^{-5} M) having different hydrogen ion concentrations and constant ionic strength, $\mu = 0.1$, were prepared using standard HCl or KOH and KCl solutions. All absorption spectra and pH measurements (Methrom 691 pH-meter) were made at 25°C. The absorption spectra were collected in the range 250–450 nm with a JASKO V-570 UV/Vis/NIR spectrophotometer guided by a personal computer.

RESULTS AND DISCUSSION

Crystal structures

Interatomic distances and bond angles are compiled in Tables 2 and 3, respectively, for [Pd(Achexim)Cl] and [Pd(Fohexim)Cl]. Atomic coordinates and displacement factor coefficients are included in the Supplementary Material. Figure 1 shows a perspective view of [Pd(Fohexim)Cl] and [Pd(Achexim)Cl] is shown in Fig. 2. The anionic Fohexim and Achexim act as tridentate ligands, which coordinate to palladium(II) centers through the pyridyl nitrogen, N(1), the azomethine nitrogen, N(2) and the thiolato sulfur atoms. The terdentate ligand, Fohexim (and Achexim), show a Z, E, Z configuration about the following bonds: C15–C16 and C35–C36, C16–N12 and C36–N22, N13–C17 and N23–C37 for the two molecules in the asymmetric unit, respectively. The palladium(II)-ligand bond distances for the two complexes are within two to three orders of magnitude of their combined estimated standard deviations although the Pd–N1 (pyridyl nitrogen) and Pd–S bonds are shorter and the Pd–N (azomethine) and Pd–Cl bonds longer for [Pd(Achexim) than for [Pd(Fohexim)Cl]. The thiosemicarbazone moieties' bond distances show even less variation between the two complexes. The coordination spheres (i.e., N1–N2–S–Pd–Cl) deviate from planarity by only 0.0354 and 0.0060 for [Pd(Achexim)Cl] and [Pd(Fohexim)Cl], respectively, and N2 shows the greatest deviation from the plane for both. The dihedral angles formed by the pyridine ring with the coordination plane is 5.10(12)° and 1.15(12)° for [Pd(Achexim)Cl] and [Pd(Fohexim)Cl], respectively.

A comparison of bond distances for the thiosemicarbazone moiety of [Pd(Fohexim)Cl] and [Pd(Achexim)Cl] with previously studied HAchexim [18] and its complexes [19, 20], palladium(II) complexes

Table 1. Crystal data and structure refinement for [Pd(Fohexim)Cl] and [Pd(Achexim)Cl]

	[Pd(Fohexim)Cl]	[Pd(Achexim)Cl]
Empirical formula	$C_{13}H_{17}ClN_4PdS$	$C_{14}H_{19}ClN_4PdS$
Formula weight	403.22	417.24
Temperature	291(2) K	291(2) K
Wavelength (Å)	0.71073	0.71073
Crystal system	Triclinic	Monoclinic
Space group	$P\bar{1}$	$P2(1)/n$
Unit Cell Dimensions		
a (Å)	7.9447(17)	7.2243(7)
b (Å)	9.6402(13)	24.937(3)
c (Å)	10.3739(18)	9.1180(11)
α (°)	79.128(12)	90
β (°)	75.104(15)	104.048(9)
γ (°)	75.558(14)	90
Volume (Å^3)	736.9(2)	1593.5(3)
Z	2	4
Calcd density (gcm^{-3})	1.817	1.739
Absorption coeff. (mm^{-1})	1.576	1.461
$F(000)$	404	840
Crystal size (mm)	$0.30 \times 0.20 \times 0.15$	$0.30 \times 0.25 \times 0.15$
θ range for data collection (°)	2.20 to 26.30	2.44 to 26.30
Index ranges	$-9 \leqslant h \leqslant 9, -11 \leqslant k \leqslant 11, -12 \leqslant l \leqslant 0$	$-9 \leqslant h \leqslant 0, 0 \leqslant k \leqslant 31, -11 \leqslant l \leqslant 11$
Reflections collected	3158	3476
Independent reflections	2982 [$R_{int} = 0.0234$]	3224 [$R_{int} = 0.0497$]
Absorption correction	Semi-empirical	Semi-empirical
Max. and min. transmission	0.970 and 0.932	0.982 and 0.882
Refinement method	Full-matrix least-squares on F^2	Full-matrix least-squares on F^2
Data/restraints/parameters	2982/0/249	3224/0/242
Goodness-of-fit on F^2	1.050	1.025
Final R indices [$I > 2\sigma(I)$]	$R_1 = 0.0264$, w$R_2 = 0.0578$	$R_1 = 0.0347$, w$R_2 = 0.0707$
R indices (all data)	$R_1 = 0.0506$, w$R_2 = 0.0631$	$R_1 = 0.0948$, w$R_2 = 0.0830$
Largest diff. peak & hole	0.388, −0.606	0.541, −0.548

Table 2. Selected bond lengths (Å) for [Pd(Achexim)Cl] and [Pd(Fohexim)Cl]

[Pd(Achexim)Cl]		[Pd(Fohexim)Cl]	
Pd–N2	1.959(3)	Pd–N2	1.951(2)
Pd–N1	2.054(4)	Pd–N1	2.070(3)
Pd–S1	2.2539(14)	Pd–S1	2.2620(10)
Pd–Cl1	2.3037(12)	Pd–Cl1	2.2984(9)
S1–C7	1.765(5)	S1–C7	1.765(3)
N2–C6	1.303(5)	N2–C6	1.292(4)
N2–N3	1.372(5)	N2–N3	1.361(3)
N1–C1	1.343(6)	N1–C1	1.336(4)
N1–C5	1.365(5)	N1–C5	1.363(4)
N3–C7	1.326(6)	N3–C7	1.335(4)
N4–C7	1.345(5)	N4–C7	1.336(4)
N4–C8	1.453(7)	N4–C13	1.468(4)
N4–C13	1.466(6)	N4–C8	1.478(4)
C5–C6	1.460(6)	C5–C6	1.444(4)
C6–C60	1.490(6)	C6–H6	0.93(4)

with other 2-acetylpyridine thiosemicarbazones [4, 5, 6], and a copper(II) complex of 2-benzoylpyridine 3-hexamethyleneiminylthiosemicarbazone [21] is given in Table 4. The thiosemicarbazone moiety bond distances are independent of both the N(4)-substituent and the metal center. Table 5 lists the palladium(II)-donor bond distances for palladium heterocyclic thiosemicarbazones having a pyridyl nitrogen as the third donor atom. Although the bulkiness of the hexim function would be expected to affect the Pd–S bond distance compared to the other two donor sites, its variation is not signifcantly different from the Pd–N distances.

Spectroscopy

Selected ^{1}H NMR data of the thiosemicarbazones and their palladium(II) complexes are shown in Table

Table 3. Selected bond angles (°) for [Pd(Achexim)Cl] and [Pd(Fohexim)Cl]

[Pd(Achexim)Cl]		[Pd(Fohexim)Cl]	
N2–Pd–N1	80.25(15)	N2–Pd–N1	81.10(10)
N2–Pd–S1	85.45(12)	N2–Pd–S1	84.14(8)
N1–Pd–S1	165.65(10)	N1–Pd–S1	165.25(7)
N2–Pd–Cl1	176.13(11)	N2–Pd–Cl1	177.49(8)
N1–Pd–Cl1	97.54(10)	N1–Pd–Cl1	96.53(8)
S1–Pd–Cl1	96.80(5)	S1–Pd–Cl1	98.22(4)
C7–S1–Pd	94.55(16)	C7–S1–Pd	95.41(11)
C6–N2–N3	119.4(4)	C6–N2–N3	119.5(3)
C6–N2–Pd	117.8(3)	C6–N2–Pd	115.8(2)
N3–N2–Pd	122.6(3)	N3–N2–Pd	124.7(2)
C1–N1–C5	118.8(4)	C1–N1–C5	118.7(3)
C1–N1–Pd	129.4(3)	C1–N1–Pd	130.6(2)
C5–N1–Pd	111.8(3)	C5–N1–Pd	110.7(2)
C7–N3–N2	112.7(4)	C6–N2–N3	119.5(3)
C7–N4–C8	122.8(4)	C7–N4–C8	119.6(3)
C7–N4–C13	120.7(4)	C7–N4–C13	120.9(3)
C8–N4–C13	115.8(4)	C8–N4–C13	119.4(3)
N2–C6–C5	114.7(4)	N2–C6–C5	117.7(3)
N2–C6–C60	122.8(4)		
C5–C6–C60	122.5(4)		
N3–C7–N4	116.3(4)	N3–C7–N4	116.5(3)
N3–C7–S1	124.6(3)	N3–C7–S1	123.6(2)
N4–C7–S1	119.1(4)	N4–C7–S1	119.8(2)
N4–C8–C9	114.5(5)	N4–C8–C9	113.1(3)
N4–C13–C12	112.7(5)	N4–C13–C12	114.1(3)

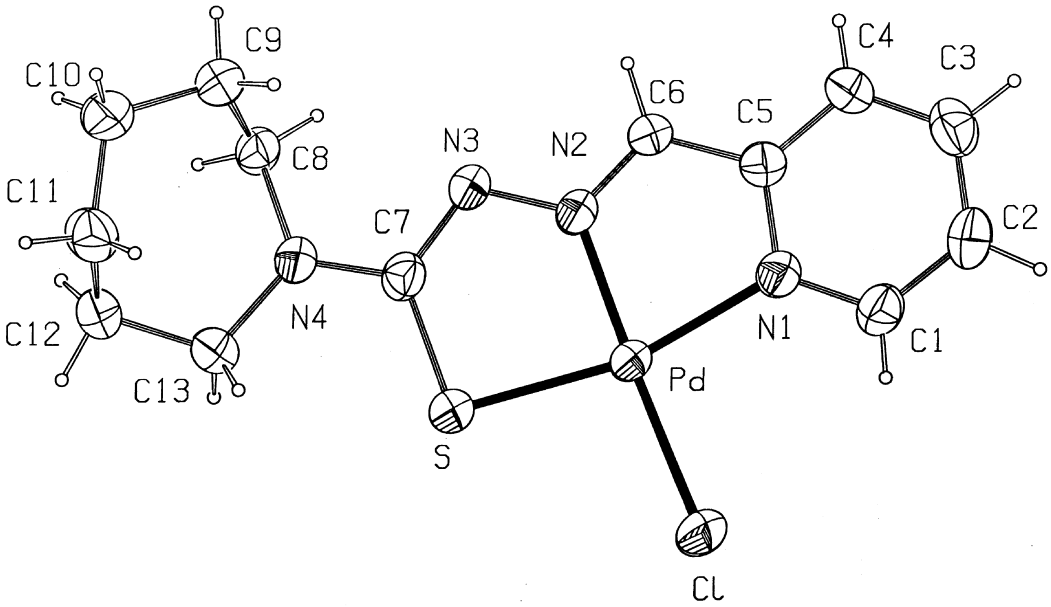

Fig. 1. An ORTEP diagram and numbering scheme for [Pd(Fohexim)Cl]

6. The main differences between the spectra of free thiosemicarbazones, HFohexim and HAchexim, and coordinated Fohexim and Achexim are the disappearance of the highest-frequency N(2)H signal and the deshielding of C(1). These changes indicate that deprotonation and metallation occurs, and the structure of the two complexes in the solid state persists in $CDCl_3$ solution. The appearance of the signal N(2)*H*

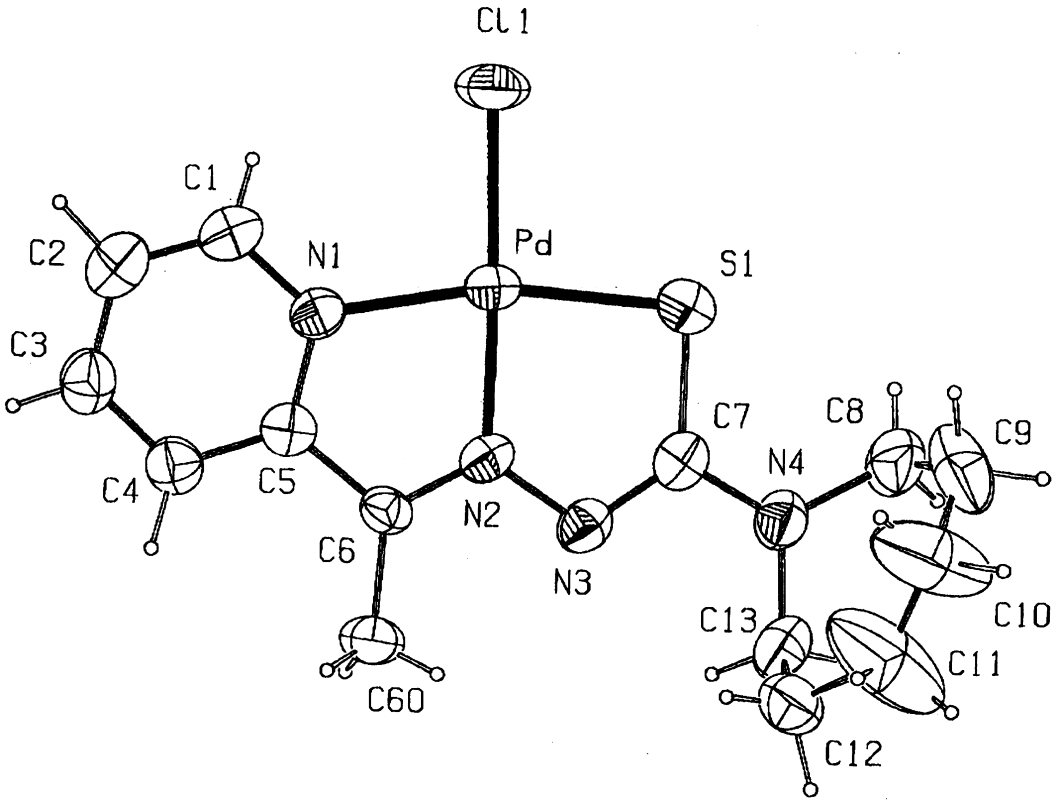

Fig. 2. An ORTEP diagram and numbering scheme for [Pd(Achexim)Cl]. Thermal ellipsoids are drawn at the 50 5 probability level

Table 4. Comparison of thiosemicarbazone moiety bond distances (Å) for complexes of HAchexim and HFohexim

Compound	C=N(2)	N(2)–N(3)	N(3)–C(S)	C–S	C(S)–N(4)	Ref.
HAchexim	1.29(1)	1.37(1)	1.36(2)	1.70(1)	1.36(1)	18
[Pd(Ac4DH)Br]	1.301(4)	1.388(4)	1.325(4)	1.746(3)	1.339(4)	4
Pd(Ac4Me)Cl]	1.307(5)	1.373(4)	1.316(5)	1.768(4)	1.336(5)	6
[Cu(Achexim)Br]	1.275(9)	1.373(7)	1.301(9)	1.759(6)	1.377(11)	19
[Cu(Bzhexim)Cl]	1.295(10)	1.358(9)	1.336(10)	1.750(9)	1.342(10)	21
[Ni(Achexim)Br]	1.33	1.37			1.33	20
[Pd(Achexim)Cl]	1.303(5)	1.372(5)	1.326(6)	1.765(5)	1.345(5)	This work
[Pd(Fohexim)Cl]	1.292(4)	1.361(3)	1.335(4)	1.765(3)	1.336(4)	This work

Table 5. A comparison of palladium-donor atom bond lengths (Å) for heterocyclic thiosemicarbazone palladium complexes

Compound	Pd–S	Pd–N(1)	Pd–N(2)	Ref.
[Pd(Ac4DH)Br]	2.245(1)	2.053(3)	1.971(3)	4
[Pd(Ac4Me)Cl]	2.256(1)	2.057(3)	1.952(3)	6
[Pd(Ac4DM)Br]	2.245(4)	2.073(11)	1.94(9)	5
[Pd(Ac4DM)$_2$]	2.258(3) 2.314(4)	2.088(10)	1.984(10)	5
[Pd(Achexim)Cl]	2.2539(14)	2.054(4)	1.959(3)	This work
[Pd(Fohexim)Cl]	2.2620(10)	2.070(3)	1.951(2)	This work

Table 6. Selected ^{1}H NMR spectra data of the ligands and complexes

Compound	Solvent	(CH_3)C(6)	C(6)*H*	C(1)*H*
HFohexim	$CDCl_3$		7.521*s*	8.579*d*
[Pd(Fohexim)Cl]	$CDCl_3$		7.518*s*	8.705*d*
HAchexim	$CDCl_3$[a]	2.52*s*		8.58*d*
	d^6-DMSO	2.48(75%)[a]		
		2.37(25%)[b]		8.720*d*
[Pd(Achexim)Cl]	$CDCl_3$	1.579*s*		8.776*d*

(a) bifurcated tautomer, designated E′ [18]; (b) E isomer with N(2)H hydrogen bonding to DMSO.

at $\delta = 15.13$ for HFohexim is due to hydrogen bonding and suggests that in $CDCl_3$ the Z isomer is prevalent while previous studies showed three forms, E, Z and the bifurcated E′ tautomer, for HAchexim, with the N(2)H resonances at $\delta = 8.52$, 15.25 and 14.95, respectively [18].

The significant IR bands of the ligands HFohexim and HAchexim and their complexes are similar to those found in other compounds with tridentate coordination [4–9]. Besides these bands the IR spectrum of [Pd(Fohexim)Cl] shows $\nu(PdN_{azo})$, $\nu(PdS)$, $\nu(PdCl)$ and $\nu(PdN_{py})$ at 460, 380, 352 and 330 cm^{-1} respectively.

Protonation constants

Because of the low solubility of HFohexim in water, spectrophotometry was used to determine its protonation constants. In aqueous solutions with pH > 2 there are three independent species ($Fohexim^-$, HFohexim and $H_2Fohexim^+$), and therefore, two distinct steps of protonation, as shown by the absorption spectra in Fig. 3(a,b). The equilibrium between the species is given by the equations (1) and (2)

$$Fohexim^- + H_3O^+ \overset{K_{a1}}{\rightleftharpoons} HFohexim + H_2O \quad (1)$$

$$HFohexim + H_3O^+ \overset{K_{a2}}{\rightleftharpoons} H_2Fohexim^+ + H_2O \quad (2)$$

The concentration protonation constants of HFohexim, K_{a1} and K_{a2}, were determined, and the 95% confidence limits for their logarithms were found to be equal to 10.80 ± 0.01 and 3.73 ± 0.02 ($n = 6$) with relative standard deviations 0.26% and 1.34%, respectively. The pK_{a2} value is lower than that of pyridine (5.0) and 2-acetylpyridine thiosemicarbazone, HAc4DH, (3.98) [4]. Compared to pyridine the lower value can be attributed to the decrease in electron density on the pyridine nitrogen caused by the electron-withdrawing effect of the azomethine function. Also, the p*Ka*1 value is lower than that of thiosemicarbazide (11.45) and 2-acetylpyridine thiose-

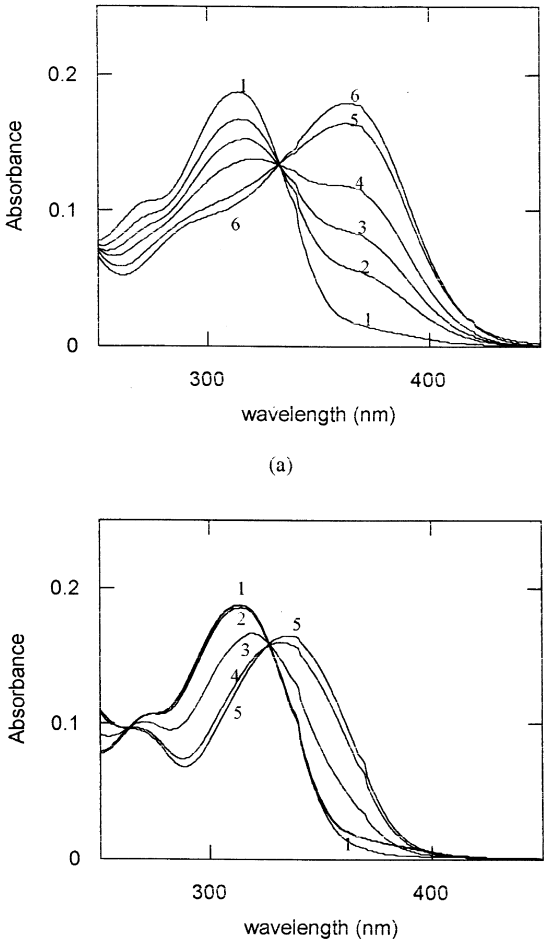

Fig. 3. Plots of absorbance data *versus* wavelength for HFohexim at 25°C in the high pH region, where the species $Fohexim^-$ and HFohexim are present (a) [pH 9.48 (1); pH 10.40 (2); pH 10.79 (3); pH 11.16 (4); pH 11.93 (5); pH = 12.92 (6)], and in the low pH region, where the species HFohexim and $H_2Fohexim^+$ are present (b) [pH 9.48 (1); pH 4.30 (2); pH 4.15 (3); pH 3.49 (4); pH 3.36 (5)].

micarbazone (11.43) and reveals that HFohexim behaves as a weak monoprotic acid. In a recent quantitave analysis of the factor controlling the acidity of N–H bonds in amide compounds, [RC(=X)NH_2], it was found that the field-inductive, polarizability and resonance effects are responsible for this acidity [22]. These three factors combine to make the N(2)*H* (hydrazinic group) more acidic than the corresponding function in HAc4DH; a similar, but smaller, decrease occurs for nitrogen in pyridine rings. When the acetyl group is compared to an aldehyde group, the latter compound is the more acidic. However, solutions of thiosemicarbazones derived from 2-acetylpyridine have been shown by NMR studies to have different mixtures of isomers and tautomers depending on the solvent so that a direct comparison is not always possible.

REFERENCES

1. Scovill, J. P., Klayman, D. L. and Franchino, C. F., *J. Med. Chem*., 1982, **25,** 1261.
2. (a) Easmon, J., Heinisch, G., Holzer, W. and Rosenwirth, B., *Arzneim. Forsch*., 1989, **39**, 1196; (b) Klayman, D. L., Scovill, J. P., Mason, C. J., Bartosevich, J. F., Bruce, J. and Lin, A. J., *Arzneim. Forsch*., 1983, **33**, 909; (c) Klayman, D. L., Scovill, J. P., Mason, C. J., Bartosevich, J. F. and Bruce, J., *J. Med. Chem*., 1983, **26**, 35.
3. Patent; Farbenfab. Bayer Ag.; NL 6612093; 1965; *Chem. Abstr*., 1968, **68**, 21850w.
4. Kovala-Demertzi, D., Domopoulou, A., Demertzis, M. A., Raptopoulou, C. P. and Terzis, A., *Polyhedron*, 1994, **13,** 1917.
5. Kovala-Demertzi, D., Domopoulou, A., Demertzis, M. A., Valdés-Martínez, J., Hernández-Ortega, S., Espinosa-Pérez, G., West, D. X., Salberg, M. M., Bain, G. A. and Bloom, P. D., *Polyhedron*, 1996, **15,** 2587; and references therein.
6. Kovala-Demertzi, D., Domopoulou, A., Demertzis, M. A., Valle, G. and Papageorgiou, A., *J. Inorg. Biochem*., 1997, **68,** 147.
7. Kovala-Demertzi, D., Domopoulou, A., and Demertzis, M. A., Presented in part at NATO Advanced Study Institute *Cytotoxic*, *Mutagenic and Carcinogenic Potential of Heavy metals Related to Human Environment*. Lucznik, Przesieka, Poland, June 15–26 (1996).
8. Papageorgiou, A., Iakovidou, Z., Mourelatos, D., Mioglou, E., Boutis, L., Kotsis, A., Kovala-Demertzi, D., Domopoulou, A., West, D. X. and Demertzis, M. A., *Anticancer Res*., 1997, **17,** 247.
9. Kovala-Demertzi, D., Domopoulou, A., Demertzis, M. A., Papageorgiou, A. and West, D. X., *Polyhedron*, 1997, **16,** 3625.
10. Hall, I. H., Rajendran, K. G., West, D. X. and Liberta, A. E., *Anticancer Drugs*, 1993, **4,** 241.
11. Scovill, J. P., *Phosphorus*, *Sulfur and Silicon*, 1991, **60,** 15.
12. Enraf-Nonius, *CAD4-Express Software*. Version 5.1. Enraf-Nonius, Delft, The Netherlands (1994)..
13. Spek, A. L., *HELENA. A Program for data reduction of CAD4 data*. University of Utrecht, The Netherlands (1997).
14. Spek, A. L., *PLATON. A Program for the automated generation of a variety of geometrical entities*. University of Utrecht, The Netherlands (1997).
15. Sheldrick, G. M., *Acta Cryst*., 1990, **A46,** 467.
16. Sheldrick, G. M., *SHELXL*97. Program for the Refinement of Crystal Structures. University of Göttingen, Germany (1997).
17. *International Tables for X-ray Crystallography*, Vol. C. Kluwer Academic Publishers: Dordrecht, The Netherlands (1995).
18. West, D. X., Bain, G. A., Butcher, R. J., Jasinski, J. P., Li, Y., Pozdniakiv, R. Y., Valdés-Martínez, J., Toscano, R. A. and Hernández-Ortega, S., *Polyhedron*, 1996, **15,** 665; and references therein.
19. Butcher, R. J. and West, D. X., *Transtion Met Chem*., 1993, **18,** 449.
20. West, D. X., Gebremedhin, H., Butcher, R. J., Jasinski, J. P. and Liberta, A. E., *Polyhedron*, 1993, **12,** 2489.
21. West, D. X., Ives, J. S., Krejci, J., Salberg, M. M., Zumbahlen, T. L., Bain, G. A., Liberta, A. E., Valdés-Martínez, J., Hernández-Ortega, S. and Toscano, R. A., *Polyhedron*, 1995, **14,** 2189.
22. Bordwell, F. G. and Ji, G. Z., *J. Am. Chem. Soc*., 1991, **113,** 8398.

Pergamon

PII: S0277-5387(98)00176-4

Polyhedron Vol. 17, No. 21, pp. 3747–3752, 1998
© 1998 Elsevier Science Ltd
All rights reserved. Printed in Great Britain
0277–5387/98 $19.00+0.00

Uranyl nitrate complexes of camphene-derived organophosphorus ligands, and the X-ray crystal structure of $[UO_2(NO_3)_2(RPO_3Me_2)_2]$ (R = *endo*-8-camphanyl)

William Henderson,[a]* Meto T. Leach,[a] Brian K. Nicholson,[a] Alistair L. Wilkins,[a] and (the late) Peter A. T. Hoye[b]

[a] Department of Chemistry, University of Waikato, Private Bag 3105, Hamilton, New Zealand

[b] International Technical Centre, Albright & Wilson Ltd., Oldbury, West Midlands, U.K.

(Received 20 October 1997; accepted 23 April 1998)

Abstract—*endo*-8-Camphanylphosphinic acid [(2,2-dimethylbicyclo [2.2.1] hept-3-ylmethyl)phosphinic acid] $camPO_2H_2$ **1** is readily oxidised to the corresponding phosphonic acid $camPO_3H_2$ **2**, the preferred reagent being SO_2 in refluxing isopropanol. Methylation of the phosphonic acid **1** with diazomethane yields the methyl ester $camPO_3Me_2$ **4**. Oxidative chlorination of $camPO_2H_2$ with $SOCl_2$ produces the phosphonic dichloride $camP(O)Cl_2$ **3**, which gives the tertiary phosphine oxide $camP(O)Ph_2$ **5** on reaction with PhMgBr. The phosphonate ester **4** and phosphine oxide **5** readily form complexes **6** and **7** respectively with uranyl nitrate. The phosphonate complex **6** has been subjected to a single-crystal X-ray diffraction study. The structure determination was not straightforward, largely as a result of the combination of a dominant scattering atom (uranium) and substantial disorder of the camphanyl groups. © 1998 Elsevier Science Ltd. All rights reserved

Keywords: phosphonate; uranyl nitrate complex; crystal structure; camphene

Compounds containing the phosphoryl (P═O) group are known to possess excellent ligand properties towards a wide range of metal centres, and the coordination chemistry of these ligands has been extensively studied [1]. Additionally, extractants containing P═O groups have also been used for many years in industrial solvent extraction (hydrometallurgical) processes for the recovery and purification of a range of metal ions [2]. Metal extractants are characteristically highly lipophilic in nature, and this property is readily conferred by the use of large, often branched, hydrocarbon moieties, such as the inexpensive 2-ethylhexyl or 2,4,4-trimethylpentyl groups [3]. Branched hydrocarbon substituents are also known to impart selectivity in metal-ion separation processes by increasing steric crowding at the metal centre [3, 4].

Recently we reported the synthesis of (2,2-dimethylbicyclo [2.2.1] hept-3-ylmethyl)phosphinic acid (*endo*-8-camphanylphosphinic acid, $camPO_2H_2$) **1**, by radical-catalysed addition of hypophosphorous acid to camphene [5, 6] and subsequently considered that the bulky, lipophilic camphanyl group might be utilisable in the synthesis of new types of organophosphorus metal extractants. Here we describe the synthesis of a number of new camphene-derived phosphorylic model ligands, together with a preliminary study of their coordination chemistry towards uranyl nitrate. Phosphorylic compounds such as trioctylphosphine oxide and tributyl phosphate are widely utilised in uranium extraction [2]. The structure of one uranyl nitrate complex is also reported.

* Author to whom correspondence should be addressed. Fax: 00 64 7 838 4219; e-mail: w.henderson@waikato.ac.nz.

RESULTS AND DISCUSSION

Ligand synthesis and characterisation

As an initial entry into the coordination chemistry of camphene-derived organophosphorus ligands, we have employed the readily-prepared *endo*-8-camphanylphosphinic acid **1** as a starting material. This is very conveniently oxidised to the corresponding phosphonic acid **2** by the use of sulfur dioxide in refluxing isopropanol, Scheme 1 [5]. In this case, the byproduct, elemental sulfur, is readily removed by simple filtration. Copper(II) nitrate in refluxing methanol also oxidises **1** to **2**, producing metallic copper as a byproduct. Alternatively, reaction of **1** with excess thionyl chloride results in oxidative chlorination, giving 8-camphanylphosphonic dichloride camP(O)Cl_2 **3**, which can subsequently be hydrolysed (by refluxing in water) to the phosphonic acid, Scheme 1. Alkaline hydrogen peroxide and concentrated nitric acid were both found to be ineffective for the oxidation of **1**.

The phosphonic acid **2** has been thoroughly characterised by ^{1}H, ^{13}C and ^{31}P NMR spectroscopy. The ^{31}P NMR chemical shift of **2** (D_2O with added NaOH, $\delta = 23.8$) compares well with other phosphonic acids, for example δ 24.8 for $MePO_3H_2$ [7]. The ^{1}H and ^{13}C-$\{^{1}H\}$ NMR spectra have been fully assigned by ^{1}H-^{1}H and ^{1}H-^{13}C COSY and nOe-difference experiments, and by comparison with the spectra of **1**; Scheme 2 shows the atom numbering scheme. The ^{1}H and COSY45 NMR spectra of camphylphosphonic acid **2** are very similar to those of the precursor phosphinic acid **1**. Consequently, resonances H_4, H_3, H_1, $H_{7''}$, $H_{5''}$, $H_{8',8''}$ and $H_{7'}$ are readily identifiable, and a complete assignment of the COSY45 spectrum is straightforward. The positions of the *exo*/*endo* protons $H_{5'}$ and $H_{5''}$ were sufficiently separated to be distinguished. The assignment results from the observation of couplings from H_4 to $H_{5'}$ (but not to $H_{5''}$), H_3 to $H_{5'}$ (but not to $H_{5''}$), and $H_{7''}$ to $H_{5''}$ (but not to $H_{5'}$) and is confirmed by the presence of an nOe from Me″ to $H_{5''}$. The other nOe enhancements are consistent with the structure shown in Scheme 2. nOe enhancements are observed from Me′ to H_3 and $H_{7''}$, and from Me″ to $H_{8',8''}$, $H_{6''}$, and $H_{5''}$, proving that the $-CH_2PO_3H_2$ group is *endo*. The negative-ion electrospray masss spectrum of **2** yielded the $[M\text{-}H]^-$ ion at m/z 217; the electrospray mass spectrometric analysis of organophosphorus acids has been described previously [8].

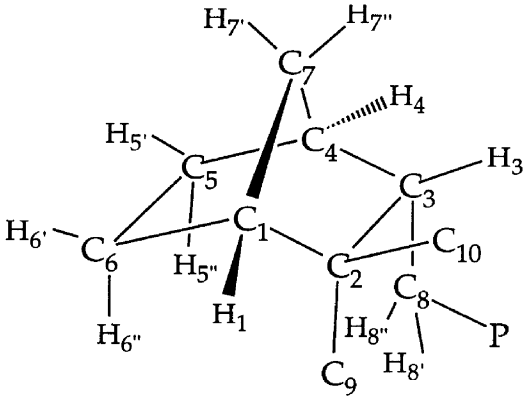

Scheme 2. Atom numbering scheme for the camphanyl-phosphorus moiety of compounds reported in this paper.

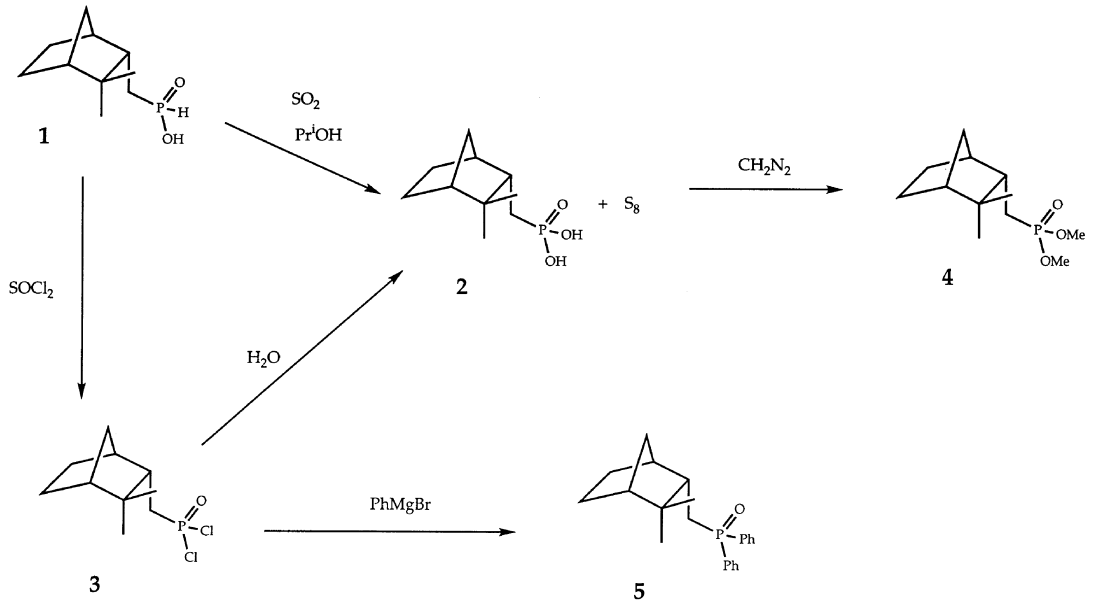

Scheme 1. Synthesis of the camphanyl organophosphorus compounds.

Camphanylphosphonic acid **2** was converted to its dimethyl ester $camPO_3Me_2$ **4** by treatment with excess diazomethane in diethyl ether, Scheme 1. Diazomethane is a convenient and well-known laboratory reagent for conversion of acids to their methyl esters, on a small scale, and was thus employed in this study so that the coordination chemistry of the esters could be investigated. The ester **3**, a colourless oil, was subsequently characterised by NMR spectroscopy and GCMS. The camphene-derived phosphine oxide ligand, $camP(O)Ph_2$ **5** was also synthesised in 75% yield by reaction of **3** with a slight excess of PhMgBr. Compound **5** shows the expected behaviour [9] for a phosphine oxide in the positive-ion electrospray mass spectrum with added KCl, yielding a range of ions of the form $[n(\mathbf{5})+\text{cation}]^+$ ($n = 1$–3, cation = H or K).

Synthesis of uranyl nitrate complexes

A wide range of uranyl(VI) nitrate complexes of the type $UO_2(NO_3)_2L_2$ has been previously prepared by the simple combination of the precursors uranyl(VI) nitrate and the phosphorylic compound (L) in an appropriate solvent, such as ethanol [10]. Similarly, the slow evaporation of a methanolic solution of the phosphonate **4** and uranyl nitrate in a 2:1 molar ratio deposits yellow crystals of the adduct **6**. An analogous complex **7** was obtained from a mixture of the phosphine oxide **5** and uranyl nitrate. Satisfactory microanalytical data were obtained for both complexes. The IR spectrum of **6** showed a U=O stretch at 933 cm^{-1}, similar to the values in other *trans*-uranyl complexes [10, 11] while the Raman spectrum showed a band at 854 cm^{-1}.

X-ray structure determination on the uranyl-phosphonate complex ***6***

A single-crystal X-ray diffraction study was carried out on complex 6. Because of disorder in the camphanyl groups, the presence of a dominant scatterer, and possible space group ambiguity the structure determination was of low quality, but does confirm the *trans* UO_2 isomer of $[UO_2(NO_3)_2(\mathbf{4})_2]$, as expected from the large number of *trans*-uranyl complexes reported in the literature [12]. Figure 1 shows the geometry of the *trans*-isomer of **6**, with some bond parameters included in the caption.

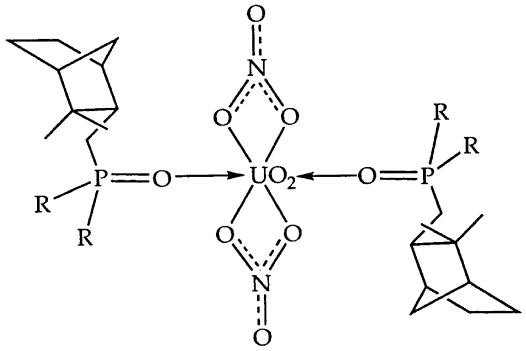

EXPERIMENTAL

^1H and ^{13}C-$\{^1H\}$ NMR spectra were recorded on a Bruker AC300P spectrometer, at 300.13 and 75.47 MHz respectively, in $CDCl_3$ (unless otherwise stated). Chemical shifts are reported relative to $CHCl_3$ (δ ^1H 7.26 and δ ^{13}C 77.06). NMR spectra of the camphene-derived ligands were fully assigned by ^1H-^1H and ^1H-^{13}C COSY and nOe-difference experiments. ^1H-^1H and ^{13}C-^1H COSY spectra were determined in absolute value mode using Bruker-supplied pulse programmes. nOe-difference spectra were obtained by subtracting a reference FID from an irradiated FID, and Fourier transforming the resulting difference-FID. ^{31}P-$\{^1H\}$ NMR spectra were recorded in CH_2Cl_2 solution on a JEOL FX90Q spectrometer at 36.23 MHz, with 85% H_3PO_4 (δ 0.0) as external reference, and a glass capillary containing D_2O used to provide a lock signal. Scheme 2 shows the atom numbering scheme for the camphanyl-phosphorus moiety.

IR spectra were recorded as KBr disks (unless otherwise specified) on a BioRad FTS-40 spectrometer. Raman spectra were recorded on powdered material contained in a glass capillary using a SPEX 1403 Ramalog spectrometer with a He/Ne laser. Melting points were recorded on a Reichert Hotstage apparatus and are uncorrected. Electrospray (ES) mass spectra were recorded on a VG Platform II instrument, with MeCN–H_2O (1:1 v/v) as the mobile phase. Nitrogen was employed as both the nebulising and drying gas, and the source temperature was 60°C. GCMS data were recorded on a HP 5890 GC interfaced to a HP 5970B mass selective detector (MSD) operated in scanning mode. A 25 m HP-1 (methyl silicone) capillary column (o.d. 0.22 mm) was used.

endo-8-Camphanylphosphinic acid **1** [5, 6] and diazomethane [13] were prepared as described previously. Uranyl nitrate hexahydrate and sulfur dioxide (BDH) were used as supplied. All solvents used in this work were of reagent grade.

Synthesis of endo-8-*camphanylphosphonic acid* ***2*** *by direct oxidation using* SO_2

endo-8-camphanylphosphinic acid **1** (77.4 g, 0.38 mol) was dissolved in a mixture of isopropanol (500 mL) and water (100 mL), the solution heated to reflux, and sulfur dioxide bubbled through for 4 hr. The reaction mixture was cooled and purged with nitrogen for 30 min. Sulfur was removed by filtration through a celite bed, and subsequent removal of most of the solvent by rotary evaporation gave *endo*-8-camphanylphosphonic acid **2** as a white crystalline solid

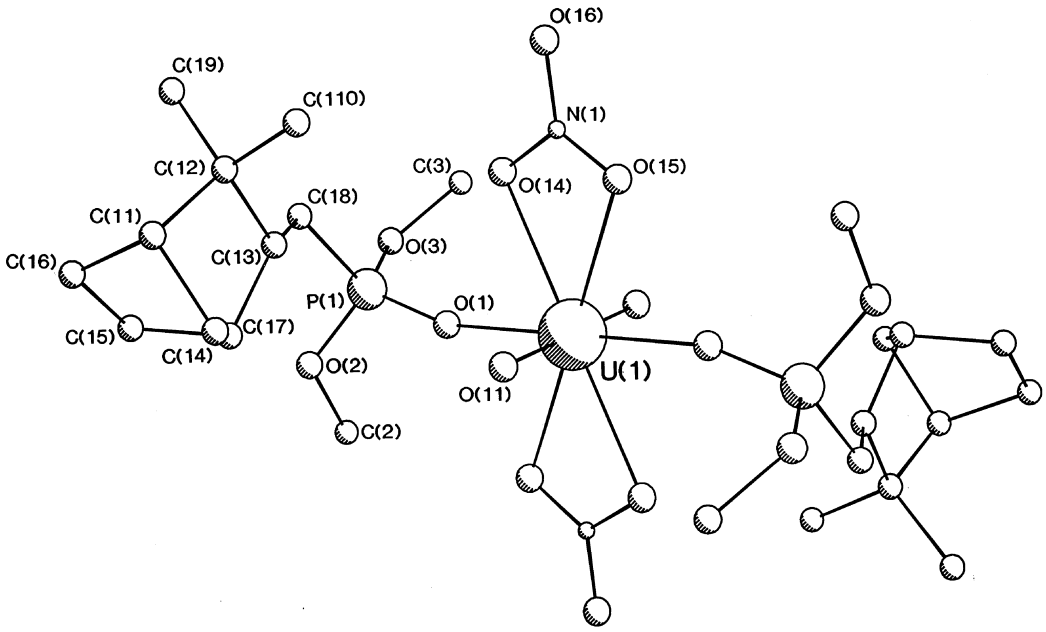

Fig. 1. Molecular structure of the camphanylphosphonate-uranyl nitrate complex **6**, together with the atom numbering scheme. Selected bond lengths (Å): U(1)–O(11) 1.668(14), U(1)–O(1) 2.345(14), U(1)–O(15) 2.51(2), U(1)–O(14) 2.52(2), P(1)–O(1) 1.52(2), P(1)–O(2) 1.557(13), P(1)–O(3) 1.57(2), P(1)–C(18) 1.74(2).

(71.0 g, 85%), m.p. 171–173°C. Found: C, 55.0; H, 8.9; P, 14.2. $C_{10}H_{19}O_3P$ requires C, 55.0; H, 8.8; P, 14.2%. ESMS (negative-ion mode); $[M\text{-}H]^-$ at *m/z* 217. NMR: ^{31}P (D_2O/NaOH) δ 23.8. ^1H NMR (CD_3OD), δ 9.97 (2H, *s*, *br*, OH), 2.38 (1H, *s*, *br*, H_4), 1.82 (1H, *m*, $H_3)_a$, 1.77 (1H, *s*, *br*, $H_1)_b$, 1.72 (1H, *m*, $H_{8'/8''})_b$, 1.66 (1H, *m*, $H_{7''})_b$, 1.65 (1H, *m*, $H_{8'/8''})_b$, 1.60 (1H, *m*, $H_{6''})_a$, 1.44 (1H, *m*, $H_{5''})_a$, 1.34 (1H, *m*, $H_{5'})_a$, 1.32 (1H, *m*, $H_{6'})_b$, 1.20 (1H, *dt*, ^2J 9.7, ^3J 1.7, $H_{7'})_a$, 0.98 (3H, *s*, Me′), 0.83 (3H, *s*, Me″). [a: partially overlapping signals; b: overlapping signals]

nOe data:

Irradiated Hydrogen	Enhanced Signal (%)
H_4	H_3 (2.0), $H_{7''}$ (1.8), $H_{5'}$ (0.6), $H_{5''}$ (1.6), $H_{7'}$ (2.3)
$H_{6''}$	H_4 (1.2), Me″ (0.7)
$H_{7'}$	H_4 (3.0), H_1 (1.7), $H_{7''}$(11.3)
Me′	H_3 (3.5), H_1 (4.3), $H_{7''}$ (4.1), Me″ (1.2)
Me″	H_1 (3.3), $H_{8'}$ (*x*) and $H_{8''}$ (*y*), $x+y=8.0$, $H_{6''}$ (7.0), $H_{5''}$ (0.9), Me′ (1.5)

^{13}C-$\{^1H\}$ NMR (CD_3OD), δ 50.1 [*d*, ^4J (P,C) 3.9, C_1], 46.0 [*d*, ^2J (P,C) 3.9, C_3], 43.5 [*d*, ^3J (P,C) 3.6, C_4], 38.3 [*d*, ^3J (P,C) 14.1, C_2], 37.8 (*s*, C_7), 32.3 (*s*, C_{10}), 25.6 (*s*, C_6), 25.2 [*d*, ^1J (P,C) 138.3, C_8], 22.3 (*s*, C_9), 21.0 (*s*, C_5). IR (liquid film, KBr disks): υ(P═O) 1122 cm^{-1} (*s*, *br*).

Synthesis of ***2*** *by oxidation with* $Cu(NO_3)_2$

Phosphinic acid **1** (2.0 g, 9.9 mmol) and $Cu(NO_3)_2{\cdot}3H_2O$ (2.39 g, 9.8 mmol) were dissolved in a mixture of methanol (70 mL) and water (10 mL). The reaction mixture was refluxed for 4.5 h, cooled and a brown precipitate (metallic Cu) was removed by filtration. Removal of the solvent by rotary evaporation gave a white solid which was found to be 8-camphanylphosphonic acid **2** (85% yield) by ^{31}P NMR spectroscopy and melting point determination.

Synthesis of $camP(O)Cl_2$ ***3***

Thionyl chloride (40 mL) was added to **1** (1.67 g, 8.2 mmol). Pyridine (10 drops) was added and the resulting yellow solution refluxed for 7.5 h. Removal of the volatiles under reduced pressure gave a light yellow oil (1.88 g, 90%). (Found: C, 47.9; H, 7.0% $C_{10}H_{17}P(O)Cl_2$ requires C, 47.2; H, 6.7%). GCMS *m/z* 254, 256 (M^+, 16% for *m/z* 254 ion). ^{31}P-$\{^1H\}$ NMR, δ 51.6 (*s*). ^1H NMR δ 2.54 (1H, *m*, *br*, $H_{8'}/H_{8''}$), 2.49 (1H, *m*, *br*, $H_{8'}/H_{8''}$), 2.34 (1H, *s*, *br*, H_4), 1.93 (1H, *m*, *br*, H_3), 1.71 (1H, *s*, *br*, H_1), 1.59 (1H, *d*, *J* 10.1, $H_{7''}$), 1.46 (2H, *m*, *br*, $H_{6''}$), 1.36 (1H, *m*, *br*, $H_{5'}$), 1.31 (1H, *m*, *br*, $H_{5''}$), 1.21 (1H, *d*, *J* 4.8, $H_{6'}$), 1.15 (1H, *d*, *J* 10.1, $H_{7'}$), 0.91 (3H, *s*, Me′), and 0.74 (3H, *s*, Me″). ^{13}C-$\{^1H\}$ NMR, δ 48.3 (*s*, C_1), 45.1 (*d*, *J* 6.5, C_3), 41.9 (*d*, *J* 5.2, C_4), 41.85 (*d*, *J* 95.7, C_8), 38.2 (*d*, *J* 17.5, C_2), 37.0 (*s*, C_7), 31.6 (*s*, C_{10}), 24.5 (*s*, C_6), 21.9 (*s*, C_9), and 20.3 (*s*, C_5).

*Synthesis of **2** by hydrolysis of **3***

To camP(O)Cl_2 **3** (0.36 g, 1.41 mmol) was added water (30 mL) and the resulting yellow solution refluxed for 6 h. The white solid which precipitated was filtered off and found to be **2** (0.24 g, 80%) by ^{31}P NMR and melting point.

Synthesis of dimethyl endo-8-*camphanylphosphonate **4***

An excess of a diethyl ether solution of diazomethane was added to **2** (0.29 g, 1.3 mmol) and the resulting solution stoppered. After 24 h the volatiles were removed under vacuum yielding **4** as a colourless oil (0.30 g, 98%). GCMS *m/z* 246 (M^+, 21%). ^{31}P-$\{^1H\}$ NMR, δ 35.8 (*s*). ^{1}H NMR, δ 3.67 [3H, *d*, OMe, J(PH) 12], 2.26 (1H, *br*, *s*, H_4), 1.73 (1H, *br*, *m*, H_3)$_a$, 1.72 (1H, *br*, *s*, H_1)$_a$, 1.72–1.66 (2H, *m*, $H_{8'/8''}$)$_b$, 1.62 (1H, *d*, ^2J 9.7, $H_{7''}$)$_a$, 1.49 (1H, *br*, *m*, $H_{6''}$), 1.31–1.20 (2H, $H_{5''/5'}$)$_b$, 1.23 (1H, *br*, *m*, $H_{6'}$)$_b$, 1.15 (1H, *d*, ^2J 9.7, $H_{7'}$), 0.92 (3H, *s*, Me′); 0.74 (3H, *s*, Me″). [a: partially overlapping signals; b: overlapping signals]

nOe data

Irradiated Hydrogen	Enhanced Signal (%)
H_4	H_3(4.2); $H_{7'}$(3.5); $H_{5'}$ and/or $H_{5''}$(5.7), H_7(3.5)
$H_{6''}$	$H_{6'}$(8.2), Me″ (5.6)
$H_{7'}$	$H_{7''}$(15.6), H_4(3.8)
Me″	Me′(1.0), H_4(*x*), $H_{8''}$(*y*), $H_{8'}$(*z*); $x+y+z=11.0$
Me′	Me″(1), H_3(3.7), $H_{7''}$(2.5)

^{13}C-$\{^1H\}$ NMR, δ 52.2 [*d*, ^2J (P,C) 6.8, OMe], 52.1 [*d*, ^2J (P,C) 6.8, OMe], 48.6 (*s*, C_1), 44.3 [*d*, ^2J (P,C) 3.7, C_3], 42.3 [*d*, ^3J (P,C) 3.9, C_4], 37.5 [*d*, ^3J (P,C) 14.3, C_2], 36.9 (*s*, C_7), 31.8 (*s*, C_{10}), 24.6 (*s*, C_6), 22.0 [*d*, ^1J (P,C) 140.1, C_8], 21.9 (*s*, C_9), 20.0 (*s*, C_5). Raman: υ(P═O) 924 cm^{-1} (s).

The phosphonate **4** was found to contain a small amount of **2**, presumably produced by the hydrolysis of **4** in air, since an excess of diazomethane was employed in the synthesis. Despite several attempts to purify this methyl ester by vacuum distillation (140°C at 0.5 mmHg) and vacuum sealing a sample for elemental analysis, satisfactory microanalytical data were not obtainable.

Synthesis of 8-*camphanyldiphenylphosphine oxide **5***

To a solution of PhMgBr (0.022 mol) in dry ether (60 mL) was added, under a nitrogen atmosphere, camP(O)Cl_2 **3** (2.94 g, 0.01 mole), and a brown oil separated. After 24 h the supernatant was removed and the residue dissolved in $CHCl_3$ (200 mL). The organic layer was washed with 10% HCl (100 mL), dried over $MgSO_4$ and evaporated to dryness to give a cream solid. This was recrystallised from hot methanol to give a colourless crystalline solid **5** (2.92 g, 75%), m.p. 171.5–173.0°C. Found: C, 77.8; H, 8.0% $C_{22}H_{27}OP$ requires C, 78.1; H, 8.1%. ESMS (positive-ion, cone voltage 80 V, with added KCl); $[M+H]^+$ (*m/z* 339), $[M+K]^+$ (*m/z* 377), $[2M+H]^+$ (*m/z* 677), $[2M+K]^+$ (*m/z* 715), and $[3M+K]^+$ (*m/z* 1053). ^{31}P-$\{^1H\}$ NMR, δ 31.4 (*s*). ^{1}H NMR, δ 7.77–7.38 (10H, *m*, 2 × Ph)$_b$, 2.22 (2H, *br*, *m*, $H_{8'/8''}$)$_b$, 2.02 (1H, *br*, *s*, H_4), 1.87 (1H, *br*, *m*, H_3), 1.69 (1H, *br*, *s*, H_1), 1.50 [1H, *d*, ^2J 9.8, $H_{7''}$]$_b$, 1.49 (1H, *br*, *m*, $H_{6''}$)$_b$, 1.21 (1H, *m*, $H_{5''}$)$_b$, 1.15 (1H, *m*, $H_{6'}$)$_b$, 1.08 (1H, *m*, $H_{5'}$)$_b$, 1.04 (1H, *d*, ^2J 9.7, $H_{7'}$)$_a$, 0.85 (3H, *s*, Me′), 0.81 (3H, *s*, Me″). ^{13}C-$\{^1H\}$ NMR, δ 131.5-128.4 (*m*, Ph), 48.4 (*s*, C_1), 44.0 [*d*, ^2J (P,C) 4.0, C_3], 42.3 [*d*, ^3J (P,C) 3.1, C_4], 37.8 [*d*, ^3J (P,C) 10.7, C_2], 37.0 (*s*, C_7), 31.6 (*s*, C_{10}), 27.3 [*d*, ^1J (P,C) 62.6, C_8], 24.7 (*s*, C_6), 22.4 (*s*, C_9), and 20.3 (*s*, C_5). [a: partially overlapping signals; b: overlapping signals]

Synthesis of $[UO_2(NO_3)_2(camPO_3Me_2)_2]$ ***6***

Phosphonate **4** (0.50 g, 2.03 mmol) and uranyl nitrate hexahydrate (0.512 g, 1.02 mmol) were dissolved in methanol (20 mL). Spontaneous evaporation to dryness at room temperature gave **6** as a yellow crystalline solid in quantitative yield, m.p. 107–111°C. Found: C, 32.5; H, 5.3; N, 3.3% $C_{24}H_{42}N_2O_{14}P_2U$ requires C, 32.6; H, 4.8; N, 3.2%. ^{31}P-$\{^1H\}$ NMR, δ 42.0 (*s*). ^{1}H NMR, δ 4.12 [*d*, 6H, OMe, $J_{(PH)}$ 11], 4.11 [*d*, 6H, OMe, J(PH) 11], 2.35 (1H, *s*, *br*, H_4)$_b$, 2.04 (1H, *m*, H_3), 2.30 (2H, *m*, $H_{8'}/H_{8''}$)$_b$, 1.75 (1H, *m*, H_1), 1.55 (1H, *d*, ^2J 9.5, $H_{7''}$)$_a$, 1.55 (1H, *m*, $H_{6''}$)$_b$, 1.43–1.20 (3H, *m*, $H_{5''}$, $H_{5'}$, $H_{6'}$)$_b$, 1.14 (1H, *d*, ^2J 9.5, $H_{7'}$), 0.94 (3H, *s*, Me′), and 0.85 (3H, *s*, Me″). [a: partially overlapping signals; b: overlapping signals] IR ν(P═O) 933 cm^{-1}.

Synthesis of $[UO_2(NO_3)_2\{camP(O)Ph_2\}_2]$ *7*

Phosphine oxide **5** (0.10 g, 0.29 mmol) and uranyl nitrate hexahydrate (0.075 g, 0.15 mmol) were dissolved in hot methanol (50 mL) and the resulting solution allowed to spontaneously evaporate at room temperature. After 3 days yellow microcrystalline **7** (0.18 g, 60%) precipitated out of solution, m.p. 226–245°C. Found: C, 49.0; H, 5.1; N, 2.5%. $C_{44}H_{54}N_2O_{10}P_2U$ requires C, 49.3; H, 5.1; N, 2.6%.

*Crystal structure determination of the uranyl nitrate-phosphonate complex **6***

Cell parameters and intensity data were collected by ω-scans on a Siemens P4 diffractometer with Mo-Kα radiation ($\lambda = 0.7107$ Å) at −143°C. The structure was solved by Patterson methods in space group C2/c (although the alternative Cc could not be excluded) and slowly developed. The camphanyl groups were difficult to define accurately because of disorder.

Refinement was full-matrix least-squares based on F^2, with all non-hydrogen atoms anisotropic, using the SHELXS86 [14] and SHELXL93 [15] programs.

Crystal Data: $C_{24}H_{46}N_2O_{14}P_2U$, M 886.60, monoclinic, C2/c, *a* 26.739(2), *b* 8.137(2), *c* 19.782(2) Å, β 127.90(2)°, U 3396.4(9) Å^3, D_c 1.734 g cm^{-3} for $Z=4$, $F(000)$ 1752, μ(Mo-Kα) 4.937 mm^{-1}. Crystal size $0.48\times0.14\times0.08$ mm. A total of 2552 data were collected, 2219 unique (R_{int} 0.0757), 1103 with $I>2\sigma(I)$, corrected for absorption based on ψ-scans.

Refinement converged with R_1 0.0723 (2σ-data), R_1 0.1486, wR_2 0.1621, GoF 0.902 (all data), no final feature $>|1.6|$e Å^{-3}. The low proportion of 'observed' reflections, and the high R_1 figure for all data, can be attributed to the occupation of a special position by the U atom, leading to the $k+l=$ odd class of reflection being systematically weak.

Acknowledgements—We thank the University of Waikato for financial support, the New Zealand Lottery Grants Board for a grant-in-aid towards a mass spectrometer, and Prof. Ward Robinson (University of Canterbury) for X-ray data collection. Dr. A. M. Cartner (University of Waikato) is acknowledged for Raman spectra.

REFERENCES

1. (a) Burford, N., *Coord. Chem. Rev.*, 1992, **112**, 1; (b) Goggin, P. L., in *Comprehensive Coordination Chemistry*, G. Wilkinson (ed-in-chief), Pergamon Press, (1987). Section 15.8.
2. (a) Peppard, D. F., *Adv. Inorg. Chem.& Radiochem.*, 1966, **9**, 1; (b) Laing, M., *Educ. in Chem.*, November (1996), p. 157; (c) Flett, D. S., *Chem. Ind.*, 1977, 706; (d) Eccles, H. and Naylor, A., *Chem. Ind.*, 1987, 174; (e) Aparna, K., Krishnamurthy, S. S. and Nethaji, M., *J. Chem. Soc., Dalton Trans.*, 1995, 2991; (f) Kannan, S. and Ferguson, G., *Inorg. Chem.*, 1997, **36**, 1724.
3. Nicol, M. J., Fleming, C. A. and Preston, J. S., *Comprehensive Coordination Chemistry*, G. Wilkinson, (ed-in-chief), Pergamon Press, (1987). Section 63.
4. (a) Mason, G. W., Bollmeier, A. F. and Peppard, D. F. *J. Inorg. Nucl. Chem.*, 1970, **32**, 1011; (b) Peppard, D. F., Mason, G. W., Bollmeister, A. F. and Lewey, S., *ibid.*, 1971, **33**, 845; (c) Mason, G. W. and Lewey, S., *ibid.*, 1971, **36**, 911.
5. Henderson, W. and Hoye, P. A. T., UK Patent (1994) 2 268 178.
6. Henderson, W., Leach, M. T., Nicholson, B. K. and Sabat, M., *J. Chem. Soc., Dalton Trans.*, 1995, 2109.
7. Tebby, J. C., in *Phosphorus*-31 *NMR Spectroscopy in Stereochemical Analysis*, J. G. Verkade and L. D. Quin, (eds.), VCH, (1987). Chapter 1.
8. Borrett, V. T., Colton, R. and Traeger, J. C., *Eur. Mass Spectrom.*, 1995, **1,** 131.
9. Henderson, W. and Olsen, G. M., *Polyhedron*, 1996, **15,** 2105.
10. *Comprehensive Inorganic Chemistry*, Pergamon Press, Oxford, (1973). Third Edition, p. 292.
11. Ruikar, P. B. and Nagar, M. S., *Polyhedron*, 1995, **14,** 3125.
12. (a) Brown, D. R., Denning, R. G. and Jones, R. H., *J. Chem. Soc., Chem. Commun.*, 1994, 2601; (b) Denning, R. G., *Struct. Bonding.*, 1992, **79**, 215.
13. *Org. Synth. Coll.*, (1943). Volume II, p. 165.
14. Sheldrick, G. M., *SHELXS*86. Program for solving crystal structures, University of Göttingen (1986).
15. Sheldrick, G. M., *SHELXL*93. Program for refining crystal structures, University of Göttingen (1993).

Pergamon

PII: S0277-5387(98)00177-6

Polyhedron Vol. 17, No. 21, pp. 3753–3758, 1998
© 1998 Elsevier Science Ltd
All rights reserved. Printed in Great Britain
0277–5387/98 $19.00+0.00

The chemistry of pyridine thiols and related ligands—8. Synthesis, NMR spectroscopy and crystal structure of first *trans*-[bis(pyridine-2-thiolato-S)-bis(triphenyl phosphine) platinum(II)]

Tarlok S. Lobana,[a]* Renu Verma[a] and Alfonso Castineiras[b]

[a]Department of Chemistry, Guru Nanak Dev University, Amritsar-143005, Punjab, India

[b]Departamento de Quimica Inorganica, Facultade de Farmacia, Universidade de Santiago, E-15706 Santiago de Compostela, Galicia, Spain

(Received 29 October 1997; accepted 22 April 1998)

Abstract—Reaction of bis(pyridine-2-thiolato-N,S)platinum(II) (**1**) in acetonitrile (obtained from $PtCl_2$ and $Na^+C_5H_4NS^-$) with two equivalents of PPh_3 forms monomeric $Pt(C_5H_4NS)_2(PPh_3)_2$ (**2**) whose X-ray structure has been determined. It crystallises from a acetonitrile–chloroform mixture and exists as a centrosymmetric square planar monomer. Pyridine-2-thiolate binds to Pt via S-atoms in a *trans*-configuration and the other two positions are occupied by P atoms of PPh_3. The interatomic important parameters are: Pt–S = 2.343(2), Pt–P = 2.3147(13), C–S = 1.739(6) Å, bond angles P–Pt–P* and S–Pt–S* each = 180.0°, P–Pt–S, P*–Pt–S = 85.24° (acute) and P–Pt–S*, P*–Pt–S = 94.76° (obtuse). It represents the first example of a structurally characterised S-bonded pyridine-2-thiolato Pt(II) complex. The NMR data (^1H, ^{13}C, ^{31}P) suggest dissociation of **2** in $CDCl_3$ as follows: $Pt(C_5H_4NS)_2(PPh_3)_2$ (**2**)→$Pt(C_5H_4NS)_2(PPh_3)$ (**2a**)+PPh_3. Both N,S- and S-bonded $C_5H_4NS^-$ moieties are confirmed from ^1H and ^{13}C NMR. © 1998 Elsevier Science Ltd. All rights reserved

Keywords: triphenyl phosphine; pyridine-2-thione; biochemically active chromophores; S-bonded platinum(II) complex; pendant pyridyl.

INTRODUCTION

In recent years, there is an upsurge in coordination chemistry of heterocyclic thiones containing chemically active chromophores of the type: –N(H)–C(=S)↔–N=C(–SH), because these ligands provide several possibilities of metal–ligand interactions and have biochemical implications [1–4]. Pyridine-2-thione(C_5H_5NS), the simplest prototype of heterocyclic thiones binds to a metal center in several ways: S-bonding(η^1), S-bridging(η^2), N,S-chelating(η^2), N,S-bridging(η^2), N,S-chelating-cum-S-bridging(η^3) and N,S-bridging-cum-S-bridging(η^3) [4–13]. For structurally characterised Pt(II or III) complexes, N,S-bridging is observed in $[Pt_2(en)_2(\mu\text{-N,S-}C_5H_4NS)_2]Cl_2{\cdot}3H_2O$ [14], $[Pt_2\{\mu\text{-N,S-}C_5H_3(4\text{-}CH_3)NS\}_2]$[15], $[Pt_2Cl_2(\mu\text{-N,S-}C_5H_4NS)_4]{\cdot}2CHCl_3$ [15], and chelation in $[Pt(\eta^2\text{-N,S-}C_5H_4NS)(PPh_3)_2](PF_6)$ [16].

As a part of our interest in coordination chemistry of C_5H_5NS or its derivatives [17–19], we report the crystal structure of $[Pt(C_5H_4NS)_2(PPh_3)_2]$ (**2**) which represents the first example of a platinum(II) complex containing monodentate S-bonded $C_5H_4NS^-$ moiety. The solid state behaviour of **2** is compared with its solution phase behaviour. In literature [20], $C_5H_4NS^-$ ligand scrambling in $Pt(C_5H_4NS)_2(PPh_3)$ has been mentioned. In this investigation, we establish both N,S- and S-bonding modes for the species [**2a**, $Pt(\eta^2\text{-N,S–}C_5H_4NS)(\eta^1\text{-S–}C_5H_4NS)(PPh_3)$] in $CHCl_3$ using multinuclear NMR (^1H, ^{13}C and ^{31}P) spectroscopy and collecting massive scans for ^{13}C NMR spectrum.

* Author to whom correspondence should be addressed. Fax: +91-183-258820; E-mail: dcse_gndu@yahoo.com

EXPERIMENTAL

General materials

Platinum(II) dichloride was procured from M/s Central Drug House Pvt (Bombay) while PPh_3 from Spectrochem. Pvt. (Bombay). 2-Hydroxypyridine was procured from M/s Sisco, Bombay. Pyridine-2-thione-(C_5H_5NS) was prepared as described previously [21, 22]. Sodium salt, $Na^+C_5H_4NS^-$ was prepared as described [17] for $Na^+C_5H_4NOS^-$. Acetonitrile was dried over P_2O_5 and other solvents dried by usual methods.

Preparation of $Pt(C_5H_4NS)_2$ (*I*) *and* $Pt(C_5H_4NS)_2(PPh_3)_2$ (*2*)

$Pt(C_5H_4NS)_2$ (**1**, yellow) was prepared from the stoichiometric reaction of $PtCl_2$ (0.186 g, 0.70 mmol) with C_5H_4NSNa (0.205 g, 1.54 mmol) in CH_3CN (25 cm^3) under reflux for *ca.* 20 h. The concentration of the solution under vacuum formed a yellow coloured solid which was treated with water to remove NaCl, recrystallised from CH_3CN and dried *in vacuo*. Yield, 40%, m.p. (°C) > 250, analytical data (%), found C, 30.4, H, 2.13, N, 6.95; required for $C_{10}H_8N_2S_2Pt$, C, 29.0, H, 1.93, N, 6.75, *IR* data (cm^{-1}), 1137s (νC═S), 426s (νPt–S), 254m (νPt–N).

$Pt(\eta^1\text{-S–}C_5H_4NS)_2(PPh_3)_2$ (**2**, yellow) was prepared by the addition of PPh_3 (0.160 g, 0.613 mmol) to $Pt(C_5H_4NS)_2$ (0.127 g, 0.306 mmol) in CH_3CN (20 cm^3) with magnetic stirring under reflux for 2 h. The excess solvent was removed under vacuum to get a yellow solid which was purified using diethylether and recrystallised from CH_3CN. Yield, 60%, m.p. (°C), 140–45, analytical data found (%), C, 58.2, H, 3.62, N, 3.02, required for $C_{46}H_{38}N_2P_2S_2$ Pt, C, 58.8, H, 4.04, N, 3.00, *IR data* (cm^{-1}), 1110s (νC═S), 430m (νPt–S).

Physical measurements

The elemental analysis for C, H and N were obtained using a Carlo-Erba 1108 microanalyser or from RSIC Chandigarh. The melting points were determined with a Gallenkamp electrically heated apparatus. The NMR spectra were recorded in $CDCl_3$ using, (i) Bruker AMX 300 spectrometer at 300.14 and 75.48 MHz probe frequencies for (^1H and ^{13}C resonances, respectively, with TMS as the internal reference) and (ii) Bruker AMX 500 spectrometer at 202.45 MHz probe frequency for $^{31}P\{^1H\}$ resonance with 85% H_3PO_4 as the external reference (δP, 27.5 ppm).

X-ray data collection and reduction

The crystal of $Pt(C_5H_4NS)_2(PPh_3)_2$ (**2**) was mounted on a glass fiber and used for data collection. Cell constants and an orientation matrix for data collection were obtained by least squares refinement of diffraction data from 25 reflections in the range of $10.60° < \theta < 18.04°$ in a ENRAF-NONIUS MACH3 automatic diffractometer [23]. Data were collected at 293 K using MoK radiation ($\lambda = 0.71073$ Å) and the ω scan technique and corrected for Lorentz and polarisation effects [24]. An empirical absorption correction was made [25]. A summary of crystal data, experimental details and refinement results are listed in Table 1.

Structure-solution and refinement

The structure was solved by direct methods [26] which revealed the position of all non-hydrogen atoms, and refined on F^2 by a full matrix least-squares procedure using anisotropic displacement parameters for all non-hydrogen atoms [27]. The hydrogen atoms were located in their calculated positions (C–H = 0.93–0.96 Å) and were refined using a riding model. After all shift/e.s.d ratios were less than 0.001, the refinement converged to the agreement factors listed in Table 1. The atomic scattering factors taken from International Tables for X-ray Crystallography [28] while molecular graphics were prepared using ZORTEP [29].

RESULTS AND DISCUSSION

Description of the crystal structure of $Pt(C_5H_4NS)_2(PPh_3)_2$ (*2*)

The selected interatomic parameters are given in Table 2 while Fig. 1 shows the molecular structure together with numbering scheme. The basic structural unit is a centrosymmetric monomer $Pt(C_5H_4NS)_2(PPh_3)_2$ (**2**). Two P atoms of PPh_3 molecules and two S atoms of $C_5H_4NS^-$ ligand coordinate to Pt atom in a square planar geometry with *trans* P–Pt–P* and S–Pt–S* angles of 180.0°, two acute (85.24°, P–Pt–S and P*–Pt–S*) and two obtuse (94.76°, P–Pt–S* and S–Pt–P*) angles. Chelation in *cis*-$[Pt(\eta^2\text{-N,S–}C_5H_4NS)(PPh_3)_2](PF_6)$ (**3**) causes more severe distortion as anticipated [e.g. *trans* S–Pt–P = 165.6°; N–Pt–P = 163.8(2)] [16]. It is significant that $C_5H_4NS^-$ can modulate the geometric positions of PPh_3 ligand as in **3** and **2** based on its coordination requirements. The Pt–P distance is normal but marginally longer than in **3** [Pt–P = 2.295, 2.253 Å] [16], while Pt–S distance [Pt–S = 2.348 Å] as well as P–C_{Ph} distance [1.832 Å] are nearly the same. The S–C(2) distance shows partial double bond character in the usual manner. The bite angle of S–C(2)–N(1) [120.7(5)°] is typical of monodentate $C_5H_4NS^-$ [117.6(7)°] as in $Hg(C_5H_4NS)_2$ [30] or is similar to the bridging $C_5H_4NS^-$ derivative [122–124°] in Pt(II) complexes [15]. Finally, the Pt–S–C(2) angle is also similar to the one in dimeric complexes [109.0(8)°]. **2** represents the first structurally characterised Pt(II) 3complex containing monodentate S-bonded $C_5H_4NS^-$ moiety. The steric effect due to

Table 1. Crystal data and structure refinement for $[Pt(C_5H_4NS)_2(PPh_3)_2]$

Empirical formula	$C_{46}H_{38}N_2P_2PtS_2$
Formula weight	939.93
Crystal system/Space group	Monoclinic/$P2_1/n$
Unit cell dimensions	$a = 10.000(2)$ Å; $\alpha = 90.00(-)^\circ$
	$b = 15.456(3)$ Å; $\beta = 97.04(2)^\circ$
	$c = 12.989(2)$ Å; $\gamma = 90.00(-)^\circ$
Volume	1992.4(7) Å^3
Z	2
Density (calculated)	1.567 Mg/m^3
Absorption coefficient	3.742 mm^{-1}
F (000)	936
Crystal description	*yellow prism*
Crystal size	$0.40 \times 0.30 \times 0.20$ *mm*
No. of reflections (*lattice*)	25
θ range (lattice)	10.60–18.04°
θ range for data collection	2.64–26.29°
Index ranges	$-12 \leqslant h \leqslant 12$, $0 \leqslant k \leqslant 19$, $0 \leqslant l \leqslant 16$
Reflections collected	4215
Independent reflections	4038 [$R_{int} = 0.0337$]
Reflections observed	2566
Criterion for observation	$>2\sigma$ (I)
Data/parameters	4037/0/317
Final R indices [$I>2\sigma$ (I)]	$R_1 = 0.0297$,
	$wR_2 = 0.0561$
Goodness-of-fit on F^2	1.000
Final R indices (all) R_1/wR_2	0.0829/0.0676
Largest diff. peak and hole	0.614 and -0.580 eÅ^{-3}
Weighting scheme	$w = [1/[S^2(F_o^2)+(0.0237P)^2+0.3454P]$
	where $P = (F_o^2+2F_c^2)/3$
Max. and min. transmission	1.000 and 0.486

bulky PPh_3 [P–Pt–P, 97.4°] and short bite angle, S–Pt–N of 68.0° in **3** appear to favour *trans*-PPh_3 and S-bonded $C_5H_4NS^-$ in **2**.

NMR spectral studies

Table 3 contains NMR data (^1H, ^{13}C, ^{31}P) for the compounds. The ^{31}P NMR spectrum of **2** (Fig. 2) shows the presence of dissociated PPh_3 in $CDCl_3$ solution according to the equation below.

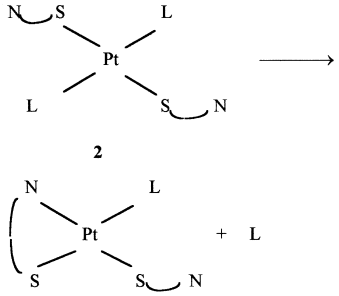

The NMR spectrum shows that dissociation is not complete, but is considerable. This means that probably **2** and **2a** are in equilibrium, however, there was no evidence for dissociation of both PPh_3 molecules. Since crystals of **2** were grown from CH_3CN, it is possible that this solvent may be acting as a stabiliser of Pt–PPh_3 bonding and as shown by ^{31}P NMR, **2** dissociates in $CHCl_3$ forming **2a** species. The lack of dissociation of **2** in CH_3CN could be attributed to the coordinating properties of CH_3CN presumably along axial sites. Alternatively CH_3CN could interact with the pendant pyridyl group via hydrogen bonding or via delocalised π-electrons on the CN group. This presumably keeps $C_5H_4NS^-$ moiety in S-bonded form with pendant pyridyl group. In contrast, in $CHCl_3$, this stabilisation of the pendant pyridyl group is not available and so it coordinates to Pt(II). It must be emphasised that due to bulky PPh_3 groups with pendant pyridyl groups in *trans* positions, the stereochemical requirements about the Pt(II) center favour dissociation of a PPh_3 group along with chelation by NS-donor set. Low field coordination shift ($\Delta\delta$P, 12.5 ppm) with $^1J_{P-Pt}$ coupling constant of 3866 Hz confirms the coordination of PPh_3 to the Pt metal center.

The absence of ^1H NMR signals due to NH in **1**

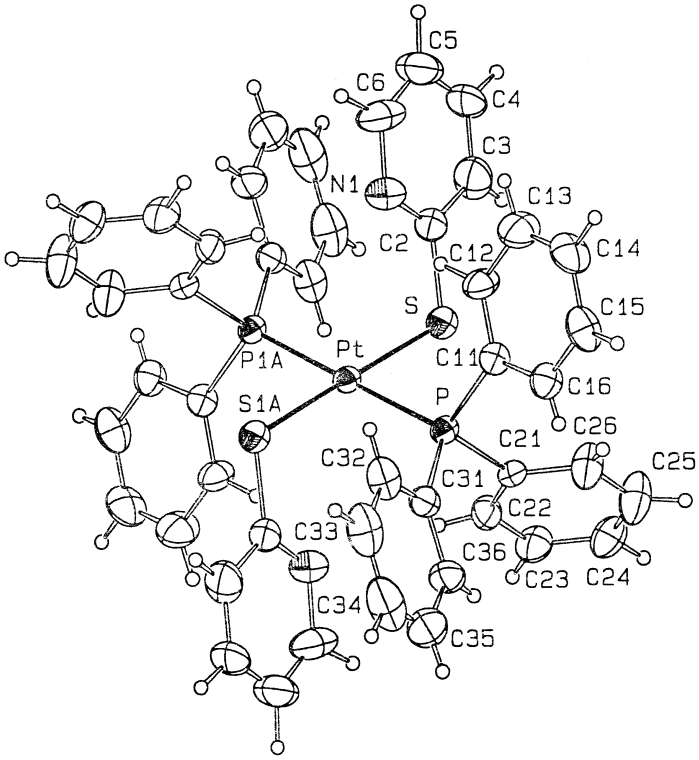

Fig. 1. Perspective view of $[Pt(C_5H_4NS)_2(PPh_3)_2]$ (**2**) molecule with the numbering scheme. The thermal ellipsoids are drawn at the 30% probability level. The hydrogen atoms are drawn with an arbitrary radius of 0.1 Å and are represented by open circles.

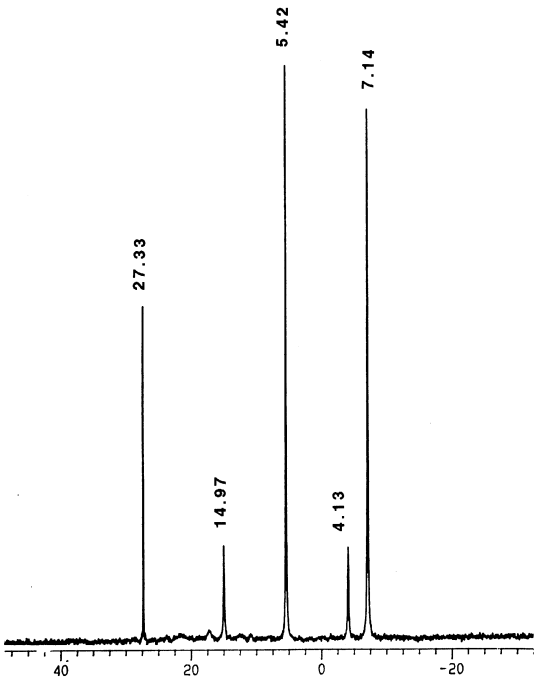

Fig. 2. The ^{31}P NMR spectrum of **2** in $CDCl_3$.

Table 2. Selected bond lengths (Å) and angles (°) for $[Pt(C_5H_4NS)_2(PPh_3)_2]$

Pt–P	2.3147(13)
Pt–S	2.343(2)
S–C(2)	1.739(6)
P–C(31)	1.825(6)
P–C(21)	1.831(5)
P–C(11)	1.841(5)
N(1)–C(2)	1.343(8)
N(1)–C(6)	1.356(8)
C(2)–C(3)	1.416(9)
C(3)–C(4)	1.348(10)
C(4)–C(5)	1.365(13)
C(5)–C(6)	1.376(12)
P–Pt–P*1	180.0
P–Pt–S*1	94.76(5)
P–Pt–S	85.24(5)
S*1–Pt–S	180.0
C(2)–S–Pt	108.2(2)
C(2)–N(1)–C(6)	117.4(7)
N(1)–C(2)–C(3)	120.7(7)
N(1)–C(2)–S	120.7(5)
C(31)–P–C(21)	105.4(3)
C(31)–P–C(11)	100.5(2)
C(21)–P–C(11)	107.1(2)
C(31)–P–Pt	119.7(2)
C(21)–P–Pt	109.8(2)
C(11)–P–Pt	113.4(2)[1]

Symmetry transformations used to generate equivalent atoms: *1 $-x, -y+1, -z$.

Table 3. The ^{1}H, ^{13}C and $^{31}P\{^{1}H\}$ NMR data (δ, ppm, J, Hz) of compounds

		H(6)	H(4)	H(3)	H(5)
1		9.10 d (J_5, 6.0)	7.36 t (J_3, 7.6, J_5, 7.6)	7.20 d (J_4, 8.1)	6.91 t (J_4, 6.6, J_6, 6.6)
2	set I	8.27 d (J_5, 3.4)	7.32 t (J_3, 7.5, J_5, 7.5)	7.37 d (J_4, 7.7)	6.82 t (J_4, 5.9, J_6, 5.9)
	set II	8.09 s[a]	6.65 t[a]	6.68 d[a] (J_4, 8.2)	6.52 s[a]
C_5H_5NS[b]		7.56 ddd (J_5, 6.3, J_4, 1.6, J_3, 0.8)	7.34 ddd (J_3, 8.7, J_5, 7.0, J_6, 1.8)	7.49 dt (J_4, 8.7, J_5, 0.8, J_6, 0.8)	6.73 td (J_4, 6.7, J_6, 6.7, J_3, 1.2)
PPh_3 signals		o-H	m- and p-H	free PPh_3	
2		7.39 m	7.56 m	7.14 m	
PPh_3		–	–	7.23 m	

^{13}C NMR		C(2)	C(6)	C(4)	C(5)	C(3)
2	set I[c]	176.5	146.9	136.8	124.9	115.7
	set II[d]	164.9	142.3	135.8	124.9	115.7
C_5H_5NS		175.6	137.0	135.9	132.8	113.1

		PPh_3 signals			
		i-C ($^{1}J_{C-P}$)	o-C ($^{2}J_{C-P}$)	m-C ($^{3}J_{C-P}$)	p-C ($^{4}J_{C-P}$)
PPh_3		132.5 (10.0)	134.2 (19.5)	128.9 (10.8)	129.1 (9.3)
2	set I	128.0 (38.5)	130.7 (6.0)	127.1 (7.5)	130.5 (n.o)
	set II	131.6 (n.o)	132.7 (6.0)	126.9 (6.8)	129.5 (n.o)[e]

$^{31}P\{^{1}H\}$	δP	$\Delta\delta P$	$^{1}J_{P-Pt}$
2	5.4[f]	12.5	3866
PPh_3	−7.14		

d, doublet; t, triplet, td, triplet of doublets; dt, doublet of triplets; ddd, doublet of doublet of doublet; s, singlet.
[a]Broad.
[b]$\delta NH = 13.40$ *v*b.
[c]N,S-chelated $C_5H_4NS^-$.
[d]S-bonded $C_5H_4NS^-$.
[e]n.o., not observed.
[f]Indicates free PPh_3 also.

and **2** confirms that in these compounds anionic $C_5H_4NS^-$ is coordinating to the Pt(II) center. The H(6) proton shows low-field shift relative to free C_5H_5NS in **1** and **2**. The coordination of PPh_3 to Pt(II) leads to a relative up-field shift in **2**. Further, two sets of H(6) proton (and for other protons) shows evidence for both N,S-chelated and S-bonded $C_5H_4NS^-$ moieties in **2a**. Since H(6), in the vicinity of nitrogen, is most sensitive to the coordination changes, the up-field shifts clearly support de-ligation of M–N bond in **2a**. Further, the fact that H(6) proton of N,S-chelated C_5H_4NS (set I) is still up field relative to that of **1**; it reveals increased Pt–N back-bonding when PPh_3 coordinates. De-ligation of Pt–N bond (set II) leads to increased aromaticity, an usual observation in metal–pyridine thiol chemistry [31].

The H(4) proton remains nearly unaffected (**1**; **2a**, set I) when $C_5H_4NS^-$ is N,S-bonded, but moves up-field when it is S-bonded only (**2**,**2a**; set II). H(3) protons also is significantly up-field when $C_5H_4NS^-$ is S-bonded only but is mildly up-field when it is N,S-bonded and finally H(5) protons are also up-field when $C_5H_4NS^-$ is S-bonded only and down-field for N,S-bonded moiety.

^{13}C NMR spectrum of **2** shows unambiguous evidence for N,S-bonded (**2a**, set I, Table 3) and S-bonded (**2**,**2a**, set II) $C_5H_4NS^-$ moieties. All pyridyl carbons except C(5) show low-field shifts (relative to free C_5H_5NS) for N,S-bonded $C_5H_4NS^-$ moiety (**2a**, set I) [31]. The upfield shift in C(2) signal with reduced shifts in positions of C(6) supports the presence of S-bonded $C_5H_4NS^-$ moiety (**2**,**2a**, set II) [31].

Acknowledgements—Financial assistance from the University Grants Commission, Delhi [Project No. F.12-47/93(SR-1)]. We are thankful to Professor J. S. Casas, University of Santiago, for instrumental facilities.

REFERENCES

1. Raper, E. S., *Coord. Chem. Rev*., 1985, **61,** 115.
2. Raper, E. S., *Coord. Chem. Rev*., 1996, **153,** 199.
3. Raper, E. S., *Coord. Chem. Rev*., 1994, **129,** 91.
4. Lobana, T. S. and Bhatia, P. K., *J. Sci. Ind. Res*., 1989, **48,** 394 (Review).
5. Deeming, A. J., Hardcastle, K. I., Meah, M. N., Bates, P. A., Dawes, H. M. and Hursthouse, M. B., *J. Chem. Soc. Dalton Trans*., 1988, 227.
6. Karagiannidis, P., Aslanidis, P., Kessissoglou, D. P., Krebs, D. and Dartmann, M., *Inorg. Chim. Acta*, 1989, **156,** 47.
7. Aslanidis, P., Hadjikakou, S. K., Karagiannidis, P., Kojic-Prodic, B. and Luic, M., *Polyhedron*, 1994, **13,** 3119.
8. Mura, P., Olby, B. G. and Robinson, S. D., *J. Chem. Soc. Dalton Trans*., 1985, 2101.
9. Rosenfield, S. G., Berends, H. P., Gelmini, L., Stephen, D. W. and Mascharak, P. K., *Inorg. Chem*., 1987, **26,** 2792.
10. Zhang, N., Wilson, S. R. and Shapley, P. A., *Organometallics*, 1988, **7,** 1126.
11. Oro, L. A., Ciriano, M. A., Viguri, F., Tiripicchio-Camellini, A. and Lahoz, F. J., *Nouv. J. Chim*., 1986, **10,** 75.
12. Deeming, A. J., Meah, M. N., Bates, P. A. and Hursthouse, M. B., *J. Chem. Soc. Dalton Trans*., 1988, 235.
13. Deeming, A. J., Karim, M., Bates, P. A. and Hursthouse, M. B., *Polyhedron*, 1988, **7,** 1401.
14. Umakoshi, K., Kinoshita, I., Fukui-Yasuba, Y., Matsumoto, K., Ooi, S., Nakai, H. and Shiro, M., *J. Chem. Soc. Dalton Trans*., 1989, 815.
15. Umakoshi, K., Kinoshita, I., Ichimura, A. and Ooi, S., *Inorg. Chem*., 1987, **26,** 3557.
16. Wang, S., Staples, R. J., Fackler, J. P. Jr., *Acta Cryst. C*, 1994, **50,** 889.
17. Lobana, T. S. and Paul, S., *Transition Met. Chem*., 1996, **21,** 300 (and references cited therein).
18. Lobana, T. S., Verma, R., Singh, R. and Castineiras, A., *Transition Met. Chem*., 1998, **23,** 25.
19. Lobana, T. S., Paul, S. and Castineiras, A., *Polyhedron*, 1997, **16,** 4023.
20. Nakatsu, Y., Nakamura, Y., Matsumoto, K. and Ooi, S., *Inorg. Chim. Acta*, 1992, **196,** 81.
21. Lobana, T. S. and Bhatia, P. K., *Indian J. Chem. Sect. A*., 1990, **29,** 1225.
22. Delarge, J., *Chem. Abstr*., 1968, **69,** 2830.
23. ENRAF-NONIUS, CAD 4-Express Software Version 5.1. Enraf-Nonius, Deft, The Netherlands, 1995.
24. Spek, A. L., HELENA, A Program for data collection of CAD4 Data. University of Utrecht, The Netherlands, 1993.
25. Walker, N. and Stuart, D., *Acta Crystallogr. Sect. A*, 1993, **39,** 158.
26. Sheldrick, G. M., *Acta Crystallogr. Sect. A*, 1990, **46,** 467.
27. Sheldrick, G. M., SHELXL 93. Program for the Refinement of Crystal Structures. University of Gottingen, Germany, 1993.
28. International Tables for X-ray Crystallography, Vol. C, Kluwer Academic Publishers. Dordrecht, The Netherlands, 1995.
29. Zsolnai, L., ZORTEP, A Program for the Presentation of Thermal Ellipsoids. University of Heidelberg, Germany, 1994.
30. Wang, S., Fackler, J. P. Jr., *Inorg. Chem*., 1989, **28,** 2615.
31. Cookson, P. D. and Tiekink, E. R. T., *J. Chem. Soc. Dalton Trans*., 1993, 259.

Pergamon

PII : S0277–5387(98)00178–8

Polyhedron Vol. 17, No. 21, pp. 3759–3764, 1998
© 1998 Elsevier Science Ltd
All rights reserved. Printed in Great Britain
0277–5387/98 $19.00+0.00

Reaction of Mo═Mo doubly-bonded complexes $(\eta^5\text{-}RC_5H_4)_2Mo_2(CO)_2(\mu\text{-}SPh)_2$ with elemental selenium. Synthesis and structural characterization of some novel sulfur/selenium quadruply-bridged molybdenum complexes

Li-Cheng Song,[a]* Ji-Quan Wang[a] and Xiao-Ying Huang[b]

[a] Department of Chemistry, Nankai University, Tianjin 300071, P.R. China

[b] State Key Laboratory of Structural Chemistry, Fuzhou 350002, P.R. China

(Received 28 January 1998 ; accepted 24 April 1998)

Abstract—The reaction of Mo═Mo doubly-bonded $(\eta^5\text{-}RC_5H_4)_2Mo_2(CO)_2(\mu\text{-}SPh)_2$ (R = MeO_2C, EtO_2C) with elemental selenium in toluene at reflux results in formation of a series of sulfur/selenium quadruply-bridged complexes *trans*/*anti*-$(\eta^5\text{-}RC_5H_4)_2Mo_2(\mu\text{-}Se)_2(\mu\text{-}SPh)_2$ (**1a**, R = MeO_2C ; **2a**, R = EtO_2C), *trans*/*syn*-$(\eta^5\text{-}RC_5H_4)_2Mo_2(\mu\text{-}Se)_2(\mu\text{-}SPh)_2$ (**1b**, R = MeO_2C ; **2b**, R = EtO_2C), and *cis*/*syn*-$(\eta^5\text{-}RC_5H_4)_2Mo_2(\mu, \eta^2:\eta^2\text{-}Se_2)(\mu\text{-}SPh)_2$ (**1c**, R = MeO_2C ; **2c**, R = EtO_2C) in 58% and 53% overall yields, respectively. The structures of all these new products have been characterized by elemental analysis, IR, ^1H NMR and MS spectroscopies, as well as for **2c** by X-ray crystallography. © 1998 Elsevier Science Ltd. All rights reserved

Keywords: Mo═Mo double bond ; selenium ; reaction ; crystal structure.

Although group 6 metal triply-bonded complexes $(\eta^5\text{-}RC_5H_4)_2M_2(CO)_4$ (M = Cr, Mo, W) have been extensively studied [1,2], the corresponding metal–metal doubly-bonded complexes $(\eta^5\text{-}RC_5H_4)_2M_2(CO)_2(\mu\text{-}SR)_2$ are little explored so far [3,4]. On the basis of our recent work concerning this project [5] and in order to further develop the chemistry of the group 6 metal doubly-bonded complexes, we carried out reaction of $(\eta^5\text{-}RC_5H_4)_2Mo_2(CO)_2(\mu\text{-}SPh)_2$ (R = MeO_2C, EtO_2C) [6] with selenium powder in refluxing toluene. Herein we report the detailed synthetic procedures and structural characterization of six novel dimolybdenum complexes prepared by the above-mentioned reaction : *trans*/*anti*-$(\eta^5\text{-}RC_5H_4)_2Mo_2(\mu\text{-}Se)_2(\mu\text{-}SPh)_2$, *trans*/*syn*-$(\eta^5\text{-}RC_5H_4)_2Mo_2(\mu\text{-}Se)_2(\mu\text{-}SPh)_2$ and *cis*/*syn*-$(\eta^5\text{-}RC_5H_4)_2Mo_2(\mu, \eta^2:\eta^2\text{-}Se_2)(\mu\text{-}SPh)_2$ (R = MeO_2C, EtO_2C). Although sulfur/sulfur and selenium/selenium quadruply-bridged transition-metal dinuclear complexes have appeared in the literature [7], such mixed sulfur/selenium quadruply-bridged dimolybdenum complexes, to the best of our knowledge, are the first examples.

* Author to whom correspondence should be addressed.

RESULTS AND DISCUSSION

It was found that reaction of Mo═Mo doubly-bonded complexes $(\eta^5\text{-}RC_5H_4)_2Mo_2(CO)_2(\mu\text{-}SPh)_2$ (R = MeO_2C, EtO_2C) [6], as a mixture of *trans*/*anti* and *trans*/*syn* isomers, with excess selenium powder in toluene at reflux for 4 h resulted in complete disappearance of the doubly-bonded starting material and in the formation of several products, as evidenced by TLC analysis. After solvent had been removed, the residue was subjected to TLC separation to give three major bands. The first blue band afforded the complexes *trans*/*anti*-$(\eta^5\text{-}RC_5H_4)_2Mo_2(\mu\text{-}Se)_2(\mu\text{-}SPh)_2$ (**1a**, R = MeO_2C ; **2a**, R = EtO_2C), the second blue band gave the complexes *trans*/*syn*-$(\eta^5\text{-}RC_5H_4)_2Mo_2(\mu\text{-}Se)_2(\mu\text{-}SPh)_2$ (**1b**, R = MeO_2C ; **2b**, R = EtO_2C), and the third yellow band produced *cis*/*syn*-$(\eta^5\text{-}RC_5H_4)_2Mo_2(\mu, \eta^2:\eta^2\text{-}Se_2)(\mu\text{-}SPh)_2$ (**1c**, R = MeO_2C ;

2c, EtO_2C), as shown in Scheme 1. Note that the terminologies of *trans* and *cis* for complexes **1a**–**c** and **2a**—**c** refer to the relative positions of the two naked Se atoms (or the two S atoms attached to phenyl group) with respect to the Mo—Mo vector, while those of *anti* and *syn* refer to the mutual orientations of the two phenyl groups with respect to their attached planar Mo_2S_2 ring for **1a**, **b** and **2a**, **b**, and to their attached butterfly Mo_2S_2 skeleton for **1c** and **2c**. All these new complexes have been characterized by elemental analysis, IR, ^1H NMR and MS spectroscopies. The ^1H NMR spectra of **1a** and **1b** displayed one singlet at ca 3.74 ppm for their methyl groups, whereas those of **2a** and **2b** exhibited one triplet at ca 1.25 ppm and one quartet at ca 4.25 ppm for their ethyl groups. In addition, they all showed three to four multiplets in the range of 6.24–7.40 ppm for the phenyl groups and the substituted cyclopentadienyl rings. The ^1H NMR spectrum of **1c** showed one singlet at 3.57 ppm for its methyl groups, one singlet at about 7 ppm for its phenyl groups and showed two broad singlets in the range of 5.24–5.52 ppm for its substituted cyclopentadienyl rings, whereas that of **2c** showed one triplet at 1.20 ppm and one quartet at 4.18 ppm for its ethyl groups, one singlet at 7.20 ppm for its phenyl groups and two broad singlets in the range 5.40–5.72 ppm for its substituted cyclopentadienyl rings. The IR spectra of **1a**–**c** and **2a**–**c** are quite similar. Besides the bands for ester carbonyl, their IR spectra all showed weak absorption bands in the range of 200–550 cm^{-1} corresponding to the stretching vibrations of Mo—S and Mo—Se bonds. In addition, the mass spectra of **1a**, **b** and **2a**, **b** demonstrated their respective molecular ion peaks and corresponding fragment ion peaks, which are in good agreement with their formulations. According to the similar reaction of the Mo=Mo doubly bonded complex $Cp_2Mo_2(CO)_2(\mu\text{-}SMe)_2$ with elemental sulfur [8], the formation of **1a**, **b** and **2a**, **b** in this kind of reaction is not unexpected; in addition, some single

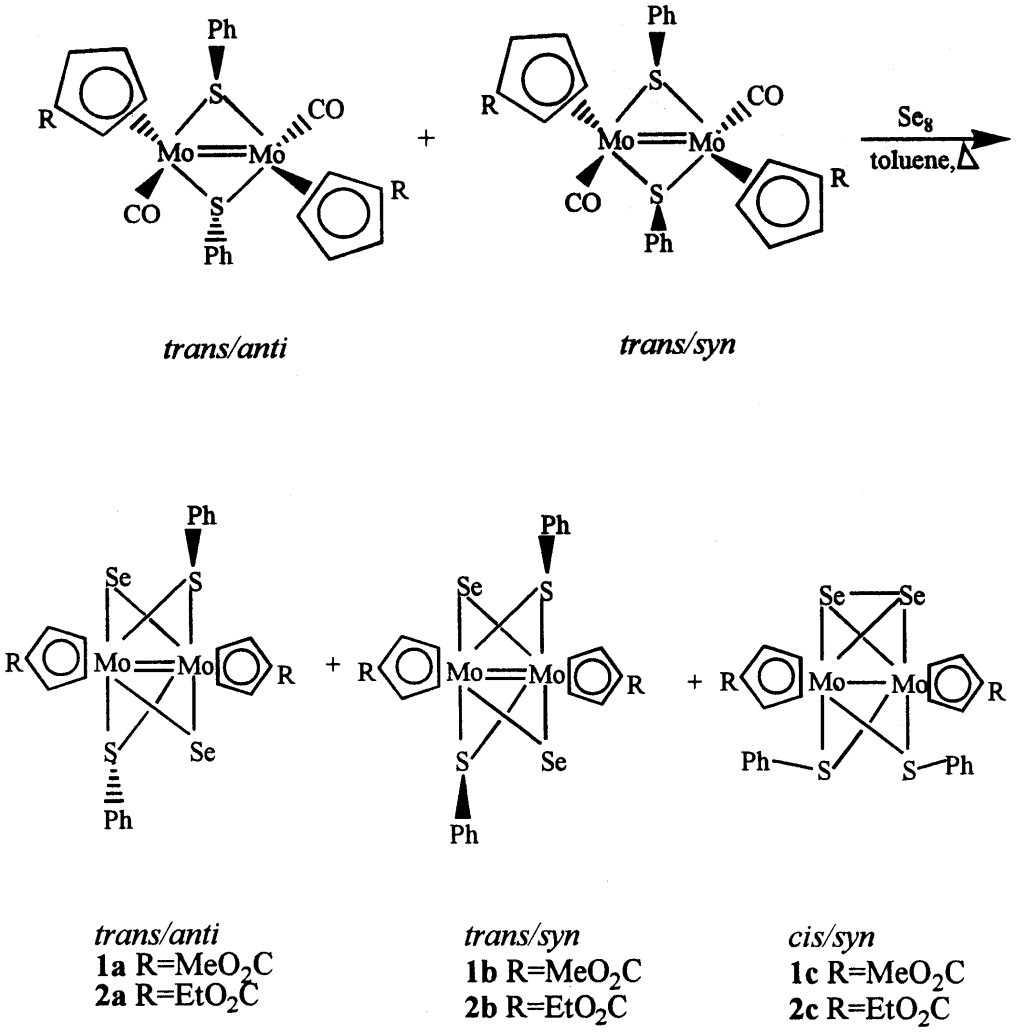

Scheme 1.

crystal structures of the compounds similar to **1a**, **b** and **2a**, **b** have been determined (see below for details). However, in this kind of reaction the formation of **1c** and **2c** is unexpected. So, in order to unambiguously confirm their structures, an X-ray diffraction analysis for **2c** was undertaken. Figures 1 and 2 represent its single crystal molecular structure and its molecular projection, respectively. Table 1 shows its selected bond distances and angles.

As seen from Figs 1 and 2 the η^5-$Et_2OCC_5H_4Mo$-$MoC_5H_4CO_2Et$-η^5 moiety is quadruply-bridged by a diselenido and two benzenethiolato ligands, and the two substituted cyclopentadienyl rings are perfectly eclipsed.

The bond distance of Se(1)—Se(2) [2.319(1) Å] in **2c** is close to that in (μ-Se_2)$Fe_2(CO)_6$ [2.293(2) Å] [9] and slightly shorter than the normal Se—Se single bond distances of 2.33(1) to 2.38(1) Å [10]. The four bridged atoms in **2c** form a plane, which is parallel to the two substituted cyclopentadienyl ring planes and

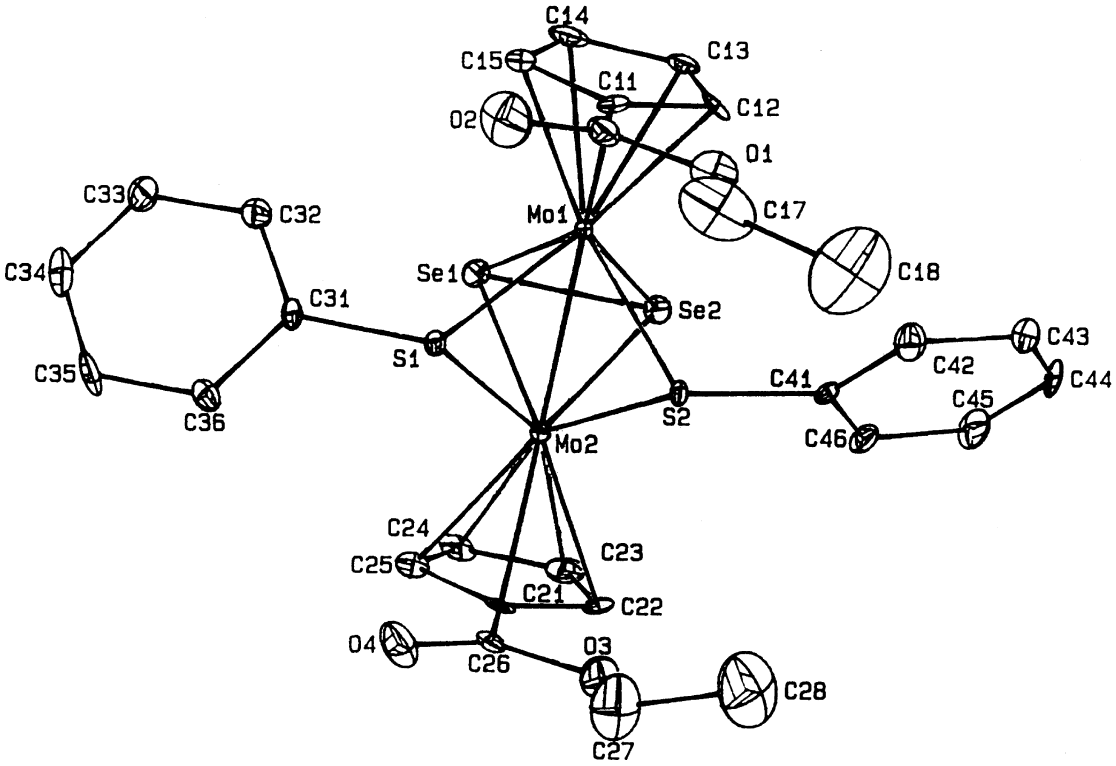

Fig. 1. ORTEP view of **2c**, drawn with 30% probability ellipsoids.

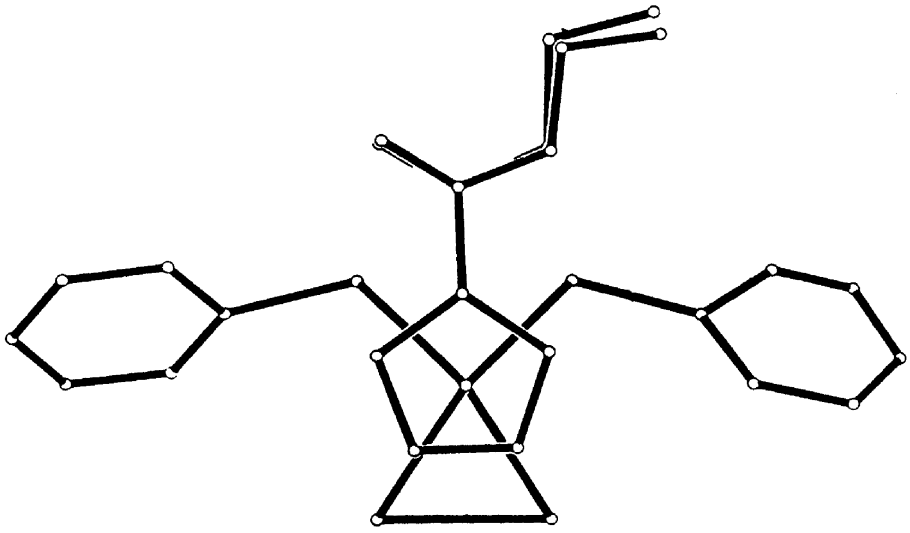

Fig. 2. The molecular projection of **2c** along its Mo—Mo bond.

Table 1. Selected bond distances (Å) and angles (°) for **2c**

Mo(1)—Mo(2)	2.661(1)	Se(1)—Se(2)	2.319(1)
Mo(1)—Se(1)	2.569(1)	Mo(1)—S(1)	2.419(2)
Mo(1)—Se(2)	2.572(1)	Mo(1)—S(2)	2.437(2)
Mo(2)—Se(1)	2.568(1)	Mo(2)—S(1)	2.436(2)
Mo(2)—Se(2)	2.558(1)	Mo(2)—S(2)	2.422(2)

S(1)—Mo(1)—Mo(2)	57.07(4)	S(2)—Mo(2)—Mo(1)	57.06(4)
S(2)—Mo(1)—Se(1)	114.30(5)	S(1)—Mo(2)—Mo(1)	56.46(5)
S(2)—Mo(1)—Se(2)	83.33(5)	Se(2)—Mo(2)—Se(1)	53.78(3)
S(2)—Mo(1)—Mo(2)	56.53(4)	Se(2)—Mo(2)—Mo(1)	59.02(3)
Se(1)—Mo(1)—Se(2)	53.62(3)	Se(1)—Mo(2)—Mo(1)	58.81(3)
Se(1)—Mo(1)—Mo(2)	58.79(3)	Se(2)—Se(1)—Mo(2)	62.89(3)
Se(2)—Mo(1)—Mo(2)	58.50(3)	Se(2)—Se(1)—Mo(1)	62.28(3)
Mo(2)—Se(1)—Mo(1)	62.40(3)	Mo(2)—Se(2)—Mo(1)	62.48(3)
Se(1)—Se(2)—Mo(2)	63.33(3)	Mo(1)—S(1)—Mo(2)	66.47(5)
Se(1)—Se(2)—Mo(1)	63.10(3)	Mo(2)—S(2)—Mo(1)	66.41(5)

bisects the Mo—Mo vector perpendicularly. The non-bonding distances between the bridged atoms are 2.839(2), 3.324(7) and 3.332(2) Å in **2c**. These distances fall in the range of the sum of van der Waals radii of corresponding S/S, S/Se atoms, and indicate a weak interaction between the bridging atoms. Complexes **1a**, **b** and **2a**, **b** are d^2–d^2 dimers and would have a $\sigma^2\delta^2$ electronic configuration [11]. This suggests a double bond present between two Mo(+IV) atoms, which is consistent with the 18-e rule. However, **1c** and **2c** are d^3–d^3 dimers with a $\sigma^2\delta^2\delta^{*2}$ electronic configuration [11], which would suggest a single bond between two Mo(+III) atoms. The single Mo—Mo bond assignment for **1c** and **2c** is also in good agreement with the 18-e rule. It is worth noting that the Mo—Mo bond length of 2.661(1) Å in **2c** is quite short for a normal single bond due to the effect of the four bridging ligands and the oxidation states of two Mo(III) atoms [12]. Some other quadruply-bridged dimolybdenum complexes in which the single Mo—Mo bond length are very close to the Mo—Mo double bond lengths are $Cp_2Mo_2(\mu\text{-SMe})_4$ [2.603(2) Å] [11] and $Cp^*_2Mo_2Br_4$ ($Cp^* = \eta^5$-1-(2,5-dimethoxyphenyl)-2,3,4,5-tetraphenylcyclo-pentadienyl] [2.691 (4) Å] [13]. The other quadruply-bridged dimolybdenum complexes with Mo═Mo double bond are *trans*/*anti*-$(\eta^5\text{-}MeC_5H_4)_2Mo_2(\mu\text{-S})_2(\mu\text{-SMe})_2$ [2.582(1) Å] [14], *trans*/*anti*-$(\eta^5\text{-}Me_5C_5)_2Mo_2(\mu\text{-S})_2(\mu\text{-SMe})_2$ [2.573(1) Å] [15], *trans*/*syn*-$(\eta^5\text{-}^iPrC_5H_4)_2Mo_2(\mu\text{-S})_2(\mu\text{-S}^tBu)_2$ [2.587(1) Å] [16] and *trans*/*syn*-$(\eta^5\text{-}C_5H_5)_2Mo_2(\mu\text{-Se})_2(\mu\text{-SePh})_2$ [2.653(2) Å] [17].

EXPERIMENTAL

All reactions were carried out under prepurified nitrogen using vacuum-line techniques. Toluene was distilled from sodium-benzophenone ketyl. Preparative TLC was carried out on glass plates (26 × 19 cm) coated with silica gel G (10–40 μm). $(\eta^5\text{-}RC_5H_4)_2Mo_2(CO)_2(\mu\text{-SPh})_2$ (R = MeO_2C, EtO_2C) were prepared according to published method [6]. IR spectra were recorded on NICOLET MAGNA FT-750 and BIO-RAD FTS-40 infrared spectrophotometers. ^{1}H NMR spectra were recorded on a JEOL FX 90Q NMR spectrometer. C/H analyses and MS determinations were performed by a 240C analyzer and an HP 5988A spectrometer, respectively. Melting points were determined on a YANACO MP-500 micro-melting point apparatus.

Preparation of **1a**, **1b** *and* **1c**

A 100 cm^3 two-necked flask fitted with a magnetic stir-bar, a rubber septum, and a reflux condenser topped with a nitrogen inlet tube was charged with 0.400 g (0.562 mmol) of $(\eta^5\text{-}MeO_2CC_5H_4)_2Mo_2(CO)_2(\mu\text{-SPh})_2$, 0.178 g (2.254 mmol) of selenium powder and 30 cm^3 of toluene. The mixt. was refluxed for 4 h. Solvent was removed at red. pres. and the residue was subjected to preparative TLC separation using CH_2Cl_2 as eluent to give three major bands (Blue, sky-blue and yellow), from which were obtained 0.120 g (26%) of **1a**, 0.070 g (15%) of **1b** and 0.080 g (17%) of **1c**, respectively. **1a**: m.p. 243–244°C. Found: C, 38.55; H, 2.71. Calc. for $C_{26}H_{24}Mo_2O_4S_2Se_2$: C, 38.34; H, 2.97%. IR (KBr, disk): 1719 vs ($\nu_{C=O}$), 502 w, 486 w, 463 w, 433 w, 426 w cm^{-1}. ^{1}H NMR ($CDCl_3$): δ 3.72 (s, 6H, $2CH_3$), 6.24–7.28 [m, 18H, 2 ($C_6H_5 + C_5H_4$)] ppm. MS (EI), *m*/*z* (rel. int.): 820 (M^+, 4.5%), 743 [$(M-Ph)^+$, 6.8], 702 [$(M-2MeO_2C)^+$, 6.7], 625 [$(M-2MeO_2C-Ph)^+$, 4.6], 574 [$(M-2C_5H_4CO_2Me)^+$, 4.8], 516 [$(C_5H_4)_2Mo_2SSe_2^+$, 3.3], 497 ($PhMo_2S_2Se_2^+$, 11.2), 484 ($C_5H_4Mo_2S_2Se_2^+$, 7.8), 468 [$(C_5H_4)_2Mo_2S_2Se^+$, 8.2], 436 [$(C_5H_4)_2Mo_2SSe^+$, 5.2], 420 ($Mo_2S_2Se_2^+$, 11.7), 388 ($Mo_2SSe_2^+$, 8.8), 356 ($Mo_2Se_2^+$, 3.5), 340 ($Mo_2S_2Se^+$, 6.9), 324 [$(C_5H_4)_2Mo_2^+$, 3.6], 308

(Mo_2SSe^+, 5.7), 260 ($Mo_2S_2^+$, 3.7), 109 (PhS^+, 16.8), 92 [$C_5H_4(CO)^+$, 45.1], 77 (Ph^+, 37.5). **1b**: m.p. 188°C (dec.). Found: 38.32; H, 2.92. Calc. for $C_{26}H_{24}Mo_2O_4S_2Se_2$: C, 38.34; H, 2.97%. IR (KBr, disk): 1720 vs ($\nu_{C=O}$), 500 w, 467 w cm^{-1}. ^1H NMR ($CDCl_3$): δ 3.77 (s, 6H, $2CH_3$), 6.50–7.00 [m, 18H, 2($C_6H_5+C_5H_4$)] ppm. MS (EI), *m/z* (rel. int.): 820 (M^+, 2.0%), 740 [$(M-Se)^+$, 2.9], 702 [$(M-2MeO_2C]^+$, 2.0], 625 [$(M-2MeO_2C-Ph)^+$, 3.5], 497 ($PhMo_2S_2Se_2^+$, 2.9), 484 ($C_5H_4Mo_2S_2Se_2^+$, 2.0), 388 ($Mo_2SSe_2^+$, 2.3), 356 ($Mo_2Se_2^+$, 1.5), 340 ($Mo_2S_2Se^+$, 1.5), 324 [$(C_5H_4)_2Mo_2^+$, 1.9], 308 (Mo_2SSe^+, 1.2), 196 (Mo_2^+, 7.3), 109 (PhS^+, 34.4), 92 [$C_5H_4(CO)^+$, 32.9], 77 (Ph^+, 100). **1c**: m.p. 217–218°C. Found: C, 38.14; H, 3.23. Calc. for $C_{26}H_{24}Mo_2O_4S_2Se_2$: C, 38.34; H, 2.97%. IR (CsI, disk): 1700 vs ($\nu_{C=O}$), 508 w, 488 w, 434 w, 369 w, 337 w, 270 w, 257 w, 229 w, 208 w cm^{-1}. ^1H NMR ($CDCl_3$): δ 3.57 (s, 6H, $2CH_3$), 5.24 [br s, 4H, 2 (H^3, H^4)], 5.52 [br s, 4H, 2 (H^2, H^5)], 7.00 (s, 10H, $2C_6H_5$) ppm.

Preparation of **2a**, **2b** *and* **2c**

The similar reaction of 0.400 g (0.540 mmol) of (η^5-$EtO_2CC_5H_4)_2Mo_2(CO)_2(\mu$-SPh)$_2$, 0.171 g (2.166 mmol) of selenium powder afforded 0.086 g (19%) of **2a**, 0.019 g (4%) of **2b** and 0.135 g (30%) of **2c**, **2a**: m.p. 237–238°C. Found: C, 39.96; H, 3.28. Calc. for $C_{28}H_{28}Mo_2O_4S_2Se_2$: C, 39.92; H, 3.35%. IR (CsI, disk): 1700 vs ($\nu_{C=O}$), 516 w, 491 w, 470 w, 432 w, 407 w, 385 w, 249 w cm^{-1}. ^1H NMR ($CDCl_3$): δ 1.20 (t, 6H, $J = 7.2$ Hz, $2CH_3$), 4.24 (q, 4H, $J = 7.2$ Hz, $2CH_2$), 6.24–7.40 [m, 18H, 2($C_6H_5+C_5H_4$)] ppm. MS (EI), *m/z* (rel. int.): 534 [$(M-2Ph-2Se)^+$, 0.8%], 484 ($C_5H_4Mo_2S_2Se_2^+$, 1.4), 436 [$(C_5H_4)_2Mo_2SSe^+$, 1.7], 420 ($Mo_2S_2Se_2^+$, 2.1), 388 ($Mo_2SSe_2^+$ 1.5), 356 ($Mo_2Se_2^+$, 2.0), 340 ($Mo_2S_2Se^+$, 1.0), 308 (Mo_2SSe^+, 1.1), 109 (PhS^+, 50.9), 92 [$C_5H_4(CO)^+$, 35.7], 77 (Ph^+, 58.6). **2b**: m.p. 155–156°C. Found: C, 39.89; H, 3.41. Calc. for $C_{28}H_{28}Mo_2O_4S_2Se_2$: C, 39.92; H, 3.35%. IR (CsI, disk): 1707 vs ($\nu_{C=O}$), 504 w, 490 w, 461 w, 380 w, 334 w, 245 w, 231 w, 216 w, 208 w cm^{-1}. ^1H NMR ($CDCl_3$): δ 1.27 (t, 6H, $J = 7.2$ Hz, $2CH_3$), 4.30 (q, 4H, $J = 7.2$ Hz, $2CH_2$), 6.54–7.08]m, 18H, 2($C_6H_5+C_5H_4$)] ppm. MS (EI), *m/z* (rel. int.): 848 (M^+, 2.0%), 771 [$(M-Ph)^+$, 3.4], 614 [$(M-2Ph-Se)^+$, 4.2], 534 [$(M-2Ph-2Se)^+$, 2.7], 516 [$(C_5H_4)_2Mo_2SSe_2^+$, 2.5], 484 ($C_5H_4Mo_2S_2Se_2^+$, 4.8), 468 [$(C_5H_4)_2Mo_2S_2Se^+$, 4.5], 436 [$(C_5H_4)_2Mo_2SSe^+$, 5.3], 420 ($Mo_2S_2Se_2^+$, 6.5), 388 ($Mo_2SSe_2^+$, 4.5), 356 ($Mo_2Se_2^+$, 5.7), 340 ($Mo_2S_2Se^+$, 3.0), 324 [$(C_5H_4)_2Mo_2^+$, 1.6], 308 (Mo_2SSe^+, 2.2), 260 ($Mo_2S_2^+$, 1.1), 196 (Mo_2^+, 2.0), 109 (PhS^+, 50.2), 92 [$C_5H_4(CO)^+$, 40.1], 77 (Ph^+, 57.1). **2c**: m.p. 190–191°C. Found: C, 40.27; H, 3.23. Calc. for $C_{28}H_{28}Mo_2O_4S_2Se_2$: C, 39.92; H, 3.35%. IR (CsI, disk): 1707 vs ($\nu_{C=O}$), 521 w, 490 w, 436 w, 429 w, 369 w, 354 w, 329 w, 228 w, 203 w cm^{-1}. ^1H NMR ($CDCl_3$): δ 1.20 (t, 6H, $J = 7.2$ Hz, $2CH_3$), 4.18 (q, 4H, $J = 7.2$ Hz, $2CH_2$), 5.40 [br s, 4H, 2(H^3, H^4)], 5.72 [br s, 4H, 2(H^2, H^5)], 7.20 (s, 10H, $2C_6H_5$) ppm. MS (EI), *m/z* (rel. int.): 659 [$(M-PhSSe)^+$, 0.6%], 470 [$(EtO_2CC_5H_4)_2Mo_2^+$, 0.9], 436 [$(C_5H_4)_2Mo_2SSe^+$, 0.5], 404 [$(C_5H_4)_2Mo_2Se^+$, 0.5], 388 ($Mo_2SSe_2^+$, 0.8), 356 ($Mo_2Se_2^+$, 0.5), 324 [$(C_5H_4)_2Mo_2^+$, 0.4], 308 (Mo_2SSe^+, 2.0), 260 ($Mo_2S_2^+$, 1.0), 196 (Mo_2^+, 1.4), 109 (PhS^+, 100), 98 (Mo^+, 2.7), 92 [$C_5H_4(CO)^+$, 21.6], 77 (Ph^+, 46.6).

Structure determination of **2c**

Suitable single crystals of **2c** for X-ray diffraction study were obtained by slow evaporation of a CH_2Cl_2/hexane solution. A single crystal with dimensions of $0.40 \times 0.30 \times 0.25$ mm for **2c** was mounted on a glass fibre with epoxy resin. Data collections were performed on a Enraf-Nonius CAD4 diffractometer equipped with a graphite monochromator at room temperature (23 ± 1°C). Details of its crystal parameters, data collections and structure refinements are summarized in Table 2. Lorentz and polarization corrections, and absorption correction were applied to the data. The structure was solved by the direct

Table 2. Details of crystal parameters, data collections and structure refinements for **2c**

Molecular formula	$C_{28}H_{28}Mo_2O_4S_2Se_2$
Molecular weight	842.45
Color and habit	yellow needle
Crystal system	monoclinic
Space group	$P2_1/n$ (No. 14)
a (Å)	11.526(3)
b (Å)	14.876(2)
c (Å)	17.057(4)
α (°)	90.00
β (°)	96.14(2)
γ (°)	90.00
V (Å^3)	2908(1)
Z	4
D_{calc} (g cm^{-3})	1.92
F(000)	1648
μ (cm^{-1})	34.92
λ(Mo–K_α) (Å)	0.71069
Scan type	$\omega/2\theta$ scan
Scan width (°)	$0.40+0.35\ tg\theta$
Scan speed (° cm^{-1})	<5.49
$2\theta_{max}$ (°)	49.9
No. of reflections measured	5618
No. of reflections, unique	5416
No. of reflections observed, *n*	4172 ($I \geqslant 3\sigma(I)$)
No. of variables, *p*	343
R	0.054
R_w	0.067
GOF	1.93
Largest Δ/σ in final cycle	0.02
$\Delta\rho$ (min/max) (e Å^{-3})	$-1.78/+1.83$

methods (MITHRIL). The final refinements were accomplished by the full-matrix least-squares method with anisotropic thermal parameters for non-hydrogen atoms. All calculations were performed on Micro VAX II computer using the TEXSAN program package.

Acknowledgements—We are grateful to the National Natural Science Foundation of China, the State Key Laboratory of Structural Chemistry and the Special Foundation of State Education Committee of China for financial support of this work.

REFERENCES

1. Curtis, M. D., *Polyhedron*, 1987, **6,** 759.
2. Song, L.-C. and Wang, J.-Q., *Youji Huaxue*, 1994, **14,** 225.
3. Gueguen, M., Petillon, F. Y. and Talarmin, J., *Organometallics*, 1989, **8,** 148.
4. Li, P. and Curtis, M. D., *J. Am. Chem. Soc.*, 1989, **111,** 8279.
5. Song, L.-C., Wang, J.-Q., Hu, Q.-M. and Huang, X.-Y., *Polyhedron*, 1996, **15,** 4295.
6. Song, L.-C., Wang, J.-Q., Hu, Q.-M. and Huang, X.-Y., *Polyhedron*, 1997, **16,** 2249.
7. (a) Wachter, J., *J. Coord. Chem.*, 1987, **15,** 219; (b) Wachter, J., *Angew. Chem. Int. Ed. Engl.*, 1989, **28,** 1613; (c) Shibahara, T., *Coord. Chem. Rev.*, 1992, **123,** 73.
8. Li, P. and Curtis, M. D., *Inorg. Chem.*, 1990, **29,** 1242.
9. Campana, C. F., Yip-Kwailo, F. and Dahl, L. F., *Inorg. Chem.*, 1979, **18,** 3060.
10. Zingaro, R. A. and Copper, W. C., *Selenium*, Van Nostrand Reinhold: New York, 1974, p. 303.
11. Connelly, N. G. and Dahl, L. F., *J. Am. Chem. Soc.*, 1970, **92,** 7470.
12. Klingler, R. J., Butler, W. M. and Curtis, M. D., *J. Am. Chem. Soc.*, 1978, **100,** 5034.
13. Saadeh, C., Colbran, S. B., Craig, D. C. and Rae, A. D., *Organometallics*, 1993, **12,** 133.
14. DuBois, M. R., VanDerveer, M. C., BuBois, D. L., Haltiwanger, R. C. and Miller, W. K., *J. Am. Chem. Soc.*, 1980, **102,** 7456.
15. Brunner, H., Meier, W., Wachter, J., Weber, P., Ziegler, M. L., Enemark, J. H. and Young, C. G., *J. Organomet. Chem.*, 1986, **309,** 313.
16. Chen, M., Bandy, J. A. and Prout, K., *Jiegou Huaxue*, 1986, **5,** 18.
17. Rakoczy, H., Schollenberger, M., Nuber, B. and Ziegler, M. L., *J. Organomet. Chem.*, 1994, **467,** 217.

Pergamon

PII: S0277-5387(98)00179-X

Polyhedron Vol. 17, No. 21, pp. 3765–3769, 1998
© 1998 Elsevier Science Ltd
All rights reserved. Printed in Great Britain
0277–5387/98 $19.00+0.00

Reaction of poly(pyrazol-1-yl)methane tetracarbonylmolybdenum (tungsten) with $RSnCl_3$(R = Ph, Cl): X-ray crystal structure of $CH_2(3,5\text{-}Me_2Pz)_2W(Cl)(CO)_3(SnCl_3)$ (Pz:pyrazolyl)

Liangfu Tang,[a] Zhihong Wang,[a] Yuming Xu,[a] Jitao Wang,[a]* Honggen Wang[b] and Xingkai Yao[b]

[a]Department of Chemistry, Nankai University, Tianjin 300071, P.R. China

[b]Central Lab. of Nankai University, Tianjin 300071, P.R. China

(Received 21 January 1998; accepted 24 April 1998)

Abstract—Bis(pyrazolyl)methane can be synthesized by the reaction of pyrazole with dibromomethane in phase transfer catalytic conditions. It reacts with $M(CO)_6$ (M = Mo, W) to give bis(pyrazolyl)methane tetracarbonylmolybdenum(0) and tungsten(0) complexes in good yield. Upon treatment of these complexes with $RSnCl_3$ (R = Ph, Cl), the seven-coordinate Mo(II) and W(II) products were obtained. The molecular structure of $CH_2(3,5\text{-}Me_2Pz)_2W(Cl)(CO)_3(SnCl_3)$ determined by X-ray crystallography showed that the six-membered W–N–N–C–N–N metallacycle was in a boat form. © 1998 Elsevier Science Ltd. All rights reserved

Keywords: poly(pyrazolyl)alkanes; bimetallic complexes; X-ray structure

INTRODUCTION

Although heterobimetallic complexes containing M–Sn (M = Mo, W) bonds have been studied for nearly three decades [1, 2], the synthesis and characterization of these complexes is still an active area of organometallic chemistry, because of their catalytic properties [3, 4]. Recently, many complexes containing Mo–Sn bonds have been reported [5–11]. The VIB metals carbonyl complexes bonded with poly(pyrazolyl)alkanes have novel structures and unusual reactivities [12–14], which encourage us to investigate M–Sn bimetallic complexes with poly(pyrazolyl)alkanes. To the best of our knowledge, there have been no reports on these complexes. In this paper, we describe a high yield synthesis of these complexes and the crystal structure of $CH_2(3,5\text{-}Me_2Pz)_2W(Cl)(CO)_3(SnCl_3)$.

* Author to whom correspondence should be addressed.

EXPERIMENTAL DETAILS

All reactions were carried out under an argon atmosphere. All solvents were dried by standard methods. ^1H NMR spectra were recorded on JEOL FT-90X and BRUKER AC-P-200 spectrometers, IR spectra data were obtained from a Nicolet-FT IR 5DX spectrometer. Elemental analyses were carried out on a Perkin-Elmer 240C analyzer. $CH_2(3,5\text{-}Me_2Pz)_2Mo(CO)_4$ [15], $CH_2(3,5\text{-}Me_2Pz)_2W(CO)_4$ [15], $C_6H_5SnCl_3$ [16] were prepared according to the literature methods. $Mo(CO)_6$ and $W(CO)_6$ were purchased from Fluka.

Synthesis of bis(pyrazolyl)methane(CH_2Pz_2)

Into a mixed solvent of benzene (60 ml) and water (25 ml) pyrazole (0.13 mol), dibromomethane (0.065 mol), tetrabutylammonium bromide (0.75 g), and sodium hydroxide (25 g) were added. The mixture was stirred and refluxed for 48 h. After cooling to the

room temperature, the benzene layer was separated and the water phase was extracted with dichloromethane (3×40 ml). The organic layers were combined and dried by $MgSO_4$. After evaporating the solvent, the residue was washed with cooled petroleum ether (2×20 ml), sublimed *in vacuo* under 100°C. Yield: 67%. m.p 109–111°C (Ref. [17]: m.p 108–111°C).

Preparation of $CH_2Pz_2Mo(CO)_4$ and $CH_2Pz_2W(CO)_4$

A solution of $Mo(CO)_6$ (2 mmol) and CH_2Pz_2 (2 mmol) in dried heptane (40 ml) was stirred and refluxed for 4 h at an argon atmosphere, during this period a yellow precipitate formed. After cooling, the precipitate was filtered off, washed with heptane, and dried *in vacuo*. Yield: 73%.

Compound $CH_2Pz_2W(CO)_4$ was obtained by a similar method described above in octane with a refluxing time of 24 h. Yield: 40%. The analytic data of $CH_2Pz_2Mo(CO)_4$ and $CH_2Pz_2W(CO)_4$ were in accordance with that of the literature [18].

Reaction of $CH_2Pz_2M(CO)_4$ with $RSnCl_3$

Due to the fact that all reactions were similar, a general procedure was described. To a stirred solution of $CH_2Pz_2M(CO)_4$ (1 mmol) suspended in 50 ml of acetonitrile, $RSnCl_3$ (1 mmol) was added by syringe. Stirring continued at room temperature for two hours, the solution became clear. After filtering, the solution was concentrated to dryness *in vacuo*. The residue was recrystallized from dichloromethane/hexane.

$CH_2Pz_2Mo(CO)_3(Cl)SnCl_2Ph$ (**I**): Yield: 74%. Yellow solid. Anal. Found: C, 28.65; H, 2.25; N, 8.38. $C_{16}H_{13}Cl_3MoN_4O_3Sn{\cdot}CH_2Cl_2$ Calcd: C, 28.51; H, 2.10; N, 7.83%. ^{1}H NMR (CD_3COCD_3): δ 8.37(d, 2, 3-H pz); 8.28(d, 2, 5-H pz); 7.98, 7.48(m, m, 2, 3, C_6H_5); 7.28, 6.89(d, d, 1, 1, CH_2); 6.70(t, 2, 4-H pz)ppm. IR (KBr): ν(CO) 2016.0(vs), 1925.8(s), 1893.0(vs); ν(pyrazole ring) 1523.8(m) cm^{-1}.

$CH_2Pz_2W(CO)_3(Cl)SnCl_2Ph$ (**II**): Yield: 68%. Yellow solid. Anal. Found: C, 26.74; H, 1.82; N, 7.87. $C_{16}H_{13}Cl_3N_4O_3SnW$ Calcd: C, 26.74; H, 1.81; N, 7.79%. ^{1}H NMR(CD_3COCD_3): δ 8.35(d, 2, 3-H pz); 8.30(d, 2, 5-H pz); 7.90, 7.47(m, m, 2, 3, C_6H_5); 7.41, 6.85(d, d, 1, 1, CH_2); 6.71(t, 2, 4-H pz)ppm. IR(KBr): ν(CO) 1999.1(vs), 1915.0(sh), 1884.8(vs); ν(pyrazole ring) 1523.8(m) cm^{-1}.

$CH_2Pz_2Mo(CO)_3(Cl)SnCl_3$ (**III**): Yield: 76%. Red solid. Anal. Found: C, 20.51; H, 1.49; N, 9.24. $C_{10}H_8Cl_4MoN_4O_3Sn$ Calcd: C, 20.37; H, 1.36; N, 9.51%. ^{1}H NMR(CD_3COCD_3): δ 8.33(d, 2, 3-H pz); 8.18(d, 2, 5-H pz); 7.27, 6.87(d, d, 1, 1, CH_2); 6.71(t, 2, 4-H pz)ppm. IR (KBr): ν(CO) 2032.4(vs), 1950.4(sh), 1884.8(vs); ν(pyrazole ring) 1515.6(m) cm^{-1}.

$CH_2Pz_2W(CO)_3(Cl)SnCl_3$ (**IV**): Yield: 54%. Yellow solid. Anal. Found: C, 17.46; H, 1.29; N, 8.56. $C_{10}H_8Cl_4N_4O_3SnW$ Calcd: C, 17.73; H, 1.18; N, 8.67%. ^{1}H NMR (CD_3COCD_3): δ 8.36(d, 2, 3-H pz); 8.15(d, 2, 5-H pz); 7.46, 6.65(d, d, 1, 1, CH_2); 6.72(t, 2, 4-H pz)ppm. IR(KBr): ν(CO) 2024.2(vs), 1948.0(sh), 1904.4(vs); ν(pyrazole ring) 1515.6(m) cm^{-1}.

Reaction of $CH_2(3,5\text{-}Me_2Pz)_2M(CO)_4$ with $RSnCl_3$

$RSnCl_3$(1 mmol) was added to a solution of $CH_2(3,5\text{-}Me_2Pz)_2M(CO)_4$ dissolved in 20 ml of dichloromethane via syringe. The color of the solution became orange–red immediately. After stirring for an hour at room temperature, the solution was concentrated to ca. 10 ml under reduced pressure, and then 10 ml of hexane was slowly added to the solution. After standing overnight, a yellow to red microcrystalline was obtained.

$CH_2(3,5\text{-}Me_2Pz)_2Mo(CO)_3(Cl)SnCl_2Ph$ (**V**): Yield: 92%. Yellow solid. Anal. Found: C, 32.73; H, 2.79; N, 7.69. $C_{20}H_{21}Cl_3MoN_4O_3Sn{\cdot}CH_2Cl_2$ Calcd: C, 32.66; H, 2.98; N, 7.26%. ^{1}H NMR (CD_3COCD_3): δ 8.05, 7.50(m, m, 2, 3, C_6H_5); 6.64, 6.12(d, d, 1, 1, CH_2); 6.20(s, 2, 4-H pz); 2.56, 2.34(s, s, 6, 6, 3 or 5-CH_3)ppm. IR (KBr): ν(CO) 1999.6(vs), 1909.4(vs), 1837.5(sh); ν(pyrazole ring) 1556.6(m) cm^{-1}.

$CH_2(3,5\text{-}Me_2Pz)_2W(CO)_3(Cl)SnCl_2Ph$ (**VI**): Yield: 71%. Yellow solid. Anal. Found: C, 30.26; H, 2.51; N, 7.26. $C_{20}H_{12}Cl_3N_4O_3SnW{\cdot}1/2CH_2Cl_2$ Calcd: C, 30.15; H, 2.70; N, 6.86%. ^{1}H NMR(CD_3COCD_3): δ 7.78, 7.47(m, m, 2, 3, C_6H_5); 6.68, 6.23(d, d, 1, 1, CH_2); 6.26(s, 2, 4-H pz); 2.58, 2.33(s, s, 6, 6, 3 or 5-CH_3)ppm. IR(KBr): ν(CO) 1991.4(vs), 1893.0(vs), 1808.3(sh); ν(pyrazole ring) 1556.6(m) cm^{-1}.

$CH_2(3,5\text{-}Me_2Pz)_2Mo(CO)_3(Cl)SnCl_3$ (**VII**): Yield: 82%. Red solid. Anal. Found: C, 25.68; H, 2.66; N, 8.89. $C_{14}H_{16}Cl_4MoN_4O_3Sn$ Calcd: C, 26.05; H, 2.48; N, 8.68%. ^{1}H NMR(CD_3COCD_3): δ 6.72, 6.20(d, d, 1, 1, CH_2); 6.39(s, 2, 4-H pz); 2.59, 2.48(s, s, 6, 6, 3 or 5-CH_3)ppm. IR(KBr): ν(CO) 2016.0(vs), 1942.2(vs), 1917.6(vs); ν(pyrazole ring) 1556.6(m) cm^{-1}.

$CH_2(3,5\text{-}Me_2Pz)_2W(CO)_3(Cl)SnCl_3$ (**VIII**): Yield: 90%. Red solid. Anal. Found: C, 22.87; H, 2.05; N, 7.48. $C_{14}H_{16}Cl_4N_4O_3SnW$ Calcd: C, 22.92; H, 2.18; N, 7.64%. ^{1}H NMR (CD_3COCD_3): δ 6.81, 6.24(d, d, 1, 1, CH_2); 6.36(s, 2, 4-H pz); 2.63, 2.48(s, s, 6, 6, 3 or 5-CH_3)ppm. IR(KBr): ν(CO) 2032.4(vs), 1958.8(vs), 1925.8(vs); ν(pyrazole ring) 1555.6(m) cm^{-1}.

Structure determination of $CH_2(3,5\text{-}Me_2Pz)_2W(Cl)(CO)_3(SnCl_3)$

Crystals suitable for X-ray analysis were grown from dichloromethane/hexane at 4°C. Crystal data are summarized in Table 1. All intensity data were collected on an Enraf-Nonius CAD4 diffractometer with graphite monochromated Mo-Kα radiation. A total of 2952 independent reflections was collected in the range of $2 \leqslant \theta \leqslant 23°$ by the $\omega/2\theta$ scan mode, of which 2725 reflections with $I \geq 3\sigma(I)$ were considered to be observed and used for subsequent refinement. A correction for empirical absorption was applied to

Table 1. Crystal data for $CH_2(3,5\text{-}Me_2Pz)_2$ W(Cl)$(CO)_3(SnCl_3)$

Formula	$C_{14}H_{16}Cl_4N_4O_3SnW$
F.W.	732.66
Crystal size (mm)	$0.2\times0.3\times0.4$
Crystal class	triclinic
Space group	P-1
Cell parameters	
a	9.984(2) Å
b	10.649(2) Å
c	10.760(2) Å
α	94.24(3)°
β	95.59(3)°
γ	104.42(3)°
V	1097(1) Å^3
Z	2
T (K)	299
Calcd density ($Mg\,m^{-3}$)	2.218
$F(000)$	688
λ (MoKα)	0.71973 Å
μ (mm^{-1})	7.0108
No. of reflections measured	3165
No. of reflections observed $I\geq 3o(I)$	2725
No. of parameters	244
Weighting scheme	$W=1/[\sigma^2(F)+0.0001F^2]$
Residuals R, Rw	0.058, 0.067

intensity data, and the structure was solved by direct methods. The final refinement by full-matrix least-squares method with anisotropic thermal parameters for non-hydrogen atoms was converged to unweighted and weighted agreement factors of 0.058 and 0.067. All calculations were performed on a PDP11/44 computer using SDP-PLUS program system.

RESULTS AND DISCUSSION

The ligand, CH_2Pz_2, has previously been synthesized by the reaction of pyrazole with dibromomethane [17]. In our work, the ligand was prepared by a similar method used for bis(3,5-dimethylpyrazolyl)methane [19]. $CH_2Pz_2Mo(CO)_4$ and $CH_2Pz_2W(CO)_4$ were synthesized by the reaction of CH_2Pz_2 and $M(CO)_6$ in toluene [18]. These compounds could also be obtained from the reaction between CH_2Pz_2 and $M(CO)_6$ in hydrocarbon solvents. Upon treatment $CH_2Pz_2M(CO)_4$ in acetonitrile, $CH_2(3,5\text{-}Me_2Pz)_2M(CO)_4$ in dichloromethane with $RSnCl_3$, the seven coordinate oxidate-addition products $CH_2Pz_2M(Cl)(CO)_3(SnCl_2R)$ and $CH_2(3,5\text{-}Me_2Pz)_2M(Cl)(CO)_3(SnCl_2R)$ were obtained in good yield, as follows:

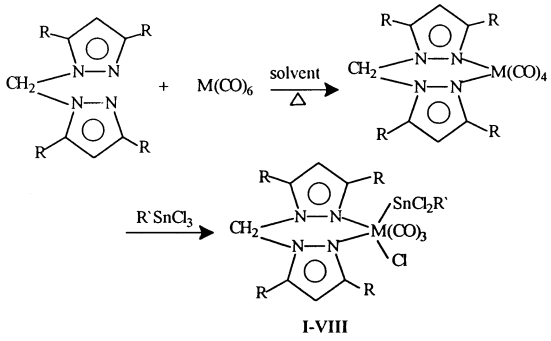

I-VIII

(R=H, CH_3; R'=Ph, Cl; M=Mo, W)

These complexes in solid form were stable in air, even in the solution, which could be stored for a period time without obvious decomposition. These complexes were yellow to red crystalline solids, which were moderate soluble in dichloromethane, but very soluble in strong polar solvents such as acetone.

Three typical infrared spectra bands in the carbonyl stretching region were observed in all complexes, which were in agreement with suggested structures. The ν(CO) frequency in the complexes containing $SnCl_3$ group was higher than that of the complexes containing $SnCl_2Ph$ group, which could be easily understood due to $SnCl_3$ group being more electronegative. The IR spectra of heterocyclic ligands at 1500–1560 cm^{-1} were hardly affected by the $SnCl_2Ph$ or $SnCl_3$ group.

The ^{1}H NMR spectra were very interesting. A typical AB system was observed. The ^{1}H NMR spectra of all complexes showed the protons of methylene group were in different environment, which exhibited two sets of resonances. These results were consistent with the boat conformation of complexes (one case shown in Fig. 1), the ^{1}H NMR spectra indicated the boat form was also maintained in solution. The fluxional process expected in these complexes must be present, but cannot give time-averaging singlet at

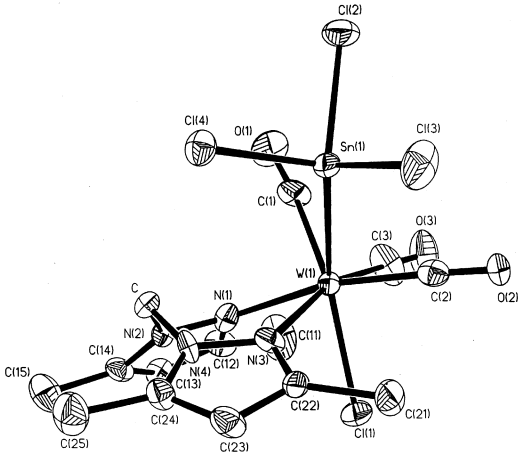

Fig. 1. The molecular structure of VIII.

room temperature on the NMR time scale. We think the presence of Cl and $SnCl_3$ groups, one below and the other above the quadrilateral face, slows the fluxional process of a boat to boat ring flip.

Selected bond lengths and bond angles for $CH_2(3,5\text{-}Me_2Pz)_2W(Cl)(CO)_3(SnCl_3)$ (**VIII**) are listed in Table 2. The crystal structure of **VIII** is presented in Fig. 1. It shows the six membered W–N–N–C–N–N metallacycle adopts the boat conformation, analogous to that in $CH_2(3,4,5\text{-}Me_3Pz)_2W(CO)_2I_2$ [14] (**1**). However, the configurations of tungsten atom are remarkable different, which is a distorted capped octahedron in **1** [14]. In present work, the tungsten atom is seven coordinate with a geometry that is best described as a distorted capped trigonal prism with a chlorine atom, Cl(1), in the unique capping position, and the W–Cl(1) bond length is 2.425 Å. The quadrilateral face consists of two carbonyl groups, C(2)O(2) and C(3)O(3), two nitrogen atoms, N(1) and N(3), which is distorted due to the two W–N bond length [W(1)–N(1) 2.248(10); W(1)–N(3) 2.243(10) Å] longer than the two W–CO distances [W(1)–C(2) 1.986(13); W(1)–C(3) 1.961(17) Å]. Thus, the configuration of tungsten atom is similar to that of $W(Cl)(SnCl_3)(CO)_3(\eta^4\text{-NBD})$ [11] (**2**). The W–Sn distance is 2.741(1) Å and is within the normal range for such bonds [19].

The environment around the tin atom is a distorted tetrahedral geometry. Three Sn–Cl bond lengths are slightly different, Sn(1)–Cl(2) at 2.348(4) Å, Sn(1)–Cl(3) at 2.331(5) Å and Sn(1)–Cl(4) at 2.379(3) Å, respectively. An interesting feature of the structure of **VIII** is that the chlorine bonded to tungsten is in the unique capping position and *trans* to $SnCl_3$ group. The Sn(1)–W–Cl(1) angle is 145.9(1)°, so, there is no chlorine atom bridge between the W–Sn bond. This feature is considerably different from that of the seven coordinated complexes containing W–Sn or Mo–Sn bond such as $W(Cl)(SnCl_3)(CO)_3(L_2)$ ($L = CH_3CN$, PPh_3, dppe, bipy, etc.) [11], $Mo(Cl)(MeSnCl_2)(CO)_3(C_{10}H_8N_2)$ [20], which was described a distorted capped octahedron geometry with a tin atom in the unique capping position and a chlorine atom bridging the W–Sn or Mo–Sn bond, and also different from that of **2** (the $SnCl_3$ group in the apical position).

Acknowledgements—This work has been supported by State Key Laboratory of Elemento-Organic Institute of Nankai University.

REFERENCES

1. Kumer, R. and Graham, W. A. G., *Inorg. Chem.*, 1968, **7,** 630.
2. Edgar, K., Johnson, B. F., Lewis, J. and Wild, S. B., *J. Chem. Soc.* A, 1968, 2851.
3. Szymanska-Buzar, T., *J. Catal.*, 1994, **93,** 137.
4. Zhang, H. X., Guibe, F. and Balavoine, G., *J. Org. Chem.*, 1990, **55,** 1857.
5. Baker, P. K. and Bury, A., *J. Organomet. Chem.*, 1989, **359,** 189.
6. Miguel, D., Perez-Martinez, J. A., Riera, V. and Garcia-Granda, S., *Polyhedron*, 1991, **10,** 1717.
7. Miguel, D., Perez-Martinez, J. A., Riera, V. and

Table 2. Selected bond lengths (Å) and bond angles (°)

W(1)–Sn(1)	2.741(1)	W(1)–C(2)	1.986(13)
W(1)–Cl(1)	2.425(3)	W(1)–C(3)	1.961(17)
W(1)–N(1)	2.248(10)	Sn(1)–Cl(2)	2.348(4)
W(1)–N(3)	2.243(10)	Sn(1)–Cl(3)	2.331(5)
W(1)–C(1)	1.972(11)	Sn(1)–Cl(4)	2.379(3)
Sn(1)–W(1)–Cl(1)	145.9(1)	W(1)–N(3)–N(4)	123.1(8)
Sn(1)–W(1)–N(1)	120.3(2)	W(1)–N(3)–C(22)	133.6(7)
Cl(1)–W(1)–N(1)	79.6(2)	W(1)–C(1)–O(1)	171.8(14)
Sn(1)–W(1)–N(3)	75.2(2)	W(1)–C(2)–O(2)	174.2(11)
Cl(1)–W(1)–N(3)	81.0(2)	W(1)–C(3)–O(3)	173.7(15)
N(1)–W(1)–N(3)	82.8(4)	Sn(1)–W(1)–C(2)	72.8(3)
Sn(1)–W(1)–C(1)	70.3(4)	Cl(1)–W(1)–C(2)	87.7(3)
Cl(1)–W(1)–C(1)	143.8(5)	N(1)–W(1)–C(2)	166.6(4)
N(1)–W(1)–C(1)	76.8(5)	N(3)–W(1)–C(2)	99.5(6)
N(3)–W(1)–C(1)	122.2(5)	C(1)–W(1)–C(2)	112.2(5)
Cl(1)–W(1)–C(3)	84.3(4)	Sn(1)–W(1)–C(3)	115.6(4)
N(1)–W(1)–C(3)	99.6(6)	W(1)–Sn(1)–Cl(3)	118.6(1)
N(3)–W(1)–C(3)	164.5(5)	Cl(2)–Sn(1)–Cl(3)	99.9(2)
C(1)–W(1)–C(3)	73.1(6)	W(1)–Sn(1)–Cl(4)	115.1(1)
C(2)–W(1)–C(3)	74.8(6)	Cl(2)–Sn(1)–Cl(4)	97.4(1)
W(1)–Sn(1)–Cl(2)	123.3(1)	Cl(3)–Sn(1)–Cl(4)	97.8(1)
W(1)–Sn(1)–Cl(3)	118.6(1)	W(1)–N(1)–N(2)	121.8(8)
Cl(2)–Sn(1)–Cl(3)	99.9(2)	W(1)–N(1)–C(12)	130.2(8)

Garcia-Granda, S., *J. Organomet. Chem.*, 1993, **455,** 121.
8. Cano, M., Panizo, M., Campo, J. A., Tornero, J. and Menendze, N., *J. Organomet. Chem.*, 1993, **463,** 121.
9. Barrado, G., Miguel, D., Perez-Martinez, J. A., Riera, V. and Garcia-Granda, S., *J. Organomet. Chem.*, 1993, **463,** 127.
10. Szymanska-Buzar, T., *J. Organomet. Chem.*, 1995, **492,** 241.
11. Szymanska-Buzar, T. and Glowiak, T., *Polyhedron*, 1997, **16,** 1599.
12. Shiu, K. B. and Liou, K. S., *J. Chin. Chem. Soc.*, 1988, **35,** 187.
13. Shiu, K. B. and Chang, C. J., *J. Chin. Chem. Soc.*, 1989, **36,** 25.
14. Shiu, K. B., Liou, K. S., Wang, S. L. and Wei, S. C., *Organometallics*, 1990, **9,** 669.
15. Shiu, K. B. and Chang, C. J., *J. Chin. Chem. Soc.*, 1987, **34,** 297.
16. Gilman, H. and Gist, L. A.<jr>Jr., *J. Org. Chem.*, 1957, **22,** 368.
17. Trofimenko, S., *J. Am. Chem. Soc.*, 1970, **92,** 5118.
18. Lobbia, G. G. and Bonati, F., *J. Organomet. Chem.*, 1989, **366,** 121.
19. Holt, M. S., Wilson, W. L. and Nelson, J. H., *Chem. Rev.*, 1989, **89,** 11.
20. Elder, M. and Hall, D., *Inorg. Chem.*, 1968, **8,** 1268.

Pergamon

PII: S0277–5387(98)00183–1

Polyhedron Vol. 17, No. 21, pp. 3771–3775, 1998
© 1998 Elsevier Science Ltd
All rights reserved. Printed in Great Britain
0277–5387/98 $19.00+0.00

Synthesis and molecular structure of (*R*,*R*/*S*,*S*)-[$PdCl_2\{1,2\text{-}(PPhCl)_2C_2B_{10}H_{10}\}$][1]

Viktor P. Balema,[a] Steffen Blaurock,[a] Vitalij K. Pecharsky,[b] Evgeny G. Rys[c] and Evamarie Hey-Hawkins[a]*

[a]Institut für Anorganische Chemie der Universität Leipzig, Talstrasse 35, D-04103 Leipzig, Germany; [b]Ames Laboratory, Iowa State University, Ames, IA 50011-3020, U.S.A.; [c]A. Nesmeyanov Institute of Organo-Element Compounds, Vavilov Str. 28, Moscow, Russia

Received 24 February 1998; accepted 23 April 1998

Abstract—The complex (*R*,*R*/*S*,*S*)-[$PdCl_2\{1,2\text{-}(PPhCl)_2C_2B_{10}H_{10}\}$] (**1**) was prepared by the reaction of (*R*,*R*/*S*,*S*)-1,2-$(PPhCl)_2C_2B_{10}H_{10}$ with [(COD)$PdCl_2$] (COD = cyclooctadiene) in CH_2Cl_2 solution and characterized by NMR spectroscopy (^{31}P, ^{11}B, ^{1}H) and X-ray structure determination (space group P^-). Due to the crystallographic center of inversion, both enantiomeric isomers (*R*,*R*) and (*S*,*S*) are present in the unit cell. The Pd atom is coordinated in a square–planar fashion by two chloro ligands and the 1,2-bis(phenylchlorophosphino)-1,2-dicarba-*closo*-dodecaborane(12). © 1998 Elsevier Science Ltd. All rights reserved

Keywords: chlorophosphino-substituted carbaborane; palladium dichloride phosphine complex; molecular structure

Transition metal complexes of functionalized phosphine ligands with reactive phosphorus–halogen bonds are rare [1–13], especially those with bidentate chlorophosphine ligands. While complexes containing bidentate tertiary phosphine ligands have been reported for most transition metals, only a limited number of compounds with chelating chlorophosphine ligands are known [6], and so far complexes that contain chlorophosphine derivatives of dicarba-*closo*-dodecaborane(12) have not been reported. Transition metal chlorophosphine complexes are suitable starting materials for the synthesis of coordinated phosphines by substitution of chloro substituents [2, 5, 8–12, 14].

We now report the synthesis of (*R*,*R*/*S*,*S*)-[$PdCl_2\{1,2\text{-}(PPhCl)_2C_2B_{10}H_{10}\}$] (**1**), which, to our knowledge, is the first transition metal complex containing a chlorophosphino-substituted carbaborane ligand and the first structurally characterized chlorophosphine–$PdCl_2$ complex with a *cis* arrangement.

Palladium complexes of general formula L_2PdCl_2 (L = phosphine) have received increasing attention as catalysts in organic syntheses [15]. However, only a limited number of Pd complexes with chlorophosphine [7–13] or dicarba-*closo*-dodecaborane(12) phosphine [16] ligands have been reported, and only two Pd complexes with chlorophosphine ligands have been structurally characterized [7, 13]. While the preparation of a $PdCl_2$ complex of the 1,2-bis(diphenylphosphino)-1,2-dicarba-*closo*-dodecaborane (12) ligand was reported as early as 1965, the product was only poorly characterized [17]. Related Pd [16] and Pt [18] complexes of dicarba-*closo*-dodecaborane(12)-substituted phosphines have only been characterized spectroscopically. For other Pt derivatives, decomposition with formation of a metal–boron bond was observed on recrystallization [19]. Thus, to date the bonding situation in dicarba-*closo*-dodecaborane(12)-phosphino complexes of $PdCl_2$ remains unknown.

Further details of the structure determination may be obtained upon request from the Cambridge Crystallographic Data Centre, giving full literature citation of the paper.

* Author to whom correspondence should be addressed.

[1] Dedicated to Professor Dr. Klaus Burger on the occasion of his 60th birthday.

RESULTS AND DISCUSSION

Synthesis and characterization of (R,R/S,S)-[$PdCl_2$\{1,2-$(PPhCl)_2C_2B_{10}H_{10}$\}] (***1***)

When (*R*,*R*/*S*,*S*)-1,2-bis(phenylchlorophosphino)-1,2-dicarba-*closo*-dodecaborane(12) (**2**) [20] is treated with [(COD)$PdCl_2$] [21] (COD = cyclooctadiene) in dichloromethane solution at room temperature, (*R*,*R*/*S*,*S*)-[$PdCl_2$\{1,2-$(PPhCl)_2C_2B_{10}H_{10}$\}] (**1**) is obtained (eq. (1)). Complex **1** is air-sensitive as a solid and in THF or toluene solution and slowly decomposes at room temperature in about two hours.

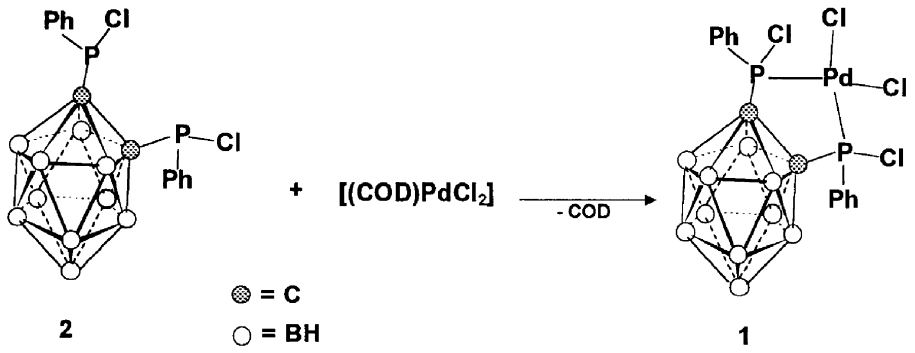

(1)

NMR spectra of ***1***

In the ^{31}P NMR spectrum, **1** exhibits a singlet at 122.7 ppm in THF (122.3 ppm in toluene), which is shifted to low-frequency relative to the free ligand **2** [$\delta(^{31}P)$: 80.54 ppm] by *ca.* 42 ppm. In the $^{11}B\{^1H\}$ NMR spectrum, three broad signals are observed for the 1,2-dicarba-*closo*-dodecaboran(12)yl-cluster at −2.5, −10.7 and −14.1 ppm (cf. **2**: 0.05, −6.4, −10.3, −11.9 ppm). On proton coupling, only the signal at −2.5 ppm splits into a doublet (J_{B-H} = 144.8 Hz), while the other signals are too broad to allow observation of B–H coupling. In the ^1H NMR spectrum, the protons of the Ph groups appear as multiplets at 7.7 and 6.9 ppm. The B–H protons are observed in the range 1.6 to 3.5 ppm as broad signals.

X-ray structural analysis of ***1***

Crystals of **1** were obtained from THF at −30°C. **1** crystallizes with two THF molecules per formula unit. The Pd atom is coordinated in a square planar fashion by two chloro ligands and the 1,2-bis(phenylchlorophosphino)-1,2-dicarba-*closo*-dodecaborane(12) (Fig. 1). Due to the crystallographic center of inversion, both enantiomeric isomers (*R*,*R*) and (*S*,*S*) are present in the unit cell. The bond lengths and angles of the 1,2-$(PPh)_2C_2B_{10}H_{10}$ fragment (Table 1) are in agreement with those observed for other phenyl-substituted derivatives of 1,2-dicarba-*closo*-dodecaborane(12) and complexes thereof [23–26]. However, the Pd–P and Pd–Cl bond lengths are much shorter than those of $PdCl_2$ complexes with tertiary phosphine or diphosphine ligands (Table 2) [7, 13, 27–29]. The only exception is [$PdCl_2$\{$Ph_2P(CH_2)_2P(CF_3)_2$\}] [28], which exhibits Pd–$P(CF_3)_2$ and Pd–Cl [trans to $P(CF_3)_2$] bond lengths comparable to those of **1**. The only other structurally characterized Pd complexes with chlorophosphine ligands, (*R*,R_P)-**3** [7] and *trans-meso*-**4** [13] also have longer Pd–P and P–

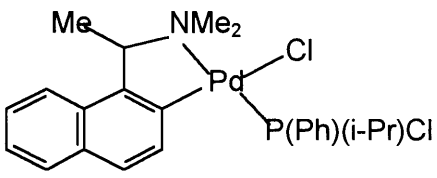

(R,R_P)-**3**

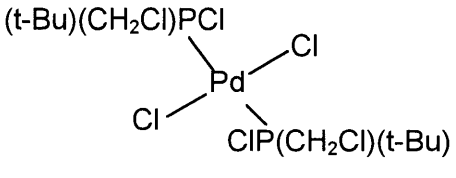

trans-meso-**4**

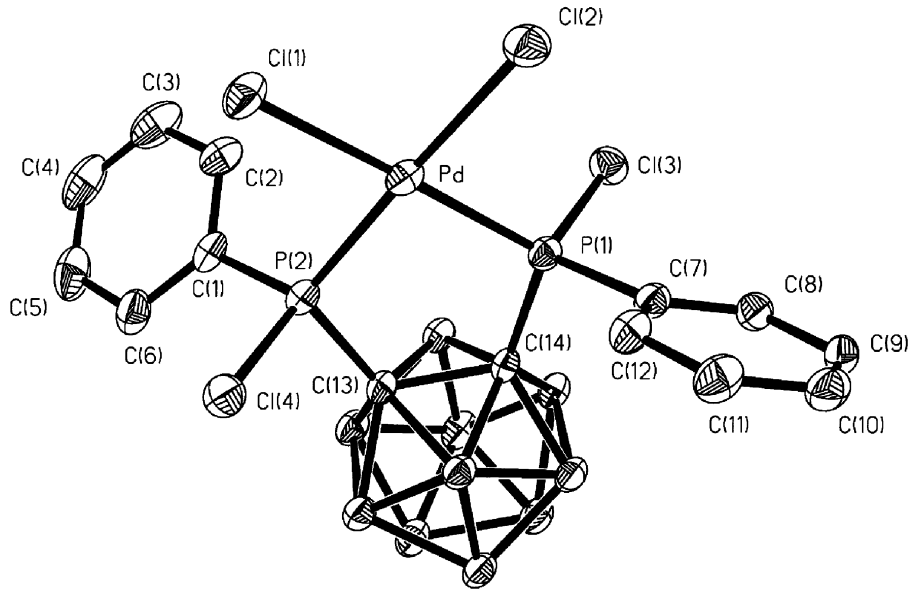

Fig. 1. Molecular structure of **1**. Only one of the present enantiomers (S,S) with its atom numbering scheme is shown (ORTEP, 30% probability, SHELXTL PLUS; XP) [22]. Hydrogen atoms have been omitted for clarity.

Table 1. Selected bond lengths (Å) and angles (deg) for **1**

Pd–P(1)	2.2069(12)	Pd–P(2)	2.2141(11)
Pd–Cl(1)	2.3278(13)	Pd–Cl(2)	2.3296(12)
Cl(3)–P(1)	2.007(2)	Cl(4)–P(2)	2.003(2)
P(1)–C(7)	1.793(3)	P(1)–C(14)	1.859(4)
P(2)–C(1)	1.798(4)	P(2)–C(13)	1.864(4)
C(13)–C(14)	1.681(5)	C(13)–B(9)	1.705(5)
C(13)–B(10)	1.706(5)	C(13)–B(1)	1.729(5)
C(13)–B(8)	1.731(5)	C(14)–B(7)	1.699(5)
C(14)–B(5)	1.707(5)	C(14)–B(8)	1.727(5)
C(14)–B(1)	1.732(5)	B–B from 1.764(6) to 1.797(6)	

P(1)–Pd–P(2)	91.90(5)	P(1)–Pd–Cl(1)	178.64(4)
P(2)–Pd–Cl(1)	86.88(5)	P(1)–Pd–Cl(2)	85.74(5)
P(2)–Pd–Cl(2)	177.62(4)	Cl(1)–Pd–Cl(2)	95.47(5)
C(7)–P(1)–C(14)	105.4(2)	C(7)–P(1)–Cl(3)	106.32(13)
C(14)–P(1)–Cl(3)	102.59(12)	C(7)–P(1)–Pd	117.88(13)
C(14)–P(1)–Pd	110.36(11)	Cl(3)–P(1)–Pd	112.93(6)
C(1)–P(2)–C(13)	106.4(2)	C(1)–P(2)–Cl(4)	106.02(14)
C(13)–P(2)–Cl(4)	102.19(12)	C(1)–P(2)–Pd	118.34(14)
C(13)–P(2)–Pd	110.32(12)	Cl(4)–P(2)–Pd	112.20(6)
C(14)–C(13)–P(2)	113.4(2)	C(13)–C(14)–P(1)	114.0(2)

Cl bonds than **1**. The Pd–Cl bond length in **1** is notably shorter than in (R,R_P)-**3** and comparable with that of the *trans*-complex **4**.

The shortening of the Pd–P and Pd–Cl bond lengths in **1** is indicative of the increased π-acceptor properties [35] of the 1,2-bis(phenylchlorophosphino)-1,2-dicarba-*closo*-dodecaborane(12) ligand (**2**) compared to phenyl-substituted tertiary phosphine or diphosphine ligands (Table 2) caused by the electron-withdrawing properties of the chloro and the 1,2-dicarba-*closo*-dodecaborane(12) groups. Their combined influence is comparable of that of two CF_3 groups.

The electron-withdrawing substituents on phosphorus increase its π-acceptor properties, and this results in a shortening of the P–Cl bond in **1** by 0.04 to 0.1 Å compared with other chlorophosphine complexes or chlorophosphines (Tab. 2) [30–34].

Table 2. Comparison of selected bond lengths in **1** with those of related palladium phosphine complexes, transition metal chlorophosphine complexes, and chlorophosphines

Compound	Pd–P (Å)	Pd–Cl (Å)	P–Cl (Å)	Ref.
1	2.2069(12, 2.2141(11)	2.3278(13) 2.3296(12)	2.007(2), 2.003(2)	This work
(R,R_P)-**3**	2.229(1)	2.394(1)	2.041(2)	[7]
trans-meso-**4**	2.3172(10)	2.2898(10)	2.0347(11)	[13]
$[PdCl_2(Ph_2PCH_2PPh_2)]$	2.234(1) 2.250(1)	2.362(1) 2.352(1)		[27]
$[PdCl_2\{Ph_2P(CH_2)_2PPh_2\}]$	2.233(2) 2.226(2)	2.361(2) 2.357(2)		[27]
$[PdCl_2\{Ph_2P(CH_2)_3PPh_2\}]$	2.244(1) 2.249(2)	2.351(1) 2.358(2)		[27]
$[PdCl_2\{Ph_2P(CH_2)_2P(CF_3)_2\}]$	2.253(4) (Ph_2P), 2.193(4) ($(CF_3)_2P$)	2.370(4)[a] 2.311(4)[b]		[28]
cis-$[PdCl_2(PMe_2Ph)_2]$	2.260(2)	2.362(3)		[29]
$[Cr(CO)_5(PCl_3)]$			2.025[d]	[30]
PCl_3[c]			2.039–2.043	[31]
cis-$[Mo(CO)_4\{PPh(Cl)NH(i\text{-}Pr)\}_2]$			2.122(1) 2.117(1)	[32]
Cl_2PCH_2Cl[e]			2.051	[33]
$[RhCl(COD)(PCl\{CH(SiMe_3)_2\}_2)]$			2.090(2)	[34]

[a] Pd–Cl *trans* to Ph_2P.
[b] Pd–Cl *trans* to $(CF_3)_2P$.
[c] In free gas phase.
[d] P–Cl average.
[e] From electron diffraction.

CONCLUSION

$[(COD)PdCl_2]$ reacts with ($R,R/S,S$)-1,2-$(PPhCl)_2C_2B_{10}H_{10}$ to give ($R,R/S,S$)-$[PdCl_2\{1,2\text{-}(PPhCl)_2C_2B_{10}H_{10}\}]$ (**1**). In **1**, the π-acceptor strength of the diphosphine ligand is increased relative to tertiary phosphine ligands.

We are presently investigating the catalytic properties and reactivity of the P–Cl bond of **1**, as well as the coordination properties of **2** towards other transition metals.

EXPERIMENTAL

All experiments were carried out under purified dry argon. Solvents were dried and freshly distilled under argon. The NMR spectra were recorded with an AVANCE DRX 400 spectrometer (Bruker), ^1H NMR: external standard TMS, internal standard solvent; ^{31}P NMR: external standard 85% H_3PO_4; ^{11}B NMR: external standard $BF_3 \cdot Et_2O$. 1,2-Bis(phenylchlorophosphino)-1,2-dicarba-*closo*-dodecaborane(12) [20] and $[(COD)PdCl_2]$ [21] were prepared according to literature procedures.

Synthesis of (R,R/S,S)-$[PdCl_2\{1,2\text{-}(PPhCl)_2C_2B_{10}H_{10}\}]$ (***1***)

($R,R/S,S$)-1,2-bis(phenylchlorophosphino)-1,2-dicarba-*closo*-dodecaborane(12) (1.25 g, 2.91 mmol) and $[(COD)PdCl_2]$ (0.865 g, 2.97 mmol) were stirred in CH_2Cl_2 (45 ml) for 4.5 h at room temperature. Then the solvent was removed *in vacuo* and the resulting solid was recrystallized from THF. At -30°C crystals of **1**·2 THF are obtained, which rapidly lose THF in vacuum to give **1** (1.53 g, 86% yield). Anal.: Calcd. for $C_{14}H_{20}B_{10}Cl_4P_2Pd$: C, 27.72, H, 3.32. Found: C, 26.73; H, 3.43. At room temperature, **1** slowly decomposes in the solid state and in solution.

*Data collection and structure refinement of **1***

Experimental data (a total of 11980 reflections) were collected at $T = 220 \pm 2$ K on a Siemens CCD (SMART) diffractometer between 3.4 and 52.3° 2Θ with monochromated Mo–Kα ($\lambda = 0.71073$ Å) radiation. This includes a total of 5765 unique reflections ($R_{int} = 0.0269$). All observed reflections (2Θ range: 3.4–52.3°) were used for determination of the unit cell parameters. A studied specimen was a white single crystal having dimensions $0.5 \times 0.4 \times 0.3$ mm. Crystal data for **1**·2 THF are as follows: $C_{14}H_{20}B_{10}Cl_4P_2Pd \cdot 2$ THF, $M = 750.75$, space group P^- (No. 2), triclinic, $a = 11.442(2)$, $b = 12.912(3)$, $c = 13.269(3)$ Å, $\alpha = 106.49(3)$, $\beta = 115.00(3)$, $\gamma = 93.44(3)^\circ$, $V = 1666.7(6)$ Å^3, at $T = 220(2)$ K, $Z = 2$, $D_c = 1.496$ g cm^{-3}, $F(000) = 756$, μ(Mo–Kα) = 0.996 mm^{-1}, no absorption correction.

Positions of Pd, Cl, and P atoms were located by using direct methods (SHELXTL PLUS) [22]. Subsequent least-squares refinement and difference electron density map calculations revealed positions of all C, B, O, and H atoms except hydrogen atoms in the molecules of the solvent (THF), which is probably due to the large thermal displacements found for both THF molecules. Therefore, coordinates of H atoms in both independent THF molecules were calculated geometrically. Final full-matrix least-squares refinement of 451 parameters with a unit weighing scheme (Pd, Cl, P, O, C, and B atoms anisotropic approximation, H atoms in B–H and Ph–H groups isotropic approximation, and H atoms in THF in calculated positions) converged to $R1 = 0.0390$, $wR2 = 0.0867$ (for reflections with $I > 2\sigma(I)$), $R1 = 0.0480$, $wR2 = 0.0924$ (all data). Atomic coordinates, bond lengths and angles, and thermal parameters have been deposited at the Fachinformationszentrum (CSD 380169).

Acknowledgements—We gratefully acknowledge support from the Fonds der Chemischen Industrie. Chemetall GmbH has provided a generous donation of lithium alkyls and Degussa AG a generous donation of $PdCl_2$. V. K. Pecharsky acknowledges support by the Office of Basic Energy Sciences, Material Science Division of the U.S. Department of Energy. E. G. Rys thanks the Deutsche Forschungsgemeinschaft for financial support (436 RUS 17/141/96).

REFERENCES

1. Fild, M. and Schmutzler, R., in *Organic Phosphorus Compounds*, Vol. 4, ed. L. Maier, G. M. Kosolapoff. John Wiley and Sons, New York, 1972, p. 65.
2. Kraihanzel, C.S., *J. Organomet. Chem.*, 1974, **73,** 137.
3. Deschamps, B., Ricard, L., Mathey, F., *Polyhedron*, 1989, **8,** 2671.
4. Salem, G., Shaw, G. B., Willis, A. C., Wild, S.B., *J. Organomet. Chem.*, 1993, **444,** 147.
5. Schumann, H., Eguren, L., *Z. Naturforsch.* **46**(b), 1991, 887 and References cited therein.
6. Bitterer, F., Brauer, D. J., Dörrenbach, F., Gol, F., Knüppel, P. C., Stelzer, O., Krüger, C., Tsay, Y.-H., *Z. Naturforsch.* **46**(b), 1991, 1131 and References cited therein.
7. Pabel, M., Willis, A. C., Wild, S. B., *Tetrahedron: Asymmetry*, 1995, **6,** 2369.
8. Lednor, P. W., Beck, W., Thiel, G., *Inorg. Chim. Acta*, 1976, **20,** L11.
9. Lednor, P. W., Beck, W., Fick, H. G., Zippel, H., *Chem. Ber.*, 1978, **111,** 615.
10. Trampisch, H., Beck, W., *Z. Naturforsch.* **38**(b), 1983, 365.
11. Wong, E. H., Bradley, F. C., *Inorg. Chem.*, 1981, **20,** 2333.
12. Berry, D. E., Beveridge, K. A., Bushnell, G. W., Dixon, K. R., *Can. J. Chem.*, 1985, **63,** 2949.
13. Machnitzki, P., Stelzer, O., Landgrafe, C., *Z. Naturforsch.* **52**(b), 1997, 1103.
14. Stelzer, O., *Top. Phosphorus Chem.*, 1977, **9,** 1.
15. Heumann, A., Jens, K.-J., Réglier, M., *Prog. Inorg. Chem.*, 1994, **42,** 483.
16. Kalinin, V. N., Usatov, A. V., Zakharkin, L. I., *J. Organomet. Chem.*, 1983, **254,** 127.
17. Zakharkin, L. I., Zhigareva, G. G., *Izv. Akad. Nauk SSSR. Ser. Khim.*, 1965, 932.
18. Hill, W. E., Rackley, B. G., Silva-Trivino, L. M., *Inorg. Chim. Acta*, 1983, **75,** 51.
19. Manojlovic-Muir, L., Muir, K. W., Solomun, T., *J. Chem. Soc. Dalton Trans.*, 1980, 317.
20. Alexander, R. P., Schroeder, H., *Inorg. Chem.*, 1963, **2,** 1107.
21. Chatt, J., Vallarino, L. M., Venanzi, L. M., *J. Chem. Soc.*, 1957, 3413.
22. SHELXTL PLUS, Siemens Analyt. X-ray Inst. Inc., 1990, XS: *Program for Crystal Structure Solution*, XL: *Program for Crystal Structure Determination*, XP: *Interactiv Molecular Graphics.*
23. Kivekäs, R., *Acta Cryst.* **51**(C), 1995, 1868.
24. Bembenek, E., Crespo, O., Gimeno, M. C., Jones, P. G., Laguna, A., *Chem. Ber.*, 1994, **127,** 835.
25. Balema, V. P., Pink, M., Sieler, J., Hey-Hawkins, E., Hennig, L., *Polyhedron*, 1998, **17,** 2087.
26. Balema, V. P., Somoza, Jr., F., Hey-Hawkins, E., *Europ. J. Inorg. Chem.*, 1998, 651; and Ref. cited therein.
27. Steffen, W. L., Palenik, G. J., *Inorg. Chem.*, 1976, **15,** 2432.
28. Manojlovic-Muir, L., Millington, D., Muir, K. W., Sharp, D. W. A., Hill, W. E., Quagliano, J. V., Vallarino, L. M., *J. Chem. Soc. Chem. Commun.*, 1974, 999.
29. Martin, L. L., Jacobson, R. A., *Inorg. Chem.*, 1971, **10,** 1795.
30. Davies, M. S., Aroney, M. J., Buys, I. E., Hambley, T. W., Calvert, J. L., *Inorg. Chem.*, 1995, **34,** 330.
31. Shell, R., Steele, D., Gates, P. N., *J. Chem. Phys.*, 1987, **87,** 2893.
32. Hill, T. G., Haltiwanger, R. C., Prout, T. R., Norman, A. D., *Inorg. Chem.*, 1989, **28,** 3461.
33. Tuzova, L. L., Naumov, V. A., *J. Struct. Chem.*, 1970, **20,** 923.
34. Murray, B. D., Hope, H., Hvoslef, J., Power, P. P., *Organometallics*, 1984, **3,** 657.
35. Manojlovic-Muir, L., Muir, K. W., *Inorg. Chim. Acta*, 1974, **10,** 47.

Pergamon

PII: SS027-7538(79)80018-55

Polyhedron Vol. 17, No. 21, pp. 3777–3784, 1998
© 1998 Elsevier Science Ltd
All rights reserved. Printed in Great Britain
0277–5387/98 $19.00+0.00

Unusual coordination modes of multidentate ligands; crystal structure of $[\{(tmhd)_3Y\}_2(hmteta)]$[tmhd = $Bu^tCOCHCOBu^t$ and hmteta = $Me_2N(CH_2CH_2NMe)_2CH_2CH_2NMe_2$]

Ian Baxter,[a] Simon R. Drake,[b] Michael B. Hursthouse,[a]* John McAleese,[b] K. M. Abdul Malik,[a] D. Michael P. Mingos,[b] David J. Otway[b,†] and John C. Plakatouras[b]

[a] Department of Chemistry, University of Wales Cardiff, P.O. Box 912, Park Place, Cardiff, CF1 3TB, U.K.

[b] Department of Chemistry, Imperial College of Science, Technology and Medicine, South Kensington, London SW7 2AY, U.K.

(Received 13 March 1998; accepted 4 May 1998)

Abstract—The reaction of the hydrated lanthanide metal β-diketonate complexes $[Ln(tmhd)_3(H_2O)]$ (tmhd = $Bu^tCOCHCOBu^t$) with hexamethyltriethylenetetramine (hmteta = $Me_2N(CH_2CH_2NMe)_2CH_2CH_2NMe_2$) in *n*-hexane at room temperature yields the anhydrous, bridged dimeric complexes, $[\{(tmhd)_3Ln\}_2(hmteta)]$, where Ln = Gd **1** or Y **2**. An X-ray study of **2** shows that only three of the four possible nitrogen atoms of the hmteta ligand are utilised in bonding to the yttrium centres. The complexes are air and moisture stable, and more importantly both have good volatility, thermal stability, and mass transport properties as demonstrated by sublimation, differential scanning calorimetry (DSC) and thermal gravimetric analysis (TGA), thus making them potential precursors for MOCVD application. © 1998 Published by Elsevier Science Ltd. All rights reserved

Keywords: gadolinium; yttrium; hmteta; β-diketonate; crystal structure

INTRODUCTION

Metal alkoxides and β-diketonates have attracted a large amount of interest because they are suitable as precursors for electronic and ceramic materials [1–8]. Metal oxides are of technological importance as solid oxide electrolytes, e.g. $Y_{0.1}Zr_{0.9}O_{1.95}$ (at 800°C) or $Ce_{0.9}Gd_{0.1}O_{1.95}$ (at *ca.* 500°C) [9–11].

Low temperature chemical vapour deposition (LPCVD) routes to a wide range of metal oxide films have been previously studied [12, 13]. Our plan was to use either bulky or chelating alkoxide, or β-diketonate ligands, thereby facilitating simple cleavage pathways and afford a reduction in the carbonaceous content of the films produced. The rational behind this technique is based on studies by Bradley, who demonstrated the dramatic effect of branching in the alkyl chain of a series of Ta and Nb alkoxides [14–17]. Small changes in the molecular architecture of the ligands will alter physical properties such as oligomerisation, volatility, and mass transport [9, 18]. It is an important requirement when designing the molecular precursors that sufficient coordinative saturation is incorporated into both ligand and chelate, such that low molecular mass

* Author to whom correspondence should be addressed. Tel.: +44-1222-874068; Fax: +44-1222-874029; E-mail: hursthouse@cardiff.ac.uk.

† E-mail: d.j.otway@ic.ac.uk

volatile species will result which are air and moisture stable. This approach is highly flexible since L–L may be varied with the use of either O or N functionalised chelates.

Herein we report that the reactions of $[Ln(tmhd)_3(H_2O)]$ (Ln = Gd or Y) with hmteta to yield the dimeric bridged complexes $[\{(tmhd)_3Ln\}_2(hmteta)]$, where Ln is Gd **1** or Y **2**. The results of the crystal structural studies for **2** are also described.

EXPERIMENTAL

General procedures and techniques

The complexes described are air and moisture stable but were routinely prepared under nitrogen using thoroughly degassed and dry solvents. The starting materials $Gd(tmhd)_3{\cdot}H_2O$ and $Y(tmhd)_3{\cdot}H_2O$ were obtained from Inorgtech. Details of procedures and instruments used were the same as described earlier [19].

Synthesis of $[\{(tmhd)_3Gd\}_2(hmteta)]$ ***1***

To a suspension of $Gd(tmhd)_3{\cdot}H_2O$ (0.313 g, 0.5 mmol) in *n*-hexane (20 ml), hmteta (0.18 ml, 1 mmol) was added. The resulting suspension was stirred until all starting material had dissolved over *ca.* 45 min. The resulting solution was then stripped to dryness to yield a colourless oil. The flask was turned to spread the oil all over the surface and then was clamped, and the product crystallized in two days. Yield: 0.34 g, 93%. M.P.: 117–121°C. Anal.: Found C, 57.08; H, 8.63; N, 3.58; $C_{78}H_{144}Gd_2N_4O_{12}$ requires C, 56.96; H, 8.84; N, 3.41%. The complex sublimed intact between 115–150°C at 5×10^{-3} Torr, m.p. of the sublimed product: 125–128°C. IR (Nujol, ν, cm^{-1}): 1589 (ms), 1575 (ms), 1537 (m), 1505 (m), 1412 (m), 1357 (m), 1281 (w), 1244 (w), 1224 (w), 1184 (w), 1137 (w), 1091 (w), 1032 (w), 1017 (w), 957 (w), 931 (w), 868 (w), 792 (w), 758(w), 737 (w), 723 (w), 600 (w), 477 (w). (Hexachlorobutadiene, ν, cm^{-1}): 2961 (s), 2901 (m, sh), 1589 (vs), 1562 (vs), 1538 (s), 1505 (vs), 1470 (m), 1452 (s), 1413 (vs), 1388 (s), 1358 (s), 1281 (w), 1244 (m), 1225 (m), 1131 (ms), 1069 (w), 1017 (w), 760 (m), 737 (w), 600 (mw). UV/visible (*n*-hexane solution, λ in nm): 306, 303, 301, 297, 294 290, 287, 284, 282, 280, 277, 275, 272, 266, 260, 210, 205, 198, 195. Mass spectrum: (EI^+; m/u^+), 706 $[Gd(tmhd)_3]^+$ (8%), 649 $[Gd(tmhd)_2(Bu^tCOCHCOH)]^+$ (51%), 523 $[Gd(tmhd)_2]^+$ (100%), 464 $[Gd(tmhd)(Bu^tCOCHCOH)]^+$ (9%).

Synthesis of $[\{(tmhd)_3Y\}_2(hmteta)]$ ***2***

$Y(tmhd)_3(H_2O)$ (0.72 g, 1.09 mmol) was dissolved in *n*-hexane (10 ml) in a flame dried Schlenk. To the clear colourless solution, hmteta (0.29 ml, 1.09 mmol) was added and stirred for 1 h. The solvent was then removed *in vacuo* and the Schlenk kept under vacuum at 65°C for 30 min. On cooling to room temperature, the Schlenk was turned to spread the oil over its surface and then clamped on its side. Large colourless blocks crystallised over a period of 2 days with the Schlenk being turned every 24 h to spread the oil and induce further crystallization. Yield: 0.76 g, 92%, m.p.: 109–112°C. Anal.: Found, C, 61.53; H, 9.51; $C_{78}H_{144}O_{12}N_4Y_2$ requires C, 62.15; H, 9.56%. The compound sublimes intact between 90–110°C at 5×10^{-3} Torr forming crystals on the cold finger and some microcrystalline powder on the sides of the vessel. The m.p. of the sublimed solid was 110–113°C. IR (Nujol, ν cm^{-1}): 2727 (vw), 1609 (m), 1590 (m), 1576 (vs), 1530 (m), 1506 (s), 1417 (s), 1306 (w), 1245 (w), 1226 (w), 1180 (w), 1141 (w), 1019 (vw), 962 (vw), 793 (vw), 759 (vw), 723 (w), 477 (vw); (hexachlorobutadiene, ν cm^{-1}): 2962 (vs), 2902 (m), 2865 (m), 1609 (s), 1590 (vs), 1539 (s), 1506 (vs), 1479 (m), 1452 (s), 1417 (vs), 1388 (s), 1359 (s), 1286 (vw), 1245 (w), 1226 (m), 1179 (m), 1141 (m), 1026 (w), 605 (vw), 476 (w). ^1H NMR (C_6D_6, 270 MHz, 20°C): δ 1.20 (s, 108H, CH_3), 2.21 (s, 6H, NCH_3), 2.34 (s, 12H, $N(CH_3)_2$), 2.59 (d, 12H, NCH_2), 5.86 (s, 6H, CH). $^{13}C\{^1H\}$ NMR (C_6D_6, 67.94 MHz, 20°C): δ 28.36 (s, CH_3), 40.32 (s, $C(CH_3)_3$), 42.55 (s, NCH_3), 45.50 (s, $N(CH_3)_2$), 54.97, 55.67, 57.49 (s, NCH_2), 90.73 (s, CH), 198.78 (s, CO). Mass spectrum: (EI^+; m/u^+), 638 $[Y(tmhd)_3]^+$ (12%), 581 $[Y(tmhd)_2(Bu^tCOCHCOH)]^+$ (64%), 455 $[Y(tmhd)_2]^+$ (100%), 397 $[Y(tmhd)(Bu^tCOCHCOH)]^+$ (6%), 272 $[Y(tmhd)]^+$ (3%).

X-ray crystallography for $[\{Y(tmhd)_3\}_2(hmteta)]$ ***2***

Crystal data $C_{78}H_{138}N_4O_{12}Y_2$, M_r 1501.74, triclinic, $a=10.274(4)$, $b=21.023(9)$, $c=21.410(9)$ Å, $\alpha=68.58(2)$, $\beta=86.19(3)$, $\gamma=82.93(3)°$, $U=4271(3)$ $Å^3$, space group $P\bar{1}$ (No. 2), $Z=2$, μ(Mo–K_α) = 14.07 cm^{-1}, $\lambda=0.71069$ Å, $T=150$ K, crystal size $0.20\times0.15\times0.13$ mm.

Crystallographic measurements were made using a Delft instruments FAST TV area detector diffractometer equipped with a rotating anode (Mo) generator by following previously described procedures [20]. Total data ($1.97\leqslant\theta\leqslant25.60°$; $-11\leqslant h\leqslant9$, $-23\leqslant k\leqslant23$, $-24\leqslant l\leqslant14$) collected 13962, 12023 unique ($R_{int}=0.0765$). The crystal was weakly diffracting and relatively few data were observed, but the structure was successfully solved by direct methods (SHELXS86) [21] and difference synthesis, and refined on F^2 by full-matrix least-squares (SHELXL93) [22]. Absorption effects were ignored. All nonhydrogen atoms were anisotropic. The hydrogen atoms were included in calculated positions (riding model) with U_{iso} tied to the U_{eq} of the parent atoms. One of the *t*-butyl groups [pivot atom C(12)] was orientationally disordered, and its three methyl groups were refined each with partial occupancies

(0.68 and 0.32). Final R_1 (on F, 1556 data with $F_o > 4\sigma(F_o)] = 0.0614$, wR_2 (on F^2, all 12023 data, 924 parameters) = 0.2789, $w = 1/[\sigma^2(F_o^2)]$. Sources of scattering factors as in Ref. [22]. The diagram was drawn with SNOOPI [23]. The calculations were done on a Pentium 200 MHz personal computer. Full details of crystallographic results have been deposited with Cambridge Crystallographic Data Centre, Ref. No. CCDC-101115.

RESULTS AND DISCUSSION

Synthesis

A range of synthetic routes has been used for the preparation of metal alkoxides or β-diketonates [24–33]. There are several features that may be noted for the synthesis of such materials, i.e. (a) the synthetic strategy of using a preformed metal β-diketonate (either anhydrous or a hydrate) leads to *water free* products [33], (b) the coordinative saturation of the metal centre by the multidentate chelate and β-diketonates leads to *air and moisture stable* precursors of known stoichiometry and is thus highly flexible since L–L may be varied with the use of either O- or N-functionalised chelates, (c) The designed synthesis of volatile molecular metal organics is possible without having to use sterically hindered ligands. The multidendate amine (L–L) forces the complex into a molecular regime, thereby removing the possible interactions between the monomers and increasing the volatility and mass transport properties of the complexes.

Physical properties

Compounds **1** and **2** are both highly soluble in a range of organic solvents. This pronounced solubility even in nonpolar aliphatic hydrocarbon solvents (i.e. *n*-hexane) is most likely to be due to the coordinative saturation of the metal atoms in these complexes. Another important property is their excellent stability to both air and moisture.

Both **1** and **2** show a significant drop (*ca.* 60°C) in their melting points on complexation with the amine ligand. Complex **1** melts at 117–121°C, whereas the parent compound $Gd(tmhd)_3{\cdot}H_2O$ melts at 170–172°C. It sublimes intact between 115–150°C at 5×10^{-3} torr over 1.5 h. The large colourless crystals obtained for compound **2** melt cleanly at 109–112°C compared with 160–165°C for $[Y(tmhd)_3(H_2O)]$ and 77–81°C for $[\{(tmhd)_3Y\}_2(triglyme)]$ (triglyme = $MeOCH_2OCH_2OCH_2OMe$) [33]. Compound **2** sublimes intact between 90–110°C at 5×10^{-3} Torr over 1 h forming crystals on the cold finger and some microcrystalline powder on the sides of the vessel.

Infrared spectra

The infrared bands for **1** and **2** (experimental section) are comparable with those in other hydrated and anhydrous β-diketonates [18, 34]. The only real difference from the spectra of the parent compounds is the presence of the amine ν(C–N) stretch at 1140 cm^{-1}; this is a shift of *ca.* 30 cm^{-1} over the free ligand and indicative of coordinated amine with relatively weak M–N bonding.

NMR spectra

The ^1H and $^{13}C\{^1H\}$ NMR spectra of **2** were run in C_6D_6 but due to large paramagnetic NMR shift of the Gd^{3+} metal nucleus no spectra could be obtained for **1**. The ^1H NMR spectrum of **2** in C_6D_6 shows both the tmhd and hmteta ligands as well resolved peaks. The hmteta protons are split into three groups; singlets for 6H $\{-NCH_3\}$ and 12H $\{-N(CH_3)_2\}$ and a doublet for 12H $\{-NCH_2-\}$. Integration for the complex gives a tmhd:hmteta ratio of 6:1. The $^{13}C\{^1H\}$ NMR spectra reveals only one environment for the tmhd and amine ligand, suggesting that either the complex exists in solution as a symmetrically bonded dimer or a rapid exchange process is occurring.

Mass spectrometry

In the mass spectra for complexes **1** and **2** the highest molecular mass ions observed for these complexes are due to the $[Ln(tmhd)_3]^+$ species at 705 and 638 amu respectively. Other intense peaks are noted in the experimental, in particular $[Ln(tmhd)_2]^+$ at 523 and 455 amu, and below this breakup of the tmhd groups is also seen. The isotope patterns of the metal containing complexes are consistent with those obtained from the natural abundance patterns or by computer simulation. The m/z ratios relate to the isotopes of greatest natural abundance, e.g. ^{157}Gd and ^{89}Y.

The above data suggest that in the vapour phase under high vacuum conditions (10^{-8} Torr) these complexes dissociate to form the oligomeric donor-Lewis base free complexes, $Ln_2(tmhd)_6$. Such behaviour is still an important observation since the materials may be used under atmospheric conditions very effectively or at low vacuum (*ca.* 10^{-3} Torr) conditions as molecular precursors for Ln_2O_3, or other ternary oxides such as $YBa_2Cu_3O_{7-x}$. The fact that the Lewis base (amine) is not coordinated to the metals under the conditions used here has been noted previously for lanthanide complexes [35, 36].

TGA/DSC studies

Both the hydrated starting materials and the amine stabilised products were subjected to thermal analysis. The results show that the addition of an amine ligand

to the hydrated species removes any coordinated water and more importantly it significantly reduces the decomposition point with respect to the parent hydrate compounds. The TGA and DSC plots for **2** are shown in Fig. 1.

The DSC of **1** shows two distinct endotherms over the range 100–300°C. The first, centred at 138.77°C (−8.61 mcal/mg), corresponds to the melting point of the compound. The second, broad peak, centred at 230.68°C (−34.15 mcal/mg), correlates well with its complete, intact sublimation observed in the TGA plot between 180 and 280°C. A very small residue of 2.75% is probably due to a small amount of carbonaceous material left.

The DSC of **2** shows an endotherm between 110–135°C (−7.38 mcal/mg) corresponding to the melting point, and two more endotherms [176–245°C (−4.86 mcal/mg) and 245–280°C] due to sublimation of the complex into the vapour phase. The TGA plot is consistent with these observations; namely a sublimation of 97.4% of the complex over the range 150–280°C leaving a final residue of 2%.

X-ray structure of [{*Y*(*tmhd*)$_3$}$_2$(*hmteta*)] ***2***

A single crystal structural study of complex **2** was undertaken to unambiguously identify its structural composition and to determine whether all of the potential N-donor sites were bound to the yttrium metal centres. The solid state structure of **2** is shown in Fig. 2 and selected bond lengths and angles are given in Table 1.

The structure is a dimer based on two Y(tmhd)$_3$ units linked by a hmteta ligand in an unusual bonding mode. The amine ligand acts simultaneously as a che-

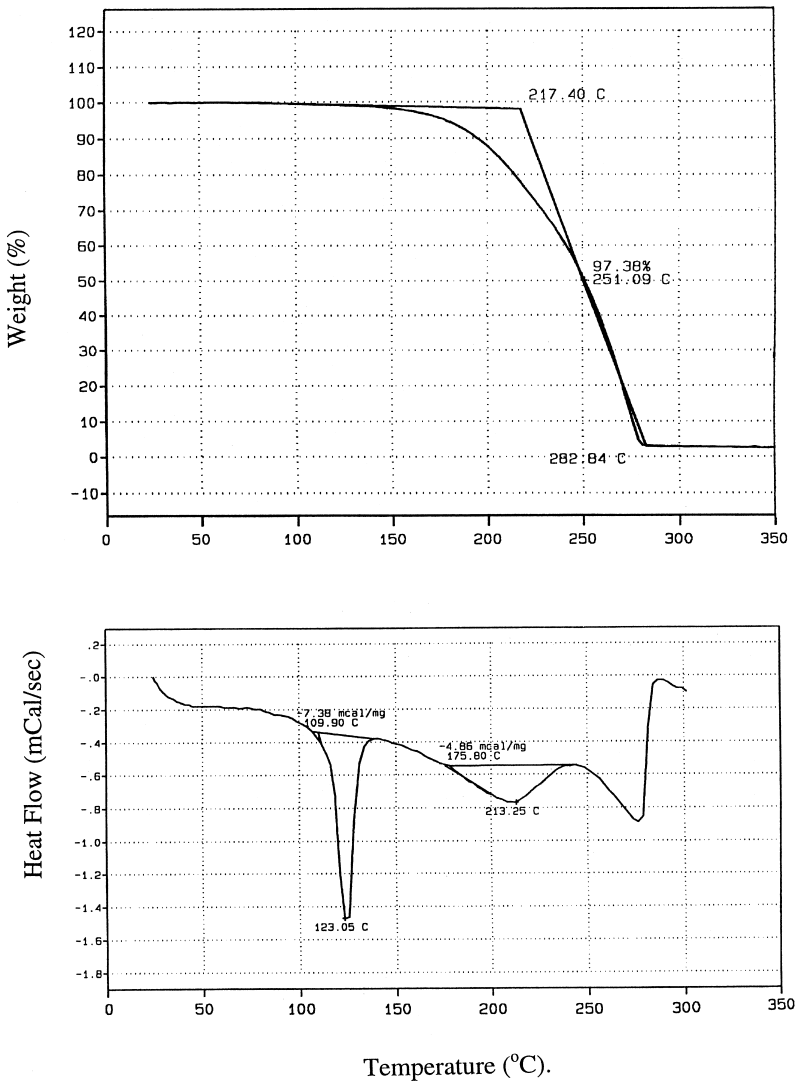

Fig. 1. The DSC and TGA plot for [{(tmhd)$_3$Y}$_2$(hmteta)] (**2**).

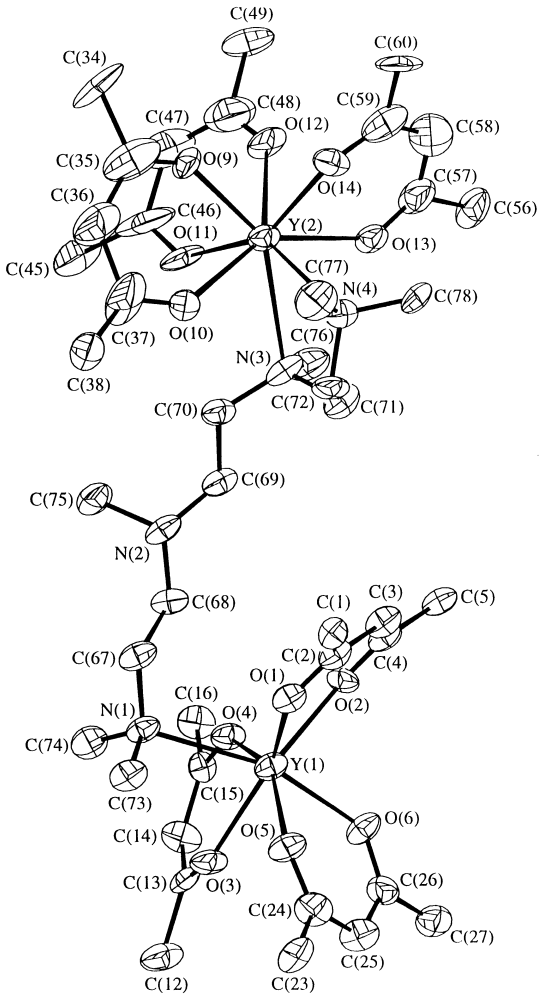

Fig. 2. X-ray structure of $[\{(tmhd)_3Y\}_2(hmteta)]$ **2**; the *tert*-butyl methyl groups are omitted for clarity. Thermal ellipsoids are drawn at 50% probability level.

late [to Y(2)], terminal ligand [to Y(1)] and as a bridging ligand via the central ethylene bridges. This mode of bonding of the potentially tetradentate hmteta ligand appears to be unique; such ligands are normally found to form two chelates involving all the four nitrogen atoms as observed in $[Ba(hfpd)_2(hmteta)]$ (hfpd = 1,1,1,5,5,5-hexafluoropentane-2,4-dionate) [32]. The binuclear structure observed for **2** does not permit utilisation of *all* the four potential nitrogen binding sites and this raises the question why the situation is different from the related triglyme bridged complex $[\{Y(tmhd)_3\}_2(triglyme)]$ [33] in which all the four oxygen atoms are involved in bonding with the metal atoms.

The environments of the two metal centres, Y(1) and Y(2), illustrated in Fig. 3, are significantly different and may be explained by the asymmetric bridging of the amine ligand. Y(1) is bonded to six oxygens from three chelating tmhd ligands and one nitrogen from the bridging hmteta ligand. This atom is seven coordinate with a geometry best described as distorted monocapped trigonal prismatic. Two of the tmhd ligands are chelated along the edges of a square face of the trigonal prism, whereas the third tmhd is chelating from the capping atom to an apex of the prism. The remaining apical site of the prism is occupied by one nitrogen atom from the amine ligand. The coordination around Y(2) consists of six oxygens from three chelating tmhd ligands, as well as two nitrogens from the hmteta ligand forming a 5-membered chelate. Y(2) is thus eight coordinate with a square antiprismatic geometry. The chelation of the ligands around this metal is interesting in that two tmhd ligands are chelating along the edges of square faces whereas the third tmhd and the hmteta ligands chelate between the two square faces. It is to be noted that yttrium resembles the lanthanide elements in most respects and can easily accommodate a high coordination number such as eight. In fact octa-coordination is a common feature observed in different yttrium complexes with β-diketonate and alkoxide ligands, and examples include species with various degrees of oligomerisation, e.g. $[Y(pd)_3(H_2O)_2]\cdot H_2O$ (monomer) (pd = pentane-1,3-dionate) [37], $[\{(tmhd)_3Y\}_2(triglyme)]$ (dimer) [33], $[Y_2(pd)_4(O_2CCH_3)_2(H_2O)_2]$ (dimer) [38] and $[Y_3(pd)_4(OCH_2CH_2OMe)_5]$ (trimer) [39]. The geometry about yttrium in all these complexes is distorted square antiprismatic. There are, however, examples of lower coordination numbers for yttrium, e.g., the hexa-coordinated oxide Y_2O_3 and the hepta-coordinated methoxyethoxide "$Y(OC_2H_4OMe)_3$". The last compound was shown to be a centrosymmetric cyclic decamer $[\{Y(OC_2H_4OMe)_3\}_{10}]$ [40], in which all the five unique yttrium atoms have pentagonal bipyramidal geometry. This compound also appears to be the highest oligomer structurally characterised for homoleptic metal alkoxides.

The Y(2)–N bond lengths are quite asymmetric [2.662(8), 2.716(8) Å], with the terminal NMe_2 group binding closer to the metal centre. In contrast, the Y(1)–N bond length involving only the terminal nitrogen from the other NMe_2 group at 2.608(8) Å is much shorter. These differences in the Y–N bond lengths can be explained by the differing coordination numbers for the two yttrium atoms and also by the steric factors. The bonding of hmteta in the present compound has no immediately accessible comparison in Ln–N chemistry, but may be contrasted with that in the barium compound $[Ba(hfpd)_2(hmteta)]$ [33]. In this compound, which is monomeric, all four nitrogen atoms of hmteta are bonded to barium forming two nearly symmetrical chelate rings [Ba–N distance 2.963(3)–3.022(10) Å], with quite acute N–Ba–N chelate angles, 62.1(3) and 61.4(3)°. The hmteta ligand can bind to barium in this way because the larger radius of Ba^{2+} (1.49 Å) supports the higher coordination number compared with Y^{3+} (1.04 Å) [41].

The Y–O bond lengths involving the β-diketonate ligands lie in the range 2.211(6)–2.338(7), average

Table 1. Selected bond lengths (Å) and angles (°) for [{(tmhd)$_3$Y}$_2$(hmteta)] **2**

Y(1)–O(6)	2.211(6)	Y(1)–O(2)	2.231(7)
Y(1)–O(4)	2.237(6)	Y(1)–O(1)	2.260(7)
Y(1)–O(5)	2.260(7)	Y(1)–O(3)	2.315(7)
Y(1)–N(1)	2.608(8)	Y(2)–O(11)	2.235(7)
Y(2)–O(9)	2.246(6)	Y(2)–O(14)	2.280(7)
Y(2)–O(13)	2.284(7)	Y(2)–O(12)	2.296(8)
Y(2)–O(10)	2.338(7)	Y(2)–N(4)	2.662(8)
Y(2)–N(3)	2.717(8)		

O(6)–Y(1)–O(2)	80.1(3)	O(6)–Y(1)–O(4)	99.3(2)
O(2)–Y(1)–O(4)	77.2(3)	O(6)–Y(1)–O(1)	114.9(3)
O(2)–Y(1)–O(1)	73.0(2)	O(4)–Y(1)–O(1)	128.9(2)
O(6)–Y(1)–O(5)	74.8(3)	O(2)–Y(1)–O(5)	128.8(3)
O(4)–Y(1)–O(5)	150.0(3)	O(1)–Y(1)–O(5)	78.4(3)
O(6)–Y(1)–O(3)	83.3(3)	O(2)–Y(1)–O(3)	143.4(2)
O(4)–Y(1)–O(3)	73.6(2)	O(1)–Y(1)–O(3)	143.4(2)
O(5)–Y(1)–O(3)	76.4(3)	O(6)–Y(1)–N(1)	162.8(3)
O(2)–Y(1)–N(1)	116.3(3)	O(4)–Y(1)–N(1)	80.5(3)
O(1)–Y(1)–N(1)	77.0(3)	O(5)–Y(1)–N(1)	96.7(3)
O(3)–Y(1)–N(1)	80.1(3)	O(11)–Y(2)–O(9)	87.1(3)
O(11)–Y(2)–O(14)	150.6(3)	O(9)–Y(2)–O(14)	74.9(3)
O(11)–Y(2)–O(13)	107.7(3)	O(9)–Y(2)–O(13)	140.7(3)
O(14)–Y(2)–O(13)	75.3(3)	O(11)–Y(2)–O(12)	74.2(3)
O(9)–Y(2)–O(12)	76.6(3)	O(14)–Y(2)–O(12)	79.1(3)
O(13)–Y(2)–O(12)	73.1(3)	O(11)–Y(2)–O(10)	79.7(3)
O(9)–Y(2)–O(10)	73.0(3)	O(14)–Y(2)–O(10)	115.6(3)
O(13)–Y(2)–O(10)	144.3(3)	O(12)–Y(2)–O(10)	140.6(3)
O(11)–Y(2)–N(4)	136.8(3)	O(9)–Y(2)–N(4)	116.0(3)
O(14)–Y(2)–N(4)	72.6(3)	O(13)–Y(2)–N(4)	78.1(3)
O(12)–Y(2)–N(4)	143.7(3)	O(10)–Y(2)–N(4)	73.8(3)
O(11)–Y(2)–N(3)	72.8(3)	O(9)–Y(2)–N(3)	145.1(3)
O(14)–Y(2)–N(3)	133.6(3)	O(13)–Y(2)–N(3)	73.7(3)
O(12)–Y(2)–N(3)	122.2(3)	O(10)–Y(2)–N(3)	75.5(3)
N(4)–Y(2)–N(3)	67.9(3)		

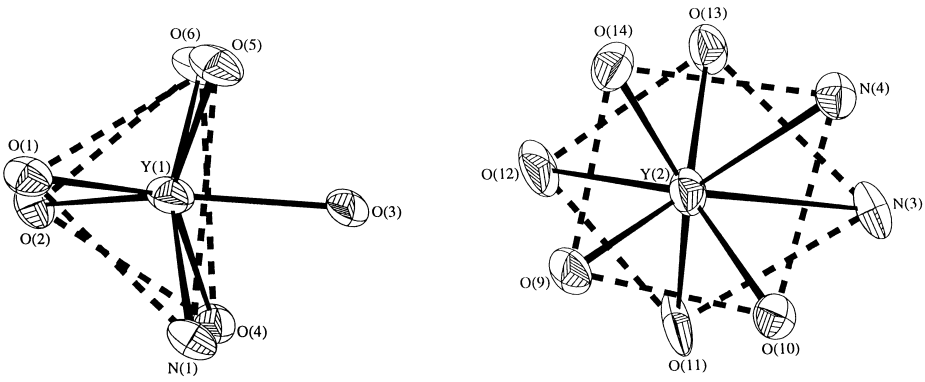

Fig. 3. The coordination sphere around [{(tmhd)$_3$Y}$_2$(hmteta)] **2**.

2.266 Å, and are close to the values in other complexes [33, 37–39, 42]. Close examination of the individual Y–O distances in **2** indicate that only one tmhd ligand [containing O(13) and O(14) and chelated to Y(2)] is nearly symmetric whilst the remaining five tmhd ligands are chelated quite asymmetrically. Not unexpectedly, the Y(2)–O distances [2.235(7)–2.338(7), average 2.28 Å] are in general longer than the Y(1)–O

distances [2.211(6)–2.314(7), average 2.25 Å] reflecting the greater steric crowding around Y(2).

The geometry parameters involving the hmteta and tmhd ligands are as expected. The hmteta chelate is nonplanar with a relative λ conformation. The OC_3O skeletons of one tmhd ligand chelated to Y(2) shows significant deviations from planarity [atomic deviations -0.089–$0.122(2)$ Å] whilst the other tmhd ligands chelated to Y(I) and Y(2) are almost planar [atomic deviations $\leqslant 0.03(2)$ Å]. The six-membered $M(O_2C_3)$ chelates are also nonplanar with fold angles of 7.9–21.7(3)° about the O···O axes. These deformations observed in coordinated tmhd ligands may be attributed to steric factors and reflect the flexible nature of such ligands.

CONCLUSION

Recent developments in organo-lanthanide chemistry have shown that the chemistry of these metals may be controlled by varying the steric environment around the metal. We have applied the above strategy to a range of lanthanides, including Y, Tb, Pr, Eu and Gd, e.g. $[\{(tmhd)_3Y\}_2(triglyme)]$ is a dimeric air stable highly volatile precursor [32]. This technique works because the lanthanide complexes are hard acids which are coordinatively unsaturated, and will react with multidendate Lewis bases which will "plug" vacant coordination sites and even displace water from hydrated species, as for yttrium above. Given that we can use either O or N functionalised chelating ligands, we are now in a position to tailor the coordination environment of the metal quite specifically.

*Acknowledgements*We thank the EPSRC (D.J.O., M.B.H., K.M.A.M. and J.C.P.), the CASE sponsor Inorgtech, and for the STA equipment, the Leverhulme Trust (J.M.), the Royal Society (for an inert atmosphere glove-box and other ancillary equipment) and B.P. for endowing D.M.P.M.'s chair.

REFERENCES

1. Bradley, D. C., *Chem. Rev.*, 1989, **89,** 1317.
2. Dorn, F. W., Krause, W. and Schroder, F., *Adv. Mater.*, 1992, **4,** 221.
3. Vaahs, T., Brÿck, M. and Bocker, W. D. G., *Adv. Mater.*, 1992, **4,** 224.
4. Adlinger, F. and Kalz, H.-J., *Angew. Chem. Int. Ed. Engl.*, 1987, **26,** 371.
5. Okamura, H. and Bowen, H. K., *Ceramics Int.*, 1986, **12,** 161.
6. Alford, N., Kendall, K., Clegg, B. and Button, T., *Phys. World*, 1991, May, 27.
7. Mackenzie, J. D. and Ulrich, D. R. (Eds.), *Ultrastructure Processing of Advanced Ceramics*. Wiley, New York, 1988.
8. Arunasalam, V.-C., Baxter, I., Darr, J. A., Drake, S. R., Hursthouse, M. B., Malik, K. M. A. and Mingos, D. M. P., *Polyhedron*, 1998, **17**(5–6), 641.
9. Steele, B. C. H., *Mat. Sci Eng. B*, 1992, **13,** 79.
10. U.K. Pat. Application 9,125,012.6 (25-11-91).
11. Proc. of Colloquium on Energy Technologies and Sustainable Development, Long Range R. and D. Opportunities, 3–7 Dec. 1991, Noordwijkerhout. Royal Netherlands Academy of Arts and Sciences, 1992.
12. Schulte, B., Maul, M., Becker, W., Elschner, S., Schlosser, E. G., Haussler, P. and Adrian, H., *Physica C*, 1991, **185-189,** 2005.
13. Cameron, D. C., Irving, L. D., Jones, G. R. and Woodward, J., *Thin Solid Films*, 1982, **91,** 339.
14. Bradley, D. C. and Thomas, I. M., *J. Chem. Soc.*, 1960, 3857.
15. Bradley, D. C. and Thomas, I. M., *Can. J. Chem.*, 1962, **40,** 1335.
16. Bradley, D. C., Chudzynska, H., Hammond, M. E., Hursthouse, M. B., Motevalli, M. and Ruowen, W., *Polyhedron*, 1992, **11,** 375.
17. Bradley, D. C., Chudzynska, H., Hursthouse, M. B. and Motevalli, M., *Polyhedron*, 1991, **10,** 1049.
18. Eisentraut, K. J. and Sievers, R. E., *J. Am. Chem. Soc.*, 1965, **87,** 5254.
19. Baxter, I., Drake, S. R., Hursthouse, M. B., Malik, K. M. A., Mingos, D. M. P., Plakatouras, J. and Otway, D. J., *Polyhedron*, 1998, **17**(5-6), 625.
20. Darr, J. A., Drake, S. R., Hursthouse, M. B. and Malik, K. M. A., *Inorg. Chem.*, 1993, **32,** 5704.
21. Sheldrick, G. M., *Acta Cryst. A*, 1990, **46,** 467.
22. Sheldrick, G. M., *SHELXL*93 *Program for Crystal Structure Refinement*. University of Göttingen, Germany, 1993.
23. K. Davies, *SNOOPI Program for Crystal Structure Drawing*. University of Oxford, U.K., 1983.
24. Mehrotra, R. C. and Batwara, J. M., *Inorg. Chem.*, 1970, **9,** 2505.
25. Vevere, I., Maijs, L. J. and Reikstina, D., *Latv. PSR Zinat. Akad. Vestis. Khim. Ser.*, 1970, 405.
26. Pavlik, I., Jacob, K. H-. and Glanz, M. Z., *Z. Anorg. Allg. Chem.*, 1989, **569,** 106.
27. Thomas, I. M., *Can. J. Chem.*, 1961, **39,** 1386.
28. Mehrotra, R. C., Misra, T. N. and Misra, S. N., *Ind. J. Chem.*, 1965, **3,** 525.
29. Mehrotra, R. C., Singh, A. and Tripathi, U., *Chem. Rev.*, 1990, **90,** 969.
30. Mehrotra, R. C., Gaur, D. P., *Metal β-Diketonates*. Academic Press, London, 1978.
31. Darr, J., Drake, S. R, Williams, D. J. and Slawin, A. M. Z., *J. Chem. Soc., Chem. Commun.*, 1993, 866.
32. Drake, S. R., Hursthouse, M. B., Malik, K. M. A. and Miller, S. A. S., *J. Chem. Soc., Chem. Commun.*, 1993, 478.
33. Drake, S. R., Hursthouse, M. B., Malik, K. M. A., Miller, S. A. S. and Otway, D. J., *Inorg. Chem.*, 1993, **32,** 4464.
34. Lee, H. Y., Cleveland, F. F., Ziomek, J. S. and Jorke, F., *Appl. Spectros.*, 1972, **26,** 251.
35. Drake, S. R., Hursthouse, M. B., Malik, K. M. A. and Otway, D. J., *J. Chem. Soc., Dalton Trans.*, 1993, 2579.

36. Cotton, S., *Lanthanides and Actinides*. MacMillllian, London, 1991.
37. Cunningham, J. A., Sands, D. E. and Wagner, W. F., *Inorg. Chem.*, 1967, **6,** 499.
38. Poncelet, O., Hubert-Pfalzgraf, L. G. and Daran, J.-C., *Polyhedron*, 1990, **9,** 1305.
39. Poncelet, O., Hubert-Pfalzgraf, L. G. and Daran, J.-C., *Inorg. Chem.*, 1990, **29,** 2885.
40. Poncelet, O., Hubert-Pfalzgraf, L. G., Daran, J.-C. and Astier, R., *J. Chem. Soc., Chem. Commun.*, 1989, 1846.
41. Huheey, J. E., *Inorganic Chemistry*: *Principles of Structure and Reactivity*, 3rd Ed. Harper and Row, NY, 1983, p. 258–259.
42. Luten, H. A., Rees, W. S. Jr. and Goedken, V. L., *Chem. Vap. Deposition*, 1996, **2,** 149.

Pergamon

PII: S0277–5387(98)00187–9

Polyhedron Vol. 17, No. 21, pp. 3785–3794, 1998
© 1998 Elsevier Science Ltd
All rights reserved. Printed in Great Britain
0277–5387/98 $19.00+0.00

Synthetic models for the glucose tolerance factor: the spectroscopic characterization and toxicity studies of monomeric and dimeric Cr(III) species

Gabriela Galuszka,[a] Maria Cieslak-Golonka,[a]* Adam Szelag,[b] Jan Starosta[a] and Agnieszka Wojciechowska[a]

[a]Institute of Inorganic Chemistry and Metallurgy of Rare Elements, University of Technology, 50-370 Wroclaw, Poland; [b]Department of Pharmacology, Medical Academy, Wroclaw, Poland

Received 11 February 1998; accepted 5 May 1998

Abstract—A number of chromium(III) complexes with glycine, cysteine, glutamic and nicotinic acids-models for biologically active Cr(III) species have been prepared and characterized with physicochemical methods (UV/Vis, IR spectra, magnetic moments). Four of them have been also tested for their toxicity. On the basis of CF calculation it was found that only the nicotinates were octahedral Cr(III) species. Other complexes exhibited a tetragonal deformations. Based upon 10 Dq values, the sequence of the ligand field strength was found to be: glycine > cysteine ≈ glutamic acid > nicotinic acid. The likely structures were proposed for the isolated compounds. The preliminary toxicity studies showed that all tested complexes appeared to be non-toxic and can be potentially applied as chromium nutrition products. © 1998 Elsevier Science Ltd. All rights reserved

Keywords: Cr(III) complexes; glucose tolerance factor; low molecular weight chromium; electronic spectra; toxicity; amino acids.

Chromium has been known to be a micronutrient for almost forty years. The essential nature of this element was recognized in 1959 by Mertz and Schwarz [1]. These authors demonstrated the role of chromium in maintaining normal glucose in rats. Later on, chromium was shown to be important for normal mammalian carbohydrate and lipid metabolism [2–4].

Despite these results very little is known about the composition and structure of the biologically active form(s) of chromium. The most conflicting results have been obtained by studying the problem of the Cr(III) relationship to the so-called glucose tolerance factor (GTF), an organic Cr(III) containing complex responsible for stimulating insulin action. The evidence obtained from the literature suggested that the GTF contained Cr(III) in the form of a complex with nicotinate (pyridine 3-carboxylate) and either glutathione or amino acids: glycine, glutamic acid and cysteine [5, 6]. However, it has also been suggested that Cr(III) may not be a component of the GTF [7–10] or that it does not play any biological role at all [8].

These results prompted many investigators to study synthetic models for the GTF [6, 11–14]. In most models two nicotinate ligands are coordinated as monodentate ligands in *trans* positions via oxygen [13, 15] or nitrogen donor atoms [11, 16, 17]. However, both biological extracts and synthetic GTF models have as yet been poorly characterized.

The other pathway in investigating the biological activity of trivalent chromium was based on Yamamoto *et al*. [18], namely isolation of naturally occurring Cr(III) containing protein of low molecular weight (LMWCr) ~1500 Da. Recently, the isolation of LMWCr in milligram quantities, together with its biochemical and physicochemical analysis, has been reported [19–22]. The composition of ligands in LMWCr is similar to the GTF. One difference is the presence of the aspartate in the former instead of the nicotinate in the latter [19]. It is postulated that in the centre of activity LMWCr contains an assembly composed of four chromium atoms bridged with oxygen, hydroxyl group, chlorine etc [19]. The oligo-

*Author to whom correspondence should be addressed. e-mail: golonka@ichn.ch.pwr.wroc.pl

peptide is probably associated with the kinase active site of the insulin receptor [22].

However, LMWCr of still unknown structure, may not be an alternative for the "old" GTF, since the latter seems to be more a nutrient in an appropriate organic form suitable for chromium deficient organisms [23]. As Cr(III) picolinate used as a dietary chromium supplement has been found to cause chromosome damage [24] other Cr(III) complexes suitable for supplementation of this ion should be investigated [22]. For example, Vincent *et al.* [22] proposed as a nutrient an inexpensive, easy to prepare Cr(III) compound containing a cationic trinuclear $[Cr_3O(O_2CCH_2)_6(H_2O)_3]^+$ species which was found to activate the insulin receptor almost identical to that of LMWCr.

With these facts in mind our studies have been focused on systematic syntheses of mono- and polymeric Cr(III) complexes with "GTF-like" ligands and investigation of their physicochemical properties and biological activity. We have prepared and spectroscopically analyzed seven Cr(III) mono and dimeric complexes with nicotinic (nic) and glutamic (glu) acids, cysteine (cys) and glycine (gly).

To the authors' knowledge, the complexes **I** and **IV** (Table 1) have been obtained for the first time. Additionally, for the previously known compound **II** [6] a new synthetic procedure has been proposed.

EXPERIMENTAL

Chemicals were used as received. Stoichiometries of the complexes were established by microanalysis (C, N, S, H), which gave satisfactory results.

Preparation of the complexes

$[Cr_2nic_2(OH)_4]\,4H_2O$ [***I***]. From the stock solutions: $Cr(NO_3)_3{*}9H_2O$ (10 g in 500 cm^3) and nicotinic acid (6.0155 g in 500 cm^3) equal volumes of 20 ml each were mixed together and warmed to 60°C under continuous stirring. The acidity had been adjusted to pH 6.0 with warm NaOH (2 M). Addition of NaOH caused the changes of colours (from green to blue) and simultaneous precipitation. After 48 h the mixture was filtered off, washed with water and ethanol.

$[Crnic_2OH]\,3H_2O$ [***II***]. $Cr(NO_3)_3\ 9H_2O$ (6 g) and nicotinic acid (3.693 g) were dissolved in a mixture of methanol (70 cm^3) and water (30 cm^3). The reagent mixture was heated to reflux for 6 h. Solid KOH (3.36 g) was added to the solution and the resulting blue precipitate was allowed to remain for 48 h in the mother liquor. The precipitate was filtered, washed with water and ethanol and dried.

$[Cr_2glu_2(OH)_2]glu\ 3H_2O$ [***III***] This compound was prepared as described elsewhere [25].

$[Crcys_2(OH)(H_2O)]\ H_2O$ [***IV***] $CrCl_3\ 6H_2O$ (1.33 g) was dissolved in a mixture of water (10 cm^3) and ethanol (2 cm^3). D,L-Cysteine (1.81 g) dissolved in water

Table 1. Analytical results

Symbol	Compound	Analytical results %							
		C		N		H		S	
		Calc.	Found	Calc.	Found	Calc.	Found	Calc.	Found
I	$[Cr_2(nic)_2(OH)_4]\cdot 4H_2O$	29.5	29.5	5.7	5.6	4.5	3.9	–	–
II	$[Cr(nic)_2(OH)]\cdot 3H_2O$	39.0	39.2	7.6	7.4	4.6	4.2	–	–
III	$[Cr_2(glu)_2(OH)_2]\cdot glu\cdot 3H_2O$	28.7	27.8	6.7	5.8	4.6	4.8	–	–
IV	$[Cr(cys)_2(OH)(H_2O)]\cdot H_2O$	20.9	21.4	8.15	8.6	3.8	3.75	18.6	17.7
V	*mer*-$[Cr(gly)_3H_2O]\cdot H_2O$	23.2	22.9	13.5	13.2	4.2	4.1	–	–
VI	*fac*-$[Cr(gly)_3H_2O]\cdot H_2O$	23.2	22.8	13.5	13.1	4.2	4.4	–	–
VII	$[Cr_2(gly)_4(OH)]_2\cdot H_2O$	21.9	22.4	12.8	12.6	4.1	5.0	–	–

($2\,cm^3$) was added and the reagent mixture was heated and evaporated to half volume. Solid KOH was added until the pH was 8. The pink violet precipitate was filtered and washed with water.

mer-[$Crgly_3$] H_2O [***V***], fac-[$Crgly_3$] H_2O [***VI***] *and* [$Cr_2(OH)_2gly_4$] H_2O [***VII***] Prepared as described in the literature [26].

The analytical results are presented in Table 1.

Physicochemical studies

Infrared spectra were recorded on a Perkin-Elmer FTIR 1600 spectrophotometer (4000–400 cm^{-1}). FIR spectra (400–70 cm^{-1}) were recorded on a Perkin-Elmer 180 spectrophotometer.

The diffuse reflectance spectra (sample in a Li_2CO_3 pressed pellet) and solution spectra (in 2 M HNO_3) were measured in the spectral range 12000–48000 cm^{-1} with a Hitachi 365 UV/Vis spectrophotometer with a IBM/PC computer. The resolution processing of the spectra was performed by applying the variable digital filter method [27–30]. The filtered spectra were used to obtain the band positions precisely and calculate the crystal field parameters, assuming first O_h symmetry and then tetragonality of the Cr(III) environment. The energy matrices were adopted from the paper by Perumareddi [31].

The magnetic measurements were carried out in the temperature range 80–300 K using a Gouy balance with $Co[Hg(SCN)_4]$ as a calibrant.

Preliminary toxicity studies

Four prepared complexes have been checked for their toxicity (**I**, **II**, **V**, **VI**). The suspensions were prepared *ex tempore*. Acute toxicity was investigated on a group of white mice *Balb C*. Mice of both sexes of 20–25 g each were studied. Three doses of the prepared compounds were administrated (in mg/kg): 100, 500 and 2000, respectively. The mice were observed for 24 h.

RESULTS AND DISCUSSION

Thermodynamically, trivalent chromium ion is the most stable oxidation state of chromium; kinetically Cr(III) compounds are inert with the half-filled t_{2g} level (d^3 conf.) in octahedral symmetry (Ref [32], and the references therein).

The prepared complexes together with their physical properties are listed in Table 2. The complexes are blue (**I–II**), violet (**III–IV**) and pinkish-red (**V–VII**). The blue complexes exhibit the presence of CrO_6 and CrO_5N chromophores, respectively. The pinkish-red ones have CrO_3N_3 chromophores with three nitrogen atoms per chromium atom. Additional nitrogen in the coordination sphere of the chromium is consistent with the blue shift of the bands manifested in the spectrochemical series (*vide infra*). In complex **III** ligand molecules are in inert and in outer coordination sphere. It was established through analysis of the infrared spectra, i.e. the presence of the hydroxide ring [25] and bidentate O,N chelation of the ligand (Table 3, vide infra). These results are in line with our findings and those of others [48] and us [49] on the observation that in one compound some organic ligands are directly bound to the central ion and some are situated outside the coordination sphere.

The effective magnetic moments (3.82–4.37 B.M.) for monomers are close to the spin only value for the d^3 system in octahedral and pseudooctahedral symmetry $^4A_2$ ground state). Lower values of the magnetic moments (<3 B.M.) were observed for the dimers.

Infrared spectra

Table 3 presents the major absorption IR frequencies of the prepared compounds. In these complexes the carboxylate groups are involved in the coordination. The values of Δ, i.e. the differences between the two frequencies ν_{as} and ν_s of the carboxyl group (Table 3) pointed to the unidentate coordination of the carboxylate ion in all complexes [33], and is in line with the results found for other Cr(III) complexes

Table 2. Physical properties of the compounds

Symbol	Substrates	Ratio M:L	Formula	Colour	μ (BM) per chromium atom	Refs. (preparation)
I	$Cr(NO_3)_2{\cdot}9H_2O$, nicotinic acid	1:2	$[Cr_2(nic)_2(OH)_4]{*}4H_2O$	blue	2.58	this work
II	$Cr(NO_3)_2{\cdot}9H_2O$, nicotinic acid	1:2	$[Cr(nic)_2(OH)]{*}3H_2O$	blue	4.37	this work
III	$CrCl_3{\cdot}6H_2O$, glutamic acid	1:3	$[Cr_2(glu)_2(OH)_2]{*}glu{*}3H_2O$	dark violet	2.57	[23]
IV	$CrCl_3{\cdot}6H_2O$, cysteine	1:3	$[Cr(cys)_2OH{*}H_2O]{*}H_2O$	pink–violet	3.82	this work
V	$CrCl_3{\cdot}6H_2O$, glycine	1:3	*mer*-$[Cr(gly)_3H_2O]{*}H_2O$	pink–violet	3.92	[24]
VI	$CrCl_3{\cdot}6H_2O$, glycine	1:6	*fac*-$[Cr(gly)_3H_2O]{*}H_2O$	pink–violet	4.34	[24]
VII	$CrCl_3{\cdot}6H_2O$, glycine	1:6	$[Cr_2(gly)_4(OH)]_2{*}H_2O$	dark red	2.35	[24]

Table 3. Important IR frequencies for Cr(III) complexes (in cm^{-1})

Compound	ν(OH)	$\nu(NH_2)$	ν(SH)	ν_{as}(COO)	ν_s(COO)	ν(C–CN)	ν(Cr–O)	ν(Cr–N)	$\Delta\nu(\nu_{as}-\nu_{as})(COO)^-$
I	3418.0s			1601.0s	1384.4s		523.0s	470.0w	216.6
II	3347.0s			1595.9s	1384.2s		527.3m		211.7
III	3441.5s	3240.0w		1635.4s	1394.5s	948.4w	539.5s	425.7m	240.9
IV	3433.3m	3244.4w	2547.0w	1646.6s	1377.2m	920.2w	559.1w	433.4w	269.4
V	3405.5m	3261.9s		1638.8s	1385.5s	915.1m	547.7s	473.3m	253.3
VI	3462.4m	3261.0s		1636.9s	1384.2s	915.7m	542.4s	473.5m	252.7
VII	3463.4s	3225.3s		1636.6s	1382.5s	919.0s	549.3m	475.1s	254.1

with the same or similar ligands [17]. The CrO stretching vibration has been found in the *ca.* 500 cm^{-1} absorption region [53]. All complexes except **II** exhibit bands at 420–470 cm^{-1}, which have been assigned to ν(CrN) vibrations [54, 55]. The proposed structures have been presented in scheme 1. Thus, the nicotinates have been found to be O-bonded (**II**) and both N- and O-bonded in one molecule (**I**). Such bonding is not very unusual in coordination chemistry [34, 35].

Electronic spectra

The spectra for the solutions and the solid state are shown in Tables 4–6.

The complexes were found to be practically insoluble in common organic solvents. As HNO_3 was used for dissolution, such spectra usually should be less reliable (i.e. changed under the acid interaction) than the solid state spectra. However, the blue shift of the bands on dissolution is *ca.* 1000 cm^{-1}, consistent with the data found in the literature for water as solvent [29] and consistent with a significant change in the environment of the central atom on dissolution. These effects are connected with a weakening of the strong hydrogen bonding system operating in the rigid solid structure [29, 36]. Thus, assuming only hydrogen bonding effects, the individuality of the complexes appeared to be larger in the solution. The {glu} complex (**III**) was found to be the only one exhibiting a very large (2000 cm^{-1}) hipsochromic shift on dissolution. We relate it to the presence of the glutamic acid molecule in the second coordination sphere (Tables 1–2) which may easily dissociate on solvent influence. This effect makes the first coordination sphere extra strong in solution. *mer*- and *fac*-Cr(III) glycine complexes contain three bidentate ligands. These complexes were the only ones with known crystal structures [36]. The chromium ion in the mono Cr(III) glycinate was found to be octahedrally coordinated with the Cr–O and Cr–N bond length 196 and 206 pm, respectively. Unusual bonding forces were present in these complexes related to the network of hydrogen bonds operating in the solid state.

In the visible absorption region two broad bands associated with the d–d Laporte forbidden quartet–quartet spin allowed transition have been observed (Tables 4–6, Fig. 1). In the near IR absorption region weak but sharp band(s) associated with the doublet–quartet spin forbidden transition(s) can be seen in the {gly} complexes (**V**–**VII**) (Table 4, Fig. 1) [46, 47]. In the rest of the compounds the positions of these bands were found on the filtration analysis (not shown in Tabs. 4–6). As this analysis (i.e. filtration) does not give the intensity values (only the energy of transitions) we were not able to discuss the magnitude of coupling between two chromium(III) nuclei in compounds **I** and **II**.

From the crystal structure results available for Cr(III) glycinate, the coordination sphere of the metal

Compound I

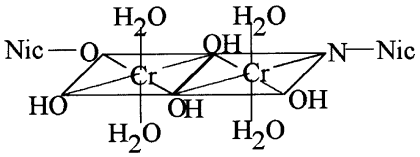

$[Cr_2(nic)_2(OH)_4]\ 4H_2O$

Compound II

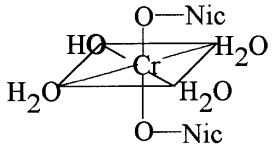

$[Cr(nic)_2OH)]\ 3H_2O]$

Compound III

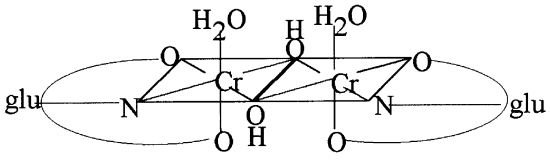

$[Cr_2(glu)_2(OH)_2(H_2O)_2]*glu*3H_2O$

Compound IV

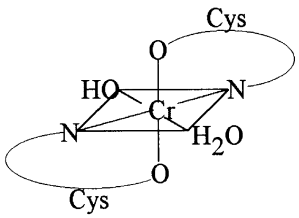

$[Cr(cys)_2(OH)(H_2O)]*H_2O$

ion is octahedral [36]. Generally, many Cr(III) complexes are octahedrally coordinated [32]. However, the fact that the complexes are dimeric with two OH bridges (**I**, **III** and **VII**), their coordination is via various donor atoms: O, N, S (**I**, **III**–**VII**) and the coordination is via oxygen atoms but from various ligands (**II**), makes the symmetry lowering possible. Thus, we have calculated crystal field parameters assuming (i) O_h symmetry and (ii) tetragonal distortion around Cr(III) ion.

The criterion of proper fitting was the RMS value found on calculation.

The results showed that the complexes belonged to two general groups:

(1) Octahedrally coordinated (the nicotinates **I** and **II**) Table 5.

Compound V

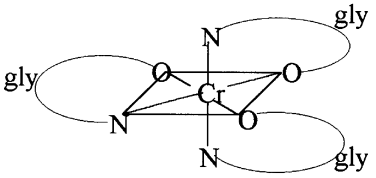

mer -$[Cr(gly)_3]*H_2O$

Compound VI

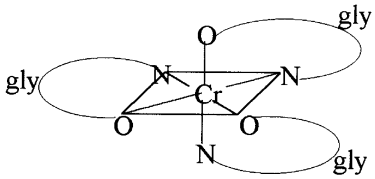

fac -$[Cr(gly)_3]*H_2O$

Compound VII

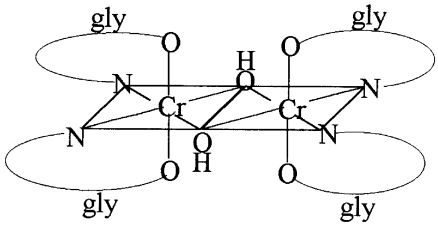

$[Cr_2(gly)_4(OH)_2]*H_2O$

Table 4. Electronic spectra of Cr(III) complexes (cm^{-1})

Compound	Spectrum		Band position		
I	Absorption		17500	24300	38000
	Diffuse reflect.		16600	23800	38000
II	Absorption		17500	24200	38500
	Diffuse reflect.		17100	23700	37800
III	Absorption		18300	25600	33500
	Diffuse reflect.		16500	24200	38800
IV	Absorption		18800	25200	33500
	Diffuse reflect.		18200	24600	38100
V	Absorption	14400	19000	25500	33400
	Diffuse reflect.	14600	18700	25600	39000
VI	Absorption	14100	18800	25200	33400
	Diffuse reflect.	14200	18900	25600	38900
VII	Absorption	14600	19200	25400	33400
	Diffuse reflect.	14800	19600	26000	38300

Table 5. The d–d band positions and crystal field parameters for Cr(III) nicotinates. (Filter parameters: step = 100, $\alpha = 300$, $N = 20$)

Compound	Chromophore	Spectrum	$^4T_{2g}(F)$	$^4T_{1g}(F)$	$^4T_{1g}(G)$	10 Dq [cm^{-1}]	B [cm^{-1}]	RMS
I	$[CrO_5N]$	Absorption	17500	24080	38080	17500	650	1.6
		Diffuse reflect	16700	23800	37200	16700	720	14.2
II	$[CrO_6]$	Absorption	17500	24200	38200	17500	665	0.9
		Diffuse reflect	16900	23600	37100	16900	667	10.7

(2) Tetragonally coordinated (the glutamate (**III**), cysteinate (**IV**) and glycinates (**V**–**VII**) Table 6.

The reasonable explanation for these results may be based on the differences in the M–L interaction between the nicotinates and the other ligands. It is manifested in the crystal field strength calculated for the absorption spectra (Tables 5–6). For the first group of the complexes the Dq values are smaller which is evidence for weaker Cr-nic interaction in comparison to the other ligands studied. However, this effect is not a very strong one. Moreover, the Dt values for complexes (**III**–**VII**) are small indicating only slight tetragonality around the Cr(III) ion. Assuming an octahedral and pseudooctahedral environment, nicotinic acid is evidently the last ligand in the spectrochemical series for the Cr(III) ion: glycine > cysteine ≈ glutamic acid > nicotinic acid.

The electronic spectroscopic data for monomeric Cr(III) species have been rationalised taking into account the 10 Dq value as a criterion (Table 4). The energy of the first spin allowed d–d transition (10 Dq) for Cr(III) monomeric complexes increases in the sequence

$$CrO_6 < CrO_4N_2 < CrO_3N_3 < CrN_6$$

The value for CrN_6 chromophore was taken from the literature [32]. This sequence also reflects the gradually changes of the colour from blue (CrO_6) through violet (CrO_4N_2) to red CrO_3N_3 (VII) and CrN_6 [32].

The grey–green colour of LMWCr concentrated solutions and the energies of two distinct visible d–d bands and UV shoulder [37] resemble water solutions of anionic type binary and ternary complexes of the $[Cr(A)(H_2O)]^{n-}$ and $[Cr(AB)]^{n-}$ type where A, B-non enzymatic cellular reductants: ascorbic acid, cysteine, glutathione [29, 30, 38]. It was found that the S-con-

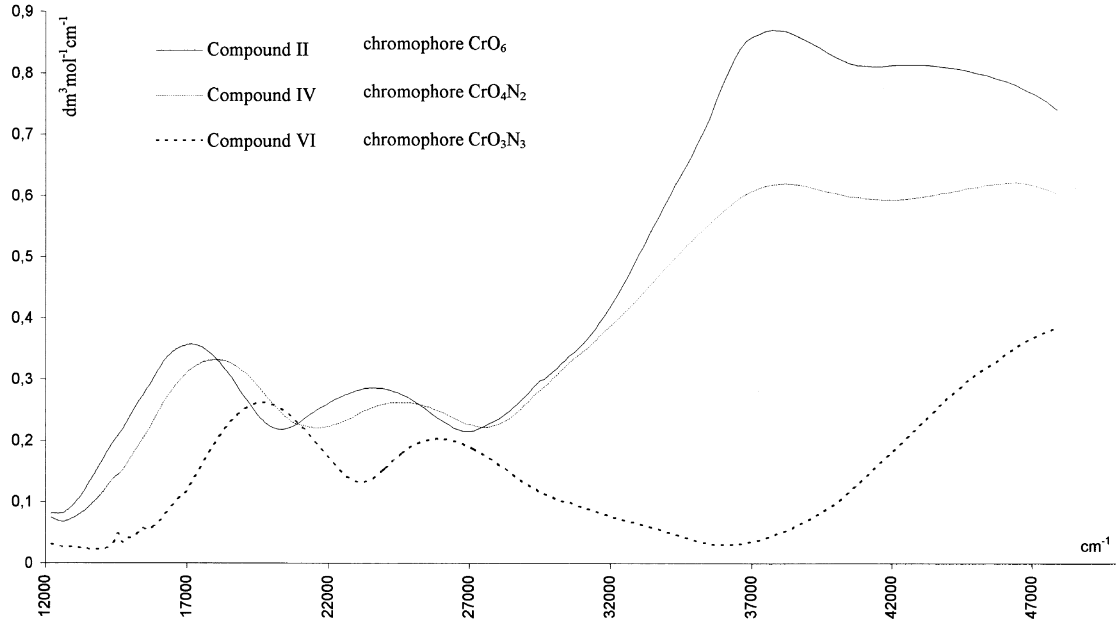

Fig. 1. Diffuse reflectance spectra of monomeric Cr(III) nicotinate (**II**), cysteinate (**IV**) and glycinate (**VI**).

Table 6. The d–d band positions and crystal field parameters of tetragonally distorted Cr(III) complexes. (Filter parameters: step = 100, $\alpha = 300$, $N = 20$)

Compound	Chromophore	Spectrum	^4E_g	$^4B_{2g}$	^4E_g	$^4A_{2g}$	$^4A_{2g}$	^4E_g	10 Dq (cm^{-1})	Ds (cm^{-1})	Dt (cm^{-1})	B (cm^{-1})	RMS
III	$[CrO_5N]$	Absorption	18100	18100	24700	27650	39500	40600	18100	640	22	740	0.0
		Diffuse reflect	16600	16600	24400	25650	38400	38700	16600	300	1.3	890	17.2
IV	$[CrO_4N_2]$	Absorption	18400	18400	24900	27650	39850	41000	18400	580	18.7	719	0.2
		diffuse reflect	16600	16600	24600	30500	39200	41000	18100	184	8.8	706	5.7
V	$[CrO_3N_3]$	absorption	18800	18800	25300	27700	40500	41500	18800	490	13	705	1.5
		Diffuse reflect	18700	18700	25500	33400	34400	51700	18700	417	8.9	723	1.5
VI	$[CrO_3N_3]$	Absorption	18800	18800	25300	27100	40500	41200	18800	400	6.7	690	0.8
		Diffuse reflect	18800	18800	25400	33200	33300	50700	18800	307	7.2	695	14.3
VII	$[CrO_2'O_2''N_2]$	Absorption	18900	18900	25350	27660	40600	41600	18900	470	12	700	0.0
		Diffuse reflect	19300	19300	25600	33300	33300	51000	19300	358	6.3	664	14

taining Cr(III) complexes exhibited the absorption in the 260 nm (*ca.* 38000 cm^{-1}) with the Cr←S [50, 51] band intensity of 3000–5000 $dm^3\,mol^{-1}\,cm^{-1}$. The 260 nm band was also found in the LMWCr [19, 37]. However, as this band was also present in the apo (i.e. Cr-free) form of the protein [19, 52] only the detailed analysis of this spectral region might explain the origin of this absorption in the LMWCr.

Toxicity

The literature data on chromium toxicity are incomplete and inconsistent [39]. The toxicity expressed by the lethal dose (LD_{50}) values is dependent on the chromium oxidation state, different species of animals and route of exposure [40–43]. Generally, oral toxicities of Cr(III) compounds appear to be 10–1000 times lower than for the hexavalent chromium compounds [38]. The toxicology of chromium(III) varies greatly among a variety of different chromium compounds [39]. For example, in genotoxical bacterial tests on a series of hexacoordinate Cr(III) complexes, out of 17 complexes 12 were positive [44].

The results of our studies are presented in Table 7. All compounds appeared to be non-toxic in this examination. The completion of the results as well as their extension into other groups of animals are under way.

SUMMARY AND CONCLUSIONS

The interaction between the Cr(III) ion and glycine, cysteine, glutamic and nicotinic acids gives a series of monomeric and dimeric complexes, models for the glucose tolerance factor (GTF). The composition of the species is strongly dependent on the metal–ligand interaction and conditions of the experiment (temperature, time, etc.). The breaking of the strong hydrogen bonding network operating in the solid state may be responsible for the blue shift of the electronic d–d bands in solution. Despite the various types of chromophores and number of the central atoms in the complexes, the coordination sphere for chromium nicotinates was found to be a full octahedron. The rest of the complexes studied can be better described assuming a tetragonally distorted octahedron. The reason for such behaviour was related to the strength of the ligand field around the central metal ion, this being weakest in the nicotinic acid.

The tentative results for the toxicity studies of the complexes are very promising. They are practically non toxic and can be potentially apply as chromium nutrition products.

Acknowledgements—The authors are indebted to Dr D. Goodall for reading the manuscript and helpful comments. Financial support from the Wroclaw University of Technology (grant No. 331-403) is gratefully acknowledged.

Table 7. LD_{50} values for Cr(III) inorganic compounds taken from the literature and the results of this work

Compound	Animal	LD_{50} (in mg/kg)	Method	Toxicity	Refs.
$[Cr_2nic_2(OH)_4]\cdot 4H_20$	mouse	>2000	intraperitoneally	non-toxic	This work
$[Crnic_2(OH)]\cdot 3H_20$	mouse	>2000	intraperitoneally	non-toxic	This work
mer-$[Crgly_3H_2O]\cdot H_2O$	mouse	>2000	intraperitoneally	non-toxic	This work
fac-$[Crgly_3H_2O]\cdot H_2O$	mouse	>2000	intraperitoneally	non-toxic	This work
$CrCl_3$	mouse	801	intravenous	slightly toxic	[45]
$CrCl_3$	frog	187	intravenous	moderately toxic	[45]
$CrCl_3$	rabbit	288	intravenous	moderately toxic	[45]
$Cr_2(SO_4)_3$	mouse	246.8	intravenous	moderately toxic	[45]
$Cr_2(SO_4)_3$	frog	37	intravenous	very toxic	[45]
$Cr_2(SO_4)_3$	rabbit	215	intravenous	moderately toxic	[45]
Cr_2O_3	dog	330	hypodermic	moderately toxic	[45]

REFERENCES

1. Mertz, W. and Schwarz, K., *Arch. Biochem. Biophys*., 1959, **85,** 292.
2. Kendrick, M. J., May, M. T., Plishka, M. J. and Robinson, K. D., *Metals in Biological Systems*. E. Horwood Series, New York/London/Toronto, 1992.
3. Mertz, W., *Biol. Trace Element Res*., 1992, **32,** 3.
4. Mertz, W., *J. Nutr*., 1993, **123,** 626.
5. Topfer, E. W., Mertz, W., Polansky, M. M., Roginski, E. E. and Wolf, W. R., *J. Agric. Food Chem*., 1977, **25,** 162.
6. Cooper, J. A., Anderson, B. F., Buckley, P. D. and Blackwell, L. F., *Inorg. Chim. Acta*, 1984, **91,** 1.
7. Haylock, S. J., Buckley, P. D. and Blackwell, L. F., *J. Inorg. Biochem*., 1983, **18,** 195; **19,** 105.
8. Da Silva, J. J. R. F. and Williams, R. J. P., *The Biological Chemistry of the Elements*. Clarendon Press, Oxford, 1991.
9. Simonoff, M., Shapcott, D., Alameddine, S., Sutter-Dub, M. T. and Simonoff, G., *Biol. Trace Elem. Res*., 1992, **32,** 25.
10. Shepherd, P. R., Elwood, C., Buckley, P. D. and Blackwell, L. F., *Biol. Trace Elem. Res*., 1992, **32,** 109.
11. Evans, G. W. and Pouchnik, P. J., *J. Inorg. Biochem*., 1993, **49,** 177.
12. Gonzales-Vergara, E., Hegenauer, J. and Saltman, P., *Inorg. Chim. Acta*, 1982, **66,** 115.
13. Green, C. A., Bianchini, R. J. and Legg, J. L., *Inorg. Chem*., 1984, **23,** 2713.
14. Evans, G. W. and Bowman, T. D., *J. Inorg. Biochem*., 1992, **46,** 243.
15. Barrett, J., Kormoh, M. K. and O'Brien, P., *Inorg. Chim. Acta*, 1985, **107,** 269.
16. Barrett, J. and O'Brien, P., *Polyhedron Rep*.1985, **9**(1), 1 and the references therein.
17. El-Shahawi, M. S., *Spectrochim. Acta*, 1995, **51A,** 161.
18. Yamamoto, A., Wada, O., Suzuki, H., *J. Nutr*., 1988, **118,** 39 and the references therein.
19. Davis, C. M. and Vincent, J. B., *Arch. Biochem. Biophys*., 1997, **339,** 335.
20. Davis, C. M., Sumrall, K. H. and Vincent, J. B., *Biochemistry*, 1996, **35,** 12963.
21. Davis, C. M. and Vincent, J. B., *Biochemistry*, 1997, **36,** 4382.
22. Davis, C. M., Royer, A. C. and Vincent, J. B., *Inorg. Chem*., 1997, **36,** 5316.
23. Vincent, J. B., *J. Nutr*., 1994, **124,** 117.
24. Stearns, D. M., Wise, J. P. Sr., Patierno, S. R. and Wetterhahn, K. E., *FASEB J*., 1995, **9,** 1643.
25. Gielzak, K. and Wojciechowski, W., *Chem. Papers*, 1994, **48**(6), 380.
26. Ley, H. and Flicken, K., *Chem. Ber*., 1912, **45,** 377.
27. Bierman, G. and Ziegler, H., *Anal. Chem*., 1986, **58,** 536.
28. Myrczek, J., *Spectrosc. Lett*., 1990, **23,** 1027.
29. Cieslak-Golonka, M., Raczko, M. and Staszak, Z., *Polyhedron*, 1992, **11,** 2549.
30. Adach, A., Janyst, J. and Cieslak-Golonka, M., *Spectrosc. Lett*., 1995, **28,** 1259.
31. Perumareddi, J. R., *J. Phys. Chem*., 1967, **71,** 3144.
32. Lever, A. B. P., *Inorganic Electronic Spectroscopy*, 2nd edn. Elsevier, Amsterdam/Oxford/New York/Tokyo, 1984.
33. Nakamoto, K., *Infrared and Raman Spectra of Inorganic and Coordination Compounds*, 3rd edn. A Wiley-Interscience Publication, New York/Chichester/Brisbane/Toronto, 1978.
34. Lomozik, L., Bolewski, L., Bregier-Jarzebowska, R., *Pol. J. Chem*., 1995, **69,** 197.
35. Bukanova, A. Y., Sidorova, T. P., Razgonaieva, G. A., Tsuvaiev, A. W. and Shubotshkin, L. K., *Zh. Neorg. Khim*., 1990, **35,** 2003.
36. Bryan, R. F., Greene, P. T., Stokely, P. F. and Wilson, E. W., *Inorg. Chem*., 1971, **10,** 1468.
37. Sumrall, K. H. and Vincent, J. B., *Polyhedron*, 1997, **16,** 4171.
38. Abdullah, M., Barrett, J. and O'Brien, P., *J. Chem. Soc. Dalton Trans*. 1985, 2085.
39. Katz, S. A. and Salem, H., *J. Appl. Toxicol*., 1993, **13,** 217.
40. Hamilton, J. W. and Wetterhahn, K. E., in *Handbook on Toxicity of Inorganic Compounds*, eds. H. G. Seiler and H. Sigel. Marcel Dekker, New York/Basel, 1987, pp. 239–250.

41. Gaur, A. and Bhattacherjee, J. W., *Water Air Soil Pollut*., 1991, **59,** 193.
42. Kargacin, B., Squibb, K. S., Cosentino, S., Zhitkovich, A. and Costa, M., *Biol. Trace Element Res*., 1993, **36,** 307.
43. Clothier, R. H., Hulme, L. M. and Smith, M., Balls, M., *Mol. Toxicol*., 1987, **1,** 571.
44. Warren, G., Schultz, P., Bancroft, D., Bennett, K., Abbott, E. H. and Rogers, S., *Mutat. Res*., 1981, **90,** 11.
45. *Handbook of Toxicology*, Vol. 1. W. B. Saunders Comp. Philadelphia–London (1956).
46. Schönherr, T., *J. Mol. Struct*., 1992, **261,** 203.
47. McCarthy, P. J. and Güdel, H. U., *Coord. Chem. Rev*., 1988, **88,** 69.
48. Czakis-Sulikowska, D. M., Radwańska-Doczekalska, J., Kuznik, B. and Malinowska, A., *Metal Chem*., 1995, **20,** 203.
49. Repka, A., Cieślak-Golonka, M., Surga, W., Żurowski, K. R., *Thermochim. Acta*, 1998, **313,** 9.
50. Santos, T. M., Pedrosa de Jesus, J. and O'Brien, P., *Polyhedron*, 1992, **11,** 1687.
51. Kaiwar, S. P., Sreedhara, A., Raghavan, M. S. S. and Rao, Ch.P., *Polyhedron*, 1996, **15,** 765.
52. Sumrall, K. H. and Vincent, J. B., *Polyhedron*, 1997, **16,** 4171.
53. Singh, D. P. and Rana, V. B., *Polyhedron*, 1995, **14,** 2901.
54. Heaster, H. and Hoggard, P. E., *Polyhedron*, 1994, **13,** 333.
55. Lee, K.-W., Eom, K.-Il, Park, S.-J., *Inorg. Chim. Acta*, 1997, **254,** 131.

Pergamon

PII: S0277-5387(98)00188-0

Polyhedron Vol. 17, No. 21, pp. 3795–3802, 1998
© 1998 Elsevier Science Ltd
All rights reserved. Printed in Great Britain
0277–5387/98 $19.00+0.00

The kinetics of the acid-catalysed decarboxylation of *cis*-[Co([15]aneN$_4$)CO$_3$]$^+$ ([15]aneN$_4$ = 1,4,8,12-tetra-azapentadecane)

Robert W. Hay* and Andrew M. Danby

School of Chemistry, University of St Andrews, St Andrews KY16 9ST, U.K.

(Received 24 October 1997; accepted 5 May 1998)

Abstract—The decarboxylation of [Co([15]aneN$_4$)CO$_3$]$^+$ in nitric acid solutions has been studied in detail over a temperature range at $I = 1.0\,\text{mol dm}^{-3}$. The reaction is biphasic, the initial reaction is the carbonato ring opening step, which is followed by very rapid decarboxylation of the monodentate carbonato intermediate. The second step is the isomerisation of *cis*-[Co([15]aneN$_4$)CO$_3$]$^+$ to the *trans*-isomer. At constant hydrogen ion concentration, values of k_{obs} for the carbonato ring opening reaction are given by $k_{obs} = k_o + k_H[H^+]$, where k_o relates to the spontaneous water hydrolysis and k_H to the acid-catalysed process. The temperature dependence of k_H gives $\Delta H^{\ddagger} = 71 \pm 2\,\text{J K}^{-1}\,\text{mol}^{-1}$ and $\Delta S^{\ddagger}_{298} = -66 \pm 6\,\text{J K}^{-1}\,\text{mol}^{-1}$. The solvent deuterium isotope effect for the acid-catalysed decarboxylation k_{D_2O}/k_{H_2O} is 2.35, which is consistent with a rapid pre-equilibrium protonation of the carbonato ring, followed by rate-determining ring opening. The mechanisms of these reactions are considered in detail. At 25°C, the rate constant for the isomerisation reaction is $4.9 \times 10^{-6}\,\text{s}^{-1}$ and is independent of the acidity in the range $[H^+] = 0.05$ to $0.5\,\text{mol dm}^{-3}$ at $I = 1.0\,\text{mol dm}^{-3}$. © 1998 Elsevier Science Ltd. All rights reserved

Keywords: macrocycle; [15]aneN$_4$; [Co([15]aneN$_4$)CO$_3$]$^+$; decarboxylation; kinetics

There have been a number of studies of the acid-catalysed decarboxylation of cobalt(III) carbonato complexes of macrocyclic tetra-amines [1–3] and many studies [4–6] of the decarboxylation of non-cyclic amine complexes. These investigations have established that the cobalt(III) complexes all undergo acid-catalysed aquation via a common mechanism involving the ring opening of the carbonato ring followed by the rapid decarboxylation of the monodentate carbonato intermediate as shown in eqs. (1–4). The conversion of the monodentate hydrogen carbonate species eq. (3) to the hydroxo-aqua complex is fast and not rate-determining. The ring opening step is catalysed both by water eq. (1) and acid eq. (2) so that k_{obs} (the observed first order rate constant at constant hydrogen ion concentration) is given by the expressions $k_{obs} = k_o + k_H[H^+]$ where k_o is the rate constant for the solvolytic pathway and k_H is the rate constant for the acid-catalysed pathway.

$$cis\text{-}[Co(L)(CO_3)]^+ + H_2O \xrightarrow{k_0} cis\text{-}[Co(L)(OH)(HCO_3)]^+ \quad (1)$$

$$cis\text{-}[Co(L)(CO_3)]^+ + H_3O^+ \xrightarrow{k_H} cis\text{-}[Co(L)(H_2O)(HCO_3)]^{2+} \quad (2)$$

$$cis\text{-}[Co(L)(H_2O)(HCO_3)]^{2+} \xrightarrow{k_1} cis\text{-}[Co(L)(OH)(H_2O)]^{2+} + CO_2 \quad (3)$$

$$cis\text{-}[Co(L)(OH)(H_2O)]^{2+} + H_3O^+ \overset{K_2}{\rightleftharpoons} cis\text{-}[Co(L)(H_2O)_2]^{3+} + H_2O \quad (4)$$

If the macrocycle is 15-membered, stable folded *cis*-complexes are only formed with chelating ligands so that the *cis*-diaqua complex formed on decarboxylation is followed by *cis-trans* isomerisation which can be observed kinetically

$$cis\text{-}[CoL(OH_2)_2]^{3+} \rightarrow trans\text{-}[CoL(OH_2)_2]^{3+}; k_i$$

* Author to whom correspondence should be addressed.

The rate constants k_H which have been reported for the acid-catalysed decarboxylation of cobalt(III) carbonato complexes vary greatly with the structure of the spectator ligand. This variation which extends over six orders of magnitude has been attributed to several factors including sterically induced strain within the carbonato ligand caused by the spectator ligand and the electron donating ability of the N_4 ligand.

Previous studies of the acid-catalysed decarboxylation of cobalt(III) macrocyclic complexes have been primarily concerned with the 14-membered ring system [2, 3, 11, 17]. We have previously studied the acid-catalysed decarboxylation of *cis*-[Co(cyclen)CO_3]$^+$ in detail [1] where cyclen is the 12-membered ring macrocycle 1,4,7,10-tetra-azacyclododecane. We have now extended this work to the 15-membered ring system and the results of this study are reported in the present paper.

EXPERIMENTAL

Synthesis

The ligand [15]aneN$_4$ (1,4,8,12-tetra-azacyclopentadecane) was prepared by a modification of Barefield's procedure [7]. Nickel(II) chloride hexahydrate (10.2 g, 0.043 mol) was dissolved in water (150 cm^3). To this solution was added 1,11-diamino-4,8-diazundecane (8 g, 0.043 mol) with stirring, followed by 30–40% aqueous glyoxal solution (10 cm^3). The blue solution was heated to 60–80°C for 2–3 hours, during which time the solution changed to a brown–red colour. The solution was then transferred to a hydrogenation bottle along with freshly prepared Raney nickel (20 g). After flushing the vessel with nitrogen, the hydrogenation apparatus was heated to 70°C under 3.5 atmospheres of hydrogen, until hydrogen uptake ceased. The violet solution was filtered to remove the catalyst and cooled in an ice bath. Sodium thiocyanate (5.2 g, 0.065 mol) dissolved in water (25 cm^3) was then added and the purple precipitate obtained filtered off. The thiocyanate complex was dissolved in water (75 cm^3), sodium cyanide (5 g, 0.1 mol) was added and the solution refluxed for 1 hr. The solution was cooled, sodium hydroxide (5 g) was added and the solution extracted several times with dichloromethane. The extracts were combined and dried over anhydrous sodium sulphate. The sodium sulphate was filtered off and the dichloromethane removed on a rotary evaporator to give the product. The ligand was recrystallised from hexane to give white, needle-like crystals and dried *in vacuo*. (Yield 4.85 g, 52%), m.p. 100°C. IR υ(NH) 3242, 3270, 3283 cm^{-1}, ^{1}H NMR ($CDCl_3$), 1.71 (6H, quintet), 1.95 (4H), 2.75 (16H, mult.).

The tetrahydrochloride of the ligand was prepared by adding an excess of concentrated hydrochloric acid to a saturated aqueous solution of the ligand (1.07 g, 5 mmol). The hydrochloride precipitated on addition of the acid and was collected by filtration (Yield 1.64 g, 91%), m.p. 220–222°C (decomp.). IR υ(NH) 3242, 3270 and 3283 cm^{-1})

The complex [Co([15]aneN$_4$)CO_3]ClO_4 was pre-

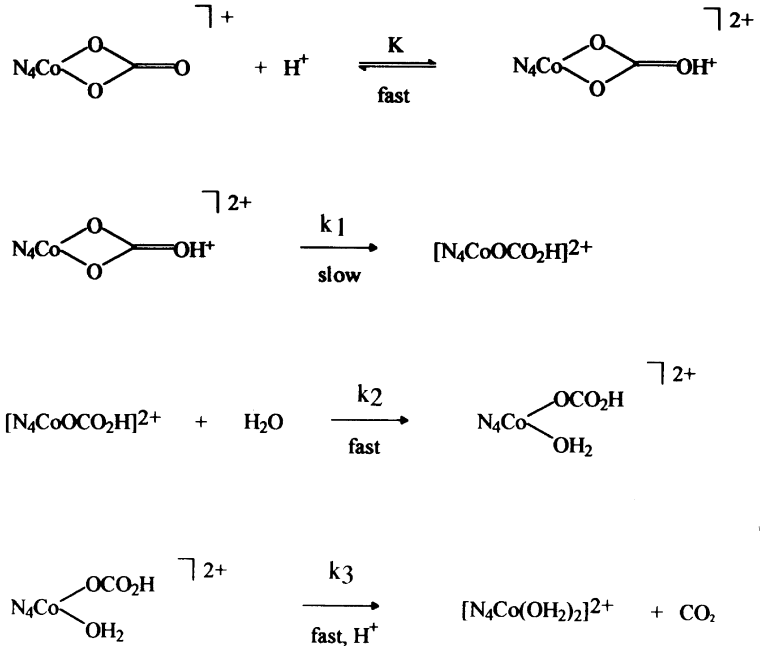

Scheme

pared as follows. The tetrahydrochloride of the ligand (1 g, 4 mmol) was mixed with an equimolar amount of sodium tris(carbonato)cobaltate(III) trihydrate, $Na_3[Co(CO_3)_3]3H_2O$ (1.45 g, 4 mmol) and the mixture ground to a fine powder in a pestle and mortar. Water (4 cm^3) was added and the resulting green paste slowly changed colour to purple. The purple material was dissolved in ethanol (50 cm^3) and the solution filtered. Sodium perchlorate (0.8 g, 6.5 mmol) was added to the filtrate and the purple perchlorate complex precipitated by the addition of ether. The complex was recrystallised from methanol and dried *in vacuo*.

(Yield 1.54 g, 90%). Found: C, 32.2; H, 5.8; N, 12.8. Calc. for $C_{12}H_{26}N_4ClCoO_7$: C, 32.3; H, 6.0; N, 12.9%). The complex has λ_{max} 528 nm ($\epsilon = 156$) and 369 nm ($\epsilon = 216\ dm^3\ mol^{-1}\ cm^{-1}$) in water.

Physical measurements

UV–vis spectra were determined with a Perkin-Elmer Lambda 5 or Lambda 14P spectrophotometer. The instruments were fitted with a Peltier cell for constant temperature measurements. IR spectra were obtained as KBr discs on a Perkin-Elmer 1710 Fourier transform infrared spectrophotometer. Conductivity measurements were made with an AGB 1000 conductivity meter outputting to a chart recorder. ^1H NMR spectra were determined at 300 MHz with a Varian Gemini instrument. Stopped-flow measurements were made with a Hi-Tech SU 51 stopped-flow spectrophotometer. Solutions of nitric acid were prepared from Volucon reagents and were standardised against sodium hydroxide which had previously been standardised using potassium hydrogen phthalate. The ionic strength in the reactions was maintained at $I = 1.0\ mol\ dm^{-3}$ using KNO_3.

RESULTS AND DISCUSSION

A typical interval scan spectrum for the reaction of *cis*-$[CoLCO_3]^+$ (L = 1,4,8,12-tetra-azacyclopentadecane) in 0.5 $mol\ dm^{-3}$ nitric acid at 35°C and $I = 1.0\ mol\ dm^{-3}$ is shown in Fig. 1. The spectra were taken at 5 minute intervals as the reaction proceeded and confirm that it is not a simple first order process. The decrease in absorbance at 540 nm does not follow a simple first order exponential decay curve. Plots of $\ln(A_t - A_\infty)$ where A_t is the absorbance at time t and A_∞ is the final absorbance against time were not linear over the full time scale and could be fitted to two exponential decays. It was possible to study the spectral changes involved in the two reactions. The complex *cis*-$[CoLCO_3]^+$ has bands at 369 and 528 nm and, as the reaction proceeds, the band at 528 nm decreases in intensity and moves to slightly lower wavelengths (*ca.* 518 nm) and the band at 369 nm disappears. These changes are accompanied by isosbestic points at 397, 477 and 587 nm.

During the second stage of the reaction, the band at 518 nm shifts to ca. 490 nm and decreases slightly in intensity. A new band of lower intensity appears at 610 nm. Good isosbestic points occur at 367, 406, 491 and 598 nm indicating that only two uniquely absorbing species are present in solution. By monitoring the reaction at 485 nm, a wavelength midway between two of the isosbestic points for each reaction, a decrease in absorbance should be observed as the first stage proceeds and should be followed by an absorbance increase as the second reaction occurs. The plot of absorbance *versus* time, Fig. 2 confirms that this is indeed the case. The absorbance *versus* time data at 485 and 540 nm was processed in a manner analogous to the treatment of radiactive decay where a daughter species is produced whose decay half life is longer than that of the parent. Good fits to the experimental results were obtained using this method. Values of $k_{obs}(1)$ and $k_{obs}(2)$ were obtained over the acidity range 0.1 to 1.0 $mol\ dm^{-3}$ $[H^+]$ at 15, 25, 30, 35, 40 and 45°C. The rate constants $k_{obs}(1)$ are summarised in Table 1. The first stage of the reaction is the conversion of *cis*-$[CoLCO_3]^+$ with λ_{max} 369 ($\epsilon = 216$) and 528 nm ($\epsilon = 156\ dm^3\ mol^{-1}\ cm^{-1}$) to the *cis*-diaqua species with λ_{max} 518 nm. Attempts to synthesize the intermediate *cis*-$[CoL(OH_2)_2]^{3+}$ were unsuccessful. However, a comparison of the spectral changes observed in the aquation of the present complex with those observed in the aquation of the analogous complexes *cis*-$[Co(cyclam)CO_3]^+$ and *cis*-$[Co(tet\ a)CO_3]^+$ provides strong confirmatory evidence that the *cis*-diaqua complex is indeed the intermediate (Table 2).

Plots of $k_{obs}(1)$ versus the nitric acid concentration are linear with a small positive intercept, Fig. 3. The rate expression takes the form $k_{obs}(1) = k_o + k_H[H^+]$ where k_o relates to the spontaneous water reaction and k_H to the acid-catalysed process. Values of k_H and k_o over a temperature range are listed in Table 3. The rate constant k_o is subject to quite large errors due to the rather small contribution which it makes to the overall reaction. The activation parameters for the spontaneous water reaction are $\Delta H^\dagger = 161.6 \pm 18.7$ kJ mol^{-1} and $\Delta S^\dagger_{298} = 211 \pm 62$ J K^{-1} mol^{-1}. Values of k_o and the activation parameters previously determined for a range of carbonato complexes are summarised in Table 4. Values of k_o cover a range of four orders of magnitude and there is a good isokinetic relationship between $\Delta H^\dagger$ and $\Delta S^\dagger_{298}$, Fig. 4, indicating that a common mechanism applies.

Activation parameters were also obtained for the acid-catalysed pathway. The values obtained are $\Delta H^\dagger = 71 \pm 1.7$ kJ mol^{-1} and $\Delta S^\dagger_{298} = -60.6 \pm 5.7$ J K^{-1} mol^{-1} and these values are compared with those previously obtained for cobalt(III) carbonato complexes in Table 5. Values of k_H range over approximately six orders of magnitude and the k_H values for the macrocyclic complexes are all some three orders of magnitude smaller than those where $L = (NH_3)_4$, $(en)_2$ or $(pn)_2$. For the macrocyclic complexes the reactivity order is L = *trans*-Me_2[14]diene > *trans*-

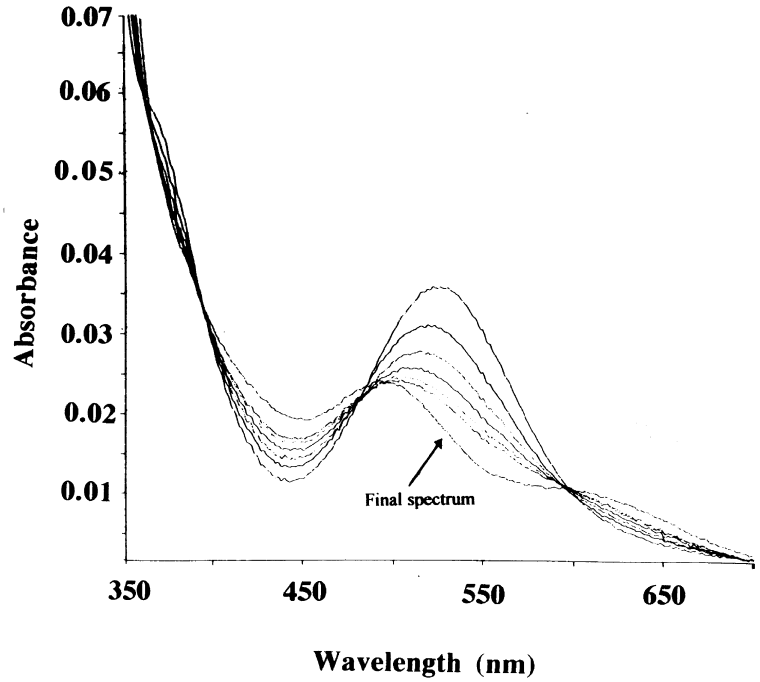

Fig. 1. Interval scan spectrum for the reaction of *cis*-$[CoLCO_3]^+$ in 0.5 mol dm^{-3} nitric acid at 35°C and $I = 1.0$ mol dm^{-3}. The time interval between scans is 5 minutes.

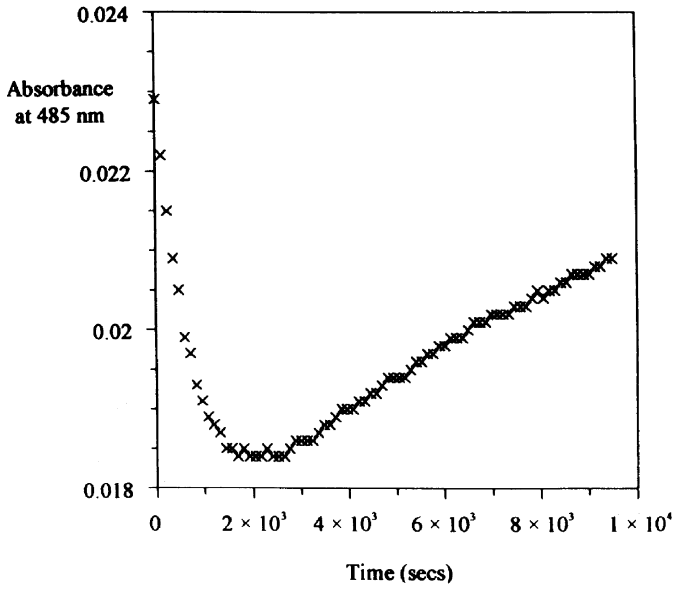

Fig. 2. Absorbance versus time plot at 485 nm for the reaction of *cis*-$[CoLCO_3]^+$ in nitric acid solution.

Me_6[14]diene > [12]aneN_4 > [15]aneN_4 > [14]aneN_4. The complex [Co[15]aneN_4)CO_3]$^+$ undergoes acid-catalysed decarboxylation some four times faster than the analogous cyclam complex at 25°C. The isokinetic plot for the acid-catalysed reactions shows considerable scatter, Fig. 5 and this probably arises in part, because k_H is the product of a rate constant and an equilibrium constant.

Francis and Jordan [8] have suggested that there is a relationship between the rate constant k_H and the average pK_a of the amine ligands in the $[CoN_4CO_3]^+$ complexes. The average pK_a of the amine ligand can

Table 1. Values of $k_{obs}(1)$ for the acid-catalysed decarboxylation of *cis*-$[CoLCO_3]^+$ at $I = 1.0\,mol\,dm^{-3}$ over the temperature range 15–45°C

$[H^+]$ (mol dm^{-3})	$10^3 k_{obs}(1)$ (s^{-1})					
	15°C	25°C	30°C	35°C	40°C	45°C
0.05	0.02	0.25	0.29	0.47	1.10	1.93
0.125	0.07	0.34	0.43	0.90	1.53	2.85
0.25	0.14	0.49	0.78	1.20	2.22	4.16
0.375	0.20	0.63	1.21	2.18	3.31	5.38
0.5	0.27	0.74	1.53	2.40	3.69	5.42

Table 2. Spectral parameters for carbonato and diaqua complexes

Complex	λ_{max} (nm)	ϵ ($dm^3\,mol^{-1}\,cm^{-1}$)	λ_{max} (nm)	ϵ ($dm^3\,mol^{-1}\,cm^{-1}$)
cis-$[Co(cyclam)CO_3]^+$	365	140	520	164
cis-$[CoLCO_3]^+$	369	182	528	138
cis-[Co (tet *b*)CO_3]$^+$	380	180	551	184
cis-$[Co(cyclam)(OH_2)_2]^+$	367	99	506	110
cis-$[CoL(OH_2)_2]^{3+}$			518	
cis-[Co(tet *b*)$(OH_2)_2$]$^{3+}$	383	133	534	91

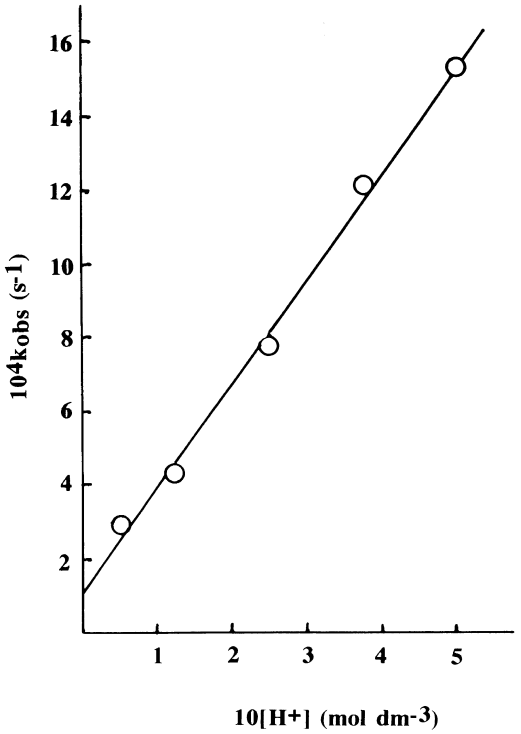

Fig. 3. Plot of $k_{obs}(1)$ for the ring opening step *versus* the nitric acid concentration.

Table 3. Values of k_o and k_H for the water and acid-catalysed decarboxylation of *cis*-$[CoLCO_3]^+$ at $I = 1.0\,mol\,dm^{-3}$

Temp (°C)	$10^3 k_H$ ($dm^3\,mol^{-1}\,s^{-1}$)	$10^4 k_o$ (s^{-1})
15	0.55 ± 0.01	0.02 ± 0.04
25	1.10 ± 0.04	1.2 ± 0.4
30	2.85 ± 0.17	1.1 ± 0.4
35	4.46 ± 0.52	2.7 ± 1.6
40	6.54 ± 0.46	8.0 ± 1.4
45	10.1 ± 1.3	10.8 ± 4.0

be used as a rough measure of the basicity and hence the electron donating ability of the nitrogen donors. As the electron donating ability decreases the residual positive charge on cobalt(III) increases and this leads to a stronger Co–O bond. The parameters listed in Table 6 indicate that an approximate relationship of this type does exist.

Mechanisms

A variety of mechanisms can be considered for the acid-catalysed decarboxylation of carbonato

Table 4. Rate constants and activation parameters for the water-catalysed reaction for a series of cobalt(III) carbonato complexes $[CoLCO_3]^+$

L	$10^4 k_o$	ΔH†	ΔS_{298}†	I	Ref
$(NH_3)_4$	1.3 ± 0.2	50 ± 4	-155 ± 79	0.5	[13]
$(en)_2$	1.2 ± 0.2	75 ± 13	-63 ± 38	0.5	[14]
$(pn)_2$	1.0 ± 0.2	75 ± 13	-63 ± 38	0.5	[14]
tren	1.7 ± 0.2	63 ± 8	-105 ± 21	0.5	[4]
$(py)_4$	1.3×10^{-2}	139 ± 3	109 ± 6	1.0	[15]
cis-$(en)_2(H_2O)_2$	710	169 ± 34	300 ± 122	1.0	[16]
trans-Me_2[14]diene	0.75	115 ± 28	65 ± 89	0.5	[11]
[15]aneN_4	1.2 ± 0.3	162 ± 19	211 ± 62	1.0	This work

Table 5. Rate constants and activation parameters for the acid catalysed decarboxylation of cobalt(III) carbonato complexes $[CoLCO_3]^+$

L	k_H ($mol\,dm^{-3}$)	$\Delta H^\dagger$ ($kJ\,mol^{-1}$)	$\Delta S^\dagger_{298}$ ($JK^{-1}\,mol^{-1}$)	I ($mol\,dm^{-3}$)	Ref
$(NH)_4$	1.5 ± 0.1	64 ± 4	-26 ± 16	0.5	[13]
$(en)_2$	0.6 ± 0.05	59 ± 13	-54 ± 38	0.5	[14]
$(pn)_2$	$0.5 + 0.05$	59 ± 13	-54 ± 38	0.5	[14]
tren	2.0 ± 0.05	46 ± 4	-84 ± 17	0.5	[14]
$(py)_4$	8.0×10^{-6}	97 ± 4	-17 ± 13	5.0	[15]
Me_6[14]diene	8.0×10^{-3}	71 ± 21	-42 ± 71	0.25	[3]
Me_2[14]diene	1.5×10^{-3}	81 ± 1	-6 ± 2	0.5	[11]
[12]aneN_4	7.0×10^{-3}	100 ± 4	$+51$	0.5	[1]
[14]aneN_4	1.3×10^{-3}	86 ± 2	-11 ± 5	0.5	[2]
[15]aneN_4	5.5×10^{-3}	71 ± 2	-61 ± 6	1.0	This work

Table 6. Average pK_a values for nitrogen containing ligands and the corresponding k_H values

Ligand	Average pK_a	k_H ($dm^3\,mol^{-1}\,s^{-1}$)
NH_3	9.3	1.5
en	8.6	0.6
pn	8.5	0.5
[15]aneN_4	7.6	5.5×10^{-3}
[14]aneN_4	6.7	1.3×10^{-3}
[12]aneN_4	6.0	7.0×10^{-3}
py	5.3	8.0×10^{-6}

complexes. The most probable mechanism which is supported by the bulk of the experimental evidence is shown in the scheme. The reaction involves a rapid pre-equilibrium protonation of the carbonato complex followed by slow rate-determining ring opening and rapid decarboxylation of the monodentate carbonato intermediate. For this mechanism, it can be readily shown that $k_{obs} = k_1 K[H^+]/(1 + K[H^+])$ and, if $K[H^+] < 1$, the expression simplifies to $k_{obs} = k_1 K[H^+]$. This latter situation applies as plots of k_{obs} *versus* $[H^+]$ are linear and show no curvature. Although some non-linear plots have been observed [4, 9, 10], these effects arise due to an enhanced ring opening reaction which is faster than the rate of decarboxylation. As a result, the decarboxylation step, which is acid independent, becomes rate-limiting at high acidities.

The solvent deuterium isotope effect for the acid-catalysed reaction was studied using $0.50\,mol\,dm^{-3}$

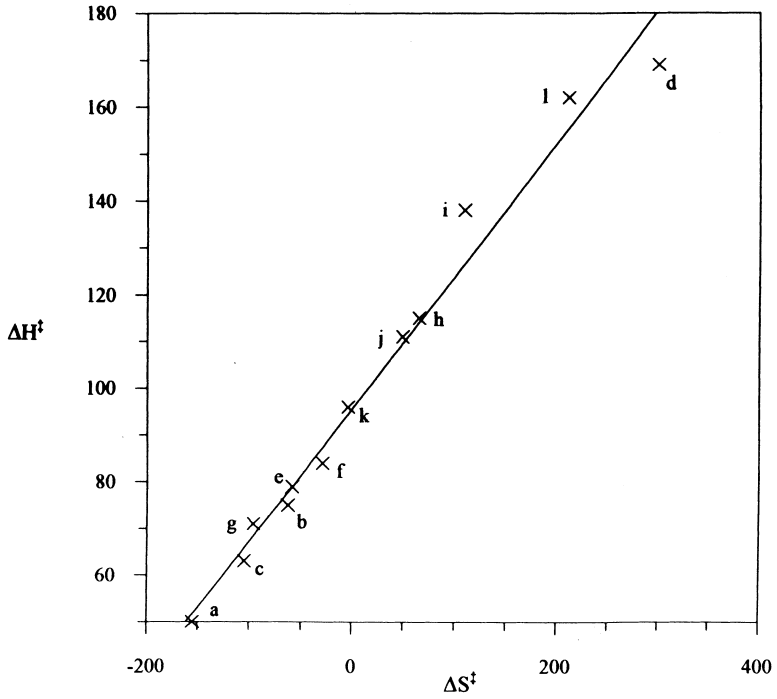

a	$[Co(NH_3)_4CO_3]^+$	g	β-$[Co(trien)CO_3]^+$
b	$[Co(en)_2CO_3]^+$	h	$[Co(Me_2[14]dieneN_4)CO_3]^+$
c	$[Co(tren)CO_3]^+$	i	$[Co(py)_4CO_3]^+$
d	*cis*-$[Co(en)(H_2O)_2CO_3]^+$	j	*cis*-$[Co(py)_2(H_2O)_2CO_3]^+$
e	*trans*-$[Co(en)(NH_3)_2CO_3]^+$	k	*cis*-$[Co(py)_2(CO_3)_2]^-$
f	α-$[Co(trien)CO_3]^+$	l	$[Co([15]aneN_4)CO_3]^+$

Fig. 4. Isokinetic plot for the spontaneous water reaction in the ring opening of cobalt(III) carbonato complexes.

DCl in D_2O at 25°C giving $k_{obs} = 1.73 \times 10^{-3}\,s^{-1}$ and an approximate value of $k_{D_2O} = 3.39 \times 10^{-3}\,dm^3\,mol^{-1}\,s^{-1}$ if the very small contribution from k_o is ignored. For the equivalent reaction involving 0.50 mol dm^{-3} HCl in H_2O at 25°C, $k_{obs} = 7.20 \times 10^{-4}\,s^{-1}$ and $k_{H_2O} = 1.44 \times 10^{-3}\,dm^3\,mol^{-1}\,s^{-1}$, giving a solvent deuterium isotope effect k_{D_2O}/k_{H_2O} for the acid catalysed reaction = 2.35 at 25°C. This value compares well with previously reported solvent deuterium isotope effects for reactions of this type. For example, 2.3 for *cis*-$[Co(en)_2CO_3]^+$ [10], 2.6 for *cis*-$[Co(Me_2[14]diene)CO_3]^+$ [11] and 2.05 for *cis*-$[Co(cyclen)CO_3]^+$ [1]. All of these values fall within the range 1.9 to 2.6 considered typical for a rapid pre-equilibrium protonation followed by a slow ring-opening reaction. As D_2O is a weaker base than water more of the protonated complex is present in D_2O and a more rapid reaction occurs. Since $k_H = k_1K$, the rate and equilibrium constants may well be affected somewhat differently by steric and electronic effects and this is the probable reason for the large scatter observed in the isokinetic plot.

Isomerisation

The second stage of the reaction involves the conversion of *cis*-$[Co([15]aneN_4)(OH_2)_2]^{3+}$ to a product with λ_{max} *ca.* 490 nm and a second less intense band at 610 nm. This spectrum corresponds to the *trans*-diaqua complex. The rate of isomerisation is independent of the acidity in the range 0.05 to 0.50 mol dm^{-3} nitric acid with $k_{isom} = 4.9 \times 10^{-6}\,s^{-1}$ at 25°C and $I = 1.0$ mol dm^{-3}. Previous studies [3, 8] of the *cis–trans* isomerisation of macrocyclic cobalt(III) complexes have shown that the mechanism is complex and involves the inversion of *sec*–NH centres in an acid or base catalysed process.

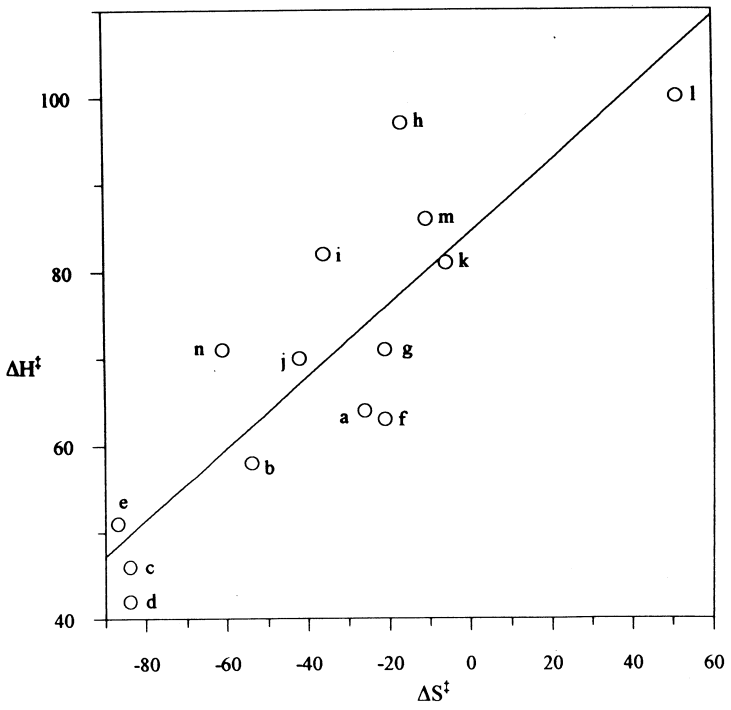

a	$[Co(NH_3)_4CO_3]^+$	h	$[Co(py)_4CO_3]^+$
b	$[Co(en)_2CO_3]^+$	i	*cis*-$[Co(py)_2(H_2O)_2CO_3]^+$
c	$[Co(tren)CO_3]^+$	j	$[Co(Me_6[14]dieneN_4)CO_3]^+$
d	*trans*-$[Co(en)(NH_3)_2CO_3]^+$	k	$[Co(Me_2[14]dieneN_4)CO_3]^+$
e	*cis*-$[Co(en)(H_2O)_2CO_3]^+$	l	$[Co(cyclen)CO_3]^+$
f	α-$[Co(trien)CO_3]^+$	m	$[Co(cyclam)CO_3]^+$
g	β-$[Co(trien)CO_3]^+$	n	$[Co([15]aneN_4)CO_3]^+$

Fig. 5. Isokinetic plot for the acid-catalysed ring opening of cobalt(III) carbonato complexes.

REFERENCES

1. Hay, R. W. and Jeragh, B., *Transition Met. Chem.*, 1979, **4,** 288.
2. Dasgupta, T., *Inorg. Chim. Acta*, 1976, **20,** 33.
3. Kernohan, J. A. and Endicott, J. F., *J. Am. Chem. Soc.*, 1969, **91,** 6977.
4. Dasgupta, T. P. and Harris, G. M., *J. Am. Chem. Soc.*, 1971, **93,** 91.
5. Buckingham, D. A. and Clark, C. R., *Inorg. Chem.*, 1994, **33,** 6171.
6. Palmer, D. A. and van Eldik, R., *Chem. Rev.*, 1983, **83,** 651.
7. Barefield, E. K., Wagner, F. and Hodges, K., *Inorg. Chem.*, 1976, **15,** 1370.
8. Francis, D. J. and Jordan, R. B., *Inorg. Chem.*, 1972, **11,** 1170.
9. van Eldik, R., Dasgupta, T. P. and Harris, G. M., *Inorg. Chem.*, 1975, **14,** 2573.
10. Harris, G. M. and Hyde, K. E., *Inorg. Chem.*, 1978, **17,** 1892.
11. Hay, R. W. and Jeragh, B., *J. Chem. Soc. Dalton Trans.*, 1979, **00,** 1343.
12. Poon, C. K. and Tobe, M. L., *Inorg. Chem.*, 1968, **7,** 2398.
13. Dasgupta, T. P. and Harris, G. M., *J. Am. Chem. Soc.*, 1969, **91,** 3207.
14. Sastri, V. S. and Harris, G. M., *J. Am. Chem. Soc.*, 1970, **92,** 2943.
15. Hyde, K. E., Fairchild, G. H. and Harris, G. M., *Inorg. Chem.*, 1976, **15,** 2631.
16. Coddington, P. M. and Hyde, K. E., *Inorg. Chem.*, 1983, **22,** 2211.
17. Endicott, J. F., Kane-Maguire, N. A. P., Rillema, D. P. and Roche, T. S., *Inorg. Chem.*, 1973, **12,** 1818.

Pergamon

PII: S0277-5387(98)00190-9

Polyhedron Vol. 17, No. 21, pp. 3803–3808, 1998
© 1998 Elsevier Science Ltd
All rights reserved. Printed in Great Britain
0277–5387/98 $19.00+0.00

Copper(II) complexes of Schiff base ligands derived from 2-(2-pyridylmethyl)-1,3-propanediamine

Harry Adams,[a] Rachel M. Bucknall,[a] David E. Fenton,[a]*
Cecilia O. Rodriguez de Barbarin,[a] Monica Garcia[b] and John Oakes[b]

Department of Chemistry, Dainton Building, The University of Sheffield, Sheffield S3 7HF, U.K.

Port Sunlight Laboratory, Unilever Research, Bebington, Wirral L63 3JW, U.K.

(Received 25 March 1998; accepted 13 May 1998)

Abstract—The synthesis and characterisation of copper(II) complexes of Schiff base ligands derived from 2-(2-pyridylmethyl)-1,3-propanediamine and substituted salicylaldehydes are reported together with the crystal structure of $CuL^2 \cdot MeOH$ in which the ligand L^2 is derived from 5-bromosalicylaldehyde is also reported. The pendant arm does not engage in inter- or intramolecular binding and inspection of the packing diagram shows that the molecules coexist as discrete van der Waals dimers. © 1998 Elsevier Science Ltd. All rights reserved

INTRODUCTION

The diamine 2-(2-pyridylmethyl)-1,3-propanediamine has been used in the construction of a series of lariat-type B_{12} model complexes [1]. Its reaction with 2,3-butanedione monoxime gave a potentially quinquedentate acyclic ligand (HL) which readily formed mononuclear complexes on reaction with cobalt compounds. The role of the pyridyl moiety as an axial coordinating pendant arm has been confirmed by X-ray structural analysis of $[ClCoL]PF_6$ and $[CH_3CoL]ClO_4/BF_4$. In this work we prepared lariat-type Schiff base ligands by reaction of 2-(2-pyridylmethyl)-1,3-propanediamine and a series of substituted salicylaldehydes in order to determine whether or not there would be an axial pendant arm interaction on reaction of these ligands with copper(II) salts.

EXPERIMENTAL

Physical measurements

Elemental analyses were carried out by the University of Sheffield Microanalytical service. Infrared spectra were recorded as KBr discs using a Perkin Elmer 1600 Fourier Transform spectrometer; NMR spectra were run on a Bruker ACF-250 spectrometer and mass spectra were obtained on a VG PROSPEC spectrometer.

Synthesis of pendant arm Schiff base ligands

2-(2-pyridylmethyl)-1,3-propane diamine was prepared according to the method given in literature [1].

H_2L^1. Salicylaldehyde (4 mmol) in methanol (50 cm^3) was added slowly to a solution of 2-(2-pyridylmethyl)-1,3-propane diamine (2 mmol) in methanol (100 cm^3). The yellow solution was stirred at room temperature for 2 h, then the solvent removed under reduced pressure to yield a viscous yellow oil in quantitative yield. MS (ES^+) 374 a.m.u.; ^1H NMR ($CDCl_3$) δ 13.45 (br), 8.55 (1H, m), 8.35 (2H, s), 7.58 (1H, m), 7.35–7.10 (6H, m), 7.00–6.85 (4H, m), 3.67 (4H, m), 2.95 (2H, d), 2.80 (1H, m); ^{13}C NMR ($CDCl_3$) δ 166.2, 161.1, 159.6, 149.5, 136.5, 132.4, 131.4, 123.9, 121.5, 118.7, 118.7, 117.0, 60.5, 40.6, 39.2

H_2L^2. The procedure for H_2L^1 was followed, using 5-bromosalicylaldehyde. The yellow oil was purified by column chromatography, eluting with dichloromethane–methanol (97:1). Yield 63%; MS. (EI^+) 531 a.m.u.; ^1H NMR ($CDCl_3$) δ 13.40 (2H, s), 8.55 (1H, m), 8.25 (2H, s), 7.60 (1H, m), 7.38 (2H, dd), 7.34 (2H, d), 7.15 (2H, m), 6.85 (2H, d), 3.77–3.58

* Author to whom correspondence should be addressed.

(4H, 2ddd), 2.92 (2H, dd), 2.82 (1H, m); ^{13}C NMR ($CDCl_3$) δ 165.0, 160.2, 159.3, 149.6, 136.6, 135.1, 133.5, 123.8, 121.6, 120.0, 119.0, 110.14, 60.6, 40.4, 39.1.

H_2L^3. The procedure for H_2L^1 was followed, using 5-chlorosalicylaldehyde, to give the product as a viscous yellow oil in quantitative yield. MS. (EI^+) 441 a.m.u.; ^{1}H NMR ($CDCl_3$) δ 13.35 (br), 8.55 (1H, m), 8.25 (2H, s), 7.60 (1H, m), 7.30–7.20 (4H, m), 7.15 (2H, m), 6.90 (2H, d), 3.70 (4H, m), 2.95 (2H, d), 2.85 (1H, m); ^{13}C NMR ($CDCl_3$) δ 165.1, 159.7, 159.3, 149.6, 136.5, 132.3, 130.5, 123.8, 123.3, 121.6, 119.4, 118.6, 60.6, 40.4, 39.1.

H_2L^4. The procedure for H_2L^1 was followed, using 2-hydroxy-5-nitrobenzaldehyde. The reaction was carried out under nitrogen and protected from light. The product was collected as a pale yellow precipitate in 80% yield. MS (EI+) 464 a.m.u.; microanalysis (%) found (required for $C_{23}H_{21}N_5O_6$): C 59.66 (59.61), H 4.47 (4.57), N 14.93 (15.11); IR (KBr disc) v(C═N) 1637 cm^{-1}, v(NO_2) 1481, 1345 cm^{-1}; ^{1}H NMR ($CDCl_3$) δ 14.30 (br), 8.75 (2H, s), 8.55 (1H, m), 8.37 (2H, d), 8.05 (2H, dd), 7.71 (1H, m), 7.29 (1H, d), 7.21 (1H, m), 6.69 (2H, d), 3.75 (4H, d), 2.90 (3H, m); ^{13}C NMR (CDCl3) δ 174.8, 167.9, 158.9, 149.7, 137.2, 135.8, 131.6, 129.2, 124.2, 122.1, 121.7, 115.4, 56.1, 39.3, 38.1.

H_2L^5. The procedure for H_2L^1 was followed, using 2-hydroxy-3-methoxybenzaldehyde, to yield a sticky yellow oil in quantitative yield. MS (EI^+) 434 a.m.u.; ^{1}H NMR ($CDCl_3$) δ 14.01 (br), 8.54 (1H, m), 8.34 (2H, s), 7.59 (1H, m), 7.19 (1H, d), 7.14 (1H, m), 6.94–6.80 (6H, m), 3.90 (6H, s), 3.67 (4H, m), 2.97 (2H, d), 2.77 (1H, m); ^{13}C NMR (CDCl3) δ 166.3, 159.4, 151.9, 149.5, 148.4, 136.5, 124.0, 123.0, 121.5, 118.5, 118.0, 113.9, 59.5, 56.1, 40.5, 38.9.

H_2L^6. A suspension of disodium salicylaldehyde-5-sulphonic acid (4 mmol) in ethanol (140 cm^3) was warmed to 60°C, then water added dropwise until a clear yellow solution formed. An ethanolic solution (15 cm^3) of 2-(2-pyridylmethyl)-1,3-propane diamine (2 mmol) was slowly added and the resulting orange solution stirred at room temperature for 2 h. The solution was left at 0°C overnight and the product precipitated as a pale yellow powder in 47% yield. Microanalysis (%) found (required for $C_{23}H_{27}N_3O_{11}S_2Na_2$): C 43.88 (43.74), H 4.18 (4.31), N 6.78 (6.65); IR(KBr disc) v(C═N) 1636 cm^{-1}; ^{1}H NMR ($CDCl_3$) δ 13.70 (br), 8.61 (2H, s), 8.53 (1H, m), 7.77–7.65 (3H, m), 7.57 (2H, dd), 7.28 (1H, d), 7.22 (1H, m), 6.79 (2H, d), 3.62 (4H, d), 2.84 (2H, m), 2.68 (1H, m); co 159.8, 149.7, 139.3, 137.0, 130.4, 129.4, 124.1, 121.9, 117.6, 116.3, 60.0, 38.9, 38.7.

Compounds H_2L^1, H_2L^2, H_2L^3, and H_2L^5 were used in complex formation without further purification.

Synthesis of pendant arm Schiff base complexes

$CuL^1 \cdot 0.5H_2O$, ***1***. A solution of cupric acetate (1 mmol) in methanol (30 cm^3) was added to a solution of ligand H_2L^1 (1 mmol) in methanol (15 cm^3). The mixture was stirred at room temperature for 2 h and the solvent removed under reduced pressure to give a green oil. Ethanol was added and a green precipitate formed, which was collected by filtration and dried to give a green powdery solid in 49% yield. Microanalysis (%) found (required for $C_{46}H_{44}N_6O_5Cu_2$): C 62.64 (62.22), H 4.98 (4.99), N 9.13 (9.46); IR (KBr disc) ν(C = N) 1616 cm^{-1}.

$CuL^2 \cdot MeOH$, ***2***. Cupric acetate (1 mmol) was added to a solution of ligand H_2L^2 (1 mmol) in methanol (25 cm^3) and the mixture stirred at room temperature for 2 h. The resulting green precipitate was collected by filtration and recrystallised from methanol to give dark blue–green crystals in 46% yield. Microanalysis (%) found (required for $C_{24}H_{23}N_3O_3Br_2Cu_1$): C 46.13 (46.14), H 3.54 (3.71), N 6.56 (6.73); IR(KBr disc): v(C═N) 1617 cm^{-1}.

$CuL^3 \cdot MeOH$, ***3***. The method for **2** was used, using ligand H_2L^3, to give a green solid in 50% yield. Microanalysis (%) found (required for $C_{24}H_{23}N_3O_3Cl_2Cu_1$): C 53.89 (53.79), H 4.12 (4.33), N 7.83 (7.84), Cl 13.35 (13.23); IR(KBr disc): v(C═N) 1616 cm^{-1}.

$CuL^4 \cdot H_2O$, ***4***. A solution of cupric acetate (0.7 mmol) in water (10 cm^3) was added to a suspension of ligand H_2L^4 (0.7 mmol) in ethanol (30 cm^3). The mixture was heated at reflux for 1.5 h and the green precipitate collected in 90% yield. Microanalysis (%) found (required for $C_{23}H_{21}N_5O_7Cu_1$): C 50.90 (50.88), H 3.74 (3.90), N 13.28 (12.90); IR(KBr disc) v(C═N) 1628 cm^{-1}, v(NO_2) 1474, 1320 cm^{-1}.

$CuL^5 \cdot 1.5H_2O$, ***5***. The method for **2** was used, using ligand H_2L^5. The resulting solution was concentrated and diethyl ether added to precipitate the product in 45% yield. Microanalysis (%) found (required for $C_{50}H_{56}N_6O_{11}Cu_2$): C 57.44 (57.52), H 5.00 (5.41), N 8.13 (8.05); IR(KBr disc): v(C═N) 1621 cm^{-1}.

$CuL^6 \cdot 5H_2O$, ***6***. 2-(2-pyridylmethyl)-1,3-propane diamine (2 mmol) in ethanol (15 cm^3) was added dropwise to a solution of cupric nitrate (2 mmol) and disodium salicylaldehyde-5-sulphonic acid (4 mmol) in water–ethanol (3:1, 150 cm^3). The solution, which became very dark green, was stirred with warming for 2 h, then ethanol added to precipitate the dark green solid in 82% yield. Microanalysis (%) found (required for $C_{23}H_{21}N_5O_7Cu_1$): C 50.90 (50.88), H 3.74 (3.90), N 13.28 (12.90); IR(KBr disc): v(C═N) 1626 cm^{-1}.

X-ray crystallography

Complex **2**, $C_{24}H_{23}Br_2CuN_3O_3 \cdot CH_3OH$ was crystallised from methanol as blue prisms. The crystallographic data are summarised in Table 1.

Three-dimensional, room temperature X-ray data were collected in the range $3.5 < 2\theta < 45^\circ$ on a Siemens P4 diffractometer by the omega scan method. Of the 3995 reflections measured, all of which were corrected for Lorentz and polarisation effects but not for absorption, 2450 independent reflections exceeded

Table 1. Crystal data and structure refinement for $CuL^2 \cdot CH_3OH$

Chemical formula	$C_{24}H_{23}Br_2CuN_3O_3$
Formula weight	624.81
Temperature	293(2) K
Radiation and wavelength	MoKα, 0.71073 Å
Crystal system, space group	monoclinic, $P2_1/n$
Unit cell dimensions	$a = 10.882(5)$ Å; $\alpha = 90^\circ$ $b = 16.228(5)$ Å; $\beta = 98.88(3)^\circ$ $c = 13.610(4)$ Å; $\gamma = 90^\circ$
Volume	2375(2) Å^3
Z	4
Density (calculated)	1.748 Mg/cm^3
Absorption coefficient μ	4.317 mm^{-1}
F(000)	1244
Crystal size	$0.80 \times 0.65 \times 0.55$ mm
θ range for data collection	1.97 to 22.51°
Index ranges	$-1 \leqslant h \leqslant 11$, $-1 \leqslant k \leqslant 17$, $-14 \leqslant l \leqslant 14$
Reflections collected	3995
Independent reflections	3103 ($R_{int} = 0.0912$)
Refinement method	full-matrix least-squares on F^2
Data/restraints/parameters	3103/0/301
Goodness of fit on F^2	1.055
Final R indices [$I > 2\sigma(I)$]	R1 = 0.0530, awR2 = 0.1367
R indices all data	$R1 = 0.0708$, $wR2 = 0.1502$
Largest diff. peak and hole	0.867 and -0.875 e Å^3

the significance level $|F|/\sigma(|F|) > 4.0$ The structure was solved by direct methods and refined by full matrix least squares on F^2. Hydrogen atoms were included in calculated positions and refined in riding mode. Refinement converged at a final $R = 0.0530$ ($wR_2 = 0.1502$, for all 3103 data, 301 parameters, mean and maximum δ/σ 0.000, 0.000), with allowance for the thermal anisotropy of all non-hydrogen atoms. Minimum and maximum final electron density -0.875 and 0.867 e Å^{-3}. A weighting scheme $w = 1/[\sigma^2(Fo^2)+(0.0906*P)^2+2.0187*P]$ where $P = (Fo^2+2*Fc^2)/3$ was used in the latter stages of refinement. Complex scattering factors were taken from the program package SHELXL93 [2] as implemented on the Viglen 486dx computer.

Supplementary material

anisotropic thermal vibrational parameters with e.s.d.s;
hydrogen atom position parameters;
observed structure amplitudes and calculated structure factors.

RESULTS AND DISCUSSION

2-(2-Pyridylmethyl)-1,3-propanediamine was prepared by the method of Gerli *et al.* [1] and reacted with a series of substituted salicylaldehydes to produce Schiff bases (H_2L^1–H_2L^6) containing a potentially pen-

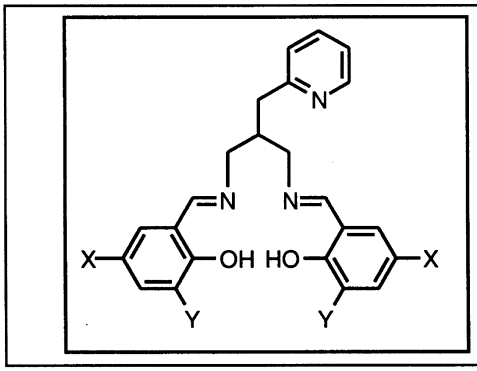

	X	Y
H_2L^1	H	H
H_2L^2	Br	H
H_2L^3	Cl	H
H_2L^4	NO_2	H
H_2L^5	H	OCH_3
H_2L^6	SO_3Na	H

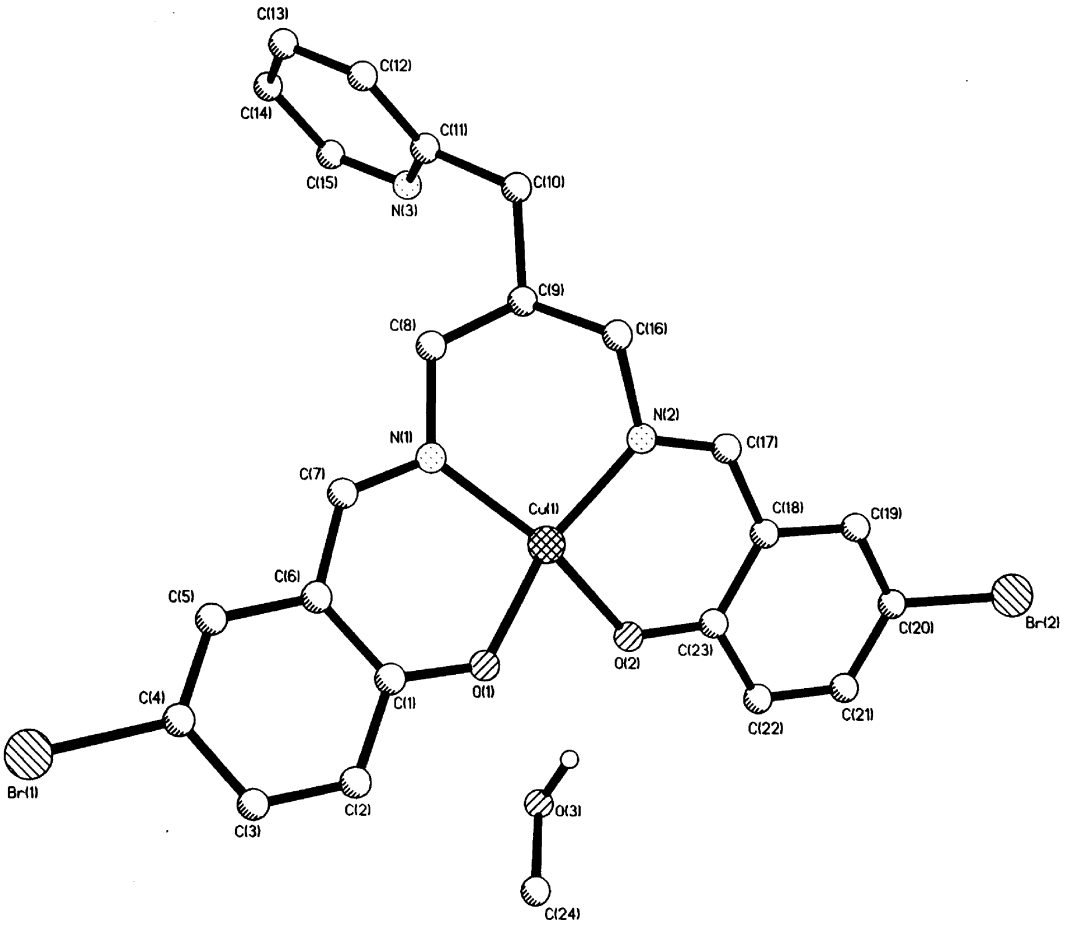

Fig. 1. The molecular structure of complex (**2**). [Selected bond lengths and angles: Cu(1)–N(1), 1.965(5); Cu(1)–N(2), 1.937(6); Cu(1)–O(1), 1.896(5); Cu(1)–O(2), 1.918(5) Å; N(1)–Cu(1)–N(2) 95.7(2), N(1)–Cu(1)–O(1) 94.5(2), O(1)–Cu(1)–O(2) 84.3(2), O(2)–Cu(1)–N(2) 92.6(2)°.]

dant pyridyl arm. The proligands were characterised via ^{1}H and ^{13}C NMR and mass spectrometry.

Synthesis of the copper(II) complexes of H_2L^1–H_2L^5 was achieved by addition of copper(II) acetate to a methanolic solution of the proligand; in the cases where X = Br, Cl and NO_2 the complexes precipitated from solution, otherwise diethylether was added to induce precipitation. The copper(II) complex of the water soluble Schiff base H_2L^6 was prepared by addition of 2-(2-pyridylmethyl)-1,3-propanediamine to a solution containing the sulphonated salicylaldehyde and copper(II) nitrate in a mixture of water and ethanol; ethanol was then added to induce precipitation of the product.

The mass spectral (FAB^+) assignments for the complexes are given in Table 2. In each case the most abundant peak was that corresponding to the parent cation with small peaks attributed to dimeric species, probably arising from aggregation in the matrix, being observed for the complexes containing bromo-, sul-

Table 2. FAB^+ mass spectral assignments for the copper(II) complexes (NOBA matrix)

Complex	*m/z* (%intensity) [ionic fragment]$^+$			
$CuL^1 \cdot 0.5H_2O$ (**1**)	435(100)	$[CuL^1H]^+$		
$CuL^2 \cdot MeOH$ (**2**)	593(100)	$[CuL^2H]^+$	1187(7)	$[Cu_2L^2{}_2H]^+$
$CuL^3 \cdot MeOH$ (**3**)	505(100)	$[CuL^3H]^+$		
$CuL^4 \cdot H_2O$ (**4**)	526(100)	$[CuL^4H]^+$		
$CuL^5 \cdot 1.5H_2O$ (**5**)	495(100)	$[CuL^5H]^+$	992(5)	$[Cu_2L^5{}_2H]^+$
$CuL^6 \cdot 5H_2O$ (**6**)	639(100)	$[CuL^6H]^+$	1279(5)	$[Cu_2L^6{}_2H]^+$

phonato-, and methoxy substituents. Peaks indicating addition and loss of Na^+ were noted at $m/z = 661$ and 617, respectively, for the sulphonato-complex.

2-(2-Pyridylmethyl)-1,3-propanediamine was employed as a spacer in the Schiff base proligands as it was thought that the pyridine nitrogen atom on the pendant arm might coordinate to the copper atom by occupying a fifth and axial coordination site as had been observed in a cobalt(III) complex of the Schiff base derived from the diamine and 2,3-butanedione monooxime [1]. Recrystallisation of the bromo-complex (**2**) from methanol gave crystals suitable for X-ray structure determination and elucidation of the structure (Fig. 1) revealed that axial ligation had not occurred. The pyridine nitrogen atom was neither coordinated to the central copper atom coordination nor to any other copper atoms in neighbouring molecules. The copper atom interacts with the two imine nitrogen atoms (1.937 and 1.965 Å) and to the two phenolate oxygen atoms (1.896 and 1.918 Å) of the ligand to attain a four-coordinate environment. This is clearly tetrahedrally distorted from a square planar geometry with the mean deviation from the plane including O(1), O(2), N(1), N(2), and Cu(1) being 0.2629 Å. The mean deviations for the planes comprising the two six-membered chelate rings Cu(1), O(1), C(1), C(6), C(7), N(1) and Cu(2), O(2), C(23), C(18), C(17), N(2) are 0.0361 and 0.0189 Å, respectively, and the angle of twist between these two planes is 28.8°. The aromatic rings are each planar (r.m.s deviations 0.008, 0.009 and 0.003 Å with Br(1) −0.015 and Br(2) 0.127 Å out of planarity). The pyridyl ring is approximately perpendicular to the phenyl rings (89° and 111°, respectively). Inspection of the packing diagram (Fig. 2) shows that the molecules coexist as discrete pairs. It has long been known from crystal

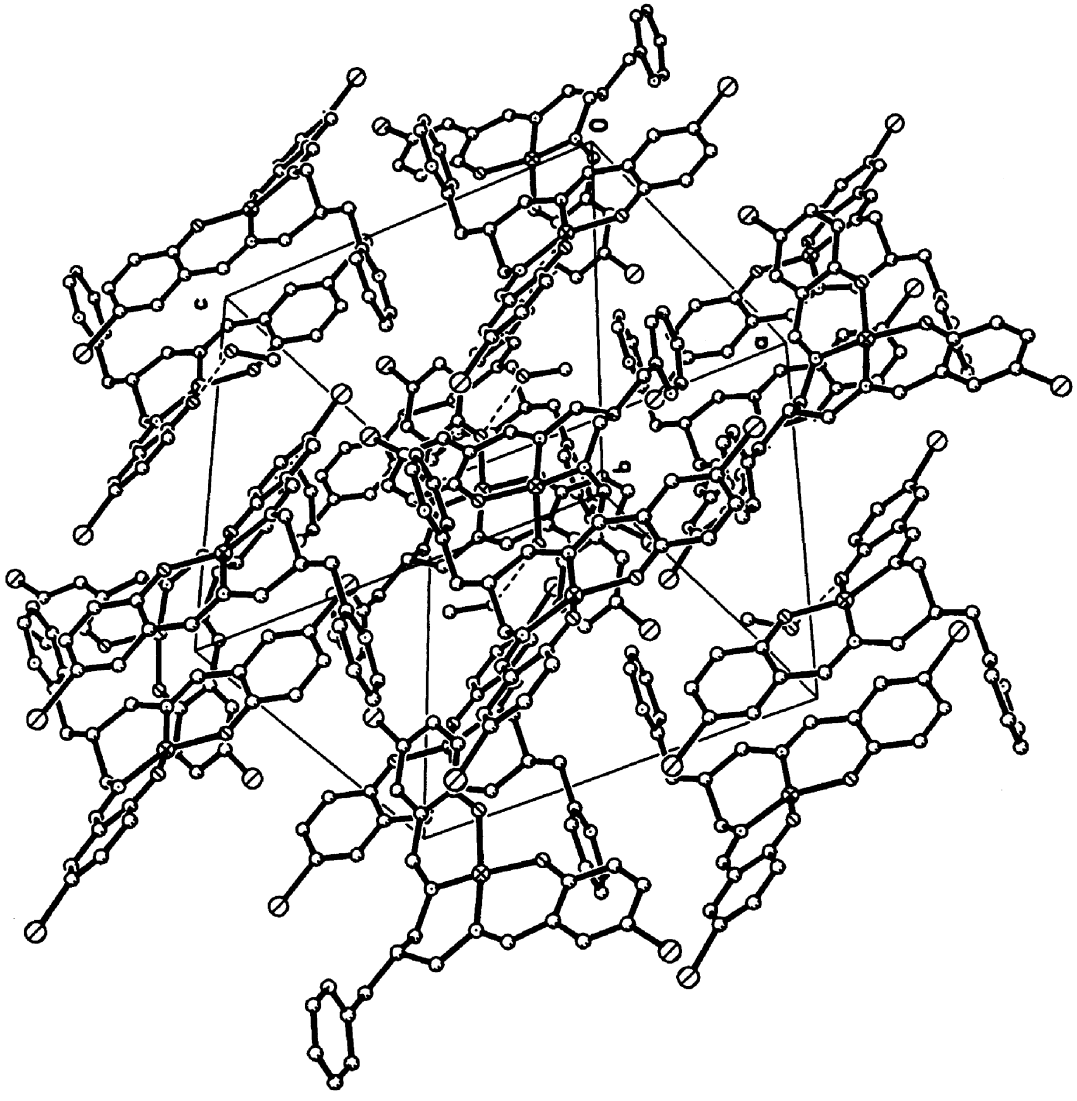

Fig. 2. The crystal packing in complex (**2**) projected along the *a* axis.

structure data that self-association can occur in copper(II) complexes of ligands such as β-diketonates [3]. Such molecules are relatively planar but pack in the crystals such that there is a weak interaction between the copper atom of one molecule and the middle carbon atoms of the chelate rings of neighbouring molecules. This is considered as arising from an interaction of the carbon p_z electrons with the neighbouring copper atom and gives rise to Cu–C separations of 3.0–3.5 Å. More recently bis(tropolonato) copper(II) has been shown to exist as dimers in the crystalline state with the two monomers stacked face to face [4]. The intermolecular nearest neighbour distances lie in the range 3.3–3.8 Å and so the dimer was said to be of the van der Waals type. In complex **2** the molecules align such that the copper atoms lie almost directly under the centroid of a neighbouring benzene ring [Cu-centroid, 3.76 Å; with a distance of 3.69 Å to the nearest edge C atom C(5) or C(19)] suggesting that there is a weak interaction between the copper and the aromatic π-cloud which reinforces, and possibly directs the stereochemical nature of, the van der Waals assisted self-association.

The structure also includes a methanol of solvation which is involved in a strong hydrogen bonding interaction to one phenolic oxygen [O(2)–HO(3) 0.938, HO(3)$\cdots$O(2) 1.903 Å, O(2)$\cdots$O(3) 2.795 Å]. Bond lengths and angles relating to the copper atom are given in the caption of Fig. 1; all other ligand bond lengths and angles were normal.

Acknowledgements—We thank Unilever Research and the University of Sheffield for support (to R. M. B) and the EPSRC and the Royal Society for funds towards the purchase of the diffractometer.

REFERENCES

1. Gerli, A., Sabat, M. and Marzilli, L.G., *J. Am. Chem. Soc*., 1992, **114,** 6711.
2. G. M. Sheldrick, SHELXL93, An integrated system for solving and refining crystal structures from diffraction data (Revision 5.1). University of Gottingen, Germany, 1993.
3. Graddon, D.P., *Coord. Chem. Rev*., 1969, **4,** 1.
4. Hasegawa, M., Inomaki, Y., Inayoshi, T., Hoshi, T. and Kobayashi, M., *Inorg. Chim. Acta*, 1997, **257,** 259.

Pergamon

PII: S0277-5387(98)00191-0

Polyhedron Vol. 17, No. 21, pp. 3809–3815, 1998
© 1998 Elsevier Science Ltd
All rights reserved. Printed in Great Britain
0277–5387/98 $19.00+0.00

Lithium-7 NMR study of the exchange kinetics of the lithium ion with cryptand C221 in methanol solution. Temperature dependence of the exchange mechanism

Mojtaba Shamsipur,[a]* Ebrahim Karkhaneei[b] and Abbas Afkhami[b]

[a] Department of Chemistry, Razi University, Kermanshah, Iran

[b] Department of Chemistry, Bouali Sina University, Hamadan, Iran

(Received 6 January 1998; accepted 7 May 1998)

Abstract—The exchange kinetics of Li^+C221 cryptate in methanol solution was studied by lithium-7 NMR line-shape analysis at a wide range of temperature. Depending on the temperature, two different exchange mechanisms were found to coexist to different extents. A dissociative pathway dominates at high temperatures (from 5 to 25°), while a bimolecular mechanism prevails at lower temperatures (from −30 to −60°C). At the temperature range of −30 to 5°C, both the dissociative and bimolecular mechanisms contribute to the metal exchange. For the dissociative pathway, the activation parameters were calculated as: $E_a = 22 \pm 2\,kJ\,mol^{-1}$; $\Delta H^{\ddagger} = 20 \pm 2\,kJ\,mol^{-1}$; $\Delta S^{\ddagger} = -144 \pm 8\,J\,mol^{-1}\,K^{-1}$. While for the bimolecular mechanism they are: $E_a = 9.9 \pm 0.4\,kJ\,mol^{-1}$; $\Delta H^{\ddagger} = 8.0 \pm 0.4\,kJ\,mol^{-1}$; $\Delta S^{\ddagger} = -146 \pm 2\,J\,mol^{-1}\,K^{-1}$. © 1998 Published by Elsevier Science Ltd. All rights reserved

Macrobicyclic polyethers (cryptands), first synthesized by Lehn and co-workers [1], in their endo–endo conformation contain an internal cavity of about spherical shape well suited for the recognition of alkali metal ions [2]. Thus, the thermodynamics of alkali cryptates in various solvent systems have been the subject of extensive research [3, 4]. Investigation of the factors affecting the thermodynamic stability and selectivity of such inclusion complexes in solution have elicited considerable interest. It has been found that the cryptands form complexes with suitable alkali metal ions which are several orders of magnitude higher than those of neutral or synthetic macrocyclic ligands [3–7], a phenomenon called the "cryptate effect" [5–7].

Moreover, a fundamental characteristic of alkali cryptate formation is the rate of cation exchange in and out of the ligand's cavity. Such kinetic studies not only result in important information on the rates and mechanisms of the complexation reactions, but also lead to a better understanding of the high stability and high selectivity of the cryptands toward different alkali cations. A number of such exchange kinetic studies have been carried out using various physico–chemical techniques [3, 4], especially proton and alkali metal NMR spectroscopy [8–17].

We have previously reported the use of line-shape analysis of the ^{7}Li [13], ^{23}Na [18], ^{133}Cs [14, 19, 20] and ^{1}H [21–24] NMR resonance lines in studies of the complexation of Li^+, Na^+, Cs^+, Pb^{2+}, La^{3+} and alkaline earth cations with different crown-ethers and cryptands in a number of different solvent systems. It has been found that the ligand structure, solvent properties, nature of counter ion, concentration of the reactants and temperature have considerable effects on the reaction rates, activation parameters and exchange mechanism of cations and macrocycles between the solvated and complexed sites. Since there was evidence for the change in the exchange mechanism of a number of metal ion–crown ether systems with temperature in methanol solution [18, 20, 23], we were interested in examining the temperature effect on the exchange kinetics of metal cryptates in this solvent. In this paper we used lithium-7 NMR line-shape analysis to determine the kinetic parameters and the mech-

* Author to whom correspondence should be addressed.

anism for the chemical exchange of Li^+ ion between the solvated and complexed sites with cryptand C221 (I) in methanol solution over a wide range of temperature (i.e. -60 to 25°C). It should be noted that the use of NMR line-shape analysis in monitoring the kinetics and mechanism of reactions involving different lithium compounds has well been documented in the pioneering work of Kaplan and Fraenkel [25].

EXPERIMENTAL

Cryptand C221 (Merck, I) was of the highest purity available and used without further purification except for vacuum drying. Reagent grade lithium perchlorate (Merck) was purified and dried as described before [26]. Spectroscopic grade methanol (Merck) was used as received. The concentration of lithium perchlorate in each solution was kept constant at 0.01 M.

All NMR measurements were done on a JEOL FX90Q FT-NMR spectrometer with a field strength of 21.13 kG. At this field, lithium-7 resonates at 34.77 MHz. The temperature of the probe was adjusted with a temperature control unit using liquid nitrogen at low temperatures and a heating element at high temperatures. To reach the equilibrium temperature, each sample tube was left in the probe for at least 15 min before measurement. At all temperatures used, the accuracy of the temperature measurements was ± 0.1°C.

The line widths of the free and complexed Li^+ ion were measured by fitting a Lorentzian function to their spectra. A complete line-shape analysis technique was used to determine the mean lifetime, τ, for the exchange processes, using the modified Bloch equations [25, 27]. The equations used were of a similar format to those used by Cahen *et al.* [10]. A non-linear least-squares program written based on the Powell technique was used to fit 100–150 points of the spectral data to the exchange equations in order to extract the τ values for the exchange system at several temperatures.

RESULTS AND DISCUSSION

From both the solid crystalline structure [28, 29] and solution studies [10, 30–32], it is well known that the cryptate complexes of alkali ions could exist either in the "inclusive" form or in the "exclusive" form. In an inclusive complex, the metal ion is located in the center of the tridimensional cavity of the cryptand, while in an exclusive structure, the metal ion resides approximately in the center of one of the poly(oxadiazacycloalkane) rings of the cryptand. In the inclusive complexes, the cryptand exists in the endo–endo conformation in which both nitrogen lone electron pairs point toward the cavity center.

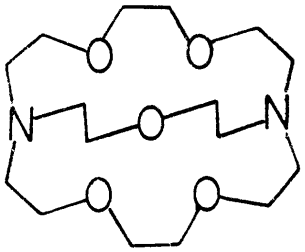

I

Lithium ion, due to its suitable size for the cavity of C211, forms a very stable inclusive Li^+C211 complex both in the crystalline state [29] and in solution [10, 31]. Lithium-7 NMR studies [10] revealed two ^{7}Li signals for the free and complexed Li^+ ion with C211, even in solvents of high donicity, the resonance of the ion inside the cryptand cavity being completely independent of the solvents. However, in the case of Li^+C221 and Li^+C222 systems, only one population averaged ^{7}Li signal was observed indicating fast Li^+ exchange between the two sites. In methanol solution, while the stability of Li^+C211 cryptate is very high ($\log K_f = 8.04$) [33], the cation forms much less stable cryptates with cryptands C221 ($\log K_f = 5.38$) [33] and, especially, C222 ($\log K_f = 2.46$) [34].

The exchange kinetics of C221 with Li^+ ion was studied in methanol solution by ^{7}Li NMR line-shape analysis at a wide range of temperature. In all cases, the concentration of lithium perchlorate salt was kept constant at 0.01 M and three solutions with C221 to Li^+ ion mole ratios <1 were prepared, so that each solution contained free and complexed Li^+ ion. The ^{7}Li NMR spectra of the resulting solutions were obtained at several different temperatures (Figure 1). At the same time, and under the same experimental conditions, the ^{7}Li NMR spectra of the solvated and complexed sites (i.e. 0.01 M solutions of $LiClO_4$ with respective ligand-to-metal ion mole ratios of 0.0 and >1) were obtained and the line widths were measured by fitting a Lorentzian function to the spectra. Interestingly, the broadening of the resonance lines of Li^+ in the solvated shell and in the cryptate form, even at very low temperatures, was found to be approximately equal. This observation, which originated from similar symmetry of the electrical field gradients in both sites, implies that the small Li^+ ion should be located in the center of the cavity of the cryptand, as is reported for the crystalline state of the alkaline cryptates [28].

Line-shape analysis to the NMR exchange equations by non-linear regressions of the 100–150 points of the spectra yielded the corresponding mean lifetimes, τ, for the exchange system used at various temperatures. The program requires evaluation of at least four parameters: amplitude, base line, zero-order phase correction and mean life time. A sample computer fit of the ^{7}Li NMR spectra is shown in Fig. 2 and all resulted τ values are collected in Table 1.

As Shchori *et al.* [35] proposed, the lithium ion may exchange between the solvated and cryptate sites by

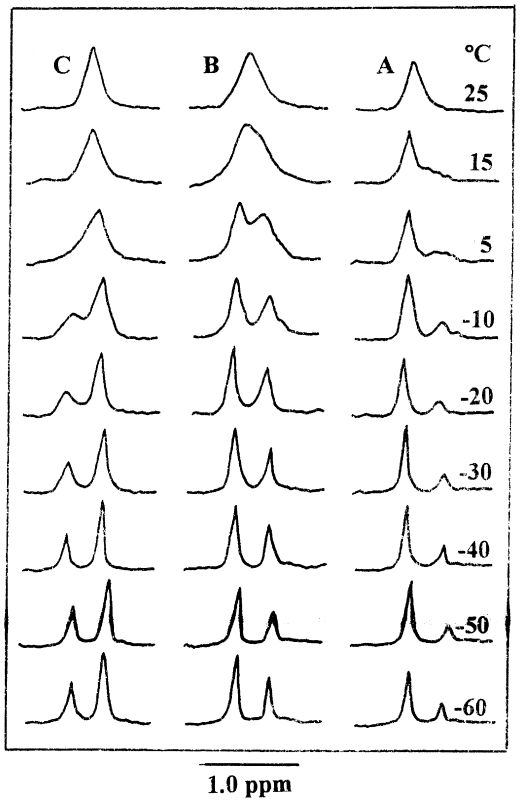

Fig. 1. ^{7}Li NMR spectra at various temperatures for 0.01 M solutions of $LiClO_4$ with C221 in methanol. The ligand-to-metal ion mole ratios are: (A) 0.30, (B) 0.45 and (C) 0.63.

Table 1. Mean lifetimes as a function of temperature for $LiClO_4$–C221 in methanol solution

T (°C)	[C221]/[$LiClO_4$]	$10^2\tau$ (s)
25	0.30	0.95
	0.45	0.78
	0.63	0.52
15	0.30	1.26
	0.45	0.99
	0.63	0.66
5	0.30	1.91
	0.45	1.45
	0.63	1.00
−10	0.30	2.74
	0.45	2.45
	0.63	1.85
−20	0.30	3.71
	0.45	3.32
	0.63	3.01
−30	0.30	4.27
	0.45	4.45
	0.63	4.28
−40	0.30	5.24
	0.45	5.25
	0.63	5.26
−50	0.30	6.27
	0.45	6.49
	0.63	6.26
−60	0.30	8.64
	0.45	8.64
	0.63	8.69

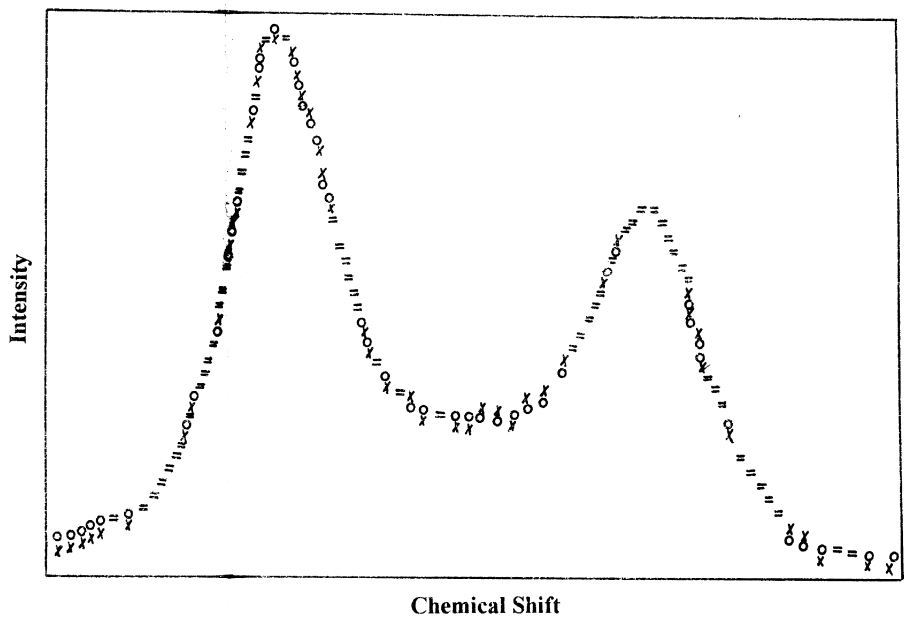

Fig. 2. Computer fit of ^{7}Li NMR spectrum obtained with a 0.01 M solution of $LiClO_4$ containing C221 in methanol with macrocycle to lithium mole ratio of 0.45 at −10°C: (×) experimental point; (○) calculated point; (=) experimental and calculated points are the same within the resolution of the plot.

either a bimolecular mechanism (I) or a dissociative pathway (II).

$$*Li^+ + Li^+C221 \xrightarrow{k_1} *Li^+C221 + Li^+ \quad (I)$$

$$Li^+ + C221 \underset{k_{-2}}{\overset{k_2}{\rightarrow}} Li^+C221 \quad (II)$$

The general expression for τ, in terms of the above mechanisms, is [13, 14, 18–20]:

$$1/\tau = k_1[Li^+]_{tot} + k_{-2}[Li^+]_{tot}/[Li^+]_{free} \quad (1)$$

where $[Li^+]_{tot}$ and $[Li^+]_{free}$ represent the total concentration and the concentration of uncomplexed lithium ion, respectively. According to eq. (1) at a given temperature, a plot of $1/\tau$ $[Li^+]_{tot}$ vs $1/[Li^+]_{free}$ determines the contribution of the two mechanisms to the exchange process. Such plots are shown in Fig. 3.

From Fig. 3, it is immediately obvious that, depending on the temperature, two different exchange mechanisms coexist to different extents. The bimolecular mechanism dominates at low temperatures (below $-30°C$) while the dissociative pathway prevails above $5°C$. However, at the temperature range between -30 to $5°C$, both the dissociative and bimolecular mechanisms contribute the metal exchange; the contributions of the two mechanisms could be obtained graphically. We have previously observed the same kind of temperature dependence of the exchange mechanism for diaza-18-crown-6-NaSCN system in THF [18], dibenzo-30-crown-10-CsSCN system in propylene carbonate and methanol [20] and 18-crown-6-$Pb(NO_3)_2$ in 70% methanol [24].

The first report on the predominance of a bimolecular mechanism was reported by Schmidt and Popov for the K^+-18-crown-6 complex in a number of non-aqueous solvents by ^{39}K NMR [36]. Since then this mechanism has been found to be operative for the chemical exchange of some other complexes of macrocyclic ligands with metal ions including Li^+ [13,

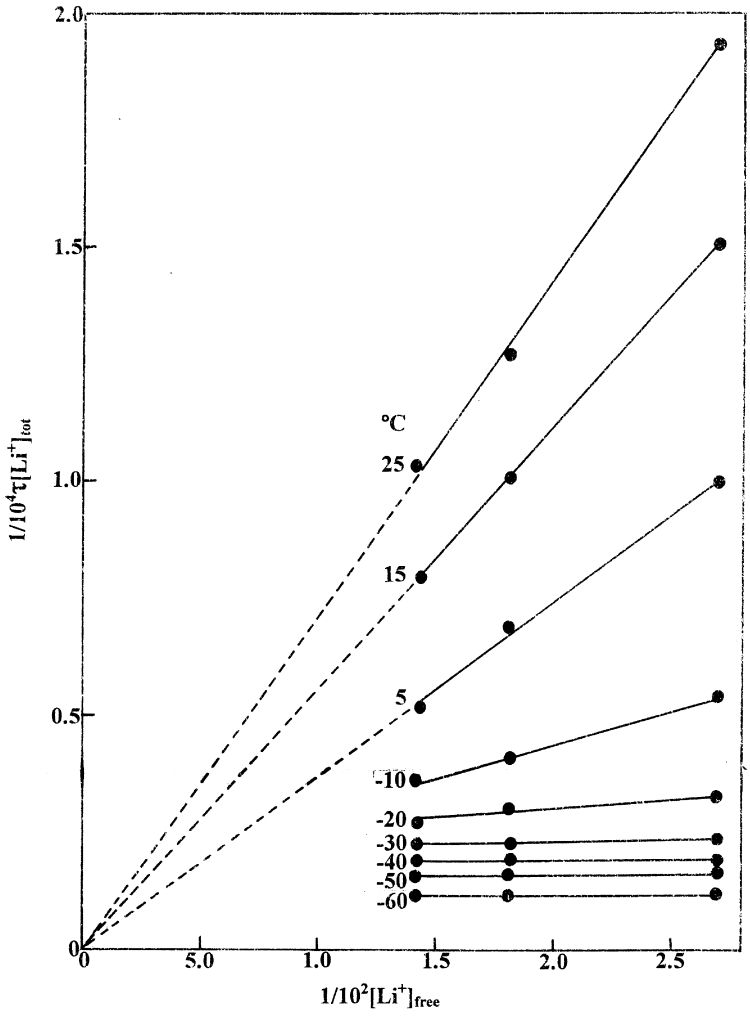

Fig. 3. Plots of $1/\tau$ $[Li^+]_{tot}$ vs $1/[Li^+]_{free}$ for Li^+–C221 system in methanol at different temperatures.

37], Na^+ [18, 38], Cs^+ [14, 19, 20], Ba^{2+} [23] and Pb^{2+} [24] ions, as studied by ^7Li, ^{23}Na, ^{133}Cs and ^1H NMR, respectively. Noteworthy, the competition between the bimolecular and dissociative mechanisms for the exchange not only depends on the temperature [18, 20, 24] but also on other experimental parameters such as the solvent properties [20, 39], nature of counter ion [40] and the concentration range studied [23, 41]. It is interesting to note that, in order for a bimolecular metal exchange to proceed in a metal-macrocycle system, the ligand should have a conformation such that the simultaneous arrival of a free cation and departure of the complexed cation can easily occur [18–20, 36].

Since in the case of both dissociative and bimolecular exchange mechanisms $1/\tau$ is proportional to k_d, it is obvious that the Arrhenius activation plots could also be obtained by plotting $\log(1/\tau)$ vs inverse temperature. Such plots for the two mechanisms, obtained at two different temperature ranges, are given in Fig. 4. Activation energies for the release of Li^+ ion from the C221 cavity were determined from the slopes of these plots and the activation parameters $\Delta H^{\ddagger}$, $\Delta S^{\ddagger}$ and $\Delta G^{\ddagger}$ were calculated by using Eryring's transition-state theory [42]. The results of these calculations are summarized in Table 2.

From the data given in Table 2, it is immediately obvious that the $\Delta G^{\dagger}$ value for a bimolecular mechanism is smaller than that for a dissociative pathway. A similar behavior has already been reported for other exchange systems [18, 20, 21]. Thus, the observed change in the exchange mechanism seems to be due to the fact that, at low temperature, the system chooses a lower energy pathway for the decomplexation step. It is interesting to note that the predominance of the bimolecular exchange mechanism over the dissociative pathway is mainly of enthalpic origin. While the $\Delta S^{\ddagger}$ values are about the same for the two exchange mechanisms, within the experimental errors, the $\Delta H^{\ddagger}$ value for the bimolecular mechanism is some 12 kJ mol^{-1} smaller than that for the dissociative pathway. The large negative entropy of activation may result from a much higher degree of solvent organization, in going from the initial complex to the transitions state,

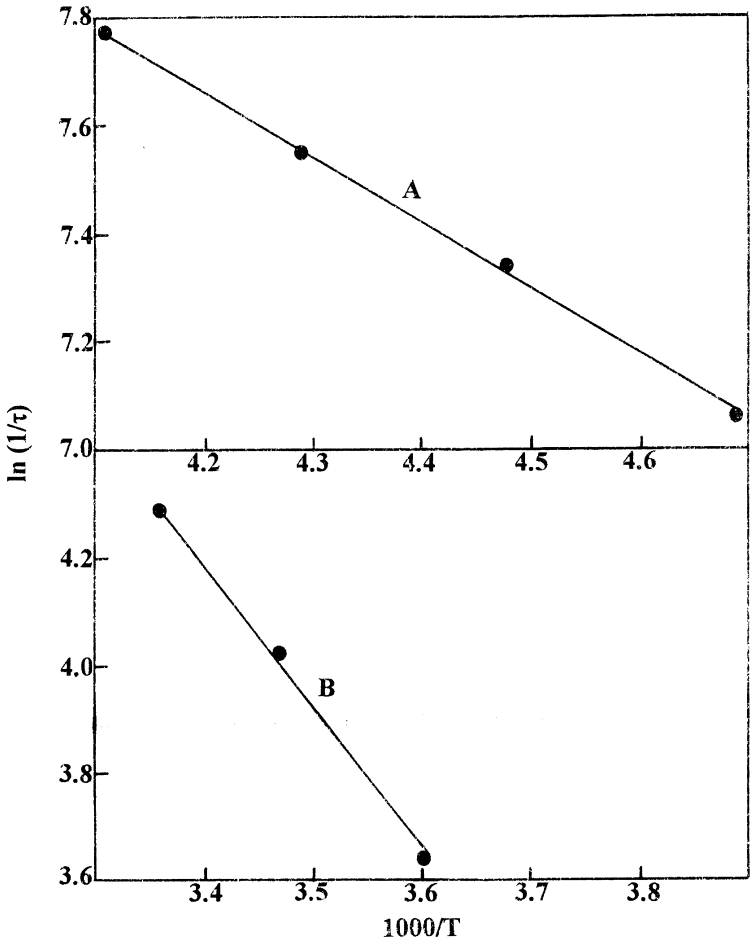

Fig. 4. Arrhenius plot of ln $(1/\tau)$ vs $1/T$ for Li^+–C221 system in methanol solution: (A) bimolecular mechanism and (B) dissociative pathway.

Table 2. Activation parameters for the metal exchange in Li^+–C221 system in methanol solution

Exchange mechanism	E_a (kJ mol^{-1})	$\Delta H^\dagger$ (kJ mol^{-1})	$\Delta S^\dagger$ (J mol^{-1} K^{-1})	$\Delta G^\dagger$ [a] (kJ mol^{-1})	k
Bimolecular	9.9 ± 0.4	8.0 ± 0.4	-146 ± 2	51.5 ± 0.2	$(2.3 \pm 0.1) \times 10$ [b]
Dissociative	22 ± 2	20 ± 2	-144 ± 8	62.9 ± 0.4	70 ± 2 [c]

[a] The standard deviation calculated by using the approximate equation $\sigma(\Delta G^\dagger) \approx |\sigma(\Delta H^\dagger) - T\sigma\Delta S^\dagger|$ [44].

[b] Unit: $M^{-1} s^{-1}$ (at $-30°C$).

[c] Unit: s^{-1} (at 25°C).

due to strong solvation of Li^+ ion with methanol [43].

The rate of dissociation of metal ion from the cryptate seems to be primarily dependent on the optimization of fit between the metal ion and the cryptand cavity [13, 16]. The Li^+ ion has just the right size for the cavity of C211 [5, 6] to form a very stable cryptate, while the cation size is too small for the cavity of C221 which results in the formation of a weaker complex, in solution [33]. Thus, it is not unexpected to observe a very low dissociation rate of the Li^+–C211 cryptate in methanol solution (i.e. $k_d = 4.4 \times 10^{-3} s^{-1}$) [33] in comparison with that obtained in this study Table 2.

REFERENCES

1. Dietrich, B., Lehn, J. M. and Sauvage, J. P., *Tetrahedron Lett*., 1969, 2885; 2889.
2. Lehn, J. M., *Pure Appl. Chem*., 1978, **30,** 871.
3. Izatt, R. M., Bradshaw, J. S., Nielsen, S. A., Lamb, J. D., Christensen, J. J. and Sen, D., *Chem. Rev*., 1985, **85,** 271.
4. Izatt, R. M., Pawlak, K., Bradshaw, J. S. and Bruening, R. L., *Chem. Rev*., 1991, **91,** 1721.
5. Lehn, J. M., *Struct. Bonding* (*Berlin*), 1973, **16,** 1.
6. Lehn, J. M. and Sauvage, J. P., *J. Am. Chem. Soc*., 1975, **97,** 6700.
7. Parham, H. and Shamsipur, M., *Polyhedron*, 1992, **11,** 987.
8. Lehn, J. M., Sauvage, J. P. and Dietrich, B., *J. Am. Chem. Soc*., 1970, **92,** 2916.
9. Ceraso, J. M. and Dye, J. L., *J. Am. Chem. Soc*., 1973, **95,** 4432.
10. Cahen, Y. M., Dye, J. L. and Popov, A. I., *J. Phys. Chem*., 1975, **79,** 1292.
11. Ceraso, J. M., Smith, P. B., Landers, J. S. and Dye, J. L., *J. Phys. Chem*., 1977, **81,** 760.
12. Lincoln, S. F., Brereton, I. M. and Spotswood, T. M., *J. Chem. Soc. Faraday Trans*., 1985, **81,** 1623.
13. Shamsipur, M. and Popov, A. I., *J. Phys. Chem*., 1986, **90,** 5997.
14. Shamsipur, M. and Popov, A. I., *J. Phys. Chem*., 1987, **91,** 447.
15. Lincoln, S. F. and Abou-Hamdan, A., *Inorg. Chem*., 1990, **29,** 358.
16. Lincoln, S. F. and Rodopoulos, T., *Inorg. Chim. Acta*, 1991, **190,** 223.
17. Whitbread, S. L., Politis, S., Stephens, A. K. W., Lucas, J. B., Dhillon, R., Lincoln, S. F. and Wainwright, K. P., *J. Chem. Soc. Dalton Trans*., 1996, 1379.
18. Szczygiel, P., Shamsipur, M., Hallenga, K. and Popov, A. I., *J. Phys. Chem*., 1987, **91,** 1252.
19. Strasser, B. O., Shamsipur, M. and Popov, A. I., *J. Phys. Chem*., 1985, **89,** 4822.
20. Shamsipur, M. and Popov, A. I., *J. Phys. Chem*., 1988, **92,** 147.
21. Amini, M. K. and Shamsipur, M., *J. Phys. Chem*., 1991, **95,** 9601.
22. Rouhollahi, A., Amini, M. K. and Shamsipur, M., *J. Solution Chem*., 1994, **23,** 63.
23. Alizadeh, N. and Shamsipur, M., *J. Solution Chem*., 1996, **25,** 1029.
24. Alizadeh, N. and Shamsipur, M., *J. Chem. Soc. Faraday Trans*., 1996, **92,** 4391.
25. Kaplan, J. I. and Fraenkel, G., *NMR of Chemically Exchanging Systems*. Academic Press, New York, 1980 (and references therein).
26. Shamsipur, M. and Popov, A. I., *Inorg. Chim. Acta*, 1980, **43,** 243.
27. Pople, J. A., Schneider, W. G. and Bernstein, H., *High Resolution Nuclear Magnetic Resonance*. McGraw-Hill, New York, 1959, p. 218.
28. Mathieu, F., Metz, B. and Moras, D., Weiss, R., *J. Am. Chem. Soc*., 1978, **100,** 4412.
29. Abou-Hamdan, A., Hounslow, A. M., Lincoln, S. F. and Hambley, T. W., *J. Chem. Soc. Dalton Trans*., 1987, 489.
30. Mei, E., Popov, A. I. and Dye, J. L., *J. Am. Chem. Soc*., 1977, **99,** 6532.
31. Popov, A. I., *Pure Appl. Chem*., 1979, **51,** 101.
32. Schmidt, E., Tremillon, J. M., Kintzinger, J. P. and Popov, A. I., *J. Am. Chem. Soc*., 1983, **105,** 7563.
33. Cox, B. G., Schneider, H. and Stroka, J., *J. Am. Chem. Soc*., 1978, **100,** 4746.
34. Buschmann, H. J., *Inorg. Chim. Acta*, 1986, **125,** 31.
35. Shchori, E., Jagur-Grodzinski, J. and Luz, Z., Shporer, H., *J. Am. Chem. Soc*., 1971, **93,** 7133.
36. Schmidt, E. and Popov, A. I., *J. Am. Chem. Soc*., 1983, **105,** 1873.
37. Briere, K. M. and Detellier, C., *J. Phys. Chem*., 1992, **96,** 2185.
38. Graves, H. P. and Detellier, C., *J. Am. Chem. Soc*., 1988, **110,** 6019.

39. Strasser, B. O. and Popov, A. I., *J. Am. Soc.*, 1985, **107,** 7921.
40. Strasser, B. O., Hallenga, K. and Popov, A. I., *J. Am. Chem. Soc.*, 1985, **107,** 789.
41. Delville, A., Stover, H. D. H. and Detellier, C., *J. Am. Chem. Soc.*, 1985, **107,** 4172.
42. Lin, S. H., Li, K. P. and Eyring, H., in *Physical Chemistry*, *an Advanced Tratise*, Vol. VII, eds. H. Eyring, D. Handerson and W. Yost. Academic Press, New York, 1977, p. 1.
43. Hinton, J. F. and Amis, E. S., *Chem. Rev.*, 1971, **71,** 627.
44. Binsch, G. and Kessler, H., *Angew. Chem. Int. Ed. Engl.*, 1980, **19,** 411.

Pergamon

PII: S0277–5387(97)00286–6

Polyhedron Vol. 17, No. 22, pp. 3817–3823, 1998
© 1998 Elsevier Science Ltd
All rights reserved. Printed in Great Britain
0277–5387/98 $19.00+0.00

Ferrocenylmethylphosphonate formation. Synthesis, spectroscopy and molecular structure

Christian J. Isaac, Mark R. J. Elsegood, William Clegg, Nicholas H. Rees, Benjamin R. Horrocks and Andrew Houlton*

Department of Chemistry, University of Newcastle upon Tyne, Newcastle upon Tyne NE1 7RU, U.K.

(Received 20 May 1997; accepted 25 June 1997)

Abstract—Reaction of ferrocenylmethanol, $FcCH_2OH$, with β-cyano-*N*,*N*-diisopropyl chlorophosphoramidite in dichloromethane yields the ferrocenylmethylphosphonate derivative, $FcCH_2P(O)(N(iPr)_2)(OCH_2CH_2CN)$, **2a**. The crystal and molecular structure of **2a** is presented. ^{31}P NMR data suggest that this is formed from $FcCH_2OP(N(iPr)_2)(OCH_2CH_2CN)$ via a Michaelis–Arbusov-type rearrangement. Similar behaviour was also observed for 1,2-phenylene chlorophosphite and diethyl chlorophosphite. © 1998 Elsevier Science Ltd. All rights reserved

Keywords: ferrocenyl; phosphonate; Arbusov; cyclic voltammetry; phosphoramidite.

INTRODUCTION

Interest in the chemistry of ferrocenyl-containing phosphines is considerable, particularly so for their co-ordination chemistry (see, for example, Refs. [1–3]). Such compounds have found application in asymmetric catalysis [4a, 4b] and reports have also been made on the biological activity of their metal complexes [5]. By contrast, there are relatively few reports [6a, 6b, 7] on other phosphorus-containing ferrocenyl derivatives, e.g. phosphonates, despite their considerable potential for synthetic applications [8]. Recently, however, the reactivity of ferrocenyl-derived alcohols, specifically 6-ferrocenylhexan-1-ol, has been utilised for the incorporation of the redox-active metallo group into oligonucleotides via reaction with β-cyano-*N*,*N*-diisopropylchlorophosphoramidite, forming initially the ferrocenylphosphoramidite before conversion to the ferrocenyl-modified nucleotide [9].

We have also been interested in the conjugation of the ferrocenyl group with nucleobases and have reported on adenine and thymine-derived examples, along with studies of their interactions with DNA [10]. In this paper we report on the reactions of ferrocenylmethanol, $FcCH_2OH$, with β-cyano-*N*,*N*-diisopropylchlorophosphoramidite and other chlorophosphites in an effort to establish the generality of such reactions.

EXPERIMENTAL

Ferrocenylmethanol was prepared from $FcCH_2NMe_3^+I^-$ as described in the literature [11]. β-cyano-*N*,*N*-diisopropylchlorophosphoramidite (Sigma), 1,2-phenylene chlorophosphite (Avocado) and diethyl chlorophosphite (Avocado) were used as supplied. Diisopropylethylamine (Aldrich) was dried over CaH_2 and distilled prior to use.

Synthesis of $FcCH_2P(O)(N(iPr)_2)(OCH_2CH_2CN)$, **2a**

Ferrocenylmethanol (0.5 g, 2.3 mmol) and dry diisopropylethylamine were dissolved in 20 m^3 of dry dichloromethane. The mixture was cooled on ice, β-cyano-*N*,*N*-diisopropylchlorophosphoramidite (0.81 m^3, 3.5 mmol) was added and the reaction mixture allowed to stand for 30 min at room temperature. Following the addition of methanol, the mixture was evaporated to give a yellow oil, which was loaded onto an alumina column and eluted with chloroform/ethylacetate/triethylamine 45:45:10. Despite evidence for at least two components in the reaction mixture,

*Author to whom correspondence should be addressed.

only the single product was isolated in pure form, **2a**. Yield 63%: m.p. 105°C. Found: C, 57.27; H; 7.15; N, 6.82, $C_{20}H_{29}FeN_2O_2P$ requires: C, 57.70; H, 7.02; N, 6.73. IR: ν(CN) at 2220 cm^{-1}, ν(P=O) at 1250 cm^{-1}.

X-ray crystallography

Crystals suitable for a single crystal X-ray structure determination were grown from a saturated solution in hexanes. Crystal data and other information on structure determination are given in Table 1. Measurements were made with graphite-monochromated Mo-Kα radiation on a Stoe-Siemens four-circle diffractometer. Unit cell parameters were refined from 2θ values (22–25°) of 51 reflections measured at $\pm\omega$ to minimize systematic errors. Intensities were measured by an on-line profile fitting procedure [12]. Absorption corrections were applied semi-empirically from azimuthal scans of sets of symmetry-equivalent reflections [13]; no corrections were required for intensity decay or extinction effects. The data sets consisted of one unique set of reflections, a complete set of Friedal opposites and a few other symmetry-equivalent reflections.

The structure was solved by direct methods and refined by full-matrix least-squares on all F^2 values, with weighting $w^{-1}=\sigma^2(F_o^2)+(0.0494P)^2+(1.2427P)$ where $P=(F_o^2+2F_c^2)/3$. All non-hydrogen atoms were refined with anisotropic displacement parameters, and isotropic H atoms were constrained with a riding model including torsional freedom for methyl groups. Residuals are defined as: $R_w=\{\Sigma[w(F_o^2-F_c^2)^2]/\Sigma[w(F_o^2)^2]\}^{1/2}$ for all data, $R=\Sigma\|F_o|-|F_c\|/\Sigma|F_o|$ for reflections with $F_o^2>2\sigma(F_o^2)$. Atomic coordinates, displacement parameters, and complete geometry have been deposited at the Cambridge Crystallographic Data Centre.

Table 1. Crystallographic data for **2a**

Formula	$C_{20}H_{29}FeN_2O_2P$
M	416.3
Crystal system	monoclinic
Space group	$P2_1/c$
a (Å)	7.5052(11)
b (Å)	18.650(3)
c (Å)	15.2048(19)
β (°)	100.283(18)
V (Å^3)	2094.0(5)
Z	4
D_c (g cm^{-3})	1.320
μ (mm^{-1})	0.81
F(000)	880
T (K)	200
Radiation; λ (Å)	MoK_α; 0.71073
Crystal size (mm)	$0.65\times0.38\times0.32$
$2\theta_{max}$ (°)	50
Maximum indices h, k, l	8, 22, 18
Reflections measured	7921
Unique reflections	3668
R_{int}	0.0161
Transmission factors	0.750–0.813
Number of refined parameters	239
R_w (all data, on F^2)	0.0876
R [3325 data with $F^2>2\sigma(F^2)$]	0.0309
Goodness of fith on F^2	1.043
Largest difference map features (e Å^{-3})	+1.06, −0.31

NMR spectroscopy

^{1}H, ^{13}C and ^{31}P NMR spectra were measured at 500.16, 125.77 and 202.47 MHz, respectively, on a Joel Lambda 500 and ^{31}P at 36.2 MHz on a Joel FX90Q NMR spectrometers. Phosphorus decoupled proton spectra, ^{1}H–^{1}H TOCSY and ^{1}H–^{13}C HSQC spectra were run using standard Joel pulse sequences. Typical 2D data sets were acquired into 1024×512 data points then zero-filled to 1024×1024 datapoints prior to Fourier transformation using a shifted sine-bell apodization function in both dimensions.

Electrochemistry

A conventional two-compartment glass cell was used with a 1mm diameter platinum disc working electrode. A silver wire was used as a quasi-reference electrode and the potential scale was established by measuring a CV of ferrocene. The electrolyte was $[N(Bu^t)_4, PF_6]$ in dimethylsulfoxide. The potentiostat was an EG&G model 263A.

RESULTS AND DISCUSSION

NMR studies

The reaction of ferrocenylmethanol with β-cyano-*N*,*N*-diisopropylchlorophosphoramidite in dichloromethane was followed at room temperature by ^{31}P NMR and data is presented in Table 2. After mixing, resonances were observed at 180 and 148 ppm. The former signal corresponds to phosphoramidite starting material, while the latter is attributed to $FcCH_2OP(N(iPr)_2)(OCH_2CH_2CN)$, **1a**. This assignment is based on comparison with analogous compounds, *viz*. $Fc(CH_2)_6OP(N(iPr)_2)(OCH_2CH_2CN)$ (^{31}P 147.7 ppm in $CDCl_3$) [9] and other non-ferrocenyl derivatives [14]. At 35 min into the experiment a resonance at 30.0 ppm begins to appear, which is due to the formation of the phosphonate $FcCH_2P(O)(N(iPr)_2)(OCH_2CH_2CN)$, **2a**. Subsequent spectra taken at regular intervals show the steady increase in the signal at 30.0 ppm with a correlated decrease of the signal at 147.7 ppm*. At reaction times greater

*It should be noted that in some reactions a small peak was observed at 13.8 ppm which we interpret as a hydrolysis product of species of type **1**. Hydrolysis of the phosphoramidite gives a product with a signal at 6.5 ppm.

Table 2. ^{31}P NMR data[a] (ppm) for the reaction of ferrocenylmethanol with β-cyano-*N*,*N*-diisopropylchlorophosphoramidite, **a**, 1,2-phenylene chlorophosphite, **b**, and diethyl chlorophosphite, **c**

	Starting material	**1**	**2**
a, β-Cyano-*N*,*N*-diisopropylchlorophosphoramidite[b]	180.0	147.7	30.0
b, 1,2-Phenylene chlorophosphite[c]	173.9	122.4	44.6
c, Diethyl chlorophosphite[b]	166.7	128.5	25.0

[a]Shifts referenced to H_3PO_4.
[b]Solvent CH_2Cl_2.
[c]Solvent $CDCl_3$.

than 4 h there remained an approximate 1:1 ratio of **1a**:**2a**.

To put these data into perspective, the reaction of β-cyano-*N*,*N*-diisopropylchlorophosphoramidite with benzylalcohol was also considered. Following the reaction using ^{31}P NMR spectroscopy revealed starting material (^{31}P 149.0 ppm in CH_2Cl_2) and a resonance at 140.1 ppm which corresponds to $PhCH_2OP(N(iPr)_2)(OCH_2CH_2CN)$. Subsequent spectra taken over 12 h showed no evidence for rearrangement.

Confirmation of the nature of product, **2a**, was made based on assignment of the ^1H and ^{13}C spectra using a combination of ^1H–^1H TOCSY and ^{31}Pe decoupling ^1H and ^1H–^{13}C HSQC experiments. The numbering scheme used here is that for the crystal structure (*vide infra*). Chemical shift and coupling constant data are given in Table 3.

The ^1H–^1H TOCSY (Fig. 1) indicated the presence of four spin systems in the ^1H spectrum. These could be assigned to the substituted cyclopentadienyl ring, the CH_2 group bridging the ferrocenyl and the phosphorous, the cyanoethyl chain and the *N*,*N*-diisopropylamido group. This left the singlet at 4.14 ppm which was assigned to the unsubstituted cyclopentadienyl ring of the ferrocenyl. A consequence of the chiral nature of the phosphorus centre is the inequivalence of the pairs of protons and carbons, (7)/(10) and (8)/(9), in the substituted cyclopentadienyl ring. The pattern of coupling indicated by the ^1H–^1H TOCSY spectrum gives the sequential ordering of the protons around the ring, but does not allow the absolute assignment. Similarly the two protons bonded to C(11) are rendered inequivalent by the chiral centre giving a typical ABX pattern, which simplified to an AB upon ^{31}P-proton decoupling. In the cyanoethyl chain the effect of the chiral centre is greatest on the C(12) protons ($\Delta\delta$ $^1H = 0.23$ ppm) which can be distinguished from the cyclopentadienyl signals by their coupling interactions with the C(13) protons at 2.62 ppm; these exhibit no discernible shift difference due to their prochiral nature. Finally the *N*,*N*-diisopropylamido group gives two signals for the methyl groups and one for the methine groups. The chiral phosphorus leads to inequivalence of the methyl pairs C(16)/C(17) and C(19)/C(20). However, the fluxionality about N(2) will lead to rapid exchange of the *N*-isopropyl groups giving rise to only one set of resonances (i.e. one methine and two methyl signals in both the ^1H and ^{13}C spectra). The ^{31}P proton spectrum indicated that only the protons attached to C(11), C(12), C(15) and C(18) had any significant coupling to phosphorus.

Alongside the ^{31}P chemical shift (23.1 ppm in $CDCl_3$) further confirmation of direct P–C bond formation involving the ferrocenylmethyl group was

Table 3. NMR data and assigment for **2a**. Spectra recorded in $CDCl_3$

	^1H	^{13}C
H–C(1–5)	4.14 (5H)	68.52
H–C(7/10)	4.26, 4.34 (2H)	69.47, 69.47
H–C(8/9)	4.13/4.11 (2H)	67.60, 67.35
H–C(11)	2.96, 2.84, J(11-11) = 15.3 Hz.	30.44, J_{P-C} = 126 Hz.
H–C(12)	3.93, 4.16, J(12-12) = 10.4 Hz.	57.63, J_{P-C} = 6 Hz.
H–C(13)	2.62, J(13-12) = 6.2 Hz.	19.73, J_{P-C} = 6 Hz.
H–C(15/18)	3.36 (2H)	45.46, J_{P-C} = 3 Hz.
H–C(16,17,19,20)	1.26, 1.16, (12H)	23.28, 22.13
C(6)		78.27, J_{P-C} = 3 Hz.
C(14)		116.89

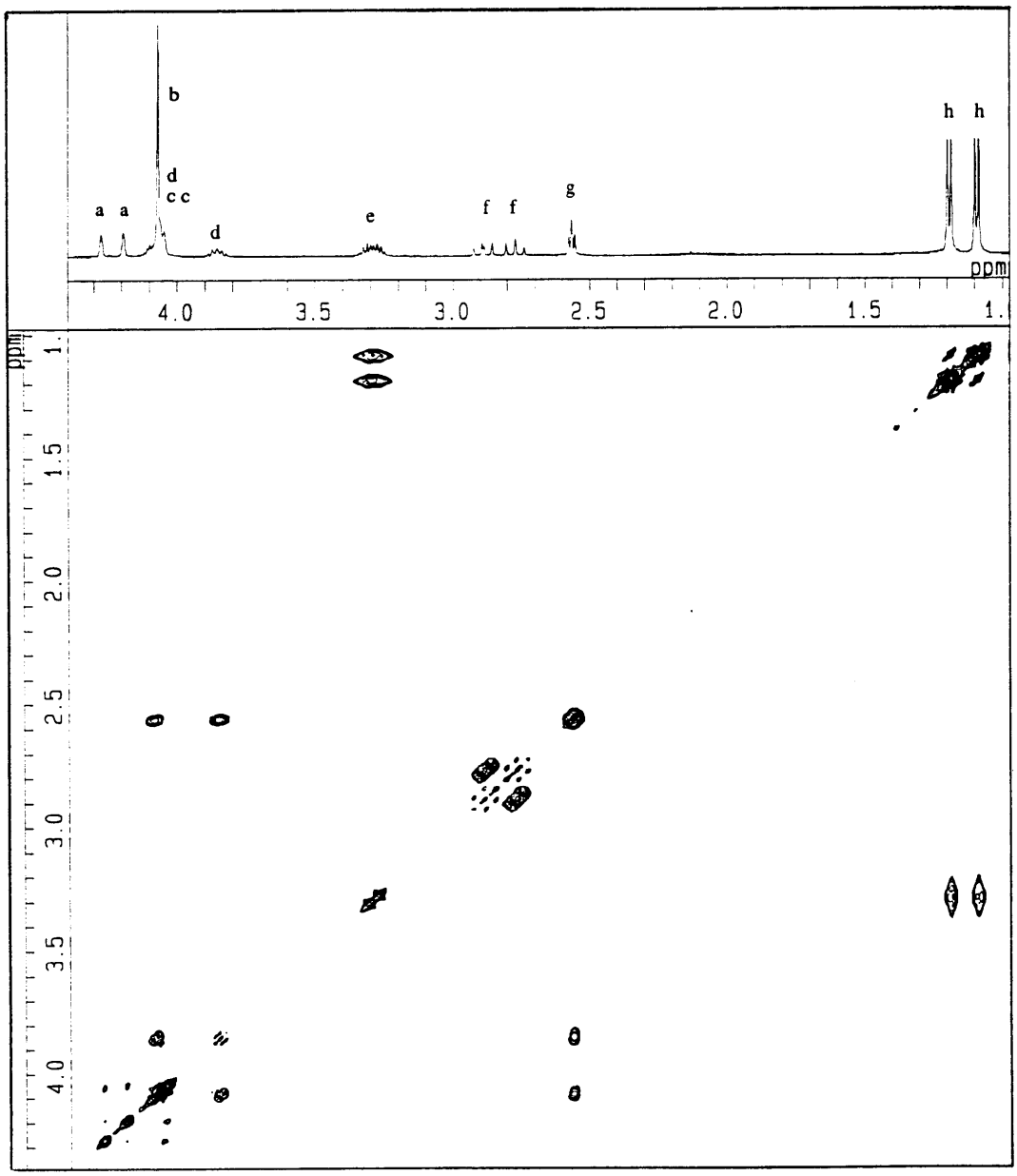

Fig. 1. ^{1}H–^{1}H TOCSY of **2a** in $CDCl_3$ at room temperature. Mixing time 25 ms. Assignments a = H(7),(10), b = H(1)–(5), c = H(8),(9), d = H(12), e = H(15),(18), f = H(11), g = H(13), h = H(16),(17),(19),(20) (see Fig. 2 and Table 3).

indicated by the magnitude of the $^{13}C(11)$–^{31}P coupling constant [$J(^{31}P$–$^{13}C) = 126$ Hz] [7, 14]. This compares with those of 3–6 Hz for the remaining ^{31}P–^{13}C coupling. These lie in the expected range for ^{2}J and ^{3}J coupling interactions for carbon to phosphorus(V) [14].

Scheme 1 depicts the proposed reaction for the formation of ferrocenylmethyl phosphonates, **2**. Following initial attack to form a ferrocenylphosphite, **1**, a Michaelis–Arbusov type rearrangement occurs to generate the corresponding ferrocenylmethylphosphonate, **2**. The rearrangement proceeds via the relatively stable ferrocenylmethyl cation [15].

In an effort to establish the general nature of this rearrangement the reaction between $FcCH_2OH$ and 1,2-phenylene chlorophosphite and diethyl chlorophosphite, respectively, were studied under the same conditions. The ^{31}P data for these are summarised in Table 2. As in the previous case with phosphoramidite, the reaction proceeds with the initial formation of a species of type **1** (Scheme 1) (^{31}P δ in the range 120–130 ppm), followed by the appearance

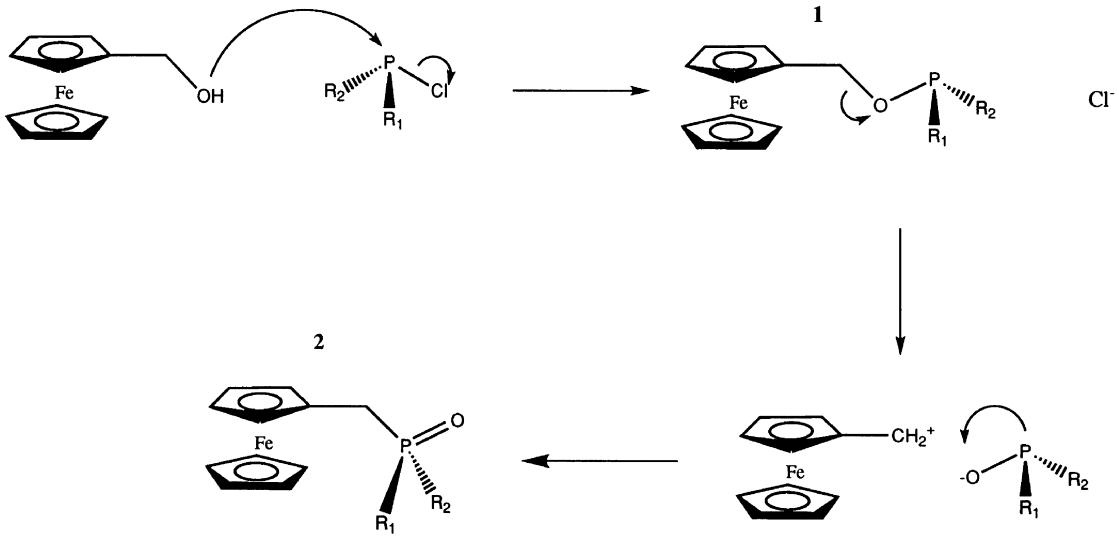

Scheme 1. Proposed reaction scheme for compounds of type **2**.

of a signal for the corresponding ferrocenylmethylphosphonate, **2** (^{31}P δ in the range 25–45 ppm). These shifts are in keeping for phosphorus with coordination spheres PO_3 and $O_2CP{=}O$, respectively. However, in both cases at reaction times over 4 h the ratio of products **1**:**2** remained at ~3:1.

In the case of 1,2-phenylene phosphorchloridite the reaction was repeated in $CDCl_3$ to allow monitoring by both ^{1}H and ^{31}P NMR. The ^{31}P showed the same features as in CH_2Cl_2, with slight differences in chemical shift. Formation of the appropriate phophonate, **2b**, based on the ^{31}P NMR was accompanied in the ^{1}H spectra by the formation of a signal at 3.14 ppm with a coupling to ^{31}P of 19 Hz indicating the formation of the $FcCH_2$–P moiety. This was confirmed by performing a selective ^{31}P-decoupling experiment irradiating at the resonant frequency of **2b** in the ^{31}P spectrum.

Crystal and molecular structure of **2a**

Crystals of **2a** suitable for study by X-ray crystallography were grown from a solution in hexane. The compound crystallises in the monoclinic space group $P2_1/c$. The molecular structure is shown in Fig. 2, which also features the atomic numbering scheme, and the selected bond lengths and angles are given in Table 4. The cyclopentadienyl groups are planar with an interplanar angle 3.79(17)° and are effectively eclipsed (7.7° twist about the line joining the ring centroids). The range of Fe–C distances is 2.039(2)–2.058(2), averaging 2.047(2) Å. The iron-ring centroid distances are 1.654(2) Å to the unsubstituted, 1.648(2) Å to the substituted rings, respectively. All of these distances are as expected, based on comparisons with other mono-substituted ferrocenyl derivatives found in the Cambridge Structural Database [16].

Table 4. Selected bond lengths (Å) and angles (°) for **2a**, with estimated standard deviations in parentheses

P(1)–O(1)	1.6006(14)	P(1)–O(2)	1.4730(15)
P(1)–N(2)	1.6444(17)	P(1)–C(11)	1.814(2)
Fe–C_{Av}	2.047(2)	Fe–Cp_{unsub}	1.654(2)
Fe–Cp_{sub} [a]	1.648(2)		
O(1)–P(1)–O(2)	114.24(8)	O(1)–P(1)–N(2)	105.79(8)
O(2)–P(1)–N(2)	112.88(9)	O(1)–P(1)–C(11)	99.29(9)
N(2)–P(1)–C(11)	109.73(9)	P(1)–N(2)–C(18)	119.17(13)
P(1)–N(2)–C(15)	122.24(14)	C(15)–N(2)–C(18)	117.44(16)
Cp–Fe–Cp	177.2(2)		

[a]Cp represents the ring centroid.

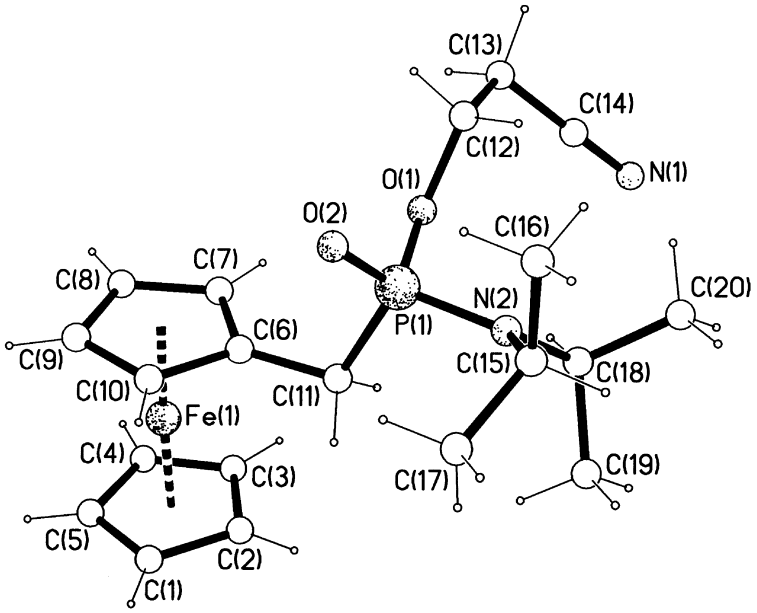

Fig. 2. Molecular structure and numbering scheme for **2a**.

A direct comparison of **2a** can be made with the analogous $FcCH_2P(O)(OPh)_2$ [7]. The Cp–CH_2 distance is 1.508(3) Å in **2a** and compares with 1.521(9) in $FcCH_2P(O)(OPh)_2$ [7]. The bonding distances around P in **2a** are; P(1)–O(1), 1.601(1); P(1)–O(2), 1.473(2); P(1)–N(2), 1.644(2) and P(1)–C(11), 1.814(2) Å. The corresponding bond distances in $FcCH_2P(O)(OPh)_2$ are P=O, 1.461; P–O_{av}, 1.590 and P–C, 1.795 Å [7]. Moreover, the bond lengths found for these ferrocenylmethylphosphonates are comparable with analogous phosphonates, such as diethyl-2-hydroxyl-1,2-diphenylethylphosphonate [17]. The geometry at phosphorus is somewhat distorted from idealised tetrahedral with bond angles around phosphorus in **2a** ranging from 99.29(9)° for O(1)–P(1)–C(11) to 114.24(8)° for O(1)–P(1)–O(2).

Previous structural characterisations of ferrocenylphosphine derivatives containing a methylene spacer attached to phosphorus include the symmetrically substituted bis(η^5-diphenylphosphinomethylcyclopentadienyl)-iron [18], its triphenylphosphinium derivatives [19] and the monosubstituted ferrocenylmethyl(triphenylphosphonium) iodide [19]. Bond lengths for the Cp–CH_2–PR_2 grouping are; C_{Cp}–CH_2, 1.493 and CH_2–P, 1.855 Å, while those for the Cp–CH_2–P+R_3 grouping are in the ranges; C_{Cp}–C, 1.485–1.501 and CH_2–P, 1.813–1.818 Å. The CH_2–P bond length in **2a** lies within the range observed for the phosphonium derivatives and together these are shorter than the equivalent distance for the phosphine.

Electrochemistry

A cyclic voltammogram reveals that **2a** exhibits a reversible one-electron wave with a formal potential, E^0, of $-0.036(5)$ V vs Fc^+/Fc and a peak current ratio of 0.84 in DMSO indicating near chemical reversibility of the redox process (scan rate 0.1 V s^{-1}). This shift in electrode potential indicates slight electron donation by the substituent group on the cyclopentadienyl ring. By contrast, the analogous $FcCH_2P(O)(OPh)_2$ derivative exhibits a slight positive shift ($E^0 = 0.058(6)$ V vs Fc^+/Fc couple) [7].

Further comparison can be made with the oxide of 1,1′-bis(diphenylphosphino)ferrocene which has a reversible ferrocene-based one-electron oxidation at $E^0 = 0.43$ V [20]. As might be expected the insertion of a methylene spacer between the ferrocenyl group and the P=O group, as in **2a** and $FcCH_2P(O)(OPh)_2$, reduces the electron withdrawing effect on the ferrocenyl moiety.

CONCLUSIONS

Reactions between ferrocenylmethanol and β-cyano-*N*,*N*-diisopropylchlorophosphoramidite leads to the formation of $FcCH_2P(O)(N(iPr)_2)(OCH_2CH_2CN)$, **2a**. ^{31}P NMR data suggest that this is formed from $FcCH_2OP(N(iPr)_2)(OCH_2CH_2CN)$ via a Michaelis–Arbusov-type rearrangement. Moreover, NMR data also reveals that this mechanism is quite general for ferrocenylmethanol and chlorophosphites.

REFERENCES

1. Togni A. and Hayashi, T., *Ferrocenes*. VCH, Weinheim, 1995.
2. Cullen, W. R. and Woolins, J. D., *Coord. Chem. Rev.*, 1981, **39,** 1.

3. Yamamoto, Y., Tanase, T., Mori, I. and Nakamura, Y., *J. Chem. Soc. Dalton Trans*, 1994, 3191.
4a. Barbaro, P. and Togni, A., *Organometallics*, 1995, **14,** 3570.
4b. Sawamura, M. and Kuwano, R., Ito, Y., *J. Am. Chem. Soc*., 1995, **117,** 9602.
5. Hill, D. T., Girard, G. R., McCabe, F. L., Johnson, R. K., Stupik, P. D., Zhang, J. H., Reiff, W. M. and Eggleston, D. S., *Inorg. Chem*., 1989, **28,** 3529.
6a. Tomas, S. and Kaluzayova, E., *Chem. Zvesti*, 1969, **23,** 540.
6b. Boev, V.I., *Zh. Obshch. Khim*., 1977, **47,** 2527.
7. Henderson, W., Oliver, A. G. and Downard, A. J., *Polyhedron*, 1996, **15,** 1165.
8. Boutagy, J. and Thomas, R., *Chem. Rev*., 1974, **74,** 87.
9. Mucic, R. C., Herrlein, M. K., Mirkin, C. A. and Letsinger, R. L., *Chem. Commun*., 1996, 555.
10. Price, C., Aslanoglu, M., Isaac, C. J., Elsegood, M. R. J., Clegg, W., Horrocks, B. R. and Houlton, A., *J. Chem. Soc. Dalton Trans*., 1996, 4115.
11. Lindsay, J. K. and Hauser, C. R., *J. Org. Chem*., 1957, **4,** 355.
12. Clegg, W., *Acta Cryst. A*, 1981, **22,** 37.
13. Sheldrick, G. M., *SHELXTL Manual*, version 5. Siemens Analytical X-ray Instruments, Madison, WI, U.S.A., 1994.
14. Verkade J. G. and Quin, L. D., *Phosphorus* 31-*NMR Spectroscopy in Stereochemical Analysis*. VCH, Florida, 1987.
15. Hill, E. A., *J. Am. Chem. Soc*., 1959, **81,** 3484.
16. Allen, F. H. and Kennard, O., *Chem. Design Automation News*, 1993, **8,** 31.
17. Angleova, O., Macicek, J., Vassilev, N. G., Momchilova, S. and Petrova, J., *J. Cryst. Spectrosc*., 1992, **22,** 253.
18. Yamamoto, Y., Tanase, T., Mori, I. and Nakamura, Y., *J. Chem. Soc. Dalton Trans*., 1994, 3191.
19. Glidewell, C., Zakaria, C. M., Ferguson, G. and Gallagher, J. F., *Acta Cryst. C*, 1994, **50,** 233.
20. Pilloni, G., Longato, B. and Corain, B., *J. Organomet. Chem*., 1991, **420,** 57.

Pergamon

PII: S0277–5387(98)00125–9

Polyhedron Vol. 17, No. 22, pp. 3825–3833, 1998
© 1998 Elsevier Science Ltd
All rights reserved. Printed in Great Britain
0277–5387/98 $19.00+0.00

Complexation in solution of magnesium(II) and cobalt(II) with purine 5′-monophosphates and pyrimide 5′-monophosphates: a potentiometric and calorimetric study

Luis A. Herrero and Angel Terrón*

Department of Chemistry, Universitat de les Illes Balears, E-07071 Palma de Mallorca, Spain

(Received 29 January 1998; accepted 25 March 1998)

Abstract—The interaction of Mg(II) and Co (II) with purine and pyrimidine nucleoside 5′-monophosphates was studied using potentiometric and calorimetric methods, with 0.1 M tetramethylammonium bromide as the background electrolyte at 25°. The presence in solution of the complexes $[Mg(AMP)_2]^{2-}$, $[Co(AMP)_2]^{2-}$, $[Co(GMP)_2]^{2-}$ $[Co(IMP)_2]^{2-}$ was observed. The relationship between enthalpies and the degree of macrochelation together with the stacking interaction between purine bases in the complexes are discussed. © 1998 Elsevier Science Ltd. All rights reserved

Keywords: magnesium; nucleotides; calorimetry.

INTRODUCTION

The bioinorganic chemistry of divalent metallic ions is a topic of great interest [1]. In this respect the role of magnesium(II) in metal-mediated hydrolysis of phosphate esters is known to be a common catalytic pathway in nucleic acid biochemistry. This role has been reviewed recently by Cowan who proposes new stoichiometries for magnesium dependent nuclease activation [[1](b)]. For this reason the knowledge of all the complexation thermodynamic magnitudes for the cellular concentration of Mg(II) (approximately 0.5 mM as free ion) seems to be relevant. It is also known that the influence on the stabilization of DNA by different 3d divalent metallic ions [[1](c)], and the activity as enzymatic cofactor of Mg(II) or Ca(II) complexes with nucleoside triphosphates or monophosphates [[1](d)].

The X-ray structures of metal-nucleotide complexes has been reviewed recently [2]. Solid state structures of the $[Co(NMP)(H_2O)_5].H_2O$ type, where NMP is guanosine 5′-monophosphate and inosine 5′-monophosphate, in which cobalt (II) ion is bound to N(7) and also, via a coordinated water molecule, to the phosphate group have been reported [[3](a)]. Other crystalline structures of the $[Co(NMP)_2]^{2-}$ type in which the metal ion is coordinated to two nucleotides in cis position, have been also described for cobalt (III) complexes with GMP and IMP. The coordination sites are identical to those of the former complex. The latter structures suggest a relevant base stacking stabilization between the purine bases in cis position, despite a butterfly-like arrangement of the two purine residues [[3](b)].

With magnesium only $[Mg(ATPH)_2]^{4-}$ structures, with coordination with the phosphate group, are known [[4](a)]. In the analogous Ca-dAMP complex only coordination of the calcium with the phosphate group are cited [[4](b)].

The interaction of the metal can also alter the hydrogen bond and stacking interactions between the bases in RNA and DNA molecules as it was pointed out by Barton [5]. In a recent publication, Marzilli has also studied by NMR [6] the possible existence of atropisomerism in complexes of the type $Pt(GMP)_2$ in solution.

The interactions of divalent 3d metallic ions with nucleotides in solution have been reviewed recently [7]. Frey and Stuehr [[7](b)] established the formation

*Author to whom correspondence should be addressed.

of the $[Ni(AMP)_2]^{2-}$, with adenosine 5′-monophosphate and adenosine 2′-monophosphate, complexes potentiometrically. Sigel [[7](a,c,d)] studied the relationship between macrochelation and the first stability constants for Co and Mg(II) (and other divalent metals) and purine nucleoside monophosphates compounds. Other studies also measured the self-association of different nucleotides by means of NMR [8].

Very few previous calorimetric studies involving divalent metallic ion and mononucleotides have been published [9] and none, to our knowledge, in which the existence of 1:2 complex has been considered for the Mg(II) and Co(II) metals. The interactions of magnesium with UMP, GMP, and AMP [[9](a,b,c)] and Co(II) with AMP [[9](d)] for the 1:1 complexes were previously published.

As a follow up of the systematic calorimetric studies carried out for the system Ni(II)- nucleoside monophosphate system [10], the aim of our this research is to confirm, by two different techniques, the existence of $[Co(NMP)_2]^{2-}$ (where N is either adenosine, guanosine or inosine) and $[Mg(AMP)_2]^{2-}$ in solution in concentrations of the order of magnitude of magnesium (II) in the cytoplasme, to determine directly their thermodynamic values, and to consider the influence of purine base stacking stabilization on these complexes.

EXPERIMENTAL

Materials

The acids H_2NMP (where N can be either adenosine, guanosine, inosine, cytidine or uridine 5′-monophosphates) used in the potentiometric experiments were purchased from Sigma and the disodium salts of nucleotides (Fig. 1) used in the calorimetric experiments were purchased from Serva.

Magnesium and cobalt (II) nitrate (analytical grade) was purchased from Merck. Tetramethylammonium bromide (analytical grade) was purchased from Aldrich. The concentrations of the nucleotide solutions were determined by weighing and then tested by UV spectrophotometry. All the solutions were prepared with deionized and then destilled water and the ionic strength was adjusted to 0.1 with tetramethylammonium bromide. The titer of the NaOH (Merck) used for the potentiometry titrations was determined with potassium hydrogen phthalate (Merck).

Potentiometric titrations

These were carried out with a potentiometer CRISON micropH 2002 and a glass electrode. The poten-

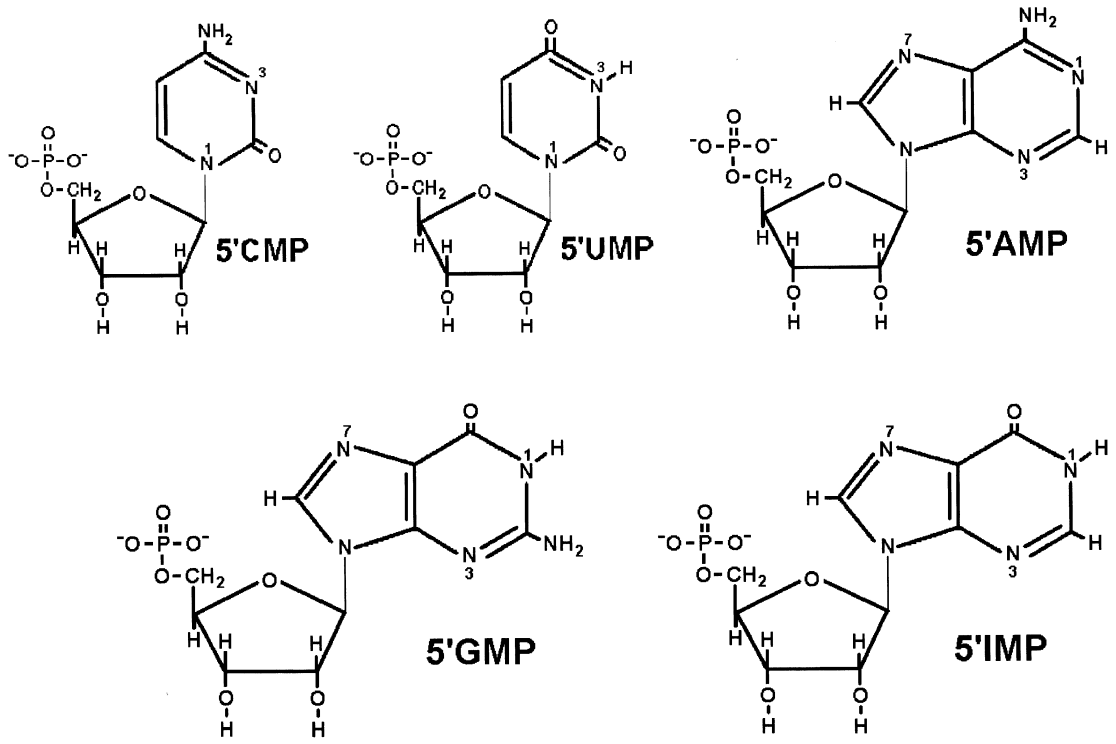

Fig. 1. Formulae and abbreviations of the purine and pyrimidine nucleoside 5′-monophosphates.

tial values were recorded on an IBM PC by means of the VALGRAN program previously described [11]. Additions of the NaOH titrant were made automatically with a CRISON MICRO BU2031 microburet. The titrations were conducted under an atmosphere of N_2 to exclude carbon dioxide in a jacketed titration vessel in which the temperature was maintained by circulating water (25 ± 0.1°C) in the jacket. Magnetic stirring was also used.

(a) Determination of CMP and UMP acidity constants. The constants for the deprotonation of the acid pyrimidine nucleotides were determined previously by titrating a known volume (about 50 ml) of H_2NMP solution with NaOH. The initial concentrations of nucleotide ranged from 6×10^{-4} to 2×10^{-3} M. The acidity constants of the puric nucleotides where determined previously [[10](c)].

(b) The determination of the constants of stability K_{MLH} and K_{ML} of the $[M(NMPH)]^+$ and [M(NMP)] complexes, respectively, was made by titrating a known volume of H_2NMP solution containing Mg(II) or Co(II) nitrate. The initial concentration of nucleotide ranged from 2×10^{-4} M to 6×10^{-4} M. The concentration ratio of metal ion to nucleotide was higher than 25:1 in all cases to avoid formation of $[M(NMP)_2]^{2-}$ complexes.

(c) The constants K_{ML2} for the complexes $[MNMP)_2]^{2-}$ were determined by titrating a known volume of nucleotide solution in the presence of metal(II) nitrate between 2.0×10^{-3} M. and 3.0×10^{-2} M. The initial nucleotide concentrations in solution varied from 1.7×10^{-2} to 2.0×0^{-2} M and the concentration of NaOH titrant was 9.37×10^{-2} M in all cases.

The main equilibria considered for the M-NMP (where M is either Mg(II) or Co(II) and NMP a nucleoside 5′-monophosphate) systems are:

$$NMPH^- + H^+ = H_2NMP\ K^H_{a2} \quad (1)$$

$$NMP^{2-} + H^+ = HNMP^-\ K^H_{a1}(Kpr)\ \text{and}\ \Delta Hpr \quad (2)$$

$$M(II) + NMP^{2-} = [M(NMP)]K_{ML}\ \text{and}\ \Delta H_{ML} \quad (3)$$

$$M(II) + NMPH^- = [M(HNMP)]^+ K_{MLH}\ \text{and}\ \Delta H_{MLH} \quad (4)$$

$$[M(NMP)] + NMP^{2-} = [(M(NMP)_2]^{2-} \quad (5)$$

$$K_{ML2}\ \text{and}\ \Delta H_{ML2}$$

Where H_2NMP is either H_2AMP H_2GMP, H_2IMP, H_2CMP or H_2UMP respectively. For the pyrimidine 5′-mononucleotides the equilibrium (5) does not necessary have to be considered.

The parameters determined and the equilibria considered for each determination are indicated below. The linear equations used to fit the experimental data were deduced from the mass balances in each case in order to establish a relationship between the measured constants with known parameters or parameters obtained during the potentiometric titration [[10](c)].

In the following expressions, A_t is the total concentration of acid hydrogens for each experimental point; K_w the water ionic product (13.72 ± 0.01 under our experimental conditions); c_{nuc} is the total concentration of the nucleotide. The K^H_{z1} values used were those previously determined by Sigel [[8](c)].

Determination of pK_{a1}.

The equilibria considered were 1 and 2. From the mass balance is obtained the following expression:

$$y/[(1-y) \times [H^+]] = K_{a1} + [(2-y) \times [H^+]]/(1-y) \times K_{a1} \times K_{a2}$$

and

$$y = \{At + (Kw/[H^+]) - [H^+]\}/c_{nuc} \quad (6)$$

Determination of K_{ML} and K_{MLH}

The equilibria considered were 1, 2, 3 and 4 and the equation to fit was:

$$(\gamma - \delta)/c_M = K_{ML} \times K_{MLH} \times \gamma \quad (7)$$

Where

$$\gamma = K_{a1} \times \beta \times [H^+]$$
$$\delta = 1 - K_{a1} \times K_{a2} \times [H^+]^2$$
$$\beta = c_{nuc} - \alpha$$
$$\alpha = A_t - [H^+] + (K_w/[H^+])$$

Determination of K_{ML2}

The equilibria considered were 1, 2, 3, 4 and 5 and the equation for the linear correlation between K_{ML2} and the experimental parameters was:

$$z/\{(1-z) \times K_{ML} \times [NMP^{2-}]\} - K_{ML} \times K_{a1} \times [H^+]/K_{ML} - 1 = \{K_{ML2} \times (2-z) \times [NMP^{2-}]\}/(1-z) \quad (8)$$

where

$z = \{c_{nuc}$-$[NMP^{2-}]$-
$K_{a1} \times [NMP^{2-}] \times [H^+] \times (1 + K_{MLH} \times [M^{2+}])\}/M_o$ and M_o is the total metal ion concentration, and $[NMP^{2-}]$ is the free deprotonated nucleotide concentration and $[M^{2+}]$ the free cobalt or magnesium(II) concentration in the equilibrium.

In our conditions, the measured standard potential from the glass electrode follows the equation:

$$E = E'^0 + g \times \log [H^+]$$

$$\text{where} \quad E'^0 = E^0 + g \times \log \gamma_H + + E_j$$

where E^0 is the standard potential (in mV) from the electrode, E_j the liquid junction potential, and γ_{H+} the proton activity coefficient and g is the Nernst constant. E'^0 can be considered constant for one potentiometric titration, and it was determined for each titration.

For calculation purposes, all the experimental results were fitted simultaneously for each system. In the calculation a first approximate value for the glass electrode standard potential in each experiment and the experimental data were used. Optimizing the values of the standard potentials with the program MINIPOT [[11](b)] and the programs POTCAL, POTPK, POTMLH and POTML2 (Adaptations of MINIPOT to our system which allow a simultaneous data treatment for various potentiometric titrations [[11](c)]) and the lineal regression of the equations (eqn (6), eqn (7) or eqn (8) for each system) the constants K_{a1}, K_{ML}, K_{MLH} and K_{ML2} were determined. The final standard potentials minimize the addition of the quadratic differences between the theoretical and experimental potentials ($\Sigma(E_t\text{-}E)^2$). The deviation for the calculated parameters are indicated as 3 σ from the lineal regression equation.

CALORIMETRIC MEASUREMENTS

The calorimetric measurements were carried out in a LKB 20001 batch microcalorimeter connected to an IBM PC for data acquisition by means of the BATCHCAL program described previously [[9](d)]. All the measurements were taken at 25.00 ± 0.01°C. The pH in equilibrium was determined by means of a CRISON micro pH 2002 with an accuracy of 0.001 pH units.

Determination of the protonation heats for CMP^{2-} and UMP^{2-} was performed by addition in independent experiences of 4 ml of 3.27 mM HCl solutions to 2 ml of nucleotide solutions (8.48 mM for CMP and 9.56 mM for UMP). The initial pH of the nucleotide solutions was 7. The determination of the protonation heat for the purine nucleotides was previously carried out [[10](c)].

The formation enthalpies ΔH_{ML} and ΔH_{ML2} for the complexes [M(NMP)] and $[M(NMP)_2]^{2-}$ were determined by mixing in independent experiments 4 ml of nucleotide solutions with 2 ml of cobalt or magnesium nitrate solutions in a calorimetric cell. The magnesium concentrations in the reaction cell at equilibrium had values comprising between 0.35 to 11 mM. The cobalt concentrations in the reaction cell at equilibrium had values comprising between 0.35 to 4.0 mM; higher concentrations were never used to prevent the formation of dimeric hydroxo-cobalt complexes [12]. The nucleotide concentration at equilibrium in the reaction and reference cells varied from 0.5 to 30 mM. Nucleotide solutions were placed in the reference cell to correct the dilution heat in all cases: the metal solution dilution heat was obtained experimentally and then subtracted from that of the reaction cell.

Table 1. Thermodynamic parameters for the purine and pyrimidine nucleoside 5′-monophosphates (at 25°C and I = 0.1 in tetramethyl ammonium bromide, the errors are indicated as 3σ)

NMP	pK_{pr}	ΔH_{pr} kJ/mol	ΔS_{pr} J/(mol × K)
AMP	6.22 ± 0.01[a]	2.0 ± 0.4 [a]	126 ± 1[a]
GMP	6.23 ± 0.01[a]	3.0 ± 0.3 [a]	129 ± 2[a]
IMP	6.22 ± 0.01[a]	2.4 ± 0.4[a]	127 ± 2[a]
CMP	6.22 ± 0.02	3.0 ± 0.3	129 ± 2
UMP	6.16 ± 0.01	3.4 ± 0.4	129 ± 2

pK_{pr}, ΔH_{pr} and ΔS_{pr}: pK_{a2}, enthalpy and entropy of protonation for the equilibrium (2) [a: from reference [10](c)].

Thermodynamic parameters for the complexes

In order to carry out the calorimetric determinations the following values are required: $\log_{KML}$, $\log K_{ML2}$, ΔH_{pr} (protonation heat of the nucleotides) (Table 1), pK_{pr} (pK_{a2}) (Table 1) and the experimental heat values (Q = experimental heat-dilution heat), the initial metal (Mo) and nucleotide (Lo) concentrations, together with the reaction and reference cells pH (pH and pHr respectively). The main equilibria considered for the M(II)-5′GMP and M(II)-5′IMP systems are 2, 3 and 5. Equilibrium 4 can be neglected in the calorimetric experimental conditions owing to the small value of K_{MLH} in comparison with K_{ML} and the low $NMPH^-$ concentration at the pH work. All these parameters either experimental (Table 1) or were determined under in the same conditions as those for the calorimetric measurements.

The total heat is a contribution of the equilibria 2, 3 and 5, and the dilution heats:

$$Q = (C_{ML} + C_{ML2}) \times \Delta H_{ML} + C_{ML2} \times \Delta H_2 + C_H \times \Delta H_p \tag{10}$$

$$Q_R = Q - C_H \times \Delta H_P$$

$$Q_1 = \Delta H_1 + X \times \Delta H_2$$

$$Q_1 = QR/(C_{ML} + C_{ML2})$$

$$X = C_{ML2}/(C_{ML} + C_{ML2})$$

$$Q_R = Q - QP \tag{11}$$

QR is the reaction heat, QP is the heat associated with eqn (2) and C_{ML} and C_{ML2} are the [M(NMP)] and $[M(NMP_2)]^{2-}$ complex amount at equilibrium respectively. The experimental values can be obtained from linear regression from eqn (11)). The values obtained are shown in Table 2. The correlation diagrams are indicated in Fig. 2.

Table 2. Thermodynamic parameters for the Mg(II)and Co(II)-purine and pyrimidine nucleoside 5′-monophosphate complexes (at 25°C and I = 0.1 with tetramnethylammonium bromide). The errors are indicated as 3σ

	AMP	**GMP**	**IMP**
K_{MgLH}	<1	<1	<1
log K_{MgL}	1.61 ± 0.01	1.71 ± 0.02	1.68 ± 0.02
log K_{MgL2}	1.84 ± 0.03	—	—
ΔH_{MgL} (kJ/mol>)	$+11.1 \pm 0.8$	$+5.3 \pm 0.8$	$+6.6 \pm 0.8$
ΔH_{MgL2} (kJ/mol)	-10.2 ± 2.2	—	—
Δ_{SMgL} (J/K × mol)	$+68 \pm 3$	-4 ± 3	1 ± 3
ΔS_{MgL2} (J/(K × mol)	$+1 \pm 8$	—	—
	CMP	**UMP**	
log K_{MgL}	1.54 ± 0.01[a]	1.56 ± 0.05[a]	
ΔH_{MgL} (kJ/Mol)	$+12.5 \pm 1.0$	$+12.0 \pm 0.4$	
ΔS_{MgL} (J/(K × mol)	$+71 \pm 4$	$+70 \pm 2$	
	AMP	**GMP**	**IMP**
K_{CoLH}	6 ± 1	18 ± 2	12 ± 2
log K_{CoL}	2.24 ± 0.01	2.68 ± 0.01	2.55 ± 0.01
ΔH_{CoL} (kJ/mol)	-3.6 ± 0.4	-14 ± 0.9	-12.2 ± 1.0
ΔH_{CoL2} (kJ/mol)	-18.2 ± 1.3	-6.1 ± 2.4	$+1.9 \pm 2.6$
Δ_{SCoL} (J/(K × mol)	$+31 \pm 2$	$+4 \pm 3$	$+8 \pm 3$
ΔS_{CoL2} (J/(K × mol)	-20 ± 5	$+20 \pm 8$	$+44 \pm 9$
	CMP	**UMP**	
log K_{CoL}	1.86[a]	1.87[a]	
ΔH_{CoL} (kJ/mol)	$+10.3 \pm 1.1$	$+10.0 \pm 0.9$	
ΔS_{CoL} (J/(K × mol)	$+70 \pm 4$	$+69 \pm 4$	

[**a**: from reference [7](d)].

The values of entropy have been calculated considering

$$\Delta G = \Delta H - T \times \Delta S$$

and $$\Delta G = -2.30 \times R \times T \times \log K.$$

RESULTS AND DISCUSSION

Thermodynamic parameters of the ligands

In the calorimetric measurements, tetramethylammonium bromide has been used as the background electrolyte instead of alkaline salts. The heat of sodium ion (or other alkaline ions) interactions with the phosphate group of nucleotides can mask calorimetric determinations. For this reason, the pK_{a2} (pK_{pr}) for the purine nucleotides [[10](c)] and pyrimidine nucleotides (in the present work) were determined in 0.1 M tetramethyl-ammonium bromide (Table 1). The values are in very good agreement with those obtained by Sigel, with sodium nitrate as background electrolyte, previously published [[7](D)]. The protonation enthalpies of the purine nucleotides [[10]c] and the pyrimidine nucleotides (in the present work) were determined by calorimetry; the calorimetric results point to an endothermic process (Table 1). The value for 5′AMP agrees with the value obtained by Antonelli calorimetrically [13].

Thermodynamic parameters and structural considerations

The constants for the formation of the cobalt and magnesium(II) with purine nucleosides obtained by potentiometry and the corresponding enthalpy and entropy measurements are indicated in Table 2. The values obtained for K_{ML} are in very good agreement with those recently described by Sigel [[7](c,d)]. For instance, for Mg(5′AMP) the constants are log $K_{MgL} = 1.60$ (Sigel at 25°C, $\mu = 0.1$ M $NaNO_3$) and log $K_{MgL} = 1.61$ (our working conditions at 25°C, $\mu = 0.1$ M tetramethyl-ammonium); the values differences are within the deviation error values. This comparison can be carried out for all the remaining metal-purine nucleotide equilibrium constant values. In the case of the pyrimidine nucleotides the constants values used were those reported by Sigel [[7](c,d)].

Sigel studied by potentiometry the degree of macrochelation of different purine nucleotides [[7](c)], discussing the equilibria between complexes where the metal is only bound to the phosphate group (open

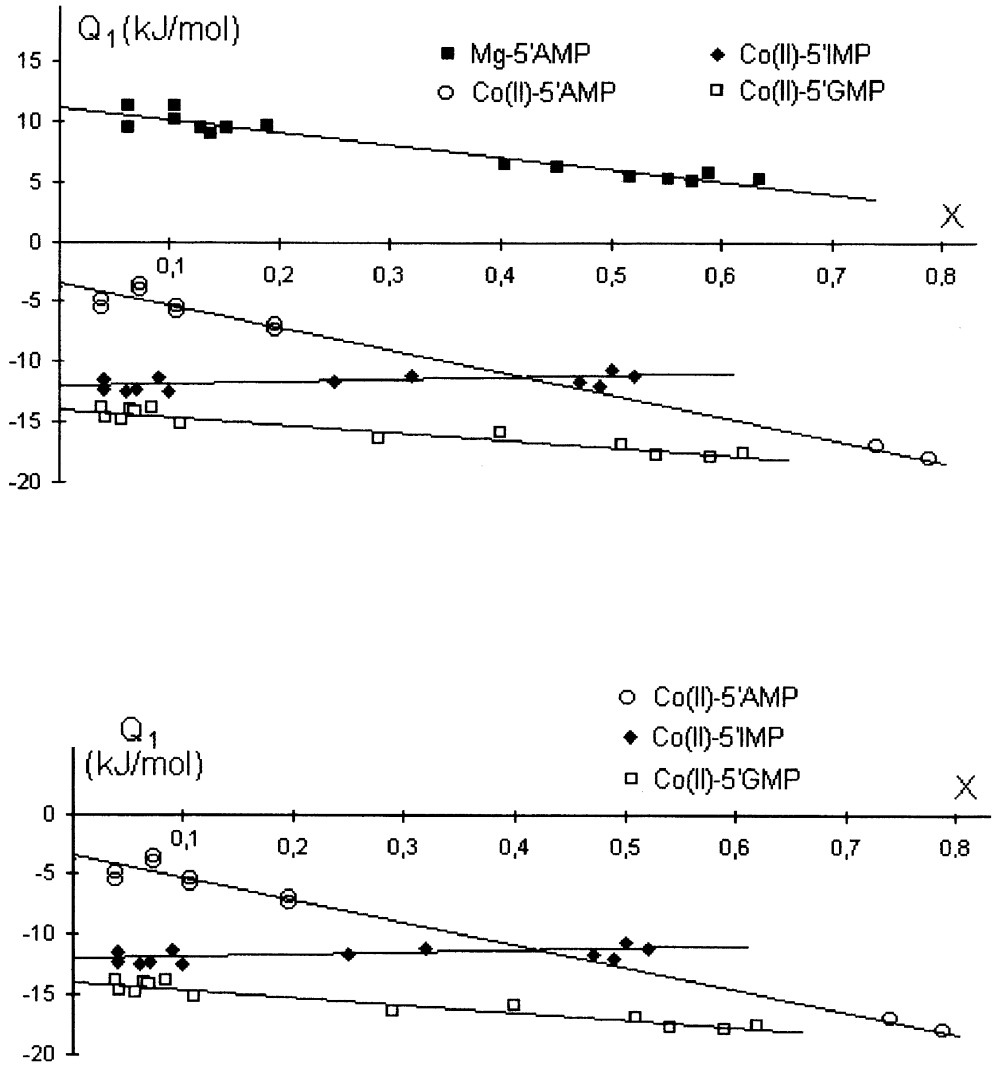

Fig. 2. Correlation diagrams for the M(II)-NMP systems.

form) and complexes were the metal is bound to the purine ring and the phosphate group (closed form)

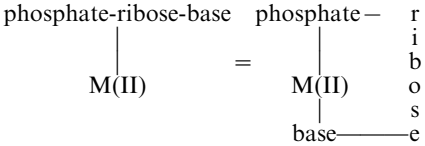

(12)

Our representation of ΔH_{ML} or ΔS_{ML} against the degree of macrochelation indicates that the higher the macrochelation the lower the value of the enthalpy and entropy. These relationships show that the macrocyclic formation is, in this case, energetically favorable and entropically unfavorable. Therefore the chelate effect does not take place, probably owing to the large number of bonds in the macrocycle.

In order to study in detail the consequences of the macrochelation on the formation enthalpies of the [M(NMP)] complexes we can consider the global reaction in two steps. In the first process the open complex is formed:

$$M(II) + NMP^{2-} = [(M(NMP)_{op}] \qquad \Delta H_{op} \quad (13)$$

And in a second step, the open complex can partially turn into the closed complex:

$$[(M(NMP)_{op}] = [(M(NMP)_{cl}] \qquad \Delta H_{cl} \quad (12a)$$

The macrochelation degree r is defined as the relation between the concentration of the closed complex [M(NMP)cl] and the total concentration of the complex [M(NMP)] in equilibrium:

$$r = [M(NMP)_{cl}]/\{[M(NMP)_{op}] + [M(NMP)_{cl}]\} \quad (14)$$

Thus the formation enthalpy for the complex can be expressed as the addition of the respective enthalpies corresponding to the two previous reactions, taking into account that the second step takes place only in part:

$$\Delta H_{ML} = \Delta H_{op} + r \times \Delta H_{cl} \quad (15)$$

In this way, it is possible to estimate the enthalpic and entropic contribution for the bonding between the cobalt(II) ion and the purine rings in these complexes, possibly through N(7) as in the solid state. Since ΔH_{ML} has been determined, and the value of ΔH_{op} for the interaction of the cobalt (II)-phosphate group ($+10.2 \pm 1.0$ kJ/mol) has been previously estimated and the values of r have been previously calculated by Sigel [[7](c,d)], the eqn (15)) can be used to obtain the values of ΔH_{cl}. The values obtained for ΔH_{cl} are approximately -28 kJ/mol for the three purine nucleotides (Table 3). Therefore this interaction is energetically favorable in these complexes. This value is of the same order than that previously described for the interaction of cobalt(II) with 9-methylpurine $\Delta H = -20.4$ kJ/mol [14].

In the case of Mg(II) the degree of macrochelation is so low that to compare degrees of macrochelation with enthalpies or entropies is unfeasible.

The same treatment can be carried out on the entropy by means of the following equation:

$$\Delta S_{ML} = \Delta S_{op} + r \times \Delta S_{cl} \quad (16)$$

The entropic values obtained for the interaction cobalt (II)-purine ring in these complexes are also very similar for the three nucleotides and show that this process is entropically unfavorable (Table 3). The rightness of our hypothesis is observed in Fig. 3, a representation of entropies and enthalpies versus r, the degree of macrochelation potentiometrically obtained by Sigel which shows the perfect correlation between the experimental and hypothetical linear parameters. Therefore, calorimetry [[10](c) and this work] supports the previous work by Sigel [[7](d)].

The potentiometric and calorimetric measurements show the existence in solution of complexes of the $[(Co(NMP)_2]^{2-}$ type, similar to those described in the solid state such for the 5′AMP, 5′GMP and 5′IMP ligands.

With the second ligand entrance the stacking phenomena could be important.

Considering the possible geometries for the complexes, four different situations can be found: a) the two nucleotides bound to the metal ion in trans position, b) the two ligands are in cis conformation without any hydrophobic interaction, c) the two nucleotides in cis position with a relevant stacking interaction and d) the second ligand is not directly coordinated to the metal ion hydrophobically interacting only with the other ligand. The known X ray structures point to structures of the type 'b', 'c' or 'd'; and no solid state structure is known, to our knowledge, in the form 'a' for nucleoside monophosphates.

The quantitative evaluation of the differences between the first and second ligand entrance can be performed by means of $\log K_{ML2} - \log K_{ML}$, $\Delta H_{ML2} - \Delta H_{ML}$ and $\Delta S_{ML2} - \Delta S_{ML}$ differences (Table 4). For the Co(II) and Mg(II) 5′AMP derivatives $\log K_{ML2}$ is similar or higher to $\log K_{ML}$, and the differences $\Delta H_{ML2} - \Delta H_{ML}$ and $\Delta S_{ML2} - \Delta S_{ML} < 0$ point to the existence of a structure of type 'c' with a hydrophobic interaction between the purine rings. This interaction could be responsible for these enthalpic and hydrophobic differences, which can be assigned on a first approach to the stacking thermodynamic parameters [[9](a,b,c,d,e,f),[10](c)], in the $[Mg(5'AMP)_2]^{2-}$ complex, the value $\Delta H_{ML2} - \Delta H_{ML}$ is approximately half the autostacking value. These values are lower than the parameters of 5′AMP autostacking ($\Delta H = -42$ kJ/mol and $\Delta S = -134 J/K \times$ mol) [[10](c)].

For the Co(II)-5′GMP and Co(II)-5′IMP the

Table 3. Enthalpies and Entropies related with the degree of macrochelation [**r** from Ref.[7](c)]

Complex	ΔH_{ML} (kJ/mol)	ΔH_{op} (kJ/mol)	r	ΔH_{cl} (kJ/mol)
Co(AMP)	-3.6 ± 0.4	$+10.2 \pm 1.0$	0.49 ± 0.09	-28 ± 8
Co(IMP)	-12.2 ± 1.0	$+10.2 \pm 1.0$	0.78 ± 0.03	-29 ± 4
Co(GMP)	-14.0 ± 0.9	$+10.2 \pm 1.0$	0.83 ± 0.02	-29 ± 3
	ΔS_{ML} (J/(mol × K))	ΔS_{op} (J/(mol × K)	r	ΔS_{cl} (J/mol × K)
Co(AMP)	$+31.0 \pm 2$	$+70 \pm 4$	0.49 ± 0.09	-79 ± 27
Co(IMP)	$+8.0 \pm 3$	$+70 \pm 4$	0.78 ± 0.03	-79 ± 13
Co(GMP)	$+4.0 \pm 3$	$+70 \pm 4$	0.83 ± 0.02	-80 ± 10

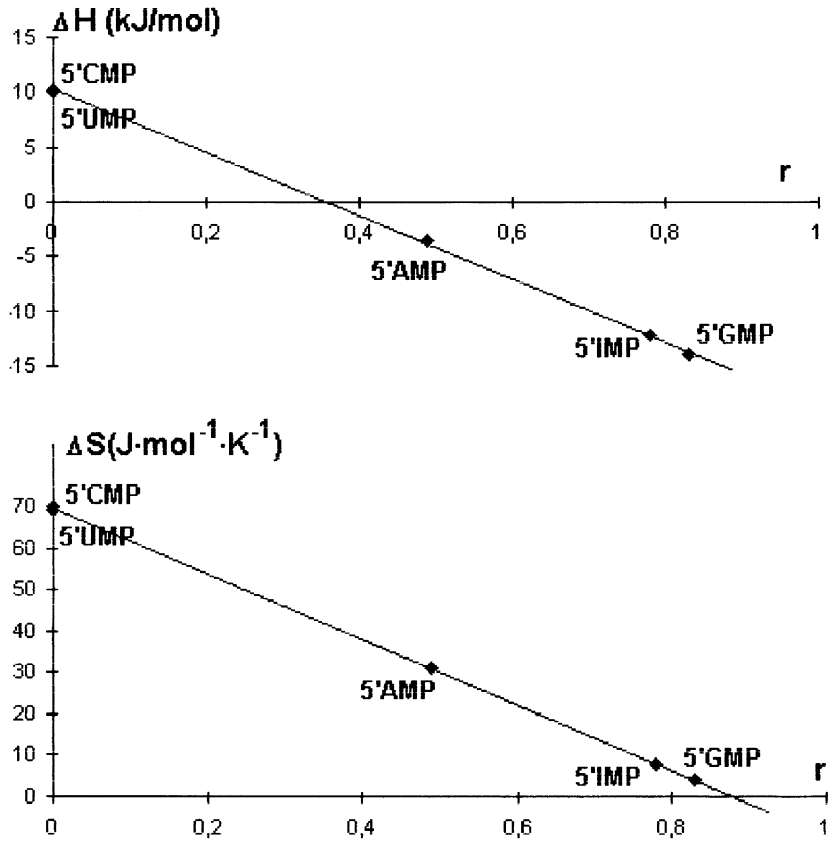

Fig. 3. Graphic representation between the values of enthalpy or entropy ΔH_{ML} and ΔS_{ML} (from this work) and the degree of macrochelation calculated by Sigel [from reference [7](c)].

differences log K_{ML2-} log $K_{ML} < 0$, $\Delta H_{ML2} - \Delta H_{ML} > 0$ and $\Delta S_{ML2} - \Delta S_{ML} > 0$ show clearly that the entrance of the second ligand is unfavorable in relation to the first ligand entrance and the process is energetically unfavorable and entropically favorable. Nevertheless a weak stacking can be masked by the degree of macrochelation, since the two effects are present.

The trend to the autostacking interaction between the purine rings in the nucleotides (5′AMP > 5′GMP > 5′IMP) [[8](a,b,c,d,e), [10](c)] is similar to that of the interaction between the nucleotides in the $[Co(NMP)_2]^{2-}$ complexes ($[Co(5'AMP)_2]^{2-} > [Co(5'GMP)_2]^{2-}$ or $[Co(5'IMP)_2]^{2-}$).

In the case of magnesium, only the $[Mg(5'AMP)_2]^{2-}$ exists due to the important stacking interactions for this nucleoside monophosphate. The latter complex could be biologically relevant to explain the affinity constants between allosteric enzymes and the magnesium-nucleotide cofactors: a) $[Mg(5'ATP)]^{2-}$ complex activates an enzyme interacting with a hydrophobic amino acid (tyrosine, phenylalanine, tryptophan); b) after the enzymatic reaction, the

Table 4. Thermodynamic parameters differences between ML_2 and ML complexes

System	$\log K_{ML2} - \log K_{ML}$	$\Delta H_{ML2} - \Delta H_{ML}$ (kJ/mol)	$\Delta S_{ML} - \Delta S_{ML2}$ (J/mol × K)
Mg(II)–AMP	+0.23	−21.3	−67
Co(II)–AMP	−0.09	−14.6	−51
Co(II)–GMP	−0.56	+7.9	+16
Co(II)–IMP	−0.65	+14.1	+36

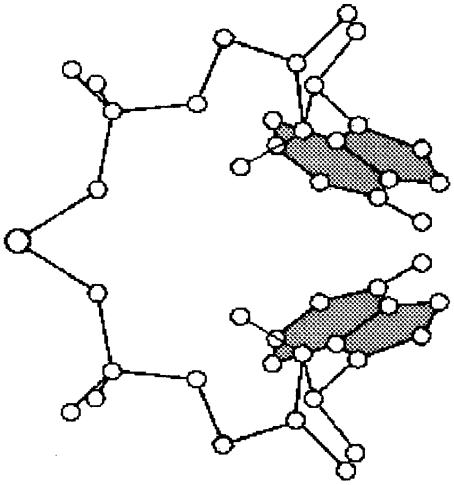

Fig. 4. Possible solution structures for the complexes $[(Mg(AMP)_2]^{2-}$.

[Mg(5′AMP)] complex is obtained, the purine ring being hydrophobically interacting with the amino acid residue has and c) could the $[Mg(5'AMP)_2]^{2-}$ complex be the species liberated from the catalytic site, compensating AMP-protein stacking with the AMP-AMP intramolecular stacking?. In this case, the former interaction in the magnesium complex could be similar to the adenine ring hydrophobic amino acid interaction. This is only a hypothesis, however, energetically balanced, and following previous results by Sigel and Yamauchi [15].

Acknowledgements—This work has received financial support from the Spanish Authorities DGICYT project number PB-94- 0922-C02-02.

REFERENCES

1. (a) Sigel, H., Sigel, A., (eds) (1988) *Metal Ions in Biological Systems*, **32**; Marcel Dekker Inc: New York. (b) Cowan, J. A., (1997) *J. Biol. Inorg. Chem*., **2** , 168–176. (c) Eichhorn, G. L., (1993) *Coord. Chem. Revs*, **128**, 167–173. (d) Black, C. K., Huang, H. W., Cowan, J. A., (1994) *Coord Chem Revs*., **135–136**, 165–202.
2. (a) Terrón, A., (1993) *Comments Inorg. Chem*., **14**, 63–88 and references therein. (b) Aoki, K., (1996) *Metal Ions in Biol. System*, **32**, 91–134., and references therein.
3. (a) Meester, P. de, Goodgame, D. M. L., Jones, T. J., Skapski, A. C., (1974) *C. R. Acad. Sci. Ser. C*, **279**, 667. (b) Poojary, M. D., Manohar, H., (1988) *J. Chem. Soc. Dalton Trans*., 1297.
4. (a) Cini, R., Burla, M. C., Nunzi, A., Polidori, G. P., Zanazzi, P. F., (1984) *J.Chem. Soc. Dalton Trans*, 2467. (b) Sato, T., (1984) *Acta Crystallogr*. sect C, **40**, 738.
5. Barton, J. (1994) *Metal/Nucleic Acid Interactions* in Bertini, I., Gray, H. B., Lippard, S. J. and Valentine, J. S.(eds) *Bioinorganic Chemistry*, University Science Books: Mill Valley, California, 505.
6. Kiser, D., Intine, F. P., Xu, Y., Natile, G. and Marzilli, L. G., *Inorg. Chem*., 1994, **33,** 4194–4198.
7. (a) Sigel, H., Song, B., (1996) *Met. Ions. Biol. Systems*, **32**, 135–205. (b) Frey, C. M., Stuehr, J. E., (1972) *J. Am. Chem. Soc*., **94**, 8898–8904. (c) Sigel, H., Massoud, S. S., Corfú, N. A., (1994) *J.Am. Chem.Soc*., **116**, 2958. (d) Sigel, H., (1993) *J.C.S. Chem. Soc. Rev*., **2**2, 255. (e) Massoud, S. S., Sigel, H., (1989) *Eur. J. Biochem*., **179**, 451–458. (f) Massoud, S. S., Sigel, H., (1988) *Inorg. Chem*., **27**, 1447–1453.
8. (a) Scheller, K. H., Sigel, H., (1983) *J.Am.Chem. Soc* , **105**, 5981–5900. (b) Mitchell, P. R., Sigel, H., (1978) *Eur. J. Biochem*., **88**, 149–154. (c) Tribolet, R., Sigel, H., (1987) *Biophys. Chem*., **27**, 119. (d) Corfú, N. A., Tribolet, R., Sigel, H., (1990) *Eur. J. Chem*., **191**, 721. (e) Neurohr, K. J., Mantsch, H. H., (1977) *Can. J. Chem*., **55**, 3620.
9. (a) Ragot, M., Sari, J. C., Belaich, J. P., (1969) *Proc. Natl. Acad. Sci. US*, **64**, 763–770. (b) Sari, J. C., Belaich, J. P., (1973) *J. Am. Chem. Soc*., **95**, 7491–7496. (c) Shanbhag, S. M., Choppin, G. R., (1987) *Inorg. Chim. Acta*, **138**, 187–192. (d) Oms, M. T., Calafat, A. M., Forteza, R., Fiol, J. J., Terrón, A., Cerdá, V., Moreno, V., (1989) *Thermochim. Acta*, **141**, 141–149.
10. (a) Herrero, L. A., Calafat, A. M., Terrón, A., (1991) *Eur.J.Biochem*., **202**, 401–404. (b) Herrero, L. A., Terrón, A., (1995), *Polyhedron*, **14**, 1771. (c) Herrero, L. A., Fiol, J. J., Mas, F., Cerdà, V., Terrón, A., (1996) *Inorg. Chem*., **13**, 3786–3791.
11. a) Cerdà, V., Maimó, J., Estela, J.M., Salvà, A., Ramis, G., (1988) *Talanta*, **35**, 667–699. b) Gazer, F., Buxbaum, P., Papp-Molnar, E., (1974) *J. Inorg. Nucl. Chem*., **36**, 849. c) Herrero, L.A. *Contribucion al Estudio Termodinámico de las Interacciones de Iones Metálicos con Nucleótidos*, Ph D. Doctoral Thesis, 1995, Universitat de les Illes Balears, 07071 Palma de Mallorca (Spain).
12. Burges, J., (1978) *Metal Ions In Solution*, Ellis Horwood, Chichester, England, 299.
13. Antonelli, M. L., Balzano, S., Carunchio, V., Cernia, E. and Purrelo, R., *J.Inorg.Biochem*., 1988, **32,** 153.
14. Arpalahti, J. and Lönnberg, H., *Inorg. Chim. Acta*, 1983, **80,** 25.
15. Yamauchi, O., Odani, A., Masuda, H. and Sigel, H., *Met. Ions Biol. Systems*., 1996, **32,** 207–270.

Pergamon

PII: S0277-5387(98)00136-3

Polyhedron Vol. 17, No. 22, pp. 3835–3839, 1998
© 1998 Elsevier Science Ltd
All rights reserved. Printed in Great Britain
0277–5387/98 $19.00+0.00

Synthesis, structure and electrochemistry of dinuclear copper(II) complex with dinucleating Schiff-base ligand

Wenxing Zhang*, Shangying Liu, Changqin Ma and Dehua Jiang

College of Chemistry, Shandong University, Jinan 250100, P.R. China

(Received 11 November 1997; accepted 18 March 1998)

Abstract—A new ligand, 1,3-di[*o*-(*o*-vanillideneimino)phenoxo]-2-propanol, H_2L, has been prepared stepwise and identified by elemental analyses (EA), IR and ^1H NMR spectra. The title complex $[Cu_2L_2](py)_2(H_2O)_2$ has been synthesized by reaction of H_2L and $Cu(OAc)_2H_2O$, and characterized by EA and IR. The redox properties of the dinuclear complex have been investigated by cyclic voltammetry. Two successive, one-electron, quasi-reversible processes indicate an interaction between two copper centers. The title complex structure is solved by X-ray diffraction. In the centro-symmetric unit $[Cu_2L_2]$, only phenolic and imino groups bind Cu atoms to form two distortional square coordination geometries, parallel to each other; and the Cu···Cu separation is 9.87 Å. © 1998 Elsevier Science Ltd. All rights reserved

Keywords: dinucleating; dinuclear; copper complex; synthesis; structure; cyclic voltammetry.

The dinucleating ligands have been classified as two series in order to study the dinuclear complexes [1]. Being more flexible than the corresponding phenoxo-compartmental ligands, the same series of hydroxo- or alkoxo-comartmental ligands have attracted more attention [2]. Dinuclear copper(II) complexes with these kinds of ligands have been magnetically characterized and structurally determined [3]. In other series of dinucleating ligands, there exist donor sets separated by an organic bridging group. Though the bridges may be non-complete conjugates, the interactions between two copper centers are indicated by the magneto- and/or electrochemical analysis results in the dinuclear complexes with these kinds of ligands [4, 5].

In this paper, the new dinucleating Schiff-base ligand, L^{2-}, belongs formally to compartmental, but in the title complex L^{2-} has selected the other coordination manner (Fig. 1), which is determined by the structural analysis. Although no three oxo atoms, linking the alkyl in the middle of the L^{2-}, coordinate to any atoms, the electro-tranfer action [6] has been confirmed by the cyclic voltammogram results.

* Author to whom correspondence should be addressed. Phone: +86 531 8563949; Fax: +86 531 8565211; E-mail: mcq@sdu.edu.cn.

EXPERIMENTAL

Materials and measurements

All starting materials were commercial products of chemical or analytic grade purity and were used without further purification. Elemental analysis, IR and ^1H NMR spectra were carried out on a Perkin-Elemer 240C microanalyser, a Nicolet 5DX FT–IR spectrophotometer as KBr disks in the range 4000–400 cm^{-1} and a Joel FX902 spectrometer in $CHCl_3$–d_1 solution, respectively.

Syntheses of H_2L

1,3-*di*-(o-*nitrophenoxy*)-2-*propanol* (*dnpp*). *o*-nitrophenol (25 g, 0.18 mol) in 30 cm^3 hot dimethylformamide (DMF) was treated with potassium carbonate (13.8 g, 0.1 mol) added slowly in ~0.5 g portions to the solution 1,3-dichloro-2-propanol (13 g, 0.1 mol) over 10 min. Gentle reflux was continued for 4 h and the resulting deep red mixture was then poured into 300 cm^3 water. The yellowish-brown granular solid was filtered out, washed with sodium hydroxide diluted anhydrous solution and water, then dried *in vacuo*. The product was recrystallized from ethanol.

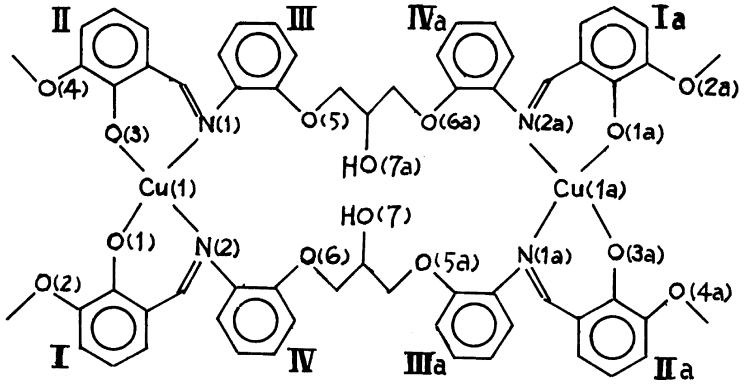

Fig. 1. coordination unit $[Cu_2L_2]$ (Cu, N and O atoms and phenyl rings are numbered).

Yield 55% (16.6 g, 0.050 mol) as yellowish needles. m.p. 127-129°C. Found: C, 53.5; H, 4.1; N, 8.6. Calc. for $C_{15}H_{14}N_2O_7$: C, 54.1; H, 3.9; N, 8.4%. IR (cm^{-1}): 3504 (s, sh, ν(OH)); 1519, 1437 (s, sh, $\nu(NO_2)$); 1254 (s, sh, ν(Ar–O–R)). ^{1}H NMR (δ): 7.80 (s, 1H(OH)); 7.20 (m, 8H(ArH)); 4.38 (s, 4H(CH_2)); 2.44 (br, 1H(CH)).

1,3-*di*(o-*aminophenoxy*)-2-*propanol* (*dapp*). dnpp (6.7 g, 20 mmol) in 100 cm^3 ethanol was refluxed with 5% palladium–carbon (0.6 g), then hydrazine hydrate (85%, 17 cm^3) was added over 30 min and the refluxing was continued until the solution become colorless (>16 h). The filtrate was distilled off *in vacuo* until the volume decreased to ~20 cm^3. The residue was abstracted with chloroform (3×10 cm^3). When the chloroform was evaporated to dryness, an oil with a little red color was obtained from the combined extracts. After several hours, the oil was naturally transformed into granular crystals. The product was recrystallized from ethanol. Yield 44% (2.4 g, 8.8 mmol) as colorless flat hexagonal prism. m.p. 95–97°C. Found: C, 65.8; H, 6.3; N, 10.2. Calc. for $C_{15}H_{18}N_2O_3$: C, 65.9; H, 6.2; N, 10.3%. IR (cm^{-1}): 3454 (s, sh, ν(OH)); 3342, 3195 (s, sh, $\nu(NH_2)$); 1269 (s, sh, ν(Ar–O–)). ^{1}H NMR (δ): 6.75 (m, 8H(ArH)); 4.10 (s, 4H(NH_2)); 3.98 (m, 4H(CH_2)).

H_2L. To a stirred solution of *o*-vanillin (2.64 g, 17.4 mmol) in 20 cm^3 hot ethanol, a solution of dapp (2.38 g, 8.7 mmol) in 20 ml hot ethanol was quickly added dropwise. After several minutes, an orange product was crystallized out. When the temperature of the mixture dropped to ambient, the micro-crystals were filtered out, washed with ethanol and dried in air. The yield (4.2 g, 7.6 mmol) of crude product was 88%, which may be sufficient for use in preparing of the complex described below. Orange colored needle crystals of $H_2L(H_2O)_{0.5}$ were obtained by recrystallization from hot ethanol. m.p. 183–185°C. Found: C, 67.2; H, 5.5; N, 5.4. Calc. for $C_{31}H_{31}N_2O_{7.5}$: C, 67.5; H, 5.6; N, 5.1%. IR (cm^{-1}): 3400 (s, br, ν(OH)); 1620 (s, sh, ν(C=N)); 1254 (s, sh, (Ar–O–R)). ^{1}H NMR (δ): 9.90 (s, 1H (OH)); 8.60 (s, 2H (ArOH)); 6.98 (m, 6H (ArH)); 6.80 (m, 8H (ArH)); 4.46 (m, 1H (CH)); 4.33 (m, 4H (CH_2)); 3.85 (s, 6H (CH_3)).

Preparation and single crystal growth of complex

H_2L (0.55 g, 1 mmol) was added slowly in portions to a stirred solution of $Cu(OAc)_2 H_2O$ (0.20 g, 1 mmol) in 50 ml methanol at room tempreture. After the mixture was refluxed for 5 h, the greater part of the solvent was distilled off. The resulted brown powder was filtered out, washed with methanol and dried *in vacuo*.

The powder was redissolved in a appropriate amount of hot pyridine. The dark red crystals $[Cu_2L_2](py)_2(H_2O)_2$, suitable for X-ray structure determination, were obtained by natural evaporation of the solvent for 1 week. Found: C, 61.2; H, 4.9; N, 6.2. Calc. for $C_{72}H_{70}N_6O_{16}Cu_2$: C, 61.6; H, 5.0; N, 6.0%. IR (cm^{-1}): 3390 (m, sh(OH)); 1639, 1610 (s, sh, ν(C=N)); 1242 (vs, sh, ν(Ar–O–R)).

Cyclic voltammetry

Apparatus and set-up. Cyclic voltammetry (CV) was performed with an MF-1A versatile voltamperemeter. Cyclic voltammograms were recorded with an X-Y recorder (LZ3). An aqueous saturated calomel electrode (SCE) as reference, platinum wire as a counter and platinum plate as a working electrode constituted a three electrode system. The platinum plate and wire electrode were immersed in a dilute solution of nitric acid before each experiment. The SCE was separated from the solution by a double bridge containing the supporting electrolyte adjacent to the SCE. Additionally, the internal resistance inherent in the used set-up, DMF and the carrier adjacent to the solution was regulated in order to minimize liquid–liquid junction potentials.

Compounding of electrolyte. DMF, dried over anhydrous magnesium sulfate and redistilled off under vacuum, was used as the solvent in the experiments. Tetrabutylammonium perchlorate (TBAP) was

employed as the supporting electrolyte in a 0.1 mol dm^{-3} concentration. TBAP was made from equivalent TBA bromide and perchloric acid in water, filtered off, washed, dried and recrystallized from ethyl acetate–*n*-hexane (1:1). The sample of $[Cu_2L_2](py)_2(H_2O)_2$ was quantitatively dissolved in the supporting electrolyte to obtained the electrolyte in 1×10^{-3} mol dm^{-3} concentration used to CV experiments. It was bubbled with nitrogen for 5 min prior to every measurement and all experiments were performed at 20 ± 0.2°C.

X-ray structure determination

Crystal data. $C_{72}H_{70}N_6O_{16}Cu_2$, Mr = 1402.47, triclinic, space group *P*1 (#2). $a = 10.154(4)$, $b = 12.061(5)$, $c = 14.449(7)$ Å, $\alpha = 104.47(3)$, $\beta = 90.57(4)$, $\gamma = 110.65(7)°$, $V = 1595(3)$Å^3, $Z = 1$, $D_c = 1.460$ g cm^{-3}, $F(000) = 730$, $\mu = 7.413$ cm^{-1}.

Data collection and refinement of crystal structure. A single crystal of dimensions $0.25\times0.3\times0.3$ mm was mounted on a glass fibre. The diffraction data were collected on an Enraf–Nonius CAD4 four-circle diffractometer with graphite-monochromated Mo–Kα radiation ($\lambda = 0.71073$ Å) using an $\omega-2\theta$ scan mode with ω scan width $0.8+0.35tg\theta$, scan rate 0.92–5.49° min^{-1}. A total of 4128 independent reflections were collected in the range $2 < \theta < 23°$, of which 2002 reflections with $I > 3\sigma(I)$ were used in the structure determination and refinement after *Lp* and empirical absorption corrections. The structure was solved by direct methods (Multan 82). All non-hydrogen atoms were located from an *E*-map and determined with successive difference Fourier syntheses. Hydrogen atoms were introduced in calculated positions but not refined. The final refinement of full matrix least-squares with anisotropic thermal parameters gave $R = 0.072$, $R_w = 0.079$ $(w = 1/\sigma^2(F_o))$, $(\Delta/\sigma)_{max} = 0.34$, $S = 2.64$. The maximum and minimum residuals had heights of 0.74 and -0.49 e Å^{-3}. All calculations were performed using the programs contained in the SDP–PLUS package.

RESULTS AND DISCUSSION

IR spectra

The symmetric and asymmetric stretching frequencies of NH_2 appear in the infrared spectrum of dapp, but none of these reappear in H_2L. As supersedure, a strong sharp peak is represent at 1620 cm^{-1}, designated as the stretching model of C═N, that means to complete the Schiff-base condensation. As contrasted with the ligand H_2L in the spectrum of the title complex $[Cu_2L_2](py)_2(H_2O)_2$, two significant changes occur: the sharpening of one absorption band at ~3400 cm^{-1} and the splitting apart of another band from 1620 cm^{-1} into 1639 and 1610 cm^{-1}. The former indicates that neither coordinated nor associated (*e.g.*, by hydrogen bond) hydroxy groups exist in the complex molecule; the latter shows that the imino group takes part in the coordination with the copper(II) atom.

Cyclic voltammetry

The cyclic voltammograms of $[Cu_2L_2](py)_2(H_2O)_2$ are drawn in Fig. 2. The redox processes of two metal centers, corresponding to two distinct couples, A and B in the curve, can be expressed as

$$\text{A}\quad \text{Cu(II)Cu(II)} \underset{-e}{\overset{+e}{\rightleftarrows}} \text{Cu(II)CuI},$$

$$\text{B}\quad \text{Cu(II)Cu(I)} \underset{-e}{\overset{+e}{\rightleftarrows}} \text{Cu(I)CuI}.$$

Relevant CV data are listed in Table 1. It was tentatively assigned that the processes are one-electron two-step successive and quasi-reversible, judging from the ΔE_p and i_{pa}/i_{pc} (≈1) values of each couple. Cathodic peak E_{pc}, anodic peak E_{pa} and approximate redox

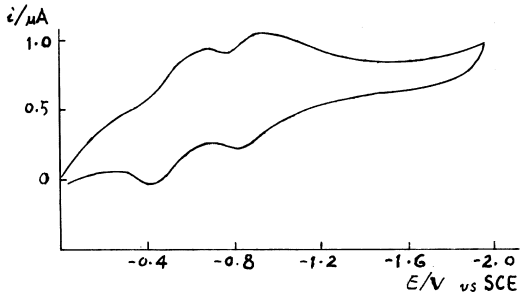

Fig. 2. Cyclic voltammetry of $[Cu_2L_2](py)_2(H_2O)_2$ in DMF at scan rate 0.1 Vs^{-1}.

Table 1. Cyclic voltammetric data of $[Cu_2L_2](py)_2(H_2O)_2$

Couple A/V				Couple B/V					
E_{pc}	E_{pa}	ΔE_p*	$E^o_{1/2}$*	E_{pc}	E_{pa}	ΔE_p*	$E^o_{1/2}$*	$\Delta E^o_{1/2}$*/V	K_{con}*
−0.66	−0.43	0.23	−0.55	−0.88	−0.80	0.08	−0.84	0.29	8.0×10^4

*$\Delta E_p = E_{pa}-E_{pc}$, $E^o_{1/2} = (E_{pa}-E_{pc})/2$, $\Delta E^o_{1/2} = E^o_{1/2}(A)-E^o_{1/2}(B)$.
$K_{con} = [Cu(II)Cu(I)]^2/[Cu(II)Cu(II)][Cu(I)Cu(I)] = \exp[nF(\Delta E^o_{1/2})/RT]$.

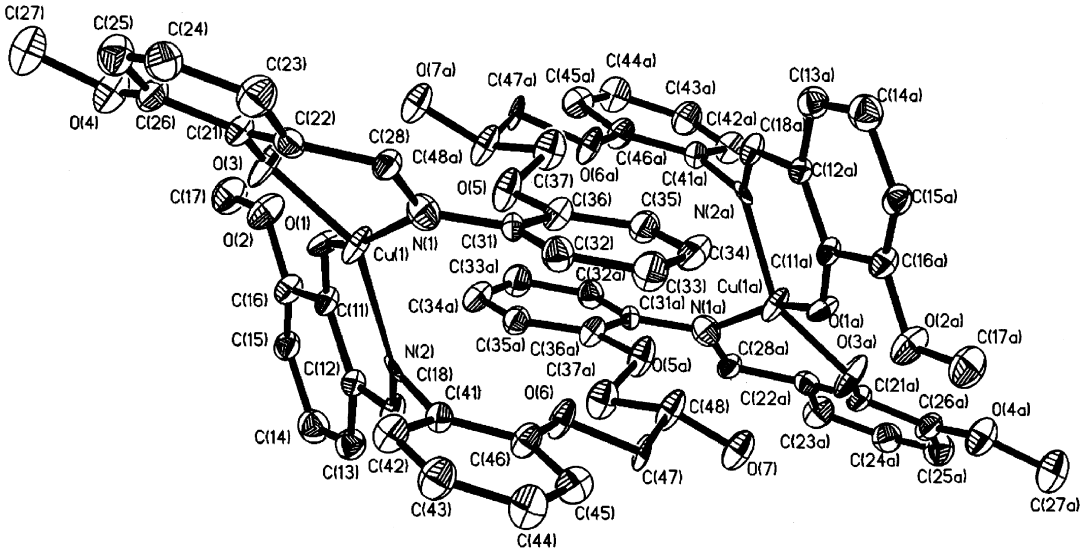

Fig. 3. The crystal structure of the dimer unit $[Cu_2L_2]$.

potential $E_{1/2}$ are all displayed within normal ranges [5, 7]; $E^0_{1/2}$ and K_{con} values, implying stability of the mixed valence state Cu(II)Cu(I), are comparable with those of the literature [7].

It is known that non interacting metal centers in similar environments do not have a $\Delta E^0_{1/2}$ separation larger than 50 mV [8]. The wave splitting magnitude of a few hundred millivolts (here it is 290 mV) should result from the weak Cu···Cu interaction in the present dinuclear complex [6].

Structure

The unit cell contains two congruent pyridine and two water molecules in the crystal, as well as a centrosymmetric dimer unit $[Cu_2L_2]$, which is displayed in Fig. 3. The geometry at each copper(II) center is best described as tetrahedral distorted square planar, being close to D_{2d}. At Cu(1), the *trans* atoms, O(1) and N(1), from two different L^{2-} lie 0.4383 Å and 0.4048 Å, respectively, above the plane, though four donor atoms (see plane V in Table 3), while O(3) and N(2) sit 0.4452 Å and 0.3979 Å, respectively, below this plane; Cu(1) is nearly in the plane, lying 0.0638 Å (Cu(1a), 6.7646 Å away) above. The shortest separation between copper atoms in the crystal lattice is 8.14 Å, but the Cu(1)···Cu(1a) distance in the same dimer is 9.87 Å. The coordinated bond lengths (see Table 2) are approximate to these of an analogous complex [9].

The alkyl group in the middle of L^{2-} are tortured to such a degree that no three oxo atoms bonding to this alkyl, O(5)–O(7), coordinate to any copper. Two phenyl rings separated by one alkyl group, plane III and IVa or IIIa and IV, are inclined at an angle of 9.9°; but two neighboring rings on the same end of one alkyl, plane I and IV or II and III, are at 112.2° or 31.7°. A common consequence of this twisting and the above torturing is that two coordination planes at Cu(1) and Cu(1a), V and Va, are parallel at an interplanar separation of 6.79 Å. It seems that this coordination configuration of the molecule induces the redox behaviors as two couples in the CV curve (*vide supra*). The literature [5] has inferred that face-to-face stacking of coordination planes may stabilize the Cu(II)Cu(I) state in a homodinuclear complex molecule.

In the discussion on CV, the existence of weak

Table 2. Coordination bond lengths (Å) and angles (°)

Cu(1)–O(1)	1.917(6)	Cu(1)–N(1)	1.965(6)
Cu(1)–O(3)	1.890(5)	Cu(1)–N(2)	1.956(6)
O(1)–Cu(1)–O(3)	88.8(2)	O(3)–Cu(1)–N(2)	150.3(2)
O(3)–Cu(1)–N(1)	91.7(2)	O(1)–Cu(1)–N(2)	92.0(2)
O(1)–Cu(1)–N(1)	158.0(2)	N(1)–Cu(1)–N(2)	98.3(2)

Table 3. Least square planes ($Ax+By+Cz+D=0$)

No.	In-plane atoms	A	B	C	D
I*	C(11)–C(16)	−0.556	0.747	−0.364	−1.776
II*	C(21)–C(26)	0.941	−0.278	−0.190	2.65
III*	C(31)–C(36)	0.721	−0.158	−0.675	4.09
IV*	C(41)–C(46)	0.677	−0.323	−0.661	1.82
V	O(1),O(3),N(1),N(2)	−0.7742	0.5875	−0.2398	1.5373
Va	O(1a),O(3a),N(1a),N(2a)	−0.7742	0.5875	−0.2398	8.3657

*I–IV have their own centrosymmetric planes Ia–IVa, respectively, that are not listed.

Cu···Cu interactions was suggested and here its contributing factor was conjectured on the face-to-face crystal structure. But another possibility should be considered: there may be a transferred structure in the electrolyte solution used for CV experiments.

Acknowledgements—The project was supported by the Natural Science Foundation of Shandong Province.

REFERENCES

1. Casellato, U., Vigato, P. A., Fenton, D. E. and Vidali, M., *Chem. Soc. Rev.*, 1979, **8,** 199.
2. Zanello, P., Tamburini, S. and Vigato, P. A., *Coord. Chem. Rev.*, 1987, **77,** 165.
3. (a) Nishida, Y., Takeuchi, M., Kida, S., *Chem.Lett.*, 1983, 1815; (b) Nishida, Y., Takeuchi, M., Kida, S., *Chem.Lett.*, 1985, 631.
4. Whitmore, B. C. and Eisemberg, R. E., *Inorg. Chem.*, 1983, **22,** 1.
5. Izumitani, T., Nakamura, M. and Okawa, H., Kida, S., *Bull. Chem. Soc. Jpn.*, 1982, **55,** 2122.
6. Zacharias, P. S. and Ramachandraiah, A., *Polyhedron*, 1985, **4,** 1013.
7. Mandal, S. K., Thompson, L. K., Nag, K., Charland, J.-P. and Gabe, E. G., *Inorg. Chem.*, 1987, **26,** 1391.
8. Ammar, F. and Saveant, J. M., *J. Electroanal. Chem.*, 1973, **47,** 115.
9. Bear, C. A., Waters, J. M. and Waters, T. N., *J. Chem. Soc.*, 1970, A2494.

Pergamon

PII: S0277–5387(98)00139–9

Polyhedron Vol. 17, No. 22, pp. 3841–3849, 1998
© 1998 Elsevier Science Ltd
All rights reserved. Printed in Great Britain
0277–5387/98 $19.00+0.00

Synthesis and structures of tris(pyrazolyl)hydroborato metal complexes as structural model compounds of carbonicanhydrase

Shengli Guo,[a] Errun Ding,[a] Yuanqi Yin*[a] and Kaibei Yu[b]

[a]Lanzhou Institute of Chemical Physics, Academia Sinica, Lanzhou 730000, P.R. China

[b]Chengdu Institute of Organic Chemistry, Academia Sinica, Chengdu 610041, P.R. China

(Received 15 July 1997; accepted 31 March 1998)

Abstract—A series of tris(pyrazoly)hydroborato metal complexes [η^3-HB(3-R^1-5-R^2pz)$_3$]MX (R^1 = Ph, 2′-thienyl, R^2 = CH_3, Ph; M = Ni, Cu, Zn, Cd; X = Cl^-, NO_3^-, CH_3COO^-) and [η^3-HB(3-Ph-5-Mepz)$_3$](3-Me-5-Phpz)Cu(PhCOO), **8**, had been synthesized and characterized. Among them, the complexes [η^3-HB(3,5-Ph_2pz)$_3$]NiCl (**3**), [η^3-HB(3-Ph-5-Mepz)$_3$]Cd(NO_3)(THF) (**4**) and **8** were analyzed by X-ray crystal structure determination, which revealed the bidentate coordination of NO_3^- in complex **4** and isomerized ligands in complex **8**. As model compounds of carbonic anhydrase (CA), the structures of these complexes were contrasted to that of the active site of CA: the derivative chloro may be the closest model compounds among them. The relationship between the coordination modes of X (X = NO_3^-, CH_3COO^-, $PhCOO^-$) in complexes and their IR spectra was also discussed. © 1998 Elsevier Science Ltd. All rights reserved

Keywords: tris(pyrazolyl)hydroborato; metal complexes; crystal structure.

INTRODUCTION

The tris(pyrazoly)hydroborato ligand, $[HB(pz)_3]^-$, has played an important role in modeling metalloenzyme active sites since 1980. Its metal complexes have been employed in the carbonic anhydrase (CA), haemocyanin, tyrosinase, non-heme iron proteins and the polymanganese site of the photo-system II oxygen-evolving center [1–5]. The active site structure of CA has two key features: one is four-coordinated distorted tetrahedral of zinc center and the other is unidentate coordination mode of bicarbonate binding to zinc, which often acts as an important intermediate in the reaction [6]: $CO_2 + H_2O \rightarrow HCO_3^- + H^+$. When bulky substituents, e.g. t-Bu, Ph and isopropyl are in the 3-position of the pyrazole ring of $[HB(pz)_3]^-$ these prevent the binding of a second equally hindered tridentate ligand and a four-coordination complex is generally formed with a single axial ligand [1, 7]. Our recent works centered on studying a series of anion X (X = Cl^-, NO_3^-, CH_3COO^-, $PhCOO^-$) derivatives of some metals [HB(pz)$_3$]MX, on the basis that structural changes would indicate the relative tendencies of different metal centers to favour unidentate vs bidentate coordination for X. In this paper, we describe the synthesis and structures of some anion (X) derivatives of certain metals that are supported by tris (pyrazolyl)hydroborato ligation (Scheme 1). In particular, the structural similarity of halide derivatives to the active site of CA, the coordination modes of X (X ≠ Cl) in the complexes will be of central importance. The activity of these model complexes to catalyze reversible hydration reaction of CO_2 is being tested in our laboratory.

EXPERIMENTAL

Materials and physical measurements

All reagents were A.R. grade and used without further purification. ^{1}H NMR spectra (δ, ppm) were rec-

* Author to whom correspondence should be addressed.

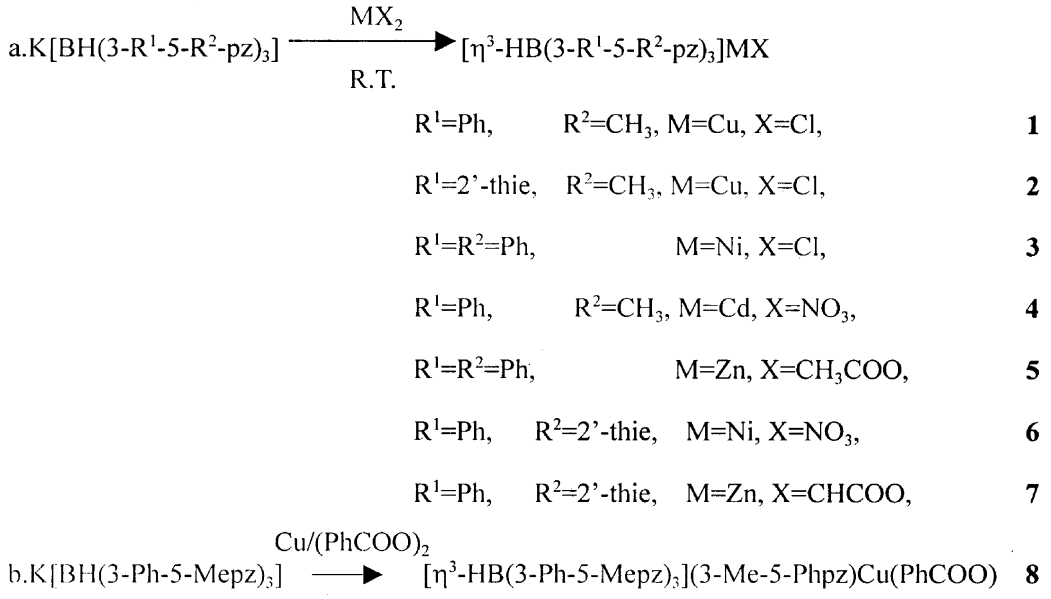

Scheme 1.

orded on a Bruker AM-400A spectrometer. IR spectra were obtained from KBr disks using a Nicolet-10DX FT-IR instrument. Elemental analyses were obtained by using a Vario EL elemental analyzer.

The tridentate ligands $K[BH(3\text{-}R^1\text{-}5\text{-}R^2\text{-}pz)_3]$ (R^1 = Ph, 2′-thienyl, R^2 = Ph, CH_3) were prepared and characterized as previously described [8].

Preparation of complexes **1**–**7**

To a solution of $K[BH(3\text{-}R^1\text{-}5\text{-}R^2\text{-}pz)_3]$ (2.0 mmol) in THF (10 cm^3) was added a solution of metal salt (2.3 mmol) in THF (20 cm^3), the mixture was stirred at room temperature for 12 h and filtered. The solvent was removed from the filtrate under reduced pressure and the residue obtained was washed with hexane, crystallized from appropriate solvents (see below) and isolated by filtration, washed and dried *in vacuo*.

(**1**) (CH_3COCH_3): IR: 2540(ν_{B-H}), 1365(δ_{CH3}), 759($\gamma_{=CH}$), 692(δ_{ring} of Ph). ^{1}H NMR ($CDCl_3$): 7.65–7.21 (m, 15H, Ph), 6.22 (s, 3H, pz), 2.62 (s, 9H, CH_3).

(**2**) (CH_3Ph/CH_3COCH_3): IR: 2528(ν_{B-H}), 1371(δ_{CH3}), 854,697(thienyl). ^{1}H NMR (CD_3CN): 7.92 (m, 3H, α H of thienyl), 7.50–7.36 (m, 5H, Ph of CH_3Ph), 7.23 (m, 6H, β H of thienyl), 6.26 (s, 3H, pz), 2.66 (s, 9H, 5-CH_3), 2.33 (s, 3H, CH_3 of CH_3Ph).

(**3**) [CH_2Cl_2/CH_3CN (2:1)]: IR: 2612(ν_{B-H}), 758($\gamma_{=CH}$ of Ph), 694(δ_{ring} of Ph). ^{1}H NMR (DMSO): 7.57 (m, 12H, ortho H of Ph), 6.97 (m, 18H, *meta*, *para* H of Ph), 6.48 (s, 3H, pz).

(**4**) (Pentane/THF): IR: 2546(ν_{B-H}), 1495[$\nu_a(NO_2)$], 1265($\nu_{N=O}$), 1028[$\nu_s(NO_2)$]. ^{1}H NMR ($CDCl_3$):7.50 (m, 6H, *ortho* H of Ph), 7.22 (m, 9H, *meta*, *para* H of Ph), 6.21 (s, 3H, pz), 3.64 (m, 4H, α H of THF), 2.56 (s, 9H, CH_3), 1.76 (m, 4H, β H of THF).

(**5**) [CH_3CN/CH_2Cl_2 (3:2)]: IR:2650(ν_{B-H}), 1550($\nu_{C=O}$), 1466(ν_{C-O}), 758($\gamma_{=CH}$ of Ph), 694(δ_{ring} of Ph). ^{1}H NMR ($CDCl_3$): 7.68 (m, 12H, *ortho* H of Ph), 7.01 (m, 18H, *meta*, *para* H of Ph), 6.48 (s, 3H, pz), 1.62 (s, 3H, CH_3COO).

(**6**) [THF/EtOH (1:1)]: IR: 2631(ν_{B-H}), 1486[$\nu_a(NO_2)$], 1281($\nu_{N=O}$), 1010[$\nu_s(NO_2)$]. ^{1}H NMR ($CDCl_3$): 7.62 (m, 6H, *ortho* H of Ph), 7.44–7.09 (m, 12H, *meta*, *para* H of Ph and α H of thienyl), 6.96 (m, 6H, β H of thienyl), 6.43 (s, 3H, pz).

(**7**) [CH_3CN/CH_2Cl_2 (1:1)]: IR: 2630(ν_{B-H}), 1569($\nu_{C=O}$), 1449(ν_{C-O}), 764($\gamma_{=CH}$ of Ph), 696(δ_{ring} of Ph). ^{1}H NMR ($CDCl_3$): 7.68 (m, 6H, *ortho* H of Ph), 7.45–7.11 (m, 12H, *meta*, *para* H of Ph and α H of thienyl), 6.98 (m, 6H, β H of thienyl), 6.44 (s, 3H, pz), 1.62 (s, 3H, CH_3COO).

Preparation of complex **8**

At room temperature, an equal amount (20 mmol) of copper (0.32 g), dibenzoyl peroxide (1.21 g), and tris[3(5)-phenyl-5(3)-methyl pyrazolyl] hydroborato potassium (0.79 g) were mixed with 200 cm^3 of acetone and stirred for 30 h. A green solid was yielded and isolated by filtration, recrystallized from ethanol, filtered, washed with benzene and dried in air. IR data: 2519(ν_{B-H}), 1593($\nu_{C=O}$), 1312(ν_{C-O}), 1389(δ_s of CH_3), 764($\gamma_{=CH}$ of Ph), 694(δ_{ring} of Ph). ^{1}H NMR ($CDCl_3$): 8.42 (m, 5H, PhCOO), 7.91 (m, 8H, *ortho* H of Ph), 7.48 (m, 12H, *meta*, *para* H of Ph), 6.21 (s, 4H, pz), 2.59 (s, 12H, CH_3).

Table 1. The physical properties and elemental analyses of the complex

No.	Colour	Yield (%)	M.p. (°C)	Found (%) (calcd. values, %)			
				C	H	N	S
1	dark green	34.7	221–222	62.04 (61.87)	4.76 (4.81)	14.35 (14.44)	–
2	yellow green	26.8	152–153	53.78 (53.76)	4.16 (4.33)	12.28 (12.14)	13.92 (13.90)
3	pale purple	28.6	>350	70.57 (70.78)	4.38 (4.46)	11.23 (11.01)	–
4	colorless	39.8	224–225 (dec.)	56.03 (55.90)	4.87 (4.93)	13.39 (13.43)	–
5	colorless	74.2	174–176 (subl.)	70.93 (71.10)	4.48 (4.66)	10.67 (10.59)	–
6	pale green	46.2	>350	57.69 (57.94)	3.39 (3.47)	12.08 (12.13)	12.13 (11.91)
7	colorless	40.8	302–303	60.74 (60.63)	3.67 (3.82)	10.41 (10.35)	11.72 (11.86)
8	green	36.2	215–216	68.27 (68.35)	5.11 (5.23)	12.87 (13.02)	–

The physical properties and elemental analyses of the complexes **1**–**8** were listed in Table 1.

Crystal structure determination

Data collection was performed with MoKα radiation ($\lambda = 0.71073$ Å) on a Siemens P4 diffractometer with data reduction using the Siemens SHELXTL program system. Experimental details for the structure determination of **3**, **4** and **8** are summarized in Table 2, while Tables 3 and 4 give a listing of selected bond lengths and angles, respectively. A perspective view of **3**, **4** and **8** are presented in Fig. 1(a), Fig. 2(a) and Fig. 3(a). The maps of crystal packing in unit cell of them are given in Fig. 1(b), Fig. 2(b) and Fig. 2(b).

RESULTS AND DISCUSSION

IR spectra

From IR spectra of the complexes, we could find the characteristic vibration peaks of BH, Me, Ph, thienyl and pyrazolyl groups, besides we may also assign certain peaks to the stretching vibration of coordinated NO_3^-, CH_3COO^- and $PhCOO^-$. According to Nakamoto's proposal [9], there is a close relation between the coordination modes of X- and its IR spectra (see Tables 5 and 6). We believe all of complex **4** and **6** conclude the bidentate coordination mode of nitrate and the last has been tested directly by X-ray crystal determination. The results revealed from Table 6, that the value of $[\nu_{(C=O)} - \nu_{(C-O)}]$ of bridged carboxylate was

Table 2. Crystal and intensity collection data

Compound No.	**3**	**4**	**8**
Chemical formula	$C_{45}H_{34}N_6BClNi$	$C_{34}H_{36}N_7BO_4Cd$	$C_{49}H_{45}N_8BO_{2.5}Cu$
Formula weight	762.9	729.9	860.3
Crystal size (mm)	$0.56 \times 0.50 \times 0.40$	$0.60 \times 0.46 \times 0.40$	$0.58 \times 0.46 \times 0.46$
Lattice	rhombohedral	triclinic	triclinic
Space group	R3	P$\bar{1}$	P$\bar{1}$
Cell constants			
a (Å)	12.9120(12)	11.3030(10)	12.722(2)
b (Å)	12.9120(12)	12.099(2)	13.068(2)
c (Å)	19.323(3)	12.607(2)	15.857(3)
α (°)	90	102.050(10)	68.090(10)
β (°)	90	91.780(10)	74.140(10)
γ (°)	120	93.620(10)	80.370(10)
V (Å^3)	2790.0(6)	1681.0(4)	2345.4(7)
Z	9	2	2
Dc (g·cm^{-3})	1.364	1.442	1.218
μ (mm^{-1})	0.636	0.698	0.513
2θ range (°)	4.2–52.0	3.3–48.0	3.86–50.0
No. of data	1318	5229	8060
No. of parameters	210	544	680
Goodness of fit on F^2	0.990	1.067	0.914
$R1$	0.0270	0.0302	0.0459
$wR2$	0.0580	0.0805	0.1152

Table 3. Selected bond lengths (Å)

	3		**4**			**8**	
Ni–Cl	2.200(2)	Cd–O(1)	2.334(3)	Cu–O(1)	1.968(2)	N(7)–N(8)	1.360(3)
Ni–N(2)	2.038(2)	Cd–O(2)	2.356(3)	Cu–N(2)	2.030(3)	N(8)–C(34)	1.334(4)
N(1)–C(7)	1.359(4)	Cd–N(1)	2.282(3)	Cu–N(4)	2.266(3)	C(4)–C(5)	1.476(4)
N(1)–N(2)	1.369(3)	Cd–N(3)	2.316(3)	Cu–N(6)	2.028(3)	C(41)–O(1)	1.267(4)
N(1)–B	1.544(3)	Cd–N(5)	2.300(3)	Cu–N(7)	2.016(3)	C(41)–O(2)	1.254(4)
N(2)–C(9)	1.350(4)	N(7)–O(3)	1.218(4)	N(1)–C(2)	1.345(4)	C(33)–C(34)	1.385(5)
C(6)–C(7)	1.475(4)	N(7)–O(1)	1.266(5)	B–N(1)	1.544(4)	C(32)–C(33)	1.393(5)
C(7)–C(8)	1.380(5)	N(7)–O(2)	1.236(5)	B–N(3)	1.526(5)	N(7)–C(32)	1.344(4)
C(8)–C(9)	1.392(5)	B–N(2)	1.550(5)	B–N(5)	1.548(5)	N(2)–C(4)	1.332(4)
C(9)–C(10)	1.475(4)	B–N(4)	1.541(5)	N(1)–N(2)	1.379(3)	C(3)–C(4)	1.400(5)
B–N(6)	1.553(5)	C(1)–C(2)	1.501(4)	C(2)–C(3)	1.364(5)		
Cd–O(4)	2.391(2)	N(3)–C(12)	1.359(4)	N(5)–C(22)	1.353(4)		

Table 4. Selected bond angles (°)

	3		**4**		**8**
N(2)–Ni–Cl	123.20(7)	O(1)–Cd–O(2)	53.78(12)	O(1)–Cu–N(7)	95.83(10)
N(2A)–Ni–Cl	123.20(7)	Cd–O(1)–N(7)	95.2(3)	O(1)–Cu–N(6)	161.79(10)
N(2B)–Ni–Cl	123.20(7)	Cd–O(2)–N(7)	95.0(3)	N(7)–Cu–N(6)	89.64(10)
N(2A)–Ni–N(2)	92.88(9)	N(1)–Cd–O(1)	162.38(12)	O(1)–Cu–N(2)	89.12(9)
N(2A)–Ni–N(2B)	92.88(9)	N(3)–Cd–O(1)	102.96(11)	N(7)–Cu–N(2)	173.89(11)
N(2B)–Ni–N(2)	92.88(9)	N(5)–Cd–O(1)	106.71(12)	N(6)–Cu–N(2)	84.57(10)
C(7)–N(1)–N(2)	109.8(2)	N(1)–Cd–O(2)	109.46(11)	O(1)–Cu–N(4)	102.30(9)
C(7)–N(1)–B	128.0(3)	N(1)–Cd–O(4)	84.11(9)	N(7)–Cu–N(4)	93.84(10)
N(2)–N(1)–B	120.0(3)	N(3)–Cd–O(4)	167.09(9)	N(6)–Cu–N(4)	94.62(10)
C(9)–N(2)–N(1)	107.0(2)	N(5)–Cd–O(4)	91.22(9)	N(2)–Cu–N(4)	88.59(10)
C(9)–N(2)–Ni	141.3(2)	O(1)–Cd–O(4)	89.91(11)	C(41)–O(1)–Cu	132.9(2)
N(1)–N(2)–Ni	111.8(2)	O(2)–Cd–O(4)	89.56(11)	N(2)–N(1)–B	121.1(2)
N(1A)–B–N(1B)	108.9(2)	N(2)–B–N(4)	109.5(3)	C(4)–N(2)–N(1)	106.6(2)
N(1A)–B–N(1)	108.9(2)	N(2)–B–N(6)	111.2(3)	C(4)–N(2)–Cu	138.0(2)
N(1B)–B–N(1)	107.4(3)	N(3)–Cd–O(2)	97.16(11)	N(4)–N(3)–B	119.6(2)
C(7)–C(8)–C(9)	106.7(3)	N(5)–Cd–O(2)	160.48(12)	C(14)–N(4)–Cu	139.3(2)
N(2)–C(9)–C(8)	109.2(3)	N(1)–Cd–N(3)	83.26(10)	N(3)–N(4)–Cu	111.5(2)
N(1)–C(7)–C(6)	123.0(3)	N(1)–Cd–N(5)	90.01(9)	C(22)–N(5)–B	131.0(3)
C(6)–C(7)–C(8)	129.6(3)	N(3)–Cd–N(5)	86.12(9)	N(6)–N(5)–B	119.4(2)
O(3)–N(7)–O(1)	119.7(5)	C(24)–N(6)–Cu	135.7(2)		
O(3)–N(7)–O(2)	124.3(5)	N(5)–N(6)–Cu	116.2(2)		
O(1)–N(7)–O(2)	116.0(3)	N(8)–N(7)–Cu	118.3(2)		
N(3)–B–N(1)	110.6(3)				
N(3)–B–N(5)	110.1(3)				
N(5)–B–N(1)	107.9(3)				

a medium between that of unidentate and bidentate were also much more accordant with his conclusion.

Origination and isomerization of ligand (3-*methyl*-5-*phenylpyrazole*) *in* **8**

The preparation of complex **8** by a similar method employed to **1**–**7** was unsuccessful and this spurred us on to find a new synthetic method. We inferred that the ligand (3-methyl-5-phenylpyrazole) in **8** may come from the very minor impurity of reactant K[BH(3-Ph-5-Mepz)$_3$].

From bond length data [N(7)–C(32) = 1.344(4) Å, N(8)–C(34) = 1.334(4) Å], we could not distinguish which N atom is 1-position of pyrazole ring formed by N(7), N(8) and other three carbon atoms. However, the structure determination shows that this is much in line with the coordination situation of nitrogen-containing heterocyclic compounds. Therefore, this ligand would be 3-methyl-5-phenyl pyrazole which was an isomer of 3-phenyl-5-methyl pyrazole existing in another ligand [η^3-HB(3-Ph-5-Mepz)$_3$]. Due to a small hindrance of the methyl group, KBH_4 preferentially attacks the NH group of isomer I, instead

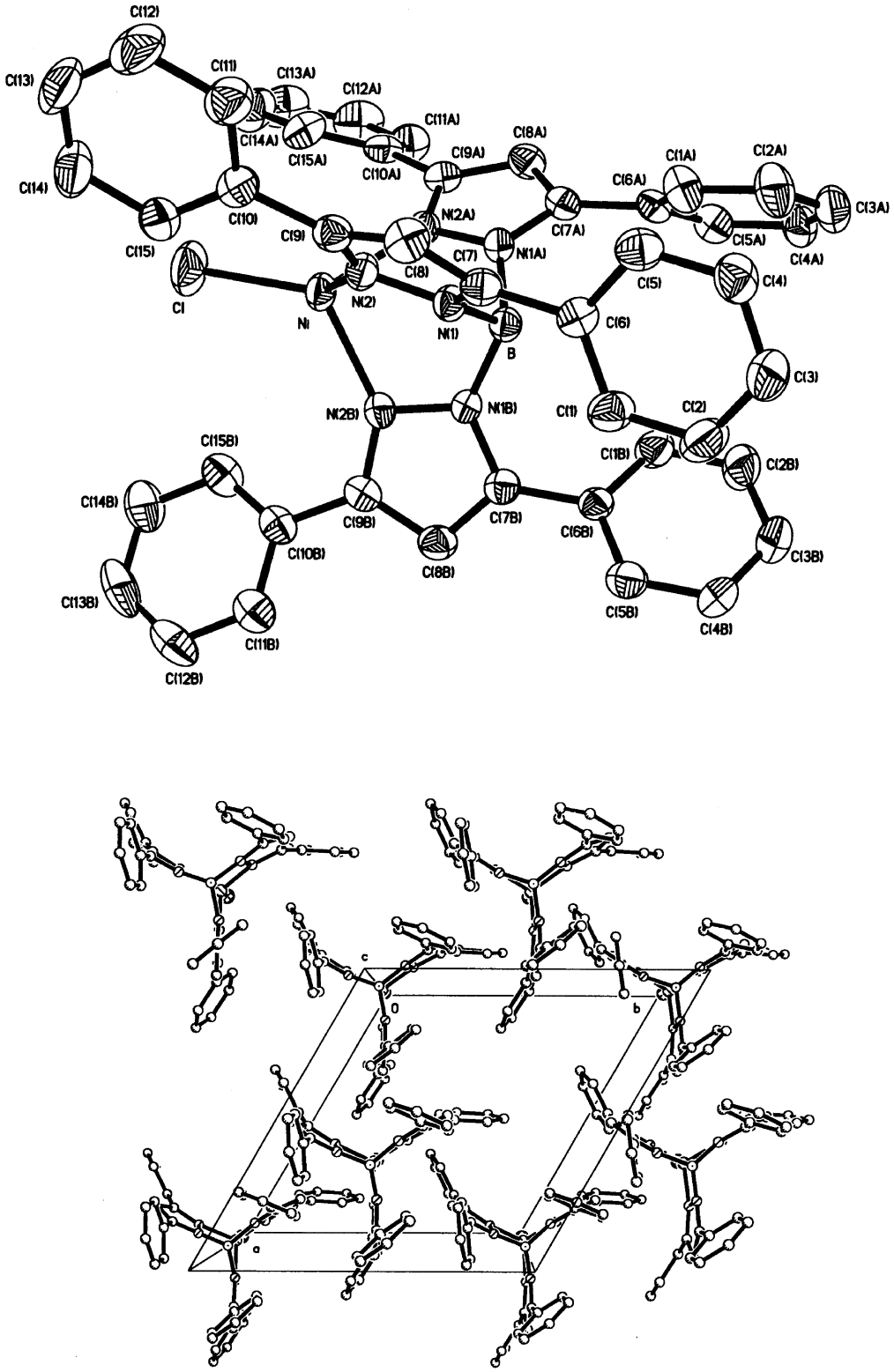

Fig. 1. (a) The molecular structure of complex **3**. (b) The map of crystal packing in unit cell for complex **3**.

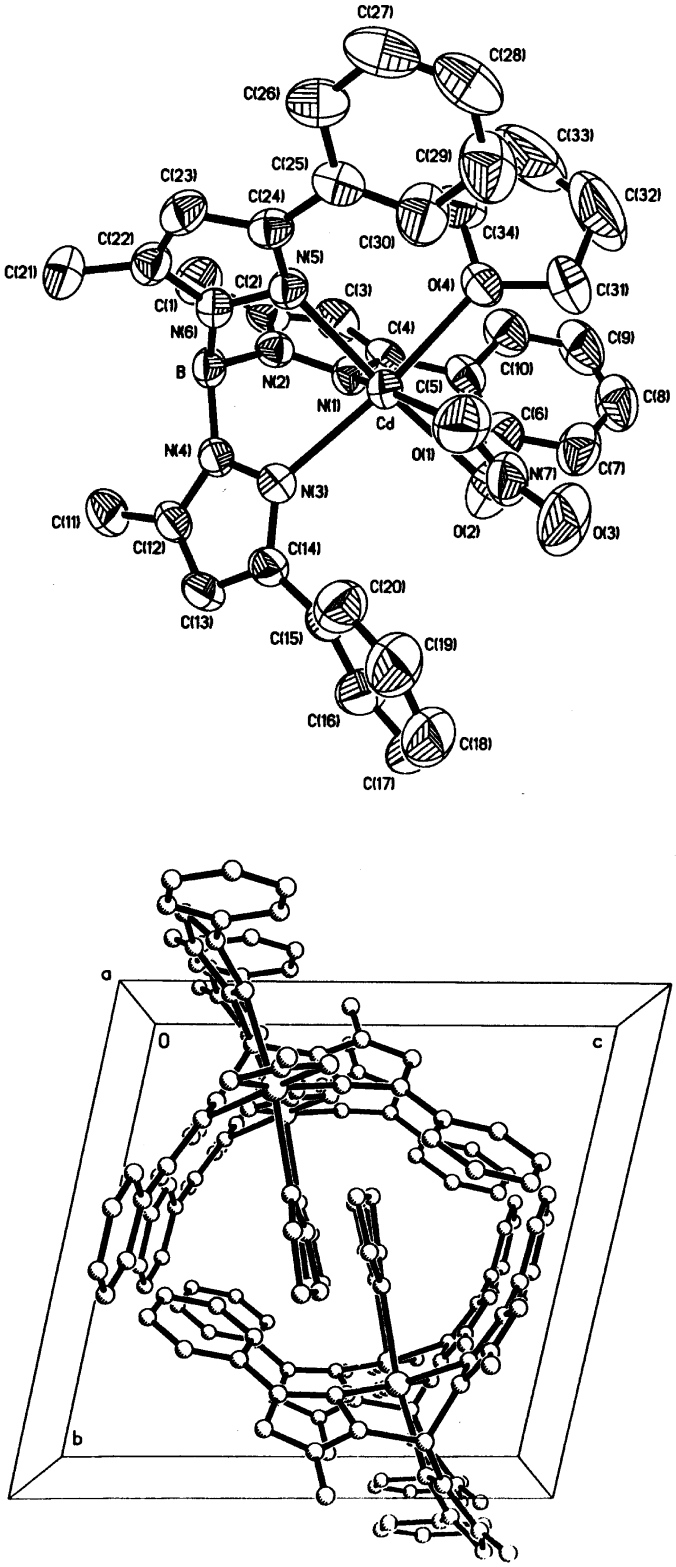

Fig. 2. (a) The molecular structure of complex **4**. (b) Unit cell packing diagram for complex **4**.

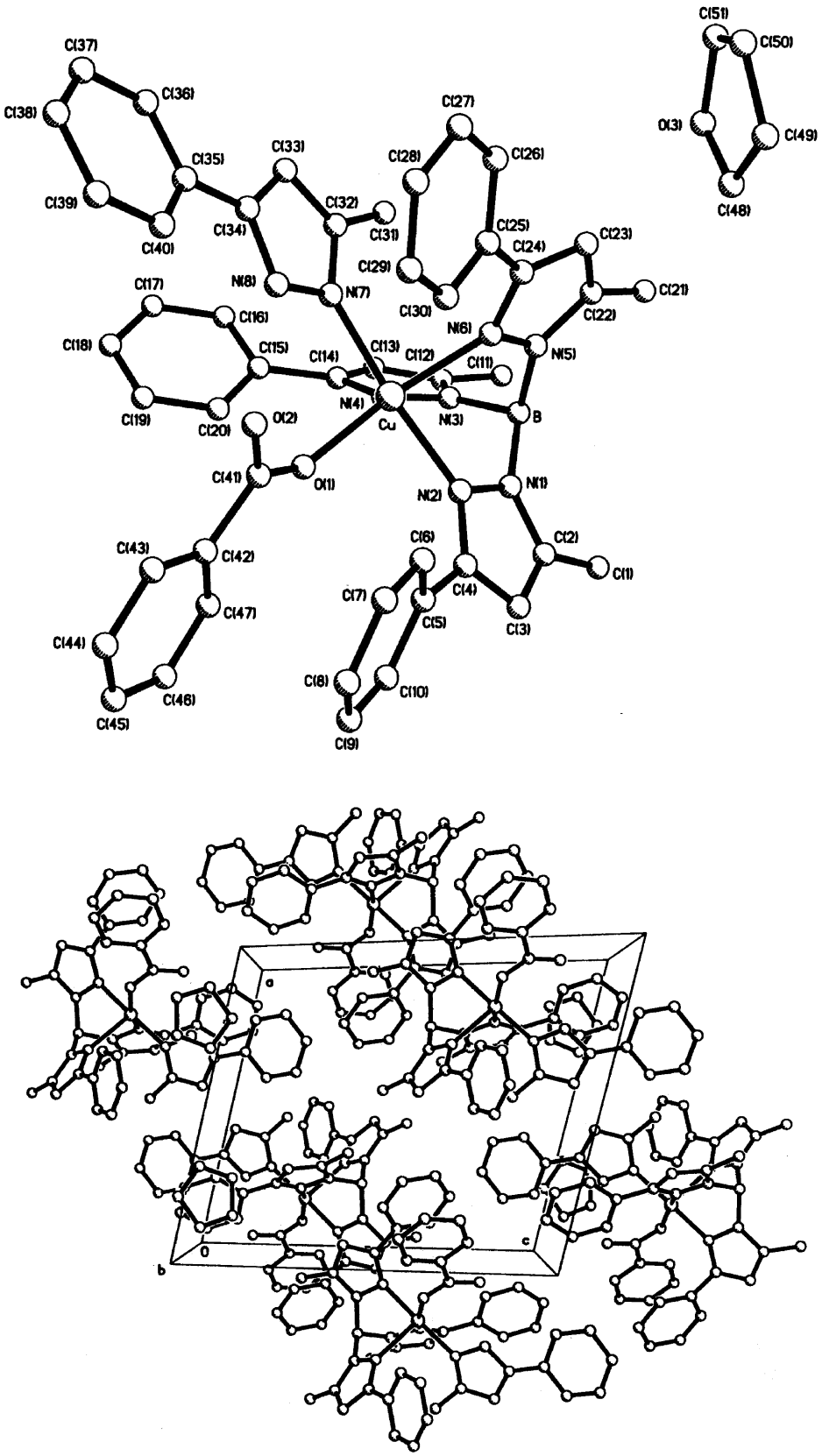

Fig. 3. (a) ORTEP diagram of **8**. (b) Unit cell packing diagram for **8**.

Table 5. The relevance of coordination mode of nitrate and its IR spectra

Complex	p_1	p_2	p_1-p_2	Coord. mode	Refs.
4	1495[$\nu_a(NO_2)$]	1265($\nu_{N=O}$)	230	bidentate	
6	1486[$\nu_a(NO_2)$]	1281($\nu_{N=O}$)	205	bidentate	
$LNi(NO_3)$	1523[$\nu_a(NO_2)$]	1279($\nu_{N=O}$)	244	bidentate	[8]
$LCu(NO_3)$	1479[$\nu_a(NO_2)$]	1267($\nu_{N=O}$)	212	bidentate	[8]
$LZn(NO_3)$	1460[$\nu_a(NO_2)$]	1286($\nu_{N=O}$)	174	anisobidentate	[8]
$[Ni(en)_2(NO_3)_2]$	1420[$\nu_a(NO_2)$]	1305[$\nu_s(NO_2)$]	115	unidentate	[10]

*p_1 denotes the highest frequency peak of NO_3, p_2 the second.
L = [η^3-HB{3-(2′-thie)-5-Mepz}$_3$].

Table 6. The relationship between the coordination mode of acetate or benzoxy and their IR spectra

Compound	$\nu_{C=O}$	ν_{C-O}	$\nu_{C=O}-\nu_{C-O}$	Mode	Refs.
CH_3COO^-, (ac)	1560	1416	144	–	
$Ru(ac)_2(CO)_2(PPh_3)_2$	1613	1315	298	unidentate	[9]
8	1593	1312	281	unidentate	
$[Pd(ac)_2(PPh_3)]_2$	1629	1314	315	unidentate	[11]
	1580	1411	169	bridged bidentate	
$Rh_2(ac)_2(CO)_3(PPh_3)$	1580	1440	140	bridged bidentate	14
$RuH(ac)(PPh_3)_2$	1526	1449	77	bidentate	[9]
5	1550	1466	84	bidentate	
7	1569	1449	120	bidentate	

of II, H_2 being eliminated and finally formed K[HB(3-Ph-5Mepz)$_3$]. So, the steric effect appears to have great influence on the formation of the complex. We found this phenomenon in our previous work [8].

I **II**

Molecular structure

The molecular structures of complexes [η^3-HB(3,5-$Ph_2pz)_3$]NiCl, [η^3-HB(3-Ph-5-Mepz)$_3$]Cd(NO_3)(THF) and [η^3-HB(3-Ph-5-Mepz)$_3$](3-Me-5-Phpz)Cu(PhCOO) are illustrated in Figs 1–3. Each of the complexes exhibits a slightly different coordination of the tris(pyrazolyl) hydroborato ligands to the metal center, the average M–N bond lengths and N–M–N interbond angles change across the series Ni, Cu, Cd: [2.038 Å, 92.88°], [2.108 Å, 89.26°], [2.299 Å, 86.46°], which is a reflection of different covalent radius of the metal (Ni < Cu < Cd). Moreover the Cd–N bond length is shorter than those in the six-coordinate sandwich complex [η^3-HB(3,5-$Me_2pz)_3$]$_2$Cd [2.36(1) and 2.43(2) Å] [10].

The molecular structure of complex **3** has a C_3 symmetry axis, containing the atoms Cl, Ni, B and H (binding to B). The nickel atom is coordinated by three nitrogen atoms and one chlorine atom, the configuration of the complex is trigonally distorted tetrahedral, as evidenced by three small N–M–N [92.88(9)°] bond angles and three large N–Ni–Cl [123.20(7)°] bond angles. The coordination environ-

ment of **3** also compares reasonably well with a theoretical calculation for the active site of CA, with bond lengths and angles of Zn–O (1.96 Å), Zn–N (2.10 Å) and O–Zn–N (117.6°) [11].

The coordination mode of nitrate in complex **4** is bidentate [2.334(3) and 2.356(3) Å], which is close to that [2.272(6) and 2.295(7) Å] of [η^3-HB(3-Bu^t-5-Mepz)$_3$]Cd(NO_3) [1], but different from our previous observed value in [η^3-HB{3-(2′-thie)-5-Mepz}$_3$]Zn(NO_3) [8], i.e. 1.966(4) and 2.463(4) Å, obviously, the different coordination mode of nitrate results from different metal centers.

As illustrated in Fig. 3, the copper atom in **8** is coordinated by four nitrogen atoms and one oxygen atom, the coordination environment around the copper center being a distorted square pyramid with N(4) at the apical position. The coordination mode of benzoxy in complex **8** is unidentate, with a Cu–O(1) bond length of 1.968(2) Å.

Since the coordination mode of nitrate and acetate in complex **4**–**7** is bidentate, benzoxy exhibits unidentate coordination in complex **8** but has four coordinated N atoms. Therefore, the coordination number of complexes **4**–**8** is five or six.

REFERENCES

1. Loonney, A., Saleh, A., Zhang, Y. and Parkin, G., *Inorg. Chem.*, 1994, **33,** 1158.
2. Kitajima, N., Fujisawa, K. and Moro-oka, Y., *J. Am. Chem. Soc.*, 1990, **112,** 3210.
3. Alsfasser, R., Trofimenko, S., Looney, A., Parkin, G. and Vahrenkamp, H., *Inorg. Chem.*, 1991, **30,** 4098.
4. Eagle, A. A., Laughlin, L. J., Young, C. G. and Tiekink, E. R. T., *J. Am. Chem. Soc.*, 1992, **114,** 9195.
5. Kitajima, N., Singh, U. P., Amagai, H., Osawa, M. and Moro-oka, Y., *J. Am. Chem. Soc.*, 1991, **113,** 7757.
6. Kitajima, N., Hikichi, S., Tanaka, M. and Moto-oka, Y., *J. Am. Chem. Soc.*, 1993, **115,** 5496.
7. Huang, J., Lee, L., Haggerty, B. S., Rheingold, A. L. and Walters, M. A., *Inorg. Chem.*, 1995, **34,** 4268.
8. Guo, S. L. and Yin, Y. Q., unpublished work.
9. Nakamoto, K., in *Infrared and Raman Spectra of Inorganic and Coordination Compounds*, 4th edn. John Wiley and Sons, New York, 1986, pp. 257–285.
10. McWhinnie, W. R., Monsef-Mirzal, Z., Perry, M. C., Shaikh, N. and Hamor, T. A., *Polyhedron*, 1993, **12,** 1193.
11. Kenneth, M. M., Hoffman, R. and Dewar, M. J. S., *J. Am. Chem. Soc.*, 1989, **111,** 5636.

Pergamon

PII: S0277–5387(98)00143–0

Polyhedron Vol. 17, No. 22 pp. 3851–3858, 1998
© 1998 Elsevier Science Ltd
All rights reserved. Printed in Great Britain
0277–5387/98 $19.00 + 0.00

Chelating properties of new series of heterocyclichydrazones. X-ray crystallography and mass spectrometry of their metal complexes

Gianluca Giorgi,*[a] Luisa Savini,[b] Luisa Chiasserini,[b] Cristina Nencini[b] and Cesare Pellerano[b]

[a]Centro Interdipartimentale di Analisi e Determinazioni Strutturali, Università degli Studi di Siena, via Aldo Moro-53100 Siena, Italy

[b]Dipartimento Farmaco Chimico Tecnologico, Università degli Studi di Siena, Banchi di Sotto, 55-53100 Siena, Italy

(Received 17 February 1998; accepted 6 April 1998)

Abstract—The chelating properties of a new series of α-N-heterocyclichydrazones (heterocycle = substituted quinoline, benzothiazole, phthalazine) have been studied. Nickel complexes have been synthesized and structurally characterized in the gas phase by mass spectrometry and tandem mass spectrometry, and in the solid state by x-ray crystallography. Each ligand (LH) acts as tridentate and it undergoes a deprotonation in the complex formation. The complexes are neutral species and they can be formulated as $[ML_2]$. The crystal structure of bis[N-(2-benzothiazolyl)-N′-(methlymethoxycarbonyl)hydrazine]nickel(II) × 0.5 H_2O has been determined. The metal shows a pseudo-octahedral polyhedron and it is coordinated to two nitrogen and to oxygen atoms in the equatorial plane, and to two hydrazone nitrogen atoms in the axial positions. © 1998 Elsevier Science Ltd. All rights reserved

Keywords: Ni^{II} complexes; hydrazone complexes; structural characterization; crystal structure; mass spectrometry.

INTRODUCTION

N-acyl- and *N*-arylhydrazones constitute important classes of organic compounds. The interest for these compounds may arise owing to their biological properties as well as for their chelating properties towards metal ions [1, 2]. As an example, 1(2*H*)-phtalazinone causes site-specific DNA damage [3] and mutagenic effects [4], and *N*-acyl- and *N*-arylhydrazones may exhibit pharmacological activities as potential antitumoral agents [5, 6]. It has been also found that complexes with essential metals, particularly first-row transition metals, may be more effective as antitumorals than the free ligands [7, 8]. Several mono and polynuclear metal complexes of hydrazone derivatives have been synthesized and characterized [2, 9–13]. In some cases these complexes are obtained as positive species, having different counter ions, such as chlorine or perchlorate [11, 12]. In other cases, deprotonation of the ligand occurs, so producing neutral metal complexes [9].

Most of these complexes have been characterized by different analytical approaches, such as infrared, UV and visible spectroscopies, nuclear magnetic resonance, magnetic measurements and x-ray crystallography. On the other hand, mass spectrometry, even if constitutes a powerful analytical tool for the characterization of organic and inorganic compounds [14], has been used only in few cases for characterizing metal complexes of hydrazone derivatives. The use of "hard" ionization methods, such as electron ionization, and "soft" desorption techniques, *e.g.* fast

* Author to whom correspondence should be addressed. E-mail: ciads@unisi.it; fax: 0039-577-227137.

atom bombardment, gives useful complementary information on the behaviour of chemical species in the gas phase.

In the ambit of a general project devoted to the characterization of heterocyclic compounds [15–17], we wish to report here on the coordination properties of new series of α-*N*-benzothiazolyl-, -quinolyl- and -phtalazinylhydrazone ligands (LH) towards Ni(II) (Scheme 1). The complexes have been characterized in the gas phase by mass spectrometry (MS) and tandem mass spectrometry (MS/MS), while x-ray crystallography was applied for the determination of the solid-state structure.

EXPERIMENTAL

Synthesis of the complexes

Metal complexes were obtained by mixing methanolic solutions of nickel acetate (1 mmol) and the appropriate ligand (2 mmol). The reaction mixture was heated under reflux for 1–2 hrs. By cooling the complexes separated as coloured solids which were filtered off, purified and dried in vacuum. Details on synthesis and yields, and other analytical data (NMR, IR) on complexes are given in ref. 6. Single crystals of **3** were obtained by dissolving 100 mg of powder in 50 ml of methanol and allowing to concentrate at room temperature. A dark brown prism of approximate dimensions $0.20 \times 0.25 \times 0.40$ mm was used for data collection.

Mass spectrometry

Mass spectra were measured on a double focusing VG 70-250S mass spectrometer (VG Analytical Ltd., Manchester, UK). Electron ionization mass spectra were obtained at electron energy of 70 eV, emission current 0.2 mA, with a source temperature of 180°C. The samples were introduced via the direct inlet system without heating. Liquid secondary ion mass spectrometry (LSIMS) experiments were carried out by bombarding a mixture of the sample and the matrix (glycerol, Fluka) with caesium ions produced by a gun operating at an anode potential and current equal to 35 kV and 2 μA, respectively. The accelerating voltage was 8 kV and the resolution was 1000 M/ΔM (10% valley). Daughter and parent ion spectra were performed to detect metastable decomposition occurring in the first field free region by appropriate linked scans. Data acquisition and analysis of the spectra were performed with a VG 11-250J data system equipped with a Digital PDP 11/83 minicomputer. Electron ionization high resolution mass measurements were performed at resolution 10000 M/ΔM (10% valley) under the data system control against perfluorokerosene standard (Fluka).

X-ray cystallography

Crystal data. **3**. $C_{22}H_{20}N_6O_5S_2Ni \times 0.51H_2O$, $M = 580.46$, Monoclinic, $a = 10.213(1)$, $b = 16.120(1)$, $c = 15.255(2)$ Å, $\beta = 102.32(1)^\circ$, $V = 2453.6(4)$ Å^3 (by least-squares refinement on diffractometer angles for 50 randomly selected and automatically centered reflections), space group $P2_1/c$ (n. 14), $Z = 4$, $F(000) = 1176$, $D_c = 1.55$ g cm^{-3}, μ(Mo–Kα) = 1.01 mm^{-1}.

The data were collected on a Siemens P4 four-circle diffractometer with graphite monochromated Mo–Kα radiation ($\lambda = 0.71069$ Å) in the range $-1 \le h \le 12$, $-1 \le k \le 19$, $-18 \le l \le 17$, ω scan mode for $1.9 \le \Theta \le 25^\circ$ scan range, scan width 1.4°, constant scan speed 2.70° min^{-1}. Three standard reflections measured every 60 min. showed no variations. 4323 unique reflections ($R_{int} = 0.028$) were collected at 22°C. Absorption correction obtained by psi scans was applied.

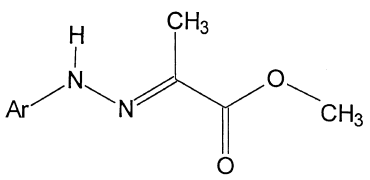

1 Ar =

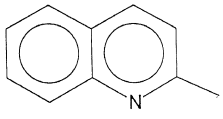

2 Ar =

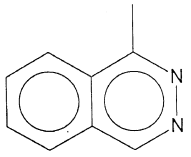

3 Ar =

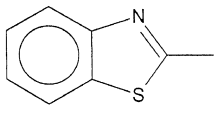

Scheme 1.

The structure was solved by direct methods implemented in SHELX-97 [18]. The refinement was carried out by full-matrix anisotropic least-squares on F^2 for all reflections for all non-H atoms by using SHELX-97 [18]. The hydrogen atoms were located on Fourier difference maps and included in the structure-factor calculations. A thermal parameter fixed at 80×10^{-3} Å^2 was used for the hydrogens of the methyl groups, while a common isotropic temperature factor, refined to 67×10^{-3} Å^2, was assigned to the other hydrogen atoms. The occupancy factor for water molecule was refined to 0.51 while it was 1 for all the other atoms.

Final refinement of 387 parameters gave $R1 = 0.042$ and $wR2 = 0.088$ for $F^2 > 2\sigma(F^2)$. Weighting scheme $w = 1/[\sigma^2(Fo)^2 + 0.0490P^2]$, where $P = (Fo^2 + 2Fc^2)/3$. Min. max height in last $\Delta\rho$ map of -0.218 and 0.450 eÅ^{-3}. Atomic scattering factors including f' and f'' were taken from ref. 18. Geometrical calculations and molecular graphics were performed by using PARST 96 [19] and SHELXTL [20] packages, respectively.

RESULTS AND DISCUSSION

Mass spectrometry

Electron ionization mass spectra of complexes **1** and **2** are reported in Fig. 1. Mass spectra of **3** obtained by electron ionization and liquid secondary ion mass spectrometry are compared in Fig. 2.

The mass spectra allow to determine the stoichiometry of the complexes. Complexes **1**, **2**, and **3** show molecular ions at *m/z* 542, 544 and 554, indicating that each specie can be formulated as $[ML_2]$. This suggests that in their formation one deprotonation for each ligand molecule occurs. It is reasonable that the exocyclic H(–N) proton is removed, as it occurs in the crystal structure of **3** (see below). Deprotonation of hydrazone ligands yielding monoanionic or dianionic species is often observed to occur in metal complex formation [2, 9, 10, 13].

The molecular ions $[ML_2]^+$ show high abundances, their relative intensities being higher than 65% (**1** and **2**) or they constitute the base peak (**3**) (Table 1). The isotopic patterns, mainly due to the five isotopes of Ni, are in good agreement with those theoretically expected. For complexes **1** and **2** the base peaks of the mass spectra are represented by the ions at *m/z* 483 and 485, respectively (Fig. 1). High-resolution data (Table 2), allowing to determine the elemental composition of ions present in the mass spectrum, have shown that these peaks are due to the loss of $^{\bullet}COOCH_3$ radical. When the carboxymethyl radical is lost, the nickel should change its coordination polyhedron, passing from a octahedron to a square pyramid. The high intensity of the ions $[ML_2\text{-}COOCH_3]^+$ suggests that also this complex is very stable in the gas phase. The loss of a further $^{\bullet}COOCH_3$ radical from the other ligand molecule is observed only for **2**, producing ions at *m/z* 426 whose relative intensity is 6.5%.

Another very intense fragment ions common to the three complexes are due to the species $[ML]^+$, producing ions at *m/z* 300 and 301 for **1** and **2**, respectively (Fig. 1; Table 1). Other fragment ions produced in the source are attributed to $[ML\text{-}CH_2O]^+$, $[L]^+$, $[ML\text{-}C_4H_5NO_2]^+$, $[L\text{-}COOCH_3]^+$.

The mass spectra of **3** obtained by electron ionization (Table 1) and LSIMS (Fig. 2) appear to be quite similar to those of **1** and **2**. Under electron ionization conditions the molecular ions $[ML_2]^{+\bullet}$ (*m/z* 554) constitute the base peak of the mass spectrum. Fragmentations occurring in the ion source resemble those described for compounds **1** and **2**. Thus the most intense fragment ions at *m/z* 495, 306, 276, 206 are attributable to the species $[ML_2\text{-}COOCH_3]^+$, $[ML]^+$, $[ML\text{-}C_4H_5NO_2]^+$, $[L]^+$.

In the LSIMS spectrum (Fig. 2, bottom) the pseudomolecular ion $[ML_2 + H]^+$ (*m/z* 555) is the base peak. The fact that the complex must add a proton to assume a positive charge suggests that in the solid state it is a neutral species. Also under *soft* conditions, like it is in LSIMS, a prominent fragmentation occurs in the source. Thus the EI and LSIMS spectra show many common fragment ions with similar abundances in the range *m/z* 300–100. One difference is represented by the ions at *m/z* 495. In fact, while in the EI spectrum of **3** they are very intense (46.2%), in LSIMS conditions their relative intensity is quite poor (10%) (Fig. 2).

Metastable daughter ion spectra, obtained by selecting the molecular ions as main beam, have shown that both the ions $[ML_2\text{-}COOCH_3]^+$ and $[ML]^+$ are produced directly by decompositions of the molecular ions (Fig. 3). It is interesting to evidence that quite different fragmentation pathways are followed by the species $[ML_2]^{+\bullet}$ and $[ML]^+$. In fact, while the elimination of the $^{\bullet}COOCH_3$ radical is highly favored from the molecular ions $[ML_2]^{+\bullet}$, both in the source (Figs 1 and 2) and in metastable processes (Fig. 3), it does not occur from the species $[ML]^+$. On the other hand, for the latter the elimination of 30 u, attributed to CH_2O, occurs and produces abundant ions in the mass spectrum and the most intense daughter ions (Fig. 3). This might be explained by considering that in the specie $[ML]^+$ only three coordination sites are available; the loss of the carbonylic oxygen will reduce them to two only. Other metastable decompositions produced by $[ML]^+$ obtained by **1** yield ions at *m/z* 242, 229, 213, 201 and 186 (Fig. 3). In particular, the ion at *m/z* 242 is attributed to $[L]^+$ due to the extrusion of the metal ion.

Crystal and molecular structure of **3**.

The asymmetric unit is constituted by two ligands N-(2-benzothiazolyl)-N′-(methylmethoxycarbonyl)

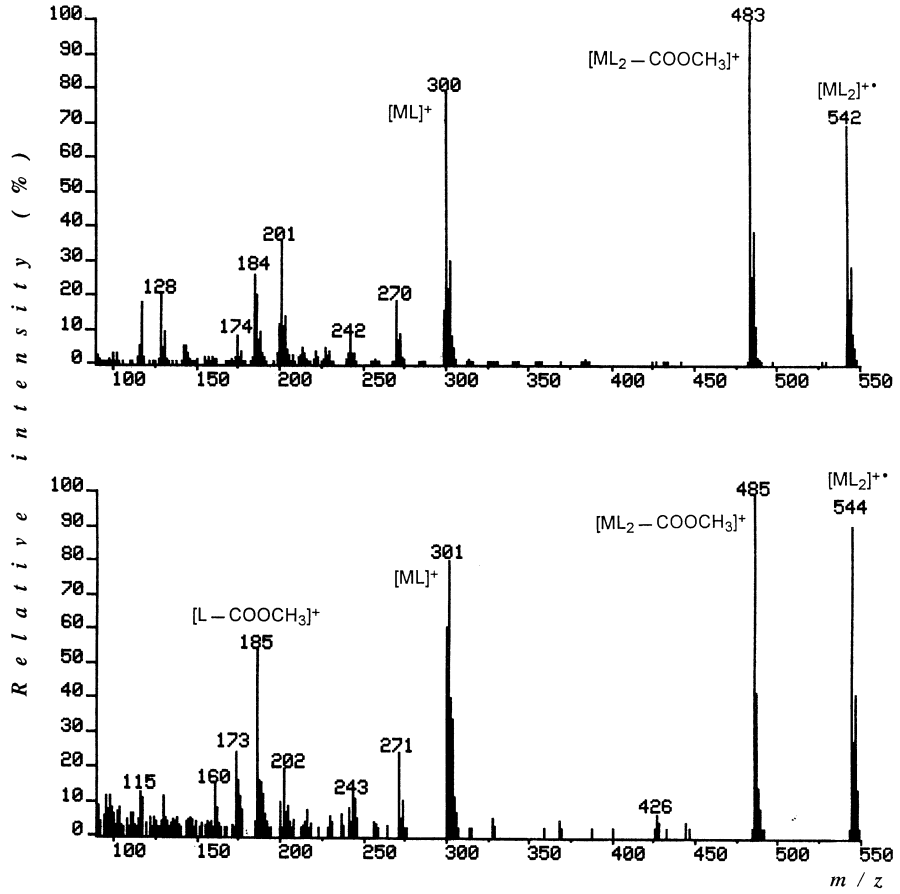

Fig. 1. Electron ionization mass spectra of complexes **1** (top) and **2** (bottom).

hydrazine bound to a nickel atom and 0.51 water molecule. The complex has no imposed crystallographic symmetry.

Each ligand molecule acts as tridentate. The metal ion shows a pseudooctahedral coordination polyhedron and it is coordinated to two oxygen (O(1), O(1A)) and to two nitrogen (N(3), N(3A)) atoms in the equatorial plane and to two hydrazone nitrogen (N(2), N(2A)) atoms in the axial positions (Fig. 4). The Ni–N distances are unequal. The two equatorial Ni–N bond lengths are 2.008(3) and 2.010(3) Å (Table 3), in agreement with Ni–N distances found in other nickel-hydrazino complexes [11, 13, 21]. The axial Ni–N bond lengths are slightly longer (2.061(3) and 2.053(3) Å). The two Ni–O distances are 2.238(3) Å (Ni–O(1)) and 2.198(3) Å (Ni–O(1A)). The octahedron is distorted with major out-of-plane deformations caused by the formation of chelate five membered rings involving both axial and equatorial ligands. As an example, the angles N(2)–Ni–O(1), N(2A)–Ni–O(1A) are equal to 75.8(1) and 76.8(1)°, while the highest in-plane deformation is due to the angles N(3)–Ni–O(1) and N(3A)Ni–O(1A) and equal to 153.9(1) and 153.8(1)°, respectively (Table 3). The nickel atom lies on the equatorial least-squares plane, while the two axial donor atoms, N(2) and N(2A), are −2.000(3) and 2.015(3) Å far from it, respectively.

In the benzothiazole moiety, the S–C bond lengths are in agreement with data previously found in analogous systems. In particular the S(1)–C(2) distance mean 1.747(3) Å in the two ligand molecules (Table 3). A search at the Cambridge Structural Database (CSD) [22] v. 5.14 for a 2-(N–N)-benzothiazolo fragment has produced 11 entries, but only for 9 entries correct geometric data are available. Only one structure is a hydrazone derivative [23], the others being mainly pyrazole and formazane derivatives. The results of the search indicate that the mean of the S(1)–C(2) bond length is equal to 1.737(7) Å, ranging from 1.710 Å in dioxo-methanol-(*β*-hydroxynaphthaldehyde-2-benzothiazolylhydrazonato)-molybdenum(VI)dimethylfor-mamide solvate [23] to 1.768 Å in azobenzene-N-(benzothiazol-2-yl)imide [24].

In the two ligand molecules, the C(2)–N(3) and N(3)–C(4) bond lengths mean 1.325(5) and 1.386(4) Å, respectively (Table 3). The mean values found in the above-cited search are equal to 1.303(8) and 1.393(5) Å, respectively. The two N–N distances in the hydrazone fragment are equal to 1.352(4) and

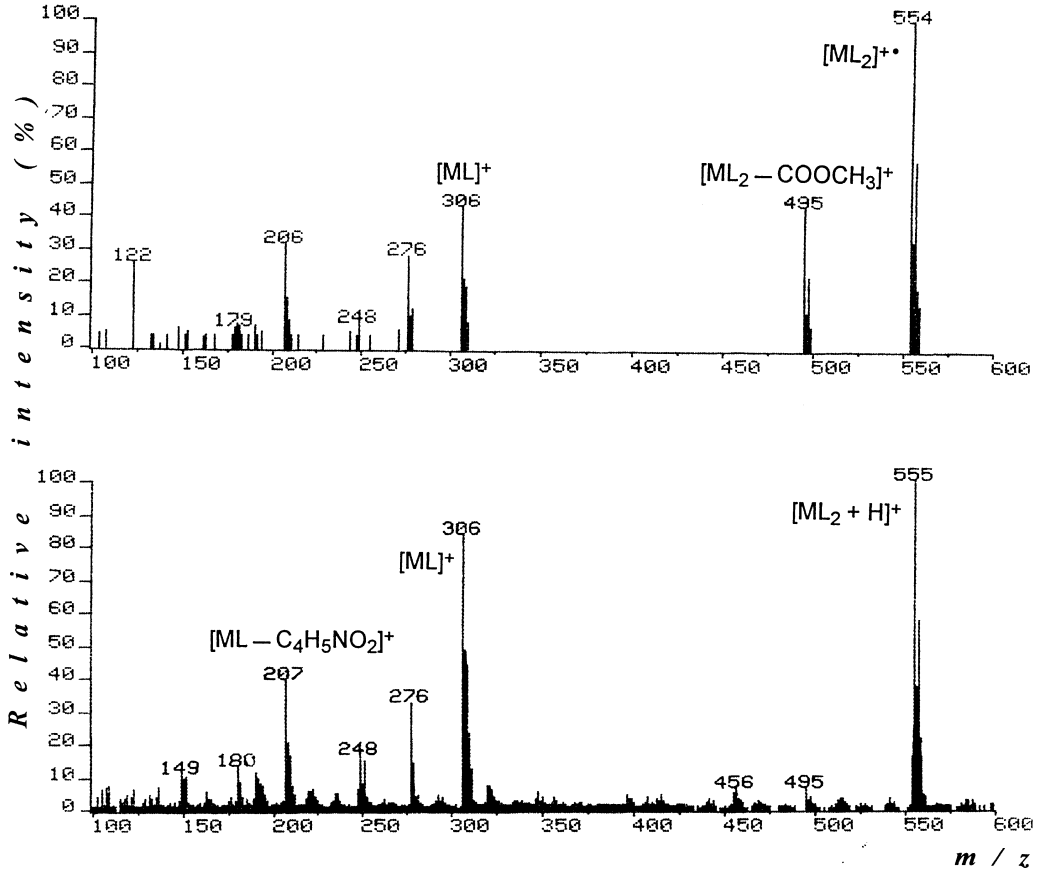

Fig. 2. Mass spectra of **3** obtained by electron ionization (top) and LSIMS (bottom).

Table 1. Electron ionization (70 eV) mass spectrometry data for compounds **1**–**3**

	m/*z* (*Relative intensity*, %)
1	546 (4.8), 545 (8.8), 544 (28.0), 543 (19.0), 542 (69.4), 487 (6.2), 486 (10.6), 485 (38.2), 484 (25.0), 483 (100), 304 (4.7), 303 (8.3), 302 (29.7), 301 (21.7), 300 (78.6), 299 (15.6), 272 (8.8), 271 (6.6), 270 (18.3), 242 (7.3), 227 (4.6), 213 (4.5), 203 (13.9), 202 (11.1), 201 (35.2), 200 (11.5), 188 (9.3), 187 (6.6), 186 (19.9), 184 (25.7), 174 (8.3), 143 (4.9), 142 (5.1), 130 (9.4), 129 (4.5), 128 (19.8), 117 (17.6), 116 (8.3), 89 (6.6)
2	548 (8.6), 547 (13.7), 546 (40.9), 545 (27.4), 544 (94.0), 489 (8.1), 488 (14.2), 487 (41.6), 486 (30.0), 485 (100), 304 (11.2), 303 (34.0), 302 (40.2), 301 (80.2), 300 (60.5), 273 (10.5), 271 (23.7), 244 (10.9), 243 (11.9), 241 (7.9), 204 (8.6), 202 (19.5), 199 (9.5), 189 (11.9), 188 (15.6), 187 (16.3), 186 (15.3), 185 (53.5), 176 (7.7), 175 (11.2), 174 (16.0), 173 (23.7), 162 (7.9), 160 (14.9), 129 (11.2), 116 (10.7), 115 (12.8), 103 (8.1), 98 (7.9), 97 (11.6), 96 (7.4), 95 (11.2), 90 (8.4), 89 (63.0)
3	558 (15.0), 557 (17.5), 556 (57.7), 555 (32.5), 554 (100), 498 (7.3), 497 (22.6), 496 (11.1), 495 (46.2), 309 (6.8), 308 (21.4), 307 (23.1), 306 (45.7), 305 (27.4), 278 (13.2), 277 (9.4), 276 (25.2), 254 (5.1), 248 (6.8), 227 (5.6), 209 (9.4), 208 (16.2) 207 (18.8), 206 (33.3), 194 (6.4), 190 (6.0), 186 (5.1), 183 (6.0), 182 (6.8), 181 (5.1), 180 (8.1), 179 (6.8), 163 (6.0), 153 (5.1), 148 (6.4), 147 (5.1), 141 (5.6), 122 (4.7), 122 (24.8), 108 (4.7), 78 (6.8)

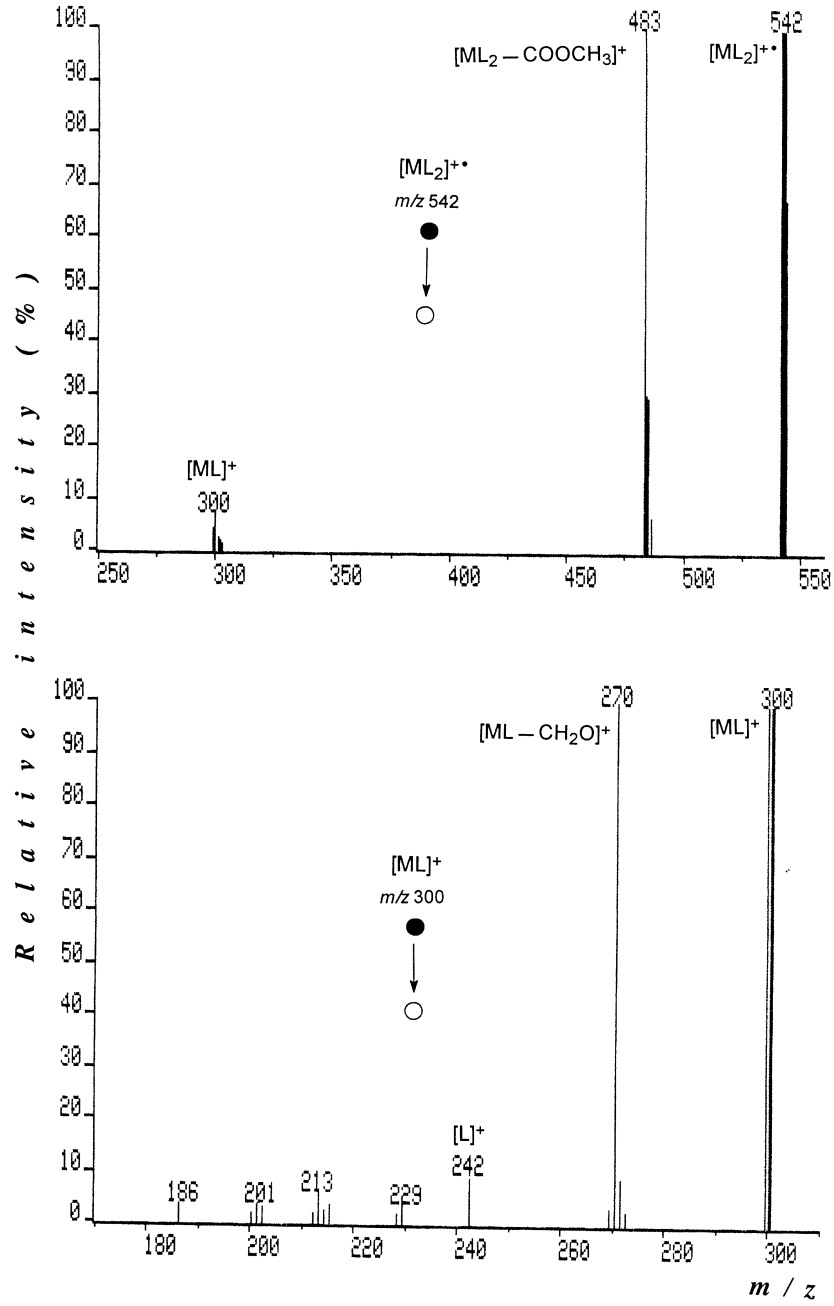

Fig. 3. Metastable daughter ion spectra of **1** by selecting the molecular ion (top) or the specie $[ML]^+$ (m/z 300, bottom) as main beam.

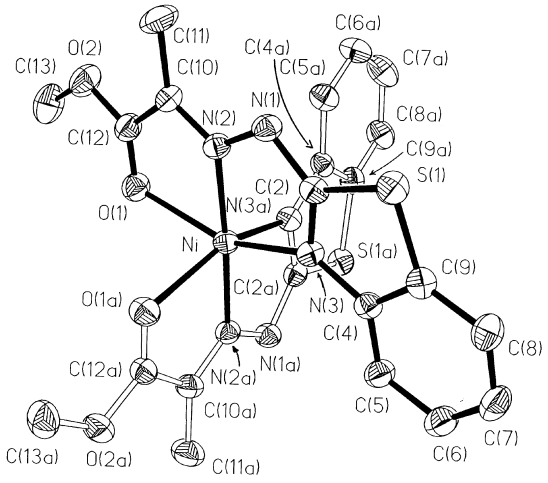

Fig. 4. Drawing of the bis[N-(2-benzothiazolyl)-N′-(methyl-methoxycarbonyl)hydrazine]nickel(II) unit of **3** showing 30% probability displacement ellipsoids. Hydrogen atoms are omitted for clarity.

Table 2. Accurate mass measurements for compound **1**

Ion	Observed mass	Error (ppm)
$[C_{26}H_{24}N_6O_4Ni]^{+\cdot}$	542.1199	2.5
$[C_{24}H_{21}N_6O_2Ni]^{+}$	483.1074	1.0
$[C_{13}H_{12}N_3O_2Ni]^{+}$	300.0292	−2.9
$[C_{12}H_{10}N_3ONi]^{+}$	270.0178	−0.4
$[C_9H_7N_2Ni]^{+}$	200.9960	1.3
$[C_{11}H_{10}N_3]^{+}$	184.0879	−2.5

1.346(4) Å. The endocyclic C–S–C angles are equal to 89.6(2) and 89.4(2)°, respectively (Table 3), in the two ligand molecules, in agreement with the values found in substituted benzothiazoles.

The two benzothiazole moieties are quite planar. In one heterocycle (S(1) ÷ C(9)) the largest deviations from the least squares plane are shown by C(2) and C(6) (0.013(4), 0.009(5) Å), while the other atoms have deviations less than 0.007 Å. The other benzothiazole (S(1A) ÷ C(9A)) shows a less degree of planarity with C(7A), C(2A) and C(4A) having deviations of 0.035(5), 0.030(3), −0.028(3) Å, respectively. The two benzothiazoles are almost perpendicular each other with dihedral angles between their least-squares planes equal to 97.3(1)°. In one ligand molecule (S(1) ÷ C(13)), the pendant group is almost coplanar with the benzothiazole. The largest deviations are due to C(13) (0.133(6) Å) and to O(1) (−0.082(3) Å). On the other hand, the other ligand molecule is quite far from the planarity. In this case, the largest deviations from the weighted least-squares planes defined by the atoms S(1A) ÷ C(13A) are due to C(13A) (0.218(5) Å), C(7A) (0.216(5) Å), while N(1A), N(3A), C(2A), C(6A), C(8A), and O(2A) show deviations larger than 0.1 Å.

Table 3. Selected bond lengths (Å) and angles (°) for bis[N-(2-benzothiazolyl)-N′-(methyl-methoxycarbonyl)hydrazine]nickel(II) × 0.51H_2O (**3**)

Ni–N(2)	2.010(3)	N(1A)–N(2A)	1.346(4)
Ni–N(2A)	2.008(3)	N(1A)–C(2A)	1.353(5)
Ni–N(3)	2.061(3)	N(2A)–C(10A)	1.297(5)
Ni–N(3A)	2.053(3)	N(3A)–C(2A)	1.323(5)
Ni–O(1)	2.238(3)	N(3A)–C(4A)	1.391(4)
Ni–O(1A)	2.198(3)	C(10A)–C(11A)	1.488(7)
S(1)–C(2)	1.746(3)	C(10A)–C(12A)	1.472(5)
S(1)–C(9)	1.744(4)	N(2)–Ni–N(3)	78.2(1)
O(1)–C(12)	1.225(5)	N(2)–Ni–O(1)	75.8(1)
O(2)–C(12)	1.318(5)	N(3)–Ni–O(1)	153.9(1)
O(2)–C(13)	1.453(7)	N(2)–N(1)–C(2)	107.8(3)
N(1)–N(2)	1.352(4)	N(3)–C(4)–C(9)	114.3(3)
N(1)–C(2)	1.357(5)	C(2)–S(1)–C(9)	89.6(2)
N(2)–C(10)	1.290(5)	N(2)–C(10)–C(12)	111.8(3)
N(3)–C(2)	1.327(5)	O(2)–C(12)–C(10)	112.7(3)
N(3)–C(4)	1.386(4)	N(2A)–Ni–N(3A)	77.5(1)
C(10)–C(11)	1.490(8)	N(2A)–Ni–O(1A)	76.8(1)
C(10)–C(12)	1.465(5)	N(3A)–Ni–O(1A)	153.8(1)
S(1A)–C(2A)	1.749(3)	N(2A)–N(1A)–C(2A)	107.1(3)
S(1A)–C(9A)	1.744(4)	N(3A)–C(4A)–C(9A)	114.5(3)
O(1A)–C(12A)	1.223(5)	C(2A)–S(1A)–C(9A)	89.4(2)
O(2A)–C(12A)	1.327(4)	N(2A)–C(10A)–C(12A)	110.8(3)
O(2A)–C(13A)	1.443(6)	O(2A)–C(12A)–C(10A)	112.5(3)

The crystal structure is stabilized by a net of hydrogen bonds involving water molecules: OW(x, y, z)... N(1)(x, 1/2 -y, -1/2+z) = 2.931(8) Å; OW(x, y, z)... N(1)(1-x, - 1/2+y, 1/2-z) = 2.997(8) Å; OW(x, y, z)... OW (1-x, -y, -z) = 3.055(9) Å. Van der Waals interactions are also present in the crystal packing.

REFERENCES

1. Attanasio, D., Fares, V. and Imperatori, P., *J. Chem. Soc. Chem. Commun*., 1986, 1476.
2. Mandal, S. K., Thomson, L. K., Newlands, M. J., Charland, J.-P. and Gabe, E. J., *Inorg. Chim. Acta*, 1990, **178,** 169.
3. Yamamoto, K. and Kawanishi, S., *Biochem. Pharmacol*., 1991, **41,** 905.
4. Toth, B., *J. Cancer Res. Clin. Oncol*., 1980, **97,** 97.
5. Savini, L., Massarelli, P., Chiasserini, L., Sega, A., Pellerano, C., Barzi, A. and Nocentini, G., *Eur. J. Med. Chem*., 1995, **30,** 547.
6. Savini, L., Massarelli, P., Chiasserini, L., Nencini, C. and Pellerano, C. *Il Farmaco*, in press.
7. Saryan, L., Ankel, E., Krishnamurti, C., Petering, D. H. and Elford, H., *J. Med. Chem*., 1979, **22,** 1218.
8. Antholine, W. E., Gunn, P. and Hopwood, L. E., *Int. J. Radiat. Oncol. Biol. Phys*., 1981, **7,** 491.
9. Attanasio, D. and Dessy, G., Fares, V., *Inorg. Chim. Acta*, 1985, **104,** 99.
10. Thompson, L. K. and Woon, T. C., *Inorg. Chim. Acta*, 1986, **111,** 45.
11. Wen, T., Thompson, L. K., Lee, F. L. and Gabe, E. J., *Inorg. Chem*., 1988, **27,** 4190.
12. Tandon, S. S., Thompson, L. K. and Hynes, R. C., *Inorg. Chem*., 1992, **31,** 2210.
13. Paolucci, G., Stelluto, S., Sitran, S., Ajò, D., Benetollo, F., Polo, A. and Bombieri, G., *Inorg. Chim. Acta*, 1992, **193,** 57.
14. *Mass Spectrometry of Metal Compounds*, (ed. J. Charalambous), Butterworths, London (1975).
15. Giorgi, G., Ponticelli, F., Czira, G. and Vékey, K., *J. Am. Soc. Mass Spectrom*., 1995, **6,** 962.
16. Giorgi, G., Anzini, M., Cappelli, A., Corelli, F. and Vomero, S., *S*., *J. Am. Soc. Mass Spectrom*., 1996, **7,** 653.
17. Giorgi, G., Salvini, L., Ponticelli, F. and Tedeschi, P., *J. Heterocyclic Chem*., 1996, **33,** 1895.
18. Sheldrick, G. SHELX-97, Program for x-ray data diffraction, Gottingen University (1997).
19. Nardelli, M. PARST96, University of Parma (1996).
20. SHELXTL™, Ver. 5, Siemens Industrial Automation Inc., Madison, WI (1994).
21. Sullivan, D. A. and Palenik, G. J., *Inorg. Chem*., 1977, **16,** 1127.
22. Allen, F. H., Davies, J .E., Galloy, J. J., Johnson, O., Kennard, O., Macrae, C. F., Mitchell, E. M., Mitchell, G. F., Smith, J. M. and Watson, D. G., *J. Chem. Inf. Comput. Sci*., 1991, **31,** 187.
23. Ilyukhin, A. B., Sergienko, V. S. and Abramenko, V. L., *Kristallografiya*, 1996, **41,** 692.
24. Potts, K. T., Elliott, A. J., Titus, G. R., Al-Hilal, D., Lindley, P. F., Boyd, G. V. and Norris, T., *Acta Cryst*., 1982, **B38,** 682.

Pergamon

PII: S0277-5387(98)00144-2

Polyhedron Vol. 17, No. 22, pp. 3859–3874, 1998
© 1998 Elsevier Science Ltd
All rights reserved. Printed in Great Britain
0277–5387/98 $19.00+0.00

Structures and properties of di-μ-oxo dimanganese(IV) complexes with bidentate Schiff bases, *N*-alkyl-substituted-salicylideneamine

Hitoshi Torayama, Hideyuki Asada, Manabu Fujiwara and Takayuki Matsushita*

Department of Materials Chemistry, Faculty of Science and Technology, Ryukoku University, Seta, Otsu 520-2194, Japan

(Received 4 November 1997; accepted 17 April 1998)

Abstract—Novel di-μ-oxo dimanganese(IV) complexes, $[Mn^{IV}(N\text{–R–X-sal})_2(\mu\text{-O})]_2$, with bidentate Schiff base ligands, *N*-alkyl-substituted-salicylideneamine, *N*–R–X-salH [R = CH_3 (Me), C_2H_5 (Et), *n*-C_3H_7 (Pr), *n*-C_4H_9 (Bu), *n*-C_6H_{13} (Hx), *n*-C_8H_{17} (Oct), *n*-$C_{10}H_{21}$ (Dec), *n*-$C_{12}H_{25}$ (Dod), or *n*-$C_{18}H_{37}$ (Octd) and X = H or 5,6-benzo], have been prepared by their reaction with potassium permanganate ($KMnO_4$) in MeCN, while stirring at room temperature. These complexes were characterized by spectroscopy, magnetic susceptibility, thermal analysis and X-ray crystallography. The structures consist of a $Mn^{IV}_2(\mu\text{-O})_2$ core with a Mn–Mn separation of 2.731(4) Å for $[Mn^{IV}(N\text{–Me-sal})_2(\mu\text{-O})]_2$, **1**, 2.769(2) Å for $[Mn^{IV}(N\text{-Et-sal})_2(\mu\text{-O})]_2$, **2**, 2.780(2) Å for $[Mn^{IV}(N\text{–Hx-sal})_2(\mu\text{-O})]_2$, **5**, 2.780(2) Å for $Mn^{IV}(N\text{-Dec-sal})_2(\mu\text{-O})]_2$, **7**, and 2.756(3) Å for $[Mn^{IV}(N\text{–Me-5,6-benzo-sal})_2(\mu\text{-O})]_2$, **10**. The complex **1** is the first di-μ-oxo dimanganese(IV) complex having asymmetrical form in which two manganese ions adopt different configurations each other. Moreover, the complexes **5** and **7** are found to exhibit the longest one among all of the Mn–Mn separation observed for the structurally characterized $Mn_2(\mu\text{-O})_2$ complexes prior to this work. The antiferromagnetic exchange interaction has been found to be $J = -83$ and -188 cm^{-1} for **1** and **7**, respectively. © 1998 Elsevier Science Ltd. All rights reserved

Keywords: photosystem II; oxygen-evolving complex; di-μ-oxo dimanganese(IV) complexes; bidentate Schiff base ligand; crystal structure, antiferromagnetic interaction.

INTRODUCTION

Manganese plays an important role in biological redox systems, which is exemplified by the oxygen-evolving complex of photosystem II (OEC of PSII) in green plants. The understanding of the structure and mechanism of OEC has grown considerably than two decades ago, however, many questions remain unanswered (i.e. how are the oxygen atoms coupled to form an O–O bond?) [1]. The possibility is that a binuclear or tetranuclear cluster forms the active site in OEC of PSII, although their precise arrangement and oxidation levels have not been determined unambiguously. X-ray absorption experiments have established the existence of at least two 2.7 Å Mn–Mn contacts within the OEC [2, 3]. Therefore, polynuclear high-valent manganese complexes having $Mn_2(\mu\text{-O})_2$ units have been investigated as functional and/or structural models for Mn-cofactor in OEC [4–19]. However, it rapidly became clear that the data from several biophysical measurements of PSII could not be well correlated with the model complexes. The models are too symmetric [20, 21].

Recently, we have reported on the properties and molecular structures of di-μ-oxo dimanganese(IV) complexes, $[Mn^{IV}(\mu\text{-salophen})(\mu\text{-O})]_2$ (salophenH_2 = *N*,*N*′-disalicylidene-1,2-diaminobenzene), **11**, $[Mn^{IV}(\mu\text{-salen})(\mu\text{-O})]_2$ (salenH_2 = *N*,*N*′-disalicylidene-1,2-diaminoethane), **12**, $[Mn^{IV}(salbn)(\mu\text{-O})]_2$ (salbnH_2 = N,N′-disalicylidene-1,4-diaminobutane), **13**, $[Mn^{IV}(salipn)(\mu\text{-O})]_2$ (salipnH_2 =

* Author to whom correspondence should be addressed. Tel.: +81-77-543-7471; Fax: +81-77-543-7483; E-mail: matusita@chem.ryukoku.ac.jp.

N,*N*′-disalicylidene-1,2-diaminopropane), **14**, and $[Mn^{IV}(N\text{–Hx-sal})_2(\mu\text{-O})]_2$, **5**, (*N*–Hx-salH = *N*-hexyl-salicylideneamine) obtained by the reaction of $KMnO_4$ with these ligands in MeCN [22–24].

In this paper, we describe the preparation and the detailed properties of novel di-μ-oxo dimanganese(IV) complexes with bidentate Schiff base ligands, $[Mn^{IV}(N\text{–R–X-sal})_2(\mu\text{-O})]_2$ {*N*–R-salH = *N*-alkyl-salicylideneamine [R = CH_3 (Me), **1**, C_2H_5 (Et), **2**, *n*-C_3H_7 (Pr), **3**, *n*-C_4H_9 (Bu), **4**, *n*-C_6H_{13} (Hx), **5**, *n*-C_8H_{17} (Oct), **6**, *n*-$C_{10}H_{21}$ (Dec), **7**, *n*-$C_{12}H_{25}$ (Dod), **8**, or *n*-$C_{18}H_{37}$ (Octd), **9**] and *N*-R-5,6-benzo-salH [CH_3 (Me), **10**, C_2H_5 (Et), *n*-C_3H_7 (Pr), *n*-C_4H_9 (Bu), *n*-C_6H_{13} (Hx), *n*-C_8H_{17} (Oct), *n*-$C_{10}H_{21}$ (Dec), *n*-$C_{12}H_{25}$ (Dod) or *n*-$C_{18}H_{37}$ (Octd)]}. These complexes have been characterized by UV-vis and IR spectra, magnetic susceptibility, thermal analysis, electrochemical analysis and X-ray crystallography.

The di-μ-oxo dimanganese(IV) complex **1** is the first example to overcome the problem that model complexes are too symmetric than OEC of PSII, and the long Mn–Mn distances of **5** and **7** may provide a good model for high oxidized S-states of OEC.

EXPERIMENTAL

Preparation of bidentate Schiff base ligands

The bidentate Schiff base ligands, *N*-alkyl-substituted-salicylideneamine, *N*–R–X-salH where R can be CH_3 (Me), C_2H_5 (Et), *n*-C_3H_7 (Pr), *n*-C_4H_9 (Bu), *n*-C_6H_3 (Hx), *n*-C_8H_{17} (Oct), *n*-$C_{10}H_{21}$ (Dec), *n*-$C_{12}H_{25}$ (Dod) or *n*-$C_{18}H_{37}$ (Octd) and X can be H or 5,6-benzo were prepared according to the method described in the literature [25].

Preparation of di-μ-oxo dimanganese complexes

$[Mn^{IV}(\text{N–}R\text{-}sal)_2(\mu\text{-}O)]_2$ (*R* = *Me*, *Et*, *Pr*, *Bu*, *Oct*, *Dec*, *Dod and Octd*). The manganese(IV) complex **1** was prepared by the reaction of *N*–Me-salH (1.35 g, 10.0 mmol) and $KMnO_4$ (0.79 g, 5.0 mmol) in MeCN (150 ml) with stirring at room temperature. The solution color changed from purple to brown and 6 h after the resulting brown solids, which correspond to manganese oxide, were filtered off. The filtrate was allowed to stand in the dark place at room temperature. Two days later the resulting brownish black crystals, **1**·2MeCN, were collected on a glass filter. They were recrystallized from MeCN (yield 1.33 g, 70%).

Other manganese(IV) complexes, $[Mn^{IV}(N\text{–R-sal})_2(\mu\text{-O})]_2$ (R = Et, Pr, Bu, Hx, Oct, Dec, Dod or Octd) were prepared in the same manner as the following preparation method. The manganese(IV) complex **5** was prepared by the reaction of *N*–Hx-salH (1.03 g, 5.0 mmol) and $KMnO_4$ (0.40 g, 2.5 mmol) in MeCN (150 ml) with stirring at room temperature. The solution color changed from purple to brown and 12 h after the resulting brown solids were collected on a glass filter and dried *in vacuo* (1.10 g). They were extracted with dichloromethane (CH_2Cl_2) (100 ml), and the solution was reprecipitated by the addition of MeCN. The resulting brown micro crystals were collected on a glass filter and dried *in vacuo*. They were recrystallized from a mixed solvent of CH_2Cl_2 and MeCN (yield 0.80 g, 67%).

$[Mn^{IV}(\text{N–}R\text{-5,6-}Benzo\text{-}sal)_2(\mu\text{-}O)]_2$ (*R* = *Me*, *Et*, *Pr*, *Bu*, *Oct*, *Dod and Octd*). The manganese(IV) complexes, $[Mn^{IV}(N\text{-R-5,6-benzo-sal})_2(\mu\text{-O})]_2$ (R = Me, Et, Pr, Bu, Oct, Dec, Dod and Octd) were prepared in the same manner above mentioned for **5**.

Single crystals of **1**·2MeCN, **2**, **5**, **7** and **10**·2MeCN have been used for X-ray crystallographic characterization.

Elemental analyses data for all of the complexes are given in Table 1.

Physical measurements

Elemental analyses were made on a Yanaco Model CHN-CORDER MT-5. UV-vis and IR spectra were recorded on a Shimadzu Model UV-3100 spectrophotometer and a Shimadzu Model IR-470 infrared spectrophotometer, respectively. Electrochemical studies were performed under argon, using a BAS Model CV-27 voltammograph equipped with a Graphtec Model WX 2400 XY recorder and a standard three-electrode assembly (glassy carbon working, Pt wire auxiliary, and Ag/AgCl MeCN 0.1 M *n*-Bu_4NClO_4, TBAP, reference electrode) with 0.1 M TBAP (*n*-Bu_4NClO_4) as the supporting electrolyte. All the redox potentials were corrected to the saturated calomel electrode (SCE). Magnetic susceptibility measurements were carried out by the Gouy method at room temperature. Variable-temperature magnetic susceptibility data were collected between 1.8 and 300 K using a Quantum Design superconducting quantum interference device (SQUID) in an applied magnetic field of 1000 G. A differential scanning calorimetry (DSC) and a thermogravimetric and differential thermal analysis (TG-DTA) were carried out by using a Rigaku TAS-200 thermal analysis system.

X-ray crystallography

Single crystals of **1**·2MeCN were obtained by recrystallization from MeCN and those of **2**, **5**, **7** and **10**·2MeCN were obtained by recrystallization from a mixed solvent of MeCN and CH_2Cl_2. The crystals were then mounted in a glass capillary and coated with silicone oil. All the data were collected on a Rigaku AFC-7R four circle automated diffractometer with graphite monochromated Cu–Kα radiation ($\lambda = 1.54178$ Å) for **1**·2MeCN and **2** or Mo–Kα radiation ($\lambda = 0.71069$ Å) for **5**, **7**, and **10**·2MeCN at room temperature. Unit-cell parameters were obtained from least square fit of 25 reflections, $18.0^\circ < 2\theta < 20.7^\circ$ for **1**, $18.2^\circ < 2\theta < 24.8^\circ$ for **2**, $6.9^\circ < 2\theta < 12.0^\circ$ for **5**,

Table 1. Elemental analyses of [Mn(*N*–R–X-sal)$_2$(μ-O)$_2$]$_2$

R, X	Formula	Analyses[a]			
		C (%)	H (%)	N (%)	Mn (%)
Me, H (**1**)·2MeCN	$Mn_2C_{36}H_{38}N_6O_6$	56.6 (56.9)	5.09 (5.04)	11.0 (11.1)	14.3 (14.5)
Et, H (**2**)	$Mn_2C_{36}H_{40}N_4O_6$	58.2 (58.9)	5.45 (5.49)	7.63 (7.63)	15.1 (15.0)
Pr, H (**3**)	$Mn_2C_{40}H_{48}N_4O_6$	60.1 (60.8)	6.10 (6.12)	7.02 (7.09)	14.0 (13.9)
Bu, H (**4**)	$Mn_2C_{44}H_{56}N_4O_6$	61.8 (62.4)	6.59 (6.67)	6.55 (6.62)	12.8 (13.0)
Hx, H (**5**)	$Mn_2C_{52}H_{72}N_4O_6$	64.4 (65.1)	7.61 (7.57)	5.81 (5.84)	11.2 (11.5)
Oct, H (**6**)	$Mn_2C_{60}H_{88}N_4O_6$	66.9 (67.3)	8.25 (8.28)	5.14 (5.23)	10.3 (10.3)
Dec, H (**7**)	$Mn_2C_{68}H_{104}N_4O_6$	69.6 (69.0)	8.91 (8.86)	4.76 (4.73)	9.31 (9.28)
Dod, H (**8**)	$Mn_2C_{76}H_{120}N_4O_6$	70.0 (70.5)	9.31 (9.34)	4.28 (4.32)	8.48 (8.48)
Octd, H (**9**)	$Mn_2C_{100}H_{168}N_4O_6$	73.2 (73.6)	10.3 (10.4)	3.43 (3.43)	6.70 (6.73)
Me, 5,6-benzo (**10**)·MeCN	$Mn_2C_{52}H_{46}N_6O_6$	64.6 (65.0)	4.91 (4.83)	8.69 (8.75)	11.8 (11.4)
Et, 5,6-benzo·2MeCN	$Mn_2C_{56}H_{54}N_6O_6$	66.0 (66.1)	5.31 (5.35)	8.22 (8.26)	10.9 (10.8)
Pr, 5,6-benzo·MeCN	$Mn_2C_{60}H_{62}N_6O_6$	66.8 (67.2)	5.80 (5.82)	7.81 (7.83)	10.1 (10.2)
Bu, 5,6-benzo	$Mn_2C_{60}H_{64}N_4O_6$	68.4 (68.8)	6.20 (6.16)	5.36 (5.35)	10.2 (10.5)
Hx, 5,6-benzo	$Mn_2C_{68}H_{80}N_4O_6$	69.9 (70.5)	6.99 (6.96)	4.79 (4.83)	9.46 (9.48)
Oct, 5,6-benzo	$Mn_2C_{76}H_{96}N_4O_6$	70.8 (71.8)	7.59 (7.61)	4.47 (4.41)	8.60 (8.64)
Dec, 5,6-benzo	$Mn_2C_{84}H_{112}N_4O_6$	72.4 (72.9)	8.15 (8.16)	4.03 (4.05)	8.13 (8.16)
Dod, 5,6-benzo	$Mn_2C_{92}H_{128}N_4O_6$	73.3 (73.9)	8.59(8.62)	3.69 (3.75)	7.35 (7.34)
Octd, 5,6-benzo	$Mn_2C_{116}H_{176}N_4O_6$	75.4 (76.0)	9.66(9.68)	3.01 (3.06)	6.01 (6.06)

[a]Required values in parentheses.

$6.6^\circ < 2\theta < 10.0^\circ$ for **7** and $6.5^\circ < 2\theta < 12.5^\circ$ for **10**·2MeCN. Three standard reflections were measured every 150 reflections; they showed no systematic decay throughout data collection. The data were corrected for Lorentz and polarization effects. All the calculations were carried out using the TEXSAN [26] crystallographic software package. The structures of the complexes were solved using direct method (SHELX86) [27] and expanded using Fourier techniques [28]. These structures were refined by the full-matrix least-squares technique with anisotropic thermal parameters for all nonhydrogen atoms. Hydrogen atoms were introduced in calculated positions but not refined. Crystallographic data for the complexes are summarized in Table 2.

Reagents

The reagents (salicylaldehyde, 5,6-benzo-salicylaldehyde, and monoamines) were obtained commercially and used without further purification. $KMnO_4$ was of the reagent grade (99.5%). MeCN was purified by distillation over P_4O_{10} twice and then distilled further before use. Other solvents were purified by usual method.

RESULTS AND DISCUSSION

Molecular structures of di-μ-oxo dimanganese complexes

The molecular structures of the di-μ-oxo dimanganese(IV) complexes **1**, **2**, **5** and **7** are shown in Figs 1–4 and these selected bond distances and angles are listed in Tables 3–6, respectively. These structures consist of two Mn(IV) centers bridged by two oxygen atoms to yield a planar Mn_2O_2 core with Mn–Mn separation of 2.731 (4) Å for **1**, 2.769(2) Å for **2**, 2.780(2) Å for **5**, and 2.780(2) Å for **7**.

For complex **1**, the unit cell contains four independent dimers, which have almost the same structure. The complex **1** is the first di-μ-oxo dimanganese(IV) complex having asymmetrical form in which two manganese ions adopt different configuration each other. On the one manganese ion (Mn1) of **1**, two phenolic oxygen atoms are located to *trans* and two imine nitrogen atoms are located to *cis* position toward a bridging μ-oxo group, which is quite similar to the structure of **5**. However, on another manganese ion (Mn2), two imine nitrogen atoms are located to *trans* and two phenolic oxygen atoms are located to *cis* position toward a bridging oxo group. It is conceivable that the formation of the asymmetric complex **1** may be caused by less steric hindrance of $-CH_3$ group of *N*–Me-sal ligand than the other *N*–R-sal ligands. **1** has distinct lengthening of the Mn–O (phenolate oxygen) and Mn–N (imine nitrogen) bond distances *trans* to the Mn–O_{oxo} bonds: Mn–O, 1.91(1) and 1.95(2) Å (*trans*) and 1.90(1) and 1.91(2) Å (*cis*); Mn–N, 2.07(2) and 2.10(2) Å (*trans*) and 2.00(2) and 2.02(2) Å (*cis*).

On the other hand, the other di-μ-oxo dimanganese(IV) complexes, **2**, **5**, and **7**, have symmetrical form. These symmetrical complexes exhibit relatively longer Mn–Mn separation than those of the di-μ-oxo dimanganese(IV) complexes with tetradentate Schiff

Table 2. Crystallographic Parameters for **1**, **2**, **5**, **7** and **10**

Compound	**1**·2MeCN	**2**	**5**	**7**	**10**·2MeCN
Chemical formula	$Mn_2C_{36}H_{38}N_6O_6$	$Mn_2C_{36}H_{40}N_4O_6$	$Mn_2C_{52}H_{72}N_4O_6$	$Mn_2C_{68}H_{104}N_4O_6$	$Mn_2C_{52}H_{46}N_6O_6$
Formula weight	760.61	734.61	959.04	1183.47	960.85
Crystal color, habit	dark brown, prism	dark brown, prism	dark brown, prism	dark brown, prism	dark brown, prism
Crystal size (mm)	$0.30 \times 0.25 \times 0.40$	$0.40 \times 0.38 \times 0.35$	$0.35 \times 0.05 \times 0.20$	$0.25 \times 0.15 \times 0.40$	$0.15 \times 0.15 \times 0.10$
a (Å)	18.525(9)	11.509(4)	12.280(4)	11.854(3)	17.318(2)
b (Å)	25.733(4)	14.105(3)	13.828(3)	14.369(2)	18.004(7)
c (Å)	15.644(2)	21.509(4)	15.336(3)	20.263(2)	15.264(4)
α (°)	101.95(1)	–	–	–	90.31(3)
β (°)	90.17(2)	–	107.59(2)	102.02(1)	120.70(1)
γ (°)	91.01(2)	–	–	–	84.27(2)
V (Å^3)	7294(3)	3491(1)	2482(1)	3404(1)	4618(1)
Z	8	4	2	2	4
Crystal system	triclinic	orthorhombic	monoclinic	monoclinic	triclinic
Space group	$P\bar{1}$	$Pccn$	$P2_1$	$P2_1$	$P\bar{1}$
D_{calc}, (g/cm^3)	1.385	1.413	1.283	1.154	1.382
$2\theta_{max}$ (°)	55.0	55.0	55.0	55.0	55.0
Total data collected	15613	2959	6143	8524	21414
Unique data	14999	2959	5931	8146	20708
Obsd data ($I > 3\sigma(I)$)	5230	1722	2641	3644	5541
R[a]	0.058	0.044	0.047	0.052	0.068
R_w[b]	0.063	0.044	0.052	0.040	0.076[2]

[a] $R = \Sigma||F_0| - F_c||/\Sigma|F_0|$. [b] $R_w = [\Sigma w(|F_0| - |F_c|)^2/\Sigma wF_0^2]^{1/2}$, $w = 4F_0^2/\sigma^2(F_0^2)$.

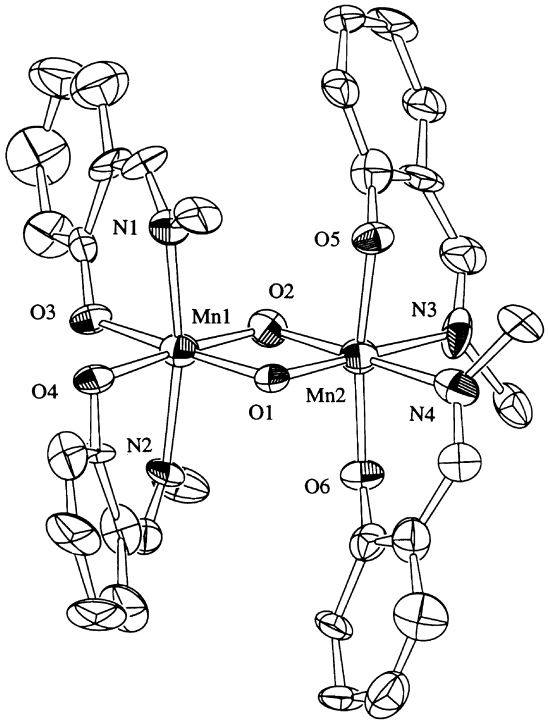

Fig. 1. Molecular structure of $[Mn^{IV}(N\text{–Me-sal})_2(\mu\text{-O})]_2$, **1**.

bases (2.688(1)–2.732(3) Å) [10, 13, 14, 19, 22–24], and the value [2.780(2) Å] observed for **5** and **7** is the longest one among all of the Mn–Mn distances observed for the structurally characterized $Mn_2(\mu\text{-O})_2$ complexes (2.580(1)–2.757(3) Å) prior to this work [5–15] [16–19]. It is considered that the long Mn–Mn distance of these complexes may be caused by the interaction of the alkyl groups of the ligands, because the complex having a longer alkyl group chain in these ligands has a longer Mn–Mn separation. In the structure of these complexes, two *N*–R-sal ligands around each manganese atom bond *via* two phenolic oxygen atoms and two imine nitrogen atoms to complete the roughly octahedral coordination environment. Adoption of this binding model of **2**, **5** and **7** places two phenolic oxygen atoms *trans* and two imine nitrogen atoms of two *N*–R-sal ligands *cis* to a bridging μ-oxo group are similar to the metal center of the di-μ-oxo dimanganese(IV) complexes with tetradentate Schiff bases, **11** and **12** [23]. The Mn–O (phenolate oxygen) and Mn–N (imine nitrogen) bond distances of **2** and **5** are almost regular: Mn–O, 1.927(4) and 1.913(4) Å for **2** and 1.950(7), 1.920(7), 1.942(7) and 1.933(7) Å for **5**; Mn–N, 2.028(4) and 2.026(4) Å for **2** and 2.025(9), 2.044(9), 2.022(9) and 2.020(9) Å for **5**. On the other hand, these bond distances of 7 are not so regular: Mn–O, 1.906(6), 1.908(6), 1.947(6) and 1.967(6) Å; Mn–N, 2.059(7), 1.991(6), 2.013(7) and 2.074(7) Å.

The molecular structure of the di-μ-oxo dimanganese(IV) complex having 5,6-benzo substituent groups **10** is shown in Fig. 5 and its selected bond distances and angles are listed in Table 7. For complex **10**, the unit cell contains two independent dimers, which have almost same structure. The complex **10** has symmetrical form, in spite of the complex **1** bearing the same alkyl group, R = Me, has an asymmetrical form. The Mn–Mn separation of **10**, 2.756(3) Å, is longer than the separation of **1**, but slightly shorter than that of **2**. It is conceivable that the symmetric complex **10** may result from the existence of the bulky 5,6-benzo substituent groups; the *N*–Me-5,6-benzo-sal ligand

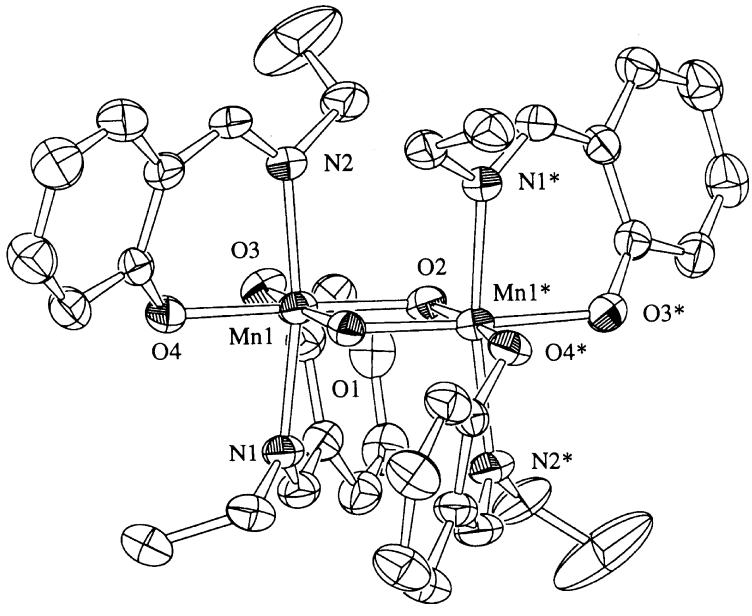

Fig. 2. Molecular structure of $[Mn^{IV}(N\text{-Et-sal})_2(\mu\text{-O})]_2$, **2**.

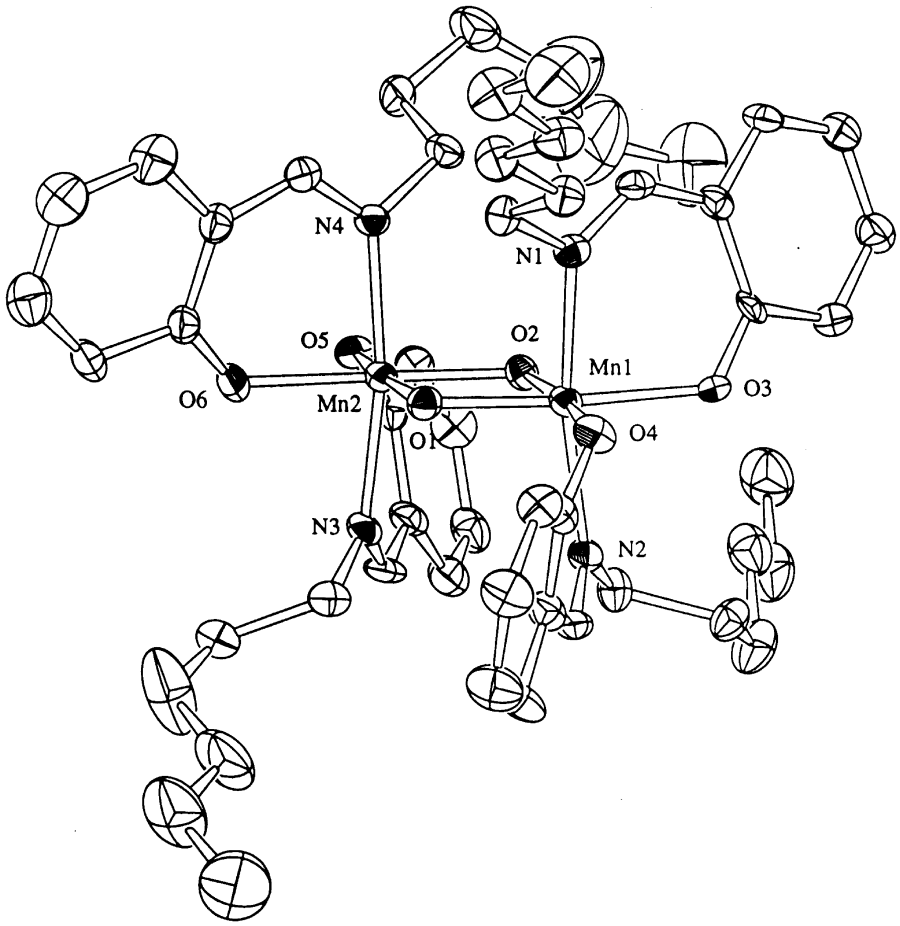

Fig. 3. Molecular structure of $[Mn^{IV}(N\text{-Hx-sal})_2(\mu\text{-O})]_2$, **5**.

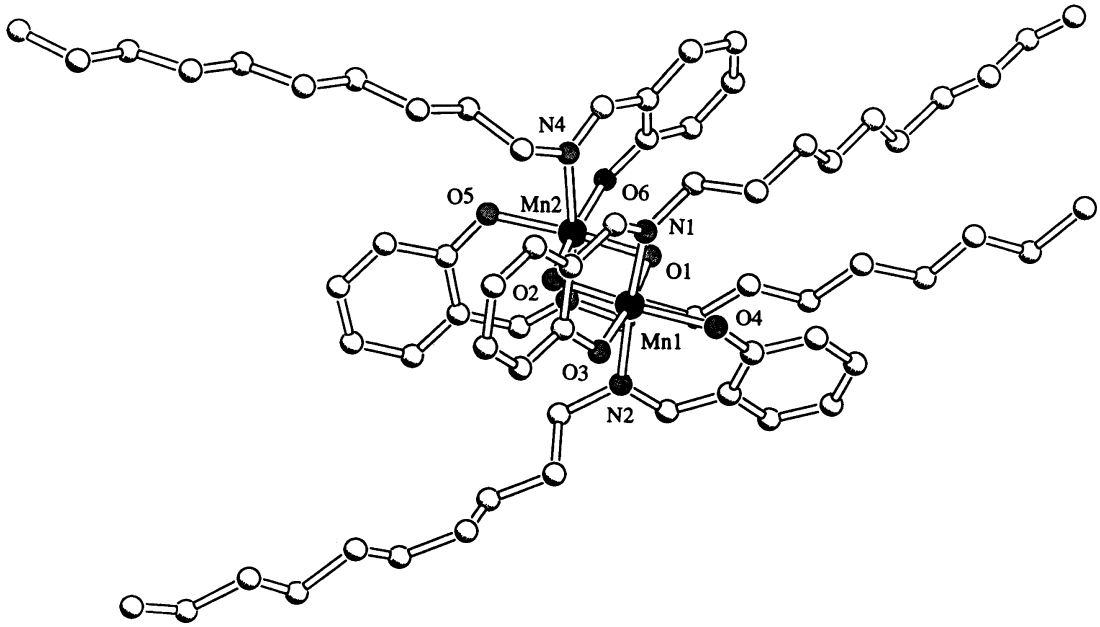

Fig. 4. Molecular structure of $[Mn^{IV}(N\text{-Dec-sal})_2(\mu\text{-O})]_2$, **7**.

Table 3. Selected interatomic distances (Å) and angles (°) for **1**

Mn1–Mn2	2.731 (4)	Mn1–O1	1.83(1)
Mn1–O2	1.83(1)	Mn1–O3	1.95(2)
Mn1–O4	1.91(1)	Mn1–N1	2.00(2)
Mn1–N2	2.02(2)	Mn2–O1	1.80(1)
Mn2–O2	1.80(1)	Mn2–O5	1.90(1)
Mn2–O6	1.91(2)	Mn2–N3	2.07(2)
Mn2–N4	2.10(2)		
Mn1–O1–Mn2	97.3(6)	Mn1–O2–Mn2	97.6(6)
O1–Mn1–O2	81.7(5)	O1–Mn2–O2	83.4(5)
O1–Mn1–O3	172.4(6)	O1–Mn1–O4	92.5(5)
O1–Mn1–N1	91.0(8)	O1–Mn1–N2	95.4(7)
O2–Mn1–O3	90.7(6)	O2–Mn1–O4	174.2(6)
O2–Mn1–N1	194.1(7)	O2–Mn1–N2	92.3(7)
O3–Mn1–O4	95.0(6)	O3–Mn1–N1	89.9(8)
O3–Mn1–N2	84.4(8)	O4–Mn1–N1	85.6(7)
O4–Mn1–N2	88.6(7)	N1–Mn1–N2	171.5(7)
O1–Mn2–O5	92.8(6)	O1–Mn2–O6	92.2(6)
O1–Mn2–N3	175.7(6)	O1–Mn2–N4	95.7(6)
O2–Mn2–O5	94.1(6)	O2–Mn2–O6	93.2(7)
O2–Mn2–N3	92.4(6)	O2–Mn2–N4	179.0(6)
O5–Mn2–O6	171.5(6)	O5–Mn2–N3	87.7(7)
O5–Mn2–N4	85.9(7)	O6–Mn2–N3	87.7(8)
O6–Mn2–N4	86.9(7)	N3–Mn2–N4	88.6(7)

Table 4. Selected interatomic distances (Å) and angles (°) for **2**

Mn1–Mn1*	2.769(2)	Mn1–O1	1.814(3)
Mn1–O2	1.820(3)	Mn1–O3	1.927(4)
Mn1–O4	1.913(4)	Mn1–N1	2.028(4)
Mn1–N2	2.026(4)		
Mn1–O1–Mn1*	99.5(2)	Mn1–O2–Mn1*	99.1(2)
O1–Mn1–O2	80.7(2)	O1–Mn1–O3	171.9(2)
O1–Mn1–O4	92.1(2)	O1–Mn1–N1	91.9(1)
O1–Mn1–N2	95.5(1)	O2–Mn1–O3	91.3(2)
O2–Mn1–O4	172.8(2)	O2–Mn1–N1	96.0(1)
O2–Mn1–N2	92.8(1)	O3–Mn1–O4	95.9(1)
O3–Mn1–N1	87.5(2)	O3–Mn1–N2	86.2(2)
O4–Mn1–N1	84.7(2)	O4–Mn1–N2	87.3(2)
N1–Mn1–N2	169.3(2)		

has much more steric hindrance than the *N*–Me-sal ligand of **1**. The Mn–O (phenolate oxygen) and Mn–N (imine nitrogen) bond distances of **10** are almost regular: Mn–O, 1.928(10), 1.927(9), 1.912(9) and 1.933(10) Å; Mn–N, 2.00(1), 2.00(1), 1.99(1) and 2.01(1) Å.

Scheme 1 shows three types of $N_2O_2(\mu\text{-}O)_2$ ligation sphere for structurally characterized di-μ-oxo dimanganese(IV) complexes with Schiff base ligands. The complexes **2**, **5**, **7** and **10** belong to type I, which has a relatively large Mn–Mn separation. Although the di-μ-oxo dimanganese(IV) complexes with tetradentate Schiff base ligands, **11**, **12** and [Mn(μ-dbsalen)(μ-O)]$_2$ (dbsalenH_2 = *N*,*N*′-di-3,5-dibromosalicylidene-1,2-diaminoethane) belong also type I, these complexes exhibit remarkably shorter Mn–Mn separations (2.688–2.718 Å) [18, 22, 23]. The type II is observed for the di-μ-oxo dimanganese(IV) complexes with several tetradentate Schiff base, **13**, **14** and [Mn(salpn)(μ-O)]$_2$ [13, 22, 23]. The Mn–Mn separation of these complexes exhibits around 2.73 Å. On the other hand, **1** is a unique complex of type III,

Table 5. Selected interatomic distances (Å) and angles (°) for **5**

Mn1–Mn2	2.780(2)	Mn1–O1	1.817(7)
Mn1–O2	1.818(7)	Mn1–O3	1.950(7)
Mn1–O4	1.920(7)	Mn1–N1	2.025(9)
Mn1–N2	2.044(9)	Mn2–O1	1.826(7)
Mn2–O2	1.815(7)	Mn2–O5	1.942(7)
Mn2–O6	1.933(7)	Mn2–N3	2.022(9)
Mn2–N4	2.020(9)		
Mn1–O1–Mn2	99.5(3)	Mn1–O2–Mn2	99.9(3)
O1–Mn1–O2	80.4(3)	O1–Mn2–O2	80.2(3)
O1–Mn1–O3	172.0(3)	O1–Mn1–O4	92.8(3)
O1–Mn1–N1	90.8(3)	O1–Mn1–N2	90.7(3)
O2–Mn1–O3	92.0(3)	O2–Mn1–O4	173.1(3)
O2–Mn1–N1	96.3(3)	O2–Mn1–N2	92.0(3)
O3–Mn1–O4	94.8(3)	O3–Mn1–N1	87.6(3)
O3–Mn1–N2	85.7(3)	O4–Mn1–N1	84.4(3)
O4–Mn1–N2	88.2(3)	N1–Mn1–N2	169.5(3)
O1–Mn2–O5	172.4(3)	O1–Mn2–O6	93.7(3)
O1–Mn2–N3	91.6(3)	O1–Mn2–N4	95.3(3)
O2–Mn2–O5	92.4(3)	O2–Mn2–O6	173.9(3)
O2–Mn2–N3	97.0(3)	O2–Mn2–N4	92.1(3)
O5–Mn2–O6	93.7(3)	O5–Mn2–N3	87.8(3)
O5–Mn2–N4	86.4(3)	O6–Mn2–N3	83.6(3)
O6–Mn2–N4	87.9(3)	N3–Mn2–N4	169.4(4)

Table 6. Selected interatomic distances (Å) and angles (°) for **7**

Mn1–Mn2	2.780(2)	Mn1–O1	1.825(6)
Mn1–O2	1.823(6)	Mn1–O3	1.906(6)
Mn1–O4	1.908(6)	Mn1–N1	2.059(7)
Mn1–N2	1.991(7)	Mn2–O1	1.810(6)
Mn2–O2	1.794(6)	Mn2–O5	1.947(6)
Mn2–O6	1.967(6)	Mn2–N3	2.013(7)
Mn2–N4	2.074(7)		
Mn1–O1–Mn2	99.7(3)	Mn1–O2–Mn2	100.5(3)
O1–Mn1–O2	79.3(2)	O1–Mn2–O2	80.5(2)
O1–Mn1–O3	172.2(3)	O1–Mn1–O4	92.6(3)
O1–Mn1–N1	90.4(3)	O1–Mn1–N2	96.8(3)
O2–Mn1–O3	93.3(3)	O2–Mn1–O4	171.7(3)
O2–Mn1–N1	94.9(3)	O2–Mn1–N2	91.1(3)
O3–Mn1–O4	94.9(3)	O3–Mn1–N1	87.8(3)
O3–Mn1–N2	85.7(3)	O4–Mn1–N1	86.7(3)
O4–Mn1–N2	88.3(3)	N1–Mn1–N2	171.4(3)
O1–Mn2–O5	173.9(3)	O1–Mn2–O6	92.5(2)
O1–Mn2–N3	93.0(3)	O1–Mn2–N4	96.9(3)
O2–Mn2–O5	93.5(3)	O2–Mn2–O6	171.9(3)
O2–Mn2–N3	97.0(3)	O2–Mn2–N4	90.6(3)
O5–Mn2–O6	93.6(2)	O5–Mn2–N3	86.8(3)
O5–Mn2–N4	84.0(3)	O6–Mn2–N3	87.3(3)
O6–Mn2–N4	86.3(3)	N3–Mn2–N4	168.4(3)

which is a novel asymmetric di-μ-oxo dimanganese(IV) complex. The bond length and angles of **1** resemble to the complex of type II. These structural differences around Mn ions are strongly correlated to electronic spectra, IR spectra, and electrochemical and magnetic properties (*vide infra*).

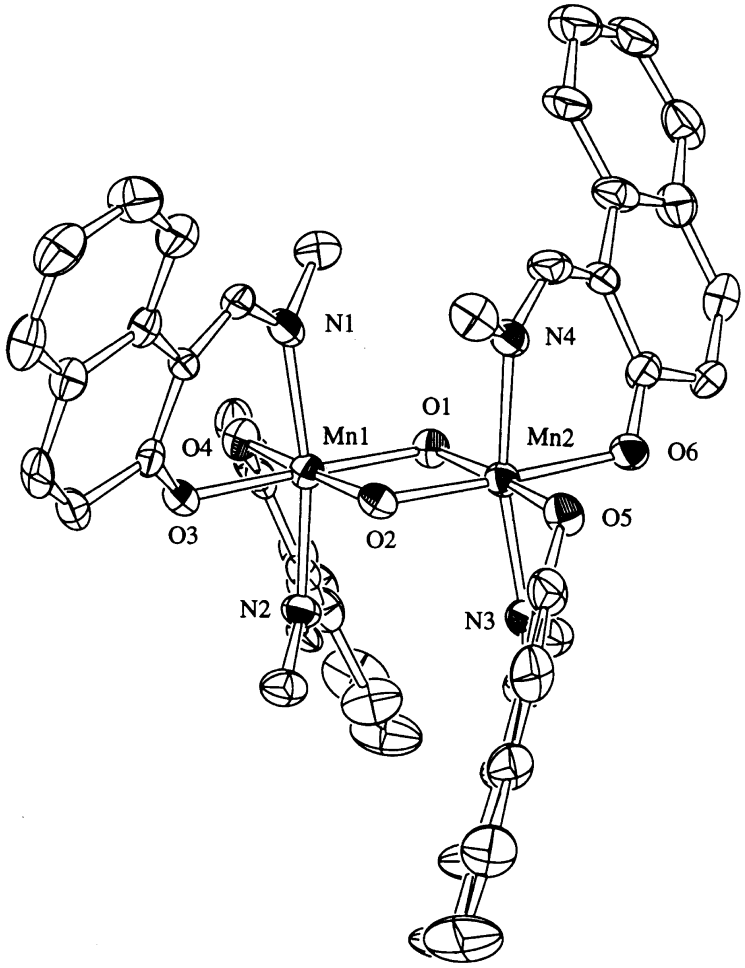

Fig. 5. Molecular structure of $[Mn^{IV}(N\text{-Me-5,6-benzo-sal})_2(\mu\text{-O})]_2$, **10**.

Electronic spectra

The electronic spectrum of the asymmetric di-μ-oxo dimanganese complex, **1**, is different from the other complexes, $[Mn^{IV}(N\text{–R-sal})_2(\mu\text{-O})]_2$ (R = Et-Dod), **2–8**. Further, the spectra of these symmetric complexes are almost the same. Figure 6 shows the electronic spectra of **1** and **8** in dichloromethane (CH_2Cl_2). The absorption bands appearing in the region 400 nm and below are thought to be associated mainly with the ligand transitions. In the visible and near-IR region, the spectra of **1** and **8** exhibit two or four absorption bands around 493 ($\varepsilon = 11100\,M^{-1}\,cm^{-1}$) and 708 nm ($\varepsilon = 477\,M^{-1}\,cm^{-1}$) for **1**, and 402 ($\varepsilon = 13150\,M^{-1}\,cm^{-1}$), 480 nm ($\varepsilon = 8760\,M^{-1}\,cm^{-1}$), 694 ($\varepsilon = 615\,M^{-1}\,cm^{-1}$), and 846 nm ($\varepsilon = 162\,M^{-1}\,cm^{-1}$) for **8**, respectively. Based on the intensities and positions, the absorption bands around 400 and 500 nm can be assigned to the ligand to metal charge-transfer transitions from oxygen atoms of the oxo groups to manganese atoms and the bands around 700 and 850 nm can be assigned to the d–d transitions. The peaks at near-IR region are characteristic to the di-μ-oxo dimanganese(IV) complexes with bidentate Schiff base ligands but not observed for the di-μ-oxo dimanganese(IV) complexes with tetradentate Schiff base ligands [24]. Particularly, the intensity and position of the d–d transition band around 850 nm for **8** resemble to the spectra of tris(bidentate ligand) manganese(III) complex, $Mn^{III}(N\text{-Dod-sal})_3$ and of tetranucler manganese(III) complex, Mn^{III}_4-(salmphen)$_6$ (salmphenH_2 = *N*,*N*′-disalicylidene-1,3-diaminobenzene) [29]. Consequently, two types between the di-μ-oxo dimanganese complexes of bidentate and tetradentate Schiff base ligands are found to be discriminative from their electronic spectra. The electronic spectrum of the symmetric complex **10** resembles to those of **2–8**. These results are consistent with those obtained from the structural analyses. On the other hand, the electronic spectrum of **9**

Table 7. Selected interatomic distances (Å) and angles (°) for **10**

Mn1–Mn2	2.756(3)	Mn1–O1	1.830(9)
Mn1–O2	1.814(9)	Mn1–O3	1.928(10)
Mn1–O4	1.927(9)	Mn1–N1	2.00(1)
Mn1–N2	2.00(1)	Mn2–O1	1.821(9)
Mn2–O2	1.831(9)	Mn2–O5	1.912(9)
Mn2–O6	1.933(10)	Mn2–N3	1.99(1)
Mn2–N4	2.01(1)		
Mn1–O1–Mn2	98.0(4)	Mn1–O2–Mn2	98.2(4)
O1–Mn1–O2	82.0(4)	O1–Mn2–O2	81.8(4)
O1–Mn1–O3	175.0(4)	O1–Mn1–O4	93.3(4)
O1–Mn1–N1	93.1(4)	O1–Mn1–N2	94.9(4)
O2–Mn1–O3	93.0(4)	O2–Mn1–O4	175.2(4)
O2–Mn1–N1	94.5(4)	O2–Mn1–N2	93.8(4)
O3–Mn1–O4	91.7(4)	O3–Mn1–N1	87.0(5)
O3–Mn1–N2	85.7(5)	O4–Mn 1–N1	86.5(4)
O4–Mn1–N2	85.7(4)	N1–Mn1–N2	169.2(5)
O1–Mn2–O5	173.6(4)	O1–Mn2–O6	93.0(4)
O1–Mn2–N3	93.9(4)	O1–Mn2–N4	94.9(4)
O2–Mn2–O5	91.8(4)	O2–Mn2–O6	174.7(4)
O2–Mn2–N3	94.9(4)	O2–Mn2–N4	94.2(4)
O5–Mn2–O6	93.4(4)	O5–Mn2–N3	86.6(5)
O5–Mn2–N4	85.5(5)	O6–Mn2–N3	86.1(4)
O6–Mn2–N4	85.6(5)	N3–Mn2–N4	168.1(5)

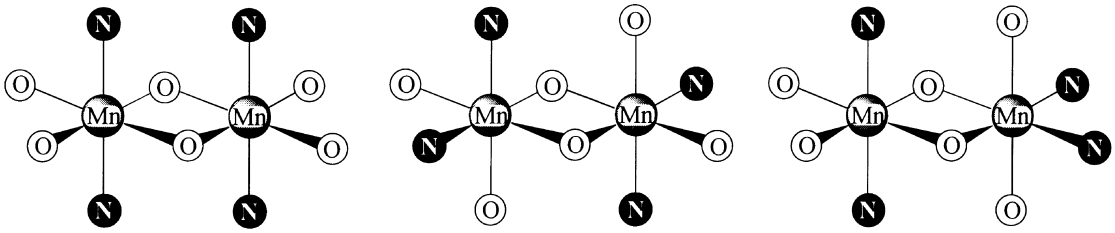

Scheme 1. Three types of $N_2O_2(\mu\text{-}O)_2$ ligation sphere for di-μ-oxo dimanganese(IV) complexes with various Schiff bases.

resembles to that of **1** compared with those observed for **2–8**. Numerical data for the electronic spectra of all the complexes are listed in Table 8.

IR spectra

It has been reported that IR spectra of the di-μ-oxo dimanganese(IV) complexes exhibit sharp absorption bands characteristic for a $Mn_2(\mu\text{-}O)_2$ core in the region around 600–700 cm^{-1}, which can be assigned to stretching vibrations of $Mn–O_{oxo}$ bonds [30]. Figure 7 shows the IR spectra of **1**, **2** and **8** in this region which exhibit an intense and two medium bands at 653, 620 and 600 cm^{-1} for **1** and two intense and one medium bands at 641, 620 and 597 cm^{-1} for **2**, and at 633, 620 and 601 cm^{-1} for **8**. The highest energy peak shifts to lower energies along with an increase in the alkyl chain length of these bidentate Schiff bases. These results are consistent with the crystallographic observations: Mn–Mn distances are separated with the same order. With exception for the intense peaks due to *n*-alkyl groups, the spectra of the complexes, **2–9**, are almost same over the region of 4000 to 400 cm^{-1}. On the other hand, in the region of 1300 to 800 cm^{-1} the spectrum of **1** is significantly different from the others. Numerical data for the IR spectra of all the complexes are listed in Table 8.

In the IR spectrum of the product obtained by heating **8** at 137°C for 1 h in vacuo, the intense band (633 cm^{-1}) disappeared without significant changes in other peaks. The resulting spectrum (Figure 7, spec-

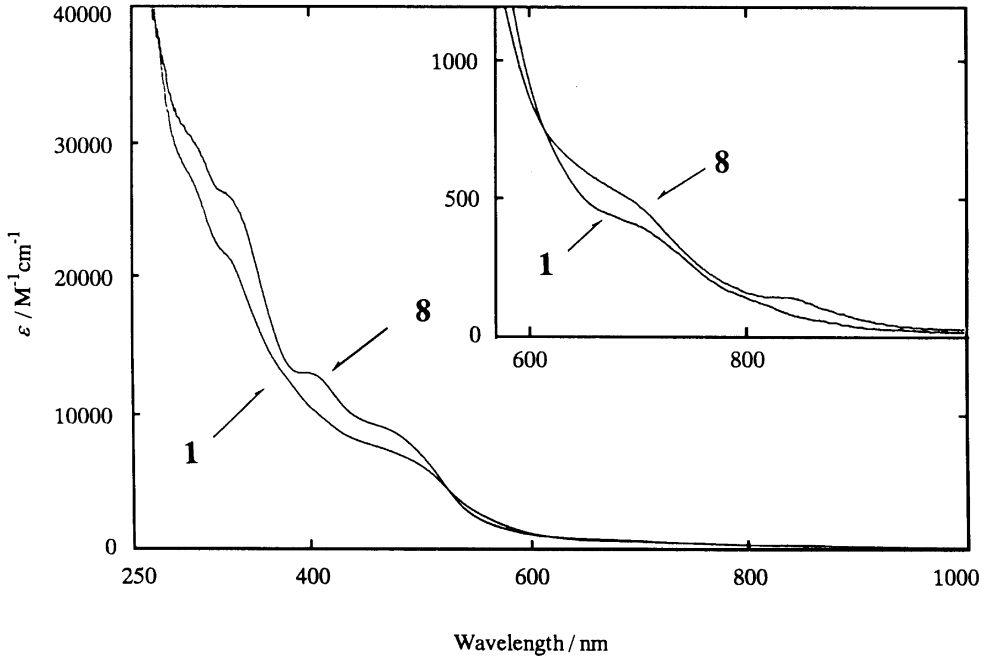

Fig. 6. Electronic absorption spectra of **1** and **8** in CH_2Cl_2.

Table 8. Physicochemical properties of $[Mn(N\text{–R-X-sal})_2(\mu\text{-O})_2]_2$

R, X	$\nu[Mn_2(\mu-O)_2]$[a] (cm^{-1})	λ_{max}[b] (nm)	μ_{eff}/Mn_2[c] (μ_B)	DSC peak[d] (°C)
Me, H (**1**)·2MeCN	653, 620, 600	298$^{(sh)}$, 333$^{(sh)}$, 493, 699	2.86	80.8[e], 126.8
Et, H (**2**)	641, 620, 597	295$^{(sh)}$, 331, 410, 481, 692$^{(sh)}$, 837	2.39	169.7
Pr, H (**3**)	634, 620, 601	298$^{(sh)}$, 336, 413, 487, 695$^{(sh)}$, 843	2.12	168.8
Bu, H (**4**)	632, 619, 600	297$^{(sh)}$, 333, 410, 483, 693$^{(sh)}$, 839	2.07	149.7
Hx, H (**5**)	632, 620, 606	302$^{(sh)}$ 334, 408, 486, 689$^{(sh)}$, 843	2.16	145.7
Oct, H (**6**)	632, 621, 602	301$^{(sh)}$, 332, 409, 488, 684$^{(sh)}$, 839	2.18	131.2
Dec, H (**7**)	632, 620, 600	300$^{(sh)}$, 333, 411, 488, 698$^{(sh)}$, 841	1.86	126.2
Dod, H (**8**)	632, 620, 601	299$^{(sh)}$, 333, 408, 486, 694$^{(sh)}$, 842	2.57	124.1
Octd, H (**9**)	629, 620, 603	300$^{(sh)}$, 334, 498$^{(sh)}$, 708$^{(sh)}$	2.53	110.8[e], 118.8
Me, 5,6-benzo·2MeCN (**10**)	649, 637, 631, 607	316, 363$^{(sh)}$, 449, 543$^{(sh)}$, 838	2.29	176.1
Et, 5,6-benzo·2MeCN	649, 635, 603	315, 363$^{(sh)}$, 442, 525$^{(sh)}$, 840	2.31	147.5
Pr, 5,6-benzo·2MeCN	649, 634, 606	316, 371$^{(sh)}$, 449, 525$^{(sh)}$, 838	2.19	152.7
Bu, 5,6-benzo·2MeCN	653, 636, 605	316, 370$^{(sh)}$, 448, 524$^{(sh)}$, 843	2.22	157.7
Hx, 5,6-benzo	654, 634, 608	317, 364$^{(sh)}$, 448, 523$^{(sh)}$, 840	2.23	157.3
Oct, 5,6-benzo	642, 625, 596	317, 369$^{(sh)}$, 455, 524$^{(sh)}$, 847	2.33	137.8
Dec, 5,6-benzo	641, 625, 596	308, 384$^{(sh)}$, 487	3.11	143.8
Dod, 5,6-benzo	641, 623, 596	308, 391$^{(sh)}$, 485	2.89	147.2
Octd, 5,6-benzo	641, 623, 595	306, 398, 421$^{(sh)}$, 491	3.29	137.5

[a]KBr pellet. [b]Measured in CH_2Cl_2. [c]Measured at room temperature (300 K). [d]With decomposition. [e]Endothermic peak.

trum A) resembled to that of $Mn^{III}(N\text{-Dod-sal})_3$ complex [29]. These results suggest that the bridging oxygen atoms were released from the di-μ-oxo dimanganese(IV) complexes by heating.

Electrochemistry

Cyclic voltammograms (CV) of these complexes were measured in CH_2Cl_2 over the range from +1.30

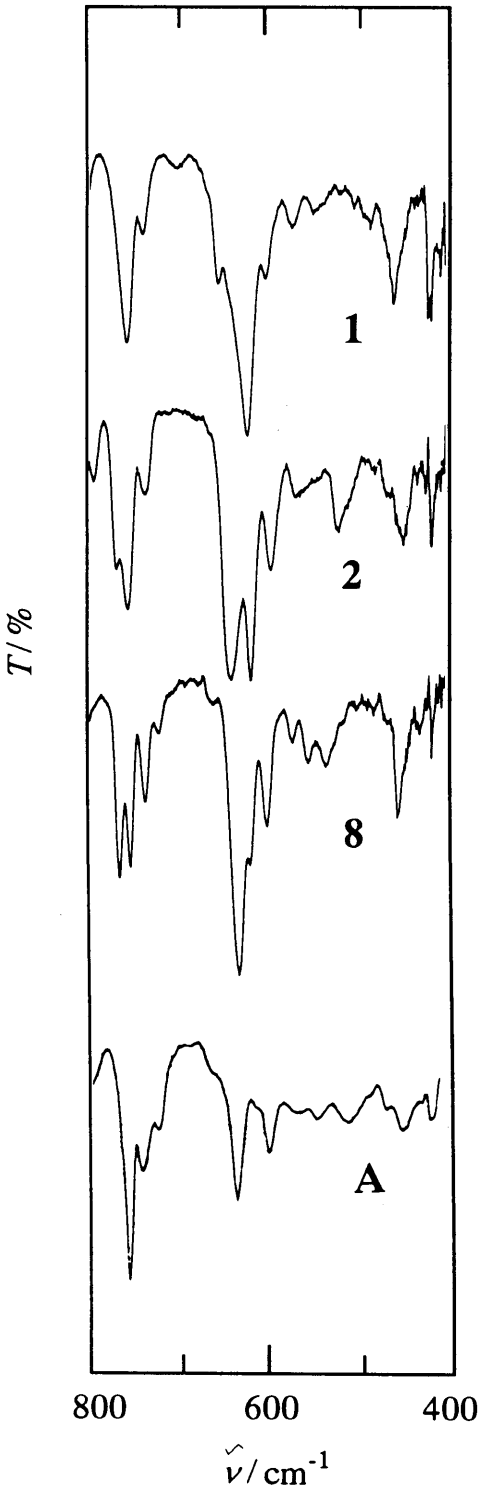

Fig. 7. IR spectra of **1**, **2**, **8** and the product obtained by heating 8 at 137°C for 1 h in *vacuo* (A).

to −1.70 V vs SCE. As shown in Fig. 8, the CVs of **1** and **5** exhibit multistage quasi-reversible redox waves and are relatively indistinct compared with those observed for the complexes with tetradentate Schiff bases [23]. Three reduction peaks are observed at the potentials of −0.24, −0.54 and −0.70 V vs SCE for 1 and −0.17, −0.41 and −0.75 V vs SCE for **5**. The CVs of other complexes, **2–8**, are almost the same feature as that of **5**. On the other hand, the CV of **9** resembles to that of **1**. These results suggest that these complexes are reduced electrochemically stepwise in a CH_2Cl_2 solution: Mn(IV)Mn(IV)→Mn(IV)Mn(III)→Mn(III)Mn(III) or Mn(IV)Mn(II)→Mn(III)Mn(II). The last reduction step may accompany with some decomposition, because this step is electrochemically irreversible.

Magnetic properties

For all the di-μ-oxo dimanganese(IV) complexes, magnetic susceptibility measurements on powdered samples were carried out at room temperature (300 K) and the magnetic moments are listed in Table 8. The temperature dependence of the effective magnetic moments of **1** and **7** are shown in Figs. 9 and 10. The effective magnetic moments (μ_{eff}) of **1** and **7** have been found to decrease from 2.86 μ_B at 300 K to 0.211 μ_B at 1.8 K for **1** and from 1.86 μ_B at 300 K to 0.226 μ_B at 1.8 K for **7**, respectively. In the temperature range 50–300 K, their magnetic moments decrease as a function of temperature. These magnetic behavior indicates that an intramolecular antiferromagnetic interaction between the two manganese(IV) ions (d^3) exists in these complexes. The anomalous magnetic behavior has been observed for the complexes below 50 K, which have arisen from paramagnetic and/or weaker antiferromagnetic impurities. Such magnetic behavior at lower temperatures may also be explained in terms of intermolecular interactions, however, which can be ruled out in the cases of the present complexes because the central manganese ions are effectively separated from other ones by alkyl groups. The magnetic data obtained for **1** and **7** (Figures 9–10) were fitted by employing an expression derived from an isotropic spin-exchange Hamiltonian $H = -2JS_1 \cdot S_2$ ($S_1 = S_2 = 3/2$) and the Van Vleck equation. The curve fitting leads to values of $J = -83\,cm^{-1}$, $g = 1.83$, $TIP = 4.0 \times 10^{-4}$ and $P = 0.16\%$ for **1** and $J = -188\,cm^{-1}$, $g = 1.81$, $TIP = 4.5 \times 10^{-4}$ and $P = 0.18\%$ for **7**, where TIP is the temperature-independence paramagnetism and P is the mole percent of paramagnetic impurities assumed to be a mononuclear manganese(III) complex. The lower J value for the complex **1** is close to those for the di-μ-oxo dimanganese(IV) complexes with tetradentate Schiff base ligands [23] and $[Mn(pic)_2(O)]_2$, picH = picolinic acid [6], which fall within the relatively narrow range of −78 to $-88\,cm^{-1}$. On the other hand, the J value for **7** is markedly higher than those reported for several other $Mn^{IV}_2(\mu\text{-}O)_2$ cores, which have J values of $-150\,cm^{-1}$ and below. Furthermore, the curve fittings of the complexes, **2**, **5** and **10** lead to values

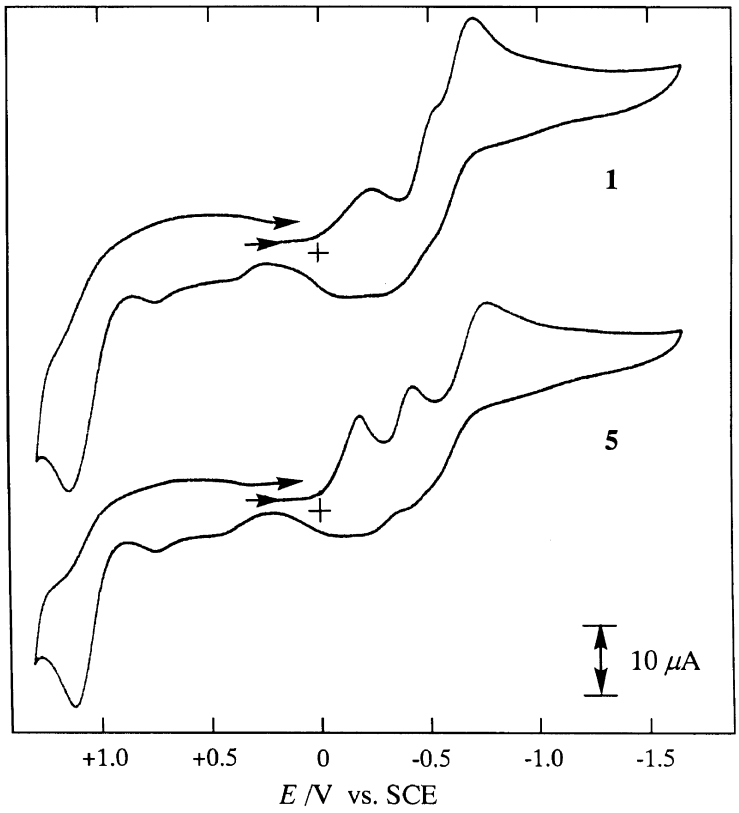

Fig. 8. Cyclic voltammograms (CV) of **1** and **5** in CH_2Cl_2.

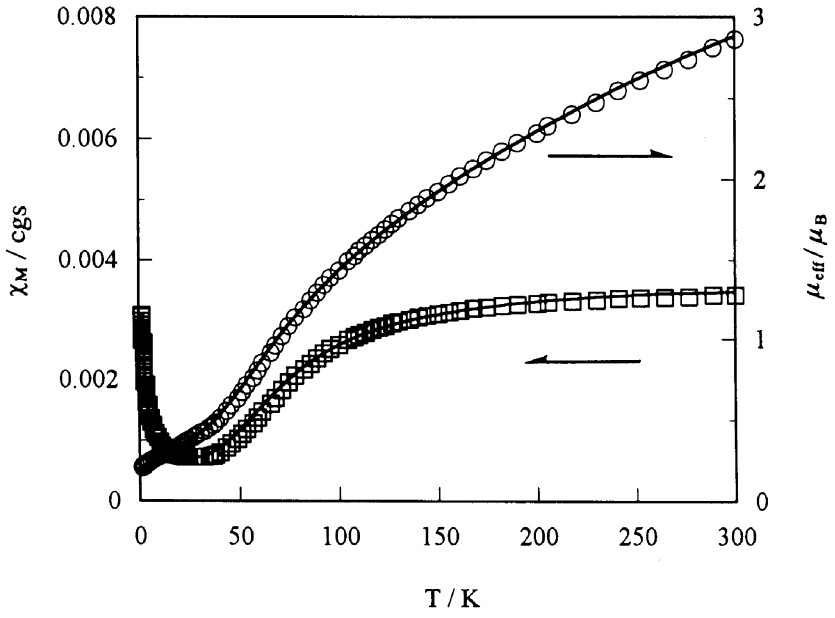

Fig. 9. Plots of χ_M and μ_{eff} of **1** per dimer vs temperature.

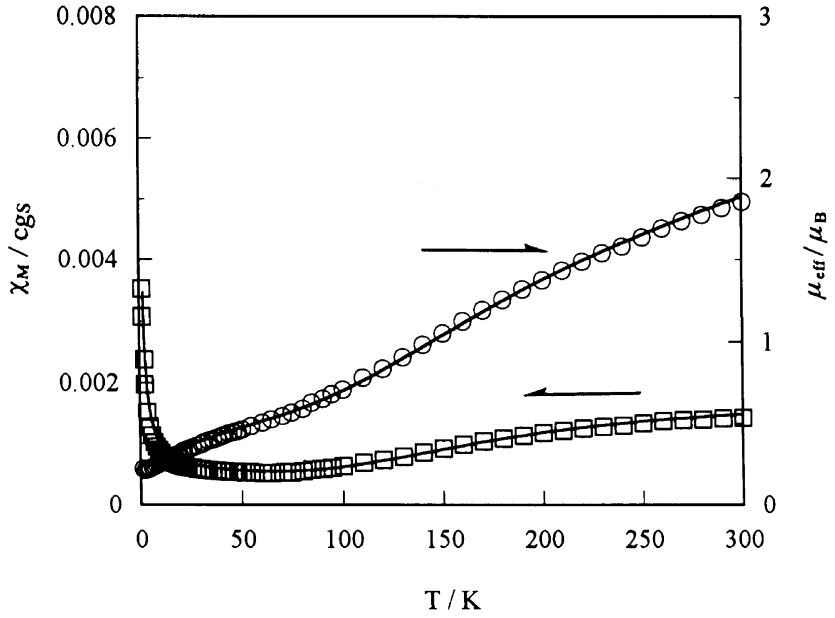

Fig. 10. Plots of χ_M and μ_{eff} of **7** per dimer vs temperature.

$J=-150\,cm^{-1}$, $g=1.90$, $P=3.5\%$ and TIP $=4.8\times10^{-4}$ for **2**, $J=-170\,cm^{-1}$, $g=1.85$, $P=0.08\%$ and TIP $=7.4\times10^{-4}$ for **5**, and $J=-119\,cm^{-1}$, $g=1.80$, $P=0.13\%$ and TIP $=2.5\times10^{-4}$ for **10**, respectively.

In the previous papers, a strong correlation between Mn–Mn distance and a magnetic exchange parameter J value for several $[Mn_2(\mu\text{-}O)_2]^{n+}$ ($n=2$, 3, 4) complexes has been discussed [4, 6, 17, 31]. However, in the case of the $Mn^{IV}{}_2(\mu\text{-}O)_2$ complex, the correlation is poor: for example, although $[Mn^{IV}(phen)_2(\mu\text{-}O)]_2^{4+}$ (phen = 1,10-phenanthroline) [5] and $[Mn^{IV}(pic)_2(\mu\text{-}O)]_2$ [6] have almost the same Mn–Mn distance [2.748(2) and 2.747(2) Å, respectively], their antiferromagnetic exchange parameters are remarkably, different, which are -144 and $-87\,cm^{-1}$, respectively. These complexes have different ligation spheres each other, and there is a limited number of the structurally characterized di-μ-oxo dimanganese(IV) complexes so far.

Table 9 shows structural data and magnetic exchange parameter J for structurally characterized di-μ-oxo dimanganese(IV) complexes with a series of bidentate or tetradentate Schiff base ligands. All of the complexes have a $N_2O_2(\mu\text{-}O)_2$ ligation sphere. The complexes with tetradentate Schiff base ligands and **1** exhibit almost same J values, within the range of -78 to $-88\,cm^{-1}$, their Mn–Mn distance, however, are appreciably different (2.705–2.732 Å). On the other hands, the complexes having large Mn–Mn separation, **2**, **5** and **7** (2.769–2.780 Å), which have strong antiferromagnetic exchange in the range of -150 to $-188\,cm^{-1}$.

From the structural data and the magnetic exchange parameter, shown in Table 8, we could suggest that the di-μ-oxo dimanganese(IV) complexes having larger antiferromagnetic exchange parameter J do have larger Mn–O_{oxo}–Mn angles. The Mn–O_{oxo}–Mn angles for the complex with tetradentate Schiff base ligand and **1** are almost constant (96.2–97.6°), although these complexes have different Mn–Mn separation. The complexes having larger antiferromagnetic exchange, **2**, **5** and **7**, do have larger Mn–O_{oxo}–Mn angles. The angles for **7** [99.7(3) and 100.5(3)°] are larger than **2** [99.1(2) and 99.5(2)°], which is consistent with the difference of J value.

These results suggest that in these compounds dose not rule out a contribution to antiferromagnetic exchange parameter J from Mn–Mn distance (direct d_{xy}–d_{xy} orbital overlap, where the x and y axes are coincident with Mn–(μ-O) bonds), although parameter J has a strong correlation with Mn–O_{oxo}–Mn angles (superexchange coupling via two bonding O atoms). A recent paper has pointed out that in the $Mn_2^{IV/IV}$ system, the longer Mn–Mn separation and the more acute Mn–O_{oxo}–Mn angle will lead to larger exchange parameters, based on the molecular orbital calculations for the di-μ-oxo manganese(IV) complexes, $[Mn(NH_3)_4(\mu\text{-}O)]_2^{n+}$ ($n=2$, 3, 4) [32]. Therefore, a systematic preparation of di-μ-oxo manganese(IV) complexes and their characterization should be needed for much more detailed discussion.

Thermal analysis (differential scanning calorimetry (DSC) and thermogravimetric and differential thermal analysis (TG-DTA))

These dimanganese(IV) complexes having linear-alkyl groups possess good solubility in organic sol-

Table 9. Inter-metal distances (Å), angles (°) and J values of di-μ-oxo dimanganese(IV) complexes with Schiff base ligands

Complex	Mn–Mn (Å)	Mn–O_{oxo} (Å)	Mn–O_{oxo}–Mn (°)	O_{oxo}–Mn–O_{oxo} (°)	J[a] (cm^{-1})	Ref.
Tetradentate Schiff bases						
[Mn(μ-salopnen)(μ-O)]$_2$	2.718(2)	1.811–1.822	96.9	83.1	−80	[24]
[Mn(μ-salen)(μ-O)]$_2$	2.705(2)	1.815–1.818	96.2	83.8	−80	[24]
[Mn(salipn)(μ-O)]$_2$	2.732(3)	1.804–1.828	97.6	82.4	−88	[24]
[Mn(salbn)(μ-O)]$_2$	2.729(1)	1.819–1.826	96.9	83.1	−78	[24]
[Mn(salpn)(μ-O)]$_2$	2.728(1)	1.816–1.822	97.2	82.8	−82	[13]
Bidentate Schiff bases						
1	2.731(4)	1.80–1.83	97.3,97.6	81.7,83.4	−83	this work
2	2.769(2)	1.814–1.820	99.5,99.1	80.7	−150	this work
5	2.780(2)	1.815–1.826	99.5,99.9	80.4,80.2	−170	this work
7	2.780(2)	1.794–1.825	99.7,100.5	79.3,80.5	−188	this work
10	2.756(3)	1.814–1.831	98.0,98.2	81.8,82.0	−119	this work

[a] Based on the spin Hamiltonian $H = -2JS_1 \cdot S_2$.

vents and relatively lower melting points with (without) some decomposition compared to those of the corresponding manganese(IV) complexes with tetradentate Schiff base ligands. Thus, the thermal properties of the present manganese(IV) complexes have been studied. The DSC curve of **9** measured over the temperature range of 25 to 250°C shows both endothermic (110.8°C) and exothermic peaks (118.8°C), which can be assigned to melting and partial decomposition of the complex, respectively. However, the DSC curves of the other symmetric complexes show only exothermic peak at 124.1 (**8**), 126.2 (**7**), 131.2 (**6**), 145.7 (**5**), 149.7 (**4**), 168.8 (**3**), and 169.7°C (**2**). On the other hand, the asymmetric complex **1**·2MeCN exhibits both endothermic (80.8°C) and exothermic peaks (126.8°C) at lower temperature than **3–6**, which can be assigned to dissociation of a crystal solvent (MeCN) and partial decomposition of the complex, respectively. It is conceivable that the lower DSC temperature may arise from its asymmetrical structure. The temperatures of the DSC peaks of all the complexes are listed in Table 8.

The TG-DTA curves of **3** shown in Fig. 11, exhibit a clear weight loss of 4.2% at 174°C) accompanying an exothermic reaction, which corresponds to the calculated value (4.05%) expected for the release of two μ-oxo oxygen atoms from the complex. Similar results were obtained for the complexes of **2** and **4**, but the corresponding weight losses for the other complexes, **5–9**, were slightly less than the calculated values for the release of two oxygen atoms: this may be caused by the difficulty in diffusion of dissociated oxygen atoms from the molten state of the complexes under the thermal analysis conditions in a stream of air. In fact, when these complexes were heated in a vacuum oven for 1 h at higher temperatures by 10°C than those of their exothermic peaks, the weight losses have been

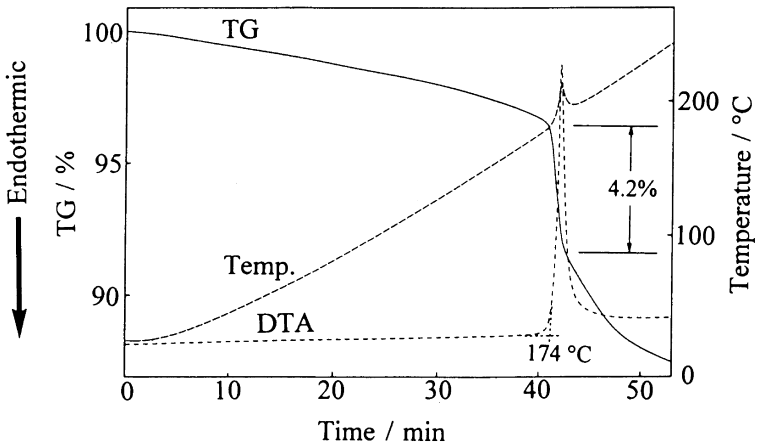

Fig. 11. TG-DTA curves of [Mn^{IV}(N-Pr-sal)$_2$(μ-O)]$_2$, **3**. Heating rate: 5°C/min in flowing air (60 ml/min).

found to correspond to the amount of two oxygen atoms per di-μ-oxo dimanganese complex.

CONCLUSIONS

In the present study, a series of di-μ-oxo dimanganese(IV) complexes with bidentate *N*-alkyl-substituted-salicylideneamine, *N*–R–X-salH, has been prepared and characterized. When R is Me (X = H), the configurations around two manganese ions have been found to be nonsymmetric toward a $Mn_2(\mu\text{-}O)_2$ core, whereas other complexes adopt a symmetric configuration. It is noteworthy that the asymmetric type is the first example, whereas all of the di-μ-oxo dimanganese(IV) complexes reported previously are a symmetrical type.

The results obtained from the X-ray structure analysis and the temperature dependent magnetic susceptibility measurements indicate that intramolecular antiferromagnetic interactions are correlated to both Mn–Mn separation and $Mn–O_{oxo}–Mn$ angles of a di-μ-oxo core. Furthermore, all of the complexes are found to release μ-oxo oxygen atoms by heating.

REFERENCES

1. Yachandra, V. K., Sauer, K. and Klein, M. R., *Chem. Rev*., 1996, **96,** 2927.
2. Pecoraro, V. L. (Ed.), *Manganese Redox Enzymes*. VCH Publishers, New York, 1992.
3. Yachandra, V. K., DeRose, V. J., Latimer, M. J., Mukerji, I., Sauer, K. and Klein, M. P., *Science*, 1993, **260,** 675.
4. Manchanda, R., Brudvig, G. W. and Crabtree, R. H., *Coord. Chem. Rev*., 1995, **144,** 1.
5. Stebler, M., Ludi, A. and Bürgi, H.-B., *Inorg. Chem*., 1986, **25,** 4743.
6. Libby, E., Webb, R. J., Streib, W. E., Folting, K., Huffman, J. C., Hendrickson, D. N. and Christou, G., *Inorg. Chem*., 1989, **28,** 4037.
7. Goodson, P. A., Glerup, J., Hodgson, D. J., Michelsen, K. and Pedersen, E., *Inorg. Chem*., 1990, **29,** 503.
8. Oki, A. R., Glerup, J. and Hodgson, D. J., *Inorg. Chem*., 1990, **29,** 2435.
9. Bossek, U., Weyhermüller, T., Wieghardt, K. and Nuber, B., Weiss, J., *J. Am. Chem. Soc*., 1990, **112,** 6387.
10. Larson, E. J. and Pecoraro, V. L., *J. Am. Chem. Soc*., 1991, **113,** 3810.
11. Sarneski, J. E., Didiuk, M., Thorp, H. H., Crabtree, R. H., Brudvig, G. W., Faller, J. W. and Schulte, G. K., *Inorg. Chem*., 1991, **30,** 2833.
12. Goodson, P. A., Glerup, J., Hodgson, D. J., Michelsen, K. and Weihe, H., *Inorg. Chem*., 1991, **30,** 4909.
13. Gohdes, J. W. and Armstrong, W. H., *Inorg. Chem*., 1992, **31,** 368.
14. Larson, E. J., Lah, M. S., Li, X., Bonadies, J. A. and Pecoraro, V. L., *Inorg. Chem*., 1992, **31,** 373.
15. Pal, S., Gohdes, J. W., Wilisch, W. C. A. and Armstrong, W. H., *Inorg. Chem*., 1992, **31,** 713.
16. Pal, S. and Armstrong, W. H., *Inorg. Chem*., 1992, **31,** 5417.
17. Pal, S., Chan, M. K. and Armstrong, W. H., *J. Am. Chem. Soc*., 1992, **114,** 6398.
18. Pal, S., Olmstead, M. M. and Armstrong, W. H., *Inorg. Chem*., 1995, **34,** 4708.
19. Bermejo, M. R., Castineiras, A., Garicia-Monteagudo, J. C., Rey, M., Sousa, A., Watkinson, M., McAuliffe, C. A., Pritchard, R. G. and Beddoes, R. L., *J. Chem. Soc*., *Dalton Trans*., 1996, 2935.
20. Wieghardt, K., *Angew. Chem. Int. Ed. Engl*., 1994, **33,** 725.
21. Wieghardt, K., *Angew. Chem. Int. Ed. Engl*., 1989, **28,** 1153.
22. Torayama, H., Nishide, T., Asada, H., Fujiwara, M. and Matsushita, T., *Chem. Lett*., 1996, 387.
23. Torayama, H., Asada, H., Fujiwara, M. and Matsushita, T., *Chem. Lett*., 1996, 1067.
24. Torayama, H., Nishide, T., Asada, H., Fujiwara, M. and Matsushita, T., *Polyhedron*, 1998, **17,** 105.
25. Matsushita, T., Hirata, Y. and Shono, T., *Bull. Chem. Soc. Jpn*., 1982, **55,** 108.
26. TEXSAN, Single crystal structure analysis package, molecular corporation, 1985 and 1992.
27. Sheldrick, G. M., in: Crystallographic Computing 3, ed. G. M. Sheldrick, C. Kruger and R. Goddard. Oxford University Press, 1985, 175.
28. Beurskens, P. T., Admiraal, G., Beurskens, G., Bosman, W. P., de Gelder, R., Israel, R., Smits, J. M. M. and Smykalla C., The DIRDIF-94 program system. Technical Report of the Crystallography Laboratory, University of Nijmegen, The Netherlands, 1994.
29. Torayama, H., Nishide, T., Asada, H., Fujiwara, M. and Matsushita, T., *Polyhedron*, 1997, **16,** 3787.
30. Matsushita, T., Spencer, L. and Sawyer, D. T., *Inorg. Chem*., 1988, **27,** 1167.
31. Thorp, H. H. and Brudvig, G. W., *New J. Chem*., 1991, **15,** 479.
32. McGrady, J. E. and Stranger, R., *J. Am. Chem. Soc*., 1997, **119,** 8512.

Pergamon

PII: S0277-5387(98)00146–6

Polyhedron Vol. 17, No. 22, pp. 3875–3880, 1998
© 1998 Elsevier Science Ltd
All rights reserved. Printed in Great Britain
0277–5387/98 $19.00+0.00

Crystal structure, magnetic properties and ESR studies of $(4\text{-apyH})_4[Cu^{II}Br_4][Cu^{I}Br_2]_2$: a novel Cu(II)/Cu(I) system containing bromocuprate(I) chains and isolated tetrabromocuprate(II) anions

Jon Sertucha,[a] Antonio Luque,[a] Francesc Lloret[b] and Pascual Román[a]*

[a]Departamento de Química Inorgánica, Facultad de Ciencias, Universidad del País Vasco, Apartado 644, E-48080 Bilbao, Spain; [b]Departament de Química Inorgànica, Facultat de Química de la Universitat de València, Dr. Moliner 50, E-46100 Burjassot Valencia, Spain

Received 11 March 1998; accepted 16 April 1998

Abstract—The synthesis, crystal structure, ESR spectra and magnetic properties are reported for the Cu(I-I)/Cu(I) compound $(4\text{-apyH})_4[Cu_3Br_8]$ (4-apyH = $C_5H_7N_2$ = 4-aminopyridinium). Single-crystals of the compound were grown by slow diffusion of *n*-hexane on an ethanolic solution of $(4\text{-apyH})_2[CuBr_4]\cdot H_2O$. The crystal structure is made up of organic cations, isolated $[Cu^{II}Br_4]^{2-}$ anions and infinite $[Cu^{I}Br_2]_n^{n-}$ chains composed of edge-sharing $Cu^{I}Br_4$ tetrahedra. N–H $\cdots$ Br hydrogen bond interactions between organic counter cations and inorganic anionic units are present and contribute to the cohesiveness of the crystal packing. Magnetic susceptibility measurements showed a good isolation of Cu(II) with a normal Curie behaviour in all the temperature range with $C = 0.44\,cm^3\,K\,mol^{-1}$ and $\theta \approx -1\,K$. ESR experiments were made at different temperatures and showed an isotropic signal ($g = 2.154$) operating at the X-band, which was resolved towards an axial-type ($g_{\parallel} = 2.31$, $g_{\perp} = 2.10$, $\langle g \rangle = 2.17$) signal at the Q-band. © 1998 Elsevier Science Ltd. All rights reserved

Keywords: bromocuprate; crystal structure; magnetic properties.

Mixed-valence inorganic systems have been of great interest to chemists for a long time because they display intriguing physical and chemical properties, provide valuable information on electron-transfer reactions and serve as possible models in a large range of chemical and biochemical catalytic systems [1]. Cu(II)/Cu(I) systems present an additional interest, because both oxidation states are labile, stereochemically flexible and show a wide range of coordination numbers and geometries. From these reasons, the chemistry of these mixed-valence compounds has been received considerable attention in the last few years and a number of Cu(II)/Cu(I) compounds have been synthesised and their structures determined by X-ray diffraction methods [2–9].

* Author to whom correspondence should be addressed. Tel.: + 34-94-464-7700; Fax: +34-94-464-8500; E-mail: qipropop@lg.ehu.es.

We report here the synthesis, X-ray crystal structure, ESR spectroscopic and magnetic characterisation of a novel Cu(II)/Cu(I) compound $(4\text{-apyH})_4[Cu_3Br_8]$ showing isolated $[Cu^{II}Br_4]^{2-}$ anions and polymeric $[CuBr_2]_n^{n-}$ chains. Crystal structures containing infinite chains of $Cu^{I}X_4$ tetrahedra sharing edges and with $[CuX_2]^-$ stoichiometry have been observed very rarely. An exhaustive search in 1997 update of Version 5.14 of the Cambridge Structural Database (CSD) [10] gave several crystal structures [11–13] with $[Cu^{I}I_2]_n^{n-}$ but no analogous chloro- or bromo-chains were found. The compounds [Cu(cnge)] $[CuBr_2]$ [14] (cnge = 1-cyanoguanidine) and $[Cu_2(\mu\text{-formate})_2(\eta\text{-2-aminoallyl})_2][Cu_2Br_4]$ [15] contain $[Cu^{I}Br_2]_n^{n-}$ chains but in both one of the bridging bromine atoms is coordinated to the cationic copper(I) complex which leads to structural features significantly different than those reported for the title compound. Three compounds containing mixed-valence [Cu^{I}

$Cu^{II}Br_4]_n^{n-}$ chains [7] and one compound with a neutral $[Cu^{II}Br_2]$ chain [16] are known.

RESULTS AND DISCUSSION

Deep violet single-crystals of a compound having the stoichiometry $(4\text{-apyH})_4[Cu_3Br_8]$ have been obtained as unique product during the slow diffusion of *n*-hexane in an ethanolic solution of the compound $(4\text{-apyH})_2[CuBr_4]\cdot H_2O$ [17]. The observed stoichiometry seems to indicate a complicated Cu(II)/Cu(I) system in which two third of the copper ions have to be present in the univalent state and the other third in the bivalent state, but does not indicate whether or not the valences are localised. However, the non-existence of significant couplings in the magnetic behaviour of the compound, as stated below, suggests the absence of direct interactions between the Cu(II) centres.

The formation of Cu(II)/Cu(I) species have been also observed in the reaction of the $CuBr_2$/HBr mixture with tris(1-pyrazolyethyl)amine [18], 6-amino-1,3-dimethyl-5[(2-carboxyphenyl)azo]uracil [6] or 3-aminopyridines [19]. It has been surmised that the Cu(I) ion may be generated by a reaction involving the decomposition of $CuBr_2$ to CuBr and Br_2. Indeed, *para*-bromination of the aromatic ring respect to the amino substituting is produced in the reaction of $CuBr_2$/HBr mixture with 2-amino-*n*-methylpyridine ($n = 3, 6$) [20, 21] and 2-aminopyridine [22], although no copper(I) is present in the final product probably due to the synthesis process takes place in an air open atmosphere which produces the reoxidation of copper(I) to copper(II). Cu(II)/Cu(I) species with brominated pyridine-ring systems have not reported in the literature and, hence, it is no possible to tied the existence of Cu(I) ion to the bromination process. In our work, *para*-bromination is not possible because the *para* position respect to the *exo*-amino group is occupied by the *endo* nitrogen atom. To the rest of our knowledge, the compound $(TEA)[Cu_2Cl_4]$ (TEA = tetraethylammonium) [4] and the compound dealt with here are the only examples so far reported of structurally characterised Cu(II)/Cu(I) species, which were synthesised from a Cu(II) complex precursor. $(TEA)[Cu_2Cl_4]$, containing a Cu(II)/Cu(I) alternative linear-chain, was prepared as a by-product of crystal growth of single crystal of $(TEA)_4[Cu_4Cl_{12}]$ by a simplified temperature gradient technique [23].

In order to determine unambiguously the actual structure and the nature of bonding interactions of the $(4\text{-apyH})_4[Cu_3Br_8]$ compound, a single-crystal X-ray diffraction analysis was undertaken. The results showed that the compound crystallises in the tetragonal system with a crystal structure composed of 4-aminopyridinium cations, discrete $CuBr_4$ tetrahedra and one-dimensional polymeric end-less chains of $CuBr_4$ tetrahedra, running along the *c*-axis of the tetragonal unit cell, in which the metal bromide tetrahedra are joined by two symmetrically equivalent bridging bromine atoms (Fig. 1). Table 1 lists selected bond lengths and angles together with the hydrogen contacts in the crystal structure.

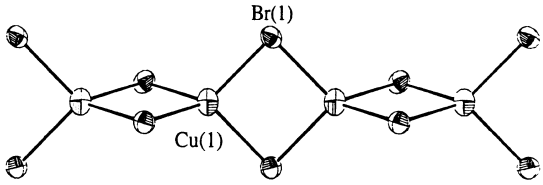

Fig. 1. Thermal ellipsoid plot (50% probability level) of the $[Cu^{I}Br]_n^{n-}$ polymeric anion in $(4\text{-apyH})_4[Cu_3Br_8]$ with the labelling scheme.

The copper atom of the edge-sharing polymeric chain, Cu(1), is located at a site of C_2 symmetry with two Cu–Br distances of 2.507(2) and 2.512(2) Å and Br–Cu–Br angles of 93.32(8), 93.55(8) and 118.04(4)°. These distances and angles are comparable with those determined for bromocomplexes containing tetrahedrically coordinated copper(I) in no-monomeric species [24–26] and are similar than those found for the Cu(I) centres in the mixed-valence $[Cu^{II}Cu^{I}Br_4]_\infty$ chains [7]. Isolated $[Cu^{I}X_4]^{3-}$ anions have not been structurally characterised in the solid state. Table 2 shows the structural parameters for monodimensional chains consisting of edge-sharing $CuBr_4$ tetrahedra. It is interesting to note that, in spite of the lower electrostatic repulsion, the intrachain Cu···Cu distance (3.44 Å) is longer that those observed in chains of edge-shared $CuBr_4$ tetrahedra with alternating and localised Cu(I) and Cu(II) sites (3.30 Å) [7] and significantly longer than that found in the neutral $[Cu^{II}_2Br_4]_\infty$ chain (3.22 Å) [16]. This fact can be explained by the similar Cu–Br–Cu angle in all the chains (84–87°) and the shorter Cu(II)–Br distances. The angle between the two $CuBr_2$ planes bisected by the chain C_2 axis is 90° and Muetterties distortion [27] from the tetrahedron is $\Delta D = 5.4\%$, these values are quite similar to those reported for the $[Cu^{I}Br_4]^{3-}$ centres within the mixed-valence $[Cu^{II}Cu^{I}Br_4]_\infty$ chains and analogous to those reported for the compound $[Cu(cnge)][CuBr_2]$ [14] and $[Cu_2(\mu\text{-formate})_2(\eta\text{-2-aminoallyl})_2][Cu_2Br_4]$ [15]. However in these two last compounds, the coordination of a bridge bromine atom to the copper(I) complex produce the increasing of the Cu–Br bond distances (longest 2.57 Å) and the decreasing of the Br–Cu–Br angles (75–80°) and as a consequence, the strong decreasing of the Cu···Cu distances (3.07–3.13 Å).

The Cu(2) atom in the isolated $CuBr_4$ unit is located on a sit of S_4 symmetry and the chromophore shows a distorted tetrahedral geometry with a Cu–Br distance of 2.371(2) Å and angles of 101.79(5) and 126.26(5)°. The distortion from the tetrahedron ($\Delta D = 15.1\%$) and the observed structural parameters are in good accordance with those usually

Table 1. Selected bond distances (Å), angles (°) and hydrogen-bonding system (Å, °) with e.s.d.s in parentheses

$[Cu^{I}Br_2]_n^{n-}$ chain				
Cu(1)–Br(1)	2.507(2)	Cu(1)–Br(1)–Cu(1)^{I}		86.57(6)
Cu(1)–Br(1)^{I}	2.512(2)	Br(1)–Cu(1)–Br(1)^{II}		93.55(8)
		Br(1)–Cu(1)–Br(1)^{III}		118.04(4)
		Br(1)^{III}–Cu(1)–Br(1)^{IV}		93.32(8)
$[Cu^{II}Br_4]^{2-}$ anion				
Cu(2)–Br(2)	2.371(2)	Br(2)–Cu(2)–Br(2)^{V}		126.26(5)
		Br(2)–Cu(2)–Br(2)^{VI}		101.79(5)
4-aminopyridinium cation				
N(1)–C(2)	1.23(6)	C(2)–N(1)–C(6)		128(3)
N(1)–C(6)	1.40(3)	N(1)–C(2)–C(3)		125(3)
C(2)–C(3)	1.46(7)	C(2)–C(3)–C(4)		113(2)
C(3)–C(4)	1.44(3)	C(3)–C(4)–C(5)		120(2)
C(4)–C(5)	1.35(2)	C(3)–C(4)–N(7)		119(2)
C(4)–N(7)	1.18(3)	C(5)–C(4)–N(7)		121(2)
C(5)–C(6)	1.54(3)	C(4)–C(5)–C(6)		124(1)
		N(1)–C(6)–C(5)		109(2)
Hydrogen-bond type		N···Br	H···Br	N–H···Br
N(1)–H(1)···Br(2)^{VI}		3.54(3)	2.54	160
N(7)–H(71)···Br(2)^{VII}		3.49(2)	2.52	163
N(7)–H(72)···Br(1)		3.54(2)	2.55	167

*Symmetry codes: I: $-y+1$, $x-1/2$, $z+1/2$; II: $-x+3/2$, $-y+1/2$, z; III: $-y+1$, $x-1/2$, $z-1/2$; IV: $y+1/2$, $-x+1$, $z-1/2$; V: $-x+1/2$, $-y+1/2$, z; VI: y, $-x+1/2$, $-z+1/2$ and VII: $-x+1$, $-y$, $-z+1$.

Table 2. Structural parameters for edge-sharing CuX_4 tetrahedra chains

Compound[a]	Centre	Cu–Br	Cu···Cu	Br–Cu–Br	Cu–Br–Cu	ΔD(%)[b]	φ[c]	Refs.
(dta)$_2$[Cu$_3$Br$_8$][Cu^{II}Br$_2$].C$_2$H$_5$OH	Cu(II)	2.394	3.214	95–120	84.2	8.1	84.9	[16]
		2.427	3.255		84.3			
(tem)[Cu^{I}Cu^{II}Br$_4$]	Cu(II)	2.387	3.308	96–141	85.9	32.3	53.8	[7]
	Cu(I)	2.469		92–119	6.1	90.0		
(dem)[Cu^{I}Cu^{II}Br$_4$]	Cu(II)	2.388	3.294	96–141	85.6	31.7	54.5	[7]
	Cu(I)	2.458		92–119	5.9	90.0		
(tea)[Cu^{I}Cu^{II}Br$_4$]	Cu(II)[d]	2.38–2.41	3.25–3.34	94–137	84–87	23–27	60–64	[7]
	Cu(I)[d]	2.44–2.49		91–129		6–7	76–82	
(4-apyH)$_4$[Cu^{II}Br$_4$][Cu^{I}Br$_2$]$_2$	Cu(I)	2.507	3.441	93–118	86.6	5.4	90.0	This work
		2.512						
[Cu(cnge)][Cu^{I}Br$_2$]	Cu(I)	2.429	3.130	102–118	80.1	3.3	88.6	[14]
		2.568[e]			75.0			
[Cu$_2$(for)$_2$(aal)$_2$][Cu$^{I}_2$Br$_4$]	Cu(I)	2.462	3.067	102–118	78.5	2.9	89.8	[15]
		2.553[e]			75.7			[2]

[a]dta = diethylammonium, tem = triethylmethylammonium, dem = diethyldimethylammonium, tea = tetraethylammonium, cnge = 1-cyanoguanidine, for = μ-formate, aal = η-2-aminoallyl, 4-apyH = 4-aminopyridinium.

[b]ΔD(%) was calculated according to: $\Delta D(\%) = (1/n)\,\Sigma_j(|\Sigma_i(\delta_i-\delta_{j1})|/|(\delta_{j1}-\delta_{j2})| \times 100$, where δ_i is the experimental dihedral angle and δ_{j1} and δ_{j2} are the theoretical dihedral angles for T_d and D_{4h}, respectively.

[c]φ = Dihedral angle between Br–Cu–Br planes bisected by the chain axis.

[d]There are three inequivalent Cu(I) and Cu(II) ions in the chain. [e]Bromide atom coordinated to the Cu(I) atom of the cationic complex unit.

found for isolated $[Cu^{II}Br_4]^{2-}$ anions [6, 17, 22]. Thus, it is clear structurally that the Cu(I) and Cu(II) ions are localized at sites Cu(1) and Cu(2), respectively, which allows us to formulate the $(4\text{-apyH})_4[Cu_3Br_8]$ compound as $(4\text{-apyH})_4[Cu^{II}Br_4][Cu^{I}Br_2]_2$, a mixed-valence compound containing 4-aminopyridinium cations, isolated $[Cu^{II}Br_4]^{2-}$ anions and an edge-sharing polymeric anionic metal bromide tetrahedra $[Cu^{I}Br_2]_n^{n-}$ chain (Fig. 2).

As far as the 4-aminopyridinium cation is concerned, bond distances and angles are normal [17]. Organic cations are inserted between the anionic units and the observed intermolecular contact distances (see end of Tab. 1) and the geometry supports the assumption of a hydrogen-bond network involving the cations and the anionic entities. One hydrogen atom of the *exo*-amino group is linked to the bromine atoms of the chain, whereas the second hydrogen atom and the *endo*-amino group one are connected to the bromine atoms of two neighbouring $[CuBr_4]^{2-}$ anions which are separated by 11.561 Å (Fig. 3). There are no other important interactions between tetrabromocuprate(II) anions, the nearest non-bonded Cu(II)···Br distance is 6.18 Å and the shortest Br(2)···Br(2) contact in the structure (5.60 Å), established between two neighbouring anions along the *c*-axis, is considerably longer than the sum of the bromine ion van der Waals radii (3.90 Å).

The cohesiveness of the crystal structure is also ensured by a face-to-face non-covalent interaction between π-systems of the pyridinic rings of the two centrosymmetric-related cations which are hydrogen-bonded to two different polymeric chains (see Fig. 2). The dihedral angle between the two adjacent rings, which are staggered in order to avoid steric hindrances, is 0°, the interplanar distance is 3.30 Å, the lateral offset is 1.4 Å and interatomic distances range from 3.3 to 3.5 Å. This structural parameters seems to indicate a significant overlapping degree.

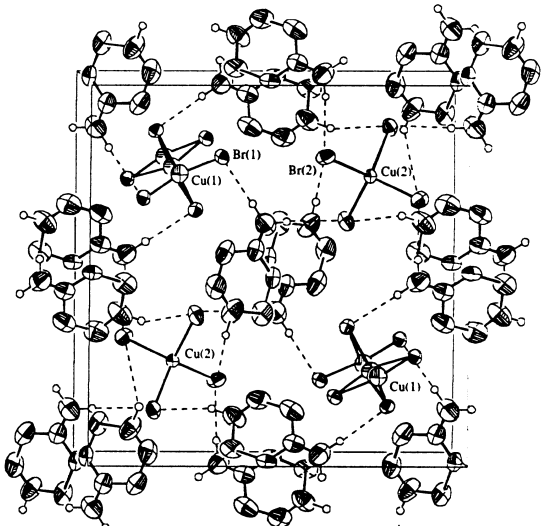

Fig. 2. Crystal packing in the $(4\text{-apyH})_4[Cu_3Br_8]$ compound. Hydrogen atoms attached to carbon were omitted for clarity.

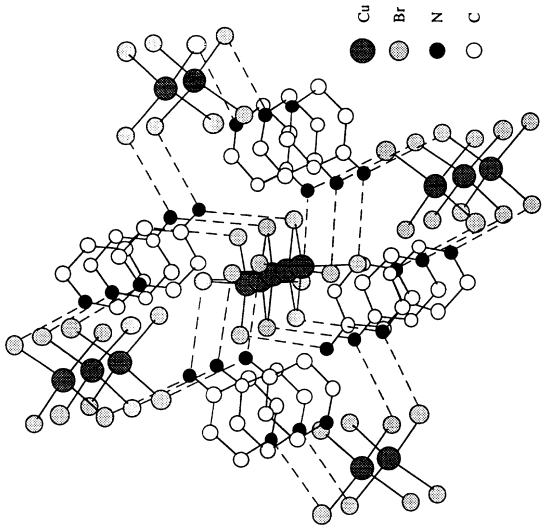

Fig. 3. View of a portion of the crystal structure of $(4\text{-apyH})_4[Cu_3Br_8]$ showing the hydrogen contacts (dashed lines) around a polymeric chain.

In the structure the Cu(II) ions are well separated, with copper–copper distances longer than 6 Å. This fact leads to a good magnetic isolation of Cu(II) as demonstrated by the thermal dependence of the $\chi_m T$ product with a nearly constant value of $\mu_{eff} = 1.88\mu_B$ within the temperature range 4.2–300 K. The susceptibility variation follows a Curie–Weiss law, with $C = 0.44\,cm^3\,K\,mol^{-1}$ and $\theta \approx -1\,K$.

In order to obtain more information about the magnetic environment of the Cu(II) centres, a polycrystalline sample was used to record the X-band ESR spectra of the compound in the range 4.2–300 K. These spectra show a broad and isotropic signal ($g = 2.154$). In attempt to search for the resolution of the spectra, Q-band spectroscopy was used. In these spectra an axial-type signal was obtained with *g*-values of $g_\parallel = 2.31$, $g_\perp = 2.10$ ($\langle g \rangle = 2.17$). Figure 4 shows the X- and Q-band spectra at room-temperature. Spectra remain practically unchanged over the work range of temperature.

EXPERIMENTAL

Reagents and physical measurements

All reagents were purchased from Fluka and Merck and were used without further purification. Microanalyses of carbon, nitrogen and hydrogen were performed on a Perkin-Elmer CHN-2400 analyser. Copper analysis was made on a Perkin-Elmer 360 Atomic Absorption/Flame emission spectrometer. The densities were measured by flotation in $CHBr_3$–CCl_4 mixtures [28]. IR spectra were recorded in the

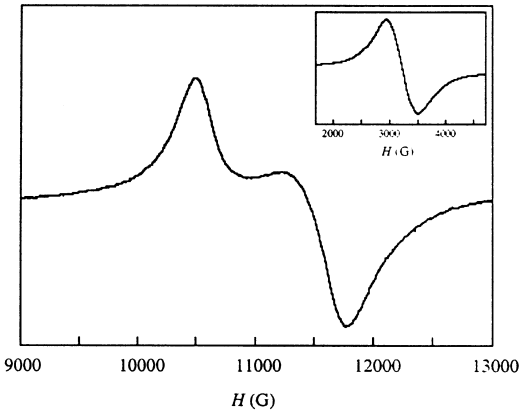

Fig. 4. Q- and X-band (inset) ESR spectra at room temperature.

4000–200 cm^{-1} range on a IR Perkin-Elmer 4200 spectrometer as KBr pellets. A Bruker ESP300 spectrometer, operating at the X- (*ca.* 9.5 GHz) and Q-band (*ca.* 34 GHz) and equipped with a standard Bruker apparatus down to liquid nitrogen and liquid helium temperatures, was used to study the ESR polycrystalline spectra between 4.2 and 300 K. The magnetic susceptibility measurements were carried out on polycrystalline samples in the temperature range 4.2–300 K with a pendulum type susceptometer/magnetometer (Manics DSM8) equipped with a helium continuous flow cryostat. Diamagnetic corrections terms were estimated from Pascal's constants [29] as -565×10^{-6} cm^{-3} mol^{-1}. Experimental magnetic susceptibility data were also corrected for temperature-independent paramagnetism (60×10^{-6} cm^3 mol^{-1} per Cu^{II}) and magnetisation of the sample holder.

Synthesis of (4-apyH)$_4$[Cu$_3$Br$_8$]

The title compound was obtained as single-crystals during the recrystallization attempts of the monohydrate 4-aminopyridinium salt of the tetrabromocuprate(II) anion. 0.12 g (0.2 mmol) of (4-apyH)$_2$[CuBr$_4$]·H$_2$O [17] was dissolved in 5 ml of ethanol. The resulting solution was transferred to a 15 mm diameter glass tube and then 20 ml of *n*-hexane was dropwise. After 3 days, dark violet prismatic single-crystals of (4-apyH)$_4$[Cu$_3$Br$_8$] were obtained. Crystals were found to be quite stable to light, air exposure and X-ray radiation. All manipulations were carried out in an open-air atmosphere. Thermogravimetric analysis indicated the no presence of water molecules in the compound composition. Yield 0.05 g, 63% based on copper (found: C, 19.88; H, 2.31; N, 9.28; Cu, 15.72. Calc. for C$_{20}$H$_{28}$Br$_8$Cu$_3$N$_8$: C, 19.85; H, 2.33; N, 9.26; Cu, 15.75%); IR data (cm^{-1}): 3480sh, 3390s, 3305s, 3265w, 3205s, 3110m, 2985m, 1645vs, 1605w, 1525vs, 1400w, 1270w, 1195s, 1101w, 995s, 815s, 650w, 580m, 500s, 226w, 218w, 209w and 207w.

The excellent agreement between the proposed stoichiometry and the elemental analysis values seems to preclude the existence of impurities or other compounds. However, the purity and homogeneity of the sample were confirmed by the comparison of the observed X-ray powder diffraction pattern and that generated from the single crystal X-ray data [30].

Crystallographic data collection and structural refinement

C$_{20}$H$_{28}$Br$_8$Cu$_3$N$_8$, $M = 1210.37$ g mol^{-1}, tetragonal, space group P4$_2$/n (No. 86), $a = b = 15.608(3)$, $c = 6.882(2)$ Å, $U = 1676.5(7)$ A^3 (by least-square refinement on diffractometer angles for 25 well-centred reflections, $18 < 2\theta < 32^\circ$), $T = 295(1)$ K, graphite-monochromated Mo–Kα radiation ($\lambda = 0.71069$ Å), $Z = 2$, $D_m = 2.40(1)$ g cm^{-3}, $D_c = 2.40$ g cm^{-3}, $F(000) = 1142$, deep violet, almost opaque, single-crystal with dimensions $0.25\times0.27\times0.30$ mm, μ(Mo–K$_\alpha$) = 114.5 cm^{-1}; Enraf-Nonius CAD4 four-circle diffractometer, ω–2θ scan mode, data collection range $2<2\theta<60^\circ$, h: 0–21, k: $\pm$15, l: 0–9; two standard reflections showed no significant variation in intensity; corrections were made for Lorentz-polarisation and for absorption (empirical correction with minimum and maximum correction coefficients of 0.874 and 1.185) [31]; 2431 reflections were measured, 1105 of which were considered as observed by applying the conditions $I\geq2\sigma(I)$. Crystal structure was solved by direct methods [32] and refined anisotropically by full-matrix least-squares methods on *F* (XRAY 76 System) [33]. Hydrogen atoms were placed at idealised positions and refined as fixed contributors. A conventional weighting scheme was used in the final refinement cycle in order to obtain flat dependence in $\langle w\Delta^2F\rangle$ vs $\langle F_o\rangle$ and vs $\langle\sin\theta/\lambda\rangle$ [34]. After the final refinement cycle, the agreement factors were $R(F_o) = 0.059$ and $wR(F_o) = 0.068$, 90 variables, $S = 1.36$, $(\Delta/\sigma)_{max} = 0.10$, $(\Delta/\sigma)_{av} = 0.01$ and $\Delta\rho_{max} = 0.98$ e Å^{-3} in the cation region. The atomic scattering factors and anomalous dispersion factors were taken from Ref.[35].

Final geometrical calculations were carried out with the PARST [36] and PLATON [37] programs. Graphical manipulations were produced using the ORTEP utility of the XTAL 3.0 system [38]. All calculations were performed on a Digital MicroVAX 4500.

Final atomic positional and thermal parameters, together with the anisotropic thermal parameters for non-hydrogen atoms, a full list of bond distances and angles, dihedral angles and a list of observed and calculated structure factors, have been deposited as supplementary material with the Cambridge Crystallographic Data Centre (CCDC).

Acknowledgements—We are grateful for financial support from the Universidad del País Vasco/Euskal Herriko Unibertsitatea (UPV/EHU) (Grant No. UPV 169.310-EA088/97). J. S. thanks the Ministerio de Educación y Ciencia of the Spanish Government for a doctoral fellowship (Grant No. AP94.42172547).

REFERENCES

1. Brown, D. B., *Mixed-Valence Compounds*, *Theory and Application in Chemistry*, *Physics*, *Geology and Biology*. Reidel, Boston, 1980.
2. Simonsen, O. and Toftlund, H., *Acta Cryst. C*, 1987, **43,** 831.
3. Mori, T., Sakai, F., Saito, G. and Inokuchi, H., *Chem. Lett*., 1987, 927.
4. Willett, R. D., *Inorg. Chem*., 1987, **26,** 3424.
5. Dunaj-Jurco, M., Ondrejovic, G., Melnik, M. and Garaj, J., *Coord. Chem. Rev*., 1988, **83,** 1.
6. Sundberg, M. R., Kivekäs, R., Ruiz, J., Moreno, J. M. and Colacio, E., *Inorg. Chem*., 1992, **31,** 1062.
7. Scott, B., Willett, R. D., Porter, L. and Williams, J., *Inorg. Chem*., 1992, **31,** 2483.
8. Blake, A. J., Dorse, R. L., Rawson, J. M. and Winpenny, R. E. P., *Polyhedron*, 1994, **13,** 2793.
9. Breeze, S. R. and Wang, S., *Inorg. Chem*., 1996, **35,** 3404.
10. Allen, F. H., Davies, J. E., Galloy, J. J., Johnson, O., Kennard, O., Macrae, C. F., Mitchell, E. M., Mitchell, G. F., Smith, J. M. and Watson, D. G., *J. Chem. Info. Comp. Sci*., 1991, **31,** 187.
11. Freckmann, B. and Tebbe, K. F., *Z. Naturforsch. B*, 1980, **35,** 1319.
12. Hartl, H., Brudgam, I., Mahdjour-Hassan-Abadi, F., *Z. Naturforsch. B*, 1983, **38,** 57.
13. Corradi, A. B., Cramarossa, M. R., Manfredini, T., Battaglia, L. P., Pelosi, G., Saccani, A. and Sandolini, F., *J. Chem. Soc. Dalton Trans*. 1993, 3587.
14. Begley, M. J., Eisenstein, O., Hubberstey, P., Jackson, S., Russell, C. E. and Walton, P. H., *J. Chem. Soc*., *Dalton Trans*. 1994, 1935.
15. Mykhalichko, B. M., Olijnyk, V. V., Myskiv, M. G., Pecharsky, V. K. and Khalil, F., *Koord. Khim*., 1994, **20,** 208.
16. Fletcher, R., Hansen, J. J., Livermore, J. and Willett, R. D., *Inorg. Chem*., 1983, **22,** 330.
17. Román, P., Sertucha, J., Luque, A. and Lezama, L., Rojo, T., *Polyhedron*, 1996, **15,** 1253.
18. Bencini, A. and Mani, F., *Inorg. Chim. Acta*, 1984, **87,** L9.
19. Willett, R. D. and Halvorson, K., *Acta Cryst. C*, 1988, **44,** 2068.
20. Place, H. and Willett, R. D., *Acta Cryst. C*, 1987, **43,** 1497.
21. Grigereit, T. E., Ramakrishna, B. L., Place, H., Willett, R. D., Pellacani, G. C., Manfredini, T., Menabue, L., Bonamartini, A. and Battaglia, L., *Inorg. Chem*., 1987, **26,** 2235.
22. Luque, A., Sertucha, J., Lezama, L., Rojo, T. and Román, P., *J. Chem. Soc. Dalton Trans*. 1997, 847.
23. Arend, H., Huber, W., Mischgofsky, F. H., Richter-Van Leeuwen, G. K., *J. Cryst. Growth*, 1978, **43,** 213.
24. Jagner, S. and Helgesson, G., *Adv. Inorg. Chem*., 1991, **37,** 1.
25. Subramanian, L. and Hoffmann, R., *Inorg. Chem*., 1992, **31,** 1021.
26. Scott, B., Willett, R., Saccani, A., Sandrolini, F. and Ramakrishna, B. L., *Inorg. Chim. Acta*, 1996, **248,** 73.
27. Muetterties, E. L. and Guggenberger, L. J., *J. Am. Chem. Soc*., 1974, **96,** 1748.
28. Román, P., Gutiérrez-Zorrilla, J. M., *J. Chem. Educ*., 1985, **62,** 167.
29. Earnshaw, A., *Introduction to Magnetochemistry*. Academic Press, London, New York, 1968.
30. Iron, K., Jeitschko, W. and Parthe, E., *LAZY PULVERIX*. Laboratoire de Crystallographie aux rayons-X, Universtite of Geneve, Switzerland, 1977.
31. Walker, N. and Stuart, D., *Acta Cryst. A*, 1983, **39,** 158.
32. Beurskens, P. T., Admiraal, G., Beurskens, G., Bosman, W. P., García-Granda, S., Gould, R. O., Smith, J. M. M. and Smykalla, C., *The DIRDIF Program System*. Tech. Rep. of the Crystallography Laboratory. University of Nijmegen, The Netherlands, 1992.
33. Stewart, J. M., Machin, P. A., Dickinson, C. W., Ammon, H. L., Heck, H. and Flack, H., *The X-RAY* 76 *System*. Tech. Rep. TR-446. Computer Science Center, University of Maryland, College Park, Maryland, U.S.A., 1976.
34. Martínez-Ripoll, M. and Cano, F. H., *PESOS. A Program for the Automatic Treatment of Weighting Schemes for Least-Squares Refinement*. Instituto Rocasolano, CSIC, Madrid, Spain, 1975.
35. *International Tables for X-Ray Crystallography*, Vol. 4. Kynoch Press, Birmingham, 1974 (present distributor: D. Reidel, Dordrecht).
36. Nardelli, M., *Comput. Chem*., 1983, **7,** 95.
37. Spek, A. L., *Acta Cryst. A*, 1990, **46,** C34.
38. Hall, S. R. and Stewart, J. M. (eds.), *XTAL*3.0 *Reference manual*. Universities of Western Australia and Maryland, 1990.

Pergamon

PII: S0277–5387(98)00147–8

Polyhedron Vol. 17, No. 22, pp. 3881–3888, 1998
© 1998 Elsevier Science Ltd
All rights reserved. Printed in Great Britain
0277–5387/98 $19.00+0.00

Some reaction chemistry of *trans*-[Fe(H)(η^2-H_2)(η^2-dppm)$_2$][BF_4]. The crystal and molecular structure of *trans*-[Fe(H)(CH_3CN)(η^2-dppm)$_2$][BF_4], dppm = bis(diphenylphosphino)methane

Yuan Gao,[a] David G. Holah,[a]* Alan N. Hughes,[a] Greg J. Spivak,[a] Matthew D. Havighurst[b] and Vincent R. Magnuson[b]

[a]Department of Chemistry, Lakehead University, Thunder Bay, Ontario, Canada, P7B 5E1.

[b]Department of Chemistry, University of Minnesota-Duluth, Duluth, Minnesota 55812, U.S.A.

(Received 21 October 1997; accepted 8 April 1998)

Abstract—Substitution of H_2 by ligands (L) in either pure *trans*-[Fe(H)(η^2-H_2)(η^2-dppm)$_2$] [BF_4], **1**, or solutions of [Fe(H)$_2$(dppm)$_2$] **2**, L and $HBF_4.Et_2O$ in which **1** is made *in situ*, produce the compounds *trans*-[Fe(H)(L)(η^2-dppm)$_2$] [BF_4] (L=CH_3CN, **3**; succinonitrile, **4**; pyridine, **5**; C_2H_4, **6**; and N_2, **7**). The order of H_2 replacement from **1** appears to be $CH_3CN > N_2 > C_2H_4 \sim$ pyridine. Evidence is presented for the protonation of the hydride ligands of **1** or **2** to produce [Fe(H_2)$_2$(η^2-dppm)$_2$] [BF_4]$_2$, **8**, although **8** could not be fully characterized nor could it be obtained in the solid state. *Trans*-[Fe(CH_3CN)$_2$(η^2-dppm)$_2$] [BF_4]$_2$, **9**, was obtained from solutions of **8** treated with acetonitrile. The coordination geometries of **3**, **9** and **4** (monodentate succinonitrile) have been confirmed by X-ray crystallography (only the gross structural features of **4** were obtained due to a poor data set from a very small crystal). © 1998 Elsevier Science Ltd. All rights reserved.

Keywords: bis(diphenylphosphino)methane; dihydrogen complexes; dihydrogen displacement reactions; iron complexes; metal hydride complexes; X-ray structures.

There is a body of literature [1–2] on metal-dihydrogen complexes in general and on cations containing Fe^{II}, hydride, dihydrogen and chelating phosphines of the type *trans*-[Fe(H)(H_2)(P-P)$_2$]$^+$ in particular. Most of these complexes have been well characterized and extensively studied by NMR methods and, to a lesser extent, by crystallography. These compounds have also been studied from the point of view of intramolecular exchange of H atoms between H^- and H_2 [1–2], the elimination and ligand substitution of H_2 [1–2], and homolytic and heterolytic splitting of dihydrogen [2]. Relative to some bis-phosphines, dppm has been used less frequently in reactions which produce such complexes although **1** and **2** were briefly reported, but not fully characterized, as being produced from reactions of Fe^{II} with dppm and $NaBH_4$ [3]. In our work on the single-step syntheses of reduced metal-phosphine complexes, we also observed [4] that Fe^{III}- and Fe^{II}-dppm mixtures are not reduced beyond Fe^{II} by $NaBH_4$ in contrast to the behaviour of high-valent Co, Ni, Pd and Pt systems. Even using $LiAlH_4$ as the reducing agent, the main product is the Fe^{II} species **2** from which **1** is derived by protonation. These were both isolated and characterized, **2** by crystallography [4]. This paper describes the substitution reactions of **1**, reactions involving the protonation of **1** and **2** and the molecular structures of three compounds.

* Author to whom correspondence should be addressed.

EXPERIMENTAL

Reagents and Solvents

Dppm, anhydrous $FeCl_3$, $HBF_4 \cdot Et_2O$, $LiAlH_4$ and $LiAlD_4$ were obtained from Aldrich. The last three reagents were stored under nitrogen. When necessary $FeCl_3$ was dried by heating the hydrated salt under reflux with $SOCl_2$ [5]. Compounds **1**, **2** and **3** were prepared by literature methods [4]. Benzene and THF were both dried before use by distilling from Na wire. All solvents were degassed prior to use by purging with nitrogen.

Physical Measurements

Both samples and reagents were handled under an inert atmosphere during weighing and data collection. Microanalyses for C, H and N were acquired in our laboratories using a Control Equipment Corporation model 240XA analyzer with V_2O_5 used as a combustion aid. Infrared spectra (for Nujol mulls between NaCl plates) were recorded on a Bruker IFS 66 FTIR spectrophotometer. ^1H and $^{31}P\{^1H\}$ NMR spectra were recorded on a Bruker AC-E 200 spectrometer. Chemical shifts are reported as δ values with positive shifts for ^1H downfield of the signal of Me_4Si (TMS) while those for ^{31}P are downfield of the signal of external 85% H_3PO_4.

Syntheses of the compounds

All the syntheses were performed in a glove box under dry (P_2O_5) nitrogen, argon, ethylene or hydrogen.

Preparation of trans-[*Fe*(*H*)(*CH*$_3$*CN*)(η^2-*dppm*)$_2$] [*BF*$_4$] (**3**)

As an alternative to the published procedure [4] for the preparation of **3**, **2** (0.21 g, 0.26 mmol) was suspended in CH_3CN (10 cm^3) and stirred at -30°C (dry ice and acetone) for 20 min. $HBF_4 \cdot Et_2O$ (200 μl, 1.36 mmol) was added dropwise to the stirred solution to form an orange red solution. Ether (50 cm^3) was added to precipitate the orange yellow solid, which was collected by filtration, dried under reduced pressure, and recrystallized from CH_2Cl_2/hexane. Yield: 86%. The spectroscopic characteristics (^{31}P and ^1H NMR; FTIR) of this product were identical to those previously published [4].

Preparation of trans-[*Fe*(*H*){*NC*(*CH*$_2$)$_2$*CN*}(η^2-*dppm*)$_2$] [*BF*$_4$] (**4**)

(a) A solution of succinonitrile (0.10 g, 1.25 mmol) in THF (4 cm^3) was added to a stirred suspension of **1** (0.13 g, 0.14 mmol) in THF (10 cm^3), and an orange red solution was formed immediately. After 40 min, ether (30 cm^3) was added and the resulting orange solid filtered off, washed twice with ether (10 cm^3 each time) and dried under reduced pressure. Yield: 80%. Recrystallization from CH_2Cl_2/hexane produced thin plates for an X-ray structural determination. Found: C, 65.7; H, 5.2; N, 2.6. Calc. for $FeF_4P_4BN_2C_{54}H_{49}$: C, 65.4; H, 4.9; N, 2.8%. IR: ν(Fe-H) 1881 (w), ν(CN) 2228 (vw), 2239 (w,b) cm^{-1}. $^{31}P\{^1H\}$ NMR (25°C, CD_2Cl_2): δ 30.3 (singlet). ^1H NMR (25°C, CD_2Cl_2): δ -13.1 (Fe-H, quintet, $^2J_{PH} = 47$ Hz); δ 4.34 and 4.81 (PCH^aH^bP, poorly resolved); δ 2.22, 1.93 (Fe-NCC$\underline{H}_2$ C$\underline{H}_2$CN, broad signals, overlapped and poorly resolved). Complex **4** is stable in air. It is soluble and stable in dichloromethane and chloroform.

(b) Alternatively, succinonitrile (0.055 g, 0.69 mmol) dissolved in THF (4 cm^3), was added to a stirred suspension of compound **2** (0.18 g, 0.22 mmol) in THF (10 cm^3). $HBF_4 \cdot Et_2O$ (200 μL, 1.36 mmol) was added dropwise. The clear yellow solution gradually became orange-red. After 20 min, ether (30 cm^3) was added and the resulting orange solid was filtered off, washed twice with ether (10 cm^3 each time) and dried under reduced pressure. Yield: 81%.

Preparation of trans-[*Fe*(*H*)(*pyridine*)(η^2-*dppm*)$_2$] [*BF*$_4$] (**5**)

Pyridine (0.1 mL, 1.24 mmol) was added to a stirred suspension of **2** (0.11 g, 0.12 mmol) in THF (10 cm^3) to produce a clear red solution. Addition of ether (30 cm^3) precipitated a blood-red solid which was washed twice with ether (10 cm^3 each time) and dried under reduced pressure. Yield: 66%. Since the solid smells strongly of pyridine, chemical analyses were unsatisfactory. Found: C, 62.5; H, 5.4; N, 2.0. Calc. for $FeF_4P_4BNC_{55}H_{45}$: C, 67.0; H, 4.6; N, 1.4%. IR: ν(Fe-H) 1853 (w) cm^{-1}. $^{31}P\{^1H\}$ NMR (25°C, deuterated pyridine): δ 22.67 (singlet). ^1H NMR (25°C, deuterated pyridine): δ -17 (Fe-H, quintet, $^2J_{PH} = 46$ Hz). In solution, **5** only has limited stability in pyridine. In acetone or methylene chloride it decomposes quickly and recrystallization attempts were unsuccessful.

Preparation of trans-[*Fe*(*H*)(η^2-*CH*$_2$=*CH*$_2$)(η^2-*dppm*)$_2$] [*BF*$_4$] $\cdot$ 0.5*CH*$_2$*Cl*$_2$(**6**)

(a) Ethylene was passed into a stirred suspension of **1** (0.091 g, 0.10 mmol) in THF (20 cm^3) at a rate of 3 bubbles/s for three h. Addition of ether (20 cm^3) precipitated an orange red product which was filtered off, washed with ether (10 cm^3) and dried under reduced pressure. Yield: 89%. The complex was recrystallized from CH_2Cl_2/hexane under Ar. Found: C, 64.5; H, 5.15. Calc. for $FeC_{52.5}H_{50}P_4BF_4Cl$: C, 64.2; H 5.1%. IR: ν(Fe-H) 1714 (w, sh) cm^{-1}. $^{31}P\{^1H\}$ NMR (25°C, $CDCl_3$): δ 32.8 (singlet). ^1H NMR (25°C, $CDCl_3$): δ -1.78 (Fe-H, quintet, $^2J_{PH} = 50.6$ Hz); δ 5.29

and 4.39 (PCH^aH^bP, poorly resolved); δ 3.18 {Fe-(η^2-$C\underline{H}_2$=$C\underline{H}_2$)}. Complex **6** is very sensitive to moisture. It is stable in dry acetone, chloroform and methylene chloride.

(b) Alternatively, $HBF_4 \cdot Et_2O$ (100 μL, 0.68 mmol) was added dropwise to **2** (0.11 g, 0.137 mmol) in THF (10 cm^3) into which ethylene was passed at a rate of 3 bubbles/s for three h. Addition of ether (20 cm^3) completed the precipitation of an orange-red solid which was filtered off, washed and dried as above. Yield: 72%.

Preparation of trans-[*Fe*(*H*)(N_2)(η^2-*dppm*)$_2$] [BF_4] (**7**)

(a) N_2 was passed at a rate of 3-5 bubbles/s for 5 h into a suspension of **1** (0.12 g, 0.13 mmol) in THF (20 cm^3). Addition of ether (20 cm^3) produced a yellow solid which was filtered off, washed twice with ether (10 cm^3 each time) and dried under reduced pressure. Yield: 77%. Recrystallization was carried out from CH_2Cl_2 under dry N_2. Found: C, 64.0; H, 4.99; N, 2.52. Calc. for $FeF_4P_4BN_2C_{50}H_{45}$: C, 63.9; H, 4.8; N, 3.0%. IR: ν(Fe-H) 1713 (vw) cm^{-1}, ν(NN) 2116 cm^{-1}. $^{31}P\{^1H\}$ NMR (25°C, CD_2Cl_2): δ 24.2 (singlet). ^1H NMR (25°C, CD_2Cl_2): δ -9.38 (Fe-$\underline{H}$, quintet, $^2J_{PH}$ = 43.6 Hz). Complex **7** gradually changes its colour in air. In solution **7** is only stable in dry CH_2Cl_2. It decomposes very quickly in acetone or chloroform.

(b) $HBF_4 \cdot Et_2O$ (100 μL, 0.68 mmol) was added dropwise to a freshly prepared stirred suspension of **2** (0.11 g, 0.13 mmol) in THF (10 cm^3). N_2 was passed into the suspension for 5 h. **7** was isolated as described above for **6** (method b). Yield: >60%.

Preparation of trans-[*Fe*(η^2-H_2)$_2$(η^2-*dppm*)$_2$] [BF_4]$_2$ (**8**)

(a) $HBF_4 \cdot Et_2O$ (15 μL, 0.1 mmol) was added dropwise with shaking to **1** (10 mg, 0.01 mmol) in CD_2Cl_2 (0.6 cm^3) under Ar or N_2 to give a clear yellow solution. $^{31}P\{^1H\}$ NMR (25°C, CD_2Cl_2): δ 3.32 (singlet). Addition of Et_2O produced only pure solid **1**, the identity of which was confirmed by ^1H and ^{31}P NMR and by IR spectroscopic examination. A similar experiment in THF under H_2 produced a solution with the same NMR spectrum (δ 3.32). Addition of Et_2O saturated with H_2 also produced only pure **1**.

(b) $HBF_4 \cdot Et_2O$ (150 μL, 1 mmol) was added dropwise to a stirred suspension of **2** (0.11 g, 0.13 mmol) in THF (10 cm^3) to give a clear yellow solution. $^{31}P\{^1H\}$ NMR (25°C): δ 3.32 (singlet). Addition of Et_2O produced **1** as above.

In spite of repeated attempts under a variety of conditions, no ^1H NMR signals upfield of TMS were observed for any solutions thought to contain **8**.

Preparation of trans-[*Fe*(CH_3CN)$_2$(η^2-*dppm*)$_2$] [BF_4]$_2 \cdot 2CH_2Cl_2$ (**9**)

To a stirred suspension of **2** (0.19 g, 0.22 mmol) in CH_3CN (6 cm^3), $HBF_4 \cdot Et_2O$ (150 μL, 1 mmol) was added to produce a clear deep-red solution. Ether (70 cm^3) was added immediately and the resulting peach-colored solid (0.21 g) was filtered off, washed with ether (10 cm^3) and dried under reduced pressure. $^{31}P\{^1H\}$ NMR (25°C, CD_2Cl_2): δ 29.8 (singlet); δ 14 (singlet); δ 12.3 (triplet) and δ 1.08 (triplet) (see discussion). The mixture of products (0.21 g) was redissolved in CH_3CN (8 cm^3) and stirred overnight. Ether (70 cm^3) was then added to precipitate out a pink solid (0.14 g) which was collected and dried as described above. CH_2Cl_2 (or CH_3CN) (4 cm^3) was added to dissolve the solid and hexane (or ether) (16 cm^3) was carefully layered over the filtrate. The final crystalline product **9**, suitable for the X-ray structure determination, was deposited within 24 h. The crystals were filtered off, washed with ether (10 cm^3) and dried under reduced pressure. Yield: 31%. Found: C, 54.1; H, 4,6; N 2.4. Calc. for $C_{56}H_{54}P_4N_2Cl_4B_2F_8Fe$: C, 53.8; H, 4.4; N, 2.2%. IR: ν(CN) 2249, 2269, 2289, 2317 cm^{-1}. $^{31}P\{^1H\}$ NMR (25°C, CD_2Cl_2): δ 14.2 (singlet). ^1H NMR (25°C, CD_2Cl_2): δ 2.37 [Fe-(NCC$\underline{H}_3$)$_2$]. Complex **9** is stable in air and is soluble and stable in methylene chloride, chloroform and acetonitrile.

The reactivity of **1** *toward propene, cis-2-butene and styrene*

When propene or *cis*-2-butene was used instead of ethylene as outlined above for the synthesis of **6** by procedure (a), or when styrene (1.62 cm^3, 14 mmol) was stirred with **1** (0.13 g, 0.14 mmol) in THF (10 cm^3), under Ar for 3 h, no evidence that **1** had reacted was detected from NMR measurements.

X-Ray Crystallography

Crystallographic data collection for **3** and **9** was carried out on an Enraf-Nonius CAD-4 diffractometer using $\mathbf{Mo}_{K\alpha}$ graphite-monochromatized radiation. Crystal structure refinement calculations were carried out on a PC Express computer with the SHELX program system [6]. NRCVAX computer programs were used for scaling and data reduction [7].

For **3**, an absorption correction was applied. The attenuation coefficient used was 1.0 and the average absorption correction factor was 0.8147. The Fe atom was located by direct methods and all remaining atoms were found by cycles of Fourier and difference Fourier calculations. Calculated ideal positions of the H atoms on the phenyl and methylene C atoms of dppm and on the methyl C of acetonitrile were included but not refined. The hydride ligand was located in the Fourier map and refined along with other atoms. The BF_4^- is disordered, with three rotationally related locations of its four fluorine atoms. All atoms, except H and F, were refined with anisotropic thermal displacement parameters. The four F atoms of each position were refined with equal

B-F distances and equal isotropic thermal displacement parameters.

Crystal data for **9**: monoclinic, $C2/c$, $a=22.5018(5)$, $b=12.3622(2)$, $c=21.6802(5)$ Å, $\beta=106.047(1)^\circ$, $Z=4$. The Fe is on a 2-fold axis so that the asymmetric unit contains the Fe, one dppm, one disordered BF_4 over two independent positions in a 0.79:0.21 ratio, and one CH_2Cl_2 which shows significant thermal motion and therefore contributes to the high residuals. R indices, as defined in ref [4] (all data): $R_1=0.1201$, $wR_2=0.2187$). Relevant bond lengths and angles are: Fe-P(1)=2.2715(14), Fe-P(2)=2.2841(13), Fe-N=1.909(4), N-C=1.1337(7), C-C in CH_3CN=1.466(8) Å; P(1)-Fe-P(2)=73.0° and the internal P-C-P angle in dppm=94.6°. These structural parameters are very similar to those reported [8] for *trans*-$[Fe(CH_3CN)_2(dppm)_2]$ $[FeI_4].2H_2O$ and the published bond lengths for the latter will be used for comparison purposes in this paper.

Crystals of **4** were exceptionally thin and consequently a poor data set allowed only confirmation of the overall structural features of **4**, namely that the succinonitrile is indeed *trans* to the H^- and is coordinated to the Fe through one of the nitrile groups [9].

Supplementary X-ray materials for **3**, including atomic coordinates and thermal parameters, have been deposited with the Cambridge Crystallographic Data Center.

RESULTS AND DISCUSSION

The synthesis of derivatives of **1** can be carried out either by the direct replacement of the dihydrogen ligand in pure **1** by several small ligands or from **1** prepared *in situ* by protonating **2** in the presence of the ligands. Care must be taken to ensure anhydrous conditions for reproducibility of the reactions. The ligands selected (CH_3CN, succinonitrile, pyridine, C_2H_4, CO [4] and N_2) have widely varying σ donor-π acceptor properties and can bind to the Fe center in an end on or side on fashion. The fact that ethylene, but not propene, *cis*-2-butene or styrene, can replace the H_2 indicates that the site is sterically constrained. Pyridine replaces the H_2 and although the resulting complex is quite unstable, the complex shows a strong singlet in the ^{31}P NMR spectrum and the expected hydride quintet in the ^1H NMR spectrum. Both pyridine and ethylene are, in turn, displaced from their respective complexes by N_2. Acetonitrile is ideally suited to the site and rapidly replaces, not only H_2, but pyridine, ethylene and N_2. The rates at which the dihydrogen is displaced varies greatly with the acetonitrile and pyridine reactions being virtually instantaneous while those involving ethylene or N_2 take several hours. A combination of infrared spectrophotometry, NMR specroscopy and X-ray crystallography confirms that, in most cases, the final product takes the form *trans*-$[Fe(H)(L)(\eta^2\text{-dppm})_2]$ $[BF_4]$ as summarized in Scheme 1.

In certain cases (Scheme 1), additional reactions occur. For example, the outcome of protonation of **2** by $HBF_4\cdot Et_2O$ (molar ratio 1:5) in acetonitrile is a function of reaction time and temperature. At -30°C, the only product is **3** while at room temperature the main product is **9**, with two *trans* acetonitrile ligands. However, ^{31}P NMR spectra reveal that, initially, three products are present since signals due to **3**, **9** and a third component which shows two triplets centered at δ 12.3 and 1.08 are observed. This third component is believed to be *cis*-$[Fe(CH_3CN)_2(dppm)_2]$ $[BF_4]_2$, **10**. The signals due to this component rapidly disappear from the spectrum as conversion of all components of the mixture into **9** occurs. The largest amounts of the *cis* isomer, **10**, obtainable in these experiments were observed (^{31}P spectrum) to be formed in fresh solutions of **2** and $HBF_4\cdot Et_2O$ (in a 1:5 molar ratio) in CH_3CN. Under these conditions, the two isomers are formed in approximately equal amounts although the relative proportion of the *trans* isomer **9** still grows rapidly with time. The Fe-dppm ring opening and rearrangement apparently required in the formation of the *cis* isomer from **2** or **3** may be facilitated by the reversible interaction of the excess of H^+ present with a P atom of dppm as has been observed [10] in studies

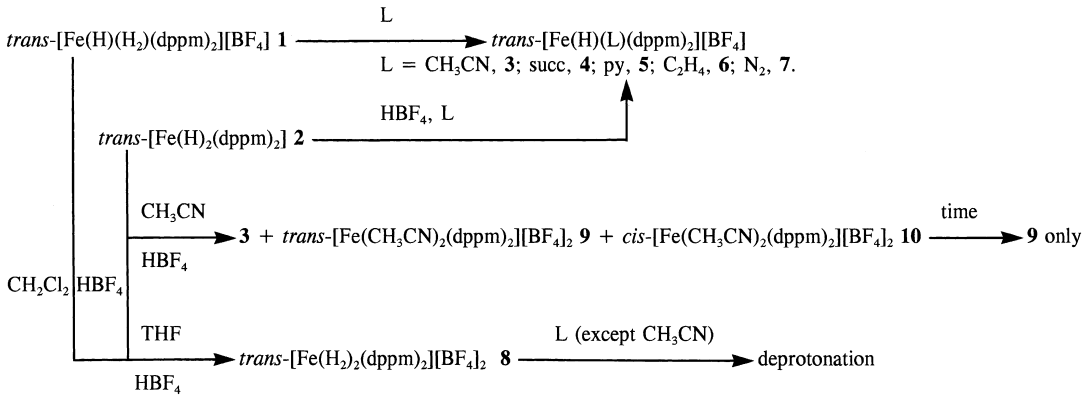

Scheme 1.

of the related reactions of [FeHX(diphosphine)$_2$] (X = Cl, Br) under acid conditions. The fact that **9** is produced from **1** or **2** in the presence of excesses of H^+ and CH_3CN implies that hydride-protonation followed by H_2 displacement is a stepwise process and that after **3** is formed, further protonation of its hydride ligand occurs, as has been observed for the process *trans*-[Os(H)(CH_3CN)(dppe)$_2$]$^+$ → *trans*-[Os(H_2)(CH_3CN)(dppe)$_2$]$^{2+}$ [11]. In the Fe case it seems that there is a second H_2 for CH_3CN exchange. This prompted an investigation of the protonation of **2** with no H_2-displacing ligand present. It was found that protonation of **2** in THF or CH_2Cl_2, or protonation of **1** in CH_2Cl_2 or CD_2Cl_2, under N_2 or argon, or in THF under H_2, produced solutions which exhibited a single ^{31}P NMR signal at δ 3.3. (Fe:HBF_4 molar ratios ranged from 1:1 to greater than 1:10). This signal is believed to be due to the bis(dihydrogen) complex **8** although repeated attempts to detect the dihydrogen signal in the ^{1}H NMR spectrum were unsuccessful due to interference from strong $HBF_4 \cdot Et_2O$ signals. This complex appears to be relatively stable towards H_2-displacing ligands in THF or CH_2Cl_2 in the presence of an excess of acid. For example, with a 10 fold molar excess of HBF_4 present, these solutions react only very slowly with acetonitrile to produce **9**, although again the *cis* isomer is present in the initial stages of the reaction. These observations support the suggestion that in the direct synthesis of **9** from **2**, the most likely intermediate is **3** rather than **8**.

In similar reactions involving protonation of a mixture of *cis*- and *trans*-[Ru(H)$_2$(dppm)$_2$] in CH_3CN using a large excess of HBF_4, only the *cis* isomer of [Ru(CH_3CN)$_2$(dppm)$_2$] [BF_4]$_2$, characterized crystallographically, was obtained [12].

All attempts to isolate solid **8** from solutions exhibiting the δ 3.3 signal in the ^{31}P spectrum resulted in spontaneous deprotonation, even under an atmosphere of H_2, and formation of **1**. This observation, in itself, is good evidence that complex **8** is certainly a symmetrical dihydrogen complex and probably a bis(dihydrogen) complex even though no dihydrogen signals are observable in the ^{1}H NMR spectra under a variety of conditions. The implication is that these signals are displaced from their usual positions and are masked by other solvent signals.

Other than a few species existing in solutions at very low temperatures [13] or in a matrix [14], few complexes containing two dihydrogen ligands are known. Among these are certain complexes of Ru [15, 16], Ir [17] and Re [16], some of which are prepared by protonating polyhydrides [16]. They are labile, the Ir complex, for example, being stable only at -80°C unless kept under an atmosphere of H_2.

Addition of ligands (other than acetonitrile) to solutions exhibiting the δ 3.3 signal in the ^{31}P spectrum resulted in deprotonation to give the corresponding monosubstituted [FeH(L)(dppm)$_2$]$^+$ system and no other bis-substituted complexes analogous to **9** could be obtained. Neither could such complexes be obtained by further protonation of monohydridic complexes such as **5**, **6** and **7** in the presence of an excess of the H_2-displacing ligand. It is possible in these cases that, after H_2 in **1** is displaced by another ligand, a combination of the strong *trans* influence of the H^- and the Lewis basic properties of the ligand leads to proton attack at another site in the molecule.

Considering now X-ray structural data for the complexes reported herein, and related complexes in the literature, *trans*-[Fe(CH_3CN)$_2$(dppm)$_2$] [FeI_4] $\cdot$ $2H_2O$, which contains the same cation as in **9**, has been prepared from FeI_2(dppm)$_2$ and CH_3CN and structurally characterized by crystallography [8]. In addition, recent work [18] has established that related complexes of the type *trans*-[$FeL_2(PP)_2$] [X]$_2$ (L = various nitriles including CH_3CN, PP = $R_2P(CH_2)_2PR_2$ with R = CH_3 or C_2H_5, and X = BF_4 or PF_6) can be synthesized either *via* protonation of $FeH_2(PP)_2$ followed by exchange of the resulting H_2 ligand or from reactions of $FeCl_2(PP)_2$ with nitriles. The structures of several of these analogues of **9** were determined [18] by X-ray crystallography. The structural parameters established by us for **9** itself are very similar to those reported [8] for *trans*-[Fe(CH_3CN)$_2$(dppm)$_2$] [FeI_4] $\cdot$ $2H_2O$ and the published bond lengths for the latter will be used for comparison purposes in this paper.

Structural information has also been acquired for **3** and **4** although due to a very small crystal, only the main structural features of **4** were confirmed (succinonitrile bound through one CN group *trans* to the H^- - see experimental section). For **3**, the crystal, data collection and refinement data are recorded in Table 1 while appropriate bond lengths and angles are summarized in Table 2. An ORTEP drawing showing the Fe coordination geometry is shown in Fig. 1. The BF_4 anion is disordered over three positions (0.40:0.34:0.26 ratio) related by rotation. As in the structures of the other complexes containing chelating dppm, distortions from octahedral geometry are due in large part to the strained 4-membered FePCP rings, with P-Fe-P angles of 73-74° and P-C-P angles of about 18° smaller than that required for a tetrahedral C atom. These, in turn, determine the non-linearity of the *trans* P-Fe-P angles [170.54(6) and 173.12(6)°]. The Fe-H distance of 1.35(6) Å is shorter than the sum of the covalent radii of Fe and H and considerably shorter than Fe-H distances of 1.5-1.6 Å, determined both by X-ray and neutron diffraction methods, found in comparable complexes [4, 19, 20, 21]. This discrepancy is probably due to the difficulties in accurately locating H atoms using X-rays, and also reflects the uncertainty in the N-Fe-H angle of 172(3)° in **3**.

In the acetonitrile ligand, the N≡C and the C-C distances are within the range found for analogous compounds containing coordinated acetonitrile [8, 18]. The most significant observation with respect to the coordinated CH_3CN concerns the Fe-N bond which is longer in **3** [1.927(4) Å] than in

Table 1. Crystal data and structure refinement for *trans*-[Fe(H)($NCCH_3$)($dppm)_2$] [BF_4] (**3**)

Empirical formula	$C_{52}H_{48}BF_4FeNP_4$(**3**)
Formula weight	943.45
Temperature (K)	293(2)
Wavelength (Å)	0.71073
Crystal system	Monoclinic
Space group	$P2_1/n$
*a*Å	12.525(3)
*b*Å	17.805(4)
*c*Å	21.540(4)
β°	92.57(3)
Volume (Å^3)	4799(2)
Z	4
D_{calc} (g cm^{-3})	1.320
Absorption coefficient (mm^{-1})	0.499
Crystal size (mm)	$0.52 \times 0.47 \times 0.26$
Crystal description	orange plate
F(000)	1976
Range (°)	1.48 to 23.98
Index ranges	$-14 <= h <= 14, 0 <= k <= 20, 0 <= 1 <= 24$
Reflections collected	7508
Independent reflections	7508 [*R*(int) = 0.0000]
Refinement method	Full-matrix least-squares on F^2
Data/restraints/parameters	7508/0/575
Goodness-of-fit on F^2	0.958
Final *R* indices*	$R1 = 0.0610$, $wR2 = 0.1345$ [$4563F_o > 4\sigma(F_o)$]
R indices (all data)	$R1 = 0.1048$, $wR2 = 0.1345$
Largest diff. peak and hole (e Å^{-3})	0.499 and −0.320

*$R1 = \sum||F_o| - |F_c||/\sum|F_o|$; $wR2 = [\sum[w(F^2_o - F^2_c)^2]/\sum[w(F^2_o)^2]]^{0.5}$

Table 2. Selected bond lengths [Å] and angles [°] for [Fe(H)($NCCH_3$)($dppm)_2$]BF_4(**3**)

Fe–P(4)	2.203(2)	P(4)–Fe–P(3)	74.16(5)
Fe–P(3)	2.203(2)	P(1)–Fe–P(2)	73.63(5)
Fe–P(1)	2.206(2)	N(1)–Fe–P(4)	96.88(12)
Fe–P(2)	2.214(2)	N(1)–Fe–P(3)	98.09(13)
Fe–H(1)	1.35(6)	N(1)–Fe–P(1)	91.36(13)
Fe–N(1)	1.927(4)	N(1)–Fe–P(2)	89.91(12)
N(1)–C(3)	1.137(6)	P(4)–Fe–H(1)	82(3)
C(3)–C(4)	1.451(8)	P(3)–Fe–H(1)	74(3)
		P(1)–Fe–H(1)	97(3)
		P(2)–Fe–H(1)	92(3)
		P(4)–Fe–P(1)	104.99(6)
		P(3)–Fe–P(1)	170.54(6)
		P(4)–Fe–P(2)	173.12(6)
		P(3)–Fe–P(2)	106.05(6)
		N(1)–Fe–H(1)	172(3)
		P(1)–C(1)–P(2)	90.8(2)
		P(3)–C(2)–P(4)	92.1(2)

[Fe($CH_3CN)_2$($dppm)_2$] [FeI_4] · $2H_2O$ [1.867(12) Å] due to the strong *trans* influence of the H^- in **3**.

The Fe-P bond lengths decrease significantly, from 2.316(3)-2.290(2) Å in *trans*-[FeCl(CO)($dppm)_2$] [BF_4] to 2.285(4)-2.281(4) Å in [Fe($CH_3CN)_2$($dppm)_2$] [FeI_4] · $2H_2O$ to 2.214(2)-2.203(1) Å in **3** to 2.172(2)-2.153(2) Å in **2**. Since the σ-bonding capabilities of the *trans* ligands increase in this order, it is possible that the corresponding strengthening of the Fe-P bond is associated with a greater involvement of Fe-P π back-

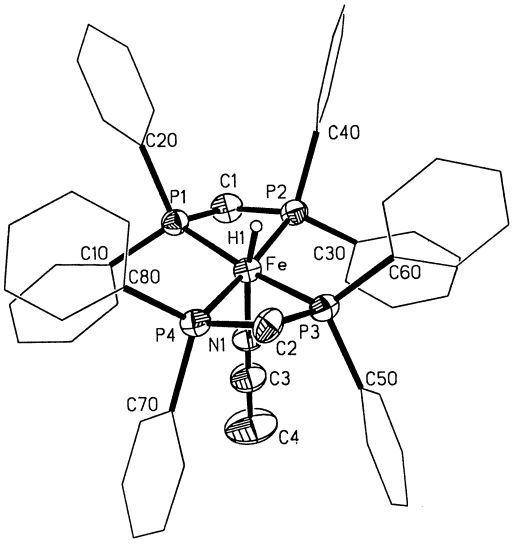

Fig. 1. ORTEP drawing of **3**.

bonding as electron density is redistributed from the Fe. It is also possible that the size of the groups in the axial positions influence the Fe-P bond lengths, with the smallest axial groups resulting in the shortest Fe-P bonds. Since several factors affect the chemical shifts of the P atoms, it is difficult to correlate δ values of 10.3, 14 (in **9**), 30 and 24, respectively, with structural parameters (see also below).

Selected spectroscopic data are summarized in Table 3 for the compounds containing the *trans* L-Fe-H arrangement reported herein together with data for the related structures *trans*-[Fe(H)(Cl)(dppm)$_2$] and *trans*-[Fe(H)(CO)(dppm)$_2$] [BF_4] [4]. There has been considerable discussion in the literature regarding the extent to which metal ions undergo π-back bonding to a dihydrogen ligand. It was hoped that the above series of compounds would allow changes in these spectral parameters to be related to changes in the Fe-ligand bonding pattern. In each case, the singlet in the ^{31}P nmr spectrum, and the upfield quintet in the ^{1}H spectrum are consistent with the *trans* H-Fe-L arrangement. υFe-H varies widely as would be expected from the large differences in the measured Fe-H bond lengths [1.35(6) Å for **3** and 1.56(8), 1.58(8) Å for **2**]. It is apparent that the IR and ^{1}H NMR data fall into two categories. First, when the Fe is coordinated to any of the four predominantly weak σ donor ligands (each with a relatively weak *trans* influence), the *trans* hydride is also strongly bound (highest υFe-H, 1853-1889 cm^{-1}) and highly shielded. In the second group, which contains the strong σ donor H^- and the good π acceptors CO and C_2H_4 (all of which have a strong *trans* influence relative to the corresponding ligands in the first group), υFe-H values indicate a weaker Fe-H bond. The hydride ligands *trans* to the good π acceptors are also the most deshielded. It appears that N_2 behaves in a similar way to C_2H_4 and CO in that there is a significant σ-π interaction as evidenced by the weakening of the N_2 bond (υN_2 reduced from 2331 in N_2 to 2116 cm^{-1} in **7**). The surprising strength of the N_2-Fe interaction is illustrated by the fact that, as mentioned earlier, N_2 displaces pyridine from **5** (rapidly) and C_2H_4 (slowly) from **6**. The Fe-H bond in **1** appears comparable in strength to others in this second group of complexes, also suggesting a σ-π interaction in these complexes consistent with the lengthening of the H-H bond from 0.8 Å in H_2 to, for example, 0.92 Å in **1** as calculated [4] from J_{HD} values. Previous work [4] interpreted the position of υFe-H in **2** as being due to the *trans* influence. It should also be noted that the H_2 ligand in **1** has little effect upon the electronic environment of the *trans* H^- compared to those in **2** and this explains why this remaining H is as susceptible to protonation as are those on the dihydride.

As noted above, there is no discernible relationship between the *trans* ligands in the various complexes and the phosphorus chemical shifts which are generally typical of P in 4-membered rings.

Acknowledgements—We thank the Natural Sciences and Engineering Research Council of Canada and the Lakehead University Senate Research Committee for financial support. We thank also G. P. A. Yap of the University of Windsor Molecular Structure Centre for the X-ray determination of the structure of complex **4** and both C. Lundeen (UMD) and V. G. Young, Jr. (University of Minnesota Crystallographic Laboratory) for the determination of the structure of **9**. A referee made several helpful suggestions.

Table 3. Selected spectroscopic properties of *trans*-[Fe(H)(L)(dppm)$_2$]$^+$ cations

Complex		**3**	**4**	**5**	**6**	**7**	**2**		**1**
L	Cl[a]	MeCN	succ	py	C_2H_4	N_2	H[a]	CO[a]	H_2[a]
υFe–H[b]	1889	1880	1881	1853	1714	1713	1711	1710	1708
δ^1H[c]	−21.2	−13.0	−13.1	−17.0	−1.8	−9.4	−7.0	−2.0	−7.2
δ^{31}P[c]	24.2	29.8	30.3	22.7	32.8	24.2	24.0	31.6	32.5

[a] ref. [4]
[b] cm^{-1}, some signals very weak;
[c] CD_2Cl_2 or CH_2Cl_2, room temp.

REFERENCES

1. Jessop, P. G. and Morris, R. H., *Coord. Chem. Rev*., 1992, **121,** 155 For an early review.
2. Morris, R. H., *Can. J. Chem*., 1996, **74,** 1907.
3. Bautista, M. T., M.Sc. Thesis, University of Toronto, cited in ref 1, 1988.
4. Gao, Y., Holah, D. G., Hughes, A. N., Spivak, G. J., Havighurst, M. D., Magnuson, V. R. and Polyakov, V., *Polyhedron*, 1997, **16,** 2797.
5. Pray, A. J., *Inorganic Syntheses*; R. J. Angelici, ed., McGraw-Hill, New York (1990) Vol. 28, p.321.
6. Sheldrick, G. M., *SHELXL*-93. *Program System for X-ray Structure Determination*. University of Cambridge, U.K., 1993.
7. Gabe, E. J., Le Page, Y., Charland, J. P., Lee, F. L. and White, P. S., PC version of the system, *J. Appl. Cryst*., 1989, **22,** 384.
8. Barclay, J. E., Evans, D. J., Hughes, D. L. and Leigh, G. J., *J. Chem. Soc*., *Dalton Trans*., 1993, 69.
9. G. P. A. Yap, unpublished results.
10. Henderson, R. A., *J. Chem. Soc*., *Dalton Trans*., 1988, 509.
11. Schlaf, M., Lough, A. J., Maltby, P. A. and Morris, R. H., *Organometallics*, 1996, **15,** 2270.
12. Holah, D. G., Hughes, A. N. and Prokopchuk, E. M., unpublished results.
13. Michos, D., Luo, X. L., Faller, J. W. and Crabtree, R. H., *Inorg. Chem*., 1993, **32,** 1370.
14. Upmacis, R. K., Polyakoff, M. and Turner, J. J., *J. Am. Chem. Soc*., 1986, **108,** 3645.
15. Moreno, B., Sabo-Etienne, S., Chaudret, B., Rodriguez-Fernandez, A., Jalon, F. and Trofimenko, S., *J. Am. Chem Soc*., 1994, **116,** 2635.
16. Christ, M. L., Sabo-Etienne, S., Chung, G. and Chaudret, B., *Inorg. Chem*., 1994, **33,** 5319 and references therein.
17. Crabtree, R. H., Lavin, M. and Bonneviot, L., *J. Am. Chem Soc*., 1986, **108,** 4032.
18. George, A. V., Field, L. D., Malouf, E. Y., McQueen, A. E. D., Pike, S. R., Purches, G. R., Hambley, T. W., Buys, I. E., White, A. H., Hockless, D. C. R. and Skelton, B. W., *J. Organomet. Chem*., 1997, **538,** 101.
19. Bianchini, C., Masi, D., Peruzinni, M., Casarin, M., Maccato, C. and Rizzi, C. A., *Inorg. Chem*., 1997, **36,** 1061.
20. Van der Sluys, L. S., Eckhert, J., Eisenstein, O., Hall, J. H., Huffman, J. C., Jackson, S. A., Koetzle, T. F., Kubas, G. J., Vergamini, P. J. and Caulton, K. G., *J. Am. Chem. Soc*., 1990, **112,** 4831.
21. Ricci, J. S., Koetzle, T. F., Bautista, M. T., Hofstede, T. M., Morris, R. H. and Sawyer, J. F., *J. Am. Chem. Soc*., 1989, **111,** 8823.

Pergamon

PII: S0277–5387(98)00167–3

Polyhedron Vol. 17, No. 22, pp. 3889–3901, 1998
© 1998 Elsevier Science Ltd
All rights reserved. Printed in Great Britain
0277–5387/98 $19.00+0.00

(2-Diphenylphosphinoethyl)cyclopentadienyl complexes of zirconium (IV): synthesis, crystal structure and dynamic behaviour in solutions

Dmitrii P. Krut'ko,*[a] Maxim V. Borzov,[a] Eduard N. Veksler,[a] Andrei V. Churakov[bc] and Judith A. K. Howard†[c]

[a]Department of Chemistry, Moscow State University, Leninskie Gory, Moscow, 119899, Russia

[b]N.S. Kurnakov Institute of General and Inorganic Chemistry, Russian Academy of Science, Leninskii prospect 31, Moscow, 117907, Russia

[c]Department of Chemistry, University of Durham, Science Laboratories, South Road, Durham, DH1 3LE, United Kingdom

(Received 7 January 1998; accepted 8 April 1998)

Abstract—The novel [η^5:η^1-(2-diphenylphosphinoethyl)cyclopentadienyl]trichlorozirconium (IV) **3** has been prepared *via* (2-diphenylphosphinoethyl)(trimethylsilyl)cyclopentadiene **2**. The structures of an adduct of **3** with tetrahydrofuran (THF) **3b** (two crystal modifications) and of an ionic complex derived from **3** and $ZrCl_4$ $\{[\eta^5{:}\eta^1-(C_5H_4CH_2CH_2PPh_2)ZrCl]_2(\mu-Cl)_3\}^+{}_2[(ZrCl_4)_2(\mu-Cl)_2]^{2-}$ **4** have been determined by an X-ray analysis. The X-ray and NMR data prove the existence of a Zr–P intramolecular coordination in **3** both in solid state and in non-solvating media within a broad range of temperatures. In THF solution the flexible equilibrium between adducts of **3** with one (**3b**) and two (**3c**) molecules of THF has been observed by variable-temperature NMR spectroscopy. The synthetic route to the simplest unsymmetrically ligated zirconocene (η^5-$C_5H_4CH_2CH_2PPh_2$)(η^5-C_5H_5)$ZrCl_2$ **5** derived from **3** has also been elaborated. © 1998 Elsevier Science Ltd. All rights reserved

Keywords: zirconium; substituted cyclopentadienes; crystal structure; NMR spectroscopy.

Transition metal complexes with ω-heteroatomsubstituted alkylcyclopentadienyl type ligands are now under intensive investigation [1]. However, only few examples of diorganophosphino-group side chain functionalized cyclopentadienyl derivatives of the Group 4 metals are known [2–6], with the only representative of monocyclopentadienyl complexes, $[\eta^5-C_5H_3-1,3-(SiMe_2CH_2PPr^i{}_2)_2]ZrCl_3$ and its alkylation products, reported [5, 6]. Meanwhile, compounds of the general type $L_nM(C_5H_4CH_2CH_2PR_2)$ with M=Ga and In [7], Fe [8], Co [4], and Rh and Ir [9] have been described. In connection with this we considered it attractive to prepare and study the structure of [η^5:η^1-(2-diphenylphosphinoethyl)cyclopentadienyl]trichlorozirconium (IV) **3**. Complex **3** was initially supposed to exhibit dynamic behaviour in solutions. To estimate the coordination ability of the diphenylphosphino group towards a Zr(IV) centre we carried out the variable-temperature NMR studies of compound **3** in CD_2Cl_2 and THF-d_8. Since the monocyclopentadienyltrihalozirconiums (IV) are precursors of unsymmetrically ligated dicyclopentadienyl complexes of Zr (IV), we were also interested in elaborating a convenient synthetic route to the simplest

*Author to whom correspondence should be addressed. E-mail: kdp@org.chem.msu.su; fax (095) 9328846.

† The second corresponding author; e-mail: J.A.K. Howard@durham.ac.uk

zirconocene of this type derived from **3**, (η^5-$C_5H_4CH_2CH_2PPh_2$)(η^5-C_5H_5)$ZrCl_2$ **5**.

RESULTS AND DISCUSSION

Synthesis of (2-diphenylphosphinoethyl)cyclopentadienyl complexes of zirconium (IV)

The Si–C bond cleavage reaction in silylated cyclopentadienes still remains among the most convenient approaches to monocyclopentadienyltrihalozirconiums (IV) derived from non-hindered cyclopentadienes [10]. Since lithium (2-diphenylphosphinoethyl)cyclopentadienide **1** is readily available [4], preparation of (2-diphenylphosphinoethyl)trimethylsilylcyclopentadiene **2** meets no problems (see Scheme 1).

Mixing of equimolar amounts of **2** and $ZrCl_4$ in toluene leads to a complete dissolution of the metal tetrahalide (supposedly caused by initial coordination of $ZrCl_4$ with the PPh_2-groups of **2**), followed by a rapid formation of a thick white precipitate. This precipitate presents crude [η^5:η^1-(2-diphenylphosphinoethyl)cyclopentadienyl]trichlorozirconium (IV) **3**. The crude product **3** can be purified both as an unsolvated form **3a** in a very low yield (fractional recrystallizations from dichloromethane) or, better, as an adduct with one molecule of tetrahydrofuran (THF) **3b** (recrystallization from THF) (see Scheme 2). Contrary to the reported for $C_5H_5ZrCl_3$ [11], adduct **3b** is thermally stable in a THF solution even at 90°C (sealed evacuated NMR-tube, 6 hours).

We suppose that the considerable amount of impurities in crude **3** and the difficulties of its purification in the unsolvated form **3a** are caused by two main factors. First of all, compound **2** presents an equilibrium mixture of isomers with allylic (**2a**) or vinylic (**2b**,**c**...) position of the Me_3Si-group. At room temperature, the ^1H NMR spectroscopically estimated molar ratio of **2a** to **2b**,**c**... is approximately 4:1 (see Scheme 1). There are certain reasons to suppose that only isomer **2a** is cleaved with $ZrCl_4$ and produces the desired complex **3**. Meanwhile, the other isomers **2b,c**.. are able to react in this manner only after their slow conversion into **2a** and may be involved into Lewis acid induced diene polymerisation. Thus, even determining of the initially required molar excess of **2** over $ZrCl_4$ presents a problem and polymeric by-products should be always expected.

Secondly, if no THF is added, the unreacted $ZrCl_4$ is hardly removable from the reaction mixture. Capturing of $ZrCl_4$ was directly confirmed by the fact, that the combined saturated mother liquors from the fractional recrystallizations of crude **3** gave after standing for 2 months at room temperature a small amount of crystalline solid $\{[\eta^5{:}\eta^1-(C_5H_4CH_2CH_2PPh_2)ZrCl]_2(\mu-Cl)_3\}_2^+[ZrCl_4)_2(\mu-Cl)_2]^{2-}$ **4**. The structure of compound **4** was established by X-ray diffraction analysis (see discussion below).

To prepare the unsymmetrically ligated zirconocene (η^5-$C_5H_4CH_2CH_2PPh_2$)(η^5-C_5H_5)$ZrCl_2$ **5** derived from **3**, we first applied the conventional cyclopentadienylation procedures. However, a reaction between **3b** and sodium cyclopentadienide either in toluene or in THF leads to inseparable mixtures of all the possible cyclopentadienyl ligand exchange products **5**–**7**. In toluene, moreover, zirconocenes **5**–**7** are formed in a statistical ratio (2:1:1, respectively) as white crystalline solids (from ether) (see Scheme 3). In contrast, the application of trimethylcyclopentadienyltin as a gentle cyclopentadienylating agent gives excellent results and pure zirconocene **5** is isolated in a good yield.

It is a well known fact that C_5H_5Na is capable of introducing more than two cyclopentadienyl ligands to Zr (IV) centre [12]. We believe that the observed ligand randomisation is caused by the traces of triscyclopentadienylzirconium (IV) species which are generated when initial **3b** and product **5** compete for $C_5H_5^-$ in the reaction mixture. When the reaction is

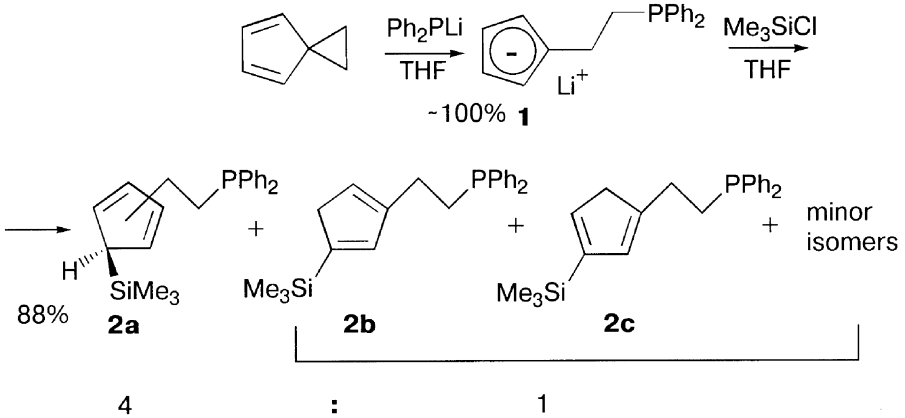

Scheme 1.

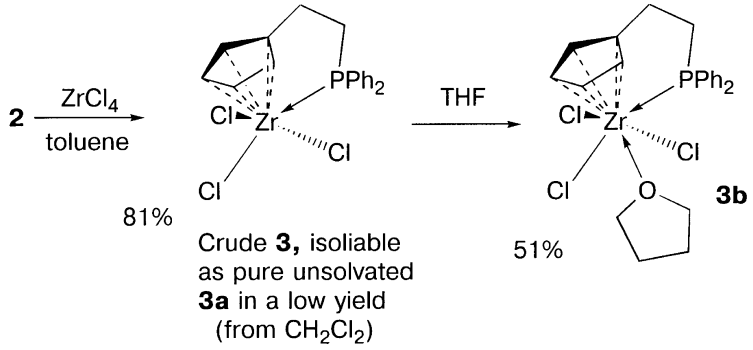

Scheme 2.

performed in toluene, the initially low solubility of C_5H_5Na increases, due to liberation of THF from **3b**. As far as **3b** is only moderately soluble in toluene, considerable excess of free cyclopentadienide appears in the solution, and, thus, cyclopentadienyl ligand exchange is complete in this case. In contrast to $C_5H_5^-$, $Me_3SnC_5H_5$ does not attack **5** at all, so triscyclopentadienylzirconium (IV) species are not generated and no products of cyclopentadienyl ligand exchange are formed.

X-RAY CRYSTAL STRUCTURE DETERMINATION OF $[\eta^5{:}\eta^1$-$(C_5H_4CH_2CH_2PPh_2)]ZrCl_3 \cdot$ THF 3b AND $\{[\eta^5{:}\eta^1-(C_5H_4CH_2CH_2PPh_2)ZrCl]_2(\mu-Cl)_3\}_2^+[(ZrCl_4)_2(\mu-Cl)_2]^{2-}$ 4

The structures of two different crystalline modifications of **3b** and ionic complex **4** were determined by X-ray analysis.

First modification of **3b** (*crystallised from* CH_2Cl_2)

The unit cell contains two independent molecules with similar geometrical parameters. These molecules seem to be related by the superposition of the rotation around the *b*-axis and 1/4-translation along the same direction. Thus, the correctness of the unit cell dimensions (doubling of axis), possibility of twinning and the space group determination have been specially checked.

The arrangement of molecules in the unit cell is such that the Zr–P directions are approximately parallel to the *b*-axis (7.8 and 5.3°). The orthogonal least-squares fitting of one independent molecule to the other, based on the positions of all non-hydrogen atoms (except carbons of THF) resulted in an r.m.s. deviation 0.07 Å. The greatest differences were observed for the conformations of the coordinated THF molecules, as far as one of them exhibits disorder of the envelope carbon atom C(83). Selected bond lengths and angles are listed in Table 1. The molecular structure of **3b** (first modification) is shown in Fig. 1.

Second modification of **3b** (crystallised from THF)

The unit cell contains only one independent molecule. The coordination environment of the central Zr atom is quite close to that found for the first crystalline modification of **3b**. However, the conformation of phosphino-substituent is completely different from the previous one (different rotations around Ph–P bond). For the first modification of **3b**, all four torsion angles between the planes of phenyl rings and exocyclic P–C bonds lie within a range 43.0–46.0°. As for the second modification, the same angles are equal to 5.7 and 90.1°. Selected bond lengths and angles are listed in Table 1. The molecular structure of **3b** (the second modification) is shown in Fig. 2.

For both modifications of **3b**, the Zr atoms possess a distorted octahedral coordination assuming that Cp-ligands occupy one site. The cyclopentadienyl rings and THF molecules lie in the apical positions while the phosphino-groups occupy equatorial ones. The mean deviation of the Zr atom from the equatorial plane towards Cp-ligand is 0.49 Å. This polyhedron is preferred for monocyclopentadienyl complexes of Zr(IV) [1, 6, 13–18], except for the cases when the latter is prohibited by the steric requirements of the substituted Cp-ligands [10c, 19]. Analysis of the Cambridge Structural Database (Release: October 1996) [20] shows that the Zr–Cl distances (2.4621(11)–2.5138(10) Å) in **3b** are of normal values for terminal Zr(IV)–Cl bonds in monocyclopentadienyl complexes (2.357–2.542 Å). The Zr–O(THF) bonds (2.350(3)–2.3613(12) Å) are noticeably shorter than it was found for the same apical bonds in $(CpR)ZrCl_3 \cdot 2THF$ (R=H, 2.393(3) Å, R=Me, 2.377(2) Å) [13].

Crystal structure of complex **4**

The crystal structure of **4** is shown in Fig. 3. Selected bond lengths and angles are listed in Tables 2 and 3,

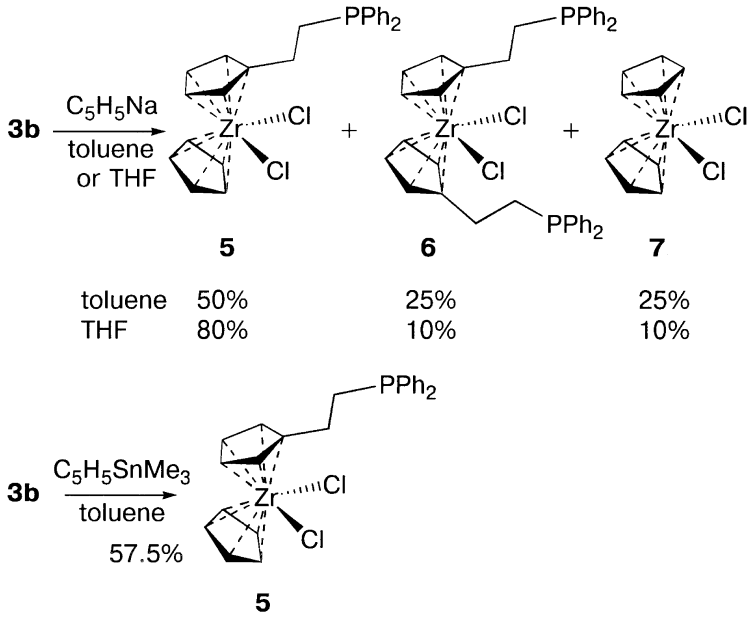

Scheme 3.

Table 1. Selected bond lengths (Å) and angles (°) for **3b**

First modification				Second modification	
Molecule A		Molecule B			
Zr(1)–O(1)	2.351(3)	Zr(2)–O(2)	2.350(3)	Zr–O	2.3613(12)
Zr(1)–Cl(12)	2.4745(11)	Zr(2)–Cl(22)	2.4621(11)	Zr–Cl(2)	2.4829(5)
Zr(1)–Cl(13)	2.4808(10)	Zr(2)–Cl(23)	2.4805(10)	Zr–Cl(3)	2.4788(5)
Zr(1)–Cl(11)	2.5138(10)	Zr(2)–Cl(21)	2.5061(10)	Zr–Cl(1)	2.4981(5)
Zr(1)–P(1)	2.8729(11)	Zr(2)–P(2)	2.8707(11)	Zr–P	2.8474(5)
Zr(1)–PL(1)*	2.229(2)	Zr(2)–PL(2)*	2.232(2)	Zr–PL*	2.236(1)
O(1)–Zr(1)–Cl(12)	81.71(7)	O(2)–Zr(2)–Cl(22)	81.53(8)	O–Zr–Cl(2)	79.50(3)
O(1)–Zr(1)–Cl(13)	78.14(7)	O(2)–Zr(2)–Cl(23)	78.00(8)	O–Zr–Cl(3)	78.98(3)
O(1)–Zr(1)–Cl(11)	76.19(7)	O(2)–Zr(2)–Cl(21)	76.53(8)	O–Zr–Cl(1)	76.69(3)
O(1)–Zr(1)–P(1)	77.87(7)	O(2)–Zr(2)–P(2)	79.25(7)	O–Zr–P	81.87(3)
Cl(12)–Zr(1)–Cl(13)	90.59(4)	Cl(22)–Zr(2)–Cl(23)	93.59(4)	Cl(3)–Zr–Cl(2)	91.87(2)
Cl(12)–Zr(1)–Cl(11)	91.62(4)	Cl(22)–Zr(2)–Cl(21)	90.55(4)	Cl(2)–Zr–Cl(1)	96.27(2)
Cl(13)–Zr(1)–Cl(11)	153.63(4)	Cl(23)–Zr(2)–Cl(21)	153.28(4)	Cl(3)–Zr–Cl(1)	152.42(2)
Cl(12)–Zr(1)–P(1)	158.66(3)	Cl(22)–Zr(2)–P(2)	158.97(3)	Cl(2)–Zr–P	161.33(2)
Cl(13)–Zr(1)–P(1)	91.25(3)	Cl(23)–Zr(2)–P(2)	90.70(3)	Cl(3)–Zr–P	83.42(2)
Cl(11)–Zr(1)–P(1)	77.59(3)	Cl(21)–Zr(2)–P(2)	76.77(3)	Cl(1)–Zr–P	80.49(2)

* PL(1) and PL(2) mean least-squares planes of the cyclopentadienyl rings.

respectively. The asymmetric unit consists of positively charged dimeric particle $\{[\eta^5{:}\eta^1\text{-}(C_5H_4CH_2CH_2PPh_2)ZrCl]_2(\mu\text{-}Cl)_3\}^+$ and a half of the centrosymmetric $[(ZrCl_4)_2(\mu\text{-}Cl)_2]^{2-}$ dianion. In addition, the crystal lattice contains disordered CH_2Cl_2 molecule. The central $\{[\eta^5{:}\eta^1\text{-}(C_5H_4CH_2CH_2PPh_2)ZrCl]_2(\mu\text{-}Cl)_3\}^+$ unit represents the second example of monocyclopentadienyl zirconium complex containing three bridging chlorine atoms [21]. However, the same $Zr_2(\mu\text{-}Cl)_3$ motif was reported for several neutral complexes of zirconium tetrachloride [22].

Both zirconium atoms have a distorted octahedral coordination. The apical bridging bonds Zr(l)–C1(5) and Zr(2)–C1(3) are significantly longer (2.7365(14) and 2.733(2) Å) than four equatorial non-terminal Zr–Cl bonds (2.5489(14)–2.6254(14) Å). Previously we have observed the same effect for similar complexes $(\eta^5{:}\eta^1\text{-}C_5Me_4CH_2CH_2EMe)ZrCl_3$, (E=S, O) [14]. Of

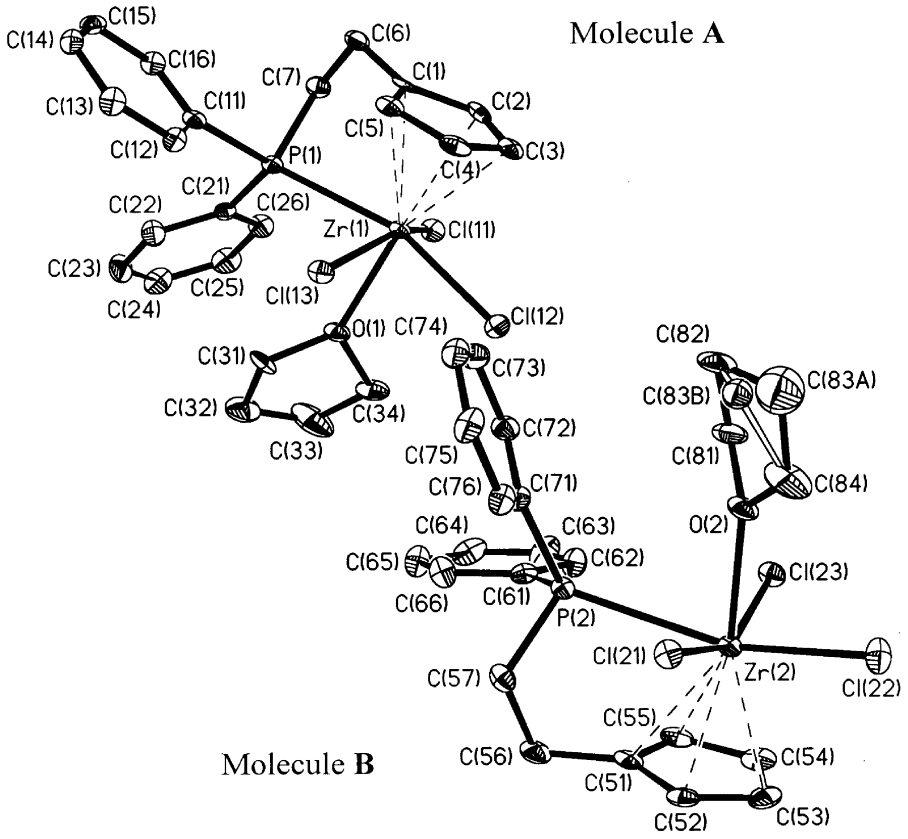

Fig. 1. Molecular structure of **3b** (first modification). Displacement ellipsoids are shown at 50% probability level. Hydrogen atoms are omitted for clarity.

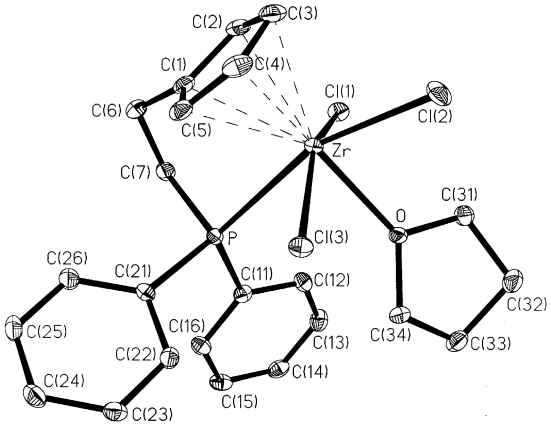

Fig. 2. Molecular structure of **3b** (second modification). Displacement ellipsoids are shown at 50% probability level. Hydrogen atoms are omitted for clarity.

interest, the longer Zr-(μ-Cl) distance (2.794(7) Å) was found in the structure of closely related anionic complex $\{[\eta^5\text{-}(C_5H_4CH_2CH{=}CH_2)ZrCl_2]_2(\mu\text{-}Cl)_3\}^-$ $[Li(DME)]^+$ [21].

The Zr–P distances (2.802(2), 2.817(2) Å) are noticeably shorter than those found in the structure of neutral complex $[\eta^5-C_5H_3-1,3-(SiMe_2CH_2PPr^i_2)_2]ZrCl_3$ (2.897(1), 2.871(1) Å) [6]. The latter can be explained by the influence of the positive charge of the $\{[\eta^5{:}\eta^1\text{-}(C_5H_4CH_2CH_2PPh_2)ZrCl]_2(\mu\text{-}Cl)_3\}^+$ unit.

NMR study of the dynamic behaviour of complex **3** *in solutions*

To determine the coordination ability of the pendant phosphine group in **3a** and **3b** in solvating and non-solvating solvents we performed the variable-temperature NMR spectroscopy investigation of the samples of **3a** in CD_2Cl_2 and **3b** both in THF-d_8 and in CD_2Cl_2. The signals in the ^1H and $^{13}C\text{-}\{^1H\}$ NMR spectra of complexes **3** and **5** (see **Experimental**) were assigned on the basis of the homonuclear Overhauser effect, coupled ^{13}C spectra and selective heteronuclear decoupling experiments.

The value of ^{31}P chemical shift is a good criterion for the presence or absence of the Zr–P coordination bond. Values close to those of free alkyldiphenylphosphines (δ *ca*-15 ppm) are characteristic of a non-coordinated PPh_2-group, while the Zr–P coordination results in the low field shifting of the signal up to δ *ca* 5–8 ppm. The similar differences

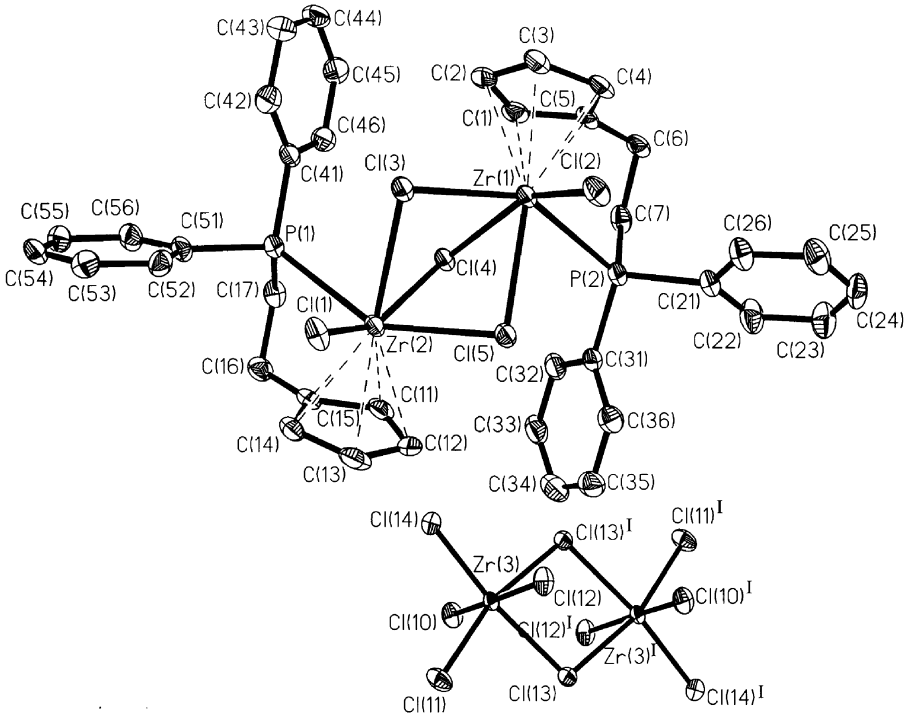

Fig. 3. Molecular structure of **4**. Displacement ellipsoids are shown at 50% probability level. Hydrogen atoms and solvent CH_2Cl_2 molecule are omitted for clarity. Superscript symbol "I" indicates symmetry equivalent atoms.

Table 2. Selected bond lengths (Å) for **4**

Zr(1)–Cl(2)	2.408(2)	Zr(2)–Cl(1)	2.411(2)
Zr(1)–C(3)	2.466(6)	Zr(2)–C(13)	2.489(6)
Zr(1)–C(2)	2.492(6)	Zr(2)–C(12)	2.495(6)
Zr(1)–C(4)	2.495(5)	Zr(2)–C(14)	2.513(6)
Zr(1)–C(1)	2.527(6)	Zr(2)–C(11)	2.525(6)
Zr(1)–C(5)	2.547(5)	Zr(2)–C(15)	2.552(6)
Zr(1)–Cl(3)	2.5489(14)	Zr(2)–Cl(3)	2.733(2)
Zr(1)–Cl(4)	2.6254(14)	Zr(2)–Cl(4)	2.6166(13)
Zr(1)–Cl(5)	2.7365(14)	Zr(2)–Cl(5)	2.5520(14)
Zr(1)–P(2)	2.817(2)	Zr(2)–P(1)	2.802(2)
P(2)–C(7)	1.830(6)	P(1)–C(51)	1.832(6)
P(2)–C(21)	1.826(6)	P(1)–C(41)	1.921(6)
P(2)–C(31)	1.831(6)	P(1)–C(17)	1.829(6)
C(1)–C(2)	1.399(9)	C(11)–C(15)	1.420(9)
C(1)–C(5)	1.426(8)	C(11)–C(12)	1.434(9)
C(2)–C(3)	1.404(9)	C(12)–C(13)	1.397(9)
C(3)–C(4)	1.402(8)	C(13)–C(14)	1.411(9)
C(4)–C(5)	1.414(8)	C(14)–C(15)	1.419(8)
C(5)–C(6)	1.510(8)	C(15)–C(16)	1.504(8)
C(6)–C(7)	1.521(8)	C(16)–C(17)	1.521(8)
Zr(3)–Cl(14)	2.383(2)	Zr(3)–Cl(12)	2.427(2)
Zr(3)–Cl(11)	2.397(2)	Zr(3)–Cl(13)[a]	2.5976(14)
Zr(3)–Cl(10)	2.416(2)	Zr(3)–Cl(13)	2.642(2)

[a]Symmetry transformation used to generate equivalent atoms: $-x+1, -y, -z$.

Table 3. Selected bond angles (°) for **4**

Cl(2)–Zr(1)–Cl(3)	94.74(5)	Cl(1)–Zr(2)–Cl(3)	78.08(5)
Cl(2)–Zr(1)–Cl(4)	152.32(5)	Cl(1)–Zr(2)–Cl(4)	152.13(5)
Cl(3)–Zr(1)–Cl(4)	77.04(4)	Cl(3)–Zr(2)–Cl(4)	74.06(4)
Cl(2)–Zr(1)–Cl(5)	78.81(5)	Cl(1)–Zr(2)–Cl(5)	95.94(5)
Cl(3)–Zr(1)–Cl(5)	76.28(4)	Cl(5)–Zr(2)–Cl(3)	76.30(4)
Cl(4)–Zr(1)–Cl(5)	73.57(4)	Cl(4)–Zr(2)–Cl(5)	76.83(4)
Cl(2)–Zr(1)–P(2)	100.33(5)	Cl(1)–Zr(2)–P(1)	100.60(5)
Cl(3)–Zr(1)–P(2)	147.57(5)	Cl(5)–Zr(2)–P(1)	147.41(5)
Cl(4)–Zr(1)–P(2)	76.32(4)	Cl(3)–Zr(2)–P(1)	79.90(4)
Cl(5)–Zr(1)–P(2)	78.70(4)	Cl(4)–Zr(2)–P(1)	75.44(4)
Zr(1)–Cl(3)–Zr(2)	89.55(4)	Zr(2)–Cl(4)–Zr(1)	90.49(4)
		Zr(2)–Cl(5)–Zr(1)	89.41(4)
C(41)–P(1)–C(17)	106.0(3)	C(21)–P(2)–C(31)	104.1(3)
C(41)–P(1)–C(51)	105.0(3)	C(21)–P(2)–C(7)	101.6(3)
C(17)–P(1)–C(51)	103.9(3)	C(31)–P(2)–C(7)	106.1(3)
C(41)–P(1)–Zr(2)	120.8(2)	C(21)–P(2)–Zr(1)	120.2(2)
C(17)–P(1)–Zr(2)	100.9(2)	C(31)–P(2)–Zr(1)	119.9(2)
C(51)–P(1)–Zr(2)	118.1(2)	C(7)–P(2)–Zr(1)	102.4(2)

in $\delta(^{31}P)$ shifts of coordinated and non-coordinated phosphino groups ($\Delta\delta$ *ca* 20 ppm) in half-sandwich complexes $[\eta^5-C_5H_3-1,3-(SiMe_2CH_2PPr^i_2)_2]ZrR_3$ (R_3=Cl_3, $Cl_2(CH_2Ph)$ and Me_3) were reported previously [6].

Both non-solvated **3a** and solvated **3b** forms of **3** in CD_2Cl_2 possess coordinated diphenylphosphino groups ($\delta(^{31}P)$ from 6 to 8 ppm, compare with $\delta(^{31}P)-14.3$ ppm for **5**, (see Table 4)). The temperature decrease down to $-70°C$ does not affect considerably the NMR spectra of both **3a** and **3b**, that points to the retention of Zr–P coordination bond over the whole temperature range studied.

Distinct deshielding of both the H^7 and C^7 signals in ^1H and ^{13}C-$\{^1H\}$ NMR spectra of **3** in respect to **5** provides an additional proof that the Zr–P coordination does take place in the half sandwich complex **3**.

All these data on the behaviour of **3** in the non-solvating CD_2Cl_2 media are in a good agreement with those on the structure of the monocyclopentadienyl complex $[\eta^5-C_5H_3-1,3-(SiMe_2CH_2PPr^i_2)_2]ZrCl_3$ in toluene solution, in which the zirconium center is hexacoordinated over a wide temperature range [6].

In a THF solution, the situation is markedly different. In this case compound **3** presents an equilibrium mixture of two forms **3b** and **3c** (see Scheme 4). The variable-temperature ^1H and ^{31}P-$^1\{H\}$ NMR spectra of compound **3** in THF-d_8 are depicted in Figs 4 and 5*. For comparison, the ^1H NMR spectrum of adduct **3b** in CD_2Cl_2 at $-70°C$ is given in Fig. 6. In this equilibrium, the participation of monoadduct **3b**

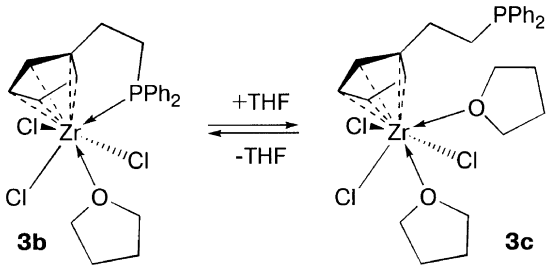

Scheme 4.

is rather evident due to the close similarity of its NMR parameters to that observed in CD_2Cl_2 (see Table 4). The second component **3c** of the equilibrium mixture exhibits no Zr–P coordination ($\delta(^{31}P)\sim -15$ ppm). As far as the adducts of $(\eta^5$-$C_5H_4R)ZrCl_3\cdot 2THF$, (R=H, Me) are well known [15], a structure of an adduct with two molecules of THF may be assigned to complex **3c** with a high degree of probability. The observed two-site exchange becomes fast on the NMR time scale at the temperatures exceeding 0°C. The content of **3c** increases from ~30% at $-30°C$ up to ~50% at $-70°C$, that may correspond to the greater negative ΔH values (and more strong bonding, respectively) of Zr-OR_2 than Zr-PR_3 coordination bond formation for cyclopentadienyltrichlorozirconiums (IV). So, the NMR spectroscopically observed exchange between **3b** and **3c** appears to be an example of a reversible solvent promoted intramolecular dissociation-coordination of a pendant side chain functionality.

We must admit here that no process of this type was observed in the cases of -OMe and -SMe side chain functionalized complexes $(\eta^5{:}\eta^1$-$C_5Me_4CH_2CH_2EMe)ZrCl_3$, (E=S, O) [14] and $(\eta^5{:}\eta^1$-

* The assignment of the signals in ^1H NMR spectra depicted in **Fig. 4** to **3b** and **3c** was performed on the basis of the homonuclear decoupling experiments and the temperature dependent changes in their relative intensities.

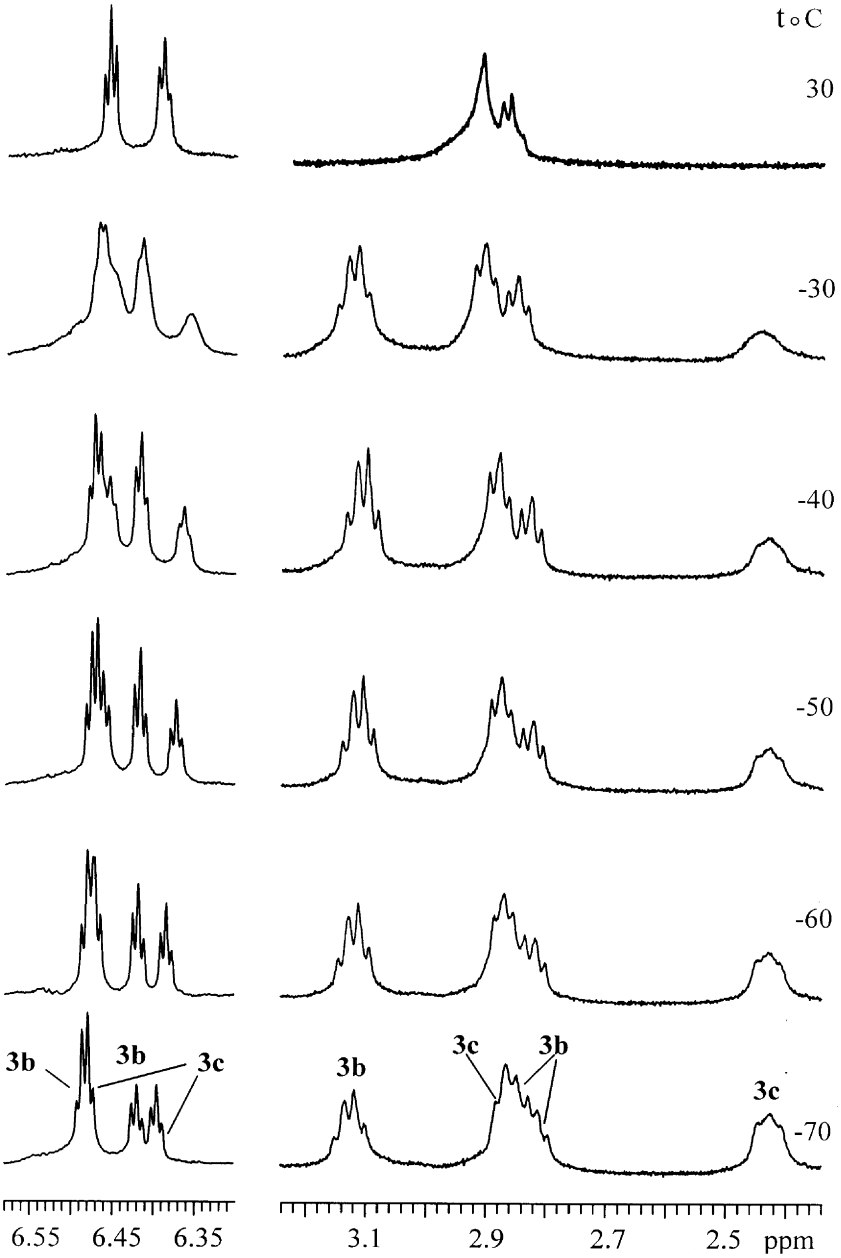

Fig. 4. Variable-temperature ^{1}H NMR spectra of **3b** and **3c** in THF-d_8. C_5H_4 and CH_2CH_2 regions are shown.

$C_5H_4CH_2CH_2OMe)ZrCl_3$ [23] in THF. Thus, the coordination ability of PPh_2-group towards Zr(IV) centre seems to be less than that of methoxy- and methylthio-groups.

EXPERIMENTAL

Initial materials and general techniques

All operations were performed in evacuated sealed glass vessels. The solvents employed (and their perdeuterated analogues) were dried with conventional agents (namely: diethyl ether and THF—with sodium benzophenone ketyl, toluene, heptane and pentane—with Na-K alloy, CH_2Cl_2 - with P_2O_5 and then with CaH_2), degassed by multiple evacuations of the frozen solvent (liq. N_2) and distilled in high vacuum directly into the reaction vessel by trapping into liq. N_2. Spiro[2,4]heptadiene-4,6 [24], trimethylcyclopentadienyltin [25] and lithium (2-diphenylphosphinoethyl)cyclopentadienide [4] **1** were prepared as described previously; lithium diphenylphosphide was prepared as a 0.6 M solution in THF by metallation of diphenylphosphine with *n*-butyl-

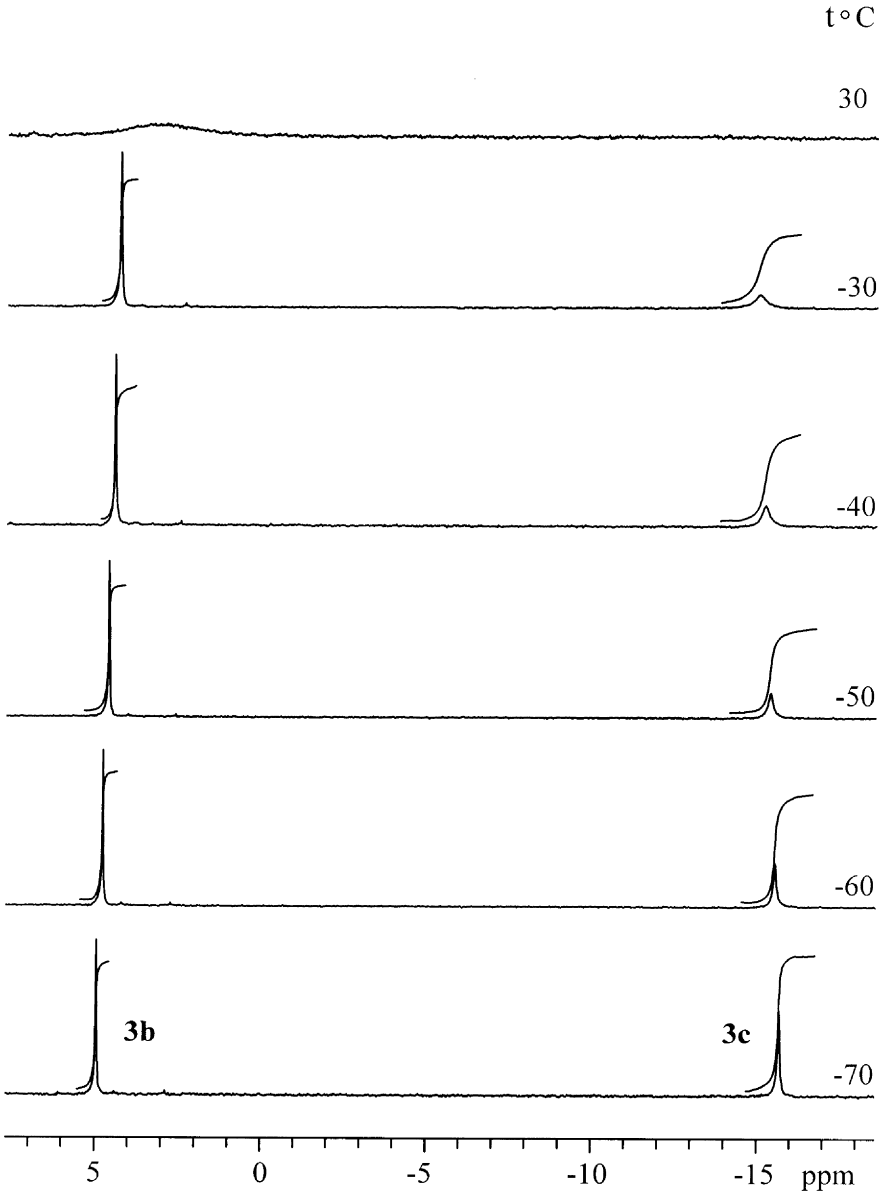

Fig. 5. Variable-temperature ^{31}P-{^{1}H} NMR spectra of **3b** and **3c** in THF-d_8.

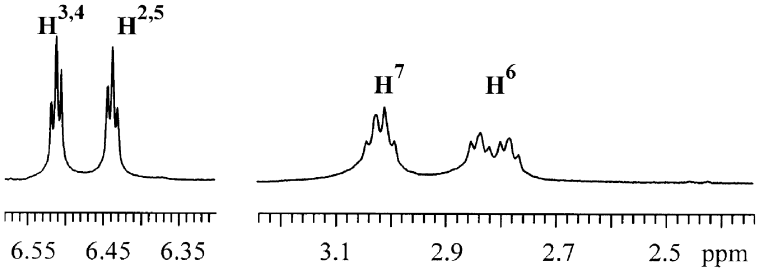

Fig. 6. ^{1}H NMR spectrum of **3b** in CD_2Cl_2 at $-70°C$. C_5H_4 and CH_2CH_2 regions are shown.

Table 4. Selected NMR parameters for **3a**–**c** and **5** at different temperatures

Complex	Solvent	t,°C	$\delta(^{31}P)$(ppm)	$\delta(H^6)$(ppm)	$\delta(H^7)$(ppm)	$\delta(C^7)$(ppm)
3a	CD_2Cl_2	30	8.3	2.98–3.10[a]		32.2
3b	CD_2Cl_2	30	6.1	2.95 (dt)	3.05 (q)	32.8
3b	CD_2Cl_2	−70	7.2	2.81 (dt)	3.02 (q)	
3b	THF-d_8	−70	5.0	2.83 (dt)	3.12 (q)	
3c	THF-d_8	−70	−15.7	2.86 (q)	2.43 (br t)	
5	THF-d_8	30	−14.3	2.78 (q)	2.38 (m)	29.3

[a]br. m, *AA′BB′*X spin system.

lithium in pentane, washing the precipitate with the same solvent and taking it up with THF. Trimethylchlorosilane was refluxed with and distilled from $AlCl_3$ onto aluminium powder, degassed and operated as it was described for the solvents. Commercially available $ZrCl_4$, diphenylphosphine and Me_3SnCl were received from Merck and Aldrich. ^1H, ^{13}C-$\{^1H\}$, and ^{31}P-$\{^1H\}$ NMR spectra were recorded on a Varian VXR-400 spectrometer at 400, 100, and 162 MHz, respectively. For ^1H and ^{13}C-$\{^1H\}$ spectra, solvent resonances [7.15 and 128.0 ppm (C_6D_6), 5.32 and 53.8 ppm (CD_2Cl_2), 1.73 and 25.3 ppm (THF-d_8)] were used as internal reference standards. For ^{31}P-$\{^1H\}$ spectra, 85% H_3PO_4 was employed as an external reference. The temperature of the spectrometer probe was calibrated by measuring the shift difference of the methanol resonance in the ^1H spectrum. The elemental analysis was performed on the Carlo-Erba automated analyzer.

Synthetic procedures

(2 - *Diphenylphosphinoethyl*)(*trimethylsilyl*)*cyclopentadiene* **2** (*a mixture of isomers*)

24.6 ml of 0.60 M solution of lithium (2-diphenylphosphinoethyl)cyclopentadienide **1** in THF (14.7 mmol) was slowly added to a cooled (−20°C) vigorously stirred solution of 1.87 ml (1.60 g, 14.7 mmol) of trimethylchlorosilane in 10 ml of THF. The reaction mixture was allowed to warm up to room temperature and left to stay overnight. On removal of the solvent by trapping it into liq. N_2, the residue was extracted with pentane, the extract evaporated and the crude product purified by distillation, that gave 4.57 g (13.04 mmol, 88.5%) of silane **2**. B.p. 154°C ($3 \cdot 10^{-2}$ torr). Anal. found: C, 75.97; H, 7.82; anal. calc. for $C_{22}H_{27}PSi$: C, 75.39; H, 7.76. NMR (listed for **2a**) (C_6D_6, 303 K) ^1H: −0.10 (*s*, 9H, $SiMe_3$), 2.34 (*m*, 2H, CH_2CH_2P), 2.64 (*q*, $^3J_{HH}=8.0$ Hz, $^3J_{HP}=8.0$ Hz, 2H, CH_2CH_2P), 3.15 (*br. s*, 1H, CH($SiMe_3$)), 6.07 (*br. s*, 1H, =CH–), 6.40 (*br. s*, 1H, =CH–), 6.48 (*br. s*, 1H, =CH–), 7.07 (*m*, 6H, *m*- and *p*-H in PPh_2), 7.46 (*m*, 4H, *o*-H in PPh_2). ^{13}C-$\{^1H\}$: −2.0 ($SiMe_3$), 26.7 (*d*, $^2J_{CP}=17.9$ Hz, CH_2CH_2P), 29.0 (*d*, $^1J_{CP}=13.1$ Hz, CH_2CH_2P), 51.1 (CH($SiMe_3$)), 127.4 (=CH–), 128.6 (*p*-C in PPh_2), 128.7 (*d*, $^3J_{CP}=6.2$ Hz, *m*-C in PPh_2) 132.3 (=CH–), 133.1 (*d*, $^2J_{CP}=18.7$ Hz, *o*-C in PPh_2), 134.2 (=CH–), 139.7 (*d*, $^1J_{CP}=15.3$ Hz, *ipso*-C in PPh_2), 145.9 (*d*, $^3J_{CP}=12.6$ Hz, $=CCH_2CH_2P$); ^{31}P-$\{^1H\}$: −14.2.

[η^5:η^1-(2-*Diphenylphosphinoethyl*)*cyclopentadienyl*] *trichloro*(*tetrahydrofuran*)*zirconium* (*IV*) **3b**

A solution of 6.29 g (17.95 mmol) of silylated cyclopentadiene **2** was added to a stirred suspension of 4.18 g (17.95 mmol) of $ZrCl_4$ in 40 ml of toluene at −20°C. The reaction mixture was allowed to warm up to room temperature, with the solid tetrachloride meanwhile dissolved. In 15 minutes a thick white precipitate formed. The reaction mixture was stirred at 50°C for an additional 2 hours and left to stay overnight. The precipitate was filtered off, washed three times with 50 ml portions of pentane and extracted with CH_2Cl_2. The combined extracts were concentrated, the precipitate filtered off, washed twice with 50 ml portions of pentane and dried in high vacuum, that yielded 6.90 g (14.5 mmol, 81%) of crude complex **3**. Recrystallization from the minimal amount of hot THF, followed by washing with ether and drying in high vacuum yielded 4.55 g (9.59 mmol, 53%) of monoadduct **3b**. Anal. found: C, 50.50; H, 4.79; anal. calc. for $C_{23}H_{26}Cl_3OPZr$ C, 50.53; H, 4.71. NMR (CD_2Cl_2, 30°C) ^1H: 1.59 (*m*, 4H, THF), 2.95 (*dt*, $^3J_{HH}=6.8$ Hz, $^3J_{HP}=21.0$ Hz, 2H, H^6), 3.05 (*q*, $^3J_{HH}=6.8$ Hz, $^2J_{HP}=6.8$ Hz, 2H, H^7), 4.02 (*m*, 4H, THF), 6.48 (virtual *t*, $^{3+4}J_{HH}=5.6$ Hz, 2H, $H^{2,5}$), 6.58 (virtual *t*, $^{3+4}J_{HH}=5.6$ Hz, 2H, $H^{3,4}$), 7.44 (*m*, 6H, *m*- and *p*-H in PPh_2), 7.67 (*m*, 4H, *o*-H in PPh_2); ^{13}C: 23.8 (*dt*, $^1J_{CH}=134$ Hz, $^2J_{CP}=9.5$ Hz, C^6), 25.4 (*t*, $^1J_{CH}=134$ Hz, THF), 32.8 (*dt*, $^1J_{CH}=136$ Hz, $^1J_{CP}=21.3$ Hz, C^7), 72.3 (*t*, $^1J_{CH}=149$ Hz, THF), 117.7 (*d*, $^1J_{CH}=178$ Hz, $C^{3,4}$), 121.7 (*d*, $^1J_{CH}=176$ Hz, $C^{2,5}$), 129.0 (*dd*, $^1J_{CH}=161$ Hz, $^3J_{CP}=8.8$ Hz, *m*-C in PPh_2), 130.8 (*d*, $^1J_{CH}=162$ Hz, *p*-C in PPh_2), 131.6 (*d*, $^1J_{CP}=25.0$ Hz, *ipso*-C in PPh_2), 133.5 (*d*, $^3J_{CP}=6.0$ Hz, C^1), 133.7 (*dd*, $^1J_{CH}=161$ Hz, $^2J_{CP}=9.4$ Hz, *o*-C in PPh_2); ^{31}P-$\{^1H\}$: 6.1.

A sample of unsolvated complex **3a** for NMR

Table 5. Crystal data, data collection, structure solution and refinement parameters for **3b** and **4**

Empirical formula	$C_{23}H_{26}Cl_3OPZr$ **3b** (first modification)	$C_{23}H_{26}Cl_3OPZr$ **3b** (second modification)	$C_{78}H_{76}Cl_{24}P_4Zr_6$ **4**
Formula weight	546.98	546.98	2535.38
Colour, habit	Colourless block	Colourless block	Colourless block
Crystal size/mm	$0.25 \times 0.20 \times 0.15$	$0.30 \times 0.25 \times 0.20$	$0.20 \times 0.20 \times 0.20$
Crystal system	Monoclinic	Monoclinic	Monoclinic
Space group	P2(1)/n	P2(1)/c	P2(1)/n
Unit cell dimensions: a/Å	7.9718(1)	8.7100(2)	11.3698(1)
b/Å	34.4298(3)	16.0401(3)	17.7818(2)
c/Å	17.1593(1)	16.7479(3)	23.7115(3)
β/°	92.435(1)	100.106(1)	102.050(1)
Volume/Å^3	4705.42(8)	2303.53(8)	4688.20(9)
Z	8	4	2
Density (calculated)/g·cm^{-3}	1.544	1.577	1.796
Absorption coefficient/mm^{-1}	0.889	0.908	1.437
F(000)	2224	1112	2504
Diffractometer		Siemens SMART CCD [26]	
Temperature/K	100.0(2)	100.0(2)	150.0(2)
Radiation (λ/Å)		graphite-monochromated Mo-Kα (0.71073)	
Scan mode	ω	ω	ω
Scan step (in ω)/°	0.3	0.3	0.3
Time per step/sec	20	15	40
θ range/°	1.18 to 26.00	1.77 to 27.48	1.44 to 27.53
Index ranges	$-10 \le h \le 8 - 40 \le k \le 44 - 22 \le l \le 20$	$-11 \le h \le 10 - 20 \le k \le 16 - 21 \le l \le 21$	$-14 \le h \le 13 - 23 \le k \le 22 - 29 \le l \le 30$
Reflections collected	30800	16258	33711
Independent reflections	9247 [$R_{int} = 0.0617$]	5281 [$R_{int} = 0.0336$]	10765 [$R_{int} = 0.1117$]
Data reduction		Siemens SAINT [27]	
Absorbtion correction		Empirical [28]	
Min. and Max. transmission	0.629 and 0.894	0.693 and 0.808	0.603 and 0.785
Solution method		Direct methods (SHELX-86) [29]	
Refinement method		Full-matrix least-squares on F^2 (SHELXL-93) [30]	
Data/restraints/parameters	9024/0/723	5048/0/367	10659/0/515
Weighting scheme $w^{-1} =$	$\sigma^2(F^2) + (0.052P)^2$	$\sigma^2(F^2) + (0.052P)^2 + 2.5057P$ where $P = (2F_c^2 + F_o^2)/3$	$\sigma^2(F^2) + 24.6532P$
Goodness-of-fit on F^2	1.067	1.087	1.225
Final R indices [$I > 2\sigma(I)$]	$R1 = 0.0456$, $wR2 = 0.0973$	$R1 = 0.0256$, $wR2 = 0.0520$	$R1 = 0.0559$, $wR2 = 0.0971$
R indices (all data)	$R1 = 0.0734$, $wR2 = 0.1145$	$R1 = 0.0335$, $wR2 = 0.0585$	$R1 = 0.1006$, $wR2 = 0.1272$
Extinction coefficient	0.00006(8)	0.00156(14)	0.00005(5)
Largest diff. Peak and hole /e$_*$Å^{-3}	0.706 and -1.517 (near Zr atoms)	0.397 and -0.319 (near Zr atom)	1.022 and -0.907 (near Zr atom)

experiments was prepared by fractional recrystallizations of a portion of crude **3** from CH_2Cl_2.

[η^5-(2-*Diphenylphosphinoethyl*)*cyclopentadienyl*](η^5-*cyclopentadienyl*)*dichlorozirconium* (*IV*) **5**

A solution of 0.31 g (1.21 mmol) of trimethylcyclopentadienyltin in 20 ml of toluene and a suspension of 0.66 g (1.21 mmol) of **3b** in 5 ml of toluene were mixed, stirred at room temperature for 3 hours and then heated at 60°C for 2 hours. The volatile components were removed in high vacuum from hot water bath (60°C) by trapping into liq. N_2. The crude product was washed on a glass filter three times with 20 ml portions of heptane, the residue was dried in high vacuum and recrystallized from ether, that gave 0.35 g (0.69 mmol, 57.5%) of zirconocene **5**. Anal. found: C, 57.41; H, 4.62; anal. calc. for $C_{24}H_{23}Cl_2PZr$ C, 57.13; H, 4.59. NMR (THF-d_8, 30°C) ^{1}H: 2.38 (*m*, 2H, H^7), 2.78 (*q*, $^3J_{HH} = 8.2$ Hz, $^3J_{HP} = 8.2$ Hz, 2H, H^6), 6.27 (virtual *t*, $^{3+4}J_{HH} = 5.2$ Hz, 2H, $H^{2,5}$), 6.38 (virtual *t*, $^{3+4}J_{HH} = 5.2$ Hz, 2H, $H^{3,4}$), 6.45 (*s*, 5H, C_5H_5), 7.29 (*m*, 6H, *m*- and *p*-H in PPh_2), 7.43 (*m*, 4H, *o*-H in PPh_2); ^{13}C: 27.4 (*dt*, $^1J_{CH} = 128$ Hz, $^2J_{CP} = 19.7$ Hz, C^6), 29.3 (*dt*, $^1J_{CH} = 128$ Hz, $^1J_{CP} = 12.3$ Hz, C^7), 113.5 (*d*, $^1J_{CH} = 174$ Hz, $C^{3,4}$), 116.5 (*d*, $^1J_{CH} = 174$ Hz, C_5H_5), 117.7 (*d*, $^1J_{CH} = 174$ Hz, $C^{2,5}$), 129.2 (*dd*, $^1J_{CH} = 160$ Hz, $^3J_{CP} = 6.0$ Hz, *m*-C in PPh_2), 129.3 (*d*, $^1J_{CH} = 160$ Hz, *p*-C in PPh_2), 133.6 (*dd*, $^1J_{CH} = 159$ Hz, $^2J_{CP} = 18.7$ Hz, *o*-C in PPh_2), 135.7 (*d*, $^3J_{CP} = 13.7$, C^1), 139.8 (*d*, $^1J_{CP} = 15.0$ Hz, *ipso*-C in PPh_2); ^{31}P-{^{1}H}: −14.3.

X-ray investigation of complexes **3b** *and* **4**

Single crystals were prepared by crystallisation from CH_2Cl_2 (the first modification of **3b**), THF (the second modification of **3b**), and saturated mother liquors from the fractional recrystallizations of crude **3** (complex **4**), mounted in inert oil on a tip of glass fibre and transferred to the cold nitrogen stream inside the diffractometer. Crystal data, data collection, structure solution and refinement parameters for **3b** and **4** are listed in Table 5.

In the case of first modification, the disordered carbon atom C(83) was refined isotropically, all other non-hydrogen atoms were refined with anisotropic thermal parameters. All hydrogen atoms were found from difference Fourier syntheses and refined isotropically, except those attached to disordered carbon atom. They were placed in calculated positions (d(C–H) = 0.96 Å) and refined using a riding model.

In the second case of **3b** all non-hydrogen atoms were refined with anisotropic thermal parameters. All hydrogen atoms were found from difference Fourier syntheses and refined in an isotropic approximation.

As for compound **4**, all non-hydrogen atoms were refined with anisotropic thermal parameters. All hydrogen atoms were placed in calculated positions (d(C–H) = 0.96 Å) and refined using a riding model.

Supplementary material available — Further details of the crystal structure determinations of **3b** and **4**, i.e tables with all atomic coordinates, thermal parameters, interatomic distances, and structure factors, are available from authors.

Acknowledgements—This investigation was supported by Russian Foundation for Basic Research (project No 96-03-34232a). A.V.C. thanks The Royal Society and The University of Durham for financial support.

REFERENCES

1. Jutzi, P. and Siemeling, U., *J. Organomet. Chem.*, 1995, **500,** 175 and references cited therein.
2. Leblanc, J. C., Moise, C., Maisonnat, A., Poilblanc, R., Charrier, C. and Mathey, F., *J. Organomet. Chem.*, 1982, **231,** C43.
3. Cuenca, T., Flores, J. C. and Royo, P., *J. Organomet. Chem.*, 1993, **462,** 191.
4. Kettenbach, R. T., Bonrath, W. and Butenschön, H., *Chem. Ber.*, 1993, **126,** 1657.
5. Fryzuk, M. D., Mao, S. S. H., Zavorotko, M. J. and MacGillivray, L. R., *J. Am. Chem. Soc.*, 1993, **115,** 5336.
6. Fryzuk, M. D., Mao, S. S. H., Duval, P. B. and Rettig, S. J., *Polyhedron*, 1995, **14,** 11.
7. Cowley, A. H., King, C. S. and Decken, A., *Organometallics*, 1995, **14,** 20.
8. Wang, T.-F., Yuang, J.-P. and Wen, Y.-S., *J. Organomet. Chem.*, 1995, **503,** 117.
9. Lee, I., Dahan, F., Maisonnat, A. and Poilblanc, R., *Organometallics*, 1994, **13,** 2743.
10. (a) Krebs, K. W., Engelhard, H. and Nischk, G. E., Ger.Offen. 1 959 322, 29.07.1971, Appl. 26.11.1969; *Chem. Abstr.*, 1971, **75**, 88768; (b) Llinás, G. H., Mena, M., Palacios, F., Royo, P. and Serrano, R., *J. Organomet. Chem.*, 1988, **340**, 37; (c) Martín, A., Mena, M. and Palacios, F., *J. Organomet. Chem.*, 1994, **480**, C10; (d) Winter, C. H., Zhou, X. X., Dobbs, D. A. and Heeg, M. J., *Organometallics*, 1991, **10**, 210.
11. Hitchcock, P. B., Lappert, M. F., Liu, D.-S. and Ryan, E. J., *Polyhedron*, 1995, **14,** 2745.
12. (a) Brajnina, E. M. and Mortikova, E. I., *Dokl. Akad. Nauk SSSR*, 1966, **169**, 335; (b) Brajnina, E. M. and Dvoryantseva, G. G., *Izv. Akad. Nauk, Ser. Khim*, 1967, 442.
13. Erker, G., Sarter, C., Albrecht, M., Dehnike, S., Kruger, C., Raabe, E., Schlund, R., Benn, R., Rufinska, A. and Mynott, R., *J. Organomet. Chem.*, 1990, **382,** 89.
14. (a) Krut'ko, D. P., Borzov, M. V., Petrosyan, V. S., Kuz'mina, L. G. and Churakov, A. V., *Russian Chemical Bulletin*, 1996, **45**, 490; (b) Krut'ko, D. P., Borzov, M. V., Petrosyan, V. S., Kuz'mina, L. G. and Churakov, A. V., *Russian Chemical Bulletin*, 1996, **45**, 1740.
15. Engelhardt, L. M., Papasergio, R. I., Raston, C. L. and White, A. H., *Organometallics*, 1984, **3,** 18.
16. Herzog, A., Liu, Feng-Quan, Roesky, H. W., Demsar, A., Keller, K., Noltemeyer, N. and Pauer, F., *Organometallics*, 1994, **13,** 1251.

17. Mu, Ying., Piers, W. E., Macgillivray, L. R. and Zaworotko, M. J., *Polyhedron*, 1995, **14,** 1.
18. Jutzi, P. and Kleimeier, J., *J. Organomet. Chem.*, 1993, **486,** 287.
19. Erker, G., Schamberger, J., van der Zeijden, A. A. H., Dehnicke, S., Kruger, C., Goddard, R. and Nolte, M., *J. Organomet. Chem.*, 1993, **459,** 107.
20. Allen, F. H. and Kennard, O., *Chemical Design Automation News*, 1993, **8,** 1.
21. Butakoff, K. A., Lemenovskii, D. A., Mountford, P., Kuz'mina, L. G. and Churakov, A. V., *Polyhedron*, 1995, **15,** 489.
22. (a) Cotton, F. A. and Kibala, P. A., *Acta Crystallogr. Sect. C*, 1991, **C47**, 270; (b) Breen, T. L. and Stephan, D. W., *Inorg. Chem.*, 1992, **31**, 4019.
23. van der Zeijden, A. A. H., Mattheis, C., Frohlich, R. and Zippel, F., *Inorg. Chem.*, 1997, **36,** 4444.
24. Zefirov, N. S., Kuznetsova, T. S., Kozhushkov, S. I., Surmina, L. S. and Raschupkina, Z. A., *Zh. Org. Khim.*, 1983, **19,** 541.
25. Jones, K. and Lappert, M. F., *J. Chem. Soc.*, 1965, 2157.
26. SMART Version 4.050. Siemens Analytical X-ray Instruments Inc., Madison, Wisconsin, USA, 1995.
27. SAINT Version 4.050. Siemens Analytical X-ray Instruments Inc., Madison, Wisconsin, USA, 1995.
28. Sheldrick, G.M., SHELXLTL-Plus. Release 4.1. Siemens Analytical X-ray Instruments Inc., Madison, Wisconsin, USA, 1991.
29. Sheldrick, G. M., *Acta Crystallogr. Sect. A.*, 1990, **A46,** 467.
30. Sheldrick, G.M., SHELXL-93. Program for the Refinement of Crystal Structures. University of Göttingen, Germany, 1993.

Pergamon

PII: S0277–5387(98)00173–9

Polyhedron Vol. 17, No. 22, pp. 3903–3908, 1998
© 1998 Elsevier Science Ltd
All rights reserved. Printed in Great Britain
0277–5387/98 $19.00+0.00

A new pathway to heteroleptic double-decker (phthalocyaninato)(porphyrinato)europium(III) complexes

Jianzhuang Jiang,[a]* Michael T. M. Choi,[b] Wing-Fong Law,[b] Ji Chen,†[a] and Dennis K. P. Ng[b1]

[a]Department of Chemistry, Shandong University, Jinan, 250100, P. R. China

[b]Department of Chemistry, The Chinese University of Hong Kong, Shatin, N.T., Hong Kong, P. R. China

(Received 11 March 1998; accepted 22 April 1998)

Abstract—Treatment of europium(III) acetylacetonate [$Eu(acac)_3 \cdot nH_2O$] with metal-free porphyrins 5,10,15,20-tetraphenylporphyrin [H_2(TPP)], 5,10,15,20-tetra(4-pyridyl)porphyrin [H_2(TPyP)], 5,10,15,20-tetrakis(4-methoxyphenyl)porphyrin [H_2(TMPP)], 5,10,15,20-tetrakis(4-chlorophenyl)porphyrin [H_2(TCPP)] or 5,10,15,20-tetrakis(4-*tert*-butylphenyl)porphyrin [H_2(TBPP)] gave the half-sandwich complexes Eu(Por)(acac) (Por = TPP, TPyP, TMPP, TCPP, TBPP), which reacted with phthalonitriles $C_6H_2R_2(CN)_2$ (R = H, C_7H_{15}, OC_5H_{11}) in the presence of 1,8-diazabicyclo[5.4.0]undec-7-ene (DBU) to give the respective heteroleptic double-decker complexes Eu[Pc*$(R)_8$](Por) (Pc* = 2,3,9,10,16,17,23,24-octasubstituted phthalocyaninate; R = H, C_7H_{15}, OC_5H_{11}) in moderate yields. All of the mixed sandwich compounds were characterized with spectroscopic methods including UV-vis, near IR, IR and mass spectrometry. © 1998 Elsevier Science Ltd. All rights reserved

Keywords: phthalocyanines; porphyrins; europium complexes; double-decker complexes.

Owing to their unique optical, electrical and other physical properties associated with the strong $\pi-\pi$ interactions, sandwich-type phthalocyaninato and porphyrinato complexes have been a subject of much current interest [1]. While numerous homoleptic compounds having the same macrocyclic ligands have been reported [[1](b)], the heteroleptic analogs are still relatively rare [[1](a)] which may be attributed to the synthetic barrier. The preparation of mixed phthalocyaninato and porphyrinato lanthanide complexes usually involves the treatment of dilithium phthalocyaninate [Li_2(Pc)] with Ln(Por)(acac) generated *in situ* from $Ln(acac)_3 \cdot nH_2O$ and H_2(Por) [2–4] or the reaction of Li_2(Pc) with $Ln(acac)_3 \cdot nH_2O$ followed by the treatment of H_2(Por) [4, 5]. These reactions normally give mixtures of the heteroleptic double-deckers Ln(Pc)(Por) and the triple-deckers Ln_2(Pc)$(Por)_2$ and $Ln_2(Pc)_2$(Por). It appears that the yields of these products depend on many factors including the nature of the lanthanide metals and the macrocycles, and the ratio of these reactants [[1](a)]. A slight variation of the reaction conditions may lead to different major product. The separation and purification of these products also require very tedious chromatographic procedure. The development of general, convenient, efficient and reproducible synthetic pathways to these mixed sandwich compounds is thus highly desirable. We have recently disclosed a new pathway to unsymmetrical bis(phthalocyaninato) europium(III) [6] and yttrium(III) [7] complexes which involves the base-catalyzed cyclic tetramerization of substituted phthalonitriles using M(Pc)(acac) (M = Eu, Y) as the templates. This synthetic strategy can be extended to give the mixed phthalocyaninato and porphyrinato double-deckers with less amounts of side products compared with the traditional methods. We describe herein the preparation of a series of europium(III)

* Author to whom correspondence should be addressed.

† Present address: Qiqihaer University, Qiqihaer, Heilongjiang, P. R. China.

[1] Alternative corresponding author.

complexes Eu[Pc*(R)$_8$](Por) using this methodology together with their spectroscopic properties. To our knowledge, heteroleptic phthalocyaninato and porphyrinato double-deckers with a substituted phthalocyaninato ligand have not been reported previously.

EXPERIMENTAL

Experimental details concerning the treatment of reagents and solvents, preparation of starting materials and physical measurements were described elsewhere [[2](c),[6]].

General procedure for the preparation of Eu[Pc(R)$_8$](Por)*

A mixture of Eu(acac)$_3 \cdot$ nH$_2$O (45 mg, 0.09 mmol) and H$_2$(Por) (0.10 mmol) in anhydrous 1,2,4-trichlorobenzene (TCB) (20 cm^3) was refluxed under nitrogen for 6 h. After removing the solvent *in vacuo*, the residue was mixed with phthalonitrile C$_6$H$_2$R$_2$(CN)$_2$ (0.60 mmol), DBU (40 mg, 0.26 mmol) and amyl alcohol (10 cm^3). The mixture was then refluxed for a further 12 h under nitrogen to give a dark green solution. The volatiles were removed under reduced pressure, then the residue was subjected to chromatography over a silica gel column to separate the protonated complex EuH[Pc*(R)$_8$](Por) from the unreacted metal-free porphyrin H$_2$(Por) and side-products including the phthalocyanine H$_2$[Pc*(R)$_8$] and the homoleptic double-decker Eu[Pc*(R)$_8$]$_2$. The protonated complexes were usually eluted out with a certain amount of unprotonated analogs Eu[Pc*(R)$_8$](Por) except for EuH(Pc)(TPyP) of which a pure sample could be isolated. Upon exposure to air for several hours (except for EuH(Pc)(TPyP), which required several days), the green/greenish-brown solutions of EuH[Pc*(R)$_8$](Por) turned to brown gradually and pure Eu[Pc*(R)$_8$](Por) could be obtained by performing column chromatography again under similar conditions and, for unsubstituted phthalocyaninato complexes **1**–**5**, followed by recrystallization from a CHCl$_3$/hexane mixture (or CHCl$_3$/MeOH for **2**). The details are summarized in Table 1.

RESULTS AND DISCUSSION

As described previously [2], treatment of Eu(acac)$_3 \cdot$ nH$_2$O with metal-free porphyrins H$_2$(Por) (Por = TPP, TPyP, TMPP, TCPP, TBPP) in refluxing TCB gave the respective half-sandwich compounds Eu(Por)(acac). These complexes prepared *in situ* were then treated with an excess of phthalonitriles C$_6$H$_2$R$_2$(CN)$_2$ (R = H, C$_7$H$_{15}$, OC$_5$H$_{11}$) in the presence of DBU in amyl alcohol to give the protonated double-deckers EuH[Pc*(R)$_8$](Por) as the initial products (Scheme 1). The compound EuH(Pc)(TPyP) was relatively stable to air and could be purified readily by column chromatography [8]. However, by leaving a CHCl$_3$ solution of this compound in air for several days, the green solution turned brown slowly and Eu(Pc)(TPyP) was produced. All other heteroleptic protonated double-deckers were rather air-sensitive. Air-oxidation already occurred during chromatography and the conversion to unprotonated counterparts Eu[Pc*(R)$_8$](Por) was essentially complete within 3 h. This procedure afforded the heteroleptic double-deckers Eu[Pc*(R)$_8$](Por) in moderate yields (Table 1) including those with a substituted phthalocyaninato ligand which, to our knowledge, have not appeared in literature so far. Compounds **1**–**5** were prepared previously by the classical methods described above [2,4]. While compounds **1** [[2](b),[4]] and **2** [[2](a)] were fully characterized, the double-deckers **3**–**5** were only produced in a very small quantity and no detailed spectroscopic data were reported [[2](c)]. For the sandwich compounds **11** and **12**, although their existence was unambiguously confirmed by their mass spectra which showed an intense MH$^+$ cluster (Table 1), their UV-Vis spectra suggested that the samples were impure and attempts to purify them with repeated chromatographic procedure were not successful.

Apart from the desired double-deckers, these reactions also produced small amounts of side products which include the metal-free phthalocyanines H$_2$[Pc*(R)$_8$] and the homoleptic double-deckers Eu[Pc*(R)$_8$]$_2$; both of which were formed by DBU-catalyzed cyclization of phthalonitriles. The former (for R = H) could be removed readily by simple filtration while the other impurities were removed by column chromatography. In contrast to the aforementioned procedures [2–5], the formation of triple-deckers was not detected in these reactions which also simplified the purification process. After the purification by repeated column chromatography, the samples were essentially pure as shown by thin layer chromatography. Satisfactory analytical data, however, could not be obtained as in the case of some other sandwich-type compounds [9].

The mixed double-deckers **3**–**12** were mass-measured using a Fourier transform ion cyclotron resonance (FTICR) mass spectrometer. The liquid secondary-ion (LSI) mass spectra of all these compounds showed an intense isotopic cluster assignable to the protonated molecular ion (MH$^+$) and the data are summarized in Table 1. Figs. 1(a) and (b) show the molecular-ion region in the spectra of **5** and **9**, respectively, in which distinct isotopic distribution can be observed. The relative abundance of the isotopic clusters is in good agreement with the corresponding simulated spectra of MH$^+$ as shown in the top-insert.

The UV-Vis and near IR spectra of the sandwich compounds **3**–**10** were also determined and the data are compiled in Table 2. The data for the known compounds **1** [4] and **2** [[2]a] are also included for

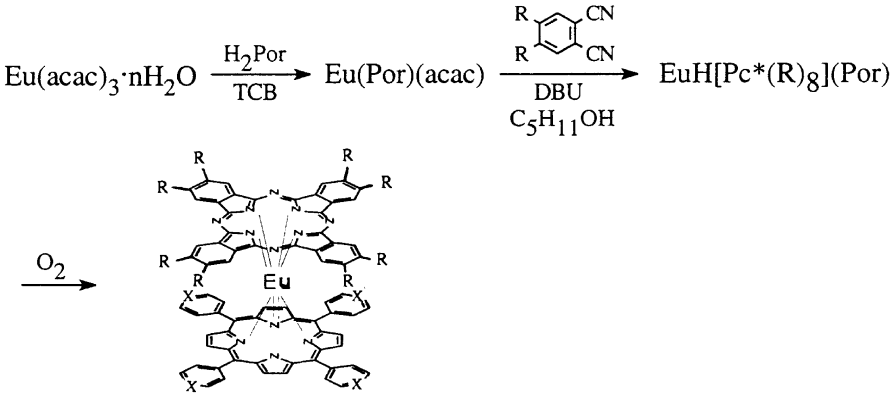

1 R = H, X = C-H
2 R = H, X = N
3 R = H, X = C-OMe
4 R = H, X = C-Cl
5 R = H, X = C-^{t}Bu
6 R = C_7H_{15}, X = C-H
7 R = C_7H_{15}, X = N
8 R = C_7H_{15}, X = C-OMe
9 R = C_7H_{15}, X = C-Cl
10 R = C_7H_{15}, X = C-^{t}Bu

Scheme 1.

Table 1. Experimental conditions, reaction yields and mass spectral data for Eu[Pc*$(R)_8$](Por)

Compound	Eluent	Yield (%)	MH^+ (expt.)[a,b] (m/z)	MH^+ (calc.)[b] (m/z)
Eu(Pc)(TPP) (**1**)	$CHCl_3$	20		
Eu(Pc)(TPyP) (**2**)	$CHCl_3$ followed with $CHCl_3$/MeOH (20:1)	69		
Eu(Pc)(TMPP) (**3**)	$CHCl_3$	43	1398.33	1398.35
Eu(Pc)(TCPP) (**4**)	$CHCl_3$/hexane (1:1)	47	1416.20	1416.15
Eu(Pc)(TBPP) (**5**)	$CHCl_3$/hexane (1:2)	21	1502.62	1502.56
Eu[Pc*$(C_7H_{15})_8$](TPP) (**6**)	$CHCl_3$/hexane (1:2)	30	2064.44	2064.19
Eu[Pc*$(C_7H_{15})_8$](TPyP) (**7**)	$CHCl_3$ followed with $CHCl_3$/MeOH (20:1)	58	2067.11	2067.17
Eu[Pc*$(C_7H_{15})_8$](TMPP) (**8**)	$CHCl_3$/hexane (1:2)	27	2183.88	2183.23
Eu[Pc*$(C_7H_{15})_8$](TCPP) (**9**)	$CHCl_3$/hexane (1:2)	42	2201.67	2201.03
Eu[Pc*$(C_7H_{15})_8$](TBPP) (**10**)	$CHCl_3$/hexane (1:2)	34	2288.97	2288.44
Eu[Pc*$(OC_5H_{11})_8$](TPP) (**11**)			1966.85	1966.89
Eu[Pc*$(OC_5H_{11})_8$](TPyP) (**12**)			1971.87	1971.88

[a] By LSI-FTICR
[b] Mass corresponding to the most abundant isotopic peak of the protonated molecular ion (MH^+)

comparison. The spectra of **3**–**5** are closely related to those of **1** and **2** and can be assigned in the same manner. By varying the Por ligand, the Pc Soret band (324–326 nm) is virtually unshifted while the Por Soret band (403–412 nm) and the first radical band (467–478 nm) shift slightly by *ca.* 10 nm. In contrast, the remaining two near IR absorptions at 978–1091 nm (another radical band) and 1218–1396 nm (ring-to-ring charge transfer band) are significantly perturbed by such variation. Fig. 2 shows the electronic absorption spectrum of **6**, which is representative for the spectra of complexes **6**–**10** containing a substituted phthalocyaninato ligand. It is worth noting that both the phthalocyanine Soret band and the radical band in the visible region are split for these compounds. The splitting of Soret band of phthalocyanine has also been observed in the spectra of M^{III}[Pc*$(R)_8]_2$ (M = Eu, Gd, Y; R = C_7H_{15}, OC_5H_{11}) [[6],[7],[9](d)]. By introducing eight alkyl chains onto the periphery of Pc, the phthalocyanine Soret band is shifted to the red while the Por Soret band remains essentially unchanged. The lowest-energy near IR band, which can be ascribed to an intramolecular ring-to-ring charge transfer transition [from Por^{2-} to Pc*$(R)_8^{\cdot -}$]

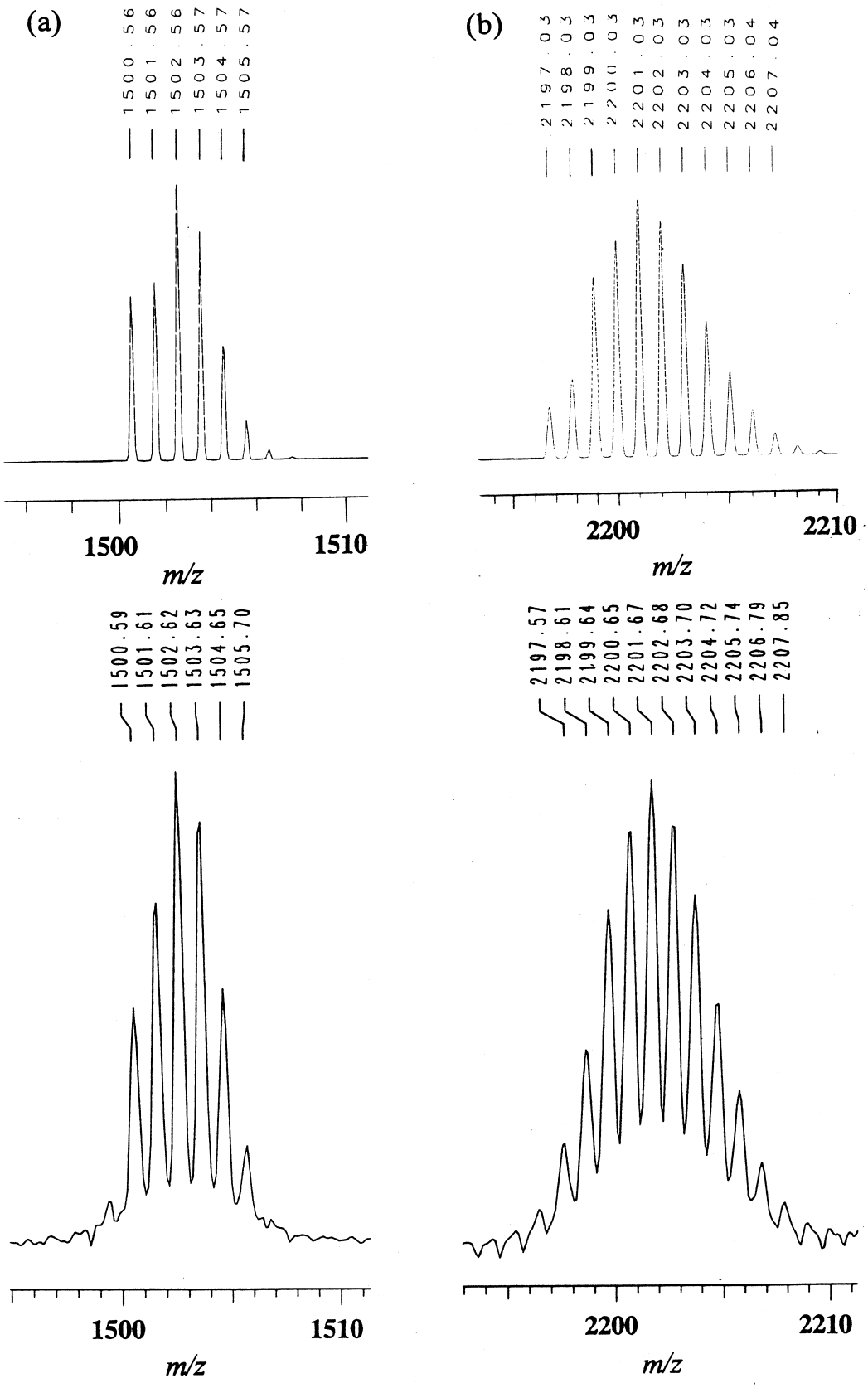

Fig. 1. Observed (bottom) and simulated (top) isotopic distribution for the protonated molecular ions of (a) Eu(Pc)(TBPP) (**5**) and (b) Eu[Pc*$(C_7H_{15})_8$](TCPP) (**9**).

Table 2. UV-vis and near IR data for compounds **1**–**10** in $CHCl_3$

Compound	λ_{max} (nm) (log ϵ)						
Eu(Pc)(TPP) (**1**) [4]	326 (4.69)		408 (5.26)	476 (4.13)		1002 (3.25)	1350 (3.41)
Eu(Pc)(TPyP) (**2**) [2a]	324 (4.78)		403 (4.90)	467 (4.51)		978	1218
Eu(Pc)(TMPP) (**3**)	324 (4.74)		412 (4.99)	477 (4.50)		1091	1396
Eu(Pc)(TCPP) (**4**)	326 (4.62)		406 (4.76)	472 (4.38)		995	1311
Eu(Pc)(TBPP) (**5**)	326 (4.73)		408 (4.95)	478 (4.50)		1019	1381
Eu[Pc*$(C_7H_{15})_8$](TPP) (**6**)	336 (5.18)	350 (5.18)	407 (5.30)	468 (4.89)	495 (4.92)	1000	1269
Eu[Pc*$(C_7H_{15})_8$](TPyP) (**7**)	344 (5.09)		405 (5.21)	473 (4.86)	497 (sh)	975	
Eu[Pc*$(C_7H_{15})_8$](TMPP) (**8**)	339 (sh)	348 (4.72)	409 (4.85)	471 (sh)	490 (4.51)	1019	1308
Eu[Pc*$(C_7H_{15})_8$](TCPP) (**9**)	339 (5.03)	356 (sh)	407 (5.15)	467 (4.81)	492 (4.78)	992	1210
Eu[Pc*$(C_7H_{15})_8$](TBPP) (**10**)	339 (sh)	352 (5.09)	408 (5.20)	470 (sh)	493 (4.83)	1012	1359

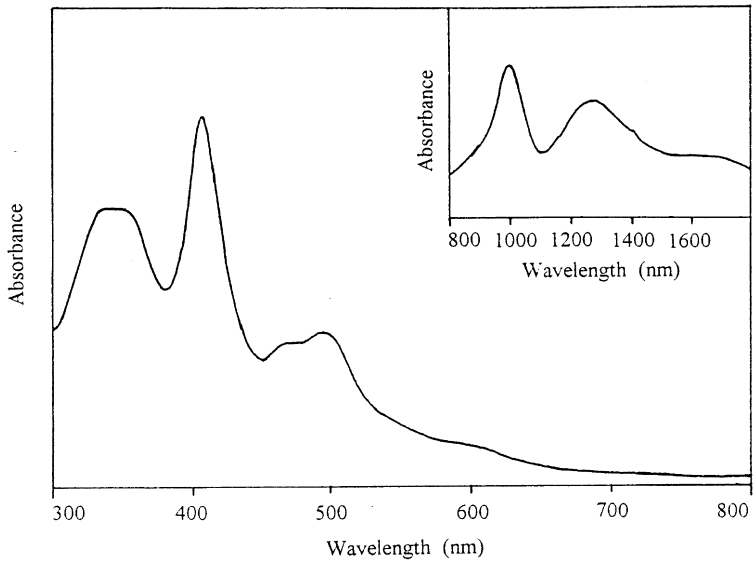

Fig. 2. UV-Vis and near IR (inset) spectra of Eu[Pc*$(C_7H_{15})_8$](TPP) (**6**) in $CHCl_3$.

[[2](a,b),[4],[5],[7]], is significantly blue-shifted. This can be attributed to the electron donating property of C_7H_{15} group which increases the energy of the singly-occupied orbital of Pc*$(C_7H_{15})_8$.

IR spectroscopy has been one of the most versatile techniques used to probe the extent of hole (de)localization in these sandwich-type compounds [[1](a)]. Similar to the double-deckers **1** and **2**, all of the complexes **3**–**10** gave a medium to strong band at 1313–1323 cm^{-1} in their IR spectra which is a diagnostic band for phthalocyanine π radical anion [Pc*$(R)_8^{\cdot -}$] [10]. This band was also observed in the IR spectra of Eu[Pc*$(R)_8]_2$ (R = H, C_7H_{15}) [[9](d)] and Eu(Pc)[Pc*$(C_7H_{15})_8$] [6]. The marker band of TPP π radical anion at 1270–1295 cm^{-1} [11] was not seen for **6**. These results might suggest that the hole in these compounds is preferentially localized on the phthalocyanine ring which is analogous to all known heteroleptic double-deckers M^{III}(Pc)(Por) [[2](a),[4]] and $[M^{IV}(Pc)(TPP)]^+$ [5, 10, 12]. That the introduction of alkyl substituents to Pc did not alter the preference of hole localization can be rationalized by the fact that the macrocycle Pc*$(C_7H_{15})_8$ is significantly easier to oxidize than unsubstituted Pc.

In conclusion, we have developed an effective pathway to heteroleptic phthalocyaninato and porphyrinato double-deckers which involves the cyclic tetramerization of phthalonitriles induced by Eu(Por)(acac). This method affords the desired double-deckers in moderate yields with relatively small amounts of side products. It is envisaged that many other novel double-decker complexes can also be prepared by using this methodology and research work along this direction is under way.

Acknowledgements—This work was supported by the Science Foundation of China (Grant No. 29701002), State Educational Committee of China, Shandong University and The Chinese University of Hong Kong.

REFERENCES

1. (a) Ng, D. K. P. and Jiang, J., *Chem. Soc. Rev.*, 1997, **26**, 433. (b) Jiang, J., Ng, D. K. P. and Kasuga, K. manuscript in preparation.
2. (a) Jiang, J., Mak, T. C. W. and Ng, D. K. P. *Chem. Ber.*, 1996, **129**, 933. (b) Jiang, J., Lau, R. L. C., Chan, T. W. D., Mak, T. C. W. and Ng, D. K. P., *Inorg. Chim. Acta*, 1997, **255**, 59. (c) Jiang, J., Liu, W., Law, W.-F. and Ng, D. K. P., *Inorg. Chim. Acta*, 1998, **268**, 49.
3. (a) Moussavi, M., De Cian, A., Fischer, J. and Weiss, R., *Inorg. Chem.*, 1986, **25**, 2107. (b) Lachkar, M., De Cian, A., Fischer, J. and Weiss, R., *New J. Chem.*, 1988, **12**, 729. (c) Chabach, D., Lachkar, M., De Cian, A., Fischer, J. and Weiss, R., *New J. Chem.*, 1992, **16**, 431.
4. Chabach, D., Tahiri, M., De Cian, A., Fischer, J., Weiss, R. and El Malouli Bibout, M., *J. Am. Chem. Soc.*, 1995, **117,** 8548.
5. Tran-Thi, T.-H., Mattioli, T. A., Chabach, D., De Cian, A. and Weiss, R., *J. Phys. Chem.*, 1994, **98,** 8279.
6. Jiang, J., Liu, W., Law, W.-F., Lin, J. and Ng, D. K. P., *Inorg. Chim. Acta*, 1998, **268,** 141.
7. Jiang, J., Xie, J., Choi, M. T. M., Yan, Y., Sun, S. and Ng, D. K. P., J. Porphyrins Phthalocyanines, in press.
8. A detailed account of the protonated double-deckers $M^{III}H(Pc)(TPyP)$ will be reported elsewhere.
9. (a) Pondaven, A., Cozien, Y. and L'Her, M., *New J. Chem.*, 1991, **15**, 515. (b) Pondaven, A., Cozien, Y. and L'Her, M., *New J. Chem.*, 1992, **16**, 711. (c) Guyon, F., Pondaven, A., Guenot, P. and L'Her, M., *Inorg. Chem.*, 1994, **33**, 4787. (d) Jiang, J., Liu, R. C. W., Mak, T. C. W., Chan, T. W. D. and Ng, D. K. P., *Polyhedron*, 1997, **16**, 515.
10. Kadish, K. M., Moninot, G., Hu, Y., Dubois, D., Ibnlfassi, A., Barbe, J.-M. and Guilard, R., *J. Am. Chem. Soc.*, 1993, **115,** 8153.
11. Shimomura, E. T., Phillippi, M. A., Goff, H. M., Scholz, W. F. and Reed, C. A., *J. Am. Chem. Soc.*, 1981, **103,** 6778.
12. Guilard, R., Barbe, J.-M., Ibnlfassi, A., Zrineh, A., Adamian, V. A. and Kadish, K. M., *Inorg. Chem.*, 1995, **34,** 1472.

Pergamon

PII: S0027-5387(98)00174-0

Polyhedron Vol. 17, No. 22, pp. 3909–3917, 1998
© 1998 Elsevier Science Ltd
All rights reserved. Printed in Great Britain
0277–5387/98 $19.00+0.00

Molecular structure and characterization of a pair of hydrate isomers for dinuclear copper(II) complexes with a 26-membered hexaazamacrocycle

Hai-Liang Zhu[a], Li-Min Zheng[a], Chun-Ying Duan[a], Xiao-Ying Huang[b], Wei-Ming Bu[a], Mei-Fang Wu[a] and Wen-Xia Tang[a]*

State Key Laboratory of Coordination Chemistry, Institute of Coordination Chemistry, Nanjing University, Nanjing 210093, P.R. China

State Key Laboratory of Structural Chemistry, Fuzhou 350002, P.R. China

(Received 6 March 1998; accepted 22 April 1998)

Abstract—A pair of seldom seen hydrate isomers with a formula of $LCu_2(CH_3COO)_2(H_2O)_2(ClO_4)_2$, where L is the dinucleating macrocyclic ligand bis-*p*-xytylBISDIEN, have been prepared and characterized by X-ray crystallography, UV/Vis spectra and magnetic measurements. The blue isomer, $[LCu_2(CH_3COO)_2(H_2O)_2](ClO_4)_2$, crystallizes in the triclinic system and the violet isomer, $[LCu_2(CH_3COO)_2](ClO_4)_2 \cdot 2H_2O$, crystallizes in the orthorhombic system. The blue complex consists of one cation $[LCu_2(CH_3COO)_2(H_2O)_2]^{2+}$ and two ClO_4^- anions. The two copper atoms are independent to each other with a separation of 6.781(9) Å. Each has a square pyramidal geometry and is five-coordinated by three N atoms from the macrocycle and two O atoms from the monodentate acetate anion and the coordinated water molecule, respectively. In violet isomer, both central copper atoms are located in an approximately square planar environment and are not coordinated by the water molecules. The isomers have different reflectance spectra due to the different coordination geometry but can rapidly interchange in solution at ambient temperature. Both compounds exhibit quite weak antiferromagnetic couplings verified by the small but negative Weiss constant ($\theta = -5.72$ K for the blue and -25.6 K for the violet isomer). © 1998 Elsevier Science Ltd. All rights reserved

Keywords: copper(II) complex; hydrate isomers; hexazamacrocycle; X-ray structure.

INTRODUCTION

Hydrate isomerism of coordination compounds is a widely known but seldom seen phenomenon. One of the most famous examples is $CrCl_3 \cdot 6H_2O$, which has three hydrate isomers [1]: the green $[Cr(H_2O)_4Cl_2]Cl \cdot 2H_2O$, the blue $[Cr(H_2O)_5Cl]Cl_2 \cdot H_2O$ and the violet $[Cr(H_2O)_6]Cl_3$. No such hydrate isomers as that the metal atoms are accommodated in a macrocycle have been reported. One of the most interesting macrocycles is the macrocyclic polyamine dinucleating ligands, which are discovered to be capable of simultaneously binding two metal ions in close proximity and are further capable of bridging bifunctional donor substrates to provide models of biological dimetallic sites. Some macrocyclic dinuclear complexes containing imidazolato [2, 3], azido [4] and carbonato [5] bridges have been described. In order to synthesize imidazolate- and acetate-bridged dinuclear copper(II)

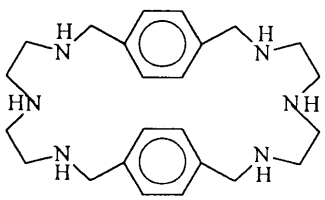

(L)

complexes, we have employed a 26-membered hexa-

* Author to whom correspondence should be addressed. Fax: +86-25-331-7761; E-mail: ccinu@netra.nju.edu.cn.

azamacrocycle L (L = bis-*p*-xylylBISDIEN) [6] as a ligand and have succeeded in synthesizing several imidazolate-bridged dicopper(II) complexes [7]. However, we failed to obtain relative acetate-bridged complexes, instead we obtained a pair of quite rarely reported hydrate isomers with formula $LCu_2(CH_3COO)_2(H_2O)_2(ClO_4)_2$. The copper atoms in both of the isomers are independent other than acetate-bridged. The metals in the blue isomer are in square pyramidal geometry with N_3O_2 chromophore and are coordinated by the water molecules; while both of the two copper atoms in the violet isomer have N_3O square planar coordination environment and are not coordinated by water molecules. Reported in this paper are the syntheses, crystal structure and magnetic properties of the two hydrate isomers.

EXPERIMENTAL

Materials

Reagents were used as obtained without further purification. Solvents were purified by standard methods before use.

Synthesis of the ligand L. L·6HBr was prepared as the similar procedure described by Martell [6]. Anal. Calcd. for $C_{24}H_{38}N_6$·6HBr: C, 32.17; H, 4.95; N, 9.38. Found: C, 32.55; H, 5.02; N, 9.11. The relative macrocyclic-polyamine was obtained according to the following method: 4.45 g L·6HBr and 2 g NaOH were dissolved in 5 ml water and cooled and then 50 ml CH_2Cl_2 was added to the mixture to extract the product. The organic phase was evaporated to dryness and was recrystallized from methanol and acetonitrile. 1.70 g white crystals were obtained. The 500 MHz ^1H NMR in D_2O of L gave (ppm from DSS) 3.66, (singlet, 8H, benzene–CH_2), 7.31 (singlet, aromatic H), 2.59 (singlet, 16H, NH–CH_2) in the ratio of 1:1:2.

Synthesis of the blue isomer: $[LCu_2(CH_3COO)_2(H_2O)_2](ClO_4)_2$. To a solution of L (103 mg, 0.25 mmol in 5 ml acetonitrile) was added a solution of $Cu(OAc)_2{\cdot}H_2O$ (100 mg, 0.5 mmol in 2 ml water) with stirring and then was added dropwise five drops of saturated aqueous solution of $NaClO_4$. The resulting solution was stored at -5°C. After 2 days, 140 mg blue prism crystals were obtained, which were filtered off, washed with water and acetonitrile and dried in a desiccator containing silica gel, yield 61%. Anal. calcd. for $C_{28}H_{48}N_6Cu_2Cl_2O_{14}$: C, 37.71; H, 5.43; N, 9.42; Cu, 14.26. Found: C, 37.59; H, 5.57; N, 8.67; Cu, 14.05.

Synthesis of the violet isomer: $[LCu_2(CH_3COO)_2](ClO_4)_2 \cdot 2H_2O$ The same procedure as for the blue isomer except that to the resulting solution was added 5 ml of *n*-butyl alcohol with stirring and was stored in a refrigerator. 2 days later, 210 mg violet crystals were obtained, yield 92%. Anal. calcd. for $C_{28}H_{48}N_6Cu_2C1_2O_{14}$: C, 37.71; H, 5.43; N, 9.42; Cu, 14.26. Found: C, 38.44; H, 5.52; N, 9.35; Cu, 14.26.

Crystallographic data collection and structure determinations

The blue isomer. A suitable crystal of the blue isomer was mounted on an Enraf-Nonius CAD4 diffractometer. Unit cell parameters were determined by a least-squares refinement of 25 reflections with $13.98 < \theta < 16.89^\circ$ using graphite-monochromatized Mo Kα with $\omega/2\theta$ scan mode. Observed reflections with $I > 3\sigma(I)$ were used for structure determination. The data were corrected for LP factors and for empirical absorption. The crystallographic data are summarized in Table 1.

The structure was solved by the Patterson method followed by Fourier syntheses and refined on F by full matrix least squares with anisotropic thermal parameters for the non-hydrogen atoms. All the hydrogen atoms were located on the difference Fourier maps and assigned isotropic thermal parameters. The O(22), O(23) and O(24) atoms of one perchlorate ion were found disordered and the site occupancy factor was fixed at 0.5 for O(22A), O(22B), O(24A), O(24B) and at 0.333 for O(23A), O(23B) and O(23C). Selected distances and angles are listed in Table 2. The calculations were performed on MICRO-VAX 3100 using the TEXSAN plus version 2.01 programs.

The violet isomer. A suitable crystal of the violet isomer was mounted on a Siemens SHELXTL P4 diffractometer equipped with graphite-monochromated Mo Kα radiation. Accurate cell parameters were derived from a least-squares fitting of the setting angles of 25 independent reflections in the range of 6–24°. The relevant crystal data and structural parameters are summarized in Table 1. The intensities were collected with a variable scan speed 5.0 to 50.0° per min in ω. The data were corrected for Lorentz and polarization effects during data reduction using XSCANS [8].

The structure was solved by the direct method and refined on F^2 by full-matrix least-squares methods using SHELXTL version 5.0 [9]. All the non-hydrogen atoms were refined anisotropically. All the hydrogen atoms were placed in calculated positions assigned fixed isotropic thermal parameters at 1.2 times the equivalent isotropic U of the atoms to which they are attached and allowed to ride on their respective parent atoms. The contribution of these hydrogen atoms were included in the structure-factors calculations. All computations were carried out on a PC-586 computer using the SHELXTL-PC Program Package [9]. Analytical expressions of neutral-atom scattering factors employed and anomalous dispersion corrections were incorporated [10]. The atoms O(2) in one water molecule, O(11), O(12), O(13), O(14), O(22), O(23) and O(24) in two perchlorate ions were refined disordered with the site occupancy factor s.o.f. = 1/2. Selected bond lengths and angles are reported in Table 3.

For both isomers, a complete listing of atomic coordinates, bond lengths, bond angles, anisotropic ther-

Table 1. Summary of crystal data, data collection and structure refinement for the violet and blue complexes

	Violet complex	Blue complex
Formula	$C_{28}H_{48}N_6Cu_2C1_2O_{14}$	$C_{28}H_{48}N_6Cu_2Cl_2O_{14}$
M	890.72	890.72
Crystal system	orthorhombic	triclinic
Space group	Pnna	P(−1)
a (Å)	15.728(3)	12.328(5)
b (Å)	24.803(5)	12.705(4)
c (Å)	10.152(2)	13.326(7)
α (°)	90	110.39(3)
β (°)	90	90.57(4)
γ (°)	90	93.39(3)
V (Å^3)	3960.3(14)	1952(2)
Z	4	2
T (°C)	293(2)	296(2)
D_c (g cm^3)	1.494	1.515
λ (Å)	0.71073	0.71073
No. of unique reflections	3580	6858
No. of observed reflections	2772 ($I \geqslant 2\sigma(I)$)	4859 ($I \geqslant 3\sigma(I)$)
2θ range (°)	3–46	0–50
F(000)	1848	1848
Crystal size	$0.28 \times 0.25 \times 0.16$	$0.50 \times 0.45 \times 0.40$
Scan mode	$\omega/2\theta$	$\omega/2\theta$
Linear abs μ (mm^{-1})	1.277	1.296
R^a, $R_w{}^b$		0.060, 0.070
R_1, $wR_2{}^c$	0.0684, 0.0614	
Goodness of fit	0.823 (on F^2)	1.90 (on F)
$\Delta\rho_{max}$ (eÅ^{-3})	0.384	0.58
$\Delta\rho_{min}$ (eÅ^{-3})	−0.407	−0.81

[a] $R = \Sigma(|F_o| - |F_c|)/\Sigma|F_o|$.
[b] $R_w = [w(F_o - |F_c|)^2/\Sigma wF_o^2]^{1/2}$, where $w = 1/\sigma^2(F)$.
[c] $w = 1/[\sigma^2F_o^2 + (0.0400P)^2 + 0.0800P]$, where $P = (F_o^2 + 2F_c^2)/3$.

Table 2. Selected bond lengths (Å) and angles (°) of the blue complex

Bond lengths			
Cu(1)–O(3)	1.911(4)	Cu(2)–O(5)	1.916(4)
Cu(1)–N(1)	1.964(5)	Cu(2)–N(4)	1.966(5)
Cu(1)–N(6)	2.041(5)	Cu(2)–N(3)	2.049(5)
Cu(1)–N(2)	2.061(5)	Cu(2)–N(5)	2.051(5)
Cu(1)–O(1)	2.496(4)	Cu(2)–O(2)	2.458(4)
O(3)–Cu(1)–N(1)	169.8(2)	O(5)–Cu(2)–N(4)	171.7(2)
O(3)–Cu(1)–N(6)	96.5(2)	O(5)–Cu(2)–N(3)	94.0(2)
O(3)–Cu(1)–N(2)	95.4(2)	O(5)–Cu(2)–N(5)	98.0(2)
O(3)–Cu(1)–O(1)	100.1(2)	O(5)–Cu(2)–O(2)	99.3(2)
N(1)–Cu(1)–N(6)	84.5(2)	N(4)–Cu(2)–N(3)	84.4(2)
N(1)–Cu(1)–N(2)	84.7(2)	N(4)–Cu(2)–N(5)	84.5(2)
N(1)–Cu(1)–O(1)	90.1(2)	N(4)–Cu(2)–O(2)	88.9(2)
N(6)–Cu(1)–N(2)	167.2(2)	N(3)–Cu(2)–N(5)	166.6(2)
N(6)–Cu(1)–O(1)	85.4(2)	N(3)–Cu(2)–O(2)	89.1(2)
N(2)–Cu(1)–O(1)	87.8(2)	N(5)–Cu(2)–O(2)	83.1(2)

Table 3. Selected bond distances (Å) and angles (°) of the violet complex

Bond lengths			
Cu(1)–O(3)	1.886(3)	Cu(1)–N(2)	2.037(5)
Cu(1)–N(1)	1.949(4)	Cu(1)–N(3)#1	2.023(4)

Bond angles			
O(3)–Cu(1)–N(1)	174.2(2)	O(3)–Cu(1)–N(3)#1	95.0(2)
N(1)–Cu(1)–N(3)#1	83.4(2)	O(3)–Cu(1)–N(2)	97.9(2)
N(1)–Cu(1)–N(2)	84.6(2)	N(3)#1–Cu(1)–N(2)	164.5(2)

mal parameters and structure factors are included as supplementary materials.

Physical measurements. ^{1}H NMR spectra were obtained at 319 K on a Bruker AM 500 spectrometer using an Aspect-3000 computer data system. Magnetic measurements on powder samples were carried out in the 77–300 K temperature range with a CAHN-2000 Farady-type magnetometer. The molar susceptibilities were corrected for the diamagnetism of the constituent atoms by using Pascal constants. The reflectance and electronic spectra were made on a Shimadzu UV-240 spectrophotometer.

RESULTS AND DISCUSSION

Description of the structure

The blue isomer: $[LCu_2(CH_3COO)_2(H_2O)_2](ClO_4)_2$. The crystal structure of the blue isomer consists of one cation, $[LCu_2(CH_3COO)_2(H_2O)_2]^{2+}$, and two perchlorate anions. The cation $[LCu_2(CH_3COO)_2(H_2O)_2]^{2+}$ results from the binding of two $(H_2O)Cu(OOCCH_3)$ units into the macrocyclic ligand L. A view of the molecule structure is given in Fig. 1. Within the macrocycle the two copper atoms are independent at the separation of 6.781 Å. Both copper atoms are in an approximately distorted square-pyramidal geometry, with the basal positions consisting of one oxygen atom [O(3)] from the coordinated acetate and three nitrogen atoms [N(1), N(2) and N(6)] from the macrocycle. The oxygen atom of the water molecule occupies the axial site and is weakly coordinated to copper atom at the distance of 2.496(4) Å [Cu(1)–O(1)] or 2.458(4) Å [Cu(2)–O(2)], which is comparable with the Cu–O(H_2) bond lengths of 2.448(6) Å in $[CuL_2(H_2O)]$ [11] and 2.571(6) Å in $[Cu(en)_2(H_2O)_2]F_2 \cdot 4H_2O$ [12]. The copper atom is at the basal plane with the deviation of 0.034 Å for Cu(1) or 0.008 Å for Cu(2). The Cu–O bond lengths between the copper atoms and the coordinated acetates [Cu(1)–O(3) = 1.911(4) Å] and [Cu(2)–O(5) = 1.916(4) Å] are in general range in copper(II) complexes with carboxylates. The angle between the copper coordination plane and the closest acetate plane is 98.15° for Cu(1) and 61.65° for Cu(2).

The intermolecular hydrogen bonds join the molecules forming a two-dimensional net structure along bc-face (see Scheme 1).

The violet isomer: $[LCu_2(CH_3COO)_2](ClO_4)_2 \cdot 2H_2O$

The crystal structure of the violet complex is presented in Fig. 2. The molecule consists of a cation,

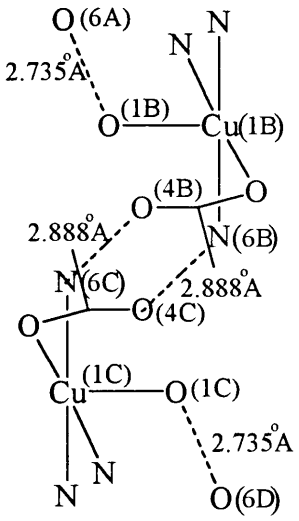

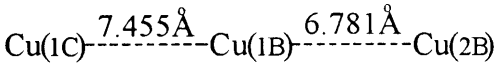

Scheme 1

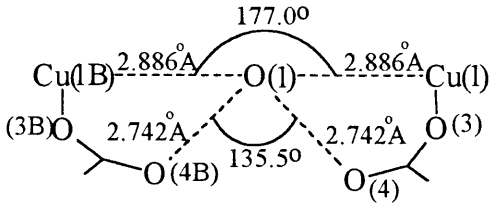

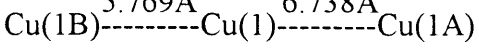

Scheme 2

The interaction between the molecules for the isomers.

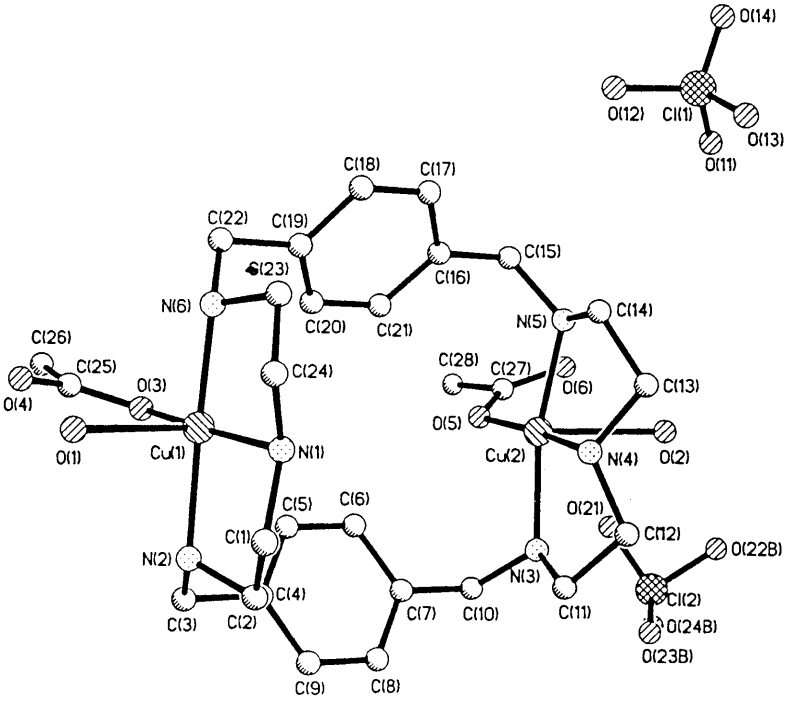

Fig. 1. Molecular structure of the blue isomer with the hydrogen atoms omitted for clarity.

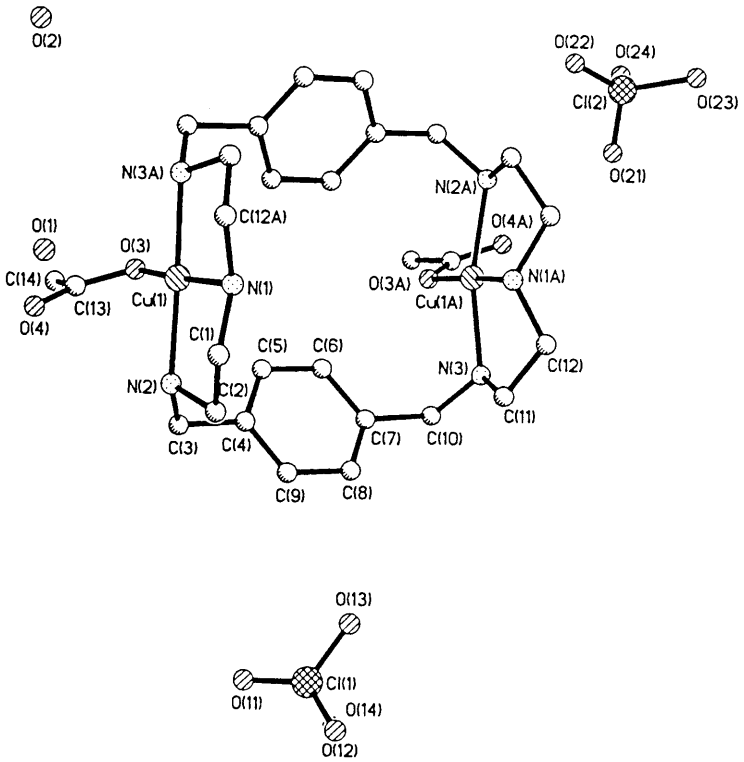

Fig. 2. Molecular structure of the violet isomer with the hydrogen atoms omitted for clarity.

$[LCu_2(CH_3COO)_2]^{2+}$, two perchlorates and two lattice water molecules. A crystallographically required two-fold axis passes through atom Cl(1) along the *z*-axis, which makes the two copper atoms equivalent. Each copper atom is in an approximately square-planar environment with copper deviating by 0.035 Å from the least-square coordination plane and is four-coordinated by three nitrogen atoms from the macrocycle and one oxygen atom from an acetate ligand. The average Cu–N bond length 2.01 Å is consistent with that of Cu(II) complexes with CuN_4 or CuN_3O chromophores. The copper–oxygen distance of 1.886(3) Å is in the general range of Cu–O bond lengths in copper complexes with carboxylates.

The metal coordination plane is nearly perpendicular to the two phenyl rings at 91.8° with one containing C(4) through C(9) and at 95.8° with the other involving C(4A) through C(9A) (symmetry operator: $-x+0.5, -y+1, z$). The angle between the basal plane of copper and the nearest acetate plane is 68.6°.

The intermolecule hydrogen bonds link the molecules along the *b*-axis forming a one-dimensional chain.

Structure comparison of the isomers. Each macrocycle in both isomers adopts a "boat"-type conformation (Figs 3 and 4), which is apparently unstrained, as indicated by the normal bond parameters. The angle between the two phenyl rings of the macrocycle is 57.67° for the blue isomer and 65.4° for the violet isomer. The angle between the two copper coordination planes is 12.9° for the blue isomer and 9.0° for the violet.

The closest intermolecular Cu···Cu separation of 7.455 Å [Cu(1B)···Cu(1C) in Scheme 1 and Fig. 3] for the blue isomer is much longer than that of 5.769 Å [Cu(1)···Cu(1B)] for the violet isomer (Scheme 2 and Fig. 4). The structurally significant difference between the isomers results from the positions of the water molecules in the complexes. For the blue isomer, the strong intermolecular hydrogen bonds (O(1B)–H···O(6A) = 2.735 Å) between the coordinated water molecules and the uncoordinated oxygen atoms of the monodentate-coordinated acetates, together with the hydrogen bonds [N(6)–H···O(4) = 2.888 Å, relative symmetry operators refer to Scheme 1 and Fig. 3], link the complex forming a two-dimensional structure along the bc-face.

Atoms Cl(2) (−0.691, 0.7500, 0.2500), O(21) (0.172, 0.7500, 0.2500), Cl(1) (0.7500, 0.5000, 0.3860) and O(1) (0.2786, 0.2500, 0.2500) of the violet isomer are in the special positions Fig. 2, one of the lattice water molecules is situated between two macrocycles and joins two uncoordinated oxygen atoms from two coordinated acetates of two neighbouring molecules by the strong hydrogen bonds [O(1)–H···O(4) =

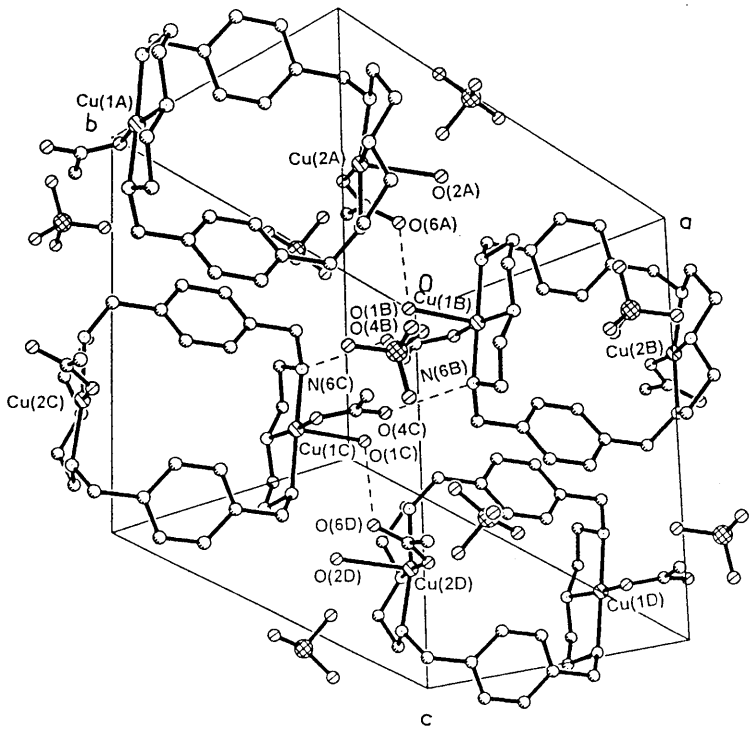

Fig. 3. A view of the crystal packing down the bc-face for the blue isomer. Symmetry operators: (A) x, y, z; (B) $-x, -y, -z$; (C) $x, y-1, z$; (D) $1-x, -1-y, 1-z$.

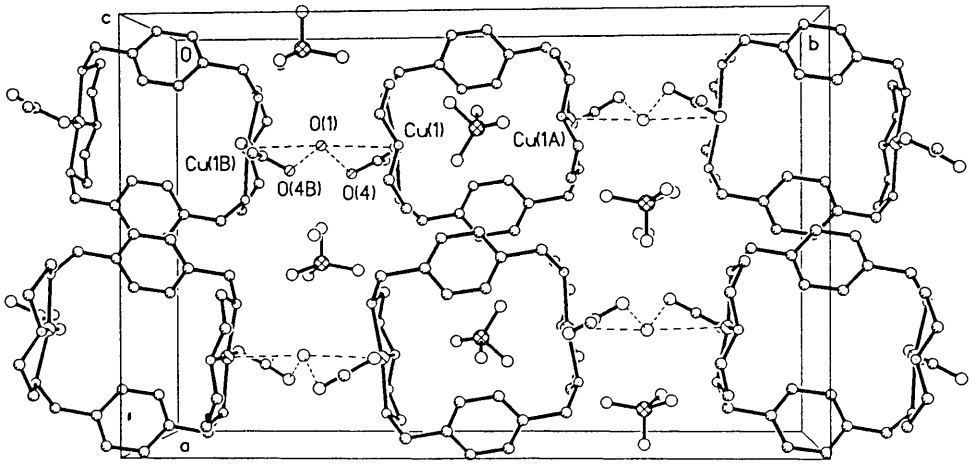

Fig. 4. A view of the crystal packing down the *b*-axis for the violet isomer.

2.742 Å], forming a one-dimensional chain (see Scheme 2 and Fig. 4) along the *b*-axis. The distance of 2.886 Å between Cu(1) and O(1) [or Cu(1B) and O(1)] is considered to be weak interaction.

uv/vis spectra

The reflectance spectra (displayed in Fig. 5) of the two isomers in visible region are quite different. There are two absorption maxima observed in the reflectance spectra for the violet complex. The band at 17.12 kK (584 nm) is assigned to $d_{z^2} \rightarrow d_{x^2-y^2}$ transitions and a resolved shoulder band at 20.24 kK (494 nm) to d_{xy}, d_{xz}, $d_{yz} \rightarrow d_{x^2-y^2}$ transitions in distorted square-planar symmetry [13], which is consistent with the crystal structure determination.

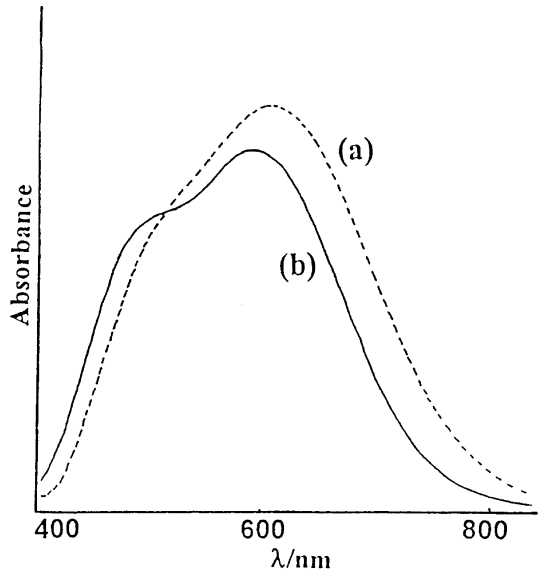

Fig. 5. Electronic reflectance spectra of $LCu_2(CH_3COO)_2(H_2O)_2(ClO_4)_2$: (a) the blue isomer and (b) the violet isomer.

Electronic spectra of copper(II) with square-pyramidal geometry have been studied extensively by Hathaway and coworkers [14, 15] and by reference to this the band at 16.50 kK (606 nm) for the blue complex is assigned to $d_{z^2} \rightarrow d_{x^2-y^2}$ transitions for a square-pyramidal system and the poorly resolved shoulder at about 19 kK (526 nm) indicates that there is some square-planar feature for the chromophore in the blue isomer, which agrees well with the result of the crystal structure determination of the complex where the axial ligation of the water molecule is quite weak (Cu–O bond length $\sim$2.5 Å) and the copper atoms are considered nearly to be with the square-planar configuration.

Magnetic susceptibility

The temperature dependence of the magnetic susceptibilities were measured in the temperature range 300 to 77 K. For the violet isomer, the plot of χ_M^{-1} vs T is linear in the range of 300–160 K (Fig. 6). The Weiss constant determined in this range is negative ($\theta = -25.6$ K), which suggests an antiferromagnetic interaction. For the blue isomer, the magnetic behavior follows the Curie–Weiss law over the measured temperature range. The Weiss constant ($\theta = -5.72$ K) is significantly smaller, indicating a much weaker antiferromagnetic interaction in the blue isomer which can be explained by their structural differences.

For the magnetic coupling between Cu(II) ions, two

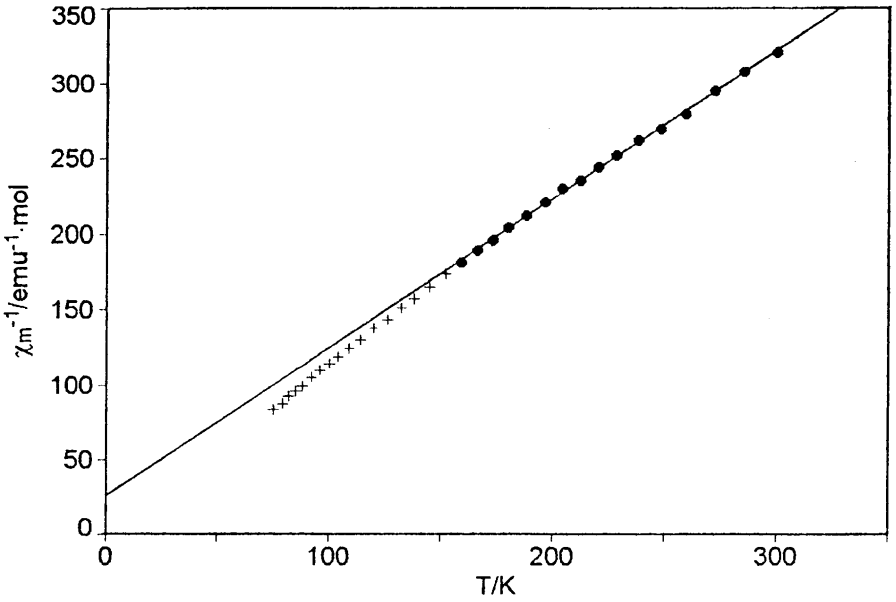

Fig. 6. Plot of χ_M^{-1} vs temperature T for the violet isomer. Dotted intercept $\theta = -25.6$ K.

exchange pathways are possible for both compounds: one is intramolecular through macrocycle ligands and the other is intermolecular through space. In both cases, the intramolecular Cu···Cu separation is very large (6.738 Å for the violet and 6.781 Å for the blue isomer, respectively). The magnetic exchange transmitted by this pathway is expected to be very small. On the other hand, the intermolecular interaction is quite different for the two compounds. In the violet isomer, the intermolecular Cu(1B)···Cu(1) separation is 5.769 Å. Between the neighboring macrocycles, there exist water molecules which "bridge" the two copper ions with Cu(1)···O(1) distance 2.886 Å (Scheme 2). Hence, a weak antiferromagnetic exchange is mediated through Cu(1B)···O(1)···Cu(1) units. The exchange is reduced due to the fact that the orientation of the magnetic orbitals of the copper ions is predominantly perpendicular to the oxygen "bridge" and, therefore, is unfavorable to propagate the interaction along Cu(1B)···O(1)···Cu(1) [16]. The susceptibility data for this compound can be analysed by a dimer model and fitted by a Bleaney–Bowers equation [17]

$$\chi_M = 2N\beta^2 g^2 (kT)^{-1} (3 + \exp(-2J/kT))^{-1}$$

where χ_M is the molar susceptibility and the other parameters have their usual meanings. A best fit, which leads to a solid line in Fig. 7, is obtained with $g = 2.19$ and $J = -1.81\,\mathrm{cm}^{-1}$.

In the blue isomer, the adjacent molecules are connected to each other through extensive hydrogen bondings. The nearest intermolecular Cu···Cu separation is 7.455(9) Å, which is much longer than that in the violet isomer (5.769(9) Å). A possible dipole–dipole or superexchange interaction between the molecules has to be ruled out, thus explains the comparatively much weaker magnetic coupling in the blue isomer.

CONCLUSION

Seldom seen hydrate isomers, the blue and the violet complexes are prepared and characterized. The difference between the isomers are the positions of the water molecules. For the blue isomer, each copper atom is five-coordinated by three N atoms from the macrocycle and by two O atoms, one of which is from the coordinated acetate and the other from the water molecule. However, the central copper atom in the violet isomer is four-coordinated by three N atoms from the macrocycle and by one O atom from the coordinated acetate and is not coordinated by the water molecules. The electronic reflectance spectra of the isomers indicate that the copper atoms are CuN_3O_2 square-pyramidal symmetry for the blue isomer and CuN_3O tetragonal environment for the violet, which is consistent with the result of the crystal structure determination. Both compounds exhibit quite weak antiferromagnetic couplings verified by the small but negative Weiss constant.

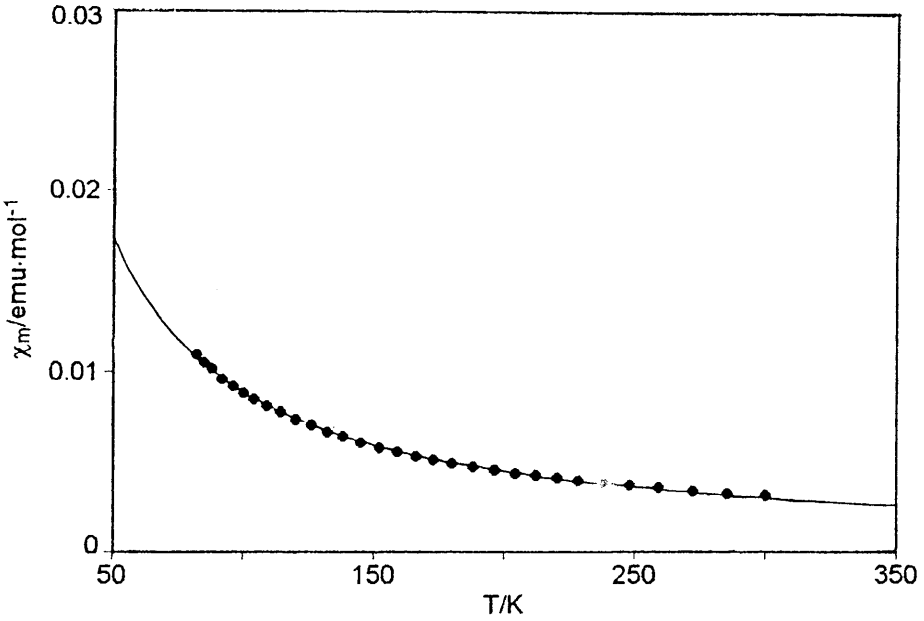

Fig. 7. Plot of the magnetic susceptibility χ_M vs temperature T for the violet isomer.

REFERENCES

1. Jones, M. M., *Elementary Coordination Chemistry*. Prentice-Hall, Englewood Cliffs, NJ, 1964, p. 48.
2. Harding, C. J., Lu, Q., Malone, J. F., Marrs, D. J., Martin, N., Mckee, V. and Nelson, J., *J. Chem. Soc. Dalton Trans.*, 1995, 1739.
3. Drew, M. G. B., Cairns, C., Lavery, A. and Nelson, S. M., *J. Chem. Soc. Chem. Commun.*, 1980, 1122.
4. Drew, M. G. B., McCann, M. and Nelson, S. M., *J. Chem. Soc. Chem. Commun.*, 1979, 481.
5. Menif, R., Reibenspies, J. and Martell, A. E., *Inorg. Chem.*, 1991, **30,** 3446.
6. Chen, D. and Martell, A. E., *Tetrahedron*, 1991, **47,** 6895.
7. Zhu, H. L., Zheng, L. M., Huang, X. Y. and Tang, W. X., *J. Inorg. Biochem.* (submitted).
8. Siemens, *SXCANS* (*Version* 2.1). Siemens Analytical X-ray Instruments, Madison, U.S.A, 1994.
9. Siemens, *SHELXTL* (*Version* 5.0). Siemens Industrial Autamation, Analytical Instrumentation, U.S.A, 1995.
10. Wilson, A. J. C. *et al.*, *International Tables for X-ray Crystallography*, Vol. C. Kluwer Academic Publishers, Dordrecht, 1992, Table 6.1.1.4 (pp. 500–502) and Table 4.2.6.8 (pp. 219–222).
11. Kamenar, B., Penavic, M., Skoric, A., Paulic, N. and Raos, N., Simeon, V., *J. Coord. Chem.*1988, **17**(1), 85.
12. Emsley, J. and Arif, M., *J. Mol. Struct.*, 1990, **220,** 1.
13. Hathway, B. J. and Billing, D. E., *Coord. Chem. Rev.*, 1970, **5,** 143.
14. Duggan, M., Ray, N. and Hathaway, B., *J. Chem. Soc. Dalton Trans.*, 1980, 1342.
15. Hathway, B. J. and Tomlinson, A. A. G., *Coord. Chem. Rev.*, 1970, **5,** 1.
16. Kahn, O., *Molecular Magnetism.* VCH Publishers, New York, 1993.
17. Bleaney, B. and Bowers, K. D., *Proc. R. Soc. London Ser. A*:, 1952, **214,** 451.

Pergamon

PII: S0277–5387(98)00181–8

Polyhedron Vol. 17, No. 22, pp. 3919–3925, 1998
© 1998 Elsevier Science Ltd
All rights reserved. Printed in Great Britain
0277–5387/98 $19.00+0.00

Two alternatives for the synthesis of non-cyclic phosphino-methanide derivatives of gold

Eduardo J. Fernández,[a] M. Concepción Gimeno,[b] Antonio Laguna,[b]* José M. López-de-Luzuriaga[a] and Elena Olmos[a]

[a] Departamento de Química, Universidad de La Rioja, Obispo Bustamante 3, 26001 Logrono, Spain

[b] Departamento de Química Inorgánica, Universidad de Zaragoza-CSIC, ICMA, 50009 Zaragoza, Spain

(Received 11 February 1998; accepted 29 April 1998)

Abstract—The reaction of phosphine–phosphonium derivatives, such as $[AuX(PPh_2CH_2PPh_2Me)]ClO_4$ or $[Au(C_6F_5)_3(PPh_2CH_2PPh_2Me)]ClO_4$, or non-cyclic bis(diphenylphosphino)methane-bridging complexes, as $[Au(C_6F_5)_2X(PPh_2CH_2PPh_2)Au(C_6F_5)]$ (X = Cl, C_6F_5) or $[Au(C_6F_5)(PPh_2CH_2PPh_2)Au(C_6F_5)]$, with acetylacetonate derivatives or gold(I) compounds leads to the synthesis of non-cyclic methanide gold complexes of the types $[AuX\{PPh_2C(AuPPh_3)_2PPh_2Me\}]ClO_4$, $[Au(C_6F_5)_2X\{PPh_2CH(AuPPh_3)PPh_2Me\}]ClO_4$, $[Au(C_6F_5)_3\{PPh_2CH–(AuPPh_3)PPh_2\}Au(C_6F_5)]$, $[N(PPh_3)_2][Au(C_6F_5)_3\{PPh_2CH–(AuX)PPh_2\}Au(C_6F_5)]$ or $[N(PPh_3)_2][\{Au(C_6F_5)_3(PPh_2CH_2PPh_2)–Au(C_6F_5)\}_2Au]$. © 1998 Elsevier Science Ltd. All rights reserved

Keywords: gold; bis(diphenylphosphino)methane; methanide; methanediide

INTRODUCTION

The chemistry of diphosphines, mainly of bis(diphenylphosphino)methane has been extensively developed in the past [1]. By deprotonation of the methylenic group an anion that can be described by different resonant forms [2] is obtained and its chemistry has been studied by several laboratories producing results that have been included in a recent revision [3]. We have contributed to this topic with the preparation of a great number of methanide or methanediide gold complexes, as for example the structurally characterized $[AuR_2\{(PPh_2)_2CH(AuR)\}]$, [4] $[AuR_2\{(PPh_2)_2C(AuPPh_3)_2\}]ClO_4$, [5] $[(RAu)HC(PPh_2AuPPh_2)_2CH(AuR)]$ [6], or $[(Ph_3PAu)_2C(PPh_2AuPPh_2)_2C(AuPPh_3)_2](ClO_4)_2$ [7] (R = C_6F_5).

However, in these products the diphosphine acts as a chelating or bridging ligand, respectively, and after the deprotonation the only possibility for further coordination is through the methanide carbon atom. Even when the free phosphine is treated with $[Au(acac)(PPh_3)]$ the eight-membered ring methanide $[CH(PPh_2AuPPh_2)_2CH]$, previously prepared by different methods by Schmidbaur [8, 8] and structurally characterized by Mingos, [9] is formed with displacement of triphenylphosphine [10]. The only examples of bridging non-cyclic methanides of gold described to date are obtained from $[Au(C_6F_5)_3(PPh_2CH_2PPh_2)]$ [11] or its calcogenide derivatives [12].

These results show that the formation of cyclic methanides is more likely than the preparation of open ones, probably due to the additional stabilization produced by the delocalization of the electronic density through the ring. This made up our minds to study the possibility of synthesizing non-cyclic gold methanide complexes and to obtain this we used two different strategies. The first one is the use of the phosphino–phosphonium ligand $PPh_2CH_2PPh_2Me^+$ that features a positive charge on the quaternary phosphorus, which increases the acidity of the methylenic protons, and where the formation of cycles is avoided because of the presence of the quaternary phosphorus. The second strategy is the employment of gold complexes, such as $[Au(C_6F_5)_2X(PPh_2CH_2PPh_2)Au(C_6F_5)]$ (X = Cl, C_6F_5) or $[Au(C_6F_5)(PPh_2CH_2PPh_2)Au(C_6F_5)]$, with a saturated coordination sphere for the metal centers, which also prevents the formation of rings.

* Author to whom correspondence should be addressed. Tel.: +34-976-761-185; Fax: +34-976-761-187; E-mail: alaguna@posta.unizar.es.

This result differs from that previously described in which although the formation of rings is avoided, the coordination was possible through two donor atoms [12].

RESULTS AND DISCUSSION

We have mentioned above two different strategies for the synthesis of open phosphino–methanide derivatives. With regard to the use of $PPh_2CH_2PPh_2Me^+$ as ligand we prepared the gold(I) complex $[AuCl(PPh_2CH_2PPh_2Me)]ClO_4$ (**1**) as starting material, by reaction of [AuCl(tht)] (tht = tetrahydrothiophene) with an equimolecular amount of $(PPh_2CH_2PPh_2Me)ClO_4$ (see Scheme 1). Complex **1** is obtained as an air and moisture stable white solid, with similar physical and spectroscopic properties to those observed for the previously described perfluorophenyl derivative **2** [13].

The use of acetylacetonate (acac) complexes has been previously reported in the synthesis of ylide or methanide complexes of gold (Refs. [10, 14, 14] and references therein). When complex **2** is treated with equimolecular amounts of [Au(acac)(PPh_3)] in dichloromethane an initial yellow colour appears, which becomes subsequently discoloured with the simultaneous formation of a white precipitate. After 1 h of reaction the solid is filtered off and $[Au(C_6F_5)(PPh_3)]$ is obtained from the solution. The analytical data for the insoluble product are in accordance with those expected for a complex with an stoichiometry $[Au(PPh_2CHPPh_2Me)]ClO_4$. Its IR spectrum shows two absorptions at 620 (m) and 1100 (vs, br) cm^{-1} [15] due to the perchlorate ion; some bands corresponding to the phosphino–phosphonium ligand at about 500 and 895 cm^{-1}, as well as a band at 586 (m) cm^{-1}, assigned to the ν(Au–C) vibration [16, 16, 16, 16, 17]. Taking these data and its insolubility into account, we propose that a polymeric complex $[Au(PPh_2CHPPh_2Me)(ClO_4)]_n$ (**3**) (probably featuring Au–P and Au–C bonds) is formed, but its low solubility did not allow us to complete its characterization.

The same result is obtained when the methanide $[Au(C_6F_5)(PPh_2CHPPh_2Me)]$ [13] is treated with $[Au(PPh_3)(tht)]ClO_4$, and no sign of formation of $[Au(C_6F_5)\{PPh_2CH(AuPPh_3)PPh_2Me\}]ClO_4$ is observed.

In contrast, when complexes **1** or **2** are treated with [Au(acac)(PPh_3)] in a 1:2 molar ratio, both methylenic protons are substituted by $[AuPPh_3]^+$ groups, affording the trinuclear species $[AuX\{PPh_2C(AuPPh_3)_2PPh_2Me\}]ClO_4$ [X = Cl (**4**), C_6F_5 (**5**)] Scheme 1. Complexes **4** and **5** are air and moisture stable solids, soluble in chlorinated solvents and acetone and non soluble in diethyl ether and hexane. Their analytical and spectroscopic data are in accordance with the proposed formulation, displaying three resonances with relative intensities 2:1:1 in their $^{31}P\{^1H\}$ NMR spectra.

Non-cyclic methanides are also obtained using phosphino–phosphonium derivatives of gold(III). Thus, reaction of $[Au(C_6F_5)_2X(PPh_2CH_2PPh_2Me)]ClO_4$ (X = Cl, C_6F_5) with $[N(PPh_3)_2](acac)$ in dichloromethane affords the previously described species $[Au(C_6F_5)_2X(PPh_2CHPPh_2Me)]$ [X = Cl (**6**), C_6F_5 (**7**)] through an alternative synthetic pathway. Their analytical and spectroscopic data agree with those previously described. [13] Treatment of the same starting products with one equivalent of [Au(acac)(PPh_3)] leads to different results than the related gold(I) compounds and the monosubstituted species $[Au(C_6F_5)_2X\{PPh_2CH(AuPPh_3)PPh_2Me\}]ClO_4$ [X = Cl (**8**), C_6F_5 (**9**)] are now easily isolated (see Scheme 2). Complexes **8** and **9** can also be prepared from the methanide compounds **6** and **7**, respectively, when reacted with the appropriate amounts of $[Au(PPh_3)(tht)]ClO_4$. Also in contrast with the behavior of the gold(I) species, the disubstituted products $[Au(C_6F_5)_2X\{PPh_2C(AuPPh_3)_2PPh_2Me\}]ClO_4$ can not be prepared even when an excess (1:3) of [Au(acac)(PPh_3)] is employed.

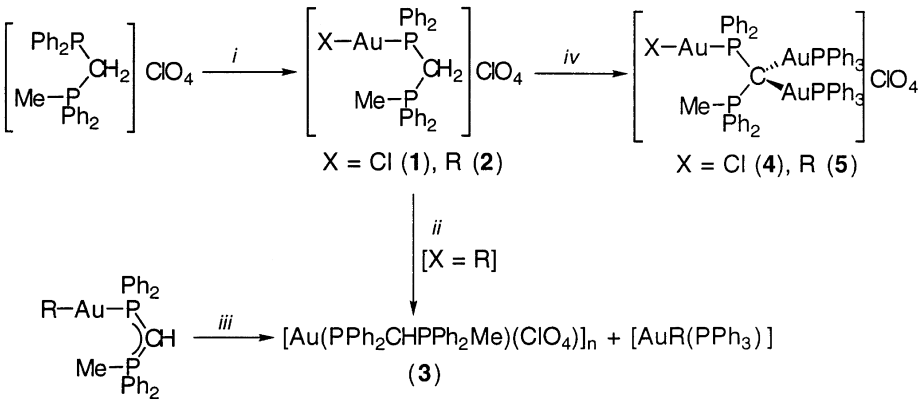

Scheme 1. R = C_6F_5; (i) [AuX(tht)]; (ii) [Au(acac)(PPh_3)]; (iii) $[Au(PPh_3)(tht)]ClO_4$; (iv) 2 [Au(acac)(PPh_3)].

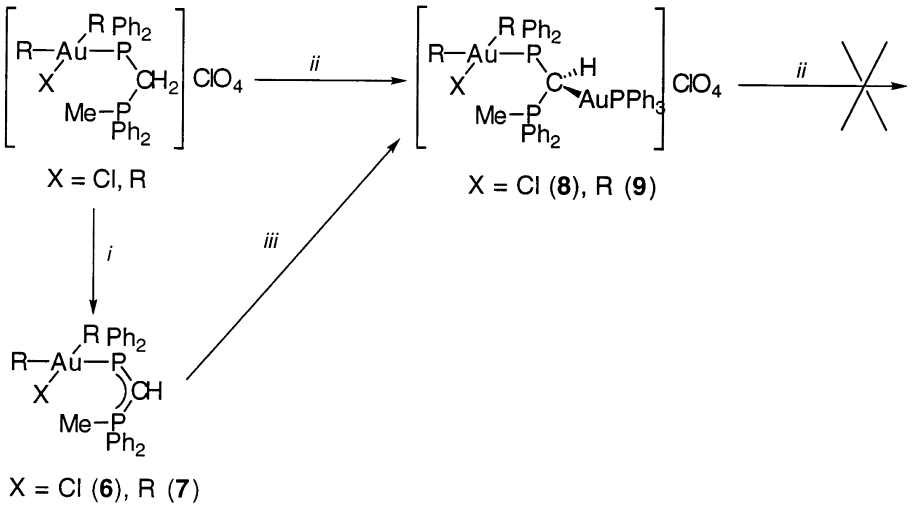

Scheme 2. R = C_6F_5; (i) $[N(PPh_3)_2](acac)$; (ii) $[Au(acac)(PPh_3)]$; (iii) $[Au(PPh_3)(tht)]ClO_4$.

Compounds **8** and **9** are obtained as white, air and moisture stable solids. Their $^{31}P\{^1H\}$ NMR spectra show three resonances with similar relative intensities, in accordance with the substitution of only one methylenic proton. This fact is also confirmed in their ^1H NMR spectra, which display one signal due to the remaining hydrogen atom, as well as a doublet corresponding to the protons of the methyl group. The ^{19}F NMR spectrum is in agreement with the *cis* position of the pentafluorophenyl groups in **8**.

Regarding the second strategy mentioned in Section 1, the use of dinuclear complexes featuring a saturated coordination sphere for the gold atoms, the employment of $[Au(C_6F_5)_3(PPh_2CH_2PPh_2)Au(C_6F_5)]$ [18] leads to the same observations than the gold(III) phosphino–phosphonium species. Thus, the reaction of this dinuclear complex with $[N(PPh_3)_2](acac)$ gives rise to the synthesis of $[N(PPh_3)_2][Au(C_6F_5)_3(PPh_2CHPPh_2)Au(C_6F_5)]$ (**10**), one of the few anionic methanides reported to date (Scheme 3).

Complex **10** is obtained as a yellow air and moisture sensitive oil, which makes its characterization difficult. In its IR spectrum a broad signal located at 1184 (m) cm^{-1}, assigned to the methanide system [3], is present. Its $^{31}P\{^1H\}$ NMR spectrum confirms the presence of the cation, because a sharp singlet at $\delta = 21.7$ ppm appears. It also shows two multiplets with the same intensity, according with the existence of two inequivalent phosphorus of the diphosphino–methanide ligand with a pentafluorophenyl group in *trans* position.

Reaction of **10** with one equivalent of $[Au(PPh_3)(tht)]ClO_4$ or $[AuX(tht)]$ (X = Cl, C_6F_5) leads to the displacement of the sulfur donor ligand and the coordination of the non-saturated methanide carbon to the gold(I) centre affording the trinuclear neutral (**11**) or anionic (**12** and **13**) derivatives, as represented in Scheme 3. Compound **11** can alternatively be synthesized directly from $[Au(C_6F_5)_3(PPh_2CH_2PPh_2)Au(C_6F_5)]$ and $[Au(acac)(PPh_3)]$ in a 1:1 molar ratio.

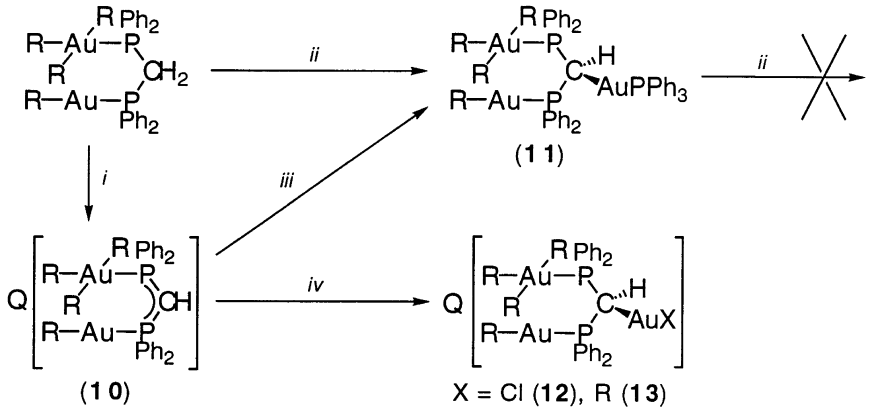

Scheme 3. R = C_6F_5; Q = $[N(PPh_3)_2]$; (i) Q(acac); (ii) $[Au(acac)(PPh_3)]$; (iii) $[Au(PPh_3)(tht)]ClO_4$; (iv) $[AuX(tht)]$.

Besides, as observed for gold(III) derivatives with $PPh_2CH_2PPh_2Me^+$, the use of an excess of [Au(acac)(PPh_3)] does not produce a double deprotonation and the monosubstituted product **11** is formed again.

Complexes **11**, **12** and **13** are obtained as white powders. They are stable in solid state and in solution, except **12**, which rapidly decomposes in solution. They are soluble in most common organic solvents, except in hexane and their analytical and spectroscopic data are in accordance with the proposed formulation (see Section 3).

In order to increase the nuclearity of the products we can use $[N(PPh_3)_2][Au(acac)_2]$, which can at once extract one methylenic proton of two different molecules of $[Au(C_6F_5)_2X(PPh_2CH_2PPh_2)Au(C_6F_5)]$ (X = Cl, C_6F_5) and coordinate both methanide units to the gold(I) center, affording the pentanuclear $[N(PPh_3)_2][\{Au(C_6F_5)_3(PPh_2CHPPh_2)Au(C_6F_5)\}_2Au]$ (**14**) (equation 1).

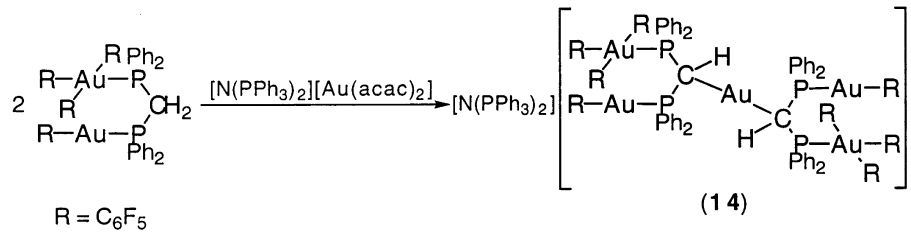

This complex is obtained as a white solid and it is air and moisture stable in solid state, but its stability decreases in solution. Its $^{31}P\{^1H\}$ NMR spectrum is similar to those registered for **10** and **12**, featuring a singlet at $\delta = 21.7$ ppm, corresponding to the cation, and two multiplets due to both types of phosphorus of the methanide unit. In spite of complex **14** having two chiral carbon atoms and thus two pairs of enantiomers which can be present at the same time (RR, SS and RS, SR), the ^{19}F and ^1H NMR spectra show only one set of signals.

Finally, we have studied the behavior of $[Au(C_6F_5)(PPh_2CH_2PPh_2)Au(C_6F_5)]$ [19]. The reaction with one equivalent of [Au(acac)(PPh_3)] gives rise to the substitution of one methylenic hydrogen, affording $[Au(C_6F_5)\{PPh_2CH(AuPPh_3)PPh_2\}Au(C_6F_5)]$ (**15**), while an excess of the acetylacetonate derivative does not lead to further substitutions, recovering always complex **15** (Scheme 4). This is a white stable solid, soluble in common organic solvents, except in hexane. Its $^{31}P\{^1H\}$ NMR spectrum shows two resonances at $\delta = 40.8$ (t) and 36.8 (d) ppm, with a relative intensity 1:2 and in its ^1H NMR spectrum a pseudotriplet of doublets centered at $\delta = 3.9$ ppm, due to the methylinic proton appears.

EXPERIMENTAL

General

NMR spectra were recorded on a Bruker ARX 300 spectrometer in $CDCl_3$ solutions. Chemical shifts are quoted relative to $SiMe_4$ (^1H, external), $CFCl_3$ (^{19}F, external) and H_3PO_4 (85%) (^{31}P, external). All experiments were carried out at room temperature and under nitrogen.

$[AuCl(PPh_2Ch_2PPh_2Me)]ClO_4$ (*1*)

To a dichloromethane solution of [AuCl(tht)] [20] (0.064 g, 0.2 mmol) was added ($PPh_2CH_2PPh_2Me$) ClO_4 (0.098 g, 0.2 mmol). After 30 min of stirring a little amount of precipitate is filtered over celite and the solution was concentrated to *ca.* 5 ml and diethyl ether was added to give complex **1** as a white solid. Yield: 80%. m.p.: 198 (dec). -$C_{26}H_{25}AuCl_2O_4P_2$ (731.30), calcd. C, 42.7; H, 3.45; found C, 42.55; H, 3.3. Λ_m: 115 Ω^{-1} cm^2 mol^{-1}. -$^{31}P\{^1H\}$NMR: δ 22.0 (d, 1P, Au–*P*Ph_2), [$^2J(PP^+) = 4.8$ Hz]) and 18.2 (m, 1P, *P*Ph_2Me); -^1H NMR δ 4.5 (dd, 2H, C*H*$_2$, [$^2J(HP) = 8.4$, $^2J(HP) = 5.4$ Hz]) and 2.4 (d, 3H, *Me*, [$^2J(HP) = 6.7$ Hz]).

$[Au(PPh_2CHPPh_2Me)]ClO_4$ (*3*)

(a) To a dichloromethane solution of **2** [13] (0.086 g, 0.1 mmol) was added [Au(acac)(PPh_3)] [21] (0.055 g, 0.1 mmol) and the solution initially turned yellow, but after a few minutes it became discoloured with the appearance of **3** as a white solid. The mixture was stirred for 1 h and complex **3** (yield: 87%) was then filtered off and [Au(C_6F_5)(PPh_3)] was isolated from the filtrate.

(b) A dichloromethane solution of [Au(C_6F_5)(PPh_2CHPPh_2Me)] [13] (0.076 g, 0.1 mmol) was treated with [Au(PPh_3)(tht)]ClO_4 [22] (0.065 g, 0.1 mmol) and a white precipitate appears. After 1 h the precipitation was complete and filtration of the

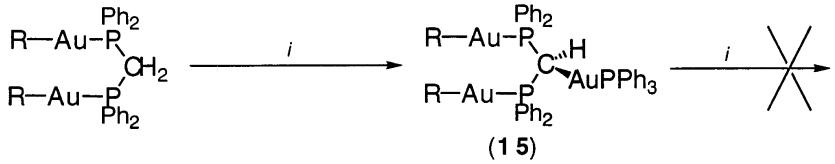

Scheme 4. R = C_6F_5; (i) [Au(acac)(PPh_3)].

solid afforded **3** (yield: 82%) while [Au(C_6F_5)(PPh_3)] was recovered from the solution. $C_{26}H_{24}AuClO_4P_2$ (694.84), calcd. C, 44.95; H, 3.5; found C, 44.75; H, 2.9.

$[Au\{PPh_2C(AuPPh_3)_2PPh_2Me\}]ClO_4$ [$X = Cl$ (***4***), C_6F_5 (***5***)]

To a solution of **1** (0.073 g, 0.1 mmol) or **2** (0.086 g, 0.1 mmol) in 20 ml of dichloromethane was added [Au(acac)(PPh_3)] (0.110 g, 0.2 mmol) and after 2 h of stirring a little amount of precipitate is filtered over celite. The solvent was then evaporated in a vacuum and 20 ml of diethyl ether was added to give complexes **4** (yield: 70%) or **5** (yield: 85%) as white solids. 4: m.p.: 130 (dec). $C_{62}H_{53}Au_3Cl_2O_4P_4$ (1647.80), calcd. C, 45.2; H, 3.25; found C, 45.25; H, 3.6. Λ_m: 95 Ω^{-1} cm^2 mol^{-1}. -^{31}P{^{1}H} NMR: δ 37.6 (dd, 2P, *P*Ph_3, [^3J(PP) = 11, ^3J(PP$^+$) = 6.3 Hz]), 32.5 (t, 1P, Au–*P*Ph_2) and 22.6 (t, 1P, *P*Ph_2Me); -^{1}H NMR: δ 2.3 (d, 3H, Me, [^2J(HP) = 13.9 Hz]). 5: m.p.: 142 (dec). -$C_{68}H_{53}Au_3ClF_5O_4P_4$ (1779.37), calcd. C, 45.8; H, 3.0; found C, 45.9; H, 2.95. Λ_m: 104 Ω^{-1} cm^2 mol^{-1}. -^{31}P{^{1}H} NMR: δ 37.6 (m, 2P, *P*Ph_3), 44.9 (m, 1P, Au–*P*Ph_2) and 23.7 (m, 1P, *P*Ph_2Me); ^{1}H NMR: δ 2.4 (d, 3H, Me, [^2J(HP) = 7.8 Hz]); -^{19}F NMR: δ −115.3 (m, 2F, *o*-F), −159.5 (t, 1F, *p*-F, [^3J(FF) = 19.5 Hz]) and −162.8 (m, 2F, *m*-F).

$[Au(C_6F_5)_2X(PPh_2CHPPh_2Me)]$ [$X = Cl$ (***6***), C_6F_5 (***7***)]

To a solution of [Au(C_6F_5)$_2$X($PPh_2CH_2PPh_2$Me)]ClO_4 [13] [0.106 g (Cl) or 0.119 g (C_6F_5), 0.1 mmol] in dichloromethane was added [N(PPh_3)$_2$](acac) (0.076 g, 0.12 mmol). After 2 h of stirring the solvent was evaporated to dryness in a vacuum and 15 ml of diethyl ether was added to precipitate the [N(PPh_3)$_2$]ClO_4 formed in the reaction, which is removed by filtration over celite. Concentration of the filtrate and addition of hexane led to complexes **6** (yield: 95%) or **7** (yield: 98%) as white solids. Their analytical and spectroscopic data agree with those previously described [13].

$[Au(C_6F_5)_2X\{PPh_2CH(AuPPh_3)PPh_2Me\}]ClO_4$ [$X = Cl$ (***8***), C_6F_5 (***9***)]

(a) A dichloromethane solution of [Au(C_6F_5)$_2$X($PPh_2CH_2PPh_2$Me)]ClO_4 [0.106 g (Cl) or 0.119 g (C_6F_5), 0.1 mmol] was treated with [Au(acac)(PPh_3)] (0.055 g, 0.1 mmol). The mixture was stirred for 2 h and the solvent was then evaporated to *ca.* 5 ml. 20 ml of diethyl ether was added to precipitate complexes **8** (yield: 90%) or **9** (yield: 65%) as white solids.

(b) To a solution of [Au(C_6F_5)$_2$X(PPh_2CHPPh_2Me)] [0.096 g (Cl) or 0.110 g (C_6F_5), 0.1 mmol] in 20 ml of dichloromethane was added [Au(PPh_3)(tht)]ClO_4 (0.065 g, 0.1 mmol) and after 30 min of stirring the solution was concentrated in a vacuum. Addition of diethyl ether gave complexes **8** (yield: 83%) or **9** (yield: 62%) as white solids. **8**: m.p.: 95 (dec). -$C_{56}H_{39}Au_2Cl_2F_{10}O_4P_3$ (1523.59), calcd. C, 44.15; H, 2.6; found C, 44.45; H, 2.35. Λ_m: 130 Ω^{-1} cm^2 mol^{-1}. -^{31}P{^{1}H} NMR: δ 39.5 ("t", 1P, *P*Ph_3, [^3N = 9.8 Hz]), 27.4 (dm, 1P, Au–*P*Ph_2) and 21.3 (dd, 1P, *P*Ph_2Me, [^2J(PP$^+$) = 29 Hz]); -^{1}H NMR: δ 5.2 ("td", 1H, C*H*, [^2J(HP) = 14.3, ^3J(HP) = 8.8 Hz]) and 2.6 (d, 3H, Me,

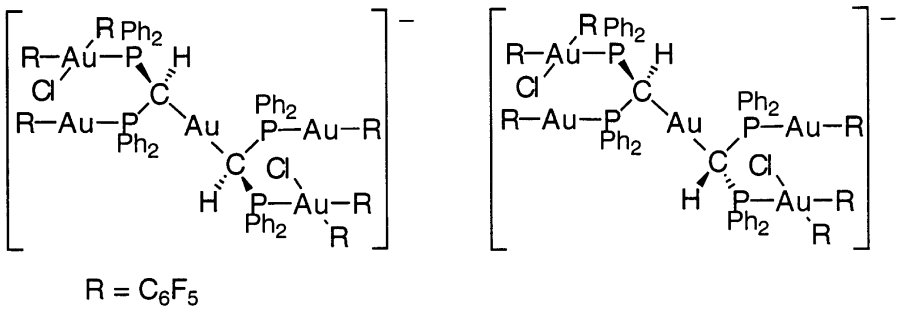

Fig. 1.

[^2J(HP) = 14.1 Hz]); -^{19}F NMR: δ-120.3 (m, 1F, *o*-F), −121.7 (m, 1F, *o*-F), −156.4 (t, 1F, *p*-F, [^3J(FF) = 19.3 Hz]), −159.4 (m, 1F, *m*-F), −160.4 (m, 1F, *m*-F), −121.8 (m, 1F, *o*-F), −122.1 (m, 1F, *o*-F), −156.5 (t, 1F, *p*-F, [^3J(FF) = 19.0 Hz]), −160.6 (m, 1F, *m*-F) and −160.8 (m, 1F, *m*-F). **9**: m.p.: 114 (dec). -$C_{62}H_{39}Au_2ClF_{15}O_4P_3$ (1655.15), calcd.: C, 45.0; H, 2.4; found C, 45.5; H, 2.45. Λ_m: 126 Ω^{-1} cm^2 mol^{-1}. -^{31}P{^{1}H} NMR: δ 38.6 (m, 1P, *P*Ph$_3$), 23.4 (m, 1P, Au–*P*Ph$_2$) and 17.4 (m, 1P, *P*Ph$_2$Me); -^{1}H NMR: δ 3.6 (m, 1H, C*H*) and 2.1 (d, 3H, Me, [^2J(HP) = 13.1 Hz]); -^{19}F NMR: δ −119.1 (m, 2F, *o*-F), −155.7 (t, 1F, *p*-F, [^3J(FF) = 19.9 Hz]), −159.6 (m, 2F, *m*-F), −120.7 (m, 2F, *o*-F), −156.5 (t, 1F, *p*-F, [^3J(FF) = 20.3 Hz]) and −160.8 (m, 2F, *m*-F).

[*N*(*PPh*$_3$)$_2$][*Au*(C$_6$F$_5$)$_3$(*PPh*$_2$*CHPPh*$_2$)*Au*(C$_6$F$_5$)] (***10***)

To a diethyl ether solution of [Au(C$_6$F$_5$)$_3$(PPh$_2$CH$_2$PPh$_2$)Au(C$_6$F$_5$)] [18] (0.144 g, 0.1 mmol) was added [N(PPh$_3$)$_2$](acac) (0.076 g, 0.12 mmol) and the solution turned yellow. After 2 h of stirring the excess of [N(PPh$_3$)$_2$](acac) was removed by filtration and the solution was dried in a vacuum giving complex **10** as a yellow oil. -^{31}P{^{1}H} NMR: δ 31.1 (m, 1P, Au(I)–*P*Ph$_2$), 18.5 (m, 1P, Au(III)–*P*Ph$_2$) and 21.7 (s, 2P, [N(*P*Ph$_3$)$_2$]$^+$).

[*Au*(C$_6$F$_5$)$_3${*PPh*$_2$*CH*(*AuPPh*$_3$)*PPh*$_2$}*Au*(C$_6$F$_5$)] (***11***)

(a) A dichloromethane solution of [Au(C$_6$F$_5$)$_3$(PPh$_2$CH$_2$PPh$_2$)Au(C$_6$F$_5$)] (0.144 g, 0.1 mmol) was treated with [Au(acac)(PPh$_3$)] (0.055 g, 0.1 mmol). The mixture was stirred for 2 h and a little amount of solid was filtered over celite. The solvent was then evaporated to *ca.* 5 ml and hexane was added to precipitate complex **11** as a white solid. Yield: 50%.

(b) To a freshly prepared solution of **10** (0.1 mmol) in dichloromethane was added [Au(PPh$_3$)(tht)]ClO$_4$ (0.065 g, 0.1 mmol) and the solution turned rapidly colourless. The solution was stirred for 30 min and the solvent was then dried in a vacuum. Addition of diethyl ether led to the precipitation of the [N(PPh$_3$)$_2$]ClO$_4$ formed in the reaction, which was removed by filtration over celite. Concentration of the filtrate and addition of hexane gave complex **11** as a white solid. Yield: 40%. m.p.: 140 (dec). -$C_{67}H_{36}Au_3F_{20}P_3$ (1904.65) calcd.: C, 42.2; H, 1.9; found C, 41.5; H, 2.0. Λ_m: 10 Ω^{-1} cm^2 mol^{-1}. -^{31}P{^{1}H} NMR: δ 39.2 ("t", 1P, *P*Ph$_3$, [*N* = 9.8 Hz]), 36.8 (m, 1P, Au(I)–*P*Ph$_2$) and 22.3 (m, 1P, Au(III)–*P*Ph$_2$); -^{1}H NMR: δ 3.6 (m, 1H, C*H*); -^{19}F NMR: δ −118.7 (m, 4F, *o*-F), −158.2 (t, 2F, *p*-F, [^3J(FF) = 20.6 Hz]), −161.1 (m, 4F, *m*-F), −121.5 (m, 2F, *o*-F), −157.9 (t, 1F, *p*-F, [^3J(FF) = 20.6 Hz]), −161.8 (m, 2F, *m*-F), −116.1 (m, 2F, *o*-F), −159.2 (t, 1F, *p*-F, [^3J(FF) = 19.3 Hz]) and −163.1 (m, 2F, *m*-F).

[*N*(*PPh*$_3$)$_2$][*Au*(C$_6$F$_5$)$_3${*PPh*$_2$*Ch*(*AuX*)*PPh*$_2$}*Au*(C$_6$F$_5$)] [*X* = *Cl* (***12***), C$_6$F$_5$ (***13***)]

To a freshly prepared solution of **10** (0.1 mmol) in dichloromethane was added [AuCl(tht)] (0.032 g, 0.1 mmol) or [Au(C$_6$F$_5$)(tht)] [23] (0.045 g, 0.1 mmol) and the solution turned rapidly colourless. After 30 min of stirring the solvent was evaporated in a vacuum and hexane was added to precipitate complexes **12** (yield: 75%) or **13** (yield: 70%) as white solids. **12**: m.p.: 63 (dec). -$C_{85}H_{51}Au_3ClF_{20}NP_4$ (2216.40), calcd. C, 46.05; H, 2.3; N, 0.6; found C, 45.8; H, 2.35; N, 0.4; **13**: m.p.: 75 (dec). -$C_{91}H_{51}Au_3F_{25}NP_4$ (2347.96), calcd.: C, 46.55; H, 2.2; N, 0.6; found C, 46.6; H, 2.4; N, 0.5. Λ_m: 81 Ω^{-1} cm^2 mol^{-1}. -^{31}P{^{1}H} NMR: δ 39.4 (m, 1P, Au(I)–*P*Ph$_2$), 22.4 (m, 1P, Au(III)–*P*Ph$_2$) and 21.7 (s, 2P, [N(*P*Ph$_3$)$_2$]$^+$); -^{1}H NMR: δ 3.55 ("t", 1H, C*H*, [*N* = 9.4 Hz]); -^{19}F NMR: δ −118.1 (m, 4F, *o*-F), −159.5 (t, 2F, *p*-F, [^3J(FF) = 21.7 Hz]), −162.4 (m, 4F, *m*-F), −120.2 (m, 2F, *o*-F), −159.3 (t, 1F, *p*-F, [^3J(FF) = 20.2 Hz]), −163.5 (m, 2F, *m*-F), −115.2 (m, 2F, *o*-F), −159.9 (t, 1F, *p*-F, [^3J(FF) = 19.5 Hz]), −164.2 (m, 2F, *m*-F), −116.2 (m, 2F, *o*-F), −160.4 (t, 1F, *p*-F, [^3J(FF) = 20.3 Hz]) and −164.7 (m, 2F, *m*-F).

[*N*(*PPh*$_3$)$_2$][{*Au*(C$_6$F$_5$)$_3$(*PPh*$_2$*CHPPh*$_2$)*Au*(C$_6$F$_5$)}$_2$*Au*] (***14***)

A dichloromethane solution of [Au(C$_6$F$_5$)$_3$(PPh$_2$CH$_2$PPh$_2$)Au(C$_6$F$_5$)] (0.144 g, 0.1 mmol) was treated with [N(PPh$_3$)$_2$][Au(acac)$_2$] [5, 24] (0.032 g, 0.05 mmol) and the solution turned rapidly yellow, which disappeared after 2 h of reaction. A little amount of solid was filtered over celite and the solution was concentrated in a vacuum. 20 ml of hexane was added to precipitate complex **14** as a white solid. Yield: 64%. m.p.: 86. -$C_{134}H_{72}Au_5F_{40}NP_6$ (3626.33), calcd. C, 44.4; H, 2.0; N, 0.4; found C, 44.55; H, 1.85; N, 0.35. Λ_m: 113 Ω^{-1} cm^2 mol^{-1}. -^{31}P{^{1}H} NMR: δ 28.0 (m, 2P, Au(I)–*P*Ph$_2$), 11.3 (m, 2P, Au(III)–*P*Ph$_2$) and 21.7 (s, 2P, [N(*P*Ph$_3$)$_2$]$^+$); -^{1}H NMR: δ 3.54 ("t", 1H, C*H*, [*N* = 9.3 Hz]); -^{19}F NMR: δ −119.1 (m, 8F, *o*-F), −154.3 (t, 4F, *p*-F, [^3J(FF) = 19.3 Hz]), −158.7 (m, 8F, *m*-F), −120.3 (m, 4F, *o*-F), −155.4 (t, 2F, *p*-F, [^3J(FF) = 19.5 Hz]), −159.6 (m, 4F, *m*-F), −114.9 (m, 4F, *o*-F), −156.5 (t, 2F, *p*-F, [^3J(FF) = 20.0 Hz]) and −161.1 (m, 4F, *m*-F).

[*Au*(C$_6$F$_5$){*PPh*$_2$*CH*(*AuPPh*$_3$)*PPh*$_2$}*Au*(C$_6$F$_5$)] (***15***)

A dichloromethane solution of [Au(C$_6$F$_5$)(PPh$_2$CH$_2$PPh$_2$)Au(C$_6$F$_5$)] (0.112 g, 0.1 mmol) was treated with [Au(acac)(PPh$_3$)] (0.055 g, 0.1 mmol). The mixture was stirred for 1 h and a little amount of solid was filtered over celite. The solvent was then evaporated to *ca.* 5 ml and hexane was added to precipitate complex **15** as a white solid. Yield: 68%. m.p.:

130 (dec). -$C_{55}H_{36}Au_3F_{10}P_3$ (1570.61), calcd. C, 42.05; H, 2.3; found C, 41.1; H, 2.7. Λ_m: 4 Ω^{-1} cm^2 mol^{-1}. - $^{31}P\{^1H\}$NMR: δ 40.8 (t, 1P, PPh_3, [^3J(PP) = 14.5 Hz]) and 36.8 (d, 2P, Au(I)–PPh_2); -^{1}H NMR: δ 3.9 (td, 1H, C*H*, [^2J(HP) = 14.4, ^3J(HP) = 7.1 Hz]); -^{19}F NMR: δ −115.3 (m, 4F, *o*-F), −160.8 (t, 2F, *p*-F, [^3J(FF) = 19.6 Hz]) and −164.2 (m, 4F, *m*-F).

Acknowledgements—We thank the Dirección General de Investigación Científica y Técnica (No. PB94-0079) for financial support.

REFERENCES

1. Puddephatt, R. J., *Chem. Soc. Rev.*, 1983, **12,** 99 and references therein.
2. Basset, J. M., Mandl, J. R. and Schmidbaur, H., *Chem. Ber.*, 1980, **113,** 1145.
3. Laguna, A. and Laguna, M., *J. Organomet. Chem.*, 1990, **394,** 743 and references therein.
4. Usón, R., Laguna, A., Laguna, M., Manzano, B., Jones, P. G. and Sheldrick, G. M., *J. Chem. Soc. Dalton Trans.*, 1984, 839.
5. Fernández, E. J., Gimeno, M. C., Jones, P. G., Laguna, A., Laguna, M. and López-de-Luzuriaga, J. M., *J. Chem. Soc. Dalton Trans.*, 1992, 3365.
6. Usón, R., Laguna, A., Laguna, M., Gimeno, M. C., Jones, P. G., Fittschen, C. and Sheldrick, G. M., *J. Chem. Soc. Chem. Commun.*, 1986, 509.
7. Fernández, E. J., Gimeno, M. C., Jones, P. G., Laguna, A., Laguna, M., López-de-Luzuriaga, J. M., *Angew. Chem. Int. Ed. Engl.*, 1994, **33,** 87.
8a. Schmidbaur, H. and Mandl, J. R., *Angew. Chem. Int. Ed. Engl.*, 1977, **16,** 640.
8b. Schmidbaur, H., Mandl, J. R., Bassett, J. M., Blaschke, G. and Zimmer-Gasser, B., *Chem. Ber.*, 1981, **114,** 433.
9. Briant, C. E., Hall, K. P. and Mingos, D. M. P., *J. Organomet. Chem.*, 1981, **229,** C–5.
10. Gimeno, M. C., Laguna, A., Laguna, M., Sanmartín, F. and Jones, P. G., *Organometallics*, 1993, **12,** 3984.
11. Fernández, E. J., Gimeno, M. C., Jones, P. G., Laguna, A., Laguna, M., López-de-Luzuriaga, J. M., *Organometallics*, 1995, **14,** 2918.
12. Alvarez, B., Fernández, E. J., Gimeno, M. C., Jones, P. G., Laguna, A. and López-de-Luzuriaga, J. M., *Polyhedron* (in press).
13. Usón, R., Laguna, A., Laguna, M., Lázaro, I., Morata, A., Jones, P. G. and Sheldrick, G. M., *J. Chem. Soc. Dalton Trans.*, 1986, 669.
14a. Vicente, J., Chicote, M. T., Saura-Llamas, I., Jones, P. G., Meyer-Bäse, K. and Erdbrügger, C. F., *Organometallics*, 1988, **7,** 997.
14b. Vicente, J., Chicote, M. T. and Lagunas, M. C., *Inorg. Chem.*, 1993, **32,** 3748.
15. Hathaway B. J. and Underhill, A. E., *J. Chem. Soc.*, 1961, 3091.
16a. Schmidbaur, H. and Franke, R., *Angew. Chem.*, 1973, **85,** 449.
16b. Schmidbaur, H. and Franke, R., *Angew. Chem. Int. Ed. Engl.*, 1973, **12,** 416.
16c. Schmidbaur, H. and Franke, R., *Inorg. Chim. Acta*, 1975, **13,** 85.
16d. Schmidbaur, H. and Franke, R., *Chem. Ber.*, 1975, **108,** 1321.
17. Usón, R., Laguna, A., Laguna, M., Usón, A. and Gimeno, M. C., *Inorg. Chim. Acta*, 1986, **114,** 91.
18. Usón, R., Laguna, A., Laguna, M., Fernández, E. J., Jones, P.G. and Sheldrick, G. M., *J. Chem. Soc. Dalton Trans.*, 1982, 1971.
19. Usón, R., Laguna, A., Vicente, J. and García, J., *Rev. Acad. Cienc. Zaragoza*, 1976, **31,** 77.
20. Allen, E. A. and Wilkinson, W., *Spectrochim. Acta*, 1972, **28A,** 2257.
21. Gibson, D., Johnson, B. F. G. and Lewis, J., *J. Chem. Soc. A*, 1970, 367.
22. Usón, R., Laguna, A., Laguna, M., Jiménez, J., Gómez, M. P., Sáinz, A. and Jones, P. G., *J. Chem. Soc. Dalton Trans.*, 1990, 3457.
23. Usón, R., Laguna, A. and Vicente, J., *J. Chem. Soc, Chem. Commun.*, 1976, 353.
24. Vicente, J., Chicote, M. T., Saura-Llamas, I. and Lagunas, M. C., *J. Chem. Soc. Chem. Commun.*, 1992, 915.

Pergamon

PII: S0277–5387(98)00182–X

Polyhedron Vol. 17, No. 22, pp. 3927–3934, 1998
© 1998 Elsevier Science Ltd
All rights reserved. Printed in Great Britain
0277–5387/98 $19.00+0.00

Cyclometallated platinum compounds with chiral imines. Crystal structure of [PtMe(2-FC_6H_3CH═N-(S)-CHMePh)(PPh_3)]

Margarita Crespo,[a]* Xavier Solans[b] and Mercè Font-Bardía[b]

[a] Departament de Química Inorgànica, Universitat de Barcelona, Diagonal 647, 08028 Barcelona, Spain

[b] Departament de Cristallografia, Mineralogia i Dipòsits Minerals, Universitat de Barcelona, Martí i Franqués s/n. 08028 Barcelona, Spain

(Received 30 January 1998; accepted 29 April 1998)

Abstract—The reactions of [$Pt_2Me_4(\mu$-$SMe_2)_2$] (**1**) with ligands ArCH═N-(*S*)-CHMePh (Ar═2-BrC_6H_4 (**2a**), 2,6-$Cl_2C_6H_3$ (**2b**), C_6F_5 (**2c**), 2-FC_6H_4 (**2d**), 2-$CF_3C_6H_4$ (**2e**)), give either cyclometallated compounds [$PtMe_2X$(RCH═N-(*S*)-CHMePh)(SMe_2)] (**3**), by intramolecular activation of C–X (X = Br, Cl or F) bonds, or compounds [PtMe(RCH═N-(*S*)-CHMePh)(SMe_2)] (**5**), by orthometallation, followed by methane elimination. The reactions of these compounds with PPh_3 result in the formation of [$PtMe_2X$(RCH═N-(*S*)-CHMePh)(PPh_3)] (**4**), or [PtMe(RCH═N-(*S*)-CHMePh)(PPh_3)] (**6**), respectively. Oxidative addition of methyl iodide to compounds **6** produces the corresponding complexes **4**. The NMR spectra of compounds **3** and **4** indicate that these are formed as two diastereomers. The X-ray structure of [PtMe(2-FC_6H_3CH═N-(*S*)-CHMePh)(PPh_3)] (**6d**) is reported. © 1998 Elsevier Science Ltd. All rights reserved

Keywords: cyclometallation; platinum; chiral imines; X-Ray crystal structure

INTRODUCTION

Cyclometallated compounds have been extensively studied because of their potential utility in organic synthesis, catalysis and asymmetric synthesis. Moreover, cyclometallated platinum complexes with N-donor ligands showing interesting photophysical, photochemical or electrochemical properties have been reported [1–5]. While relatively few examples of cycloplatination of chiral N-donor ligands have been described [6, 7], predetermination of helical chirality at the metal center has been achieved for both square–planar platinum(II) and octahedral platinum(IV) cyclometallated compounds, by the use of adequate ligands [8].

Following our interest in cyclometallated platinum complexes containing bidentate (C, N) ligands [9, 10], we now describe new cyclometallated compounds obtained by the reaction of [$Pt_2Me_4(\mu$-$SMe_2)_2$] and imines ArCH═N-(*S*)-CHMePh, derived from (*S*)-α-methylbenzylamine. According to previous results [9, 10], for Ar═2-BrC_6H_4, 2,6-$Cl_2C_6H_3$ and C_6F_5, the formation of octahedral platinum(IV) compounds in which the metal atom becomes a chiral center is expected, arising from activation of C–Br, C–Cl or C–F bonds, respectively. Interestingly, resolution of platinum(II) in a trigonal bipyramidal environment has been achieved by using the enantiomeric imine 2-(CH═N-(*S*)-CH(Me)Ph)-6-MeC_5H_3N [11]. For imines containing the aryl groups 2-$CF_3C_6H_4$ or 2-FC_6H_4, C–H bond activation, followed by CH_4 elimination, is expected to lead to formation of chiral-at-ligand cyclometallated platinum(II) compounds. These complexes may undergo oxidative addition reactions to yield octahedral platinum compounds. Fluorinated substituents were selected for this study because ^{19}F NMR spectroscopy has been reported to be one of the most sensitive techniques for detecting diastereomers [12].

RESULTS AND DISCUSSION

Ligands ArCH═N-(*S*)-CHMePh (Ar═2-BrC_6H_4 (**2a**), 2,6-$Cl_2C_6H_3$ (**2b**), C_6F_5 (**2c**), 2-FC_6H_4 (**2d**), 2-

* Author to whom correspondence should be addressed.

$CF_3C_6H_4$ (**2e**)) were prepared from the condensation reaction of (*S*)-α-methylbenzylamine and the appropriate aldehyde, carried out in refluxing ethanol. The reactions of $[Pt_2Me_4(\mu\text{-}SMe_2)_2]$ (**1**) with iminic ligands ArCH=N-(*S*)-CHMePh (**2a**–**2e**) were carried out in acetone and the results are shown in Scheme 1.

For imines **2a** and **2b** formation of platinum(IV) cyclometallated compounds $[PtMe_2Br(C_6H_4CH{=}N\text{-}(S)\text{-}CHMePh)(SMe_2)]$ (**3a**) and $[PtMe_2Cl(2\text{-}ClC_6H_3CH{=}N\text{-}(S)\text{-}CHMePh)(SMe_2)]$ (**3b**) by activation of a C–Br or a C–Cl bond, respectively, was achieved. Such processes have been reported for analogous ligands derived from benzylamine [9, 10] or *N*,*N*-dimethylethylenediamine [13–15] and, in all cases, a *fac*-PtC_3 stereochemistry is adopted which makes the octahedrally coordinated platinum(IV) a chiral center. As ligands **2** are optically active, platinum (IV) compounds **3a** and **3b** consist of a mixture of two diastereomers (*C*,*S*) and (*A*,*S*), in which *C*/*A* represents the absolute stereochemistry (clockwise and anticlockwise) [16] at the platinum and *S* describes the chirality at carbon. The reaction of $[Pt_2Me_4(\mu\text{-}SMe_2)_2]$ (**1**) with imine $C_6F_5CH{=}N\text{-}(S)\text{-}CHMePh$ (**2c**) gave a complex mixture which could not be identified.

The reactions of compounds **3a** and **3b** with triphenylphosphine yielded cyclometallated platinum(IV) compounds $[PtMe_2Br(C_6H_4CH{=}N\text{-}(S)\text{-}CHMePh)(PPh_3)]$ (**4a**), and $[PtMe_2Cl(2\text{-}ClC_6H_3CH{=}N\text{-}(S)\text{-}CHMePh)(PPh_3)]$ (**4b**).

Although compound $[PtMe_2F(C_6F_4CH{=}N\text{-}(S)\text{-}CHMePh)(SMe_2)]$ (**3c**) could not be obtained in a pure form from the reaction of **1** with imine $C_6F_5CH{=}N\text{-}(S)\text{-}CHMePh$ (**2c**), addition of PPh_3 to the reaction mixture gave $[PtMe_2F(C_6F_4CH{=}N\text{-}(S)\text{-}CHMePh)(PPh_3)]$ (**4c**). Activation of a C–F bond has been confirmed by NMR spectroscopy.

Imines **2d** and **2e** yielded cyclometallated platinum (II) compounds $[PtMe(2\text{-}FC_6H_3CH{=}N\text{-}(S)\text{-}CHMePh)(SMe_2)]$ (**5d**) and $[PtMe(2\text{-}CF_3C_6H_3CH{=}N\text{-}(S)\text{-}CHMePh)(SMe_2)]$ (**5e**), respectively, by C–H bond activation with loss of methane. The reaction of compounds **5d** and **5e** with one equivalent of triphenylphosphine in acetone yielded cyclometallated platinum(II) compounds $[PtMe(2\text{-}FC_6H_3CH{=}N\text{-}(S)\text{-}CHMePh)(PPh_3)]$ (**6d**) and $[PtMe(2\text{-}CF_3C_6H_3CH{=}N\text{-}(S)\text{-}CHMePh)(PPh_3)]$ (**6e**).

The reactions of **6d** and **6e** with methyl iodide were also studied. Oxidative addition of alkyl halides to square–planar platinum(II) complexes is well documented; in particular, studies concerning compounds $[PtMe_2(NN)]$ (where NN is a bidentate nitrogen donor ligand) have been reported and experimental evidence points to *trans* stereochemistry in the resulting platinum compounds [17–20]. Upon addition of an excess of methyl iodide to solutions of compounds **6** in acetone, the color of the solution faded and compounds $[PtMe_2I(2\text{-}FC_6H_3CH{=}N\text{-}(S)\text{-}CHMePh)(SMe_2)]$ (**4d**) and $[PtMe_2I(2\text{-}CF_3C_6H_3CH{=}N\text{-}(S)\text{-}CHMePh)(SMe_2)]$ (**4e**) were isolated as a mixture of two diastereomers (*C*,*S*) and (*A*,*S*). Therefore, analogous results are obtained by intermolecular oxidative addition of methyl iodide to cyclometallated platinum(II) compounds and by intramolecular oxidative addition of C–Br, C–Cl or C–F bonds.

The NMR spectra of compounds **3** and **4** clearly revealed two diastereomers in nearly equal amounts. No epimerization was observed when the solution was left to stand. Attempts to separate the diastereomers by crystallization in several solvents were unsuccessful, which suggests similar solubility properties for both isomers.

In the ^1H NMR spectra, two methylplatinum resonances, coupled to ^{195}Pt, appear for each isomer, as singlets for compounds **3**, and as doublets, due to coupling with one phosphorus atom, for compounds **4**. The small value for the coupling constant of the axial methyl with platinum suggest a *trans* arrangement of this group and the PPh_3 ligand, as previously reported for analogous compounds [21]. Relative proportions of the isomers, averaged from all the signals, are 1: 0.90 (**4a**), 1: 0.95 (**4b**), 1: 0.85 (**4c**), 1: 0.80 (**4d**) and 1: 0.85 (**4e**).

^{31}P NMR spectra of compounds **4** confirm the presence of two diastereomers since two signals appear, both coupled to ^{195}Pt. Similarly, two fluorine resonances appear in the ^{19}F NMR of compounds **4d** and **4e**. Moreover, in the ^{19}F NMR of **4c**, ten distinct resonances were observed, eight of them in the aromatic region and two at higher field (*ca.* −280 ppm, $J(FPt) = 195$ Hz, $J(FP) = 28$ Hz), which were assigned to platinum bound fluorine atoms, on the basis of previously reported data [10, 14]. A better diastereomeric peak separation (*ca.* 4 ppm) is observed for the F–Pt than for the aromatic fluorine (*ca.* 0.5 ppm) resonances.

In the ^1H NMR spectra of cyclometallated platinum(II) compounds, the resonance for the methylplatinum group appears as a singlet for compounds **5** and as a doublet, due to coupling with one phosphorus atom, for compounds **6**. In both cases, the value of J(Me–Pt) is larger than that obtained for compounds **3** and **4**, which is consistent with the corresponding oxidation states of platinum.

Compound **6d** was also characterized crystallographically. Suitable crystals were grown in acetone solution. The crystal structure is composed of discrete molecules separated by van der Waals interactions. The structure is shown in Fig. 1, and molecular dimensions are listed in Table 1. The platinum atom displays a tetrahedral distorted planar coordination and the following displacements (Å) are observed from the least-squares plane of the coordination sphere: Pt, 0.0338; P, −0.1107; N, 0.1039; C(3), −0.1425; C(16), 0.1155.

In contrast to the results reported for cyclopalladated analogues [22], the PPh_3 ligand and the aryl carbon occupy mutually *trans* positions. Thus, the tendency of phosphines to avoid coordinating *trans* to carbon donor ligands in palladium complexes [23] does not apply to platinum.

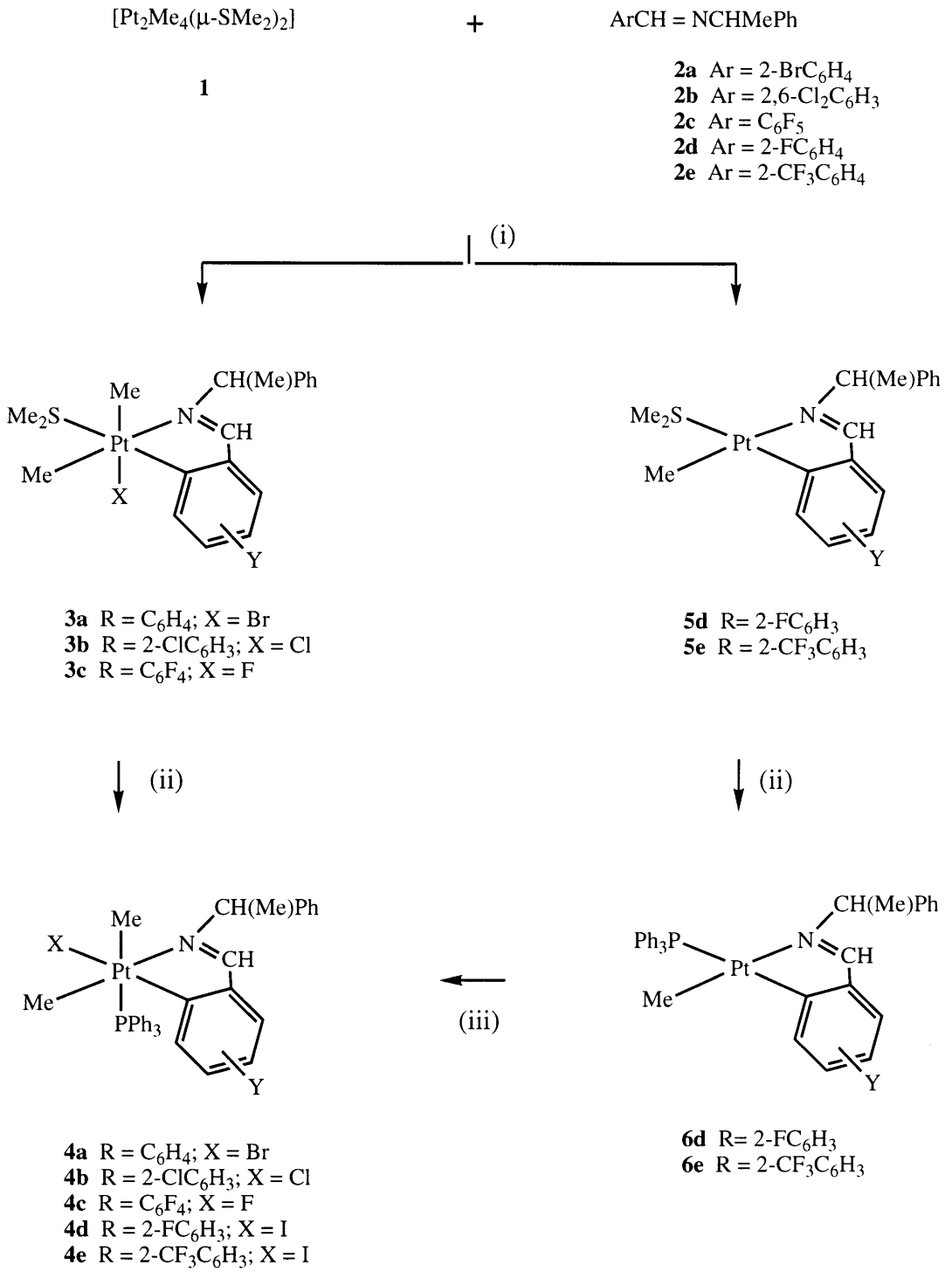

Scheme 1. (i) Acetone, room temperature, 16 h; (ii) $+PPh_3$ (1:1), acetone, room temperature; (iii) +MeI, acetone, room temperature, 2 h.

The metallacycle displays an envelope conformation with the N, C(1), C(2), C(3) moiety planar and the platinum atom displaced from the plane by −0.214 Å. The angle between the coordination plane and the planar metallacycle moiety is 11.29°. The angles between adjacent atoms in the coordination sphere of platinum lie in the range 79.9(2)–105.11(13)°, the smallest angles corresponding to the

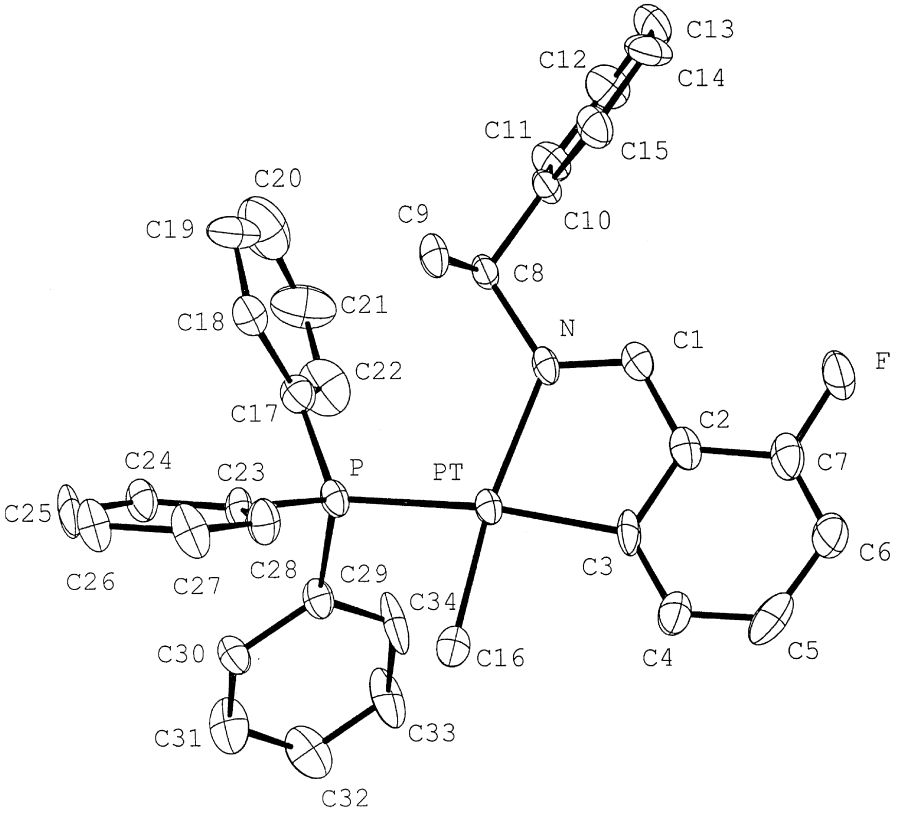

Fig. 1. Molecular structure of **6d**.

Table 1. Selected bond lengths (Å) and angles (deg) for compound **6d**

Pt–C(3)	2.057(6)	Pt–C(16)	2.058(7)
Pt–N	2.119(5)	Pt–P	2.305(2)
P–C(29)	1.791(7)	P–C(23)	1.828(6)
P–C(17)	1.834(7)	N–C(1)	1.293(7)
N–C(8)	1.541(7)	F–C(7)	1.358(10)
C(1)–C(2)	1.416(9)	C(2)–C(3)	1.429(9)
C(2)–C(7)	1.440(9)	C(3)–C(4)	1.370(10)
C(4)–C(5)	1.351(11)	C(5)–C(6)	1.433(14)
C(6)–C(7)	1.315(13)	C(8)–C(9)	1.473(8)
C(8)–C(10)	1.513(7)		
C(3)–Pt–C(16)	90.5(3)	C(3)–Pt–N	79.9(2)
C(16)–Pt–N	169.2(3)	C(3)–Pt–P	170.3(2)
C(16)–Pt–P	85.1(2)	N–Pt–P	105.11(13)
C(29)–P–C(23)	106.2(3)	C(29)–P–C(17)	102.4(3)
C(23)–P–C(17)	103.2(3)	C(1)–N–C(8)	120.9(5)
C(1)–N–Pt	114.2(4)	C(8)–N–Pt	124.6(3)
N–C(1)–C(2)	116.6(5)	C(1)–C(2)–C(3)	118.6(5)
C(9)–C(8)–C(10)	114.7(5)	C(9)–C(8)–N	106.4(5)
C(10)–C(8)–N	110.9(4)		

metallacycle. Bond lengths in the coordination sphere of platinum are in the range reported for analogous cyclometallated platinum compounds [21, 24–27].

In conclusion, the results reported here show that intramolecular activation of C–X bonds of chiral imines at platinum gives either optically active cyclometallated platinum(II) compounds (X = H), or platinum(IV) compounds (X = F, Cl or Br). The latter, and

the products obtained upon oxidative addition to the platinum(II) compounds, as well as their phosphine derivatives, are formed as a pair of diastereomers in nearly equimolecular amounts.

EXPERIMENTAL

^1H, ^{31}P–$\{^1H\}$ and ^{19}F NMR spectra were recorded by using Varian Gemini 200 (^1H, 200 MHz), Bruker DRX-250 (^{31}P, 101.3 MHz), and Varian XL 300FT (^{19}F, 282.2 MHz) spectrometers, and referenced to $SiMe_4$ (^1H), H_3PO_4 (^{31}P), and $CFCl_3$ (^{19}F). δ values are given in ppm and J values in Hz. Microanalyses were performed by the Serveis Científico–Tècnics de la Universitat de Barcelona.

Preparation of the compounds

The complex $[Pt_2Me_4(\mu\text{-}SMe_2)_2]$ (**1**) was prepared by the method reported in the literature [28].

Compounds **2** were prepared by the reaction of 5 mmol of the corresponding aldehyde ArCHO and the equimolar amount of (*S*)-α-methylbenzylamine in 25 mL of ethanol [29]. The mixture was refluxed for two hours and the solvent was removed in a rotary evaporator to yield imines **2a**–**2d** as yellow oils, which were used without any further purification.

2-*$BrC_6H_4CHNCHMePh$* (***2a***) Yield 1.2 g (83%). ^1H NMR ($CDCl_3$), δ = 1.60 [d, ^3J(HMe) = 6, Me], 4.62 [q, ^3J(HMe) = 6, CH*Me*], {7.25–7.57 [m, 8H], 8.11 [d, ^3J(HH) = 7, 1H], aromatics}, 8.74 [s, CH═N].

2,6-*$Cl_2C_6H_3CHNCHMePh$* (***2b***) Yield 1.0 g (72%). ^1H NMR ($CDCl_3$), δ = 1.65 [d, ^3J(HMe) = 7, Me], 4.62 [q, ^3J(HMe) = 7, CH*Me*], 7.10–7.50 [m, aromatics], 8.52 [s, CH═N].

$C_6F_5CHNCHMePh$ (***2c***) Yield 1.2 g (80%). ^1H NMR ($CDCl_3$), δ = 1.63 [d, ^3J(HMe) = 7, Me], 4.57 [q, ^3J(HMe) = 7, CH*Me*], {7.36–7.40 [m], aromatics}, 8.47 [s, CH═N]. ^{19}F NMR ($CDCl_3$), δ = −164.6 [m, F^a], −153.9 [m, F^c], −145.0 [m, F^b].

2-*$FC_6H_4CHNCHMePh$* (***2d***) Yield 1.0 g (89%). ^1H NMR ($CDCl_3$), δ = 1.59 [d, ^3J(HMe) = 7, Me], 4.60 [q, ^3J(HMe) = 7, CH*Me*], {7.05–7.46 [m, 8H], 8.08 [td, J(HH) = 8; 2, 1H], aromatics}, 8.71 [s, CH═N]. ^{19}F NMR ($CDCl_3$), δ = −122.96 [ddd, J(HF) = 13; 8; 5].

2-*$CF_3C_6H_4CHNCHMePh$* (***2e***) Yield 1.1 g (79%). ^1H NMR ($CDCl_3$), δ = 1.60 [d, ^3J(HMe) = 7, Me], 4.62 [q, ^3J(HMe) = 7, CH*Me*], {7.21–7.69 [m], 8.28 [d, 1H], aromatics}, 8.74 [q, J(H–F) = 3, 1H, CH═N]. ^{19}F NMR ($CDCl_3$), δ = −57.9 [s].

Compounds **3a**, **3b**, **5d** and **5e** were prepared by reaction of 100 mg (0.17 mmol) of $[Pt_2Me_4(\mu\text{-}SMe_2)_2]$ (**1**) with 0.35 mmol of the corresponding imine in acetone (25 mL). The mixture was stirred for 16 h and the solvent was removed in a rotary evaporator. The oily residue was washed with hexane (3 × 5 mL) and dried *in vacuo*.

[*$PtMe_2Br(C_6H_4CHNCHMePh)(SMe_2)$*] (***3a***) Yield 150 mg (75%). ^1H NMR(acetone-d^6), isomer 1 (major): δ = 0.74 [s, ^2J(HPt) = 71, Me–Pt], 1.16 [s, ^2J(HPt) = 69, Me–Pt], 1.66 [s, ^3J(HPt) = 13, SMe_2], 8.61 [s, ^3J(HPt) = 48, CH═N]; isomer 2 (minor): δ = 0.97 [s, ^2J(HPt) = 71, Me], 1.19 [s, ^2J(HPt) = 69, Me], 1.75 [s, ^3J(HPt) = 13, SMe_2], 8.47 [s, ^3J(HPt) = 46, CH═N].

[*$PtMe_2Cl$*(2-*$ClC_6H_3CHNCHMePh$*)(*SMe_2*)] (***3b***) Yield 120 mg (61%). ^1H NMR(acetone-d^6), isomer 1 (major): δ = 0.97 [s, ^2J(HPt) = 70, Me–Pt], 1.19 [s, ^2J(HPt) = 68, Me–Pt], 1.90 [s, ^3J(HPt) = 15, SMe_2], 8.80 [s, ^3J(HPt) = 47, CH═N]; isomer 2 (minor): δ = 0.76 [s, ^2J(HPt) = 71, Me], 1.18 [s, ^2J(HPt) = 68, Me], 1.82 [s, ^3J(HPt) = 15, SMe_2], 8.89 [s, ^3J(HPt) = 48, CH═N].

[*PtMe*(2-*$FC_6H_3CHNCHMePH$*)(*SMe_2*)] (***5d***) Yield 150 mg (87%). ^1H NMR(acetone-d^6), δ = 0.87 [s, ^2J(HPt) = 83, Me–Pt], 1.75 [d, ^3J(H–Me) = 7, Me], 1.94 [s, ^3J(HPt) = 28, SMe_2], 5.54 [q, ^3J(H–Me) = 7, CH*Me*], {6.59 [m], 7.10–7.29 [m], aromatics}, 9.10 [s, ^3J(HPt) = 57, CH═N]. ^{19}F NMR ($CDCl_3$), δ = −113.93 [dd, J(FPt) = 60, J(HF) = 10; 6].

[*PtMe*(2-*$CF_3C_6H_3CHNCHMePh$*)(*SMe_2*)] (***5e***) Yield 160 mg (84%). ^1H NMR(acetone-d^6), δ = 0.90 [s, ^2J(HPt) = 82, Me–Pt], 1.77 [d, ^3J(HMe) = 7, Me], 1.98 [s, ^3J(HPt) = 28, SMe_2], 5.63 [q, ^3J(H–Me) = 7, CH*Me*], {7.35 [m], 7.90 [m], aromatics}, 9.11 [s, ^3J(HPt) = 59, CH═N]. ^{19}F NMR ($CDCl_3$), δ = −58.26 [s].

Compounds **4a** and **4b** were prepared by reaction of 50 mg of the corresponding compounds **3a** (0.064 mmol) and **3b** (0.065 mmol) with 17 mg (0.065 mmol) of PPh_3 in acetone (10 mL). Within one hour, the color of the solution faded and after addition of hexane, the yellow–white solid was collected by filtration, washed with hexane and dried *in vacuo*.

Compound **4c** was prepared by the reaction of 100 mg (0.17 mmol) of $[Pt_2Me_4(\mu\text{-}SMe_2)_2]$ (**1**) with 104 mg (0.35 mmol) of imine **2c** in acetone (10 mL). The mixture was stirred for 5 h and 90 mg (0.35 mmol) of PPh_3 were added. After one hour, hexane (10 mL) was added and the resulting precipitate was collected by filtration, washed with hexane, and dried *in vacuo*.

[*$PtMe_2Br(C_6H_4CHNCHMePH)(PPh_3)$*] (***4a***) Yield 50 mg (74%). ^1H NMR(acetone-d^6), isomer 1 (major) δ = 0.56 [d, ^2J(HPt) = 60, ^3J(HP) = 8, Me–Pt], 1.32 [d, ^2J(HPt) = 70, ^3J(HP) = 7.5, Me–Pt], 1.08 [d, ^3J(HH) = 7, Me], 6.13 [q, CH*Me*], {6.46 [d, J(HPt) = 40, J(HH) = 7.5], 6.75 [t, J(HH) = 7.5], 6.99 [t, J(HH) = 7.5], aromatics}, 8.96 [s, ^3J(HPt) = 48, CH═N], isomer 2 (minor) δ = 1.10 [d, ^2J(HPt) = 58, ^3J(HP) = 7.5, Me–Pt], 1.42 [d, ^2J(HPt) = 69, ^3J(HP) = 8, Me–Pt], 1.85 [d, ^3J(HH) = 6.5, Me], 5.80 [q, J(HH) = 7, CH*Me*], {6.42 [d, J(HPt) = 40, J(HH) = 8], 6.68 [t, J(HH) = 7.5], 6.85 [t, J(HH) = 7.5], aromatics}, 7.93 [s, ^3J(HPt) = 48, CH═N]. ^{31}P NMR(acetone-d^6), isomer 1 (major) δ = −7.21 [s, ^1J(PPt) = 984], isomer 2 (minor) δ = −7.93 [s, ^1J(PPt) = 1019]. Anal. calc. for $C_{35}H_{35}BrNPPt$: C, 54.20; H, 4.55; N, 1.80. Found, C, 54.4; H, 4.7; N, 1.6%.

[*$PtMe_2Cl$*(2-*$ClC_6H_3CHNCHMePh$*)(*PPh_3*)] (***4b***)

Yield 50 mg (74%). ^{1}H NMR(acetone-d^6), isomer 1 (major) $\delta = 1.02$ [d, ^2J(HPt) = 60, ^3J(HP) = 8, Me–Pt], 1.34 [d, ^2J(HPt) = 69, ^3J(HP) = 8, Me–Pt], 1.90 [d, ^3J(HH) = 7, Me], 5.78 [q, J(HH) = 7, CH*Me*], {6.52 [d, J(HPt) = 40, J(HH) = 8], 6.70 [t, J(HH) = 7], 6.81 [d, J(HH) = 7.5], aromatics}, 9.12 [s, ^3J(HPt) = 50, CH═N], isomer 2 (minor) $\delta = 0.46$ [d, ^2J(HPt) = 60, ^3J(HP) = 8, Me–Pt], 1.25 [d, ^2J(HPt) = 68, ^3J(HP) = 8.5, Me–Pt], 1.17 [d, ^3J(HH) = 7, Me], 6.13 [q, J(HH) = 7, CH*Me*], {6.56 [d, J(HPt) = 40, J(HH) = 8], 6.74 [t, J(HH) = 8], 6.94 [d, J(HH) = 8], aromatics}, 8.26 [s, ^3J(HPt) = 51, CH═N]. ^{31}P NMR(acetone-d^6), isomer 1 (major) $\delta = -6.79$ [s, ^1J(PPt) = 1002], isomer 2 (minor) $\delta = -6.13$ [s, ^1J(PPt) = 978]. Anal. calc. for $C_{35}H_{34}Cl_2NPPt$: C, 54.90; H, 4.48; N, 1.83. Found, C, 54.6; H, 4.1; N, 1.7%.

[$PtMe_2F(C_6F_5CHNCHMePH)(PPh_3)$] (***4c***) Yield 140 mg (51%). ^{1}H NMR(acetone-d^6), isomer 1 (major) $\delta = 0.42$ [dd, ^2J(HPt) = 58, ^3J(HP) = 8, ^3J(HF) = 7, Me–Pt], 1.60 [q, ^2J(HPt) = 65, ^3J(HP) = J(HF^d = J(HF^e) = 8, Me–Pt], 1.21 [d, ^3J(HH) = 7, Me], 5.48 [q, J(HH) = 7, CH*Me*], 8.27 [s, ^3J(HPt) = 49, CH═N], isomer 2 (minor) $\delta = 1.01$ [dd, ^2J(HPt) = 58, ^3J(HP) = 8, ^3J(HF) = 7, Me–Pt], 1.72 [q, ^2J(HPt) = 67, ^3J(HP) = J(HF^d) = J(HF^e) = 8, Me–Pt], 1.86 [d, ^3J(HH) = 7, Me], 5.65 [q, J(HH) = 7, CH*Me*], 9.16 [s, ^3J(HPt) = 50, CH═N]. ^{19}F NMR($CDCl_3$), isomer 1 (major) $\delta = -144.0$ [t, J(F^{a}F^b) = J(F^{a}F^d) = 21, F^a]; −166.5 [t, J(F^{a}F^b) = J(F^{b}F^c) = 20, J(F^{b}Pt) = 15, F^b], −149.9 [t, J(F^{c}F^d) = J(F^{c}F^b) = 21, F^c], −128.7 [m, F^d], −279.8 [d, J(F^{e}P) = 28, J(F^{e}Pt) = 195, F^e], isomer 2 (minor) $\delta = -143.6$ [t, J(F^{a}F^b) = J(F^{a}F^d) = 21, F^a]; −166.1 [t, J(F^{a}F^b) = J(F^{b}F^c) = 20, J(F^{b}Pt) = 15, F^b], −149.4 [t, J(F^{b}F^c) = J(F^{c}F^d) = 21, F^c], −128.3 [m, F^d], −276.0 [d, J(F^{e}P) = 28, J(F^{e}Pt) = 195, F^e]. ^{31}P NMR(acetone-d^6), isomer 1 (major) $\delta = -0.48$ [d, ^1J(PPt) = 950, ^2J (PF) = 30], isomer 2 (minor) $\delta = 1.08$ [d, ^1J(PPt) = 975, ^2J(PF) = 29]. Anal. calc. for $C_{35}H_{31}F_5NPPt$: C, 53.43; H, 3.97; N, 1.78. Found, C, 52.9; H, 3.6; N, 1.6%.

Compounds **6d** and **6e** were prepared by reaction of 50 mg of the corresponding compounds **5d** (0.10 mmol) and **5e** (0.091 mmol) with 26 mg (0.10 mmol) of PPh_3 in acetone (10 mL). The mixture was stirred for two hours and the solvent was removed *in vacuo*. Upon addition of hexane (15 mL), the yellow–white solid was collected by filtration, washed with hexane (3 × 5 mL) and dried *in vacuo*.

[$PtMe$(2-$FC_6H_3CHNCHMePh$)(PPh_3)] (***6d***) Yield 60 mg (86%). ^{1}H NMR(acetone-d^6), $\delta = 0.71$ [d, ^2J(HPt) = 84, ^3J(HP) = 7, Me–Pt], 1.17 [d, ^3J(HH) = 7, Me], 4.55 [m, CH*Me*], {6.88 [m, 2H], 7.19 [m], 7.38 [m], 7.47 [m], 7.77 [m], aromatics}, 8.82 [s, ^3J(HPt) = 58, CH═N]. ^{19}F NMR ($CDCl_3$), $\delta = -114.02$ [ddd, J(FPt) = 46, J(HF) = 14; 5, J(FP) = 8]. ^{31}P NMR (acetone-d^6), $\delta = 32.10$ [s, ^1J(PPt) = 2231, J(FP) = 8]. Anal. calc. for $C_{34}H_{31}FNPPt$: C, 58.45; H, 4.47; N, 2.00. Found, C, 58.7; H, 4.8; N, 1.9%.

[$PtMe$(2-$CF_3C_6H_3CHNCHMePH$)(PPh_3)] (***6e***) Yield 60 mg (88%). ^{1}H NMR (acetone-d^6), $\delta = 0.71$ [d, ^2J(HPt) = 82, ^3J(HP) = 7, Me–Pt], 1.15 [d, ^3J(HH) = 7, Me], 4.54 [m, CH*Me*], {6.92 [m, 2H], 7.24 [m], 7.44 [m], 7.71 [m], 7.99 [m], aromatics}, 8.82 [s, ^3J(HPt) = 58, CH═N]. ^{19}F NMR ($CDCl_3$), $\delta = -58.43$ [s]. ^{31}P NMR (acetone-d^6), $\delta = 31.85$ [s, ^1J(PPt) = 2231]. Anal. calc. for $C_{35}H_{31}F_3NPPt$: C, 56.15; H, 4.17; N, 1.87. Found, C, 55.7; H, 4.2; N, 1.8%.

Compounds **4d** and **4e** were prepared by reaction of 50 mg of the corresponding compounds **6d** and **6e** with an excess of methyl iodide (0.1 mL) in acetone (10 mL). The mixture was stirred at room temperature for 2 h. On addition of hexane (10 mL), light yellow crystals were formed, and they were collected by filtration, washed with hexane (3 × 5 mL) and dried *in vacuo*.

[$PtMe_2I$(2-$FC_6H_3CHNCHMePh$)(PPh_3)] (***4d***) Yield 50 mg (83%). ^{1}H NMR(acetone-d^6), isomer 1 (major) $\delta = 0.78$ [d, ^2J(HPt) = 61, ^3J(HP) = 7, Me–Pt], 1.46 [d, ^2J(HPt) = 70, ^3J(HP) = 8, Me–Pt], 1.23 [d, ^3J(HH) = 7, Me], 6.43 [q, ^3J(HH) = 7, CH*Me*], {6.35 [d, J(HF) = 8, J(HPt) = 49], 6.63 [m], 6.98 [m], aromatics}, 9.05 [s, ^3J(HPt) = 54, CH═N], isomer 2 (minor) $\delta = 1.29$ [d, ^2J(HPt) = 60, ^3J(HP) = 7, Me–Pt], 1.56 [d, ^2J(HPt) = 70, ^3J(HP) = 8, Me–Pt], 1.89 [d, ^3J(HH) = 7, Me], 6.00 [q, ^3J(HH) = 7, CH*Me*], {6.27 [d, J(HF) = 8, J(HPt) = 43], 6.77 [m], 6.90 [m], aromatics}, 8.19 [s, ^3J(HPt) = 48, CH═N]. ^{19}F NMR($CDCl_3$), isomer 1 (major) $\delta = -117.0$ [dd, J(FPt) = 40, J = 10; 6], isomer 2 (minor) $\delta = -117.1$ [dd, J(FPt) = 39, J = 9; 6]. ^{31}P NMR(acetone-d^6), isomer 1 (major) $\delta = -7.87$ [s, ^1J (PPt) = 960], isomer 2 (minor) $\delta = -8.74$ [s, ^1J (PPt) = 996]. Anal. calc. for $C_{35}H_{34}FINPPt$: C, 50.01; H, 4.08; N, 1.67. Found, C, 49.6; H, 4.0; N, 1.7%.

[$PtMe_2I$(2-$CF_3C_6H_3CHNCHMePh$)(PPh_3)] (***4e***) Yield 45 mg (76%). ^{1}H NMR(acetone-d^6), isomer 1 (major) $\delta = 0.74$ [d, ^2J(HPt) = 61, ^3J(HP) = 7, Me–Pt], 1.47 [d, ^2J(HPt) = 71, ^3J(HP) = 7, Me–Pt], 1.22 [d, ^3J(HH) = 7, Me], 6.56 [q, ^3J(HH) = 7, CH*Me*], {6.87 [d, J(HF) = 8, J(HPt) = 44], 7.06 [t, J(HH) = 7], aromatics}, 8.98 [s, ^3J(HPt) = 49, CH═N]. isomer 2 (minor) $\delta = 1.25$ [d, ^2J(HPt) = 60, ^3J(HP) = 7, Me–Pt], 1.58 [d, ^2J(HPt) = 70, ^3J(HP) = 8, Me–Pt], 1.91 [d, ^3J(HH) = 7, Me], 6.05 [q, ^3J(HH) = 7, CH*Me*], {6.70 [d, J(HH) = 8, J(HPt) = 44], 6.93 [t, J(HH) = 7], aromatics}, 8.26 [s, ^3J(HPt) = 49, CH═N]. ^{19}F NMR($CDCl_3$), isomer 1 (major) $\delta = -60.62$ [s], isomer 2 (minor) $\delta = -60.04$ [s]. ^{31}P NMR(acetone-d^6), isomer 1 (major) $\delta = -9.05$ [s, ^1J(PPt) = 956], isomer 2 (minor) $\delta = -10.11$ [s, ^1J(PPt) = 995]. Anal. calc. for $C_{36}H_{34}F_3INPPt$: C, 48.55; H, 3.85; N, 1.57. Found, C, 48.0; H, 4.1; N, 1.6%.

X-ray structure analysis. Data collection

A prismatic crystal was selected and mounted on an Enraf–Nonius CAD4 diffractometer. Unit cell parameters were determined from automatic centering of 25 reflections ($12^\circ < \theta < 21^\circ$) and refined by least-

Table 2. Crystallographic data and details of the refinements for compound **6d**

Formula	$C_{34}H_{31}FNPPt$
FW	698.66
Cryst. syst.	monoclinic
Space group	$P2_1$
a, b, c, Å	12.425(2), 9.218(3), 12.609(2)
α, β, γ, deg	90, 94.093(11), 90
V, Å^3	1440.5(5)
D_c, g cm^{-3}	1.611
Z	2
$F(000)$	688
Cryst. size, mm^3	$0.1 \times 0.1 \times 0.2$
λ(Mo, K$_\alpha$), Å	0.710 69
T, K	293(2)
no. of reflections collected	4428
$R[I > 2\sigma(I)]$, $Rw(F^2)$	0.0287, 0.0691
R[all data], $Rw(F^2)$	0.0363, 0.0833
no. of refined parameters.	345
max. shift/esd	0.0
max. and min. diff. peaks, eÅ^{-3}	0.968 and −0.945

squares method. Intensities were collected with graphite monochromatized MoKα radiation, using $\omega/2\theta$ scan-technique. 4428 reflections were measured in the range $2.22^\circ \leqslant \theta \leqslant 29.97^\circ$; 3934 were assumed as observed applying the condition $I > 2\sigma(I)$. Three reflections were measured every two hours as orientation and intensity controls; significant intensity decay was not observed. Lorentz polarization and absorption corrections were made. Further details are given in Table 2.

Structure solution and refinement

The structure was solved by Patterson synthesis, using SHELXS Computer Program [30], and refined by the full-matrix least-squares method, with the SHELX93 computer program [31]. The function minimized was $\Sigma w \| F_o|^2 - |F_c|^2|^2$, where $w = [\sigma^2(I) + (0.1194P)^2]^{-1}$, and $P = (|F_o|^2 + 2|F_c|^2)/3$. f, f' and f'' were taken from international tables of X-ray crystallography [32]. The extinction coefficient was 0.0000(5). The chirality of the structure was defined from the Flack coefficient [33], which is equal to 0.001(9) for the given results. All hydrogen atoms were computed and refined with an overall isotropic temperature factor using a riding model. Further details are given in Table 2.

Acknowledgements—We acknowledge financial support from the DGICYT (Dirección General de Investigación Científica y Técnica, Ministerio de Educación y Cultura, Spain, PB 96-0164 project) and from the Generalitat de Catalunya (1995-SGR-0044 project).

REFERENCES

1. Maestri, M., Deuschel-Cornioley, C. and von Zelewsky, A., *Coord. Chem. Rev.*, 1991, **111,** 117.
2. Maestri, M., Sandrini, D., von Zelewsky, A., Deutschel-Cornioley, C., *Inorg. Chem.*, 1991, **30,** 2476.
3. Minghetti, G., Pilo, M. I., Sanna, G., Seeber, R., Stoccoro, S. and Laschi, F., *J. Organomet. Chem.*, 1993, **452,** 257.
4. von Zelewsky, A., Suckling, A. P. and Stoeckli-Evans, H., *Inorg. Chem.*, 1993, **32,** 4585.
5. Jolliet, P., Gianini, M., von Zelewsky, A., Bernardinelli, G. and Stoeckli-Evans, H., *Inorg. Chem.*, 1996, **35,** 4883.
6. Minghetti, G., Cinellu, M. A., Chelucci, G. and Gladiali, S., *J. Organomet. Chem.*, 1986, **307,** 107.
7. Ranatunge-Bandarage, P. R. R., Duffy, N. W., Johnston, S. M., Robinson, B. H. and Simpson, J., *Organometallics*, 1994, **13,** 511.
8. Gianini, M., Forster, A., Haag, P., von Zelewsky, A. and Stoecki-Evans, H., *Inorg. Chem.*, 1996, **35,** 4889.
9. Crespo, M., Martinez, M., Sales, J., Solans, X. and Font-Bardía, M., *Organometallics*, 1992, **11,** 1288.
10. Crespo, M., Martinez, M. and Sales, J., *Organometallics*, 1993, **12,** 4297.
11. Albano, V., Braga, D., DeFelice, V., Panunzi, A. and Vitagliano, A., *Organometallics*, 1987, **6,** 517.
12. Cuvinot, D., Mangeney, P., Alexakis, A., Notmant, J. F. and Lellouche, J. P., *J. Org. Chem.*, 1989, **54,** 2420.
13. Anderson, C. M., Crespo, M., Jennings, M. C., Lough, A. J., Ferguson, G. and Puddephatt, R. J., *Organometallics*, 1991, **10,** 2672.
14. Anderson, C. M., Crespo, M., Ferguson, G., Lough, A. J. and Puddephatt, R. J., *Organometallics*, 1992, **11,** 1177.

15. López, O., Crespo, M., Font-Bardia, M. and Solans, X., *Organometallics*, 1997, **16,** 1233.
16. Block, B. P., Powell, W. H., Fernelius W. C., in *Inorganic Chemical Nomenclature*, *Principles and Practice*. American Chemical Society, Washington, DC, 1990, ch. 16.
17. Scott, J. D. and Puddephatt, R. J., *Organometallics*, 1985, **4,** 1221.
18. Scott, J. D. and Puddephatt, R. J., *Organometallics*, 1986, **5,** 1538.
19. Crespo, M. and Puddephatt, R. J., *Organometallics*, 1987, **6,** 2548.
20. Crespo, M., *Polyhedron*1996, **15**(12), 1981.
21. Crespo, M., Solans, X. and Font-Bardía, M., *J. Organomet. Chem*., 1994, **483,** 187.
22. Albert, J., Granell, J., Mínguez, J., Muller, G., Sainz, D. and Valerga, P., *Organometallics*, 1997, **16,** 3561.
23. Vicente, J., Arcas, A., Bautista, D. and Jones, P. G., *Organometallics*, 1997, **16,** 2127.
24. Stoccoro, S., Cinellu, M. A., Zucca, A., Minghetti, G. and Demartin, F., *Inorg. Chim. Acta*, 1994, **215,** 17.
25. Canty, A. J., Minchin, N. J., Patrick, J. M., White, A. H., *J. Chem. Soc., Dalton Trans*. 1983, 1253.
26. Navarro-Ranninger, C., López-Solera, I., Alvarez-Valdés, A., Rodríguez-Ramos, J. M., Massaguer, J. R., García-Ruano, J. L. and Solans, X., *Organometallics*, 1993, **12,** 4104.
27. Crespo, M., Solans, X. and Font-Bardía, M., *Organometallics*, 1995, **14,** 355.
28. Scott, J. D. and Puddephatt, R. J., *Organometallics*, 1983, **2,** 1643.
29. Bigelow, L. A., Ealough, H., in *Organic Syntheses*, Vol. 1, ed. A. H. Blatt. J. Wiley, New York, 1944.
30. Sheldrick, G. M., *Acta Cryst. A*, 1990, **46,** 467.
31. Sheldrick, G. M., SHELX 93. *A computer program for crystal structure refinement*, University of Gottingen, Germany, 1993.
32. *International Tables of X-Ray Crystallography*, Vol. IV, Kynoch, Birmingham, 1974, pp. 99–100 and 149.
33. Flack, H. D., *Acta Cryst. A*, 1983, **39,** 876.

Pergamon

PII: S0277–5387(98)00184–3

Polyhedron Vol. 17, No. 22, pp. 3935–3945, 1998
© 1998 Elsevier Science Ltd
All rights reserved. Printed in Great Britain
0277–5387/98 $19.00+0.00

Catalysis of esterification reactions by oxo-molybdenum-alkoxides: X-ray structures of $Cl_2(O)Mo(\mu\text{-}^nPr)_2(\mu\text{-}HO^nPr)Mo(O)Cl_2$ and $Cl_2(O)Mo(\mu\text{-}OEt)_2(\mu_2\text{-}\eta^1\eta^1\text{-}HOCH_2CH_2OH)Mo(O)Cl_2$

Marc Hunger, Christian Limberg* and László Zsolnai

Anorganisch-Chemisches Institut, Universität Heidelberg, Im Neuenheimer Feld 270, 69120 Heidelberg, Germany

(Received 19 January 1998; accepted 5 May 1998)

Abstract—The compound $Cl_2(O)Mo(\mu\text{-}OEt)_2(\mu\text{-}HOEt)Mo(O)Cl_2$, **1**, has been shown to catalyse esterification reactions. The reaction rates increase with decreasing acidity of the carboxylic acids employed. The steric effects observed are the same as in catalysis by Brønsted acids, but catalysis by **1** can also be applied in esterifications of protected amino acids. **1** is modified under the catalytic conditions yielding a species which coordinates and thereby activates the carboxylic acids in the rate-determining step. Subsequently an alkoxide ligand, probably originating in the coordination sphere of Mo centres, attacks the carboxylic centre producing the corresponding ester. Other oxo molybdenum(V) compounds do catalyse esterifications, too, but **1** is significantly more efficient as a precatalyst, even in comparison with closely related compounds, like $Cl_2(O)Mo(\mu\text{-}OEt)_2(\mu_2\text{-}\eta^1\eta^1\text{-}HOCH_2CH_2OH)Mo(O)Cl_2$, **4**, in which the labile EtOH bridge had been replaced by $HOCH_2CH_2OH$. The crystal structures of the compounds **4** and $Cl_2(O)Mo(\mu\text{-}O^nPr)_2(\mu\text{-}HO^nPr)Mo(O)Cl_2$, **2**, which possesses a propanol bridge, are discussed. © 1998 Elsevier Science Ltd. All rights reserved

Keywords: catalysis; molybdenum oxides; alkoxides; esterification; alcohol bridge; binuclear complexes

INTRODUCTION

Studies involving transition-metal alkoxides have become an integral part of inorganic and organometallic chemistry [1–8]. Oxo-alkoxides of metals obviously constitute an interesting series of intermediates between alkoxides and oxides of metals [9]. Concerted efforts initiated to elucidate the basic chemistry of the manifold applications of oxo-alkoxides are enhancing the efficacy of such applications [10, 11].

While exploiting the chemistry of the molybdenum-oxo-alkoxide **1** we found that this complex with the unusual ethanol bridge spanning two molybdenum centres catalyses esterification reactions [12].

Usually such reactions are promoted by Brønsted acids catalysing forward and backward reaction by activating the carbonyl group. However, there are cases in which acid catalysis cannot be applied because of the sensitivity of the particular substrates (like protected amino acids, for instance) to protonic attack. Consequently stoichiometric reagents are employed then to achieve esterification [13].

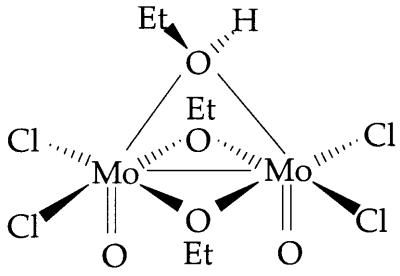

1

* Author to whom correspondence should be addressed.

Bearing these problems in mind we were interested in determining the scope of applicability of **1** in esterifications and the mechanism of action to see whether it can act as a general catalyst for such reactions. The results of this investigation are presented below.

EXPERIMENTAL

All manipulations were carried out with a vacuum line (at a background pressure $< 10^{-4}$ mbar) or else, in a glove-box, or by means of Schlenk-type techniques involving the use of a dry argon atmosphere. Solvents were dried according to standard procedures; microanalyses were performed by the Analytische Laboratorien des Organisch-Chemischen Institutes der Universität Heidelberg. IR spectra were recorded with a Bruker IFS 66 FT IR spectrometer. ^{1}H NMR spectra of solutions were recorded using a Bruker AC 200 instrument operating at 200 MHz. The X-ray diffraction measurements were made on single crystals on a Siemens P4 R3m/V four-circle diffractometer with graphite-monochromated Mo-Kα radiation. **1** was produced by the published procedure [12]. $MgSO_4$ had been dried by heating to 80°C under continuous pumping overnight.

Single crystal structures of $2{\cdot}^n PrOH$ *and* $4{\cdot}(C_2H_5)_2O{\cdot}0.75\ EtOH$

Crystals of **2** and **4** grown by cooling of dichloromethane and diethylether solutions, respectively, were suspended in an oil in the glove box, quickly selected under the microscope, loaded on top of a fibre and frozen to 200 K.

In the case of **2**, 4031 reflections were measured ($\theta_{max} = 50.2°$); all unique. 3069 reflections with $I > 2\sigma(I)$ were used in all calculations. The structure was solved by direct methods and refined by full-matrix least-squares procedures based on F^2, SHELXL-97 [14], with anisotropic thermal parameters for all non-hydrogen atoms apart from the C8 and C9 atoms of the disordered PrOH bridge and the C atoms of the disordered solvent molecule (PrOH) included in the cell. All hydrogen atoms were calculated by the use of a riding model. The final difference synthesis maximum and minimum were 1.094 and -1.014 eÅ^{-3}, respectively.

In the case of **4**, 5552 reflections were measured ($\theta_{max} = 50.1°$); 5207 unique. $R_{int} = 0.0679$, 2907 reflections with $I > 2\sigma(I)$ were used in all calculations. The structure was solved by direct methods and refined by full-matrix least-squares procedures based on F^2, SHELXL-97 [14] with anisotropic thermal parameters for all non-hydrogen atoms apart from those of the solvent molecules. All hydrogen atoms were calculated by the use of a riding model. The final difference synthesis maximum and minimum were 1.357 and -0.829 eÅ^{-3}, respectively. The crystallographic data for $\mathbf{2}{\cdot}^n$PrOH and $4{\cdot}(C_2H_5)_2O{\cdot}0.75$EtOH are given in Table 1.

Catalytic esterifications In general the carboxylic acid (typically 0.02 mol) was dissolved under an argon atmosphere in an excess of freshly distilled alcohol in a Schlenk-tube. Two spatulas of dry $MgSO_4$ were

Table 1. Crystallographic data of **2** and **4**

	2	**4**
Formula	$C_9H_{22}Mo_2Cl_4O_5{\cdot}CH_3CH_2CH_2OH$	$C_6H_{16}Mo_2Cl_4O_6{\cdot}0.75$ $CH_3CH_2OH{\cdot}O(CH_2CH_3)_2$
Crystal size (mm)	$0.3 \times 0.3 \times 0.3$	$0.3 \times 0.3 \times 0.25$
Crystal system	orthorhombic	monoclinic
Space group	*P*bca	$P2_1/n$
a (Å)	13.565 (3)	9.205 (2)
b (Å)	17.482 (3)	16.111 (7)
c (Å)	19.086 (3)	19.911 (8)
β (°)	90.000 (0)	92.48 (2)
V (Å^3)	4526 (1)	2950 (2)
D_c (g cm^{-3})	1.773	1.406
Z	8	4
F (000)	2416	1246
μ (cm^{-1})	16.02	12.36
R	0.0422	0.0848
Rw	0.0973	0.2354
S	1.282	1.211
Weighing scheme	0.046700	0.142300

added and the suspension heated to 80°C for 2 h under stirring (the Schlenk tube was sealed by means of a pressure-relief valve). Subsequently, after cooling of the mixture to room temperature 1 mol.% of **1**, weighted out and loaded into a separate vessel in a glove box, were added in a stream of argon and the mixture heated for another 4 h. After filtering the volatiles were removed under vacuum and the residue investigated ^{1}H NMR spectroscopically. The ratios of the integrals of selected signals of acids and esters gave the yields of the corresponding esterification.

In the cross experiment 1.50 g (0.011 mol) of phenyl acetic acid, 2.35 g (0.011 mol) of diphenyl acetic acid, 1.02 g (0.022 mol) of ethanol and 1.33 g (0.022 mol) of isopropanol were dissolved in toluene and heated to 80°C for 4 h in the presence of $MgSO_4$ and **1** ($2{\cdot}10^{-4}$ mol). After the reaction a 1 N NaOH solution was added and the esters extracted by diethylether. After filtering over basic alox the ester solution was investigated by GC/MS measurements.

The experiments under variation of the ethanol concentration were performed in CH_2Cl_2 solutions in flame-sealed glass tubes. When the ratio of employed phenyl acetic acid and ethanol was increased to 1 the yield with respect to the ester was still 85% (compare the yield of 90% obtained in ethanol as the solvent).

Synthesis of ***2*** 2 g ($4{\cdot}10^{-3}$ mol) of **1** were dissolved in freshly distilled *n*-propanol and heated to 80°C for 4 h. After removal of the volatiles an orange solid was obtained which was crystallised from CH_2Cl_2 and proved to consist of **2**·^{n}PrOH by comparison with the published data [15]. On prolonged pumping the crystals loose their solvent and become amorphous.

Reaction of ***1*** *with acetic acid* 0.59 g ($1.19{\cdot}10^{-3}$ mol) of **1** was dissolved in dry acetic acid [1.44 g (0.024 mol)] and heated to 80°C for 4 h in the presence of $MgSO_4$. Afterwards all volatiles were distilled off the solids and investigated NMR spectroscopically.

Synthesis of ***4*** 1.00 g ($1.9{\cdot}10^{-3}$ mol) of **1** were loaded into a Schlenk tube in a glove box, dissolved in toluene and reacted with freshly distilled ethylene glycol [0.11 ml (0.0019 mol)] introduced into the tube via a syringe. A dark brown viscous oil and an orange solid precipitated which were separated from each other by decanting the suspension from the oil. The solid was filtered off the solution and dried under vacuum. After drying of the solid it is only marginally soluble in pure diethylether, while the solubility of the freshly filtered solid is high enough (because of the EtOH included) to recrystallise it from ether. Yield: 47%; $C_6H_{16}Cl_4Mo_2O_6$ M = 517.89 g/mol; found: C, 13.76; H, 3.06; Cl, 26.21; Mo, 38.17%; calc.: C, 13.91; H, 3.09; Cl, 27.38; Mo, 37.00%; IR ν/cm^{-1}: 3410m, 2974w, 2955w, 1438s, 1362w, 1352s, 1262w, 1000vs, 890vs, 870sh, 540s, 530s (KBr).

IR solution studies A solution of the acid (0.5 mmol) in 15 ml CH_2Cl_2 was prepared in a high pressure tube equipped with a teflon valve, which already contained an excess of $MgSO_4$. After recording of an IR spectrum of the solution in a cell furnished by NaCl windows equimolar amounts of **1** were added. Again a sample was investigated IR spectroscopically and subsequently the whole reaction vessel was heated to 80°C for 1 h. After cooling a further IR spectrum was recorded.

RESULTS AND DISCUSSION

First it was important to employ carboxylic acids with varying acidities and sterical demands in order to compare their yields in the esterification reactions catalysed by **1**. Since each reaction was stopped after 4 h, although the yields could have been improved on further reaction time, accordingly not really yields rather than reaction rates are considered. To guarantee comparability of the results a standard procedure was established being applicable to most of the acids investigated.

Electronic and steric effects

To study the influence of the electronic properties of the acids on the esterification yield, derivatives of acetic acid were reacted with ethanol at 80°C. Acetic acid itself ($K_s = 1.7{\cdot}10^{-5}$) [16] is quantitatively converted into ethyl acetate during the 4 h reaction time while the yield decreases to 90% on substitution of one H atom by phenyl (phenyl acetic acid has a K_s of $4.9{\cdot}10^{-5}$) [16] and to 80% on substitution by 4-nitrophenyl (4-nitro phenyl acetic acid has a K_s of $14.1{\cdot}10^{-5}$) [16]. This makes quite clear that electronic effects do not have a great influence on the reaction rates. However, the effect observed is inverse to the one found for protonic catalysis: the weaker the acid, the faster it can be converted into the corresponding ester. Provided that the catalysis proceeds via activation of the carbonyl groups by coordination to Mo centres this finding must be related to the coordination properties of carboxylic acids or the corresponding carboxylates with respect to hard oxo-molybdenum(V) centres in dependence on their acidity, as discussed later.

In the next step alcohols and carboxylic acids with varying sterical demands were employed. Table 2 shows the yields obtained in esterification reactions of carboxylic acids with varying degrees of substitution at the α-carbon using ethanol as the reagent. From those it can be deduced that, as expected, the reaction rates decrease drastically when the bulk near to the carboxylic group is increased. If in the esterification of phenyl acetic acid ethanol is replaced by *i*-propanol the yield decreases from 90 to 30% while no reaction occurs on employment of *t*-butanol confirming that the sterical demand of the alcohols is relevant to the reaction rates, too.

Surprisingly, no derivative of benzoic acid could be converted into the corresponding ester (no detectable quantities were produced) via catalysis with **1**. Steric reasons for this finding are not obvious since even

adamantanoic acid with its highly branched α-C atom could be esterificated in 39% yield. However, neither electronic effects can be made responsible since all derivatives tried also failed to react, independently of the K_s values (4-nitro-, 3,4-dihydroxy-, 4-methyl-, 4-methoxy-, 4-aminobenzoic acid as well as benzoic acid itself were employed spanning a K_s range of $36 \cdot 10^{-5}$–$1.4 \cdot 10^{-5}$ [16, 18]; compare the K_s values of the acids which had successfully been reacted before). This raised the question of whether such compounds deactivate **1** as a catalyst and suggested a further experiment: an attempt was made to catalyse the esterification of phenylacetic acid by ethanol in the presence of **1** *and* benzoic acid. Indeed the yield decreased from 90 to 54% which means that benzoic acid coordinates strongly (though reversibly) to the catalyst but it cannot be esterificated for unknown reasons thereby deactivating the catalyst. Any explanation probably involves a very special property of benzoic acid derivatives like for instance the hindered rotation of the aryl residue in order not to loose favourable resonance providing such acids with a very special "steric bulk" in comparison to acids like adamantanoic acid. It is not obvious, however, how this should come into play during esterification without knowing the detailed mechanism and the catalytically active species.

Activation of the carboxylic function

In order to explain some of the peculiarities described above it was important to obtain more detailed information concerning the individual steps of this catalytic esterification. Assumed that the acid or its conjugated base coordinates to the catalyst first and subsequently reacts with the alcohol employed (producing the ester which dissociates subsequently), the question of which step should be assigned as being the rate determining one arises. To decide between the two possibilities an experiment was performed in which two different acids and two different alcohols were present in the reaction mixture. The reagents chosen differed in their sterical demands, the acids additionally in their K_s values.

As a result four different esters were obtained whose relative yields, as shown in eq. (1), were determined by means of GC/MS measurements. They strongly suggest that the coordination of the acid is indeed the rate determining step: $PhCH_2C(O)O^iPr$ and Ph_2CH-C(O)OEt are formed in 21 and 9% yield, respectively, although the ethyl ester should have been formed predominantly in comparison to the *i*-propyl ester according to the results shown in Table 2 and under the assumption that both esters have the same chance to get esterificated by one alcohol or another [19]. Additional support for this conclusion comes from experiments under variation of the ethanol concentration in the esterification of $PhCH_2COOH$: lowering of the alcohol/acid ratio from an alcohol excess to a 1:1 ratio had only a small effect on the esterification rate, consistent with a fast reaction of the alcohol.

Alkoxide transfer and exchange; crystal structure of $Cl_2(O)Mo(\mu\text{-}O^nPr)_2(\mu\text{-}HO^nPr)Mo(O)Cl_2$, ***2***

The question remains, whether the alcohol reacts directly with the activated carboxylic acid or with the catalyst which then acts as an alkoxide transfer mediator. The Mo–OH functions resulting from such a reaction would then be replaced by alcoholate ligands via reaction with the corresponding alcohols and the water produced trapped by the $MgSO_4$ added. A first hint to an intramolecular alkoxide transfer gives the fact that on heating of preparative amounts of **1** with an excess of acetic acid 80% of its alkoxide/alcohol ligands are found in form of ester functions after the reaction. In addition the ethanol and ethoxide ligands in **1** proved to be easily exchangeable by other alcoholate ligands. Heating of **1** in *n*-propanol to 80°C for 4 h exclusively yields the *n*-propoxy derivative of **1**, **2** [15] (compare eq. (2)).

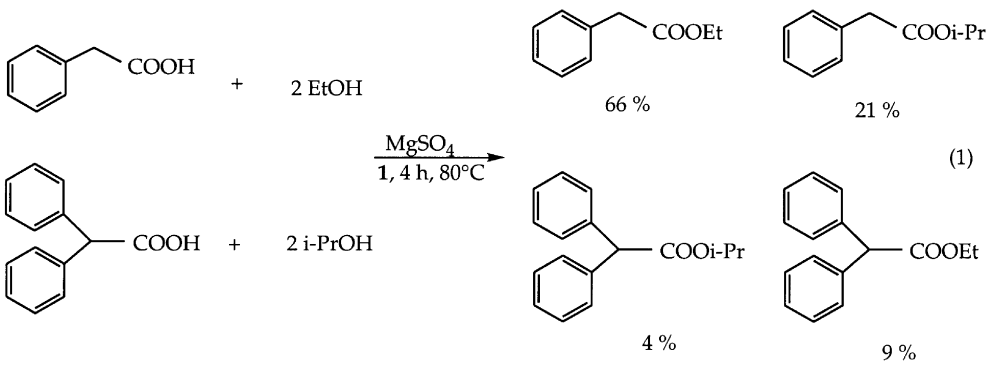

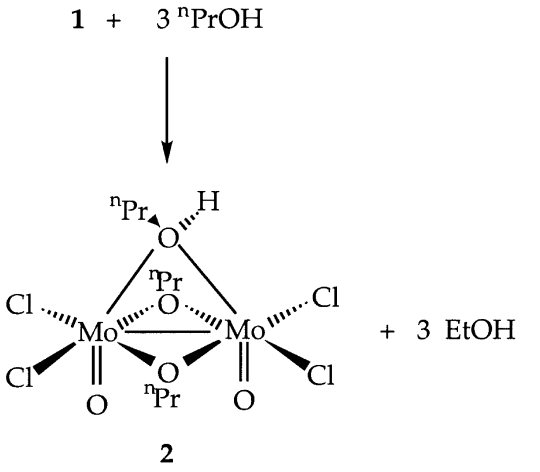

(2)

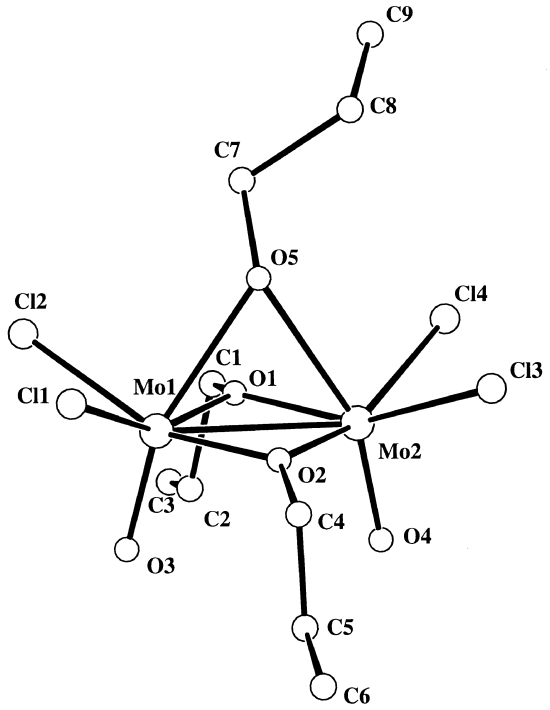

Fig. 1. The molecular structure of **2**; all protons have been omitted in the interest of clarity.

Single crystals of **2** were investigated by X-ray diffraction yielding the structure shown in Fig. 1. The orthorhombic cell contains 8 molecules of **2** each of which forms a hydrogen bond via a hydrogen of the bridging ^{n}PrOH to a solvated PrOH molecule (not shown in Fig. 1). Selected bond distances and angles are listed in Table 3. **2** consists of two O=$MoCl_2$ units bridged by two propoxy groups and one propanol molecule. The Mo(μ-O^{n}Pr)$_2$Mo moiety contains a planar Mo_2O_2 heterocycle. Each Mo atom is therefore placed in a distorted octahedral environment. While the metal atoms are formally in the +5 oxidation state (d^1) the diamagnetism of the complex implies that the two d electrons form a Mo–Mo single bond (d(Mo–Mo) = 2.6760(8) Å). As **1**, **2** contains an unusual bridging alcohol unit. The Mo–O(μ-HO^{n}Pr) bond lengths [2.413(4), 2.435(4) Å] are 0.41 Å larger than the average Mo–O(μ-O^{n}Pr) length [2.006(4) Å] while being only lightly shorter than those found in **1** for Mo–O(μ-EtOH) [2.48(2) Å]. All other bond lengths and angles compare well with those of **1**.

*Applications for **1** as a precatalyst in esterifications*

After the investigations described above had provided an idea of the functioning of the catalyst, attempts were made to employ **1** in esterifications which are more difficult to perform experimentally, i.e. those of substances which are sensitive to Brønsted acids. Protected amino acids of the type S–NR–CH_2COOH (S = protecting group) belong to this class of substances, since the S–N bonds are cleaved in an acidic milieu. Consequently, in order to achieve their esterification, which can be very important to (i) mask acidic protons, (ii) protect the carboxylic group against nucleophilic attack, (iii) vary their solubility and volatility or (iv) protect the carboxylic group with regard to reduction, stoichiometric condensing or alkoxylating reagents have to be used [13]. Dicyclohexylcarbodiimide and BOP–Cl/NEt_3 belong to the first category while $Me_2NCH(OR')_2$ is an effective alkoxide transfer reagent. However, none of these procedures is as simple as the catalysis by protons producing water as the only side product. Accordingly it was attempted to *catalytically* convert such acids into the corresponding esters using **1**. The amino acids

Table 2. Catalytical esterifications of carboxylic acids (RCOOH) with varying degrees of substitution at the α-carbon atoms by alcohols (R′OH). The yields shown have been obtained after 4 h at 80°C in the presence of **1**

R = CH_2Ph;	R′ = Et	$K_s = 4.9 \times 10^{-5}$ [16]	90% yield
R = $CHPh_2$;	R′ = Et	$K_s = 4.76 \times 10^{-5}$ [16]	45% yield
R = adamantyl;	R′ = Et	$K_s = 1.25 \times 10^{-5}$ [17]	39% yield
R = CH_2Ph;	R′ = $CH(CH_3)_2$	$K_s = 4.9 \times 10^{-5}$ [16]	30% yield
R = CH_2Ph;	R′ = $C(CH_3)_3$	$K_s = 4.9 \times 10^{-5}$ [16]	0% yield

Table 3. Selected bond lengths (Å) and bond angles (°) of **2**

Mo(1)–Mo(2)	2.6760(8)	O(2)–Mo(1)–O(1)	96.41(14)
Mo(1)–O(3)	1.645(4)	O(2)–Mo(1)–O(5)	68.13(14)
Mo(1)–O(2)	2.002(4)	O(1)–Mo(1)–O(5)	68.84(13)
Mo(1)–O(1)	2.007(4)	O(2)–Mo(2)–O(1)	96.24(14)
Mo(1)–O(5)	2.413(4)	O(2)–Mo(2)–O(5)	67.62(14)
Mo(1)–Cl(1)	2.339(2)	O(1)–Mo(2)–O(5)	68.33(13)
Mo(1)–Cl(2)	2.349(2)	Mo(1)–O(1)–Mo(2)	83.54(14)
Mo(2)–O(1)	2.010(4)	Mo(1)–O(2)–Mo(2)	83.80(13)
Mo(2)–O(2)	2.005(3)	Mo(1)–O(5)–Mo(2)	67.01(10)
Mo(2)–O(4)	1.641(4)		
Mo(2)–O(5)	2.435(4)		
Mo(2)–Cl(4)	2.335(2)		
Mo(2)–Cl(3)	2.340(2)		

shown in Table 4 were reacted with EtOH in the presence of catalytic amounts of **1** under the usual conditions. As can be seen, these experiments were successful although the yields obtained after 4 h reaction time varied drastically from case to case. Since the K_s values of these carboxylic acids as their steric demands are expected to be quite similar, the reasons for the differing yields are not quite clear. One possibility would be a concurrence of the N-atoms in the complexation reaction of the carboxylic functions to the catalyst in dependence on the electronic conditions of the groups S.

The catalytically active species

In order to obtain more detailed information about the reasons for the substrate selectivity observed and the functioning of the catalyst the next point which had to be addressed was the characterisation of the catalytically active species in solution. Considering the chemical properties of **1** [20, 21] it cannot be expected that this compound is more than a precatalyst being modified in the presence of carboxylic acids under the reaction conditions. In fact it is not possible to isolate **1** back after the catalysis. If not catalytic rather than preparative amounts of **1** are employed in esterifications, after removal of all volatiles brown oils are obtained showing a Mo/Cl ratio of 1/2 according to elemental analysis. This finding rules out the possibility that the observed catalytic activity is merely a result of protonation of **1** by the acids, thereby delivering HCl which is responsible for catalysing the esterification. In addition the latter would also be contradictory to the fact that protected amino acids could and benzoic acid could not be converted into the corresponding ester in the presence of **1**. The observation that no colour change from orange to green can be observed during the esterification suggests (not proves though) that the metal–metal bond remains intact during the reaction [22]. Therefore an intermediate with the metal fragment shown below is imaginable, the carboxylic acid being activated in the rate-determining step by coordination to the two metal centres located in close proximity.

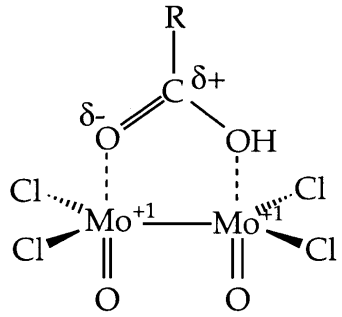

There is a precedent case [23] where such a coordination mode has been proved by X-ray crystallography and if this was relevant to the present case, too, the success of catalysis would be linked to

Table 4. Esterification catalysis of protected amino acids by EtOH in the presence of **1**. The yields shown have been obtained after 4 h at 80°C

S–NR–CH_2–COOH	S–N–R = phthaloyl	25% yield
	S = tosyl; R = H	100% yield
	S = acetyl; R = H	27% yield
	S = *t*-butyl oxycarbonyl; R = H	100% yield

the availability of a binuclear Lewis acidic species with free coordination sites (or labile ligands). To test this hypothesis the reaction of phenylacetic acid with ethanol was performed in the presence of catalytical amounts of the compound $PPN^+NEt_3H^+$ $[Cl_2(O)Mo(\mu_2\text{-}O)_2Mo(O)Cl_2]^{2-}$ [20] whose anion possesses two Mo(V) centres with free coordination sites. However, the esterification yield was only 29%, probably because of the lower lewis acidity of the metal centres as compared to those of the catalyst generated from **1** (note that $[Cl_2(O)Mo(\mu_2\text{-}O)_2Mo(O)Cl_2]^{2-}$ is stable inspite of vacant coordination sites, probably because of electron donation by the O bridges, while it is not possible to remove EtOH from **1** without simultaneously inducing aggregation processes [20, 21]). To further study the modification of **1** under the catalytic conditions several experiments were carried out in which **1** was reacted with equimolar amounts of carboxylic acids under standard conditions (EtOH (exc.), 80°C). By isolation and characterisation of the resulting molybdenum complexes it was hoped to get hints to the catalytically active species in solution. Removal of the volatiles after such experiments, however, yielded in most cases insoluble oils which could naturally not be investigated as thoroughly as necessary to derive definite conclusions. In the case of tosyl glycine a red brown oil was obtained which was soluble in diethyl ether. After cooling of such a solution to −25°C the resulting red solid could be identified as **3**, which had previously been isolated after the reaction of **1** with PMe_3 [20, 21].

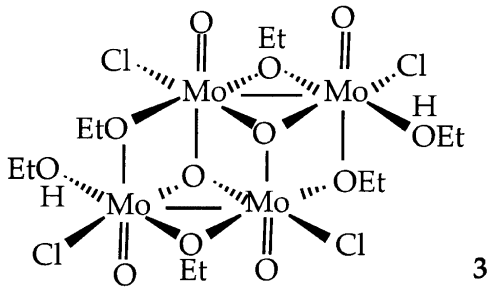

3

Since **3** had been produced under the conditions of the catalysis (it is not formed if **1** is just heated to 80°C for 4 h) it was tempting to consider this compound, at least in the case of tosyl glycine, as the catalyst in question being furnished with two labile EtOH ligands suitable to provide free coordination sites. To probe this suggestion **3** itself was tested as a catalyst in esterification reactions under the conditions as described above. The standard reagent, phenylacetic acid, could be converted into the corresponding ethyl ester in 55% yield. From this finding it can be concluded that indeed **3** has the right properties to act as a catalyst in esterification reactions (*vide supra*) but that it is probably not the active species in catalyses with **1** since there the yield was much higher. From the fact that **3** is not capable of coordinating a carboxylic acid as shown above for a binuclear species it follows that a binuclear coordination is not a necessary condition for this type of catalysis and that appropriate electronic conditions on Mo oxo centres in combination with free coordination sites are probably sufficient to provide the corresponding compounds with some catalytic activity.

However, **3** cannot be the sole compound resulting from **1** under catalytic conditions since, as mentioned above, in the raw non-volatile material isolated after such reactions the Mo/Cl ratio still amounts to 1/2. Therefore, if **3** (with a Mo/Cl ratio of 1) is formed, a product with a higher content in Cl must be generated, too. This led us to investigate the catalytic properties of $O{=}MoCl_3(PMe_3)(O{=}PMe_3)$ [21] in the esterification of phenylacetic acid with ethanol, which were yet again less pronounced (50% yield) as compared to those of the species resulting from **1**. In summary, the latter was superior to all model compounds tried with respect to catalytic activity and therefore seems to have special advantageous qualities. Regardless, the above investigation has shown so far that activation of the carboxylic function can be achieved making use of just one Mo=O centre with the right properties (electronically and coordinatively) and that the alkoxy ligands found in the esters after the reactions are probably mediated by such centres, too. Accordingly the rate determining step, the coordination of carboxylic acids to Mo=O centres, might proceed under formation of a favourable 6-membered ring as shown below decomposing again on intra-

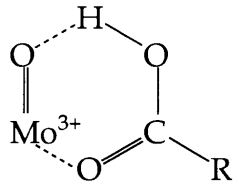

molecular attack of an alkoxy ligand. The ester thereby produced is not able to coordinate in this fashion and therefore leaves the Mo centre making room for a new acid molecule. In an attempt to obtain direct information about the stage *preceeding* this rate determining step, i.e. the interaction of the carboxylic functions with **1** producing the catalytically active species, IR solution studies were performed. Equimolar amounts of **1** and acetic acid/benzoic acid/*p*-nitro-phenylacetic acid were reacted at room temperature in CH_2Cl_2 solution.

Acetic acid Addition of **1** to a CH_2Cl_2 solution of acetic acid causes the ν(C=O) bands of the solution IR spectrum belonging to the free acid to decrease by *ca.* 90%. Apart from new bands belonging to the alkoxide groups of the oxomolybdenum alkoxide species resulting from **1** new features can be noticed

at 1659 and 1630 cm^{-1}. These could have their origins in a η^1-O–C(Me)=O ligand (the corresponding ν_s modes being masked by the bands of alkoxide ligands; a broad band at 1404 cm^{-1} can be observed in form of a shoulder) being formed by addition of the carboxylic OH group to a Mo–μ-OEt bond, the EtOH thereby delivered remaining coordinated. Heating of this mixture to 80°C for 1 h caused no spectral change. However, heating for 0.5 h after addition of two equivalents of EtOH resulted in the formation of free acid (proving that the corresponding complex coexists with free acetic acid in an equilibrium) as well as ethyl acetate. Further heating for 2 h lead to a complete conversion to ethyl acetate. If a 1:1 mixture of **1** and acetic acid is heated in pure EtOH after the removal of all volatiles and redissolution of the residue in dichloromethane an IR spectrum is obtained which is basically identical with the one displayed by **1** at least in the region 900–1900 cm^{-1}. No bands belonging to carboxylate ligands or acids can be detected anymore.

Benzoic acid As in the case of acetic acid on addition of equimolar amounts of **1** to a solution of benzoic acid the ν(C=O) bands of the free acid decrease by *ca.* 90% while a band of medium intensity at 1607 cm^{-1} and a strong complex band centred at 1382 cm^{-1} (with a shoulder at 1410 cm^{-1}) appear. These could be due to ν_s and ν_{as} of a carboxylate ligand and their large separation strongly supports a η^1-O–C(Ph)=O coordination mode [24, 25] of the latter being formed by addition of the OH group of benzoic acid to a Mo–μ-OEt–Mo unit yielding Ph(O)C–O–Mo–Mo–O(H)Et entities (no formation of free EtOH is observed). As above no spectral change is observed upon heating. On isolation of the species a ^{13}C NMR spectrum shows signals for at least four different CH_3CH_2O-groups but for only one benzoate ligand. This is in contrast to the IR spectra which seemed to support the existence of more than one benzoate group. An explanation should be sought in very fast exchange, rearrangement or isomerisation processes which can only be detected on the time scale of the IR spectroscopy. Such processes are not unusual for alkoxide compounds [1–8]. If two equivalents of EtOH are added to a 1:1 mixture of the acid and **1** the bands attributed to the η^1-O–C(Ph)=O ligands decrease somewhat in favour of bands belonging to free acid as well as two new bands which probably have their origin in an η^2-O–C(Ph)=O ligand as indicated by their frequency separation [24, 25] (1525 and 1415 cm^{-1}). In contrast to the acetic acid experiment (*vide supra*) and in agreement with the results of the catalysis experiments the IR spectrum of this mixture remained unchanged after heating to 80°C for 1 h.

p-*Nitrophenylacetic acid* In order to determine the effect of acidity on the observations as outlined above a third acid, *p*-nitrophenylacetic acid, was employed which has a higher K_s value ($14.1 \cdot 10^{-5}$) than both benzoic acid ($6.3 \cdot 10^{-5}$) and acetic acid ($1.75 \cdot 10^{-5}$) but which, in contrast to benzoic acid, can be esterificated in 80% yield under standard conditions. Indeed, also in this case a sharp decrease of the ν(C=O) bands could be observed while, as for benzoic acid, new bands at 1624 (m), 1444 (w), 1410 (sh) and 1383 (s) appeared. The carboxylate regions of the IR spectra are very similar in the cases of *p*-nitrophenylacetic and benzoic acid.

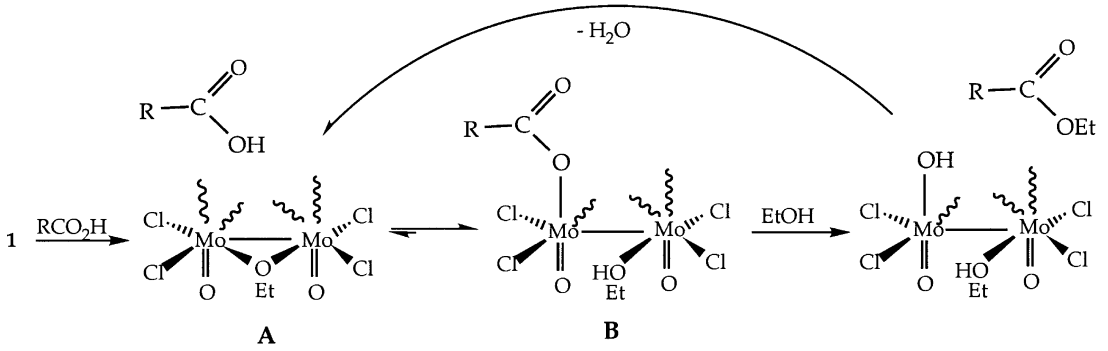

These results have to be interpreted as follows (compare eq. (3)): the IR spectra discussed above belong to the catalytically active species, which can be isolated and probably consists of a complex oxo molybdenum alkoxide **B** (with at least four magnetically different alkoxide groups) containing η^1-O–C(R)=O ligands according to the IR spectra. Addition of a further equivalent of the acid in the cases of benzoic and *p*-nitrophenylacetic acid did not lead to a significant alteration of the IR spectra (the additional equivalent is not consumed) so that the species under discussion is formed via a 1:1 reaction between **1** and the carboxylic acids. All acids react the same way and to the same extent in the first step independently of their acidities, just in the case of acetic acid a species with a further type of carboxylate ligand seems to be present in the equilibrium as indicated by an

additional weak band at 1659 cm^{-1}. Since the reactions between **1** and carboxylic acids are almost quantitative already at r.t. the rate determining step still has to follow. The latter involves either a change in coordination mode of the carboxylate ligands or the intermediate coordination of further acid molecules (possibly of the type as shown above) at higher temperatures being followed by a rapid conversion into the corresponding ester by alkoxide or alcohol ligands in close proximity. The fact that species **B** behaves inert at 80°C in the case of acetic acid but decomposes under formation of the ethylester when EtOH or excess of acid (compare with Section 3.3) had been added previous to heating suggests that its reactivity depends on the presence of donor ligands which can occupy free coordination sites generated by ester formation. The alkoxide transfer step does not seem to be possible in the case of benzoic acid derivatives for one reason or another. Any attempt to give reasons for this finding (compare with Section 3.1), however, would be purely speculative without knowing the constitution of the corresponding Mo-species **B** in solution and is therefore avoided here. **B** had an oily consistence after isolation in all cases and was insoluble when amino acids had been employed as the reagents. In cases where **B** showed sufficient solubility to enable a spectroscopic investigation in solution the available spectroscopic data naturally did not allow to draw conclusions about its constitution (due to its complex nature and constitution).

*Modification of **1**; crystal structure of* $Cl_2(O)Mo(\mu\text{-}OEt)_2(\mu_2\text{-}\eta^1\eta^1\text{-}HOCH_2CH_2OH)Mo(O)Cl_2$, ***4***

Although representing an efficient precatalyst, employment of **1** as such is hampered by its high sensitivity to atmospheric water. Therefore attempts were made to modify this compound with respect to an easier handling. The most labile part of the molecule is the weak ethanol bridge spanning the two Mo centres. Removal of this bridge is the primary step in most of the reactions of **1** [20, 21]. This suggested experiments to stabilise the molecule via replacement of the ethanol by a bifunctional alcohol thereby making use of the chelating effect. The reaction of **1** with ethylene glycol yielded an orange solid which was no longer soluble in solvents like toluene and dichloromethane, making its NMR spectroscopic characterisation difficult. However, IR-spectroscopy and elemental analyses suggested that the initial aim of generating $Cl_2(O)Mo(\mu\text{-}OEt)_2(\mu_2\text{-}\eta^1\eta^1\text{-}HOCH_2CH_2OH)Mo(O)Cl_2$, **4**, had been successful and an X-ray structure analysis of a single crystal obtained from an diethylether solution confirmed the presence of a $\mu_2\text{-}\eta^1\eta^1\text{-}HOCH_2CH_2OH$ bridge in **4**, as shown in Fig. 2 (selected bond lengths and angles are listed in Table 5). The asymmetric unit of the monoclinic cell contains one molecule of **4**, a disordered diethylether molecule and a partially occupied (0.75) disordered EtOH molecule. While the $Cl_2(O)Mo(\mu\text{-}OEt)_2Mo(O)Cl_2$ frame in **4** is in principal the same as in **1** the octahedral environ-

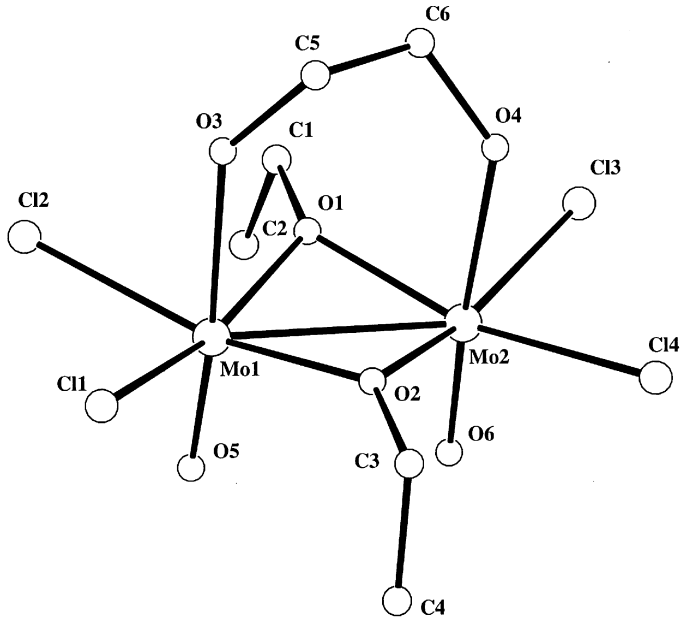

Fig. 2. The molecular structure of **4**; all protons have been omitted in the interest of clarity.

Table 5. Selected bond lengths (Å) and bond angles (°) of **4**

Mo(1)–O(5)	1.644(8)	O(5)–Mo(1)–O(2)	100.0(4)
Mo(1)–O(2)	1.991(9)	O(5)–Mo(1)–O(1)	99.8(4)
Mo(1)–O(1)	2.010(7)	O(5)–Mo(1)–Cl(2)	95.7(4)
Mo(1)–O(3)	2.291(8)	O(5)–Mo(1)–Cl(1)	97.2(3)
Mo(1)–Cl(2)	2.350(4)	O(9)–Mo(1)–Cl(1)	163.0(3)
Mo(1)–Cl(1)	2.371(3)	O(5)–Mo(1)–Mo(2)	91.7(3)
Mo(1)–Mo(2)	2.751(2)	O(6)–Mo(2)–Mo(1)	90.9(3)
Mo(2)–O(6)	1.648(8)		
Mo(2)–O(1)	2.007(8)		
Mo(2)–O(2)	2.019(8)		
Mo(2)–O(4)	2.284(7)		
Mo(2)–Cl(4)	2.365(4)		
Mo(2)–Cl(3)	2.371(3)		
O(3)–C(5)	1.38(2)		
O(4)–C(6)	1.413(14)		

ment of the Mo atoms in **4** is far less distorted than in **1** and **2**. The bond lengths in that core do not differ significantly from those in **1** and **2**. However, the O5–Mo1–Cl1/2 angles [97.2(3), 95.7(4)°] for instance are about 7° smaller than those in **1** approaching 90°. The O6–Mo2–Mo1 and O5–Mo1–Mo2 angles [90.9(3), 91.7(3)°] are even closer to the right angle but the O5–Mo1–O1/2 angles are slightly larger than those in **1** so that the Mo_2O_2 heterocycle is no longer planar (dihedral angles: 156°). At the vacant sites of the core the ethylene glycol bridge coordinates forming O6–Mo2–O4 and O5–Mo1–O3 angles of almost 180° [175.2(4) and 176.7(4)°]. Since each O atom of the bridge coordinates to only one Mo atom naturally the Mo–O bond lengths [2.2844(7), 2.291(7) Å] are much shorter (0.2 Å) than those in **1**.

As hoped in contrast to **1**, **4** can be handled in air for short periods so that in the next step its catalytic properties were investigated. However, the higher resistivity of **4** to air in comparison to **1** goes along with a lower activity as a catalyst (or precatalyst) so that an esterification yield of only 50% was found for the reaction of phenylacetic acid with ethanol. Accordingly the weakly bound EtOH bridge in **1** seems to play a decisive role in the formation of the catalytically active species from **1**.

CONCLUSIONS

In conclusion it appears that certain O═Mo(V) compounds are suitable to catalyse esterification reactions. Our investigation suggests that this process probably proceeds via coordination and activation of the carboxylic acids in the rate determining step followed by intramolecular alkoxide transfer. Compound **1** has unique properties as a precatalyst in this respect, producing species of very high activity in solution under the reaction conditions, which are able to even convert protected amino acids into the corresponding esters. The decreasing reaction rates on employment of the related compound **4** highlights the fine tuning of the properties of these catalytically active species by the nature of the precatalyst. While the usual influence of steric effects on the reaction rates is observed, in contrast to protonic catalysis the rates increase with decreasing acidity of the carboxylic acids. Future research will concern the investigation of the passivating effects of benzoic acid derivatives and the behaviour of other metal oxides.

Acknowledgements—We are grateful to Professor Dr G. Huttner for his permanent, generous support and the Deutsche Forschungsgemeinschaft as well as the Fonds der Chemischen Industrie for providing scholarships (to C. L.).

REFERENCES

1. Hubert-Pfalzgraf, L. G., *N. J. Chem.*, 1987, **11,** 663.
2. Livage, J., *J. Solid State Chem.*, 1986, **64,** 322.
3. Dislich, H., *J. Non-Cryst. Solids*, 1985, **73,** 599.
4. Bradley, D. C., *Chem. Rev.*, 1989, **89,** 1319.
5. Herrmann, W. A., Huber, N. W. and Runte, O., *Angew. Chem.*, 1995, **107,** 2371–2390, *Angew. Chem., Int. Ed. Engl.*, 1995, **34,** 2187–2206.
6. Chisholm, M. H., Rothwell, I. P., *Comprehensive Coordination Chemistry*, Vol. 2, ed. G. Wilkinson. Pergamon, New York, pp. 335–364.
7. Mehrotra, R. C., *Adv. Inorg. Chem. Radiochem.*, 1983, **26,** 26.
8. Mayer, J. M., *Polyhedron*, 1995, **14,** 3273–3292.
9. Mehrotra, R. C. and Singh, A., *Chem. Soc. Rev.*, 1996, 1–13.
10. Hubert-Pfalzgraf, L. G., *Polyhedron*, 1994, **13,** 1181.
11. Sonika, Narula, A. K., Vermani, O. P. and Sharma, H. K., *J. Organometal. Chem.*, 1994, **470,** 67 and references therein.
12. Limberg, C., Parsons, S., Downs, A. J. and Watkin, D. J., *J. Chem. Soc. Dalton Trans.*, 1994, 1169.
13. Greene, T. W. and Wuts, P. G. M., *Protective*

Groups in Organic Synthesis, 2nd edn. Wiley-Interscience, 1991.
14. Sheldrick, G. M., *SHELXL*-97, *A Program for Crystal Structure Refinement*. University of Göttingen, 1997.
15. Limberg, C., Boese, R. and Schiemenz, B., *J. Chem. Soc. Dalton Trans.*, 1997, 1633.
16. Morrison, R. T. and Boyd, R. N., *Lehrbuch der Organischen Chemie*, 2nd edn. VCH-Verlag, Weinheim, 1978, p. 889.
17. Heller, A., *J. Am. Chem. Soc.*, 1989, **111,** 6767.
18. Simon, A., *Helv. Chim. Acta*, 1957, **40,** 1918–1921.
19. Hoffman, R. W., *Aufklärung von Reaktionsmechanismen*. Thieme Verlag, Stuttgart, 1976.
20. Limberg, C., Downs, A. J., Parsons, S. and Blake, A. J., *Inorg. Chem.*, 1996, **35,** 4439.
21. Limberg, C., Büchner, M., Heinze, K. and Walter, O., *Inorg. Chem.*, 1997, **36,** 872.
22. Stiefel, E. I., *Prog. Inorg. Chem.*, 1965, **4,** 867.
23. Rao, J. K. M. and Viswamitra, M. A., *Acta Crystallogr. B*, 1972, **28,** 1484.
24. Robinson, S. D. and Uttley, M. F., *J. Chem. Soc. Dalton Trans.*, 1973, 1912.
25. Deacon, G. B. and Phillips, R. J., *Coord. Chem. Rev.*, 1980, **33,** 227.

Pergamon

PII: S0277–5387(98)00186–7

Polyhedron Vol. 17, No. 22, pp. 3947–3953, 1998
© 1998 Elsevier Science Ltd
All rights reserved. Printed in Great Britain
0277–5387/98 $19.00+0.00

Synthesis and NMR investigation on *mer*-[$Re^{III}Cl_3(L)_3$] and *mer*-[$Re^{III}Cl_3(L)_2(PPh_3)$] complexes (L = pyridine-like ligand). X-ray structure of *mer*-[$Re^{III}Cl_3(3,5\text{-lut})_3$]

Francesco Tisato,[a] Fiorenzo Refosco,[a] Alessandro Dolmella[b] and Giuliano Bandoli[b,*]

[a]Istituto di Chimica e Tecnologie Inorganiche e dei Materiali Avanzati, C.N.R., Corso Stati Uniti 4, 35020 Padova, Italy; [b]Dipartimento di Scienze Farmaceutiche, Università di Padova, Via Marzolo 5, 35131 Padova, Italy

Received 24 February 1998; accepted 4 May 1998

Abstract—The co-ordination geometry of the monomeric rhenium complexes *mer*-[$Re^{III}Cl_3(L)_3$] (L = py **1**, 3,5-lut **2**, 4-pic **3**) has been determined in the solid state by single X-ray diffraction of the representative complex **2** and in solution by proton NMR spectroscopy. Only a single stable conformation has been found in the solid state and in solution, under the experimental conditions utilised. The NMR spectra of the related complexes *mer*-[$Re^{III}Cl_3(L)_2(PPh_3)$] (L = py **4**, 3,5-lut **5**, 4-vinpy **6**) have also been reported for comparison purposes.
© 1998 Elsevier Science Ltd. All rights reserved

Keywords: rhenium; pyridine; crystal structure; NMR.

INTRODUCTION

In the past the long established inorganic chemistry of rhenium has provided a useful framework for understanding and expanding the field of technetium co-ordination chemistry [1]. Then, in the eighties, basic inorganic chemistry of the long-lived isotope *i.e.*, ^{99g}Tc has been extensively developed, primarily because of the relevance of the short-lived isotope ^{99m}Tc to diagnostic nuclear medicine [2]. More recently, the advent of ^{186}Re and ^{188}Re therapeutic radiopharmaceuticals [3–5] has made this metal of intrinsic value to nuclear medicine. In this work we have re-visited some rhenium chemistry, including monomeric complexes of the type *mer*-[$Re^{III}Cl_3(L)_3$] (L = py **1**, 3,5-lut **2**, 4-pic **3**) and *mer*-[$Re^{III}Cl_3(L)_2(PPh_3)$] (L = py **4**, 3,5-lut **5**, 4-vinpy **6**) [py = pyridine, 3,5-lut = 3,5-dimethylpyridine, 4-pic = 4-methylpyridine, 4-vinpy = 4-vinylpyridine], previously described by Wilkinson *et al*. [6]. During the synthetic work we have isolated and structurally characterised, for the first time, a monomeric rhenium(III) complex with pyridine-type ligands, namely *mer*-[$ReCl_3(3,5\text{-lut})_3$] **2**. The meridional arrangement of the solid state is retained also in the solution state, as established by proton NMR studies.

RESULTS

Syntheses

Substitution reaction operated by pyridine ligands onto labile [$ReCl_3(MeCN)(PPh_3)_2$] [6], afforded *mer*-[$Re^{III}Cl_3(L)_2(PPh_3)$] derivatives as major product and *mer*-[$Re^{III}Cl_3(L)_3$] in fairly low yields. The crude solid collected from the reaction mixture after 2 h of reflux in the relevant pyridine was loaded onto a silica gel column. Elution with $CHCl_3$ evidenced the existence of three products. The first band contained the par-

Additional material, available from the Cambridge Crystallographic Data Centre (CCDC reference number 101419), comprises final atomic fractional co-ordinates, bond lengths, bond angles, anisotropic thermal parameters and H-atoms co-ordinates.

* Author to whom correspondence should be addressed.

tially substituted *mer*-[$Re^{III}Cl_3(L)_2(PPh_3)$] derivative, and the second one *mer*-[$Re^{III}Cl_3(L)_3$], whereas a major impurity (up to 40% of the total rhenium content), then characterised as the oxidised dioxo *trans*-$[ReO_2(L)_4]^+$ complex was retained on silica. The prolonged contact of the crude material with the air and the presence of moisture in the chloroform solution were most likely responsible for the oxidation of Re(III) species to the thermodynamically stable dioxo-Re(V) derivatives.

Structural commentary

The crystal structure of *mer*-[$ReCl_3(3,5\text{-lut})_3$] **2** is built up of two independent molecules [labelled (**A**) and (**B**)] in the asymmetric unit, which also comprises a MeOH hemimolecule solvent. The relative orientation of molecules (**A**) and (**B**) is depicted in Fig. 1, which also shows the thermal vibration ellipsoids of the non-hydrogen atoms. The co-ordination about rhenium is distorted octahedral and the two groups of ligands are arranged in a meridional fashion. The angles between *cis*-ligands vary between 87.8 and 91.7° (Table 1), while the *trans*-angles are between 176.4 and 179.3°, so that the departure from the ideal octahedron, which is usually ascribed to the mutual repulsion of the ligands is very limited, as shown also by the dihedral angle between the N_3 of 3,5-lut_3 and the Cl_3 triangles [90.5 and 88.8° in (**A**) and (**B**), respectively]. The two independent molecules differ slightly, the r.m.s. being of 0.13 Å when the fitting [7] involves 13 atoms (those of the "inner core" plus the two nearest lutidine carbons). The unique differences lie in (i) Cl(2)–Re(1)–Cl(3) angle (91.7°), to compare with Cl(5)–Re(2)–Cl(6) (87.8°) [Cl(5) and Cl(6) atoms interact, in some way, with the solvent molecule, so that Cl(6)––O and Cl(5)––O separations are 3.39 and 3.67 Å, respectively]; (ii) the lutidine rings make, each other, dihedral angles of 115.7, 95.3 and 53.4° in (**A**) to compare with the corresponding values 116.9, 89.5, and 60.6° in (**B**). To our knowledge this structure represents the first example of a mononuclear ReX_3N_3 complex (where X = halide and N is a unidentate pyridine-like N-donor) to be characterised by X-ray crystallography. On the other hand, the X-ray structure of a strictly related technetium compound, namely *mer*-[$TcCl_3(4\text{-pic})_3$], has been recently reported [8]. The Re–N and Re–Cl bond lengths in *mer*-[$ReCl_3(3,5\text{-lut})_3$], compared with those in closely related compounds collected in Table 2, show that: (i) the values of $Re–N_{py}$ distances (in the range 2.06 ÷ 2.17 Å) shorten as the formal oxidation state of the metal is lowered, while the distances become longer when the *trans*-influence is operating, as in

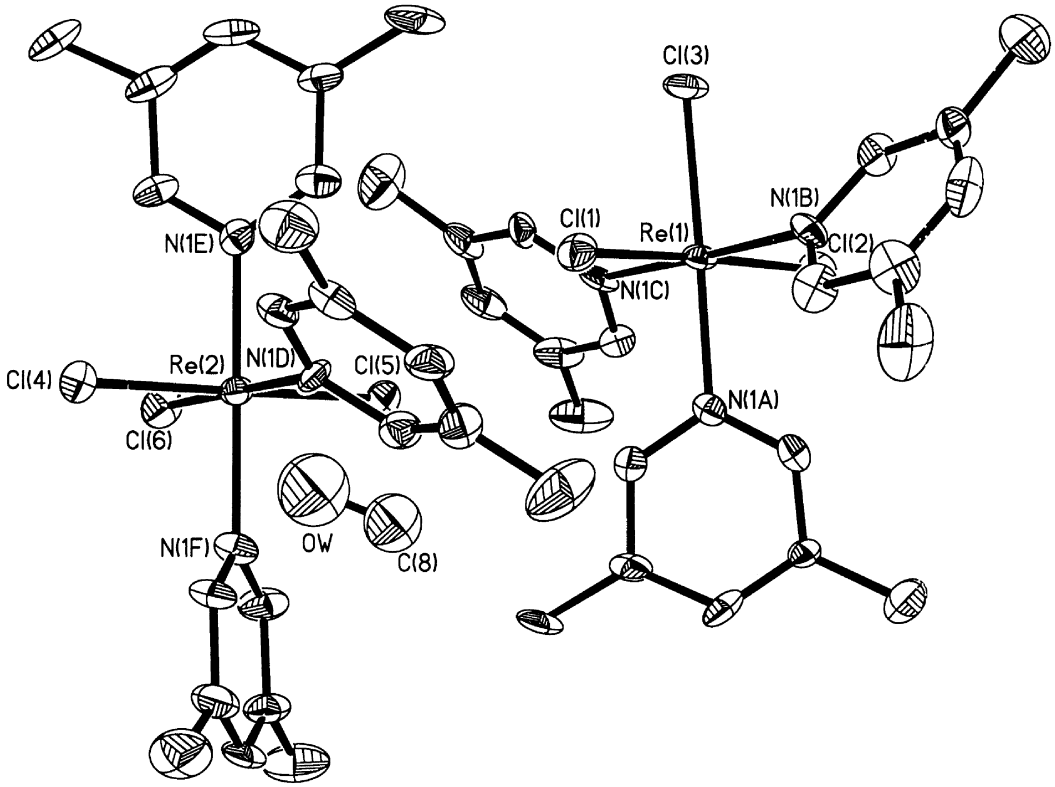

Fig. 1. Relative orientation of the two molecules (**A**) and (**B**) in the asymmetric unit along with the MeOH molecule in **2**. Thermal vibration ellipsoids scaled to include 50% probability.

Table 1. Selected bond lengths (Å) and angles (deg) for **2**

Re(1)–Cl(1)	2.356 (4)	Re(2)–Cl(4)	2.348 (4)
Re(1)–Cl(2)	2.362 (4)	Re(2)–Cl(5)	2.351 (4)
Re(1)–Cl(3)	2.402 (4)	Re(2)–Cl(6)	2.396 (4)
Re(1)–N(1A)	2.13 (1)	Re(2)–N(1D)	2.12 (1)
Re(1)–N(1B)	2.13 (1)	Re(2)–N(1E)	2.12 (1)
Re(1)–N(1C)	2.12 (1)	Re(2)–N(1F)	2.13 (1)
Cl(1)–Re(1)–Cl(2)	176.4 (1)	Cl(4)–Re(2)–Cl(5)	179.3 (1)
Cl(1)–Re(1)–Cl(3)	91.5 (1)	Cl(4)–Re(2)–Cl(6)	91.6 (1)
Cl(2)–Re(1)–Cl(3)	91.7 (1)	Cl(5)–Re(2)–Cl(6)	87.8 (1)
N(1A)–Re(1)–N(1B)	90.2 (4)	N(1D)–Re(2)–N(1E)	89.4 (4)
N(1A)–Re(1)–N(1C)	90.8 (4)	N(1D)–Re(2)–N(1F)	88.6 (4)
N(1B)–Re(1)–N(1C)	179.0 (4)	N(1E)–Re(2)–N(1F)	177.6 (4)
Cl(3)–Re(1)–N(1A)	178.9 (3)	Cl(6)–Re(2)–N(1D)	177.8 (3)

Table 2. Comparison of Re–N_{py} and Re–Cl bond lengths (Å) in mononuclear octahedral Re complexes with unidentate N-donor py-like ligands

Compound	o.n.[a]	Re–N	Re–Cl	Ref.
Trans-$[ReO_2(dmap)_4]^{2+}$[b]	VI	2.11; 2.12		[9, 10]
Trans-$[ReO_2(py)_4]^+$	V	2.14 ÷ 2.17		[11]
$[ReOCl_2(OEt)(py)_2]$	V	2.13; 2.14	2.37; 2.44	[12]
$[ReOCl_2(OSiMe_3)(py)_2]$	V	2.13; 2.13	2.39; 2.41	[13]
Trans-$[ReO_2(4\text{-pic})_4]^+$	V	2.11 ÷ 2.15		[14]
Cis-$[ReO_2(bpy)(py)_2]^+$	V	2.14		[15]
Mer-$[ReCl_3(3,5\text{-lut})_3]$	III	2.12 ÷ 2.13	2.35 ÷ 2.40	Present work
Cis-$[Re(bpy)_2Cl_2]^+$	III	2.095	2.36	[16]
Trans-$[ReCl_4(NO)(py)]^-$	II	2.22	2.35 ÷ 2.38	[17]
$[Re(bpy)_3]^+$	I	2.06		[16]

[a] o.n. = oxidation number; [b] dmap 4-(dimethylamino)py.

$[ReCl_4(NO)(py)]^-$ [17]; (ii) the Re–Cl distances are comprised in the rather narrow range 2.35–2.41 Å and the "abnormal" value of 2.44 Å in $[ReOCl_2(OEt)(py)_2]$ is caused by steric repulsion [12]; (iii) the Re–Cl bond length *trans* to the pyridine ligand is longer than the mutually *trans* Re–Cl distances by 0.04 Å. A similar trend is observed in the above mentioned isostructural *mer*-$[TcCl_3(4\text{-pic})_3]$ complex: the chloride ligand *trans* to the picoline donor is lengthened by 0.13 Å compared to the mutually *trans*-ones, whereas the variation of the Tc–N_{pic} distances is within the experimental error [8].

Proton NMR characterisation

Proton NMR data for synthesised *mer*-Re(III) complexes are summarised in Table 3. In addition, the proton spectrum of the representative complex *mer*-$[ReCl_3(4\text{-vinpy})_2(PPh_3)]$ **6** is depicted in Fig. 2. In spite of the paramagnetism of the low-spin d^4 ion, all of the Re(III) complexes can be conveniently characterised in solution by proton NMR spectroscopy. The two unpaired electrons are responsible for the spreading of the signals over a wide ppm range, but successful observation of proton NMR spectra (with multiplicity retention) is due to the extremely short electron-spin-relaxation time ($T_{1e} < 10^{-11}$ s) of the Re(III) centre [18]. The meridional configuration established in the solid state for *mer*-$[ReCl_3(3,5\text{-lut})_3]$ is retained in solution, as revealed, for example, by the appearance of two A_2B_2C pyridine proton systems, of relative integration 1:2, in $[ReCl_3(py)_3]$. Such a pattern does not undergo detectable modification in the range -50 to $+50\,^{\circ}C$ in chloroform-*d* solutions. Two types of pyridine protons are likewise detected in *mer*-$[ReCl_3(py)_2(PPh_3)]$, along with a further A_2B_2C set arising from the phenyl groups of PPh_3. This pattern is in accordance with two *cis*-positioned pyridine ligands, facing a chloride and a phosphine phosphorus, respectively. Such a distorted octahedral environment with two *cis*-positioned pyridine ligands

Table 3. NMR chemical shifts (ppm) of the pyridine ring protons for *mer*-$[ReCl_3(L)_3]$ and *mer*, *cis*-$[ReCl_3(L)_2(PPh_3)]$ complexes in chloroform-*d* solutions

	Trans-py donor	α	β	γ
py		8.30	6.97	7.36
$[ReCl_3(py)_3]$ **1**	N-py	5.94 (−2.36)	16.93 (+9.96)	3.16 (−4.20)
	Cl	−0.32 (−8.62)	14.24 (+7.27)	−1.47 (−8.83)
3,5-lut		8.22	2.27 (Me)	7.27
$[ReCl_3(3,5\text{-lut})_3]$ **2**	N-lut	5.43 (−2.79)	0.94 (−1.33)	0.7 (−7.20)
	Cl	−0.64 (−8.86)	−0.84 (−3.11)	−2.15 (−9.42)
4-pic		8.28	6.23	2.15 (Me, s)
$[ReCl_3(4\text{-pic})_3]$ **3**	N-pic	5.62 (−2.66)	16.21 (+9.98)	16.14 (+13.99)
	Cl	−1.39 (−9.67)	13.70 (+7.47)	14.91 (+12.76)
$[ReCl_3(py)_2(PPh_3)]$[a] **4**	P-PPh_3	13.28 (+4.98)	16.71 (+9.74)	7.89 (+0.53)
	Cl	−3.28 (−11.58)	12.45 (+5.48)	1.43 (−5.93)
$[ReCl_3(3,5\text{-lut})_2(PPh_3)]$[a] **5**	P-PPh_3	13.02 (+4.80)	−0.51 (−2.78)	7.45 (+0.18)
	Cl	−4.28 (−12.50)	−0.84 (−3.11)	0.74 (−6.53)
$[ReCl_3(4\text{-vinpy})_2(PPh_3)]$[a] **6**	P-PPh_3	17.14 (+8.58)	13.23 (+5.96)	12.11 (+5.45)
				5.33 (−0.64)
				5.09 (−0.40)
	Cl	12.79 (+4.23)	−3.61 (+10.88)	9.00 (+2.34)
				3.42 (−2.55)
				2.42 (−3.07)
4-vinpy		8.56	7.27	6.66 (H_{gem})
				5.97 (H_{cis})
				5.49 (H_{trans})

[a] The Phenyl protons of PPh_3 resonate at $\delta = 13.55$ (a), 8.85 (b) and 8.50 (g) ppm for **4**, at $\delta = 13.54$ (a), 8.81 (b) and 8.48 (g) for **5**, and at $\delta = 13.52$ (a), 8.83 (b) and 8.49 (g) ppm for **6**.

has been established recently in the solid state by Beauchamp and coworkers [19].

3 DISCUSSION

The chemistry of low-valent technetium and rhenium species is dominated by the presence in the coordination sphere of moderate to strong π-acid ligands such as alkyl- and aryl-phosphines, isocyanides or carbon monoxide [20–22]. However, the search for a substitution-active low-valent species, which may be of great interest as labile starting material at "carrier free" level, has prompted some synthetic groups to develop complexes with "electron-rich" metal centres surrounded by weak π-acid ligand environments. Among these, polypyridyl ligands have appeared to be suitable substrates for stabilising mononuclear M^{III}, M^{II} and M^{I} complexes (M = Tc, Re) [23, 24]. Moreover, the ability of pyridine to function as both a good σ-donor and a moderate π-acid ligand has provided a rare structural comparison of a transition metal in three different oxidation states contained within a nearly identical ligand field. The peculiar electronic flexibility of pyridine-like ligands turned out to be properly investigated also in the solution state by proton NMR spectroscopy for *mer*-$[ReCl_3(L)_3]$ complexes. In *mer*-$[ReCl_3(py)_3]$ compounds the alternating sign pattern of the ring position chemical shift (the α- and γ-protons are shifted upfield while the β-protons are shifted downfield, see Table 3), and the lack of attenuation of the isotropic shifts with the increasing distance from the metal seems to support that spin delocalisation occurs *via* the aromatic ligand π-system [25]. This behaviour parallels that shown by the second-row congener complex *mer*-$[TcCl_3(py)_3]$ [26]. In this connection the upfield shift experienced by α- and γ-protons is in agreement also with a significant π-back donation operating from the "electron rich" d^4 metal system to the pyridine ligands. Back-bonding to the unique pyridine protons (the unique pyridine is the ligand facing the chloride donor) appears to be stronger; indeed, they receive larger electron density from the metal than do either of the mutually *trans* pyridines, which compete against each other. A greater competition is experienced by the coordinated pyridine facing the more efficient π-acid system PPh_3 in *mer*-$[ReCl_3(py)_2(PPh_3)]$ (Table 3). In this pyridine α- and γ-proton signals move even downfield, whereas the pyridine protons positioned *trans* to the chloride donor retain the usual alternating sign pattern of the ring position chemical shift. Substitution of the γ-proton with a methyl group, as in $[ReCl_3(4\text{-pic})_3]$, determines a downfield shift of the methyl signals (the opposite side than that of the original γ-proton) [27]. Analogously, the methyl groups at the β-positions of the lutidine backbones in *mer*-$[ReCl_3(3,5\text{-lut})_3]$ are upfield shifted, which is again the opposite side than that of the β-protons. The same

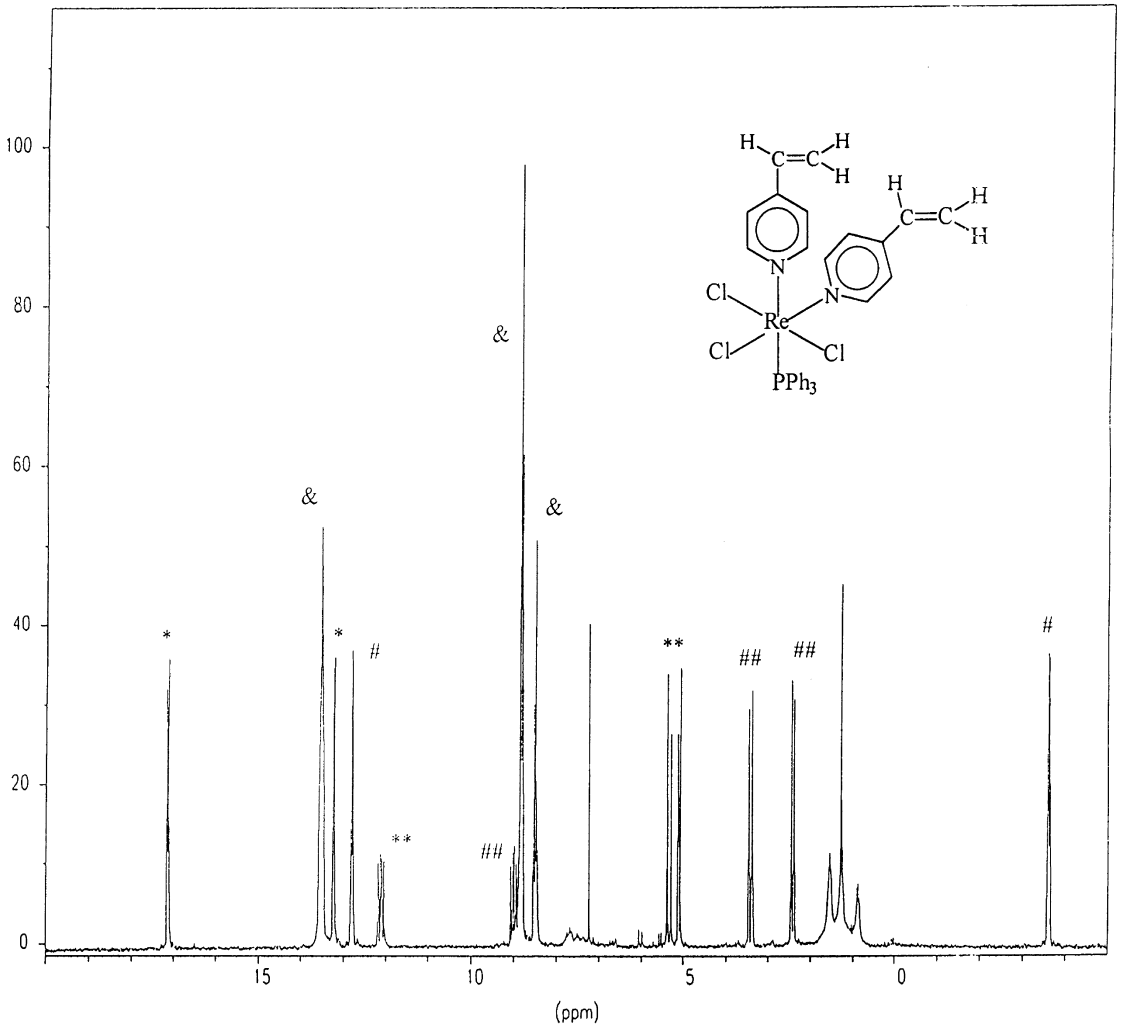

Fig. 2. Proton NMR spectrum of [$ReCl_3$(4-vinpy)$_2$(PPh_3)] **6** over the $+20 \div -5$ ppm region. * Denotes signals arising from the 4-vinyl-pyridine coordinated *trans* to PPh_3 (** protons from the vinyl group), whereas # denotes signals from the 4-vinyl-pyridine coordinated *trans* to Cl (## protons from the vinyl group). & denotes PPh_3 signals.

trend is encountered in the related complex [$ReCl_3$(4-vinpy)$_2$(PPh_3)] **6**, where a vinyl group is incorporated in the *para*-position and a PPh_3 substitutes a pyridine ligand. As above described for *mer*-[$ReCl_3$(py)$_2$(PPh_3)], the two *cis*-positioned vinyl-pyridines face distinct chemical environments, a chloride and a triphenylphosphine donor, which induce different chemical shift values for pyridine protons. However, in both pyridines the vinyl protons at C_α are downfield shifted, whereas those at C_β are upfield shifted (Fig. 2 and Table 3). This recurring behaviour further substantiates the occurrence of π-spin delocalisation through hyperconjugation between the methyl (or vinyl) group and the aromatic ring [9, 10].

In summary, the syntheses and characterisation of *mer*-[$Re^{III}Cl_3(L)_3$] and *mer*-[$ReCl_3(L)_2(PPh_3)$] complexes have provided the first X-ray structure determination of a monomeric polypyridyl Re(III) complex *mer*-[$ReCl_3$(3,5-lut)$_3$]. The meridional configuration found in the solid state originates at least two different types of lutidine ligands. However, the presence of two independent entities in the unit gives rise to significant steric constraints. As a consequence, each one of the three lutidines display a different orientation. The *mer* configuration is retained in solution, where the pyridine protons originate two different set of signals, whose integration ratio is correctly 1:2. No sign of further splitting of pyridine signals is observed in chloroform solutions in the range -50 to $+50\,^{\circ}C$.

EXPERIMENTAL

Apparatus

Microanalyses were carried out with a Fisons EA1108 elemental analyser. The IR spectra were recorded in KBr pellets with a Mattson 3030 Fourier-

transform spectrometer (4000–400 cm^{-1}). Proton NMR spectra were recorded on a Bruker AC-200 spectrometer and were referenced to the resonances of residual protons in the deuterated solvent. Other active NMR nuclei are theoretically detectable in our compounds, including isotopes of ^{187}Re ($I = 5/2$). However, the lack of spherical symmetry in diamagnetic $Re^{V}O_2^{+}$ species make conditions very unfavourable for signal detection [20, 21], whereas solubility problems bar the availability of the potentially useful ^{13}C probe. The proton NMR investigations were performed at 295 K on 10^{-3}–5×10^{-4} M solutions and unambiguous proton assignments were made through relative integration, spin–spin splitting, homo-nuclear decoupling and two-dimensional experiments [28–30]. Fast-atom bombardment mass spectra in the positive mode (FAB^{+}) were recorded by using a 3-nitrobenzyl alcohol matrix on a VG ZAB-2F spectrometer. Xenon was used as the primary beam gas, and the ion gun was operated at 8 keV. Data were collected over the mass range 100–1300 at 0.7 s per scan.

Materials

Unless otherwise stated, all chemicals were of reagent grade. Pyridine and substituted pyridines were purchased from Aldrich Chimica and used as received. $[ReCl_3(MeCN)(PPh_3)_2]$ was obtained according to the published procedure [6].

Syntheses of Re(III) complexes

mer-$[ReCl_3(py)_3]$ **1**. The following modification of the reported preparation was used [6]. In a two-necked flask equipped with a refluxing condenser, solid $[ReCl_3(MeCN)(PPh_3)_2]$ (0.107 g, 0.125 mmol) was dissolved in neat pyridine (11.0 ml) under a dinitrogen atmosphere. The reaction mixture was refluxed for 4 h and then *n*-hexane (200 ml) was added to the cooled solution, which was placed in the refrigerator overnight. A dark precipitate was isolated by filtration, washed with a few drops of Et_2O. Then it was dissolved in 3 ml of $CHCl_3$ and loaded onto a silica-gel chromatography column (20 × 2 cm), which was eluted with $CHCl_3$ yielding the desired product (second band); the solution was then reduced to dryness by rotary evaporation and the solid dried *in vacuo* overnight. Yield 14 mg, 21%. (Found: C, 34.3; H, 3.0; N, 7.7. $C_{15}H_{15}N_3Cl_3Re$ requires C, 34.00; H, 2.85; N, 7.93%). FAB mass spectrum: m/z 530, $[M]^{+}$.

mer-$[ReCl_3(L)_3]$ (L = 3,5-lut **2**, 4-pic **3**). These complexes were prepared as above detailed for **1**. **2**: yield 18%. (Found: C, 41.3; H, 4.6; N, 6.6. $C_{21}H_{27}N_3Cl_3Re$ requires C, 41.08; H, 4.43; N, 6.84%). FAB mass spectrum: m/z 614, $[M]^{+}$. **3**: yield 17%. (Found: C, 38.2; H, 3.7; N, 7.2. $C_{21}H_{27}N_3Cl_3Re$ requires C, 37.80; H, 3.70; N, 7.35%). FAB mass spectrum: m/z 572, $[M]^{+}$.

mer-$[ReCl_3(L)_2(PPh_3)]$ (L = py **4**, 3,5-lut **5**, 4-vinpy **6**) were prepared as reported [6].

Crystallography

$C_{21}H_{27}N_3Cl_3Re \cdot 1/2CH_3OH$, **2**·1/2MeOH, $M = 630.03$, Monoclinic, $a = 13.410(6)$, $b = 20.975(8)$, $c = 17.889(7)$ Å, $\beta = 99.84(5)^{\circ}$, $U = 4958(3)$ $Å^3$, $D_c = 1.688$ g cm^{-3}, $Z = 8$, $F(000) = 2472$, space group $P2_1/n$, Mo–K_α radiation, $\lambda = 0.71073$ Å, μ(Mo–K_α) = 52.4 cm^{-1}. The dark red crystal sample, obtained from a MeOH solution, was an elongated polyhedron of dimensions 0.10 × 0.15 × 0.50 mm. The intensity measurements were carried out on a Nicolet Siemens R3m/V automated four-circle diffractometer; the intensities (up to $2\theta = 45^{\circ}$) were corrected for Lorentz-polarisation effects and absorption, using an empirical method based on the ψ-scans of five reflections at $\chi \cong 90^{\circ}$. Transmission factors were found in the range 0.58–0.81. After removing all the reflections having $I_o < 2\sigma$ (I_o), a final set of 4529 independent data was used in the solution and refinement of the structure performed on F^2. All the non-hydrogen atoms were refined anisotropically, while O and C(8) atoms of MeOH molecule were treated isotropically. The final agreement indices R and $wR2$ $\{ = [\Sigma w(F_o^2 - F_c^2)^2 / \Sigma w(F_o^2)^2]^{1/2}\}$ were 0.046 and 0.114, respectively. The atomic scattering factors were taken from *International Tables for X-ray Crystallography* [31] and all calculations were performed with the SHELXTL/PC and SHELXL93 structure analysis packages [32, 33].

REFERENCES

1. Davison, A., in *Technetium in Chemistry and Nuclear Medicine*, Vol. 1, ed. E. Deutsch, M. Nicolini and H. N. Wagner Jr. Cortina International, Verona, Italy, 1983, p. 3.
2. Deutsch, E., Nicolini, M. and Wagner, H. N. Jr. ed., *Technetium in Chemistry and Nuclear Medicine*, Vol. 1. Cortina International, Verona, Italy, 1983.
3. Deutsch, E., Libson, K., Vanderheyden, J.-L., Ketring, A. R. and Maxon, H. R., *Nucl. Med. Biol.*, 1986, **13,** 465.
4. Jurisson, S., Berning, D., Jia, W. and Ma, D., *Chem. Rev.*, 1993, **93,** 1137.
5. Dilworth, J. R. and Parrott, S. J., *Chem. Soc. Rev.*, 1998, **27,** 43.
6. Rouschias, G. and Wilkinson, G., *J. Chem. Soc.* (*A*), 1967, 993.
7. Nyburg, S. C., *Acta Cryst. B*, 1974, **30,** 251.
8. Lu, J., Yamano, A. and Clarke, M. J., *Inorg. Chem.*, 1990, **29,** 3483.
9. Eaton, D. R., Josey, A. D., Phillips, W. D. and Benson, R. E., *J. Chem. Phys.*, 1962, **37,** 347.

10. Eaton, D. R., Josey, A. D., Benson, R. E., Phillips, W. D. and Cairns, T. L., *J. Am. Chem. Soc.*, 1962, **84,** 8100.
11. Brewer, J. C., Thorp, H. H., Slagle, K. M., Brudvig, G. W. and Gray, H. B., *J. Am. Chem. Soc.*, 1991, **113,** 3171.
12. Lock, C. J. L. and Turner, G., *Acta Cryst. B*, 1978, **34,** 923.
13. Lock, C. J. L. and Turner, G., *Can. J. Chem.*, 1977, **55,** 333.
14. Schmid, S. and Strähle, J., *Z. Kristallogr.*, 1992, **198,** 49.
15. Johnson, J. W., Brody, J. F., Ansell, G. B. and Zentz, S., *Inorg. Chem.*, 1984, **23,** 2415.
16. Ciani, G., Giusto, D., Manassero, M. and Sansoni, M., *J. Chem. Soc. Dalton Trans.*, 1978, 798.
17. Backbourn, R. L., Jones, L. M., Ram, M. S., Sabat, M. and Hupp, J. T., *Inorg. Chem.*, 1990, **29,** 1791.
18. Keller, H. J. and Schwarzhans, K. E., *Angew. Chem. Int. Ed. Engl.*, 1970, **9,** 196.
19. Pearson, C. and Beauchamp, A. L., *Can. J. Chem.*, 1997, **75,** 220.
20. Davison, A., Kronauge, J. F., Jones, A. J., Pearlstein, R. M. and Thornback, J. R., *Inorg. Chem.*, 1988, **27,** 3245.
21. O'Connell, L. A., Pearlstein, R. M., Davison, A., Kronauge, J. F., Thornback, J. R. and Jones, A. J., *Inorg. Chim. Acta*, 1989, **161,** 39.
22. Tisato, F., Refosco, F. and Bandoli, G., *Coord. Chem. Rev.*, 1994, **135–136,** 325.
23. Wilcox, B. E., Ho, D. M. and Deutsch, E., *Inorg. Chem.*, 1989, **28,** 3917.
24. Helberg, L. E., Orth, S. D., Sabat, M. and Harman, W. D., *Inorg. Chem.*, 1996, **35,** 5584.
25. Rohrscheid, F., Erns, R. E. and Holm, R. H., *J. Am. Chem. Soc.*, 1967, **89,** 6472.
26. Breikss, A. I., Davison, A. and Jones, A., *Inorg. Chim. Acta*, 1990, **170,** 75.
27. Forman, A., Murell, J. N. and Orgel, L. E., *J. Chem. Phys*, 1959, **31,** 1129.
28. Jeener, J., *Ampere Summer School*. Basko Polje, Yugoslavia, 1971.
29. Aue, W. P., Bartholdi, E. and Ernst, R. R., *J. Chem. Phys.*, 1976, **64,** 2229.
30. Ernst, R. R., Bodenhausen, G. and Wokaum, A., *Principles of Nuclear Magnetic Resonance in One and Two Dimensions*. Clarendon, Oxford, 1987.
31. International Tables for X-ray Crystallography, Vol. IV. Kynoch Press, Birmingham, 1974, p. 202.
32. Sheldrick, G. M., SHELXTL/PC, version 5.3. Siemens Analytical X-ray Instruments Inc., Madison, WI, U.S.A., 1990.
33. Sheldrick, G. M., SHELXL93. *Program for the Refinement of Crystal Structures*. University of Göttingen, Germany, 1993.

Pergamon

PII: S0277-5387(98)00189-2

Polyhedron Vol. 17, No. 22, pp. 3955–3961, 1998
© 1998 Elsevier Science Ltd
All rights reserved. Printed in Great Britain
0277–5387/98 $19.00+0.00

Synthesis and characterization of bis-chelated nickel(II) complexes of the methylpyruvate Schiff bases of S-alkyldithiocarbazates and the X-ray crystal structure of the $[Ni(ONSMe)_2]$ complex

Mohammad Akbar Ali,[a]* Mohamed Nazimuddin,[b] Rina Shaha,[b] Ray J. Butcher[c] and Jeffrey C. Bryan[d]

[a]Department of Chemistry, University of Brunei Darussalam, Brunei Darussalam, BSB 2028, Brunei

[b]Department of Chemistry, University of Chittagong, Chittagong, Bangladesh

[c]Department of Chemistry, Howard University, Washington, DC, U.S.A.

[d]Chemical and Analytical Sciences Division, Oak Ridge national Laboratory, Oak Ridge, TN 37831-6119, U.S.A.

(Received 27 January 1998; accepted 5 May 1998)

Abstract—New nickel(II) complexes of general empirical formula, $[Ni(ONS)_2]$ (ONS^- is the anionic form of tridentate ligands formed from methylpyruvate and S-methyl- and S-benzyldithiocarbazates) have been synthesized and characterized by magnetic and spectroscopic techniques. The complexes are six-coordinate and octahedral. The crystal and molecular structure of $[Ni(ONSMe)_2]$ ($ONSMe^-$ is the anionic form of the methylpyruvate Schiff base of S-methyldithiocarbazate) has been determined by X-ray diffraction which shows that the nickel(II) complex has a distorted octahedral structure with the ligands coordinated to the nickel(II) ion as uninegatively charged tridentate chelating agents via the carbonyl oxygen, the azomethine nitrogen and the mercaptide sulphur atoms. The distortion from regular octahedral geometry is attributed to the restricted bite angles of the planar ONS tridentate ligands. © 1998 Elsevier Science Ltd. All rights reserved

Keywords: nickel(II) complexes; Schiff bases; S-alkyldithiocarbazates; crystal structure; methylpyruvate Schiff bases; octahedral nickel(II) complexes

INTRODUCTION

Metal complexes of sulphur–nitrogen chelating agents derived from S-alkyl esters of dithiocarbazic acid have attracted considerable attention over the past few years [1–12] in view of their interesting physico-chemical properties [9, 10] and potentially useful therapeutic properties [13]. Thus, the nickel(II) complex of the 2-acetylpyridine Schiff base of S-methyldithiocarbazate, [Ni(NNS)CI] has been shown to exhibit marked activity in the P388 Lymphocytic Leukaemmia test system [14]. Some Schiff bases of S-alkyl esters of dithiocarbazic acid and their copper(II) complexes have also been shown to display antifungal and antibacterial properties [3, 4, 8]. Although in the past several synthetic and spectral characterization of metal-dithiocarbazate complexes have been reported in the literature, structural work by X-ray crystallography on such complexes are few in number. As part of our ongoing work on metal chelates of dithiocarabazic acid and its derivatives, we report here the preparation and magnetic and spectroscopic characterization of two bis-chelated nickel(II) com-

* Author to whom correspondence should be sent.

plexes of the methylpyruvate Schiff bases of S-methyl- and S-benzyldithiocarbazates, together with the X-ray crystal structure determination of the $[Ni(ONSMe)_2]$ complex.

EXPERIMENTAL

All physical measurements and analytical procedures were similar to those described previously [3].

Synthesis of the ligands

The two Schiff bases were prepared by the same general method.

The appropriate S-alkyldithiocarbazate (2 mmol) dissolved in abs. ethanol (100 cm^3) was mixed with a hot solution of methyl pyruvate (2 mmol) in the same solvent (100 cm^3) and the mixture was refluxed for *ca.* 2 h and then left to stand overnight. The volume of the solution was then reduced to about 50 cm^3 whereupon the crystals which had formed were collected by filtration and recrystallized from abs. ethanol to obtain pale yellow needle-shaped crystals. HONSMe (the Schiff base of methylpyruvate with S-methyldithiocarbazate): yield, 80%, m.p. 97°C; found: C, 35.1; H, 4.7; N, 13.7. calc. for $C_6H_{10}N_2S_2$: C, 34.9; H, 4.9; N, 13.6%.

HONSBz (the Schiff base of methylpyruvate with S-benzyldithiocarbazate): yield, 75%. m.p. 109°C; found: C, 51.2; H, 5.1; N, 10.0%; calc. for $C_{12}H_{14}N_2S_2O_2$: C, 5 1.0; H, 5.0; N, 9.9%.

General method of preparation of the complexes

The appropriate Schiff base (2 mmol) was dissolved in a mixture of boiling methanol (50 cm^3) and 2,2-dimethoxypropane (5 cm^3). To the solution, a hot solution of nickel(II) nitrate hexahydrate (1 mmol) in the same mixture of solvents (50 cm^3) was added and the mixture was allowed to stand overnight during which time beautiful brown crystals of the complexes formed. These were filtered off, washed with methanol and dried in a vacuum desiccator over anhydrous silica gel.

Found: C, 30.8; H, 3.7; N, 12.0; calc. for $C_{12}H_{18}N_4O_4S_4Ni$: C, 30.7; H, 3.9; N, 11.9%. Found: C, 46.3; H, 4.0; N, 8.7; calc. for $C_{24}H_{26}N_4S_4O_4Ni$: C, 46.4; H, 4.2 N, 9.0%.

X-ray crystal structure analysis

The intensity data were obtained by means of an Enraf-Nonius CAD4 diffractometer at 293 K. Intensities were corrected for Lorentz and polarization effects and empirical absorption corrections were applied based on a set of ψ scans. Calculations were carried out using XCAD49 (data reduction) SHELXTL (absorption correction, structure solution/refinement and molecular graphics). All hydrogen atoms were placed in calculated positions, refined using a riding model and given an isotropic displacement parameter equal to 1.2(CH, CH_2) or 1.5(CH_3) times the equivalent isotropic displacement parameter of the atom to which it is attached. When warranted, methyl hydrogen atomic positions were allowed to rotate about the C–C bond. Full-matrix least-squares refinement of all data against F^2 of the quantity $w(F_o^2–F_c^2)$ was used to adjust the position and anisotropic thermal parameters of all non-hydrogen atoms. Unit cell dimensions were refined by use of the settings of 25 accurately determined reflections widely separated in reciprocal space. Intensities were measured by ϖ scans. The structure was solved by direct methods [15] and subsequent Fourier syntheses were used to determine remaining non-hydrogen atomic positions. A summary of crystallographic data, experimental details and refinement results is given in Table 1.

RESULTS AND DISCUSSION

The Schiff bases of S-methyldithiocarbazate and S-benzyldithiocarbazate with methylpyruvate (Figure 1), hereinafter abbreviated as HONSMe and HONSBz, respectively, can exhibit thione (1a) and thiol (1b) tautomerism, since they have a thioamide function –NH–C(═S)SR.

The IR spectra of these compounds, however, do not exhibit any ν(S–H) band at *ca.* 2700 cm^{-1}, but display the ν(NH) bands at *ca.* 3200 cm^{-1} indicating that, in the solid state, they remain as the thioketo tautomeric form (**1a**). However, in solution and in the presence of nickel(II) ion, they quickly change to the thiol form with the concomitant formation of nickel(II) complexes of the deprotonated thiolate forms of the ligands. The related thiosemicarbazone ligands have been found to coordinate to metal ions in both protonated [16] and deprotonated [17] forms. However, there are two unique examples of thiosemicarbazone complexes, one of which is a bis-ligand chromium(III) complex [18] and the other is a bis-ligand copper(II) complex [19] where the two tridentate NNS thiosemicarbazone ligands are present as both protonated and deprotonated forms in the same complexes. However, so far as the complexes of Schiff bases of S-alkyldithiocarbazates are concerned, there has not been a single example as yet, where these Schiff bases coordinate to a metal ion as the protonated thione form. Our attempts so far, to obtain nickel(II) complexes of the protonated forms of these ligands have also been unsuccessful.

The present Schiff bases react readily with nickel(II) nitrate to yield the bis-ligand complexes of formula, $[Ni(ONSR)_2]$. Attempts to prepare mono-ligated complexes of the type [Ni(ONS)X] (X = Cl, Br, NCS) have been unsuccessful.

The IR spectra of the free ligands display a very

Table 1. Crystal data, data collection and structure refinement parameters for the [Ni(ONSMe)$_2$] complex

Compound	[Ni(ONSMe)$_2$]
Empirical formula	$C_{12}H_{18}N_4NiO_4S_4$
Formula weight	469.25
Temperature	293(2) K
Wavelength	0.71073 Å
Crystal system	Monoclinic
Space group	$P2_1/c$
Unit cell dimension	$a=8.0070(10)$ Å, $\alpha=90^\circ$ $b=12.8440(10)$ Å, $\beta=91.21^\circ$ $c=18.988(2)$ Å, $\gamma=90^\circ$
V	1952.3(4) Å^3
Z	4
Density (calculated)	1.596 mg/m^3
Absorption coefficient	1.446 mm^{-1}
F(OOO)	968
Crystal size	$0.22\times0.72\times0.27$ mm
Θ range for data collection	2.54 to 27.49°
Index ranges	$0\leqslant h\leqslant8$, $0\leqslant k\leqslant16$, $-24\leqslant m\leqslant24$
Reflections collected	4455
Independent reflections	4143 ($R_{int}=0.0216$)
Absorption correction	semi-empirical from ψ-scans
Max. and min. transmission	0.2898 and 0.2313
Refinement method	full-matrix least-squares on F^2
Data/restraints/parameters	4143/0/250
Goodness-of-fit on F^2	1.050
Final R indices [$I>2\sigma(I)$]	$R_1=0.0345$, $wR_2=0.0860$
R indices (all data)	$R_1=0.0481$, $wR_2=0.0941$
Largest diff. peak and hole	0.445 and −0.332 e Å^{-3}

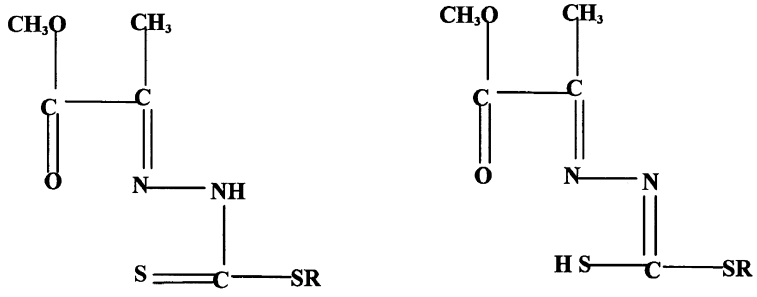

(1a; the thione form; R = CH_3, CH_2 C_6H_5) **(1b; thiol form)**

Fig. 1. The thione (a) and the thiol (b) forms of the ligand.

strong band at 1710 cm^{-1} which is assigned to the ν(C═O) of the carbonyl group. This band is shifted to *ca.* 1655 cm^{-1} in the spectra of the complexes, indicating that the ligands coordinate to the nickel(II) ion via the carbonyl group. The ν(NH) bands of the free ligands at 3220 cm^{-1} completely disappear in the spectra of the complexes indicating that they deprotonate while coordinating with the nickel(II) ion. The azomethine ν(C═N) bands of the ligands at 1610 cm^{-1} undergo a shift to lower frequencies (Table 2) supporting coordination through the azomethine nitrogen atom. The above IR results support that the ligands coordinate to the nickel(II) ion as ONS tridentate chelating agents. This is further supported by the X-ray results discussed later.

The nickel(II) complexes reported here are non-

Table 2. Selected IR bands and electronic spectral data for the ligands and their nickel(II) complexes

Compound	IR bands				Electronic spectral bands[a]	
	ν(N–H)	ν(C=O)	ν(C=N)	ν(N–N)	state	λ_{max} (nm)
HONSMe	3200s	1710s	1610s	1075s	Nujol	388, 300, 255
	3140sh				CH_2Cl_2	385 (3.1), 311 (4.4), 248 (3.5)
HONSBZ	3260s	1710s	1605m	1080s	Nujol	395, 320, 255
					CH_2Cl_2	316 (4.4), 231 (3.7)
$[Ni(ONSMe)_2]$	–	1655s	1560s	1040s	Nujol	915, *ca.* 550sh, 433, 311, 253
					CH_2Cl_2	902 (1.7), 400sh, 342 (4.4), 237 (4.10)
$[Ni(ONSBz)_2]$	–	1655s	1570s	1038s	Nujol	800, *ca.* 500sh, 360, 249
					CH_2Cl_2	915 (1.9), 420sh, 346 (4.5), 233 (4.4)

[a] Log ε ($l\,mol^{-1}\,cm^{-1}$) are in parentheses.

electrolytes in dichloromethane {Λ (Ω^{-1} cm^2 mol^{-1}) <1}, indicating that they coordinate to the nickel(II) ion as uninegatively charged ligands. The brown colours of the complexes may seem to suggest a low-spin configuration for the nickel(II) ion but their room-temperature magnetic moments {2.93BM for $[Ni(ONSMe)_2]$ and 2.94BM for $[Ni(ONSBz)_2]$} indicate that they are of the high-spin type. This is strong evidence that these complexes are six-coordinate and probably octahedral.

Their electronic spectra, in addition to showing intraligand bands at *ca.* 390, 320 and 255 mn, exhibit a ligand to metal charge transfer band at *ca.* 400 nm. The d–d bands were observed at 915 and 550 nm for the $[Ni(ONSMe)_2]$ complex and at 800 and 500 nm for the $[Ni(ONSBz)_2]$ complex. These bands may be assigned to the $^3A_{2g} \Rightarrow {}^3T_{2g}$ and $^3A_{2g} \Rightarrow {}^3T_{1g}$ transitions of octahedral nickel(II), respectively. The third expected band corresponding to the transition, $^3A_{2g} \Rightarrow {}^3T_{1g}(P)$ could not be located probably due to the interference of the intense charge transfer band.

The X-ray crystal and molecular structure of $[Ni(ONSMe)_2]$

The structure of the complex together with the atom numbering scheme used, is shown in Fig. 2. The selected bond lengths and bond angles are listed in Table 3. The complex contains discrete six-coordinate nickel(II) ions with the ligands coordinated to the nickel(II) ion as uninegatively charged ONS tridentate chelating agents via the carbonyl oxygen atom, the azomethine nitrogen atom and the thiolate sulphur atom. The ligand is present as the deprotonated mercaptide form. The deprotonation of the ligand is accompanied by tautomerization to the imino thiolate form. While coordinating in the iminothiolate form, the negative charge on the sulphur atom (generated by deprotonation) is delocalized in the C–N–N–C system as indicated by their intermediate bond distances: C(5A)–N(2A) = 1.315(3) Å, N(2A)–N(1A) = 1.377(3) Å; C(3A)–N(1A) = 1.292(3) Å; C(5B)–N(2B) = 1.312 Å, N(2B)–N(1B) = 1.373(3) Å, C(3B)–N(1B) = 1.295(3) Å. The two Schiff bases are coordinated to the nickel(II) ion in the meridional configurations (the sulfur and carbonyl oxygen atoms *cis* to each other and the azomethine nitrogen *trans*). Bis-chelated nickel(II) complexes of tridentate ligands whose structures are known, have almost always been found to have similar *mer* arrangements of ligands around nickel(II) [11, 20, 21]. The two Ni–N(imine) bond lengths {2.014(2) and 2.013(2) Å} compare well with those of other octahedral nickel(II) complexes of sulphur–nitrogen ligands [11, 20, 21]. The two Ni–S bonds are, however, relatively short compared with other octahedral nickel(II) complexes of related ligands (Table 4). The shorter Ni–S bond lengths in the present complex, compared with those in analogous complexes, are attributed to a stronger nickel–sulphur interaction in this complex. The C–S bond distances in the complexes are longer than those reported for free thiosemicarbazones 1.678 ± 0.002 Å in 4-formylpyridinethiosemicarbazone [22] and 1.684 ± 0.004 Å in 2-keto-3-ethoxybutyraldehydebis(thiosemicarbazone) [23]. The lengthening of the C–S bond can be ascribed to the enethiolization process that occurs prior to coordination of the ligands with the nickel(II) ion. For the purpose of comparison, the nickel(II) donor atom distances in some octahedral nickel(II) complexes of related ligands, whose structures have been determined by diffraction, are shown in Table 4. The data indicate that, bond distances in most octahedral nickel(II) complexes of planar tridentate ligands compare well with each other excepting the Ni–S bond in the present complex, which is much shorter than those in related complexes. In the meridional configuration, the two cis-bonded sulphur atoms are expected to repel each other resulting in longer Ni–S bonds. The electronic effects probably dictate the shorter Ni–S distances in this complex.

The stereochemistry around the nickel(II) ion in the $[Ni(ONSMe)_2]$ complex is a distorted octahedron. The

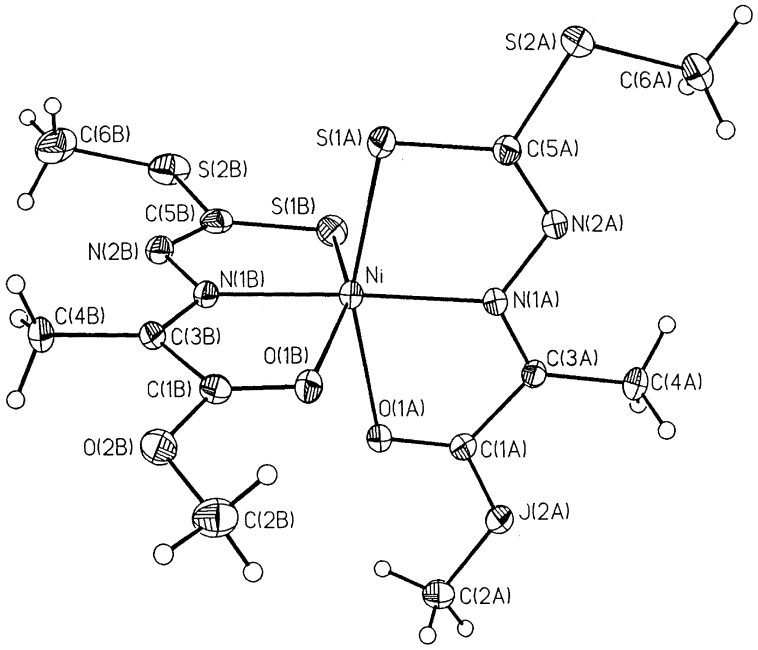

Fig. 2. The structure of $[Ni(ONSMe)_2]$.

Table 3. Selected bond lengths (Å) and bond angles (°) for $[Ni(ONSMe)_2]$

Ni–N(1B)	2.013(2)	Ni–N(1A)	2.014(2)
Ni–O(1A)	2.218(2)	Ni–O(1B)	2.263(2)
Ni–S(1B)	2.3583(9)	Ni–S(1A)	2.3607(8)
C(5A)–S(1A)	1.721(3)	C(5B)–S(1B)	1.715(3)
C(5A)–N(2A)	1.315(3)	C(5B)–N(2B)	1.312(4)
N(2A)–N(1A)	1.377(3)	N(2B)–N(1B)	1.373(3)
N(1A)–C(3A)	1.292(3)	N(1B)–C(3B)	1.295(3)
C(3A)–C(1A)	1.487(3)	C(1B)–C(3B)	1.489(4)
C(1A)–O(1A)	1.223(3)	C(1B)–O(1B)	1.221(3)
N(1B)–Ni–N(1A)	176.94(8)	N(1B)–Ni–O(1A)	100.48(7)
N(1A)–Ni–O(1A)	76.48(7)	N(1B)–Ni–O(1B)	76.22(7)
N(1A)–Ni–O(1B)	103.57(7)	O(1A)–Ni–O(1B)	81.06(7)
N(1B)–Ni–S(1B)	93.55(6)	O(1B)–Ni–S(1B)	156.95(5)
N(1B)–Ni–S(1A)	100.12(6)	N(1A)–Ni–S(1A)	82.94(6)
O(1A)–Ni–S(IA)	157.54(5)	O(1B)–Ni–S(1A)	95.31(5)
S(1B)–Ni–S(1A)	97.78(3)	N(1A)–Ni–S(1B)	96.82(6)

Table 4. Comparison of nickel(II)-donor atom bond lengths (Å) in some six-coordinate nickel(II) complexes of tridentate sulfur–nitrogen chelating agents

Compound	Ni–S(1A)	Ni–S(1B)	Ni–N(1A)	Ni–N(1B)	Ni–X(1A)[a]	Ni–X(1B)[a]	Ref.
$[Ni(pytsc)_2]$[b]	2.440(2)	2.409(2)	2.004(6)	2.056(6)	2.125(7)	2.106(7)	[20]
$[Ni(isoqtsc)_2]$[c]	2.424(2)	2.412(2)	2.013(5)	2.026(5)	2.110(6)	2.114(6)	[21]
$[Ni(NNSMe)_2]$[d]	2.420(3)	2.412(3)	2.056(6)	2.016(6)	2.224(7)	2.166(7)	[11]
$[Ni(ONSMe)_2]$[e]	2.3607(8)	2.3583(9)	2.014(2)	2.013(2)	2.218(2)	2.263(2)	This work

[a] X is carbonylic oxygen or pyridine nitrogen donor.
[b] pytsc is the pyridine-2-carboxaldehydethiosemicarbazone.
[c] isoqstc is isoquinoline-2-carboxaldehyde thiosemicarbazone.
[d] NNSMe is the 6-methyl-2-formylpyridine Schiff base of S-methyldithiocarbazate.
[e] ONSMe is the methylpyruvate Schiff base of S-methyldithiocarbazate.

Table 5. Comparison of selected bond angles (°) for some bis-chelated nickel(II) complexes of tridentate Schiff base ligands

Angle[a]	[Ni(pytsc)2][b]	[Ni(isoqtsc)$_2$][c]	[Ni(NNSMe)$_2$][d]	[Ni(ONSMe)$_2$][e]
S(1B)–Ni–N(1B)	80.7(0.2)	81.3(2)	81.0(2)	82.85(6)
S(1B)–Ni–N(1A)	102.8(0.2)	100.4(2)	93.8(2)	96.82(6)
N(1A)–Ni–S(1A)	79.3(0.3)	81.2(2)	80.6(2)	82.94(6)
N(1A)–Ni–N(1B)	169.0(0.2)	177.5(2)	172.8(3)	176.94(8)
X(1A)–Ni–S(1B)	93.2(0.2)	91.5(2)	90.7(2)	93.55(6)
X(1B)–Ni–S(1B)	158.1(0.2)	159.0(2)	158.1(2)	156.95(5)
X(1A)–Ni–S(1A)	156.9(0.2)	159.0(2)	157.6(2)	157.54(5)
X(1A)–Ni–N(1A)	78.1(0.2)	78.2(2)	77.6(3)	76.48(7)

[a] X is carbonyl oxygen or pyridine nitrogen.
[b] pytsc is the pyridine-2-carboxaldehydethiosemicarbazone [20].
[c] isoqtsc is the isoquinoline-2-carboxaldehydethiosemicarbazone [21].
[d] NNSMe is the 6-methyl-2-pyridinecarboxaldehyde Schiff base of S-methyldithiocarbazate [11].
[e] ONSMe is the methyl pyruvate Schiff base of S-methyldithiocarbazate [this work].

S(1A)–Ni–S(1B) angle is 97.78(3)° which is larger than the ideal value of 90°, expected for a perfect octahedron. The twelve angles subtended at the nickel(II) ion by adjacent donor atoms range from 76.22(7)° for the N(1B)–Ni–O(1B) angle to 103.57(7)° for the N(1A)–Ni–O(1B) angle, indicating appreciable distortion from idealized geometry. The distortion from an ideal octahedral geometry is attributed to the restricted bite angles imposed by the planar tridentate ligands. For the purpose of comparison, the bond angles of [Ni(ONSMe)$_2$] and those of other related bis-ligand six-coordinate nickel(II) complexes are listed in Table 5. The data show that none of the bond angles in these complexes are close to the idealized values expected for a regular octahedral structure. From the limited structural data available on octahedral bis-chelated nickel(II) complexes of sulphur–nitrogen chelating agents, it can be safely stated that distortion is a common phenomenon in six-coordinate nickel(II) complexes of planar tridentate SN donor ligands.

Acknowledgements—Financial support from the University of Brunei Darussalam is gratefully acknowledged.

REFERENCES

1. Akbar Ali, M., Guan, T. S., Bhattacharjee, P., Butcher, R. J., Jasinski, J. P., Li Yu, *Trans. Met. Chem.*, 1996, **21,** 351.
2. Akbar Ali, M., Fernando, K. R., Palit, D. and Nazimuddin, M., *Trans. Met. Chem.*, 1995, **20,** 19.
3. Hossain, M. E., Alam, M. N., Akbar Ali, M., Nazimuddin, M., Smith, F. E. and Hynes, R. C., *Polyhedron*, 1996, **15,** 973.
4. Hossain, M. E., Alam, M. N., Akbar Ali, M., Nazimuddin, M., Begum, J., Smith, F. E. and Hynes, R. C., *Inorg. Chim. Acta*, 1996, **249,** 207.
5. Akbar Ali, M., Haroon, C. M., Nazimuddin, M., Majumder, S. M. M. H., Tarafder, M. T. H. and Khair, M. A., *Trans. Met. Chem.*, 1992, **17,** 133.
6. Zhou, Z., Yu, K., Gou, S. and You, X., Xu, Z., *Polyhedron*, 1991, **10,** 371.
7. Bhattacharjee, S. and Bhattacharjee, R. G., *J. Chem. Soc. Dalton Trans.*, 1992, 1357.
8. Nazimuddin, M., Akbar Ali, M. and Smith, F. E., *Trans. Met. Chem.*, 1992, **17,** 74.
9. Abu-Raqabah, A., Davies, G., El-Sayed, M. A., El-Toukhy, A., Shaikh, S. N. and Zubeita, J., *Inorg. Chim. Acta*, 1992, **193,** 43.
10. Onan, K. D., Davies, G., El-Sayed, M. A. and El-Toukhy, A., *Inorg. Chim. Acta*, 1986, **119,** 121.
11. Akbar Ali, M., Majumder, S. M. M. H., Butcher, R. J., Jasinski, J. P. and Jasinski, J. M., *Polyhedron*, 1997, **16,** 2749.
12. Majumder, S. M. M. H., Akbar Ali, M. and Smith, F. E., *Polyhderon*, 1987, **6,** 1653.
13. Akbar Ali, M., Hossain, G., Majumder, S. M. M. H. and Nazimuddin, M., *Polyhedron*, 1987, **6,** 1653.
14. Das, M. and Livingstone, S. E., *Br. J. Cancer*, 1978, **37,** 101.
15. Gilmore, C. J., *J Appl. Cryst.*, 1984, **17,** 42.
16. Gronbaek-Hazell, R., *Acta Chem. Scand.*, 1992, **26,** 1653.
17. Cravalca, L., Nardelli, M. and Fava, G., *Acta Cryst.*, 1962, **15,** 1139.
18. Tiumken, M. D., Wilson, S. R. and Hendrickson, D., *Inorg. Chem.*, 1985, **24,** 3450.

19. Souza, P., Matesanz, A. I. and Fernandez, V., *J. Chem. Soc. Dalton Trans.*, 1996, 3011.
20. Clark, G. R. and Palenik, G. J., *Cryst. Struct. Comm.*, 1980, **9,** 449.
21. Mathew, M. and Palenik, G. J., *J. Am. Chem. Soc.*, 1969, **91,** 6310.
22. Restivo, R. J. and Palenik, G. J., *Acta Cryst. B*, 1970, **26,** 1397.
23. Gabe, E. J., Taylor, M. R., Pickworth Glusker, J., Minkin, J. A. and Patterson, A. L., *Acta Cryst. B*, 1969, **25,** 1620.

Pergamon

PII: S0277-5387(98)00194-6

Polyhedron Vol. 17, No. 22, pp. 3963–3967, 1998
© 1998 Elsevier Science Ltd
All rights reserved. Printed in Great Britain
0277–5387/98 $19.00+0.00

Synthesis, photochemical and conducting properties of oligo(digermanylene–phenylene)s and related compounds

Kunio Mochida,[a]* Shigeru Maeyama,[a] Masanobu Wakasa[b] and Hisaharu Hayashi[b]

[a]Department of Chemistry, Faculty of Science, Gakushuin University, 1-5-1 Mejiro, Tokyo 171-8588, Japan

[b]The Institute of Physical and Chemical Research (Riken), Wako, Saitama 351-0106, Japan

(Received 16 March 1998; accepted 7 May 1998)

Abstract—Oligo(digermanylene–phenylene)s and related oligomers were prepared by treatment of di-Grignard reagents of the corresponding aryl dibromides with 1,2-dichlorotetramethyldigermane. Upon ultraviolet irradiation of films of oligo(digermanylene–phenylene) and related oligomer in air, the germanium–germanium bond in the oligomer films changed into a digermoxane chain probed by XPS. The laser flash photolysis of the oligo(digermanylene–phenylene) film showed the formation of an oligogermyl radical as a reactive intermediate during photodegradation. Iodine doping of the oligomers showed the conductivities of the order of 10^{-4} S cm^{-1}.
© 1998 Elsevier Science Ltd. All rights reserved

Keywords: polygermane; photolysis; laser flash photolysis; XPS spectra conductivity.

INTRODUCTION

Considerable interest has been focussed on polymers having a regular alternating arrangement of a group 14 element σ unit and a π-electron system in the backbone in view of their novel properties and potential applications [1, 2, 2–5, 5, 6, 6–9]. These polymers strongly absorb light in the ultraviolet (UV) and near-UV regions, owing to σ–π conjugation. Bleaching of the absorption band is caused by a decomposition of the group 14 element–group 14 element bond under UV irradiation. Therefore, the polymers are quite photosensitive and have an attractive possibility to be used as photoresists. This polymer also shows conducting properties when the polymer is doped with an oxidizing agent such as antimony pentafluoride. While the synthesis and properties of poly(disilanylene-π electron system)s have been amply investigated, there have been few reports on those of poly(digermanylene-π electron system)s [7, 10, 11]. As part of our problem to explore the synthesis and properties of new classes of polygermanes [11–13], we herein describe the synthesis, photochemical and conducting properties of oligo(digermanylene–phenylene)s and related oligomers.

RESULTS AND DISCUSSION

Oligo(digermanylene-π electron system)s were prepared by treatment of di-Grignard reagents obtained from 1,2-, 1,3-, 1,4-dibromobenzene and 2,5-dibromothiophene with 1,2-dichlorotetramethyldigermane. The oligo-(digermanylene-π electron system)s were fractionated by precipitation from toluene with 2-propanol. The molecular weights (M_w) of the oligomers were measured by gel permeation chromatography (GPC) using polystyrene sample for calibration. The oligomers had a narrow molecular weight distribution (M_w/M_n) but were in relatively low yields.

The M_w, M_w/M_n, UV data and ionization potentials (IP's) of the oligomers are summarized in Table 1.

Oligo(digermanylene-1,2-phenylene) (**1**), oligo (digermanylene-1,3-phenylene) (**2**), oligo(digermanylene-1,4-phenylene) (**3**) and oligo(digermanylene-2,5-thienylene) (**4**) have characteristic electronic absorp-

* Author to whom correspondence should be addressed.

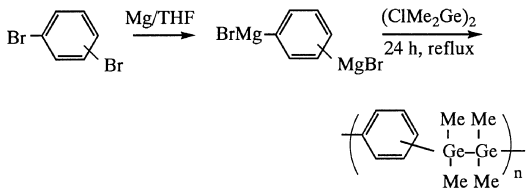

tion bands. The oligomers **1**–**4** have a more intense broad absorption from 200 nm ($\varepsilon < 10^4$ at 250 nm), tailing down into the visible region. The very high extinction coefficients of oligomers **1**–**4** may be attributed to an extension of the Ge–Ge σ conjugation effects into π systems. The values of IP's of oligomers **1**–**4** were in the 5.00–5.78 eV range.

The oligomers **1**–**4** are isolated as colorless or pale yellow solids and moderately light-sensitive molecules. The oligomers **1**, **2** and **4** are soluble in common organic solvents such as chloroform, benzene, toluene and THF and show film-forming properties. The oligomer **3** is little soluble.

Thin films of the oligomer **1**, **4** were prepared by spin-coating from a 5–10% THF solution. The film was deposited on a quartz plates and dried under a vacuum at room temperature. The film thickness of the oligomer, which was determined by UV-VIS spectrometry, was 0.4–0.6 μm [14]. As expected, an oligomer film is quite light sensitive. Figure 1 shows the bleaching of a film of oligomer **1**, **4** by irradiation with a 110-W low-pressure Hg arc lamp ($\lambda = 254$ nm) at room temperature in air. The decrease of the absorbance of the oligomer upon irradiation is caused by a Ge–Ge chain scission [13, 15, 16]. After UV irradiation for 5 min, the oligogermane films were dissolved in THF and their M_w's were determined by GPC analysis. GPC spectra showed an almost constant of M_w for the oligomer. Thus, these UV and GPC results show that the Ge–Ge bonds in films of oligogermanes change into a digermoxane chain after UV irradiation.

In addition to UV observation, the process of photodegradation of the oligomer film was observed by X-ray photoelectron spectroscopy (XPS) [17]. The XPS spectra of the Ge 3d region for the oligomer **1**, **4** film were observed both before and after UV irradiated at 254 nm, as shown in Fig. 2. The XPS spectra before UV irradiation shows a peak at 33 eV attributed to the Ge–Ge structure. After UV irradiation in air for 1 h, the peak of Ge–Ge almost disappears and the peak at 38 eV, assigned to the Ge–O–Ge structure, increases. These results of XPS spectra showed that the Ge–Ge bonds in films of oligogermanes changed into Ge–O–Ge chains after UV irradiation.

To obtain information about reactive intermediates in the photodegradation of an oligo(digermanylene-1,2-phenylene) film **1**, the laser flash photolysis ($\lambda = 266$ nm) of the oligomer film **1** was carried out in air [16]. To avoid the thermal and photodegradation of the oligomer film induced by the intense pulsed laser light, measuring spot on the film was shifted after each excitation. The laser flash photolysis of the oligomer film **1** at 293 K gave a transient absorption peak at *ca.* 310 nm, as shown in Fig. 3. The transient peak at *ca.* 310 nm has been assigned to that of the oligogermyl radicals by comparing its spectral characteristics with those for similar previously reported polygermyl radicals in solutions and films [16, 18]. No transient peaks assigned to germylenes (420–450 nm) were observed. Thus, the key intermediate is oligogermyl radicals generated by a Ge–Ge bond scission in the photodegradation of the oligo(digermanylene-1,2-phenylene) film **1** in air.

In general, oligogermanes composed of an alternating digermanylene unit and π electron system are insulators (10^{-9} S cm^{-1}). However, when the oligomers are treated with an oxidizing agent such as SbF_5 and I_2, they become conducting. Thus, when thin films of oligomers **1**–**4** and related compounds were exposed to iodine vapor under reduced pressure (1 mm Hg), the conductivity of the films increased steadily and reached almost constant values after 1 h of doping. The conductivity at this point was determined to be $(1.0–1.3) \times 10^{-4}$ S cm^{-1} by the direct current four-probed method. Germanium-containing polymers and oligomers show similar conductivity as compared with the corresponding silicon analogues [7, 9,

Table 1. Properties of oligo(digermanylene-π electron system)s **1**–**4**

Oligomer		M_w (10^3)	M_w/M_n	λ_{max} (nm) (ε)[a]	IP (eV[b])	Yield (%)
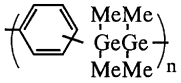	1,2-(**1**)	4.0	1.3	260 (17600)	5.19	24.0
	1,3-(**2**)	4.7	1.6	235 (15400)	5.26	20.0
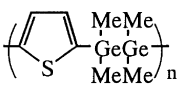	1,4-(**3**)	3.0	1.2	249 (12200)	5.00	12.0
	(**4**)	2.6	1.1	263 (17000)	5.78	20.0

[a] In THF.
[b] Retarding-field UPS.

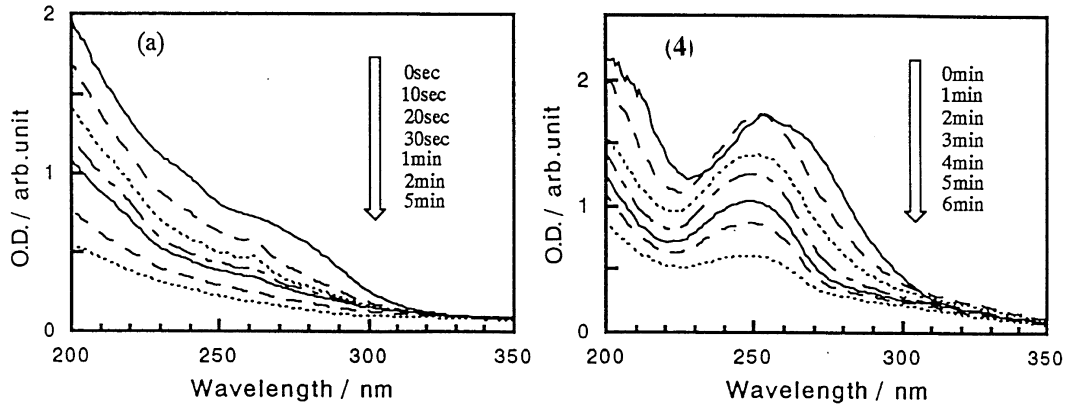

Fig. 1. UV spectra of films of oligomers **1**, **4** with successive UV irradiation.

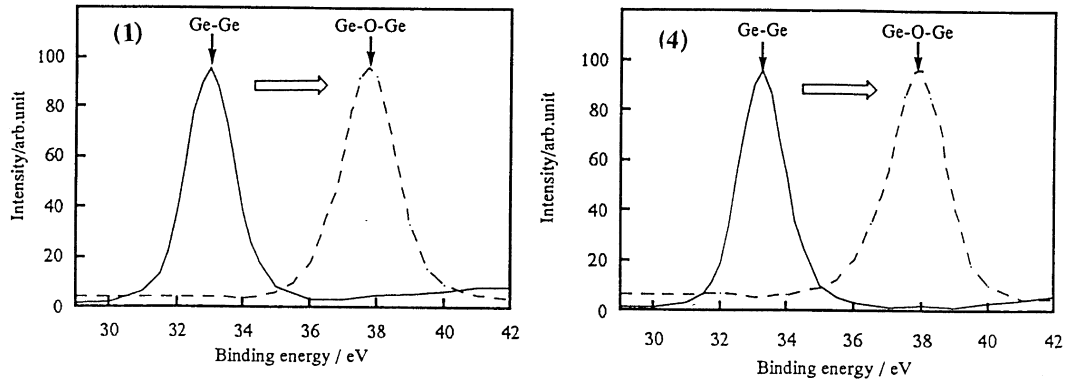

Fig. 2. XPS spectra of films of oligomers **1**, **4** before UV irradiation (———) and after UV irradiation (· · ·) in the air.

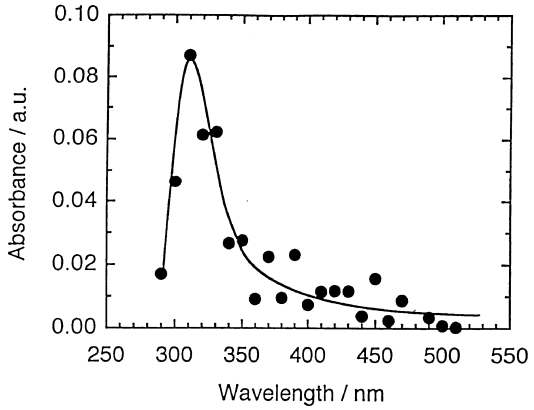

Fig. 3. Transient absorption spectrum obtained by laser flash photolysis of oligomer **1** in the air after excitation at 0.2 μs.

Table 2. Conductivity of oligomer **1**–**4** and related compounds with I_2 vapor

		Conductivity (S/cm)[a]	
Oligomer	M_w	pristine (10^{-9})	doped (10^{-4})
1		6.8	1.1
2		2.8	1.2
3		1.4	1.3
4		27.0	1.1
$(PhMeGe)_n$	5400	8.2	1.7
$(PhGe)_n$	1700	2.0	0.2

[a]In vacuum.

19]. The conductivity of the polymer and oligomer shown in Table 2 are in the same range (10^{-4} S cm^{-1}).

EXPERIMENTAL

^{1}H and ^{13}C NMR spectra were recorded with a Varian Unity-Inova 400 MHz NMR. The GC-MS spectra were recorded using a JEOL JMS-DX 303 mass spectrometer. The UV and UV-VIS spectra were recorded on a Shimadzu UV 2200 spectrometer. Interference spectra were observed with a Hitachi U-3500 UV-VIS spectrometer. Gas chromatography was done on a Shimadzu GC8A with 1 m 20% SE30 and 30% Apiezon L columns. Liquid chromatography

was done on a Twincle with an Asahipak GS 310 column.

Preparation of oligo(digermanylene-1,3-phenylene)

Oligo(digermanylene-1,2-phenylene) and oliogo-(digermanylene-1,3-phenylene) were prepared as described [10]. Oligo(digermanylene-1,4-phenylene) and oligo(digermanylene-2,5-thienylene) were prepared in the same manner by treatment of di-Grignard reagents obtained from *p*-dibromobenzene and 2,5-dibromothiophene, respectively, with 1,2-dichlorotetramethyldigermane as described [7, 10]. As a representative example, the preparation of oliogo (digermanylene-1,3-phenylene) is described. Magnesium (0.97 g, 40 mmol) and *m*-dibromobenzene (4.72 g, 20 mmol) in THF (5 cm^3) were added to a dry Ar inlet, pressure-equalizing dropping funnel and a mechanical stirrer. Distilled 1,2-dichlorotetramethyldigermane (5.52 g, 20 mmol) was added via a funnel to a di-Grignard reagent. The reaction mixture was added and stirred with refluxing for 20 h. After hydrolysis with water, the organic layer was extracted with toluene. The organic layer was washed copiously with water and dried over anhydrous sodium sulfate. The solvent was removed on a rotary evaporator and the residue was recrystallized with ethanol. The solid was dried at 80°C in a vacuum oven for 5 h (20% yield). ^{1}H NMR ($CDCl_3$) δ 0.46 (s, 3 H), 7.30 (m, 4H); ^{13}C NMR ($CDCl_3$) δ −3.51, 127.50, 132.97, 138.39, 140.89; IR (cm^{-1}, KBr) 2970, 827, 787, 780, 596. Anal. Calcd. for $C_{10}H_{16}Ge_2$: C, 42.68%; H, 5.73%. Found: C, 42.92%; H, 6.18%. Oliogo(digermanylene-1,2-phenylene): ^{1}H NMR ($CDCl_3$) δ 0.41 (s, 3 H), 7.27 (m, 4H); ^{13}C NMR ($CDCl_3$) δ −3.00, 116.62, 123.68, 130.00; IR (cm^{-1}, KBr) 2899, 1414, 1261, 1230, 1095, 1022, 827, 752, 698, 588, 559. Anal. Calcd. for $C_{10}H_{16}Ge_2$: C, 42.68%; H, 5.73%. Found: C, 43.08%; H, 6.05%. Oligo(digermanylene-1,4-phenylene): ^{1}H NMR ($CDCl_3$) δ 0.41 (s, 3 H), 7.26 (m, 4H); ^{13}C NMR ($CDCl_3$) δ −2.90, 130.50, 141.90; IR (cm^{-1}, KBr) 2932, 1377, 1234, 1230, 1111, 827, 773, 600, 572, 480. Anal. Calcd. for $C_{10}H_{16}Ge_2$: C, 42.68%; H, 5.73%. Found: C, 43.22%; H, 6.32%. Oligo (digermanylene-2,5-thienylene): ^{1}H NMR ($CDCl_3$) δ 0.57 (s, 3 H), 7.16 (m, 2H); ^{13}C NMR ($CDCl_3$) δ −1.89, 133.98, 143.82; IR (cm^{-1}, KBr) 2903, 1485, 1402, 1267, 1234, 1199, 979, 941, 831, 790, 734, 603, 572, 495. Anal. Calcd. for $C_8H_{14}SGe_2$: C, 32.30%; H, 5.28%. Found: C, 32.78%; H, 5.76%.

Photochemical reactions of oligo(digermanylene–phenylene)s film by UV

A thin film of oligo(digermanylene–phenylene) was prepared by spin-coating from a 5–10% THF solution. The film was deposited on quartz plates ($10 \times 30 \times 1$ mm) and dried under a vacuum (10^{-3} mm Hg, 1 mm Hg = 133.322 Pa) at room temperature. The film thickness was determined by UV-VIS spectrometer (0.4–0.6 μm). The film was irradiated with a 110-W low-pressure Hg arc lamp (Sen Tokushu Kogen Co.) at room temperature. The absorption spectrum of the film was recorded by UV and UV-VIS spectrometry.

Time-resolved optical absorption

Laser flash photolysis experiments were performed at room temperature by using the fourth harmonic ($\lambda = 266$ nm) of a Quanta-Ray (GCR-130) Nd:YAG laser as an excitory light source. The sample was a thin film of oligo(digermanylene–phenylene) on a quartz plate. The laser pulse was about 6 ns; details concerning the laser-photolysis apparatus and manipulation have been published elsewhere [16].

Conductivity measurement for oligomer films doped with I_2

A thin film of an oligomer was prepared in the same manner as described above. The film was exposed to saturated I_2 vapor under reduced pressure (1 mm Hg) in a glass vessel. The conductivity of the films increased steadily with increasing time of doping and reached almost constant values after 1 h. The conductivities in vacuum at this point were determined by the direct current four-probe method.

Acknowledgements—The authors thank Dr Koichi Handa of Nissan Auto Co. for measuring the XPS of oligo (digermanylene-π electron system)s. We also thank Mitsubisi Material Co. for providing us with germanium tetrachloride. This work was in part supported by a Grant-in-Aid for Scientific Research from the Ministry of Education, Science and Culture (No. 08554024).

REFERENCES

1. Fujino, M. and Isaka, H., *J. Chem. Soc. Chem. Commun.*, 1989, 466.
2a. Hu, S. and Weber, W. P., *Polym. Bull.*, 1989, **21,** 133.
2b. Hong, H. H. and Weber, W. P., *Polym. Bull.*, 1989, **22,** 363.
3. Hengge, E. and Baumegger, A., *J. Organomet. Chem.*, 1989, **369,** C39.
4. Iwahara, T. and Hayase, S., West, R., *Macromolecules*, 1990, **23,** 1298.
5a. Ijadi-Maghsoodi, S., Pang, Y. and Barton, T. J., *J. Polym. Sci. A*, 1990, **28,** 955.
5b. Ijadi-Maghsoodi, S. and Barton, T. J., *Macromolecules*, 1990, **23,** 4485.
6a. Brefort, J. L., Corriu, R. J. P., Gerbier, P., Guerin, C., Henner, B. J. L., Jean, A., Kuhlmann, T., Garnier, F. and Yassar, A., *Organometallics*, 1992, **11,** 2500 and references cited therein.
6b. Chicart, P., Corriu, R. J. P., Moreau, J. J. E., Garnier, F. and Yassar, A., *Inorganic and Organometallic Polymers with Special Porperties*, ed. R.

H. Laine. Kluwer Academic, Dordrecht, The Nethreland, 1992, p. 179.
7. Hayashi, T., Uchimaru, Y., Reddy, N. P. and Tanaka, M., *Chem. Lett*., 1992, 647.
8. Fang, M.-C., Watanabe, A. and Matsuda, M., *J. Organomet. Chem*., 1995, **489,** 15.
9. Kunai, A., Ueda, T., Horata, K., Toyoda, E., Nagamoto, I., Ohshita, J., Ishikawa, M. and Tanaka, K., *Oragnometallics*, 1996, **15,** 2000 and references cited therein.
10. Mochida, K., Nagano, S., Maeyama, S., Kodaira, T., Watanabe, A. and Ito, O., Matsuda, M., *Bull. Chem. Soc. Jpn*., 1997, **70,** 713.
11. Mochida, K., Shibayama, N. and Goto, M., *Chem. Lett*., 1998 (in press).
12. Mochida, K. and Chiba, H., *J. Organomet. Chem*., 1994, **473,** 45.
13. Mochida, K., Ohkawa, T., Kawata, H., Watanabe, A. and Ito, O., Matsuda, M., *Bull. Chem. Soc. Jpn*., 1996, **69,** 2993.
14. Tolansky, S., *Multiple-Beam Interferometry of Surfaces and Films*. Clarendon, 1948.
15. Miller, R. D. and Sooriyakumaran, R., *J. Polym. Sci. Polym. Chem. Ed*., 1987, **25,** 111.
16. Mochida, K., Nagano, S., Kawata, H., Wakasa, M. and Hayashi, H., *J. Organomet. Chem*., 1997, **542,** 75.
17. Avery, N. R., *Vibrationary Spectroscopy of Molecular on Surfaces*, eds. J. T. Yates, Jr., and T. E. Madey. Plenum, 1987.
18. Mochida, K., Kimijima, K., Chiba, H., Wakasa, M. and Hayashi, H., *Organometallics*, 1994, **13,** 404.
19. Kunai, A., Toyoda, E., Horata, K. and Ishikawa, M., *Organometallics*, 1995, **14,** 714.

Pergamon

PII: S0277-5387(98800195-8

Polyhedron Vol. 17, No. 22, pp. 3969–3975, 1998
© 1998 Elsevier Science Ltd
All rights reserved. Printed in Great Britain
0277–5387/98 $19.00+0.00

One-dimensional co-ordination polymers formed by crown ether metal cation bridges: synthesis and crystal structure of nickel(II) dithiolene complexes $[\{Na(benzo\text{-}15\text{-}crown\text{-}5)\}_2 Ni(i\text{-}mnt)_2]_n \cdot nCH_2Cl_2$ and $[\{Na(benzo\text{-}15\text{-}crown\text{-}5)\}_2Ni(mnt)_2]_n$

De-Liang Long,* Yong Cui, Jiu-Tong Chen, Wen-Dan Cheng and Jin-Shun Huang*

State Key Laboratory of Structural Chemistry, Fujian Institute of Research on the Structure of Matter, Chinese Academy of Sciences, Fuzhou, Fujian 350002, PR China

(Received 13 January 1998; accepted 7 May 1998)

Abstract—Reaction of $NiCl_2 \cdot 6H_2O$, Na_2[i-mnt] and benzo-15-crown-5 in CH_3OH/CH_2Cl_2 at room temperature leads to $[\{Na(benzo\text{-}15\text{-}crown\text{-}5)\}_2Ni(i\text{-}mnt)_2]_n \cdot nCH_2Cl_2$ (**1**). The same reaction with Na_2[mnt] instead of Na_2[i-mnt] affords $[\{Na(benzo\text{-}15\text{-}crown\text{-}5)\}_2Ni(mnt)_2]_n$ (**2**). Both complexes were isolated as crystalline products. X-ray diffraction analyses reveal that the main segments of **1** and **2** are infinite "train" structures, in which the building blocks $Ni(i\text{-}mnt)_2$ or $Ni(mnt)_2$ in end-to-end arrangements act as "body frames" and crown cycles standing by the body frames play the role of "cartwheel". They are joined with each other through sodium ions. © 1998 Elsevier Science Ltd. All rights reserved

Keywords: crown ether; nickel(II) dithiolate; crystal structure; co-ordination polymer.

INTRODUCTION

Crown ether compounds have been well known for their co-ordination ability to alkali, alkaline earth and rare earth metal ions to form various types of structures [1, 2]. Benzo-15-crown-5 with five oxygen atoms on its cycle and suitable diameter of cavity reacting with sodium ions affords very usually the sandwiched structure $[Na(benzo\text{-}15\text{-}crown\text{-}5)_2]^+$ (I, see Scheme 1) [3–7]. In a few cases the mono crown cycle-capped sodium cation $[Na(benzo\text{-}15\text{-}crown\text{-}5)]^+$ (II) with remaining co-ordination positions that can accept other donors were detected. Of this type of structure are examples such as $[Na(benzo\text{-}15\text{-}crown\text{-}5)ClO_4]$ reported by Owen [7] and $[Na(benzo\text{-}15\text{-}crown\text{-}5)C_6H_2N_3O_7]$ by Ward *et al.* [8]. It is possible for one

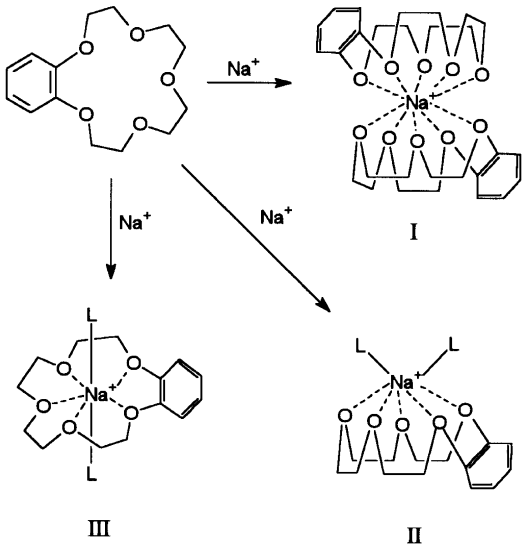

Scheme 1.

* Author to whom correspondence should be addressed. E-mail: ldl@ms.fjirsm.ac.cn.

to use $[Na(benzo\text{-}15\text{-}crown\text{-}5)]^+$ as building blocks to construct low dimensional co-ordination polymer. Herrmann *et al.* [9] reported the one-dimensional structure of $[Na(benzo\text{-}15\text{-}crown\text{-}5)(ReO_4)]_n$, which was characterised by sodium ion in a nearly planar crown ether environment (III) and tetrahedral perrhenate. These subunits are joined with each other resulting in helical perrhenate sodium chains of pentagonal bipyramidal configuration around sodium cations. In this paper we present two novel structures that $[Na(benzo\text{-}15\text{-}crown\text{-}5)]^+$ use its two collateral positions (II) to joint complex anions $[Ni(i\text{-}mnt)_2]^{2-}$ and $[Ni(mnt)_2]^{2-}$ to form infinite chain-like co-ordination polymers, where $[i\text{-}mnt]^{2-}$ and $[mnt]^{2-}$ are conjugated ligands isomalenonitriledithiolate and malenonitriledithiolate, respectively.

The ligand $[i\text{-}mnt]^{2-}$ is a versatile and classic ligand in the synthesis of complexes and cluster compounds, about which a number of research reports were raised in the last two decades [10–16]. Metal complexes with $[mnt]^{2-}$ and its analogous, well known for their reversible redox behaviour and extensive ground-state π-electron delocalisation, had been a subject of considerable attention. Investigation in this area had stimulated much interest of synthetic and materials chemists [17–19]. Recently there is much interest in the search for new and improved synthetic molecular metals and many of these are based on Group 10 metals and planar organic donor molecules such as $[mnt]^{2-}$ [20]. It was thought that other metal ions, for example alkali and alkaline earth metal ions or transition metal ions, could connect the complex anions of $[i\text{-}mnt]^{2-}$ and $[mnt]^{2-}$ ligands by bonding to their cyano groups to build new type of conjugated co-ordination polymer [21]. Up to date the case of low dimensional polymer of these ligands in N-coordinated fashion are very rare. The sole example is $[\{Ni(NH_3)_4\}Ni(S_2C{=}C(CN)\}_2]_\infty$ reported by Zhu *et al.* [22]. However only one cyano group of a $[i\text{-}mnt]^{2-}$ ligand in this compound is co-ordinated to nickel cation $[Ni(NH_3)_4]^{2+}$ and in consideration of the hydrogen bondings this compound has in fact a three-dimensional structure.

EXPERIMENTAL

Material and methods

All reagents and solvents purchased were A.R. or C.P. grade and used without further purification. Na_2[i-mnt] [23] and Na_2[mnt] [24] were prepared as described in the literature. Carbon, hydrogen and nitrogen analyses were carried out on a Perkin-Elmer 240C elemental analyser. The infrared spectra (4000–400 cm^{-1}) and far-infrared spectra (650–100 cm^{-1}) were recorded as KBr and CsI pellets on a Nicolet Magna 750 FT-IR spectrometer.

Preparation of complexes

Solid Na_2[*i*-mnt] (0.37 g, 2 mmol) was added to a solution of $NiCl_2{\cdot}6H_2O$ (0.24 g, 1 mmol) in methanol (20 ml) with stirring. The solution colour immediately turned to yellowish-green. After stirring for 30 min, a dichloromethane solution (20 ml) containing benzo-15-crown-5 (0.54 g, 2 mmol) was added dropwisely. The solution was stirred for another hour and its colour gradually changed to slightly reddish brown. The insoluble substance was filtered off and the solvent was removed by distillation to leave about 10 ml solution. Reddish brown crystals of **1** were obtained. Yield 0.72 g. Anal. calc. for $C_{37}H_{42}Cl_2N_4Na_2NiO_{10}S_4$: C, 44.2; H, 4.2; N, 5.6%. Found: C, 43.9; H, 4.1; N, 5.6%. IR (cm^{-1}) 2208vs ($\nu_{C\equiv N}$), 1597w, 1500s, 1454m ($\nu_{C=C}$, Ph), 1400s, 1377vs, ($\nu_{C=C}$, *i*-mnt), 1252s, 1209s, 1122vs ($\nu_{C\text{–}O\text{–}C}$), 1097s, 1047m, 949s, 941s, 897s ($\nu_{C\text{–}S}$), 748m, 740m, 730m, 480m, 380m, 301m, 210m ($\nu_{Ni\text{–}S}$).

$[\{(Benzo\text{-}15\text{-}crown\text{-}5)Na\}_2Ni(mnt)_2]_n$ **2** was prepared using the similar procedure as above with Na_2[mnt] instead of Na_2[i-mnt]. Deep red crystals of **2** were obtained in yield 0.65 g. Anal. calc. for $C_{36}H_{40}N_4Na_2NiO_{10}S_4$: C, 46.9; H, 4.4; N, 6.1%. Found: C, 46.7; H, 4.3; N, 6.0%. IR (cm^{-1}) 2218m, 2195vs, 2152w ($\nu_{C\equiv N}$), 1597w, 1504s, 1456m ($\nu_{C=C}$, Ph), 1481s ($\nu_{C=C}$, mnt), 1357w, 1257s, 1209s, 1124vs ($\nu_{C\text{–}O\text{–}C}$), 1090m, 1045m, 943s ($\nu_{C\text{–}S}$), 906s, 744m, 735m, 515m, 360m, 224m ($\nu_{Ni\text{–}S}$), 206m.

Crystal structure determination

Single crystals for structure determinations were obtained from methanol solution by slow evaporation of the solvent in air.

The crystal data for compound **1** and **2** are summarised in Table 1, together with some experimental details. Intensity data for compound **1** were obtained on a Siemens Smart/CCD area-detector diffractometer with graphite-monochromated Mo–Kα ($\lambda = 0.71073$ Å) radiation. Measurements was made by using an ω scan mode with a scan speed of 10 second/frame and 0.3°/frame in the range of $1.89 < \theta < 23.28$. Data reductions and cell refinements were performed with Smart-CCD software [25]. The cell parameters were obtained by a least-squares fit of 5639 reflections ($1.89 < \theta < 23.28$). Structure solution and refinement were carried out on an Indy workstation of Silicon Graphics using SHELXTL program package [26]. The structure was solved by direct method. All non-hydrogen atoms were located on the E-map or successive difference Fourier syntheses. The structure was refined by full-matrix least-squares techniques on F^2 with anisotropic thermal parameters for all non-hydrogen atoms. Hydrogen atoms were located theoretically and not refined. The final cycle of full-matrix least-squares refinement converged with $R = \Sigma(|F_o| - |F_c|)/\Sigma|F_o| = 0.040$ and $wR = [\Sigma[w(F_o^2 - F_c^2)^2]/\Sigma[w(F_o^2)^2]]^{1/2} = 0.099$, $w = 1/[\sigma^2(F_o^2) + (0.0599P)^2]$, where $P = (F_o^2 + 2F_c^2)/3$. Single crystal of **2** was scanned on a Enraf Nonius CAD-4 diffractometer with graphite-monochromated Mo-Kα ($\lambda = 0.71073$ Å) radiation. Intensity data were collected by using $\omega/2\theta$ scan mode with

Table 1. Crystal parameter, data collection and structure refinement details

Chemical formula	$C_{37}H_{42}Cl_2N_4Na_2O_{10}NiS_4$	$C_{36}H_{40}N_4Na_2O_{10}NiS_4$
Formula weight	1006.58	921.69
Crystal system	triclinic	triclinic
Space group	*P*-1	*P*-1
a (Å)	10.7382(4)	10.524(2)
b (Å)	11.0193(5)	10.671(3)
c (Å)	19.7752(8)	19.359(6)
α (°)	99.107(1)	76.22(2)
β (°)	95.833(1)	86.52(2)
γ (°)	96.939(1)	88.07(2)
V (Å)	2276.1(2)	2107.0(9)
Z	2	2
D_c (g cm^{-3})	1.469	1.450
Absorption coefficient (cm^{-1})	8.03	7.3
Crystal size (mm^3)	$0.50 \times 0.23 \times 0.22$	$0.80 \times 0.70 \times 0.32$
Absorption correction	SADABS [25]	empirical (ψ-scan)
Transmission factors	0.66–1.00	0.35–1.00
Reflections collected	8806	7394
No. unique data	6270	7394
No. obs. with $I > n\sigma(I)$	4654 ($n=2$)	5912 ($n=3$)
Residuals: *R*; *wR*(*Rw*)	0.040, 0.099	0.060, 0.071
Max. shift in final cycle	0.000	0.004
Peaks in final diff. map	0.51 to -0.63	0.73 to -0.24

Details in common: temperature, 293 K.

a scan speed of 5.5°/min in the range of $2\theta < 50°$. The cell parameters were obtained by a least-squares fit of setting angles for 25 reflections ($11 < \theta < 17$). Structure of **2** was solved by direct method and refined by full-matrix least-squares techniques on *F* with anisotropic thermal parameters for all of the non-hydrogen atoms. Hydrogen atoms were located theoretically and not refined. The final full-matrix least-squares refinement converged with unweighted and weight agreement factors $R = \Sigma(|F_o| - |F_c|)/\Sigma|F_o| = 0.060$ and $Rw = [\Sigma w(|F_o| - |F_c|)^2/\Sigma w|F_o|^2]^{1/2} = 0.071$, $w = 1/[\sigma^2(F_o) + (0.020F_o)^2 + 1.0]$. All calculations were performed on a COMPAQ 486 computer using MOLEN/PC program package [27].

RESULTS AND DISCUSSION

Synthesis

Benzo-15-crown-5 with suitable cavity for Na^+ ion can form complexes in three fashions I, II and III as demonstrated in Scheme 1. The most probable way is I with the sodium ion sandwiched by two ligand molecules. In the synthesis process of **1** and **2**, the reactant ratios were held carefully. The excessive benzo-15-crown-5 may lead to discrete ionic product characterised as $[Na(benzo\text{-}15\text{-}crown\text{-}5)_2]_2[Ni(i\text{-}mnt)_2]$ and $[Na(benzo\text{-}15\text{-}crown\text{-}5)_2]_2[Ni(mnt)_2]$ [28]. Crystals of complex **1** with CH_2Cl_2 molecules included in are easily effloresced by losing the solvents. Crystals of **2** are very stable when exposed to air. Both the complex polymers are soluble in CH_3OH, CH_3CN, DMF and DMSO and barely dissolved in $CHCl_3$ and water. Complex anion $[Ni(mnt)_2]^{2-}$ in solution is easily oxidised to $[\{Ni(mnt)_2\}_2]^{2-}$ as reported in literature [20]. When the solution of complex **2** was evaporated slowly in air for single crystal growth, a little amount of black crystals was obtained and characterised as $[Na_2(H_2O)_2(benzo\text{-}15\text{-}crown\text{-}5)_3][\{Ni(i\text{-}mnt)_2\}_2]$ by X-ray diffraction, which has nickel(III) dithiolene complex anions and interesting triple-decker crown ether sodium dications [28].

Description of the structure

The labelling scheme and ORTEP diagram of the asymmetric unit for **1** and **2** are shown in Figs 1 and 2. The structures of the moieties [Na(benzo-15-crown-5)] in both **1** and **2** are similar to that of $[Na(benzo\text{-}15\text{-}crown\text{-}5)ClO_4]$ reported by Owen [7] and that of $[Na(benzo\text{-}15\text{-}crown\text{-}5)(C_6H_2N_3O_7)]$ by Ward *et al.* [8]. Each of the sodium ions is half-capped by one benzo-15-crown-5 cycle through co-ordinated oxygen atoms. The Na^+ ions lie about 1.0 Å towards the complex anions from the plane of the five O atoms of associated crown cycles. The oxygen atoms are coplanar to within not larger than 0.5 Å. The Na–O distances in the two structures fall in the range from 2.375(5) to 2.544(4) Å and have a mean value of 2.452(5) Å. Both the lower and upper limits occur at Na(2) in **2**. The selected bond distances and angles are listed in Tables 2 and 3 together with the average Na^+–O bond dis-

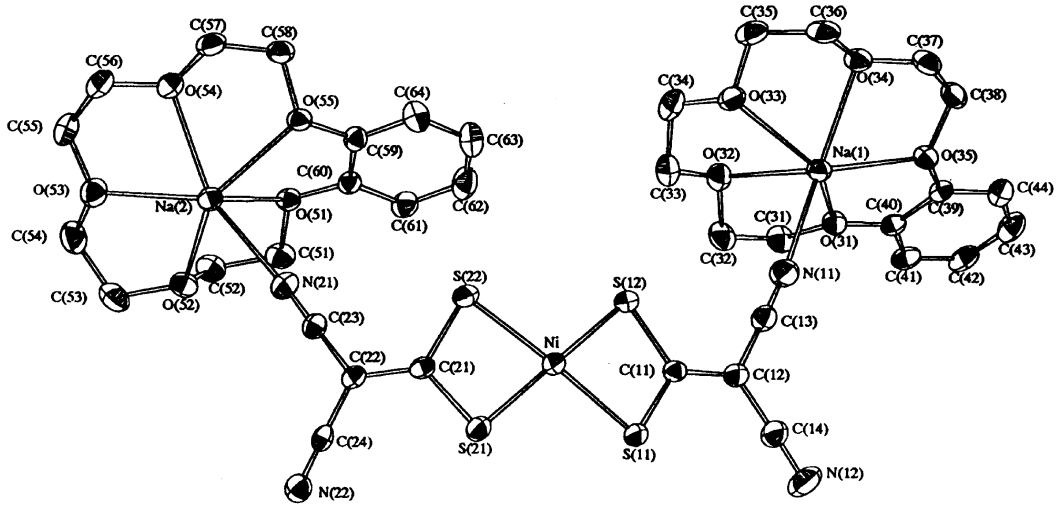

Fig. 1. ORTEP drawing of the molecular structure and labelling scheme for the main segment of **1**. Displacement ellipsoids are shown at the 25% probability level and hydrogen atoms have been omitted for clarity.

tances for individual sodium ions. From the sum of the van der Waals radii [29] 1.40 Å for O and the effective ionic radii 1.02 Å for Na^+, one may expect distance Na^+–O of 2.42 Å. The mean value for the twenty Na^+–O distances in **1** and **2** is in perfect agreement with predicted values and is comparable to 2.399(5) Å (average) observed in [Na(benzo-15-crown-5)ClO_4] [7] and 2.430(3) Å in [Na(benzo-15-crown-5)($C_6H_2N_3O_7$)] [8].

The remarkable structural feature for **1** is the four Na^+–NC bonds and for **2** is the three Na^+–NC bonds and a weak Na^+–S interaction. These contacts link the $[Na(benzo\text{-}15\text{-}crown\text{-}5)]^+$ cations and $[Ni(i\text{-}mnt)_2]^{2-}$ or $[Ni(mnt)_2]^{2-}$ anions to form infinite -Ni-(i-mnt)-$[Na(benzo\text{-}15\text{-}crown\text{-}5)]_2$-(i-mnt)- or -Ni-(mnt)-$[Na(benzo\text{-}15\text{-}crown\text{-}5)]_2$-(mnt)- chains. For the asymmetrical unit, there exist two inversion centres located at the midway between Na(1) and Na(1^i) as well as Na(2) and Na(2^{ii}) (symmetry code for **1**, *i*: $1-x, 1-y, 1-z$; ii: $2-x, -y, -z$ and for **2**, i: $1-x, 1-y, -z$; ii: $2-x, 1-y, 1-z$). From the sum of the van der Waals radii (1.50 Å for N and 1.8 Å for S) [29] and the effective ionic radii for Na^+, the expected distances for Na^+–N and Na^+–S are 2.52 and 2.82 Å, respectively. The Na(1)–N(11), Na(2)–N(21) and Na(2)–N(22^{ii}) in **1** and Na(1)–N(11), Na(2)–N(21) in **2** are all shorter than the predicated value of 2.52 Å, which indicates the genuine bonds between sodium ions and those cyano groups. Na(2)–N(21^{ii}) in **1** and Na(1)–N(12^i), Na(2)–S(22^{ii}) in **2** are slightly longer

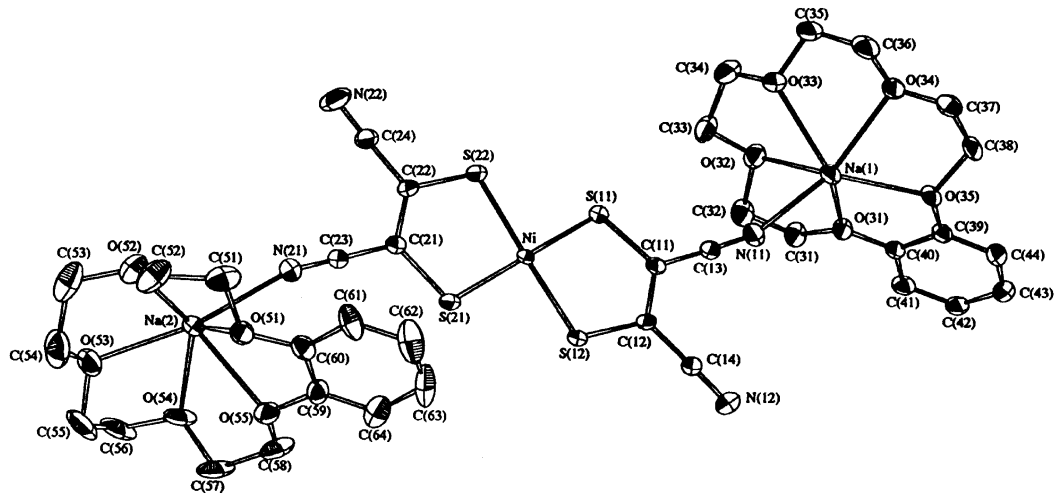

Fig. 2. ORTEP drawing of the molecular structure and labelling scheme for the anion portion of **2**. Displacement ellipsoids are shown at the 25% probability level and hydrogen atoms have been omitted for clarity.

Table 2. Selected bond distances (Å) and angles (°) of $[\{Na(benzo\text{-}15\text{-}crown\text{-}5)\}_2Ni(i\text{-}mnt)_2]_n(CH_2Cl_2)_n$, **1**

Ni–S(11)	2.203(1)	Ni–S(21)	2.201(1)
Ni–S(12)	2.205(1)	Ni–S(22)	2.212(1)
Na(1)–O(31)	2.411(3)	Na(2)–O(51)	2.449(2)
Na(1)–O(32)	2.505(3)	Na(2)–O(52)	2.407(2)
Na(1)–O(33)	2.434(3)	Na(2)–O(53)	2.441(3)
Na(1)–O(34)	2.425(2)	Na(2)–O(54)	2.462(3)
Na(1)–O(35)	2.417(2)	Na(2)–O(55)	2.426(2)
Na(1)–O (average)	2.438(3)	Na(2)–O (average)	2.438(3)
Na(1)–N(11)	2.469(4)	Na(2)–N(21)	2.496(3)
Na(1)–N(12^{i})	2.995(5)	Na(2)–N(22^{ii})	2.502(3)
S(11)–C(11)	1.716(3)	S(21)–C(21)	1.724(3)
S(12)–C(11)	1.714(3)	S(22)–C(21)	1.722(3)
N(11)–C(13)	1.141(4)	N(21)–C(23)	1.146(4)
N(12)–C(14)	1.135(5)	N(22)–C(24)	1.142(4)
C(11)–C(12)	1.379(4)	C(21)–C(22)	1.381(4)
C(12)–C(14)	1.418(5)	C(22)–C(23)	1.417(5)
C(12)–C(13)	1.428(5)	C(22)–C(24)	1.427(5)
S(11)–Ni–S(12)	78.88(3)	S(21)–Ni–S(11)	100.45(3)
S(11)–Ni–S(22)	172.45(4)	S(21)–Ni–S(12)	178.27(4)
S(12)–Ni–S(22)	100.88(4)	S(21)–Ni–S(22)	79.57(3)
N(11)–Na(1)–N(12^{i})	73.4(2)	N(21)–Na(2)–N(22^{ii})	82.3(2)
S(12)–C(11)–S(11)	109.4(2)	S(22)–C(21)–S(21)	110.1(2)
C(13)–N(11)–Na(1)	174.6(3)	C(23)–N(21)–Na(2)	172.7(3)
C(14)–N(12)–Na(1^{i})	111.0(4)	C(24)–N(22)–Na(2^{ii})	114.2(3)

Symmetry code i: $1-x, 1-y, 1-z$; ii: $2-x, -y, -z$.

Table 3. Selected bond distances (Å) and angles (°) of $[\{(benzo\text{-}15\text{-}crown\text{-}5)Na\}_2Ni(mnt)_2]_n$, **2**

Ni–S(11)	2.177(1)	Ni–S(21)	2.169(1)
Ni–S(12)	2.169(1)	Ni–S(22)	2.166(1)
Na(1)–O(31)	2.403(4)	Na(2)–O(51)	2.544(4)
Na(1)–O(32)	2.543(4)	Na(2)–O(52)	2.464(5)
Na(1)–O(33)	2.477(5)	Na(2)–O(53)	2.375(5)
Na(1)–O(34)	2.421(4)	Na(2)–O(54)	2.471(4)
Na(1)–O(35)	2.435(4)	Na(2)–O(55)	2.528(5)
Na(1)–O (average)	2.456(5)	Na(2)–O (average)	2.476(5)
Na(1)–N(11)	2.510(5)	Na(2)–N(21)	2.477(5)
Na(1)–N(12^{i})	2.986(6)	Na(2)–S(22^{ii})	3.176(2)
S(11)–C(11)	1.715(5)	S(21)–C(21)	1.719(5)
S(12)–C(12)	1.723(5)	S(22)–C(22)	1.734(5)
N(11)–C(13)	1.149(6)	N(21)–C(23)	1.142(7)
N(12)–C(14)	1.154(8)	N(22)–C(24)	1.127(8)
C(11)–C(12)	1.397(6)	C(21)–C(22)	1.363(6)
C(11)–C(13)	1.421(6)	C(21)–C(23)	1.434(7)
C(12)–C(14)	1.421(8)	C(22)–C(24)	1.428(8)
S(11)–Ni–S(12)	91.88(5)	S(12)–Ni–S(21)	87.88(5)
S(11)–Ni–S(21)	177.67(5)	S(12)–Ni–S(22)	174.25(5)
S(11)–Ni–S(22)	88.65(5)	S(21)–Ni–S(22)	91.82(5)
N(11)–Na(1)–N(12^{i})	73.8(1)	S(22)–Na(2)–N(21^{ii})	89.4(1)
Na(1)–N(11)–C(13)	163.5(4)	Na(2)–N(21)–C(23)	161.9(4)
Na(1)–N(12)–C(14^{i})	125.6(4)		

Symmetry code i: $1-x, 1-y, -z$; ii: $2-x, 1-y, 1-z$.

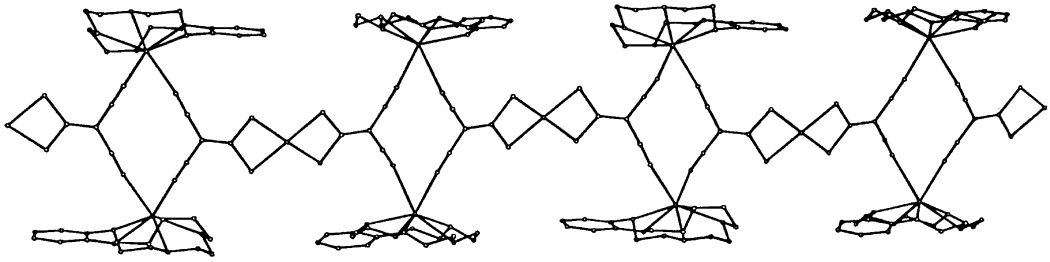

Fig. 3. A drawing of the polymer chain for the main segment of **1**.

than the predicted values showing weaker interactions between these atoms. If all these contacts are taken into consideration, the formation of chain-like polymers are obvious. Typical Na^+–N distances reported are Na^+–$NCCH_3$ 2.523(10) Å in $(NaI)_2(CH_3CN \cdot H_2O)_3$ [30], Na^+–NCS 2.396(2) Å in $Na(C_{12}H_{24}O_5S)(SCN)$ ($C_{12}H_{24}O_5S$ = crown thioether) [31] and Na^+–NC 2.532(15) and 2.568(14) Å in $NaAg(CN)_2$ [32]. A sodium-sulphur co-ordination is primarily found in inorganic compounds with Na^+–S distances in the range 2.8–3.1 Å [33]. The Na^+–N and Na^+–S contacts in Na_2[i-mnt] [34] were found to be 2.616(5) and 2.943(2) Å (average), respectively. The polymer chain structures of **1** and **2** can be described in terms of infinite "train" for the end-to-end arrangements of the complex anions that are considered to be the "body frames". Thus the crown cycles standing by the "body frames" act as "cartwheels" and that joint the body-frame and cartwheels are the sodium ions. Drawings of polymer chain of **1** and **2** are demonstrated in Figs 3 and 4.

For the crystal structures of **1** and **2**, there are two polymer chains in a cell, related to each other through the cell centre (1/2, 1/2, 1/2). One Ni atom was found in the asymmetrical unit co-ordinated by four S atoms of two i-mnt or mnt units. The NiS_4 grouping in both the structures is essentially planar. Notable deviations from planarity are found however when the whole $[Ni(i\text{-}mnt)_2]^{2-}$ and $[Ni(mnt)_2]^{2-}$ units are considered and probably due to the packing force. Na(1) and Na(2) are separately within planes of the nearest ligands with deviations not larger than 0.1 Å. The Ni–S distances in **1** are regularly in the range of 2.201(1) to 2.213(1) Å and are comparable to 2.106(4) Å found in $[\{Ni(NH_3)_4\}Ni(S_2C{=}C(CN)\}_2]_\infty$ [22]. The geometry of the i-mnt ligands in **1** is nearly the same as those detected in this compound. The average C–S bond distance of 1.719(5) shows some double-bond character, which is near the value of 1.713(3) Å observed in Na_2[i-mnt] [34] and is slightly shorter than 1.78(2) Å in the complex $[\{Ag(PPh_3)_2\}_2Ni(i\text{-}mnt)_2]$, in which the sulphur atoms co-ordinate to both Ni and Ag atoms tetrahedrally [35]. For compound **2** the Ni–S separations are slightly shorter than the corresponding values in **1** indicating the difference of cycle intension affecting on bond distances between a five-membered ring and a four-membered one. Structure details with mnt in **2** are similar to those found in $[NBu_4]_2[Ni(mnt)_2]$ [36] and $[\{Ag(PPh_3)_2\}_2Ni(mnt)_2]$ [35]. Compared with the values in free ligand $[i\text{-}mnt]^{2-}$ and $[mnt]^{2-}$ before complexation, no significant changes for the C–C, C=C, C≡N bond distances in both the two structures were found. This indicates that the bondings in the complex polymers are similar to those in free ligands with the delocalization of the π system.

Acknowledgements—This work was supported by grants from the National Natural Science Foundation of China. Dr Long acknowledges the funds from the Postdoctoral Research Foundation of China.

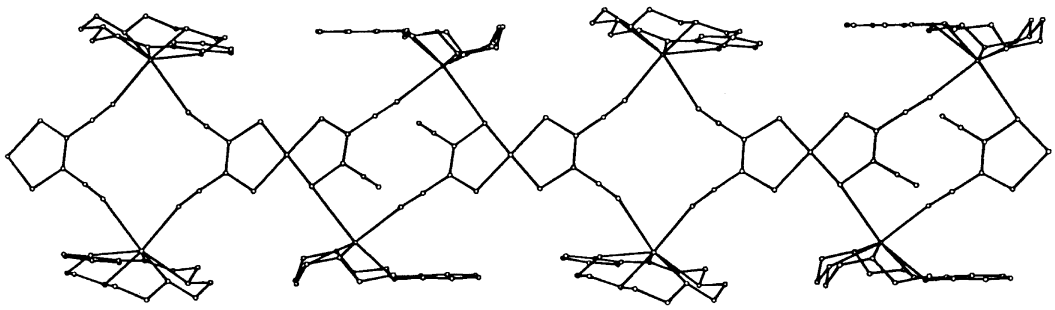

Fig. 4. A drawing of the polymer chain of **2**.

REFERENCES

1. Poonia, N. S., Bagdi, P. and Sidhu, K. S., *J. Inclusion Phenom.*, 1986, **4,** 43.
2. Bock, H., Hauck, T., Naether, C. and Havlas, Z., *Angew. Chem. Int. Ed. Engl.*, 1997, **36,** 638.
3. Long, D.-L., Jin, Q.-H., Xin, X.-Q. and Yu, K.-B., *Acta Cryst. C*, 1997, **C53,** 554.
4. Bush, M. A. and Truter, M. R., *J. Chem. Soc. Perkin Trans.*, 1972, **2,** 341.
5. Dreissig, W., Dauter, Z., Cygan, A. and Biernat, J. F., *Inorg. Chim. Acta*, 1985, **96,** 21.
6. Moody, D. C. and Ryan, R. R., *Cryst. Struct. Commun.*, 1979, **8,** 933.
7. Owen, J. D., *J. Chem. Soc. Dalton Trans.*, 1980, 1066.
8. Ward, D. L., Popov, A. I. and Poonia, N. S., *Acta Cryst. C*, 1984, **40,** 238.
9. Herrmann, W. A., Kucher, J. G., Weichselbaumer, G., Herdtweck, E. and Kiprof, P., *J. Organomet. Chem.*, 1989, **372,** 351.
10. Long, D., Zheng, H., Xin, X., Sakane, G. and Shibahara, T., *Polyhedron*, 1997, **16,** 4305.
11. Hummel, H.-U., *Trans. Met. Chem.*, 1987, **12,** 172.
12. Li, H. Y. and Amma, E. L., *Inorg. Chim. Acta*, 1990, **177,** 5.
13. Hummel, H.-U. and Meske, H., *J. Chem. Soc. Dalton Trans.*, 1989, 627.
14. Khan, Md. N. I., Wang, S., Fackler, Jr., J. P., *Inorg. Chem.*, 1989, **28,** 3579.
15. Fackler, Jr., J. P., Richard, J. S. and Zerihun, A., *J. Chem. Soc. Chem. Commun.*, 1994, 431.
16. Liu, C. W., McNeal, C. J., Fackler, Jr., J. P., *J. Cluster Sci.*, 1996, **7,** 385.
17. Miller, J. S. and Epstein, A. J., *Prog. Inorg. Chem.*, 1975, **20,** 1.
18. Anderson, H. L., Martin, S. J. and Bradley, D. D. C., *Angew. Chem. Int. Ed. Engl.*, 1994, **33,** 655.
19. Hanack, M. and Deger, S., Lange, A., *Coord. Chem. Rev.*, 1988, **83,** 115.
20. Clemenson, P. I., *Coord. Chem. Rev.*, 1990, **106,** 171.
21. Long, D.-L., Chen, J.-T., Cui, Y. and Huang, J.-S., *Chem. Lett.*, 1988, 171.
22. Zhu, R., Lu, S., Huang, X., Wu, Q. and Yu, R., Huang, J., *Acta Cryst. C*, 1995, **51,** 1515.
23. Hatchard, W. R., *J. Org. Chem.*, 1964, **29,** 660.
24. Davsion, A. and Holm, R. H., *Inorg. Synth.*, 1967, **10,** 8.
25. Siemens, *SMART Version* 4.0. *Users Manual*. Siemens Analytical X-Ray Instruments, Madison, Wiscosin, U.S.A., 1994.
26. Siemens, *SHELXTL Version* 5.0. *Reference Manual*. Siemens Analytical X-Ray Instruments, Madison, Wiscosin, U.S.A., 1994.
27. Fair, C. K. *MOLEN*, *An interactive Structure Solution Procedure*. Enraf-Nonius, Delft, The Netherlands, 1990.
28. Long, D.-L. and Huang, J.-S. (to be published).
29. Bondi, A., *J. Phys. Chem.*, 1964, **68,** 441.
30. Hill, I. R., Irish, D. E., Nicholas, N. J. and Toogood, G. E., *Acta Cryst. C*, 1986, **42,** 404.
31. Campbell, M. L., Larson, S. B. and Dalley, N. K., *Acta Cryst. B*, 1981, **37,** 1741.
32. Range, K.-J., Kuehnel, S. and Zabel, M., *Acta Cryst. C*, 1989, **45,** 1419.
33. Mereiter, K., Preisinger, A. and Guth, H., *Acta Cryst. B*, 1989, **35,** 19.
34. Hummel, H.-U., *Acta Cryst. C*, 1987, **43,** 41.
35. Coucouvanis, D. N., Baenziger, C. and Johnson, S. M., *Inorg. Chem.*, 1974, **13,** 1191.
36. Kobayashi, A. and Sasaki, Y., *Bull. Chem. Soc. Jpn.*, 1977, **50,** 2650.

Pergamon

PII: S0277-5387(98)00201-0

Polyhedron Vol. 17, No. 22, pp. 3977–3978, 1998
© 1998 Elsevier Science Ltd
All rights reserved. Printed in Great Britain
0277–5387/98 $19.00+0.00

Comments: "pH-Independent decomposition reactions of L-ascorbic acid in aqueous metal solutions—I. Formation and structures of Co(II) and Gd(III) oxalates"

Synthesis and Structure of $[Ln(H_2O)_3]_2(C_2O_4)_3$ with Ln = Eu, Gd, Tb and Dy

D. Trollet, S. Roméro, A. Mosset and J. C. Trombe*

C.E.M.E.S., 29, Rue J. Marvig, F-31055 Toulouse Cedex 4, France

(Received 20 January 1998; accepted 22 February 1998

In their paper *'pH-Independent decomposition reactions of* L-ascorbic acid in aqueous metal solutions—I. Formation and structures of Co(II) and Gd(III) oxalates', C. Ünaleroglu *et al.* claim to have synthesized the gadolinium oxalate 'hexahydrate' and solved its structure by X-ray diffraction on a single crystal [1]. Although the R values were acceptable ($R = 0.055$, $wR = 0.067$) and, moreover, the residuals in the electron map were weak ($\Delta\rho_{max} = 0.11\ eÅ^{-3}$), such a structural determination appears, to us, as being questionable because of its similarity with the well-known gadolinium oxalate 'decahydrate'.

The lanthanide oxalates have been the object of many structural studies. There were two series of lanthanide oxalate hydrate:

—$[Ln(H_2O)_3]_2(C_2O_4)_3.4H_2O$ with Ln = La ... Er (including yttrium), known as 'decahydrate', crystallizing in the monoclinic system, space group $P2_1/c$ or $P2_1/a$ [2–9].

—$[Ln(H_2O)_2]_2(C_2O_4)_3.2H_2O$ with Ln = Ho ... Lu (including yttrium and scandium), known as 'hexahydrate', crystallizing in the triclinic system, space group $P\bar{1}$ [10–12].

Both series have a similar layered structure. Lanthanide elements and oxalate ligands build a layer parallel to (010) for the first series and to $(1\bar{1}0)$ for the second one. The only major difference is the number of water molecules either free or linked to the lanthanide. Three or two water molecules are bounded to the lanthanide for the first or the second series, respectively; that is, the result of the well-known 'lanthanide contraction'. The number of free water molecules also differs, four or two per formula, respectively. Free water molecules are located into the interlayer space and, particularly for the first series, they are disordered. However, they contribute to the cohesion of the lattice through hydrogen bonds.

Usually, gadolinium belongs to the first series. To our knowledge, Ollendorf *et al.* are the first ones to describe gadolinium oxalate 'decahydrate' [5]. The cell constants, reported by these latter authors, are $a = 11.042$ Å, $b = 9.631$ Å, $c = 10.097$ Å, $\beta = 114.14°$; $V = 979.9$ Å^3, and $Z = 2$ (per formula), space group $P2_1/c$. These parameters are very close to those observed by Ünaleroglu, $a = 10.075(1)$ Å, $b = 9.634(1)$ Å, $c = 11.049(1)$ Å, $\beta = 65.8(1)°$; $V = 978.4(1)$ Å^3, space group $P2_1/a$: the parameters a and c are inverted and β must be the supplementary angle $180 - 65.8° = 114.2°$ in order to transform the space groups from $P2_1/a$ to $P2_1/c$.

Thus, it is likely that Ünaleroglu *et al.* have forgotten the free water molecules and, in fact, they are dealing with gadolinium oxalate 'decahydrate'. If the formula stated by these authors were true, the loss of eight free water molecules per unit-cell would result in a very open framework, about 20% in volume (*vide infra*) and, as these last molecules strengthen the framework, their departure would certainly causes a collapse of the lattice.

By contrast, we have clearly shown the existence of

* Author to whom correspondence should be addressed.

such a hexa-aquo di-gadolinium tris-oxalate, $[Gd(H_2O)_3]_2(C_2O_4)_3$ [12–14]. This last complex crystallizes in the monoclinic system, space group $P2_1/c$, with $a = 8.371(1)$ Å, $b = 9.748(4)$ Å, $c = 9.417(4)$ Å, $\beta = 90.26(2)^\circ$; $V = 768.5(4)$ Å^3 and $Z = 2$ (per formula). Indeed, the loss of free water molecules leads to a difference in the cell volume, $979.9 - 768.5 = 211.4$ Å^3, a value which is in agreement with the departure of 8 molecules (2×4) by taking V_{H_2O} as being equal to 26.4 Å^3. The structure is also layered but the frame differs largely from those observed in the 'decahydrate' and the 'hexahydrate'. This structure has been extended from europium to dysprosium.

REFERENCES

1. Ünaleroglu, C., Zümreoglu-Karan, B., Zencir, Y. and Hökelek, T., *Polyhedron*, 1997, **16,** 2155.
2. Hansson, E., *Acta Chem. Scand.*, 1970, **24,** 2969.
3. Hansson, E., *Acta Chem. Scand.*, 1973, **27,** 2852.
4. Hansson, E. and Albertsson, J., *Acta Chem. Scand.*, 1968, **22,** 1682.
5. Ollendorf, W. and Weigel, V. F., *Inorg. Nucl. Chem. Letters*, 1969, **5,** 263.
6. Weigel, V. F. and Ollendorf, W., *Acta Cryst.*, 1967, **22,** 923.
7. Huang, S.-H., Zhou, G.-D. and Mak, T. C. W., *J. Crystallo. Spectros. Res.*, 1991, **21,** 127.
8. Michaelides, A., Soulika, S. and Aubry, A., *Polyhedron*, 1988, **23,** 579.
9. Beagley, B. and Pritchard, R. G., *Acta Cryst.*, 1988, **C44,** 174.
10. Hansson, E., *Acta Chem. Scand.*, 1972, **26,** 1337.
11. Hansson, E., *Acta Chem. Scand.*, 1973, **27,** 823.
12. Trollet, D., Diplôme d'Etude Supérieures. Université P. Sabatier, Toulouse, 1994.
13. Roméro, S., Thèse. Université P. Sabatier, Toulouse, 1997.
14. Trollet, D., Roméro, S., Mosset, A. and Trombe, J. C., *C.R. Acad. Sci., Série II b*, 1997, **325,** 663.

Pergamon

PII: S0277-5387(98)00202-2

Polyhedron Vol. 17, No. 22, pp. 3979–3980, 1998
© 1998 Elsevier Science Ltd
All rights reserved. Printed in Great Britain
0277–5387/98 $19.00+0.00

Comments: "Synthesis and structure of $[Ln(H_2O)_3]_2(C_2O_4)_3$ with Ln = Eu, Gd, Tb and Dy"

C. Ünaleroğlu[a], B. Zümreoğlu-Karan[a], Y. Zencir[a] and T. Hökelek[b]

[a]Department of Chemistry, Hacettepe University, Beytepe Campus, 06532, Ankara, Turkey

[b]Department of Physics, Hacettepe University, Beytepe Campus, 06532, Ankara, Turkey

(Received 20 March 1998; accepted 19 May 1998

In their comment [1], "Synthesis and Structures of $[Ln(H_2O)_3]_2(C_2O_4)_3$ with Ln = Eu, Gd, Tb and Dy", Trollet *et al*. criticize our published paper, "pH-Independent decomposition reactions of L-ascorbic acid in aqueous metal solutions-I. Formation and structures of Co(II) and Gd(III) oxalates" [2]. They claim we have forgotten the free water molecules and in fact have dealt with gadolinium oxalate 'decahydrate' instead of gadolinium oxalate 'hexahydrate' which we reported. They also claim that the absence of free water molecules in this structure, which are assumed to strengthen the framework, would certainly cause a collapse of the lattice.

In our paper, we have reported the crystal structure of gadolinium oxalate 'hexahydrate' obtained by the very slow decomposition of gadolinium ascorbate complex. The crystals were air-dried and stored in a closed vessel for about two months before performing the chemical, thermogravimetrical and X-ray analyses. The crystals were large enough for single crystal work. All analyses were done using samples from the same batch. Chemical analysis results clearly indicate the hexahydrate composition (10.6%C, 1.4%H). As shown by Wendlandt [3], the hydrate water of gadolinium oxalate decahydrate begins to come off at 45°C, at 120°C hexahydrate composition is reached and anhydrous oxalate is obtained at 315°C which then rapidly decomposes beyond 375°C. Our sample starts to dehydrate at 120°C (Fig. 1) and the mass loss of 16% (15.7%, theoretical) in the dehydration step is consistent with the hexahydrate composition. These results undoubtedly indicate the absence of free water. It is also a well known fact that the number of water molecules depends on the preparation conditions [3, 4]. The varying water content obtained for the compounds $M_2(C_2O_4)_3 \cdot nH_2O$ might be explained by the inclusion of different amounts of water in the cavities depending on the conditions such as temperature and the metal ionic radii. It should be noted that our sample has been obtained by the very slow decomposition of gadolinium ascorbate complex rather than by precipitating from aqueous oxalate solutions as for most oxalate hydrates [5, 6] or by heating the decahydrate structure with $Na_2C_2O_4$ at 150°C as reported by Trollet *et al*. [7].

The precise experimental CAD-4 diffractometer measurements of our gadolinium oxalate 'hexahydrate' showed that it crystallized in the monoclinic system, space group $P2_{1/a}$ with $a = 10.075(1)$ Å, $b = 9.634(1)$ Å, $c = 11.049(1)$ Å, $\beta = 65.8(1)°$, $V = 978.4(1)$ Å^3, $Z = 4$, $D_x = 2.33$ Mg·m^{-3}. The final refinement values were $R = 0.055$, $wR = 0.067$, $S = 1.08$ and $\triangle\rho\,(\max) = 0.11$ eÅ^{-3}, which are the most powerful evidence of the correctness of the structure determination. If there were forgotten free water molecules in the structure, then the residual electron density would be higher, and we would expect large values of R, wR and S (goodness of fit).

The structure of $Nd_2(C_2O_4)_3 \cdot 10.5H_2O$ isotypic with $Gd_2(C_2O_4)_3 \cdot 10H_2O$ was studied by Hansson [4] who showed that the two oxalate ligands link the metal atoms in chains running parallel to a-axis and the third oxalate links these chains together to form a network. The cavities were assumed to be occupied by free water molecules. The metal oxalate layers are held together directly by hydrogen bonds formed between the oxygens coordinated to metal atoms of adjacent layers and indirectly *via* the water molecules in the cavities. The following low-temperature work by Hansson [6] on the determination of the previously unlocated free water molecules in $Nd_2(C_2O_4)_3 \cdot 10.5H_2O$, reveals that the main function of these molecules seems to be of filling space and they should be only weakly attached to the surrounding atoms and

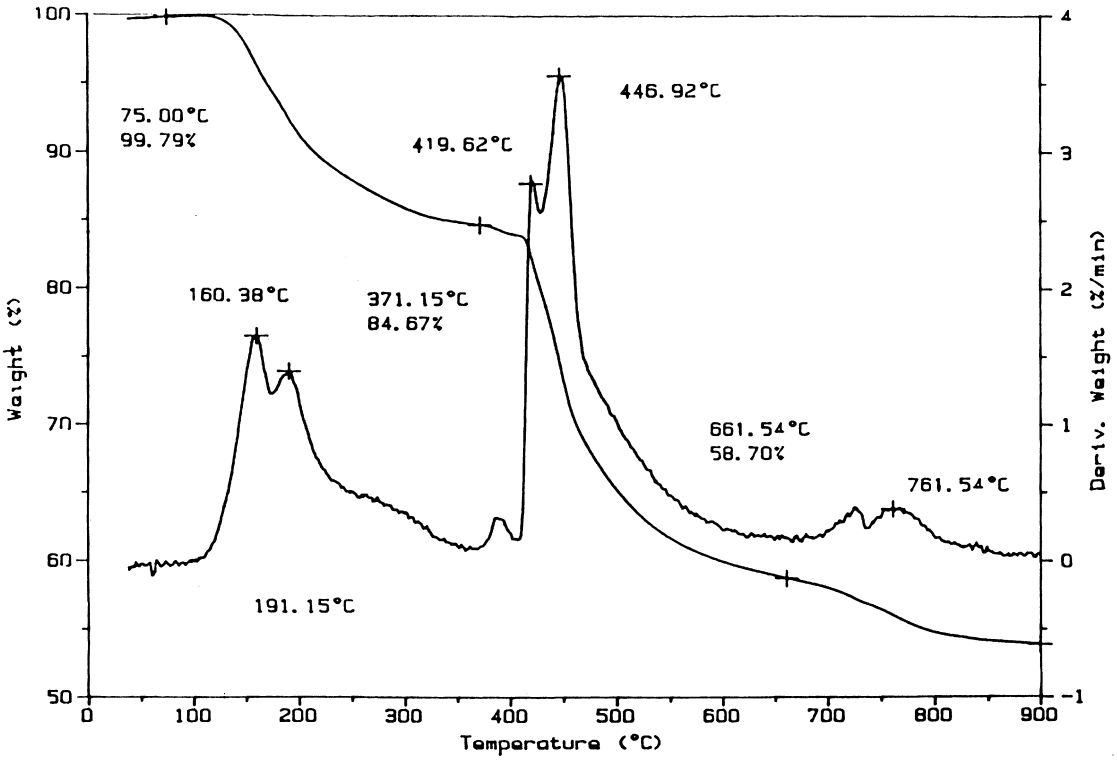

Fig. 1. Thermal decomposition curve of gadolinium oxalate hexahydrate.

each other. The same interaction was reported for the $Sc_2(C_2O_4)_3 \cdot 6H_2O$ structure [8]. It appears that the hydrogen bonds which hold the lattice are those between water molecules coordinated to the metal ion and the carboxylic oxygens in adjacent layers. So, leaving off the free water molecules which can be expected to be thermally labile due to weak hydrogen or Van der Waals bonds from the cavities of such a zeolite-like structure neither causes a collapse of the lattice nor changes the structure and the unit cell volume as determined [9] and reported by us [2].

REFERENCES

1. Trollet, D., Romero, S., Mosset, A. and Trombe, J. C., *Polyhedron*, in print.
2. Ünaleroğlu, C., Zümreoğlu-Karan, B., Zencir, Y. and Hökelek, T., *Polyhedron*, 1997, **16,** 2155.
3. Wendlandt, W. W., *Analyt. Chem.*, 1958, **30,** 58.
4. Hansson, E., *Acta Chem. Scand.*, 1970, **24,** 2969.
5. Ollendorff, W. and Weigel, F., *Inorg. Nucl. Chem. Lett.*, 1969, **5,** 263.
6. Hansson, E., *Acta Chem. Scand.*, 1973, **27,** 823.
7. Trollet, D., Romero, S., Mosset, A. and Trombe, J. C., *C. R. Acad. Sci., Serie II b*, 1997, **325,** 663.
8. Hansson, E., *Acta Chem. Scand.*, 1972, **26,** 1337.
9. Amiraslanov, I. E., Nadzhafov, G. N., Usubaliev, B. T., Musaev, A. A., Movsumov, E. M. and Mamedov, Kh. S., *Zh.Strukt.Khim.*, 1980, **27,** 140.

Pergamon

PII: S0277-5387(98)0019-X

Polyhedron Vol. 17, No. 23–24, pp. 3981–3987, 1998
© 1998 Elsevier Science Ltd
All rights reserved. Printed in Great Britain
0277–5387/98 $19.00+0.00

2,6-Bis(diphenylphosphinosulfide)pyridine (L) as a facial terdentate ligand: synthesis and characterisation of the tricarbonylrhenium(I) complexes *fac*-$[Re(CO)_3L]^+$ $[Re_2(CO)_6(\mu\text{-}X)_3]^-$ (X = Cl, Br or I) and *fac*-$[Re(CO)_3L]^+$ $[SbF_6]^-$

Peter J. Heard[a]* and Abil E. Aliev[b]

[a]Department of Chemistry, Birkbeck College, Gordon House, 29 Gordon Square, London WC1H 0PP, U.K.

[b]Department of Chemistry, University College London, Christopher Ingold Laboratories, 20 Gordon Street, London WC1H 0AJ, U.K.

(Received 3 April 1998; accepted 12 May 1998)

Abstract—The halogenopentacarbonylrhenium(I) compounds react with 2,6-bis(diphenylphosphinosulfide) pyridine (L) under mild conditions to yield ionic complexes of general formulae, *fac*-$[Re(CO)_3L]^+$ $[Re_2(CO)_6(\mu\text{-}X)_3]^-$ (X = Cl, Br or I), in which the ligand adopts a facial terdentate bonding mode. A synthesis of $[Re(CO)_3L]^+$ $[SbF_6]^-$ was carried out to establish the presence of the cation, *fac*-$[Re(CO)_3L]^+$, in the complexes. The character of the anions was confirmed by negative ion MALDI-TOF mass spectrometry. The cation is fluxional; the P–phenyl rings oriented towards the metal moiety exhibit restricted rotation at low temperature. The free energy of activation, $\Delta G^{\dagger}$, for hindered rotation is *ca.* 47 kJ mol^{-1} for all complexes. Solid-state ^{31}P NMR data are reported for the free ligand and for the complexes, $[Re(CO)_3L][SbF_6]$ and $[Re(CO)_3L][Re_2(CO)_6(\mu\text{-}X)_3]$ (X = Cl, Br or I). © 1998 Elsevier Science Ltd. All rights reserved

Keywords: tricarbonylrhenium(I); solid-state NMR; phosphine ligands.

INTRODUCTION

Metal complexes of ligands that have uncoordinated donor atoms are now well established as fluxional species. The classical example of this type of fluxional behaviour is exhibited by transition metal complexes of 2,2′:6′,2″-terpyridine (terpy), in which terpyridine is restricted to a bidentate bonding mode [1, 2]. Other potentially terdentate ligands, such as 2,6-bis(oxazolinyl)pyridines [3, 4] and 2,6-bis(sulfanyl)pyridines [5, 6], also display fluxional behaviour when coordinated to a metal in a bidentate fashion. As part of our on-going interest in the dynamic stereochemical behaviour exhibited by transition metal complexes of this type, we chose to investigate the tricarbonylrhenium(I) halide complexes of 2,6-bis (diphenylphosphinosulfide)pyridine (L). It was expected that, under mild conditions, the ligand would react with the halogenopentacarbonylrhenium(I) compounds, to form complexes of general formulae *fac*-$[ReX(CO)_3L]$ (X = Cl, Br or I), with the ligand bound in a bidentate fashion via the N donor of the pyridine ring and one of the sulfur donors. However, analytical and spectroscopic data indicate that ionic complexes of the type *fac*-$[Re(CO)_3L]^+$ A^- (where A is the counter ion) are formed, with the ligand adopting a facial terdentate bonding mode. Accordingly, we report here on the synthesis and characterisation of the complexes *fac*-$[Re(CO)_3L]^+$ $[Re_2(CO)_6(\mu\text{-}X)_3]^-$ (X = Cl, Br or I) and *fac*-$[Re(CO)_3L]^+$ $[SbF_6]^-$.

* Author to whom correspondence should be addressed. E-mail: p.heard@chem.bbk.ac.uk.

EXPERIMENTAL

Syntheses

All manipulations were carried out under an atmosphere of dry oxygen-free nitrogen, using standard Schlenk techniques [7]. Solvents were dried [8] and degassed before use. The pentacarbonylrhenium(I) halides [9] were prepared using previously published procedures and the ligand, 2,6-bis(diphenylphosphinosulfide)pyridine (L) was prepared by Professor W. McFarlane [10]. The three complexes $[Re(CO)_3L]^+[Re_2(CO)_6(\mu\text{-}X)_3]^-$ (X = Cl, Br or I) were prepared similarly, as illustrated by the procedure for $[Re(CO)_3L]^+[Re_2(CO)_6(\mu\text{-}Br)_3]^-$. The hexafluoroantimonate complex was prepared by treatment of $[Re(CO)_5(thf)]^+$ $[SbF_6]^-$ with 2,6-bis(diphenylphosphinosulfide)pyridine, and from $[Re(CO)_3L]^+$ $[Re_2(CO)_6(\mu\text{-}Br)_3]^-$, by treatment with $AgSbF_6$, as described.

$[Re(CO)_3L][Re_2(CO)_6(\mu\text{-}Br)_3]$

Pentacarbonylrhenium(I) bromide (120 mg, 0.295 mmol) and 2,6-bis(diphenylphosphinosulfide) pyridine (150 mg, 0.293 mmol) were heated under reflux in 20 cm^3 of a 50:50 (v/v) mixture of benzene–petroleum ether (b.p. 60–80°C) for *ca.* 18 h. The resulting orange solid was isolated by filtration, and recrystallised from dichloromethane. Yield: 77 mg, 50%.

$[Re(CO)_3L][SbF_6]$

Method A $[ReBr(CO)_5]$ (50 mg, 0.123 mmol) and $AgSbF_6$ (30 mg, 0.127 mmol) were refluxed in 15 cm^3 of tetrahydrofuran (thf) for *ca.* 2 h. The resulting solution was filtered (to remove AgBr) and then added to a stirred solution of 2,6-bis(diphenylphosphinosulfide)pyridine (70 mg, 0.137 mmol in 5 cm^3 of thf). The reaction mixture was refluxed for *ca.* 18 h, then the solvent removed *in vacuo*, to yield a yellow–orange solid. Recrystallisation from dichloromethane–pentane yielded 60 mg (48%) of yellow $[Re(CO)_3L][SbF_6]$.

Method B $[Re(CO)_3L][Re_2(CO)_6(\mu\text{-}Br)_3]$ (100 mg, 0.06 mmol) and $AgSbF_6$ (25 mg, 0.106 mmol) were stirred at ambient temperature for *ca.* 24 h, in 20 cm^3 of CH_2Cl_2. The resulting yellow solution was filtered (to remove AgBr) and evaporated to dryness *in vacuo*. The crude yellow product was crystallised from dichloromethane–pentane. Yield: 64 mg, 98%.

Physical methods

Infrared spectra were recorded in CH_2Cl_2, using matched CaF_2 solution cells on a Nicolet 205 FT-IR spectrometer operating in the region 4000–400 cm^{-1}. Elemental analyses were carried out at University College London. Mass spectra were obtained at the London School of Pharmacy. Fast atom bombardment (FAB) mass spectra were carried out on a VG Analytical ZAB-SE instrument, using Xe^+ ion bombardment at 8 kV energy. Matrix assisted laser desorption/ionisation time of flight (MALDI-TOF) mass spectra were obtained on a Fisons TofSpec instrument, with a linear flight path of 0.9 m, operating in the negative ion mode. The laser was fired fifty times at minimal energy, to produced the averaged spectra. The matrix used was 5-chloro-2-mercaptobenzothioazole. X-Ray powder patterns were obtained by Dr I. P. Parkin, University College London, on a Siemens D5000 X-ray powder diffractometer, using Ge monochromated Cu-K_α radiation ($\lambda = 1.5406$ Å).

Solution-state ^1H, ^{19}F and ^{31}P NMR spectra were recorded in CD_2Cl_2 or $CDCl_3$ on a Bruker AMX400 Fourier transform spectrometer, operating at 400.13, 376.45 and 161.98 MHz, respectively. Chemical shifts are reported relative to tetramethylsilane (^1H), $CFCl_3$ (^{19}F) and 85% aqueous H_3PO_4 (^{31}P). NMR probe temperatures were controlled by a standard B-VT 2000 unit; probe temperatures were periodically checked (100% MeOH) and are considered accurate to within ± 1°C.

High-resolution solid-state ^{31}P NMR spectra were recorded at 121.5 and 242.9 MHz on Bruker MSL300 and AMX600 Fourier transform spectrometers, respectively, equipped with standard Bruker magic angle spinning probes. Spectra were measured at ambient temperature (298 K), on polycrystalline powders in zirconia rotors with a 4 mm external diameter. Chemical shifts are quoted relative to 85% aqueous H_3PO_4. Spectra were recorded using a "single-pulse" sequence with magic angle spinning and high-power ^1H decoupling. The isotropic peaks were identified by varying the MAS frequencies (3–11 kHz) and the principal components of the ^{31}P CSA tensor (δ_{11}, δ_{22} and δ_{33}) were determined using the Herzfeld–Berger method [11] [prior to the spinning side-band analyses, the overlapping resonances were deconvoluted using the NUTS (Acorn NMR) line fitting subroutine]. The chemical shielding anisotropy, $\Delta\sigma$, and the asymmetry parameter, η, are defined as [12]: $\Delta\sigma = [(\delta_{11} + \delta_{22})/2] - \delta_{33}$ and $\eta = (\delta_{11} - \delta_{22})/(\delta_{iso} - \delta_{33})$, where $\delta_{iso} = (\delta_{11} + \delta_{22} + \delta_{33})/3$.

RESULTS AND DISCUSSION

Treatment of the halogenopentacarbonylrhenium(I) compounds with a stoichiometric quantity of 2,6-bis(diphenylphoshinosulfide)pyridine (L) (Fig. 1) under moderate conditions was expected to yield complexes of general formulae *fac*-$[ReX(CO)_3L]$ (X = Cl, Br or I), with the ligand bound to the metal in a bidentate fashion [structure (**II**), Fig. 1]. However, microanalytical data indicated the formation of complexes of molecular formulae $Re_3(CO)_9X_3L$. The fast atom bombardment (FAB) mass spectra of all three

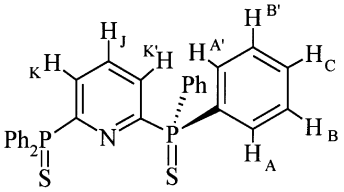

Free ligand (L)

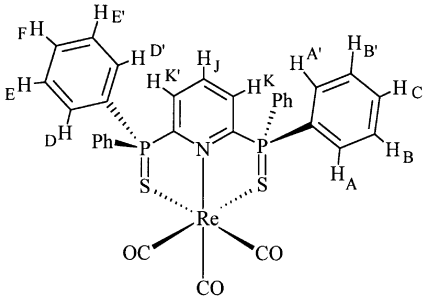

(I)

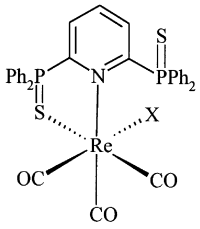

(II)

Fig. 1. The structures of the free ligand (L), the $[Re(CO)_3L]$ cation (**I**) and the expected complexes, $[ReX(CO)_3L]$ (**II**). The hydrogen atom labelling schemes for the ligand and (**I**) are shown alongside.

complexes displayed a molecular ion at $m/z^+ = 782$, which corresponds to the species $[Re(CO)_3L]^+$ [structure (**I**), Fig. 1] (the observed and calculated isotope patterns are consistent). Since rhenium-halide bonds in halogenotricarbonylrhenium(I) complexes usually remain intact on ionisation [13], FAB mass spectral data indicate the formation of a cationic species, in which the ligand acts in a terdentate bonding mode. As the cation stoichiometry is $Re(CO)_3L$, the counter ions must have the molecular formulae (from the C, H and N analyses) $Re_2(CO)_6X_3$ (X = Cl, Br or I). Complex anions of this stoichiometry are know; namely the triply halide-bridged dirhenium anions, $[Re_2(CO)_6(\mu\text{-}X)_3]^-$ (X = Cl, Br or I) [14, 15]. Negative ion mass spectrometry (using the MALDI-TOF technique) was carried out on the complexes to confirm the nature of the anions; molecular ions were observed for the three complexes at $m/z^- = 645$ (X = Cl), 779 (X = Br) and 920 (X = I), due to the proposed anions. Analytical data are reported in Table 1.

Attempts to prepare the desired complexes, $[ReX(CO)_3L]$, by treatment of the rheniumpentacarbonyl halides with 2,6-bis(diphenylphoshinosulfide)pyridine under milder conditions (CH_2Cl_2; ambient temperature) were unsuccessful; the ionic species, $[Re(CO)_3L][Re_2(CO)_6(\mu\text{-}X)_3]$ (X = Cl, Br or I), were again isolated (although reaction times were significantly longer).

To confirm the presence of the $[Re(CO)_3L]^+$ cation in the complexes isolated (see above), an explicit synthesis of the hexafluoroantimonate salt, $[Re(CO)_3L]^+[SbF_6]^-$ was carried out. Reaction of $[ReBr(CO)_5]$ with $AgSbF_6$ in tetrahydrofuran (thf), followed by treatment of the $[Re(CO)_5(thf)]^+$ cation with a stoichiometric quantity of 2,6-bis(diphenylphoshinosulfide)pyridine (L), yielded $[Re(CO)_3L][SbF_6]$ as a yellow solid (see above). Treatment of $[Re(CO)_3L][Re_2(CO)_6(\mu\text{-}Br)_3]$ with $AgSbF_6$ also yielded $[Re(CO)_3L][SbF_6]$. Data (FAB-MS, IR and NMR) for the cation in $[Re(CO)_3L][SbF_6]$ were the same as for the proposed cation in the complexes, $[Re(CO)_3L][Re_2(CO)_6(\mu\text{-}X)_3]$ (X = Cl, Br or I). Attempts were made to grow single crystals for X-ray crystallographic studies in order to confirm unambiguously the terdentate bonding mode of the ligand; suitable crystals could not be obtained.

All four complexes, $[Re(CO)_3L][Re_2(CO)_6(\mu\text{-}X)_3]$ (X = Cl, Br or I) and $[Re(CO)_3L][SbF_6]$, are stable in the solid-state under ambient conditions, and are soluble in moderately polar solvents (e.g. CH_2Cl_2). In coordinating solvents, such as acetone and methanol, the complexes quickly decompose; infrared spectroscopy indicates the formation of the $[Re(CO)_3(solvent)_3]^+$ cation and a quantitative yield of the free ligand is recovered.

The infrared spectrum of $[Re(CO)_3L][SbF_6]$ displayed three bands in the carbonyl stretching region, characteristic of a *fac*-octahedral coordination geometry, with local C_s symmetry, for the $Re(CO)_3$ moiety [16]. The free ligand displays a strong band at 647 cm^{-1} due to the P═S stretching mode [10]. Although no band assignable unambiguously to the P═S stretch in the cation, $[Re(CO)_3L]^+$, was observed, the band at 647 cm^{-1} is absent in the IR spectrum of the complex; infrared data therefore clearly indicate that the ligand, 2,6-bis(di-

Table 1. Analytical data for the complexes $[Re(CO)_3L][Re_2(CO)_6(\mu\text{-}X)_3]$ (X = Cl, Br or I) and $[Re(CO)_3L][SbF_6]$

		ν(CO)[a] (cm^{-1})				Analyses[d]		
Complex	Colour	cation	anion[e]	m/z^+ [b]	m/z^- [c]	C	H	N
$[Re(CO)_3L][Re_2(CO)_6(\mu\text{-}Cl)_3]$	orange	2036 1949 1920	2024 (2030) ~1920 (1917)	782	645	31.94 (31.94)	1.38 (1.62)	0.91 (0.98)
$[Re(CO)_3L][Re_2(CO)_6(\mu\text{-}Br)_3]$	orange	2036 1949 1920	2023 (2028) 1910sh (1915)	782	779	29.27 (29.22)	1.38 (1.48)	0.84 (0.90)
$[Re(CO)_3L][Re_2(CO)_6(\mu\text{-}I)_3]$	orange	2036 1949 1920	2018 (2012) 1905sh (1914)	782	920	26.96 (26.80)	1.19 (1.36)	0.77 (0.82)
$[Re(CO)_3L][SbF_6]$	yellow	2036 1949 1920		782	234	36.88 (37.77)	2.05 (2.28)	1.36 (1.38)

[a] Infrared data; spectra recorded in CH_2Cl_2 solution.
[b] FAB mass spectral data (cation).
[c] Negative ions mass spectral data.
[d] Calculated values in parentheses.
[e] Literature value given in parentheses (see Ref. [14]); sh = shoulder.

phenylphoshinosulfide)pyridine, is acting in a *fac*-terdentate bonding mode with the S atoms coordinated to the metal. The IR spectra of the complexes $[Re(CO)_3L][Re_2(CO)_6(\mu\text{-}X)_3]$ (X = Cl, Br or I) each displayed three bands due to the CO stretching modes of the cation (these were in identical positions to those observed for the SbF_6 salt), plus additional bands due to the counter ions, $[Re_2(CO)_6(\mu\text{-}X)_3]^-$ (X = Cl, Br or I). No band assignable to the free P═S stretching mode (see above) was observed. The isolated $[Re_2(CO)_6(\mu\text{-}X)_3]^-$ anions have local D_{3h} symmetry and are therefore expected to exhibit two IR active carbonyl stretching modes (A_2'' and E′). The sharp A_2'' bands are clearly observed to slightly lower frequency of the A_1 band of the cation. The E′ bands tend to overlap with the cation band at 1920 cm^{-1}; however, the E′ bands of the bromo- and iodo-species are observable. The CO stretching frequencies for the anions are close to those reported previously for the complexes $[Et_4N][Re_2(CO)_6(\mu\text{-}X)_3]$ (X = Cl, Br or I), in the same solvent (CH_2Cl_2) [14]. Infrared data are reported in Table 1.

NMR studies

The ambient temperature (298 K) $^{31}P\{^1H\}$ NMR spectra of the complexes $[Re(CO)_3L][Re_2(CO)_6(\mu\text{-}X)_3]$ (X = Cl, Br or I) and $[Re(CO)_3L][SbF_6]$ in CD_2Cl_2 are, as expected, identical. The spectra display a single resonance at $\delta \approx 67.0$ [cf. $\delta = 38.4$ for the free ligand (in $CDCl_3$)], indicating that either (i) both P are equivalent, as a result of the ligand adopting a symmetrical bonding mode or (ii) the ligand is undergoing some rapid fluxional process that leads to the averaging of different P environments. To try to distinguish between these two possibilities spectra were recorded at low temperature (190 K), in an attempt to "freeze-out" any dynamic stereochemical processes. No spectral changes were observed, indicating a stereochemically rigid molecule, with the two P atoms in identical chemical positions. Solution ^{31}P NMR data therefore indicate the formation of complex, in which both S(=PPh_2) atoms of the ligand are bound to the metal centre. This was confirmed by solid-state ^{31}P NMR spectroscopy (see below).

The solid-state ^{31}P spectrum of the free ligand, 2,6-bis(diphenylphoshinosulfide)pyridine, displays two isotropic resonances, with spinning side-bands, in a 1:1 intensity ratio at $\delta = 41$ and 38, as a result of the two P atoms being crystallographically inequivalent. The spectra also indicate the presence of residual dipolar coupling between the nitrogen (^{14}N nuclide) of the pyridine ring and the phosphorus nuclides. We are currently undertaking a full analysis of the solid-state NMR spectra of 2,6-bis(diphenylphoshinosulfide)pyridine and the related oxide and selenide compounds, and will report the results of these studies shortly.

The solid-state ^{31}P NMR spectra of the complexes $[Re(CO)_3L][Re_2(CO)_6(\mu\text{-}X)_3]$ (X = Cl, Br or I) also display two isotropic resonances (with spinning side-bands), in a 1:1 (integral) intensity ratio at *ca.* $\delta = 65$ and 62. The small chemical shift differences between the signals indicate that they arise as a result of the P

atoms being crystallographically inequivalent, rather than as a result of chemical inequivalence. This clearly supports the hypothesis of the ligand bonding in a symmetrical fashion, with both S atoms coordinated. The hexafluoroantimonate salt, $[Re(CO)_3L][SbF_6]$, displays two isotropic signals, in a 1:1 intensity ratio, at *ca.* $\delta = 71$ and 66. The different chemical shifts of the isotropic resonances of the $[SbF_6]^-$ complex compared to those of the other three complexes (see above) presumably arise because of different packing in the solid-state. This interpretation is supported by the results of X-ray powder diffraction studies on the four complexes. The powder patterns obtained for the complexes $[Re(CO)_3L][Re_2(CO)_6(\mu\text{-}X)_3]$ (X = Cl, Br or Br) are essentially identical, but are different from that obtained for $[Re(CO)_3L][SbF_6]$. The solid-state ^{31}P NMR spectrum of $[Re(CO)_3L][Re_2(CO)_6(\mu\text{-}Br)_3]$ is shown in Fig. 2 and ^{31}P NMR data for the ligand, 2,6-bis(diphenylphosphinosulfide)pyridine and the four complexes, $[Re(CO)_3L][Re_2(CO)_6(\mu\text{-}X)_3]$ (X = Cl, Br or I) and $[Re(CO)_3L][SbF_6]$ are reported in Table 2.

The ambient temperature (298 K) ^1H NMR spectra of the complexes $[Re(CO)_3L][Re_2(CO)_6(\mu\text{-}X)_3]$ (X = Cl, Br or I) and $[Re(CO)_3L][SbF_6]$ [L = 2,6-bis(diphenylphosphinosulfide)pyridine] in CD_2Cl_2 are essentially identical. The spectra displayed eight distinct chemical shifts in the region $\delta = 7.2$–8.2 and are indicative of the ligand bonding in a symmetrical fashion. The signals of the pyridine-H nuclides, H_J, H_K and $H_{K'}$ Fig. 1, show the characteristic pattern of an ABB′ sub-set of an ABB′XX′ spin system (the P atoms being the XX′ sub-set). The signal from H_J is readily assigned because the $^4J_{PH}$ coupling (≈ 3.8 Hz) is approximately half that of the $^3J_{HH}$ coupling (≈ 7.8 Hz); thus H_J gives rise to a pseudo septet. The signal from $H_K/H_{K'}$ is then readily identified from a ^1H–^1H COSY experiment (see below).

If rotation about the P–C(phenyl) bonds is assumed to be rapid at ambient temperature (298 K), as appears apparent from the ^1H NMR spectra, the hydrogen nuclides of the P–phenyl rings would be expected to give rise to three resonances, characteristic of an AA′BB′C spin system. Thus the six remaining chemical shifts (see above) must result from inequivalence of pairs of phenyl rings. This inequivalence arises because two phenyl rings point towards the metal moiety and two away from it Fig. 1. If the inequivalence arose as a result of an unsymmetrical mode of co-ordination, then all four P–phenyl rings would be expected to be inequivalent (see Fig. 1) and twelve distinct chemical shifts would result. Ambient temperature ^1H NMR data are therefore consistent with either (i) a symmetrical bonding mode for the ligand or (ii) the presence of rapid fluxional process that leads to a time-averaging of pairs of phenyl rings. The latter possibility can be excluded to the basis of the ^{31}P NMR data (see above) and the results of a low temperature ^1H NMR study (see below). The resonances of the *ortho*-hydrogens of the phenyl rings are readily identified by their couplings to the phosphorus nuclides ($^3J_{PH} \approx 14$–15 Hz). The remaining signals (Table 3) can then be assigned on the basis of a single ^1H–^1H COSY experiment. The assignment of the two sets of phenyl–H signals to the two pairs of phenyl rings was based on the low temperature ^1H NMR spectra (see below). The ^1H NMR spectrum of $[Re(CO)_3L][Re_2(CO)_6(\mu\text{-}Cl)_3]$ at 298 K is shown in Fig. 3 and data are reported in Table 3.

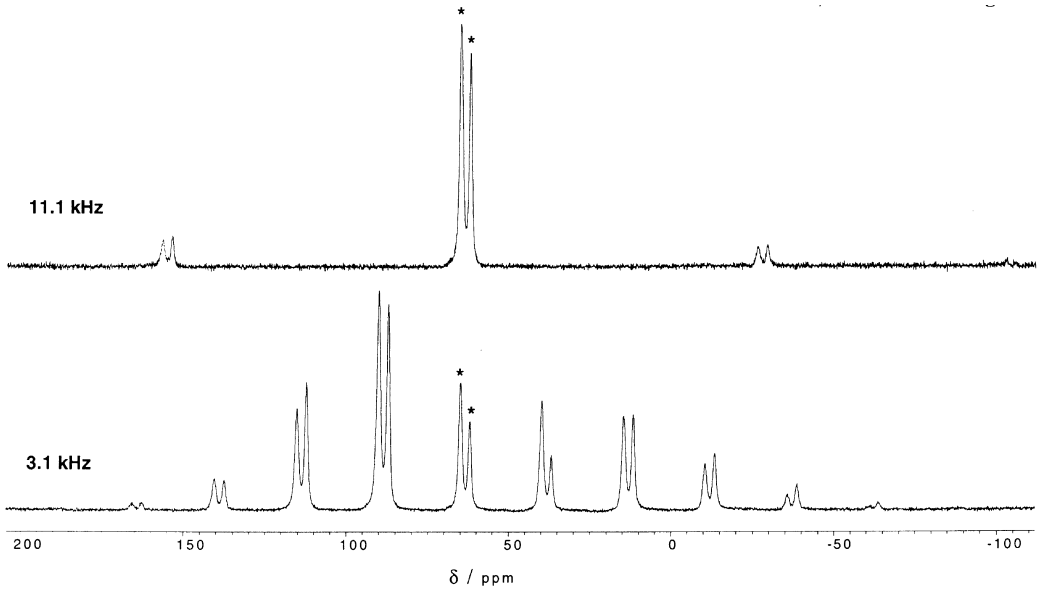

Fig. 2. The 121 MHz solid-state ^{31}P NMR spectrum of $[Re(CO)_3L][Re_2(CO)_6(\mu\text{-}Br)_3]$ at two different MAS frequencies. The MAS frequencies are shown alongside and the isotropic peaks are denoted *.

Table 2. Phosphorus-31 NMR data[a] for L and the complexes $[Re(CO)_3L][Re_2(CO)_6(\mu\text{-}X)_3]$ (X = Cl, Br or I) and $[Re(CO)_3L][SbF_6]$

Compound	δ^b	δ_{iso}	δ_{11}	δ_{22}	δ_{33}	$\Delta\sigma$	η
Ligand	38.4 (37.7)[c]	41	102	98	−77	177	0.03
		38	98	98	−82	180	0.00
$[Re(CO)_3L][Re_2(CO)_6(\mu\text{-}Cl)_3]$	67.0	65	143	86	−35	150	0.57
		62	134	102	−49	167	0.29
$[Re(CO)_3L][Re_2(CO)_6(\mu\text{-}Br)_3]$	67.1	65	144	86	−35	150	0.59
		62	131	106	−51	169	0.22
$[Re(CO)_3L][Re_2(CO)_6(\mu\text{-}I)_3]$	66.8	65	141	84	−29	142	0.61
		62	133	104	−50	168	0.26
$[Re(CO)_3L][SbF_6]$	66.8	71	145	84	−18	133	0.69
		66	145	79	−27	139	0.71

[a] Ambient temperature (298 K) solid-state NMR data except for [b]; CSA tensors assigned according to the Haeberlen convention (Ref. [12]).

[b] Ambient temperature (298 K) solution NMR data; spectra recorded in $CDCl_3$ or CD_2Cl_2 (see text).

[c] Literature value give in parentheses [see Ref. [10] (solvent not reported)].

A variable temperature ^1H NMR study of the complexes was undertaken, between ambient temperature (298 K) and *ca.* 200 K, to help confirm the stereochemical rigidity of the complexes, and thence the symmetrical bonding mode of the ligand, 2,6-bis(diphenylphosphinosulfide)pyridine. Although the ^1H NMR spectra are temperature dependent (see below), there was no evidence to indicate the slowing of an oscillatory rearrangement, that would be expected if the ligand were bound in a bidentate fashion [1–6]. The low temperature ^1H NMR spectra are therefore consistent with a stereochemically rigid symmetrical bonding mode for the ligand. Band shape changes indicative of restricted rotation about the P–C(phenyl) bonds of *one pair* of phenyl rings were observed on cooling. If it is assumed that the phenyl rings oriented towards the metal moiety have the higher magnitude for the free energy of activation ($\Delta G^{\dagger}$) for the P–C (phenyl) bond rotation, as a consequence of steric interactions with the metal moiety, a full assignment of the phenyl–H resonances to the two pairs of rings can be made. Assignments were made on this basis (Table 3). A full analysis of the variable temperature spectra was not undertaken. Approximate values for the free energies of activation were determined [17] at the temperature of initial line broadening ($T_i \approx 203$ K)

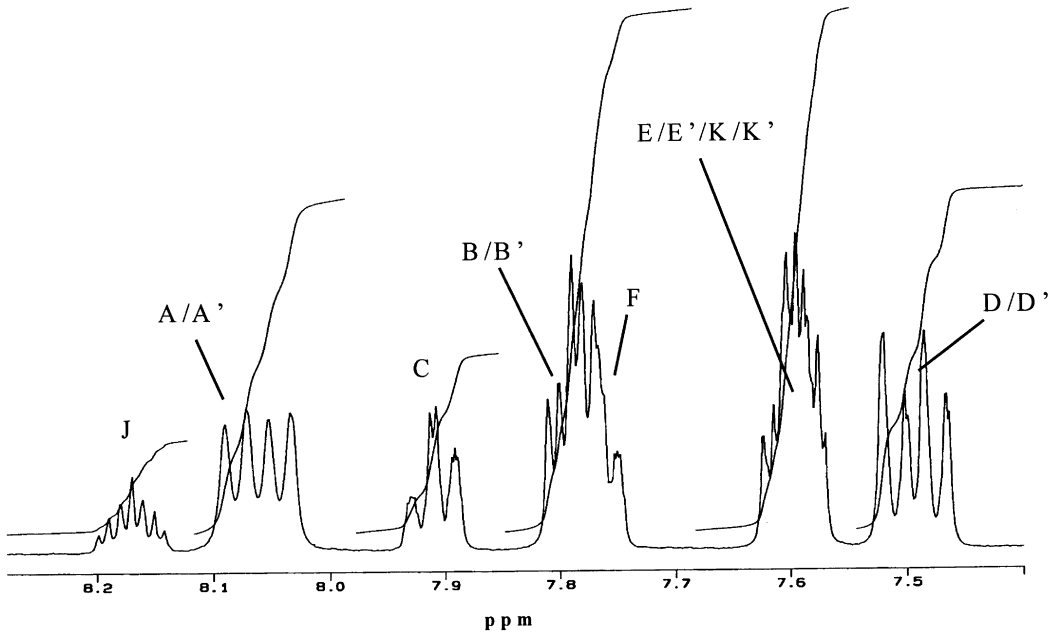

Fig. 3. The ambient temperature 400 MHz ^1H NMR spectrum of $[Re(CO)_3L][Re_2(CO)_6(\mu\text{-}Cl)_3]$. See Fig. 1 for labelling.

Table 3. Hydrogen-1 NMR data[a] for L and the cation, $[Re(CO)_3L]^+$

Compound[b]	$\delta(H_A/H_{A'})$	$\delta(H_B/H_{B'})$	$\delta(H_C)$	$\delta(H_D/H_{D'})$	$\delta(H_E/H_{E'})$	$\delta(H_F)$	$\delta(H_K/H_{K'})$	$\delta(H_J)$
Ligand	7.60 (7.5[c], 0.8[c], 13.3 [d])	7.30 (7.5[c], 2.8[d])	7.50 (7.5[c], 0.8[c], 1.2[d])				8.71 (7.8[c], 14.1[d])	8.07 (7.8[c], 3.8[d])
$[Re(CO)_3L]^+ A^-$	8.07 (7.6[c], 0.8[c], 15.1[d])	7.79 (7.6[c], 3.6[d])	7.91 (7.6[c], 0.8[c], 1.9[d])	7.50 (7.4[c], 0.8[c], 14.1[d])	[e]	7.76 (7.4[c], 0.8[c], 1.8[d])	[e]	8.16 (7.7[c], 3.7[d])

[a]Data recorded at 298 K; ^{1}H chemical shifts quoted relative to tetramethylsilane; spectra of the complexes were recorded in CH_2Cl_2; spectrum of the ligand recorded in $CDCl_3$; see Fig. 1 for labelling.

[b]$A^- = [Re_2(CO)_6(\mu\text{-}X)_3]^-$ (X = Cl, Br or I) or $[SbF_6]^-$.

[c]$^nJ_{HH}$ (Hz).

[d]$^nJ_{PH}$ (Hz).

[e]$H_E/H_{E'}$ and $H_K/H_{K'}$ overlap, giving a complex multiplet centred at *ca.* 7.6 ppm.

and from band coalescence ($T_c \approx 243$ K); $\Delta G^\dagger \approx 47$ kJ mol^{-1} at both T_i and T_c. The apparent temperature independence of $\Delta G^\dagger$ indicates that the entropy of activation, $\Delta S^\dagger$, is approximately zero, as expected for an intramolecular process. The activation energies measured were the same for all four complexes, consistent with the presence of the same cation in each case.

Although the ^{1}H and ^{31}P NMR data clearly show that the ligand is co-ordinated to the metal centre in a symmetrical fashion, via both S atoms, data do not exclude the possibility that the ligand is bound in a bidentate fashion, with the N donor of the pyridine ring uninvolved in bonding. This is considered highly unlikely on chemical grounds, and is inconsistent with the mass spectral and IR data (see above). The orange/yellow colour of the complexes (which is indicative of tricarbonylrhenium(I)–pyridine complexes [3, 13]) is also consistent with the pyridine ring being bound.

The ^{19}F NMR spectrum of the hexafluoroantimonate complex, $[Re(CO)_3L][SbF_6]$, was obtained to confirm the presence of the $[SbF_6]^-$ anion. The ambient temperature ^{19}F spectrum (in CD_2Cl_2) comprises two overlapping sub-spectra (at $\delta = -123.4$), due to coupling to ^{121}Sb ($I = 5/2$, 57.25%) and ^{123}Sb ($I = 7/2$, 42.75%); $^1J[^{121}Sb\text{–}F] = 1945$ Hz, $^1J[^{123}Sb\text{–}F] = 1050$ Hz. Data are consistent with those reported previously for the $[SbF_6]^-$ anion [18].

Acknowledgements—We are grateful to Birkbeck College for financial support, to Professor W. McFarlane for the synthesis of the ligand and to the University of London for access to the solid-state NMR facilities at University College London and Queen Mary and Westfield College and the 400 MHz solution NMR service at Kings College. Dr B. C. Smith and Dr G. Hogarth are acknowledged for helpful discussions.

REFERENCES

1. Abel, E. W., Long, N. J., Orrell, K. G., Osborne, A. G., Pain, H. M. and Šik, V., *J. Chem. Soc. Chem. Commun.*, 1992, 303.
2. Abel, E. W., Orrell, K. G., Osborne, A. G., Pain, H. M., Šik, V., Hursthouse, M. B. and Malik, K. M. A., *J. Chem. Soc. Dalton Trans.*, 1994, 3441 and references therein.
3. Heard, P. J. and Jones, C., *J. Chem. Soc. Dalton Trans.*, 1997, 1083.
4. Heard, P. J. and Tocher, D. A., *J. Chem. Soc. Dalton Trans.* (in press).
5. Abel, E. W., Ellis, D. and Orrell, K. G., *J. Chem. Soc. Dalton Trans.*, 1992, 2243.
6. Abel, E. W., Heard, P. J., Orrell, K. G., Hursthouse, M. B. and Mazid, M. A., *J. Chem. Soc. Dalton Trans.*, 1993, 3795.
7. Shriver, D. F., *Manipulation of Air-Sensitive Compounds*. McGraw-Hill, New York, 1969.
8. Perrin, D. D. and Armarego, W. L. F., *Purification of Laboratory Chemicals*. Pergamon, Oxford, 1988.
9. Schmidt, S. P., Trogler, W. C. and Basolo, F., *Inorg. Synth.*, 1979, **28,** 160.
10. McFarlane, H. C. E., McFarlane, W. and Muir, A. S., *Polyhedron*, 1990, **9,** 1757.
11. Herzfeld, J. and Berger, A. E., *J. Chem. Phys.*, 1980, **73,** 6021.
12. Haeberlen, U., *Adv. Magn. Reson.* (Suppl. 1). Academic Press, 1976.
13. Heard, P. J., Ph. D. Thesis, University of Exeter, 1994 and references therein.
14. Brisdon, B. J., Edwards, D. A. and White, J. W., *J. Organomet. Chem.*, 1978, **161,** 233.
15. Hrung, C. P., Tsutsui, M., Cullen, D. L., Meyer, E. F. and Morimoto, C. N., *J. Am. Chem. Soc.*, 1978, **100,** 6068.
16. Edwards, D. A. and Marshalsea, J., *J. Organomet. Chem.*, 1977, **131,** 73.
17. Faller, J. W., *Encyclopaedia of Inorganic Chemistry*, ed. R. B. King. Wiley, New York, 1994, p. 3914 *et seq.*
18. Harris, R. K., *NMR and the Periodic Table*, eds. R. K. Harris and B. E. Mann. Academic Press, 1978, p. 381 and references therein.

Pergamon

PII: S0277–5387(98)00197–1

Polyhedron Vol. 17, No. 23–24, pp. 3989–3997, 1998
© 1998 Elsevier Science Ltd
All rights reserved. Printed in Great Britain
0277–5387/98 $19.00+0.00

Coordination chemistry of 5,5″-disubstituted 2,2′:6′,2″-terpyridines

Edwin C. Constable,*[a] John E. Davies,[b] David Phillips[b] and Paul R. Raithby[b]

[a]Institut für Anorganische Chemie, Spitalstrasse 51, 4056 Basel, Switzerland

[b]University Chemical Laboratory, Lensfield Road, Cambridge CB2 1EW, U.K.

(Received 2 April 1998; accepted 7 May 1998)

Abstract—Two 2,2′:6′,2″-terpyridine ligands bearing substituents in the 5 and 5″-positions have been prepared and their iron(II) complexes studied to investigate the influence of substituents in these positions. A synergistic interplay between σ- and π-bonding effects, involving conjugation of the substituents with the central ring, means that, in contrast to 4′-substituted 2,2′:6′,2″-terpyridines, the metal–ligand interactions cannot be simply correlated with the electron-donor or -acceptor properties of the substituents. The crystal structure of the complex $[Fe(\mathbf{3})_2][PF_6]_2 \cdot 2MeCN$ (**3** = 5,5″-bis(propoxy)-2,2′:6′,2″-terpyridine) is reported. In addition, cobalt(II) and ruthenium(II) complexes of 5,5″-bis(propoxy)-2,2′:6′,2″-terpyridine were prepared and characterised.
© 1998 Elsevier Science Ltd. All rights reserved

Keywords: metal complexes; 2,2′:6′,2″-terpyridine; ligand reactions; metallosupramolecular chemistry; oligopyridines.

1. INTRODUCTION

Oligopyridines are widely utilised as metal binding domains for metallosupramolecular chemistry [1–3]. The two earliest members of the series, 2,2′-bipyridine and 2,2′:6′,2″-terpyridine (tpy, **1**) have been most investigated and we have concentrated our attention upon derivatives of **1**. It is synthetically facile to incorporate a wide variety of electron-releasing or withdrawing substituents, in addition to functional components such as redox- or photoactive substituents, into the 4′-position of a 2,2′:6′,2″-terpyridine and we have systematically investigated the effects of such changes upon the coordination chemistry of the ligands and the properties of their metal complexes [4–6]. Surprisingly little is known about the effect of substituents in other positions on the coordination behaviour of derivatives of **1**, although substitution in the 5 and 5″-positions has been shown to lead to topologically novel supramolecular species [7, 8]. In this paper we describe our detailed studies of representative 5,5″-disubstituted 2,2′:6′,2″-terpyridines bearing electron-withdrawing and electron-releasing substituents.

* Author to whom correspondence should be addressed. Tel.: +41-61-267-1001; Fax: +41-61-267-1015; E-mail: constable@ubaclu.unibas.ch

2. EXPERIMENTAL

^{1}H NMR spectra were recorded on Brüker WM250, AM400 and DPX500 spectrometers; positive ion fast atom bombardment (FAB), fast ion bombardment (FIB) and electron impact (EI) mass spectra were recorded on a Kratos MS50 spectrometer using a 3-nitrobenzyl alcohol matrix for the FAB and FIB spectra. IR spectra were recorded on Perkin-Elmer 1710, Perkin-Elmer Paragon 1000 or a Philips PU9624 Fourier Transform spectrophotometers with the samples in compressed KBr disks. Electronic spectra were obtained using Kontron Instruments Uvikon 810P or Perkin-Elmer Lambda 12 spectrophotometers. Electrochemical measurements were carried out using an Autolab PGSTAT20 voltammetric analyser. A conventional three-electrode configuration was used, with platinum bead working and auxiliary electrodes and a silver wire pseudo-reference electrode. All measurements were performed in acetonitrile (distilled from CaH_2 then P_4O_{10}) with a supporting electrolyte of

0.1 M $[NBu^n_4][BF_4]$ (recrystallized from ethanol/water and rigorously dried) with a scan rate of $50\,mV\,s^{-1}$. Potentials are quoted vs ferrocene/ferrocinium ($Fc/Fc^+ = 0.0$ V) couple as measured from ferrocene which was added at the end of each experiment as an internal reference. The compound 5,5″-dinitro-2,2′:6′,2″-terpyridine (**2**) was prepared by the method in Refs [9, 10].

2.1. 5,5″-*Bis*(*propoxy*)-2,2′:6′,2″-*terpyridine*, **3**

Propan-1-ol (0.95 mmol, 57 mg) and **2** (150 mg, 0.464 mmol) were added sequentially to a slurry of powdered KOH (300 mg, 5.4 mmol) in dmso ($8\,cm^3$) and the mixture stirred for 24 h at 50°C. After this period, the reaction mixture was treated with water ($70\,cm^3$) to give an off-white precipitate of **3** (97 mg, 60%). This was recrystallised from $CHCl_3$/MeOH to give **3** as an analytically pure white crystalline material. Yield: 81 mg (50%). Mp. 122–126°C. (Found: C, 71.0; H, 7.2; N, 11.7% $C_{21}H_{23}N_3O_2 \cdot 1/3H_2O$ requires: C, 71.0; H, 6.7; N, 11.8%). IR (KBr): 1565 s, 1561 s, 1472 s, 1446 m, 1493 m, 1286 w, 1262 m, 1219 m, 1133 m, 1020 s, 811 s, 754 w, 719 m, 624 $m\,cm^{-1}$. Mass spectrum (+ve FAB): *m/z* 349 (M), 307 (M-C_3H_7), 265 (M-2(C_3H_7)). ^{1}H NMR ($CDCl_3$): δ 8.52 (d, 2H, H^3), 8.35 (d, 2H, H^6), 8.27 (d, 2H, $H^{3'}$), 7.87 (t, 1H, $H^{4'}$), 7.32 (dd, 2H, H^4), 4.03 (t, 2H, C$\mathbf{H}_2$O), 1.85 (m, 2H, C$\mathbf{H}_2$CH$_3$), 1.06 (d, 3H, C$\mathbf{H}_3$).

2.2. $[Co(\mathbf{2})_2][PF_6]_2$ *and* $[Fe(\mathbf{2})_2][PF_6]_2$

Ligand **2** (100 mg, 0.309 mmol) was added to a solution of $CoCl_2 \cdot 6H_2O$ (37 mg, 0.155 mmol) or $FeCl_2 \cdot 4H_2O$ (31 mg, 0.155 mmol) in methanol ($40\,cm^3$) and the mixture stirred at 50°C for 30 min. After this period, the reaction mixture was cooled to room temperature, filtered and the filtrate treated with an excess of ammonium hexafluorophosphate. The resultant precipitates were dissolved in acetonitrile and recrystallised by the diffusion of ether vapour into the solution to give the desired complexes analytically pure.

2.2.1. $[Co(\mathbf{2})_2][PF_6]_2$*: brown crystals*. Yield: 77 mg (50%). (Found: C, 35.3; H, 1.7; N, 13.5. $C_{30}CoH_{18}N_{10}O_8P_2F_{12}$ requires: C, 36.2; H, 1.8; N, 14.0%). IR (KBr): 1617 s, 582 w, 1540 m, 1452 m, 1356 s, 1292 m, 1257 m, 1129 w, 841 s, 755 m, 559 $s\,cm^{-1}$. Mass spectrum (+ve FAB): *m/z* 851 $\{Co(\mathbf{2})_2(PF_6)\}$, 705 $\{Co(\mathbf{2})_2\}$, 382 $\{Co(\mathbf{2})\}$. ^{1}H NMR (CD_3CN): δ 123, 67.1, 66.0, 25.0, 7.5. UV/VIS (MeCN): λ_{max}/nm ($\varepsilon/10^3\,dm^3\,mol^{-1}\,cm^{-1}$) 520 sh (0.65), 330 (32.2), 282 sh (46.2), 269 (50.3), 208 (46.8).

2.2.2. $[Fe(\mathbf{2})_2][PF_6]_2 \cdot H_2O$*: purple crystals*. Yield: 95 mg (61%). (Found: C, 35.1; H, 1.8; N, 13.3. $C_{30}FeH_{20}N_{10}O_9P_2F_{12}$ requires: C 35.7; H 2.0; N 13.9%). IR (KBr): 1619 m, 1576 w, 1534 s, 1450 m, 1355 s, 1279 m, 842 s, 756 m, 559 $s\,cm^{-1}$. Mass spectrum (+ve FAB): *m/z* 869 $\{Fe(\mathbf{2})_2(PF_6)(H_2O)\}$, 847 $\{Fe(\mathbf{2})_2(PF_6)\}$, 702 $\{Fe(\mathbf{2})_2\}$, 379 $\{Fe(\mathbf{2})\}$. ^{1}H NMR (CD_3CN): δ 8.72 (d, 4H, H^3), 9.23 (d, 4H, $H^{3'}$), 8.61 (dd, 4H, H^4), 8.95 (t, 2H, $H^{4'}$), 7.54 (d, 4H, H^5). UV/VIS (MeCN): λ_{max}/nm ($\varepsilon/10^3\,dm^3\,mol^{-1}\,cm^{-1}$) 582 (5.4), 395 sh (8.9), 334 (64.6), 289 (72.3), 266 (71.4).

2.3. $[Ru(\mathbf{2})_2][PF_6]_2$

Ligand **2** (100 mg, 0.309 mmol) and $RuCl_3 \cdot 3H_2O$ (40 mg, 0.155 mmol) were suspended in ethane-1,2-diol ($15\,cm^3$) and the mixture heated to 150°C for 15 min. After this period, the reaction mixture was cooled to room temperature and treated with methanol ($20\,cm^3$) and treated with an excess of ammonium hexafluorophosphate. The precipitate was dissolved in acetonitrile and recrystallised by the diffusion of ether vapour into the solution to give $[Ru(\mathbf{2})_2][PF_6]_2$ as a dark orange–brown microcrystalline solid. Yield: 72 mg (45%). (Found: C, 33.8; H, 1.6; N, 12.9. $C_{30}H_{18}N_{10}O_8P_2RuF_{12}$ requires: C 34.73; H 1.75; N 13.50%). IR (KBr): 1618 m, 1577 m, 1535 s, 1452 m, 1356 s, 1280 m, 1257 w, 841 s, 755 m, 559 s cm^{-1}. Mass spectrum (+ve FAB): *m/z* 892 $\{Ru(\mathbf{2})_2(PF_6)\}$, 748 $\{Ru(\mathbf{2})_2\}$, 424 $\{Ru(\mathbf{2})\}$. ^{1}H NMR (CD_3CN): δ 8.74 (d, 4H, H^3), 9.04 (d, 4H, $H^{3'}$), 8.65 (dd, 4H, H^4), 8.66 (t, 2H, $H^{4'}$), 7.90 (d, 4H, H^6). UV/VIS (MeCN): λ_{max}/nm ($\varepsilon/10^3\,dm^3\,mol^{-1}\,cm^{-1}$) 499 (6.1), 328 (43.0), 286 (49.9), 265 (41.8), 218 (39.9).

2.4. $[Fe(\mathbf{3})_2][PF_6]_2$

$FeCl_2 \cdot 4H_2O$ (28 mg, 0.141 mmol) was added to a methanolic solution of **3** (98.4 mg, 0.282 mmol) and the mixture was stirred for 30 min at 50°C. The resulting purple solution was filtered and the complex precipitated by the addition of excess methanolic $[NH_4][PF_6]$. Recrystallisation from MeCN/Et_2O gave purple crystals of $[Fe(\mathbf{3})_2][PF_6]_2 \cdot 2H_2O$. Yield: 120 mg (80%). (Found: C, 46.3; H, 4.7; N, 7.65. $FeC_{42}H_{50}N_6O_6P_2F_{12}$ requires: C, 46.7; H, 4.7; N, 7.8%). IR (KBr): 1603 m, 1570 m, 1459 m, 1400 m, 1302 m, 1242 m, 1113 w, 1014 m, 842 s, 802 w, 558 $s\,cm^{-1}$. Mass spectrum (+ve FAB): *m/z* 900 $\{Fe(\mathbf{3})_2(PF_6)\}$, 755 $\{Fe(\mathbf{3})_2\}$. ^{1}H NMR (CD_3CN): δ 8.34 (d, 4H, H^3), 8.64 (d, 4H, $H^{3'}$), 7.38 (dd, 4H, H^4), 8.54 (dd, 2H, $H^{4'}$), 6.57 (d, 4H, H^6), 3.75 (t, 8H, C$\mathbf{H}_2$O), 1.56 (m, 8H, C$\mathbf{H}_2$CH$_3$), 0.83 (d, 12H, C$\mathbf{H}_3$). UV/VIS (MeCN): λ_{max}/nm ($\varepsilon/10^3\,dm^3\,mol^{-1}\,cm^{-1}$) 529 (5.8), 337 (37.8), 273 (76.9), 216 (37.6).

2.5. *Crystal structural determination of* $[Fe(\mathbf{3})_2][PF_6]_2 \cdot 2MeCN$

Red blocks of the compound were obtained by the slow diffusion of diethyl ether vapour into an acetonitrile solution of the complex. A single crystal was mounted in a capillary tube and all geometric and

intensity data were taken from this crystal using a AFC7-R diffractometer. Pertinent crystallographic data are given in Table 1. Intensity data, gathered by the ω–2θ method were reduced by routine procedures. Structure solution used SHELXS-86 and the structure was refined using SHELXL-93. Empirical absorption corrections (ψ-scans) were applied.

The structure was solved by direct methods and refined by alternating cycles of least squares refinement and difference-Fourier synthesis. The Fe, C, N and O atoms of the cation and the P atoms of the anions were refined anisotropically. Refinement was carried out on F^2 for all reflections except for two with very negative F^2 values or flagged by the user for potential systematic errors. One of the two hexafluorophosphate counterions is extensively disordered and the propoxy chains show high thermal parameters. Selected bond angles and bond distances are given in Table 2.

3. RESULTS AND DISCUSSION

3.1. *Ligand synthesis*

Our aim was to prepare a suite of 2,2′:6′,2″-terpyridine ligands with varying substituents in the 5,5″-positions in order to investigate the effect of electron-releasing and electron-withdrawing groups in these positions. We selected the 5,5″-dinitro compound **2** and the 5,5″-alkoxy derivative **3** as representatives with electron-withdrawing and electron-releasing groups, respectively. The substituted ligand **2** was prepared by the literature method [9, 10] and was obtained as a pale brown microcrystalline solid. All spectroscopic and physical properties were in accord with the structure and with those previously reported. Surprisingly, although **2** has been known for a number of years, the coordination chemistry does not seem to have been systematically investigated.

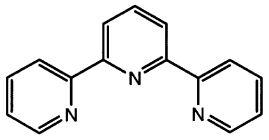

1

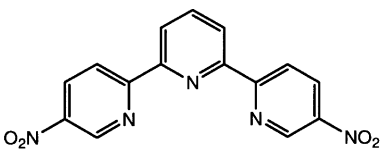

2

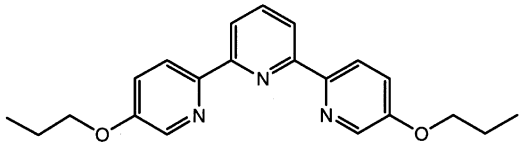

3

Although 4-nitropyridines are known to be activated towards attack by) nucleophiles with concomitant displacement of nitrite and the formation of 4-substituted derivatives, such reactions are not well-established for 5-nitropyridines, in which the negative charge which develops on the ring in the associative intermediate cannot be localised onto the more electronegative nitrogen atom of the pyridine ring. However, we have found that **2** reacts smoothly with nucleophiles under forcing conditions to give excellent yields of 5,5″-disubstituted-2,2′:6′,2″-terpyridines. The reaction of **2** with propan-1-ol in dmso containing solid potassium hydroxide resulted in a smooth displacement of nitrite to give **3** in 60% yield. We believe that the ease of displacement represents the availability of resonance-stabilised intermediates in which the charge is localised upon the nitrogen atom of an *adjacent* pyridine ring (Scheme 1.

The new ligand **3** was obtained as a white crystalline solid in 50% yield and was fully characterised by conventional methods. A parent ion is observed in the mass spectrum and the ^{1}H NMR spectrum [Fig. 1(a)] is characteristic of a 5,5″-disubstituted 2,2′:6′,2″-terpyridine. The most obvious feature in the ^{1}NMR spectrum is the observation of H^6 as a doublet ($^3J_{4,6}$ 2.75 Hz). The expected signals assigned to the propoxy groups were observed in the aliphatic region of the spectrum. The electronic effects of the nitro and propoxy substituents may be qualitatively evaluated by a comparison of their ^{1}H NMR spectra. The most remarkable feature is that the chemical shifts of the protons on the central pyridine ring are dramatically affected by the nature of substituents in the 5 and 5″-positions of the two terminal rings. For example, $H^{3'}$ and $H^{4'}$ are found at δ 8.46 and 7.97, respectively, in **1**, whereas they are shifted upfield to δ 8.27 and 7.87 in **3** and markedly downfield to δ 8.66 and 8.09 in **2**. Similar effects are seen for the terminal rings; H^6 shifts upfield from δ 8.63 in **1** to δ 8.52 in **3** and downfield to δ 8.81 in **2**. All of these shifts suggest that the electronic effects of substituents in the 5 and 5″-positions will have a dramatic effect upon the properties of the 2,2′:6′,2″-terpyridine structure and are in marked contrast with the behaviour of 4′-substituted 2,2′:6′,2″-terpyridine where the chemical shifts of the protons on the terminal rings are effectively independent of the nature of the 4′-substituent [4, 5, 6].

3.2. *Iron(II) complexes of* **2** *and* **3**

The reaction of two equivalents of **2** or **3** with iron(II) chloride in methanol yielded deep purple solu-

Table 1. Crystal data and structure refinement for $[Fe(3)_2, PF_6]_2 \cdot 2MeCN$

Empirical formula	$C_{46}H_{52}F_{12}FeN_8O_4P_2$
Formula weight	1126.75
Temperature	293(2) K
Wavelength	0.71069 Å
Crystal system	Triclinic
Space group	$P\bar{1}$
Unit cell dimensions	$a = 14.725(6)$ Å, $b = 14.795(7)$ Å, $c = 12.967(4)$ Å, $\alpha = 95.18(3)^\circ$, $\beta = 104.29(3)^\circ$, $\gamma = 112.080(3)^\circ$
Volume	2484(2) Å^3
Z	2
Density (calculated)	1.507 Mg/m^3
Absorption coefficient	0.465 mm^{-1}
F(000)	1160
Crystal size	$0.30 \times 0.25 \times 0.20$ mm
θ range for data collection	2.59 to 22.51°
Index ranges	$0 \leq h \leq 15$, $-15 \leq k \leq 14$, $-13 \leq l \leq 13$
Reflections collected	6780
Independent reflections	6481 ($R_{init} = 0.0553$)
Absorption correction	Semi-empirical from ψ-scans
Max. and min. transmission	1.000 and 0.945
Refinement method	Full-matrix least-squares on F^2
Data/restraints/parameters	6479/34/858
Goodness-of-fit on F^2	1.649
Final R indices [$I > 2\sigma(I)$]	$R1 = 0.1066$, wR2 = 0.2581
R indices (all data)	$R1 = 0.1611$, wR2 = 0.2866
Largest diff. peak and hole	1.473 and -1.177 e Å^{-3}

Table 2. Selected bond lengths (Å) and angles (°) for $[Fe(3)_2, PF_6]_2 \cdot 2MeCN$

Fe(1)–N(5)	1.876(7)	Fe(1)–N(2)	1.895(7)
Fe(1)–N(1)	1.960(7)	Fe(1)–N(6)	1.982(7)
Fe(1)–N(3)	1.975(8)	Fe(1)–N(4)	1.994(7)
N(5)–Fe(1)–N(2)	77.0(3)	N(5)–Fe(1)–N(1)	101.4(3)
N(2)–Fe(1)–N(1)	81.5(3)	N(5)–Fe(1)–N(6)	81.3(3)
N(2)–Fe(1)–N(6)	99.3(3)	N(1)–Fe(1)–N(6)	91.0(3)
N(5)–Fe(1)–N(3)	96.1(3)	N(2)–Fe(1)–N(3)	81.0(3)
N(1)–Fe(1)–N(3)	62.5(3)	N(6)–Fe(1)–N(3)	91.0(3)
N(5)–Fe(1)–N(4)	80.9(3)	N(2)–Fe(1)–N(4)	98.6(3)
N(1)–Fe(1)–N(4)	90.1(3)	N(6)–Fe(1)–N(4)	62.1(3)
N(3)–Fe(1)–N(4)	93.4(3)		

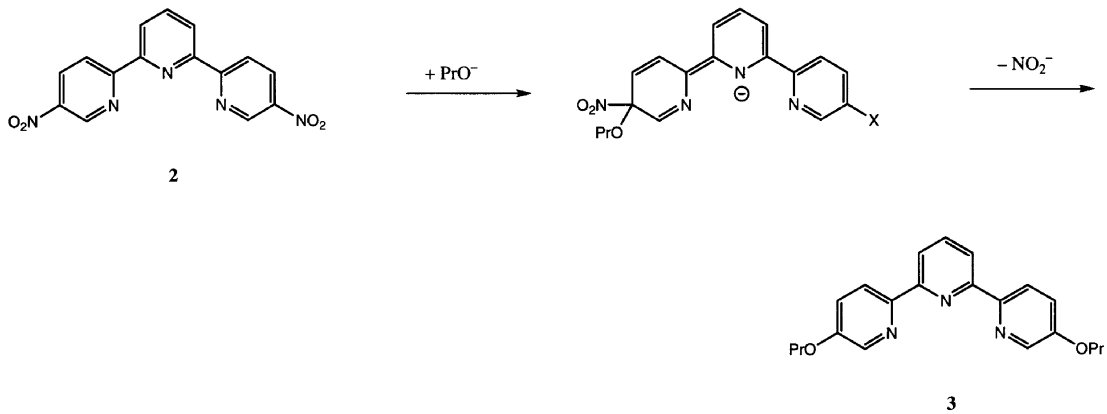

2 **3**

Scheme 1.

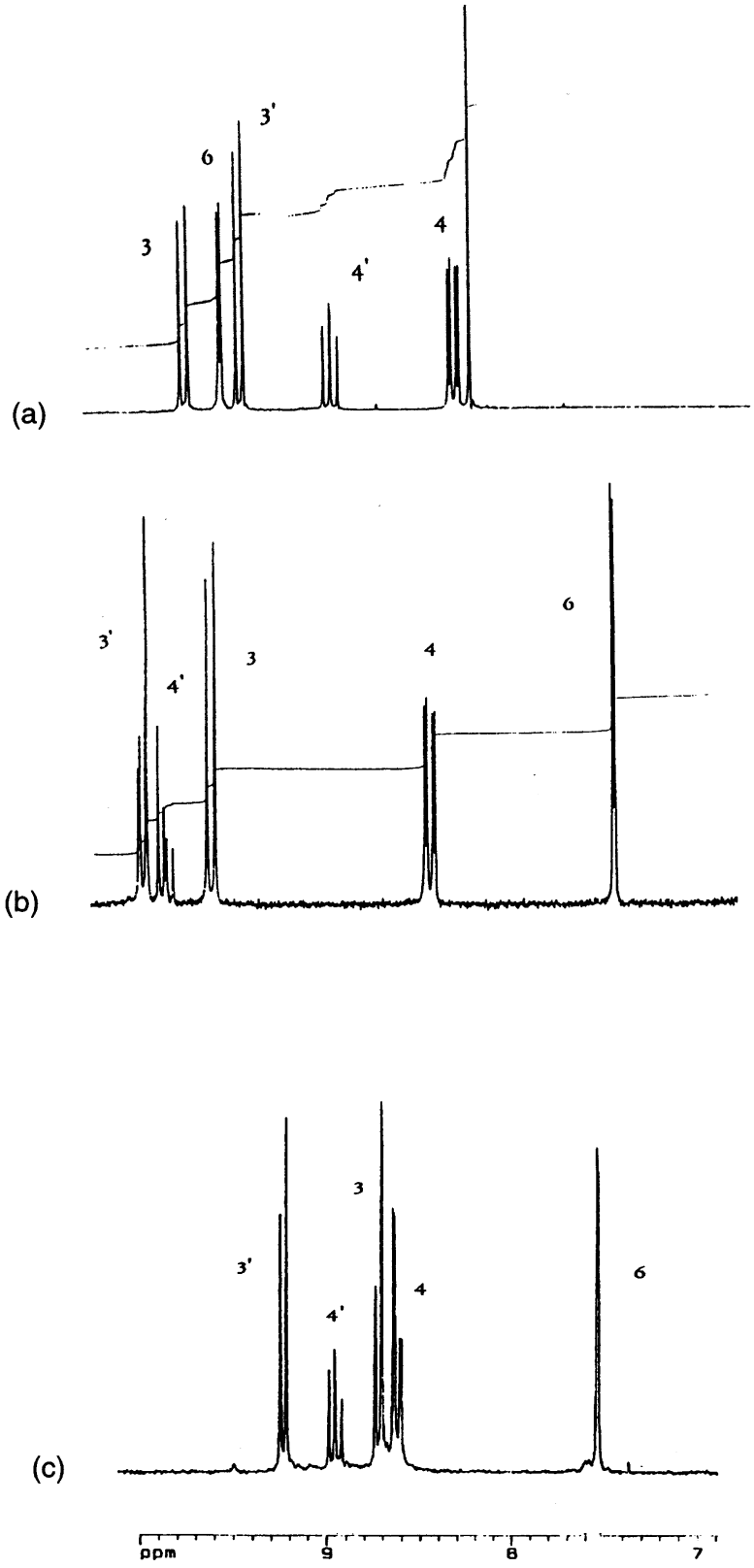

Fig. 1. ^{1}H NMR spectra (250 MHz) of (a) a $CDCl_3$ solution of **3**, (b) a CD_3CN solution of $[Fe(\mathbf{3})_2][PF_6]_2$, and (c) a CD_3CN solution of $[Fe(\mathbf{2})_2][PF_6]_2$.

tions from which the purple salts $[FeL_2][PF_6]_2 \cdot nH_2O$ (L = **2** or **3**) were precipitated with ammonium hexafluorophosphate. In each case, FAB mass spectra of the complexes revealed peaks assigned to $\{[FeL_2, PF_6]\}^+$ and $\{[FeL_2]\}^+$. The differing electronic effects in the two complexes were assessed by a variety of spectroscopic means. We note at this point, that although substituents at the 5 position are not expected to significantly influence the nature of the interaction of the metal ion with the *terminal* rings, the electronic effects may be efficiently transmitted to the *central* ring (Scheme 2).

The electronic spectra of the iron complexes contain a dominant MLCT absorption in the visible region which gives rise to the purple colour (see Section 2). The observed variation in the extinction coefficients represents differing band widths for the various overlapping components of the MLCT processes. The variation in absorption maximum is marked and we have discussed previously the origins of such effects [11]. The nitro substituents in $[Fe(\mathbf{2})_2][PF_6]_2$ result in a shift to lower energy as a result of the lowering of the ligand LUMO energy. Similarly, the electron-releasing substituent in **3** raises the energy of the LUMO and leads to an increase in the energy of the MLCT transition whilst the electron-withdrawing substituent lowers its energy. Semi-empirical calculations (MOPAC, AM1) on the free ligands and the model complexes $[ZnL_2]^{2+}$ (L = **1**, **2** or **3**) fully confirm this model, as do electrochemical studies (see below) which show a reasonable correlation between the MLCT energy and the difference between the metal-centred process and the first ligand reduction.

The electronic effects of the various ligands may be further quantified by a consideration of the redox behaviour of the various complexes. In each case a reversible or quasi-reversible iron(II)/(III) process is observed. In the case of $[Fe(\mathbf{2})_2][PF_6]_2$ these processes are observed at +1.18, −0.90, −1.10, −1.57 and −1.73 V whereas in $[Fe(\mathbf{3})_2][PF_6]_2$ it is found at 0.73, −1.74 and −1.81 V (all potentials quoted vs internal ferrocene/ferrocenium; $[Fe(\mathbf{1})_2][PF_6]_2$ 0.74, −1.64, −1.82 V). We had expected that ligand **2** would destabilise the iron(II) state and shift the iron(II)/(III) couple to more positive potential, as indeed it does. The electron-releasing substituents in **3** play-a multiple role. The raising of the LUMO energy makes **3** a less good π-acceptor than either **1** or **2**. However, this is compensated by a **3** being a better σ-donor. The balance of these two effects is such that the iron(II)/(III) potential for $[Fe(\mathbf{3})_2][PF_6]_2$ is essentially the same as observed for $[Fe(\mathbf{1})_2][PF_6]_2$. These observation stress once again the difficulty in predicting the precise effects of varying ligand structure when synergistic back-bonding is involved [12].

A further measure of the electronic effects within the complexes is found from a study of the ^{1}H NMR spectra of CD_3CN solutions. The ^{1}H NMR spectra of these diamagnetic complexes are sharp and well-resolved and chemical shift data are presented in Table 3 and Fig. 1(b) and (c). Although the individual chemical shifts are quite variable, we have shown previously [4] that $\Delta\delta$ coordination shift values (δ free ligand, $CDCl_3$–δ complex, CD_3CN) are characteristic and, in the 4′-substituted-2,2′:6′,2″-terpyridine series, virtually independent of the substituents. The $\Delta\delta$ values presented in Table 3 indicate that the electronic effects in **1**, **2** and **3** are variable and that they differ in such a way as to give rather different contributions to the coordination shift. The most interesting feature is the relatively large variation in coordination shifts associated with the central ring. This provides further support for our model involving the transmission of electronic effects to the metal through this ring.

We have also determined the crystal structure of the complex $[Fe(\mathbf{3})_2][PF_6]_2 \cdot 2MeCN$ in an attempt to further quantify the electronic interactions between the metal centre and the ligand. The structure of the cation as observed in the solid state is presented in Fig. 2. One of the propoxy groups is disordered with the terminal methyl group occupying two sites. Only one of the conformations is presented in Fig. 2. The

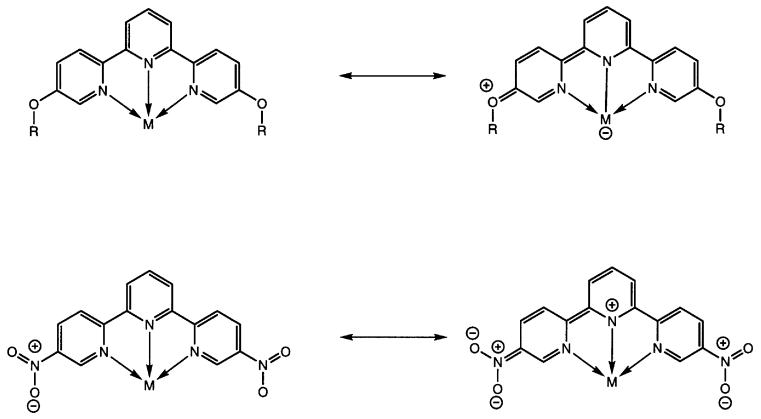

Scheme 2.

Table 3. ^{1}H NMR spectroscopic data for CD_3CN solutions of iron(II) complexes

Complex $[FeL_2, PF_6]_2$, L =	Proton chemical shift/coordination shift[a]					
	3	4	5	6	3′	4′
1	8.47	7.87	7.06	7.06	8.91	8.54
	+0.16	−0.01	+0.28	+1.64	−0.51	−0.71
2	8.72	8.61	–	7.54	9.23	8.95
	+0.10	+0.04	–	+1.98	−0.57	−0.86
3	8.34	7.38	–	6.57	8.64	8.54
	+0.18	−0.06	–	+1.78	−0.37	−0.67

[a] $\Delta\delta = \delta$ free ligand, $CDCl_3$–δ complex, CD_3CN.

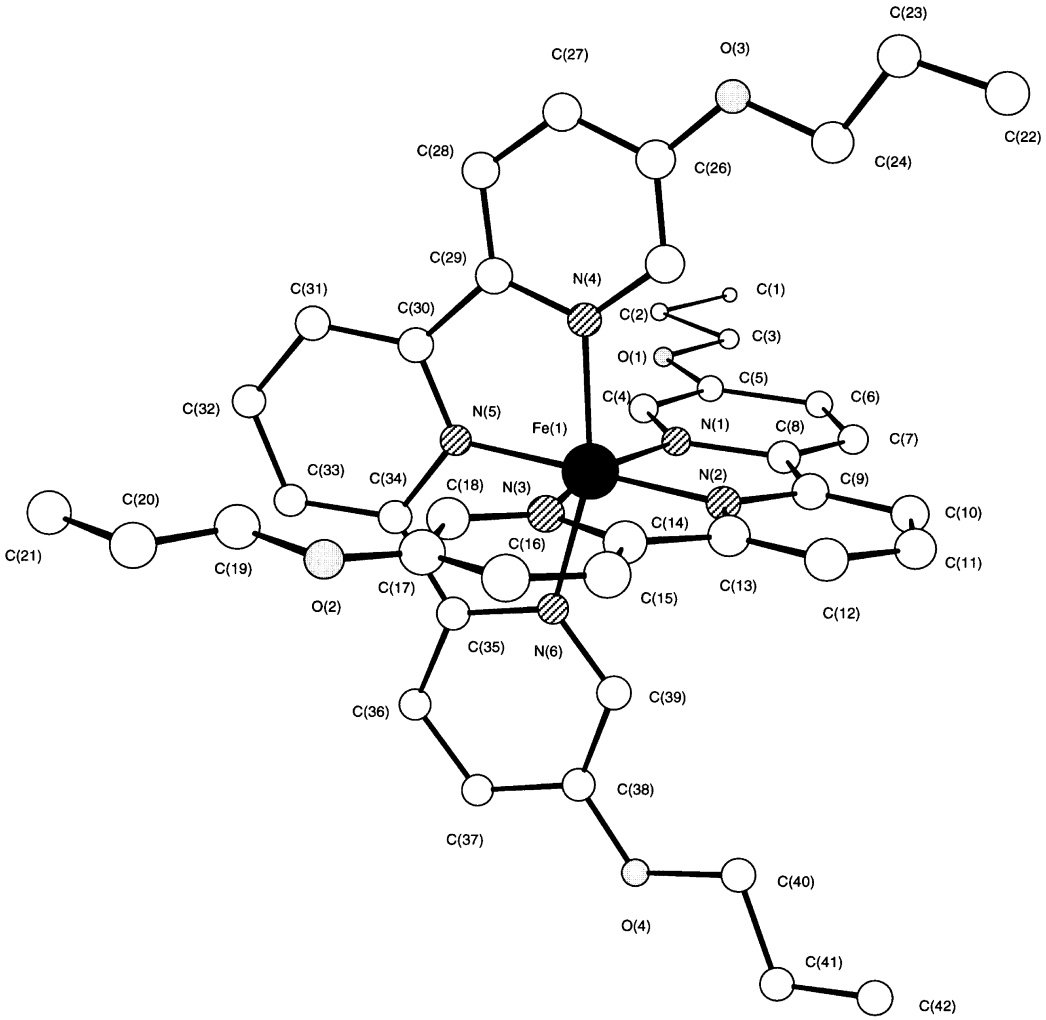

Fig. 2. The $[Fe(\mathbf{3})_2]^{2+}$ cation present in $[Fe(\mathbf{3})_2][PF_6]_2 \cdot 2MeCN$ showing the labelling scheme adopted.

solid state structural determination confirms the presence of the expected cation which adopts approximately D_{2d} symmetry. There are no short contacts between the cations and the anions or the lattice acetonitrile molecules. The tpy domains of the two ligands are approximately planar. Abnormal metal–ligand interactions are expected to be expressed in the Fe–N distances (Table 2). However, the Fe–N distances and bite angles are identical within standard deviations to those of other $[Fe(\mathbf{1})_2]^{2+}$ salts which have been reported [13, 14]. In the crystal lattice the cations form channels with the PF_6^- anions and acetonitrile molecules between them, as indicated in Fig. 3. This appears to confirm our conclusions from the electrochemical studies that the synergism is such that the increased σ-donor and reduced π-acceptor properties of **3** cancel each other out.

3.3. *Cobalt(II) and ruthenium(II) complexes of* 2

For comparison, the complexes $[M(\mathbf{2})_2][PF_6]_2$ (M = Ru or Co) were also prepared, The brown complex $[Co(\mathbf{2})_2][PF_6]_2$ was prepared by the direct reaction of **2** with cobalt acetate in methanol whereas orange $[Ru(\mathbf{2})_2][PF_6]_2$ was obtained by the reaction of **2** with ruthenium trichloride in ethane-1,2-diol. In each case the microanalysis confirmed the formulation of the products and the FAB mass spectrum exhibited ions corresponding to $\{M(\mathbf{2})_2(PF_6)\}^+$, $\{M(\mathbf{2})_2\}^+$ and $\{M(\mathbf{2})\}^+$.

As expected the cobalt(II) complex is paramagnetic and exhibits a typical paramagnetically shifted ^{1}H NMR spectrum with resonances observed at δ 123, 67.1, 66.0, 25.0, 7.5. Although $[Co(\mathbf{1})_2]^{2+}$ complexes show spin crossover behaviour in the solid state, the solution behaviour is better defined. All of the $[Co(Xtpy)_2]^{2+}$ species that we have studied show one of the two ^{1}H NMR spectroscopic behaviours; the lowest field peak is in the range δ 200 to 230 or in the range δ 90 to 130. These values are typical of a low-spin cobalt(II) species, indicating that the introduction of the 5,5″-substituents does not affect the spin state; in solution $[Co(\mathbf{1})_2]^{2+}$ salts are always low spin, whereas the introduction of even a single substituent at the 6-position of the tpy results in high-spin species [15]. The ^{1}H NMR spectrum of the ruthenium complex is typical of a bis(tpy) complex; the resonances of the H^6 and H^4 protons are shifted down-field with respect to $[Ru(\mathbf{1})_2][PF_6]_2$ (0.57 ppm for H^6 and 0.74 ppm for H^4) whilst H^3 experiences only a modest shift of 0.26 ppm. The π-conjugation between the central ring and the nitro substituents is important, and the protons on the central ring also exhibit significant shifts with respect to $[Ru(\mathbf{1})_2][PF_6]_2$ (0.30 ppm for $H^{3'}$ and 0.26 ppm for $H^{4'}$).

The absorption spectrum of the ruthenium complex showed the same trend as the iron analogue with a

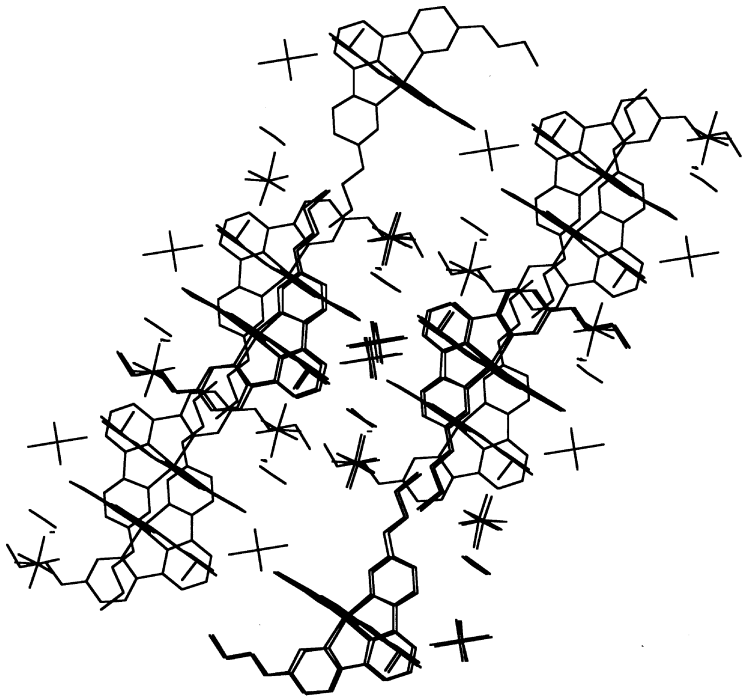

Fig. 3. Packing diagram of $[Fe(\mathbf{3})_2][PF_6]_2 \cdot 2MeCN$ showing the formation of channels between the cations in which the anions and lattice solvent molecules are located.

shift of the MLCT to lower. This behaviour is also paralleled in the electrochemical activity. The complex $[Co(\mathbf{2})_2][PF_6]_2$ exhibited a quasi reversible (ΔE 107 mV) cobalt(II)/(III) process at +0.42 V vs ferrocene/ferrocenium, shifted to more positive potential than that of $[Co(\mathbf{1})_2][PF_6]_2$ (−0.05 V). The ruthenium complex behaves similarly and shows a quasi-reversible ruthenium(II)/(III) process at +1.30 V, shifted 380 mV to more positive potential than $[Ru(\mathbf{1})_2][PF_6]_2$.

4. CONCLUSIONS

The introduction of substituents onto the 5- and 5″-positions of a 2,2′:6′,2″-terpyridine affects the electronic properties of the metal complexes. However, the interactions are complex and cannot be explained simply in terms of the overall electron-releasing or -donating properties of the substituents. The σ- and π-effects act synergistically and conjugation between the substituents on the terminal rings and the central ring is a dominant factor. We are currently extending these observations to other 5,5″-disubstituted ligands.

Acknowledgements—We gratefully acknowledge the Schweizerischer Nationalfonds zur Förderung der wissenschaftlichen Forschung and Ciba-Geigy plc for support.

REFERENCES

1. Constable, E. C., *Prog. Inorg. Chem.*, 1994, **42,** 67.
2. Constable, E. C., *Tetrahedron*, 1992, **48,** 10013.
3. Constable, E. C., in *Comprehensive Supramolecular Chemistry*, Vol. 9, ed. J.-M. Lehn. Pergamon, Oxford, 1996, p. 213.
4. Constable, E. C., Cargill Thompson, A. M. W., Tocher, D. A. and Daniels, M. A. M., *New J. Chem.*, 1992, **16,** 855.
5. Constable, E. C., Cargill Thompson, A. M. W. and Tocher, D. A., in *Supramolecular Chemistry*, eds. V. Balzani and L. De Cola. Kluwer Academic Press, Dordrecht, 1992, p. 219.
6. Constable, E. C., in *Transition Metals in Supramolecular Chemistry*, eds. L. Fabbrizzi and A. Poggi. Kluwer, Dordrecht, 1994, p. 81.
7. Crane, J. D. and Sauvage, J.-P., *New J. Chem.*, 1992, **16,** 649.
8. Constable, E. C. and Phillips, D., *Chem. Commun.*, 1997, 827.
9. Matsumura, E. and Ariga, M., Tohda, Y., *Bull. Chem. Soc. Jpn.*, 1979, **52,** 2413.
10. Tohda, Y., Eiraku, M. T., Nakagawa, Y., Usami, Y., Ariga, M., Kawashima, T., Tani, K., Watanabe, H. and Mori, Y., *Bull. Chem. Soc. Jpn.*, 1990, **63,** 2820.
11. Maestri, M., Armaroli, N., Balzani, V., Constable, E. C., Cargill Thompson, A. M. W., *Inorg. Chem.*, 1995, **34,** 2759.
12. Constable, E. C., Neuburger, M., Smith, D. R. and Zehnder, M., *Inorg. Chim. Acta*, in press.
13. Baker, A. T. and Goodwin, H. A., *Aust. J. Chem.*, 1985, **38,** 207.
14. Laine, P., Gourdon, A. and Launay, J.-P., *Inorg. Chem.*, 1995, **34,** 5156.
15. Constable, E. C., Kulke, T., Neuburger, M. and Zehnder, M., *New J. Chem.*, 1997, **21,** 1091.

Pergamon

Polyhedron Vol. 17, No. 23–24, pp. 3999–4009, 1998
© 1998 Elsevier Science Ltd
All rights reserved. Printed in Great Britain
0277–5387/98 $19.00+0.00

PII: S0277-5387(98)00198-3

Structural characterization and luminescence studies of new lanthanide(III) complexes with nicotinic and isonicotinic acid *N*-oxides

Jiang-Gao Mao[a,1], Hong-Jie Zhang[b], Jia-Zuan Ni[b], Shu-Bin Wang[b] and Thomas C. W. Mak[a]*

Department of Chemistry, The Chinese University of Hong Kong, Shatin, New Territories, Hong Kong, P.R. China

Laboratory of Rare Earth Chemistry and Physics, Changchun Institute of Applied Chemistry, The Chinese Academy of Sciences, Changchun 130022, P.R. China

(Received 19 January 1998; accepted 14 May 1998)

Abstract—Four new polymeric lanthanide(III) complexes of nicotinic acid *N*-oxide and isonicotinic acid *N*-oxide have been synthesized and structurally determined. In the isomorphous compounds $[\{Ln(L^1)_3(H_2O)_2\}_n]\cdot 4nH_2O$ (HL^1 = nicotinic acid *N*-oxide; Ln = Eu, **1**; Ln = Er, **2**) the lanthanide(III) ions form infinite double chains along the *b* direction through the coordination of bridging carboxylate and *N*-oxide groups. The chains are cross-linked through hydrogen bonds between aqua ligands and uncoordinated *N*-oxide groups and between aqua ligands and lattice water molecules, to form a three-dimensional network. $[\{Eu(L^2)_2(H_2O)_4\}_n](NO_3)_n\cdot nH_2O$ (HL^2 = isonicotinic acid *N*-oxide, **3**) has a polymeric structure in which the europium (III) ions are connected into infinite chains by pairs of *syn–syn* carboxylate groups. Adjacent chains are inter-linked by hydrogen bonds between aqua ligands and *N*-oxide groups to form a layer parallel to the (100) plane, and such layers are connected by hydrogen bonds between nitrate anions and aqua ligands, and between oxide groups and lattice water molecules, into a three-dimensional network. In $[\{Er_2(L^2)_4(H_2O)_{10}\}](NO_3)_2\cdot H_2O$, **4**, dinuclear units are inter-linked into a three-dimensional network through hydrogen bonding between aqua ligands and *N*-oxide groups of both bidentate bridging and unidentate L^2 ligands. Factors affecting the formation of coordination chains and dinuclear units are discussed. Luminescence properties of **1** and **3** have also been studied. © 1998 Elsevier Science Ltd. All rights reserved

Keywords: lanthanide complex; coordination polymer; crystal structure; luminescence.

INTRODUCTION

Lanthanide complexes of three isomers of pyridine carboxylic acid, namely nicotinic acid, isonicotinic acid and picolinic acid, have been extensively investigated [1–13]. Pyridine carboxylic acid *N*-oxides have an oxygen atom in place of the nitrogen donor site, but studies on ligand behavior toward lanthanides are limited [14–19], as so far only one dimeric lanthanum complex of 6-methyl-picotinic acid *N*-oxide has been structurally determined [19]. *N*-oxide functionalization of nicotinic acid and isonicotinic acid should increase the flexibility of the resulting ligands in addition to enhancement of their capacities for coordination and or hydrogen bonding and, hence, their lanthanide complexes are expected to exhibit different characteristics as compared with the corresponding lanthanide nicotinates and isonicotinates. In this paper, we describe the preparation and structural characterization of four new lanthanide(III) complexes of nicotinic acid *N*-oxide and isonicotinic acid *N*-oxide, namely isomorphous $[\{Ln(L^1)_3(H_2O)_2\}_n]\cdot 4nH_2O$ (HL^1 = nicotinic acid *N*-oxide; Ln = Eu, **1**; Ln = Er, **2**) with a polymeric double-chain structure, $[\{Eu(L^2)_2(H_2O)_4\}_n](NO_3)_n\cdot nH_2O$ (HL^2 = isonicotinic

[1] On sabbatical leave from Fujian Institute of Research on the Structure of Matter, The Chinese Academy of Sciences, Fuzhou 350002, P.R. China.

* Author to whom correspondence should be addressed. Fax: +86-852-2603-5057; E-mail: tcwmak@cuhk.hk.

acid *N*-oxide, **3**) whose metal ions are linked into an infinite chain by pairs of bridging carboxylate groups, and a dinuclear complex, $[\{Er_2(L^2)_4(H_2O)_{10}\}](NO_3)_2 \cdot 4H_2O$ (**4**). Luminescence properties of the two europium(III) complexes have also been studied.

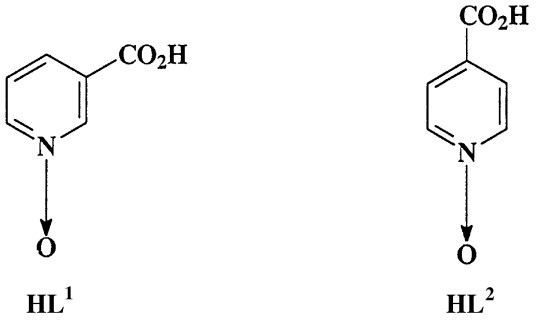

EXPERIMENTAL

IR spectra were obtained from KBr pellets with a Nicolet Magna-IR 550 spectrometer. Electronic spetra in the UV-visible range were recorded at room temperature with a Hitachi U-2000 spectrophotometer. Excitation and emission spectral measurements were performed on a Hitachi MPF-4 fluorescence spectrophotometer at room temperature. Luminescence measurements were carried out using solid samples at 298 K and corrections for the lamp response and PMT (type R928 operating in photon counting mode) were applied.

Synthesis of complexes 1–4

Nicotinic acid *N*-oxide (or isonicotinic acid *N*-oxide) (1.0 mmol) was completely dissolved in 10 cm^3 of distilled water by slow addition of aqueous ammonia (2 N) to form a clear solution, to which $Ln(NO_3)_3 \cdot nH_2O$ (0.5 mmol) (Ln = Eu or Er) was added under stirring. The resultant solution was filtered off. Storage of the solution in a desiccator charged with drierite for several days yielded crystals of complexes **1–4**. IR data: of $[\{Eu(L^1)_3(H_2O)_2\}_n] \cdot 4nH_2O$, **1**, 3416s, 3100w, 1656s, 1589s, 1555s, 1387s, 1226s, 1132m, 1085w, 1025w, 944m, 815m, 775m, 669m, 581m cm^{-1}; $[\{Er(L^1)_3(H_2O)_2\}_n] \cdot 4nH_2O$, **2**, 3442s, 3079w, 1670s, 1607s, 1562s, 1418s, 1384s, 1233s, 1139m, 1090w, 1022w, 948m, 818m, 772m, 669m, 601w cm^{-1}; $[\{Eu(L^2)_2(H_2O)_4\}_n](NO_3)_n \cdot nH_2O$, **3**, 3382s, 3098w, 2470w, 2427w, 1664s, 1605s, 1564s, 1480m, 1412s, 1384s, 1300m, 1226s, 1119m, 1025w, 945m, 815s, 772s, 689m, 671m, 584m, 450m cm^{-1}; $[\{Er_2(L^2)_4(H_2O)_{10}\}](NO_3)_2 \cdot 4H_2O$, **4**, 3443s, 3095w, 2426w, 1941w, 1668s, 1635s, 1553s, 1490m, 1409s, 1218s, 1183s, 1151s, 1109m, 1046m, 882m, 868s, 827m, 784s, 682m, 636s, 570m, 472m cm^{-1}.

Crystal structure determination

Information concerning crystallographic data and structure refinement of the four complexes is summarized in Table 1. Raw intensities of complex **1** was collected at 293 K on a MSC/Rigaku RAXIS-IIC imaging plate system with a rotating anode Mo-*K*α X-ray source ($\lambda = 0.71073$ Å, 50 kV, 150 mA) [20, 21] and corrected for absorption using the ABSCOR program [22]. Data collection of complexes **2**, **3** and **4** were performed on a Siemens R3m/V diffractometer in the variable ω-scan mode [23] using Mo-Kα radiation ($\lambda = 0.71073$ Å) at 294 K. Unit-cell parameters were calculated from least-squares fitting of 2θ angles for 25 reflections. Crystal stability was monitored by recording three check reflections at intervals of 197 data measurements, and no significant variation was detected. The raw data were processed with a learnt-profile procedure [24], and empirical absorption corrections based on ψ-scan data were also applied.

All calculations were performed on a PC 486 computer with the SHELXTL-PC program package [25, 26] and SHELXL-93 program package [27]. Each crystal structure was solved with the Patterson superposition method. The non-hydrogen atoms were refined anisotropically. The water O(2w) and nitrate O(21) and O(22) atoms in complex **3** are disordered over the imposed mirror plane and their site occupancy factors are reduced to one-half. All hydrogen atoms were generated geometrically, assigned fixed isotropic thermal parameters and included in the structure factor calculations. Analytical expressions of neutral-atom scattering factors were employed [28], and anomalous dispersion corrections were incorporated.

RESULTS AND DISCUSSION

Crystal structure of $[Ln(L^1)_3(H_2O)_2]_n \cdot 4nH_2O$ (Ln = Eu, ***1***; Ln = Er, ***2***)

These two complexes are isostructural and the structure of the europium(III) complex is shown in Fig. 1(a). The Ln(III) atom is eight-coordinated by six oxygen atoms from four L^1 ligands and two aqua ligands. The carboxylate groups are involved in three different coordination modes: a common bidentate chelating mode [Eu(1)–O(1)–C(6) 91.9(4)° and Eu(1)–O(2)–C(6) 93.5(4)° for **1**; Er(1)–O(1)–C(6) 91.5(2)° and Er(1)–O(2)–C(6) 93.2(2)° for **2**], a bidentate bridging mode in the *syn–syn* configuration [Eu(1)–O(3)–C(12)–C(7) 135.0° and C(7)–C(12)–O(4)–Eu(1a) −140.4° in **1**; Er(1)–O(3)–C(12)–C(7) 134.2° and C(7)–C(12)–O(4)–Er(1a) −141.4° in **2**], as well as a unidentate mode [Ln(1)–O(5)–C(18) = 149.5(5) and 148.7(2)°, respectively, for complexes **1** and **2**]. The mean Ln–O(aqua) distances are 2.426(5) and 2.365(3) Å, respectively, for complexes **1** and **2**. The Ln–O(carboxylate) distances are in the order Ln–O(chelating) > Ln–O(bridging) > Ln–O(unidentate) (Table 2. Most lanthanide complexes of nicotinic acid are dimeric in which the metal ions are bridged by four carboxylate groups and each metal ion is further

Table 1. Data collection and processing parameters for complexes **1**–**4**

Complex	**1**	**2**	**3**	**4**
Formula	$C_{18}H_{24}N_3O_{15}Eu$	$C_{18}H_{24}N_3O_{15}Er$	$C_{12}H_{18}N_3EuO_{14}$	$C_{12}H_{22}N_3O_{16}Er$
FW	674.4	689.7	580.25	631.6
Colour, habit	colourless block	pink prism	colorless block	pink prism
Crystal size (mm)	$0.23\times0.25\times0.37$	$0.11\times0.16\times0.52$	$0.32\times0.28\times0.50$	$0.12\times0.08\times0.58$
Crystal system	triclinic	triclinic	orthorhombic	triclinic
Space group	$P\bar{1}$ (No. 2)	$P\bar{1}$ (No. 2)	*Cccm* (No. 66)	$P\bar{1}$ (No. 2)
a (Å)	8.205(2)	8.190(2)	10.558(1)	9.233(2)
b (Å)	9.867(2)	9.758(2)	16.829(2)	10.491(2)
c (Å)	15.948(3)	15.848(3)	10.491(3)	12.185(2)
α (°)	80.29(3)	80.36(3)	90	77.48(3)
β (°)	81.35(3)	81.09(3)	90	74.86(3)
γ (°)	80.64(3)	80.53(3)	90	70.76(3)
U (Å^3)	1245.6(6)	1221.0(6)	1864.0(5)	1064.6(5)
Z	2	2	4	2
F(000)	672	682	1144	622
D(calcd) (g cm^{-3})	1.798	1.876	2.068	1.970
μ (mm^{-1})	2.594	3.516	3.447	4.026
Collection range; $2\theta_{max}$	$\pm h$, $-k$, $\pm l$, 52.0°	h, $\pm k$, $\pm l$, 52.0°	h, k, l, 52.0°	h, $\pm k$, $\pm l$, 52.0°
Unique data measured	3860	5643	1132	4907
Observed data [$F>4.0\sigma$ (F)], n	3797	5144	803	4655
No. of variables, p	334	334	88	289
$R1$, $wR2$ (for observed data)	0.052, 0.139	0.026, 0.066	0.045	0.039, 0.100
$R1$, $wR2$ (for all data)	0.053, 0.141	0.030, 0.068	0.109	0.040, 0.105
S (goodness-of-fit)	1.075	1.028	1.072	1.085
Maximum residual in final difference map (e Å^{-3})	1.47 (0.92 Å from Eu(1))	0.83	1.82 (1.12 Å from Eu(1))	1.55 (0.92 Å from Er(1))

$R1 = \Sigma\|F_o|-|F_c\|/\Sigma|F_o|$, $wR2=\{\Sigma w[(F_o)^2-(F_c)^2]^2/\Sigma w[(F_o)^2]^2\}^{1/2}$, $S=[\Sigma w[(F_o)^2-(F_c)^2]^2/(n-p)]^{1/2}$, $w = 1/[\Sigma(|F_o|^2)^2+(aP)^2+bP]$ where $P = [\max(|F_o|^2, 0)+2(F_o)^2]/3$ a, b = 0.0987, 2.68 for **1**; 0.0435, 0.67 for **2**; 0.0575, 40.54 for **3** and 0.0773, 0.97 for **4**.

coordinated to one bidentate chelating carboxylate group and two aqua ligands [2, 3, 5–8]. Higher coordination numbers for the light lanthanide(III) ions can be achieved with two bridging carboxylate groups adopting the terdentate bridging and chelating coordination mode [4]. Under acidic condition, Ho(III) nicotinate comprises polymer chains made up of lanthanide(III) ions alternately linked by four and two carboxylate groups [4]. The unidentate mode of the carboxylate group is so far only observed in mononuclear europium phenanthroline nicotinate [8]. The significant difference between the structures of lanthanide complexes of nicotinic acid *N*-oxide and those of lanthanide nicotinates is due to the coordination of the *N*-oxide group to the metal ions. In complexes **1** and **2**, one *N*-oxide group bonds to the metal ion [N(2)–O(22)–Eu(1b) 127.1(4)° in **1** and N(2)–O(22)–Er(1b) 127.6(2)° in **2**]; the Ln–O(*N*-oxide) distance is slightly longer than those of Ln–O(carboxylate, bridging) and Ln–O(carboxylate, unidentate), but much shorter than Ln–O(carboxylate, chelating) Table 2. The other two *N*-oxide groups are only involved in hydrogen bonding with both coordinated and lattice water molecules Table 2. Each pair of lanthanide ions are bridged by two bidentate *syn–syn* carboxylate groups with Ln...Ln separation of 5.606(1) and 5.540(1) Å for **1** and **2**, respectively. These dimeric units are linked through Ln–O(*N*-oxide) bonds to form infinite double chains directed along the *b* axis [Fig. 1(b)]. The latter are cross-linked through hydrogen bonds between aqua ligands and uncoordinated oxide groups, and between aqua ligands and cyclic $(H_2O)_4$ units to form a three-dimensional network [Table 2, Fig. 1(b)].

The coordination geometry of the Eu(III) atom is best described as a strongly distorted square-antiprism. The least-squares plane fitted to atoms O(1), O(3), O(4a) and O(2w) has a mean deviation of 0.448 Å, whereas another face defined by O(2), O(22b), O(1w) and O(5) has a mean deviation of 0.416 Å. The dihedral angle between these two least-squares planes is *ca.* 5.5°. The Eu(III) atom is displaced 1.262 and 1.241 Å, respectively, from the above two faces.

Crystal structures of $[\{Eu(L^2)_2(H_2O)_4\}_n](NO_3)_n\cdot nH_2O$, ***3***, and $[Er_2(L^2)_4(H_2O)_{10}](NO_3)_2\cdot 4H_2O$, ***4***

Complex **3** contains europium(III) carboxylate chains built of bis(carboxylato-O,O′)-bridged centrosymmetric dimeric subunits. As illustrated in Fig.

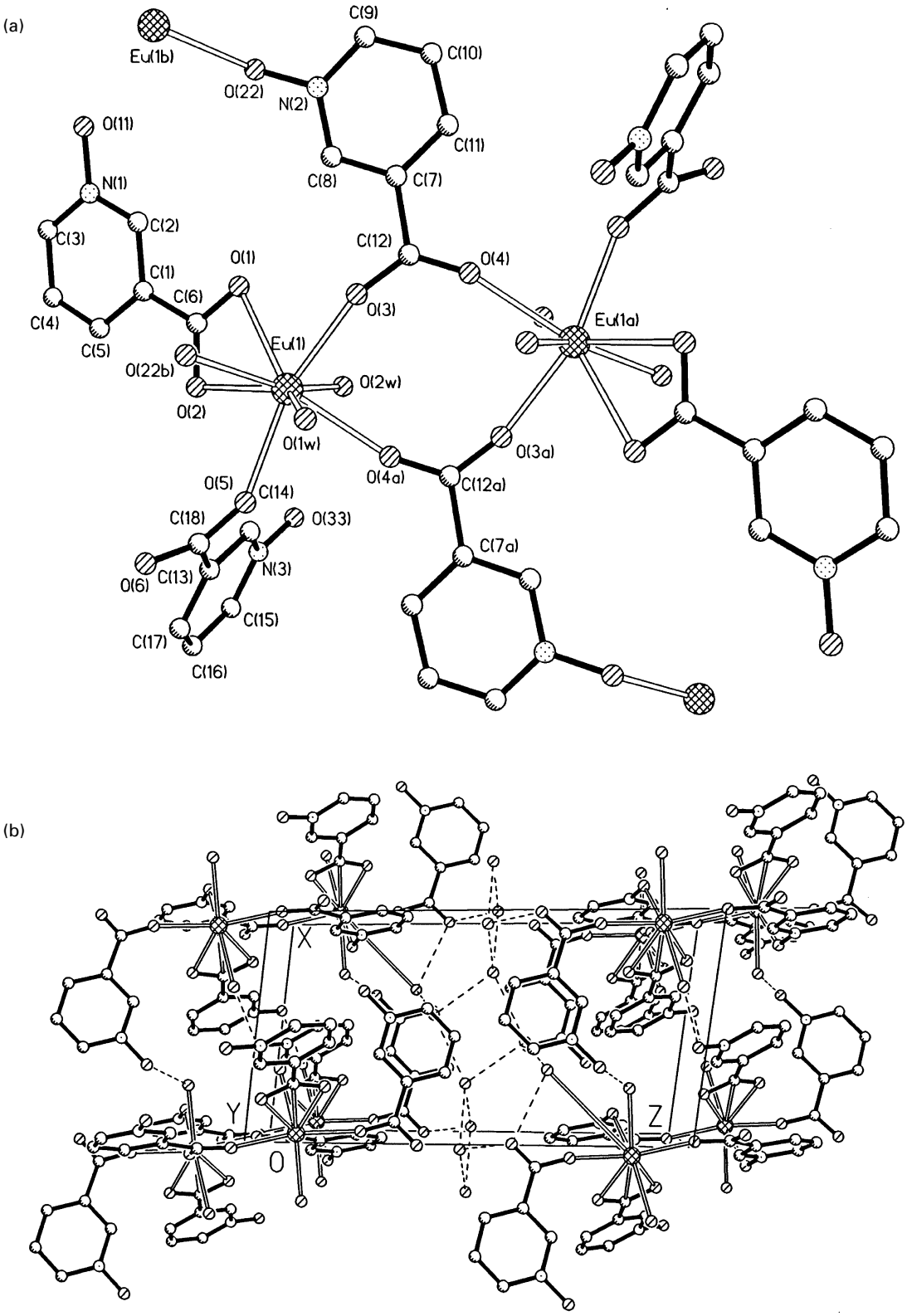

Fig. 1. (a) Perspective view showing the asymmetric unit of complex **1** with the atom labeling scheme (the lattice water molecules have been omitted for clarity). (b) Packing drawing showing the linkage of metal carboxylate double chains through hydrogen bonds between aqua ligands and lattice water molecules.

Table 2. Selected bond lengths (Å) and bond angles (°)

$[\{Eu(L^1)_3(H_2O)_2\}_n]\cdot 4nH_2O$, **1**

Eu(1)–O(5)	2.303(4)	Eu(1)–O(3)	2.309(5)	Eu(1)–O(4a)	2.358(4)
Eu(1)–O(22b)	2.379(5)	Eu(1)–O(2W)	2.411(5)	Eu(1)–O(1W)	2.440(5)
Eu(1)–O(2)	2.501(5)	Eu(1)–O(1)	2.546(5)	O(4)–Eu(1a)	2.358(4)
O(22)–Eu(1b)	2.379(5)	Eu(1)···Eu(1a)	5.606(1)		
Hydrogen bonding					
O(1W)...O(11b)	2.835	O(1W)···O(22b)	2.701	O(1W)···O(33c)	2.649
O(2W)···O(11d)	2.810	O(2W)···O(1We)	2.686	O(3W)···O(4W)	2.810
O(4W)...O(5W)	2.825	O(4W)...O(5Wf)	2.809	O(5W)...O(6W)	2.858
O(5W)...O(6Wg)	2.866				

O(5)–Eu(1)–O(3)	160.6(2)	O(5)–Eu(1)–O(4a)	77.7(2)
O(3)–Eu(1)–O(4a)	86.4(2)	O(5)–Eu(1)–O(22b)	89.9(2)
O(3)–Eu(1)–O(22b)	96.0(2)	O(4a)–Eu(1)–O(22b)	142.1(2)
O(5)–Eu(1)–O(2W)	97.7(2)	O(3)–Eu(1)–O(2W)	87.0(2)
O(4a)–Eu(1)–O(2W)	69.6(2)	O(22b)–Eu(1)–O(2W)	148.3(2)
O(5)–Eu(1)–O(1W)	84.2(2)	O(3)–Eu(1)–O(1W)	80.9(2)
O(4a)–Eu(1)–O(1W)	74.9(2)	O(22b)–Eu(1)–O(1W)	68.2(2)
O(2W)–Eu(1)–O(1W)	143.1(2)	O(5)–Eu(1)–O(2)	73.7(2)
O(3)–Eu(1)–O(2)	125.6(2)	O(4a)–Eu(1)–O(2)	129.2(2)
O(22b)–Eu(1)–O(2)	79.0(2)	O(2W)–Eu(1)–O(2)	73.8(2)
O(1W)–Eu(1)–O(2)	140.3(2)	O(5)–Eu(1)–O(1)	125.2(2)
O(3)–Eu(1)–O(1)	74.2(2)	O(4a)–Eu(1)–O(1)	139.4(2)
O(22b)–Eu(1)–O(1)	76.5(2)	O(2W)–Eu(1)–O(1)	74.0(2)
O(1W)–Eu(1)–O(1)	133.8(2)	O(2)–Eu(1)–O(1)	51.8(2)
C(6)–O(1)–Eu(1)	91.9(4)	C(6)–O(2)–Eu(1)	93.5(4)
C(12)–O(3)–Eu(1)	160.6(5)	C(12)–O(4)–Eu(1a)	160.0(5)
C(18)–O(5)–Eu(1)	149.5(5)	N(2)–O(22)–Eu(1b)	127.1(4)

$[\{Er(L^1)_3(H_2O)_2\}_n]\cdot 4nH_2O$, **2**

Er(1)–O(5)	2.245(2)	Er(1)–O(3)	2.251(2)	Er(1)–O(4a)	2.294(2)
Er(1)–O(22b)	2.310(2)	Er(1)–O(2W)	2.345(3)	Er(1)–O(1W)	2.385(3)
Er(1)–O(2)	2.461(3)	Er(1)–O(1)	2.497(2)		
O(22)–Er(1b)	2.310(2)	Er(1)...Er(1a)	5.540(1)		
Hydrogen bonding					
O(1W)···O(11b)	2.823	O(1W)...O(22b)	2.630	O(1W)···O(33c)	2.648
O(2W)···O(11d)	2.795	O(2W)···O(1We)	2.681	O(3W)···O(4W)	2.770
O(4W)···O(5W)	2.817	O(4W)···O(5Wf)	2.838	O(5W)···O(6W)	2.849
O(5W)···O(6Wg)	2.835				

O(5)–Er(1)–O(3)	159.8(1)	O(5)–Er(1)–O(4a)	77.7(1)
O(3)–Er(1)–O(4a)	86.1(1)	O(5)–Er(1)–O(22b)	90.4(1)
O(3)–Er(1)–O(22b)	95.0(1)	O(4a)–Er(1)–O(22b)	141.8(1)
O(5)–Er(1)–O(2W)	97.6(1)	O(3)–Er(1)–O(2W)	88.1(1)
O(4a)–Er(1)–O(2W)	70.2(1)	O(22b)–Er(1)–O(2W)	147.9(1)
O(5)–Er(1)–O(1W)	84.4(1)	O(3)–Er(1)–O(1W)	79.6(1)
O(4a)–Er(1)–O(1W)	74.6(1)	O(22b)–Er(1)–O(1W)	68.1(1)
O(2W)–Er(1)–O(1W)	143.4(1)	O(5)–Er(1)–O(2)	73.6(1)
O(3)–Er(1)–O(2)	126.6(1)	O(4a)–Er(1)–O(2)	129.6(1)
O(22b)–Er(1)–O(2)	79.1(1)	O(2W)–Er(1)–O(2)	73.6(1)
O(1W)–Er(1)–O(2)	140.2(1)	O(5)–Er(1)–O(1)	126.1(1)
O(3)–Er(1)–O(1)	74.1(1)	O(4a)–Er(1)–O(1)	139.1(1)
O(22b)–Er(1)–O(1)	76.6(1)	O(2W)–Er(1)–O(1)	73.6(1)
O(1W)–Er(1)–O(1)	133.4(1)	O(2)–Er(1)–O(1)	52.7(1)
C(6)–O(1)–Er(1)	91.5(2)	C(6)–O(2)–Er(1)	93.2(2)
C(12)–O(3)–Er(1)	159.6(2)	C(12)–O(4)–Er(1a)	160.5(2)
C(18)–O(5)–Er(1)	148.7(2)	N(2)–O(22)–Er(1b)	127.6(2)

Table 2—*continued.*

Eu(1)–O(1a)	2.352(6)	Eu(1)–O(1b)	2.352(6)	Eu(1)–O(1)	2.352(6)
Eu(1)–O(1c)	2.352(6)	Eu(1)–O(1Wb)	2.462(6)	Eu(1)–O(1W)	2.462(6)
Eu(1)–O(1Wc)	2.462(6)	Eu(1)–O(1Wa)	2.462(6)	O(1)–C(1)	1.229(7)
C(1)–O(1d)	1.229(7)	C(1)–C(2)	1.507(13)	C(2)–C(3d)	1.35(2)
Hydrogen bonding					
O(1W)···O(21)	2.684	O(11)···O(2W)	2.606	O(1W)···O(1Wc)	2.693
O(1W)···O(22e)	2.739	O(11)···O(2Wf)	2.606		

O(1a)–Eu(1)–O(1b)	149.9(3)	O(1a)–Eu(1)–O(1)	88.5(3)
O(1b)–Eu(1)–O(1)	99.2(3)	O(1a)–Eu(1)–O(1c)	99.2(3)
O(1b)–Eu(1)–O(1c)	88.5(3)	O(1)–Eu(1)–O(1c)	149.9(3)
O(1a)–Eu(1)–O(1Wb)	138.0(2)	O(1b)–Eu(1)–O(1Wb)	72.0(2)
O(1)–Eu(1)–O(1Wb)	77.9(2)	O(1c)–Eu(1)–O(1Wb)	77.0(2)
O(1a)–Eu(1)–O(1W)	77.0(2)	O(1b)–Eu(1)–O(1W)	77.9(2)
O(1)–Eu(1)–O(1W)	72.0(2)	O(1c)–Eu(1)–O(1W)	138.0(2)
O(1Wb)–Eu(1)–O(1W)	132.8(3)	O(1a)–Eu(1)–O(1Wc)	77.9(2)
O(1b)–Eu(1)–O(1Wc)	77.0(2)	O(1)–Eu(1)–O(1Wc)	138.0(2)
O(1c)–Eu(1)–O(1Wc)	72.0(2)	O(1Wb)–Eu(1)–O(1Wc)	136.2(3)
O(1W)–Eu(1)–O(1Wc)	66.3(3)	O(1a)–Eu(1)–O(1Wa)	72.0(2)
O(1b)–Eu(1)–O(1Wa)	138.0(2)	O(1)–Eu(1)–O(1Wa)	77.0(2)
O(1c)–Eu(1)–O(1Wa)	77.9(2)	O(1Wb)–Eu(1)–O(1Wa)	66.3(3)
O(1W)–Eu(1)–O(1Wa)	136.2(3)	O(1Wc)–Eu(1)–O(1Wa)	132.8(3)
C(1)–O(1)–Eu(1)	155.8(6)		

$[Er_2(L^2)_4(H_2O)_{10}](NO_3)_2{\cdot}4H_2O$, **4**

Er(1)–O(3)	2.278(3)	Er(1)–O(3W)	2.283(3)	Er(1)–O(5W)	2.315(3)
Er(1)–O(4a)	2.334(3)	Er(1)–O(2)	2.379(3)	Er(1)–O(4W)	2.386(3)
Er(1)–O(1W)	2.420(3)	Er(1)–O(2W)	2.434(3)	O(4)–Er(1a)	2.334(3)
Er(1)...Er(1a)	4.804(1)				
Hydrogen bonding					
O(1W)···O(1)	2.613	O(1W)···O(32)	2.814	O(2W)···O(3W)	2.670
O(2W)···O(4W)	2.839	O(2W)···O(22b)	2.784	O(2W)···O(7W)	2.783
O(3W)···O(11b)	2.667	O(3W)···O(11c)	2.676	O(4W)···O(5W)	2.885
O(4W)···O(22b)	2.776	O(5W)···O(22d)	2.697	O(5W)···O(6We)	2.664
O(6W)···O(31)	2.738	O(6W)···O(31f)	2.845		

O(3)–Er(1)–O(3W)	146.8(1)	O(3)–Er(1)–O(5W)	86.7(1)
O(3W)–Er(1)–O(5W)	95.8(1)	O(3)–Er(1)–O(4a)	106.5(1)
O(3W)–Er(1)–O(4a)	90.8(1)	O(5W)–Er(1)–O(4a)	144.0(1)
O(3)–Er(1)–O(2)	76.7(1)	O(3W)–Er(1)–O(2)	72.9(1)
O(5W)–Er(1)–O(2)	71.7(1)	O(4a)–Er(1)–O(2)	143.4(1)
O(3)–Er(1)–O(4W)	71.6(1)	O(3W)–Er(1)–O(4W)	141.0(1)
O(5W)–Er(1)–O(4W)	75.7(1)	O(4a)–Er(1)–O(4W)	77.1(1)
O(2)–Er(1)–O(4W)	135.2(1)	O(3)–Er(1)–O(1W)	78.8(1)
O(3W)–Er(1)–O(1W)	80.4(1)	O(5W)–Er(1)–O(1W)	144.7(1)
O(4a)–Er(1)–O(1W)	71.3(1)	O(2)–Er(1)–O(1W)	73.7(1)
O(4W)–Er(1)–O(1W)	127.7(1)	O(3)–Er(1)–O(2W)	142.8(1)
O(3W)–Er(1)–O(2W)	68.9(1)	O(5W)–Er(1)–O(2W)	76.6(1)
O(4a)–Er(1)–O(2W)	72.9(1)	O(2)–Er(1)–O(2W)	126.6(1)
O(4W)–Er(1)–O(2W)	72.2(1)	O(1W)–Er(1)–O(2W)	131.9(1)
C(6)–O(2)–Er(1)	139.1(3)	C(12)–O(3)–Er(1)	175.2(3)
C(12)–O(4)–Er(1a)	123.6(3)		

Symmetry codes: For **1**–**2**: (a) $1-x, 1-y, 1-z$, (b) $1-x, -y, 1-z$, (c) $1+x, y, z$, (d) $x, 1+y, z$, (e) $-x, -y, 1-z$, (f) $2-x, -y, -z$, (g) $1-x, -y, -z$. For **3**: (a) $-x, y, -z+1/2$, (b) $-x, -y, z$, (c) $x, -y, -z+1/2$, (d) $x, y, -z$, (e) $-x+1/2, -y+1/2, z$, (f) $-x, 1-y, -z$. For **4**: (a) $-x, -y, -z$, (b) $x, y-1, z$, (c) $-x, 1-y, -1-z$, (d) $-1-x, 1-y, -z$, (e) $x-1, y+1, z$, (f) $1-x, -1-y, -1-z$.

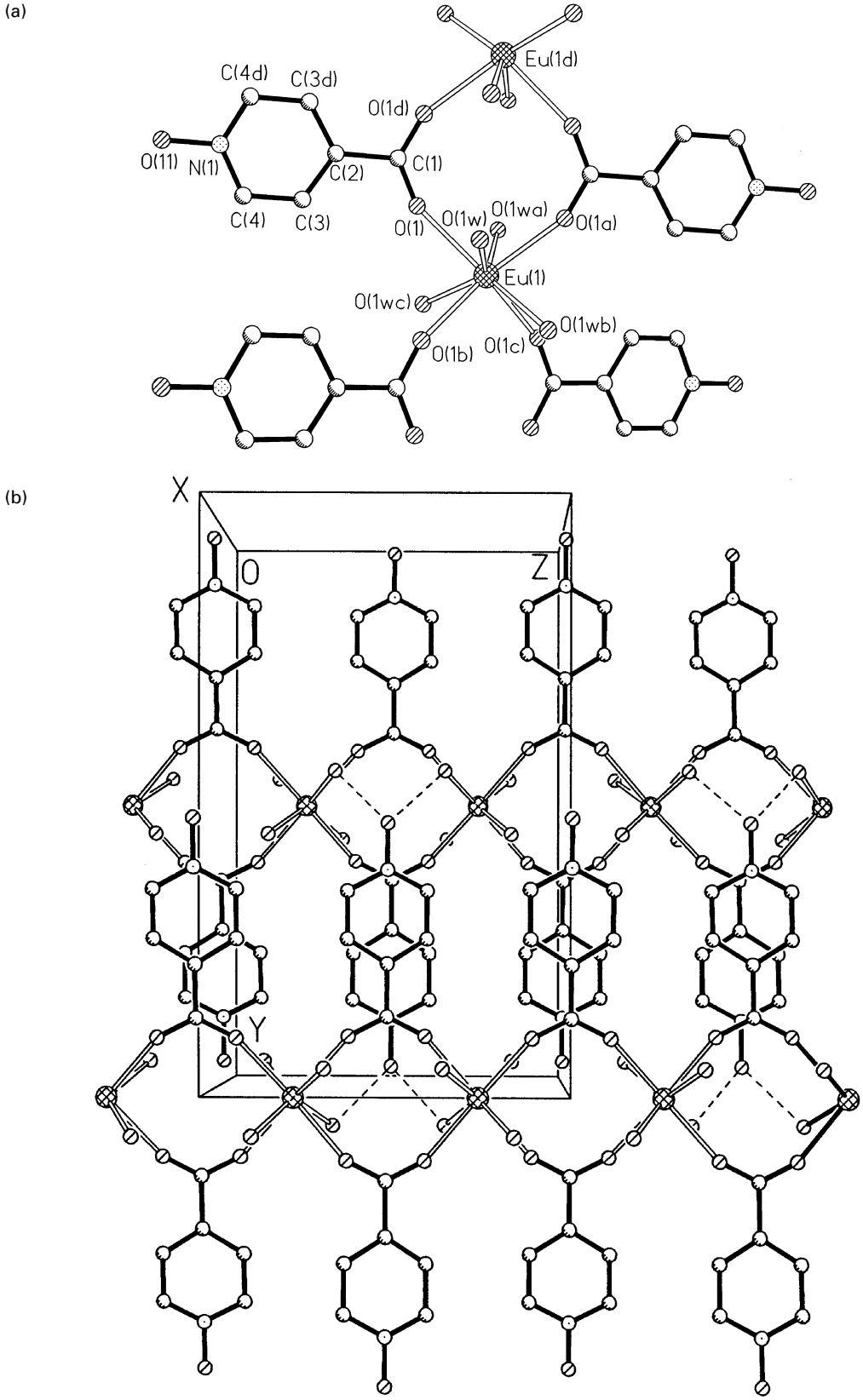

Fig. 2. (a) Perspective view showing the *syn–syn* carboxylato-O,O′ bridged dimeric unit of complex **3** (the lattice water molecules and nitrate anion have been omitted for clarity). (b) Packing drawing showing the three dimensional network of complex **3**.

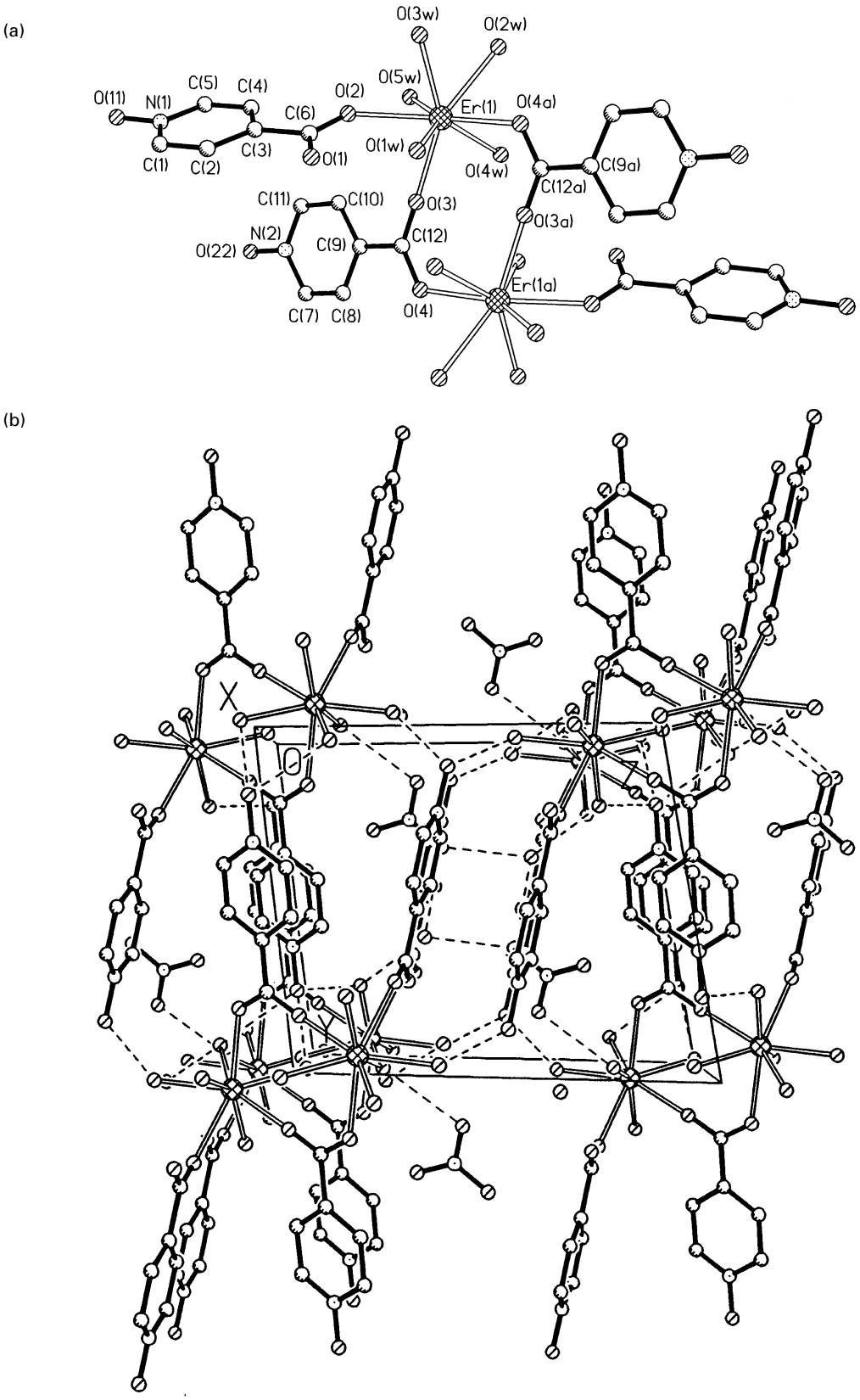

Fig. 3. (a) Perspective view showing the dimeric unit of complex **4** with the atom labeling scheme (the lattice water molecules and discrete nitrate anions have been omitted for clarity). (b) Packing drawing showing the three dimensional network built from dimeric units of complex **4** through hydrogen bonds between aqua ligands and *N*-oxide groups, and between uncoordinated carboxylate groups and aqua ligands.

2(a), the europium(III) ion resides on a site of symmetry 222; it is eight-coordinated by four equivalent oxygen atoms of L^2 ligands and four equivalent aqua ligands with Eu–O(aqua) and Eu–O(carboxylate) bond distances of 2.462(6) and 2.352(6) Å, respectively. The carboxylate group is only involved in the bidentate *syn–syn* bridging mode (C(2)–C(1)–O(1)–Eu(1) −157.4° and C(2)–C(1)–O(1d)–Eu(1d) 157.4°). Each europium(III) ion is linked with its two neighbors through pairs of bridging carboxylate groups with an Eu. . .Eu separation of 5.245(1) Å, forming an infinite chain of symmetry 2 along the *b* direction [Fig. 2(b)]. The *N*-oxide oxygen atoms are not coordinated to the europium(III) ion but form hydrogen bonds with coordinated aqua ligands belonging to neighboring chains Table 2. These hydrogen bonds link the metal carboxylate chains into layers parallel to the *bc* plane [Fig. 2(b)]. The layers are held together by hydrogen bonds between nitrate anions and aqua ligands, and between oxide groups and lattice water molecules, to form a three-dimensional network Table 2. The coordination geometry at the Eu(III) center is a slightly distorted square antiprism. One square face comprises atoms O(1w), O(1wa), O(1) and O(1a) with a mean deviation of 0.269 Å and the other least-squares plane is defined by atoms O(1wb), O(1wc), O(1b)

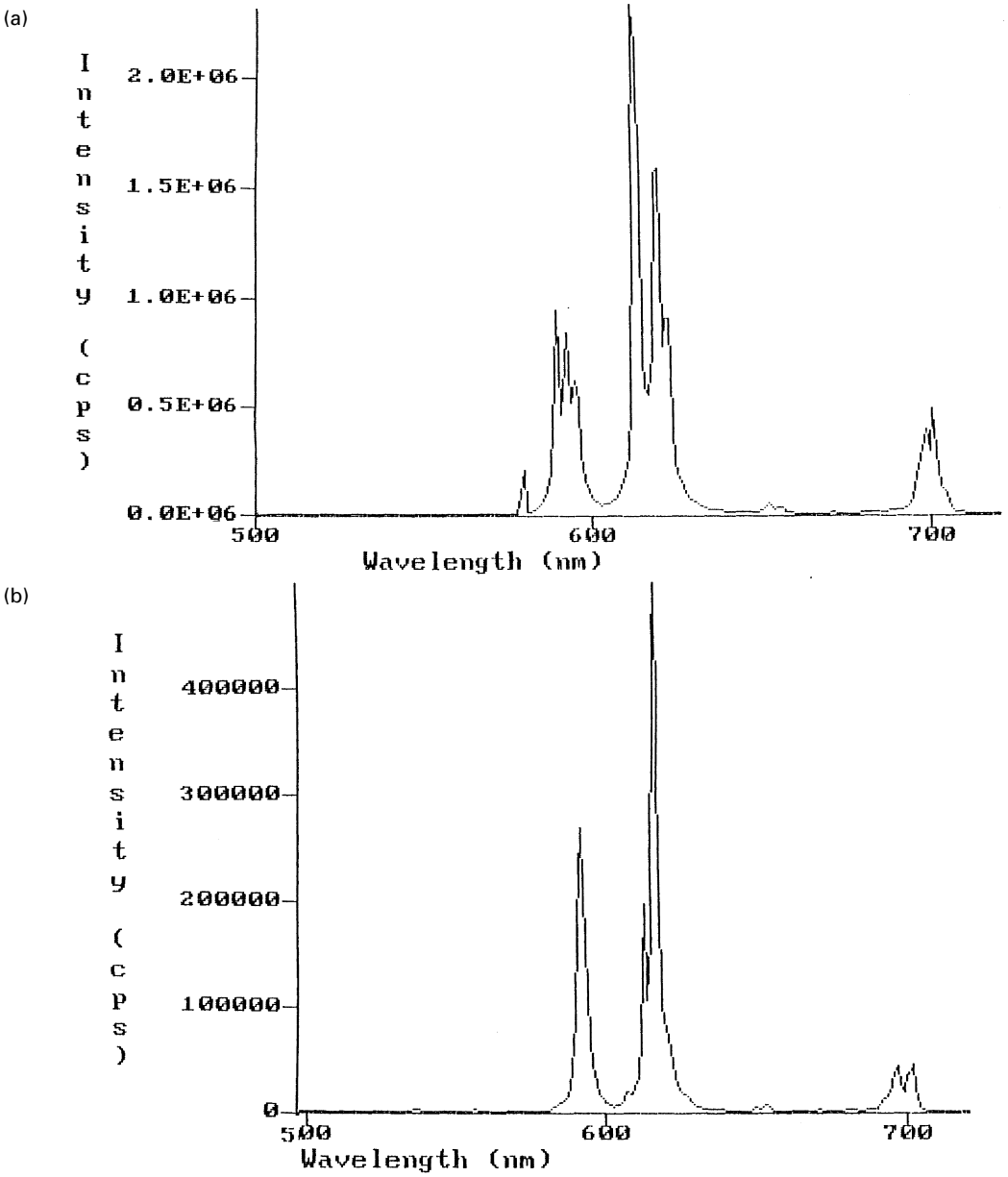

Fig. 4. (a) Emission spectrum of complex **1** for excitation at 333 nm. (b) Emission spectrum of complex **3** for excitation at 337 nm.

and O(1c) with the same deviation. These two faces are parallel to each other. The europium(III) ion resides exactly in the center of the square antiprism, being displaced 1.254 Å from the above two planes.

Due to the smaller ionic radius of the erbium(III) ion as compared to the europium(III) ion, the crystal structure of complex **4** exhibits different features. It comprises a packing of dimeric cations, nitrate anions and lattice water molecules. As shown in Fig. 3(a), the erbium(III) ion is eight-coordinated by three carboxylate oxygen atoms from two L^2 ligands and five aqua ligands with mean Er–O(aqua) and Er–O (carboxylate) distances of 2.363(3) and 2.330(3) Å, respectively. One L^2 ligand acts in the bidentate *syn–anti* carboxylate bridging coordination mode [Er(1)–O(3)–C(12)–C(9) -31.8° and C(9)–C(12)–O(4)–Er(1a) 171.2°], but the carboxylate group of the other L^2 ligand adopts the unidentate coordination mode [Er(1)–O(2)–C(6) 139.1(3)°], leaving the uncoordinated O(1) oxygen atom to form a strong intramolecular hydrogen bond with O(1w) with a separation of 2.613 Å. The distance between the two erbium(III) ions in the dimeric unit is 4.804(1) Å, being much shorter than the Eu...Eu separation in complex **3**. As in the case of complex **3**, the *N*-oxide groups are not directly coordinated to the lanthanide ions, but hydrogen-bonded to both aqua ligands and lattice water molecules Table 2, thereby linking the dimeric units into a three-dimensional network [Fig. 3(b)]. The nitrate anions also participate in hydrogen bonding Table 2.

The reason why complex **4** is dimeric while complex **3** is polymeric arises from the difference of the ionic radii of the relevant lanthanide(III) ions. The heavy Er(III) ion has a smaller ionic radius than the lighter Eu(III) ion and hence is more likely to be hydrated [29]. As the aqua ligands compete with the carboxylate groups for coordination sites of the metal ion, the replacement of one carboxylate oxygen by an aqua ligand in the coordination sphere of the Er(III) ion suffices to breaks up the polymeric chain into dimeric units.

It is notable that hydrogen bonding between coordinated aqua ligands and *N*-oxide groups of L^2 ligands brings the pyridine rings closer and nearly parallel to each other [Fig. 2(b) and Fig. 3(b)], so that the resulting aromatic packing effect further enhances the thermal stability of complexes **3** and **4**.

Luminescence properties of $[\{Eu(L^1)_3(H_2O)_2\}_n]\cdot 4nH_2O$, ***1***, *and* $[\{Eu(L^2)_2(H_2O)_4\}_n](NO_3)_n\cdot nH_2O$, ***3***

The excitation spectrum of **1** ($\lambda_{em} = 617$ nm) exhibits a strong ligand absorption band at 333 nm and the characteristic absorption bands of the europium(III) ion (362, 367, 376, 382, 384, 395(max), 398(shoulder), 417, 465 and 474 nm), whereas the excitation spectrum of **3** ($\lambda_{em} = 614$ nm) shows a relatively weak ligand absorption peak at 337 nm and characteristic absorption peaks of the europium(III) ion (362, 367, 376, 381, 385, 395(max), 417, 465 and 473 nm). The luminescence spectra for ligand excitation are exhibited in Fig. 4(a) and (b), respectively, for complexes **1** and **3**. The luminescence data for the two complexes are summarized in Table 3. From the spectra, it is noticed that the bands originated from the $^5D_0 \rightarrow {}^7F_3$ transition are weak. The appearance of the $^5D_0 \rightarrow {}^7F_0$ transition and presence of three components in the $^5D_0 \rightarrow {}^7F_1$ transition of complex **1** points to the europium(III) ion having a structural environment of low symmetry [Fig. 4(a)] [30, 31]. From structural analysis its site symmetry was assigned to be C_1. For complex **3**, the $^5D_0 \rightarrow {}^7F_0$ transition is not observed and the $^5D_0 \rightarrow {}^7F_j$ ($j = 1, 2$) transition has fewer components [Fig. 4(b)]. Thus the europium(III) ion in complex **3** should reside on a highly symmetric lattice site. This is in good agreement with the results of crystal structure determination. From the results of crystal structural analysis, the chemical and structural environment

Table 3. Luminescence data of complexes **1** and **3**

Complex **1**				Complex **3**			
E (cm^{-1})	λ (nm)	E_0 (cm^{-1})	Assignment	E (cm^{-1})	λ (nm)	E_0 (cm^{-1})*	Assignment
17241	580	0	$^5D_0 \rightarrow {}^7F_0$				
16949	590	292	$^5D_0 \rightarrow {}^7F_1$	16892	592	349	$^5D_0 \rightarrow {}^7F_1$
16863	593	378					
16807	595	434					
16287	614	954	$^5D_0 \rightarrow {}^7F_2$	16313	613	928	$^5D_0 \rightarrow {}^7F_2$
16155	619	1086		16207	617	1034	
16077	622	1164					
15337	652	1904	$^5D_0 \rightarrow {}^7F_3$	15385	650	1856	$^5D_0 \rightarrow {}^7F_3$
14306	699	2935	$^5D_0 \rightarrow {}^7F_4$	14347	697	2894	$^5D_0 \rightarrow {}^7F_4$
14265	701	2976		14245	702	2996	

*Calculation based on the $^7F_0$ energy level in complex **1**.

around the europium(III) ion has a symmetry close to D_{2d}. The Eu($^5D_0$) lifetime of complex **3** (0.69 ms for $\lambda_{ex,em} = 338, 617$ nm; 0.73 ms for $\lambda_{ex,em} = 395, 617$ nm) is much shorter than that of complex **1** (1.38 ms for $\lambda_{ex,em} = 333, 614$ nm; 1.44 ms for $\lambda_{ex,em} = 395, 613$ nm). This can be explained by the fact that complex **3** has more aqua ligands in the coordination sphere of the europium(III) ion.

Acknowledgements—This work is supported by a Hong Kong Research Grants Council Earmarked Grant (Ref. No. CUHK 303/96P).

REFERENCES

1. Abdul'minev, I. K., Aslanov, L. A., Porai-Koshits, M. A. and Chupakhina, R. A., *Zh. Strukt. Khim.*, 1973, **14,** 383.
2. Aslanov, L. A., Abdul'minev, I. K. and Porai-Koshits, M. A., *Zh. Strukt. Khim.*, 1972, **13,** 468.
3. Aslanov, L. A., Kiekbaev, I. D., Abdul'minev, I. K. and Porai-Koshits, M. A., *Kristallografiya*, 1974, **19,** 179.
4. Kay, J., Moore, J. W. and Glick, M. D., *Inorg. Chem.*, 1972, **11,** 2818.
5. Prout, K., Marin, J. M., Hutchison, C. A. Jr., *J. Am. Chem. Soc.*, 1972, **94,** 1858.
6. Zhang, Z.-S., Wu, J.-G. and Deng, R.-W., *Gaodeng Xuexiao Huaxue Xuebao*, 1990, **11,** 7 [In Chinese].
7. Li, L.-S., Chen, D. G. and Jin, S. P., *Zhongguo Xitu Xuebao*, 1993, **11,** 101 [In Chinese].
8. Palkina, K. K., Kuz'mina, N. E., Myasnikov, O. E., Orlova, I. M. and Shchelokov, R. N., *Russ. J. Coord. Chem.*, 1995, **21,** 67.
9. Starynowicz, P., *Acta Crystallogr. C*, 1993, **1895,** C49.
10. Starynowicz, P., *Acta Crystallogr. C*, 1991, **47,** 294.
11. Starynowicz, P., *Acta Crystallogr. C*, 1991, **47,** 32.
12. Ma, J.-F., Jin, Z.-S. and Ni, J.-Z., *Polyhedron*, 1995, **14,** 563.
13. Ma, J.-F., Hu, N.-H. and Ni, J.-Z., *Polyhedron*, 1996, **15,** 1797.
14. Navaneetham, N. S. and Soundarajan, S., *Indian J. Chem. A*, 1981, 93.
15. Manning, P. G., *Can. J. Chem.*, 1966, **44,** 1471.
16. Boyd, S. A., Kohrman, R. E. and West, D. X., *Inorg. Nucl. Chem. Lett.*, 1976, **12,** 603.
17. Boyd, S. A., Kohrman, R. E. and West, D. X., *Inorg. Nucl. Chem. Lett.*, 1977, **13,** 129.
18. De Sa, G. F., e Silva, F. R. G. and Malta, O. L., *J. Alloys Compd.*, 1994, **207,** 457.
19. Yan, L., Liu, J.-M., Wang, X., Yang, R.-D. and Song, F.-L., *Polyhedron*, 1995, **14,** 3545.
20. Sato, M., Yamamoto, M., Imada, K., Katsube, N., Tanaka, Y. and Higashi, T., *J. Appl. Cryst.*, 1992, **25,** 348.
21. Tanner, J. and Krause, K. L., *Rigaku J.*, 1992, **11,** 4.
22. Higashi, T., *ABSCOR*: *An Empirical Absorption Correction Based on Fourier Coefficient Fitting*. Rigaku Corporation, Tokyo, 1995.
23. Sparks, R. A., in *Crystallographic Computing Techniques*, ed. F. R. Ahmed. Munksgaard, Copenhagen, 1976, p. 452.
24. Kopfmann, G. and Huber, R., *Acta Cryst. A*, 1968, **24,** 348.
25. Sheldrick, G. M., in *Computational Crystallography*, ed. D. Sayre. Oxford University Press, New York, 1982, p. 506.
26. Sheldrick, G. M., in *Crystallographic Computing* 3: *Data Collection*, *Structure Determination*, *Proteins and Databases*, eds. G. M. Sheldrick, C. Kruger and R. Goddard. Oxford University Press, New York, 1985, p. 175.
27. Ibers, J. A. and Hamilton, W. C. (eds.), *International Tables for X-ray Crystallography*, Vol. 4. Kynock Press, Birmingham (now distributed by Kluwer Academic Press, Dordrecht), 1974, pp. 55, 99 and 149.
28. Sheldrick, G. M., *SHELXL* 93, *a Program for the Refinement of Crystal Structure*. University of Göttingen, Germany, 1993.
29. Goldman, S. and Morss, L. R., *Can. J. Chem.*, 1975, **53,** 2695.
30. Piguet, C., Bünzli, J.-C. G., Bernardinelli, G., Hopfgartner, G. and Williams, A. F., *J. Am. Chem. Soc.*, 1993, **115,** 8197.
31. Jin, L.-P., Lu, S.-X. and Lu, S.-Z., *Polyhedron*, 1996, **15,** 4069.

Pergamon

Polyhedron Vol. 17, No. 23–24, pp. 4011–4014, 1998
© 1998 Elsevier Science Ltd
All rights reserved. Printed in Great Britain
0277–5387/98 $19.00+0.00

PII: S0277–5387(98)00192–2

Crystal and molecular structure of $(TMEDA)_2Li_2Se_4$

Timothy A. J. Worden,[a] Dominic S. Wright[a] and Alexander Steiner[b,*]

[a]Department of Chemistry, University of Cambridge, Lensfield Road, Cambridge CB2 1EW, U.K.

[b]Department of Chemistry, University of Liverpool, Crown Street, Liverpool L69 7ZD, U.K.

(Received 25 August 1997; accepted 13 May 1998)

Abstract—X-ray crystal structure determination shows that both terminal selenium centres of the Se_4^{2-}-chain in $(TMEDA)_2Li_2Se_4$ (TMEDA = *N*,*N*,*N*′,*N*′-tetramethylethylenediamine) are bridging both lithium centres, while the central Se-atoms are loosely coordinated towards the metal centres, resulting in a distorted trigonal prismatic Li_2Se_4 core. © 1998 Elsevier Science Ltd. All rights reserved

Keywords: lithium; selenium; polychalcogenides; nitrogen ligands; X-ray structure.

INTRODUCTION

It is well known that inorganic lithium salts form discrete molecular complexes in the presence of polydentate ligand systems [1]. Lithium polychalcogenides solvated by bi- or tridentate nitrogen chelates exist in the solid state as monomeric complexes of the general composition $L_2Li_2X_n$ (X = S or Se) [2–4]. Scheme 1 illustrates their different structure types. If the tridentate PMDETA (*N*,*N*,*N*′,*N*″,*N*″-pentamethyldiethylenetriamine) is used as in $(PMDETA)_2Li_2S_4$ (**1a**) and $(PMDETA)_2Li_2Se_5$ (**1b**) zig–zag chains with terminally coordinated lithium centres are obtained. In contrast, the presence of the bidentate TMEDA (*N*,*N*,*N*′*N*′-tetramethylethylenediamine) as utilised in $(TMEDA)_2Li_2S_6$ (**2a**) leads to a bridging coordination behaviour of the bent chalcogenide chain [3, 4]. An equal structure pattern is observed in the presence of the more bulky bidentate TEEDA (tetraethylethylenediamin) [2]. Here we report the crystal and molecular structure of the TMEDA solvated selenium derivative $(TMEDA)_2Li_2Se_4$ (**2b**).

EXPERIMENTAL

Preparation of $(TMEDA)_2Li_2Se_4$ (**2b**)

All manipulations were performed under dry argon using Schlenk, vacuum-line and glove-box techniques. $[(CyNH)_2PN]_3$ (1.00 g, 1.38 mmol) was dissolved in 20 ml of THF. To this solution six equivalents of *n*-butyllithium (5.52 ml, 1.5 M in hexane) were added. After stirring this solution for 1 h, selenium powder (654 mg, 8.28 mmol) was added at once. The dark red solution was heated to reflux (5 min) and then stirred for 30 min at room temperature. All solvents were removed *in vacuo* and subsequently the residual dark red oil was dissolved in a mixture of 20 ml diethylether and 1 ml TMEDA. Storage of the filtered solution for 1 day yielded 270 mg of dark red crystals. The physical properties of the obtained crystals correspond with those reported by Tatsumi *et al.* [2].

Side products regarding the phosphazene components, which are formed by the reaction could not be characterised so far. The ^{31}P NMR spectrum of the reaction mixture shows a very complex signal pattern, which cannot be assigned to distinct species.

X-ray structure determination of $(TMEDA)_2Li_2Se_4$ (**2b**)

Data were collected on a STOE four circle diffractometer equipped with MoKα radiation (graphite monochromator, $\lambda = 0.71073$ Å) using an oil-coated crystal, employing the ω–θ scan technique. The data set was corrected for Lorentz, polarisation and absorption (ψ-scans) effects. Crystal data are listed in Table 1. The structure was solved by direct method [5] and refined by full-matrix least-squares procedures using all data on F^2 [6]. All nonhydrogen atoms were

*Author to whom correspondence should be addressed. Tel.: +44-151-794-3544; fax: +44-151-794-3588; e-mail: aggi@liv.ac.ak

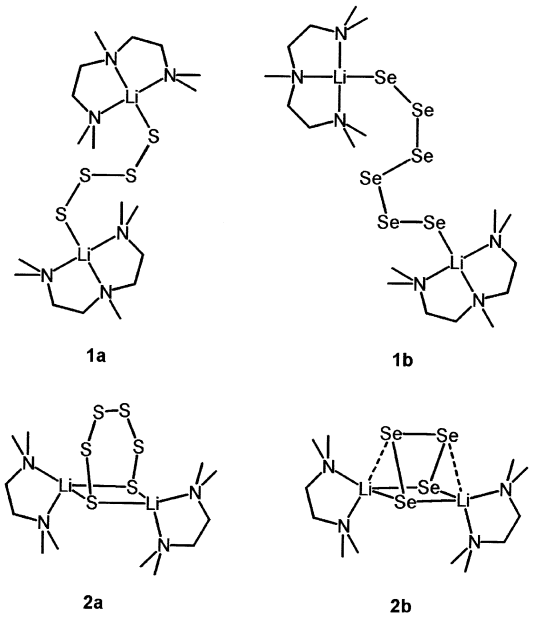

Scheme 1.

Table 1. Crystallographic data for $(TMEDA)_2Li_2Se_4$ (**2b**)

Empirical formula	$C_{12}H_{32}Li_2N_4Se_4$
Formula weight	562.14
Temperature (K)	153(2)
Crystal system	triclinic
Space group	$P\bar{1}$
Unit cell dimensions	
a (Å)	8.576(3)
b (Å)	11.847(5)
c (Å)	12.534(5)
α (°)	90.85(3)
β (°)	110.26(3)
γ (°)	107.45(3)
Volume (Å^3)	1129.6(8)
Z	2
Density (calc.) (g cm^{-3})	1.653
Absorption coefficient (mm^{-1})	6.494
F(000)	548
Crystal size (mm)	$0.52 \times 0.45 \times 0.15$
2θ Range for data collection (°)	8–45
Index ranges	$-9 \geqslant h \geqslant 9,\ -12 \geqslant k \geqslant 12,\ -11 \geqslant l \geqslant 13$
Reflections collected	3313
Independent reflections	2947 ($R_{int} = 0.104$)
Max., min. transmission	0.787, 0.201
Data/parameters	2943/199
$R1$ [$I > 2\sigma(I)$]	0.083
$wR2$ (all data)	0.266
Largest difference peak, hole (eÅ^{-3})	1.51, −1.72

refined anisotropically and hydrogen atoms were set geometrically. $R1 = \Sigma|F_o - F_c|/\Sigma|F_o|$ and $wR2 = \{\Sigma[w(F_o^2 - F_c^2)^2]/\Sigma[w(F_o^2)^2]\}^{0.5}$ with a weighting scheme of the form $w^{-1} = \sigma(F_o^2) + (0.1500P)^2 + 13.7123P$, with $P = (F_o^2 + 2F_c^2)/3$.

RESULTS AND DISCUSSION

In our ongoing studies investigating the reduction properties of multianionic phosphazenates [7, 8], we reacted hexalithiated hexakis(cyclohexylamino)-cyclotriphosphazene, which exists as the THF-solvated dimeric complex $[(THF)_4Li_{12}\{(CyN)_6P_3N_3\}_2]$ (Cy = cyclohexyl) in the solid state [7], with six equivalents of elemental selenium in THF. Recrystallisation of the crude product from Et_2O/TMEDA solution gave dark red crystals of **2b** which were suitable for single crystal X-ray structure analysis. An alternative synthetic route was reported by Tatsumi *et al*. reacting elemental lithium and selenium in liquid ammonia and recrystallising the crude product using a mixture of toluene/TMEDA [2].

The molecular structure of **2b** is illustrated in Fig. 1. Selected interatomic distances and angles are listed in Table 2. The solid state structure of **2b** is composed of monomeric molecular units in which both lithium cations are bridged by the terminally arranged selenium centres of the chelating Se_4^{2-}-chain in a similar way as the lithium centres in the TMEDA-solvated polysulfide **2a**. Li–Se(terminal) bond distances are 2.63 Å on average and in correspondence with those observed in the PMDETA coordinated derivative **1b**. Each lithium centre in **2b** is saturated in a bidentate manner by one TMEDA ligand [Li–N (av.) 2.11 Å] and in addition loosely coordinated by one of the centrally arranged selenium centres Li(1)···Se(2) = 3.09(3) and Li(2)···Se(3) = 3.08(2) Å, resulting in a distorted trigonal prismatic geometry for the central Li_2Se_4 core. The overall geometry of the molecular unit can be described as of non-crystallographic C_2-symmetry. Structural features of the Se_4^{2-}-chain in **2b** are in accordance with those observed in corresponding systems providing highly ionic environments such as [Ba–4en][Se_4] (**3a**) [9], [Ba–222Crypt][Se_4] (**3b**) [10] and $[PPN]_2[Se_4] \cdot 4CH_3CN$ (**3c**) [11]. As in agreement with the structural observations in these systems, the terminal Se–Se-distances in **2b** are slightly shorter [Se1–Se2 2.336(3) and Se3–Se4 2.326(3) Å] than the central one [Se2–Se3 2.376(3) Å]. While the Se_4^{2-}-chains in **3a** and **3c** exist as non-coordinated ion-separated units, **3b** contains a Se_4^{2-}-chain which connects two barium centres in the same fashion as it connets both lithium centres in the PMDETA derivative **1b**. Due to the bridging nature of the terminal Se-centres, the Se1–Se2–Se3–Se4 torsion angle in **2b**, which is 42.5(1)°, is significantly tighter as those observed in **3a**–**c**.

The structural similarities of the TMEDA solvated lithium polychalcogenides **2a** and **2b** on one hand and of the PMDETA solvated derivatives **1a** and **1b** on the other hand show, that the hapticity of the hard nitrogen base directs the overall coordination mode of the resulting complexes. The bidentate TMEDA is leaving two coordination sites at the tetrahedrally complexed lithium centre for the soft polychalcogenide ligands, while the tridentate PMDETA is providing only one coordination site at the metal centre for an additional donor system. Therefore a

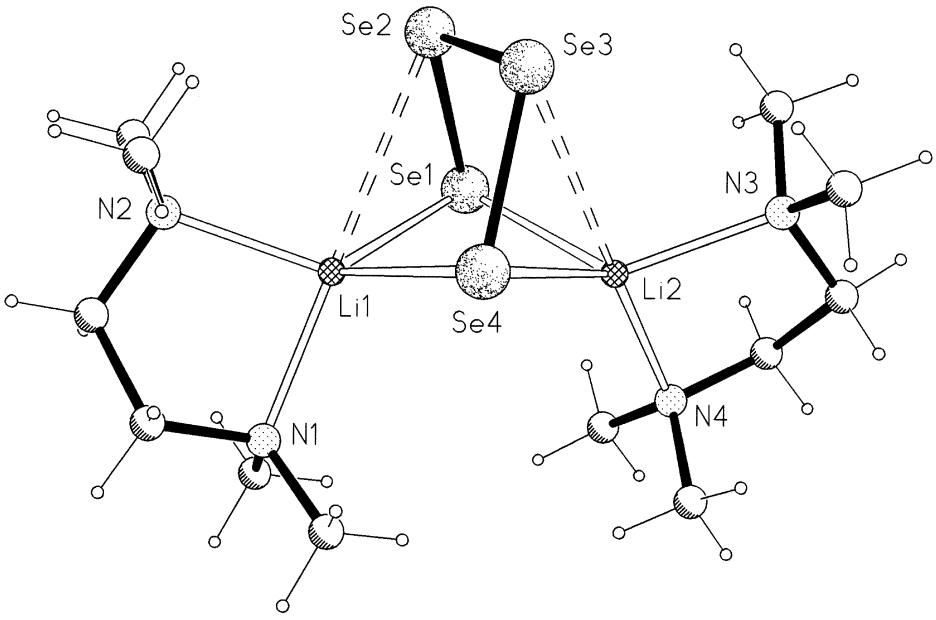

Fig. 1. The crystal structure of **2b**.

Table 2. Selected interatomic distances (Å) and angles (°) for $(TMEDA)_2Li_2Se_4$ (**2b**)

Se(1)–Se(2)	2.336(3)	Se(4)–Li(1)	2.65(3)
Se(2)–Se(3)	2.376(3)	Se(4)–Li(2)	2.61(2)
Se(3)–Se(4)	2.326(3)	Li(1)–N(1)	2.14(3)
Se(1)–Li(1)	2.59(3)	Li(1)–N(2)	2.09(3)
Se(1)–Li(2)	2.66(2)	Li(2)–N(3)	2.09(2)
Se(2)–Li(1)	3.09(3)	Li(2)–N(4)	2.12(3)
Se(3)–Li(2)	3.08(2)		

Se(2)–Se(1)–Li(1)	77.4(6)	Se(4)–Se(3)–Li(2)	55.7(4)
Se(2)–Se(1)–Li(2)	92.7(5)	Se(2)–Se(3)–Li(2)	82.1(5)
Li(1) –Se(1)–Li(2)	79.4(8)	Se(3)–Se(4)–Li(2)	76.9(5)
Se(1)–Se(2)–Se(3)	103.84(9)	Se(3)–Se(4)–Li(1)	92.1(6)
Se(1)–Se(2)–Li(1)	54.9(5)	Li(2)–Se(4)–Li(1)	79.1(8)
Se(3)–Se(2)–Li(1)	81.1(6)	N(2)–Li(1)–N(1)	87.0(11)
Se(4)–Se(3)–Se(2)	105.03(9)	N(3)–Li(2)–N(4)	87.5(10)

bicyclic arrangement with bent X_n^{2-}-chains is favoured in the case of TMEDA, whereas acyclic zig–zag chains with terminally arranged lithium centres are obtained using PMDETA.

REFERENCES

1. Snaith, R. and Wright, D. S. in *Lithium Chemistry*: *a Theoretical and Experimental Overview*, ed. A. -M. Sapse and P. v. R. Schleyer. Wiley, New York, 1995, p. 227.
2. Tatsumi, K., Kawaguchi, H., Inoue, K., Tani, K. and Cramer, R.E., *Inorg. Chem.*, 1993, **32,** 4317.
3. Tatsumi, K., Inoue, Y., Nakamura, A., Cramer, R. E., VanDoome, W. and Gilje, J.W., *Angew. Chem. Int. Ed. Engl.*, 1990, **29,** 422.
4. Banister, A. J., Barr, D., Brooker, A. T., Clegg, W., Cunnington, M. J., Doyle, M. J., Drake, S. R., Gill, W. R., Manning, K., Raithby, P. R., Snaith, R., Wade, K. and Wright, D. S. *J Chem. Soc. Chem. Commun.*, 1990, 105.
5. Sheldrick, G. M. *SHELXS*-86, *Program for Crystal Structure Solution*. Universität Göttingen, 1986.
6. Sheldrick, G. M. *SHELXL*-93, *Program for crystal structure refinement*. Universität Göttingen, 1993.
7. Steiner, A. and Wright, D.S., *Angew. Chem. Int. Ed. Engl.*, 1996, **35,** 636.
8. Steiner, A. and Wright, D. S. *J Chem. Soc. Chem. Commun.*, 1997, 283.
9. König, T., Eisenmann, B. and Schäfer, H., *Z. Naturforsch.*, 1982, **37b,** 1245.
10. König, T., Eisenmann, B. and Schäfer, H., *Z. Anorg. Allg. Chem.*, 1983, **498,** 99.
11. Brese, N. E., Randall, C. R. and Ibers, J. A., *Inorg. Chem.*, 1988, **27,** 940.

Pergamon

Polyhedron Vol. 17, No. 23–24, pp. 4015–4021, 1998
© 1998 Elsevier Science Ltd
All rights reserved. Printed in Great Britain
0277–5387/98 $19.00+0.00

PII: S0277-5387(98)00200-9

Isopropyltetramethylcyclopentadienyl samarium chemistry: structural studies of divalent $(C_5Me_4{}^iPr)_2Sm(THF)$ and mixed valent $[(C_5Me_4{}^iPr)_2Sm]_2(\mu\text{-Cl})$

William J. Evans*, Kevin J. Forrestal and Joseph W. Ziller

Department of Chemistry, University of California, Irvine, CA 92697, U.S.A.

(Received 15 December 1997; accepted 3 May 1998)

Abstract—The isopropyltetramethylcyclopentadienyl samarium complexes $(C_5Me_4{}^iPr)_2Sm(THF)$, **1**, and $[(C_5Me_4{}^iPr)_2Sm]_2(\mu\text{-Cl})$, **2**, have been isolated and structurally characterized. Divalent **1** crystallizes from hot toluene as a monosolvate in space group $P3_121$ with $a=b=15.494(2)$ Å, $c=9.7724(7)$ Å, $\alpha=\beta=90^\circ$, $\gamma=120^\circ$, $V=2031.6(5)$ Å^3 and $D_{calcd}=1.346$ g/cm^3, $Z=3$ and $T=163$ K. **1** has a 141.6° ring centroid–Sm–ring centroid angle and an average Sm–C distance of 2.80(3) Å. **2** crystallizes from hot toluene in space group P1 with $a=9.616(2)$ Å, $b=15.479(2)$ Å, $c=17.844(1)$ Å, $\alpha=111.671(4)^\circ$, $\beta=93.488(8)^\circ$, $\gamma=107.494(9)^\circ$, $V=2309.3(5)$ Å^3 and $D_{calcd}=1.423$ g/cm^3, $Z=2$ and $T=163$ K. The two bent metallocene units in **2** are connected by an asymmetrical chloride bridge which has a 169.88(4)° Sm(1)–Cl–Sm(2) angle and 2.678(1) Å Sm(1)–Cl and 2.891(1) Å Sm(2)–Cl distances. The 2.69(2) Å average Sm(1)–C($C_5Me_4{}^iPr$) distance is characteristic of Sm(III) and the 2.80(2) Å average Sm(2)–C($C_5Me_4{}^iPr$) distance is characteristic of Sm(II). © 1998 Elsevier Science Ltd. All rights reserved

Keywords: samarium; peralkylcyclopentadienyl; mixed valence; metallocene; bridging chloride

INTRODUCTION

The pentamethylcyclopentadienyl ligand has been very effective in providing crystallographically characterizable complexes for the study of organometallic Sm(II) and Sm(III) chemistry and an important body of structural data is available [1–4]. Less symmetrically substituted polyalkylated cyclopentadienyl ligands are also useful in the study of organosamarium chemistry, but only a limited amount of crystallographic data is available on such compounds [5]. As part of a project to make sterically crowded $(C_5Me_4R)_3Sm$ complexes [5, 6], we have prepared and isolated the first example of a structurally characterized isopropyltetramethylcyclopentadienyl samarium complex, $(C_5Me_4{}^iPr)_2Sm(THF)$. In the course of these studies $[(C_5Me_4{}^iPr)_2Sm]_2(\mu\text{-Cl})$ was also isolated. These complexes allow structural comparisons with C_5Me_5 samarium complexes and the chloride complex is a rare example of a mixed valence bimetallic organosamarium compound.

* Author to whom correspondence should be addressed. Tel.: +1-949-824-5174; Fax: +1-949-824-2210; E-mail: wevans@uci.edu.

EXPERIMENTAL

The compounds described below are extremely air and moisture sensitive. Therefore, all procedures were conducted using standard inert atmosphere techniques in a nitrogen-filled glovebox and solvents were distilled under nitrogen from sodium or potassium benzophenone ketyl as previously described [7].

Preparation of $C_5Me_4{}^iPrH$

$C_5Me_4{}^iPrH$ was prepared for the first time to our knowledge following the procedure successful for C_5Me_5H [8]. A 250 ml three-neck round bottom flask was equipped with a stir bar, gas inlet adapter and a reflux condenser. The flask was placed under an atmosphere of nitrogen and ^{i}PrMgCl (0.1 mol, 50 ml

of 2.0 M solution in diethyl ether) was added to the flask followed by an additional 100 ml of diethyl ether. The flask was then placed in an ice bath and 2,3,4,5-tetramethyl-2-cyclopentenone (10 g, 0.072 mol) was added dropwise over a 2 h period. The solution was allowed to warm to room temperature and stirred overnight. Any remaining ^{i}PrMgCl was then destroyed by slow dropwise addition of MeOH (5 ml) followed by H_2O (20 ml). The ether solution was washed with an aqueous solution containing NH_4Cl (13 g), concentrated HCl (20 ml) and H_2O (100 ml). This aqueous solution was back-extracted with ether and the ether solutions were combined. The ether solution was stirred for 1 h with 2 ml of 6 N HCl to ensure complete elimination of water. The organic layer was then washed with 5% $NaHCO_3$ and dried over K_2CO_3. Rotary evaporation of the solvent yielded 8.0 g of a pale yellow, viscous liquid which was purified by vacuum distillation at 35–40°C and 0.025 Torr. The ^{1}H NMR spectrum indicated that a mixture of isomers was present.

Preparation of $K(C_5Me_4{}^{i}Pr)$

In the glovebox $C_5Me_4{}^{i}PrH$ (2.0 g, 12.3 mmol) was added dropwise to a slurry of KH (0.40 g, 10.0 mmol) in THF (100 ml) and the reaction was allowed to stir for 24 h. $KC_5Me_4{}^{i}Pr$ is insoluble in THF and was filtered, washed with hexane and isolated as a white, flocculent powder (1.33 g, 65% yield).

Preparation of $(C_5Me_4{}^{i}Pr)_2Sm(THF)$, ***1***

In the glovebox $SmI_2(THF)_2$ (0.67 g, 1.23 mmol), $KC_5Me_4{}^{i}Pr$ (0.50 g, 2.47 mmol) and THF (15 ml) were placed into a vial. The THF solution immediately appeared purple and white insoluble material was present throughout the reaction. The solution was allowed to stir for 12 h at room temperature. Filtration and removal of solvent by rotary evaporation yielded $(C_5Me_4{}^{i}Pr)_2Sm(THF)$ as a purple powder (0.485 g, 72% yield). ^{1}H NMR (C_6D_6, 25°C, 300 MHz) δ 27.6 (6 H, CH_3), 10.3 (6 H, CH_3), 7.32 (4 H, THF), −3.37 (4 H, THF), −9.39(6 H, CH_3). ^{13}C NMR (THF-d_8, 25°C, 500 MHz) δ 95.0 (-*C*H(CH_3)$_2$), 93.0 (CH_3), 81.0 (CH_3), 59.0 (CH_3), −44.0 (C_5R_5), −62.4 (C_5R_5), −66.5 (C_5R_5). Anal. Calcd. for $SmC_{28}H_{46}O$: Sm 27.4. Found: Sm 25.6. Purple crystals suitable for X-ray diffraction were grown from hot toluene.

Preparation of $(C_5Me_4{}^{i}Pr)_2Sm(OEt_2)$

This compound was made in analogy to the preparation of $(C_5Me_5)_2Sm(OEt_2)$ [5, 9]. Diethyl ether (15 ml) was added to desolvated SmI_2 (0.50 g, 1.23 mmol) and $KC_5Me_4{}^{i}Pr$ (0.50 g, 2.47 mmol) in a Schlenk flask. The ether solution immediately appeared very dark green and white insoluble material was present throughout the reaction. The solution was allowed to stir for 12 h at room temperature. Filtration and removal of solvent under vacuum yielded $(C_5Me_4{}^{i}Pr)_2Sm(OEt_2)$ as a dark green powder (0.413 g, 68% yield). ^{1}H NMR (C_6D_6, 25°C, 300 MHz) δ 12.6, 6.53, 3.89, −0.55, −7.85, −8.82.

X-ray data collection, structure determination, and refinement for $(C_5Me_4{}^{i}Pr)_2Sm(THF)$, ***1***

A purple crystal of approximate dimensions $0.20 \times 0.26 \times 0.33$ mm was coated with Paratone oil, mounted on the tip of a glass fiber and transferred to a Siemens P4 diffractometer. The determination of Laue symmetry, crystal class, unit cell parameters and the crystal's orientation matrix were carried out according to standard procedures [10]. Intensity data were collected at 163 K using a 2θ–ω scan technique with MoKα radiation. The raw data were processed with a local version of CARESS [11] which employs a modified version of the Lehman–Larsen algorithm to obtain intensities and standard deviations from the measured 96-step peak profiles. All subsequent calculations were carried out using the SHELXL program [12]. All 3802 data were corrected for absorption and for Lorentz and polarization effects and were placed on an approximately absolute scale. The crystal class is trigonal and the space group is $P3_121$.

The structure was solved by direct methods and refined on F^2 by full-matrix least-squares techniques. The analytical scattering factors for neutral atoms were used throughout the analysis [13]. Hydrogen atoms were included using a riding model. The molecule is located on a two-fold rotation axis ($Z = 3$). At convergence, $wR2 = 0.0733$ and GOF = 1.067 for 143 variables refined against all 2399 unique data. [As a comparison for refinement on F, $R1 = 0.0302$ for those 1961 data with $F > 4.0\sigma(F)$.] Refinement of the Flack parameter [14] was used to determine the absolute structure (i.e. the space group $P3_121$ was chosen over the enantiomeric space group $P3_221$).

X-ray data collection, structure determination, and refinement for $[(C_5Me_4{}^{i}Pr)_2Sm]_2(\mu\text{-Cl})$, ***2***

Dark red crystals of **2** were isolated from a hot toluene solution of the product obtained by treating $(C_5Me_4{}^{i}Pr)_2Sm(OEt_2)$ with a mixture of $Pb(C_5Me_4{}^{i}Pr)_2$ [15] and $PbCl_2$ in toluene (cf. [5]). A red crystal of **2** of approximate dimensions $0.27 \times 0.27 \times 0.33$ mm was handled as described above for **1**. All 10668 data were corrected for absorption and for Lorentz and polarization effects and were placed on an approximately absolute scale. There were no systematic absences nor any diffraction symmetry other than the Friedel condition. The centrosymmetric triclinic space group $P\bar{1}$ was assigned and later determined to be correct. The structure was solved and refined as described for **1**. At convergence, $wR2 = 0.0821$ and GOF = 1.038 for 460

variables refined against all 10064 unique data. [As a comparison for refinement on F, $R1 = 0.0324$ for those 8422 data with $F > 4.0\sigma(F)$].

RESULTS AND DISCUSSION

Reaction chemistry

$C_5Me_4{}^iPrH$ can be made in a straightforward manner from tetramethylcyclopentenone and ^iPrMgCl following the general route to C_5Me_5H from tetramethylcyclopentenone and MeLi [8]. $C_5Me_4{}^iPrH$ can be deprotonated with KH and the resulting salt reacts with $SmI_2(THF)_2$ to form a purple complex in a manner analogous to the reaction of samarium diiodide with KC_5Me_5 which forms $(C_5Me_5)_2Sm(THF)_2$ [16]. Crystallization of the product of this reaction gives the monosolvate $(C_5Me_4{}^iPr)_2Sm(THF)$, **1** (Fig. 1), which was characterized by analytical, spectroscopic and X-ray diffraction methods (Table 1).

The ^1H NMR spectrum of **1** in C_6D_6 contains a broad resonance at 27.6 ppm ($\nu_{1/2} = 145$ Hz) as well as resonances at 10.3 and -9.39 ppm with line widths ($\nu_{1/2} = 58$ and 46 Hz, respectively) similar to those found in $(C_5Me_5)_2Sm(THF)_2$ [17], which contains the ring methyl resonance between 2.0–3.0 ppm depending on the concentration. A pattern of ring methyl resonances split to high and low field has been observed for the related C_5Me_4R compound $(C_5Me_4Et)_2Sm(THF)_2$ [17], which has ring methyl resonances at 4.54 and 0.10 ppm. Hence, the 10.3 and the -9.39 resonances are attributed to the ring methyl groups and the broad resonance to an unresolved doublet for the isopropyl methyl groups. This assignment is consistent with the 1:1:1 integration ratio for these three resonances. The isopropyl methine proton was not located. The chemical shifts of the remaining two peaks in the spectrum arise from coordinated THF and are highly concentration dependent.

The ^{13}C NMR spectrum of **1** in C_6D_6 has the same type of unusual shifts as observed for $(C_5Me_5)_2Sm(THF)_2$ [16] and other divalent samarocenes. The methyl carbon resonances as well as the isopropyl carbon attached to the ring are shifted downfield of the usual position to 59–95 ppm. The ring carbons are shifted upfield into the -44 to -67 ppm region. This type of ^{13}C NMR spectrum is a hallmark of organosamarium(II) complexes [18].

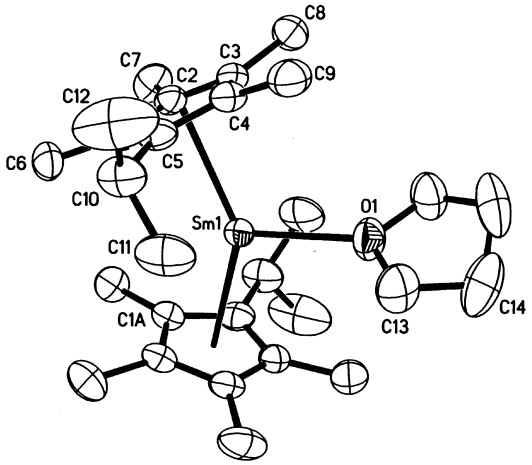

Fig. 1. Thermal ellipsoid plot of $(C_5Me_4{}^iPr)_2Sm(THF)$, **1**, with ellipsoids drawn at the 50% level and hydrogen atoms omitted for clarity.

Crystallographic studies

The structure of **1** is shown in Fig. 1. $(C_5Me_4{}^iPr)_2Sm(THF)$ has a bent metallocene structure with a 141.6° (ring centroid)–Sm–(ring centroid) angle. In comparison, $(C_5Me_5)_2Sm(THF)_2$ [16] has a 136.7° (ring centroid)–samarium–(ring centroid) angle and the analogous monosolvate, $(C_5Me_5)_2Sm(THF)$, **3** [19], has a 138.5° angle. Although the angle is larger in **1**, the 2.80(3) Å average Sm–C distance is equivalent within experimental error to the 2.816(4) Å average in **3**. The 2.540(5) Å Sm–O distance in **1** is also similar to the 2.569(3) Å distance in **3** (Table 2).

Complexes **1** and **3** differ, however, in the position of the THF molecule. In **1**, the THF is positioned symmetrically: the Sm–O bond lies on a two-fold rotation axis. In this central position, it is in the sterically least crowded position. In contrast the THF molecule in **3** is not located symmetrically with respect to the bent metallocene: the Sm–O(THF) vector makes a 37° angle with the plane defined by the samarium and the two ring centroids. In the related complexes $(C_5Me_5)_2Sm(OC_5H_{10})$ [20] and $[C_5H_2(SiMe_3)_3][C_5H_3(SiMe_3)_2]Sm(THF)$ [19] the analogous angles are 30° and 20°. Calculations on the hypothetical d^0 bent metallocene, $[(C_5H_5)_2TiH]^+$, indicated that a 65° angle would be orbitally optimal [21]. The variable 0–37° angles observed in these samarocene complexes are consistent with limited orbital control of this parameter in lanthanide complexes.

One other unusual feature in the structure of **1** is the orientation of the isopropyl methyl carbon C(11) toward Sm. Since the metal center in this monosolvated compound is likely to be sterically unsaturated, it is conceivable that some long range interactions with the isopropyl methyl groups could occur. Agostic interactions involving distant parts of ligands are common in organometallic complexes of the electrophilic lanthanides when they are sterically unsaturated [22–39]. Indeed, the 3.31 Å Sm···C(11) distance is less than the sum of the van der Waals radii of a methyl group and samarium [40]. Although nonbonded Ln–C distances shorter than their van der Waals radii have been observed for divalent lanthanide bis(trimethylsilyl)amide compounds [41–44], e.g. $[(Me_3Si)_2N]_2Sm(THF)_2$ [41] has four non-bonded Sm···C interactions in the 3.32(1)–3.46(1) Å range

Table 1. Experimental data for the X-ray diffraction study of $(C_5Me_4{}^iPr)_2Sm(THF)$, **1**, and $[(C_5Me_4{}^iPr)_2Sm]_2(\mu\text{-Cl})$, **2**

Compound	**1**	**2**
Formula	$C_{28}H_{46}Sm$	$C_{48}H_{76}ClSm_2$
FW	549.00	989.24
Temperature (K)	163	163
Crystal system	trigonal	triclinic
Space group	$P3_121$	$P\bar{1}$
a (Å)	15.494(2)	9.616(2)
b (Å)	15.494(2)	15.479(2)
c (Å)	9.7724(7)	17.8436(13)
α (°)	90	111.671
β (°)	90	93.488
γ (°)	120	107.494
Volume (Å^3)	2031.6(5)	2309.3(5)
Z	3	2
D_{calcd} (Mg/m^3)	1.346	1.423
Diffractometer	Siemens P4	Siemens P4
Radiation	MoKα ($\lambda = 0.710730$ Å)	MoKα ($\lambda = 0.710730$ Å)
Monochomator	highly oriented graphite	highly oriented graphite
Data collected	$+h, \pm k, \pm l$	$+h, \pm k, \pm l$
Scan type	2θ–ω	2θ–ω
Scan range (°)	1.20 plus α_1, α_2 separation	1.20 plus α_1, α_2 separation
Scan speed (° min^{-1} (in ω)]	3.0	3.0
2θ range (°)	2.58 to 25.0	2.24 to 27.5
μ(MoKα) (mm^{-1})	2.183	2.605
Absorption correction	semi-empirical (Ψ-scan method)	semi-empirical (Ψ-scan method)
Reflections collected	3802	10668
Reflections with $\lvert F_o\rvert > 4.0\sigma(\lvert F_o\rvert)$	1961	8422
No. of variables	143	460
R_F	6.7%	7.6%
R_{wF}	7.3%	8.2%
Goodness of fit	1.067	1.038

Table 2. Selected bond distances (Å) and angles (°) for $(C_5Me_4{}^iPr)_2Sm(THF)$, **1**

Sm(1)–O(1)	2.540(5)	Sm(1)–C(1)	2.789(5)
Sm(1)–C(2)	2.842(5)	Sm(1)–C(3)	2.834(4)
Sm(1)–C(4)	2.788(5)	Sm(1)–C(5)	2.747(5)
Sm(1)–Cnt(1)	2.531		
Cnt1–Sm(1)–Cnt1A#1	141.6	Cnt1–Sm(1)–O(1)	109.2

and $(C_5Me_5)_2Sm$ has an intermolecular Sm–C(Me) contact of 3.22 Å [45], this appears to be the first intramolecular Ln···C contact of this type for a crystallographically characterized divalent $(C_5R_5)_2Sm$ compound. The agostic interactions observed in lanthanide and yttrium organometallic compounds typically involve distorted angles in the ligand system. In this case the numerical value of the 112.3(5)° C(5)–C(10)–C(11) involving C(11) is more acute than the analogous 114.3(5)° C(5)–C(10)–C(12) angle involving the methyl group away from the samarium, but the values are indistinguishable within the error limits.

The structure of $[(C_5Me_4{}^iPr)_2Sm]_2(\mu\text{-Cl})$, **2**, Fig. 2, allows further evaluation of the metrical parameters of the $C_5Me_4{}^iPr$ ligand since it contains both divalent and trivalent samarium. Crystals of this compound were obtained fortuitously from a hot toluene solution of $(C_5Me_4{}^iPr)_2Sm(OEt_2)$, $(C_5Me_4{}^iPr)_2Pb$ [15] and $PbCl_2$ and the structure is included here since it provides data on the $C_5Me_4{}^iPr$ ligand with samarium in two oxidation states. The mixed valence nature of **2** is shown not only by its composition of five anionic ligands with the two metals, but also by the bond distances which show that this is a class I mixed valence system [46] in which the metals exist in distinct oxidation states. The two distinct $(C_5Me_4{}^iPr)_2Sm$ bent metallocene units have very different Sm–C($C_5Me_4{}^iPr$) bond distance ranges. The Sm(1)–C distances range from 2.650(3)–2.714(4) Å and average 2.69(2) Å, which are typical for a *trivalent*, 7-coordinate, C_5Me_5-ligated Sm complex [18, 47]. The Sm(2)–C distances range from 2.778(4)–2.830(4) Å and average 2.80(2) Å, which is identical to that of divalent **1** above and is slightly shorter than normal for a *divalent*, 7-coordinate, C_5Me_5-ligated Sm complex. The extensive data available on pentamethylcyclopentadienyl samarium

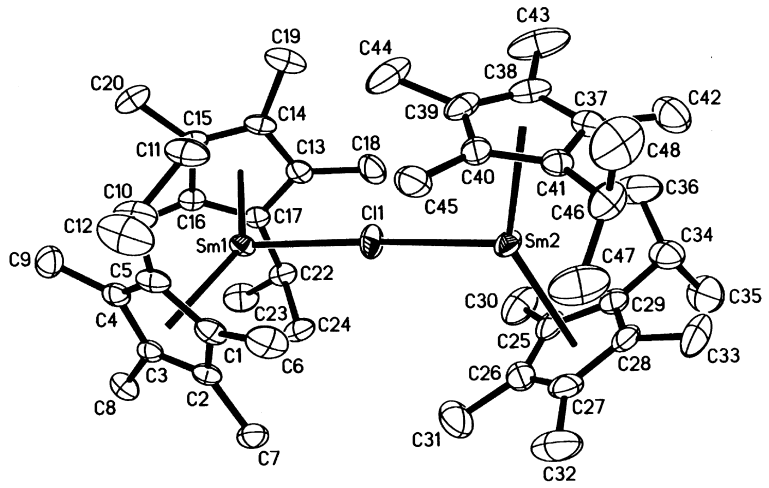

Fig. 2. Thermal ellipsoid plot of $[(C_5Me_4{}^tPr)_2Sm]_2(\mu\text{-Cl})$, **2**, with ellipsoids drawn at the 50% level and hydrogen atoms omitted for clarity.

complexes show that divalent complexes typically have Sm–C average distances 0.1 Å larger than trivalent complexes. In the mixed valence complex, $(C_5Me_5)_2Sm(\mu\text{-}C_5H_5)Sm(C_5Me_5)_2$ [18], the difference in average Sm–C(C_5Me_5) bond distances is 0.048 Å, however.

The Sm–Cl bond distances in **2** are also consistent with the different oxidation states. Hence, the 2.678(1) Å Sm(1)–Cl distance involving the trivalent metal is much smaller than the 2.891(1) Å Sm(2)–Cl distance involving the divalent center. These distances are not as definitive for the mixed valence formulation since bridging halide to lanthanide bond distances vary over a much wider range than Sm–C(C_5Me_5) bond lengths, particularly in asymmetrically bridged complexes. For example, in the complexes $[(C_5Me_5)_2Sm(\mu\text{-Cl})]_3$ and $\{[(C_5Me_5)_2ClSm]_2(\mu\text{-Cl})\}^-$ $\{[(C_5Me_5)_2ClSm](\mu\text{-Cl})[(C_5Me_5)_2Sm](\mu\text{-tetraglyme})[(C_5Me_5)_2Sm]\}^+$, **4**, the trivalent Sm–(μ-Cl) distances vary from 2.76(1)–2.89(1) Å (Table 3) [48].

There are relatively few structurally characterized organometallic samarium compounds of general formula $[(C_5R_5)_2Sm]_2(\mu\text{-X})$. However, the series X = O, S, Se, Te where R is Me and both metals are trivalent has been crystallographically characterized and is available for comparison [49, 50]. The Sm–X–Sm angle for the oxide bridged complex is 180° while the angles in the S, Se, and Te compounds are 170.2(1)°, 169.7(1)° and 170.0(1)°, respectively. The 169.8° angle in $[(C_5Me_4{}^iPr)_2Sm]_2(\mu\text{-Cl})$ closely resembles those of the S, Se and Te compounds. This angle is also similar to the 165.1(4)° and 164.8(4)° Sm–Cl–Sm angles in **4** [48]. Comparison with the ytterbium compounds $[(C_5Me_5)_2Yb]_2(\mu\text{-Se})$, **5** [9], and $[(C_5Me_5)_2Yb]_2(\mu\text{-F})$, **6** [51], can also be made. Complex **5** has a Yb–Se–Yb angle of 171.09(6)° while the smaller bridging fluoride atom in **6** results in a linear 180° Yb–F–Yb angle in order to minimize steric repulsion of the $(C_5Me_5)_2Yb$ units.

Table 3. Selected bond distances (Å) and angles (°) for $[(C_5Me_4{}^iPr)_2Sm]_2(\mu\text{-Cl})$, **2**

Sm(1)–C(17)	2.650(3)	Sm(1)–C(5)	2.662(4)
Sm(1)–C(1)	2.671(4)	Sm(1)–C(16)	2.673(3)
Sm(1)–C1(1)	2.6782(10)	Sm(1)–C(13)	2.686(4)
Sm(1)–C(2)	2.700(3)	Sm(1)–C(4)	2.701(4)
Sm(1)–C(15)	2.706(4)	Sm(1)–C(14)	2.714(3)
Sm(1)–C(3)	2.714(4)	Sm(1)–Cnt1	2.404
Sm(1)–Cnt2	2.400		
Sm(2)–C(25)	2.778(4)	Sm(2)–C(40)	2.778(4)
Sm(2)–C(29)	2.780(4)	Sm(2)–C(41)	2.782(4)
Sm(2)–C(39)	2.800(4)	Sm(2)–C(26)	2.804(4)
Sm(2)–C(28)	2.813(4)	Sm(2)–C(37)	2.817(4)
Sm(2)–C(38)	2.820(4)	Sm(2)–C(27)	2.830(4)
Sm(2)–C1(1)	2.8912(10)	Sm(2)–Cnt3	2.530
Sm(2)–Cnt3	2.528		
Cnt1–Sm(1)–C1(1)	110.8	Cnt2–Sm(1)–C1(1)	108.2
Cnt1–Sm(1)–Cnt2	141.0	Cnt3–Sm(2)–C1(1)	106.3
Cnt4–Sm(2)–C1(1)	109.4	Cnt3–Sm(2)–Cnt4	143.3
Sm(1)–C1(1)–Sm(2)	169.88(4)		

Examination of the positions of the isopropyl methyl carbon atoms with respect to the metals shows that neither methyl group attached to the rings on divalent Sm(2) is within 3.9 Å of Sm(2), but C(11) and C(24) are located 3.26 and 3.18 Å, respectively, from Sm(1). Taking into account a radial difference of about 0.1 Å between divalent and trivalent samarium, these Sm–C distances are in the range of the 3.31 Å Sm···C(11) distance found in **1**. Similarly, the 109.6(3)° C(17)–C(22)–C(24) and 110.9(4)° C(5)–C(10)–C(11) angles are more acute than their analogs involving the other methyl carbons: C(17)–C(22)–C(23) is 115.8(4)° and C(5)–C(10)–C(12) is 114.6(4)°. However, the pairs of C–C–C angles involving the isopropyl groups which are not oriented toward Sm(2) also have this type of angular disparity: C(29)–C(34)–C(35) is 110.9(4)° and

C(29)–C(34)–C(36) is 114.6(5)°; C(41)–C(46)–C(48) is 110.4(4)° and C(41)–C(46)–C(47) is 115.0(4)°.

The 141.6° (ring centroid)–Sm–(ring centroid) angle in **1** and the 141.0° and 143.3° (ring centroid)–Sm–(ring centroid) angles for Sm(1) and Sm(2) in **2** are the largest observed to date in any organometallic samarium complex [47]. This indicates that increased steric bulk on the cyclopentadienyl rings can affect the ring centroid–Sm–ring centroid angles, which could in turn lead to different reactivity patterns when compared to the C_5Me_5 ligand.

CONCLUSION

Complexes **1** and **2** show that samarium metallocenes are accessible with the sterically more demanding $C_5Me_4{}^iPr$ ligand in both divalent and trivalent oxidation states. In comparison to C_5Me_5, the isopropyl-substituted group increases the (ring centroid)–metal–(ring centroid) angles in the complexes, but it does not affect the metal ligand bond distances significantly. The specific orientation of the isopropyl group in **1** suggests that long distance lanthanide hydrocarbon interactions can be studied using appropriately substituted C_5Me_4R moieties.

Acknowledgements—We thank the National Science Foundation for support for this research and the U.S. Department of Education Graduate Assistance in Areas of National Need program for a fellowship to K. J. F.

REFERENCES

1. Evans, W. J., *Polyhedron*, 1987, **6,** 803.
2. Marks, T. J. and Ernst, R. D., in *Comprehensive Organometallic Chemistry*, Vol. 3, Chap. 21, eds. F. G. A. Stone, G. Wilkinson and E. W. Abel. Pergamon Press, Oxford, 1982.
3. Schaverien, C. J., *Adv. Organomet. Chem.*, 1994, **36,** 283.
4. Schumann, H., Meese-Marktscheffel, J. A. and Esser, L., *Chem. Rev.*, 1995, **95,** 865.
5. Evans, W. J., Forrestal, K. J., Leman, J. T. and Ziller, J. W., *Organometallics*, 1996, **15,** 527.
6. Evans, W. J., Gonzales, S. L. and Ziller, J. W., *J. Am. Chem. Soc.*, 1991, **113,** 7423.
7. Evans, W. J., Grate, J. W. and Doedens, R. J., *J. Am. Chem. Soc.*, 1985, **107,** 1671.
8. Fendrick, C. M., Schertz, L. D., Mintz, E. A. and Marks, T. J., *Inorg. Synth.*, 1992, **29,** 193.
9. Berg, D. J., Burns, C. J., Andersen, R. A. and Zalkin, A., *Organometallics*, 1989, **8,** 1865.
10. *XSCANS Software Users Guide*, Version 2.1. Siemens Industrial Automation, Madison, WI, 1994.
11. Broach, R. W., Argonne National Laboratory, Illinois, 1978.
12. Sheldrick, G. M., Siemens Analytical X-Ray Instruments, Madison, WI, 1994.
13. *International Tables for X-Ray Crystallography*, Vol. C. Kluwer Academic Publishers, Dordrecht, 1992.
14. Flack, H. D., *Acta Cryst. A*, 1983, **39,** 876.
15. Evans, W. J., Forrestal, K. J., Clark, R. D. and Ziller, J. W. (to be submitted).
16. Evans, W. J., Grate, J. W., Choi, H. W., Bloom, I., Hunter, W. E. and Atwood, J. L., *J. Am. Chem. Soc.*, 1985, **107,** 941.
17. Evans, W. J., Bloom, I., Hunter, W. E. and Atwood, J. L., *Organometallics*, 1985, **4,** 112.
18. Evans, W. J. and Ulibarri, T. A., *J. Am. Chem. Soc.*, 1987, **109,** 4292.
19. Evans, W. J. and Ulibarri, T. A., *Polyhedron*, 1989, **8,** 1007.
20. Evans, W. J., Kociok-Kohn, G., Foster, S. E., Ziller, J. W. and Doedens, R. J., *J. Organomet. Chem.*, 1993, **444,** 61.
21. Lauher, J. W. and Hoffmann, R., *J. Am. Chem. Soc.*, 1976, **98,** 1729.
22. Jeske, G., Lauke, H., Mauermann, H., Swepston, P. N., Schumann, H. and Marks, T. J., *J. Am. Chem. Soc.*, 1985, **107,** 8091.
23. Evans, W. J., Drummond, D. K., Bott, S. G. and Atwood, J. L., *Organometallics*, 1986, **5,** 2389.
24. Den Haan, K. H., De Boer, J. L. and Teuben, J. H., *J. Organomet. Chem.*, 1987, **327,** 31.
25. Heeres, H. J., Renkema, M., Booij, J., Meetsma, A. and Teuben, J. H., *Organometallics*, 1988, **7,** 2495.
26. Booij, M. H., Kiers, N. H., Meetsma, A., Teuben, J. H., Smeets, W. J. J. and Spek, A. L., *Organometallics*, 1989, **8,** 2454.
27. Heeres, H. J., Meetsma, A., Teuben, J. H., Smeets, W. J. J. and Spek, A. L., *Organometallics*, 1989, **8,** 2637.
28. Booij, M., Kiers, N. H., Meetsma, A. and Teuben, J. H., *Organometallics*, 1989, **8,** 2454.
29. Heeres, H. J., Meetsma, A. and Teuben, J. H., *Organometallics*, 1989, **8,** 2637.
30. Booij, M., Meetsma, A. and Teuben, J. H., *Organometallics*, 1991, **10,** 3246.
31. Evans, W. J., Keyer, R. A. and Ziller, J. W., *Organometallics*, 1993, **12,** 2618.
32. Booij, M., Deelman, B.-J., Duchateau, R., Postma, D. S., Meetsma, A. and Teuben, J. H., *Organometallics*, 1993, **12,** 3531.
33. Duchateau, R., van Wee, C. T., Meetsma, A. and Teuben, J. H., *J. Am. Chem. Soc.*, 1993, **115,** 4931.
34. Hasinoff, L., Takats, J. and Zhang, X. W., *J. Am. Chem. Soc.*, 1994, **116,** 8833.
35. Giardello, M. A., Conticello, V. P., Brard, L., Sabat, M., Rheingold, A. L., Stern, C. L. and Marks, T. J., *J. Am. Chem. Soc.*, 1994, **116,** 10212.
36. Sun, Y., McDonald, R., Takats, J., Day, V. W. and Eberspacher, T. A., *Inorg. Chem.*, 1994, **33,** 4433.
37. Sun, Y., Takats, J., Eberspacher, T. and Day, V. W., *Inorg. Chim. Acta*, 1995, **229,** 315.
38. Zhang, X., McDonald, R. and Takats, J., *N. J. Chem.*, 1995, **19,** 573.
39. Duchateau, R., van Wee, C. T. and Teuben, J. H., *Organometallics*, 1996, **15,** 2291.
40. Pauling, L., *The Nature of the Chemical Bond*, 3rd edn. Cornell University Press, Ithaca, NY, 1969.
41. Evans, W. J., Drummond, D. K., Zhang, H. and Atwood, J. L., *Inorg. Chem.*, 1988, **27,** 575 and references therein.
42. Tilley, T. D., Andersen, R. A. and Zalkin, A., *J. Am. Chem. Soc.*, 1982, **104,** 3725.

43. Tilley, T. D., Andersen, R. A. and Zalkin, A., *Inorg. Chem.*, 1984, **23,** 2271.
44. Boncella, J. M. and Andersen, R. A., *Organometallics*, 1985, **4,** 205.
45. Evans, W. J., Hughes, L. A. and Hanusa, T. P., *Organometallics*, 1986, **5,** 1285.
46. Robin, M. B. and Day, P., *Adv. Inorg. Chem. Radiochem.*, 1967, **10,** 247.
47. Evans, W. J. and Foster, S. E., *J. Organomet. Chem.*, 1992, **433,** 79.
48. Evans, W. J., Drummond, D. K., Grate, J. W., Zhang, H. and Atwood, J. L., *J. Am. Chem. Soc.*, 1987, **109,** 3928.
49. Evans, W. J., Grate, J. W., Bloom, I., Hunter, W. E. and Atwood, J. L., *J. Am. Chem. Soc.*, 1985, **107,** 405.
50. Evans, W. J., Rabe, G. W., Ziller, J. W. and Doedens, R. J., *Inorg. Chem.*, 1994, **33,** 2719.
51. Burns, C. J. and Andersen, R. A., *J. Chem. Soc. Chem. Commun.*, 1989, 136.

Pergamon

Polyhedron Vol. 17, No. 23–24, pp. 4023–4031, 1998
© 1998 Elsevier Science Ltd
All rights reserved. Printed in Great Britain
0277–5387/98 $19.00+0.00

PII: S0277-5387(98)00204-6

Synthesis of tris(quinoxaline-2,3-dithiolato)manganese(IV) and its reaction with $[Cu(CH_3COO)_2H_2O]_2$. Crystal structure of $[Mn^{II}(DMF)_4(H_2O)_2][Cu^{III}(qdt)_2]_2$

José A. Ayllón[a,1], Isabel C. Santos[a], Rui T. Henriques[a,b,*], Manuel Almeida[a], Luís Alcácer[b] and Maria T. Duarte[b]

Departamento de Química, Instituto Tecnológico e Nuclear, 2686 Sacavém, Portugal

Departamento de Engenharia Química, Instituto Superior Técnico, 1096 Lisbon, Portugal

(Received 6 March 1998; accepted 18 May 1998)

Abstract—Tris(quinoxaline-2,3-dithiolato)manganese(IV) was synthesised and isolated as two different salts, $(PPh_4)_2[Mn^{IV}(qdt)_3]\cdot 1/2CHCl_3$, **1**, and $(HNEt_3)_2[Mn^{IV}(qdt)_3]\cdot 2H_2O$, **2** (qdt = quinoxaline-2,3-dithiolate). The magnetic behaviour of **1** is the typical of a high spin d^3 system, presenting an effective magnetic moment of 3.85 μ_B at room temperature. The reaction of **2** with copper(II) acetate in DMF (*N*,*N*-dimethylformamide) solution involves redox and ligand exchange processes and produces the new salt $[Mn^{II}(DMF)_4(H_2O)_2][Cu^{III}(qdt)_2]_2$, **3**. The crystal structure of compound **3** consists of sequences of two layers of $[Cu^{III}(qdt)_2]^-$ anions and one of $[Mn^{II}(DMF)_4(H_2O)_2]^{2+}$ cations. Each cation is linked to four anions through O–H···N hydrogen bonds between the water ligand of the cation and one nitrogen atom of qdt ligand in the anion. Magnetic isolation of the Mn(II) centres in **3** is confirmed by magnetic susceptibility measurements. © 1998 Elsevier Science Ltd. All rights reserved

Keywords: quinoxaline-2,3-dithiolate; copper(III) complexes; manganese(IV) complexes; crystal structure; magnetic susceptibility; dimethylformamide

INTRODUCTION

The ligand quinoxaline-2,3-dithiolate (qdt) appears to be particularly interesting and its complexes with several transition metals, Co(III), Cu(II), Cu(III), Fe(III), Fe(IV), Ni(II), Pd(II), Pt(II), Zn(II), have been studied [1–6]. The use of qdt as an analytical reagent [7] and the utilisation of qdt complexes as ion-active substances of membrane electrodes have been reported [8]. Molybdenum complexes have been investigated for modelling of molybdenum hydroxylase enzymes [9–11]. More recently the photophysical properties of the platinum complexes, specially their luminescence, have been studied [12, 13]. Complexes of quinoxaline-2,3-dithiolate are analogous to metal-bisdithiolenes, but although tris(dithiolene)manganese (IV) compounds are known [14, 15], no previous isolation and characterisation of a quinoxaline-2,3-dithiolate complex of manganese has been done.

One or both nitrogen atoms of the qdt ligand in their complexes could be reversible protonated, as observed in the Pt(II) [13], Ni(II) [1, 6] or Mo(IV) complexes [10], for example. To our knowledge, the participation of this group in the direct co-ordination of an "outer" metal has been established only in the binuclear complex, (2,3-dithioquinoxalato)bis(η^5-cyclopentadienyl)titanium(III), $[Cp_2Ti(qdt)TiCp_2]$, where the qdt ligand acts as a bridge [16]. There is some controversy regarding the viability of the pyrazine bridges for mediating electron transfer [17, 18]. Aiming at contributing to establish whether the pyrazine rings may be used to produce magnetically interacting salts M[M′(qdt)2], we used the triethylammonium salts of qdt complexes of Cu(III), Fe(III) and Mn(IV)

[1] Present address: Departamento de Química, Edificio Cn, Universidad Autónoma de Barcelona, 08193 Bellaterra, Spain.

* Author to whom correspondence should be addressed.

combining them with copper(II) salts. Products of these reactions are microcrystalline powders very insoluble in common solvents and were not characterised, except for Mn(IV), from which we have produced monocrystals of a salt, $[Mn^{II}(DMF)_4(H_2O)_2][Cu^{III}(qdt)_2]$, with the added/outside metal solvated, with no direct interaction with the nitrogen atoms of the qdt ligand. We present here the preparation of Mn(IV) qdt complexes and the synthesis and crystal structure of this new salt, **3**.

EXPERIMENTAL SECTION

Solvents and reagents were obtained from commercial sources and used without further purification unless otherwise stated. All the reactions were carried out in an open vessel. The ligand H_2qdt was prepared starting from 2,3-dichloroquinoxaline (Aldrich) by the procedure of Theriot *et al.* [2]. Elemental analysis, using a Perkin-Elmer 240 elemental analyser, were made at the analytical service of our laboratory.

Preparation of $(PPh_4)_2[Mn^{IV}(qdt)_3]\cdot 1/2CHCl_3$

H_2qdt (272 mg, 1.40 mmol) was dissolved in a solution of NaOH (112 mg, 2.80 mmol) in methanol (100 ml). A solution of $MnCl_2{\cdot}4H_2O$ (135 mg, 0.68 mmol) in methanol (50 ml) was slowly added with vigorous stirring. After 20 min, a solution of $(PPh_4)Br$ (300 mg, 0.72 mmol) in methanol (70 ml) was added, followed by 50 ml of water. The resultant solution is allowed to stand overnight in an open vessel and the day after green microcrystals appeared which were filtered and washed with water and diethyl ether. The crude compound was recrystallised in chloroform–hexane. Yield, 60%. Found: N, 6.16; C, 63.14; H, 3.45. Calcd. for $C_{72.5}H_{52.5}Cl_{1.5}MnN_6O_6P_2S_6$: N, 6.13; C, 63.55; H, 3.86.

Preparation of $(HNEt_3)_2[Mn^{IV}(qdt)_3]\cdot 2H_2O$

H_2qdt (272 mg, 1.40 mmol), $MnCl_2{\cdot}4H_2O$ (135 mg, 0.68 mmol) and an excess of triethylamine (0.5 ml, 3.6 mmol) were refluxed in methanol during one hour. The mixture obtained was filtered and allowed to stand overnight in an open vessel. The day after green monocrystals were collected by the procedure used for **1**. Yield, 70%. Found: N, 12.87; C, 49.64; H, 5.50. Calcd for $C_{36}H_{48}MnN_8O_2S_6$: N, 12.85; C, 49.58; H, 5.55. The crude compound could be recrystallised in dichloromethane–hexane.

Preparation of $[Mn^{II}(DMF)_4(H_2O)_2][Cu^{III}(qdt)_2]_2$

$(HNEt_3)_2[Mn^{IV}(qdt)_3]\cdot 2H_2O$ (50 mg, 0.057 mmol) was dissolved in 10 ml of DMF (dimethylformamide) and a solution of $[Cu(CH_3COO)_2H_2O]_2$ (12 mg, 0.060 mmol Cu) in 10 ml of DMF was added. The dark solution obtained was allowed to stand for a week in an open vessel where dark green monocrystals grew. They were filtered and washed with DMF and diethyl ether. Yield, 20%. Found: N, 12.61; C, 40.53; H, 2.92. Calcd for $C_{44}H_{48}N_{12}O_6S_8MnCu_2$: N, 13.13; C, 41.30; H, 3.78.

X-ray crystallography

A dark-green crystal of approximate dimensions $0.28\times0.08\times0.06\,mm^3$ was mounted in a glass capillary on a goniometer head and transferred to an Enraf-Nonius CAD-4 automatic diffractometer where X-ray data were collected at room temperature with graphite monochromated Mo Kα radiation ($\lambda=0.71069$ Å). Unit cell dimensions and a crystal orientation matrix were obtained from square refinement of the setting angles of 25 reflections in the $10^\circ<\theta<13^\circ$ range. The data set was collected in a ω–2θ scan mode [$\Delta\omega=(0.80+0.35\tan\theta)^\circ$]. The intensities were corrected for Lorentz and polarisation effects and an empirical absorption correction (ψ scan) was made (maximum and minimum transmission factors were 0.9660 and 0.9990). The MoLEN program was used for data reduction. The structure was solved by standard Patterson methods using SHELX86 [19], and subsequently completed by Fourier recycling using SHELX93 [20]. All non-hydrogen atoms were refined anisotropically. The hydrogen atoms were set in calculated positions. The final refinement on F_o^2 by full-matrix least-square techniques, with anisotropic thermal displacement parameters for the non-hydrogen atoms converged at $R=0.0330$, $R_w=0.0756$ and $S=1.075$. A difference Fourier synthesis revealed residual densities between 0.379 and $-0.350\,e/Å^3$. Scattering factors and anomalous dispersion factors used were those supplied in SHELX93. The drawings were made with ORTEP [29].

Magnetic susceptibility

Magnetic susceptibility measurements were performed in the range 4.2–300 K using a longitudinal Faraday system (Oxford Instruments) with a 7 T superconducting magnet. Polycrystalline samples (8.6 mg for **1** and 9.2 mg for **3**) were placed in a thin-wall Teflon bucket, previously measured. The magnetic fields used were 2 T and force was measured with a microbalance (Sartorius S3D-V) applying forward and reverse gradients of 5 T/m. Paramagnetic susceptibility was calculated from the raw susceptibility data correcting for diamagnetism that was estimated from tabulated Pascal's constants [21] as -727×10^{-6} emu/mol for **1** and -550×10^{-6} emu/mol for **3**.

RESULTS AND DISCUSSION

Manganese(II) chloride reacts with the quinoxaline-2,3-dithiolate ligand, in basic media, giving a green

manganese(IV) complex. Many reasons could explain the change in the oxidation state of the manganese. The qdt ligand favours the stabilisation of transition metal cations in a high oxidation state as observed in many cases. This is a metal centred process, electrochemically observable for instance for the $[Ni^{III}(qdt)_2]^-$–$[Ni^{II}(qdt)_2]^{2-}$ couple in DMF solution [6]. The Cu(III) is air stable; this complex is easily obtained by air oxidation of the Cu(II) complex in solution [2]. The cobalt(II) complex must be prepared under a nitrogen atmosphere [3] but the cobalt(III) one is relatively air stable. Starting from iron(III) chloride, and without any special requirement, an iron(IV) air stable complex is obtained [3]. The molybdenum(IV) complex treated with iodine, a soft oxidant, produces the molybdenum(V) species [11]. In all the reported tris-dithiolene manganese complexes, the Mn is in the +IV oxidation state [14, 15]. These complexes are always green and in some cases are prepared starting from manganese (II) salts in open recipients with no other oxidant addition.

On the other hand, manganese(II) is poorly represented in the chemistry of dithiolenes. Oxidation of the thiol compound of Mn(II) to Mn(III) occurs so readily that Mn(II) compounds have to be prepared anaerobically. In addition, it is well known that the alkaline solutions that contain Mn(II) species are usually not stable in regard to the oxidation to Mn(IV) compounds, the MnO_2 precipitate being formed in many cases.

Although we started from a 2:1 qdt:Mn molar ratio, the elemental analysis of **1** indicates that a 3:1 complex was obtained. This stoichiometry is the observed one for the high oxidation state cation: tris(quinoxaline-2,3-dithiolato) complexes of cobalt(III) and iron(IV) [3], molybdenum(IV) [10, 21] and molybdenum(V) [11] have been characterised. X-ray powder patterns are identical to those of the Fe analogue, suggesting that $(AsPh_4)_2[Mn(mnt)_3]$ has the same octahedral structure defined for the Fe compound [14, 15].

The magnetic behaviour of **1** is typical of a high spin d^3 system (Fig. 1): it presents a μ_{eff} of 3.85 μ_B at room temperature. The isolation of the magnetic centres can also be inferred from the susceptibility data. All the tris(dithiolene)manganese complexes have magnetic moments near 4 μ_B, typical of high spin d^3 systems [14, 15]. Therefore, on the basis of the experimental data and reported values for other Mn compounds in the literature, the assignment of the +IV oxidation state to the two obtained manganese compounds is justified.

In the synthesis of **1** we utilised the much usual route to the qdt complexes, starting from the sodium or potassium salt of the ligand, obtained by the reaction of the slightly acidic H_2qdt with NaOH (or KOH). These salts react with the metal chloride or nitrate to produce a complex. When anionic complexes are obtained, a salt of a bulk cation must be added to precipitate the anionic complex. Basic media must be assured when the complex is still in solution to prevent the protonation of the nitrogen atoms.

$(HNEt_3)_2[Mn^{IV}(qdt)_3]\cdot 2H_2O$ was obtained by a different route based on the addition of an excess of triethylamine to a mixture of H_2qdt and a metallic salt, manganese(II) chloride in this case. The amine acts as a base, to deprotonate the slightly acidic H_2qdt, giving then an ammonium cation suitable to precipitate the anionic complex. Using this method, we have obtained the Mn(IV) complex described here and also salts of other known qdt complexes as $(HNEt_3)_2[Fe^{III}(qdt)_2]_2\cdot 2H_2O$ and $(HNEt_3)[Cu^{III}(qdt)_2]\cdot 2H_2O$. Although the amine can promote the precipitation of metal hydroxide, amine excess helps the formation of soluble species able to react with the qdt ligand to give the desired complex.

These triethylammonium salts, with a cation that

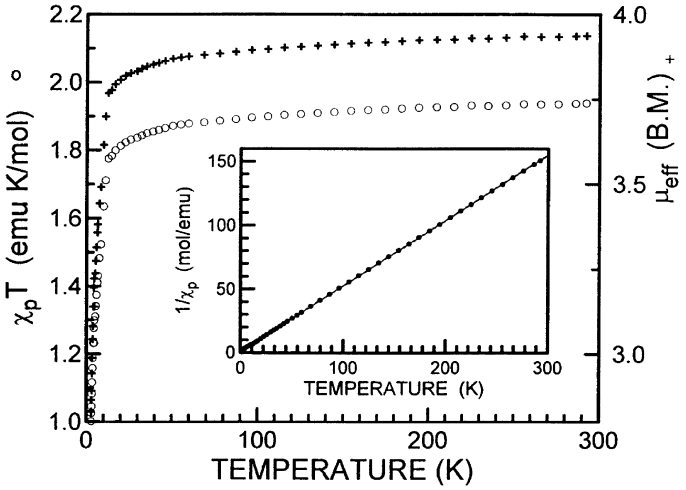

Fig. 1. Experimental χ_pT (crosses, left scale) and effective magnetic moment (open circles, right scale) as a function of temperature for $(PPh_4)_2[Mn^{IV}(qdt)_3]_2$; the inset shows the plot of χ_p^{-1} vs T.

has an acidic nature, are specially appropriate for reacting with other metal compounds in which the ligand has a basic nature (such as the acetates), in order to obtain bimetallic salts of stoichiometry $M^{y}_{(2n-x)/y}[M^{x}(qdt)_n]$. If the ability of solvent co-ordination to M^y is less than the one of the nitrogen atom in the pyrazine rings, both metals may be connected via qdt ligand and the formation of two or three-dimensional networks could be anticipated. These intermetallic contacts could favour interactions between the unpaired electrons of both metals, M^y and M^x, that must originate interesting magnetic properties.

The reaction between $(HNEt_3)_2[Mn^{IV}(qdt)_3]\cdot 2H_2O$ and $[Cu(CH_3COO)_2H_2O]_2$ in DMF produces a monocrystalline compound, $[Mn^{II}(DMF)_4(H_2O)_2][Cu^{III}(qdt)_2]$, **3**. X-ray data allowed the identification of the copper and manganese in **3**. This reaction involves a complete reorganisation of the co-ordination sphere of both metals that also change their oxidation states, whose assignment is reinforced by the magnetic susceptibility data. The manganese is not bonded to the dithiolene function, but is solvated by DMF and water. No direct contact between the pyrazine and the manganese is observed, but they are hydrogen-bond connected through the water ligand (a detailed discussion of the structure is given below).

This reaction must be done in an open container; **3** was not obtained when a closed vessel was employed. This indicates that the intervention of the atmospheric oxygen may be a requirement. The synthesis of **3** from the reaction of Mn(II) perchlorate with $(PPh_4)[Cu^{III}(qdt)_2]$ in DMF was not successful (Scheme 1).

DMF is an aprotic solvent which acts as an oxygen-donor ligand. A number of metal complexes containing DMF, in addition to other different ligands have been synthesised and their structures reported, but the number of homoleptic complexes characterised are reduced. The DMF is *a priori* a weak ligand: anionic ligands with any significant co-ordinating power can compete with amides for co-ordination sites so that the products isolated from reactions of amides with transition metal halides usually contain co-ordinated halide. In all the co-ordination compounds of DMF that have been characterised by X-ray studies, the bonding is through oxygen. Water is also a competitor with them for co-ordination and consequently when dry conditions have not been used, products containing both amide and water are obtained [22].

The magnetic susceptibility measurements for **3** agree with the existence of isolated Mn(II) centres, a classic d^5 system. No contribution to the paramagnetism from the $[Cu^{III}(qdt)_2]^-$ square planar d^8 system must be expected since its tetraphenylphosphonium salt has been reported as diamagnetic [2]. Upon cooling from room temperature, the susceptibility increases, closely following a Curie law until the lowest temperature measured. As shown in Fig. 201, the $\chi_p T$ product curve exhibits a wide plateau (20–300 K) corresponding to an effective magnetic moment of 5.8 μ_B, close to the value due to a $S = 5/2$ spin, which is 5.92 μ_B by the spin-only formula.

CRYSTAL STRUCTURE OF $[Mn^{II}(DMF)_4(H_2O)_2][Cu^{III}(qdt)_2]_2$

The crystal structure of $[Mn^{II}(DMF)_4(H_2O)_2][Cu^{III}(qdt)_2]_2$ consists of two sheets of $[Cu^{III}(qdt)_2]^-$ anions alternating with $[Mn^{II}(DMF)_4(H_2O)_2]^{2+}$ cations (Figs 3 and 4) almost parallel to the *bc* plane. For the $[Cu^{III}(qdt)_2]^-$ anion, the distances and angles are very similar to those found in $(PPh_4)[Cu^{III}(qdt)_2]$ (which contain two independent anions) or $(perylene)_2[Cu^{III}(qdt)_2]$ [23]. In particular, their Cu–S bond distances (2.18 Å average) confirm the charge of the anion (average Cu–S bond distances of 2.26 Å for $[Cu^{II}(qdt)_2]^{2-}$ and 2.18 Å $[Cu^{III}(qdt)_2]^-$ has been measured in their PPh_4 salts [5]).

The qdt ligand is not symmetrically bonded to the copper atom and the two Cu–S bond distances in this compound are quite identical to corresponding ones in similar salts, as indicated in Table 1. In **3**, the two ligands of each $[Cu^{III}(qdt)_2]^-$ anion are also not equivalent as a consequence of the intermolecular

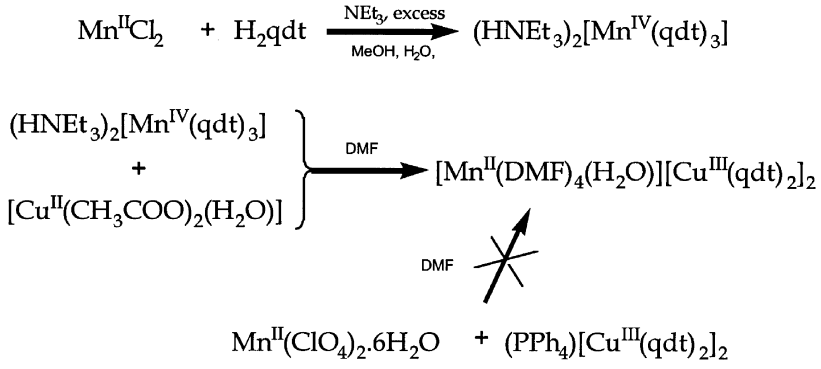

Scheme 1.

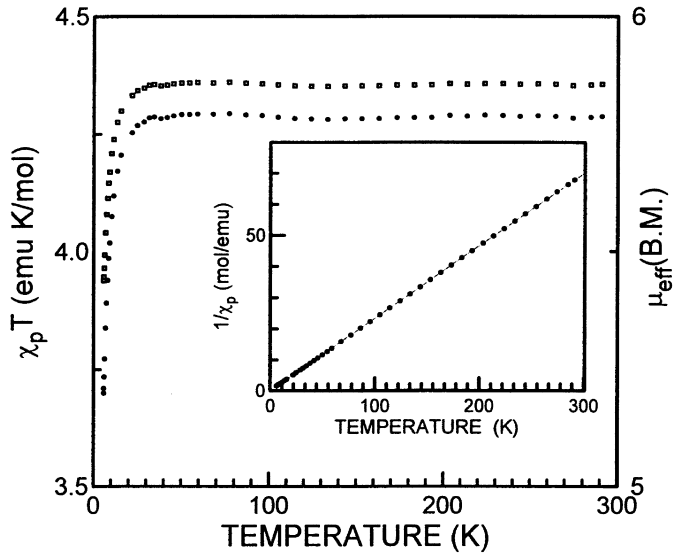

Fig. 2. Experimental $\chi_p T$ (full circles, left scale) and effective magnetic moment (open squares, right scale) as a function of temperature for $[Mn^{II}(DMF)_4(H_2O)_2][Cu^{III}(qdt)_2]_2$; the inset shows the plot of $\chi_p{}^{-1}$ vs T.

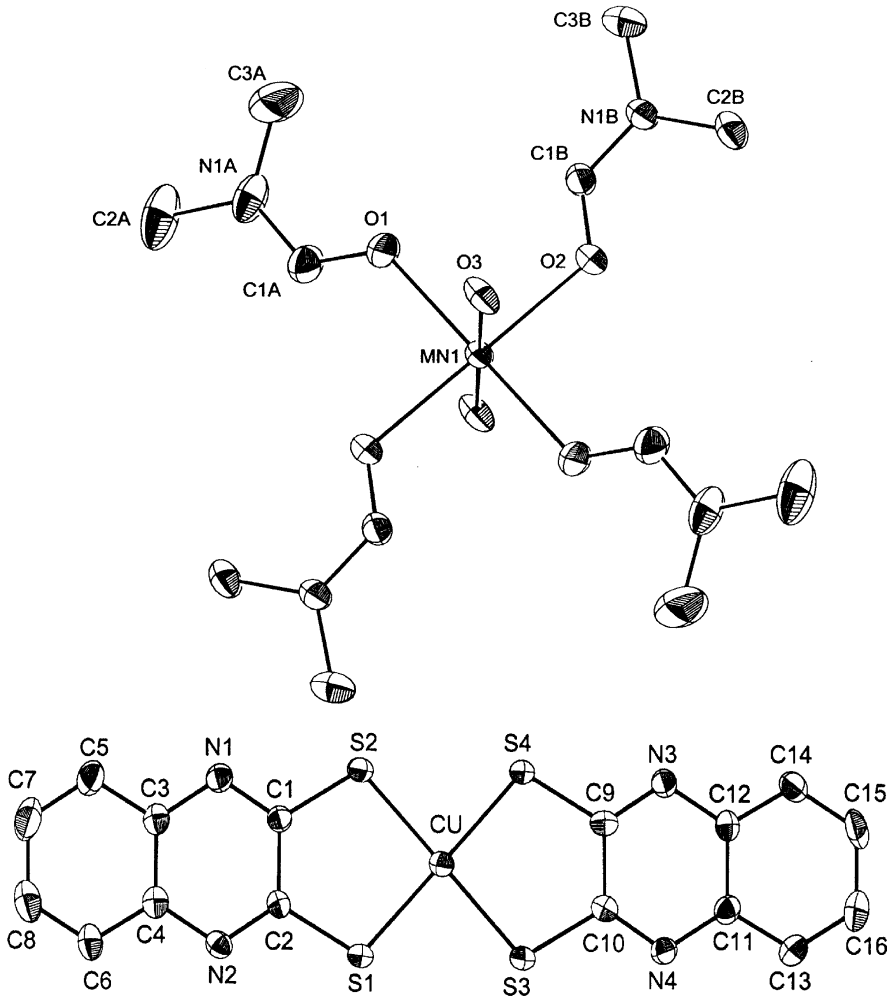

Fig. 3. ORTEP plot of the species $[Mn^{II}(DMF)_4(H_2O)_2]^{2+}$ and $[Cu^{III}(qdt)_2]^-$, showing the labelling scheme for the atoms.

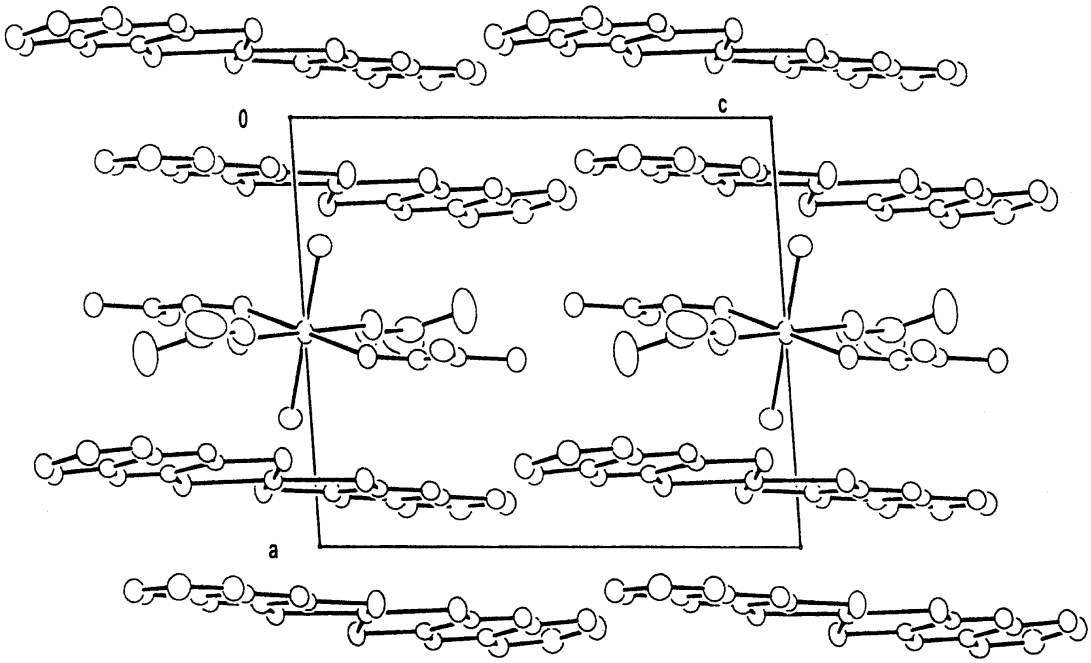

Fig. 4. ORTEP projection onto the *ac* plane of the $[Mn^{II}(DMF)_4(H_2O)_2][Cu^{III}(qdt)_2]_2$ structure. Hydrogen atoms are omitted for clarity.

interactions: this explains some differences in "symmetrical" bond lengths and angles on the two sides of the molecule. In fact, the $[Cu^{III}(qdt)_2]^-$ deviates from planarity: the angle between the CuS_4 plane and each of the mean planes of the ligands is 5.21(2)° and 4.14(2)° for S1S2...C7C8 and S3S4···C15C16, respectively, and it is 8.31(2)° between the two ligands (Table 2–4).

This is the first characterisation of the $[Mn^{II}(DMF)_4(H_2O)_2]^{2+}$ cation. A search of the January 1998 release of the Cambridge Structural Database showed no previous determination of this anion, $[Mn^{II}(DMF)_6]^{2+}$ or other manganese related cation.

The $[Mn^{II}(DMF)_4(H_2O)_2]^{2+}$ cation has two DMF and one water independent molecules. The Mn(II) cation being located on a centre of symmetry, has a pseudo octahedral environment defined by four oxygen atoms of four DMF molecules, located in a plane

Table 1. Angles and bond lengths (average values) for different $Cu(qdt)_2$ complexes. "a1", average angle between the CuS_4 and $C_8N_2S_2$ planes; other angles and distances are indicated in the figure

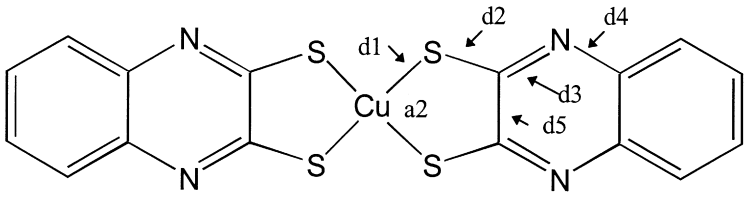

Compound	Ref.	a1	a2	d1	d2	d3	d4	d5
$[Mn^{II}(DMF)_4(H_2O)_2][Cu^{III}(qdt)_2]_2$	This paper	4.7	92.4	2.18	1.74	1.30	1.37	1.44
$(PPh_4)_2[Cu^{II}(qdt)_2]$	[5]	10.0	90.5	2.26	1.74	1.31	1.37	1.46
$(PPh_4)[Cu^{III}(qdt)_2]$*	[5]	21.4	92.2	2.18	1.75	1.31	1.37	1.44
		24.0	91.5	2.19	1.75	1.31	1.37	1.44
$(Perylene)_2[Cu^{III}(qdt)_2]$	[23]	1.5	92.8	2.18	1.74	1.31	1.37	1.44

*This compound contains two independent anions.

Table 2. Crystallographic data for $[Mn^{II}(DMF)_4(H_2O)_2][Cu^{III}(qdt)_2]_2$

Formula	$C_{44}H_{48}Cu_2MnN_{12}O_6S_8$	d_{calc} (Mg/m^3)	1.570
fw	1279.44	T (K)	293(2)
a (Å)	10.185 (1)	Wavelength (Å)	0.71069
b (Å)	11.662 (2)	μ (Mo Kα) (mm^{-1})	1.374
c (Å)	12.073(2)	Space group	P$\bar{1}$
α (°)	71.451(2)	V (Å^3)	1353.58(4)
β (°)	85.107(1)	R^a	0.0330
γ (°)	86.393(1)	$R_w{}^b$	0.0756
Z	1	S^c	1.075
Crystal system		triclinic	
F(000)		655	
Theta range for data collection		1.78 to 27.96°	
Index ranges		$-13<h<13$, $-14<k<15$, $0<l<15$	
Reflections collected		6817	
Independent reflections		6509 ($R_{int}=0.0117$)	
Data/restraints/parameters		5693/0/405	
Largest difference peak and hole (e/Å^3)		0.379/−0.350	

[a] $R=\Sigma\|F_o|-|F_c|/\Sigma|F_o|$.
[b] $R_w=[\Sigma[w(F_o^2-F_c^2)^2]/\Sigma[w(F_o^2)^2]]1/2$.
[c] $S=\Sigma[[w(F_o^2-F_c^2)^2]/(n-p)]1/2$; $w=1/[\sigma^2F_o^2+(0.0722P)+0.15P]$; $P=(\max(F_o^2+2F_c^2))/3$.
n = number of observations; p = number of parameters.

Table 3. Selected bond distances (Å) for $[Mn^{II}(DMF)_4(H_2O)_2][Cu^{III}(qdt)_2]_2$

Mn(1)–O(1)	2.145 (2)	Mn(1)–O(2)	2.182 (2)
Mn(1)–O(3)	2.156 (2)		
O(1)–C(1A)	1.228 (4)	C(1A)–N(1A)	1.300 (4)
N(1A)–C(2A)	1.438 (5)	N(1A)–C(3A)	1.458 (6)
O(2)–C(1B)	1.235 (3)	C(1B)–N(1B)	1.305 (3)
N(1B)–C(2B)	1.447 (4)	N(1B)–C(3B)	1.454 (4)
Cu(1)–S(1)	2.1901 (7)	Cu(1)–S(2)	2.1823 (7)
Cu(1)–S(3)	2.1782 (7)	Cu(1)–S(4)	2.1843 (7)
S(1)–C(2)	1.738 (2)	S(2)–C(1)	1.744 (3)
S(3)–C(10)	1.747 (2)	S(4)–C(9)	1.742 (3)
C(1)–N(1)	1.302 (3)	C(1)–C(2)	1.443 (3)
C(2)–N(2)	1.307 (3)	N(1)–C(3)	1.370 (3)
N(2)–C(4)	1.372 (3)	C(3)–C(5)	1.406 (4)
C(3)–C(4)	1.413 (3)	C(4)–C(6)	1.404 (4)
C(5)–C(7)	1.367 (4)	C(6)–C(8)	1.373 (4)
C(7)–C(8)	1.400 (4)	C(9)–N(3)	1.309 (3)
C(9)–C(10)	1.434 (3)	C(10)–N(4)	1.299 (3)
N(3)–C(12)	1.375 (3)	N(4)–C(11)	1.370 (3)
C(11)–C(13)	1.406 (4)	C(11)–C(12)	1.410 (3)
C(12)–C(14)	1.406 (4)	C(13)–C(16)	1.365 (4)
C(14)–C(15)	1.362 (4)	C(15)–C(16)	1.402 (4)

(that necessarily contain the manganese atoms), and the two oxygen atoms of the water molecules. The $(H_2)O$–Mn–$O(H_2)$ axis is almost orthogonal to the former equatorial plane (87.90°). This plane defined by the four O atoms of DMF bonded to the Mn atom and the plane defined by the anions, are roughly parallel to the *bc* plane.

The DMF ligand is planar and the intramolecular bond lengths and angles are in good agreement with those found in other DMF metal-bonded complexes: $[Ni(DMF)_6][ClO_4]_2$ [24], $[Fe(DMF)_6][ClO_4]_2$ [25, 26] or $[Fe(DMF)_6][ClO_4]_3$ [27], for instance. The conformation of the two kinds of DMF molecules are different, as denoted by the different angles between their plane and the plane MnO_4 (O = oxygen from DMF) or the different dihedral angles between the carbonyl bond of one DMF ligand and the Mn–O bonds of the remaining ligands. The interaction between the H atoms of the methyl groups of the DMF ligands and the sulphur atoms may play a significant role in the determination of the different conformations. The torsion angles are 150.0(3)° (O3–Mn–O1–C1A) and 1.0(2)° (O3–Mn–O2–C1B).

Interactions between the anionic and cationic species exist, as denoted by several N···H and S···H contacts below or in the range of the sum of the van der Waals radii. Each $[Mn^{II}(DMF)_4(H_2O)_2]^{2+}$ cation is connected to four neighbouring anions by hydrogen bonding between the water ligand and the nitrogen of the pyrazine ring of the qdt ligand at the distances: O–H···N (O(3)–H···N(3)′, 2.80 Å; O(3)–H·N(2)′, 2.82 Å. On the other hand, each $[Cu^{III}(qdt)_2]^-$ anion interacts with two cations. S···H interactions contact the thiolate function with the one hydrogen of the methylene group (CH_3) of the DMF (S(2)···H(3C)′, 2.92 Å). If we consider this network of hydrogen bonds, the structure can be described as layers of ''sandwiches'' composed by two sheets of $[Cu^{III}(qdt)_2]^-$ anions surrounding one sheet of

Table 4. Selected angles (°) for $[Mn^{II}(DMF)_4(H_2O)_2][Cu^{III}(qdt)_2]_2$

O(1)–Mn(1)–O(3)	90.70 (9)	O(1)–Mn(1)–O(2)	88.54 (8)
O(2)–Mn(1)–O(3)	93.56 (7)		
C(1A)–O(1)–Mn(1)	125.7 (2)	O(1)–C(1A)–N(1A)	123.8 (3)
C(1A)–N(1A)–C(2A)	122.3 (4)	C(1A)–N(1A)–C(3A)	119.9 (3)
C(2A)–N(1A)–C(3A)	117.5 (4)	C(1B)–O(2)–Mn(1)	124.6 (2)
O(2)–C(1B)–N(1B)	124.8 (3)	C(1B)–N(1B)–C(2B)	121.5 (3)
C(1B)–N(1B)–C(3B)	122.0 (3)	C(2B)–N(1B)–C(3B)	116.6 (3)
S(1)–Cu(1)–S(2)	92.53 (3)	S(1)–Cu(1)–S(3)	87.54 (3)
S(1)–Cu(1)–S(4)	172.89 (3)	S(2)–Cu(1)–S(3)	177.72 (3)
S(2)–Cu(1)–S(4)	87.89 (3)	S(3)–Cu(1)–S(4)	92.32 (3)
C(2)–S(1)–Cu(1)	104.09 (8)	C(1)–S(2)–Cu(1)	104.10 (8)
C(10)–S(3)–Cu(1)	104.60 (9)	C(9)–S(4)–Cu(1)	104.26 (9)
N(1)–C(1)–C(2)	122.3 (2)	N(1)–C(1)–S(2)	118.2 (2)
C(2)–C(1)–S(2)	119.5 (2)	N(2)–C(2)–C(1)	121.3 (2)
N(2)–C(2)–S(1)	119.1 (2)	C(1)–C(2)–S(1)	119.6 (2)
C(1)–N(1)–C(3)	117.1 (2)	C(2)–N(2)–C(4)	117.6 (2)
N(1)–C(3)–C(5)	119.3 (2)	N(1)–C(3)–C(4)	121.0 (2)
C(5)–C(3)–C(4)	119.7 (2)	N(2)–C(4)–C(6)	119.9 (2)
N(2)–C(4)–C(3)	120.6 (2)	C(6)–C(4)–C(3)	119.5 (2)
C(7)–C(5)–C(3)	119.6 (3)	C(8)–C(6)–C(4)	119.8 (3)
C(5)–C(7)–C(8)	120.9 (3)	C(6)–C(8)–C(7)	120.5 (3)
N(3)–C(9)–C(10)	121.3 (2)	N(3)–C(9)–S(4)	118.9 (2)
C(10)–C(9)–S(4)	119.8 (2)	N(4)–C(10)–C(9)	122.8 (2)
N(4)–C(10)–S(3)	118.2 (2)	C(9)–C(10)–S(3)	119.0 (2)
C(9)–N(3)C(12)	117.1 (2)	C(10)–N(4)C(11)	116.9 (2)
N(4)–C(11)C(13)	119.6 (2)	N(4)–C(11)C(12)	120.8 (2)
C(13)–C(11)C(12)	119.6 (2)	N(3)–C(12)C(14)	119.7 (2)
N(3)–C(12)C(11)	120.9 (2)	C(14)–C(12)C(11)	119.4 (2)
C(16)–C(13)C(11)	119.9 (3)	C(15)–C(14)C(12)	119.8 (3)
C(14)–C(15)C(16)	121.1 (3)	C(13)–C(16)C(15)	120.3 (3)

$[Mn^{II}(DMF)_4(H_2O)_2]^{2+}$ cations. This situation resembles the $(PPh_4)_2[Mo^{IV}(qdt)_3]$ structure, where the $[Mo^{IV}(qdt)_3]^{2-}$ anions are linked by hydrogen bonding via the quinoxaline nitrogen atoms through water molecules (distances N···O, 3.6 Å) [10] and a similar network is found in $(NEt_4)_2[Ni(qdt)_2]\cdot 2H_2O$ [28].

CONCLUSION

In the present work we showed the possibility of obtaining compounds containing $M(qdt)_2$ complexes and a second metal. However, for getting the latter metal co-ordinated to the outer sphere of the quinoxaline ring further work is necessary in order to eliminate competition from the co-ordinating power of solvents.

Supplementary material available

Complete lists of atomic coordinates, bond parameters and tables of thermal parameters and hydrogen atom coordinates have been deposited at the Cambridge Crystallographic Data Centre (CCDC, deposition number 101599) and are available from the authors on request (21 pages).

Acknowledgements—This work was partially supported by the Human Capital and Mobility Program of the European Union (J. A. A., contract number CHRX-CT93-0148) and by Fundação para a Ciência e a Tecnologia under contract PRAXIS/2/2.1/QUI/203/94.

REFERENCES

1. Rignedoli, A., Peyronel, G. and Malavasi, W., *J. Inorg. Nucl. Chem.*, 1963, **1976,** 38.
2. Theriot, L. J., Ganguli, K. K., Kavarnos, S. and Bernal, I., *J. Inorg. Nucl. Chem.*, 1969, **31,** 3133.
3. Ganguli, K. K., Carlisle, G. O., Hu, H. J., Theriot, L. J. and Bernal, I., *J. Inorg. Nucl. Chem.*, 1971, **33,** 79.
4. Dalziel, J. A. W., Donaldson, J. D., Mehtta, B. D. and Tricker, M. J., *J. Inorg. Nucl. Chem.*, 1973, **35,** 811.
5. Boyde, S., Garner, C. D. and Clegg, W., *J. Chem. Soc. Dalton Trans.*, 1987, 1083.

6. Mukhopadhyay, S. and Ray, D., *J. Chem. Soc. Dalton Trans*., 1993, 1159.
7. Burke, R. W. and Deardoff, E. R., *Talanta*, 1970, **17,** 255.
8. Ryabushko, O. P., Pilipenko, A. T., Batkovskaya, L. A. and Savin, Y. S., *Ukr. Khim. Zh*., 1988, **54,** 1172.
9. Boyde, S., Garner, C. D., Enemark, J. H. and Ortega, R. C., *Polyhedron*, 1986, **5,** 377.
10. Boyde, S., Garner, C. D., Enemark, J. H. and Ortega, R. B., *J. Chem. Soc. Dalton Trans*., 1987, 297.
11. Boyde, S., Garner, C. D., Enemark, J. H., Bruck, M. A. and Kristofzski, J. G., *J. Chem. Soc. Dalton Trans*., 1987, 2267.
12. Cummings, S. D. and Eisenberg, R., *Inorg. Chem*., 1995, **34,** 2007.
13. Cummings, S. D. and Eisenberg, R., *Inorg. Chem*., 1995, **34,** 3396.
14. McCleverty, J. A., in *Progress in Inorganic Chemistry*, Vol. 10, ed. F. A. Cotton. Interscience, New York, 1968, p. 49.
15. Burns, R. D. and McAuliffe, C. A., in *Advances in Inorganic Chemistry and Radiochemistry*, Vol. 22, ed. H. J. Emeleus and A. G. Sharpe. Academic Press, London, 1979, p. 303.
16. Corbin, D. R., Francesconi, L. C., Hendrickson, D. N. and Stucky, G. D., *Inorg. Chem*., 1981, **20,** 2084.
17. Bunker, B. C., Drago, R. S., Hendrickson, D. W., Kessel, S. L. and Richman, R., *J. Am. Chem. Soc*., 1978, **100,** 3805.
18. Hush, N. S., Edgar, A. and Beattie, J. K., *Chem. Phys. Lett*., 1980, **69,** 128.
19. Sheldrick, G. M., *SHELX* 86, *Program for Crystal Structure Solution*. University of Göttingen, 1986.
20. Sheldrick, G. M., *SHELX* 93, *Program for Crystal Structure Solution*. University of Göttingen, 1993.
21. Kahn, O., *Molecular Magnetism*. VCH Pub., NY, 1993.
22. Bull, W. E., Madan, S. K. and Willis, J. E., *Inorg. Chem*., 1963, **2,** 303.
23. Santos, I. C., Ayllón, J. A., Henriques, R. T., Almeida, M., Alcacer, L. and Duarte, M. T., *Acta Cryst. C*, 1997, **53,** 1764.
24. Mckee, V., Metcalfe, T. and Wikaira, J., *Acta Cryst. C*, 1996, **52,** 1139.
25. Baumgartner, O., *Z. Kristallogr*., 1986, **174,** 253–263.
26. Young, A. C. M., Walters, M. A. and Dewan, J. C., *Acta Cryst. C*, 1989, **45,** 1733.
27. Holt, E. M., Alcock, N. W., Sumner, R. H. and Asplund, R. O., *Cryst. Struct. Commun*., 1979, **8,** 255.
28. Pignedoli, A., Peyronel, G. and Antolini, L., *Acta Cryst. B*, 1974, **30,** 2181.
29. Johnson, C. K., *ORTEP II*. Report ORNL-5138. Oak Ridge National Laboratory, Oak Ridge, TN, 1976.

Pergamon

Polyhedron Vol. 17, No. 23–24, pp. 4033–4039, 1998
© 1998 Elsevier Science Ltd
All rights reserved. Printed in Great Britain
0277–5387/98 $19.00+0.00

PII: S0277-5387(98)00205-8

Comparative X-ray crystallographic characterization of the mono- and bimetallic complexes of rhenium(I) tricarbonyl chloride with 2,3-bis(2-pyridyl)pyrazine

J.R. Kirchhoff* and K. Kirschbaum

Department of Chemistry, The University of Toledo, Toledo, OH 43606, U.S.A.

(Received 8 February 1998; accepted 3 May 1998)

Abstract—Comparative X-ray crystallographic characterization of $[Re(dpp)(CO)_3Cl]$ and $[Re(CO)_3Cl]_2dpp$, where dpp is 2,3-bis(2-pyridyl)pyrazine, has been conducted to examine the structural consequences resulting from sequential coordination of two $[Re(CO)_3Cl]$ molecular fragments to dpp. Addition of one metal center results in the coordinating portion of dpp adopting a relatively planar configuration. The dihedral angle between the pyrazine ring and the coordinated N(1)-pyridyl ring is 15.3(4)°, while the dihedral angle between the pyrazine ring and the uncoordinated N(2)-pyridyl ring is 45.8(3)°. The dpp ligand in the bimetallic complex is found to twist to accommodate the second metal center as manifested by a two-fold increase in the N(1)-pyridyl and pyrazine dihedral angle [29.7(4)°] and a decrease for the N(2)-pyridyl and pyrazine dihedral angle [31.6(3)°]. The direct structural consequence is an increase in the distortion of the central pyrazine moiety upon addition of each $[Re(CO)_3Cl]$ fragment. This observation confirms previously reported spectroscopic results that inferred the differences in electronic structure between $[Re(dpp)(CO)_3Cl]$ and $[Re(CO)_3Cl]_2dpp$ were due to the dpp ligand adopting a nonplanar geometry in the bimetallic complex. © 1998 Elsevier Science Ltd. All rights reserved

Keywords: rhenium; X-ray crystallography; 2,3-bis(2-pyridyl)pyrazine; bimetallic complexes.

INTRODUCTION

The photochemical and photophysical properties of metal-to-ligand charge-transfer (MLCT) excited state(s) of complexes of the type $[Re(NN)(CO)_3X]$, where NN is a chelating α,α′-diimine ligand and X is for example a halide, MeCN, PhCN, pyridine, piperidine, $SnPh_3$, $GePh_3$, have attracted significant attention since the initial characterization of the luminescence properties by Wrighton and co-workers [1–3] and the demonstration that $[Re(bpy)(CO)_3X]$ (bpy = 2,2′-bipyridine; X = Cl, Br) complexes acted as combination photosensitizers and electrocatalysts for the reduction of CO_2 to CO [4–11].

A recent aspect of transition metal photochemistry has focused on the characterization of multimetallic or supramolecular complexes as multielectron redox reagents or models for intermolecular electron-transfer [12, 13]. One approach to the design and development of supramolecular complexes utilizes a multidentate bridging ligand as a template to which monometallic molecular fragments are attached to build the multimetallic system. For example in rhenium(I) systems the neutral molecular fragment, $[Re(CO)_3Cl]$, has been exploited to build bimetallic complexes around a variety of α,α′-diimine based bridging ligands (BL) [14–24]. Interestingly, monometallic complexes such as $[Re(BL)(CO)_3Cl]$ with bidentate BL ligands are in general emissive in fluid solution while emission from the bimetallic counterparts, $[Cl(CO)_3Re(BL)Re(CO)_3Cl]$, is rarely observed.[1] In contrast, bimetallic rhenium(I) complexes of the type $[(NN)(CO)_3Re(BL')Re(CO)_3(NN)]$,

[1] Emissive bimetallic complexes of this type have been reported for $[Re(CO)_3Br]_2QP$ (QP = 5,5′,3″,5‴-tetramethyl-2,2′:6′,2″:6″2‴-quaterpyridine) [15], $[Re(CO)_3Cl]_2$Mebpy-Mebpy (Mebpy-Mebpy = 1,2-bis(4′-methyl-2,2′-bipyridyl-4-yl)ethane) [19] and $[Re(CO)_3(CH_3CN)]_2ppz$ (ppz = 4′7′-phenanthrolino-5′6′:5,6-pyrazine) [24].

* Author to whom correspondence should be addressed.

where BL′ links the metal centers by unidentate coordination to each metal center, have been found to be highly emissive in fluid solution [25–30]. The photophysical behavior of these rhenium(I) complexes has been rationalized by a model invoking the energy gap law [20–22, 24–29]. However, it has been recently noted that this model may be oversimplified in some cases and the extent of delocalization of the excited electron and the rigidity of the acceptor ligand should also be considered [31].

For bimetallic complexes of the type $[Cl(CO)_3Re(BL)Re(CO)_3Cl]$, the loss of emission as compared to the monometallic complexes has been described as due to the lowering of the energy of the π^* orbitals on the bridging ligand, which is manifested by the structural changes required to accommodate the addition of a second $[Re(CO)_3Cl]$ fragment [16, 19–22, 24]. In particular, comparative NMR studies of monometallic and bimetallic $[Re(CO)_3Cl]$ complexes with dpp (2,3-bis(2-pyridyl)pyrazine) and ppz (4′7′-phenanthrolino-5′,6′:5,6-pyrazine) as bridging ligands have suggested that the coordinating part of dpp adopts a planar geometry in the monometallic complex while the bimetallic complex requires a puckered or twisted arrangement in order to incorporate the second metal center [19, 24]. In this report, X-ray crystallographic analysis of $[Re(dpp)(CO)_3Cl]$ and $[Re(CO)_3Cl]_2dpp$ has been used to directly examine the structural consequences that result upon the addition of a second $[Re(CO)_3Cl]$ subunit to $[Re(dpp)(CO)_3Cl]$.

EXPERIMENTAL

Materials

$[Re(dpp)(CO)_3Cl]$ and $[Re(CO)_3Cl]_2dpp$ were prepared from $Re(CO)_5Cl$ (Aldrich) and dpp (Aldrich) by slight modification of literature procedures [3, 17]. All other reagents were of ACS grade and used without further purification. X-ray quality crystals were obtained by slow evaporation of a methanol solution of each complex.

Crystallographic determination of $[Re(dpp)(CO)_3Cl]$

A pyramidal-shaped orange–red crystal of $[Re(dpp)(CO)_3Cl]$ with approximate dimensions of $0.20 \times 0.20 \times 0.08$ mm was mounted on a fine glass fiber with glue. Preliminary examination and data collection were carried out at room temperature on a Siemens SMART Platform diffractometer. Intensity data were collected using 0.3° ω-scans at three different ϕ-settings corresponding to a nominal hemisphere of data. The cell constants were obtained from the setting angles of 4873 reflections in the range $4^\circ < \theta < 27^\circ$. The intensities of 6317 reflections with $2\theta < 60^\circ$ were corrected for absorption (semi-empirical, ψ-scans). Equivalent reflections were averaged, and the remaining 4352 unique reflections were used for further calculations. The structure was solved by direct methods (SHELXS-86) [32]. All non-hydrogen atoms were refined with anisotropic thermal parameters by full matrix least-squares on F^2 using all unique data (SHELXL-93) [33]. The hydrogen atoms were calculated on idealized positions ($CH_{ar.} = 0.93$ Å, $U_H = 1.2 \times U_C$) and included in the refinements as riding atoms.

Crystallographic determination of $[Re(CO)_3Cl]_2dpp$

A column-shaped red crystal of $[Re(CO)_3Cl]_2dpp$ with approximate dimensions of $0.33 \times 0.20 \times 0.15$ mm was mounted on a glass fiber with glue. Data collection was conducted at room temperature on an Enraf-Nonius CAD4 diffractometer with the ω–2θ scan technique to a maximum 2θ of 52°. The cell constants and an orientation matrix for data collection were obtained from the setting angles of 25 reflections in the range $10^\circ < \theta < 14^\circ$. A total of 5066 reflections were measured and 4809 were found to be unique. Anisotropic decay and semi-empirical absorption (ψ-scan) corrections were applied to the data set; equivalent reflections were averaged. 3906 reflections met the condition $F_o^2 > 3.0\sigma(F_o^2)$ and were used for further calculations. A starting model for the structure was provided by direct methods with MULTAN [34] and further developed to a final structure model with anisotropic thermal parameters for non-hydrogen atoms and isotropic thermal parameters for hydrogen atoms. Refinement was accomplished by the full-matrix least-squares technique on F using all observed data [35].

A summary of the crystal data for both complexes is given in Table 1. Selected bond distances, bond angles and torsion angles are given in Tables 2–4, respectively.

RESULTS AND DISCUSSION

The ORTEP diagrams of $[Re(dpp)(CO)_3Cl]$ and $[Re(CO)_3Cl]_2dpp$ with the atom numbering schemes are shown in Figs. 1 and 2. The local coordination geometry about each rhenium(I) metal center in both complexes can be described as a distorted octahedron. In $[Re(CO)_3Cl]_2dpp$, two $[Re(CO)_3Cl]$ molecular fragments are linked by the dpp bridging ligand through bidentate nitrogen chelation. An approximate C_2 axis bisects the pyrazine ring between C(6) and C(9) with no significant differences between the corresponding bond distances and angles in each half of the molecule. The distortion from octahedral coordination geometry is evident from the significant reduction of the N–Re–N angles from 90° in the idealized polyhedron to $74.5(2)^\circ$ in $[Re(dpp)(CO)_3Cl]$, and $75.1(2)^\circ$ and $75.3(2)^\circ$ in $[Re(CO)_3Cl]_2dpp$, which results from the small bite angles of the dpp ligand. The *trans* angles about rhenium in the monometallic and bimet-

Table 1. Summary of crystal data for $[Re(dpp)(CO)_3Cl]$ and $[Re(CO)_3Cl]_2dpp$

	$[Re(dpp)(CO)_3Cl]$	$[Re(CO)_3Cl]_2dpp$
Formula	$ReC_{17}H_{10}N_4O_3Cl$	$Re_2C_{20}H_{10}N_4O_6Cl_2$
Formula weight	539.94	845.63
Crystal system	monoclinic	monoclinic
a (Å)	6.5802(1)	10.985(4)
b (Å)	17.4273(2)	18.849(5)
c (Å)	7.8027(2)	11.794(4)
β (deg)	100.400(1)	103.87(3)
V (Å^3)	880.08(3)	2371(3)
Space group	$P2_1$	$P2_1/n$
Z	2	4
ρ_{calcd} (g/cm^3)	2.038	2.37
μ (Mo Kα) (mm^{-1})	7.080	10.61
Radiation λ (Å)	Mo Kα, 0.71073	Mo Kα, 0.71073
Refinement	F^2, all data	F (3906 refl. with $I>3\sigma(I)$)
$R_1(F)$[a], observed data	0.0269 (4073 refl. with $I > 2\sigma(I)$)	0.033 (3906 refl. with $I > 3\sigma(I)$)
$R_1(F)$[a], all data	0.0312	0.045
$wR_1(F)$[b], observed data	n.a.	0.042
$wR_2(F^2)$[c], all data	0.0609	n.a.
$S(F)$[d]	n.a.	1.45 (3906 refl. with $I > 3\sigma(I)$)
$S(F^2)$[e], all data	1.125	n.a.

[a] $R_1(F) = \Sigma\|F_o|-|F_c\|/\Sigma|F_o|$.
[b] $wR_1(F) = [\Sigma w(|F_o|-|F_c|)^2/\Sigma w|F_o|^2]^{1/2}$.
[c] $wR_2(F^2) = [\Sigma w(F_o^2-F_c^2)^2/\Sigma w(F_o^2)^2]^{1/2}$.
[d] $S(F) = [\Sigma w(|F_o|-|F_c|)^2/(N_{data}-N_{parameter})]^{1/2}$.
[e] $S(F^2) = [\Sigma w(F_o^2-F_c^2)^2/(N_{data}-N_{parameter})]^{1/2}$.

Table 2. Selected bond distances (Å) for $[Re(dpp)(CO)_3Cl]$ and $[Re(CO)_3Cl]_2dpp$

Atom 1	Atom 2	$[Re(dpp)(CO)_3Cl]$	$[Re(CO)_3Cl]_2dpp$
Re(1)	Cl(1)	2.478(2)	2.478(2)
Re(1)	N(1)	2.178(5)	2.176(5)
Re(1)	N(4)	2.175(5)	2.152(6)
Re(1)	C(15)	1.906(8)	1.925(8)
Re(1)	C(16)	1.925(8)	1.911(7)
Re(1)	C(17)	1.912(7)	1.908(7)
Re(2)	Cl(2)		2.473(2)
Re(2)	N(2)		2.171(6)
Re(2)	N(3)		2.155(6)
Re(2)	C(18)		1.902(6)
Re(2)	C(19)		1.926(7)
Re(2)	C(20)		1.918(8)
N(1)	C(1)	1.343(7)	1.349(9)
N(1)	C(5)	1.359(7)	1.345(9)
N(2)	C(14)	1.349(9)	1.323(9)
N(2)	C(10)	1.352(8)	1.368(9)
N(3)	C(8)	1.323(9)	1.332(8)
N(3)	C(9)	1.361(8)	1.368(8)
N(4)	C(6)	1.366(7)	1.373(8)
N(4)	C(7)	1.334(7)	1.327(8)
C(9)	C(10)	1.497(9)	1.459(9)
C(6)	C(5)	1.483(7)	1.466(9)

allic complexes range from 171.2(3)° to 179.4(2)° and from 172.1(2)° to 174.8(2)°, respectively. The carbonyl groups assume a *fac* geometry about the metal center in both complexes with an average Re–CO bond distance of 1.914(8) Å ($n = 3$) and 1.915(7) Å ($n = 6$). The average Re–Cl distance is 2.476(2) Å for $[Re(CO)_3Cl]_2dpp$ as compared to 2.478(2) Å for $[Re(dpp)(CO)_3Cl]$. In the monometallic complex the pyridyl and pyrazine Re–N distances are essentially identical with an average distance of 2.177(5) Å ($n = 2$), while in the bimetallic complex the average Re–N distance is 2.164(6) Å ($n = 4$) with the pyridyl Re–N distances slightly longer than the pyrazine Re–N distances. These observed values are in the range for Re-ligand distances and angles in related structurally characterized $[Re(NN)(CO)_3X]$ complexes [29, 30, 36–48].

Sequential addition of $[Re(CO)_3Cl]$ molecular fragments to dpp produces several interesting structural effects. Huang *et al*. have determined the structure of the uncoordinated dpp ligand and found the average deviation from planarity for the pyrazine and pyridine moieties to be only 0.007 and 0.001 Å, respectively [49]. In addition, the pyridyl groups in the free ligand rotate about the C(9)–C(10) and the C(5)–C(6) axes to alleviate a potential steric interaction between H(11) and H(4) [50]. Consequently, dihedral angles of 42.2° between the pyrazine and pyridyl rings are

Table 3. Selected bond angles (deg) for $[Re(dpp)(CO)_3Cl]$ and $[Re(CO)_3Cl]_2dpp$

Atom 1	Atom 2	Atom 3	$[Re(dpp)(CO)_3Cl]$	$[Re(CO)_3Cl]_2dpp$
Cl(1)	Re(1)	N(1)	84.00(13)	82.3(1)
Cl(1)	Re(1)	N(4)	83.94(13)	82.3(1)
Cl(1)	Re(1)	C(15)	90.5(3)	92.2(2)
Cl(1)	Re(1)	C(16)	179.4(2)	174.8(2)
Cl(1)	Re(1)	C(17)	92.8(2)	95.7(2)
N(1)	Re(1)	N(4)	74.5(2)	75.1(2)
N(1)	Re(1)	C(15)	98.1(3)	98.6(3)
N(1)	Re(1)	C(16)	95.9(2)	92.9(2)
N(1)	Re(1)	C(17)	173.2(2)	172.6(3)
N(4)	Re(1)	C(15)	171.2(3)	172.1(2)
N(4)	Re(1)	C(16)	95.4(2)	94.7(3)
N(4)	Re(1)	C(17)	99.2(2)	97.6(3)
C(15)	Re(1)	C(16)	90.1(3)	90.4(3)
C(15)	Re(1)	C(17)	87.9(3)	88.6(3)
C(16)	Re(1)	C(17)	87.2(3)	88.8(3)
Cl(2)	Re(2)	N(2)		82.5(1)
Cl(2)	Re(2)	N(3)		81.9(1)
Cl(2)	Re(2)	C(18)		172.8(2)
Cl(2)	Re(2)	C(19)		98.6(2)
Cl(2)	Re(2)	C(20)		93.0(2)
N(2)	Re(2)	N(3)		75.3(2)
N(2)	Re(2)	C(18)		90.5(3)
N(2)	Re(2)	C(19)		173.4(3)
N(2)	Re(2)	C(20)		99.1(3)
N(3)	Re(2)	C(18)		94.8(3)
N(3)	Re(2)	C(19)		98.4(3)
N(3)	Re(2)	C(20)		172.9(3)
C(18)	Re(2)	C(19)		88.3(3)
C(18)	Re(2)	C(20)		89.6(3)
C(19)	Re(2)	C(20)		87.3(3)

Table 4. Selected torsion angles (deg) for $[Re(dpp)(CO)_3Cl]$ and $[Re(CO)_3Cl]_2dpp$

	$[Re(dpp)(CO)_3Cl]$	$[Re(CO)_3Cl]_2dpp$
N(1)–pyridyl–pyrazine	15.3(4)	29.7(4)
N(2)–pyridyl–pyrazine	45.8(3)	31.6(3)
N(1)–C(5)–C(6)–N(4)	10.6(9)	−20.5(8)
N(2)–C(10)–C(9)–N(3)		−15.6(8)
Cl(1)–Re(1)–Re(2)–C(18)		−42.3(2)

observed. Addition of one $[Re(CO)_3Cl]$ fragment locks in bidentate coordination through the N(1)-pyridyl and N(4)-pyrazine atoms and reduces the dihedral angle between these two rings to 15.3(4)°. In contrast, the uncoordinated N(2)-pyridyl ring maintains a dihedral angle with respect to the pyrazine ring of 45.8(3)°. Concomitantly, the corresponding torsion angle in $[Re(dpp)(CO)_3Cl]$ is found to be +10.6(9)° as compared to a torsion angle of 136.1° in the free ligand [49]. In related $[Re(NN)(CO)_3X]$ complexes, where NN is 2,2′-bipyridine [29, 30, 39, 41, 43], 2,2′-bipyrimidine [42] and η^2-2,2′:6′,2″-terpyridine [45–47], the analogous torsion angle ranges from −3.3° to +9.83°. In all cases bidentate coordination of a NN-based ligand with one $[Re(CO)_3Cl]$ fragment drives the coordinating part of the NN ligand toward planarity.

Coordination of the second $[Re(CO)_3Cl]$ fragment to $[Re(dpp)(CO)_3Cl]$ reverses this trend. To accommodate both metal centers in a stable complex, the pyridyl rings twist in opposite directions. This causes an increase in the dihedral angle between the N(1)-pyridyl and the pyrazine ring [29.7(4)°] and a decrease

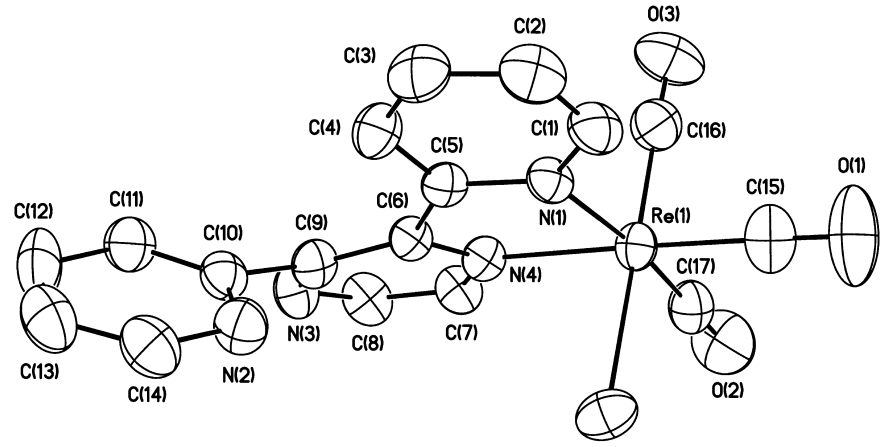

Fig. 1. ORTEP diagram of $[Re(dpp)(CO)_3Cl]$ showing 50% probability ellipsoids.

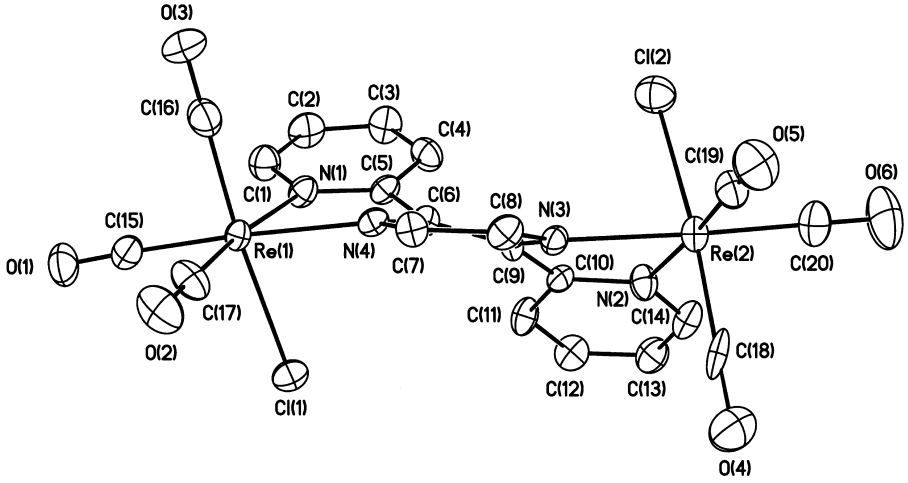

Fig. 2. ORTEP diagram of $[Re(CO)_3Cl]_2dpp$ showing 50% probability ellipsoids.

for the dihedral angle between the N(2)-pyridyl and the pyrazine ring [31.6(3)°]. A further consequence of the increased twist of the dpp ligand in the bimetallic complex is seen in the Cl(1)–Re(1)–Re(2)–C(18) torsion angle [−42.3(2)°]. Thus, looking down the axis defined by the Re(1) and Re(2) atoms, the ligands on the $[Re(CO)_3Cl]$ fragments are arranged in a staggered configuration. The deviation from planar coordination is also demonstrated by the larger torsion angles in $[Re(CO)_3Cl]_2dpp$ in comparison to $[Re(dpp)(CO)_3Cl]$: N(2)–C(10)–C(9)–N(3), −15.6(8)°; N(1)–C(5)–C(6)–N(4), −20.5(8)°. This is further manifested by the shortening of the N(3)- and N(4)-pyrazine to Re bond lengths in the bimetallic complex, and the observation that Re(1) and Re(2) are located −0.462 and 0.376 Å from the best plane defined by the atoms of the central pyrazine ring in comparison to 0.255(9) Å for Re(1) in $[Re(dpp)(CO)_3Cl]$. Bimetallic coordination also brings into play the potential steric interaction of H(11) and H(4) on the pyridyl rings. The X-ray structure for $[Re(CO)_3Cl]_2dpp$ is consistent with the theoretical description necessary to achieve a stable bimetallic complex with a bridging dpp ligand [50]. The calculated H(11) ⋯ H(4) distances are 3.72 Å in $[Re(dpp)(CO)_3Cl]$ and 3.01 Å in $[Re(CO)_3Cl]_2dpp$, which are both well above the minimum theoretical distance of 1.8 Å [50].

Of particular interest are the localized structural distortions that occur within the central pyrazine ring of dpp upon metal coordination. In comparison to the free ligand (0.007 Å) [49], the average deviation from planarity for a single atom in the pyrazine moiety increases to 0.037(5) Å in $[Re(dpp)(CO)_3Cl]$ and to 0.062(6) Å in $[Re(CO)_3Cl]_2dpp$. The largest deviations from planarity within the pyrazine ring occur at C(6) and C(9): $[Re(dpp)(CO)_3Cl]$, C(6) −0.060(4) Å; C(9) 0.053(4) Å and $[Re(CO)_3Cl]_2dpp$, C(6) 0.101(6) Å; C(9) −0.108(6) Å. Coordination of the metal centers clearly requires the dpp ligand to twist, which induces a buckling of the pyrazine ring (Fig. 2). In contrast, the

planarity for the pyridyl rings is only slightly changed upon metal coordination as are the internal bond distances and angles within dpp.

The X-ray structures of $[Re(dpp)(CO)_3Cl]$ and $[Re(CO)_3Cl]_2dpp$ provide direct and quantitative evidence of the degree to which the dpp ligand must twist to accommodate the second $[Re(CO)_3Cl]$ molecular fragment. This result confirms the previous NMR investigations of $[Re(CO)_3Cl]_2BL$ complexes and the resonance Raman study of $[Ru(dpp)(bpy)_2]^{2+}$ and $[(bpy)_2Ru]_2dpp^{4+}$ which inferred the dpp ligand in the bimetallic complexes requires a puckered or non-planar conformation to bind two metal centers [19, 24, 51]. The X-ray structures further reveal the most important structural consequences are borne by the central pyrazine ring as each metal center is added. It is reasonable to believe the structural distortion of the pyrazine ring is a major contributing factor that influences the electronic structure of $[Re(CO)_3Cl]_2dpp$ and results in the corresponding reduction in emission intensity and excited state lifetime relative to $[Re(dpp)(CO)_3Cl]$ [19, 20, 52]. Such structural distortions are most likely absent in bimetallic complexes with the planar ppz bridging ligand. As a result, room temperature emission has been observed in $[Re(CO)_3CH_3CN]_2ppz$ and has been attributed to a decrease in the nonradiative decay rates relative to the dpp bimetallic complex [24].

SUPPLEMENTARY MATERIAL AVAILABLE

Tables of the final values of all refined and calculated atomic coordinates with esd's and a complete listing of bond lengths, bond angles, anisotropic thermal parameters, and the structure factors are available as an X-ray crystallographic file in CIF format from the Cambridge Crystallographic Data Centre, 12 Union Road, Cambridge CB2 1EZ, U.K. by quoting the complete journal citation.

Acknowledgements—Financial support from the Donors of The Petroleum Research Fund, administered by the American Chemical Society (Grant No. 23968-G3), and The University of Toledo is gratefully acknowledged. Funding for the Ohio Crystallography Consortium at The University of Toledo from the College of Arts and Sciences and the Ohio Board of Regents is also acknowledged. We also thank Paul Szalay for the synthesis of $[Re(dpp)(CO)_3Cl]$ and David R. McMillin for helpful suggestions. We are also indebted to A. Alan Pinkerton for the use of his diffractometer, which was obtained with funding from The Department of Navy (Grant No. N00014-97-1-0409).

REFERENCES

1. Luong, J. C., Faltynek, R. A. and Wrighton, M. S., *J. Am. Chem. Soc.*, 1980, **102,** 7892.
2. Fredericks, S. M., Luong, J. C. and Wrighton, M. S., *J. Am. Chem. Soc.*, 1979, **101,** 7415.
3. Wrighton, M. S. and Morse, D. L., *J. Am. Chem. Soc.*, 1974, **96,** 998.
4. Hawecker, J., Lehn, J.-M. and Ziessel, R., *J. Chem. Soc., Chem. Commun.*, 1983, 536.
5. Hawecker, J., Lehn, J.-M. and Ziessel, R., *J. Chem. Soc., Chem. Commun.*, 1984, 328.
6. Hawecker, J., Lehn, J.-M. and Ziessel, R., *Helv. Chim. Acta*, 1986, **69,** 1990.
7. Kutal, C., Weber, M. A., Ferraudi, G. and Geiger, D., *Organometallics*, 1985, **4,** 2161.
8. Kutal, C., Corbin, A. J. and Ferraudi, G., *Organometallics*, 1987, **6,** 553.
9. Sullivan, B. P., Bolinger, C. M., Conrad, D., Vining, W. J. and Meyer, T. J., *J. Chem. Soc., Chem. Commun.*, 1985, 1414.
10. O'Toole, T. R., Margerum, L. D., Westmoreland, T. D., Vining, W. J., Murray, R. W. and Meyer, T. J., *J. Chem. Soc., Chem. Commun.*, 1985, 1416.
11. Johnson, F. P. A., George, M. W., Hartl, F. and Turner, J. J., *Organometallics*, 1996, **15,** 3374.
12. Scandola, F., Indelli, M. T., Chiorboli, C. and Bignozzi, C. A., *Top. Curr. Chem.*, 1990, **158,** 73.
13. Balzani, V. and Scandola, F., *Supramolecular Photochemistry*, Ellis Horwood, New York, 1991.
14. Vogler, A. and Kisslinger, J., *Inorg. Chim. Acta*, 1986, **115,** 193.
15. Juris, A., Campagna, S., Bidd, I., Lehn, J.-M. and Ziessel, R., *Inorg. Chem.*, 1988, **27,** 4007.
16. Sahai, R., Rillema, D. P., Shaver, R. J., Van Wallendael, S., Jackman, D. C. and Boldaji, M., *Inorg. Chem.*, 1989, **28,** 1022.
17. Ruminski, R. and Cambron, R. T., *Inorg. Chem.*, 1990, **29,** 1575.
18. Kalyanasundaram, K. and Nazeeruddin, M. K., *J. Chem. Soc., Dalton Trans.*, 1990, 1657.
19. Van Wallendael, S., Shaver, R. J., Rillema, D. P., Yoblinski, B. J., Stathis, M. and Guarr, T. F., *Inorg. Chem.*, 1990, **29,** 1761.
20. Baiano, J. A., Carlson, D. L., Wolosh, G. M., DeJesus, D. E., Knowles, C. F., Szabo, E. G. and Murphy, W. R. Jr., *Inorg. Chem.*, 1990, **29,** 2327.
21. Baiano, J. A. and Murphy, W. R. Jr., *Inorg. Chem.*, 1991, **30,** 4594.
22. Baiano, J. A., Kessler, R. J., Lumpkin, R. S., Munley, M. J. and Murphy, W. R. Jr., *J. Phys. Chem.*, 1995, **99,** 17690.
23. Kaim, W. and Kohlman, S., *Inorg. Chem.*, 1990, **29,** 2909.
24. Yoblinski, B. J., Stathis, M. and Guarr, T. F., *Inorg. Chem.*, 1992, **31,** 5.
25. Tapolsky, G., Duesing, R. and Meyer, T. J., *J. Phys. Chem.*, 1989, **93,** 3885.
26. Tapolsky, G., Duesing, R. and Meyer, T. J., *Inorg. Chem.*, 1990, **29,** 2285.
27. Lin, R. and Guarr, T. F., *Inorg. Chim. Acta*, 1990, **167,** 149.
28. Lin, R., Guarr, T. F. and Duesing, R., *Inorg. Chem.*, 1990, **29,** 4172.
29. Lin, R., Fu, Y., Brock, C. P. and Guarr, T. F., *Inorg. Chem.*, 1992, **31,** 4346.
30. Yam, V. W.-W., Lau, V. C.-Y. and Cheung, K.-K., *J. Chem Soc., Chem. Commun.*, 1995, 259.
31. Treadway, J. A., Loeb, B., Lopez, R., Anderson, P. A., Keene, F. R. and Meyer, T. J., *Inorg. Chem.*, 1996, **35,** 2242.
32. Sheldrick, G. M., *Acta Cryst. A*, 1990, **46,** 467.

33. Sheldrick, G. M., University of Göttingen, 1993.
34. Main, P., Fiske, S. J., Hull, S. E., Lessinger, L., Germain, G., Declercq, J. P. and Woolfson, M. M., MULTAN80. University of York, England, 1980.
35. Fair, C. K., *MolEN, An Interactive Intelligent System for Crystal Structure Analysis*. Enraf-Nonius, Delft, The Netherlands, 1990.
36. Tikkanen, W., Kaska, W. C., Moya, S., Layman, T. and Kane, R., *Inorg. Chim. Acta*, 1983, **76,** L29.
37. Wallace, L., Woods, C. and Rillema, D. P., *Inorg. Chem.*, 1995, **34,** 2875.
38. Connick, W. B., Di Bilio, A. J., Hill, M. G., Winkler, J. R. and Gray, H. B., *Inorg. Chim. Acta*, 1995, **240,** 169.
39. Horn, E. and Snow, M. R., *Aust. J. Chem.*, 1980, **33,** 2369.
40. Calabrese, J. C. and Tam, W., *Chem. Phys. Lett.*, 1987, **133,** 244.
41. Chen, P., Curry, M. and Meyer, T. J., *Inorg. Chem.*, 1989, **28,** 2271.
42. Winslow, L. N., Rillema, D. P., Welch, J. H. and Singh, P., *Inorg. Chem.*, 1989, **28,** 1596.
43. Guilhem, J., Pascard, C., Lehn, J.-M. and Ziessel, R., *J. Chem. Soc., Dalton Trans.*, 1989, 1449.
44. Moya, S. A., Guerrero, J., Pastene, R., Schmidt, R., Sariego, R., Sartori, R., Sanz-Aparicio, J., Fonseca, I. and Martínez-Ripoll, M. M., *Inorg. Chem.*, 1994, **33,** 2341.
45. Anderson, P. A., Keene, F. R., Horn, E. and Tiekink, R. T., *Appl. Organomet. Chem.*, 1990, **4,** 523.
46. Abel, E. W., Dimitrov, V. S., Long, N. J., Orrell, K. G., Osborne, A. G., Pain, H. M., Šik, V., Hursthouse, M. B. and Mazid, M. A., *J. Chem. Soc., Dalton Trans.*, 1993, 597.
47. Civitello, E. R., Dragovich, P. S., Karpishin, T. B., Novick, S. G., Bierach, G., O'Connell, J. F. and Westmoreland, T. D., *Inorg. Chem.*, 1993, **32,** 237.
48. Bardwell, D. A., Barigelletti, F., Cleary, R. L., Flamigni, L., Guardigli, M., Jeffrey, J. C. and Ward, M. D., *Inorg. Chem.*, 1995, **34,** 2438.
49. Huang, N.-T., Pennington, W. T. and Peterson, J. D., *Acta Cryst. C*, 1991, **47,** 2011.
50. Escuer, A., Vicente, R., Comas, T., Ribas, J., Gomez, M., Solans, X., Gatteschi, D. and Zanchini, C., *Inorg. Chim. Acta*, 1991, **181,** 51.
51. Knorrs, C., Gafney, H. D., Baker, A. D. and Braunstein, C., *J. Raman Spectrosc.*, 1983, **14,** 32.
52. Lee, Y. F., Kirchhoff, J. R., Berger, R. M. and Gosztola, D., *J. Chem. Soc., Dalton Trans.*, 1995, 3677.

Pergamon

Polyhedron Vol. 17, No. 23–24, pp. 4041–4048, 1998
© 1998 Elsevier Science Ltd
All rights reserved. Printed in Great Britain
PII: SS027-7538(79)80020-6X
0277–5387/98 $19.00+0.00

Crystal structures of the Ba–Cu(I) alkoxides $Ba_4Cu_6(O)(OCEt_3)_{12}$ and $BaCu_6(OCEt_3)_8$

Andrew P. Purdy* and Clifford F. George

Chemistry Division (Code 6120) and Laboratory for the Structure of Matter (Code 6030), Naval Research Laboratory, Washington, DC 20375, U.S.A.

(Received 22 December 1997; accepted 3 May 1998)

Abstract—A single crystal of the Ba–Cu(I) oxo-alkoxide $Ba_4Cu_6(O)(OCEt_3)_{12}$ (**1**) was isolated from the reaction of $Ba_2Cu_4(OCEt_3)_8$ (**2**) with oxygen. Oxo-alkoxide **1** crystallizes in the cubic space group I23 with the four Ba atoms distributed tetrahedrally around the central oxide ion and six $Cu(OCEt_3)_2^-$ units bridging each Ba atom to the three others. The Ba–Cu(I) alkoxides $[BaCu(OCEt_3)_3]_n$ (**3**) and $BaCu_6(OCEt_3)_8$ (**4**) were also synthesized. Crystals were not obtained for **3**, but the easily crystallized **4** has two $Cu_3(OCEt_3)_4^-$ moieties coordinated to a central Ba atom, and disproportionates in solution to many products. © 1998 Elsevier Science Ltd. All rights reserved. © 1998 Elsevier Science Ltd. All rights reserved

Keywords: heterometallic alkoxide; barium copper alkoxide; copper (I); oxide; oxo-alkoxide; disproportionation

INTRODUCTION

Heterometallic alkoxides are of interest as precursors to ceramic materials [1–3]. Although many such compounds have been characterized by X-ray crystallography, only a small number of structurally characterized bimetallic Cu(I) alkoxides are known. From the nine examples reported to date, some common structural features are apparent. In all such compounds, the Cu(I) atoms are 2-coordinate and nearly linear. Compounds can have $Cu(OR)_2^-$ ions, which typically bridge two metal atoms. Examples of this configuration include $Li_4Cu_4(OCMe_3)_8$ and $Na_4Cu_4(OCEt_3)_8$, [4] $L_2Ba_2Cu_4(OCRMe_2)_8$ ($L=Me_3PO$, Me_3NO; $R=CH_3$, CF_3) [5–7] and $(THF)_2Ba_2Cu_2(OCMe(CF_3)_2)_6$ [7]. Three examples of Cu_2O_3 moieties bridging two other metal atoms have also been reported, these include $Ba_2Cu_4(OCEt_3)_8$ [4], $Zr_2Cu_2(OCHMe_2)_{10}$ [8] and $Zr_4Cu_4(O)(OCHMe_2)_{18}$ [9]. In the former two compounds, a $Cu_2(OR)_3^-$ ion is the bridging unit and in the latter it is a $^-(RO)_2Cu_2OCu_2(OR)_2^-$ ion. In all except $L_2Ba_2Cu_4(OCRMe_2)_8$, the electropositive metal ($M=Li$, Na, Ba, Zr) is part of a $[M(OR)_n]_2$ ring structure. In this work we report the structures of two new Ba–Cu(I) alkoxides with $OCEt_3$ ligands that exhibit some new structural features. Thus we add to the knowledge base of how stoichiometery and identity of the R group affects the structure of mixed metal alkoxides.

EXPERIMENTAL

General comments

All manipulations were performed under a helium atmosphere in a Vacuum-Atmospheres Dri-Lab, in a Pyrex bulb equipped with a stirbar and a Kontes valve or on the vacuum line. Anhydrous ammonia (Air Products) was used as received. All non-deuterated solvents (Aldrich) were dried by distillation from sodium benzophenone ketyl before use and C_6D_6 was distilled from Na/K. The compounds $CuOCEt_3$ and $Ba(NH_2)_2$ were prepared as described previously [10–12]. NMR spectra were recorded on a Bruker AC-300 instrument. X-ray powder patterns were recorded on a Phillips diffractometer with a graphite crystal monochromator using Cu Kα radiation. Elemental analyses were performed by E+R Microanalytical Laboratories, Corona, NY.

Synthesis of $Ba(OCEt_3)_2$

A mixture of $Ba(NH_2)_2$ (1.63 g, 9.6 mmol), an excess of $HOCEt_3$ (3.1 g, 27 mmol) and pyridine (20 ml) was

* Author to whom correspondence should be addressed.

stirred in a H-tube for 16 h at 80°C. The mixture was filtered and the solids were dried *in vacuo* at 150°C to remove all solvent. A 71% yield of the white solid was isolated (2.52 g). Anal. found (calcd) for $C_{14}H_{30}O_2Ba$: C, 45.74 (45.73); H, 8.17 (8.22); Ba, 37.60 (37.35). ^{13}C NMR: (NMP) δ 9.54 (Me), 33.96 (CH_2), 74.06 (C).

*Isolation of $Ba_4Cu_6(O)(OCEt_3)_{12}$ (**1**) crystal*

In a previously reported experiment, a benzene solution of $Ba_2Cu_4(OCEt_3)_8$ (**2**) was filtered through dry talc and the solvent was stripped from the filtrate to afford **2** [4]. A C_6H_6/THF mixture was then washed through the filter and the second filtrate was oxidized by bubbling with oxygen for a minute, affording a brown, soluble material. The solvents were removed *in vacuo* and the brown solid was redissolved in heptane and allowed to stand in the dri-lab in a stoppered vial for 16 months. Slow evaporation of the solvent deposited a crystal of **1**.

*Attempts to synthesize **1***

(a) A mixture of $Ba(OCEt_3)_2$ (1.40 g, 3.8 mmol) and $CuOCEt_3$ (1.02 g, 5.7 mmol) was stirred in THF (10 ml) at 75°C for 4 h and at room temperature for a week. The mixture was filtered through dry talc and the solvent was removed *in vacuo*, affording 2.4 g of "$Ba_2Cu_3(OCEt_3)_7$". A 236 mg sample of the latter was mixed with 5 mL of toluene in a small H-tube and stirred overnight. The mixture was filtered, the solids were washed twice with re-condensed solvent and all solvents were removed *in vacuo*. A total of 60 mg of the white, toluene insoluble $[BaCu(OCEt_3)_3]_n$ (**3**) was isolated. NMR (D8-THF) ^1H, 0.88 (m, CH_3), 1.30 (br,s, CH_2), 1.42 (q), 1.49 (q); ^{13}C, (δ) 9.42, 9.53 (Me), 34.79, 34.49 (CH_2), 76.98, 76.11, 75.04 (C). Anal found (Calcd) for $C_{21}H_{45}O_3BaCu$: C, 46.19 (46.16); H, 8.51 (8.30); Cu, 11.37 (11.63); Ba, 25.11 (25.13).

(b) A solution of "$Ba_2Cu_3(OCEt_3)_7$" (0.65 g) in THF (8 ml) was prepared in a reaction bulb. A septum cap was put on the bulb and 4.8 μl of H_2O was added with stirring and stirred 3 days. Solvent was removed *in vacuo* and an NMR spectrum of the product in C_6D_6 showed mostly **2** in solution with several other components. All attempts to grow crystals were unsuccessful.

(c) Partially hydrolyzed $Ba(OCEt_3)_2$ was obtained from stirring Et_3COH (1.47 g, 12.6 mmol) and $Ba(NH_2)_2$ (1.07 g, 6.32 mmol) in pyridine (10 ml) for 3 h at 70°C, removal of all volatile materials under vacuum, addition of fresh pyridine, condensation of 1.60 mmol H_2O into the flask at −196°C and 12 h stirring at room temperature. This mixture was added to a four-fold excess of $CuOCEt_3$ (6.81 g, 38.1 mmol) in THF (30 ml), followed by 3 h stirring at 80°C. All solvents were removed *in vacuo*, followed by the addition of warm toluene and filtration. The solvent was stripped off the filtrate *in vacuo* and the resulting solids were recrystallized from heptane. The large, colorless crystals were washed 3 times with heptane and dried *in vacuo* affording $BaCu_6(OCEt_3)_8$ (**4**) [2.66 g (39%)]. Anal. found (calcd) for $C_{56}H_{120}BaCu_6O_8$: C, 46.78 (46.70); H, 8.33 (8.40); Ba, 9.06 (9.54); Cu, 26.14 (26.47). NMR (C_6D_6): ^1H, 0.997 (t), 1.09 (t), 1.49 (q), 1.66 (q); ^{13}C, 8.82, 9.43 (CH_3), 34.73, 34.89 (CH_2), 77.31, 77.34 (C); other peaks from disproportionation, see Fig. 1.

$Ba(OCEt_3)_2 + 3CuOCEt_3$

$Ba(OCEt_3)_2$ (0.30 g, 0.82 mmol) and $CuOCEt_3$ (0.44 g, 2.5 mmol) were stirred in 10 ml THF for 5 h at 70°C and the solvent was removed. The mixture was redissolved in toluene, filtered and the solvent was removed *in vacuo* affording a light tan solid, which was recrystallized by slow evaporation from heptane.

*$BaCu_6(OCEt_3)_8$ (**4**)*

$Ba(OCEt_3)_2$ (0.14 g, 0.38 mmol) and an excess of $CuOCEt_3$ (0.50 g, 2.8 mmol) was stirred in 5 ml THF at 80°C for 4 h, the mixture was filtered and the solvent was removed *in vacuo*. The mixture was redissolved in heptane and the solvent was allowed to evaporate slowly by placing the container into a vessel containing mineral oil. The crystals were washed with heptane and allowed to dry, affording 0.10 g of **4** (19%). Most of the yield was lost during the heptane wash step, and there is little doubt that the synthesis of **4** could be further optimized.

*Hydrolysis of **4***

A sample of **4** (1.0 g, 0.7 mmol) was dissolved in 5 ml THF in an H-tube and frozen at −196°C. Water (0.10 g, 5.5 mmol) was condensed into the H-tube, the mixture was allowed to warm to room temperature and stirred as soon as possible. An initial yellow color quickly turned to deep orange. The mixture was filtered in 30 min, the solids were washed with recondensed solvent and dried *in vacuo* for 16 h affording 369 mg of orange solid. A 136 mg sample of the latter was heated *in vacuo* at 250°C for 1.5 h resulting in 115 mg orange–brown solid.

*Crystal structures of **1** and **4***

Suitable crystals of **1** and **4** were mounted in thin walled glass capillaries under inert gas atmosphere. Data were collected in the $\Theta/2\Theta$ mode on an automated Siemens P4 diffractometer equipped with an incident beam graphite monochromator and the data were corrected for Lorentz and polarization effects. Corrections were made for a linear decay of 9.8% for **4**. In each case the structures were determined by

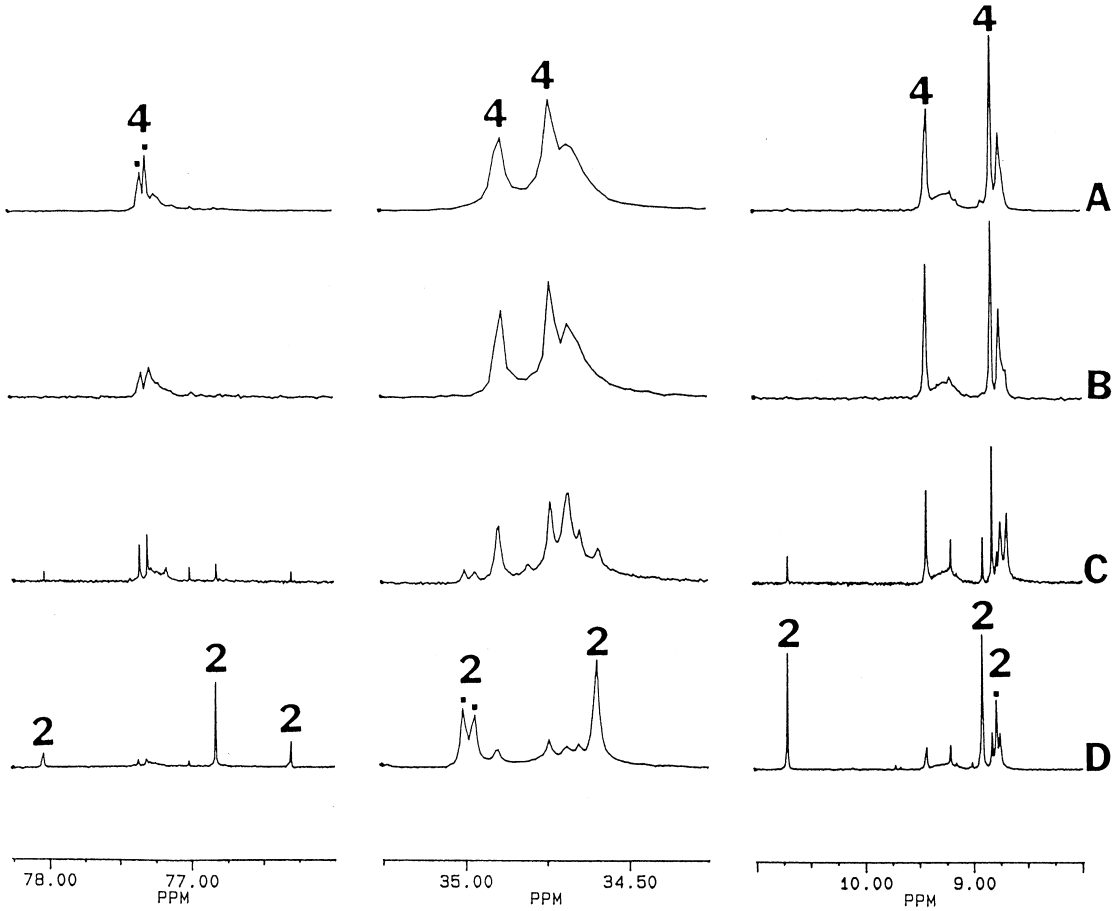

Fig. 1. ^{13}C NMR spectra of $BaCu_6(OCEt_3)_8$ (**4**), $A = 0.40$ M, $B = 0.12$ M, $C = 0.012$ M and D = a 3:1 mixture of $CuOCEt_3$ and $Ba(OCEt_3)_2$.

direct methods and refined using full matrix least-squares methods as implemented by the program SHELXL-PC [13]. For **1** the parameters refined included the coordinates and anisotropic thermal parameters for all but the hydrogen atoms. For **4** only the Ba, Cu and O atoms were refined anisotropically. The carbon atoms in **4** were refined with isotropic thermal parameters and the C–C bonds were constrained to 1.50(1) Å. Hydrogen atoms were placed in idealized positions (C–H = 0.96 Å) and the coordinate shifts for carbon were applied to the bonded hydrogens. The isotropic thermal parameters for the hydrogens were fixed. Additional data collection and refinement parameters are given in Table 1 and selected distances and angles in Table 2. Atom coordinates are available from the Cambridge Crystallographic Database, refcodes 101455 and 101456.

RESULTS AND DISCUSSION

Synthesis and reactivity

Only one crystal of the oxo-alkoxide $Ba_4Cu_6(O)(OCEt_3)_{12}$ (**1**) was isolated from the a mixture obtained from oxidation of impure $Ba_2Cu_4(OCEt_3)_8$ (**2**). The isolation of only one crystal prevented NMR, IR, or elemental analysis from being done on **1**. Some efforts were made to synthesize **1** deliberately, without success. The two binary alkoxides, $CuOCEt_3$ and $Ba(OCEt_3)_2$ were dissolved in a 3:2 ratio in THF. An NMR spectrum of the THF solution (in C_4D_8O) was relatively simple, but showed the presence of **2**. When this THF soluble product was washed with aromatic solvents, the **2** was removed and an insoluble (in PhMe) white solid was left behind. The latter was identified as $[BaCu(OCEt_3)_3]_n$ (**3**) by elemental analysis. However, attempts to obtain crystals of **3** from THF solution were unsuccessful. Since the simple combination of $CuOCEt_3$ and $Ba(OCEt_3)_2$ in a 3:2 ratio did not afford **1**, we thought that a hydrolysis step may be necessary to form the oxide ion in the center of the alkoxide. Addition of a stoichiometric amount of water to a THF solution of "$Ba_2Cu_3(OCEt_3)_7$" afforded a complex mixture from which no crystals were isolated, although one cannot exclude the possibility that **1** was present. In one attempt to prepare **1**, an inadvertent fourfold excess of $CuOCEt_3$ was added. A ternary alkoxide with a Cu:Ba ratio of

Table 1. Summary of crystal data and refinement parameters

Compound	**1**	**4**
Empirical formula	$C_{84}H_{180}O_{13}Ba_4Cu_6$	$C_{56}H_{120}O_8BaCu_6$
Crystal habit	irregular	translucent plate
Crystal system	cubic	triclinic
Space group	I23	P-1
a (Å)	17.636(1)	11.868(2)
b (Å)	17.636(1)	15.825(2)
c (Å)	17.636(1)	19.623(3)
α (°)	90	91.58(1)
β (°)	90	105.56(1)
γ (°)	90	90.34(1)
V (Å^3)	5485.8(5)	3548.7(9)
Z	2	2
Formula weight/F(000)	2328.9/2372	1440.1/1500
r(calc) (g cm^{-3})	1.410	1.348
Radiation, wavelength (Å)	0.71073	0.71073
Temperature (K)	293	293
Crystal dim. (mm)	$0.32 \times 0.27 \times 0.22$	$0.42 \times 0.36 \times 0.32$
m, absorption coefficient (mm^{-1})	2.600	2.351
2θ max. (°)	55.0	45.0
2θ scan range (°)	$3.6+\Delta\alpha1\alpha2$	$2.4+\Delta\alpha1\alpha2$
2θ scan speed (°/min)	variable 5.0 to 30	variable 10.0 to 30
h, k, l collected	1 to 22, 0 to 16, 0 to 13	0 to 12, −17 to 17, −21 to 20
Data collected	1342	10117
Independent data/$R_{int.}$	645 (0.02)	9267(0.03)
Observed data ($I>2\sigma I$)	471	3648
Absorp. correction	semi-empirical psi scans	semi-empirical psi scans
Max and Min transmission	0.29, 0.22	0.48, 0.42
Parameters refined/restraints	645/83	9263/360
R-factors, obs. data ($R1$[a], $wR2$[b])	0.060, 0.157	0.102, 0.215
R-factors, all data	0.088, 0.184	0.249, 0.302
Goodness of fit, all data	1.10	1.06
Fourier differences (eÅ^{-3})	−0.48, 0.75	−0.59, 0.84

[a] $\Sigma\|\|F_o|-|F_c\|\|/\Sigma|F_o|$.
[b] $[\Sigma(w\Delta^2)/\Sigma[w(F_o^2)^2]]^{1/2}$.
[c] $[\Sigma w(\Delta^2)/(N_o-N_p)]^{1/2}$ where $\Delta=(F_o^2-F_c^2)$.

6:1 ($BaCu_6(OCEt_3)_8$, **4**) was isolated in good yield from the latter reaction and identified by its crystal structure. This Cu rich Ba–Cu alkoxide disproportionates in C_6D_6 to many products, of which only **2** and $CuOCEt_3$ were positively identified by their NMR spectra. The intensities of the lines are concentration dependent and most of the same products are present in a solution with a Cu:Ba ratio of 3:1. Since **4** should have 2 peaks in a 1:1 ratio for each of its 3 types of carbon atoms and **4** should be present in the greatest amounts in the most concentrated solutions, a tentative peak assignment for **4** can be made. Representative ^{13}C NMR spectra are displayed in Fig. 1 with assignments indicated. Apparently, any combination of $Ba(OCEt_3)_2$ and $CuOCEt_3$ with a Cu:Ba ratio of greater than 2:1 produces a complex equilibrium of products in aromatic solvents. A similar observation was made with $(THF)_2Ba_2Cu_2(OR)_6$ and $(Me_3NO)_2Ba_2Cu_4(OR)_8$ where reaction with additional $[Cu(OR)]_4$ produced mixtures of products [7].

Upon slow evaporation, the 3:1 $CuOCEt_3$:$Ba(OCEt_3)_2$ solution afforded crystals of **2**, whose identity was confirmed by NMR. The crystals were however, a new polymorph with a unit cell volume about half that reported previously [4][1]. The quality of the crystals were too poor to make a full structure solution worthwhile.

An experiment was performed to determine whether **4** would act as a precursor to any new, copper-rich inorganic phases. When **4** was hydrolyzed in THF solution an orange precipitate was formed. That precipitate was converted to a mixture of the known phases Cu_2O and $BaCu_2O_2$ on heating to 250°C as determined by the X-ray powder pattern [14, 15].

[1] Triclinic, $a=12.034(1)$, $b=12.359(1)$, $c=12.914(2)$, $\alpha=77.03(1)$, $\beta=75.59(1)$, $\gamma=78.525(9)$, $V=1791.8(6)$ Å^3.

Table 2. Selected bond lengths and angles for **1** and **4**

1

Ba1–O1	2.54(1)	O1–Ba1–O1E	112.5(2)	Ba1–O2–Ba1A	109.5
Ba1–O2	3.167(2)	O1–Ba1–O2	106.2(3)	C1–O1–Cu1	116(1)
Cu1–O1	1.84(1)	O1–Cu1–O1A	174.7(7)	C1–O1–Ba1	133(1)
Ba1···Cu1	3.566(2)	Cu1–O1–Ba1	107.9(5)		

4

Ba1–O5	2.54(1)	Cu1–O1	1.81(1)	Cu3–O3	1.81(1)	Cu5–O6	1.82(2)
Ba1–O1	2.54(1)	Cu1–O2	1.83(1)	Cu3–O4	1.83(1)	Cu5–O7	1.81(1)
Ba1–O4	2.56(1)	Cu2–O3	1.78(2)	Cu4–O6	1.81(1)	Cu6–O7	1.82(1)
Ba1–O8	2.58(1)	Cu2–O2	1.81(2)	Cu4–O5	1.81(1)	Cu6–O8	1.82(1)
	Ba1···Cu	3.512(3)–3.571(3)			Cu···Cu	2.714(4)–2.794(4)	

O5–Ba1–O1	99.4(4)	O3–Cu2–O2	172.9(7)	Cu4–O5–Ba1	108.4(6)
O5–Ba1–O4	110.5(4)	O3–Cu3–O4	172.5(7)	Cu6–O8–Ba1	107.2(5)
O1–Ba1–O4	102.7(5)	O6–Cu4–O5	171.9(7)	Cu2–O2–Cu1	100.0(7)
O5–Ba1–O8	100.4(4)	O6–Cu5–O7	170.9(7)	Cu2–O3–Cu3	98.3(8)
O1–Ba1–O8	113.1(4)	O7–Cu6–O8	173.0(6)	Cu4–O6–Cu5	97.2(7)
O4–Ba1–O8	127.4(4)	Cu1–O1–Ba1	106.7(6)	Cu6–O7–Cu5	100.5(6)
O1–Cu1–O2	173.7(7)	Cu3–O4–Ba1	104.9(6)		

Crystal structures

The oxo-alkoxide $Ba_4Cu_6(O)(OCEt_3)_{12}$ (**1**) crystallizes in the cubic crystal system with the O^{2-} ion at the origin (Figure 2). All four Ba and all six Cu atoms are, respectively, equivalent by symmetry. The Ba atoms are distributed around the oxide ion in a tetrahedral arrangement with a Ba–O2 distance of 3.167(2) Å, which is very long for a bond between a four-coordinate oxide ion and barium. For example, the complex $Ba_4(O)(O\text{-tamp})_6C{\cdot}3PhMe$ has a similar geometry around a μ_4-oxo atom with Ba–O distances of 2.65(2)–2.675(7) Å [16]. Even the μ-6 oxo atom in $H_4Ba_6(\mu_6\text{-O})(OCH_2CH_2OMe)_{14}$ has shorter Ba–O distances around 2.9 Å [17]. Essentially, O2 is only weakly bonded to the bariums with its interaction being primarily ionic in nature. Each of the Ba atoms is also connected by a nearly linear $Cu(OR)_2^-$ unit [O–Cu–O = 174.7(7)°] to every other Ba, making the barium atoms four-coordinate. Efforts to refine O2 as something heavier than oxygen were unsuccessful. The Cu atoms form the vertices of an octahedron centered on O2 and are 6.0 Å apart. Each Ba atom has an approximately tetrahedral coordination environment [O–Ba–O = 112.5(2) and 106.2(3)°]. Apparently, the Ba–O1–Cu cage prevents the four Ba atoms from making a closer approach to O2.

The heterometallic alkoxide $BaCu_6(OCEt_3)_8$ (**4**) has no molecular symmetry (Figure 3). Two $Cu_3(OCEt_3)_4^-$ units coordinate the barium. Each $Cu_3(OCEt_3)_4^-$ moiety is shaped approximately like a rectangle with a side removed and can be thought of as a $(Cu(OR))_4$ molecule [18] with one copper atom missing. These $Cu_3(OR)_4^-$ ions are almost planar, as the deviations of the O atoms from the Cu1–Cu2–Cu3 and Cu4–Cu5–Cu6 planes range from 0.05 to 0.2 Å. The Cu1–Cu2–Cu3 plane makes a dihedral angle of 20° to the Cu4–Cu5–Cu6 plane. The coordination environment around Ba is tetrahedral to a rough approximation with O–Ba–O angles ranging from 99.4(4) to 127.4(4)° and averaging 108.9°. Some interaction may be present between the Cu atoms in each $Cu_3(OCEt_3)_4^-$ unit, as their average separation is only 2.75 Å. Copper–copper separations range from 2.646(2) to 2.771(3) Å in $[CuOCMe_3]_4$ and are 2.652(2) Å in $Cu_2Zr_2(OCHMe_2)_{10}$.

The Ba–OR distances of both **1** and **4** [2.54(1) to 2.58(1)] are normal for four-coordinate Ba, which for example are 2.414(8) and 2.579(8) Å in $Ba[O\text{-}C_6H_3(CMe_3)_2Me]_2[HMPTA]_2$ [19] and range from 2.51(1) to 2.59(1) Å in **2**. However, the Ba–O distances in the $L_2Ba_2Cu_4(OCRMe_2)_8$ compounds, which have 5-coordinate Ba, are slightly longer, averaging 2.61 Å. The Ba–O–Cu angles in **1** and **4** fall in a fairly narrow range from 104.9(6) to 108.4(6), in which the Ba–O–Cu angles of $Ba_2Cu_4(OCEt_3)_8$ [105.4(4) and 106.4(5)°] also fall. In the *t*-butoxy complexes, $L_2Ba_2Cu_4(OCRMe_2)_8$, the Ba–O–Cu angles range from 103.5 to 110.9° [5–7]. One fluorinated complex, $(THF)_2Ba_2Cu_2(OMe(CF_3)_2)_6$, has smaller Ba–O–Cu angles of 96.9 to 101.7°, however this molecule may be distorted by the extensive Ba–F coordination [7]. A greater range is found for Cu–O–Cu angles (within a Cu_2O_3 or Cu_3O_4 moiety) which vary from 91.7(5)° in $[CuOCMe_3]_4$ to 110.4(3)° in **2** and range from 97.2(7) to 100.5(6) in **4**.

CONCLUSIONS

With seven Ba–Cu(I), two Zr–Cu(I) and two alkali–Cu(I) alkoxides structurally characterized, some gen-

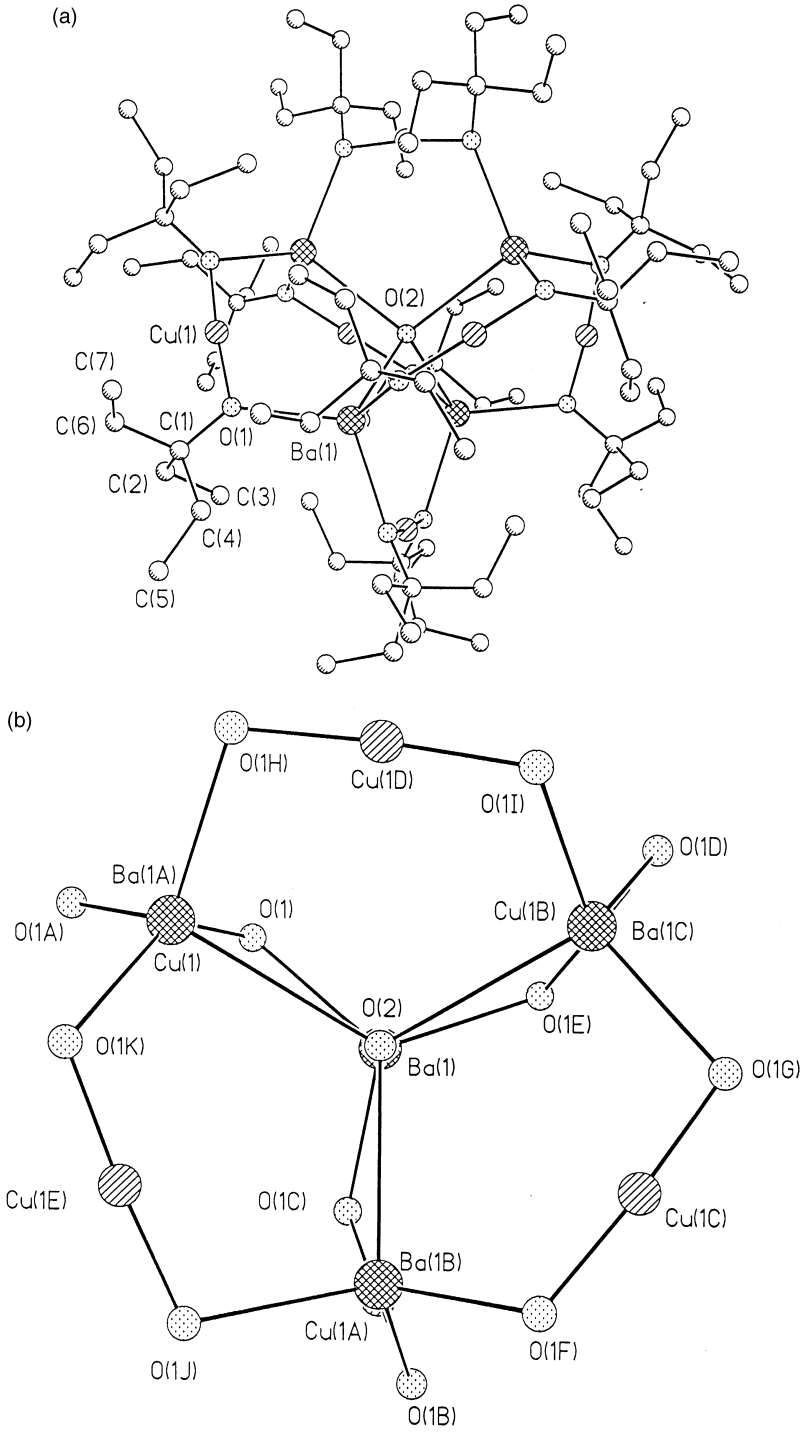

Fig. 2. (a) Structure of $Ba_4Cu_6(O)(OCEt_3)_{12}$ (**1**). (b) A view of the $Ba_4Cu_6O_{13}$ core down a threefold axis. Some Cu atoms are hidden by Ba atoms.

eralizations can be drawn. First, all three examples of Ba–Cu(I) alkoxides with $OCEt_3$ groups have 4-coordinate Ba, whereas the $OCRMe_2$ compounds have at least 5-coordinate Ba and therefore require an extra ligand to afford a soluble molecular compound. Most other Ba alkoxides with $OCMe_3$ groups have at least 6-coordinate Ba (see, for example, Refs. [20, 21]). Second, the Cu–O and Ba–O distances and the O–Cu–O, Cu–O–Cu and Ba–O–Cu angles vary over fairly narrow ranges, with the Cu–O–Cu angle being the most flexible. This means that each $Cu_n(OR)_{n+1}$ moiety has a relatively well defined range of bite sizes

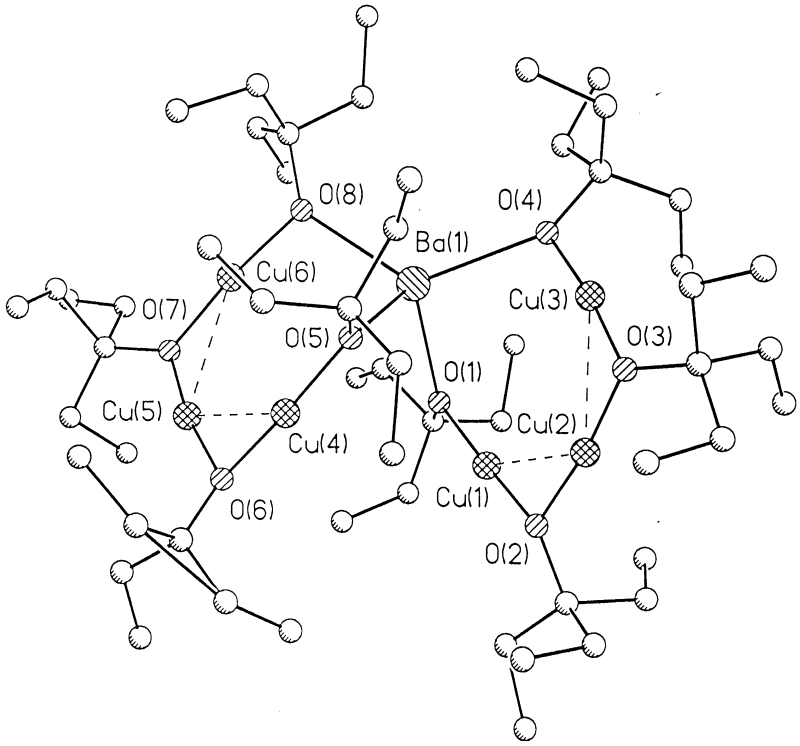

Fig. 3. Structure of $BaCu_6(OCEt_3)_8$ (**4**). Labeling of carbon atoms was omitted for clarity.

and its geometric limits can be readily estimated by calculation, or by using scale molecular models. Thus, a bidentate $Cu(OR)_2^-$ unit can coordinate two Ba atoms separated by 4 to 5.5 Å (Ba···Ba = 5.2 Å in **1**), while $Cu_2(OR)_3^-$ can accommodate Ba–Ba separations from 2.5 to 9 Å and $Cu_3(OR)_4^-$ can coordinate a single Ba atom as it does in **4** or 2 Ba atoms separated by up to 8 Å. Clearly, $Cu(OR)_2^-$ is the most geometrically constrained and $Cu_3(OR)_4^-$ is the most flexible. As observed previously, Ba–Cu(I) alkoxides are highly flexible systems and can have a wide variety of molecular species in solution, especially when copper-rich. The ability to isolate particular solid compounds is probably more related to how lattice energies and packing forces correlate to complex solution equilibria rather than any general preference for a particular stoichiometry.

Acknowledgements—We thank the ONR for financial support.

REFERENCES

1. Mehrotra, R. C., Singh, A. and Sogani, S., *Chem. Soc. Rev.*, 1994, 215.
2. Mehrotra, R. C. and Singh, A., *Chem. Soc. Rev.*, 1996, 1.
3. Caulton, K. G., Hubert-Pfalzgraf, L. G., *Chem. Rev.*, 1990, **90,** 969.
4. Purdy, A. P. and George, C. F., *Polyhedron*, 1995, **14,** 761.
5. Borup, B., Huffman, J. C. and Caulton, K. G., *J. Organomet. Chem.*, 1997, **536,** 109.
6. Borup, B., Folting, K. and Caulton, K. G., *Chem. Mater.*, 1997, **9,** 1021.
7. Borup, B., Streib, W. E. and Caulton, K. G., *Inorg. Chem.*, 1997, **36,** 5058.
8. Vaartstra, B. A., Samuels, J. A., Barash, E. H., Martin, J. D., Streib, W. E., Gasser, C. and Caulton, K. G., *J. Organomet. Chem.*, 1993, **449,** 191.
9. Samuels, J. A., Chiang, W., Huffman, J. C., Trojan, K. L., Hatfield, W. E., Baxter, D. V. and Caulton, K. G., *Inorg. Chem.*, 1994, **33,** 2167.
10. Purdy, A. P., George, C. F. and Callahan, J. H., *Inorg. Chem.*, 1991, **30,** 2812.
11. Purdy, A. P., Berry, A. D. and George, C. F., *Inorg. Chem.*, 1997, **36,** 3370.
12. Purdy, A. P. and George, C. F., *Main Group Chem.*, 1996, **1,** 229.
13. Sheldrick, G. M., *SHELXTL-PC*, Release 5.03. Siemens Analytical X-ray Instruments, Madison, Wisconsin, U.S.A., 1994.
14. Klassen, H. and Hoppe, R., *Z. Anorg. Allg. Chem.*, 1982, **485,** 101 (JCPDS cards 36-1074 and 22-1370).
15. Teske, C. L. and Muller-Buschbaum, H., *Z. Naturforsch.*, 1972, **27b,** 296 (JCPDS card 39-245).
16. Tesh, K. F. and Hanusa, T. P., *J. Chem. Soc. Chem. Commun.*, 1991, 879.
17. Caulton, K. G., Chisholm, M. H., Drake, S. R.

and Huffman, J. C., *J. Chem. Soc. Chem. Commun.*, 1990, 1498.
18. Greiser, T. and Weiss, E., *Chem. Ber.*, 1976, **109,** 3142.
19. Belderrain, T. R., Espinos, J. P. Fernandez, A., Gonzalez-Elipe, A. R., Leinen, D., Monge, A., Peque, M., Ruiz, C. and Carmona, E., *J. Chem. Soc. Dalton Trans.* 1995, 1529.
20. Borup, B., Samuels, J. A., Streib, W. E. and Caulton, K. G., *Inorg. Chem.*, 1994, **33,** 994.
21. Caulton, K. G., Chisholm, M. H., Drake, S. R. and Folting, K., *J. Chem. Soc. Chem. Commun.* 1990, 1349.

Pergamon

Polyhedron Vol. 17, No. 23–24, pp. 4049–4058, 1998
© 1998 Elsevier Science Ltd
All rights reserved. Printed in Great Britain
0277–5387/98 $19.00+0.00

PII: S0277–5387(98)00208–3

Syntheses, crystal structures and properties of Zn(II) and Cd(II) complexes derived from *N*-(*o*-nitrophenyl)-*N*′-(methoxycarbonyl) thiourea(H_2omt) and 2,2′-bipyridine(bpy) or *o*-phenanthroline(phen)

Xu Shen,*[a] Xianfa Shi,[a] Beisheng Kang,[b], Yu Liu,[b] Yexiang Tong,[b], Hualiang Jiang[c] and Kaixian Chen[c]

[a]Department of Chemistry, Tongji University, Shanghai 200092, People's Republic of China

[b]Department of Chemistry, Zhongshan University, Guangzhou 510275, People's Republic of China

[c]Shanghai Institute of Materia Medica, Chinese Academy of Sciences, Shangahi 200031, People's Republic of China

(Received 7 January 1998; accepted 18 May 1998)

Abstract—The chelating properties of *N*-(*o*-nitrophenyl)-*N*′-(methoxycarbonyl)thiourea (H_2omt) were investigated through the study of the crystal structures of Cd(Homt)$_2$(bpy), **1**, Zn(Homt)$_2$(phen), **2** and H_2omt (bpy = 2,2′-bipyridine, phen = *o*-phenanthroline). The cadmium(II) ion in **1** is in a distorted octahedral geometry contributed by the two N atoms from bipyridine and the two S and the two deprotonated amine N atoms from two Homt groups [Cd–N(bpy) = 2.329(3), Cd–N(amine) = 2.360(3) and Cd–S = 2.690(1) Å]. The Zn(II) ion in complex **2** is four-coordinated by the two N atoms from the *o*-phenanthroline and the two deprotonated amine N atoms from two Homt groups in a distorted tetrahedral fashion, in which the binding of S atom to the metal is not involved [Zn–N(phen) = 2.088(4), Zn–N(amine) = 1.998(3) Å]. © 1998 Elsevier Science Ltd. All rights reserved

Keywords: syntheses; crystal structures; cadmium(II) complex; zinc(II) complex; *N*′-(*o*-nitrophenyl)-*N*′-(methoxycarbonyl)thiourea; bipyridine; *o*-phenanthroline.

INTRODUCTION

Recently, the derivative *N*-(*o*-nitrophenyl)-*N*′-(ethoxycarbonyl)thiourea (H_2oet) was isolated from the leaves of resistant *Pyricuiria oryzae cav*. rice variety [1] and the preliminary pharmacological tests showed its high antibacterial activity. In our previous work [2], several ligands similar to the basic structure of H_2oet were prepared and their Cu(I) complexes were prepared and crystallographically characterized. It is interesting to find that copper(I) complexes can be obtained from the copper(II) salts by *in situ* reduction in the presence of these thiourea derivatives. In fact, the biological activities of complexes with thiourea derivatives have been well documented and thiourea derivatives have been successfully screened for various biological actions [3–6] and some *N*-substituted-*N*′-alkoxycarbonyl thioureas have been used in commercial fungicides. To date, plenty of transition metal complexes with such thiourea derivatives have been reported and the structures with O,S-binding to the metal ions were well proposed in alkaline media based on a series of physicochemical properties [7–9]. Now, it has been a common knowledge that complexation with metal ions may enhance the biological activity of a wide variety of organic compounds. For example, the copper(II) complex of 2-ace-

* Author to whom correspondence should be addressed.

tyloxybenzoic acid (aspirin), a ligand used as an analgesic since the last century, was reported to be significantly more active as an anti-inflammatory agent than the free ligand (Refs [10,11]. and references cited therein). Complexes of metal ions containing a bidentate organic compound such as 2,2′-bipyridine (bpy) and phenanthrolinine (phen) have been well reported [12,13] and they serve as interesting models for the understanding enzyme–metal ion–substrate relationship, thus playing an important role in metalloenzyme-catalyzed biochemical reactions [14,15]. In our previous work, the chloroform solvated Cd(II) complex with the ligand *N*-(*o*-nitrophenyl)-*N*′-(methoxycarbonyl)thiourea (H_2omt) and *o*-phenanthroline was reported [16] and Zn(II) and other transition metal complexes [e.g. Cu(II), Co(II)] with H_2omt and bipyridine (bpy) were synthesized [17]. To make such work more complete, in this paper we report the crystal structures of Zn(II) and Cd(II) complexes with H_2omt and bpy for Cd(II) and phen for Zn(II).

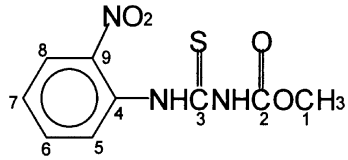

N-(*o*-nitrophenyl)-N'-(methoxycarbonyl)thiourea (H_2omt) (**m. f.** $C_9H_9O_4N_3S$)
(carbon atoms labelling is for ^{13}C NMR assignments)

EXPERIMENTAL

Chemicals

All reactants were reagent grade and used without further purification.

Physical measurements

C, H and N analyses were carried out on a Carlo Erba 1106 elemental analyzer. IR spectra were recorded on a Magna 750 spectrometer, UV spectral data were collected by a Shimadzu UV-300 spectrometer. NMR (^1H and ^{13}C) spectra were determined with a Bruker AM 500 instrument in DMSO-d_6 solution. Cyclic voltammetry was performed with a HDV-7B Potentiostat and LZ3Q-204 *X*–*Y* recorder with an electrochemical cell containing a Pt wire working electrode, a Pt plate auxiliary electrode and an SCE reference electrode.

X-ray crystallography

Pertinent crystal data, basic information about the data collection and structure refinement of the crystals of **1**, **2** and H_2omt are given in Table 1.

The structures were all solved by direct methods. Refinements were carried out by full-matrix least squares using anisotropic thermal parameters for all the non-hydrogen atoms. The hydrogen atoms were included as fixed contributions in structure factor calculations but not refined. All calculations were performed on a Compaq computer using the TEXSAN program package.

Biological activity

The antibacterial and antifungal activities of the ligand H_2omt and the metal complexes against the standard strains of *B. subtilis* 6633, *S. lutea*, *S. aureus* 209p, *P. diploccus*, *E. coli* and *P. aeruginosa* x313 and *S. Yake Sake* were determined using the plate method [18]. Each of the compounds was prepared at a concentration of 0.55 mM during the tests and the results are listed in Table 6.

Preparations

N-(o-Nitrophenyl)-N′-(methoxycarbonyl)-thiourea (*H_2omt*). The preparation of the ligand H_2omt was according to our previous method [7–9].

General preparation method for Cd(Homt)$_2$(bpy), **1**, *and Zn(Homt)$_2$(phen)*, **2**. A solution of $M(ClO_4)_2 \cdot 6H_2O$ (M = Cd and Zn) (3 mmol) in 20 cm^3 of methanol was added slowly to a methanolic solution of 2,2′-bipyridine or *o*-phenanthroline (3 mmol in 15 cm^3). This was warmed by stirring at 40–45°C for 30 min to give a clear solution which was cooled to room temperature and to it was added the clear methanolic solution (20 cm^3) containing H_2omt (6 mmol) and NaOH (6 mmol). A large amount of yellowish solids were precipitated, this resulting mixture was stirred at room temperature for a further 3 h and the solids were collected by filtration, washed thoroughly with water

Table 1. Summary of crystallographic data and structural parameters of the compounds H_2omt, **1** and **2**

Compound	H_2omt	**1**	**2**
Formula	$C_9H_9N_3O_4S$	$C_{28}H_{24}N_8O_8CdS_2$	$C_{30}H_{22}N_8O_8S_2Zn$
M	255.25	777.08	752.05
Crystal size (mm^3)	$0.25\times0.20\times0.15$	$0.45\times0.45\times0.25$	$0.25\times0.15\times0.15$
Crystal color and shape	yellow, prism	yellow, prism	yellow, prism
Crystal system	monoclinic	monoclinic	monoclinic
Space group	C2/c (# 15)	C2/c (# 15)	C2/c (# 15)
a (Å)	31.420 (5)	22.463 (5)	20.911 (5)
b (Å)	4.672(2)	9.681(4)	10.848(4)
c (Å)	15.226(2)	15.312(5)	15.508(4)
β (°)	97.47(1)	112.64(3)	113.50(2)
V ($Å^3$)	2216(1)	3073 (2)	3226(3)
Z	8	4	4
D_c ($g\cdot cm^{-3}$)	1.530	1.68	1.548
F(000)	1056	1568	1536
μ (cm^{-1})	2.86	8.99	9.63
Diffractometer	Rigaku AFC5R	Enraf-Nonius CAD4	Enraf-Nonius CAD4
2θ max. (°)	50.0	49.9	49.9
Scan width (°)	$0.85+0.35\tan\theta$	$0.95+0.35\tan\theta$	$0.85+0.45\tan\theta$
Scan speed (min^{-1})	<12.0	<5.85	<7.84
No. of unique reflections	2217	2888	3014
No. of observations	1460 [$I>2\sigma(I)$]	2326 [$I>3\sigma(I)$]	1927 [$I>2\sigma(I)$]
No. of variables	154	250	222
Temperature (°)	23	23	23
R	0.041	0.033	0.051
Rw	0.059	0.041	0.053
GOF	1.62	1.26	1.25
Max. shift in final cycle	0.002	0.00	0.0004
$\Delta\rho$ max., min. ($e\,Å^{-3}$)	0.21, −0.24	0.93, −0.60	0.29, −0.37

and methanol and dried *in vacuo*. Complex **1**, m.p. 243°C (decomp.). Yield, 89%. Found: C, 43.6; H, 4.1; N, 14.6. Calc. for $C_{28}H_{24}N_8O_8CdS_2$: C, 43.2; H, 3.1; N, 14.4%. Complex **2**, m.p. 227°C (decomp). Yield, 91%. Found: C, 47.8; H, 10; N, 14.6. Calc. for $C_{30}H_{22}N_8O_8S_2Zn$: C, 47.9; H, 2.9; N, 14.9%.

Single crystals suitable for X-ray analyses were obtained by slow diffusion of diethyl ether into the solution of **1** or **2** in chloroform over several weeks.

RESULTS AND DISCUSSION

Crystal structures

The structure of complex $Cd(Homt)_2(bpy)$, **1**, is depicted in Fig. 1, which shows that the Cd(II) ion is six-coordinated by two N atoms from bipyridine and two S and two N atoms from two Homt groups. Selected atomic distances and bond angles are listed in Table 2.

The bond lengths Cd–S(1) of 2.690(1) Å and Cd–N(1) of 2.360(3) Å are well within the range of the published results dealing with Cd–S (thiocarbonyl) [19] and Cd–N(amine) [20] and are also comparable to Cd–S (thiocarbonyl) [2.687(2) Å] and Cd–N(amine) [2.326(4), 2.330(4) Å] in our previous work [16]. The structural data within the 2,2′-bypyridine molecule are normal and Cd–N(4) of 2.329(3) Å is comparable to the reported values of Cd–N(bipy) elsewhere [21, 22]. The geometry of the six-coordinated cadmium(II) atom is distorted with the bond angles N(1)–Cd–S(1) = 61.59(7)°, N(1)–Cd–N(4) = 99.2(1)° and N(1)–Cd–N(4a) = 100.2(1)°. The molecule contains two four-membered (from Homt) and one five-membered chelate rings (from phen) and the metal ion deviates by 0.0313(2) Å from the plane N(1)C(2)S(1)Cd. The dihedral angle between the least squares planes N(1)C(2)S(1)Cd and N(4)C(14)C(14a)N(4a)Cd is 100.38(7)°.

The structure of complex $Zn(Homt)_2(phen)$, **2**, is shown in Fig. 2, and selected bond distances and angles are also listed in Table 2. The Zn(II) atom is four-coordinated by the two N atoms from the *o*-phenanthroline molecule and the two deprotonated amine N atoms from two Homt groups in a distorted tetrahedral geometry with N(4)–Zn–N(1) = 115.8°, N(4)–Zn–N(4a) = 79.8(3)° and N(1)–Zn–N(1a) = 128.9(2)°. The Homt ligand is monodentately coordinated to Zn(II) atom with the deprotonated amine nitrogen atom where the S atom does not bind to the metal ion, which is different from that in complex **1**. As Zn(II) ion is a harder acid relative to Cd(II) and

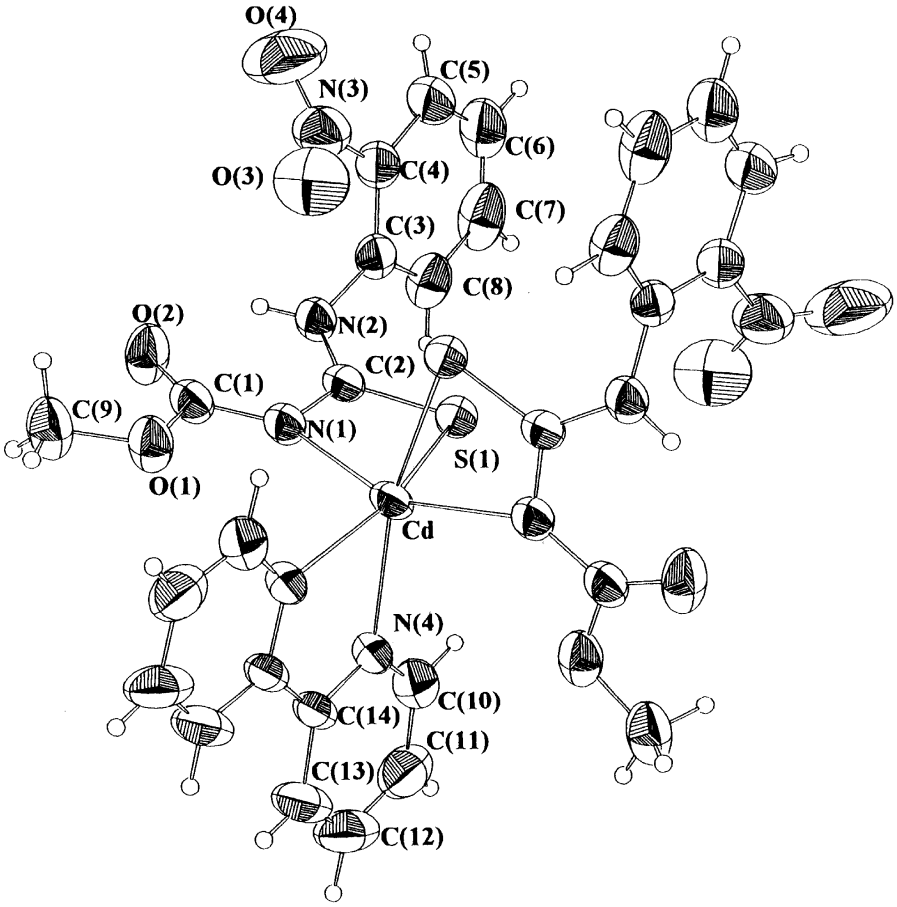

Fig. 1. ORTEP drawing of complex **1** with ellipsoids at 35% probability.

Table 2. Selected bond lengths (Å) and angles (°) of complexes **1** and **2**

1					
N(1)–Cd	2.360(3)	N(4)–Cd	2.329(3)	S(1)–Cd	2.690(1)
N(1)–Cd–N(1a)	156.2(1)	N(4)–Cd–N(1a)	100.3(1)	C(1)–N(1)–Cd	135.8(2)
N(1)–Cd–N(4)	99.2(1)	N(4)–Cd–N(4a)	70.0(1)	C(2)–S(1)–Cd	80.0(1)
N(1)–Cd–S(1)	61.59(7)	N(4)–Cd–S(1)	101.21(8)	C(2)–N(1)–Cd	100.8(2)
N(1a)–Cd–S(1)	101.07(8)	N(4)–Cd–S(1a)	159.13(7)	C(10)–N(4)–Cd	122.8(3)
S(1a)–Cd–S(1)	92.89(5)			C(14)–N(4)–Cd	118.2(2)
2					
Zn–N(1)	1.998(3)	Zn–N(4)	2.088(4)		
N(1)–Zn–N(4)	115.8(1)	N(4)–Zn–N(1)i	103.0(2)	C(1)–N(1)–Zn	122.9(3)
N(1)–Zn–N(4)i	103.1(2)	N(4)–Zn–N(4)i	79.8(3)	C(2)–N(1)–Zn	113.1(3)
N(1)–Zn–N(1)i	128.9(2)			C(10)–N(4)–Zn	128.6(4)
				C(15)–N(4)–Zn	112.7(4)

Symmetry operator: a: $1-x$, y, $1/2-z$; i: $1-x$, $-y$, $-z$.

thus less thiophilic, the Homt ligand tends to ligate only through the N atoms with Zn–N(1) 1.998(3) Å like a normal Zn–N(amine) bond [23]. The structural data within the phenanthroline molecule are without much change and the bond Zn–N(4) of 2.088(4) Å is well within the values Zn–N(phen) [24].

The structure of the ligand H_2omt is shown in Fig. 3. The coordination behavior of the Homt group is

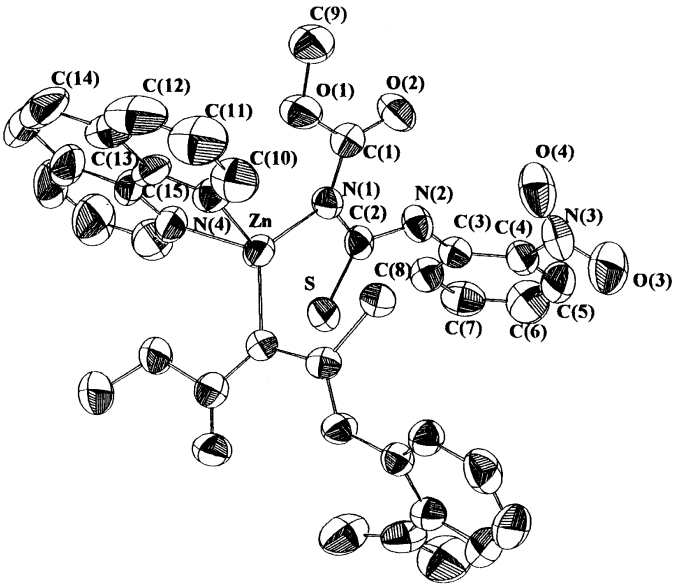

Fig. 2. ORTEP drawing of complex **2** with ellipsoids at 35% probability.

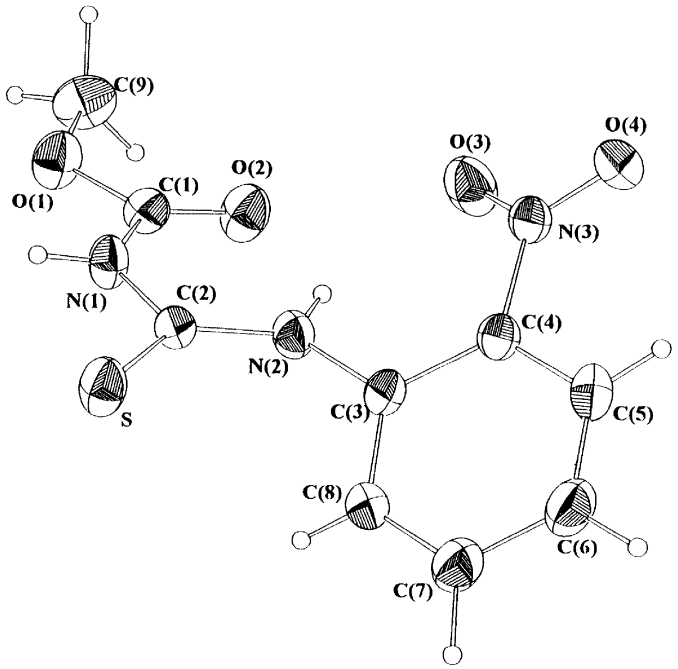

Fig. 3. ORTEP drawing of H_2omt with ellipsoids at 50% probability.

different in each of the complexes, with either mono- or bidentate coordination. In the free ligand H_2omt, the thiourea moiety SO(1)O(2)N(1)N(2)C(1)C(2)C(9) is almost planar and N(3) is in the plane of the phenyl group, these two planes form a dihedral angle of 44.37°. In complex **1**, N(2) is also in the plane of the phenyl group, and the dihedral angle between this plane and the least squares plane SO(1)O(2)N(1)N(2)C(1)C(2) is 70.51°. With respect to complex **2**, the dihedral angle between the plane of N(2) and the phenyl group and the plane O(1)O(2)N(1)C(1)C(2)C(9) is 54.55°. Comparative bond distances and angles involving Homt group for the free ligand H_2omt and complexes **1** and **2** are listed

Table 3. Comparative bond distances (Å) and angles (°) involving Homt group for the compounds H_2omt, **1** and **2**

	H_2omt	**1**	**2**
C(9)–O(1)	1.444(4)	1.428(5)	1.433(6)
O(1)–C(1)	1.322(3)	1.341(4)	1.340(5)
C(1)–O(2)	1.200(3)	1.211(4)	1.210(5)
C(1)–N(1)	1.374(3)	1.366(4)	1.363(6)
N(1)–C(2)	1.374(3)	1.345(4)	1.361(5)
C(2)–S	1.666(3)	1.710(3)	1.674(4)
C(2)–N(2)	1.342(3)	1.347(4)	1.348(5)
N(2)–C(3)	1.421(3)	1.421(4)	1.396(5)
C(3)–C(4)	1.402(4)	1.385(5)	1.390(6)
C(4)–C(5)	1.385(4)	1.382(5)	1.374(7)
C(5)–C(6)	1.379(4)	1.360(7)	1.354(8)
C(6)–C(7)	1.383(5)	1.361(7)	1.361(8)
C(7)–C(8)	1.376(4)	1.392(6)	1.363(7)
C(8)–C(3)	1.379(4)	1.375(5)	1.393(6)
C(4)–N(3)	1.471(3)	1.455(5)	1.464(7)
N(3)–O(3)	1.225(3)	1.212(5)	1.214(6)
N(3)–O(4)	1.217(3)	1.210(5)	1.222(5)
C(9)–O(1)–C(1)	116.1(2)	116.0.(3)	117.3(4)
O(1)–C(1)–O(2)	124.9(3)	121.9(3)	122.5(4)
O(1)–C(1)–N(1)	109.9(2)	108.5(3)	108.0(4)
O(2)–C(1)–N(1)	125.2(3)	129.7(3)	129.4(4)
C(1)–N(1)–C(2)	128.5(2)	121.6(3)	123.0(4)
N(1)–C(2)–S	118.2(2)	116.2(2)	117.2(3)
N(1)–C(2)–N(2)	115.1(2)	122.1(3)	119.0(4)
N(2)–C(3)–C(4)	121.7(2)	121.1(3)	122.4(4)
N(2)–C(3)–C(8)	121.2(2)	121.3(3)	120.6(4)
C(3)–C(8)–C(7)	121.9(3)	119.8(4)	120.7(5)
C(8)–C(7)–C(6)	120.1(3)	121.0(4)	120.7(5)
C(7)–C(6)–C(5)	119.8(3)	120.4(4)	120.5(5)
C(6)–C(5)–C(4)	119.3(3)	118.6(5)	119.5(5)
C(5)–C(4)–C(3)	121.7(2)	122.5(4)	121.6(5)
C(3)–C(4)–N(3)	122.1(2)	120.9(3)	120.6(4)
C(5)–C(4)–N(3)	116.2(2)	116.5(4)	117.8(5)
C(4)–N(3)–O(3)	119.0(2)	118.8(4)	117.3(5)
C(4)–N(3)–O(4)	118.0(3)	117.3(4)	118.3(5)
O(3)–N(3)–O(4)	122.9(2)	123.8(4)	124.3(5)
S–C(2)–N(2)	126.6(2)	121.6(2)	123.7(3)
C(8)–C(3)–C(4)	117.1(3)	117.7(3)	117.0(4)
C(2)–N(2)–C(3)	126.3(2)	123.4(3)	129.5(4)

in Table 3. As shown in Table 3, there is general agreement of the values. The shorter bond N(1)–C(2) for complex **1** can be caused by the formation of S–Cd bond. For the same reason, complex **1** has the longest C(2)–S bond. The different conformation of the compounds arising from the binding of the metal ions to H_2omt gives rise to the following bond angles sequences: (i) O(1)–C(1)–O(2): (H_2omt) > (**1**) ≈ (**2**); (ii) O(2)–C(1)–N(1): (H_2omt) < (**1**) ≈ (**2**); (iii) C(1)–N(1)–C(2): (H_2omt) > (**1**) > (**2**); (iv) N(1)–C(2)–N(2): (H_2omt) < (**2**) < (**1**); (v) S–C(2)–N(2): (H_2omt) > (**2**) > (**1**); (vi) C(2)–N(2)–C(3): (**2**) > (H_2omt) > (**1**).

Spectroscopic properties of the compounds

IR and UV spectra For the compounds of H_2omt, **1** and **2**, the bands at *ca.* 3140 cm^{-1} are usually attributed to the stretching frequency ν(NH), while for complex **3**, the band above 3100 cm^{-1} was not observed, indicating the absence of NH group. The intense band arising from the amide-I stretching vibration at 1732 cm^{-1} for H_2omt is red-shifted when ligation occurs in the Cd(II) (1648 cm^{-1}) and Zn(II) (1661 cm^{-1}) complexes. The C=S band at 867 cm^{-1} for the free ligand H_2omt has shifted to 855 cm^{-1} in complex **1**, indicative of the binding via the thiolato sulfur atom to Cd(II) ion, which is also indicated by the presence of a band of 310 cm^{-1}, assignable to ν(Cd–S) [25]. Therefore, the nearly unchanged ν(C=S) band at 868 cm^{-1} in complex **2** implicates the non-coordination of thiolate sulfur, in agreement with the X-ray crystallographic results. In addition, the coordination of nitrogen atom to Cd(II) or Zn(II) ion in complex **1** or **2** is observed by the presence of bands at *ca.* 320 ~ 335 cm^{-1}, assignable to ν(Cd–N) or ν(Zn–N) [26].

The UV spectra of the ligand H_2omt and complexes **1** and **2** are shown in Fig. 4. For all three compounds, the bands at about 278 nm are ascribed to ^{1}L(b) absorption of the aromatic ring. The signals around

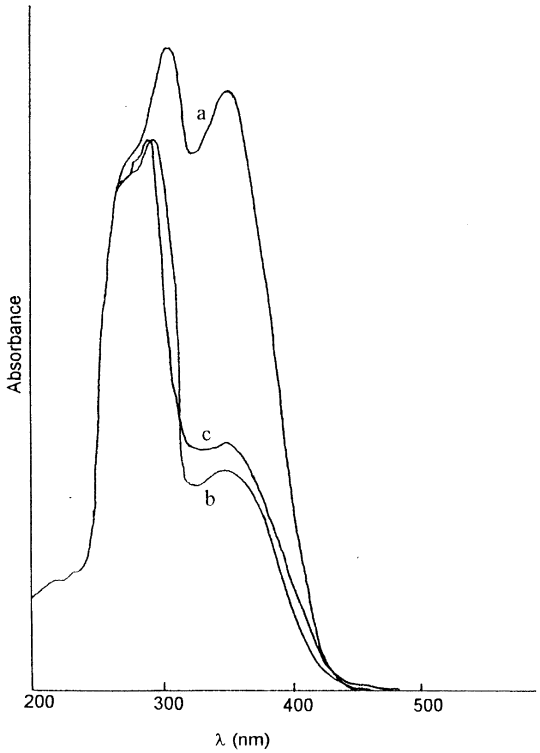

Fig. 4. UV spectra of the compounds in chloroform (a, H_2omt; b, **1**; c, **2**).

Table 4. ^{1}H NMR spectra of compounds H_2omt, **1** and **2** (in ppm)

Compound	Assignment[a]			
	Ar–NHC(S)	HNC(O)	OCH_3	aromatic ring
H_2omt	12.52 (s, 1H)	8.3 (s, 1H)	3.9 (s, 3H)	7.39 ~ 8.47 (m, 4H)
1	12.81 (s, 1H)	–	3.5 (s, 3H)	7.27 ~ 9.06 (m, 12H)
2	12.95 (s, 1H)	–	3.3 (s, 3H)	7.24 ~ 9.58 (m, 12H)

[a] s = single, m = multiple.

300 nm are attributed to the absorption of the NO_2 group. As for the $n\rightarrow\pi^*$ absorptions of C=O, they are near 345 nm. All the absorptions shown a bathochromical shift for the complexes relative to those of the free ligand are caused by the coordination of metal ions to the ligand. The $n\rightarrow\pi^*$ excitation of C=S is not observed in any of the compounds, in agreement with that reported by Barret *et al*. [27].

^{1}H and ^{13}C NMR spectra The ^{1}H and ^{13}C NMR spectra of the ligand H_2omt and complexes **1** and **2** are listed in Tables 4 and 5, respectively.

As shown in Table 4, most of their proton signals are observed to shift to down fields in complexes **1** and **2** relative to those of the free ligand due to the binding of the metal ions. The absence of δ(NH) [s, 1H, HN–C(O)] in the complexes shows the coordination of deprotonated amine to Cd(II) or Zn(II) ion.

In comparison with the ^{13}C NMR spectrum of the ligand H_2omt (Table 5), C_2 has shifted to a lower field at δ 186.34 for **1** and 186.98 for **2**; C_3 to δ 159.31 (**1**) and 159.14 (**2**). However, C_1 is found to have shifted to a higher field at δ 51.85 for **1** and 51.68 for **2**.

Electrochemical studies

The cyclic voltammograms of the compounds H_2omt, **1** and **2** are shown in DMF and CH_3CN solutions at a scan rate of 0.1 V s^{-1} in the scan ranges 0 to +1.8 and −1.8 to 0 V are shown in Figs 5 and 6, respectively. As can be seen from Fig. 5, it is found that each of three compounds exhibit two irreversible cathodic peaks with −0.43 and −1.53 V for H_2omt, −0.30 and −1.40 V for **1** as well as −0.53 and −1.57 V for **2**, and one reversible redox couples at −1.13 and −1.08 V for H_2omt, −0.93 and −0.90 V for **1** and −1.13 and −1.05 V for **2**. Thus, it is tentatively suggested that all these peaks are ascribed to the reduction and oxidation process of the Homt group. In terms of the cyclic voltammograms of the compounds in CH_3CN solution as shown in Fig. 6, each of the compounds display an anodic peak (H_2omt, 1.28 V; **1**, +1.39 V; **2**, +1.39 V) one cathodic peak (H_2omt, −0.83 V; **1**, −0.55 V; **2**, −0.5 V) and one reversible redox couple (H_2omt, −1.15 and −1.13 V; **1**, −0.90 and −0.85 V; **2**, −0.92 and −0.87 V). In addition, it is interesting to find that there is a cathodic peak appearing at −1.50 V for H_2omt, while such a peak is absent for either of the two complexes, suggesting that the cyclic voltammogramms of the compounds are affected by the solvent.

Biological activities

The antibacterial and antifungal activities of the compounds are listed in Table 6, showing that the free

Table 5. ^{13}C NMR spectra of the compounds H_2omt, **1** and **2** (in ppm)

Compound	Assignment[a]								
	C_1[b]	C_2	C_3	C_4	C_5	C_6	C_7	C_8	C_9
H_2omt	53.78	178.68	152.48	142.21	125.15	133.49	126.73	128.16	132.48
1	51.85	186.34	159.31	141.96	124.69	135.04	125.39	128.40	133.05
2	51.68	186.98	159.14	141.76	124.69	134.91	126.61	128.52	132.97

[a] The signals of 2,2′-bipyridinyl ring for **1** appear at δ 150.71, 149.96, 139.37, 121.15 and 120.74, while the ones of *o*-phenanthrolinyl ring for **2** are observed at δ 149.76, 140.98, 138.27, 132.16, 125.07 and 124.60.

[b] The positions of the carbon atoms are denoted in the structure of the free ligand H_2omt.

Table 6. Antibacterial and antifungal activity of the compounds H_2omt, **1** and **2**[a]

Bacterium or fungus	H_2omt	**1**	**2**
B. subtilis 6633	0	5.3	3.8
S. lutea	0	7.5	7.4
S. aureus 209p	0	9.5	11.1
P. diploccus	0	9.2	6.5
E. coli	5.0	7.1	7.7
P. aeruginosa x313	0	9.3	9.3
S. Yake Sake	3.2	6.0	6.9

[a](1) The concentration of each tested compound was given in 0.55 mM. (2) The inhibition zone was given in mm.

ligand H_2omt was inactive against *B. subtilis* 6633, *S. lutea*, *S. aureus* 209p, *P. diploccus* and *P. aeruginosa* x313, but slightly active against *E. coli* and *S. Yake Sake*. Both the metal complexes exhibited inhibition activities against the tested bacteria and fungus, indicating that the enhancement of the biological activities of the complexes is related to the coordination of the metal ion and the bpy or phen molecule.

Acknowledgements—The financial supports from the NNSF of China, Developing Foundation of Tongji University and the Natural Science Foundation of Guangdong Province are appreciated.

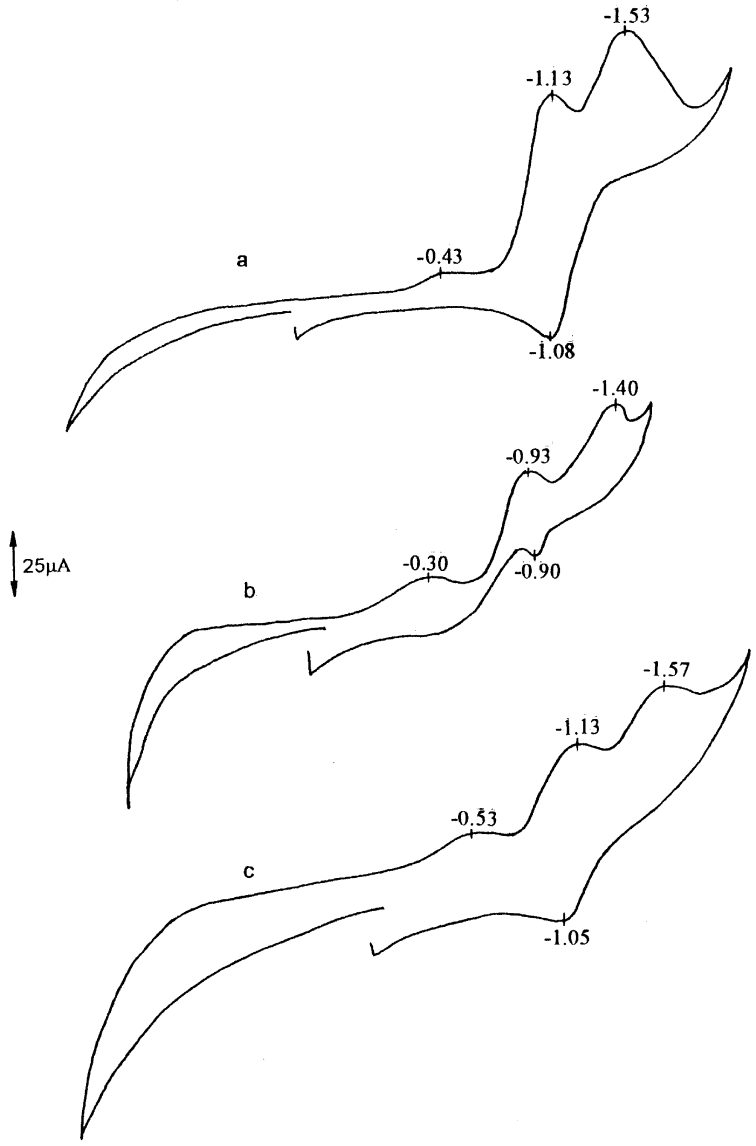

Fig. 5. Cyclic voltammograms of compounds H_2omt (a), **1** (b), **2** (c). (Measured in DMF, 1×10^{-4} mol · dm^{-3}, scan rate 100 mV · s^{-1}).

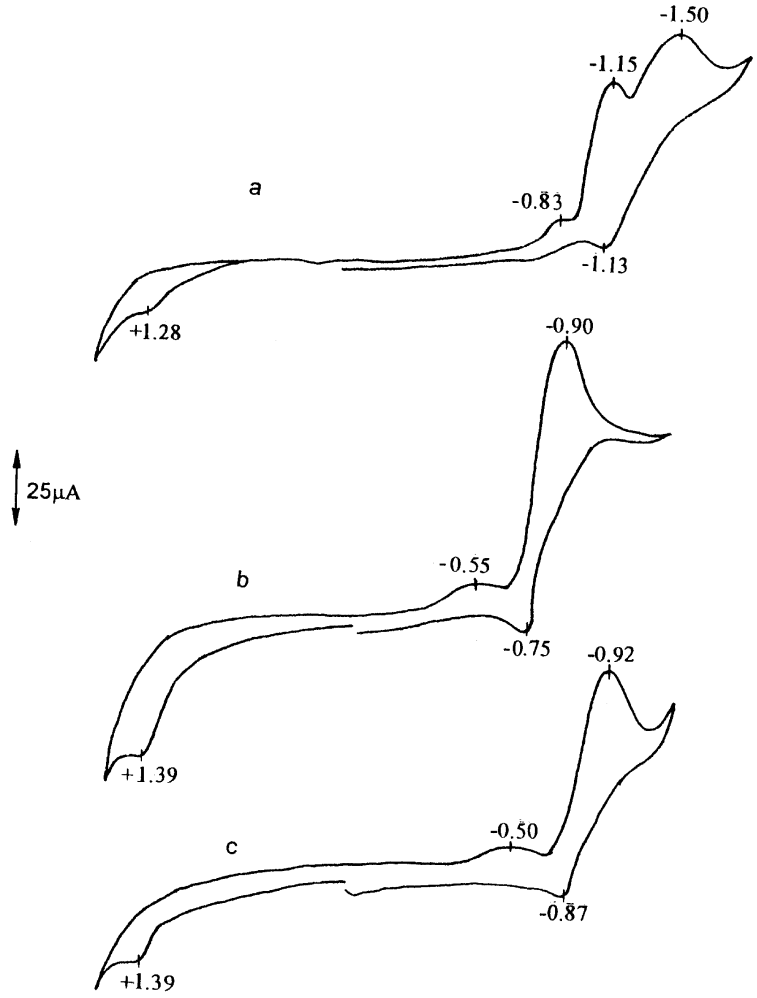

Fig. 6. Cyclic voltammograms of compounds H_2omt (a), **1** (b), **2** (c). (Measured in CH_3CN, 1×10^{-4} mol · dm^{-3}, scan rate 100 mV · s^{-1}).

REFERENCES

1. Huang, Z., Wu, L., Xiao, J., Huang, Q., Liu, Y. and Gu, L., *Youji Huaxue*, 1995, **15,** 221.
2. Shen, X., Wen, T. B., Liu, Q. T., Huang, X. Y., Kang, B. S., Wu, X. L., Huang, Z. S. and Gu, L. Q., *Polyhedron*, 1997, **16,** 2605.
3. French, F. A., Blanz, E. J., Amaral, J. R. D. and French, D. A., *J. Med. Chem.*, 1970, **13,** 1117.
4. Mohapatra, B. B., Guru, S. and Mohapatra, B. K., *J. Inorg. Nul. Chem.*, 1977, **39,** 2291.
5. Antholine, W. and Taketa, F., *J. Inorg. Biochem.*, 1982, **16,** 145.
6. Petering, D. H., *Metal Ions in Biological Systems*, Vol. 11, Chap. 4, ed. H. Sigel. Marcel Dekker, New York, 1980.
7. Shoukry, M. M., Mahgoub, A. S. and Elnagdi, M. H., *J. Inorg. Nul. Chem.*, 1980, **42,** 1171.
8. Mohamadou, A., Dechamps-Olivier, I. and Barbier, J. P., *Polyhedron*, 1994, 13, 1363 and 3277.
9. Guilion, E., Mohamadou, A., Dechamps-Olivier, I. and Barbier, J. P., *Polyhedron*, 1996, **15,** 947.
10. Ranford, J. D., Sadler, P. J. and Tocher, D. A., *J. Chem. Soc. Dalton Trans.*, 1993, 3393.
11. Korolkiewicz, Z., Hac, E., Gagalo, L., Gorezyca, P. and Lodzinska, A., *Agents Actions*, 1989, **26,** 355.
12. Sundberg, R. J. and Martin, R. B., *Chem. Rev.*, 1974, **46,** 571.
13. Abdel-Rahman, L. H., Battaglia, L. P. and Mahmoud, M. R., *Polyhedron*, 1996, **15,** 327.
14. Bradshaw, R. A., Shearer, W. T. and Gurd, P. R. N., *J. Biol. Chem.*, 1968, **243,** 3817.
15. Freedmann, T. B., Loehr, J. S. and Loehr, T. M., *J. Am. Chem. Soc.*, 1976, **98,** 2809.
16. Shen, X., Kang, B. S., Liu, Y., Gu, L. Q. and Huang, X. Y., *J. Coord. Chem.* In press.
17. Shen, X., Shi, X. F., Liu, Y. S. and Kang, B. S., *Chem. J. Chin. Uni.* In press.
18. Gerhardt, P., *Manual of Methods for General Bacteriology*, ed. R. N. Castello. American Society for Micrology, 1981, pp. 65–208.

19. Castro, J. A., Romero, J., Garcia-Vazquez, J., Sousa, A., Zubieta, J. and Chang, Y., *Polyhedron*, 1996, **15,** 2741.
20. Castro, R., Duran, M. L., Garcia-Vazquez, J. A., Sousa, A., Castineiras, A., Hiller, W. and Strahle, J., *Z. Naturforsch*., 1992, **47b,** 1067.
21. Santos, R. A., Koch, E. S. and Harbison, G. S., *J. Am. Chem. Soc*., 1990, **112,** 9257.
22. Dakternieks, D., *Aust. J. Chem*., 1982, **35,** 469.
23. Zhang, W. X., Ma, C. Q., Wang, X. N., Yu, Z. G., Jing, D. H. and Zheng, J. M., *Chin. J. Struct. Chem*., 1996, **15,** 404.
24. Baggio, R., Baggio, S., Pardo, M. I. and Garland, M. T., *Acta Cryst. C*, 1996, **52,** 820.
25. Speca, A. N., Karayannis, N. M. and Pytlewski, L. L., *Inorg. Chim. Acta*, 1976, **17,** 29.
26. Noboru, O. and Nakamoto, K., *Inorg. Chem*., 1975, **10,** 798.
27. Barret, J. and Deghaidy, F. S., *Spectrochim. Acta*, 1975, **31A,** 707.

Pergamon

Polyhedron Vol. 17, No. 23–24, pp. 4059–4064, 1998
© 1998 Elsevier Science Ltd
All rights reserved. Printed in Great Britain
0277–5387/98 $19.00+0.00

PII: S0277–5387(98)00209–5

Conformation and electrochemistry of some β-[alkyl-bridged biferrocenyl]-α,β-unsaturated ketones

Yao-feng Yuan,[a]†Ling-yun Zhang,[a] Ai-guo Hu,[a] Ji-tao Wang[a] and Wan-yi Liu[b]

[a]National Key Laboratory of Elemento-Organic Chemistry, Department of Chemistry, Nankai University, Tianjin 300071, People's Republic of China

[b]Department of Chemistry, Ningxia University, Yinchuan 750021, People's Republic of China

(Received 30 July 1997; accepted 18 May 1998)

Abstract—The geometrical and conformational isomerism of some β-[alkyl-bridged biferrocenyl]-α,β-unsaturated ketones was discussed on the basis of their IR and ^{1}HNMR spectra. They exist in *s-cis* conformation. The electrochemistry of the title compounds was also studied using cyclic voltammetry. Two distinct consecutive pairs of one-electron reversible redox peaks centered on the two non-equivalent ferrocenyl fragments were observed. © 1998 Elsevier Science Ltd. All rights reserved

Keywords: β-[alkyl-bridged biferrocenyl]-α,β-unsaturated ketones; conformational study; electrochemistry.

INTRODUCTION

Binuclear ferrocene derivatives have aroused many researches in recent years as redox active entities with potential application in fields such as materials for molecular electronics and as biologically active compounds [1–3]. Zanello's group has done some work on alkyl-bridged biferrocene compounds [4, 5]. As a continuation of our previous studies on alkyl-bridged biferrocene [6], we now report here the condensation reactions of alkyl-bridged biferrocenyl formaldehyde with aryl ketones, which afford several β-[alkyl-bridged biferrocenyl]-α,β-unsaturated ketones (Scheme 1). Their conformational and electrochemical properties are discussed as well.

EXPERIMENTAL

2,2-Diferrocenyl propane, 2,2-diferrocenyl butane and the corresponding formaldehyde derivatives were prepared as before [6]. Other chemicals were of analytical grade. The instruments used were the same as those described in the literature [6]. Cyclic voltammetric experiments were performed on a BAS-100B electrochemical analyzer equipped with a three electrode assembly with 0.1 mol/l -*n*-Bu_4NPF_6 as support electrolyte and CH_2Cl_2 as solvent. The working electrode was a platinum disk of 1.5 mm in diameter embedded in a cobalt glass seal and was polished consecutively with polishing alumina and diamond suspensions between runs. The reference electrode was a KCl saturated calomel electrode. A platinum filament was used as an auxiliary electrode. The solutions were saturated and blanketed with N_2 before the first scan. Measurements were made at room temperature.

Synthesis of β-[alkyl-bridged biferrocenyl]-α,β-unsaturated ketones

Taking compound **1** as an example: A solution of 2,2-propinyl-bridged biferrocene formaldehyde (4.84 g, 1.1 mmol) and *p*-aminopheylmethylketone (2.97 g, 2.2 mmol) in 95% EtOH (35 cm^3) was stirred at room temperature for 8–12 h in the presence of KOH (0.168 g, 3 mmol). The reaction mixture was then extracted by CH_2Cl_2, washed to neutral by water

†Author to whom correspondence should be addressed. Tel.: +86-22-2350-9163; Fax: +86-22-2350-4853; E-mail: yuanyfz@public1.tpt.tj.cn

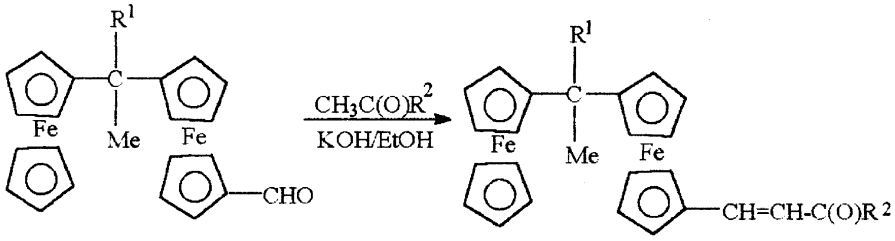

1. R^1=CH_3, R_2=*p*-$NH_2C_6H_4$; 2. R^1=CH_3, R_2=C_6H_5; 3. R^1=C_2H_5, R_2=*p*-$NH_2C_6H_4$
4. R^1=C_2H_5, R_2=C_6H_5 ; 5. R^1=C_2H_5, R_2=Fc.

Scheme 1. The preparation of the title compounds.

and dried with anhydrous Na_2SO_4. After removal of the solvent under reduced pressure, the dark red residue was dissolved in a minimum amount of benzene and chromatographed on alumina using C_6H_6 and C_6H_6–Et_2O (2:3) as eluents successively. The resulting product was recrystallized by EtOH–H_2O. **2**–**5** are synthesised analogously. Yield >90%.

RESULTS AND DISCUSSION

All the *β*-[alkyl-bridged biferrocenyl]-*α*,*β*-unsaturated ketones are red solids stable in the air. Their analytical and melting points are listed in Table 1. Their IR, ^{1}H NMR and UV spectra data are listed in Tables 2–4, respectively.

IR spectra

The KBr disk IR spectra of the *β*-[alkyl-bridged biferrocenyl]-*α*,*β*-unsaturated ketones show two strong bands at about 1650 and 1590 cm^{-1}, due to the carbonyl and ethylenic stretching vibration respectively. The two peaks in the region 1000–1077 cm^{-1} were allocated as $\delta_{CH=CH}$ of olefin with a *trans* configuration [7]. While in CCl_4 solution, $\nu_{C=O}$ and $\nu_{C=C}$ bands split, indicating the existence of an equilibrium between *s-cis* and *s-trans* conformation. Their IR spectral data in CCl_4 solution were listed in Table 2.

In compounds **1**–**5**, a conformational equilibrium may occur by the rotation around both C(1′)–C(*β*) and C(*α*)–C(CO) bonds. There are two favored coplanar forms, *s-cis* (**1**) and *s-trans* (**2**), as illustrated in Scheme 2. IR spectra is often used to study the equilibrium between *s-cis* and *s-trans* [8, 9]. Investigation of many substituted monoferrocene analogues have been reported [10, 11].

The *s-cis* form is preferred because there may be strong steric repulsion between H(*β*) and the *ortho*-hydrogens on the phenyl group in *s-trans* conformation. There are sharp carbonyl bands and intensified $\nu_{C=CH}$ bands in the IR spectra of their CCl_4 solutions. On the basis of the empirical rules suggested by Shorter and Hayes *et al.* [8, 9], the existence of the equilibrium and the predominance of the *s-cis* conformation in solution could be inferred. This conclusion is also supported by their ^{1}H NMR spectra.

^{1}H NMR *spectra*

^{1}H NMR spectra of the new compounds are recorded at room temperature. As the cyclopentadienyl protons are in almost the same chemical environment, their signals overlap and form an multiplet. In the ^{1}H NMR spectra of the title compounds, the olefinic protons give a doublet, corresponding to an AB type absorption. The coupling constant is 15 Hz, indicating they exist in *trans*-configuration, in which the biferrocenyl and the carbonyl groups take the opposite

Table 1. Physical properties and elemental analyses data for the title compounds

Compounds	M.p. (°C)	Found (calcd) (%)		
		C	H	N
1	180–181	69.0 (69.0)	5.6 (5.3)	2.9 (2.5)
2	83–84	70.9 (71.2)	5.6 (6.1)	–
3	35–37	69.0 (68.4)	6.3 (5.5)	2.4 (2.4)
4	40–41	71.0 (70.4)	6.2 (6.3)	–
5	82–83	66.7 (67.1)	5.8 (5.8)	–

Table 2. IR Data in CCl_4 solution for the title compounds (cm^{-1})

Compounds	*s-cis*		*s-trans*		
	$\nu_{C=O(1)}$	$\nu_{C=C(1)}$	$\nu_{C=O(2)}$	$\nu_{C=C(2)}$	$\delta_{CH=CH}$
1	1676 (s)	1552 (vs)	1620 (s)	1585 (vs)	1003 (s)
2	1686 (s)	1558 (vs)	1661 (s)	1593 (s)	1002 (vs)
3	1659 (s)	1549 (s)	1651 (vs)	1580 (s)	1014 (vs)
4	1716 (s)	1551 (vs)	1657 (vs)	1596 (s)	
5	1648 (s)	1551 (s)	1610 (vs)	1605 (s)	
FcCH=CHC(O)Bu-*n*[a]	1685	1600	1663	1617	
FcCH=CHC(O)Ph	1661	–	1635	–	
FcCH=CHC(O)C_6H_4-4-Me[a]	1659	–	1636	–	

[a]From Ref.[10].

Table 3. ^{1}H NMR data for the title compounds (δ, ppm)

Compounds	Bridged alkyl	Cp	Olefinic		Ph	NH_2
			α	β		
1	1.9 (s, 6H)	4.1–4.6 (m, 17H)	7.0 (d, 1H)	7.6 (d, 1H)	7.2 (m,2H), 7.9 (m,2H)	3.8 (s, 2H)
2	1.3–1.6 (m, 6H)	3.9–4.6 (m, 17H)	7.0 (d, 1H)	7.7 (d, 1H)	7.2–7.9 (m, 5H)	
3	0.7 (m, 3H), 1.6 (s, 3H), 1.9 (m, 2H)	4.1–4.6 (m, 17H)	7.0 (d, 1H)	7.6 (d, 1H)	7.2–7.8 (m, 4H)	3.8 (s, 2H)
4	0.8 (m, 3H), 1.6 (s, 3H), 1.9 (m, 2H)	4.1–4.7 (m, 17H)	7.0 (d, 1H)	7.6 (d, 1H)	7.2 (m,2H), 7.8 (m,3H)	
5	0.8 (m, 3H), 1.6 (s, 3H), 1.9 (m, 2H)	4.1–4.4 (m, 26H)	6.8 (d, 1H)	7.6 (d, 1H)		

Table 4. UV absorptions of the title compounds and their related precursors (λ_{max}, nm)

Compounds	π–π^*(ε_{max})			d–d(ε_{max})
1	202 (88610)	249 (16750)	367 (32790)	505 (4580)
2	204 (139800)	252 (63830)	322 (44370)	482–541 (7570–7060)
3	202 (86540)	255 (18200)	369 (35760)	504 (6910)
4	204 (145600)	253 (59630)	330 (46280)	488–540 (7580–6140)
5	204 (204600)		332 (113520)	483–505 (4830–2690)
$FcC(Me)_2FcCHO$	204 (130100)		275 (62710)	437–467 (7570–6550)
FcC(Me)(Et)CHO	204 (128900)		282 (59670)	437–472 (7260–6680)

position of the double bond. This is in accordance with their monoferrocenyl analogues reported in the literature [10]. Both H(α) and H(β) signals are shifted upfield. If the *s-trans* rotamer is favored, H(α) is in the shielding area of the carbonyl group and H(β) is closer to the aryl ring, whose anisotropy would increase the shielding about H(β). Their δ values could not be so high. Consequently, the *s-cis* conformation is the favored conformation.

UV spectra

The UV spectra of the title compounds were recorded in 95% EtOH and are summarized in Table 4,

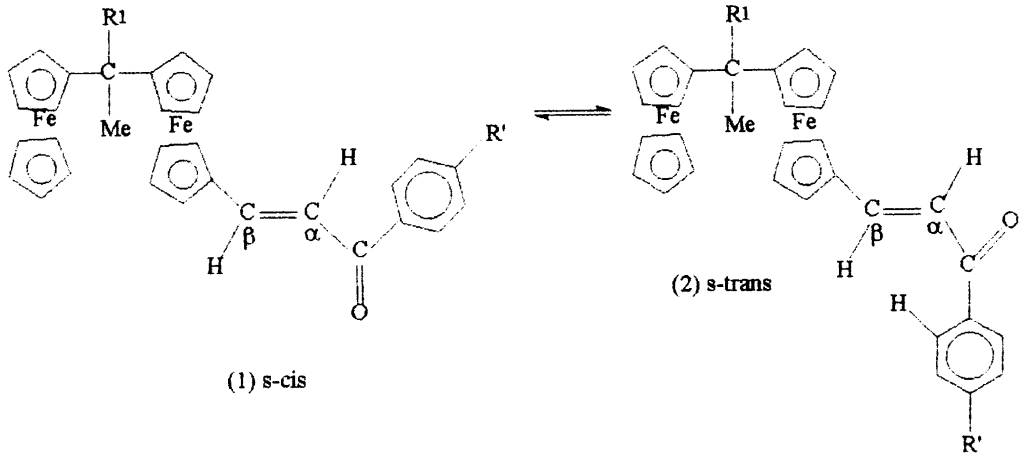

Scheme 2. Conformational equilibrium of the title compounds.

together with some related literature reported ferrocene derivatives. The strongest absorption bands at 322–369 nm can be assigned to the π–π^* transition of the α,β-unsaturated ketone conjugated with the ferrocene nucleus. The d–d transition, appears at a longer wavelength in the region 482–541 nm as a broad peak. The two ferrocenyl groups are indistinguishable by UV spectra. The large bathochromic shifts are ascribed to the extensive conjugation of α,β-unsaturated ketone with the ferrocenyl moiety and the interaction of the nonbonding d-orbital of iron with the substituents on the ferrocenyl group. In addition, such large bathochromic shifts may also involve the bridging alkyl group, which play some role in electronic interactions. This could be inferred from their electrochemical behavior also.

Electrochemical studies

The cyclic voltammetric behaviours of the compounds were studied using CH_2Cl_2 as solvent and 0.1 mol l^{-1} TBAFB(Bu_4NBF_4) as supporting electrolyte. The measurements were carried out at 13°C. The scan rate was 100 mV s^{-1}. The $\overline{E_{p1}}$ [$\overline{E_{p1}} = 1/2(E_{pa1} + E_{pc1})$], $\overline{E_{p2}}$ [$\overline{E_{p2}} = 1/2(E_{pa2} + E_{pc2})$] and their differences $\Delta\overline{E_p} = \overline{E_{p2}} - \overline{E_{p1}}$, together with the K_{con} and Robin–Day classification [12, 13, 14] are given in Table 5. For comparison, ferrocene, 2,2-diferrocenylpropane (DFP), 2,2-diferrocenyl butane (DFB), diferrocenylketone (DFK) [4] and bisferrocene (BF) [4] were also included in the measurements and the results are listed in Table 5. The CV curves of **1** and **5** are illustrated in Figs 1 and 2.

The following could be inferred from Table 5.

1. There are two pairs of redox peaks in the cyclic voltammograms of all the compounds studied.
2. The $\overline{E_{p1}}$ values of the first redox peak are all lower than that of ferrocene. This is attributed to the monosubstituted ferrocenyl group. The bridging alkyl and the other ferrocenyl group exert mainly an electron-donating effect, which makes it easier to be oxidized.

Table 5. Electrochemical characteristics for the oxidation process of the title compounds and related molecules with the Robin–Day classification of the relevant mix-valent species

Compounds	$\overline{E_{p1}}$ (V)	$E_{pc1} - E_{pa1}$ (mV)	$\overline{E_{p2}}$ (V)	$E_{pc2} - E_{pa2}$ (mV)	$\Delta\overline{E_p}$ (V)	K_{con} ($\times 10^4$)	Robin–Day class
1	0.355	89	0.548	75	0.193	0.18	II
2	0.359	103	0.553	71	0.194	0.19	II
3	0.386	72	0.671	78	0.285	6.6	II–III
4	0.389	80	0.676	73	0.281	7.0	II–III
5	0.376	63	0.628	75	0.262	2.7	II–III
DFP	0.355	81	0.551	76	0.196	0.20	II
DFB	0.328	74	0.551	73	0.223	0.59	II
DFK[a]	0.55		0.74		0.19	0.10	II
BF[a]	0.44		0.79		0.35	80	III
Ferrocene	0.44	99					

[a] From Ref.[4].

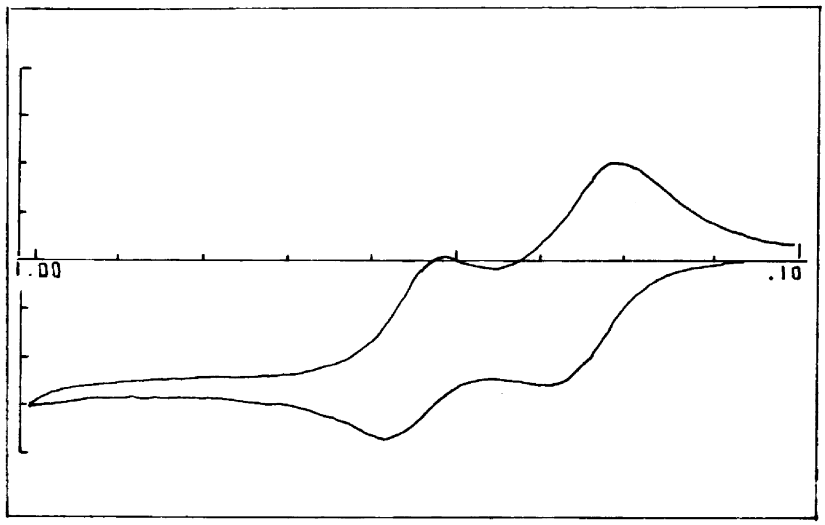

Fig. 1. Cyclic voltammogram obtained in CH_2Cl_2 (0.1 mol/l Bu_4NBF_4) at room temperature at a potential sweep rate of 100 mV s^{-1} for **1**. The initial potential was set at 0.100 V and the switching potential was 1.000 V.

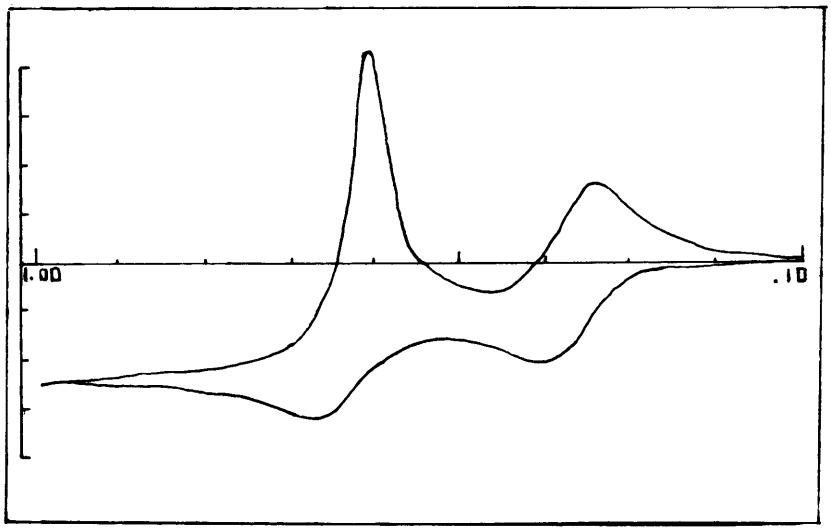

Fig. 2. Cyclic voltammogram obtained in CH_2Cl_2 (0.1 mol/l Bu_4NBF_4) at room temperature at a potential sweep rate of 100 mV s^{-1} for **5**. The initial potential was set at 0.100 V and the switching potential was 1.000 V.

3. The $\overline{E_{p2}}$ value of the second redox peak increases in the order 1→2→5→3→4 and $\Delta\overline{E_p}$ increases in the same order, indicating the more deformation from tetrahedral configuration the parent compounds [15] is, the more non-equivalent the two ferrocenyl groups are. The amino group is an electron-donating group and, as a result, **1** and **3** are oxidized slightly easier than **2** and **4**.
4. The $\Delta\overline{E_p}$ values of **1** and **2** reveal that the interaction between the two Fe sub-units is slight, the monocation is a slightly delocalized, weakly interacting class II mix valent species according to Robin–Day classification [4, 12, 13]. While in **3**–**5**, the two subunits interact more, thus causing extensive delocalization. They are classified between the weakly-interacting class II and strong-interacting class III within the Robin–Day classification.
5. For the redox of compounds with two or more ferrocenyl groups, a number of factors affecting the behavior of the ferrocenyl moieties concur. In the occurrence of two waves, through-space and through-bridge interactions and substituent effects coexist. The through-bridge interactions, however, seemed to be predominant. The more deformation

from regular tetrahedral configuration caused by the bridging group, the larger the difference in the electrochemical behaviors of the ferrocenyl groups.

Acknowledgements—This work was supported by the National Natural Science Foundation of China and the National Key Laboratory of Elemento-Organic Chemistry, Nankai University.

REFERENCES

1. Desbois, M. H. and Astruc, D., *Organometallics*, 1989, **8,** 1841.
2. Houlton, A., Jasim, N., Robert, R. M. G., Silver, J., Cunningham, D., McArdle, P. and Hggins, T., *J. Chem. Soc., Dalton Trans.*, 1992, 2235.
3. Neuse, E. W., Meirim, M. G. and Blom, N. F., *Organometallics*, 1988, **7,** 2562.
4. Ferguson, G., Glidewell, C., Opromolla, G., Zakaria, C. M. and Zanello, P., *J. Organomet. Chem.*, 1996, **517,** 183.
5. Osbome, A. G., Silva, M. W., Hursthouse, M. B., Malik, K. M. A., Opromolla, G. and Zanello, P., *J. Organomet. Chem.*, 1996, **516,** 167.
6. Yao-feng Yuan, Ling-yun Zhang, Wei-qing Qian, Ji-tao Wang, Wan-yi Liu, *Trans. Met. Chem.*1998, **23**(1), 21–24.
7. Eglinton, G., *Physical Methods in Organic Chemistry*, ed. J. C. P. Schwartz. Oliver and Boyd, Edinburgh, 1964, p. 65.
8. Shorter, J., *Quart. Rev.*, 1970, **24,** 433.
9. Hayes, W. P. and Timmons, C. J., *Spectra Acta A*, 1968, **24,** 323.
10. Kono, H., Shiga, M., Motoyama, I. and Hata, K., *Bull. Chem. Soc. Jpn.*, 1970, **43,** 1435.
11. Nagy, A. G. and Sohar, P., *J. Organomet. Chem.*, 1990, **390,** 217.
12. Robin, M. B. and Day, P., *Adv. Inorg. Chem. Radiochem.*, 1967, **10,** 247.
13. Gagne, R. R., Koval, C. A., Smith, T. J. and Cimolino, M. C., *J. Am. Chem. Soc.*, 1979, **101,** 4571.
14. Dimmok, J. R., Carter, P. L. and Ralph, P. D., *J. Chem. Soc. B*, 1968, 698.
15. Sun, Z., Hu, Y. C. and Li, Z., Huang, S., *Chin. J. Struct. Chem.*, 1988, **7,** 339.

Pergamon

Polyhedron Vol. 17, No. 23–24, pp. 4065–4070, 1998
© 1998 Elsevier Science Ltd
All rights reserved. Printed in Great Britain
0277–5387/98 $19.00+0.00

PII: S0277–5387(98)00210–1

Unexpected N-configurations in a Ni^{2+} complex of a mono-N-functionalized macrocycle

Claudio Schmid,*[a] Markus Neuburger,[a] Margareta Zehnder,[a] Thomas A. Kaden[a]† and Thomas Hübner[b]

[a]Institute of Inorganic Chemistry, Spitalstr. 51, 4056 Basel, Switzerland

[b]Molecular Simulations, Karl-Böhm-Str. 1, 85598 Baldham, Germany

(Received 20 January 1998; accepted 18 May 1998)

Abstract—The X-ray diffraction study of the Ni^{2+} complex with 1,4-dimethyl-1,4,8,11-tetraazacyclotetradec-8-yl-(2-ethane sulfonic acid) reveals a distorted *cis*-octahedral geometry around the metal ion The four nitrogen atoms of the macrocycle, the sulfonate group of the side chain and a water molecule are the six donor groups. Interesting is that in the crystals we find two relatively unexpected N-configurations of the macrocycle: the *cis*-II and the *cis*-V arrangement. Their relative energies and structures have been calculated using molecular modeling. (density functional theory, DFT). © 1998 Elsevier Science Ltd. All rights reserved. © 1998 Elsevier Science Ltd. All rights reserved

Keywords: structure; mono-N-functionalized; tetraazamacrocycle; Ni(II) complex; isomers.

1. INTRODUCTION

The functionalization of polyazamacrocycles has produced a large number of new and interesting compounds [1–3]. On one side the introduction of pendant chains can modify the solubility of the macrocycle, i.e. it can make it more lipophilic and thus one can extract metal ions from aqueous solution into an organic phase [4, 5]. On the other side the pendant chain can be used to covalently attach a macrocycle to a solid support and thus make ion exchangers [6–8] or to a protein such as a monoclonal antibody and thus label it with radioisotopes for nuclear medical applications [9, 10]. Furthermore functional groups, which have donor properties can enhance the complexation properties and selectivity of the macrocyclic moiety. So for example, the introduction of four acetate groups into 1,4,7,10-tetraazacyclododecane has produced an extremely powerful ligand such as DOTA [11], which because of its very high stability constants with Gd^{3+} has applications as contrast agent in magnetic resonance imaging [12].

Especially interesting in this regard are structural studies of metal complexes of such functionalized polyazamacrocycles, since they allow correlation of the molecular structures and coordination geometries [13]. In the case of mono-N-functionalized derivatives of 1,4,8,11-tetraazacyclotetradecane pentacoordination [14, 15] or *trans*-octahedral geometry [16, 17] have been observed depending on whether all nitrogens are tertiary or not. For di-N-functionalized compounds *trans*-octahedral species have been reported [16, 17].

In continuation of such studies we have now introduced a 2-ethanesulfonate group as a side chain into the tetraazamacrocycle **1** to give **2** and studied the structure of its Ni^{2+} complex.

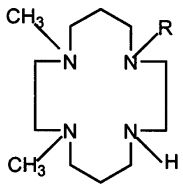

1 R = H,
2 R = $-CH_2CH_2SO_3H$

* Present address: Molecular Simulations, Karl-Böhm-Str. 1, 85598 Baldham, Germany.

† Author to whom correspondence should be addressed. Tel: +41-61-267-1006; Fax: +41-61-267-1020.

2. EXPERIMENTAL

^{1}H-NMR and ^{13}C-NMR spectra were run on a Gemini 300 using tetramethylsilane as an internal standard.

Compound **1** (1 mM) [18, 19], dissolved in EtOH (30 ml), was added dropwise at 5°C under nitrogen to a mixture of LiOH (4 mM) and sodium-2-chloroethanesulfonate (3 mM) in water (40 ml). The solution was then heated to 60°C for 20 h. After cooling to RT it was filtered and rotatory evaporated. The raw material was taken up in absolute EtOH so that the inorganic salts could be removed by filtration. The solvent was evaporated and the orange–brown oil was dried under high vacuum. ^{1}H-NMR showed that it is a mixture of **1** and **2**. Beside the signals belonging to **1** the following resonances were observed and tentatively assigned to (**2**): ^{1}H- and ^{13}C-NMR (D_6-DMSO) 1.52–1.68 (quint. CH_2–CH_2–CH_2); 2.10, 2.13 (2s, MeN); 2.30–2.43, 2.47–2.52, 2.56–2.72 (3m, CH_2N and CH_2SO_3H); 3.80 (br, NH). ^{13}C-NMR (D_6-DMSO): 24.80 ($CH_2CH_2CH_2$); 45.16, 45.39 (MeN); 47.24, 49.44, 51.25, 52.02, 52.16, 53.46, 54.20, 58.84, 55.15, 55.88 (CH_2N and CH_2SO_3).

A solution of this mixture in EtOH was treated with a slight excess of $Ni(ClO_4)_2 \cdot 6H_2O$, heated to reflux for 30 min and stirred overnight. The precipitated complex was collected by filtration, washed with absolute EtOH and Et_2O and finally dried in the desiccator. The blue complex was characterized by FAB.MS: 393 [complex-ClO_4]$^+$ and X-ray diffraction (see Section 2.1.).

2.1. *X ray crystallography*

[Ni(**2**)]ClO_4 crystallizes in the monoclinic space group P 21/a as cube-shaped, blue crystals (Table 1). A sample was glued on a glass fiber and mounted on the diffractometer.

Unit cell parameters were determined by the carefully centering of 25 independent, strong reflections with $23^\circ \leq \theta \geq 45^\circ$. Data collection has been carried out at 293 K using an Enraf-Nonius CAD4 diffractometer equipped with a Cu Kα fine focus sealed tube and with a graphite monochromator. Three reflections monitored every 2 h showed an intensity loss of 5.97%. The usual corrections were applied. Absorption correction was carried out using psi-scans (minimum and maximum transmission: 0.44/1.00). The structure was solved by direct methods using the program SIR92 [21]. Anisotropic least squares full matrix refinement was carried out on all non-hydrogen atoms using the program CRYSTALS [22]. The hydrogen atoms are in calculated positions. One part of the macrocyclic ligand and the counterion is disordered.

Table 1. Crystal data and parameters of data collection for [Ni(**2**)ClO_4]

Formula	$C_{14}H_{33}ClN_4NiO_8S$ ($C_{14}H_{31}N_4NiO_3 \cdot H_2O \cdot ClO_4$)
Mol. weight	511.66
Crystal system	monoclinic
Spacegroup	P 21/a
a (Å)	13.1296(12)
b (Å)	11.3594(8)
c (Å)	14.1155(13)
α (°)	90.000
β (°)	93.710(7)
γ (°)	90.000
volume (Å^3)	2100.8(3)
Z	4
F(000)	1080
Density (g cm^{-3})	1.62
μ (mm^{-1})	3.87
Crystal size (mm)	$0.18 \times 0.40 \times 0.55$
Temperature (K)	293
Radiation	Cu Kα ($\lambda = 1.54180$)
Scan type	$\Omega/2\theta$
θ max (°)	77.50
No. of measured reflections	4560
No. of independent reflections	4223
No. of reflections in refinement	3911
No. of variables	375
Final R	0.0458
Final R_w	0.0532
Weighting scheme	Chebychev polynomial [20]
Last max/min in diff. map	$0.48/-0.44$

Appropriate restraints have been set up to refine these parts. The refinement of 375 parameters including 3911 reflections with $I > 4.00\sigma(I)$ lead to a residual of 0.0458 ($R_w = 0.0532$). Scattering factors have been taken from the *International Tables* [23]. The fractional coordinates have been deposited at the Cambridge Crystallographic Data Center.

2.2. *Molecular modelling*

All DFT calculations were performed using the DMol program [24]. A double numeric basis set (DND) and a medium integration grid were used. Both structures were geometry optimized using the gradient corrected Vosko–Wilk–Nusair (BVWN) functional to an SCF convergence criteria of 5×10^{-4} a.u. and a maximum geometry gradient < 0.005 a.u.

3. RESULTS AND DISCUSSION

Generally the alkylation of 1,4-dimethyl-1,4,8,11-tetraazacyclotetradecane (**1**) with two ore more equivalents of alkylating agent gives difunctionalized products [18, 19, 25]. In the case of $ClCH_2CH_2SO_3Na$, however, a mixture of the starting compound **1** and the mono derivative **2** resulted. Since attempts to isolate the pure ligand failed, we tried a purification by addition of Ni^{2+} to the raw product. By selective crystallization the Ni^{2+} complex of **2**, besides a small amount of that with **1**, was obtained.

The crystal structure of [Ni(**2**)]ClO_4 (Fig. 1) is disordered in the propylene bridge between N(1) and N(2) and in the ethylene bridge between N(2) and N(3). The structure can be regarded as a superimposition of two N-conformers in the ratio 15:85 one being the *cis*-V the other the *cis*-II form according to the nomenclature of Bosnich *et al.* [26].

In both species the Ni^{2+} is octahedrally coordinated by the four nitrogens of the macrocycle, one oxygen of the sulfonate group and a water molecule. The two oxygens are *cis* to each other and the macrocycle is folded along the N(1)–Ni–N(3) axis. Bonds are in their normal range: 2.11–2.16 Å for Ni–N and 2.09–2.16 Å for Ni–O (Table 2). The angles around the Ni^{2+} ion are somewhat distorted from the ideal octahedral ones (Table 2).

The *cis*-arrangement found here is somewhat unusual for mono-N-functionalized derivatives,

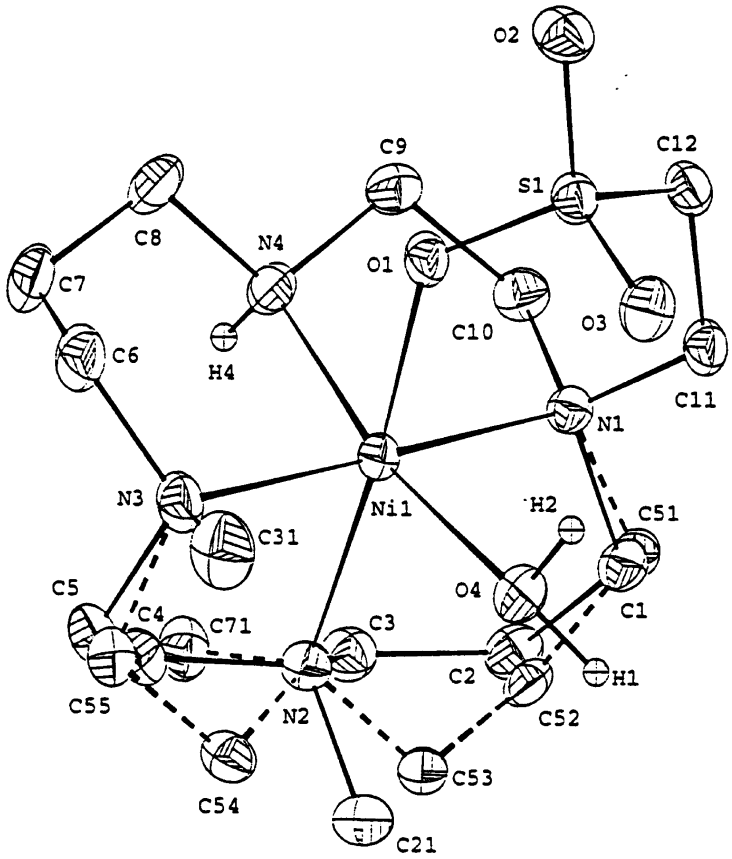

Fig. 1. ORTEP plot of the Ni^{2+} complex with **2**, showing the disorder in the propylene bridge between N(1) and N(2) and in the ethylene bridge between N(2) and N(3).

Table 2. Selected bonds (Å) and angles (°) in the structure of [Ni(**2**)](ClO$_4$) · H$_2$O

Ni(1)–N(1)	2.146(2)
Ni(1)–N(2)	2.134(2)
Ni(1)–N(3)	2.157(2)
Ni(1)–N(4)	2.112(2)
Ni(1)–O(1)	2.089(1)
Ni(1)–O(4)	2.161(2)
N(1)– Ni(1)–N(2)	94.98(6)
N(1)– Ni(1)–N(3)	177.68(7)
N(2)– Ni(1)–N(3)	83.76(7)
N(1)– Ni(1)–N(4)	83.70(7)
N(2)– Ni(1)–N(4)	96.08(7)
N(3)– Ni(1)–N(4)	94.49(8)
N(1)– Ni(1)–O(1)	92.87(6)
N(2)– Ni(1)–O(1)	172.11(6)
N(3)– Ni(1)–O(1)	88.43(6)
N(4)– Ni(1)–O(1)	85.64(7)
N(1)– Ni(1)–O(4)	89.57(6)
N(2)– Ni(1)–O(4)	92.59(6)
N(3)– Ni(1)–O(4)	92.43(7)
N(4)– Ni(1)–O(4)	169.44(7)
O(1)– Ni(1)–O(4)	86.59(6)

which generally give either pentacoordinated [14, 15] or *trans*-octahedral geometries [16, 17].

Also interesting is the fact that two N-configurations (*cis*-II and *cis*-V) are present in the same crystal (Fig. 2). For metal complexes of derivatives of 1,4,8,11-tetraazacyclotetradecane generally the *trans*-I and *trans*-III arrangement are found for square planar, pentacoordinated or *trans*-octahedral coordination geometries, whereas *cis*-V has been observed only in a few cases [27].

Since to our knowledge the *cis*-II arrangement has not been found up to now it was interesting to compare the relative energy of the two species by molecular modeling. The energy difference between *cis*-II and *cis*-V is 2.8 kcal/mol according to the molecular modeling calculation. The difference does not explain the 85:15 ratio found in the crystals, but the coincidence between the calculated and experimentally found structures are good with $R = 0.14$ and $R = 0.13$ for *cis*-II and *cis*-V, respectively (Fig. 2).

In the unit cell there is an extended network of intra [for example O(3) . . . H(2) . . . O(4)] and intermolecular

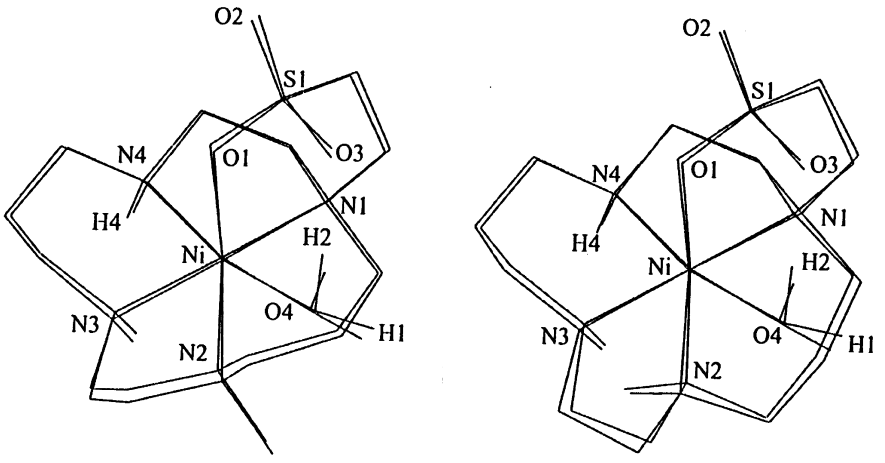

Fig. 2. Superimposition of the experimental and calculated structure of isomer *cis*-II (a) and *cis*-V (b).

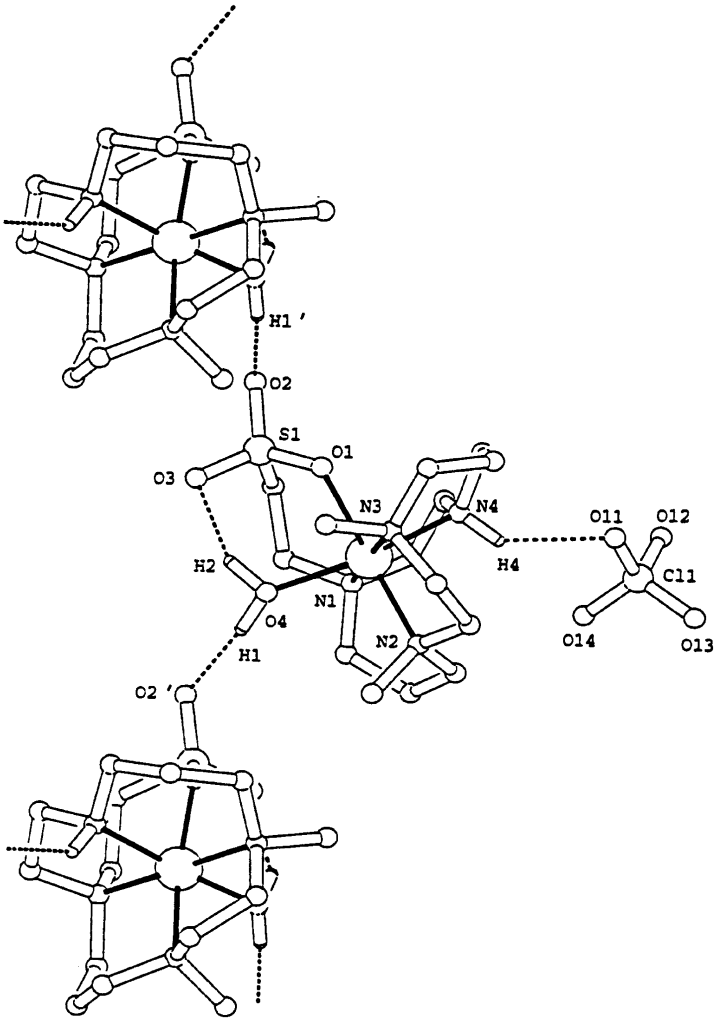

Fig. 3. Inter- and intramolecular hydrogen bonds in the unit cell of $[Ni(\mathbf{2})](ClO_4) \cdot H_2O$.

[O(4)...H(1)...O(2) or N(4)...H(4)...O(11)] hydrogen bonds (Fig. 3).

Whether these are responsible for the stabilization of the two N-configurations in the solid state is difficult to say.

Acknowledgements—This work was supported by the Bundesamt für Bildung und Wissenschaft in the context of a COST-D1 project.

REFERENCES

1. Kaden, Th. A., *Topics Curr. Chem.*, 1984, **121,** 157.
2. Bernhardt, P. and Lawrence, G. A., *Coord. Chem. Rev.*, 1990, **104,** 297.
3. Kaden, Th. A., in *Advances in Supramolecular Chemistry*, Vol. 3, ed. G. W. Gokel. JAI Press, Greenwich, 1993, p. 65.
4. Muller, F. R. and Handel, H., *Tetrahedron Lett.*, 1982, **23,** 2769.
5. Di Casa, M., Fabbrizzi, L., Perotti, A. and Tundo, P., *Inorg. Chem.*, 1985, **24,** 1610.
6. Blain, S., Appriou, P., Chaumeil, H. and Handel, H., *Anal. Chim. Acta*, 1990, **232,** 331.
7. Chaumeil, H. and Handel, H., *Eur. Polymer J.*, 1991, **27,** 269.
8. Schmid, I. and Sintra, R., *Topics Curr. Chem.*, 1984, **121,** 105.
9. Liu, Y. F. and Wu, C. C., *Pure Appl. Chem.*, 1991, **63,** 427.
10. Parker, D., *Chem Soc. Rev.*, 1990, **19,** 271.
11. Stetter, H., Frank, W. and Mertens, R., *Tetrahedron*, 1981, **37,** 767.
12. Meyer, D., Schaefer, M. and Bonnemain, B., *Invest. Radiol.*, 1988, **23,** 232.
13. Kaden, Th. A., *Comm. Inorg. Chem.*, 1990, **10,** 25.
14. Tschudin, D., Riesen, A. and Kaden, Th. A., *Helv. Chim. Acta*, 1989, **72,** 131.

15. Studer, M., Riesen, A. and Kaden, Th. A., *Acta Cryst. C*, 1990, **46,** 741.
16. Chapman, J., Ferguson, G., Gallagher, J. F., Jennings, M. C. and Parker, D., *J. Chem. Soc. Dalton Trans.*, 1992, 345.
17. Helps, I. M., Parker, D., Chapman, J. and Ferguson, G., *J. Chem. Soc. Chem. Commun.*, 1988, 1094.
18. Barefield, E. K., Wagner, F. and Hodges, U. D., *Inorg. Chem.*, 1976, **15,** 1370.
19. Wagner, F. and Barefield, E. K., *Inorg. Chem.*, 1976, **15,** 408.
20. Carruthers, J. R. and Watkin, D. J., *Acta Cryst. A*, 1979, **35,** 698.
21. Altomare, A., Cascarano, G., Giacovazzo, G., Guagliardi, A., Burla, M. C., Polidori, G. and Camalli, M., *J. Appl. Cryst.*, 1994, **27,** 435.
22. Watkin, D. J., Carruthers, R. J. and Betteridge, P., *Crystals*. Chemical Crystallography Laboratory, Oxford, U.K., 1985.
23. *International Tables for Crystallography*, Vol. IV. Kynoch Press, Birmingham, 1974, Table 2.2B.
24. *DMol Version* 960. Molecular Simulations, San Diego, CA, 1996.
25. Schibler, W. and Kaden, Th. A., *J. Chem. Soc. Chem. Commun.*, 1981, 603.
26. Bosnich, B., Poon, C. K. and Tobe, M. L., *Inorg. Chem.*, 1965, **4**, 1102 and 1109.
27. Boyens, I. C. A. and Dobson, S. M., in *Stereochemical and Stereophysical Behaviour of Macrocycles*, Vol. 2, ed. I. Bernal. Elsevier, Amsterdam, 1987, p. 1.

Pergamon

Polyhedron Vol. 17, No. 23–24, pp. 4071–4077, 1998
© 1998 Elsevier Science Ltd
All rights reserved. Printed in Great Britain
0277–5387/98 $19.00+0.00

PII: S0277–5387(98)00211–3

Coordination complexes of the hydroxymethylphosphine $FcCH_2P(CH_2OH)_2$ [Fc = (η^5-C_5H_5)Fe(η^5-C_5H_4)] and the X-ray crystal structure of the cationic gold bis(phosphine) complex $[Au\{FcCH_2P(CH_2OH)_2\}_2]Cl$

Nicholas J. Goodwin and William Henderson*

Department of Chemistry, University of Waikato, Private Bag 3105, Hamilton, New Zealand

(Received 21 April 1998; accepted 19 May 1998)

Abstract—Platinum(II) and palladium(II) complexes MCl_2L_2 and the gold(I) complex $[AuL_2]Cl$ of the air-stable ferrocene-derived hydroxymethylphosphine $FcCH_2P(CH_2OH)_2$ (L) have been synthesised by ligand substitution reactions, and the η^6-*p*-cymene ruthenium(II) complex $RuCl_2(\eta^6$-$C_{10}H_{14})L$ has been synthesised by a chloride bridge-splitting reaction of the dimer $[RuCl_2(\eta^6$-$C_{10}H_{14})]_2$. The cationic gold complex has been the subject of a single-crystal X-ray diffraction study, which shows the presence of the expected linearly coordinated bis(phosphine)gold cation, hydrogen-bonded to the chloride counterion and a lattice water molecule. © 1998 Elsevier Science Ltd. All rights reserved

Keywords: ferrocene; phosphine; hydroxymethyl; metal phosphine complexes; crystal structure.

INTRODUCTION

Hydroxymethylphosphines, containing P–CH_2OH functional groups, together with their metal complexes, have been known for some years [1]. However, in recent years there has been a renewed interest in the chemistry of these ligands ([2], see for example [3, 4]). Transition metal complexes of a variety of monodentate [5, 6], bidentate [7–11] and tridentate [12] hydroxyalkyl-phosphines have been recently reported, including zerovalent complexes of platinum, palladium and nickel [13, 14]. There is general interest in water-soluble phosphines in areas such as catalysis (see for example [15, 16]) and the development of new metal-based drugs [2, 9, 17]. The versatile reactivity of the hydroxymethylphosphine group towards primary and secondary amines (Mannich-type condensation) [18] allows the synthesis of a wide range of aminomethylphosphines [19–22]. Phosphines such as tris(2-cyanoethyl)phosphine [23–26] and phosphatriaza-adamantane (PTA) (for recent references see [27–30]) are synthesised starting from $P(CH_2OH)_3$, and are attracting interest in their own right. Such Mannich-type chemistry of Ph_2PCH_2OH has also been exploited in the synthesis of organophosphine dendrimers and complexes thereof [31–35].

Recently, we reported the high-yield synthesis (from inexpensive and readily-available $(FcCH_2NMe_3)I$ and $P(CH_2OH)_3$) of the air-stable ferrocene-derived hydroxymethylphosphine $FcCH_2P(CH_2OH)_2$ **1** [36]. Full details of the synthesis of this phosphine, together with some derivatives, have been reported [37]. Ferrocene-containing phosphines are being intensively investigated for their coordination chemistry (particularly 1,1′-bis(diphenylphosphino)ferrocene, dppf) [38], and applications to homogeneous catalysis [39–41]. The presence of the redox-active ferrocene centre provides additional interest in such ligands. We have also shown that **1** can be used to synthesise the completely air-stable and crystalline primary alkylphosphine $FcCH_2PH_2$ [42]. In this present paper we report some initial studies on the coordination chemistry of **1**,

*Author to whom correspondence should be addressed. Fax: +64-7-838-4219; E-mail: w.henderson@waikato.ac.nz

towards platinum group metal centres, gold, and ruthenium.

RESULTS AND DISCUSSION

Synthesis, NMR spectroscopy and electrospray mass spectrometry

Platinum(II) *cis*-$PtCl_2[FcCH_2P(CH_2OH)_2]_2$ **3**, palladium(II) $PdCl_2[FcCH_2P(CH_2OH)_2]_2$ **4**, gold(I) $[Au\{FcCH_2P(CH_2OH)_2\}_2]Cl$ **5** and η^6-*p*-cymene ruthenium(II), $RuCl_2(\eta^6\text{-}C_{10}H_{14})[FcCH_2P(CH_2OH)_2]$ **6**, complexes of the bis(hydroxymethyl)phosphine **1** have been prepared. The complexes were synthesised by standard procedures for this type of metal–phosphine–halide complex, involving displacement of the labile 1,5-cyclo-octadiene (COD) ligand from $MCl_2(COD)$ (M = Pd or Pt), by reaction of the *t*-butylisocyanide complex Au(CNBu^t)Cl with two equivalents of phosphine, or by the bridge-splitting reaction of **1** with $[RuCl_2(\eta^6\text{-}C_{10}H_{14})]_2$. The platinum and palladium complexes show relatively low solubilities in dichloromethane, and can be isolated as powders, and washed with dichloromethane to remove any excess ligand and liberated COD. Satisfactory elemental microanalytical data were obtained for all complexes.

NMR data for the complexes **3** and **4** suggest that they both have a *cis* configuration. Evidence for this is seen in the large $^1J(PtP)$ splitting of the ^{31}P NMR signal of **3** at δ 7.8 (3428 Hz) [43]. Also, the multiplets for ^{13}C NMR signals from the CH_2 groups in **3** exhibit a 5-line pattern which has been established as being characteristic of *cis* configuration for compounds of this sort, where there is an $A[X]_2$ spin system with virtual coupling [44, 45]. ^{31}P NMR of **4** indicates this Pd complex exists as only one isomer in solution. The multiplets for the ^{13}C NMR signals of the CH_2 groups in **4** are not as well defined as for **3**, but consist of broad doublets, which have also been identified as indicative of *cis* conformation in this type of compound [44, 45].

The gold complex **5** was initially thought to be the monophosphine complex $[Au\{FcCH_2P(CH_2OH)_2\}]Cl$ (and was reported as such in the initial communication [36]), but after further subsequent characterisation it has been reformulated as the bis(phosphine) complex **5**. Even if the reaction is performed with a 1:1 mole ratio of the reagents, this complex will form in preference to the monophosphine complex. The monophosphine complex can be prepared by reaction of **5** with AuCl(tetrahydrothiophene), but is unstable and degrades in solution.

Electrospray mass spectrometry [46, 47] has been used to provide additional characterisation data for complexes **5** and **6**. The gold complex **5** shows strong peaks for the parent cation $(L)_2Au^+$ (m/z 780.9) (L = **1**), as well as the mono-phosphine complex $(L)Au^+$ (m/z 489.0) (Fig. 1). Gold(I) phosphine complexes have been the subject of a detailed electrospray mass spectrometry study [48], and ions of the type observed in this work were reported previously. The stable carbocation $FcCH_2^+$ was observed at m/z 199.5; this ion is also observed as a fragment ion for the parent phosphine **1** [37], together with other $FcCH_2X$ type compounds [49]. Under the conditions employed for analysis of compound **6**, one peak was observed, arising from the exchange of a chloride ligand for an acetonitrile solvent molecule, i.e. $[M - Cl + MeCN]^+$ at m/z 604.3.

X-ray structure determination of $[Au\{FcCH_2P(CH_2OH)_2\}_2]Cl$ (**5**)

A variety of metal complexes of hydroxymethylphosphines have been structurally characterised previously, all being reported relatively recently. Reported examples [7, 8, 13, 50–52] include *cis*-$PtCl_2(Ph_2PCH_2OH)_2$ [5], the palladium [10], platinum [11] and rhenium complexes [9] of $(HOCH_2)_2PC_6H_4P(CH_2OH)_2$, and the rhenium complex of $(HOCH_2)_2PCH_2CH_2P(CH_2OH)_2$ [9]. Of greater relevance to the present study are the very recently reported compounds $[Au\{(HOCH_2)_2PC_6H_4P(CH_2OH)_2\}_2]Cl_2$ [53], $[Au_2\{(HOCH_2)_2PCH_2CH_2P(CH_2OH)_2\}_2]Cl_2$, $[Au\{P(CH_2OH)_3\}_4]Cl$ [54] and $[Au(Ph_2PCH_2OH)_3]Cl$ [54].

Single crystals of the gold bis(phosphine) complex **5** were obtained by recrystallisation from methanol/diethyl ether and subjected to a single-crystal X-ray diffraction study. The lattice contains the cation $[Au\{FcCH_2P(CH_2OH)_2\}_2]^+$, consisting of the two-coordinate gold(I) centre linearly coordinated by two phosphine ligands **1**, with P(1)–Au(1)–P(2) 176.51(6)°. The structure of the cation of **5** is given in Fig. 2, together with the atom numbering scheme, and selected bond lengths and angles are summarised in Table 1. As well as the cation, the lattice also contains a chloride counterion, and a water molecule of crystallisation. The shortest Au···Cl distance, Au(1)···Cl(1), is 3.436(2) Å, a distance which approximates the sum of the van der Waals radii (3.41 Å); any bonding interaction between the gold and chlorine atoms in the crystal must therefore be very weak. Additionally, the shortest gold–gold distance in the lattice is 5.8587(5) Å, which excludes the possibility of any bonding interactions between gold atoms. Of the gold–hydroxymethylphosphine structures previously reported, the only one displaying linear coordination at the gold atom is $[Au_2\{(HOCH_2)_2PCH_2CH_2P(CH_2OH)_2\}_2]Cl_2$ [53]. However, unlike compound **5** this compound seems to display strong auriophilic interactions. The structure of **5** is disordered at two points: The chloride ion occupies two positions, one on an inversion centre (not the source of disorder), and another position which has 50% occupancy, and the oxygen O(2) shows around 70% occupancy with an alternative position labelled O(2a) around 30% filled.

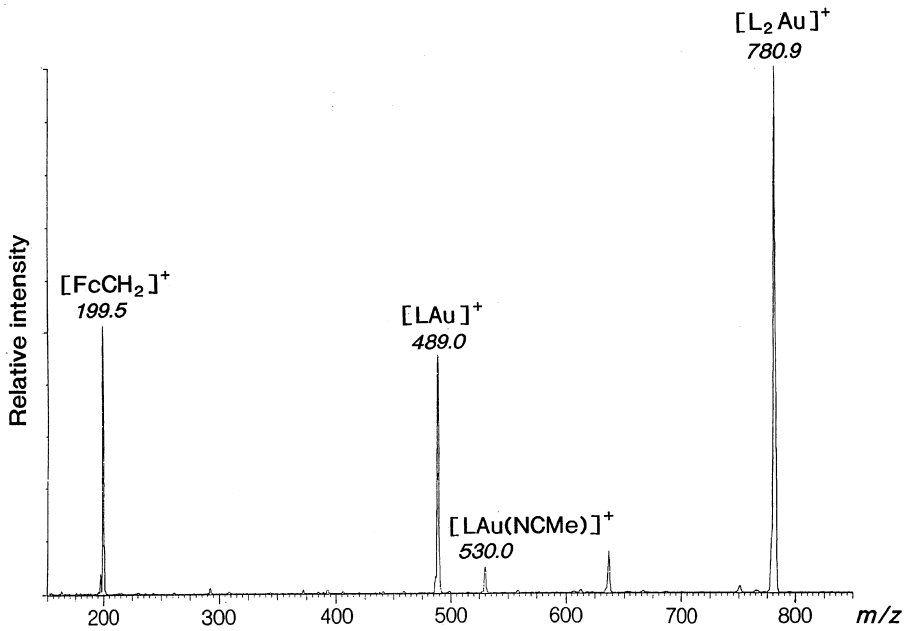

Fig. 1. Positive-ion ESMS spectrum of the gold phosphine complex **5** ($=(L_2Au)^+Cl^-$; L = **1**) in MeCN–H_2O at a cone voltage of 100 V, showing ion assignments.

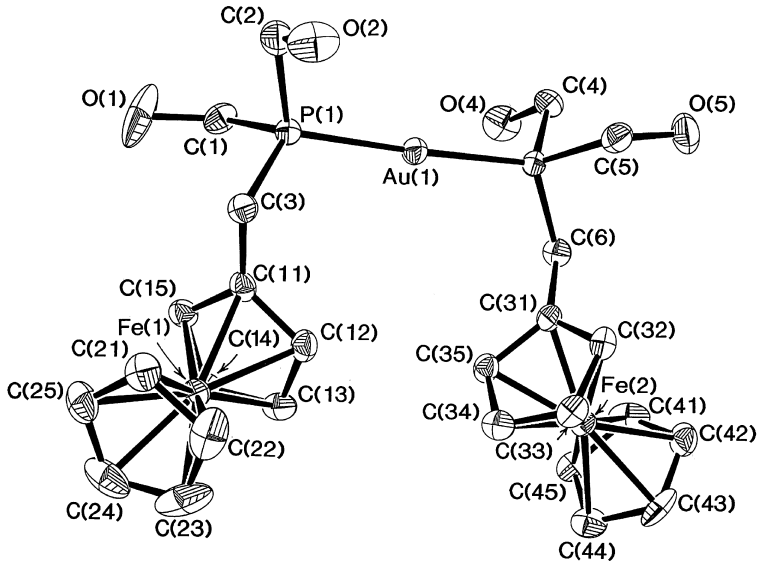

Fig. 2. ORTEP diagram of the $[Au\{FcCH_2P(CH_2OH)_2\}_2]^+$ cation of **5**, showing the atom numbering scheme.

No hydroxyl hydrogen atoms could be located in the final difference map, but consideration of interatomic distances in the structure suggests hydrogen-bonding in the lattice consists of a two-dimensional network in the plane of the *a* and *b* axes. In the direction of the *a* axis, hydrogen-bonding is probable between O(4), O(6) (that is, the water of crystallisation) and O(2) (or O(2a)) of the adjacent molecule ($O(4)\cdots O(6) = 2.707$ Å, $O(6)\cdots O(2a) = 2.748$ Å, $O(6)\cdots O(2) = 3.135$ Å). In the direction of the *b* axis, a hydrogen bond is probable between O(4) and O(5) of adjacent molecules ($O(4)\cdots O(5) = 2.636$ Å). Interatomic distances also suggest some hydrogen-bonding from O–H functions to both Cl(1) and Cl(2) is possible, with a number of $O\cdots Cl$ distances of around 3 Å.

Table 1. Selected bond lengths (Å) and angles (deg) for $[Au\{FcCH_2P(CH_2OH)_2\}_2]Cl \cdot H_2O$ (**5**)

Au(1)–P(2)	2.310(2)	Au(1)–P(1)	2.311(2)
P(1)–C(3)	1.821(6)	P(1)–C(1)	1.830(7)
P(1)–C(2)	1.839(7)	P(2)–C(6)	1.822(6)
P(2)–C(5)	1.831(7)	P(2)–C(4)	1.835(7)
O(1)–C(1)	1.428(9)	O(2)–C(2)	1.391(10)
O(4)–C(4)	1.432(9)	O(5)–C(5)	1.419(9)
C(3)–C(11)	1.505(9)	C(6)–C(31)	1.508(8)

P(2)–Au(1)–P(1)	176.51(6)	C(3)–P(1)–C(1)	105.0(3)
C(3)–P(1)–C(2a)	103.2(3)	C(1)–P(1)–C(2)	103.9(3)
C(3)–P(1)–Au(1)	117.0(2)	C(1)–P(1)–Au(1)	114.0(2)
C(2)–P(1)–Au(1)	112.4(2)	C(6)–P(2)–C(5)	105.6(3)
C(6)–P(2)–C(4)	102.4(3)	C(5)–P(2)–C(4)	101.0(3)
C(6)–P(2)–Au(1)	117.3(2)	C(5)–P(2)–Au(1)	114.2(2)
C(4)–P(2)–Au(1)	114.4(2)	O(2)–C(2)–P(1)	112.4(5)
O(1)–C(1)–P(1)	113.1(5)	C(11)–C(3)–P(1)	112.7(4)
O(4)–C(4)–P(2)	110.9(4)	O(5)–C(5)–P(2)	112.2(5)
C(31)–C(6)–P(2)	112.7(4)	C(12)–C(11)–C(3)	126.2(6)
C(15)–C(11)–C(3)	126.5(6)	C(3)–C(11)–Fe(1)	125.2(4)
C(32)–C(31)–C(6)	126.8(6)	C(35)–C(31)–C(6)	126.1(6)
C(6)–C(31)–Fe(2)	126.4(4)		

Fe–C, range 2.026(7)–2.060(7); average 2.046(7) Å.
C–C bonds of Cp ligands, range 1.386(11)–1.430(9), average 1.417(10).

Anti-tumour activity

The platinum, palladium and gold hydroxymethylphosphine complexes **3**–**5** each contain a metal with known anticancer activity [55], as well as phosphine and ferrocene units, which can both also show anti-tumour properties (in the case of ferrocene as the ferricinium ion). Consideration was given to the possibility that in these complexes the combined effect of the sub-units might make them useful anti-tumour agents. However, both **4** and **5** are too insoluble in methanol or water to be tested, while **3** was tested for cytotoxicity and found to be inactive, with an IC_{50} of 250,051 $\mu g\,ml^{-1}$ using the P388 anti-tumour assay.

Conclusion

In conclusion, the hydroxymethylphosphine **1** appears to show typical phosphine ligand properties towards precious metal centres. We are currently investigating the synthesis of metal complexes derived from the primary phosphine **2**, together with the electrochemistry of complexes of **1** and **2**; results will be reported in due course.

EXPERIMENTAL

Reactions were carried out in solvents of LR grade or better, in air unless otherwise stated. Light petroleum refers to the fraction boiling in the range 40–60°C.

^1H and ^{13}C–$\{^1H\}$ NMR spectra were recorded in either DMSO-d_6 or $CDCl_3$ solution (as indicated) on a Bruker AC300P spectrometer at 300.13 and 75.47 MHz, respectively, relative to $SiMe_4$ (δ 0.0). Scheme 1 depicts the labelling system employed for assignment of ferrocenyl NMR signals. ^{31}P–$\{^1H\}$ NMR spectra were recorded on the same instrument at 121.51 MHz with 85% H_3PO_4 (δ 0.0) as external reference. IR spectra were recorded as KBr discs on a BioRad FTS40 spectrometer, and melting points were determined using a Reichert Hotstage apparatus, and are uncorrected.

Electrospray mass spectra were obtained in positive-ion mode with a VG Platform II mass spectrometer using a 1:1 v/v acetonitrile–water mobile phase. The compounds were dissolved in the mobile

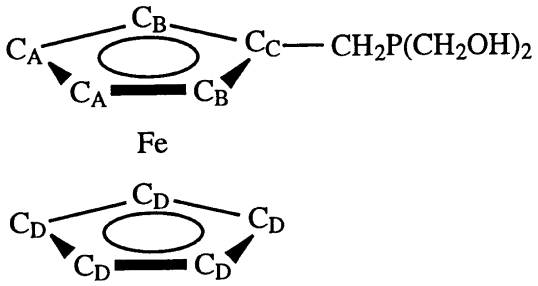

Scheme 1. Atom labelling used in NMR assignments of the ferrocenyl rings, shown for compound **1**.

phase to give a solution typically of approximate concentration 0.1 mM. The diluted solution was injected into the spectrometer via a Rheodyne injector fitted with a 10 μl sample loop. A Thermo Separation Products SpectraSystem P1000 LC pump delivered the solution to the mass spectrometer source (60 EC) at a flow rate of 0.01 ml min^{-1}, and nitrogen was employed both as a drying and nebulising gas. Cone voltages were typically varied from 10 to 100 V, in order to investigate the effect of higher voltages on fragmentation of the parent ions. Excellent agreement between observed and calculated isotope distribution patterns was observed for all major peaks. Theoretical isotope patterns were calculated using the *Isotope* program [56]. The complexes $PtCl_2$(COD) [57], $PdCl_2$(COD) [58], AuCl(CNBu*t*) [59], AuCl(tetrahydrothiophene) [60] and $[RuCl_2(\eta^6\text{-}C_{10}H_{14})]_2$ [61] and the ligand $FcCH_2P(CH_2OH)_2$ [37] were prepared by literature methods.

Anti-tumour testing of compound **5** was carried out at the Chemistry Department of the University of Canterbury, Christchurch, New Zealand.

Synthesis of cis-$PtCl_2[FcCH_2P(CH_2OH)_2]_2$ (**3**)

Phosphine **1** (0.100 g, 0.343 mmol) and $PtCl_2$(COD) (0.064 g, 0.172 mmol) were dissolved in CH_2Cl_2 (10 ml, LR grade) and stirred for 30 min. The resulting precipitate was removed by vacuum filtration, and dried under vacuum, giving **3** as a yellow powder (0.128 g, 0.151 mmol, 88%), M.P. ca. 210°C (dec). Found: C, 37.1; H, 4.5%. Calcd for $C_{26}H_{34}Cl_2Fe_2O_4P_2Pt$: C, 36.7; H, 4.0%. IR ($cm^{-1}$): 3410 (s), 3093 (w), 2919 (w), 2853 (w), 1462 (w), 1427 (m), 1405 (m), 1386 (m), 1237 (w), 1173 (w), 1105 (m), 1038 (s), 1028 (s), 1002 (m), 924 (w), 878 (m), 832 (m), 747 (w), 501 (m), 484 (m), and 452 (m). $^{31}P\text{–}\{^1H\}$ NMR (DMSO-d_6): δ 7.8 (s, $^1J(PtP) = 3428$ Hz). ^1H NMR (DMSO-d_6): δ 3.25 (FcCH_2P, d, $J = 5.2$ Hz, 2H), 4.04–4.19 (C_A–H, C_D–H, and PCH_2O, m, 11H), and 4.34 (C_B–H, unresolved t, 2H). $^{13}C\text{–}\{^1H\}$ NMR (DMSO-d_6): δ 25.51 (FcCH_2P, m), 58.62 (PCH_2O, m), 71.49 (C_A), 72.57 (C_D), 73.70 (C_B), and 83.65 (C_C).

Synthesis of $PdCl_2[FcCH_2P(CH_2OH)_2]_2$ (**4**)

Phosphine **1** (0.1248 g, 0.427 mmol) and $PdCl_2$(COD) (0.051 g, 0.214 mmol) were dissolved in CH_2Cl_2 (5 ml) and stirred for 15 min. The solution was cooled to 4°C before the precipitate was removed by filtration, washed with CH_2Cl_2, and dried under vacuum. Product **4** was obtained as an orange/brown powder insoluble in most common organic solvents (0.145 g, 0.191 mmol, 89%), M.P. ca. 185°C (dec). Found: C, 41.7; H, 4.4%. Calcd for $C_{26}H_{34}Cl_2Fe_2O_4PdP_2$: C, 41.0; H, 4.5%. IR ($cm^{-1}$): 3389 (s), 3094 (m), 2918 (w), 2852 (w), 1462 (w), 1427 (m), 1405 (m), 1386 (m), 1299 (w), 1237 (w), 1175 (w), 1105 (m), 1139 (s), 1126 (s), 1103 (m), 923 (w), 879 (m), 858 (m), 829 (m), 594 (w), 500 (m), 484 (m), and 444 (m). $^{31}P\text{–}\{^1H\}$ NMR (DMSO-d_6): δ 32.4 (s). ^1H NMR (DMSO-d_6): δ 3.24 (FcCH_2P, d, $J = 7.1$ Hz, 2H), and 4.04–4.44 (C_A–H, C_B–H, C_D–H, and PCH_2O, m, 13H). $^{13}C\text{–}\{^1H\}$ NMR (DMSO-d_6): δ 24.26 (FcCH_2P, m), 57.67 (PCH_2O, m), 69.49 (C_A), 70.48 (C_D), 71.33 (C_B), and 81.64 (C_C).

Synthesis of $[Au\{FcCH_2P(CH_2OH)_2\}_2]Cl$ (**5**)

Phosphine **1** (0.093 g, 0.314 mmol) and AuCl(CNBu′) (0.050 g, 0.159 mmol) were dissolved in CH_2Cl_2 (5 ml) and the solution stirred for 15 min. Petroleum spirits (b.p. 40–60°C) (10 ml) was added and the resulting precipitate removed by vacuum filtration to give **5** as a yellow powder, which was dried under vacuum to give the product **5** (0.105 g, 0.129 mmol, 80.6%). Recrystallisation by cooling a hot MeOH/diethyl ether solution to ca. −30°C yielded golden needles suitable for X-ray structural analysis (0.069 g, 0.084 mmol, 53%). M.P. 127–134°C. Found: C, 37.1; H, 3.9%. Calcd for $C_{26}H_{34}AuClO_4P_2Fe_2 \cdot H_2O$: C, 37.4%; H, 4.3%. IR (cm^{-1}): 3259 (s, br), 1408 (m), 1386 (m), 1298 (w), 1242 (w), 1185 (w), 1106 (m), 1038 (s), 1027 (s), 1002 (m), 926 (w), 887 (m), 804 (m), 595 (w), 504 (m), 483 (m), and 445 (w). ESMS (cone voltage 100 V) *m*/*z*: 780.9 $[L_2Au]^+$, 489.0 $[LAu]^+$, 199.5 $[FcCH_2]^+$ (L = **1**). $^{31}P\text{–}\{^1H\}$ NMR (DMSO-d_6): δ 36.2 (s). ^1H NMR (DMSO-d_6): δ 3.14 (FcCH_2P, s, 2H), 4.05–4.08 (PCH_2O, m, 4H), 4.20 (C_A–H, t, $J = 1.7$ Hz, 2H), 4.24 (C_D–H, s, 5H), and 4.26 (C_B–H, t, $J = 1.7$, 2H). $^{13}C\text{–}\{^1H\}$ NMR ($CDCl_3$): δ 24.90 (FcCH_2P, m), 59.53 (PCH_2O, m), 71.73 (C_A), 72.69 (C_D), 73.15 (C_B), and 84.48 (C_C).

Synthesis of $RuCl_2(\eta^6\text{-}C_{10}H_{14})[FcCH_2P(CH_2OH)_2]$ (**6**)

$[RuCl_2(\eta^6\text{-}C_{10}H_{14})]_2$ (0.070 g, 0.114 mmol) was dissolved in CH_2Cl_2 (10 ml) which was purged and placed under nitrogen before addition of **1** (0.066 g, 0.227 mmol). The mixture was refluxed for 20 min and the solvent removed under vacuum to give the crude product as a dark oil in quantitative yield. Vapour diffusion recrystallisation from CH_2Cl_2/EtOH with pentane yielded the product as a brown powder which was dried under vacuum (0.093 g, 0.155 mmol, 68%). M.P. = 181–188°C. Found: C, 46.2; H, 5.5%. Calc. for $C_{23}H_{31}Cl_2FeO_2PRu$: C, 46.2; H, 5.2%. IR (cm^{-1}): 3398 (s), 3174 (m), 3082 (m), 3043 (s), 2964 (m), 2873 (m), 1498 (w), 1467 (m), 1441 (m), 1384 (m), 1105 (m), 1036 (s), 1023 (s), 1002 (m), 924 (m), 890 (m), 864 (m), 823 (m), 811 (m), 777 (w), 508 (s), 479 (s), 460 (m), 444 (s), 426 (m). ESMS (cone voltage 60 V) *m*/*z*: 604.3 $[M - Cl + CH_3CN]^+$. $^{31}P\text{–}\{^1H\}$ NMR ($CDCl_3$-d_6): δ 25.9 (s). ^1H NMR ($CDCl_3$-d_6): δ 1.23 ($CH(CH_3)_2$, d, $J = 7$ Hz, 6H), 2.05 (CH_3, s, 3H), 2.78 ($CH(CH_3)_2$, hept., $J = 7$ Hz, 1H), 3.24 (FcCH_2P, d, $J = 8$ Hz, 2H), 4.16 (C_D–H, s, 5H), 4.18–4.19 (PCH_2O and C_A–H, m, 6H), 4.29 (C_B–H, s, 2H), 5.44 ($CH_3C(CH)_2$, d,

$J = 6$ Hz, 2H), 5.50 ($Pr^iC(CH)_2$, d, $J = 6$ Hz, 2H). ^{13}C–$\{^1H\}$ NMR ($CDCl_3$): δ 18.36 (CH_3, s), 22.21 ($CH(CH_3)_2$, s), 24.88 ($FcCH_2P$, d, $J = 19$ Hz), 30.75 ($CH(CH_3)_2$, s), 58.34 (PCH_2O, d, $J = 31$ Hz), 68.46 (C_A, s), 69.23 (C_D, s), 69.69 (C_B, s), 80.66 (C_C, s), 85.51 ($CH_3C(CH)_2$, d, $J = 4$ Hz), 87.98 ($Pr^iC(CH)_2$, d, $J = 4$ Hz), 96.41 ($CH_3C(CH)_2$, s), 107.11 ($Pr^iC(CH)_2$, s).

X-ray crystal structure of $[Au\{FcCH_2P(CH_2OH)_2\}_2]Cl \cdot H_2O$

Crystal data: $C_{26}H_{36}AuClFe_2O_5P_2$, $M_r = 834.60$; monoclinic, space group P2/c, $a = 12.3838(2)$ Å, $b = 6.3295(1)$ Å, $c = 36.8279(2)$ Å, $\beta = 92.360(1)^\circ$, $V = 2884.24(7)$ Å^3, $D_c = 1.922$ g cm^{-3} for $Z = 4$. $F(000) = 1640$, μ(Mo Kα) = 1.29 mm^{-1}, λ(Mo Kα) = 0.71073 Å, $T = -70^\circ$C, crystal size = 0.54 × 0.20 × 0.02 mm, yellow plate. A total of 16938 reflections were collected in the range $1.11 < \theta < 26.40^\circ$, corresponding to 6338 unique data ($R_{int} = 0.0409$, $T_{max,min}$ 0.91027, 0.6960).

The unit cell dimensions and intensity data were obtained on a Siemens SMART CCD diffractometer. The data collection nominally covered over a hemisphere of reciprocal space, by a combination of three sets of exposures; each set had a different ϕ angle for the crystal and each exposure covered 0.3° in ω. The crystal to detector distance was 5.0 cm. The data sets were corrected empirically for absorption using SADABS [62].

The structure was solved by Patterson methods and developed routinely. Full-matrix least squares refinement was based on F^2. Oxygen O(2) was disordered over two positions and was refined as O(2) and O(2a), with occupancies refined to 70.8% and 29.2%, respectively while temperature factors for the two atoms were restrained to 0.05. Temperature factors were subsequently allowed to refine without constraint, while occupancy was fixed. Only half the Cl(2) sites were occupied, and so refinement was carried out with occupancy set to 50%. Since Cl(1) occupied an inversion centre between two gold cations, the combined effect of the two chlorine atom positions was to provide one negative charge for each Au(I) atom. Refinement was carried out with all non-hydrogen atoms except O(2a) anisotropic and with hydrogen atoms included in calculated positions with isotropic temperature factors 1.2 times that of the U_{iso} of the atom to which they are bonded. Hydrogen atoms of the OH groups and the water molecule could not be found in the difference map and so were not included in the refinement. Refinement converged at $R_1 = 0.0419$ [for 4910 reflections with $F_o > 4\sigma(F_o)$] and $wR_2 = 0.0912$ (all data) ($w = [\sigma^2(F_o^2) + (0.0295P)^2 + 8.96P]^{-1}$ where $P = (\max(F_o^2, 0) + 2F_c^2)/3$); final GoF = 1.149). The final difference map showed no peak greater than $+1.172$ e Å^{-3} and no hole larger than -1.391 e Å^{-3} [both close to Au(1)]. Programs used for structure solution and refinement were SHELXS-86 [63] and SHELXL-93 [64].

Complete lists of atomic coordinates, bond parameters and tables of thermal parameters and hydrogen atom coordinates have been deposited at the Cambridge Crystallographic Data Centre (CCDC).

Acknowledgements—We thank the University of Waikato and the New Zealand Lottery Grants Board for financial support of this work. We thank Assoc. Professor C. E. F. Rickard and Dr L. J. Baker (University of Auckland) for collection of the X-ray data set, Johnson–Matthey PLC for a generous loan of platinum, and Wendy Jackson for technical assistance. We also thank Professor B. K. Nicholson (University of Waikato) for assistance with the X-ray crystallography. NJG thanks the William Georgetti Trust for a scholarship.

REFERENCES

1. Chatt, J., Leigh, G. J. and Slade, R. M., *J. Chem. Soc.*, 1973, 2021.
2. Katti, K. V., *Curr. Sci.*, 1996, **70,** 219.
3. Pringle, P. G. and Smith, M. B., *Platinum Metals Rev.*, 1990, **34,** 74.
4. Downing, J. H., Gee, V. and Pringle, P. G., *Chem. Commun.*, 1997, 1527.
5. Davies, D. L., Neild, J., Prouse, L. J. S. and Russell, D. R., *Polyhedron*, 1993, **12,** 2121.
6. Komiya, S., Awata, H., Ishimatsu, S. and Fukuoka, A., *Inorg. Chim. Acta*, 1994, **217,** 201.
7. Baxley, G. T., Miller, W. K., Lyon, D. K., Miller, B. E., Nieckarz, G. F., Weakley, T. J. R. and Tyler, D. R., *Inorg. Chem.*, 1996, **35,** 6688.
8. Nieckarz, G. F., Weakley, T. J. R., Miller, W. K., Miller, B. E., Lyon, D. K. and Tyler, D. R., *Inorg. Chem.*, 1996, **35,** 1721.
9. Reddy, V. S., Berning, D. E., Katti, K. V., Barnes, C. L., Volkert, W. A. and Ketring, A. R., *Inorg. Chem.*, 1996, **35,** 1753.
10. Reddy, V. S., Katti, K. V. and Barnes, C. L., *J. Chem. Soc., Dalton Trans.*, 1996, 1301.
11. Reddy, V. S., Katti, K. V. and Barnes, C. L., *Inorg. Chim. Acta*, 1995, **240,** 367.
12. Smith, C. J., Reddy, V. S. and Katti, K. V., *Chem. Commun.*, 1996, 2557.
13. Ellis, J. W., Harrison, K. N., Hoye, P. A. T., Orpen, A. G., Pringle, P. G. and Smith, M. B., *Inorg. Chem.*, 1992, **31,** 3026.
14. Hoye, P. A. T., Pringle, P. G., Smith, M. B. and Worboys, K., *J. Chem. Soc., Dalton Trans.*, 1993, 269.
15. Cornils, B. and Kuntz, E. G., *J. Organomet. Chem.*, 1995, **502,** 177.
16. Kalck, P. and Monteil, F., *Adv. Organomet. Chem.*, 1992, **34,** 219.
17. Herbowski, A. and Deutsch, E. A., *J. Organomet. Chem.*, 1993, **460,** 19.
18. Frank, A. W., Daigle, D. J. and Vail, S. L., *Textile Res. J.*, 1982, **52,** 678.
19. Fawcett, J., Hoye, P. A. T., Kemmitt, R. D. W., Law, D. J. and Russell, D. R., *J. Chem. Soc., Dalton Trans.*, 1993, 2563.
20. Fawcett, J., Kemmitt, R. D. W., Russell, D. R. and Serindag, O., *J. Organomet. Chem.*, 1995, **486,** 171.

21. McLain, S. J., *J. Am. Chem. Soc*., 1983, **105,** 6355.
22. McLain, S. J., *Inorg. Chem*., 1986, **25,** 3124.
23. Khan, M. N. I., King, C., Fackler, J. P. Jr. and Winpenny, R. E., *Inorg. Chem*., 1993, **32,** 2502.
24. Al-Arfaj, A. R., Hussain, M. S., Isab, A. A. and Akhtar, M. N., *Acta Cryst. C*, 1996, **52,** 550.
25. Liu, C. W., Pan, H., Fackler, J. P., Jr., Wu, G., Wasylishen, R. E. and Shang, M., *J. Chem. Soc*., *Dalton Trans*., 1995, 3691.
26. Orpen, A. G., Pringle, P. G., Smith, M. B. and Worboys, K., *J. Organomet. Chem*., 1998, **550,** 255.
27. Joó, F., Nádasdi, L., Bényei, A. C. and Darensbourg, D. J., *J. Organomet. Chem*., 1996, **512,** 45.
28. Darensbourg, D. J., Stafford, N. W., Joó, F. and Reibenspies, J. H., *J. Organomet. Chem*., 1995, **488,** 99.
29. Darensbourg, D. J., Decuir, T. J., Stafford, N. W., Robertson, J. B., Draper, J. D. and Reibenspies, J. H., *Inorg. Chem*., 1997, **36,** 4218.
30. Alyea, E. C., Ferguson, G. and Kanna, S., *Polyhedron*, 1997, **16,** 3533.
31. Slany, M., Bardajf, M., Casanove, M.-J., Caminade, A.-M., Majoral, J.-P. and Chaudret, B., *J. Am. Chem. Soc*., 1995, **117,** 9764.
32. Larre, C., Caminade, A.-M. and Majoral, J.-P., *Angew. Chem. Int. Ed. Engl*., 1997, **36,** 596.
33. Slany, M., Caminade, A.-M. and Majoral, J.-P., *Tetrahedron Lett*., 1996, **37,** 9053.
34. Bardaji, M., Kustos, M., Caminade, A.-M., Majoral, J.-P. and Chaudret, B., *Organometallics*, 1997, **16,** 403.
35. Lartigue, M.-L., Caminade, A.-M. and Majoral, J.-P., *Tetrahedron Asym*., 1997, **8,** 2697.
36. Goodwin, N. J., Henderson, W. and Sarfo, J. K., *Chem. Commun*., 1996, 1551.
37. Goodwin, N. J., Henderson, W., Nicholson, B. K., Sarfo, J. K., Fawcett, J. and Russell, D. R., *J. Chem. Soc*., *Dalton Trans*., 1997, 4377.
38. Gan, K. S., and Hor, T. S. A., in *Ferrocenes*, ed. A. Togni and T. Hayashi. VCH, Weinheim, 1995, p. 1.
39. Hayashi, T., in *Ferrocenes*, ed. A. Togni and T. Hayashi. VCH, Weinheim, 1995, p. 105.
40. Hayashi, T. and Kumada, M., *Acc. Chem. Res*., 1982, **15,** 395.
41. Abbenhuis, H. C. L., Burckhardt, U., Gramlich, V., Kollner, C., Pregosin, P. S., Salzmann, R. and Togni, A., *Organometallics*, 1995, **14,** 759.
42. Goodwin, N. J., Henderson, W. and Nicholson, B. K., *Chem. Commun*., 1997, 31.
43. Appleton, T. G., Clark, H. C. and Manzer, L. E., *Coord. Chem. Rev*., 1973, **10,** 335.
44. Redfield, D. A. and Nelson, J. H., *Inorg. Nucl. Chem. Lett*., 1974, **10,** 727.
45. Redfield, D. A., Cary, L. W. and Nelson, J. H., *Inorg. Chem*., 1975, **14,** 50.
46. Hop, C. E. C. A. and Bakhtiar, R., *J. Chem. Educ*., 1996, **73,** A162.
47. Colton, R., D'Agostino, A. and Traeger, J. C., *Mass Spectrom. Rev*., 1995, **14,** 79.
48. Colton, R., Harrison, K. L., Mah, Y. A. and Traeger, J. C., *Inorg. Chim. Acta*, 1995, **231,** 65.
49. Henderson, W., Oliver, A. G. and Downard, A. J., *Polyhedron*, 1996, **15,** 1165.
50. Harrison, K. N., Hoye, P. A. T., Orpen, A. G., Pringle, P. G. and Smith, M. B., *J. Chem. Soc*., *Chem. Commun*., 1989, 1096.
51. Hope, H., Olmstead, M. M., Power, P. P. and Viggiano, M., *Inorg. Chem*., 1984, **23,** 326.
52. Bartsch, R., Hietkamp, S., Morton, S., Peters, H. and Stelzer, O., *Inorg. Chem*., 1983, **22,** 3624.
53. Berning, D. E., Katti, K. V., Barnes, C. L., Volkert, W. A. and Ketring, A. R., *Inorg. Chem*., 1997, **36,** 2765.
54. Berning, D. E., Katti, K. V., Barnes, C. L. and Volkert, W. A., *Chem. Ber./Recueil*, 1997, **130,** 907.
55. S. P. Fricker (ed.), *Metal Compounds in Cancer Therapy*. Chapman and Hall, London, 1994.
56. Arnold, L. J., *J. Chem. Educ*., 1992, **69,** 811.
57. McDermott, J. X., White, J. F. and Whitesides, G. M., *J. Am. Chem. Soc*., 1976, **98,** 6521.
58. Drew, D. and Doyle, J. R., *Inorg. Synth*., 1972, **13,** 52.
59. Schneider, W., Angermaier, K., Sladek, A. and Schmidbaur, H., *Z. Naturforsch. b*, 1996, **51,** 790.
60. Uson, R., Laguna, A. and Laguna, M., *Inorg. Synth*., 1989, **26,** 85.
61. Bennett, M. A., Huang, T.-N., Matheson, T. W. and Smith, A. K., *Inorg. Synth*., 1982, **21,** 74.
62. Blessing, R. H., *Acta Cryst. A*, 1995, **51,** 33.
63. Sheldrick, G. M., SHELXS 86, Program for Solving Crystal Structures, University of Göttingen, 1986.
64. Sheldrick, G. M., SHELXL 93, Program for Refining Crystal Structures, University of Göttingen, 1993.

Pergamon

Polyhedron Vol. 17, No. 23–24, pp. 4079–4089, 1998
© 1998 Elsevier Science Ltd
All rights reserved. Printed in Great Britain
0277–5387/98 $19.00+0.00

PII: S0277-5387(98)00243-5

Syntheses and structural characterization of the one dimensional polymers: $^{1}_{\infty}[Rh_2(OAc)_4(NCPhCN)\cdot S]$; $S = CH_3COCH_3$, CH_3OH, C_2H_5OH, C_4H_8O and C_6H_6

Tianyan Niu, Jian Lu, Gerardo Crisci and Allan J. Jacobson*

Department of Chemistry, University of Houston, Houston, TX 77204-5641, U.S.A.

(Received 12 January 1998; accepted 15 May 1998)

Abstract—The syntheses and characterization of five compounds obtained by the reaction of dirhodium(II)tetraacetate with 1,4-dicyanobenzene in different solvent systems are described. The structures of $Rh_2(OAc)_4(NCPhCN)\cdot CH_3COCH_3$ (**1**), $Rh_2(OAc)_4(NCPhCN)\cdot 2CH_3OH$ (**2**), $Rh_2(OAc)_4(NCPhCN)\cdot C_4H_8O$ (**4**) and $Rh_2(OAc)_4(NCPhCN)\cdot C_6H_6$ (**5**) were determined by single crystal X-ray diffraction. All structures contain one dimensional polymeric chain, comprised of dirhodiumtetraacetate units bridged by 1,4-dicyanobenzene molecules. Solvent molecules are located between the chains in each structure and three different packing arrangements of the polymer chains result from the inclusion of these different solvent molecules. Compounds **1**, **2** and **3** crystallize in space group C2/c with similar cell parameters. Compound **4** also crystallizes in the same space group, but its structure is significantly different from those of **1**, **2** and **3**. Compound **5** crystallizes in space group $P\bar{1}$ and contains an unusual polymer chain structure. © 1998 Elsevier Science Ltd. All rights reserved

Keywords: coordination polymer; one dimensional polymer chains; dirhodiumtetraacetate; 1,4-dicyanobenzene; synthesis; crystal structure

INTRODUCTION

The coordination chemistry of dinuclear tetra-carboxylates of the transition metals has been a focus of several previous investigations. Adducts such as $Cr_2(OAc)_4(py)_2$ [1] and several polymers such as: $Cr_2(OAc)_4\cdot(pyz)_2$ [1], $Mo_2(O_2CCH_3)_4\cdot L$ (L = pyrazine, 4,4′-bipyridine, 1,4-diazabicyclo[2.2.2]octane) [2], $[Ru_2(O_2CC_2H_5)_4(phz)]BF_4$ [3] and $Cu_2(OAc)_4(pyz)$ [4] have been studied in detail. Several reactions of the Rh(II) tetra-acetate dimer with organic or organometallic ligands have been reported [5–8]. With some ligands, for example bis(4-pyridinecarbonitrile) [9] and pyridine, $M_2(O_2CR)_4L_2$ [10] metal cluster complexes are formed. One and two dimensional polymers are obtained by reactions with 2-(aminomethyl)pyridine [11], TCNE [12] and 4-amino-5-(aminomethyl)-2-methylpyrimidine [13] and $K_3Co(CN)_6$ [14]. Polymers containing $Rh_2(O_2CR)_4$ dimers with different R groups, for example, $Rh_2(O_2CEt)_4$ [15] or $Rh_2(O_2CCF_3)_4$ [16, 17], bridged by suitable organic ligands have also been reported.

Although extensive studies have focused on the formation of coordination polymers of the $Rh_2(O_2CR)_4$ dimer with linear-bidentate nitrogen ligands, the role of specific solvent molecules in the formation and crystallization of such polymers has not been investigated. In the present work, we report the syntheses and structures of compounds formed by the reaction of $Rh_2(OAc)_4$ with 1,4-dicyanobenzene in different solvents. Five new one dimensional coordination polymers have been obtained: $Rh_2(OAc)_4(NCPhCN)\cdot CH_3COCH_3$ (**1**), $Rh_2(OAc)_4(NCPhCN)\cdot 2CH_3OH$ (**2**), $Rh_2(OAc)_4(NCPhCN)\cdot xC_2H_5OH$ ($x \cong 1$) (**3**), $Rh_2(OAc)_4(NCPhCN)\cdot C_4H_8O$ (**4**) and $Rh_2(OAc)_4(NCPhCN)\cdot C_6H_6$ (**5**).

The structures of **1**, **2**, **4** and **5** were determined by analyses of single crystal X-ray diffraction data. The polymers all consist of one dimensional chains of $Rh_2(OAc)_4$ dimers bridged by 1,4-dicyanobenzene ligands, with the cavities between the chains filled by

* Author to whom correspondence should be addressed.

different solvent molecules. Packing of specific solvent molecules and the chains determines the final crystal structure. For **3**, only the unit cell dimensions and space group were determined and indicate that **3** is isostructural with **1** and **2**.

EXPERIMENTAL

Reagents and apparatus

Rhodium(II)acetate (STREM Chemical) and 1,4-dicyanobenzene (Aldrich) were used as received. Acetone, methanol, ethanol, benzene and tetrahydrofuran (THF) were dried over molecular sieves (4 Å). Infrared data were collected on a Galaxy FTIR 5000 series spectrometer, using the KBr pellet method. X-ray powder diffraction measurements were carried out using a Scintag XDS 2000 automated powder diffractometer (Cu Kα radiation, θ–θ, flat plate geometry). The Cerius 2 program [18] was used to simulate X-ray powder diffraction patterns from the single crystal X-ray data. Thermogravimetric analyses were carried out by using a TA Instruments 2100 thermal analyzer in a flowing nitrogen atmosphere at a heating rate of 1°C/min.

Syntheses

$Rh_2(OAc)_4(NCPhCN)\cdot CH3COCH3$ (***1***). $Rh_2(OAc)_4$ (10 mg, 0.023 mmol) and 1,4-dicyanobenzene (5 mg, 0.039 mmol) were dissolved in 25 ml acetone. The solution was stirred for 30 min and then slowly evaporated. Dark red crystals in the form of long columns or thin plates crystallized from the solution after 6 d. IR bands (cm^{-1}): 3443 (s), 3092 (w), 3046 (w), 2986 (w), 2934 (w), 2396 (w), 2301 (w), 2234 (m), 1588 (s), 1506 (w), 1437 (s), 1417 (s), 1358 (m), 1279 (w), 1051 (w), 924 (w), 845 (m), 702 (s), 629 (w), 561 (m).

$Rh_2(OAc)_4(NCPhCN)\cdot 2CH_3OH$ (***2***). A solution of 1,4-dicyanobenzene (15.2 mg, 0.119 mmol) in THF (30 ml) was added to a suspension of $Rh_2(OAc)_4$ (35 mg, 0.08 mmol) in methanol (40 ml). The mixture was stirred for about 1 h at room temperature. Slow evaporation produced small, red rod-shaped crystals in about 1 week in 95.9% yield. The compound is insoluble in water, but soluble in acetonitrile, THF and methanol. IR bands (cm^{-1}): 3443 (s), 3090 (w), 3044 (w), 2930 (w), 2233 (w), 1591 (s), 1435 (s), 1416 (s), 1385 (m), 1352 (w), 1277 (w), 1219 (w), 1051 (w), 858 (w), 812 (w), 702 (m), 629 (w), 565 (w).

$Rh_2(OAc)_4(NCPhCN)\cdot C_2H_5OH$ (***3***). The same procedure was used as described above for **1**, with ethanol replacing acetone. The dark red crystals were irregular multifaceted prisms. IR bands (cm^{-1}): 3447 (s), 3435 (s), 3098 (w), 3054 (w), 2363 (w), 2234 (m), 1588 (s), 1506 (w), 1437 (s), 1418 (s), 1358 (m), 1277 (w), 1051 (w), 922 (w), 845 (m), 704 (s), 629 (w), 598 (w), 561 (m).

$Rh_2(OAc)_4(NCPhCN)\cdot C_4H_8O$ (***4***). The reaction was carried out as described above for **1**, using THF as the solvent in place of acetone. Dark red diamond-shaped plates formed in 7 days. IR bands (cm^{-1}): 3495 (s), 3422 (s), 3100 (w), 3054 (w), 2971 (w), 2930 (w), 2855 (w), 2361 (w), 2234 (m), 1935 (w), 1588 (s), 1506 (w), 1437 (s), 1416 (s), 1356 (m), 1279 (w), 1057 (m), 845 (s), 799 (w), 698 (s), 629 (w), 596 (w), 561 (s).

$Rh_2(OAc)_4(NCPhCN)\cdot C_6H_6$ (***5***). A solution of 1,4-dicyanobenzene (5 mg, 0.039 mmol) in 10 ml THF was added to a suspension of $Rh_2(OAc)_4$ (10 mg, 0.023 mmol) in 10 ml benzene. The solid dissolved completely after being stirred for 1 h. Two distinct habits of lilac coloured crystals were observed after a week of slow evaporation. The majority of the product consisted of very large multifaceted blocks, while the remainder were square columns. A square column crystal was used for the data collection since the large blocks appeared to be polycrystalline. Subsequently, a small fragment cut from a large block verified that it was indeed the same phase as the crystal used for data collection. IR bands (cm^{-1}): 3449 (s), 3424 (s), 3096 (w), 3054 (w), 3005 (w), 2926 (w), 2390 (w), 2234 (m), 1588 (s), 1437 (s), 1416 (s), 1385 (m), 1356(m), 1279(w), 1045(w), 845(m), 696(s), 629(w), 598(w), 561(m).

All of the compounds show the expected IR stretching frequencies from the $Rh_2(OAc)_4$·dicyanobenzene polymer and the specific solvent molecule. Coordination of the dicyanobenzene is indicated by a CN stretching frequency at 2234 cm^{-1}, which is slightly blue-shifted from the CN stretching frequency (2232 cm^{-1}) of neat 1,4-dicyanobenzene.

Structure determinations

For **1**, **3** and **5**, X-ray data were collected using a Nicolet R3m/V automatic diffractometer (graphite-monochromated Mo-Kα radiation). Data for **2** and **4** were collected using an Enraf-Nonius CAD-4, four circle diffractometer also with Mo-Kα radiation.

A crystal of **1** with dimensions $0.10 \times 0.35 \times 0.45$ mm was mounted on a glass fiber and transferred to the diffractometer. The crystal was cooled to 223 K in a stream of cold nitrogen gas. Lattice parameters were determined from the angles of 25 reflections in the range $16.3° < 2\theta < 30.3°$. Crystal data and details of the data collection and refinement are presented in Table 1. Data were collected in ω–2θ mode. Intensity data for 2386 reflections (2121 unique) were collected in the range $4° < 2\theta < 50°$. Two standard reflections were monitored after every two h or every 100 data collected and these showed a 12% linear decay over the course of the experiment. A normalization factor as a function of X-ray exposure time was applied to account for this. During data reduction, Lorentz and polarization corrections and a semi-empirical absorption correction based on ten

Table 1. Crystallographic data for **1**, **2**, **3**, **4** and **5**

Solvent	Acetone (**1**)	Methanol (**2**)	Ethanol (**3**)[d]	THF (**4**)	Benzene (**5**)
Formula	$C_{19}H_{22}N_2O_9Rh_2$	$C_{18}H_{24}N_2O_{10}Rh_2$		$C_{20}H_{24}N_2O_9Rh_2$	$C_{22}H_{22}N_2O_8Rh_2$
FW	628.21	634.24		642.23	648.24
a (Å)	23.122(7)	23.113(3)	23.336(8)	22.735(5)	8.062(2)
b (Å)	12.382(7)	12.290(3)	12.248(4)	8.162(10)	8.400(2)
c (Å)	8.518(3)	8.503(1)	8.527(3)	14.660(8)	10.354(2)
α (°)	90	90	90	90	95.16(2)
β (°)	97.82(2)	97.54(2)	98.223	116.16(2)	99.14(2)
γ (°)	90	90	90	90	118.18(2)
Z	4	4	4	4	1
V (Å^3)	2416	2395	2412	2442	599
Crystal system	monoclinic	monoclinic	monoclinic	monoclinic	triclinic
Space group	C2/c (No. 15)	C2/c (No. 15)	C2/c (No. 15)	C2/c (No. 15)	$P\bar{1}$ (No. 2)
T (K)	223	298	223	298	223
λ (Å)	0.71073	0.71073	0.71073	0.71073	0.71073
$D_{calc.}$ (g cm^{-3})	1.727	1.760		1.747	1.796
μ (Mo-Kα) (mm^{-1})	1.415	1.431		1.402	1.426
F(000)	1248	1280		1280	322
Data collection, θ (°)	2.96 to 25.05	2.97 to 24.98		2.00 to 27.91	2.80 to 25.05
Index ranges	$-27 \leqslant h \leqslant 27$	$-27 \leqslant h \leqslant 26$		$-29 \leqslant h \leqslant 26$	$0 \leqslant h \leqslant 9$
	$0 \leqslant k \leqslant 14$	$0 \leqslant k \leqslant 14$		$0 \leqslant k \leqslant 10$	$-9 \leqslant k \leqslant 8$
	$-10 \leqslant l \leqslant 0$	$0 \leqslant l \leqslant 10$		$0 \leqslant l \leqslant 19$	$-12 \leqslant l \leqslant 11$
Reflections collected	2280	2269		2714	2112
Independent reflections	2121	1964		2714	2102
Number of parameters	147	143		150	198
$R(F)$[a] (%)[c]	5.86	4.75		3.39	1.77
$wR2(F)$[b] (%)[c]	15.75	13.14		9.38	4.32
$\Delta\rho_{max.}$, $\Delta\rho_{min}$ (eÅ^{-3})	1.784, −2.343	1.128, −1.396		0.740, −1.188	0.527, −0.353
Goodness-of-fit (F^2)	1.057	1.124		1.049	0.993

[a] $R = \Sigma \| F_0 | - | F_c \| / \Sigma | F_0 |$.
[b] $wR2 = [\Sigma[w(F^2_0 - F^2_c)^2] / \Sigma[w(F^2_0)^2]]^{1/2}$.
[c] $[F_0 > 4\sigma(F_0)]$.
[d] Only unit cell determined.

reflections having χ values between 70 and 90° were applied. The structure was solved in space group C2/c by direct methods and standard difference Fourier techniques using SHELXS-96 [19]. Refinement on F^2 was carried out by full-matrix least-squares procedures using SHELXL-96 beta [19]. All nonhydrogen atoms were refined with anisotropic thermal parameters. Hydrogen atoms were included in calculated positions riding on their carrier atoms, with fixed isotropic thermal parameters related to the value of the equivalent isotropic thermal parameter of their carrier atoms by a factor of 1.5 for the methyl hydrogen atoms and a factor of 1.2 for the other hydrogen atoms. Weights were optimized in the final refinement cycles.

The data collection and refinement of **5** were carried out in the same way as for **1**. A lilac square column with dimensions $0.08 \times 0.12 \times 0.40$ mm was used. Twenty-five reflections in the range $18° < 2\theta < 42°$ were centered, giving a triclinic cell. Intensity data were collected in the ω–2θ mode with a range of $4 < 2\theta < 50°$. A semi-empirical absorption correction based on ψ scans was applied to the data during data reduction. The structure was determined and refined in space group $P\bar{1}$ using the same programs as **1**.

For **2** and **4**, suitable crystals with dimensions $0.31 \times 0.11 \times 0.10$ and $0.15 \times 0.3 \times 0.3$ mm, respectively, were mounted with epoxy glue on the tip of a glass fiber and transferred to the diffractometer. 25 reflections were used to determine the unit cell and data were collected using the ω–2θ scan method in both cases. Intensities were corrected for Lorentz and polarization effects, as well as for absorption (ψ scans). Intensities of three standard reflections showed no variations greater than those predicted by counting statistics. In both cases, space group C2/c was chosen and confirmed by successful structure refinement. The structure solution and refinement were carried out similarly as the other compounds. For **3**, only the unit cell dimensions and space group were determined (223 K). Selected bond distances and angles for **1**, **2**, **4** and **5** are given in Table 2.

Table 2. Selected bond distances (Å) and angles (°) for **1**, **2**, **4** and **5**

Acetone (**1**)			
Rh(1)–O(4)	2.029(4)	Rh(1)–O(1)	2.031(4)
Rh(1)–O(3)	2.035(5)	Rh(1)–O(2)	2.049(5)
Rh(1)–N(1)	2.239(5)	Rh(1)–Rh(1)[a]	2.3910(10)
O(1)–C(1)	1.267(8)	O(2)–C(2)[a]	1.273(8)
O(3)–C(2)	1.250(8)	O(4)–C(1)[a]	1.266(8)
N(1)–C(11)	1.128(8)	C(1)–C(3)	1.498(9)
C(2)–C(4)	1.511(11)	C(11)–C(12)	1.448(8)
C(12)–C(14)	1.382(9)	C(12)–C(13)	1.409(10)
C(13)–C(14)[b]	1.353(10)		
O(4)–Rh(1)–O(1)	175.8(2)	O(4)–Rh(1)–O(3)	89.6(2)
O(1)–Rh(1)–O(3)	90.4(2)	O(4)–Rh(1)–O(2)	90.4(2)
O(1)–Rh(1)–O(2)	89.2(2)	O(3)–Rh(1)–O(2)	175.8(2)
O(4)–Rh(1)–N(1)	91.2(2)	O(1)–Rh(1)–N(1)	93.1(2)
O(3)–Rh(1)–N(1)	91.4(2)	O(2)–Rh(1)–N(1)	92.9(2)
O(4)–Rh(1)–Rh(1)[a]	87.92(13)	O(1)–Rh(1)–Rh(1)[a]	87.85(12)
O(3)–Rh(1)–Rh(1)[a]	87.76(12)	O(2)–Rh(1)–Rh(1)[a]	88.01(12)
N(1)–Rh(1)–Rh(1)[a]	178.7(2)		
C(1)–O(1)–Rh(1)	119.8(4)	C(2)[a]–O(2)–Rh(1)	118.7(4)
C(2)–O(3)–Rh(1)	120.2(4)	C(1)[a]–O(4)–Rh(1)	119.9(4)
C(11)–N(1)–Rh(1)	178.1(5)	O(1)–C(1)–O(4)[a]	124.5(6)
O(3)–C(2)–O(2)[a]	125.2(7)	N(1)–C(11)–C(12)	179.1(7)
CH_3OH (**2**)			
Rh–O(3)	2.024(4)	Rh–O(1)	2.033(4)
Rh–O(2)	2.049(5)	Rh–O(4)	2.050(4)
Rh–N	2.236(4)	Rh–Rh[c]	2.3910(8)
O(1)–C(11)	1.248(7)	O(2)–C(13)	1.265(7)
O(3)–C(11)[c]	1.262(7)	O(4)–C(13)[c]	1.246(7)
N–C(1)	1.122(7)	C(1)–C(2)	1.462(7)
C(2)–C(4)[d]	1.375(8)	C(2)–C(3)	1.391(9)
C(3)–C(4)	1.392(8)	C(11)–C(12)	1.519(8)
C(13)–C(14)	1.499(9)		
O(3)–Rh–O(1)	175.48(14)	O(3)–Rh–O(2)	90.1(2)
O(1)–Rh–O(2)	89.4(2)	O(3)–Rh–O(4)	90.1(2)
O(1)–Rh–O(4)	90.0(2)	O(2)–Rh–O(4)	175.4(2)
O(3)–Rh–N	91.3(2)	O(1)–Rh–N	93.2(2)
O(2)–Rh–N	92.4(2)	O(4)–Rh–N	92.1(2)
O(3)–Rh–Rh[c]	87.76(11)	O(1)–Rh–Rh[c]	87.74(11)
O(2)–Rh–Rh[c]	87.95(11)	O(4)–Rh–Rh[c]	87.50(11)
N–Rh–Rh[c]	179.00(13)	C(11)–O(1)–Rh	119.5(4)
C(13)–O(2)–Rh	119.2(4)	C(11)[c]–O(3)–Rh	119.6(3)
C(13)[c]–O(4)–Rh	120.1(4)	C(1)–N–Rh	177.8(5)
N–C(1)–C(2)	179.2(7)	O(1)–C(11)–O(3)[c]	125.5(5)
O(4)[c]–C(13)–O(2)	125.1(6)		
THF (**4**)			
Rh(1)–O(4)	2.029(3)	Rh(1)–O(2)	2.039(3)
Rh(1)–O(1)	2.040(3)	Rh(1)–O(3)	2.040(3)
Rh(1)–N(1)	2.226(3)	Rh(1)–Rh(1)[a]	2.3830(10)
O(1)–C(1)	1.263(4)	O(2)–C(2)	1.265(5)
O(3)–C(1)[a]	1.258(4)	O(4)–C(2)[a]	1.253(4)
N(1)–C(11)	1.140(5)	C(1)–C(4)	1.489(5)
C(2)–C(3)	1.506(6)	C(11)–C(12)	1.434(4)
C(12)–C(13)	1.374(5)	C(2)–C(14)	1.388(5)
C(13)–C(14)[e]	1.376(5)	O(21)–C(21)	1.401(11)
C(21)–C(22)[g]	1.306(13)	C(22)–C(22)[f]	1.42(2)
O(4)–Rh(1)–O(2)	175.98(9)	O(4)–Rh(1)–O(1)	89.47(12)
O(2)–Rh(1)–O(1)	89.94(11)	O(4)–Rh(1)–O(3)	90.45(12)
O(2)–Rh(1)–O(3)	89.86(11)	O(1)–Rh(1)–O(3)	176.06(9)
O(4)–Rh(1)–N(1)	91.37(12)	O(2)–Rh(1)–N(1)	92.64(12)

(*continued*)

Table 2—*continued*

O(1)–Rh(1)–N(1)	93.97(12)	O(3)–Rh(1)–N(1)	89.96(11)
O(4)–Rh(1)–Rh(1)[a]	88.17(8)	O(2)–Ph(1)–Rh(1)[a]	87.84(7)
O(1)–Rh(1)–Rh(1)[a]	88.13(8)	O(3)–Rh(1)–Rh(1)[a]	87.94(7)
N(1)–Rh(1)–Rh(1)[a]	177.85(8)	C(11)–N(1)–Rh(1)	168.7(3)
O(3)[a]–C(1)–O(1)	125.7(3)	O(3)[a](C1)–C(4)	117.8(3)
O(1)–C(1)–C(4)	116.6(3)	O(4)[a](C2)–O(2)	125.7(3)
O(4)[a]–C(2)–C(3)	117.9(4)	O(2)–C(2)–C(3)	116.3(4)
N(1)–C(11)–C(12)	178.2(4)	C(21)[f]–O(21)–C(21)	106.4(13)
C(22)[g]–C(21)–O(21)	106.4(9)	(C21)[h]–C(22)–C(22)[f]	106.0(8)
Benzene (**5**)			
Rh–O(3)[i]	2.0348(14)	Rh–O(4)	2.0360(14)
Rh–O(1)	2.0360(12)	Rh–O(2)[i]	2.0369(13)
Rh–N(1)	2.237(2)	Rh–Rh[i]	2.3887(4)
O(1)–C(1)	1.264(2)	O(2)–C(1)	1.260(2)
O(3)–C(3)	1.263(2)	O(4)–C(3)	1.265(2)
N(1)–C(5)	1.137(3)	C(1)–C(2)	1.502(2)
C(3)–C(4)	1.503(3)	C(5)–C(6)	1.446(3)
C(6)–C(8)[b]	1.380(3)	C(6)–C(7)	1.389(3)
C(7)–C(8)	1.382(3)	C(9)–C(11)[j]	1.336(10)
C(9)–C(10)	1.399(10)	C(10)–C(11)	1.371(10)
C(9′)–C(10′)	1.340(11)	C(9′)–C(11′)[j]	1.407(11)
C(10′)–C(11′)	1.399(11)		
O(3)[i]–Rh–O(4)	176.01(5)	O(3)[i]–Rh–O(1)	89.84(5)
O(4)–Rh–O(1)	90.44(5)	O(3)[i]–Rh–O(2)[i]	89.82(5)
O(4)–Rh–O(2)[i]	89.63(5)	O(1)–Rh–O(2)[i]	175.98(5)
O(3)[i]–Rh–N(1)	98.32(6)	O(4)–Rh–N(1)	85.65(6)
O(1)–Rh–N(1)	92.03(5)	O(2)[i]–Rh–N(1)	91.99(5)
O(3)[i]–Rh–Rh[i]	87.90(4)	O(4)–Rh–Rh[i]	88.13(4)
O(1)–Rh–Rh[i]	187.97(4)	O(2)[i]–Rh–Rh[i]	88.01(4)
N(1)–Rh–Rh[i]	173.78(4)	C(1)–O(1)–Rh	119.18(11)
C(1)–O(2)–Rh[i]	119.17(11)	C(3)–O(3)–Rh[i]	119.39(12)
C(3)–O(4)–Rh	119.06(12)	C(5)–N(1)–Rh	150.6(2)
O(2)–C(1)–O(1)	125.7(2)	O(3)–C(3)–O(4)	125.5(2)
N(1)–C(5)–C(6)	176.2(2)		

Symmetry transformations used to generate equivalent atoms:[a] $-x+1/2, -y+1/2, -z$; [b] $-x+1, -y+1, -z+1$; [c] $-x+1/2, -y+3/2, -z$; [d] $-x+1, -y+2, -z+1$; [e] $-x+1, -y, -z+1$; [f] $-x+1, y, -z+1/2$; [g] $-x+1, y-1, -z+1/2$; [h] $-x+1, y+1, -z+1/2$; [i] $-x, -y+1, -z+2$; [j] $-x, -y, -z+1$.

RESULTS AND DISCUSSION

Preparation

The characteristics of the compounds obtained from the reaction of rhodium(II)acetate dimer with 1,4-dicyanobenzene vary with the different solvents used. Two methods were used for the synthesis of the five compounds. **1**, **3** and **4** were synthesized with only one type of solvent. The solvent served to dissolve the starting materials and was subsequently incorporated into the structure within a channel formed by stacking of the polymer chains. For **2** and **5**, two types of solvents were involved in the synthesis. One served to dissolve the starting material and the other one was incorporated into the structure. THF was used as the solvent but was not observed in the final structures. Excess 1,4-dicyanobenzene was used in all of the five reactions. The structure and composition of the final products were insensitive to changes in the stoichiometry of the reactants.

Structures

All of the polymeric structures contain one dimensional chains comprised of rhodiumacetate dimers bridged by 1,4-dicyanobenzene (see Fig. 1 for **1**). Each compound has different solvent molecules located between the polymer chains and each solvent causes significant variations in the crystal structures that are adopted.

Figure 1 shows the local coordination of compound **1** with the atoms labelled. Figures 2 and 3 show different views of the spatial relationship between the linear chains. In Fig. 2, the acetate ligands have been omitted

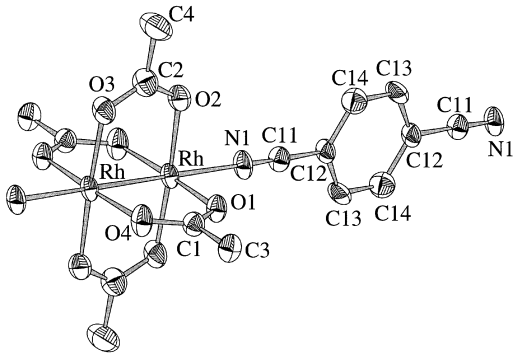

Fig. 1. Ortep drawing of the local coordination of **1** with thermal ellipsoids at the 50% probability level, the solvent acetone is not shown.

for clarity. The dinuclear $Rh^{4+}{}_2$ carboxylate core remains intact, with a Rh–Rh distance of 2.391(1) Å. The Rh–O distances range from 2.029(4) to 2.049(5) Å. The octahedral coordination sphere of Rh is completed by axial coordination to the nitrogen atom of the organic ligand at a distance of 2.239(5) Å. The Rh–N–C linkage is nearly linear, with an angle of 178.1(5)°. The chains stack together with an average separation of 3.8 Å, Fig. 2. The phenylrings from the alternating chains are not parallel to each other and the closest contact between adjacent phenylrings is 3.559 Å (C12 from one ring and C14 from another ring). Adjacent chains are oriented at an angle of 56.3° with respect to each other when projected on the **ab** plane, Fig. 3. Part of the extended structure of **1** is shown in Fig. 3. The intersections of the chains define channels in the structure that are occupied by the solvent molecules.

The acetone molecules in **1** are severely disordered and are difficult to locate in difference maps. One acetone molecule was refined with an occupancy factor of 0.276, while four additional atom sites designated as carbon were also located and refined with fixed occupancies of 0.3. From thermogravimetric analysis data (see Section 3.3), one acetone molecule per dirhodium unit is present.

The arrangement of the polymer chains in the structure of **2** is the same as in **1**. Adjacent chains are oriented at an angle of 56.0° with respect to each other, when projected on the **ab** plane. This angle is essentially the same as observed in **1** (56.3°). The average Rh–O, Rh–N and Rh–Rh bond distances in the two compounds are the same within errors. The methanol solvent molecules in **2** are also disordered. The positions of two methanol molecules could be refined, albeit with high thermal parameters. The exact number of methanol molecules could not be determined from the X-ray data, however thermogravimetric analysis indicates that two methanol molecules per dirhodium unit are present.

In **4**, the THF solvent molecules are ordered and a significant change in the arrangement of the polymeric chains [Fig. 4(a)–(c)] is observed. In **1** and **2** the chains are nearly linear, but in **4** the C–N–Rh angle is reduced to 168.7(3)°. The Rh–Rh–N and N–C–C angles in **4** are still close to 180°. The N–Rh distance [2.226(3) Å]

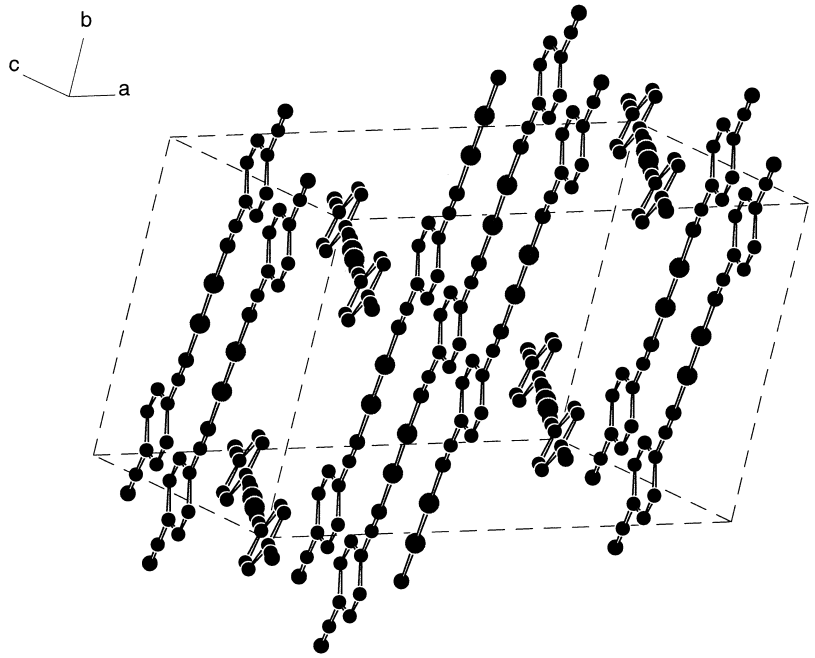

Fig. 2. View of the structure of **1** showing the stacking of the chains. For clarity, the acetate groups of the Rh dimer are not shown.

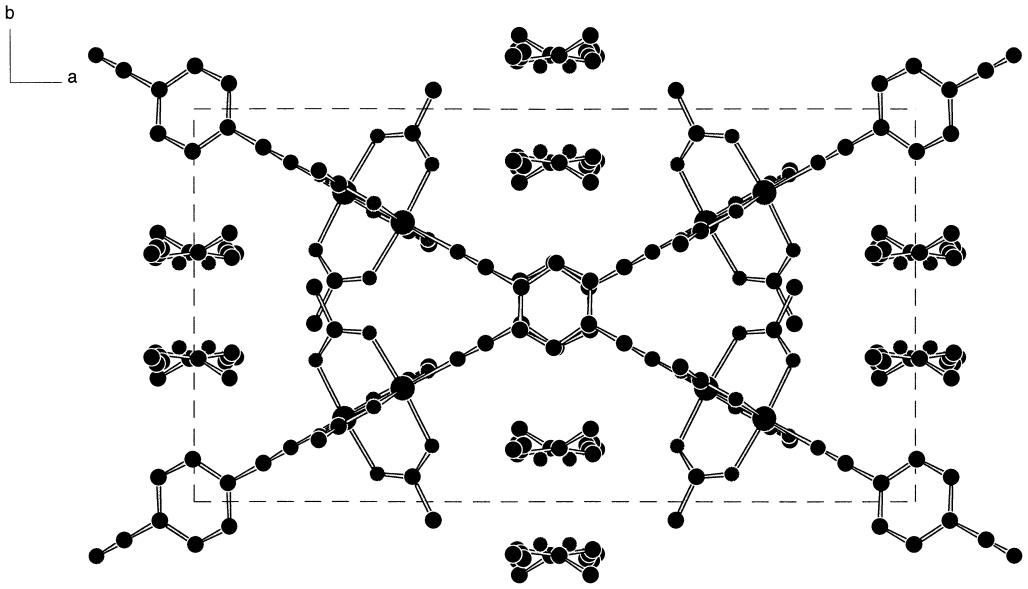

Fig. 3. Projection of the structure of **1** along *c*. Disordered acetone molecules are shown between the chains.

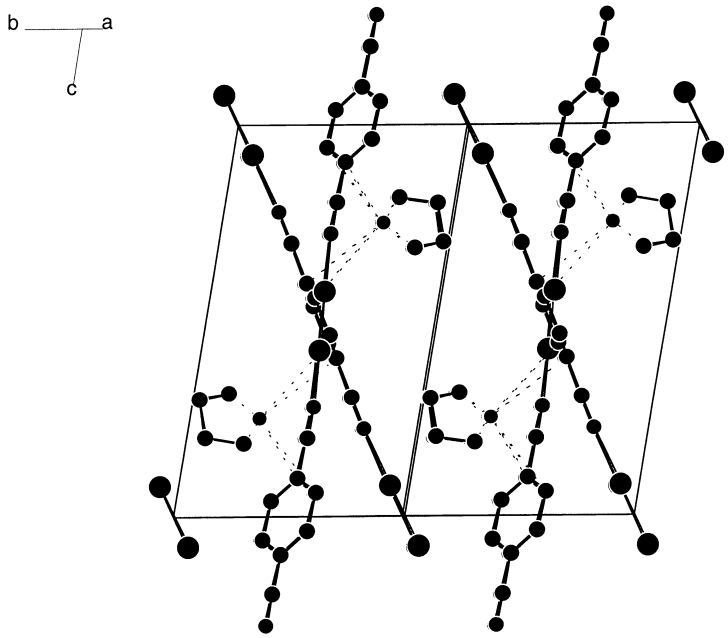

Fig. 4. (a) View of the structure of **4** showing the stacking of the chains and the THF molecules. For clarity, the acetate groups of the Rh dimer are not shown. (b) Local coordination of **4** showing the attraction between oxygen of the THF and the phenylrings in the chains. For clarity, the acetate groups of the Rh dimer are not shown. The dotted lines indicate the closest contact between the THF and phenylrings. (c) View of the structure of **4** showing the attraction between oxygen of the THF and the phenylrings in the chains. For clarity, the acetate groups of the Rh dimer are not shown. The dotted lines indicate the closest contact between the THF and phenylrings.

is similar to the distance in **1** and **2**. The change in angle at the N atom, however, imparts a slight zigzag geometry to the chains as can be seen in Fig. 4. The stacking of the polymer chains in **4** is similar to that observed in **1** and **2**, but the alternating chains make an angle of 39.50° (projected on **ab** plane). The arrangement of THF molecules between adjacent chains suggests a weak interaction through the oxygen lone electron pairs. This interaction may be responsible for reducing the dihedral angle between the

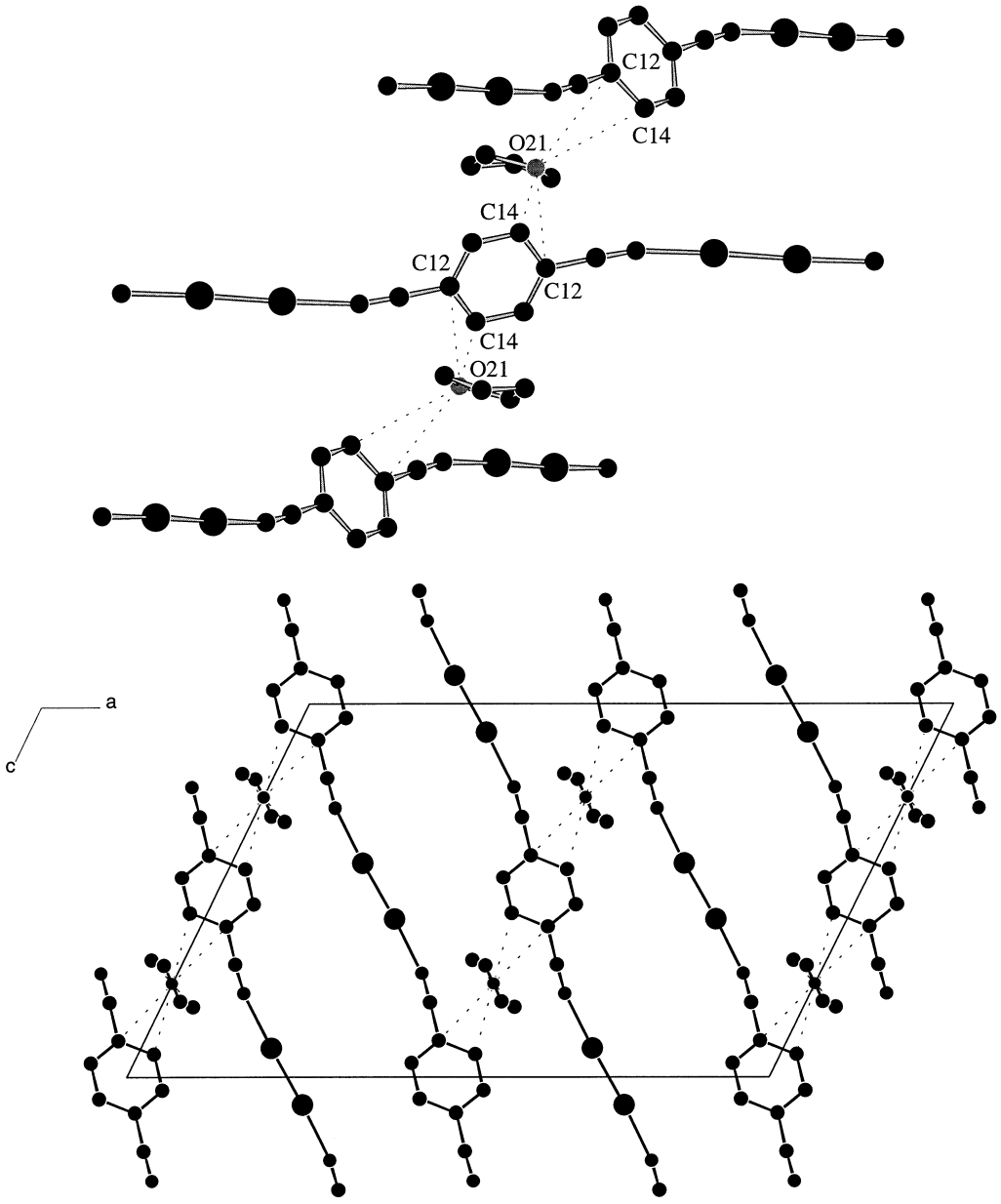

Fig. 4—continued.

chains by ~17°. The distances between the THF oxygen atom and the chains (O21–C14 and O21–C12) are 3.381 and 3.434 Å, respectively. The bridging geometry is symmetric because THF lies on a crystallographic two-fold axis.

A different structure is observed when benzene molecules are trapped between the polymer chains. Crystals of **1**, **2**, **3** and **4** all have the same dark red color, while crystals of **5** are lilac. In **5**, all of the chains in the crystal are parallel to each other (Figure 5). Every polymeric chain zigzags as in **4**, with a C–N–Rh angle of 150.6(2)°, which is much further from linear than the corresponding angle in **4** [168.7(3)°]. The benzene molecules that sandwich each phenylring in the chain are parallel to each other and are separated by a distance of 8.461 Å. The phenylring in the chain and the benzenering are not parallel and the closest contact between them is 3.483 Å (C6–C9), while the distance from C5 of the cyanide group to C9 of the benzenering is 3.352 Å. The spacing between the phenylrings is too large to imply any strong electronic interaction. The benzene molecules are disordered over two different positions, rotated at roughly 30° to each other about a common crystallographic inversion center. Analysis of the isotropic thermal parameters showed a 50% occupancy for each orientation.

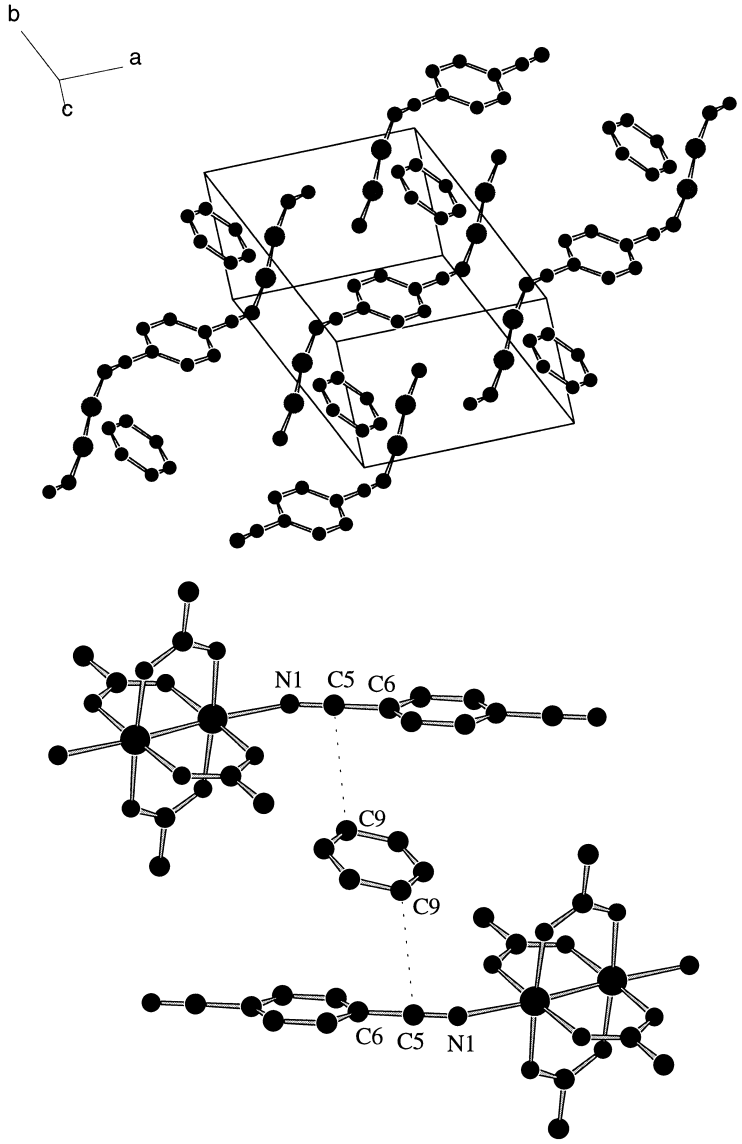

Fig. 5. (a) View of the structure of **5** showing the stacking of the chains and the benzene molecules. For clarity, the acetate groups of the Rh dimer are not shown and only one position of the disordered benzene molecule is shown. (b) Local coordination of **5** showing the attraction between the benzene molecules and the phenylrings in the chains. The dotted lines indicate the closest contact between the benzene molecule with the chains. (c) View of the structure of **5** along *a* showing the stacking of the chains.

All five crystal structures have solvent "channels" leading directly to the surface: **1**, **2**, **3** and **4** have channels along the *c* axis, while **5** has a channel along *a*. In TGA measurements on heating, acetone, methanol and ethanol are all removed near their boiling points. However, THF and benzene are lost at temperatures significantly higher than their boiling points and the removal of the solvent molecules is not well resolved in temperature from the temperature at which the dicyanobenzene molecules are removed. The TGA data suggest some weak interaction between the solvent molecules and the frameworks of **4** and **5**. The structure of **4**, suggests some interaction between the oxygen lone pair electrons in THF and the chains, whereas in **5** the benzene molecules may have some π–π interactions with the phenylrings in the chain.

Thermogravimetric analysis

Each of **1**, **2**, **3**, **4** and **5** was heated to 400°C in nitrogen to determine the solvent contents and thermal stabilities (Figure 6). For **1**, the first two weight losses at $T < 118$°C corresponded to the loss of one

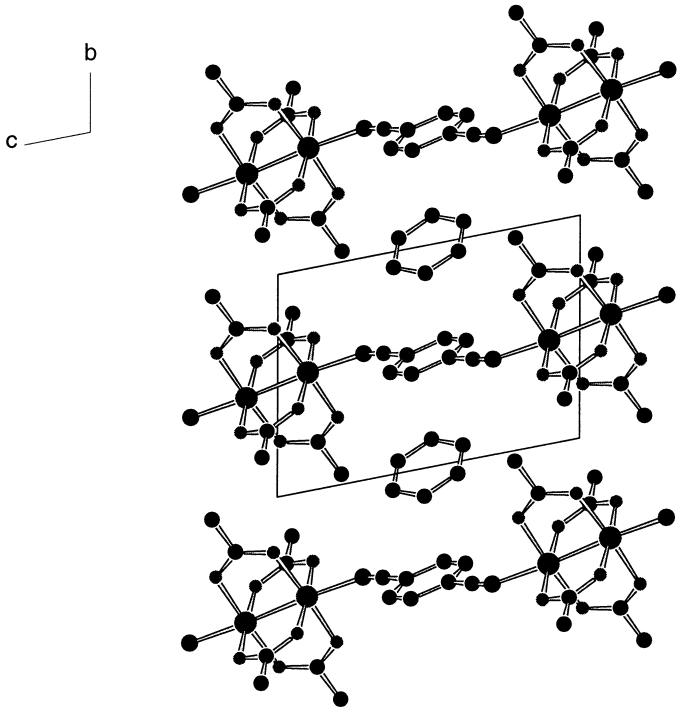

Fig. 5—*continued.*

molecule of acetone (observed 9.67%, calculated 9.25%). From 118 to 175°C, a second weight loss corresponded to removal of one dicyanobenzene molecule (observed 21.99%, calculated 20.40%). The final weight loss occurred between 227 and 246°C and corresponded to the loss of the four acetate groups. No further decomposition was observed above 246°C. X-ray powder diffraction confirmed that the black residue was pure Rh (observed 31.20%, calculated 32.76%). Interestingly the original shape of the crystal was preserved after decomposition.

The thermal decomposition behaviors of **2** and **3** were similar to that of **1**. In both cases, the loss of solvent molecules was completed at relatively low temperature (62°C for **2** and 113°C for **3**). The weight losses corresponding to the loss of dicyanobenzene molecules and the four acetate groups occurred in similar temperature ranges in **2** and **3** and they were not significantly different from those of **1**. The solvent losses indicated a composition of two methanol molecules per dirhodium unit per unit cell in **2** and one ethanol molecule per dirhodium unit per unit cell in **3**.

Compound **4** showed no thermal decomposition until 100°C. This temperature is significantly higher than observed for **1**, **2** and **3**, which lose solvent molecules immediately on heating. The removal of THF and the dicyanobenzene molecules were not well resolved in temperature but the sum of the losses (observed 31.35%, calculated 31.18%) indicated only one THF molecule per formula unit. The weight loss corresponding to the four acetate groups was similar to the value observed for the other compounds. The thermal decomposition of **5** showed three-steps in the weight loss below 178°C, the total weight loss corresponded to the removal of one benzene and one dicyanobenzene molecule (observed 31.81%, calculated 31.82%). The remaining weight losses was similar to other compounds.

4. CONCLUSIONS

Five new one dimensional coordination polymers formed by dirhodium(II)tetraacetate bridged by 1,4-dicyanobenzene have been synthesized and characterized. Each compound has a different solvent molecule filling the cavities between the polymeric chains. The type of solvent apparently plays an important role in the crystallization process and determines the separation and orientation of the polymeric chains. We are currently investigating other solvents that can be introduced between the chains and further work will focus on studying the extensions to 2D and 3D polymers by using multifunctional organic bridging ligands.

Acknowledgements—We thank the National Science Foundation (DMR-9214804) and the Robert A. Welch Foundation for support of this work and Dr James Korp for help with crystallography.

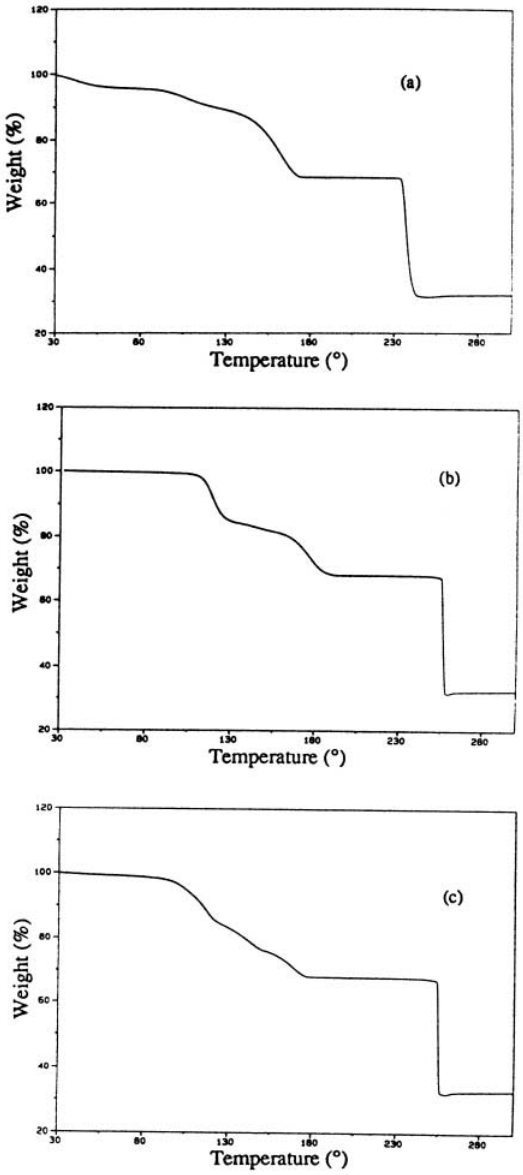

Fig. 6. Thermogravimetric analysis data for **1** (a), **4** (b) and **5** (c).

REFERENCES

1. Cotton, F. A. and Felthouse, T. R., *Inorg. Chem.*, 1980, **19,** 328–331.
2. Handa, M., Yamada, K., Nakao, T. and Kasuga, K., *Chem. Lett.*, 1993, 1969–1972.
3. Cotton, F. A. and Kim, Y., Ren, T., *Inorg. Chem.*, 1992, **31,** 2723–2726.
4. Morosin, B., Hughes, R. C. and Soos, Z. G., *Acta Cryst. B*, 1975, **31,** 762.
5. Cotton, F. A., Deboer, B. G., Pipal, M. D. and Ucko, D. A., *Acta Cryst. B*, 1971, **27,** 1664.
6. Christoph, G. G. and Koh, Y.-B., *J. Am. Chem. Soc.*, 1979, **101,** 1422.
7. Koh, Y. B. and Christoph, G. G., *Inorg. Chem.*, 1979, **18,** 1122.
8. Cotton, F. A. and Felthouse, T. R., *Inorg. Chem.*, 1980, **19,** 323–328.
9. Cotton, F. A. and Felthouse, T. R., *Acta. Cryst. C*, 1984, **40,** 42–45.
10. Koh, Y. B. and Christoph, G. G., *Inorg. Chem.*, 1978, **17,** 2590–2596.
11. Crawford, C. A., Day, E. F., Streib, W. E., Huffman, J. C. and Christou, G., *Polyhedron*, 1994, **13,** 2943–2993.
12. Cotton, F. A. and Kim, Y., Lu, J., *Inorg. Chim. Acta*, 1994, **221,** 1–4.
13. Aoki, K. and Yamazaki, H., *J. Am. Chem. Soc.*, 1984, **106,** 3691–3692.
14. Lu, J., Harrison, W. T. A. and Jacobson, A. J., *Chem. Commun.*, 1996, 399–400.
15. Cotton, F. A. and Felthouse, T. R., *Inorg. Chem.*, 1981, **20,** 600–608.
16. Cogne, A., Grand, A. and Rey, P., Subra, R., *J. Am. Chem. Soc.*, 1989, **111,** 3230–3238.
17. Cotton, F. A. and Kim, Y., *J. Am. Chem. Soc.*, 1993, **115,** 8511–8512.
18. *Cerius*2, *Version* 2.0. BIOSYM/Molecular Simulations, 1995.
19. Sheldrick, G. M., *SHELXS*-96 *beta and SHELXL*-96 *beta*, *Program Package for Structure Solution and Refinement*. Universität Göttingen, Göttingen, 1996.

Pergamon

Polyhedron Vol. 17, No. 23–24, pp. 4091–4099, 1998
© 1998 Elsevier Science Ltd
All rights reserved. Printed in Great Britain
0277–5387/98 $19.00+0.00

PII: S0277–5387(98)00214–9

Persulfurated complexes of palladium(II) and platinum(II) with fluorinated aryl-thiolates. X-ray structure of $[Pt(SC_6F_5)_2(CH_3SCH(CH_3)CH(CH_3)SCH_3)]$

Erika Martin,*[a] Beatriz Toledo,[a] Hugo Torrens,[a] Fernando J. Lahoz[b] and Pilar Terreros[c]

[a]DEPg., F. Química, UNAM, 04510, Mexico D.F., Mexico

[b]Depto. de Química Inorgánica, ICMA-CSIC, Universidad de Zaragoza, 50009 Zaragoza, Spain

[c]ICP-CSIC, Cantoblanco, 28049 Madrid, Spain

(Received 12 February 1998; accepted 21 May 1998)

Abstract—The syntheses of the persulfurated $[M(SR_F)_2(CH_3SCH(CH_3)CH(CH_3)SCH_3)]$, M = Pd or Pt; $R_F = C_6F_5$ or C_6F_4H-4 compounds allow the separation of two diastereomers and the NMR detection of five conformers (three *anti* and two *syn*) of each compound. ^1H, ^{19}F and ^{195}Pt NMR data have been used to assign each conformer and to obtain their relative populations as well as to follow their equilibrium at high temperatures. The X-ray diffraction molecular and crystalline structure of $[Pt(SC_6F_5)_2(CH_3SCH(CH_3)CH(CH_3)SCH_3)]$ has been determined. © 1998 Elsevier Science Ltd. All rights reserved

Keywords: persulfurated; crystal structure; fluorothiolates; palladium; platinum; sulfur inversion.

1. INTRODUCTION

The chemistry of co-ordination compounds with metal centres surrounded exclusively by sulfur donor ligands has been extensively examined. The interest in this area is due to its relevance to *i.a.* catalysis, bio-inorganics and structural chemistry [1–6].

For complexes containing chiral three co-ordinated sulfur atoms, several structural and kinetic studies have been undertaken with regard to the inter-conversion of isomers that arises from configuration inversion at the sulfur atoms [7,8].

However, for those complexes with three or more possible NMR-observable conformers [9,10], since there is no conclusive evidence to distinguish among spectroscopic signals arising from different conformers, seldom is a precise assignment accomplished [11–13].

Previously [14–16] we were interested in the chemistry of metal centres surrounded exclusively by sulfur atoms and as part of the research done, in this paper we report the syntheses of $[M(SR_F)_2(CH_3SCH(CH_3)CH(CH_3)SCH_3)]$, M = Pd, $SR_F = SC_6F_5$, **1**; $SR_F = SC_6RH$-4, **2**; M = Pt, $SR_F = SC_6F_5$, **3**; $SR_F = SC_6F_4H$-4, **4**; the separation of two sets of isomers for each complex and the X-ray diffraction crystal structure of a diastereomer of $[Pt(SC_6F_5)_2(CH_3SCH(CH_3)CH(CH_3)SCH_3)]$. The separation of both diastereomers allows, for the first time, a direct identification of the stereoisomers present in solution by ^1H, ^{19}F and ^{195}Pt NMR.

2. EXPERIMENTAL

$[MCl_2\{(meso,rac)\text{-}CH_3SCH(CH_3)CH(CH_3)SCH_3\}]$, M = Pd or Pt [17], $Pb(SC_6F_5)_2$ [18] and $Pb(SC_6F_4H\text{-}4)_2$ [19] were prepared according to published methods.

After $[MCl_2\{(meso,rac)\text{-}CH_3SCH(CH_3)CH(CH_3)SCH_3\}]$, M = Pd or Pt (1.2 mmol) and $Pb(SC_6F_5)_2$ or $Pb(SC_6F_4H\text{-}4)_2$ (1.2 mmol) were dissolved in 60 ml of

* Author to whom correspondence should be addressed.

acetone, the resulting suspensions were magnetically stirred for 2 h at room temperature. $PbCl_2$ was then filtered off and the clear orange or yellow solutions were evaporated to dryness (yields: **1** = 90%, **2** = 84%, **3** = 96% and **4** = 91%).

0.75 g of silica-gel were added to the solids (*ca.* 0.15 g) after they were dissolved in *ca.* 15 ml of acetone. For each compound, the solvent was evaporated and the impregnated silica was placed on top of a chromatographic column and eluted with chloroform:acetone (10:1) to obtain solutions of *cis* [R_f = 3.8, **1**-*cis* (23.5%); R_f = 3.6, **2**-*cis* (47.9%); R_f = 3.1, **3**-*cis* (41.3%); R_f = 3.0, **4**-*cis* (43.2%)] and *trans* [R_f = 4.9, **1**-*trans* (10.9%); R_f = 4.7, **2**-*trans* (25.43%); R_f = 4.4, **3**-*trans* (48.9%); R_f = 4.2, **4**-*trans* (51.8%)] isomers.

Slow evaporation of these solutions at room temperature afforded orange powders or yellow crystals. Analytical data were determined by Galbraith Laboratories, U.S.A.

Infrared spectra were recorded over the 4000–200 cm^{-1} range as CsI pellets on a Perkin-Elmer 1330 instrument equipped with a data station.

^1H, ^{19}F and ^{195}Pt NMR spectra were measured with a SDS-360 MHz and a modified NT-360 spectrometer operating at 360, 282.23 and 77.1 MHz, respectively, by Spectral Data Services (IL, U.S.A.). Chemical shifts are relative to TMS, $\delta = 0$ (^1H); $CFCl_3$, $\delta = 0$ (^{19}F) and $Na_2[PtCl_4]/D_2O$, $\delta = 0$ (^{195}Pt). A standard variable temperature unit was used to control the probe temperature, which was checked periodically by a thermocouple to ensure that temperature readings were kept within ± 1°C. Palladium complexes were studied in $(CD_3)_2CO$ from -37 to 40°C and platinum complexes were studied in $(CD_3)_2CO$ at room temperature and in $(CD_3)_2SO$ at high temperatures.

Crystallographic data for $[Pt(SC_6F_5)_2(CH_3SCH(CH_3)CH(CH_3)SCH_3)]$ **3**-*cis*: $C_{18}H_{14}F_{10}PtS_4$, M = 743.61, a = 7.102(1), b = 19.066(3), c = 16.799(3) Å, β = 94.71(2)°, U = 2267.0(6) $Å^3$, T = 295 K, space group $P2_1/n$, Z = 4, ρ = 2.179 g cm^{-3}, μ = 66.93 cm^{-1}. A crystal of dimensions 0.17 × 0.12 × 0.18 mm was used for indexing and intensity data collection in the scan mode by using graphite monochromatized Mo-Kα radiation in a Siemens AED diffractometer using $\omega/2\theta$ scans ($3 \leq 2\theta \leq 50$°). They were corrected for Lorentz, polarisation and absorption effects. The structure was solved by the Patterson method. All non-hydrogen atoms were anisotropically refined (SHELX-76) [20] and hydrogen atoms were included in the observed positions. Final R and R_w values were 0.024 for 3171 observed reflections [$F \geq 5\sigma(F)$].

3. RESULTS AND DISCUSSION

Methathetical reactions of $[MCl_2\{(meso, rac)\text{-}CH_3SCH(CH_3)CH(CH_3)SCH_3\}]$, M = Pd or Pt with the anionic pseudohalogens $(SC_6F_5)^-$ or $(SC_6F_4H\text{-}4)^-$ in acetone proceeded as expected to give $[M(SR_F)_2\{(meso, rac)\text{-}CH_3SCH(CH_3)CH(CH_3)SCH_3\}]$, M = Pd, $SR_F = SC_6F_5$, **1**; $SR_F = SC_6F_4H$-4, **2**; M = Pt, $SR_F = SC_6F_5$, **3**; $SR_F = SC_6F_4H$-4, **4**; as orange–red (**1** and **2**) or yellow crystalline (**3** and **4**), air stable complexes which are soluble in acetone and dichloromethane. Analytical data consistent with the given formulation have been deposited as supplementary data.

Infrared spectra show characteristic absorption bands of the fluorinated moieties: 1515, 1480, 1085, 975 and 855 cm^{-1} for $SR_F = SC_6F_5$ and 1480, 1430, 1165 and 910 cm^{-1} corresponding to $SR_F = SC_6F_4H$-4 [19]. Other infrared frequencies agree with the dithiolate ligand expected absorptions, but have been omitted since they are of limited value to the following discussion.

From each compound **1** to **4**, two isomers were separated by dry column chromatography on silica-gel by using a chloroform–acetone mixture as eluent as described in Section 2.

Single crystals of the **3**-*cis*, were isolated by slow evaporation of chloroform:acetone solutions at room temperature. The X-ray diffraction structure of **3**-*cis* is shown in Fig. 1 and selected geometric data are collected in Table 1.

The molecules exhibit a slightly distorted square-planar arrangement around the platinum centre, with four co-ordinated sulfur atoms showing a clear sp^3 hybridisation. The racemic mixture of the *cis* isomer crystallise as the conformer with a formal alternate chiral configuration, *RSRS* or *SRSR*, in the chiral atoms of the chelated thioether ligand $CH_3S\text{-}CH(CH_3)CH(CH_3)SCH_3$. The molecular structure of **3**-*cis* corresponds to isomer **A** (see Fig. 4 below).

Sharp *et al.* [21] have found a closely related structure for $[PtCl_2(CH_3SCH(CF_3)CH(CF_3)SCH_3)]$ in which the trifluomethyl groups lie on the opposite side of the chelate ring from the methyl substituents.

The observed mean values for the Pt–S (Pt–SR_F 2.317 and Pt–SC_2 2.291 Å) and S–C [S–C(sp^2) 1.765 and S–C(sp^3) 1.817 Å] bond distances are similar to those found on the related *trans*-$[Pt(SC_6F_5)(SEt_2)_2]$ [16] [Pt–SR_F 2.323, Pt–SC_2 2.302; S–C(sp^2) 1.760, S–C(sp^3) 1.808 Å].

For $[PtCl_2(CH_3SCH(CF_3)CH(CF_3)SCH_3)]$ [21] the platinum–sulfur mean distance is slightly shorter (Pt–SC_2 2.237 Å) probably reflecting a lower *trans*-influence of the chloride ligand as compared with that of the $SC_6F_5^-$ moiety [22]. In general, sulfur–carbon lengths agree satisfactorily with the ranges described for this type of bond distance [23].

The isomers separated from these complexes can be explained simply in terms of the relative orientation of the substituents on methine groups (*cis* and *trans* diastereomers). As shown in Fig. 2, the ring is puckered at the carbon atoms but, as is the case with five membered rings at room temperature, there is fast ring inversion in all species investigated to date. At low temperature, however, few conformers have been previously identified in solution [17].

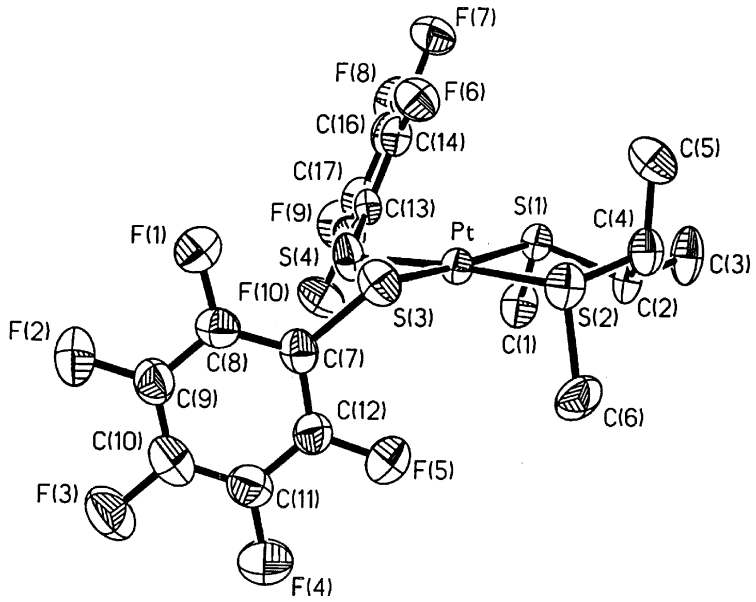

Fig. 1. X-ray structure of $[Pt(SC_6F_5)_2(CH_3SCH(CH_3)CH(CH_3)SCH_3)]$, **3**-*cis*.

Table 1. Selected molecular dimensions (bond lengths in Å, angles in °) for $[Pt(SC_6F_5)_2(CH_3SCH(CH_3)CH(CH_3)SCH_3)]$ **3**-*cis* with e.s.d.s. in parentheses

Pt–S(1)	2.293(1)	Pt–S(2)	2.289(1)
Pt–S(3)	2.323(1)	Pt–S(4)	2.310(1)
S(1)–C(1)	1.806(5)	S(1)–C(2)	1.839(5)
S(2)–C(4)	1.827(6)	S(2)–C(6)	1.797(6)
S(3)–C(7)	1.761(5)	S(4)–C(13)	1.768(5)
S(3)–Pt–S(4)	89.95(5)	S(2)–Pt–S(4)	173.76(5)
S(2)–Pt–S(3)	84.81(5)	S(1)–Pt–S(4)	96.93(5)
S(1)–Pt–S(3)	171.56(5)	S(1)–Pt–S(2)	88.59(5)
Pt–S(1)–C(2)	102.63(2)	Pt–S(1)–C(1)	110.70(2)
Pt–S(2)–C(6)	104.81(2)	Pt–S(2)–C(4)	103.35(2)
Pt–S(3)–C(7)	108.83(2)	Pt–S(4)–C(O)	110.97(2)

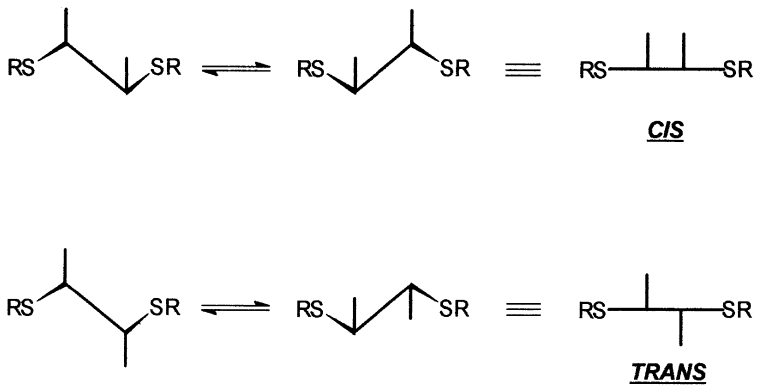

Fig. 2. Diagram representing compounds $[M(SR_F)_2(CH_3SCH(CH_3)CH(CH_3)SCH_3)]$. The $M(SR_F)_2$ unit lies perpendicular to the paper and in the plane defined by the sulfur atoms.

NMR spectra of compounds *cis* and *trans* revealed the expected presence of further isomeric forms arising from the relative position of the methyl substituents on the sulfur atoms with respect to the plane of the metal co-ordination, giving rise to *anti* and *syn* isomers, as exemplified in Fig. 3.

Anti and *syn* conformers can undergo an interconversion process through inversion of configuration at the sulfur centers. These conformational changes of the sulfur substituents are slow enough as to be detected by NMR experiments.

All together, the relative orientations of both sulfur and carbon substituents can, therefore, generate two different sets of non-interconvertable isomers (*cis* and *trans*) with three NMR-detectable and interconvertable conformers in each set, as shown on Fig. 4.

Therefore, in terms of NMR spectroscopy, both methyl substituents on the sulfur atoms (CH_3–S) are equivalent in isomers **A**, **C**, **D** and **F**, whereas isomers **B** and **E** bear pairs of magnetically non-equivalent CH_3–S moieties. Exactly the same is valid when the CH_3–C and R_F–S fragments are considered.

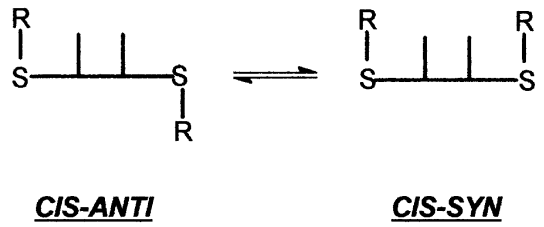

Fig. 3. *Anti* and *syn* isomers of $[M(SR_F)_2(CH_3SCH(CH_3)CH(CH_3)SCH_3)]$.

3.1. *Cis-diastereomers*

NMR selected parameters for compounds **1**-*cis* to **4**-*cis* are collected in Table 2.

^{1}H NMR spectra of isomers *cis* show three doublets arising from the CH_3–C fragments. In all cases two of these doublets have exactly the same intensity, which suggests that they arise from two non-equivalent methyls attached to the same molecule. These absorptions can, therefore, be assigned unambiguously to isomer **B** in Fig. 4. The third doublet arises from an isomer with magnetically equivalent methyl substituents, which is the case of either **A** or **C**; no definite assignment can be made at this point, however.

Proton NMR spectra also show a complicated overlap of signals due to the -CH–CH- skeleton and, as before, three signals for the CH_3–S substituents which, for compounds **3** and **4**, exhibit satellites characteristic of magnetic coupling with platinum (^{195}Pt, 34% abundance). J_{Pt-H}(**3**-*cis*) = 42.1 Hz and J_{Pt-H}(**4**-*cis*) = 42.1 Hz.

In addition, when $R_F = C_6F_4H$-4 (*cis*-compounds **2** and **4**), three triplets of triplets, characteristic of the X part of two distinct A_2B_2X magnetic systems, are detected.

This fact is of interest and seldom observed since practically all spectroscopic studies on this type of compound focus on the neutral ligand. Very few of the anionic ligands used before are suitable for NMR observation. The fluorothiolates involved in this work thus allow the distinction between magnetic non-equivalence brought up by the molecular asymmetry.

The presence of distinguishable thiolates is also reflected on the ^{19}F NMR spectra, showing three doublets for the *ortho*-fluorine atoms, a complicated multiplet of overlapping signals due to *meta*-fluorine

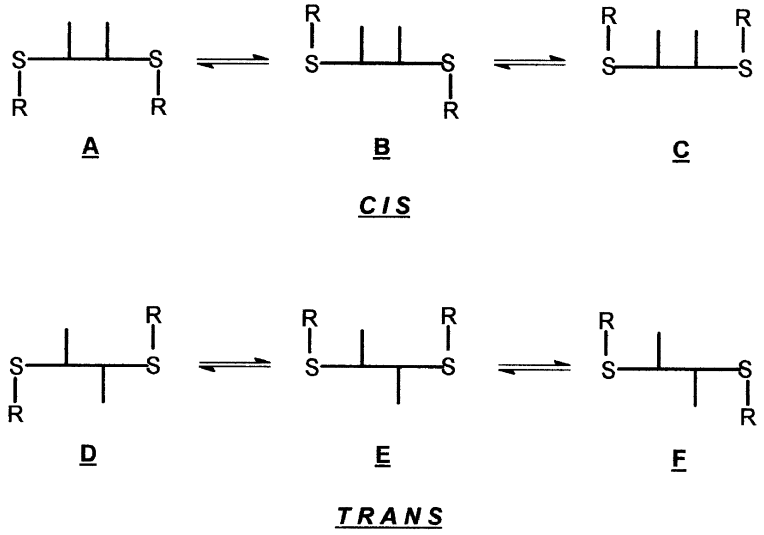

Fig. 4. *Cis* and *trans* isomers of $[M(SR_F)_2(CH_3SCH(CH_3)CH(CH_3)SCH_3)]$.

Table 2. NMR selected parameters for *cis*-diastereomers of $[M(SR_F)_2(CH_3SCH(CH_3)CH(CH_3)SCH_3)]$ **1**–**4**, M = Pd, $(CD_3)_2CO$ at 237 K; M = Pt, $(CD_3)_2CO$ at 298 K

	δ's				J's		
	Pt	H_p	F_o	F_p	$^3J_{Fo}-F_m$	$^3J_{Fm}-F_p(H)$	$^4J_{Fo}-F_p(H)$
1							
A			−131.95d	−162.03t			
					27.9	20.4	–
B			−132.30d	−162.63t			
			−132.63d	−162.65t			
2							
A		7.30tt	−132.73m				
					–	10.2	7.5
B		7.28tt	−133.06m				
		7.31tt	−133.27m				
3							
A	−4253s		−130.91dd	−161.34tt			
					28.0	21.3	7.9
B	−4251s		−131.16dd	−161.64t			
			−131.42dd	−161.76t			
4							
A	−4340s	7.07tt	−132.62m				
					–	10.3	7.2
B	−4339s	7.06tt	−132.88m				
		7.08tt	−133.77m				

atoms and, for complexes **1** and **3**, three triplets arising from the fluorine atoms in the *para* position of the fluorinated ring [Fig. 5(a)].

This spectroscopic information is consistent with the presence of only two out of the three, **A**, **B** and **C** possible isomers. Considering the multiplicity observed on the NMR signals, isomer **B** can be recognised unambiguously, but a distinction between **A** and **C** (Fig. 4) is not evident.

Further evidence for the presence of a single pair of isomers was able to be gained from $^{195}Pt-\{^1H\}$ NMR spectra of compounds **3**-*cis* and **4**-*cis* at room temperature. **3**-*cis* shows two singlets at $\delta_{Pt} = -4253$ and −4251 ppm with a relative proportion of 5.9 to 1. **4**-*cis* shows two absorptions at $\delta_{Pt} = -4340$ and −4339 ppm with 3.5 to 1 relative intensities.

Molecular models indicate extensive steric interactions between the sulfur and carbon substituents and they appear to be in the order **A** < **B** < **C**. In agreement with this order in which the least hindered isomers are predicted to have equivalent methyl–sulfur substituents, it is reasonable to assume that the most abundant isomer is **A**, while **C** has the lowest, unobservable, concentration. Assignment of signals at $\delta_{Pt} = -4253$ (**3**-*cis*) and −4340 (**4**-*cis*) ppm to isomers **A** rather than to isomers **C**, seems further supported by the fact that the structure found in the solid state for $[Pt(SC_6F_5)_2(CH_3SCH(CH_3)CH(CH_3)SCH_3)]$ is in fact that of isomer **A**.

According to that assignment, the relative population of isomers **A** and **B** (Fig. 4), for compounds **1** to **4**, are given in Table 3.

3.2. *Trans-diastereomers*

NMR selected parameters for compounds **1**-*trans* to **4**-*trans* are collected in Table 4.

^1H NMR spectra of complexes *trans* show a complex, ill-defined multiplet on the CH_3–C region. Four signals, however, arising from the CH_3–S fragments, were clearly observed.

For compounds **3** and **4**, these signals exhibit satellites characteristic of $^1H-^{195}Pt$ magnetic coupling with platinum (^{195}Pt, 34% abundance). J_{Pt-H}(**3**-*trans*) = 41.4 Hz and J_{Pt-H}(**4**-*trans*) = 42.5 Hz.

For all compounds **1** to **4**, two of these signals have exactly the same intensity, suggesting that they arise from two non-equivalent methyls attached to the same molecule. These absorptions can, therefore, be assigned unambiguously to isomer **E** in Fig. 4. The remaining two signals are resonances from isomers **D** and **F**, both having magnetically equivalent methyl substituents.

Proton NMR spectra also display a complex multiplet of overlapping signals due to the -CH–CH- skeleton. In addition, when $R_F = C_6F_4H$-4 (*trans*-compounds **2** and **4**), four signals characteristic of the X

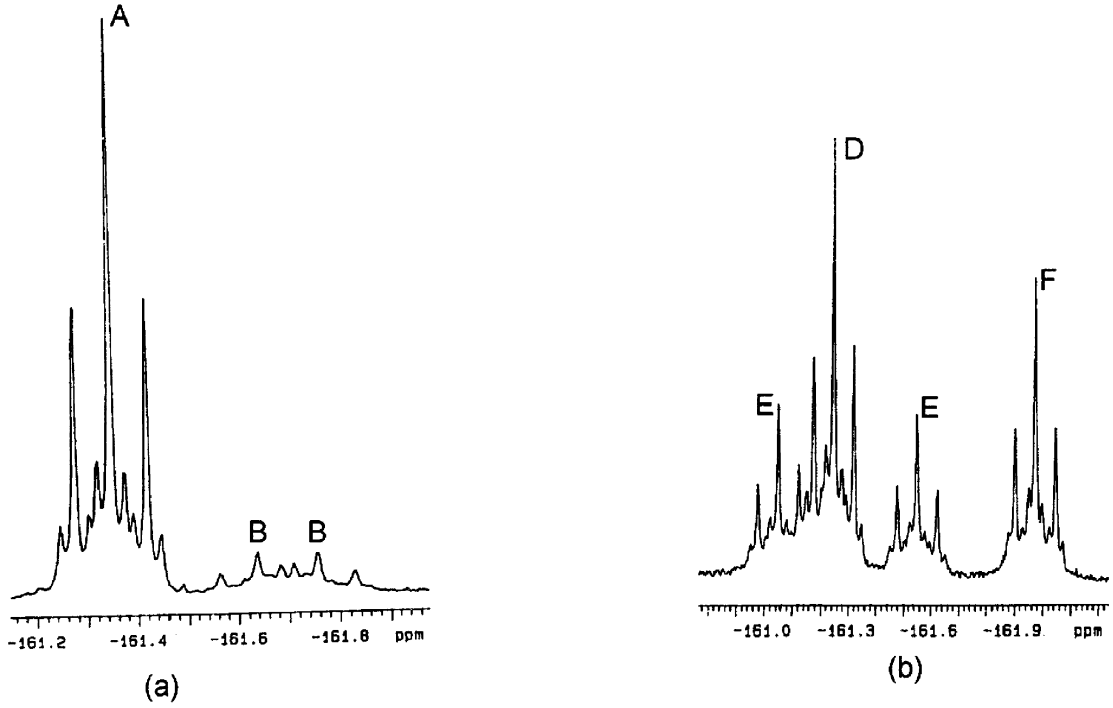

Fig. 5. ^{19}F NMR of *para*-fluorine region of $[Pt(SC_6F_5)_2(CH_3SCH(CH_3)CH(CH_3)SCH_3)]$ **3**-*cis* (a) and **3**-*trans* (b).

Table 3. Relative isomeric populations for $[M(SR_F)_2(CH_3SCH(CH_3)CH(CH_3)SCH_3)]$, M = Pd (237 K), $R_F = C_6F_5$ **1**; C_6F_4H-4 **2**; M = Pt(298 K), $R_F = C_6F_5$ **3**; C_6F_4H-4 **4**

	Cis			*Trans*		
	A	**B**	**C**	**D**	**E**	**F**
1	6.3	1	–	1.1	1.4	1
2	5.6	1	–	1.1	1.3	1
3	5.9	1	–	1.3	1.1	1
4	3.5	1	–	1.2	1.1	1

part of three different A_2B_2X magnetic systems, are detected.

^{19}F NMR spectra show four doublets for the *ortho*-fluorine atoms, a complicated multiplet of overlapping signals due to *meta*-fluorine atoms and, for complexes **1** and **3**, four triplets of triplets arising from the fluorine atoms in the *para* position of the fluorinated ring [Fig. 5(b)]. No ^{19}F–^{195}Pt magnetic couplings were observed.

The available spectroscopic information is consistent with the presence of isomers **D**, **E** and **F** (Fig. 4) in solution of compounds **1**-*trans* to **4**-*trans*.

Further evidence of such an isomeric distribution is gained from ^{195}Pt–$\{^1H\}$ NMR spectra of compounds **3**-*trans* and **4**-*trans* which show, at room temperature, three singlets at $\delta_{Pt} = -4252$, -4257 and -4261 ppm and $\delta_{Pt} = -4339$, -4342 and -4343 ppm, respectively. The relative intensities of these signals are 1.3:1.1:1 for **3**-*trans* and 1.2:1.1:1 for **4**-*trans*.

As seen before, molecular models indicate considerable steric interactions between the sulfur and carbon substituents, which appear to be in the order **D** < **E** < **F**. In agreement with this order in which the least hindered isomers are predicted to have *anti* and equivalent sulfur substituents, the most abundant isomer is probably **D**, whereas **F** appears to be the least abundant.

The relative populations assigned to *trans*-isomers **D**, **E** and **F** (Fig. 4), for compounds **1** to **4**, are given in Table 3.

Conformers **A** and **B**, on the one hand, as well as **D**, **E** and **F**, on the other, are involved in dynamic equilibria due to a configuration inversion at the thioether sulfur atoms. The pyramidal inversion is a relatively slow process suitable for detection within the NMR time scale as the individual absorptions from each isomer coalesce into a single averaged resonance.

As expected, the thiolate ligands seem to have fast free rotation and, at room temperature and higher, do not participate in the fluxionality of these molecules.

For comparable compounds, palladium derivatives show lower coalescence temperatures than does platinum. This can be attributed to the more effective 3p(S)–4d(Pd) overlap compared with the 3p(S)–5d(Pt)

Table 4. NMR selected parameters for *trans*-diastereomers of $[M(SR_F)_2(CH_3SCH(CH_3)CH(CH_3)SCH_3)]$ **1**–**4**, M = Pd, $(CD_3)_2CO$ at 237 K; M = Pt, $(CD_3)_2CO$ at 298 K

	δ's				J's		
	Pt	H_p	F_o	F_p	$^3J_{Fo}-F_m$	$^3J_{Fm}-F_p(H)$	$^4J_{Fo}-F_p(H)$
1							
D			−131.87d	−162.19t			
E			−131.78d	−161.75t	27.1	21.0	–
			−131.95d	−162.29t			
F			−132.45d	−162.91t			
2							
D		7.30tt					
			−132.70m				
E		7.29tt			–	10.2	7.5
		7.28tt					
			−133.09m				
F		7.26tt					
3							
D	−4252s		−130.88dd	−161.26tt			
E	−4257s		−130.80dd	−161.05tt	28.2	22.6	8.5
			−130.92dd	−161.55tt			
F	−4261s		−131.44dd	−161.98tt			
4							
D	−4339s	7.08tt					
			−132.97m				
E	−4342s	7.06tt			–	10.3	7.2
		7.07tt	−132.57m				
F	−4343s	7.04tt					

overlap, which allows an easier access to the transition state in the case of palladium complexes [24]. In fact, palladium derivatives show slow sulfur inversion at 237 K while platinum derivatives show it at 298 K in $(CD_3)_2CO$ solutions.

For palladium complexes we have measured coalescence temperatures by observing the ^{19}F NMR spectra of the thiolate moieties. For platinum complexes, coalescence temperatures were determined directly from the variable temperature ^{195}Pt NMR spectra. Coalescence temperatures are collected in Table 5.

Cis-compounds **1** to **4** show a single coalescence of signals in agreement with the fast interconversion **A**⇔**B**. On the other hand, *trans*-compounds **1** to **4** give rise to two consecutive temperatures of coalescence, in agreement with a process involving three species: **D**⇔**E**⇔**F** for which two different energies of inversion are reasonably to be expected (Fig. 6).

In summary, NMR studies of each diastereomer of complexes **1** to **4** show the presence of three conformers of the *trans* isomers but only two of the *cis* isomer. In general, NMR spectra are quite similar and only slight changes in the relative isomeric populations were observed. As expected, relative abundances can be detected regardless of the observed nuclei.

Table 5. Coalescence temperatures of the compounds **1** to **4**

Compound[a]	Isomer	CT1[b]	Isomer	CT1[b]	CT2[b]
1 $[Pd(SC_6F_5)_2L]$	*cis*	283	*trans*	283	308
2 $[Pd(SC_6F_4H\text{-}4)_2L]$	*cis*	283	*trans*	283	308
3 $[Pt(SC_6F_5)_2L]$	*cis*	333	*trans*	343	363
4 $[Pt(SC_6F_4H\text{-}4)_2L]$	*cis*	333	*trans*	343	383

[a]$L = CH_3SCH(CH_3)CH(CH_3)SCH_3$.
[b]Coalescence temperature (CT) in K.

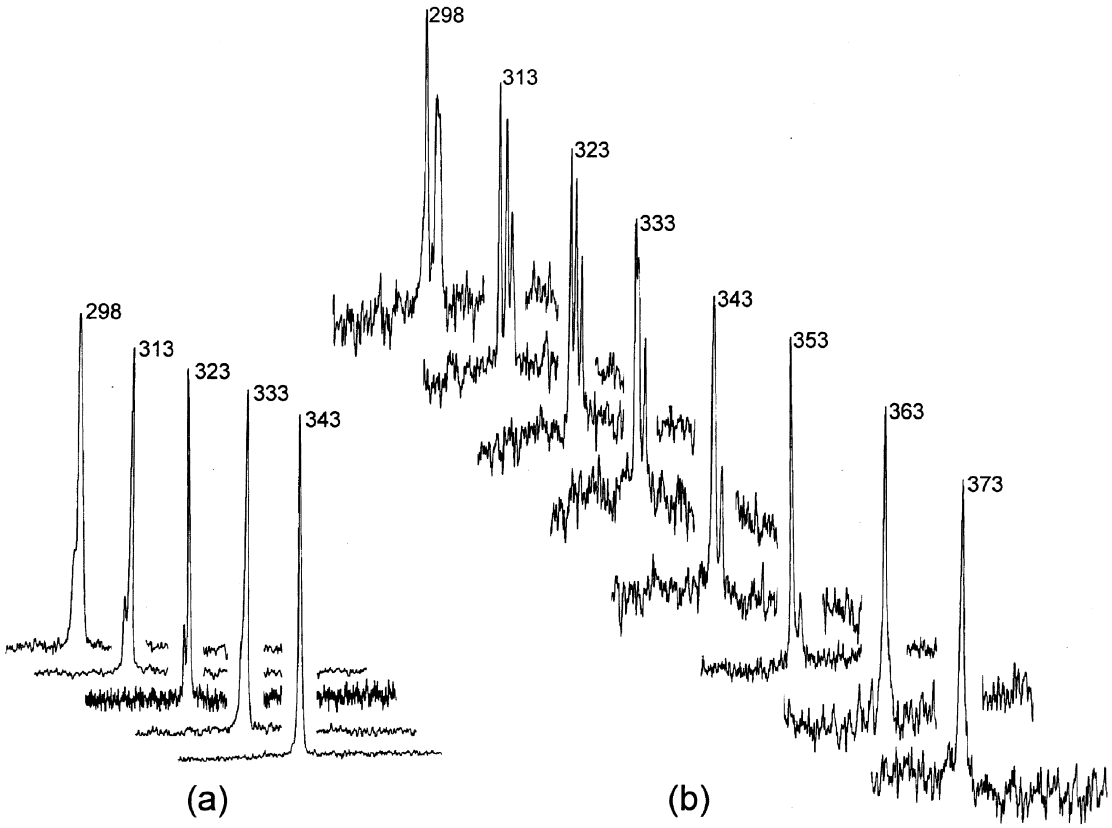

Fig. 6. Variable temperature ^{195}Pt NMR spectra of [Pt(SC_6F_5)$_2$($CH_3SCH(CH_3)CH(CH_3)SCH_3$)] **3**-*cis* (a) and **3**-*trans* (b).

4. SUPPLEMENTARY MATERIAL AVAILABLE

Tables of analytical data are shown in Appendix A. Crystal and intensity measurement data, positional parameters of calculated hydrogen atoms, anisotropic thermal parameters and bond distances and angles have been deposited at Cambridge Crystallographic Data Centre, deposition code: 101590.

Acknowledgements—We wish to thank DGAPA-UNAM, PADEP-UNAM and CONACYT for financial support and to Dr Sylvain Bernès for his helpful assistance.

REFERENCES

1. Stephan, D. and Nadasdi, T., *Coord. Chem. Rev.*, 1996, **147,** 147.
2. Krebs, B. and Henkel, G., *Angew. Chem. Int. Ed. Engl.*, 1991, **30,** 769.
3. Blower, P. and Dilworth, J., *Coord. Chem. Rev.*, 1987, **76,** 121.
4. Black, J. R., Champness, N. R., Levason, W. and Reid, G., *J. Chem. Soc. Dalton Trans.*, 1995, 3439.
5. Black, J. R., Champness, N. R., Levason, W. and Reid, G., *J. Chem. Soc. Chem. Commun.*, 1995, 1277.
6. Black, J. R. and Levason, W., *J. Chem. Soc. Dalton Trans.*, 1994, 3225.
7. Abel, E. W., Bhargava, S. K. and Orrell, K. G., *Prog. Inorg. Chem.*, 1984, **32,** 1.
8. Orrell, K. G., *Coord. Chem. Rev.*, 1989, **96,** 1.
9. Orrell, K. G., Šik, V., Brubaker, C. and McCulloch, B., *J. Organomet. Chem.*, 1984, **276,** 267.
10. Abel, E. W., Khan, R., Kite, K., Orrell, K. G. and Šik, V., *J. Chem. Soc. Dalton Trans.*, 1980, 1175.
11. Abel, E. W., Coston, T. P., Higgins, K. M., Orrell, K. G., Šik, V. and Cameron, T. S., *J. Chem. Soc. Dalton Trans.*, 1989, 701.
12. Abel, E. W., Moss, I., Orrell, K. G., Šik, V., Stephenson, D., Bates, P. A. and Hursthouse, M. B., *J. Chem. Soc. Dalton Trans.*, 1988, 521.
13. Mao, X.-A., Yao, J.-Z., Tian, B.-S. and Chen, Y.-Y., *Magn. Reson. Chem.*, 1996, **34,** 109.
14. Cruz-Garritz, D., Leduc, B., López-Tercero, J., Martin, E. and Torrens, H., *Rev. Soc. Quim. Méx.*, 1990, **34,** 76.
15. García, J., Martin, E., Morales, D., Torrens, H. and Del Río, F., *Inorg. Chim. Acta*, 1993, **207,** 93.
16. Cruz-Garritz, D., Martin, E., Torrens, H. and Mayoh, K., Smith, A., *Trans. Met. Chem.*, 1991, **16,** 236.
17. Cross, R. J., Rycroft, D. S., Sharp, D. W. A. and Torrens, H., *J. Chem. Soc. Dalton Trans.*, 1980, 2434.

18. Peach, M. E., *Can. J. Chem.*, 1968, **46,** 2699.
19. Bertran, A., Garcia, J., Martin, E., Sosa, P. and Torrens, H., *Rev. Soc. Quim. Mex.*, 1993, **37,** 185.
20. Sheldrick, G. M., *SHELX Systems Report*. University of Cambridge, 1976.
21. Hunter, W. N., Muir, K. W. and Sharp, D. W. A., *Acta Cryst. C*, 1984, **40,** 37.
22. Cruz-Garritz, D., Chamizo, J. A., Cruz, M. and Torrens, H., *Rev. Soc. Quim. Mex.*, 1989, **33,** 18.
23. Orpen, A. G., Brammer, L., Allen, F. H., Kennard, O., Watson, D. G. and Taylor, R., *J. Chem. Soc. Dalton Trans.*, 1989, 31.
24. Abel, E. W., Evans, D. G., Koe, J. R., Šik, V., Bates, P. A. and Hursthouse, M. B., *J. Chem. Soc. Dalton Trans.*, 1989, 985.

APPENDIX A

SUPPLEMENTARY ANALYTICAL DATA

The analytical data of **1**–**4** *meso*/*rac*-complexes are given in Table 6. The analytical data of *cis* and *trans* complexes are given in Table 7.

Table 6. Analytical data of **1**–**4** *meso*/*rac*-complexes

Compound[a]	Analyses (%)[b]		
	C	H	S
1 $[Pd(SC_6F_5)_2L]$	32.6 (33.0)	2.3 (2.2)	19.2 (19.6)
2 $[Pd(SC_6F_4H\text{-}4)_2L]$	34.4 (34.9)	2.8 (2.6)	20.4 (20.7)
3 $[Pt(SC_6F_5)_2L]$	28.9 (29.1)	1.7 (1.9)	17.3 (17.3)
4 $[Pt(SC_6F_4H\text{-}4)_2L]$	30.1 (30.6)	2.4 (2.3)	17.9 (18.1)

[a] $L = CH_3SCH(CH_3)CH(CH_3)SCH_3$.
[b] Calculated values in parentheses.

Table 7. Analytical data of *cis* and *trans* complexes

Compound[a]	Analyses (%)[b]		
	C	H	S
1-*cis* $[Pd(SC_6F_5)_2L]$	32.8 (33.0)	2.3 (2.2)	19.5 (19.6)
1-*trans* $[Pd(SC_6F_5)_2L]$	32.9 (33.0)	2.2 (2.2)	19.4 (19.6)
2-*cis* $[Pd(SC_6F_4H\text{-}4)_2L]$	34.7 (34.9)	2.6 (2.6)	20.5 (20.7)
2-*trans* $[Pd(SC_6F_4H\text{-}4)_2L]$	34.8 (34.9)	2.5 (2.6)	20.8 (20.7)
3-*cis* $[Pt(SC_6F_5)_2L]$	28.9 (29.1)	1.8 (1.9)	17.3 (17.3)
3-*trans* $[Pt(SC_6F_5)_2L]$	29.0 (29.1)	2.0 (1.9)	17.4 (17.3)
4-*cis* $[Pt(SC_6F_4H\text{-}4)_2L]$	30.4 (30.6)	2.4 (2.3)	17.9 (18.1)
4-*trans* $[Pt(SC_6F_4H\text{-}4)_2L]$	30.5 (30.6)	2.3 (2.3)	18.2 (18.1)

[a] $L = CH_3SCH(CH_3)CH(CH_3)SCH_3$.
[b] Calculated values in parentheses.

Pergamon

Polyhedron Vol. 17, No. 23–24, pp. 4101–4108, 1998
© 1998 Elsevier Science Ltd
All rights reserved. Printed in Great Britain
0277–5387/98 $19.00+0.00

PII: S0277–5387(98)00215–0

N-bridged and H-bridged aminoalanes: Single-crystal X-ray structure determinations for the planar dimer $\{[(Me_3Si)_2N]_2Al(\mu\text{-}H)\}_2$ and the puckered four-membered ring compound $(Me_3Si)_2N(Me_2N)Al(\mu\text{-}NMe_2)_2Al(H)N(SiMe_3)_2$

Jerzy F. Janik,*[a] Richard L. Wells,†[a] Arnold L. Rheingold[b] and Ilia A. Guzei[b]

[a]Paul M. Gross Chemical Laboratory, Department of Chemistry, Duke University, Durham, NC 27708-0346, U.S.A.

[b]Department of Chemistry, University of Delaware, Newark, DE 19716, U.S.A.

(Received 23 March 1998; accepted 21 May 1998)

Abstract—The known bis(bis(trimethylsilyl)amino)alane $\{[(Me_3Si)_2N]_2Al(\mu\text{-}H)\}_2$ (**1**) is obtained from disproportionation of the base-stabilized monomeric bis(trimethylsilyl)aminoalane $[(Me_3Si)_2NAlH_2]\cdot NMe_3$ in refluxing toluene. The single-crystal X-ray structure determination for **1** provides a H-bridged planar dimer with exo-cyclic $N(SiMe_3)_2$ groups. The combination of **1** with $HNMe_2$ in a 1:1 ratio results in competing aminolysis at the Al–H site and transamination at the Al–$N(SiMe_3)_2$ site of **1**, as illustrated by the molecular structure of $(Me_3Si)_2N(Me_2N)Al(\mu\text{-}NMe_2)_2Al(H)N(SiMe_3)_2$ (**2**) which is isolated from this system. The characteristic structural feature of **2** is a puckered {Al–N–Al–N} ring with different ligands on two aluminum atoms.
© 1998 Elsevier Science Ltd. All rights reserved

Keywords: alanes; trimethylsilylamines; disproportionation; transamination; aminolysis; precursors.

INTRODUCTION

In the solid state, some alane amine adducts show dimeric connectivities $[H_3Al\cdot L]_2$ (for example, $L=NMe_3$ [1], NMe_2CH_2Ph [2]) with five-coordinated aluminum atoms and somewhat counterintuitive unsymmetrical Al–H–Al bridges while, on the other hand, others seem to favor a monomeric mode with four-coordinated Al in $H_3Al\cdot L$ (for example, $L=N(n\text{-}Bu)_3$ [3], quinuclidine [4]) or five-coordinated Al having a N–$Al(H_3)$–N bond sequence as in trigonal bipyramidal $H_3Al\cdot 2NMe_3$ [5]. This span of bonding preferences in the alane adducts is generally interpreted as a manifestation of the ligand's steric hindrance and is not an exclusive property of amine Lewis bases. The latter is illustrated by examples of the Al–H–Al bridged dimer $[H_3Al\cdot THF]_2$ and trigonal bipyramidal $H_3Al\cdot 2THF$ with an O–$Al(H_3)$–O axis [6]. Even more complex bonding environments are encountered in some polymeric structures containing AlH_3 units [7]. Finally, ionic bonding is displayed by rare species of the type $(H_2AlL)^+(AlH_4)^-$ where L is a tri- or tetradentate amine ligand [8]. The progress in the chemistry of Lewis base adducts of alane and gallane has recently been reviewed [9].

The aminoalanes, $\{H_nAl(NR_2)_{3-n}\}$ ($n=0$, 1, 2), appear to exhibit similar diversity of bonding as outlined above for alane amine adducts but relatively shorter Al–N bond lengths in the former make the steric factor play a more obvious role. For example, the dimethylaminoalane, $(H_2AlNMe_2)_3$, is a N-bridged trimer in solution [10] and in the solid state [11] but both bis(dimethylamino)alane, $[HAl(NMe_2)_2]_2$ [12], and tris(dimethylamino)alane, $[Al(NMe_2)_3]_2$ [13, 14], are N-bridged dimers. Even

* On leave from the University of Mining and Metallurgy, Krakow, Poland.

† Author to whom correspondence should be addressed.

larger NR_2 groups may result in N-bridged dimeric cores such as found in 2,6-dimethylpiperidinoalane, $[H_2Al(dmp)]_2$ [15]. A further increase of the bulkiness of the piperidino ligand, in the absence of NMe_3 as in the reaction between $LiAlH_4$ with $(tmpH) \cdot HCl$, yields a postulated H-bridged trimer 2,2,6,6-tetramethylpiperidinoalane, $[H_2Al(tmp)]_3$, or, even in the presence of NMe_3 in the reaction between $H_3Al \cdot NMe_3$ with 2 equivalents of tmpH, gives the authenticated H-bridged dimer bis(2,2,6,6-tetramethylpiperidino)alane, $[HAl(tmp)_2]_2$ [15]. On the other hand, an extreme bulkiness of $N(SiMe_3)_2$ coupled with a latent N-basicity in this group is thought to be responsible for the kinetic stabilization of the unassociated $Al[N(SiMe_3)_2]_3$ [16].

In addition to the formation of the N- or H-bridged aminoalanes, stabilization of the aminoalane unit by an available Lewis base may sometimes also be favorable. In systems utilizing the convenient form of alane, $H_3Al \cdot NMe_3$, trimethylamine as a potent Lewis base is found in a few cases to play that role. It was originally reported that the monomeric aminoalane, stabilized by coordination of NMe_3 at the Al-site, $[H_2AlN(SiMe_3)_2] \cdot NMe_3$, was formed from the reaction between $H_3Al \cdot NMe_3$ and $HN(SiMe_3)_2$ [17, 18]. This finding was later confirmed in a parallel study, which additionally provided a structural proof for the related $[H(Cl)AlN(SiMe_3)_2] \cdot NMe_3$ [19]. Further, a 1:1 ratio reaction between $H_3Al \cdot NMe_3$ and tmpH afforded $[H_2Al(tmp)] \cdot NMe_3$ [20], which can be compared with the previously discussed H-bridged trimer $[H_2Al(tmp)]_3$ [15] obtained in the absence of trimethylamine. One should be aware that this kind of adduct stabilization extends into other group 13–group 15 systems and, for example, is also found in the pnictinoalanes $[H_2AlEMes_2] \cdot NMe_3$ (E = P, As) [21] and $[H_2AlAs(SiMe_3)_2] \cdot NMe_3$ [22].

The original reports by Paine and coworkers on the preparation of $[H_2AlN(SiMe_3)_2] \cdot NMe_3$ [17, 18] indicated that thermal decomposition of this compound resulted in the formation of new bis(bis-(trimethylsilyl)amino)alane $\{[(Me_3Si)_2N]_2Al(\mu\text{-}H)\}_n$ of an undetermined degree of oligomerization; some analytical evidence, however, supported the presence of Al–H–Al bridges in this product [18]. This was contrary to what the parallel report by Raston and coworkers claimed about the thermal behavior of $[H_2AlN(SiMe_3)_2] \cdot NMe_3$ [19], namely, decomposition to elemental aluminum presumably along a reductive coupling pathway with dihydrogen evolution and, here, additionally, with concurrent release of NMe_3. In this regard, one has to be aware that reductive coupling is not the only thermally induced decomposition pathway for aminoalanes and it has long been known that their ligand disproportionation chemistry is of equal importance [12, 23]. Herein, we confirm the originally reported disproportionation of $[H_2AlN(SiMe_3)_2] \cdot NMe_3$ and describe the single-crystal X-ray diffraction study for the resulting H-bridged dimer, bis(bis(trimethylsilyl)amino)alane $\{[(Me_3Si)_2N]_2Al(\mu\text{-}H)\}_2$ (**1**). We also outline the reaction of **1** with $HNMe_2$ and the isolation of an unsymmetrically substituted product $(Me_3Si)_2N(Me_2N)Al(\mu\text{-}NMe_2)_2Al(H)N(SiMe_3)_2$ (**2**) for which a single-crystal structure is presented.

EXPERIMENTAL

General techniques

All experiments were carried out using standard vacuum/Schlenk techniques. Solvents were dried and distilled from Na benzophenone ketyl or Na/K alloy prior to use. $HNMe_2$ was obtained from Aldrich and used as received. $[H_2AlN(SiMe_3)_2] \cdot NMe_3$ and $\{[(Me_3Si)_2N]_2Al(\mu\text{-}H)\}_2$ were prepared by the literature methods [18]; the synthesis and characterization of the latter is also described in more detail below. ^1H and $^{13}C\{^1H\}$ NMR spectra were acquired on a Varian Unity 400 spectrometer at 25°C from toluene-d_8 solutions and referenced vs $SiMe_4$ by generally accepted methods. Mass spectra were collected on a JEOL JMS-SX 102A spectrometer operating in the EI mode at 20 eV. IR spectra of solids and oily products were acquired using KBr pellets and NaCl plates, respectively, on a BOMEM Michelson MB-100 FT-IR spectrometer. A calibrated manifold was used for volume estimations of reaction gases. Melting behavior (uncorrected) was determined with a Thomas-Hoover Uni-melt apparatus for samples flame-sealed in glass capillaries. Single-crystal X-ray diffraction studies for **1** and **2** were performed at the Department of Chemistry and Biochemistry, University of Delaware, Newark, DE, on a Siemens P4/CCD diffractometer, using Mo Kα radiation ($\lambda = 0.71073$ Å). All calculations were carried out with the help of SHELXTL 5.03 programs [24]; the structures were solved by direct methods.

Preparation of $\{[(Me_3Si)_2N]_2Al(\mu\text{-}H)\}_2$ (**2**)

A sample of $[H_2AlN(SiMe_3)_2] \cdot NMe_3$, 1.24 g or 5.0 mmol, was dissolved in about 10–15 mL of toluene, stirred and refluxed overnight under nitrogen. Typically, elemental aluminum precipitated on the sides of reaction flask in the form of agglomerates but, sometimes, aluminum would form as a colloidal suspension. The mixture was concentrated by evacuation to about 5–10 mL and refluxed for an additional 24 h. Subsequently, it was filtered, the volatiles evacuated from the filtrate and the resulting residue dissolved in a few mL of hexane. The concentrated hexane solution, after storage at −30°C, afforded abundant colorless crystals of **1**, 0.48 g or 55% yield based on eqn (1) (*vide infra*). More crystalline product could be recovered from the solution by further concentrating and repeating the low temperature crystallization. M.p. 95–97°C. ^1H NMR: δ 0.34 (36H; $SiMe_3$), 4.4 (1H, br; AlH). $^{13}C\{^1H\}$ NMR: δ 6.0 ($SiMe_3$). MS: *m*/*e* (inten-

sity) (ion): peak clusters around: 695 (1) ($\{[(Me_3Si)_2N]_2Al(\mu\text{-}H)\}_2$–*H* or *M*–*H*), 667 (1) (*M*–2Me + H), 596 (1) (M–$SiMe_3$ + 3H), 552 (2) (M–2$SiMe_3$ + 2H), 536 (2) (M–*N*$(SiMe_3)_2$), 492 (3) (M–*N*$(SiMe_3)_2$–3Me + H), 461 (2) (M–*N*$(SiMe_3)_2$–5Me) 421 (5) (M–*N*$(SiMe_3)_2$–$SiMe_3$–3Me + 3H), 347 (3) ($[(Me_3Si)_2N]_2AlH$–*H* or *M**–*H*), 331 (2) (*M**–Me–2H), 300 (2) (*M**–3Me–3H), 275 (3) (*M**–$SiMe_3$), 202 (3) (*M**–2$SiMe_3$), 161 (20) ($HN(SiMe_3)_2$), 146 (100) ($HN(SiMe_3)_2$–Me), 130 (10) ($HN(SiMe_3)_2$–2Me–H), 74 (9) ($HSiMe_3$). IR (KBr pellet/Nujol mull): *v*(Al–H) range, 1882/1880 cm^{-1}. We note that these Al–H stretching frequencies significantly differ from that of a weak band at 1790 cm^{-1} originally reported for **1** [18]. In the present study, the medium intensity band at about 1880 cm^{-1} was reproducible, but its intensity was decreasing fast in the course of measurements due to deterioration of the sample. At this point, we are inclined to think that the band reported earlier might have been recorded for a significantly decayed sample.

Reactions of $\{[(Me_3Si)_2N]_2Al(\mu\text{-}H)\}_2$ *with* $HNMe_2$. *Isolation of* $(Me_3Si)_2N(Me_2N)Al(\mu\text{-}NMe_2)_2Al(H)N(SiMe_3)_2$ (**2**)

0.10 g of **1** (0.14 mmol) was dissolved in about 10 mL of toluene and the reaction flask was freeze-pump-thawed three times. Onto this, using a calibrated vacuum line, 0.29 mmol of $HNMe_2$ was deposited at −78°C. The mixture was stirred at room temperature overnight and non-condensables, H_2, were measured, 0.04 mmol. The solution was then stored for a few days at −30°C. At the end of this period, the volatiles were removed yielding an oil/solid product. IR (neat): weak to medium band in the *v*(N–H) range at 3310 cm^{-1}; medium band in the *v*(Al–H) range at 1833 cm^{-1}. A toluene-d_8 NMR sample of this product was run immediately, 1 day, 2 weeks and 7 weeks after preparation.

Immediately: ^1H NMR (intensity) (group assignment): $SiMe_3$ region: δ 0.08 (9) ($HN(SiMe_3)_2$), 0.27 (23), 0.31 (24), 0.33 (100); NMe_2 region: δ 1.88 (9), 1.89 (9) and several small intensity peaks (<1) in this region at 2.29, 2.32, 2.41, 2.42, 2.51, 2.60, 2.76; AlH region: δ 4.0 (very broad), 4.51. $^{13}C\{^1H\}$ NMR (intensity) (group assignment): $SiMe_3$ region: δ 2.6 (7) ($HN(SiMe_3)_2$), 5.0 (3), 6.2 (100), 6.5 (16), 6.8 (4); NMe_2 region: δ 37.9 (24), 40.4 (1), 41.6 (2), 42.0 (3), 43.2 (2), 43.5 (7).

1 day after: ^1H NMR (intensity) (group assignment): $SiMe_3$ region: δ 0.08 (100) ($HN(SiMe_3)_2$), 0.27 (50), 0.31 (80), 0.33 (35); NMe_2 region: δ 1.88 (1), 1.89 (1), 2.42 (15), 2.51 (1), 2.60 (8), 2.76 (2); no unequivocally measurable broad feature in the AlH region except for the sharp resonance at δ 4.51. $^{13}C\{^1H\}$ NMR (intensity) (group assignment): $SiMe_3$ region: δ 2.6 (90) ($HN(SiMe_3)_2$), 4.9 (55), 6.2 (70), 6.5 (100), 6.8 (14); NMe_2 region: δ 37.9 (13), 40.4 (15), 41.6 (5), 42.0 (10), 43.2 (10), 43.5 (70).

2 weeks after: ^1H NMR (intensity) (group assignment): $SiMe_3$ region: δ 0.08 (100) ($HN(SiMe_3)_2$), 0.27 (55), 0.31 (83), 0.33 (6); NMe_2 region: δ 1.88 (1), 1.89 (1), 2.42 (16), 2.52 (3), 2.60 (8), 2.76 (4); AlH region: δ 4.1 (broad), 4.51. $^{13}C\{^1H\}$ NMR (intensity) (group assignment): $SiMe_3$ region: δ 2.6 (83) ($HN(SiMe_3)_2$), 4.9 (63), 6.2 (35), 6.5 (100), 6.8 (32); NMe_2 region: δ 37.9 (1), 40.4 (20), 41.6 (16), 42.0 (19), 43.2 (17), 43.5 (65).

7 weeks after: The NMR spectra were identical to those obtained after 2 weeks. The oily/solid product was redissolved in a small amount of toluene and, subsequently, volatiles were allowed to evaporate at −30°C in the course of several days. After almost complete removal of volatiles, a small quantity of a colorless crystalline product was isolated. A single-crystal X-ray structure determination provided $(Me_3Si)_2N(Me_2N)Al(\mu\text{-}NMe_2)_2Al(H)N(SiMe_3)_2$ (**2**). ^1H NMR for a freshly prepared sample (intensity) (group assignment): $SiMe_3$ region: 0.281 (85), 0.284 (100), 0.29 (63), 0.30 (77), 0.31 (52), 0.32 (71), 0.33 (58); NMe_2 region: δ 2.42 (14), 2.52 (12), 2.66 (25), 2.77 (19), 2.78 (16); AlH region: no discernible feature between δ 3.0–5.0. This sample was also run two days after preparation and showed an even more complex spectrum indicating continuing changes in the solution. IR (KBr pellet): *v*(Al–H) range, medium to strong band at 1860 cm^{-1}.

Structural determinations for **1** *and* **2**

Specimens of **1** were obtained in the form of thin colorless needles from recrystallization in toluene at −30°C and mounted in capillaries prior to determination. The systematic absences in the diffraction data were consistent with monoclinic space groups $P2_1/m$ and $P2_1$ but only the latter yielded computationally stable results and refinement. The structure was solved using direct methods, completed by subsequent difference Fourier syntheses and refined by full-matrix least-square procedures. All non-hydrogen atoms were refined with anisotropic displacement coefficients. All C-hydrogen atoms were treated as idealized contributions. The Al-hydrogen atoms were located from the difference map and were refined with fixed thermal parameters and fixed Al–H distances, 1.727(1) Å. The geometry of the {Al–H–Al–H} ring was not constrained. There are two symmetry independent, but chemically similar, molecules in the asymmetric unit and the thermal ellipsoid diagram of molecule 1 is shown in Fig. 1. The thermal ellipsoid diagram of molecule 2 is available in the Supporting Information. Specimens of **2** were obtained as blocky colorless crystals from slow evaporation of toluene at −30°C and mounted in capillaries prior to determination. The data were consistent with the monoclinic space group $P2_1/n$. The structure was solved using direct methods, completed by subsequent difference Fourier syntheses and refined by full-matrix

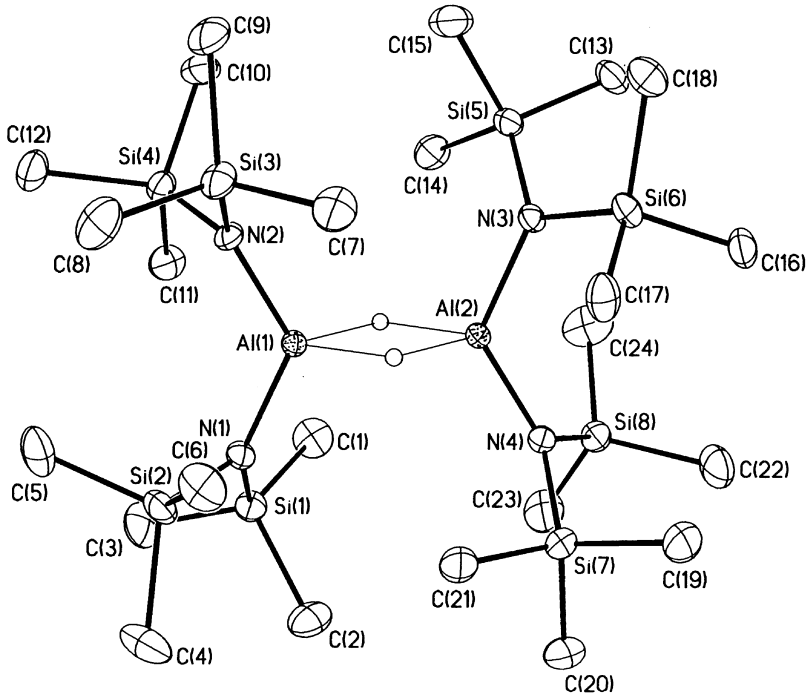

Fig. 1. Thermal ellipsoid diagram (30% probability ellipsoids) showing the molecular structure of **1** (independent molecule 1). All C-hydrogen atoms are omitted for clarity.

least-square procedures. Semi-empirical absorption corrections were not required because there was less than 10% variation in the integrated Ψ-scan intensity data. The Si–N distances were restrained to an average N–Si distance of 1.74 Å. All non-hydrogen atoms were refined with anisotropic displacement coefficients. The hydrogen atom on Al(1) was placed in an idealized position with the fixed Al–H distance of 1.50 Å. All other hydrogen atoms were treated as idealized contributions. The residuals for **2** are rather high due to marginal quality of the specimen. However, the metric parameters and their esd's around aluminum atoms appear to be of acceptable quality. The thermal ellipsoid diagram of **2** is shown in Fig. 2. Details of the

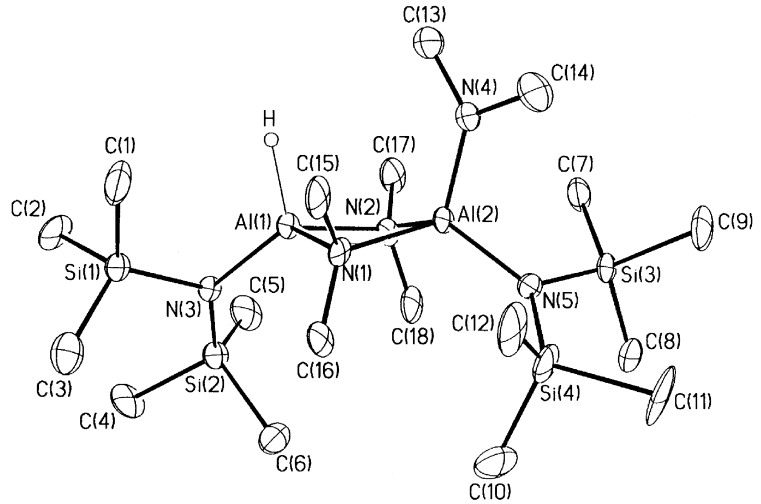

Fig. 2. Thermal ellipsoid diagram (30% probability ellipsoids) showing the molecular structure of **2**. All C-hydrogen atoms are omitted for clarity.

data collection for **1** and **2** are summarized in Table 1, and Table 2 shows selected bond distances and angles.

RESULTS AND DISCUSSION

Bis(bis(trimethylsilyl)amino)alane $\{[(Me_3Si)_2N]_2Al(\mu\text{-}H)\}_2$ (**1**) was obtained from disproportionation of the based-stabilized monomeric aminoalane $[H_2AlN(SiMe_3)_2]\cdot NMe_3$ as described by the following idealized equation [18]:

$$2[H_2AlN(SiMe_3)_2]\cdot NMe_3 \xrightarrow[\text{toluene}]{\text{reflux}} H_3Al\cdot NMe_3 + 1/2\{[(Me_3Si)_2N]_2Al(\mu\text{-}H)\}_2 \quad (1)$$
$$\downarrow$$
$$Al + 3/2H_2 + NMe_3$$

The anticipated formation of the alane trimethylamine byproduct, $H_3Al\cdot NMe_3$, would have been associated with its decomposition under toluene reflux conditions and precipitation of elemental aluminum [25], which was indeed observed. We found this disproportionation reaction to be crucially dependent on the substrate's concentration. For example, dilute toluene solutions did not show signs of the precipitation of elemental aluminum even after a several day-long reflux. On the other hand, appropriately concentrated solutions appeared to react as above in the course of several hours while intermediate removal of some toluene by evacuation accelerated the reaction's progress and resulted in increased yields. The isolation of **1**, after filtering out aluminum, was accomplished by low temperature recrystallization from hexane in which it was much less soluble than was unreacted $[H_2AlN(SiMe_3)_2]\cdot NMe_3$.

The characterization data acquired for **1** in this study were consistent with its chemical make-up as originally reported [18]. In particular, the mass spectrum showed the parent ion for the dimer and other logically derived fragmentation ions. A few higher than dimer *m/e* fragments of extremely low intensity (<1%) were also detected. This indicated that the dimeric association via H-bridges generally survived the heated probe and electron impact conditions in the MS experiment. The ^1H and $^{13}C\{^1H\}$ NMR spectra were in agreement with the original NMR data for **1** and, based on their simplicity, supported a symmetrical environment for the $N(SiMe_3)_2$ groups while excluding a possible rigid, N-bonded structure.

The crystallographic determination for **1** provided two symmetry independent, but chemically similar, molecules in the asymmetric unit. Fig. 1 shows the structure of one of the molecules. The molecule of **1** is a H-bridged dimer which is structurally very similar although not isomorphous with the H-bridged dimer bis(2,2,6,6-tetramethylpiperidino)alane, $[HAl(tmp)_2]_2$ [15], or related F-bridged dimer $[(tmp)_2AlF]_2$ [26]. For example, the wide average N–Al–N angle in **1**, 124.6°, can be compared with the same angles in $[HAl(tmp)_2]_2$,

Table 1. Crystallographic data and measurements for **1** and **2**

	1	**2**
Molecular formula	$C_{24}H_{74}Al_2N_4Si_8$	$C_{18}H_{55}Al_2N_5Si_4$
Formula weight	697.55	507.99
Crystal system	monoclinic	monoclinic
Space group	$P2_1$	$P2_1/n$
a (Å)	13.7119(2)	9.1715(5)
b (Å)	18.3400(3)	22.9239(13)
c (Å)	17.8971(4)	15.0291(9)
β (°)	91.4750(9)	96.088(2)
V (Å^3)	4499.20(18)	3139.9(3)
Z	4	4
μ (mm^{-1})	0.297	0.260
Temperature (K)	223(2)	198(2)
D_{calcd} (g/cm^3)	1.030	1.075
Crystal dimensions (mm)	0.10 × 0.10 × 0.10	0.40 × 0.35 × 0.25
Θ range for data collection (°)	1.14–28.21	1.63–22.50
No. of reflections collected	29387	7735
Independent reflections	17056 (R_{int} = 0.0584)	3809 (R_{int} = 0.1028)
Data/restraints/parameters	17056/9/697	3499/5/266
R [$I>2\sigma(I)$];[a] wR2[b]	0.0596; 0.1136	0.1220; 0.2918
R (all data);[a] wR2[b]	0.1110; 0.1356	0.1708; 0.3411
Goodness-of-fit[c]	1.027	0.975
Final max/min $\Delta\rho$ (e/Å^{-3})	0.320/−0.337	0.774/−0.923

[a] $R = \Sigma\Delta/\Sigma(F_0)$, $\Delta = |F_0| - |F_c|$.
[b] $wR2 = \Sigma[w(F_0^2 - F_c^2)^2]/\Sigma[(wF_0^2)^2]^{1/2}$.
[c] $GooF = [\Sigma[w(|F_0| - |F_c|)^2]/(n-p)]^{1/2}$.

Table 2. Selected bond distances (Å) and angles (°) for **1** and **2** with estimated standard deviations in parentheses

1		**2**	
Bond lengths			
Al–*exo*-N (av)	1.824	Al(1)–*exo*-N(3)	1.836(4)
Al–*exo*-N; min/max	1.811(4)/1.844(4)	Al(2)–*exo*-*N*(5)	1.842(4)
		Al(2)–*exo*-*N*(4)	1.782(8)
		Al(1)–*endo*-N(2)	1.966(8)
		Al(1)–*endo*-N(1);	1.948(7)
		Al(2)–*endo*-N(1)	1.985(8)
		Al(2)–*endo*-N(2)	1.987(7)
Al–*endo*-H	1.727(1)	Al–*exo*-H (assumed)	1.50
Al–Al (av)	2.661	Al(1)–Al(2)	2.829(3)
Si–N (av)	1.755	Si–N (av)	1.743
Si–N; min/max	1.749(5)/1.765(5)	Si–N; min/max	1.7426(10)/1.7430(10)
Si–C (av)	1.874	Si–C (av)	1.87
Si–C; min/max	1.850(7)/1.900(6)	Si–C; min/max	1.834(14)/1.889(10)
Bond angles			
N–Al–N (av)	124.6	N(1)–Al(1)–N(2)	86.1(3)
N–Al–N; min/max	124.2(2)/125.1(2)	N(1)–Al(2)–N(2)	84.5(3)
N–Al–Al (av)	117.7	Al(1)–N(1)–Al(2)	92.0(3)
N–Al–Al; min/max	115.19(14)/120.5(2)	Al(1)–N(2)–Al(2)	91.4(3)
Si(2)–N(1)–Al(1)	115.0(2)	N(3)–Al(1)–N(1)	116.4(3)
Si(1)–N(1)–Al(1)	125.9(3)	N(3)–Al(1)–N(2)	122.4(3)
Si(2)–N(1)–Si(1)	118.7(2)	N(4)–Al(2)–N(5)	111.3(3)
		N(4)–Al(2)–N(1)	110.2(4)
		N(4)–Al(2)–N(2)	114.0(4)
		N(5)–Al(2)–N(2)	114.9(4)
		N(5)–Al(2)–N(1)	119.5(3)

126.9(1)° and $[(tmp)_2AlF]_2$, 128.6(1)° and they all may reflect similar steric demands of the amino groups in these compounds. The environment around each N-atom in **1** is planar (2Si, N and Al connected atoms lie in the same plane; sum of relevant angles is close to 360°) and, although it is tempting to associate this property with a mostly dΠ(Si)–pΠ(N) interaction in the $N(SiMe_3)_2$ ligand, a planar environment appears to exist in the similar {2C, N, Al} fragment in $[HAl(tmp)_2]_2$ which is lacking such an interaction.

The average Al–N bond length in **1**, 1.824 Å, belongs to short distances of this type and its magnitude seems to be a consequence of a tetracoordinate Al atom bonded to a sterically congested tricoordinate N atom. This is strikingly supported by comparison with the Al–N distances in the relevant cases of the previously discussed $[HAl(tmp)_2]_2$, 1.835(3) Å, and $[(tmp)_2AlF]_2$, 1.832(2) Å, as well as of $[H(Cl)AlN(SiMe_3)_2]\cdot NMe_3$ [19], 1.823(4) Å [for $Al–N(SiMe_3)_2$]. Shorter Al–N distances are found in tricoordinate Al/tricoordinate N structures, for example, monomeric $Al[N(SiMe_3)_2]_3$, 1.78(2) Å [16], or six-membered planar ring $[MeAlN(2,6\text{-}iPr_2C_6H_3)]_3$, 1.782(4) Å [27], but in the extremely congested monomeric *t*-$Bu_2AlN(SiPh_3)_2$ this distance is 1.880(4) Å [28]. On the other hand, in tetracoordinate Al/tetracoordinate N ring or cluster structures these lengths typically span the 1.9 to 2.0 Å range, for example, as in cubane $(PhAlNPh)_4$, 1.914(5) Å [29], dimer $[(Me_3Si)_2AlNH_2]_2$, 1.955 Å [30] and trimer $(t\text{-}Bu_2AlNH_2)_3$, 2.008 Å [31], although in the dimer $\{[(Me_3Si)_2N]_2AlNH_2\}_2$ this bond length is much shorter, 1.841 Å (av) [32]. These trends are illustrated by the structure of $(Me_3Si)_2N(Me_2N)Al(\mu\text{-}NMe_2)_2Al(H)N(SiMe_3)_2$ (**2**) (*vide infra*) that contains Al atoms connected to both tricoordinate N atoms (terminal congested $N(SiMe_3)_2$ and noncongested NMe_2) and tetracoordinate N atoms (bridging NMe_2).

The Al–H distance of 1.727(1) Å in **1** is one of the longest among similar symmetrical Al–H bridging distances, possibly indicating a loose association of the monomers in the solid state. However, this can not be reconciled in a straightforward way with the dimer parent ion in the gas phase detected by mass spectrometry. This distance can be compared with the average Al–H lengths in the previously discussed symmetrical dimer $[HAl(tmp)_2]_2$, 1.68 Å or trimer (*t*-$Bu_2AlH)_3$, 1.726(5) Å [33]. For the unsymmetrically H-bridged dimer of the $[H_3Al\cdot L]_2$ type of alane adducts, $[H_3Al\cdot N(Me_2)CH_2CH_2CH_2Cl]_2$, the following Al–H distances are found that span almost the entire range of observable distances of this type, namely, two different ring distances, 1.84(3) and 1.99(5) Å, and two different terminal distances, 1.20(7) and 1.40(6) Å [34]. Of particular interest also is the average Al–Al distance of 2.661 Å. It can be compared with this sep-

aration in other symmetrical dimers such as $(HAlMe_2)_2$, 2.62 Å [35] and $[HAl(tmp)_2]_2$, 2.680(2) Å. More importantly, this distance is in the range of the Al–Al bonding distances in structurally authenticated, neutral, monomeric dialanes $[(Me_3Si)_2CH]_4Al_2$, 2.660(1) Å [36] and $[(i\text{-}Pr_3C_6H_2)]_4Al_2$, 2.647(3) Å [37] or tetrameric cluster $[Al(C_5Me_5)]_4$, 2.769 Å (av) [38]. Based on that, some bonding interaction along the Al–Al axis is thus probable in **1**.

A 1:1 ratio reaction of **1** and $HNMe_2$ was performed to test preferences of the two possibly competing reactions, namely, aminolysis at the Al–H site with the formation of dihydrogen and transamination at the Al–$N(SiMe_3)_2$ site(s) with the formation of $HN(SiMe_3)_2$. These types of reactions were observed to occur simultaneously in the combination of $[H_2AlN(SiMe_3)_2] \cdot NMe_3$ and NH_3, and yielded a rare benzene soluble polymeric precursor that was used to make transparent AlN coatings on alumina substrates [18]. Surprisingly, only minute quantities of H_2 were measured several hours past addition indicating very slow aminolysis. This was further supported by an IR spectrum for raw products that showed a N–H stretching band at 3310 cm^{-1} consistent with coordinated $HNMe_2$ by **1** at this stage of reaction. The NMR spectra for the reaction mixture were run in the course of several weeks following addition and showed a multitude of slowly formed products. This was accompanied by increased quantities of evolved H_2 (sharp ^1H NMR resonance at δ 4.51 [39]) and $HN(SiMe_3)_2$ consistent with a relatively slow aminolysis and transamination in the system, respectively.

Compound **2** was isolated in small quantities after several days of a low temperature storage of the reaction mixture accompanied by a slow evaporation of volatiles. The NMR data obtained for a fresh solution of **2** in toluene-d_8 were complex and subject to changes with time. These changes might be indicative of slow equilibration processes and formation of more stable symmetrical products in the solution but, also of some on-going chemical interactions. Interestingly, the IR spectrum for the freshly isolated product showed only a single, well defined but, alas, broad band in the ν(Al–H) range at 1860 cm^{-1}.

The molecular structure of **2** is shown in Fig. 2. It features a puckered {Al–N–Al–N} ring with unsymmetrical (different) ligands on the aluminum atoms, and can be visualized as a Me_2N-bridged, two-site adduct of the different monomeric aminoalanes $Al(NMe_2)_2[N(SiMe_3)_2]$ and $HAl(NMe_2)[N(SiMe_3)_2]$. The $N(SiMe_3)_2$ groups on two different Al ring atoms are in the *cis* position to each other. Potentially increased steric congestion due to the *cis* configuration is apparently counterbalanced by ring puckering, which has the effect of moving apart the $N(SiMe_3)_2$ groups on the congested side of the ring and getting the neighboring small H and NMe_2 ligands closer on the other side of the ring with a concurrent decrease of the Al–Al distance. The latter distance of 2.829(3) Å seems to be, however, outside the range of any significant aluminum–aluminum bonding interaction (*vide supra*). The ring puckering as defined by the angle between the N(1)–Al(1)–N(2) and N(1)–Al(2)–N(2) planes amounts to 25.5°. The N and Al atoms in the ring are four-coordinate; although the hydrogen atom is not resolved on Al(1), its presence is supported by both structural [pyramidal Al(1) atom] and chemical evidence [IR band in the ν(Al–H) range at 1860 cm^{-1}].

Despite the relatively high values of the residuals for **2**, the quality of the numerical data is good enough to address some of the molecule's structural aspects. The aluminum–nitrogen bonds in **2** represent a comprehensive range of bond configurations including ring and different exocyclic bonds, all in one molecule. The average Al–N distance in the ring (Al–*endo*-NMe_2), 1.972 Å, can be compared with the average distances of this type in some of the Me_2N-bridged dimers such as $[Al(NMe_2)_3]_2$, 1.965 Å [14] (or 1.970 Å [13]) and $[HAl(NMe_2)_2]_2$, 1.966 Å [13] or trimer $(H_2AlNMe_2)_3$, 1.950 Å [13]. The Al–*exo*-NMe_2 distance of 1.782(8) Å in **2** belongs, in general, to very short Al–N bond lengths. For example, the following Al–*exo*-NMe_2 distances are found in the dimers $[Al(NMe_2)_3]_2$, 1.800 Å (av) [15] [or 1.814 Å (av) [13]], $[HAl(NMe_2)_2]_2$, 1.804(2) Å [13] and $[(Me_2N)_2Al\{\mu\text{-}N(H)1\text{-adamantanyl}\}]_2$, 1.793 Å [15], while the apparently shortest to-date Al–N bond lengths are reported for monomeric $Al[N(SiMe_3)_2]_3$, 1.78(2) Å [16], and six-membered planar ring $[MeAlN(2,6\text{-}iPr_2C_6H_3)]_3$, 1.782(4) Å [27]. The other exocyclic AlN distance(s) in **2**, i.e. Al–*exo*-$N(SiMe_3)_2$, 1.839 Å (av), falls well within the range of similar terminal bonds. This is exemplified by comparison of this distance with the respective average lengths in **1**, 1.824 Å, $\{[(Me_3Si)_2N]_2AlNH_2\}_2$, 1.841 Å [32], or $\{[(Me_3Si)_2N]_2Al(NH_2)_2\}_3Al$, 1.850 Å [32]. The Al–*exo*-$N(SiMe_3)_2$ lengths are generally longer than the Al–*exo*-NMe_2 lengths and this may reflect the congestion effect of the bulkier $N(SiMe_3)_2$ group.

In summary, the structure of **2** illustrates the occurrence of both the aminolysis (absence of H on one of the Al atoms) and transamination [singular $N(SiMe_3)_2$ groups on each Al atom] taking place in the reaction between **1** and $HNMe_2$. Similar combinations of $[H_2AlN(SiMe_3)_2] \cdot NMe_3$ and NH_3 were also reported to proceed via concerted ammonolysis and transamination and resulted in a soluble polymeric precursor to aluminum nitride [11]. The data presented here are consistent with complex elimination chemistry in these systems and suggest that the new $\{[(Me_3Si)_2N]_2Al(\mu\text{-}H)\}_2$ may be a valuable precursor for conversion to aluminum nitride materials.

Acknowledgements—R. L. W. wishes to thank the Office of Naval Research for its financial support. The University of Delaware acknowledges the National Science Foundation (CHE09628768) for their support of the purchase of the CCD-based diffractometer.

REFERENCES

1. Atwood, J. L., Bennett, F. R., Elms, F. M., Jones, C., Raston, C. L. and Robinson, K. D., *J. Am. Chem. Soc.*, 1991, **113,** 8183.
2. Andrews, P. C., Gardiner, M. G., Raston, C. L. and Tolhurst, V.-A., *Inorg. Chim. Acta*, 1997, **259,** 249.
3. Lobkovski, E. B. and Semenenko, K. N., *Zh. Strukt. Khim.*, 1975, **16,** 150.
4. Atwood, J. L., Butz, K. W., Gardiner, M. G., Jones, C., Koutsantonis, G. A., Raston, C. L. and Robinson, K. D., *Inorg. Chem.*, 1993, **32,** 3482.
5. Heitsch, C. W., Nordman, C. E. and Parry, R. W., *Inorg. Chem.*, 1963, **2,** 508.
6. Gorrell, I. B., Hitchcock, P. B. and Smith, J. D., *J. Chem. Soc., Chem. Commun.*, 1993, 189.
7. Andrews, P. C., Raston, C. L., Skelton, B. W. and White, A. H., *Chem. Commun.*, 1997, 245.
8. Atwood, J. L., Robinson, K. D., Jones, C. and Raston, C. L., *Chem. Commun.*, 1991, 1697.
9. Gardiner, M. G. and Raston, C. L., *Coord. Chem. Rev.*, 1997, **166,** 1.
10. Ruff, J. K. and Hawthorne, M. F., *J. Am. Chem. Soc.*, 1960, **82,** 2141.
11. Semenenko, K. N., Lobkovskii, A. L. and Dorosinskii, A. L., *Zh. Strukt. Khim.*, 1972, **13,** 743.
12. Kovar, R. A. and Ashby, E. C., *Inorg. Chem.*, 1971, **10,** 893.
13. Ouzounis, K., Riffel, H., Hess, H., Kohler, U. and Weidlein, J., *Z. Anorg. Allg. Chem.*, 1983, **504,** 67.
14. Waggoner, K. M., Olmstead, M. M. and Power, P. P., *Polyhedron*, 1990, **9,** 257.
15. Klein, C., Nöth, H., Tacke, M. and Thomann, M., *Angew. Chem. Int. Ed. Engl.*, 1993, **32,** 886.
16. Sheldrick, G. M. and Sheldrick, W. S., *J. Chem. Soc. A*, 1969, 2279.
17. Janik, J. F. and Paine, R. T., *XVth Int. Conf. on Organometallic Chemistry*. Warsaw, Poland, Aug. 1992, p. 113.
18. Janik, J. F., Duesler, E. N. and Paine, R. T., *J. Organomet. Chem.*, 1997, **539,** 19.
19. Gardiner, M. G., Koutsantonis, G. A., Lawrence, S. M., Lee, F.-C. and Raston, C. L., *Chem. Ber.*, 1996, **129,** 545.
20. Atwood, J. L., Koutsantonis, G. A., Lee, F.-C. and Raston, C. L., *J. Chem. Soc. Chem. Commun.*, 1994, 91.
21. Atwood, D. A., Contreras, L., Cowley, A. H., Jones, R. A. and Mardones, M. A., *Organometallics*, 1993, **12,** 17.
22. Janik, J. F., Wells, R. L. and White, P. S., *Inorg. Chem.*, 1998, **37,** 3561.
23. Nöth, H. and Wiberg, E., *Fortschr. Chem. Forsch.*, 1967, **8,** 323.
24. SHELXTL V5.03. Siemens Industrial Automation, Madison, WI.
25. Gladfelter, W. L., Boyd, D. C. and Jensen, K. F., *Chem. Mater.*, 1989, **1,** 339.
26. Krossing, I., Nöth, H., Tacke, C., Schmidt, M. and Schwenk, H., *Chem. Ber./Recueil*, 1997, **130,** 1047.
27. Waggoner, K. M., Hope, H. and Power, P. P., *Angew. Chem. Int. Ed. Engl.*, 1988, **27,** 1699.
28. Petrie, M. A., Ruhlandt-Senge, K. and Power, P. P., *Inorg. Chem.*, 1993, **32,** 1135.
29. McDonald, T. R. R. and McDonald, W. S., *Acta Cryst.*, 1972, **328,** 1619.
30. Janik, J. F., Duesler, E. N. and Paine, R. T., *Inorg. Chem.*, 1987, **26,** 4341.
31. Interrante, L. V., Sigel, G. A., Garbauskas, M., Hejna, C. and Slack, G. A., *Inorg. Chem.*, 1989, **28,** 252.
32. Paciorek, K. J. L., Nakahara, J. H., Hoferkamp, L. A., George, C., Flippen-Anderson, J. L., Gilardi, R. and Schmidt, W. R., *Chem. Mater.*, 1991, **3,** 82.
33. Uhl, W., *Z. Anorg. Allg. Chem.*, 1989, **570,** 37.
34. Andrews, P. C., Gardiner, M. G., Raston, C. L. and Tolhurst, V.-A., *Inorg. Chim. Acta*, 1997, **259,** 249.
35. Almenningen, A., Anderson, G. A., Forgaard, F. R. and Haaland, A., *Acta Chem. Scand.*, 1972, **26,** 2315.
36. Uhl, W., *Z. Naturforsch. B*, 1988, **43,** 1113.
37. Wehmschulte, R. J., Ruhlandt-Senge, K., Olmstead, M. M., Hope, H., Sturgeon, B. E. and Power, P. P., *Inorg. Chem.*, 1993, **32,** 2983.
38. Dohmeier, C., Tacke, M. and Schnöckel, H., *Angew. Chem. Int. Ed. Engl.*, 1991, **30,** 564.
39. Pulham, C. R., Downs, A. J., Goode, M. J., Rankin, D. W. H. and Robertson, H. E., *J. Am. Chem. Soc.*, 1991, **113,** 5149 and references therein.

Pergamon

Polyhedron Vol. 17, No. 23–24, pp. 4109–4114, 1998
© 1998 Elsevier Science Ltd
All rights reserved. Printed in Great Britain
0277–5387/98 $19.00+0.00

PII: S0277–5387(98)00216–2

Studies on some reactions of cyclopalladated azobenzenes with N,O-chelators

K. Bag, T. K. Misra and C. Sinha*

Department of Chemistry, The University of Burdwan, Burdwan 713104, India

(Received 16 January 1998; accepted 25 May 1998)

Abstract—The synthesis and characterization of new planar mixed chelates of the type [Pd(A)(N,O)] (A = *ortho*-metallated azobenzene or its substituted derivatives, A_1 to A_5, N,O = 2-picolinato (pic), quinaldato (qnd), 8-quinolinolato (q) and 2-methyl-5-sulphonic-8-quinolinolato (msq)) are achieved by splitting the halogeno-bridge in $[Pd_2(A)_2Cl_2]$ by aqueous $AgNO_3$ solution followed by the addition of N,O-chelator. $[Pd(A_2)(N,O)]$ occurs as isomer $[Pd(A_3)(N,O)]$ and the composition have been established using ^1H NMR data. The complex composition is supported by elemental analyses and IR data. Cyclic voltammetric studies suggest two successive redox responses correspond to azo reduction. © 1998 Elsevier Science Ltd. All rights reserved

Keywords: cyclopalladated; mixed chelates; N,O-donor; spectral studies; electrochemistry.

INTRODUCTION

Cyclopalladated compounds of transition metals have attracted a great deal of attention in recent times [1–8]. Many reviews concerning their synthesis and reactivities appear in literature [9–14]. We have extensively studied the cyclopalladation reactions of many substituted azobenzenes and Schiff bases [15–19]. Azobenzene becomes palladated at the azo-nitrogen and *ortho*-carbon atom and produces bridged dimeric species [20–22]. The bridge splitting reactions of the dimer with neutral ligands such as tertiary phosphines [23–25], pyridines [26] and anionic ligands such as acetylacetonate [27], arylazooximate [28] gave large number of planar mixed organopalladium complexes. In the present paper we report a further new type (**2**) of mixed cyclopalladated complexes of azobenzenes with (N,O)-chelators. We have chosen monoanionic N,O-chelator: picolinic acid (Hpic), quinaldic acid (Hqnd), 8-quinolinol (Hq) and its derivative 2-methyl-5-sulphonic-8-quinolinol (Hmsq) (H stands for the phenolic hydrogen) as the capping ligand. They form five membered chelate ring with cyclopalladated Pd(C,N) fragment (**1**).

* Author to whom correspondence should be addressed.

RESULTS AND DISCUSSION

The complex (**2**) is abbreviated as Pd(A)(N,O) where A represents the azobenzenes. A_1 to A_5 are the specific abbreviations of the ligand A depending on substituents and binding mode as set out in Scheme 1.

The chloro-bridged cyclopalladated azobenzenes $[Pd_2(A)_2Cl_2]$ in acetone were treated with aqueous $AgNO_3$ and refluxed for a few hours. To the filtrate (N,O)-chelators were added in equivalent amount (1:1 mole ratio). The picolinato [Pd(A)(pic)], quinaldato [Pd(A)(qnd)] and 8-quinolinolato [Pd(A)(q)] and [Pd(A)(msq)] derivatives were precipitated as orange solid. The complexes are non-electrolytic in nature and suggest covalent binding of the chelators. The composition of the complexes are supported by elemental analyses data (Table 1).

The complexes display spectral characteristics corresponding to ν(N=N) at 1360–1385 cm^{-1}. The assignment of all bands has not been attempted. However, a comparison of the spectra with those of the respective chloro-bridged dimers and of free (N,O)-chelator affords useful information. Picolinato [Pd(A)(pic)] and quinaldato [Pd(A)(qnd)] derivatives exhibit strong stretching due to ν_{as}(COO) and ν_s(COO) at $\sim$1650 and 1340 cm^{-1} respectively which appears in the free ligand at 1720 cm^{-1}. The difference in stret-

Table 1. Microanalytical[a] and UV–VIS spectral data[b]

Complex	Elemental			UV–VIS spectral data λ_{max} (nm) ($10^{-3}\varepsilon$, $dm^3\,mol^{-1}\,cm^{-1}$)
	C(%)	H(%)	N(%)	
[Pd(A_1)(pic)]	52.7 (52.8)	3.0 (3.2)	10.4 (10.3)	478(3980)[c], 448(3360), 382(7000)
[Pd(A_2)(pic)]	54.0 (53.9)	3.4 (3.5)	9.9 (9.9)	480(4220)[c], 450(4340), 385(7890)
[Pd(A_4)(pic)]	55.0 (54.9)	3.9 (3.9)	9.5 (9.6)	483(4600)[c], 454(5320), 387(9810)
[Pd(A_5)(pic)]	45.1 (45.2)	2.3 (2.3)	8.7 (8.8)	485(5840)[c], 452(5080), 385(8940)
[Pd(A_1)(qnd)]	57.8 (57.5)	3.3 (3.3)	9.2 (9.1)	480(3060)[c], 450(3640), 383(7850)
[Pd(A_2)(qnd)]	58.1 (58.3)	3.5 (3.6)	9.0 (8.9)	485(5430)[c], 450(6340), 380(9560)
[Pd(A_4)(qnd)]	59.2 (59.1)	3.9 (3.9)	8.7 (8.6)	484(7245)[c], 454(8580), 387(16520)
[Pd(A_5)(qnd)]	49.8 (50.0)	2.6 (2.5)	7.8 (8.0)	485(6460)[c], 452(8540), 385(10360)
[Pd(A_1)(q)]	58.5 (58.4)	3.4 (3.5)	9.6 (9.7)	484(3280)[c], 451(4020), 386(8240)
[Pd(A_2)(q)]	59.2 (59.3)	3.9 (3.8)	9.5 (9.4)	480(4230)[c], 450(5226), 380(9370)
[Pd(A_4)(q)]	60.2 (60.1)	4.0 (4.1)	9.0 (9.1)	483(5280)[c], 454(6140), 387(11620)
[Pd(A_5)(q)]	50.3 (50.4)	2.5 (2.6)	8.5 (8.4)	484(4650)[c], 452(5840), 380(9240)
[Pd(A_1)(msq)]	50.1 (50.3)	3.3 (3.2)	8.2 (8.0)	488(4480)[c], 448(5660), 385(8450)
[Pd(A_2)(msq)]	51.3 (51.2)	3.6 (3.5)	7.9 (7.8)	486(5030)[c], 450(6890), 380(9460)
[Pd(A_4)(msq)]	52.2 (52.0)	3.9 (3.8)	7.4 (7.6)	482(4940)[c], 454(6330), 385(8020)
[Pd(A_5)(msq)]	44.2 (44.4)	2.3 (2.5)	7.3 (7.1)	485(4780)[c], 450(6260), 380(7940)

[a] Calculated values are in parentheses.
[b] In $CHCl_3$ except [Pd(A)(msq)] derivatives, those are recorded in DMSO.
[c] Shoulder.

ching frequency ($\Delta\nu = 290\,cm^{-1}$) suggests unidentate carboxylato coordination [29, 30, 31]. Additional bands are observed at 860–840, 720–700 and 680–660 cm^{-1} and support the coordinated picolinate ion. Similarly quinolinolato [Pd(A)(q)] and [Pd(A)(msq)] exhibit two characteristic band at 1560–1580 and 1490–1505 cm^{-1} along with ring deformation at $\sim 400\,cm^{-1}$ supporting the presence of N,O-chelator in the cyclopalladated moiety. All the complexes exhibit stretching at 520–530 and 350–380 cm^{-1} corresponding to ν(Pd–O) and ν(Pd–N), respectively.

The solution electronic spectra of the complexes were recorded in $CHCl_3$ and the transitions are assigned on the basis of reported literature [18–22, 28]. The transition around 500 nm is assigned to charge transfer transition in the metallated fragment [20–22, 28] and the higher energy transitions are referred to intraligand charge transfer transitions.

For asymmetrical azobenzene (A_2/A_3) the cyclopalladated complex occurs as a mixture of isomers but in no case they are separated by chromatography. Because of bad solubility of the chloro-bridged species in common organic solvents direct isomer assessment by ^{1}H NMR is not easily achieved [32]. Different other methods [33, 34] like gas chromatographic analysis of the products obtained by exhaustive carbonylation of the dimer had been used. The ^{1}H NMR spectral technique had been employed in a limited area [28] for the product analysis obtained by bridge splitting reactions using PPh_3, arylazooximes etc. We are also using ^{1}H NMR technique for the assessment of isomer population (Table 2). For symmetrical azobenzenes (A_1, A_4, A_5) no such isomerism is observed. The bridge splitting reaction followed by chelation using N,O-chelator may produce, in principle, two geometric isomers (B and C) for symmetrical and four isomers for asymmetrical azobenzenes, respectively. The isomers could not be isolated by chromatography on silica gel or alumina. There are many bridge splitting reactions [23–27] of cyclopalladated azobenzenes, Schiff bases with pyridines or phosphines where the base occupies *trans*-position to azo/azomethine-N. 2-Picolinic acid is also used as bridge splitter in a cyclopalladated α-naphthylethylamine where heterocyclic-N occupies *trans* to amine nitrogen. This may provide a guide to consider single isomer (B) from the symmetrical azobenzenes and two isomers from asymmetrical azobenzene.

The ^{1}H NMR spectra of free ligands and the cyclopalladated complexes of symmetrical azobenzenes are the guide lines to the signal assignment. In cases, where the metallation of both substituted and unsubstituted rings occurs, the population of the isomer having metallation in the substituted ring is higher, in line with the electrophilic nature of the palladation reaction. Symmetrical azobenzenes yield single mixed chelate complex which is supported by two Me signals of [Pd(A_4)(N,O)] in ^{1}H NMR spectra, in line with the electrophilic nature of the palladation reaction. Asymmetrical ligand in [Pd(A_2)(N,O)] gives closely spaced δ_{Me} signal. Originally cyclopalladated complex exists in two isomeric forms and at least two mixed chelates will appear in the product. The observed ratio of [Pd(A_2)(N,O)]:[Pd(A_3)(N,O)] is 3:2. The results are in agreement with those obtained by the bridge splitting reaction using PPh_3 and pyridine.

Table 2. ^{1}H NMR data of complexes in [Pd(A)(N,O)]

Complex	δ (ppm)													
	2-H[a]	3-H	4-H	5-H	6-H	7-H	8-H	9-H	10-H	11-H	12-H[a]	14, 18-H	15, 17-H	Me
[Pd(A_1)(pic)]	—	8.65[a]	8.08[b]	7.90[b]	8.25[a]	—	—	7.64[a]	7.36[a]	7.36[b]	7.8	7.89	7.58[c]	
[Pd(A_2)(pic)]	—	8.63[a]	8.03[b]	7.86[b]	8.23[a]	—	—	7.48[d]	—	7.09[a]	7.62	7.80	7.49[c]	2.44[e]
[Pd(A_4)(pic)]	—	8.61[a]	8.00[b]	7.85[b]	8.27[a]	—	—	7.44[d]	—	7.04[a]	7.63	7.7	7.26[a]	2.52, 2.4
[Pd(A_5)(pic)]	—	8.68[a]	8.04[b]	7.88[b]	8.25[a]	—	—	7.77[d]	—	7.58[a]	7.89	7.96	7.68[a]	
[Pd(A_1)(qnd)	—	8.78[a]	8.55[b]	8.08[c]	7.81[c]	7.81[c]	8.48[a]	7.67[a]	7.39[b]	7.39[b]	7.84	7.96	7.63[c]	
[Pd(A_2)(qnd)	—	8.70[a]	8.50[b]	8.08[c]	7.81[c]	7.81[c]	8.52[a]	7.47[d]	—	7.08[a]	7.59	7.82	7.54[c]	2.45[e]
[Pd(A_4)(qnd)	—	8.70[a]	8.51[b]	8.09[c]	7.79[c]	7.79[c]	8.50[a]	7.48[d]	—	7.07[a]	7.66	7.75	7.31[a]	2.48, 2.4
[Pd(A_5)(qnd)	—	8.84[a]	8.61[b]	8.13[c]	7.84[c]	7.84[c]	8.52[a]	7.81[d]	—	7.61[a]	7.93	8.0	7.73[a]	
[Pd(A_1)(q)	8.94	8.12[b]	8.42[c]	7.69[c]	7.83[c]	7.60[a]	—	7.58[a]	7.33[b]	7.33[b]	7.75	7.8	7.51[c]	
[Pd(A_2)(q)	8.92	8.11[b]	8.34[c]	7.70[c]	7.81[c]	7.60[a]	—	7.40[d]	—	7.09[a]	7.64	7.74	7.45[c]	2.50
[Pd(A_4)(q)	8.90	8.08[b]	8.36[c]	7.65[c]	7.80[c]	7.56[a]	—	7.37[d]	—	7.02[a]	7.6	7.65	7.21[a]	2.50, 2.3
[Pd(A_5)(q)	8.95	8.10[b]	8.45[c]	7.72[c]	7.87[c]	7.64[a]	—	7.79[d]	—	7.55[a]	7.85	7.91	7.65[a]	
[Pd(A_1)(msq)[g]	—	7.83[a]	8.34[a]	—	8.05[a]	7.72[a]	—	7.50[a]	7.26[b]	7.26[b]	7.7	7.74	7.46[c]	2.84[f]
[Pd(A_2)(msq)[g]	—	7.80[a]	8.33[a]	—	8.03[a]	7.71[a]	—	7.30[d]	—	6.97[a]	7.58	7.68	7.42[c]	2.84[f], 2.5
[Pd(A_4)(msq)[g,h]	—	7.80[a]	8.30[a]	—	8.01[a]	7.69[a]	—	7.31[d]	—	7.00[a]	7.56	7.6	7.17[a]	2.82[f], 2.51

[a] Doublet.
[b] Triplet.
[c] Multiplet.
[d] Singlet.
[e] Isomeric δ_{Me}, 2.38 ppm.
[f] δ_{Me} of msq.
[g] Solvent: $CDCl_3$, except [Pd(A)(msq)] where DMSO-d_6 is used.
[h] The concentration of [Pd(A_5)(msq)] is very low to get well defined ^{1}H NMR in DMSO-d_6.

The heterocyclic ring protons appear in general at the downfield region relative to arylazo protons. The proton numbering pattern is shown in Scheme 1. The signals are assigned on the basis of spin–spin interaction and change therein on substitution. In picolinato derivatives the most downfield doublet is 3-H ($\sim$8.6 ppm) followed by 6-H ($\sim$8.2 ppm) signal. The protons 4-H and 5-H appear relatively at upfield position $\sim$8.0 and 7.8 ppm respectively. The quinaldato derivatives [Pd(A)(qnd)] similarly exhibit resonances in downfield region for 3-H to 8-H at 8.7 to 7.8 ppm. 8-Quinolinolato complexes [Pd(A)(q)] exhibit 2-H signal at most downfield region ($\sim$8.9 ppm); the pyridinic ring protons appear in downfield region (2-H to 4-H, 8.9 to 8.4 ppm) and phenolic ring protons appear at relatively upfield region (5-H to 7-H, $\sim$7.6 to 7.8 ppm). Arylazo ring protons appear relatively in upfield position (7.0 to 7.7 ppm) and the signal position is highly sensitive to the substituent in the aryl ring. In A_2/A_3, A_4 and A_5 singlet resonance is due to 9-H proton. Metallated ring protons appear in more downfield region than non-metallated ring ones. Other ring protons appear at usual position and the signal movement is in accordance with the electronic effect of the substituents [35].

Electrochemistry

Cyclic voltammetric data were collected under N_2 environment using glassy carbon working electrode in acetonitrile versus saturated calomel electrode (SCE) in presence of tetrabutylammonium perchlorate (TBAP). The iR compensation was applied internally in the instrument. All the complexes display two redox responses and the data are collected in Table 3. The peak potentials are nearly invariant with scan rate (50–500 mV s^{-1}) and the cathodic peak current (i_{pc}) is proportional to $v^{1/2}$ and i_{pa}/i_{pc} lies at 0.9–1.02 suggesting reversibility of the redox process. The current height measurement shows one-electron redox type and the peak-to-peak separation (ΔE_p) suggests quasireversible character of the couples. Palladium(II) reduction in mixed complexes of cyclopalladated azobenzenes were reported at very high potential and a two-electron quasireversible reduction process followed by chemical reaction [28]. In the present series of complexes the couples are one-electron reduction type at relatively lower value and stable on repetitive cyclic operation. This excludes the metal reduction. Ligand reduction is believed to occur primarily at the azo-function who can accommodate up to two electrons [28] at the LUMO. The coulometric experiment for the first couple confirms one-electron reduction at the azo-centre. The experiment was performed in one case [Pd(A_1)(q)] at -1.4 V vs SCE in MeCN and coulomb count ($\eta = Q/Q' = 0.94$ where Q and Q' are observed and calculated coulomb) suggests just one-electron reduction. On reduction the solution colour has changed from orange red to brown red

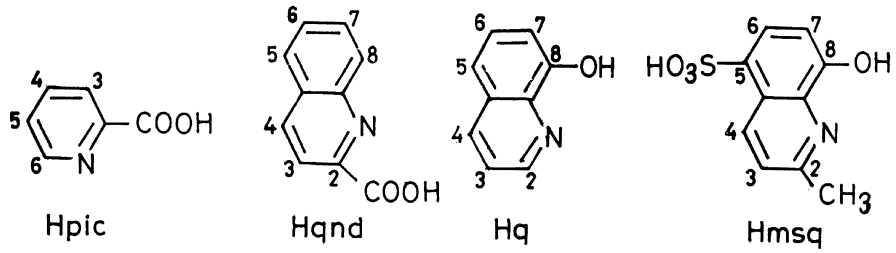

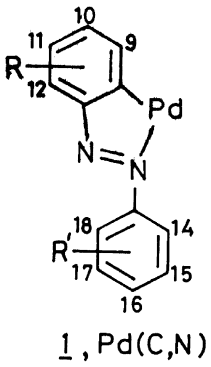

Isomeric modes of Pd(C,N) fragment

	R	R′
A_1	H	H
A_2	10-Me	H
A_3	H	16-Me
A_4	10-Me	16-Me
A_5	10-Cl	16-Cl

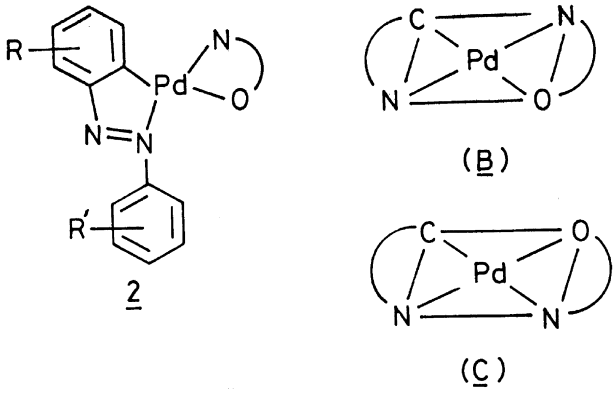

Scheme 1.

and in the UV–VIS spectra the shoulder at 484 nm is eliminated while new band appears at 510 nm. The ESR spectra of the reduced product shows interesting behaviour; at room temperature a broad signal is observed at $g = 2.005$ with peak-to-peak separation 45 G. The spectrum at liquid-nitrogen temperature (77 K) shows hyperfine splitting pattern. Detail investigation is under scrutiny. The observation supports the literature report [36, 37] and suggests that the first reduction is believed to occur at the azo-function of the ligand. The effect of the substitution on reduction potential data again supports the assignment. Change of substituents (*para*-to-azo group in aryl ring) in the metallated ring brings about in increasing cathodic shift of $E_{1/2}$ in the order Cl > H > Me as expected from Hammett relation [38]. The second couple ($E_{1/2}{}^2$) varies irregularly and does not confirm to the second step reduction, of azo-function. The reduction of heterocyclic coligand is not ruled out which may need comparatively higher energy to accommodate electrons at the antibonding orbital. There may be a certain degree of involvement of coligand π^*-orbital in conjunction with azo-antibonding orbital.†

EXPERIMENTAL

The solvents used in the reactions were of reagent grade and were dried by reported procedures [15, 16]. 2-Picolinic acid (Hpic), quinaldic acid (Hqnd) (Fluka), 2-methyl-5-sulfonic-8-quinolinol (Hmsq) (Aldrich) and 8-quinolinol (BDH) were recrystallized before use from ethanol–water (2:1, v/v). Palladium chloride was

† One of the Referees has suggested in this manner.

Table 3. Cyclic voltammetric data of [Pd(A)(N,O)] in acetonitrile at 298 K

Compound[a]	Reduction Potentials[b] $-E_{1/2}^1(\Delta E_p)$	$-E_{1/2}^2(\Delta E_p)$
[Pd(A_1)(pic)]	1.055(100)	1.441(160)
[Pd(A_2)(pic)]	1.117(90)	1.514(140)
[Pd(A_4)(pic)]	1.15(80)	1.585(100)
[Pd(A_5)(pic)]	0.942(90)	1.365(140)
[Pd(A_1)(qnd)]	1.150(140)	1.384(180)
[Pd(A_2)(qnd)]	1.200(100)	1.435(140)
[Pd(A_4)(qnd)]	1.270(100)	1.545(130)
[Pd(A_5)(qnd)]	1.041(110)	1.309(150)
[Pd(A_1)(q)]	1.160(140)	1.550(120)
[Pd(A_2)(q)]	1.237(120)	1.644(140)
[Pd(A_4)(q)]	1.316(110)	1.805(160)
[Pd(A_5)(q)]	0.992(90)	1.276(120)
[Pd(A_1)(msq)]	1.105(80)	1.425(110)
[Pd(A_2)(msq)]	1.165(90)	1.500(120)
[Pd(A_4)(msq)]	1.214(120)	1.610(160)
[Pd(A_5)(msq)]	0.955(100)	1.376(120)

[a] Meaning of the symbols are as in the text.

[b] Potentials are 0.5 ($E_{pc} + E_{pa}$); E_{pc} and E_{pa} are cathodic and anodic peak potentials respectively, unit in V and ΔE_p in mV (reference to SCE), scan rate 50 mV s^{-1}, solute concentration $\sim 10^{-3}$ M in MeCN, [NBu_4, ClO_4] is supporting electrolyte (0.1 M).

received from Arrora Matthey, Calcutta, India. Disodium tetrachloropalladate was prepared by reported procedure [15, 16]. Azobenzenes were synthesized by condensing nitroaromatics and aromatic amines in hot glacial acetic acid as reported earlier [20–22]. All other chemicals and solvents were reagent grade and were used as received.

IR spectra were recorded on Perkin Elmer 783 and 883 spectrophotometers. ^{1}H NMR data were collected from Bruker 300 MHz FT NMR spectrometer in $CDCl_3$. UV–VIS spectra were obtained using Shimadzu 160A spectrophotometer. Elemental analyses were obtained using Perkin Elmer 2400 CHNS/O analyser.

Synthesis of complexes

Complexes [$Pd_2(A)_2Cl_2$] were prepared according to reported methods [20–22, 28]. The mixed ligand complexes [Pd(A)(N,O)] were synthesized by a general procedure and representative case is detailed below.

2-(*Picolinato*)(7-*phenylazophenyl-C*^{8},*N*)*palladium*(*II*), [*Pd*(*A*)(*pic*)]

To acetone solution (10 cm^3) of [$Pd_2(A_1)_2Cl_2$] (0.2 g, 0.31 mmol) was added aqueous $AgNO_3$ (0.11 g, 0.65 mmol) solution. The mixture was refluxed for 2 h. The precipitated AgCl was filtered at hot condition through G-4 sintered crucible. To this orange solution 2-picolinic acid (0.08 g, 0.65 mmol) in acetone (10 cm^3) was added dropwise with continuous stirring. The colour of the solution turned to orange-red and the precipitate appeared slowly on evaporation in air. The volume of the solution was reduced to half and the precipitate was filtered, washed with water, and recrystallized from chloroform–hexane via diffusion. The product was dried over $CaCl_2$. The yield was 70%.

The yield of other compounds varied between 65 and 80%.

Acknowledgements—Financial assistance from Department of Science and Technology, and University Grants Commission, New Delhi are thankfully acknowledged. One of the authors (K. B.) is indebted to Professor B. R. De, Department of Chemistry, Vidyasagar University, Midnapore for his help, T. K. M. thanks to the Council of Scientific and Industrial Research, New Delhi for giving him a fellowship.

REFERENCES

1. Omae, I., *Organometallic Intramolecular Coordination Compounds*. Elsevier, New York, 1986.
2. Wilkinson, G., Stone, F. G. A. and Abel, E. W. (eds), *Comprehensive Organometallic Chemistry*, Vol. 6. Pergamon, New York, 1982.
3. Crabtree, R. H., *Chem. Rev*., 1985, 245.
4. Singh, H. B., Sudha, N., West, A. A. and Hamor, H., *J. Chem. Soc. Dalton Trans*., 1990, 907.
5. Crispini, A. and Ghedini, M., *J. Chem. Soc. Dalton Trans*., 1997, 75.
6. Ryabov, A. D., Kuzmina, L. G., Dvotsova, N. V., Stufkenes, D. J. and van Eldrik, R., *Inorg. Chem*., 1993, **32,** 3166.
7. Leung, P. H., Loh, S.-K., Mox, K. F., White, A. J. P. and Williams, D. J., *J. Chem. Soc. Dalton Trans*., 1996, 4443.
8. Wu, Y. J., Liu, W. H. and Yang, L., Zhu, O., *Polyhedron*, 1997, **16,** 335.
9. Spencer, J., Pfeffer, M., Kyritsakar, N. and Fischer, J., *Organometallics*, 1995, **14,** 2214.
10. Dunina, V. V., Zalevskaya, O. A. and Potapov, V. M., *Russ. Chem. Rev*., 1988, **57,** 434.
11. Ryabov, A. D., *Synthesis*, 1985, 233.
12. Omae, I., *Chem. Rev*., 1979, **79,** 287.
13. Anderson, G. K., *Synlett*, 1995, 681.
14. Byers, P. K., Canty, A. J. and Honeyman, R. T., *Adv. Organomet. Chem*., 1992, **34,** 1.
15. Chattopadhyay, P., Nayak, M. K., Bhattacharya, S. P. and Sinha, C., *Polyhedron*, 1997, **16,** 1291.
16. Basuli, F., Chattopadhyay, P. and Sinha, C., *Polyhedron*, 1996, **15,** 2439.
17. Sinha, C., *Polyhedron*, 1993, **12,** 2363.
18. Chattopadhyay, S., Sinha, C., Chowdhury, S. B. and Chakravorty, A., *J. Organomet. Chem*., 1992, **427,** 111.
19. Chattopadhyay, S., Sinha, C., Basu, P. and Chakravorty, A., *J. Organomet. Chem*., 1991, **414,** 42 and references therein.

20. Mahapatra, A. K., Bandyopadhyay, D., Bandyopadhyay, P. and Chakravorty, A., *Inorg. Chem.*, 1986, **25,** 2214.
21. Elder, R. C., Curea, R. D. P. and Morrison, R. F., *Inorg. Chem.*, 1976, **15,** 1623.
22. Cope, A. C. and Siekman, R. W., *J. Am. Chem. Soc.*, 1965, **87,** 3272.
23. Vila, J. M., Gayoso, M., Fernandez, J. J., Ortigueira, J. M. and Suarez, A., *Polyhedron*, 1990, **9,** 2741.
24. Albert, J., Cadena, J. M. and Granell, J., *Tetrahedron Asymm.*, 1997, **8,** 991.
25. Vicente, J., Arcas, A., Bantista, D. and Jones, P. G., *Organometallics*, 1997, **16,** 2127.
26. Selvakumar, K. and Vancheesan, S., *Polyhedron*, 1996, **15,** 3979.
27. Suarez, A., Vila, J. M., Pereira, M. T., Gayoso, E. and Gayoso, M., *J. Orgranomet. Chem.*, 1987, **335,** 359.
28. Bandyopadhyay, P., Mascharak, P. K. and Chakravorty, A., *J. Chem. Soc. Dalton Trans.*, 1982, 675.
29. Hoare, J. L., Cavell, K. J., Hecker, R., Skelton, B. W. and White, A. H., *J. Chem. Soc. Dalton Trans.*, 1996, 2197 and references therein.
30. Poruies, J., Navarro, F. and Sicilia, V., *Polyhedron*, 1988, **7,** 2659.
31. Jones, R., Purcell, T. G., Williams, D. J. and Woollins, J. D., *Polyhedron*, 1988, **7,** 647.
32. Cross, R. J. and Tennet, N. H., *J. Organomet. Chem.*, 1976, **15,** 1623.
33. Takahasi, H. and Tsuji, J., *J. Organomet. Chem.*, 1967, **10,** 511.
34. Bruce, M. I., Goodall, B. L. and Stone, F. G. A., *J. Chem. Soc. Chem. Commun.*, 1973, 558.
35. Chattopadhyay, P. and Sinha, C., *Polyhedron*, 1994, **13,** 2689.
36. Krejcik, M., Zalis, S., Klima, J., Sykora, D., Matheis, W. and Klein, A., Kaim, W., *Inorg. Chem.*, 1993, **32,** 3362.
37. Johnson, C. S. Jr. and Chang, A., *J. Chem. Phys.*, 1965, **43,** 3183.
38. Boto, K. G. and Thomas, F. G., *Aust. J. Chem.*, 1971, **24,** 975.
39. Hockless, D. C. R., Mayadunne, R. C. and Wild, S. B., *Tetrahedron Asymm.*, 1995, **6,** 3031.

Pergamon

Polyhedron Vol. 17, No. 23–24, pp. 4115–4119, 1998
© 1998 Elsevier Science Ltd
All rights reserved. Printed in Great Britain
0277–5387/98 $19.00+0.00

PII: S0277–5387(98)00217–4

Coordination and self-assembly in the crystal structure of $K[AsMe_2S_2] \cdot 2H_2O$

Sofia Pascu,[a] Luminita Silaghi-Dumitrescu,[a] Alexander J. Blake,[b] Ionel Haiduc[a] and D. Bryan Sowerby[b]*

[a]Department of Chemistry, Babes-Bolyai University, R-3400 Cluj-Napoca, Romania

[b]Department of Chemistry, University of Nottingham, Nottingham NG7 2RD, U.K.

(Received 29 April 1998; accepted 25 May 1998)

Abstract—A major feature of the crystal structure of $K[AsMe_2S_2] \cdot 2H_2O$, which contains two independent formula units, is the presence of infinite sheets formed by edge sharing between two different types of $K(H_2O)_4S_2$ octahedra in which the sulfurs occupy either *cis* or *trans* positions. Although the four independent arsenic–sulfur distances all fall between those for single and double bonds, one sulfur at each arsenic is coordinated to potassium and the As–S distance here is longer [mean 2.140(2) Å] than that to the second sulfur [mean 2.111(5) Å] which is effectively free. The structure also contains a series of weak O–H . . . S hydrogen bonds.
© 1998 Elsevier Science Ltd. All rights reserved

Keywords: arsenic(III); dithioarsinate; dimethyldithioarsinate; crystal structure; sheet structure.

INTRODUCTION

Although the coordination properties of dithiophosphorus based ligands, i.e. dithiophosphates, dithiophosphonates and dithiophosphinates [1, 2], have been extensively studied, there are relatively few reports on the behaviour of the corresponding arsenic based ligands. Both main group and transition metal derivatives are known but few compounds have been investigated by X-ray methods. Such ligands should, and apparently do, show the same coordination versatility that is well established with the phosphorus analogues and examples where the ligands are monodentate [3, 4], chelating [5–7], bridging [8, 9] and tridentate (chelating–bridging) [10] are known. Any discussion of such structures requires information on the As–S separations in simple compounds such as the free acids to define As–S and As=S distances and simple salts to define the separation when the π-component is delocalised. Although free dithioarsinic acids, e.g. $AsR_2S(SH)$, where R = Me or Ph, are not known nor is structural information available on simple dithioarsinate salts, As–S single and double bond distances, ca. 2.25 and 2.07 Å, respectively, have been established from other compounds [4, 11, 12]. During the course of our work on arsenic–sulfur compounds, we prepared $K[AsMe_2S_2] \cdot 2H_2O$ and report here the results of a crystal structure determination.

RESULTS AND DISCUSSION

Alkali metal dimethyldithioarsinates were first prepared from cacodyl disulfide [13] but in the present case hydrogen sulfide was passed through a concentrated equimolar solution of hydrated dimethylarsinic acid and potassium hydroxide in ethanol using a modification of a literature method [14]; the product was isolated as a dihydrate. ^{1}H NMR spectroscopy in dmso-d_6 showed the expected two signals in a 3:2 ratio at 1.64 ppm for the methyl and 3.39 ppm for the water protons and there was a single ^{13}C signal at 31.68 ppm. Signals for the methyl protons varied with solvent and were at 1.85 and 1.96 ppm for solutions in $CDCl_3$ and D_2O, respectively. Symmetric and antisymmetric As–S stretching modes gave strong bands at 428 and 456 cm^{-1} in the IR spectrum of a nujol mull; the As–C stretches were at 616 and 651 cm^{-1} with methyl deformation modes at 913, 1360 and 1406 cm^{-1}. There was also a further broad band

* Author to whom correspondence should be addressed.

between 3300 and 3500 cm^{-1} associated with the hydrate water.

The X-ray determination shows the presence of two independent formula units in the asymmetric unit for this compound. Important bond distances and angles are collected in Table 1 and a diagram showing the asymmetric unit and the atom numbering scheme is in Fig. 1. Each arsenic atom shows distorted tetrahedral coordination with bond angles ranging between 104.8(6) and 114.6(1)° and as expected the smallest angles are those between methyl groups and the largest between two sulfur atoms. Although the As–S distances (mean 2.126 Å) fall between those for single

Table 1. Important bond distances (Å) and angles (°)

K1–O1[a]	2.719(9)
K1–O2	2.762(10)
K1–O3[a]	2.655(8)
K1–O4[b]	2.836(9)
K1–S1	3.218(4)
K1–S2	3.262(4)
K2–O1	2.760(9)
K2–O2	2.753(9)
K2–O3	2.826(9)
K2–O4	2.656(8)
K2–S1[c]	3.243(4)
K2–S2	3.217(4)
As1–S1	2.139(3)
As 1–S3	2.106(3)
As1–C11	1.930(11)
As1–C12	1.907(12)
As2–S2	2.141(3)
As2–S4	2.116(3)
As2–C21	1.929(11)
As2–C22	1.926(11)
O3[a]–K1–O1[a]	93.2(3)
O3[a]–K1–O2	109.2(3)
O1[a]–K1–O2	93.2(3)
O3[a]–K1–O4[b]	84.3(2)
O1[a]–K1–O4[b]	76.1(3)
O2–K1–O4[b]	163.5(3)
O3[a]–K1–S1	111.4(2)
O1[a]–K1–S1	152.4(2)
O2–K1–S1	90.2(2)
O4[b]–K1–S1	93.62(19)
O3[a]–K1–S2	157.3(2)
O1[a]–K–S2	84.5(2)
O2–K1–S2	93.5(2)
O4[b]–K1–S2	73.23(19)
S1–K1–S2	68.03(10)
C12–As1–C11	104.8(6)
C12–As1–S3	109.0(4)
C11–As1–S3	110.8(4)
C12–As1–S1	109.5(4)
C11–As1–S1	107.8(4)
S3–Asl–S1	114.57(14)
As1–S1–K1	105.48(13)
As1–S1–K2[b]	114.82(13)
K1–S1–K2[b]	76.03(10)
C22–As2–C21	105.5(6)
C22–As2–S4	110.1(4)
C21–As2–S4	109.3(4)
C22–As2–S2	108.0(4)
C21–As2–S2	109.2(4)
S4–As2–S2	114.36(13)
As2–S2–K2	105.73(13)
As2–S2–K1	114.44(12)

Table 1—*continued*

K2–S2–K1	76.20(10)
O4–K2–O2	87.7(3)
O4–K2–O1	106.5(3)
O2–K2–O1	160.2(3)
O4–K2–O3	160.6(3)
O2–K2–O3	74.9(3)
O1–K2–O3	88.7(3)
O4–K2–S2	112.3(2)
O2–K2–S2	94.7(2)
O1–K2–S2	92.8(2)
O3–K2–S2	78.07(18)
O4–K2–S1[c]	96.6(2)
O2–K2–S1[c]	86.0(2)
O1–K2–S1[c]	78.7(2)
O3–K2–S1[c]	74.25(18)
S2–K2–S1[c]	151.12(12)
K1[d]–O1–K2	88.9(3)
K2–O2–K1	92.9(3)
K1[d]–O3–K2	88.8(2)
K2–O4–K1[c]	92.8(3)

Various symmetry transformations were used to generate equivalent atoms.

[a] Symmetry transformation: $x, y+1, z$.

[b] Symmetry transformation: $x-1, y+1, z$.

[c] Symmetry transformation: $x+1, y-1, z$.

[d] Symmetry transformation: $x, y-1, z$.

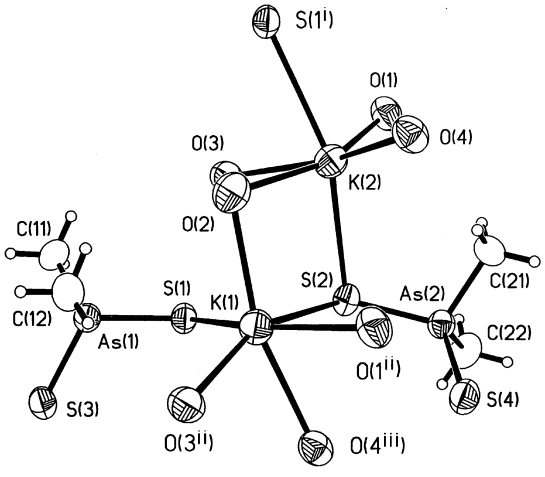

Fig. 1. The asymmetric unit, with completed potassium coordination spheres, for $K[AsMe_2S_2]\cdot 2H_2O$ and the atom numbering scheme. Symmetry operations are: (i) $1+x, 1-y, z$; (ii) $x, 1+y, z$; (iii) $x-1, 1+y, z$.

(*ca.* 2.25 Å) and double (*ca.* 2.07 Å) bonds, implying delocalisation of the π component, one distance at each arsenic is shorter [2.106(3) and 2.116(3) Å to S(3) and S(4), respectively] than the other [2.139(3) and 2.141(3) Å, to S(1) and S(2), respectively)] This is a consequence of the fact that the latter are coordinated to potassium ions while S(3) and S(4) make no other major contacts and are effectively free.

Each potassium ion is in distorted octahedral coordination to two sulfur and four oxygen atoms [*trans* angles range between 151.1(1) and 163.5(3)°] and this unit appears to be the major structure determining factor. Although each potassium coordination sphere contains the same atoms, the sulfurs are *cis* at K(1) [S(1)–K(1)–S(2) 68.0(1)°] but *trans* at K(2) [S(1^{i})–K(2)–S(2) 151.1(1)°]. K–S distances fall between 3.217(4) and 3.262(4) Å [mean 3.24(2) Å] with K–O distances between 2.655(8) and 2.836(9) Å.

For clarity, the overall structure can be considered to arise by sharing O(4)–S(1) and O(2)–S(2) edges between K(1) and K(2) octahedra to give infinite zigzag chains, which are then interlinked into sheets in the *ab* plane by sharing O(1)–O(3) edges. One view of part of the sheet is shown in Fig. 2 while Fig. 3 shows more clearly the edge sharing octahedra. A series of weak hydrogen bonds, all within a given sheet (see Table 2), between hydrogens of the four water molecules and the four sulfur atoms completes the structure.

This crystal structure can be described as a self-organised supramolecular structure, generated by electrostatic interactions and hydrogen bonds. The arrangement of the basic units is dictated by these forces, rather than by the simple packing of ions, and water molecules participate fully in the structure rather than simply occupying interstices or channels. As illustrated in Figs 2 and 3, the structure contains interlinked hexanuclear units, suggesting that under appropriate conditions such units may be isolable as discrete species.

There are strong similarities between this structure and that of $Na[PEt_2S_2] \cdot 2H_2O$ [15] where the asymmetric unit is a single formula unit. Sodium is coordinated by four oxygens and two *cis* sulfurs, as for K(1) in the present structure, and edge sharing between these octahedral NaO_4S_2 units gives related infinite sheets in the *ab* plane. The fact that there are two different coordination arrangements about

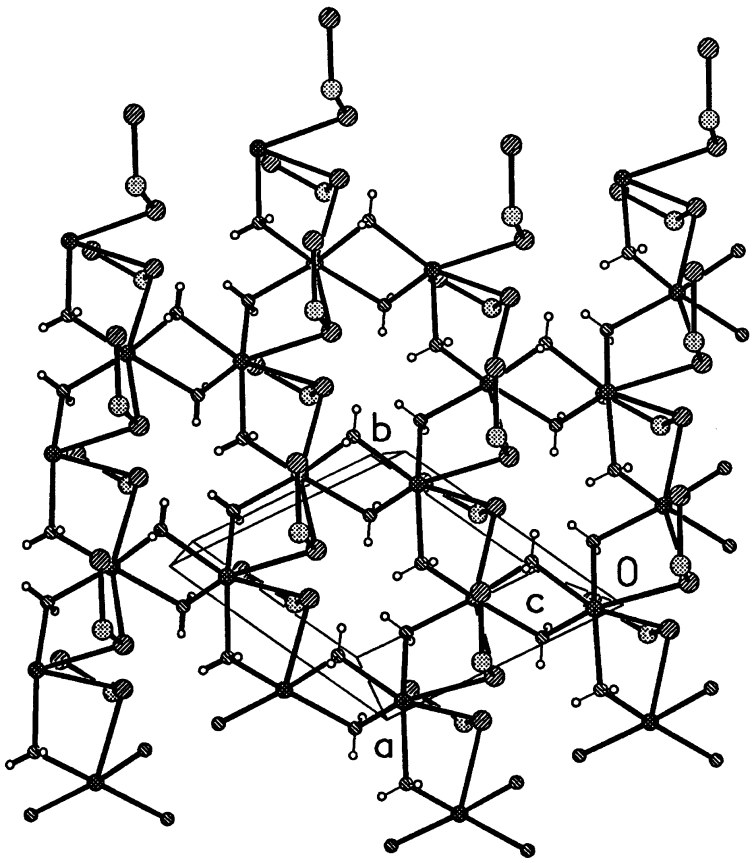

Fig. 2. Part of the sheet structure in the *ab* plane (methyl substituents at arsenic have been omitted for clarity).

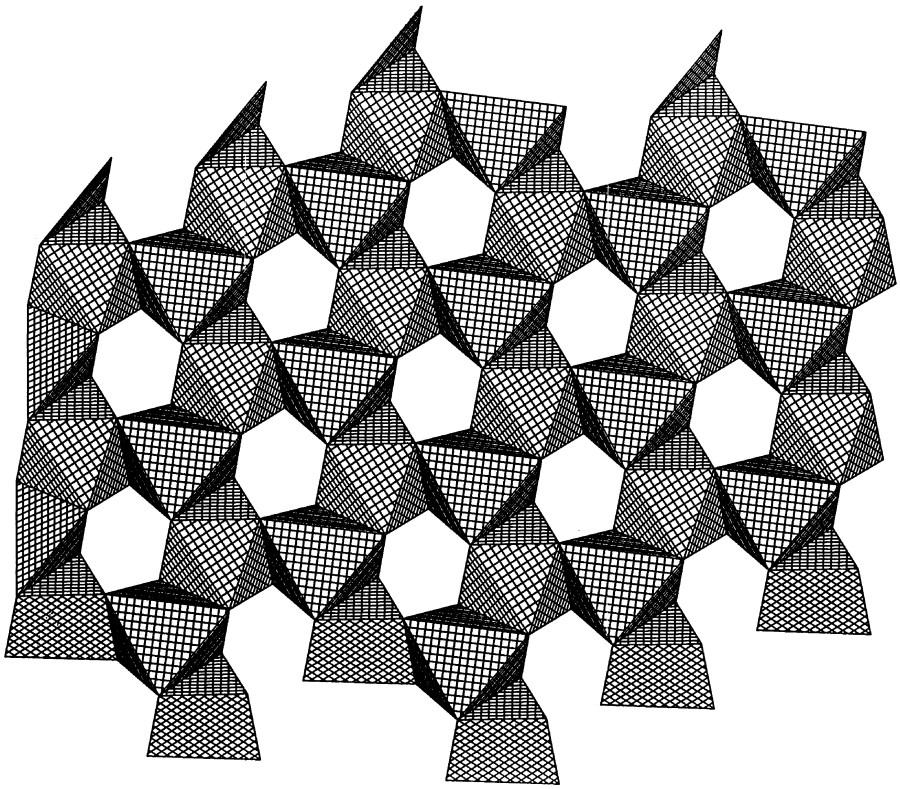

Fig. 3. Packing of the KO_4S_2 octahedra in the *ab* plane.

Table 2. O–H . . . S hydrogen bond parameters

	O . . . S (Å)	H . . . S (Å)	O–H . . . S (°)	As–S . . . H (°)
O(1)–H(1A) . . . S(4)–As(2[a])	3.27(1)	2.48	157	100
O(1)–H(1B) . . . S(2)–As(2[b])	3.25(1)	2.58	137	103
O(2)–H(2A) . . . S(1)–As(I[c])	3.27(1)	2.61	135	104
O(2)–H(2B) . . . S(3)–As(1[b])	3.31(1)	2.52	154	103
O(3)–H(3A) . . . S(3)–As(1)	3.23(1)	2.44	157	97
O(3)–H(3B) . . . S(1)–As(1)	3.28(1)	2.49	154	109
O(4)–H(4A) . . . S(4)–As(2[b])	3.26(1)	2.46	157	97
O(4)–H(4B) . . . S(2)–As(2[c])	3.28(1)	2.49	155	110

Various symmetry transformations were used to generate equivalent atoms.
[a] Symmetry transformation: $x, y-1, z$.
[b] Symmetry transformation: $1+x, y-1, z$.
[c] Symmetry transformation: $1+x, y-1, z$.

potassium in the present structure, however, leads to no major difference in the sheet structure resulting from edge sharing.

EXPERIMENTAL

Preparation of potassium dimethyldithioarsinate

The compound was obtained by passing hydrogen sulfide for two hours into a solution of hydrated dimethylarsinic acid (500 mg, 3.16 mmol) and potassium hydroxide (170 mg, 3.16 mmol) in ethanol (35 cm^3). On cooling the solution to 0°C, a white precipitate of the required compound as the dihydrate was obtained in almost quantitative yield. Crystallisation from a mixture of dichloromethane and hexane (1/1) gave air stable colourless crystals of the compound, suitable for X-ray crystallography. M.Pt 95°C. Found: C, 9.8; H, 4.1. $C_2H_{10}AsKO_2S_2$ calc.: C, 10.1; H, 4.0%.

Crystal structure determination

Crystal data $C_4H_{20}As_2K_2O_4S_4$, $M=488.5$, triclinic, space group $P\bar{1}$, $a=6.623(3)$, $b=6.694(2)$, $c=24.658(13)$ Å, $\alpha=84.45(4)$, $\beta=87.73(6)$, $\gamma=60.56(2)^\circ$, $V=947.5(7)$ Å^{-3}, $Z=2$, $D_c=1.712$ g cm^{-3}, $F(000)=488$, $\mu=4.402$ mm^{-1}, Mo-Kα radiation, $\lambda=0.71073$ Å, crystal size $=0.47\times0.35\times0.20$ mm.

Data for 3519 reflections ($-7<h<7$, $-7<k<7$, $-18<k<29$) were collected on a Stoe Stadi-4 diffractometer: of these 3295 [$R_{int}=0.133$] were unique and 2678 had $I>2\sigma(I)$. The structure was solved by direct methods (SHELXS-86) [16] and difference Fourier syntheses and refined by least squares on F^2 (SHELXL-93) [17]. Nonhydrogen atoms were assigned anisotropic thermal parameters and hydrogen atoms were placed at calculated positions and refined using a riding model. Refinement converged (3295 data, 146 parameters, GOF 1.248) at R_1 0.0482, wR_2 0.1025 (observed data) and R_1 0.0837, wR_2 0.1657 (all data). Full details of the atomic parameters and bond lengths and angles have been deposited with the Cambridge Crystallographic Data Centre.

REFERENCES

1. Haiduc, I., Sowerby, D. B. and Lu, S. F., *Polyhedron*, 1995, **14,** 3389.
2. Haiduc, I. and Sowerby, D. B., *Polyhedron*, 1996, **15,** 2469.
3. Silaghi-Dumitrescu, L., Haiduc, I. and Weiss, J., *J. Organomet. Chem.*, 1984, **263,** 158.
4. Camerman, N. and Trotter, J., *J. Chem. Soc.*, 1964, 219.
5. Silaghi-Dumitrescu, L., Haiduc, A., Cervantes-Lee, F. and Pannell, K. H., *Rev. Roum. Chem.*, 1997, **42,** 587.
6. Silaghi-Dumitrescu, L., Haiduc, I., Toscano, A. and Cea-Olivares, R., *Polyhedron*, submitted for publication.
7. Cea-Olivares, R., Ebert, K., Silaghi-Dumitrescu, L. and Haiduc, I., *Heteroatom. Chem.*, 1997, **8,** 317.
8. Silvestru, C., Silaghi-Dumitrescu, L., Haiduc, I., Begley, M. J., Nunn, M. and Sowerby, D. B., *J. Chem. Soc., Dalton Trans.*, 1986, 1031.
9. Sowerby, D. B., Begley, M. J., Silaghi-Dumitrescu, L., Silaghi-Dumitrescu, I. and Haiduc, I., *J. Organomet. Chem.*, 1994, **469,** 45.
10. Abel, E. W., Beckett, M. A., Bates, P. A. and Hursthouse, M. B., *Polyhedron*, 1988, **7,** 1855.
11. Silaghi-Dumitrescu, L., Gibbons, M. N., Silaghi-Dumitrescu, I., Zukerman-Schpector, J., Haiduc, I. and Sowerby, D. B., *J. Organomet. Chem.*, 1996, **517,** 101.
12. Silaghi-Dumitrescu, L., Pascu, S., Silaghi-Dumitrescu, I., Haiduc, I., Gibbons, M. N. and Sowerby, D. B., *J. Organomet. Chem.*, 1997, **549,** 187.
13. Bunsen, R., *Liebieg's Ann. Chem.*, 1843, **46,** 21.
14. Baratova, Z. R., Solozhenikin, P. M. and Semenov, E. V., *Dokl. Akad. Nauk SSSR*, 1977, **236,** 1137.
15. Svensson, G. and Albertson, J., *Acta Crystallogr.*, 1989, **C45,** 395.
16. Sheldrick, G. M., *Acta Crystallogr. Sect. A*, 1990, **46,** 467.
17. Sheldrick, G. M., *SHELXL*-93. Institut für Anorganische Chemie der Universität Göttingen, Germany, 1993.

Pergamon

Polyhedron Vol. 17, No. 23–24, pp. 4121–4130, 1998
© 1998 Elsevier Science Ltd
All rights reserved. Printed in Great Britain
0277–5387/98 $19.00+0.00

PII: S0277–5387(98)00219–8

Some metal complexes containing diphenylphosphinoacetic acid as a P-bonded neutral ligand. Crystal structures of [AuCl($Ph_2PCH_2CO_2H$)] and *trans*-[$PdCl_2(Ph_2PCH_2CO_2H)_2$]$0.33H_2O \cdot 0.33C_2H_5OH$

Dennis A. Edwards,† Mary F. Mahon and Timothy J. Paget

Department of Chemistry, University of Bath, Claverton Down, Bath BA2 7AY, U.K.

(Received 13 March 1998; accepted 29 May 1998)

Abstract—Diphenylphosphinoacetic acid (HA) reacts as a neutral *P*-donor ligand with a variety of transition metal compounds to generate the new complexes [$CuCl(HA)_x$] ($x=1$ or 3), *trans*-[$PdCl_2(HA)_2$], *cis*-[$PtCl_2(HA)_2$], [AuCl(HA)] and *cis*-[$Mo(CO)_4(HA)_2$]. The crystal structure of [AuCl(HA)] involves a linear Cl–Au–P arrangement [179.0(1)°], neighbouring molecules forming hydrogen-bonded dimers in the lattice array. The hydrogen-bonding is of the planar type commonly found in free carboxylic acids with intermolecularly bonded pairs of [AuCl(HA)] molecules being related by an inversion centre. Recrystallisation of *trans*-[$PdCl_2(HA)_2$] from ethanol yields crystals of the solvate *trans*-[$PdCl_2(HA)_2$]$\cdot 0.33H_2O \cdot 0.33C_2H_5OH$. The asymmetric unit contains 1.5[$PdCl_2(HA)_2$] molecules along with water and ethanol molecules exhibiting only half site occupancy. For every three [$PdCl_2(HA)_2$] molecules two are hydrogen-bonded to neighbours using carboxylic acid groups to form chains. The third molecule differs in that hydrogen-bonding occurs between one oxygen of a carboxylic acid group and the lattice water, the oxygen of which further hydrogen-bonds to the lattice ethanol. © 1998 Elsevier Science Ltd. All rights reserved

Keywords: diphenylphosphinoacetic acid; gold(I); palladium(II); carboxylic acid; hydrogen bonding.

INTRODUCTION

A vast range of metal complexes containing coordinated acetate anions have been prepared and characterised over many years but complexes containing the parent acetic acid are quite rare. Examples include $[M(CH_3CO_2H)_6]^{2+}$ (M = Mg, Ca, Mn, Co, Ni, Cu and Zn) [1] and a crystal structure determination of the nickel cation as its tetrafluoroborate confirms that the ligands are *O*-unidentate [2, 3]. A similar picture emerges on consideration of substituted acetic acids and their anions as ligands where the substituent contains a group 15 donor atom. The additional group 15 donor atoms may compete with the carboxylic acid donor oxygens for coordination to metal centres, increasing the number of possible coordination modes and providing differentiation between hard and soft metal–ligand interactions. Taking the simplest amino-acid as an example, glycine forms many complexes involving *N*,*O*-chelating glycinate anions but rather few containing glycine itself and these display a range of coordination types. For example, glycine is zwittterionic and *O*,*O*′-bridging in [$Ag_2(O_2CCH_2NH_3)_2](NO_3)_2$ [4], *O*-unidentate in [$(\eta\text{-}C_5H_5)_2Ti(O_2CCH_2NH_3)_2]Cl_2$ [5] and *N*-unidentate in *cis*-[$PtX_2(NH_2CH_2CO_2H)_2$] (X = Cl or Br) [6].

Metal complexes derived from phosphine-substituted acetic acids are less well known. Considering the ligand used in this work, diphenylphosphinoacetic acid $Ph_2CH_2CO_2H$, (abbreviated as HA with the anion as A^-), structure determinations of [$Pd(A)_2$] [7], [PtBr(A)(HA)]$\cdot H_2O$ [8], [Rh(CO)(A)(HA)] [9], [$Rh(A)_3]\cdot PhNO_2\cdot H_2O$ [10], [RhCl(H)(A)$(HA)_2$] [10] and [Et_4N][$W(CO)_4$(A)] [11] confirm that the anion is *O*,*P*-chelating in all cases, although it is tridentate both bridging and chelating through the carboxylate

†Author to whom correspondence should be addressed. Fax: +44-1225-826-231; E-mail: d.a.edwards@bath.ac.uk

unit only in [Ca(A)$_2$] [12]. Three of the above complexes also contain HA as a ligand and in each case it is bonded in a *P*-unidentate manner, this coordination mode also having been established for *trans*-[PdBr$_2$(HA)$_2$] [13] and [Hg$_2$Br$_2$(μ-Br)$_2$(HA)$_2$] [14]. Thus the parent acid HA can behave as a ligand in the manner of a diphenylalkylphosphine. We report here the syntheses of a number of new examples and include discussion of two crystal structure determinations.

EXPERIMENTAL

Diphenylphosphinoacetic acid was prepared by a variation of the method of Jarolim and Podlahova [15] (found: C, 68.9; H, 5.39. $C_{14}H_{13}O_2P$ requires C, 68.9; H, 5.36%). NMR ($CDCl_3$), ^{1}H δ 3.11 (s, CH_2, 2H), 7.33–7.48 (m, Ph, 10H), 11.50 (br s, O*H*, 1H); ^{13}C{^{1}H} δ 35.1 (d, $^1J_{CP}$ = 23.2, *C*H$_2$), 128.4 (d, $^3J_{CP}$ = 6.6, C_{meta}), 129.0 (s, C_{para}), 132.4 (d, $^1J_{CP}$ = 19.9, C_{ipso}), 136.7 (d, $^2J_{CP}$ = 14.3, C_{ortho}), 177.2 (d, $^2J_{CP}$ = 8.8, *C*O$_2$H); ^{31}P{^{1}H} δ −15.1. IR (cm^{-1}) 1700 vs $\nu(CO_2)_{asym}$, 1301, 1291 s $\nu(CO_2)_{sym}$.

The starting materials [Mo(CO)$_4$(nbd)], [PdCl$_2$(PhCN)$_2$], [PtCl$_2$(PhCN)$_2$] and [AuCl(tht)] (nbd = norbornadiene, tht = tetrahydrothiophene) were prepared by standard literature methods. Microanalyses were carried out using a Carlo-Erba microanalysis system. Jeol GX 270 and EX 400 spectrometers were used to obtain ^{1}H, ^{13}C and ^{31}P NMR spectra. Infrared spectra were recorded as Nujol or hexachlorobutadiene mulls using Nicolet 510P or Perkin-Elmer 597 spectrophotometers. Positive and negative ion FAB mass spectra were recorded on Vacuum Generators 7070E and Autospec instruments using 3-nitrobenzyl alcohol matrices. The *m*/*z* values reported below are based on ^{35}Cl, ^{63}Cu, ^{98}Mo, ^{106}Pd and ^{197}Au, peak intensities being expressed relative to the strongest metal-containing fragment. Reactions and subsequent manipulations were carried out under an atmosphere of dry nitrogen as required.

Tetracarbonylbis(diphenylphosphinoacetic acid)molybdenum(0)

A solution of [Mo(CO)$_4$(nbd)] (1.00 g, 3.3 mmol) and HA (1.60 g, 6.7 mmol) in dichloromethane (20 cm^3) was stirred at room temperature for 18 h. The resulting colourless precipitate was removed by filtration, washed with dichloromethane and dried *in vacuo*. Yield 2.2 g, 96% (found: C, 55.1; H, 3.72. $C_{32}H_{26}MoO_8P_2$ requires C, 55.2; H, 3.76%). NMR [(CD$_3$)$_2$CO], ^{1}H δ 3.25 (virtual t, CH_2, 4H), 7.39 and 7.51 (m, Ph, 20H); ^{13}C{^{1}H} δ 37.8 (s, *C*H$_2$), 129.0 (d, $^2J_{CP}$ = 17.6, C_{ortho}), 130.4 (s, C_{para}), 133.1 (d, $^3J_{CP}$ = 12.1, C_{meta}), 137.3 (d, $^1J_{CP}$ = 33.1, C_{ipso}), 169.4 (s, *C*O$_2$H), 210.2 (d, $^2J_{CP}$ = 9.9, *C*O), 216.1 (d, $^2J_{CP}$ = 17.6, *C*O); ^{31}P{^{1}H} δ +25.0. IR (cm^{-1}) 2027 vs, 1921 vs, 1910 sh, 1897 vs ν(CO), 1701 s $\nu(CO_2)_{asym}$, 1296 m $\nu(CO_2)_{sym}$. FAB-MS (*m*/*z*), 698 (15% [M]$^+$), 670 (6% [M–CO]$^+$), 642 (40% [M–2CO]$^+$), 614 (3% [M–3CO]$^+$), 586 (21% [M–4CO]$^+$), 454 (100% [M–(HA)]$^+$), 426 (50% [M–(HA)–CO]$^+$).

trans-Dichlorobis(diphenylphosphinoacetic acid)palladium(II)

HA (0.32 g, 1.30 mmol) and [PdCl$_2$(PhCN)$_2$] (0.25 g, 0.65 mmol) were allowed to react for 24 h in stirred dichloromethane (10 cm^3). The resulting yellow–green precipitate was collected, washed with dichloromethane and dried *in vacuo*. Yield, 0.40 g, 92% (found: C, 50.1; H, 3.88. $C_{28}H_{26}Cl_2O_4P_2Pd$ requires C, 50.5; H, 3.94%). NMR (CD_3CN), ^{1}H δ 3.71 (d, CH_2, 4H, $^2J_{PH}$ = 12.5), 7.31, 7.54, 7.83 (m, Ph, 20H); ^{13}C{^{1}H} δ 129.6, 132.1, 133.7, 134.6; ^{31}P{^{1}H} δ +12.4. IR (cm^{-1}) 1732 s, 1707 s $\nu(CO_2)_{asym}$, 1350 m $\nu(CO_2)_{sym}$, 330 m ν(PdCl). FAB-MS (*m*/*z*), 629 (46% [M–Cl]$^+$), 593 (100% [M–2Cl–H]$^+$), 350 (20% [M–2Cl–(HA)]$^+$).

Recrystallisation from ethanol gave yellow cube-like crystals suitable for an X-ray structure determination. The crystals were found to contain one ethanol and one water solvate molecule for every three $PdCl_2(HA)_2$ molecules (found: C, 50.1; H, 4.57. $C_{86}H_{86}Cl_6O_{14}P_6Pd_3$ requires C, 50.6; H, 4.20%).

cis-Dichlorobis(diphenylphosphinoacetic acid)platinum(II)

A solution of HA (0.090 g, 0.37 mmol) in dichloromethane (1.0 cm^3) was added to a solution of [PtCl$_2$(PhCN)$_2$] (0.087 g, 0.18 mmol) in dichloromethane (2.0 cm^3). A further 1.0 cm^3 of dichloromethane was added and the mixture stirred for 10 min. The colourless solution was allowed to stand for 18 h before collecting the precipitated product, washing with dichloromethane and drying *in vacuo*. Yield, 0.103 g, 76% (found: C, 45.2; H, 3.49. $C_{28}H_{26}Cl_2O_4P_2Pt$ requires C, 44.6; H, 3.47%). NMR (CD_3CN), ^{1}H δ 3.63 (d, CH_2, 4H, $^2J_{PH}$ = 11.7), 7.28–7.67 (m, Ph, 20H); ^{13}C{^{1}H} δ 33.2 (s, *C*H$_2$), 129.4, 132.4, 134.7; ^{31}P{^{1}H} δ +3.0 [^1J(^{195}Pt–^{31}P) = 3790]. IR (cm^{-1}), 1734 sh, 1696 s $\nu(CO_2)_{asym}$, 1300 m $\nu(CO_2)_{sym}$, 332 m, 303 m ν(PtCl).

Chloro(diphenylphosphinoacetic acid)copper(I)

Copper(I) chloride (0.20 g, 2.0 mmol) was added to a stirred solution of HA (0.50 g, 2.0 mmol) in dichloromethane (10 cm^3) and any reaction allowed to proceed for 24 h at room temperature. The resulting colourless precipitate was filtered, washed with dichloromethane and dried *in vacuo*. Yield, 0.43 g, 63% (found: C, 49.1; H, 3.80. $C_{14}H_{13}ClCuO_2P$ requires C, 49.0; H, 3.82%). NMR (CD_3CN), ^{1}H δ 3.66 (d, CH_2, 2H, $^2J_{PH}$ = 13.5), 7.46, 7.68, 7.78–7.83 (m, Ph, 10H); ^{13}C{^{1}H} δ 34.7 (d, *C*H$_2$, $^2J_{CP}$ = 12.2), 129.6 (d,

$^3J_{CP}=8.8$, C_{meta}), 131.2 (s, C_{para}), 131.6 (d, $^2J_{CP}=9.9$, C_{ortho}), 133.5 (d, $^1J_{CP}=15.4$, C_{ipso}), 170.1 (s, CO_2H); $^{31}P\{^1H\}$ δ −13.3. IR (cm^{-1}), 1705 vs $\nu(CO_2)_{asym}$, 1294 s $\nu(CO_2)_{sym}$. FAB-MS (m/z), FAB$^+$ 1333 (1% $[M_4–Cl]^+$), 649 (60% $[M_2–Cl]^+$), 551 (100% $[M–Cl+(HA)]^+$), 405 (34% $[M_2–Cl–(HA)]^+$), 342 (10% $[M]^+$); FAB$^-$ 1368 (2% $[M_4]^-$), 1124 (7% $[M_4–(HA)]^-$), 878 (27% $[M_4–2(HA)–2H]^-$), 635 (45% $[M_4–3(HA)–H]^-$), 537 (100% $[M_3–2(HA)–H]^-$), 341 (92% $[M–H]^-$).

Chlorotris(diphenylphosphinoacetic acid)copper(I)

Copper(I) chloride (0.075 g, 0.76 mmol) slowly dissolved when added to a stirred solution of HA (0.563 g, 2.31 mmol) in dichloromethane (10 cm^3). The reaction was allowed to proceed for 24 h at room temperature before removal of some of the solvent *in vacuo* to yield a colourless crystalline product. Yield, 0.33 g, 52% (found: C, 59.9: H, 4.75. $C_{42}H_{39}ClCuO_6P_3$ requires C, 60.7; H, 4.73%). NMR ($CDCl_3$), ^1H δ 3.16 (s, CH_2, 6H), 7.13, 7.32 (m, Ph, 30H), 10.07 (br, CO_2H, 3H); $^{13}C\{^1H\}$ δ 33.5 (s, CH_2), 128.3 (d, $^3J_{CP}=6.6$, C_{meta}), 129.8 (s, C_{para}), 131.5 (d, $^1J_{CP}=23.2$, C_{ipso}), 132.4 (d, $^2J_{CP}=14.4$, C_{ortho}), 171.9 (s, CO_2H); $^{31}P\{^1H\}$ δ −9.5. IR (cm^{-1}), 1725 sh, 1700 vs $\nu(CO_2)_{asym}$, 1290 m $\nu(CO_2)_{sym}$, 247 w ν(CuCl). FAB-MS (m/z) 795 (2% $[M–Cl]^+$), 551 (100% $[M–Cl–(HA)]^+$), 263 (50% $[M–Cl–2(HA)–CO_2]^+$).

Chloro(diphenylphosphinoacetic acid)gold(I)

A solution of HA (0.15 g, 0.60 mmol) in dichloromethane (2.0 cm^3) was added to a solution of chloro (tetrahydrothiophene)gold(I) (0.20 g, 0.60 mmol) in dichloromethane (3.0 cm^3). The mixture was stirred overnight at room temperature giving a yellow solution. Removal of the solvent *in vacuo* gave a yellow crystalline solid which was recrystallised from dichloromethane before drying *in vacuo*. Yield, 0.25 g, 87% (found: C, 35.2; H, 2.70. $C_{14}H_{13}AuClO_2P$ requires C, 35.3; H, 2.75%). NMR ($CDCl_3$), ^1H δ 3.83 (d, CH_2, 2H, $^2J_{PH}=12.5$), 7.62, 7.82 (m, Ph, 10H); $^{13}C\{^1H\}$ δ 35.0 (d, $^1J_{CP}=37.4$, CH_2), 129.9 (d, $^1J_{CP}=61.7$, C_{ipso}), 130.3 (d, $^3J_{CP}=12.1$, C_{meta}), 133.3 (s, C_{para}), 134.2 (d, $^2J_{CP}=14.3$, C_{ortho}), 168.7 (s, CO_2H); $^{31}P\{^1H\}$ δ +25.0. IR (cm^{-1}), 1700 vs $\nu(CO_2)_{asym}$, 1300 s $\nu(CO_2)_{sym}$, 335 vs ν(AuCl). FAB-MS (m/z) 917 (22% $[M_2–Cl]^+$), 685 (3% $[M–Cl+(HA)]^+$), 476 (7% $[M]^+$), 441 (100% $[M–Cl]^+$).

X-ray crystallography

Crystal data, data collection and refinement details are given for *trans*-$[PdCl_2(Ph_2CH_2CO_2H)_2]\cdot 0.33C_2H_5OH\cdot 0.33H_2O$ and for $[AuCl(Ph_2PCH_2CO_2H)]$ in Table 1. Selected bond lengths and angles are reported for each compound in Tables 2 and 3, respectively. Additional information for each structure is available from the Cambridge Crystallographic Data Centre and comprises final fractional atomic coordinates, thermal parameters, hydrogen atom coordinates and complete listings of bond lengths and angles. The contents of the unit cell of the palladium compound, produced using ORTEX [16], is shown in Fig. 1 along with the labelling scheme. Views of the supramolecular structure highlighting the hydrogen-bonding motifs are shown in Figs 2 and 3. The asymmetric unit of the gold compound is given in Fig. 4, also produced using ORTEX [16].

Data were collected at room temperature on a CAD-4 diffractometer using graphite-monochromated Mo-Kα radiation. The diffraction intensities were corrected for Lorentz and polarisation effects. An absorption correction was applied for the gold compound (transmission factor extrema 1.000, 0.230). The structures were solved using SHELX86 [17] and refined using SHELX93 [18]. In the final least squares cycles all atoms were allowed to vibrate anisotropically. For the palladium compound, hydrogen atoms were included at calculated positions on carbon atoms, where relevant. Hydrogens associated with the carboxylic acid moieties, the hydroxyls of the ethanol molecules and the lattice waters could not be located, even by examining a difference Fourier synthesis based on low Bragg data. For the gold compound, hydrogen atoms were included at calculated positions where relevant, except on the carboxylic acid moieties.

RESULTS AND DISCUSSION

Six new complexes all involving diphenylphosphinoacetic acid, abbreviated as HA, as a neutral *P*-donor ligand have been prepared and characterised. In these compounds the ligand is primarily acting as an alkyldiarylphosphine, although additional intermolecular hydrogen-bonding employing the carboxylic acid function is likely to be present in all cases as established by X-ray crystallography for the palladium and gold examples (*vide infra*). The complexes have been prepared either by direct reaction of the acid with a metal chloride as for $[CuCl(HA)_x]$ ($x=1$ or 3), or by displacement of a suitable labile ligand from a metal complex. Thus the syntheses of $[MCl_2(HA)_2]$, (M = Pd or Pt), $[Mo(CO)_4(HA)_2]$ and [AuCl(HA)] have been achieved from $[MCl_2(PhCN)_2]$, $[Mo(CO)_4(nbd)]$ and [AuCl(tht)], respectively (nbd = norbornadiene; tht = tetrahydrothiophene). Characterisation of products has been carried out using ^1H, ^{13}C and ^{31}P NMR, IR and FAB-MS (selected data are given in Section 2) and for the palladium and gold complexes, single crystal X-ray structure determinations.

The ^1H NMR spectra of the six complexes are very

Table 1. Crystal data and data collection details for *trans*-$[PdCl_2(Ph_2PCH_2CO_2H)_2]\cdot 0.33EtOH\cdot 0.33H_2O$ and for $[AuCl(Ph_2PCH_2CO_2H)]$

Empirical formula	$C_{43}H_{43}Cl_3O_7P_3Pd_{1.5}$	$C_{14}H_{13}AuClO_2P$
Formula weight	1030.63	476.63
Crystal system	triclinic	monoclinic
Space group	$P\bar{1}$ (No. 2)	$P2_1/n$
a (Å)	9.881(2)	9.296(1)
b (Å)	15.684(6)	9.479(1)
c (Å)	15.716(4)	17.534(2)
α (°)	87.27(3)	
β (°)	79.61(2)	97.05(1)
γ (°)	85.78(2)	
V (Å^3)	2387.6(11)	1533.4(3)
Z	2	4
D_c (Mg m^{-3})	1.434	2.065
μ (mm^{-1})	0.885	9.866
$F(000)$	1044	896
Crystal dimensions (mm)	$0.3\times0.3\times0.25$	$0.2\times0.2\times0.25$
Theta range for data collection (°)	2.10 to 23.93	2.34 to 23.92
hkl ranges	0 to 11, −17 to 17, −17 to 17	−10 to 10, 0 to 10, 0 to 20
Reflections collected	7952	2396
Independent reflections (R_{int})	7461 (0.0146)	2396 (0.0000)
Data, restraints, parameters	7440, 0, 542	2396, 0, 173
Goodness of fit on F^2	1.117	1.099
Final R_1, wR_2 indices $[I>2\sigma(I)]$	0.0353, 0.1014	0.0338, 0.0801
(All data)	0.0645, 0.1327	0.0641, 0.0948
Largest residuals (e Å^{-3})	0.846, −0.420	1.330, −1.044
Weighting scheme, w	$1/[\sigma^2(F_o^2)+(0.0605P)^2+3.2051P]$ where $P=(F_o^2+2F_c^2)/3$	$1/[\sigma^2(F_o^2)+(0.0511P)^2+5.0094P]$ where $P=(F_o^2+2F_c^2)/3$

similar to that of diphenylphosphinoacetic acid itself. The methylene resonance appears as a doublet (^{2}J *ca.* 12 Hz) for the palladium, platinum and gold complexes as a result of coupling to phosphorus while that of the molybdenum tetracarbonyl appears as a virtual triplet, with a quite broad central peak, resulting from the two phosphorus nuclei being strongly coupled to each other. Detection of the carboxylic acid proton was only achieved for the ligand itself and for $[CuCl(HA)_3]$.

Apart from the palladium and platinum species the remainder show the expected six ^{13}C resonances (a methylene, a carboxylic acid and four phenyl signals) at quite similar chemical shifts to those of the free ligand. Only partial data were obtained for the palladium and platinum compounds, as a result of low solubilities in non-reacting solvents. Additional carbonyl carbon resonances at 210.2 and 216.1 ppm, with appropriate ^{31}P–^{13}C coupling constants, confirms the anticipated *cis*-octahedral geometry of the molybdenum product. The ^{31}P chemical shift values are invariably downfield relative to the free ligand as a result of bonding by the ligand through phosphorus. However, the coordination shifts, $\Delta\delta$, vary significantly from compound to compound, the molybdenum and gold complexes both showing shifts of 40.1 ppm whereas those of the two copper(I) complexes are much smaller, being only 1.8 and 5.6 ppm for the mono- and tris-ligand complexes, respectively. These coordination shifts are very much of the same magnitude as those of related metal-alkyldiphenylphosphine or -triphenylphosphine complexes e.g. *cis*-$[Mo(CO)_4(PPh_2Bu^n)_2]$, $\Delta\delta=42.9$ ppm [19]; $[AuCl(Ph_2PCH_2CONHMe)]$, $\Delta\delta=41.9$ ppm [20]; $[CuCl(PPh_3)_3]\cdot MeCN$, $\Delta\delta=2.3$ ppm [21]. The coordination shifts for *trans*-$[PdCl_2(HA)_2]$ and *cis*-$[PtCl_2(HA)_2]$ are intermediate in magnitude being 27.5 and 18.1 ppm, respectively. These $\Delta\delta$ values can be compared with those of the analogous *trans*-$[PdCl_2(PPh_2Bu^n)_2]$ [22] and *cis*-$[PtCl_2(PPh_2Bu^n)_2]$ [19] which are 33.4 and 24.1 ppm, respectively. The large $^1J(^{195}Pt–^{31}P)$ coupling constant of 3790 Hz observed for the platinum complex is indicative of *cis*-square planar geometry, a useful comparison [19] being the values for *cis*- and *trans*-$[PtCl_2(PPh_2Bu^n)_2]$ of 3641 and 2531 Hz, respectively. It appears, therefore, from these $\Delta\delta$ and J values that our preparative route leads to the *trans*-isomer for the palladium compound, as has been established by crystallography for $[PdBr_2(HA)_2]$ [13], whereas the platinum compound is isolated as the *cis*-isomer. Further evidence supporting this proposal comes from infrared spectroscopic and, for the palladium complex, crystallographic results (*vide infra*).

The infrared-active asymmetric and symmetric carboxylate stretches are little changed from those of the free acid indicating the lack of coordination to the

Table 2. Selected bond lengths (Å) and angles (°) for *trans*-$[PdCl_2(Ph_2PCH_2CO_2H)_2]\cdot 0.33EtOH\cdot 0.33H_2O$

Pd(1)–Cl(1)	2.305(1)	Cl(1)–Pd(1)–P(1)	93.24(4)
Pd(1)–P(1)	2.326(1)	Cl(1)–Pd(1)–P(1′)	86.76(4)
P(1)–C(7)	1.816(5)	C(7)–P(1)–C(1)	101.8(2)
P(1)–C(1)	1.821(4)	C(7)–P(1)–C(13)	104.5(2)
P(1)–C(13)	1.839(5)	C(1)–P(1)–C(13)	103.8(2)
O(1)–C(14)	1.255(6)	O(1)–C(14)–O(2)	122.4(4)
O(2)–C(14)	1.262(6)		
Pd(2)–Cl(2)	2.303(1)	Cl(2)–Pd(2)–P(2)	86.45(5)
Pd(2)–P(2)	2.309(1)	Cl(2)–Pd(2)–P(2′)	93.55(5)
P(2)–C(15)	1.807(5)	C(15)–P(2)–C(21)	104.6(2)
P(2)–C(21)	1.814(5)	C(15)–P(2)–C(27)	103.8(2)
P(2)–C(27)	1.830(5)	C(21)–P(2)–C(27)	105.3(2)
O(3)–C(28)	1.215(6)	O(3)–C(28)–O(4)	122.4(5)
O(4)–C(28)	1.314(6)		
Pd(3)–Cl(3)	2.295(1)	Cl(3)–Pd(3)–P(3′)	90.90(5)
Pd(3)–P(3)	2.337(2)	Cl(3)–Pd(3)–P(3)	89.10(5)
P(3)–C(35)	1.808(6)	C(35)–P(3)–C(29)	106.9(3)
P(3)–C(29)	1.807(5)	C(35)–P(3)–C(41)	107.0(3)
P(3)–C(41)	1.847(6)	C(29)–P(3)–C(41)	101.8(3)
O(5)–C(42)	1.264(9)	O(6)–C(42)–O(5)	124.4(7)
O(6)–C(42)	1.212(9)		
O(5)–O(8)	2.67(2)	O(1)–O(2′)	2.614(6)
O(7)–O(8)	2.91(2)	O(3)–O(4′)	2.686(5)
O(6)–O(8)	3.39(2)		

All P–Pd–P and Cl–Pd–Cl angles are exactly 180.0° as dictated by symmetry.

Symmetry transformations used to generate equivalent atoms: P(1′) $-x$, $-y+1$, $-z$; P(2′) $-x+1$, $-y$, $-z$; P(3′) $-x+1$, $-y+1$, $-z+1$; O(2′) $1-x$, $1-y$, z; O(4′) $-x$, $-y$, $-z$.

Table 3. Selected bond lengths (Å) and angles(°) for $[AuCl(Ph_2PCH_2CO_2H)]$

Au(1)–P(1)	2.220(2)	Au(1)–Cl(1)	2.270(3)
P(1)–C(1)	1.808(8)	C(14)–O(1)	1.237(10)
P(1)–C(7)	1.803(8)	C(14)–O(2)	1.265(11)
P(1)–C(13)	1.824(9)	C(13)–C(14)	1.514(12)
O(1)–O(2′)	2.618(9)		
P(1)–Au(1)–Cl(1)	179.0(1)	C(1)–P(1)–C(7)	106.6(4)
C(1)–P(1)–Au(1)	114.4(3)	C(7)–P(1)–C(13)	101.5(4)
C(7)–P(1)–Au(1)	113.4(3)	C(13)–P(1)–C(1)	106.4(4)
C(13)–P(1)–Au(1)	113.5(3)	O(1)–C(14)–O(2)	122.5(8)

Symmetry transformations used to generate O(2′): $1-x$, $1-y$, $2-z$.

metals *via* this part of the ligand but not excluding the likelihood of carboxylic acid hydrogen-bonding which is also present in the free acid [23]. The molybdenum tetracarbonyl complex exhibits four strong ν(CO) stretches as predicted for a *cis*-octahedral species, the frequencies being very similar to those of *cis*-$[Mo(CO)_4(PPh_3)_2]$ [24]. The copper(I) tris-ligand complex shows a ν(CuCl) stretch at 247 cm^{-1} which compares well with that of $[CuCl(PPh_3)_3]\cdot MeCN$ [21] at 249 cm^{-1}. A similar band for the mono-ligand complex has not been detected but would be below the lower limit of our spectrometer (200 cm^{-1}) if it possesses, as we believe on the basis of mass spectrometry evidence, a cubane-type $[CuCl(HA)]_4$ arrangement. The gold complex has ν(AuCl) at 335 cm^{-1}, a similar frequency [25] to that of linear $[AuCl(PPh_3)]$, 325 cm^{-1}. The palladium complex has one band which can be assigned to ν(PdCl) at 330 cm^{-1} whereas the platinum complex has two bands assignable to ν(PtCl) at 332 and 303 cm^{-1}. This is in line with the respective suggestions above of *trans*- and *cis*-square planar geometries and also in agreement with the known structure of *trans*-$[PdBr_2(HA)_2]$ [13] and the stereochemistry of the recrystallised material *trans*-$[PdCl_2(HA)_2]\cdot 0.33EtOH\cdot 0.33H_2O$ produced in this study.

Positive and negative ion FAB mass spectra have been obtained for all except the platinum compound. Generally only the major metal-containing positive ions are given in Section 2. One particularly novel fragmentation involves the decarboxylation of coordinated diphenylphosphinoacetic acid generating methyldiphenylphosphine as the successor ligand. As expected, stepwise loss of four carbonyl ligands is observed for the molybdenum complex. Both positive and negative ion fragments are listed for [CuCl(HA)] only, because significant fragment ions of correct isotopic distribution to be derived from Cu_4Cl_4 units are detected. This strongly suggests that a tetrameric cubane-type structure akin to that of $[CuCl(PPh_3)]_4$ or a step-type stucture as shown by $[CuBr(PPh_3)]_4\cdot 2CHCl_3$ is taken up [26, 27]. The mass spectrum of the gold complex contains few fragments but a dimer parent ion and the dimer less one chloride ligand are both detected in agreement with the solid state structure discussed below.

Recrystallisation of *trans*-$[PdCl_2(HA)_2]$ from ethanol gave crystals of *trans*-$[PdCl_2(HA)_2]\cdot 0.33EtOH\cdot 0.33H_2O$ showing rather different IR band frequencies to those of the unsolvated complex [e.g. $\nu_{asym}(CO_2)$ 1705, 1694 and $\nu_{sym}(CO_2)$ 1302 cm^{-1}]. The crystal stucture is quite involved, the asymmetric unit containing three half molecules of the complex together with one molecule each of water and ethanol, both at half site occupancy, i.e. 1 H_2O and 1 EtOH for every 3 palladiums. Three independent square planar *trans*-$[PdCl_2(HA)_2]$ species are present in the structure, all three metal atoms being located at inversion centres intrinsic to the space group symmetry. Fig. 1 shows a portion of the overall structure with the asymmetric unit delineated by those labelled atoms which are unprimed. Two of the *trans*-$[PdCl_2(HA)_2]$ units, those involving Pd(1) and Pd(2), are similar and are involved in the formation of a one-dimensional polymeric array along the *a* axis *via* two-fold hydrogen bonding to lattice neighbours through carboxylic acid groups (see Fig. 2). This form of hydrogen bonding is directly related to that found in carboxylic acids themselves,

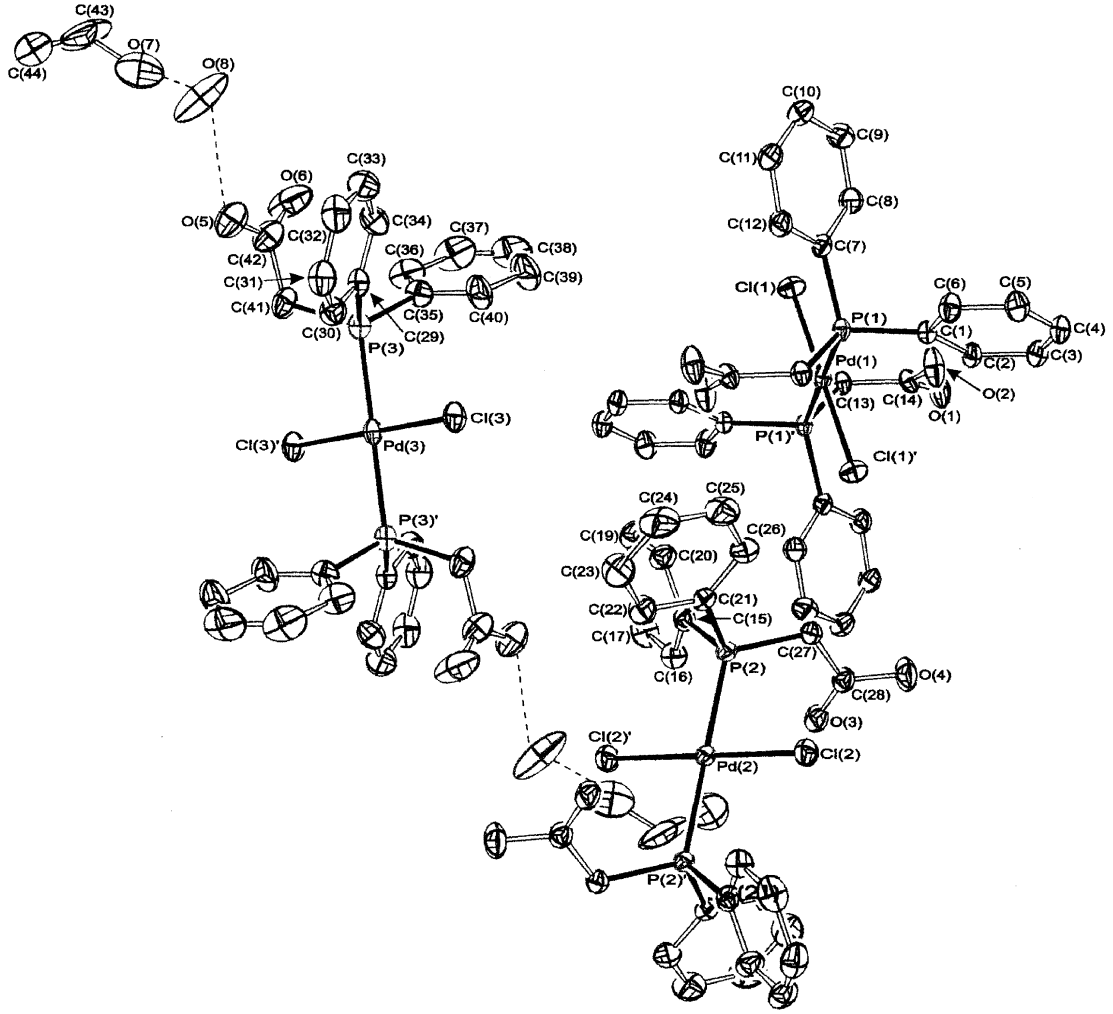

Fig. 1. The unit cell contents of $[PdCl_2(Ph_2PCH_2CO_2H)_2] \cdot 0.33EtOH \cdot 0.33H_2O$ showing the labelling scheme. The asymmetric unit comprises the atoms with unprimed labels. Thermal ellipsoids are at the 30% probability level.

e.g. acetic acid [28]. These polymers are stacked in the *b* direction and alternate between Pd(1)- and Pd(2)-containing molecules at half unit cell intervals. The *trans*-$[PdCl_2(HA)_2]$ moieties containing Pd(3) are different, (see Fig. 3). These molecules are not involved in carboxylic acid derived hydrogen bonding to generate polymeric arrays. Rather, discrete hydrogen-bonded entities are formed by interaction of the -OH of each carboxylic acid unit with the oxygen of each water molecule present. The water molecules are then further hydrogen-bonded to the ethanol solvent molecules. Given that the protons associated with $-CO_2H$, H_2O and ethanol hydroxyl groups could not be located in the crystallographic study, the presence of the various types of hydrogen bonding was inferred from short O . . . O distances.

Despite the fact that all three metal atoms are situated at inversion centres, thus rendering all P–Pd–P and Cl–Pd–Cl angles with a value of 180° where each metal centre is co-planar with its attached donor atoms, the metal centres have, nonetheless, slightly different coordination environments. For example, the three individual Pd–Cl bond lengths are quite consistent [2.295(1), 2.303(1) and 2.305(1) Å] whereas the Pd–P bond lengths vary significantly [2.326(1), 2.309(1) and 2.337(2) Å]. However, the mean of the Pd–P bond lengths exactly matches that determined for *trans*-$[PdBr_2(HA)_2]$, 2.332 Å [13]. Also, whereas the species containing Pd(3) has Cl–Pd–P angles close to the ideal 90° [89.10(5)°], the corresponding angles associated with Pd(1) and Pd(2) show some deviation [86.76(4) and 86.45(5)°, respectively]. Although a Pd . . . O separation of 3.171(6) Å was regarded as evidence of a weak additional interaction in the structure of *trans*-$[PdBr_2(HA)_2]$ [13], the shortest Pd . . . O contact in the present structure is 3.26 Å between Pd(1) and O(2) and we do not feel that this is significant. For all three molecules, the P–CH_2CO_2H bond lengths

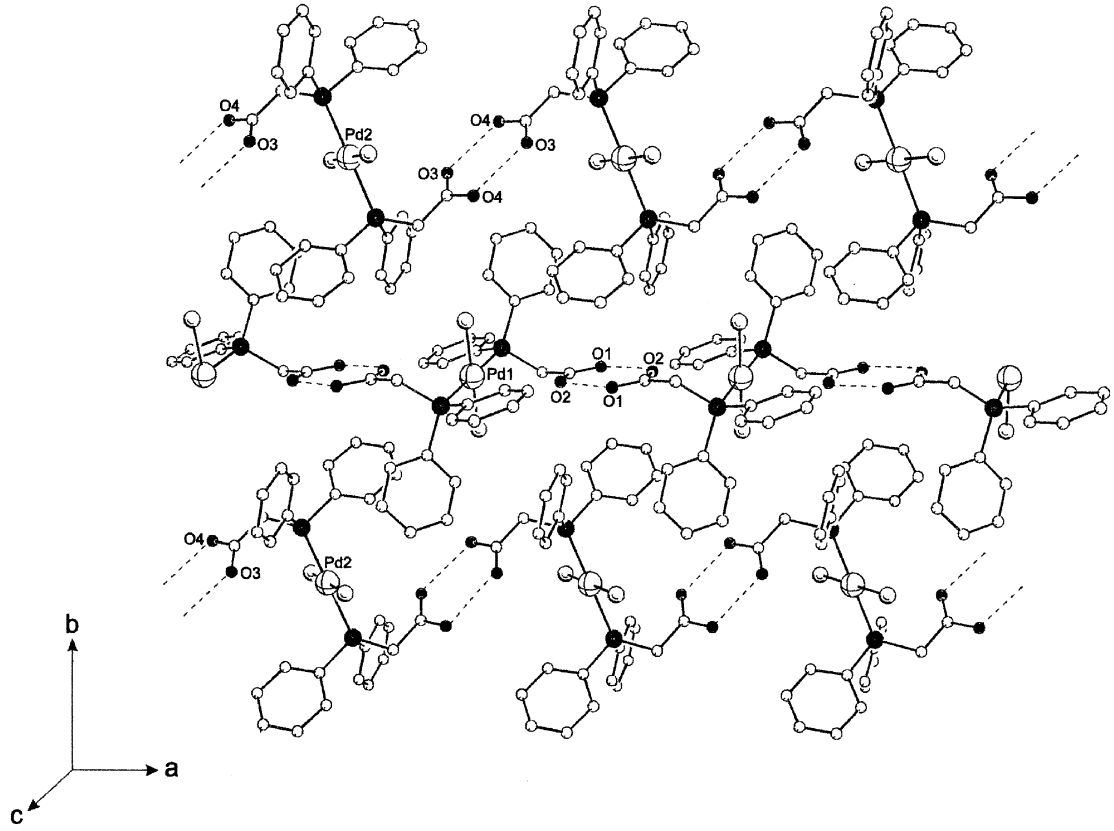

Fig. 2. View down the *c* axis of the palladium compound showing the one-dimensional chains formed by hydrogen bonded carboxylic acid groups.

are noticeably longer than the P–C(aryl) bond lengths, a feature much less apparent in *trans*-[$PdBr_2(HA)_2$]. Conversely, within the -CH_2CO_2H groups, the mean C–C bond length of 1.492 Å is rather shorter than that of *trans*-[$PdBr_2(HA)_2$] at 1.523 Å. The three molecules show quite different carboxylic acid C–O bond lengths, the distinction between the formal C–OH and C=O bonds being most obvious in the molecules containing Pd(2) [difference 0.099(6) Å], which is very similar to that of *trans*-[$PdBr_2(HA)_2$] [difference 0.095(9) Å] [13]. This difference is less significant in the molecules containing Pd(3) [difference 0.052(9) Å] and essentially absent in molecules containing Pd(1) [difference 0.007(6) Å]. This unexpected observation may relate to the type, degree of asymmetry and extent of the hydrogen bonding for each molecular species. Differences between the three molecules are also marked when the various Pd–P–C, P–C–C and C–P–C angles are considered, although details will not be given here. The O–C–O angles in each of the three molecules are slightly greater than 120° [122.4(4), 122.4(5) and 124.4(7)°], the largest angle being associated with molecules containing Pd(3).

The intermolecular hydrogen bonding involving molecules containing Pd(1) and Pd(2) generates two sets of one-dimensional polymeric chains (Fig. 2). The O . . . O distances of molecules involving Pd(2) centres, 2.686(5) Å, are similar to those found in *trans*-[$PdBr_2(HA)_2$] [13], *cis*-[PtBr(A)(HA)] [8], *cis*-[Rh(CO)(A)(HA)] [9] and, indeed, in the free acid [23], being 2.710(7), 2.620(6), 2.67 and 2.660(7) Å, respectively. The hydrogen bonding involved in linking molecules containing Pd(1) is of the same type with a slightly shorter O . . . O interaction of 2.614(6) Å. The hydrogen bonding associated with molecules containing Pd(3) does not generate a polymer as a consequence of only 50% site occupancy of the water and ethanol solvate molecules. The O . . . O contacts between O(5) of the complex containing Pd(3) and O(8) of H_2O and between O(8) of H_2O and O(7) of EtOH are 2.67(2) and 2.91(2) Å, respectively, the latter therefore indicating a much weaker form of hydrogen bonding than that of the carboxylic acid variety in the molecular structure. The final carboxyl oxygen, O(6) is unique among the six carboxylic acid oxygens in not being involved in intermolecular hydrogen bonding, as is evident from the long O(6) . . . O(8) separation of 3.39(2) Å.

In the complex [AuCl(HA)], the gold displays linear coordination [Cl–Au–P 179.0(1)°] with two individual molecules linked into a dimer (Fig. 4) again with two sets of O . . . O interactions of 2.618(9) Å, which are

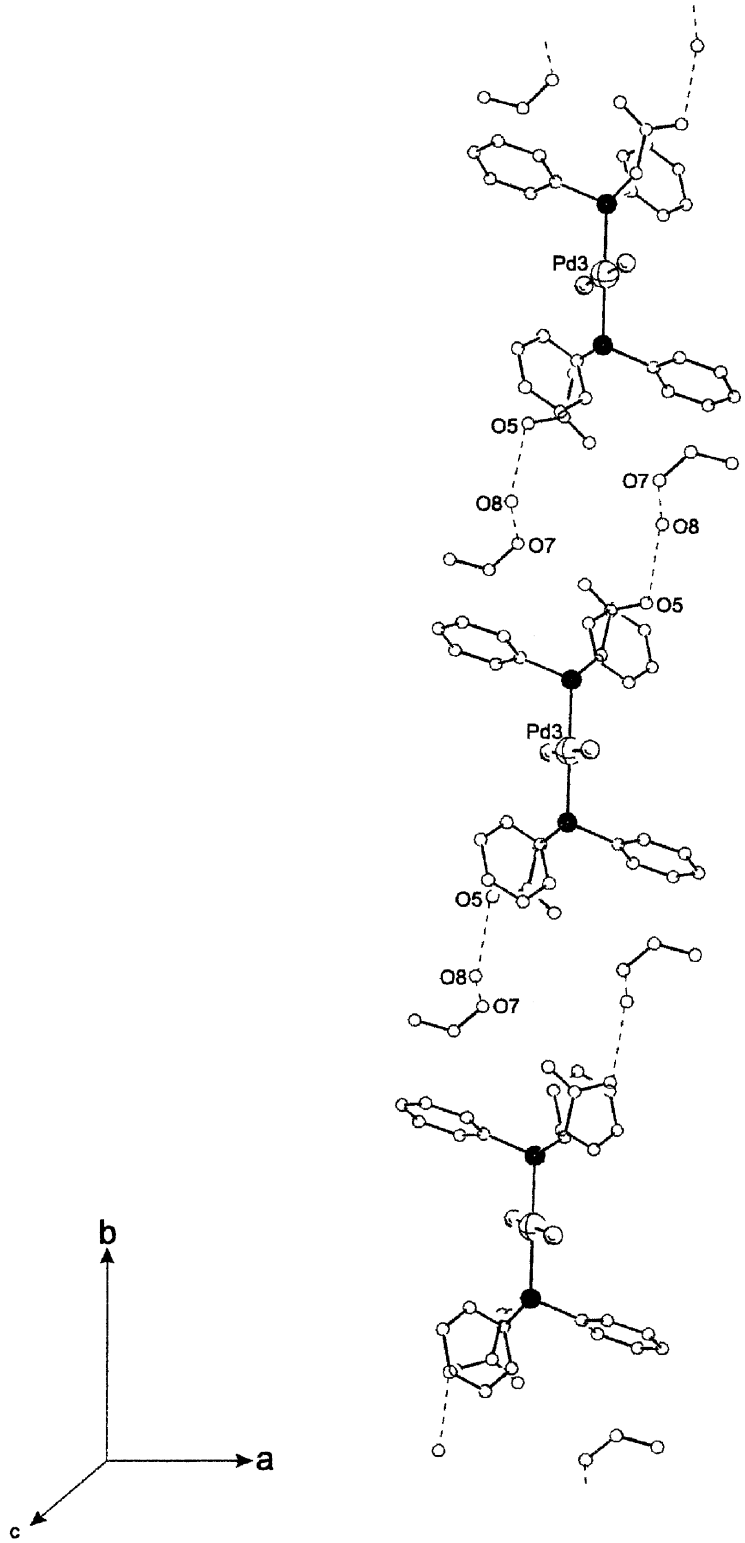

Fig. 3. View down the *c* axis of the palladium compound showing the discrete hydrogen bonding involving carboxylic acid, water and ethanol molecules. Only 50% occupancy of the positions of the solvent molecules is observed.

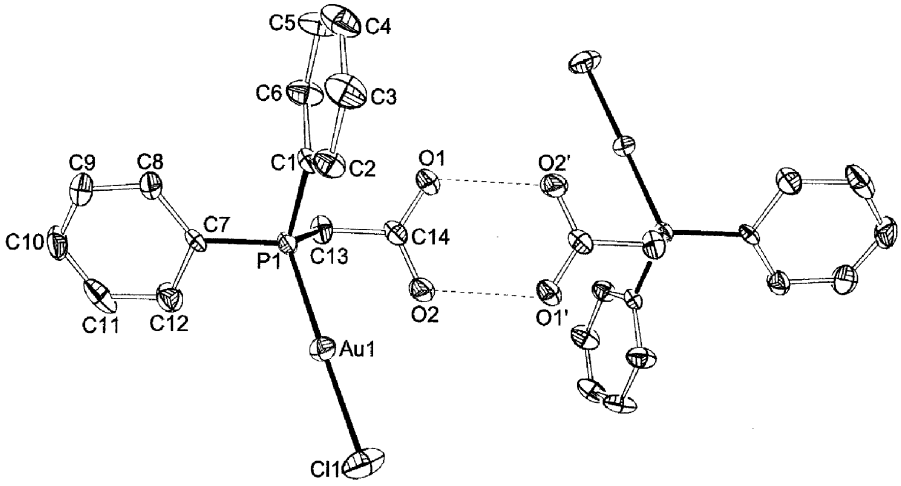

Fig. 4. ORTEX plot of the hydrogen bonded dimer of [AuCl($Ph_2PCH_2CO_2H$)] showing the labelling scheme. Thermal ellipsoids are at the 30% probability level.

slightly shorter than those for the palladium compound noted above. The individual C–O bond lengths of 1.237(10) and 1.265(11) Å suggest that the carboxylic acid protons are not quite symmetrically placed in the hydrogen bonding array, being more closely associated with O(2) rather than O(1). The hydrogen bonded dimers are formed by assembling neighbouring molecules in the lattice which are spatially related by an inversion centre. Typically, O(1) and O(2) of the molecule as presented are hydrogen bonded to O(2′) and O(1′), respectively, of the neighbouring molecule generated *via* the operator $1-x$, $1-y$, $2-z$. The OCO angle of 122.5(8)° compares to that of 122.2(4)° for the free acid [23] which displays a similar hydrogen bonding arrangement. The hydrogen bonding system holds the AuCl units well apart prohibiting intra-dimer aurophilic Au . . . Au contacts which have been identified in the structures of some linear gold(I) compounds [29].

The Au–Cl bond length of 2.270(3) Å is very similar to those of [AuCl(PPh_3)] [30] and [AuCl{$Ph_2PCH_2C(O)NHMe$}] [20] [2.279(3) and 2.275(2) Å, respectively] and the Au–P bond length of 2.220(2) Å also compares well with those of the above two complexes [2.235(3) and 2.221(1) Å, respectively]. The P–CH_2CO_2H bond length is, as found for the palladium complex, slightly longer than the P–C(aryl) bond lengths but the mean P–C bond lengths (1.812 Å) and C–P–Au and C–P–C bond angles (113.8 and 104.8°, respectively) are closely similar to those of [AuCl(PPh_3)] [30] (1.820 Å, 113.5° and 105.1°, respectively) showing that substitution of a phenyl ring for a -CH_2CO_2H group has little effect structurally, apart from the generation of an additional hydrogen bonding array.

Acknowledgements—We thank EPSRC for a maintenance grant (to T. J. P.).

REFERENCES

1. van Leeuwen, P. W. N. M. and Groeneveld, W. L., *Rec. Trav. Chim. Pays-Bas*, 1968, **87,** 86.
2. van Doorne, W. and Hannink, M., *Synth. React. Inorg. Metal-Org. Chem.*, 1981, **11,** 15.
3. Cramer, R. E., van Doorne, W. and Dubois, R., *Inorg. Chem.*, 1975, **14,** 2462.
4. Mohana Rao, J. K. and Viswamitra, M. A., *Acta Cryst. B*, 1972, **28,** 1484.
5. Klapotke, T. M., Kopf, H., Tornieporth-Oetting, I. C. and White, P. S., *Organometallics*, 1994, **13,** 3628.
6. Baidina, I. A., Podberezskaya, N. V., Borisova, S. V., Shestakova, N. A., Kuklina, U. F. and Malchikov, G. D., *Zhur. Strukt. Khim.*, 1979, **20,** 548.
7. Civis, S., Podlahova, J., Loub, J. and Jecny, J., *Acta Cryst. B*, 1980, **36,** 1395.
8. Hazell, A. C., Hazell, R. G., Kratochvil, B. and Podlahova, J., *Acta Cryst. B*, 1981, **37,** 2068.
9. Jegorov, A., Kratochvil, B., Langer, V. and Podlahova, J., *Inorg. Chem.*, 1984, **23,** 4288.
10. Jegerov, A., Podlaha, J., Podlahova, J. and Tureecek, F., *J. Chem. Soc. Dalton Trans.*, 1990, 3259.
11. Darensbourg, D. J., Draper, J. D. and Reibenspies, J. H., *Inorg. Chem.*, 1997, **36,** 3648.
12. Podlahova, J., Podlaha, J. and Cisarova, I., *Z. Krist.*, 1990, **192,** 67.
13. Podlahova, J., Loub, J. and Jecny, J., *Acta Cryst. B*, 1979, **35,** 328.
14. Podlahova, J., Kratochvil, B., Loub, J. and Paulus, H., *Acta Cryst. C*, 1986, **42,** 415.
15. Jarolim, T. and Podlahova, J., *J. Inorg. Nuclear Chem.*, 1976, **38,** 125.
16. McArdle, P., *J. Appl. Cryst.*, 1994, **27,** 438.
17. Sheldrick, G. M., *Acta Cryst. A*, 1990, **46,** 467.
18. Sheldrick, G. M., *SHELX*93, *A Computer Program for Crystal Structure Refinement*. University of Göttingen, 1993.
19. Pregosin, P. S. and Kunz, R. W., ^{31}P *and* ^{13}C *NMR*

of Transition Metal Phosphine Complexes. Springer-Verlag, Berlin, 1979.
20. Lange, P., Schier, A. and Schmidbaur, H., *Inorg. Chim. Acta*, 1995, **235,** 263.
21. Krauter, T. and Neumuller, B., *Polyhedron*, 1996, **15,** 2851.
22. Mann, B. E., Masters, C., Shaw, B. L., Slade, R. M. and Stainbank, R. E., *Inorg. Nucl. Chem. Lett*., 1971, **7,** 881.
23. Shkol'nikova, L. M., Masyuk, A. A., Dyatlova, N. M. and Podlahova, J., *Zhur. Strukt. Khim*., 1987, **28,** 156.
24. Cotton, F. A., *Inorg. Chem*., 1964, **3,** 702.
25. McAuliffe, C. A., Parish, R. V. and Randall, P. D., *J. Chem. Soc. Dalton Trans*., 1979, 1730.
26. Churchill, M. R. and Kalra, K. L., *J. Am. Chem. Soc*., 1973, **95,** 5772.
27. Barron, P. F., Dyason, J. C., Engelhardt, L. M., Healy, P. C. and White, A. H., *Inorg. Chem*., 1984, **23,** 3766.
28. Scheuerman, R. F. and Suss, R. L., *Acta Cryst*., 1962, **15,** 1244.
29. Schmidbaur, H., *Gold Bull*., 1990, **23,** 11.
30. Baenziger, N. C., Bennett, W. E. and Soboroff, D. M., *Acta Cryst. B*, 1976, **32,** 962.

Pergamon

Polyhedron Vol. 17, No. 23–24, pp. 4131–4138, 1998
© 1998 Elsevier Science Ltd
All rights reserved. Printed in Great Britain
0277–5387/98 $19.00+0.00

PII: S0277–5387(98)00220–4

Photoinduced intramolecular electron transfer in Schiff-base bridged Ruthenium(II)-quencher molecules

Chun-Ying Duan,[a]† Zhong-Lin Lu,[a] Xiao-Zeng You,[a] Zhong-Yuan Zhou,[b] Thomas C.W. Mak,[b] Qin Luo[c] and Jing-Ying Zhou[c]

[a]Coordination Chemistry Institute and The State Key Laboratory of Coordination Chemistry, Nanjing University, Nanjing, 210093, P. R. China

[b]Department of Chemistry, The Chinese University of Hong Kong, Hong Kong P. R. China

[c]The Laser Institute, Zhong-shan University, Guang-zhou, 5100275, P. R. China

(Received 11 November 1997; accepted 30 May 1998)

Abstract—A series of Schiff-base bridged polypyridine ruthenium(II)-quencher [here after abbreviated as Ru-Q] molecules have been prepared and characterized, where the functional groups Q were dimethylamino(-$N(CH_3)_2$, methyloxyl(–OCH_3), hydroxyl(–OH) and nitro group(NO_2). Steady state and time resolved luminescence measurements of these ruthenium complexes show that the luminescence properties of the Ru(II) MLCT excited state of Ru–OCH_3 is only slightly modified from that of $Ru(bpy)_3^{2+}$, whereas the quenchers group Q in the Ru–$N(CH_3)_2$, Ru–OH and Ru–NO_2 complexes can quench the yield and lifetime of the Ru MLCT emission. Electrochemistry measurement suggests that the quenching processes were the long-range intramolecular electron transfer reductive quenching for the Ru–OH and Ru–$N(CH_3)_2$ and oxidative quenching for the Ru–NO_2, respectively. Single crystal structure analysis of the Ru–$N(CH_3)_2$ complex revealed that the coordination geometry of the ruthenium is a slightly distorted octahedron with four nitrogen atoms of the two bipyridine molecule and two nitrogen atoms from the L-$N(CH_3)_2$ ligands, p-dimethylamionbenzaldehyde 4, 5-diazafluorene-9-hydrazone. The Ru–N distances are in agreement with those in the other polybipyridine ruthenium complexes. © 1998 Elsevier Science Ltd. All rights reserved

Keywords: Crystal structure; ruthenium(II) complexes; quenching process; electron transfer

Over the last 30 years, a considerable amount of effort has been devoted to probe the mechanism of long range electron transfer, and detailed theoretical treatments have gradually emerged [1–3]. However, experiments have been hampered by the inherent difficulties of designing systems in which each variable can be controlled independently. In comparison to the numerous studies that have focused on the distance dependence of ET rates[4–10], little quantitative information regarding the reaction driving force is available.

In order to gain better understanding of the ET fundamentals in such systems we have designed and synthesized a series of molecules containing an inorganic chromophore and an organic quencher, separated by a long range bridging ligand [11, 12]. In most of these complexes, tris(2, 2′-bipyridine) ruthenium was always chosen as the chromophore, since it can demonstrate the combined attributes of a significantly absorption in the visible spectral region, the relative longevity of the metal-to-ligand charge transfer and capture of the metal center in a variety of oxidation states and the rapidity of the redox reactions involving the excited state (quench). The lowest excited state properties of the complexes of this gene are controlled by the pattern of low-lying electronic levels which are ligand-dependent [13–15]. By changing the ligand around the ruthenium center, it is possible to "fine tune" the redox and photophysical properties of the ground and excited states of these polypyridinyl ruthenium(II) complexes.

†Author to whom correspondence should be addressed.

The Ru-Q systems (see Scheme) described here

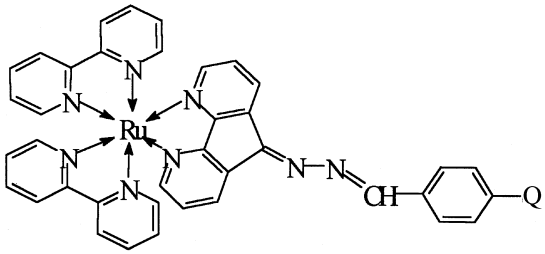

possess several features relevant to the study of intramolecular photoinduced electron transfer phenomenon, the most important of which is that the direction and free energy of electron transfer can be controlled simply by changing the redox potential of the functional group Q. This not only allows for the study of electron transfer versus transfer mechanism in fine details, but also offers the opportunity to more fully explore the interplay between the reaction driving force and the electron transfer rate [1, 13].

EXPERIMENTAL

Physical measurements

Elemental analyses were performed on a Perkin–Elmer 240C analytical instrument. IR spectra were recorded on a Nicolet FT-IR-170SX instrument (KBr discs) in the 4000–400 cm^{-1} range. The solution electronic spectra were obtained on a Shimadzu 240 spectrophotometer in CH_3CN solution. ^{1}H-NMR spectra were recorded on a Bruker Aspect AM300 spectrometer at ambient temperature in DMSO-d_6 using TMS as an internal reference.

Preparations

4,5-diazafluorene-9-hydrazine and $[Ru(bpy)_2Cl_2]\cdot {}_2H_2O$ were prepared according to the literature [16, 17]. All other chemicals were reagent grade and used without further purification.

p-Dimethylaminobenzaldehyde 4, 5-*diazafluorene*-9-*hydrazone* (L–$N(CH_3)_2$)

4–5 drops of acetic acid were added to an ethanol solution of 4,5-diazafluorene-9-hydrazine (1.0 mmol, 0.196 g) and p-dimethylaminobenzaldehyde (1.0 mmol, 0.89 g). A red solid formed after refluxing for 3 hours was isolated. Yield 0.31 g (90%). Anal. calcd for $C_{20}H_{17}N_5\cdot H_2O$: C, 69.5; H, 3.5; N, 20.3. Found: C, 69.0. H, 3.2; N, 19.7. IR(cm^{-1}): ν(C═N) 1628, 1564; ν(C═C), 1508, 1397; δ(C–H) 750(diazafluorene), 695(phenyl). ^{1}H-MNR, 8.74(*s*, 1H, N═CH); (4,5-diazafluorne ring): 9.00(*d*, 1H), 8.75(*d*, 1H), 8.73(*d*, 1H), 8.26(*d*, 1H), 7.55(*t*, 1H), 7.53(*t*, 1H); (phenyl ring) 7.90(*d*, 2H), 6.87(*d*, 2H); methyl group: 2.17(*d*, 6H). Uv-vis(nm) (logϵ). 248(2.14), 325(2.19).

p-Methoxylbenzaldehyde 4,5 *diazafluorene*-9-*hydrazone* (L-OCH_3)

The compound was synthesized by similar procedure but by using p-methoxylbenzaldehyde (1.0 mmol, 0.136 g) instead of p-dimethylaminobenzaldehyde, yield 0.24 g(85%) of yellow solid. Anal. calcd for $C_{19}H_{14}N_4O$: C, 68.6. H, 4.8; N, 16.7. Found: C, 69.0; H, 4.6; N, 16.4. IR (cm^{-1}) ν(C═N) 1605, 1565; ν(C═C), 1512, 1395, ν(C–O) 1153, 1060, δ(C–H) 749 (diazafluorene), 693(phenyl). ^{1}H-NMR, 8.69(*s*, 1H, N═CH); (4,5-diazafluorne ring) 8.97(*d*, 1H), 8.71(*d*, 1H), 8.69(*d*, 1H), 8.33(*d*, 1H), 7.53(*t*, 1H), 7.48(*t*, 1H); (phenyl ring) 7.96(*d*, 2H), 7.11(*d*, 2H); methyl group: 2.63(*d*, 3H) Uv-vis(mm) (logϵ) 254(1.69), 377(2.75).

p-Hydroxylbenzaldehyde 4,5-*diazafluorene*-9-*hydrazone* (L-OH)

The compound was synthesized by similar procedure but by using p-hydroxylbenzaldehyde (1.0 mmol, 0.14 g) instead of p-dimethylaminobenzaldehyde. Yield 0.25 g(87%) of orange solid. Anal. calcd for $C_{18}H_{12}N_4O\cdot H_2O$: C, 67.9; H, 4.4; N, 17.6. Found: C, 68.2; H, 4.6; N, 17.1 IR(cm^{-1}) 1615, 1565, ν(C═C), 1504, 1395; ν(C–O), 1020; δ(C–H) 753 (diazafluorene), 705 (phenyl). ^{1}H-NMR: 8.69(*s*, 1H N═CH); (diazafluorne ring) 9,04(*d*, 1H), 8.71(*d*, 1H), 8.68(*d*, 1H), 8.36(*d*, 1H), 7.54(*t*, 1H), 7.47(*t*, 1H), (phenyl ring) 7.90(*d*, 2H), 6.96(*d*, 2H). Uv-vis(nm) (logϵ) 252(1.60), 282(2.80)

p-Nitrobenzaldehyde 4,5-*diazafluorene*-9-*hydrazone* (L–NO_2)

The compound was synthesized by similar procedure but by using p-Nitrobenzaldehyde (1.0 mmol, 0.15 g) instead of p-dimethylaminobenzaldehyde, yield 0.28 g (90%) of yellow product, Anal. calcd for $C_{18}H_{11}N_5O_2\cdot H_2O$: C, 62.2; H, 3.8; N, 20.2. Found: C, 62.5; H, 4.0; N, 19.8. IR (cm^1) ν(C═N) 1598, 1565, ν(C═C), 1508, 1394, ν(N–O), 1394. δ(C–H) 750 (diazafluorene), 695 (phenyl). ^{1}H-NMR: 8.69(*s*, 1H N═CH), (diazafluorne ring) 9,03(*d*, 1H), 8.72(*d*, 1H), 8.67(*d*, 1H), 8.32(*d*, 1H), 7.51(*t*, 1H), 7.47(*t*, 1H); (phenyl ring) 7.80(*d*, 2H), 6.97(*d*, 2H). Uv-vis(nm) (logϵ). 252(2.71), 262(2.48)

Ru–$N(CH_3)_2$)

To an ethanol solution of $[Ru(bpy)_2Cl_2]\cdot {}_2H_2O$ (2 mmol, 1.04 g) was added ligand L-$N(CH_3)_2$ (2.2 mmol, 0.56 g). After refluxing under nitrogen for 8 h in the dark, the mixture was filtered into a methanol solution containing 0.4 g hexafluoro-

phosphate. The dark-brown solid formed was isolated and dried under vacuum. Yield: 1.6 g(75%). Anal. calcd. for $C_{40}H_{33}N_9RuP_2F_{12}$ C, 46.6; H, 3.2; N, 12.2. Found: C, 46.6; H, 3.5: N, 12.0. IR(cm^{-1}): ν(C═N) 1628, 1564; ν(C═C), 1508, 1397; ν(PF), 842; ν(C–H), 750 (diazafluorene), 695 (phenyl); ν(Ru–N), 558. ^{1}H-NMR 8.87(*s*, 1H, N═CH); (bipyridine ring): 8.55(*d*, 2H), 8.40(*d*, 2H), 8.28(*t*, 2H), 8.24(*t*, 2H), 7.97(*t*, 2H), 7.93(*t*, 2H), 7.65(*d*, 2H), 7.62(*d*, 2H); (4.5-diazafluorne ring): 9.08(*d*, 1H), 8.87(*d*, 1H), 8.85(*t*, 1H), 8.45(*d*, 1H), 7.74(*t*, 1H), 7.47(*d*, 1H); (phenyl ring): 8.02(*d*, 2H), 6.91(*d*, 2H); methyl: 2.17(*d*, 6H). Uv-vis(nm) (logϵ). 215(3.00), 234 (3.66), 284(6.26), 440(2.94).

Ru–OCH_3

The compound was prepared according to same procedure using ligand (L-OCH_3) (0.73 g, 2.2 mmol) instead of ligand L-N(CH_3)$_2$. Yield 1.5 g(76%). Anal. calcd for $C_{39}H_{3O}F_{12}N_8OP_2Ru \cdot H_2O$: C, 45.22; H, 3.11; N, 10.82. Found: C, 45.20; H, 2.98; N, 10.47. IR(cm^{-1}): ν(C═N) 1605, 1560; ν(C═C), 1512, 1412; ν(C–O) 1163, 1023; ν(P–F), 840; δ(C-H), 742(diazafluorene), 685 (phenyl); ν(Ru–N), 557. ^{1}H-NMR, 8.83(*s*, 1H, N═CH); (bipyridine ring): 8.48(*d*, 2H), 8.30(*d*, 2H), 8.13(*t*, 211), 8.08(*t*, 2H), 8.02(*t*, 2H), 7.62(*t*, 2H), 7.59(*d*, 2H), 7.47(*d*, 2H) (4, 5-diazafluorne ring): 8.88(*d*, 1H), 8.87(*d*, 1H), 8.85(*t*, 1H), 8.45(*d*, 1H), 774(*t*, 1H), 8.47(*d*, 1H); (phenyl ring): 8.02(*d*, 2H), 6.91(*d*, 2H); methyl: 2.67(*d*, 3H). Uv-vis(nm) (logϵ). 215(3.00), 234(3.66), 284(6.26), 440(2.94).

Ru–OH

The compound was prepared according to same procedure using ligand (L-OH) (0.71 g, 2.2 mmol) instead of ligand L-N(CH_3)$_2$. Yield 1.4 g(72%). Anal. calcd. for $C_{38}H_{28}F_{12}N_8OP_2Ru \cdot H_2O$: C, 44.7; H, 2.9; N, 10.9. Found: C, 45.0; H, 3.3; N, 10.3. IR(cm^{-1}): ν(C═N) 1604, 1587; ν(C═C), 1512, 1419; ν(C–O) 1168; ν(P–F), 843; δ(C–H), 741(diazafluorene), 692(phenyl); ν(Ru–N), 558. ^{1}HNMR, 8.80(*s*, 1H, N═CH); (bipyridine ring): 8.50(*d*, 2H), 8.45(*d*, 2H), 8.14(*t*, 2H), 8.07(*t*, 2H), 7.98(*t*, 2H), 7.61(*t*, 2H), 7.45(*d*, 2H), 7.37(*d*, 2H); (4, 5-diazafluorne ring): 8.84(*d*, 1H), 8.50(*d*, 1H), 8.46(*t*, 1H), 8.29(*d*, 1H), 7 53(*t*, 1H), 7.45(*d*, 1H); (phenyl ring): 7.89(*d*, 2H), 7.01(*d*, 2H); Uv-vis(nm) (logϵ) 210(3.13), 235(3.88), 282(6.37), 385(2.94), 412(2.93).

Ru–NO_2

The compound was prepared according to same procedure using ligand (L-NO_2) (0.77 g, 2.2 mmol) instead of ligand L-N(CH_3)$_2$ Yield 1.8 g(85%). Anal. calcd. for $C_{38}H_{28}F_{12}N_8OP_2Ru \cdot H_2O$: C, 44.7; H, 2.9; N, 10.9. Found: C, 45.0; H, 3.3; N, 10.3. IR(cm^{-1}): ν(C═N) 1604, 15893, ν(C═C), 1520, 1417; ν(N–O) 1345; ν(P–F), 841; δ(C–H), 762(diazafluorene), 672(phenyl), ν(Ru–N), 558. ^{1}H-MNR, 8.97(*s*, 1H, N═CH); (bipyridine ring): 8.82(*d*, 2H), 8.50(*d*, 2H), 8.23(*t*, 2H), 8.12(*t*, 2H), 7.96(*t*, 2H), 7.73(*t*, 2H), 7.55(*d*, 2H), 7.36(*d*, 2H). (4, 5-diazafluorne ring): 8.84(*d*, 1H), 8.60(*d*, 1H), 8.42(*t*, 1H), 8.29(*d*, 1H), 7.61(*t*, 1H), 7.52(*d*, 1H); (phenyl ring): 7.87(*d*, 2H), 7.15(*d*, 2H); Uv-vis(nm) (logϵ). 208(2.58), 236(4.01), 285(6.58), 390(2.80), 430(1.00).

Electrochemistry

Differential-pulse voltammetry was done with an EG and GPAR model 273 instrument, which has a 50 ms pulse width, with current sampled 40 ms after the pulse was applied. A sweep rate of 2 mV/s was used in all pulse experiments with a drop time of 0.5 s. Cyclic voltammetry were also performed using EG and GPAR model 273 potentiostats in a three-electrodes cell. The cell was fitted with purged N_2 inlet and outlet and comprise of a platinum-wire working electrode, a platinum auxiliary electrode and a Ag/AgCl reference electrode. Current-potential curves were displayed on am IBM computer using model 270 electrochemical analysis software. Data were recorded on a Hewlett-Packard recorder. The voltammograms of the complexes were obtained in dichloromethane with n-Bu_4NClO_4 (0.1 mol dm^{-3}) as the electrolyte.

Caution! Although no problems were encountered in this work, the salt perchlorates are potentially explosive. They should be prepared in small quantities and handled with care.

Luminescence studies

Steady luminescence intensities were measured on Perkin Elmer LS50 spectrofluometer in acetonitrile at room temperature with irradiation at 440 nm. Sample concentrations were $\approx 1 \times 10^5$ M. The Uv-vis absorption spectra of the solutions used in luminescence experiments were measured before and after the collection of steady state and time resolved data. In every case the spectra were identical before and after the experiments, indicating that sample degradation did not occur during data acquisition. Emission intensities for vacuum degassed solution of all the four complexes were measured with respect to Ru(bipy)$_3$(ClO_4)$_2$ in CH_3CN solution (concentration $= 1.0 \times 10^{-5}$ M, $\phi_{em} = 0.062$) [13]. Correction was made for the difference in absorption of the sample at the excited wavelength.

Time-resolved emission decay were measured following excitation by a FL2002 dye laser pumped by an EMG 201 quasimolecular laser. Lasing at 450 nm was achieved by coumarine 460(Excitation). Emission was monitored at right angle to the excitation by using a Hamamastsu R3896 PMT (photo multiplier tube) coupled to a Macpherson 272 scanning mono-

chromator. The output of the PMT was processed by a Lecroy 7200A transient digitizer interfaced to an IBM-PC. Transient decays were fitted to single-exponential functions.

Crystallography

A prismatic crystal with dimensions of $0.34 \times 0.18 \times 0.12$ of Ru–N$(CH_3)_2$ was mounted on a glass fibre and used for data collection. Cell constants were obtained by least-square refinements on the 275 reflections in the range $2\theta_{max} = 55.0^\circ$. The intensities were collected at 294 K on a Rigaku RAXIS-IIC imaging-plate diffractmeter using MoKα radiation ($\lambda = 0.71073$ Å) from a rotating-anode generator operating at 50 kV and 90 mA ($2\theta_{max} = 55.0^\circ$) with 60 oscillation frames and in the range of $0 \sim 180^\circ$, exposure 8 min per frame [18, 19]. Absorption corrections were made using the ABSCOR program based on Fourier-coefficient fitting to the intensities of symmetry-equivalent reflections [20].

The Ru–N$(CH_3)_2$, $C_{40}H_{33}N_9Ru\ P_2F_{12}$ was crystallized in triclinic space group P-1 with cell dimensions of $a = 18.353(1)$, $b = 19.761(1)$, $c = 13.450(1)$ Å, $\alpha = 100.29(1)$, $\beta = 97.43(1)$, $\gamma = 90.44(1)$, $V = 4757(2)$Å, $Z = 4$, $Mr = 1010.8$, $Dc = 1.439\ gcm^{-3}$. The structure was solved by the direct methods. All non-hydrogen atoms were refined anisotropically by full-matrix least-squares method. Hydrogen atoms of the ligand and solvent molecule were placed in calculated positions (C–H 0.96 Å), assigned fixed isotropic thermal parameters and allowed to ride on their respective parent atoms. The contributions of these hydrogen atoms were include in the structure-factor calculations. Of 16455 reflection measured, 7662 were unique (Rint = 0.09%) and used in the structure determination and refinement. Final cycles of refinement converged with discrepancy indices of $R = 0.073$ and $R_w = 085$, with the weighting scheme being $[\sigma^2(F) + 0.0003F^2]^{-1}$. The Goodness of Fit is 1.33. The final difference Fourier map revealed only one peak above $1e/Å^3$, lying 0.85 Å from Ru(1). A maximum shift and shift/esd in the final cycles were 0.009 and 0.006, respectively. The atoms in two of the PF_6 anions were disordered and were refined with s.o.f = 0.5 for F(11), F(12), F(13), F(11′), F(12′) and F(13′); P(5), F(52) and F(54); and s.o.f = 0.25 for F(51), F(53), F(55), F(56), F(51′), F(53′), F(55′) and F(56′).

All computation were carried out on a PC-486 computer using the SHELXL-PC program [21] package. Additional materials available from the Cambridge Crystallographic Data Center comprise of the complete lists of atomic coordinates, thermal parameters and bond lengths and angles.

RESULTS AND DISCUSSION

Synthesis and spectral characterization

The ligands (see Scheme) were prepared by treating 4,5-diazafluorene-9-hydrazone with equivalent substituted benzaldehydes in refluxing ethanol solution. On refluxing of the $[Ru(bpy)_2Cl_2]\cdot 2H_2O$ with 1:1 molar equivalent of the ligands in ethanol and with purged nitrogen gas inlet and outlet, the corresponding ruthenium(II) complexes were produced.

IR spectra of the ligand and ruthenium complexes are consistent with their structures, the bands near $1620\ cm^{-1}$ for free ligand and Ru(II) complexes can be assigned to C═N vibration of conjunction π system, the band at *ca* $760\ cm^{-1}$ is safely assigned to the δ(C–H) of the bipyridine and the 4,5-diazaflorene ring. The band at *ca* $560\ cm^{-1}$ which is not present in the IR spectra of the ligand is assigned to the Ru–N (bipy) stretching vibration of *cis*-configuration. The bands due to PF^-_6 and water molecules are present at $840\ cm^{-1}$ and $3400\ cm^{-1}$ respectively.

Proton NMR spectroscopy can play an important role in determining the purity and coordination geometry of ruthenium complexes. For the free ligands, it should be noted that there are six types of protons in the 4,5-diazafluorene ring, indicating the asymmetrical electron density on the two pyridine rings. The two multiplets can be assigned to the protons in the *m*-position of the azonitrogen atoms. Two doublets are assigned to the protons next to the azonitrogen atoms, while other doublets at the lower field should be assigned to the protons near hydrazone moieties. After formula complexes, the chemical shift of azomethine proton shifted to lower field [22, 23]. However, it is very difficult to assign each proton precisely.

The free ligands show two distinctive bands near 250 nm and 270 nm in the Uv-vis spectra, which can be assigned to the transition of $\pi \rightarrow \pi^*$ of the larger π-conjugated system in the these compounds. The π^* levels of bpy and ligand are at different energies. For the ruthenium complexes, new bands at *ca* 450 nm and 243 nm might be assigned to the charge transfer from the filled $d\pi$ (Ru^{II}) levels to low lying π^* (ligand levels) [26, 27] as $d\pi \rightarrow \pi_1^*$ and $d\pi \rightarrow \pi_2^*$, respectively. The broadening of the band at *ca* 450 nm might be contributed to the significant triplet character coupled in single MLCT transition and the mixing of separated MLCT transitions occurring in the Schiff-base ligand and the bipyridine molecules [26, 27].

Steady state and time-resolved luminescence spectra

Table 1 contains a summary of emission maxima and relative quantum yields of the Ru complexes in vacuum degassed CH_3CN solution. It is interesting to note that the emission energy and band shapes (Fig. 1) are nearly identical for each of the complexes indicating that the luminescence is from a $d\pi$ Ru$\rightarrow\pi^*$ bpy MLCT excited state like that of $Ru(bpy)^{2+}_3$ [28–30]. However, a number of distinctive differences between $Ru(bpy)^{2+}_3$ and the complexes are also observed: firstly, the emission maxima of the complexes are found at lower energy than that of $Ru(bpy)^{2+}{}_3$ and

Table 1. The lifetime, quantum yield, emission wavelength and the redox potentials

Complex	$E_{Ru(III)/Ru(II)}$	[a]$E_{1/2}$	$E_{Ru(II)/Ru(I)}$	E^{0-0}	[b]λ_{em}(nm)	Φ_{em}	τ_0(ns)
[c]$Ru(bpy)_3^{2+}$	1.27		−1.13	2.10	626	0.062	920
$Ru–N(CH_3)_2$	1.30	0.83	−1.15	2.06	686	0.010	265
$Ru–OCH_3$	1 29		−1.12	2.05	691	0.041	605
Ru–OH	1.33	0.73	−1.13	2.14	688	0.002	169
$Ru–NO_2$	1.33	−0.69	−1.21	2.10	686	0.012	223

[a]Redox potential (vs AgCl/Ag) were measured in acetontrilc (1.0×10^{-3} M) 0.1 M Bu_4NClO_4 as electrohyte with scaning rate 50 mV/s

[b]measured under the stead state, excited at 440 nm in acetontrile (1.0×10^{-5} M)

[c]Ref: [13].

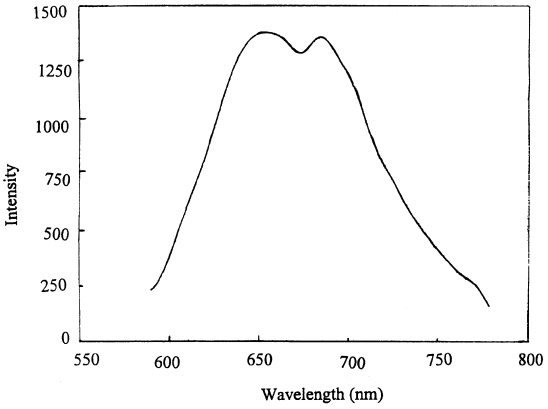

Fig. 1. The Emission spectrum of $Ru–N(CH_3)_2$ (excited at 440 nm in acetontrile).

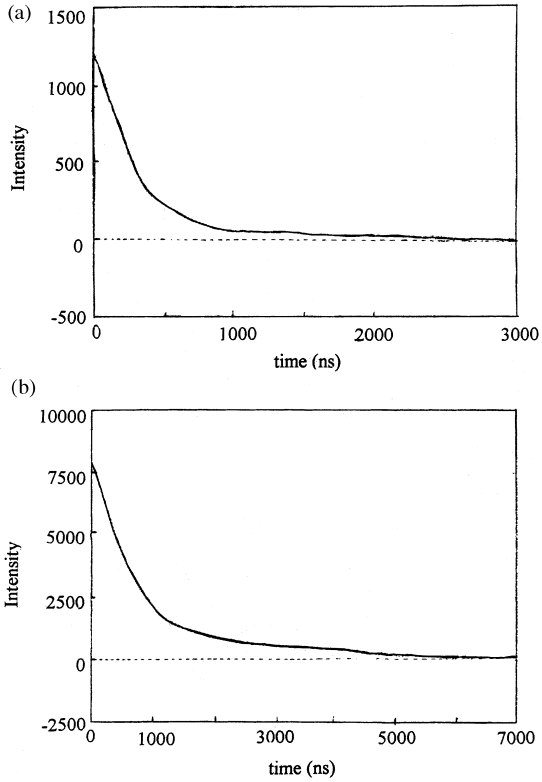

Fig. 2. Time-resolved emission spectral measured at 686 nm for $Ru–OCH_3$ (a) and $Ru–N(CH_3)_2$(b).

shows one shoulder near 685 nm; secondly the quantum yield became smaller and are dependent on the substitution of the phenyl ring. These differences might be contributed to the quenching of the MLCT excited state of ruthenium moieties by the functional group Q. However, considering the much higher quantum yield of the CH_3O substituted ruthenium complex than the other ruthenium complexes, it can be suggested that the CH_3O functional group does not quench the MLCT excited state. This suggestion is also consistent with the predictions from the electrochemical experiments. The lower quantum yield noted for the $Ru–OCH_3$ relative to $[Ru(bpy)_2(phen)]^{2+}$ [13] is attributed to an effect of the long π-system upon the nonradiative decay rate of MLCT excited state.

Table 1 also listed the lifetimes of the MLCT luminescence for the four ruthenium(II) complexes $Ru(bpy)^{2+}{}_3$. The decay plot of the Ru-OCH_3 [Fig. 2(a)] is described well by a single exponential function with a lifetime of 620 ns. The lowering in quantum yield of the Ru-OCH_3 complex compared to that of $Ru(bpy)^{2+}{}_3$ is likely due to an effect of the OCH_3 group upon the non-radiative decay rate of the Ru MLCT excited state [31]. The experimental emission decays of the other ruthenium complexes are fitted using single-exponential functions, e.g. that for the $RuN(CH_3)_2$ is shown if Fig. 2(b). The emission lifetimes of the three complexes, which range from 350 to 150 ns, are all lower than those of $Ru–OCH_3$. The attenuation in emission lifetimes observed for the three Ru-Q complexes is attributed to quenching of the Ru MLCT excited state by intramolecular electron transfer between the Ru moiety and the functional group Q.

Mechanism of intramolecular electron transfer

Based on the quantum yield and the emission lifetime of these Ru-Q complexes, it is clear that the Ru MLCT excited state are efficiently quenched by the functional group, $-N(CH_3)_2$, –OH and $-NO_2$. Several possible quenching mechanisms must be considered: first, these Ru-Q complexes might undergo intermolecular electron transfer, but this possibility is unlikely, since the experiments are done at very low concentration and the observed quenching rate is too rapid to be ascribed to a bimolecular reaction, second quenching mode of the Ru MLCT excited state may involve energy transfer from ruthenium moieties to the functional group, however, this pathway is also considered unlikely because the spectral overlap between the Ru MLCT emission and absorption of the Schiff-base ligands is so small that energy transfer emission *via* coulombic mechanism can be effectively ruled out [32]; further evidence against an energy transfer mechanism in this system is provided by the sensitivity of the quenching rate to the redox potentials of the functional group Q. For these reasons, we believe that quenching occurs by intramolecular electron transfer.

Cyclic voltammetry and differential-pulse voltammetry of the four ruthenium complexes reveal that the first oxidation and reducation potentials for the Ru center common to each of the complexes are at *ca* 1.30 and -1.15 V(vs AgCl/Ag) on the average (Table 1). According to the emission and Uv-vis spectra of these ruthenium complexes, the MLCT excited state energy of these complexes can be calculated [12] as *ca.* 2.1 eV in an average (Table 1), which is compared to the MLCT excited state energy of $Ru(bpy)^{2+}{}_3$ (2.1 eV) [33] the average excited state potentials might be calculated as $E_{1/2}LRu(III)/*Ru(II)] = -0.80$ V, $E_{1/2}[*Ru(II)/Ru(II)] = 0.95$ V [34]. It follows that the *Ru MLCT is at the same time a good electron acceptor and a good electron donor (eq. 1) Table 2

$$*Ru(II) + Q \rightarrow Ru(III) + Q^{-} \text{ oxidative quenching}$$

$$*Ru(II) + Q \rightarrow Ru(I) + Q^{+} \text{ reductive quenching}$$

These potentials also indicates that an electron acceptor with a reduction potential > -0.80 V or an electron donor with an oxidation potential > 0.95 V will quench the MLCT excited state by electron transfer.

Cyclic voltammetry on the $Ru–OCH_3$ complex reveals that the CH_3O- functional group is not redox active within the potential -1.0 V to $+1.0$ V. This indicates that the CH_3O- functional group cannot quench the Ru MLCT excited state by thermodynamically favorable electron transfer.

Cyclic voltammetry of the $Ru–N(CH_3)_2$ and Ru–OH complexes reveals that in addition to the characteristic waves for the Ru complex, an irreversible cathodic wave is observed at Ep = 0.85 V and 0.76 V for the $–N(CH_3)_2$ and –OH functional group, respectively. The irreversibility indicates that the chemical reactions of the functional group are significant on the tune scale of the electrochemical experiment. Under these conditions the peak potential for the observed wave only approximates the true thermodynamic potential for the electrode process. However, differential pulse voltammetry reveals that the $E_{1/2}$ for the two oxidation reactions are 0.83 and

Table 2. Selected bond lengths (Å) and bond angles (°) of the ligand* $L–N(CH_3)_2$ and the ruthenium complex $Ru–N(CH_3)_2$

$L–N(CH_3)_2$		$Ru–N(CH_3)_2$			
		Bond distances			
		Ru(1)–N(11)	2.065(5)	Ru(2)–N(21)	2.056(4)
		Ru(1)–N(12)	2.038(4)	Ru(2)–N(22)	2.048(4)
		Ru(1)–N(13)	2.048(4)	Ru(2)–N(23)	2.049(4)
		Ru(1)–N(14)	2.060(4)	Ru(2)–N(24)	2.050(4)
		Ru(1)–N(15)	2.149(4)	Ru(2)–N(25)	2.122(4)
		Ru(1)–N(16)	2.105(5)	Ru(2)–N(26)	2.123(4)
C(31)–N(17)	1.295(3)	C(31)–N(17)	1.323(7)	C(71)–N(27)	1.273(6)
N(17)–N(18)	1.401(3)	N(17)–N(18)	1.376(5)	N(27)–N(28)	1.388(6)
N(18)–C(32)	1.295(3)	N(18)–C(32)	1.293(7)	N(28)–C(72)	1.290(7)
		Bond angles			
		N(11)–Ru(1)–N(12)	79.6(2)	N(21)–Ru(2)–N(24)	173.9(2)
		N(11)–Ru(1)–N(14)	175.2(2)	N(21)–Ru(2)–N(22)	79.5(2)
		N(13)–Ru(1)–N(15)	171.8(2)	N(23)–Ru(2)–N(24)	79.0(2)
		N(13)–Ru(1)–N(14)	79.2(2)	N(23)–Ru(2)–N(25)	170.0(2)
		N(15)–Ru(1)–N(16)	83.0(2)	N(22)–Ru(2)–N(26)	170.7(2)
		N(12)–Ru(1)–N(16)	170.9(2)	N(25)–Ru(2)–N(26)	82.2(2)

*Reference [35].

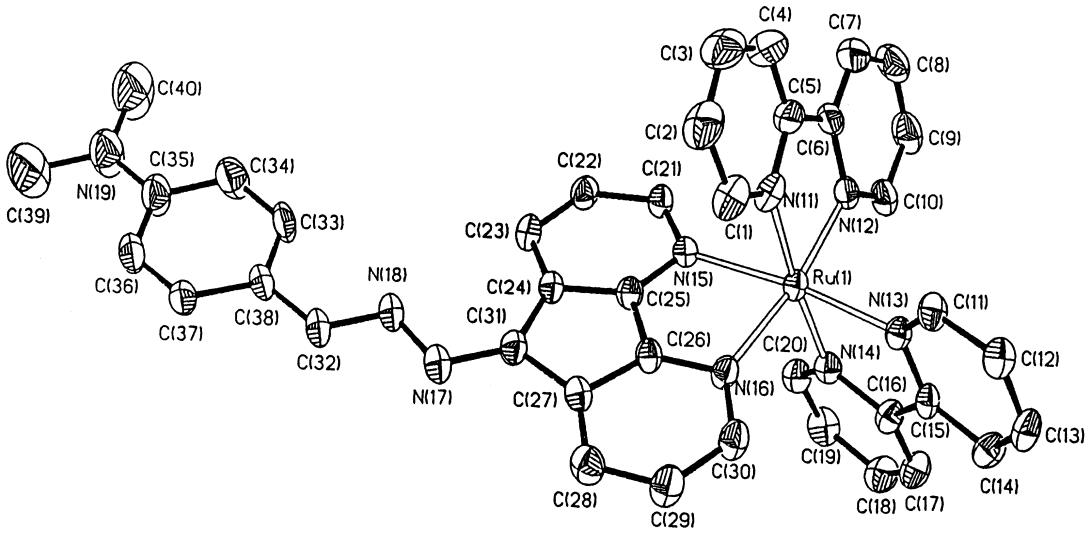

Fig. 3. Molecular structure with atomic numbering scheme of Ru-N$(CH_3)_2$ cation. The thermal ellipsoids are drawn at the 30% probability level.

0.73 V, respectively. From this potential along with the excited state oxidation potentials for the Ru complex described above, the *Ru(II) was quenched through reductive quenching process in the Ru–N$(CH_3)_2$ and Ru–OH complexes. The free energy for *Ru to oxidise the functional groups is estimated to be -0.08 V and -0.28 V for Ru–N$(CH_3)_2$ and Ru-OH complexes respectively.

Cyclic voltammetry of the Ru–NO_2 complex also reveals that in addition to the characteristic waves for the Ru complex, an irreversible cathodic wave is observed at Ep $= -0.65$ V for the NO_2 functional group. Differential-pulse voltammetry reveals that the $E_{1/2}$ for the reduction reaction is -0.59 V. From this potential along with the excited state oxidation potentials for the Ru complex, the *Ru MLCT was quenched through oxidative quenching process in the Ru–NO_2 complex. The free energy for *Ru to reduced the functional group is estimated to be -0.18 eV.

Description of crystal structures

In most references, the mechanism of electron transfer and the relationship between the rate constant and the donor-acceptor separation can not be discussed fully because of the flexibility of the bridging ligand and the uncertainty of the D–A separation. In this case, the crystal structure of the molecular is efficient for a detailed discussion of the photoinduced electron transfer studies. In our earlier studies, the crystal structure of the free ligand L-N$(CH_3)_3$ has been reported [35]. In this paper, we discussed the crystal structure of the Ru–N$(CH_3)_2$ complex.

There are two slightly different Ru(II) moieties in the asymmetric unit (Fig. 3). In each moiety, the coordination geometry of the ruthenium ion is a slightly distorted octahedron with four pyridine nitrogen atoms from the two bipyridine molecules, and two nitrogen atoms from the Schiff-base ligand, *p*-dimethylaminobenzaldehyde 4-5-dizafluorene-9-hydrazone. The Ru–N(bpy) distances of 2.04–2.06 Å are good in agreement with the value of 2.056 Å found in $[Ru(bpy)_3](PF_6)_2$ [36] and similar bis(bipyridyl) ruthenium complexes [37–41].

The bite angles of the two bipyridine ligands are 79.6(2), 79 2(2)° for Ru(1) and 79.5(2), 79.0(2)° for Ru(2), respectively. While the bite angle of the Schiff-base ligand, L-N$(CH_3)_2$, are 83.0(2) for Ru(1) and 82.2 (2) for Ru(2), respectively, these angles are somewhat bigger in keeping with the increased size of the chelating ring, The two *trans* angles associated with the Schiff-base ligand are 171.8(2), 170.9(2) for Ru(1) and 170.0(2), 170.7(2) for Ru(2), respectively. These values are quite different from the *trans* angles associated to the bipyridine nitrogen atoms. (175.2(2) for Ru(1) and 173.9(2) for Ru(2), respectively). The bond lengths and angles of the ligand L-N$(CH_3)_2$ in the complex are in normal range and consistent with those of the free ligand.

Acknowledgements—This work is supported by the State Science and Technology Commission and National Nature Science Foundation of China.

REFERENCES

1. Marcus, R. A. and Sutin, N., *Biochem. Biophys. Acta.*, 1995, **811,** 265.
2. Kavarnos, G. J. and Turro, N. J., *Chem. Rev.*, 1986, **86,** 401.
3. Guarr, T. F. and McLendon, G., *Coord. Chem. Rev.*, 1985, **68,** 1.

4. Joran, A. D., LeLand, B. A., Felker, P. M., Zewail, A. H., Hopfiled, J. J. and Dervan, P. B., *Nature*, 1987, **327,** 508.
5. Miller, J. R., Beitz, J. V. and Huddleston, R. K., *J. Am. Chem. Soc.*, 1984, **106,** 5057.
6. Sessler, J. L., Capuano, V. L. and Burrell, A. K., *Inorg. Chim. Acta.*, 1993, **204,** 93.
7. Bolger, J., Gourdon, G., Ishow, E. and Launay, J. P., *J. Chem. Soc., Chem. Commun.*, 1995, **00,** 1799.
8. Grosshenny, V., Harriman, A., Grosshenny, V., Harrhnan, A. and Ziessel, R., *Angew. Chem., Int. Ed. Engl.*, 1995, **34,** 1100.
9. Collin, J.-P., Harriman, A., Heitz, V., Odobel, F. and Sauvage, J. P., *J. Am. Chem. Soc.*, 1994, **116,** 5679.
10. Harriman, A., Odobel, F. and Sauvage, J. P., *J. Am. Chem. Soc.*, 1995, **117,** 9461.
11. Duan, C. Y., Shen, X. Q., Zhu, L. G. and You, X. Z., *Polyhedron*, 1994, **13,** 321.
12. Zhu, L. G., Wang, Y. X., Duan, C. Y., Xia, X. B. and You, X. Z., *Science Bulletin*, 1991, **35,** 345 (in Chinese).
13. Juris, A., Barigelletti, S., Campagna, S., Balzani, V., Belser, P. and von Zelewsky, A., *Coord. Chem. Rev.*, 1988, **85,** 84.
14. Balzani, V. and Scandola, F., (1991), *Supramolecular Photochemistry*, Horwood: Chechestter, UK.
15. Johnson, S. R., Westmoreland, T. D., Caspar, J. V., Barqawi, K. R. and Meyer, T. J., *Inorg. Chem.*, 1988, **27,** 3195.
16. Molochoski, J. and Szule, Z., *Pol. J. Chem.*, 1983, **67,** 33.
17. Sullivan, B. P., Salmon, D. J. and Meyer, T. J., *Inorg. Chem.*, 1978, **17,** 3334.
18. (a) Tanner, J. and Krause K. L., *The Rigaku Journal*, 1994, 11, **4**; (b) ibid, 1990, **7**, 28.
19. Krause, K. L. and Phillips, G. N., *J. Appl. Cryst.*, 1992, **25,** 146.
20. Higashi, T, (1995), ABSCOR Rigaku Corporation, Tokyo.
21. Sheldrick, G. M., (1982), in *Computational Crystallography*, D. Sayre (Ed.) pp. 506-514; Oxford University Press, New York.
22. Ibers, J. and Hamilton, W. C., (Eds.), (1974), in *International Tables for X-ray Crystallography*, pps. 25, 99, 149; Kynock Press, Birmingham (now distributed by Kluwer Academic Press, Dordrecht).
23. Predieri, G., Vignali, C., Denti, G. and Serroni, S., *Inorg. Chim. Acta.*, 1993, **205,** 145.
24. Rutherford, T. J., Reitsma, D. A. and Keene, F. R., *J. Chem. Soc., Dalton Trans.*, 1994, **00,** 3659.
25. Anderson, P. A., Deacon, G. B., Harrmann, K. H., Keene, F. R., Meyer, T. J., Reitsma, D. A., Skelton, B. W., Strouse, G. F., Thomas, N. C., Treadway, J. A. and White, A. H., *Inorg. Chem.*, 1995, **34,** 6145.
26. Kober, E. M. and Meyer, T. J., *Inorg. Chem.*, 1983, **22,** 1614.
27. Riesen, H. and Krauz, E., *J. Chem. Phy.*, 1993, **99,** 7614.
28. Calvert, J. M., Caspar, J. V., Binstead, R. A., Westmoreland, T. D. and Meyer, T. J., *J. Am. Chem. Soc.*, 1982, **104,** 3335.
29. Caspar, J. V., Kober, E. M., Sullivan, B. P. and Meyer, T. J., *J. Am. Chem Soc.*, 1982, **104,** 630.
30. Schoonover, J. R., Chen, P. Y., Bates, W. D., Dyer, R. B. and Meyer, T. J., *Inorg. Chem.*, 1994, **33,** 793.
31. (This hypothcsis is based on the observation that the radiative decay rate, calculated by ϕ/τ is almost same for the OCH_3 functional Ru complex and the $Ru(bpy)^{3+}{}_3$ in the same condition.).
32. Turro, N. J., *Modern Molecular Photochemistry*, Benjamin/Cumming, Menlo Park, CA. 1978. .
33. Schanze, K. S. and Sause, K., *J. Am. Chem. Soc.*, 1988, **110,** 1180.
34. (The equations used for calculation of the excited state potentials are as follows: $E_{1/2}$*Ru(III)/*Ru(II)] = $E_{1/2}$[Ru(III)/Ru(II)]-E_{MLCT}, $E_{1/2}$[*Ru(II)/[*Ru(II)/Ru(I)] = $E_{1/2}$[Ru(II)/Ru(II)] + E_{MLCT}).
35. Lu, Z.-L., Duan, C.-Y., Tian, Y.-P., You, X.-Z., Fun, H.-K. and Sivakumar, K., *Acta Crystallogr. C.*, 1996, **52,** 1507.
36. Biner, M., Burgi, H. B. and Ludi, A., Rohr, C., *J. Am. Chem. Soc.*, 1992, **114,** 5197.
37. Rillema, D. P., Jones, D. S. and Levy, H. A., *J. Chem. Soc. Chem. Commun.*, 1979, **00,** 197.
38. Rillema, D. P., Taghdiri, D. G., Jones, D. S., Keller, C. D., Worl, L. A., Meyer, T. J. and Levy, H. A., *Inorg. Chem.*, 1987, **26,** 578.
39. Buchanan, B. E., Vos, J. G., Kaneko, M., von der Putten, W. J. M., Kelly, J. M., Hage, R., de Graaff, R. A. G., Prins, R., Haasnoot, J. G. and Reedijk, J., *J. Chem. Soc. Dalton, Trans.*, 1990, **00,** 2425.
40. Holligan, B. M., Jeffery, J. C., Norgett, M. K., Schatz, E. and Ward, M. D. J., *J. Chem. Soc, Dalton, Trans.*, 1992, **00,** 3345.
41. Wong, K. Y., Che, C. M., Liu, C. K., Chiu, W. H., Zhou, Z. Y. and Mak, T. C. W., *J. Chem. Soc. Chem. Commun.*, 1992, **00,** 754.

Pergamon

Polyhedron Vol. 17, No. 23–24, pp. 4139–4143, 1998
© 1998 Elsevier Science Ltd
All rights reserved. Printed in Great Britain
0277–5387/98 $19.00+0.00

PII: S0277–5387(98)00221–6

2,2′-Bipyridyl and 1,10-phenanthroline adducts of the diborane(4) compound $B_2(1,2\text{-}S_2C_6H_4)_2$

Chaoyang Dai,[a] Stuart M. Johnson,[b] Fiona J. Lawlor,[c] Philip Lightfoot,[d] Todd B. Marder,[a,e,*] Nicholas C. Norman,[b,c,*] A. Guy Orpen,[b,*] Nigel L. Pickett,[c] Michael J. Quayle[b] and Craig R. Rice[b]

[a]Department of Chemistry, The University of Waterloo, Waterloo, Ont., Canada N2L 3G1

[b]School of Chemistry, The University of Bristol, Bristol BS8 1TS, U.K.

[c]Department of Chemistry, The University of Newcastle, Newcastle upon Tyne NE1 7RU, U.K.

[d]Department of Chemistry, The University of St. Andrews, St Andrews Fife KY16 9ST, U.K.

[e]Science Laboratories, Department of Chemistry, The University of Durham, South Road, Durham DH1 3LE, U.K.

(Received 13 March 1998; accepted 31 May 1998)

Abstract—The syntheses and structures of the 2,2′-bipyridyl and 1,10-phenanthroline adducts of the diborane(4) compound $B_2(1,2\text{-}S_2C_6H_4)_2$ are described. In both cases, the bidentate nitrogen donor ligands bridge the B–B bond, one nitrogen being bonded to each boron. © 1998 Elsevier Science Ltd. All rights reserved

Keywords: diborane(4); ligand adducts.

INTRODUCTION

Diborane(4) compounds, B_2R_4 (for a recent overview containing key references, see Ref. [1]), have been the focus of renewed interest in recent years, not least because of their importance as reagents in transition metal catalysed diboration reactions [2], and as part of our own interest in such compounds, we have recently reported results relating to the Lewis acidity of the boron centres [3, 4]. Specifically, we noted that the compounds $B_2(cat)_2$ (**1**) (cat = 1,2-$O_2C_6H_4$) and $B_2(thiocat)_2$ (**2**) (thiocat = 1,2-$S_2C_6H_4$) [5, 6] formed both *mono* and *bis*-adducts with 4-picoline [3, 4], whilst **2** also formed *mono* and *bis*-adducts with tertiary phosphines consistent with a greater degree of Lewis acidity for the sulphur substituted boron centres [4]. Herein, we describe the adducts formed between **2** and 2,2′-bipyridyl and 1,10-phenanthroline.

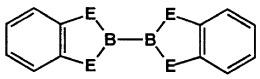

1, E = O; **2**, E = S

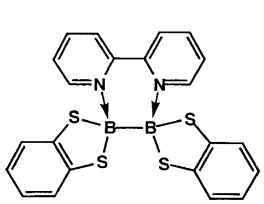

3

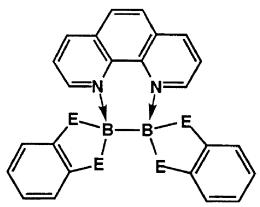

4, E = S; **5**, E = O

RESULTS AND DISCUSSION

Reactions between **2** and one equivalent of either 2,2′-bipyridyl (bipy) or 1,10-phenanthroline (phen) in CH_2Cl_2 solution led to the immediate formation of a

* Authors to whom correspondence should be addressed.

coloured (pale red in the case of **3** and red in the case of **4**) solution. After addition of an overlayer of toluene and subsequent solvent diffusion over a period of days at -30°C, dark red (almost black in the case of **4**) crystals were obtained, analytical data for which were in accord with the formulae $[B_2(thiocat)_2(bipy)]$ (**3**) and $[B_2(thiocat)_2(phen)]$ (**4**) (in both cases, with some solvent of crystallisation: see Experimental section).

Single crystals of both **3** and **4**, although of relatively poor quality, were suitable for X-ray crystallography, the results of which are shown in Figs 1 and 2 with selected bond lengths and angles given in Table 1. Compound **3** (Fig. 1) crystallises as a CH_2Cl_2 solvate with two molecules of **3** and two of CH_2Cl_2 in the asymmetric unit. The independent molecules of **3** are essentially identical (they are related by a pseudo-inversion centre; see Experimental section) and consist of units of **2** with the bipy ligand bridging the B–B bond, one nitrogen centre being bonded to each boron. The two B–B distances [B(1)–B(2) 1.65(5) and B(3)–B(4) 1.61(4) Å] are the same within experimental error and similar both to the B–B distance in **2** itself [1.673 Å average for two independent molecules] [6] and to the corresponding bond lengths in the related *bis*-adduct compounds of **2** $[B_2(thiocat)_2(4\text{-picoline})_2]$ [B–B 1.715(10) Å] and $[B_2(thiocat)_2(PMe_2Ph)_2]$ [B–B 1.750(4) Å] [4]. The B–S distances in **3** (average 1.916 Å) are similar to those found in $[B_2(thiocat)_2(4\text{-picoline})_2]$ and $[B_2(thiocat)_2(PMe_2Ph)_2]$ and the B–N bond lengths (average 1.65 Å) are also similar to those found in both the *mono* and *bis*-4-picoline adducts of **1** and **2** described in Refs. [3, 4]. All boron atoms in **3** are tetrahedrally coordinated with angles which do not deviate markedly from ideal values; any deviations which are present are likely to arise from constraints imposed by the five and six-membered rings. The coordination of the bipy ligands does, however, result in a significant twisting about the B–B bond leading to an ethane-like conformation for the $(BS_2N)_2$ unit. Thus the torsion angles defined by taking the coordinates of the mid-point of the S–S vectors in each thiocat group and the two boron atoms are 64.9 and 51.4°. The $B_2N_2C_2$ six-membered rings are markedly non-planar [τ(NBBN) = 50.2 and 50.4°; τ(NCCN) = 14.2 and 29.2°, maximum deviation from $B_2N_2C_2$ plane is 0.32 Å for B(2) and 0.35 Å for B(4)].

Compound **4** crystallises as a CH_2Cl_2 and toluene solvate with molecules of **4** lying on a crystallographic C_2 axis. The molecular structure of **4** (Fig. 2) is similar to that of **3** in that the phen ligand bridges the B–B bond of the $B_2(thiocat)_2$ unit. The B–B [1.707(13) Å], B–S [B(1)–S(1) 1.903(7) and B(1)–S(2) 1.930(7) Å] and B–N [B(1)–N(1) 1.620(8) Å] distances are all in expected ranges when compared with those of **3** and the compounds described in Ref. [4] and the twisting about the B–B bond seen in **3** is also present here [equivalent torsion angles and interplanar angles defined as above are: 38.1° for "S''BB"S"; τ(NBBN) = 35.2°; τ(NCCN) = 7.1°, maximum deviation from $B_2N_2C_2$ plane is 0.22 Å for B(1) and B(1a)].

Perhaps the most unusual feature about **3** and **4** is the observation that the bipy and phen ligands bridge an element–element bond. This type of bridging coordination is extremely rare for these ligands, the only previously known examples being the double quat-

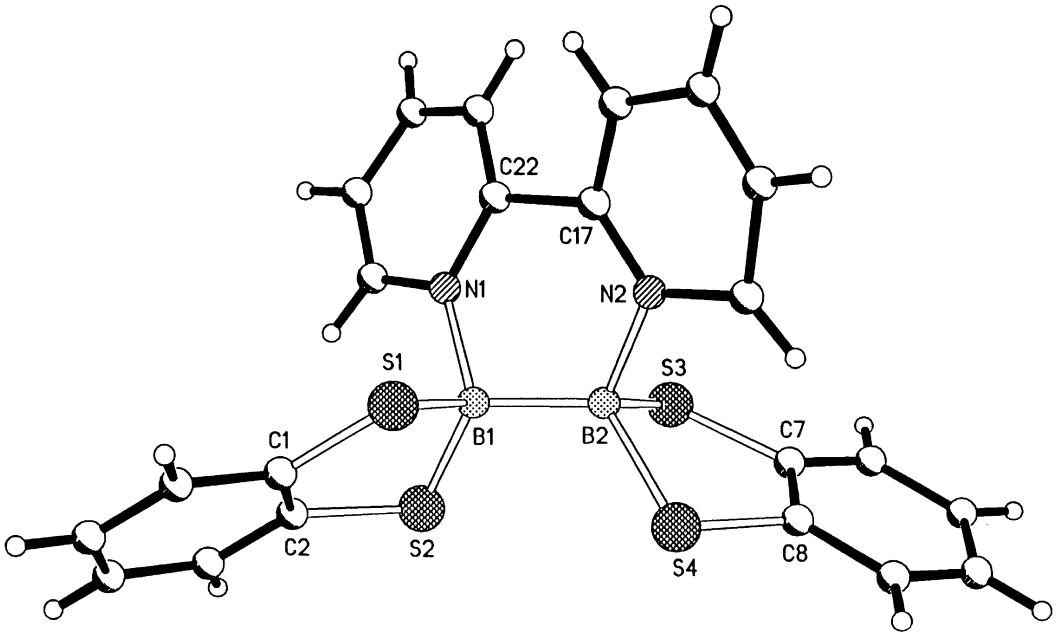

Fig. 1. A view of the molecular structure of one of the two crystallographically independent molecules of **3** showing the atom numbering scheme. Hydrogen atoms are omitted for clarity.

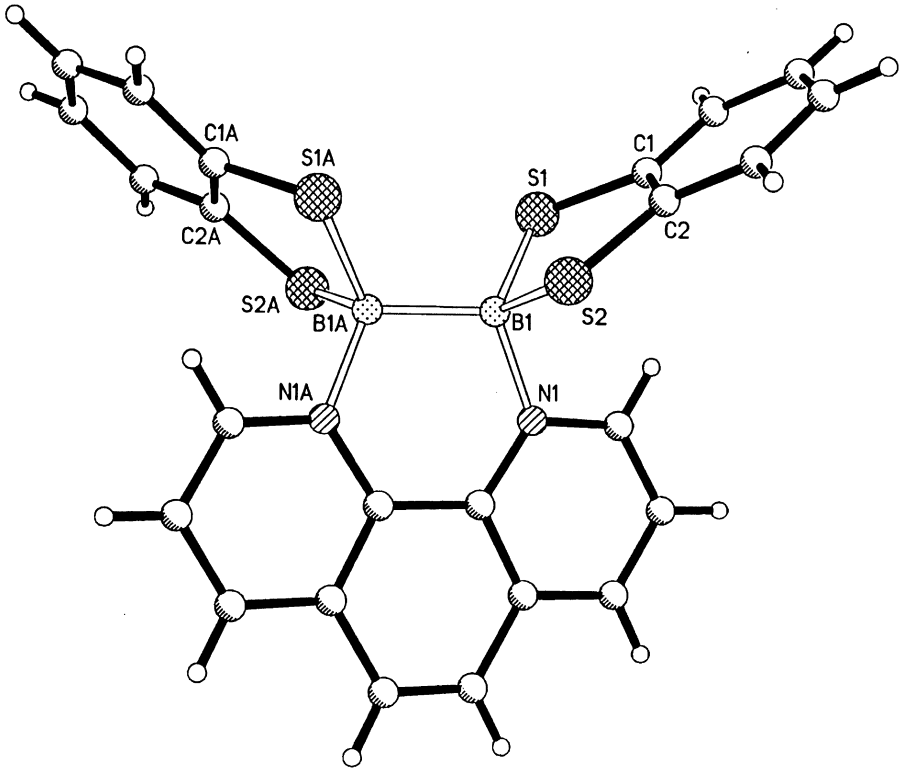

Fig. 2. A view of the molecular structure of **4** showing the atom numbering scheme. Hydrogen atoms are omitted for clarity.

Table 1
Selected bond lengths and angles for compounds **3** and **4**

3[a]		**3**[a]		**4**	
Bond lengths					
B(1)–B(2)	1.65(5)	B(3)–B(4)	1.61(4)	B(1)–B(1a)	1.707(13)
B(1)–S(1)	1.95(4)	B(3)–S(5)	1.93(3)	B(1)–S(1)	1.903(7)
B(1)–S(2)	1.83(4)	B(3)–S(6)	1.90(3)	B(1)–S(2)	1.930(7)
B(1)–N(1)	1.65(4)	B(3)–N(3)	1.68(4)	B(1)–N(1)	1.620(8)
B(2)–S(3)	1.95(3)	B(4)–S(7)	1.94(3)		
B(2)–S(4)	1.95(3)	B(4)–S(8)	1.94(3)		
B(2)–N(2)	1.68(3)	B(4)–N(4)	1.61(3)		
Bond angles					
B(2)–B(1)–S(1)	113(2)	B(4)–B(3)–S(5)	117(2)	B(1a)–B(1)–S(1)	110.6(4)
B(2)–B(1)–S(2)	115(2)	B(4)–B(3)–S(6)	115(2)	B(1a)–B(1)–S(2)	114.5(5)
B(2)–B(1)–N(1)	105(2)	B(4)–B(3)–N(3)	106(2)	B(1a)–B(1)–N(1)	110.2(3)
N(1)–B(1)–S(1)	104(2)	N(3)–B(3)–S(5)	106(2)	N(1)–B(1)–S(1)	111.1(4)
N(1)–B(1)–S(2)	114(2)	N(3)–B(3)–S(6)	108(2)	N(1)–B(1)–S(2)	105.5(4)
S(1)–B(1)–S(2)	106(2)	S(5)–B(3)–S(6)	103.6(14)	S(1)–B(1)–S(2)	104.8(3)
B(1)–B(2)–S(3)	113(2)	B(3)–B(4)–S(7)	116(2)		
B(1)–B(2)–S(4)	118(2)	B(3)–B(4)–S(8)	115(2)		
B(1)–B(2)–N(2)	111(2)	B(3)–B(4)–N(4)	109(2)		
N(2)–B(2)–S(3)	107(2)	N(4)–B(4)–S(7)	106(2)		
N(2)–B(2)–S(4)	106(2)	N(4)–B(4)–S(8)	108(2)		
S(3)–B(2)–S(4)	100.5(13)	S(7)–B(4)–S(8)	101.8(12)		

[a] Two crystallographically independent molecules.

ernary, *N*,*N*′-dialkyl species formed by reaction between either bipy or phen and 1,2-dibromoethane [7].

Also interesting is the colour of these two complexes. All of the *mono* and *bis*-picoline adducts of **1** and **2** described in Refs. [3, 4] are colourless or very pale yellow in contrast to the red colours seen here. These are presumably charge-transfer transitions from filled orbitals in the B_2(thiocat)$_2$ unit to empty π*-orbitals of the bipy or phen ligands. That the colours persist in solution indicates that association between **2** and either bipy or phen is present in solution as well as in the solid state although we were not able to confirm this by ^{1}H or ^{11}B NMR studies owing to the very poor solubility of both **3** and **4**.

As a final point, we note that **1** also forms a red solution in $CHCl_3$ when one equivalent of 1,10-phenanthroline is added, with red crystals being isolated after work-up. On the basis of the colour of the solution and solid, a similar structure to **4** is likely but since the crystals were not of X-ray quality, any structural formulation must remain tentative although analytical data were consistent with the formation of a 1:1 adduct albeit as a $CHCl_3$ solvate.

EXPERIMENTAL

General procedures

All reactions were performed using standard Schlenk techniques under an atmosphere of dry, oxygen-free dinitrogen. All solvents were distilled from appropriate drying agents immediately prior to use (sodium for toluene and hexanes and CaH_2 for CH_2Cl_2). Microanalytical data were obtained at the University of Bristol and UV-visible spectra were obtained on a Perkin-Elmer Lambda 2 spectrophotometer.

Compounds **1** and **2** were prepared by the literature methods [5]. 2,2′-bipyridyl and 1,10-phenanthroline were procured commercially but were dried by azeotropic distillation of toluene in a Dean and Stark apparatus before use.

Preparations

[B_2(*thiocat*)$_2$(*phen*)] (***4***) A solution of dried 1,10-phenanthroline (0.029 g, 0.16 mmol) in CH_2Cl_2 (2 cm^3) was added to a stirred solution of **2** (0.050 g, 0.16 mmol) in CH_2Cl_2 (2 cm^3) resulting in the immediate formation of a red solution. Addition of an overlayer of toluene (3 cm^3), cooling to -30°C and subsequent solvent diffusion over a period of two days afforded **4** as dark red (almost black) crystals which were then washed with hexane (2×2 cm^3) (0.089 g, 84%). One of these crystals was used for X-ray crystallography which revealed the presence of one molecule of CH_2Cl_2 and one molecule of toluene per molecule of **4**. $C_{24}H_{16}N_2B_2S_4{\cdot}CH_2Cl_2{\cdot}C_6H_5CH_3$ requires C, 58.30; H, 4.00; N, 4.20%. Found: C, 56.10; H, 3.70; N, 4.80. Some loss of solvent of crystallisation occurred accounting for the poor quality analytical data. UV-VIS (CH_2Cl_2), 509.8 nm, $\varepsilon_0 = 26$.

Compound **3** was prepared in an analogous manner and in similar yield using 2,2′-bipyridyl in place of 1,10-phenanthroline. X-ray crystallography revealed the presence of CH_2Cl_2 of crystallisation. $C_{22}H_{16}N_2B_2S_4{\cdot}CH_2Cl_2$ requires C, 50.90; H, 3.35; N, 5.15%. Found: C, 50.65; H, 3.15; N, 5.05. The pale red colour of solutions of **3** in CH_2Cl_2 were not of a sufficient intensity to obtain satisfactory solution UV-VIS data.

Compound **5** was also prepared similarly but using $CHCl_3$ rather than CH_2Cl_2. Analytical data were consistent with a 1:1 adduct of **1** and 1,10-phenanthroline with one molecule of $CHCl_3$ of crystallisation present. $C_{24}H_{16}N_2B_2O_4{\cdot}CHCl_3$ requires C, 55.90; H 3.20; N, 5.20%. Found: C, 55.05; H, 3.00; N, 4.45. UV-VIS (CH_2Cl_2), $\lambda = 425.0$ nm, $\varepsilon_0 = 540$.

It is important that the 2,2′-bipyridyl and 1,10-phenanthroline used in these reactions is dry and that none of the hydrates are present. Any traces of water lead to extensive decomposition products, one of which, in the reaction which afforded **5**, was identified by X-ray crystallography as the salt [phenH]$^+$[B(cat)$_2$]$^-$ [8].

X-ray crystallography

Crystal data for ***3*** $\cdot CH_2Cl_2$ $C_{23}H_{18}B_2Cl_2N_2S_4$, $M = 543.15$, orthorhombic, $a = 16.828(3)$, $b = 14.553(3)$, $c = 20.069(4)$ Å, $U = 4914.9(17)$ Å^3, $T = 220(1)$ K, space group $Pna2_1$ (No. 33), $Z = 8$, $\mu = 0.62$ mm^{-1}, 3062 reflections measured, 2475 unique ($R_{int} = 0.0970$). Final $R_1 = 0.0830$ for 1849 reflections $I > 2\sigma(I)$.

X-ray diffraction measurements were made on a single crystal mounted on a glass fibre with graphite-monochromated Mo-K$_\alpha$ X-radiation ($\bar{\lambda} = 0.71073$ Å) using a Rigaku AFC7S diffractometer. Unit cell constants and an orientation matrix were obtained from a least-squares refinement using the setting angles of 18 carefully centred reflections in the range $7.31° < \theta < 11.49°$. Intensity data were collected using the ω–2θ scan technique. Azimuthal scans of several reflections indicated no need for an absorption correction. Data were integrated using teXsan [9] and were corrected for Lorentz and polarisation effects. Intensities were weak and collected to only $\theta = 20.26°$. The structure was solved by direct methods and refined by full-matrix least squares against F^2 for all data with $I > -3\sigma(I)$. The structure was solved and refined in the acentric space group $Pna2_1$ with two molecules of **3** and two dichloromethane solvent molecules per asymmetric unit. There appears to be a local pseudo inversion centre between the molecules of **3** although this does not hold for the solvent molecules and is not a true inversion centre. Chlorine, sulphur and nitrogen atoms were refined anisotropically and

hydrogens were assigned fixed isotropic displacement parameters and were constrained to idealised geometries. The aromatic rings of the $BS_2C_6H_4$ groups were restrained to D_{6h} symmetry. The absolute structure parameter [10] was determined by refinement to be $-0.10(40)$.

Crystal data for $\mathbf{4}\cdot 1.0CH_2Cl_2 1.0C_6H_5Me$ $C_{16}H_{13}BClNS_2$, $M=329.65$, monoclinic, $a=12.332(3)$, $b=10.1552(13)$, $c=12.259(2)$ Å, $\beta=90.108(10)^\circ$ $U=1535.1(4)$ Å^3, $T=173(2)$ K, space group $P2/c$ (No. 13), $Z=4$, $\mu=0.51$ mm^{-1}, 9230 reflections measured, 3498 unique ($R_{int}=0.0308$). Final $R_1=0.0898$ for 2974 reflections $I>2\sigma(I)$.

Many of the details of the structure analyses are the same as those for $\mathbf{3}\cdot CH_2Cl_2$. X-ray diffraction measurements on a single crystal coated in a hydrocarbon oil mounted on a glass-fibre under argon were made using a Siemens SMART diffractometer. Intensity data were collected by 0.3° width ω steps accumulating area detector frames spanning a hemisphere of reciprocal space. Data were integrated using the SAINT [11] program and corrected for Lorentz, polarisation and long-term intensity fluctuations. The asymmetric unit contained half a molecule of **4**, CH_2Cl_2 and C_6H_5Me, with molecules of **4** lying over a crystallographic C_2 axis. The toluene and dichloromethane solvates were disordered over an inversion centre. Since the β angle was 90.108° the structure was refined to test the possibility that it may be twinned with a pseudo-orthorhombic cell, using the twin law (1 0 0, 0 −1 0, 0 0 −1). However, the twin component parameter refined to 0.012(2) indicating a marginal amount of twinning and resulted in no significant improvement in the *R*-factor. An extinction parameter, x, of the form $F_c' = F_c/[1+0.001xF_c^2\lambda^3/\sin(2\theta)]^{-0.25}$ was refined to 0.014(2). All calculations were made with programs of the SHELXTL system [12]. Complex neutral-scattering factors were taken from Ref. [13].

Acknowledgements—T. B. M. thanks the NSERC of Canada, N. C. N. thanks the EPSRC, Laporte and The Royal Society and A. G. O. thanks EPSRC for research support and for a studentship (M. J. Q.). T. B. M. and N. C. N. also thank NSERC and The Royal Society for supporting this collaboration via a series of Bilateral Exchange Awards and F. J. L. and N. L. P. thank the British Council (Ottawa, Canada) for scholarships supporting their travel to Waterloo.

REFERENCES

1. Lesley, G., Marder, T. B., Norman, N. C. and Rice, C. R., *Main Group Chem. News*, 1997, **5,** 4.
2. Marder, T. B. and Norman, N. C., *Topics in Catal.*, Vol. 5, eds. W. Leitner and D. G. Blackmond. Baltzer Science Publishers, Amsterdam, 1998, p. 63.
3. Nguyen, P., Dai, C., Taylor, N. J., Power, W. P., Marder, T. B., Pickett, N. L. and Norman, N. C., *Inorg. Chem.*, 1995, **34,** 4290.
4. Clegg, W., Dai, C., Lawlor, F. J., Marder, T. B., Nguyen, P., Norman, N. C., Pickett, N. L., Power, W. P. and Scott, A. J., *J. Chem. Soc. Dalton Trans.*, 1997, 839.
5. Lawlor, F. J., Norman, N. C., Pickett, N. L., Robins, E. G., Nguyen, P., Lesley, G., Marder, T. B., Ashmore, J. A. and Green, J. C., *Inorg. Chem.* (in press).
6. Clegg, W., Elsegood, M. R. J., Lawlor, F. J., Norman, N. C., Pickett, N. L., Robins, E. G., Scott, A. J., Nguyen, P., Taylor, N. J. and Marder, T. B., *Inorg. Chem.* (in press).
7. Hofbauer, M., Mobius, M., Knoch, F. and Benedict, R., *Inorg. Chim. Acta*, 1996, **247,** 147.
8. Clegg, W., Dai, C., Elsegood, M. R. J., Lawlor, F. J., Marder, T. B., Norman, N. C., Pickett, N. L. and Scott, A. J., *Acta Cryst. C* (submitted).
9. *teXsan. Crystal Structure Analysis Package*. Molecular Structure Corporation, 1985 and 1992.
10. Bernardinelli, G. and Flack, H.D., *Acta Cryst. A*, 1985, **41,** 500.
11. *SAINT* (*Siemens Area Detector INTegration*) *program*. Siemens Analytical X-ray, Madison, WI, U.S.A., 1995.
12. *Siemens SHELXTL*, *Revision* 5.03. Siemens Analytical X-ray, Madison, WI, U.S.A., 1995.
13. *International Tables for Crystallography*, Vol. C. Kluwer, Dordrecht, 1992.

Pergamon

Polyhedron Vol. 17, No. 23–24, pp. 4145–4154, 1998
© 1998 Elsevier Science Ltd
All rights reserved. Printed in Great Britain
0277–5387/98 $19.00+0.00

PII: S0277–5387(98)00222–8

Coordination compounds derived from first-row transition metal salts. Synthesis, analytical, spectroscopic and structural characterization. Crystal structure of [{bis(3,4,5-trimethylpyrazol-1-yl)methane}$ZnBr_2$]

Claudio Pettinari,[a]† Fabio Marchetti,[a] Augusto Cingolani,[a] Dante Leonesi,[a] Marcello Colapietro[b] and Serena Margadonna[b]

[a]Dipartimento di Scienze Chimiche, Università degli Studi di Camerino, via S. Agostino 1, 62032 Camerino MC, Italy

[b]Dipartimento di Chimica, Università di Roma "La Sapienza", P.le A. Moro 5, 00185, Rome, Italy

(Received 31 March 1998; accepted 1 June 1998)

Abstract—The interaction between bis(4-methylpyrazol-1-yl)methane or bis(3,4,5-trimethylpyrazol-1-yl)methane and several MX_2 salts (M = Mn, Fe, Co, Ni or Cu; X = Cl; M = Mn, Co, Ni or Cu, X = NO_3; M = Zn, X = Br) gives 1:1 and 2:1 adducts depending on counter-ion, molar ratio of reagents and solvent of reaction employed. Structural conclusions are drawn from IR, far-IR, UV, magnetic susceptibility and conductivity data. In the crystal structure of the title compound the zinc atom is found in a strongly distorted tetrahedral coordination [N–Zn–N: 92.2(6); Br–Zn–Br: 119.1(1)°]. The Zn–N [2.075(19) and 2.078(15) Å] and Zn–Br [2.350(3) and 2.372(3) Å] bond distances are longer than those reported for related compounds owing to steric hindrance of the N_2-donor. © 1998 Elsevier Science Ltd. All rights reserved

Keywords:

INTRODUCTION

Bis(pyrazol-1-yl)alkanes are a versatile class of neutral N_2-donor ligands which form stable chelates with transition and main group elements [1–7]. They can be prepared readily and contain two pyrazole rings, which are generally very stable toward chemical attack, for example against both oxidizing and reducing agents.

The coordinating behaviour of these molecules is often very different from that shown by the isosteric and isoelectronic anionic poly(pyrazol-1-yl)borates, for which a number of papers [8–13] devoted to their coordination chemistry has been published and also from that shown by 2,2′-bipyridine and 1,10-phenanthroline chelating planar donors, extensively used in the field of the coordination chemistry [14–17]. While 2,2′-bipyridine and 1,10-phenanthroline adducts are likely to contain an approximately planar five membered M–N–C–C–N moiety, upon coordination of bis(pyrazolyl)methanes, six-membered cycle are formed for which a boat conformation is forecast (Fig. 1). It is noteworthy that the bis(pyrazol-1-yl)alkanes, with steric constraints, may impose unusual stoichiometries and geometries on transition metal ions [18–20].

Nevertheless there had been no systematic study on the derivatives of this class of ligands with typical and transition elements, so that an investigation into this area was began, and after working on zinc [21], cadmium [21], mercury [21], tin(IV) and organotin(IV) [22], silver(I) [23] and copper(I) [24] derivatives, we were prompted, by the results obtained, to continue to prepare other new bis(pyrazol-1-yl)alkanes metal derivatives.

It has been previously observed that different substituents on the azole ring can produce reliable chan-

†Author to whom correspondence should be addressed.

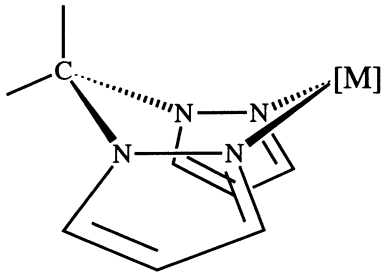

Fig. 1. The six-membered cycle formed by bis(pyrazol-1-yl) alkanes upon complexation.

ges on spectroscopic properties and structures of both transition and post-transition metal derivatives [25, 26], but at this moment the importance of a methyl group in the 4-position of the pyrazole has not been completely realized, so that after the investigation on the coordinating properties of the donor bis(4-methylpyrazol-1-yl)methane (L^M) and bis(3,4,5-trimethylpyrazol-1-yl)methane (L^T) towards group 12 [18, 19, 20, 27] and 14 [22] metal derivatives, it seemed to us opportune to extend the study to interaction between these donors and first-row transition salts.

Here we report the synthesis, analytical (magnetic susceptibility and conductivity) and spectroscopic characterization (IR, UV) of some adducts between L^M or L^T and Mn(II), Fe(II), Co(II), Ni(II) Cu(II) and Zn(II) salts and also the X-ray crystal structure of the zinc(II) bromide adduct of bis(3,4,5-trimethylpyrazol-1-yl)methane.

EXPERIMENTAL

All the chemicals were purchased from Alfa (Karlsruhe) and Aldrich (Milwaukee) and used as received. The samples for microanalysis were dried *in vacuo* to constant weight (20°C, *ca.* 0.1 Torr). Elemental analyses (CHN) were carried out in the house with Fisons Instruments 1108 CHNS-O Elemental analyzer. IR spectra were recorded from 10000 to 100 cm^{-1} with a Perkin-Elmer instrument System 2000 FT-IR. Melting points were taken on an IA 8100 Electrothermal instrument. Electronic spectra were recorded from 800 to 200 nm in CH_3CN solution with an HP 8452 Diode Array Spectrophotometer. The electric resistance of solutions was measured with a Crison CDTM 522 conductimeter at room temperature. The magnetic susceptibilities were measured at room temperature (20°C) by the Gouy method, with a Sherwood Scientific Magnetic Balance MSB-Auto, using $HgCo(NCS)_4$ as calibrant and correcting for diamagnetism with the appropriate Pascal constants. The magnetic moments (in B.M.) were calculated from the equation $\mu_{eff} = 2.84(X_M^{corr} \cdot T)^{1/2}$.

Reagents

Preparation of bis(4-methylpyrazol-1-yl)methane (L^M) and bis(3,4,5-trimethylpyrazol-1-yl)methane. The donors bis(4-methylpyrazol-1-yl)methane ($\mathbf{L}^M$) and bis(3,4,5-trimethylpyrazol-1-yl)methane ($\mathbf{L}^T$) were prepared according to Claramunt's procedure [28].

Synthesis of the metal derivatives

Bis(4-methylpyrazol-1-yl)methanedichloromanganese(II)(H_2O) **1**. Compound **1** was obtained upon mixing $MnCl_2 \cdot 4H_2O$ (0.099 g, 0.5 mmol) in dichloromethane (20 ml) with bis(4-methylpyrazol-1-yl)methane ($\mathbf{L}^M$) (0.176 g, 1.0 mmol) in the same solvent (10 ml). The colorless precipitate immediately formed was filtered after 2 h and washed several times with diethyl ether (0.123 g, yield 77%). M.p.: 216–220°C dec. Anal. Calcd for $C_9H_{14}Cl_2MnN_4O$; C, 33.8; H, 4.4; N, 17.5. Found: C, 34.0; H, 4.6; N, 17.9%.

Bis{bis(4-methylpyrazol-1-yl)methane}dichloromanganese(II)(H_2O) **2**. Compound **2** was obtained upon mixing $MnCl_2 \cdot 4H_2O$ (0.195 g, 1.0 mmol) in diethyl ether (20 ml) with bis(4-methylpyrazol-1-yl)methane ($\mathbf{L}^M$) (0.352 g, 2.0 mmol) in the same solvent (10 ml). The colorless precipitate immediately formed was filtered after 2 h and washed several times with diethyl ether (0.322 g, yield 65%). M.p.: 228°C dec. Anal. Calcd for $C_{18}H_{26}Cl_2MnN_8O$; C, 43.6; H, 5.3; N, 22.6. Found: C, 43.2; H, 5.2; N, 22.3%.

Bis(4-methylpyrazol-1-yl)methanedichloroiron(II)(H_2O) **3**. Compound **3** was obtained upon mixing $FeCl_2 \cdot 4H_2O$ (0.099 g, 0.5 mmol) in ethanol (20 ml) with bis(4-methylpyrazol-1-yl)methane ($\mathbf{L}^M$) (0.176 g, 1.0 mmol) in the same solvent (10 ml). The brown precipitate immediately formed was filtered after 2 h and washed several times with ethanol (0.131 g, yield 82%). M.p.: 273–276°C dec. Anal. Calcd for $C_9H_{14}Cl_2FeN_4O$; C, 33.7; H, 4.4; N, 17.4. Found: C, 33.6; H, 4.4; N, 17.2%.

Bis{bis(4-methylpyrazol-1-yl)methane}dichloroiron(II)(H_2O)$_2$ **4** Compound **4** was obtained upon mixing $FeCl_2 \cdot 4H_2O$ (0.197 g, 1.0 mmol) in diethyl ether (20 ml) with bis(4-methylpyrazol-1-yl)methane ($\mathbf{L}^M$) (0.353 g, 2.0 mmol) in the same solvent (10 ml). A pale-brown precipitate was formed immediately, filtered after 2 h and washed several times with diethyl ether (0.464 g, yield 90%). M.p.: 268–270°C dec. Anal. Calcd for $C_{18}H_{28}Cl_2FeN_8O_2$; C, 42.0; H, 5.5; N, 21.7. Found: C, 41.7; H, 5.5; N, 21.7%.

Bis{bis(4-methylpyrazol-1-yl)methane}dichlorocobalt(II)(H_2O)$_2$ **5**. Compound **5** was obtained upon mixing $CoCl_2$ (0.130 g, 1.0 mmol) in diethyl ether (20 ml) with bis(4-methylpyrazol-1-yl)methane ($\mathbf{L}^M$) (0.354 g, 2.0 mmol) in the same solvent (10 ml). The pale-rose precipitate immediately formed was filtered after 4 h and washed several times with diethyl ether (0.373 g, yield 72%). M.p.: 253–255°C dec. Anal. Calcd for $C_{18}H_{28}Cl_2CoN_8O_2$; C, 41.7; H, 5.5; N, 21.7. Found: C, 41.5; H, 5.7; N, 21.6%.

Bis{*bis*(4-*methylpyrazol*-1-*yl*)*methane*}*dichloronickel*(*II*)(*H*$_2$*O*) **6** Compound **6** was obtained upon mixing $NiCl_2$ (0.130 g, 1.0 mmol) in ethanol (20 ml) with bis(4-methylpyrazol-1-yl)methane ($\mathbf{L}^M$) (0.423 g, 2.4 mmol) in the same solvent (10 ml). The sky-blue precipitate formed was filtered after 24 h and washed several times with ethanol and diethyl ether (0.390 g, yield 78%). M.p.: 326°C dec. Anal. Calcd for $C_{18}H_{26}Cl_2N_8NiO$; C, 41.8; H, 5.5; N, 21.7. Found: C, 41.5; H, 5.7; N, 21.6%.

Bis(4-*methylpyrazol*-1-*yl*)*methanedichlorocopper* (*II*) **7**. Compound **7** was obtained upon mixing $CuCl_2 \cdot 2H_2O$ (0.138 g, 0.8 mmol) in ethanol (20 ml) with bis(4-methylpyrazol-1-yl)methane ($\mathbf{L}^M$) (0.405 g, 2.3 mmol) in the same solvent (10 ml). The green precipitate immediately formed was filtered after 2 h and washed several times with ethanol and diethyl ether. (0.191 g, yield 77%). M.p.: 265–268°C dec. Anal. Calcd for $C_9H_{12}Cl_2CuN_4$; C, 34.8; H, 3.9; N, 18.0. Found: C, 35.0; H, 4.0; N, 18.1%.

Bis{*bis*(4-*methylpyrazol*-1-*yl*)*methane*}*dinitromanganese*(*II*)(*H*$_2$*O*)$_2$ **8**. Compound **8** was obtained upon mixing $Mn(NO_3)_2 \cdot 6H_2O$ (0.220 g, 0.76 mmol) in dichloromethane (20 ml) with bis(4-methylpyrazol-1-yl)methane ($\mathbf{L}^M$) (0.221 g, 1.25 mmol) in the same solvent (10 ml). The colorless precipitate formed was filtered after 4 days and washed several times with dichloromethane and diethyl ether (0.319 g, yield 74%). M.p.: 176–180°C dec. Anal. Calcd for $C_{18}H_{28}MnN_{10}O_8$; C, 38.1; H, 5.0; N, 24.7. Found: C, 37.8; H, 4.8; N, 24.4%.

Bis{*bis*(4-*methylpyrazol*-1-*yl*)*methane*}*dinitrocobalt* (*II*)(*H*$_2$*O*)$_2$ **9**. Compound **9** was obtained upon mixing $Co(NO_3)_2 \cdot 6H_2O$ (0.226 g, 0.77 mmol) in dichloromethane (20 ml) with bis(4-methylpyrazol-1-yl)methane ($\mathbf{L}^M$) (0.303 g, 1.72 mmol) in the same solvent (10 ml). The pale rose precipitate formed was filtered after 3 days and washed several times with dichloromethane and diethyl ether (0.351 g, yield 80%). M.p.: 157–160°C dec. Anal. Calcd for $C_{18}H_{28}CoN_{10}O_8$; C, 37.8; H, 4.9; N, 24.5. Found: C, 37.6; H, 5.1; N, 24.3%.

Bis{*bis*(4-*methylpyrazol*-1-*yl*)*methane*}*dinitronickel* (*II*)(*EtOH*) **10**. Compound **10** was obtained upon mixing $Ni(NO_3)_2 \cdot 6H_2O$ (0.290 g, 1.0 mmol) in ethanol (20 ml) with bis(4-methylpyrazol-1-yl)methane ($\mathbf{L}^M$) (0.35 g, 2.0 mmol) in the same solvent (10 ml). The lilac precipitate formed was filtered after 2 days and washed several times with ethanol and diethyl ether (0.511 g, yield 88%). M.p.: 246–249°C dec. Anal. Calcd for $C_{20}H_{30}N_{10}NiO_7$; C, 41.3; H, 5.2; N, 24.1. Found: C, 41.6; H, 5.1; N, 24.3%.

Bis{*bis*(4-*methylpyrazol*-1-*yl*)*methane*}*dinitrocopper* (*II*)(*H*$_2$*O*)$_2$ **11**. Compound **11** was obtained upon mixing $Cu(NO_3)_2 \cdot 2.5H_2O$ (0.186 g, 0.80 mmol) in dichloromethane (20 ml) with bis(4-methylpyrazol-1-yl)methane ($\mathbf{L}^M$) (0.300 g, 1.70 mmol) in the same solvent (10 ml). The dark-blue precipitate formed was filtered after 3 days and washed several times with dichloromethane and diethyl ether (0.433 g, yield 94%). M.p.: 237–238°C dec. Anal. Calcd for $C_{18}H_{28}CuN_{10}O_8$; C, 37.5; H, 4.9; N, 24.3. Found: C, 37.6; H, 5.0; N, 24.2%.

Bis(3,4,5-*trimethylpyrazol*-1-*yl*)*methanedichloro manganese*(*II*)(*H*$_2$*O*) **12**. Compound **12** was obtained upon mixing $MnCl_2 \cdot 4H_2O$ (0.099 g, 0.5 mmol) in diethyl ether (20 ml) with bis(3,4,5-trimethylpyrazol-1-yl)methane ($\mathbf{L}^T$) (0.23 g, 1.0 mmol) in the same solvent (10 ml). The colorless precipitate formed was filtered after 2 days and washed several times with diethyl ether (0.165 g, yield 88%). M.p.: 334°C dec. Anal. Calcd for $C_{13}H_{22}Cl_2MnN_4O$; C, 41.6; H, 5.9; N, 14.9. Found: C, 41.4; H, 5.7; N, 14.7%.

Bis(3,4,5-*trimethylpyrazol*-1-*yl*)*methanedichloroiron* (*II*)(*H*$_2$*O*) **13**. Compound **13** was obtained upon mixing $FeCl_2 \cdot 4H_2O$ (0.064 g, 0.3 mmol) in dichloromethane (20 ml) with bis(3,4,5-trimethylpyrazol-1-yl)methane ($\mathbf{L}^T$) (0.23 g, 1.0 mmol) in the same solvent (10 ml). The pale-brown precipitate formed was filtered after 1 day and washed several times with diethyl ether (0.087 g, yield 77%). M.p.: 312–314°C dec. Anal. Calcd for $C_{13}H_{22}Cl_2FeN_4O$; C, 41.4; H, 5.9; N, 14.9. Found: C, 41.7; H, 6.0; N, 14.4%.

Bis(3,4,5-*trimethylpyrazol*-1-*yl*)*methanedichlorocobalt*(*II*) **14**. Compound **14** was obtained upon mixing $CoCl_2$ (0.129 g, 1.0 mmol) in ethanol (20 ml) with bis(3,4,5-trimethylpyrazol-1-yl)methane ($\mathbf{L}^T$) (0.23 g, 1.0 mmol) in the same solvent (10 ml). The dark-blue precipitate formed was filtered after 1 day and washed several times with diethyl ether (0.225 g, yield 62%). M.p.: >360°C dec. Anal. Calcd for $C_{13}H_{20}Cl_2CoN_4$; C, 43.1; H, 5.6; N, 15.4. Found: C, 43.0; H, 5.8; N, 15.4%.

Bis(3,4,5-*trimethylpyrazol*-1-*yl*)*methanedichlorocopper*(*II*) **15**. Compound **15** was obtained upon mixing $CuCl_2 \cdot 2H_2O$ (0.138 g, 0.8 mmol) in ethanol (20 ml) with bis(3,4,5-trimethylpyrazol-1-yl)methane ($\mathbf{L}^T$) (0.23 g, 1.0 mmol) in the same solvent (10 ml). After 24 h diethyl ether was added. The light-green precipitate formed was filtered after 2 days and washed several times with diethyl ether (0.243 g, yield 83%). M.p.: 215–220°C dec. Anal. Calcd for $C_{13}H_{20}Cl_2CuN_4$; C, 42.6; H, 5.5; N, 15.3. Found: C, 42.2; H, 5.4; N, 15.1%.

Bis{*bis*(3,4,5-*trimethylpyrazol*-1-*yl*)*methane*}*dinitrocobalt*(*II*)(*H*$_2$*O*) **16**. Compound **16** was obtained upon mixing $Co(NO_3)_2 \cdot 6H_2O$ (0.226 g, 0.77 mmol) in ethanol (20 ml) with bis(3,4,5-trimethylpyrazol-1-yl) methane ($\mathbf{L}^T$) (0.46 g, 2.0 mmol) in the same solvent (10 ml). The violet precipitate was formed, which was filtered after 3 days and washed several times with ethanol and diethyl ether (0.461 g, yield 90%). M.p.: 276–277°C dec. Anal. Calcd for $C_{26}H_{42}CoN_{10}O_7$; C, 46.9; H, 6.4; N, 21.0. Found: C, 47.2; H, 6.5; N, 20.9%.

Bis{*bis*(3,4,5-*trimethylpyrazol*-1-*yl*)*methane*}*dinitronickel*(*II*) **17**. Compound **17** was obtained upon mixing $Ni(NO_3)_2 \cdot 6H_2O$ (0.290 g, 1.0 mmol) in dichloromethane (20 ml) with bis(3,4,5-trimethylpyrazol-1-yl)methane ($\mathbf{L}^T$) (0.46 g, 2.0 mmol) in the same solvent

(10 ml). The light-blue precipitate formed upon addition of diethyl ether was filtered after 3 days and washed several times with dichloromethane and diethyl ether (0.427 g, yield 66%). M.p.: 320°C dec. Anal. Calcd for $C_{26}H_{40}N_{10}NiO_6$; C, 48.3; H, 6.2; N, 21.7. Found: C, 48.0; H, 6.4; N, 21.5%.

Bis(3,4,5-*trimethylpyrazol*-1-*yl*)*methanedibromozinc*(*II*) **18**. Compound **18** was obtained upon mixing $ZnBr_2$ (0.225 g, 1.0 mmol) in diethyl ether (20 ml) with bis(3,4,5-trimethylpyrazol-1-yl)methane ($\mathbf{L}^T$) (0.23 g, 1.0 mmol) in the same solvent (10 ml). The colorless precipitate immediately formed was filtered after 2 h and washed several times with diethyl ether and recrystallized from dichloromethane/diethyl ether (0.415 g, yield 90%). The spectroscopic and analytical data are in accordance with those reported in literature [27].

X-ray crystallography

Crystal and experimental data are summarized in Table 1. A crystal of $C_{13}H_{20}Br_2N_4Zn$, obtained from a chloroform/diethyl ether solution was mounted on a CS automatic four-circle diffractometer equipped with a Huber goniometer using graphite monochromatized Mo-$K\alpha$ radiation ($\lambda = 0.71069$ Å). The cell parameters were refined by least squares from the angular positions of 32 reflections in the range $5 < 2\theta < 28°$. The data were collected at room temperature for $3 < 2\theta < 60°$ from colorless crystal of approximate $0.1 \times 0.2 \times 0.2$ mm using an ω scan technique. The scan rate was automatically chosen according to the peak intensity in the range 2.0–30.0° min^{-1}. Background counts were taken with stationary crystal with an offset of 0.6° at each end of the scan, and a total background to scan time ratio of 0.5. The intensities of three standard reflections, monitored every 97 reflections during the data collections don't show decay. Data were corrected for Lorentz and polarization effects. A total of 1802 independent reflections having $|F_o| > 6\sigma|F_o|$ were used in all subsequent calculations.

Table 1. Crystal data of compound **18**

Formula	$C_{13}H_{20}Br_2N_4Zn$
Formula weight	457.5
Crystal system	monoclinic
Space group	C 2/c
a (Å)	15.057(5)
b (Å)	16.486(5)
c (Å)	15.973(5)
β (°)	116.390(5)
V (Å^{-3})	3485(2)
Z	8
D_c (g cm^{-3})	1.745
μ (cm^{-1})	5.992
F (000)	1808.0
No. of measured reflections	5044
No. of unique reflections	2290
No. of observed reflections, $\|F_o\| > 6\sigma\|F_o\|$, n	1802
Function minimized	$\Sigma w(\|F_o\| - \|F_c\|)^2$
Variables refined, m	181
a, b and c values in the weighting function[a]	8.387, 0.095, 0.018
R[b]	5.8
R_w[c]	7.5
Goodness of fit, S[d]	1.054

[a] $w = 1.0/(a + b|F_o| + c|F_o|^2)$.
[b] $R = \Sigma(|F_o|^2 - |F_c|^2)/\Sigma F_o^2$.
[c] $R_w = \Sigma w(|F_o| - |F_c|)^2/\Sigma w F_o^2$.
[d] $S = \Sigma w(|F_o| - |F_c|)^2/(n - m)$.

The structure was solved by direct methods. All non-hydrogen atoms were refined by full matrix least-squares methods with anisotropic thermal parameters. The hydrogen atom was assigned the equivalent isotropic temperature factor of the parent carbon atom and allowed to ride on it. Atomic scattering factors were taken from Ref.[29]. All calculations were done on a PC using the SIR CAOS structure determination package [30].

RESULTS AND DISCUSSION

Derivatives **1**–**18** were synthesized from interaction between the ligands bis(pyrazol-1-yl)alkanes (L in general; in detail: L^M = (bis(4-methylpyrazol-1-yl) methane, L^T = bis(3,4,5-trimethylpyrazol-1-yl) methane) and the appropriate metal salt $MX_2 \cdot xH_2O$ (M = Zn, X = Br, M = Mn, Fe, Co, Ni or Cu, X = Cl; M = Ni, Co or Cu, X = NO_3) in accordance with the following:

$$nL + MX_2 \cdot xH_2O \xrightarrow{S} [(L)_nMX_2] \cdot xH_2O \cdot zS \quad (1)$$

A 2:1 adduct is always the product from metal nitrates also when a different metal to ligand molar ratio was employed, while 1:1 or 2:1 adduct are found with metal halides, depending not only on the donor but also on the solvent and on the molar ratio used in the synthesis.

It is interesting to note that the donor bis(4-methylpyrazol-1-yl)methane L^M gives with $MnCl_2$ and $FeCl_2$ acceptors both 1:1 and 2:1 adducts, whereas the more basic bis(3,4,5-trimethylpyrazol-1-yl)methane, L^T gives only 1:1 adducts. The greater steric hindrance of L^T with respect to L^M causes this different behaviour. No reaction was observed between L^T and $Mn(NO_3)_2 \cdot 6H_2O$ and $Cu(NO_3) \cdot 2.5H_2O$, the starting materials being always recovered.

All the compounds **1**–**18** were identified through elemental analyses (Section 2), solid-state infrared spectra (Table 2), magnetic and conductivity data (Table 3) and electronic spectra (Table 4).

With exception of compounds **2**, **6**, **12** and **17** which melt with decomposition, our adducts have sharp melting points. All the complexes are insoluble in water, diethyl ether, aromatic and aliphatic hydro-

Table 2. Selected IR and far-IR (nujol) data of derivatives **1**–**17**

Compound	No.	ν(OH), δ(OH)	β(ring)	ν(C_{ring}–H)	δ(ring)	ν(M–N)	Other data
L^M			1574s	3149m	640vs		
				3084m	608s		
$(L^M)MnCl_2 \cdot H_2O$	1	3250br	1574m	3106m	640vs	218m	301s, ν(Mn–Cl), 196s,
		1630m			607s		ν(Mn–Cl–Mn)
$(L^M)_2MnCl_2 \cdot H_2O$	2	3440br	1573m	3148m	649s	231vs	310s, ν(Mn–Cl)
		1665m		3088m	634vs	223s	
					607s		
$(L^M)FeCl_2 \cdot H_2O$	3	3220br	1575m	3095w	639s	365s	377vs, ν(Fe–Cl), 210s,
		1654m			606m	321m	ν(Fe–Cl–Fe)
$(L^M)_2FeCl_2 \cdot 2H_2O$	4	3260br	1576m	3084w	639s	345m	363s, ν(Fe–Cl)
		1636m			608m		
$(L^M)CoCl_2 \cdot 2H_2O$	5	3140br	1576m		640s	236m	298m, ν(Co–Cl), 185s,
		1644m			608m		ν(Co–Cl–Co)
$(L^M)_2NiCl_2 \cdot H_2O$	6	3220br	1577s		642s	301s	376s, ν(Ni–Cl)
		1643s			609s	264m	
$(L^M)CuCl_2$	7		1572m	3124m	637s	389m	302s, 293s, ν(Cu–Cl)
				3093m	606s	365m	
$(L^M)_2Mn(NO_3)_2 \cdot 2H_2O$	8	3390br	1574m	3106m	642s	226m	296m, ν(Mn–O),
		1658s			606s		1779w, 1766w, 1747,
							($\nu_1+\nu_4$, NO_3)
$(L^M)_2Co(NO_3)_2 \cdot 2H_2O$	9	3180br	1575s		642s	244s	369vs, ν(Co–O), 1748w,
		1652m			605s		1732w, ($\nu_1+\nu_4$, NO_3)
$(L^M)_2Ni(NO_3)_2 \cdot EtOH$	10	3360br	1576m	3093m	641vs	292vs	303s, ν(Ni–O), 1768w,
		1654m			606s	263m	1747w, 1707w, ($\nu_1+\nu_4$,
							NO_3)
$(L^M)_2Cu(NO_3)_2 \cdot 2H_2O$	11	3290br	1575m	3122m	639s	376m	308vs, ν(Cu–O), 1748w,
		1674s			605s		1733w, ($\nu_1+\nu_4$, NO_3)
L^T			1585s		641m		
			1515m		618m		
$(L^T)MnCl_2 \cdot H_2O$	12	3380br	1581m		634m	252s	302vs, ν(Mn–Cl), 175s,
		1628m	1506w		619m		ν(Mn–Cl–Mn)
$(L^T)FeCl_2 \cdot H_2O$	13	3240br	1579m		636m	386sh	354vs, 309s, ν(Fe–Cl)
		1630m	1510m		618m	378v	
$(L^T)CoCl_2$	14		1580m		636m	247m	349vs, 314s, ν(Co–Cl)
			1510m		618m	232m	
$(L^T)CuCl_2$	15		1575m		632s	398vs	281s, ν(Cu–Cl), 195s,
			1505m		620m	369m	185s, ν(Cu–Cl–Cu)
$(L^T)_2Co(NO_3)_2 \cdot H_2O$	16	3430br	1578m		632s	244s	369vs, ν(Co–O), 1760w,
		1652m	1510w		624m		1746w, 1722w, ($\nu_1+\nu_4$,
							NO_3)
$(L^T)_2Ni(NO_3)_2$	17		1579m		632m	301s	373vs, ν(Ni–O), 1769w,
			1508w		624m		1746w, 1722w, ($\nu_1+\nu_4$,
							NO_3)

carbons, poorly soluble in chlorinate solvents and acetone, generally soluble in acetonitrile and nitromethane. Derivatives **1**, **2** and **6** were soluble only in the latter solvent. Electronic spectra and conductivity measurements were performed in acetronitrile and nitromethane, respectively.

Several derivatives contain one or two molecules of water of crystallization notwithstanding addition of the dehydrating agent $HC(OEt)_3$ to reactions solutions [31].

The halide adducts **1**, **2**, **5**, **7**, **12** and **13** are non-electrolytes in nitromethane solution, thus ruling out self-ionization or displacement of the anion by the solvent, i.e.

$$2[(L)MX_2] \rightleftharpoons [(L)_2M]^{2+} + [MX_4]^{2-} \quad (2)$$

$$[(L)_nMX_2] + n\ \text{solvent} \rightleftharpoons [(L)_nM(\text{solvent})_n]^{2+} + 2[X]^- \quad (3)$$

Derivatives **3**, **4**, **8**, **14** and **15** seem to be only partially dissociated or not completely electrolytes in nitromethane (Λ_m in the range 24.7–43.3 $\Omega^{-1}\,cm^2\,mol^{-1}$) whereas the derivatives **6**, **9**–**11**, **16** and **17** are 1:1 electrolytes (Λ_m in the range 60–80 $\Omega^{-1}\,cm^2\,mol^{-1}$).

Table 3. Magnetic and conductance data of derivatives **1**–**17**

Compound (empirical formula)	No.	F.W.	χ_M^{corr}	μ_{eff}[a]	Solvent	Concentration[b]	Λ_m^c
$(L_M)MnCl_2 \cdot H_2O$ $C_9H_{14}Cl_2MnN_4O$	**1**	320.1	$1.30 \cdot 10^{-2}$	5.51	CH_3NO_2	$0.44 \cdot 10^{-3}$	12.5
$(L_M)_2MnCl_2 \cdot H_2O$ $C_{18}H_{26}Cl_2MnN_8O$	**2**	496.3	$1.54 \cdot 10^{-2}$	6.00	CH_3NO_2	$0.53 \cdot 10^{-3}$	14.1
$(L_M)FeCl_2 \cdot H_2O$ $C_9H_{14}Cl_2FeN_4O$	**3**	321.0	$0.85 \cdot 10^{-2}$	4.48	CH_3NO_2	$1.38 \cdot 10^{-3}$	43.3
$(L_M)_2FeCl_2 \cdot 2H_2O$ $C_{18}H_{28}Cl_2FeN_8O_2$	**4**	515.2	$1.20 \cdot 10^{-2}$	5.30	CH_3NO_2	$0.58 \cdot 10^{-3}$	26.0
$(L_M)CoCl_2 \cdot 2H_2O$ $C_9H_{16}Cl_2CoN_4O_2$	**5**	342.1	$0.64 \cdot 10^{-2}$	3.86	CH_3NO_2	$1.55 \cdot 10^{-3}$	11.7
$(L_M)_2NiCl_2 \cdot H_2O$ $C_{18}H_{26}Cl_2N_8NiO$	**6**	500.1	$0.46 \cdot 10^{-2}$	3.28	CH_3NO_2	$1.06 \cdot 10^{-3}$	52.3
$(L_M)CuCl_2$ $C_9H_{12}Cl_2CuN_4$	**7**	310.7	$0.17 \cdot 10^{-2}$	2.00	CH_3NO_2	$0.83 \cdot 10^{-3}$	10.1
$(L_M)_2Mn(NO_3)_2 \cdot 2H_2O$ $C_{18}H_{28}MnN_{10}O_8$	**8**	567.4	$1.68 \cdot 10^{-2}$	6.29	CH_3NO_2	$0.79 \cdot 10^{-3}$	31.6
$(L_M)_2Co(NO_3)_2 \cdot 2H_2O$ $C_{18}H_{28}CoN_{10}O_8$	**9**	571.4	$0.99 \cdot 10^{-2}$	4.81	CH_3NO_2	$1.38 \cdot 10^{-3}$	62.7
$(L_M)_2Ni(NO_3)_2 \cdot EtOH$ $C_{20}H_{30}N_{10}NiO_7$	**10**	581.2	$0.37 \cdot 10^{-2}$	3.03	CH_3NO_2	$1.08 \cdot 10^{-3}$	81.6
$(L_M)_2Cu(NO_3)_2 \cdot 2H_2O$ $C_{18}H_{28}CuN_{10}O_8$	**11**	576.0	$0.15 \cdot 10^{-2}$	1.89	CH_3NO_2	$1.16 \cdot 10^{-3}$	70.4
$(L_T)MnCl_2 \cdot H_2O$ $C_{13}H_{23}Cl_2MnN_4O$	**12**	376.2	$1.55 \cdot 10^{-2}$	6.03	CH_3NO_2	$1.47 \cdot 10^{-3}$	3.5
$(L_T)FeCl_2 \cdot H_2O$ $C_{13}H_{23}Cl_2FeN_4O$	**13**	377.1	$1.17 \cdot 10^{-2}$	5.24	CH_3NO_2	$0.80 \cdot 10^{-3}$	16.9
$(L_T)CoCl_2$ $C_{13}H_{26}Cl_2CoN_4$	**14**	362.2	$1.06 \cdot 10^{-2}$	5.00	CH_3NO_2	$0.23 \cdot 10^{-3}$	24.7
$(L_T)CuCl_2$ $C_{13}H_{26}Cl_2CuN_4$	**15**	367.8	$0.83 \cdot 10^{-2}$	1.39	CH_3NO_2	$1.32 \cdot 10^{-3}$	29.5
$(L_T)_2Co(NO_3)_2 \cdot H_2O$ $C_{26}H_{44}CoN_{10}O_7$	**16**	667.6	$1.02 \cdot 10^{-2}$	4.88	CH_3NO_2	$0.67 \cdot 10^{-3}$	70.6
$(L_T)_2Ni(NO_3)_2$ $C_{26}H_{42}N_{10}NiO_6$	**17**	649.4	$0.43 \cdot 10^{-2}$	3.16	CH_3NO_2	$0.95 \cdot 10^{-3}$	68.4

[a] μ_{eff} are in B.M. (Bohr magnetons).
[b] Concentrations are in mol/l.
[c] $\Omega^{-1}\,cm^2\,mol^{-1}$.

Magnetic moments of the derivatives of manganese(II), iron(II), cobalt(II), nickel(II) and copper(II) are typical of high spin d^5, d^6, d^7, d^8 and d^9 metal complexes, respectively, containing five, four, three, two and one decoupled electrons, respectively.

Derivatives **1**, **3**, and **5** show values of μ_{eff} slightly smaller than appropriate theoretical μ_s, likely due to partial extinction of magnetic moment caused by formation of chloro or nitro-bridged dimers, oligomers or polymers containing weak M···M interactions. In fact, it has been previously observed that many transition metal derivatives containing bis(pyrazol-1-yl)alkane donors adopt binuclear geometries with chloro-bridged metal atoms [2, 4].

In the IR spectra of complexes **1**–**6**, **8**–**13** and **16**, the appearance of broad bands of variable intensity centred at 3200–3400 and 1630–1670 cm^{-1} due to ν(OH) and δ(OH) vibrations, respectively, confirms the presence of water.

The medium band at *ca.* 1570 cm^{-1}, in the derivatives of L^M and those at *ca.* 1570 and 1510 cm^{-1} in the derivatives of L^T, due to breathing of the pyrazole rings [32, 33], do not undergo any notable shift upon coordination. Moreover two strong absorption bands at 640 and 610 cm^{-1} have been assigned to ring deformation modes [34, 35].

In the IR spectra of nitrato derivatives straightforward assignments of the two highest-frequency bands ν_1 and ν_5 of NO_3 groups are not possible due to the presence of nujol and of many overlapped ligand bands in the region 1200–1500 cm^{-1}.

However in the overtone region several weak bands

Table 4. UV–Visible data of derivatives **1**–**17**

Compound	No.	Solvent	Concentration (mol/l)	λnm (cm^{-1})	ε $(mol/l)^{-1}\,cm^{-1}$	Assignment
L^M		CH_3CN	$1.29 \cdot 10^{-3}$	224 (44643)	2550	ligand
$(L^M)MnCl_2 \cdot H_2O$	1	insoluble				
$(L^M)_2MnCl_2 \cdot H_2O$	2	insoluble				
$(L^M)FeCl_2 \cdot H_2O$	3	CH_3CN	$1.58 \cdot 10^{-3}$	242 (41322)	5020	ligand
				310 (32258)	3570	CT
				360 (27778)	3300	CT
				1733 (5770)*		d–d
$(L^M)_2FeCl_2 \cdot 2H_2O$	4	CH_3CN	$1.29 \cdot 10^{-3}$	232 (43103)	5650	ligand
				310 (32258)	3000	CT
				358 (27933)	2300	CT
				1039 (9625)*		d–d
				1120 (8930)*		d–d
$(L^M)CoCl_2 \cdot 2H_2O$	5	CH_3CN	$1.01 \cdot 10^{-3}$	230 (43478)	6700	ligand
				256 (39062)	2300	CT
				300 (33333)	290	CT
				592 (16892)	130	d–d
				652 (15337)	150	d–d
				678 (14749)	180	d–d
				1044 (9580)*		d–d
$(L^M)_2NiCl_2 \cdot H_2O$	6	insoluble		1053 (9500)*		d–d
$(L^M)CuCl_2$	7	CH_3CN	$0.71 \cdot 10^{-3}$	234 (42735)	10420	ligand
				270 (37037)	9870	CT
				406 (24630)	1140	CT
				690 (14493)	140	d–d
$(L^M)_2Mn(NO_3)_2 \cdot 2H_2O$	8	CH_3CN	$0.85 \cdot 10^{-3}$	228 (43860)	7200	ligand
				272 (36765)	350	CT
				602 (16611)	15	d–d
$(L^M)_2Co(NO_3)_2 \cdot 2H_2O$	9	CH_3CN	$1.02 \cdot 10^{-3}$	232 (43103)	6870	ligand
				292 (34247)	1000	CT
				500 (20000)	50	d–d
				1064 (9400)*		d–d
$(L^M)_2Ni(NO_3)_2 \cdot EtOH$	10	CH_3CN	$1.07 \cdot 10^{-3}$	228 (43860)	6230	ligand
				268 (37313)	660	CT
				1064 (9400)*		d–d
$(L^M)_2Cu(NO_3)_2 \cdot 2H_2O$	11	CH_3CN	$0.90 \cdot 10^{-3}$	228 (43860)	7400	ligand
				284 (35211)	1530	CT
				336 (29762)	780	CT
				690 (14493)	60	d–d
				1059 (9440)*		d–d
L^T		CH_3CN	$1.58 \cdot 10^{-3}$	218 (45872)	3350	ligand
$(L^T)MnCl_2 \cdot H_2O$	12	CH_3CN	$0.68 \cdot 10^{-3}$	218 (45872)	3350	ligand
				272 (36765)	230	CT
$(L^T)FeCl_2 \cdot H_2O$	13	CH_3CN	$1.07 \cdot 10^{-3}$	234 (42735)	7000	ligand
				306 (32680)	2380	CT
				358 (27933)	2060	CT
				596 (16778)	120	CT
				1499 (6670)*		d–d
				1706 (5860)*		d–d
$(L^T)CoCl_2$	14	CH_3CN	$1.77 \cdot 10^{-3}$	234 (42735)	4100	ligand
				290 (34483)	860	CT
				566 (17668)	340	d–d
				612 (16340)	360	d–d
				668 (14970)	410	d–d
				1069 (9350)*		d–d
				1333 (7500)*		d–d
				1675 (5970)*		d–d
$(L^T)CuCl_2$	15	CH_3CN	$0.91 \cdot 10^{-3}$	230 (43478)	7800	ligand
				272 (36765)	2360	CT
				352 (28409)	770	CT
				440 (22727)	330	CT
				750 (13333)	100	d–d

Table continued on next page

Table 4.—*continued*

Compound	*No.*	*Solvent*	*Concentration (mol/l)*	*λ*nm (cm^{-1})	*ε* $(mol/l)^{-1}\,cm^{-1}$	Assignment
$(L^T)_2Co(NO_3)_2 \cdot H_2O$	16	CH_3CN	$0.81 \cdot 10^{-3}$	236 (42373)	8600	ligand
				295 (33898)	1360	CT
				500 (20000)	70	d–d
				1067 (9370)*		d–d
$(L^T)_2Ni(NO_3)_2$	17	CH_3CN	$0.81 \cdot 10^{-3}$	230 (43378)	8500	ligand
				1081 (9250)*		d–d

*The data are from near IR (nujol) spectra.

at 1700–1800 cm^{-1}, due to $\nu_1 + \nu_4$ combination bands, have been detected which can help in distinguishing ionic or coordinate nitrates [36].

Derivatives **9** and **11** exhibit two weak bands and the splitting Δ is 16 and 15 cm^{-1}, respectively, in accordance with an unidentate nitrate group in the solid state, whereas in the spectra of derivatives **8**, **10**, **16** and **17** three weak absorptions have been detected in the same region, indicative of the existence of both ionic and coordinate nitrate. These derivatives likely contain a six-coordinate metal atom surrounded by four nitrogen atoms and two oxygen atoms.

We have assigned some medium-to-strong absorption bands in the 200–400 cm^{-1} range to *ν*(M–Cl), *ν*(M–N) and *ν*(M–O) vibrations modes [37]. In the chloro derivatives **1**, **3** and **5** besides *ν*(M–Cl) stretching frequencies in the region 300–400 cm^{-1}, we have always detected also a strong absorption between 180 and 220 cm^{-1}, likely due to *ν*(M–Cl–M) vibration, in accordance with magnetic results which suggest a dinuclear or polynuclear structure. Only one IR-active *ν*(M–Cl) stretching band is found in the far-IR spectrum of derivatives **2** and **6** in accordance with octahedral N_4Cl_2Mn and N_4Cl_2Ni central cores, respectively, where the Cl atoms occupy *cis* positions. In the spectra of anhydrous derivatives **7**, **13** and **14** two strong *ν*(M–Cl) and two strong *ν*(M–N) vibration modes appeared below 400 cm^{-1} which are indicative of distorted tetrahedral geometries.

The near-IR and visible absorption bands give further support to the hypothesized geometries for our derivatives. The $FeCl_2$ adduct **13** (C_{2v} structure), shows a band at 6670 cm^{-1} with a shoulder at 5860 cm^{-1} assignable to $^5T_{2g} \leftarrow {}^5E_g$ transition with additional fine structure due to the loss of degeneracy of the $^5T_{2g}$ state [38], whereas the likely dinuclear derivative **3** shows only a band at 5770 cm^{-1}.

In the spectrum of compound **4** two absorption at 8930 and 9625 cm^{-1}, respectively, are in accordance with an octahedral distorted geometry (pseudo-D_{4h} symmetry) having a ground state $(t_{2g})^4(e_g)^4$ ($^5T_{2g}$) and the only spin allowed excited state $(t_{2g})^3(e_g)^3$, (^5E_g) being split into $^5A_1 + {}^5B_1$ [39, 40].

In the blue pseudo-tetrahedral cobalt derivative **14** the $^4T_1(F) \leftarrow {}^4A_2$ and $^4T_1(P) \leftarrow {}^4A_2$ transitions appear as multiple absorptions both in the near IR (5970, 7500 and 9350 cm^{-1}) and in the visible (566, 612, 668 nm) regions [31]. Instead the likely dinuclear pink cobalt derivative **5** exhibits a broad band at 9590 cm^{-1} in the near IR and three absorptions at 592, 652 and 678 nm in the visible region as previously observed in high spin five-coordinate Co(II) systems having a structure intermediate between square pyramidal and trigonal bipyramidal [41, 42, 43].

High-spin cobalt nitrate derivatives **9** and **16** are likely six-coordinated with a ionic NO_3 group and the other NO_3 linked to metal in the O_2-bidentate form [31, 44].

Apparent absence of visible absorptions for derivatives **10** and **17** is likely due to their very low energy transitions [45].

The copper nitrato derivative **11** exhibits in the near IR spectrum a band at 9440 cm^{-1} likely due to transitions to z^2 from x^2–y^2 and a band at 690 nm in the visible region which arises from a double degenerate (*xz* and *yz*) level, respectively, in accordance with a *cis*-octahedral geometry [46].

The structure of the compound [bis(3,4,5-trimethylpyrazol-1-yl)methanedibromozinc(II)] **18** with the numbering scheme is given in Fig. 2. Selected bond distances and angles are listed in Table 5. In the unit cell of the adduct **18** there are eight molecules which are monomeric with no short intramolecular contacts and are kept together by van der Waals interactions.

Table 5. Selected crystal data of compound **18**

Bond distances			
Zn–Br(1)	2.372(3)	Zn–Br(2)	2.350(3)
Zn–N(1)	2.078(15)	Zn–N(3)	2.075(19)
Bond angles			
Br(1)–Zn–Br(2)	119.1(1)	Br(1)–Zn–N(1)	107.0(4)
Br(2)–Zn–N(1)	113.7(4)	Br(1)–Zn–N(3)	108.2(4)
Br(2)–Zn–N(3)	113.3(5)	N(1)–Zn–N(3)	92.2(6)
Zn–N(1)–N(2)	116.6(12)	Zn–N(1)–C(3)	136.1(11)
Zn–N(3)–N(4)	118.7(15)	Zn–N(3)–C(10)	133.1(12)

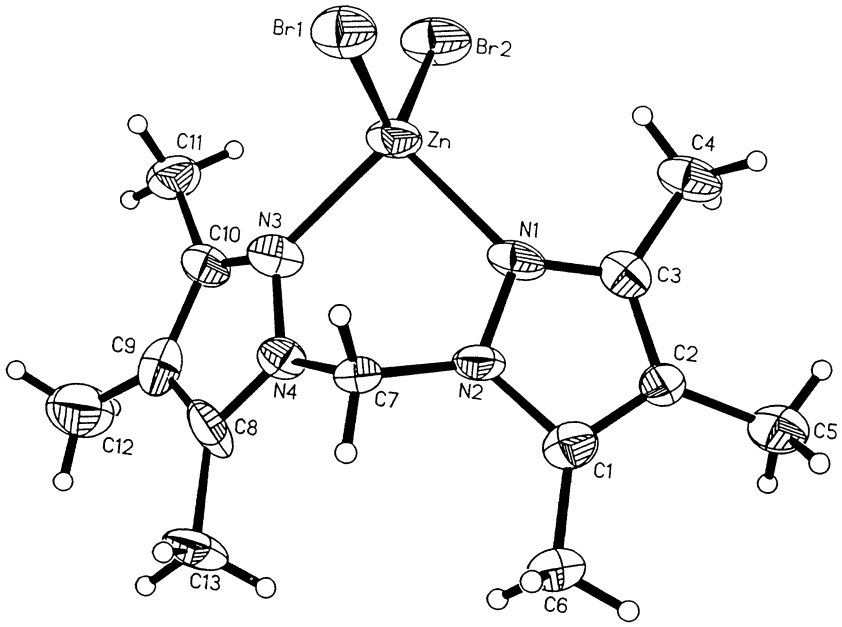

Fig. 2. An ORTEP view of complex $[L^TZnBr_2]$ (**18**).

The two pyridinic nitrogens of the donor L^T and two bromine atoms are arranged around the zinc atom in a strongly distorted environment: the N–Zn–N and Br–Zn–Br angles are 92.2(6) and 119.1(1)°, respectively, whereas the N–Zn–Br angles ranges from 107.0(4) to 113.7(4)°. The six-membered $C(N–N)_2Zn$ ring adopts an inverted boat conformation: the molecule is "butterfly" shaped; in fact the angle formed by the plane passing through each of the pyrazole rings and the plane passing through the central six-membered ring are about 27°. The N–Zn–N angle found in this compound lies out of the upper limit (89°) found for the metal derivatives of bis(pyrazol-1-yl)alkanes [7]. This further confirms the well-known greater flexibility of this family of ligands with respect to 2,2′-bipyridine and 1,10-phenanthroline donors which have a "fixed" bite. The Zn–N distances are longer than those found in similar dibromozinc(II) derivatives [25] and support the steric misfit between the N_2-donor L^T and the tetrahedral zinc ion. On the other hand the Zn–Br distances are in the range found for tetrahedral dibromozinc(II) complexes [25, 47].

CONCLUSIONS

The combined evidence from measurements carried out in solid state and in solution (IR, conductivity, magnetic susceptibility, UV spectra, X-ray crystal structure determination) gives here a picture which is different from that obtained when other poly(pyrazol-1-yl)alkanes were considered [1–7].

The bis(4-methylpyrazol-1-yl)methane seems to be a better donor toward transition metal acceptors with respect to other bis(pyrazol-1-yl)alkanes [1–7]: the ligand/metal ratio *r*, frequently a measure of the donating ability, is 2 not only with good acceptors such as $M(NO_3)_2$ but also with MCl_2 salts; *r* is strongly dependent not only from the solvent but also from the molar ratio employed in the synthesis. We have found a marked difference between the behavior of bis(4-methylpyrazol-1-yl)methane and that of bis(3,4,5-trimethylpyrazol-1-yl)methane.

The donating ability can be easily correlated to basicity and steric hindrance of the heterocyclic ring: the bis(4-methylpyrazol-1-yl)methane also if is less basic than bis(3,4,5-trimethylpyrazol-1-yl)methane, however is less sterically hindered and a better donor ligand.

Polynuclear derivatives are also possible in the case of metal chloride acceptors such as $MnCl_2$, $FeCl_2$ and $NiCl_2$: this behavior is analogous to those previously found [2, 4].

SUPPLEMENTARY MATERIAL

Tables of atomic coordinates and isotropic equivalent thermal parameters, tables of structures factors, a full list of bond lengths and angles and tables of anisotropic displacement parameters are available on request from one of the authors.

Acknowledgements—We thank the MURST, CNR-Rome and the Universities of Camerino and Rome for financial help.

REFERENCES

1. Mesubi, M. A. and Ekemenzie, P. I., *Trans. Met. Chem.*, 1984, **9,** 91.
2. Reedijk, J. and Verbiest, J., *Trans. Met. Chem.*, 1978, **3,** 51.
3. Canty, A. J., Lee, C. V., Chaichit, N. and Gatehouse, B. M., *Acta Cryst. B*, 1982, **38,** 743.
4. Jansen, J. C., van Koningsveld, H., van Ooijen, J. A. C. and Reedijk, J., *Inorg. Chem.*, 1980, **19,** 170.
5. Mani, F., *Inorg. Chim. Acta*, 1980, **38,** 97.
6. Gioia Lobbia, G., Bonati, F., Cingolani, A., Leonesi, D. and Lorenzotti, A., *J. Organomet. Chem.*, 1989, **359,** 21.
7. Lorenzotti, A., Bonati, F., Cingolani, A., Gioia Lobbia, G., Leonesi, D. and Bovio, B., *Inorg. Chim. Acta*, 1990, **170,** 199.
8. Trofimenko, S., *Inorg. Synth.*, 1970, **12,** 99.
9. Trofimenko, S., *Acc. Chem. Res.*, 1971, **4,** 17.
10. Trofimenko, S., *Chem. Rev.*, 1972, **72,** 497.
11. Shaver, A., *J. Organomet. Chem. Library*, 1977, **3,** 157.
12. Trofimenko, S., *Progr. Inorg. Chem.*, 1986, **34,** 115.
13. Trofimenko, S., *Chem. Rev.*, 1993, **93,** 943.
14. McWhinnie, W. R. and Miller, J. D., *Adv. Inorg. Chem. Radiochem.*, 1969, **12,** 135.
15. McKenzie, E. D., *Coord. Chem. Rev.*, 1971, **6,** 187.
16. Schilt, A. A., *Applications of* 1,10-*Phenanthroline and Related Compounds*. Pergamon Press, 1969.
17. McBryde, W. A., *A Critical Review of Equilibrium Data for Proton and Metal Complexes of* 1,10-*Phenanthroline*, 2,2′-*Bipyridil and Related Compounds*. Pergamon Press, 1978.
18. Trofimenko, S., *J. Am. Chem. Soc.*, 1970, **92,** 5118.
19. Clark, H. C., Ferguson, G., Jain, V. K. and Parvez, M., *Organometallics*, 1983, **2,** 806.
20. Canty, A. J., Lee, C. V., Chaichit, N. and Gatehouse, B. M., *Acta Crystallogr. B*, 1982, **38,** 743.
21. Pettinari, C., Santini, C., Leonesi, D. and Cecchi, P., *Polyhedron*, 1994, **13,** 1553.
22. Pettinari, C., Lorenzotti, A., Sclavi, G., Cingolani, A., Rivarola, E., Colapietro, M. and Cassetta, A., *J. Organomet. Chem.*, 1995, **496,** 69.
23. Pettinari, C., Lorenzotti, A., Cingolani, A., Leonesi, D., Marra, M. and Marchetti, F., *Gazz. Chim. Ital.*, 1993, **123,** 481.
24. Bonati, F., Cingolani, A., Gioia Lobbia, G., Leonesi, D., Lorenzotti, A. and Pettinari, C., *Gazz. Chim. Ital.*, 1990, **120,** 341.
25. Pettinari, C., Cingolani, A. and Bovio, B., *Polyhedron*, 1996, **15,** 115.
26. Pettinari, C., Lorenzotti, A., Pellei, M. and Santini, C., *Polyhedron*, 1997, **16,** 3435.
27. Pettinari, C., Gioia Lobbia, G., Lorenzotti, A. and Cingolani, A., *Polyhedron*, 1995, **14,** 793.
28. Claramunt, R. M., Hernandez, H., Elguero, J. and Julia, S., *Bull. Soc. Chim. Fr.*, 1982, **2,** 5.
29. *International Tables for X-ray Crystallography*, Vol. IV. Kynoch Press, Birmingham, 1974, pp. 99–149.
30. Camalli, M., Capitani, D., Cascarano, G., Cerrini, S., Giacovazzo, C. and Spagna, R., Italian Patent No. 35403c/86. SIR CAOS User Guide, Istituto di Strutturistica Chimica CNR.
31. Reedijk, J. and Verbiest, J., *Trans. Met. Chem.*, 1979, **4,** 239.
32. Vos, J. G. and Groeneveld, W. L., *Inorg. Chim. Acta*, 1977, **24,** 123.
33. Nieuwpoort, G., Vos, J. G. and Groeneveld, W. L., *Inorg. Chim. Acta*, 1978, **29,** 117.
34. Reedijk, J., *Rec. Trav. Chim.*, 1969, **88,** 1451.
35. Mesubi, M. A. and Anumba, F. O., *Trans. Met. Chem.*, 1985, **10,** 5.
36. Lever, A. B. P., Mantovani, E. and Ramaswamy, B. S., *Can. J. Chem.*, 1957, **1971,** 49.
37. Nakamoto, K., *Infrared Spectra of Inorganic and Coordination Compounds*, ed. K. Nakamoto. John Wiley and Sons, New York, 1986.
38. Quagliano, J. V., Banerjee, A. K., Goedkin, V. L. and Vallarino, L. M., *J. Am. Chem. Soc.*, 1970, **92,** 482.
39. Madeja, K. and Konig, E., *J. Inorg. Nucl. Chem.*, 1963, **25,** 377.
40. Little, B. F. and Long, G. J., *Inorg. Chem.*, 1978, **17,** 3401.
41. Dori, Z., Eisenberg, R. and Gray, H. B., *Inorg. Chem.*, 1967, **6,** 483.
42. Dori, Z. and Gray, H. B., *Inorg. Chem.*, 1968, **7,** 889.
43. Burmeister, J. L., O'Sullivan, T. P. and Johnson, K. A., *Inorg. Chem.*, 1971, **10,** 1803.
44. Lever, A. B. P., *Inorganic Electronic Spectroscopy*, 2th edn. Elsevier, Amsterdam, The Netherlands, 1984, pp. 480–490.
45. Lever, A. B. P., *Inorganic Electronic Spectroscopy*, 2th edn. Elsevier, Amsterdam, The Netherlands, 1984, pp. 507–520.
46. Hathaway, B. J. and Billing, D. E., *Coord. Chem. Rev.*, 1970, **5,** 143.
47. Yoon, K. and Parkin, G., *J. Am. Chem. Soc.*, 1991, **113,** 8414.

Pergamon

Polyhedron Vol. 17, No. 23–24, pp. 4155–4162, 1998
© 1998 Elsevier Science Ltd
All rights reserved. Printed in Great Britain
0277–5387/98 $19.00+0.00

PII: S0277-5387(98)00223-X

Synthesis and redox properties of ferrocenylquinoxalines

Piero Zanello[a], Marco Fontani[a], S. Zaka Ahmed[b] and Christopher Glidewell[b]*

[a] Dipartimento di Chimica dell'Università di Siena, Pian dei Mantellini, 44, 53100 Siena, Italy

[b] School of Chemistry, University of St. Andrews, St. Andrews, Fife KY16 9ST, U.K.

(Received 30 March 1998; accepted 1 June 1998)

Abstract—The ferrocenyl 1,2-diketone [$(C_5H_5)Fe(C_5H_4)COCOPh$] when condensed with aromatic 1,2-diamines forms a range of ferrocenyl-substituted quinoxalines: when the diamine is unsymmetrically substituted the quinoxaline is formed as a mixture of two regio-isomers, which can in some cases be separated by careful chromatography. Electrochemical studies show that these present ferrocenylquinoxalines undergo the expected reversible one-electron oxidation centred on the ferrocenyl moiety and a two-electron reduction process centred on the quinoxalyl fragment, which is accompanied by chemical complications. The oxidation of the ferrocenyl group occurs at potentials slightly higher than that of unsubstituted ferrocene (by about 100–150 mV, depending on the substituents) indicating that the quinoxalyl substituent is slightly electron-withdrawing with respect to ferrocene. © 1998 Elsevier Science Ltd. All rights reserved

Keywords: cyclic voltammetry; electrochemistry; ferrocene; quinoxaline.

INTRODUCTION

The reaction between 1,2-diketones and 1,2-diamines to form quinoxalines, well-known as a characteristic reaction for both components, has been successfully exploited as a polymer-forming process when applied to combinations of bis(1,2-diketones) and bis(1,2-diamines) [1–3]. For polymer synthesis, the reaction can generally be performed under solvent-free (melt-phase) conditions, when the sole by-product is water which distills from the reaction mixture at the melting temperature of the components. It is the removal of the water by-product, along with the *in situ* formation of new heteroaromatic rings, which drives the process to completion. The effectiveness of this reaction [1–3] makes it an attractive route for the synthesis of organometallic polymers, for example by reaction of 1,1′-ferrocenediylbis(1,2-diketones) with bis(1,2-diamines). We have recently described effective routes to a range of ferrocenyl 1,2-diketones [4, 5] and here we present the results of a study of reactions of a representative ferrocenyl diketone, FcCOCOPh [4, 6] [$Fc = (C_5H_5)Fe(C_5H_4)$] with a range of 1,2-diamines, to form the corresponding ferrocenylquinoxalines, along with an electrochemical study of their redox properties. Monomeric ferrocenylquinoxalines are themselves potentially of interest and importance: a number of quinoxalines are powerful antibiotics and some examples show potential as anti-cancer drugs [7] and their action in this respect is dependent on their binding to DNA by intercalation [8]. At the same time, some rather simple ferricinium salts have been shown to exhibit powerful anti-tumour activity against a range of human tumour types [9]: the introduction of ferrocenyl substituents onto the quinoxaline framework could perhaps provide, in a single molecular species, a powerful combination of these two actions.

RESULTS AND DISCUSSION

Syntheses of ferrocenylquinoxalines

Reaction of 1-ferrocenyl-2-phenylethanedione, FcCOCOPh, **1**, with 1,2-diaminobenzene, **2**, yields the corresponding 2-ferrocenyl-3-phenylquinoxaline, **3**. When the reaction is conducted in the absence of solvent by melting together the two components under

* Author to whom correspondence should be addressed.

an inert atmosphere, the yield of the deep-purple product is generally somewhat less than 50%, after chromatographic purification. However, if the two reactants are first mixed in dioxan solution and then slowly heated first in solution and, subsequently, after all the solvent has evaporated, as a melt, the yield of purified product is consistently around 65%.

The product **3** is readily characterised by its analytical data and its ^{1}H and ^{13}C NMR spectra. The ^{1}H NMR spectrum contains, as well as characteristic signals from the monosubstituted ferrocenyl fragment, well-separated resonances arising from the phenyl and quinoxalyl fragments: the ^{13}C spectrum again shows the characteristic resonances from the ferrocenyl fragment, together with seven CH and five quaternary resonances in the aromatic region. A single-crystal X-ray diffraction analysis of **3**, prepared in this manner, has been published [10]. Because of the significantly enhanced yield obtained when the reactants were first heated in dioxan (b.p. 101°C) prior to the melt-phase condensation, the reactions of **1** with other aromatic 1,2-diamines were all conducted under similar conditions; in all these reactions, the choice of solvent was influenced by a combination of reactant solubility and solvent volatility. As with compound **3**, nearly all the resulting quinoxalines were isolated after chromatography on silica or alumina as hydrates, either monohydrates or hemihydrates.

Thus, when the ferrocenyl diketone **1** was reacted with 3,4-diaminobenzoic acid **4**, initially in chlorobenzene (b.p. 132°C), the quinoxaline **5** was obtained in *ca.* 80% yield after chromatographic purification. However, both the ^{1}H and ^{13}C NMR spectra indicated the presence of the two regio-isomers **5a** and **5b**, arising from the alternative orientations of the reactants in the condensation process: integration of the ^{1}H spectrum in the ferrocenyl region indicated a major:minor isomer ratio of 2:1.

No chromatographic conditions could be found under which the isomers were separable and consequently the assignment of the major and minor isomers as either **5a** or **5b** was not possible. However, it was possible, despite some peak overlap, to analyse completely for each isomer the quinoxalyl region of the ^{1}H NMR spectrum in terms of an ABX pattern having a J_{AX} ($= {}^{5}J_{HH}$) of zero. Similarly, with the 4-nitrodiamine **6**, the two regio-isomers **7a** and **7b** of the corresponding nitroquinoxaline are formed, with in this case a major:minor isomer ratio of 3:1; again, the quinoxalyl region of the ^{1}H NMR spectrum was analysed in terms of two ABX patterns each with a J_{AX} of zero.

From the condensation of the diketone **1** with 2,3-diaminotoluene, again a mixture of two regio-isomers **8a** and **8b** was formed, with a major:minor ratio of 3:2 as judged from the ^{1}H NMR spectrum, but on this occasion the two isomers were separable by careful chromatography on silica. On the other hand, the two regio-isomers **9a** and **9b** obtained using 2,3-diaminopyridine were not separable on silica, but were found to be separable on alumina provided that pure dichloromethane was employed as eluent: even the slightest increase in the polarity of the mobile phase caused the isomers to elute together.

In the quinoxaline-forming condensations involving substituted diamines, the modest regio-selectivity is determined by the relative nucleophilicities of the two amino groups in the diamine component, and the relative electrophilicities of the two carbonyl carbon atoms in the diketone **1**. It is assumed that the more nucleophilic amino group reacts faster with the more electrophilic carbonyl. In diamines **4** and **6**, in which the substituent R is electron-withdrawing, the amino group *meta* to R will be the more nucleophilic, while the carbonyl adjacent to the phenyl ring in **1** will be the more electrophilic, because of the strong electron-donating character of the ferrocenyl fragment. Hence, it is to be expected that **5b** is the more abundant isomer of **5**; similarly for **7**, the ferrocenyl fragment is preferentially *para* to the deactivating substituent. In 2,3-diaminotoluene, the amino group *ortho* to methyl is the more nucleophilic, so that **8b** is expected to predominate, while the strong deactivation of the 2-amino group in 2,3-diaminopyridine leads to the expectation of **9a** as the major isomer.

Use of the bis-1,2-diamine, **10**, under the reaction conditions employed for the formation of quinoxalines **3**, **5**, **7**, **8** and **9** and using dioxan as solvent

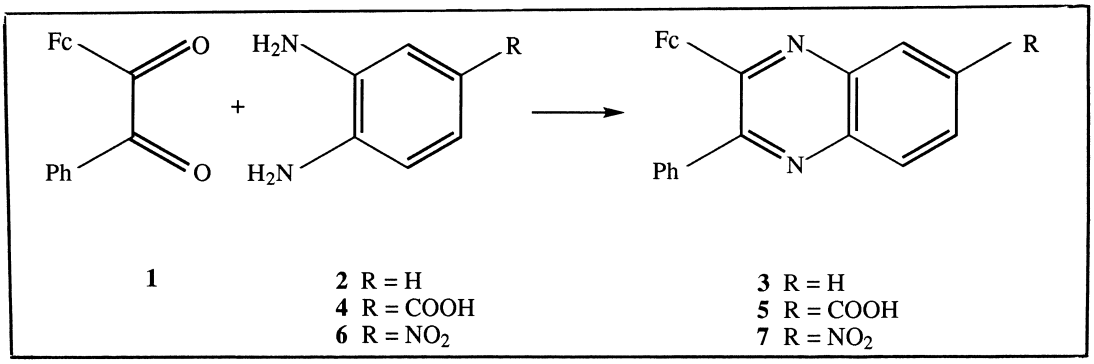

1

2 R = H
4 R = COOH
6 R = NO_2

3 R = H
5 R = COOH
7 R = NO_2

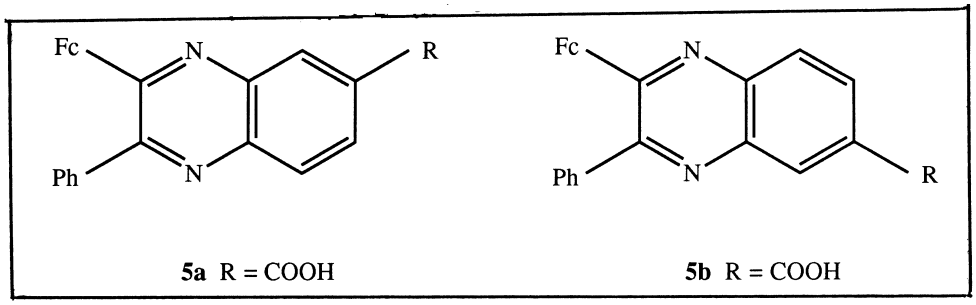

5a R = COOH **5b** R = COOH

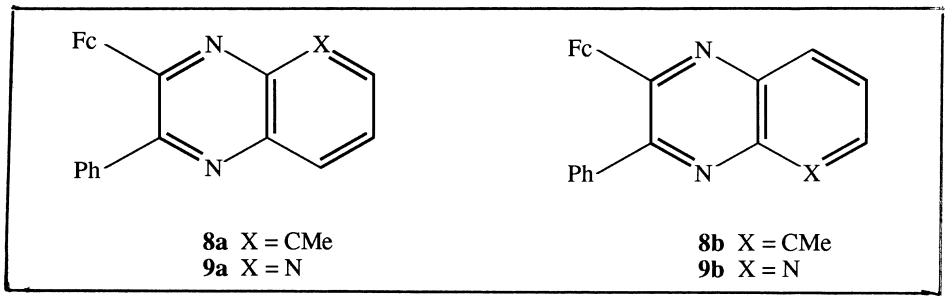

8a X = CMe
9a X = N

8b X = CMe
9b X = N

gave, as a mixture of regio-isomers, the expected bis-product **11**. However, when the ferrocenyl diketone **1** and the bis-diamine **10** were reacted together in alkaline aqueous solution [11], the predominant product was the monoquinoxaline **12**, accompanied by only a trace of **11**.

Electrochemistry

Figure 1, which refers to compound **3**, shows the typical cyclic voltammogram exhibited by the present compounds in dichloromethane solution. Both an oxidation process possessing features of chemical reversibility and an apparently irreversible reduction process, which is about twice greater in height than the oxidation step, are apparent.

Controlled-potential coulometric investigation of the anodic process ($E_w = +0.7$ V) show the consumption of one electron/molecule. Upon exhaustive one-electron oxidation the original ruby-red solution of **3** turns jade-green and displays an absorption in the visible region at $\lambda_{max} = 692$ nm. In confirmation of the chemical reversibility of the ferrocene/ferricenium oxidation, cyclic-voltammetric tests performed on the oxidised green solution display voltammetric profiles entirely complementary to that shown in Fig. 1.

Analysis [12] of the cyclic-voltammetric anodic responses with scan rates varying from 0.02 to 1.00 V s^{-1} show parameters which are diagnostic of a one-electron removal which is essentially reversible from the electrochemical viewpoint. As a matter of fact, the i_{pc}/i_{pa} ratio is constantly equal to unity, the current function $i_{pa}/v^{1/2}$ remains constant and the peak-to-peak separation progressively increases from 70 to 170 mV. Such a slight departure from the constant value of 59 mV expected for an electrochemically-reversible one-electron process neatly parallels that observed for the one-electron oxidation of unsubstituted ferrocene, so that it may be attributed to uncompensated solution resistances.

So far as the reduction process is concerned, it was not possible to perform macroelectrolysis investigations because of the closeness of the solvent reduction. Based on the relative heights, we assign it to a single two-reduction process, which is however complicated by subsequent reactions, as yet uncharacterised. As the inset of Fig. 1 shows, when the scan rate was increased beyond 2.00 V s^{-1}, a reoxidation appears directly associated to the reduction process. This means that the rate of the chemical complication falls within the cyclic voltammetry time window, allowing estimation of *ca.* 0.05 s as the half-life of the electrogenerable $[\mathbf{3}]^{2-}$ anion [13].

Table 1 presents for all the compounds studied the formal electrode potentials of the redox changes discussed above and, for comparison, the corresponding data for the unsubstituted 2-ferrocenylquinoxaline (**13**) are also reported. The electrogenerated ferricenium species $[\mathbf{5}]^+$, $[\mathbf{9}]^+$ and $[\mathbf{13}]^+$ proved to be not fully stable and to undergo slow decomposition.

In comparison with unsubstituted ferrocene itself, the ferrocenylquinoxalines oxidise at potential values some 100–150 mV higher, thus indicating that the quinoxaline exerts a significant electron-withdrawing

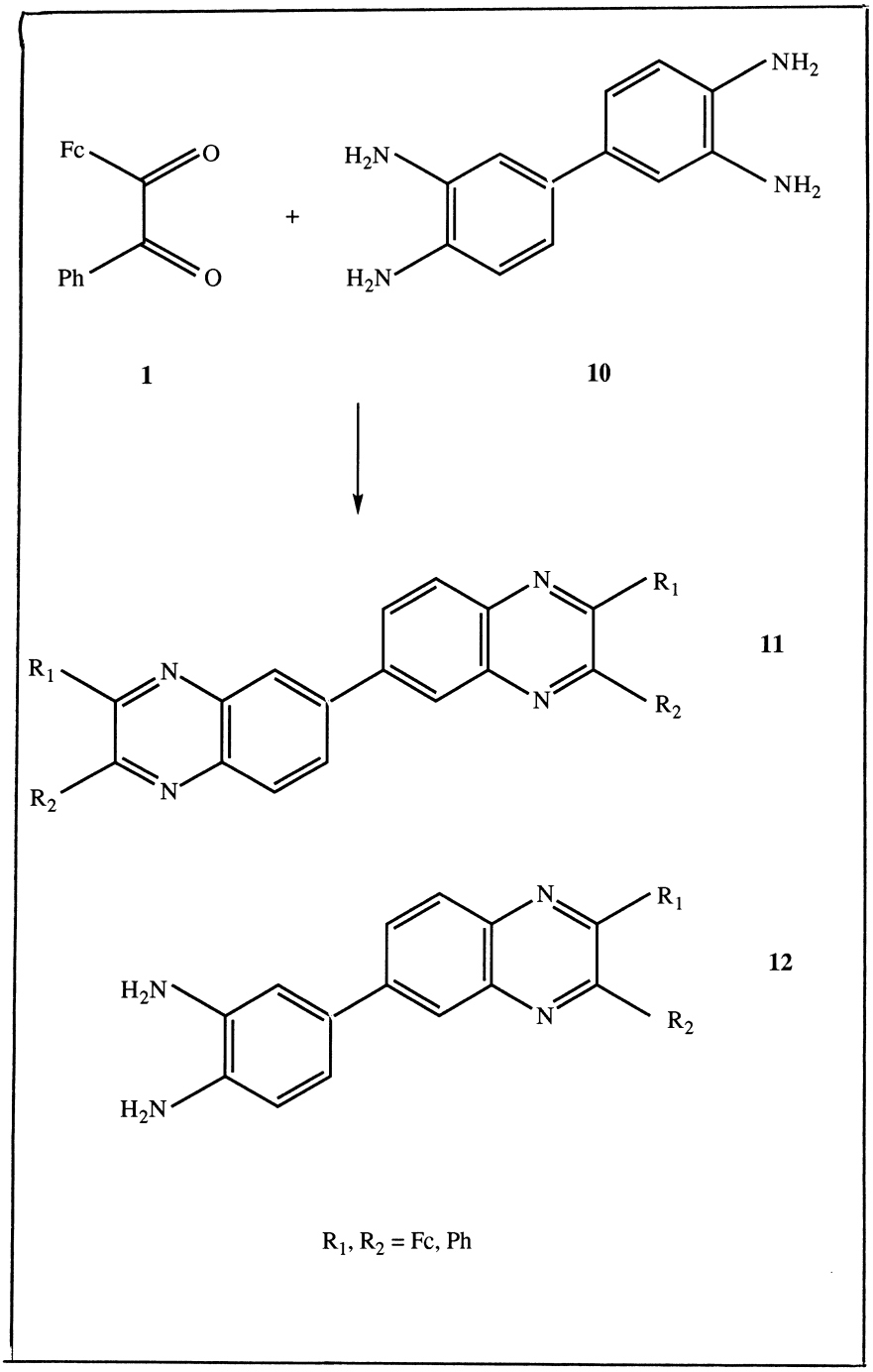

effect. However, the effects of the substituents on the quinoxaline ring are always readily interpreted. Comparison between **13** and **3**, indicates that the 3-phenyl substituent, which might have been expected to make the oxidation more difficult, in fact makes the oxidation slightly easier, suggesting that resonance effects predominate over inductive effects. This could also explain the absence of inductive effects exerted by the methyl group in **8**, or the carboxyl group in **5**, compared with **3**. On the other hand, the strongly electron-withdrawing NO_2 group in **7** generates its expected effect.

The redox behaviour of the biferrocene complex **11** merits comment. It exhibits a single oxidation process, but unfortunately, because of its very low solubility satisfactory controlled-potential coulometry was not possible. However, in view of the absence of further oxidation processes up to $+1.2$ V, it may be specu-

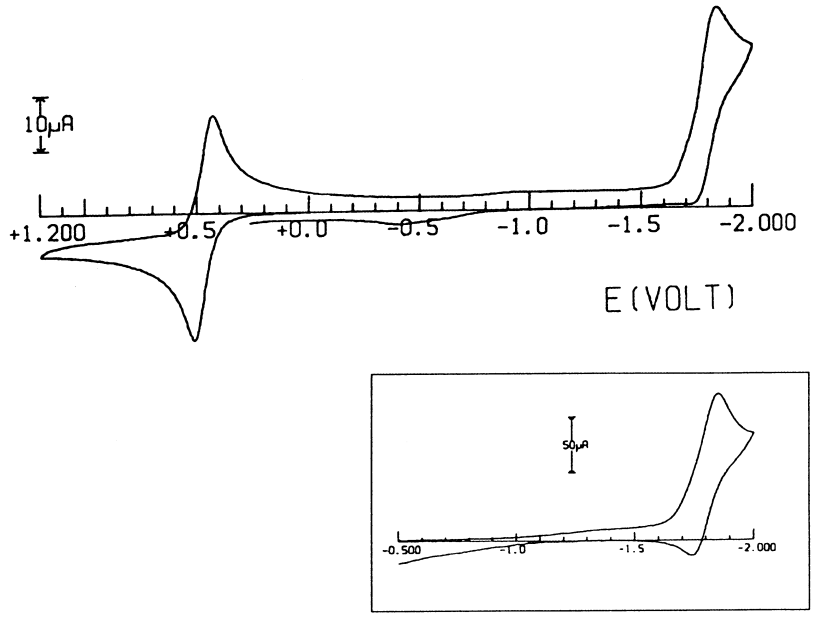

Fig. 1. Cyclic voltammogram recorded at a platinum electrode on a CH_2Cl_2 solution containing **3** (1.3×10^{-3} mol dm^{-3}) and $[NBu_4][PF_6]$ (0.2 mol dm^{-3}). Scan rates: main figure, 0.20 V s^{-1}; inset, 2.00 V s^{-1}.

Table 1. Formal electrode potentials (in V, vs S.C.E.), peak-to-peak separations (in mV) and spectroscopic data (in nm) for the redox changes exhibited by the present ferrocenylquinoxalines in dichloromethane solution.

Complex	$E^0_{0/1+}{}'$	ΔE_p[a]	λ_{max}[b]	$E^0_{0/2-}{}'$
3	+0.47	80	692	−1.80[c]
5	+0.49	97	680	—
7	+0.55	75	660	−1.55[d,e]
8	+0.49	79	705	−1.80[d]
9	+0.55	75	681	−1.51[c]
11	+0.46[f]	70	—	—
13	+0.53	95	675	−1.79[d]
FcH	+0.39	84	620	—

[a] Measured at 0.1 V s^{-1}.
[b] Absorption band of the oxidized species.
[c] Measured at 2.0 V s^{-1}.
[d] Peak potential value.
[e] A preceding reduction centred on the NO_2 group is present at $E^{0\prime} = -0.95$ V.
[f] Two-electron step.

lated that this is due to a single two-electron step. Were this to be so, it would imply that no electronic communication occurs between the two quinoxalyl units.

Finally, as far as the presence of isomeric species is concerned, as noted above for compounds **5**, **7**, **8**, **9** and **11**, it may be pointed out that only in the case of compound **5** was the presence of two almost overlapping oxidation processes observed, which could account for the somewhat greater peak-to-peak separation in **5** compared with the other species.

EXPERIMENTAL

The diketone FcCOCOPh was prepared as previously described [4]. Aromatic diamines were obtained from commercial sources and were purified using published methods [14]. NMR spectra were recorded at ambient temperatures, in $CDCl_3$ solution unless stated otherwise, on a Bruker AM-300 spectrometer operating at 300.135 MHz for ^{1}H and 75.469 MHz for ^{13}C. Diethyl ether and light petroleum (b.p. 40–60°C) were dried over sodium wire. Elemental analyses were by the Microanalytical Laboratory of this School.

Synthesis of 2-ferrocenyl-3-phenylquinoxaline

Melt-phase reaction Ferrocenylphenylethanedione **1** (0.2 g, 0.63 mmol) and 1,2-diaminobenzene **2** (0.1 g, 0.93 mmol) were taken in a Pyrex glass test tube with a side arm and fitted with a bubbler. The mixture was heated to melting in an oil bath at 140°C under nitrogen for 30 min, water vapours were observed condensing on the walls of tube. After cooling the crude material was dissolved in dichloromethane and checked by TLC; this showed one purplish-red spot almost at the same R_f value as ferrocenylphenylethanedione. This crude product was chromatographed on silica gel using dichloromethane as the eluting solvent, concentrated and crystallised to

give dark purple crystals of 2-ferrocenyl-3-phenylquinoxaline **3** (0.11 g, 45%).

Reaction in dioxan solution Ferrocenylphenylethanedione **1** (0.2 g, 0.63 mmol), 1,2-diaminobenzene **2** (0.1 g, 0.93 mmol) were dissolved in 1,4-dioxan (3 cm^3) in a Pyrex glass test tube with a side arm and fitted with a bubbler. This mixture was heated in an oil bath at 110°C under a gentle stream of nitrogen until dryness. The temperature of the bath was raised to 140°C and held at this temperature for 20 min. The crude product was purified as for the melt-phase reaction. Weight of chromatographed product 0.16 g (65%).

The products from these two processes were found to be identical by TLC and by ^1H and ^{13}C NMR. Anal. found C 72.2, H 4.4, N 6.9; $C_{24}H_{18}FeN_2$ requires C 73.9, H 4.7, N 7.2%; $C_{24}H_{18}FeN_2.0.5H_2O$ requires C 72.2, H 4.8, N 7.0%. M.p. 208–210°C (lit. 208–209°C [4]). NMR δ(H) 4.00. (5H, s, C_5H_5); 4.35 (2H, m) and 4.55 (2H, m) (C_5H_4); 7.50–7.55 (5H, m, Ph); 7.72 (2H, m) and 8.08 (2H, m) (quinoxalyl); δ(C) 69.9 (d, C_5H_5); 70.1 (d), 70.8 (d) and 82.3 (s) (C_5H_4); 128.4 (d), 128.8 (d), 128.9 (d), 129.0 (d), 129.2 (d), 129.3 (d), 129.9 (d), 139.8 (s), 140.3 (s), 141.9 (s), 154.1 (s) and 154.1 (s) (phenyl and quinoxalyl).

Synthesis of ferrocenylphenylquinoxalylcarboxylic acid

In a similar manner, ferrocenylphenylethanedione **1** (0.5 g, 1.57 mmol), 3,4-diaminobenzoic acid **4** (0.26 g, 1.7 mmol) and chlorobenzene (5 cm^3) were heated in a silicone oil bath at 140°C under a gentle stream of nitrogen; after 1 h. TLC showed that no unreacted diketone remained. During the reaction time the colour of the mixture also changed from dark red to dark purple. The mixture was then heated to dryness. After cooling, the solid residue was dissolved in dichloromethane, filtered, washed with water, dried (Na_2SO_4), concentrated and chromatographed over silica gel using diethyl ether as the mobile phase to yield ferrocenylphenylquinoxalylcarboxylic acid **5** (0.55 g, 81%) as a dark purple solid. The ^1H NMR spectrum showed the presence of two regio-isomers. The relative yield of the regio-isomers as calculated from the ^1H NMR integration is 2:1. Anal. found C 66.9, H 4.7, N 5.7; $C_{25}H_{18}FeN_2O_2$ requires C 69.1, H 4.2, N 6.5; $C_{25}H_{18}FeN_2O_2.H_2O$ requires C 66.4, H 4.5, N 6.2%. NMR δ(H) (major isomer) 4.01 (5H, s, C_5H_5); 4.38 (2H, m) and 4.58 (2H, m) (C_5H_4); 7.4–7.7 (5H, m, Ph); 8.15 (1H, d; *J*, 8.8), 8.35 (1H, dd; *J*, 8.8 and 1.6) and 8.92 (1H, d; *J*, 1.6) (quinoxalyl);. (minor isomer) 4.03 (5H, s, C_5H_5); 4.40 (2H, m) and 4.60 (2H, m) (C_5H_4); 7.4–7.7 (5H, m, Ph); 8.15 (1H, d; *J*, 8.8), 8.38 (1H, dd; *J*, 8.8 and 1.6) and 8.91 (1H, d; *J*, 1.6) (quinoxalyl); δ(C) (major isomer) 68.4_7 (d, C_5H_5); 69.0 (d), 69.5 (d) and 80.1 (s) (C_5H_4); (minor isomer) 68.5_3 (d, C_5H_5); 69.3 (d), 69.6 (d) and 80.4 (s) (C_5H_4); (both isomers) 126.9_3 (d), 126.9_6 (d), 127.0_5 (d), 127.1_6 (d), 127.6_3 (d), 127.7_2 (d), 127.7_8 (d), 128.3 (d), 129.6 (d), 129.8 (d), 130.1 (d), 131.1 (d), 137.3 (s), 138.1_7 (s), 138.2_4 (s), 139.4 (s), 140.0 (s), 142.0 (s), 152.4 (s), 153.0 (s), 153.6 (s) and 154.6 (s) (phenyl and quinoxalyl); 166.2 (s) COOH. The resolution of the aromatic resonances requires resolution enhancement. Both the carboxyl carbons appear at the same position, and two of the quaternary carbons of the aromatic/quinoxaline moieties are superimpose on other peaks in that region and hence are not visible in the spectrum.

Synthesis of ferrocenylphenylnitroquinoxaline

Ferrocenylphenylethanedione **1** (0.22 g, 0.69 mmol), 4-nitro-1,2-diaminobenzene **6** (0.12 g, 0.76 mmol) and toluene (5 cm^3) were refluxed, as above, under a gentle stream of nitrogen for 3 h; the reaction was monitored by TLC. The solvent was evaporated after this time. After cooling, the solid residue was redissolved in dichloromethane, filtered, concentrated and chromatographed over silica gel using dichloromethane as the mobile phase to yield ferrocenylphenylnitroquinoxaline **7** (0.22 g, 73%) as a dark purple solid. The compound crystallises as a hemi-hydrate as shown by the elemental analysis and integration of the ^1H NMR spectrum gave an isomer ratio of 3:1. An attempt to separate the two isomers on silica using dichloromethane as eluent yielded a pure fraction of the more abundant isomer, together with a mixture of both the isomers. Anal. found (isomer mixture) C 65.1, H 3.9, N 9.1; $C_{24}H_{17}FeN_3O_2$ requires C 66.2, H 3.9, N 9.6; $C_{24}H_{17}FeN_3O_2.0.5H_2O$ requires C 64.9, H 4.1, N, 9.4%. NMR (major isomer pure, minor isomer from spectrum of mixture) δ(H) (major isomer) 4.01 (5H, s, C_5H_5); 4.40 (2H, m) and 4.57 (2H, m) (C_5H_4); 7.5–7.6 (5H, m, Ph); 8.18 (1H, d; *J*, 9.5), 8.44 (1H, dd; *J*, 9.5 and 2.4) and 8.98 (1H, d; *J*, 2.4) (quinoxalyl); (minor isomer) 4.00 (5H, s, C_5H_5); 4.43 (2H, m) and 4.60 (2H, m) (C_5H_4); 7.5–7.6 (5H, m, Ph); 8.16 (1H, d; *J*, 9.4), 8.48 (1H, dd; *J*, 9.4 and 2.4) and 8.98 (1H, d; *J*, 2.4) (quinoxalyl); δ(C) (major isomer) 69.9 (d, C_5H_5); 70.8 (d), 71.1 (d) and 80.8 (s) (C_5H_4); 121.8 (d), 124.7 (d), 128.4 (d), 128.9_0 (d), 129.5 (d), 130.5 (d), 138.9 (s), 140.4 (s), 142.0 (s), 147.9 (s), 144.8 (s) and 157.1 (s) (phenyl and quinoxalyl); (minor isomer) 70.0 (d, C_5H_5); 71.2_5 (d), 71.2_8 (d) and 80.7 (s) (C_5H_4); 123.2 (d), 125.6 (d), 128.2 (d), 128.8_7 (d), 129.4 (d), 129.6 (d), 138.0 (s), 138.9 (s), 144.1 (s), 146.7 (s), 145.2 (s) and 158.1 (s) (phenyl and quinoxalyl).

Synthesis of ferrocenylphenylmethylquinoxaline

In a similar manner, ferrocenylphenylethanedione **1** (0.5 g, 1.57 mmol), 2,3-diaminotoluene (0.22 g, 1.8 mmol) and chlorobenzene (5 cm^3) were refluxed in an oil bath at 150°C under a gentle stream of nitrogen. The reaction was monitored by TLC and after 4 h the reaction was complete. The two regio-isomers had distinguishable R_f values, but the less polar isomer

had almost the same value as the diketone, so that it was sometimes difficult to differentiate between diketone and this isomer of the product. When the reaction was complete, the solvent was removed and the solid residue was redissolved in dichloromethane, filtered, concentrated and chromatographed over silica gel using dichloromethane/petrol as the mobile phase to yield ferrocenylphenylmethylquinoxaline **8** (0.6 g, 95%) as a dark purple solid. The relative yield of the regioisomers as calculated from the ^{1}H NMR integration is 3:2. Another column was run to separate the two isomers from each other; this yielded first the pure less-polar isomer, then the mixture of two isomers and finally a small portion of the more-polar isomer. Anal. found C 74.0, H 5.0, N 6.7; $C_{25}H_{20}FeN_2$ requires C 74.3, H 5.0, N 6.9%. NMR δ(H) (major isomer) 2.95 (3H, s, CH_3); 4.02 (5H, s, C_5H_5); 4.32 (2H, m) and 4.55 (2H, m) (C_5H_4); 7.4–7.7 (7H, m) and 7.94 (1H, d) (phenyl and quinoxalyl); (minor isomer) 2.82 (3H, s, CH_3); 4.00 (5H, s, C_5H_5); 4.32 (2H, m) and 4.55 (2H, m) (C_5H_4); 7.4–7.7 (7H, m) and 7.94 (1H, d) (phenyl and quinoxalyl); δ(C) (major isomer) 17.1 (q, CH_3); 69.7 (d, C_5H_5); 69.7 (d), 70.8 (d) and 82.9 (s) (C_5H_4); 126.8 (d), 128.1 (d), 128.5_0 (d), 128.5_5 (d), 129.1 (d), 129.5 (d), 136.5 (s), 139.6 (s), 139.8 (s), 140.8 (s), 152.1 (s) and 152.4 (s) (phenyl and quinoxalyl); (minor isomer) 17.0 (q, CH_3); 69.6 (d, C_5H_5); 69.6 (d), 70.7 (d) and 82.7 (s) (C_5H_4); 126.2 (d), 127.9 (d), 128.4 (d), 128.6 (d), 129.2 (d), 129.4 (d), 137.3 (s), 138.8 (s), 140.2 (s), 141.4 (s), 151.4 (s) and 152.9 (s) (phenyl and quinoxalyl).

Synthesis of 2-*ferrocenyl*-3-*phenyl*-5-*azaquinoxaline*

Ferrocenylphenylethanedione **1** (0.32 g, 1.0 mmol), 2,3-diaminopyridine (0.22 g, 2.0 mmol) and 1,4-dioxan (2 cm^3) were heated, as above, in an oil bath at 110°C under a slow stream of nitrogen until dryness. The temperature was then increased to 150°C and held for 30 min. After cooling, the mixture was dissolved in dichloromethane, filtered, concentrated and chromatographed on silica gel to give pure ferrocenylphenylazaquinoxaline **9** (0.26 g, 67%) as a dark purple solid. The product contained both regio-isomers of the azaquinoxaline, confirmed by ^{1}H and ^{13}C NMR. The two isomers which were not separable on silica gel were found to be separable on alumina by very careful elution using dichloromethane as eluting solvent. Any slight increase in the polarity of the mobile phase (e.g. one drop of methanol in 100 cm^3 of dichloromethane) elutes both the isomers at the same time. Integration of the ^{1}H NMR spectrum gave an isomer ratio of *ca.* 3:2. Anal. found C 69.8, H 4.6, N 10.1; $C_{23}H_{17}FeN_3$ requires C 70.6, H 4.4, N 10.7%. NMR δ(H) (major isomer) 4.02 (5H, s, C_5H_5); 4.38 (2H, m) and 4.62 (2H, m) (C_5H_4); 7.4–7.7 (6H, m, phenyl and quinoxalyl), 8.42 (1H, d × d) and 9.10 (1H, d) (quinoxalyl); (minor isomer) 4.06 (5H, s, C_5H_5); 4.40 (2H, m) and 4.68 (2H, m) (C_5H_4); 7.4–7.8 (6H, m, phenyl and quinoxalyl), 8.46 (1H, d × d) and 9.15 (1H, d) (quinoxalyl); δ(C) (major isomer) 69.6 (d, C_5H_5); 70.2 (d), 70.8 (d) and 81.8 (s) (C_5H_4); 124.8 (d), 127.8 (d), 128.9 (d), 129.2 (d), 136.2 (s), 136.8 (d), 138.8 (s), 148.4 (s), 152.5 (d), 155.3 (s) and 155.5 (s) (phenyl and quinoxalyl); (minor isomer) 69.8 (d, C_5H_5); 70.7 (d), 71.0 (d) and 80.5 (s) (C_5H_4); 123.7 (d), 128.2 (d), 128.7 (d), 128.9 (d), 134.2 (s), 137.7 (d), 139.2 (s), 150.0 (s), 153.6 (d), 154.1 (s), 157.8 (s) (phenyl and quinoxalyl).

Synthesis of di(*ferrocenyl*)*diphenylbiquinoxaline*

In a similar manner, ferrocenylphenylethanedione **1** (0.30 g, 0.94 mmol), 3,3′,4,4′-biphenyltetramine **10** (0.40 g, 1.87 mmol) and 1,4-dioxan (2 cm^3) were heated in an oil bath at 110°C under a gentle stream of nitrogen until all the solvent had evaporated. The temperature of the oil bath was then raised to 150°C and the mixture was kept at this temperature for 45 min. After cooling, the solid residue was dissolved in dichloromethane. TLC analysis showed the presence of two purple quinoxaline spots. As three regioisomers of the product **11** could be formed in this reaction, it is possible that the two of these isomers have virtually identical R_f values. As the R_f values of the two distinguishable components are very closely similar, attempts to separate the isomers have not so far been successful.

Synthesis of ferrocenyl-phenyl-6-(3′,4′-*diaminophenyl*)*quinoxaline*

Ferrocenylphenylethanedione **1** (0.10 g, 0.314 mmol), 3,3′,4,4′-biphenyltetramine (0.13 g, 0.61 mmol), sodium sulfite (0.06 g, 0.48 mmol) and potassium carbonate (0.06 g, 0.43 mmol) were dissolved in 50% (v/v) aqueous ethanol (50 cm^3). The mixture was refluxed with stirring for 2 h. After this time, TLC of the organic extract showed two highly polar components of very similar R_f values, in addition to traces of the bis-quinoxaline **11** and unreacted biphenyltetramine. During the course of the reaction some solid product precipitated out; this was filtered off and the filtrate extracted with diethyl ether. The combined solids were purified by chromatography on neutral alumina using 20% (v/v) methanolic diethyl ether as eluent to yield ferrocenylphenyl-6-(3′,4′-diaminophenyl)quinoxaline **12** (0.12 g, 77%). Anal. found C 71.6, H 4.8, N 11.0; $C_{30}H_{24}FeN_4$ requires C 72.6, H 4.9, N 11.3%; $C_{30}H_{24}FeN_4.0.5(H_2O)$ requires C 71.3, H 5.0, N 11.1%.

Electrochemistry

materials and apparatus for electrochemistry have been described elsewhere [13, 15]. All the potential

values are referred to the saturated calomel electrode (S.C.E.).

Acknowledgements—P. Z. gratefully acknowledges the financial support of the University of Siena (ex quota 60%) and the technical assistance of Mrs Giuseppina Montomoli. S. Z. A. thanks the Committee of Vice-Chancellors and Principals (U.K.) and the University of St. Andrews for financial support.

REFERENCES

1. Stille, J. K. and Williamson, J. R., *J. Polym. Sci. A*, 1964, **2,** 3867.
2. Stille, J. K., Williamson, J. R. and Arnold, F. E., *J. Polym. Sci. A*, 1965, **3,** 1013.
3. Stille, J. K. and Arnold, F. E., *J. Polym. Sci. A-1*, 1966, **4,** 551.
4. Glidewell, C., Ahmed, S. Z., Gottfried, M., Lightfoot, P., Royles, B. J. L., Scott, J. P. and Wonnemann, J., *J. Organomet. Chem.*, 1997, **530,** 177.
5. Ahmed, S. Z., Glidewell, C. and Lightfoot, P., *J. Organomet. Chem.*, 1997, **542,** 81.
6. Ferguson, G., Glidewell, C., Gottfried, M. and Trotter, J., *Acta Cryst. C*, 1996, **52,** 773.
7. Sheldrick, G. M., Heine, A., Schmidt-Bäse, K., Pohl, E., Jones, P. G., Paulus, E. and Waring, M. J., *Acta Cryst. B*, 1995, **51,** 987.
8. Waring, M. J. and Wakelin, L. P. G., *Nature* (*London*), 1974, **252,** 653.
9. Köpf-Maier, P. and Köpf, H., *Chem Rev.*, 1987, **87,** 1137.
10. Ferguson, G., Glidewell, C. and Scott, J. P., *Acta Cryst. C*, 1996, **52,** 770.
11. Jones, R. G. and McLaughlin, K. C., *Org. Synth.*, 1950, **30,** 86.
12. Brown, E. R. and Sandifer, J., in *Physical Methods of Chemistry*: *Electrochemical Methods*, eds. B. W. Rossiter and J. F. Hamilton, Vol. 2, Chap. 4. Wiley, New York, 1986.
13. Togni, A., Hobi, M., Rihs, G., Rist, G., Albinate, A., Zanello, P. and Zech, D., Keller, H., *Organometallics*, 1994, **13,** 1224.
14. Perrin, D. D. and Armarego, W. L. F., *Purification of Laboratory Chemicals*, 3rd edn. Pergamon, Oxford, 1988.
15. Zanello, P., Fabrizi de Biani, F., Glidewell, C., Koenig, J. and Marsh, S. J., *Polyhedron*, 1998, **17,** 1795.

Pergamon

Polyhedron Vol. 17, No. 23–24, pp. 4163–4167, 1998
© 1998 Elsevier Science Ltd
All rights reserved. Printed in Great Britain
0277–5387/98 $19.00+0.00

PII: S0277–5387(98)00224–1

Organometallic gold derivatives with the [1-Si^{t}BuMe$_2$-1,2-$C_2B_{10}H_{10}$]-carboranyl ligand. Crystal structure of [1-{Au(PPh$_3$)}-2-Si^{t}BuMe$_2$-1,2-$C_2B_{10}H_{10}$]

Olga Crespo, M. Concepción Gimeno, Antonio Laguna* and Ana M. Peña

Departamento de Química Inorgánica, Instituto de Ciencia de Materiales de Aragón, Universidad de Zaragoza-CSIC, 50009 Zaragoza, Spain

(Received 16 March 1998; accepted 2 June 1998)

Abstract—Reaction of 1-Li-2-Si^{t}BuMe$_2$-1,2-$C_2B_{10}H_{10}$ with [AuClL] (L = PPh$_3$, PPh$_2$Me, AsPh$_3$) in molar ratio 1:1 affords the organometallic gold complexes [1-AuL-2-Si^{t}BuMe$_2$-1,2-$C_2B_{10}H_{10}$]. The complex PPN[Au{2-Si^{t}BuMe$_2$-1,2-$C_2B_{10}H_{10}$}$_2$] (PPN = N(PPh$_3$)$_2$) has also been synthesised by reaction of PPN[AuCl$_2$] with 1-Li-2-Si^{t}BuMe$_2$-1,2-$C_2B_{10}H_{10}$ in molar ratio 1:2. The crystal structure of [1-{Au(PPh$_3$)}-2-Si^{t}BuMe$_2$-1,2-$C_2B_{10}H_{10}$] has been established by X-ray diffraction. © 1998 Elsevier Science Ltd. All rights reserved

Keywords: gold; carborane

INTRODUCTION

The synthesis of carboranyl derivatives has been extensively studied because in some aspects they resemble organic compounds with electron-accepting groups [1–4]. During the past decade investigations in the field of C-substituted carboranes have involved the creation of new models to be used in theoretical investigations [5], the preparation of organic and organometallic carboranyl compounds for the production of polymeric materials [6–8] (and references cited therein) and biological and medical investigations [9]. These compounds have proved particularly useful in the boron neutron capture therapy (BNCT) for cancer [10–13].

It is known that *o*-carborane derivatives form unusually strong Au–C bonds. Nevertheless, examples of closo-carboranes σ-bonded to gold by 2c–2e σ-bonds are relatively rare (as opposed to the most studied nido-carboranes interacting gold via cluster bonding) [14–18].

The first report was made by Mitchel and Stone [19, 20], who prepared the complexes [Au(2-R-1,2-$C_2B_{10}H_{10}$)(PPh$_3$)] [R = H, Me, Ph]. More recently species of stoichiometry [Au(2-R-1,2-$C_2B_{10}H_{10}$)L] [R = CH$_2$OCH$_3$, Ph; L = PPh$_3$, P(*o*-tol)$_3$, PCy$_3$, PEt$_3$, AsPh$_3$] have been reported by Reid and Welch [21] whereas in the work published by Hawthorne *et al.* [22] dimetallated species of *o*-carborane and bis(*o*-carborane) have been synthesised.

We have reported recently on the synthesis of the first *m*-carborane derivatives bonded to gold by 2c–2e σ-bond [23] as part of our studies with carborane derivatives [24–30]. Our contribution this time is related to some new organometallic gold(I) derivatives with the carboranyl group [1-Si^{t}BuMe$_2$-1,2-$C_2B_{10}H_{10}$]$^-$. This carboranyl derivative has been described as a good precursor in the synthesis of monosubstituted carborane derivatives [31].

RESULTS AND DISCUSSION

The treatment of 1-Si^{t}BuMe$_2$-1,2-$C_2B_{10}H_{11}$ with Li^{n}Bu leads to the lithiated derivative 1-Li-2-Si^{t}BuMe$_2$-1,2-$C_2B_{10}H_{10}$ (**1**) which is not isolated; further reaction of **1** with the organochloro complexes [AuClL] affords the organometallic derivatives [1-

* Author to whom correspondence should be addressed. Tel.: +34-976-761-185; Fax: +34-976-761-187; E-mail: alaguna@posta.unizar.es.

(AuL)-2-Si^{t}BuMe$_2$-$C_2B_{10}H_{10}$] [L = PPh_3 (**2**), PPh_2Me (**3**) and $AsPh_3$ (**4**)] (Scheme 1).

Complexes **2**–**4** behave as nonconductors in acetone solutions. In their IR spectra the υ(BH) absorptions appear at 2592 (br, vs), (**2**), 2664 (br, vs) (**3**) and 2566 (br, vs) (**4**) cm^{-1}, respectively.

The positive liquid secondary-ion mass spectra (LSIMS) of complexes **2**–**4** show the molecular peaks at m/z = 716 (**2**, 50%), 597 (**3**, 5%) and 760 (**4**, 40%), although the most intense ones correspond to the fragments $[AuL_2]^+$ [m/z 721 (**2**), 597 (**3**) and 809 (**4**)].

Compounds **2** and **3** exhibit only one signal in their $^{31}P\{^1H\}$ NMR spectra downfield referred to the starting materials ($\Delta\delta$ = 4.8 (**2**) and 5.5 (**3**) ppm).

In the ^{1}H NMR spectra of **2**–**4** a multiplet and a broad signal appear which correspond to the phenylic protons (7–7.8 ppm) and the BH protons (1–3 ppm) respectively. All of them exhibit two resonances due to the Si^{t}BuMe$_2$ fragment at about 1.0 and 0.5 ppm. In addition to this pattern, compound **3** displays one doublet due to the methyl protons of the phosphine ligand.

Complex **2** has been characterised by X-ray diffraction studies and the structure is shown in Fig. 1. Selected bond lengths and angles are collected in Table 1. In the molecule the gold centre exhibits a distorted linear geometry, P–Au–C(1) = 171.3(12)°, although there are no obvious reasons for this distortion, it may be possible that because the bulky nature of the Si^{t}BuMe$_2$ group there is some steric hindrance. This distorted geometry is not observed in [Au(2-CH_2O–CH_3)-1,2-$C_2B_{10}H_{10}$)($AsPh_3$)] [As–Au–C = 177.05(2)°] [21].

The Au–P distance of 2.2718(13) Å is of the same order than those found in another *o*-carboranyl compounds such as [Au(2-H-1,2-$C_2B_{10}H_{10}$)(PPh_3)] (2.271(2) Å) [22] or in the *m*-carboranyl derivative [23] [Au_2(μ-1,7-$C_2B_{10}H_{10}$)(PPh_3)$_2$] (2.265(2), 2.271(2) Å) and can also be compared with those found in complexes of the type [AuR(PPh_3)] (R = C_6F_5, 2.27(1) Å) [32].

The Au–C(1) distance, 2.050(4) Å, is of the same order as those obtained for the complexes commented below (2.054(7), 2.047(7) Å for the *m*-carborane derivative; 2.039(8) and 2.039(8) Å for the mono and disubstituted *o*-carborane derivatives respectively). It has been shown that the Au–C distances depend on the hybridisation state of the carbon atom. The distances found in the commented *o*-carboranyl and *m*-carboranyl complexes are clearly characteristic values of a carbon with sp^2 hybridisation [20], which range from 2.05 to 2.09 Å. These short Au–C distances in carborane derivatives support Stone's observations that the unusual stability of auracarboranes is attributed to the electron withdrawing influence of the cage. The fact that a similar stability is observed in gold-perfluoroalkyl compounds, with the Au–C distances only slightly longer, but in the range of an sp^2 hybridisation, is coherent with such a conclusion.

No organometallic derivative of this ligand has been reported as far as we know, but no appreciably distortion is expected for the Si^{t}BuMe$_2$ group from one compound to another, thus the Si–C(2) distance 1.924(5) Å compares well with those found in 1,2-(1-SiMe$^t{}_2$Bu-1,2-$C_2B_{10}H_{10})_2$-C_6H_4 [1.951(4), 1.956 Å] [33] as well as the C(1)–C(2) distance 1.706(6) Å in complex **2**, 1.714(6), 1.707(7) Å in the related species.

Reaction of **1** with PPN[$AuCl_2$] [PPN = N(PPh_3)$_2$] in molar ratio 2:1 affords a compound which contains two carboranyl groups: PPN[Au{2-Si^{t}BuMe$_2$-1,2-$C_2B_{10}H_{10}$}$_2$] (**5**) (Figure 1).

Compound **5** behaves as 1:1 electrolyte in acetone solutions. In the IR spectrum of **5** the υ(BH) absorption appears at 2632 cm^{-1}. Its LSIMS (+) spectrum

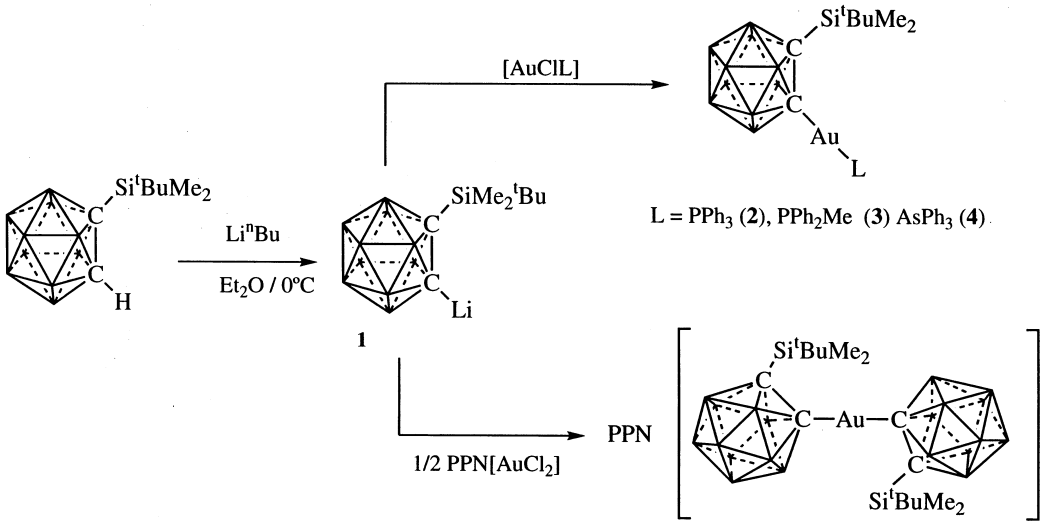

Scheme. 1.

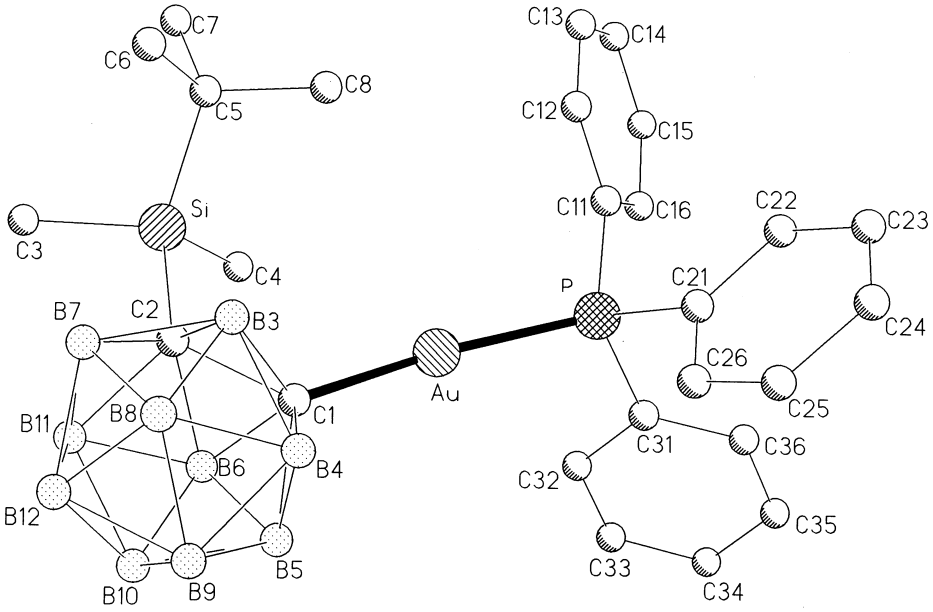

Fig. 1. The molecule of complex **2** in the crystal showing the atom-numbering scheme, radii are arbitrary. H atoms are omitted for clarity.

Table 1. Selected bond lengths (Å) and angles (°) for **2**

Au–C(1)	2.050(4)	Au–P	2.2718(13)
Si–C(3)	1.859(5)	Si–C(4)	1.863(5)
Si–C(5)	1.897(5)	Si–C(2)	1.924(5)
P–C(11)	1.813(5)	P–C(31)	1.814(4)
P–C(21)	1.822(4)	C(1)–C(2)	1.706(6)
C(1)–Au–P	171.34(12)	C(3)–Si–C(4)	109.1(3)
C(3)–Si–C(5)	109.2(3)	C(4)–Si–C(5)	109.9(2)
C(3)–Si–C(2)	106.1(2)	C(4)–Si–C(2)	107.9(2)
C(5)–Si–C(2)	114.6(2)	C(11)–P–C(31)	105.9(2)
C(11)–P–C(21)	106.3(2)	C(31)–P–C(21)	104.4(2)
C(11)–P–Au	116.7(2)	C(31)–P–Au	113.1(2)
C(21)–P–Au	109.6(2)	C(2)–C(1)–Au	126.1(3)
B(5)–C(1)–Au	117.7(3)	B(3)–C(1)–Au	118.7(3)
B(6)–C(1)–Au	122.5(3)	B(4)–C(1)–Au	115.6(3)
B(7)–C(2)–Si	119.1(3)	C(1)–C(2)–Si	121.9(3)
B(11)–C(2)–Si	118.6(3)	B(3)–C(2)–Si	120.2(3)
B(6)–C(2)–Si	118.7(3)	C(8)–C(5)–Si	111.4(3)
C(7)–C(5)–Si	106.2(3)	C(6)–C(5)–Si	113.9(3)
C(16)–C(11)–P	121.9(4)	C(12)–C(11)–P	118.9(4)
C(26)–C(21)–P	118.2(4)	C(22)–C(21)–P	122.4(4)
C(36)–C(31)–P	121.1(3)	C(32)–C(31)–P	119.4(4)

presents the molecular peak as the most intense at $m/z = 712$. The ^{1}H NMR spectrum of **5** exhibits a similar pattern to those commented above for **2** and **4**.

EXPERIMENTAL

Infrared spectra were recorded in the range from 4000 to 200 cm^{-1} on a Perkin-Elmer 883 spectrophotometer using Nujol mulls between polyethylene sheets. Conductivities were measured in ca. 5×10^{-4} mol dm^{-3} solution with a Philips PW 9509 conductimeter. C and H analyses were carried out with a Perkin–Elmer 2400 microanalyser. Mass spectra were recorded on a VG Autospec, with the liquid secondary ion mass spectrometry (LSIMS +) technique using nitrobenzylalcohol as matrix. NMR spectra were recorded on a Varian Unity 300 and Bruker

ARX 300 spectrometer in $CDCl_3$. Chemical shifts are cited relative to 85% H_3PO_4 (external, ^{31}P) and $SiMe_4$ (external, ^1H).

Starting materials

o-carborane was from Desxil Corporation and Si^{t}BuMe$_2$Cl was from Aldrich, both of them were used as given. Compounds 1-Si^{t}BuMe$_2$-1,2-$C_2B_{10}H_{11}$ [31], [AuCl(PPh_3)], [AuCl(PPh_2Me)], [AuCl($AsPh_3$)] [34] and PPN[$AuCl_2$] [35] were synthesised according to the literature procedures.

Preparation of [1-(*AuL*)-2-*Si^{t}BuMe$_2$*-1,2-$C_2B_{10}H_{10}$] [*L* = *PPh$_3$* (**2**), *PPh$_2$Me* (**3**), *AsPh$_3$* (**4**)]

To a solution of 1-Si^{t}BuMe$_2$-1,2-$C_2B_{10}H_{11}$ (77.4 mg, 0.3 mmol) in dried diethyl ether (30 cm^3) at 0°C and under nitrogen atmosphere Li^{n}Bu was added (0.3 mmol, 0.48 ml and 0.62 M). After stirring the mixture for 30 min [AuCIL] was added [0.3 mmol, L = PPh_3, 14.8 mg; L = PPh_2Me, 12.9 mg; L = $AsPh_3$, 15.9 mg]. The suspension was stirred for another 30 min and allowed to warm. After filtration of the suspension over celite and concentration to ca. 5 cm^3 complexes **2** (76%), **3** (48%) and **4** (57%) as white solids are obtained by addition of *n*-hexane (ca. 10 cm^3). **2** Anal. (%) Found: C, 43.05; H, 5.35. Calc. for $C_{26}H_{40}AuB_{10}PSi$: C, 43.55; H, 5.6. $\Lambda_M = 28\,\Omega^{-1}\,cm^2\,mol^{-1}$. ^1H NMR: 0.25 (s, 6H, CH_3), 0.88 (s, 9H, ^{t}Bu), 7–7.6 (m, br, 15H, Ph). $^{31}P\{^1H\}$ NMR: 38.4 (s). **3** Anal. (%) Found: C, 38.35; H, 5.6. Calc. for $C_{21}H_{38}AuB_{10}PSi$: C, 38.55; H, 5.85. $\Lambda_M = 14\,\Omega^{-1}\,cm^2\,mol^{-1}$. ^1H NMR: 0.35 (s, 6H, CH_3), 0.99 (s, 9H, ^{t}Bu), 1.95 (d, J(PH) = 8.4 Hz, 3H, CH_3), 7.2–7.6 (m, br, 10H, Ph). $^{31}P\{^1H\}$ NMR: 22.8 (s). **4** Anal. (%) Found: C, 41.05; H, 5.3. Calc. for $C_{26}H_{40}AsAuB_{10}Si$: C, 41.35; H, 5.4. $\Lambda_M = 9\,\Omega^{-1}\,cm^2\,mol^{-1}$. ^1H NMR: 0.32 (s, 6H, Me), 0.95 (s, 9H, ^{t}Bu), 7.0–7.51 (m, br, 15H, Ph).

Preparation of PPN[*Au*{2-*Si^{t}BuMe$_2$*-1,2-$C_2B_{10}H_{10}$}$_2$] (**5**)

To a solution of 1-Si^{t}BuMe$_2$-1,2-$C_2B_{10}H_{11}$ (77.4 mg, 0.3 mmol) in dry diethyl ether (30 cm^3) at 0°C and under nitrogen atmosphere Li^{n}Bu was added (0.3 mmol, 0.48 ml, 0.62 M). After stirring the mixture for 30 min PPN[$AuCl_2$] was added [0.15 mmol, 12 mg]. The suspension was stirred for another 30 min and allowed to warm. After filtration of the suspension over celite and concentration to ca. 5 cm^3 complex **5** (68%) is afforded by addition of *n*-hexane (ca. 10 cm^3). Anal. (%) Found: C, 50.65; H, 6.5; N, 1.15. Calc. for $C_{52}H_{80}AuB_{20}NP_2Si_2$: C, 49.95; H, 6.45; N, 1.1. $\Lambda_M = 134\,\Omega^{-1}\,cm^2\,mol^{-1}$. ^1H NMR: 0.39 (s, 12H, Me), 1.02 (s, 18H, ^{t}Bu), 7.46–7.65 (m, br, 30H, Ph). $^{31}P\{^1H\}$ NMR: 21.2 (s).

X-ray crystal structure determination of **2**

Crystal Data: **2**, $C_{26}H_{40}AuB_{10}PSi$, Mr = 716.71, triclinic, space group $P\bar{1}$, $a = 10.164(2)$, $b = 12.557(3)$, $c = 14.200(2)$ Å, $\alpha = 115.680(10)$, $\beta = 93.040(10)$, $\gamma = 102.700(10)$, $U = 1570.5(5)$ Å^3, $Z = 2$, $D_c = 1.516$ Mg m^{-3}, λ (Mo-Kα) = 0.71073 Å, $\mu = 4.79$ mm^{-1}, $F(000) = 708$, $T = -100$°C. Single crystals were obtained by a slow diffusion of *n*-hexane into a dichloromethane solution of complex **2**. A colourless prism $0.50 \times 0.40 \times 0.30$ mm was used to collect 5561 intensities to $2\theta_{max} = 50°$ (Siemens P4 diffractometer, monochromated Mo-Kα radiation) of which 5119 were independent ($R_{int} = 0.032$). An absorption correction based on Ψ-scans was applied with transmission factors 0.599–0.863. Cell constants were refined from setting angles of 64 reflections in the range 2θ from 10 to 25°. The structure was solved by the heavy-atom method and subjected to full-matrix least-squares refinement on F^2 (SHELXL-93); all the atoms were refined anisotropically, H atoms were included using a riding model. Refinement proceed to $wR(F^2) = 0.074$ for 5117 reflections and 357 parameters, conventional $R(F) = 0.029$, $S(F^2) = 1.022$, maximum $\Delta\rho$ 2.4 e Å^{-3}.

REFERENCES

1. Grimes, R. N., *Carboranes*. Academic Press, New York, 1970.
2. Matteson, D. S., *J. Organomet. Chem*., 1981, **207,** 13.
3. *Gmelin Handbook of Inorganic Chemistry*, 3rd Supplement, Vol. 4, 80th edn. Springer, Berlin, 1988.
4. Bregadze, V. I., *Chem. Rev*., 1992, **92,** 209.
5. Wu, S. and Jones, M. Jr., *Inorg. Chem*., 1988, **27,** 2005.
6. Mayes, M., Greene, J. and Cohen, M. S., *J. Polym. Sci. A*, 1967, **5,** 365.
7. Pappeti, S., Schaeffer, B. B., Grey, A. P. and Heying, T. L., *J. Polym. Sci. A*, 1966, **4,** 1623.
8. Brown, D. A., Colquhoun, H. M., Daniels, J. A., MacBride, J. A. H., Stephenson, I. R. and Wade, K., *J. Mater Chem*., 1992, **2,** 793.
9. Paxton, R. J., Beatty, B. G., Hawthorne, M. F., Varadarajan, A., Williams, L. E., Curtis, F. L., Knobler, C. B. and Shively, J. E., *Proc. Natl. Acad. Sci. U.S.A*., 1991, **88,** 3387.
10. Barth, R. F., Soloway, A. H. and Fairchild, R. G., *Cancer Res*., 1990, **50,** 1061.
11. Shelly, K., Feakes, D. A., Hawthorne, M. F., Schmidt, P. G., Krisch, T. A. and Bauer, W. F., *Proc. Natl. Acad. Sci. U.S.A*., 1992, **89,** 9039.
12. Hawthorne, M. F., *Pure Appl. Chem*., 1991, **63,** 327.
13. Hawthorne, M. F., *Angew. Chem*., 1993, **32,** 950.
14. Howard, J. A. K., Jeffery, J. C., Jellis, P. A., Sommerfeld, T. and Stone, F. G. A., *J. Chem. Soc., Chem. Commun*., 1991, 1664.
15. Jeffery, J. C., Jellis, P. A. and Stone, F. G. A., *J. Chem. Soc., Dalton Trans*., 1993, 1073.

16. Jeffery, J. C., Jellis, P. A. and Stone, F. G. A., *Inorg. Chem.*, 1993, **32,** 3943.
17. Jeffery, J. C., Jellis, P. A. and Stone, F. G. A., *Organometallic*, 1994, **13,** 2651.
18. Gopher, J. C., Goals, P. A. and Stone, F. G. A., *J. Chem. Soc., Dalton Trans.*, 1994, 25.
19. Mitchell, C. M. and Stone, F. G. A., *J. Chem. Soc., Chem. Commun.*, 1970, 1263.
20. Baukova, T. V., Ku'zmina, L. G., Dvortsova, N. V., Poraikoshits, M. A., Kravtsov, D. M. and Perevalova, E. G., *Organomet. Chem. USSR*, 1989, **2,** 580.
21. Reid, B. D. and Welch, A. J., *J. Organomet. Chem.*, 1992, **438,** 371.
22. Harwel, D. E., Mortimer, M. D., Knobler, C. B., Anet, F. A. L. and Hawthorne, M. F., *J. Am. Chem. Soc.*, 1996, **118,** 2679.
23. Crespo, O., Gimeno, M .C., Jones, P. G. and Laguna, A., *J. Organomet. Chem.*, 1997, **531,** 87.
24. Crespo, O., Gimeno, M. C., Laguna, A. and Jones, P. G., *J. Chem. Soc., Dalton Trans.*, 1992, 1601.
25. Crespo, O., Gimeno, M. C., Jones, P. G. and Laguna, A., *J. Chem. Soc., Chem. Commun.*, 1993, 1696.
26. Bembeneck, E., Crespo, O., Gimeno, M. C., Jones, P. G. and Laguna, A., *Chem. Ber.*, 1994, **127,** 835.
27. Crespo, O., Gimeno, M. C., Jones, P. G. and Laguna, A., *Inorg. Chem.*, 1994, **33,** 6128.
28. Crespo, O., Gimeno, M. C., Jones, P. G. and Laguna, A., *Inorg. Chem.*, 1996, **35,** 1361.
29. Artigas, M. M., Crespo, O., Gimeno, M. C., Jones, P. G., Laguna, A. and Villacampa, M. D., *Inorg. Chem.*, 1997, **36,** 6454.
30. Crespo, O., Gimeno, M. C., Jones, P. G., Laguna, A. and Villacampa, M. D., *Angew. Chem. Int. Ed. Engl.*, 1997, **36,** 993.
31. Jiang, W., Chizhevsky, I. T., Mortimer, M. D., Chen, W., Knobler, C. B., Johnson, S. E., Gomez, F. A. and Hawthorne, M. F., *Inorg. Chem.*, 1996, **35,** 5417.
32. Baker, R. W., Pauling, P. J., Ramsay, W., Foster, R. and Ingold, C., *J. Chem. Soc., Dalton Trans.*, 1972, 2264.
33. Gomez, F. A., Johnson, S. E. and Hawthorne, M. F., *J. Am. Chem. Soc.*, 1991, **113,** 5917.
34. Uson, R. and Laguna, A., *Inorg. Synth.*, 1982, **21,** 71.
35. Nesmenayov, A. N., Perevalova, E. G., Struchkov, T. Yu., Antipin, M. Yu., Grandberg, K. I. and Duachenko, V. P., *J. Organomet. Chem.*, 1980, **201,** 343.
36. Sheldrick, G. M., *SHELX*-93: *a Program for Crystal Structure Refinement*. University of Göttingen, Germany, 1993.

Pergamon

Polyhedron Vol. 17, No. 23–24, pp. 4169–4177, 1998
© 1998 Elsevier Science Ltd
All rights reserved. Printed in Great Britain
0277–5387/98 $19.00+0.00

PII: S0277–5387(98)00225–3

Self association in the structures of two copper(II)–Azo-dye complexes

Harry Adams,[a] Rachel M. Bucknall,[a] David E. Fenton,[a]* Monica Garcia[b] and John Oakes[b]

[a]Department of Chemistry, Dainton Building, The University of Sheffield, Sheffield S3 7HF, U.K.;
[b]Port Sunlight Laboratory, Unilever Research, Bebington, Wirral L63 3JW, U.K.

Received 25 March 1998; accepted 2 June 1998

Abstract—The structures of the copper(II) complexes of two azo-dyes, 1-(2-pyridylazo)-2-naphthol (HPAN) and 2,2′-dihydroxyazobenzene (H_2DAB), Cu(PAN)NO_3 and Cu(DAB)·pyr are reported. In the former the molecules exist as discrete van der Waals pairs whereas in the latter an unusual trimeric unit is found which is held together by long bonding interactions between the copper atom in one molecule and one of the hydroxy oxygen atoms from the adjacent molecule: Cu(2)–O(1B), 2.517; Cu(3)–O(2C), 2.566, Cu(1)– O(2B), 2.622 and Cu(3)–O(1A), 2.768 Å. © 1998 Elsevier Science Ltd. All rights reserved

Keywords:

Although terdentate complexing agents containing an azo-group and a hydroxy group *ortho* to the azo-group have been used as spectrophotometric and titrimetric reagents, in solvent-extraction studies and as dyes, there is a general lack of information about the structures of metal complexes of *o*-hydroxy-*o*-azo-dyes [1]. In the course of a study designed to investigate the factors influencing the solid state assembly of such complexes we have determined the structures of the copper(II) complexes of two azo-dyes, 1-(2-pyridylazo)-2-naphthol (HPAN) and 2,2′-dihydroxyazobenzene (H_2DAB) both of which exist as oligomers.

EXPERIMENTAL

Synthesis

1-(2-pyridylazo)-2-naphthol (HPAN) and 2,2′-dihydroxyazobenzene (H_2DAB) were purchased from Aldrich and used without further purification. Positive ion fast atom bombardment mass spectra (FAB+) were recorded using a VG PROSPEC spectrometer with 4-nitrobenzyl alcohol (NOBA) as the matrix.

Preparation of Cu(PAN)(NO_3)

A solution of copper(II) nitrate (2.04 mmol) in methanol (10 cm^3) was added to a suspension of the red dye, 1-(2-pyridylazo)-2-naphthol, (2.04 mmol) in methanol (50 cm^3). The resulting purple solution was heated at reflux temperature for 30 min, filtered hot and then left to cool overnight. The dark precipitate was collected to yield a purple–brown solid on drying *in vacuo* (76% yield). Recrystallisation from methanol gave crystals suitable for X-ray structure determination. Found: C, 48.4: H, 2.3: N, 15.1%. Calculated for $C_{15}H_{10}CuN_4O_4$: C, 48.2: H, 2.7: N, 15.0%. M.s. (FAB+: NOBA matrix) 311 [Cu(PAN)]; 622 $[Cu(PAN)]_2$.

Preparation of Cu(DAB)·pyr

2,2′-dihydroxyazobenzene (2.3 mmol) was dissolved in methanol (70 cm^3) with warming and the orange solution filtered. To the clear solution was added a solution of copper(II) acetate (2.3 mmol) in methanol (50 cm^3) and a gelatinous precipitate formed. The mixture was heated at reflux temperature for 2 h and the resulting brown solid collected. Vapour phase diffusion of petroleum ether into a solution of the brown solid in pyridine gave shiny green crystals suitable for X-ray structure determination. Found: C,

*Author to whom correspondence should be addressed.

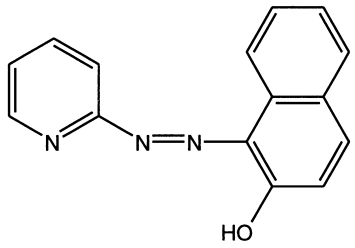

HPAN

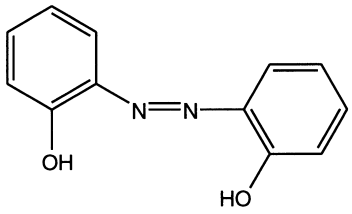

H_2DAB

57.3: H, 3.9: N, 11.5%. Calculated for $C_{17}H_{13}CuN_3O_2$: C, 57.5: H, 3.7: N, 11.8%.

X-ray crystallography

For both structures three-dimensional, room temperature X-ray data were collected in the range $3.5 < 2\theta < 45^\circ$ on a Siemens P4 diffractometer by the omega scan method. Complex scattering factors were taken from the program package SHELXL93 [2] as implemented on the Viglen 486dx computer. Anisotropic thermal vibrational parameters with e.s.d's, hydrogen atom position parameters and observed structure amplitudes and calculated structure factors are available from the authors by request.

Cu(PAN)NO_3, $C_{15}H_{10}CuN_4O_4$, was crystallised from methanol as blue prisms; the crystallographic data is summarised in Table 1. Of the 4442 reflections measured, all of which were corrected for Lorentz and polarisation effects but not for absorption, 1568 independent reflections exceeded the significance level $|F|/\sigma(|F|) > 4.0$. The structure was solved by direct methods and refined by full matrix least squares on F^2. Hydrogen atoms were included in calculated positions and refined in riding mode. Refinement converged at a final $R = 0.0327$ ($wR_2 = 0.0825$, for all 1863 data, 217 parameters, mean and maximum δ/σ 0.000, 0.000), with allowance for the thermal anisotropy of all non-hydrogen atoms. Minimum and maximum final electron density -0.384 and $0.375\,e\,Å^{-3}$. A weighting scheme $w = 1/[\sigma^2(F_o^2) + (0.0309*P)^2 +$

Table 1. Crystal data and structure refinement for Cu(PAN)NO_3 and Cu(DAB)·pyr

Compound	Cu(PAN)NO_3	Cu(DAB)·pyr.
Chemical formula	$C_{15}H_{10}CuN_4O_4$	$C_{17}H_{13}CuN_3O_2$
Formula weight	373.81	354.84
Temperature (K)	293(2)	293(2)
Radiation and wavelength	Mo-Kα, 0.71073 Å	Mo-Kα, 0.71073 Å
Crystal system, space group	monoclinic, $P2_1/n$	monoclinic, $P2_1$
Unit cell dimensions	$a = 9.058(2)$ Å, $\alpha = 90^\circ$, $b = 11.896(3)$ Å, $\beta = 108.65(2)^\circ$, $c = 14.013(2)$ Å, $\gamma = 90^\circ$	$a = 11.176(2)$ Å, $\alpha = 90^\circ$, $b = 16.215(3)$ Å, $\beta = 100.11(3)^\circ$, $c = 12.180(4)$ Å, $\gamma = 90(2)^\circ$
Volume (Å^3)	1430.7(6)	2173.0(7)
Z	4	6
Density (calculated) (Mg/cm^3)	1.735	1.627
Absorption coefficient, μ (mm^{-1})	1.557	1.521
$F(000)$	756	1086
Crystal size (mm)	$0.35 \times 0.30 \times 0.22$	$0.31 \times 0.22 \times 0.15$
θ range for data collection ($^\circ$)	2.30 to 22.50	1.85 to 25.03
Index ranges	$-1 \leqslant h \leqslant 9$, $-12 \leqslant k \leqslant 12$, $-15 \leqslant l \leqslant 14$	$-12 \leqslant h \leqslant 11$, $-17 \leqslant k \leqslant 17$, $-13 \leqslant l \leqslant 10$
Reflections collected	4442	9673
Independent reflections	1863 ($R_{int} = 0.0457$)	6157 ($R_{int} = 0.0555$)
Refinement method	full-matrix least-squares on F^2	full-matrix least-squares on F^2
Data/restraints/parameters	1863/0/217	6157/18/631
Goodness of fit on F^2	1.069	0.934
Final R indices [$I > 2\sigma(I)$]	$R_1 = 0.0327$, $wR_2 = 0.0779$	$R_1 = 0.0450$, $wR_2 = 0.1011$
R indices all data	$R_1 = 0.0429$, $wR_2 = 0.0825$	$R_1 = 0.0543$, $wR_2 = 0.1035$
Largest diff. peak and hole	0.375 and -0.384 e Å^3	0.838 and -0.338 e Å^3

$1.0241*P]$ where $P = (F_o^2 + 2*F_c^2)/3$ was used in the latter stages of refinement.

Cu(DAB)·pyr, $C_{17}H_{13}CuN_3O_2$, was crystallised by vapour diffusion of petroleum ether into a pyridine solution of the complex giving green blocks; the crystallographic data is summarised in Table 1. Of the 9673 reflections measured, all of which were corrected for Lorentz and polarisation effects but not for absorption, 4932 independent reflections exceeded the significance level $|F|/\sigma(|F|) > 4.0$. The structure was solved by direct methods and refined by full matrix least squares on F^2. Hydrogen atoms were included in calculated positions and refined in riding mode. Refinement converged at a final $R = 0.0450$ ($wR_2 = 0.1035$, for all 6157 data, 631 parameters, mean and maximum δ/σ 0.000, 0.000), with allowance for the thermal anisotropy of all non-hydrogen atoms with the exception of N(1Ca) and N(2Cb). The atoms N(1Ca), N(2Ca) and N(1Cb), N(2Cb) were refined to an occupancy of 44 and 56%, respectively. Minimum and maximum final electron density -0.338 and $0.838\,e\,\text{Å}^{-3}$. A weighting scheme $w = 1/[\sigma^2(F_o^2) + (0.0485*P)^2 + 0.4503*P]$ where $P = (F_o^2 + 2*F_c^2)/3$ was used in the latter stages of refinement.

RESULTS AND DISCUSSION

[1-(2-*Pyridylazo*)-2-*naphtholato*]*copper*(*II*), [*Cu*(*PAN*)]NO_3

The reaction of HPAN with copper(II) nitrate in methanol yielded a purple–brown solid which analysed as $[Cu(PAN)]NO_3$ [3]; recrystallisation from the same solvent gave crystals suitable for structural analysis. The FAB+ mass spectrum showed a parent peak at m/z 311 attributable to $[Cu(PAN)]^+$ and a further peak at 622 attributable to a dimeric species, $[Cu(PAN)]_2$. In order to determine whether this was due to a genuine molecular association the molecular structure was determined. This shows (Fig. 1) that the azo-nitrogen atom furthest from the pyridine ring coordinates to the copper atom leading to the formation of two five-membered chelate rings; the double

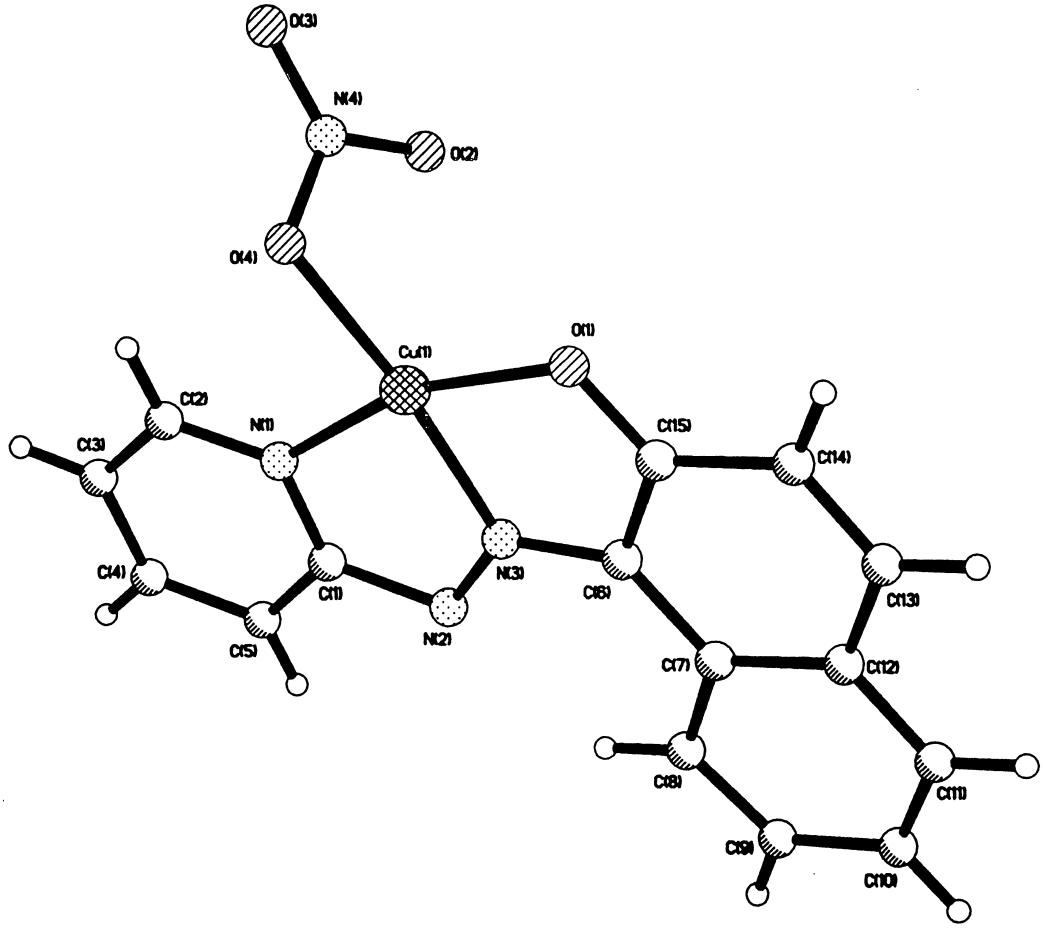

Fig. 1. The molecular structure of $[Cu(PAN)]NO_3$.

bond character of the azo-group is preserved. The fourth equatorial coordination position is occupied by an oxygen atom from the monodentate nitrate anion. Although the angles around the copper atom deviate from 90° the geometry nevertheless is close to square co-planar [the mean deviation for the plane

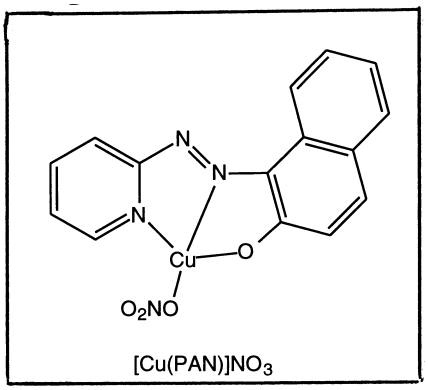

including O(1), N(3), N(1) and O(4) is 0.0244 Å and for that including the copper atom, O(1), N(3), N(1), O(4) and Cu is 0.0098 Å. The structure therefore is similar to that previously described for the complex $[Cu(PAN)(H_2O)]ClO_4$ [4]; the significant difference being that there is a water molecule bound to the copper in $[Cu(PAN)(H_2O)]ClO_4$ reflecting the weakly coordinating ability of the perchlorate anion relative to that of the nitrate anion. A comparison of the bond lengths and of the angles at the copper is given in Table 2.

Inspection of the packing diagram (Fig. 2) shows that the molecules exist as discrete pairs and this confirms the dimeric structure implied by the FAB+ mass spectrum. It has long been known from crystal structure data that self-association can occur in copper(II) complexes of ligands such as β-diketonates [5]. Such molecules are relatively planar and pack such that there is a weak interaction between the copper atom of one molecule and the central carbon atoms of the chelate rings of neighbouring molecules. More recently, an investigation concerning bis(tropolonato)copper(II) has clearly shown that this complex forms a sandwich-type van der Waals dimer in the crystalline state [6]. In the present case there is no evidence for interaction involving the copper atom or any π-stacking effects but the interatomic distance between a nitrate oxygen atom, O(2), and the C(5)H group on the adjacent molecule, 2.877 Å, suggests that there a weak hydrogen bonding interaction between these pairs might assist in augmenting the alignment of the present van der Waals dimer.

[2,2′-*Dihydroxyazobenzene*(-2)]*copper*(*II*), *pyridine*, *Cu*(*DAB*)·pyr

A brown gelatinous precipitate was produced when copper(II) acetate was added to a solution of H_2DAB in methanol [3]. Vapour diffusion of diethyl ether into a solution of the precipitate in pyridine gave shiny green crystals of Cu(DAB)·pyr. Unsuccessful attempts were made to record the FAB+ mass spectrum of both the powder and the crystals in NOBA matrices; in each case very protracted ranges of weak intensity peaks were detected and no discrete pattern emerged. It was thought that oligomerisation had occurred and so a crystal structure was determined in order to resolve this problem.

Table 2. A comparison of the bond lengths and bond angles in $[Cu(PAN)]NO_3$ and $[Cu(PAN)(H_2O)ClO_4$

	$[Cu(PAN)]NO_3$	$[Cu(PAN)(H_2O)]ClO_4$[a]
Bond length (Å)		
Cu(1)–N(1)	1.980(3)	1.97
Cu(1)–N(3)	1.950(3)	1.95
Cu(1)–O(1)	1.948(2)	1.97
Cu(1)–O(4)	1.987(3)	1.98
N(2)–N(3)	1.297(4)	1.27
Bond angle(°)		
N(3)–Cu(1)–O(1)	82.65(11)	83
N(3)–Cu(1)–N(1)	79.43(11)	80
N(1)–Cu(1)–O(4)	96.70(11)	98
O(1)–Cu(1)–O(4)	100.99(11)	99

[a]This data was taken from Ref. [4].

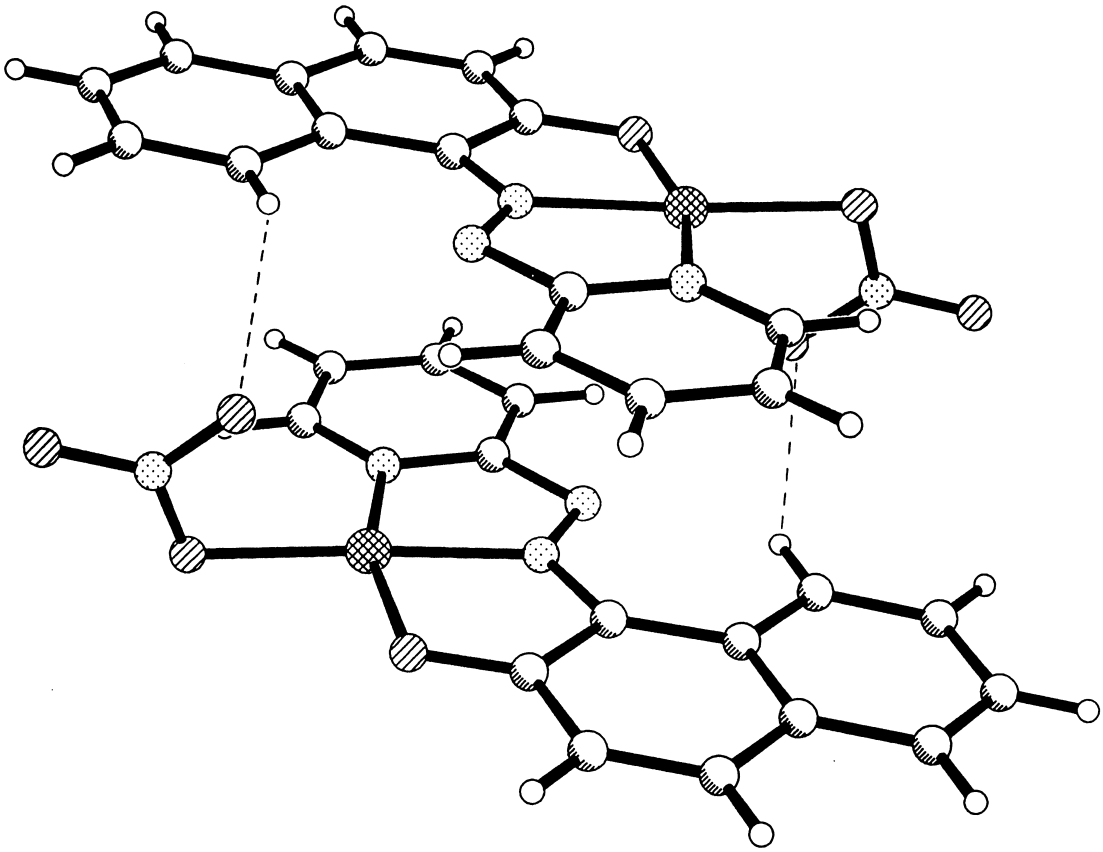

Fig. 2. The dimeric unit found for $[Cu(PAN)]NO_3$.

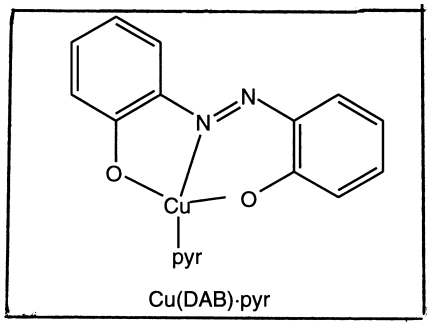

The crystal structure (Figs 3 and 4) revealed that the complex had crystallised in trimeric units, each consisting of three copper-dye molecules. This was unexpected as trinuclear copper(II) complexes are less extensively found than dinuclear complexes and examples of trinuclear complexes arising from self association are rare [7]. The trimers may be described as resembling triple-decker sandwiches in which the outer layers have grown stale and curled back from the central layer. Alternatively they may be viewed as being composed of two dimers with one common unit. Interestingly one pair of molecules lies "head to head", in parallel, with the pyridines adjacent to each other whereas the second set lies "head to tail", or inverted, with the pyridines at opposite ends of the dimer. It is likely that the deviation from planarity of the terminal units, N(3C)–Cu(2)–N(1C), 154.7° and N(3a)–Cu(1)–N(1A), 161.4° as compared with N(3B)–Cu(3)–N(1B), 174.1° for the central unit, leads to the construction of trimers rather than to the formation of stacks as would be anticipated if all three units were planar but it is not obvious why the two terminal units are twisted at 180° to each other.

Copper–ligand bonds have been classified as short interactions [Cu–L, 1.9–2.1 Å], intermediate interactions [Cu–L, 2.1–2.4 Å] and long interactions [Cu–L, 2.4–3.0 Å] [7]. In the present structure the trimer is held together by long bonding interactions between the copper atom in one molecule and one of the hydroxy oxygen atoms from the adjacent molecule: Cu(2)–O(1B), 2.517; Cu(3)–O(2C), 2.566, Cu(1)–O(2B), 2.622 and Cu(3)–O(1A), 2.768 Å. The shorter pair of distances are associated with the "head to tail" dimer and the longer pair with the "head to head" dimer. The copper–copper separations between the copper atoms Cu(2)–Cu(3) and Cu(1)–Cu(3) are 3.361 and 3.473 Å, respectively, with the shorter distance again associated with the "head to tail" dimer.

Although the aromatic rings lie above each other in the "head to head" dimer (Fig. 5) the separations of the centroids are rather long for π–π interactions,

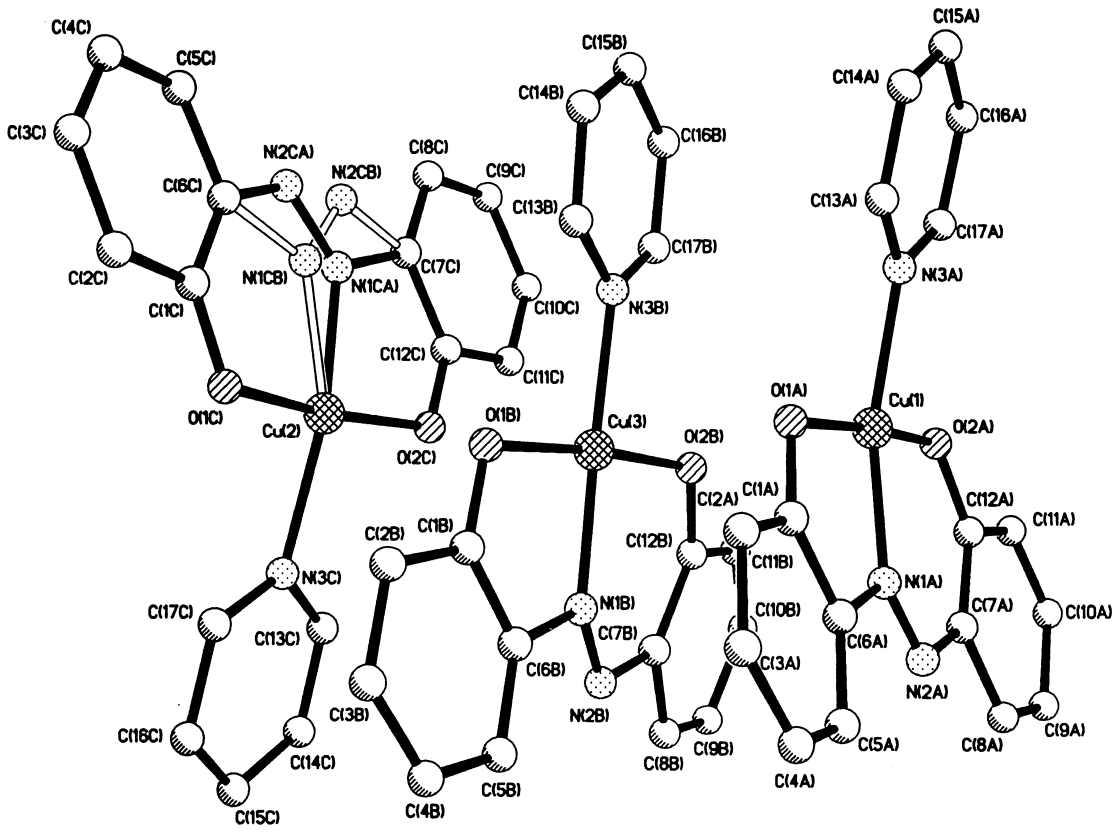

Fig. 3. The trimeric structure of Cu(DAB)·pyr. [Long bonding interactions at the copper atoms are: Cu(2)–O(1B), 2.517; Cu(3)–O(2C), 2.566, Cu(1)– O(2B), 2.622 and Cu(3)–O(1A), 2.768 Å. The intermetallic separations are: Cu(2)–Cu(3), 3.361 and Cu(1)–Cu(3), 3.473 Å].

pyridine[N(3A)–C(17A)]–pyridine[N(3B)–C(17B)], 3.760 A$\mathring{\beta}$; benzene[C(7A)–C(12A)]–benzene[C(7B)–C(12B)], 4.079 Å, and benzene[C(1A)–C(6A)]–benzene[C(1B)–C(6B)], 3.967 Å. Furthermore the benzene rings, which are coplanar having mean deviations from the planes composed of C(1A)–C(6A), C(7A)–C(12A), C(1B)–C(6B) and C(7B)–C(12B) of 0.0034, 0.0084, 0.0147 and 0.0038° respectively, are tilted away from each other, both intramolecularly and intermolecularly. The rings associated with Cu(1), C(1A)–C(6A) and C(7A)–C(12A), have an interplanar angle of 5.1° and those with Cu(3), C(1B)–C(6B) and C(7B)–C(12B), have an interplanar angle of 21.2°. Ring C(7A)–C(12A) and ring C(7B)–C(12B) are tilted away from each other at an angle of 22.6° and rings C(1A)–C(6A) and C(1B)–C(6B) tilt away from each other at an angle of 9.2°.

In the trimer each copper(II) atom is coordinated to the oxygen atoms of both deprotonated hydroxy groups from the dye and to one of the azo-group nitrogen atoms such that five- and six-membered chelate rings were formed. The fourth coordination position at each copper(II) atom was occupied by a molecule of pyridine. Bond lengths and angles at the metal atoms are given in Table 3 and if only these short interactions are considered then as the angles at the copper atoms deviate from 90° the geometry at each copper atom may be regarded as distorted square planar. If consideration is made of the long interactions observed between each copper atom and one of the hydroxy oxygen atoms from an adjacent molecule; Cu(1)–O(2B), Cu(2)–O(1B), Cu(3)–O(1A) and Cu(3)–O(2C) then the central copper atom, Cu(3), can be considered as distorted octahedral with the two terminal copper atoms in square pyramidal environments. Cu(1) has a τ value of 0.215 and Cu(2) a mean τ value of 0.26 where τ is an index of the degree of trigonality within the structural continuum between square pyramidal and trigonal pyramidal geometries [$\tau = (\beta - \})/60$ where β = O(2)–Cu–O(1) and α = N(3)–Cu–N(1)] [8]. For perfect square pyramidal and trigonal pyramidal geometries the values of τ are zero and unity, respectively.

The azo-N atoms binding to Cu(2), N(1C) and N(2C) were found to be disordered and the atoms N(1Ca), N(2Ca) and N(1Cb), N(2Cb) were refined to an occupancy of 44 and 56%, respectively. A similar occurrence has been noted in the structure of the analogous Schiff base complex *N*-(2-hydroxyphenyl)-salicylaldiminato-pyridine-copper(II), Cu(HSP), which

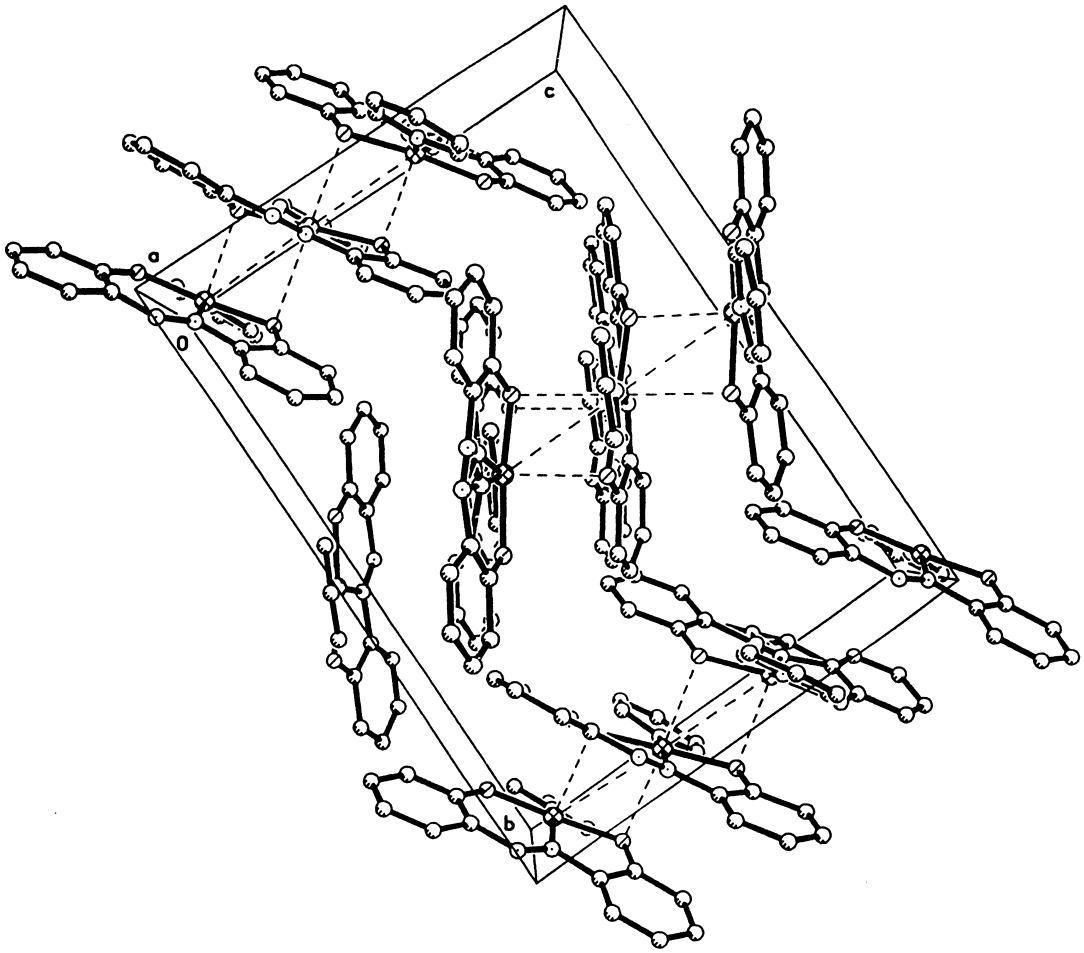

Fig. 4. The crystal packing in Cu(DAB) · pyr viewed along the *a* axis.

Table 3. Bond lengths (Å) and angles (°) found in the complex Cu(DAB) · pyr. (Ligand A, B and C refer to the atom numbering.) Details for the complex Cu(HSP) are also given

	Cu(1) ligand A	Cu(2) ligand C	Cu(3) ligand B	Cu(HSP)[a]
Bond length (Å)				
Cu–N(1)	1.946(6)	1.939(9); 2.00(2)	1.968(5)	2.023[b]
Cu–N(3)	2.040(4)	2.039(4)	2.021(4)	2.064
Cu–O(1)	1.933(5)	1.908(5)	1.951(4)	1.881
Cu–O(2)	1.880(5)	1.924(5)	1.902(4)	1.819
Bond angle (°)				
N(3)–Cu–O(1)	93.2(2)	92.7(2)	94.3(2)	109.4
N(3)–Cu–O(2)	91.0(2)	93.0(2)	90.9(2)	105.3
O(2)–Cu–N(1)	94.3(2)	77.3(4); 98.2(4)	91.8(2)	92.1[b]
O(1)–Cu–N(1)	82.9(2)	99.7(4); 78.4(4)	82.9(2)	90.4[b]

[a]Data taken from Ref. [9].
[b]N(imine) replaces N(1).

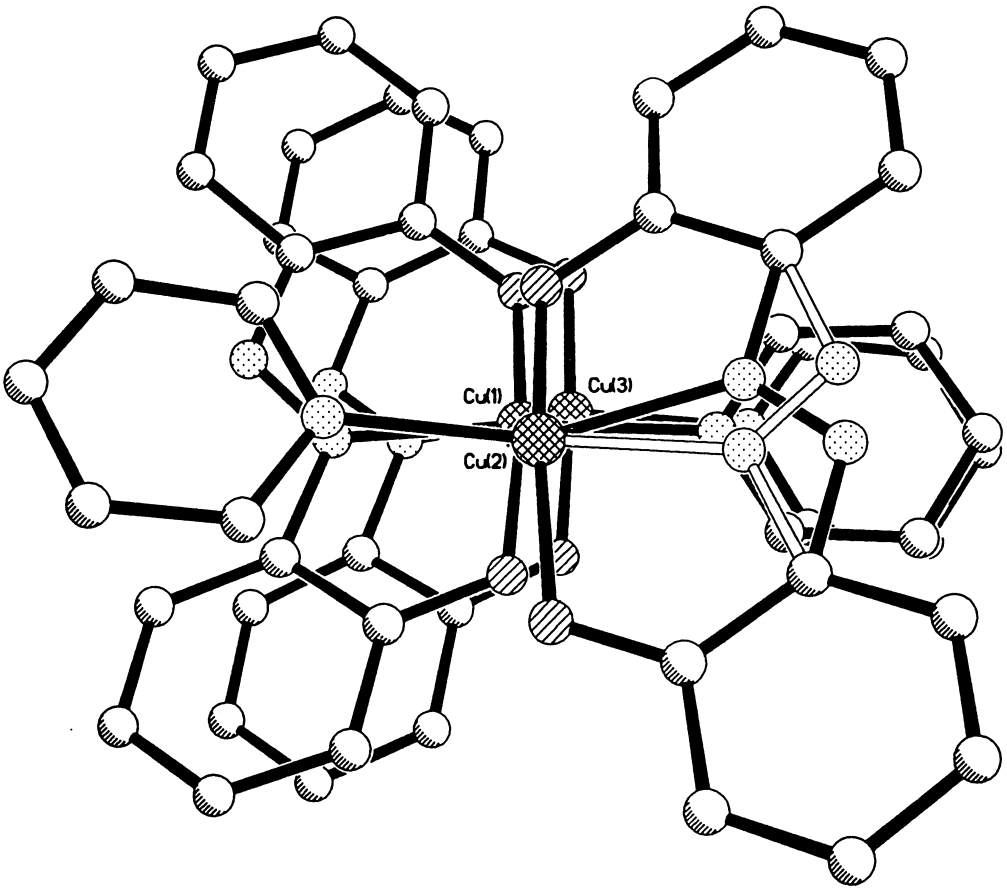

Fig. 5. The trimeric structure of Cu(DAB) · pyr as viewed down the Cu(2)–Cu(1)–Cu(3) axis.

has been reported and shows only discrete molecules of the complex [9]. The bond lengths and angles at the copper in Cu(HSP) are given in Table 3 and show that whereas the copper–nitrogen interactions are slightly longer the copper–oxygen interactions are slightly shorter than for the corresponding distances in Cu (DAB) · pyr.

If Cu(HSP) had been isolated in the absence of pyridine then the copper(II) would have been three-coordinate and coordinatively unsaturated [10]. A

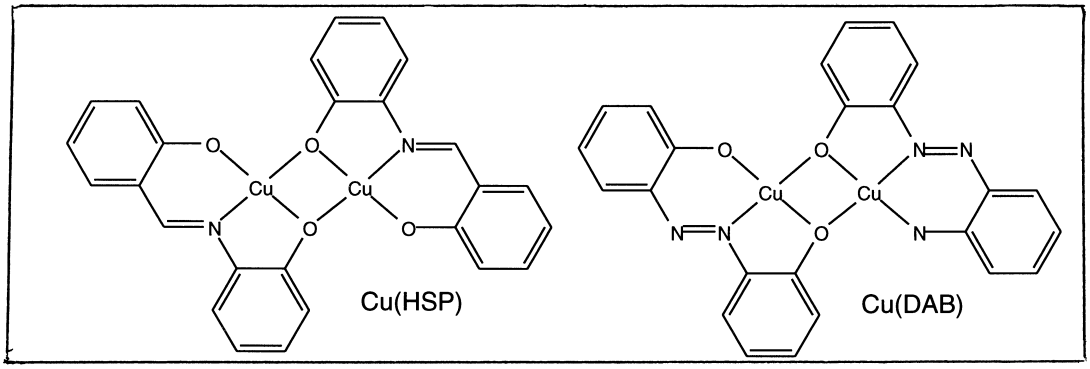

magnetic susceptibility study of *N*-(2-hydroxyphenyl)-salicylaldiminato-copper(II) revealed a subnormal magnetic moment which was attributed to antiferromagnetic coupling arising from dimer formation. Dissolution of this dimer in pyridine led to the formation of Cu(HSP)·pyr. The complex Cu(DAB) was originally isolated as a gelatinous material which dried to an amorphous solid. By analogy with the Schiff base it is proposed that the amorphous material is at least dimeric, but as there are present other donor facilities oligomerisation could occur. Dissolution in protic solvents gives the gelatinous material which could be a mixture of oligomers and of four coordinate species using the solvent as an additional donor.

Acknowledgements—We thank Unilever Research and the University of Sheffield for support (to R. M. B) and the EPSRC and the Royal Society for funds towards the purchase of the diffractometer.

REFERENCES

1. Price, R., in *Comprehensive Coordination Chemistry*, Vol. 6, Chap. 58, eds. G. Wilkinson, R. D. Gillard and J. A. McCleverty. Pergamon Press, Oxford, 1987, p. 35.
2. Sheldrick, G. M., *SHELXL*93, *An Integrated System for Solving and Refining Crystal Structures from Diffraction Data*, Revision 5.1. University of Göttingen, Germany, 1993.
3. Bucknall, R. M., Ph.D. Thesis, University of Sheffield, 1996.
4. Ooi, S., Carter, D. and Fernando, Q., *Chem. Comm.*, 1967, 1301.
5. Graddon, D. P., *Coord. Chem. Rev.*, 1969, **4,** 1.
6. Hasegawa, M., Inomaki, Y., Inayoshi, T., Hoshi, T. and Kobayashi, M., *Inorg. Chim. Acta*, 1997, **257,** 259.
7. Hathaway, B. J., in *Comprehensive Coordination Chemistry*, Vol. 5, Chap. 53, eds. G. Wilkinson, R. D. Gillard and J. A. McCleverty. Peragmon Press, Oxford, 1987, p. 533.
8. Addison, A. W., Rao, T. N., Reedijk. J., van Rijn, J. and Vershoor, G. C., *J. Chem. Soc. Dalton Trans.*, 1984, 1349.
9. Elmali, A., Atakal, O., Svoboda, I. and Fuess, H., *Z. Kristall.*, 1993, **205,** 146.
10. Kishita, M. and Muto, Y., Kubo, M., *Austr. J. Chem.*, 1957, **10,** 386.

Pergamon

Polyhedron Vol. 17, No. 23–24, pp. 4179–4187, 1998
© 1998 Elsevier Science Ltd
All rights reserved. Printed in Great Britain
0277–5387/98 $19.00+0.00

PII: S0277-5387(98)00226-5

Chiral Schiff base complexes of copper(II), vanadium(IV) and nickel(II) as oxidation catalysts. X-ray crystal structures of [Cu(*R*-salpn)(OH_2)] and [Cu(±-busalcx)]

Siona Bunce, Ronald J. Cross,* Louis J. Farrugia, Sam Kunchandy, Linette L. Meason, Kenneth W. Muir, Maureen O'Donnell, Robert D. Peacock, Diane Stirling and Simon J. Teat[1]

Chemistry Department, University of Glasgow, Glasgow G12 8QQ, U.K.

(Received 20 April 1998; accepted 5 June 1998)

Abstract—Several new complexes of chiral and achiral tetradentate Schiff bases with copper(II), nickel(II) and oxovanadyl(IV) ions have been synthesised and characterised and the structures of [Cu(*R*-salpn)(OH_2)] and [Cu(±-busalcx)] have been elucidated by X-ray analysis. [Cu(*R*-salpn)(OH_2)] is essentially square pyramidal with an unusually long bond [2.494(4) Å] from Cu to the oxygen of the apical water molecule. Molecules are linked by hydrogen bonding between the coordinated water and the salpn oxygens of neighbouring molecules. A long contact between a salpn CH_2 hydrogen and a neighbouring copper atom [H(3B)...Cu = 2.966(1) Å] might be regarded as a CH···Cu hydrogen bond and completes a pseudo-octahedral coordination about copper. [Cu(±-busalcx)] displays tetrahedrally-distorted planar coordination about the copper atom and has no significant intermolecular contacts. The copper, nickel and vanadyl complexes were screened as homogeneous catalysts for the oxidation by Bu^tOOH or H_2O_2 of PhMeS to PhMeSO. All of them are active catalysts but of the chiral complexes only [Cu(*R*,*R*-busalcx)] produced a reasonable enantiomeric excess (14%). Supporting the complexes on silica improved the enantioselectivity of the less sterically hindered [Cu(*R*-salpn)(OH_2)] (from 2 to 10%), but diminished that of the more hindered [Cu(*R*,*R*-busalcx)], probably by slowing the reaction to such an extent that the uncatalysed oxidation could compete effectively. Finally [Cu(salen)], [Cu(*R*-salpn)] and [Ni(*R*-salpn)] were synthesised in the pores of zeolites X and Y. These were shown to be active heterogeneous catalysts for the sulfide to sulfoxide oxidations, but no significant e.e. resulted from the use of the chiral catalysts. © 1998 Elsevier Science Ltd. All rights reserved.

Keywords: chiral; oxidation catalysis; Schiff bases; copper; nickel; vanadium; zeolites; crystal structures.

INTRODUCTION

The favourable ligand properties of tetradentate Schiff bases like salen [ethylenebis(salicylideneiminate); **1**] have ensured continued interest in their complexes for many years. [Ni(salen)] and [Pd(salen)] have recently been investigated as hydrogenation catalysts, both homogeneously and heterogeneously in the cages of zeolites X and Y [1–3]. It has also been claimed that zeolite-encapsulated [Cu(salen)]catalyses the oxidation of cyclohexanol to cyclohexanone [4], the epoxidation of norbornene and the hydroxylation of 1-naphthol [5], all under mild conditions. Of the several chiral examples of complexes of these types, perhaps the most celebrated is the highly sterically crowded Jacobsen's catalyst, [MnCl(busalcx)] (busalcx is ligand **6**), which achieves high enantioselectivity as an alkene epoxidation catalyst [6]. This type of complex, too, has recently been assembled and trapped inside the hypercages of zeolite EMT [7].

We describe here the syntheses and structures of chiral and achiral complexes of copper(II), nickel(II)

[1] Chemistry Department, University of Newcastle, Newcastle-upon-Tyne, U.K.

* Author to whom correspondence should be addressed.

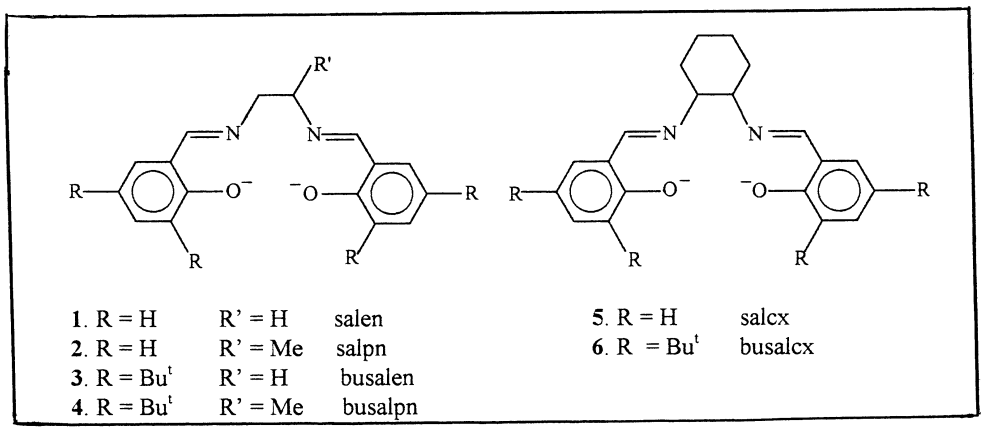

and vanadium(IV) with Schiff base ligands **1**–**6** and an examination of their potential as oxidation catalysts for the conversion of sulfides RR'S to sulfoxides.

RESULTS AND DISCUSSION

The copper complexes [Cu(*R*-salpn)(OH_2)], [Cu(*R*,*R*-salcx)], [Cu(busalen)], [Cu(*R*-busalpn)], [Cu(*R*,*R*-busalcx)] and [Cu(±-busalcx)], nickel complexes [Ni(*R*-salpn)], [Ni(*R*,*R*-salcx)], [Ni(busalen)], [Ni(*R*-busalpn)], [Ni(*R*,*R*-busalcx)] and [Ni(±-busalcx)] and vanadyl complexes [VO(*R*-busalpn)] and [VO(*R*,*R*-busalcx)] were prepared by refluxing together the relevant Schiff bases with $Cu(NO_3)_2 \cdot 3H_2O$, $NiCl_2 \cdot 6H_2O$ or $VO(SO_4)$, respectively, and an appropriate base.

The copper *R*-salpn complex was obtained by us as its monohydrate. It has previously been isolated either anhydrous or hydrated [8, 9]. Its structure was confirmed by X-ray crystallographic analysis and is shown in Fig. 1. Salient bond lengths and angles are presented in Table 1 and represent a marked improvement in accuracy over an early two-dimensional X-ray analysis of this material [10]. The compound is essentially square pyramidal in structure with an unusually long bond to the water molecule [2.494(4) Å] in the apical position, located on the opposite side of the square to the propyl CH_3 group. More typical Cu–O bond lengths to apical water molecules in such square pyramidal molecules are the value of 2.355(3) Å found in [Cu(tetraL)(OH_2)] [11] (tetraL is a tetramethylcyclam derivative) and 2.328(3) Å reported in aqua(dimethylpyrazole)(*N*-salicylildeneglycinato)copper(II) [12]. The water molecule in [Cu(salpn)(OH_2)] is hydrogen bonded to both salpn oxygens of a neighbouring molecule [Fig. 2; $O(3)\cdots O(1)' = 2.958(5)$ Å, $O(3)\cdots O(2)' = 2.788(5)$ Å] and a salpn CH_2 hydrogen occupies the pseudo-

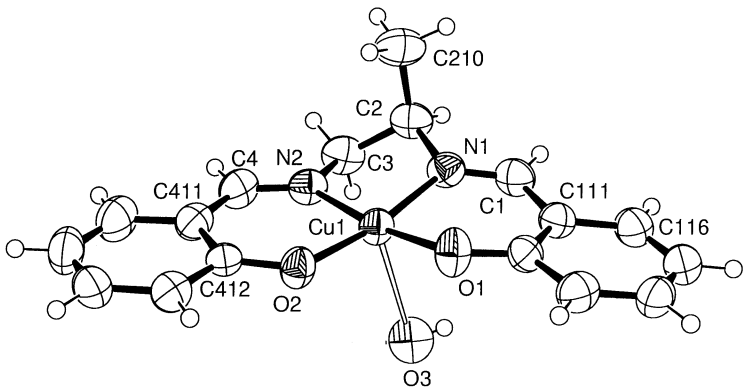

Fig. 1. A view of a molecule of [Cu(*R*-salpn)(OH_2)]. 50% probability ellipsoids are shown, except for hydrogen atoms which are represented by spheres of arbitrary size.

Table 1. Salient bond lengths (Å) and angles (°) for [Cu(*R*-salpn)(OH_2)]

Cu(1)–O(2)	1.916(2)	Cu(1)–O(1)	1.929(2)
Cu(1)–N(1)	1.949(3)	Cu(1)–N(2)	1.952(3)
Cu(1)–O(3)	2.494(4)		
O(2)–Cu(1)–O(1)	91.06(10)	O(2)–Cu(1)–N(1)	169.57(12)
O(1)–Cu(1)–N(1)	91.92(12)	O(2)–Cu(1)–N(2)	92.43(12)
O(1)–Cu(1)–N(2)	171.29(12)	N(1)–Cu(1)–N(2)	83.29(12)
O(2)–Cu(1)–O(3)	99.29(12)	O(1)–Cu(1)–O(3)	87.97(14)
N(1)–Cu(1)–O(3)	90.81(13)	N(2)–Cu(1)–O(3)	99.33(14)

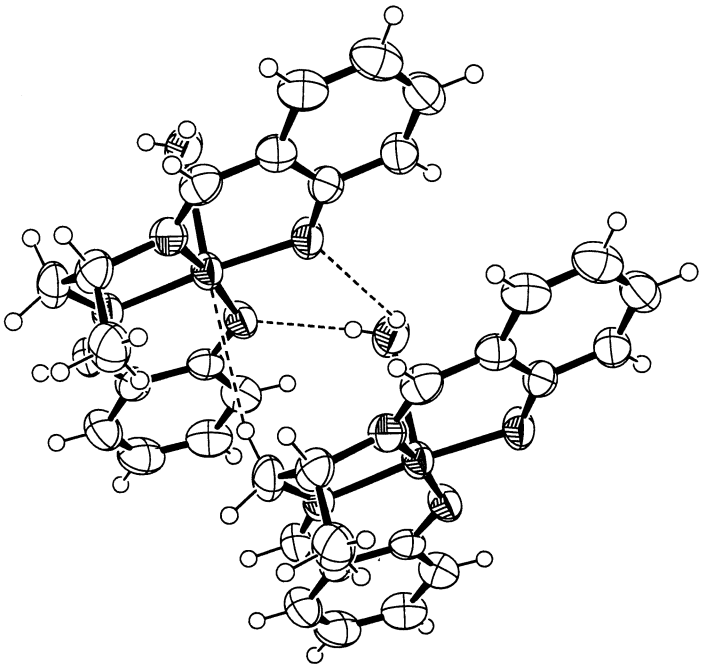

Fig. 2. Intermolecular interactions between molecules of [Cu(*R*-salpn)(OH_2)].

octahedral site of the copper atom of this molecule, with a C–H···Cu distance of 2.966(1) Å. Though extremely long, we note that this arrangement fulfills the criteria proposed for C–H···M hydrogen bonds [13].

Although the slight tendency to form 5-coordinate compounds is also evident in [Cu(salen)], which crystallises in dimeric oxygen-bridged units [14, 15], none of our other copper complexes was obtained as a hydrate. The structure of [Cu(salcx)] has been described previously and is a distorted square plane [16]. The compounds with Bu^t substituents were consistently obtained as feathery needles unsuitable for crystallographic analysis. Using a racemic form of the ligand, however, [Cu(±-busalcx)] was finally obtained as fine needles from which a structure determination was possible using synchrotron radiation. This structure is shown in Fig. 3 with salient bond lengths and angles presented in Table 2. The analysis confirms the *trans*-diamino stereochemistry of the cyclohexyl ring despite the presence of disorder. Each molecular site is occupied with equal probability by *RR* and *SS* diastereomers (only the former is shown in Fig. 3). Although alternative atomic sites are obvious only for C(31), C(33), C(34) and C(36) it is possible that systematic error may affect the positions of other atoms, most notably N(1) and N(2).

Molecules of [Cu(±-busalcx)] have close to C_2 point symmetry, with the two approximately planar O(*n*)N(*n*)C(*n*1)–C(*n*7) units ($n = 1$, 2) defining a dihedral angle of 28.5°. The copper atom displays tetrahedrally distorted square planar coordination characterised by *trans*-O–Cu–N angles of 165°. The Cu–O distances are close to the value (1.893 Å) [16]

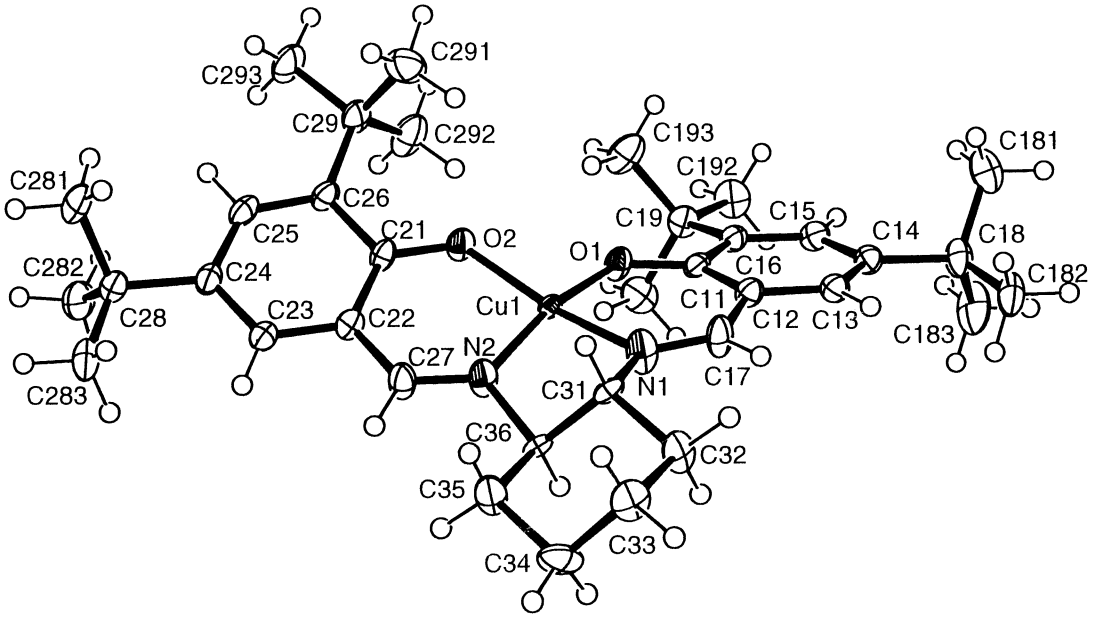

Fig. 3. A view of a molecule of [Cu(±-busalcx)]. 50% probability ellipsoids are shown, except for hydrogen atoms which are represented by spheres of arbitrary size. Only one of the two alternative sites occupied by disordered atoms C(31), C(33), C(34) and C(36) is displayed.

Table 2. Salient bond lengths (Å) and angles (°) for [Cu(±-busalcx)]

Cu(1)–O(1)	1.886(3)	Cu(1)– O(2)	1.887(3)
Cu(1)–N(2)	1.904(4)	Cu(1)–N(1)	1.915(4)
O(1)–Cu(1)–O(2)	91.47(12)	O(1)–Cu(1)–N(2)	165.16(17)
O(2)–Cu(1)–N(2)	94.12(14)	O(1)–Cu(1)–N(1)	94.11(14)
O(2)–Cu(1)–N(1)	165.06(17)	N(2)–Cu(1)–N(1)	83.90(16)

typical of bonds between O and four-coordinate Cu^{II}. The Cu–N bond lengths are on average 0.04 Å shorter than the mean Cu–N distance of 1.954 Å found in related Schiff base complexes [17]. The six-membered chelate rings are nearly flat (Cremer–Pople puckering parameter $Q = 0.123$ and 0.128 Å) [18] whereas the Cu(1)–N(1)–C(31)–C(36)–N(2) ring has $Q = 0.58$ Å and $\varphi = 270.3°$, equal to the ideal half-chair value of 270° to within experimental error. The cyclohexyl ring ($Q = 0.71$ Å and $\theta = 177°$) has a close to ideal chair conformation. The shortest intermolecular contacts involving the metal atom, Cu···H distances of 3.3 Å, are clearly non-bonding.

Thus the tetrahedrally-distorted square planar configuration resembles those of the related complexes [Cu(salcx)] [16], **7** [19] and **8** [20]. In all of these 4-coordinate compounds the Cu–O bonds are shorter than Cu–N and both types are shorter than in the 5-coordinated (or pseudo-octahedral; see above) [Cu(salpn)(OH_2)]. The distortions from planar coordination in [Cu(sal-1,3-pn)], with its additional CH_2 bridging unit in the central chelate ring, are noticeably greater than in the others [21].

The nickel compounds are all diamagnetic and hence best described as square planar. Nevertheless an appreciable distortion from planarity is evident in the structure of [Ni(salcx)] [22], although [Ni(salen)] itself, though dimeric, consists of nearly planar molecules [23]. The butyl derivatives again formed fibrous crystals. The vanadyl complexes [VO(*R*-busalpn)] and [VO(*R*,*R*-busalcx)] also formed as feathery crystals unsuitable for X-ray analysis. Their structures are presumably based on the familiar square pyramids, typified by [VO(salen)] [24].

OXIDATION REACTIONS

Homogeneous oxidations

Several copper(II), nickel(II) and vanadium(IV) complexes are known to be effective catalysts for a

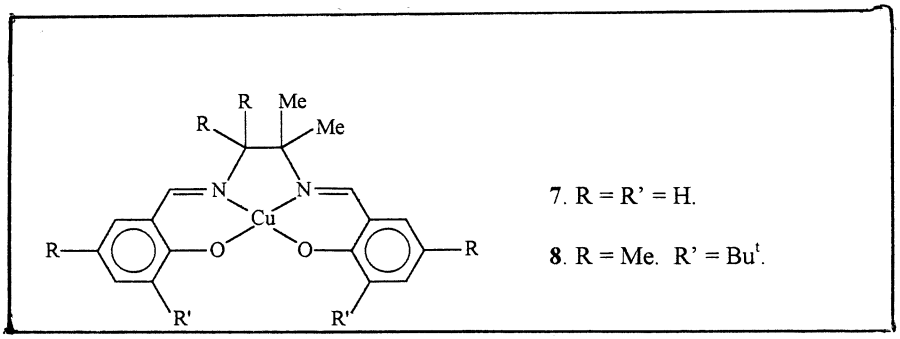

7. R = R' = H.

8. R = Me. R' = Bu^t.

number of oxidation reactions. For example, the Baeyer–Villiger oxidation of cyclic ketones to lactams has been successfully catalysed homogeneously by [Cu(OAc)$_2$] or [Ni(OAc)$_2$] [25, 26] and heterogeneously by Cu^{2+} in hydrotalcite clays [27]. The oxidation of prochiral sulfides to sulfoxides has been catalysed by a range of chiral vanadyl complexes [28] including Schiff base complexes [29]. Moderate enantiomeric excesses were also reported from the use of vanadium-containing pillared clays modified by diethyltartrate [30]. Our intention was to probe the effects of sterically hindered complexes as enantioselective catalysts, as our previous experience indicates that greater steric bulk can improve the enantiomeric excess of the products [31]. The oxidation of prochiral PhMeS to its sulfoxide, PhMeSO, by the action of 5% aqueous Bu^{t}OOH in CH_2Cl_2 or acetonitrile at 0° was catalysed by adding 10 mol.% of the molecular complex. It was necessary to maintain the low temperature throughout to suppress the competing, non-catalysed reaction which could only lead to racemic product. In the presence of [Cu(*R*-salpn)] or [Cu(*R*,*R*-salcx)] the reactions proceed smoothly to produce 60% of the sulfoxide in 5 h, but with negligible (<2%) e.e. These observations parallel those previously reported with the use of [VO(salpn)] as catalyst [29]. An explanation advanced for the low e.e.s from that system was that the substrate and/or oxidant could approach the metal from the methyl side or the opposite side of the planar salpn ligand with similar ease. No sulfone was observed from our reactions.

Using the sterically-hindered complexes [Cu(*R*-busalpn)], [Cu(*R*,*R*-busalcx)], [VO(*R*-busalpn)] or [VO(*R*,*R*-busalcx)] as catalysts under the same conditions produced only 10% of products over the same time period. Once again, however, no significant enantiomeric excess was produced. The reactions were repeated using aqueous H_2O_2 as oxidant instead of Bu^{t}OOH in case hindrance between catalyst and oxidant was preventing the reaction from proceeding enantioselectively. These reactions proceeded even more slowly, presumably due to the two-phase solvent system, but [Cu(*R*,*R*-busalcx)] led to a 14% e.e., with [VO(*R*,*R*-busalcx)] producing a 4% e.e.

The nickel complexes [Ni(*R*-salpn)] and [Ni(*R*,*R*-busalcx)] also catalysed the conversion of sulfide to sulfoxide, but without generating any measurable e.e.

Silica supported complexes

The copper complexes [Cu(*R*-salpn)] and [Cu(*R*,*R*-busalcx)] were impregnated onto silica (Gasil 35 M) and the silica-supported complexes tested as catalysts for the H_2O_2 oxidation of PhMeS under conditions similar to above. In both cases the production of coloured solutions testified to some leaching of the complex into solution during the reaction, but the catalytic performance of the [Cu(*R*-salpn)] was improved, producing a 10% e.e. in a 20% reaction over 5 h. This is strongly indicative that despite the leaching problem, the oxidation reaction has taken place predominantly at the surface. The more hindered complex performed less well, reaching only 2% reaction after 5 h with a 4% e.e., indicating that under these conditions at least, restricted access to the chiral centre was not helpful. A possible explanation is that under these extremely slow reaction conditions the non-catalysed process competes more effectively.

Zeolite-encapsulated complexes

In an attempt to utilise the improved performance of the copper catalysts in contact with silica and to overcome the problem of complex leaching, we have synthesised [Cu(salen)], [Cu(*R*-salpn)] and [Ni(*R*-salpn)] in the pores of zeolites X and Y (the pores of these zeolites are not large enough to accommodate our more bulky ligands). These were prepared by standard methods [1–5] by introducing Cu^{2+} or Ni^{2+} into the zeolite by ion exchange, treating this material with salen or salpn (the use of CH_2Cl_2 or CH_3CN solutions for this step proved less efficient than employing molten ligand), then removing excess ligand by prolonged extraction with CH_2Cl_2. Finally, the materials were subjected to further ion exchange with Na^+ to remove any uncomplexed copper ions. (This last stage is of considerable importance, since we established in a control experiment that zeolite-supported copper

ions themselves are excellent catalysts for sulfide oxidations).

Microanalytical results indicated that the zeolites held close to the expected one molecule per cage. The UV/visible spectra of the zeolite materials were similar to those of the copper complexes themselves.

The oxidation of thioanisole to PhMeSO by hydrogen peroxide was indeed catalysed by all three of the zeolite-encapsulated molecules but no significant enantiomeric excess resulted from the use of the chiral materials. Moreover the rate of the reactions was very slow, presumably due to the need for the reactants to diffuse into the zeolite pores. The history of the zeolite encapsulated catalyst could be of importance. It has been reported that Cu(salen)/zeolite-Y is green and inactive towards norbornene or 1-naphthol oxidations after refluxing in CH_2Cl_2, but red and active after MeCN treatment [5]. The differences are assigned to changes in the anchoring of the complex to the cage walls. We note that our Cu(salpn)/zeolites are also colour-sensitive, changing from yellow–green after CH_2Cl_2 reflux to orange after prolonged MeCN treatment, but discerned no change in catalytic ability between the two types.

Overall we conclude that the use of our chiral complexes as homogeneous oxidation catalysts is similar to, but no better than, the less sterically-hindered vanadium(IV) complexes described in the literature [29]. On the other hand there is a real enhancement of selectivity if the catalysts are supported on silica, although catalyst leaching into solution prevents effective exploitation of this method. Encapsulating the smaller compounds in zeolites overcomes the leaching problems under our reaction conditions, but the reactions in the pores are slow and non-selective.

EXPERIMENTAL

1,2-diaminopropane and 1,2-cyclohexyldiamine were resolved by literature methods [32, 33]. Schiff bases were prepared by refluxing the above diamines or 1,2-diaminoethane with salicylaldehyde or 3,5-di-*tert*-butyl salicylaldehyde. Typical syntheses of the copper, nickel and vanadyl complexes are given below. Table 3 lists analytical data on new compounds.

Synthesis of [Cu(R-salpn)(OH_2)]

To a solution of *R*-salpnH_2 (5.9 g, 21 mmol) in ethanol (60 ml) was added $Cu(NO_3)\cdot 3H_2O$ (5.0 g, 21 mmol) in ethanol (30 ml). The mixture was heated and 42 ml of 1 M aqueous NaOH was added. The purple solution was cooled to yield dark purple X-ray-quality crystals of the product [2.9 g, 98%: M.pt. 229–231°. $[\alpha]_D$ +625° (EtOH, $c = 0.66$ mmol·lit^{-1})].

Synthesis of [Ni(R-salpn)]

This was prepared similarly from salpnH_2 and $NiCl_2\cdot 6H_2O$ to yield deep orange crystals of the product [67%: $[\alpha]_D$ 954° (EtOH, 1.0 mmol·lit^{-1}). Found, C, 60.2; H, 4.7; N, 8.45%: req. for $C_{17}H_{16}N_2NiO_2$, C, 60.23; H, 4.75; N, 8.27%].

Synthesis of [Ni(R-*busalpn*)]

$Ni(NO_3)_2\cdot 3H_2O$ (0.861 g; 2.96 mmol) was added to an ethanol (100 ml) solution of *R*-busalpnH_2 (1.5 g; 2.96 mmol) and the mixture refluxed for 1 h. The product was formed as a pale brown precipitate. It was washed with ethanol and recrystallised from acetone (yield, 75%).

Synthesis of [VO(R,R-*busalcx*)]

To a hot solution of [$VO(SO_4)$] (0.163 g; 1 mmol) in methanol (45 ml) was added a slurry of *R*,*R*-busalcxH_2 (0.546 g; 1 mmol) in MeOH (15 ml) and pyridine (2 ml). The green precipitate of product was filtered off and recrystallised from a MeOH/$CHCl_3$ 1:1 mixture.

Homogeneous oxidations

In a typical procedure, thioanisole (0.62 ml; 5.3 mmol) and [Cu(salpn)OH_2] (0.14 g; 0.38 mmol) were dissolved in acetonitrile (25 ml) at 0°. A mixture of Bu^{t}OOH 0.88 ml of 5.5 molar aq. solution (5.3 mmol) in a further 25 ml of acetonitrile at 0° was added and the mixture stirred for 5 h. The clear reaction mixture turned purple. After quenching with aqueous sodium sulfite solution, the organic layer was separated, dried (anhydrous Na_2SO_4) and analysed by HPLC (Chiracel OB column with 10% isopropanol/90% hexane mobile phase, eluted at a flow rate of 0.5 ml/min).

In other variations the Bu^{t}OOH was replaced by aqueous H_2O_2 and the reaction mixture treated in the same way.

Silica-supported complexes

In a typical procedure, 5 g of Gasil 35 M silica was oven dried at 110° for 24 h then added to a solution of [Cu(salpn)(OH_2)] (3.117 g; 8.62 mmol) in $CHCl_3$ (50 ml). After stirring the mixture for 24 h, the solvent was removed by rotary evaporation and pumping under vacuum. The catalyst was kept overnight at 110° prior to use.

0.14 g of this catalyst was placed in a flask with $CHCl_3$ (25 ml) and thioanisole (0.62 ml; 5.3 mmol) and cooled to 0°. To this was added 0.54 ml of 30% aqueous hydrogen peroxide and the mixture stirred for 5 h at this temperature. A purple colour in the solvent indicated that some of the complex had dissolved. The

Table 3. Analytical data on new compounds

	Found			Calculated		
Compound	%C	%H	%N	%C	%H	%N
(busalen)H_2	78.05	9.75	5.7	77.94	9.74	5.68
(*R*-busalpn)H_2	78.2	9.5	5.4	78.21	9.95	5.53
(*R*,*R*-busalcx)H_2	78.9	10.0	5.2	79.08	9.95	5.12
($\pm$-busalcx)H_2	79.0	9.7	5.1	79.08	9.95	5.12
Cu(busalen)	69.3	8.45	4.8	69.35	8.36	5.06
Cu(*R*-busalpn)	69.5	8.4	5.0	69.75	8.51	4.93
Cu(*R*,*R*-busalcx)	71.1	8.6	4.7	71.08	8.61	4.61
Cu($\pm$-busalcx)	70.55	8.6	4.5	71.08	8.61	4.61
Ni(busalen)	69.7	8.4	5.05	69.95	8.44	5.09
Ni(*R*-busalpn)	70.4	8.55	4.8	70.35	8.59	4.97
Ni(*R*,*R*-busalcx)	71.1	8.5	4.7	71.65	8.68	4.64
Ni($\pm$-busalcx)	70.75	8.7	4.4	71.65	8.68	4.64
VO(*R*-busalpn)	69.25	8.3	4.9	69.33	8.46	4.90
VO(*R*,*R*-busalcx)	71.1	8.8	4.7	70.68	8.59	4.58

mixture was treated by aqueous (50 ml) sodium sulfite (0.67 g; 5.3 mmol) and the organic layer extracted into chloroform, filtered and dried (anhydrous $MgSO_4$). After removal of the chloroform under vacuum, the product was diluted by hexane and analysed as above by HPLC.

Zeolite-encapsulated materials

The complexes were prepared as described for [Cu(salen)] in zeolite–Na X and zeolite–Na Y in CH_2Cl_2 solvent [4, 5]. Any non-encapsulated complex was removed by Soxhlet extraction with dichloromethane or acetonitrile for several hours and uncomplexed copper ions were replaced by sodium ions by treatment with NaCl.

In a typical experiment, 0.14 g of Cu(salpn)/zeolite X was placed in a flask with thioanisole (0.62 ml; 5.3 mmol) in CH_2Cl_2 (20 ml) at 0°. To this was added 0.54 ml of 30% aqueous hydrogen peroxide and the mixture stirred for 5 h at this temperature. The mixture was then treated by aqueous (50 ml) sodium sulfite (0.67 g; 5.3 mmol) and the organic layer extracted into chloroform, filtered and dried (anhydrous $MgSO_4$). After removal of the chloroform under vacuum, the product was diluted by hexane and analysed as before by HPLC.

X-ray structure determination of [*Cu*(*salpn*)(*OH*$_2$)]

Details of data collection procedures and structure are given in Table 4. A single crystal of suitable size was attached to a glass fibre using acrylic resin and mounted on a goniometer head in a general position. Data were collected in bisecting mode on an Enraf-Nonius TurboCAD4 diffractometer, running under CAD4-Express software and using graphite monochromated X-radiation. Precise unit cell dimensions were determined by refinement of the setting angles of 25 high-angle reflections which were flagged during data collection. Standard reflections were measured every 2 h during data collection and no significant variation in intensities was noted. Lorentz-polarization corrections were then applied to the reflection data. The ψ-scan data which were collected indicated that no absorption correction was necessary, and none was applied. The structures were solved by direct methods (SHELXS-97) [34]. All non-H atoms were allowed anisotropic thermal motion. Aliphatic CH hydrogen atoms were included at calculated positions, with C–H = 0.96 Å, while the OH protons were found from a difference map and were freely refined. Refinement (SHELXL-97) [35] was by full-matrix least-squares on F^2, using all the unique data and the weighting scheme $w = [\sigma^2(F_o)^2 + (AP)^2 + BP]^{-1}$ where $P = [F^2_o/3 + 2F^2_c/3]$ and $A = 0.0412$, $B = 0.1607$. $\sigma(F_o)^2$ was estimated from counting statistics. Neutral atom scattering factors, coefficients of anomalous dispersion and absorption coefficients were obtained from Ref. [36]. The absolute configuration was confirmed by the refinement of the Flack absolute structure parameter, which refined to zero within error. Calculations using PLATON [37] indicated that there were no voids in the lattice capable of containing any solvent molecules. Thermal ellipsoid plots were obtained using the program ORTEP-3 for Windows [38].

X-ray structure determination of [*Cu*($\pm$-*busalcx*)]

Details of data collection procedures and structure are given in Table 4. The crystals grew as long, extremely fine brown needles which gave no dis-

Table 4. Experimental details of the crystallographic studies

Compound formula	$C_{17}H_{18}CuN_2O_3$	$C_{36}H_{52}CuN_2O_2$
Compound number		
Compound colour	dark green	brown
M_r	361.87	608.34
Space group	$P2_12_12_1$	P-1
Crystal system	orthorhombic	triclinic
a (Å)	5.149(1)	9.882(2)
b (Å)	13.320(3)	13.573(1)
c (Å)	22.947(6)	14.843(2)
α (°)	90	62.897(1)
β (°)	90	73.205(1)
γ (°)	90	78.801(1)
V (Å^{-3})	1573.8(6)	1692.0(4)
λ (Å)	0.71073	0.6870
Z	4	2
D_{calc} (g cm^{-3})	1.527	1.194
$F(000)$	748	654
μ(Mo-K$_\alpha$) (mm^{-1})	1.404	0.677
Scan mode	$\varpi/2\theta$	n/a
ω scan angle (°)	$0.91+0.47\tan(\theta)$	n/a
θ range (°)	3.1–25.0	2.1–26.8
Crystal size (mm)	$0.5\times0.3\times0.3$	$0.25\times0.04\times0.02$
No. of data collected	2368	9775
No. of unique data	2134	6856
Temperature (K)	291(2)	160(2)
hkl range	$-6\rightarrow1$; $-2\rightarrow15$; $-27\rightarrow2$	$-12\rightarrow12$; $-17\rightarrow13$; $-19\rightarrow18$
R_{int}	0.017	0.028
No. of data in refinement	2134	6856
No. of refined parameters	218	419
Final R $[I>2\sigma(I)]$ (all data)	0.029 (0.036)	0.065 (0.078)
R^2_w $[I>2\sigma(I)]$ (all data)	0.067 (0.070)	0.161 (0.166)
Goodness of fit, S	1.071	1.201
Flack absolute structure parameter	0.01(2)n/a	
Largest remaining feature in electron density map (eÅ^{-3})	0.33 (max), −0.19 (min)	0.72 (max), −0.48 (min)
Shift, esd in last cycle (max)	0.001	0.001

$R=\Sigma(\|F_o\|-\|F_c\|)/\Sigma(F_o)$; $wR2=\{\Sigma(w(F_o^2-F_c^2)^2)/\Sigma(w(F_o^2)^2)\}^{1/2}$.
$R_{int}=\Sigma|F_o^2-F_o^2(\text{mean})|/\Sigma F_o^2$ (summation is carried out only where more than one symmetry equivalent is present).

cernable diffraction with a conventional X-ray source. However, it proved possible to make satisfactory measurements on a Siemens SMART CCD diffractometer mounted on the single crystal diffraction station (9.8) at the Daresbury Laboratory Synchrotron Radiation Source, U.K. The intensities of 9775 reflections were averaged to give 6856 unique reflections (85% of those accessible). 5720 unique reflections were deemed observed $[I>2\sigma(I)]$. The data were corrected for Lp and decomposition effects by the standard SAINT software. The structure was solved by Patterson and Fourier methods and refined (SHELXL-97) [35] using all the unique data to convergence on F^2 with $w=[\sigma^2(F^2)+(0.044P)^2+4.5P]^{-1}$ where $P=[F^2_o/3+2F^2_c/3]$. All non-H atoms were allowed anisotropic thermal motion. H atoms rode on their parent C atoms and an orientation parameter was successfully refined for each of the 12 methyl groups. The cyclohexyl ring is disordered so that atoms C(31), C(33), C(34) and C(36) are each distributed over two sites with occupancy 1/2 roughly related by reflection in the CuN_2 plane. The ring C–C bonds were restrained to the value 1.545(6) Å. Mass attenuation coefficients and dispersion corrections (for $\lambda=0.7107$ Å) and atomic scattering factors were those incorporated in SHELXL-97 [35]. The WinGX

package [39] and ORTEP-3 for Windows [38] were used for other calculations.

SUPPORTING INFORMATION AVAILABLE

Tables of atomic parameters, a complete geometry listing and observed and calculated structure factors are available from the authors. The structure will be deposited in the Cambridge Structural Database.

*Acknowledgements*We wish to express our gratitude to Professor William Clegg for making time on the Daresbury SMART-CCD diffractometer available to us. We also thank EPSRC (U.K.) and the University of Glasgow for support.

REFERENCES

1. Chatterjee, D., Bajaj, H. C., Das, A. and Bhatt, K., *J. Mol. Catal.*, 1994, **92,** L235.
2. zu Altenschidesche, H. M. and Nesper, R., *Stud. Surf. Sci. Catal.*, 1995, **98,** 120.
3. Kowalak, S., Weiss, R. C. and Balkus, K. J., *J. Chem. Soc. Chem. Commun.*, 1991, 57.
4. Ratnasamy, C., Murugkar, A. and Padhye, S., *Indian J. Chem.*, 1996, **35A,** 1.
5. Koner, S., *J. Chem. Soc. Chem. Commun.*, 1998, 593.
6. Jacobsen, E. N., Zhang, W., Muci, A. R., Ecker, J. R. and Deng, L., *J. Am. Chem. Soc.*, 1991, **113,** 7063.
7. Ogunwumi, F. B. and Bein, T., *J. Chem. Soc. Chem. Commun.*, 1997, 901.
8. Gillard, R. D. and Wilkinon, G., *J. Chem. Soc.*, 1963, 5399.
9. Gillard, R. D., Laurie, S. H. and Ugo, R., *J. Inorg. Nucl. Chem.*, 1971, **33,** 997.
10. Llewellyn, F. J. and Waters, T. N., *J. Chem. Soc.*, 1960, 2639.
11. Tahirov, T. H., Lu, T.-H., Liao, F.-L., Wang, S.-L., Chen, B.-H., Chi, T.-Y. and Chung, C.-S., *Acta Cryst. C*, 1996, **52,** 2687.
12. Warda, S., Friebol, C., Sivy, J., Plesch, G. and Svajlenova, O., *Acta Cryst. C*, 1996, **52,** 2763.
13. Brammer, L., Zhao, D., Ladipo, F. T. and Braddock-Wilking, J., *Acta Cryst. B*, 1995, **51,** 632.
14. Baker, E. N., Hall, D. and Waters, T. N., *J. Chem. Soc. A*, 1970, 406.
15. Bhadbhade, M. M. and Srinivas, D., *Inorg. Chem.*, 1993, **32,** 6122.
16. Bernardo, K., Leppard, S., Robert, A., Commenges, G., Dahan, F. and Meunier, B., *Inorg. Chem.*, 1996, **35,** 387.
17. *International Tables for Crystallography*, Vol. C. International Union of Crystallography, Kluwer Academic Publishers, Dordrecht, 1992, pp. 714–778.
18. Cremer, D. and Pople, J. A., *J. Am. Chem. Soc.*, 1975, **97,** 1354–1359.
19. Lo, J.-M., Yao, H.-H., Liao, F.-L., Wang, S.-L. and Lu, T.-H., *Acta Cryst. C*, 1997, **53,** 848.
20. Valko, M., Boca, R., Klement, R., Kozisek, J., Mazur, M., Pelikan, P., Morris, H. and Eias, H., Muller, L., *Polyhedron*, 1997, **16,** 903.
21. Xiong, R. G., Song, B.-L., Zuo, J.-L. and You, X.-Z., *Polyhedron*, 1996, **15,** 903.
22. Wojtczak, A., Szlyk, E., Jaskolski, M. and Larsen, E., *Acta Chem. Scand.*, 1997, **51,** 274.
23. Shol'nikova, L. M., Yumal, E., Shugam, E. A. and Voblikova, V. A., *J. Struct. Chem.*, 1970, **11,** 819.
24. Riley, P. E., Pecoraro, V. L., Carrano, C. J., Bonadies, J. A. and Raymond, K. N., *Inorg. Chem.*, 1986, **25,** 154.
25. Yamada, T., Takahashi, K., Kato, K., Takai, T., Inoki, S. and Mukaiyama, T., *Chem. Lett.*, 1991, 641.
26. Bolm, C., Schlinggloff, G. and Weickhardt, K., *Tetrahedron Lett.*, 1993, **34,** 3405.
27. Kaneda, K., Ueno, S. and Imanaka, T., *J. Mol. Catal.*, 1995, **102,** 135.
28. Bolm, C. and Bienewald, F., *Angew. Chem.* (*Int. Edn.*), 1995, **34,** 2640.
29. Nakajima, K., Kojima, K., Kojima, M. and Fujita, J., *Bull. Chem. Soc. Jpn.*, 1990, **63,** 2620.
30. Choudary, B. M. and Rani, S. S., *J. Mol. Catal.*, 1992, **75,** L7.
31. Cross, R. J., Farrugia, L. J., Newman, P. D., Peacock, R. D. and Stirling, D., *J. Chem. Soc. Dalton Trans.*, 1996, 4449.
32. Dwyer, F. P., Gorvan, F. L. and Shalman, A., *J. Am. Chem. Soc.*, 1959, **81,** 290.
33. Galsbol, F., Steenbol, P. and Sorensen, B. S., *Acta Chem. Scand.*, 1972, **26,** 3605.
34. Sheldrick, G. M., *SHELXS*-97: *A Program for Automatic Solution of Crystal Structures by Direct Methods*. University of Göttingen, Germany, 1997.
35. Sheldrick, G. M., *SHELXL*-97: *A Program for Crystal Structure Refinement*, Release 97-2. University of Göttingen, Germany, 1997.
36. *International Tables for Crystallography*, Vol. C. Kluwer, Dordrecht, 1995, Tables 4.2.4.2, 4.2.6.8 and 6.1.1.4.
37. Spek, A. L., *Acta Crystallogr. A*, 1990, **46,** C34.
38. Farrugia, L. J., *J. Appl. Cryst.*, 1997, **30,** 565.
39. Farrugia, L. J., *WinGX*: *A Program System for X-ray Analysis*. University of Glasgow, U.K., 1996.

Pergamon

Polyhedron Vol. 17, No. 23–24, pp. 4189–4193, 1998
© 1998 Elsevier Science Ltd
All rights reserved. Printed in Great Britain
0277–5387/98 $19.00+0.00

PII: S0277–5387(98)00227–7

Synthesis, crystal and molecular structure of a new heterometallic oxo-2-methoxyethoxide, $BaMo_2O_5(OC_2H_4OMe)_4(HOC_2H_4OMe)$

Vadim G. Kessler,*[a] Nataliya Ya. Turova,[a] Andrei N. Panov,[a] Zoya A. Starikova,[b] Alexandr I. Yanovsky,[b] Yuri T. Struchkov[b] and David Benlian[c]

[a]The Department of Chemistry, Lomonosov Moscow State University, Vorobjovy Gory, 119899 Moscow, Russia

[b]The A.N. Nesmeyanov Institute of Organoelement Compounds, 28 Vavilov Street, 117813 Moscow, Russia

[c]Laboratoire de Chimie de Coordination, Universite de Provence, 13397 Marseille, France

(Received 30 March 1998; accepted 2 June 1998)

Abstract—The colorless needle-shaped crystals of a new heterometallic 2-methoxyethoxide, $BaMo_2O_5(OC_2H_4OMe)_4(HOC_2H_4OMe)$ (**1**), have been obtained by the saturation of barium 2-methoxyethoxide solution in 2-methoxyethanol with the crystalline $MoO_2(OC_2H_4OMe)_2$. The precipitation started when the Ba:Mo ratio achieved a 1:2 value and the precipitate formed contained $BaMoO_4$ as an admixture thus indicating that the formation of oxo species led partially even to formation of inorganic molybdates. Molecules of **1** involve the metal–oxygen framework quite typical of trinuclear homo- and heterometallic alkoxide species. The rather high coordination number of the barium atom (10) and the lengths of the observed interatomic distances permit to suggest that this atom in **1** forms predominantly ionic bonds and, therefore, complex **1** can be formulated as $[Ba(HOC_2H_4OMe)]^{2+}[Mo_2O_5(OC_2H_4OMe)_4]^{2-}$. © 1998 Elsevier Science Ltd. All rights reserved

Keywords: heterometallic oxo-2-methoxyethoxide; barium 2-methoxyethoxide; crystalline $MoO_2(OC_2H_4OMe)_2$

INTRODUCTION

Pursuing our systematic program of investigation of heterometallic alkoxides of molybdenum, we turned to the studies of stabilization of the molybdenum alkoxide derivatives of alkaline earth metals by application of functional alcohols. Such stabilization was needed to avoid the ether elimination reaction that led in the case of the derivatives of aliphatic alcohols to the formation of $M^{II}MoO_4$ on interaction of the corresponding alkoxides. The only compounds isolated so far were bimetallic magnesium–molybdenum methoxides [1], whose stability was presumably due to the reluctance of the methoxy group to form the corresponding R^+ cation, which is considered to be the first step of the ether elimination mechanism. It has also been shown earlier for the sodium derivatives that the use of 2-methoxyethoxide as an alkoxide ligand can lead to stabilization of heterometallic complexes of molybdenum and tungsten. Thus, instead of unstable complexes with a 1:1 composition, involving aliphatic radicals and existing only in solution, the stable crystalline product $NaMoO_2(OC_2H_4OMe)_3$ was obtained. It had reproducible solubility in the parent alcohol even in the presence of excess of NaOR [2].

In the present paper we report the application of this approach for the isolation and structural charac-

*Author to whom correspondence should be addressed. Present address: Department of Chemistry, Swedish University of Agricultural Sciences, Box 7015, 75007 Uppsala, Sweden.

terization of a mixed-metal barium–molybdenum compound, $BaMo_2O_5(OC_2H_4OMe)_4(HOC_2H_4OMe)$ (**1**).

EXPERIMENTAL

All compounds described in this work are highly sensitive to moisture and oxygen and therefore all operations with them were carried out in argon atmosphere using a vacuum line or a dry box. Dehydration of 2-methoxyethanol used was performed by boiling it under reflux over magnesium alkoxide with subsequent distillation. Carbon, hydrogen and the incombustible residue content in the samples was determined using conventional combustion technique at the Laboratory of Organic Microanalysis at the Moscow State University.

IR spectra were registered with Specord IR 75 for nujol mulls. Crystalline solids were identified using powder diffractometry (DRON 3M).

Isolation of $BaMo_2O_5(OC_2H_4OMe)_4(HOC_2H_4OMe)$ (**1**)

To the solution prepared by dissolution of 0.496 g (3.6 mmol) of barium metal in 10 ml of 2-methoxyethanol was added on continuous stirring 2.057 g (7.4 mmol) of $MoO_2(OC_2H_4OMe)_2$. The precipitation started immediately and the mixture became non-transparent. It was then warmed to 60°C, but remained turbid in appearance, while no bulky solid precipitate could be observed. It was left for crystallization in a refrigerator at 0°C overnight. The resulting solution did not become clear but from the mixture obtained, 1.216 g of precipitate could be isolated. The latter consisted of regularly shaped transparent crystals and fine particles of a white powder. The attempt to recrystallize the precipitate from 5 ml of pure 2-methoxyethanol at 50°C resulted in the formation of a turbid solution over the unchanged white powder (the transparent crystals were dissolved completely). The insoluble residue was separated by centrifugation and dried *in vacuo* (yield 0.036 g). X-ray powder diffraction study showed it to be a well-formed $BaMoO_4$-phase. The attempt to isolate the other product in a pure form failed as on cooling and storage of the turbid solution, the coprecipitation of the white powder with the regularly shaped transparent crystals occurred constantly. As slow cooling permitted the isolation of quite large crystals (up to approximately $2.0 \times 0.8 \times 0.3$ mm in size), they were separated from the mixture by a needle and analyzed. Found: C, 22.78; H, 4.41; incombustible residue, 56.8. Calc. for $C_{15}H_{36}BaMo_2O_{15}$ (**1**): C, 22.91; H, 4.58; incombustible residue, 56.2. IR, cm^{-1}: 405 w, 468 m, 490 m, 556 s, 575 s, 596 s, 615 s, 812 s, 885 s, 900 s br, 915 s, 925 sh, 3400 s v. br. The exact chemical composition of **1** was established by the X-ray single crystal study. The identity of the single crystal studied and the bulk sample was proved by complete indexing (except for the lines that belonged to $BaMoO_4$) of the X-ray powder pattern of the latter using the X-ray single crystal parameters obtained for **1**.

Crystal data for **1**

$C_{15}H_{36}O_{15}Mo_2Ba$, M = 785.7, monoclinic, space group Cc, at 293 K; $a = 18.353(5)$, $b = 8.947(5)$, $c = 18.236(5)$ Å, $\beta = 116.49(2)^\circ$, $V = 2680(1)$ Å^3, $Z = 4$, $D_c = 1.947$ g cm^{-3}. The X-ray diffraction experiment was carried out with Siemens P3/PC diffractometer ($T = 293$ K, graphite monochromated Mo-Kα radiation, $\lambda = 0.71073$ Å, θ–2θ scan technique, $\theta \leq 33^\circ$). The structure was solved by direct methods using SHELXTL PLUS 5 programs (gamma version) [3]. The positions of all non-hydrogen atoms were refined anisotropically by full-matrix least-squares technique, the H(1) atom position was first determined from the difference Fourier synthesis and then refined isotropically. All other hydrogen atoms were included in the final refinement in calculated positions with the temperature factors $U_{iso} = 1.2U_{eq}(C_i)$, where C_i is the carbon atom to which the correspondent hydrogen atom is bonded). The final discrepancy factors were $R_1 = 0.0354$ [for 4386 observed reflections with $I \geq 2\sigma(I)$], $wR_2 = 0.0970$ (for all 4809 reflections used in refinement; total of 302 refined parameters). No absorption correction was applied. Atomic coordinates, a full list of bond lengths and angles and thermal parameters have been deposited at the Cambridge Crystallographic Data Center.

RESULTS AND DISCUSSION

The interaction of homometallic alkoxides (barium 2-methoxyethoxide prepared by dissolution of barium metal in parent alcohol and $MoO_2(OC_2H_4OMe)_2$ synthesized by the electrochemical method described in Ref.[4]) was studied using the following procedure: the solutions of barium 2-methoxyethoxide in 2-methoxyethanol with approximately 10 wt% concentration were saturated on continuous stirring at room temperature with the solid molybdenum 2-methoxyethoxide. At the beginning no changes could be observed and the solutions remained clear and transparent, but when the metal ratio reached the value of Mo:Ba = 2:1, the precipitation of white powder started immediately. On heating of a portion of the mixture thus obtained it was found that the precipitate could only partially be redissolved in either mother liquor or pure 2-methoxyethanol. The examination of the sediment under the optical microscope has shown it to be a mixture of tiny white non-transparent particles (almost insoluble in alcohol) and regular shaped transparent crystals (long parallelepipeds, nearly needles) that could be extracted with the excess of 2-methoxyethanol. The X-ray powder diffraction showed the first to be a highly disperse powder of

well-formed $BaMoO_4$ phase. The nature of the other product was determined by X-ray single crystal investigation.

The latter has shown that the crystals in question are built up of triangular $BaMo_2O_4(\mu\text{-O})(\mu_3,\eta^2\text{-}OC_2H_4OMe)_2(\mu_2,\eta^2\text{-}OC_2H_4OMe)_2(\eta^2\text{-}HOC_2H_4OMe)$ aggregates (Fig. 1, Table 1), possessing a nearly spherical shape. The aggregates are linked into infinite chains along the *b*-axis of the crystal via hydrogen bonds O–H...O [O(15)...O(5) 2.625(6) Å, H(1)–O(15) 0.55(8) Å, H(1)...O(5) 2.19(8) Å, O(15)H(1)O(5) 137(10)°], formed by the OH group of the alcohol moiety and μ_2-oxo atom that binds the molybdenum atoms together. The coordination polyhedron of the barium atom (coordination number 10) is a severely distorted bicapped tetragonal antiprism (Fig. 2), its coordination sphere including all oxygen atoms of four alkoxogroups and of one solvating alcohol molecule, which means that all OC_2H_4OMe groups in the structure of **1** have η^2 chelate function. The basal planes of the antiprism [O(9)O(13)O(11)O(14) and O(12)O(7)O(10)O(8)] are nearly parallel [they form the dihedral angle 4.5(1)°] and are rotated by 27° relative to each other. The position of the barium atom in relation to the basal planes is considerably asymmetric: it is displaced by 0.993 Å and 1.537 Å from the O(9)O(13)O(11)O(14) plane and O(12)O(7)O(10)O(8) plane, respectively. The O(15) and O(6) atoms are in the capping positions above and below the bases of antiprism, the corresponding bond angle O(15)Ba(1)O(6) being 163.7(2)°. The arrangement of the chelate cycles conforms with the general pattern typical of *cis*-isomers of $[M(L)_5]$ complexes with bidentate L ligand [5], having the geometry of bicapped antiprism, e.g.$[Ba(MeCONHCOMe)_5](ClO_4)_2$ [6]. It is to be mentioned that significant non-systematic variations of the bond lengths within each group of chemically identical Ba–O bonds are observed in the structure of **1**. Thus the Ba–μ_3-OR [Ba(1)–O(6) 2.773(4), Ba(1)–O(7) 2.709(4) Å], Ba–μ_2-OR [Ba(1)–O(10) 2.788(5), Ba(1)–O(12) 2.861(5) Å] and Ba–O(ether) [Ba(1)–O(11) 2.978(6), Ba(1)–O(14) 2.934(6), Ba(1)–O(8) 2.844(5), Ba(1)–O(9) 2.802(5), Ba(1)–O(13) 2.951(7) Å] bonds differ significantly within each group, although in general Ba–O(alkoxo) distances are still noticeably shorter than Ba–O(ether) bond lengths, the corresponding average values being equal to 2.776 and 2.882 Å. Such irregularity in coordination in combination with the high coordination number and long interatomic distances (approximately equal to the sum of the corresponding ionic radii [7]), permits treatment of the bonding of the

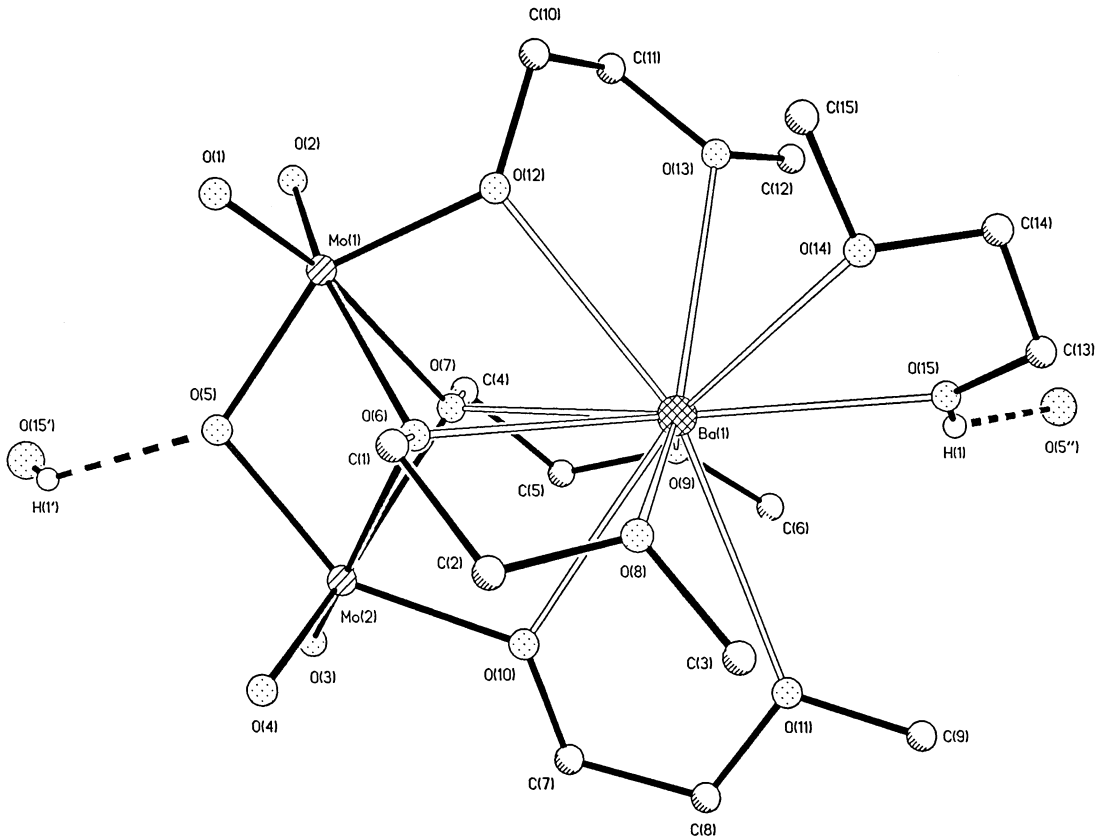

Fig. 1. The structure of the $[Ba(ROH)]^{2+}[Mo_2O_5(OR)_4]^{2-}$ ($R = C_2H_4OMe$) aggregate in the crystal of **1**. Primed and doubly primed atoms are derived from the reference atoms by symmetry operations $x, 1-y, 0.5+z$ and $x, 1-y, z-0.5$, respectively.

Table 1. Selected bond lengths (Å) and angles (°) in the structure of $[Ba(ROH)]^{2+}[Mo_2O_5(OR)_4]^{2-}$ ($R = C_2H_4OMe$)

Ba(1)–O(7)	2.709(4)	Ba(1)–O(8)	2.844(5)
Ba(1)–O(15)	2.746(5)	Ba(1)–O(12)	2.861(5)
Ba(1)–O(6)	2.773(4)	Ba(1)–O(14)	2.934(6)
Ba(1)–O(10)	2.788(5)	Ba(1)–O(13)	2.951(7)
Ba(1)–O(9)	2.802(5)	Ba(1)–O(11)	2.978(6)
Mo(1)–O(2)	1.705(6)	Mo(2)–O(4)	1.695(6)
Mo(1)–O(1)	1.714(6)	Mo(2)–O(3)	1.703(6)
Mo(1)–O(5)	1.955(5)	Mo(2)–O(5)	1.958(5)
Mo(1)–O(12)	1.978(5)	Mo(2)–O(10)	1.966(5)
Mo(1)–O(6)	2.189(4)	Mo(2)–O(7)	2.255(4)
Mo(1)–O(7)	2.274(4)	Mo(2)–O(6)	2.261(5)
O(7)–Ba(1)–O(15)	143.1(2)	O(2)–Mo(1)–O(1)	104.5(3)
O(7)–Ba(1)–O(6)	53.06(13)	O(1)–Mo(1)–O(6)	97.8(3)
O(15)–Ba(1)–O(6)	163.7(2)	O(2)–Mo(1)–O(7)	91.3(3)
O(7)–Ba(1)–O(10)	58.31(14)	O(6)–Mo(1)–O(7)	66.6(2)
O(15)–Ba(1)–O(10)	126.8(2)	O(1)–Mo(1)–O(5)	99.2(3)
O(7)–Ba(1)–O(9)	61.1(2)	O(2)–Mo(1)–O(5)	100.8(3)
O(15)–Ba(1)–O(14)	57.6(2)	O(1)–Mo(1)–O(12)	99.5(3)
O(12)–Ba(1)–O(13)	56.4(2)	O(2)–Mo(1)–O(12)	98.1(3)
O(10)–Ba(1)–O(11)	55.9(2)	O(5)–Mo(1)–O(12)	149.1(2)
O(10)–Ba(1)–O(12)	107.35(14)	O(1)–Mo(1)–O(7)	163.8(3)
O(13)–Ba(1)–O(11)	137.0(2)	O(2)–Mo(1)–O(6)	157.7(3)
O(9)–Ba(1)–O(14)	133.8(2)	Mo(2)–O(5)–Mo(1)	105.6(2)
O(10)–Ba(1)–O(14)	145.6(2)	Mo(1)–O(6)–Mo(2)	89.0(2)
O(7)–Ba(1)–O(8)	110.12(14)	Mo(2)–O(7)–Mo(1)	87.02(14)

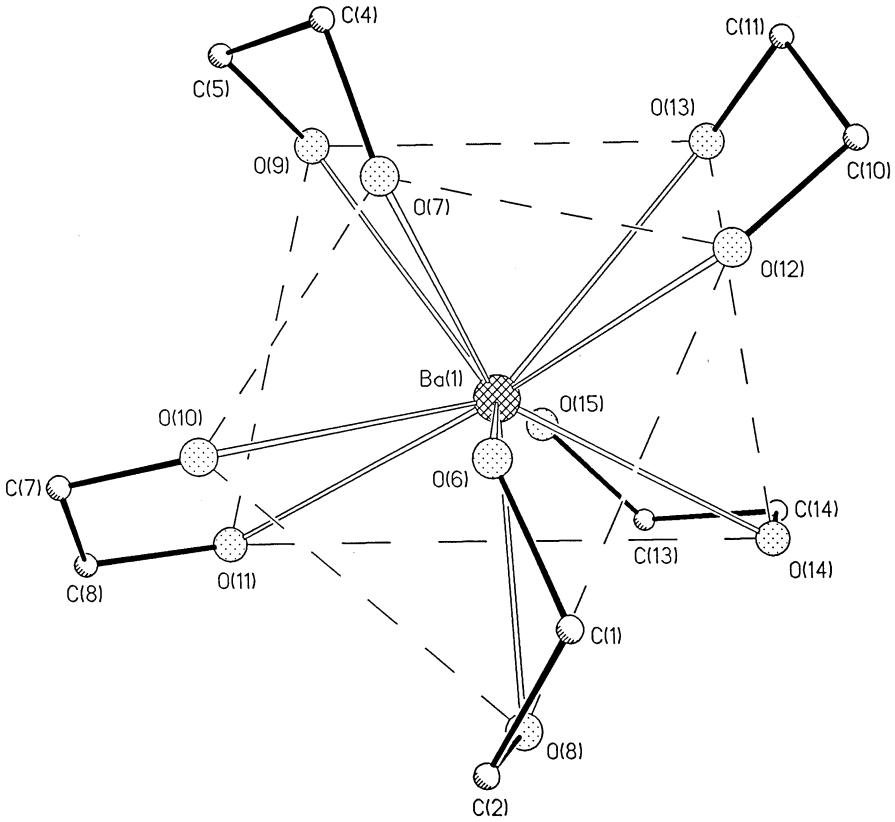

Fig. 2. The coordination polyhedron of Ba atom in the structure of **1** [the projection on O(9)O(13)O(11)O(14) basal plane].

barium atoms as predominantly ionic. The neutral aggregates observed can thus be considered as close ion pairs, consisting of $[Ba(HOR)]^{2+}$ cations and $[Mo_2O_5(OR)_4]^{2-}$ anions ($R = C_2H_4OMe$). It is to be noted that no direct analogy to the described barium coordination can be provided by the structures of known homo- or heterometallic barium oxo-2-methoxyethoxides. All barium atoms in the structure of $H_4Ba_6(\mu_6\text{-}O)(OC_2H_4OMe)_{14}$ [8] have very similar coordination with eight rather than ten neighbours. Their coordination polyhedra are rather irregular, while the values of the corresponding Ba–O distances are very close to those observed for **1** [2.90–2.93 for Ba–O(oxo), 2.67–2.82 for Ba–μ_3-O, 2.71–2.81 for Ba–O(H)R (terminal) and 2.83–2.97 Å for Ba–O(ether)] apparently due to the same nature of bonding in this aggregate. Of the same order of magnitude are also the lengths of corresponding Ba–O distances in the structure of $Ba_4Ti_{13}O_{18}(OC_2H_4OMe)_{24}$ [9] [the average values are: 2.908(9) for Ba–O(ether), 2.693(9) for Ba–O(OR) and 3.07(2) Å for Ba–O(oxo) bonds] while the coordination number of barium atoms in this structure is 12. The same coordination number as in **1** demonstrate the barium atom in the structure of $BaCu_4(thd)_4(OC_2H_4OMe)_6$ [10], however, its coordination environment in this case cannot be attributed to some of the known canonical polyhedra as in **1**. In contrast to **1** only two of eight 2-methoxyethoxide groups surrounding the central atom in this structure are chelating. This peculiarity probably accounts for the rather high variation of bond length within the groups of chemically identical bonds observed in the structure of the Ba–Cu derivative [2.68–3.08 for Ba–μ_3-O(R), 2.73–3.02 for Ba-μ_2-O(R) and 2.85–2.89 Å for Ba–O(ether) functions].

The structure of the dimolybdenum moiety is very close to that described for the $[Mo_2O_5(O_2R)_2]^{2-}$ anion (where O_2R is the pyrocatecholate residue) [11]. The Mo=O [Mo(1)–O(1) 1.714(6), Mo(1)–O(2) 1.705(6), Mo(2)–O(3) 1.703(6), Mo(2)–O(4) 1.695(6) Å], Mo–μ-O [Mo(1)–O(5) 1.955(5), Mo(2)–O(5) 1.958(5) Å], Mo–μ_2-O(R) [Mo(1)–O(12) 1.978(5), Mo(2)–O(10) 1.966(5) Å] and Mo–μ_3-O(R) [Mo(1)–O(6) 2.189(4), Mo(1)–O(7) 2.274(4), Mo(2)–O(6) 2.261(5), Mo(2)–O(7) 2.255(4) Å] bond lengths in **1** lie within the limits usually observed for octahedrally coordinated Mo atoms. The IR spectrum of the complex is in good agreement with the structure of **1** described above.

It is to be noted that this product as well as the bimetallic molybdenum isopropoxides described in the literature [1] belong to those alkoxide systems, which have more oxoligands than the molybdenum species from which they are derived, i.e. $MoO_2(OC_2H_4OMe)_2$. This fact in combination with the inevitable precipitation of $BaMoO_4$ on both synthesis and recrystallization of the product from parent alcohol shows that the application of the functional ligand such as 2-methoxyethanol provides only partial protection from the ether elimination reaction in this particular case.

Acknowledgements—The authors express their gratitude to INTAS (Grant 94-771) and the Russian Foundation for Basic Research (Projects 94-03-08338 and 96-33553) for financial support.

REFERENCES

1. Antipin, M., Struchkov, Yu. T., Shilov, A. and Shilova, A., *Gazz. Chim. Ital.*, 1993, **123,** 265.
2. Turova, N. Ya., Kessler, V. G. and Kucheiko, S. I., *Polyhedron*, 1991, **10,** 2617.
3. Robinson, W. and Sheldrick, G. M., *Crystallographic Computing Techniques and New Technologies*, eds. N. W. Isaacs and M. R. Taylor. Oxford University Press, 1988.
4. Kessler, V. G., Turova, N. Ya., Korolev, A. V., Yanovsky, A. I. and Struchkov, Yu. T., *Mendeleev Commun.*, 1991, 89.
5. Kepert, D., *Inorganic Stereochemistry*. Mir Publishers, Moscow, 1985 (Russian translation).
6. Gentile, P. S., White, J. and Haddad, S., *Inorg. Chem.*, 1975, **13,** 149.
7. Shannon, R. D., *Acta Crystallogr.*, 1976, **32A,** 751.
8. Caulton, K. G., Chisholm, M. H., Drake, S. R. and Huffman, J. C., *J. Chem. Soc. Chem. Commun.*, 1990, 1498.
9. Campion, J.-F., Payne, D., Chae, H. K., Maurin, J. K. and Wilson, S. R., *Inorg. Chem.*, 1991, **30,** 3245.
10. Bidell, W., Shklover, V. and Berke, H., *Inorg. Chem.*, 1992, **31,** 5561.
11. Tkachev, V. V. and Atovmyan, L. O., *Sov. J. Coord. Chem.* (*Russ.*), 1976, **2,** 110.

Pergamon

Polyhedron Vol. 17, No. 23–24, pp. 4195–4201, 1998
© 1998 Elsevier Science Ltd
All rights reserved. Printed in Great Britain
0277–5387/98 $19.00+0.00

PII: S0277–5387(98)00229–0

New studies in the copper(II) acyclovir (acv) system. NMR relaxation studies and the X-ray crystal structure of $[Cu(acv)_2(H_2O)_2](NO_3)_2$

Iztok Turel,[a]* Bjørn Andersen,[b] Einar Sletten,[b] Andrew J. P. White[c] and David J. Williams[c]

[a]Faculty of Chemistry and Chemical Technology, University of Ljubljana, Aškerčeva 5, 1000 Ljubljana, Slovenia

[b]Department of Chemistry, University of Bergen, Allegt. 41, 5007 Bergen, Norway

[c]Department of Chemistry, Imperial College of Science, Technology and Medicine, London SW7 2AY, U.K.

(Received 20 March 1998; accepted 3 June 1998)

Abstract—The crystal structure of $[Cu(acv)_2(H_2O)_2]$ $(NO_3)_2$ is reported; there is a pseudo-chelate N(7)/O(6) bonding of a purine to the metal and it contains the shortest Cu–O(6) distance [2.698(2) Å] so far reported for a simple copper(II)-nucleoside. This unusual bonding is due to the hydrophobic medium (absolute methanol) used for crystallisation. ^{1}H NMR spectra of the complex recorded both in methanol and in aqueous solution confirm N(7) as the main copper coordination site and that the acyclic chain is not involved in binding. © 1998 Elsevier Science Ltd. All rights reserved

Keywords: acyclovir; copper(II) complex; crystal structure; NMR spectroscopy; pseudo-chelate bonding.

INTRODUCTION

For many years the coordination of purines to metal ions has been investigated by several researchers (Refs [1–4]. and references therein). It has been suggested that purines act as chelating ligands to metals through N(7) and the exocyclic atom attached to C(6) [5]. However, in aqueous systems, true chelation has only been observed in 6-thiopurines. The typical bonding pattern in the metal complexes of 6-oxopurines can best be described as indirect chelation where a water molecule in the coordination sphere forms interligand hydrogen bonds to the exocyclic substituent at C(6). In a few cases, when no hydrogen bond donors were available, 6-oxopurines have been found to form weak N(7)/O(6) chelates, though with N(7) remaining as the primary binding site. It has been proposed that such N(7)/O(6) chelation is an intermediate in a critical step of a possible mechanism of action for Pt antitumor drugs and this is the main reason that this topic has been so thoroughly studied [6,7].

It has been calculated that if the M–O(6) and M–N(7) lengths were each of *ca*. 2 Å (normal values for first-row transition metals), the C(5)–N(7)–M angle would be approximately 90°; the maximum overlap of available orbitals on the metal with the hybrid orbitals on N(7), however, occurs when this angle is 135° [8]. This could explain why chelate formation is so rare in this system. On the other hand, a few years ago a semiempirical calculation showed that N(7)/O(6) chelation is possible in the Pt–guanine system [9].

We have previously shown that the antiherpes drug acyclovir (acv = 9-{(2-hydroxyethoxy)methyl}guanine) (Scheme 1) can form various species with Cu(II) ions with bonding occurring typically through N(7) [10,11]. Three copper–acv complexes (including the title compound) have been tested for antiviral efficacy against Herpes Simplex viruses (HSV 1, HSV 2) and were found to exhibit differing activities perhaps due

* Author to whom correspondence should be addressed. Fax: +386-61-1258-220; E-mail: iztok.turel@uni-lj.si

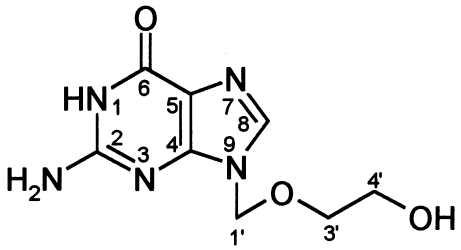

Scheme 1.

to the varying coordination mode of the acv ligands [12].

Here we report an example of N(7)/O(6) copper(II) bonding to 6-oxopurine with the shortest Cu–O(6) distance in a simple copper(II) nucleoside system observed so far. An NMR study of the proton relaxation times (T_1 and T_2) was also performed in the copper(II)–acyclovir system. Our aim was to check for any differences in relaxation times between aqueous and methanolic media which could suggest the presence of different bonding modes.

EXPERIMENTAL

Acyclovir (Sigma) and copper nitrate(V) trihydrate (Merck, p.a. quality, min. 99.5%) were used without further purification. Deuterated solvents were supplied by Fluorochem (D_2O, 99.9% D) and Norell (CH_3OD, 99%). Complex $[Cu(acv)_2(H_2O)_2](NO_3)_2$ (diaquabis[9-{(2-hydroxyethoxy)-methyl}guanine] copper(II) nitrate(V)) was prepared by dissolving $Cu(NO_3)_2 \cdot 3H_2O$ (1.33 mmol) in absolute methanol (30 ml) followed by slow addition of acv (1.33 mmol). After a few days dark green needles were grown from the solution. Found: C, 28.29; H, 3.62; N, 25.01. $C_{16}H_{26}N_{12}O_{14}Cu$ requires C, 28.49; H, 3.90; N, 24.93%. Similar to our previous syntheses [10,11,13] described before, it was necessary to use an excess of metal salt to prevent the precipitation of acv due to its low solubility. It is interesting to note that when a (1:1) methanol–water solvent mixture was used the complex $[Cu(acv)_2(H_2O)_3](NO_3)_2 \cdot H_2O$ was the product [11].

Crystal data for $C_{16}H_{26}N_{12}O_{14}Cu$: $M_r = 674.0$, monoclinic, space group $P2_1/n$ (No. 14), $a = 4.865(1)$, $b = 14.253(1)$, $c = 19.036(1)$ Å, $\beta = 92.48(1)^\circ$, $V = 1318.8(2)$ Å^3, $Z = 2$ (the molecule has crystallographic C_i symmetry), $D_c = 1.697$ g cm^{-3}, μ(Cu-K$_\alpha$) = 20.1 cm^{-1}, $F(000) = 694$. A green platy needle of dimensions $0.37 \times 0.20 \times 0.07$ mm was used. Data were measured on a Siemens P4/PC diffractometer with Cu-K$_\alpha$, radiation (graphite monochromator) using ω-scans. 2176 independent reflections were measured ($2\theta \leq 127^\circ$) of which 1994 had $|F_o| > 4\sigma(|F_o|)$ and were considered to be observed. The data were corrected for Lorentz and polarisation factors, but not for absorption. The structure was solved by direct methods and all the non-hydrogen atoms were refined anisotropically. The nitrate anion was found to exhibit slight rotational disorder (*ca.* 35°) about one of the N–O bonds; this was resolved into two alternate partial occupancy orientations (60:40) for two of the oxygen atoms. (The quoted hydrogen bonding geometries refer only to the major occupancy oxygen atoms.) The N–H and O–H hydrogen atoms were located from a ΔF map and refined isotropically subject to a distance constraint (0.90 Å). The positions of the remaining hydrogen atoms were idealised, assigned isotropic thermal parameters, $U(H) = 1.2U_{eq}(C)$ and allowed to ride on their parent atoms. Refinement was by full-matrix least squares based on F^2 to give $R_1 = 0.036$, $wR_2 = 0.101$ for the observed data and 239 parameters. The maximum and minimum residual electron densities in the final ΔF map were 0.36 and -0.36 eÅ^{-3}, respectively. The mean and maximum shift/error ratios in the final refinement cycle were 0.000 and 0.003, respectively. Computations were carried out using the SHELXTL PC program system [14], CCDC reference number 101706.

^{1}H *NMR spectroscopy*

The ^{1}H NMR experiments were performed on a Bruker DRX spectrometer operating at 600 MHz. All NMR experiments were recorded at 298 K. The solvent peak was suppressed by a 3-9-19 WATERGATE pulse sequence. One-dimensional spectra were recorded into 64K complex points with a 22 ppm spectral width, a 12 μs pulse width and a recycling delay of 2 s. The T_1 measurements were carried out using an inversion recovery sequence, in which the WATERGATE suppression sequence was incorporated. A list of 13 different delays in the range 0.01 to 10 s were used. The NMR data were processed on a PC (Pentium, 133 MHz) using WIN-NMR version 960901.2 (Bruker). The spectra were multiplied by an exponential window function prior to Fourier transformation. Typically, 1 Hz was added to the line width. The 1D spectra were zero filled to 128 K. No base line correction was needed. The proton spectra were referenced to the H_2O/D_2O-resonance in water at 4.76 ppm at 298 K and the methyl resonance in methanol at 3.40 ppm at 298 K.

To a 0.40 mM solution of acv in CH_3OD successive aliquots of *ca.* 4.0 mm $Cu(NO_3)_2$ were added by a micropipette. The analogous titration was also carried out in aqueous solution in order to study the influence of hydration on the coordination geometry. The pH values of the starting solutions were 6.3.

RESULTS AND DISCUSSION

The X-ray analysis of the crystals from the reaction mixture reveals (Fig. 1) a complex in which two acv ligands are bound "monodentately" via N(7) in a *trans*, C_i symmetric arrangement to the copper centre

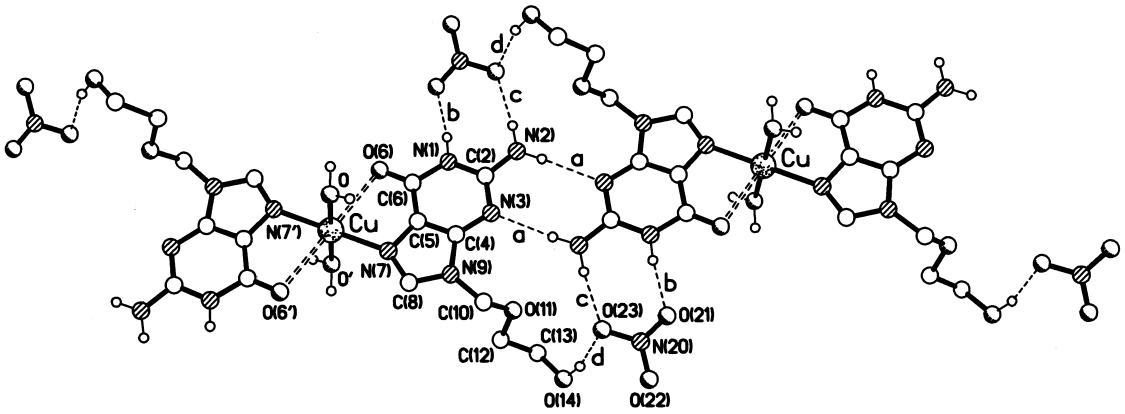

Fig. 1. Perspective drawing of $[Cu(acv)_2(H_2O)_2]$ $(NO_3)_2$ showing the pseudo octahedral geometry at copper. Part of one of the hydrogen-bonded ribbons formed by N–H . . . N "base-pair" links between the purine units and between the terminal hydroxyl and the nitrate anion in the title compound is also shown. Hydrogen bonding geometries [X . . . Y, H . . . Y distances (Å) and X–H . . . Y angles (°)]: (a) 3.04, 2.15, 168; (b) 2.85, 1.96, 172; (c) 2.88, 1.98, 173; (d) 2.78, 1.91, 164 [all X–H distances normalised to 0.90 Å]. Note that the crystallographic numbering scheme is slightly different from the conventional numbering used in Scheme 1 and in Figs 2 and 3.

[2.004(2) Å, Table 1]. The geometry at copper is slightly distorted square planar, the other two coordination sites being occupied by aqua ligands [1.953(2) Å]. This arrangement is in contrast to the square pyramidal geometry observed when the reaction is performed in water alone [11]. The planes of the purine rings are inclined by *ca.* 75° to the copper coordination plane, thus directing the ligand carbonyl oxygen atoms towards the vacant Cu octahedral sites at a distance of 2.698(2) Å. This secondary coordination interaction is clearly significant as evidenced by a severe distortion in the Cu–N(7)–C(8) angle which is enlarged to 143.3(2)°, cf. a normal value of *ca.* 125° [11], and a concomitant contraction of the Cu–N(7)–C(5) angle to 111.5(1)° (cf. *ca.* 130°) [11]. The ligand is thus acting in a pseudo-bidentate fashion with an O–Cu–N bite angle of 77.13(6)°. Precedents for a purine ligand acting in this manner are rare,

Table 1. Selected bond lengths (Å) and angles (°) for $[Cu(acv)_2(H_2O)_2]$ $(NO_3)_2$

Cu–O	1.953(2)	Cu–N(7)	2.004(2)
Cu–O(6)	2.698(2)	N(1)–C(6)	1.378(3)
N(1)–C(2)	1.389(3)	C(2)–N(2)	1.327(3)
C(2)–N(3)	1.329(3)	N(3)–C(4)	1.347(3)
C(4)–C(5)	1.368(3)	C(4)–N(9)	1.378(3)
C(5)–N(7)	1.387(3)	C(5)–C(6)	1.406(3)
C(6)–O(6)	1.243(3)	N(7)–C(8)	1.310(3)
C(8)–N(9)	1.372(3)		
O–Cu–N(7′)	88.69(7)	O–Cu–N(7)	91.31(7)
O′–Cu–O(6)	97.87(6)	O–Cu–O(6)	82.13(6)
N(7′)–Cu–O(6)	102.87(6)	N(7)–Cu–O(6)	77.13(6)
O–Cu–O′	180	O(6)–Cu–O(6′)	180
N(7)–Cu–N(7′)	180	C(6)–N(1)–C(2)	123.9(2)
N(2)–C(2)–N(3)	120.4(2)	N(2)–C(2)–N(1)	115.9(2)
N(3)–C(2)–N(1)	123.6(2)	C(2)–N(3)–C(4)	112.8(2)
N(3)–C(4)–C(5)	126.8(2)	N(3)–C(4)–N(9)	127.9(2)
C(5)–C(4)–N(9)	105.3(2)	C(4)–C(5)–N(7)	110.8(2)
C(4)–C(5)–C(6)	120.6(2)	N(7)–C(5)–C(6)	128.5(2)
O(6)–C(6)–N(1)	123.1(2)	O(6)–C(6)–C(5)	124.9(2)
N(1)–C(6)–C(5)	112.0(2)	C(6)–O(6)–Cu	96.8(1)
C(8)–N(7)–C(5)	104.9(2)	C(8)–N(7)–Cu	143.3(2)
C(5)–N(7)–Cu	111.5(1)	N(7)–C(8)–N(9)	112.1(2)
C(8)–N(9)–C(4)	106.9(2)		

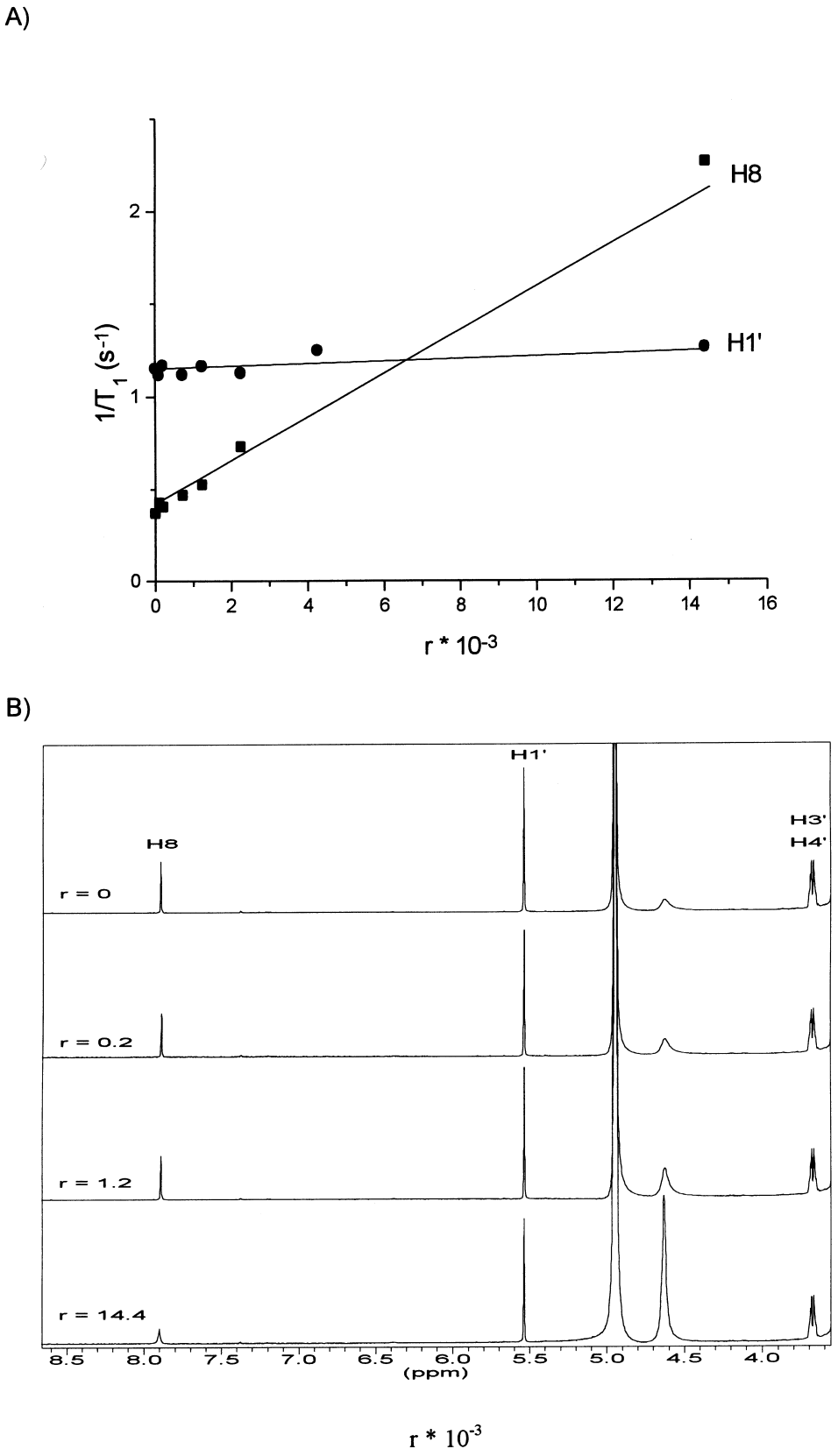

Fig. 2. (A) Effect of Cu(II) concentration on spin-lattice relaxation rates ($1/T_1$) in methanolic solutions of acv [$r = n$(Cu(II)/n(acv), c(acv) = 0.40 mM]. (B) Stacked plot showing the effect of increasing amount of Cu(II) ions on the line width of proton resonances in acv methanolic (CH_3OD) solutions [$r = n$(Cu(II)/n(acv), c(acv) = 0.40 mM].

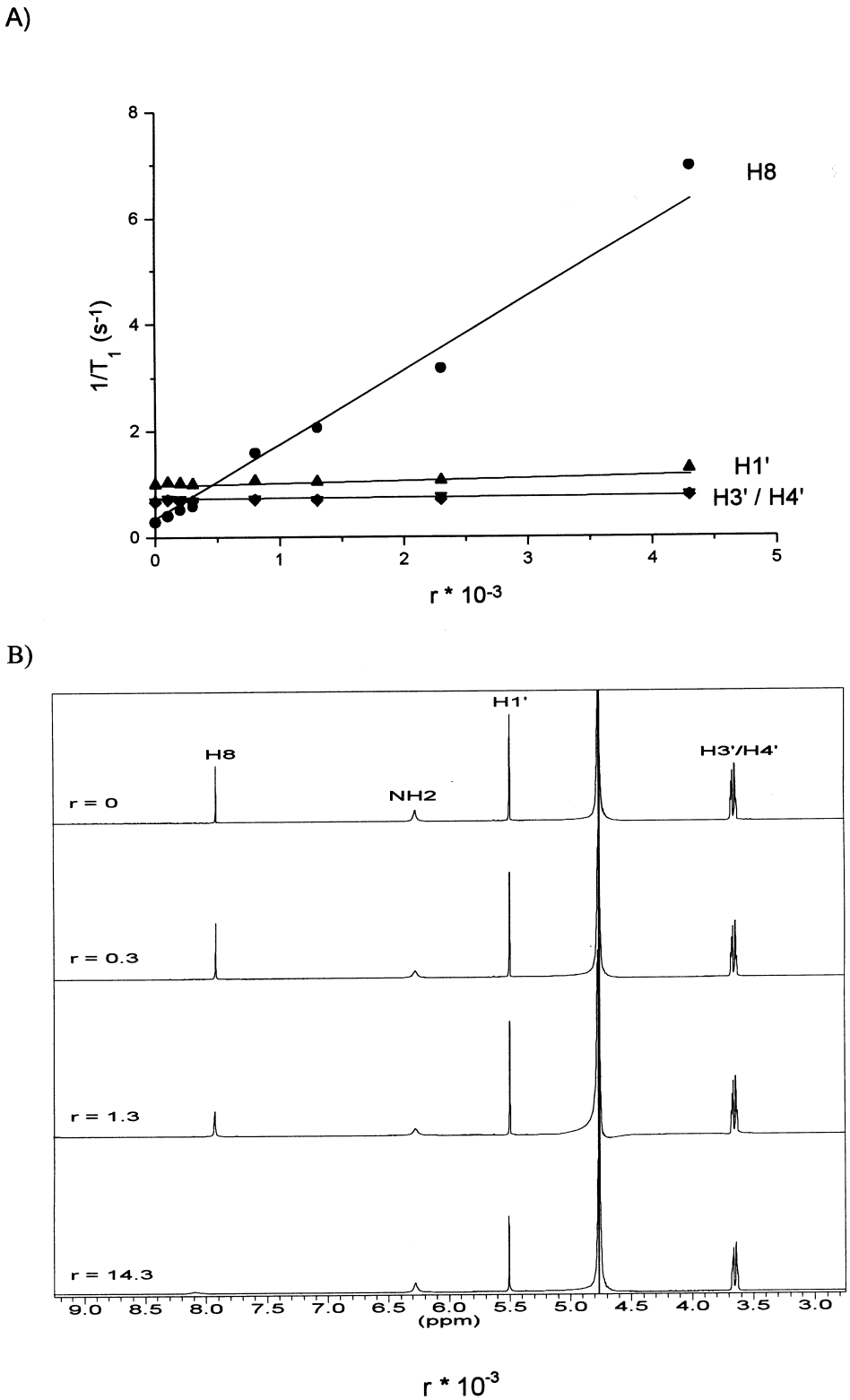

Fig. 3. (A) Effect of Cu(II) concentration on spin-lattice relaxation rates ($1/T_1$) in water solutions of acv [$r = n$(Cu(II))/n(acv), c(acv) = 0.40 mM]. (B) Stacked plot showing the effect of increasing amount of Cu(II) ions on the line width of proton resonances in acv water solutions [$r = n$(Cu(II))/n(acv), c(acv) = 0.40 mM].

there being only a few previously published examples where the metal (platinum [15], titanium [16,17] and rhodium [18])–oxygen distance is shorter than that observed here. There are two other examples of purine acting as a pseudo-bidentate ligand to copper, but in both of these other cases the Cu–O distance is noticeably longer, at 2.83 [19] and 2.92 Å [20], though each exhibit an appreciable enlargement of the external angles at N(7) (142 and 139°, respectively). The hydroxyethoxymethyl side-chain of an acv molecule has an extended geometry with a *gauche* relationship for the two oxygen atoms.

An inspection of the packing of the molecules reveals (Fig. 1) a pattern of C_i symmetric "base-pair" recognition between one of the amino N–H hydrogen atoms of one purine and the N(3) nitrogen of another and vice versa to form ribbons that extend in the crystallographic *b* direction. The other amino hydrogen atom and the imino and hydroxy H-atoms are hydrogen bonded to the nitrate anion. This dihydrogen bond formation between guanine and an oxyanion has been observed in several other X-ray structures of guanine salts of oxyanions [21]. The aqua ligands cross-link these ribbons via O–H . . . O hydrogen bonds to the carbonyl oxygen O(6) (O . . . O 2.68, H . . . O 1.82 Å; O–H . . . O 160°) and the terminal hydroxyl oxygen O(14) (O . . . O 2.62, H . . . O 1.73 Å; O–H . . . 0 170°) creating a series of parallel, corrugated sheets (O–H distances normalised to 0.90 Å). This pattern of hydrogen bonding is in marked contrast to that observed for the complex crystallised from water [11], demonstrating how major changes in the hydrogen bonding preferences can be influenced by changes in the solvent mixture.

It is obvious that the type of solvent is crucial for the mode of acv–metal coordination in the solid state. Whereas in the product isolated from water typical bonding through N(7) was observed, in methanol a rare example of N(7)/O(6) bonding takes place but the isolated compound may not be representative of the main species present in solution. The very elaborate network of hydrogen bonding in the crystal may also influence the coordination pattern. In order to eliminate these possible packing effects the complexation was followed by NMR titrations in both aqueous and methanolic media.

The effect of paramagnetic line broadening of proton signals by adding an aqueous solution of $Cu(NO_3)_2$ to acv dissolved in methanol and the corresponding effect on spin-lattice relaxation rates ($1/T_1$) versus Cu(II) concentration are shown in Fig. 2. It can easily be seen that the H(8) signal (7.91 ppm) is dramatically broadened due to a dipolar interaction between the unpaired electron on Cu(II) coordinated at N(7) and the adjacent H(8) nucleus. There is almost no observable effect on the methylene proton resonances (3.67 and 3.68 ppm) confirming that the Cu(II) ions do not interact with either the ether oxygen or the hydroxy group. The intensity of the residual HOD resonance at 4.76 ppm is seen to increase during the titration due to the addition of aliquots of aqueous $Cu(NO_3)_2$. Since the observed paramagnetic line broadening may be influenced by scalar (non-geometric) factors the spin-lattice relaxation rates were also measured. These data which mainly contain through-space dipolar effects corroborate the conclusion based on line broadening measurements and, furthermore, are in accordance with the crystal structure as far as N(7) binding is concerned.

The NMR measurements (T_1 and T_2) carried out in aqueous solution (Fig. 3) are shown to be comparable to those obtained in methanol regarding the non-exchangeable protons. The signals from the exchangeable protons (N–H and NH_2) show no paramagnetic broadening ruling out any Cu(II)-binding to N(3). Unfortunately, proton NMR spectroscopy was not able to distinguish between a normal hexacoordinated structure and a chelate structure in solution. In conclusion we confirm that both in aqueous and methanolic media N(7) is the dominant binding site and that the atoms of the acyclic chain are not involved in metal ion coordination.

Acknowledgements—The Royal Society and Slovenian Academy of Sciences and Arts are thanked for financial support (ESEP grant for I. T.). B. A. gratefully acknowledges a fellowship from the Norwegian Research Council.

REFERENCES

1. Hodgson, D. J., in *Prog. Inorg. Chem.*, Vol. 23, ed. S. J. Lippard. John Wiley and Sons, New York, 1977, p. 211.
2. Tu, A. T. and Heller, M. J., in *Metal Ions in Biological Systems*, Vol. 1, ed. H. Sigel. Marcel Dekker, New York, 1974, p. 1.
3. Aoki, K., in *Metal Ions in Biological Systems*, Vol. 32, ed. H. Sigel. Marcel Dekker, New York, 1996, p. 91.
4. Terrón, A., *Comm. Inorg. Chem.*, 1993, **14,** 63.
5. Harker, T. R. and Freiser, H., *J. Am. Chem. Soc.*, 1958, **80,** 1132.
6. Marzilli, L. G., Kistenmacher, T. J. and Eichhorn, G. L., *Met. Ions Biol.*, 1980, **1,** 179.
7. Barton, J. K. and Lippard, S. J., *Met. Ions Biol.*, 1980, **1,** 31.
8. Sletten, E., *Chem. Commun.*, 1971, 558.
9. Lipinski, J., *Inorg. Chim. Acta*, 1988, **152,** 151.
10. Blažič, B., Turel, I., Bukovec, N., Bukovec, P. and Lazarini, F., *J. Inorg. Biochem.*, 1993, **51,** 737.
11. Turel, I., Bukovec, N., Goodgame, M. and Williams, D. J., *Polyhedron*, 1997, **16,** 1701.
12. Panteva, M., Varadinova, T. and Turel, I., *Metal Based Drugs*, 1998, **5,** 19.
13. Turel, I., Leban, I. and Gruber, K., *J. Inorg. Biochem.*, 1996, **63,** 41.
14. *SHELXTL PC*, version 5.03. Siemens Analytical X-Ray Instruments, Madison, WI, 1994.
15. Cozak, D., Mardhy, A., Olivier, M. J. and Beauchamp, A. L., *Inorg. Chem.*, 1986, **25,** 2600.
16. Beauchamp, A. L., Belanger-Gariepy, F.,

Mardhy, A. and Cozak, D., *Inorg. Chim. Acta*, 1986, **124,** L23.
17. Lorbeth, J., Massa, W., Essawi, M. E. and Labib, L., *Angew. Chem. Int. Ed. Engl.*, 1988, **27,** 1160.
18. Chen, H. H., Olmstead, M. M., Smith, D. P., Maestre, M. F. and Fish, R. H., *Angew. Chem. Int. Ed. Engl.*, 1995, **34,** 1514.
19. Colacio, E., Suárez-Varela, J., Dominguez-Vera, J. M., Avila-Rosón, J. C., Hidalgo, M. A. and Martín-Ramos, D., *Inorg. Chim. Acta*, 1992, **202,** 219.
20. Szalda, D. J., Kistenmacher, T. J. and Marzilli, L. G., *J. Am. Chem. Soc.*, 1976, **98,** 8371.
21. Sletten, E. and Erevik, G., *Acta Crystallogr. B*, 1977, **33,** 1633.

Pergamon

Polyhedron Vol. 17, No. 23–24, pp. 4203–4212, 1998
© 1998 Elsevier Science Ltd
All rights reserved. Printed in Great Britain
0277–5387/98 $19.00+0.00

PII: S0277–5387(98)00230–7

X-ray crystal structures of $Mo_3S_4(DTP)_3(salicylate)(CH_3CN)$ and $[Mo_3S_4(DTP)_3(phthalate)(Py)]_2 \cdot EtOH \cdot CH_2Cl_2$: intramolecular H-bonds and S–S interactions in trinuclear molybdenum cluster compounds

Ling Wu, Jibo Xia, Changneng Chen, Xiaoying Huang, Yuangen Yao† and Jiaxi Lu

State Laboratory of Structural Chemistry, Fujian Institution of Research on the Structure of Matter, Chinese Academy of Sciences, Box 143, Fuzhou, 350002, P.R. China

(Received 14 January 1998; accepted 8 June 1998)

Abstract—Two new molybdenum cluster compounds, $Mo_3S_4(DTP)_3(salicylate)(CH_3CN)$ and $[Mo_3S_4(DTP)_3(phthalate)(Py)]_2 \cdot EtOH \cdot CH_2Cl_2$, have been rationally synthesized by the ligand substitutional reaction of $Mo_3S_4(DTP)_4(H_2O)$ with salicylic acid and phthalic acid, respectively. Their crystal structures have been determined. A molecular-design method for Mo_3S_4 cluster compounds was developed. Two incomplete cuboidal molybdenum cluster units can be linked by intramolecular H-bonds. © 1998 Elsevier Science Ltd. All rights reserved

Keywords: synthesis; X-ray structure; H-bond; S–S interaction; aromatic carboxylate; NMR.

INTRODUCTION

Since the trinuclear molybdenum cluster compound $Mo_3S_4(\mu\text{-DTP})(DTP)_3(L)$, where L = loosely-coordinated ligand, DTP = diethyldithiophosphate, (**I**) was reported [1], several new clusters formulated as $Mo_3S_4(\mu\text{-}RCO_2)(DTP)_3(L)$ (**II**) were synthesized by substitution reactions [2]. It is now well established that this Mo_3S_4 precursor **I**, unlike its aqueous analogous cation $[Mo_3S_4(H_2O)_9]^{4+}$, has three different substitutional sites: bridging DTP, terminal DTP [3] and the loosely-coordinated ligand L. By choosing ligands of different chemical properties for the precursor **I**, we can now control the molecular fragmentation to design molybdenum cluster molecules suitable for potential applications, for example, in the exploitation of catalytic reactions promoted at a metal site embedded in metal–sulfur aggregates [4, 5]; in the synthesis of new optical limiting materials [6]. Aromatic carboxylic acids, which can bond with various functional groups, were considered in this paper as the substituting reagents for the bridging DTP ligand.

In our preliminary experiments, the reaction of **I** with benzoic acid yielded a brown powder which was difficult to dissolve in any solvent, making the crystal structure determination impossible. However, we isolated well-formed crystals of $Mo_3S_4(DTP)_3(salicylate)(CH_3CN)$ (**III**) and $[Mo_3S_4(DTP)_3(phthalate)(Py)]_2 \cdot EtOH \cdot CH_2Cl_2$ (**IV**) by the reaction with salicylic acid and phthalic acid, respectively. Compared with the earlier experimental results, this paper provides a further molecular-design method for Mo_3S_4 cluster compounds.

EXPERIMENTAL

General procedure

$Mo_3S_4(DTP)_4(H_2O)$ was obtained by the method of literature [3]. HDTP was purified before used by vacuum distillation [7]. Phthalic acid, salicylic acid, dichloromethane and pyridine are commercially avail-

†Author to whom correspondence should be addressed.

able A.R. grade reagents which are used without further purification. The whole experiments were handled free of water. IR spectra were recorded on Nicolet Magna 750 and FTS-40 spectrometers in KBr pellets. ^{31}P NMR spectra were measured on an Varian Unity-500 NMR spectrometer in deuterated acetone [3] with reference to 85% H_3PO_4. Spectra were first recorded in 100.0 kHz width and then enlarged to a suitable scale.

Preparation of $Mo_3S_4(DTP)_3$(salicylate)(CH_3CN) (**III**): in a flask, 0.3 g $Mo_3S_4(DTP)_4(H_2O)$ was dissolved in 40 cm^3 of mixed solvent of ethanol and acetonitrile (v/v = 3:1). 0.03 g salicylic acid was then added while stirring. When refluxed over an oil bath at 100°C for an hour, the hot dark brown solution was filtered into another flask. Rectangular black crystals precipitated in 10 days. Yield: 0.18 g, 60%. Found: Mo, 25.18; C, 21.76; H, 3.31; N, 1.06; Calc. for $C_{21}H_{38}Mo_3NO_9P_3S_{10}$: Mo, 25.03; C, 21.94; H, 3.33; N, 1.22.

Preparation of $[Mo_3S_4(DTP)_3$(phthalate)(Py)$]_2 \cdot EtOH \cdot CH_2Cl_2$ (**IV**): 0.20 g of $Mo_3S_4(DTP)_4H_2O$ was dissolved in 30 cm^3 dichloromethane and 20 cm^3 ethanol. The solution was then refluxed over an oil bath at 100°C with 0.03 g phthalic acid and 0.2 cm^3 pyridine for an hour. When filtered and cooled to room temperature, this black solution gave well-shaped rectangular black crystals in two weeks. Yield 0.15 g (70%). Found: Mo, 22.30; C, 24.25; H, 3.21; N, 1.06; Calc. for $C_{53}H_{88}Cl_2Mo_6N_2O_{21}P_6S_{20}$: Mo, 22.46; C, 24.84; H, 3.46; N, 1.09.

X-ray structure determinations

The crystal data for compounds **III** and **IV** are summarized in Table 1. The important bond lengths and angles for the complex **III** and **IV** are given in Tables 2 and 3. Single crystals for **III** and **IV** were carefully chosen, coated with epoxy resin and mounted on glass fibers. Data collections and cell dimension measurements were performed on Siemens SMART CCD diffractometer with graphite-monochromatized Mo–Kα radiation ($\lambda = 0.71073$ Å) at 21 ± 2°C. Intensity data for all crystals were obtained in the range $3.08 < 2\theta < 46.6^\circ$ by using an ω scan technique. The data reductions and structural analysis were performed on a silicon computer station with Smart CCD software and the structure were refined on F^2 through the use of the SHELXL-PC programs [8, 9, 10]. Empirical absorption corrections were applied. The positions of the molybdenum atoms were determined by direct methods, and successive difference electron density maps located the remaining nonhydrogen

Table 1. Crystallographic data and some experimental details for complexes **III** and **IV**

Compound	Complex **III**	Complex **IV**
Chemical formula	$C_{21}H_{38}Mo_3NO_9P_3S_{10}$	$C_{53}H_{88}Cl_2Mo_6N_2O_{21}P_6S_{20}$
Formula weight	1149.80	2562.87
Color	black	black
Crystal dimension (mm)	$0.10 \times 0.15 \times 0.20$	$0.15 \times 0.15 \times 0.20$
Crystal system	triclinic	triclinic
Space group	P$\bar{1}$	P$\bar{1}$
F (000)	1132	2560
a (Å)	13.506(3)	15.692(0)
b (Å)	13.546(3)	15.707(8)
c (Å)	15.026(3)	22.603(3)
α (°)	72.64(3)	99.395(1)
β (°)	65.96(3)	93.164(1)
γ (°)	60.67(3)	115.883(1)
V (Å^3)	2171.84(0)	4894.85(11)
Z	2	2
D_{calc} (g cm^{-3})	1.74(6)	1.73(6)
Temp (K)	296(2)	293(2)
μ (mm^{-1})	1.380	1.383
No. of refl. collected	8569	19117
No. of refl. observed	5102($>4\sigma$)	11272($>2\sigma$)
R	0.0530	0.0553
R_w	0.0713	0.1286
Goodness of fit. S	1.88	1.138
Parameters refined	400	903
Largest shift	0.025	0.024
Largest different peak (e Å^{-3})	0.91	1.29

$R = \Sigma \| F_0| - |F_c| / \Sigma |F_0|$. $R_w = [\Sigma w(|F_0| - |F_c|)^2 / \Sigma w |F_0|^2]^{1/2}$.

Table 2. Selected bond length (Å) and angles (°) for the complex **III**

Mo(1)–Mo(2)	2.763(1)		
Mo(1)–Mo(3)	2.765(1)		
Mo(1)–S	2.339(2)		
Mo(1)–S(1)	2.302(3)		
Mo(1)–S(2)	2.282(2)		
Mo(1)–N	2.269(7)		
Mo(2)–Mo(3)	2.693(2)		
Mo(2)–S(3)	2.289(2)		
Mo(2)–S	2.350(3)		
Mo(2)–S(1)	2.294(2)		
Mo(2)–O(2)	2.244(6)		
Mo(3)–S(3)	2.290(3)		
Mo(3)–S	2.346(2)		
Mo(3)–S(2)	2.297(2)		
Mo(3)–O(1)	2.252(5)		
O(2)–C	1.29(2)		
O(1)–C	1.26(1)		
O(3)–H(3A)	0.850		
O(3)–C(2)	1.35(2)	Mo(1)–Mo(3)–S(3)	97.0(1)
Mo(2)–Mo(1)–Mo(3)	58.3(1)	S(3)–Mo(3)–S	108.5(1)
Mo(2)–Mo(1)–S	54.1(1)	Mo(1)–Mo(3)–S(2)	52.6(1)
Mo(3)–Mo(1)–S	53.9(1)	Mo(2)–Mo(3)–S(2)	98.7(1)
Mo(2)–Mo(1)–S(1)	52.9(1)	S(3)–Mo(3)–S(2)	93.2(1)
Mo(3)–Mo(1)–S(1)	97.7(1)	S–Mo(3)–S(2)	104.8(1)
S–Mo(1)–S(1)	105.2(1)	Mo(2)–S(3)–Mo(3)	72.1(1)
Mo(2)–Mo(1)–S(2)	97.1(1)	Mo(1)–S–Mo(2)	72.2(1)
Mo(3)–Mo(1)–S(2)	53.1(1)	Mo(1)–S–Mo(3)	72.3(1)
S–Mo(1)–S(2)	105.5(1)	Mo(2)–S–Mo(3)	70.0(1)
S(1)–Mo(1)–S(2)	97.2(1)	Mo(1)–S(1)–Mo(2)	73.9(1)
Mo(1)–Mo(2)–Mo(3)	60.9(1)	Mo(1)–S(2)–Mo(3)	74.3(1)
Mo(1)–Mo(2)–S(3)	97.1(1)	Mo(2)–Mo(3)–S(3)	54.0(1)
Mo(3)–Mo(2)–S(3)	54.0(1)	Mo(1)–Mo(3)–S	53.7(1)
Mo(1)–Mo(2)–S	53.7(1)	Mo(2)–Mo(3)–S	55.1(1)
Mo(3)–Mo(2)–S	54.9(1)	S–Mo(2)–S(1)	105.1(1)
S(3)–Mo(2)–S	108.4(1)	Mo(1)–Mo(3)–Mo(2)	60.8(1)
Mo(1)–Mo(2)–S(1)	53.2(1)	O(1)–C–C(1)	118.5(1)
Mo(3)–Mo(2)–S(1)	100.0(1)	O(2)–C–C(1)	116.7(9)
S(3)–Mo(2)–S(1)	94.3(1)		

atoms. All the nonhydrogen atoms except some disordered C atoms of DTP ligand were refined anisotropically. Least-squares refinements were performed by fullmatrix procedures. Crystal structure plots were drawn using ORTEP II [11] software. The positions of all hydrogen atoms were generated geometrically (C–H bond fixed at 0.96 Å), assigned isotropic thermal parameters and allowed to ride on their respective parent C atoms before the final cycle of least-squares refinement. Hydrogen atoms coordinating O were included at idealized positions with an assumed O–H distance of 0.85 Å. Intermolecular S–S distances and dihedral angles were calculated using Molen programs software. The highest peak on the final difference Fourier map in **III** has a height of 1.293 e $Å^{-3}$, which is located at a position 0.738 Å away from Cl2 (chlorine 2).

RESULTS AND DISCUSSION

Crystal structure

$Mo_3S_4(DTP)_3$(salicylate)(CH_3CN) (**III**). The main structural feature of **III** (shown in Fig. 1) is similar to that of the typical incomplete cubane-type Mo_3S_4 clusters with DTP as the ligand [12]. The bond length of Mo1–N 2.269(7) Å is shorter than the corresponding one in $Mo_3OS_3(DTP)_4(CH_3CN)$, 2.274(6) Å [13]. The substitution of salicylate for bridging DTP decreases its bridged Mo2–Mo3 bond from 2.734(1) Å [14] to 2.693(2) Å, which is almost the same as the average Mo–Mo 2.690 Å when bridged by aliphatic carboxylates [2]. However, the average Mo–μ-S bond 2.292(3) Å of **III** (2.293(2) Å of **IV**, see below) is longer than that of the corresponding ali-

Table 3. Selected bond length (Å) and angles (°) for the complex **IV**

Mo(1)–S(3)	2.290(2)
Mo(1)–S(1)	2.295(2)
Mo(1)–S(4)	2.336(2)
Mo(1)–N(1)	2.358(7)
Mo(1)–Mo(2)	2.7551(10)
Mo(1)–Mo(3)	2.7628(10)
Mo(2)–O(2)	2.215(5)
Mo(2)–S(3)	2.293(2)
Mo(2)–S(2)	2.296(2)
Mo(2)–S(4)	2.345(2)
Mo(2)–Mo(3)	2.6913(9)
Mo(3)–O(1)	2.252(5)
Mo(3)–S(2)	2.292(2)
Mo(3)–S(1)	2.293(2)
Mo(4)–O(5)	2.267(5)
Mo(4)–S(5)	2.294(2)
Mo(4)–Mo(6)	2.6935(11)
Mo(5)–Mo(6)	2.7559(10)
Mo(6)–O(6)	2.235(6)
C8–O3	1.272(10)
C8–O4	1.254(10)
C08–O7	1.253(10)
C08–O8	1.267(11)

S(3)–Mo(1)–S(1)	96.56(8)	C(7)–O(1)–Mo(3)	121.4(5)
S(3)–Mo(1)–S(4)	105.50(7)	C(7)–O(2)–Mo(2)	122.6(5)
S(1)–Mo(1)–S(4)	105.10(7)	C(07)–O(5)–Mo(4)	122.3(5)
S(3)–Mo(1)–Mo(2)	53.10(5)	C(07)–O(6)–Mo(6)	122.8(5)
S(1)–Mo(1)–Mo(2)	96.72(6)	O(2)–C(7)–O(1)	126.8(7)
S(4)–Mo(1)–Mo(2)	54.09(5)	O(2)–C(7)–C(1)	116.1(7)
N(1)–Mo(1)–Mo(2)	93.4(2)	O(1)–C(7)–C(1)	117.0(7)
S(3)–Mo(1)–Mo(3)	97.82(6)	C(1)–C(6)–C(5)	118.9(8)
S(1)–Mo(1)–Mo(3)	52.94(5)	C(1)–C(6)–C(8)	122.5(7)
S(4)–Mo(1)–Mo(3)	53.61(5)	C(5)–C(6)–C(8)	118.4(8)
N(1)–Mo(1)–Mo(3)	134.8(2)	O(4)–C(8)–O(3)	124.5(8)
Mo(2)–Mo(1)–Mo(3)	58.38(2)	O(4)–C(8)–C(6)	119.9(8)
O(2)–Mo(2)–S(3)	172.7(2)	O(3)–C(8)–C(6)	115.6(8)
O(2)–Mo(2)–S(2)	83.5(2)	O(6)–C(07)–O(5)	126.1(8)
S(3)–Mo(2)–S(2)	94.56(8)	O(6)–C(07)–C(01)	116.3(7)
O(2)–Mo(2)–S(4)	82.2(2)	O(5)–C(07)–C(01)	117.6(8)
S(3)–Mo(2)–S(4)	105.13(8)	O(7)–C(08)–O(8)	124.6(9)
S(2)–Mo(2)–S(4)	108.00(7)	O(7)–C(08)–C(06)	118.9(8)
O(2)–Mo(2)–Mo(3)	84.80(14)	O(8)–C(08)–C(06)	116.2(8)
S(3)–Mo(2)–Mo(3)	99.79(6)	S(1)–Mo(3)–S(4)	105.35(8)
S(2)–Mo(2)–Mo(3)	54.01(6)	O(1)–Mo(3)–Mo(2)	84.2(1)
S(4)–Mo(2)–Mo(3)	54.62(5)	S(2)–Mo(3)–Mo(2)	54.15(6)
O(2)–Mo(2)–Mo(1)	134.2(1)	S(1)–Mo(3)–Mo(2)	98.56(6)
S(3)–Mo(2)–Mo(1)	53.00(6)	S(4)–Mo(3)–Mo(2)	55.10(5)
S(2)–Mo(2)–Mo(1)	97.46(6)	O(1)–Mo(3)–Mo(1)	133.3(1)
S(4)–Mo(2)–Mo(1)	53.81(5)	S(2)–Mo(3)–Mo(1)	97.34(6)
Mo(3)–Mo(2)–Mo(1)	60.95(2)	S(1)–Mo(3)–Mo(1)	53.01(6)
O(1)–Mo(3)–S(2)	83.4(2)	S(4)–Mo(3)–Mo(1)	53.80(5)
O(1)–Mo(3)–S(1)	173.0(2)	Mo(2)–Mo(3)–Mo(1)	60.66(2)
S(2)–Mo(3)–S(1)	92.93(8)	S(2)–Mo(3)–S(4)	108.61(7)
O(1)–Mo(3)–S(4)	81.5(2)		

phatic carboxylate-substituted clusters(Mo–μ-S, 2.28 Å) [15, 16, 17], showing the effect on the Mo_3S_4 core from the bridging ligand and its substituents.

It is structurally unusual [18, 19] that those atoms in **III**, Mo3, Mo2, O1, O2, C, C1, C2, C3, C4, C5, C6 and O3 share a large plane with good coplanarity, as shown by the data listed in Table 4; the dihedral angle between the plane 2 and the plane 3 is 7(2)°. The bond

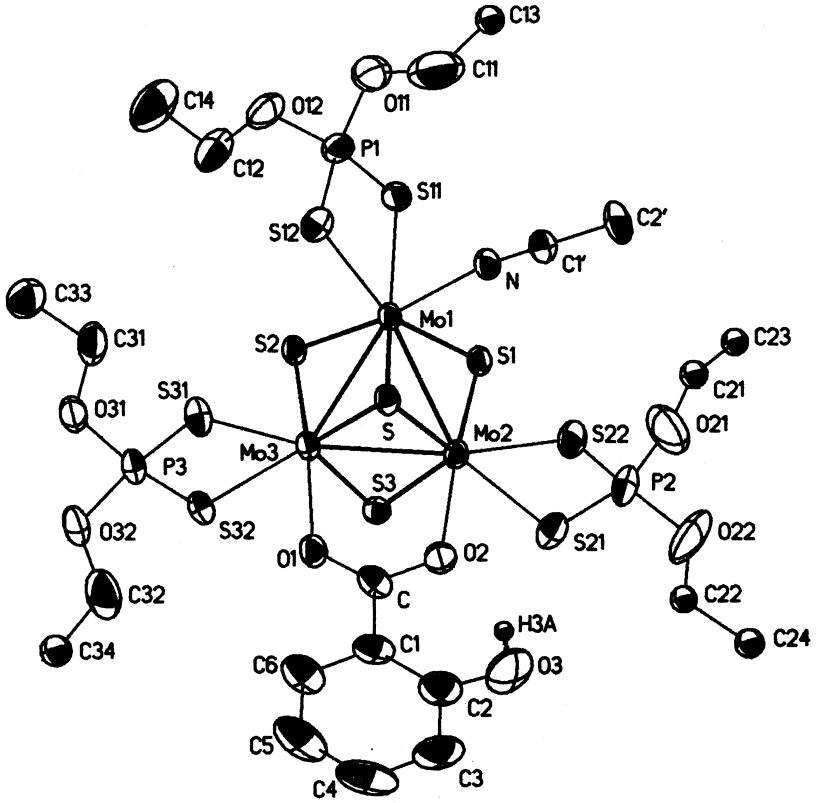

Fig. 1. The ORTEP drawing of compound **III** with a 30% probability level.

Table 4. Dihedral angles calculated for complex **III** and **IV**

Plane No.	Atoms	Plane No.	Dihedral angle (°)
	Complex **III**		
1	Mo1, Mo2, Mo3	2	145.8(1)
2	Mo2, Mo3, O2, O1, C, C1	3	7(2)
3	C, C1, C2, C3, C4, C5, C6	1	139.6(4)
	Complex **IV**		
1	Mo2, Mo3, O1, O2, C1, C7	2	47.6(2)
2	C1, C2, C3, C4, C4, C6, C7, C8	4	92.0(2)
3	Mo4, Mo6, O5, O6, C07, C01	4	46.7(2)
4	C01, C02, C03, C04, C05, C06, C07, C08	5	45.8(2)
5	O3, O4, C8, H3B, O7, O8, C08, H8A	2	46.8(3)

lengths Mo2–O2, Mo3–O1 and bond angles O2–C–C1, O1–C–C1 are different, showing higher asymmetry for plane 2 and 3. These structural details result from the intramolecular H-bond formed between O2 and O3 (distance between O1 and O3 is 2.57 Å). The H-bond, which is coplanar to the phenyl group, forces O3 closer to O1, fixing and tilting the phenyl group to O3 side. As a result, the salicylate ligand has more asymmetry and more coplanarity with Mo2 and Mo3. A dihedral angle of 145.77(14)° between the plane 1 and the plane 2 shows the heavily distorted octahedral coordination of Mo in **III**.

$[Mo_3S_4(DTP)_3(Phthalate)(Py)]_2 \cdot EtOH \cdot CH_2Cl_2$ (**IV**). It is interesting to find that the spare –COOH groups in cluster **IV** still have the capability of forming a dimeric carboxylic acid via H-bonding. The cluster **IV**, as shown in Fig. 2, consists of two incomplete cubane-type $[Mo_3S_4(DTP)_3(phthalate)(Py)]$ units

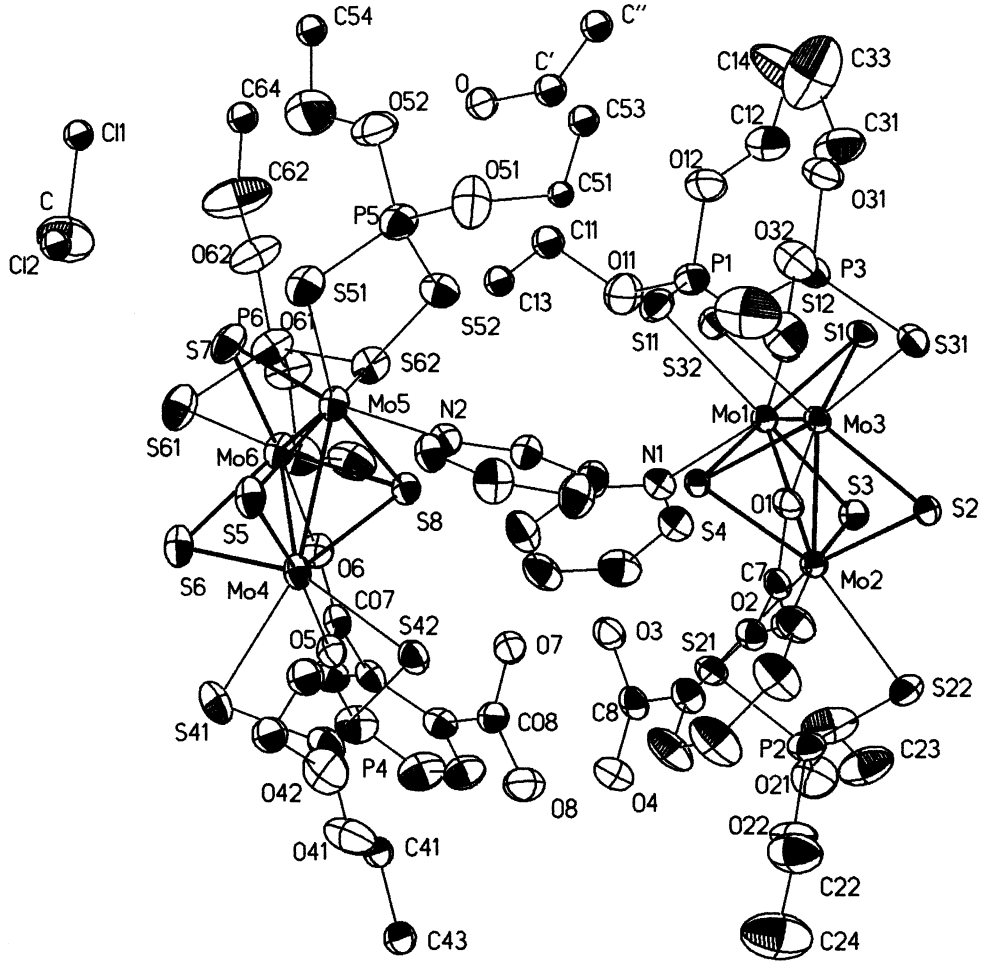

Fig. 2. The ORTEP drawing of compound **IV** with a 30% probability level.

linked together by the intramolecular H-bonds. Two solvent molecules, EtOH and CH_2Cl_2, are situated in the unit cell.

Structural data and dihedrals indicated that two pendant –COOH groups from two phthalate molecules constructed a highly symmetrical rigid plane via intermolecular H-bonding. The structure of this plane was shown in Fig. 3. Although these two H

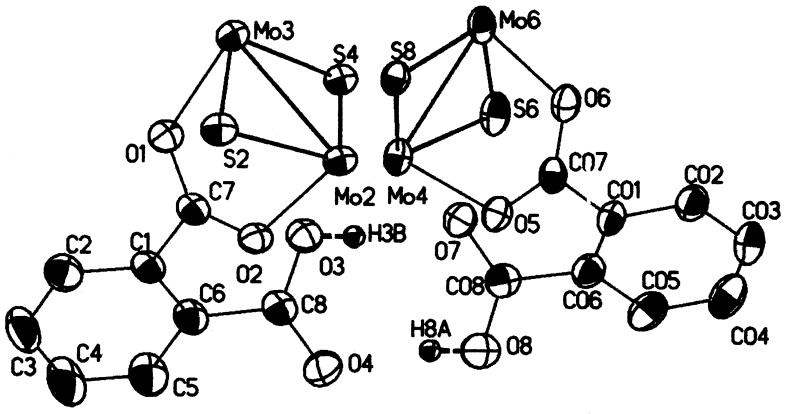

Fig. 3. The ORTEP drawing of two –COOH groups of compound **III** with a 30% probability level.

atoms were theoretically added to the adjacent O atoms (O3–H3B and O4–H8A distances are 0.85 Å, O7–H3B and O4–H8A are 1.84 Å), according to the distance (2.69 Å) of both O3–O7 and O4–O8, we can deduce that the two H atoms H3B and H8A are roughly linear and situated in the same plane with the four O atoms and strong H-bonds are formed. The IR spectra for clusters **III** and **IV** were measured [20] as listed in Table 5. A broad absorption at 3200 cm^{-1} was assigned to ν_{OH} for compound **III** and a sharp absorption at 2978 cm^{-1}, which overlaps with the phenyl absorption, was assigned to the ν_{OH} for **IV**. This is consistent with the crystal structural results that the H-bond in **IV** is linear and much stronger than that in **III**. The dihedral angles calculated between the two phenyl planes (plane 2 and 4) is 92.0(2)° as shown in Table 4, indicate that the two phenyl planes are aligned perpendicularly in the lattice.

The mean Mo–O bond length 2.242(5) Å (to phthalate ligands) in **IV** is longer than that of the similar aliphatic carboxylate cluster compounds [19] and these four Mo–O bonds, listed in Table 3, differ considerably from each other. This difference is even greater than that of the corresponding Mo–O in cluster **III** as shown in Table 2. This distortion of the coordinated –COO groups is caused by crystalline packing effects. The alignment of the bulky Mo_3S_4 core and the neighboring DTP ligand distort Mo2Mo3O1C7O2 and Mo4Mo6O6CO7O5 planes and also twist the H-bonding plane as shown by the following data: O4O8O3 124.5(8)° ≈ O7OO8O8 124.6(9)°, C8–O3 (1.272(10) Å) ≈ C08–O8 (1.267(11) Å) and C8–O4 (1.254(10) Å) ≈ C08–O7 (1.253(10) Å). As reflected by the dihedral angles between plane 1 and 2, 3 and 4 (Table 4), the RCO_2 group is no longer coplanar as opposed to the case in cluster **III**.

S–S interactions

The intramolecular S–S interactions [21, 22] in $[Mo_3S_4]$-type (M = Mo, W) clusters are important in crystal packing along with the ligand substitutional effect discussed above. For both **III** and **IV**, S–S interactions, which are all considerably shorter than the corresponding van der Waals contacts [22, 23], were calculated as shown in Fig. 4 and were listed in Table 6. In cluster **III**, the S–S interactions favor the opposite alignment of the two molecules in the cell. On the other side of the molecule, the phenyl ring sterically hinders μ-S atom to form further superamolecular interaction [14], so the two molecules of **III** are packed into the cell with a symmetric center [24]. Similarly, six S–S interactions are found in **IV**. S1, as well as S6, can form two S–S interactions with another two S atoms.

^{31}P NMR

^{31}P NMR spectra of **III** and **IV**, (Fig. 5), were measured in acetone-d_6. The assignment of the ^{31}P resonances is consistent with the literature [3]. The resonance (T_1) at 110.08 ppm for **III** was assigned to the two coalesced DTP ligands coordinated to Mo2 and Mo3, respectively; the other resonance (T_2) at 111.33 ppm was assigned to the DTP coordinated to Mo1. Similarly, the resonance (T_1) at 110.82 ppm in **IV** was assigned to the four DTP ligands coordinated to Mo2 and Mo3, Mo4 and Mo6; the other resonance (T_2) at 110.20 ppm was assigned to the DTP ligand coordinated to Mo1, Mo5.

Experimentally, the loosely coordinated ligand L affects the NMR spectrum by its dynamic dissociation in the solution and the carboxylate does so by the long-distance electron delocalization. Normally, the pyridine substitution for acetonitrile will broaden NMR linewidths considerably [3], so significant line-broadening in the spectra of compound **IV** is expected.

For this series of trinuclear clusters, the relative position of T_1 and T_2 is determined by the type of the loosely coordinated ligand L. For compound **III**, L = CH_3CN, T_2 is situated at the lower field to T_1; on the contrary, T_2 is situated at the higher field in the spectra of compound **IV**, L = pyridine. Nevertheless, L can only affect the chemical shift of T_2 considerably, it does little to the chemical shift of T_1, so the chemical shift differences between T_1 and T_2 are mainly attributed to aromatic substituents –OH and $-CO_2H$. This leads to the conclusion that the Mo_3S_4 core and the superconjugation translate the electron effect to DTP ligands [25]. A more systematic ^{31}P NMR spectroscopic study on more cluster compounds will soon follow.

Acknowledgments—We are grateful for the financial support to the Foundation of the Chinese National Natural Sciences (No. 29303025), the Foundation of Fujian Provincial Natural Sciences (No. 970133) and the Foundation of the Chinese State Key Laboratory of Structural Chemistry (No. 970095).

Table 5. IR vibration of complexes **III** and **IV** (cm^{-1})

		NνMo–(μ_3 – S)	νMo–(μ-S)	νMo–(μ-O)	ν(O–H)	ν(C–O)	νC_6H_6
III	IR	452	480	641	3200	1169	3000–3030
IV	IR	451	482	642	2978	1159	3000–3050

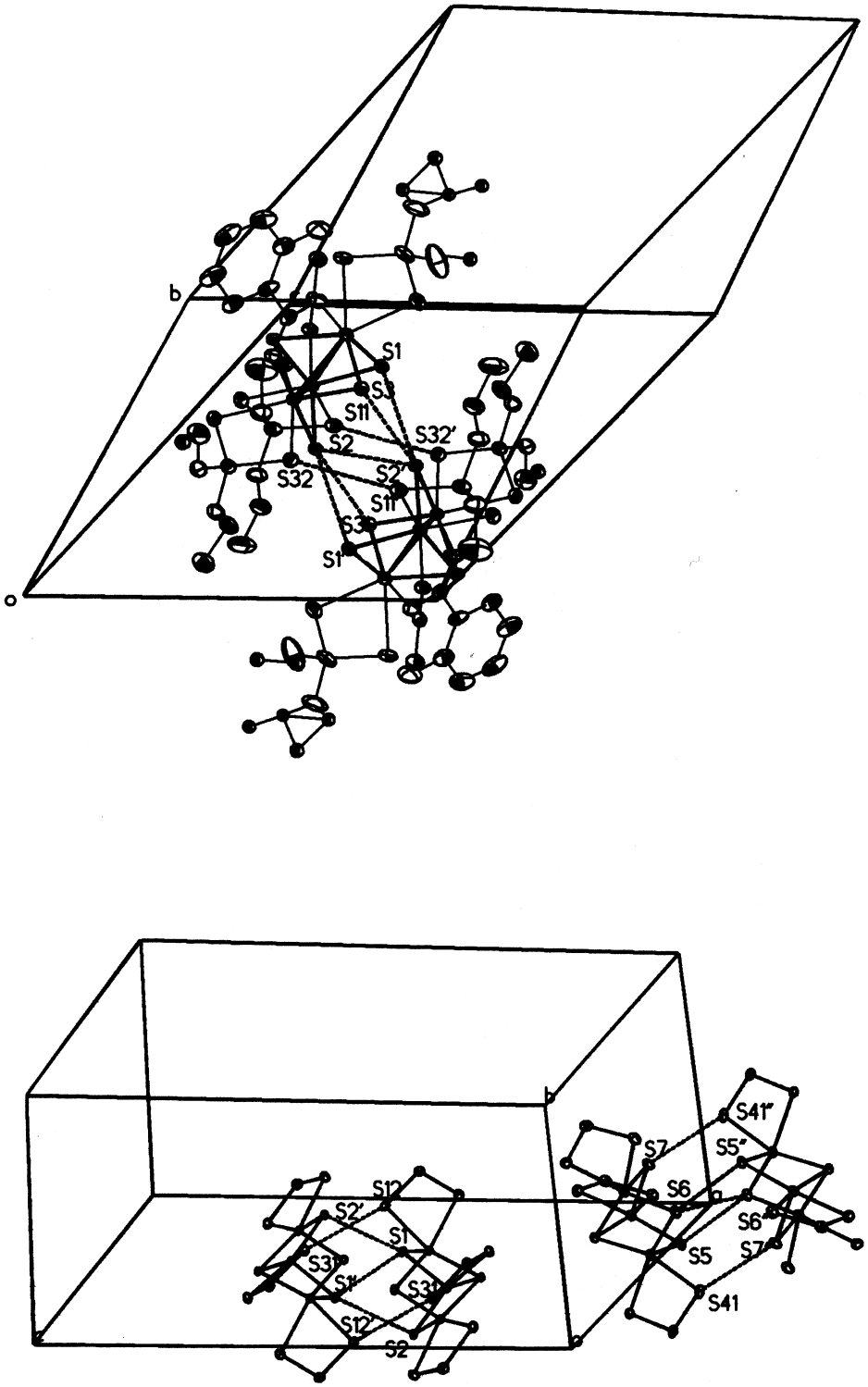

Fig. 4. The ORTEP drawing of S–S interactions in compound **III** and **IV** with a 15% probability level.

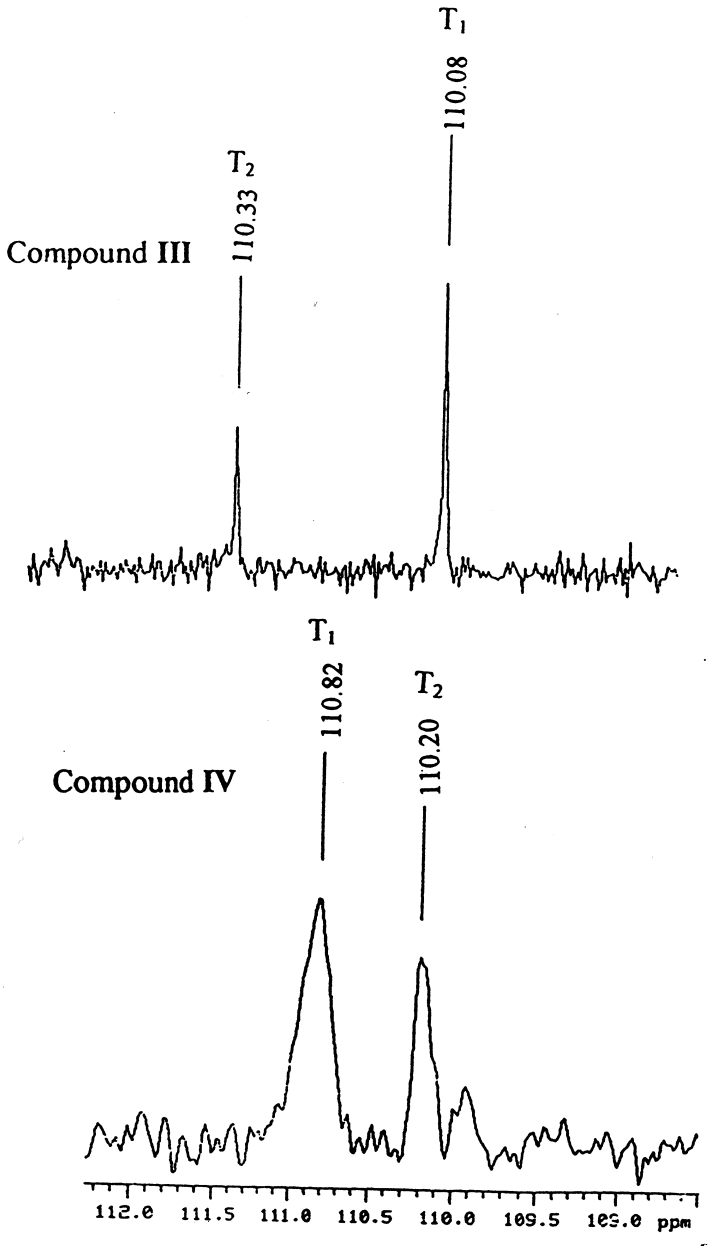

Fig. 5. Decoupled ^{31}P NMR spectra of compound **III** and **IV**.

Table 6. S–S interactions of complex **III** and **IV**

	Complex **III**		Complex **IV**	
Symmetry operations	S atoms	distance (Å)	S atoms	distance (Å)
$(1-x, 1-y, 1-z)$	S1–S2′	3.646(2)	S1–S1′	3.229(3)
	S2–S2′	3.264(3)	S1–S2′	3.416(3)
	S2–S3′	3.364(2)	S12–S13′	3.611(4)
	S11–S32′	3.529(7)		
$(2-x, -y, -z)$			S5–S6″	3.450(4)
		S6–S6″	3.419(4)	
			S7–S41″	3.667(4)

The authors also wish to express their appreciation to Professor M. C. Hong, Dr J. T. Chen and Mr Q. M. Wang for the data collection and structure analysis.

REFERENCES

1. Keck, H., Kuchen, W., Mathow, J. and Wunderlich, H., *Angew. Chem. Int. Ed. Engl.*, 1982, **12,** 929.
2. Huang, J.-Q., Huang, J.-L., Shang, M.-Y., Lu, S.-F., Lin, X.-T., Lin, Y.-H., Huang, M.-D., Zhuang, H.-H. and Lu, J.-X., *Pure Appl. Chem.*, 1988, **60,** 1185–1192.
3. Yao, Y.-G., Akashi, H., Sakane, G., Shibahara, T. and Ohtaki, H., *Inorg. Chem.*, 1995, **34,** 42–48.
4. Murata, T., Gao, H., Mizobe, Y., Nakano, F., Motomura, S., Tanase, T. and Yano, S., Hidai, M., *J. Am. Chem. Soc.*, 1992, **114,** 8287–8288.
5. Murata, T., Mizobe, Y., Gao, H., Ishii, Y., Wakabayashi, T., Nakano, F., Tanase, T., Yano, S., Hidal, M., Echizen, I., Nanikawa, H. and Motomura, S., *J. Am. Chem. Soc.*, 1992, **116,** 3389–3398.
6. Shi, S. and Ji, W., Tang, H., *J. Am. Chem. Soc.*, 1994, **116,** 3615–3616.
7. Bacon, W. E. and Lesure, W. M., *J. Am. Chem. Soc.*, 1954, **76,** 670–676.
8. Sheldrick, G. M., *SHEXLXTL/PC. Users Manual*, Siemens Analytical X-ray Instruments, Madison, WI, 1990.
9. Sheldrick, G. M., in *Computational Computing* 3. *Data Collection, Structure Determination, Proteins and Databases*, ed. G. M. Sheldrick, C. Kreuger and R. Goddard. Oxford University Press, New York, 1985, pp. 175–189.
10. Sheldrick, G. M., *SHELXLT-Plus. PC Version*, Siemens Analytical X-ray Instruments, Madison, WI, 1987.
11. Johnson, C. K., *ORTEP II. Report ORNI*-5138. Oak Ridge National Laboratory, 1976.
12. Shibahara, T., *Adv. Inorg. Chem.*, 1991, **37,** 143–173.
13. Shibahara, T., private communication.
14. Lin, X.-T., Lin, Y.-H., Huang, J.-Q. and Huang, J.-Q., *Kexue Tongbao*, 1986, **7,** 509.
15. Lu, S.-F., Shang, M.-Y., Huang, J.-Q., Huang, J.-L. and Lu, J.-X., *Sci. Sin. B*, 1988, **XXXI,** 147.
16. Birnbanum, A., Cotton, F. A., Dori, Z., Kapon, M., Marler, D., Reisner, G. M. and Schwotzer, W., *J. Am. Chem. Soc.*, 1985, **107,** 2405.
17. Wu, D.-M., Zhuang, H.-H., Zheng, J.-J., Huang, J.-L., Lu, J.-X. and Huang, J.-Q., *Sci. Sin. B*, 1985, **7,** 589.
18. Lu, S.-F., Huang, J.-Q., Huang, X.-Y. and Wu, Q.-J., *JieGou HuaXue* (*Chin. J. Struct. Chem.*), 1995, **14,** 482–487.
19. Lu, S.-F., Huang, J.-Q., Huang, M.-D. and Huang, J.-L., *Acta Chim. Sin. Engl. Ed.*, 1989, **1,** 24.
20. Huang, J.-L., Huang, J.-Q., Shang, M.-Y. and Lu, J.-X., *Adv. Sci. China Chem.*, 1990, **3,** 155–180.
21. Fedin, V. P., Sokolov, M. N. and Virovets, A. V., *Inorg. Chim. Acta.*, 1992, **194,** 195.
22. Cotton, F. A. and Wilkinson G., *Advanced Inorganic Chemistry*, John Wiley and Sons, 1962, p. 104.
23. Casas, J. S., Castineirtas, A., Haiduc, I., Sonchez, A. and Sordo, J., *Polyhedron*, 1994, **13,** 1805–1809.
24. Lu, S.-F., Wu, Q.-J., Chen, H.-B., Yu, R.-M. and Huang, J.-Q., *JieGou HuaXue* (*Chin. J. Struct. Chem.*), 1994, **13,** 389–396.
25. Lu, J.-X., *JieGou HuaXue* (*Chin. J. Struct. Chem.*), 1989, **8,** 327–339.

Pergamon

Polyhedron Vol. 17, No. 23–24, pp. 4213–4217, 1998
© 1998 Elsevier Science Ltd
All rights reserved. Printed in Great Britain
PII: S0277–5387(98)00231–9
0277–5387/98 $19.00+0.00

Preparation and structures of two anionic antimony(III) mixed halides, Hpy[$SbBr_2Cl_2$] and [Hpy]$_8$[$Sb_4Br_{12}Cl_8$]

Michael Nunn, Alexander J. Blake, Michael J. Begley and D. Bryan Sowerby†

Department of Chemistry, University of Nottingham, Nottingham NG7 2RD, U.K.

(Received 6 March 1998; accepted 6 June 1998)

Abstract—Structures are reported for two anionic antimony(III) bromide chlorides, Hpy[$SbBr_2Cl_2$] and [Hpy]$_4$[$Sb_4Br_{12}Cl_8$], both of which are subject to halogen disorder. The first compound has an infinite chain structure in which antimony coordination is raised to six by the formation of double halogen bridges by atoms with high bromine content. The structure of the second compound is based on a distorted square of antimony atoms, again in distorted octahedral coordination. The antimony atoms are linked together by single bromine bridges and chlorine atoms or atoms with high chlorine content occupy the *trans* positions. The pattern of Sb–Br bridging distances suggests that the structure is derived by interconnection of two singly bridged $[Sb_2Br_5Cl_4]^{3-}$ units by two bridging Br^- ions. © 1998 Elsevier Science Ltd. All rights reserved

Keywords: antimony(III) halide anions; mixed halides; crystal structure; halogen disorder.

INTRODUCTION

The well known Lewis acidity of antimony(III) halides leads in the presence of added halide ion to species with the stoichiometries $[SbX_4]^-$, $[SbX_5]^{2-}$, $[SbX_6]^{3-}$ and $[Sb_2X_9]^{3-}$ [1]. Although a monomeric form of the pentahalide is known in $(NH_4)_2[SbCl_5]$ [2] and $K_2[SbCl_5]$ [3], because of coordinative unsaturation at antimony(III) and the availability of lone pair density on the halogens, intermolecular bridging is possible. This leads to both dimeric and chain polymeric forms for the $[SbX_4]^-$ stoichiometry in $(NBu_4)_2[Sb_2Cl_8]$ [4] and $\{(Hpy)[SbCl_4]\}_n$ [5], respectively, and tetrameric and polymeric forms for the $[SbX_5]^{2-}$ stoichiometry in $\{(2,2'\text{-bipyH}_2)[SbCl_5]\}_4$ [6] and $\{(4,4'\text{-bipyH}_2)[SbCl_5]\}_n$, respectively. A dimeric alternative for the latter stoichiometry has been identified in the potassium and ammonium salts of $[Bi_2Br_{10}]^{4-}$ [7]; the corresponding antimony analogue is currently unknown.

We have been interested in the structures of antimony(III) haloanions, both those which are purely inorganic [8] and those also incorporating phenyl groups [9], and now report an extension of this work to species containing both bromine and chlorine. Our interests are in the degree of polymerisation that results and in which of the two halogens occupy any bridging positions. Few compounds containing two of the heavier halides have been investigated but we have previously described the bioctahedral structure of $(NMe_4)_3[Sb_2Br_3Cl_6]$ [8], which contains bridging bromine atoms. In related anionic antimony(III) mixed chloride or bromide fluorides [1], the heavier halogen also occupies the bridging positions. This paper reports the preparation and structures of two further mixed bromide chlorides with the stoichiometries $[SbBr_2Cl_2]^-$ and $[SbBr_3Cl_2]^{2-}$, respectively.

EXPERIMENTAL

Preparation of Hpy[$SbBr_2Cl_2$]

This compound was prepared as described previously [8] by recrystallising [Hpy]$_3$[Sb_2Cl_9] from hot concentrated hydrobromic acid solution and recrystallised from ethanol. (Found: C, 13.8; H, 1.4; N, 3.3; Br, 36.9. Calc for $C_5H_6Br_2Cl_2NSb$: C, 13.9; H, 1.4; N, 3.2; Br, 36.9%).

†Authr to whom correspondence should be addressed.

Preparation of $[Hpy]_8[Sb_4Br_{12}Cl_8]$

A solution of pyridinium chloride (3.2 g, 0.028 mol) in anhydrous ethanol was added to a solution of antimony(III) bromide (5.0 g, 0.014 mol) in the same solvent. The pale yellow precipitate which formed immediately was redissolved by heating and on cooling yellow crystals of $[Hpy]_8[Sb_4Br_{12}Cl_8]$ were obtained. M.p. 160° (dec). (Found: C, 19.9; H, 2.0; N, 4.6; Br, 40.8. Calc for $C_{40}H_{48}Br_{12}Cl_8N_8Sb_4$: C, 20.2; H, 2.0; N, 4.7; Br, 40.5%).

Crystal structure determinations

Crystals of $Hpy[SbBr_2Cl_2]$ and $[Hpy]_8[Sb_4Br_{12}Cl_8]$ suitable for X-ray diffraction were obtained by slow recrystallisation from ethanol.

$Hpy[SbBr_2Cl_2]$. Crystal data: $C_5H_6Br_2Cl_2NSb$, $M=432.6$, monoclinic, space group C2/c, $a=11.631(4)$, $b=12.788(4)$, $c=7.543(2)$ Å, $\beta=92.88(4)°$, $U=1120.5$ Å^3, $Z=4$, $D_c=2.56$ g cm^{-3}, $F(000)=792$, $\mu=10.46$ mm^{-1}, Mo-Kα radiation (graphite monochromated), $\lambda=0.71073$ Å, $T=295$ K, crystal size $0.5\times0.3\times0.3$ mm^3.

Intensity data were collected on a Hilger and Watts four-circle diffractometer for 1040 reflections in the range $0°<\theta<25°$ ($-13<h<13$, $0<k<15$, $0<l<9$) of which 783 unique reflections with $I>3\sigma(I)$ were considered observed. The data were corrected for Lorentz and polarisation effects and for absorption [10]. Crystallographic calculations used the CRYSTALS programs [11] and scattering factors, including anomalous dispersion contributions, were those for neutral atoms [12]. The antimony atom, lying on a two fold axis, was located from a Patterson synthesis and the remaining non-hydrogen atoms were revealed by a series of full-matrix least squares refinements and difference Fourier syntheses. The nitrogen and *para* carbon atoms of the cation lie on the two fold axis. After refinement with anisotropic thermal parameters, the hydrogen atoms were placed at their calculated positions but were not further refined. Because the bromine/chlorine disorder has been observed in related antimony mixed halide species, the occupation factors of the bromine and chlorine atoms were allowed to refine. Final refined values gave the following Br/Cl fractions: Br 0.68 [Cl′ 0.32] and Cl 0.68 [Br′ 0.32]. Application of a four coefficient Chebyshev weighting scheme led to final convergence (54 least squares parameters, maximum shift/esd 0.07) at $R=0.053$ ($R_w=0.064$).

$[Hpy]_8[Sb_4Br_{12}Cl_8]$. Crystal data: $C_{40}H_{48}Br_{12}Cl_8N_8Sb_4$, $M=2370.4$, orthorhombic, space group $Cmc2_1$, $a=14.654(3)$, $b=34.041(2)$, $c=13.681(2)$ Å, $U=6825(2)$ Å^3, $Z=4$, $D_c=2.307$ g cm^{-3}, $F(000)=4416$, $\mu=8.94$ mm^{-1}, Mo-Kα radiation (graphite monochromated), $\lambda=0.71073$ Å, $T=220(2)$ K, crystal size $0.62\times0.28\times0.19$ mm^3.

Diffraction data were collected on a Stoe Stadi four-circle diffractometer at 220 K (ω/θ scan mode and on-line profile fitting [13]). A total of 8380 reflections was collected to θ_{max} 25° and after applying a numerical absorption correction (T range, 0.095–0.224) merging gave 3263 unique data (R_{int}, 0.128) which were used in subsequent calculations. Of these 2833 had $F_o>4\sigma(F_o)$.

Direct methods [14] followed by difference Fourier syntheses located all non-hydrogen atoms and of these, Sb, Br and Cl were refined anisotropically [15]. Hydrogen atoms were placed at their calculated positions and allowed to ride on their parent atoms. The bridging atoms were ordered bromines but there was extensive disorder in the terminal atoms, except for Cl(4). The disorder was modelled as Br and Cl components having coincident positions and identical anisotropic thermal parameters and their linked occupancies were refined. Additional restraints based on the known Br/Cl ratio (3:2) were also employed. As the pyridinium cations were relatively poorly defined, with most disordered about the crystallographic mirror planes, carbon and nitrogen atoms could not be distinguished and geometric restraints were applied to the intramolecular cation geometry. The weighting scheme, $w^{-1}=\sigma^2(F_o^2)+0.127P^2+16.90P$; where $P=1/3[\mathrm{Max}(F_o^2, 0)+2F_c^2]$, led to final convergence at R_1 $[F_o>4\sigma(F_o)]=0.0688$, wR_2 (all data) $=0.1899$,

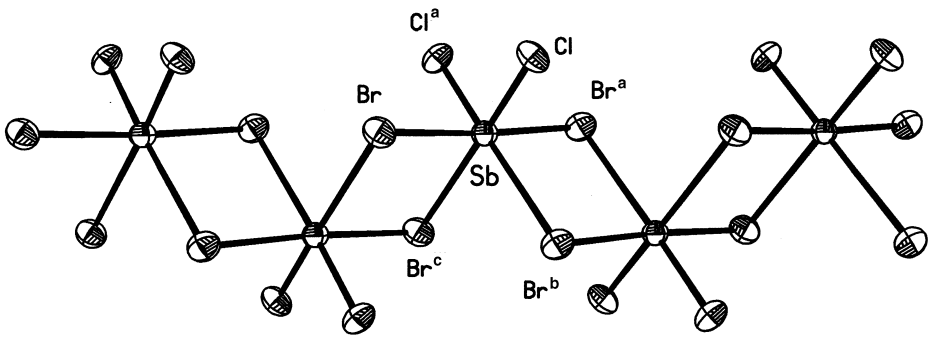

Fig. 1. Structure of $Hpy[SbBr_2Cl_2]$, showing the atom numbering scheme. Both halogen atoms are disordered and the atom label identifies the major component. See text for discussion.

Table 1. Selected bond lengths (Å) and angles (°) for $Hpy[SbBr_2Cl_2]$

Sb–Br	2.778(2)
Sb–Br[b]	3.213(2)
Sb–Cl	2.463(2)
Br–Sb–Br[a]	176.67(9)
Br–Sb–Br[b]	96.10(5)
Br–Sb–Br[c]	86.30(5)
Br–Sb–Cl	87.87(7)
Br–Sb–Cl[a]	89.87(7)
Br[b]–Sb–Br[c]	88.08(7)
Br[b]–Sb–Cl	88.80(8)
Br[b]–Sb–Cl[a]	173.06(7)
Cl–Sb–Cl[a]	95.0(1)
Sb–Br–Sb[a]	93.70(5)

Symmetry transformations used to generate equivalent atoms: [a] $-x, y, 0.5-z$; [b] $x, -y, 0.5+z$; [c] $-x, -y, -z$.

$S=1.05$ for 232 refined parameters and 44 restraints. An extinction correction refined to 0.00018(6) [16], the Flack absolute structure parameter was 0.07(3) and a final difference Fourier synthesis showed no peaks above $+2.61$ or below $-2.75\,e\text{Å}^{-3}$, which were located close to the antimony atoms.

Tables of atomic coordinates, bond distances and angles, anisotropic thermal parameters and hydrogen atom positions for both compounds have been deposited with the Cambridge Crystallographic Data Centre.

RESULTS AND DISCUSSION

Structure of $Hpy[SbBr_2Cl_2]$

The infinite chain structure of the anion in this compound is shown in Fig. 1 and bond distances and angles are listed in Table 1. In this compound antimony coordination is raised to six by formation of four asymmetric halogen bridges giving distorted octahedral coordination about antimony and stereochemical inactivity for the lone pair of electrons on antimony. From the space group symmetry, only one bromine and one chlorine atom are unique. This chain structure, orientated along the *c* axis, is one of the variants expected for the $[MX_4]^-$ stoichiometry and has been found previously for other Group 15 anions with this stoichiometry, including $Hpy[SbCl_4]$ [5] and $Hpy[SbBr_4]$ [17]; the present compound is, in fact, isostructural with the latter.

We have noted in previous structure determinations on antimony(III) mixed bromide-chlorides that there is a strong possibility of halogen disorder. For example, although the bridging atoms in both $[SbBr_3Cl_6]^{3-}$ [8] and $[Sb_2OBr_4Cl_2]^{2-}$ [18] are truly bromine, those in $[Sb_2OBr_2Cl_4]^{2-}$ have only 0.53 bromine content with the remaining bromine content associated with the four, predominantly chlorine, terminal atoms. Terminal halogens in $[Sb_2OBr_4Cl_2]^{2-}$, formally two bromine and two chlorine atoms, are similarly subject to halogen disorder [18]. On the other hand, in antimony(III) systems containing fluorine and a heavier halogen, e.g. $Na[SbBrF_3(H_2O)]$ [19] and $(NH_4)[SbCl_3F_2]$ [20], etc. such disorder does not occur

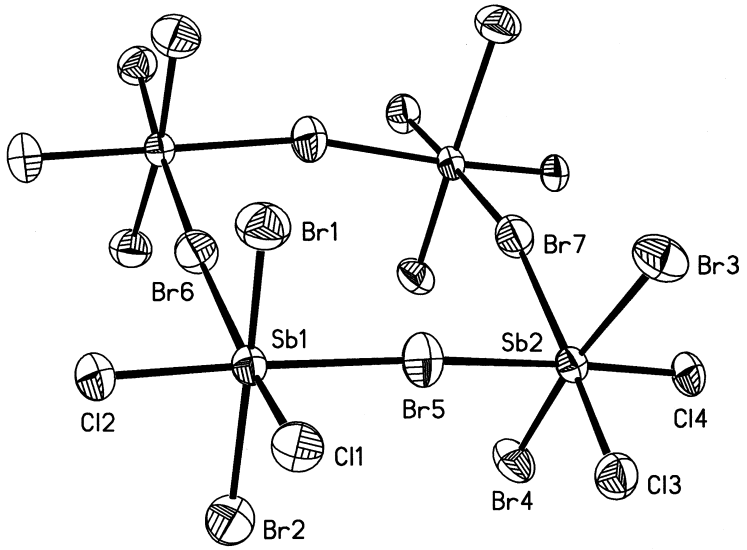

Fig. 2. Structure of $[Hpy]_8[Sb_4Br_{12}Cl_8]$, showing the atom numbering scheme. With the exception of Br(5), Br(6), Br(7) and Cl(4) which are ordered, all other halogen atoms are subject to disorder. The atom label identifies the major component; see text for discussion.

and bridging positions are occupied uniquely by the heavier halogen.

In the present compound, bridging positions are occupied by atoms with 0.68 bromine content and terminal positions by atoms with 0.68 chlorine character and the disorder is reflected in the bond distances. For example, the asymmetric bridge bonds are shorter [2.772(2) and 3.213(2) Å] than those in the corresponding tetrabromide [2.822(3) and 3.234(4) Å] [13] and the terminal atom separation [2.463(2) Å] longer than that for the tetrachloride [2.380(3) Å] [5].

Any anion–cation contacts are expected to involve hydrogen bonding between the pyridinium group and the most electronegative anion site and there are short N...Cl contacts [3.384(7) Å] probably representing a weak, bifurcated hydrogen bond. Such bonding has also been suggested in $Hpy[SbBr_4]$ [17] where the shortest N...Br contact is 3.44 Å, but in the corresponding chloride, the pyridinium cation is disordered with a two-fold axis passing through opposite C–C bonds and the closest contact between a ring atom and the terminal chlorine is 3.56 Å [5].

Structure of $[Hpy]_8[Sb_4Br_{12}Cl_8]$

This compound, with the stoichiometry $[SbBr_3Cl_2]^{2-}$, shows neither the monomeric, square pyramidal structure of $M_2[SbCl_5]$, where $M = NH_4$ [2] or K [3], nor the dimeric, doubly bridged, octahedral structure previously found for $M_4[Bi_2Br_{10}]$ [7]. The observed structure, with a mirror plane passing through Br(4) and Br(5), is shown in Fig. 2 together with the atom numbering scheme and is a tetrameric variant, similar to that of the corresponding 2,2′-bipyridinium salt [6]. Selected distances and angles in the anion are collected in Table 2. As with the compound above, this also showed halogen disorder, but atoms designated as Br(5), Br(6), Br(7) and Cl(4) are ordered. For the remainder, refinement gave the following Br/Cl fractions: Br(1) 0.68(2) [Cl(1′) 0.32(2)], Br(2) 0.80(2) [Cl(2′) 0.20(2)], Br(3) 0.93(2) [Cl(3′) 0.07(2)], Br(4) 0.68(2) [Cl(4′) 0.32(2)], Cl(1) 0.77(2) [Br(1′) 0.23(2)], Cl(2) 0.54(2) [Br(2′) 0.46(2)], Cl(3) 0.74(2) [Br(3′) 0.26(2)].

Antimony atoms are again at the centres of distorted octahedral SbX_6 units with presumed stereochemically inactivity for the lone pair and occupy the corners of a distorted square. They are interlinked by Br(5), Br(6) and Br(7), the latter two lying on a mirror plane. All three bromine bridges are almost linear [Sb–Br–Sb angles of 167.33(11), 176.65(13) and 162.33(11)° at Br(5), Br(6) and Br(7), respectively], with the smallest angle at Br(7) *trans* to the largest angle at Br(6). Ring angles at antimony are also different [94.99(9)° at Sb(1) and 92.95(8) at Sb(2)].

The four independent Sb–Br distances within the eight-membered ring fall into two sets, i.e. those to Br(6) and Br(7), the atoms on the mirror plane, are "long" [3.2277(13) and 3.2303(13) Å] and those to Br(5) which are substantially shorter [3.040(3) and 3.081(3) Å]. The structure could therefore be considered as arising by interconnecting two symmetry related singly bridged $[Br_2Cl_2Sb(1)Br(5)Sb(2)Br_2Cl_2]^{3-}$ units by bromide ions Br(6) and Br(7).

Atoms with high chlorine content, which varies from fully ordered for Cl(4) to 0.54 for Cl(2), occupy positions *trans* to bridging bromines and the observed

Table 2. Selected bond lengths (Å) and angles (°) for $[Hpy]_8[Sb_4Br_{12}Cl_8]$

Sb1–Cl1	2.458(4)
Sb1–Cl2	2.582(3)
Sb1–Br1	2.647(3)
Sb1–Br2	2.896(3)
Sb1–Br5	3.040(3)
Sb1–Br6	3.2277(13)
Sb2–Cl4	2.445(4)
Sb2–Cl3	2.491(4)
Sb2–Br4	2.598(3)
Sb2–Br3	2.953(3)
Sb2–Br5	3.081(3)
Sb2–Br7	3.2303(13)
Br6–Sb1[a]	3.2277(13)
Br7–Sb2[a]	3.2303(13)
Cl1–Sb1–Cl2	93.07(13)
Cl1–Sb1–Br1	87.93(11)
Cl2–Sb1–Br1	90.04(11)
Cl1–Sb1–Br2	84.87(11)
Cl2–Sb1–Br2	86.25(10)
Br1–Sb1–Br2	171.71(10)
Cl1–Sb1–Br5	84.76(12)
Cl2–Sb1–Br5	177.40(9)
Br1–Sb1–Br5	91.31(10)
Br2–Sb1–Br5	92.12(9)
Cl1–Sb1–Br6	172.11(12)
Cl2–Sb1–Br6	87.35(9)
Br1–Sb1–Br6	84.19(9)
Br2–Sb1–Br6	103.02(8)
Br5–Sb1–Br6	94.99(9)
Cl4–Sb2–Cl3	89.54(14)
Cl4–Sb2–Br4	90.27(14)
Cl3–Sb2–Br4	88.68(12)
Cl4–Sb2–Br3	85.15(14)
Cl3–Sb2–Br3	86.48(11)
Br4–Sb2–Br3	173.36(10)
Cl4–Sb2–Br5	174.42(13)
Cl3–Sb2–Br5	85.30(11)
Br4–Sb2–Br5	91.72(9)
Br3–Sb2–Br5	92.41(9)
Cl4–Sb2–Br7	92.23(12)
Cl3–Sb2–Br7	178.12(12)
Br4–Sb2–Br7	90.68(9)
Br3–Sb2–Br7	94.30(8)
Br5–Sb2–Br7	92.95(8)
Sb1–Br5–Sb2	167.33(11)
Sb1–Br6–Sb1[a]	176.65(13)
Sb2–Br7–Sb2[a]	162.33(11)

Symmetry transformation used to generate equivalent atoms: [a] $-x, y, z$.

"Sb–Cl" distances varying from 2.445(4) to 2.582(3) Å broadly correlate with the halogen content. The remaining *trans* related atoms, occupying the fifth and sixth octahedral positions above and below the Sb_4Br_4 ring plane, have bromine contents ranging between 0.53 and 0.93 and again the Sb–Br separations correlate well with bromine content.

Any discussion of antimony(III)–halogen bond lengths, even in neutral species, is fraught with problems resulting from secondary bond formation [21]. This is a consequence of the Lewis acidity of antimony(III) and occurs with halogens of either neighbouring neutral molecules or, in the case of halogenoanions, with added halide ions. One of the most satisfactory models for describing this type of interaction is to consider it occurring via σ^* orbitals of primary Sb–halogen bonds; this necessarily leads to a correlation between the lengths of the *trans* related bonds so formed [22]. Two extremes can be considered. At the first, one bond will be effectively single and the second a van der Waals contact while at the other, the bond lengths will be equal and equivalent to a "half bond"; any combination between these extremes is theoretically possible. By analysing crystallographic data for compounds where such secondary bonding occurs [23], values of 2.32 and 2.62 Å can be assigned to single and half Sb–Cl bonds and 2.46 and 2.79 Å to single and half Sb–Br bonds. The Sb–Cl and Sb–Br van der Waals contacts are *ca.* 4.0 and 4.2 Å, respectively, and the separation limits are then defined. The compounds currently under consideration, however, present further complications as (a) neither is mononuclear and in some cases one of the atoms of a *trans* related pair is also a bridging atom to a second antimony, inevitably modifying the separations, and (b) there is bromine/chlorine disorder, which again inevitably influences the bond lengths.

REFERENCES

1. Fisher, G. A. and Norman, N. C., *Adv. Inorg. Chem.*, 1994, **41,** 233.
2. Edstrand, M., Inge, M. and Ingri, N., *Acta Chem. Scand.*, 1974, **13,** 122.
3. Wismer, R. K. and Jacobson, R. A., *Inorg. Chem.*, 1974, **13,** 1678.
4. Ensinger, U., Schwarz, W. and Schmidt, A., *Z. Naturforsch. B*, 1982, **37,** 1584.
5. Porter, S. K. and Jacobson, R. A., *J. Chem. Soc. A*, 1970, 1356.
6. Lipka, A., *Z. Naturforsch. B*, 1983, **38,** 1615.
7. Lazarini, F., *Acta Cryst. B*, 1977, **33,** 1954.
8. Hall, M., Nunn, M., Begley, M. J. and Sowerby, D. B., *J. Chem. Soc. Dalton Trans.*, 1986, 1231.
9. Hall, M. and Sowerby, D. B., *J. Organomet. Chem.*, 1988, **347,** 59.
10. Stewart, J. M. and Hall, S. R., *The XTAL System of Crystallographic Programs*, *Users Manual*. University of Maryland, 1985.
11. Watkin, D., Carruthers, J. R. and Betteridge, D. W., *CRYSTALS Users Guide*. Chemical Crystallography Laboratory, University of Oxford, 1985.
12. *International Tables for X-ray Crystallography*, Vol. 4. Kynoch Press, Birmingham, 1974.
13. Clegg, W., *Acta Cryst. A*, 1981, **37,** 22.
14. Sheldrick, G. M., *Acta Cryst. A*, 1990, **46,** 467.
15. Sheldrick, G. M., *SHELXL*-97. University of Göttingen, Germany, 1997.
16. Sheldrick, G. M., *SHELXTL/PC*, version 5.03. Siemens Analytical Instruments, Madison, WI, U.S.A., 1995.
17. DeHaven, P. W. and Jacobson, R. A., *Cryst. Struct. Commun.*, 1976, **5,** 31.
18. Begley, M. J., Hall, M., Nunn, M. and Sowerby, D. B., *J. Chem. Soc. Dalton Trans.*, 1986, 1735.
19. Ducourant, M. B., Bonnet, B., Fourcade, R. and Mascherpa, G., *Acta Cryst. B*, 1977, **33,** 3693.
20. Udovenko, A. A., Volkova, L. M. and Davidovich, R. L., *Koord. Khim.*, 1978, **4,** 305.
21. Alcock, N. W., *Adv. Inorg. Radiochem.*, 1972, **15,** 1.
22. Carmalt, C. J. and Norman, N. C., in *Chemistry of Arsenic Antimony and Bismuth*, ed. N. C. Norman. Blackie, 1998, p. 27.
23. Hall, M., Ph.D. Thesis, University of Nottingham, 1980.

Pergamon

Polyhedron Vol. 17, No. 23–24, pp. 4219–4226, 1998
© 1998 Elsevier Science Ltd
All rights reserved. Printed in Great Britain
0277–5387/98 $19.00+0.00

PII: S0277–5387(98)00232–0

Mixed sulphur/oxygen diethoxy-diphenyl-imidodiphosphinates

Domineco C. Cupertino,[a] Robin W. Keyte,[b] Alexandra M. Z. Slawin[b] and J. Derek Woollins[b]*

[a]Zeneca Specialties Division, Blackley, Manchester M9 8ZS, U.K.

[b]Department of Chemistry, Loughborough University, Loughborough, LE11 3TU, U.K.

(Received 16 April 1998; accepted 8 June 1998)

Abstract—Reaction of $(EtO)_2P(S)NH_2$ with $ClP(O)Ph_2$ gives $(EtO)_2P(S)NHP(O)Ph_2$ (**1**) similarly reaction of $ClP(S)Ph_2$ yields $(EtO)_2P(O)NHP(S)Ph_2$ (**2**). The X-ray structures of **1** and **2** reveal P═O...H–N hydrogen bonded structures with distinct differences in packing and conformation. Thus **1** exists with the P═S and P═O groups in a *gauche* or *cisoid* orientation with SP...PO torsion angles of 79.5 and −69° for the two independent molecules which form a hydrogen bonded chain whereas **2** is a *transoid* dimer with an SP...PO torsion of 172° in the solid state. ML_2 (M = Zn, Pd, Pt) complexes derived from **1** and **2** are also described and the X-ray structure of $Zn[(EtO)_2P(O)NP(S)Ph_2]_2$ is reported. © 1998 Elsevier Science Ltd. All rights reserved

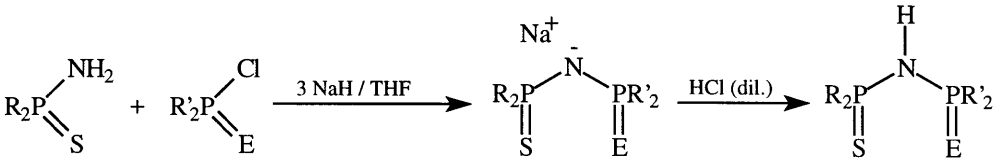

for R = Ph, R' = EtO. R = EtO, R' = Ph. E = S / O

Keywords:

INTRODUCTION

Mixed donor imidophosphinates can be easily prepared and show interesting structural differences.

There is considerable interest in the co-ordination of metals by monoanionic, bidentate ligands. For example, acetylacetonate, *acac*, and its derivatives form a large class of complexes which have been extensively studied [1]. The dithio- and deseleno-imidodiphosphinate ligands $Ph_2P(E)NHP(E)Ph_2$ may be considered to be main group analogues of *acac*. They are readily prepared and offer the opportunity to vary both the donor atoms and the R-group more easily than is the case of acac, and so are amenable to fine tuning for specific metal complexation [2]. A number of complexes of these types of ligands (including variation of phenyl groups for Me and ^{i}Pr) have been described [2–11] though less work has been reported on alkoxy based systems and mixed systems. There has recently been a report on the preparation of a mixed R, R′ system [12] but little work has been reported on mixed donor systems. Here we describe the preparation of $(EtO)_2P(S)NHP(O)Ph_2$ (**1**) and $(EtO)_2P(O)NHP(S)Ph_2$ (**2**). The X-ray structures and some coordination complexes of **1** and **2** are also reported.

EXPERIMENTAL

General

Unless stated otherwise, all reactions were performed under an atmosphere of oxygen-free nitrogen using standard Schlenk procedures. All glassware was

*Author to whom correspondence should be addressed. Tel.: +44-1509-222565; fax: +44-1509-223925; e-mail: j.d.woollins@lboro.ac.uk.

oven dried at 100°C or flame dried under vacuum before use.

All solvents and reagents were purchased from Aldrich, BDH or Fisons and used as received. In addition toluene, thf, Et_2O and petroleum ether (60–80) were distilled from sodium-benzophenone under nitrogen, and CH_2Cl_2 from CaH_2. $CDCl_3$ (99+ atom% D) was as supplied.

^{31}P (36.2, 101.25 MHz) were recorded on JEOL FX90Q, or Bruker AC250 spectrometers. Chemical shifts are reported relative to 85% H_3PO_4. Infra-red spectra were recorded as KBr discs a Perkin Elmer System 2000 FTIR spectrometer. Raman spectra were recorded on Perkin Elmer System 2000 FT spectrometer with a diode pumped Nd/YAG laser. Microanalyses were carried out by the respective microanalytical services of Loughborough University and Zeneca Specialties Research Centre. FAB +ve mass spectra were recorded by the EPSRC mass spectrometry service at Swansea and the mass spectrometry service at the Zeneca Specialties Research Centre.

Syntheses

$Ph_2P(S)Cl$ $Ph_2P(S)Cl$ was formed by refluxing diphenylchlorophosphine (12.30 g, 10.0 ml, 0.053 mol) with sulphur (1.70 g, 0.053 mol) overnight in toluene (30 ml) under N_2. The solvent was removed *in vacuo* off to give a clear oil (13.31 g; $^{31}P–\{^1H\}$ NMR ($CDCl_3$): δ 79.4 ppm).

$Ph_2P(C)NH_2$ $Ph_2P(S)NH_2$ was formed by bubbling NH_3 through a solution of $Ph_2P(S)Cl$ (4.0 g, 15.84 mmol) in ether (100 ml) for 20 min. After filtering the reaction mixture through celite, the filtrate was evaporated to dryness giving a white solid (3.62 g; $^{31}P–\{^1H\}$ NMR ($CDCl_3$): δ 59.7 ppm).

$(EtO)_2P(S)NH_2$ $(EtO)_2P(S)NH_2$ was formed by bubbling ammonia gas through a solution of diethylchlorothiophosphate (24.0 g, 20.0 ml, 0.127 mol) in ether (100 ml) for 20 min. After filtering the reaction mixture through celite, the filtrate was evaporated to dryness to give a clear oil (21.36 g; $^{31}P–\{^1H\}$ NMR ($CDCl_3$): δ 74.2 ppm).

$(EtO)_2P(S)NHP(S)Ph_2$ ***1*** $(EtO)_2P(S)NH_2$ (1.80 g, 10.6 mmol) was dissolved in thf (50 ml) and 3 molar equivalents of NaH (60% dispersion in paraffin oil 1.26 g, 31.2 mmol) was added slowly at 0°C. The mixture was allowed to warm to room temperature and stirred for 30 min, then $Ph_2P(O)Cl$ (2.50 g, 10.6 mmol) was added dropwise at 0°C. The mixture was stirred overnight at room temperature. Methanol (5 ml) was added dropwise to destroy any excess sodium hydride. The mixture was reduced by half under vacuum before 2 M aqueous HCl (50 ml) was added, producing a white precipitate which was extracted with dichloromethane (3×20 ml). The dichloromethane solution was dried over $MgSO_4$ then evaporated to dryness to give a yellow oil which was recrystallised from the minimum of dichloromethane and petroleum ether (40–60) yielding colourless crystals upon cooling (2.87 g, 7.77 mmol, 73.1% yield, mp 84°C). Microanalysis calculated for $C_{16}H_{21}NO_3P_2S$: C 52.0; H 5.7; N 3.8%. Observed: C 52.5; H 5.7; N 3.6%. $^{31}P–\{^1H\}$ NMR ($CDCl_3$): $\delta(P_1)$ 64.1(d), $\delta(P_2)$ 19.7 ppm. $^2J(^{31}P_1–^{31}P_2)$ 17.6 Hz. FTIR (dichloromethane solution, CsI plates at 100 microns): ν(N–H) 3342 cm^{-1}; (KBr disc): ν(N–H) not observed, δ(N–H) 1344; ν(PNP) 936, 913, 787; ν(PO) 1196, 1128; ν(PS) 607 cm^{-1}.

$(EtO)_2P(O)NHP(S)Ph_2$ ***2*** $Ph_2P(S)NH_2$ (3.62 g, 15.54 mmol) was dissolved in thf (50 ml) and 3 molar equivalents of NaH (60% dispersion in paraffin oil, 1.86 g, 46.61 mmol) was added slowly at 0°C. The mixture was allowed to warm to room temperature and stirred for 30 min, then $(EtO)_2P(O)Cl$ (2.68 g, 2.25 ml, 15.54 mmol) was added dropwise at 0°C. The mixture was stirred overnight to destroy any excess sodium hydride. The mixture was reduced by half under vacuum before 2 M aqueous HCl (50 ml) was added, producing a white precipitate which was extracted with dichloromethane (3×20 ml). The dichloromethane solution was dried over $MgSO_4$ then evaporated to dryness to give a yellow oil which was recrystallised from the minimum of dichloromethane yielding colourless crystals upon cooling (4.62 g, 12.52 mmol, 80.6% yield, mp 174°C). Microanalysis calculated for $C_{16}H_{21}NO_3P_2S$: C 52.0; H 5.7; N 3.8%. Observed: C 51.4; H 5.5; N 3.6%. $^{31}P_1–^{31}P_2$) 13.2 Hz. FTIR (dichloromethane solution, CsI plates at 100 microns): ν(N–H) 3334 cm^{-1}; (KBr disc): δ(N–H) 1315; ν(PNP) 754; ν(PO) 1186; ν(PS) 630 cm^{-1}. FT Raman (capillary sample): ν(PO) 1159; ν(PS) 616 cm^{-1}.

$Zn[(EtO)_2P(S)NP(S)Ph_2]_2$ ***3*** A solution of **1** (0.050 g, 0.135 mmol), KO^tBu (0.015 g, 0.134 mmol) and $ZnCl_2$ (0.010 g, 0.073 mmol) in thf (20 ml) was stirred for 1 hour. The mixture was then evaporated to dryness and dichloromethane added. The resulting mixture was filtered and the filtrate evaporated to dryness yielding a colourless oil. Microanalysis calculated for $C_{32}H_{40}N_2O_6P_4S_2Zn$: C 47.9; H 5.0; N 3.5%. Observed: C 46.9; H 4.9; N 3.3%. $^{31}P–\{^1H\}$ NMR ($CDCl_3$): $\delta(P_1)$ 43.4(d), $\delta(P_2)$ 21.6(d) ppm. $^2J(^{31}P_1–^{31}P_2)$ 24.2 Hz. FTIR (KBr disc): ν(PNP) 1262, 1182, 747; ν(PO) 1161, 1127; ν(PS) 562; δ(NPS) 402 cm^{-1}. FAB +ve MS: m/z 801 corresponds to $\{Zn[(EtO)_2P(S)NP(O)Ph_2]_2\}^+$.

$Zn[(EtO)_2P(O)NP(S)Ph_2]_2$ ***4*** A solution of **2** (0.050 g, 0.135 mmol), KO^tBu (0.015 g, 0.134 mmol) and $ZnCl_2$ (0.010 g, 0.073 mmol) in thf (20 ml) was stirred for 1 hour. The mixture was then evaporated to dryness and dichloromethane added which was filtered and the filtrate evaporated to dryness yielding a colourless oil. Microanalysis calculated for $C_{32}H_{40}N_2O_6S_2Zn$: C 47.9; H 5.0; N 3.5%. Observed: C 47.0; H 4.8; N 3.5%. $^{31}P–\{^1H\}$ NMR ($CDCl_3$): $\delta(P_1)$ 5.4(d), $\delta(P_2)$ 35.6(d) ppm. $^2J(^{31}P_1–^{31}P_2)$ 22.0 Hz. FTIR (KBr disc); ν(PO) 1112; ν(PS) 583; δ(NPS)

421 cm^{-1}. FAB +ve MS: *m/z* 801 corresponds to $\{Zn[(EtO)_2P(O)NP(S)Ph_2]_2\}^+$.

Pd$[(EtO)_2P(S)NP(O)Ph_2]_2$ ***5*** $Pd(cod)Cl_2$ (0.019 g, 0.067 mmol) was added to a solution of **1** (0.0.50 g, 0.136 mmol) and KO^{t}Bu (0.0.15 g, 0.134 mmol) in thf (20 ml) and stirred for 1 hour, changing colour from yellow to red/orange. The mixture was then evaporated to dryness and dichloromethane added. After filtration the filtrate was evaporated to dryness giving a dark red oil. Microanalysis calculated for $C_{32}H_{40}N_2O_6P_4S_2Pd$: C 45.6; H 4.8; N 3.3%. Observed: C 45.4; H 5.0; N 3.1%. $^{31}P-\{^1H\}$ NMR ($CDCl_3$): $\delta(P_1)$ 58.6(d), $\delta(P_2)$ 21.8(d) ppm. $^2J(^{31}P_1-^{31}P_2)$ 13.4 Hz. FTIR (KBr disc): *v*(PNP) 1240; *v*(PO) 1126; *v*(PS) 547 cm^{-1}. FAB +ve MS: *m/z* 843 corresponds to $\{Pd[(EtO)_2P(S)NP(O)Ph_2]_2\}^+$.

Pt$[(EtO)_2P(S)NP(O)Ph_2]_2$ ***6*** $Pt(cod)Cl_2$ (0.020 g, 0.053 mmol) was added to a solution of **1** (0.039 g, 0.106 mmol) and KO^{t}Bu (0.012 g, 0.107 mmol) in thf (20 ml) and refluxed for 1 hour, changing colour from colourless to a yellow solution. The mixture was then evaporated to dryness and dichloromethane added. After filtration the filtrate was evaporated to dryness giving a yellow oil. Microanalysis calculated for $C_{32}H_{40}N_2O_6P_4S_2Pt$: C 41.3; H 4.3; N 3.0%. Observed: C 41.9; H 4.3; N 2.6%. $^{31}P-\{^1H\}$ NMR ($CDCl_3$): $\delta(P_1)$ 65.3(d), $\delta(P_2)$ 19.7(d) ppm. $^2J(^{31}P_1-^{31}P_2)$ 18.7 Hz. No $^2J(^{31}P-^{195}Pt)$ coupling was observed that could confidently be assigned or calculated. FTIR (KBr disc): *v*(PNP) 1259, 1161; *v*(PO) 1125; *v*(PS) 548 cm^{-1}. FAB +ve MS: *m/z* 932 corresponds to $\{Pt[(EtO)_2P(S)NP(O)Ph_2]_2\}^+$.

Pd$[(EtO)_2P(O)NP(S)Ph_2]_2$ ***7*** $Pd(cod)Cl_2$ (0.019 g, 0.067 mmol) was added to a solution of **2** (0.050 g, 0.136 mmol) and KO^{t}Bu (0.015 g, 0.134 mmol) in thf (20 ml) and stirred for 1 hour, changing colour from yellow to red/orange. The mixture was then evaporated to dryness and dichloromethane added. The mixture was filtered and the filtrate evaporated to dryness giving a dark red oil. Microanalysis calculated for $C_{32}H_{40}N_2O_6P_4S_2Pd$: C 45.6; H 4.8; N 3.3%. Observed: C 45.4; H 4.9; N 3.1%. $^{31}P-\{^1H\}$ NMR ($CDCl_3$). Two sets of AX spectra. $\delta(P_1)$ 3.9(d), $\delta(P_2)$ 28.4(d) ppm. $^2J(^{31}P_1-^{31}P_2)$ 24.5 Hz. $\delta(P_{A2})$ 3.6(d), $\delta(P_{X2})$ 27.4(d) ppm. $^2J(^{31}P_{A2}-^{31}P_{X2})$ 29.7 Hz. FTIR (KBr disc): *v*(PNP) 1231, 1165; *v*(PO) 1112; *v*(PS) 570 cm^{-1}. FAB +ve MS: *m/z* 843 corresponds to $\{Pd[(EtO)_2P(O)NP(S)Ph_2]_2\}^+$.

Pt$[(EtO)_2P(O)NP(S)Ph_2]_2$ ***8*** $Pt(cod)Cl_2$ (0.020 g, 0.053 mmol) was added to a solution of **2** (0.039 g, 0.106 mmol) and KO^{t}Bu (0.012 g, 0.107 mmol) in thf (20 ml) and stirred for 1 hour, changing colour from colourless to a yellow solution. The mixture was then evaporated to dryness and dichloromethane added. The mixture was filtered and the filtrate evaporated to dryness giving a yellow oil. Microanalysis calculated for $C_{32}H_{40}N_2O_6P_4S_2Pt$: C 41.3; H 4.3; N 3.0%. Observed: C 41.9; H 4.5; N 2.5%. $^{31}P-\{^1H\}$ NMR ($CDCl_3$): $\delta(P_1)$ 0.4(d), $\delta(P_2)$ 24.9(d) ppm. $^2J(^{31}P_1-^{31}P_2)$ 23.4 Hz. No $^2J(^{31}P-^{195}Pt)$ coupling was observed that could confidently be assigned or calculated. FTIR (KBr disc): *v*(PNP) 1240, 1164; *v*(PO) 1181; *v*(PS) 551 cm^{-1}. FAB +ve MS: *m/z* 932 corresponds to $\{Pt[(EtO)_2P(O)NP(S)Ph_2]_2\}^+$.

Crystallography

Details of crystallographic parameters are summarised in Table 1. Crystals were mounted on quartz fibres using araldite. Data were collected using Cu–Kα radiation and ω scans at room temperature with a Rigaku AFC7S diffractometer. Intensities were corrected for Lorentz-polarisation and for absorption. In **1** there are two independent molecules, one of which exhibits some slight disorder in the positions of the oxygen and its adjacent carbon atom in one of the ethoxy groups; the disorder was resolved into two sites (occupancies 70/30) and the lower occupancy sites were refined isotropically. The remaining non-H atoms were refined anisotropically. The positions of the C–H hydrogen atoms were idealised whilst the N–H atoms were allowed to refine isotropically. Refinements were by full matrix least squares based on *F* using teXsan [13]. The weighting scheme is as previously reported [3].

RESULTS AND DISCUSSION

The synthesis of **1** and **2** are based upon a literature preparation [14] for compounds with mixed substituent groups. The amine and halide are "clipped"

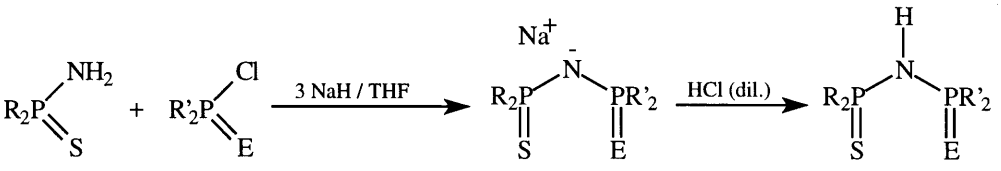

for R = Ph, R' = EtO. R = EtO, R' = Ph. E = S / O

together with sodium hydride in thf. Silvestru and coworkers recently reported [12] the use of BuLi for this reaction but we have found that NaH is more convenient, less costly and allows for the reactions to be more readily scaled up. It should be noted that (in contrast to S,S systems) the mixed S/O compounds are unstable to heat. Characteristic bands [11] were observed in the FTIR, ν(NH) *ca.* 3300, δ(NH) 1344–1315, ν(PO) 1196–1186, ν(PNP) 976–936, 787–754 and ν(PS) 646–630 cm^{-1}.

The ^{31}P NMR spectra ($CDCl_3$, Table 2) are of the AX type. As expected the δ values of the $R_2P(S)$ part of **1** and **2** are quite close to those of the starting amines. Furthermore changing P═S for P═O results in a shift to lower frequency (as is the case in EPR_3 systems) though this is far more pronounced for the EtO substituted phosphorus than for the Ph substituted phosphorus atom. The larger differences seen in the case of **2** may be due to the greater electron withdrawing effect of the EtO group or it may reflect some difference in the tautomeric form in solution. Another noticeable difference between **1** and **2** is in the magnitude of the $^2J(^{31}P–^{31}P)$ coupling which is considerably less in **2** and this may relate to the P–N–P angle which is smaller (and closer to trigonal) in the crystal structure of **1**.

In the solid state structure of **1** there are two crystallographically independent molecules. In both of these the P═S and P═O groups are in a *gauche* or *cisoid* orientation (Figure 1, Table 3) with SP...PO torsion angles of 79.5 and -69° (i.e. the P═O and P═S groups are rotated in opposite directions in the two crystallographically independent molecules). The molecules form a hydrogen bonded chain similar to that observed in ($^iPR_2P(S)NHP(S)^iPr$ [11]. On electronic grounds the hydrogen bonding is through the oxygen but the factors that favour chain rather than dimer formation (as was the case in $Ph_2P(S)NHP(S)Ph_2$) are not obvious. The P(2)–S(1) bond lengths at 1.895(3)/1.921(2) Å are slightly shorter than previously observed P–S bonds [2] and the P(2)–N(1) bond length average value of 1.66 A is normal for these type of systems. The P(1)–O(1) bond lengths are 1.476(3)/1.484(3) Å and the P–N–P angles are 122.6(2) and 127.2(2)°; the former angle is the smallest P–N–P angle observed by us for any imidodiphosphinate. As mentioned above the molecules pack into chains with the two molecules in the asymmetric unit alternating throughout the chain length; the details of the H-bonding in the chain are given in Table 3.

2 was found to be a typical *trans* dimer (Figure 2, Table 3) with an SP...PO torsion angle of 172.3°. As expected on both steric and electronic grounds the hydrogen bonding contact to form the dimer is thorough the P═O oxygen atoms, with the phenyls substituents on the pendant phosphorus. The P(1)–S(1) bond length is 1.931(1) Å and the P(2)–O(1) bond length is 1.475(2) Å. The P(2)–N(1) bond length of

Table 1. Details of the X-ray crystal structure data collections and refinements

	$(EtO)_2P(S)NHP(O)Ph_2$ (**1**)	$(EtO)_2P(O)NHP(S)Ph_2$ (**2**)	$Zn[(EtO)_2P(O)NP(S)Ph_2]_2$ (**4**)
Empirical formula	$C_{16}H_{21}NO_3P_2S$	$C_{16}H_{21}NO_3P_2S$	$C_{32}H_{40}O_6P_4S_2N_2Zn$
M	369.35	369.35	802.07
Crystal colour, habit	clear, block	clear, block	clear, block
Crystal dimensions/mm	$0.15\times0.15\times0.40$	$0.26\times0.30\times0.32$	$0.10\times0.10\times0.33$
Space group	P-1 (#2)	$P2_1/n$ (#14)	$C2/c$ (#15)
a (Å)	10.196(4)	9.275(3)	19.614(4)
b (Å)	19.301(2)	8.688(3)	10.468(1)
c (Å)	10.080(1)	23.438(2)	19.780(2)
α (°)	102.93(1)	90	90
β (°)	98.40(2)	98.54(1)	108.32(1)
γ (°)	83.25(2)	90	90
U (Å^3)	1905.4(8)	1867.8(8)	3855.6(9)
D_c (g cm^{-3})	1.287	1.313	1.382
μ (mm^{-1})	3.2	3.3	3.8
2θ max (°)	110.2	120.1	120.1
F(000)	776.00	776.00	1664.00
Measured reflections	5168	3205	3161
Independent reflections (R_{int})	4800 (0.064)	2999 (0.093)	3058 (0.122)
Observed reflections [$I>3.0\sigma(I)$]	3717	2232	2322
Reflection/parameter ratio	8.77	10.68	10.85
Minimum/maximum transmission	0.68/1.00	0.80/1.00	0.67/1.00
Final R,R'	0.057, 0.050	0.043, 0.043	0.044, 0.039
Maximum Δ/σ	0.58	0.06	0.28
Largest difference peak hole/eÅ^{-3}	0.30	0.35	0.31

Table 2. ^{31}P NMR ($CDCl_3$) for **1**–**8**. P_1 denotes the ethoxy and P_2 denotes the phenyl substituted phosphorus atoms

	δ (ppm)		$^2J(^{31}P–^{31}P)$ (Hz)
	P_1	P_2	$[P_1–P_2]$
$(EtO)_2P(S)NHP(O)Ph_2$ **1**	64.1	19.7	17.6
$(EtO)_2P(O)NHP(S)Ph_2$ **2**	0.1	53.3	13.2
$Zn[(EtO)_2P(S)NP(O)Ph_2]_2$ **3**	43.4	21.6	24.2
$Zn[(EtO)_2P(O)NP(S)Ph_2]_2$ **4**	5.4	35.6	22.0
$Pd[(EtO)_2P(S)NP(O)Ph_2]_2$ **5**	58.6	21.8	13.4
$Pt[(EtO)_2P(S)NP(O)Ph_2]_2$ **6**	65.3	19.7	18.7
$Pd[(EtO)_2P(O)NP(S)Ph_2]_2$ **7**[a]	3.9	27.4	24.5
$Pt[(EtO)_2P(O)NP(S)Ph_2]_2$ **8**	0.4	24.9	23.4

[a] In addition there was another AX type spectrum, δ 28.4, 3.6 $^2J(^{31}P–^{31}P)$ 29.7 Hz.

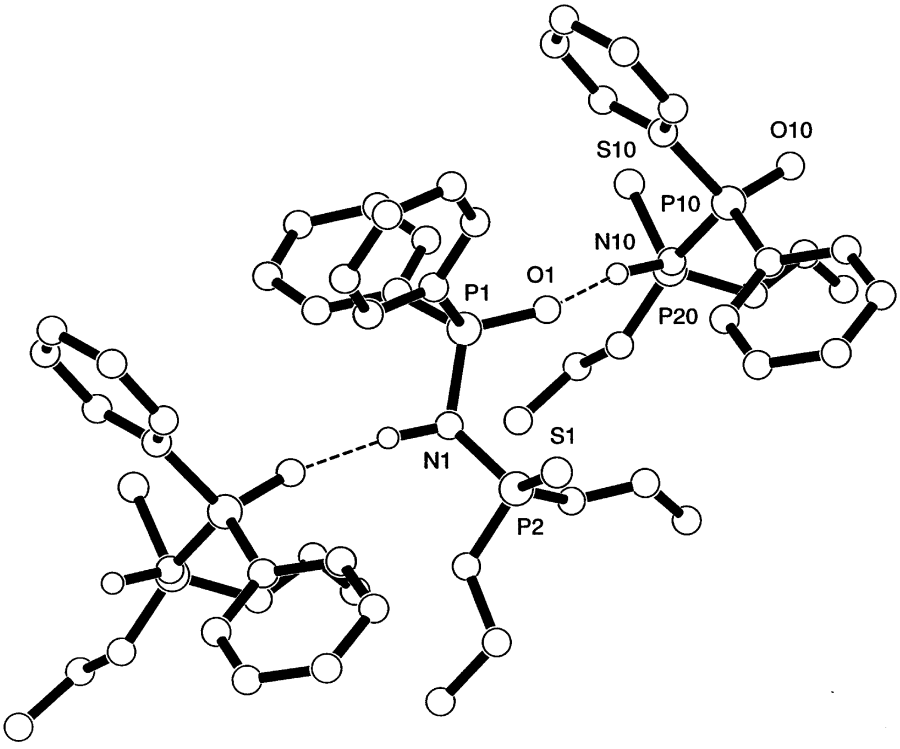

Fig. 1. The solid state structure of $(EtO)_2P(S)NHP(O)Ph_2$ **1** showing the H-bonded chain structure.

1.632(3) Å is short compared to the P(1)–N(1) length of 1.679(3) Å and suggests that there may be some degree of localisation — this would be in accord with the ^{31}P NMR observations mentioned above. As one would expect from the P═O...P═S torsion angle, the molecules in **2** pack into dimer pairs via N–H...O–H-bonds.

It is interesting to note (Table 3) how short the P–S bond length is for **1** (1.90 Å) in comparison to those for the other compounds (*ca.* 1.94 Å) and this can be rationalised as a consequence of the electron withdrawing ethoxy groups. Further support for this argument is that the shortest P–O bonds are observed in **2**. The varying S–P...P–E torsion angles in these types of system cannot be readily explained by steric effects alone, both $(EtO)_2P(S)NHP(S)Ph_2$ and **2** contain phenyl substituted phosphorus with a sulphur donor atom, yet their torsion angles are 87.0 and 172.3° in contrast to the angle of 79.5 and −69° for **1**. Further MO and molecular modelling studies are in progress.

Table 3. Selected bond lengths (Å) and angles (°) for $(EtO)_2P(S)NHP(S)Ph_2$ $(EtO)_2P(O)NHP(S)Ph_2$ **1** and $(EtO)_2P(S)NHP(O)Ph_2$ (**1** contains two crystallographically independent molecules)

	$(EtO)_2P(S)NHP(S)Ph_2$	**1** $(EtO)_2P(S)NHP(O)Ph_2$		**2** $(EtO)_2P(O)NHP(S)Ph_2$
S–P(1)	1.937(1)	–		1.931(1)
S–P(2)	1.920(2)	1.895(3)	1.921(2)	–
O(1)–P(1)	–	1.476(3)	1.484(3)	–
O(1)–P(2)	–	–		1.457(2)
P(1)–N(1)	1.681(3)	1.673(4)	1.661(4)	1.679(3)
P(2)–N(1)	1.667(3)	1.662(4)	1.653(3)	1.632(3)
P(1)–N(1)–P(2)	129.9(2)	122.6(2)	127.2(2)	130.5(1)
S–P...P–E	87.0	79.5	−69	172.3
H...O		H(1*n*)...O(10) 1.73; H(1O*n*)...O(1) 1.60		1.88
O...N		N(1)...O(10*) 2.79; N(10)...O(1) 2.72		2.80
N–H...O		N(1)–H(1*n*)...O(10*) 172; N(10)–H(10*n*)...O(1) 168		175

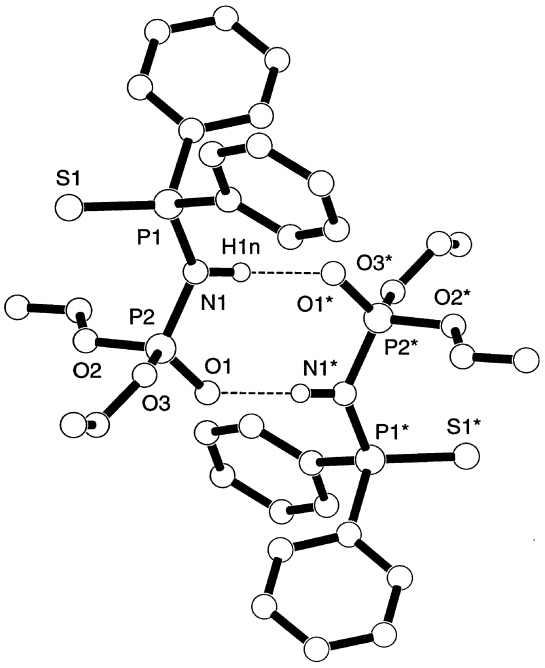

Fig. 2. The solid state structure of $(EtO)_2P(O)NHP(S)Ph_2$ **2** showing the H-bonded dimer.

One mole of zinc chloride and two moles of KO^{t}Bu were stirred at room temperature with two moles of **1** or **2** in thf. The solvent was then evaporated off, dichloromethane added and the mixture was filtered. The filtrate was evaporated to dryness yielding in each case an opaque white oil. For $Zn[(EtO)_2P(O)NP(S)Ph_2]_2$ (**4**) the oil yielded a small amount of crystals from the minimum of dichloromethane at −10°C which were subsequently studied by single crystal analysis. All complexes gave reasonable elemental analyses and the FAB +ve mass spectra revealed the expected parent ions for **3** $Zn[(EtO)_2P(S)NP(O)Ph_2]_2$. Characteristic bands were observed in the FTIR. Again the characteristic shifts in the ν(PNP) vibration from around 950 to 1239–1262 cm^{-1}, the ν(PO) band from around 1190 to 1050 cm^{-1} and the ν(PS) vibration from 640 to 552–583 cm^{-1} all signify the change in bond order within the ligand due to the delocalisation of the negative charge (Table 4).

The ^{31}P NMR Table 2 are of the AX type. The shift of the ethoxy substituted phosphorus of **4** increases by 5 ppm upon coordination/deprotonation. Furthermore the ^{2}J phosphorus coupling in **4** increases by 9 Hz relative to **2**. In contrast the shift of the phenyl substituted phosphorus of **3** has increased by only 1 ppm and the ^{2}J phosphorus coupling increases by 6.5 Hz.

The X-Ray structure of **4** (Figure 3) reveals the expected tetrahedral coordination at zinc (the zinc atom lies on a crystallographic twofold axes and the molecule has crystallographic twofold symmetry). The P–S and P–O bonds lengthen and the P–N bonds shorten upon deprotonation/coordination (as expected from the increase in the frequency of the ν(PNP) vibration in the FTIR). The Zn–S bond is *ca.* 0.025 Å shorter for **4** than for $Zn(^iPr_2P(S)NP(S)iPr_2)_2$ [11] whilst the S–P–N angles compare well. The S–P–N and O–P–N angles for **4** are equal to each other whilst the P–N–P angle increased by 4° upon coordination. The Zn–S–P angle is 98.0(1)°, unexpectedly low for this type of ring in a tetrahedral complex, [9° less than the analogous angle is in $Zn(^iPr_2P(S)NP(S)iPr_2)_2$]. Such a small angle has only previously been observed for square planar complexes with an MS_2P_2N ring in the "chair" conformation. In contrast the Zn–O–P angle at 129.0(2)° is very large. The six-membered ring is folded, with the Zn–P(1)–

Table 4. Selected bond lengths (Å) and angles (°) for $Zn[(EtO)_2P(O)NHP(S)Ph_2]_2$ **4** and $Zn(^iPr_2P(S)NP(S)iPr_2)_2$ [11] (this latter compound is in the space group $I4_1/a$

	4 $Zn[(EtO)_2P(O)NP(S)Ph_2]_2$	$Zn(^iPr_2P(S)NP(S)iPr_2)_2$ [11]
P(1)–S(1)	2.013(2)	2.032(1)
P(2)–O(1)	1.479(3)	
P(1)–N(1)	1.579(3)	1.581(2)
P(2)–N(1)	1.551(3)	
Zn–S(1)	2.318(1)	2.345(1)
Zn–O(1)	1.946(3)	
S(1)–P(1)–N(1)	118.4(1)	118.5(1)
O(1)–P(2)–N(1)	118.5(2)	
P(1)–N(1)–P(2)	134.1(2)	140.5(3)
S(1)–Zn–O(1)	107.5(1)	
S(1)–Zn–O(1*)	109.5(1)	
O(1)–Zn–O(1*)	104.7(2)	
S(1)–Zn–S(1*)	117.4(1)	108.0(1)
Zn–S(1)–P(1)	98.0(1)	107.1(1)
Zn–O(1)–P(2)	129.0(2)	

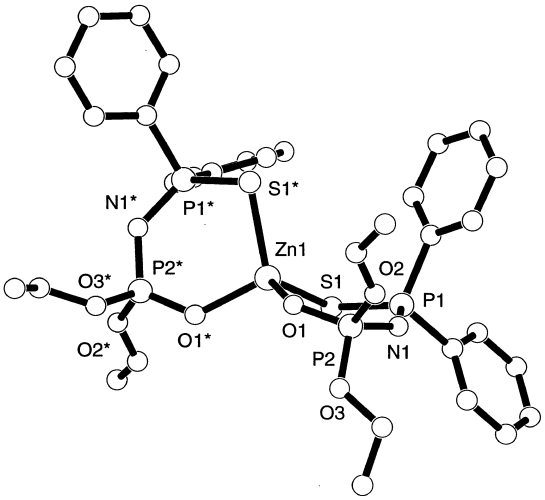

Fig. 3. Solid state structure of $Zn[(EtO)_2P(O)NP(S)Ph_2]_2$ **4**.

S(1) plane being inclined by 33° to the Zn–P(1)–N(1)–P(2)–O(1) plane [max deviation from this plane is 0.05 A for N(1)] and unlike most previous examples is not readily categorised as "chair" or "boat".

One mole of $M(cod)Cl_2$ (M = Pd, Pt) and two moles of KO^tBu were stirred at room temperature with two moles of **1** or **2** in thf. The solvent was then evaporated off and after the addition of dichloromethane the mixture was filtered. The filtrate was evaporated to dryness yielding deep red oils for the palladium complexes and yellow oils for the platinum complexes. Satisfactory elemental analyses were observed for all complexes and expected parent ions in the FAB +ve mass spectra were observed for the palladium complexes $Pd[(EtO)_2P(S)NP(O)Ph_2]_2$ (**5**) and $Pd[(EtO)_2P(O)NP(S)Ph_2]_2$ (**7**) at 843 m/z, and the platinum complexes $Pt[(EtO)_2P(S)NP(O)Ph_2]_2$ (**6**) and $Pt[(EtO)_2P(O)NP(S)Ph_2]_2$ (**8**) at 932 m/z. Bands observed in the FTIR for ν(PNP) were 1206–1259 cm^{-1}, ν(PS) were 539–570 cm^{-1}. The ^{31}P NMR of **5**–**8** are of the simple AX type and the chemical shifts follow the pattern seen in **3** and **4** except in the case of **7** which contains two AX spectra. Possible structures are shown in Fig. 4; the most likely explanation is the presence of *cis* and *trans* isomers of the square planar complex. However we cannot exclude a "chair"/"boat" equilibrium of the PdS_2P_2N rings or the possibility that coordination occurs through the sulphur and nitrogen atoms Fig. 4, similar to the reported palladium complex $Pd[(PhO)_2P(S)NP(O)(OPh)_2]_2$ [15].

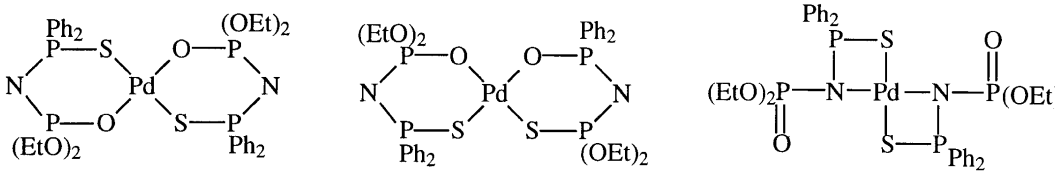

Fig. 4. Possible structures for $Pd[(EtO)_2P(O)NP(S)Ph_2]_2$.

REFERENCES

1. See, for example; Katoh, M., Miki, K., Tanaka, N. and Kasai, N., *Bull. Chem. Soc. Jpn.*, 1981, 54, 611.
2. Woollins, J. D., *J. Chem. Soc., Dalton Trans.*, 1996, 2893.
3. Bhattacharyya, P., Novosad, J., Phillips, J., Williams, D. J. and Woollins, J. D., *J. Chem. Soc., Dalton Trans.* , 1995, 1607.
4. Bhattacharyya, P., Slawin, A. M. Z., Smith, M. B. and Woollins, J. D., *Inorg. Chem.*, 1996, **35,** 3675.
5. Nouaman, M., Zak, Z., Herrmann, E. and Navratil, O., *Z. Anorg. Allg. Chem.*, 1993, **619,** 1147.
6. Cea-Olivares, R. and Noth, H., *Z. Naturforsch.*, 1987, **42B,** 1507.
7. Slawin, A. M. Z., Ward, J., Williams, D. J. and Woollins, J. D., *J. Chem. Soc. Chem. Commun.*, 1994, 421.
8. Cea-Oliveras, R., Novosad, J., Slawin, A. M. Z., Woollins, J. D., Garcia-Montalvo, V., Espinosa-Perez, G. and Garcia, P. G. Y., *J. Chem. Soc. Chem. Commun.*, 1996, 519.
9. Garcia-Montalvo, V., Novosad, J., Kilian, P., Woollins, J. D., Slawin, A. M. Z., Garcia, P. G. Y., Lopez-Cardoso, M., Espinosa-Perez, G. and Cea-Olivares, R., *J. Chem. Soc. Dalton Trans.*, 1997, 1025.
10. Silvestru, C., Rosler, R., Haiduc, I., Cea-Olivares, R. and Espinosa-Perez, G., *Inorg. Chem.*, 1995, **34,** 3352.
11. Cupertino, D., Keyte, R. W., Slawin, A. M. Z., Williams, D. J. and Woollins, J. D., *Inorg. Chem.*, 1996, **35,** 2695.
12. Silvestru, C., Rosler, R., Drake, J. E., Yang, J., Espinosa-Perez, G. and Haiduc, I., *J. Chem. Soc. Dalton Trans.*, 1998, 73.
13. teXsan: Crystal Structure Analysis Package, Molecular Structure Corporation (1985 and 1992).
14. Meznick, L. and Marecek, A., *Z. Chem.*, 1981, **8,** 294.
15. Navratil, O., Herrmann, E., Grossmann, G. and Teply, J., *Collect. Czech. Chem. Commun.*, 1990, **55,** 364.

Pergamon

Polyhedron Vol. 17, No. 23–24, pp. 4227–4235, 1998
© 1998 Elsevier Science Ltd
All rights reserved. Printed in Great Britain
0277–5387/98 $19.00+0.00

PII: S0277-5387(98)00233-2

EPR characterisation of nickel(III) complexes with N_2O_2 Schiff base ligands derived from naphthaldehyde and their pyridine adducts

Cristina Freire and Baltazar de Castro*

CEQUP/Departamento de Química, Faculdade de Ciências, Universidade do Porto, 4150 Porto, Portugal

(Received 30 April 1998; accepted 8 June 1998)

Abstract—Nickel(II) complexes with quadridentate N_2O_2 Schiff base ligands derived from naphthaldehyde have been synthesised and their oxidative chemistry was studied in *N*,*N*′-dimethylformamide and in dimethylsulfoxide. Electrochemical and EPR data for the oxidised solutions have revealed that in these strong co-ordinating solvents, only the complexes with aliphatic imine bridges were oxidised to low spin six-coordinate nickel(III) complexes, in a $^2A_1(d_{z^2})$ ground state, formulated as $[Ni(III)(L)\cdot S_2]^+$, where S stands for a solvent molecule. Upon addition of pyridine to fluid solutions of $[Ni(III)(L)\cdot S_2]^+$, new species were formed that on the basis of their EPR spectra can be formulated as $[Ni(III)(L)\cdot py_2]^+$. Extensive electronic characterisation of the Ni(III) compounds was made by coupling EPR and electronic spectroscopic data. © 1998 Elsevier Science Ltd. All rights reserved

Keywords: nickel(II); nickel(III); Schiff base complexes; oxidative chemistry; EPR

INTRODUCTION

High and low valent nickel chemistry has attracted increased attention as it has become clear that these oxidation states are biologically significant [1–3] and their complexes may also be used as catalysts in several redox reactions [4–8]. We have been interested in the study of nickel(I) and (III) complexes with polydentate ligands with mixed co-ordination spheres [9–16], the main purposes of the ongoing work centres on the identification of the factors that control the oxidation/reduction site in these complexes, the determination of their redox potentials and the characterisation of their electronic structure.

Nickel(II) complexes with quadridentate N_2O_2 Schiff base ligands have been know for a long time [17] and our interest in the chemistry and reactivity of their +3 oxidation state has led us to perform a systematic investigation on their oxidative chemistry. In a previous paper we reported the redox properties and electronic characterisation of a series of nickel(II) complexes with salicylaldehyde based ligands [9]. We have now extended this study to a group of nickel(II) complexes with Schiff base ligands derived from naphthaldehyde, in order to assess the contribution of unsaturation in the aldehyde moiety to the strength of equatorial/axial ligand fields, and to the stabilisation of the +3 oxidation state for nickel.

In the present work we report the preparation of nickel(II) complexes with ligands derived from naphthaldehyde with aromatic imine bridges, and on the oxidative chemistry of these and similar complexes with aliphatic amine bridges studies in *N*,*N*′-dimethylformamide and dimethylsulfoxide; the complexes were oxidised by controlled potential electrolysis and their pyridine adducts were also prepared. Extensive electronic characterisation of the Ni(III) species was obtained by coupling EPR and electronic spectroscopic data and the results are compared with those for similar complexes with ligands derived from salicylaldehyde [9] (Scheme 1).

RESULTS AND DISCUSSION

Structural and electronic structure for nickel(II) complexes

The X-ray structure and electronic characterisation, in nujol and Me_2SO, of the complexes [Ni(napen)]

* Author to whom correspondence should be addressed. Fax.: +351-2-608-2959; E-mail: bcastro@fc.up.pt.

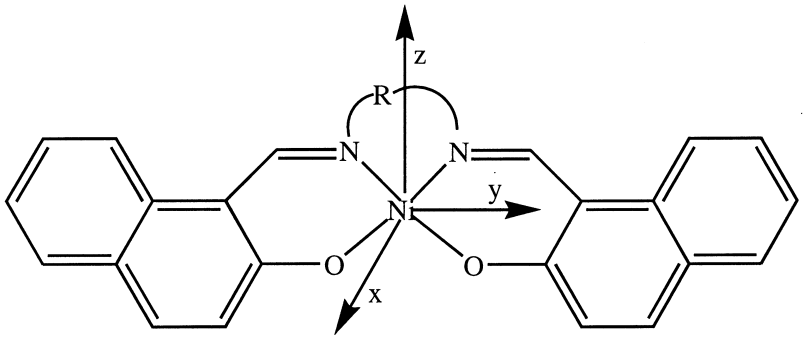

R= $(CH_2)_2$	(1)	[Ni(napen)]
R=C $(CH_2)_2$C $(CH_2)_2$	(2)	[Ni(naptMe)]
R=$(CH_2)_3$	(3)	[Ni(nappd)]
R=Ph	(4)	[Ni(napoph)])
R=4,5-Cl_2Ph	(5)	[Ni(napophCl_2)]

Scheme 1.

[11, 18], [Ni(nappd)] [11, 19] and [Ni(naptMe)] [11] have already been published and the results are included to provide a coherent framework for the overall study reported here. The co-ordination geometry around the metal atom is square planar, with the ligand bound through the nitrogen and oxygen atoms in a N_2O_2 *cis*-configuration. The coordination sphere is unchanged in Me_2SO for [Ni(napen)] and [Ni(naptMe)], but incipient axial co-ordination of solvent molecules occurs for [Ni(nappd)] upon solubilization, as suggested by the bathochromic shift observed for the *d–d* bands [11]. Electronic spectra of [Ni(napen)] and [Ni(naptMe)] in DMF are similar to those in Me_2SO and also suggest the invariance of their structure in this solvent, but for [Ni(nappd)] a similar shift of the band maxima is observed, implying that incipient axial co-ordination also occurs in DMF.

No crystals of diffractometric quality could be obtained for [Ni(napph)] and [Ni(napphCl_2)]; however, we propose a square planar sphere in solid and in solution for these complexes, as for the ones with salicylaldehyde based ligands on the basis of the similar absorption spectra [11, 12, 20].

Spectra of all complexes, in both solvents and in the solid, show several very intense bands at low wavelengths that are assigned to charge transfer transitions [21–23]. Those of complexes with aliphatic bridges show also a weaker band 530–600 nm, that is assigned to the unresolved transitions from the four low-lying d orbitals to the empty d_{xy} orbital [21–23]. This latter band is not observed for complexes with aromatic bridges, as it is masked by the high intensity charge transfer transitions that, due to the larger planar π-system of the ligands, occur at longer wavelengths.

The energy of the *d–d* transitions can provide a rough estimate of ligand field strength, since one of the electronic transitions comprised in the band envelope is $d_{xy} \leftarrow d_{x^2-y^2}$ and the energy associated with this transition is 10 Dq-C [21–23]. Analysis of the energy of *d–d* transitions for complexes with aliphatic bridges, shows that an increase in the number of bridging carbon atoms is associated with a decrease in ligand field. In this context, as [Ni(nappd)] has the largest Ni–N and Ni–O distances of all structures, the weaker equatorial ligand field must be responsible for the axial co-ordination of solvent molecules.

As the energies of *d–d* transitions are similar to those of the homologous complexes with ligands derived from salicylaldehyde [9], the ligand field for both type of complexes is of the same magnitude. However, charge transfer bands occur at longer wavelengths for the complexes reported in this work, a consequence of the replacement of the salicylaldehyde by the naphthaldehyde moiety.

Cyclic voltammetry of nickel(II) complexes

In Table 1 is summarised the electrochemical data for all complexes, including those for [Ni(napen)], [Ni(naptMe)] and [Ni(nappd)] in Me_2SO, which have been published previously [11]. In both solvents, [Ni(napph)] is irreversibly oxidised and [Ni(napphCl_2)] does not show any charge transfer process within the potential range studied; no further studies were pursued with these complexes. The other compounds exhibit in DMF one oxidation process in the potential window studied, with $E_{1/2}$ (vs Ag/AgCl) varying from 0.78 to 0.95 V. With increasing scan rate

Table 1. Cyclic voltammetric results for nickel(II) complexes in DMF and Me_2SO (0.1 mol dm^{-3} TEAP) at 25°C[a]

Complex	In DMF						In Me_2SO					
	Ag/AgCl (1 mol dm^{-3} NaCl)				Fc^+/Fc		Ag/AgCl (1 mol dm^{-3} NaCl)				Fc^+/Fc	
	E_{pa}	E_{pc}	ΔE	$E_{1/2}$	$E_{1/2}$	i_{pc}/i_{pa}[b]	E_{pa}	E_{pc}	ΔE	$E_{1/2}$	$E_{1/2}$	i_{pc}/i_{pa}[b]
[Ni(napen)][c]	0.91	0.79	0.12	0.85	0.38	1.00	0.84	0.72	0.12	0.79	0.23	0.97
[Ni(nappd)][c]	0.83	0.73	0.12	0.78	0.31	0.90	0.69	0.56	0.13	0.63	0.15	1.00
[Ni(naptMe)][c]	1.00	0.90	0.1	0.945	0.48	0.95	0.95	0.85	0.10	0.90	0.42	0.94
[Ni(napoph)]	1.03	[d]					1.07	[d]				
[Ni(napophCl_2)]	[e]						[e]					

[a] All potentials in V. Solute concentration $\approx 10^{-3}$ mol dm^{-3}; scan rate = 0.05 V s^{-1}; E_{pa} and E_{pc} are the anodic and the cathodic peak potentials, respectively; $\Delta E = E_{pa} - E_{pc}$; $E_{1/2} = 1/2(E_{pa} + E_{pc})$. Under the conditions used, $E_{1/2}$ (Fc^+/Fc) is 0.50 V in DMF and 0.48 V in Me_2SO.

[b] The ratio i_{pc}/i_{pa} in DMF decreases for scan rates lower than 0.04 V s^{-1}, while in Me_2SO this behavior is observed only for scan rates lower than 0.01 V s^{-1}.

[c] Data in Me_2SO from Ref. [11].

[d] Cyclic voltammograms do not show the corresponding cathodic wave.

[e] No electrochemical processes were detected in the potential range used.

(v) a linear dependence is observed between i_p and $v^{1/2}$ and between E_p and i_p; moreover, the anodic–cathodic peak potential separation [ΔE(DMF) = 0.10–0.12 V] is similar to that observed for the couple Fc^+/Fc, for which a diffusion controlled one electron reversible process is assumed. Furthermore, the ratio i_{pc}/i_{pa} is scan rate dependent and reaches values near 1 only for scan rates faster than 0.04 V s^{-1}.

Electrochemical data in DMF is consistent with the one electron reversible oxidation process Ni(II)→ Ni(III) (see below), which is followed by a chemical decomposition path of the electrogenerated Ni(III) species [24], as has been observed in Me_2SO [11, 13]. However, in DMF the decomposition rates of oxidised species are faster than in Me_2SO, as supported by the observation that the ratio i_{pc}/i_{pa} approaches 1 only for scan rates faster than in Me_2SO.

Dependence of redox potentials on the solvent As has been found for salicylaldehyde related complexes [9, 10], redox potentials show a cathodic shift with an increase in the donor capacity of the solvent, due to the co-ordination of solvent molecules that occurs concomitantly with oxidation of the square planar Ni(II) complexes. The cathodic shift in the redox potentials on going from DMF to Me_2SO is thus attributed to stronger axial bonds that are established between nickel(III) and the molecules of the better donor and this helps to stabilise the high oxidation state of the metal (see below).

Dependence of redox potentials on the ligand For complexes with aliphatic imine bridges no significant differences are observed between $E_{1/2}$ for complexes derived from naphthaldehyde and salicylaldehyde, implying that the change of the aldehyde moiety apparently does not induce great changes in the metal electronic density. However, when the imine bridge is aromatic, the electrochemical behaviour changes significantly: complexes with ligands derived from naphthaldehyde do not show any reversible oxidation process, in contrast with their related *saloph* derivatives [9]. This behaviour can be accounted for by invoking larger π delocalization in the former complexes that would (i) ease electron-density delocalisation from the metal to the ligand and (ii) impart higher rigidity to the planar four-dentate ligand system, thus hindering a contraction of the hole cavity, and making it harder to oxidise the metal ion [25–28].

Introduction of methyl groups in the imine bridge, produces an anodic shift in the redox potential relative to that of [Ni(napen)] as was observed in the homologous compounds derived from salicylaldehyde [9]. Based on X-ray data obtained for [Ni(naptMe)] this observation is consistent with the interpretation that steric hindrance on axial binding sites, imposed by the axially oriented methyl groups of the imine bridge, decreases stabilisation of Ni(III) by co-ordinated solvent molecules [11, 29].

Electronic data for [Ni(nappd)] indicate incipient axial co-ordination of solvent molecules takes place and accordingly the low $E_{1/2}$ values for this complex can be explained by invoking its greater tendency to bind axial solvent molecules in the +2 oxidation state, thus facilitating the oxidation process/formation of six-coordinate Ni(III) complexes.

EPR spectra of electrogenerated nickel species and pyridine adducts

Electrochemical oxidation of the Ni(II) complexes produces a change in solution colour from reddish to dark brown, implying formation of new species. EPR

spectra of fluid electrolysed solutions exhibit a single broad line, with g_{iso} in the range 2.197–2.210 in DMF and 2.182–2.192 in Me_2SO, an indication of a metal-centred oxidation process and consequently of the presence of Ni(III) species in solution. Oxidised complex solutions decay, at room temperature, to EPR silent solutions; the decomposition rates are dependent on the ligand, but are always faster in DMF (half-lives of ≈ 7 min) than in Me_2SO (half-lives up to 30 min). The decay in DMF is significantly reduced at $-20^{\circ}C$, at which temperature half-lives similar to those in dimethylsulfoxide are observed. Samples are stable in both solvents for several days when kept frozen in liquid nitrogen.

Frozen solution EPR spectra of electrolytically generated nickel Ni(III) complexes show rhombic symmetry and large g tensor anisotropy and are typical of low-spin ($S=1/2$) Ni(III) complexes [30–38]. No hyperfine splitting could be detected in any of the three g regions [Figure 1(a)].

In the absence of EPR crystal data for the Ni(III) complexes studied, the observed similarity between their g features and those of analogous nickel(III) and cobalt(II) compounds [9–13, 39] can be extended to support the following orientation scheme for the tensor axes of the nickel complexes: $g_1=g_x, g_2=g_y, g_3=g_z$, where g_1 and g_3 refer to the lowest and highest magnetic field g values, respectively. EPR data for Ni(III) species in DMF and in Me_2SO are summarised in Table 2.

Addition of pyridine to freshly prepared solutions of Ni(III) complexes in Me_2SO, at room temperature and in DMF at temperatures just above the softening point of the frozen glass, originates new species in solution as can be inferred from the rapid colour change of the solutions to yellow red in the first solvent and to yellow brown in the latter solvent.

Frozen solutions of pyridine adducts are EPR silent in Me_2SO, but in DMF they exhibit EPR spectra of rhombic type, although with less rhombicity than the parent complexes, with g_{av} in the range 2.130–2.142, and with hyperfine couplings in all g regions. The existence of one well resolved quintuplet ($a=2.14$–2.27 mT) in the region of higher magnetic field and of

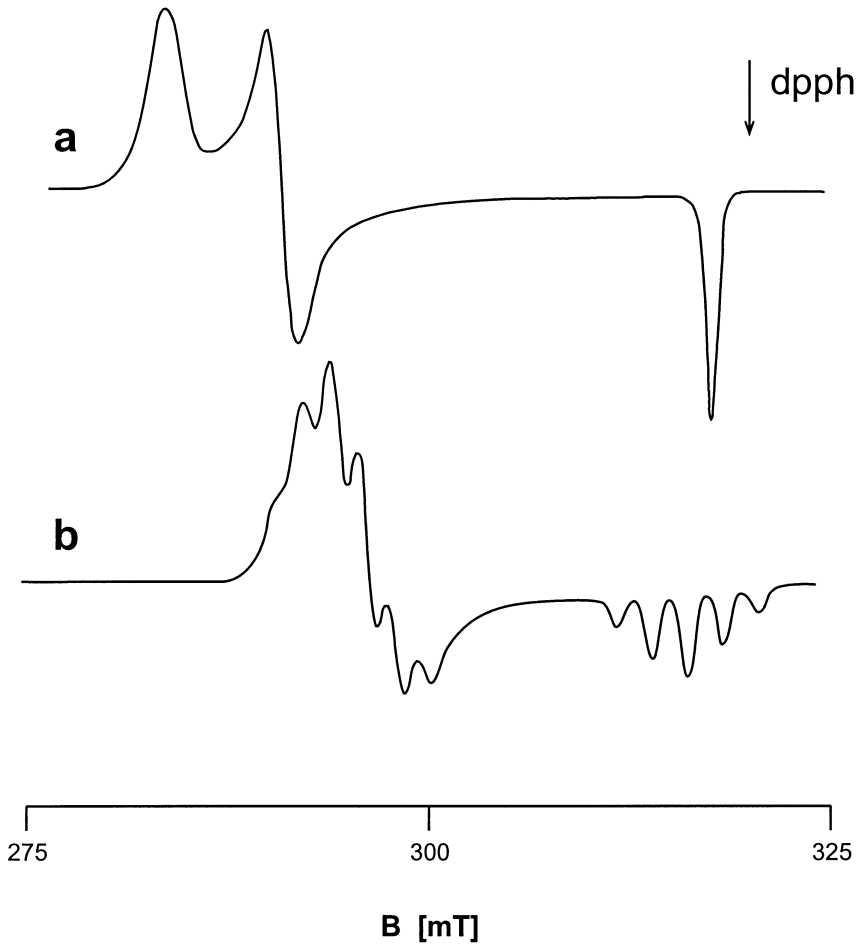

Fig. 1. Frozen solution X-band EPR spectra at $-140^{\circ}C$ of (a) electrochemically oxidised solution of [Ni(napen)] in DMF and (b) the correspondent pyridine adduct.

Table 2. EPR parameters for $[Ni(L)(DMF)_2]^+$ and $[Ni(L)\{(Me_2SO\}_2]^+$ complexes

Complex	Experimental g values					Coefficients[a]			Energy of excited states (cm^{-1})		
	g_x	g_y	g_z	g_{av}[b]	g_{iso}[c]	C_1	C_2	C_3	Δ^2B_1	Δ^2A_2	ΔQ[d]
$[Ni(napen)(DMF)_2]^+$	2.269	2.211	2.018	2.166	2.207	0.0330	0.0423	0.1004	11917	9297	3917
$[Ni(napen)(Me_2SO)_2]^+$ [e]	2.269	2.211	2.018	2.166	2.192	0.0330	0.0423	0.1004	11917	9297	3917
$[Ni(napen)(py)_2]^+$	2.202	2.167	2.022	2.130	[f]	0.0246	0.0303	0.1050	15986	12979	3745
$[Ni(nappd)(DMF)_2]^+$	2.262	2.219	2.027	2.169	2.210	0.0328	0.0397	0.1199	10899	9005	2982
$[Ni(nappd)\{(Me_2SO)_2]^+$ [e]	2.264	2.222	2.029	2.172	2.184	0.0329	0.0397	0.1240	10866	9005	2883
$[Ni(nappd)(py)_2]^+$	2.198	2.171	2.030	2.133	[f]	0.0239	0.0283	0.1220	14958	12633	2930
$[Ni(naptMe)(DMF)_2]^+$	2.274	2.218	2.017	2.170	2.197	0.0344	0.0434	0.0985	11432	9061	3992
$[Ni(naptMe)(Me_2SO)_2]^+$ [e]	2.268	2.221	2.018	2.169	2.182	0.0347	0.0422	0.1007	11333	9319	3905
$[Ni(naptMe)(py)_2]^+$	2.225	2.180	2.020	2.142	[f]	0.0272	0.0345	0.1017	14458	11399	3867

[a] Obtained from McGarvey equations, see text.
[b] The value of g_{av} was calculated as $1/3(g_x+g_y+g_z)$.
[c] g_{iso} was obtained from fluid solution EPR spectra at 233 K.
[d] ΔQ is the difference between the average energy of the quartet states and the ground state.
[e] g values from Ref. [11].
[f] It was not possible to obtain fluid solution EPR spectra, see text.

two non-resolved quintuplets in the two other g regions, imply the existence in DMF of six-co-ordinate Ni(III) species with two pyridines molecules bound axially [Figure 1(b)]. The similarity between the g patterns of these species with those obtained in the absence of pyridine, supports the same orientation scheme for the tensor axes of the pyridine adducts. EPR parameters for $[Ni(L)\cdot py_2]^+$ are summarised in Tables 2–3.

No EPR signals could be detected in fluid solutions of pyridine/DMF, even at temperatures just above the freezing point of the solution. This result combined with the observation that pyridine adducts in Me_2SO are also EPR silent indicate that Ni(III) pyridine adducts have very short life times in fluid solutions.

Electronic spectra of nickel(III) species

Electronic spectral data for Ni(III) species in Me_2SO are included in Table 4; no data are included for DMF solutions, as decomposition of the Ni(III) species is faster in this solvent and only very weak bands could be observed.

Room temperature electronic spectra of oxidised solutions are very similar to those of Ni(III) complexes with ligands derived from salicylaldehyde [9, 10] and show a very broad band in the near-IR region, $880\,nm < \lambda_{max} < 1040\,nm$, with molar extinction coefficient values in the range 850 to 900 $l\,mol^{-1}\,cm^{-1}$. For some complexes, a band at higher energies could also be observed ($640\,nm < \lambda_{max} < 680\,nm$, $\varepsilon = 790$–

Table 3. Nitrogen-14 superhyperfine coupling constants and spin densities for $[Ni(L)\cdot py_2]^+$ complexes[a]

Complex	Experimental superhyperfine coupling[a]					Anisotropic super-hyperfine tensor		Spin densities on ^{14}N			
	A_x	A_y	A_z	A_{av}[b]	A_{iso}[b]	$A_{xx,yy}$	A_{zz}	C^2_{2s}	C^2_{2p}	total[c] (%)	λ^2
$[Ni(napen)(py)_2]^+$	1.74	1.74	2.30	1.74	1.93	−2.0	3.6	0.035	0.109	28.7	3.1
$[Ni(nappd)(py)_2]^+$	1.60	1.66	2.09	1.63	1.78	−1.5	2.9	0.032	0.087	23.9	2.7
$[Ni(naptMe)(py)_2]^+$	1.80	1.71	2.22	1.75	1.91	−1.6	3.0	0.034	0.091	25.0	2.6

[a] The A values are expressed in mT.
[b] A_{iso} could not be obtained for the adducts and A_{av} values are used instead, with $\langle A_{av}\rangle = 1/3(A_x+A_y+A_z)$.
[c] Spin density delocalized onto the two axial nitrogen atoms.

Table 4. Electronic spectral data for $[Ni(L)\cdot(Me_2SO)_2]^+$ complexes[a]

Complex	Experimental values[a]		Calculated values[b]			ξ[c]
$[Ni(napen)(Me_2SO)_2]^+$	880, (880); br	640, (820); s	850	990	640	393
$[Ni(nappd)(Me_2SO)_2]^+$	1040, (850); br	[d]	960	1100	[d]	357
$[Ni(naptMe)(Me_2SO)_2]^+$	960, (900); br	680, (790); s	900	1080	680	393

[a] Band maxima expressed in nm; molar extinction coefficients, in parenthesis, expressed in $mol^{-1}\,dm^3\,cm^{-1}$; br = broad; s = shoulder.

[b] Values obtained by deconvolution of the experimental absorption spectra.

[c] ξ values calculated to get the best fit between the transition energies obtained from electronic spectra and calculated from EPR parameters.

[d] Obscured by high intensity charge transfer bands.

$8201\,mol^{-1}\,cm^{-1}$), but only discernible as a shoulder on a very intense charge transfer absorption band ($380\,nm < \lambda_{max} < 420\,nm$, $\varepsilon = 6800$–$7500\,l\,mol^{-1}\,cm^{-1}$) No electronic spectra for $[Ni(L)\cdot py_2]^+$ could be obtained under the experimental conditions used, since their lifetimes in fluid solution were not long enough to allow the recording of electronic spectra.

Electronic structure of the nickel(III) species

We assume that Ni(III) pyridine adducts have an almost planar equatorial N_2O_2 environment [C_{2v}(x) symmetry], as in the Ni(II) square planar precursor complexes [22, 23]. From the observations that $g_z < g_x$, g_y and that the larger N-hyperfine splittings (Nhfs) are observed in the g_z component, it can be concluded that the unpaired electron must lie in an orbital which is predominantly $d^2{}_z$, implying a $^2A_1$ ground state; since in this symmetry $^2A_1 = a d_{z^2} + b d_{x^2-y^2}$, then $a \gg b$ [40].

This ground state has been observed in the majority of known six-co-ordinate Ni(III) complexes [9–12, 30–38] and the same ground state is assumed for nickel(III) complexes in pure solutions of DMF and Me_2SO, as the patterns of g values are very similar to those of $[Ni(L)\cdot py_2]^+$; nickel(III) complexes in pure solutions are thus formulated as $[Ni(L)\cdot S_2]^+$ [S = DMF, Me_2SO].

None of the Ni(III) species exhibit EPR spectra in which hyperfine splitting due to in-plane nitrogen ligand atoms could be observed. The same is found for analogous Ni(III) and Co(II) complexes and has been interpreted as to imply that these are only weak delocalisation of unpaired spin density to the π system of the equatorial ligand [39–41].

Electronic band assignment was made using the d-orbital ordering $d_{xy} > d_{z^2} > d_{xz}, d_{yz} > d_{x^2-y^2}$ proposed by Hitchman *et al.* for the related Co(II) *salen* complexes [41, 42], which has been used in Ni(III) complexes derived from salicylaldehyde [9, 10] and assuming that: (i) the high intensity bands in the visible region is due to allowed charge transfer transitions from ligand to Ni(III) (superimposed on charge transfer bands to nickel(II), as the electrolysis were not complete; see above) and (ii) the two medium intensity bands in the near infrared region can be assigned to Ni(III) *d–d* transitions. Deconvolution of the broad band yielded two bands at slightly different energies Table 4 that are assigned to the electronic transitions, $d_{xz} \leftarrow d_{z^2}$ ($^2B_1 \leftarrow {}^2A_1$) and $d_{yz} \leftarrow d_{z^2}$; ($^2A_2 \leftarrow {}^2A_1$). The shoulder in the visible region must correspond to the $d_{xy} \leftarrow d_{z^2}$ ($^2B_2 \leftarrow {}^2A_1$) transition.

Analysis of the EPR parameters using the model developed by McGarvey for d^7 systems with a $^2A_1(d_{z^2})$ ground state [40], in conjunction with the approximation suggested by Raynor [43, 44] can provide additional information on the electronic structure of Ni(III) species. The equations for the g tensor are [10]:

$$g_z = 2.0023 + 2C^2{}_3 + 3C_1C_2 - 3C^2{}_2 - 3C^2{}_1 \quad (1a)$$

$$g_x = 2.0023 + 2C^2{}_3 - 3C_1C_2 - 3C^2{}_1 + 6C_2 \quad (1b)$$

$$g_y = 2.0023 + 2C^2{}_3 - 3C_1C_2 - 3C^2{}_2 + 6C_1 \quad (1c)$$

where $C_1 = \xi/\Delta(^2B_1)$, $C_2 = \xi/\Delta(^2A_2)$ and $C_3 = \xi/\Delta(^4B_2)$; $\Delta(^n\Gamma_i)$ is the energy difference between the $^n\Gamma_i$ excited state and the ground state ($^2A_1$) and ξ is the one electron spin orbit coupling constant. C_1 and C_2 yield approximate values for the energies of the excited states $^2B_1$ and $^2A_2$ relative to that of the ground state $^2A_1$.

An estimate for the spin orbit coupling constant can be obtained by finding the value of ξ that minimises the differences between the values of $\Delta(^2B_1)$ and $\Delta(^2A_1)$ obtained by EPR spectra analysis and those from the electronic spectra. In Me_2SO, the values so obtained indicate a reduction of the spin orbit coupling constant of 50% for complexes with *nappd*, and of 55% for the other complexes (Table 4). Values for the latter complexes are comparable with those with ligands derived from salicylaldehyde with aliphatic bridges, whereas ξ for [Ni(nappd)] is similar to those of salicylaldehyde with aromatic bridges [9, 10].

For complexes with axially bound DMF and pyri-

dine, it was not possible to estimate spin orbit coupling constants using the procedure described above, as their electronic spectra could not be recorded and the energy of excited states was calculated using the spin orbital coupling constants in Me_2SO.

A knowledge of ξ and C_3 enables an estimate of the (average) energy of low-lying excited quartet states (ΔQ) and in Table 2 are included the calculated values of $\Delta(^2B_1)$, $\Delta(^2A_1)$ and ΔQ for $[Ni(L)\cdot(DMF)_2]^+$, $[Ni(L)\cdot\{Me_2SO)\}_2]^+$ and $[Ni(L)\cdot(py)_2]^+$. The importance of quartet states to the spin Hamiltonian parameters must be stressed, as their calculated (average) values are non-negligible, typically in the range of 2880–3990 cm^{-1} above the ground state.

As in a previous paper [9], we will use the results of Hitchman [41, 42] to analyse the factors that affect the electronic structure of nickel(III) complexes with ligands derived from naphthaldehyde. Data in Tabs. 2–3 show the energy of the doublets to be more dependent on the axial ligand, whereas that of quartet states on the equatorial ligand, as predicted by Hitchman.

Effect of the axial co-ordination on the energy of excited states No correlation between the energy of excited quartets and axial ligation could be found. The energy of the doublets does not change significantly when the solvent is varied from DMF to Me_2SO, but co-ordination of pyridine increases significantly the energy of the excited doublets, due to stronger interaction of the axial ligands with the d_{z^2} orbital. In fact, raising the energy of d_{z^2} relative to d_{yz} and d_{xz} would decrease C_2 and C_1 and, neglecting second-order terms, eqs. (1a, 1b, 1c) can be expressed as $g_x = 2.0023 + 6C_2$ and $g_y = 2.0023 + 6C_1$, and thus accounts for the observed decrease in g_x and g_y.

Effect of the equatorial ligand on the energy of excited states Data in Table 2 reveal, that for each axial ligand, $[Ni(nappd)\cdot L]^+$ has the lowest energy for both doublet and quartet states, $[Ni(napen)\cdot L]^+$ has the highest energy doublets and $[Ni(naptMe)\cdot L]^+$ exhibits the highest energy quartet states. Furthermore, as the energy of the quartet states are directly related to the in-plane ligand field [41, 42], it is possible to infer that $[Ni(nappd)\cdot L]^+$ and $[Ni(naptMe)\cdot L]^+$ exhibit the weaker and stronger equatorial ligand field, respectively.

To circumvent the lack of structural data for Ni(III) complexes needed to support the aforementioned correlation we will make use of the corresponding data of the Ni(II) precursor complexes. [Ni(naptMe)] has the shortest Ni–N and Ni–O bond distances [11], therefore the smaller cavity, whereas [Ni(nappd)] has the longest bond lengths [19] and the larger cavity. As oxidation of the metal centre induces a decrease in ionic radius, it is to be expected that ligands with large bite will be less prone to adjust the hole cavity to the size of the metal ion, and therefore the same pattern for bond lengths is expected for the Ni(III) complexes. In fact, structural data for the homologous Ni(II) complexes correlate with the observation that $[Ni(naptMe)\cdot L]^+$ and $[Ni(nappd)\cdot L]^+$ have the stronger and weaker equatorial ligand field, respectively. On the other hand, the steric constraint imposed by the methyl groups of the imine bridge on the axially coordinate solvent molecules explain the higher energy for the doublets of $[Ni(napen)\cdot L]^+$, as compared with those of $[Ni(naptMe)\cdot L]^+$.

As the energy of the excited states for the Ni(III) complex with *napen* and *naptMe* are slightly larger than those of the homologous complexes with ligands derived from salicylaldehyde, it can be concluded that the in-plane ligand fields of the naphthaldehyde based complexes are stronger. The excited state energy pattern for *nappd* and the values of ξ are similar to those of salicylaldehyde based complexes with aromatic imine bridges. It is tempting to relate these similarities with structural data from the precursor Ni(II) complexes. In [Ni(nappd)] and in complexes with *saloph*-derived ligands, Ni–N bond lengths (1.871 Å) are longer than Ni–O (1.866 Å), as opposed to what is found in naphthaldehyde- and *salen*-based compounds, for which $d(Ni–N) < d(Ni–O)$ [11, 12, 45–48]. Stronger O-donor in-plane interaction with Ni(III) can thus be invoked for [Ni(nappd)], in contrast to the latter complexes for which the stronger in-plane interaction occur with N-donor atoms.

Nitrogen hyperfine tensor and spin density on nitrogen atoms of axial bound pyridines

The 2s and 2p spin densities, the ratio p:s ($\lambda^2 = C^2_{2p}/C^2_{2s}$) and the total spin density delocalised onto the axially bounded pyridine have been calculated by procedures described elsewhere [9, 10, 49], and are reported in Table 3. The highest values for C^2_{2s}, C^2_{2p} and total spin density are observed for [Ni(napen)], whereas [Ni(nappd)] has the lowest. The values of these parameters for naphthaldehyde-based complexes are slightly higher than those of homologous complexes with *salen*-based ligands, but significantly lower than those with aromatic bridges. We have shown [9] that the total spin density delocalised onto the axial N atoms in complexes with salicylaldehyde is greater for those with aromatic bridges, a consequence of the extensive delocalised π equatorial ligands that act as stronger π donors to nickel(III).

The results reported in this work imply that an increase in ligand unsaturation by the replacement of the salicylaldehyde by the naphthaldehyde moiety does not increase significantly π donation to nickel(III). The influence of aromatic imine bridge in naphthaldehyde based complexes, for which π delocalisation encompasses the aldehyde moieties and the imine bridge as with salicylaldehyde based complexes with aromatic bridges, could not be assessed, as these ligands do not stabilise the +3 oxidation state.

CONCLUSIONS

The oxidation process of nickel(II) complexes with ligands derived from naphthaldehyde in DMF and

Me_2SO is similar to that of their homologous salicylaldehyde based complexes and proceeds through oxidation of the metal centre, originating Ni(III) species with solvent molecules axially co-ordinated, except for complexes with aromatic bridges for which no Ni(III) species could be obtained.

The importance of axial co-ordination in the stabilisation of the +3 oxidation state became evident (i) from the cathodic shift observed for $E_{1/2}$ as the donating ability of the solvent increases; (ii) from the observation that [Ni(naptMe)], which exhibits axial steric hindrance, shows one of the more positive oxidation potentials and finally (iii) by noting that the complex with the lowest $E_{1/2}$, [Ni(nappd)], is the one that exhibits greater tendency to bind solvent molecules in the +2 oxidation state.

Electronic characterisation of nickel(III) naphthaldehyde based complexes has revealed also that the energy of the low lying excited doublets is largely dependent on the axially co-ordinated ligand, whereas that of the excited quartets shows greater dependence on the equatorial ligand. This latter observation allowed us to propose that complexes with *nappd* and *naptMe* have the weaker and stronger in-plane ligand field, respectively; moreover, structural data for the related nickel(II) complexes was used to propose that the strong/weak in-plane ligand strength in Ni(III) complexes is related to small/large ligand bite. Finally, comparison of electrochemical and spectroscopic data of the reported complexes with those of salicylaldehyde based complexes showed that the increase of unsaturation in the aldehyde moiety has only significant changes in the physicochemical properties of Ni(II)/Ni(III) complexes when the ligand has an aromatic imine bridge.

EXPERIMENTAL

The reagents were obtained from commercial sources and used as received, except 2,3-dimethyl-2,3-butanediamine that was prepared by the method of Sayre [50]. Tetraethylammonium perchlorate [51], the ligands and the nickel(II) complexes [17, 52] were prepared by standard methods.

Synthesis and spectroscopic characterisation in Me_2SO of compounds **1**–**3** have been published previously [11]. Electronic spectra (250–1200 nm) of **1**–**3** in DMF are similar to those in Me_2SO. Details on the electrochemical synthesis of nickel(III) complexes and the preparation of their pyridine adducts have been described in Ref. [9].

4: [Ni(napoph)]: $C_{28}H_{20}N_2O_2Ni \times H_2O$: calcd. C 68.5, H 4.0, N 5.7; found C 68.6, H 3.9, N 5.7. ^{1}H NMR ([D_6]DMSO, 297 K): $\delta = 7.05$–8.58 (16 H, aromatic H), 9.70 (2H, =CH). Electronic spectra (250–1200 nm): $\lambda_{max}(\varepsilon) = 495$ (9900), 485 (10500), 435 (30100), 400 nm (21000 $mol^{-1}\,dm^3\,cm^{-1}$) in Me_2SO; $\lambda_{max} = 540$, 505, 440, 410 nm in nujol.

5: [Ni(napophCl_2)]: $C_{28}H_{18}N_2O_2Cl_2Ni$: calcd C 62.0, H 3.0, N 5.2; found: C, 61.6; H, 2.9; N, 5.0. ^{1}H NMR ([D_6]DMSO, 297 K): $\delta = 7.05$–8.60 (14 H, aromatic H), 9.69 (2H, =CH). Electronic spectra (250–1200 nm): $\lambda_{max}(\varepsilon) = 505$ (11100), 490 (13200), 410 (32500), 390 nm (24200 $mol^{-1}\,dm^3\,cm^{-1}$) in Me_2SO; $\lambda_{max} = 530$, 510, 440, 405 nm in nujol.

Physical measurements

Elemental analyses were performed at the Microanalytical Laboratory, University of Manchester. ^{1}H NMR spectra were recorded on a Bruker AC200 spectrometer at 200 MHz (298 K). Chemical shifts are reported in ppm referred to TMS as an internal standard. Electronic spectra of Ni(II)/Ni(III) complexes were recorded with a Cary 17DX spectrophotometer at room temperature. Molar extinction coefficients for the nickel(III) electronic bands were estimated by double integration of EPR spectra, including baseline and Aasa and Vänngard corrections [53], using Me_2SO solutions of copper(II) nitrate as concentration standards. EPR spectra were obtained with an X-band Varian E 109 spectrometer at 77 K. Spectra were calibrated with diphenylpicrylhydrazyl (dpph; $g = 2.0037$) and the magnetic field was calibrated by use of Mn^{2+} in MgO. The reported EPR parameters were obtained by computer simulation [54]; linewidths (x, y, z) were typically 0.3–0.5 mT. The solvents for syntheses were of reagent grade and those for electrochemical measurements of analytical grade; all solvents were used as received.

Electrochemical measurements were made with a VA-Detector E 611, a VA-Scanner E 612 and a Coulometer E 524 (all from Metrohm) using DMF or Me_2SO solutions 1 mmol dm^{-3} in Ni(II) complex and 0.1 mol dm^{-3} Et_4NClO_4. Cyclic voltammetry was performed using a platinum microsphere as working electrode, a platinum wire as counter electrode, and an Ag/AgCl (1 mol dm^{-3} NaCl) reference electrode. All potentials are reported relative to that of the Ag/AgCl (1 mol dm^{-3} NaCl) reference electrode and to $E_{1/2}$ of the Fc^+/Fc couple; under the experimental conditions used (scan rate 0.05 Vs^{-1}) $E_{1/2}$ for the Fc^+/Fc couple: 0.50 V in DMF [$\Delta E(Fc^+/Fc) = 0.10$ V] and 0.48 V in Me_2SO [$\Delta E(Fc^+/Fc) = 0.09$ V]. Measured potentials were not corrected for liquid junction potentials. Scan rates from 0.01 to 0.10 V s^{-1} were used and the low and high potential limits were 0.30 and 1.30 V. Electrolysis were carried out at controlled potential, at a value 0.05 V higher than the anodic peak potential, using a Pt gauze as working electrode, a platinum foil as counter electrode and an Ag/AgCl (1 mol dm^{-3} NaCl) as reference electrode. The time elapsed during electrolysis in either solvent was typically 15 min and this time corresponds roughly to the moment when formation of the oxidised species becomes slower than their decomposition, as can be inferred by following the variation of the intensity of the derivative EPR bands with electrolysis time. Concentration of the

Ni(III) compounds at the end of electrolysis was comprised between 30 and 50% (molar basis) of total nickel in solution.

Acknowledgements—This work was partially supported by the Fundação para a Ciência e Tecnologia (Lisboa) through projects Praxis/2/2.1/QUI/316/94 and Praxis/3/3.1/MMA/1780/95.

REFERENCES

1. Kolodziej, A. F., *Prog. Inorg. Chem.*, 1994, **41,** 493.
2. Cammack, R., *Adv. Inorg. Chem.*, 1988, **32,** 297.
3. Lancaster, J. R., Jr., ed., *Bioinorganic Chemistry of Nickel*. VCH, New York, 1988.
4. Yoon, H., Wagler, T. R., O'Connor, K. and Burrows, C. J., *J. Am. Chem. Soc.*, 1990, **112,** 4568.
5. Gosden, C., Healy, K. P. and Pletcher, D., *J. Chem. Soc. Dalton Trans.*, 1978, 972.
6. Bakac, A. and Espenson, J. H., *J. Am. Chem. Soc.*, 1986, **108,** 719.
7. Collin, J. P. and Sauvage, J. P., *Coord. Chem. Rev.*, 1989, **93,** 245.
8. Amatore, C. and Jutand, A., *J. Am. Chem. Soc.*, 1991, **113,** 2819.
9. Freire, C. and de Castro, B., *J. Chem. Soc. Dalton Trans.*, 1998, 1491.
10. de Castro, B. and Freire, C., *Inorg. Chem.*, 1990, **29,** 5113.
11. Carrondo, M. A. A. de C. T., de Castro, B., Coelho, A. M., Domingues, D., Freire, C. and Morais, J., *Inorg. Chim. Acta*, 1993, **205,** 157.
12. Azevedo, F., Carrondo, M. A. A. de C. T., de Castro, B., Convery, M., Domingues, D., Freire, C., Duarte, M. T., Nielson, K. and Santos, I., *Inorg. Chim. Acta*, 1994, **219,** 43.
13. de Castro, B., Freire and C., Pereira, E., *J. Chem. Soc. Dalton Trans.*, 1994, 571.
14. Pereira, E., Gomes, L. and de Castro, B., *Inorg. Chim. Acta*, 1998, **271,** 83.
15. Pereira, E., Gomes, L. and de Castro, B., *J. Chem. Soc. Dalton Trans.*, 1998, 629.
16. Valente, M., Freire, C. and de Castro, B., *J. Chem. Soc. Dalton Trans.* (accepted).
17. Holm, R. H., Everett, G. W. Jr. and Chakravorty, A., *Prog. Inorg. Chem.*, 1966, **7,** 183.
18. Akhtar, F., *Acta Cryst. B*, 1981, **37,** 84.
19. Akhtar, F. and Drew, M. G. B., *Acta Cryst. B*, 1982, **38,** 1149.
20. Radha, A., Seshasayee, M., Ramalingam, K. and Aravamudar, G., *Acta Cryst. C*, 1985, **37,** 1169.
21. Lever, A. B. P., *Inorganic Electronic Spectroscopy*, 2nd edn. Elsevier, New York, 1984.
22. Maki, G., *J. Chem. Phys.*, 1958, **28,** 651.
23. Maki, G., *J. Chem. Phys.*, 1958, **29,** 1129.
24. Astruc, D., *Electron Transfer and Radical Processes in Transition Metal Chemistry*. VCH, New York, 1995.
25. Busch, D. H., *Acc. Chem. Res.*, 1978, **11,** 392.
26. Lovecchio, F. V., Gore, E. S. and Busch, D. H., *J. Am. Chem. Soc.*, 1974, **96,** 3109.
27. Streeky, J. A., Pillsbury, D. G. and Busch, D. H., *Inorg. Chem.*, 1980, **19,** 3148.
28. Kadish, K. M., *Prog. Inorg. Chem.*, 1986, **34,** 435.
29. Averill, D. F. and Broman, R. F., *Inorg. Chem.*, 1978, **17,** 3389.
30. Buttafava, A., Fabbrizi, L., Perotti, A., Poggi, A. and Poli, G., Seghi, B., *Inorg. Chem.*, 1986, **25,** 1456.
31. Bencini, A., Fabbrizi, L. and Poggi, A., *Inorg. Chem.*, 1981, **20,** 2544.
32. Krüger, H.-J. and Holm, R. H., *Inorg. Chem.*, 1989, **28,** 1148.
33. Krüger, H.-J., Peng, G. and Holm, R. H., *Inorg. Chem.*, 1991, **30,** 734.
34. Gore, E. S. and Busch, D. H., *Inorg. Chem.*, 1973, **12,** 1.
35. Bemtgen, J. M., Gimpert, H. R. and von Zelewsky, A., *Inorg. Chem.*, 1983, **22,** 3576.
36. Desideri, A., Raynor, J. B. and Poon, C. K., *J. Chem. Soc. Dalton Trans.*, 1977, 2051.
37. Bossu, F. P. and Margerum, D. W., *Inorg. Chem.*, 1975, **14,** 881.
38. Mehne, L. F. and Wayland, B. B., *Inorg. Chem.*, 1975, **14,** 881.
39. Daul, C., Schlapfer, C. W. and von Zelewsky, A., *Struct. Bonding* (*Berlin*), 1970, **36,** 129.
40. McGarvey, B. R., *Can. J. Chem.*, 1975, **53,** 2498.
41. Hitchman, A., *Inorg. Chem.*, 1985, **1977,** 16.
42. Hitchman, A., *Inorg. Chim. Acta*, 1970, **26,** 237.
43. Labause, G. and Raynor, J. B., *J. Chem. Soc. Dalton Trans.*, 1980, 2388.
44. Labause, G. and Raynor, J. B., *J. Chem. Soc. Dalton Trans.*, 1981, 590.
45. Manfredotti, A. G. and Guastini, C., *Acta Cryst. C*, 1983, **39,** 863.
46. Drew, M. G. B., Prasad, R. N. and Sharma, R. P., *Acta Cryst. C*, 1985, **41,** 1755.
47. Radha, A., Seshasayee, M., Ramalingam, K. and Aravamudan, G., *Acta Cryst. C*, 1985, **41,** 1169.
48. Akhtar, F., *Acta Cryst. B*, 1981, **37,** 84.
49. Goodman, B. A. and Raynor, J. B., *Adv. Inorg. Chem. Radiochem.*, 1970, **13,** 135.
50. Sayre, R., *J. Am. Chem. Soc.*, 1955, **77,** 6689.
51. Donald, S. T., Jr., *Experimental Electrochemistry for Chemistry*. Wiley, New York, 1974.
52. McAuliffe, C. A., Parish, R. V., Ashmawy, F. M., Issa, R. M. and Amer, S. A., *J. Chem. Soc. Dalton Trans.*, 1987, 2009.
53. Pool, C. P., Jr., *Electron Spin Resonance*, 2nd edn. Wiley, New York, 1983.
54. Pilbrow, J. R. and Winfield, M. E., *Mol. Phys.*, 1973, **25,** 1073.

Pergamon

Polyhedron Vol. 17, No. 23–24, pp. 4237–4247, 1998
© 1998 Elsevier Science Ltd
All rights reserved. Printed in Great Britain
0277–5387/98 $19.00+0.00

PII: S0277–5387(98)00234–4

Synthesis, characterization and crystal structures of three diverse copper(II) complexes with thiophene-2,5-dicarboxylic acid and 1,10-phenanthroline

Bang Lin Chen[a], K. F. Mok[a]*, Siu-Choon Ng[a], Yun-Long Feng[b] and Shi-Xiong Liu[b]

[a]Department of Chemistry, National University of Singapore, Singapore 119260, Singapore

[b]Department of Chemistry, Fuzhou University, Fujian 350002, P.R. China

(Received 7 January 1998; accepted 9 June 1998)

Abstract—Three copper(II) complexes with thiophene-2,5-dicarboxylic acid (H_2Tda) and 1,10-phenanthroline (phen) ligands have been synthesized and structurally characterized: $[Cu(Tda)(phen)(H_2O)_2]\cdot 3H_2O$ (**1**), $[Cu(Tda)(phen)_2]\cdot 1/2H_2Tda\cdot 2H_2O$ (**2**) and $[\{Cu(Tda)(phen)(H_2O)\}_n]$ (**3**). The Cu atom in all of the three complexes is in five coordinate, distorted square pyramidal environments. The thiophene-2,5-dicarboxylate molecule is monodentate in **1** and **2** in which the molecular structure is stabilized by intermolecular aromatic ring stacking interaction between the thiophene ring and the aromatic rings in the 1,10-phenanthroline molecule and hydrogen bondings. In **3** the thiophene-2,5-dicarboxylate ion is bis-monodentate and bridges the $[Cu(phen)(H_2O)]$ units to form a one-dimensional polymer. Complex **2** shows quasi-reversible one-electron redox of Cu^{2+}/Cu^{+} at 0.001 V vs SCE. Coordination environments of copper(II) in the reported complexes and stacking interactions in **1** and **2** are compared with those in the copper(II) site of galactose oxidase (GOase). © 1998 Elsevier Science Ltd. All rights reserved

Keywords: crystal structures; copper(II) complexes; thiophene derivatives; stacking interactions

INTRODUCTION

Thiophene derivatives have been known to show biological activities [1]. Yet relatively very few of their metal complexes have so far been reported [2–7]. Thiophene-2,5-dicarboxylic acid (H_2Tda) is reported to be a potential anti-cancer agent [8]. Four lanthanide complexes with formula $Ln_2(Tda)_3\cdot nH_2O$ (Ln = La,Gd,Dy) and $Sm(Tda)OH\cdot H_2O$ have been synthesized, but only their IR data were reported. The coordination modes of thiophene-2,5-dicarboxylate in these complexes are still unknown [9]. Thiophene-2,5-dicarboxylate can potentially be a monodentate, a bidentate and a tridentate ligand; it can also be a bridging or chelating ligand.

Five-coordinate copper(II) complexes are not uncommon; the geometry around the metal ion is trigonal bipyramidal or square pyramidal. Many biologically active copper-containing molecules have five-coordinate metal centres. For example, the active site in the structure of galactose oxidase (GOase, copper-containing enzyme) has been determined [10, 11]. The geometry around the monomeric copper(II) centre is square pyramidal (see Fig. 1) in which the copper(II) ion is coordinated to four amino acid residues from the protein chain and one exogenous acetate anion (pH 4.5) or one water molecule (pH 7.0). One tyrosine oxygen atom, two histidine nitrogen atoms and an acetate oxygen atom (or an oxygen of water) form the square base while the apical position is occupied by a further tyrosine oxygen atom. The structure reveals a novel biological modification of the equatorial tyrosine 272, which is covalently linked by a thioether bond to the sulfur atom of cysteine 228. This thioether linkage very likely contributes to lowering the redox

* Author to whom correspondence should be addressed.

potential of the Tyr272 free radical. This new observation has stimulated research on synthesising small molecule complexes as models for the copper biosite present in this enzyme [12–16].

Among interactions between nucleic acids and amino acids, hydrogen bonding and aromatic-ring stacking are two of the four possibly important interactions in biological systems [17] and such interactions are known to occur in a number of copper(II) complexes of biological significance [17–32]. The existence of stacking interactions in copper(II) complexes with nucleotides and a second ligand (an aromatic base such as 1,10-phenanthroline and 2,2′-dipyridine), which stabilises the formed complexes, greatly influences the coordination of nucleotides where metal–nucleotide interactions take place predominantly at the phosphate group and the nucleotide base is not bound to the metal ion but stacked with the aromatic ring of the second ligand [19–25]. In the GOase copper site, the unusual thioether bond between Tyr272 and Cys228 is stacked with the indole ring of Trp290 as shown in Fig. 1. These strong interactions seem to stabilize the Tyr272 free radical and are probably involved in the catalytic mechanism [10, 11]. Our selection of 1,10-phenanthroline as the second ligand is based on the consideration that 1,10-phenanthroline is known to be an important aromatic base involved in stacking interactions and may possibly stabilise the formed copper(II) complexes with thiophene-2,5-dicarboxylate by chelate effect and stacking interactions. Here we report the synthesis and crystal structure of three copper(II) complexes with thiophene-2,5-dicarboxylic acid and 1,10-phenanthroline: $[Cu(Tda)(phen)(H_2O)_2]\cdot 3H_2O$ (**1**), $[Cu(Tda)(phen)_2]\cdot 1/2H_2Tda\cdot 2H_2O$ (**2**) and $[\{Cu(Tda)(phen)(H_2O)\}_n]$ (**3**).

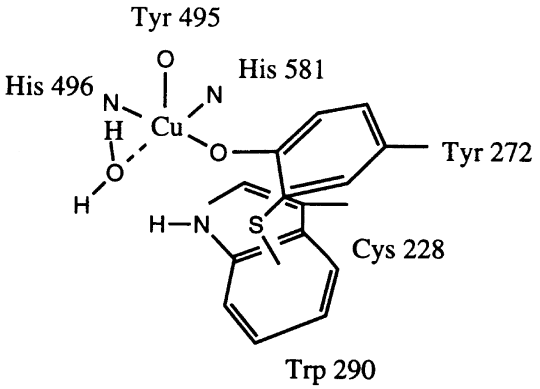

Fig. 1. Coordination environments of galactose oxidase copper site.

EXPERIMENTAL

General

All chemicals were reagent grade and used without further purification.

Elemental analyses were carried out by the Microanalytical Laboratory of the Department of Chemistry, National University of Singapore. Solution pH values of the reaction mixture were measured using a Metrohm 691 pH Meter. IR spectra were recorded as KBr discs using a Perkin Elmer 1600 Fourier-transform IR spectrometer (4400–450 cm^{-1}), UV-Vis spectra were recorded on a Shimadzu UV-240 UV-visible spectrophotometer using Nujol mulls for solid samples and in $EtOH/H_2O$(1:1) for solution samples. Cyclic voltammetry studies of the complexes were performed on a EG&G 273 Potentiostat/Galvanostat using EG&G 270/250 Research Electrochemical Software 4.0. The single-compartment electrochemical cell was equipped with a platinum foil working electrode (0.5 cm^2), a saturated calomel electrode (SCE) and a platinum wire counter electrode. Scans were done at 50 mV s^{-1} in $EtOH/H_2O$(1:1) that contained 0.10 M $(NEt_4)ClO_4$ as the supporting electrolyte. The concentration of the metal complexes were 1×10^{-3} M. Solutions were purged with dry argon prior to data collection. Emf values are reported vs SCE. Thermogravimetric and differential thermoanalysis data were obtained on a Universal V1.5B TA Instrument in air flux with a heating rate of 10°C min^{-1}. Thiophene-2,5-dicarboxylic acid was synthesized by a modified literature method [33].

Synthesis of $[Cu(Tda)(phen)(H_2O)_2]\cdot 3H_2O$ (*1*) *and* $[Cu(Tda)(phen)_2]\cdot 1/2H_2Tda\cdot 2H_2O$ (*2*)

2 cm^3 of 0.1 M $Cu(NO_3)_2$ aqueous solution and 2 cm^3 of 0.1 M H_2Tda–Phen (1:1 molar ratio) ethanol solution were mixed in a 10 cm^3 capped bottle (vial); then 0.6 cm^3 of 0.1 M NaOH aqueous solution was added. The resulting solution with a pH of 3.46 was set aside. Several days later, light green crystals and dark blue crystals were formed. The light green and the dark blue crystals were separated. The light green crystals were complex **1** (15 mg, yield 15% based on Cu). Anal. calcd for $C_{18}H_{20}CuN_2O_9S$: C, 42.90; H, 4.00; N, 5.56; S, 6.36; Cu, 12.61%. Found: C, 42.93; H, 4.22; N, 5.68; S, 6.20; Cu, 12.72%. IR (KBr disc, cm^{-1}): 1571, 1560 (ν_{as} COO^-), 1386, 1356 ($\nu_s COO^-$). UV-Vis [λ_{max} (nm), ε ($dm^3\,mol^{-1}\,cm^{-1}$) in parentheses]: 276, 656 (d–d*) (solid); 204 (5982), 222 (3900), 270 (5380), 735 (226). The dark blue crystals were those of **2** (20 mg, yield 14% based on Cu). Anal. calcd for $C_{33}H_{24}CuN_4O_8S_{1.5}$: C, 55.34; H, 3.38; N, 7.82; S, 6.71; Cu, 8.87%. Found: C, 55.39; H, 3.47; N, 7.89; S, 6.68; Cu, 8.91%. IR (KBr disc, cm^{-1}): 1691 (ν_{as} COOH), 1583 (ν_{as} COO^-), 1353 ($\nu_s COO^-$). UV-Vis [λ_{max} (nm), ε ($dm^3\,mol^{-1}\,cm^{-1}$) in parentheses]: 290, 640 (d–d*) (solid); 204 (9400), 222 (6110), 268 (8460), 728 (250).

Synthesis of $[\{Cu(Tda)(phen)(H_2O)\}_n]$ (**3**)

2 cm^3 of 0.1 M $CuCl_2$ aqueous solution and 2 cm^3 of 0.1 M H_2Tda–Phen (1:1 molar ratio) ethanol solution were mixed in a 10 cm^3 capped bottle (vial); then 0.9 cm^3 of 0.1 M NaOH aqueous solution was added. The resulting solution with a pH of 3.65 was put aside. After several days, green crystals were formed. The green crystals were collected as **3** (28 mg, yield 32% based on Cu). Anal. calcd for $C_{18}H_{12}CuN_2O_5S$: C, 50.05; H, 2.80; N, 6.48; S, 7.42; Cu, 14.71%. Found: C, 49.87; H, 2.67; N, 6.46; S, 7.23; Cu, 14.78%. IR (KBr disc, cm^{-1}): 1590, 1576 (ν_{as} COO^-), 1364 ($\nu_s COO^-$). UV-Vis (λ_{max}/nm): 288, 680 (d–d*) (solid).

X-ray structure determination

X-ray diffraction data for **1** and **3** were collected on a Rigaku AFC5R diffractometer at room temperature with graphite-monochromated Mo-Kα radiation ($\lambda = 0.71069$ Å), using ω–2θ scan mode. Cell dimensions were obtained from 25 reflections in the 2θ range of 20–30° for each compound. Lp and DIFABS corrections were made for all reflections. Data reduction and structure refinement were performed using the TEXSAN packages [34]. The structures of **1** and **3** were solved by the Patterson and direct methods, respectively. All non-hydrogen atoms were refined anisotropically by least-squares methods. Hydrogen atoms for **1** and **3** were located by a combination of difference Fourier map and HYDROGEN program, their positions were not refined. X-ray diffraction data for **2** were collected on a Siemens R3m/V diffractometer using graphite-monochromated Mo-Kα radiation ($\lambda = 0.71073$ Å). Unit cell parameters were determined by a least-squares fit of 25 independent reflections, which were obtained by automatic random search. Semi-empirical absorption corrections were applied. The structure was solved by direct methods on a Digital Equipment Corporation Micro VAX II computer. Refinements by full matrix least-squares were carried out on a PC by using SHELXTL PLUS (PC version) software package [35] and final refinement was run using SHELXL-93 [36]. All non-hydrogen atoms were refined anisotropically. Hydrogen atoms were introduced at calculated positions (C–H = 0.96 Å). A summary of the crystallographic data is given in Table 1.

RESULTS AND DISCUSSION

Thiophene-2,5-dicarboxylic acid is a dibasic acid with acidity constants of pK_{a1} 3.18 and pK_{a2} 4.28 in

Table 1. Crystal data and refinement details for complexes **1**, **2** and **3**

Compound	**1**	**2**	**3**
Formula	$C_{18}H_{20}CuN_2O_9S$	$C_{33}H_{24}CuN_4O_8S_{1.5}$	$C_{18}H_{12}CuN_2O_5S$
Formula weight	503.97	716.19	431.91
Crystal system	monoclinic	monoclinic	monoclinic
Space group	C 2/c (#15)	C 2/c (#15)	P 2_1/c(#14)
a (Å)	26.551(8)	26.615(5)	10.452(2)
b (Å)	7.886(3)	16.045(3)	16.841(2)
c (Å)	27.368(7)	15.776(3)	10.454(3)
β(°)	133.45(2)	113.45(3)	108.69(2)
V (Å^3)	4160(5)	6181(3)	1743(1)
Z	8	8	4
D_c (mg·cm^{-3})	1.61	1.54	1.65
μ (mm^{-1})	1.99	0.87	1.40
F(000)	2070	2936	876
Crystal dimensions (mm)	0.25 × 0.20 × 0.10	0.15 × 0.25 × 0.28	0.20 × 0.20 × 0.15
Index range, h	0–31	0–31	0–12
Index range, k	−9–9	0–19	0–20
Index range, l	−32–32	−18–17	−12–12
Independant reflections	5210	5496	3575
Observed reflections	3146 [$I > 3\sigma(I)$]	3521 [$I > 2\sigma(I)$]	2512 [$I > 3\sigma(I)$]
No. of variables	282	432	245
Residual electron density (e·Å^{-3}) (max, min)	0.44; −0.42	0.34; −0.40	0.37; −0.36
R[a]	0.044	0.042	0.039
Rw	0.055[b]	0.100[c]	0.051[b]
S	1.32	0.84	1.40
(Δ/σ)max	0.021	0.001	0.017

[a] $R = \Sigma w|F_o - F_c|/\Sigma(F_o)$.
[b] $Rw = \{[\Sigma w|F_o - F_c|^2/\Sigma w(F_o)^2]\}^{1/2}$.
[c] $wR_2 = \{\Sigma w[(F_o^2 - F_c^2)^2]/\Sigma wF_o^4\}^{1/2}$.

aqueous EtOH (30%) solution and pK_{a1} 4.14 in aq. EtOH (50%) [37, 38]. It exists as an equilibrium mixture of H_2Tda, $HTda^-$ and Tda^{2-} in solutions of different pHs. Hence the complexation reactivity of this ligand depends on its degree of protonation, i.e. the pH of the solution. When the pH of the reaction mixture (pH 3.46) was carefully controlled by addition of 0.6 cm^3 0.1 M NaOH aqueous solution to 4 cm^3 of $Cu(NO_3)_2$ and a H_2Tda–phen mixture, complexes **1** and **2** were obtained simultaneously. Reaction of 2 cm^3 of 0.1 M $CuCl_2$ aqueous solution and 2 cm^3 of 0.1 M H_2Tda–phen ethanol solution, at a pH of 3.65, produced complex **3**. Crystals suitable for X-ray crystallographic determination were obtained directly from the above reaction mixture.

*Structures of **1**, **2** and **3***

The structure of **1** consists of monomeric [Cu(Tda)(Phen)$(H_2O)_2$] units linked by water molecules through hydrogen bonding. The structure of **2** contains discrete neutral units of [Cu(Tda)$(Phen)_2$], thiophene-2,5-dicarboxylic acid molecules and water molecules of crystallization; the uncoordinated H_2Tda molecule is linked to the central complex by hydrogen bonds. In **1** and **2** thiophene-2,5-dicarboxylate is monodentate and the molecular packing is determined mainly by hydrogen bonding and aromatic ring-stacking interactions as depicted in Figs 2 and 3. Selected bond distances and angles are given in Tables 2 and 3. In $[\{Cu(Tda)(phen)(H_2O)\}_n]$ (**3**), [Cu(phen)(H_2O)] units are bridged by thiophene-2,5-dicarboxylate anions which act as bridging bis-monodentate ligands to form one-dimensional polymer chains running in a zig-zag manner. The partial molecular packing is shown in Fig. 4 together with the atomic labelling scheme. Selected bond length and angle are listed in Table 4. Intramolecular Cu···Cu separation along the chain is 10.76 Å, comparable with those bridged by terephathates [39].

The common structural feature of complexes **1**, **2** and **3** is that the copper atom in all of the three com-

Table 2. Selected bond distances (Å) and angles (°) for **1**

Cu(1)–O(1)	1.928(3)	Cu(1)–O(5)	1.962(3)
Cu(1)–N(1)	2.014(3)	Cu(1)–N(2)	2.014(4)
Cu(1)–O(6)	2.272(3)		
O(1)–Cu(1)–O(5)	92.5(1)	O(1)–Cu(1)–N(1)	88.8(1)
O(1)–Cu(1)–N(2)	168.7(1)	O(1)–Cu(1)–O(6)	98.0(1)
O(5)–Cu(1)–N(1)	164.5(1)	O(5)–Cu(1)–N(2)	95.2(1)
O(5)–Cu(1)–O(6)	90.8(1)	N(1)–Cu(1)–N(2)	81.6(1)
N(1)–Cu(1)–O(6)	104.3(1)	N(2)–Cu(1)–O(6)	90.2(1)

Table 3. Selected bond distances (Å) and angles (°) for **2**

Cu(1)–O(1)	1.993(3)	Cu(1)–N(1)	2.054(3)
Cu(1)–N(2)	2.006(3)	Cu(1)–N(3)	1.995(3)
Cu(1)–N(4)	2.223(3)		
O(1)–Cu(1)–N(1)	163.3(1)	O(1)–Cu(1)–N(2)	90.9(1)
N(1)–Cu(1)–N(2)	81.5(1)	O(1)–Cu(1)–N(3)	93.7(1)
N(1)–Cu(1)–N(3)	93.8(1)	N(2)–Cu(1)–N(3)	175.3(1)
O(1)–Cu(1)–N(4)	96.5(1)	N(1)–Cu(1)–N(4)	99.6(1)
N(2)–Cu(1)–N(4)	100.6(1)	N(3)–Cu(1)–N(4)	79.6(1)

Table 4. Selected bond distances (Å) and angles (°) for **3**

Cu(1)–O(1)	1.932(2)	Cu(1)–O(5)	1.971(2)
Cu(1)–N(1)	2.014(3)	Cu(1)–N(2)	2.014(3)
Cu(1)–O(3a)	2.184(2)		
O(1)–Cu(1)–O(5)	94.6(1)	O(1)–Cu(1)–N(1)	89.7(1)
O(1)–Cu(1)–N(2)	166.1(1)	O(1)–Cu(1)–O(3a)	98.3(1)
O(5)–Cu(1)–N(1)	165.9(1)	O(5)–Cu(1)–N(2)	91.3(1)
O(5)–Cu(1)–O(3a)	93.3(1)	N(1)–Cu(1)–N(2)	81.7(1)
N(1)–Cu(1)–O(3a)	99.4(1)	N(2)–Cu(1)–O(3a)	93.9(1)

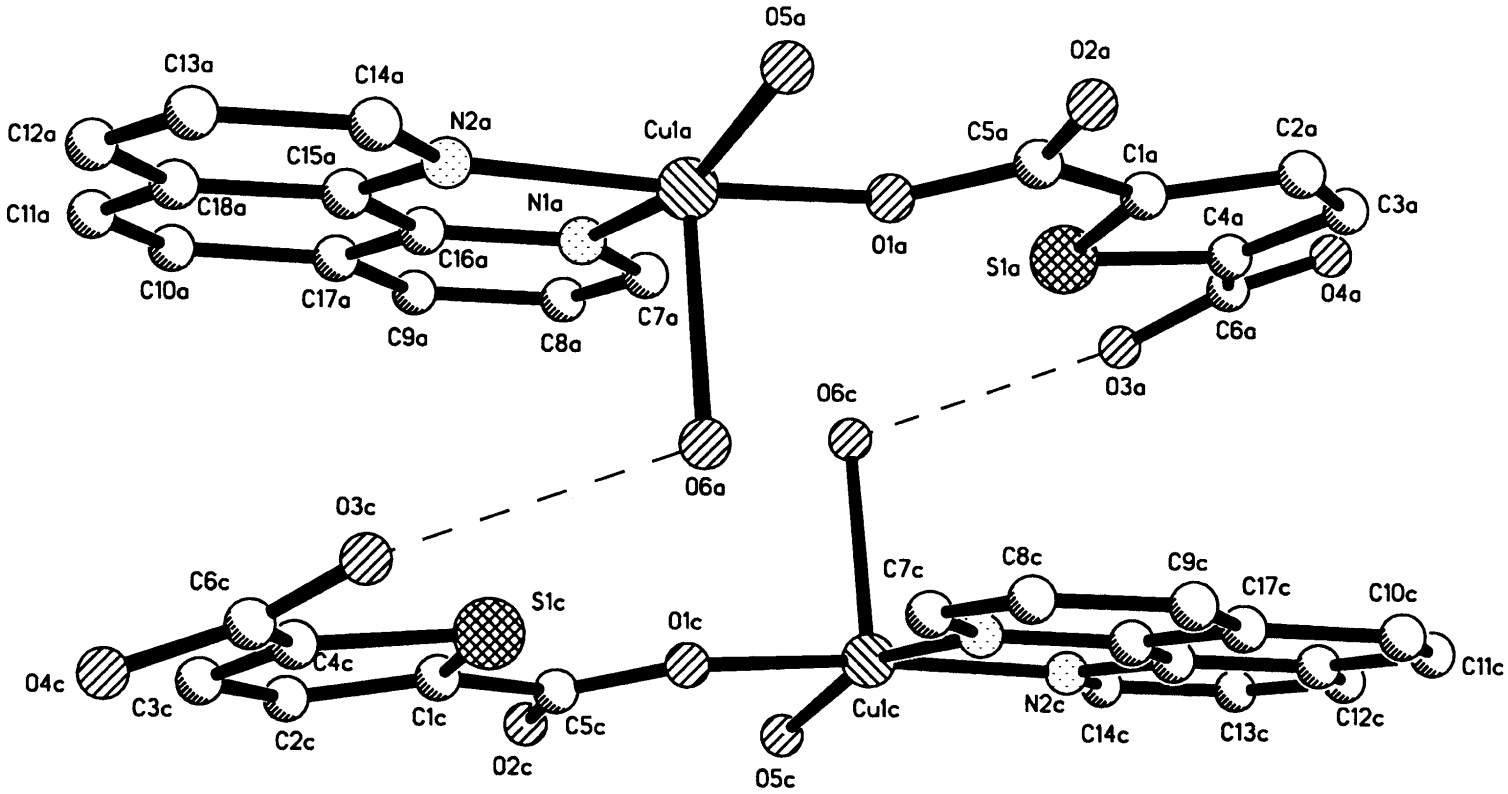

Fig. 2. Partial packing diagram of **1** with atomic labelling scheme showing the stacking interactions and hydrogen bonding.

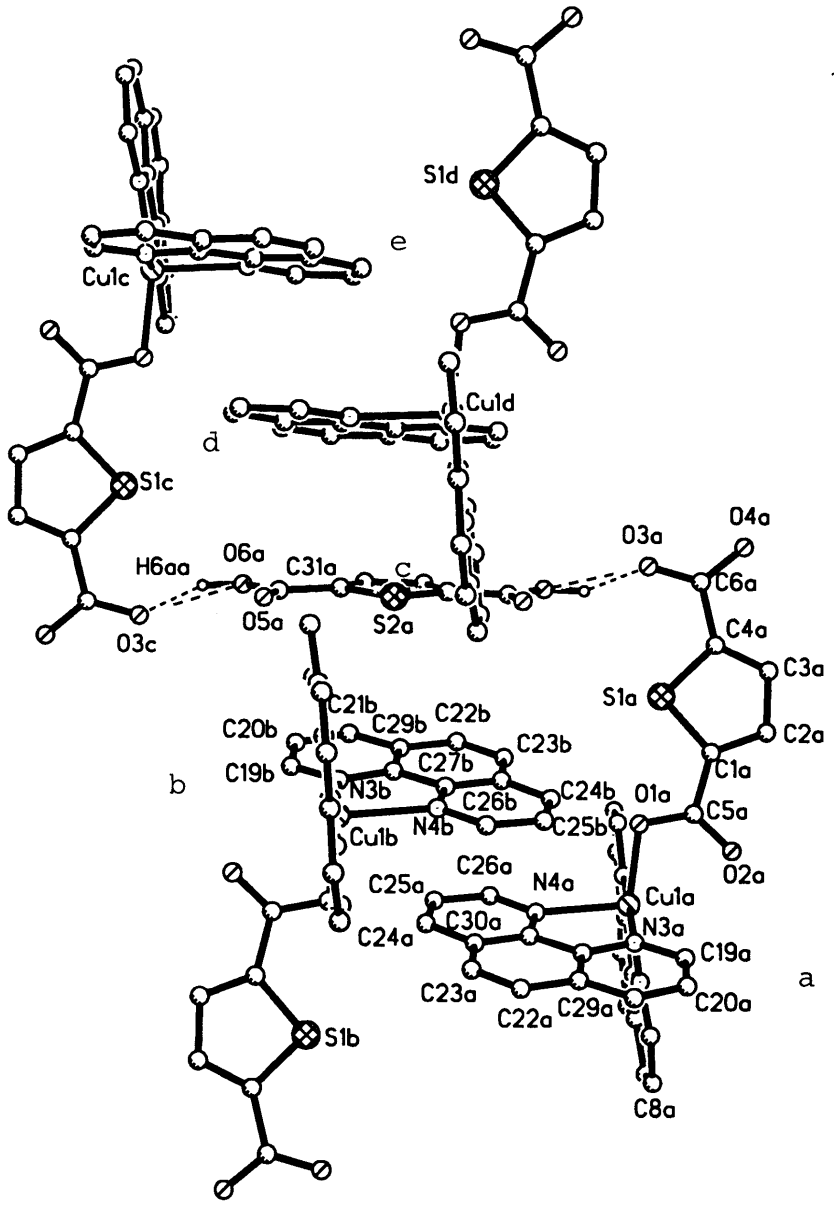

Fig. 3. Partial packing diagram of **2** with atomic labelling scheme showing the stacking interactions and hydrogen bonding.

plexes is in a five coordinate, distorted square pyramidal environment. Figure 5 shows the comparison of copper(II) coordination environments together with the coordination environment of the active GOase site. Some structural parameters of these complexes are listed in Table 5. In the present three complexes the geometries around copper(II) are best described as distorted square pyramidal with small trigonal-bipyramidal component from $\tau = 0.003$ to 0.20 [40].

Observed Cu–N(phen), Cu–O(water) and Cu–O(carboxylate) bond distances are comparable with literature values [27–29, 41–44]. The Cu–O(carboxylate) bond length in **2** [1.993(3) Å] is longer than that in **1** [1.928(3) Å] and 1.932(1) Å in **3** indicating that the coordination of thiophene-2,5-dicarboxylate to copper(II) in **2** is weaker than those in **1** and **3**, possibly due to the steric effects resulting from the presence of two phenanthroline molecules. All the carboxylate coordination to copper is in *syn* mode which is the preferred coordination mode of a carboxylate in small complex molecules [45] and for proteins containing carboxylate–metal ion interactions [46]. The thiophene-2,5-dicarboxylate molecule is nearly planar in all of the three complexes.

A further interesting structural feature which needs to be emphasised is the intermolecular aromatic ring-stacking interactions between the thiophene ring and

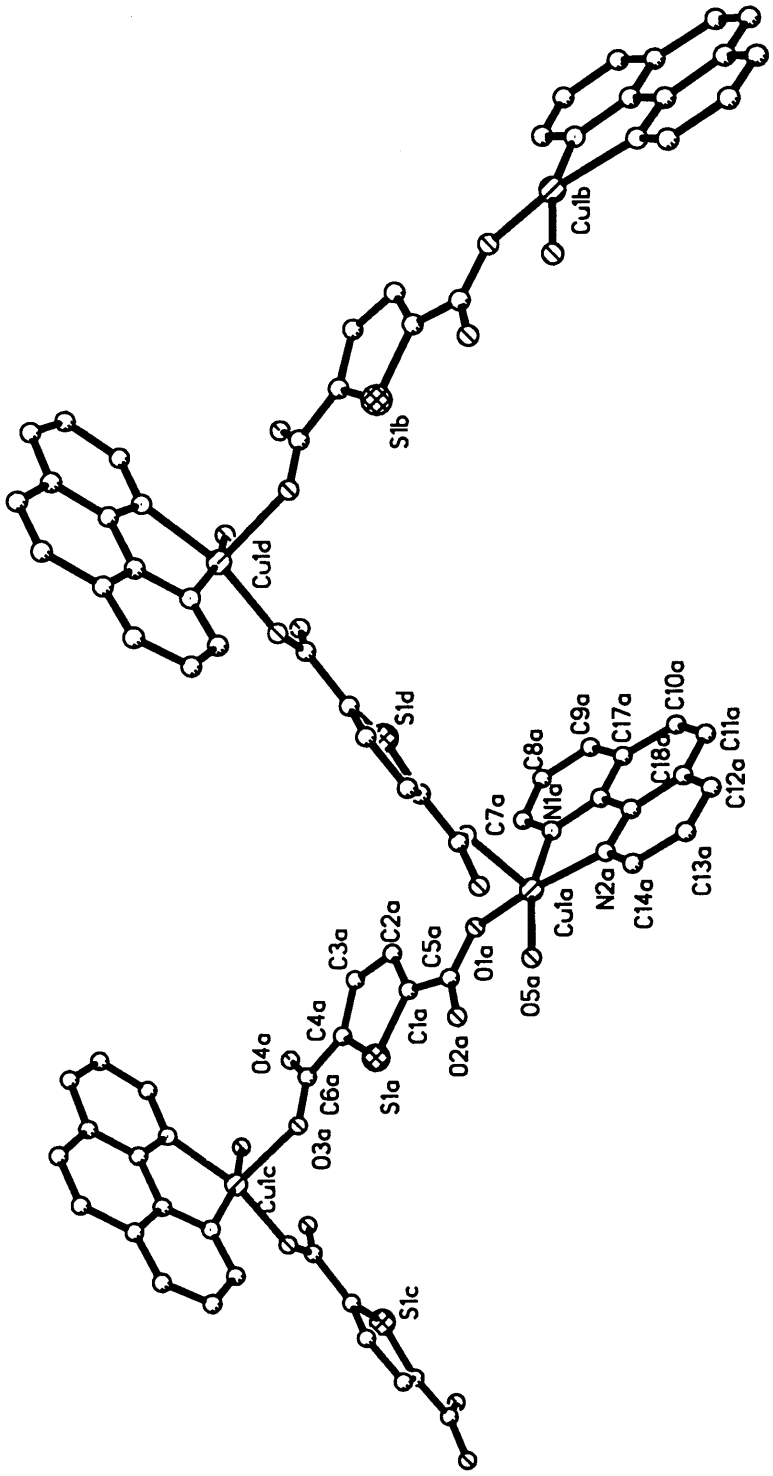

Fig. 4. Partial packing diagram of 3.

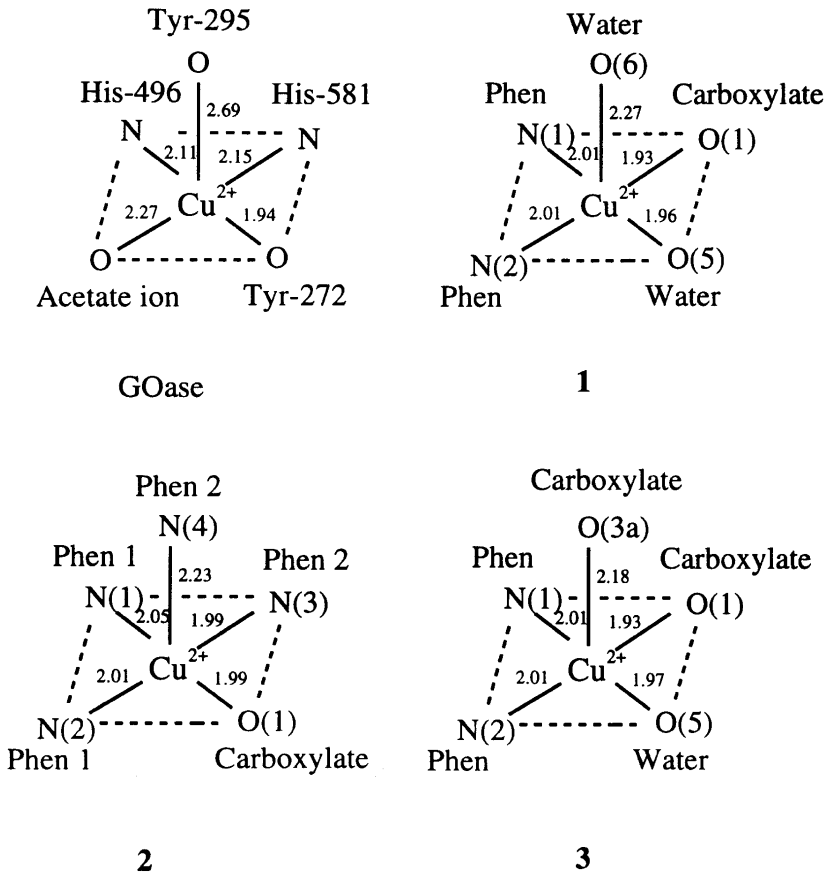

Fig. 5. Comparison of copper(II) coordination environments.

Table 5. Comparison of some structural parameters for copper(II) coordination spheres

Complex	τ^*	R.m.s deviation of basal plane (Å)	Deviation of Cu above plane (Å)	Axial bond length (Å)
1	0.07	0.071	0.20	2.272
2	0.20	0.116	0.11	2.225
3	0.003	0.011	0.21	2.184

*For perfect tetragonal and trigonal-bipyramidal geometries the values of τ are zero and unity, respectively; $\tau = (\beta - \alpha)/60$, being an index of the degree of tetragonality within the structural continuum between square-planar and trigonal-bipyramidal geometries [40].

1,10-phenanthroline rings in **1** and **2** as shown in Figs. 2–3. It has been established that stacking interactions, observed either in solution or in the solid state, are recognized as enhancing the stability of mixed ligand complexes, but more importantly, as creating specific structures [19–25]. The stacking interactions probably also stabilize the structure of **1** and **2**. The dihedral angle between the mean thiophene plane and the mean plane of 1,10-phenanthroline in an adjacent molecule is 9.7° and the average distance between the two planes is about 3.65 Å in **1**. Atom S1c is just below the phenanthroline rings with more overlap with the ring formed by N1a, C7a, C8a, C9a, C17a and C16a. Figure 3 shows the partial packing diagram of the structure of **2**. Planes a, b, d and e are the corresponding phenanthroline molecular planes from four different molecules while plane c is that of the neutral thiophenedicarboxylic acid. Planes b and d (also a and e) are symmetrically displaced with respect to plane c. The dihedral angles between plane b and plane c is 11.2° and separation between the two planes is 3.70 Å. Planes a and b (also d and e) are strictly parallel with

Table 6.Comparison of parameters involved in stacking interactions

Compounds	Dihedral angle (°)	Planes separation (Å)	Distances from sulfur to the atoms at the stacked plane (Å)
1	9.7	3.65	3.46 (N1a), 3.95 (C15a), 3.49 (C16a), 3.82 (C17a) (from S1c)
2	11.2	3.70	3.85 (C21b), 4.04 (C22b) 3.94 (C28b), 3.68(C29b) (from S2a)
GOase	1.8	3.4	3.84 (S to six carbons of Trp290)

a separation of 3.5 Å. S2a is exactly above the centre of the rings formed by N3b, C19b, C20b, C21b, C22b, C30b, C27b, C28b, C29b and C30b. In the GOase copper active site, the thioether bond between Tyr272 and Cys228 is stacked with the indole ring of Trp290 as shown in Fig. 1. The six-membered ring of indole ring of Trp290 located exactly above the sulfur atom [the distances between the sulfur and these six carbons of Trp290 are all 3.84(4) Å]. The "best" plane defined by all the side-chain atoms of Tyr272 and Cys228 makes an angle of 1.8°, nearly perfectly parallel, with the plane of the side-chain atoms of Trp290. The two planes are 3.4 Å apart. A comparison of some of the parameters involved in stacking interactions in **1**, **2** and GOase is listed in Table 6.

Physical, electrochemical and thermal properties

Complexes **1** and **2** can be dissolved in methanol, ethanol, dmf, etc. by ultrasonic shaking and gentle heating, while **3** is insoluble in common solvents.

The infrared spectrum of the free ligand, H_2Tda, shows ν(C═O) of COOH at 1665 cm^{-1} as a strong band indicating that there is intermolecular hydrogen bonding of the type C═O···H–O in the uncoordinated thiophene-2,5-dicarboxylic acid molecules. This is commonly observed in the case of carboxylic acids [47]. After deprotonation and coordination to a copper atom, this band disappears and is replaced by very strong bands in the 1560–1590 and 1350–1390 cm^{-1} regions, which correspond to the asymmetric and symmetric vibrations of the COO^- moiety, respectively. In complex **2**, a strong band at 1690 cm^{-1} indicates that the carbonyl oxygen in H_2Tda is not involved in hydrogen bonding and this is confirmed by the structure determination.

The solid state room-temperature electronic spectra of **1**, **2** and **3** exhibit a broad d–d band with a maximum at 656, 640 and 680 nm, respectively, which is typical for square-pyramidal coordination of copper(II) complexes [12–16, 41, 42]. **1** and **2** exhibit broad absorptions at 735 and 728 nm, respectively, in ethanol–water (1:1) solution. The lower-energy bands suggest that changes have occurred in the geometry around copper(II) and probably indicate the presence of a more trigonal-bipyramidal element in solution [13, 48, 49].

The cyclic voltammogram of **1** and **2** was measured in ethanol–water (1:1) solution contained 0.10 M $(NEt_4)ClO_4$ as the supporting electrolyte. A selected voltammogram is shown in Fig. 6. The complexes are electrochemically active and display irreversible one-electron reduction waves with $E_{1/2}$ −0.126 V ($i_{pa}/i_{pc}=0.85$, $\Delta E_p=162$ mV) for **1** and quasi-reversible one-electron reduction waves with $E_{1/2}$ 0.001 V ($i_{pa}/i_{pc}=1.04$, $\Delta E_p=96$ mV) for **2** vs SCE, which are assigned to Cu^{2+}/Cu^+ one-electron redox. SCE is 0.242 V vs NHE [50], so $E_{1/2}$ is 0.116 V for **1** and 0.243 V for **2** vs NHE, comparable to 0.15 V for Cu^{2+}(aq)/Cu^+(aq) and 0.17 V for $Cu^{2+}(phen)_2$/$Cu^+(phen)_2$ redox potentials (Ref. [44] and references therein).

A water molecule of crystallization can be distinguished from a coordinated water molecule in a complex by means of differential thermoanalysis. The TGA–DTA result shows that **1** first loses water of crystallization between 40–150°C with a total loss of three water molecules (calcd weight lost: 10.7%; found: 10.3%). The complex began losing the two coordinated water molecules at 150°C. In complex **2** the two water molecules of crystallization were lost in the 75–160°C temperature range (calcd weight lost: 5.4%, found: 5.0%). **3** began to lose water at 160°C, a relatively high temperature indicating the absence of water of crystallization; the eventual total weight lost corresponds to the loss of one coordinated water molecule (calcd weight lost: 4.1%, found: 4.2%). In a similar square pyrimidal [Cu(L-glu)(phen)(H_2O)]·$3H_2O$ complex [27], the coordinated water molecule is lost in the 110–150°C temperature range, indicating the bond strength of the coordinated water molecule in this complex is weaker than those in **1** and **3**.

Acknowledgements—We thank the National University of Singapore for the research scholarship to B.-L.C. and Ms T.-T. Ong for her assistance in the electrochemical experiments.

REFERENCES

1. Press, J. B., in *The Chemistry of Heterocyclic Compounds*, Vol. 44, Part 4, Chap. 3, ed. Salo Gronowitz. Wiley, New York, 1992.
2. Angelici, R. J., *Coord. Chem. Rev.*, 1990, **105,** 27.
3. Rauchfuss, T. B., *Prog. Inorg. Chem.*, 1991, **39,** 259.

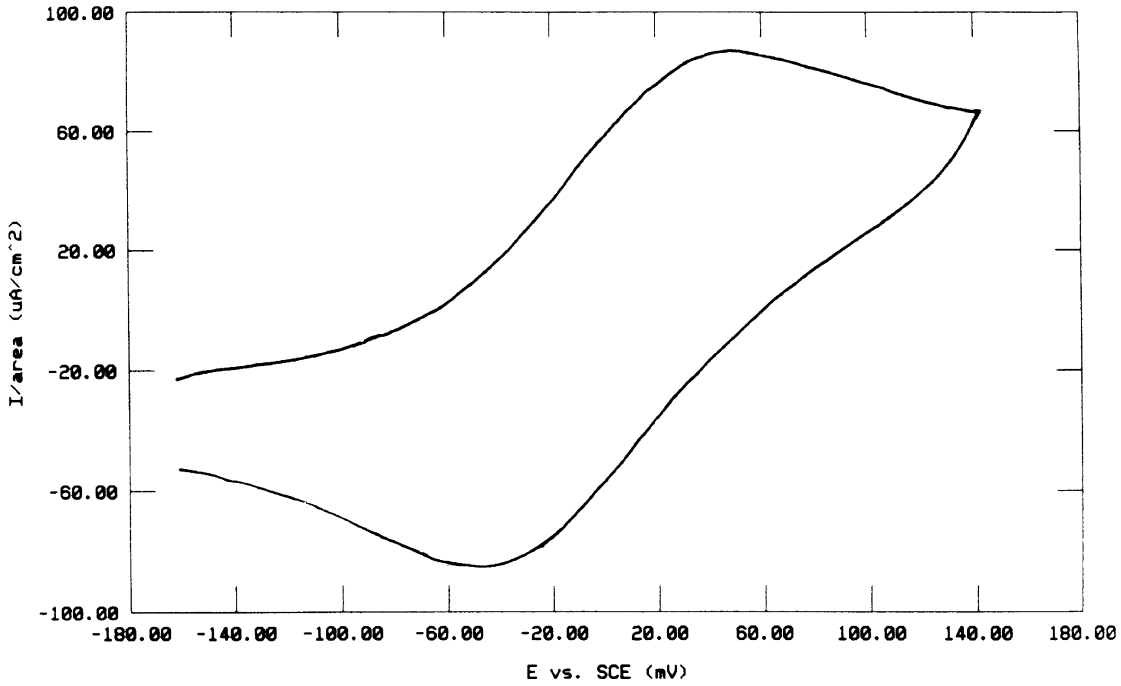

Fig. 6. Cyclic voltammogram of **2** in 1:1 $EtOH/H_2O$ solution (0.1 M TEAP) at a scan rate of $50\,mV\,s^{-1}$. The solution concentration was 10^{-3} M.

4. Bailey, N. A., Eddy, M. M., Fenton, D. E., Moss, S., Mukhopadhyay, A. and Jones, G., *J. Chem. Soc. Dalton Trans.*, 1984, 2281.
5. Alvarez, M., Lugan, N. and Mathieu, R., *Inorg. Chem.*, 1993, **32,** 5652.
6. Modder, J. F., Leijen, R. J., Vrieze, K., Smeets, W. J. J., Spek, A. L. and Koten, G. van, *J. Chem. Soc. Dalton Trans.*, 1995, 4021.
7. Drew, M. G. B., Harding, C. J., Howarth, O. W., Lu, Q., Marrs, D. J., Morgan, G. G., McKee, V. and Nelson, J., *J. Chem. Soc. Dalton Trans.*, 1996, 3021.
8. Sahasrabudhe, M. B., Nerurkar, M. K., Nerurkar, M. V., Tilak, B. D. and Bhavasar, M. D., *Br. J. Cancer*, 1960, **14,** 547.
9. Guerriero, P., Casellato, U., Sitran, S., Vigato, P. A. and Graziani, R., *Inorg. Chim. Acta*, 1987, **133,** 337.
10. Ito, N. V., Phillips, S. E., Stevens, C., Ogel, Z. B., McPherson, M. J., Keen, J. N., Yadav, K. D. S. and Knowles, P. F., *Nature* (*London*), 1991, **350,** 87.
11. Ito, N., Phillips, S. E. V., Yadav, K. D. S. and Knowles, P. F., *J. Mol. Biol.*, 1994, **238,** 794.
12. Adams, H., Bailey, N. A., Campbell, I. K., Fenton, D. E. and He, Q.-Y., *J. Chem. Soc. Dalton Trans.*, 1996, 2233.
13. Adams, H., Bailey, N. A., Rodriguez de Barbarin, C. O., Fenton, D. E. and He, Q.-Y., *J. Chem. Soc. Dalton Trans.*, 1995, 2323.
14. Uma, R., Viswanathan, R., Palaniandavar, M. and Lakshminarayanan, M., *J. Chem. Soc. Dalton Trans.*, 1994, 1219.
15. Whittaker, M. M., Duncan, W. R. and Whittaker, J. W., *Inorg. Chem.*, 1996, **35,** 382.
16. Halfen, J. A., Young, V. G. Jr. and Tolman, W. B., *Angew. Chem. Int. Ed. Engl.*, 1996, **35,** 1687.
17. Sigel, H., Fischer, B. E. and Farkas, E., *Inorg. Chem.*, 1983, **22,** 925.
18. Fischer, B. E. and Sigel, H., *J. Am. Chem. Soc.*, 1980, **102,** 2998.
19. Sigel, H., *Angew. Chem. Int. Ed. Engl.*, 1975, **14,** 394.
20. Mitchell, P. R. and Sigel, H., *J. Am. Chem. Soc.*, 1978, **100,** 1564.
21. Fischer, B. E. and Bau, R., *J. Chem. Soc. Chem. Commun.*, 1977, 272.
22. Aoki, K., *J. Am. Chem. Soc.*, 1978, **100,** 7106.
23. Wei, C. Y., Fischer, B. E. and Bau, R., *J. Chem. Soc. Chem. Commun.*, 1978, 1053.
24. Fischer, B. E. and Bau, R., *Inorg. Chem.*, 1978, **17,** 27.
25. McCann, S., McCann, M., Casey, M. T., Devereux, M., McKee, V., McMichael, P. and McCrea, J. G., *Polyhedron*, 1997, **16,** 4247.
26. Sheldrick, W. S., *Z. Naturforsch B:*, 1982, **37,** 863.
27. Antolini, L., Marcotrigiano, G., Menabue, L., Pellacani, G. C., Saladini, M. and Sola, M., *Inorg. Chem.*, 1985, **24,** 3621.
28. Dubler, E., Haring, U. K., Scheller, K. H., Baltzer, P. and Sigel, H., *Inorg. Chem.*, 1984, **23,** 3785.
29. Antolini, L., Battaglia, L. P., Bonamartini Corradi, A., Marcotrigiano, G., Menabue, L., Pellacani, G. C., Saladini, M. and Sola, M., *Inorg. Chem.*, 1986, **25,** 2901.

30. Orioli, P., Cini, R., Donati, D. and Mangani, S., *J. Am. Chem. Soc.*, 1981, **103,** 4446.
31. Sugimori, T., Shibakawa, K., Masuda, H., Odani, A. and Yamauchi, O., *Inorg. Chem.*, 1993, **32,** 4951.
32. Yamauchi, O., Odani, A., Kohzuma, T., Masuda, H., Toriumi, K. and Saito, K., *Inorg. Chem.*, 1989, **28,** 4066.
33. Bauner, W., Fischer, R., Keil, S., Noll, B. and Weinelt, H., *Ger.* (*East*), 1978, 129448.
34. Molecular Structure Corporation, *TEXSAN. Single Crystal Structure Analysis Software*. MSC, 3200 Research Forest Drive, The Woodlands, TX 77381, U.S.A., 1989.
35. *SHELXTL PLUS* (*PC Version*). Siemens Analytical X-ray Instruments, Madison, Wadison, WI, 1989.
36. Sheldrick, G. M., *SHELXL*-93: *A Program for Structure Refinement*. University of Göttingen, Germany, 1993.
37. Oae, S., Furukawa, N., Watanabe, T., Otsuji, Y. and Hamada, M., *Bull. Chem. Soc. Jpn.*, 1965, **38,** 1247.
38. Butler, A. R., *J. Chem. Soc. B*, 1970, 867.
39. Cano, J., Munno, G. D., Sanz, J. L., Ruiz, R., Faus, J., Lloret, F., Julve, M. and Caneschi, A., *J. Chem. Soc. Dalton Trans.*, 1997, 1915.
40. Addison, W., Rao, J. N., Reedijk, J., van Rijn, J. and Versheoor, G. C., *J. Chem. Soc. Dalton Trans.*, 1984, 1349.
41. Lim, M. C., Sinn, K. and Martin, R. B., *Inorg. Chem.*, 1976, **15,** 807.
42. Battaglia, L. P., Bonamartini Corradi, A., Ianelli, S., Zoroddu, M. A. and Sanna, G., *J. Chem. Soc. Faraday Trans.*, 1991, **87,** 3863.
43. Maccarrone, G., Nardin, G., Randaccio, L., Tabbi, G., Rosi, M., Sgamellotti, A., Rizzarelli, E. and Zangrando, E., *J. Chem. Soc. Dalton Trans.*, 1996, 3449.
44. Hathaway, B. J., in *Comprehensive Coordination Chemistry*, Vol. V, Chap. 53, eds. G. Wilkinson, R. D. Gillard and J. A. McCleverty. Pergamon Press, Oxford, 1987.
45. Carrell, C. J., Carrell, H. L., Eelebacher, J. and Glusker, J. P., *J. Am. Chem. Soc.*, 1988, **110,** 8651.
46. Chakrabarti, P., *Protein Eng.*, 1990, **4,** 49.
47. Bellamy, L. J., in *The Infra-red Spectra of Complex Molecules*, 3rd edn. John Wiley, New York, 1975.
48. Tyagi, S. and Hathaway, B. J., *J. Chem. Soc. Dalton Trans.*, 1981, 2029.
49. Tyagi, S. and Hathaway, B. J., *J. Chem. Soc. Dalton Trans.*, 1983, 199.
50. Bard, A. J. and Faulkner, L. R., in *Electrochemical Methods*: *Fundamentals and Applications*. John Wiley, New York, 1980.

Pergamon

Polyhedron Vol. 17, No. 23–24, pp. 4249–4256, 1998
© 1998 Elsevier Science Ltd
All rights reserved. Printed in Great Britain
0277–5387/98 $19.00+0.00

PII: S0277–5387(98)00235–6

Reactions of coordinated alcohol as a route to mixed-metal La–Zn alkoxides: molecular structure of $LaZn_3(\mu\text{-}OBu^t)_6[N(SiMe_3)_2]_3$

Stephane Daniele,[a] Liliane G. Hubert-Pfalzgraf*[a] and Jacqueline Vaissermann[b]

[a]Laboratoire de Chimie Moléculaire, URA-CNRS, Université de Nice-Sophia Antipolis, Parc Valrose, 06108 Nice Cedex 2, France

[b]Laboratoire de Chimie des Métaux de Transition, URA-CNRS, Place Jussieu, 75230 Paris Cedex 05, France

(Received 20 March 1998; accepted 9 June 1998)

Abstract—The reactions between $La_3(OBu^t)_9(HOBu^t)_2$ and $Zn[N(SiMe_3)_2]_2$ have been investigated as a means to access to La–Zn species. A volatile complex $LaZn_3(\mu\text{-}OBu^t)_6[N(SiMe_3)_2]_3$ (**1**) was obtained at room temperature together with $La_4Zn_2O(OBu^t)_{13}[N(SiMe_3)_2]$ (**2**) and $[La_4O(OBu^t)_{10}]_2$ (**3**). The reaction was more selective under reflux although retention of the $Zn–N(SiMe_3)_2$ bond was still observed giving $La_4Zn_2(OBu^t)_{15}[N(SiMe_3)_2]$ (**4**). No La–Zn species were obtained if the La_3 solvate was refluxed with either $Zn(OBu^t)[N(SiMe_3)_2]$ or $[Zn(OBu^t)_2]_m$; $La_5(\mu_5\text{-}O)(OBu^t)_{13}$ was isolated in the latter case. The various compounds were characterized by elemental analysis, FTIR, ^1H NMR. **1** was also characterized by single crystal X-ray diffraction; its molecular structure is based on a central 6-coordinate lanthanum with 3-coordinate zinc atoms. © 1998 Elsevier Science Ltd. All rights reserved

Keywords: mixed-metal alkoxides; zinc; lanthanum; sol–gel; MOCVD; amides.

INTRODUCTION

A large variety of electrooptical ceramics are based on lanthanum oxides. Complex oxides such as (Pb, La)(Zn, Nb, Zr, Ti)O_3 (PBLNZT) or $La_2Zn_2SnO_7$ are examples of current formulations and show that lanthanum is associated to zinc [1]. Chemical routes such as sol-gel or MOCVD techniques are crucial for the control of the properties, of the microstructure and for the processing of these materials as films [2, 3]. These techniques depend of the availability of soluble or volatile, homo- or heterometallic oxide precursors. "Single-source" precursors have been shown to improve the properties of high tech materials [3]. Despite the importance of lanthanum in the formulation of advanced materials, mixed-metal oxide precursors involving lanthanum remain scarce. No simple species based on lanthanum and alkaline metals and which could be used as a synthon is available. The mixed-metal species reported so far for lanthanum are isopropoxide derivatives in which the rare earth is associated with niobium [4, 5], with molybdenum [6] or with zirconium [7]. By contrast with most metal alkoxides, zinc derivatives are relatively inert and, as a result, the formation of mixed-metal species requires less classical routes [8]. We recently reported the formation of mixed-metal oxoalkoxides based on zinc and tantalum by metathesis reaction between ZnI_2 and $KTa(OiPr)_6$ or by ultrasonic activation between the homometallic alkoxides [9]. A large number of metal alkoxides are obtained as solvates with alcohol molecules [10, 11]. The enhanced acidity of the coordinated alcohol molecules turns these ligands into functional groups able to react with labile species or even electropositive metals [12–14] allowing the built up of mixed-metal species.

The structurally characterized lanthanum tertiary butoxide solvate $La_3(\mu_3\text{-}OBu^t)_2(\mu\text{-}OBu^t)_3(OBu^t)_4(HOBu^t)_2$, appeared as an attractive synthon [15] for this strategy and thus for a convenient route to

*Author to whom correspondence should be addressed. New address: Université de Lyon 1 ESI, bâtiment 731, boulevard du 11 Nov 1918, 69622 Villeurbanne Cedex, France. E-mail: Hubert@cismsun.univ-lyon1.fre

La–M species. We report here the results of the investigations between $La_3(OBu^t)_9(HOBu^t)_2$ and zinc bis-trimethylsilylamide $Zn[N(SiMe_3)_2]_2$. By contrast with the reactions between $La_3(OBu^t)_9(HOBu^t)_2$ and other metal bis-trimethylsilylamide derivatives [16], the reaction with $Zn[N(SiMe_3)_2]_2$ is less selective probably as a result of a lower lability of the $Zn–N(SiMe_3)_2$ bond. Mixed-metal La–Zn oxo and nonoxo derivatives displaying $LaZn_3$ and La_4Zn_2 stoichiometries and the lanthanum oxoalkoxide $[La_4O(OBu^t)_{10}]_m$ were obtained depending on the experimental conditions. They were characterized by elemental analysis, FTIR, ^{1}H NMR and by a single crystal X-ray diffraction study for $LaZn_3(\mu\text{-}OBu^t)_6[N(SiMe_3)_2]_3$.

EXPERIMENTAL SECTION

All manipulations were routinely performed under argon using Schlenk tubes and vacuum line techniques with solvents purified by standard methods. $La_3(OBu^t)_9(HOBu^t)_2$ and $Zn[N(SiMe_3)_2]_2$ were obtained according to the literature [15, 17]. NMR(^{1}H, ^{13}C) and IR spectra were run on Bruker AC-200 and IR-FTS 45 spectrometers, respectively. IR spectra were obtained as Nujol mulls. Analytical data were obtained from the Centre de Microanalyses du CNRS.

Synthesis of $LaZn_3(OBu^t)_6[N(SiMe_3)_2]_3$ (**1**), $La_4Zn_2O(OBu^t)_{13}[N(SiMe_3)_2]$ (**2**) and $[La_4O(OBu^t)_{10}]_2$ (**3**)

0.278 cm^3 (0.74 mmol) of $Zn[N(SiMe_3)_2]_2$ in 5 cm^3 of toluene were added to $La_3(OBu^t)_9(HOBu^t)_2$(0.90 g, 0.74 mmol) in 25 cm^3 of toluene. Stirring was maintained for 20 h at room temperature. Evaporation to dryness gave a white solid, which was redissolved in 20 cm^3 of toluene. The solution was concentrated and cooled to 4°C. Crystals of **1** were obtained after 24 h 0.16 g (52%/Zn, 6%/La). Anal. Found: C, 40.8, H, 8.92, N, 3.45; La, 11.02; Zn, 15.42 Calc. for $C_{42}H_{108}O_6N_3LaSi_6Zn_3$, C, 40.2; H, 8.67; N, 3,35; La, 11.09; Zn, 15.65%. IR (cm^{-1}): 1366 s; 1250 sh, 1247 s, ν(Si–C), 1175 s; 972 vs, 925 w, 904 vs, 883 vs, 847 s, 832 vs, 815 s, 756 m, 671 m, 613 w; 559 s, 476 m, 466 m, 408 s, 385 s ν(M–O). ^{1}H NMR ($CDCl_3$, ppm): 1.50 s (9H, μ-OBut), 0.14 s (18H, $SiMe_3$). $^{13}C\{^1H\}$ NMR ($CDCl_3$, ppm): 73.2 (OC), 35.0 (CMe_3), 6.0 (SiMe_3).

Further concentration of the solution gave crystals of **2** (0.18 g, 28%/Zn, 18%/La) after 24 h at 4°C. Anal. Found: C, 38.53, H, 7.62, N 0.80, La, 30.50; Zn, 7.30 Calc. for $C_{58}H_{135}O_{14}NLa_4Si_2Zn_2$ C, 38.42; H, 7.50; N, 0.77, La, 30.67; Zn, 7.22%. IR (cm^{-1}): 1360 s; 1240 s ν(Si–C), 1199 vs; 1021 w, 973 vs, 934 vs, 906 s, 889 sh, 831 m, 766 m; 674 w, 614 w ν(Zn–N); 559 s, 511 s, 481 s, 385 vs ν(M–O). ^{1}H NMR ($CDCl_3$, ppm): 1.66 s, (9H, μ_3-OBut), 1.58 s, (18H, μ_3-OBut), 1.47 s, (9H, μ-OBut), 1.45 s (36H, μ-OBut), 1.21 s (18H, μ-OBut, 1.09 s (18H, LaOBut), 1.06 s (9H, *Z*nOBut), 0.08 s (18H, $SiMe_3$).

The last crop of crystals corresponds to **3** (0.54 g, 56%/La). Anal. Found: C, 36.23, H, 6.77, La, 42.76 Calc. for $C_{40}H_{90}O_{11}La_4$: C, 36.88, H, 6.93, La, 42.59%. IR (cm^{-1}): 1220 m, 1197 s; 976 s, 960 m, 936 s, 905 m, 831 w, 766 w; 564 m, 482 s, 387 s (νLa–OR). ^{1}H NMR ($CDCl_3$, ppm): 1.71 s (54H, μ_3-OBut), 1.51 s (72H, μ-OBut), 1.27 s (18H, OBut), 1.16 s (36H, OBut).

Synthesis of $La_4Zn_2(OBu^t)_{15}[N(SiMe_3)_2]$ (**4**)

A similar procedure but in refluxing conditions applied to 0.263 cm^3 (0.70 mmol) of $Zn[N(SiMe_3)_2]_2$ in 5 cm^3 of toluene and to $La_3(OBu^t)_9(HO^tBu)_2$ (0.85 g, 0.70 mmol) in 25 cm^3 of toluene gave **4** (0.62 g, 91%/Zn, 61%/La). Anal. Found: C, 43.97, H, 8.55, La, 28.42; Zn, 6.36 Calc. for $C_{66}H_{153}O_{15}NLa_4Si_2Zn_2$: C, 43.07, H, 8.38, La, 28.62; Zn, 6.73%. IR (cm^{-1}): 1362 s; 1247 s ν(Si–C); 1219 s, 1197 vs ν(C–O); 1021 w, 992 s, 973 vs, 955 s, 934 vs, 913 m, 905 m, 885 m, 828 m, 798 sh, 767 m; 672 w, 604 w ν(Zn–N); 585 w, 571 w, 508 m, 495 s, 386 vs (νM–OR). ^{1}H NMR ($CDCl_3$, ppm): 1.73 s (18H, μ_3-OtBu), 1.55 s (9H, μ_3-OBut), 1.53 s (9H, μ3), 1.52 s (36H, μ-OtBu), 1.37 s (18H, μ-OBut), 1.27 s (9H, ZnOtBu), 1.16 s (36H, LaOBut), 0.08 s (18H, $SiMe_3$).

All compounds were pale yellow, soluble in toluene and in THF but insoluble in hexane.

Synthesis of $La_5(\mu_5\text{-}O)(OBu^t)_{13}$

0.323 g (0.264 mmol) of $La_3(OBu^t)_9(HOBu^t)_2$ in 15 ml of toluene were added to a suspension of 56 mg (0.264 mmol) of $Zn(OBu^t)^2$ in 10 ml of toluene. The reaction medium was stirred at room temperature for 23 h and refluxed for 6 h. The precipitate isolated by filtration corresponded to Zn ter-butoxide (quantitative amount). The filtrate was evaporated to dryness, the crude solid was recrystallized in THF, colorless crystals were obtained at −25°C (0.145 g, 55%). The same compound was obtained by reflux for 6 h in the absence of the zinc alkoxide. IR (cm^{-1}): 971 vs, 934 vs, 913 m, 827 m, 766 m; 570, 508 m, 484 s, 385 vs (νLa–OR). ^{1}H NMR ($CDCl_3$, ppm): 1.69 s (36H), 1.51 s (36H), 1.15 s (45H).

Crystallography of $LaZn_3(OBu^t)_6[N(SiMe_3)_2]_3$ (**1**)

Suitable crystals of **1** were grown directly from the reaction medium. 3185 data ($4 < 2\theta < 32°$) were collected at −80°C on a CAD-4 diffractometer using the graphite monochromatized Mo-Kα radiation ($\lambda = 0.71070$ Å). The crystals were unstable. The intensities of three standard reflections monitored every hour decayed uniformly to final values about 10% of the initial ones. The data were scaled accordingly. The decay in intensities accounts for the limited range of 2θ, several attempts with various crystals did not improve the data. Basic information is collected in Table 1.

Computations were performed by using CRYS-

TALS adapted on a Micro Vax II [18]. The structure was solved by Patterson methods and subsequent Fourier maps. Of the 3185 unique refections, 2085 with $I > 3\sigma(I)$ were used to solve and refine the structure. All atoms were refined anisotropically. Least squares refinements with approximation in three blocks to the normal matrix were carried out minimizing the function $w(|F_0|-|F_c|)^2$, were F_0 and F_c are the observed and calculated structure factors. Unit weight was used. Models reached convergence with $R=(|F_0|-\Sigma|F_c|)/\Sigma|F_0|$ and $R_w=[\Sigma w(|F_0|-|F_c|^2)/\Sigma(F_0)^2]^{1/2}$ of 0.127 and 0.141 respectively for 246 variables. Criteria for a satisfactory complete analysis were the ratios of rms shift to standard deviation being less than 0.1 and no significant features in the final difference map. Anomalous dispersions terms were applied. Empirical absorption corrections were made [19].

Atomic coordinates, nonessential bond lengths and angles and thermal parameters have been deposited at the Cambridge Crystallographic Data Centre.

RESULTS AND DISCUSSION

Synthesis and characterization

The reaction between $La_3(OBu^t)_9(HOBu^t)_2$ and $Zn[N(SiMe_3)_2]_2$ (1:1 stoichiometry) proceeds smoothly in toluene at room temperature (Scheme 1) giving different species which were separated by their solubility properties. While a compound having a La_3Zn stoichiometry was expected with a strategy based on the reactivity of the coordinated alcohol molecules the first compound isolated (in modest yield 6%/La) was actually a species having the opposite stoichiometry, $LaZn_3(OBu^t)_6[N(SiMe_3)_2]_3$ (**1**). Further crystallizations afforded the heterometallic oxoalkoxide $La_4Zn_2O(OBu^t)_{13}[N(SiMe_3)_2]$ (**2**) (yield 18%/la) and, as the last crop and major species (yield 56%/La), the homometallic $[La_4O(OBu^t)_{10}]_2$ oxoalkoxide **3**. Compound **1** is formed at room temperature, independently of the stoichiometry used (molar ratio from 1 to 5). The preceding reaction is more selective if it is achieved in refluxing toluene over 20 h. The nonoxo species $La_4Zn_2(OBu^t)_{15}[N(SiMe_3)_2]$ (**4**) is the only one isolated (yield 61%/La). IR and ^{1}H NMR data confirm the presence of trimethylsilylamide ligands for compounds **1**, **2** and **4**. This is evidenced by ν(Si–C) absorption bands at $\sim 1250\,cm^{-1}$ in the FTIR spectra while resonances at high field (0.14 or 0.08 ppm) are detected in the proton NMR spectra. The poor reactivity of the Zn–$N(SiMe_3)_2$ bond is in agreement with other observations [20]. No evidence for solvating alcohol molecules was found either by FTIR or by NMR (absence of a peak due to hydroxyls by contrast with the solvated La_3 butoxide). The heterometallic character for the various compounds was supported by elemental analyses and by a X-ray structure determination for **1**.

Table 1. Crystallographic data for $LaZn_3(\mu\text{-}OtBu)_6[N(SiMe_3)_2]_3$

Chemical formula	$C_{42}H_{126}O_6N_3Si_6Zn_3La$
fw	1273
Crystal system	triclinic
Space group	*P*-1
Z	2
a (Å)	11.442(4)
b (Å)	13.202(2)
c (Å)	22.685(4)
α (°)	75.29(1)
β (°)	83.75(2)
γ (°)	85.75(2)
V (Å^3)	3289(2)
ρ (calculated) (g cm^{-3})	1.28
μ (Mo-Kα) (cm^{-1})	18.91
Diffractometer	CAD4
Monochromator	graphite
Radiation	Mo-Kα(0.71070)
Scan type	ω/2θ
Scan range θ (°)	$1.2+0.34\tan\theta$
2θ Range (°)	4–32
Reflection collected	3185
Reflection used (criteria)	2085[$I>3\sigma(I)$]
R	0.127
R_w [a]	0.141
I.s. parameters	246

[a] $R_w=\Sigma iWi(F_0-F_c)^2/\Sigma iWiF_0^2]^{1/2}$.

*Molecular structure of $LaZn_3(OBu^t)_6[N(SiMe_3)_2]_3$ (**1**)*

The crystals of **1** are built up by $LaZn_3(\mu\text{-}OBu^t)_6N(SiMe_3)_2]_3$ molecules possessing a pseudo third order symmetry axis. Lanthanum and zinc are 6- and 3-coordinate respectively (Fig. 1). Selected bond lengths and angles are collected in Table 2. The central lanthanum atom is surrounded by six tertiary butoxide ligands [La–μ-OR av. 2.45(2) Å] leading to a trigonal prismatic geometry. The La–OR bond lengths fall in the range commonly observed [2, 3, 15]. The OR ligands act as assembling ligands between lanthanum and trigonal planar zinc atoms still bearing a trimethylsilylamide ligand. The Zn–N bond distances [av. 1.90(3) Å] are comparable to the Zn–OR ones [av. 1.92(3) Å]. The bond lengths and the angles O–Zn–N [av. 135.5(12)°] and O–Zn–O [av. 89.1(10)°] are similar to these observed for $\{Zn(\mu\text{-}OCEt_3)_2[N(SiMe_3)_2]\}_2$ [21]. The framework of **1** is related to that of other tetrametallic lanthanide species namely $[LnAl_3(OPr^i)_{12}]$ [22], $[LaM_3(BINOL)_3]$ (M = Li, Na, BINOL = binaphtol) [23–25], $Ln(\mu\text{-}OtBu)_3(\mu\text{-}Me)_3(AlMe_2)_3$ (Ln = Y, Nd, Pr) [26] or $[Nd(NMe_2)_3(MMe_3)_3]$ (M = Al, Ga) [27].

The ^{1}H NMR spectra give evidence that the structure of **1** is retained in solution. All butoxide and silylamide groups are equivalent. Compound **1** is vol-

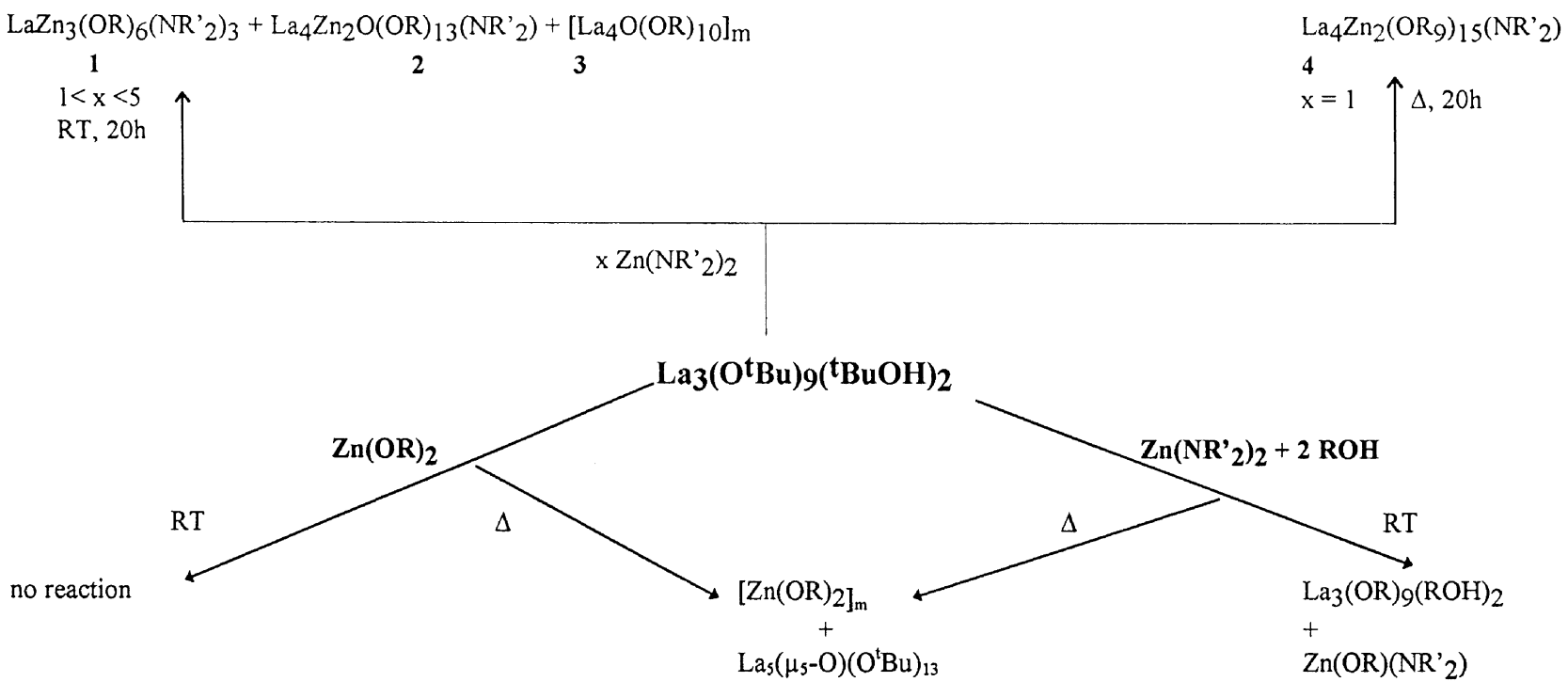

Scheme 1. Reactivity of La_3 $(OtBu)_9(tBuOH)_2$ toward zinc derivatives (R = *t*Bu, $NR_2' = N(SiMe_3)_2$, all reactions in toluene.

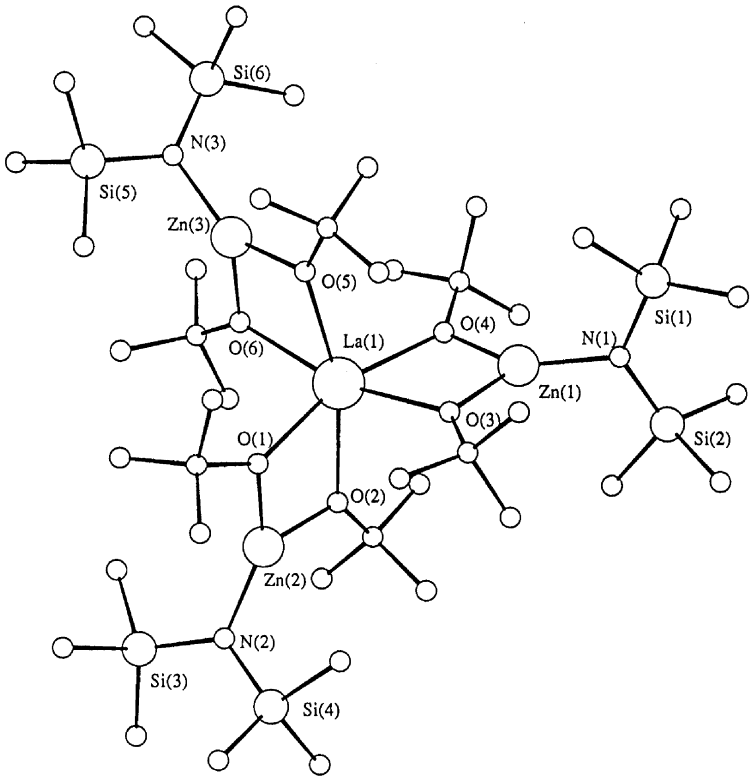

Fig. 1. Molecular structure and atom-labelling scheme for La(μ-O*t*Bu)$_6${Zn[N(SiMe$_3$)$_2$]$_2$}$_3$.

Table 2. Selected interatomic distances (Å) and angles (°) for LaZn$_3$(μ-O*t*Bu)$_6$[N(SiMe$_3$)$_2$]$_3$

La(1)–Zn(1)	3.424(5)	La(1)–Zn(3)	3.410(5)
La(1)–Zn(2)	3.411(5)		
La(1)–O(1)	2.39(2)	La(1)–O(4)	2.42(2)
La(1)–O(2)	2.50(3)	La(1)–O(5)	2.46(3)
La(1)–O(3)	2.46(2)	La(1)–O(6)	2.48(2)
Zn(1)–O(3)	1.92(2)	Zn(1)–O(4)	1.91(2)
Zn(2)–O(1)	1.92(3)	Zn(2)–O(2)	1.94(3)
Zn(3)–O(5)	1.91(2)	Zn(3)–O(6)	1.90(3)
Zn(1)–N(1)	1.90(3)	Zn(2)–N(2)	1.92(3)
Zn(3)–N(3)	1.87(3)		
O(2)–La(1)–O(1)	67.3(10)	O(5)–La(1)–O(3)	101.2(8)
O(3)–La(1)–O(1)	102.1(7)	O(5)–La(1)–O(4)	93 5(7)
O(3)–La(1)–O(2)	93.0(7)	O(6)–La(1)–O(1)	90.7(7)
O(4)–La(1)–O(1)	163.4(8)	O(6)–La(1)–O(2)	101.3(7)
O(4)–La(1)–O(2)	100.6(8)	O(6)–La(1)–O(3)	163.7(7)
O(4)–La(1)–O(3)	66.1(7)	O(6)–La(1)–O(4)	103.1(7)
O(5)–La(1)–O(1)	100.5(9)	O(6)–La(1)–O(5)	66 2(8)
O(5)–La(1)–O(2)	163.1(7)		
O(4)–Zn(1)–O(3)	88.0(9)	O(6)–Zn(3)–O(5)	90.3(10)
O(2)–Zn(2)–O(1)	89.0(12)		
Zn(1)–O(3)–La(1)	102.0(9)	Zn(2)–O(2)–La(1)	99.5(13)
Zn(1)–O(4)–La(1)	103.8(8)	Zn(3)–O(5)–La(1)	101.8(11)
Zn(2)–O(1)–La(1)	104.3(13)	Zn(3)–O(6)–La(1)	101.6(9)
O(3)–Zn(1)–N(1)	134.8(11)	O(2)–Zn(2)–N(2)	131.2(13)
O(4)–Zn(1)–N(1)	137.2(11)	O(5)–Zn(3)–N(3)	134.6(12)
O(1)–Zn(2)–N(2)	139.8(13)	O(6)–Zn(3)–N(3)	135.1(11)

atile (165°C/10^{-3} mm of Hg), it is thus a potential precursor for MOCVD applications. No evolution of the OBu*t*/N(SiMe$_3$)$_2$ ratio is observed by adding three equivalents of tertiary butanol to a solution of **1** in toluene at room temperature. The Zn–N bonds display thus a quite reduced reactivity toward free alcohol.

Although no crystals suitable for X-ray studies were obtained for **2**–**4**, ^{1}H NMR data allow, by comparison with these of La$_3$(OBu*t*)$_9$(HOBu*t*)$_2$, to suggest structures. All compounds displayed chemical shifts of the tertbutoxide groups spreading over the range 1.7–1.0 ppm accounting for magnetically nonequivalent alkoxide ligands namely triply-bridging, doubly-bridging and terminal ones [15]. FTIR and NMR data are in agreement with the retention of the original trinuclear La$_3$(OR)$_9$ core, structures A, B and C which are consistent with the experimental data display the common coordination numbers for the metals, namely 6-coordinated lanthanum and 3-coordinated zinc.

Compound **4** displays seven types of OR signals in a 2:1:1:4:2:1:4 integration ratio. Structure B is in agreement with the experimental data, it can be described as a La$_3$(OR)$_9$ unit associated to LaZn$_2$(OR)$_6$[N(SiMe$_3$)$_2$] which is a fragment of **1**. Seven peaks are observed as well for the proton NMR spectra of compound **2**, they are present in a 1:2:1:4:2:2:1 integration ratio. These data favor a structure of type B.

Zn(OR)$_2$ units. **1** can be seen as the association between La(OR)$_3$ and three Zn(OR)[N(SiMe$_3$)$_2$] species. Alkoxysilylamides seem to have a special stability for zinc, as illustrated by the characterization of {Zn(μ-OCEt$_3$)$_2$[N(SiMe$_3$)$_2$]}$_2$ in the solid state [21].

The tendency to form oxo species is well documented for lanthanide alkoxides. Tetranuclear lanthanide oxoalkoxide units have been stabilized in heterometallic species such as [Y$_4$(μ_3-OBu*t*)$_2$(μ-OBu*t*)$_4$(OBu*t*)$_4$(μ_4-O)(μ-Cl)$_2$Li$_4$(μ-OBu*t*)$_2$] [28] and [Sm$_4$Ti(μ_5-O)(OPr^i)$_{14}$] [29]. Their structures derive from the assembly of two trinuclear Ln$_3$(OR)$_9$ moieties along a face. Praseodymium alkoxides display a tendency to form oxo derivatives based on tetranuclear units namely Pr$_4$O(OR)$_{10}$ or Pr$_4$O$_2$(OR)$_8$ (R = Np) [30]. However, the larger size of praseodymium requires higher coordination numbers and thus frameworks different from these established for the other lanthanides. The hydroxo-oxo cluster Lu$_4$(μ_4-O)(μ_3-OH)(μ_3-OR)(μ-OR)$_4$(OR)$_4$ (R = CMe$_2$CH$_2$OMe) represents another example of a tetranuclear framework [31]. Compound **3** displays a quite simple NMR spectrum with four types of OR ligands which resonate in a 6:8:2:4 integration ratio. These data are compatible with structure C assuming that the signals of all triply-bridging and all doubly-bridging OR are degenerate. **3** can formally be considered as resulting from the assembly of two La$_3$(OR)$_9$ units via two LaO(OR)

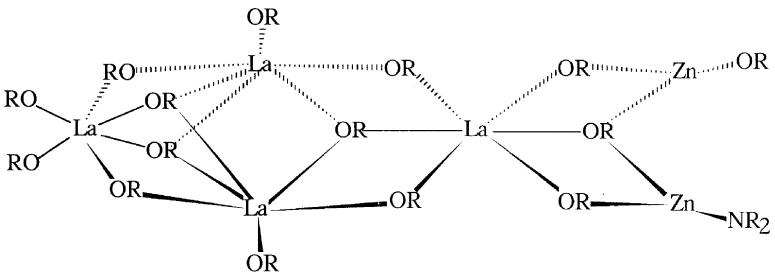

A(4)

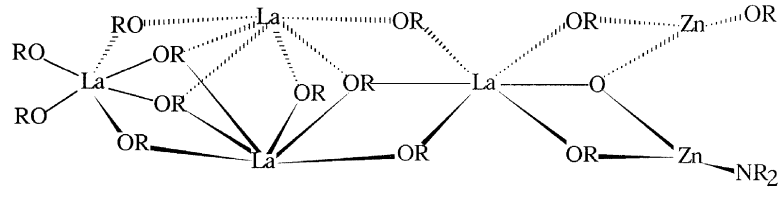

B(2)

Compounds **2** and **4** have similar formulaes, formally they differ only by replacement of two OBu*t* ligands by an oxo one. The various LaZn species can actually be formally considered as resulting from the assembly of La(OR)$_3$ and Zn(OR)[N(SiMe$_3$)$_2$] or moieties. The overall structure is thus somehow reminiscent to that of Gd$_6$(μ_4-O)(OR)$_{16}$ (R = C$_2$H$_4$OMe) in which two triangular units are assembled orthogonally via a μ_4-O oxo ligand with a tetrahedral surrounding [32].

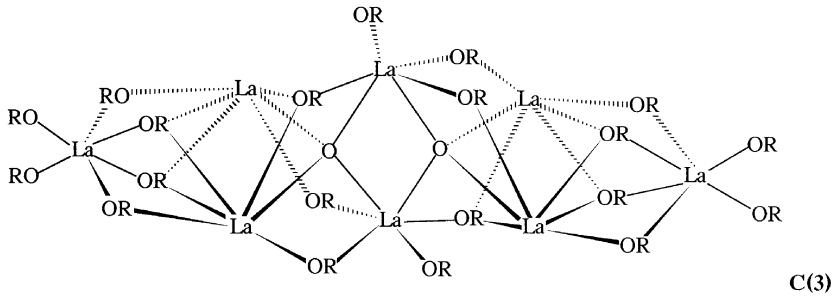

The reactivity of the tertiary butanol molecules of $La_3(OBu^t)_9(HOBu^t)_2$ toward metal trimethylsilylamides (M = Pb, Ba) was shown to proceed with retention of the trinuclear lanthanum core thus giving compounds with the anticipated stoichiometry between the metals and complete substitution of the $N(SiMe_3)_2$ ligands [16]. The results reported here show the unique behavior of zinc bis-trimethylsilylamide. The obtaining of several species at room temperature — by contrast to the reaction achieved under reflux — suggests the presence of competing reactions. The reaction at room temperature is characterized by the formation of oxo-species, La–Zn or La ones, the latter being the predominant one.

The poor selectivity and/or control of the LaZn stoichiometry raised the question of whether the reaction proceeded via coordinated or free alcohol molecules (the latter resulting from dissociation reactions of the La_3 solvate). Low temperature ^1H NMR spectra of $La_3(OBu^t)_9(HOBu^t)_2$ were reported to show several types of alkoxide ligands, which were attributed to triply-bridging, doubly-bridging and terminal groups. Additional peaks in the spectra registered at 230 K were attributed to some minor, unidentified species [15]. We observed no reaction between $[Zn(OBu^t)_2]_m$ and $La_3(OBu^t)_9(Bu^tOH)_2$, attempts to induce a reaction by heating afforded $La_5(\mu_5\text{-}O)(O^tBu)_{13}$ having a structure similar to that of the pentanuclear lanthanide oxoisopropoxides as shown by single crystal X-ray diffraction [33] while zinc tertbutoxide was totally recovered. No La–Zn species were formed either at room temperature by mixing $Zn[N(SiMe_3)_2]_2$, terbutanol and $La_3(OBu^t)_9(Bu^tOH)_2$ (only partial alcoholysis of $Zn[N(SiMe_3)_2]_2$ giving $Zn(OR)[N(SiMe_3)_2]$ occurs in such conditions). Heating the reaction medium under reflux ended up with the same homometallic species, namely $La_5(\mu_5\text{-}O)(O^tBu)_{13}$, as for the reaction with $[Zn(OBu^t)_2]_m$ as the reagent. These observations indicate that both $[Zn(OBu^t)_2]_m$ and $Zn(OBu^t)[N(SiMe_3)_2]$ are inert toward the La_3 solvate thus confirming that the building up of LaZn species proceed via the coordinated alcohol molecules. Our findings also account for a limited stability of $La_3(OBu^t)_9(Bu^tOH)_2$ with respect to its evolution into oxoalkoxides such as $La_5(\mu_5\text{-}O)(O^tBu)_{13}$ and $[La_4O(OBu^t)_{10}]_2$ which are inert toward $[Zn(OBu^t)_2]_m$. The La_2Zn stoichiometry of compounds **2** and **4** might be useful for low temperature routes to the La_2ZnO_4 oxide.

REFERENCES

1. Haertling G. H., in *Electronic Ceramics*, ed. L. M. Levinson. M. Dekker, New-York, 1988.
2. Hubert-Pfalzgraf, L. G., *New J. Chem.*, 1987, **11**(10), 663.
3. Hubert-Pfalzgraf, L. G., *New J. Chem.*, 1995, **19**(5–6), 727.
4. Kessler, V. G., Ya Turova, N., Pamov, A. N., Yanovsky, A. I., Pisarevsky, A. P. and Struchkov, Yu. T., *Polyhedron*, 1996, **15,** 335.
5. Kessler, V. G., Hubert-Pfalzgraf, L. G., Halut, S. and Daran, J. C., *J. Chem. Soc. Chem. Commun.*, 1994, **0,** 705.
6. Turevskoya, E. P., Turova, N. Ya., Korolev, A. V., Yanovsky, A. I. and Struchkov, Yu. T., *Polyhedron*, 1995, **14,** 1531.
7. Mehrotra, R. C., Tripathi, U. M. and Singh, A., *Polyhedron*, 1991, **10**(9), 949.
8. Caulton, K. G., Hubert-Pfalzgraf, L. G., *Chem. Rev.*, 1990, **90,** 969.
9. Boulmaaz, S., Hubert-Pfalzgraf, L. G., Halut, S. and Daran, J.C., *J. Chem. Soc. Chem. Commun.*, 1994, **0,** 601.
10. Bradley D. C., Mehrotra R. C. and Gaur D. P., *Metal Alkoxides*. Academic Press, London, 1978.
11. Vaarstra, B. A., Huffmann, J. C., Gradeff, P. S., Hubert-Pfalzgraf, L. G., Daran, J. C., Parraud, S., Yanly, K. and Caulton, K. G., *Inorg. Chem.*, 1990, **29,** 3126.
12. Vaarstra, B. A., Streib, W. E. and Caulton, K. G., *J. Am. Chem. Soc.*, 1990, **112,** 8593.
13. Vaarstra, B. A., Huffman, J. C., Streib, W. E. and Caulton, K. G., *Inorg. Chem.*, 1991, **30,** 3068.
14. Hubert-Pfalzgraf, L. G. and Sirio, C., Halut, S., *Polyhedron*, 1998, **16,** 1129.
15. Bradley, D. C., Chudzynska, H., Hursthouse, M. B. and Motevalli, M., *Polyhedron*, 1991, **10,** 1049.
16. Daniele, S., Ph.D. thesis, Nice, 1995.
17. Burger, H., Sawodny, W. and Wannaghat, H., *J. Organometal. Chem.*, 1965, **3,** 113.
18. Watkin D. J., Carruthers D. J. and Bettridge T. W., *CRYSTALS*, *User's Guide*, *Crystallographic Program System*. Chemical Crystallography Laboratory, University of Oxford, Oxford, 1988.

19. Walker, N. and Stuart, D., *Acta Cryst*., 1983, **39,** 158.
20. Gerts, R. L., Huffman, J. C., Weistersberg, D. E., Folting, K. and Caulton, K. G., *Nouv. J. Chim*., 1988, **12,** 455.
21. Goel, S. C., Chiang, M. Y. and Buhro, W. E., *Inorg. Chem*., 1990, **29,** 4646.
22. Wijk, M., Norrestam, R., Nygren, M. and Westin, G., *Inorg. Chem*., 1996, **35,** 1077.
23. Sasai, H., Suzuki, T., Itoh, N. and Shibasaki, M. R., *Appl. J. Organometal. Chem*., 1995, **9,** 421.
24. Arai, T., Yamada, Y. M. A., Yamamoto, N., Sasai, H. and Shibasaki, M., *Chem Eur. J*., 1996, **2,** 1368.
25. Shibasaki, M., Sasai, H. and Takayoshi, A., *Angew. Chem. Int. Ed*., 1997, **36,** 1236.
26. Biagini, P., Lugli, G., Abis, L. and Millini, R., *J. Organometal. Chem*., 1994, **474,** C16.
27. Evans, W. J., Anwander, R., Doedens, R. J. and Ziller, W. Z., *Angew. Chem. Int. Ed*., 1994, **33,** 1641.
28. Evans, W. J., Sollberger, M. S. and Hanusa, T. P., *J. Am. Chem. Soc*., 1988, **110,** 1841.
29. Daniele, S., Hubert-Pfalzgraf, L. G. and Daran, J. C., *Polyhedron*, 1994, **13,** 927.
30. Hubert-Pfalzgraf, L. G., Daniele, S., Bennaceur, A., Daran, J. C. and Vaissermann, J., *Polyhedron*, 1957, **16,** 1223.
31. Anwander, R., Munck, F. C., Priermeier, T., Scherer, W., Runte, O. and Herrmann, W. A., *Inorg. Chem*., 1997, **36,** 3545.
32. Daniele, S., Hubert-Pfalzgraf, L. G. and Daran, J. C., *Polyhedron*, 1996, **15,** 1063.
33. Daniele, S., to be published.

Pergamon

Polyhedron Vol. 17, No. 23–24, pp. 4257–4264, 1998
© 1998 Elsevier Science Ltd
All rights reserved. Printed in Great Britain
PII: S0277–5387(98)00236–8
0277–5387/98 $19.00+0.00

Synthesis and characterization of aluminum ethyl-(*S*)-lactate complexes and VT NMR studies of $[Bu_2^iAl((S)\text{-}(-)\text{-}\mu_2\text{-}OC(H)(Me)C(O)OEt))]_2$

Bao-Tsan Ko,[a] Fa-Cherng Wang,[a] Yih-Lu Sun,[a] Chia-Her Lin,[a] Chu-Chieh Lin[a]† and Chen-Yuan Kuo[b]

[a]Department of Chemistry, National Chung-Hsing University, Taichung 402, Taiwan, R.O.C.

[b]Department of Chemical Engineering, Yung-Ta Industrial Commercial College, Pingtung 909, Taiwan, R.O.C.

(Received 30 March 1998; accepted 9 June 1998)

Abstract—The reactions of ethyl-(*S*)-(−)-lactate with R_3Al in diethyl ether yield the pentacoordinated complexes $[R_2Al((S)\text{-}(-)\text{-}\mu_2\text{-}OC(H)(Me)C(O)OEt))]_2$ (**1**: R = Me; **2**: R = Et; **3**: R = Bu^i). These compounds have been characterized by spectroscopic studies as wells as crystallographic method. These structures show dimeric features containing unusual 5.4.5-fused rings with an Al_2O_2 core and the ester group bonded to Al through the C=O. VT NMR studies of compound **3** suggest that the weak (C=O)→M dative bond may undergo dissociation in solution, giving rise to the equilibrium with a four-coordinate species among two five-coordinate species at ambient temperature. © 1998 Elsevier Science Ltd. All rights reserved

Keywords: aluminum; alkoxide; ethyl-(*S*)-lactate; fluxional.

INTRODUCTION

Although compounds containing Al–O bonds have been extensively studied for many years [1, 2], the recognition that aluminum alkoxides may enhance regioselective and stereoselective organic synthesis has recently led researchers to great interest in this area again [3–10]. For example, the first reported highly enantioselective Diels–Alder reaction is the reaction of acrylate ester with 5-benzyloxymethyl-cyclopentadiene in the presence of aluminum trichloride catalyst [11]. *Cis*-dihydropyrone can be obtained in 90% yield with 97% ee by the treatment of a mixture of benzaldehyde and siloxydiene in toluene under the catalysis of a bulky chiral organoaluminum complex prepared from (*R*)-3,3′-bis(tris-arylsilyl)binaphthol and trimethylaluminum [12]. Recently we reported the crystal structure of $[Al\{(S)\text{-}(-)\text{-}\mu_2\text{-}OC(H)(Me)C(Ph)_2OH\}Cl_2]_2$ [13] prepared from the reaction of aluminum trichloride with (*S*)-(−)-1,1-diphenyl-1,2-propane diol that has shown excellent catalytic activities in the Diels–Alder reactions between cyclopentadiene and acrolein or methyl acrylate [14]. In continuation of this study, we present here the preparation and characterization of four aluminum (*S*)-lactate complexes and the variable temperature NMR studies of $[Bu_2^iAl((S)\text{-}(-)\text{-}\mu_2\text{-}OC(H)(Me)C(O)OEt)]_2$. These compounds contain an interesting structure with 5.4.5-fused rings in which two five- and one four-membered rings are coplanar. VT NMR results indicate that $[Bu_2^iAl((S)\text{-}(-)\text{-}\mu_2\text{-}OC(H)(Me)C(O)OEt))]_2$ is dynamic in solution in which slow exchange occurs among two five-coordinate species at ambient temperature.

†Author to whom correspondence should be addressed.

EXPERIMENTAL SECTION

General

All manipulations were carried out under dry nitrogen atmosphere. Solvents were dried by refluxing at least 24 h over sodium/benzophenone (toluene, hexane, ether) and freshly distilled prior to use. Deuterated solvents (Aldrich) were dried over molecular sieves. $AlMe_3$ (2.0 M in toluene) and ethyl-(*S*)-(−)-lactate were purchased from Aldrich and used without further purification. $AlEt_3$ (15% in hexane), $Al(Bu^i)_3$ (15% in hexane) and Et_2AlCl (15% in hexane) were purchased from TCI and used without further purification. Melting points were determined with a Buchi 535 digital melting point apparatus. ^1H and ^{13}C NMR spectra were recorded on a Varian VXR-300 (300 MHz) or a Gemini-200 (200 MHz) spectrometer with chemical shifts given in ppm from the internal TMS. Mass spectra were recorded on a Jeol Jms-HX 110. Microanalyses were performed using a Heraeus CHN-O-RAPID instrument. Infrared spectra were obtained from a Brucker Equnox 55 spectrometer.

Preparation of complex **1**

To an ice cold (0°C) solution of ethyl-(*S*)-(−)-lactate (0.23 ml, 2.0 mmol) in ether (20 ml), Me_3Al (2.0 M in toluene, 1.2 ml, 2.4 mmol) was added slowly. After all of the later solution was added, the mixture was stirred for 2 hours. Volatile materials were removed under vacuum. The residue was extracted with 20 ml of warm ether, then allowed to cool to 25°C to yield white powder. After filtered, the filtrate was then dried *in vacuo* to give an addition portion of white powder. Both portions of powder exhibited identical ^1H NMR spectra. Yield: 0.32 g (91%). Found: C, 48.28, H, 8.84. Calcd for $C_{14}H_{30}Al_2O_6$: C, 48.27; H, 8.68%. ^1H NMR ($CDCl_3$): δ 4.47 (q, 1H, CH, $J_{H-H}=6.9$ Hz), 4.39 (q, 2H, OCH_2CH_3, $J_{H-H}=7.2$ Hz), 1.45 (d, 3H, CH_3, $J_{H-H}=6.9$ Hz), 1.36 (t, 3H, O–Et, $J_{H-H}=7.2$ Hz), −0.97 (s, 6H, $AlCH_3$). ^{13}C NMR ($CDCl_3$, ppm): 181.84 (COOEt), 66.70 (COOEt), 64.55(OCHMe), 20.37 (COOEt), 13.96 ($OCH(CH_3)$), −9.21 (Al–CH_3). IR (KBr, cm^{-1}): 2997.6, 2942.5, 1699.0, 1471.6, 1384.0, 1345.8, 1278.2, 11.87.1, 1148.6, 1066.5, 1014.4. Mp: 152–154°C.

Preparation of **2**

To an ice cold (0°C) solution of ethyl-(*S*)-(−)-lactate (0.23 ml, 2.0 mmol) in hexane (10 ml), Et_3Al (15% in hexane, 2.6 ml, 2.4 mmol) was added slowly. The mixture was stirred for 2 hours after the addition of Et_3Al and then was dried under vacuum. The residue was extracted with 5 ml of hot hexane and then was cooled to −20°C. Colorless crystals were obtained after 24 h. Yield: 0.18 g (45%). Found: C, 53.03, H, 9.36; Calcd for $C_{18}H_{38}Al_2O_6$: C, 53.45; H, 9.47%. ^1H NMR ($CDCl_3$, ppm): δ 4.50 (q, 2H, $J_{H-H}=7.0$, CH), 4.41 (q, 4H, $J_{H-H}=7.20$ Hz, CH_2 (Et_2O)), 1.48 (d, 6H, $J_{H-H}=7.0$ Hz, CH_3), 1.38 (t, 6H, $J_{H-H}=7.2$ Hz, CH_3), 0.93 (t, 12H, $J_{H-H}=8.2$ Hz, CH_3(AlEt)), −0.28 (q, 8H, $J_{H-H}=8.2$ Hz, CH_2(AlEt)). ^{13}C NMR ($CDCl_3$, ppm): 181.92 (CO), 67.09 (OCH_2CH_3), 64.56 (OCHMe), 20.24 ($OCH(CH_3)$), 14.02 (OCH_2CH_3), 9.77 (CH_2CH_3 (AlEt)), 1.19 (CH_2CH_3(AlEt)). IR (KBr, cm^{-1}): 2995.3, 2941.8, 2861.7, 1687.6, 1455.5, 1388.2, 1346.7, 1315.4, 1272.4, 1139.7. Mp: 93–94°C.

Preparation of **3**

To an ice cold (0°C) solution of ethyl-(*S*)-(−)-lactate (0.46 ml, 4.0 mmol) in ether (20 ml), $(Bu^i)_3Al$ (15% in hexane, 8.0 ml, 4.6 mmol) was added slowly. After all of the later solution was added, the mixture was stirred for 2 more hours. The volatile materials were removed *in vacuo*. The residue was extracted with 30 ml of hexane and then concentrated to *ca.* 5 ml. Colorless crystals were obtained after cooling at 4°C for 24 h. Yield: 0.75 g (73%). Found: C, 59.59; H, 10.61. Calcd for $C_{26}H_{54}Al_2O_6$: C, 60.44; H, 10.53%. ^1H NMR ($CDCl_3$, ppm): δ 4.496 (q, 1H, HCOAl, $J_{H-H}=7.0$ Hz), 4.375 (t, 2H, OCH_2CH_3, $J_{H-H}=7.2$ Hz), 1.687 (m, 1H, CH), 1.488 (d, 3H, CH_3CHOAl, $J_{H-H}=7.0$ Hz), 1.376 (t, 3H, CH_2CH_3, $J_{H-H}=7.2$ Hz), 0.865, 0.854 (dd, 6H, $(CH_3)_2CH$, $J_{H-H}=6.6$ Hz), −0.210, −0.221 (dd, 2H, CH_2Al, $J_{H-H}=6.6$ Hz). ^{13}C NMR ($CDCl_3$, ppm): 182.12 (C=O), 67.01 (HCOAl), 64.68 (OCH_2CH_3), 28.57, 28.21 ($(CH_3)_2CH$), 26.33 (CH), 24.12 (CH_2Al), 20.12 (CH_3COAl), 14.03 (CH_2CH_3). IR (KBr, cm^{-1}): 2943.6, 2859.7, 1687.6, 1457.0, 1408.3, 1347.6, 1264.7, 1142.3, 1066.5, 1014.7, 943.3. Mp: 87–89°C.

Preparation of **4**

To an ice cold (0°C) solution of ethyl-(*S*)-(−)-lactate (0.46 ml, 4.0 mmol) in ether (20 ml), Et_2AlCl (15% in hexane, 5.8 ml, 5.0 mmol) was added slowly. After all of the later solution was added, the mixture was stirred for 2.5 hours and then was dried under vacuum. The residue was extracted with 5 ml of ether and then was cooled to −20°C. Colorless crystals were obtained after 7 days. Yield: 0.40 g (48%). Found: C, 39.81, H, 6.48. Calcd for $C_{14}H_{28}Al_2Cl_2O_3$: C, 40.30; H, 6.76%. ^1H NMR ($CDCl_3$, ppm): 4.95 (q, 2H, $J_{H-H}=7.0$ Hz, CH), 4.56 (q, 4H, $J_{H-H}=7.20$ Hz, CH_2(OEt), 1.64 (d, 6H, $J_{H-H}=7.0$ Hz, CH_3), 1.51 (t, 6H, $J_{H-H}=7.2$ Hz, CH_3), 0.97 (t, 6H, $J_{H-H}=8.2$ Hz, CH_3(AlEt)), −0.08 (q, 4H, $J_{H-H}=8.2$ Hz, CH_2(AlEt)). ^{13}C NMR ($CDCl_3$, ppm): 185.3 (CO), 67.5 (OCH_2CH_3), 67.3 (OCHMe), 19.2 ($OCH(CH_3)$), 13.7 (OCH_2CH_3), 9.1 (CH_2CH_3(AlEt)), 0.8 (CH_2CH_3(AlEt)). IR (KBr, cm^{-1}): 2988.5, 2943.9, 2905.1, 2865.1, 1665.3, 1476.3, 1460.3, 1427.6, 1389.8, 1352.6, 1286.0, 1136.7, 1007.1. Mp: 103–106°C.

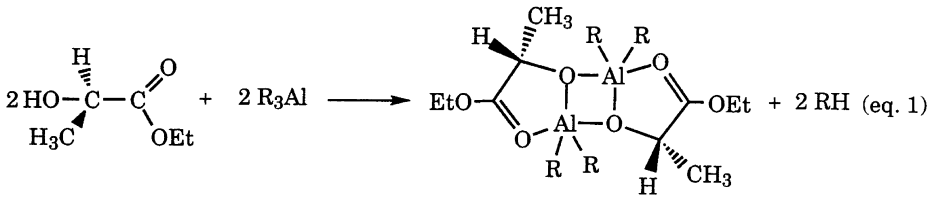

(**1**: R = CH_3, **2**: R = Et, **3**: R = Bu^i)

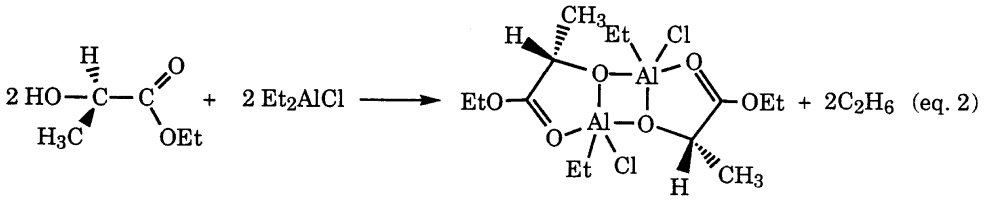

(**4**)

X-ray crystallographic studies

Suitable crystals of **1**, **2**, **3** and **4** were sealed in thin-walled glass capillaries under nitrogen atmosphere and mounted on a Siemens P4 diffractometer. The crystallographic data were collected using a θ–2θ scan mode with Mo Kα radiation. The space group determination was based on a check of the Laue symmetry and systematic absences, and was confirmed by the structure solution. The structure was solved by direct methods using Siemens SHELXTL PLUS package [15]. All non-H atoms were located from successive Fourier maps. Anisotropic thermal parameters were used for all non-H atoms and fixed isotropic for H atoms that were refined using riding model† [15]. Crystallographic data of **1**, **2**, **3** and **4** are summarized in Table 1.

RESULTS AND DISCUSSION

Preparation of **1**, **2**, **3** *and* **4**

The reactions of R_3Al with one equivalent of ethyl-(*S*)-(−)-lactate in diethyl ether lead to the formation of five-coordinated complexes $[R_2Al((S)\text{-}(-)\text{-}\mu_2\text{-}OC(H)(Me)C(O)OEt)]_2$ (**1**: R = Me; **2**: R = Et; **3**: R = Bu^i) (eq. 1). Ethyl-(*S*)-(−)-lactate reacts with Et_2AlCl to afford the product $[(Et)(Cl)Al((S)\text{-}(-)\text{-}\mu_2\text{-}OC(H)(Me)C(O)OEt))]_2$ (**4**) (eq. 2). All of these compounds are air and moisture sensitive colorless solid. The ^{1}H NMR spectra of compounds **1**, **2** and **4** taken at 20°C are essentially as expected. There is no OH resonance indicating loss of the hydroxyl proton which is proved by IR spectroscopic studies. Examination of the ^{1}H NMR of these three compounds shows that the alkyl groups bound to the metal atoms in a given complex are equivalent at ambient temperature. This phenomenon is consistent with most five-coordinate aluminum complexes reported by Oliver [17]. However, $[Me_2Al(O\text{-}(R)\text{-}CHC_6H_5((S)\text{-}CH((S)\text{-}NHCH_3)CH_3)]_2$ demonstrate inequivalence in solution at 25°C [18].

Molecular structures of **1**, **2** *and* **3**

Suitable crystals for structure determination of **1** was obtained from an ether solution at 25°C. Compounds **2** and **3** were recrystallized from a hexane solution at 4°C. Their molecular structures have been determined by X-ray crystallography and are shown in Fig. 1. All three structures are similar with the difference only in the alkyl groups bonded to aluminum. The structure of **1** was originally solved in the space group $P4_3$. However, after carefully examining its absolute configuration, the space group $P4_1$ was finally chosen. The structure of **1** shows a dimeric feature which contains 5.4.5-fused rings with an Al_2O_2 core and the ester group bonded to Al through the

† Hydrogen atoms were ride on carbons or oxygens in their idealized positions and held fixed with the C–H distances of 0.96 Å and the O–H distances of 0.85 Å.

Table 1. Crystallographic data of complex **1**, **2**, **3** and **4**

	1	**2**	**3**	**4**
Formula	$C_{14}H_{30}Al_2O_6$	$C_{18}H_{38}Al_2O_6$	$C_{26}H_{54}Al_2O_6$	$C_{14}H_{28}Al_2Cl_2O_6$
F_w	348.4	404.5	516.7	417.2
Crystal system	tetragonal	monoclinic	monoclinic	monoclinic
Space group	$P4_1$	$P2_1$	$P2_1$	$P2_1$
a (Å)	7.613(2)	8.835(2)	9.159(2)	8.047(2)
b (Å)	9.475(2)	18.432(4)	14.378(3)	
c (Å)	35.011(4)	14.969(2)	9.676(2)	9.846(2)
β (°)		92.49(2)	91.86(2)	98.16(2)
V (Å^3)	2029.2(8)	1251.9(4)	1632.6(6)	1127.6(4)
Z	4	2	2	2
$D_{calcd.}$, Mg · m^{-3}	1.140	1.073	1.051	1.229
λ(Mo Kα) (Å)	0.71073	0.71073	0.71073	0.71073
Absorption coefficient (mm^{-1})	0.164	0.141	0.121	0.388
2θ Range, deg	4.0 to 48.0°	4.0 to 45.0°	4.0 to 43.0°	3.5 to 45.0°
Scan type	θ–2θ	θ–2θ	θ–2θ	θ–2θ
Reflections collected	2009	3648	4086	3264
Observed reflections	1569 ($F>4.0\sigma(F)$)	1722 ($F>4.0\sigma(F)$)	2435 ($F>4.0\sigma(F)$)	2029 ($F>4.0\sigma(F)$)
No. of refined parameter	199	235	307	271
R[a] for significant reflections	0.0570	0.0684	0.0858	0.0523
Rw[b] for significant reflections	0.0608	0.0703	0.0868	0.0570
GoF[c]	1.63	1.71	1.74	1.44

[a] $R=|\Sigma(|F_o-F_c|)/\Sigma|F_o||$.
[b] $Rw=|\Sigma\sqrt{w}(|F_o-F_c|)/\Sigma\sqrt{w}F_o||$. $w=1/[\sigma^2(F)+0.001)F^2]$ for **1**, **2**, and **4** and $w=1/[\sigma^2(F)+0.002)F^2]]$ for **3**.
[c] $GoF=[\Sigma w(|F_o|-|F_c|)^2/(N_{rflns}-N_{params})]^{1/2}$.

C═O in which Al_2O_2 core is essentially coplanar. Similar fused rings have been found in many cases [13, 17, 19]. However, the interesting feature is that each of the mean planes of these two five-member rings are almost coplanar with the Al_2O_2 core with the dihedral angles between 5 and 4-membered rings are only 3.4 and 4.4°, respectively. The coplanarity of these 5.4.5-fused rings is depicted in Fig. 2. The constraints of the fused 5.4.5 ring system result in the rather small O(1)–Al(1)–O(2) and O(1)–Al(1)–O(21) angles of 77.7(2) and 75.7(3)°, respectively. The coordination polyhedron of the central five-coordinated aluminum atom in **1** is somewhat distorted from perfect trigonal bipyramidal geometry with two carbons and one of two bridging oxygen atoms siting on equatorial positions. The aluminum atom, two ligating carbon atoms, and one bridging oxygen atom are almost coplanar. The two equatorial Al–C bonds average 1.959(9) Å that are similar to normal Al–C bonds in four-coordinated complexes. However, the dative O→Al (ester) bonds at 2.154(6) Å are 0.26 Å longer than the longest dative bond from an oxygen to a four-coordinated aluminum for an ester group [20, 21, 22]. The Al–O bonds in Al_2O_2 ring are asymmetric with Al–O distances ranging from 1.837(6) to 1.948(5). The Al–O–Al and O–Al–O bond angles are within the range reported for a Al_2O_2 ring system [23, 24, 25]. Selected bond lengths and bond angles of **1**, **2**, **3** and **4** are given in Table 2. There are five different possible modes of the coordination of ester groups to aluminum centers shown as in Scheme 1 [22, 26]. The average angle of Al–O–C (ester) is 111.4(5)° in **1** and Al(1) is only 0.003 Å above the C(2)C(3)O(2)O(3) plane. Therefore it belongs to type II mode where all atoms of the ester group and aluminum are in the same plane. Ab initio calculations for $H_3Al(O{=}CH_2)$ suggest that type II is the energetically favored geometry [27].

Crystal structure of **4**

Suitable crystals for structure determination of compound **4** were obtained from an ether solution at −20°C. The crystal structure of **4** (shown as in Fig. 3) which is resembling to the structure of **1** also demonstrates dimeric feature with an Al_2O_2 core and an ester group bonded to Al through the C═O group. Both chloride and carbon of ethyl group positions are disordered with respect to chloride/ethyl occupancy, and therefore the least-square refinement was carried out so that for each chloride and ethyl atom site a single set of coordinates and temperature factors was used, but the site occupancy was refined as a fraction of a chlorine atom and a fraction of a ethyl atom such that two fractions summed to unity. This resulted in values of *ca.* 0.75 Cl and 0.25 C for Cl(1)/C(6′) and Cl(2)/C(16′) positions and vice versa 0.75 C and 0.25 Cl for Cl(1′)/C(6) and Cl(2′)/C(16). The average bond distance of Al–O in the Al_2O_2 core of 1.864 Å is within

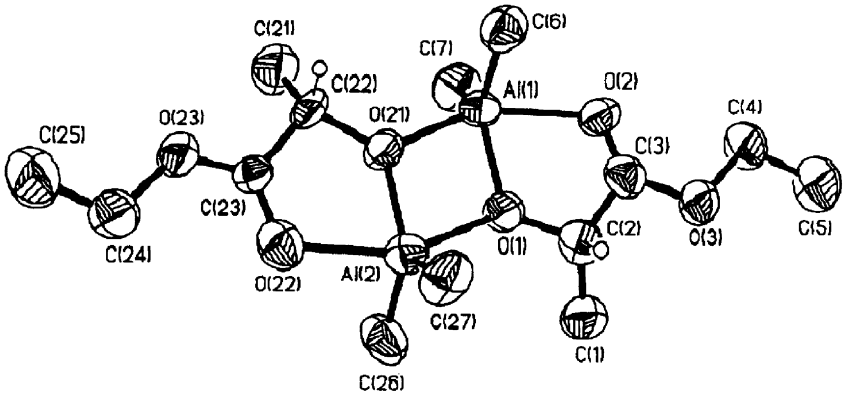

(a)

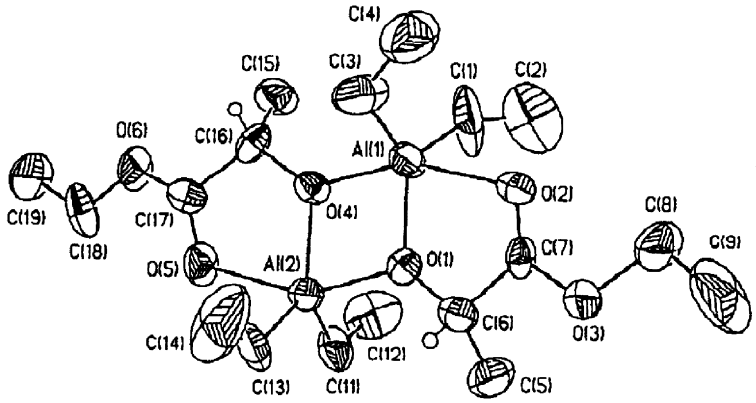

(b)

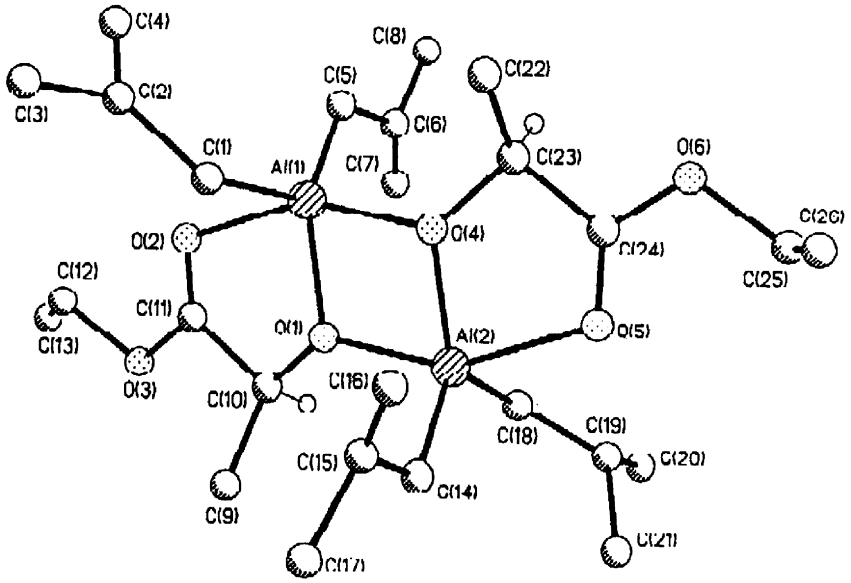

(c)

Fig. 1. Molecular structures of (a) $[Me_2Al((S)\text{-}(-)\text{-}\mu_2\text{-}OC(H)(Me)C(O)OEt)]_2$ (**1**) (b) $[Et_2Al((S)\text{-}(-)\text{-}\mu_2\text{-}OC(H)(Me)C(O)OEt)]_2$ (**2**) and (c) $[Bu^i_2Al((S)\text{-}(-)\text{-}\mu_2\text{-}OC(H)(Me)C(O)OEt)]_2$ (**3**).

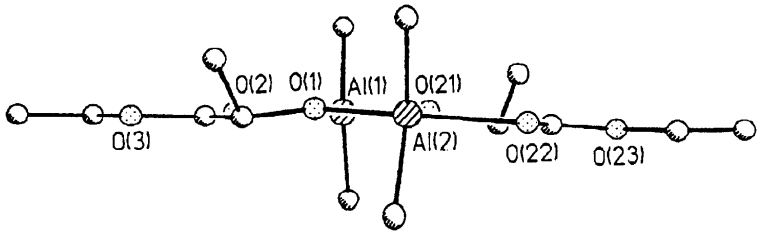

Fig. 2. Molecular structures of $[Me_2Al((S)\text{-}(-)\text{-}\mu_2\text{-}OC(H)(Me)C(O)OEt)]_2$ (**1**): viewed along the Al_2O_2 plane.

Table 2. Selected bond distances (Å) and bond angles (°) of **1**, **2**, **3**, and **4**

Compound	**1**	**2**	**3**	**4**
Al–O (bridged, ave.)	1.840(6)	1.843(8)	1.829(6)	1.825(5)
	1.931(5)	1.930(8)	1.907(7)	1.904(5)
Al–O (lactate, ave.)	2.154(6)	2.171(10)	2.137(9)	2.027(6)
Al–C (ave.)	1.959(9)	1.941(13)	1.955(14)	2.121(29)
Al–Cl (ave.)				2.141(8)
Al–Al	2.982(3)	2.985(4)	2.941(4)	2.955(3)
Al–O–Al (Al_2O_2, ave.)	104.5(3)	104.6(4)	103.8(3)	104.9(2)
O–Al–O (Al_2O_2, ave.)	76.8(3)	76.4(3)	76.2(3)	75.9(2)
Al–O–C (bridged, ave.)	126.7(5)	127.2(6)	127.2(6)	126.8(5)
Al–O–C (lactate, ave.)	111.4(5)	113.3(8)	111.8(9)	113.4(5)

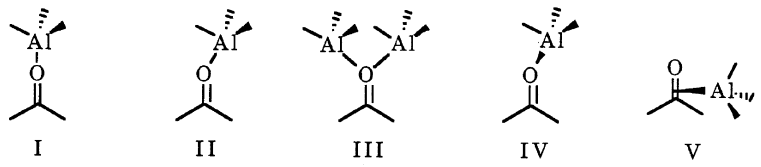

Scheme 1.

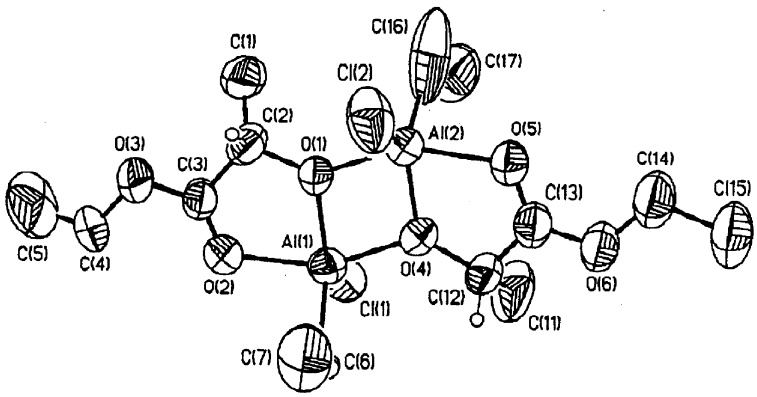

Fig. 3. Molecular structure of $[(Et)(Cl)Al((S)\text{-}(-)\text{-}\mu_2\text{-}OC(H)(Me)C(O)OEt)]_2$ (**4**).

a normal range for an Al_2O_2 ring. The Al–C and Al–Cl bond distances and C–Al–Cl bond angle are not reliable due to the disordered problem.

VT NMR studies of **3**

It is interesting to note that although the crystal structure of **3** is similar to that of **1** and **2**. However the ^{1}H NMR spectrum of compound **3** taken at room temperature shows two doublets at δ 0.866/0.848 and 0.855/0.833 ppm corresponding to $(CH_3)_2CH$ indicating that these two methyl groups on an iso-butyl group bonded to aluminum are chemically nonequivalent. This phenomenon is in contrast to the results observed for **1** and **2** where only one set of Al–R resonance is found in complexes containing five-coordinate aluminum centers. However in the $[Et_2Al(8\text{-quinolinolato})]_2$ [28] and $[R_2AlOCH_2\text{-}2\text{-}C_5H_4N]_2$ [29] dimer nonequivalence of the methylene groups only appears at low temperature where exchange is slow. In order to probe the structure in solution of **3**, variable-temperature NMR studies in d_8-toluene were performed and the selected spectra are shown in Fig. 4. VT NMR studies demonstrate that the chemical shifts of the various groups on Bu^i group are temperature dependent. At 20°C, two doublets at δ 1.266, 1.243 and 1.255, 1.233 ppm respectively indicating two nonequivalent methyl groups (Me_a and Me_b) of Al–Bu^i. However these two doublet peaks become closer as the temperature was raised. At 92°C these two doublet peaks merge as one set doublet at δ 1.172, and 1.151 ppm indicating that these two methyl groups are chemical equivalent. The above VT NMR studies suggest that the weak (C=O)→M dative bond may undergo dissociation in solution, giving rise to the equilibrium with a four-coordinate species shown in Scheme 2 in which slow exchange occurs among two five-coordinate species at ambient temperature. However a rapid exchange takes place at high temperature above 92°C.

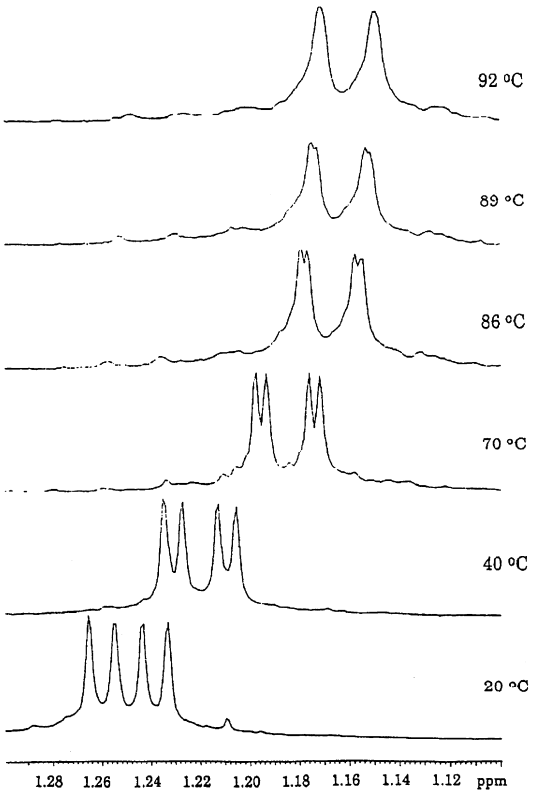

Fig. 4. A variable-temperature ^{1}H NMR spectrum in the methyl region of the Al–Bu^i of **3**.

Infrared spectra studies

The Infrared spectra of free lactate, **1**, **2**, **3**, and **4** in the 1600 to 1700 cm^{-1} range are compared in Table 3. A strong (C=O) absorption due to the lactate was observed at 1687 cm^{-1} for **2** and 1665 cm^{-1} for **4**. There is a decrease in carbonyl stretching frequency in the IR spectrum of the aluminum complexes when compared to the free carbonyls (1738 cm^{-1}). However, its magnitude drop ranges from 39–73 cm^{-1} which is much smaller than those found for four-coordinated aluminum ester complexes (85–125 cm^{-1}) [20, 21, 22]. That the C=O stretching frequency decreases as the substituted group changes from an electron donating group, ethyl group, to the electron withdrawing chloride resulting from a more positive charge on the aluminum center in **4** compared to that in **2** is due to the electronic effect. The result is consistent with the crystal structure data that Al–(O=C) distance of 2.171 Å for **2** is longer than the Al–O distance of 2.027 Å for **4**.

CONCLUSIONS

These structures show dimeric feature containing unusual 5.4.5-fused rings with an Al_2O_2 core and the ester group bonded to Al through C=O. These 5- and 4-membered rings are coplanar. The dative O→Al (ester) bonds at 2.154(6) Å are 0.26 Å longer than the longest dative bond from oxygen to four-coordinate aluminum for an ester group. VT NMR studies of **3** suggest that the weak (C=O)→M dative bond may undergo dissociation in solution, giving rise to the equilibrium with a four-coordinate species in which slow exchange occurs among two five-coordinate species at ambient temperature. However a rapid exchange takes place at high temperature above 92°C. Further studies using these compounds as catalyst in Diels–Alder reactions are proceeding.

Supplementary materials

Tables given full details of the crystal data, data collection, structure solution parameters, atomic

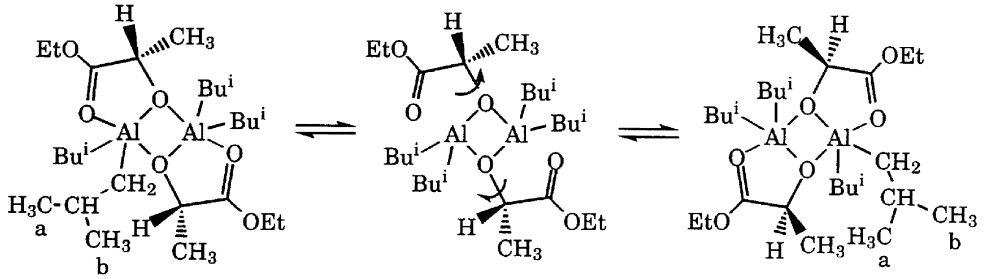

Scheme 2.

Table 3. The comparison of infrared spectra of free lactate, **1**, **2**, **3**, and **4**

Compounds	C=O stretching (cm^{-1})
Free lactate	1738
1	1699
2	1687
3	1688
4	1665

coordinates of all atoms, bond distances, bond angles, anisotropic thermal parameters of nonhydrogen atoms and isotropic thermal parameters of hydrogen atoms.

Acknowledgements—Financial support from the National Science Council of the Republic of China is gratefully acknowledged.

REFERENCES

1. Oliver, J. P., *Adv. Organomet. Chem.*, 1970, **8,** 167.
2. Taylor, M. J., in *Comprehensive Coordination Chemistry*, ed., G. Wilkinson. 1987, Ch. 25.1.
3. Pindur, U. and Lutz, G., Otto, C., *Chem. Rev.*, 1993, **93,** 741.
4. Renaud, P., Bourquard, T., Gerster, M. and Moufid, N., *Angew. Chem. Int. Ed. Engl.*, 1994, **33,** 1601.
5. Hashimoto, S., Komeshima, N. and Koga, K., *J. Chem. Soc. Chem. Commun.* 1979, 437.
6. Bartley, D. W. and Kodadek, T. J., *Tetrahedron Lett.*, 1990, **31,** 6303.
7. Danishefsky, S. and DeNinno, M. P., *Angew. Chem. Int. Ed. Engl.*, 1987, **26,** 15.
8. Corey, E. J., Sarshar, S. and Lee, D.-H., *J. Am. Chem. Soc.*, 1994, **116,** 12089.
9. Corey, Et .J. and Letavic, M. A., *J. Am. Chem. Soc.*, 1995, **117,** 9616.
10. Noyori, R., Tomino, I., Tanimoto, Y. and Nishizawa, M., *J. Am. Chem. Soc.*, 1984, **106,** 6709.
11. Corey, E. J. and Ensley, H. E., *J. Am. Chem. Soc.*, 1975, **97,** 6908.
12. Maruoka, K., Itoh, T., Shirasaka, T. and Yamamoto, H., *J. Am. Chem. Soc.*, 1988, **110,** 310.
13. Ko, B.-T., Lee, M.-D. and Lin, C.-C., *J. Chin. Chem. Soc.*, 1997, **44,** 163–168.
14. Rebiere, F., Riant, O. and Kagan, H. B., *Tetrahedron: Asymmetry*, 1990, **1,** 199.
15. Sheldrick, G. M. (1991). SHELXTL PLUS User's Manual. Revision 4.1 Nicolet XRD Corporation, Madison, WI.
17. Hendershot, D. G., Barber, M., Kumar, R. and Oliver, J. P., *Organometallics*, 1991, **10,** 3302.
18. Sierra, M. L., de Mel, V. S. J. and Oliver, J. P., *Organometallics*, 1989, **8,** 2486.
19. Duff, A. W., Hitchcock, P. B., Lappert, M. F. and Taylor, R. G., *J. Organomet. Chem.*, 1985, **293,** 271.
20. Oliver, J. P., Kumar, R. and Taghiof, M., in *Coordination Chemistry of Aluminum*, ed., G. H. Robinson. 1993, Ch. 5.
21. Shreve, A. P., Mulhaupt, R., Fultz, W., Calabrese, J., Robbins, W. and Ittel, S. D., *Organometallics*, 1988, **7,** 409.
22. Power, M. B., Bott, S. G., Atwood, J. L. and Barron, A. R., *Organometallics*, 1990, **9,** 3086.
23. Mason, M. R., Smith, J. M., Bott, S. G. and Barron, A. R., *J. Am. Chem. Soc.*, 1993, **115,** 4971.
24. Kumar, R., Sierra, M. L., de Mel, V. S. J. and Oliver, J. P., *Organometallics*, 1990, **9,** 484.
25. Schulz, S., Roesky, H. W., Noltemeyer, M. and Schmidt, H.-G., *J. Chem. Soc. Dalton Trans.* 1995, 177.
26. Healy, M. D., Power, M. B. and Barron, A. R., *Coord. Chem. Rev.*, 1994, **130,** 63.
27. LePage, T. J. and Wiberg, K. B., *J. Am. Chem. Soc.*, 1992, **114,** 7931.
28. Dzugan, S. T. and Goedken, V. L., *Inorg. Chim. Acta*, 1988, **54,** 169.
29. van Vliet, M. R. P., Buysingh, P., van Koten, G., Vrieze, K., Kojic-Prodic, B. and Spek, A. L., *Organometallics*, 1985, **4,** 1701.

Pergamon

Polyhedron Vol. 17, No. 23–24, pp. 4265–4273, 1998
© 1998 Elsevier Science Ltd
All rights reserved. Printed in Great Britain
0277–5387/98 $19.00+0.00

PII: S0277–5387(98)00237–X

Syntheses, X-ray structures, spectroscopic and magnetic studies of two new polymeric copper(II) azide complexes; $[Cu(3\text{-ethylpyridine})_2(N_3)_2]_n$ and $[Cu(4\text{-ethylpyridine})_2(N_3)_2]_n$

Mohamed A. S. Goher,*[a] Albert Escuer,[b] Morsy A. M. Abu-Youssef[c] and Franz A. Mautner*[c]

[a]Department of Chemistry, Faculty of Science, Kuwait University, P.O. Box 5969 Safat, 13060 Kuwait

[b]Departament de Química Inorgànica, Universitat de Barcelona, Diagonal 647, 08028 Barcelona, Spain

[c]Institut für Physikalische und Theoretische Chemie, Technische Universität Graz, A-8010 Graz, Austria

(Received 16 February 1998; accepted 10 June 1998)

Abstract—Two new 1:2 polymeric complexes of copper(II) azide with 3-ethylpyridine (**1**) and 4-ethylpyridine (**2**), have been synthesized and characterized by spectroscopic and crystallographic methods. The structure of complex (**1**) contains a dimeric $[Cu(3\text{-Etpy})_2(N_3)_2]_2$ unit and a monomeric $[Cu(3\text{-Etpy})_2(N_3)_2]$ unit. Each copper atom in the dimeric unit attains a five coordination environment, whereas the copper atom in the second unit has an elongated octahedral geometry. In complex (2), each copper atom in the asymmetric unit is coordinated to the end nitrogens of two μ_2-1,3 azido ligands, a pair of *trans* 4-Etpy molecules and a nitrogen atom of a terminal azide group. This same nitrogen atom further links a neighboring copper atom at a long Cu–N distance of 2.920(7) Å, thus connecting the asymmetric units giving rise to a 2D structure. The IR and electronic spectra are reported. Strong absorption bands due to $N_3 \rightarrow Cu^{II}$MLCT transitions are observed in spectra of solids and solutions of both complexes. Magnetic susceptibility and EPR data of both complexes are presented and discussed. © 1998 Elsevier Science Ltd. All rights reserved

Keywords: copper(II) azide complexes; 3-, and 4-ethylpyridine; X-ray crystal structures; electronic spectra; infrared spectra; magnetic measurements

INTRODUCTION

A substantial array of copper(II) azido complexes of neutral pyridine derivative ligands have been prepared, structurally characterized and shown to have a wide variety of stoichiometries, solid state stereochemistries and varying degrees of oligomerization. Thus neutral complexes of copper(II) azide: ligand ratios of 1:1 [1–9], 1:2 [10–14] and 3:2 [15, 16], in addition to $[CuL_4(N_3)]^+$ cationic complexes [17] have been synthesized and characterized. In these complexes different types of bonding of azido ligands have been demonstrated. Thus, the 1:2 complexes of 4-picoline, which features oligomeric edge-sharing chains of polyhedra, contains terminal and μ_2-1,1 bridging azido ligands, the corresponding complex of 3-picoline contains both μ_2-1,1 and μ_2-1,3 bridging azides, whereas the 1:2 complex of 3-benzoylpyridine [18] possesses only μ_2-1,3 azido ligands. On the other hand, while the polymeric complex $[Cu(N_3)_2(DENA)]$ (DENA = diethylnicotinamide) contains μ_2-1,1 and μ_3-1,1,3 groups, the 3:2 complex of 2-benzoylpyridine possesses μ_2-1,1 and μ_3-1,1,1 bridging azides [16]. These examples demonstrate the versatility of the azide ligand. Moreover, this ver-

* Authors to whom correspondence should be addressed.

satility reflects itself in the variety of magnetic behavior of the metal azido complexes from strong anti-ferromagnetic [19–21] to strong ferromagnetic [22–25] including ferro–antiferromagnetic [26, 27] depending upon the nature of the bridging azido ligand. We now isolated two new complexes of the formula $CuL_2(N_3)_2$, where L = 3-, and 4-ethylpyridine (hereafter abbreviated as 3-, and 4-Etpy), of related structures. The synthesis and characterization of these complexes as elucidated by X-ray crystallography, spectroscopic and magnetic methods are presented in this paper.

EXPERIMENTAL

3-, and 4-ethylpyridine were purchased from Aldrich company and other chemicals were of analytical grade quality.

Preparation of polymeric $[Cu(3\text{-}ethylpyridine)_2(N_3)_2]_n$ *complex* (*I*)

Copper(II) nitrate trihydrate (0.72 g, 3 mmol) dissolved in *ca.* 30 cm^3 acetone and 3-Etpy (0.75 g, 7 mmol) were mixed together, followed by addition of an aqueous solution (*ca.* 5 cm^3) of NaN_3 (0.52 g, 8 mmol). After filtration of the brown solution mixture, several drops of 3-Etpy were added to prevent the co-precipitation of the 1:1 complex. The final mixture was allowed to stand in an open beaker over *ca.* three weeks until black well-shaped crystals of the complex were separated along with a blue crystalline material. Yield, 40% with respect to copper. Anal.; Found; C, 46.3; H, 4.9; N, 30.6; Cu, 17.8. Calc.: C, 46.5; H, 5.0; N, 30.9; Cu, 17.6%.

Preparation of polymeric $[Cu(4\text{-}ethylpyridine)_2(N_3)_2]_n$ *complex* (*2*)

Copper(II) nitrate trihydrate (0.72 g, 3 mmol) and 4-ethylpyridine (1.07 g, 10 mmol) were mixed together in 40 cm^3 acetone. To this mixture, an aqueous solution (*ca.* 5 cm^3) of NaN_3 (0.48 g, 7.5 mmol) was added with continuous stirring. The green precipitate was filtered off and then dissolved in DMF, followed by addition of several drops of 4-Etpy. The final mixture was filtered off and the filtrate allowed to stand in an open beaker over several weeks until dark green crystals of the complex deposited. Yield, 50%. Anal.; Found; C, 46.6; H, 5.0; N, 30.0; Cu, 17.4. Calc.: C, 46.5; H, 5.0; N, 30.9; Cu, 17.6%.

Caution: both compounds are very sensitive to grinding and explode upon heating and friction.

Physical measurements

The experimental procedures and instruments used for different physical measurements are as described previously [18, 26, 27].

X-ray crystal structure analyses

A modified STOE four circle diffractometer was used for single crystal X-ray measurements. Orientation matrix and lattice parameters were obtained by least-squares refinement of the diffraction data from 40 (compound **1**) and 65 (compound **2**) reflections in the 2θ range 10–32°. Data were collected at 293(2) K using graphite crystal monochromatized Mo–Kα radiation ($\lambda = 0.71069$ Å) and the ω-scan technique. The intensities were corrected for Lorentz-polarization effects, for absorption and also for intensity decay (intensities of two standard reflections dropped continuously during data collection by 19% and 9%, respectively). Crystallographic data and processing parameters are given in Table 1.

The structures were solved by direct methods and subsequent Fourier analyses. Anisotropic displacement parameters were applied to non-hydrogen atoms in full-matrix least-squares refinements based on F^2. The hydrogen atoms were assigned with isotropic displacement factors and included in the final refinement cycles by use of geometrical restraints. Analytical expressions of neutral-atom scattering factors were employed, and anomalous dispersion corrections were incorporated. The program DIFABS [28], and the SHELXTL/PC [29] program package were used for computations. Selected bond distances and bond angles are given in Tables 2 and 3. Supplementary data consisting of fractional atomic coordinates, displacement parameters, observed and calculated structure factors and complete lists of bond distances and bond angles have been deposited, CCDC deposition numbers 101853 and 101854.

RESULTS AND DISCUSSION

3-ethylpyridine as well as 4-ethylpyridine interact with the copper(II) ions in presence of azide ions producing complexes of general formula $CuL_2(N_3)_2$. In case of 3-Etpy, crystals of the 1:2 azide complex were co-precipitated with blue crystals of a 1:2 nitrate complex. The sizes of both types of crystals are sufficient to separate them from each other after filtration and dryness. Both azide complexes are insoluble in non-polar solvents, e.g. benzene, carbontetrachloride, etc., and some polar solvents, e.g. methyl alcohol, chloroform and water. They are slightly soluble in acetone and ethanol but soluble in DMF and DMSO, giving non-conducting solutions. The colors of these complexes change to brown immediately in the last two solvents.

Structures

Figures 1 and 2 illustrate the principle structural features of complex (**1**), for which selected bond distances and bond angles are collected in Table 2. The structure contains two different subunits; [Cu(3-

Table 1. Crystallographic data and processing parameters

Compound	**1**	**2**
Molecular formula	$C_{14}H_{18}CuN_8$	$C_{14}H_{18}CuN_8$
Molecular weight	361.90	361.90
Color	black	deep green
System, space group	monoclinic, $P2_1/n$	monoclinic, $P2_1/n$
a (Å)	11.996(3)	14.653(6)
b (Å)	14.703(3)	8.076(3)
c (Å)	15.094(3)	15.114(7)
α (°)	90	90
β (°)	111.77(2)	109.56(3)
γ (°)	90	90
V (Å^3)	2472.4(9)	1685(1)
Z	6	4
μ(MoKα) (mm^{-1})	1.337	1.308
Normal. transmission factors	1.000–0.440	1.000–0.189
D_{calc}/D_{obs} (Mg/m^3)	1.458/1.46(2)	1426/1.43(2)
Approx. crystal size (mm)	$0.55 \times 0.30 \times 0.30$	$0.62 \times 0.48 \times 0.08$
θ range of data collection (°)	3.06–26.00	2.86–27.00
Reflections collected	5342	3506
Independ. refl./R_{int}	4525/0.0423	2785/0.0546
Parameters	324	212
Goodness-of-Fit on F^2_o	1.074	1.065
R_1/wR_2	0.0519/0.1054	0.0811/0.1599
Weighting factors*: a/b	0.0457/0.0186	0.0652/1.6958
Largest peak/hole (eÅ^{-3})	0.309/−0.358	0.354/−0.360

* $w^{-1} = [\sigma^2(F^2_o) + (aP)^2 + bP]$ and $P = (F^2_o + 2F^2_c)/3$.

Table 2. Selected bond distances (Å) and angles (°) of **1**

Cu(1)...Cu(1a)	3.323(1)	Cu(1)...Cu(2)	5.979(2)
Cu(2)...Cu(1a)	6.459(2)	Cu(1)–N(21)	1.981(4)
Cu(1)–N(1)	2.005(3)	Cu(1)–N(11a)	2.020(3)
Cu(1)–N(2)	2.030(3)	Cu(1)–N(11)	2.409(3)
Cu(1)–N(33)	3.509(4)	Cu(2)–N(31)	1.992(4)
Cu(2)–N(3)	2.018(3)	Cu(2)–N(13a)	2.658(3)
N(11)–N(12)	1.201(4)	N(11)–Cu(1a)	2.020(3)
N(12)–N(13)	1.154(4)	N(21)–N(22)	1.180(5)
N(22)–N(23)	1.152(5)	N(31)–N(32)	1.195(5)
N(32)–N(33)	1.162(5)		
N(21)–Cu(1)–N(1)	92.80(14)	N(21)–Cu(1)–N(11a)	175.4(2)
N(1)–Cu(1)–N(11a)	91.81(13)	N(21)–Cu(1)–N(2)	86.9(2)
N(1)–Cu(1)–N(2)	167.85(13)	N(11a)–Cu(1)–N(2)	88.59(13)
N(21)–Cu(1)–N(11)	96.11(14)	N(1)–Cu(1)–N(11)	95.80(12)
N(11a)–Cu(1)–N(11)	83.16(12)	N(2)–Cu(1)–N(11)	96.31(12)
N(11)–Cu(1)–N(33)	155.6(1)	N(31)–Cu(2)–N(3)	90.82(14)
N(3)–Cu(2)–N(13a)	89.2(1)	N(31)–Cu(2)–N(13a)	91.8(1)
N(12)–N(11)–Cu(1a)	126.9(3)	N(12)–N(11)–Cu(1)	120.8(3)
Cu(1a)–N(11)–Cu(1)	96.84(12)	N(13)–N(12)–N(11)	177.8(4)
N(22)–N(21)–Cu(1)	125.8(3)	N(23)–N(22)–N(21)	177.4(5)
Cu(1)–N(33)–N(32)	136.3(3)	N(32)–N(31)–Cu(2)	119.6(3)
Cu(2a)–N(13)–N(12)	129.1(3)	N(33)–N(32)–N(31)	177.6(4)

symmetry codes: (a) $-x, -y, -z$; (b) $-x-1, -y, -z$.

Table 3. Selected bond distances (Å) and angles (°) of **2**

Cu(1)...Cu(1a)	3.813(3)	Cu(1)...Cu(1b)	6.283(2)
Cu(1)–N(11)	1.972(6)	Cu(1)–N(21)	1.990(6)
Cu(1)–N(2)	2.010(5)	Cu(1)–N(1)	2.027(5)
Cu(1)–N(21a)	2.920(7)	Cu(1)–N(13b)	2.675(8)
N(11)–N(12)	1.190(9)	N(12)–N(13)	1.149(9)
N(21)–N(22)	1.183(8)	N(22)–N(23)	1.139(8)
N(11)–Cu(1)–N(21)	169.1(3)	N(11)–Cu(1)–N(2)	89.2(2)
N(21)–Cu(1)–N(2)	92.7(2)	N(11)–Cu(1)–N(1)	87.8(2)
N(21)–Cu(1)–N(1)	90.8(2)	N(2)–Cu(1)–N(1)	175.6(2)
N(1)–Cu(1)–N(21a)	92.2(2)	N(2)–Cu(1)–N(21a)	91.1(2)
N(11)–Cu(1)–N(21a)	89.4(3)	N(21)–Cu(1)–N(21a)	79.9(3)
N(1)–Cu(1)–N(13b)	86.9(2)	N(2)–Cu(1)–N(13b)	90.3(2)
N(11)–Cu(1)–N(13b)	99.2(3)	N(21a)–Cu(1)–N(13b)	171.3(2)
N(12)–N(11)–Cu(1)	123.3(5)	Cu(1)–N(21)–Cu(1a)	100.1(3)
N(13)–N(12)–N(11)	176.1(8)	N(22)–N(21)–Cu(1)	121.5(5)
N(23)–N(22)–N(21)	176.2(8)		

symmetry codes: (a) $-x+1, -y, -z+1$; (b) $-x+3/2, y+1/2, -z+3/2$.

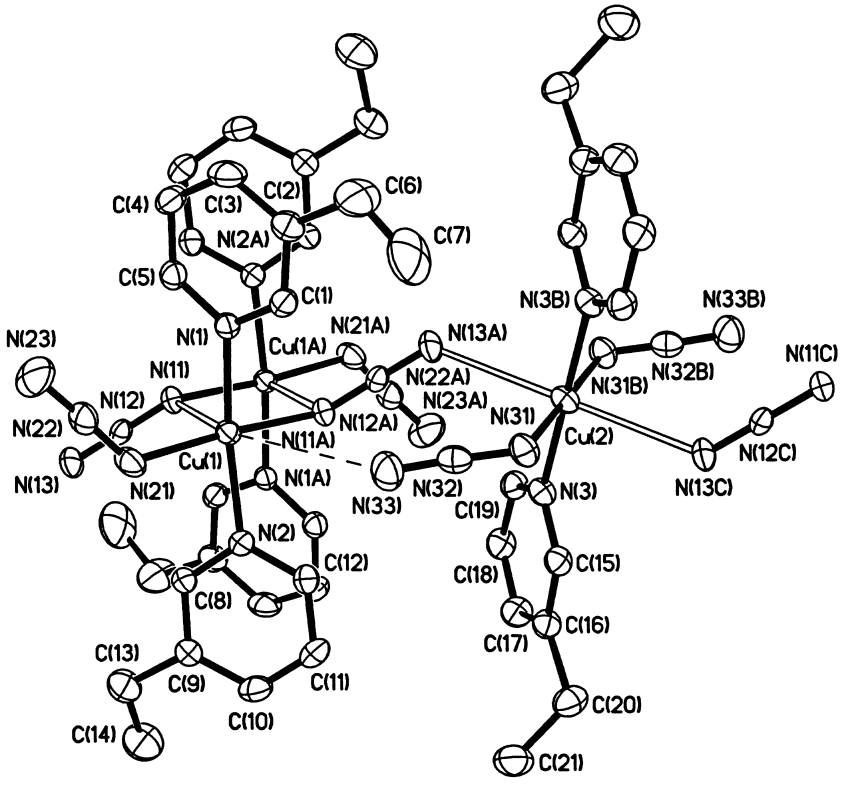

Fig. 1. $[Cu(3\text{-ethylpyridine})_2(N_3)_2]_n$, **1**: Molecular geometry and atom labelling scheme of the trinuclear unit. Hydrogen atoms are omitted. Open stick bonds indicate Cu–N bonds within the range 2.20–2.80 Å; broken lines are Cu–N distances >2.80 Å.

$Etpy)_2(N_3)_2]_2$ (I) and $[Cu(3\text{-}Etpy)_2(N_3)_2]$ (II). Each copper atom in the dimeric unit (I) is coordinated by pairs of trans 3-Etpy molecules, terminal azido groups [N(21)–N(22)–N(23) and N(21a)–N(22a)–N(23a)] and nitrogen atoms of μ_3-1,1,3 bridging azido ligands [N(11)–N(12)–N(13) and N(11a)–N(12a)–N(13a)]. Thus each copper atom is pentacoordinated by four short Cu–N distances [from 1.981(4) to 2.030(3) Å]

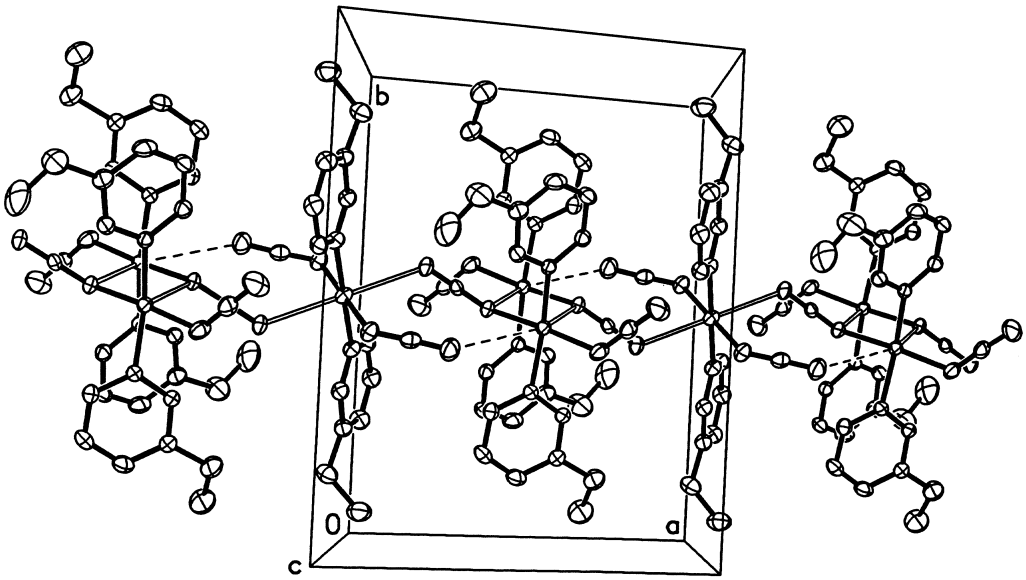

Fig. 2. [Cu(3-ethylpyridine)$_2$(N$_3$)$_2$]$_n$, **1**: One-dimensional chain of copper polyhedra oriented along the *a*-axis of the unit cell.

and a fifth long Cu–N bond length of 2.409(3) Å, adopting a distorted square pyramidal geometry with N(11) at the apical site. The metal center, Cu(2), in unit (II), which is located at an inversion center, binds two azido ligands [N(31)–N(32)–N(33) and N(31b)–N(32b)–N(33b)], two 3-Etpy molecules and the other end nitrogen of the two μ_3-1,1,3 azido ligands at a long Cu–N distances of 2.658(3) Å, giving rise to a (2+2+2) elongated distorted octahedral geometry. The distances between copper atoms of the two units, Cu(2)...Cu(1) and Cu(2)...Cu(1a) are 5.979(2) and 6.459(2) Å, respectively. The terminal azide groups [N(31)–N(32)–N(33) and N(31b)–N(32b)–N(33b)] from unit (II) have very long distances of 3.509(4) Å, between the other end nitrogen atoms and copper atoms of neighboring dimeric units on both sides. The Cu...Cu distance of 3.323(1) Å within the Cu_2N_2 ring of the dimeric unit (I) is longer than corresponding values [3.120(2) and 3.071(2) Å] found in the structure of [Cu(pyridine–N–oxide)(N$_3$)$_2$]$_n$ [14], shorter than that reported for [Cu(3-pic)$_2$(N$_3$)$_2$]$_n$ of 3.546(2) Å [12], but comparable with that found [3.326(2) Å] in the structure of [Cu(3-acetylpyridine)$_2$(N$_3$)$_2$]$_n$ [14].

Figure 3 is a perspective drawing showing the principle structural features of complex (**2**) along with the atom labelling scheme. Selected bond lengths and bond angles are collected in Table 3. The coordination polyhedron around copper atoms may be described as (4+1+1) with four short bonds with N(1) and N(2) from 4-Etpy molecules and N(11) and N(21) from two azido ligands [Cu–N, av = 2.0 Å] and nitrogen atom N(13a) of asymmetric μ_2-1,3 azido group which occupies an apical position at a long Cu–N distance of 2.658(3) Å. Such tetragonal pyramids are connected to zig-zag chains. N(21) further links the former chains of polyhedra at a very long distance, Cu(1)–N(21a) = 2.920(7) Å. Thus azido ligand N(21)–N(22)–N(23) behaves as μ_2-1,1 bridging group and asymmetric di-μ_2-1,1 of such azides form Cu_2N_2 cyclic rings giving rise to sheets of poyhedra (Figure 4). Although the structure of complex (**2**) differs from that of complex (**1**), steric and packing effects are operative and cause the connection of the chains of tetragonal polyhedra through such very long Cu–N distances giving rise to a two-dimensional structure.

The structures of the title complexes (**1**) and (**2**) are closely related to those of diazido-2,2′-bipyridine copper(II) [30] and [(2-aminoethyl)pyridine]copper(II) azide [1]. In the former the copper is described as being square-planar with two additional long bonds [Cu–N: 2.682 and 2.680 Å] leading, through semi-coordination, to polymerization in the *x* direction. In the latter, the coordination geometry around the copper atom is distorted from square planar by a tetrahedral twist of 28°. The copper coordination polyhedron is completed by short interactions, both above and below the mean plane, to the bonded azide nitrogen atoms of adjacent molecules related by the *c*-glide symmetry [Cu–N: 2.88 and 2.66 Å].

Long Cu–N distances are also observed in the linear systems: Cu(4-pic)$_2$(N$_3$)$_2$ [Cu–N: 2.52(2)–2.79(2) Å] [10]; [Cu(DENA)(N$_3$)$_2$] [2.755(5) and 2.841(5) Å] [4, 5]; Cu(3-pic)$_2$(N$_3$)$_2$ [Cu–N: 2.625–2.679 Å] [12]; Cu(3,4-lut)(N$_3$)$_2$ [Cu–N: 2.638(3) Å] [15]; both modifications of Cu(py)$_2$(N$_3$)$_2$ [Cu–N: 2.50–2.76 Å] [31, 32]; Cu(NH$_3$)$_2$(N$_3$)$_2$ [Cu–N: 2.56(1) and 2.67(1) Å] [33]; KCu(picolinato)(N$_3$)$_2$]$_n$ [Cu–N: 2.649(4) Å] [34] and copper azido complex with tridentate ligand 1-(imidazol-4-yl)-2-(2-pyridylmethylene)-amino)-ethane [Cu–N: 2.797 and 2.804 Å] [35]. Sheets of polyhedra are formed in case of copper complexes with the (3-

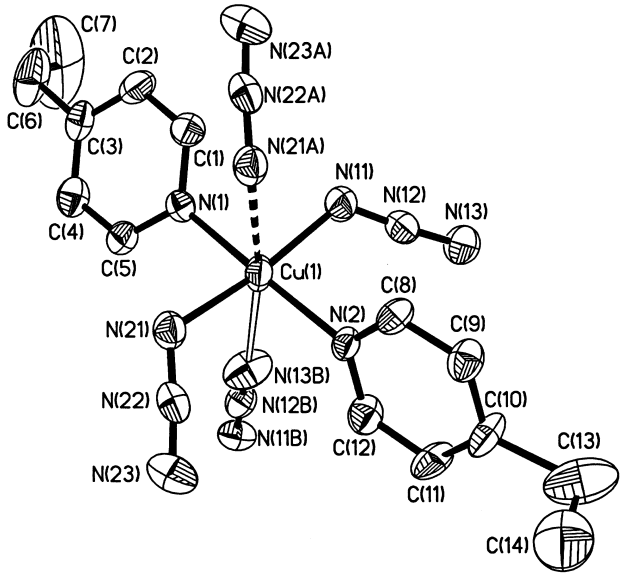

Fig. 3. $[Cu(4\text{-ethylpyridine})_2(N_3)_2]_n$, **2**: Molecular geometry and atom labelling scheme. Hydrogen atoms are omitted. Open stick bonds indicate Cu–N bonds within the range 2.20–2.80 Å; broken lines are Cu–N distances > 2.80 Å.

aminopropyl)oxamidato ligand [Cu–N: 2.564(3) and 2.859(4) Å] [36] and $[Cu_2(bpym)(N_3)_4]$ (bpym = 2,2′-bipyrimidine) [Cu–N: 2.480(2) and 2.743(3) Å] [37], whereas Cu–N distances of 2.60(2) and 2.70(2) Å are observed in $Cu(N_3)_2$ [38] and a long Cu–N distance of 2.627(6) Å in the 3:2 complex with 2-benzoylpyridine [16]. In case of the three copper azido complexes with tridentate ligand 1,4,7-trimethyl-1,4,7-triazacyclononane dimeric units are formed by taking into account Cu–N distances from 2.709 to 2.944 Å [21].

IR spectra

X-ray structure determination showed complex (**1**) to have three asymmetric azides with δd values of 0.047, 0.033 and 0.028 Å, and complex (**2**) to contain two asymmetric azido ligands with δd values of 0.044 and 0.041 Å. While the number of $\nu_{as}N_3$ bands are two (Table 4) as expected in case of complex (**2**), the appearance of only one $\nu_{as}N_3$ sharp band is unexpected for complex (**1**). However, this result is not unusual. For example, the IR spectrum of $Cu(pyridine)_2(N_3)_2$, with two asymmetric azido groups showed only one ν_{as} band at 2040 cm^{-1} [32]. For complex (**2**) the positions of the $\nu_{as}N_3$ absorption bands are not consistent with the δd verses $\nu_{as}N_3$ relationship given earlier [39, 40] which suggests two bands around 2040 cm^{-1}. It is possible that some coincidence of the vibrations related to the azides with such very close δd values leads to some sort of resonance or configuration interactions. It is noteworthy to mention that the markedly strong band usually appeared around 1285 cm^{-1} associated with ν_sN_3 in copper(II) azido complexes containing one ore more di-μ_2-1,1 bridging azido systems [4–7], is not observed in the IR spectra of both complexes (**1**) and (**2**). Instead, a weak to medium band appears around 1284–1289 cm^{-1}.

Electronic spectra

The electronic spectra of the title complexes, **1** and **2**, measured as Nujol mulls are given in Table 5. These spectra exhibit d–d transitions as a broad band centered around 14700 and 15350 cm^{-1}, for **1** and **2**, respectively, suggesting a distorted six-coordinate copper(II) environment [41, 42] for both complexes. The spectra of these complexes also show at least three strong bands in the ranges 33000–22000 cm^{-1} and 31000–18400 cm^{-1}, for **1** and **2**, respectively. These bands are due to $N_3 \rightarrow Cu^{II}$ LMCT transitions. While two and four azide-to-copper charge transfer transitions have been predicted [43] for terminal and μ_2-1,1 or μ_2-1,3 bridging azido ligands in copper(II) complexes, respectively, only one feature is observed for terminal copper(II) azide monomers and two bands are reported for μ_2-1,3 or μ_2-1,1 dimers [36]. The present structure with terminal azides, μ_3-1,1,3 and μ_2-1,1 or μ_2-1,3 azides show at least three $N_3 \rightarrow Cu^{II}$ LMCT bands. In DMF and DMSO both complexes show a very strong band in the range 25250–24000 cm^{-1} due to $N_3 \rightarrow Cu^{II}$ CT transitions, in addition to the d–d absorption around 14000 cm^{-1} for DMF and 13000 cm^{-1} for DMSO. Thus these complexes in DMF and DMSO show only one LMCT absorption band and the d–d transition is shifted to lower wave numbers. The change of color of these complexes in both solvents from green to brown could be associated with a partial reduction of Cu(II) to Cu(I) leading to

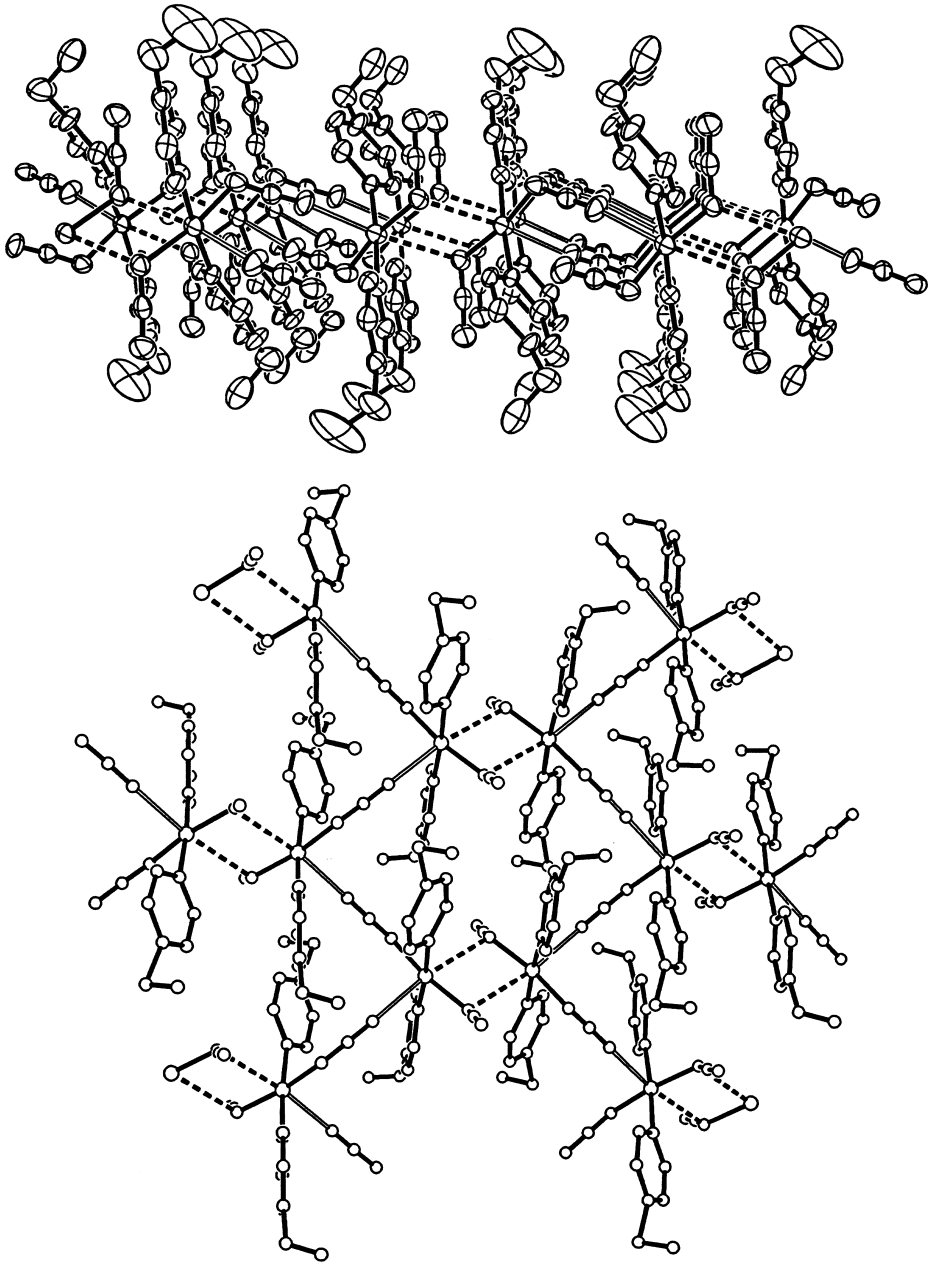

Fig. 4. $[Cu(4\text{-ethylpyridine})_2(N_3)_2]_n$, **2**: Two-dimensional arrangement of the copper polyhedra. Top: front view; bottom: view onto the sheet of copper polyhedra. Bond types as in Fig. 3.

mixed-valence compounds which are well known to exhibit such brownish color. In EtOH, however, complex **2** retains its identity as suggested by its color and the position of the d–d absorption band at $14880\,cm^{-1}$, a little lower value than of the solid sample.

Magnetic properties

$\chi_M T$ verses T plot, (referred to the *three* coppers molecular weight), of compound **1** and the $\chi_M T$ verses T plot (for *two* copper atoms), of compound **2** are shown in Fig. 5. For **1**, the $\chi_M T$ plot shows a practically constant value close to $1.2\,cm^3{\cdot}K{\cdot}mol^{-1}$ in the temperature range 300–25 K, decreasing slightly at low temperature. The 4 K value reaches $0.93\,cm^3{\cdot}K{\cdot}mol^{-1}$. This magnetic behavior indicates a very weak overall antiferromagnetic interaction. Compound **2** shows a room temperature $\chi_M T$ value of $0.86\,cm^3{\cdot}K{\cdot}mol^{-1}$, which increases up to $0.94\,cm^3{\cdot}K{\cdot}mol^{-1}$ at 20 K, decreasing slightly at lower temperatures, indicating a dominating weak fer-

Table 4.Azide and copper-ligand frequencies in complexes $[Cu(3\text{-}Etpy)_2(N_3)_2]_n$ (**1**) and $[Cu(4\text{-}Etpy)_2(N_3)_2]_n$ (**2**)

Frequency (cm^{-1})		Assignments
1	**2**	
2030 vs[a]	2072 vs	$\nu_{as}N_3$
	2040 vs	
1325 wm	1337 wm	ν_sN_3
1284 wm	1289 wm	
607 m	615 wm	δN_3
365 ms	374 ms	νCu–N_3
260 ms	265 ms	νCu–N(L)

[a] s = strong, m = medium, w = weak, v = very.

Table 5. Electronic spectral data

Complex	Solvent	$N^-{}_3 \rightarrow Cu^{II}(CT(\xi)$[a]	d–d(ξ)[a]
1	NM	33000	14700 br
		29760	
		22720 br	
	DMF	24750 (2222)	13774 (145)
	DMSO	25252 (2660)	13192 (152)
2	NM	30850	15360 br
		23866	
		18416	
	DMF	24038 (3560)	14144 (270)
	DMSO	24271 (2800)	12836 (180)
	EtOH	24213 (1200)	14880 (120)

[a] In cm^{-1}, NM = Nujol mull, br = broad.

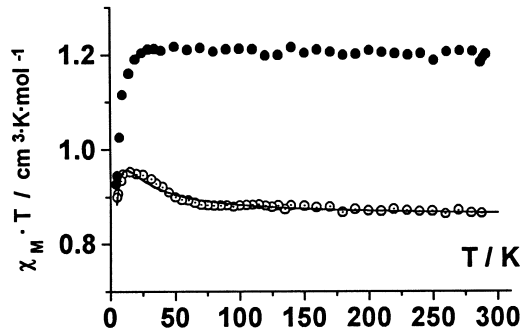

Fig. 5. $\chi_M T$ verses T plots for **1** (solid circles) and **2** (dot center circles). Solid line show best fit obtained for **2** (explanations see text).

romagnetic interaction in the 300–20 K temperature range and a weak antiferromagnetic coupling at low temperature.

From the structural data, the two compounds show the azide bridges between equatorial-apical sites of square pyramidal or octahedral copper(II) environments. The unpaired electronic density is then largely localized in the *xy* plane, and all interactions involving the non-active $d^2{}_z$ atomic orbital should be very weak or even negligible.

Compound **1** shows the unusual μ_3-1,1,3 azide bridges between each three copper atoms unit, for which two interactions of opposite sign may be expected: the double μ_2-1,1 bridges between Cu(1)–Cu(1a) may afford ferromagnetic coupling, whereas for the end-to-end bridges between Cu(1)/Cu(1a) and Cu(2) antiferromagnetic coupling may be expected. Moreover, all the azide bridges involve at least one axial coordination site of the corresponding copper environments: N(11) acts as a bridge between an equatorial Cu(1) and an axial Cu(1a) sites, as occurs for the Cu(1)–N(11)–N(12)–N(13)···Cu(2), whereas the interaction trough Cu(1a)···N(11)–N(12)–N(13)···Cu(2) involves two large axial sites. From these data, the magnetic behavior of the compound **1** may be reasonably assumed as very weak ferro–antiferro competing interactions which allows to an apparently non-coupled system, with a dominant antiferromagnetic interaction, evidenced at low temperature. Due to the small decay at low temperature, try to evaluate the J values of this system has no sense, and only the qualitative discussion of the observed properties was made.

For compound **2**, the interaction provided by the end-to-end bridge should be quasi-negligible due to the very large Cu(1)–N(13b)–N(12b) bond angle of 172.7(6)°, according to previous MO calculations [26, 27]. Experimental magnetic data have been fitted as a dimeric CuCu ferromagnetic entity including a z"J" parameter to evaluate the weak antiferro–magnetic interactions [44], $S = 1/2$ systems. The best fit parameters, referred to the Hamiltonian $H = -JS_1S_2$ were $J = -12.4(5)\,cm^{-1}$, $g = 2.137$ and $J' = -0.37(3)\,cm^{-1}$.

EPR spectra

The X-band EPR spectra of solid samples of both complexes at room temperature consist of the typical axial copper(II) signals, with $g_{par.} = 2.19$, $g_{perp.} = 2.07$ for **1** and $g_{par.} = 2.17$, $g_{perp.} = 2.09$ for **2**. Absence of half-field signals for the two compounds reinforced the assumption of very weak superexchange interactions.

Acknowledgements—Financial supports by the Kuwait University Research Administration Project (no. SC 077) and the Department of Chemistry General Facility Projects (Analab); CICYT grant PB096/163; and Jubiläumsfonds der Österreichischen Nationalbank (project 6630) are gratefully acknowledged. The authors thank Professor Kratky, Dr. Belaj (Univ. Graz) and Dr. Gatterer (TU Graz) for assistance.

REFERENCES

1. Baily, N. A., Fenton, D. E. and McLean, C. H., *Inorg. Chim. Acta*, 1991, **197,** 1.

2. Goher, M. A. S. and Mak, T. C. W., *Inorg. Chim. Acta*, 1984, **85,** 117.
3. Goher, M. A. S. and Mak, T. C. W., *Inorg. Chim. Acta*, 1984, **89,** 119.
4. Mak, T. C. W. and Goher, M. A. S., *Inorg. Chim. Acta*, 1986, **115,** 17.
5. Goher, M. A. S., Wang, R.-J. and Mak, T. C. W., *J. Mol. Struct*., 1991, **243,** 179.
6. Goher, M. A. S. and Mautner, F. A., *Z. Naturforsch*., 1991, **46(b),** 687.
7. Mautner, F. A. and Goher, M. A. S., *Polyhedron*, 1993, **12,** 2823.
8. Goher, M. A. S., Al-Salem, N. A. and Mautner, F. A., *Polyhedron*, 1996, **15,** 4513.
9. Goher, M. A. S., Mautner, F. A. and Al-Salem, N. A., *Polyhedron*, 1997, **16,** 2239.
10. Goher, M. A. S. and Mautner, F. A., *Cryst. Res. Technol*., 1992, **27,** 817.
11. Mautner, F. A., Goher, M. A. S. and Abdou, A. E. H., *Polyhedron*, 1993, **12,** 2815.
12. Mautner, F. A. and Goher, M. A. S., *Polyhedron*, 1992, **11,** 2537.
13. Goher, M. A. S. and Mautner, F. A., *Polyhedron*, 1996, **15,** 5.
14. Goher, M. A. S. and Mautner, F. A., *Polyhedron*, 1995, **14,** 1751.
15. Mautner, F. A. and Goher, M. A. S., *Polyhedron*, 1994, **13,** 2141.
16. Goher, M. A. S. and Mak, T. C. W., *Inorg. Chim. Acta*, 1985, **99,** 223.
17. Mautner, F. A. and Goher, M. A. S., *Polyhedron*, 1996, **15,** 1133.
18. Goher, M. A. S. and Mautner, F. A., *Polyhedron*, accepted.
19. Sikorav, S., Bkouche-Waksman, K. and Kahn, O., *Inorg. Chem*., 1984, **23,** 490.
20. Commarmond, J., Plumere, P., Lehn, J. M., Agnus, Y., Louis, R., Weiss, R., Kahn, O., Morgenstern-Badarau, I., *J. Am. Chem. Soc*., 1982, **104,** 6330.
21. Chaudhuri, P., Oder, K., Wieghardt, K. and Nuber, B., Weiss, J., *Inorg. Chem*., 1986, **25,** 2818.
22. Kahn, O., Sikorav, S., Gouteron, J., Jeannin, S. and Jeannin, Y., *Inorg. Chem*., 1983, **22,** 2877.
23. Tuczek, F. and Bensch, W., *Inorg. Chem*., 1995, **34,** 1482.
24. Charlot, M. F., Kahn, O., Chaillet, M. and Larrieu, C., *J. Am. Chem. Soc*., 1986, **108,** 2574.
25. Escuer, A., Vicente, R., Ribas, J., El-Fallah, M. S., Solans, X. and Font-Bardia, M., *Inorg. Chem*., 1993, **32,** 3727.
26. Escuer, A., Vicente, R., Goher, M. A. S. and Mautner, F. A., *Inorg. Chem*., 1996, **35,** 6386.
27. Escuer, A., Vicente, R., Mautner, F. A. and Goher, M. A. S., *Inorg. Chem*., 1997, **36,** 1233.
28. Walker, N. and Stuart, D., *Acta Cryst. A*, 1983, **39,** 158.
29. SHELXTL/PC v. 5.03, Siemens Analytical Automation Inc., Madison, WI (1995).
30. Bushnall, G. W. and Khan, M. A., *Can. J. Chem*., 1974, **52,** 3125.
31. Mautner, F. A. and Goher, M. A. S., *Polyhedron*, 1995, **14,** 1809.
32. Agrell, I., *Acta Chem. Scand*., 1969, **23,** 1667.
33. Agrell, I., *Acta Chem. Scand*., 1966, **20,** 1281.
34. Goher, M. A. S. and Mautner, F. A., *Polyhedron*, 1995, **14,** 1439.
35. Matsumoto, K., Ooi, S., Nakatsuka, K., Mori, W., Suzuki, S., Nakara, A. and Nakao, Y., *J. Chem. Soc., Dalton Trans*. 1985, 2095.
36. Chen, Z. N., Tang, W. X. and Yu, K. B., *Polyhedron*, 1994, **13,** 783.
37. de Munno, G., Real, J. A., Julve, M. and Munoz, M. C., *Inorg. Chim. Acta*, 1993, **211,** 227.
38. Agrell, I., *Acta Chem. Scand*., 1967, **21,** 2647.
39. Agrell, I., *Acta Chem. Scand*., 1971, **25,** 2865.
40. Goher, M. A. S., *Acta. Chim. Hung*., 1990, **127,** 213.
41. Kohout, J., Quastlerova-Hvastijova, M., Kohoutova, M. and Gazo, J., *Monatsh. Chem*., 1971, **102,** 350.
42. Hathaway, B. J., *J. Chem. Soc., Dalton Trans*. 1972, 1196.
43. Pate, J. E., Ross, P. K., Thamann, T. J., Reed, C. A., Karlin, K. D., Sorrell, T. N. and Solomon, E. J., *J. Am. Chem. Soc*., 1989, **111,** 5198.
44. Kahn, O. *Molecular Magnetism*, VCH Publishers, New York, 1993.

Pergamon

Polyhedron Vol. 17, No. 23–24, pp. 4275–4289, 1998
© 1998 Elsevier Science Ltd
All rights reserved. Printed in Great Britain
0277–5387/98 $19.00+0.00

PII: S0277–5387(98)00238–1

Synthesis, coordination chemistry and crystal structures of [2+2] macrocycles incorporating 2,6-bis(thiomethyl)pyridine sub-units

Edwin C. Constable,*[a] Adam C. King[b] and Paul R. Raithby[b]

[a]Institut für Anorganische Chemie, Universitat Basel, Spitalstrasse 51, 4056 Basel, Switzerland

[b]University Chemical Laboratory, Lensfield Road, Cambridge CB2 1EW, U.K.

(Received 25 May 1998; accepted 10 June 1998)

Abstract—A series of potentially dinucleating [2+2] macrocyclic ligands with two *SNS* metal-binding domains separated by a variable polymethylene chain have been prepared. Two examples of these ligands have been structurally characterised. These ligands form polymeric adducts with $[Rh_2(O_2CCMe_3)_4]$ in which the ligands are thought to act as exocyclic *S*-donors to the axial sites of the dinuclear complex. In contrast, reaction with $[(CO)_2Rh(\mu\text{-}Cl)_2Rh(CO)_2]$ resulted in the formation of dinuclear complexes in which two Rh(CO) units are bound to each macrocyclic ligand. © 1998 Elsevier Science Ltd. All rights reserved

Keywords: macrocycles; synthesis; X-ray structure; rhodium complexes.

1. INTRODUCTION

We have been interested in the properties of ligands incorporating both hard and soft donor sites for a number of years and have developed a number of ligand systems incorporating both (hard) nitrogen and (soft) sulfur donors into oligoaromatic [1–8], open chain [9, 10] and macrocyclic [11, 12] ligands. The design of macrocyclic ligands capable of binding two or more metal ions is of current interest and in this paper we show how the inversion of a synthetic strategy allows the formation of [2+2] as opposed to [1+1] macrocyclic ligands. These ligands were designed as they offer the possibility of binding two interacting mononuclear sites or a dinuclear component within a single macrocyclic ligand.

2. EXPERIMENTAL

^{1}H NMR spectra were recorded on Brüker WM250 or AM400 spectrometers; positive ion fast atom bombardment (FAB) and electron impact (EI) mass spectra were recorded on A.E.I. MS12 or Kratos MS50 spectrometers using a 3-nitrobenzyl alcohol matrix for the FAB spectra. IR spectra were recorded on Perkin-Elmer 1483 or 983 spectrophotometers with the samples in compressed KBr disks, as nujol mulls or as liquid films between CsI plates. Melting points were determined using unsealed capillary tubes and are uncorrected. 2,6-Bis(bromomethyl)pyridine **1** [13] and $[(CO)_2Rh(\mu\text{-}Cl)_2Rh(CO)_2]$ [14] were prepared by the literature methods.

2.1. 2,6-*Bis*(*mercaptomethyl*)*pyridine*, **2**

2,6-Bis(bromomethyl)pyridine (4.0 g, 15.2 mmol) and thiourea (2.3 g, 30.4 mmol) were dissolved in EtOH (50 cm^3) and the mixture heated to reflux for 5 h, after which the solution was evaporated to dryness *in vacuo* to give a white precipitate of solid thiouronium salt which was then treated with a solution of $NaHCO_3$ (2.12 g, 30.4 mmol) in water (100 cm^3) to give a clear solution. This solution was then boiled for 45 min under N_2, cooled to room temperature and extracted with CH_2Cl_2 (3×50 cm^3). The extracts were combined, washed with a saturated aqueous NaCl, dried over $MgSO_4$ and the solvent removed *in vacuo* to give a dark yellow oil. Kugelrohr distillation of this

*Author to whom correspondence should be addressed. Tel.: +41-61-267-1001; Fax: +41-61-267-1015; E-mail: constable@ubaclu.unibas.ch

oil gave **2** as a colourless liquid. Yield: 70–80%. B.p. 96–100°C/0.2 mm Hg. (Found: C, 49.2; H, 5.1; N, 8.2% $C_7H_9NS_2$ requires: C, 49.08; H, 5.30; N, 8.18%). IR (liquid film): 3060 w, 2931 w, 2546 w br, 1598 s, 1572 s, 1452 s, 1219 m, 1160 w, 1088 m, 822 m cm^{-1}. Mass spectrum (+ve FAB): *m/z* 171 {**2**}. ^{1}H NMR (CD_3OD): δ 7.60 (t, 1H, H^4), 7.25 (d, 2H, $H^{3,5}$), 3.75 (s, 4H, CH_2).

2.2. 2,3,12,13-*Tetrathia*-[4.4](2,6)-*pyridinophane*, **5**

2.2.1. *Method* 1 As in Section 2.1 to give the thiouronium salt which was then boiled with a saturated aqueous solution of $NaHCO_3$ in air (100 cm^3) for 45 min; the solution was then cooled extracted with CH_2Cl_2 (3 × 50 cm^3), the extracts combined, washed with a saturated aqueous NaCl, dried ($MgSO_4$) and concentrated to give **5** as a cream powder. M.p. 151–152 (lit.[15], 150–152°C). (Found: C, 49.82; H, 4.17; N, 8.36% $C_7H_9NS_2$ requires: C, 49.67; H, 4.17; N, 8.28%). IR (liquid film): 3050 w, 2964 w, 1588 s, 1572 s, 1452 s, 1205 m, 1084 m, 993 w, 815 m, 753 m cm^{-1}. Mass spectrum (EI): *m/z* 338 {**5**}. ^{1}H NMR (CF_3CO_2D): δ 8.30 (t, 2H, H^4), 7.73 (d, 4H, $H^{3,5}$), 4.12 (s, 8H, CH_2).

2.2.2. *Method* 2 A solution of **2** (0.1 g, 0.55 mmol) in MeOH (5 cm^3) was mixed with aqueous NaOH (0.2 g in 5 cm^3) and the mixture left in air for 4 days at 4°C. The white precipitate was collected by filtration and dried to give analytically pure **5**. Yield: 0.04 g (40%).

2.3. [2 + 2] *Macrocycles*

A solution of **2** (100 mg, 0.55 mmol) and the appropriate α,ω-dibromoalkane (0.55 mmol) in EtOH (25 cm^3) was heated to reflux and then treated with solid NaOH (200 mg). The mixture was heated to reflux for 2 h, after which period a white precipitate had formed. The reaction mixture was cooled, the white solid collected by filtration, washed with EtOH (3 × 10 cm^3) and separated by thin layer chromatography on alumina plates using 1:1 PhMe/CH_2Cl_2 as eluent.

2.3.1. 2,8,17,23-*Tetrathia*-[9.9](2,6)-*pyridinophane*, **6** Colourless crystals. Yield: 14 mg (10%). R_f = 0.17. (Found: C, 60.22; H, 7.18; N, 5.92% $C_{24}H_{34}N_2S_4$ requires: C, 60.20; H, 7.16; N, 5.85%). IR (KBr): 2928 m, 2856 w, 1587 s, 1571 s, 1463 s, 1451 m, 1384 w, 1156 w, 1080 w, 993 w, 818 w cm^{-1}. Mass spectrum (EI): *m/z* 478 {**6**}. ^{1}H NMR (CD_2Cl_2): δ 7.60 (t, 2H, H^4), 7.20 (d, 4H, $H^{3,5}$), 3.75 (s, 8H, pyCH_2S), 2.45 (t, 8H, CH_2C**H**$_2$S), 1.50 (m, 8H, C**H**$_2$$CH_2$S), 1.33 (m, 4H, CH_2C**H**$_2$$CH_2$).

2.3.2. 2,9,18,25-*Tetrathia*-[10.10](2,6)-*pyridinophane*, **7** Colourless crystals. Yield: 16 mg (11%). R_f = 0.20. (Found: C, 61.89; H, 7.40; N, 5.81% $C_{26}H_{38}N_2S_4$ requires: C 61.61; H 7.56; N 5.53%). IR (KBr): 2920 m, 2850 w, 1591 s, 1573 s, 1465 s, 1453 m, 1383 w, 1137 w, 1088 w, 993 w, 818 w cm^{-1}. Mass spectrum (EI): *m/z* 506 {**7**}. ^{1}H NMR (CD_2Cl_2): δ 7.60 (t, 2H, H^4), 7.20 (d, 4H, $H^{3,5}$), 3.75 (s, 8H, pyCH_2S), 2.45 (t, 8H, CH_2C**H**$_2$S), 1.50 (m, 8H, C**H**$_2$$CH_2$S), 1.34 (m, 8H, C**H**$_2$$CH_2$$CH_2$S).

2.3.3. 2,10,19,27-*Tetrathia*-[11.11](2,6)-*pyridinophane*, **8** Colourless crystals. Yield: 17 mg (11%). R_f = 0.24. (Found: C, 62.67; H, 7.85; N, 5.52% $C_{28}H_{42}N_2S_4$ requires: C 62.87; H 7.91; N 5.24%). IR (KBr): 2925 s, 2852 m, 1591 s, 1574 s, 1461 s, 1452 m, 1384 w, 1157 w, 1087 w, 993 w, 817 w cm^{-1}. Mass spectrum (EI): *m/z* 534 {**8**}. ^{1}H NMR (CD_2Cl_2): δ 7.60 (t, 2H, H^4), 7.20 (d, 4H, $H^{3,5}$), 3.75 (s, 8H, pyCH_2S), 2.45 (t, 8H, CH_2C**H**$_2$S), 1.50 (m, 8H, C**H**$_2$$CH_2$S), 1.32 (m, 12H, C**H**$_2$C**H**$_2$$CH_2$$CH_2$S).

2.3.4. 2,11,20,29-*Tetrathia*-[12.12](2,6)-*pyridinophane*, **9** Colourless crystals. Yield: 20 mg (12%). R_f = 0.30. (Found: C, 64.35; H, 8.41; N, 5.01% $C_{30}H_{46}N_2S_4$ requires: C 64.01; H 8.24; N 4.98%). IR (KBr): 2920 s, 2851 m, 1588 m, 1572 m, 1466 m, 1453 m, 1385 w, 1137 w, 1084 w, 993 w, 823 w cm^{-1}. Mass spectrum (EI): *m/z* 562 {**9**}. ^{1}H NMR (CD_2Cl_2): δ 7.60 (t, 2H, H^4), 7.20 (d, 4H, $H^{3,5}$), 3.75 (s, 8H, pyCH_2S), 2.45 (t, 8H, CH_2C**H**$_2$S), 1.52 (m, 8H, C**H**$_2$$CH_2$S), 1.25 (m, 16H, C**H**$_2$C**H**$_2$$CH_2$$CH_2$S).

2.3.5. 2,12,21,31-*Tetrathia*-[13.13](2,6)-*pyridinophane*, **10** Colourless crystals. Yield: 26 mg (15%). R_f = 0.36. (Found: C, 64.93; H, 8.45; N, 4.51% $C_{32}H_{50}N_2S_4$ requires: C 65.03; H 8.53; N 4.74%). IR (KBr): 2918 s, 2848 m, 1589 m, 1571 m, 1465 m, 1451 m, 1382 w, 1156 w, 1074 w, 993 w, 818 w cm^{-1}. Mass spectrum (EI): *m/z* 590 {**10**}. ^{1}H NMR (CD_2Cl_2): δ 7.60 (t, 2H, H^4), 7.20 (d, 4H, $H^{3,5}$), 3.75 (s, 8H, pyCH_2S), 2.45 (t, 8H, CH_2C**H**$_2$S), 1.52 (m, 8H, C**H**$_2$$CH_2$S), 1.25–1.28 (m, 20H, C**H**$_2$C**H**$_2$C**H**$_2$ $CH_2$$CH_2$S).

2.3.6. 2,13,22,33-*Tetrathia*-[14.14](2,6)-*pyridinophane*, **11** Colourless crystals. Yield: 27 mg (16%). R_f = 0.40. (Found: C, 66.10; H, 8.75; N, 4.66% $C_{34}H_{54}N_2S_4$ requires: C, 65.96; H, 8.79; N, 4.53%). IR (KBr): 2919 s, 2849 m, 1587 m, 1574 m, 1465 m, 1453 m, 1385 w, 1137 w, 1084 w, 993 w, 820 w cm^{-1}. Mass spectrum (EI): *m/z* 618 {M}, 585 {MH–S}, 557 {M–CH_2SH}, 529 {M–$(CH_2)_4SH$}, 447 {MH–$(CH_2)_{10}SH$}. ^{1}H NMR (CD_2Cl_2): δ 7.60 (t, 1H, H^4), 7.25 (d, 2H, $H^{3,5}$), 3.75 (s, 4H, CH_2). ^{1}H NMR (CD_2Cl_2): δ 7.60 (t, 2H, H^4), 7.20 (d, 4H, $H^{3,5}$), 3.75 (s, 8H, pyCH_2S), 2.45 (t, 8H, CH_2C**H**$_2$S), 1.52 (m, 8H, C**H**$_2$$CH_2$S), 1.25–1.30 (m, 24H, C**H**$_2$C**H**$_2$C**H**$_2$$CH_2$$CH_2$S).

2.4. *Tetrakis*(μ-*pivalato*)*dirhodium*

Tetrakis(μ-acetato)dirhodium (0.2 g, 0.45 mmol) and pivalic acid (4.0 cm^3) were heated at 130°C for 1 h, after which the solution was allowed to cool and then dried *in vacuo* over P_4O_{10} for 5 days. The solid pale green product was then dried in air at 140°C and used without further purification. Yield: 0.15 g (55%). IR (KBr): 2961 m, 2930 m, 2872 m, 1598 s, 1565 s,

1497 m, 1485 m, 1460 m, 1416 s, 1375 m, 1363 m, 1222 m, 897 w cm^{-1}. Mass spectrum (+ve FAB): *m/z* 610 {**M**}. ^{1}H NMR ($CDCl_3$): δ 0.98 (s).

2.5. $\{[Rh_2(O_2CCMe_3)_4]\}_2(L)$

A solution of *tetrakis*(μ-pivalato)dirhodium (25 mg, 0.041 mmol) in CH_2Cl_2 (5 cm^3) was added to a solution of the [2+2] macrocycle (0.041 mmol) in CH_2Cl_2 (5 cm^3) and the mixture stirred at room temperature for 30 min, after which time the colour had changed from green to purple and a purple oil had separated. The supernatant liquid was decanted and the purple oil was washed with CH_2Cl_2 (3 × 30 cm^3) and the residue dried *in vacuo* to give the $\{[Rh_2(O_2CCMe_3)_4]\}_2$(L) complexes as deep purple powders.

2.5.1. $\{[Rh_2(O_2CCMe_3)_4]\}_2$(**11**) Yield: 17 mg (42%). (Found: C, 48.60; H, 7.03; N, 1.55% $C_{74}H_{126}N_2O_{16}S_4Rh_4$ requires: C, 48.32; H, 6.90; N, 1.50%). IR (KBr): 2958 m, 2926 m, 2855 m, 1584 s, 1548 w, 1484 m, 1455 w, 1415 s, 1376 m, 1362 m, 1223 m, 1164 w, 1137 w, 897 w, 802 w, 780 w, 636 m cm^{-1}. Mass spectrum (+ve FAB): *m/z* 1228 $\{Rh_2(piv)_4$(**11**)$\}$. ^{1}H NMR (CD_3SOCD_3): δ 7.60 (t, 2H, H^4), 7.20 (d, 4H, $H^{3,5}$), 3.75 (s, 8H, $pyCH_2S$), 2.50 (CH_2CH_2S, isochronous with solvent residual resonance), 1.52 (m, 8H, CH_2CH_2S), 1.24–1.30 (m, 24H, $CH_2CH_2CH_2CH_2CH_2S$), 0.92 (s, 72H, CH_3).

2.5.2. $\{[Rh_2(piv)_4]\}_2$(**6**) Yield: 12 mg (45%). R_f = 0.40. (Found: C, 45.18; H, 6.12; N, 1.70% $C_{64}H_{106}N_2O_{16}S_4Rh_4$ requires: C, 45.20; H, 6.20; N, 1.60%). IR (KBr): 2958 m, 2926 m, 2855 m, 1584 s, 1548 w, 1484 m, 1455 w, 1415 s, 1376 m, 1362 m, 1223 m, 1164 w, 1137 w, 897 w, 802 w, 780 w, 636 m cm^{-1}. Mass spectrum (+ve FAB): *m/z* 1088 $\{Rh_2(piv)_4$(**6**)$\}$. ^{1}H NMR (CD_3SOCD_3): δ 7.60 (t, 2H, H^4), 7.20 (d, 4H, $H^{3,5}$), 3.74 (s, 8H, $pyCH_2S$), 2.50 (CH_2CH_2S, isochronous with solvent residual resonance), 1.50 (m, 8H, CH_2CH_2S), 1.33 (m, 4H, $CH_2CH_2CH_2S$), 0.92 (s, 72H, CH_3).

2.6. $[(CO)Rh(L)Rh(CO)][PF_6]_2$

A suspension of the appropriate [2+2] ligand (0.065 mmol) in methanol (2 cm^3) was added to a solution of freshly sublimed $[(CO)_2Rh(\mu\text{-}Cl)_2Rh(CO)_2]$ (20 mg, 0.65 mmol) in methanol (2 cm^3) and the mixture stirred at room temperature for 30 min under dinitrogen. The solution was filtered under dinitrogen and the clear yellow filtrate treated with ammonium hexafluorophosphate (100 mg) in methanol (5 cm^3). The coloured precipitates were collected by filtration, washed well with methanol (3 × 10 cm^3) and dried *in vacuo* to give the products in quantitative yield.

2.6.1. $[(CO)Rh$(**11**)$Rh(CO)][PF_6]_2$ Light yellow powder. (Found: C, 36.70; H, 4.65; N, 2.41% $C_{36}H_{54}N_2O_2S_4Rh_2P_2F_{12}$ requires: C, 36.93; H, 4.65; N, 2.39%). IR (KBr): 2924 m, 2852 m, 1996 s, 1600 w, 1563 w, 1466 w, 839 vs, 559 m cm^{-1}. Mass spectrum (+ve FAB): *m/z* 1026 $\{Rh_2$(**11**)$(CO)_2PF_6\}$. ^{1}H NMR (CD_3CN): δ 7.96 (t, 2H, H^4), 7.60 (d, 4H, $H^{3,5}$), 4.66 (br d, 8H, $pyCH_2S$), 3.04 (t, 8H, CH_2CH_2S), 1.86 (m, 8H, CH_2CH_2S), 1.25–1.60 (m, 24H, $CH_2CH_2CH_2CH_2CH_2S$).

2.6.2. $[(CO)Rh$(**10**)$Rh(CO)][PF_6]_2$ Light yellow powder. (Found: C, 35.95; H, 4.61; N, 2.55% $C_{34}H_{50}N_2O_2S_4Rh_2P_2F_{12}$ requires: C, 35.74; H, 4.41; N, 2.45%). IR (KBr): 2925 m, 2853 w, 1991 s, 1601 w, 1562 w, 1466 w, 839 vs, 559 m cm^{-1}. Mass spectrum (+ve FAB): *m/z* 997 $\{Rh_2$(**10**)$(CO)_2PF_6\}$. ^{1}H NMR (CD_3CN): δ 7.96 (t, 2H, H^4), 7.60 (d, 4H, $H^{3,5}$), 4.66 (br d, 8H, $pyCH_2S$), 3.04 (t, 8H, CH_2CH_2S), 1.86 (m, 8H, CH_2CH_2S), 1.30–1.60 (m, 20H, $CH_2CH_2CH_2CH_2CH_2S$).

2.6.3. $[(CO)Rh$(**9**)$Rh(CO)][PF_6]_2$ Yellow powder. (Found: C, 34.25; H, 4.10; N, 2.30% $C_{32}H_{46}N_2O_2S_4Rh_2P_2F_{12}$ requires: C, 34.48; H, 4.16; N, 2.51%). IR (KBr): 2922 m, 2849 w, 1993 s, 1600 w, 1563 w, 1465 w, 839 vs, 559 m cm^{-1}. Mass spectrum (+ve FAB): *m/z* 969 $\{Rh_2$(**9**)$(CO)_2PF_6\}$. ^{1}H NMR (CD_3CN): δ 7.96 (t, 2H, H^4), 7.60 (d, 4H, $H^{3,5}$), 4.66 (br d, 8H, $pyCH_2S$), 3.04 (t, 8H, CH_2CH_2S), 1.86 (m, 8H, CH_2CH_2S), 1.31–1.58 (m, 16H, $CH_2CH_2CH_2CH_2S$).

2.6.4. $[(CO)Rh$(**8**)$Rh(CO)][PF_6]_2$ Burgundy red powder. (Found: C, 33.22; H, 4.11; N, 2.62% $C_{30}H_{42}N_2O_2S_4Rh_2P_2F_{12}$ requires: C, 33.16; H, 3.90; N, 2.58%). IR (KBr): 2925 m, 2850 w, 2005 s, 1600 w, 1565 w, 1464 w, 839 vs, 558 m cm^{-1}. Mass spectrum (+ve FAB): *m/z* 941 $\{Rh_2$(**8**)$(CO)_2PF_6\}$. ^{1}H NMR (CD_3CN): δ 7.96 (t, 2H, H^4), 7.60 (d, 4H, $H^{3,5}$), 4.66 (br d, 8H, $pyCH_2S$), 3.04 (t, 8H, CH_2CH_2S), 1.90 (m, 8H, CH_2CH_2S, isochronous with solvent residual resonance), 1.34–1.57 (m, 12H, $CH_2CH_2CH_2CH_2CH_2S$).

2.6.5. $[(CO)Rh$(**7**)$Rh(CO)][PF_6]_2$ Burgundy red powder. (Found: C, 31.98; H, 3.64; N, 2.66% $C_{28}H_{38}N_2O_2S_4Rh_2P_2F_{12}$ requires: C, 31.77; H, 3.62; N, 2.65%). IR (KBr): 2925 w, 2852 w, 2006 s, 1600 w, 1566 w, 1467 w, 839 vs, 559 m cm^{-1}. Mass spectrum (+ve FAB): *m/z* 913 $\{Rh_2$(**7**)$(CO)_2PF_6\}$. ^{1}H NMR (CD_3CN): δ 7.96 (t, 2H, H^4), 7.60 (d, 4H, $H^{3,5}$), 4.66 (br d, 8H, $pyCH_2S$), 3.04 (t, 8H, CH_2CH_2S), 1.90 (m, 8H, CH_2CH_2S, isochronous with solvent residual resonance), 1.45–1.68 (m, 8H, $CH_2CH_2CH_2S$).

2.6.6. $[(CO)Rh$(**6**)$Rh(CO)][PF_6]_2$ Orange–red powder. (Found: C, 30.00; H, 3.20; N, 2.79% $C_{26}H_{34}N_2O_2S_4Rh_2P_2F_{12}$ requires: C, 30.30; H, 3.33; N, 2.72%). IR (KBr): 2927 w, 2853 w, 2009 s, 1602 w, 1569 w, 1466 w, 839 vs, 559 m cm^{-1}. Mass spectrum (+ve FAB): *m/z* 885 $\{Rh_2$(**6**)$(CO)_2PF_6\}$. ^{1}H NMR (CD_3CN): δ 7.96 (t, 2H, H^4), 7.60 (d, 4H, $H^{3,5}$), 4.66 (AB q, 8H, $pyCH_2S$), 3.04 (t, 8H, CH_2CH_2S), 1.90 (m, 8H, CH_2CH_2S, isochronous with solvent residual resonance), 1.49–1.74 (m, 4H, $CH_2CH_2CH_2S$).

2.7. $[(CO)Rh$(**10**)$Rh(CO)][RhCl_2(CO)_2]_2$

A suspension of the appropriate **10** (20 mg, 0.0338 mmol) in methanol (10 cm^3) was added to a

solution of $[(CO)_2Rh(\mu\text{-}Cl)_2Rh(CO)_2]$ (26.2 mg, 0.676 mmol) in methanol (5 cm^3) to give a yellow solution. After stirring at room temperature for 15 min the solution had turned orange and a deep orange solid had been precipitated. The mixture was stirred for an additional 30 min and the solid collected by filtration, washed with methanol (3×5 cm^3) and dried *in vacuo* to give [(CO)Rh(**10**)Rh(CO)][$RhCl_2(CO)_2$]$_2$. Yield: 41 mg (92%). (Found: C, 34.48; H, 3.76; N, 2.07% $C_{38}H_{50}N_2O_6Cl_4S_4Rh_4$ requires: C, 34.77; H, 3.84; N, 2.13%). IR (KBr): 2929 m, 2853 w, 2061 s, 1993 vs, 1977 m, 1603 w, 1564 w, 1466 w cm^{-1}. Mass spectrum (+ve FAB): *m/z* 824 {Rh_2(**10**)(CO)}. ^{1}H NMR (CD_3CN): δ 7.96 (t, 2H, H^4), 7.60 (d, 4H, $H^{3,5}$), 4.66 (br d, 8H, $pyCH_2S$), 3.04 (t, 8H, $CH_2C\mathbf{H}_2S$), 1.86 (m, 8H, $C\mathbf{H}_2CH_2S$), 1.30–1.60 (m, 20H, $C\mathbf{H}_2C\mathbf{H}_2C\mathbf{H}_2CH_2CH_2S$).

2.8. *Crystal structural determination of* **6** *and* **10**

Transparent blocks of the compounds were obtained by the slow evaporation of CH_2Cl_2 solutions and were mounted on glass fibres. All geometric and intensity data were taken from these crystals. Pertinent crystallographic data are given in Table 1. Intensity data, gathered were reduced by routine procedures. Structure solution used SHELXTL or SHELXTL PLUS.

The structures were solved by direct methods and refined by alternating cycles of least squares refinement and difference-Fourier synthesis. All non-H atoms were refined anisotropically; in the case of **6** the H-atoms were all given a common isotropic displacement coefficient, whereas for **10** the aromatic and aliphatic H-atoms were given different thermal parameters. Refinement was carried out on F^2 for all reflections. Selected bond angles and bond distances are given in Table 2.

3. RESULTS AND DISCUSSION

3.1. *Ligand synthesis*

Our aim was to prepare a suite of macrocyclic ligands with bridging groups linking two 2,6-bis(thiomethyl)pyridine sub-units in the generic [2 + 2] structure **3** in which L represents the bridging unit. Somewhat to our surprise, examples of such structures in the literature proved to be sparse [11, 12, 16–20]. In contrast, examples of the [1 + 1] congeners **4** are abundant and a large variety of spacer groups have been incorporated [16–18, 21–35]. One feature which struck us forcibly was that with the exception of those systems incorporating diazacrown ether spacers [21] and one thioether exchange reaction [22–24] all of the known [1 + 1] macrocyclic systems were prepared from the action of α,ω-dithiols on the dibromo compound **1** (or its chloro analogue). We were particularly interested in the use of relatively flexible linker groups and decided to adopt an alternate strategy in which 2,6-bis(mercaptomethyl)pyridine **2** was reacted with α,ω-dihalo compounds. The rationale for this strategy came from our eventual hope to use template methods for the synthesis of the macrocycles. A templated reaction seemed to be more likely if the sulfur-containing component had the *SNS* donor set of **2** rather than a flexible, and possibly non-chelating S_2 donor set of an α,ω-dithiol.

The intermediate dibromo compound **1** was prepared in 43% yield as a white crystalline solid using a slight modification of the literature method in which commercially available 2,6-bis(hydroxymethyl) pyridine is treated with concentrated hydrobromic acid [13]. The dithiol **2** was prepared from **1** by reaction with thiourea followed by basic hydrolysis of the intermediate thiouronium salt with $NaHCO_3$ solution in a modified literature procedure [36, 37]. Purification by distillation yielded **2** as a colourless oil with the expected spectroscopic and analytic properties.

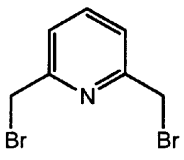

1

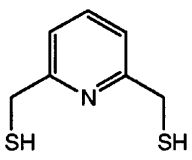

2

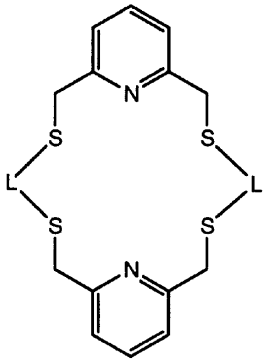

3

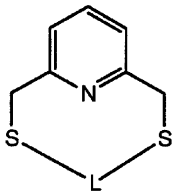

4

In the course of our preparative work, we noted that it was critical to add only two molar equivalents of $NaHCO_3$ during the hydrolysis step. If an excess of $NaHCO_3$ were added, we found that smooth conversion to the cyclic disulfide **5** occurred even with exclusion of atmospheric dioxygen. Compound **5** was initially identified by its IR spectrum which generally resembled that of **2** but lacked the S–H stretching mode in the 2500–2600 cm^{-1}; a parent ion was observed at m/z 338 in the mass spectrum. The properties of **5** corresponded to those of a cyclic dimer which had previously been reported [15].

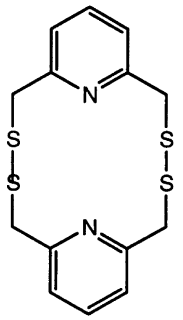

5

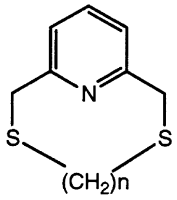

12 n = 5
13 n = 6
14 n = 7
15 n = 8
16 n = 9
17 n = 10

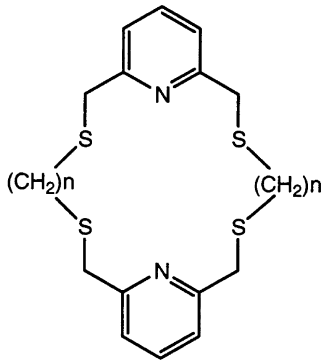

6 n = 5
7 n = 6
8 n = 7
9 n = 8
10 n = 9
11 n = 10

The dithiol **2** was reacted with the α,ω-dibromo compounds $Br(CH_2)nBr$ (n = 5–10) in EtOH in the presence of sodium hydroxide under dinitrogen. In the absence of NaOH, no reaction occurred. When NaOH was added, a white solid precipitated from the reaction mixture over the course of several hours at reflux. This material was indefinitely air-stable in the solid state. The ^1H NMR spectra of $CDCl_3$ solutions of the crude products (after filtration to remove poorly soluble material) showed single aromatic environments consisting of the expected doublets and triplets, but *two* py-CH_2S environments in an approximate ratio of 1:2. Thin layer chromatography over alumina using 1:1 CH_2Cl_2:PhMe as eluent allowed the separation of small amounts (<5%) of a fast running compound and 10–15% of a slower running component in each case. There were also significant amounts of baseline polymeric material.

In each case, the IR spectra of the two isolated components were identical and the most pertinent feature was the absence of any S–H stretching modes. The mass spectra of the products indicated that the faster running components should be formulated as the [1+1] macrocycles and the slower running, more abundant species as the [2+2]. The [1+1] ligands **12**–**15** have been previously reported [17, 30] and as our interest lay in the dinucleating systems, they were not further investigated.

The dinucleating [2+2] compounds were obtained as white crystalline solids with almost identical IR and ^1H NMR spectroscopic properties. The ^1H NMR spectra only differed in the intensity of the aliphatic methylene resonances. In order to fully confirm the formation of the [2+2] ligands and to probe the spatial relationships of the *SNS* donor sets, we have determined the solid state X-ray structures of **6** and **10**.

3.2. *X-ray structures of* **6** *and* **10**

The X-ray structure determination of **6** confirmed the gross structure of the [2+2] macrocycle and revealed the presence of two conformers within the crystal lattice as shown in Fig. 1. In one of the conformers, all four of the sulfur atoms are oriented with exocyclic lone pairs, whereas in the other one sulfur at each *SNS* unit is exocyclic whilst the other is endocyclic. The C–S–C bond angles at the endocyclic sulfur atoms are slightly smaller than those at the exocyclic [98.0(3) vs 101.1(2)–102.7(2)°]. All C–S bond distances are within the usual range and lie between 1.788(6)–1.820(4) Å. The packing of the molecules within the lattice is of some interest. The molecules of **6** form columns in which the two conformations alternate

Table 1. Crystal data and structure refinement for **6** and **10**

	6	**10**
Empirical formula	$C_{24}H_{34}N_2S_4$	$C_{32}H_{50}N_2S_4$
Formula weight	478.8	591.0
Diffractometer	Stoe AED4/V	Siemens R3m/V
Temperature (K)	290	290
Radiation, λ (Å)	graphite monochromated Mo	Kα, 0.71069
Crystal system	triclinic	triclinic
Space group	P$\bar{1}$	P$\bar{1}$
a (Å)	9.225(5)	5.291(2)
b (Å)	12.644(9)	8.104(3)
c (Å)	12.949(9)	19.362(6)
α (°)	64.37(3)	91.42(3)
β (°)	75.23(3)	91.96(3)
γ (°)	68.66(3)	100.95(3)
Volume (Å^3)	1259.8(14)	814.1(5)
Z	2	1
Density (calc.) (Mg m^{-3})	1.262	1.205
Absorption coefficient (mm^{-1})	0.375	0.302
F(000)	512	320
Crystal size (mm)	$0.30 \times 0.32 \times 0.35$	$0.10 \times 0.18 \times 0.38$
2θ range for data coll. (°)	5.0 to 45.0	5.0 to 42.0
Scan type	ω/θ	2θ–θ
Index ranges	$0 \le h \le 10$	$-5 \le h \le 5$
	$-13 \le k \le 15$	$-8 \le k \le 8$
	$-14 \le l \le 15$	$0 \le l \le 19$
Reflections collected	4674	1866
Independent reflections	4381 ($R_{\text{init}} = 0.0671$)	1734 ($R_{\text{init}} = 0.051$)
Observed reflections	3392 ($F > 4.0\sigma(F)$)	906 ($F > 4.0\sigma(F)$)
Structure solution	SHELXTL	SHELXTL PLUS
Refinement method	full-matrix least-squares	full-matrix least-squares
Goodness-of-fit	1.84	1.08
Final R indices [$F > 4\sigma(F)$]	$R = 0.0869$, $wR = 0.1227$	$R = 0.0561$, $wR = 0.0703$
R indices (all data)	$R = 0.1004$, $wR = 0.1302$	$R = 0.1218$, $wR = 0.0925$
Largest diff. peak, hole (eÅ^{-3})	0.96, -0.45	0.24, -0.27
Weighting scheme	$w^{-1} = \sigma^2(F) + 0.0035F^2$	$w^{-1} = \sigma^2(F) + 0.0023F^2$

(Fig. 2). The columns are arranged such that the pyridine rings of adjacent columns are approximately parallel with an interplanar stacking distance of ≈ 3.4 Å.

The structural determination of **10** also confirmed the formation of the [2 + 2] macrocycle and the molecular structure is presented in Fig. 3. In contrast to the structure of **6**, only a single conformer is present in the lattice, with one endocyclic and one exocyclic oriented sulfur at each *SNS* unit. All bond lengths and angles within the molecule are typical. The two pyridine rings of each macrocycle are coplanar and the molecules form a columnar arrangement in which graphitic packing occurs between molecules within the column, as opposed to *between* columns with **6** (Fig. 4). Details of the crystal structure determinations are presented in Table 1 and selected geometrical parameters are given in Table 2.

3.3. *Reactions with Rh–Rh bonded dinuclear rhodium complexes*

One of the principal aims that we had in preparing this series of ligands was to investigate metal–metal interactions in a series of dinuclear complexes in which the distance between the metal-binding domains was varied in a controlled manner. We were encouraged to note that mononuclear rhodium(I) complexes of a related [1 + 1] macrocycle exhibited short (3.32 Å) Rh . . . Rh interactions [22, 23, 24] and considered that the incorporation of two *SNS* donor sets in a ligand would allow these to be maximised. In the first instance, we investigated the behaviour of the representative ligands **6** and **11** with dinuclear metal–metal bonded species to see whether it would be possible for the ligands to fold around a dimetal core.

We chose the complex *tetrakis*(μ-pivalato) dirhodium [$Rh_2(O_2CCMe_3)_4$] with a Rh–Rh single bond as our starting material on the grounds of its good solubility in organic solvents and the characteristic and intense resonance for the *tert*-butyl groups in the ^{1}H NMR spectrum. The reaction of emerald green CH_2Cl_2 solutions of [$Rh_2(O_2CCMe_3)_4$] with CH_2Cl_2 solutions of **6** or **11** at a 1:1 stoichiometry resulted in the deposition of purple oils which gave dark purple solids upon drying. The IR spectra of

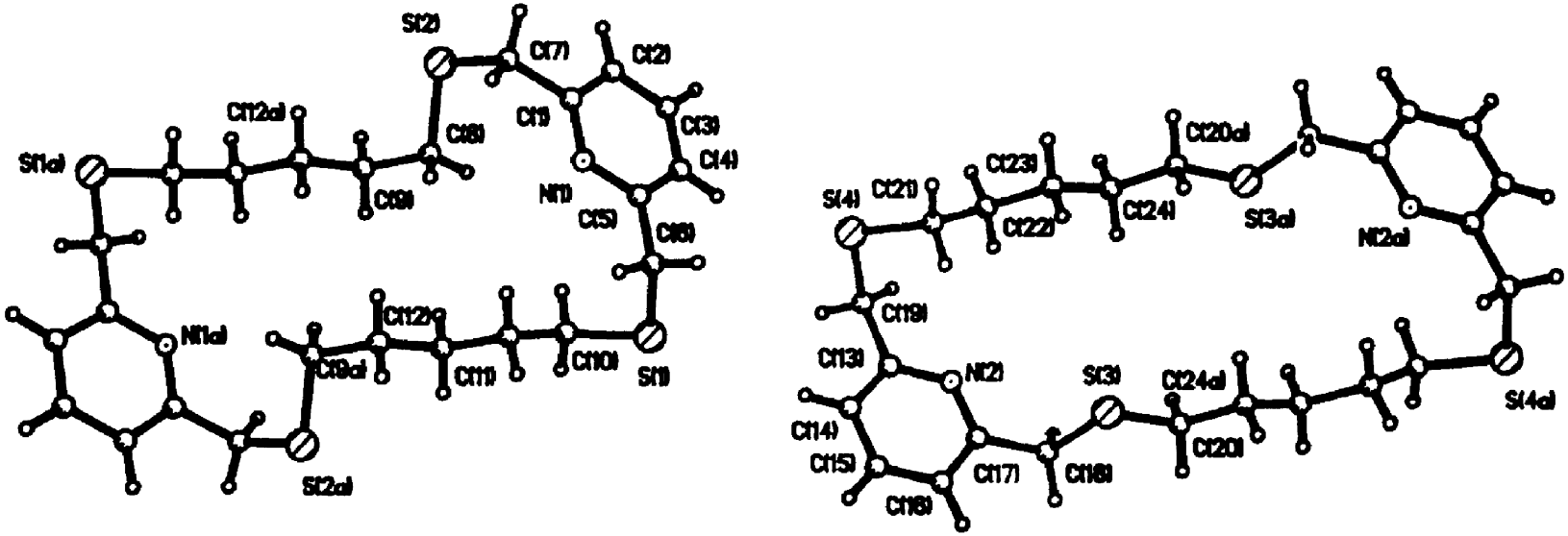

Fig. 1. The crystal and molecular structure of the two conformers of **6** which are present in the crystal lattice and showing the numbering scheme adopted.

Table 2. Selected bond lengths (Å) and angles (°) for **6** and **10**

6		**10**	
N(1)–C(1)	1.323(6)	N(1)–C(1)	1.365(11)
N(1)–C(5)	1.351(5)	N(1)–C(5)	1.355(10)
C(6)–S(1)	1.805(5)	C(6)–S(1)	1.794(10)
S(1)–C(10)	1.808(5)	S(1)–C(8)	1.797(10)
C(7)–S(2)	1.820(4)	C(7)–S(2)	1.808(8)
S(2)–C(8)	1.803(6)	S(2)–C(14)	1.809(9)
N(2)–C(13)	1.331(6)		
C(18)–S(3)	1.788(6)		
C(19)–S(4)	1.811(5)		
N(2)–C(17)	1.329(6)		
S(3)–C(20)	1.787(7)		
S(4)–C(21)	1.796(6)		
C(5)–C(6)–S(1)	115.8(3)	C(1)–C(6)–S(1)	111.6(6)
C(1)–C(7)–S(2)	114.0(3)	C(6)–S(1)–C(8)	99.8(4)
C(17)–C(18)–S(3)	110.8(3)	C(5)–C(7)–S(2)	114.9(6)
C(13)–C(19)–S(4)	113.6(3)	C(7)–S(2)–C(14)	101.7(4)
S(2)–C(8)–C(9)	109.7(3)	S(1)–C(8)–C(9)	112.8(7)
S(4)–C(21)–C(22)	116.1(3)	S(2)–C(14)–C(15)	116.9(7)
C(6)–S(1)–C(10)	102.7(2)		
C(7)–S(2)–C(8)	101.1(2)		
C(18)–S(3)–C(20)	98.0(3)		
C(19)–S(4)–C(21)	102.7(2)		
S(1)–C(10)–C(11)	116.7(3)		
S(3)–C(20)–C(24A)	114.2(4)		

these products exhibited absorptions at 1584 and 1425 cm^{-1} characteristic of bridging carboxylate together with absorptions at 1484 and 1455 cm^{-1} typical of the macrocyclic ligands and suggested the formation of adducts in which the dirhodium core remains intact. The FAB mass spectra of the purple products showed highest mass peaks assigned to 1:1 adducts together with a series of fragmentation peaks corresponding to sequential loss of pivalate.

The purple compounds were insoluble in chlorinated solvents and it was only possible to obtain ^1H NMR spectra in CD_3SOCD_3 solution. The complexes are unstable in this solvent and the spectrum corresponds to a superimposition of the spectra of the macrocycle and $[Rh_2(O_2CCMe_3)_4]$ in the same solvent. However, the ratio of the *tert*-butyl singlet to the peaks arising from the macrocycles clearly indicated that products of stoichiometry $\{[Rh_2(O_2CCMe_3)_4]\}_2(L)$ (L = **6** or **11**) had been formed, a fact confirmed by partial microanalysis of the purple solids. The 2:1 stoichiometry argues against the inclusion of the dinuclear units within the macrocyclic cavity, particularly in the case of **6**, and we propose a polymeric structure with an exocyclic bonding mode (Fig. 5). The polymeric formulation is in accord with the insolubility of the product.

The formation of *tetrakis*(carboxylato)dirhodium species with two axial sulfur donor thioether ligands has been previously established [38, 39]. In view of the extreme insolubility of these materials, we have not further investigated their constitution.

3.4. *Reactions with* $[(CO)_2Rh(\mu\text{-}Cl)_2Rh(CO)_2]$

As it had not proved possible to directly incorporate a dirhodium unit into the macrocyclic cavity, we decided to try to incorporate two mononuclear fragments with the hope that the imposed proximity would lead to metal–metal interactions. The presence of two *SNS* metal-binding domains suggested that a square-planar rhodium(I) centre bearing one additional ligand would be appropriate. Accordingly, we investigated the interaction of the [2 + 2] macrocycles with $[(CO)_2Rh(\mu\text{-}Cl)_2Rh(CO)_2]$.

Suspensions of the [2 + 2] macrocycles in methanol reacted slowly with deep red $[(CO)_2Rh(\mu\text{-}Cl)_2Rh(CO)_2]$ to give bright yellow solutions. In each case, the addition of ammonium hexafluorophosphate to these yellow solutions resulted in the precipitation of coloured products. Surprisingly, the colour of these microcrystalline precipitates varied considerably, depending upon the macrocycle used. In the case of ligands **9**, **10** and **11** the addition of ammonium hexafluorophosphate yielded yellow solids, but in the case of **6** an orange precipitate was obtained and with **7** and **8**, striking burgundy red solids were obtained. The red and orange solids dissolved in dichloromethane, acetonitrile or acetone to give yellow solutions with identical electronic spectra exhibiting maxima at 221 and 277 nm with a long tail into the visible. The products exhibited a single terminal carbonyl stretching mode in their IR spectra in the range 1996–2009 cm^{-1} together with bands at $\approx$1565 and 1600 cm^{-1} charac-

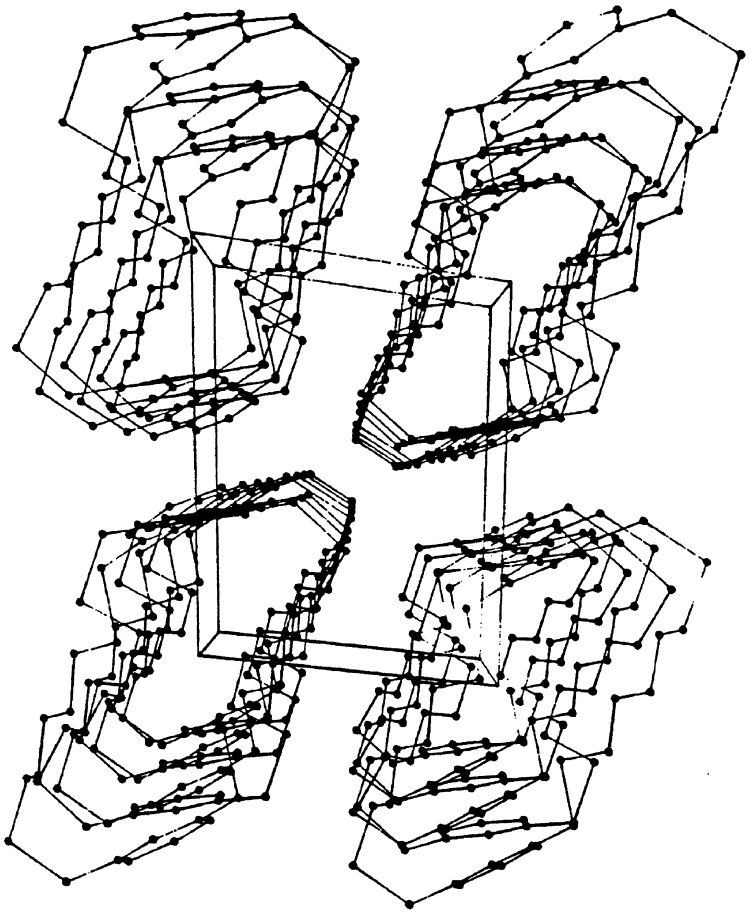

Fig. 2. The packing of the two conformers of **6** in the crystal lattice showing the formation of columns with intercolumnar π-stacking.

teristic of a pyridine coordinated to rhodium(I) [17]. In each case, FAB mass spectrometry gave peaks corresponding to $\{[(CO)Rh(L)Rh(CO)][PF_6]\}^+$ and microanalysis indicated dinuclear formulations $[(CO)Rh(L)Rh(CO)][PF_6]_2$ to be appropriate. These data are all consistent with the formation of dinuclear complexes in which each *SNS* domain is coordinated to a Rh(CO) moiety in a manner similar to that found with related mononucleating [1 + 1] complexes and we propose the structures indicated in Fig. 6.

The variation of colour within these systems is of some interest and is thought to relate to the degree of intermetallic interaction between the square-planar metal centres. The precise origin is somewhat unclear. The observation that the colour differences are only a solid state phenomenon, argues that the interactions are intermolecular and arising by the overlap of metal orbitals directed along the *z* axis (rhodium square plane defining *x* and *y*). However, the variation within the series is more consistent with an intramolecular interaction, in which the macrocyclic ring size controls the interaction of metal centres within the same macrocycle. Of course, conformational changes upon dissolution could also result in the loss of the Rh . . . Rh interactions. Electrochemical studies of solutions of the complexes revealed no oxidative processes and only ligand based reductions.

In an attempt to obtain higher nuclearity complexes, we also investigated the interaction of the representative ligand **10** with two equivalents of $[(CO)_2Rh(\mu\text{-}Cl)_2Rh(CO)_2]$ in methanol. Upon stirring, the reaction mixture changed from red, to yellow and finally to orange with the simultaneous precipitation of a deep orange solid. The IR spectrum was very similar to those of the products above, but in addition to the expected carbonyl mode at 1993 cm^{-1} also showed two additional carbonyl absorptions at 2061 and 1977 cm^{-1}. The ^1H NMR spectrum of a solution of the orange product was identical to that of $[(CO)Rh(\mathbf{10})Rh(CO)][PF_6]_2$ and the highest mass peak in the FAB mass spectrum was assigned to $\{Rh_2(\mathbf{10})(CO)\}$. Microanalysis indicated a formulation $[(CO)Rh(\mathbf{10})Rh(CO)][RhCl_2(CO)_2]_2$; the $[RhCl_2(CO)_2]^-$ anion is known to be formed from the reaction of $[(CO)_2Rh(\mu\text{-}Cl)_2Rh(CO)_2]$ with chloride (in this case, released in the formation of the $[(CO)Rh(\mathbf{10})Rh(CO)]^{2+}$

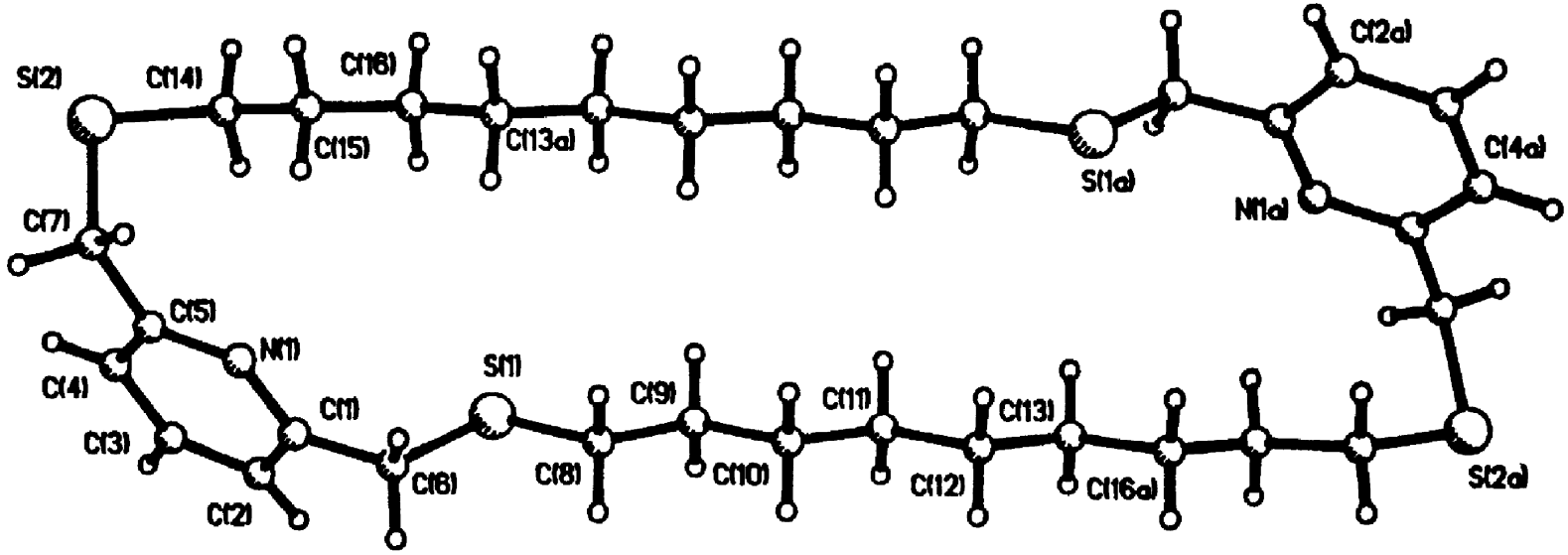

Fig. 3. The crystal and molecular structure of **10** showing the numbering scheme adopted.

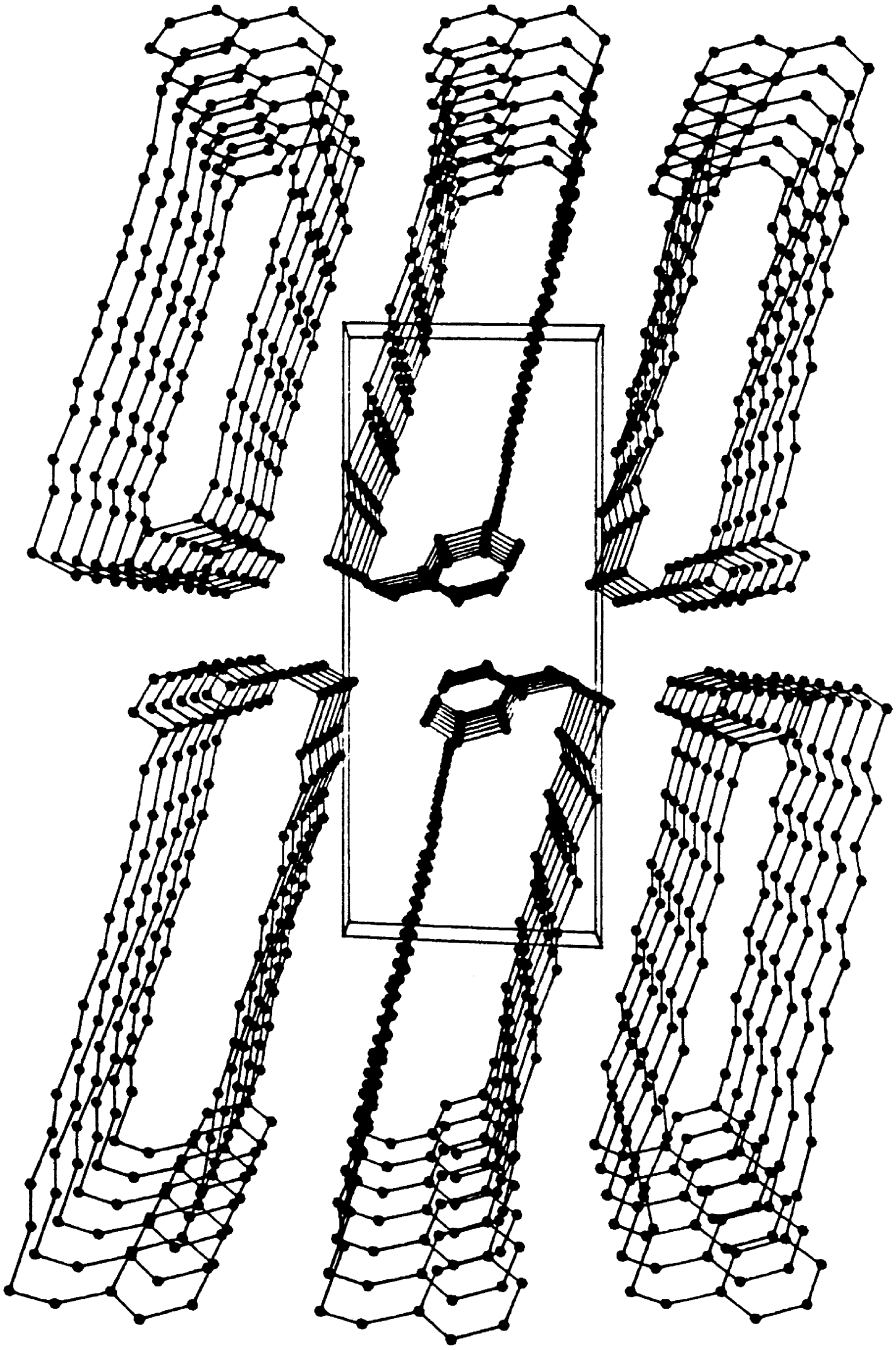

Fig. 4. The packing of **10** in the crystal lattice showing the formation of columns with intracolumnar π-stacking.

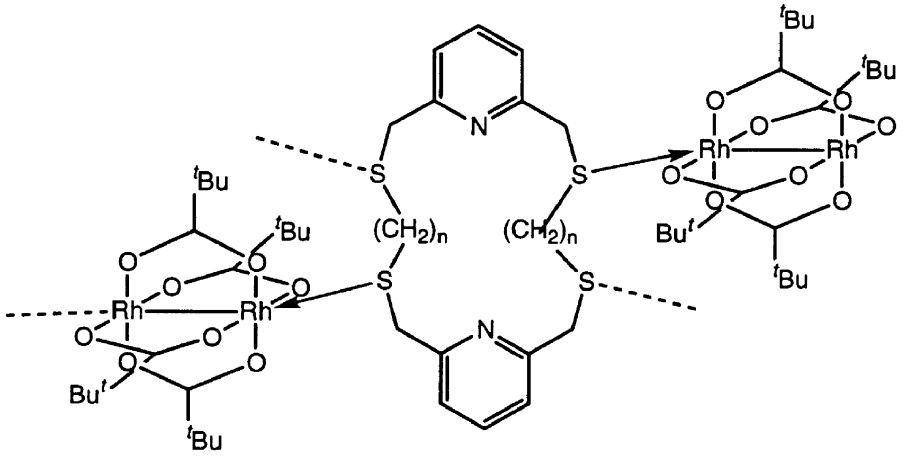

Fig. 5. Proposed structures for the polymeric materials of 2:1 stoichiometry obtained from the reaction of the [2+2] macrocyclic ligands with $[Rh_2(O_2CCMe_3)_4]$.

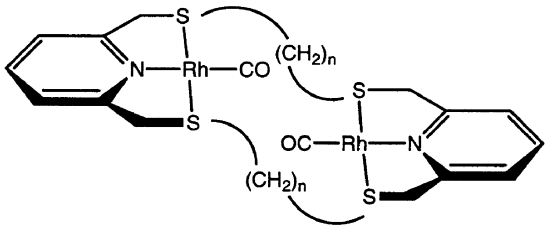

Fig. 6. Proposed structures for the dinuclear complexes obtained from the reaction of the [2+2] macrocyclic ligands with $[(CO)_2Rh(\mu\text{-}Cl)_2Rh(CO)_2]$.

cation) and the IR bands are fully in accord with this species [39–41]. The overall stoichiometry of the reaction is thus:

$$2[(CO)_2Rh(\mu\text{-}Cl)_2Rh(CO)_2] + \mathbf{10} \rightarrow [(CO)Rh(\mathbf{10})Rh(CO)][RhCl_2(CO)_2]_2$$

Treatment of methanol suspensions of $[(CO)Rh(\mathbf{10})Rh(CO)][RhCl_2(CO)_2]_2$ with ammonium hexafluorophosphate resulted in the formation of yellow $[(CO)Rh(\mathbf{10})Rh(CO)][PF_6]_2$.

3.5. ^{1}H *NMR studies of* $[(CO)Rh(L)Rh(CO)][PF_6]_2$ *complexes*

In each case, the $[(CO)Rh(L)Rh(CO)][PF_6]_2$ complexes dissolved in acetonitrile to give yellow solutions in CD_2Cl_2 or CD_3CN, the ^{1}H NMR spectra of which resembled those of the free ligands in terms of the number of resonances, but with some peaks broadened and all shifted to lower field. The most significant observation was that the $pyCH_2S$ protons now appeared as broadened doublets rather than as singlets. The appearance of diastereotopic protons for this methylene group is a natural consequence of the coordination of the *SNS* domain to the metal centre and provides evidence for the formulation in Fig. 6. Only in the case of the complex with **6** was the spectrum well resolved and the $pyCH_2S$ protons observed as a sharp AB quartet.

This phenomenon has been observed previously with related [1+1] macrocycles [17, 18, 22, 23, 24] and the dynamic process is assigned to inversion at the sulfur (Fig. 7). The complex $[(CO)Rh(\mathbf{9})Rh(CO)][PF_6]_2$ was taken as representative and variable temperature ^{1}H NMR spectra for CD_3CN solutions over the temperature range 255 to 315 K are presented in Fig. 8. These data may be analysed using a simple two site exchange model and lead to an activation free energy of 64.4 ± 0.2 kJ mol^{-1}, which is comparable to that reported for the related complexes with [1+1] macrocycles.

4. CONCLUSIONS

A range of [2+2] macrocyclic ligands have been prepared from 2,6-bis(mercaptomethyl)pyridine. Reaction with rhodium–rhodium bonded dinuclear complexes resulted only in an exocyclic bonding mode rather than incorporation of the dimer into the macrocyclic cavity. In contrast, reaction with $[(CO)_2Rh(\mu\text{-}Cl)_2Rh(CO)_2]$ allowed the introduction of two Rh(CO) units into the macrocyclic cavity. We are currently extending these studies to macrocycles derived from 2,6-dimercaptopyridine.

Acknowledgements—We gratefully acknowledge the Schweizerischer Nationalfonds zur Förderung der wissenenschaftlichen Forschung and EPSRC (U.K.) for support.

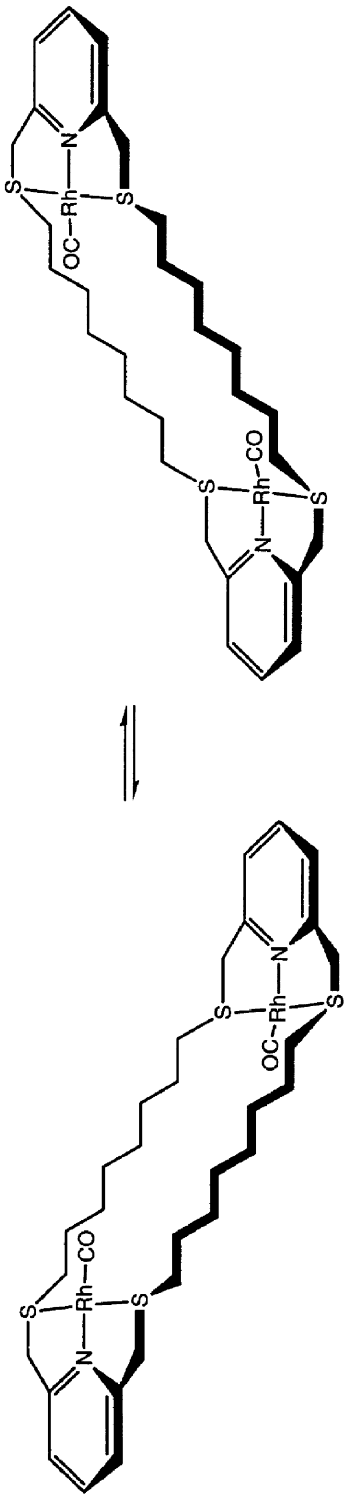

Fig. 7. The dynamic process involving inversion at sulfur observed for $[(CO)Rh(L)Rh(CO)][PF_6]_2$ and other complexes.

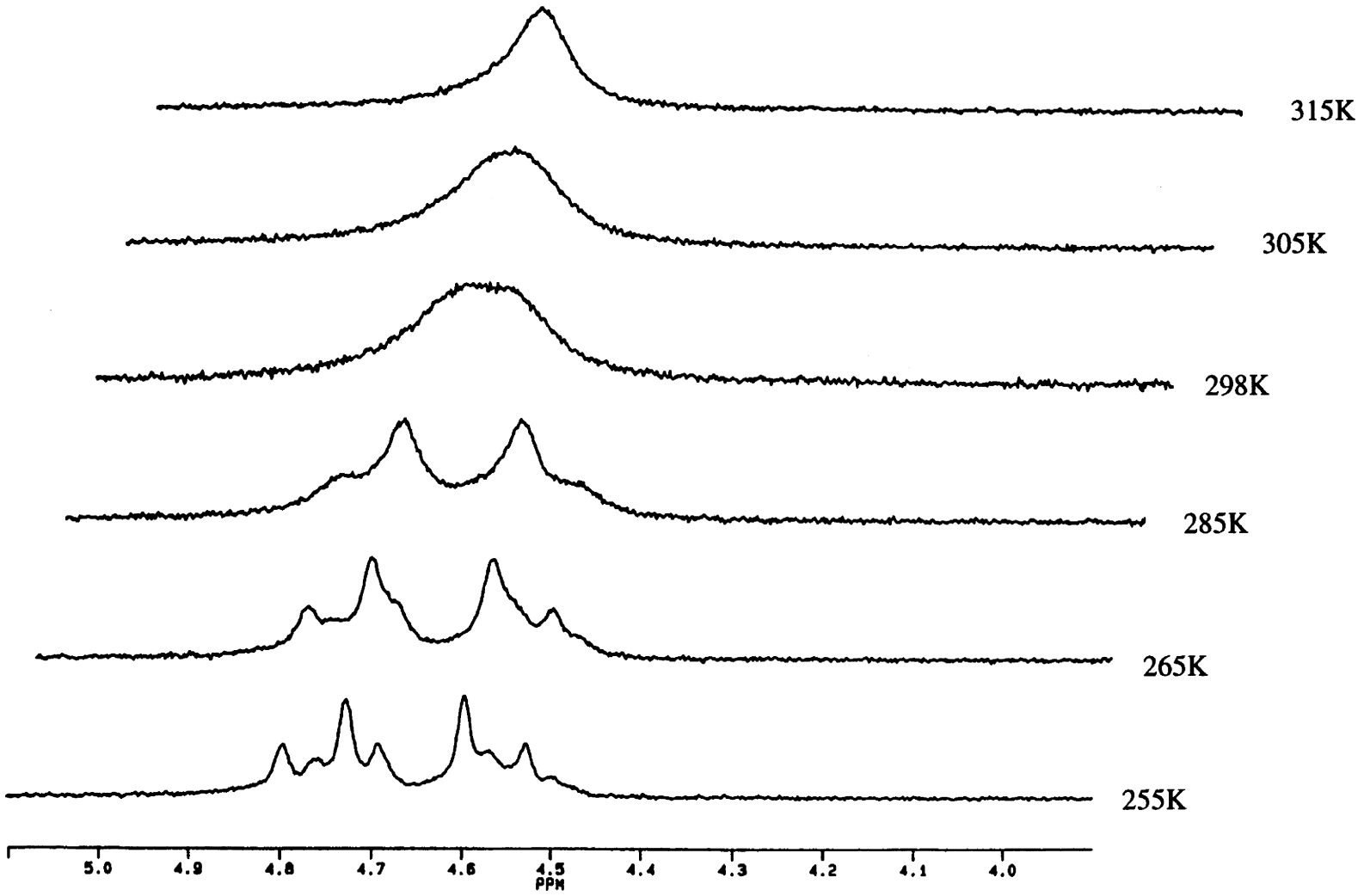

Fig. 8. 250 MHz ^{1}H NMR variable temperature spectra of CD_3CN solutions of [(CO)Rh(**9**)Rh(CO)][PF_6]$_2$.

REFERENCES

1. Constable, E. C., Henney, R. P. G. and Tocher, D. A., *J. Chem. Soc., Chem. Commun.*, 1989, 913.
2. Constable, E. C., Henney, R. P. G. and Tocher, D. A., *J. Chem. Soc., Dalton Trans.*, 1991, 2335.
3. Constable, E. C., Henney, R. P. G. and Tocher, D. A., *J. Chem. Soc., Dalton Trans.*, 1992, 2467.
4. Constable, E. C., Henney, R. P. G. and Leese, T. A., *J. Organomet. Chem.*, 1989, **361,** 277.
5. Constable, E. C. and Sousa, L. R., *J. Organomet. Chem.*, 1992, **427,** 125.
6. Constable, E. C., Henney, R. P. G., Raithby, P. R. and Sousa, L. R., *J. Chem. Soc., Dalton Trans.*, 1992, 2251.
7. Constable, E. C., Dunne, S. J., Rees, D. G. F. and Schmidt, C. X., *Chem. Commun.* 1996, 1169.
8. Dunne, S. J. and Constable, E. C., *Inorg. Chem. Commun.*, 1998, **1,** 167.
9. Constable, E. C., Stotereau, P. J. and Drew, M. G. B., *Inorg. Chim. Acta*, 1988, **145,** 3.
10. Constable, E. C., Stotereau, P. J. and Drew, M. G. B., *Polyhedron*, 1989, **8,** 2749.
11. Constable, E. C., Sacht, C., Palo, G., Tocher, D. A. and Truter, M. R., *J. Chem. Soc., Dalton Trans.*, 1993, 1307.
12. Constable, E. C., Lewis, J., Marquez, V. E. and Raithby, P. R., *J. Chem. Soc., Dalton Trans.*, 1986, 1747.
13. Baker, W. O., Buggle, K. M., McOmie, J. F. W. and Watkin, D. A. M., *J. Chem. Soc.*, 1958, 3594.
14. McCleverty, J. A. and Wilkinson, G., *Inorg. Synth.*, 1972, **13,** 211.
15. Galuszko, K., *Rocz. Chem.*, 1975, **49,** 1597.
16. Weber, E. and Vögtle, F., *Liebigs Ann. Chem.*, 1976, 891.
17. Parker, D., Lehn, J.-M. and Rimmer, J., *J. Chem. Soc., Dalton Trans.*, 1985, 1517.
18. Helps, I. M., Matthes, K. E., Parker, D. and Ferguson, G., *J. Chem. Soc., Dalton Trans.*, 1989, 915.
19. Salata, C. A., van Engen, D. and Burrows, C. J., *J. Chem. Soc., Chem. Commun.*, 1988, 579.
20. Modica, G., Maffi, S., Montoneri, E., Giuffre, L. and Grassi, A., *Angew. Chem.*, 1987, **99,** 149.
21. Carroy, A. and Lehn, J.-M., *J. Chem. Soc., Chem. Commun.*, 1986, 1232.
22. Ferguson, G., Matthes, K. E. and Parker, D., *J. Chem. Soc., Chem. Commun.*, 1987, 1350.
23. Ferguson, G., Matthes, K. E. and Parker, D., *Acta Cryst. C*, 1989, **45,** 741.
24. Ferguson, G., Matthes, K. E. and Parker, D., *Angew. Chem. Int. Ed. Engl.*, 1987, **26,** 1162.
25. Weber, E. and Vögtle, F., *Chem. Ber.*, 1976, 1803.
26. Vögtle, F. and Weber, E., *Angew. Chem.*, 1974, 126.
27. Escriche, L., Sanz, M., Casabo, J., Teixidor, F., Molins, E. and Miravitlles, C., *J. Chem. Soc., Dalton Trans.*, 1989, 1739.
28. Lehn, J.-M., Schmidt, F. and Vigneron, J.-P., *Tetrahedron Lett.*, 1988, **29,** 5255.
29. Newkome, G. R., Pappalardo, S. and Fronczek, F. R., *J. Am. Chem. Soc.*, 1983, **105,** 5152.
30. Bryan, D., *J. Coord. Chem.*, 1976, **6,** 97.
31. Weber, G., Jones, P. G. and Sheldrick, G. M., *Acta Cryst. C*, 1983, **39,** 389.
32. Reddy, P. J., Ravichandran, V., Chacko, K. K., Weber, E. and Saenger, W., *Acta Cryst. C*, 1989, **45,** 1871.
33. Lemmerz, R., Nieger, M. and Vögtle, F., *Chem. Ber.*, 1994, **127,** 1147.
34. Fukazawa, Y., Usui, S., Shiokawa, T. and Tsuchiya, J., *Chem. Lett.*, 1986, 641.
35. Girmay, B., Kilburn, J. D., Underhill, A. E., Varma, K. S., Hursthouse, M. B., Harman, M. E., Becher, J. and Bojesen, G., *J. Chem. Soc., Chem. Commun.*, 1989, 1406.
36. Bristol-Myers Co., U.S. Patent 3 290 319/1966. *Chem. Abstr.*, 1967, **66**, 115609k.
37. Banya Pharmaceutical Co. Ltd., Jpn. Patent 72 17 778/1972. *Chem. Abstr.*, 1972, **77**, 151979s.
38. Clark, R. J. H., Hempleman, A. J., Dawes, H. M., Hursthouse, M. B. and Flint, C. D., *J. Chem. Soc., Dalton Trans.*, 1985, 1775.
39. Cotton, F. A. and Felthouse, T. R., *Inorg. Chem.*, 1980, **19,** 323.
40. Vallarino, L. M., *Inorg. Chem.*, 1965, **4,** 161.
41. Griffith, W. P., *J. Chem. Soc. A*, 1970, 2788.

Pergamon

Polyhedron Vol. 17, Nos. 25, 26, pp. 4291–4313, 1998
© 1998 Elsevier Science Ltd
All rights reserved. Printed in Great Britain
PII: S0277–5387(98)00246–0
0277–5387/98 $19.00 + 0.00

POLYHEDRON REPORT NUMBER 64

Applications of electrospray mass spectrometry in organometallic chemistry

William Henderson,* Brian K. Nicholson and Louise J. McCaffrey

Department of Chemistry, University of Waikato, Private Bag 3105, Hamilton, New Zealand

CONTENTS

1. INTRODUCTION 4291

2. THE ELECTROSPRAY IONISATION TECHNIQUE 4292
2.1. Principles 4292
2.2. Solvents 4294
2.3. Ionisation processes 4294
2.4. Fragmentation processes 4297
2.5. Ion assignment 4297
2.6. Instrument maintenance 4297

3. METAL–ALKYL AND –ARYL COMPLEXES 4299
3.1. Metal–alkyl complexes 4299
3.2. Metal–aryl complexes 4300

4. METAL CARBONYL COMPLEXES AND METAL CLUSTERS 4301
4.1. Ionic metal carbonyl species 4301
4.2. Neutral metal carbonyl complexes 4303

5. METAL–CYCLOPENTADIENYL COMPLEXES, INCLUDING METALLOCENES 4306

6. OTHER COMPLEXES 4307

7. PHOSPHINES, ARSINES AND THEIR ONIUM SALTS 4308

8. MISCELLANEOUS APPLICATIONS 4309
8.1. Organometallic functionalisation of peptides and proteins for mass spectrometric analysis 4309
8.2. Fullerenes 4309

9. FUTURE SCOPE 4310

1. INTRODUCTION

Mass spectrometry is one of the oldest instrumental analytical techniques. Since the earliest use for determining the isotopic composition of the elements, it has been extensively developed. In particular, new ionisation

† Author to whom correspondence should be addressed. Fax: +64-7-838-4219; E-mail: w.henderson@waikato.ac.nz

methods have extended the range of samples which can be examined. Electron-impact (EI) ionisation has long been used for converting volatile, neutrally-charged substrates to cations (and less frequently, anions) so that their mass spectra can be examined [1]. This rather harsh method usually induces extensive fragmentation, which can of course be useful in characterising compounds, but which often prevents the detection of the parent ions. The main limitation for this method is the need for the sample to have significant vapour pressure at temperatures below the decomposition point. This has been a handicap in inorganic chemistry for ionic or high-molecular mass samples and for thermally-fragile organometallic (and bio-inorganic) species.

The introduction of fast atom bombardment (FAB) ionisation partially overcame this limitation, so that the use of mass spectrometry could be extended to new areas of inorganic and organometallic chemistry [2, 3]. However, this too is a harsh ionisation technique and only the more robust samples survive the ionisation process intact, and complications arising from recombination of fragments, or interactions with the matrix, are commonplace.

More recently, matrix-assisted laser desorption ionisation (MALDI) has been used to provide gas-phase ions for a range of substrates [4–6], including metal–carbonyl complexes and clusters [7–9] and organogermanium dendrimers [10]. However, this technique is often characterised by aggregation of analytes, giving high molecular mass signals.

A new method of ionisation was introduced in the mid-1980's, largely by Fenn and co-workers [11, 12]. This was termed electrospray mass spectrometry (ESMS) and essentially involves spraying a solution of the sample to be analysed into the source of a mass spectrometer and stripping away the solvent. Solubility rather than volatility then becomes the critical factor and since the ionisation occurs under very mild conditions, as discussed below, molecular ions of fragile molecules can be routinely observed. The method was quickly exploited by researchers working with biomolecules because proteins and other high-mass, thermally-sensitive substrates could be readily analysed; a large number of reviews and compilations have appeared in this area [13–20]. There has also been extensive use of ESMS as the detector for an LC-MS system [21]. The capabilities of the current range of commercial instruments have recently been summarised for those wishing to purchase an instrument [22].

The enormous scope of the ESMS technique in inorganic and organometallic chemistry has only recently become apparent and this is reflected in that to date there has only been one major review of the application of ESMS in inorganic chemistry [23], together with others of more limited scope [13, 24]. This present review describes some of the applications of ESMS in organometallic chemistry, with a particular emphasis on illustrating the types of compounds which can be successfully analysed. We have not attempted to be fully comprehensive in our coverage of the literature, but have tried to present illustrative examples over as wide an area as possible. It is our hope that this account will encourage readers to apply the versatile ESMS technique to their own area(s) of research.

2. THE ELECTROSPRAY IONISATION TECHNIQUE

2.1. *Principles*

Full details of the principles behind the electrospray process fall outside the scope of this review and can be found in the comprehensive reviews in this area [13, 15, 18–21, 23, 25, 26]. However, the basic features are summarised here in order to provide a basic framework for the subsequent discussion.

A diagrammatic representation of an ES mass spectrometer is shown in Fig. 1. Exact details vary with different commercial instruments, but the overall processes are typically similar. The sample, dissolved in the appropriate solvent, is injected as a fine spray at a low flow rate from a capillary held at a high voltage (e.g. 3000–4000 V) into a chamber at atmospheric pressure. This is shown schematically in Fig. 2. The nature of this electrospray, and the mechanism by which it generates ions, has been well debated [28]. Two basic ideas have emerged. The first approach is an electrophoretic one in which it is assumed the charged tip leads to partial separation of positive and negative ions, giving an excess of positive ions (in the positive-ion mode) at the liquid surface as it emerges from the tip [25]. This encourages fine, charged droplets to cleave off. The second approach regards the electrospray process as an unconventional electrochemical cell, with part of the current being carried by the charged droplets [29]. The chamber into which the sample is sprayed is purged with a drying gas (usually nitrogen) which evaporates the solvent from the charged droplets†. As the droplets get smaller the charge density increases and ions are transferred to the gas-phase either by extrusion from the

† Some reports have questioned the importance of evaporation (see Ref. [30]).

surface, or by a "Coulombic explosion" once the charge density exceeds some critical value. The ions formed in this process are then pumped through skimmer cones or similar, each at successively higher vacuum, before transferring to any of the normal mass analysers (i.e. magnetic sector, quadrupole, time-of-flight or to Fourier Transform ion cyclotron resonance (FTICR) [31, 32] or quadrupole [33] ion traps).

Typical flow rates are 0.01 ml min^{-1} and concentrations of a few ppm are ample, so very small samples are required, as with other mass spectral methods. The development of the "nanospray" technique is allowing analysis of even smaller samples [34, 35].

Since the sample is delivered as a solution, the technique allows the direct analysis of reaction solutions. In almost every case where independent evidence for the nature of species present in solution is available (such as NMR spectroscopy or electrochemistry), the information obtained by ESMS is generally in good agreement [23]. For studies of labile systems, ESMS can be particularly effective, since it can typically be used in the analysis of systems inaccessible by techniques such as NMR spectroscopy, due to paramagnetism or lack of a readily observed nucleus. The measurement of ESMS spectra at room temperature is also experimentally more convenient than low temperature NMR.

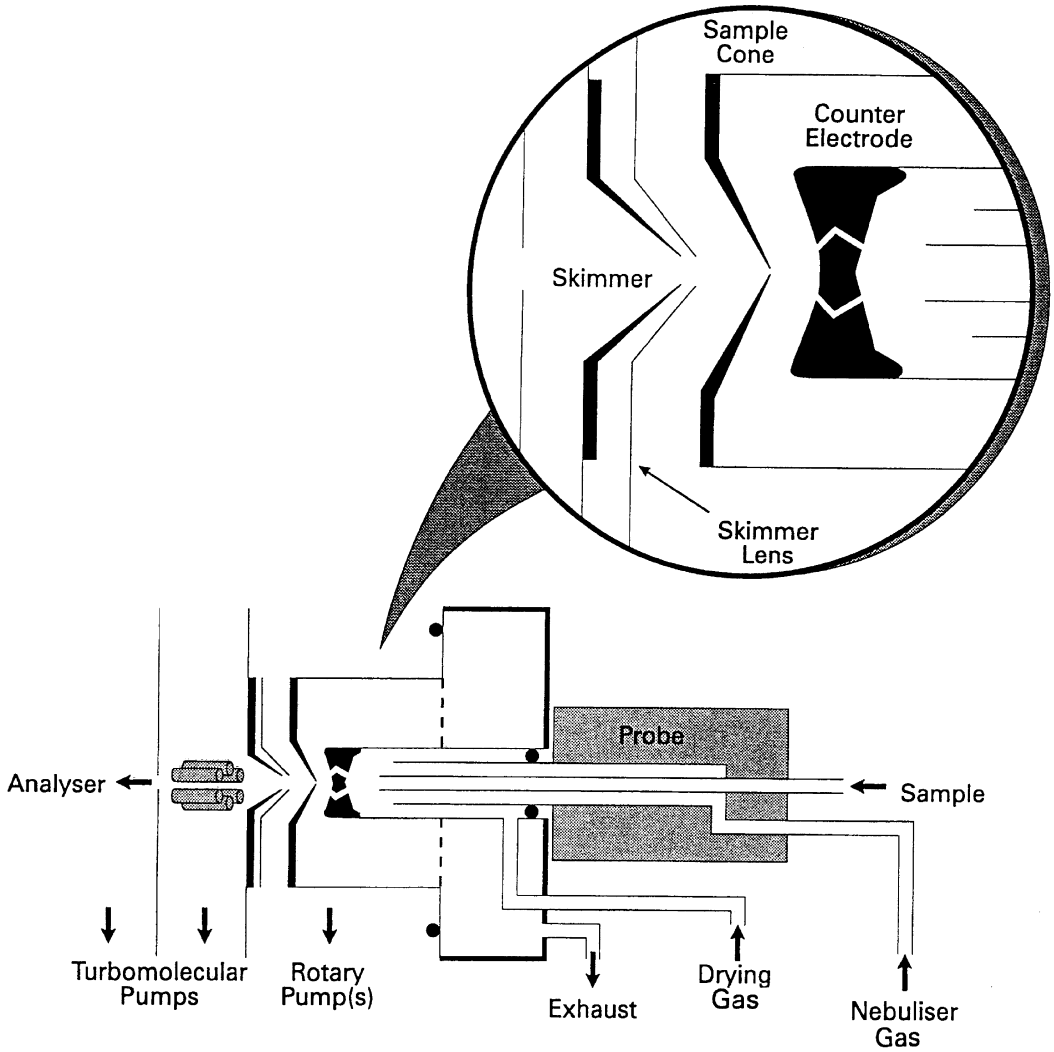

Fig. 1. Schematic diagram of a typical electrospray mass spectrometer. The positioning of the skimmer cone, used in providing fragmentation of the various ions generated in the source, can be clearly seen. (Used with permission from Micromass Australia.)

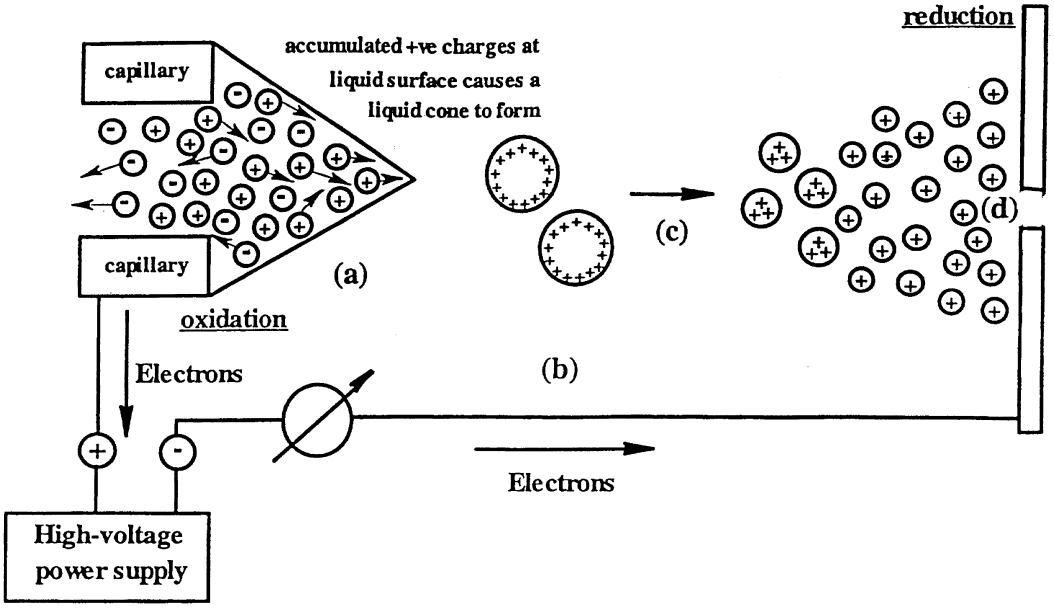

Fig. 2. A schematic representation of the ionisation mechanism in an electrospray mass spectrometer, operating in positive-ion mode. At (a) the high charge drives positive ions to the liquid surface so that the droplets emitted at (b) have a nett charge. Desolvation processes (c) then generate individual ions that pass through an orifice (d) in the negative electrode towards the mass analyser (taken from Ref. [27]).

2.2. *Solvents*

The choice of solvent is largely dictated by the solubility and stability of the compound to be analysed, together with the ionisation mechanism being used (see Section 2.3). A mixture of acetonitrile and water (often 1:1 v/v) is probably the most common mobile phase since it provides sufficient solubility for a wide range of polar and non-polar substrates, and can donate or accept protons. For ionic compounds, non-protic solvents may be used, including tetrahydrofuran, dichloromethane, chloroform, among others. For neutral compounds containing protonatable atoms (see Section 2.3) the use of a protic solvent (e.g. water, alcohols), or solvent combination (e.g. methanol–water, acetonitrile–water) provides sufficient H^+ ions to facilitate protonation, and so allows observation of $[M+H]^+$ parent ions, where M is the parent molecule. Relatively involatile solvents such as ethylene glycol can also be used [30].

For compounds which show either moisture and/or air-sensitivity, then ES analysis is still possible with appropriate precautions for handling the compounds concerned. As an illustration of this, a number of highly moisture-sensitive metal alkoxides typified by $Zr(OR)_4$ have been successfully analysed in rigorously-dried alcohol solvent [36]. Other examples of the ESMS analysis of air-sensitive metal carbonyls are given in Section 4.

2.3. *Ionisation processes*

As with other MS techniques, only ions can be detected, though in ESMS both anions and cations can be analysed equally conveniently. For samples which already contain ions, no further ionisation is needed. The solvated ions in the spray droplets are stripped of the solvent to give gas-phase ions (cations or anions) which are fed directly into the mass analyser. As a typical example, Fig. 3 shows the spectrum obtained for the dianion cluster $[Os_{10}C(CO)_{24}]^{2-}$; signal-to-noise levels of this quality are readily achieved [37].

For highly-charged species, association with counterions is common. For example the anionic cluster $Na_6[Ru_3(CO)_{10}\{P(C_6H_4SO_3)_3\}_2]$ ($\equiv Na_6X$) gives signals in the negative-ion mode which correspond to $[X+Na]^{5-}$, $[X+2Na]^{4-}$, $[X+3Na]^{3-}$ and $[X+4Na]^{2-}$ [38]. Peaks arising from ions with some solvent molecules still attached are also often found. It is charge-density and not total charge *per se* which determines stability; proteins and other large biomolecules typically yield highly-charged ions (but with a low charge density), the resulting relatively low m/z values allowing their analysis by quadrupole analysers with a limited mass range (e.g. 0–3000 Da).

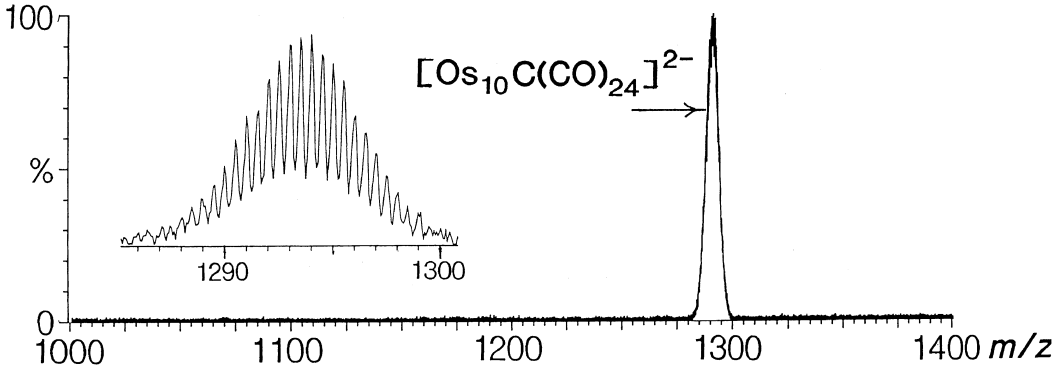

Fig. 3. The negative ion electrospray mass spectrum of $[N(PPh_3)_2]_2[Os_{10}C(CO)_{24}]$, showing the quality of spectra possible for anionic clusters. The inset shows the isotope pattern, with the mass separation of m/z 0.5 confirming the 2- charge (taken from Ref. [37]).

For neutral species some means of ionisation is required for detection and this is where ingenuity is sometimes needed, particularly for organometallic complexes. The commonest process is for the sample to abstract a proton from the solvent to give a $[M+H]^+$ ion, but for this to happen the sample needs to have a site of sufficient basicity to attach the H^+ to. Ionisation takes place with substrates that would normally not be considered strong Brønsted–Lowry bases, so that strong bonds to H^+ are not necessary. Typically, oxygen or nitrogen atoms provide very effective protonation sites, present in functional groups such as ethers, carbonyl compounds (ketones, amides etc), sulfoxides, phosphine oxides, amines and the like. Similarly, species containing -COOH or -OH groups can lose a proton to generate the corresponding negative ion which is detected as $[M–H]^-$. Indeed for many samples both the $[M+H]^+$ and $[M–H]^-$ ions can be detected in positive- or negative-ion modes, respectively, differing by two mass units. To encourage these processes, small quantities of an acid (e.g. HCOOH or CF_3COOH) or base (e.g. NH_3) can be added.

Association of the substrate with other ions is also common and other peaks in the spectrum (which can have variable intensity) in addition to $[M+H]^+$ often include $[M+NH_4]^+$, $[M+Na]^+$ or $[M+K]^+$ from the traces of cations often present in even HPLC-grade solvents. These assignments can be readily confirmed by the deliberate addition of the appropriate ion. Higher aggregates are also common, with some substrates giving $[2M+H]^+$ or even $[4M+NH_4]^+$, for example. The use of metal ions such as Na^+, K^+ or Ag^+ to form ions by association with neutral substrates is sometimes more successful than added H^+ and allows the technique to be extended into non-protic solvents [39, 40]. Silver(I) salts such as $AgClO_4$ are reasonably soluble in aprotic solvents such as benzene, and the Ag^+ ion has a strong propensity for binding to "soft" ligand centres. Accordingly, silver(I) salts have been used in the successful analysis of phosphines [41, 42], arsines [43], thioethers [44], arenes [45] and metal carbonyls [37, 46] by ESMS. Another example of the successful use of an ionisation agent is the addition of methoxide (and other alkoxide ions) to neutral metal carbonyl compounds to allow detection as the $[M+OMe]^-$ species [37, 47]. Further details on this technique are given in Section 4.

In rather rare cases, electrochemical processes occurring in the charged probe tip [29] oxidise electron-rich substrates to generate $[M]^+$ ions rather than protonated $[M+H]^+$ ions [48, 49]. The $[M]^{\ddagger}$ and $[M+H]^+$ ions can be distinguished readily since the instruments have resolution which reliably discriminates between species one mass unit apart. These oxidations are somewhat unpredictable and appear to be instrument- and compound-dependent. For example, analysis of $M[B_3H_8]$ ($M=Me_4N$ and Cs) in methanol solutions resulted in electrochemical conversion to $[B(OMe)_4]^-$ ions [50]. This conversion was not observed in MeCN solvent, or in bulk MeOH solution. Porphyrins also sometimes give $[M]^{\ddagger}$ ions [51].

Among organometallic complexes, the metallocenes are perhaps the most common species to demonstrate this electrochemical behaviour, discussed further in Section 5. Indeed the incorporation of ferrocene moieties into compounds provides a route for ionisation by electrochemical oxidation. Ferroceneboronic acid, $FcB(OH)_2$ [$Fc=(\eta^5\text{-}C_5H_5)Fe(\eta^5\text{-}C_5H_4)$] and ferrocenoyl azide, $FcC(O)N_3$ are two reagents which have been used for the derivatisation of alcohols for ESMS analysis [52]. Fullerenes have a high electron affinity and are also relatively easily oxidised, and the direct analysis of the fullerene C_{60} can be carried out, with the radical ions $C_{60}^{\cdot -}$ and $C_{60}^{\cdot +}$ being observed [53, 54].

The addition of a chemical oxidant such as $NOBF_4$ can generate cations from neutral substrates, such as metal–diethyldithiocarbamate complexes [55]. Recently there have been successful attempts to include an electrochemical cell into the electrospray source to induce oxidative ionisation prior to infusion into the source

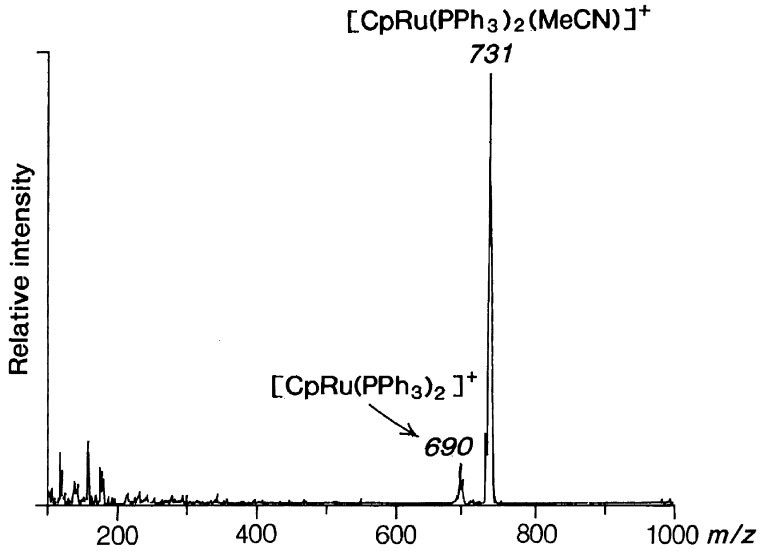

Fig. 4. The positive ion mass spectrum of $CpRuCl(PPh_3)_2$ in $MeCN/H_2O$, showing peaks assigned to $[M–Cl+MeCN]^+$ and $[M–Cl]^+$.

[56, 57]. This is a modification to the basic ES technique which should find many useful applications in organometallic chemistry.

A further ionisation mechanism which can occur for formally neutral substrates is loss of an anionic ligand, typically halide, which may result in the formation of solvated or unsolvated cations. This mechanism appears to be a reasonably general one for coordination and organometallic complexes containing halide ligands. As an illustrative example, Fig. 4 shows the positive-ion spectrum of $[CpRuCl(PPh_3)_2]$ in $MeCN–H_2O$ solution, which gives the ion $[CpRu(PPh_3)_2(MeCN)]^+$ at a low cone voltage and the desolvated ion $[CpRu(PPh_3)_2]^+$ at a higher cone voltage [58]. Other organometallic complexes showing the same general behaviour include *trans*-$[Pt(CH_3)I(PPh_3)_2]$, *trans*-$[IrCl(CO)(PPh_3)_2]$, *cis*-$[PtCl(CH_2COCH_2R)(PPh_3)_2]$ (R = H or Cl) [58] and the organogold(III) halide complexes **1** [59]. The formation of positive ions of this type can generally be enhanced, and the spectra simplified, by adding a volatile donor ligand of better donor ability than the solvent, such as pyridine (py), whereupon ions of the type $[M–halide+py]^+$ ions are readily observed in most cases, at low to moderate cone voltages. The use of pyridine as an ionisation reagent for metal halide complexes is beneficial, since in its absence misleading relative ion intensities may occur. As an illustration, the gold dihalide complex **1a** showed a significant ion at m/z 525 in its positive-ion ESMS spectrum, which is assigned as the bis(cyclometallated) species **2**. Addition of pyridine to the solution however gave the expected $[M–Cl+py]^+$ as the major ion. The species **2** was not observed in the ^1H NMR spectrum and so the strong peak in the absence of pyridine results from a high ionisation efficiency relative to the dichloro complex [59].

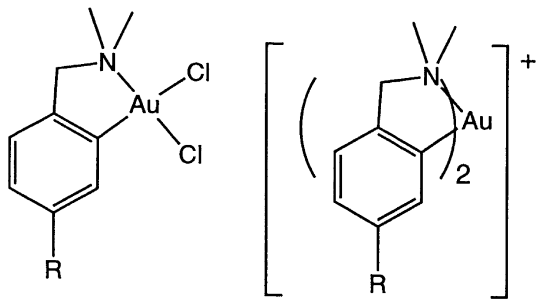

1a, R = OMe
1b, R = H

2

2.4. *Fragmentation processes*

The ionisation processes described above are essentially chemical ionisation and are gentle in nature, typically resulting in intact "parent" ions being observed under the normal operating conditions. This is one of the major advantages of the ESMS technique over EI or FAB techniques. However, fragmentation can often be induced by applying a voltage (typically 10–100 V) across the skimmer cones (refer to Fig. 1), the so-called cone voltage. This has the effect of encouraging collisions between ions and between ions and neutral species (such as the gas used), resulting in fragmentation. In general, it is this parameter that has the most dramatic effect on the ions observed in an ES mass spectrum. Other types of mass spectrometer achieve fragmentation in different ways, such as in a Fourier transform ion cyclotron resonance (FTICR) mass spectrometer [31, 32]. Fragmentation can be very useful in determining functional groups, although fragmentation processes are different to those that are found in EI mass spectrometry. Higher values of the cone voltage are also useful for minimising aggregates of ions with solvent molecules. The actual cone voltage required to induce fragmentation is very much dependent on the sample, but the technique can be used in a qualitative sense, for example to determine the most weakly-bonded ligands on a metal centre. It appears that more highly-charged species fragment more extensively under given conditions, presumably because of more energetic collisions induced by the drift voltage between the cones [38, 60]. The effect of varying cone voltage is illustrated for a typical organometallic example in Fig. 5, which shows a series of $[Os_3(CO)_n+OMe]^-$ ions observed from a solution of $[Os_3(CO)_{12}]$ with added methoxide ionisation agent (refer to Section 4) [37, 47].

2.5. *Ion assignment*

Unambiguous assignment of ions observed in ESMS analysis can be achieved by comparing the experimental and calculated isotope distribution patterns. The former can be routinely obtained by recording the spectrum of the ion concerned in high resolution mode, while the latter can be simulated with programs such as the *Isotope* program for the Macintosh, details of which have been published [61]. Many metals, and a number of other elements commonly found in ligands in organometallic systems (e.g. Cl, Br, Se), have several isotopes providing valuable information. The isotope pattern also reveals the charge on the ion, by the m/z separation between adjacent peaks. Using a standard quadrupole mass analyser, we have been able to routinely obtain isotope patterns for ions with up to four charges (in which case adjacent peaks in the isotope pattern are separated by 0.25 Da). As an illustration we refer to Fig. 2, which gives the isotope distribution pattern for the $[Os_{10}C(CO)_{24}]^{2-}$ cluster anion, with peaks separated by 0.5 m/z units.

2.6. *Instrument maintenance*

The commercial instruments now available are remarkably robust. Routine operation is well within the expertise of graduate students, so that continuous specialist technical support is not needed, placing the technique firmly in the instrumental armoury of the practicing synthetic chemist. Since the ionisation chamber is at atmospheric pressure, routine cleaning can be carried out without breaking the vacuum in the rest of the spectrometer, so that a source-clean usually involves less than an hour of down-time.

As a final comment in this section, we note that cross-contamination can occur from some species which have a tendency to linger in the mass spectrometer (specifically, in the capillary systems and injector system). The bis(triphenylphosphine)iminium $[N(PPh_3)_2]^+$, (PPN^+) cation, which is widely used in organometallic chemistry has a marked propensity to linger, giving characteristic m/z 538 signals in subsequent samples. In a similar fashion, the cation $[CpRu(PPh_3)_2]^+$ (m/z 691, refer to Fig. 4) is also remarkably persistent. If silver(I) salts have been used to effect ionisation, they too can linger in the spectrometer for some time, generating unexpected $[M+Ag]^+$ ions in subsequent spectra of compounds with soft donor atoms which favour coordination to Ag^+. Flushing the system with a good donor ligand for silver, for example pyridine, can minimise prolonged contamination. Sodium iodide and caesium iodide are used as mass calibrants in ES spectrometers [62] and can cause problems with halide exchange reactions in metal chloride complexes for example. Polyethers are also used for positive-ion calibration and can be problematical when used in high concentrations. Formic acid, which can be used as a cleaning solution, may linger for some period of time, effecting protonolysis reactions and in some cases the observation of metal–formate complexes. For these reasons, it is useful to maintain a detailed log-book of all samples analysed so that possible sources of contamination from previous samples can be monitored.

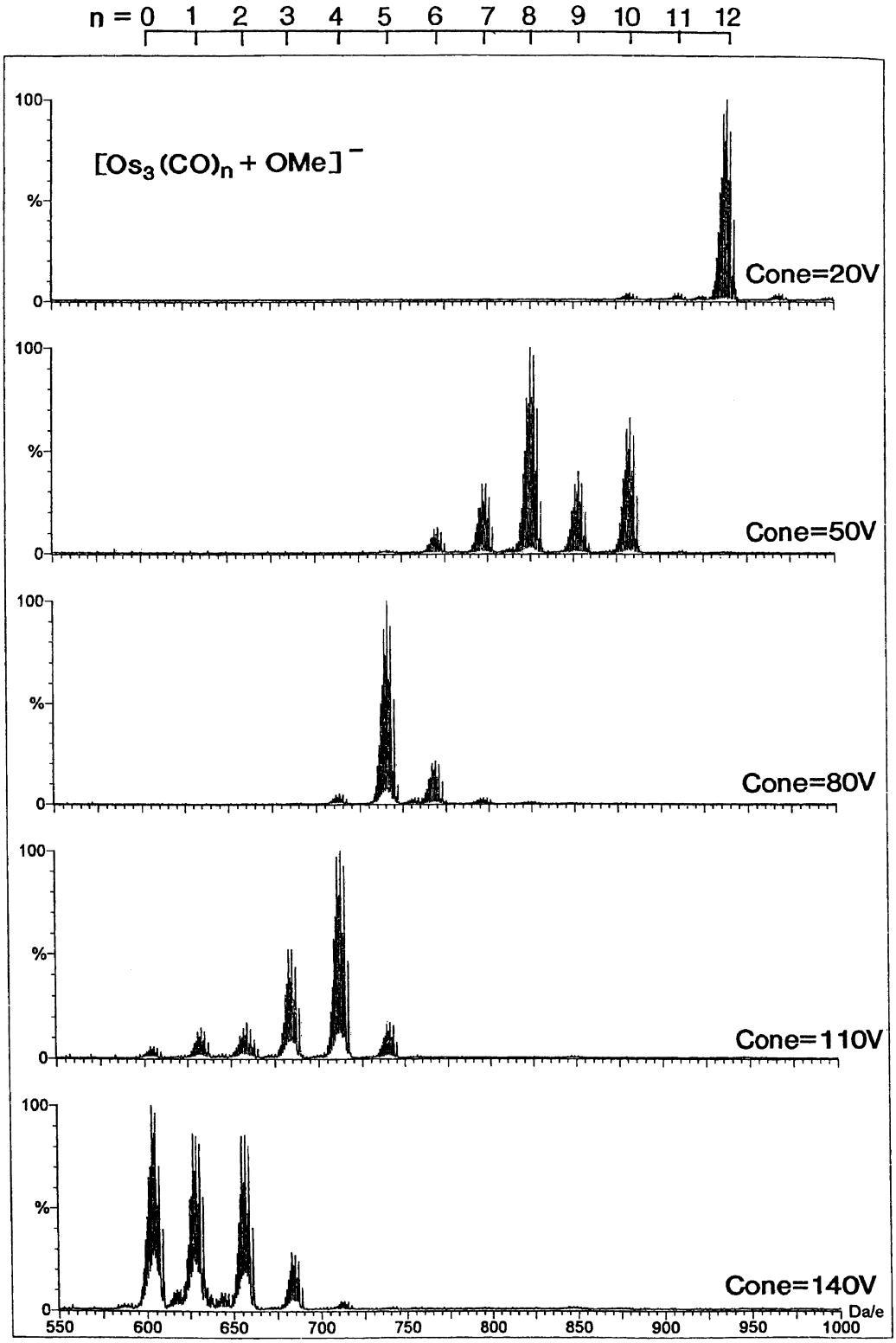

Fig. 5. Cone voltage induced CO fragmentation in the ESMS of the adduct of OMe^- with $Os_3(CO)_{12}$ in MeOH (taken from Ref. [47]).

3. METAL–ALKYL AND –ARYL COMPLEXES

3.1. *Metal–alkyl complexes*

ESMS studies of metal alkyls have to date centred largely on main-group and late transition-metal derivatives, which provide the more stable examples. Reports cover the metal–alkyl complexes of tin, germanium, silicon, arsenic, mercury, platinum, palladium, gold, indium and thallium.

Organotin compounds, especially the organotin halides, have been the subject of several studies. The chemical and toxicological properties exhibited by organotin compounds depend on the speciation of the tin complex and this is conveniently monitored by ESMS. The hydrolysis products of Ph_3SnBr, Ph_3SnCl, Ph_2SnCl_2, Me_3SnCl and $^nBu_3SnCl$ have been investigated by ESMS in both positive- and negative-ion modes, in aqueous acetonitrile solvent [63]. Species observed in positive-ion mode included aggregate ions of the type $[(R_3Sn)_n(OH)_{n-1}]^+$ with intensity decreasing with increased n. The solvated $[R_3Sn(MeCN)_{1\text{ or }2}]^+$ ions were also observed, with the solvating MeCN groups being lost at higher cone voltages. In the negative ion spectra several different types of species could be identified; solutions of Ph_3SnX (X = Cl or Br) yielded $[Ph_3SnX_2]^-$, $[Ph_3SnX(OH)]^-$, $[Ph_3SnO]^-$ and $[Ph_3SnOSnPh_3X]^-$, while Ph_2SnCl_2 yielded primarily $[Ph_2SnCl_3]^-$. The various mixed-halide ions $[^nBu_3SnXY]^-$ (X, Y = halide) were all observed in solutions of $^nBu_3SnCl$ with mixed halides. Other work has been done on organotin compounds to investigate an alternative method (to GC–MS employing EI ionisation) for identification [64]. Mixtures of organotin compounds have also been studied [65]. In this study, carried out in methanol solvent, tin-methoxy species were also detected. Tin has the record number of natural isotopes (10) and the characteristic pattern allows for unambiguous assignment of peaks and clear identification of any dimers which may form. Tributyltin (TBT) species are the most important in the marine environment and have been studied using ionspray mass spectrometry/mass spectrometry (a technique related to ESMS) as part of a trace metal analysis [66]. By means of selected reaction monitoring of a daughter ion pair (m/z 179/291) in the spectrum of TBT, quantitative estimates of the concentration of tin present at low levels were able to be made.

Larger tin aggregates have also been studied by ESMS. The mixed-alkyl distannoxane $[^tBu_2(Cl)SnOSn(Cl)Me_2]$ has been studied by positive-ion ESMS in methanol–water, giving a series of tri-tin species, which presumably arise by reaction with the solvent system [67]. The compound $[(BuSn)_{12}O_{14}(OH)_6]Cl_2$ has been characterised by X-ray crystallography and NMR spectroscopy, and positive-ion ESMS revealed that the cation retained its integrity in dichloromethane–methanol solution, giving a single peak at m/z 1218 [68]. Over time, two hydroxyl groups were replaced by methoxide ions (from methanol in the mobile phase) to give a peak in the spectrum at m/z 1232. Further experiments demonstrated the use of ESMS as a means for monitoring such substitution reactions.

Certain silicon and germanium compounds are also amenable to ESMS analysis. Electrospray tandem mass spectrometry has led to deduction of the structure of a germanium compound, Ge-132 (bis-carboxyethyl germanium sesquioxide) and to some interesting conclusions about its fragmentation pathway [69]. The confirmation of the identity of some silicon-containing heteroboranes was also achieved using electrospray [70]. Moisture-sensitive $H_2N(CH_2)_3Si(OEt)_3$ has been analysed by ESMS in dry ethanol mobile phase [36]. The first three generations of an organo-silatrane-containing dendrimeric wedge have recently been synthesised and characterised by positive-ion ESMS [71]. At low cone voltages, compounds containing a residual tri-alkanolamine moiety predominantly show multiply-charged ions of the type $[M + H + xNH_4]^{(x+1)+}$ ($x = 0$–3), while compounds with residual epoxy groups show strong $[M + xNH_4]^{x+}$ ions, where $x = 1$–4. The observation of such multiply-charged ions for these compounds containing multiple protonation sites is reminiscent of the classical behaviour of larger peptides and proteins in ESMS [19].

ESMS has been employed for the study of various other organoarsenic compounds. Arsenobetaine ($Me_3AsCH_2CO_2$), arsenocholine ($Me_3AsCH_2CH_2OH$), tetramethylarsonium iodide $[Me_4As]I$, methylarsonic acid ($MeAsO_3H_2$) and dimethylarsinic acid (Me_2AsO_2H) were examined by positive-ion ESMS [72]. In a separate study, the quantification of ten organoarsenic compounds (including those listed above, in addition to various arylarsonic acids and trimethylarsine oxide, $Me_3As{=}O$) was described using a reversed-phase microbore HPLC separation coupled with ESMS [73]. Additionally, Ag^+ ions have been used in the analysis of a range of tertiary arsine ligands [43].

The organometallic complex between mercury(II) and the nucleobase dimethyluracil (Hdmura), (1,3-dimethyluracil-5-yl)mercury(II) nitrate **3**, has been analysed as DMSO and H_2O solutions, giving hydrolysed ions of the type $[Hg_6(dmura)_6O_2]^{2+}$, $[Hg_6(dmura)_6O_2(NO_3)]^+$ and $[Hg(dmura)(Me_2SO)]^+$ [74]. A series of methylmercury(II) derivatives (each of which give intact ions in their ESMS spectra) has been investigated for their participation in ligand exchange reactions in solution, and electrospray was found to be a convenient technique by which to follow these reactions [75]. Each compound was a complex of a neutral nitrogen base which was seen to be easily displaced by a variety of other ligands yielding new methylmercury complexes. The methylmercury cation has also been reacted with some amino acids as well as glutathione [76] to give products

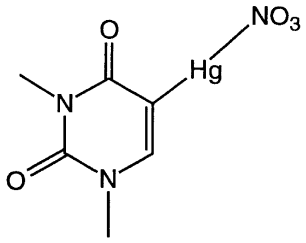

3

(observed using ESMS) of the form $[(MeHg)_2(AA–H)]^+$ (AA = amino acid e.g. glycine, histidine) when the reactant was added in 1:1 stoichiometry. The interaction of $MeHg^+$ with a range of proteins and peptides has also been investigated and is discussed in greater detail in Section 8.

Examples of organoplatinum(IV) and -palladium(IV) compounds have been investigated using ESMS [77] to yield results consistent with chemical properties already known about the compounds. The Pt(IV) complexes [78] were more stable towards fragmentation, while the palladium compounds of the type $[Me_2(C_3H_5)Pd(mim\text{-}_2pyCH)]I$ (mim_2pyCH = methylimdazolyl-derived ligand) routinely lost methyl ligands at low cone voltages. A number of ionic Pd(II) compounds have also been analysed and each gave intact cation signals. The platinum(II) acetylide complex $[Pt_2(CC^tBu)_3(\mu\text{-dppm})_2]^+$ (dppm = $Ph_2PCH_2PPh_2$) gives the expected $[M]^+$ ion in its ES spectrum and the fragment ion $[(dppm)Pt(CC^tBu)]^+$ was also observed [79]. The bis-chelate complex $[Pt(CH_2PPh_2CH_2PPh_2)_2]^{2+}$ has been synthesised by reaction of the bis(chloromethyl) complex $[Pt(CH_2Cl)_2(dppm)]$ with one equivalent of dppm and the ESMS spectrum yielded the $[M]^{2+}$ cation [79]. In contrast, the FAB spectrum of the same complex gave both the $[M]^+$ and $[M]^{2+}$ ions, as a result of the FAB ionisation process being more reducing than the ES ionisation process. Fragment ions observed were assigned on the basis of CH_2 expulsions/ring contraction processes.

Gold(III), indium(III) and thallium(III) all form dimethyl derivatives incorporating neutral polydentate nitrogen donor ligands but the indium and thallium compounds tend to have highly variable structures in the solid-state [80]. All the gold complexes exhibited intact cations in their positive mass spectra but this is not always the case for the indium and thallium compounds. The indium compounds are known to be fluxional in solution and reversible ligand dissociation was demonstrated.

Carbon–hydrogen bond activation by transition-metal complexes has been directly observed by ESMS [81, 82]. The cationic complexes $[CpIr(PMe_3)Me]^+$ and $[Cp^*Ir(PMe_3)Me]^+$ undergo C–H bond activation depending on the cone voltage.

3.2. *Metal–aryl complexes*

Enantioselective fragmentation of palladium–aryl complexes has recently been demonstrated by ESMS [83]. Fragmentation for the (*R*,*R*) enantiomer **4** was more pronounced than that for the (*R*,*S*) enantiomer **5**. A number of metallodendrimers, derived from the palladium–aryl building block **6**, have been synthesised and subsequently characterised by ESMS [84]. The compound **6** yielded the $[M–Cl]^+$ ion in the positive-ion ES spectrum, as found for other metal–halide complexes (*vide infra*).

Reactive palladium–aryl intermediates have been detected by ESMS. Catalytic intermediates observed in the palladium(0) catalysed coupling reaction between aryl halides and arylboronic acids (the Suzuki reaction) have been detected by ESMS [85]. In this study, pyridyl halides were used in place of phenyl derivatives so that a protonatable group was present in complexes which otherwise could be invisible to the ES ionisation technique. In another study, intermediates in the palladium catalysed intramolecular arylation of enamines have been observed [86]. These studies suggest the potential of ESMS for the detection of intermediates in other reaction solutions.

Copper(I) salts in conjunction with organolithium reagents are widely used synthetic reagents; ESMS data for mixtures of copper(I) iodide or -cyanide with lithium halides have been reported, and it was indicated that negative ion ESMS data on the organometallic thienyl cuprate 2-ThCu(CN)Li have been obtained, though full details do not yet appear to have been published [87].

Finally, a number of cyclometallated benzylamine gold(III) complexes containing ureylene [88], thiosalicylate [59] and sulfido [89] ligands have been characterised by positive ion ESMS. The gold metallacycles were found

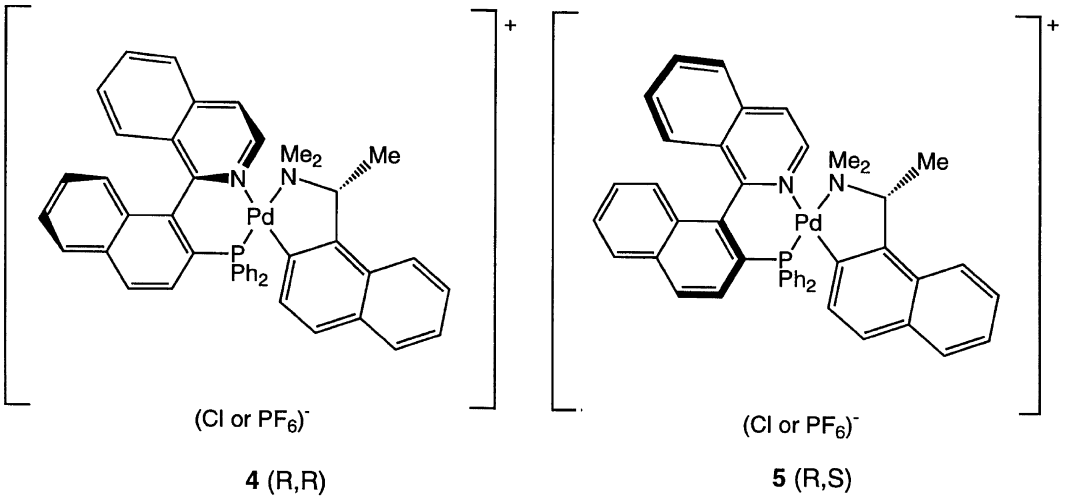

4 (R,R) **5** (R,S)

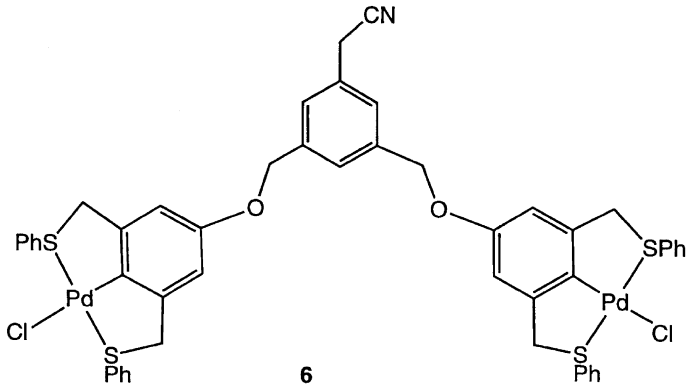

6

to be generally stable towards cone voltage induced fragmentation. Monocationic sulfido-silver–gold-halide aggregates were the product of a thiourea reaction with **1** in the presence of silver ions [89].

4. METAL CARBONYL COMPLEXES AND METAL CLUSTERS

4.1. *Ionic metal carbonyl species*

The carbonyl ligand is very widespread among organometallic complexes; it may be the sole ligand or may be present in conjunction with other ligands such as phosphines, alkyl groups or π-hydrocarbons. For metal–carbonyl complexes which are charged, the ES process is ideally suited for the analysis of such species, transferring solution ions into the gas phase for direct analysis. The positively-charged chromium(I) species *trans*-$[Cr(CO)_2(dppe)_2]^+$ (dppe = $Ph_2PCH_2CH_2PPh_2$) illustrates this, giving an intact ion in the positive-ion ES spectrum [90, 91]. Cations of the type $[M(CO)_2(P–P)_2X]^+$ (M = Mo, W; P–P = dppe, $Ph_2PCH_2PPh_2$ (dppm); X = F, Cl, Br and I) [92], and *cis*/*mer*-$[Re(CO)_2Br(Ph_2PCH_2PPh_2Me)(dppm)]^+$ [90] have also been successfully observed using ESMS. Related ions $[Re(CO)_2(P_2P')X]^+$ ($P_2P' = Ph_2P(CH_2)_2P(Ph)(CH_2)_2PPh_2$; X = Cl, Br) have been investigated in another study [93]. The amount of deuteration of the complex $[Mo(CO)_2(dppe)_2D]^+$ has been determined by ESMS [94]. Anionic complexes of the types $[M(CO)_5X]^-$ (M = Cr, Mo, W; X = Cl, Br, I) and *cis*-$[M^*(CO)_4X_2]^-$ (M^* = Mn, Re; X = Cl, Br, I) have also been observed [92]. The general feature of all these spectra is the appearance of the intact carbonyl complex ion, which in some cases loses CO ligands when the skimmer (cone) voltage is increased. A comparative study involving ES, FAB and FD (field desorption) mass spectra of a large range of cationic π-hydrocarbon metal carbonyl complexes of the types [(η^5-(dien-

yl)Fe(CO)$_3$]BF$_4$, [CpFe(CO)$_2$(η^2-alkene)]BF$_4$ or [η-(C$_7$H$_7$)M(CO)$_3$]BF$_4$ (M = Cr, Mo, W) concluded that ESMS is the most convenient and informative of the three techniques for compounds of this type [95].

ESMS has been used to identify an unstable rhenium complex which occurs as a reaction intermediate of CO_2-photofixation using the complex [Re(bipy)(CO)$_3$(PPh$_3$)]$^+$ [96, 97]. The parent cation shows the expected strong [M]$^+$ ion at low cone voltages, with loss of a single CO ligand at higher cone voltage (40 V). Upon irradiation in a DMF-triethanolamine (TEOA) solution under a CO_2 atmosphere, the final product was the formate complex [Re(bipy)(CO)$_3$(OCOH)], but two intermediate complexes were identified, by HPLC, one of which was found and confirmed by ESMS to be [Re(bipy)(CO)$_3$(TEOA)]$^+$. The DMF complex was not observed and it was postulated that this is due to the poor donor ability of DMF compared to TEOA.

Polynuclear metal cluster anions can also be characterised by ESMS, though the list is still limited. As expected, charged clusters yield strong and generally simple ES spectra as illustrated earlier for [Os$_{10}$C(CO)$_{24}$]$^{2-}$ (Fig. 2); [Ru$_6$C(CO)$_{16}$]$^{2-}$ also gives pleasing ESMS spectra [37]. Anionic transition-metal clusters of the type (Ph$_4$P)[Fe$_3$(CO)$_{10}$(μ-CO){μ-Hg(M)}] [M = CpMo(CO)$_3$, Co(CO)$_4$, CpFe(CO)$_2$, CpW(CO)$_3$, and Mn(CO)$_5$], having the general structure **7**, have been studied and it was concluded that ESMS was the most appropriate method (when compared to FAB-MS) by which to control ion fragmentation [98]. The most intense peak at a cone voltage of 50 V was the [M–CO]$^-$ species, though the [M]$^-$ ions were also observed. Lower cone voltages than 50 V were not reported, but it would be anticipated that more intense parent ions would be seen at very low (e.g. 10 V) cone voltages. The cluster complex (Et$_4$N)[Fe$_6$C(CO)$_{16}$(AuPPh$_3$)] was also studied by ESMS [98]; the parent anion was the largest peak at a cone voltage of 50 V, and the second-largest was the ion formed by loss of one CO ligand. Related monoanionic complexes [Fe$_4$C(CO)$_{12}${μ-Hg(M)}] formed by reaction of (PPN)$_2$[Fe$_4$C(CO)$_{12}$] [PPN = N(PPh$_3$)$_2^+$] with ClHg(M) [M = as for **7** below] also give the monoanions as the base peaks in the negative-ion ES spectra [99].

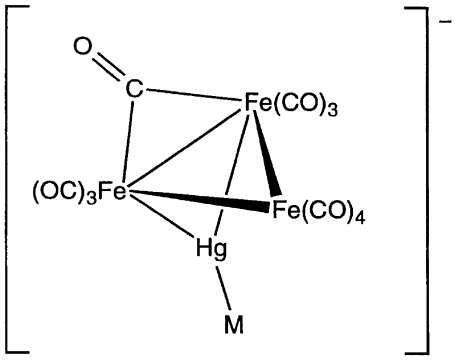

7 **M**

CpMo(CO)$_3$
CpW(CO)$_3$
CpFe(CO)$_2$
Mn(CO)$_5$
Co(CO)$_4$

The ESMS spectrum of the highly air-sensitive platinum carbonyl cluster (Ph$_4$P)$_2$[Pt$_{12}$(CO)$_{24}$] has been described, giving [(Ph$_4$P)(Pt$_{12}$(CO)$_{24}$)]$^-$ (m/z 3351), formed by ion aggregation and [Pt$_{12}$(CO)$_{11}$]$^{2-}$ (m/z 1324) as the two most intense ions [24]. Several Pt$_9$ ions, [(Ph$_4$P)$_2$(Pt$_9$(CO)$_{18}$)]$^-$, [(Ph$_4$P)$_2$(Pt$_9$(CO)$_{13}$)]$^-$ and [Pt$_9$(CO)$_8$]$^{2-}$, are formed by loss of one of the Pt$_3$ triangles. Only preliminary details of this work have so far been reported. Another air-sensitive anionic cluster which has been analysed by ESMS is the species [Ni$_{10}$(BiMe)$_2$(CO)$_{18}$]$^{2-}$; for this species the parent ion was not observed, but instead gave eight peaks corresponding to [M–2Me–nCO]$^{2-}$, as a result of both CO and methyl loss [100]. The related organoantimony species [Ni$_{10}$(SbPr^i)$_2$(CO)$_{18}$]$^{2-}$ showed the parent dianion, together with other fragments formed by CO and propyl loss [101]. These results demonstrated the stability of the Ni$_{10}$Sb$_2$ and Ni$_{10}$Bi$_2$ clusters and the greater strength of the Sb–C versus Bi–C bonds.

The anionic clusters [Ru$_3$(CO)$_{12-n}$L$_n$]$^{3n-}$(n = 1–3), [H$_4$Ru$_4$(CO)$_{11}$L]$^{3-}$ and [Ru$_6$C(CO)$_{16}$L]$^{3-}$ (where L is the water-soluble phosphine [P(m-C$_6$H$_4$SO$_3$)$_3$]$^{3-}$ as the Na$^+$ salt) are readily examined by ESMS in water or

MeOH. They give aggregate peaks containing varying numbers of sodium counter-ions, with the most highly-charged species observed being $[Ru_3(CO)_{10}L_2+Na]^{5-}$ [38].

ESMS has also been used in the identification of the product of CO reduction of Na_2PtCl_6 and $RhCl_3$ on an MgO support [102]. The product cluster anion was extracted from the support and negative-ion ESMS revealed the anion $[PtRh_5(CO)_{15}]^-$ as the major ion, together with the fragment ions $[PtRh_5(CO)_{14}]^-$ and $[PtRh_5(CO)_{13}]^-$.

4.2. *Neutral metal carbonyl complexes*

For neutral metal carbonyl complexes, techniques for study by ESMS have not been available until very recently. Coordinated CO contains a formal lone-pair of electrons on oxygen, but this atom is not readily protonated in solution, although interactions of the CO-oxygen with hydrogen-bond donors in the solid-state occurs [103–106]. This means that "normal" ESMS studies on metal carbonyl complexes are only possible when the co-ligand has suitable functional groups; examples of this type include η^4-(diene)$Fe(CO)_3$ or η^6-(arene)$Cr(CO)_3$ where the organic ligand has $>C{=}O$, $-NH_2$ or ${=}N(R)$ groups that allow ready formation of $[M+H]^+$ ions [107].

More generally, homoleptic metal carbonyls and mixed-ligand complexes which contain only non-protonatable groups must be subjected to alternative ionisation processes. The most successful and general method found to date is to dissolve the metal carbonyl in an alcohol solvent, and to add a small quantity of the corresponding sodium alkoxide (easily generated by adding a small piece of the metal to a separate portion of the alcohol) [37]. Nucleophilic attack of the resulting alkoxide on a coordinated CO ligand then occurs:

$$L_nM\text{–}CO+OR^-\rightarrow[L_nM\text{–}CO_2R]^- \quad (1)$$

The resulting $[M+OR]^-$ ions are readily analysed in negative-ion mode. This derivatisation process is useful since the reactions are general for many metal carbonyls, are rapid and are characterised by large equilibrium constants favouring the charged product. A range of alcohols can be used, but methanol is preferred. A competing ionisation, if hydride ligands are present, may be deprotonation giving $[M\text{–}H]^-$ ions. An illustrative list of the metal carbonyl complexes which have successfully given ions using this ionisation technique is in Table 1, where the generality of the method can be easily seen. It is equally effective for mononuclear complexes and for high molecular mass polynuclear clusters [37, 47, 108, 109].

For direct comparison of techniques there is a recent report of the use of UV laser-desorption mass spectrometry to analyse the hexanuclear ruthenium carbide clusters $[Ru_6C(CO)_{17}]$, $[Ru_6C(CO)_{14}(\eta^6\text{-}C_6H_5Me)]$ and $[Ru_6C(CO)_{12}(\eta^6\text{-}C_6H_4Me_2)(\mu\text{-}C_6H_7Me)]$ and $[Ru_6C(CO)_{14}(C_{16}H_{16})]$ (Fig. 6) [8, 9]. Positive-ion spectra showed abundant singly-charged positive ions, together with CO loss from the parent clusters and a series of high molecular weight clusters formed by aggregation of the intact hexaruthenium carbide cores, observed by a time-of-flight detector. Interpretation of the ESMS spectra is much more straightforward.

Examples discussed so far have been for characterisation of single compounds. ESMS also has valuable application in monitoring reactions. One of the classical routes to high-nuclearity clusters has been the pyrolysis of smaller clusters, but such reactions are typically non-specific. The products isolated and characterised have generally been those which crystallise, often after laborious chromatographic separation. There is no doubt that other clusters remain uncharacterised, especially those that are charged so cannot easily be purified by traditional chromatographic methods. For monitoring cluster reactions ESMS is complementary to, but more sensitive than, IR spectroscopy, since the latter technique can suffer from overlap of bands due to two or more species. As an illustration of the potential of ESMS in this area, Fig. 7 shows the negative-ion ESMS spectrum of pyrolysed (210°C) $Os_3(CO)_{12}$, after extraction with ethyl acetate and derivatisation with NaOMe, yielding osmium carbonyl clusters of a range of metal nuclearities [37].

The addition of OMe^- to derivatise neutral metal carbonyl compounds for ESMS observation involves

Table 1. A representative range of the neutral metal carbonyl compounds that show clean $[M+OMe]^-$ ions in their ESMS spectra when run in MeOH with added NaOMe. For a more complete list see Ref. [37]

$[Fe(CO)_5]$	$[W(CO)_6]$	$[Re_2(CO)_{10}]$
$[Mo(CO)_3Cp]_2$	$[Os_3(CO)_{12}]$	$[Fe_3(CO)_{11}(CNBu^t)]$
$[Ru_3(CO)_{11}(PPh_3)]$	$[Ru_3H(C_2Bu^t)(CO)_9]$	$[Cp(CO)_3Mo\text{–}(C{\equiv}C)_2\text{–}C_6H_5]$
$[Ir_4(CO)_{12}]$	$[Ru_4H_4(CO)_{12}]$	$[NiRu_3H_3(CO)_9Cp]$
$[Ru_5(CO)_9(C_6H_5Me)]$	$[Ru_6C(CO)_{17}]$	$[Ru_6C(CO)_{14}(C_6H_5Me)]$

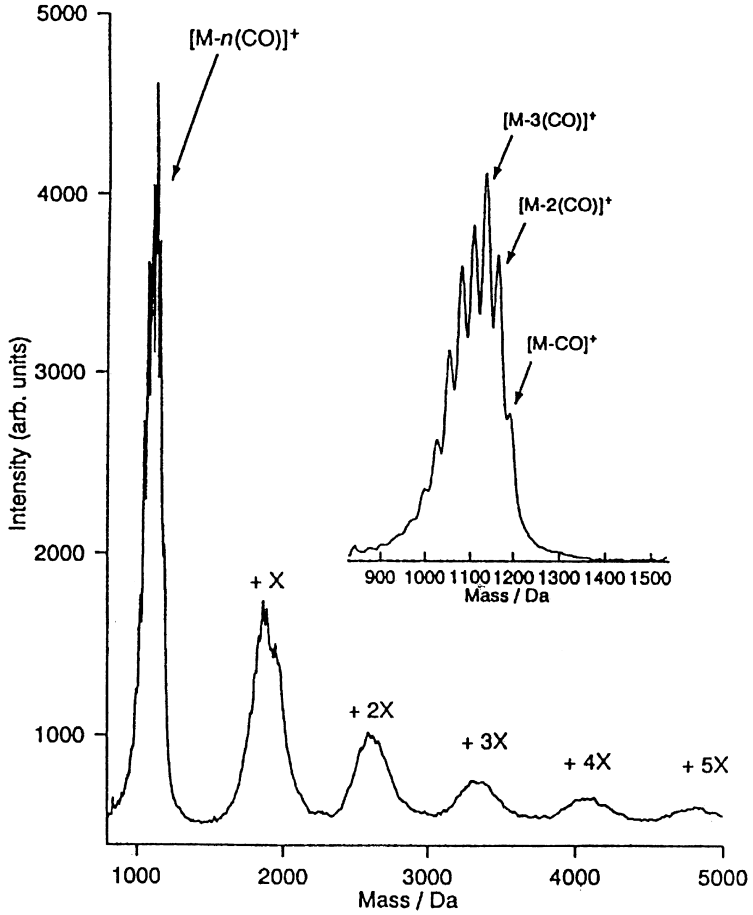

Fig. 6. The laser desorption mass spectrum of $[Ru_6C(CO)_{14}(C_{16}H_{16})]$ (taken from Ref. [9]).

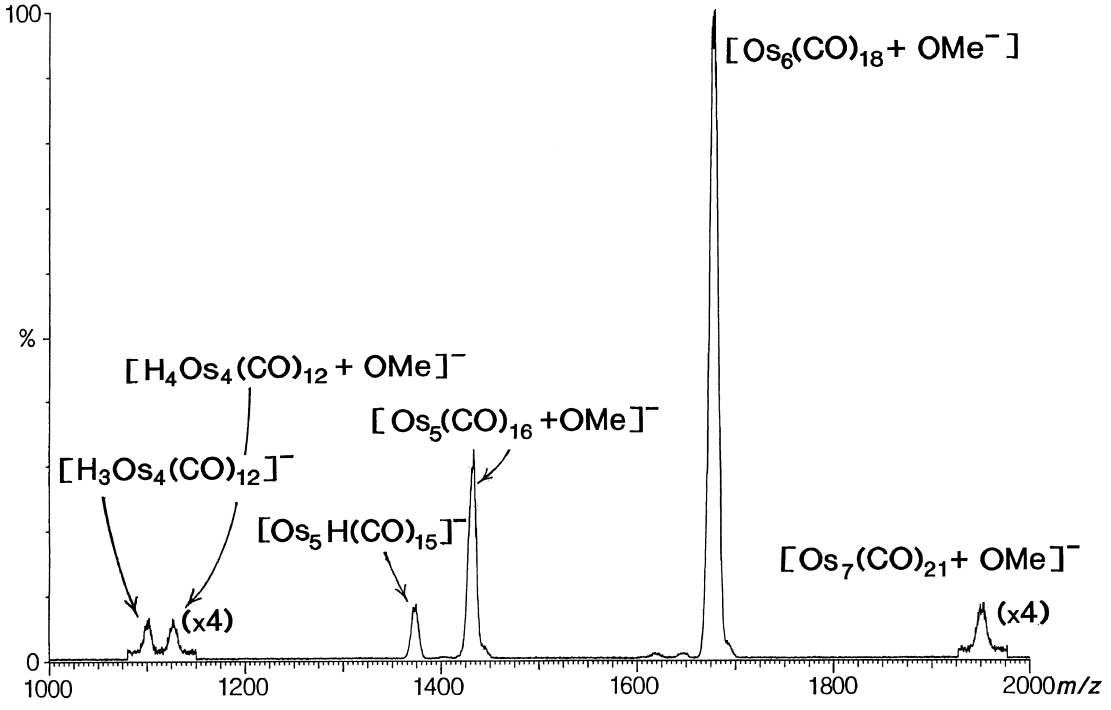

Fig. 7. The negative-ion mass spectrum of an extract of the crude product from the pyrolysis of $Os_3(CO)_{12}$ after treatment with NaOMe in MeOH, showing products of nuclearity 4–7 (taken from Ref. [37]).

nucleophilic attack at a coordinated CO. Another example of this type which is less well studied involves corresponding attack by the azide ion, which usually proceeds via the overall process shown in eqn (2) presumably via the initial addition of N_3^- to a coordinated CO followed by loss of N_2:

$$L_nM\text{–}CO + N_3^- \rightarrow [L_nM\text{–}NCO]^- + N_2 \quad (2)$$

ESMS has provided the first direct evidence for an intermediate azide-addition product and serves as a rapid screening technique on a small scale to assess which substrates are most suitable for subsequent preparative-scale reactions [110].

Examples so far discussed have involved formation of negative ions from the neutral metal carbonyl species. An alternative procedure involves attachment of a positively charged species to the substrate. As discussed above, protons do not generally add to give $[M+H]^+$ ions, but in some cases mono-charged ions such as Na^+, Cs^+ or Ag^+ are useful ionisation aids. A series of rhenium–bipyridine complexes of the type *fac*-$[Re(X_2bipy)(CO)_3Y]$ (X_2bipy = 4,4′-X_2-2,2′-bipyridine; X = H, Me, CF_3; Y = CN, Cl, Br, OCHO) yielded no ions of the form $[Re(X_2bipy)(CO)_3]^+$ in methanol solution, but addition of $NaNO_3$ yielded $[Re(X_2bipy)(CO)_3Y+Na]^+$ ions [111]. When X was OH, the methoxy complex $[Re(X_2bipy)(CO)_3OMe+Na]^+$ was observed, but no adduct was observed for $[Re(CO)_5Cl]$ using this method. An $[M+Na]^+$ adduct has also been observed for the complex [*fac*-Re(bipy)$(CO)_3$CN] in the presence of $NaNO_3$ ionisation agent, indicating that it is a general ionisation method for this class of compound [112].

The sodium ionisation method can be applied to other complexes, such as ruthenium–nitrosyl complexes of the type $[Ru(NO)Cl_3(EPh_3)_2]$ (*E* = P, As, Sb), which with added alkali metal cations result in the observation of [M + cation]$^+$ ions [113]. Similarly $[M+Na]^+$ ions are sometimes observed with metal carbonyl clusters that have been treated with NaOMe [37].

For all of these examples it appears that attachment is via an iso-carbonyl (or iso-nitrosyl) link of the type $L_nM\text{–}C{\equiv}O\ldots Na^+$. In support of this, $[M+Na]^+$ ions are usually only found with metal carbonyl clusters that are electron-rich with electron-donating co-ligands. For example $Ru_3(CO)_9(PPh_3)_3$ gives a clean $[M+Na]^+$ signal but the parent $Ru_3(CO)_{12}$ does not [37].

An alternative ionisation technique uses silver(I) ions in a range of solvents and gives $[M+Ag(solvent)_n]^+$ type ions (n = 0 or 1, depending on cone voltage) [37, 46]. Metal carbonyl complexes which give successful ions by this technique include $Ru_3(CO)_{12}$, $Os_3(CO)_{12}$, $Re_2(CO)_{10}$ and $SiFe_4(CO)_{16}$ but overall it is a less general method. Here the ionisation mechanism appears to involve addition of the Ag^+ to a M–M bond rather the isocarbonyl-type interaction assumed for the other metal cations [37]. This method of ionisation is also successful for analysing poly-yne compounds with metal carbonyl end-groups, although here attachment of the Ag^+ via the C≡C bonds seems probable [109].

A more drastic formation of cations from neutral metal carbonyl species comes from a study of the neutral rhenium carbonyl complexes [(ind)$Re(CO)_3$] (ind = η^5-indenyl), and [$CpRe(CO)_3$] in MeCN solution. These give rise to $[Re(CO)_3(MeCN)_3]^+$ ions in the ES analysis, though the original species are stable in bulk solution [114]. It was suggested that oxidation of the parent compound generates seventeen-electron cations, which are labile, resulting in the loss of the cyclopentadienyl or indenyl ligands. In contrast, the complexes [(ind)Re$(CO)_2$(butyne)] and [$CpRe(CO)_2$(butyne)] did not lose the aromatic hydrocarbon ligand on ES analysis and the predominant ions observed were [(ind)Re(CO)(MeCN)(butyne)]$^+$ and [CpRe(CO)(MeCN)(butyne)]$^+$ [114].

Another approach which we are taking in the analysis of metal carbonyl complexes, is to incorporate ancillary protonatable phosphine ligands [115]. Examples of these "electrospray-friendly" analogues of the ubiquitous triphenylphosphine ligand are **8**. These ligands are chemically and electronically similar to triphenylphosphine, yet the methoxy group facilitates ionisation by protonation (Section 2.3). A number of complexes of these ligands have been prepared and examples include $Fe(CO)_3P^*_2$ and $Mo(CO)_4(P^{***})_2$; all complexes of this type yield strong $[M+H]^+$ ions whereas the triphenylphosphine analogues do not.

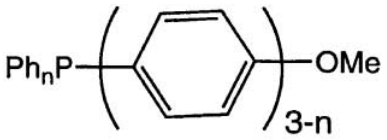

8a; n = 2, P*
8b; n = 1, P**
8c; n = 0, P***

5. METAL–CYCLOPENTADIENYL COMPLEXES, INCLUDING METALLOCENES

The cyclopentadienyl ligand itself is not protonatable under ES conditions and therefore the behaviour of such complexes is strongly dependent on the nature of the ancillary ligands present.

The archetypal metallocene, ferrocene, Cp_2Fe, is an accepted standard in the measurement of electrode potentials for non-aqueous redox systems and the ease of oxidation of metallocenes results in them being ideal candidates for ESMS study. As described earlier in Section 2, the ES capillary is able to act as an electrochemical cell, resulting in substrate oxidation. The ferricinium ion, in the form of the salt $[Cp_2Fe]BF_4$ generated by oxidation of ferrocene with $NOBF_4$, has been analysed by ESMS and the parent Cp_2Fe^+ ion was observed with high intensity at m/z 186 [90]. A study of collision-induced dissociation (CID) caused by increasing the (skimmer) cone voltage produced two extra peaks corresponding to loss of one and both Cp ligands. These fragments are also the major ions observed upon analysis of ferrocene using EI mass spectrometry.

While chemical oxidation is certainly effective, it is certainly not the only ionisation pathway available for metallocene complexes. Ruthenocene and osmocene have been investigated and each gave the oxidised metallicinium ion $[Cp_2M]^+$ without the addition of an oxidising agent [116]. However, in the case of osmocene, the increased basicity of the metal in this complex resulted in competitive protonation occurring, giving $[Cp_2OsH]^+$. The protonated decamethylosmocene cation $[Cp^*_2OsH]^+$ was observed in the positive ion ESMS spectrum of $[Cp^*_2OsH][Os_2Br_8]$, formed by reaction of H_2OsBr_6 with Cp*H and ethanol [117].

For other metallocene-derived compounds, protonation and oxidation may compete with each other to be the dominant ionisation pathway, the relative amounts of each depending on the redox potential of the metallocene centre, the basicity of the attached substituents, and also on instrumental parameters such as the solvent flow rate. (A slower flow rate results in a greater residence time in the metal capillary and more oxidation). Thus for the ferrocenyl-amine $FcCH_2NMe_2$, only the protonated $[M+H]^+$ ion was observed due to the high basicity of the NMe_2 moiety; the compound $[FcCH_2NMe_3]I$ also gave an intense peak due to the cation [118]. For the phosphonate $FcCH_2P(O)(OPh)_2$, both protonated $[M+H]^+$ and oxidised $[M]^+$ ions were observed, reflecting the lower basicity of the P=O moiety compared to the amine [118]. At higher cone voltages, the unsubstituted ligand was selectively lost and this is interpreted in terms of intramolecular stabilisation of the resulting cation formed. The compounds $FcCH_2OH$ [118], $FcCH_2P(CH_2OH)_2$ [119], and $FcCH_2PH_2$ [120] have also been studied by ESMS (including the addition of silver ions to the phosphines, refer to Section 8). For all of these compounds containing the $FcCH_2E$ moiety (where E is N or P), the ion $[FcCH_2]^+$ is a commonly observed stabilised carbocation, with its ease of formation reflecting the ability of the E moiety to act as a leaving group. The formation of this ion was therefore maximum for $FcCH_2NMe_3^+$, which can readily lose Me_3N. The ferrocene-derived thiolate anion $FcCO_2(CH_2)_{16}S^-$ (together with a number of other thiolate anions) has been studied by negative-ion ESMS, which gives the expected $[M]^-$ ion; the ion $FcCO_2^-$ was also observed as a fragment ion [121].

A number of titanocene(IV) complexes of β-diketonates of the type $[Cp_2Ti(\beta\text{-diketonate})]PF_6$, formed by oxidation of the corresponding titanium(III) complexes with $[Cp_2Fe]PF_6$, gave the expected parent ions in their positive-ion ESMS spectra [122].

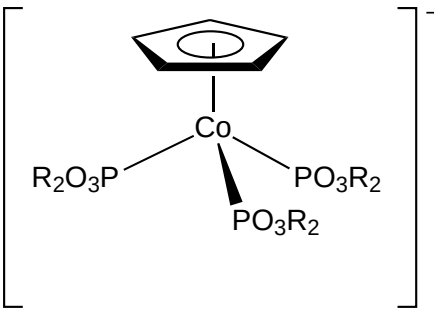

9

Uninegative tripodal oxygen ligands L of the type **9** have attracted much attention for their coordination chemistry, being analogous in many respects to the cyclopentadienyl ligand. Complexes of these ligands (R = Me, Et, ^{i}Pr) with alkali metals have been studied by negative-ion ESMS [123]. Ions of the type $[NaL_2]^-$, $[Na_2L_3]^-$ and $[Na_3L_4]^-$ were observed and related to the known trimeric and polymeric structures of the sodium salts of these ligands. Addition of alkali metal halides (e.g. NaCl) to solutions of these ligands yields

ions of the type $\{[L]^- + n(NaCl)\}$ ($n = 1$–9) and $\{[NaL_2]^- + n(NaCl)\}$ ($n = 1$–8). These results were contrasted with the uninegative tripodal nitrogen ligand $[HB(pz)_3]^-$ (pz = pyrazolyl), which yielded only $[HB(pz)_3]^-$ and $K\{[HB(pz)_3]\}_2^-$ ions, and no adducts with alkali metal halides.

There have been several studies on complexes containing metallocene-derived phosphine ligands. A range of ferrocene-derived phosphine ligands has been surveyed by ESMS, including application of various ionisation reagents for such compounds (refer to Section 7) [42]. ESMS has been used in a study of C–S bond insertion reactions of thiazolium salts with platinum(0) diphosphine complexes containing the ligand $(Ph_2PC_5H_4)_2Fe$ (dppf) [124]. A number of bis(diphenylphosphino)ruthenocene (dppr) complexes of ruthenium, which also contain a coordinated Cp ligand, have been studied by ESMS [125]. The complexes [Ru(Cp)Cl(dppr)] and $[Ru(Cp)(dppr)(MeCN)]PF_6$ both yield the ion $[Ru(Cp)(dppr)(MeCN)]^+$ when analysed by ESMS and the MeCN ligand is lost at relatively low cone voltages. Loss of the CO ligand from $[Ru(Cp)(dppr)(CO)]^+$ required much higher cone voltages, indicating higher stability. The vinylidene complex $[Ru(Cp)(dppr)(=C=CHPh)]^+$ gives the expected molecular ion, together with the dication $[Ru(Cp)(dppr)(=C=CHPh)]^{2+}$, formed by electrochemical oxidation of the ruthenocene moiety in the capillary (refer to Section 2.3).

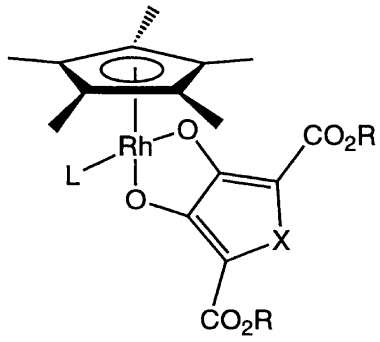

10
L = pyridine, PPh_3;
X = O, S;
R = Me, Et

A series of pentamethylcyclopentadienyl (Cp*) complexes of rhodium containing dioxolene ligands of the type **10** have been synthesised and characterised by ESMS [126]. The lability of the ancillary PPh_3 ligand was readily ascertained by means of cone voltage-induced fragmentation and by *in situ* reactions with reagents such as hydrogen peroxide and elemental sulfur or selenium, which react with the labilised PPh_3 ligand, generating $Ph_3P{=}E$ ligands (E = O, S or Se), which coordinate to the Rh centre to differing extents. The cyclic trimer $[Cp^*Rh(2'\text{-deoxyadenosine})]_3^{3+}$ has been used in the gas-phase molecular recognition of aromatic acid and aromatic carboxylic acid guests [127]. The supramolecular recognition is believed to occur via non-covalent π–π interactions.

The Cp* tungsten complex $[Cp^*WS_2(SCH_2CH_2Br)]$ has been successfully analysed in THF solution by ESMS, using LiCl as the ionisation reagent [40]. In positive-ion mode, ions of the type $[M + Li]^+$, $[M + Li(THF)]^+$ and $[2M + Li]^+$ were observed, while in negative-ion mode, $[M + Cl]^-$ is seen; these observations illustrate the effective use of a combination of an aprotic solvent and metal salt ionisation reagent in the analysis of sensitive organometallic complexes, as described in Section 2. The cluster $[Cp^*_2Mo_2Fe_2S_4]_3(\mu\text{-}S_4)_3$ has also been analysed in THF solution, to which a small amount of acetic acid was added, giving $[M + H]^+$ and $[M + 2H]^{2+}$ ions, indicating that the species is very readily protonated [128].

Finally in this section, the large star-shaped molecule **11** containing $[Ru(bipy)_3]^{2+}$ type units and a central (arene)$FeCp^+$ moiety has been analysed by positive-ion ESMS, which gave the 4+, 5+ and 6+ ions formed by aggregation with varying numbers of PF_6^- counterions, corresponding to the parent species of mass 5912 Da [129].

6. OTHER COMPLEXES

Silver(I) ions have a propensity to bind with soft electron density donor groups and thus this metal is well-known to form π-complexes with molecules such as alkenes, alkynes and arenes. This can be exploited in the analysis of such compounds by ESMS.

The tungsten tetra-ynyl complex $[CpW(CO)_3\text{-}C_8\text{-}W(CO)_3Cp]$ (M) when analysed at a low cone voltage with

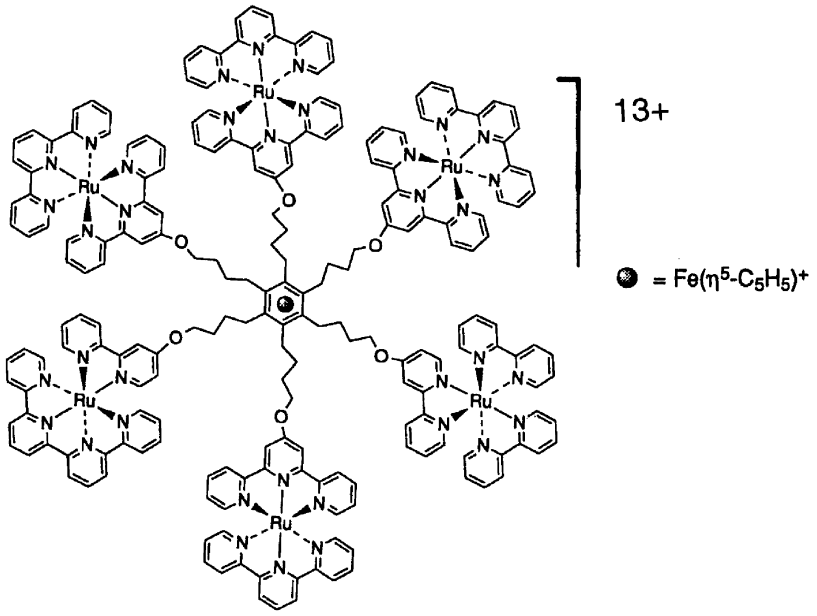

11

added $AgNO_3$ yielded the ions $[M_2Ag]^+$ (*m*/*z* 1631) and $[MAg(MeCN)]^+$ (*m*/*z* 911), while at higher cone voltages, fragmentation by successive loss of CO ligands from the parent ion was observed [109].

A wide range of platinum(II) complexes containing cyclo-octa-1,5-diene (COD) or phosphines, together with various other ligands such as thiosalicylate [130], ureylene [131], β-propiolactam monoanion [132] and thiourea dianion [133] have all been routinely analysed by positive-ion ESMS and all species give strong ions of the type $[M+H]^+$ and $[M+NH_4]^+$. All of these complexes contain ancillary N or O atoms which can act as protonation sites. ESMS was also used to investigate the cone voltage-induced fragmentation pathways of these complexes. Formation of cyclometallated triphenylphosphine species is a common theme for these complexes when subjected to high cone voltages, though complexes containing chelating phosphine ligands [e.g. $Ph_2PCH_2CH_2PPh_2$ (dppe) or $(Ph_2PC_5H_4)_2Fe$ (dppf)] undergo this process much less readily. For the thiourea complexes and the azetidinone complexes, the *in situ* coordination chemistry with Ag^+ ions and with a range of metal cations respectively, was also investigated [133].

Host–guest complexes can also be readily identified by ESMS and there have been extensive studies in this area. A series of calixarenes and paracyclophane molecules, which are conformationally both rigid and defined, have been studied with various metal cations [134]. Complexes of a paracyclophane with Li^+, Na^+ and K^+ were scarcely detectable by either secondary ion mass spectrometry (SIMS), but those with Rb^+ and Cs^+ were very intense and studies suggested that the cavity was optimised for binding of the Cs^+ ion. Although the Ag^+ ion has an affinity for π electron density, it does not bind in the cavity because of its size, which is comparable to K^+.

A number of allyl complexes have been studied by ESMS. The platinum–cyclopentadienyl complex, also containing a π-allyl ligand, $[Pt(C_5H_4Me)(\eta^3\text{-}C_3H_6)]$ has been examined by positive-ion ESMS and found to give an $[M]^+$ ion by oxidation, with a contribution from the protonated ion $[M+H]^+$; the only fragment ion observed was $[M\text{-allyl}]^+$ ([i.e. $(C_5H_4Me)Pt]^+$), though other aggregate ions were observed, including species containing up to six platinums [135]. Complexes of the type $[Pt(\eta^3\text{-}C_3H_6)(PPh_3)X]$ (X = Cl, Br, I) have also been studied and gave the ion $[Pt(C_3H_6)PPh_3]^+$, together with various solvated Pt complexes, including bis(triphenylphosphine) complexes [136].

7. PHOSPHINES, ARSINES AND THEIR ONIUM SALTS

Phosphines (R_3P) and arsines (R_3As) are very widely used as ligands in organometallic chemistry and accordingly they deserve mention in this review. Such compounds, exemplified by PPh_3, are not readily protonated in the absence of other functional groups (such as methoxy substituents, refer to Section 4) and therefore pre-ionisation is necessary. This may be achieved in a number of ways:

(i) Quaternisation to the respective onium salt, for example with methyl iodide. A range of mono-, di- and tri-phosphines have been converted to their methylphosphonium salts in this way and characterised by positive-ion ESMS [137]. In early studies in the ESMS of inorganic species, Colton and Traeger reported that the organic salts $[PhCH_2PPh_3]Cl$ and $[Bu_4N]PF_6$ yield the cations as the base peaks in their positive-ion spectra.

(ii) Conversion to the hydroxymethylphosphonium salt $[R_3P(CH_2OH)]^+$, using a mixture of formaldehyde and hydrochloric acid. A range of phosphines has been analysed by ESMS in this way [41, 42].

(iii) Oxidation to the phosphine oxide (using, for example H_2O_2). The resulting phosphine oxide then yields strong $[M+H]^+$ ions in the positive-ion ESMS spectrum when analysed in a protic solvent [41, 42].

(iv) Addition of silver(I) or copper(I) ions (see Section 2.3). These metal ions form stable complexes with a wide range of phosphine, arsine and stibine (among other) ligands and in the positive-ion ESMS spectra, ions of the type $[n\mathrm{M}+\mathrm{cation}]^+$ (cation = Cu or Ag; M = ligand; $n = 1$–4 depending on metal–ligand combination) are observed [41, 42].

The use of "electrospray-friendly" phosphine ligands **8** has been discussed earlier in this review (Section 4.2) [115]. Additionally, sulfonated aryl phosphines, which are attracting current interest for their applications in transition-metal catalysed biphasic reactions, yield strong negative-ion spectra, and selected examples have been cited earlier [38, 42].

8. MISCELLANEOUS APPLICATIONS

8.1. *Organometallic functionalisation of peptides and proteins for mass spectrometric analysis*

The affinity of organomercury compounds for thiols has been exploited for the derivatisation of cysteine-containing peptides and proteins. Interactions of Hg^{2+}, $MeHg^+$ and $PhHg^+$ cations with the thiol group of cysteine, glutathione and a 27-residue polypeptide containing one cysteinyl sulfur have been studied by positive-ion ESMS [138]. The $MeHg^+$ cation shows a greater affinity for cysteinyl sulfur, whereas $PhHg^+$ also forms isomeric species in which the mercury is bonded to an amino or carboxylic acid group. *p*-Hydroxymercuribenzoic acid has also been used to form derivatives analysed by MALDI-MS. The mass shift before and after derivatisation allows the total number of sulfhydryl groups in the protein to be determined [139]. The ions $MeHg^+$ and $PhHg^+$ have been evaluated (together with a wide range of other metal cations) as ionisation reagents for the proteins myoglobin and ubiquitin [140] while $MeHg^+$ has been investigated with horse heart cytochrome *C* [141]. One practical application of ESMS involves organometallic compounds as an aid in the analysis of peptides [142]. The study used an ionic species, $[(\eta^5\text{-}C_6H_7)Fe(CO)_3]^+$ (Fed^+), to form adducts with various nucleophilic peptides in a 50% methanol solution. These are produced in a similar manner to adducts between such cations and other nucleophilic reagents such as imidazoles or tertiary phosphines. The results showed a high adduction rate with Fed^+ for several peptides including N-acetylhistidine, and glutathione. The pH change was recorded for each peptide solution when the cation was added (*in situ*, in a specific mole ratio) and this yielded valuable information such as possible deprotonation sites in the histidine residues present. In all cases an ion corresponding to $[Fed]^+$ (m/z 219) and $[\mathrm{peptide}+Fed]^+$ was observed at a skimmer cone voltage of 20 V, along with various other protonated species. The only evidence of fragmentation in the ESMS of these organometallic adducts was the presence of weak intensity ions (1% intensity) in the spectra of two of the peptides which were assigned to $[\mathrm{peptide}+\text{Fed-CO}]^+$ in each case. Peptides investigated were *N*-acetylhistidine, *p*-Glu-His-Pro, *p*-Glu-His-Gly-NH_2, glutathione, *p*-Glu-His-Trp-Ser-Try-Gly-Leu-Arg-Pro-Gly and *p*-Glu-His-Trp-Ser-Try-Gly-Leu-Arg-Pro-Gly-Cys. Cysteine and histidine residues show preference for binding. It was concluded that ESMS is a versatile technique for the identification of adducts between peptides and organometallic reagents.

8.2. *Fullerenes*

Fullerenes, typified by the archetypal C_{60}, are of intense current interest in the chemical community, and a wide range of metal derivatives, including organometallic complexes, have been synthesised. Accordingly, development of techniques for their analysis by ESMS is of some interest, particularly since these molecules are characteristically non-polar and have low solubility in many solvents. In addition, the use of the soft-ionisation ESMS is likely to provide more useful information on higher homologues, which may fragment under more vigorous ionisation conditions. A number of indirect approaches have been reported which involve prior derivatisation, including incorporation of crown ether groups [143, 144, 145] and amination [146]. Oxidation or reduction using chemical redox agents has also been studied, using a variety of oxidants and reductants [147, 148, 149]. ESMS analysis of fullerenes is in fact directly achievable, as a result of either electrochemical oxidation or reduction in the ES capillary, which can act as an electrochemical cell. A number of studies have appeared in this area. A mixture of C_{60} and C_{70} ("fullerite") was analysed in dichloromethane

solution and found to yield radical anions ($C_{60}^{\cdot-}$ and $C_{70}^{\cdot-}$) in the negative-ion spectrum. No corresponding radical cations were observed in the positive-ion spectrum in this study. Prior electrochemical reduction of the fullerite sample, followed by ESMS analysis, yielded a more complex and irreproducible spectrum, though the fullerene radical anions were observed [54]. It was concluded that a compound should be directly analysable by ESMS providing its redox potential lies within the range -0.8 and $+1.0$ V vs SCE in CH_2Cl_2 solution. C_{60} and a number of derivatives were subsequently analysed directly in toluene solution, yielding the radical ions $C_{60}^{\cdot+}$ and $C_{60}^{\cdot-}$ in positive- and negative-ion modes, respectively [150]. The spectra were characterised by the presence of strong molecular ions with little or no fragmentation, though minor ions assigned as $C_{60}O^-$ and $C_{60}(PhCH_2)^-$ were also observed.

9. FUTURE SCOPE

The ESMS technique is uniquely suited to the analysis of polar, high molecular weight, involatile, thermally labile and rapidly-exchanging systems, providing they are soluble and stable in some solvent and can be ionised by some appropriate method. The wide variety of examples given in this review demonstrate that the technique has found an important role in the armoury of techniques employed by the organometallic chemist. The vast majority of the references quoted in this review have appeared in the past 4 years, showing applications are multiplying rapidly. There is still great scope for further development of this technique in many areas of chemistry. It is our hope that this review has inspired those organometallic chemists not already *au fait* with the technique to apply it to their own field of research, or to develop new fields, previously inaccessible due to the absence of suitable definitive analytical techniques. Many new and exciting developments in inorganic and organometallic electrospray mass spectrometry are anticipated in the near future.

Acknowledgements—We thank the University of Waikato for supporting our research in electrospray mass spectrometry, together with our co-workers whose names appear in the references cited, in particular Scott McIndoe, Maarten Dinger, Corry Decker and Nick Goodwin. The New Zealand Lottery Grants Board is also acknowledged for a grant-in-aid towards the purchase of our mass spectrometer. We also thank Professor M.I. Bruce for helpful comments.

REFERENCES

1. Litzow, M. R. and Spalding, T. R., *Mass Spectrometry of Inorganic and Organometallic Compounds*. Elsevier, Amsterdam, 1973.
2. Miller, J. M., *Adv. Inorg. Chem. Radiochem.*, 1984, **28,** 1.
3. Bruce, M. I. and Liddell, M. J., *Appl. Organomet. Chem.*, 1987, **1,** 191.
4. Weller, R. R., MacMahon, T. J. and Freiser, B. S., in *Laser and Mass Spectrometry*, ed. D. M. Lubman. Oxford Series on Optical Science, Oxford University Press, Oxford, U.K., 1990, p. 249.
5. Loo, J. A., *Bioconjugate Chem.*, 1995, **6,** 644.
6. Hillenkamp, F., Karas, M., Beavis, R. C. and Chait, B. T., *Anal. Chem.*, 1991, **63,** 1193.
7. Dale, M. J., Dyson, P. J., Suman, P. and Zenobi, R., *Organometallics*, 1997, **16,** 197.
8. Dale, M. J., Dyson, P. J., Johnson, B. F. G., Langridge-Smith, P. R. R. and Yates, H. T., *J. Chem. Soc. Dalton Trans.*, 1996, 771.
9. Dale, M. J., Dyson, P. J., Johnson, B. F. G., Martin, C. M., Langridge-Smith, P. R. R. and Zenobi, R., *J. Chem. Soc. Chem. Commun.*, 1995, 1689.
10. Huc, V., Boussaguet, P. and Mazerolles, P., *J. Organomet. Chem.*, 1996, **521,** 253.
11. Fenn, J. B., Mann, M., Meng, C. K., Wong, S. F. and Whitehouse, C. M., *Mass Spectrom. Rev.*, 1990, **9,** 37.
12. Fenn, J. B., Mann, M., Meng, C. K., Wong, S. F. and Whitehouse, C. M., *Science*, 1989, **246,** 64.
13. Cole, R. B. (ed.), *Electrospray Ionisation Mass Spectrometry*; *Fundamentals*, *Instrumentation and Applications*. Wiley-Interscience, New York, 1997.
14. Langley, G. J. and Mills, G. A., *Educ. Chem.*, 1997, 14.
15. Snyder, A. P., *Biochemical and Biotechnological Applications of Electrospray Ionization Mass Spectrometry*, ACS Symposium Series, No. 619. American Chemical Society, Washington, D.C., 1996.
16. Bakhtiar, R., Hofstadler, S. A. and Smith, R. D., *J. Chem. Educ.*, 1996, **73,** A118.
17. Przybylski, M. and Glocker, M. O., *Angew. Chem. Int. Ed. Engl.*, 1996, **35,** 807.
18. Mann, M., *Org. Mass Spectrom.*, 1990, **25,** 575.
19. Mann, M. and Wilm, M., *Trends Biochem. Sci.*, 1995, **20,** 219.
20. Smith, R. D., Loo, J. A., Edmonds, C. G., Barinaga, C. J. and Udseth, H. R., *Mass Spectrom. Rev.*, 1991, **10,** 359.
21. Whitehouse, C. M., Dreyer, R. N., Yamashita, M. and Fenn, J. B., *Anal. Chem.*, 1985, **57,** 675.
22. Whitehouse, C. M., Dreyer, R. N., Yamashita, M. and Fenn, J. B., *Anal. Chem.*, 1997, **69,** 427A.
23. Colton, R., D'Agostino, A. and Traeger, J. C., *Mass Spectrom. Rev.*, 1995, **14,** 79.
24. Hop, C. E. C. A. and Bakhtiar, R., *J. Chem. Educ.*, 1996, **73,** A162.

25. Kebarle, P. and Tang, L., *Anal. Chem.*, 1993, **65,** 972A.
26. Hofstadler, S. A., Bakhtiar, R. and Smith, R. D., *J. Chem. Educ.*, 1996, **73,** A82.
27. Depree, C. V., M.Sc. Thesis, University of Waikato, 1995.
28. Fenn, J. B., *J. Am. Soc. Mass Spectrom.*, 1993, **4,** 524.
29. Blades, A. T., Ikonomou, M. G. and Kebarle, P., *Anal. Chem.*, 1991, **63,** 2109.
30. Guevremont, R., Le Blanc, J. C. Y. and Siu, K. W. M., *Org. Mass Spectrom.*, 1993, **28,** 1345.
31. McLuckey, S. A., Van Berkel, G. J., Goeringer, D. E. and Glish, G. L., *Anal. Chem.*, 1994, **66,** 689A.
32. Amster, I. J., *J. Mass Spectrom.*, 1996, **31,** 1325.
33. Kofel, P., Reinhard, H. and Schlunegger, U. P., *Org. Mass Spectrom.*, 1991, **26,** 463.
34. Wilm, M. and Mann, M., *Int. J. Mass Spectrom. Ion Process.*, 1994, **136,** 167.
35. Wilm, M. and Mann, M., *Anal. Chem.*, 1996, **68,** 1.
36. Løver, T., Henderson, W., Bowmaker, G. A., Seakins, J. M. and Cooney, R. P., *J. Mater. Chem.*, 1997, 1553.
37. Henderson, W., McIndoe, J. S., Nicholson, B. K. and Dyson, P. J., *J. Chem. Soc. Dalton Trans.*, 1998, 519.
38. Bryce, D. J. F., Dyson, P. J., Nicholson, B. K. and Parker, D. G., *Polyhedron* (in press).
39. Saf, R., Mirtl, C. and Hummel, K., *Tetrahedron Lett.*, 1994, **35,** 6653.
40. Ohnishi, S., Kawaguchi, H. and Tatsumi, K., unpublished results.
41. Henderson, W. and Olsen, G. M., *Polyhedron*, 1996, **15,** 2105.
42. Henderson, W. and Olsen, G. M., *Polyhedron*, 1998, **17,** 577.
43. Fitzpatrick, M. G., Hanton, L. R., Henderson, W., Kneebone, P. E., Levy, E. G., McCaffrey, L. J. and McMorran, D. A., *Inorg. Chim. Acta*, 1998, **281,** 101.
44. Colton, R., Mitchell, S. and Traeger, J. C., *Inorg. Chim. Acta*, 1995, **231,** 87.
45. Canty, A. J. and Colton, R., *Inorg. Chim. Acta*, 1994, **220,** 99.
46. Henderson, W. and Nicholson, B. K., *J. Chem. Soc. Chem. Commun.*, 1995, 2531.
47. Henderson, W., McIndoe, J. S., Nicholson, B. K. and Dyson, P. J., *Chem. Commun.*, 1996, 1183.
48. Van Berkel, G. J. and Zhou, F., *Anal. Chem.*, 1995, **67,** 2916.
49. Van Berkel, G. J. and Zhou, F., *Anal. Chem.*, 1995, **67,** 3958.
50. Hop, C. E. C. A., Saulys, D. A. and Gaines, D. F., *J. Am. Soc. Mass Spectrom.*, 1995, **6,** 860.
51. Van Berkel, G. J., McLuckey, S. A. and Glish, G. L., *Anal. Chem.*, 1992, **64,** 1586.
52. Van Berkel, G. J., Quirke, J. M. E., Tigani, R. A., Dilley, A. S. and Covey, T. R., *Anal. Chem.*, 1998, **70,** 1544.
53. Liu, T.-Y., Shiu, L.-L., Luh, T.-Y. and Her, G.-R., *Rapid Commun. Mass Spectrom.*, 1995, **9,** 93.
54. Dupont, A., Gisselbrecht, J.-P., Leize, E., Wagner, L. and Van Dorsselaer, A., *Tetrahedron Lett.*, 1994, **35,** 6083.
55. Bond, A. M., Colton, R., D'Agostino, A., Harvey, J. and Traeger, J. C., *Inorg. Chem.*, 1993, **32,** 3952.
56. Zhou, F. and Van Berkel, G. J., *Anal. Chem.*, 1995, **67,** 3643.
57. Bond, A. M., Colton, R., D'Agostino, A., Downard, A. J. and Traeger, J. C., *Anal. Chem.*, 1995, **67,** 1691.
58. Evans, C. and Henderson, W., unpublished results.
59. Dinger, M. B. and Henderson, W., *J. Organomet. Chem.*, 1998, **560,** 233.
60. Løver, T., Henderson, W., Bowmaker, G. A., Seakins, J. and Cooney, R. P., *Inorg. Chem.*, 1997, **36,** 3711.
61. Arnold, L. J., *J. Chem. Educ.*, 1992, **69,** 811.
62. Hop, C. E. C. A., *J. Mass Spectrom.*, 1996, **31,** 1314.
63. Henderson, W. and Taylor, M. J., *Polyhedron*, 1957, **1996,** 15.
64. Lawson, G., Dahm, R. H., Ostah, N. and Woodland, E. D., *Appl. Organomet. Chem.*, 1996, **10,** 125.
65. Stewart, I. I. and Horlick, G., *Trends Anal. Chem.*, 1996, **15,** 80.
66. Siu, K. W. M., Gardner, G. J. and Berman, S. S., *Anal. Chem.*, 1989, **61,** 2320.
67. Dakternieks, D., Jurkschat, K., van Dreumel, S. and Tiekink, E. R. T., *Inorg. Chem.*, 1997, **36,** 2023.
68. Dakternieks, D., Zhu, H., Tiekink, E. R. T. and Colton, R., *J. Organomet. Chem.*, 1994, **476,** 33.
69. Lamb, J. H. and Sweetman, G. M. A., *Rapid Commun. Mass Spectrom.*, 1996, **10,** 594.
70. Dopke, J. A., Bridges, A. N., Schmidt, M. R. and Gaines, D. F., *Inorg. Chem.*, 1996, **35,** 7186.
71. Kemmitt, T. and Henderson, W., *J. Chem. Soc. Perkin Trans.*, 1997, **1,** 729.
72. Florencio, M. H., Duarte, M. F., de Bettencourt, A. M. M., Gomes, M. L. and Vilas Boas, L. F., *Rapid Commun. Mass Spectrom.*, 1997, **11,** 469.
73. Pergantis, S. A., Winnik, W. and Betowski, D., *J. Anal. Atom. Spectrom.*, 1997, **12,** 531.
74. Zamora, F., Sabat, M., Janik, M., Siethoff, C. and Lippert, B., *Chem. Commun.*, 1997, 485.
75. Canty, A. J. and Colton, R., *Inorg. Chim. Acta*, 1994, **215,** 179.
76. Canty, A. J., Colton, R., D'Agostino, A. and Traeger, J. C., *Inorg. Chim. Acta*, 1994, **223,** 103.
77. Canty, A. J., Traill, P. R., Colton, R. and Thomas, I. M., *Inorg. Chim. Acta*, 1993, **210,** 91.
78. Byers, P. K., Canty, A. J., Skelton, B. W. and White, A. H., *Organometallics*, 1990, **9,** 826.
79. Bergamini, P., Bortolini, O., Curcuruto, O. and Hamdan, M., *J. Mass Spectrom.*, 1995, S77.
80. Canty, A. J., Colton, R. and Thomas, I. M., *J. Organomet. Chem.*, 1993, **455,** 283.
81. Hinderling, C., Plattner, D. A. and Chen, P., *Angew. Chem. Int. Ed. Engl.*, 1997, **36,** 243.
82. Hinderling, C., Feichtinger, D., Plattner, D. A. and Chen, P., *J. Am. Chem. Soc.*, 1997, **119,** 10793.

83. Aplin, R. T., Doucet, H., Hooper, M. W. and Brown, J. M., *Chem. Commun*., 1997, 2097.
84. Huck, W. T. S., van Veggel, F. C. J. M. and Reinhoudt, D. N., *Angew. Chem. Int. Ed. Engl*., 1996, **35,** 1213.
85. Aliprantis, A. O. and Canary, J. W., *J. Am. Chem. Soc*., 1994, **116,** 6985.
86. Ripa, L. and Hallberg, A., *J. Org. Chem*., 1996, **61,** 7147.
87. Lipshultz, B. H., Stevens, K. L., James, B., Pavlovich, J. G. and Snyder, J. P., *J. Am. Chem. Soc*., 1996, **118,** 6796.
88. Dinger, M. B. and Henderson, W., *J. Organomet. Chem*., 1998, **557,** 231.
89. Dinger, M. B., Henderson, W., Nicholson, B. K. and Robinson, W. T., *J. Organomet. Chem*., 1998, **560,** 169.
90. Colton, R. and Traeger, J. C., *Inorg. Chim. Acta*, 1992, **201,** 153.
91. Bond, A. M., Colton, R., Cooper, J. B., Traeger, J. C., Walter, J. N. and Way, D. M., *Organometallics*, 1994, **13,** 3434.
92. Ahmed, I., Bond, A. M., Colton, R., Jurcevic, M., Traeger, J. C. and Walter, J. N., *J. Organomet. Chem*., 1993, **447,** 59.
93. Bond, A. M., Colton, R., Gable, R. W., Mackay, M. F. and Walter, J. N., *Inorg. Chem*., 1997, **36,** 1181.
94. Marken, F., Bond, A. M. and Colton, R., *Inorg. Chem*., 1995, **34,** 1705.
95. Kane-Maguire, L. A. P., Kanitz, R. and Sheil, M. M., *J. Organometal. Chem*., 1995, **486,** 243.
96. Hori, H., Johnson, F. P. A., Koike, K., Takeuchi, K., Ibusuki, T. and Ishitani, O., *J. Chem. Soc. Dalton Trans*., 1997, 1019.
97. Hori, H., Ishitani, O., Koike, K., Takeuchi, K. and Ibusuki, T., *Anal. Sci*., 1996, **12,** 587.
98. Ferrer, M., Reina, R., Rossell, O., Seco, M. and Segalés, G., *J. Organomet. Chem*., 1996, **515,** 205.
99. Reina, R., Riba, O., Rossell, O., Seco, M., Gómez-Sal, P. and Martín, A., *Organometallics*, 1997, **16,** 5113.
100. Mlynek, P. D. and Dahl, L. F., *Organometallics*, 1997, **16,** 1655.
101. Mlynek, P. D. and Dahl, L. F., *Organometallics*, 1997, **16,** 1641.
102. Xu, Z., Kawi, S., Rheingold, A. L. and Gates, B. C., *Inorg. Chem*., 1994, **33,** 4415.
103. Braga, D. and Grepioni, F., *Acc. Chem. Res*., 1997, **30,** 81.
104. Braga, D., Grepioni, F., Tedesco, E., Biradha, K. and Desiraju, G. R., *Organometallics*, 1996, **15,** 2692.
105. Braga, D., Grepioni, F. and Desiraju, G. R., *J. Organomet. Chem*., 1997, **548,** 33.
106. Braga, D. and Grepioni, F., *Chem. Commun*., 1996, 571.
107. Kane-Maguire, L. A. P., Kanitz, R. and Sheil, M. M., *Inorg. Chim. Acta*., 1996, **245,** 209.
108. Bruce, M. I., Skelton, B. W., White, A. H. and Zaitseva, N. N., *Aust. J. Chem*., 1997, **50,** 163.
109. Bruce, M. I., Ke, M. and Low, P. J., *Chem Commun*., 1996, 2405.
110. McIndoe, J. S. and Nicholson, B. K., *J. Organomet. Chem*. (accepted).
111. Hori, H., Ishihara, J., Koike, K., Takeuchi, K., Ibusuki, T. and Ishitani, O., *Chem. Lett*., 1997, 273.
112. Hori, H., Ishihara, J., Koike, K., Takeuchi, K., Ibusuki, T. and Ishitani, O., *Chem. Lett*., 1997, 1249.
113. Chand, S., Coll, R. K. and McIndoe, J. S., *Polyhedron*, 1998, **17,** 507.
114. Hop, C. E. C. A., Brady, J. T. and Bakhtiar, R., *J. Am. Soc. Mass Spectrom*., 1997, **8,** 191.
115. Decker, C., Henderson, W. and Nicholson, B. K., unpublished results.
116. Xu, X., Nolan, S. P. and Cole, R. B., *Anal. Chem*., 1994, **66,** 119.
117. Gross, C. L., Wilson, S. R. and Girolami, G. S., *Inorg. Chem*., 1995, **34,** 2582.
118. Henderson, W., Oliver, A. G. and Downard, A. J., *Polyhedron*, 1996, **15,** 1165.
119. Goodwin, N. J., Henderson, W., Nicholson, B. K., Sarfo, J. K., Fawcett, J. and Russell, D. R., *J. Chem. Soc. Dalton Trans*., 1997, 4377.
120. Goodwin, N. J., Henderson, W. and Nicholson, B. K., *Chem. Commun*., 1997, 31.
121. McCarley, T. D. and McCarley, R. L., *Anal. Chem*., 1997, **69,** 130.
122. Bond, A. M., Colton, R., Englert, U., Hügel, H. and Marken, F., *Inorg. Chim. Acta*, 1995, **235,** 117.
123. Colton, R., D'Agostino, A., Traeger, J. C. and Kläui, W., *Inorg. Chim. Acta*, 1995, **233,** 51.
124. Smith, V. C. M., Aplin, R. T., Brown, J. M., Hursthouse, M. B., Karalulov, A. I., Malik, K. M. A. and Cooley, N. A., *J. Am. Chem. Soc*., 1994, **116,** 5180.
125. Yeo, S. P., Henderson, W., Mak, T. C. W. and Hor, T. S. A., *J. Chem. Soc. Dalton Trans*. (submitted).
126. Henderson, W., Fawcett, J., Kemmitt, R. D. W. and Russell, D. R., *J. Chem. Soc. Dalton Trans*., 1995, 3007.
127. Bakhtiar, R., Chen, H., Ogo, S. and Fish, R. H., *Chem. Commun*., 1997, 2135.
128. Kawaguchi, H., Yamada, K., Ohnishi, S. and Tatsumi, K., *J. Am. Chem. Soc*., 1997, **119,** 10871.
129. Marvaud, V. and Astruc, D., *Chem. Commun*., 1997, 773.
130. McCaffrey, L. J., Henderson, W., Nicholson, B. K., Mackay, E. J. and Dinger, M. B., *J. Chem. Soc. Dalton Trans*., 1997, 2577.
131. Dinger, M. B., Henderson, W., Nicholson, B. K. and Wilkins, A. L., *J. Organomet. Chem*., 1996, **526,** 303.
132. Henderson, W. and Sabat, M., *Polyhedron*, 1997, **16,** 1663.
133. Henderson, W. and Nicholson, B. K., *Polyhedron*, 1996, **15,** 4015.
134. Inouchi, F., Miyahara, Y., Inazu, T. and Shinkai, S., *Angew. Chem. Int. Ed. Engl*., 1995, **34,** 1364.
135. Carta, G., Rossetto, G., Borella, L., Favretto, D. and Traldi, P., *Rapid Commun. Mass Spectrom*., 1997, **11,** 1315.

136. Favaro, S., Pandolfo, L. and Traldi, P., *Rapid Commun. Mass Spectrom.*, 1997, **11,** 1859.
137. Colton, R., Traeger, J. C. and Harvey, J., *Org. Mass Spectrom.*, 1992, **27,** 1030.
138. D'Agostino, A., Colton, R., Traeger, J. C. and Canty, A. J., *Eur. Mass Spectrom.*, 1996, **2,** 273.
139. Zaluzec, E. J., Gage, D. A. and Watson, J. T., *J. Am. Soc. Mass Spectrom.*, 1994, **5,** 359.
140. D'Agostino, A., Colton, R. and Traeger, J. C., *Eur. Mass Spectrom.*, 1995, **1,** 243.
141. Bond, A. M., Colton, R., D'Agostino, A., Traeger, J. C., Downard, A. J. and Canty, A. J., *Inorg. Chim. Acta*, 1998, **267,** 281.
142. Bennett, K. L., Carver, J. A., David, D. M., Kane-Maguire, L. A. P. and Sheil, M. M., *J. Coord. Chem.*, 1995, **34,** 351.
143. Wilson, S. R. and Wu, Y., *J. Am. Soc. Mass Spectrom.*, 1993, **4,** 596.
144. Wilson, S. R. and Wu, Y., *J. Am. Chem. Soc.*, 1993, **115,** 10334.
145. Wilson, S. R. and Lu, Q., *Tetrahedron Lett.*, 1993, **34,** 8043.
146. Wilson, S. R. and Wu, Y., *Org. Mass Spectrom.*, 1994, **29,** 186.
147. Anacleto, J. F., Quilliam, M. A., Boyd, R. K., Howard, J. B., Lafleur, A. L. and Yadav, T., *Rapid Commun. Mass Spectrom.*, 1993, **7,** 229.
148. Hiraoka, K., Kudaka, I., Fujimaki, S. and Shinohara, H., *Rapid Commun Mass Spectrom.*, 1992, **6,** 254.
149. Fujimaki, S., Kudaka, I., Sato, T., Hiraoka, K., Shinohara, H., Saito, Y. and Nojima, K., *Rapid Commun. Mass Spectrom.*, 1993, **7,** 1077.
150. Liu, T.-Y., Shiu, L.-L., Luh, T.-Y. and Her, G.-R., *Rapid Commun. Mass Spectrom.*, 1995, **9,** 93.

Pergamon

Polyhedron Vol. 17, Nos. 25, 26, pp. 4315–4326, 1998
© 1998 Elsevier Science Ltd
All rights reserved. Printed in Great Britain
0277–5387/98 $19.00+0.00

PII: S0277–5387(98)00168–5

Synthesis, spectral and electrochemical characteristics of asymmetrical iron(II) tris-dioximates

Yan Z. Voloshin,*[a] Oleg A. Varzatskii,[b] Aleksei V. Palchik,[b] Ernest V. Polshin,[b] Yurii A. Maletin[b] and Nataly G. Strizhakova[b]

[a]Karpov Institute of Physical Chemistry, Moscow 103064, Russia

[b]Institute of General and Inorganic Chemistry, Kiev 252142, Ukraine

(Received 11 November 1997; accepted 21 April 1998)

Abstract—Meridianal- and axial-asymmetrical clathrochelate tris-dioximates of the $FeD_2D'(BF)_2$ and $FeD_3(BX)(Y)$ types (where D,D′ = dioximes dianions, X = C_6H_5, F; Y = BF, B*n*-C_4H_9, $SnCl_3$) have been prepared by a stepwise synthesis from a planar-square macrocyclic precursors in the first case and from a semiclathrochelate compounds immobilized on the sorbent surface in the second one. The composition and structure of the isolated compounds have been established from elemental analysis data, polynuclear NMR, ^{57}Fe Mössbauer and FAB mass spectra. The structure parameters of α-benzyldioximate $FeBd_3(BF)(Bn\text{-}C_4H_9)\cdot C_6H_5CH_3\cdot\frac{1}{2}C_8H_{16}$ (Fe–N distance – 1.89 Å, bite angle – 38.6°, polyhedron distortion angle – 17.9°) were determined by X-ray crystallography. The electrochemical properties of the obtained complexes and their dependence on the nature of a ligand have been determined by cyclic voltammetry. © 1998 Elsevier Science Ltd. All rights reserved

Keywords: cage compounds; ^{57}Fe Mössbauer spectra; electrochemistry; X-ray structure.

INTRODUCTION

In most cases syntheses of macrobicyclic iron(II) tris-dioximates occur via a one-step procedure enabling one to obtain only complexes with identical dioxime fragments and capping groups [1–7]. It is not expedient to utilize mixtures of dioximes or capping agents with similar properties in these processes to produce asymmetrical compounds because of the formation of a mixture of products that is close to a statistical one. The formation of predominantly symmetrical complexes has been observed even when the dioximes and capping agents used differ significantly in their properties. The former case can be accounted for by the difference of non-macrocyclic tris-dioximates, described in [8–12] as first intermediate, stability constants (in case $\beta^{[Fe(H_2D)_3]^{2+}} \gg \beta^{[Fe(H_2D)(H_2D')]^{2+}}$) predominantly formed symmetrical $[Fe(H_2D)_3]^{2+}$ complex capping for different cross-linking agents due to the symmetrical clathrochelate. Similarly, in the second case, when the capping agents display an essentially different activity, a second intermediate, being of a semiclathrochelate nature, will preferably be formed by the strongest of them and will be presumably capped at a statistic ratio, since the second capping is not a rate-controlling step [8–12]. Additionally, a higher crystal lattice energy for symmetrical compounds as compared to that for asymmetrical ones is observed: in most cases clathrochelates are obtained in a solid state in the course of reaction and, therefore, an increase in the crystal lattice energy leads to a shift in equilibrium in the direction of the symmetrical product formation. When asymmetrical dioximes such as phenylglyoxime or methylglyoxime are employed as the starting ligand, a mixture of *fac*- and *mer*-isomers was obtained. However, in some cases one of them was isolated individually [13]. In spite of the fact that clathrochelates are produced by a multistage mechanism through the formation of semiclathrochelate products, the latter have not been isolated because of their lability. At the same time, a

* Author to whom correspondence should be addressed.

directed synthesis of clathrochelates containing difference dioximate fragments and capping agents allows one to produce functionally substituted precursors suitable for further functionalization, as well as to vary rather finely the physico-chemical properties of the products obtained. The present study was undertaken to develop new methods for the synthesis of meridianal- and axial-asymmetrical complexes and to determine their physico-chemical properties.

EXPERIMENTAL

The reagents used, $FeCl_2 \cdot 4H_2O$, $Fe(BF_4)_2 \cdot 6H_2O$, $BF_2 \cdot O(C_2H_5)_2$, $SnBr_4$, sorbents, *n*-butyl and phenylboronic acids, dioximes, bases, as well as organic solvents, were obtained commercially. The starting dioximes designations are shown in Table 1.

The analyses for the carbon, hydrogen and nitrogen content were carried out with a Carlo Erba model 1106 microanalyser. Iron and tin were determined spectrophotometrically.

To take FAB spectra, a high-resolution double-focusing MX-1310 mass-spectrometer (electrostatic and magnetic sectors) was used. The substance to be investigated was dissolved in tricyanoethoxypropane. A sample of 5–10 ml of the solution was bombarded by an argon atom beam with an energy of 3.5 keV. The calibration of the mass number scale in the mass-spectrometer under FAB conditions was performed against the peaks of cluster ions. The analyzer peak resolution under FAB conditions was usually 10,000.

The relative intensities of the isotope peaks of molecular and fragment ions were calculated from the data on the abundance of natural isotopes of all the elements forming a part of these ions. The composition of molecular or fragment ions in the experimental mass spectra is confirmed by comparing the

Table 1. ^{57}Fe Mössbauer spectra parameters (mm/s) of macrobicyclic iron(II) dioximates

Compound	Starting dioxime	IS	QS	φ predicted (deg)
$FeNx_3(BC_6H_5)(BF)$	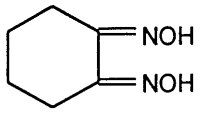 nioxime, H_2Nx	0.32	0.78	12–17
$[FeNx_3(BC_6H_5) \cdot (AlOH)]$	H_2Nx	0.37	0.36	17–22
$((n\text{-}C_4H_9)_4N)[FeNx_3(BC_6H_5)(SnCl_3)]$	H_2Nx	0.33	0.0	27–32
$FeBd_3(BF)(Bn\text{-}C_4H_9)$	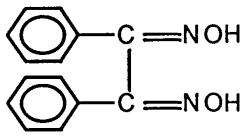 α-benzyldioxime, H_2Bd	0.32	0.28	17.9[a]
$FeDm_3(BC_6H_5)(BF)$	$CH_3—C(=NOH)$ | $CH_3—C(=NOH)$ dimethylglyoxime, H_2Dm	0.32	0.54	17–22
$FeDm_2Bd(BF)_2$	H_2Dm, H_2Bd	0.34	0.47	20–25
$FeBd_2Gm(BF)_2$	H_2Bd, H_2Gm	0.32	0.44	20–25
$FeDm_2Gm(BF)_2$	H_2Dm, H_2Gm	0.33	0.67	14–19
$FeBd_2Dm(BF)_2$	H_2Dm, H_2Bd	0.31	0.37	22–27
$FeBd_2Nx(BF)_2$	H_2Bd, H_2Nx	0.33	0.58	17–22
$FeNx_3(BF)_2$ [4]	H_2Nx	0.33	0.68	14–19
$FeNx_3(BC_6H_5)_2$ [17]	H_2Nx	0.29	0.61	17–22
$(HDEA)_2[FeNx_3(SnCl_3)_2]$ [5, 18]	H_2Nx	0.37	(−)0.20	37.5[a]
$FeGm_3(BF)_2$ [4]	H—C—C(=NOH) | H—C—C(=NOH) glyoxime, H_2Gm	0.31	0.56	17–22
$FeGm_3(Bn\text{-}C_4H_9)_2$ [19]	H_2Gm	0.32	0.84	10.9[a]
$FeDm_3(BF)_2$ [20]	H_2Dm	0.31	0.90	13.3[a]
$FeDm_3(Bn\text{-}C_4H_9)_2$ [17]	H_2Dm	0.33	0.57	17–22
$FeBd_3(BF)_2$ [21]	H_2Bd	0.32	0.25	29.3[a]
$FeBd_3(Bn\text{-}C_4H_9)_2$ [17]	H_2Bd	0.29	0.28	27–33

[a] X-ray structure data.

isotope peak series of these ions with the calculated ones.

The IR spectra of solid samples (CsI and KBr tablets) were recorded in the range from 200 to 4000 cm^{-1} on a Specord M-80 spectrophotometer. The bands were assigned using the previous results. The UV–VIS spectra of solutions in chloroform were recorded in the range from 200 to 800 nm on a Lambda 9 Perkin Elmer spectrophotometer. The individual Gauss components of these spectra were calculated using the SPECTRA program. The ^{1}H, ^{13}C, ^{11}B and ^{119}Sn NMR spectra of the solutions in $CDCl_3$ were recorded on a AC-200 Bruker FT-spectrometer.

^{57}Fe Mössbauer spectra were obtained on YGRS-4M spectrometer with a constant acceleration mode. The spectra were collected on 256 multichannel amplitude analyzer. The isomer shift was measured relatively to sodium nitroprusside and α-Fe foil was used for the velocity scale calibration. ^{57}Co in Cr matrix was used as a source, which was always kept at room temperature. The minimum absorption line width in the spectrum of a standard sample of sodium nitroprusside was 0.24 mm/s.

Cyclic voltammograms were recorded in acetonitrile under argon atmosphere using a PI-50-1 potentiostat coupled with a B7-45 tera-ohmic potentiometer as a current–voltage convertor. Tetrabutylammonium tetrafluoroborate (0.1 M) was used as a supporting electrolyte. A platinum microelectrode of 10 μm in diameter, thoroughly polished and rinsed before measurements, was chosen as a working electrode. A platinum wire was applied as an auxiliary electrode. An SCE reference electrode was connected to the cell via a salt bridge. All potentials were referred to the redox potential of the ferrocene (Fc^{+}/Fc) couple as an internal standard. This potential is at +0.400 V vs SCE under the present experimental conditions.

Syntheses of complexes

$[FeDm_2(BF_2)_2(CH_3CN)_2]$, $[FeBd_2(BF_2)_2(CH_3CN)_2]$ and $[Fe(H_2Nx)_3]Cl_2$ complexes were obtained as described previously [14, 15].

$FeDm_2Bd(BF)_2$ $[FeDm_2(BF_2)_2(CH_3CN)_2]$ (4.64 g, 10 mmol) was dissolved/suspended in dry acetonitrile (30 ml) which had been degassed with argon. Then H_2Bd (4.8 g, 20 mmol) and *N*,*N*-diisopropylethyl amine (3.6 ml, 20 mmol) were added to the stirred reaction mixture. The red–violet solution was heated at 40–50°C for 10 min, then $BF_3 \cdot O(C_2H_5)_2$ (2.8 ml, 22 mmol) and *N*,*N*-diisopropylethyl amine (3.6 ml, 20 mmol) were added dropwise. After a reaction time of 30 min, $BF_3 \cdot (C_2H_5)_2O$ (2.8 ml, 22 mmol) was added, the reaction mixture was heated to 80°C, stirred for 20 min and filtered.

The filtrate was treated in a three-fold volume of water and the product was extracted with chloroform (50 ml). The extract was washed with a 5% NaOH aqueous solution, water and dried with anhydrous $CaCl_2$. After evaporation of chloroform to 20 ml, a solid product was precipitated by addition of a four-fold volume of hexane. The solid was dissolved in a benzene–diethyl ether (5:1) mixture. The solution was dried with CaH_2 and precipitated with hexane. The resulting orange product was additionally purified by reprecipitation from a concentrated chloroform solution with methanol, washed with a small amount of methanol, diethyl ether, hexane and dried *in vacuo*; yield 1.16 g, 20%. Found: C, 45.4; H, 4.0; N, 14.3; Fe, 9.6. Calc. for $C_{22}H_{22}N_6O_6B_2F_2Fe$: C, 45.4; H, 3.8; N, 14.4; Fe, 9.6%.

$FeBd_2Dm(BF)_2$ This complex was synthesized like the previous one except $[FeBd_2(BF)_2(CH_3CN)_2]$ (3.68 g, 5 mmol) and H_2Dm (1.16 g, 10 mmol) were used instead of $[FeDm_2(BF)_2(CH_3CN)_2]$ and H_2Bd; yield 0.88 g, 25%. Found: C, 59.2; H, 3.8; N, 12.0; Fe, 7.8. Calc. for $C_{32}H_{26}N_6O_6B_2F_2Fe$: C, 59.4; H, 3.7; N, 12.0; Fe, 7.9%.

$FeDm_2Gm(BF)_2$ This complex was synthesized like the $FeDm_2Bd(BF)_2$ except H_2Gm (1.8 g, 20 mmol) was used instead of H_2Bd; yield 0.43 g, 10%. Found: C, 27.8; H, 3.2; N, 19.3; Fe, 13.2. Calc. for $C_{10}H_{14}N_6O_6B_2F_2Fe$: C, 27.9; H, 3.3; N, 19.5; Fe, 13.0%.

$FeBd_2Gm(BF)_2$ This complex was synthesized like the $FeBd_2Dm(BF)_2$ except H_2Gm (0.88 g, 10 mmol) was used instead of H_2Dm and the reaction was realized at room temperature; yield 0.47 g, 14%. Found: C, 53.2; H, 3.2; N, 12.4; Fe, 8.2. Calc. for $C_{30}H_{22}N_6O_6B_2F_2Fe$: C, 53.1; H, 3.2; N, 12.4; Fe, 8.2%.

$FeBd_2Nx(BF)_2$ This complex was synthesized like the $FeBd_2Dm(BF)_2$ except H_2Nx (0.71 g, 5 mmol) was used instead H_2Dm and the reaction was realized at room temperature; yield 1.17 g, 32%. Found: C, 55.6; H, 3.7; N, 11.4; Fe, 7.6. Calc. for $C_{34}H_{28}N_6O_6B_2F_2Fe$: C, 55.8; H, 3.8; N, 11.5; Fe, 7.6%.

$FeNx_3(BC_6H_5)(BF)_2$ Preliminarily immobilized semiclathrochelate $FeNx_3(BC_6H_5) \cdot (AlO(OH))n$ complex was obtained. Specially prepared aluminium oxide hydroxide was produced by dissolving an aluminium foil (54 g, 2 mol) in 1.5 l absolute *iso*-propanol after activation with $HgCl_2$. The resulted solution was treated with a water–*iso*-propanol mixture (200 and 250 ml, respectively), stirred for 2 h, filtered and the precipitate was dried *in vacuo* at 150°C. 20 g AlO(OH) obtained as described above was placed under argon stream into a solution of $FeCl_2 \cdot 4H_2O$ (2.4 g, 12 mmol) and H_2Nx (8.5 g, 60 mmol) in 200 ml of acetonitrile. The suspension was stirred for 30 min and the solution of phenylboronic acid (2.44 g, 20 mmol) and dicyclohexyl amine (4 ml, 20 mmol) in 50 ml acetonitrile was added dropwise. The reaction mixture was left overnight at 40°C and filtered. The precipitate was washed with acetonitrile (200 ml), chloroform (250 ml), 150 ml of methylene dichloride with phenylboronic acid (1.22 g, 10 mmol) and extracted with methylene dichloride in a Soxhlet extractor for about 60 h to decolored of extragent. The solid after extraction was dried in air; yield ~25 g.

The product obtained (10 g) was suspended in a mixture of ethyl acetate (20 ml) and $BF_3 \cdot O(C_2H_2)_2$ (5 ml), stirred for 1 h, filtered and the filtrate was washed with aqueous sodium carbonate. The solid was washed with ethyl acetate (20 ml) and this filtrate was added to the first one.

The resulted solution was washed with water, dried with Na_2SO_4 and evaporated to dryness. The product obtained was washed with a small amount of diethyl ether, reprecipitated from methylene dichloride with heptane and dried *in vacuo*; yield 0.1 g, 3.5%. Found: C, 48.5; H, 4.8; N, 14.3; Fe, 9.3. Calc. for $C_{24}H_{29}N_6O_6B_2FFe$: C, 48.6; H, 4.9; N, 14.2; Fe, 9.4%.

The $[FeNx_3(BC_6H_5) \cdot Al(OH)]$ complex was also obtained from the above-mentioned immobilized complex by basic decomposition with NaOH and $((n\text{-}C_4H_9)_4N)OH$ followed by extraction with a benzene–THF (1:2) mixture. The resulted solution was precipitated with heptane and reprecipitated from a THF–diethyl ether (1:3) mixture with heptane and dried *in vacuo*.

The $FeNx_3(BC_6H_5)(BF)$ complex can also be obtained from $FeNx_3(BC_6H_5)_2$. This compound (2 g, 3 mmol) and triethyloxonium fluoroborate (1.84 g, 10 mmol) were suspended/dissolved in 15 ml of methylene dichloride and stirred for 50 h at room temperature. The reaction mixture was washed with aqueous $NaHCO_3$, monoethanolamine, water, dried with K_2CO_3, evaporated to ~10 ml and precipitated with heptane. The solid was separated by chromatography on Silasorb C-300 (eluent: chloroform–*iso*-propanol (100:1)) and the products were isolated ($FeNx_3(BC_6H_5)_2$: 0.3 g, $FeNx_3(BC_6H_5)(BF)$: 0.25 g, $FeNx_3(BF)_2$: 0.23 g).

$FeDm_3(BC_6H_5)(BF)$ This complex was synthesized like the previous one except H_2Dm (7.0 g, 60 mmol) was used instead of nioxime; yield 0.12 g, 5%. Found: C, 42.0; H, 4.3; N, 16.2; Fe, 10.7. Calc. for $C_{18}H_{23}N_6O_6B_2FFe$: C, 41.9; H, 4.5; N, 16.3; Fe, 10.8%.

$FeBd_3(BF)(B\text{n-}C_4H_9)$ The starting $Fe(HBd)_2(H_2Bd)$ complex was obtained by reflux of suspension/solution of $FePy_4Cl_2$ (8.86 g, 20 mmol) and H_2Bd (14.4 g, 60 mmol) in 120 ml ethanol. The reaction mixture was filtered and water (400 ml) was added to the filtrate. After precipitation the solid was filtered, washed with water and aqueous ethanol (20%) and dried *in vacuo*; yield 10.5 g, 70%.

Immobilized semiclathrochelate $FeBd_3(Bn\text{-}C_4H_9) \cdot (AlO(OH))n$ was obtained using AlO(OH) sorbent, prepared as described above.

[Fe(HBd)(H_2Bd)] complex (5.0 g, 6.5 mmol) and the above-mentioned sorbent (10 g) were stirred for 30 min in acetonitrile (100 ml) at 40°C and a solution of *n*-butylboronic acid (0.92 g, 10 mmol) in acetonitrile (25 ml) was added dropwise. The reaction mixture was stirred for 4 h at 50°C, filtered and the solid was treated as described for $FeNx_3(BC_6H_5) \cdot (AlO(OH))n$; yield 13.4 g.

The obtained product (2.5 g) was suspended in chloroform (25 ml) and a solution of $BF_3 \cdot O(C_2H_5)_2$ (5 ml) in acetonitrile (5 ml) was added. The reaction mixture was stirred for 20 min, filtered and the solid was washed with chloroform. The filtrate was added to the first one and the solution was washed with aqueous Na_2CO_3, water, dried with $CaCl_2$, evaporated to ~2 ml and precipitated with heptane. The solid was reprecipitated from chloroform with heptane and dried *in vacuo*; yield 0.37 g, 39%. Found: C, 60.5; H, 4.8; N, 10.4; Fe, 6.8. Calc. for $C_{40}H_{39}N_6O_6B_2FFe$: C, 60.4; H, 4.9; N, 10.6; Fe, 7.0%.

$((n\text{-}C_4H_9)_4N)[FeNx_3(BC_6H_5)(SnCl_3)]$ The solution of $[Fe(H_2Nx)_3]Cl_2$ (4.5 g, 8 mmol), nioxime (0.9 g, 6 mmol) and aluminium oxide (neitral, Brockman I, 45 g) in acetonitrile (150 ml) was stirred for 10 h and filtered. The solid was washed with acetonitrile and dried *in vacuo*. Reflux of the obtained product with phenylboronic acid (3.7 g, 30 mmol) and nioxime (0.4 g, 3 mmol) in benzene (200 ml) for 3 h resulted in a solid, which was filtered, washed with benzene (100 ml), chloroform (300 ml) and acetonitrile (250 ml) and dried *in vacuo*; yield 50 g.

The solid was suspended in an acetonitrile–chloroform (1:1) mixture (300 ml) and a solution of $SnCl_4$ (10 ml, 8.6 mmol) in chloroform (50 ml) was added dropwise under vigorous stirring. After a reaction time of 15 min at room temperature the solution was filtered, washed at 0°C with $((n\text{-}C_4H_9)_4N)Cl$ aqueous solution (10%, 50 ml, two times) and water (100 ml, two times) and dried with anhydrous $MgSO_4$. The mixture of solid $((n\text{-}C_4H_9)_4N)_2[FeNx_3(SnCl_3)_2]$ and $((n\text{-}C_4H_9)_4N)[FeNx_3(BC_6H_5)(SnCl_3)]$ complexes was obtained by precipitation from chloroform extract with heptane.

The precipitate was dissolved in THF and the former complex was precipitated with a two-fold volume of diethyl ether. The filtrate, containing the latter one, was treated with a five-fold volume of pentane. The obtained solid product was reprecipitated, washed with a small amount of diethyl ether, pentane and dried *in vacuo*; yield 0.8 g, 10%. Found: C, 46.8; H, 6.2; N, 9.5; Fe, 5.4; Sn, 11.7. Calc. for $C_{40}H_{65}N_7O_6BCl_3FeSn$: C, 46.5; H, 6.3; N, 9.5; Fe, 5.4; Sn, 11.5%.

RESULTS AND DISCUSSION

Meridianal-asymmetrical iron(II) clathrochelates were obtained by the cycloaddition of α-dioximes (H_2D) to preliminarily synthesized planar-square macrocyclic iron(II) bis-dioximates by the following reaction:

$$[FeD_2(BF_2)_2(CH_3CN)_2] + H_2D' \rightarrow FeD_2D'(BF)_2 + 2HF.$$

It is obvious that this reaction is favored by binding the HF acid released during its course, i.e., in the presence of H^+ and F^- ion acceptors. A weakly coordinating sterically hindered *N,N*-diisopropylethyl amine and boron trifluoride etherate were used as H^+ ion acceptor and electrophilic agent to remove F^-

ions, respectively. In addition, $BF_3 \cdot O(C_2H_5)_2$ has prevented the side elimination reactions of capping boronfluoride groups (Scheme 1).

The above reaction proceeds under more rigid conditions and takes more time than a direct template condensation on the iron(II) ion that can be accounted for by the fact that the overall mechanism of clathrochelate synthesis involves, as mentioned above, an intermediate tris-complex formation step [8–12]. It is evident that macrocyclic planar-square iron(II) bis-dioximates are relatively kinetically stable, and the addition of a third dioxime molecule involves not only detachment of an axially coordinated solvate ligand, but also considerable rearrangements in the nearest coordination environment, which is, naturally, accompanied by an appreciable consumption of energy.

In the absence of F^- ion acceptors, a clathrochelate is not formed and the reaction completes at a stage of *cis*-addition of the protonated dioxime to a planar-square macrocycle. In the absence of the base B with certain dioximes (H_2Nx and H_2Dm), the reaction yields a mixture of symmetrical clathrochelates. In other cases, only a mixture of decomposition products has been formed.

A direct synthesis of axial-asymmetrical tris-dioximate iron(II) clathrochelates via the formation of semiclathrochelate complexes of type II, without application of protecting groups, could not be realized even in a great excess of complex I since a compound of type II readily disproportionates to give I and III (Scheme 2).

We have managed to obtain an axial-asymmetrical $FeNx_3(BC_6H_5)(BF)$ complex, along with the symmetrical products, via a "re-boronating" reaction from the preliminarily formed $FeNx_3(BC_6H_5)_2$ attacked by triethyloxonium fluoroborate, the complex was isolated using chromatography (Scheme 3).

This, however, cannot be a general method. Our attempts to prepare the $FeDm_3(BC_6H_5)(BF)$ complex by an analogous scheme have not been successful: only a symmetrical $FeDm_3(BF)_2$ complex has been formed.

The synthesis of axial-asymmetrical clathrochelate iron(II) dioximates were realized through a stepwise "assembling" on the sorbent surface (Scheme 4).

A chemical immobilization of a nonmacrocyclic tris-complex on the matrix surface has enabled us to protect one of its two triangular planes formed by oxime groups (Ia) and to obtain the immobilized semiclathrochelates via capping by Lewis acids. The desorption of these semiclathrochelates (IIa) with the help of another capping agent leads to the formation of asymmetrical clathrochelate (IIIa).

The success of the synthesis carried out by this procedure is governed by a sorbent aptitude for a specific binding of the starting tris-complex (Ia) and the subsequent desorption of a semiclathrochelate (IIa) affected by a capping agents.

We have examined more than ten sorbents based on aluminium, titanium, silicon oxides and hydroxides. Different sorbents, based on silicon dioxide, adsorb nonmacrocyclic iron(II) tris-dioximates yielding complexes of type Ia which, after the first capping, are

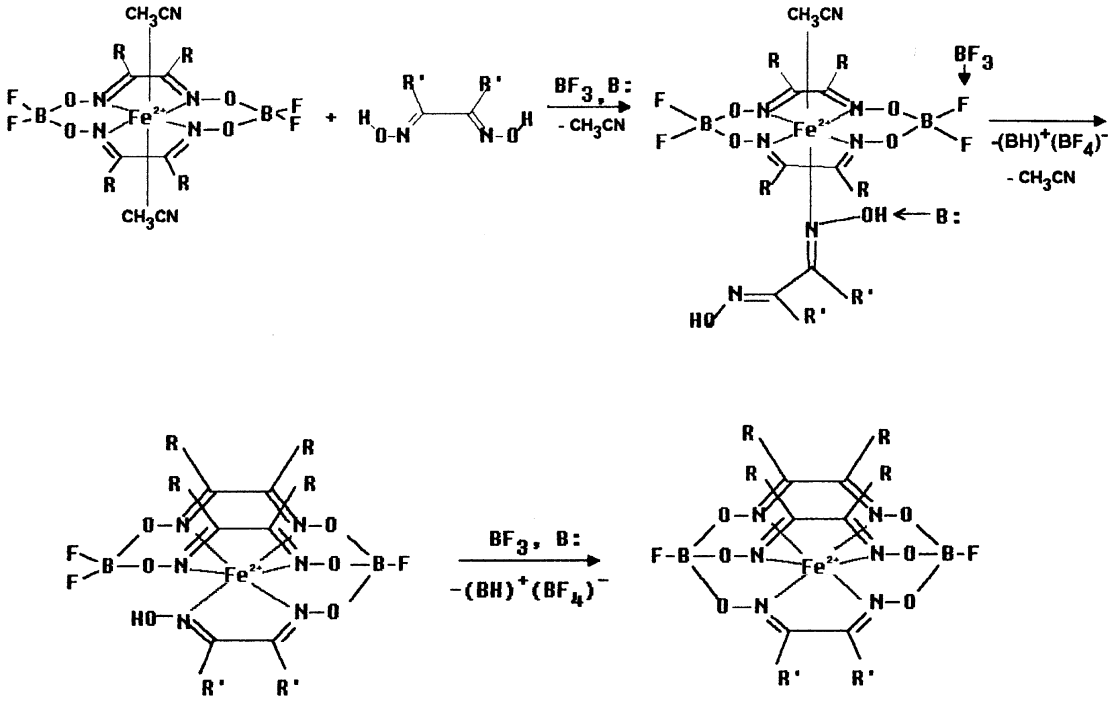

Scheme 1.

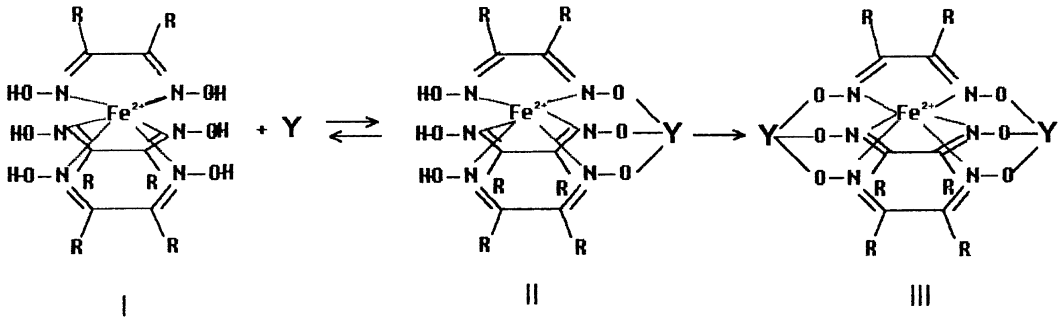

Scheme 2.

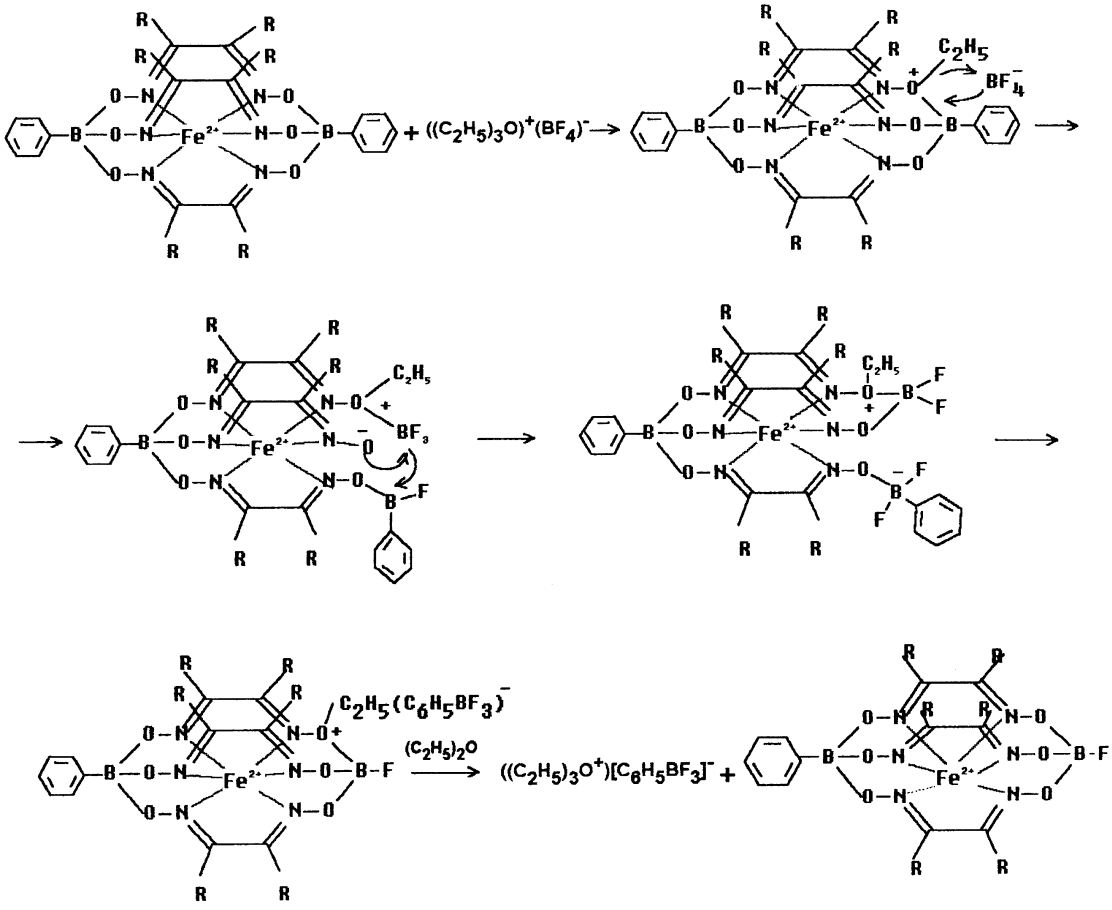

Scheme 3.

desorbed by $BF_3 \cdot O(C_2H_5)_2$ to give clathrochelates of type IIIa. However, they display a low sorbtion capacity towards Ia. With silicon(IV) hydroxide, obtained by hydrolysis of silicon(IV) tetraethoxyde, no compounds of type IIa have been formed. The titanium(IV) hydroxide resulted from hydrolysis of titanium(IV) tetrabutoxyde exhibits a very high sorption capacity towards Ia. The latter is, however, apt to desorption to give IIIa, when treated with capping agents.

Aluminium(III) oxides show results depending, to a great extent, on the method of sorbents formation and treatment. As a whole, however, the degrees of both desorption and purity of the formed product IIIa

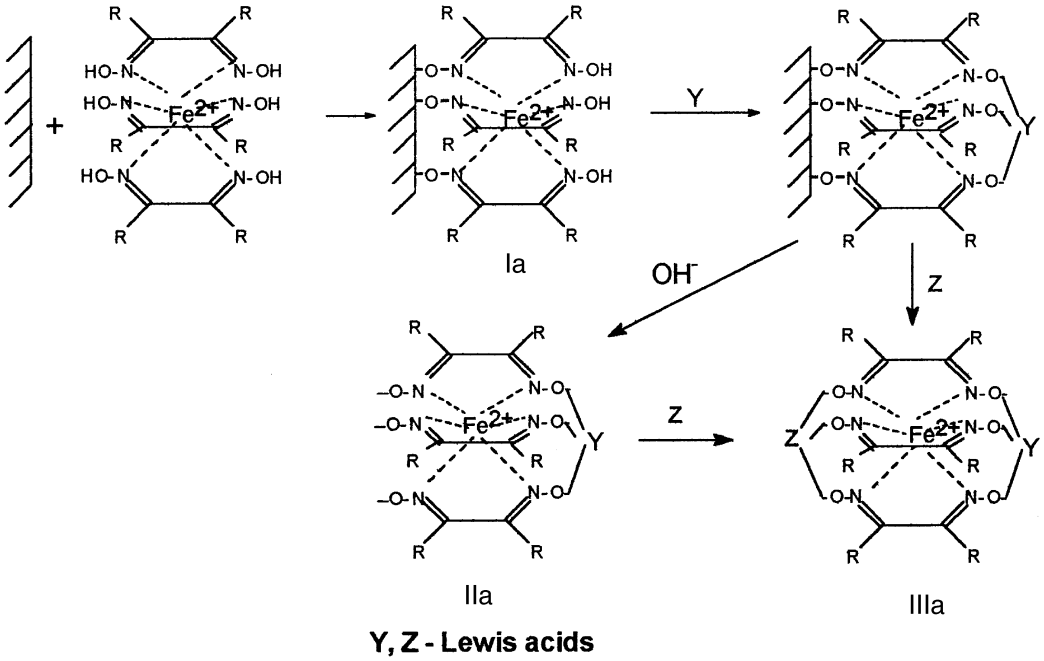

Scheme 4.

are low. The aluminium(III) hydroxide resulted from corrosion of amalgamated aluminium does not tend to the formation of complexes of type IIa.

The best results were obtained with aluminium hydroxide resulted from hydrolysis of aluminium(III) *iso*-propylate. A high sorption capacity (*ca.* 10%) of compounds Ia, a high degree of desorption of complexes IIa and the purity of clathrochelates IIIa formed make aluminium(III) hydroxide the most suitable agent for the synthesis of targeted compounds.

A hydrolytic decomposition of the immobilized nioximate $FeNx_3(BC_6H_5)\cdot(AlO(OH))n$ semi-clathrochelate by a mixture of aqueous NaOH and $((n\text{-}C_4H_9)_4N)OH$ solutions enables one to isolate the product having a hypothetical composition as $[FeNx_3(BC_6H_5)\cdot(AlOH)]$ detectable in FAB mass spectrum, and to obtain clathrochelates quantitatively by reactions with Lewis acids. Unfortunately, we failed to isolate and characterize this product as a pure one with no admixtures because it readily disproportionates and oxidizes.

For all synthesized compounds (except the mixed borontin-containing one) the most intensive $[M+H^+]^+$ molecular ions were detected in FAB mass spectra.

The main spectral parameters of the synthesized clathrochelates are typical for clathrochelate iron(II) tris-dioximates [4, 5]. The isomer shift (IS) values in ^{57}Fe Mossbauer spectra (Table 1), which is determinated by the s-electron density on the iron nucleus, are characteristic for low-spin iron(II) complexes and markedly lower than those for analogous non-macrocyclic tris-dioximates. This phenomenon reflects a so-called "macrocyclic" effect of ligand field increase upon formation of a clathrochelate structure [4].

A quadrupole splitting (QS) in the ^{57}Fe Mossbauer spectra, which characterize the electric field gradient on the iron nucleus, characterizes a twist angle φ of a coordination polyhedron intermediate between a trigonal prism (TP, $\varphi = 0^\circ$, QS $\sim +1$ mm/s) and a trigonal antiprism (TAP, $\varphi = 60^\circ$, QS ~ -0.3 mm/s). The φ value for each complex may be predicted with the help of a correlation curve "QS vs φ" proposed in [4] or calculated from a new version of the partial quadrupole splitting concept [16].

In the clathrochelate ligand field, binding t_{2g}-level of iron(II) with an electronic d^6 configuration splits into e_1 and a_1 levels. In case of TP geometry, the energy of the e_1 level is higher than that of a_1 and the QS sign is positive. For TAP geometry, e_1 is lower in energy than a_1 and the QS sign is negative. The inversion of these levels takes place at $\varphi \approx 30^\circ$. All boron-containing macrobicyclic tris-dioximates of known structure have a TP geometry [16] and, hence, a positive QS value. There are good reasons to believe that the QS in the synthesized boron-containing complexes has also a positive sign. This fact is confirmed by an appreciable QS absolute value in the majority of the synthesized compounds and allows one to predict the φ values listed in Table 1. The QS values for meridianal-asymmetrical clathrochelates are intermediate between those for the corresponding symmetrical complexes of the known structure.

The introduction of some "new" dioximate frag-

ments into the clathrochelate cage, as a rule, exerts much more on the QS and φ values than in the case when a second such fragment is introduced. The above statements are clearly shown for α-benzydioxime in Table 2.

A similar phenomenon was observed upon introduction of glyoximate and nioximate fragments into the clathrochelate framework instead of α-benzyldioximate and dimethylglyoximate ones.

For axial-asymmetrical complexes, just like for symmetrical boron-containing iron(II) tris-dioximates [4, 16], distinct dependencies of QS and φ values on the nature of a substituent at the boron atom have been obtained.* The QS value in a mixed borontin-containing clathrochelate is equal to zero which is in agreement with the above statements too: the QS value in the corresponding trigonal-prismatic boron-containing $FeNx_3(BC_6H_5)_2$ complex has a positive sign, while the corresponding trigonal-antiprismatic tin-containing clathrochelate, according to the data reported in [5, 18], is characterized by a negative QS value. A superposition of these two contributions gives a twist angle φ close to 30° and, hence, the QS value is zero.

The UV–VIS spectra for synthesized meridianal-asymmetrical compounds in solution indicate a more complex chromophore system than that of symmetrical clathrochelates, while the spectra for boron-containing axial-asymmetrical compounds closely resemble those of the corresponding symmetrical compounds. It should be noted that the UV–VIS spectra for the latter with the same dioxime and different boron-containing capping fragments are practically identical [4, 17]. The spectrum for a mixed borontin-containing $((n\text{-}C_4H_9)_4N)[FeNx_3(BC_6H_5)(SnCl_3)]$ clathrochelate alone essentially differs from that for the $FeNx_3(BC_6H_5)_2$ complex: apart from a singlet band about 460 nm characteristic for boron-containing compounds, a more intense band appears about 500 nm detectable in the UV–VIS spectrum for a tin-chloride tris-dioximate $[FeNx_3(SnCl_3)_2]^{2-}$ dianion. The intensities of these bands are redistributed (Table 3).

An analogous phenomenon was also observed in the spectra of some meridianal-asymmetrical clathrochelates ($FeDm_2Bd(BF)_2$, $FeBd_2Dm_3(BF)_2$ and $FeBd_2Nx_2(BF)_2$). The intense $Md \rightarrow L\pi^*$ charge transfer band in the UV–VIS spectra of these compounds proved to be a superposition of two bands with maxima slightly shifted to the long-wavelength range as compared to the corresponding symmetrical complexes ($(FeDm_3(BF)_2$, $FeBd_3(BF)_2$ and $FeNx_3(BF)_2$), but at an unusual and unexpected ratio of the intensities of these bands takes place.

The UV–VIS spectrum for the $FeBd_2Gm(BF)_2$ complex proved also to be quite unexpected since it contains only one band with the intermediate value of $\lambda_{max} = 464$ nm, rather than two bands at approximately 440 and 480 nm. With this complex, maximal tension in π-systems of different dioxime fragments is presumably observed. Since UV–VIS spectral characteristics of $FeDm_3(BF)_2$ and $FeGm_3(BF)_2$ complexes are identical in the visible part, the charge transfer band in the spectrum for an asymmetrical $FeDm_2Gm(BF)_2$ clathrochelate is nearly the same as that for the first two complexes. In this case the band positions of intraligand π–π^* transitions differ from that for symmetrical compounds.

The asymmetry of the synthesized complexes manifests itself in their IR and NMR spectra (Tables 3 and 4). The C=N and N–O stretching vibrations in the dioxime fragments of meridianal-asymmetrical clathrochelates and in the mixed borontin-containing axial-asymmetrical complex proved to be the most sensitive ones. These vibrations may be assigned to the corresponding dioximate groups or their fragments bound to a certain type of an capping groups. In particular, the stretching vibrations of the C=N band in the spectrum of the $FeDm_2Gm(BF)_2$ complex are a superposition of two signals: one about 1560 cm^{-1}, which may be assigned to a glyoximate fragment (for the $FeGm_3(BF)_2$ clathrochelate, it is detected at 1559 cm^{-1}) and at 1583 cm^{-1}, which may be assigned to dimethylglyoximate fragments (for the $FeDm_3(BF)_2$ clathrochelate, it is detected at 1585 cm^{-1}). The same vibration in the IR spectrum

---

* After sending this paper to the Editor the structure of one axial-asymmetrical complex (Fig. 1) was solved [20]. Single crystals of the $FeBd_3(BF)(Bn\text{-}C_4H_9)\cdot C_6H_5CH_3\cdot\frac{1}{2}C_8H_{16}$ complex were obtained by slow evaporation of the saturated solution in a toluene–cyclooctane (1:3) mixture for several weeks. Due to the partial decay of the sample it turned out to be impossible to get a larger data set. Moreover one of the phenyl rings is disordered, the rest were refined in a "rigid-body" approximation. However, the structure is the first example of asymmetric clathrochelates and the data obtained allow to analyze the coordination environment of the central atom. $C_{57}H_{55}B_2FFeN_6O_6$, crystal size $0.36\times0.28\times0.22$ mm, $M = 1015.74$, triclinic, space group $P\bar{1}$, $a = 10.852(2)$, $b = 14.071(3)$, $c = 17.050(3)$ Å, $\alpha = 87.63(3)^\circ$, $\beta = 87.46(3)^\circ$, $\gamma = 80.20(3)^\circ$, $U = 2561.5(9)$ Å^3, $Z = 2$, $D_c = 1.112$ g cm^{-3}, $\mu = 0.345$ mm^{-1}, $F(000) = 1020.2892$ independent reflections were collected at 293 K on a CAD4 diffractometer using Mo-Kα radiation ($\lambda = 0.71073$ Å) with $\theta/2\theta$ scans ($1.86^\circ < \theta < 19.98^\circ$). The structure was solved by the heavy-atom method, refinement was made by a full-matrix least squares an F^2 for all data with anisotropic displacement parameters for non-hydrogen atoms and isotropic for hydrogen atoms; goodness-of-fit = 1.078, final R indices ($I > 2\sigma(I)$) $R1 = 0.0792$, $wR2 = 0.2114$, $w^{-1} = \sigma^2(F_o^2) + (0.152P)^2 + 16.974P$, $P = (F_o^2 + 2F_c^2)/3$. The main parameters of the iron(II) coordination polyhedron (Fe–N distance is 1.89 Å and N–Fe–N bite (chelate) angle is 39.5°) are characteristic for macrobicyclic iron(II) tris-dioximates. The smaller distortion angle value ($\varphi = 17.9^\circ$) than estimated from ^{57}Fe Mössbauer parameters (Table 1, for analogous $FeBd_3(BF)_2$ complex with similar QS value distortion angle significantly higher, $\varphi = 29.3^\circ$) accounted for the electron–donor effect of *n*-butyl substituent at boron atom rather than an electron-acceptor effect of the fluorine substituent.

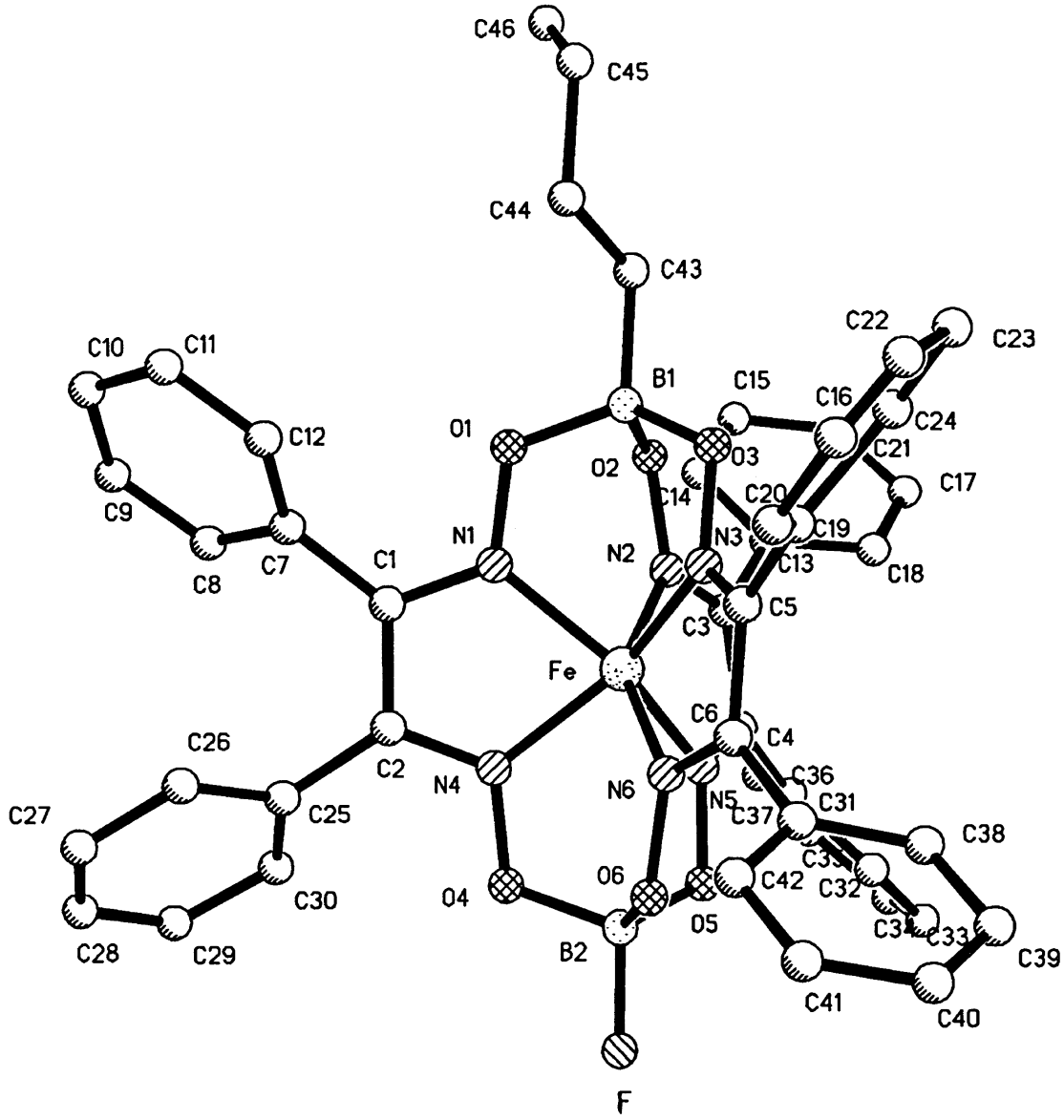

Fig. 1. Molecular structure of the $FeBd_3(BF)(Bn\text{-}C_4H_9)$ complex. Hydrogen atoms are omitted and one of the two disordered phenyl groups C(19)–C(24) are shown.

Table 2.

	$FeDm_3(BF)_2$	$FeDm_2Bd(BF)_2$	$FeDmBd_2(BF)_2$	$FeBd_3(BF)_2$
QS (mm/s)	0.90	0.47	0.37	0.25
ΔQS (mm/s)	0.22 (increment Dm→Bd)	0.43	0.10	0.12
φ (deg)	13.3	20–25	22–27	29.3

for the mixed borontin-containing compound appears in the form of a band at 1565 cm^{-1} (for the $(HDEA)_2[FeNx_3(SnCl_3)_2]$ complex $\nu(C{=}N) = 1568$ cm^{-1} [5]) and a band at 1573 cm^{-1} (for the $FeNx_3(BC_6H_5)_2$ complex $\nu(C{=}N) = 1580$ cm^{-1} [17]), which can be attributed to the oxime fragments bound to

Table 3. IR (cm^{-1}) and UV–VIS spectra parameters of macrobicyclic iron(II) dioximates

Compound	ν(C=N)	ν(N–O)	ν(B–O)	λ (nm) ($\varepsilon \times 10^3\,mol^{-1}1\,cm^{-1}$)
$FeNx_3(BC_6H_5)(BF)$	1580	958, 1061	1194m	278(7.4), 243(2.4), 352(1.7), 447(16)
$FeDm_3(BC_6H_5)(BF)$	1577m	933, 940, 1093	1197m	226(11), 243(3.7), 266(6.8), 307(2.1), 440(14)
$FeBd_3(BF)(Bn\text{-}C_4H_9)$	1583m	932, 941, 1062	1205m	264(31), 292(17), 321(3.9), 417(4.1), 481(29)
$((n\text{-}C_4H_9)_4N)[FeNx_3(BC_6H_5)(SnCl_3)]$	1565, 1573	957, 1050, 1056	1196m 316 ($SnCl_3$)	284(12), 325(3.7), 358(1.3), 463(3.9), 497(7.4)
$FeDm_2Bd(BF)_2$	1582m	932, 950, 1052m, 1107	1196m	262(12), 283(15), 369(2.5), 454(12), 493(10)
$FeBd_2Dm(BF)_2$	1583, 1602	930, 943, 1061, 1080sh	1197m	260(47), 289(18), 298(4.6), 455(18), 492(13)
$FeBd_2Nx(BF)_2$	1582, 1588	933, 955, 1060,	1197m	258(26), 290(16), 310(4.2), 459(19), 493(12)
$FeDm_2Gm(BF)_2$	1560sh, 1583	930sh, 946, 1085m	1190m	260(10), 342(2.0), 441(14)
$FeBd_2Gm(BF)_2$	1562, 1587	731, 945, 1063, 1084		256(35), 281(7.6), 374(3.9), 464(23)
$FeNx_3(BOH)_2$ [4]	1584	965, 1070	1190m	276(5.6), 297(2.2), 406(3.3), 446(15)
$FeBd_3(BF)_2$ [4]	1582	946, 1065	1212m	257(38), 290(7.2), 408(4.2), 479(23)
$FeDm_3(BF)_2$ [4]	1585	949, 1094	1194m	266(6.0), 391(2.3), 440(15)
$FeGm_3(Bn\text{-}C_4H_9)_2$ [19]	1559	945, 1097	1207m	287(8.2), 297(4.0), 394(4.3), 439(13)
$(HDEA)_2[FeNx_3(SnCl_3)_2]$ [5]	1568	968, 1046	310 ($SnCl_3$)	298(17), 479(7.2), 558(6.2)

tin- and boron-containing capping fragments, respectively. The IR spectrum obtained for the later clathrochelate also clearly shows intense characteristic bands of stretching vibrations for both capping fragments (ν(B–O) at approximately 1200 and ν(Sn–Cl) at approximately 320 cm^{-1} [4, 5]). It should also be stressed that for a distorted TAP α-benzyldioximate $FeBd_3(BF)_2$, the ν(B–O) bands have been observed at a higher frequency (1212 cm^{-1}) than for its meridianal-asymmetrical derivatives (for $FeBd_2Dm(BF)_2$ and $FeDm_2Bd(BF)_2$ complexes ν(B–O) = 1197 and 1196 cm^{-1}, respectively) with a geometry close to TP (see above). For the trigonal-prismatic $FeDm_3(BF)_2$ complex this band was detected at 1194 cm^{-1} [4].

The use of the polynuclear NMR spectroscopy has allowed us to confirm the composition of the asymmetrical clathrochelates obtained with the help of the integral intensity ratios of the signals in the ^1H NMR spectra for the protons in the dioxime fragments, substituents at the boron atom and the tetrabutylammonium cation (for the mixed borontin-containing compound). The spectrum for the axial-asymmetrical $FeDm_3(BC_6H_5)(BF)$ dimethylglyoximate also reveals the nonequivalence of methyl substituents. The nonequivalence of dioximate ring fragments in axial-asymmetrical clathrochelates is still more pronounced in the $^{13}C\{^1H\}$ NMR spectra (Table 4). The ^{11}B NMR spectra for these complexes (except for the mixed borontin-containing clathrochelate) reveal signals for the both caps: a broadened singlet of alkyl- or arylborate and a doublet of boronfluoride tetrahedral (judging from the $\delta^{11}B$ value) fragments. The value of a spin–spin coupling constant ($J^{11}B$–^{19}F is approximately 15 Hz) indicates a high symmetry for the BO_3F fragment. The same symmetry of capping boronfluoride fragments was detected in meridianal-asymmetrical clathrochelates (Table 4). In the ^{119}Sn NMR spectrum for the mixed compound in solution, an octahedral SnO_3CI_3 fragment manifests itself as a singlet ($\delta^{119}Sn = -660$ ppm) which is slightly different from the chemical shift value in the case of a symmetrical $[FeNx_3(SnCl_3)_2]^{2-}$ dianion ($\delta^{119}Sn = -640$ ppm).

The above mentioned nonadditivity effect of the introduction of α-benzyldioximate fragments instead of dimethyldioximate ones in the series of ^1H NMR spectral characteristics of meridianal-asymmetrical complexes with α-benzyldioxime and dimethylglyoxime was clearly observed: the introduction of the first fragment increases chemical shifts in the methyl protons by approximately 0.2 ppm, while the appearance of the second diphenyl chelate ring only by 0.06 ppm (Table 4).

The cyclic voltammograms of synthesized iron(II) clathrochelates demonstrate the quasi-reversible waves assigned to Fe^{2+}/Fe^{3+} couple in the anodic range [22]. The position and shape of the waves do not practically depend on the scan rate within the

Table 4. NMR (^{1}H, ^{13}C{^{1}H}, ^{11}B) spectra of macrobicyclic iron(II) dioximates

Compound	^{1}H relative TMS (ppm)		^{13}C relative TMS (ppm)			^{11}B rel. $NaB(C_6H_5)_4$ (^{119}Sn rel. $Sn(CH_3)_4$)
	$\delta(R_1$ [a])	$\delta(R_2$ [a])	$\delta(R_1$ [a])	$\delta(R_2$ [a])	δ(C=N)	
$FeNx_3(BC_6H_5)(BF)$	1.79m	2.92m	21.5, 21.6	26.1, 26.2	151.7, 151.8	7.9 (BF, $J^{11}B-^{19}F=14$ Hz), 9.2 (BC_6H_5)
$FeDm_3(BC_6H_5)(BF)$	2.45	2.46	13.35	13.50	151.9, 152.7	8.2 (BF, $J^{11}B-^{19}F=14$ Hz), 9.7(BC_6H_5)
$FeBd_3(BF)(Bn\text{-}C_4H_9)$	7.27m, 7.42m		127.6, 129.4, 130.7	127.8, 129.7, 130.9	154.9, 156.4	7.6 (BF, $J^{11}B-^{19}F=15$ Hz), 9.8 ($Bn\text{-}C_4H_9$)
$((n\text{-}C_4H_9)_4N)[FeNx_3(BC_6H_5)(SnCl_3)]$	1.70m	3.01m	21.2, 21.3	25.7, 25.9	154.1, 155.1	15.9 (BC_6H_5), 660 ($SnCl_3$)
$FeDm_2Bd(BF)_2$	2.46	7.26m	13.6	127.8, 129.6, 130.6	153.7, 153.8	8.5 ($J^{11}B-^{19}F=13.5$ Hz)
$FeBd_2Dm(BF)_2$	2.52	7.28m, 7.35m, 7.38m	13.8	127.8, 129.8, 130.8	154.8, 155.7	
$FeBd_2Nx(BF)_2$	1.87m, 3.02m	7.28m, 7.31m, 7.38m	21.2, 26.5	127.8, 129.8, 130.8	155.2, 155.4	7.9 ($J^{11}B-^{19}F=15.3$ Hz)
$FeDm_2Gm(BF)_2$	2.45	7.75	13.6		140.2, 153.5	
$FeBd_2Gm(BF)_2$	8.00	7.27m, 7.31m, 7.38m	127.9, 130.2, 130.7		142.2, 156.2	
$FeGm_3(BF)_2$ [4]	8.27				145.1	10.3 ($J^{11}B-^{19}F=15.7$ Hz)
$FeNx_3(BF)_2$ [4]	1.74	2.81	20.7, 25.8		152.5	10.4 ($J^{11}B-^{19}F=13.7$ Hz)
$FeDm_3(BF)_2$ [4]	2.26		13.1		153.2	10.4 ($J^{11}B-^{19}F=14.2$ Hz)
$FeBd_3(BF)_2$ [4]	7.37		127.8, 129.6, 138.8		156.6	10.2 ($J^{11}B-^{19}F=11.7$ Hz)

[a] R_1, R_2 are different types of substituents or different fragments of these substituents in the dioxime moieties.

Table 5. Electrochemical characteristics of meridianal- and axial-asymmetrical iron(II) clathrochelates in acetonitrile

Compound	$E_{1/2}$ (mV)[a]	ΔE (mV)[b]
$FeDm_3(BF)_2$	0.785	60
$FeDm_2Bd(BF)_2$	0.850	70
$FeDmBd_2(BF)_2$	0.900	70
$FeBd_3(BF)_2$	0.940	70
$[FeNx_3(SnCl_3)_2]^{2-}$	0.240	120
$[FeNx_3(BC_6H_5)(SnCl_3)]^-$	0.385	65
$FeNx_3(BC_6H_5)_2$	0.635	60
$FeNx_3(BF)(BC_6H_5)$	0.710	85
$FeNx_3(BF)_2$	0.745	80
$FeBd_3(BF)(Bn\text{-}C_4H_9)$	0.880	70
$FeBd_3(Bn\text{-}C_4H_9)_2$	0.760	60
$Fe(HBd)_2(H_2Bd)$	0.140	80

[a] Vs Fc^+/Fc inner standard.
[b] The Tomeš criterion: $\Delta E = E_{3/4} - E_{1/4}$.

interval of 5–100 mV s^{-1} but depend on the substituents in the ligand dioxime fragments and capping groups. Table 5 lists the half-wave oxidation potentials for meridianal-asymmetrical mixed dimethylglyoximate–α-benzyldioximate complexes. A decrease in the electron-donating effect of phenyl groups as compared to methyl groups must lead to the reduction in electron density on the iron atom and shift the oxidation potential to the anode range. As can be seen from Table 5, the observed shifts in the oxidation potential really decrease with increasing the number of α-benzyldioximate fragments in the complex, but there appears a nonadditivity of shifts, which correlates with the ^{57}Fe Mössbauer, UV–VIS and NMR spectroscopic evidences indicating the major changes in the complex structure upon introduction of the first α-benzyldioximate fragment.

Table 5 also represents the results of a cyclic voltammetric study of axial-asymmetrical clathrochelates. In this case, a certain rise in $E_{1/2}$ potential was observed with increasing the inductive Taft constant (δ_I) [23] of the substituent at the boron atom in the n-C_4H_9 (−0.06) < C_6H_5 (0.10) < F (0.52) series.

Tin-containing compounds are also worth to be considered: an appreciable effect of negatively charged SnO_3Cl_3 fragments is evident, though it was not determined experimentally. In this case the appearance of the first substituent with +I-effect has a far greater influence on the magnitude of $E_{1/2}$ than the introduction of the second one (Table 5; for nioxime: $(BC_6H_5)_2 \rightarrow (BC_6H_5)(BF)$ (+0.075 V) $\rightarrow (BF)_2$ (+0.035 V); $(SnCl_3)_2 \rightarrow (SnCl_3)(BC_6H_5)$ (+0.145 V) $\rightarrow (BC_6H_5)_2$ (+0.250 V); for α-benzyldioxime: $(Bn\text{-}C_4H_9)_2 \rightarrow (Bn\text{-}C_4H_9)(BF)$ (+0.080 V) $\rightarrow (BF)_2$ (+0.060 V)).

In the case of meridianal-asymmetrical complexes the nonadditivity of the shifts in the iron oxidation potentials has also been observed in passing from

dimethylglyoximates to α-benzyldioximates $Dm_3 \rightarrow Dm_2Bd$ (+0.065 V)→$DmBd_2$ (+0.050 V)→Bd_3 (+0.040 V).*

Acknowledgements—Support of the Russian Fund of Fundamental Researches (Grant N96-03-33512a) is gratefully acknowledged.

REFERENCES

1. Jackels, S. C. and Rose, N. J., *Inorg. Chem.*, 1972, **12,** 1232.
2. Johnson, J. N. and Rose, N. J., *Inorg. Synth.*, 1982, **21,** 112.
3. Rai, H. C., Jena, A. K. and Sahoo, B., *Inorg. Chim. Acta*, 1979, **35,** 29.
4. Voloshin, Y. Z., Kostromina, N. A. and Nazarenko, A. Y., *Inorg. Chim. Acta*, 1990, **170,** 181 and references therein.
5. Voloshin, Y. Z., Kostromina, N. A., Nazarenko, A. Y. and Polshin, E. V., *Inorg. Chim. Acta*, 1991, **185,** 83.
6. Voloshin, Y. Z. and Polshin, E. V., *Polyhedron*, 1992, **11,** 457.
7. Voloshin, Y. Z., Nazarenko, A. Y. and Polshin, E. V., *Polish J. Chem.*, 1997, **71,** 428.
8. Voloshin, Y. Z., Kostromina, N. A., Nazarenko, A. Y., Polshin, E. V. and Tyukhtenko, S. I., *Theor. Exp. Khim.*, 1989, **25,** 322.
9. Voloshin, Y. Z., Kostromina, N. A. and Nazarenko, A. Y., *Ukr. Khim. Zh.*, 1993, **59,** 451.
10. Voloshin, Y. Z. and Noskov, Y. G., *Ukr. Khim. Zh.*, 1993, **59,** 347.
11. Voloshin, Y. Z., Noskov, Y. G., Terekhova, M. I. and Kron, T. E., *Ukr. Khim. Zh.*, 1993, **59,** 231.
12. Voloshin, Y. Z., Noskov, Y. G., Terekhova, M. I. and Kron, T. E., *Polish J. Chem.*, 1996, **70,** 1229.
13. Zavodnik, V. E., Belsky, V. K., Voloshin, Y. Z. and Varzatsky, O. A., *J. Coord. Chem.*, 1993, **23,** 97.
14. Thompson, D. W. and Stynes, D. V., *Inorg. Chem.*, 1990, **29,** 3815.
15. Turta, K. I., Stukan, R. A., Bulgak, I. I., Batyr, L. G. and Ozol, L. D., *Koord. Khim.*, 1978, **4,** 1391.
16. Nazarenko, A. Y., Polshin, E. V. and Voloshin, Y. Z., *Mendeleev Commun.*, 1993, 45.
17. Voloshin, Y. Z., Dr. Sc. (Prof.) Thesis, Ivanovo, 1993.
18. Lindeman, S. V., Struchkov, Y. T. and Voloshin, Y. Z., *J. Coord. Chem.*, 1993, **28,** 319.
19. Lindeman, S. V., Struchkov, Y. T. and Voloshin, Y. Z., *Polish J. Chem.*, 1993, **67,** 1575.
20. Zavodnik, V. E., unpublished results.
21. Lindeman, S. V., Struchkov, Y. T. and Voloshin, Y. Z., *Inorg. Chim. Acta*, 1991, **184,** 107.
22. Robbins, M. K., Naser, D. W., Heiland, J. L. and Grzybowski, J. J., *Inorg. Chem.*, 1985, **24,** 3381.
23. Gordon, A. T. and Ford, R. A., *The Chemist's Companion*. Wiley Interscience, New York, 1972.

* Complete tables of atomic coordinates, thermal parameters, bond length and angles have been deposited at the Cambridge Crystallographic Data Centre (CCDC) and also are available from Professor Y. Z. Voloshin on request.

Pergamon

Polyhedron Vol. 17, Nos. 25, 26, pp. 4327–4330, 1998
© 1998 Elsevier Science Ltd
All rights reserved. Printed in Great Britain
0277–5387/98 $19.00+0.00

PII: S0277–5387(98)00193–4

The inclusion behavior of benzo-15-crown-5 with hydrated transition metal picrates

Baoming Ji,[a]* Zhixian Zhou,[b] Kuiling Ding[b] and Yanzhong Li[b]

[a]Department of Chemistry, Luoyang Teacher's College, Luoyang 471022, People's Republic of China

[b]Department of Chemistry, Zhengzhou University, Zhengzhou 450052, People's Republic of China

(Received 11 March 1998; accepted 7 May 1998)

Abstract—Six kinds of benzo-15-crown-5 (L) adducts having the stoichiometric formula $M(Pic)_2 \cdot L \cdot xH_2O$ (M = Mn, Cu, $x = 2$; M = Co, Ni, Zn, Cd, $x = 4$; Pic means picrate anion) have been synthesized and characterized by EA, IR, UV and molar conductance. The X-ray crystal structural analysis of the benzo-15-crown-5 adduct with hydrated copper(II) picrate revealed that the benzo-15-crown-5 molecule virtually acts as a second-sphere ligand, which associates with the copper(II) ion by hydrogen bonding of the coordinating water molecule. By the comparison of the IR, UV spectra and molar conductance of the new adducts prepared, it can be deduced that the other adducts exhibit the similar coordination environment to that of the copper adduct. © 1998 Elsevier Science Ltd. All rights reserved

Keywords: copper(II); picrate; crown ether; X-ray; hydrogen bond; crystal structure.

INTRODUCTION

In the process of the chemical extraction of metal ions with crown ether species, picrate is usually used as a hydrophobic counter-anion to carry the host–guest complexes into the organic phase. The extraction mechanism is closely related to the interaction pattern of the picrate complexes of the metal ions with crown ethers. The establishment of the crystal and molecular structures of these complexes indicated that the alkali and alkaline earth metal ions coordinate directly with the crown ether molecules. Nakagawa et al. demonstrated that the solvent extract abilities of aqueous lanthanide picrates with common crown ethers, such as 15-crown-5, 18-crown-6 and their benzo or cyclohexano derivatives, are much lower than those of aqueous alkali- and alkaline-earth–metal picraes, in spite of the apparent matching of the host cavity size and the diameter of the naked lanthanide cation. The low extract abilities are attributed to incomplete dehydration of trivalent lanthanide ions upon extraction [1, 2, 3]. Recently, in the course of our study on the extraction mechanism of hydrated lanthanide picrates with benzo-15-crown-5 (B15C5), a new series of crystalline extracted complexes of hydrated lanthanide picrates with B15C5 have been obtained. X-ray crystal structural analysis revealed that the B15C5 molecules do not coordinate directly with lanthanide ions, but act as a second-sphere ligand which is associated with lanthanide picrates by hydrogen bonding of coordinating water molecules [4, 5, 6]. These interesting results motivated us to extend our study of the second-sphere coordination of metal crown ether chemistry. In the present paper, we report the synthesis and the characterization of the B15C5 adducts with hydrated transition metal (Mn, Co, Ni, Cu, Zn and Cd) picrates and the crystal structure of the B15C5 adduct with hydrated copper(II) picrate.

EXPERIMENTAL

Reagents

All the chemicals used were of reagent grade. B15C5 was recrystallized from *n*-heptane (m.p 79–80°C). Hydrated transition metal (M = Mn, Co, Ni, Cu, Zn and Cd) picrates were prepared by the reaction of picric acid and the corresponding metal carbonates in good yields. Their general formula was determined to be $M(Pic)_2 \cdot 6H_2O$ by elemental analysis.

*Author to whom correspondence should be addressed.

Chemical and physical measurements

Melting points were measured on a WC-1 apparatus and are uncorrected. Transition metal ion contents were determined by EDTA complexometric titration method. Microanalyses (C, H and N) of the adducts were carried out on a Carlo-Erba 1106 elemental analyzer. The IR spectra were recorded on a Shimadzu 435 spectrometer in KBr pellets. UV–VIS spectra were measured with a Shimadzu UV-2100 spectrometer. Conductivity measurements were performed with a DDS-11A conductometer with acetone as solvent at 25°C.

General procedure for the preparation of the adducts

The adducts were prepared by dissolving a 1:2 molar ratio of hydrated metal picrate and B15C5 in a 2:2:1 (v/v/v) mixed solvent of MeCN, EtOH and H_2O, and the resulting solutions were filtered and allowed to stand over several days until the crystalline products of the adducts were separated. A green single crystal of copper(II) adduct suitable for X-ray structural analysis was obtained by recrystallization using the same mixed solvent.

X-ray crystal structure determination of Cu adduct

All measurements were made on a Rigaku AFC7R diffractometer with graphite monochromated MoKα radiation and a 12 kW rotating anode generator. Cell constants and orientation matrix for data collection were obtained from a least-squares refinement using the setting angles of 19 carefully centered reflections in the range of $23.23 < 2\theta < 26.73°$. The data were corrected for Lorentz and polarization effects and empirical absorption.

The structure was solved by direct methods and expanded using Fourier techniques. The nonhydrogen atoms were refined anisotropically. Hydrogen atoms were included but not refined. All calculations were performed on a Micro VAX3100 computer using teXsan crystallographic software package of Molecular Structure Corporation (1985 and 1992). Neutral atom scattering factors were taken from Cromer and Waber. Atomic coordinates and anisotropic temperature factors for all nonhydrogen atoms were refined by full-matrix least-squares.

The crystallographic data and refinement parameters are listed in Table 1. The selected bond distances and angles are given in Table 2

Table 1. The crystallographic data and refinement parameters

Empirical formula	$C_{26}H_{28}N_6O_{21}Cu$
Formula weight	824.08
Crystal color, habit	green, prismatic
Crystal dimensions (mm)	$0.20 \times 0.20 \times 0.30$ mm
Omega scan peak width at half-height (°)	0.32
a (Å)	13.542(3)
b (Å)	17.034(7)
c (Å)	7.572(1)
α (°)	90.41(2)
β (°)	100.54(1)
γ (°)	108.31(2)
V (Å^{-3})	1626.4(8)
Space group	$p\bar{1}$ ($\#2$)
Z	2
D_{calc} (g cm^{-3})	1.683
$F(000)$	846.00
μ (MoKα) (cm^{-1})	7.74
$2\theta_{max}$ (°)	45.0
Total No. of reflections measured	4160
No. observations [$I > 3.00\ \sigma\ (I)$]	3612
R	0.032
R_w	0.049
Maximum peak (e$^-$Å^{-3})	0.50
Minimum peak (e$^-$Å^{-3})	−0.41

RESULTS AND DISCUSSION

The elemental analysis data as shown in Table 3 indicate that all the adducts prepared have a 1:1 metal picrate–ligand stoichiometry with two or four water molecules, although a mixture of the hydrated transition metal picrate and ligand in a molar ratio of 1:2 was used.

All the adducts possess similar IR spectra, indicating that they have similar coordination pattern. The IR spectra of the adducts revealed that the molecular symmetric vibration absorption of the ligand at *ca.* 980 cm^{-1} disappears and that the ν_{AR-O-C} absorption at 1250 cm^{-1} does not undergo any changes in the adducts. The intensity of the $\nu_{as(C-O-C)}$ absorption at 1120 cm^{-1} for the adducts decreases obviously in comparison with that of the free ligand. These results implied that some interaction between hydrated transition metal picrates and aliphatic ether oxygen atoms rather than the phenolic ether oxygen atoms occurs in the adducts. This conclusion will be further confirmed by the X-ray crystal structure analysis of the copper(II) adduct. The strong absorption bands at 3200–3500 cm^{-1} in the adducts show the presence of the water molecules, which is consistent with that of microanalysis.

The measurements of the UV–VIS spectra of the adducts show that all the adducts possess the similar absorption pattern. The absorption for the picrate anion at 320–330 nm does not show much difference before and after the formation of the adducts. This implies that the coordination pattern of the hydrated transition metal picrates does not undergo a pronounced conformational change after the adducts were formed and as a result the central transition

Table 2. Selected bond lengths and angles for the Cu adduct (estimated standard deviations in parentheses)

	Bond length (Å)		
Cu–O6	1.941(2)	O4–C11	1.433(4)
Cu–O7	1.916(2)	O8–H21	0.92
Cu–O8	1.948(2)	O8–H22	0.95
Cu–O9	1.937(2)	O9–H23	0.81
O1–C1	1.425(4)	O9–H24	0.85
O1–C14	1.411(4)	O4–H21	1.759
O4–C10	1.426(4)	O1–H22	1.921
	Bond angle (°)		
O6–Cu–O7	159.84(8)	O7–Cu–O9	94.04(8)
O6–Cu–O8	91.13(8)	O8–Cu–O9	160.11(9)
O6–Cu–O9	87.40(8)	H21–O8–H22	112.7
O7–Cu–O8	94.13(8)	H23–O9–H24	106.1

Table 3. Synthesis, analytical and molar conductivity data of the adducts

Adduct[a]	Yield (%)	M.p. (°C)	Anal. Found (calcd) (%)				Conductivity[b] ($\Omega^{-1}\,cm^2\,mol^{-1}$)
			C	H	N	M	
$Mn(Pic)_2 \cdot L \cdot 2H_2O$	75	186–188	38.27 (38.29)	3.44 (3.44)	10.38 (10.31)	6.49 (6.74)	35.12 (37.81)
$Co(Pic)_2 \cdot L \cdot 4H_20$	68	164–166	36.45 (36.49)	3.75 (3.74)	9.79 (9.83)	6.49 (6.89)	34.44 (36.48)
$Ni(Pic)_2 \cdot L \cdot 4H_20$	71	142–144	36.53 (36.50)	3.72 (3.74)	9.89 (9.83)	7.01 (6.87)	34.30 (36.62)
$Cu(Pic)_2 \cdot L \cdot 2H_2O$	73	176–178	37.87 (37.86)	3.42 (3.40)	10.18 (10.19)	7.75 (7.72)	15.30 (19.50)
$Zn(Pic)_2 \cdot L \cdot 4H_20$	64	168–170	36.41 (36.22)	3.69 (3.71)	9.83 (9.75)	7.68 (7.59)	20.19 (25.58)
$Cd(Pic)_2 \cdot L \cdot 4H_2O$	65	122–124	34.40 (34.34)	3.51 (3.52)	9.31 (9.25)	12.03 (12.37)	33.43 (36.01)

[a]Pic is picrate anion, L is benzo-15-crown-5.

[b]Measured in 10^{-3}M acetone solutions at 25°C; the conductivity values of corresponding hydrated transition metal picrates are shown in parentheses.

metal ions may not take part in the direct interaction with the oxygen atoms of crown ether.

The molar conductivity values (as shown in Table 3) for these adducts in acetone are in the range of 15.3–35.2 $\Omega^{-1}\,cm^2\,mol^{-1}$, which is the indication of nonelectrolytes for the adducts [7]. Therefore, the transition metal ions in the adducts do not coordinate with the B15C5 molecule directly and no free picrate anion was released, which further supports the results obtained by UV–VIS spectral measurements.

The molecular structure of the Cu adduct is shown in Fig. 1. The adduct consists of two parts, $Cu(Pic)_2 \cdot 2H_2O$ and B15C5. In the former part, two phenolic oxygen atoms (O6 and O7) in picrate anions and two oxygen atoms (O8 and O9) in water molecules coordinate with central Cu cation, and as result, the coordination number for Cu(II) is 4. The bond lengths for Cu–O6, Cu–O7, Cu–O8 and Cu–O9 are 1.941(2), 1.916(2), 1.948(2) and 1.937(2) Å, respectively. The bond angles of 91.13(8), 94.13(8), 94.04(8) and 87.40(8)° for O6–Cu–O8, O8–Cu–O7, O7–Cu–O9 and O9–Cu–O6, respectively, are near to 90° and the bond angles of 159.84(8) and 160.11(9)° for O6–Cu–O7 and O8–Cu–O9 are less than 180°. Therefore, the coordination about the Cu atom can be considered as a distorted square planar. It is obvious that the latter part, B15C5, does not take part in the coordination with the Cu cation directly. However, it was included in the adduct by hydrogen bonding between one of the coordinating water molecules and two aliphabic ether oxygen atoms (O1 and O4). Two phenolic oxygen atoms in B15C5 do not participate in the formation of hydrogen bond, which is consistent with the result obtained by IR determination. The distance for O1–H22 and O4–H21 are 1.921 and 1.759 Å, respectively, which is the indication of the formation of typical hydrogen bonds [8]. Therefore, the water molecule in the adduct virtually acts as a bridge to associate the copper(II) picrate with B15C5 molecule through hydrogen bonding. This kind of inclusion phenomenon of B15C5 is similar to the results of our previous studies on the complexation of hydrated lanthanide picrates with B15C5 [4, 5, 6]. However, it is completely different from the complexation patterns

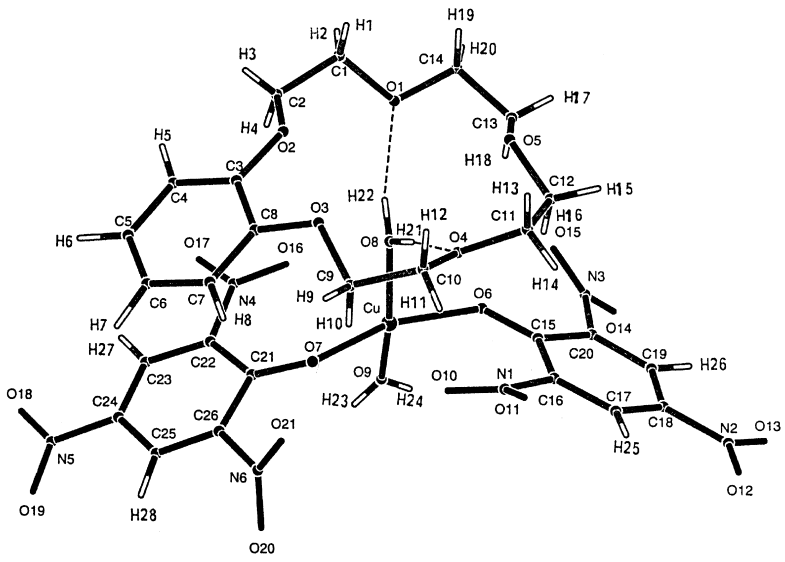

Fig. 1. Molecular structure of $Cu(Pic)_2 \cdot B15C15 \cdot 2H_2O$.

of $CuCl_2$ and hydrated $Cu(ClO_4)_2 \cdot 6H_2O$ with B15C5, where copper(II) cation was included in the cavity of the B15C5 by direct coordination of crown ether oxygen atoms with Cu(II) ion [9, 10].

On the basis of the crystal structure analysis of the copper adduct and the investigation of IR, UV–VIS spectra and molar conductance of the title adducts, it can be concluded that the coordination ability of the water molecules and picrate anion with transition metal ions are stronger than that of B15C5 molecule, and as a result the hydrated transition metal picrate rather than the transition metal crown ether cationic complex is formed predominately. Due in part to the steric hindrance of the bulky picrate anion and coordinating water molecules around the transition metal ion, the cavity of B15C5 molecule can not accommodate the copper(II) or other transition metal ions directly, although the cavity size of the B15C5 molecule is close to the size of these transition metal ions [9, 10]. Consequently, the B15C5 molecule adopts a special association mode in order to combine with them, i.e. the B15C5 molecule virtually acts as a second-sphere ligand which associates with the hydrated transition metal picrates by hydrogen bonding of coordinating water molecule.

REFERENCES

1. Nakagawa, K., Okada, S., Inoue, Y. and Tai, A., Hakushi, T., *Anal. Chem*., 1988, **60,** 2527.
2. Nakagawa, K., Inoue, Y. and Hakushi, T., *J. Chem. Res*., 1990, **348,** 2625.
3. Nakagawa, K., Inoue, Y. and Hakushi, T., *J. Chem. Res*., 1992, **268,** 2122.
4. Zhou, Z. X., Du, C. X., Zhou, Z. H., Yu, K. B. and Zhou, Z. Y., *Yingyong Huaxue*., 1993, **10**(6), 31.
5. Mao, Z. H., Zhou, Z. H., Zhou, H., Zhou, Z. X., Li, J. W. and Du, C. X., *Sichuan Daxue Xuebao* (*Ziran Kexue Ban*), 1995, **32**(3), 319.
6. Zhou, Z. X., Zheng, W. C. and Li, Y. Z., *Polyhedron*, 1996, **15,** 3519.
7. Geary, W. J., *Coord. Chem. Rev*., 1971, **7,** 81.
8. Grossie, D. A., Watson, W. H., Vogtle, F. and Muller, W. M., *Acta Cryst. B*, 1982, **38,** 3157.
9. Sakurai, T., Kobayashi, K., Tsuboyama, S., Kohno, Y., Azuma, N. and Ishizu, K., *Acta Cryst. C*, 1983, **39,** 206.
10. You, X., Li, Z., Yang, X., Li, C. and Wang, D., Huang, J., *Kexue Tongbao*., 1985, **30**(1), 66.

Pergamon

Polyhedron Vol. 17, Nos. 25, 26, pp. 4331–4337, 1998
© 1998 Elsevier Science Ltd
All rights reserved. Printed in Great Britain
PII: S0277-5387(98)00199-5
0277–5387/98 $19.00+0.00

Study of kinetics and mechanism of the acid dissociation of copper(II) complex of novel C-functionalized macrocyclic dioxotetraamines[1]

Huakuan Lin*, Shourong Zhu, Appolin Bave Kondiano, Xuncheng Su, Fuping Kou and Yunti Chen

Department of Chemistry, Nankai University, Tianjin, 300071, People's Republic of China

(Received 25 August 1997; accepted 14 May 1998)

Abstract—The kinetics of the acid dissociation of copper(II) complexes of novel C-functionalized macrocyclic dioxotetraamines has been studied by means of a stopped-flow spectrophotometer. The acid dissociation rate follows the law $V_d = C_{com}kK_1K_2H^2/(1+K_1H+K_1K_2H^2)$. From the experimental facts we have obtained, the dissociation kinetics are interpreted by a mechanism involving the negatively charged carbonyl oxygen of the complex being rapidly protonated in a pre-equilibrium step, the rate-determining step being intramolecular hydrogen (enolic tautomer) migration (to imine nitrogen). The dissociation rate reached a plateau in the strongly acidic solution. By means of temperature coefficient method, ΔH^{ϕ}, ΔS^{ϕ} of the pre-equilibrium step and $\Delta H^{\neq}$, $\Delta S^{\neq}$ of the rate-determining step were obtained. The results of 13-membered macrocyclic dioxotetraamines have been discussed. The influence of the substituents to the acid dissociation rates has also been discussed. The Bronsted type linear free energy relationships do also exist in these C-functionalized dioxotetraamine copper(II) complexes. © 1998 Elsevier Science Ltd. All rights reserved

Keywords: macrocyclic dioxotetraamines; acid dissociation; kinetics; mechanism; copper(II) complex.

INTRODUCTION

Acid-assisted dissociation kinetics of open-chain polyamine complexes has been extensively studied [1–12], and many of these works have been reviewed [11]. Recently, there has been considerable interests in the kinetics and mechanism of the acid dissociation of macrocyclic polyamine complexes [13–18]. Most of the previous work concerns mainly the macrocyclic complex without substituents. In general, due to the thermodynamic and kinetic macrocyclic effect, macrocyclic complexes are substantially thermodynamically stable and kinetically inert, the rates of dissociation of metal complexes with tetraazacycloalkanes are relatively slow. In some instances they are so slow that one can study them even under extreme conditions, such as in 10 M $HClO_4$ [13]. Dioxoteraamine macrocycles are unique metal chelators, their structures bear the dual feature of macrocyclic polyamine and oligopeptides [19–25]. Macrocyclic dioxotetraamine complexes display interesting properties from the point of view of the redox activity and stability. Hay *et al*. [26] described the kinetics of the dissociation of copper(II) and nickel(II) complexes with 1,4,8,11-tetraazacyclotetradecane-5,7-dione(dioxocyclam) in the pH region 4–5, in which the analogous complexes with 14-aneN4(cyclam) give no sign of dissociation. Because of electron withdrawing of the carbonyl group, the decrease of electron density on the nitrogen atom of the amido group reduces the strength of the C–N bond and causes the macrocyclic dioxopolyamine complexes to dissociate easier than the corresponding macrocyclic polyamine complexes. The replacement of amino group by amide can greatly increase the acid-dissociation rate of the complexes [26]. In the study of the complex formation of dioxotetraamine, Kimura [25] considered the existence of non-deprotonated or singly deprotonated copper(II) complex unlikely. That is, the dioxotetraamine dissociates both its amide hydrogen atoms simultaneously when coordinated to a 3d metal ion. By

[1] Project 29671020 supported by National Nature Science Foundation of China.

* Author to whom correspondence should be addressed.

means of pH potential titration and spectrum titration Siegfried and Kaden [27] considered, however, that the existence of a non-deprotonated and singly deprotonated complex is possible. Under conditions of non-release of a hydrogen ion on amido nitrogen the metal ion can still coordinate with the amido nitrogen, but there was no definite experimental evidence indicating it to be true. Recently, Siegfried *et al.* [28] obtained the structure of the monocrystal of copper(II) complex with 1,4,8,11-tetraazacyclo-tetradecane-5-one(oxocyclam), and indicated that there were non-released hydrogen ions in these complexes and the positions of protonation were on the carbonyl oxygen atoms. We have obtained the monocrystal of the copper(II) complex of C-functionalized macrocyclic dioxotetraamines [23] which further indicated that singly deprotonated complex MLH_{-1} does exist in the course of formation of the complex MLH_{-2}. Non-deprotonated copper(II) complexes of dioxotetraamine macrocycles had been prepared [21]. From the above mentioned fact, we believe that when the amido-macrocyclic ligands coordinate with the metal ion, the protons on the amide group can transfer to the carbonyl oxygen atoms first and then dissociate stepwise from the complex. Siegfried and Kaden [27] and Hay *et al.* [26] suggested a different acid dissociation tendency, but there is no evidence to support their mechanism. It stimulates us to further investigate the acid dissociation kinetics and mechanism.

We have reported the kinetics and mechanism of the acid dissociation of copper(II) complexes of 6-(2′-hydroxy-3′,5′-substituted benzyl)-1,4,8,11-tetraazatetradecane-5,7-dione previously [29]. In this paper we further investigate the acid dissociation of copper(II) complexes of 12-(2′-hydroxy-3′,5′-substituted benzyl)-1,4,7,10-tetraazacyclo-tridecane-11,13-dione in order to understand how the ring size influenced the rate of acid dissociation of the complex in C-functionalized macrocyclic dioxotetraamines copper(II) complexes.

EXPERIMENTAL

Reagents

All the reagents used were of reagent grade. KNO_3 and chloroacetic acid were recrystallized before use. Redistilled water was used for preparation of all the solutions. The 12-(2′-hydroxy-3′,5′-substituted benzyl)-1,4,7,10-tetraazacyclotridecane-11,13-dione were prepared according to the methods in Ref. [22] (Scheme 1).

Instructions

Electronic spectra were recorded on a Shimadzu UV-240 spectrophotometer. Stability constants of the macrocyclic dioxotetraamine copper(II) complexes were determined as reported previously [22]. The pH values were measured by means of a Beckman Φ71 pH meter. Kinetic measurement was made by Union Giken RA-401 stopped flow spectrophotometer.

Kinetic measurements

The complex and buffer solutions were prepared and the ion strength of solutions was maintained at $0.1\,mol\,dm^{-3}$, pH values of the solutions were adjusted with $1\,mol\,dm^{-3}$ KOH or HNO_3. Complex solutions were prepared by mixing equimolar quantities of ligand and $Cu(NO_3)_2$, followed by adjustment of pH to 7 with KOH, at which the complex is fully in the form of $[CuH_{-2}L]$. The course of dissociation was followed at their absorption maxima, i.e., 510 nm (L_1), 502 nm (L_2), 498 nm (L_3), 489 nm (L_4), and 520 nm (L_5), respectively. Apparent first order rate constants were obtained with at least 3 half-lives and represent the average of three runs. Reproducibility of the values of k_{obs} was better than $\pm 5\%$.

RESULTS AND DISCUSSION

All these complexes have a d–d absorption band at ~ 500 nm, but the free ligands have no absorption in this region. In acid dissociation measurement, the absorption at 500 nm disappeared without any interference, whereas the hydrogen ion concentration was maintained constant by means of buffer solutions, a first-order reaction with respect to the concentration of the copper(II) complex was observed, that is, the kinetics of the acid dissociation of the copper(II) complexes follow the rate law $V_d = k_{obs}C_{com}$, where C_{com} is the total concentration of the complex and k_{obs} is the pseudo-first-order rate constant. The relationship of

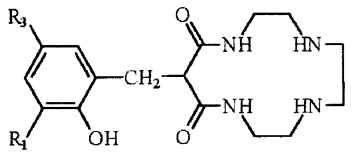

L_1:$R_1 = OCH_3$, $R_2 = H$; L_2:$R_1 = R_2 = H$

L_3:$R_1 = H$, $R_2 = Br$; L_4:$R_1 = R_2 = Br$

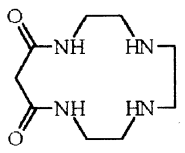

L_5

Scheme 1. Structure of the ligands.

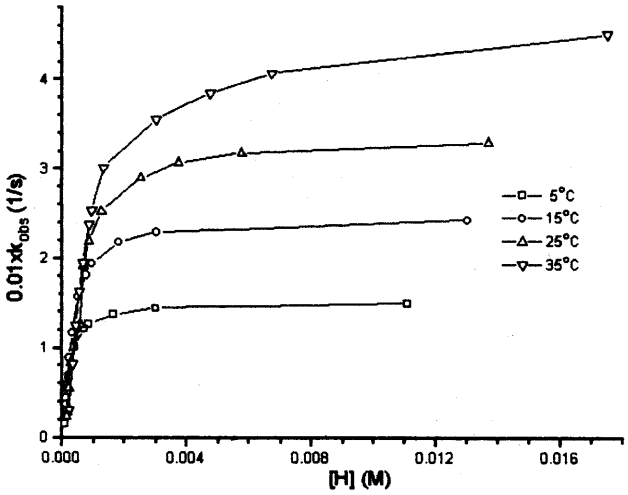

Fig. 1. Plot of acid dissociation apparent constant (k_{obs}) of CuL13(H) complexes; $k_{obs} \sim [H]$.

k_{obs} values vs the hydrogen ion concentration, $[H^+]$, and temperature were plotted in Figs 1 and 2.

From Figs 1 and 2, the same phenomena have been seen with one reported previously [29], we can see that k_{obs} increased rapidly with the increase of $[H^+]$ at low hydrogen concentration, but with further increase of $[H^+]$, k_{obs} increases slowly, until reaching a plateau, i.e., k_{obs} stays unchanged with the increase of $[H^+]$. This work again indicated that the mechanism proposed in a previous paper [29] was reasonable. As yet we have not obtained the crystal structure of the singly-deprotonated 13-membered macrocyclic dioxotetraamine copper(II) complex, but we have reason to believe the protonation of negatively charged amido oxygen atoms of the investigated 13-membered macrocyclic dioxotetraamine copper(II) complex can proceed stepwise. As the rates are very rapid, these processes are considered as pre-equilibrium ones. The third step would be the migration of protons from the amido oxygen to the amido nitrogen with concomitant release of copper(II). This process is the rate-determining step. The fourth step would be very fast protonation of the free ligand obtained in the third step (Scheme 2).

The observed reaction rate is of first-order with respect to the complex concentration C_{com}

$$V_d = k_{obs} C_{com} \tag{1}$$

From the following stoichiometric equation

$$C_{com} = [ML] + [MH_{-1}L] + [MH_{-2}L] \tag{2}$$

we have

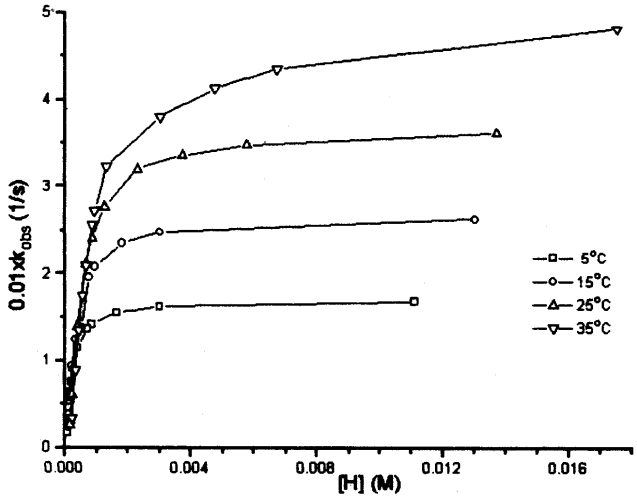

Fig. 2. Plot of acid dissociation apparent constant (k_{obs}) of CuL13(OCH_3) complexes; $k_{obs} \sim [H]$.

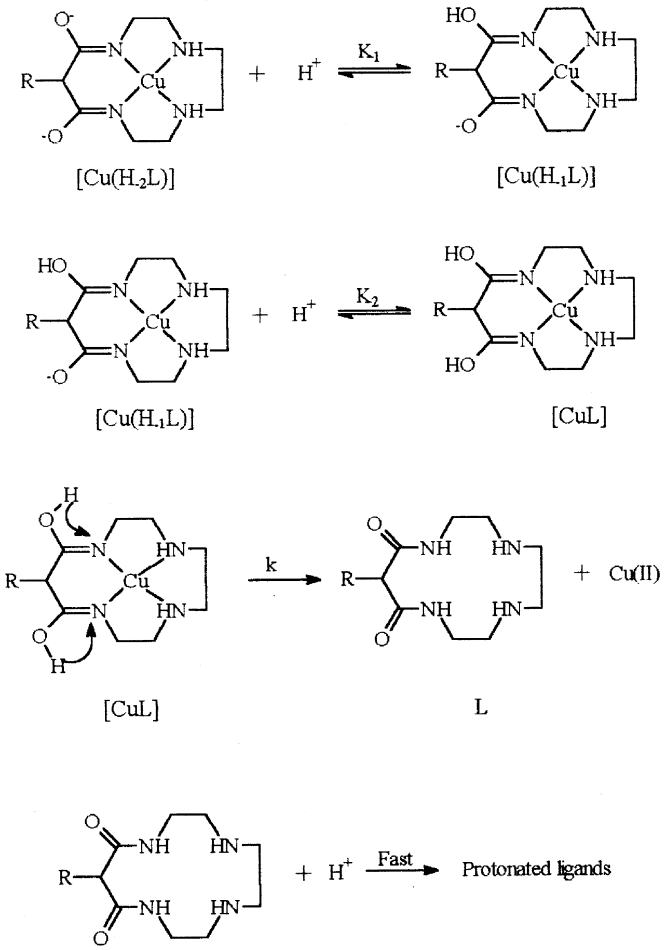

Scheme 2. Proposed acid-dissociation mechanism.

$$C_{com} = [ML](1 + K_1[H] + K_1K_2[H^2])/K_1K_2[H]^2 \quad (3)$$

Accord to the mechanism,

$$V_d = k[ML] = C_{com}kK_1K_2[H]^2/(1 + K_1[H] + K_1K_2[H]^2) \quad (4)$$

therefore

$$k_{obs} = kK_1K_2[H]^2/(1 + K_1[H] + K_1K_2[H]^2) \quad (5)$$

From non-linear least-square fitting of the experimental points using eq. (5), we can obtain the values of κ, K_1 and K_2 which are listed in Tables 1–33, respectively.

From the Eyring equation

$$\ln(k/T) = -\Delta H_m^{\neq}/RT + \Delta S_m^{\neq}/R + \ln(R/N_a h) \quad (6)$$

The activation parameters $\Delta H_m^{\neq}$ and $\Delta S_m^{\neq}$ of the rate-determining step can be obtained.

K_1 and K_2 are equilibrium constants of first and second pre-equilibrium steps, respectively:

$$MH_{-2}L + H = MH_{-1}L, \quad K_1 = [MH_{-1}L]/[MH_{-2}L][H] \quad (7)$$

$$MH_{-1}L + H = ML, \quad K_2 = [ML]/[MH_{-1}L][H] \quad (8)$$

By the following thermodynamic equations:

$$\ln K = -\Delta H_m^{\phi}/RT + \Delta S_m^{\phi}/R \quad (9)$$

The thermodynamic parameters ΔH_m^{ϕ}, ΔS_m^{ϕ} can be obtained.

The activation parameters $\Delta H_m^{\neq}$ and $\Delta S_m^{\neq}$ are listed in Table 1 with the rate-constant k, the thermodynamic parameters ΔH_m^{ϕ} ΔS_m^{ϕ} are also listed in Tables 2–3 with corresponding equilibrium constants, respectively. For comparison, the rate constant k and $\Delta H_m^{\neq}$, $\Delta S_m^{\neq}$ of corresponding 14-membered systems are also listed in Table 1 and the stability constants of binary systems Cu(II)-RTADO-13 [30] and Cu(II)-RTADO-14 [31] are listed in Table 4.

From Table 1 it is seen that the rate constant κ decreases with the change of ligands from $CuH_{-2}L_1$ to $CuH_{-2}L_4$ (the substituents change from CH_3O to

Table 1. The rate constant k and $\Delta H_m^{\neq}$, $\Delta S_m^{\neq}$, $I = 0.1\,\mathrm{mol\,dm^{-3}}$ KNO_3

Complex	5°C	15°C	25°C	35°C	45°C	$\Delta H_m^{\neq}$ ($kJ\,mol^{-1}$)	$\Delta S_m^{\neq}$ ($J\,K^{-1}\,mol^{-1}$)	γ
				13-membered				
$CuH_{-2}L_1$	171.3	268.8	371.3	498.8		-22.78 ± 1.33	-119.4 ± 4.5	-0.9966
$CuH_{-2}L_2$	152.0	247.3	338.1	464.8		-23.76 ± 1.63	-116.8 ± 5.6	-0.9953
$CuH_{-2}L_3$	145.7	229.5	327.0	442.2		-23.88 ± 1.20	-116.8 ± 4.1	-0.9975
$CuH_{-2}L_4$	129.5	219.7	309.0	436.3		-26.04 ± 1.76	-109.9 ± 6.0	-0.9955
$CuH_{-2}L_5$	84.85	168.1	306.4	532.9		-41.16 ± 0.58	-59.3 ± 2.0	-0.9998
				14-membered				
$CuH_{-2}L_1$		8.05	13.89	25.06	43.89	-40.73 ± 1.14	-86.1 ± 3.8	-0.9992
$CuH_{-2}L_2$		9.45	16.75	29.54	49.15	-39.52 ± 0.32	-88.8 ± 1.1	-0.9999
$CuH_{-2}L_3$		6.49	11.74	21.34	37.05	-41.86 ± 0.50	-83.9 ± 1.7	-0.9999
$CuH_{-2}L_4$		5.08	9.47	17.42	32.37	-44.45 ± 0.92	-77.0 ± 3.0	-0.9996
$CuH_{-2}L_5$		11.32	19.54	35.24	56.99	-38.94 ± 0.84	-89.4 ± 2.8	-0.9995

Table 2. The pre-equilibrium constant of first step K_1, ΔH_1^{ϕ} and ΔS_1^{ϕ}, $I = 0.1$

Complex	5°C	15°C	25°C	35°C	ΔH_1^{ϕ} ($kJ\,mol^{-1}$)	ΔS_1^{ϕ} ($J\,K^{-1}\,mol^{-1}$)	γ
$CuH_{-2}L_1$	6227	4340	2731	1775	-30.08 ± 1.59	-35.2 ± 5.5	0.9972
$CuH_{-2}L_2$	6266	4340	2822	1762	-30.12 ± 1.82	-35.3 ± 6.2	0.9964
$CuH_{-2}L_3$	4785	3851	2722	1753	-23.82 ± 3.03	-14.6 ± 10.4	0.9842
$CuH_{-2}L_4$	4630	3571	2604	1733	-23.17 ± 2.17	-12.8 ± 7.4	0.9914
$CuH_{-2}L_5$	5650	7098	2381	1600	-30.78 ± 2.41	-38.4 ± 8.2	0.9939

Table 3. The pre-equilibrium constant of second step K_2, ΔH_2^{ϕ} and ΔS_2^{ϕ}, $I = 0.1$

Complex	5°C	15°C	25°C	35°C	ΔH_1^{ϕ} ($kJ\,mol^{-1}$)	ΔS_1^{ϕ} ($J\,K^{-1}\,mol^{-1}$)	γ
$CuH_{-2}L_1$	5028	4055	1805	1252	-35.39 ± 5.80	-55.5 ± 19.8	0.9742
$CuH_{-2}L_2$	5107	3317	2459	1824	-24.19 ± 1.17	-16.2 ± 4.0	0.9977
$CuH_{-2}L_3$	3719	2625	1910	1161	-27.06 ± 2.50	-28.6 ± 8.5	0.9916
$CuH_{-2}L_4$	2534	2128	1609	1091	-19.89 ± 2.84	-5.8 ± 9.7	0.9802
$CuH_{-2}L_5$	4096	2982	1294	905	-38.18 ± 5.19	-67.5 ± 17.7	0.9820

Table 4. Stability constants of binary systems Cu(II)-RATO-14 and Cu(II)-RTADO-13, $I = 0.1\,\mathrm{mol\,dm^{-3}}$ KNO_3, 25 ± 0.1°C

Ligands		L_1	L_2	L_2	L_4
$\log\beta_{11-2}$	RTADO-14 [31]	2.03	1.83	1.47	1.12
	RTADO-13 [30]	1.57	1.58	1.07	-0.67
$\log\beta_{11-1}$	RTADO-14	10.23	10.02	9.54	9.05
	RTADO-13	7.22	7.01	6.63	4.83
$\log\beta_{11-0}$	RTADO-14	14.35	14.17	13.75	13.33

2Br). That is, values of the rate constant κ decrease with the decrease of base-strength of the macrocyclic dioxotetraamine ligands. The larger the electron density on the nitrogen atoms of amido group of the macrocyclic dioxotetraamine ligands, the faster the intramolecular hydrogen migration. The linear regression of the rate constants $\log\kappa$ to the protonation constant $\log\beta_1$ [$L_1(CH_3O)$ 10.26; $L_2(H)$ 10.01; $L_3(Br)$ 9.78; $L_4(2Br)$ 9.39 [30]] gives the following equations:

$$\log\kappa = 1.898 + 0.06364\log\beta_1,$$

$$(25^\circ\text{ C, except for } CuH_{-2}L_1), \quad \gamma = 1.000 \quad (11)$$

The linear regression of the rate constants $\log k$ to the pre-equilibrium constants $\log K_1$ also gives the following equations:

$$\log k = -1.353 + 1.125\log K_1,$$

$$(25^\circ\text{ C, except for } CuH_{-2}L_1), \quad \gamma = 0.9961 \quad (11)$$

In above two linear relationships $CuH_{-2}L_1$ (CH_3O) point deviates the straight line, i.e. the straight line turns the corner at $CuH_{-2}L_2$ (H) point. It is possible due to the different influence of the electron-drawing group and electron-repelling group to this linear relationship. It shows that Bronsted type linear free energy relationships do exist in these C-functionalized dioxotetraamine copper(II) complexes. From Table 1 it is also seen that the rate constants k of 13-membered systems are larger than those of the 14-membered systems, that is, the acid-dissociation of 13-membered complexes is faster than of the 14-membered complexes. This is because the ring size of the 14-membered macrocyclic dioxotetraamine is larger than that of the 13-membered macrocyclic dioxotetraamine and the cavity of the 14-membered ring fits better with the copper(II) ion than that of the 13-membered ring. The stability of Cu(II) complexes of 14-membered systems is higher than 13-membered systems (see Table 4). Therefore, the rate constants k of acid-dissociation of 13-membered Cu(II) complexes is larger than of 14-membered complexes.

From Tabs. 2–3, it is seen that ΔH_1^ϕ, ΔH_2^ϕ, ΔS_1^ϕ and ΔS_2^ϕ have negative values. It implies that the first and second pre-equilibrium steps are exothermic processes with decrease of entropy. This is due to the fact that the first and second pre-equilibrium steps are the protonation of negatively charged carbonyl oxygens (neutralization reaction). It is also seen that the K values, the equilibrium constants of the pro-equilibrium steps which are determined kinetically, agree better with those obtained by pH titration method.

From the above results, we can also understand that the stability of Cu(II) complexes of macrocyclic dioxotetraamine is smaller than that of the corresponding Cu(II) complexes of macrocyclic tetraamines (saturated and analogs) (see Table 4). This is because the electron withdrawing ability of carbonyl oxygen considerably diminishes the density of the electron cloud on the nitrogen atom of amide and thus reduces the stability of the Cu(II) complexes. Therefore, acid-dissociation of Cu(II) complexes of macrocyclic dioxotetraamines takes place much easier than the saturated analogs. In fact, it is very difficult for the Cu(II) complexes of saturated macrocyclic tetraamine to undergo acid dissociation under the investigated conditions reported in this paper.

REFERENCES

1. Margerum, D. W., Roracacher, D. B. and Clake, F. G., *Inorg. Chem.*, 1963, **2,** 667.
2. Ahmed, A. K. S. and Wilkins, R. G., *J. Chem. Soc.*, 1960, 2901.
3. Melson, G. A. and Wilkins, R. G., *J. Chem. Soc.*, 1962, 2662.
4. Melson, G. A. and Wilkins, R. G., *J. Chem. Soc.*, 1962, 4475.
5. Ahmed, A. K. S. and Wilkins, R. G., *Proc. Chem. Soc.*, 1959, 399.
6. Ahmed, A. K. S. and Wilkins, R. G., *J. Chem. Soc.*, 1959, 3700.
7. Ahmed, A. K. S. and Wilkins, R. G., *J. Chem. Soc.*, 1960, 2859.
8. Childers, R. F. and Wentworth, R. A. D., *Inorg. Chem.*, 1969, **8,** 2218.
9. Weatherburn, D. C., Billo, E. J., Jones, J. P. and Margerum, D. W., *Inorg. Chem.*, 1970, **9,** 1557.
10. Koiski, G. B. and Margerum, D. W., *Inorg. Chem.*, 1969, **8,** 1129.
11. Margerum, D. W., Cayley, G. R., Weatherburn, D. C. and Pagenkopf, G. K., *ACS Monogr.*, 1978, **174,** 1.
12. Read, R. A. and Margerum, D. W., *Inorg. Chem.*, 1981, **20,** 3143.
13. Pondit, A. K., Das, A. K. and Barerjia, D., *Trans. Met. Chem.*, 1988, 437.
14. Chang, C. C. and Chung, C. S., *J. Chem. Soc., Dalton Trans.*, 1991, 1965.
15. Liang, B. F. and Chung, C. S., *Inorg. Chem.*, 1983, **22,** 1017.
16. Liang, B. F. and Chung, C. S., *Inorg. Chem.*, 1981, **20,** 2152.
17. Chen, I. H. and Chung, C. S., *Inorg. Chem.*, 1988, **27,** 1880.
18. Chen, J. W., Wu, D. S. and Chung, C. S., *Inorg. Chem.*, 1986, **25,** 1940.
19. Luo, Q. H., Zhu, S. R., Shen, M. C., Dai, A. B., Liu, A. D., Gu, H. C., Li, F. M. and Di, S. J., *Kexue Tongbao*, 1992, 1288.
20. Shen, M. C., Luo, Q. H., Zhu, S. R., Tu, Q. Y., Dai, A. B., Liu, A. D., Gu, H. C., Li, F. M. and Di, S. J., *Chem. J. Chin. Univ., Series B*, 1990, **6,** 354.
21. Luo, Q. H., Zhu, S. R., Shen, M. C., Yu, S. Y., Zhang, Z., Huang, X. Y. and Wu, Q. J., *J. Chem. Soc., Dalton Trans.*, 1994, 1873.
22. Zhu, S. R., Lin, H. K., Lin, C. C., Kou, F. P. and Chen, Y. T., *Inorg. Chim. Acta*, 1995, **228,** 225.
23. Kou, F. P., Zhu, S. R., Lin, H. K., Chen, Y. T., Wang, H. G. and Yao, X. K., *J. Chem. Soc., Chem. Commun.*, 1996, 59.

24. Lin, H. K., Zhu, S. R., Gu, Z. X., Chen, Y. T., *J. Chem. Soc.*, *Dalton Trans*., 1995, 1879.
25. Kimura, E., *J. Coord. Chem.*, 1986, **15,** 1.
26. Hay, R. W., Pujari, M. P. and Mclaren, F., *Inorg. Chem*., 1984, **23,** 3033.
27. Siegfried, L. and Kaden, T. A., *J. Phys. Org. Chem*., 1992, **5,** 549.
28. Siegfried, L., Neuburger, M., Zehnder, M. and Kaden, T. A., *J. Chem. Soc. Chem. Commun*., 1994, 951.
29. Kou, F., Zhu, S., Lin, H., Chen, W. and Chen, Y., Lin, M., *Polyhedron*, 1997, **16,** 2021.
30. Xian, J.-C., Zhu, S.-R., Lin, H.-K. and Chen, Y.-T., *Chem. J. Chin. Univ*., 1994, **15,** 163.
31. Lin, H.-K., Zhu, S.-R., Appolin, B. K., Kou, F.-P. and Chen, Y.-T., *Acta Physico-Chimica Sinica*, 1997, **13,** 417.

Pergamon

Polyhedron Vol. 17, Nos. 25, 26, pp. 4339–4345, 1998
© 1998 Elsevier Science Ltd
All rights reserved. Printed in Great Britain
PII: S0277–5387(98)00203–4
0277–5387/98 $19.00+0.00

Synthesis of tetrahedral heteronuclear MoCoFe(μ_3-E) (E=S, Se) clusters via isolobal displacement and functional transformation reactions. The crystal molecular structure of η^5-$MeCOC_5H_4MoCoFe(\mu_3\text{-}Se)(CO)_8$

Li-Cheng Song[a,*], Yu-Bin Dong[a], Qing-Mei Hu[a] and Jie Sun[b]

[a]Department of Chemistry, Nankai University, Tianjin 300071, People's Republic of China

[b]Laboratory of Organometallic Chemistry, Shanghai 200032, People's Republic of China

(Received 31 March 1998; accepted 1 September 1998)

Abstract—The dppe-bridged Mo–Mo singly-bonded dimers (μ-dppe)(η^5-$RC_5H_4)_2Mo_2(CO)_4$ (dppe $=Ph_2PCH_2CH_2PPh_2$; **1a**, R=H; **1b**, R=MeCO; **1c**, $R=MeO_2C$) prepared by reaction of Mo–Mo triply-bonded dimers (η^5-$RC_5H_4)_2(CO)_2Mo_2(CO)_4$ and dppe, reacted with μ_3-Se cluster $Co_2Fe(\mu_3\text{-}Se)(CO)_9$ to give single clusters η^5-$RC_5H_4MoCoFe(\mu_3\text{-}Se)(CO)_8$ (**2a**, R=H; **2b**, R=MeCO; **2c**, $R=MeO_2C$), whereas the disodium salt [(μ-dppe)(η^5-$MeO_2CC_5H_4)_2Mo_2(CO)_4]Na_2$ (**3**) prepared by reaction of **1c** and 1% Na/Hg, reacted with μ_3-S cluster $Co_2Fe(\mu_3\text{-}S)(CO)_9$ to afford single cluster η^5-$MeO_2CC_5H_4MoCoFe(\mu_3\text{-}S)(CO)_8$ (**4**) and double cluster (μ-dppe)[(η^5-$MeO_2CC_5H_4MoCoFe(\mu_3\text{-}S)(CO)_7]_2$ (**5**). Further treatment of **2b** with $NaBH_4$ gave a single cluster containing hydroxyl group η^5-$MeCH(OH)C_5H_4MoCoFe(\mu_3\text{-}Se)(CO)_8$ (**6**), which reacted with Et_3OBF_4 to give single cluster η^5-$MeCH(OEt)C_5H_4MoCoFe(\mu_3\text{-}Se)(CO)_8$ (**7**) and double cluster [η^5-$C_5H_4CH(Me)O(Me)CHC_5H_4$-$\eta^5$][$MoCoFe(\mu_3\text{-}Se)(CO)_8]_2$ (**8**) both containing ether functionality. All the new clusters have been characterized by elemental analysis and spectroscopic methods, as well as by X-ray diffraction analysis for cluster **2b**. © 1998 Elsevier Science Ltd. All rights reserved

Keywords: Mo≡Mo triple bond; MoCoFeS clusters; MoCoFeSe clusters; synthesis; reactions; crystal structure.

INTRODUCTION

Since the 1970s heteronuclear transition metal cluster complexes have been attracting considerable attention, largely due to their potential applications such as in catalysis, as well as the novelty and diversity of their reactions and structures [1–4]. Among the reactions studied so far, the isolobal displacement [5, 6] and functional transformation reactions [6] are of great interest and particularly useful for the rational synthesis of such transition metal clusters. As an extension of our project related to those mentioned above [6–9] we wish to report herein: (i) the synthesis of some new single and double tetrahedral MoCoFe(μ_3-E)(E=S, Se) clusters through the isolobal displacement reactions of two new types of dppe-bridged isolobal reagents with parent clusters $Co_2Fe(\mu_3\text{-}E)(CO)_9$. (ii) A series of functional transformation reactions starting from one of the clusters mentioned above to give additional new single and double MoCoFe(μ_3-Se) clusters containing functionally substituted cyclopentadienyl ligands. (iii) The X-ray crystal diffraction analysis for single cluster η^5-$MeCOC_5H_4MoCoFe(\mu_3\text{-}Se)(CO)_8$.

*Author to whom correspondence should be addressed.

RESULTS AND DISCUSSION

Preparation of **1a–c** *and in situ reaction with* $Co_2Fe(\mu_3\text{-}Se)(CO)_9$; *synthesis and characterization of* **2a–c**

Similar to the preparation of (μ-dppm)$Cp_2Mo_2(CO)_4$ [10], an equimolar amount of triply-bonded dimers $(\eta^5\text{-}RC_5H_4)_2Mo_2(CO)_4$ (R = H, COMe, CO_2Me) reacted with dppe ligand in anhydrous THF at 0°C under nitrogen to give a purple solution of (μ-dppe)$(\eta^5\text{-}RC_5H_4)_2Mo_2(CO)_4$ (**1a**, R = H; **1b**, R = MeCO; **1c**, R = MeO_2C); Since dppe-bridged complexes **1a–c** were very air-sensitive and hard to separate, we treated them *in situ* with two molar equivalents of parent cluster $Co_2Fe(\mu_3\text{-}Se)(CO)_9$ at room temperature, affording three new single tetrahedral MoCoFe(μ_3-Se) cluster complexes η^5–$RC_5H_4MoCoFe(\mu_3\text{-}Se)(CO)_8$ (**2a**, R = H; **2b**, R = MeCO; **2c**, R = MeO_2C), as shown in Scheme 1.

Clusters **2a–c** are deeply colored air-stable solids, which have been characterized by elemental analysis and spectroscopic techniques.

The IR spectra of **2a–c** all showed several absorption bands in the range of 2073–1868 cm^{-1} for their carbonyl ligands attached to transition metals, whereas those of **2b** and **2c** showed one additional absorption band at 1688 and 1721 cm^{-1} for their respective ketonic and ester carbonyls. The ^1H spectrum of **2a** exhibited one singlet at 5.36 ppm for its parent cyclopentadienyl ring, whereas those of **2b** and **2c** exhibited one singlet at 2.44 and 3.92 ppm for their methyl groups of the substituents on cyclopentadienyl ligands, respectively. In addition, the ^1H spectra of **2b** and **2c** showed one multiplet at 5.40–5.72 ppm for H^3 and H^4 protons remote from the substituent and one multiplet at 5.85–6.04 ppm for H^2 and H^5 protons close to the substituent on the substituted cyclopentadienyl rings, since the substituents are electron-withdrawing. Although the mass spectrum of **2a** showed its molecular ion M^+ peak, those of **2b** and **2c** exhibited only a series of reasonable fragment peaks generated from their fragment ions such as M^+-*n*CO (*n* = 1–8).

Crystal structure of **2b**

In order to further confirm the structures of single clusters **2a–c**, a single-crystal structure of **2b** was determined by X-ray diffraction methods. In the unit cell of **2b** there are two independent molecules **A** and **B**, whose structures are shown in Fig. 1. Since the geometric parameters of **A** and **B** are very similar, only the selected bond lengths and angles of **A** are given in Table 1.

As seen from Fig. 1, the molecule of **2b** consists of a distorted tetrahedral MoCoFeSe cluster core, on which there are one acetylcyclopentadienyl and two CO's ligands coordinated to Mo atom as well as two sets of three CO's coordinated to Fe and Co atoms, respectively. Actually, the single tetrahedral cluster **2b** is very similar. to the half of the double tetrahedral cluster $[(\eta^5\text{-}C_5H_4C(O)CH_2]_2[MoCoFe(\mu_3\text{-}S)(CO)_8]_2$ [6] and thus in both clusters the corresponding geometric parameters are comparable. For instance, the bond lengths of Mo–Fe, Mo–Co,Fe–Co are 2.7749(8), 2.8230(9) and 2.570(1) Å in **2b**, whereas the corresponding those are 2.801(1), 2.790(2) and 2.580(2) Å in $[\eta^5\text{-}C_5H_4C(O)CH_2]_2[MoCoFe(\mu_3\text{-}S)(CO)_8]_2$ [6], respectively. The distance of the Mo atom to the substituted Cp centroid is 1.983 Å in **2b**, whereas the corresponding one is 2.001 Å [6]. Among the eight carbonyls of **2b**, seven carbonyls, i.e. C(1)–O(1) through C(7)–O(7), are terminal and one carbonyl,

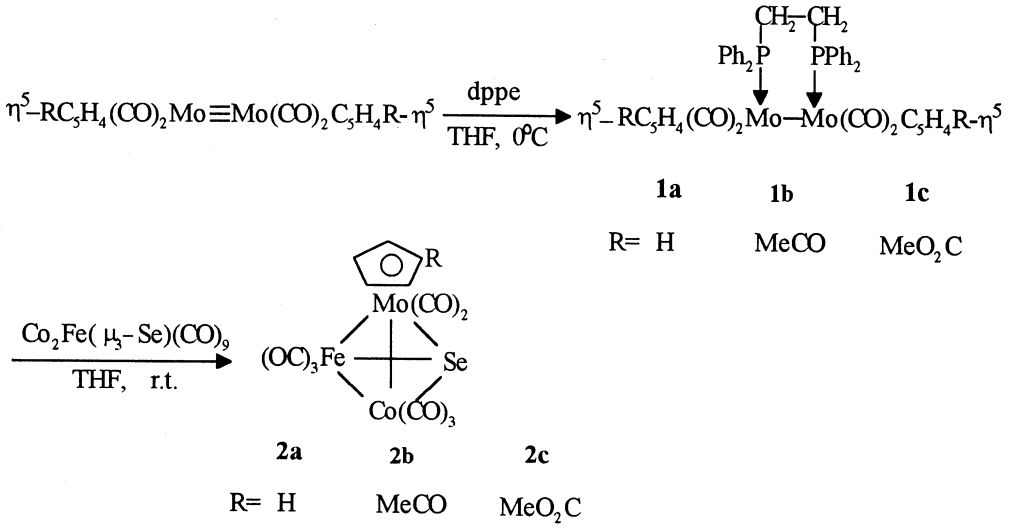

Scheme 1.

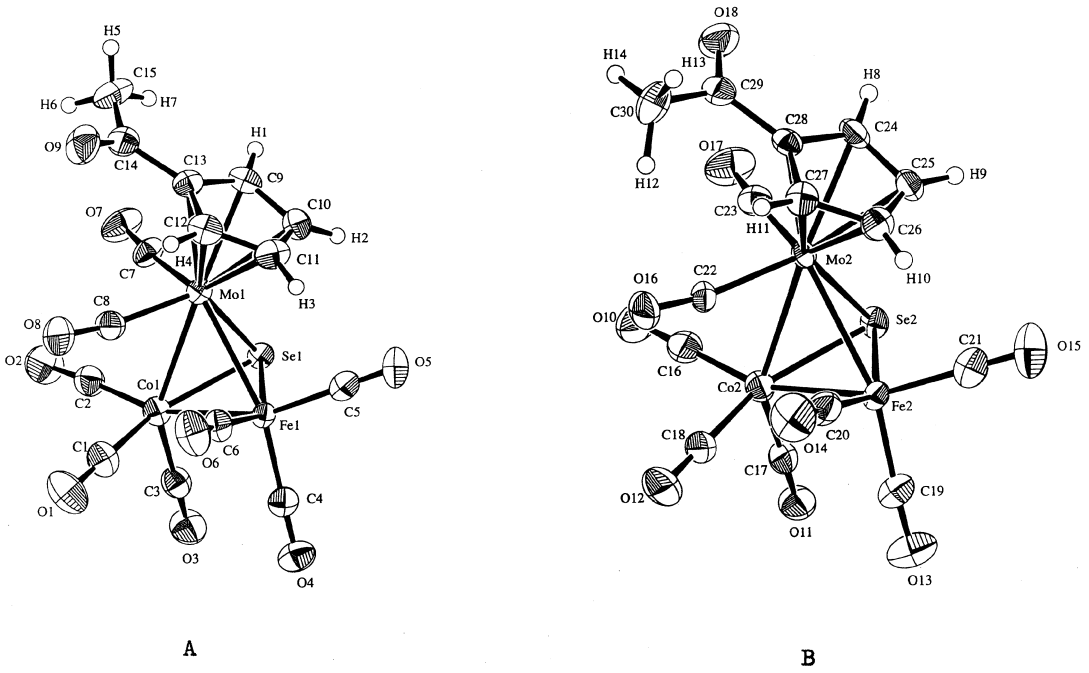

Fig. 1. An ORTEP plot of 2b.

Table 1. Selected bond lengths (Å) and angles (°) for molecule **A** of **2b**

Mo(1)–Se(1)	2.4870(7)	Mo(1)–CO(1)	2.8230(9)
Mo(1)–Fe(1)	2.7749(8)	Mo(1)–C(7)	1.981(6)
Mo(1)–C(8)	1.984(6)	Se(1)–Fe(1)	2.307(9)
Se(1)–Co(1)	2.3164(9)	Co(1)–C(1)	1.788(6)
Co(1)–Fe(1)	2.570(1)	Fe(1)–C(5)	1.7931(6)
O(1)–C(1)	1.145(7)	O(8)–C(8)	1.150(7)
O(5)–C(5)	1.142(7)	O(7)–C(7)	1.148(7)
O(9)–C(14)	1.197(8)	C(9)–C(10)	1.399(8)

Se(1)–Mo(1)–Co(1)	51.25(2)	Se(1)–Mo(1)–Fe(1)	51.66(2)
Se(1)–Mo(1)–C(7)	83.3(2)	Se(1)–Mo(1)–C(8)	120.0(2)
Co(1)–Mo(1)–C(7)	79.3(2)	Co(1)–Mo(1)–Fe(1)	54.65(2)
Co(1)–Mo(1)–C(8)	68.8(2)	C(9)–Mo(1)–C(10)	35.0(2)
Mo(1)–Se(1)–Co(1)	71.89(3)	Mo(1)–Se(1)–Fe(1)	70.62(3)
Co(1)–Se(1)–Fe(1)	67.55(3)	Mo(1)–Co(1)–Fe(1)	61.72(3)
Mo(1)–Co(1)–Se(1)	56.86(2)	Mo(1)–Co(1)–C(2)	101.5(2)
Mo(1)–Co(1)–C(1)	108.3(2)	Mo(1)–Fe(1)–Co(1)	63.63(3)
Mo(1)–Fe(1)–Se(1)	57.72(2)	Se(1)–Fe(1)–Co(1)	56.40(3)
Mo(1)–Fe(1)–C(4)	154.0(2)	Mo(1)–C(8)–O(8)	168.9(5)

i.e. C(8)–O(8) attached to Mo atom is semi-bridging. This is due to its asymmetric parameter $\alpha = d_2 - d_1/d_1 = 0.41$ [d_2 = CO(1)...C(8) = 2.80 Å, d_1 = Mo(1)–C(8) = 1.984 Å], which falls well into the range of α value defined for semi-bridging CO's by Curtis [11]. Since the angle of Mo(1)–C(8)–O(8) is 168.9(5)° and the angle of Co(1)–Mo(1)–C(8) is 68.8(2)°, the semi-bridging C(8)–O(8) is bridged across on the Mo(1)–Co(1) bond. The presence of both terminal and semi-bridging carbonyls in **2b** is consistent with its IR spectral data.

Preparation of **3** *and subsequent reaction with* $Co_2Fe(\mu_3\text{-}S)(CO)_9$; *synthesis and characterization of* **4** *and* **5**

More interestingly, we found that reaction of **1c** with an excess amount of 1% amalgam in THF at

0°C, after filtration, gave a yellow solution of another new type of isolobal reagent, [(μ-dppe)(η^5-$MeO_2CC_5H_4)_2Mo_2(CO)_4$]$Na_2$ (**3**). Further treatment of the solution of **3** *in situ* with two molar equivalents of parent cluster $Co_2Fe(\mu_3\text{-}S)(CO)_9$, initially at room temperature and then at reflux, afforded both single cluster η^5-$MeO_2CC_5H_4MoCoFe(\mu_3\text{-}S)(CO)_8$ (**4**) and double cluster (μ-dppe)(η^5-$MeO_2CC_5H_4)_2Mo_2Co_2Fe_2(CO)_{14}$ (**5**) (Scheme 2).

While single cluster **4** was previously prepared by another procedure [6], double cluster **5** is new and has been characterized by elemental analysis and spectroscopic methods. In the IR spectrum of **5** there was one ester carbonyl absorption band at 1729 cm^{-1} and four absorption bands in the range of 2049–1877 cm^{-1}, characteristic of its carbonyls attached to transition metals. The ^1H NMR spectrum of **5** indicated the presence of all the organic groups. For example, the multiplet at 2.04–2.52 ppm could be assigned to the ethylene group of dppe ligand, the two singlets at 3.82 and 3.86 ppm might be attributed to methyl groups of the substituted cyclopentadienyl ligands. Similar to **2a**–**c** the four protons on each substituted cyclopentadienyl ring showed two multiplets, one at a higher field ascribed to H^3 and H^4 protons and the other at a lower field assigned to H^2 and H^5 protons. Double cluster **5** is the only example in which two subcluster cores are connected through a dppe bridge, although a series of double clusters containing biscyclopentadienyl bridges such as [η^5-$C_5H_4C(O)CH_2]_2$[$MCoFe(\mu_3\text{-}S)(CO)_8]_2$ (M = Mo, W) [6] are known.

Functional reactions starting from **2b**; *synthesis and characterization of* **6**–**8**

Functional transformation reactions have proved to be a very useful method for preparation of transition metal cluster complexes [6]. For example, treatment of **2b** with an excess amount of $NaBH_4$ in methanol at room temperature gave an acetyl reduced product **6** in 65% yield. Further treatment of **6** with an excessive amount of triethyloxonium tetrafluoroborate in CH_2Cl_2 at room temperature gave both alkylating and condensation products **7** and **8** in 24 and 36% yields, respectively (Scheme 3).

Single and double clusters **6**–**8** are air-stable red–brown oils, which have been characterized by elemental analysis, IR and ^1H NMR spectroscopy. The C/H analysis is consistent with their respective compositions. The IR spectra of **6**–**8** showed their carbonyl absorption bands in the range of 2071–1886 cm^{-1} and hydroxyl and ether group absorption bands at 3441, 1103 and 1119 cm^{-1}, respectively. The ^1H NMR spectra of **6**–**8** showed their respective functionally substituted cyclopentadienyl ligands. For example, the doublet at 1.52 ppm is for the methyl group of **6**, the triplet and quartet at 1.20 and 3.48 ppm is for the ethyl group of **7**. However, the protons on substituted cyclopentadienyl ligands of **6**–**8**, in contrast to those of their starting cluster **2b**, exhibited only one multiplet in the range of 5.04–5.68 ppm, obviously caused by the newly generated chiral α-carbon atoms in clusters **6**–**8** through the functional transformation reactions.

EXPERIMENTAL

All reactions were carried out under highly prepurified tank nitrogen. TLC was performed on 25 × 20 cm glass plates coated with silica gel G (10–40 μm). THF was distilled from Na/benzophenone ketyl. (η^5-$RC_5H_4)_2Mo_2(CO)_4$ (R = H, COMe, MeO_2C)

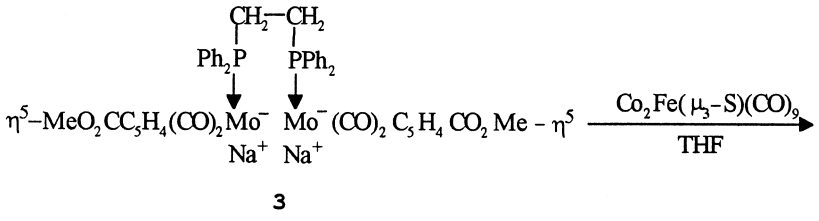

3

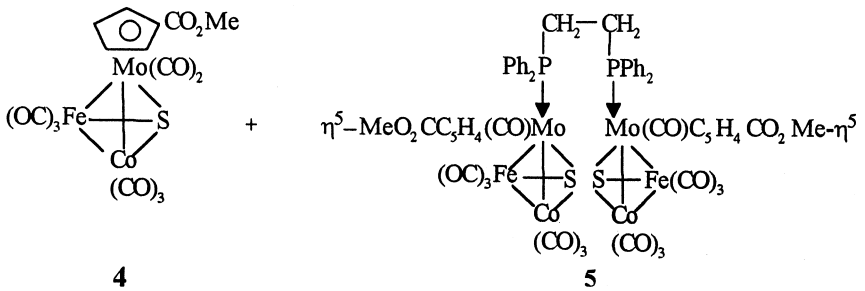

4 **5**

Scheme 2.

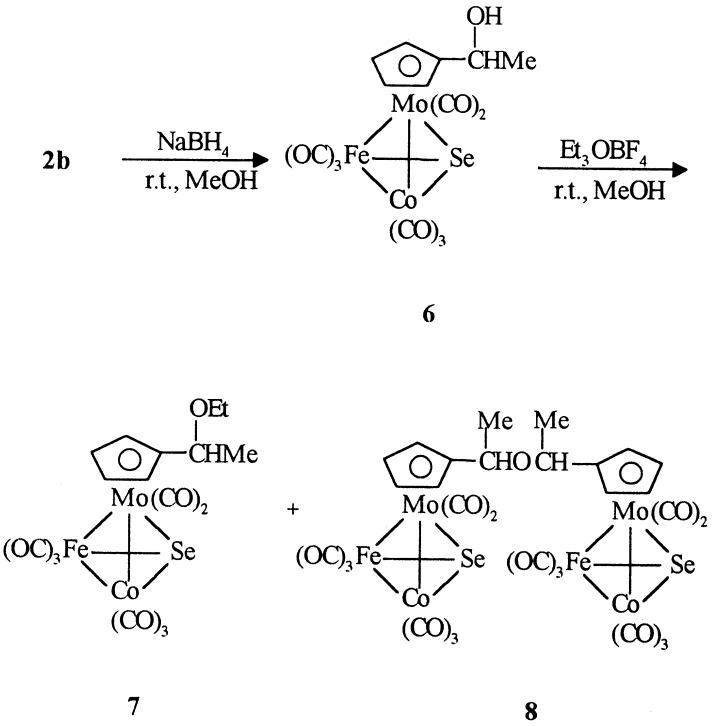

Scheme 3.

[12–14], $Co_2Fe(\mu_3\text{-}E)(CO)_9$(E = S, Se) [15] and Et_3OBF_4 [16] were prepared according to the published methods. $Mo(CO)_6$, $Ph_2PCH_2CH_2PPh_2$ (dppe) were purchased from Strem Chemicals. IR and ^1H spectra were recorded on a Nicolet FT-IR 5DX spectrophotometer and a JEOL FX 90Q or Brucker AC-P 200 NMR spectrometer, respectively. Mass spectra and elemental analyses were obtained with an HP 5988A and Perkin-Elmer 240C analyzer, respectively. Melting points were determined on a Yanaco MP-500 apparatus and were uncorrected.

Preparation of η^5-$C_5H_5MoCoFe(\mu_3\text{-}Se)(CO)_8$ (**2a**) *via* (μ-dppe)(η^5-$C_5H_5)_2Mo_2(CO)_4$ (**1a**)

To a 100 cm^3 two-necked flask were added (η^5-$C_5H_5)_2Mo_2(CO)_4$(0.283 g, 0.67 mmol) and THF (20 cm^3). The mixture was stirred and cooled to 0°C to give a deep-red THF solution of (η^5-$C_5H_5)_2Mo_2(CO)_4$. To the solution were added dppe (0.267 g, 0.67 mmol) and the mixture was stirred for an additional 10 min to give a purple THF solution of **1a**. $Co_2Fe(\mu_3\text{-}Se)(CO)_9$ (0.676 g, 1.34 mmol) was added to the solution of **1a** and the mixture was stirred for 4 h at room temperature. The solvent was removed under reduced pressure and the residue was extracted with CH_2Cl_2. The extracts were subjected to TLC separation using CH_2Cl_2/petroleum ether (1:3) as eluent. From the main band was obtained **2a** (0.172 g, 22%) as a red–brown solid. **2a**: m.p. 75°C (dec). Found: C, 26.9; H, 0.9. Calc. for $C_{13}H_5CoFeMoO_8Se$; C, 27.0; H, 0.9%. IR (KBr, disc): ν_{CO}, 2073 s, 2024 vs, 1983 vs, 1893 s cm^{-1}. ^1H NMR($CDCl_3$, δ, ppm): 5.36 (s, 5H, C_5H_5). MS(EI): m/z (^{98}Mo) 582 (M^+, 0.5%), 554 (M^+–CO, 0.6), 526 (M^+–2CO, 0.4), 498 (M^+–3CO, 0.8), 470 (M^+–4CO, 0.8), 442 (M^+–5CO, 2.6), 414 (M^+–6CO, 2.4), 386 (M^+–7CO, 1.6), 358 (M^+–8CO, 3.2), 293 (Mo $FeCoSe^+$, 0.8), 219 [$C_5H_5Mo(CO)_2^+$, 1.0], 65 ($C_5H_5^+$, 2.1).

Preparation of η^5-$MeCOC_5H_4MoCoFe(\mu_3\text{-}Se)(CO)_8$ (**2b**) *via* (μ-dppe)(η^5-$MeCOC_5H_4Mo_2(CO)_4$ (**1b**)

The same procedure as that for **1a** was followed, but (η^5-$MeCOC_5H_4)_2Mo_2(CO)_4$ (0.347 g, 0.67 mmol) was used instead of (η^5-$C_5H_4)_2Mo_2(CO)_4$ to give a purple THF solution of **1b**. $Co_2Fe(\mu_3\text{-}Se)(CO)_9$ (0.676 g, 1.34 mmol) was added to the solution of **1b** and the mixture was stirred for 4 h at room temperature. The same workup as that for **2a** was followed. From the main band was obtained **2b** (0.126 g, 15%) as a red–brown solid. **2b**: m.p. 95–96°C. Found: C, 29.0; H, 1.2. Calc. for $C_{15}H_7CoFeMoO_9$ Se; C, 29.0; H, 1.1%. IR (KBr, disc): ν_{CO}, 2073 vs, 2032 vs, 2008 vs, 1975 vs, 1909 s, 1868 s; $\nu_{C=O}$ 1688 s cm^{-1}. ^1H NMR ($CDCl_3$, δ, ppm): 2.44 (s, 3H, CH_3). 5.44–5.72 (m, 2H, H^3, H^4), 5.85–6.04 (m, 2H, H^2, H^5). MS(EI): m/z (^{98}Mo) 596 (M^+–CO, 1.6%), 568 (M^+–2CO, 3.9), 540 (M^+–3CO, 3.6), 512 (M^+–4CO, 3.5), 484 (M^+–5CO, 7.5), 456 (M^+–6CO, 13.8), 428 (M^+–7CO, 7.7), 400 (M^+–

8CO, 11.2), 357 ($C_5H_4MoFeCo\ Se^+$, 1.3), 293 (Mo $FeCoSe^+$, 2.2), 261 [$MeCOC_5H_4Mo(CO)_2^+$, 1.6], 205 ($MeCOC_5H_4\ Mo^+$, 2.7), 107 ($MeCOC_5H_4^+$, 1.4).

Preparation of η^5-$MeO_2CC_5H_4MoCoFe(\mu_3\text{-}Se)(CO)_8$ (**2c**) *via* (μ-dppe)(η^5-$MeO_2CC_5H_4Mo_2(CO)_4$ (**1c**)

The same procedure as that for **1a** was followed, but (η^5-$MeO_2CC_5H_4)_2Mo_2(CO)_4$ (0.367 g, 0.67 mmol) was used instead of (η^5-$C_5H_5)_2Mo_2(CO)_4$ to give a purple THF solution of **1c**. $Co_2Fe(\mu_3\text{-}Se)(CO)_9$ (0.676 g, 1.34 mmol) was added to the solution of **1b** and the mixture was stirred for 4 h at room temperature. The same workup as that for **2a** was followed. From the main band was obtained **2c** (0.122 g, 14%) as a red–brown solid. **2c**: m.p. 55–56°C. Found: C, 28.2; H, 1.1. Calc. for $C_{15}H_7CoFeMoO_{10}Se$; C, 28.3; H, 1.1%. IR (KBr, disc): ν_{CO}, 2073 vs, 2024 vs, 1991 vs, 1893 s; $\nu_{C=O}$ 1721 s cm^{-1}. ^1H NMR($CDCl_3$, δ, ppm): 3.92 (s, 3H, CH_3). 5.40–5.68 (m, 2H, H^3, H^4), 5.90–6.02 (m, 2H, H^2, H^5). MS(EI): *m*/*z* (^{98}Mo) 612 (M^+–CO, 1.0), 584 (M^+–2CO, 3.0), 556 (M^+–3CO, 2.4), 528 (M^+–4CO, 4.6), 500 (M^+–5CO, 9.6), 472 (M^+–6CO, 20.6), 444 (M^+–7CO, 11.6), 416 (M^+–8CO, 11.9), 357 ($C_5H_4MoFeCoSe^+$, 15.1), 293 ($MoFeCoSe^+$, 8.2), 277 ($MeO_2CC_5H_4Mo(CO)_2^+$, 1.7), 221 ($MeO_2CC_5H_4Mo^+$, 3.3), 123 ($MeO_2CC_5H_4^+$, 2.2).

Preparation of η^5-$MeO_2CC_5H_4MoCoFe(\mu_3\text{-}S)(CO)_8$ (**4**) *and* (μ-dppe)[(η^5-$MeO_2CC_5H_4MoCoFe(\mu_3\text{-}S)(CO)_7]_2$ (**5**) *via* [(μ-dppe)(η^5-$MeO_2CC_5H_4)_2Mo_2(CO)_4]Na_2$ (**3**)

The above flask was charged with (η^5-$MeO_2CC_5H_4)_2Mo_2(CO)_4$ (0.301 g, 0.55 mmol) and THF (20 cm^3). The stirred mixture was cooled to 0°C to give a deep-red THF solution of (η^5-$MeO_2CC_5H_5)_2Mo_2(CO)_4$. To the solution was added dppe (0.219 g, 0.55 mmol) and the mixture was stirred for additional 10 min to give a purple THF solution of **1c**. To the solution of **1c** at 0°C was added amalgam (1%, 23 g) and the mixture was stirred for an additional 20 min at this temperature, after filtration to give a yellow solution of **3**. To the solution of **3** was added $Co_2Fe(\mu_3\text{-}S)(CO)_9$ (0.504 g, 1.10 mmol) and the mixture was stirred for 1 h at room temperature and then refluxed for 2 h. After removal of the solvent under reduced pressure, the residue was extracted with CH_2Cl_2 and the extracts were subjected to TLC separation using CH_2Cl_2/petroleum ether (1:1) as eluent. From the brown band, **4** was obtained, which was identified by comparison of its IR and ^1H NMR spectra with those of the authentic sample [6]. From the black band, **5** (0.076 g, 9%) was obtained as a black solid. **5**: m.p. 101°C (dec). Found: C, 42.5; H, 2.8. Calc. for $C_{54}H_{38}Co_2Fe_2Mo_2O_{18}P_2S_2$; C, 42.6; H, 2.5%. IR(KBr, disc): ν_{CO}, 2049 s, 1991 vs, 1967 vs, 1877 s; $\nu_{C=O}$ 1729 s cm^{-1}. ^1H NMR ($CDCl_3$, δ, ppm): 2.04–2.52 (m, 4H, PCH_2CH_2P), 3.82, 3.86 (s, s, 6H, CH_3), 5.50–5.68 (m, 4H, H^3, $H^{3'}$; H^4, $H^{4'}$), 5.80–6.12 (m, 4H, H^2, $H^{2'}$; H^5, $H^{5'}$), 7.04–7.72 (m, 20H, $4C_6H_5$).

Preparation of η^5-$MeCH(OH)C_5H_4MoCoFe(\mu_3\text{-}Se)(CO)_8$ (**6**)

The above flask was charged with (η^5-$MeCOC_5H_4MoCoFe(\mu_3\text{-}Se)(CO)_8$ (**2b**) (0.308 g, 0.49 mmol), $NaBH_4$ (0.021 g, 0.55 mmol) and MeOH (10 cm^3). The mixture was stirred overnight at room temperature. The solvent was removed under vacuum and the residue was extracted with CH_2Cl_2. The extracts were subjected to TLC separation using CH_2Cl_2/petroleum ether (1:1) as eluent. From the main brown band was obtained **6** (0.200 g, 65%) as a red–brown oil. Found: C, 29.3; H, 1.3. Calc. for $C_{15}H_9CoFeMoO_9Se$: C, 28.9; H, 1.5%. IR (KBr, disc): ν_{OH}, 3441 m, ν_{CO} 2070 s, 2021 s, 1889 s cm^{-1}. ^1H NMR($CDCl_3$, δ, ppm): 1.52 (d, J = 7.2 Hz, 3H, CH_3), 1.76–2.02 (br, 1H, OH), 4.52–4.80 (m, 1H, CH), 5.10–5.52 (m, 4H, C_5H_4).

Preparation of η^5-$MeCH(OEt)C_5H_4MoCoFe(\mu_3\text{-}Se)(CO)_8$ (**7**) *and* η^5-$C_5H_4CH(Me)O(Me)CHC_5H_4$-$\eta^5$)[$MoCoFe(\mu\text{-}Se)(CO)_8]_2$ (**8**)

The above flask was charged with η^5-$MeCH(OH)C_5H_4MoCoFe(\mu_3\text{-}Se)(CO)_8$ (**6**) (0.150 g, 0.24 mmol) Et_3OBF_4 (0.185 g, 0.97 mmol) and CH_2Cl_2 (7 cm^3). The mixture was stirred at room temperature for 9 h. After removal of solvent under reduced pressure, the residue was subjected to TLC separation using CH_2Cl_2/petroleum ether (1:1) as eluent. The first band is tiny and thus had not been collected. From the second band **7** (0.038 g, 24%) was obtained as a red oil. **7**: found: C, 31.6; H, 1.7. Calc. for $C_{17}H_{13}CoFeMoO_9Se$: C, 31.4; H, 2.0%. IR (KBr, disc): ν_{CO}, 2071 vs, 2021 vs, 1886 s; ν_{C-O} 1103 m cm^{-1}. ^1H NMR ($CDCl_3$, δ, ppm): 1.20 (t, J = 7.2 Hz, 3H, CH_2CH_3), 1.44 (d, J = 7.2 Hz, 3H, $CHCH_3$), 3.48 (q, J = 7.2 Hz, 2H, CH_2), 4.22 (q, J = 7.2 Hz, 1H, CH), 5.12–5.52 (m, 4H, C_5H_4). From the third band **8** (0.053 g, 36%) was obtained as a red oil. **8**: found: C, 29.6; H, 1.8. Calc. for $C_{30}H_{16}Co_2Fe_2Mo_2O_{17}Se_2$: C, 29.4; H, 1.3%. IR (KBr, disc): ν_{CO}, 2069 vs, 2022 vs, 1893 s; ν_{C-O} 1119 s cm^{-1}. ^1H NMR ($CDCl_3$, δ, ppm): 1.32–1.64 (m, 6H, $2CH_3$), 4.28–4.60 (m, 2H, 2CH), 5.04–5.68 (m, 8H, $2C_5H_4$).

Structure determination of **2b**

The single crystals of **2b** were grown in its CH_2Cl/hexane solution at *ca.* −20°C, from which a single crystal with dimensions 0.20 × 0.20 × 0.30 mm was chosen for X-ray diffraction analysis. Diffraction data were collected on a Rigaku. AFC7R CAD4 diffractometer with Mo-Kα radiation using the $\omega/2\theta$

Table 2. Summary of crystallographic data for **2b**

Empirical formula	$C_{15}H_7CoFeMoO_9Se$
Formula weight	1241.79
Crystal system	orthorhombic
Space group	*Pbca* (#61)
a (Å)	26.322(4)
b (Å)	18.027(2)
c (Å)	16.012(3)
V (Å^3)	7597(3)
Z	16
D_{calc} (g cm^{-1})	2.171
F(000)	4768.00
Absorption coefficient, μ (cm^{-1})	42.27
Radiation (Å)	Mo-Kα (λ = 0.71069)
Temperature (°C)	20.0
$(2\theta)_{max}$ (°)	47.0
Observed reflections $I > 3.00\sigma I$	4424
No. of variables	504
R	0.027
Rw	0.040
GOF	1.19
$(\Delta/\sigma)_{max}$	0.22
$\Delta\rho_{max}$ (e Å^{-3})	0.47
$\Delta\rho_{min}$ (e Å^{-3})	−0.63

scan mode. Crystallographic data for **2b** are summarized in Table 2. The structure was solved by the direct method (SAPI 91) using TEXSAN package.

Acknowledgements—We are grateful to the National Natural Science Foundation of China, the State Key Laboratory of Structural Chemistry at Fujian Institute of Research on Structure of Matter and the Laboratory of Organometallic Chemistry at Shanghai Institute of Organic Chemistry for financial support of this project.

REFERENCES

1. Roberts, D. A. and Geoffroy, G. L., in *Comprehensive Organometallic Chemistry*, Vol. 6, eds. G. Wilkinson, F. G. A. Stone and E. W. Abel. Pergamon Press, Oxford, England, 1982, p. 763.
2. Adams, R. D., in *Comprehensive Organometallic Chemistry II*, Vol. 10, eds. E. W. Abel, F. G. A. Stone and G. Wilkinson. Pergamon Press, Oxford, England, 1995, p. 1.
3. Vahrenkamp, H., in *Transition Metal Chemistry-Current Problems of General, Biological and Catalytic Relevance*, eds. A. Muller and E. Diemann. Verlag Chemie, 1981, p. 35.
4. Salto, T., in *Early Transition Metal Clusters with π-Donor Ligands*, Chap. 3, ed. M. H. Chisholm. VCH, New York, 1995.
5. Hoffmann, R., *Angew. Chem. Int. Ed. Engl.*, 1982, **21,** 711.
6. Song, L.-C., Shen, J.-Y., Hu, Q.-M. and Huang, X.-Y., *Organometallics*, 1995, **14,** 98.
7. Song, L.-C., Shen, J.-Y., Hu, Q.-M., Wang, R.-J. and Wang, H.-G., *Organometallics*, 1993, **12,** 408.
8. Song, L.-C., Shen, J.-Y., Hu, Q.-M. and Qin, X.-D., *Polyhedron*, 1995, **14,** 2079.
9. Song, L.-C., Dong, Y.-B., Hu, Q.-M., Huang, X.-Y. and Sun, J., *Organometallics*, 1997, **16,** 4540.
10. Riera, V., Ruiz, M. A. and Villafane, F., *Organometallics*, 1992, **11,** 2854.
11. Curtis, M. D., Han, K. R. and Butler, W. M., *Inorg. Chem.*, 1980, **19,** 2096.
12. Curtis, M. D., Fotinos, N. A., Messerle, L. and Sattelberger, A. P., *Inorg. Chem.*, 1983, **22,** 1559.
13. Song, L.-C., Wang, J.-Q., Zhao, W.-J., Hu, Q.-M., Fang, Y.-Q. and Zhang, S.-J., *J. Organomet. Chem.*, 1993, **453,** 105.
14. Song, L.-C., Shen, J.-Y., Wang, J.-Q., Hu, Q.-M., Wang, R.-J. and Wang, H.-G., *Polyhedron*, 1994, **13,** 3235.
15. Cowie, M., Dekock, R. L., Wagenmaker, T. R., Seyferth, D., Henderson, R. S. and Gallagher, M. K., *Organometallics*, 1989, **8,** 119.
16. Merrwein, H., *Org. Synth.*, 1966, **46,** 113.

Pergamon

Polyhedron Vol. 17, Nos. 25, 26, pp. 4347–4352, 1998
© 1998 Elsevier Science Ltd
All rights reserved. Printed in Great Britain
PII: S0277–5387(98)00207–1
0277–5387/98 $19.00+0.00

Transition metal complexes of the tripodal ligand 4-(2′-pyridylmethyl)-4-azaheptane-1,7-diamine. Crystal structures of $[CuLCl]ClO_4$ and $[NiL(MeCN)_2](ClO_4)_2$

Robert W. Hay*, Thomas Clifford and Philip Lightfoot

School of Chemistry, University of St Andrews, St Andrews KY16 9ST, U.K.

(Received 19 January 1998; accepted 18 May 1998)

Abstract—The tripodal ligand 4-(2′-pyridylmthyl)-4-azaheptane-1,7-diamine has been prepared by reaction of 2-aminemethyl pyridine with acrylonitrile, followed by the reduction of the nitrile groups. Copper(II), nickel(II), zinc(II), cobalt(III) and chromium(III) complexes of the ligand have been prepared and characterized and the crystal structures of the complexes $[CuLCl]ClO_4$ and $[NiL(MeCN)_2](ClO_4)_2$ determined. The copper complex is five coordinate with approximate square pyramidal stereochemistry with the apical position occupied by a primary amine donor. The nickel complex is octahedral with the pyridine nitrogen donor lying *trans* to an acetonitrile ligand. © 1998 Elsevier Science Ltd. All rights reserved

Keywords: tripodal ligand; copper(II); nickel(II); zinc(II); cobalt(III); chromium(III); crystal structures.

INTRODUCTION

There are a limited number of tripodal amine ligands, important examples are tren $[N(CH_2CH_2NH_2)_3]$ and trpn $[N(CH_2CH_2CH_2NH_2)_3]$. Cobalt(III) complexes of trpn have recently attracted considerable attention as the complex $[Co(trpn)(OH)(OH_2)]^{2+}$ promotes the hydrolysis of unactivated carboxylic esters such as methyl acetate [1a, 1b], the hydrolysis of amides [2] and the hydrolysis of phosphate esters [3a, 3b]. The complex $[Co(tren)(OH)(OH_2)]^{2+}$ is also known to promote the hydrolysis of amino acid esters and peptides [4]. In addition tren and trpn have been used as intermediates in the synthesis of a range of macrocycles and cryptand ligands such as (**1**) in which a variety of dialdehydes can be used as "spacers" [5]. For this reason we have been interested in the chemistry of tripodal amine ligands which may be of value in catalytic studies and as intermediates in the synthesis of macrocyclic ligands. In the present paper we discuss the synthesis and characterization of a variety of transition metal complexes of the tripodal ligand 4-(2′-pyridylmethyl)-4-azaheptane-1,7-diamine (**2**).

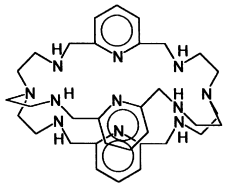

(1)

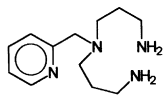

(2)

EXPERIMENTAL

Physical measurements

Infrared spectra were recorded on a Perkin Elmer 1710 Fourier Transform spectrophotometer as KBr discs or as liquid film. UV–VIS spectra were recorded on a Lambda 14P spectrophotometer. The NMR spectra were obtained at 200 MHZ using a Varian Gemini FT spectrometer.

Synthesis

1,5-Dicyano-3-(2′-pyridyln-ethyl)-3-azapentane was prepared by the Michael addition of 2-ami-

*Author to whom correspondence should be addressed. Tel.: +44-1334-463-827; fax: +44-1334-463-808.

nomethyl pyridine to acrylonitrile, essentially as previously described [17]. It was found that cyanoethylation of 2-aminomethyl pyridine does not require the presence of acetic acid as a catalyst.

4-(2′-*Pyridylmethyl*-4-*azaheptane* (*L*)

The amine was prepared by the reduction of the dinitrile with hydrogen and Raney nickel essentially using the procedure described by Chin *et al*. [3b] for the preparation of the ligand tris(3-aminopropyl)amine.

Moore *et al*. [17] have also described a procedure using Raney nickel and $NaBH_4$ as the reducing agent. The amine was purified by vacuum distillation (b.p. 153–154°C at 0.05 mm Hg). A forerun of the monoalkylated product b.p. 105°C was discarded. Found: C, 64.5; H, 10.2; N, 25.0. Calc. for $C_{12}H_{22}N_4$: C, 64.8; H, 10.0; N, 25.2%. Electron impact mass spectrum [M^+] 222 (calc. 222). ^{1}H NMR ($CDCl_3$) 8.55 (1H,d), 7.70 (1H,t), 7.45 (1H,d), 7.17 (1H,t), 3.72 (2H,s), 2.70 (4H,t), 2.55 (4H,t), 1.75 (4H,br), 1.60 (4H,Pent). The ligand tetrahydrobromide was prepared by the dropwise addition of concentrated HBr to a solution of the amine in ethanol.

[CuLCl]ClO_4

The ligand (0.5 g, 2.25 mmol) was dissolved in ethanol (10 cm^3) and added to copper(II) chloride dihydrate (0.38 g, 2.25 mmol). Addition of isopropanol gave a sticky solid which was dissolved in hot ethanol (*ca*. 10 cm^3). Addition of sodium perchlorate (0.5 g) in ethanol (20 cm^3) gave an immediate pale-blue precipitate. The complex was filtered off washed with ethanol then diethyl ether and recrystallized from boiling acetonitrile (0.42 g, 39%). Found: C, 34.7; H, 5.2; N, 13.5. Calc. for $C_{12}H_{22}N_4O_4Cl_2Cu$: C, 34.25; H, 5.3; N, 13.3%. $\Lambda_M = 116\ S\,cm^2\,mol^{-1}$ in $MeNO_2$. λ_{max}/nm (ε_{max}/$dm^3\,mol^{-1}\,cm^{-1}$) 736 (98), 822 (100) in water, 721 (121), 849sh(108) in acetonitrile.

[ZnL]$(ClO_4)_2$

A boiling solution of the ligand (0.30 g, 1.35 mmol) in ethanol (10 cm^3) was added dropwise to a solution of zinc(II) perchlorate hexahydrate (0.50 g, 1.35 mmol) in boiling ethanol (5 cm^3). On cooling, a small amount of oil was separated from the solution, then colourless blades formed. The complex was filtered off and washed with ethanol, then recrystallized from the minimum volume of boiling ethanol (0.49 g, 74%). Found: C, 29.6; H, 4.0; N, 11.3. Calc. for $C_{12}H_{22}N_4O_8Cl_2Zn$: C, 29.6; H, 4.6; N, 11.5%. $\Lambda_M = 193\ S\,cm^2\,mol^{-1}$ in nitromethane at 25°C.

[NiL$(MeCN)_2$]$(ClO_4)_2$

A boiling solution of the ligand (0.30 g, 1.35 mmol) in ethanol (10 cm^3) was added dropwise to a solution of nickel(II) perchlorate hexahydrate (0.49 g, 1.35 mmol) in boiling ethanol (5 cm^3). The green nickel(II) solution turned blue on addition of the amine and on cooling a blue oil formed. The oil was dissolved in boiling acetonitrile (15 cm^3). On cooling purple blocks formed (0.56 g, 82%). Found: C, 33.9; H, 4.8; N, 14.7. Calc. for $C_{16}H_{28}N_6O_8Cl_2Ni$: C, 34.2; H, 5.0; N, 14.95%. $\Lambda_M = 227\ S\,cm^2\,mol^{-1}$ in nitromethane at 25°C. λ_{max}/nm (ε_{max}/$dm^3\,mol^{-1}\,cm^{-1}$) 524(11) 888(8) in acetonitrile and 569(8) 900sh(7) in water.

[CoLBr_2]Br

The ligand tetrahydrobromide (1 g) was ground together with $Na_3[Co(CO_3)_3]\cdot 3H_2O$ [7] (0.66 g). Water (1 cm^3) was added and after the vigorous effervescence had subsided, the mixture was heated on a hot plate for *ca*. 20 min to give a burgundy red solution. The sticky red solid was dissolved in methanol (10 cm^3) and HBr added with gentle heating until the solution became brown–green. Isopropyl alcohol (25 cm^3) was then added to give a pale green–brown precipitate. The precipitate was dissolved by the addition of methanol (10 cm^3) and gentle heating. Dark brown crystals formed on cooling. The crystals were filtered off and washed with ethanol (1 cm^3) then diethyl ether ($2 \times 2\ cm^3$). Yield 0.5 g. Found: C, 27.5; H, 3.9; N, 10.6. Calc. for $C_{12}H_{22}N_4Br_3Co$: C, 27.7; H, 4.25; N, 10.75%). The complex has $\Lambda_M = 421\ S\,cm^2\,mol^{-1}$ in water at 25°C and $\lambda_{max} = 468$ nm ($\varepsilon = 567\ dm^3\,mol^{-1}\,cm^{-1}$) in methanol.

[CrLCl_2]Cl

The ligand (1 g; 4.5 mmol) and chromium(III) chloride hexahydrate (4.5 mmol) were both dissolve separately in DMF (20 cm^3) and brought to the boil on a hot plate. After boiling for some 20 min the chromium solution became rose–pink due to complete dehydration and was added dropwise to the boiling solution of the ligand. A dark-brown solution formed and the purple complex began to crystallize. Additional product could be obtained by removal of half of the solvent under reduced pressure.

The crude complex was recrystallized from 1 mol dm^{-3} HCl (5 cm^3). Found: C, 37.4; H, 5.8; N, 14.6. Calc. for $C_{12}H_{22}N_4Cl_3Cr$: C, 37.9; H, 5.8; N, 14.7%). The complex has $\Lambda_M = 98\ S\,cm^2\,mol^{-1}$ in water at 25°C. The visible spectrum in aqueous solution has λ_{max} 404 ($\varepsilon = 72$) and 541 nm ($\varepsilon = 59\ dm^3\,mol^{-1}\,cm^{-1}$).

Crystallography

Crystal data. $C_{12}H_{22}N_4CuCl_2O_4$, [CuLCl]ClO_4, M = 420.78, primitive orthorhombic, space group

$P2_12_12_1$ (No.19), $a=9.172(2)$, $b=23.090(2)$, $c=8.270(1)$ Å, $U=1751.4(4)$ Å^3, $F(000)=868$, $Z=4$, $D_c=1.596\,g\,cm^{-3}$, MoKα radiation, $\lambda=0.71069$ Å, $\mu(MoK\alpha)=15.75\,cm^{-1}$, $T=290$ K. Blue block crystal grown by vapour diffusion of diethyl ether into a methanol solution of the complex.

$C_{16}H_{28}N_6NiCl_2O_8$.[NiL(MeCN)$_2$](ClO$_4$)$_2$, $M=562.04$, primitive orthorhombic, space group $Pna2_1$ (No. 33), $a=15.974(3)$, $b=8.054(4)$, $c=19.371(4)$ Å, $U=2491(2)$ Å^3, $F(000)=1168$, $Z=4$, $D_c=1.498$ g cm^{-3}, MoKα radiation, $\lambda=0.71069$ Å, $\mu(MoK\alpha)=10.44\,cm^{-1}$, $T=290$ K. Purple block crystal grown by slow recrystallization from methanol.

Data collection and processing. [CuLCl](ClO$_4$)$_2$. A blue crystal of approximate dimensions $0.20\times0.15\times0.30$ nm was mounted on a glass fibre. The unit cell parameters were obtained by least squares refinement of 25 automatically centred reflections in the range $27.2<2\theta<33.4°$. Rigaku AFC7S diffractometer, ω–2θ scan type with ω scan width $(0.89+0.35\tan\theta)$, ω scan speed $16.0°\,min^{-1}$ (up to 4 scans), 1809 reflections measured (max $2\theta=50.0°$). No decay correction was made, but an absorption correction was required (transmission coefficients 0.8653–1.0000). Corrections were made for Lorentz and polarization effects.

[NiL(MeCN)$_2$](ClO$_4$)$_2$. A purple crystal of approximate dimensions $0.20\times0.10\times0.30$ mm was mounted on a glass fibre. The unit cell parameters were obtained by least squares refinement of 15 automatically centred reflections in the range $6.62<2\theta<11.15°$. Rigaku AFC7S diffractometer, ω–2θ scan type with ω scan width $=(0.84+0.35\tan\theta)$, ω scan speed $16.00°\,min^{-1}$ (up to 4 scans), 2532 reflections measured (max $2\theta=50.0°$). No decay correction was made, but an absorption correction was required (transmission coefficients 0.9057–1.0000). Corrections were made for Lorentz and polarization effects.

Structure analysis and refinement

[CuLCl](ClO$_4$)$_2$. Direct methods [8] were employed and expanded using Fourier techniques [9]. All nonhydrogen atoms were refined anisotropically. Hydrogens are included but not refined. The final cycle of full-matrix least squares refinement was based on 1528 observed reflections [$I>3.00\sigma(I)$] and 208 variable parameters and converged with unweighed agreement factors of $R=0.045$ and $R'=0.040$ ($R=\Sigma\|F_o|-|F_c\|/\Sigma|F_o|$; $R'=(\Sigma(|F_o|-|F_c|)^2/\Sigma w|F_o|^2)^{1/2}$. The standard deviation of an observation of unit weight [10] was 2.96. The maximum and minimum peaks in the final difference Fourier map correspond to 0.56 and -0.45 eÅ^{-3}, respectively. The perchlorate anion was refined anisotropically and inspection of the ORTEP thermal ellipsoids indicated considerable disorder of the perchlorate oxygen atem. Attempts to model the disorder on the basis of a number of partially occupied positions around the chlorine atom did not give a significant reduction in the R value. All calculations were performed using the TEXSAN [10] crystallographic software package of the Molecular Structure Corporation.

[NiL(MeCN)$_2$](ClO$_4$)$_2$. As described above, direct methods were employed and expanded using Fourier techniques. All nonhydrogen were refined anisotropically except for the oxygens of one perchlorate group. Hydrogens were included but not refined. The full cycle of least squares refinement was based on 1633 observed reflections [$I>3.00\sigma(I)$] and 277 variable parameters and converged with unweighed agreement factors of $R=0.072$ and $R'=0.061$. The standard deviation of unit weight was 3.94. The weighting scheme was based on counting statistics and included a factor ($p=0.001$) to downweight the intense reflections. Plots of $w(\Sigma|F_o|-|F_c|)^2$ vs. $|F_o|$, reflection order in data collection, $\sin\theta/\lambda$ and various classes of indices showed no unusual trends. The maximum and minimum peaks in the final difference Fourier map corresponded to 0.64 and -0.57 eÅ^{-3} respectively. Attempts to model the disorder of the perchlorate oxygen atoms on the basis of a number of partially occupied positions around the chlorine atom did not produce a significant reduction in the value of R.

RESULTS AND DISCUSSION

The tripodal ligand 4-(2′-pyridylmethyl)-4-azaheptane-1,7-diamine (2 = L) was readily prepared by the reactions outlined in the Scheme. It was found that

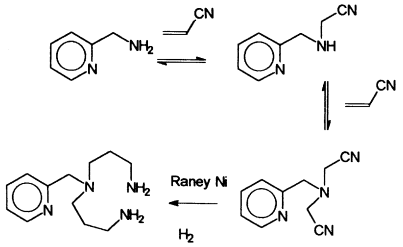

cyanoethylation of 2-aminomethyl pyridine does not require the presence of an acid catalyst. Even under the reaction condition employed (a large excess of acrylonitrile) some monoalkylated species are formed. The cyanoethylated product was not purified since distillation led to appreciable decomposition. After reduction the mono- and dialkylated and amines could readily be separated by vacuum distillation.

A variety of metal complexes with copper(II), nickel(II), zinc(II), cobalt(III) and chromium(III) were readily characterized and the crystal structures of the copper and nickel complexes determined.

The $[CuLCl]^+$ cation is five-coordinate with an N_4Cl donor set, Fig. 1. The geometry is best described as distorted square pyramidal, and selected bond lengths and angles are summarized in Table 1. The crystal structure of the analogous complex [Cu(tren)NCS]SCN [11] establishes that with the symmetrical

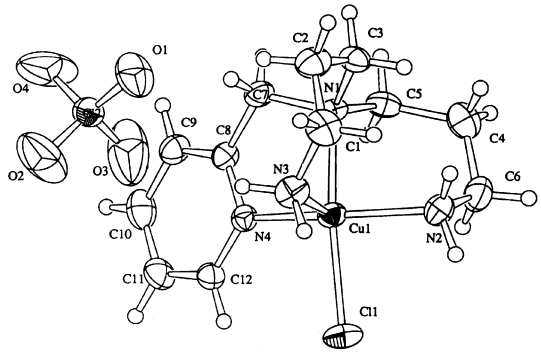

Fig. 1. ORTEP of the complex $[CuLCl]ClO_4$ with the atom numbering scheme.

Table 1. Selected bond distances (Å) and angles (°) in $[CuLCl]ClO_4$ with estimated standard deviations in parenthesis

Cu(1)–N(1)	2.069(6)	N(1)–Cu(1)–N(2)	89.2(3)
Cu(1)–N(2)	2.004(6)	N(3)–Cu(1)–N(1)	93.6(3)
Cu(1)–N(3)	2.192(7)	N(1)–Cu(1)–N(4)	82.2(3)
Cu(1)–N(4)	2.033(6)	N(3)–Cu(1)–N(2)	101.4(3)
Cu(1)–CI(1)	2.300(2)	N(1)–Cu(1)–Cl(1)	166.0(2)
		N(3)–Cu(1)–Cl(1)	100.4(2)
		N(2)–Cu(1)–N(4)	151.5(3)
		N(3)–Cu(1)–N(4)	106.3(3)
		N(2)–Cu(1)–Cl(1)	87.6(2)
		N(4)–Cu(1)–Cl(1)	94.2(2)

tripodal tren ligand copper has a trigonal bipyramidal geometry. In the present complex there is a large N4–Cu–N2 bond angle of 151.5° and acute angles of 106.3 and 101.4° for N4–Cu–N3 and N3–Cu–N2, respectively. The donors N1, N2, N4 and Cl may be considered to form the base of the pyramid with copper sitting some 0.5 Å above the plane and N3 occupying the apical position. Two isomers (**3**) and (**4**) are possible in square pyramidal geometry. Isomer

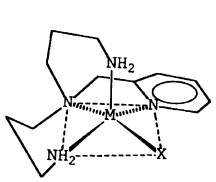

(**3**)

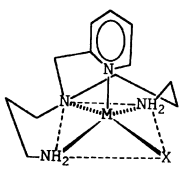

(**4**)

(**3**) is found in this structure with a primary amino group in the apical site. The primary amine in the apical position (N3) has a somewhat longer bond (2.192 Å) to copper than the in-plane amine (2.004 Å). The pyridine nitrogen to copper bond length of 2.033(6) Å is close to that typically observed in pyridine complexes (*ca.* 1.98 Å) and the Cu–Cl bond length also falls within the expected limits for 5-coordinate complexes. The pyridine ring is planar (torsion angles are $0.3 \pm 0.2°$) and the carbon–carbon bond distances in the alkyl chains show no unusual features (1.51 ± 0.02 Å).

The blue cation $[NiL(MeCN)_2]^{2+}$ is as expected six-coordinate and octahedral, Fig. 2, with the two acetonitrile ligands in *cis*-positions. Two isomers (**5**) and (**6**) are possible for an $[MLX_2]$ type complex. Isomer

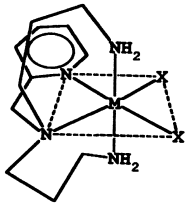

(**5**)

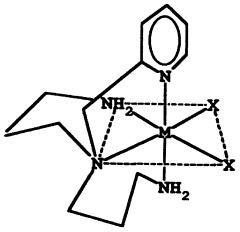

(**6**)

(**5**) has the pyridine donor *trans* to the group X, while isomer (**6**) has the pyridine *trans* to a primary amino donor. The present complex has the isomer (**5**) geometry with the pyridine donor *trans* to an acetonitrile. Selected bond lengths and angles are summarized in Table 2. The nickel–amine and nickel–pyridine bond distances are all fairly similar with slightly shorter bonds to the tertiary nitrogen donor and the pyridine donor, presumably due to the smaller bite angle of the five-membered chelate ring. The average Ni–N bond length of 2.10(4) Å is quite typical for high spin nickel(II) complexes. The Ni–N bond lengths for the acetonitrile ligands are close to the average values noted in previously published structures [12a, 12b, 12c, 12d, 12e]. The Ni–N–C bond angle (167 and 156°) is distorted from the expected value of 180°. The C–N bond lengths of 1.17 and

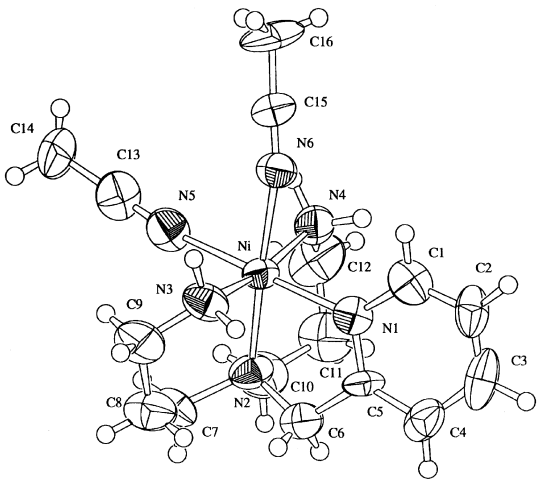

Fig. 2. ORTEP of the complex $[NiL(MeCN)_2](ClO_4)_2$ with the atom numbering scheme.

Table 2. Selected bond distances (Å) and angles (°) in $[NiL(CH_3CN)_2](ClO_4)_2$ with estimated standard deviations in parenthesis

Ni(1)–N(1)	2.02(1)	N(1)–Ni(1)–N(2)	82.3(5)
Ni(1)–N(2)	2.09(1)	N(1)–Ni(1)–N(3)	95.5(6)
Ni(1)–N(3)	2.07(1)	N(1)–Ni(1)–N(4)	90.1(5)
Ni(1)–N(4)	2.15(1)	N(1)–Ni(1)–N(5)	174.8(6)
Ni(1)–N(5)	2.10(2)	N(1)–Ni(1)–N(6)	96.3(6)
Ni(1)–N(6)	2.14(2)	N(3)–Ni(1)–N(4)	168.0(6)
N(6)–C(15)	1.17(2)	N(5)–Ni(1)–N(6)	86.8(6)
N(5)–C(13)	1.19(2)	Ni(1)–N(6)–C(15)	156(1)
		Ni(1)–N(5)–C(13)	167(1)

1.19 Å compare well with the literature values [13] for coordinated acetonitrile and are quite close to the value found in free acetonitrile 1.157 Å. Coordinated acetonitrile is known to hydrolyse quite rapidly in a number of metal complexes to give coordinated acetamide [14]. This result has been attributed to the Lewis acidity of the metal ion leading to polarization of the C=N bond. It is clear from the crystallographic studies that ground state effects are quite small and presumably indicate that the major role of the metal ion in the hydrolytic reaction occurs in stabilising the transition state of the hydrolysis.

The disordered perchlorate anions are located between layers of the complexes and are hydrogen bonded to the primary amino protons as shown in the crystal packing diagram, Fig. 3. The copper(II) complex does not display this type of hydrogen bonding to the perchlorate anions and there are no unusual packing features.

The cobalt(III) and chromium(III) complexes are expected to have the normal octahedral geometry found with complexes of these metal ions. They are also expected to have the isomer (**5**) geometry observed in the nickel(II) complex. Cobalt(III) complexes of trpn of the type $[Co(trpn)X_2]^+$ (X = Cl, Br) are known to aquate very rapidly in aqueous solution to give the $[Co(trpn)(OH_2)_2]^{3+}$ cation [15]. Rapid aquation of the chloride ligands in $[CoLCl_2]^+$ was also observed. The complex is a 3:1 electrolyte in aqueous solution ($\Lambda_M = 421\ S\,cm^3\,mol^{-1}$) indicating rapid loss of the chloride ligands. The much less reactive $[CrLCl_2]Cl$ has $\Lambda_M = 98\ S\,cm^2\,mol^{-1}$ in water consistent with a 1:1 electrolyte. The chromim(III) complex has λ_{max} 404 nm ($\varepsilon = 72$) and 541 nm ($\varepsilon = 59\ dm^3\,mol^{-1}\,cm^{-1}$) values which are quite typical for a *cis*-CrN_4Cl_2 chromophore.

The copper(II) complex $[CuLCl]ClO_4$ has two bands in the visible spectrum in aqueous solution at 736 nm ($\varepsilon = 98$) and 822 nm ($\varepsilon = 100\ dm^3\,mol^{-1}\,cm^{-1}$) consistent with the five-coordinate structure found in the solid state. Hathaway *et al.* [16] have noted two bands in the solid state spectrum of $[Cu(bipy)_2X]X$ complexes which have a trigonal bipyramidal structure in the solid state and in solution.

The $[ZnL](ClO_4)_2$ complex is a 2:1 electrolyte in the noncoordinating solvent nitromethane ($\Lambda_M = 193$ S $cm^2\ mol^{-1}$), suggesting that the complex is 4-coordinate with probably a tetrahedral structure.

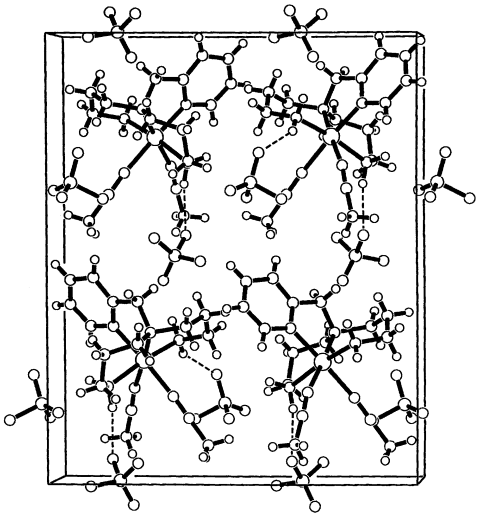

Fig. 3. Packing diagram for the complex $[NiL(MeCN)_2](ClO_4)_2$ showing hydrogen bonding between N3–H...O(3) of the perchlorate anion.

REFERENCES

1. (a) Chin, J. and Banaszczyk, M., *J. Am. Chem. Soc.*, 1989, **111,** 2724; (b) Chin, J., *Acc. Chem. Res.*, 1991, **24,** 145.
2. Chin, J., Jubian, V. and Mrejan, K., *J. Chem. Soc. Chem. Comun.*, 1990, 1326.
3. (a) Milburn, R. M., Massoud, S. S. and Taffese, F., *Inorg. Chem.*, 1985, **24,** 2591; (b) Chin, J., Banaszczyk, M. and Jubian, V., Zou, X., *J. Am. Chem. Soc.*, 1989, **111,** 186.
4. Kimura, E., Young, S. and Collman, J. P., *Inorg. Chem.*, 1970, **9,** 1183.
5. Ngwenya, M. P., Martell, A. E. and Reibenspies, J., *J. Chem. Soc. Chem. Comnun.*, 1990, 1207.
6. Billica, H. R. and Adkins, H., *J. Am. Chem. Soc.*, 1948, **70,** 695.
7. Bauer, H. F. and Drinkard, W. C., *J. Am. Chem. Soc.*, 1960, **82,** 5031.
8. Altomare, A., Burla, M. C., Camalli, M., Cascarano, M., Giacovazzo, C., Guagliardi, A. and Polidori, G., *J.Appl. Crystallogr.*, 1993, **26,** 343.
9. Beurkens, P. T., Admiraal, G., Beurkens, G., Bossman, W. P., de Gelder, R., Israel, R. and Smits, J. M. M., The DIRDIF-94 Program System. Technical report of the Crystallography Laboratory, University of Nijmegen, Netherlands.
10. Crystal Structure Analysis Package. Molecular Structure Corporation, Houston TX, 1985 and 1992.

11. Jain, P. C. and Lingafelder, E. C., *J. Am. Chem. Soc.*, 1967, **89,** 724.
12. (a) Jircitano, A. J. and Mertes, K.B., *Inorg. Chem.*, 1983, **22,** 1828; (b) Freeman, G. M., Barefield, E. K. and Van Derveer, D.G., *Inorg. Chem.*, 1984, **23,** 3092; (c) Constable, E. C., Elder, S. M., Healey, J. and Tocher, D. A., *J. Chem. Soc. Dalton Trans.*, 1990, 1669; (d) Zhuang, Z. J., Matsumoto, N., Okawa, H. and Kida, S., *J. Chem. Soc. Dalton Trans*, 1989, 2095; (e) Adhikary, B., Liu, S. and Lucas, C.R., *Inorg. Chem.*, 1993, **32,** 5957.
13. Weiss, M. C., Bursten, B., Peng, S.-M. and Goedken, V. L., *J. Am. Chem. Soc.*, 1976, **98,** 8021.
14. (a) Barnard, P. F. B., *J. Chem. Soc. A*, 1969, 2140; (b) Breslow, R., Fairweather, R. and Keana, J., *J. Am. Chem. Soc.*, 1967, **89,** 2135; (c) Bennett, M. A., Robertson, G. B., Whimp, P. O. and Yoshida, T., *J. Am. Chem. Soc.*, 1973, **95,** 5649; (d) Buckingham, D. A., Keene, F. R. and Sargeson, A.M., *J. Am. Chem. Soc.*, 1973, **95,** 5649; (e) Curtis, N. J. and Sargeson, A.M., *J. Am. Chem. Soc.*, 1984, **106,** 625; (f) Clark, C. R. and Hay, R. W., *J. C. S. Dalton*, 1974, 4960; (g) Hay, R. W. and Nolan, K. B., *J. C. S. Dalton*, 1974, 914; (h) Zanella, A. W. and Ford, P.C., *Inorg. Chem.*, 1975, **14,** 42; (i) Chin, J. and Kim, J.H., *Angew. Chem. Int. Ed. Engl.*, 1990, **29,** 523.
15. Massoud, S. S. and Milburn, R. M., *Polyhedron*, 1989, **8,** 275.
16. Harrison, W. D., Kennedy, D. M., Power, M., Sheahan, R. and Hathaway, B. J., *J. Chem. Soc. Dalton Trans.*, 1981, 199.
17. Grant, S. J., Moore, P., Omar, H. A. A. and Alcock, N. W., *J. Chem. Soc. Dalton Trans.*, 1994, 485.

Pergamon

PII: S0277-5387(98)00218-6

Polyhedron Vol. 17, Nos. 25, 26, pp. 4353–4364, 1998
© 1998 Elsevier Science Ltd
All rights reserved. Printed in Great Britain
0277–5387/98 $19.00+0.00

Analysis of ^{183}W and ^{17}O NMR chemical shifts in polyoxometalates by extended Hückel MO calculations

Leonid P. Kazansky,[a]* Patrick Chaquin,[b] Michel Fournier[c] and Gilbert Hervé[d]

[a]Institute of Physical Chemistry, Russian Academy of Sciences, 31 Leninski pr., Moscow 114071, Russia

[b]Laboratoire de Chimie Organique Theorique, (URA 506 CNRS) Université Pierre et Marie Curie, 4 Place Jussieu, 75252 Paris Cedex 05, France

[c]Laboratoire de Catalyse hétérogéne et homogéne (402) USTL, 59655 Villeneuve d'Ascq, France

[d]Laboratoire d'Electrochimie et Chimie inorganique, LECSI, Versailles, France

(Received 27 February 1998; accepted 29 May 1998)

Abstract—The extended Hückel molecular orbital (EHMO) calculations have been carried out using cluster approach to polyoxo anions, i.e. calculations have been done for a single octahedron MO_6 of different symmetry and results have been used to analyze ^{183}W and ^{17}O NMR spectra. Using five d→d* energy differences for the individual WO_6 the sum $\Sigma 1/(E_d \rightarrow E_d^*)$ have been calculated and plotted against the ^{183}W chemical shift (from +258 to −670 ppm) for corresponding type of tungsten atom and practically a linear correlation between two parameters have been observed. This points out the electronic nature of the ^{183}W chemical shift. Similar correlation have been found for the ^{17}O NMR chemical shifts (−90 to +800 ppm) when the plotted against product of the R^{-3} $\Sigma 1/(E_p \rightarrow E_p^*)$ where the R^{-3} bond length of the corresponding W–O bond. Increasing the ^{183}W nuclear magnetic shielding with the calculated electron population on tungsten atom for closely related anions has been observed, but no general tendency between δ and the calculated electronic charge if the symmetry of polyhedron is changed is expected. © 1998 Elsevier Science Ltd. All rights reserved

Keywords: polyoxometalates; Hückel molecular orbital calculations; ^{183}W and ^{17}O NMR.

INTRODUCTION

NMR is a very important method for determining the structure of polyoxometalates both in solution and sometimes in the solid state [1–6]. It is also valuable for studying the electronic structure of this rather important class of inorganic complexes from the scientific and practical points of view [1–8]. However, in many cases the interpretation of the results lacks understanding the nature of the chemical shifts of the ^{17}O, ^{59}Mo and ^{183}W NMR, the nuclei which constitute a polyoxoanion.

There are various approaches for calculation of the magnetic shielding and *ab initio* is considered as the most reliable method to calculate the paramagnetic and diamagnetic terms, but it is limited to rather small molecules [9]. The ^{95}Mo NMR chemical shifts and charges on atoms have been calculated for simple and mixed tetrahedral anions $MoX^{2-}{}_4$ where $X=O^{2-}$, S^{2-} and Se^{2-}, including *ab initio* approach [9–15] and the gradual increase of the paramagnetic term with increasing number of S has been found. Though the *ab initio* results did not agree with each other, the calculations have shown the importance of the charge transfer transitions from bonding to antibonding MOs involving mainly the d-orbitals of the molybdenum atom [9–11]. However, large discrepancies in the calculated and observed values have also been

* Author to whom correspondence should be addressed. E-mail: leo@surface.phyche.msk.su.

found if the coordination polyhedron MoX_n changes [14]. The use of the *ab initio* method for the calculation of the chemical shifts for large molecules and particularly the ones having a heavy nucleus such as the ^{183}W one in a distorted polyhedron, seems to present a cumbersome problem, especially if the relativistic correction is needed [16].

It is known that the chemical shift of nuclei, other than proton is mainly determined by the change of the paramagnetic contribution which may be estimated by the Jameson–Gutowsky equation involving the mean excitation energy ΔE and the imbalance of the electrons in the valence shell [17]. In a case of d^0 cations ΔE corresponds to the lowest charge transfer (LCT) band.

Importance of the paramagnetic contribution determining the changes in the observed ^{17}O and ^{183}W NMR chemical shifts has been shown by linear correlation between the ^{17}O NMR shifts for polyoxometalates (Ta, Nb, W, Mo, V) [18] and ^{183}W chemical shifts for a number of polyoxotungstates $XW_{12}O_{40}^{x-8}$ with the Keggin structure [19] and the wavelength of LCT band observed in the UV-spectra of solutions for the corresponding polyoxoanion.

Earlier, an analysis of the ^{183}W NMR shifts and geometry parameters [20] of known structures enabled to find the following general tendency: decreasing the averaged bondlength of individual distorted octahedron having one W═O terminal bond and increasing the number of the vertex bridging oxygen atoms result in larger shielding and in decreasing the ^{183}W NMR shifts. But the data for some other geometry do not follow the observed trend and moreover both the ^{17}O and ^{183}W chemical shifts for polyoxotungstates other than Keggin structure do not correlate with the LCT wavelength [18, 19].

Keeping in mind that according to *ab initio* method the ^{95}Mo NMR chemical shift is inversely proportional to the calculated energy separation between the ground and the excited states or between bonding to antibonding MOs ($d \rightarrow d^*$ transitions) [10–12] we have calculated MO energy diagrams with the extended Hückel MO (EHMO) method for MoX^{2-}_4 (where $X = O^{2-}$, S^{2-}, Se^{2-}) and obtained practically linear correlation between the observed ^{95}Mo NMR chemical shifts and the sum $\Sigma 1/E_n$ where E_n is the energy separation between bonding and five antibonding MOs, like it has been found in the *ab initio* calculations [10–12]. We believe it is not surprising at first, because often the step-like substitution of one ligand by other results in the gradual change of the MO energies which will correlate with the observed chemical shifts. Moreover, the observed ^{95}Mo NMR chemical shifts correlates with the averaged M–X bondlengths, as well. Second, the correlation shows that use the energy separation may be good substitute for the actual excited states which are important in the paramagnetic shielding. From this we have assumed that using EHMO calculations for understanding the ^{183}W NMR chemical shifts may be useful. What is more important is to follow the trend in the ^{183}W NMR chemical shifts within range of -700 to 260 ppm, if the geometric configuration is changed with the *same* type of ligand. In the chemical shift pattern there are some peculiarities which are difficult to explain without understanding its nature.

In this paper we would like to show the possibility to find a general trend in the ^{183}W and ^{17}O NMR chemical shifts characteristic for different types of octahedron WO_6 which may be encountered in the polyoxotungstates using the parameters calculated by the extended Hückel MO method. Surprisingly, such an easy approach has given rather fair correspondence between the observed ^{183}W and ^{17}O chemicals shifts and the calculated parameters for the corresponding type of distorted WO_6 octahedra which constitute a large polyoxoanion. Moreover, the calculation may be extended to consideration of the chemical shifts upon reduction when two electrons are introduced into heteropolyanion whose structure rests unchanged.

MO DIAGRAMS FOR THE DISTORTED OCTAHEDRA WO_6

The EHMO calculations have been carried out using the ICON program [21–23]. The parameters for the calculations are presented in Table 1.

In some attempts to understand the electronic structure of polyoxometalates the EHMO method had been applied for a single regular octahedron (or combination of several octahedra) or for large molecules [24–28]. The present MO diagrams have been calculated for isolated *distorted* octahedra using the real bondlengths and angles found from the X-ray diffraction studies and results of calculations are compared with NMR data.

The isolation of a single octahedron may be justified because in many cases polyoxometalates spectroscopically behave as a sum of several octahedra [29].

In all structures of polyoxo anions the octahedra are strongly distorted because of formation of one or two (practically never three in polyoxo anions) multiple bonds $M{=}O_t$ ($R = 1.69$–1.76 Å), where O_t is the terminal oxygen atom, that, by *trans*-effect, substantially weakens a bond ($M–O_i$) ($R = 2.20$–2.45 Å) in *trans*-position (Figure 1I). When an octahedron has the only terminal $W{=}O_t$ bond, its symmetry is close to C_{4v}. Such configuration is characteristic for complexes of the d^1 cations and for the d^0 and d^1 cations in many polyoxoanions, especially in polyoxotungstates.

However, for most of Mo^{6+} and W^{6+} monomeric complexes the symmetry of MO_6 octahedra is close to C_{2v}, (Figure 1II) resulting from the formation of two *cis* O_2M bonds as more stable configuration using all three d_π orbitals [30].

The distances between the tungsten cation and the bridging oxygen atoms O_c (vertex or corner shared)

Table 1. Ionization potentials, exponents and coefficients

Atom	Orbital	Energy, (eV)	Exponent (coefficient)	Exponent (coefficient)
Tungsten	s	−8.260	1.8900 (1.0000)	
	p	−5.170	1.8500 (1.0000)	
	d	−10.370	0.6454 (1.544)	0.5636 (1.0000)
Oxygen	s	−32.300	2.275 (1.000)	
	p	−12.275	2.270 (1.000)	
Hydrogen	s	−13.600	1.300 (1.000)	

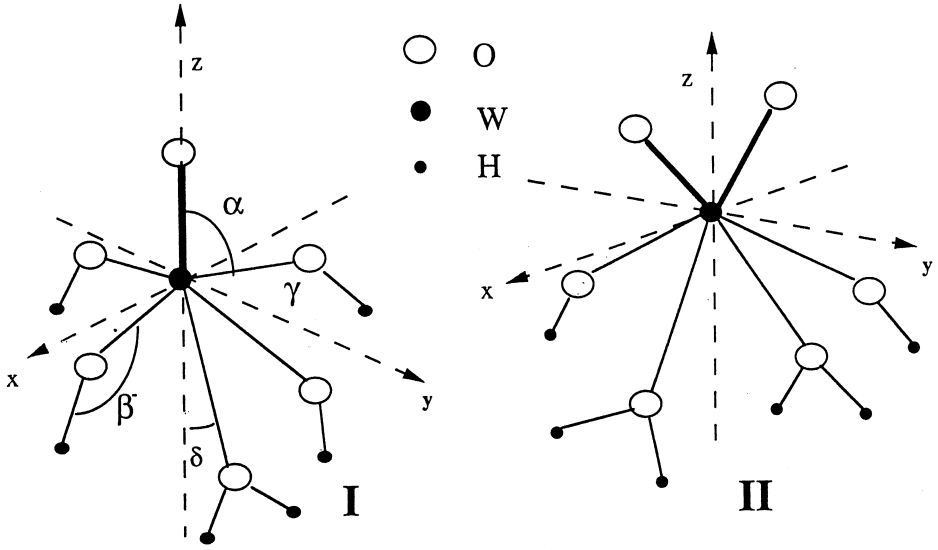

Fig. 1. MO_6 octahedra of C_{4v} (I) and C_{2v} (II) symmetries.

and O_e (edge shared) are in the range of $R = 1.8$–2.0 Å with the angle W–O–W being equal to 150–180° for O_c and 114–125° for O_e, respectively. In the isolated octahedron WO_6 these bridging oxygen atoms are replaced by OH groups ($R_{OH} = 0.94$ Å) to compensate the lack of the adjacent tungsten atoms with the conservation of the angle. The internal oxygen atom O_i is replaced by water molecule. Such presentation may fairly well represent an octahedron in the polyoxometalate frame work. This is confirmed by further EHMO computations using large molecules, though a general gradual stabilization of all antibonding levels has been observed.

The calculation for WO_4^{2-} reveals the expected $d_\pi^* \rightarrow d_\sigma^*$ separation in the MO diagram for tetrahedral configuration. When tetrahedron is converted into a distorted octahedron, its LUMO is stabilized (Figure 2, diagram 0) showing a decrease of HOMO-LUMO separation. Moreover, the calculation for octahedral $OWO(OH)_4OH_2O$ with all bonds (mean for each type) at 90° to each other has showed the difference between the calculated MO diagram with a sequence $d_{xy}^* < d_{xz}^*$, $d_{yz}^* < d_{z^2}^* < d_{x^2-y^2}^*$ and well known and usually accepted MO diagram proposed by Ballhausen and Gray [31] for treating "*yl*" complexes of V, Mo, W (d^1) in the weak ligand field. In their diagram the antibonding orbitals, consisting mostly of metallic *d*-orbitals are found to be in the following order: $d_{xy}^* < d_{xz}^*$, $d_{yz}^* < d_{x^2-y^2}^* < d_{z^2}^*$. Using the geometry adopted in their study, our calculation for $VO(H_2O)_5$ fairly well reproduces the known MO diagram with the coefficient for d_{xy}^* orbital being very close to 1.0. However, in polyoxovanadates as well as in other polyoxometalates, the bond lengths in the bridges M–O–M are much shorter than the V–OH_2 distance as supposed for *penta*aquavanadyl and as a consequence, the position of some MO levels may be changed. The diagram 0 is characteristic for all five cations (V^{5+}, Mo^{6+}, W^{6+}, Nb^{5+}, Ta^{5+}) in the MO_6 octahedron having symmetry close to C_{4v}. The ordering of the energies of the d*-orbitals comes from both the choice of the ligands and the geometry of a polyhedron MO_n.

Actually, the symmetry of each octahedron is deviated from C_{4v}, tungsten atom comes out from the square of the bridging oxygen atoms giving the angle

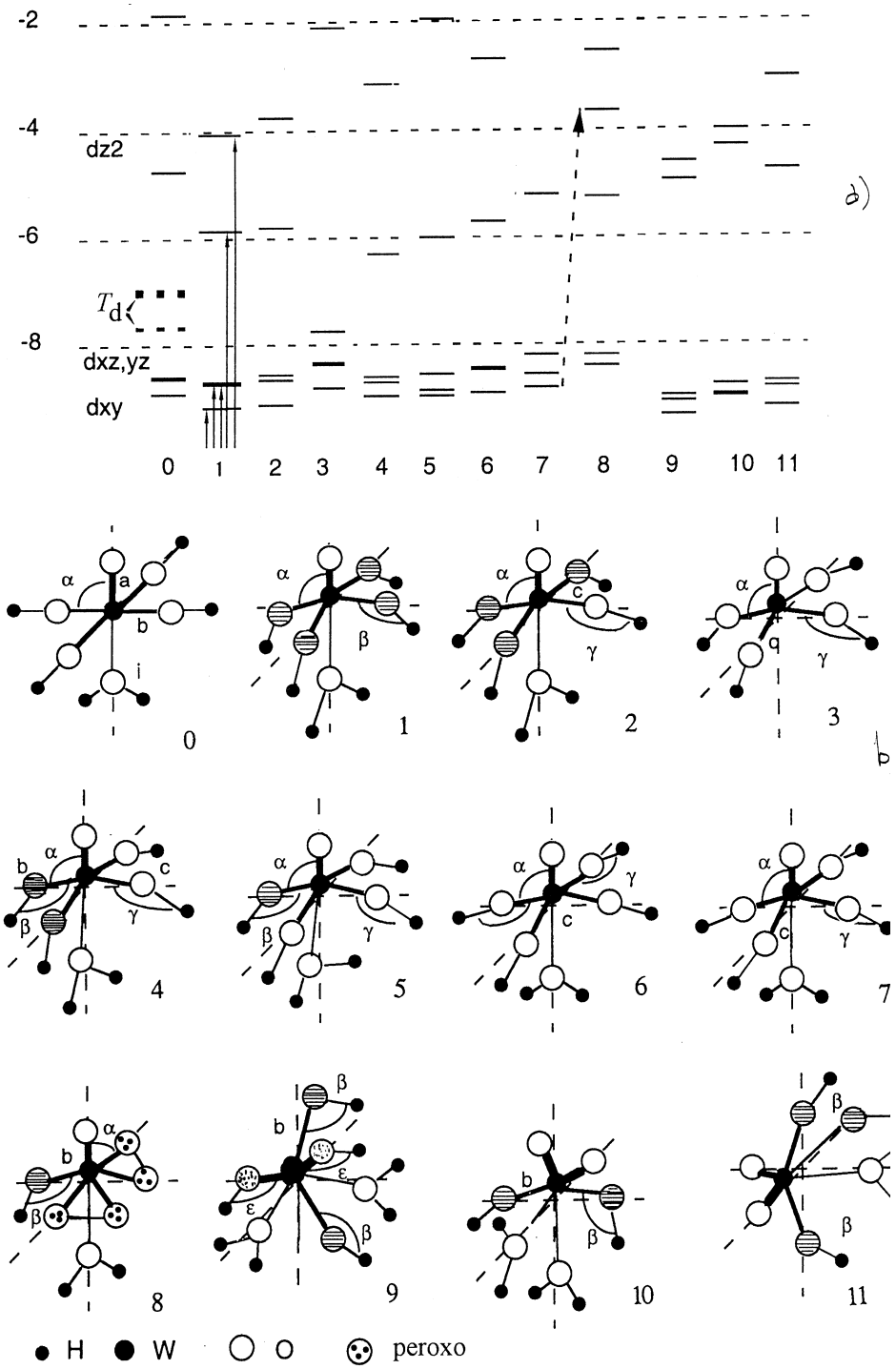

Fig. 2. Calculated MO diagrams (only the virtual antibonding MOs involving mainly the d-orbitals are shown) (a) and distorted polyhedra (b) (α-angle between terminal and bridging (shaded circles for edge-shared and open ones for corner-shared) oxygen atoms, β and γ- angles W–O–W in edge and corner sharing bridges, respectively): (0) for WO_6 – idealized C_{4v} symmetry (broken lines are for WO_4^{2-}); (1) for WO_6 like in $W_6O_{19}^{2-}$ (vertical lines show the transitions from the average bonding to five antibonding levels), (2) for WO_6 in $LnW_{10}O_{36}^{8-}$; (3) for WO_5 like in $P_2W_{21}O_{71}^{6-}$; (4) for WO_6 in $PW_{12}O_{40}^{3-}$, (5) for WO_6 like in the belts of $P_2W_{18}O_{62}^{6-}$, (6) for WOO_4OH_2 in $P_2W_{21}O_{71}^{6-}$; (7) for WO_6 in $P_5W_{30}O_{110}^{14-}$; (8) for WO_7 in peroxotungstates (arrow shows the change of the d_{xy}* position due to substantial interaction with *p*-orbitals of oxygen lying in the plane perpendicular to the *z*-axis; 9, 10, 11) for WO_6 of C_{2v} symmetry $W_7O_{24}^{6-}$-unique W_I with two *pseudo*-terminal bonds (dotted circles) (9), one of four W_{II} (10) and one of two W_{III} (11).

O═W–$O_{c,e}$ larger than 90°. On the other hand, the long bond W–O_i may not be aligned with the axis z, giving the angle ε. Thus the distances W–O and the angles between them are taken from real structures for each type of octahedron with $O_{c,e}$–H direction being aligned with the direction of $O_{c,e}$–W to the neighboring atom, the angles β and γ, respectively.

The change of polyhedron and its symmetry results in the variation of the energies of the antibonding MO levels. The positions of the nonbonding and bonding orbitals are only slightly changing from one case to other with HOMO energy staying fairly constant (Table 2). Therefore, in Fig. 2 only the virtual orbitals, consisting of the metallic d*-orbitals with some admixture of the O2p orbitals and which are more important, are shown.

Without discussing the details of the change in the calculated positions of MOs depending on the geometry we may note that even small deviations from the symmetry close to C_{4v} may change the levels an a result cannot be predicted without calculation. It has been noted as well that the distances noticeably affects the nuclear shieldings calculated by *ab initio* method [14].

Diagram 1 Fig. 2 represents the sequence of MO for an octahedron isolated from highly symmetrical structure $W_6O_{19}^{2-}$ having only edge-shared octahedra [32]. It can be noticed that increasing the angle α between the terminal and bridging oxygen atoms results in decreasing all unoccupied MOs. In the structure of $LnW_{10}O_{36}^{9-}$, there are two types of the tungsten atoms and one which is bound to Ln is taken for calculation (Figure 2, diagram 2) [33]. Each equivalent octahedron WO_6 in the Keggin structure $PW_{12}O_{40}^{3-}$ has two corner and two edge sharing oxygen atoms (Figure 2, diagram 4) [34]. Otherwise, in the Dawson structure $P_2W_{18}O_{62}^{6-}$ two sets (6:12) of WO_6 octahedra [35] one like in the Keggin anion and the other (one of the twelve ones forming two belts) has three corner bridging oxygen atoms. For the latter the MO diagram 5 shows notable change in the position of MOs (Figure 2, diagram 5). The MO diagram 7, calculated for the WO_6 octahedron (all bridging oxygen atoms are used in the corner sharing) which has been found in $NaP_5W_{30}O_{110}^{14-}$ complex, [36] shows large destabilization of MOs.

A peculiar *penta*configuration for one type of tungsten has been found in $As_2W_{21}O_{71}^{6-}$ with rather short W═O_t and four W–O_c bonds [37]. The calculation shows, that such configuration induces the substantial destabilization of all antibonding orbitals, except the $d_{z^2}*$ (Figure 2, diagram 3). As it can be seen, a removal of oxygen from the *trans*-position to O_t stabilizes $d_{z^2}*$ orbital.

In some heteropoly complexes of the types $As_2W_{21}O_{71}^{6-}$, $P_2W_{21}O_{71}^{6-}$ two Keggin fragments may coordinate the tungsten atoms forming WO_6 with four bridging oxygen atoms in the corner positions [37, 38]. A water molecule is really located in *trans*-position to the terminal oxygen atom. This configuration resem-

Table 2. The energies for antibonding MOs, for the effective bonding MO E_{eff} and Λ calculated for different octahedra and ^{183}W NMR data for the corresponding polyoxotungstes

Type*	1	2	3	4	5	6	7	8	9	10	11
$-E$ (eV) W5d*	4.04	3.76	2.01	3.16	1.96	2.71	1.46	2.56	4.59	4.00	3.04
	5.84	5.78	7.76	6.32	6.00	5.70	5.2	3.66	4.96	4.32	4.75
	8.70	8.56	8.36	8.60	8.56	8.46	8.21	5.28	8.94	8.74	8.70
	8.70	8.64	8.36	8.72	8.88	8.46	8.56	8.18	9.04	8.96	8.8
	9.38	9.10	8.80	8.96	8.96	8.90	8.81	8.40	9.29	8.96	9.12
E_{eff}, W5d	15.52	15.43	15.40	15.53	15.51	15.47	15.43	15.15	15.48	15.47	15.59
Λ	0.646	0.640	0.639	0.633	0.626	0.619	0.613	0.560	0.657	0.633	0.619
^{183}W (ppm)	58	−10	−40	−93	−175	−210	−290	−690	269	−92	−179

* Type of polyhedron WO_n in different polyoxotungstates (see text).

bling the idealized one (Figure 2, diagram 0) results in the MO diagram 6.

Finally, the MO diagram 8 is presented for the peroxocomplex of tungsten, where seven coordinations with two peroxogroups located in a plane perpendicular to the W=O$_t$ bond are found [39]. The most noticeable feature is the strong interaction of the W5d$_{xy}$ orbital with the corresponding O2p orbitals, lying in the *xy*-plane. This induces the strong destabilization of the d$_{xy}$* (noted by an arrow).

Thus, changing of a polyhedron geometry results in the variation in energy levels. The calculated data may be compared with the observed chemical shifts.

ENERGY DIFFERENCE BETWEEN OCCUPIES AND UNOCCUPIED MO AND ^{183}W NMR CHEMICAL SHIFTS IN POLYOXOTUNGSTATES

Nuclear magnetic shielding is usually represented as a sum of the diamagnetic, σ^{dia} and paramagnetic, σ^{para} terms [9]. The change in NMR chemical shifts is determined mainly by the paramagnetic term that depends on the excited states of a molecule [9–11]. This is clearly seen in Fig. 3 where ^{193}W chemical shifts for the Keggin anions and ^{17}O chemicals shifts for the terminal and bridging oxygen atoms are plotted against the LCT wavelength (O→M transition) measured in the UV spectra of the Keggin $XM_{12}O_{40}^{x-8}$ anions and isopolyanions $M_6O_{19}^{n-}$. However, if the anions having different structures are compared, no correlation is observed, showing that this optical transition does not contribute much to the observed chemicals shifts.

According to the sum-over-state perturbation theory the paramagnetic term is determined by [10, 11]

$$\sigma_{para} = -\frac{\mu_0 e^2}{8\pi m^2}\sum_n \langle 0|\sum_k r^{-3}{}_k L_{kl}|n\rangle\langle n|\sum_k L_{ku}|0\rangle + \langle 0|\sum_k L_{ku}|n\rangle\langle n|\sum_k r^{-3} L_{kl}|0\rangle/(E_n - E_0),$$

where $|0>$ and $|n>$ denote the ground and excited states wave functions, respectively and E_0 and E_n their energy with r and L being the distance of an electron from the origin and the angular momentum operator around nucleus under study. As Nakatsuji *et al.* [10, 11] have shown, the denominator is the most important in the ^{95}Mo shifts. Thus, σ^{para} is determined by the magnetically dipole-allowed d→d* transitions (the charge transfer from the bonding MO involving d$_\pi$ and d$_\sigma$ metallic orbitals to antibonding MO involving d$_\pi$* and d$_\sigma$*), which usually lie in the far UV-region and do not correspond to HOMO-LUMO separation. For rather distorted MO_6 configuration many transitions are possible, resulting in different contributions to the paramagnetic term and hence to the observed chemical shift. Therefore this should bring about great difficulties in the calculation of the magnetic nuclear shielding. Though EHMO cannot afford the excited states, we believe that the energy separation between the bonding and antibonding levels may fairly represent the excited states of a molecule. So in our case we have simplified the problem and calculated the weight average energy, E_d, of the "effective" bonding MO orbital involving both d$_\pi$ and d$_\sigma$ atomic orbitals using their coefficients and the corresponding calculated energy. As showed calculations, the difference between these bonding *d* orbitals much less then between the antibonding orbitals, so called the ligand field splitting. Then five transitions from this d orbital to five antibonding MO involving W5*d** orbitals (E_d→E(d$_{xy}$), E_d→E(d$_{xz}$), E_d→E(d$_{yz}$), E_d→E(d$_{z^2}$) and E_d→E(d$_{x^2-y^2}$) have been calculated and taken into account.

So in simplified form the paramagnetic term will be proportional [40]

$$\sigma_{para} \propto -r^{-3}\sum \Delta E^{-1}\langle 0|L^2|0\rangle = -r^{-3}\Lambda\langle 0|L^2|0\rangle$$

where $\langle 0|L^2|0\rangle$ is the angular imbalance of the charge and $\Lambda = \Sigma\Delta E^{-1}$ is the sum of five inverse energy separation between the occupied MO (d) orbital and five antibonding MOs involving W5d* Table 2. At present we accept that r^{-3} does not change much throughout a series because the mean bond length R_{W-O} for each octahedron is only slightly changed [20].

Since the antibonding MO's participate both in the magnetic and optical dipole-allowed transitions, for very closely related molecules the chemical shifts may fairly well correlate with the wavelength, λ, or $1/E_{gap}$ (HOMO-LUMO separation). That is why linear correlation between the chemical shifts, δ and λ have been found for MX4n- anions [13, 14] and for polyoxoanions (Fig. 3). But as we have mentioned some points do not fit the correlations because the HOMO-LUMO separation is not important contribution to the paramagnetic term for different symmetries. So for all studied polyhedrons with one terminal bond the Λ values have been calculated and compared with the observed ^{183}W NMR chemical shifts.

The most deshielded tungsten (58 ppm) is observed in $W_6O_{19}^{2-}$ where each WO_6 is linked only by edges. [41] The replacement of one bent W–O–W by W–O–Ln with larger angle in $LnW_{10}O_{36}^{n-}$ results in shielding. [42] Further shielding is observed with increasing the number of the corner sharing oxygen atoms in the Keggin [18, 41], the Dawson [19] and $NaP_5W_{30}O_{110}^{14-}$ anions. [36] The most shielded W is observed in peroxocomplexes with the chemical shift reaching −690 ppm [39]. *Penta*coordinated tungsten atom gives the resonance line in the common range at −40 ppm [37, 39].

Practically linear correlation between the calculated Λ for the individual octahedra, as well as for *penta*- and *hepta*coordinations and the ^{183}W NMR chemical shifts, δ, measured for the corresponding polyoxotungstates is observed [Fig. 4(a)]. It is noteworthy,

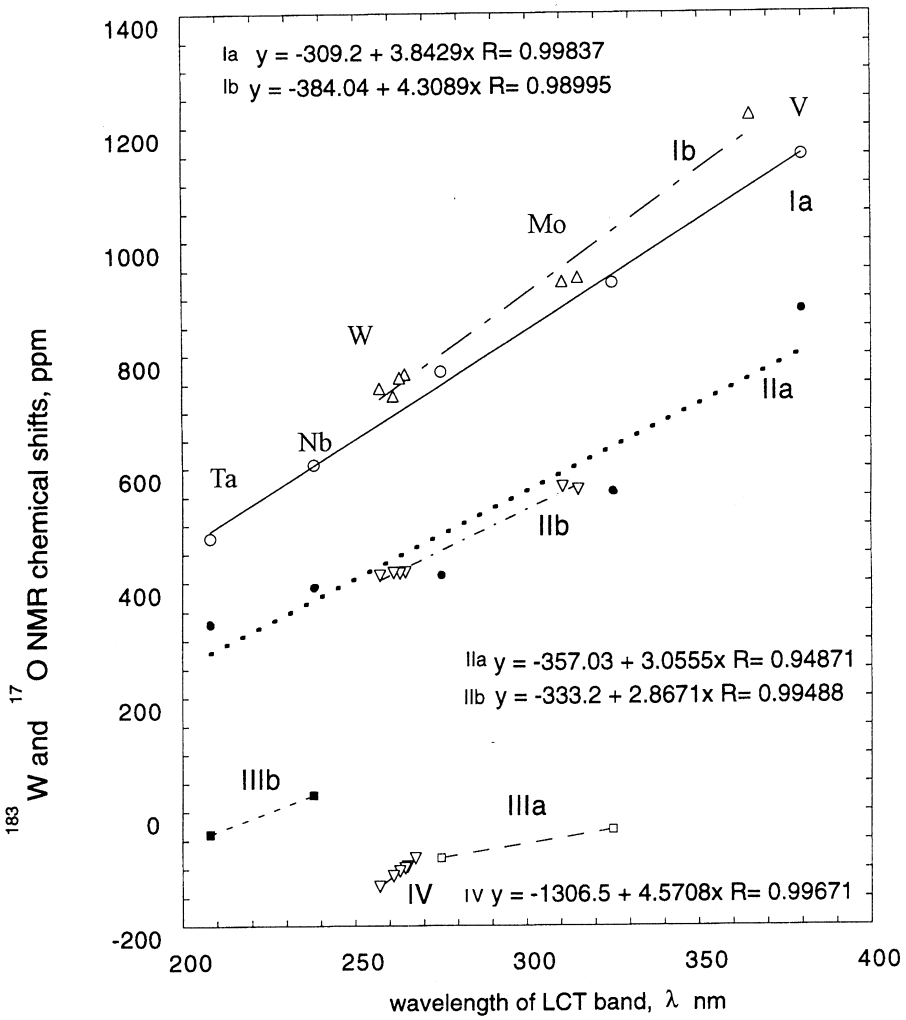

Fig. 3. Correlations between ^{17}O and ^{183}W NMR chemical shifts of different polyoxoanions and the wavelength, λ, of the lowest charge transfer observed in the UV spectra. (Trends Ia and IIa; the chemical shifts for the terminal and bridging oxygen atoms for M6O19*n*-anions, IIIa and IIIb-trends for the internal oxygen atoms in Mo, W and Nb, Ta anions, respectively. Trends Ib and IIb; ^{17}O NMR chemical shifts for the terminal and bridging oxygen atoms of the Keggin anions $XW_{12}O_{40}^{n-}$ and trend IV, ^{183}W NMR in $XW_{12}O_{40}^{n}$ anions, respectively).

that using only the lowest energy separation, for example $d \rightarrow d_{xy}^*$ for any type of octahedron, or the sum of two lowest transitions do not result in the nice correlation. So the paramagnetic term, if we want to compare different symmetries, should include all five transitions and not only the lowest ones, though they certainly dominate.

Additional confirmation of the importance of the $d \rightarrow d^*$ transitions in the chemical shifts has been obtained from MO calculations for the individual octahedra WO_6 with two terminal oxygen atoms (*cis*-MO_2 and symmetry close to C_{2v} as shown in Fig. 2II). Such WO_6 with different degree of distortion are observed in $W_7O_{24}^{6-}$ [43–45], and other polyoxotungstates. The former gives three lines with the 1:4:2 intensity ratio in the ^{183}W NMR spectrum [46, 47]. Corresponding MO diagrams 9–11 Fig. 3 reflect the changes in the coordination sphere with the unique WO_6 (diagram 9) which has two *pseudo*-terminal bonds W=O and reveals the highest chemical shift observed for this type of octahedron (+259 ppm). As we can see, these two points satisfy the correlation except for the unique type of tungsten, whose chemical shift is slightly above, but nevertheless the correlation reasonably explains unusual large shift for this unique tungsten in $W_7O_{24}^{6-}$.

It is encouraging that such a simple approach gives the possibility to assign the observed NMR lines when crystallographic parameters are known and allow to explain some trends in ^{183}W NMR chemical shifts.

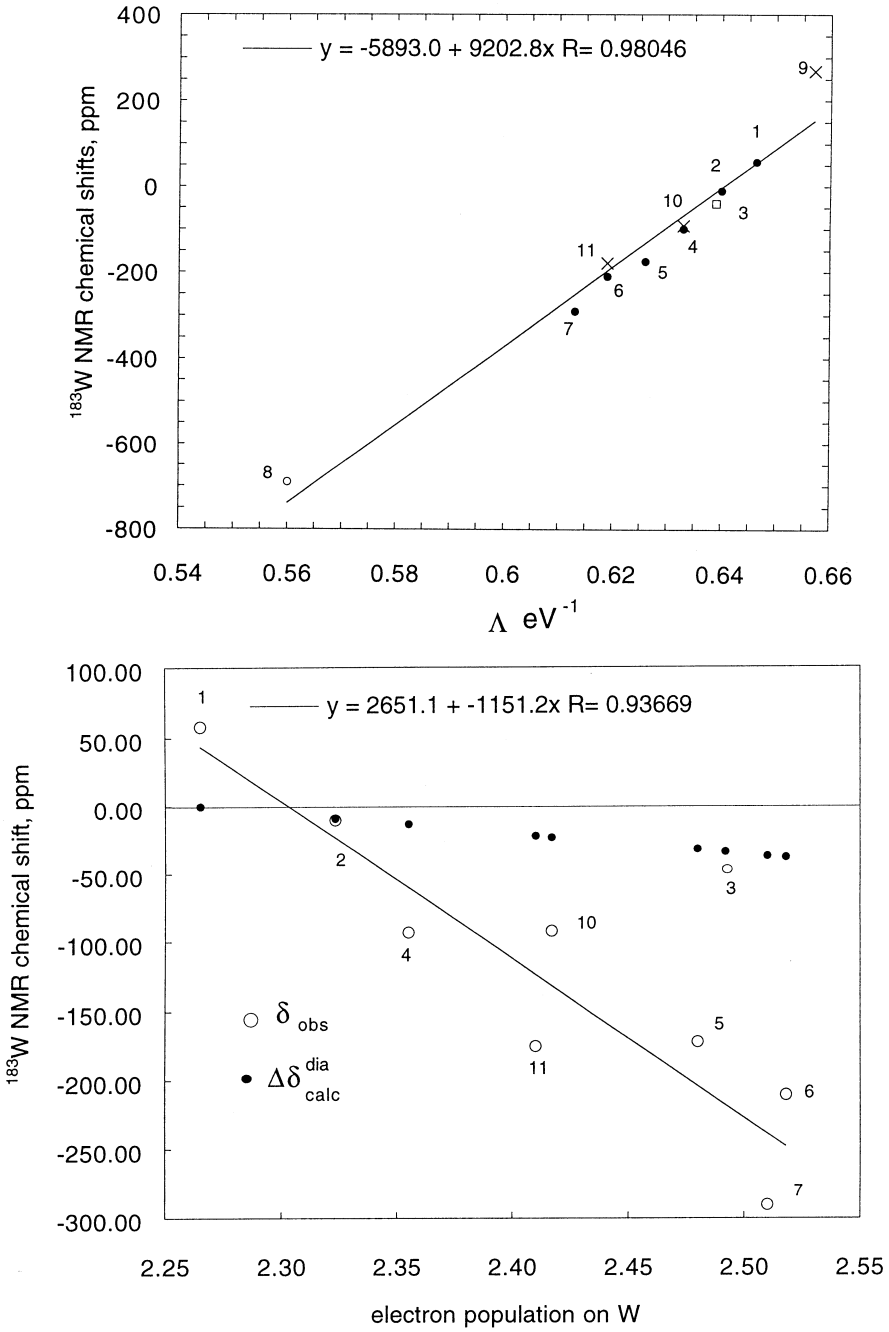

Fig. 4. (a) Correlation of ^{183}W NMR chemical shifts (δ) and the calculated $\Sigma E^{-1}(\Lambda)$ involving separation between occupied and vacant MO (d−d*), involving mainly the W5d and O2p orbitals. (b) Plot between the ^{183}W NMR chemical shifts (δ) and the change of the calculated diamagnetic term, (black circles) against the calculated electron population q, on tungsten atoms.

THE CHEMICAL SHIFTS AND THE CHARGE ON THE TUNGSTEN ATOM

The correlation clearly shows that the excited states contribute considerably to the observed ^{183}W chemical shifts. In some way, the correlation between the ^{183}W shifts, δ and the mean bond length W–O in WO_6 points out a certain dependence of the excited states on the ground state [20]. We may assume that in some extent the ground state determines the excited states and therefore a correlations between δ and a certain ground state property may be observed.

In this connection we have plotted of the measured ^{183}W shifts, δ and the calculated electron population

on tungsten atoms [Fig. 4(b)]. In general, an increase of the negative charge on tungsten results in its shielding that goes parallel to decreasing Λ. Despite some approximations in the calculations of the electron population given by EHMO method, these trends may be used in discussing the chemical shifts of different atoms in complex molecules. For estimation of the effect of the charge we may use the calculated charges and formula given by Malli and Froese [48]. The possible changes in the diamagnetic shielding may be reach 30 ppm. [Fig. 4(b), black points].

Ab initio [10, 11, 14, 15] and EHMO calculations of the charges on molybdenum for $MoO_{4-x}S_x^{2-}$ result in the opposite trend, increasing a gross electron population in the Mo4d orbitals results in the nuclear deshielding. On the contrary, the ^{17}O NMR shifts increase with decrease of the negative charge on oxygen. [13, 14] However, it should be mentioned that the correlation between the chemical shifts and the charges for nuclei other than protons, like presented here and elsewhere [13–15] may be fortuitous and sometimes misleading. The real $\Delta\delta$ depending on the charge may be quite small and may monotonically increases or decreases within a consecutive series adding to or subtracting from much larger values induced by the paramagnetic shielding. The points 3, 11 and 12 in Fig. 4(b) do not fit a general trend found for octahedra of similar symmetry. No general correspondence between ^{77}Se NMR chemical shifts and computed charges has been found in *ab initio* computation of the chemical shifts [49]. Though certain dependence of the ^{55}Mn NMR shifts on the population in d* orbitals had been shown [50].

^{17}O NMR CHEMICAL SHIFTS AND EHMO CALCULATED PARAMETERS

The approach which has been used in analysis of the ^{183}W NMR shifts may be applied for analyzing the ^{17}O NMR chemical shifts, though some limitations should be born in mind because in the calculation we have used an isolated octahedron, whose bridging oxygen atoms are represented by the corresponding OH group. Nevertheless it is appropriate to consider them because the excited states really determine the paramagnetic contribution, as shown by correlation in Fig. 3. Some strengthening of the terminal bond in the Keggin anions compared with hexametalates is clearly seen from the upper position of line IIa in the plot. It shows that the chemical shift is also depended on the metal–oxygen distance. Usually the exponential dependence between the chemical shifts and bondlength for V–O, Mo–O and W–O is usually found [51–53].

For each oxygen atom the weight-averaged energy of the "effective" O2p orbital has been calculated using the appropriate atomic coefficients and the energies. (Table 3) These values do not change much and therefore the values Λ when the separations between this orbital of a given oxygen atom and antibonding MOs are used, are close to each other for the same octahedron. This explains the three dependencies of the chemical shifts on the same wavelength presented in Fig. 3. So in this case we should take into account the bond distances R_{W-O}. In some extent a change in $R_{W-O}{}^{-3}$ is assumed to be proportional to the r^{-3} value of O2p orbital [54]. Therefore for each oxygen atom we multiply the Λ value by the corresponding R^{-3} Table 3 and the observed chemical shifts of three different anions, $W_6O_{19}^{2-}$, $LnW_{10}O_{36}^{9-}$, $PW_{12}O_{40}^{3-}$ and $W_7O_{24}^{6-}$ are plotted against product ΛR^{-3} [Fig. 5(a)]. Once again we have got a fairly linear correlation between two values showing the importance of the electronic origin in the change of the ^{17}O NMR chemical shift. Here we can compare some puzzling results when the shielding of both ^{183}W and ^{17}O nuclei is increasing when passing from $W_6O_{19}^{2-}$ to $LnW_{10}O_{36}^{9-}$ with decreasing Λ, but for $PW_{12}O_{40}^{3-}$ increasing the tungsten shielding (less Λ) corresponds to decreasing oxygen shielding. Namely the term R^{-3} brings about larger values of $R^{-3}\Lambda$ explaining such unexpected trend.

From this position we can come back to Fig. 3 and replot the actual data on the ^{17}O chemical shifts against λR^{-3}, (bondlength W–O and the LCT band with the maximum wavelength, λ, for a number of polyoxotungstates). Linear correlation is observed [Fig. 5(b)] and it validates using this isolated octahedron approach. Extrapolation of the plot $\delta/\lambda R^{-3}$ to zero gives the diamagnetic contribution which is close to the calculated one -350 ppm [48]. It is noteworthy that the point for WO_4^{2-} lies within the observed trend, showing the small influence of the neighboring tungsten atoms of a polymeric structure on the diamagnetic contribution.

As for the charges on the oxygen atoms, their values should be considered when the calculated data for the whole anions are available. It is noteworthy that the internal oxygen atoms reveal some effect on the chemical shifts depending on the overall charge on the polyoxometalates $M_6O_{19}^{n-}$ Fig. 3. Increasing from -2 for W and Mo anions (trend IIIa) to -8 for Ta and Nb anions (trend IIB) results in the positive shift, but it needs special consideration.

CONCLUSIONS

The present calculations of the electronic structure using individual WO_6 octahedra of different symmetries have shown a substantial influence of the local geometry on the position mainly of the antibonding levels. Strong interaction between oxygen and tungsten markedly destabilizes the d_π* and d_σ* orbitals. Despite certain limitations and approximations the practical linear dependence ^{183}W and ^{17}O NMR chemical shifts on the sum of the inverse energies of the five transitions from bonding to antibonding MO points out the electronic nature of the chemical shifts.

Table 3. The LCT wavelength λ (nm), bondlength R_{W-O} (Å), ^{17}O NMR chemical shifts (ppm) and calculated Λ for polyoxotungstates

	λ	O_{term}			$O_{briding}$			O_{intern}		
		R	δ	Λ	R	δ	Λ	R	δ	Λ
$W_6O_{19}^{2-}$	275	1.693	772	0.6534	1.924	413	0.6646	2.325	−61	0.6628
	Ep (eV)			15.42			15.32			15.34
$LaW_{10}O_{36}^{9-}$	256[a]	1.73	656	0.6400	1.93	340	0.6488	2.32	−34	0.6463
	Ep (eV)			15.43	1.91	326	15.33			15.35
	247[a]	1.73	637							
$PW_{12}O_{40}^{3-}$	264.5	1.70	769	0.6480	1.905	418	0.6456	2.45	70	0.6377
	Ep (eV)			15.43			15.38			15.40
$H_2W_{12}O_{40}^{6-}$	261.1	1.72	723		1.92	417		2.22	80	
$W_7O_{24}^{6-}$	WI	1.77	590	0.6802	1.89	254	0.6852	2.26	70	0.6852
	Ep (eV)			15.23			15.18			15.18
	WII	1.74	648	0.6457	1.945	316	0.6493	2.17	70	0.6529
					1.978	295	0.6493	2.28	254	
	Ep (eV)			15.32			15.28			15.24
	WIII	1.745	624	0.6444	1.90	295	0.6462	2.195	70	0.6507
		1.748	603	0.6444						
	Ep (eV)			15.34			15.27			15.22

[a] Broad shoulder in the UV-spectrum deconvoluted into two components and assigned to different W atoms, with 256 nm being attributed to 8 WO_6 linked to La.

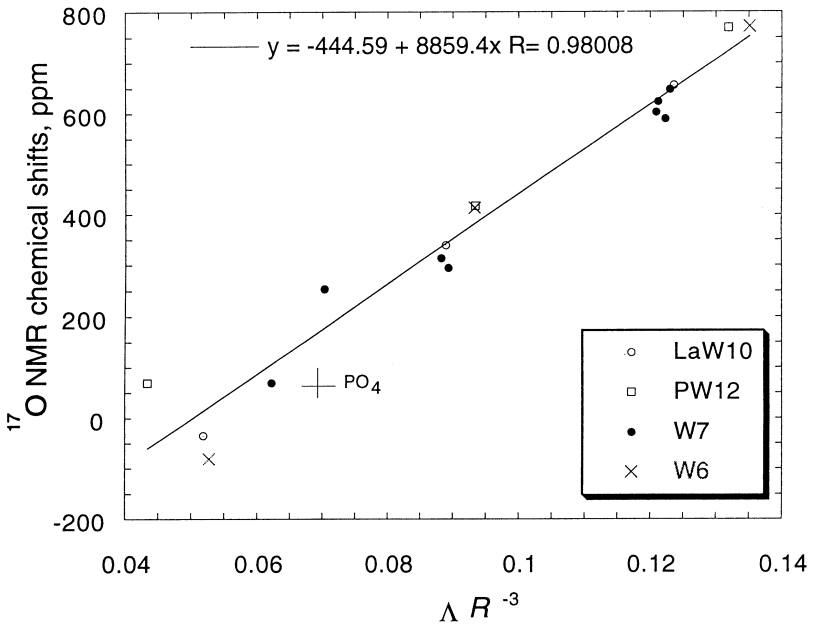

Fig. 5. (a) Correlation between the observed ^{17}O NMR chemical shifts and calculated $R^{-3}\Lambda$ for different types of the oxygen atoms in $W_6O_{19}^{2-}$, $LaW_{10}O_{36}^{9-}$, $PW_{12}O_{40}^{3-}$ and $W_7O_{24}^{6-}$. (b) Plot of the observed ^{17}O chemical shifts and the value $\lambda x R^{-3}$, where λ is the wavelength of the observed lowest charge transfer, O–W (x for WO_4^{2-}) for $W^6O_{19}^{2-}$ (W_6), $PW_{12}O_{40}^{3-}$ and $H_2W_{12}O_{40}^{6-}$ (XW_{12}) and $LaW_{10}O_{36}^{9-}$ (LaW_{10}) anions.

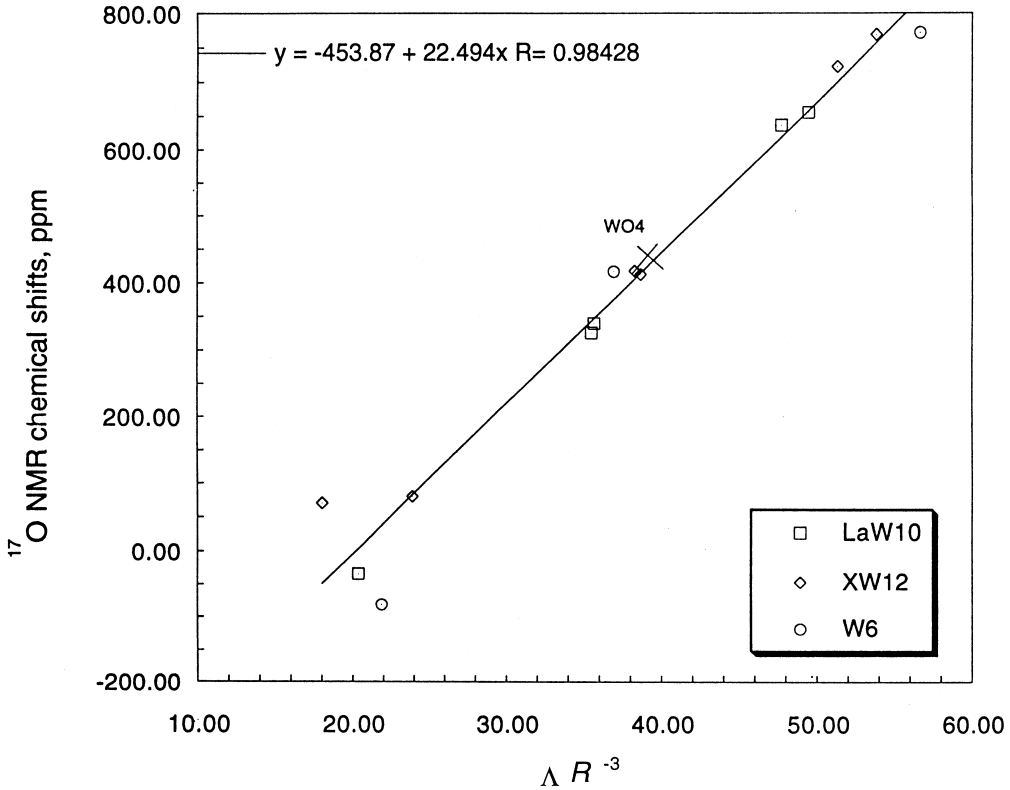

Fig. 5—*continued.*

Even using a distorted polyhedron isolated from a polymeric structure may explain some unexpected chemical shifts. The similar situation has been observed when a cluster approach is used to study the ^{51}V NMR shift in polyoxovanadate with the help of the SOS density functional perturbation theory [55]. We currently try to apply the EHMO for large polyoxoanions to get more insight in the nature of the chemical shifts. Heteropolyanions present an interesting case when one or several addenda cation may be reduced to 5+ or 4+ oxidation states. This reduction may induce large deshielding of the metal nuclei and this case using EHMO approach will be considered elsewhere.

As calculations show, that local geometry of individual in large anions such as $CeW_{10}O_{36}^{8-}$, $W_{10}O_{32}^{4-}$ and $W_7O_{24}^{6-}$ markedly affects the antibonding MO levels, revealing expected trends obtained from the calculations using single octahedron approach. That is why the isolation of one octahedron with its real geometrical characteristics with the linear correlation between the observed chemical shifts and the calculated parameters may be a fairly justifying approach for the qualitative estimation of the chemical shift of a given atom in a molecule. Moreover, using the average energy approach in the calculation made for large polyoxoanions allows to understand some mute points in the chemical shift pattern.

As *ab initio* calculations have shown that the paramagnetic shielding is very critical to the input parameters and by adjusting one may get the full compatibility of the observed and calculated chemicals shielding, especially in a gradual substitution of one ligand atom for other one. So we believe that using "good" input data which may give full correspondence with the observed transitions in the optical spectra, the correlation like we have observed will be much better.

Acknowledgements—L. P. K. is grateful to CNRS for financial support during his work in 1993 at Université Pierre et Marie Curie (Paris).

REFERENCES

1. Pope, M. T., *Hetero and Isopoly Oxometalates*. Springer, Berlin, 1983.
2. Pope, M. T. and Müller, A., *Angew. Chem. Int. Ed. Engl.*, 1991, **30,** 34.
3. Pope, M. T. and Müller A. (Eds), *Polyoxometalates: from platonic solids to antiretroviral activity*. Kluver Academic Publishers, 1993.
4. Black, J. B., Clayden, N. J., Griffiths, L. and Scott, J. D., *J. Chem. Soc. Dalton Trans.*, 1984, 2765.

5. Kozhevnikov, I. V., Sinnema, A., van Bekkum, H. and Fournier, M., *Catal. Lett*., 1996, **41,** 153.
6. Knight, C. T. G., Turner, G. L., Kirpatrick, R. J. and Oldfield, E., *J. Am. Chem. Soc*., 1986, **108,** 7426.
7. Maksimovskaya, R. I., Bondareva, V. M. and Litvak, G. S., *Zh. Neorgan. Khim*., 1996, **41,** 1173.
8. Maksimovskaya, R. I., *Kinet. Katal*., 1995, **36,** 910.
9. Tossel, J. A. (Ed.), *Nuclear magnetic shielding and molecular structure*. NATO ASI Series Reidel, Dordrecht, 1993.
10. Nakatsuji, H., Sugimoto, M. and Saito, S., *Inorg. Chem*., 1990, **29,** 1221.
11. Nakatsuji, H., Sugimoto, M. and Saito, S., *Inorg. Chem*., 1990, **29,** 3095.
12. Nakatsuji, H. in *Nuclear magnetic shielding and molecular structure*, ed. J. A. Tossel. NATO ASI Series, Reidel, Dordrecht, 1993.
13. Combariza, J. E., Enemark, J. H., Barfield, M. and Facelli, J. C., *J. Am. Chem. Soc*., 1989, **111,** 7619.
14. Combariza, J. E., Barfield, M. and Enemark, J. H., *J. Phys. Chem*., 1991, **95,** 5463.
15. Teruel, H. and Sierralta, A., *Polyhedron*, 1996, **15,** 2215.
16. Hada, M., Kaneko, H. and Nakatsuji, H., *Chem. Phys. Lett*., 1996, **261,** 7.
17. Jameson, C. J. and Gutowsky, H. S., *J. Chem. Phys*., 1964, **40,** 1714.
18. Kazanskii, L. P., *Koord. Khim*., 1977, **3,** 327.
19. Acerete, R., Hammer, C. F. and Baker, L. C. W., *J. Am. Chem. Soc*., 1982, **104,** 5384.
20. Kazansky, L. P., *Chem. Phys. Lett*., 1994, **223,** 289.
21. Hoffman, R. and Lipscomb, W. H., *J. Chem. Phys*., 1962, **36,** 2179.
22. Hoffman, R. and Lipscomb, W. H., *J. Chem. Phys*., 1962, **37,** 2872.
23. Hoffman, R. and Lipscomb, W. H., *J. Chem. Phys*., 1963, **39,** 1397.
24. Moffat, J. B., *J. Mol. Catal*., 1984, **26,** 385.
25. Masure, D., Chaquin, P., Louis, C., Che, M. and Fournier, M., *J. Catal*., 1989, **119,** 415.
26. Weber, R. S., *J. Phys. Chem*., 1994, **98,** 2999.
27. Jensen, S. A., Singh, D. J. and Wang, S. H., *Chem. Mater*., 1994, **6,** 146.
28. Chen, T. L., Ji, J., Xiao, S. H., Cai, T. X. and Yan, G. S., *Int. J. Quantum Chem*., 1992, **44,** 1015.
29. So, H. and Pope, M. T., *Inorg. Chem*., 1973, **11,** 1441.
30. Porai-Koshits, M. A. and Atovmian, L. O., *Koord. Khim*., 1975, **9,** 1271.
31. Ballhausen, C. J. and Gray, G. B., *Inorg. Chem*., 1962, **1,** 111.
32. Krylov, N. I. and Kolomnikov, I. S., *Koord. Khim*., 1977, 1895, 3.
33. Ozeki, T. and Yamase, T., *Acta Cryst. C*, 1993, **49,** 1574–1577.
34. Brown, G. M., Noe-Spirlet, M. R., Busing, W. R. and Levy, H. A., *Acta Cryst. B*, 1977, **33,** 1038.
35. Sergienko, V. S., Porai-Koshitz, M. A., Kiselev, S. V., Butman, N. A. and Chuvaev, V. F., *Zh. Neorg. Khim*., 1983, **28,** 1187.
36. Alizadeh, M. H., Harmalker, S. P., Jeannin, Y., Martin-Frére, J. and Pope, M. T., *J. Am. Chem. Soc*., 1985, **107,** 2662.
37. Martin-Frére, J. and Jeannin, Y., *Inorg. Chem*., 1984, **23,** 3394.
38. Tourné, C. M., Tourné, G. F. and Weakley, T. J. R., *J. Chem. Soc. Dalton Trans*., 1986, 2237.
39. Salles, L., Aubry, C., Thouvenot, R., Robert, F., Doremieux-Morin, C., Chottard, G., Ledon, H., Jeannin, Y. and Bregeau, J. M., *Inorg. Chem*., 1994, **33,** 871.
40. Mason, J., *Chem. Rev*., 1987, **87,** 1299.
41. Gansow, O., Ho, R. K. C. and Klemperer, W. G., *J. Organomet. Chem*., 1980, **187,** 27.
42. Fedotov, M. A., Samokhvalova, E. M. and Kazansky, L. P., *Polyhedron*, 1996, **15,** 3341.
43. Burtseva, K. G., Chernaya, T. S. and Sirota, M. I., *Dokl. AN SSSR*, 1978, **243,** 104.
44. Fuchs, J. and Flindt, E.-P., *Z. Naturforsch. b*, 1979, **34,** 412.
45. Ikenoue, S., Mikuriya, M., Miyachi, O., Nukada, R. and Yagasaki, A., *Bull. Chem. Soc. Jpn*., 1994, **67,** 2590.
46. Maksimovskaya, R. I. and Burtseva, K. G., *Polyhedron*, 1985, **4,** 1559.
47. Hastings, J. J. and Howarth, O. W., *J. Chem. Soc. Dalton Trans*., 1992, 209.
48. Malli, G. and Froese, C., *Int. J. Quantum Chem*., 1967, **1,** 95.
49. Buhl, M., Thiel, W., Fleischer, U. and Kutzelnigg, R., *J. Phys. Chem*., 1995, **99,** 4000.
50. Clayton, T. W. and Bursten, B. E., *New J. Chem*., 1991, **15,** 713.
51. Maksimovskaya, R. I., Fedotov, M. A. and Kazansky, L. P., *Reakt. Kimet. Catal. Letts*, 1981, **16,** 185.
52. Fedotov, M. A. and Maksimovskaya, R. I., *Dokl. Akad. Nauk. SSSR*, 1978, **240,** 128.
53. Fedotov, M. A., Kazansky, L. P. and Spitsyn, L. V. I., *Dokl. Akad. Nauk SSSR*, 1983, **272,** 1179.
54. Nakatsuji, H., Hada, M., Tejima, T., Nakajima, T. and Sugimoto, M., *Chem. Phys. Lett*., 1996, **249,** 284.
55. Malkin, W. G., Malkina, O. L., Casida, M. E. and Salahub, D. R., *J. Am. Chem. Soc*., 1994, **116,** 5898.
56. Ramsay, N. F., *Phys. Rev*., 1950, **78,** 699.

Pergamon

Polyhedron Vol. 17, Nos. 25, 26, pp. 4365–4377, 1998
© 1998 Elsevier Science Ltd
All rights reserved. Printed in Great Britain
0277–5387/98 $19.00+0.00

PII: S0277–5387(98)00239–3

Ruthenium(II/III)–bipyridine complexes with four-membered sulphur donor co-ligands: synthesis, metal valence preference, spectroscopic and electron-transfer properties

Shilpa S. Kulkarni, Bidyut Kumar Santra, Pradip Munshi and Goutam Kumar Lahiri*

Department of Chemistry, Indian Institute of Technology, Powai, Bombay, Mumbai 400076, India

(Received 15 April 1998; accepted 11 June 1998)

Abstract—A group of stable ruthenium(II) and (III) mixed-ligand tris-chelated complexes of the type $[Ru^{n+}(bpy)(L)_2]^{z+}$ (**1**–**8**, $n=2$, $Z=0$; **9**, $n=3$, $Z=1$) have been synthesized and characterized (bpy = 2,2′-bipyridine; L = anionic form of the ligands, ROC(S)SK, (R = Me, Et, ^{n}Pr, ^{i}Pr, ^{n}Bu, ^{i}Bu, $-CH_2-$Ph) or $(EtO)_2P(S)SNH_4$ or $(Et)_2NC(S)SNa$). The complexes **1**–**8** are diamagnetic and electrically neutral and the complex **9** is one-electron paramagnetic and behaves as 1:1 electrolyte in acetonitrile solvent. The complexes **1**–**8** and **9** display two MLCT transitions near 530, 370 nm and 663, 438 nm respectively. Intra-ligand bipyridine based π–π^* transition is observed near 300 nm. The complexes **1**–**8** exhibit room-temperature emission from the highest energy MLCT band (~370 nm). At room temperature the lifetime of the excited states for the complexes **2** and **8** are found to be 90 and 95 ns respectively. In acetonitrile solution the complexes **1**–**9** show a reversible ruthenium(III)–ruthenium(II) couple in the range $-0.08 \rightarrow 0.40$ V and irreversible ruthenium(III)–ruthenium(IV) oxidation in the range 1.19–1.45 V vs Ag/AgCl. One reversible bipyridine reduction is observed for each complex in the range $-1.70 \rightarrow -1.85$ V vs Ag/AgCl. The presence of trivalent ruthenium in the oxidized solution for one complex **1** is evidenced by the axial EPR spectrum at 77 K. The isolated trivalent complex **9** also exhibits an axial EPR spectrum at 77 K. The EPR spectra of the trivalent ruthenium complexes ($\mathbf{1}^+$ and **9**) have been analyzed to furnish values of distortion parameters ($\Delta(cm^{-1}) \rightarrow \mathbf{1}^+$, 3689; **9**, 3699) and energies of the two expected ligand field transitions ($v_1(cm^{-1}) \rightarrow \mathbf{1}^+$, 3489; **9**, 3497 and $v_2(cm^{-1}) \rightarrow \mathbf{1}^+$, 4339; **9**, 4348) within the t_2 shell. One of the ligand field transitions has been experimentally observed at 4673 cm^{-1} for complex **9** and which close to the computed v_2 value (4348 cm^{-1}).© 1998 Elsevier Science Ltd. All rights reserved

INTRODUCTION

Since the discovery of important photo-redox properties of ruthenium–bipyridine complexes, there has been continuous research activity in this area [1–12]. Here the main thrust has been primarily focused on the development of newer ruthenium–bipyridine systems with the perspective of interesting physico-chemical properties. Basic strategies behind all these activities are either to incorporate selective groups within the bipyridine moiety itself or use other types of donor sites along with the ruthenium--bipyridine core to generate mixed-ligand mononuclear or polynuclear complexes to modulate the photo-redox activities of this class of complexes [13–28]. The present work originates from our interest in preparing new mixed-ligand ruthenium–bipyridine complexes of type $[Ru(bpy)(L)_2]$, where L is a sulphur donor ligand which can form a four-membered chelate ring on coordination and in studying the effect of sterically hindered S,S donor ligands L on the redox and spectroscopic properties of the Ru–bpy core. As a part of our program here we have chosen dithiocarbonate, $ROC(S)S^-$; dithiophosphate, $(RO)_2P(S)S^-$ and dithiocarbamate $(R)_2NC(S)S^-$ as ligand L. Herein we report the synthesis of three classes of complexes having RuN_2S_4 chromophore, their spectroscopic and

* Author to whom correspondence should be addressed.

electrochemical properties, spectroelectrochemical correlation and preliminary photophysical aspects. To the best of our knowledge this work demonstrates the first example of $[Ru(bpy)(L)_2]$ complexes where L is a sterically hindered four-membered sulphur donor ligand.

RESULTS AND DISCUSSION

Synthesis

Three types of S,S donor ligands, potassium salt of dithiocarbonate (KL^{1-7}), ammonium salt of dithiophosphate (NH_4L^8) and sodium salt of dithiocarbamate (NaL^9) are used for the present study.

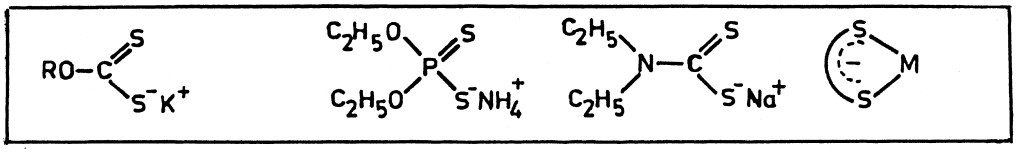

The anionic form of the ligands (L^-) bind to the metal ion as bidentate S,S coordinators forming a four-membered chelate ring (ML).

The complexes, $[Ru^{II}(bpy)(L^{1-8})_2]$ (**1**–**8**) and $[Ru^{III}(bpy)(L^9)_2]^+$ (**9**) (bpy = 2,2′-bipyridine) have been synthesized from $[Ru(bpy)Cl_3]$ following the general dechlorination route shown in Scheme 1.

The reactions of potassium salt of dithiocarbonate ligands (KL^{1-7}) with the starting complex $Ru(bpy)Cl_3$ spontaneously result in red colored complexes **1**–**7** at room temperature, whereas the reaction of ammonium salt of dithiophosphate NH_4L^8 with the $Ru(bpy)Cl_3$ requires slight heating to yield the violet colored complex **8**. The crude products **1**–**8** were purified by column chromatography using silica gel column.

The reaction of sodium salt of diethyl dithiocarbamate with the $Ru(bpy)Cl_3$ under stirring condition at room temperature yields green colored cationic complex **9**. The cationic complex **9** has been isolated as perchlorate salt, $[Ru^{III}(bpy)(L^9)_2]ClO_4$.

Although dithiocarbonate (L^{1-7}) and dithiophosphate (L^8) ligands stabilize the ruthenium ion in the complexes **1**–**8** in bivalent Ru(II) state, the corresponding dithiocarbamate complex **9** stabilizes the trivalent Ru(III) state. The chemically and electrochemically generated trivalent Ru(III) congeners of complexes **1**–**8** and bivalent Ru(Il) congener of complex **9** are unstable at room temperature (see later). The bipyridine ligand is known to stabilize the bivalent ruthenium due to its strong π-acidic nature [13–28]. Since all the three types of complexes (**1**–**7**, **8** and **9**) consist of one bipyridine ligand common, the observed metal oxidation state preference in the complexes (**1**–**9**) is therefore naturally originated from the inducted dithio ligands (L^{1-9}).

The stabilization of Ru(III) state in the case of dithiocarbamate complex (**9**) is not clearly under-

$$Ru(bpy)Cl_3 + KL^{1-7} \xrightarrow{(i)} [Ru^{II}(bpy)(L^{1-7})_2]$$
1–7

$$Ru(bpy)Cl_3 + NH_4L^8 \xrightarrow{(ii)} [Ru^{II}(bpy)(L^8)_2]$$
8

$$Ru(bpy)Cl_3 + NaL^9 \xrightarrow{(iii)} [Ru^{III}(bpy)(L^9)_2]^+$$
9

Ligand	Complex
L^1	→ **1**
L^2	→ **2**
L^3	→ **3**
L^4	→ **4**
L^5	→ **5**
L^6	→ **6**
L^7	→ **7**
L^8	→ **8**
L^9	→ **9**

Scheme 1. (i) MeOH, stirring, (ii) MeOH, heat and (iii) MeOH, stirring.

stood, however, the inherent electronegativity difference between the N atom of L^9 and oxygen atom of L^{1-7} and the π-acceptor nature of the phosphorus of L^8 might be responsible for the above valence state preference in the complexes **1**–**9**.

The microanalytical data of the complexes are shown in Table 1. The results are in good agreement with the calculated values thus confirming the composition of the mixed-ligand tris-chelates [Ru(bpy)$(L^{1-8})_2$] (**1**–**8**)] and [Ru(bpy)$(L^9)_2$]ClO_4 (**9**). In acetonitrile solution the complexes **1**–**8** do not show any conductivity whereas the complex **9** exhibits 1:1 conductivity (Λ_M, 150 $\Omega^{-1}\,cm^2\,M^{-1}$). Solid state magnetic moment measurements at 298 K indicate that the complexes **1**–**8** are essentially diamagnetic (t_{2g}^6, idealized $S=0$) and complex **9** is one-electron paramagnetic ($\mu_{eff}=1.91\,\mu\beta$) as expected for the 3+ state of ruthenium (low-spin d^5, $S=1/2$).

Spectral study

IR spectra FTIR spectra of the complexes (**1**–**9**) were recorded as KBr discs. Direct comparisons of the IR spectra of **1**–**9** with that of the starting complex [Ru(bpy)Cl_3] indicate that the ν_{Ru-Cl} vibrations near 330 cm^{-1} [29] are absent in the former complexes and new vibrations due to the coordinated ligands L are systematically present in the complexes (**1**–**9**). A very strong and broad vibration at 1098 cm^{-1} and a strong and sharp band at 624 cm^{-1} are observed for the complex **9** due to the presence of ionic perchlorate.

^1H *NMR spectra* In $CDCl_3$ solvent, all the complexes (**1**–**8**) display well resolved ^1H NMR spectra. The spectral data are listed in Table 2 and two representative spectra are shown in Fig. 1. The assignment of the individual proton resonances are made on the basis of their relative intensity and spin–spin structure [30]. All the complexes (**1**–**8**) should have plane of symmetry and this makes each half of the molecule equivalent. In view of the imposed symmetry around the ruthenium center aromatic region of the spectra of complexes (**1**–**6** and **8**) displaying systematically four signals having equal intensities (two doublets and two triplets) (Fig. 1) correspond to one pyridine ring of bipyridine ligand. In the case of complex **7** aromatic region of the spectrum shows additional peaks due to phenyl ring attached to the dithiocarbonate ligand (L^7) (Table 2). The phenyl ring protons are not resolved properly and all the five protons have appeared as one complex signal centered at 7.36 ppm (Table 2), which precluded unequivocal assignment of the signals as doublets or triplets. However, the presence of five phenyl ring protons is clearly observable from the relative intensity of the peaks. Depending on the nature of L aliphatic region of the spectra display distinct signals for O–CH_3, O–CH_2, O–CH, –CH, –CH_2 and –CH_3 protons correspond to one ligand (L) as imposed symmetry makes the two

Table 1. Microanalytical, electronic absorption and emission data

Compound	Elemental analysis (%)[a]			Electronic spectral data[b] λ_{max} (nm) (ε[c], $M^{-1}\,cm^{-1}$)	Emission data[b]	
	C	H	N		λ_{max} (nm)	λ_{max} (nm)
1	35.55 (35.66)	2.89 (2.97)	5.82 (5.94)	531(4480), 401(6750)[d], 365(7660), 299(13870)	365	429
2	38.56 (38.47)	3.51 (3.60)	5.75 (5.61)	537(4500), 401(5750)[d], 370(6720), 298(12300),	370	423
3	40.84 (40.97)	4.13 (4.17)	5.25 (5.31)	538(3860), 399(5500)[d], 374(6000), 298(11820)	374	420
4	40.82 (40.97)	4.22 (4.17)	5.46 (5.31)	540(6280), 403(8000)[d], 374(9420), 299(13620)	374	430
5	43.37 (43.23)	4.75 (4.68)	5.16 (5.04)	537(4810), 400(6750)[d], 370(8050), 299(13400)	370	421
6	43.32 (43.23)	4.61 (4.68)	4.92 (5.04)	539(6760), 403(8000)[d], 373(9280), 299(13400)	373	424
7	50.19 (50.07)	3.65 (3.53)	4.33 (4.49)	524(3400), 407(5600)[d], 365(6250), 299(12810)	365	433
8	34.55 (34.44)	4.52 (4.46)	4.37 (4.46)	528(3080), 380(5160), 299(13010)	380	429
9	36.82 (36.77)	4.17 (4.29)	8.71 (8.58)	663(1610), 438(3150), 340(8000)[d], 301(13950)	–	–

[a] Calculated values are in parentheses.
[b] In acetonitrile solution.
[c] Extinction coefficient.
[d] Shoulder.

Table 2. ^{1}H NMR spectral data in $CDCl_3$

Compound	δ (J/Hz)[a]											
	6H	3H	4H	5H	$-OCH_3$	$-OCH_2$	–OCH	–CH	$-CH_2(1)$	$-CH_2(2)$	$-CH_3$	–ph
1	9.45 (7.20)[b]	8.04 (9.30)[b]	7.67 (7.5)[c] (7.5)	7.35 (6.5)[c] (6.5)	4.12[d]	–	–	–	–	–	–	–
2	9.46 (7.69)[b]	8.03 (9.73)[b]	7.65 (9.73)[c] (8.76)	7.34 (8.11)[c] (8.11)	–	4.60 (7.08)[e] (7.08) (7.08)	–	–	–	–	1.44 (7.32)[c] (7.32)	–
3	9.46 (7.67)[b]	8.02 (7.06)[b]	7.64 (7.06)[c] (7.06)	7.33 (7.06)[c] (7.06)	–	4.50 (7.10)[c] (7.10)	–	–	1.84[f]	–	1.01 (7.06)[c] (7.06)	–
4	9.46 (7.69)[b]	8.01 (9.73)[b]	7.64 (8.92)[c] (9.72)	7.32 (8.11)[c] (8.91)	–	–	5.56[f]				1.43 (6.00)[b] 1.37 (6.00)[b]	–
5	9.44 (7.69)[b]	8.01 (7.94)[b]	7.62 (7.94)[c] (7.94)	7.31 (6.17)[c] (7.02)	–	4.53 (7.50)[c] (6.50)	–	–	1.78[f]	1.43[f]	0.92 (8.18)[c] (8.18)	–
6	9.45 (7.69)[b]	8.00 (7.10)[b]	7.63 (7.71)[c] (7.71)	7.33 (6.85)[c] (7.71)	–	4.30 (7.69)[b]	–	2.12[f]			1.02 (7.06)[b] 0.95 (6.17)[b]	–
7	9.40 (7.90)[b]	8.01 (8.10)[b]	7.65 (7.92)[c] (7.87)	7.45 (8.10)[c] (7.65)		5.59 (9.37)[e] (9.37) (9.37)						7.36[g]
8	9.94 (8.50)[b]	7.96 (6.80)[b]	7.61 (6.85)[c] (7.50)	7.35 (8.20)[c] (7.60)	–	4.22 (7.60)[e] (3.91) (8.30)[e]	–	–	–	–	1.34 (6.43)[c] (6.48) 1.23 (6.72)[c] (6.72)	–

[a] Tetramethyl silane is the internal standard.
[b] Doublet.
[c] Triplet.
[d] Singlet.
[e] Quartet.
[f] Multiplet, center value is given.
[g] Overlapping phenyl protons, center value is given.

ligands (L) equivalent in the complexes. In fact the upfield region of the spectra displaying excellent distribution pattern of the aliphatic proton signals (Table 2). In all cases experimentally observed relative ratio of aromatic protons to aliphatic protons matches very well with the calculated values.

Electronic spectra The solution electronic spectra of the complexes (**1**–**9**) were recorded in acetonitrile solvent in the UV–visible region (200–900 nm). The spectral data are listed in Table 1 and the representative spectra are shown in Fig. 2. The absorption spectra of all the complexes **1**–**8** are similar and showing one intense transition in the UV region and two moderately intense transitions in the visible region near 530 and 370 nm. The 370 nm band is associated with a shoulder at the lower energy part near 400 nm (Table 1). The lowest energy bands near 530 and 400 nm can be attributed to $d\pi(Ru) \rightarrow \pi^*(bpy)$ (symmetric) and $d\pi(Ru) \rightarrow \pi^*(bpy)$ (antisymmetric) MLCT transitions [31–36]. The next higher energy band near 370 nm may be due to $d\pi(Ru) \rightarrow L(MLCT)$ transition. The absorption at 300 nm is assigned to π–π^* ligand centered (bpy) transition. It may be noted that the lowest energy MLCT transition of $[Ru(bpy)_3]^{2+}$ appears at 452 nm [37] gets substantially shifted to a lower energy ($\sim$530 nm) on substituting

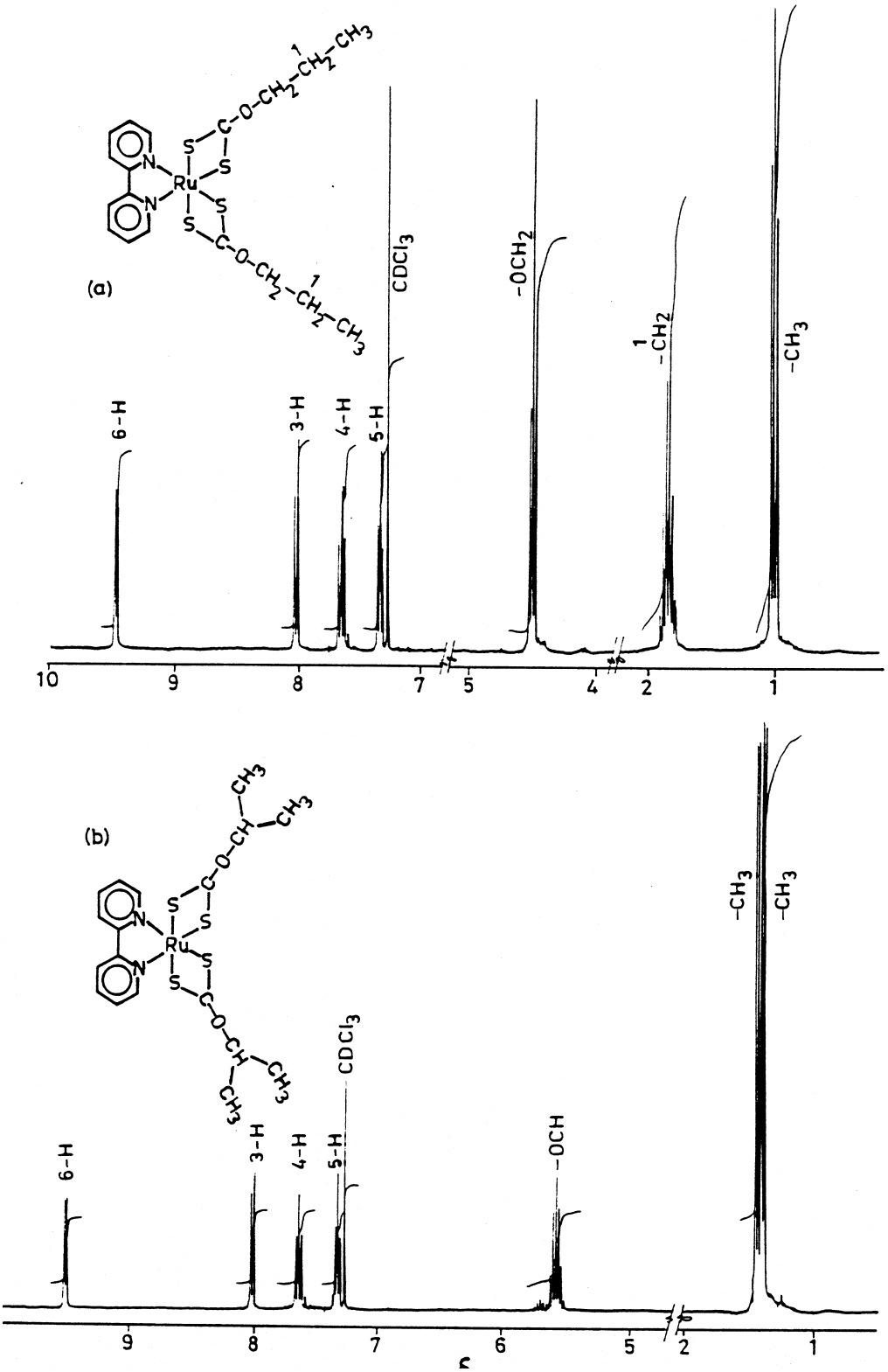

Fig. 1. ^{1}H NMR spectra of (a) $[Ru^{II}(bpy)(L^3)_2]$, **3** and (b) $[Ru^{II}(bpy)(L^4)_2]$, **4** in $CDCl_3$.

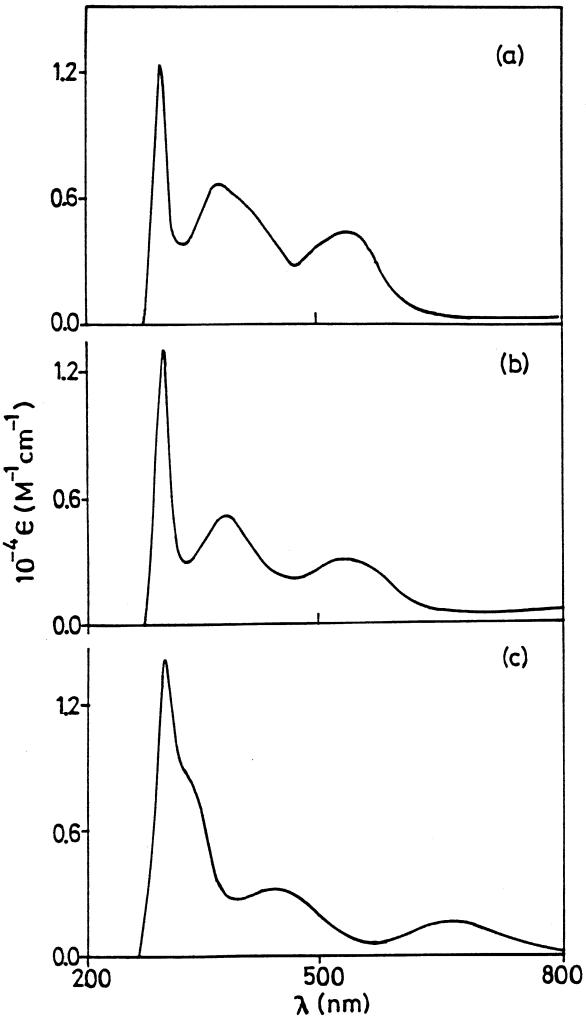

Fig. 2. Electronic spectra of (a) $[Ru^{II}(bpy)(L^2)_2]$, **2**, (b) $[Ru^{II}(bpy)(L^8)_2]$, **8** and (c) $[Ru^{III}(bpy)(L^9)_2]$ ClO_4, **9** in acetonitrile at 298 K.

bpy with dithio ligands, which is in consonance with greater σ-donor and weaker π-acceptor property of L relative to bpy. The electronic spectrum of trivalent ruthenium complex **9** also showing similar three bands but the first two bands are shifted to further lower energy (Table 1). The lowest energy transition at 663 nm is assigned to be the ligand to metal charge-transfer (LMCT) transition as expected for the Ru(III) complexes [38].

Room-temperature emission spectra Emission properties of the complexes (**1**–**8**) were studied in acetonitrile solution at room temperature. The spectral data are listed in Table 1 and the representative spectra are shown in Fig. 3. Excitations of the complexes **1**–**8** near 530 nm (peak position of the lowest energy MLCT band) exhibit very weak emissions, however, excitations near 370 nm (corresponding peak position of the second lowest energy band) result in moderately strong emissions in between 420 to 430 nm (Table 1). The origin of the emissions was further confirmed by the corresponding excitation spectrum of the same solution. It may be noted that the free ligands (KL^{1-7} and NH_4L^8) also showing emissions near 400 nm.

Since both the free ligands (KL^{1-7} and NH_4L^8) and the complexes (**1**–**8**) exhibit emissions around the same positions, the observed emissions for the complexes may therefore be originated from the MLCT band involving primarily the co-ordinated ligands (L).

The lifetime of the excited states of two representative complexes (**2** and **8**) have been determined and are found to be 90 and 95 ns respectively, at room temperature.

Redox properties

All the complexes are electroactive with respect to metal as well as ligand centers. Redox properties of

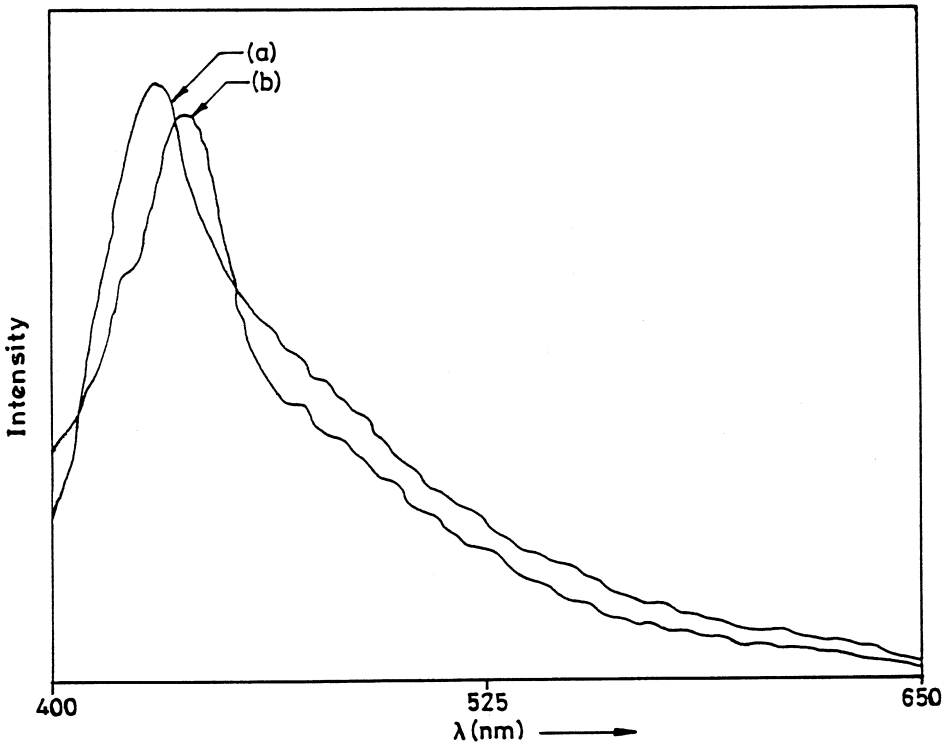

Fig. 3. Emission spectra of (a) $[Ru^{II}(bpy)(L^{8})_2]$, **8** and (b) $[Ru^{II}(bpy)(L^{7})_2]$, **7** in acetonitrile at 298 K.

the complexes have been studied in acetonitrile solvent by cyclic voltammetry (CV) using a platinum working electrode. The complexes (**1**–**9**) display three redox processes in the potential range ± 2.0 V vs Ag/AgCl (tetraethylammonium perchlorate used as an electrolyte, 298 K). Representative voltammograms are shown in Fig. 4. The peak-to-peak separations of the couples lie in the range of 70–90 mV. Reduction potentials data are listed in Table 3.

The ruthenium(III)–ruthenium(II) couple

The complexes **1**–**8** display one reversible oxidation process in the range 0.2–0.4 V and complex **9** exhibits one reversible reduction process at -0.08 V vs Ag/AgCl (Fig. 4) which are assigned to be the ruthenium(III)–ruthenium(II) couple eqn (1) [39].

$$[Ru^{III}(bpy)(L)_2]^{+} + e^{-} \rightleftharpoons [Ru^{II}(bpy)(L)_2] \qquad (1)$$

The one-electron nature of the responses is established by current height and constant potential coulometric data. The presence of trivalent ruthenium in the oxidized solutions of **1**–**8** is confirmed by characteristic EPR spectrum of the ruthenium(III) congener (see later). The formal potential of the couple (eqn (1)) varies depending on the nature of ligands L. Although ruthenium ion in the complexes having dithiocarbonate (**1**–**7**) and dithiophosphate (**8**) ligands stabilizes in 2+ oxidation state, the corresponding dithiocarbamate complex (**9**) stabilizes the trivalent ruthenium ion. The low ruthenium(III)–ruthenium(II) potential ($E_{298}{}^{0} = -0.08$ V) of complex **9** can account for its stabilization in the trivalent state rather than the bivalent state under atmospheric conditions. Thus the electrochemically as well as chemically generated bivalent congener of **9** is unstable in presence of air, spontaneously oxidized to the trivalent complex **9**. Since the reaction takes place particularly under atmospheric conditions the oxygen in air might be responsible for the stabilization of trivalent ruthenium in the complex **9**.

Under identical experimental conditions, the ruthenium(III)–ruthenium(II) reduction potential of $[Ru(bpy)_3]^{2+}$ appears at 1.27 V [31–35]. Thus substitutions of well known π-acidic bpy ligands from the $[Ru(bpy)_3]^{2+}$ core by two dithio ligands, L in the complexes (**1**–**9**) result in decrease of ruthenium(III)–ruthenium(II) potential by 0.9–1.4 V depending on the nature of ligands L. The monoanionic dithio ligands L^{-} decrease the overall charge of the complex cation 2+ in $[Ru(bpy)_3]^{2+}$ to zero in the present complexes (**1**–**9**) and that reduction of overall charge provides further electrostatic stabilization of the oxidized trivalent Ru^{III}–L species. This is possibly developed due to the σ-donor character of the dithio ligands [39]. This substantial decrease in Ru^{III}–Ru^{II} potential while moving from $[Ru(bpy)_3]^{2+}$ to $[Ru(bpy)(L)_2]$ (**1**–**8**) and the reversible nature of the voltammograms (Fig. 4)

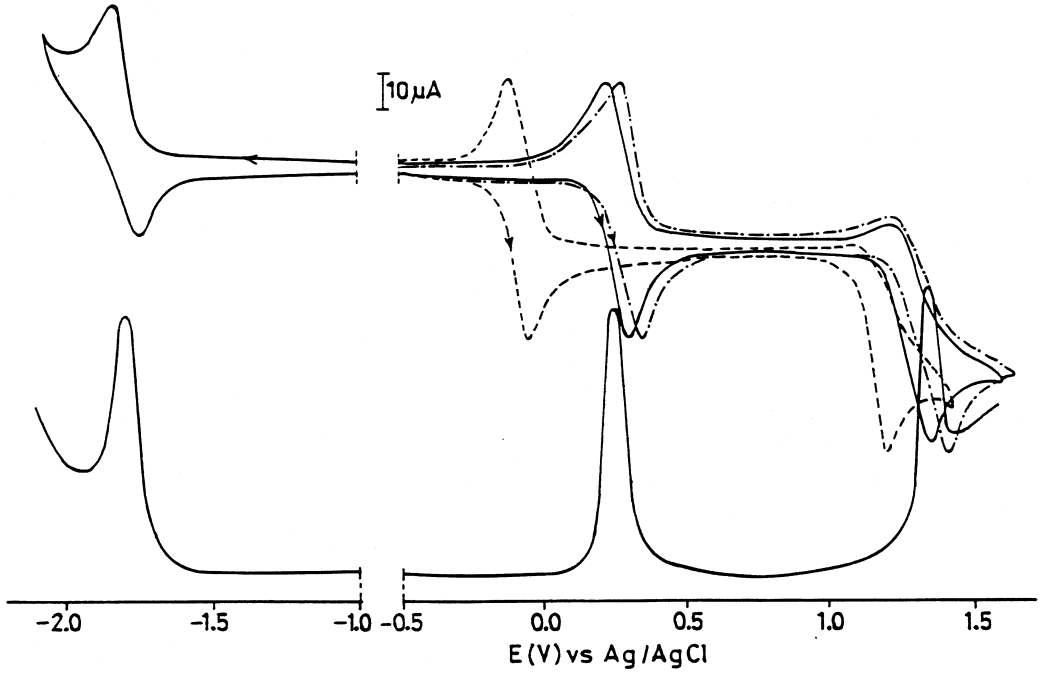

Fig. 4. Cyclic voltammograms of $\sim 10^{-3}$ M solution of $[Ru^{II}(bpy)(L^2)_2]$, **2**, (———), (b) $[Ru^{II}(bpy)(L^8)_2]$, **8** (– · –) and (c) $[Ru^{III}(bpy)(L^9)_2]\,ClO_4$, **9** (- - -) in acetonitrile at 298 K. Differential pulse voltammograms and bipyridine reduction (———) are only shown for complex **2**.

Table 3. Electrochemical data at 298 K[a]

Compound	Ru^{III}–Ru^{II} couple $E_{298}{}^0$ (V) (ΔEp (mV))	n[b]	Ru^{III}–Ru^{IV} E_{pa}[c] (V)	Ligand reduction $E_{298}{}^0$ (V) (ΔE_p (mV))	ΔE^0 (mV)[d]	ν_{MLCT} (cm^{-1})	
						calc.[e]	obs.[f]
1	0.23 (70)	0.97	1.28	−1.79 (90)	2.02	19291	18832
2	0.25 (80)	0.96	1.34	−1.77 (80)	2.02	19291	18622
3	0.30 (70)	1.05	1.38	−1.73 (80)	2.03	19372	18587
4	0.28 (70)	1.02	1.36	−1.75 (90)	2.03	19372	18519
5	0.34 (80)	1.06	1.42	−1.72 (80)	2.06	19614	18622
6	0.32 (80)	0.95	1.40	−1.72 (80)	2.04	19453	18553
7	0.40 (70)	1.10	1.45	−1.70 (90)	2.10	19936	19084
8	0.30 (80)	1.07	1.40	−1.75 (90)	2.05	19533	18939
9	−0.08 (70)	0.95	1.19	−1.85 (90)	–	–	–

[a] Condition: solvent, acetonitrile; supporting electrolyte, TEAP; reference electrode, Ag/AgCl; solute concentration, $\sim 10^{-3}$ M; working electrode, platinum wire.

[b] $n = Q/Q'$, where Q' is the calculated Coulomb count for $1e^-$ transfer and Q is the Coulomb count found after exhaustive electrolysis of $\sim 10^{-2}$ M solution of the complex.

[c] E_{pa} values are considered due to the irreversible nature of the voltammograms.

[d] Calculated by using eqn (4) of text.

[e] Calculated by using eqn (3) of text.

[f] In acetonitrile solution.

indicate the possibility of isolating the trivalent congeners of **1**–**8** under the present mixed-ligand environment.

Although the ruthenium(II)–ruthenium(III) oxidation potentials for the complexes (**1**–**8**) are appreciably low (Table 3), the oxidized trivalent congeners are not stable enough to be isolated (see later).

The complexes (**1**–**9**) exhibit a second irreversible oxidation process in between 1.19–1.45 V vs Ag/AgCl (Fig. 4, Table 3). Although the current height of this

irreversible process is higher than the previous one-electron Ru^{III}–Ru^{II} process, the one-electron nature of the second irreversible oxidation process is established with the help of differential pulse voltammetry (Fig. 4). The second one-electron oxidation process could be due to either Ru^{III}–Ru^{IV} oxidation or oxidation of the thiolato group. Since the potential difference (1.10–1.27 V, Table 3) between the two successive processes ($Ru^{II/III}$–second irreversible oxidation process) in the complexes (**1**–**9**) is comparable well with the reported observed potential difference between the two successive redox processes for the ruthenium center ($Ru^{II/III}$–$Ru^{III/IV}$) in mononuclear systems [40, 41], it may therefore be reasonable to assume the second irreversible oxidation as ruthenium(III)–ruthenium(IV) oxidation. However, the possibility of oxidation of the coordinated thiol group cannot be ruled out. The irreversible nature of the process has precluded its further characterization.

Ligand reduction

All the complexes (**1**–**9**) display one reversible reduction in the range $-1.72 \rightarrow -1.85$ V (Table 3, Fig. 4). The one-electron nature of this couple has been established by the current height and differential pulse voltammetry (Fig. 4). Since the free ligands (KL^{1-7}, NH_4L^8, NaL^9) do not exhibit any ligand reduction within the above mentioned potential range, the observed reduction is therefore considered to be reduction of the coordinated bpy ligand. 2,2′-bipyridine is a well known electron-acceptor center and each bpy can accept two electrons in one electrochemically accessible lowest unoccupied molecular orbital (LUMO) [42–45]. Although two successive one-electron bpy reductions are expected for each of the complexes, in practice one reduction corresponding to eqn (2) has been observed within the experimental potential range (-2 V). The other expected reduction could not be detected presumably due to solvent cut-off.

$$\underset{z=0,\mathbf{1}\text{–}\mathbf{8};\,z=1,\mathbf{9}}{[Ru(bpy)(L)_2]^z} + e^- \rightleftharpoons \underset{z=-1,\mathbf{1}\text{–}\mathbf{8};\,z=0,\mathbf{9}}{[Ru(bpy)(L)_2]^z} \qquad (2)$$

Spectroelectrochemical correlation

Complexes **1**–**8** display lowest energy MLCT transitions of the type $t_2(Ru) \rightarrow$ ligand LUMO (where LUMO is dominated by the diimine function of the bpy ligand) in the range 524–540 nm (Table 1). The reversible ruthenium(III)–ruthenium(II) reduction potentials and the ligand (bpy) reductions are appeared in the ranges $0.23 \rightarrow 0.40$ V and $-1.72 \rightarrow -1.79$ V respectively. Here the MLCT transition involves excitation of the electron from the filled t_{2g}^6 orbital of ruthenium(II) to the lowest π^* orbital of the diimine function. The energy of this band can be predicted from the experimentally observed electrochemical data with the help of eqns (3) and (4) [46, 47].

$$\nu_{MLCT} = 8065(\Delta E^0) + 3000 \qquad (3)$$

$$\Delta E^0 = E_{298}{}^0(Ru^{III} - Ru^{II}) - E_{298}{}^0(L) \qquad (4)$$

Here $E_{298}{}^0$ (Ru^{III}–Ru^{II}) is the formal potential (in V) of the reversible ruthenium(III)–ruthenium(II) couple, $E_{298}{}^0$ (L) that of the ligand reduction and ν_{MLCT} is the frequency or energy of the charge transfer band in cm^{-1}. The factor 8065 is used to convert the potential difference ΔE from V into cm^{-1} unit and the term 3000 cm^{-1} is of empirical origin. The calculated and experimentally observed ν_{MLCT} transitions are listed in Table 3 and there is a linear relationship between the ν_{MLCT} and ΔE (Fig. 5). Here, the calculated values for all the complexes lie within the 900 cm^{-1} of the experimentally observed charge-transfer energies, which are in good agreement with the previously observed correlation in the other mixed-ligand ruthenium–bipyridine and related systems [48–50].

Electrogeneration of trivalent ruthenium congener and distortion parameters

Chemical oxidations of the complexes (**1**–**8**) in acetonitrile solvent by aqueous ceric ammonium sulphate resulted in green solution initially corresponding to the trivalent congeners of the complexes ($\mathbf{1}^+$–$\mathbf{8}^+$). The oxidized complexes are not stable enough to be isolated in the solid state as it get decomposed to an unidentified product.

Coulometric oxidations of the complexes (**1**–**8**) at a potential 200 mV positive to the corresponding E_{pa} of Ru^{II}/Ru^{III} couple in acetonitrile solution at 298 K generated the same green colored trivalent ruthenium-(III) complexes. The observed Coulomb count corresponds to $1e^-$-transfer for all the complexes (Table 3). The resulting oxidized solutions ($\mathbf{1}^+$–$\mathbf{8}^+$) display voltammograms which are superposable on those of the corresponding bivalent complexes (**1**–**8**) which imply that the oxidations here may be stereoretentive in nature. Electrochemically generated oxidized complexes ($\mathbf{1}^+$–$\mathbf{8}^+$) are not stable enough, eventually decomposed to an unidentified product which has precluded their further characterizations. However, in the case of complex $\mathbf{1}^+$ we have been succeeded to record the EPR spectrum by quick freezing the green colored oxidized solution in liquid N_2 (77 K). It exhibits an axial EPR spectrum. The axial nature of the EPR spectrum (Fig. 6) ($g_1 = 2.424$, $g_2 = 2.424$, $g_3 = 1.752$) is characteristic of trivalent ruthenium(III) in axially distorted octahedral environment (low-spin Ru^{III}, $t_{2g}{}^5$, $S = 1/2$) [51, 52].

The green colored isolated trivalent ruthenium-(III)–dithiocarbamate complex **9** also exhibits similar axial EPR spectrum (Fig. 6) ($g_1 = 2.405$, $g_2 = 2.405$, $g_3 = 1.756$). The electrochemical reduction of complex **9** at -0.25 V vs Ag/AgCl resulted in a red-brown colored complex corresponding to the bivalent

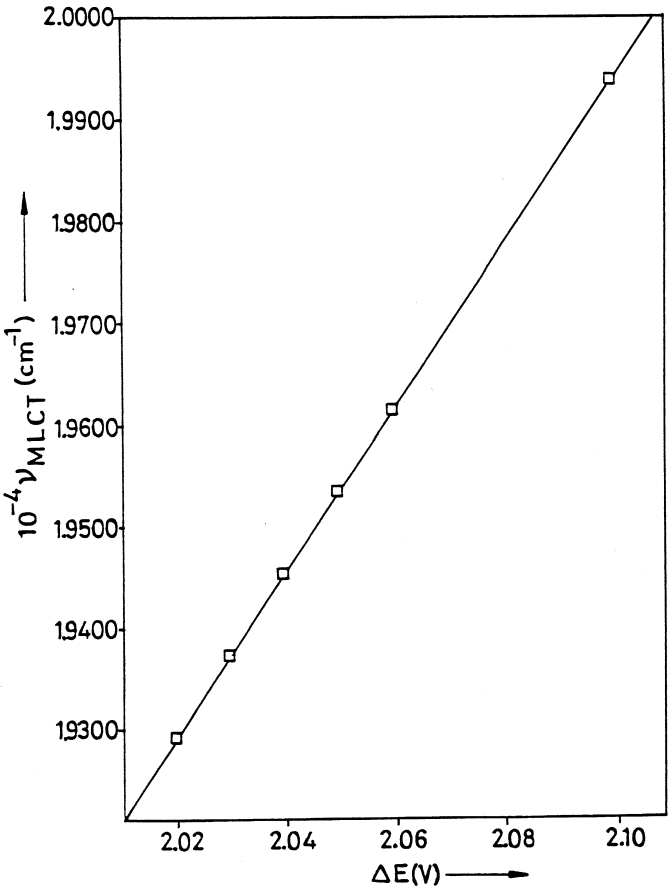

Fig. 5. Least squares plot of the lowest energy metal-to-ligand charge-transfer band (ν_{MLCT}, cm^{-1}) vs the difference in potential (ΔE, V) between $Ru^{II/III}$ couple and the bipyridine reduction.

ruthenium(II) congener ($\mathbf{9}^-$). The reduced species ($\mathbf{9}^-$) shows a voltammogram which is superposable on that of the corresponding trivalent complex **9** which indicates the stereoretentive nature of the reduction process. When the same red-brown reduced solution was coulometrically reoxidized at 0.1 V vs Ag/AgCl, the green colored trivalent complex **9** was formed quantitatively. The chemical reduction of **9** by hydrazine hydrate can also generate the bivalent complex $\mathbf{9}^-$ immediately. The reduced species is unstable under atmospheric conditions, spontaneously oxidizes to trivalent complex **9**.

The theory of EPR spectra of low-spin d^5 complexes are documented in literature [53–57]. The distortion of pseudo octahedral complexes is expressed as the sum of axial (Δ) and rhombic (V) components. The t_2 orbital consists of the components $t_2^0(xy)$, $t_2^+(xz)$, $t_2^-(yz)$. The degeneracy of t_2 orbital is partially removed by axial distortion (Δ), which placed t_2^0 (b) above t_2^+/t_2^- (e). The superimposed (V) then further splits (e) into t_2^+ and t_2^-.

The distortion parameters (Δ and V) and the energies of two optical transitions (ν_1 and ν_2) from ground to upper Kramers doublets can be obtained from the analysis of EPR spectrum using the g tensor theory of low-spin d^5 ions.

The EPR spectrum provides only the absolute g values and so neither their signs nor the correspondence of g_1, g_2 and g_3 to g_x, g_y and g_z are known. There are forty-eight possible combinations based on the labeling (x,y,z) and signs chosen for the experimentally observed g values. For the present case we have chosen the combination $-g_1 = -g_2 > g_3$ (due to axial nature of the spectra g_1 and g_2 are same, Fig. 6) as this particular set gives the orbital reduction factor, $k < 1.0$ The computed values of orbital reduction factor (k), axial distortion (Δ/λ) and the two ligand-field optical transitions (ν_1/λ and ν_2/λ) for the complexes $\mathbf{1}^+$ and **9** are listed in Table 4. The value of spin–orbit coupling constant (λ) of ruthenium(III) is taken as 1000 cm^{-1} [53–57]. In view of the axial nature of the EPR spectra of the complexes, rhombic distortion (V) is found to be zero.

The low energy near-IR spectrum (maximum wavelength scan up to 2500 nm) of the complex **9** (near-IR spectrum of the complex $\mathbf{1}^+$ cannot be checked due to its unstable nature) has been checked and it displays one weak transition at 2140 nm (ε, $M^{-1}\,cm^{-1}$, 60). In

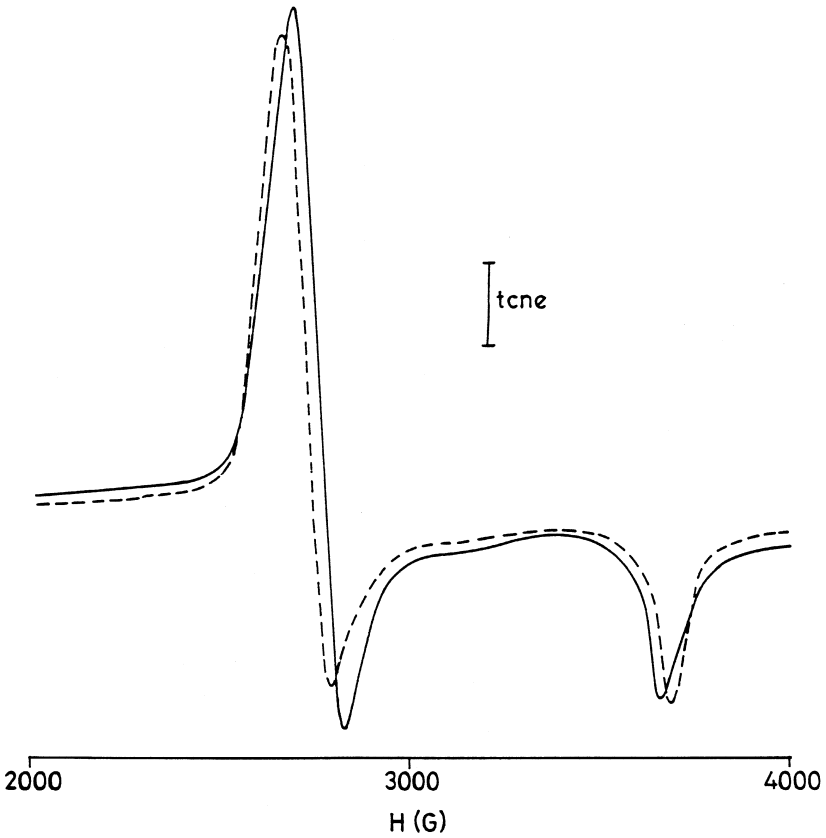

Fig. 6. X-band EPR spectra of coulometrically oxidized complex $[Ru^{III}(bpy)(L^1)_2]^+$, $\mathbf{1}^+$ (- - -) and $[Ru^{III}(bpy)(L^9)_2]\,ClO_4$, **9** (———) in acetonitrile solution at 77 K.

Table 4. The EPR g values[a] and distortion parameters[b]

	Compound	
	$\mathbf{1}^+$	**9**
g_1	−2.424	−2.405
g_2	−2.424	−2.405
g_3	1.752	1.756
k	0.889	0.857
Δ/λ	3.689	3.699
V/λ	0.000	0.000
v_1/λ	3.489	3.497
v_2/λ	4.339	4.348

[a] In acetonitrile solution at 77 K.
[b] Meanings are given in the text.

view of the involved approximations in the theory, the agreement between the experimentally observed v_2 and calculated v_2 value is excellent. Due to instrumental limitation (maximum wavelength scan up to 2500 nm) it has not been possible to compare the v_1 band.

CONCLUSIONS

We have thus observed that the dithiocarbamate ligand (L^9) along with bipyridine preferentially stabilizes ruthenium(III) in the complex **9**. However, the similar dithiocarbonate (L^{1-7}) and dithiophosphate (L^8) ligands selectively stabilize ruthenium(II) in the complexes **1**–**7** and **8**. Although the reduced ruthenium(II) congener of the complex **9** and the oxidized ruthenium(III) congeners of the complexes **1**–**8** have been observed in the cyclic voltammetric time scale, the reduced and the oxidized species are not stable enough to be isolated using bulk electrolysis as well as by chemical means. The bivalent complexes **1**–**8** exhibit moderately strong emissions at room temperature which are possibly originated from the dithio ligand based MLCT transitions.

EXPERIMENTAL

Materials

Commercially available ruthenium trichloride (S.D. Fine Chemicals, Bombay, India) was converted to

$RuCl_3 \cdot 3H_2O$ by repeated evaporation to dryness with concentrated hydrochloric acid. The [Ru(bpy)Cl_3] was prepared according to the reported procedure [29]. Other chemicals such as 2,2′-bipyridine, diethyl dithio carbamate and solvents were reagent grade and used as received. Silica gel (60–120 mesh) used for the column chromatography was purchased from S.D. Fine Chemicals, Bombay, India. For Spectroscopic and electrochemical studies HPLC grade solvents were used. Commercial tetraethyl ammonium bromide was converted to pure tetraethyl ammonium perchlorate (TEAP) by following an available procedure [58].

Physical measurements

Solution electrical conductivity was checked using a Systronic conductivity bridge, 305. Electronic spectra (900–200 nm) were recorded using a Shimadzu UV 160 spectrophotometer. Near-IR spectrum was recorded by using a Hitachi 330 spectrophotometer. Infrared spectra were taken on a Nicolet spectrophotometer with samples prepared as KBr pallets. Magnetic susceptibility was checked with a PAR vibrating sample magnetometer. ^{1}H NMR spectra were obtained with the use of 300 MHz Varian FT-NMR Spectrometer. Cyclic voltammetry and coulometric measurements were carried out using a PAR model 273A electrochemistry system. A platinum wire working electrode, a platinum wire auxiliary electrode and an Ag/AgCl reference electrode were used in a three-electrode configuration. TEAP was the supporting electrolyte and the solution concentration was $\sim 10^{-3}$ M. The half wave potential $E_{298}{}^0$ was set equal to 0.5 ($E_{pa} + E_{pc}$), where E_{pa} and E_{pc} are anodic and cathodic cyclic voltammetric peak potentials respectively. The scan rate used was 50 mV s^{-1}. A platinum wire gauze working electrode was used in coulometric experiments. All electrochemical experiments were carried out under dinitrogen atmosphere and are uncorrected for junction potentials. EPR measurements were made with a Varian model 109 E-line X-band spectrometer fitted with a quartz dewar for measurements at 77 K (liquid nitrogen). The spectrum was calibrated by using tetracyanoethylene (tcne) ($g = 2.0023$). The elemental analyses were carried out with a Carlo Erba (Italy) elemental analyzer. Solution emission properties were checked using a SPEX-fluorolog spectrofluorometer.

CAUTION! Perchlorate salts of metal complexes are generally explosive. Care should be taken while handling such complexes.

Treatment of EPR data

An outline of the procedure can be found in our recent publications [38, 59]. We would like to note that a second solution also exists that is different from the chosen one, having small Δ, γ_1 and γ_2 values. The experimentally observed near-IR result clearly eliminates this solution as unacceptable.

Synthesis of ligands and complexes

The ligands KL^{1-7} and NH_4L^8 were prepared by following the reported procedures [60, 61].

The complexes **1**–**7** were synthesized using a general method. Yields varied in the range 80–85%. Specific details are given for one representative case.

(2,2′-*bipyridine*) *bis*(*O-ethyl dithiocarbonate*) *ruthenium*(*II*) [Ru(bpy)$(L^2)_2$] (**2**). Ru(bpy)Cl_3 (100 mg, 0.275 mmol) was dissolved in 20 cm^3 of methanol and stirred for 10 min. To this solution, the ligand KL^2 (132 mg, 0.825 mmol) was added. The initial brown solution of Ru(bpy)Cl_3 immediately turned to red color. The progress of the reaction was monitored periodically by TLC. The solvent was then evaporated under reduced pressure and the crude product was then purified by chromatography on a silica gel (60–120 mesh) column. The pure complex (**2**) was eluted with benzene. On removal of the solvent under reduced pressure fine crystalline complex [Ru(bpy)$(L^2)_2$] was obtained. Yield: 82%.

The complex [Ru(bpy)$(L^8)_2$] (**8**) was prepared by following the above procedure except it requires heating for approximately 30 min after the addition of NH_4L^8 ligand in the starting complex. Yield was 85%.

(2,2′-*bipyridine*) *bis*(*diethyldithiocarbamate*) *ruthenium*(*III*) *perchlorate* [Ru(bpy)$(L^9)_2$]ClO_4 (**9**) Ru(bpy)Cl_3 (100 mg, 0.275 mmol) was dissolved in 20 cm^3 of methanol and stirred for 10 min. To this solution, the ligand NaL^9 (180 mg, 0.825 mmol) was added. The resultant mixture was stirred for 30 min. Initial brown solution of Ru(bpy)Cl_3 was gradually changed to green. The progress of the reaction was monitored periodically by TLC. The crude product was then purified by column chromatography on a silica gel (60–120 mesh) column. The pure complex **9** was eluted with a 4:1 ratio of dichloromethane and acetonitrile solvents. On removal of the solvent mixture under reduced pressure a gummy mass was obtained. It was redissolved in minimum volume of acetonitrile and the concentrated solution was treated with an excess of saturated aqueous $NaClO_4$ solution. The resulting mixture was allowed to stand for 30 min at 273 K. The green colored precipitate thus obtained was collected by filtration and washed thoroughly with ice-cold water. The solid mass was then dried in vacuo over P_4O_{10} Yield: 80%.

Acknowledgements—Financial support received from the Department of Science and Technology, New Delhi, India is gratefully acknowledged. Special acknowledgement is made to the Regional Sophisticated Instrumentation Center, RSIC, IIT Bombay for providing NMR and EPR facilities.

REFERENCES

1. Coe, B. J., Friessen, D. A., Thompson, D. W. and Meyer, T. J., *Inorg. Chem.*, 1996, **35,** 4575.

2. Milkevitch, M., Brauns, E. and Brewer, K. J., *Inorg. Chem.*, 1996, **35,** 1737.
3. Ward, M. D., *Inorg. Chem.*, 1996, **35,** 1712.
4. Rasmussen, S. C., Thompson, D. W., Singh, V. and Petersen, J. D., *Inorg. Chem.*, 1996, **35,** 3449.
5. Cargill Thompson, A. M. W., Jeffery, J. C., Liard, D. J. and Ward, M. D., *J. Chem. Soc. Dalton Trans.*, 1996, 879.
6. Greaney, M. A., Coyle, C. L., Harmer, A. J. and Stiefel, E. I., *Inorg. Chem.*, 1989, **28,** 912.
7. Kroner, R., Heeg, M. J. and Deutsch, E., *Inorg. Chem.*, 1988, **27,** 558.
8. Rao, P. S., Thakur, G. A. and Lahiri, G. K., *Indian J. Chem.*, 1996, **35A,** 946.
9. Santra, B. K., Menon, M., Pal, C. K. and Lahiri, G. K., *J. Chem. Soc. Dalton Trans.*, 1997, 1387.
10. Mukherjee, R. N. and Chakravorty, A., *J. Chem. Soc. Dalton Trans.*, 1983, 2197.
11. Howard, C. A. and Ward, M. D., *Angew. Chem. Int. Ed. Engl.*, 1992, **31,** 1028.
12. Hossain, M., Chattopadhyay, B. K. and Ghosh, S., *Polyhedron*, 1997, **16,** 4313.
13. Sprintschnik, G., Sprintschnik, H. W., Kirsch, P. P. and Whitten, D. G. J., *J. Am. Chem. Soc.*, 1976, **98,** 2337.
14. Gilbert, J. A., Eggleston, D. S., Murphy, W. R. Jr., Gaselowitz, D. A., Gersten, S. W., Hodgson, D. J. and Meyer, T. J., *J. Am. Chem. Soc.*, 1985, **107,** 3855.
15. Gersten, S. W., Samuels, G. J. and Meyer, T. J., *J. Am. Chem. Soc.*, 1982, **104,** 4029.
16. Gilbert, J. A., Geselowitz, D. and Meyer, T., *J. Am. Chem. Soc.*, 1986, **108,** 1493.
17. Honda, K. and Frank, A. J., *J. Chem. Soc. Chem. Commun.*, 1984, 1635.
18. Ellis, C. D., Gilbert, J. A., Murphy, W. R. Jr. and Meyer, T. J., *J. Am. Chem. Soc.*, 1983, **105,** 4842.
19. Vining, W. and Meyer, T. J., *J. Electroanal. Chem. Interfacial Electrochem.*, 1985, **195,** 183.
20. Tanaka, K., Morimoto, M. and Tanaka, T., *Inorg. Chim. Acta*, 1981, **56,** L61.
21. Rillema, D. P., Dressick, W. J. and Meyer, T. J., *J. Chem. Soc. Chem. Commun.*, 1980, 247.
22. Durham, B., Dressick, W. J. and Meyer, T. J., *J. Chem. Soc. Chem. Commun.*, 1979, 381.
23. Dressick, W. J., Meyer, T. J., Durham, B. and Rillema, D. P., *Inorg. Chem.*, 1982, **21,** 345.
24. Gleria, M., Minto, F., Beggiato, G. and Bortolus, P. J., *J. Chem. Soc. Chem. Commun.*, 1978, 285.
25. Durham, B., Caspar, J. V., Nagle, J. K. and Meyer, T. J., *J. Am. Chem. Soc.*, 1982, **104,** 4803.
26. Durham, B., Wilson, S. R., Hodgson, D. J. and Meyer, T. J., *J. Am. Chem. Soc.*, 1980, **102,** 600.
27. Sullivan, B. P., Salmon, D. J. and Meyer, T. J., *Inorg. Chem.*, 1978, **17,** 3334.
28. Casper, J. V. and Meyer, T. J., *Inorg. Chem.*, 1983, **22,** 2444.
29. Anderson, S. and Seddon, K. R., *J. Chem. Res. (S)*, 1979, 74.
30. Pesce, B., *Nuclear Magnetic Resonance in Chemistry*. Academic Press, New York, 1965, p. 174.
31. Ceulemansm, A., Vanquickenborne, L. G., *J. Am. Chem. Soc.*, 1981, **103,** 2238.
32. Root, M. J. and Deutsch, E., *Inorg. Chem.*, 1985, **14,** 1464.
33. Alsfasser, R. and Eldik, R. V., *Inorg. Chem.*, 1996, **35,** 628.
34. Coe, B. J., Meyer, T. J. and White, P. C., *Inorg. Chem.*, 1995, **34,** 593.
35. Juris, A., Balzani, V., Barigelletti, F., Campagna, S., Belser, P., von Zelewsky, *Coord. Chem. Rev.*, 1988, **84,** 85.
36. Lees, A. J., *Chem. Rev.*, 1987, **87,** 711.
37. Brown, G. M., Weaver, T. R., Keene, F. R. and Meyer, T. J., *Inorg. Chem.*, 1976, **15,** 190.
38. Lahiri, G. K., Bhattacharya, S., Ghosh, B. K. and Chakravorty, A., *Inorg. Chem.*, 1987, **26,** 9324.
39. Santra, B. K., Lahiri, G. K., *J. Chem. Soc. Dalton Trans.*, 1997, 129.
40. Bag, N., Lahiri, G. K., Bhattacharya, S., Falvello, L. R. and Chakravorty, A., *Inorg. Chem.*, 1988, **27,** 4396.
41. Lahiri, G. K., Bhattacharya, S., Mukherjee, M., Mukherjee, A. K. and Chakravorty, A., *Inorg. Chem.*, 1987, **26,** 3359.
42. Bhattacharya, S., *Polyhedron*, 1993, **12,** 235.
43. Elliott, C. M., *J. Chem. Soc. Chem. Commun.*, 1980, 261.
44. Tokel-Takvoryan, N. E., Hemingway, R. E. and Bard, A. J., *J. Am. Chem. Soc.*, 1973, **95,** 6583.
45. Morris, D. E., Hanck, K. W. and DeArmond, M. K., *Inorg. Chem.*, 1985, **24,** 977.
46. Goswami, S., Mukherjee, R. N. and Chakravorty, A., *Inorg. Chem.*, 1983, **22,** 2825.
47. Ghosh, B. K. and Chakravorty, A., *Coord. Chem. Rev.*, 1989, **95,** 239.
48. Sullivan, B. P., Caspar, J. V., Johnson, S. R. and Meyer, T. J., *Organometallics*, 1984, **3,** 1241.
49. Dodsworth, E. S. and Lever, A. B. P., *Chem. Phys. Lett.*, 1986, **124,** 152.
50. Greaney, M. A., Coyle, C. L., Harmer, H. A., Jordan, A. and Stiefel, E. I., *Inorg. Chem.*, 1989, **28,** 912.
51. Chattopadhyay, S., Bag, N., Basu, P., Lahiri, G. K. and Chakravorty, A., *J. Chem. Soc. Dalton Trans.*, 1990, 3389.
52. Pramanik, A., Bag, N., Lahiri, G. K. and Chakravorty, A., *J. Chem. Soc. Dalton Trans.*, 1990, 3823.
53. Hill, N. J., *J. Chem. Soc. Faraday Trans.*, 1972, **2,** 427.
54. Bleaney, B. and O'Brien, M. C. M., *Proc. Phys. Soc. London B*, 1956, **69,** 1216.
55. Griffith, J. S., *The Theory of Transition Metal Ions*. Cambridge University Press, London, 1972, p. 364.
56. Daul, C. and Goursot, A., *Inorg. Chem.*, 1985, **24,** 3554.
57. Mahapatra, A. K., Datta, S., Goswami, S., Mukherjee, M., Mukherjee, A. K. and Chakravorty, A., *Inorg. Chem.*, 1986, **25,** 1715.
58. Sawyer, D. T., Sobkowiak, A. and Roberts, J. L., Jr., *Electrochemistry for Chemists*, 2nd edn. Wiley, New York, 1995.
59. Bag, N., Lahiri, G. K. and Chakravorty, A., *J. Chem. Soc. Dalton Trans.*, 1990, 1557.
60. Vogel, A. I., *Text Book of Practical Organic Chemistry*. ELBS, Longman, London, 1978, p. 588.
61. Lefferts, J. L., Mollouy, K. C., Zuckerman, J. J., Haituc, I., Guta, C. and Ruse, D., *Inorg. Chem.*, 1980, **19,** 1662.

Pergamon

PII: S0277–5387(98)00240–X

Polyhedron Vol. 17, Nos. 25, 26, pp. 4379–4391, 1998
© 1998 Elsevier Science Ltd
All rights reserved. Printed in Great Britain
0277–5387/98 $19.00 + 0.00

Interaction between peroxide ion and phenol group which are coordinated to the same iron(III) ion

Sayo Ito,[a] Yoshihiro Ishikawa,[a] Satoshi Nishino,[a] Teruyuki Kobayashi,[a] Shigeru Ohba[b] and Yuzo Nishida[a,†]

[a]Department of Chemistry, Faculty of Science, Yamagata University, Yamagata 990, Japan

[b]Department of Chemistry, Faculty of Science and Technology, Keio University, Yokohama 223, Japan

(Received 23 March 1998; accepted 12 June 1998)

Abstract—We have prepared several new iron(III) complexes with ligands which contain a phenol group; these are tetradentate [(X-phpy)H, X and H(phpy) represent the substituents on the phenol ring and *N*,*N*-bis(2-pyridylmethyl)-*N*-(2-hydroxybenzyl)amine, respectively] and pentadentate ligands [(R-enph-X)H; R = ethyl(Et) or methyl(Me) derivative and H(Me-enph) denotes *N*,*N*-bis(2-pyridylmethyl)-*N*″-methyl-*N*″-(2″-hydroxylbenzylamine)ethylenediamine] and have determined the crystal structures of Fe(phpy)Cl_2, Fe(5-NO_2-phpy)Cl_2, and Fe(Me-enph)ClPF_6, which are of a mononuclear six-coordinate iron(III) complex with coordination of one or two chloride ion(s). These compounds are highly colored (dark violet) due to the coordination of phenol group to an iron(III) atom. When hydrogen peroxide was added to the solution of the iron(III) complex, a color change occurs with bleaching of the violet color, indicating that oxidative degradation of the phenol moiety occurred in the ligand system. The bleaching of the violet color was also observed by the addition of *t*-butylhydroperoxide. The rate of the disappearance of the violet color is highly dependent on the substituent on the phenol ring; introduction of an electron-withdrawing group in the phenol ring decreases the rate of bleaching, suggesting that disappearance of the violet band should be due to a chemical reaction between the phenol group and a peroxide adduct of the iron(III) species with an η^1-coordination mode and that in this reaction the peroxide adduct acts as an electrophile towards phenol ring. The *intramolecular* interaction between the phenol moiety and an iron(III)-peroxide adduct may induce activation of the peroxide ion, and this was supported by several facts that the solution containing an iron(III) complex and hydrogen peroxide exhibits high activities for degradation of nucleosides and albumin. © 1998 Elsevier Science Ltd. All rights reserved

Keywords: Iron(III)-peroxide adduct; interaction of peroxide ion and phenol group; activation of peroxide; degradation of nucleoside; degradation of albumin.

INTRODUCTION

Peroxoiron(III) complexes are increasingly being considered as potential intermediates in oxidations catalyzed by both non-heme [1–5] and heme iron centers [6–10]. For example, electrospray mass spectrometry have revealed that an "activated bleomycin" is a monomeric iron(III)-peroxide adduct with an η^1-coordination mode [10]. Although several binuclear iron(III)-peroxide adducts have been characterized by their absorption [11–15], resonance Raman spectra [11, 12, 14], and crystal structure determinations [these are all of (μ-η^1:η^1-peroxo)diiron(III) structure] [16–18], however, evidence for the formation of a monomeric iron(III)-peroxide adduct with an η^1-coordination mode is scarce [19] and their reactivities are unknown [2, 3, 20]. In this study we have prepared several mono-

†Author to whom correspondence should be addressed. Present address: Institute for Molecular Science, Okazaki 444-8585, Japan.

meric iron(III) compounds with ligands containing substituted phenols shown below in order to obtain chemical evidence for formation of a monomeric iron(III)-peroxide adduct and also to obtain information on the reactivity of the peroxide adduct [21].

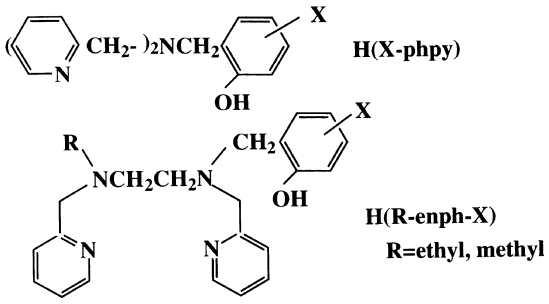

Structure 1.

EXPERIMENTAL

Materials

Hydrogen peroxide (30%) and *t*-butylhydroperoxide (70%) were obtained commercially.

Synthesis of ligands

By adding $NaBH_4$ into the methanol solution containing salicyclaldehyde and 2-aminomethylpyridine, white solid, *N*-(2-hydroxybenzyl)-2-amino-methylpyridine was obtained. According to the procedure by Toftlund *et al* [22], the ligand, H(phpy), was obtained as oil (illustrated below). For the iron(III) complex preparation, the oil was used without further purification. Other ligands, H(X-phpy), where X = 3-OMe, 5-NO_2, 3-NO_2, 3,5-Br_2, were also obtained as oil according to the same way as described for H(phpy).

In a similar manner, the ligands H(R-enph) were obtained as oil and used for metal complex preparation without further purification (shown below). The substituted forms, H(R-enph-X), were also obtained as oil in a similar manner.

Synthesis of iron(III) complex

The methanol solution of the ligand (0.001 mol) was mixed with a methanol solution of ferric chloride six-hydrate (0.001 mol) and the precipitated violet crystals were filtered and once recrystallized from an acetonitrile/methanol solution. In the case of Fe(III) with

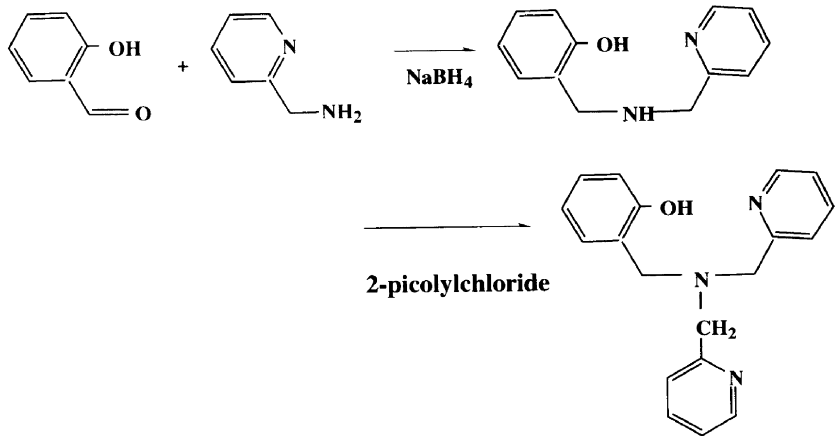

Structure 2.

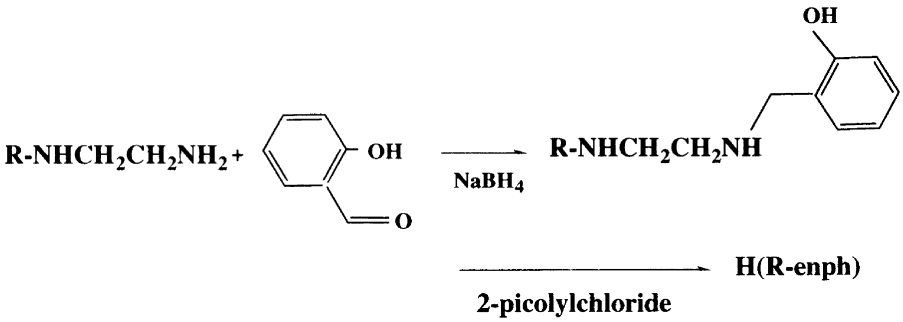

Structure 3.

Table 1. Crystal data of the compounds

Compound	**I**	**II**	**III**
Formula	$C_{19}H_{18}Cl_2FeN_3O \cdot C_2H_3N$	$C_{19}H_{17}Cl_2FeN_4O_3 \cdot C_2H_3N$	$C_{23}H_{25}ClFeN_4OPF_6 \cdot 2H_2O$
Molecular weight	472.18	517.18	633.76
monoclinic	triclinic	monoclinic	
Space group	P21/c	$P\bar{1}$	P21/c
a (Å)	9.343(8)	11.944(2)	15.567(3)
b (Å)	12.034(3)	13.736(1)	9.008(2)
c (Å)	19.971(4)	7.029(1)	19.507(2)
a (°)	90	98.73(1)	90
b (°)	103.82(3)	100.65(1)	93.93(1)
g (°)	90	88.85(1)	90
V (Å^3)	2180.4(18)	1120.2(3)	2729.0(8)
Z	4	2	4
Dx (Mg m^{-3})	1.438	1.533	1.543
μ (mm^{-1})	0.956	0.945	0.782
Scan	θ–2θ	θ–2θ	θ–2θ
Reflections (independent)	3137	5144	6268
Observed reflections [$F_o > 3\sigma(F_o)$]	2030	3779	3326
Parameters	262	306	397
R	0.0527	0.0476	0.0706
ωR*	0.0440	0.0447	0.0573
$(\Delta/\sigma)_{max}$	0.03	0.024	0.05
$\Delta\rho_{max}$ (e Å^{-3})	0.39	0.49	0.62
$\Delta\rho_{min}$ (e Å^{-3})	−0.32	−0.58	−0.57
S	1.35	1.19	1.47

*$\omega = 1/[\sigma^2(F) + 0.000225F^2]$.

H(R-enph-X) complexes, $NaClO_4$ or NH_4PF_6 was added to the solution. Satisfactory analysis was obtained and analytical data of the new compounds are available on request from the authors.

Crystal structure determinations

Crystals of Fe(phpy)$Cl_2 \cdot CH_3CN$, **I**, and Fe(5-NO_2-phpy)$Cl_2 \cdot CH_3CN$, **II**, were grown from acetonitrile solutions and Fe(Me-enph-H)$ClPF_6 \cdot 2H_2O$, **III**, from aqueous methanol solution. Crystal data are listed in Table 1. X-ray diffraction intensities were measured up to $2\theta = 55°$ using MoKα radiation ($\lambda = 0.71073$ Å) on a Rigaku four-circle diffractometer AFC-5 at Keio University. Structure analysis was carried out using CRYSTAN-GM software version 6.3.3 on a SUN Park-10 workstation. Details of the structure analyses were deposited with the CCDC, Union Road, Cambridge.

Degradation of albumin by iron(III) complex and hydrogen peroxide

In a typical run, to the solution containing iron(III) complex (5 μl, 0.15–0.6 mmol dm^{-3}), Tris–HCl buffer (5 μl, 0.1 M, pH = 7.8) and hydrogen peroxide (5 μl, 6.25–100 mmol dm^{-3} solution) was added albumin solution (5 μl, 0.11 mmol dm^{-3}) and after 1 h mixing, the reaction solution was mixed with solution containing 2-mercaptoethanol and electrophoresed; denatured samples were analyzed on 12.5% sodium dodecylsulfate-polyacrylamide gel electrophoresis [2]. Products were visualized by Coomasie Blue and the band intensities were quantified on an ATTO Densitograph Model AE-6920-M/W/V (for Mac).

Degradation of nucleosides by iron(III) complex and hydrogen peroxide

To an aqueous solution of iron(III) complex containing nucleic acid or nucleoside, was added hydrogen peroxide solution (10 cm^3, 1/10 M) and the degradation of the nucleic acid or nucleoside were assessed in terms of HPLC according to a similar manner to that reported by Kasai and Nishimura [23]. The nucleosides used are adenine, 2′-deoxyadenosine, 2′-deoxyguanosine, 7-methylguanine, cytosine, deoxycytidine, thymine and deoxythymidine.

Molecular orbital calculations on ligand system

MOPAC calculations (MNDO/AM1) [4] were performed on the substituted 2-(dimethylamino)phenol, illustrated on next page.

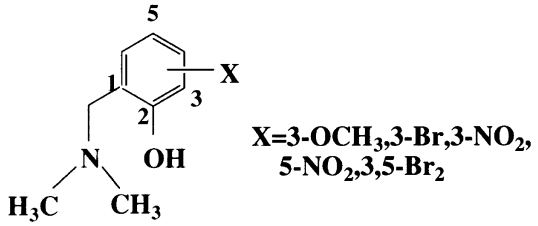

Structure 4.

Physical measurements

Absorption spectra were obtained with a Shimazdu UV-2200 at 298 K.

RESULTS AND DISCUSSION

Crystal structure

The ORTEP drawing of the iron(III) compounds, Fe(phpy)Cl_2, Fe(5-NO_2-phpy)Cl_2 and Fe(Me-enph)Cl^+ are illustrated in Figs 1–3 and the selected bond lengths and bond angles are listed in Table 2. The structural features of the first two compounds are essentially the same to each other; both compounds are of a distorted six-coordinate structure. The introduction of nitro-group at 5-position induces the lengthening of the Fe–O (phenolic oxygen) bond by $\sim$0.03 Å.

In the case of Fe(Me-enph)Cl^+ complex, Fe–O (phenol oxygen) is 1.869(5) Å, which are shorter than those observed for the Fe(phpy)Cl_2 compounds, which may be due to higher Lewis acidity of the iron(III) atom in the former complex with positive charge(see Table 3). This is also reflected in the shorter bond length of Fe–Cl atom.

Absorption spectra

In Fig. 4, the absorption spectra of a series of Fe(X-phpy)Cl_2 complexes in acetonitrile are shown; a strong absorption band observed in the range 535–647 nm is attributed to the charge transfer band from phenol to an iron(III) atom [24]. The band positions of the compounds are highly dependent on the substituents on the phenol ring, X; absorption energy is the highest for the compounds containing nitro-group, the compound with 3-OMe exhibits the absorption maximum with the lowest energy (see Table 4). This may also be explained in terms of the energies of the HOMO of the phenol moiety; as shown in the Table 5, energy of HOMO of the compound containing nitro-group is the lowest among the ligands used in this study and the ligand containing 3-OMe group has the highest HOMO. Since the absorption band around 500 nm has been attributed to the charge-transfer from the

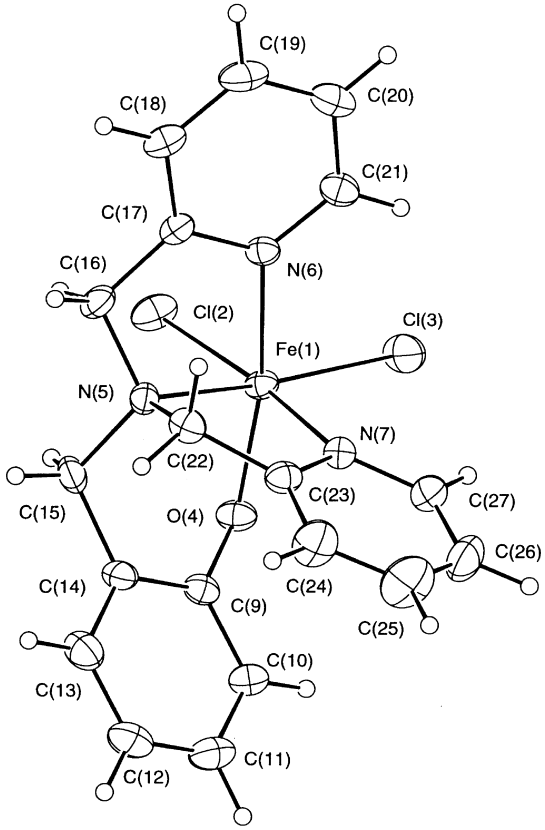

Fig. 1. ORTEP drawing of Fe(phpy)Cl_2.

Table 2. Comparison of structural features of Fe(phpy)Cl_2 and Fe(5-NO_2-phpy)Cl_2 compounds

	Fe(phpy)Cl_2		Fe(5-NO_2-phpy)Cl_2
Fe–O4 (phenol) (Å)	1.892(3)		1.923(2)
Fe–N7 (pyridine) (Å)	2.207(4)	Fe–N9	2.207(2)
Fe–N6 (pyridine) (Å)	2.197(4)	Fe–N8	2.193(2)
Fe–N5 (Å)	2.227(5)	Fe–N7	2.232(2)
Fe–Cl2 (Å)	2.336(2)		2.319(1)
Fe–Cl3 (Å)	2.293(2)		2.282(1)

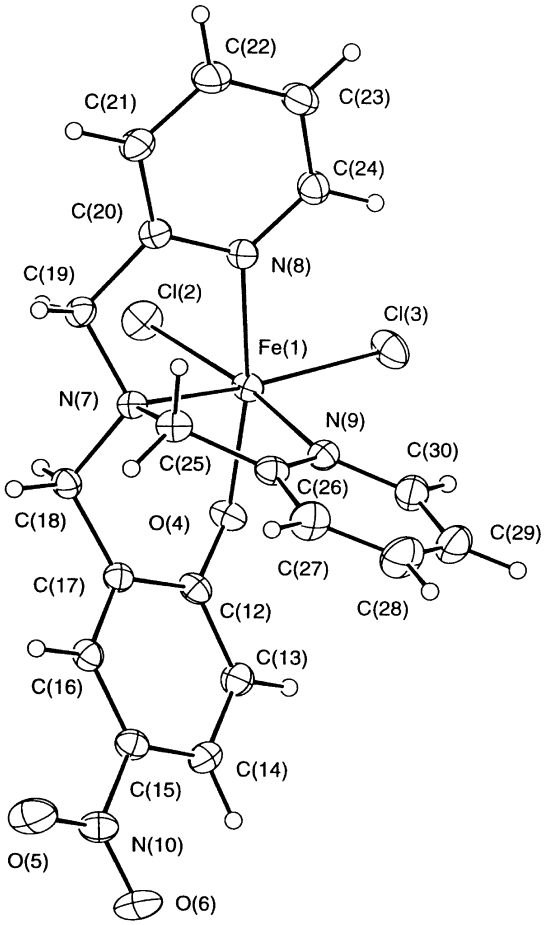

Fig. 2. ORTEP drawing of Fe(5-NO_2-phpy)Cl_2.

HOMO of the phenol to the dπ-orbital of the iron atom, the observed phenomenon can be reasonably explained. A similar shift of the absorption maximum was also observed for the series of Fe(R-enph-X)Cl^+ compounds (see Table 4).

Table 4. Absorption maximum of the CT bands (phenol to iron(III)) of the Iron(III) compounds (in acetonitrile, 298 K)

	Absorption maximum (nm)
Fe(phpy)Cl_2	589.5
Fe(3-OMe-phpy)Cl_2	647.0
Fe(5-Br-phpy)Cl_2	589.0
Fe(3,5-Br_2-phpy)Cl_2	583.0
Fe(3-NO_2-phpy)Cl_2	535.5
Fe(5-NO_2-phpy)Cl_2	541.0
Fe(Et-enph)ClPF_6	616.5
Fe(Et-enph-3-OMe)ClClO_4	688.0
Fe(Et-enph-5-Br)ClPF_6	617.5

Table 5. Energies of HOMO and LUMO of substituted 2-(dimethylamino)phenol

X	HOMO (eV)	LUMO (eV)
3-OMe	−8.59	0.60
H	−8.94	0.37
3-Br	−9.09	0.01
3,5-Br_2	−9.17	−0.23
3-NO_2	−9.68	−0.90
5-NO_2	−9.80	−0.94

The absorption spectra of the compounds are dependent on the solvent used, as shown in Fig. 5; the change of the spectrum in water from that in acetonitrile should be attributed to the displacement of the chloride ion by hydroxide ion in an aqueous solution; this is confirmed by ion spray mass spectroscopy done for the Fe(Et-enph)Cl^+ compound. As shown in Fig. 6, in the acetonitrile solution chloride ion is coordinated to an iron(III) atom ($m/z = 465.8$),

Table 3. Selected bond distances (Å) and angles (°) of compound **III**

Bond distance (Å)			
Fe1–Cl2	2.271(3)	Fe1–O16	1.869(5)
Fe1–N19	2.228(6)	Fe1–N20	2.222(6)
Fe1–N21	2.171(6)	Fe1–N22	2.172(6)
Bond angle (°)			
Cl2–Fe1–O16	102.1(2)	Cl2–Fe1–N19	167.2(2)
Cl2–Fe1–N20	96.8(2)	Cl2–Fe1–N21	91.0(2)
Cl2–Fe1–N22	91.9(2)	O16–Fe1–N19	84.1(2)
O16–Fe1–N20	157.9(2)	O16–Fe1–N21	92.9(3)
O16–Fe1–N22	97.8(3)	N19–Fe1–N20	79.7(2)
N19–Fe1–N21	99.8(3)	N19–Fe1–N22	76.1(3)
N20–Fe1–N21	75.3(3)	N20–Fe1–N22	92.8(3)
N21–Fe1–N22	168.1(3)		

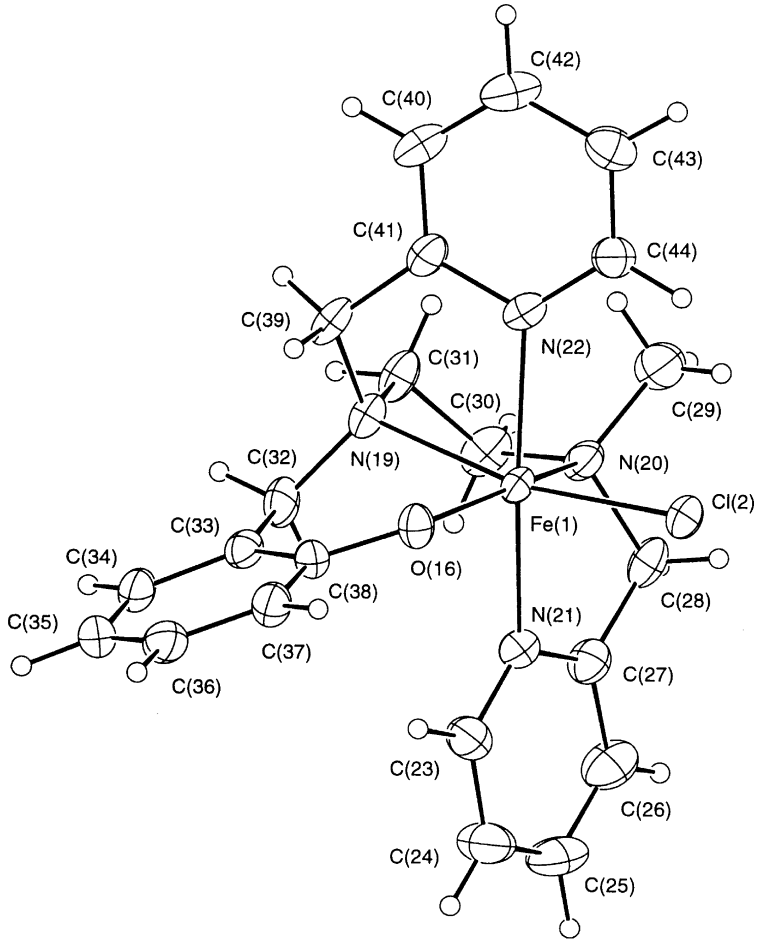

Fig. 3. ORTEP drawing of Fe(Me-enph)Cl^{+}.

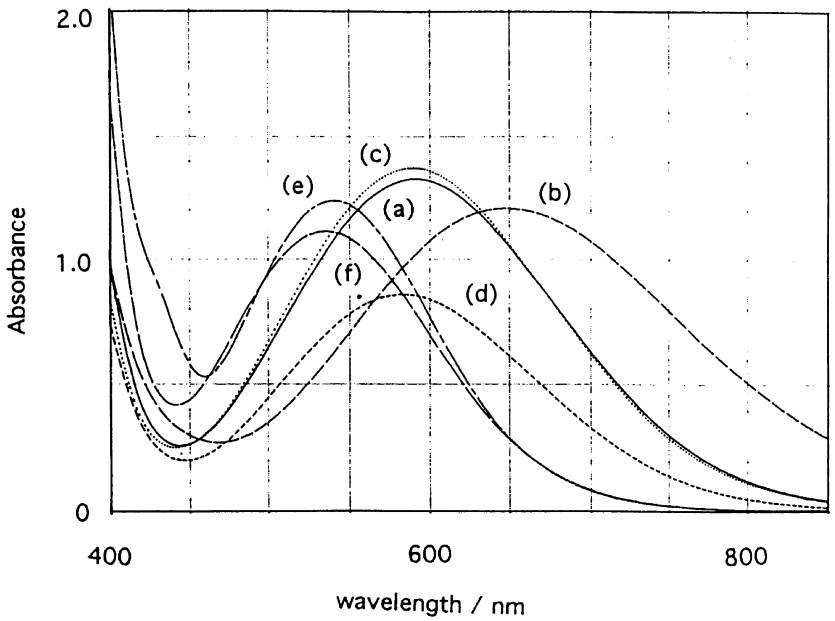

Fig. 4. Absorption spectra of Fe(X-phpy)Cl_2 complexes (in CH_3CN; 5×10^{-4} mol dm^{-3}; 298 K): (a) X = H; (b) X = 3-OMe; (c) X = 5-Br; (d) X = 3,5-Br_2; (e) 3-NO_2 and (f) X = 5-NO_2.

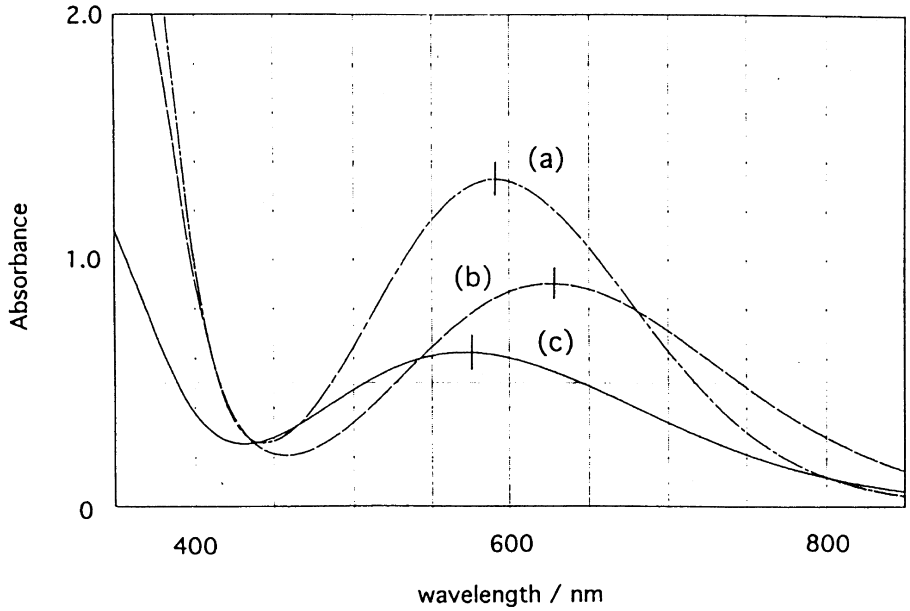

Fig. 5. Absorption spectra of Fe(phpy)Cl_2 in various solvents (5×10^{-4} mol dm^{-3}, 298 K): (a) in CH_3CN; (b) in CH_3OH and (c) in H_2O.

however in the presence of water, OH^- coordinates to an iron(III) instead of chloride ion ($m/z = 448.1$).

When hydrogen peroxide solution was added to the iron(III) compounds, interesting changes were observed in the spectra; one example, the change of the spectrum of the Fe(phpy)Cl_2 system, was shown in Fig. 7. This indicates that disappearance of the absorption band due to phenol to iron(III) charge transfer band occurs during this time, leaving a yellow solution. Similar spectral changes were also observed for other compounds, but the rate of bleaching of the absorption bands are highly dependent on the X on the phenol ring; the order of the bleaching is (see Fig. 8):

$$\text{3-OMe} > \text{H} > \text{5-Br} > \text{3,5-Br}_2 \gg \text{3-NO}_2$$

This order is roughly consistent with the order of energy of HOMO of the ligand system. A similar spectral change was also observed for the Fe(R-enph-X)Cl^+ compounds (data, not shown), the order of the rate of disappearance of the absorption band is also; 3-OMe > H > 5-Br.

It should be noted here that bleaching of the absorption band was also found when *t*-butylhydroperoxide solution was added to a solution of an iron(III) compound, as an example the case of the Fe(phpy)Cl_2 is shown in Fig. 9. It should be noted here that the rate of bleaching by *t*-butylhydroperoxide is much slower than that observed for the case of hydrogen peroxide, although the order of the disappearance of the absorption was the same as that observed for the hydrogen peroxide;

$$\text{3-OMe} > \text{H} > \text{3,5-Br}_2 \approx \text{5-Br} > \text{3-NO}_2.$$

Origin of the change of absorption bands in the visible region

On the addition of hydrogen peroxide to an iron(III) complex solution, a peroxide-adduct formation may occur at the position coordinated by the chloride ion. The rate of disappearance of the absorption band increases with increasing ratio of water vs acetonitrile in the solvents used indicates that formation of hydroxide species is necessary for a facile peroxide adduct formation, as shown in Scheme 1.

There are two reasons to explain the fact that charge transfer bands due to the electronic transition from phenol ring to an iron(III) atom disappeared on the addition of hydrogen peroxide; (1) change of the valence state of the iron(III) ion to Fe(IV) or Fe(V) and (2) change of the electronic structure of the phenol ring through interaction with a peroxide adduct in the Scheme. Since the yellow solution resulting after 1 h does not change anymore for several days, it is undoubtedly true that oxidative degradation of the phenol moiety has proceeded in the reaction course. Formation of Fe(V)=O may be also likely and some researchers have proposed the formation of an iron(IV) or iron(V) state in the reaction cycle in cytochrome P-450 or methane monooxygenase [25, 26]. However, the slower rate of disappearance of the absorption bands in the solution containing *t*-butylhydroperoxide than that in the hydrogen peroxide may suggest that at least the disappearance of the absorption band is not directly related with formation of a high valent iron-oxo species, because it is generally accepted that *t*-butylhydroperoxide exhibits a stronger oxidation power than that of hydrogen per-

A

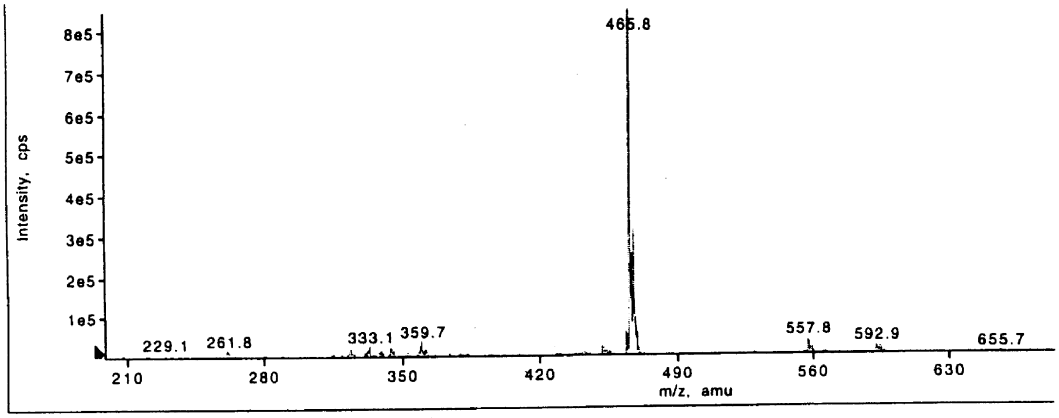

B

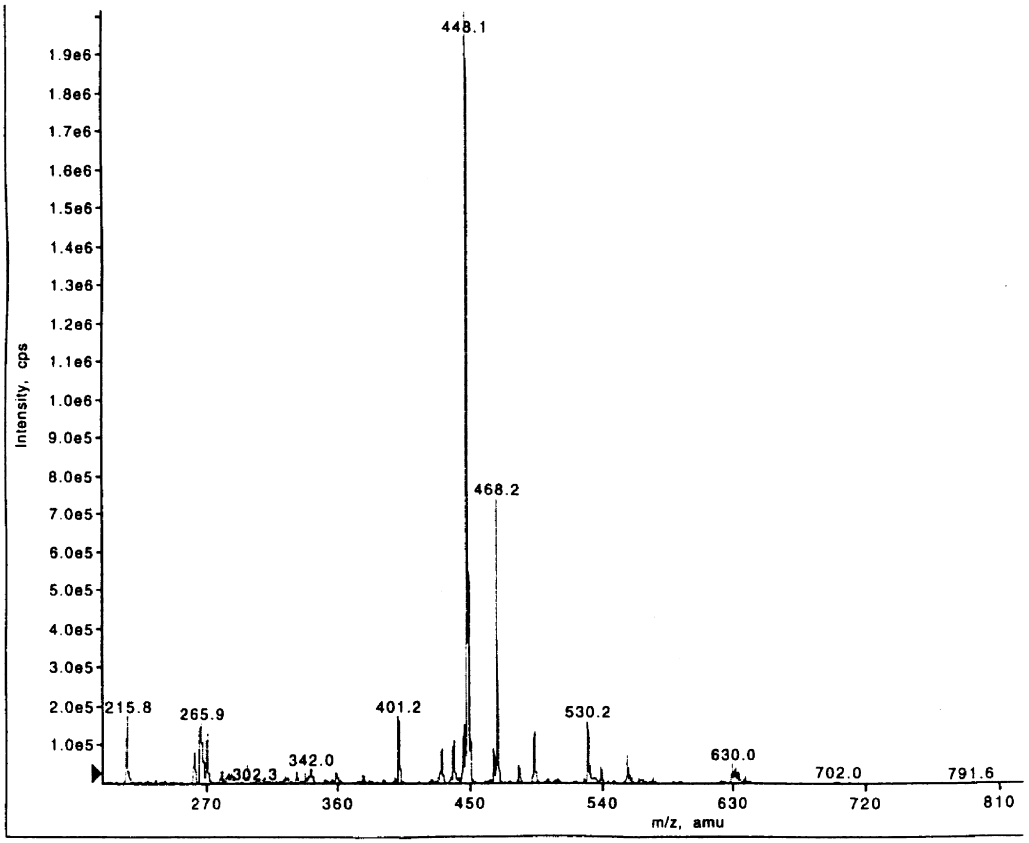

Fig. 6. Ion spray mass spectroscopy of Fe(Et-enph)ClClO$_4$. (A) In acetonitrile and (B) in water.

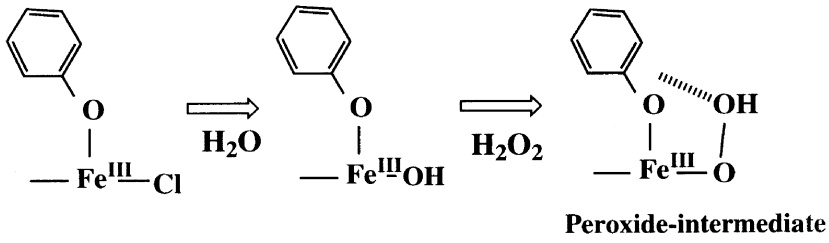

Scheme 1.

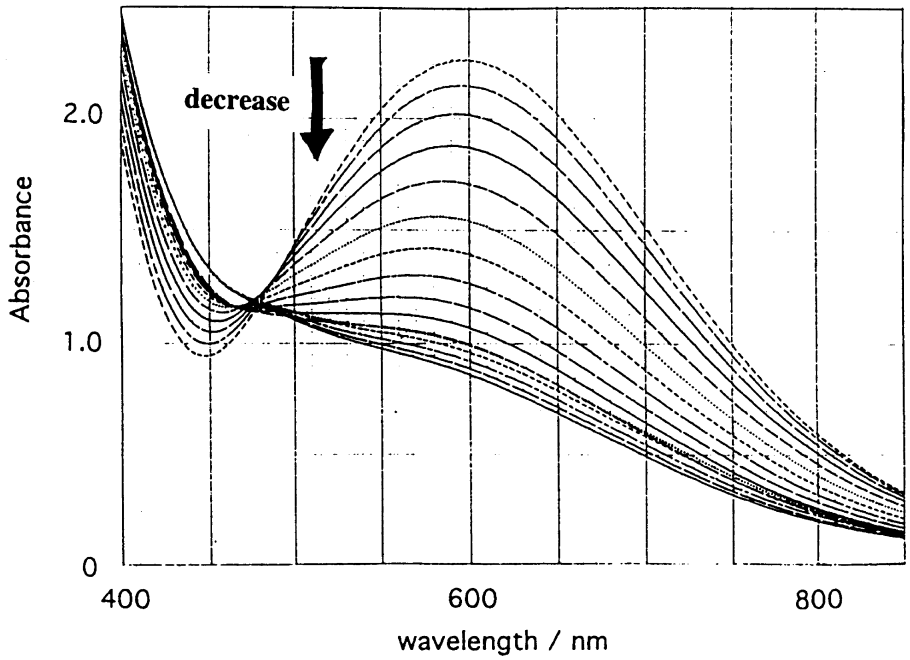

Fig. 7. Time course of absorption spectra of the system containing $Fe(phpy)Cl_2$ and hydrogen peroxide (solvent; $H_2O/CH_3CN = 1/4$, $[Fe^{3+}] = 2 \times 10^{-3}$ mol dm^{-3}, $[H_2O_2] = 2 \times 10^{-2}$ mol dm^{-3}, 298 K. Measurements were performed every 2 min after addition of hydrogen peroxide solution).

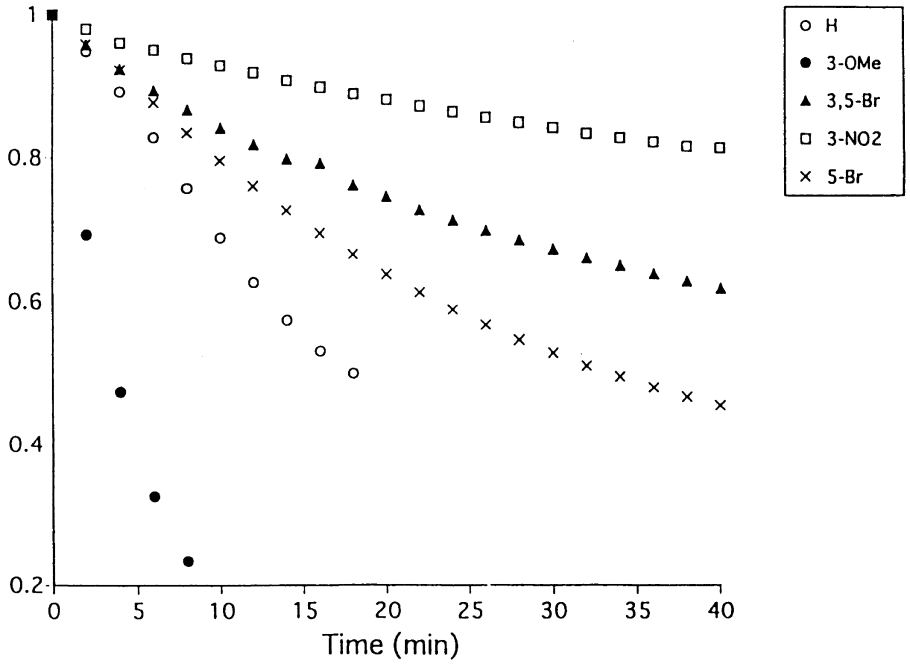

Fig. 8. Time course of absorption maximum of the $Fe(X\text{-}phpy)Cl_2$ complex (in water/acetonitrile = 1/4 solution, 298 K).

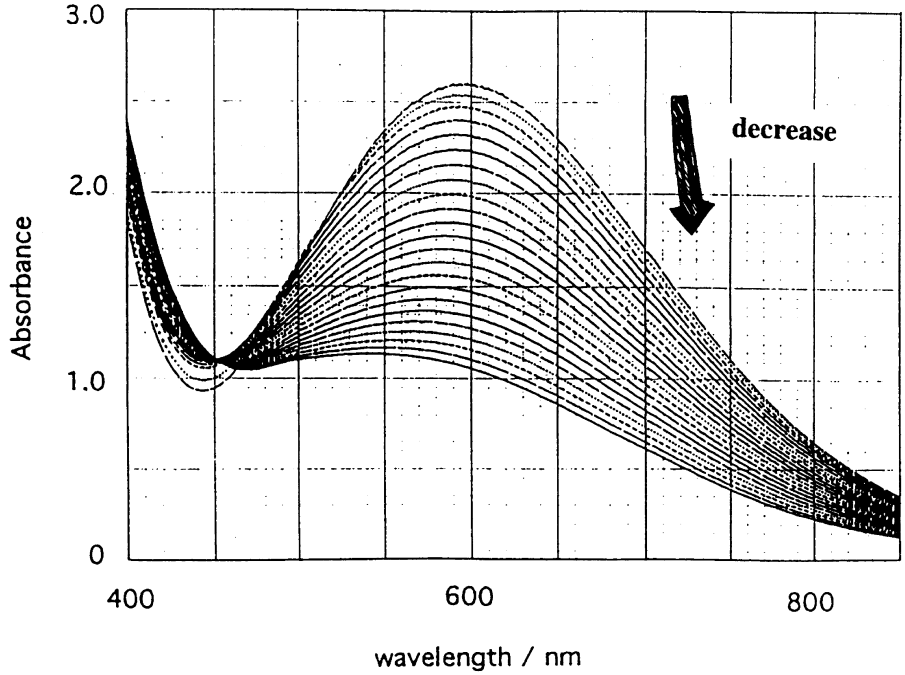

Fig. 9. Time course of absorption spectra of the system containing $Fe(phpy)Cl_2$ and *t*-butylhydroperoxide (solvent; $H_2O/CH_3CN = 4/1$, $[Fe^{3+}] = 2 \times 10^{-3}$ mol dm^{-3}, [*t*-Bu-OOH] $= 4 \times 10^{-2}$ mol dm^{-3}, 298 K. Measurements were performed every 15 min after addition of hydrogen peroxide solution).

oxide [27, 28]. As the rate of bleaching of the absorption band is not dependent on the concentration of an iron(III) ion, it seems most likely that the degradation of the phenol moiety was induced by the *intramolecular* attack of a terminal oxygen atom of the peroxide adduct with η^1-coordination mode, as shown in the Scheme. The large bulky substituent of the *t*-butylhydroperoxide may prevent the approach of the oxygen atom to the phenol ring (see below), which may reasonably explain the much slower rate of bleaching of the absorption bands observed in this study.

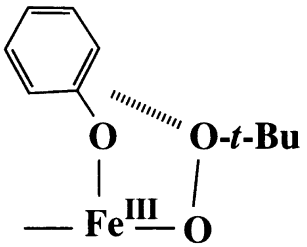

Structure 5.

In our previous papers [3, 4], we have investigated the reactivity of an iron(III)-peroxide adduct with η^1-coordination mode and have reported that this species exhibits electrophilic reactivity at both the O1 and O2 positions, which is confirmed by several examples [4, 21, 29]. In the present case, the reactivity at the O2 position is important.

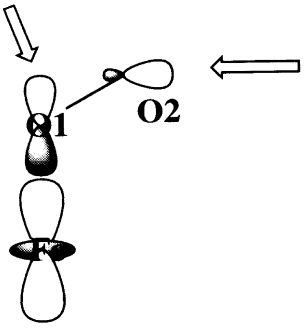

Structure 6.

Since the peroxide adduct shows electrophilic nature at the O2 position, it is anticipated that the phenol moiety of 3-OMe derivative shows the highest affinity towards the peroxide adduct, because the energy of the HOMO is the highest among the compounds as shown below and this is quite consistent with the experimental results as described before. The *intramolecular* interaction between the peroxide adduct and the phenol moiety may give an oxygenated or oxidized product associated with the disappearance of the absorption band in the visible region, however the details on oxygenation products of the phenol moiety are not clear at present. However, as men-

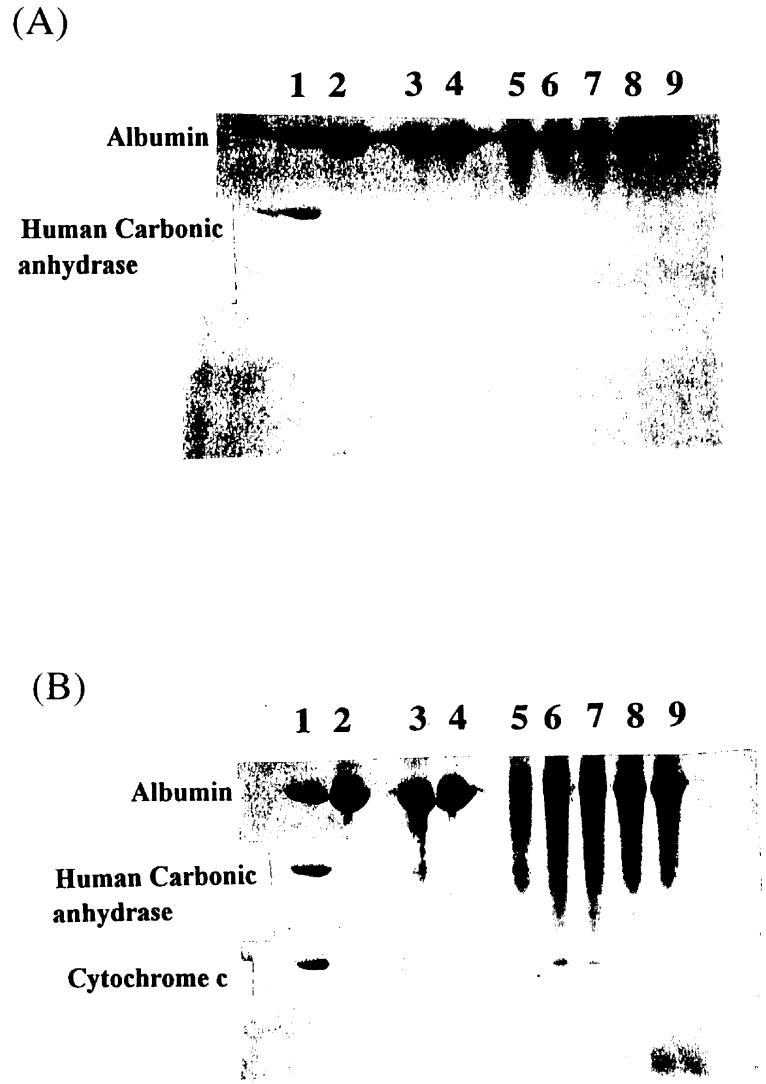

Fig. 10. Degradation of albumin by iron(III) complex in the presence of hydrogen peroxide; concentration of iron(III) complex is 0.5 mmol dm^{-3} (see <secr id=‡2‡>). (A) $Fe(tpa)Cl_2^+$ lane 1, albumin and human carbonic anhydrase I (HCA); lane 2, albumin, only; lane 3, albumin and iron(III) complex; lane 4, albumin and H_2O_2 (100 mmol dm^{-3} solution); lane 5, albumin + iron(III) complex + H_2O_2 (100 mmol dm^{-3} solution); lane 6, albumin + iron(III) complex + H_2O_2 (50 mmol dm^{-3} solution); lane 7, albumin + iron(III) complex + H_2O_2 (25 mmol dm^{-3} solution); lane 8, albumin + iron(III) complex + H_2O_2 (12.5 mmol dm^{-3} solution); lane 9, albumin + iron(III) complex + H_2O_2 (6.25 mmol dm^{-3} solution). (B) $Fe(phpy)Cl_2$: lane 1, albumin, human carbonic anhydrase I (HCA); lane 2, albumin, only; lane 3, albumin and iron(III) complex; lane 4, albumin and H_2O_2 (100 mmol dm^{-3} solution); lane 5, albumin + iron(III) complex + H_2O_2 (100 mmol dm^{-3} solution); lane 6, albumin + iron(III) complex + H_2O_2 (50 mmol dm^{-3} solution); lane 7, albumin + iron(III) complex + H_2O_2 (25 mmol dm^{-3} solution); lane 8, albumin + iron(III) complex + H_2O_2 (12.5 mmol dm^{-3} solution); lane 9, albumin + iron(III) complex + H_2O_2 (6.25 mmol dm^{-3} solution).

tioned in previous papers [3, 4], the interaction between the phenol ring (π-electron) and the peroxide adduct with η^1-coordination mode in the intermediate (see below) induces more activation of hydrogen peroxide [4], leading to facile heterolytic cleavage of the O–O bond and to formation of an Fe(III)–O (atomic oxygen)–OH^- species. This Fe(III)–O (atomic oxygen), which is alternately written as Fe(V)=O, is assumed to exhibit high activity for oxidation and oxygenation of the organic compounds, which is consistent with several experimental facts as shown below.

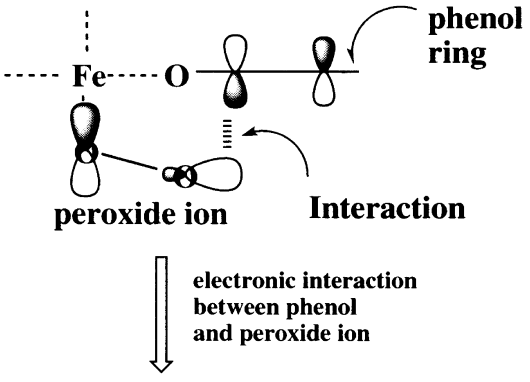

Structure 7.

Reactivity of the iron(III)-complexes containing phenol derivatives

In this study we have observed that Fe(phpy)Cl_2 complex exhibits high activity for degradation of deoxyadenosine, but its activity of the (tpa)-complex is negligible. Similar facts were also observed for the other nucleosides and nucleic acids such as cytosine and deoxyguanosine, etc. (data, not shown). Quite high activity of the H(phpy)-complex to that of the (tpa)-complex was also observed for the degradation of albumin in the presence of hydrogen peroxide, as shown in Fig. 10; serious degradation of albumin was detected at low concentration of hydrogen peroxide (6.26 mmol dm^{-3}) in the case of the Fe(phpy)Cl_2 complex, whereas no degradation was found for the (tpa)-complex under the same experimental conditions [see lanes 6–9 of both (A) and (B) in Fig. 10]. The high activity of the H(phpy)-complex also can be attributed to the activated form of the peroxide ion through interaction with the phenol group. Little activity observed for the Fe-(tpa) complex can be explained by the fact that Fe(tpa)Cl_2^+ complex has no phenol moiety and the activation of the peroxide ion by the pyridine ring is negligible (see below) [3, 4].

Acknowledgements—The present work was supported by a Foundation of P&G. Ion Spray Mass Spectroscopy was obtained by Professor K. Tatsumi at Nagoya University.

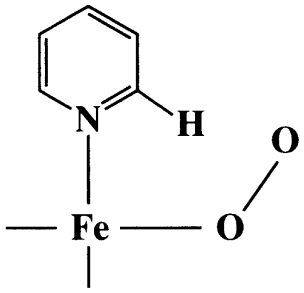

Structure 8.

REFERENCES

1. Nishida, Y. and Takeuchi, M., *Z. Naturforsch.*, 1987, **42B,** 52.
2. Rana, T. M. and Meares, C. F., *Proc. Natl. Acad. Sci. U.S.A.*, 1991, **88,** 10578.
3. Ito, S., Okuno, T., Matsushima, H., Tokii, T. and Nishida, Y., *J. Chem. Soc. Dalton Trans.*, 1996, 4479.
4. Ito, S., Okuno, T., Itoh, H., Ohba, S., Matsushima, H., Tokii, T. and Nishida, Y., *Z. Naturforsch.*, 1997, **52B,** 719.
5. Lubben, M., Meetsma, E. C., Wilkinson, E. C., Feringa, B. and Que, L. Jr., *Angew. Chem. Int. Ed. Engl.*, 1995, **34,** 1512.
6. White, R. E. and Coon, C. J., *Annu. Rev. Biochem.*, 1980, **49,** 315.
7. Pratt, J. M., Ridd, T. I. and King, L. J., *J. Chem. Soc. Chem. Commun.*, 1995, 2297.
8. Robichaud, P. E., Shyadehi, A. Z., Wright, J. N., Akhtar, E. and Akhtar, T., *Biochemistry*, 1995, **34,** 14104.
9. Vaz, A. D. N., Pernecky, S. J., Raner, G. M. and Coon, M. J., *Proc. Natl. Acad. Sci. U.S.A.*, 1996, **93,** 4644.
10. Sam, J. W., Tang, X.-J. and Peisach, J., *J. Am. Chem. Soc.*, 1994, **116,** 5250.
11. Nishida, Y., Shimo, H., Takeuchi, M. and Kida, S., *Inorg. Chim. Acta*, 1984, **96,** 115.
12. Murch, B. P., Bradley, F. C. and Que, L. Jr., *J. Am. Chem. Soc.*, 1986, **108,** 5027.
13. Brenann, B. A., Chen, Q., Garcia, C. J., True, A. E., O'Connor, C. J. and Que, L. Jr., *Inorg. Chem.*, 1937, **1991,** 30.
14. Nishida, Y., Nasu, M. and Akamatsu, T., *Z. Naturforsch.*, 1992, **47B,** 115.
15. Feig, A. L., Becker, M., Schindler, S., Edlik, R. and Lippard, S., *J. Inorg. Chem.*, 1996, **35,** 2590.
16. Kim, K. and Lippard, S. J., *J. Am. Chem. Soc.*, 1996, **118,** 4914.
17. Dong, Y., Yan, S., Young, V. G. and Que, L. Jr., *Angew. Chem. Int. Ed. Engl.*, 1996, **35,** 618.
18. Ookubo, T., Sugimoto, H., Nagayam, T., Masuda, H., Sato, T., Tanaka, K., Maeda, Y., Okawa, H., Hayashi, Y., Uehara, A. and Suzuki, M., *J. Am. Chem. Soc.*, 1996, **118,** 701.
19. Harris, D. L. and Loew, G. H., *J. Am. Chem. Soc.*, 1994, **116,** 11671.
20. Nishida, Y., Itoh, H. and Yamazaki, A., *Polyhedron*, 1994, **13,** 2473.

21. Ito, S., Suzuki, M., Kobayashi, T., Itoh, H., Harada, A., Ohba, S. and Nishida, Y., *J. Chem. Soc. Dalton Trans.*, 1996, 2579.
22. Toftlund, H. and Andersen, S. Y., *Acta Chem. Scand.*, 1981, **35A,** 575.
23. Kasai, H. and Nishimura, S., *Nucl. Acids Res.*, 1984, **12,** 2137.
24. Que, L. Jr., *Coord. Chem. Rev.*, 1983, **50,** 73.
25. Sono, M., Roach, M. P., Coulter, E. D. and Dawson, J. H., *Chem. Rev.*, 1996, **96,** 2841.
26. Wallar, B. J. and Lipscomb, J. D., *Chem. Rev.*, 1996, **96,** 2625.
27. Plesnicar, B., *The Chemistry of Peroxides*, Chap. 17, ed. S. Patai. John Wiley and Sons, New York, 1983.
28. Nyuyen, C., Guajardo, R. J. and Maschrak, P. K., *Inorg. Chem.*, 1996, **35,** 6273.
29. Torpey, J., Lee, D. A., Smith, K. M., Ortiz de Montellano, P. R., *J. Am. Chem. Soc.*, 1996, **118,** 9172.

Pergamon

Polyhedron Vol. 17, Nos. 25, 26, pp. 4393–4402, 1998
© 1998 Elsevier Science Ltd
All rights reserved. Printed in Great Britain
0277–5387/98 $19.00+0.00

PII: S0277–5387(98)00242–3

Crystal structure of tetraethylammonium bis(tetracarbonylmolybdenum)-tetrathiotungstate, $[Et_4N]_2[(OC)_4MoS_2WS_2Mo(CO)_4]$ and synthesis, infrared spectra, ^{95}Mo NMR spectra and cyclic voltammetry of new linear trinuclear Mo(W)–S carbonyl clusters containing mixed-valence metal atoms $[(OC)_4MS_2M'SM(CO)_4]^{2-}$ (M, M′ = Mo or W)

Botao Zhuang,* Peihua Yu, Lingjie He, Liangren Huang and Guohua Pan

State Key Laboratory of Structural Chemistry, Fujian Institute of Research on the Structure of Matter, Chinese Academy of Sciences, Fuzhou, Fujian 350002, China

(Received 6 March 1998; accepted 15 June 1998)

Abstract—Four trinuclear molybdenum(tungsten)-sulfur carbonyl cluster compounds, $[Et_4N]_2[(OC)_4MoS_2MoS_2Mo(CO)_4]$ (**1**), $[Et_4N]_2[(OC)_4WS_2WS_2W(CO)_4]$ (**2**), $[Et_4N]_2[(OC)_4MoS_2WS_2Mo(CO)_4]$ (**3**), $[Et_4N]_2[(OC)_4WS_2MoS_2W(CO)_4]$ (**4**) have been prepared by both reaction of $[M(CO)_4(S_2CNEt_2)]^-$ with $M'S_4^{2-}$ in MeOH and reaction of MeCN solution of $M(CO)_6$ with $M'S_4^{2-}$ in MeOH (M = Mo, W; M′ = Mo, W). These complexes has been characterized by routine elemental analysis and spectroscopy and the structures of **1** and **3** have been determined by X-ray crystallography. The structure study reveals that the anion of **3** contains a heteronuclear Mo–W–S trimetallic core, $[MoS_2WS_2Mo]^{2-}$, consisting of two perpendicular rhombic MoS_2W units sharing a tungsten atom. The Mo–W bond distances are 3.028(2) and 3.031(2) Å and the Mo–W–Mo angle is 176.04(5)°. The average bond lengths of W–S and Mo–S are 2.21 and 2.54 Å, respectively. The X-ray, structure, IR, CV (cyclic voltammetry) and ^{95}Mo NMR studies on these four cluster complexes indicated that these cluster complexes possess wide separated oxidation states of metal atoms and exhibit the charge transfer, $M^L \rightarrow M^HS_4$ (M^L represents a low-valance metal atom and M^H a high valence metal atom), between the two different valence metallic centers in the cluster complexes. It has been found that the charge transfer, $M^L \rightarrow M^HS_4$, in the complexes are: **1** > **4**, **3** > **2**, **1** > **3**, **4** > **2**, **1** > **2** and **3** ~ **4** implying the electron-donation ability of low-valence metal atoms in the complexes is $Mo^0 > W^0$ and the electron-accepted ability of the high valence metal atoms in the complexes is $Mo^{VI} > W^{VI}$. © 1998 Elsevier Science Ltd. All rights reserved

Keywords: mixed-valence Mo(W)–S cluster; synthesis; structure; IR; ^{95}Mo NMR; CV.

1. INTRODUCTION

The chemistry of molybdenum–sulfur cluster compounds and mixed-valence-containing metal cluster complexes has increasingly attracted the attention from chemists and bioinorganic chemists because of the existence of molybdenum–sulfur bonding in a variety of Mo-containing enzymes, among them nitrogenase [1–3] and hydrodesulfurization catalysts containing molybdenum and sulfur atoms [4] and also because of the great importance of mixed-valence in biosystems and catalysis systems. As a part of our studies on complexes with low-valence molybdenum atoms [5, 6, 7, 8]. We have found and developed a new Mo(W)S cluster compound family containing low- and mixed-valence metal atoms, $[\{(OC)_4M\}xM'S_4]^{2-}$ (M = Mo, W; M′ = Mo, W; x = 1,2) [9, 10, 11, 12],

* Author to whom correspondence should be addressed.

which corresponds to the linear Mo–Fe–S cluster complexes, $[(FeL_2)xMS_4]^{2-}$ (L = SR, Cl; $x = 1,2$ and M = Mo, W) [13] that have been studied as modeling compounds for the active center of nitrogenase, In our previous publications several dinuclear members and a trinuclear member of this family, the tetraethylammonium salts of $[(OC)_4MoS_2WS_2]^{2-}$ [9], $[(OC)_4MoS_2MoS_2]^{2-}$ [11] $[(OC)_4WS_2WS_2]^{2-}$ [10] and $[(OC)_4MoS_2MoS_2Mo(CO)_4]^{2-}$ (**1**) [12] have been reported. Herein, we present the synthesis of the new trinuclear members including homo- and heteronuclear ones, $[Et_4N]_2[(OC)_4WS_2WS_2W(CO)_4]$ (**2**), $[Et_4N]_2[(OC)_4MoS_2WS_2Mo(CO)_4]$ (**3**) and $[Et_4N]_2[(OC)_4WS_2MoS_2W(CO)_4]$ (**4**), the crystal structure of **3** and the investigation on the charge transfer in this series of compounds including **1** by IR spectra, CV and ^{95}Mo NMR spectra studies.

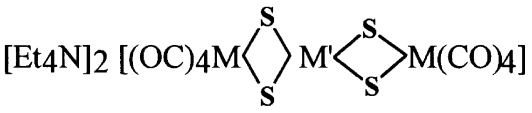

1, M=M'=Mo; **2**, M=M'=W;
3, M=Mo, M'=W; **4**, M=W, M'=Mo

2. EXPERIMENTAL

2.1. *Materials and methods*

All procedures including synthetic reaction, structure determination, physical and chemical measurements were carried out under nitrogen atmosphere by using standard Schlenk technique and all solvents and reagents were dried and degassed before use. Acetonitrile was distilled from CaH_2. Methanol and isopropanol were dried by distillation with magnesium methoxide. $Mo(CO)_6$, $W(CO)_6$ and NaS_2CNEt_2 were purchased from Alfa (U.S.A.) and the Shanghai Chemical Reagent Company, respectively. The complexes, $[Et_4N][Mo(CO)_4(S_2CNEt_2)]$ [14], $[Et_4N]_2[MS_4]$(M = Mo, W) [15] and $[Et_4N][W(CO)_4(S_2CNEt_2)]$ [10] were prepared by the literature methods.

IR spectra were recorded on a Perkin-Elmer 577 IR spectrometer and Digilab FTS-20E/D-V Foudet IR spectrometer. Elemental analysis were performed on a Carlo Erba instrumentation elemental analyzer MOD 1106; ^{95}Mo NMR spectra of the samples in MeCN were measured on Varin Unit 500 NMR spectrometer (U.S.A.) with a relative solution of 2 M Na_2MoO_4 in D_2O sealed in a capillary.

Cyclic voltammetry (CV) measurements were performed with a three-electrode cell using 0.1 M Bu_4NBF_4 as the supporting electrolyte and MeCN as solvent. The working electrode was glass carbon, the reference electrode was an aqueous SCE separated from the sample solution by a salt bridge and the auxiliary electrode is platinum wire. Solutions were deoxygenated and blanketed with a nitrogen atmosphere and the potentiostat was a CV-B from BAS (Bioanalytical System).

2.2. *Syntheses of complexes*

2.2.1. $[Et_4N]_2[(OC)_4MoS_2MoS_2Mo(CO)_4]$ (**1**) **1** was prepared by reaction of $[Et_4N]_2MoS_4$ with $[Et_4N][Mo(CO)_4(S_2CNEt_2)]$ in MeOH or MeCN according to the literature method [12].

2.2.2. $[Et_4N]_2[(OC)_4WS_2WS_2W(CO)_4]$ (**2**) (i) A mixture of $[Et_4N]_2[WS_4]$ (0.50 g, 0.874 mmol) and $[Et_4N][W(CO)_4(S_2CNEt_2)]$ (1.30 g, 2.26 mmol) in 60 ml of MeCN were stirred at 60–65°C for 3 days resulting in a deep red solution with brown–red precipitate in it. After cooling to room temperature, 0.50 g brown–red product **2** was obtained by filtration, washed with MeOH and dried *in vacuo*, yield: 50%. Analysis: calcd. for $C_{24}H_{40}N_2O_8S_4W_3$, C, 24.74; H, 3.44; N, 2.41; S, 10.99; W, 47.42%. Found: C, 24.47; H, 3.58; N, 2.87; S, 10.98; W, 47.85%. IR (KBr pellet): 2000 s, 1876 s, 1861 s, 1818 s cm^{-1} ($\nu_{WC=O}$); 580 m, 566 m cm^{-1} (δ_{W-C-O}); 465 w, 436 w ($\nu_{W(VI)-Sb}$), ~415 sh ($\nu_{W(O)-Sb}$) and 349 ($\nu_{W(O)-C}$) cm^{-1}. After collecting the **2** product the filtrate was cooled at 4°C. 0.04 g of red microcrystalline product, which was recognized as dinuclear compound $[Et_4N]_2[(OC)_4WS_2WS_2]$ [10] by IR spectrum, was obtained.

(ii) A mixture of $[Et_4N]_2[WS_4]$ (0.572 g, 1 mmol) and $[Et_4N][W(CO)_4(S_2CNEt_2)]$ (0.58 g, 1 mmol) in 50 ml of MeCN were stirred at 55–60°C for 24 h. After treating by the same procedures as in (i), 0.13 g of **2** (yield, 22% based on the amount of $[Et_4N][W(CO)_4(S_2CNEt_2)]$ used) and 0.09 g of red crystalline product of dinuclear compound $[Et_4N]_2[(OC)_4WS_2WS_2]$ [10] (yield: 10%) were obtained.

2.2.3. $[Et_4N]_2[(OC)_4MoS_2WS_2Mo(CO)_4]$ (**3**) (i) A mixture of $[Et_4N]_2WS_4$ (0.572 g, 1 mmol) and $[Et_4N][Mo(CO)_4(S_2CNEt_2)]$ (0.972 g, 2 mmol) in 45 ml of MeOH was stirred at 55°C for 24 h resulting in much deep red microcrystalline precipitate. 0.60 g of **3** were obtained after cooling to room temperature, filtered, washed with MeOH and dried *in vacuo*, yield, 61%. Analysis: calcd. for $C_{24}H_{40}Mo_2N_2O_8S_4W$, C, 29.15; H, 4.05; N, 2.83; Mo, 19.43; S, 12.96; W, 18.62%. Found: C, 28.42; H, 4.17; N, 2.90; Mo, 19.02; S, 12.56. W, 18.89%. IR (KBr pellet): 2004 s, 1895 s, 1865 s, 1815 s cm^{-1} ($\nu_{MoC=O}$); 595 m, 580 m, 570 m cm^{-1} (δ_{M-C-O}); 450 w (ν_{W-Sb}), 428 w (ν_{Mo-Sb}), 340 (ν_{Mo-C}) cm^{-1}. The filtration was cooled at 4°C; a small amount of red crystal product (0.15 g) which is recognized as dinuclear compound $[EtN]_2[(OC)_4MoS_2WS_2]$ [9] by its IR spectrum.

(ii) A mixture of $[Et_4N]_2WS_4$ (0.572 g, 1 mmol) and $Mo(CO)_6$(0.258 g, 2 mmol) in 50 ml of MeCN was stirred at 45–50°C for 3 h and then, at 82°C for 18 h, resulting in a deep red solution. After cooling to room

temperature the reaction mixture was concentrated to the volume of 15 ml by vacuum and 50 ml of EtOH was added leading to a small amount of precipitate. Filtering off the residue, the filtrate was cooled at 4°C resulting in precipitation of a brown solid (~0.23 g) which is an impure mixture judged by its IR spectra. Removing the brown solid, the filtrate was continued to be cooled at 4°C for several days, 0.24 g of red crystalline product, **3**, was collected. Yield: 25%. Crystals suitable for X-ray crystal structure determination of **3** were obtained from a mixed solution of MeOH and MeCN.

2.2.4. $[Et_4N]_2[(OC)_4WS_2MoS_2W(CO)_4]$ (**4**) (i) A mixture of $[Et_4N][W(CO)_4(S_2CNEt_2)]$ (1.15 g, 2 mmol) and $[Et_4N]_2MoS_4$ (0.48 g, 1 mmol) in 50 ml of MeOH was stirred at 45–50°C for 24 h resulting in the precipitation of a brown microcrystalline product. After cooling to room temperature, 0.54 g of microcrystalline **4** were obtained by filtration, washed with MeOH and dried *in vacuo*; yield: 50.2%. Analysis: calcd. for $C_{24}H_{40}MoN_2O_8S_4W_2$, C, 26.77; H, 3.72. N, 2.60; Mo, 8.92. S, 14.90; W, 34.20%. Found: C, 27.09; H, 4.01; N, 3.06; Mo, 8.45; S, 15.02; W, 34.80%. IR (KBr pellet): 2000 s, 1882 s, 1860 s, 1822 s cm^{-1} ($\nu_{WC=O}$); 572 m, 572 m, 562 m cm^{-1} (δ_{W-C-O}), 459 w, 442 w (ν_{Mo-Sb}), 417 w (ν_{W-Sb}), 345 (ν_{W-C}) cm^{-1}.

(ii) A mixture of $[Et_4N][W(CO)_4(S_2CNEt_2)]$ (1.15 g, 2 mmol) and $[Et_4N]_2MoS_4$ (0.48 g, 1 mmol) in 50 ml of MeCN was stirred at 45–50°C for 24 h resulting in a brown–green solution. The resulting reaction mixture was concentrated to a volume of 25 ml and 50 ml of isopropanol was added. A small amount of precipitate was filtered off and the filtrate was cooled at 4°C. 0.33 g of brown crystalline **4** was obtained after filtration, washed with MeOH and dried *in vacuo*. yield: 31%.

2.3. *X-ray crystal structure determination*

A dark plate crystal of **3** with approximate dimensions of $0.20 \times 0.30 \times 0.40$ mm coated with epoxy resin was mounted on a glass fiber in a random orientation. Diffraction measurements were made on an Enraf-Nonius CAD4 computer controlled κ-axis diffractometer equipped with a graphite crystal incident beam monochromator. Unit cell parameters were obtained from a least-squares fit of 25 reflections in the range of $11 < \theta < 13°$ and given in Table 1. The intensity data were recorded using a ω–2θ scan technique to a maximum 2θ of 52.0° with a variable scan speed. A total of 3931 reflections, of which 3688 were unique, were collected. An isotropic decay correction was applied and the correction factors ranged from 0.967 to 1.143. Lorentz and polarization correction were applied to the data. An empirical absorption correction based on a series of psi-scans was applied to the data. Relative transmission coefficients ranged from 0.590 to 1.000. An empirical DIFABS [17] absorption correction was made after structure refinement with isotropic thermal parameters. The maximum and minimum absorption corrections were 1.0204 and 0.9633, respectively. The structure was solved by direct methods with MULTAN-83 program. A total of three atoms were located from the E-map and the remaining atoms were located in succeeding difference Fourier syntheses. Hydrogen atoms were not included in the calculations. Only the 2155 reflections with $I > 3.0\,\sigma(I)$ were used in the refinements. The final cycle of refinement included 267 variable parameters and converged (largest parameter shift was 0.53) with unweighted and weighted agreement factors of 0.054 and 0.060, respectively. The e.s.d. of observations of unit weight was 0.59, the highest peak in the final difference Fourier was 1.23 e/Å^3, the minimum negative peak was -0.21 e/Å^3.

All calculations were performed on a VAX computer using MOLEN/PC [18].

A list of atomic coordinates and calculate thermal parameters have been deposited at the Cambridge Crystallographic Data Centre.

3. RESULTS AND DISCUSSION

3.1. *Synthesis of* $[Et_4N]_2[(OC)_4MS_2M'S_2M(CO)_4]$ (M = Mo, W; M = Mo, W)

$[M(CO)_4(S_2CNEt_2)]^-$ reacts with $[M'S_4]^{2-}$ (2:1 in mol. ratio) in solvents such as MeOH MeCN, affording trinuclear Mo–W–S cluster complexes, $[Et_4N]_2[(OC)_4MS_2M'S_2M(CO)_4]$ (M = M′ = Mo; (**1**); M = M′ = W, (**2**); M = Mo, M′ = W, (**3**) and M = W, M′ = Mo, (**4**) by the two step synthetic reaction (1) and (2) as reported in our previous paper [12].

$$[M'S_4]^{2-} + [M(CO)_4(S_2CNEt_2)]^- \rightarrow [(OC)_4MS_2MS_2]^{2-} + (S_2CNEt_2)^- \quad (1)$$

$$[(OC)_4MS_2MS_2]^{2-} + [M(CO)_4(S_2CNEt_2)]^- \rightarrow [(OC)_4MS_2M'S_2M(CO)_4]^{2-} + (S_2CNEt_2)^- \quad (2)$$

The reactions in eqns (1) and (2) take place almost simultaneously and because of the small solubility of the trinuclear products in MeOH the trinuclear products precipitated as soon as the reaction in eqn (1) took place, therefore, the yield is higher when the solvent MeOH is used. Nevertheless, in the solution MeCN, besides the reactions in eqns (1) and (2) there is the reaction in eqn (3) [9, 10] between dinuclear and trinuclear products.

$$[(OC)_4MS_2M'S_2M(CO)_4]^{2-} \rightleftarrows [(OC)_4MS_2M'S_2]^{2-} + M(CO)_4(MeCN)_2. \quad (3)$$

This leads to a decrease in the yield of trinuclear products. So, the kind of solvent greatly influences the yield of the trinuclear products. As shown in Table 2,

Table 1. Crystallographic data for $[Et_4N]_2[(OC)_4MoS_2WS_2Mo(CO)_4]$ (**3**)

Formula	$C_{24}H_{40}Mo_2N_2O_8S_4W$	d_c (g cm-3)	1.87
fw	988.58	radiation λ (Å)	MoKα
Cryst. Syst.	monoclinic		($\lambda = 0.71073$)
Space group	$P2_1/m$.	abs. coeff.μ (cm^{-1})	42.9
T (°C)	23 ± 1	R[a]	0.054
a (Å)	8.809(2)	Rw[b]	0.060
b (Å)	8.676(2)	function minimized	$\Sigma w(\|F_o\|-\|F_c\|)^2$
c (Å)	22.853(4)	w	$1/[\sigma^2(F_o^2)+(0.010\,F_o)^2+1.000]$[c]
β (°)	94.18(2)		
V (Å^3)	1758.0		
Z	2		

[a] $R = \Sigma||F_o|-|F_c||/\Sigma|F_o|$.
[b] $Rw = [\Sigma w(|F_o|-|F_c|)^2/\Sigma|F_o|^2]^{1/2}$.
[c] See Ref. [16].

Table 2. Influence of solvents on the yield of products

Compounds	$[M(CO)_4(S_2CNEt_2)]$-/$[M'S_4]^{2-}$	Solvents	T (°C)	Yield (%)
1	2:1	MeOH	55	80[a]
	2:1	MeCN	45–50	57[a]
2	2.6:1	MeOH	60–65	50
	1:1	MeOH	55–60	20
3	2:1	MeOH	~55	61
	2:1	MeCN	~50, 82	25
4	2:1	MeOH	45–50	50.2
	2:1	MeCN	45–50	31

[a] See Ref.[12].

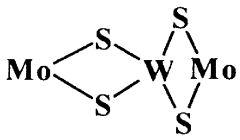

A

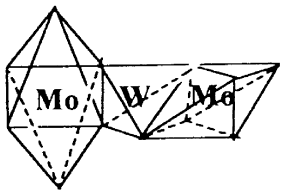

B

the yield of trinuclear products are higher in MeOH than in MeCN.

According to the synthetic reaction of this series of trinuclear compounds, it can be predicted that two new members of heterometal compounds $[(OC)_4MoS_2MoS_2W(CO)_4]^{2-}$ and $[(OC)_4WS_2WS_2Mo(CO)_4]^{2-}$, can be synthesized by control of the ratio of M(O) compounds and M(VI) compounds used.

3.2. *Structure of* $[Et_4N]_2[(OC)_4MS_2M'S_2M(CO)_4]$ (**3**) *and the existence of widely separated oxidation states of metal atoms in the compounds*

The selected bond distances and angles of **3** are listed in Table 3 and the structure of the anion of **3** is depicted in Fig. 1. **3** comprised two cations Et_4N^+ and a trinuclear dianion $[(OC)_4MoS_2WS_2Mo(CO)_4]^{2-}$, as shown in Table 3 and Fig. 1, the anion of **3** contained a trinuclear mixed metallic core, $[MoS_2WS_2Mo]^{2-}$ which was composed of two rhombic units, MoS_2W, sharing the high valence tungsten atom in perpendicular arrangement (**A**).

The central tungsten located in the center of a tetrahedron with four bridging sulfur atoms and the geometry of each terminal molybdenum atom in low oxidation state is an octahedron with two bridging sulfur atoms and four carbon atoms from four terminal carbonyls. In another word, the whole geometry

Table 3. Selected bond distances (Å) and angles (°) of **3**

W–MO(1)	3.028(2)	Mo(2)–C(22)	2.00(3)
W–Mo(2)	3.031(2)	Mo(2)–C(23)	2.02(3)
W–s(1)	2.207(5)	O(11)–C(11)	1.19(4)
W–S(2)	2.200(5)	O(12)–C(12)	1.15(3)
W–S(3)	2.218(4)	O(13)–O(13′)	1.25(4)
Mo(1)–S(1)	2.537(5)	O(13)–C(13′)	1.61(4)
Mo(1)–S(2)	2.533(6)	O(13)–C(13)	1.24(4)
Mo(1)–C(11)	1.92(2)	O(13′)–C(13′)	1.10(5)
Mo(1)–C(12)	1.96(3)	O(21)–C(21)	1.16(3)
Mo(1)–C(13′)	1.97(4)	O(22)–C(22)	1.17(3)
Mo(1)–C(13)	2.04(4)	O(23)–C(23)	1.15(3)
Mo(2)–S(3)	2.556(4)	C(13′)–C(13)	0.74(5)
Mo(2)–C(21)	1.96(2)		
Mo(1)–W–Mo(2)	176.04(5)	C(12)–Mo(1)–C(13)	97.0(8)
MO(1)–W–S(1)	55.3(1)	C(13′)–Mo(1)–C(13′)	153(1)
Mo(1)–W–S(2)	55.3(1)	C(13′)–Mo(1)–C(13)	173(1)
Mo(1)–W–S(3)	124.4(2)	C(13′)–Mo(1)–C(13)	21(1)
Mo(2)–W–S(1)	128.6(1)	C(13)–Mo(1)–C(13)	163(1)
Mo(2)–W–S(2)	120.8(2)	W–Mo(2)–S(3)	45.8(1)
Mo(2)–W–S(3)	55.7(2)	W–Mo(2)–C(21)	135.2(5)
S(1)–W–S(2)	110.6(2)	W–Mo(2)–C(22)	94.5(6)
S(1)–W–S(3)	108.6(1)	W–Mo(2)–C(23)	87.9(6)
S(2)–W–S(3)	108.9(1)	S(3)–Mo(2)–S(3)	91.5(1)
S(3)–W–S(3)	111.2(2)	S(3)–Mo(2)–C(21)	89.5(5)
W–Mo(1)–S(1)	45.7(1)	S(3)–Mo(2)–C(21)	178.8(5)
W–Mo(1)–S(2)	45.5(1)	S(3)–Mo(2)–C(22)	91.1(5)
W–mo(1)–C(11)	136.5(7)	S(3)–Mo(2)–C(23)	90.6(4)
W–Mo(1)–C(12)	133.0(8)	C(21)–Mo(2)–C(21)	89.6(6)
W–Mo(1)–C(13′)	103.0(9)	C(21)–Mo(2)–C(22)	88.2(6)
W–Mo(1)–C(13)	82.0(9)	C(21)–Mo(2)–C(23)	90.1(6)
S(1)–Mo(1)–S(2)	91.2(2)	C(22)–Mo(2)–C(23)	177.6(9)
S(1)–Mo(1)–C(11)	177.8(8)	W–S(1)–MO(1)	79.0(2)
S(1)–Mo(1)–C(12)	87.3(8)	W–S(2)–Mo(1)	79.2(2)
S(1)–Mo(1)–C(13′)	101.0(9)	W–S(3)–Mo(2)	78.5(1)
S(1)–Mo(1)–C(13)	85.9(8)	O(13′)–O(13)–C(13′)	43(2)
S(2)–Mo(1)–C(11)	91.0(8)	O(13′)–O(13)–C(13)	69(2)
S(2)–Mo(1)–C(12)	178.6(8)	C(13)–O(13)–C(13)	26(2)
S(2)–Mo(1)–C(13′)	97.1(8)	O(13)–O(13′)–C(13′)	86(3)
S(2)–Mo(1)–C(13)	82.9(8)	O(13)–C(13′)–O(13′)	51(2)
C(11)–Mo(1)–C(12)	90(2)	O(13)–C(13′)–C(13)	47(4)
C(11)–Mo(1)–C(13′)	78.7(9)	O(13′)–C(13′)–C(13)	98(5)
C(11)–Mo(1)–C(13)	94.4(9)	O(13)–C(13)–C(13′)	107(5)
C(12)–Mo(1)–C(13′)	83.2(8)		

C(13), C(13′), O(13) and O(13′) are statistic distributions.

of the dianion of **3** may be described as **B**, which consists of two terminal octahedrons with low valence molybdenum atom in the center and a medial tetrahedron with central high valence tungsten atom sharing two edges (two perpendicular S . . . S lines). There is a symmetric mirror with Mo1, W, Mo2, S1, S2, C11, C12, C22, C23 O11, O12, O22 and O23 atoms in it and the C13, C13′ and O13, O13′ atoms are statistic distribution. W–Mo bond lengths and MoWMo angles are 3.028, 3.031 Å and 176.04(5)°, respectively, indicating metal–metal interaction. Four W–S bond lengths are basically, equivalent (2.21 Å) and the corresponding Mo–S bond distances are 2.535 (Mo–S1, Mo–S2) and 2.556 Å (Mo–S3) and Mo–C bond lengths are 1.97(Mo1–C) and 1.99 Å (Mo2–C).

Although the formal oxidation states of the two Mo and the W atoms in **3** are zero and VI, respectively, the somewhat longer distance of Mo–C showed that the real oxidation state of the two Mo atoms are higher than zero if comparing with the Mo–C distance (1.965 Å) of Mo(0)complex, $[Mo(CO)_4(S_2CNEt_2)]^-$ [14]. Considering the W–S bond distances, it is obvious that the average W–S bond length of **3** is longer than that of W^{VI} complex, WS_4^{2-} (W–S, 2.17 Å) [19] indicating that the real oxidation state of tungsten atom in **3** is somehow lower than VI. Apparently, the

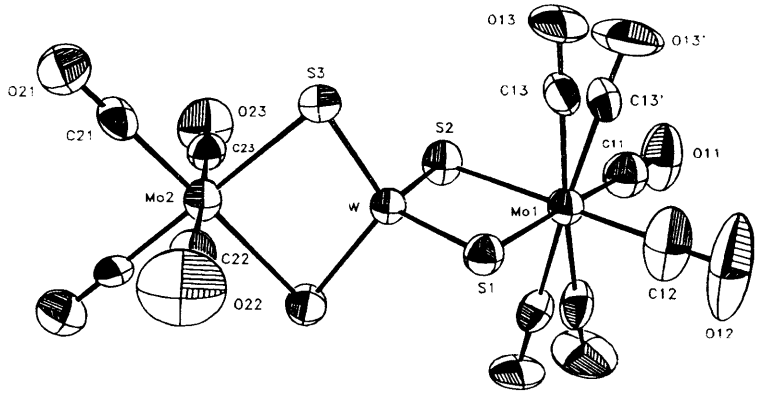

Fig. 1. The structure of the anion of **3**, $[(OC)_4MoS_2WS_2Mo(CO)_4]^{2-}$. The atoms C13, O13 and C13′, O13′ are statistically distributed and the occupancy of each of them is 50%.

existence of mixed valence metal atoms in **3** would lead to the occurrence of charge transfer between the different valence metal centers, $Mo^0 \rightarrow W^{VI}$, resulting in a partial oxidation of Mo^0 and partial reduction of W^{VI} in terms of the suggestion that Fe→M charge transfer is evident in the Fe–M–S (M=Mo or W) complexes when the mean values of the iron–ligand bond lengths and of the M–S bond distances in the MS_4^{2-} ligands are taken into account [13]. However, the electron delocalization takes place only partly, thus, the two kinds of metal atoms (Mo and W) in **3** still exist wide separated oxidation states. Inviting the structural parameters of **1** [12] for comparison (Table 4), it can be found that the Mo–S and Mo–C bond lengths of **1** are shorter and longer than that of **3**, respectively, implying that the oxidation states of the two terminal Mo atoms in **1** are somehow higher than that in **3**. This shows that the charge transfer $Mo^0 \rightarrow W^{VI}$ in **3** is smaller than the transfer $Mo^0 \rightarrow Mo^{VI}$ in **1**. The extent of the charge transfer $M^L \rightarrow M^H$ (M^L and M^H are lower valence and higher valence metal atoms, respectively) should depend on the electron-donation ability of M^L and electron-accepted ability of M^H. The result that the charge transfer $Mo^0 \rightarrow Mo^{VI}$, in **1** is larger than the charge transfer $Mo^0 \rightarrow W^{VI}$ in **3** seems to show that the electron accepted ability of Mo^{VI} is stronger than that of W^{VI}. Of cause, the M^L–M^H–M^L angle, which determines the extent of offset effect [20, 21] between the two $M^L \rightarrow M^H$ charge transfers in opposite direction, also influence on the extent of each $M^L \rightarrow M^H$ charge transfer in complex. The Mo–W–Mo angle of **3** is somewhat bigger than the Mo–Mo–Mo angle in **1** implying the somewhat larger offset effect of charge transfer in **3**. It should be pointed out that the two terminal Mo^0 atoms in **3** are more different than those in **1**. This is, perhaps, due to the statistics distribution of the carbonyl group (C13–O13) in axial position of one Mo atom (Mo1) in **3**. It could be estimated that the structures of the **2** and **4** are similar to that of **1** and **3**. As a matter of fact, the similarity of their IR spectra, cyclic voltammogram and ^{95}Mo NMR spectra support this point (see Sections 3.3–3.5).

Table 4. Selected structural parameters of **1** and **3**

	1	**3**
M^L-M^H (Å)	3.0003, 2.9978	3.031(2), 3.028(2)
M^L-M^H-M^L (°)	174.46	176.04
M^H-S_b (Å)	2.220, 2.216, 2.219, 2.228	2.207, 2.200, 2.218, 2.218
mean	2.22	2.21
M^L-S_b (Å)	2.521, 2.530	2.533, 2.537
mean	2.526	2.535
	2.534, 2.533	2.556, 2.556
mean	2.533	2.556
M^L-C (Å)	2.01, 2.00	1.99, 1.97

3.3. *Infrared spectra*

IR spectra of **1**, **2**, **3** and **4** are very similar. They showed four strong bands in the range of 1600–2010 cm^{-1}, three medium absorption peaks in 500–600 cm^{-1}, two peaks in 430–470 cm^{-1}, one peak at ~350 cm^{-1} and a somewhat weak absorption in 402–417 cm^{-1} (see Table 5). The former four kinds of absorptions are known to be the characteristic vibration frequencies of $\nu_{M(0)C-O}$, $\delta_{M(0)-C-O}$, $\nu_{M(VI)-Sb}$ and $\nu_{M(0)-C}$, respectively [22] and the latter somewhat weak peak should be assigned to the $\nu_{M(0)-Sb}$ because they are observed in the molybdenum(0)compound $[Mo(CO)_4(S_2CNEt_2)]^-$ [14] and $[Mo_2(SPh)_2(CO)_8]^{2-}$ [7].

Referring to the IR data of $[MS_4]^{2-}$(M=Mo, W) [15] and $[M(CO)_4(S_2CNEt_2)]^-$ (M=Mo, W)[10, 14], it can be found that the $\nu_{M(0)C-O}$ and $\nu_{M(0)-Sb}$ in all the four complexes are 13–60 and 9–10 cm^{-1} higher than that of $[M(CO)4(S_2CNEt_2)]^-$, respectively, and the $\nu_{M(VI)-Sb}$ of all the complexes are 5–27 cm^{-1} lower than that of $[MS_4]^{2-}$. This implies that the coordination of

Table 5. IR spectra data of **1**–**4**

Compound	$\nu_{M(0)C-O}$	$\delta_{M(0)-C-O}$	$\nu_{M(VI)-Sb}$[a]	$\nu_{M(0)-C}$	$\nu_{M(0)-Sb}$[a]
1	2005 m	589 m	451 m	343 m	417w
	1900 s	578 m	438 m		
	1870 s	568w			
	1825 s				
2	2000 m	580 m	465w	349 m	415 sh
	1876 s	566 m	436 m		
	1861 s				
	1818 s				
3	2004 m	594 m	459w	344 m	416 sh
	1895 s	579 m	434 m		
	1865 s	570 m			
	1815 s				
4	2000 m	572 m	459w	345 m	427w
	1882 s	562 m	446 m		
	1860 s				
	1822 s				

[a]Sb = bridging sulfur atom.

$[M^{VI}S_4]^{2-}$ to $M^0(CO)_4$ moiety leads to increase of the oxidation state of M^0 (partial oxidation of M^0) and decrease of the valence of M^{VI} (partial reduction of M^{VI}) indicating, evidently, the existence of charge transfer of $M^0 \rightarrow M^{VI}$. Carefully inspecting the values of $\nu_{M(0)C-O}$ and $\nu_{M(VI)-Sb}$ listed in Table 5, it is apparent that the $\nu_{M(0)C-O}$ of **1** is larger than that of **3** and the $\nu_{W(0)C-O}$ of **4** is larger than that of **2**; the $\nu_{Mo(VI)-Sb}$ of **4** is higher than that of **1** and the $\nu_{W(VI)-Sb}$ of **2** is larger than that of **3** implying that the real valences of Mo^L atoms in **1** are higher than that in **3**, the real valences of W^L atoms in **4** are higher than that in **2**, the real oxidation state of Mo^H atom in **4** is higher than that in **1** and the real oxidation state of W^H atom in **2** is higher than that in **3**. Thus, the extents of $M^0 \rightarrow M^{VI}$ charge transfers in **1**–**4** can be summarized as following Scheme 1.

Interestingly, a relationship between $Fe^{II} \rightarrow M^{VI}$ charge transfer and $\Delta\nu$ ($\nu_{M(VI)-Sb}$-$\nu_{Fe(II)-Sb}$) found in linear Fe–Mo–S cluster compounds $[(FeL_2)xS_2MS_2]^{2-}$ (L = Cl, SR; M = Mo, W; $x = 1$, 2) [23] also exists in this series Mo–W–S cluster complexes. i.e. the value of $\Delta\nu$ is inversely proportional to that of charge transfer. $\Delta\nu$ ($\nu_{M(VI)-Sb}$-$\nu_{M(0)-Sb}$) of **1**–**4** are 34, 50, 43 and 42, respectively, Obviously, the exact same result of scheme 1 can be obtained based on the $\Delta\nu$ values. It is worth pointing out that employing the $\Delta\nu$ values, the comparison of charge transfers between **1** and **2** and between **3** and **4** can be further made. The $\Delta\nu$ value of **1** is smaller than that of **2** and the $\Delta\nu$ value of **3** is similar to that of **4** indicating the charge transfer of $M^0 \rightarrow M^{VI}$ in **1** is larger than that in **2** and **3** has similar charge transfer as **4**. In general, the existence of charge transfer between two mixed valence metal atoms is dependent on the electron donation ability of the lower valence metal atom and the electron accepted ability of the higher valence metal atom, therefore, the results obtained above should imply that the electron donation ability of Mo^0 is larger than that of W^0 and the electron accepted ability of Mo^{VI} is also larger than that of W^{VI}. In fact, this is consistent with the larger binding energy of W-4f than Mo-3d [24]. If considering the electron configurations between the Mo atom ($3d^5S^1$) and the W atom ($4d^4S^2$) and the fact that W compounds are more inert than Mo compounds, this result is also reasonable.

3.4. *Cyclic voltammetry*

The cyclic voltammograms of **1**–**4** in acetonitrile were shown in Fig. 2 and the cyclic voltammetry data were listed in Table 6. As is shown in Fig. 2 and Table 6, all the four complexes (**1**–**4**) possessed two similar electrochemical events. One is a pseudo reversible redox couple at -1.65–-1.99 V vs SEC (E_1) and one is an irreversible oxidation peak at $+0.19$–$+0.21$ V vs SCE (E_2). The values of E_1 are analogous to the redox potentials of MoS_4^{2-} (-1.08 V vs SCE) [28] and (o-xyl-S_2)$FeMS_4^{2-}$(M = Mo, -1.8 V; M = W, -1.8 V) [29, 30], which was evidenced to be the redox of M(VI)/M(V) by EPR study and the E_2 were very similar to that of $[M(CO)_4(S_2CNEt_2)]^-$ (M = Mo, $+0.14$ [14]; M = W, $+0.15$ V [10]) and $[Mo(CO)_5SR]^-$ ($+0.17$ V) [5]. This apparently indicates that E_1 and E_2 events resulted from the redox of the $M^0(CO)_4$- and $M^{VI}S_4$ centers in the complexes, respectively. In terms of the voltammetric peak current parameters $i_p/v^{1/2}AC$ of E_1 and E_2 similar to that (observed in identical conditions) of Cp_2Fe which was known to be one-

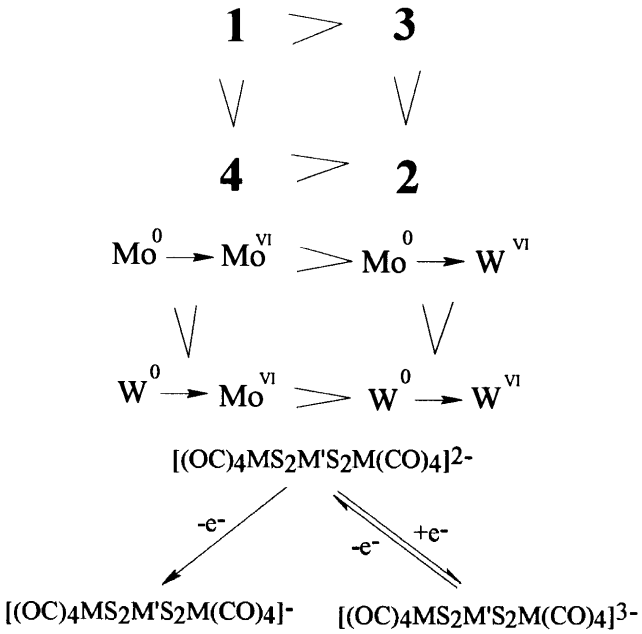

Scheme 1.

electron redox process, both E_1 and E_2 events are one-electron redox processes. Thus the electrochemical behavior of the four complexes can be expressed as shown in Scheme 1.

In comparing the E_1 and E_2 with the redox potentials of related M^{VI} compounds, MoS_4^{2-} and M^0 compounds, $[M(CO)_4(S_2CNEt_2)]^-$ (M = Mo and W), (see Table 6) it is easy to find that E_1 values of all the complexes are more negative than the redox potential of MoS_4^{2-} indicating that the oxidation states of the high valence metal atoms M^H in all the four compounds are lower than VI and the E_2 of all the compounds are more positive than the redox potential of $[M(CO)_4(S_2CNEt_2)]^-$ (M = Mo and W) showing that the oxidation states of the low-valence metal atoms M^L in all the compounds are higher than zero. This implies a partial electron delocalization from M^0 to M^{VI} atoms in the mixed-valence metal cluster compounds. In other words, a charge transfer, $M^0 \rightarrow M^{VI}$, takes place between the mixed-valence metallic centers. Carefully examining the E_1 and E_2 values of **1**–**4**, it could be seen that the E_1 of **3** and **1** are more negative than that of **2** and **4**, respectively, indicating that the oxidation states of the high valence metal atoms M^H in **2** and **4** are higher than that in **3** and **1**, respectively and the E_2 of **1** and **4** are more positive than that of **3** and **2**, respectively, meaning that the low valence metal atoms M^L in **1** (Mo) and in **4** (W) have higher oxidation states than those in **3** (Mo) and **2** (W), respectively. Thus, for the extents of charge transfer $M^0 \rightarrow M^{VI}$ we have the results. **1** > **3**, **4** > **2**, **1** > **4** and **3** > **2**. This result is exactly the same as that shown in Scheme 1 obtained from the IR spectra studies.

Table 6. Cyclic voltammetry data (V/SCE) of **1**–**4** and related Mo^0, W^0, Mo^{VI} and W^{VI} compounds

Compounds	E_1	E_2	Refs.
1	−1.72	+0.21	this work
2	−1.90	+0.19	this work
3	−1.99	+0.19	this work
4	−1.65	+0.20	this work
$Mo(CO)_4(S_2CNEt_2)^-$		+0.14	[14]
$W(CO)_4(S_2CNEt_2)^-$		+0.15	[10]
MoS_4^{2-}	−1.08		[25, 26]
$[(o\text{-xyl-}S_2)FeMS_4]^{2-}$	−1.6(Mo)		
	−1.8(W)		[27]

3.5. ^{95}Mo *NMR spectra*

The ^{95}Mo NMR spectra of **1**, **3** and **4** are shown in Fig. 3 and the chemical shift data are listed in Table 7. The ^{95}Mo NMR spectra of **1**, **3** and **4** contain two kinds of ^{95}Mo chemical shifts, δ_1 at down field and δ_2 at up field. Referring to the ^{95}Mo chemical shifts of Mo^0 compound, $Mo(CO)_6$ (−1856 ppm [31]) and Mo^{VI} compound, MoS_4^{2-} (2209 ppm), δ_1 and δ_2 are, respectively, related to the MoS_4 and $Mo(CO)_4$ centers, in **1**, **3** and **4**. Obviously, the δ_1 are lower than that of MoS_4^{2-} and the δ_2 are higher than that of $Mo(CO)_6$ showing Mo atom of MoS_4 center in the complexes has somewhat more shielding than that of MoS_4^{2-} and the Mo atoms of $Mo(CO)_4$ centers in the

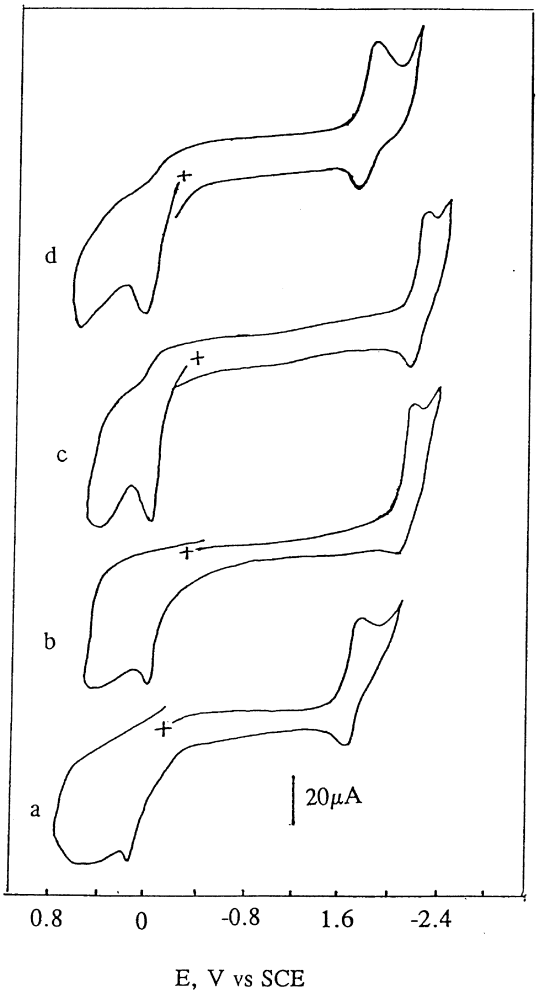

Fig. 2. The cyclic voltammograms of **1**(a), **2**(c), **3**(b) and **4**(d), in MeCN, sample concentration, 0.002 M; scan rate, 100 mV s^{-1}.

complexes have less shielding than that of $Mo(CO)_6$. This is consistent with the results from structure, IR and CV studies that the oxidation states of Mo atom of the MoS_4 center in the complexes are somewhat lower than +6 and the valences of Mo atoms of $Mo(CO)_4$ centers in the complexes are somewhat higher than zero. Such a shift in oxidation state implies the existence of charge transfer between the two different valence metal centers in the complexes. In comparison to the down field δ_1 values of **1** with **4**, it could be found that δ_1 of **1** is larger than the one of **4**. In terms of the "chemical shift-oxidation state relationship" hold in the di- and trinuclear Mo–W– series complexes with an M–M bond: the shielding increases (NMR signal shift to upfield) with an increase in the oxidation state [25, 26], the oxidation state of the Mo atom in a MoS_4-center of **1** would be lower than that of **4**, thus, the larger shift in oxidation state of **1** indicates that the charge transfer in **1** is larger than that in **4**. This is consistent with the results from IR and CV studies mentioned above. Interestingly, according to the X-ray crystallography, IR and CV studies, the oxidation state of the Mo atom in a $Mo(CO)_4$ center of **1** is higher than that in **3**, but the δ_2 of **1** more shifts to downfield than that of **3**. This indicates that, in contrast with δ_1, the δ_2 shows the normal "chemical shift-oxidation state relationship: the shielding increases (NMR signal shift to upfield) with a decrease of oxidation state" as monomeric complexes of molybdenum do [31, 27].

Table 7. ^{95}Mo chemical shifts of **1**, **3**, **4** and related Mo^0 and Mo^{VI} complexes

Complexes	δ_1 (ppm)	δ_2 (ppm)
1	1614.1	−1470.2
3		−1577.1
4	1592.9	
MoS_4^{2-}	2209.3	
$Mo(CO)_6$		−1856

4. SUMMARY

1. Reaction of M^0-carbonyl such as $M(CO)_6$ and $[M(CO)_4(S_2CNEt_2)]^-$ with tetrathiometallate, MS_4^{2-}, results in a series of mixed-valence metal cluster compounds $[(OC)_4MS_2M'S_2M(CO)_4]^{2-}$ (M = Mo or W; M′ = Mo or W) by control of the ratio of reactants and use of different solvents.
2. Trinuclear cluster compounds contain an $MS_2M'S_2M$ skeleton with metal atoms in widely separated formal oxidation states (zero and plus six).
3. X-ray crystal structure, IR, CV and ^{95}Mo NMR studies reveal the existence of mixed valence metal atoms and charge transfer $M^0 \rightarrow M^{VI}$ in all the four cluster complexes.
4. The extent of charge transfer $M^0 \rightarrow M^{VI}$ for all the complexes are: **1** > **4**, **1** > **3**, **4** > **2** and **3** > **2**. This implies the charge transfer extents: $Mo^0 \rightarrow Mo^{VI} > W^0 \rightarrow Mo^{VI}$, $Mo^0 \rightarrow W^{VI} > W^0 \rightarrow W^{VI}$, $Mo^0 \rightarrow Mo^{VI} > Mo^0 \rightarrow W^{VI}$ and $W^0 \rightarrow Mo^{VI} > W^0 \rightarrow W^{VI}$, thus, it appears that the electron-donation ability of Mo^0 is larger than that of W^0 and the electron-accepted ability of Mo^{VI} is also larger than that of W^{VI}. In other words, Mo^0 is more easily oxidized than W^0 and Mo^{VI} is more easily reduced than W^{VI}.

Acknowledgements—We acknowledge the grants from NNSFC and CPNKPFR for support in this research and thank Dr Zong Chen from Xiamen University and Daxu Wu from the State Key Laboratory of Structural Chemistry for their assistance in carrying out the ^{95}Mo NMR spectra measurements and useful discussions.

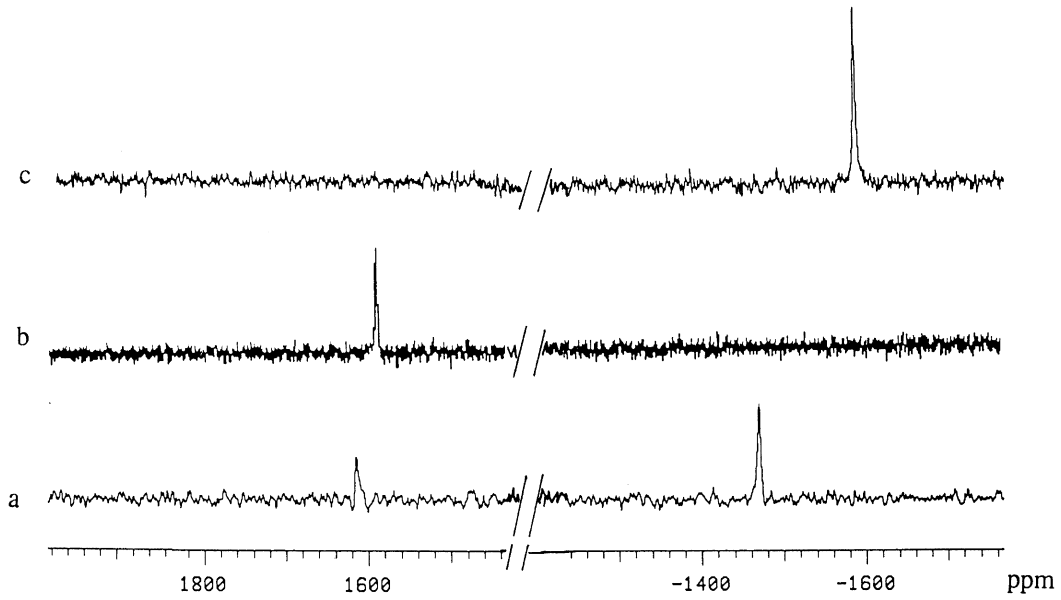

Fig. 3. The ^{95}Mo NMR spectra of **1**(a), **4**(b) and **3**(c).

REFERENCES

1. Ganner, S. P., Hodgson, K. O., Gillum, W. O. and Mortenson, L. E., *J. Am. Chem. Soc.*, 1978, **100,** 3399.
2. Ganner, S. P., Gillum, W. O., Hodgson, K. O., Mortenson, L. E., Stiefel, E. I., Chisnell, J. R., Brill, W. J. and Shah, V. K., *J. Am. Chem. Soc.*, 1978, **100,** 3314.
3. Zimmermen, R., Hunck, E., Brill, W. J., Shah, V. K., Henzl, M. T., Ravlings, J. and Orme-Johnson, W. H., *Biochim. Biophys. Acta*, 1978, **557,** 185.
4. Anzenhofer, K. and de Boer, J. J., *Acta Cryst.*, 1969, **25B,** 1419.
5. Zhuang, B., Mcdonald, J. W., Schultz, F. A. and Newton, W. E., *Organometallics*, 1984, **3,** 934.
6. Zhuang, B., Huang, L., He, L., Chen, W. and Yang, Y., Lu, J., *Acta Chim. Sin.*, 1986, **4,** 294.
7. Zhuang, B., Huang, L., He, L. and Yang, Y., Lu, J., *Inorg. Chim. Acta*, 1989, **157,** 85.
8. Zhuang, B., Huang, L. and He, L., Lu, J., *Inorg. Chim. Acta*, 1989, **160,** 229.
9. Zhuang, B., Yu, P. and Huang, L., Lu, J., *Inorg. Chim. Acta*, 1989, **162,** 127.
10. Zhuang, B., Yu, P., Huang, L. and He, L., Lu, J., *Inorg. Chim. Acta*, 1990, **177,** 239.
11. Zhuang, B., Yu, P. and Huang, L., Lu, J., *Jiegou Huaxue*, 1992, **11,** 354.
12. Zhuang, B., Yu, P., Huang, L. and He, L., Lu, J., *Polyhedron*, 1994, **13,** 125.
13. Coucouvanis, D., *Accts. Chem. Res.*, 1981, **14,** 201.
14. Zhuang, B., Huang, L., He, L. and Yang, Y., Lu, J., *Inorg. Chim. Acta*, 1988, **145,** 225.
15. McDonald, J. W., Frieson, G. D., Rosenhein, L. D. and Newton, W. E., *Inorg. Chim. Acta*, 1983, **72,** 205.
16. Killean, R. C. G. and Lawrence, J. L., *Acta Cryst. B*, 1969, **25,** 1750.
17. Walker, N. and Stuart, D., *Acta Cryst. A*, 1983, **39,** 159.
18. Molen, *An Interactive Structure Solution Procedure*. Enraf-Nonius, Delft, 1990.
19. Sasvari, K., *Acta Cryst.*, 1963, **16,** 716.
20. Coucouvanis, D., Baenziger, N. C., Simhon, E. D., Stremple, P., Swenson, A., Kostikas, A., Simopoulos, A., Petronleas, V. and Papaefthmious, V., *J. Am. Chem. Soc.*, 1980, **102,** 1730.
21. Zhuang, B., Huang, L., Lan, A., He, L. and Zhao, X., Lu, J., *Polyhedron*, 1992, **11,** 2557.
22. Muller, A., Diemann, E., Jostes, R. and Bogge, H., *Angew. Chem. Ed. Engl.*, 1981, **20,** 934.
23. He, L. and Zhang, L., Lu, J., *Huaxue Xuebao*, 1987, **8,** 44.
24. Wang, B., Sasaki, Y., Nagasawa, A. and Ito, T., *J. Coord. Chem.*, 1988, **18,** 45.
25. Nagasawa, A., Sasaki, Y., Wang, B., Ikari, S. and Ito, T., *Chem. Lett.*, 1987, 1271.
26. Wang, B., Sasaki, Y., Nagasawa, A. and Ito, T., *J. Coord. Chem.*, 1988, **18,** 45.
27. Grieves, R. A. and Mason, J., *Polyhedron*, 1986, **18,** 415.
28. You, J. and Wu, D., Liu, H., *Polyhedron*, 1986, **5,** 535.
29. Losenhein, L. D. and McDonald, J. W., *Inorg. Chem.*, 1987, **26,** 3414.
30. Friesen, G. D., McDonald, J. W. and Newton, W. E., *Inorg. Chim. Acta*, 1982, **67,** L1.
31. Minelli, M., Enemark, J. H., Brownlee, R. T. C., O'Connor, M. J. and Wedd, A. G., *Coord. Chem. Rev.*, 1985, **68,** 169.

Pergamon

Polyhedron Vol. 17, Nos. 25, 26, pp. 4403–4413, 1998
© 1998 Elsevier Science Ltd
All rights reserved. Printed in Great Britain
PII: S0277–5387(98)00243–5
0277–5387/98 $19.00+0.00

Potentiometric and spectroscopic studies of the copper(II) complexes with some aminodiphosphonic acids in aqueous solution

Barbara Kurzak,[a]* Anna Kamecka,[a] Krzysztof Kurzak,[a] Julia Jezierska[b] and Paweł Kafarski[c]

[a]Institute of Chemistry, Pedagogical University, 08-110 Siedlce, Poland

[b]Faculty of Chemistry, University of Wroclaw, 50-383 Wroclaw, Poland

[c]Institute of Organic Chemistry, Biochemistry and Biotechnology, Technical University, 50-370 Wroclaw, Poland

(Received 27 March 1998; accepted 15 June 1998)

Abstract—The stoichiometries and stability constants of the copper(II) complexes with seven aminodiphosphonates [R–N($CH_2PO_3H_2$)$_2$, L] containing iminomethylenephosphonate moieties have been determined pH-metrically at 25°C and at an ionic strength of 0.20 mol dm^{-3} (KCl). The results suggest for L = **1**–**6** only equimolar species: [Cu(H_2L), [Cu(HL), [CuL] and two hydroxo [CuH$_{-1}$L] and [CuH$_{-2}$L], in the pH range of 2–11.5, the only difference is the presence of an additional [Cu(H_3L)] species (~15%) at low pH for N-3-picolyliminodi(methylenephosphonic) acid. For L = **7** the model contains protonated and non-protonated 1:2 species. From the comparative analysis of the stability and the spectroscopic (UV–VIS and EPR) data it has been established that the ligands in [CuHL] and [CuL] are tridentate; the formation of two five-membered chelate rings leads to very stable complexes. The LMCT bands from O$^-$ (PO_3^{2-}) and N_{imino} to Cu^{2+} are at 225–231 and 302–277 nm. © 1998 Elsevier Science Ltd. All rights reserved

Keywords: potentiometry; stability constants; copper(II) complexes; aminopolyphosphonates; EPR spectra; UV–VIS spectra.

INTRODUCTION

The aminopolyphosphonates are analogues of aminopolycarboxylates in which the carboxyl groups (CO_2^-) are substituted by phosphonate moieties (PO_3^{2-}). Among the most widely commercially used of aminoalkylphosphonic acids [1–5] is diethylenetriamine-N,N,N′,N″,N″-pentamethylenephosphonic acid; available under various trade names such as "DEQUEST" and "BRIQUEST". An investigation of the interaction of the phosphonic groups with metal ions may provide useful information on the behaviour of these type of compounds. Studies on the simpler aminomethylenephosphonic acids serve as models for understanding the behaviour of more complex systems [6].

Aminopolyphosphonic acids and their derivatives have also received considerable attention because of their interesting biological activity. For example, N,N′-di(phosphonomethyl)glycine is an active component of Polaris®, known plant growth regulator [7], whereas N-(phosphonomethyl)glycine is an active ingredient of a popular herbicide Roundup® [8, 9].

Metal aminophosphonate (aminopolyphosphonate) chemistry is attracting increasing interest because of the variety of properties than can be introduced via the phosphonate ligand [10, 11]. The complex-formation equilibria have been reported for several kinds of C- or N-substituted derivatives of iminodimethylenebis(phosphonic acid) [12–16]. The

* Author to whom correspondence should be addressed. Fax: +4825-44-20-45; E-mail: bkurzak@wsrp.siedlce.pl

complex formation of N,N-dimethyliminodi(methylenephosphonic) acid and N,N-dimethylaminomethylphosphonic acid with alkaline-earth and divalent transition metals have been investigated by Sawada *et al.* [17]. Thermodynamic parameters for chelate complexes of some aminopolyphosphonates–alkaline-earth metal ions have been studied by calorimetric titrations also by Sawada *et al.* [18]. Kozlowski *et al.* [19] report pH-metric and spectroscopic studies for the proton and copper(II) complexes of a series of ambidentate N-(phosphonomethyl)amino acids containing both iminomethylenecarboxylate and iminomethylenephosphonate moieties. Potentiometric and spectroscopic studies on the coordination ability of biologically important pyridine mono- and bis-phosphonates have shown that, when sterically possible, these compounds undergo tridentate coordination with copper(II) and the complexes are very stable [20].

Thus, although metal complexes of aminophosphonic (aminopolyphosphonic) acids have been studied fairly extensively in solution, their solution chemistry is still not well understood [21, 22]. Moreover, bisphosphonic acid derived herbicides are frequently inactive if applied in natural environment. There are two possible explanations of the lack of their activity: either they may be fast and effectively degraded by soil microflora or strongly bound by soil (most probably as metal ion complexes) and thus inactivated. So, for better understanding and interpretation of the biological findings more detailed knowledge about complexing abilities of this type of compounds is indispensable.

The aim of this work was to study (in aqueous solution) the protonation equilibria, coordination modes and the stability of the complexes of Cu^{II} with a large group of iminodiphosphonic acids which secondary amine moiety substituted by various functional groups (see Scheme 1).

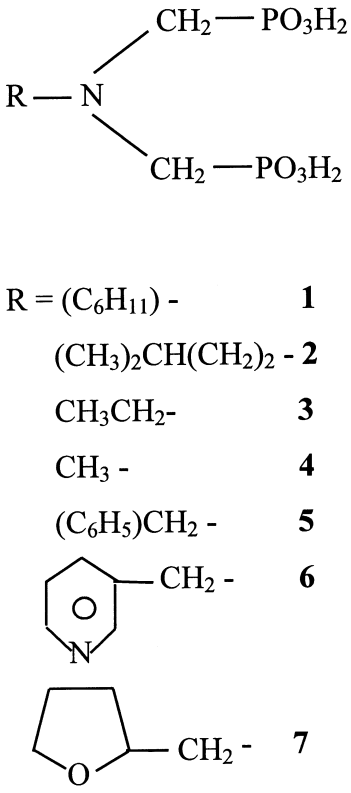

Scheme 1.
N-cyclohexyliminodi(methylenephosphonic) acid **1**, N-isopentyliminodi(methylenephosphonic) acid **2**, N-*n*-propyliminodi(methylenephosphonic) acid **3**, N-methyliminodi (methylenephosphonic) acid **4**, N-benzyliminodi(methylenephosphonic) acid **5**, N-3-picolyliminodi(methylenephosphonic) acid **6**, N-2-methyltetrahydrofuryliminodi (methylenephosphonic) acid **7**.

2. EXPERIMENTAL

2.1. *Materials*

Diphosphonic acids used in this paper were obtained according to previously described procedures [23, 24]. The purity and the exact concentrations of the solutions of the ligands used for potentiometric studies were determined by the Gran method [25]. The concentration of copper(II) chloride stock solution was standardized by complexometric ethylenedinitrilotetraacetate (EDTA) titration. Carbonate-free potassium hydroxide (the titrant) was prepared and standardized against a standard potassium hydrogenphthalate solution.

2.2. *Potentiometry*

The stability constants of the proton and copper(II) complexes were determined by pH-metric titration of $2\,cm^3$ samples. The ligand concentration was $2\times10^{-3}\,mol\,dm^{-3}$ and the metal ion:ligand ratio was 0:1; 1:1.5; 1:2 or 1:3. The ionic strength was adjusted to $0.2\,mol\,dm^{-3}$ with KCl in each case. The titrations were performed over the range pH 2.5–11.5 with KOH solution. All titration solutions were thermostated at $25\pm0.1^{\circ}C$ using a constant-temperature waterbath.

The pH was measured with a MOLSPIN automatic titration system using a micro combination pH electrode (Mettler-Toledo, Type 2). The electrode system was calibrated by periodic titrations of HCl solution ($7.5\times10^{-3}\,mol\,dm^{-3}$ in KCl) against standard KOH solution. The resulting titration data were used to calculate the standard electrode potentials, E^0, and the dissociation constant for water ($pK_w=13.74$). These values were then used to calculate the hydrogen-ion concentration $[H^+]$ from emf readings [26]; number of titration, 3; calculations, SUPERQUAD computer program [27].

For clarity, the charges of the complexes are omitted in the text and tables. It has to be mentioned,

however, that the fully deprotonated forms have charges L^{4-}.

2.3. *Spectroscopic measurements* (*UV/VIS and EPR*)

The UV–VIS absorption spectra were obtained at room temperature on a SPECORD M40 spectrophotometer. The spectra were recorded digitally ($20\,cm^{-1}$) over the range 11000–50000 cm^{-1}. The spectral data at selected *ca*. 1000 wavenumbers over the range 28000–50000 cm^{-1} (or 24000–50000 cm^{-1}) were employed for analysis and resolved into Gaussian components. The metal ion concentration was 3×10^{-4} mol dm^{-3} for UV and 3×10^{-3} mol dm^{-3} for VIS. The spectra were fitted with Gaussian bands using the CFP program [28] based on the Slavič [29] numerical algorithm, which for the last a few years has been successfully applied by us to the deconvolution of d–d (ligand field) spectra [30, 31, 32] (and references therein).

Electron paramagnetic resonance (EPR) spectra were performed on a Bruker ESP 300E spectrometer at the X-band frequency (9.45 GHz) at 77 K in ethylene glycol–water (1:1 v/v) solutions. The ligand concentration was 4.0×10^{-3} mol dm^{-3} and the concentration ratio of metal–ligand was 1:2. The spectra were analysed by computer simulation program [33] based on resonance fields calculated according to method of Sakaguchi *et al*. [34].

3. RESULTS AND DISCUSSION

3.1. *Potentiometric and EPR studies*

Protonation constants were calculated first assuming ligand concentrations as calculated from the titration curves and secondly, after allowing ligand and proton concentrations to "float" in SUPERQUAD. It was found that the concentrations never changed by more than 1% and calculated constants remained constant within the calculated errors. These observations confirmed the purity of the aminodiphosphonic acids studied. The list of these compounds is shown in Scheme 1.

The fully protonated forms of the ligands **1**–**5** and **7** contain five dissociable protons (H_5L^+) (two at each phosphonic function and one at the imino nitrogen, N_{imino}), and six protons in the case of ligand **6** (H_6L^{2+}) (due to additional proton at the pyridine nitrogen atom).

The acid–base properties of the aminodiphosphonic acids differ from those of aminomonophosphonates. The latter have three protonation constants with $\log K_{NH_3^+}\approx10$–11, $\log K_{PO_3H^-}\approx5$–6 and $\log K_{PO_3H_2}\approx1$ [35, 36] and give not only equimolar species. The presence of the second phosphonic group ($\log K_{PO_3H^-}\approx5$) in the case of aminodiphosphonates **1**–**6** leads to equimolar species only and to the formation of additional protonated Cu^{II} complexes.

It is evident from Table 1 that the change of pK values calculated for compounds **1**–**7** is consistent with electronic effects of the substituents attached to the imino nitrogen. Thus, substitution of the methyl by more electrodonating izopentyl group increases an electron density on the nitrogen atom; this density is partly transferred to the phosphorous atoms. This effect makes the amino and the PO_3H^- groups more basic and pK values for **2** is higher than this for **4**. On the other hand, the presence of acid strengthening aromatic rings decreases pK(NH^+) values for **5** and **6** as compared to **4**; the highest acidity of the NH^+ group corresponds to stronger electron withdrawing effect of pyridine than that manifested by benzene ring.

The pK values characteristic for the dissociation of the two protons from the two $-PO_3H_2$ groups are $\sim$1.5–2, and thus they are fully deprotonated in the pH range studied and do not take part in metal coordination equilibria. Only the highest pK can be unambiguously assigned (due to proton dissociation from the imino nitrogen, NH^+). The further deprotonation of the phosphonic groups may cause overlapping of each other what means that the $pK_{PO_3H^-}$ macroconstants are not characteristic feature of real acidity of these groups. This means that the microscopic acid dissociation constants must be determined to clarify the acid–base properties of the studied ligands but this was beyond the scope of the present work. The acidic deprotonation site with pK of 2.94 for **6** seems to be localized at the pyridine ring nitrogen.

The ligands **1**–**6** exhibit similar Cu^{II}-coordination pattern (Table 1). The model contains protonated complexes but neither a 1:2 species nor any polynuclear ones. This finding was what is additionally proved by the EPR studies (Table 2). The formation of the bis complexes seems to be generally hindered because studied ligands are generally tridentate yielding two five-membered chelate rings. The electrostatic repulsion of the negatively charged phosphonate groups precludes coordination of the second ligand; the charge of the bis complex would be $6-$. Hence, only 1:1 complexes are formed and data collected in Table 1 indicate high chelating ability of the ligands towards Cu^{II}. The chemical model for system of ligand **7** with copper(II) is different if comparing with all the others studied systems. This model contains protonated and non protonated 1:2 species (Table 1) which result from the presence of the additional coordination site.

The metal complex speciations derived from potentiometric calculations for compounds **1**–**6** do not differ considerably. The Cu^{II}/ligand **5** system presented in Fig. 1 exhibits, in general, approximately the same distribution curves as those observed for the other ones, and thus is representative for all the group. Three complexes: [$Cu(H_2L)$], [Cu(HL)], [CuL] and two hydroxo [$CuLH_{-1}$] and [$CuLH_{-2}$], are formed in the pH range of 2–11.5, with the single difference found

Table 1. Protonation constants of the ligands ($\log \beta^{H}$) and stability constants of the copper(II) complexes ($\log \beta$) at 25°C and $I = 0.2\,\mathrm{mol\,dm^{-3}}$ (KCl)

Assignments	Compound						
	1	**2**	**3**	**4**	**5**	**6**	**7**
$\log \beta_1^H$	12.5[a]	12.3[a]	12.2[a]	11.75(1)	11.32(1)	10.40(1)	11.46(1)
$\log \beta_2^H$	18.59(2)	18.51(2)	18.24(3)	17.70(1)	17.51(1)	16.49(2)	17.59(2)
$\log \beta_3^H$	23.29(2)	23.38(2)	22.93(3)	22.49(1)	22.24(1)	21.42(2)	22.38(3)
$\log \beta_4^H$	–	–	–	–	–	24.36(4)	–
$\log K^H(PO_3H^-)$	6.10	6.26	6.01	5.95	6.19	6.09	6.13
$\log K^H(PO_3H^-)$	4.70	4.87	4.69	4.79	4.73	4.93	4.79
$\log K^H(NH_{pyr}^+)$	–	–	–	–	–	2.94	–
$\log \beta[Cu(H_3L)]$	–	–	–	–	–	23.98(3)	–
$\log \beta[Cu(H_2L)]$	21.28(5)	21.81(1)	21.15(4)	21.54(1)	21.11(1)	21.06(1)	22.23(2)
$\log \beta[Cu(HL)]$	17.41(1)	18.13(1)	17.60(1)	18.03(1)	17.55(1)	17.31(1)	19.00(1)
$\log \beta[CuL]$	12.69(1)	13.49(1)	13.26(1)	13.82(1)	13.06(1)	12.41(1)	14.81(1)
$\log \beta[CuLH_{-1}]$	3.09(2)	3.21(1)	3.02(2)	3.44(1)	2.88(1)	1.97(2)	4.54(4)
$\log \beta[CuLH_{-2}]$	−8.64(6)	−8.91(6)	−9.47(10)	−8.88(3)	−8.94(2)	−10.03(3)	−6.41(3)
$\log \beta[Cu(HL)_2]$	–	–	–	–	–	–	34.65(6)
$\log \beta[Cu(HL)L]$	–	–	–	–	–	–	29.46(2)
$\log \beta[CuL_2]$	–	–	–	–	–	–	19.57(4)
$pK_{[Cu(H_2L)]}$	3.87	3.68	3.55	3.51	3.56	3.75	3.23
$pK_{[Cu(HL)]}$	4.72	4.64	4.34	4.21	4.49	4.90	4.19
$pK_{[CuL]}$	9.60	10.28	10.24	10.38	10.18	10.44	10.27
$Cu^{2+} + HL_{PO_3H^-} \rightleftarrows Cu(HL)$[b]	12.71	13.26	12.91	13.24	12.82	12.38	14.21
$\log K_{[CuL]} - \Sigma pK$	−10.60	−9.89	−9.67	−8.67	−9.18	−9.01	−7.57

The standard deviations are given in parentheses. Charges omitted for simplicity.
[a]From NMR measurements, unpublished data.
[b]$\log K = \log \beta_{[Cu(HL)]} - pK_{PO_3H^-}$.

for complexes of compound **6**, namely the presence of an additional $[Cu(H_3L)]$ species (~15%) at low pH (Fig. 1).

The deprotonation constant, pK_{CuH_3L}, of the corresponding equilibrium: $[Cu(H_3L)] \rightleftarrows [Cu(H_2L)] + H^+$, is 2.92. This value is almost identical with that obtained for the ligand itself (Table 1) supporting that N_{pyr} is not involved in the coordination. In this case the pyridine nitrogen is unable to coordinate the metal ion due to steric reasons. Thus, for the first species the propose binding mode is (PO_3^{2-}, PO_3H^-) with N_{pyr} and N_{imino} protonated. This may be supported by the d–d transition at around 773 nm. For a species with two monoprotonated phosphonic functions this transition should be around 800 nm [20]. This fact is in good agreement with the EPR spectral properties of the species $[Cu(H_3L)]$ (at pH 2.6). The values of $A_\parallel$ and $g_\parallel$ (Table 2) imply that the coordination sphere around Cu^{II} in plane consists of oxygen atoms as only donors.

Deprotonation of $[Cu(H_2L)]$ leads to the formation of [Cu(HL)]. This process is not accompanied by a significant shift of the d–d band (Table 2). It is interesting that all the first deprotonation constants of $[CuH_2L]$, pK_{CuH_2L}, are of the same order of magnitude and considerably lower than the corresponding deprotonation constants of the free ligands (see Table 1). It seems that in $[Cu(H_2L)]$ the Cu^{II} is coordinated to the N_{imino} and PO_3H^- chelate donor system, whereas the second phosphonic group, PO_3H^-, remains uncoordinated. Taking into account a strong affinity of Cu^{II} to nitrogen donors it is much more likely that a protonation occurs via the phosphonate O^-.

EPR parameters, $g_\parallel$ and $A_\parallel$, of the species formed with ligands **1**–**6** existing at pH 3.6 (Table 2) are apparently different from those found for Cu^{II} ions coordinated by oxygen donors of phosphonic groups as the only ligands [37, 38] (in which $g_\parallel = 2.400$ and $A_\parallel = 143 \times 10^{-4}\,\mathrm{cm^{-1}}$). This fact confirms participation of the imino nitrogen and PO_3H^- group in the chelate ring of $[Cu(H_2L)]$. Furthermore, EPR spectral parameters, for the first $[Cu(H_3L)]$ species for L = **6** at pH about 2.6 are evidently dissimilar in comparison with those observed for the remaining ligand systems and their values are consistent with the smallest strength of metal–ligand interaction.

The deprotonation of the imino group starts above pH 5.0 and may overlap with deprotonation of PO_3H^- groups. Therefore, in [Cu(HL)] the $\{PO_3^{2-}$, N_{imino}, $PO_3H^-\}$ set can be active. The tridentate character of the donor set results in a small but detectable increase in $A_\parallel$ and decrease in $g_\parallel$ (Table 2). Taking into account the difference in acidity of the coordinating donor PO_3H^- group equilibrium constant

Table 2. Spectroscopic parameters for the Cu(II) complexes

Ligand	Species	EPR[a]		UV/VIS[b]
		$A_{\parallel}$ (10^{-4} cm^{-1})	$g_{\parallel}$	λ (nm) ε (dm^3 mol^{-1} cm^{-1})
1	$[Cu(H_2L)]$	**a**	**a**	–
	[Cu(HL)]	156	2.325	–
	[CuL]	157	2.315	681(73)
				302.0(1306)
				230.7(2582)
	$[CuLH_{-1}]$	160	2.290	671(75)
2	$[Cu(H_2L)]$	147	2.345	755(57)
	[Cu(HL)]	152	2.333	755(52)
	[CuL]	157	2.325	714(65)
				287.5(1705)
				225.6(3151)
	$[CuLH_{-1}]$	167	2.287	700(64)
3	$[Cu(H_2L)]$	**a**	**a**	–
	[Cu(HL)]	153	2.235	749(48)
	[CuL]	156	2.327	726(63)
				283.4(1502)
				225.1(2992)
	$[CuLH_{-1}]$	**b**	**b**	715(60)
4	$[Cu(H_2L)]$	**a**	**a**	–
	[Cu(HL)]	150	2.340	749(47)
	[CuL]	158	2.328	727(57)
				277.3(1610)
				224.3(3272)
	$[CuLH_{-1}]$	**b**	**b**	715(55)
5	$[Cu(H_2L)]$	146	2.345	751(62)
	[Cu(HL)]	153	2.337	749(50)
	[CuL]	157	2.325	716(65)
				288.3(1967)
				230.9(3641)
	$[CuLH_{-1}]$	167	2.290	689(71)
6	$[Cu(H_3L)]$	145	2.355	773 (60)
	$[Cu(H_2L)]$	151	2.340	746(53)
	[Cu(HL)]	–	–	733 (63)
	[CuL]	157	2.328	706(66)
				285.9(1883)
				229.7(3707)
	$[CuLH_{-1}]$	166	2.295	701(64)
7	$[Cu(H_2L)]$	147	2.344	–
	[Cu(HL)]	150	2.316	–
	[CuL]	152	2.313	763(62)
				284.1(1407)
				224.7(2622)
	[Cu(HL)L]	158	2.280	749(66)
	$[CuL_2]$	160	2.279	755(68)
	$[CuLH_{-1}]$	–	–	759(73)

[a]**a**: the EPR spectrum of $[Cu(H_2L)]$ for L = **1** and **3** was not found to be in agreement with its smaller contribution than that found for the same complex formed by L = **2** and **5**. It is also difficult to distinguish the spectra at low pH in the case of the systems with L = **1**, **3**, **4** and **6** in accordance with a too small separation between the maxima corresponding to the contribution of $[Cu(H_2L)]$ and [Cu(HL)] species; **b**: the stepwise transition to $[Cu(OH)_4]^{2-}$ is reached after one day, in contrast to the remaining complexes which appeared to be more stable.

[b]The VIS absorption bands presented in the table arise from distribution-corrected absorption spectra and their positions are approximately estimated from experimental spectra. The UV absorption data arise from Gaussian analysis of the experimental spectrum.

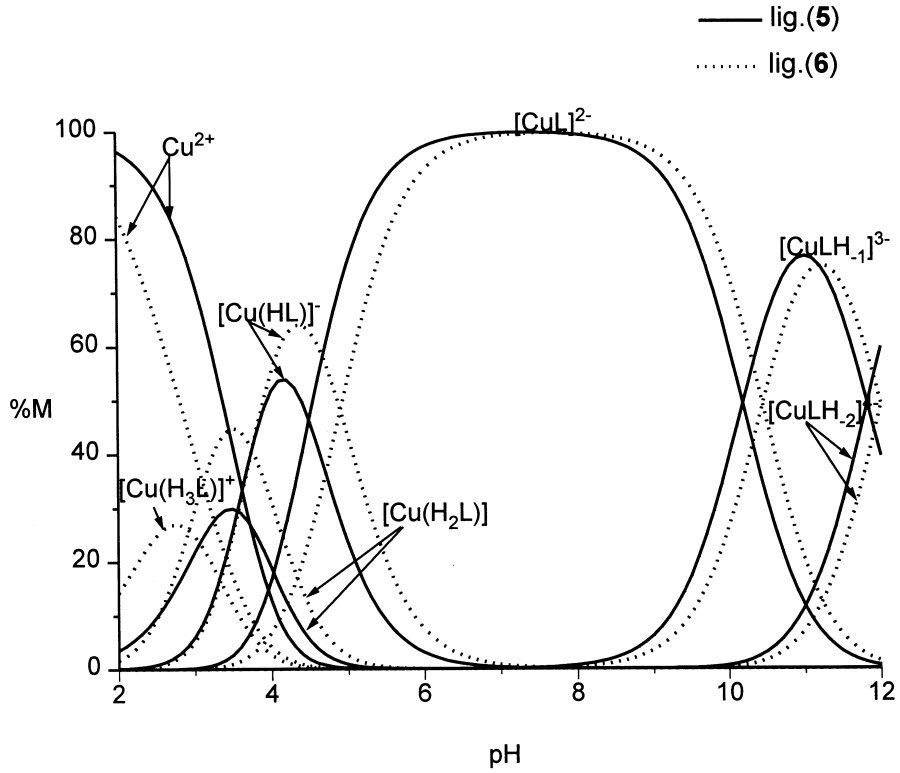

Fig. 1. Species distribution curves for the complexes formed in the Cu^{II}/ligand **5** (full line) and Cu^{II}/ligand **6** (dotted line) systems as a function of pH; $c_{Cu^{2+}} = 3 \times 10^{-3}$ mol dm^{-3}; $c_L = 5 \times 10^{-3}$ mol dm^{-3}.

$\log K_{CuHL} = \log \beta_{Cu(HL)} - pK_{PO_3H^-}$, is about of the same order of magnitude as stability constant, $\log K_{CuL}$ (Table 1). This fact suggests the same O,N,O-tridentate binding mode of the ligands in these two species.

The formation of [CuL] follows the liberation of the proton from weakly coordinated $-PO_3H^-$ group, which consequently becomes more strongly bound to Cu^{II}. The proposed bonding mode for [CuHL] and [CuL] (Scheme 2) should be favoured by the stability increase due to the simultaneous presence of two five-membered chelate rings in the molecule. The sterically possible simultaneous binding of the phosphonate–O^- of both phosphonic groups and imino nitrogen [39] of these tridentate ligands to Cu^{II} is reflected in a high stability constant of [CuHL] and [CuL] (Table 1). An evident increase in $A_{\|}$ and decrease in $g_{\|}$ values can be treated as a further indication that Cu^{II} coordination is realized by the $\{PO_3^{2-}, N_{imino}, PO_3^{2-}\}$ donor set. It is noteworthy that the spectrum of [Cu(HL)] for L = **7** is observed at distinctly lower pH than for the remaining ligands. This result is in a good agreement with the calculated species distribution. Ligand **7** is a more effective chelating agent than other ones. This is reflected in the higher basicity-adjusted stability constant, $\log K_{[CuL]} - \Sigma pK$ (Table 1) and also in the pH value of complexation of 20% of Cu^{II}, which is $\sim$5% for other ligands (Figs. 1 and 2). A comparison of the copper complexes of **5** and **7** (these ligands have the same basicity) shows significant differences. Basicity-adjusted stability constants, $\log K_{[CuL]} - \Sigma pK$, are -9.18 and -7.57 for **5** and **7**, respectively. Taking this into account, comparison of [Cu(**5**)] and [Cu(**7**)] complexes still reveals a difference in stabilities of about 1.6 log units, suggesting strong interaction between Cu^{II} and the furyl oxygen atom (Scheme 3). The proposed bonding mode for [CuHL] and [CuL] (L = **7**) should be favoured by the stability increase due to the simultaneous presence of three five-membered chelate rings in the molecule. The sterically possible simultaneous binding of the phosphonate–O^- of both phosphonic groups, imino nitrogen and furyl oxygen to Cu^{II} is reflected in a very high stability constant of [CuHL] and [CuL].

A comparison of the EPR spectra as a function of pH for the Cu^{II}/ligand **7** system with those e.g. for the Cu^{II}/ligand **3** system (Fig. 3) indicates the 2*N* coordination in the former system, which means that 1:2 species are formed. It also results in a distinct shift in the d–d transition to higher energies if comparing spectra of 1:1 and 1:2 species for the former system. Moreover, the EPR spectra show equilibrium between these species in wide pH range (in contrast to lone [CuL] species observed in the case of **1**–**6** ligands) again confirming unique distribution of the species postulated for Cu^{II}/ligand **7** system.

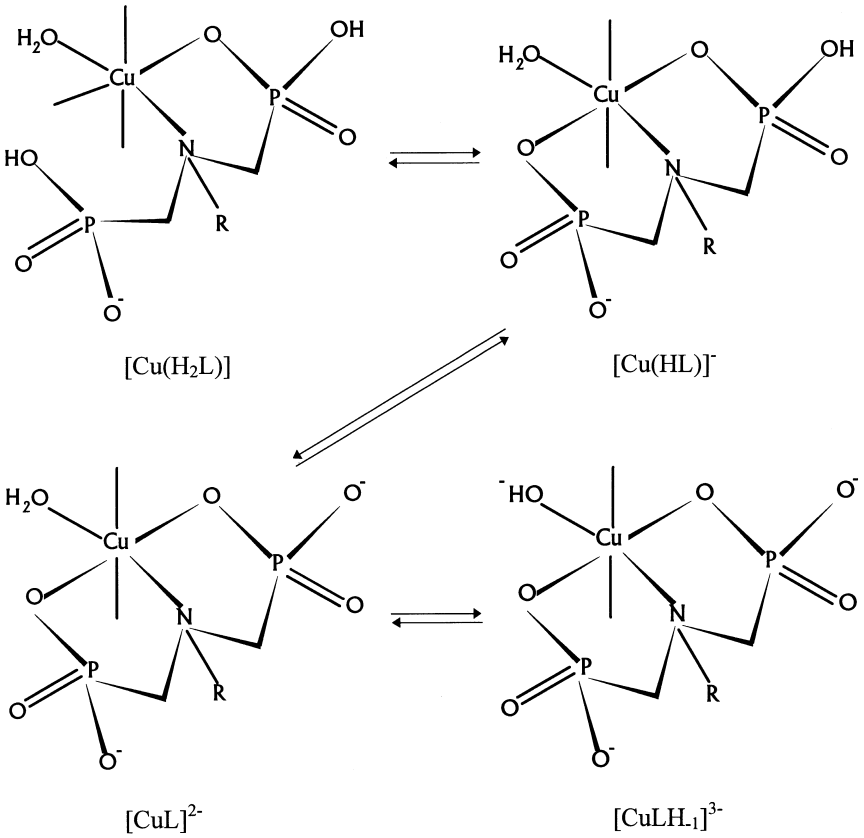

Scheme 2. Proposed structures of complexes formed by ligands **1**–**6** with copper(II).

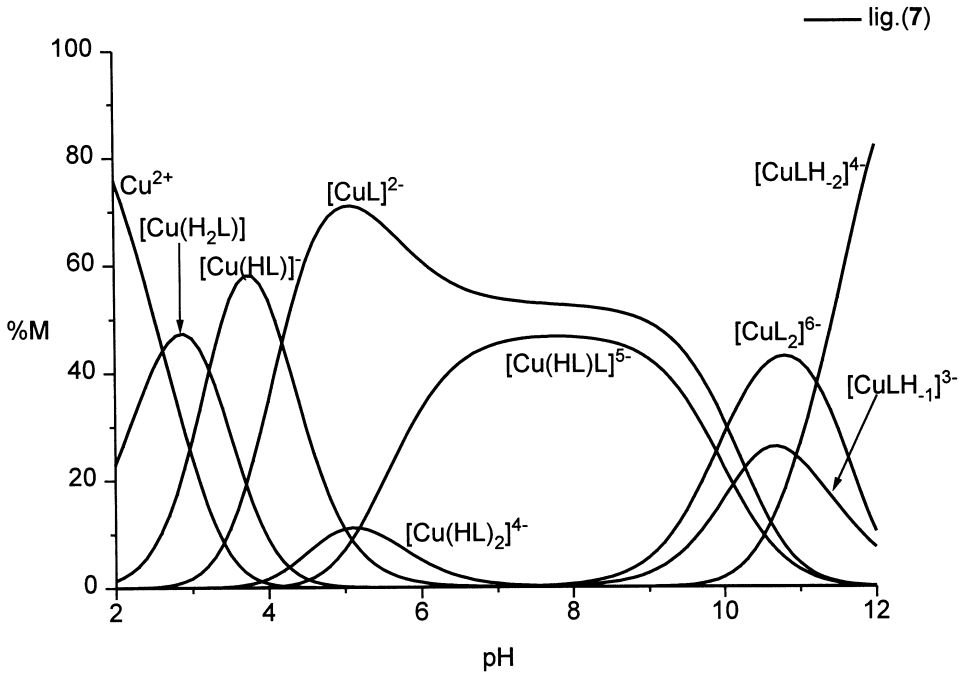

Fig. 2. Species distribution curves for the complexes formed in the Cu^{II}/ligand **7** system as a function of pH; $c_{Cu^{2+}} = 3 \times 10^{-3}$ mol dm^{-3}; $c_L = 5 \times 10^{-3}$ mol dm^{-3}.

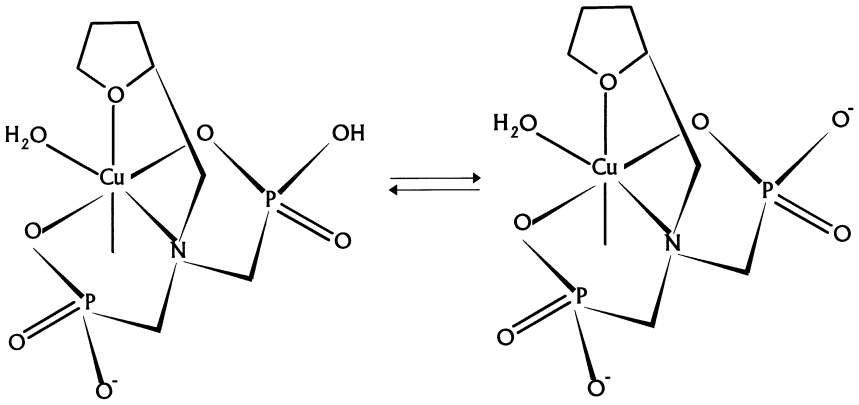

Scheme 3. Proposed structures of the $[Cu(HL)]^{-}$ and $[CuL]^{2-}$ complexes formed by ligand **7**.

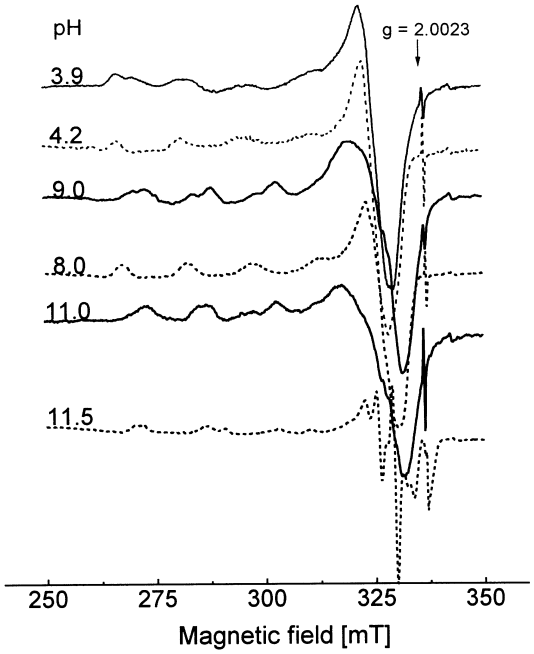

Fig. 3. The comparison between the EPR spectra of the complexes formed by ligand **7** (solid line) and **3** (dashed line) as a function of pH; $c_{Cu^{2+}} = 2 \times 10^{-3}$ mol dm^{-3}; $c_L = 4 \times 10^{-3}$ mol dm^{-3}.

The basicity-adjusted stability constants ($\log K_{[CuL]} - \Sigma pK$) varies in the sequence (Table 1):

$$[Cu(\mathbf{1})] < [Cu(\mathbf{2})] < [Cu(\mathbf{3})] < [Cu(\mathbf{5})] \approx [Cu(\mathbf{6})] < [Cu(\mathbf{4})] < [Cu(\mathbf{7})].$$

This can be explained, in part, by the significant changes of the amine substituent size. It is interesting that the sequence of the basicity-adjusted stability constants of the [Cu(**4**)] and [Cu(**1**)] species is an opposite to the basicity of the free ligands. Probably, in this case the stability increase due to the increase in basicity of the coordinating donor groups is overcompensated by steric (R-group size) and electrostatic effects [40]. This presumably also appears in the spectral parameters of [CuL] (see below).

Two further deprotonation processes of [CuL] leading to the formation of $[CuLH_{-1}]$ and $[CuLH_{-2}]$ are detected in potentiometry and correspond to the subsequent dissociation of the protons from coordinated water molecules. The first $[CuLH_{-1}]$ complex exhibits slightly blue-shifted d–d band and is observed in the EPR spectrum. The characteristic change of the EPR parameters (Table 2) is consistent with replacement of a water molecule by an OH^{-} group in the metal plane.

3.2. *Spectrophotometrical studies*

Absorption spectra of the Cu^{II}/ligand **2** system presented in Fig. 4 exhibit, in general, approximately the same changes vs pH as those observed for the other above-mentioned systems. Even at the pH level where the distribution of the species has a maximum, the other complexes coexist in a greater or smaller extent. Therefore, in the absorption spectra measured even at this pH level the contributions from the other species would be included. To extract the ligand-field absorption spectrum of each species, the experimental spectrum, measured at a pH value where each species exhibits maximal contribution, was resolved into the components spectra corresponding to the individual species existing at that pH. The molecular absorptivity for the individual species was then calculated taking into account their distribution. The distribution-corrected curves for the Cu^{II}/ligand **2** system are shown in Fig. 5. In some cases this method has not given satisfactory results for species which contribution was too small in the system.

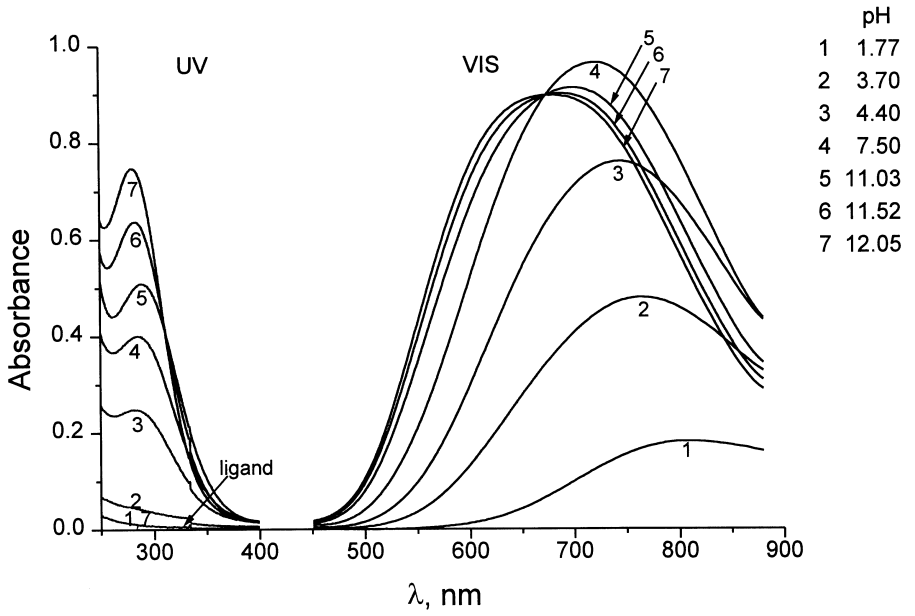

Fig. 4. pH-varied absorption spectra of the Cu^{II}/ligand **2** system: $c_{Cu^{2+}} = 3 \times 10^{-4}$ mol dm^{-3}; $c_L = 5 \times 10^{-4}$ mol dm^{-3} (UV-1 cm cells); $c_{Cu^{2+}} = 3 \times 10^{-3}$ mol dm^{-3}; $c_L = 5 \times 10^{-3}$ mol dm^{-3} (VIS-5 cm cells).

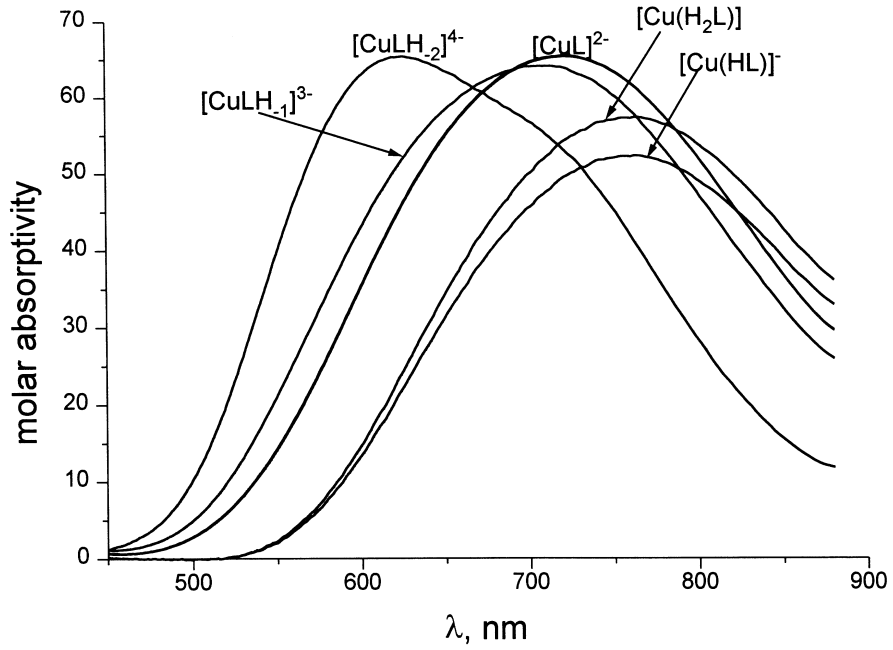

Fig. 5. Distribution-corrected absorption spectra for [Cu(H_2L)], [Cu(HL)], [CuL], [Cu(LH_{-1})] and [Cu(LH_{-2})] in the Cu^{II}/ligand **2** system.

3.3. *Ultraviolet spectroscopic studies*

All the band maxima reported in this work are derived from Gaussian analysis of the experimental curves in the ultraviolet region. In general, the unique procedure (see Section 2) which starts with Gaussian analysis, through assignment of the bands, to calculation of the chemically useful parameters, is based on two assumptions: the symmetry of compound is known, and theoretical model (e.g. ligand field model for the complexes and orbital molecular model for the ligands) is adequate for the calculation of the spectral

parameters. Unfortunately, the systems presented in this work are rather complex. Different structures of the particular ligands are the reason that above mentioned interpretation makes for considerable difficulties. Thus, each system studied should be analysed. separately. Therefore, the Gaussian analysis of the ultraviolet spectra in this work provides the bands which can be really conclusively distinguished from the experimental (observed) spectrum. The numerical spectra $\varepsilon_i = f(\nu_i)$ and full Gaussian analysis results of all spectra are available from the authors on request. Fig. 6(a),(b) presents (as representative example) ultraviolet spectra ($\varepsilon_i = f(\nu_i)$) along with Gaussian components for Cu^{II}/ligand **4** and Cu^{II}/ligand **6** systems.

Because ligands **1**–**4** have not bands in the UV region, observed two bands correspond to the CT transitions (for example: Cu^{II}/ligand **4** system in Fig. 6(a)). Although compounds **5**, **6** and **7** have their own UV absorption spectra, two new bands are easily seen when their spectra are compared with those for the complexes (for example: Cu^{II}/ligand **6** system in Fig. 6(b)). A number of respective bands indicates clearly diversity of the metal-bond donor set. The CT band at 288 nm is not observed for the Cu^{II}/ligand **8** system **8** = 1-hydroxy-3-methylbutylphosphonic acid $(CH_3)_2CHCH_2CH(OH)PO_3H_2$) (Fig. 6(c)). In this case the coordination of phosphonate oxygen atoms to copper(II) is beyond doubt. Thus, the band at 302–277 nm observed for the copper(II)–**1**–**6** and **7** systems corresponds most likely to the $N_{imino} \rightarrow Cu^{II}$ LMCT transition (a similar range of energy was found for the copper(II)-N-iminodi(methylenephosphonic) acid system [20]. The second band are seen in these seven systems at 225–231 nm. This band is similar to this observed for the Cu^{II}/ligand **8** system and $[Cu(H_2O)_6]Cl_2$ complex (212 nm) (Fig. 6(c),(d)) and can be reasonably assigned to the transition from PO_3^{2-} oxygen to copper(II) i.e. LMCT transition.

From the data collected in Table 2 we conclude that the energy order of the lower energetically CT transition displays hipsochromic effect (i.e. increasing energy)

$$[\mathrm{Cu}(\mathbf{1})] < [\mathrm{Cu}(\mathbf{5})] < [\mathrm{Cu}(\mathbf{6})] \approx [\mathrm{Cu}(\mathbf{7})] \approx [\mathrm{Cu}(\mathbf{3})] < [\mathrm{Cu}(\mathbf{2})] \ll [\mathrm{Cu}(\mathbf{4})].$$

This effect depends predominantly on the size of the fragment R (Scheme 1) bonded to the nitrogen donor. These fragments are directly influencing the nitrogen donor–metal bonding. The highest energy is observed when R = methyl group and the lowest when R

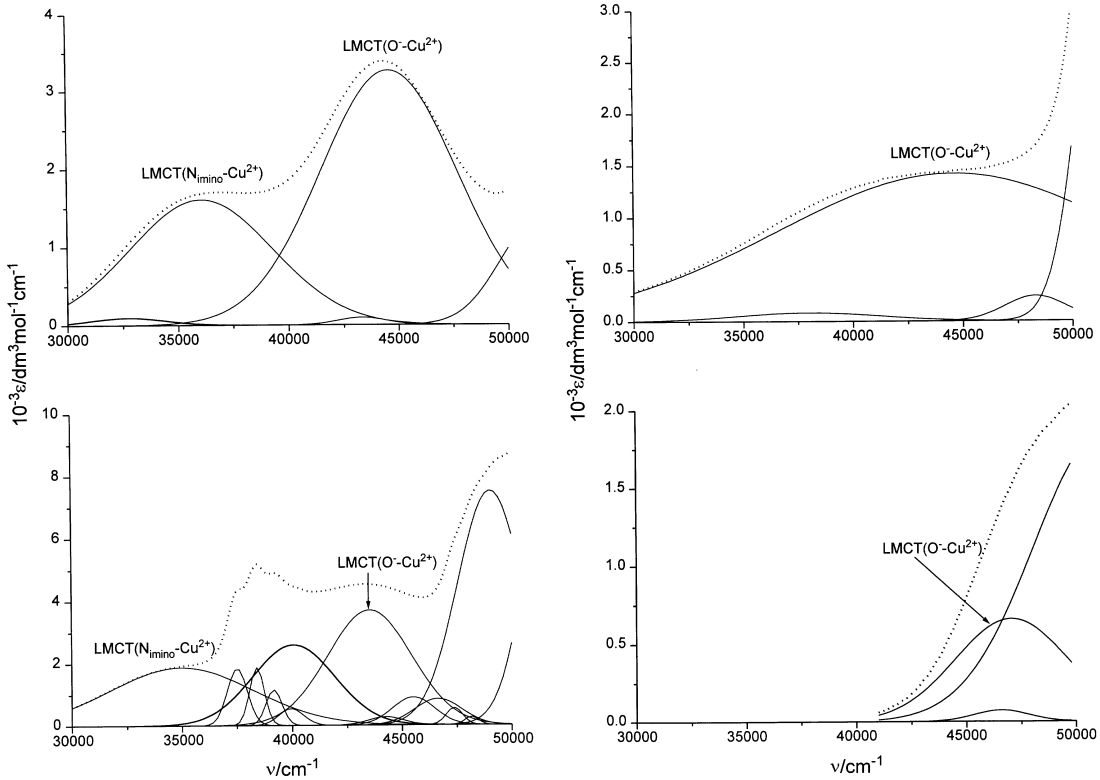

Fig. 6. Ultraviolet spectra and Gaussian line-shape analysis for: [CuL]; L = **4** (a), L = **6** (b); pH 7.5; L = $(CH_3)_2CHCH_2CH(OH)PO_3H_2$ (c); $[Cu(H_2O)]Cl_2$ (d). (· · ·) experimental spectrum, (———) component bands.

involves a cyclohexyl ring. A similar energy relation is observed for the second CT transition.

4. CONCLUSION

The ligands **1**–**6** exhibit the model contains protonated complexes but neither a 1:2 species nor any polynuclear ones. From the comparative analysis of the stability and the spectroscopic (UV–VIS and EPR) data it has been established that the coordination in [CuHL] and [CuL] is realized by the $\{PO_3^{2-}$, N_{imino} $PO_3^{2-}\}$ donor set. Ligand **7** is a more effective chelating agent than other ones. The EPR spectra for the Cu^{II}/ligand **7** system indicate the 2*N* coordination so, 1:2 species are formed. It also results in a distinct shift in the d–d transition to higher energies if comparing spectra of [CuL] and [CuL_2]. A comparison of the basicity-adjusted stability constants, $\log K_{[CuL]} - \Sigma pK$, suggests strong interaction between Cu^{II} and the furyl oxygen atom.

Acknowledgements—The authors gratefully thank Dr Andre Ożarowski of the University of California (ozarowsk @indigo.ucdavis.edu) for allowing use of his simulation program for EPR spectra. The work was financially supported by the Polish State Committee for Scientific Research (KBN, grant #2P303 055 07).

REFERENCES

1. *Chem. Abstr*. 115, 258475e.
2. *Chem. Abstr*. 100, 123537w.
3. *Chem. Abstr*. 107, 119312w.
4. Bligh, S. W. A., Harding, C. T., McEwen, A. B. and Sadler, P. J., *Polyhedron*, 1994, **13,** 1937.
5. Fedurov, V. V., Orlovskii, A. A., Alistratov, A. V., Solodenko, V. A., Kasheva, G. N., Kolodyazhnyi, O. I. and Kukhar, V. P., *Dokl. Akad. Nauk Ukr. SSSR*, 1991, **154**.
6. Choi, N., Constantinou, M., Hyatt, D., Matthews, R. W., McPartlin, M. and Scowen, I. J., *Polyhedron*, 1997, **16,** 355.
7. Solvin, J. P. and Tobin, E. M., *Biochim. Biophys. Acta*, 1981, **177,** 637.
8. *Roundup Herbicide by Monsato*. Monsato, St. Louis, MO, 1985, p. 9.
9. Hoagland, R. E. and Duke, S. O., *ACS Symp. Ser*., 1982, 189.
10. Lejczak, B., Kafarski, P. and Zygmunt, J., *Biochemistry*, 1989, **28,** 3549.
11. Grobelny, D., Goli, U. B. and Galardy, R. E., *Biochemistry*, 1989, **28,** 4948.
12. Moedritzer, K. and Irani, R. R., *J. Org. Chem*., 1966, **31,** 1603.
13. Carter, R. P., Carroll, R. L. and Irani, R. R., *Inorg. Chem*., 1967, **6,** 939.
14. Motikaitis, R. J. and Martell, A. E., *Inorg. Chem*., 1980, **19,** 1646.
15. Belskii, F. I., Goryunova, I. B., Petrovskii, P. V., Medved, T. Ya. and Kabachnik, M. I., *Izv. Akad. Nauk SSSR*, 1982, **31,** 103.
16. Motikaitis, R. J. and Martell, A. E., *J. Coord. Chem*., 1985, **14,** 139.
17. Sawada, K., Kanda, T., Naganuma, Y. and Suzuki, T., *J. Chem. Soc. Dalton Trans*., 1993, 2557.
18. Sawada, K., Miyagawa, T., Sakaguchi, T. and Doi, K., *J. Chem. Soc. Dalton Trans*., 1993, 3777.
19. Jeżowska-Bojczuk, M., Tamas, K., Kozłowski, H., Decock, P. and Barycki, P., *J. Chem. Soc. Dalton Trans*., 1994, 811.
20. Boduszek, B., Dyba, M., Jeżowska-Bojczuk, M., Kiss, T. and Kozlowski, H., *J. Chem. Soc. Dalton Trans*., 1997, 973.
21. Matczak-Jon, E., Kurzak, B., Sawka-Dobrowolska, W., Kafarski, P. and Lejczak, B., *J. Chem. Soc. Dalton Trans*., 1996, 3455.
22. Kurzak, B., Matczak-Jon, E. and Hoffmann, M., *J. Coord. Chem*., 1998, **43,** 243.
23. Soroka, M. and Mastalerz, P., *Pol. J. Chem*., 1976, **50,** 661.
24. Oleksyszyn, J., Gruszecka, E., Kafarski, P. and Mastalerz, P., *Monatsch. Chem*., 1982, **113,** 1138.
25. Gran, G., *Acta Chem. Scand*., 1950, **4,** 599.
26. Molina, M., Melios, C., Tognalli, J. O., Luchiari, L. C. and Jafelicci, M. Jr., *J. Electroanal. Chem*., 1979, **105,** 237.
27. Gans, P., Sabatini, A. and Vacca, A., *J. Chem. Soc. Dalton Trans*., 1985, 1195.
28. Kurzak, K. Ph.D. Thesis, Technical University of Wrocław, Wrocław, 1983.
29. Slavič, I. A., *Nucl. Instrum. Methods*, 1976, **34,** 285.
30. Kurzak, K., *Spectrochim. Acta*, 1991, **47A,** 1041.
31. Kurzak, K., *Wiad. Chem*., 1991, **45,** 425 in Polish.
32. Kurzak, K., Kołkowicz, A., *Spectrosc. Lett*.1997, **30**(5), 805.
33. Ożarowski, A., unpublished program.
34. Sakaguchi, U., Arata, Y. and Fujiwara, S., *J. Magn. Reson*., 1973, **9,** 118.
35. Kiss, T., Balla, J., Nagy, G., Kozłowski, H. and Kowalik, J., *Inorg. Chim. Acta*, 1987, **138,** 25.
36. Kiss, T., Farkas, E., Kozłowski, H., *Inorg. Chim. Acta*, 1989, **155,** 281.
37. Trochimczuk, A. and Jezierska, J., *Polymer*, 1997, **38,** 2431.
38. Vishnevskaya, G. P., Molochnikov, L. S. and Safin, P. Sh., *EPR in Ion Exchangers*. Nauka, Moscow, 1992.
39. Makaranets, B. I., Polynova, T. N., Mitrofanova, N. D. and Porai-Koshits, M. A., *Zh. Struct. Khim*., 1991, **32,** 116.
40. Bal, W., Bertini, I., Kozłowski, H., Monnani, R., Scozzafava, A. and Siatecki, Z., *J. Inorg. Biochem*., 1990, **40,** 227.

Pergamon

Polyhedron Vol. 17, Nos. 25, 26, pp. 4415–4423, 1998
© 1998 Elsevier Science Ltd
All rights reserved. Printed in Great Britain
0277–5387/98 $19.00+0.00

PII: S0277–5387(98)00244–7

Interaction of nitric oxide with cobalt(II) phthalocyanine: kinetics, equilibria and electrocatalytic studies

Sibulelo L. Vilakazi and Tebello Nyokong†

Department of Chemistry, Rhodes University, Grahamstown 6140, South Africa

(Received 20 April 1998; accepted 16 June 1998)

Abstract—The coordination of nitric oxide (NO) to cobalt(II) phthalocyanine (CoPc) in dimethyl sulphoxide (DMSO) has been studied. CoPc coordinates with NO in a 1:1 ratio, forming a CoPc(NO) species. The IR band observed at 1680 cm^{-1} is assigned to the coordinated NO. In the presence of excess NO, pseudo first order kinetics were followed. The observed rate constant, k_f, was determined to be $15.0 \pm 0.3\ dm^{-3}\ mol^{-1}\ s^{-1}$ and the equilibrium constant was $K = 5.4 \pm 0.4 \times 10^4 dm^3\ mol^{-1}$. Solution or adsorbed CoPc catalyses the reduction of NO. The products of reduction include NH_3 and NH_2OH. © 1998 Elsevier Science Ltd. All rights reserved

Keywords: cobalt; phthalocyanine; nitric oxide; catalysis; kinetics; equilibria.

INTRODUCTION

Nitric oxide (NO) has been found to be an essential component of many physiological processes. NO is believed to have a wide range of functions including regulation of blood pressure, neurotransmission and ability to kill intracellular parasites and tumorous cells [1–4]. NO readily forms complexes with transition metal ions, including those found in metalloproteins. Studies into the binding of NO by metalloporphyrins have aided in the understanding of how NO interacts with haem containing biomolecules such as haemoglobin and myoglobin. NO has been shown to have a high affinity for ferrous haem [3]. Both iron(II) and iron(III) porphyrins have been shown to coordinate NO, forming $Fe^{II}P(NO)$ and $Fe^{III}P(NO)$ complexes, respectively [5–7]. Autoreduction of the $Fe^{III}P(NO)$ complex to the $Fe^{II}P(NO^+)$ species has been reported [4, 6]. NO adducts of cobalt substituted myoglobin and haemoglobin have been reported [8], hence the substitution of iron by cobalt in synthetic porphyrins has gained considerable attention. Studies into the coordination of NO to cobalt porphyrin (CoP) complexes are of interest. $Co^{II}P$ readily binds NO forming the $(NO)Co^{II}P$ species. Cobalt(III) tetrakis(*N*-methyl-2-pyridyl)porphine ($[Co^{III}(2\text{-}TMPyP)]^{5+}$) is known to bind with NO through reductive nitrosylation with the formation of the $[(NO)Co^{II}(2\text{-}TMPyP)]^{4+}$ species [9]. Exposure of the $[(NO)Co^{II}(2\text{-}TMPyP)]^{4+}$ species to air rapidly converts it to $[(NO_2^-)Co^{III}(2\text{-}TMPyP)]^{4+}$. Metallophthalocyanine (MPc) complexes have a similar structure to the metalloporphyrins and have been used to mimic the properties of the naturally occurring metalloporphyrin complexes. MPc have an added advantage in that they are more stable to degradation than metalloporphyrin complexes. $Fe^{II}Pc$ has been shown to reversibly bind NO in dimethylsulphoxide (DMSO) according to eq. (1) [10, 11]

$$(DMSO)_2Fe^{II}Pc + NO \rightleftarrows (DMSO)(NO)Fe^{II}Pc + DMSO. \quad (1)$$

Axial coordination of NO to solid MnPc, CoPc and ZnPc has also been reported [12, 13]. Results from X-ray photoelectron spectroscopy showed that coordination of NO to MnPc, FePc and CoPc was accompanied by some electron transfer between the central metal and the NO molecule [13]. We report in this work on the kinetics and equilibria of the coordination of NO to CoPc in solution. It has recently been demonstrated that NO bonds to nickel(II) tetrasulphophthalocyanine ($[Ni^{II}TSPc]^{4-}$) in aqueous solu-

†Author to whom correspondence should be addressed. E-mail: chtn@warthog.ru.ac.za

tion. It was suggested that autooxidation of the $[Ni^{II}TSPc]^{4-}$ occurred following coordination of NO with the formation of a $[Ni^{III}TSPc(NO^{-})]^{4-}$ species [14]. Interestingly, in all the studies on the coordination of NO to metalloporphyrin or MPc complexes, only one mole of NO coordinates to one mole of the metalloporphyrin or MPc complex. However, it has been shown that axial ligand substitutions in MPc complexes occur in a stepwise manner, with the consecutive coordination of the two ligands [15].

Even though there are reports on the binding of NO to CoPc complexes, kinetic or equilibria information on this binding has not been reported. Binding of NO or NO_2^- to CoPc is of importance for analysis of these species, since ring substituted cobalt phthalocyanine complexes have demonstrated an excellent selectivity toward the electroreduction of nitrite ion [16].

There are a number of reports on the use of metalloporphyrin complexes [7, 17–24] and haemoglobin [25] for the electrochemical detection of NO and as electrocatalysts for the reduction of NO to ammonia and other products [9, 26]. Reports on the use of MPc complexes for the detection of NO are limited [27]. Selective reduction of NO to NH_3 has been reported [27] for CoPc adsorbed on a glassy carbon electrode. However, very low yields of NH_3 were observed at pH > 4 [27]. It is important to understand the role played by the MPc complexes during the electrocatalytic reactions. It has been suggested that electron transfer reactions mediate electrochemical detection of NO, using metalloporphyrin complexes [7]. Metal and ring-based reduction and oxidation processes can occur in CoPc complexes. In this work, we study the electrocatalytic ability of CoPc (in solution or adsorbed onto the electrode) for the reduction of NO.

EXPERIMENTAL

Materials

Cobalt(II) and iron(II) phthalocyanine (CoPc and FePc, respectively) were purchased from Aldrich and used without further purification. The solid complex between NO and CoPc was prepared by stirring CoPc in dimethylformamide (DMF) in an NO atmosphere for 4 h, then evaporating the solvent to dryness. NO was prepared by adding saturated sodium nitrite dropwise to a 0.2 mol dm^{-3} H_2SO_4 solution under nitrogen atmosphere. The NO produced was bubbled into nitrogen saturated deionized water or passed through a drying agent into nitrogen saturated, dimethylsulphoxide (DMSO). NO solutions in water or DMSO were prepared freshly before use and kept in a glass flask fitted with a rubber septum. The concentration of NO in DMSO was determined by the method proposed by Ascenzi *et al.* [11], using the reaction of NO with FePc in DMSO. The concentration of NO in DMSO could also be calculated using its solubility of 3.0×10^{-3} mol dm^{-3} [11]. NO concentration in water was calculated using the reported solubility of 2.2×10^{-3} mol dm^{-3} [11].

Electrochemical methods

Electrochemical data were collected with the Bioanalytical Systems (BAS) model CV-50 W voltammetric analyser. For cyclic voltammetry, a glassy carbon electrode (3.0 mm diameter) was used as a working electrode and a platinum wire as an auxiliary electrode. For nonaqueous studies, the reference electrode was the BAS nonaqueous reference electrode containing a silver wire immersed in a 0.01 mol dm^{-3} $AgNO_3$ and containing 0.1 mol dm^{-3} tetraethylammonium perchlorate (TEAP) in DMSO. The electrolyte was TEAP for all electrochemical experiments in nonaqueous solutions. For cyclic voltammetry in aqueous solutions, the reference electrode was the Ag/AgCl(3 mol dm^{-3} KCl). Concentrations of CoPc in DMSO for cyclic voltammetry were in the 10^{-4}–10^{-3} mol dm^{-3} range.

For electrocatalytic reactions, a glassy carbon electrode modified with CoPc (CoPc–GCE) was employed as a working electrode. The GCE was modified by the drop dry method, in which a drop of a saturated ($\sim 1 \times 10^{-3}$ mol dm^{-3}) solution of CoPc in pyridine was placed on the GCE and dried in air. Prior to coating with the CoPc complex, the GCE was polished with alumina on a Buehler felt pad, followed by soaking in dilute nitric acid and rinsing in water, acetone and the solvent of interest. For bulk electrolysis, a two compartment cell was employed, with a platinum plate of area 2.2 cm^2 as counter electrode and a Ag/AgCl (3 mol dm^{-3} KCl) reference electrode. The working electrodes consisted of a carbon rod (area = 0.2 cm^2) coated with CoPc using the drop dry method. Electrical contact with the working electrode was established via a copper wire. Phthalate buffer, pH 4, was used for studies of NO in aqueous solutions. A nitrogen atmosphere was maintained for all electrochemistry experiments. Yields of ammonia were determined by the Nessler method [28] and by monitoring the absorbance at 400 nm. Hydroxylamine was determined spectroscopically using the specific test described in the literature [9].

Kinetics and equilibria

Kinetic and equilibrium studies were run at 20°C and monitored with the Cary 1E UV–VIS spectrophotometer. We monitored the appearance of the spectra due to the product formed following the addition of NO to solutions of the CoPc in DMSO. Typically, a known volume of the DMSO solution of CoPc was added to a 1 cm path length cell and deaerated using nitrogen. Then a known volume of a deaerated solution of NO in DMSO was added to the cell

and the spectra monitored with time. Bubbling of nitrogen into the cell was continued while adding the NO solution. NO is readily oxidized by oxygen, hence the cell was fitted with a stopper to avoid oxygen affecting the reaction. Concentrations of the CoPc were kept constant at 4.5×10^{-6} mol dm $^{-3}$, while NO concentrations were varied from 6.2×10^{-5} to 1.2×10^{-4} mol dm^{-3}. Since the concentration of the NO was larger than that of CoPc by a factor of at least 10, pseudo-first order conditions were assumed for kinetic studies.

Infra red spectra were recorded with the Perkin Elmer Spectrum 2000 IR spectrophotometer, using CaF_2 windows and dichloromethane as the solvent.

RESULTS AND DISCUSSION

Spectral characterization

In DMSO solutions, CoPc is known to be a six coordinate complex [29], hence the starting complex for our studies is expected to be the $(DMSO)_2CoPc$ species. The *Q* band of the $(DMSO)_2CoPc$ species is centred at 660 nm. Figure 1 shows the absorption spectral changes observed when DMSO solutions of NO (1.1×10^{-4} mol dm $^{-3}$) were added to solutions of $(DMSO)_2CoPc$. On addition of NO, the *Q* band of the $(DMSO)_2CoPc$ species shifts isosbestically from 660 to 666 nm. An isosbestic point was observed at 657 nm. The presence of an isosbestic point is a clear indication that only two species are absorbing in the *Q* band region of the spectra. X-ray photoelectron spectroscopy studies [13] have shown that electron transfer from the metal to NO occurs following coordination of NO to CoPc. On the other hand, reductive nitrosylation has been reported for the coordination of NO to Co^{II} porphyrin complexes [9]. We investigated the possibility of the oxidation of $Co^{II}Pc$ to the $Co^{III}Pc$ species, following addition of NO to $(DMSO)_2CoPc$ in solution. When NO was added to solutions of chemically generated $Co^{III}Pc$ species in DMSO, the *Q* band of the resulting complex was observed at 665 nm, a wavelength very close to that obtained in Fig. 1(b) following addition of NO to $Co^{II}Pc$. It is thus likely that the $Co^{III}Pc$ species is formed in Fig. 1. Based on the absorption spectral data and on the X-ray photoelectron spectroscopic data, we represent the complex formed following coordination of NO to $Co^{II}Pc$ as the $Co^{III}Pc(NO)$ species. We used IR spectroscopy to study the interaction between NO and $Co^{II}Pc$. For IR studies, dichloromethane and not DMSO was employed as a solvent due to the strong IR vibrations of the latter in the region of NO vibrations. The IR spectra of $Co^{II}Pc$ in CH_2Cl_2 showed a new IR band at 1680 cm^{-1} in the presence of NO. The IR spectra of free NO was observed at 1847 cm^{-1}. The IR spectra of cobalt(II) porphyrins in CH_2Cl_2 and in the presence of NO, show the ν_{NO} in the 1681–1695 cm^{-1} region [30]. Thus, the IR band observed at 1680 cm^{-1} is assigned to bound NO. Vibrational frequencies of NO greater than 1700 cm^{-1} have been associated [14] with the electron

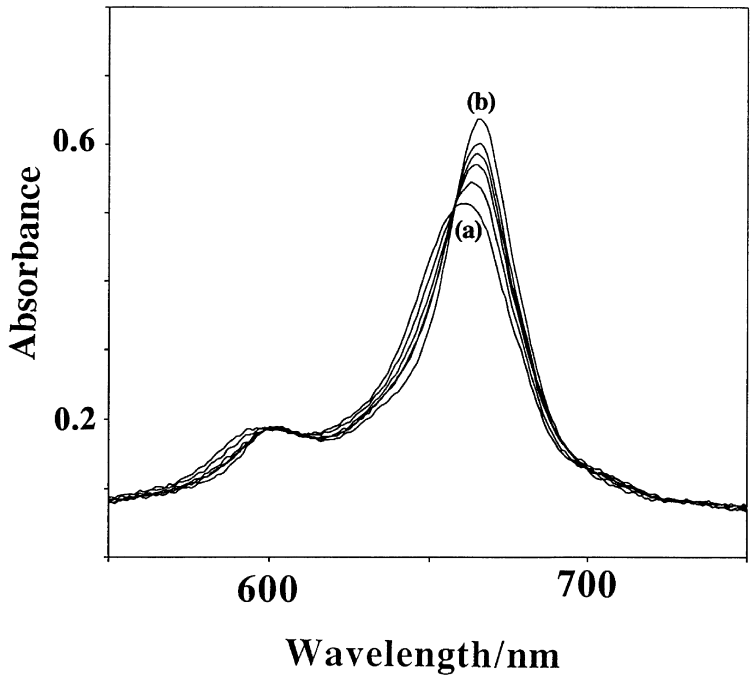

Fig. 1. Absorption spectral changes observed on addition of NO (1.1×10^{-4} mol dm^{-3}) to $(DMSO)_2CoPc$ in DMSO. (a) spectra before addition of NO (b) spectra 18 min after addition of NO.

transfer from NO to the central metal and NO vibrational frequencies less than 1700 cm^{-1}, to the metal to NO electron transfer [14]. Thus, the observation of an NO frequency lower than 1700 cm^{-1} for the complex formed when NO is added to $Co^{II}Pc$, supports the formation of the $(NO)Co^{III}Pc$ species as a result of electron transfer from the central metal to NO. Attempts to synthesize solid (NO)CoPc species by bubbling NO to solutions of CoPc in dimethylformamide, then evaporating off the solvent resulted in the formation of a complex that was more soluble in organic solvents than the original species. Absorption spectral studies of the (NO)CoPc complex showed the presence of a $Co^{III}Pc$ species.

Kinetic and equilibrium studies

Kinetic and equilibria data for the coordination of NO to CoPc were determined by monitoring the formation of the (NO)CoPc species. The increase in the Q band of this species at 666 nm was monitored for kinetic and equilibrium measurements. Equilibrium data were determined by standard spectroscopic techniques using eq. (2)

$$\log[(A_{eq}-A_0)/(A_\infty-A_{eq})]=\log K+n\log[NO]. \quad (2)$$

In eq. (2), A_{eq} is the equilibrium absorbance at 666 nm, A_0 is the absorbance before addition of NO and A_∞, the absorbance after complete formation of the (NO)CoPc complex, was determined from the final absorbance at 666 nm. Figure 2 shows a plot of $\log[(A_{eq}-A_0)/(A_\infty-A_{eq})]$ vs log[NO]. A linear plot with a slope near unity ($n=0.9\pm0.1$) was obtained, showing that only one mole of NO is coordinated to the CoPc species. The linearity of the plot confirms the coordination of NO to the CoPc complex. Least square analysis gave an equilibrium constant of, $K=5.4\pm0.4\times10^4\ dm^3\ mol^{-1}$.

Plots of the observed rate constant, k_{obs}, vs the concentration of NO were linear, Fig. 3, showing that the coordination is first order in NO. Axial ligand substitution reactions in metallophthalocyanines are dissociative with the formation of a highly reactive five-coordinate intermediate [15, 31]. The axial ligand substitution in $(DMSO)_2CoPc$ may thus be represented by the reactions of eqs. (3) and (4)

$$(DMSO)_2CoPc \underset{k_{-1}}{\overset{k_1}{\rightleftharpoons}} (DMSO)CoPc + DMSO \quad (3)$$

$$NO + (DMSO)CoPc \underset{k_{-2}}{\overset{k_2}{\rightleftharpoons}} [(DMSO)(NO)CoPc \quad (4)$$

The rate law for axial ligand exchange reactions in MPc complexes shown by the reactions of eqs. (3) and (4) is generally given by eq. (5)

$$k_{obs}=k_f[NO]+k_r, \quad (5)$$

where k_f, the rate constant for the forward reaction, is given by $k_1k_2/k_{-1}[DMSO]$ and k_r is the rate constant for the reverse reaction. Least square analysis of the data presented in Fig. 3 gave $k_f=15.0\pm0.3\ dm^{-3}\ mol^{-1}\ s^{-1}$ from the slope and from the intercept, $k_r=3.1\pm0.1\times10^{-4}\ s^{-1}$ was obtained. Using these values of rate constants, the value of the equi-

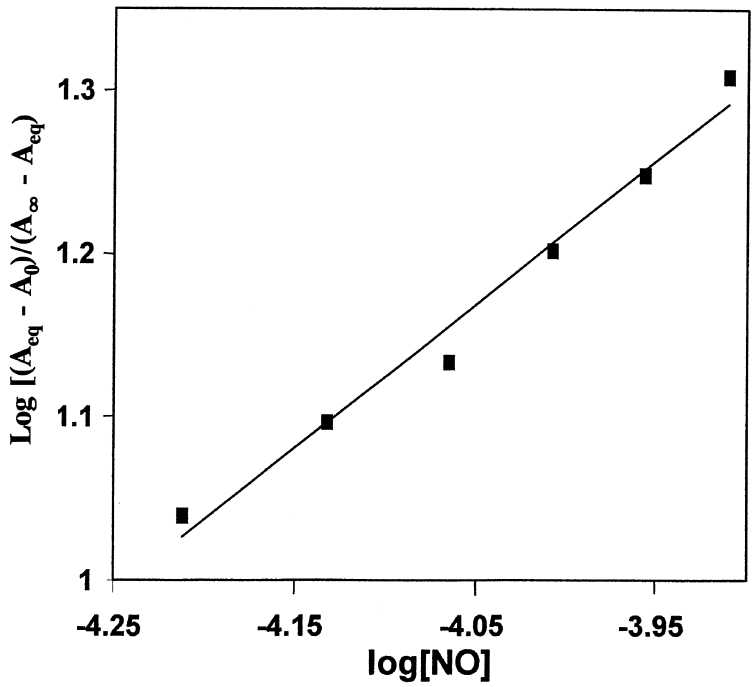

Fig. 2. Plot of $\log[(A_{eq}-A_0)/(A_\infty-A_{eq})]$ vs log[NO] for the formation of the (NO)CoPc species.

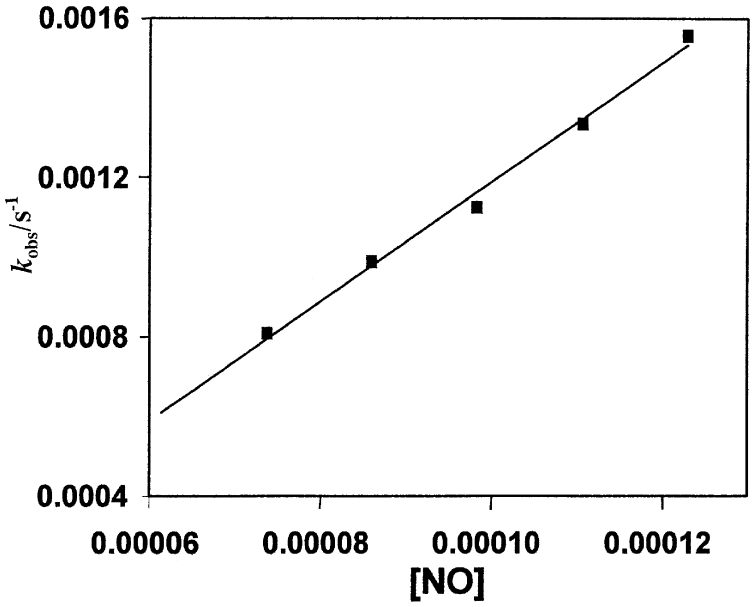

Fig. 3. Plot of the observed rate constant, k_{obs}, vs the concentration of NO for the formation of the (NO)CoPc species.

librium constant for NO coordination to CoPc was estimated to be $K_1 = 4.8 \times 10^4\,dm^3\,mol^{-1}$ from the relationship, $K_1 = k_f/k_r$, in excellent agreement with the value determined above from the equilibrium data.

For the coordination of NO to $(DMSO)_2FePc$, Ascenzi *et al.* [10] obtained an equilibrium constant of $1.1 \times 10^6\ dm^3\ mol^{-1}$ and $k_f = 2.2 \times 10^4\ dm^3\ mol^{-1}\,s^{-1}$. These values are much larger than the values obtained in this work for the coordination of NO to $(DMSO)_2$ CoPc. The coordination of pyridine in $(DMSO)_2$ FePc also occurred [32] with much larger equilibrium and rate constants than the coordination of pyridine in $(DMSO)_2$CoPc. This implies that the five coordinate (DMSO)FePc species are more reactive than the corresponding (DMSO)CoPc. The equilibrium constants observed for coordination of NO to CoPc are of the same order of magnitude as the equilibrium constants reported for the coordination of NO to cytochrome C and metmyoglobin [6]. The rate constant for the coordination of NO to CoPc is similar to the rate constants reported for the coordination of NO to Mn porphyrin complexes [26].

Electrocatalytic reduction of NO

Cyclic voltammetry of CoPc in donor solvents such as DMSO is well documented [33]. Figure 4(a) shows the cyclic voltammogram of CoPc in DMSO in the absence of NO. The first reduction in CoPc is known [33] to occur at the central Co^{II} metal to form the $Co^{I}Pc$ species. Subsequent reductions occur at the phthalocyanine ring. Thus, the reduction labelled I in Fig. 4(a) is assigned to $Co^{II}Pc(-2)/Co^{I}Pc(-2)$. The metal reduction in $Co^{II}Pc$ in dimethylacetamide was observed at -0.2 V vs saturated calomel electrode [33]. The rest of the reductions in Fig. 4(a) are then due to ring-based processes. The half-wave potentials for couples I, II, III and IV were respectively found to be -0.08, -0.36, -0.66 and -0.93 V vs Ag/AgCl.

On addition of NO to solutions of CoPc in DMSO, the cyclic voltammogram shown in Fig. 4(b) was obtained. Following the discussion above, the cyclic voltammogram in Fig. 4(b) should be due to the $(NO)Co^{III}Pc$ species in DMSO. Three quasi-reversible reduction couples were obtained in Fig. 4(b). The reduction couples were enhanced relative to the reduction couples for CoPc in the absence of NO. Also the reduction couples in Fig. 4(b) are observed at slightly different potentials than the potentials for the reduction of $(DMSO)_2Co^{II}Pc$. A considerable enhancement in the cathodic currents was observed for the fourth reduction, labelled IV in Fig. 4(b) on addition of NO to $(DMSO)_2$CoPc. There was no corresponding return peak for IV following addition of NO. The large increase in cathodic current relative to the anodic currents is typical behaviour for catalytic reduction. The catalytic peak was observed at -0.93 V vs Ag/AgCl. The potential for the catalytic peak shifted to more negative potentials, with increase in NO concentration. The catalytic currents for the reduction of NO increased with increase in concentration as shown in Fig. 5, clearly showing that the peak (IV) is due to the reduction of NO. The catalytic peak currents also increased linearly with increase in the square root of scan rate, for scan rates ranging from 50 to $500\,mV/s^{-1}$, confirming a diffusion controlled process for the reduction of NO.

It is expected that the reduction of $Co^{II}Pc$ species

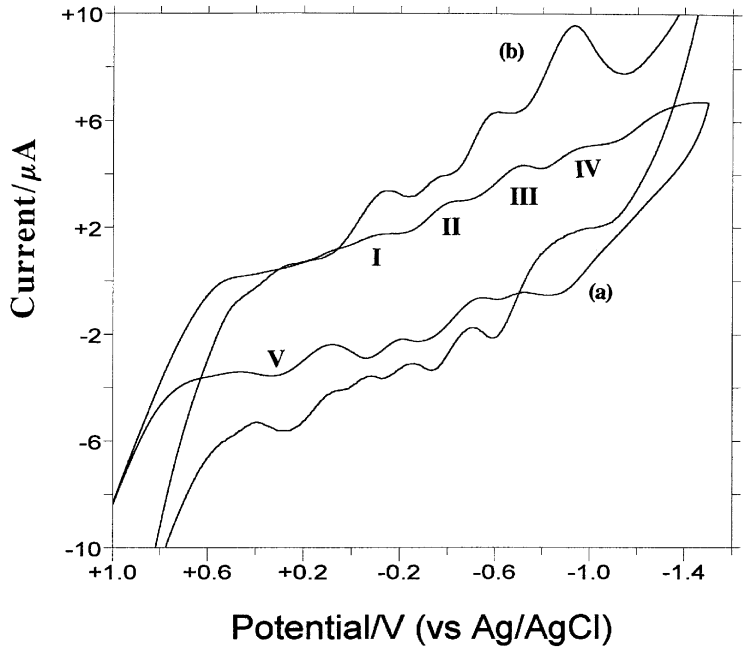

Fig. 4. Cyclic voltammogram of CoPc in DMSO (a) before and (b) after addition of NO (1.1×10^{-4} mol dm^{-3}) to the same concentration of CoPc as in (a). Electrolyte is 0.1 mol dm^{-3} TEAP and the scan rate 100 mV/s.

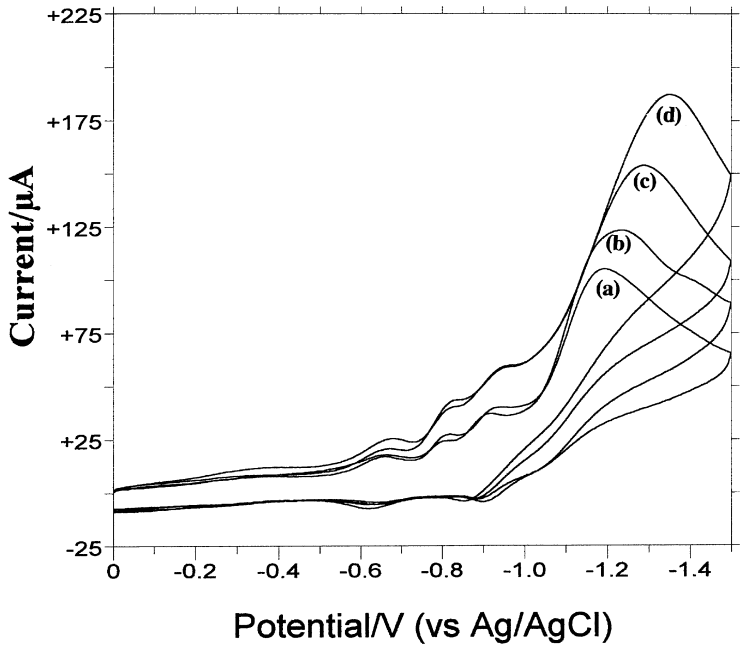

Fig. 5. Cyclic voltammograms of CoPc in DMSO, in the presence of increasing concentrations of NO: (a) 4.6×10^{-4}; (b) 5.7×10^{-4}; (c) 6.7×10^{-4} and (d) 8.3×10^{-4} mol dm^{-3}. Electrolyte is 0.1 mol dm^{-3} TEAP and the scan rate 100 mV/s.

would occur by consecutive one-electron reductions. The reduction occurs first at the central metal to give a $Co^{I}Pc$ species. Subsequent reductions are expected to occur at the phthalocyanine ring. The reduction labelled IV is at the potentials reported [33] for ring reductions of the CoPc species. The fact that we observe an enhancement in the cathodic currents of the peaks associated with phthalocyanine ring-based reductions on addition of NO to CoPc, suggests that it is these reductions that are involved in catalysing the reduction of NO. In many reductions involving CoPc as a catalyst, metal-based reduction processes

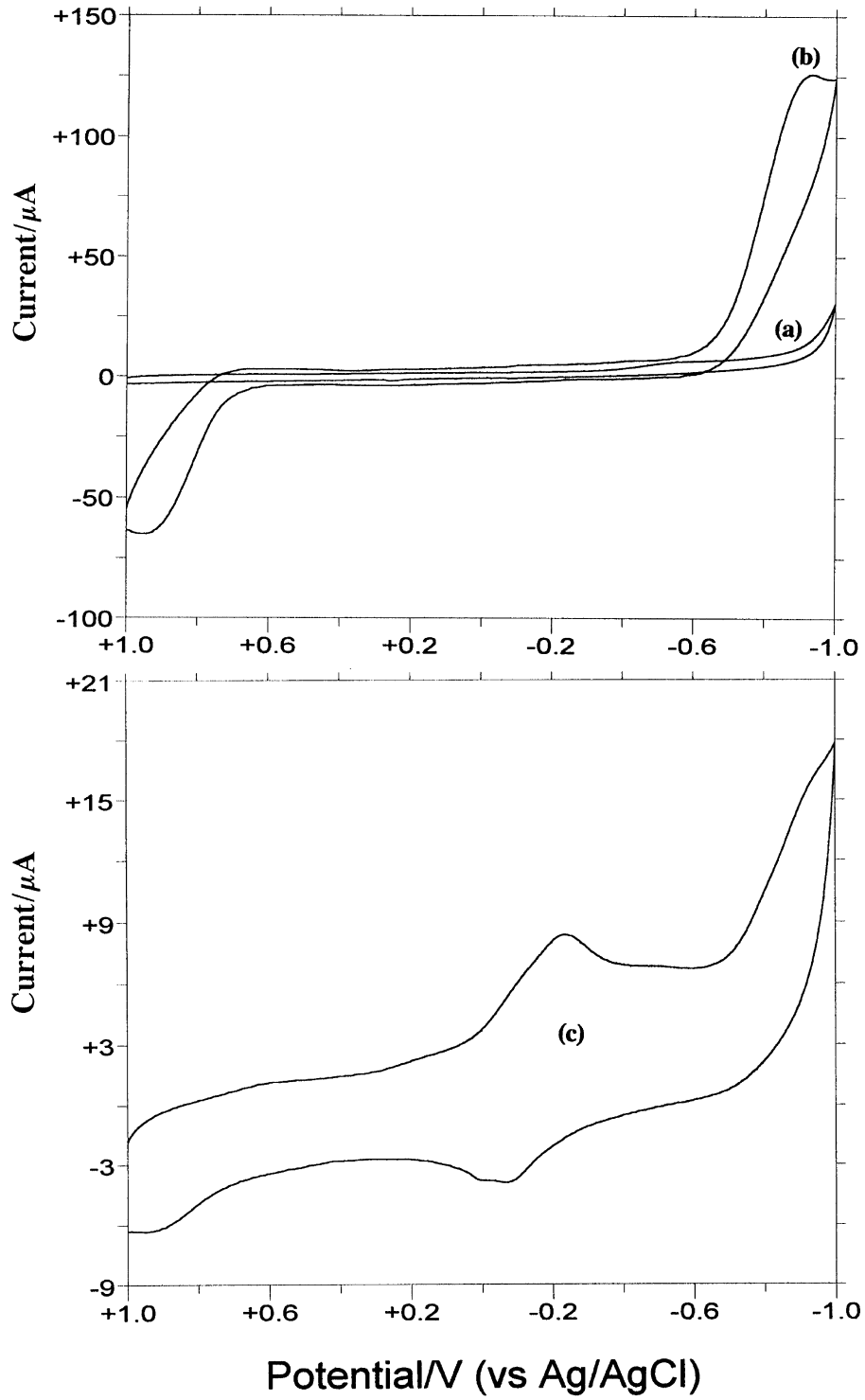

Fig. 6. Cyclic voltammograms of NO (7.0×10^{-4} mol dm^{-3}) on (a) unmodfied glassy carbon electrode and (b) CoPc modified glassy carbon electrode. (c) cyclic voltammogram of CoPc–GCE in buffer alone. Electrolyte pH 4 buffer. The scan rate is 100 mV/s.

have been suggested as playing a major role [12]. This work, however shows that ring-based processes may be involved in the catalytic reduction of NO using CoPc. The following mechanism is thus proposed for the reduction of NO using CoPc in solution:

$$Co^{II}Pc(-2) + NO \rightarrow (NO)Co^{III}Pc(-2) \quad (6)$$

$$(NO)Co^{III}Pc(-2) + e^- \rightarrow (NO)Co^{II}Pc \quad (7)$$

$$(NO)Co^{II}Pc(-2) + e^- \rightarrow (NO)Co^{I}Pc(-2) \quad (8)$$

$$(NO)Co^{I}Pc(-2) + e^- \rightarrow (NO)Co^{I}Pc(-3) \quad (9)$$

$$(NO)Co^{I}Pc(-3) + ne^- \rightarrow NH_3 \text{ and other products.} \quad (10)$$

The DMSO solvent and the overall charge have been left out of the above equations for clarity. Following the formation of the reduction products it is expected that the $Co^{II}Pc$ species would be regenerated.

Figure 6 shows the cyclic voltammograms of NO reduction on unmodified glassy carbon electrode and on a glassy carbon electrode modified with CoPc. In the absence of NO the reduction peaks due to adsorbed CoPc are observed near -0.15 V vs Ag/AgCl, Fig. 6(c). Reduction peaks observed for adsorbed CoPc have been assigned to Co^{III}/Co^{II} and Co^{II}/Co^{I} [12]. In the presence of NO, a catalytic reduction current rose sharply from about -0.6 V and showed a reduction peak at -0.93 V. The catalytic currents did not decrease significantly with subsequent scan on the same CoPc–GCE, indicating that the electrode was not deactivated by the adsorption of the reduction products. The catalytic currents observed in Fig. 6(b) for NO on CoPc–GCE, were much higher than the reduction currents observed for NO on an unmodified glassy carbon electrode, Fig. 6(a). Catalytic currents were also observed for the oxidation of NO on CoPc–GCE, with a peak at 0.94 V vs Ag/AgCl. The reduction currents at -0.93 V increased linearly with increase in the concentration of NO, Fig. 7. The reduction peak for the reduction of NO on a glassy carbon electrode modified with CoPc was observed before at -0.8 V in a citric acid–hydrochloric acid solution [27].

Bulk electrolysis of a solution containing NO in a pH 4 buffer at potentials of the catalytic reduction currents (-0.95 V), gave $n=5$, where $n=$number of moles of electrons involved in the reaction. Since reduction of NO to ammonia requires five electrons, the value of $n=5$ confirms that NH_3 is one of the reduction products of NO, as has been observed before. Analysis of the solution following bulk electrolysis gave a 35% yield of ammonia (with respect to NO) after 2 h of electrolysis of 10 cm^3 solution containing 2.1×10^{-3} mol dm^{-3} NO. Hydroxylamine was also detected as one of the reduction products.

In conclusion, we have shown in this work that NO coordinates to CoPc in DMSO solutions, forming a (NO)CoPc species. The equilibrium and rate constants for this interaction are lower than reported for the interaction of NO with FePc. There was evidence for electron transfer from the central Co ion to NO, with the formation of the $(NO)Co^{III}Pc$ species. Axial ligand exchange reactions in metallophthalocyanine and complexes normally involve the exchange of both ligands in $(L)_2Mpc$ complexes. The coordination of

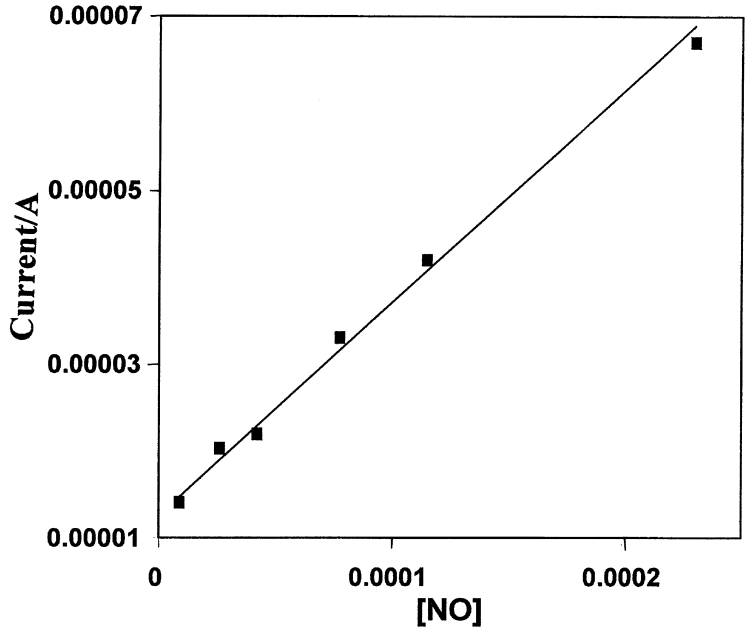

Fig. 7. Plot of [NO] vs catalytic reduction currents for the reduction of NO on CoPc–GCE. Electrolyte is pH 4 buffer and the scan rate 100 mV/s.

the second NO ligand to CoPc was not observed. Cyclic voltammetry studies showed that phthalocyanine ring-based reductions of the CoPc species catalyse the reduction of NO.

Acknowledgements—This work was supported by Rhodes University and by the Foundation of Research Development in South Africa. S. L. V. wishes to thank the University of the North for a graduate scholarship.

REFERENCES

1. Pitsillides, A., Rawlinson, S. C. F., Suswillo, R. F. L., Bourrin, S., Zaman, G. and Lanyon, L. E., *FASEB J*., 1995, **9,** 1614.
2. Galea, E., Reis, D. J., Xu, H. and Feinstein, D. L., *FASEB J*., 1995, **9,** 1632.
3. Butler, A. R. and Williams, D. L. H., *Chem. Soc. Rev*., 1993, 233.
4. Davies, N. A., Wilson, M. T., Slade, E., Fricker, S. P., Murrer, B. A., Powell, N. A. and Henderson, G. R., *Chem. Comm*., 1997, 47.
5. Bedioui, F., Trevin, S. and Devynck, J., *Electroanalysis*, 1996, **8,** 1085.
6. Hoshino, M., Ozawa, K., Seki, H. and Ford, P. C., *J. Am. Chem. Soc*., 1993, **115,** 9568.
7. Laverman, L. E., Hoshino, N. and Ford, P. C., *J. Am. Chem. Soc*., 1997, **119,** 12663.
8. Hori, H., Ikeda-Saito, M., Leigh, J. S. and Yonetami, T., *Biochemistry*, 1982, **21,** 1431.
9. Cheng, S.-H. and Su, Y. O., *Inorg. Chem*., 1994, **33,** 5847.
10. Ascenzi, P., Brunori, M., Pessesi, G., Ercolani, C. and Monacelli, F., *J. Chem. Soc. Dalton Trans*., 1987, 369.
11. Ascenzi, P., Fruttero, R., Ercolan, C. I. and Monacelli, F., *Analusis*, 1996, **24,** 316.
12. Zagal, J. H., *Coord. Chem. Rev*., 1992, **119,** 89.
13. Uchida, K., Soma, M., Onishi, T. and Tamaru, K., *J. Chem. Soc. Faraday Trans*. 1, 1979, **75,** 2839.
14. Zilbermann, I., Hayon, J., Katchalski, T., Raveh, O., Rishpon, J., Shames, A. I. and Bettelheim, A., *J. Electrochem. Soc*., 1997, **144,** L228.
15. Nyokong, T., *J. Chem. Soc. Dalton Trans*., 1993, 3601.
16. Li, J.-Z., Pang, X.-Y. and Yu, R.-Q., *Anal. Chim. Acta*, 1994, **297,** 437.
17. Mesároš, Š., Grunfeld, S., Mesárošova, A., Bustin, D. and Malinski, T., *Anal. Chim. Acta*, 1997, **339,** 265.
18. Malinski, T., Taha, Z., Grunfeld, S., Burewicz, A. and Tomboulian, P., *Anal. Chim. Acta*, 1993, **279,** 135.
19. Trévin, S., Bedioui, F. and Devynck, J., *Talanta*, 1996, **43,** 303.
20. Hayon, J., Ozer, D., Rishpon, J. and Bettelheim, A., *J. Chem. Soc. Chem. Comm*., 1994, 619.
21. Bedioui, F., Trevin, S., Albin, V., Villegas, M. G. G. and Devynck, J., *Anal. Chim. Acta*, 1997, **341,** 177.
22. Malinski, T. and Taha, Z., *Nature*, 1992, **358,** 676.
23. Trévin, S., Bedioui, F. and Devynck, J., *J. Electroanal. Chem*., 1996, **408,** 261.
24. Ciszewski, A., Kubaszewski, E., Łożyński, M., *Electroanalysis*, 1996, **8,** 293.
25. Yu, A.-M., Zhang, H.-L. and Chen, H.-Y., *Anal. Lett*., 1997, **30,** 1013.
26. Yu, C.-H. and Su, Y. O., *J. Electroanal. Chem*., 1994, **368,** 323.
27. Ogura, K. and Yamasaki, S., *J. Appl. Electrochem*., 1985, **15,** 279.
28. Bassett, J., Denney, R. C., Jeffery, G. H. and Mendham, J., *Vogel's Textbook of Quantitative Inorganic analysis*, Longman, New York, 1981.
29. Stillman, M. J. and Nyokong, T., in *Phthalocyanines*: *Properties and Applications*, ed. C. C. Leznoff and A. B. P. Lever, VCH, New York, 1989.
30. Richter-Addo, G. B., Hodge, S. J., Yi, G. B., Khan, M. A., Ma, T., Caemelbacke, E. V., Guo, N. and Kadish, K. M., *Inorg. Chem*., 1996, **35,** 6530.
31. Ascenzi, P., Brunori, M., Pennesi, P., Ercolani, C. and Monacelli, F., *J. Chem. Soc. Dalton Trans*., 1990, 105.
32. Nyokong, T., *Polyhedron*, 1995, **14,** 2325.
33. Lever, A. B. P., Milaeva, E. R. and Speier, G., in *Phthalocyanines*: *properties and applications*, ed. C. C. Leznoff and A. B. P. Lever, Vol. 3, VCH, New York, 1993.

Pergamon

Polyhedron Vol. 17, Nos. 25, 26, pp. 4425–4431, 1998
© 1998 Elsevier Science Ltd
All rights reserved. Printed in Great Britain
0277–5387/98 $19.00+0.00

PII: S0277–5387(98)00248–4

Synthesis and X-ray crystal structures of new trirhenium nonachloride chalcogenide clusters

Robert W. McGaff, Randy K. Hayashi, Douglas R. Powell and Paul M. Treichel*

Department of Chemistry, University of Wisconsin-Madison, 1101 University Avenue, Madison, WI 53706, U.S.A.

(Received 21 January 1998; accepted 2 June 1998)

Abstract—The acetone adduct of trirhenium nonachloride, $Re_3Cl_9(acet)_3$, where acet = acetone, reacts in acetone solution at room temperature with tetrabutylammonium chalcogenides $[N(C_4H_9)_4]_2E$, where E = S, Se and Te, producing the tetrabutylammonium salts of the new cluster anions $[Re_3(\mu_3\text{-}E)(\mu_2\text{-}Cl)_3Cl_6]^{2-}$. In the crystallographically determined structures of these compounds, triangles of rhenium atoms are capped by single chalcogen atoms, giving anions of near C_{3v} symmetry. The compound where E = S is also formed in the reaction of Re_3Cl_9 with $[N(C_4H_9)_4]_2[MoS_4]$ by sulfide transfer. © 1998 Elsevier Science Ltd. All rights reserved

Keywords: rhenium; metal clusters; sulfur; selenium; tellurium; crystal structures

INTRODUCTION

Our research efforts are centered on finding rational low- or ambient-temperature synthetic routes to Re(III) cluster compounds. To this end, we carried out the reaction of $Re_3Cl_9(acet)_3$ with the tetrathiomolybdate ion, $[MoS_4]^{2-}$, in acetone solution. Rather than isolating a Re–Mo mixed-metal cluster with bridging sulfide ligands, however, a previously unknown cluster dianion, $[Re_3(\mu_3\text{-}S)(\mu_2\text{-}Cl)_3Cl_6]^{2-}$ was obtained. This new species, isolated as a tetrabutylammonium salt, was formed via sulfide transfer from $[MoS_4]^{2-}$, well known behavior for this species.

The same dianion was then synthesized by the more logical direct reaction of $Re_3Cl_9(acet)_3$ with a stoichiometric amount of $[(C_4H_9)_4N]_2S$. Generalizing, this direct reaction was next used to synthesize other members of the homologous series of compounds $[(C_4H_9)_4N]_2$ $[Re_3(\mu_3\text{-}Se)(\mu_2\text{-}Cl)_3Cl_6]$, **2**, and $[(C_4H_9)_4N]_2[Re_3(\mu_3\text{-}Te)(\mu_2\text{-}Cl)_3Cl_6]$, **3**, using $[(C_4H_9)_4N]_2Se$ and $[(C_4H_9)_4N]_2Te$, respectively. This paper describes the synthesis and structural characterization of these three compounds.

* Author to whom correspondence should be addressed.

EXPERIMENTAL

Materials

Acetone was dried by refluxing over $CaSO_4$. Tetrahydrofuran and diethyl ether were dried by refluxing over Na/benzophenone. These solvents were distilled immediately prior to use. Sodium sulfide, ammonium tetrathiomolybdate (99.97%), selenium powder (100 mesh, 99.5%), trirhenium nonachloride, lithium (3.2 mm wire, 98%), tellurium powder (200 mesh), sodium and anhydrous ethanol were obtained from commercial sources and used as received. Tetra-*n*-butylammonium chloride monohydrate (98%) was obtained from a commercial source; prior to use, it was recrystallized twice from anhydrous ethanol/diethyl ether to remove as much water as possible. All manipulations were carried out under an atmosphere of dry nitrogen using standard Schlenk techniques [1].

Spectroscopic measurements

Electronic spectra were measured on a Cary 4Bio spectrophotometer. Matrix assisted laser desorption/ionization (MALDI) mass spectra were recorded on a Bruker Reflex II spectrometer equipped with a

N_2 laser operating with an accelerating voltage of -20 kV and a reflectron voltage of -21.2 kV. Spectra were obtained in the negative ion mode, using a dithranol matrix and are the sum of 50 shots. Samples for MALDI analysis were dissolved in acetone and then mixed with the matrix in tetrahydrofuran prior to deposition onto the target. Ion signals in the spectra were assigned based both on m/z values and distinctive isotopic patterns which accurately match calculated patterns. The relevant information from these spectra was the presence of a peak whose mass corresponded to the parent anionic mass lacking one Cl^-, $[M–Cl]^-$ (and the lack of any peaks at other masses that could be assigned to other clusters). The observed pattern was predicted based on ongoing MALDI studies in our group on anionic rhenium clusters [2].

Structure determination and refinement

Crystals used in the crystallographic study were mounted on glass fibers. Intensity data were collected at 133 K on a Siemens P4 diffractometer equipped with a CCD detector using phi scan frames with a range of 0.3° in phi. Graphite monochromated Mo-Kα radiation ($\lambda = 0.71069$ Å) was utilized. Absorption corrections were calculated by a semi-empirical method and applied to the data. Hydrogen atom positions were refined by use of a riding model. Data collection [3] and reduction [4] were accomplished on a Silicon Graphics computer using software standard in the crystallography laboratory at the University of Wisconsin-Madison. Structures were solved by direct methods and refined by full-matrix least-squares on F^2 using the SHELXTL Version 5 software [5]. Neutral atom scattering factors were taken from standard tables [6]. Other details regarding the crystallographic experiments are contained in Table 1.

Reaction of $[(C_4H_9)_4N]_2S$ *with* $Re_3Cl_9(acet)_3$

A 50 ml Schlenk flask was charged with 19.2 mg (0.246 mmol) Na_2S and 136.8 mg (0.526 mmol) $[(C_4H_9)_4N]Cl$. Acetone (20 ml) was added and the contents of the flask were stirred at room temperature for 1 h. Another 50 ml Schlenk flask was charged with a solution of $Re_3Cl_9(acet)_3$ (formed *in situ* from 215.9 mg (0.246 mmol) of $[Re_3Cl_9]_x$ and 20 ml of acetone) [7]. This solution was transferred by cannula into the flask containing the sulfide ion. The reaction mixture was stirred overnight (approximately 12 h). The solution was then filtered to separate a dark precipitate (discarded). The dark red–orange filtrate was concentrated to *ca.* 5 ml and then approximately 4 ml of the concentrated solution was filtered into a 22 mm O.D. Schlenk tube. The remaining solution was filtered into a 12 mm O.D. Schlenk tube. Both samples were layered carefully with diethyl ether. Over several days, dark red crystals formed in both tubes. Crystals of $[Bu_4N]_2[Re_3(\mu_3\text{-}S)(\mu_2\text{-}Cl)_3Cl_6]$, **1**, from the larger Schlenk tube were collected and weighed (95.2 mg). The estimated overall yield, correcting to account for the solution used for growing crystals for X-ray analysis was 34%. The MALDI mass spectrum of **1** contained a peak at $m/e = 874.4$ (calc. 874.6), corresponding to the parent ion minus one chloride ligand, $[Re_3Cl_8S]^{1-}$. The electronic spectrum of this sample contained peaks at 343 nm ($\varepsilon = 2800\ M^{-1}\ cm^{-1}$), 372 nm (sh), 470 nm ($\varepsilon = 1900\ M^{-1}\ cm^{-1}$) and 563 nm (sh).

Crystals of **1** from the smaller tube, containing one acetone molecule per formula unit, were used for an X-ray structural determination. Details regarding the crystallography and structure of **1** are contained in Tables 1–3; the structure of the anionic portion of **1** is shown in Fig. 1.

Reaction of $[(C_4H_9)_4N]_2Se$ *with* $Re_3Cl_9(acet)_3$

The same reaction conditions and workup procedures were used to prepare dark red crystalline $[(C_4H_9)_4N]_2[Re_3(\mu_3\text{-}Se)(\mu_2\text{-}Cl)_3Cl_6]$, **2**, from $Re_3Cl_9(acet)_3$ and $[(C_4H_9)_4N]_2Se$. The estimated yield was 20%. A literature method [8] was used to prepare Li_2Se, which was converted to $[(C_4H_9)_4N]_2Se$ by metathesis with $[(C_4H_9)_4N]Cl$. The MALDI mass spectrum of **2** contained a peak at $m/e = 920.8$ (calc. 920.5) corresponding to the parent ion minus one chloride ligand, $[Re_3Cl_8Se]^{1-}$. The electronic spectrum of this sample showed peaks at 329 nm ($\varepsilon = 13000\ M^{-1}\ cm^{-1}$), 372 nm (sh), 456 nm ($\varepsilon = 3400\ M^{-1}\ cm^{-1}$), and 541 nm (sh). Crystals of **2**, which also contain one acetone molecule per formula unit and belong to the same space group as **1**, were isolated. Details regarding the crystallographic experiment and structure of **2** are contained in Tables 1–3; the anionic portion of **2** is isostructural to the anion in **1**.

Reaction of $[(C_4H_9)_4N]_2Te$ *with* $Re_3Cl_9(acet)_3$

Similar reaction conditions and workup procedures were used to prepare **3** from $Re_3Cl_9(acet)_3$ and $[(C_4H_9)_4N]_2Te$. Li_2Te was synthesized by an adaptation of a published procedure [8], substituting lithium wire for potassium, and converted to $[(C_4H_9)_4N]_2Te$ by metathesis with $[(C_4H_9)_4N]Cl$. (A purple color in the reaction mixture indicated that there was some polytelluride in the solution.) Compound **3** did not crystallize as readily as **1** or **2**; most of the sample came out of solution as a thick paste. However, a few dark red crystals of $[(C_4H_9)_4N]_2[Re_3(\mu_3\text{-}Te)(\mu_2\text{-}Cl)_3Cl_6]$, **3**, were isolated. The MALDI mass spectrum of **3** showed a peak at $m/e = 970.6$ (calc. 970.5) corresponding to the parent ion minus one chloride ligand, $[Re_3Cl_8Te]^{1-}$. The electronic spectrum of this sample showed peaks at 338, 351 (sh), 457 and 547 nm (sh). Extinction coefficients were not measured for **3**, due to the small amount of pure sample.

Table 1. Crystal data for compounds **1**, **2** and **3**

Formula	$C_{32}H_{72}N_2Re_3Cl_9S(C_3H_6O)$	$C_{32}H_{72}N_2Re_3Cl_9Se(C_3H_6O)$	$C_{32}H_{72}N_2Re_3Cl_9Te$
Formula weight	1452.70	1499.60	1490.17
Crystal dimensions (mm)	$0.30\times0.25\times0.25$	$0.25\times0.25\times0.25$	$0.45\times0.20\times0.05$
Crystal color, habit	dark red prism	dark red prism	red plate
Crystal system	triclinic	triclinic	monoclinic
Space group	$P\bar{1}$	$P\bar{1}$	C2/c
a (Å)	11.0271(2)	11.1638(2)	36.7373(5)
b (Å)	12.6618(2)	12.7107(2)	14.5950(2)
c (Å)	20.3972(3)	20.3242(2)	19.3974(3)
α (°)	73.668(2)	74.187(2)	90
β (°)	75.260(2)	78.753(2)	110.462
γ (°)	77.150(2)	76.822(2)	90
V (Å^3)	2607.91(7)	2674.46(7)	9744.3(2)
Z	2	2	8
Peaks to determine cell	7386	8192	7838
Θ range for cell peaks (°)	3.0 to 25.0	3.0 to 25.0	3.0 to 25.0
μ (mm^{-1})	7.474	7.929	8.539
Θ range for data collection (°)	2.36 to 29.01	2.37 to 28.86	2.63 to 25.00
Scan time (s/frame)	20	30	30
Index ranges (h)	$-14\leqslant h\leqslant14$	$-14\leqslant h\leqslant13$	$-41\leqslant h\leqslant50$
Index ranges (k)	$-17\leqslant k\leqslant16$	$-17\leqslant k\leqslant16$	$-19\leqslant k\leqslant8$
Index ranges (l)	$-27\leqslant l\leqslant20$	$-20\leqslant l\leqslant27$	$-25\leqslant l\leqslant14$
Reflections collected	28162	28373	17499
Independent reflections	12261	12311	8254
Reflections with $I>2\sigma(I)$	9947	10584	6857
Restraints	92 (cation)	40 (cation)	15 (cation)
Parameters	460	460	422
Goodness-of-fit on F^2	1.038	1.087	1.052
Maximum transmission	0.357	0.493	0.264
Minimum transmission	0.274	0.358	0.133
$R1$ [$I>2\sigma(I)$]	0.0447	0.0509	0.1050
$wR2$ (all data)	0.1866	0.1249	0.2839
Largest difference peak (e Å^{-3})	2.709	3.190	12.589
Largest difference hole (e Å^{-3})	−2.986	−2.880	−2.624
Largest and mean Δ/esd	−0.002 and 0.000	−0.012 and 0.000	−0.014 and 0.001

Although the quality of the crystals of **3** was poor, it was possible to determine with certainty the presence of the core structure of three rhenium atoms capped by a tellurium atom in the anion. Crystals of **3** formed in the space group C2/c and did not contain solvent. Details regarding the crystallographic experiment and structure of **3** are contained in Tables 1–3. The anionic portion of **3** is isostructural to the anions in **1** and **2**.

Reaction of $[MoS_4]^{2-}$ *with* $Re_3Cl_9(acet)_3$

A 50 ml Schlenk flask was charged with 41.3 mg (0.159 mmol) $[NH_4]_2MoS_4$ and 54 mg (0.208 mmol) $[(C_4H_9)_4N]Cl$. Acetone (15 ml) was added to the flask and the contents were stirred at room temperature for 2 h, resulting in an orange–red solution and a white solid (presumably ammonium chloride). Another 50 ml Schlenk flask was charged with 140 mg (0.159 mmol) of $[Re_3Cl_9]_x$ and acetone (15 ml). After the solid dissolved, forming $Re_3Cl_9(acet)_3$, this solution was transferred by cannula into the flask containing the MoS_4^{2-}. The combined contents were allowed to stir overnight. A dark solid (discarded) was separated from the red–orange solution by filtration. Approximately 2 ml of this solution was transferred, using a filter-tipped cannula, into a Schlenk tube. Diethyl ether was carefully added in a layer above the solution. Dark red crystals of **1** formed on standing. Identification as compound **1** was verified by a match of unit cell data (space group $P\bar{1}$) with identical unit cell dimensions to the product obtained by the reaction described above). The yield of **1** in this reaction was low.

RESULTS AND DISCUSSION

The syntheses of compounds **1**, **2** and **3** were accomplished by the general reaction shown in eq. (1), where E = S, Se, or Te. These three compounds, dark

Table 2. Selected bond distances (Å) for compounds **1**, **2** and **3** (E = S, Se, or Te)

	$[Re_3Cl_9S]^{2-}$	$[Re_3Cl_9Se]^{2-}$	$[Re_3Cl_9Te]^{2-}$
Re(1)–Re(2)	2.4317(4)	2.4370(5)	2.418(1)
Re(1)–Re(3)	2.4337(4)	2.4341(4)	2.406(1)
Re(2)–Re(3)	2.4359(4)	2.4323(5)	2.408(1)
Re(1)–E(1)	2.419(2)	2.5559(8)	2.728(2)
Re(1)–Cl(1)	2.467(2)	2.474(2)	2.464(6)
Re(1)–Cl(2)	2.334(2)	2.340(2)	2.316(6)
Re(1)–Cl(3)	2.407(2)	2.416(2)	2.410(7)
Re(1)–Cl(9)	2.409(2)	2.410(2)	2.386(6)
Re(2)–E(1)	2.425(2)	2.5595(8)	2.718(2)
Re(2)–Cl(4)	2.434(2)	2.459(2)	2.445(7)
Re(2)–Cl(5)	2.314(2)	2.336(2)	2.312(7)
Re(2)–Cl(3)	2.409(2)	2.411(2)	2.425(8)
Re(2)–Cl(6)	2.414(2)	2.418(2)	2.394(8)
Re(3)–E(1)	2.419(2)	2.5527(8)	2.726(2)
Re(3)–Cl(7)	2.456(2)	2.467(2)	2.463(7)
Re(3)–Cl(8)	2.339(2)	2.343(2)	2.211(9)
Re(3)–Cl(6)	2.403(2)	2.413(2)	2.404(7)
Re(3)–Cl(9)	2.416(2)	2.418(2)	2.411(6)

red in color, were isolated in crystalline form and characterized by a combination of X-ray crystallography and mass spectrometry. Moderate yields of the first two compounds were obtained; however **3** was only obtained in low yield.

$$Re_3Cl_9(acet)_3 + [(C_4H_9)_4N]_2E \rightarrow [(C_4H_9)_4N]_2[Re_3(\mu_3\text{-}E)(\mu_3\text{-}Cl)_3Cl_6] + 3\text{acetone} \quad (1)$$

The synthetic procedure used here is viewed as well suited to the formation of these species: the chalcogenide ion's preferred mode of coordination is to bridge three metals, while the uncharged rhenium complex contains three weakly bonded and readily displaced acetone ligands.

The rhenium–chalcogen core of the anions in compounds **1**, **2** and **3** is isostructural; the structure of the anionic portion of **1** is shown in Fig. 1. The crystal lattices of both **1** and **2** contained acetone and crystals of both compounds are quite sensitive to solvent loss. Crystals of **3** were of poorer quality than those of **1** and **2**; thus, the *R* value for **3** is quite high. Still, there can be no doubt as to the core structure of the anion; that is, three rhenium atoms capped by a μ_3-Te atom. MALDI mass spectrometric results and the similarity of the electronic structure of **3** to those of **1** and **2** serve to further confirm the identity of **3**.

The anions in **1**, **2** and **3** with a triangle of rhenium atoms capped by the chalcogen atom have approximate C_{3v} symmetry. Similar to all other triangular clusters of rhenium (III), bridging chloride ions lie in the plane of the three metal atoms. Rhenium–rhenium distances are approximately 2.4 Å, typical of Re–Re double bonds (Ref. [9] and references therein). The average Re–chalcogen distance increases from 2.421 Å in **1** to 2.556 Å in **2** and 2.724 Å in **3**, a predictable variation based on atomic radii of the chalcogens. Lists of selected bond distances and angles are given in Tables 2–3, respectively. A complete listing of bond lengths and angles is given as supplementary material.

Rhenium(III) cluster species have been known for more than thirty years. Trirhenium clusters have been widely studied and many derivatives with this core structure have been reported [9, 10]. Thus the existence of a new series of compounds with relatively simple structures and their relatively straightforward synthesis, was surprising. Perhaps this is a consequence of the fact that derivatives of $[Re_3Cl_9]_x$ with sulfur ligands are not very common [9, 10].

Although **1**, **2** and **3** represent the first examples of triangular rhenium(III) halide clusters capped by single chalcogen atoms with halide ligands on all other rhenium positions, there are some interesting structural comparisons to be made with clusters of other nuclearities and with rhenium compounds in which the metals are in an oxidation state other than +3. A number of hexanuclear rhenium species having an octahedron of metal atoms with face bridging sulfide ions are known [10]. The species $Re_3S_7Cl_7$ [11], $Re_3S_7Cl_6AlCl_4$ [12] and $Re_3S_7Br_7$ [12] contain Re_3 triangles capped by sulfur atoms, but in contrast to **1**, **2** and **3**, rhenium atoms are in the +5 oxidation state in these species. In accordance with the higher oxidation state, longer Re–Re bonds in these clusters (about 2.7 Å) match single bond distances. Rhenium triangles capped by sulfur are also seen in the mixed valent, rhenium(III)–rhenium(IV) complex $Re_3S_4Br_3(PEt_3)_4$

Table 3. Selected bond angles (°) for compounds **1**, **2** and **3** (E = S, Se, or Te)

	$[Re_3Cl_9S]^{2-}$	$[Re_3Cl_9Se]^{2-}$	$[Re_3Cl_9Te]^{2-}$
Re(3)–Re(1)–Re(2)	60.09(1)	59.91(1)	59.90(4)
Re(1)–Re(2)–Re(3)	60.00(1)	59.99(1)	59.79(4)
Re(1)–Re(3)–Re(2)	59.92(1)	60.10(1)	60.31(4)
Re(1)–E(1)–Re(2)	60.27(4)	56.90(2)	52.74(2)
Re(1)–E(1)–Re(3)	60.40(5)	56.91(2)	52.35(4)
Re(2)–E(1)–Re(3)	60.38(4)	56.82(2)	52.52(4)
Re(1)–Cl(3)–Re(2)	60.66(4)	60.64(4)	60.0(2)
Cl(3)–Re(1)–Re(2)	59.70(5)	59.58(5)	60.3(2)
Cl(3)–Re(2)–Re(1)	59.64(5)	59.78(5)	59.7(2)
Re(2)–Cl(6)–Re(3)	60.76(5)	60.46(4)	60.3(2)
Cl(6)–Re(2)–Re(3)	59.39(5)	59.66(6)	60.1(2)
Cl(6)–Re(3)–Re(2)	59.85(5)	59.88(6)	59.6(2)
Re(3)–Cl(9)–Re(1)	60.58(5)	60.55(4)	60.2(1)
Cl(9)–Re(1)–Re(3)	59.83(5)	59.88(5)	60.4(2)
Cl(9)–Re(3)–Re(1)	59.58(4)	59.57(5)	59.4(2)
E(1)–Re(1)–Cl(1)	94.37(7)	94.62(7)	95.3(2)
E(1)–Re(1)–Cl(3)	88.90(7)	89.22(6)	88.4(2)
E(1)–Re(1)–Re(2)	59.99(4)	61.62(2)	63.42(4)
E(1)–Re(1)–Re(3)	59.81(4)	61.48(2)	63.77(4)
E(1)–Re(1)–Cl(9)	89.09(7)	89.07(6)	88.8(2)
Cl(2)–Re(1)–Cl(1)	90.38(8)	90.03(9)	87.4(3)
Cl(2)–Re(1)–Cl(3)	91.34(8)	90.2(1)	92.7(3)
Cl(2)–Re(1)–Re(2)	116.22(6)	114.18(7)	113.3(2)
Cl(2)–Re(1)–Re(3)	116.17(5)	114.97(7)	111.9(2)
Cl(2)–Re(1)–Cl(9)	90.74(7)	91.5(1)	90.4(3)
E(1)–Re(2)–Cl(4)	94.18(7)	94.50(7)	95.9(2)
E(1)–Re(2)–Cl(6)	89.51(7)	89.17(6)	89.6(2)
E(1)–Re(2)–Re(3)	59.70(4)	61.45(2)	63.91(4)
E(1)–Re(2)–Re(1)	59.74(5)	61.48(2)	63.86(4)
E(1)–Re(2)–Cl(3)	88.72(6)	89.24(6)	88.3(2)
Cl(5)–Re(2)–Cl(4)	89.56(8)	89.3(1)	88.7(3)
Cl(5)–Re(2)–Cl(6)	90.67(7)	91.1(1)	91.8(4)
Cl(5)–Re(2)–Re(3)	117.34(6)	115.53(8)	113.0(2)
Cl(5)–Re(2)–Re(1)	117.07(6)	115.24(7)	111.5(2)
Cl(5)–Re(2)–Cl(3)	91.10(7)	90.5(1)	90.4(3)
E(1)–Re(3)–Cl(7)	93.88(7)	94.35(6)	95.7(2)
E(1)–Re(3)–Cl(9)	88.94(6)	88.98(6)	88.3(2)
E(1)–Re(3)–Re(1)	59.79(5)	61.61(2)	63.88(4)
E(1)–Re(3)–Re(2)	59.92(4)	61.73(2)	63.58(4)
E(1)–Re(3)–Cl(6)	89.90(7)	89.44(7)	89.2(2)
Cl(8)–Re(3)–Cl(7)	89.82(7)	90.37(8)	92.2(3)
Cl(8)–Re(3)–Cl(9)	89.76(8)	90.0(1)	90.8(3)
Cl(8)–Re(3)–Re(1)	116.45(6)	113.90(7)	109.0(2)
Cl(8)–Re(3)–Re(2)	117.79(6)	114.95(8)	110.3(2)
Cl(8)–Re(3)–Cl(6)	91.41(9)	91.6(1)	91.8(3)

[13] and the rhenium(IV) complexes $Re_3S_4Cl_4(PEt_3)_3$ [13], and $Re_3NiS_4Cl_6(PEt_3)_4$ [14]. Capping oxygen atoms on rhenium triangles are observed in the crystallographically determined structures of the organometallic compounds $[NEt_4]_2[Re_3H_3(\mu_3\text{-}O)(CO)_9]$ [15], $[NEt_4][Re_3H_3(\mu_3\text{-}OH)(CO)_9]$ [16] (which exists as a hydrogen-bonded trimethylamine adduct), and $[NEt_4][Re_3H_3(\mu_3\text{-}OEt)(CO)_9]$ [17]. A capping sulfur atom occurs in the structure of the triangular organometallic rhenium compound $[NEt_4][Re_3H_3(\mu_3\text{-}SBu^t)(CO)_9]$ [18]. In these compounds Re–Re distances of 2.7–3 Å are found, corresponding to single bonds between rhenium atoms. Triangular rhenium complexes with capping selenium and tellurium atoms have not been structurally characterized before this report.

As noted in Section 1, compound **1** was also prepared by the reaction of $[(C_4H_9)_4N]_2[MoS_4]$ with

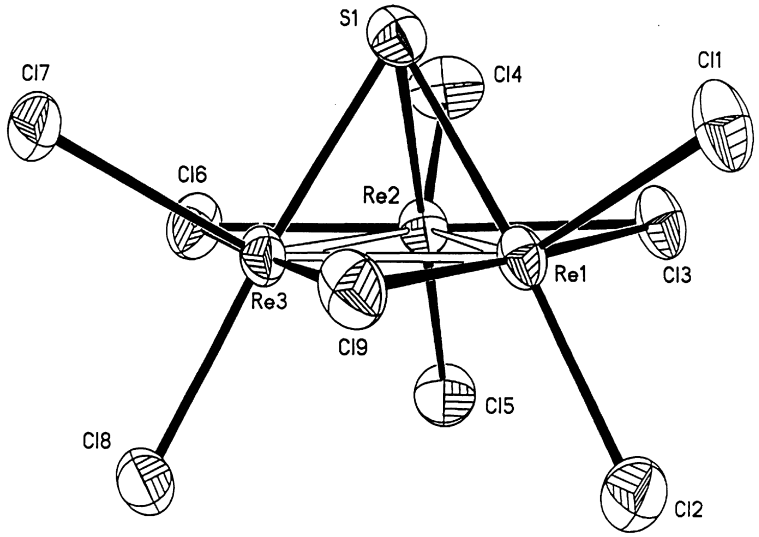

Fig. 1. The crystallographically determined structure of the anion in **1**.

$Re_3Cl_9(acet)_3$ eq. (2). Donation of sulfide ion is one of the general reaction types known for $[MoS_4]^{2-}$.

$$Re_3Cl_9(acet)_3 + [(C_4H_9)_4N]_2[MoS_4] \rightarrow [(C_4H_9)_4N]_2[Re_3(\mu_3\text{-}S)(\mu_2\text{-}Cl)_3Cl_6] + \text{byprod.} \quad (2)$$

Analogous reactions include those of $[NH_4]_2[MoS_4]$ with sulfates of copper, nickel and cobalt to produce mixtures of the corresponding metal sulfides and MoS_3 [19]. Other examples of this reaction type are seen in the hydrolysis of $[NH_4]_2[MoS_4]$ to give MoS_3, NH_4OH and H_2S [20, 21] and in the reaction of $[MoS_4]^{2-}$ with H^+ to give MoS_3 and HS^- as products [21].

Supplementary material available: crystal data, structure refinement description, data collection parameters, complete listing of atomic coordinates, thermal displacement parameters (isotropic and anisotropic), bond lengths and angles and torsion angles for **1**, **2** and **3**.

Acknowledgements—We wish to acknowledge Research Corporation for support of this work. We also acknowledge the NSF (Grants CHE-9310428 and CHE-9520868) and the University of Wisconsin-Madison for major instrumentation grants. Additionally, we thank Nancy Carter Dopke for assistance in obtaining MALDI mass spectra.

REFERENCES

1. Shriver, D. F. and Drezdzon, M. A., *The Manipulation of Air Sensitive Compounds*, 2nd edn. Wiley, New York, 1986.
2. Dopke, N. C., Treichel, P. M. and Vestling, M. M., *Inorg. Chem.*, 1998, **37,** 1272.
3. *SMART Software Reference Manual*. Siemens Analytical X-ray Instruments, 6300 Enterprise Dr., Madison, WI 53719-1173, U.S.A., 1994.
4. *SAINT Version* 4 *Software Reference Manual*. Siemens Analytical X-ray Instruments, 6300 Enterprise Dr., Madison, WI 53719-1173, U.S.A., 1995.
5. Sheldrick, G. M., *SHELXTL Version* 5 *Reference Manual*. Siemens Analytical X-ray Instruments, 6300 Enterprise Dr., Madison, WI 53719-1173, U.S.A., 1994.
6. *International Tables for Crystallography*, Vol. C. Kluwer, Boston, 1995, Tables 6.1.1.4, 4.2.6.8 and 4.2.4.2, .
7. Cotton, F. A. and Mague, J. T., *Inorg. Chem.*, 1964, **3,** 1402.
8. Brauer, G. (ed.), *Handbook of Preparative Inorganic Chemistry*, 2nd edn. Academic Press, New York, 1963.
9. Cotton, F. A. and Walton, R. A., *Multiple Bonds between Metal Atoms*, 2nd edn. Clarendon Press, Oxford, 1993.
10. Lee, S. C. and Holm, R. H., *Angew. Chem. Int. Ed. Engl.*, 1990, **29,** 840.
11. Timoshchenko, N. N., Kolesnichenko, V. L., Volkov, S. V., Slovokhotov, Yu. L. and Struchkov, Yu. T., *Sov. J. Coord. Chem.*, 1991, **16,** 567 (English translation).
12. Aslanov, L. A., Volkov, S. V., Kolesnichenko, V. L., Mischanchuk, T. B., Rybakov, V. B. and Timoshchenko, N. I., *Sov. Prog. Chem.*, 1991, **57,** 1 (English translation).
13. Yamada, S., Miyake, N., Imoto, H. and Saito, T., *Chem. Lett.*, 1997, 671.
14. Miyake, N., Imoto, H. and Saito, T., *Chem. Lett.*, 1997, 631.
15. Ciani, G., Sironi, A. and Albano, V. G., *J. Chem. Soc. Dalton Trans.*, 1977, 1667.
16. Beringhelli, T., D'Alfonso, G., Freni, M., Ciani, G. and Molinari, H., *J. Organomet. Chem.*, 1986, **311,** 177.
17. Ciani, G., D'Alfonso, G., Freni, M., Romiti, P.

and Sironi, A., *J. Organomet. Chem.*, 1981, **219,** C23.
18. Bonfichi, R., Ciani, G., D'Alfonso, G., Romiti, P. and Sironi, A., *J. Organomet. Chem.*, 1982, **231,** C35.
19. Clark, G. M. and Doyle, W. P., *J. Inorg. Nucl. Chem.*, 1966, **28,** 381.
20. Bernard, J. C. and Tridot, G., *Bull. Soc. Chim. France*, 1961, 818.
21. Müller, A., Glemser, O., Diemann, E. and Hofmeister, H., *Z. Anorg. Allgem. Chem.*, 1969, **371,** 74.

Pergamon

Polyhedron Vol. 17, Nos. 25, 26, pp. 4433–4441, 1998
© 1998 Elsevier Science Ltd
All rights reserved. Printed in Great Britain
PII: S0277–5387(98)00249–6
0277–5387/98 $19.00 + 0.00

Complexation of cobalt(II), nickel(II), and zinc(II) ions with mono and binucleating azo compounds: A potentiometric and spectroscopic study in aqueous solution

Gabriela A. Ibañez and Graciela M. Escandar*

Departamento de Química Analítica, Facultad de Ciencias Bioquímicas y Farmacéuticas, Universidad Nacional de Rosario, Suipacha 531 (2000) Rosario, Argentina

(Received 21 January 1998; accepted 2 June 1998)

Abstract—The interaction of Co(II), Ni(II) and Zn(II) ions with a series of aromatic α-hydroxy azo compounds, 1,4-*bis*-*p*-sulfonylazo-2,3-dihydroxy naphthalene, 4-(2-hydroxy-1-phenylazo)-benzenesulfonate, 4-(2-hydroxy-1-naphthylazo)-benzenesulfonate, and 4-(9-hydroxy-10-phenanthrylazo)-benzenesulfonate, has been studied in aqueous solution. While both mono and binuclear chelates were found in the complex systems formed by the first azo compound, the existence of mononuclear chelates with different degrees of protonation was verified in the systems formed by the other ones. The equilibrium constants for all metal complexes were evaluated using a combination of potentiometric and spectrophotometric titration data. Within the mononucleating ligands, the magnitudes of the complexes equilibrium constants were to be found similar, even when their aromaticities are different. Both the metal coordination sites and the tautomeric structures of the ligand in each complex have been inferred through spectroscopic analysis. © 1998 Elsevier Science Ltd. All rights reserved

Keywords: coordination chemistry; spectroscopy and potentiometry; aromatic hydroxy azo compounds

INTRODUCTION

Azo compounds play an important role in analytical chemistry as chromogenic agents [1]. Furthermore, from a biological point of view, the study of the binding properties of organic chelating ligands containing both mono- and binucleanting aromatic α-hydroxy azo groups is significant due to their use as models for certain metal-enzyme interactions and also for the possible transport of metal ions in biological media [2–5]. Specifically, the study of binuclear complexes for developing small model compounds for the active sites of biomolecules may contribute to the better understanding of the original systems [6]. On the other hand, it has been proved that polydentate chelating agents can remove the metal ions from metalloenzymes through the formation of ternary complexes between the metal, the ligand and the apoenzyme. As an example, the inhibition of carbonic anhydrase by acetazolamide which is able to bind Zn(II) ion can be cited [7]. A substantial number of works have been performed, in the solid state and in solvent mixtures, with both Schiff bases and aromatic hydrazones which are structurally related with the presently studied compounds [2, 3]. However, azo compounds have the advantage of being soluble and stable in water solutions, allowing a more suitable understanding of biological processes [7]. We have previously reported a study of the coordination abilities of aromatic α-hydroxy azo compounds towards the copper (II) ion [8, 9]. We have now extended the study to other transition metal ions of interest, such as bivalent Co(II), Ni(II) and Zn(II). Specifically, the ligands analyzed are: 1,4-*bis*-*p*-sulfonylazo-2,3-dihydroxy naphthalene (SADN), 4-(2-hydroxy-1-phenylazo)-benzenesulfonate (HPBS), 4-(2-hydroxy-1-naphthylazo)-benzenesulfonate (HNBS) and 4-(9-hydroxy-10-phenanthrylazo)-benzenesulfonate (HPTBS) (Scheme 1). These compounds show interesting prototropic properties and are represented in Scheme 1 in their more stable tautomeric forms [8, 9].

* Author to whom correspondence should be addressed.

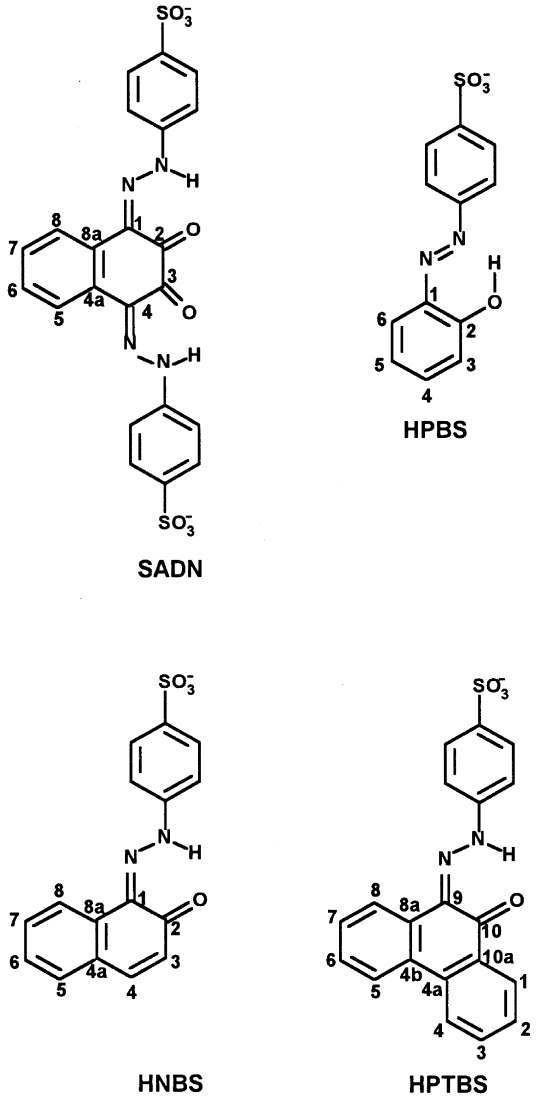

Scheme 1.

The study has been carried out taking into account the tautomeric properties of these ligands and correlating them with their chelating behavior.

EXPERIMENTAL

Reagents

The ligands were prepared as previously described, using standard procedures [8–10]. Their purities were checked by elemental analysis, ^{1}H NMR and potentiometric titrations. Stock solutions of about 0.01 M of Zn(II), Co(II) and Ni(II) were prepared by dissolving the corresponding nitrates (AR) in doubly distilled water. The metal concentrations were determined by titrations with previously standardized ethylenediamine-N,N,N′,N′-tetraacetic acid solution in the presence of appropriate indicators [11]. Solutions of carbonate-free NaOH and HNO_3 were standardized against potassium hydrogenphthalate and sodium carbonate, respectively.

Potentiometric equipment and measurements

Potentiometric titrations were carried out under nitrogen atmosphere at 20.0 ± 0.1°C, with the ionic strength (μ) adjusted to 0.10 M with $NaNO_3$. Prior to each experiment, the Metrohm 713 pH meter used was fitted with glass and reference electrodes and calibrated to read pH directly with freshly prepared solutions of standard HNO_3, standard NaOH and standard acetic acid. Thus, the term pH is in this work defined as $-\log[H^+]$. The initial concentrations of metal and ligand in the 1:1 system were in the range 7×10^{-4}–1×10^{-3} M. In the solutions used to investigate 1:2 and 2:1 metal–ligand ratios the concentrations of ligand or metal were doubled, as required. Equilibrium pH values were determined at every incremental addition of NaOH or HNO_3 to the experimental solutions. For each system three or more replicate measurements were carried out. Since the complexes studied were not fully formed at low pH, their stability constants could be determined by potentiometric titrations without the need of using competitive methods. The computational program for processing the potentiometric data was Best [12]. The selection of the chemical model for each investigated system was done according to previously known similar systems. Refinements were considered satisfactory when the value of σ_{fit} was lower than 0.04 [13]. Standard deviations for the reported constants refer only to random errors [14].

Spectrophotometric determinations

These measurements were performed with a Beckman DU 640 spectrophotometer, using 1.00 cm quartz microcells, at 20.0°C and $\mu = 0.10$ M ($NaNO_3$). The initial concentrations of metal and ligand in the 1:1 system were in the range 1×10^{-5}–6×10^{-5} M. Conformity of Beer's law was verified in all cases. In the experimental solutions employed to investigate 1:2 and 2:1 metal–ligand ratios the concentrations of ligand or metal were doubled, as required. The spectrophotometric titrations were carried out following procedures which are described in detail elsewhere [9]. Briefly, small increments of NaOH *ca.* 0.02 M were added to the nitrogen bubbled solution, which contained the metal and ligand in the corresponding ratio. For each pH point a known aliquot of solution was extracted and the absorption spectrum was read. The obtained profile of absorbances at the wavelength of the absorption maximum vs pH in each run was used to calculate the equilibrium constants of the complexes formed in each system. These calculations were performed with the aid of the program Epsilon

(FTP://WWW.FBIOYF.UNR.EDU.AR/CIENTIFICO/QUIMICA.ZIP) [15]. Standard deviations for the reported constant values refer only to random errors [14].

The hydrolysis constants for the investigated cations were calculated from the data of Baes and Mesmer [16]. The log of the overall metal hydrolysis constants used in both potentiometric and spectrophotometric computations were:

$K_{ZnH_{-1}} = -9.15$, $K_{Zn_2H_{-1}} = -8.89$, $K_{ZnH_{-3}} = -28.4$, $K_{ZnH_{-4}} = -40.7$, $K_{CoH_{-1}} = -9.85$, $K_{Co_2H_{-1}} = -10.95$, $K_{CoH_{-3}} = -31.5$, $K_{CoH_{-4}} = -45.8$, $K_{NiH_{-1}} = -10.06$, $K_{Ni_2H_{-1}} = -10.45$, $K_{NiH_{-3}} = -30.0$, $K_{NiH_{-4}} = -43.5$.

All these values correspond to 25°C and $\mu = 0.10$ M. The log K_w value used throughout this work was -13.87 (20°C, $\mu = 0.10$ M) [16].

RESULTS AND DISCUSSION

The values of both the deprotonation constants and extinction coefficients for the ligands studied in this work were those previously reported [8, 9] and are summarized in Table 1. The equilibrium constant values for the complexes formed in each system are listed in Table 2 and are discussed below. They were evaluated spectrophotometrically at wavelengths which are similar to those in the corresponding deprotonation constant determinations.

SADN systems

While potentiometry may be considered as the most accurate method for the evaluation of complex equilibrium constants, spectrophotometric determinations are useful when the former cannot be employed, for example when insoluble species are formed at the concentrations typical of potentiometric techniques [17]. However, if the spectrophotometric method is applied, certain intrinsic limitations should be taken into account, namely the fact that association reactions are not favored at low concentrations, and therefore that the species found may be different that those detected at higher metal–ligand concentrations. Further, the errors associated with the formation constants calculated from spectrophotometric data are larger than those obtained from potentiometry [15]. On the other hand, there are advantages from a qualitative point of view, since the spectra of the complex systems are informative with respect to the structure of the complexes formed.

Conforming to the position of the binding groups of SADN, both mono- and binuclear species could be formed. The study of mononuclear complexes should be the first step to evaluating binuclear chelates. In general, the experimental data from both potentiometric and spectrophotometric titrations in the mononucleating SADN systems could be described by considering eqns (1)–(3):

$$M^{2+} + H_2L^{2-} = [ML]^{2-} + 2H^+ \quad (1)$$

$$M^{2+} + H_2L^{2-} = [MH_{-1}L]^{3-} + 3H^+ \quad (2)$$

$$M^{2+} + H_2L^{2-} = [MH_{-2}L]^{4-} + 4H^+. \quad (3)$$

Notice that negative charges for the ligand (H_2L^{2-}) correspond to those of sulfonate groups, and that H_{-n} represents the protons released upon complex formation, in addition to those of the ligand. On the other hand, the equilibria implicated in the binuclear complexes formation can be, in general, represented by eqns (4) and (5):

$$2M^{2+} + H_2L^{2-} = [M_2L] + 2H^+ \quad (4)$$

$$2M^{2+} + H_2L^{2-} = [M_2H_{-2}L]^{2-} + 4H^+. \quad (5)$$

In addition to these reactions, deprotonation of $[M_2H_{-2}L]^{2-}$ may occur at very high pH. The presence of these binuclear complexes is not only required by the refinement, but by the fact that hydroxide precipitation is not observed in alkaline media in neither

Table 1. Deprotonation constants and spectral characteristics of the studied compounds[a]

Compounds	log K	ε ($M^{-1}cm^{-1}$)[b]			
		H_2L^{-2}	HL^{-3}	HL^-	L^{2-}
SADN[c]	−10.24	22400 (402)	10000 (402)		
	−12.66				
HPBS[d]	−2.02				
	−8.11			25400 (351)	5500 (351)
HNBS[d]	−11.28			21300 (483)	10300 (483)
HPTBS[d]	−12.7			21800 (478)	11400 (478)

[a] Values at 20.0°C and 0.10 M ionic strength ($NaNO_3$).
[b] Wavelengths between parenthesis.
[c] Ref. [8].
[d] Ref. [9].

Table 2. Log of equilibrium constant values for metal complexes, $\mu = 0.10$ M ($NaNO_3$), $t = 20.0$ °C[a]

Ligand	Quotient	Co(II)		Ni(II)		Zn(II)		Cu(II)[b]
		P	*S*	*P*	*S*	*P*	*S*	
SADN (H_2L)	$[H]^2[ML]/[M][H_2L]$	−12.88(0.02)	−12.88(0.04)	−11.26(0.02)	−11.4(0.1)	−12.12(0.04)	−12.9(0.3)	−5.91
	$[H]^3[MH_{-1}L]/[M][H_2L]$	−23.69(0.04)		−22.8(0.2)		−20.35(0.04)		
	$[H]^4[MH_{-2}L]/[M][H_2L]$					−31.4(0.1)		
	$[H]^2[M_2L]/[M]^2[H_2L]$	−9.32(0.02)		−7.92(0.02)				−2.74
	$[H]^4[M_2H_{-2}L]/[M]^2[H_2L]$	−27.11(0.02)		−25.51(0.03)		−25.32(0.05)		−15.62
	$[H]^5[M_2H_{-3}L]/[M]^2[H_2L]$					−36.4(0.2)		
HPBS (HL)	$[H][ML]/[M][HL]$			−5.36(0.01)				
	$[H]^2[MH_{-1}L]/[M][HL]$			−14.1(0.1)		−13.0(0.1)		−7.8
HNBS (HL)	$[H][ML]/[M][HL]$	−5.08(0.04)						−2.71
	$[H]^2[MH_{-1}L]/[M][HL]$	−13.75(0.03)	−14.1(0.1)		−14.0(0.1)	−12.07(0.02)		−7.60
HPTBS (HL)	$[H]^2[MH_{-1}L]/[M][HL]$		−13.8(0.1)		see text		−11.6(0.1)	−7.2

[a] Charges are omitted, random error between parenthesis. [b] From Refs [8, 9]. *P* = potentiometry. *S* = spectrophotometry.

of the studied metallic systems. It is necessary to point out that the binuclear complexes were only detected in potentiometric concentrations.

Co(II)

The potentiometric equilibrium profile of pH vs *a* (*a*: mol of base added per mol of ligand) for the 1:1 Co(II)–SADN system, shown in Fig. 1, shows one break at $a = 2$, which is followed by a flattening of the curve. The reverse curve displayed a similar behavior. The curve could only be satisfactorily fitted by considering both $[CoL]^{2-}$ and $[CoH_{-1}L]^{3-}$ species formation (Table 2). In the spectrophotometric titration experiments only $[CoL]^{2-}$ was found. According to the species distribution for this system, the latter complex begins to form at pH 8 and reaches a maximum of 95% at pH 11. With the purpose of obtaining structural information, the complex spectrum was analyzed. An absorption corrected spectrum at pH 11 was obtained by subtracting from the latter the spectrum of the ligand at the same pH and at the corresponding free concentration of SADN (Fig. 2). The resulting spectrum resembles that of SADN in the diketo tautomer, with an absorption band at 530 nm [8]. In principle, two different deprotonation schemes may be proposed for the ligand in $[CoL]^{2-}$. If the ligand releases one proton, and a coordinated water molecule the other one, the most probable structure is **f** (Scheme 2). On the other hand, if the ligand loses both protons, the fully deprotonated structure of the chelating agent in the complex would be **k** (Scheme 2). According to these statements, the structures A and B of Scheme 3 represent feasible coordinations for Co(II) in the $[CoL]^{2-}$ species. Because a high metal coordination would involve a strong steric strain, as in other metal systems formed by related compounds, a tetracoordinated metal ion is suggested [3, 8].

The potentiometric curve corresponding to the 2:1 metal–ligand system exhibits two inflections (Fig. 1), the first at $a = 2$ and the second one at $a = 4$. These results could be explained on the basis of the formation of analogous binuclear complexes proposed above for the Cu(II)–SADN system (i.e., $[M_2L]^{2-}$ and $[M_2H_{-2}L]^{4-}$) [8]. The complexes being more stable in the latter case. As previously mentioned, in the 2:1 system and under spectrophotometric conditions, only the 1:1 complex was found.

Ni(II)

In both 1:1 and 2:1 potentiometric systems, the behavior of Ni(II) ion towards SADN is similar to that of Co(II) ion (Fig. 1 and Table 2). The $[NiL]^{2-}$ complex is also detected in the 1:1 system from spectrophotometric data. Its structure was analyzed according to the spectrum at pH 11, in the similar way to the Co(II) complex. In this case, the spectrum (Fig.

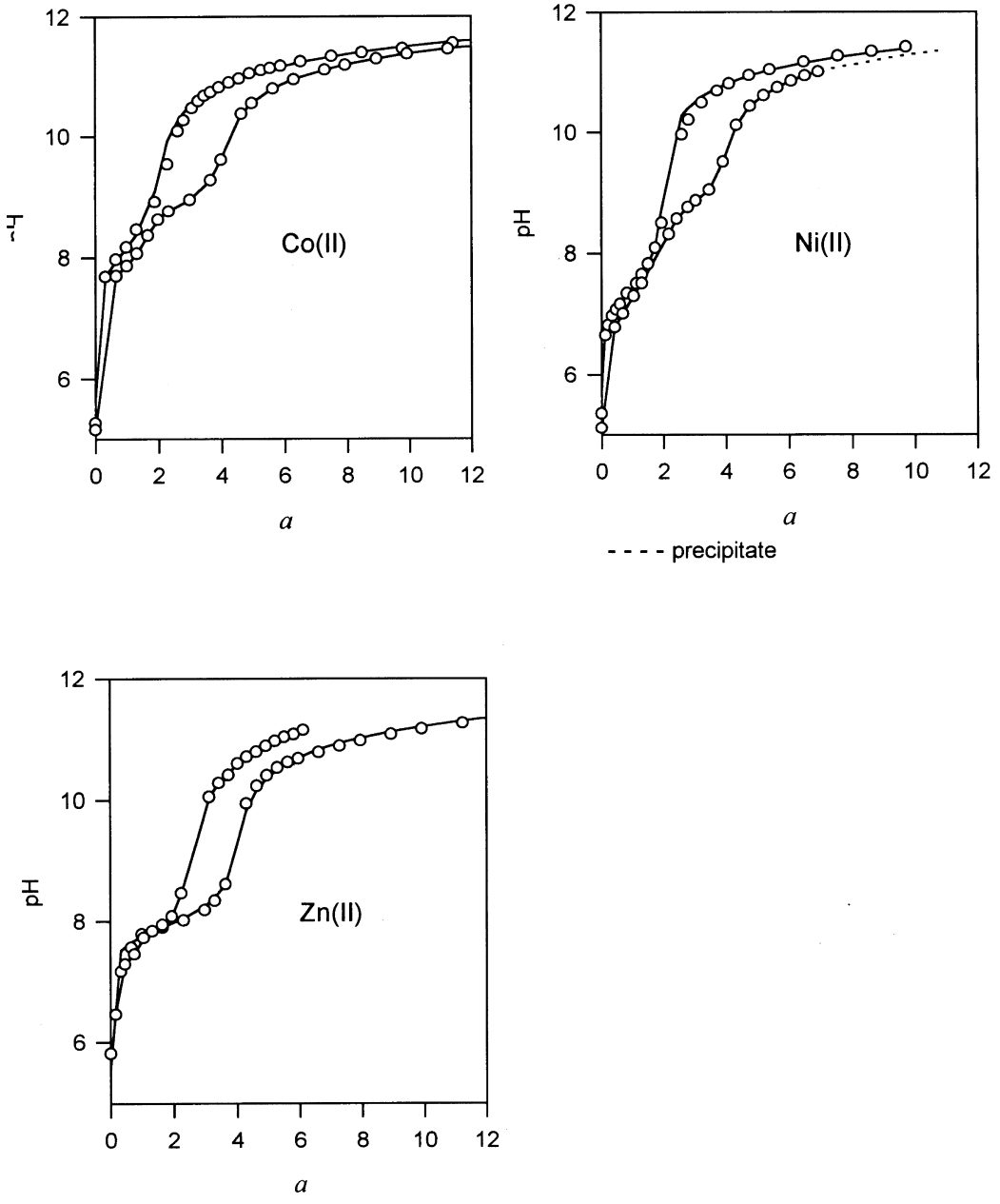

Fig. 1. Comparison of experimental (○) and calculated (———) pH values vs a (moles of base per mol of ligand or cation) in the case of 1:1 and 2:1 metal–SADN systems.

2) displays an absorption band at 548 nm (corresponding to either structure A or B of Scheme 3) and a shoulder at 430 nm. This shoulder could be related with a slight contribution of a dicatecholate-type structure.

Zn(II)

A typical potentiometric profile corresponding to a 1:1 Zn(II)–SADN system is presented in Fig. 1, along with the calculated pH values. In contrast to the Co(II) and Ni(II) systems, this curve presents an inflection at $a=3$, and the flattening beyond this value suggests an additional equilibrium corresponding to the formation of a more deprotonated complex. Therefore, the discrepancies between the measured and calculated pH values were minimized by considering the species $[ZnL]^{-2}$, $[ZnH_{-1}L]^{-3}$ and $[ZnH_{-2}L]^{-4}$. Only the $[ZnL]^{-2}$ complex was spectrophotometrically detected, between pH 8 and 10.5, in concentrations not higher than 67% with respect to the total metal

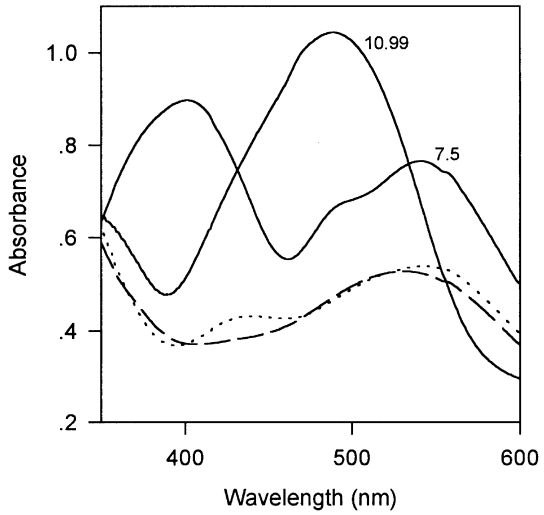

Fig. 2. Absorption spectra of: (———) SADN (H_2L) at indicated pH values ($C = 4.09 \times 10^{-5}$ M), (- - -) $[CoL]^{2-}$ ($C = 3.58 \times 10^{-5}$ M) and (· · ·) $[NiL]^{2-}$ ($C = 3.71 \times 10^{-5}$ M).

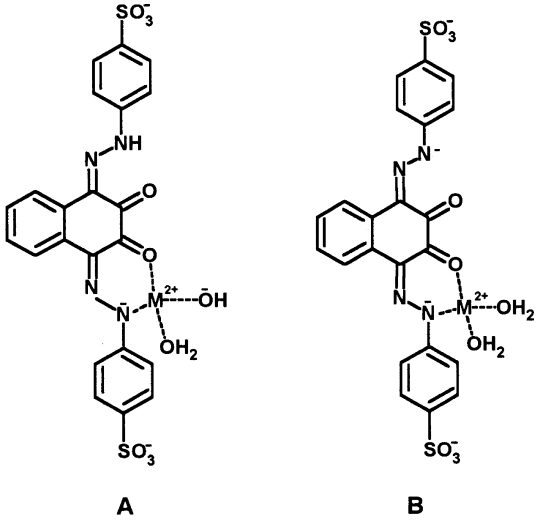

Scheme 3.

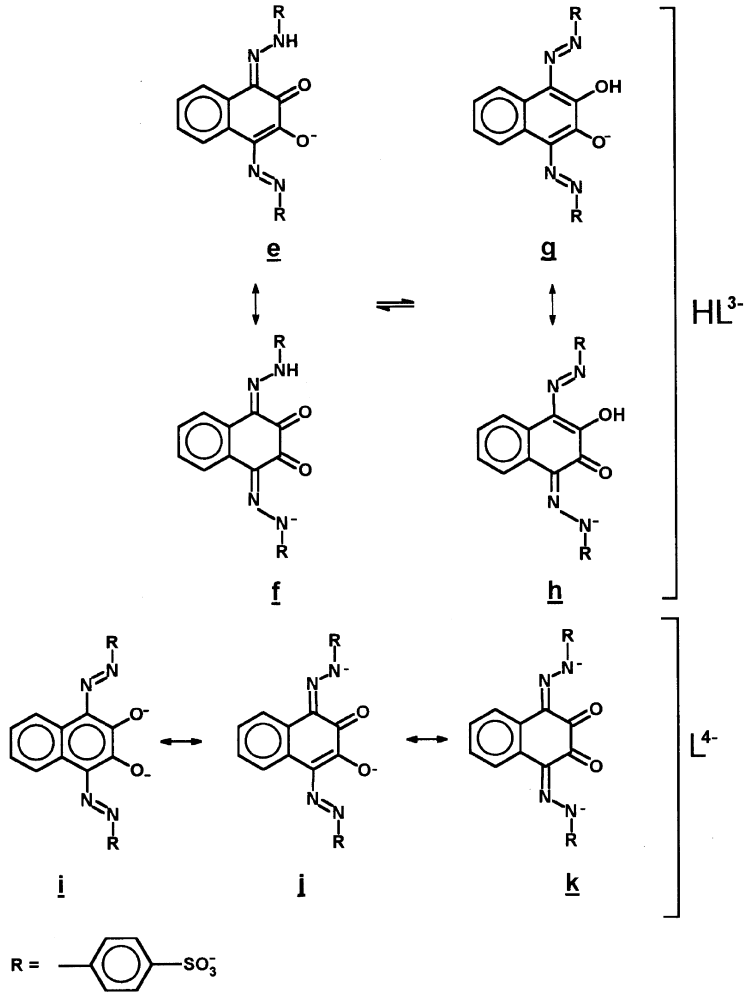

Scheme 2.

concentration. At pH higher than 11 the hydrolytic species are dominant, and the spectra correspond to those of free ligand in its monoprotonated keto–enol form (Fig. 2).

The potentiometric profile for a typical 2:1 Zn(II)–SADN solution (Fig. 1), is also different than those in the analogous Co(II) and Ni(II) systems. It only shows a jump at $a=4$. In this case the species found were $[Zn_2H_{-2}L]^{2-}$ and $[Zn_2H_{-3}L]^{3-}$. Although a structural analysis cannot be performed due to the dominance of hydrolytic species at high pH, it is likely that both in mononuclear and binuclear zinc complexes the coordination would take place with N(1) and one of the aromatic oxygen atoms. Because the metal ions here analyzed are "borderline" cations, they should be preferentially complexed by "borderline" bases, such as unsaturated nitrogen donors rather than negatively charged oxygen donors [18]. Furthermore, this type of coordination provides additional stabilization by a six membered ring formation.

HPBS, HNBS and HPTBS systems

The complexes formation in these mononucleating systems would involve the following equilibria:

$$M^{2+}+HL^{-}=[ML]+H^{+} \quad (6)$$

$$M^{2+}+HL^{-}=[MH_{-1}L]^{-}+2H^{+} \quad (7)$$

$$M^{2+}+HL^{-}=[MH_{-2}L]^{2-}+3H^{+}. \quad (8)$$

Again, the negative charge on the ligand represents that of the sulfonate group. The species formed resemble those of the mononuclear complexes of SADN. However, it should be taken into account that the same chelate stoichiometries do not necessarily correspond to the same structures, since SADN has an additional ligand proton.

The first mole of the released proton (eqn (6)) can be attributed to dissociation of the ligand. According to the azocompound analyzed, this H may have more phenolic or hydrazonic character (Scheme 1). The additional protons might be attributed to the deprotonation of water molecules coordinated to the metal. In each system, the presence of either of the above mentioned equilibria should be related with both the hydrolytic tendency of the metal and with the characteristics of the coordinating compound. In neither case was there any indication of the formation of 1:2 metal–ligand complexes.

Co(II)

While no complexation was detected in the Co(II)–HPBS systems in our working conditions, complex formation was found when the ligand was HNBS. The species formed are insoluble at the concentrations used in the 1:1 metal–ligand potentiometric experiments, even at low pH. However, on using higher ligand to metal ratios, and performing reverse titrations, no solid was observed. The solution appears to be stable, yet supersaturated with respect to the insoluble species. Therefore, and according to the suggestion of Martell [19], the data were considered as corresponding to equilibrium and the constant values were determined (Table 2). A precipitate slowly formed after the experiment. As can be appreciated, two complexes were found: [CoL] and $[CoH_{-1}L]^{-}$. The previously mentioned solid phase is ascribed to the latter complex, with the negative charge of the sulfonate group being neutralized with a counter-ion of the supporting electrolyte.

The spectrophotometric curves at different values of pH for the 1:1 Co–HNBS system exhibit isosbestic points (539 and 387 nm) above pH 9. Values of pH higher than 10.5 could not be analyzed because of the presence of a fine precipitate, even at the low concentrations used. From the profile of absorbance vs pH (Fig. 3) $[CoH_{-1}L]^{-}$ was found. The spectra also show that when the complex concentration is increased, the band at 483 nm (previously assigned to the keto form of HNBS) [9] decreases but does not shift. This fact suggests that the complexes formed would display a keto-hydrazonic structure, with the metal ion binding to N(1), to the lone pair electrons of the oxygen atom and to hydroxy groups from coordinated water molecules.

Due to the low solubility of the compound HPTBS, their systems could not be potentiometrically evaluated and therefore results from spectrophotometric determinations were obtained. The refinement of the spectrophotometric titration curves also indicates the presence of $[CoH_{-1}L]^{-}$ as the major species in alkaline

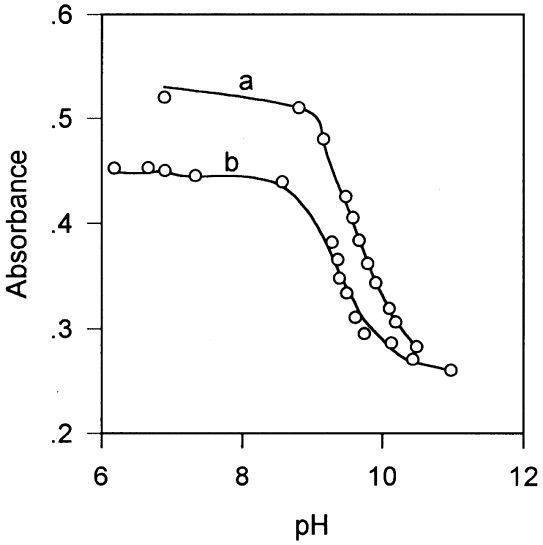

Fig. 3. Experimental (○) and calculated (———) absorbance values vs pH in (a) Co(II)–HNBS system, initial $C_{NHBS}=2.57\times10^{-5}$ M, initial $C_{Co}=2.53\times10^{-5}$ M; (b) Co(II)–HPTBS system, initial $C_{HPTBS}=2.06\times10^{-5}$ M, initial $C_{Co}=2.24\times10^{-5}$ M. $\mu=0.10$ M, $t=20.0$°C.

media. In this case the spectra also suggest a keto tautomer for the ligand in the complex, with a band at 478 nm [9].

Ni(II)

Ni(II) ion forms weak complexes with the phenolic derivative HPBS (Table 2), and $Ni(OH)_2$ precipitation is observed in basic media. No complexes were detected under spectrophotometric conditions.

Due to the insolubility of the systems, the complexes formed with both the naphtholic and phenanthrolic derivatives could not be potentiometrically studied. However, from spectrophotometric titrations, the species $[NiH_{-1}L]^-$ was found in the HNBS system. This species forms a fine precipitate above pH 10. The spectra show an isosbestic point at 528 nm above pH 9. This fact would be in accordance with the simultaneous presence of two absorbing species (protonated ligand and complex). These spectra also suggest a keto-hydrazonic structure for this complex.

In the Ni(II)–HPTBS system, the absorbance curves are modified above pH 8 with respect to that of the free ligand. This fact would be indicative of a complex formation, but a turbidity in the working solution at this point precluded the equilibrium constant determination.

Zn(II)

As in the Co(II) and Ni(II) systems, and according to both electrochemical and spectrophotometric data, the Zn(II) ion shows a weak interaction with HPBS. In the potentiometric experiment only the $[ZnH_{-1}L]^-$ complex was detected, reaching a maximum of 14% with respect to the total analytical metal ion concentration, before precipitation is observed at $pH \approx 7.6$. Since at this pH value the concentration of free Zn(II) ion is enough to form $Zn(OH)_2$, the solid phase is attributed to this latter species. At the low concentrations of reagents used in the spectrophotometric titration, no hydroxide formation was detected and zinc hydrolytic species are predominant at high pH. However, the low concentration of $[ZnH_{-1}L]^-$ complex does not allow us to determine spectrophotometrically its equilibrium constant, without incurring in large errors in the calculated value. For the same reason, the complex structure was not assigned.

The same type of complex was detected in the Zn(II)–HNBS system from potentiometric measurements. In this case the former is more stable with respect to that formed by the phenyl derivative, but this fact does not avoid hydroxide precipitation in alkaline media. Under spectrophotometric conditions, no complex formation was detected.

A stable $[ZnH_{-1}L]^-$ formed with HTPBS was spectrophotometrically found. This complex is the predominant species at alkaline medium and begins to precipitate at pH 10. Its structure, inferred from the spectra, is in agreement with a keto-hydrazonic form.

CONCLUSIONS

By using potentiometric and spectrophotometric methods, the interaction of a series of aromatic α-hydroxy azo compounds with bivalent metal ions of biological interest has been established. Thus, the equilibrium constants were evaluated, confirming the existence of chelates with different degrees of deprotonation. SADN forms mono- and binuclear complexes with the analyzed metal ions. In both types of complexes, the metal center would be bonded to a ligand oxygen, a nitrogen and hydroxyl groups. In the systems containing HPBS, HNBS and HPTBS, the formation of the $[MH_{-1}L]^-$ complex (insoluble at high concentrations) was always detected. The magnitudes of the complexes equilibrium constants are not significantly different within this series of compounds, even when the aromaticity increases in going from HPBS to HPTBS. Within the complexes, these ligands appear to exist in the keto-hydrazonic form, with the metal ion also coordinated to oxygen, nitrogen N(1) and hydroxyl groups. The equilibrium constant values for $[ML]^{2-}$ complexes of SADN are, for most systems, significantly larger than those for analogous $[MH_{-1}L]^-$ complexes of HNBS. This fact could be attributed to the presence of an additional aromatic oxygen in SADN, which favors a negative charge distribution over the other binding oxygen. It can be appreciated that the ligands herein studied form more stable complexes with the bivalent Cu(II) ion.

Acknowledgements—We thank University of Rosario and CONICET for financial support.

REFERENCES

1. Shibata, S. in *Chelates in Analytical Chemistry*, ed. Flaschka, H. and A. J. Barnard, Jr., Marcel Dekker, New York, 1972, vol. 4.
2. Costamagna, J., Vargas, J., Latorre, R., Alvarado, A. and Mena, G., *Coord. Chem. Rev.*, 1992, **119,** 67 and references therein.
3. Ledesma, G. N., Gonzalez Sierra, M. and Escandar, G. M., *Polyhedron*, 1998, **17,** 1517.
4. Fenton, D. E. in *Advances in Inorganic and Bioorganic Mechanisms*, ed. Sykes, A. J., Academic Press, London, 1983, vol. 2.
5. Crane, J. D., Fenton, D. E., Latour, J. M. and Smith, A. J., *J. Chem. Soc., Dalton Trans.*, 1991, 2979.
6. Göbel, M. W., *Angew. Chem. Int. Ed. Engl.*, 1994, **33,** 1141.
7. Burger, K. (ed.), *Biocoordination Chemistry: Coordination Equilibria in Biologically Active Systems*, Ellis Horwood, New York, 1990.
8. Ibañez, G. A., Olivieri, A. C. and Escandar, G. M., *J. Mol. Struc.*, 1997, **435,** 199.

9. Ibañez, G. A., Olivieri, A. C. and Escandar, G. M., *J. Chem. Soc. Faraday Trans*., 1997, **93,** 545.
10. Vogel, A. I., *Practical Organic Chemistry*, 3rd edn, Longmans, London, 1961, p. 625.
11. Schwarzenbach, G., *Complexometric Titrations*, Interscience, New York, 1960, pp. 78–79 and 83.
12. Martell A. E. and Motekaitis, R. J., *The Determination and Use of Stability Constants*, 2nd. edn., VCH, New York, 1992, p. 143.
13. Motekaitis, R. J. and Martell, A. E., *Can. J. Chem*., 1982, **60,** 2403.
14. Olivieri, A. C. and Escandar, G. M., *Anal. Lett*., 1997, **30,** 1967.
15. Araujo, C. L., Ibañez, G. A., Ledesma, G. N., Escandar, G. M. and Olivieri, A. C., *Computers Chem*., 1998, **22,** 161.
16. Baes, C. F., Jr. and Mesmer, R. E., *The Hydrolysis of Cations*, Robert E. Krieger Publishing Company, Malabar, FL, 1986.
17. Martell A. E. and Motekaitis, R. J., *The Determination and Use of Stability Constants*, 2nd. edn., VCH, New York, 1992, ch. 3.
18. Hancock, R. D. and Martell, A. E., *Chem. Rev*., 1989, **89,** 1875.
19. Martell A. E. and Motekaitis, R. J., *The Determination and Use of Stability Constants*, 2nd. edn., VCH, New York, 1992, p. 101.

Pergamon

Polyhedron Vol. 17, Nos. 25, 26, pp. 4443–4450, 1998
© 1998 Elsevier Science Ltd
All rights reserved. Printed in Great Britain
PII: S0277–5387(98)00250–2
0277–5387/98 $19.00+0.00

Convenient, rapid synthesis of rare earth orthochromites $LnCrO_3$ by self-propagating high-temperature synthesis

Maxim V. Kuznetsov[a] and Ivan. P. Parkin[b],*

[a] Department of Physics and Astronomy, University College London, Gower Street, London WC1E 6BT, U.K.

[b] Department of Chemistry, Christopher Ingold Laboratories, University College London, 20 Gordon Street, London WC1H OAJ, U.K.

(Received 13 May 1998; accepted 17 June 1998)

Abstract—Lanthanide orthochromites of general formula $LnCrO_3$ (Ln = La, Ce, Pr, Nd, Sm, Eu, Gd, Tb, Dy, Ho, Er, Tm, Tb, Lu) and $YCrO_3$ have been made by self-propagating high-temperature synthesis (SHS). Four different SHS reactions were found to form $LnCrO_3$: reaction of Ln_2O_3, Cr and CrO_3 with $NaClO_4$ or $Ba(ClO_4)_2$ in air; reaction of Ln_2O_3, Cr and CrO_3 in oxygen; reaction of $LnCl_3$, $CrCl_3$ and NaO_2 or Na_2O_2 in air and reaction of $Ln(NO_3)_3$, Cr and melamine in air. Reactions were studied by DTA and TGA experiments which showed exotherms and weight losses associated with the initiation temperatures (*ca.* 350°C) of the SHS reactions. Maximum reaction temperature T_c and propagation velocity U_c were measured for selected reactions. X-ray powder diffraction showed a single phase orthorhombic perovskite structure was produced in all reactions. Systematic changes in the lattice parameters, cell volume and pycnometrical densities were seen as a function of lanthanide atomic number. SHS prepared $LnCrO_3$ samples were all shown to be weak antiferromagnets. IR spectra for the $LnCrO_3$ materials showed bands at 635, 480, 440, 350 and 180 cm^{-1}. © 1998 Elsevier Science Ltd. All rights reserved

Keywords: lanthanide; orthochromite; SHS

INTRODUCTION

Lanthanide orthochromites have the general formula $LnCrO_3$ and adopt the perovskite crystal structure [1]. These materials have been widely studied as refractory conducting ceramics because of their electrical conductivity, oxidation resistance and high melting points (>2400°C). These properties have lead to applications in high-temperature furnace heating elements and interconnects in solid oxide fuel cells [2–5]. Substituted $LnCrO_3$ also show potential in gas sensing applications [6]. Lanthanide orthochromites have been made in air at 1200°C by combination of the appropriate metal oxides [7–9], however the process also involves multiple heating and regrinding steps to help overcome the solid state diffusion barrier. Alternative synthesis strategies have been employed including nitrate decomposition [10], hydrothermal reaction [11], co-precipitation [12], the hydrazine method [13] and decomposition of molecular precursors such as $La[Cr(CH_2(COO)_2)_3]$ [14]. All of these reactions give some improvement in synthesis time and product quality by allowing mixing of the precursors at the molecular level. These methods often involve multiple stages and the precursor always requires heating in a furnace to *ca.* 1200°C. We have shown that it is possible to form $LnCrO_3$ by a metathesis reaction [15],

$$LnCl_3 + CrCl_3 + 3Li_2O \rightarrow LnCrO_3 + 6LiCl. \quad (1)$$

This reaction is exothermic and is driven by the lattice energy of the coproduced lithium chloride. In this particular case the reaction required heating at 800°C for 2 h to produce $LnCrO_3$ and the reaction did not proceed with a synthesis wave or thermal flash. Solid state metathesis reactions have been utilised for the

* Author to whom correspondence should be addressed.

formation of a range of inorganic materials [16]. When the metathesis reaction is sufficiently exothermic, a powder of the green mixture can be ignited at one end with a heated filament. This produces a solid flame that moves out from the point of initiation through the whole material. Such reactions proceed in a matter of seconds, producing crystalline products which do not require furnace heating or further treatment other than simply washing with water to remove byproduct salt. Solid state metathesis reactions are a subclass of self-propagating high-temperature synthesis (SHS). SHS is a the name given to a general process where an exothermic chemical reaction replaces the requirement to heat the reagents; energy for the transformation primarily comes from the reaction enthalpy. SHS reactions are typically of the oxidation–reduction type, two well known examples are the thermite reaction ($Al+Fe_2O_3$), which produces iron metal and is used in welding, and the Goldsmidt reaction ($Al+Cr_2O_3$), which is used to form chromium metal [16]. Here we report the rapid synthesis of lanthanide and yttrium orthochromites by four different SHS reactions.

EXPERIMENTAL

All reagents were obtained from Aldrich (U.K.) and Saint Gobain (France) and used as supplied. Milling operations were carried out in a FRITSCH 05.102 ball mill (Germany) using Halsedon containers and balls. Combustion temperatures were measured using an optical pyrometer (Promin-M1) and tungsten–rhenium (5% and 20% Re) thermocouples. X-ray powder diffraction was performed on a DRON 3M spectrometer using Ni filtered $CuK_{\alpha 1}$ radiation ($\lambda = 1.54056$ Å). Phases were identified and indexed using the ASTM system. Pycnometrical densities were measured by standard methods using toluene; magnetic measurements were made on an EG&G PARC 4500 (U.S.A.); TGA and DTA experiments were carried out on SETARAM TAG24 (France) using alumina standards. FT-IR spectra were obtained on a Bruker IFS 307 in the reflection mode. SEM/EDAX were determined on a Hitachi S300 instrument. Coefficients of linear expansion were measured by dilatometric techniques.

Preparation of $LnCrO_3$ from reaction of Ln_2O_3, Cr and $NaClO_4$; Ln = La, Ce, Pr, Nd, Sm, Eu, Gd, Tb, Dy, Ho, Er, Tm, Th, Lu and Y

The same reaction scale and procedure was adopted for all the lanthanides illustrated here for Ln = La.

La_2O_3 (15.00 g, 0.045 mmol), chromium metal (4.67 g, 0.090 mol) and sodium perchlorate (4.13 g, 0.0375 mol) were ground for 1 h in a ball mill. The mixture was pressed (30 kg/cm^3) into a 2 cm by *ca.* 4 cm cylindrical pellet. Small holes were drilled through the pellet and W–Re thermocouples inserted. The pellet was supported on a ceramic boat and the reaction ignited by an electrically heated nicrome wire filament at one end. This produced an orange–yellow propagation wave that proceeded through the solid at *ca.* 2–4 mm s^{-1}. This produced a green solid which was ground in a pestle and mortar, washed with distilled water (3×200 ml) filtered through a Buchner funnel and dried in air at 80°C for 4 h. Yields were essentially quantitative. The solid was analysed by X-ray powder diffraction, VSM, and for selected samples by coefficient of linear expansion (Table 1). FT-IR spectra for all $LnCrO_3$ were identical showing five

Table 1. Lattice parameters *a*, *b* and *c*, unit cell volume, angles between the planes (110) and (−110), pycnometrical densities *d* (g/cm^3), specific magnetisation σ_s (G cm^3/g at 83 K and 10 kOe) and average coefficient of linear expansion α (400–1000 K, K^{-1}) of lanthanide chromites produced by self-propagating high-temperature synthesis.

Compound	*a* (Å) (±0.004)	*b* (Å) (±0.004)	*c* (Å) (±0.004)	*V* (Å^3)	(110)(110) (±2′)	*d*	σ_s	$\alpha \cdot 10^7$
$LaCrO_3$	5.502	5.481	7.761	234.04	89°46′	6.50	0.106	82
$CeCrO_3$	5.495	5.486	7.717	232.63	89°54′	6.68	0.296	–
$PrCrO_3$	5.458	5.458	7.709	229.65	90°00′	6.78	2.019	80
$NdCrO_3$	5.315	5.563	7.547	223.14	92°36′	6.91	0.770	74
$SmCrO_3$	5.213	5.559	7.664	222.10	93°40′	7.17	0.581	67
$EuCrO_3$	5.254	5.538	7.620	221.72	93°01′	7.28	0.486	–
$GdCrO_3$	5.302	5.499	7.581	221.03	92°05′	7.41	1.839	65
$TbCrO_3$	5.281	5.503	7.548	219.36	92°21′	7.60	5.778	–
$DyCrO_3$	5.248	5.525	7.536	218.51	92°56′	7.77	6.897	–
$HoCrO_3$	5.245	5.521	7.536	218.22	92°56′	7.96	9.402	–
$ErCrO_3$	5.258	5.523	7.486	217.39	93°48′	8.06	6.498	–
$YbCrO_3$	5.224	5.430	7.474	212.01	92°12′	8.19	1.516	84
$LuCrO_3$	5.168	5.510	7.404	210.83	93°40′	8.37	0.899	–
$YCrO_3$	5.226	5.534	7.531	217.80	93°16′	5.57	0.885	73

bands in the region 700–200 cm^{-1}. SEM showed uniform micron sized agglomerates. EDAX showed consistent Ln to Cr (1:1) ratios across all surface spots. Similar reactions were also studied by replacing $NaClO_4$ with $Ba(ClO_4)_2$. This gave comparable samples.

Preparation of $LnCrO_3$ from reaction of Ln_2O_3, Cr and oxygen (Ln = La, Sm, Dy)

The same reaction scale and procedure was adopted for all lanthanides illustrated here for Ln = La.

La_2O_3 (15.00 g, 0.045 mol) and chromium metal (4.67 g, 0.090 mol) were ground for 1 h in a ball mill. The resulting powder was supported on a ceramic boat (15 cm by 3 cm) and placed inside of a 5 cm i.d. quartz tube. Oxygen was admitted through the tube (10 l/min) and the reaction ignited at one end by an electrically heated filament (800°C). This initiated a yellow–white propagation wave that travelled through the solid at *ca.* 4 mm s^{-1}. The resultant yellow–green powder was collected (after *ca.* 15 min) and analysed by X-ray powder diffraction ($a = 5.500$ Å, $b = 5.480$ Å, $c = 7.762$ Å; $\gamma = 89.46°$) and FT-IR which showed single phase $LaCrO_3$ was produced. Yields from the reaction were essentially quantitative.

Preparation of $LnCrO_3$ from the reaction of $LaCl_3$, $CrCl_3$ and Na_2O_2 (Ln = La, Ce, Gd, Ho)

All the manipulations and weighings were performed inside of an inert atmosphere (N_2) glove box, the same procedure was followed for all lanthanides illustrated here for Ln = La.

Anhydrous $LaCl_3$ (8.00 g, 0.0326 mol), $CrCl_3$ (5.17 g, 0.0326 mol) and Na_2O_2 (7.64 g, 0.098 mol) were ground together inside a ball mill for 1 h. The resulting powder was supported on a ceramic boat (15 cm, by 3 cm) and an SHS reaction initiated by a heated filament (800°C) in air. This produced a synthesis wave that travelled through the solid at *ca.* 2 mm s^{-1}. The reaction was left for 10 min and the products were washed with distilled water (2×1 l) and filtered in air using a Buchner funnel. The resultant green powder was analysed by X-ray powder diffraction ($a = 5.501$ Å, $b = 5.481$ Å, $c = 7.760$ Å; $\gamma = 89.44°$) and FT-IR. These techniques showed that the product was single phase $LaCrO_3$. Yields were essentially quantitative.

Reaction of NaO_2 with $LaCl_3$ and $CrCl_3$ proceeded in the same manner as that outlined above except the molar ratios of the starting materials were adjusted to salt balance the sodium and chlorine.

Reaction of lanthanide nitrate, melamine and chromium powder were investigated under the same conditions as previously reported [17].

Caution

Solid state metathesis reactions and self-propagating high-temperature synthesis can eject material from the initiation zone. Some of these reactions have been known to self-initiate on grinding and mixing the reagents (although this was not observed for the reactions studied here), especially when strong oxidising ($NaClO_4$) and reducing agents are present. New systems should be studied on a small scales using suitable safety screens.

RESULTS AND DISCUSSION

Synthesis and characterisation

Four separate types of SHS reaction were studied for the formation of $LnCrO_3$,

$$0.5Ln_2O_3 + Cr + 0.375NaClO_4 \rightarrow LnCrO_3 + 0.375NaCl, \quad (2a)$$

$$0.5Ln_2O_3 + xCr + (1-x)CrO_3 + (0.75x - 0.375)NaClO_4 \rightarrow LnCrO_3 + (0.75x - 0.375)NaCl, \quad (2b)$$

$$0.5Ln_2O_3 + xCr + (1-x)CrO_3 + (0.375x - 0.1875)Ba(ClO_4)_2 \rightarrow LnCrO_3 + (0.375x - 0.1875)BaCl_2, \quad (2c)$$

$$0.5Ln_2O_3 + Cr + 0.75O_2 \rightarrow LnCrO_3, \quad (3)$$

$$LnCl_3 + CrCl_3 + 3Na_2O_2 \rightarrow LnCrO_3 + 6NaCl + 1.5O_2, \quad (4a)$$

$$LnCl_3 + CrCl_3 + 6NaO_2 \rightarrow LnCrO_3 + 6NaCl + 4.5O_2, \quad (4b)$$

$$Ln(NO_3)_3 + Cr + C_3N_6H_6 \rightarrow LnCrO_3 + 2NH_3 + 3CO_2 + 2N_2. \quad (5)$$

The products from all of the reactions (after trituration with water in the case of eqs. (2a, 2b, 2c, 4a, 4b)) were analysed by X-ray powder diffraction Table 1, VSM Table 1 and FT-IR. Selected samples from reaction (2a) and (4a) were analysed by SEM which showed micron sized aggregates, EDAX on these samples gave consistent Ln to Cr ratios over all of the surface spots.

The IR spectra of all the lanthanide orthochromites (Equations (2a, 2b, 2c, 3–4a, 4b, 5)) were measured in the reflection mode. These showed five broad bands at *ca.* 635 480, 440, 350 and 180 cm^{-1}. All of the materials showed similar IR patterns consistent with an isostructural series. Some slight shifts (*ca.* 5–10 cm^{-1}) in frequency were observed between samples dependent on the lanthanide although no clear pattern of shift with lanthanide atomic weight was observed.

The band at 635 cm^{-1} is due to a Cr–O stretching vibration [13]. The IR spectra do not show any evidence for incorporation of starting materials or the $LnCrO_4$ phase (dominant IR bands at 900–700 cm^{-1}). The $LnCrO_4$ phase has been observed as an intermediate and a contaminant in the traditional synthesis of $LnCrO_3$ [13].

X-ray investigations of the SHS prepared lanthanide chromites indicated that they are all isostructural and have an orthorhombic unit cell with the exception of $PrCrO_3$ which was tetragonal. The lattice parameters were consistent between samples prepared by different reactions (2–5), the data reported in Table 1 is for reaction (2a) only. There have been a number of reports concerning the crystal structures of lanthanide chromites. For example $LaCrO_3$ has been reported with both monoclinic and rhomohedral structures [18, 19] and $PrCrO_3$ with a tetragonal space group (as also observed here) [20]. Despite this, most authors agree that the data can be best fitted to an isostructural series of materials with orthorhombic symmetry [17, 21, 22] akin to the structure also adopted by gadolinium ferrite [23]. As noted above all the SHS prepared materials show orthorhombic symmetry. A steady decrease in the *a* and *c* parameters and unit cell volume was observed with increasing lanthanide atomic number. This is consistent with a contraction in size of the lanthanide cation across the series. There is no detectable pattern in the variations of the *b* unit cell parameters with lathanide atomic number. Some variation in angle between the (110) and (−110) planes is observed within each lanthanide subgroup. In the La–Eu subgroup an increase in angle is observed from 89°46′ for $LaCrO_3$ to 93°40′ for $SmCrO_3$ Table 1. The variation in angle is also observed in the Gd–Lu subgroup. A plot of variation in angle and *c*-cell parameter against rare earth atomic radius is shown in Fig. 1. The SHS prepared lanthanides had in most cases (Ln = La, Ce, Pr, Gd, Tb, Dy, Ho, Er, Tm, Yb, Lu and Y) indexing within error limits of traditionally prepared materials and literature standards [12–16, 21, 22]. This is shown in Fig. 2 which plots unit cell volume and pycnometrical density against lanthanide ionic radius for SHS and conventionally prepared materials. The unit cell volumes are extremely similar for the lanthanides of large and small radius (within 1 $Å^3$), however a discontinuity was observed for Nd and Sm where the SHS prepared materials had a slightly smaller unit cell volume. Considering the error in the measured lattice

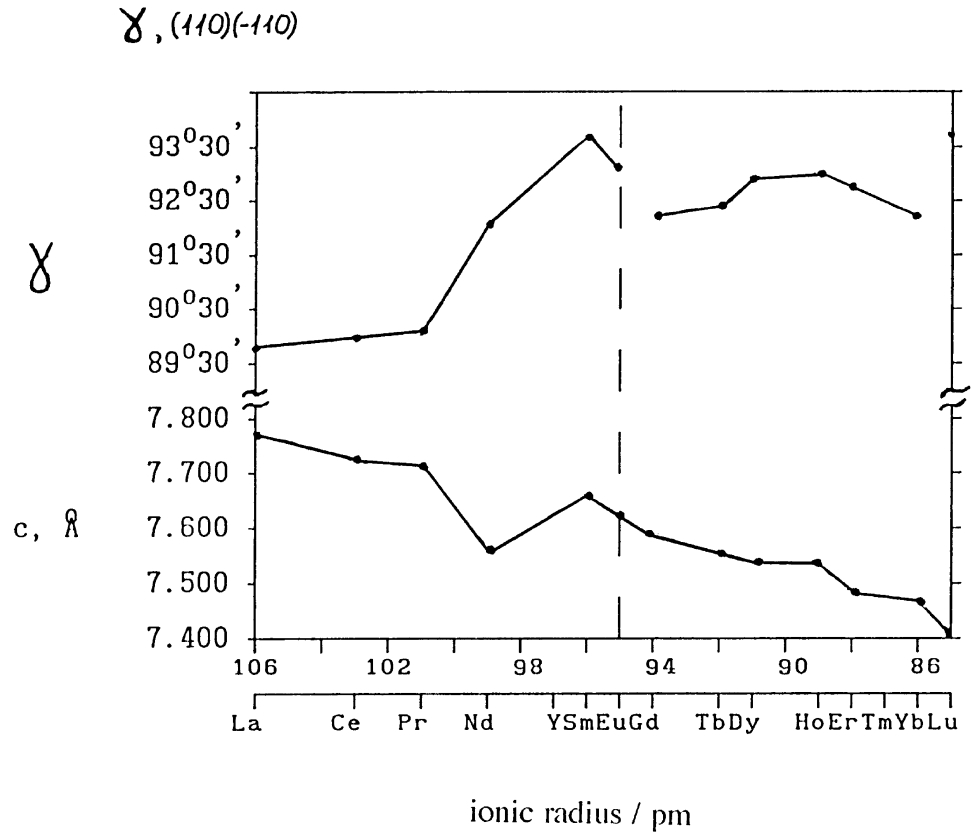

Fig. 1. Changes of orthorhombic parameter *c* and angle of rhombic distortion of lanthanide chromites prepared by self-propagating high-temperature synthesis against lanthanide ionic radius [24].

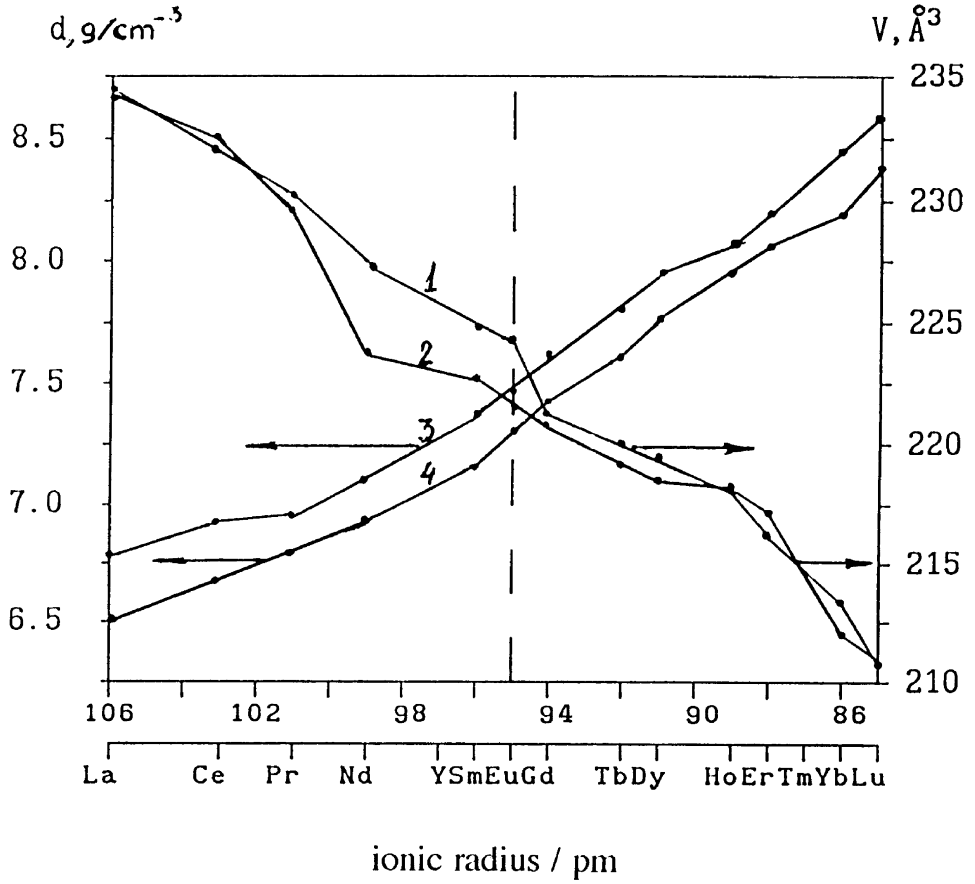

Fig. 2. Plots of unit cell volume (lines 1, 2) and pycnometrical density lines (3, 4) against lanthanide ionic radius [24] for SHS prepared (reaction 2a, lines 2, 4) and conventionally prepared materials (lines 1, 3).

parameters, this difference is significant and not easily accountable. The pycnometrical densities of the SHS prepared lanthanide orthochromites are less than the densities produced by conventional methods [22] Fig. 2. This can be readily accounted as a huge gas evolution occurs during the SHS process, producing a porous materials [23]. It has been shown previously that densification of samples is possible during SHS if a compressive force or controlled constricted environment is used, however this was not investigated for $LnCrO_3$ [25]. For traditionally prepared $LnCrO_3$ materials the maximum rhombohedral distortion (b/a) of the lattice in La–Lu series was 1.059 for $LuCrO_3$ [22]. For the SHS prepared materials the rhombohedral distortion was maximised for both $SmCrO_3$ and $LuCrO_3$ at 1.066.

The magnetic characteristics of the SHS prepared rare-earth chromites were determined Table 1. These indicated that all the materials are antiferromagnets with weak spontaneous magnetic moments. The specific magnetisation values within the La–Eu and Gd–Lu subgroups were different. Measurements at $T = 83$ K and 10 kOe indicated that within both subgroups maxima were observed at the middle of the series Table 1. For the La–Eu group the maximum value is for $PrCrO_3$ – 2.019 and for the Gd–Lu series $HoCrO_3$ – 9.402. These measurements were directly comparable to previous conventionally prepared materials [10–14, 24].

All of the energy (apart from the small amount required to initiate the reaction) for the SHS formation of $LnCrO_3$ comes from an exothermic chemical reaction. In reactions (2a)–(2c) the oxidation of chromium metal provides the driving force for the reaction and the oxygen comes from the solid oxidisers $NaClO_4$ and $Ba(ClO_4)_2$. In reaction (3) the oxidation of chromium metal by gaseous oxygen provides the fuel source for the reaction. In reaction (4a) and (4b) the SHS reaction is promoted by the metathetical exchange of ions and the production of six moles of sodium chloride. In reaction (5) the SHS reaction of $Ln(NO_3)_3$ and Cr is promoted by the exothermic decomposition of melamine $C_3N_6H_6$. Thermochemical data for lanthanide chromites is lacking [26–28]. However one report for $CeCrO_3$ indicates a heat of formation of -1527.2 kJ/mol [29]. Assuming similar heats of formation for all of the lanthanides and using Hesses law this gives heats of reaction for (2a)

of *ca.* $-670\,kJ\,mol^{-1}$; for (3) of $-640\,kJ\,mol^{-1}$ and of (4a) of $-830\,kJ\,mol^{-1}$. These heats of reaction are sufficient to heat up the reactants and drive the transformation. In some cases (2a–2c, 4a, 4b) coproduced NaCl is produced and this in part is vapourised from the reaction. This vapourisation acts as a heat break and limits the reaction temperature to *ca.* 1400°C [16]. It should be noted that the SHS reactions cool relatively quickly and that within 10 min the samples are close to room temperature.

The SHS reaction of Ln_2O_3, xCr, $(1-x)CrO_3$ and $NaClO_4$ proceeded by a steady combustion wave of velocity U_c 2.0 mm/s. The reaction was very sensitive to the ratio of Cr metal to CrO_3. Chromium metal provides the fuel for the reaction and chromium oxide acts in part as a dilutent to absorb some of the reaction energy. Thermocouple measurements indicated that the maximum reaction temperature inside of the reaction was 1900–2300°C. Optical pyrometry measurements indicate a surface reaction temperature in the range of 1000–1150°C. Combustion velocity and temperature seemed largely independent on which lanthanide was used. The maximum reaction temperature and propagation velocity were observed to decrease with x eq. (2b). An SHS reaction proceeded for $x = 1$ to $x = 0.55$ (Table 2). The reaction failed to propagate for values of x below 0.55 as insufficient chromium fuel was present. This meant that the reaction is insufficiently exothermic to allow spread of reaction away from the source of initiation [30, 31]. Combined DTA and TGA data (Figure 3) indicates that for $x = 1$ the reaction initiated at $T = 330$°C and the maximum heat flow from the reaction occurred at 450°C. This corresponds with the decomposition temperature of $NaClO_4$ releasing oxygen which combines with the chromium metal to produce the large exotherm.

The reaction of lanthanide oxide with chromium metal also propagates using oxygen gas instead of an internal intimately mixed solid oxidiser. The propagation velocity and temperature of both reactions are comparable providing sufficient oxygen gas is used in the reaction. At slow flows of oxygen and if the reaction is conducted in air, the propagation velocity is dramatically curtailed and the propagation wave can falter. The limiting step in this reaction is the diffusion of oxygen through the powder. This also explains why the reaction of Ln_2O_3 with Cr and oxygen does not work on a compressed pellet.

Combination of the anhydrous halides and sodium superoxide or peroxide supported an SHS reaction and formed single phase $LnCrO_3$ (Ln = La, Ce, Gd, Ho). One difficulty of this route is that the reagents are hydroscopic and required prior grinding in an inert atmosphere. The driving force for this reaction is the formation of NaCl and $LnCrO_3$. The maximum temperature observed in this reaction was lower than that observed in reactions (2a) and (2c). This is because the coproduced NaCl partly vapourises during the reaction and acts as an internal heat break to soak up some of the reaction enthalpy. The final products were readily obtained after washing off the coproduced NaCl with water.

Lanthanide orthochromites can also be made by combustion of chromium metal and lanthanide nitrate providing an exothermic co-reaction is present within the green mixture. A mixture of the lanthanide nitrate and chromium metal does not ignite in air because the reaction is insufficiently exothermic [30, 31] (*ca.* $300\,kJ\,mol^{-1}$) to propagate between adjacent layers. When a combustion additive is placed in the green mixture two effects occur. Firstly the combustion additive provides heat and dramatically raises the temperature of the starting reagents, in effect it is a form of "chemical oven". Secondly the decomposition of the additive produces large quantities of gas. This gas expansion can be detrimental to the SHS process because it spreads the product and consequently lowers the overall reaction temperature. In the reactions studied here, melamine ($C_3N_6H_6$) was used as a combustion aid (*ca.* $300\,kJ\,mol^{-1}$). Despite producing large quantities of gas on melamine decomposition, the reaction did propagate rapidly. Notably despite addition of the combustion aid no impurities were detected in the product. This indicates that the melamine is completely converted into gaseous products during the reaction (NH_3, CO_2, N_2). The use of a combustion aid does increase the overall cost of the

Table 2. Dependence of combustion temperature on quantity of chromium metal in the system $0.5La_2O_3 + x\text{Cr} + (1-x)CrO_3$.

x	T_{max} (°C) (optical pyrometer)	T_{max} (°C) (thermocouple)	Cr (mass %)
1.00	1000	1900	24.20
0.90	960	1860	21.30
0.80	930	1830	18.53
0.70	890	1800	15.88
0.65	870	1770	14.59
0.60	840	1750	13.33
0.55	800	1710	12.09
<0.55	no combustion	no combustion	<12.09

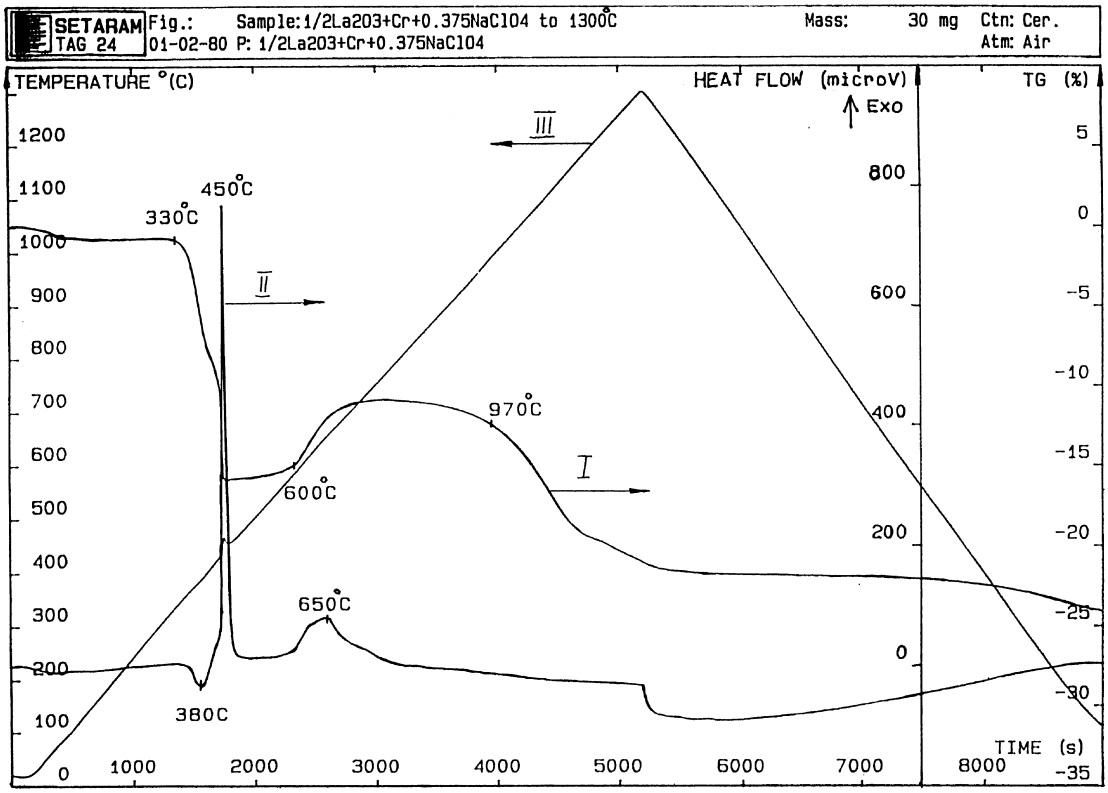

Fig. 3. TGA (line I) and DTA curves (line II) of the SHS reaction of $0.5La_2O_3+Cr+0.375NaClO_4$. Line III represents the oven ramping temperature.

SHS reaction, indeed the combustion aid is often more expensive than the ingredients of the SHS process.

All of the SHS reactions produced single phase $LnCrO_3$ in minutes without the need to externally heat the reaction. In practical terms the reaction of lanthanide oxide and chromium metal using perchlorate solid oxidisers are the easiest to perform. The SHS reactions are all somewhat easier to perform than conventional synthesis in that they require no prior chemistry and do not require heating in a furnace. In many previously reported SHS reactions a second stage of thermal post treatment of the powders is required because the initial synthesis wave only promotes about 90% conversion [30, 31]. In the SHS reactions studied here only single phase $LnCrO_3$ was obtained despite the very short heating times invoked by the reaction. The large exothermicity of the SHS reactions studied (all $>600\,kJ\,mol^{-1}$), the extremely high reaction temperatures (1400°–2200°C), relatively large reaction scale and the premilling of reagents helped to promote single phase formation. It is also notable that by using solid oxidisers the reactions can be promoted in air, this is relatively unusual for an SHS reaction to form a metal oxides where special reaction containers and an oxygen atmosphere are normally required [32].

CONCLUSIONS

Lanthanide chromites with general formula $LnCrO_3$ were synthesised by four separate self-propagating high-temperature syntheses. All the reactions produced single phase orthorhombic $LnCrO_3$ which were weak antiferromagnets. The SHS prepared $LnCrO_3$ show uniform changes in lattice parameters and unit cell volume with lanthanide atomic number. The SHS materials are equal in quality to traditionally prepared materials and require relatively simple synthesis conditions without recourse to use of a furnace.

Acknowledgements—Dr M. Ktiznetsov thanks the Royal Society for an FSU fellowship. Dr I. P. Parkin thanks the Royal Society for an FSU Joint Project grant. Dr Q. A. Pankhurst is thanked for useful discussions on related systems. Dr Y. Morozov is thanked for help with the magnetic measurements.

REFERENCES

1. Geller, S., *Acta Cryst.*, 1957, **10,** 243.
2. Meadowcroft, D. B., Meier, P. G. and Warren, A. C., *Energy Conversion*, 1972, **12,** 145.

3. Minh, N. Q., *J. Am. Ceram. Soc.*, 1993, **75,** 563.
4. Kleinschmager, H. and Relch, A., *Z. Naturforsch.*, 1972, **27,** 363.
5. Kilbourn, B. T., *A Lanthanide Lanthology*. Molycorp Inc., White Plains, NY, 1993.
6. Haung, R. F. and Wowng, W. Y., *J. Mater. Res.*, 1996, **11,** 3077.
7. Bansal, K. P., Kumari, S., Das, B. K. and Jain, G. C., *Trans. J. Brit. Ceram. Soc.*, 1981, **80,** 215.
8. Anderson, H. U., *Mater. Sci. Res.*, 1978, **11,** 469.
9. Song, S. T., *Ceram. Int.*, 1984, **10,** 143.
10. Matveichuk, V. T. and Tresvyatskii, S. G., *Spectroscopy of Atoms and Molecules*. Naukova Durnka, Kiev, 1969, p. 393.
11. Yoshimura, M. and Song, S., Somiya, S., *J. Ceram. Soc. Jpn.*, 1982, **90,** 91.
12. Inagaki, M., Yamamoto, O. and Hirohara, M., *J. Ceram. Soc. Jpn.*, 1990, **98,** 675.
13. Kikkawa, T., Yoshinaka, M., Hirota, K. and Yamaguchi, O., *J. Mater. Sci. Lett.*, 1995, **14,** 1071.
14. Nakayarna, S. and Sakamoto, M., *J. Ceram. Soc. Jpn.*, 1992, **100,** 342.
15. Parkin, I. P., Kornarov, A. V. and Fang, Q., *Polyhedron*, 1996, **15,** 3117.
16. I. P. Parkin, *Chem. Soc. Rev.*, 1996, 199.
17. Vereshagin, A. L. and Sviridov, V. V., *Dokl. Acad. Nauk. SSSR*, 1978, **240,** 602.
18. Bents, U. H., *Phys. Rev.*, 1957, **106,** 225.
19. Wold, A. and Ward, R., *J. Am. Chem. Soc.*, 1954, **76,** 1029.
20. Schwartz, H., *Z. Anorg. Allg. Chem.*, 1963, **322,** 1.
21. Zaitseva, Z. A., Litvin, A. L. and Ostapenko, S. S., *Ukr. Acad. Sci. Dokl.*, 1977, **12,** 1095.
22. Zaltseva, Z. A., Litvin, A. L. and Shevchenko, A., *Ukr. Acad. Sci. Dokl.*, 1973, **8,** 1099.
23. I. P. Parkin, *Chem. Ind.*, 1997, **16,** 725.
24. Babichev, A. P., Babushkina, N. A. and Bratovski, A. M., *Physical Values Handbook*. Viniti, Moscow, 1991, p. 1232.
25. Merzhanov, A. G., *Int. J. SHS*, 1995, **4,** 323.
26. Glushko, V. P., *Thermal constants of compounds*, Vol. 11. VINITI, Moscow, 1970–1982.
27. Ryabin, V. A., Kireeva, M. V. and Berg, N. A., *Inorganic compounds of chromium*. Bolshova, Leningrad, 1981, p. 208.
28. I. L. Knunyants, *Chemical Encyclopaedia*, Vol. 5. Soviet Encyclopaedia, Moscow, 1988–1996.
29. Wayman, D. D., Evans, W. H., Parker, V. B., Schumm, R. H., Halow, J., Bailey, S. M., Chumey, K. C. and Nuttal, R. L., *The NBS Tables of Chemical Thermodynamic Properties*. American Chemical Society, Washington, DC, 1982.
30. MerManov, A. G., *Adv. Mater.*, 1992, **4,** 294.
31. Merzhanov, A. G., *Int. J. SHS*, 1995, **5,** 909.
32. Kuznetsov, M. V., Morozov, Y. G. and Nersesyan, M. D., *Inorg. Mater.*, 1997, **33,** 1249.

Pergamon

Polyhedron Vol. 17, Nos. 25, 26, pp. 4451–4456, 1998
© 1998 Elsevier Science Ltd
All rights reserved. Printed in Great Britain
0277–5387/98 $19.00+0.00

PII: S0277–5387(98)00251–4

Synthesis, characterization and crystal structure of a 6,8,15,17-tetramethyldibenzo[*b*,*i*][1,4,8,11]tetraaza[14]-annulene yttrium(III) complex

Zenglin Wang, Kazunori Sakata* and Mamoru Hashimoto

Department of Chemistry, Faculty of Engineering, Kyushu Institute of Technology, Tobata-ku, Kitakyushu 804-8550, Japan

(Received 21 April 1998; accepted 18 June 1998)

Abstract—In this study, the sandwich complex of tmtaa, Y(tmtaa)(Htmtaa)·2THF (H_2tmtaa = 6,8,15,17-tetramethyldibenzo[*b*,*i*][1,4,8,11]tetraaza[14]annulene, THF = tetrahydrofuran) was synthesized and characterized by IR, UV, mass and NMR spectra as well as DSC measurement. The crystal structure of the complex was determined by X-ray crystal diffraction. The yttrium(III) is coordinated though 8 nitrogen atoms of a dianionic macrocyclic ligand, tmtaa, and of an anionic macrocyclic ligand, Htmtaa, to form an octacoordinated complex which has a sandwich structure. The average bond lengths of Y–N for tmtaa and Htmtaa are 2.40(2) and 2.47(2) Å, respectively. The distances of the yttrium to the planes of the 4 nitrogen atoms for tmtaa and Htmtaa are 1.44(2) and 1.51(2) Å, respectively. © 1998 Elsevier Science Ltd. All rights reserved

Keywords: macrocycles; crystal structures; yttrium(III) complexes; tmtaa complexes; sandwich complexes; NMR spectra

INTRODUCTION

Since 6,8,15,17-tetramethyldibenzo[*b*,*i*][1,4,8,11]-tetraaza[14]annulene, usually abbreviated with H_2tmtaa, was first synthesized by Jaeger [1], there has been considerable research activity concerning the syntheses and structural characterization of metal complexes with H_2tmtaa [2–23]. There are three reasons for this phenomenon: (a) H_2tmtaa has a structure and property similar to porphyrins and phthalocyanines and such systematic research provides a great help to model some biological phenomena [2–10]; (b) metal complexes of tmtaa, electron-rich compounds, have strong functions to stabilize metal–carbon bonds and so some metal complexes with H_2tmtaa, called organic–metal blocks, are prepared as an initial materials for the organic–metal syntheses [11–17]; (c) the 7,16-positions of H_2tmtaa and its metal complexes have been found to act as nucleophilic centres and many electrophilic reagents could react with these positions, which provide an opportunity for preparing more complex compounds employed as models for biologically significant macrocyclic systems [18–23]. However, there are a few papers reporting on rare earth complexes of H_2tmtaa, but the crystal structures of [Li(THF)][Ce(tmtaa)$_2$]·THF [24] and [K(THF)$_3$][Sm$_2$(tmtaa)$_2$]·4THF [25] were determined by Magull and Simon. As a continuation of our research work, an yttrium complex with H_2tmtaa has been synthesized and characterized and its structure has been determined by X-ray diffraction.

EXPERIMENTAL

Materials and methods

All chemicals were reagent grade and were used without further purification except as noted. All solvents were distilled from their sodium–benzophenone blue solution (THF, benzene, hexane and diethylether) or from phosphorus pentoxide (dichloromethane, acetonitrile) under a nitrogen atmosphere. All reaction operations were performed in a dry box

* Author to whom correspondence should be addressed.

under an argon atmosphere. The H_2tmtaa was prepared according to the literature [26, 27]. $YCl_3(THF)_3$ was also prepared according to literature [28] and recrystallized from dichloromethane/hexane.

Infrared spectra in the 400–4000 cm^{-1} region were taken on a Hitachi 260-30 spectrophotometer at room temperature. KBr disk and Nujol mull techniques were employed. Ultraviolet and visible spectra covering the 14000–37000 cm^{-1} range were recorded on a Shimadzu UV-200S double beam spectrophotometer for benzene solutions at room temperature. ^1H NMR measurements were taken on a JEOL JNM-A500 spectrometer operating in a Fourier transform mode. The NMR spectra were run in benzene-d_6 and chemical shifts were given in ppm relative to tetramethylsilane as an internal reference standard. FAB mass spectra were carried out with a JEOL JMS-SX102A gas chromatograph–mass spectrometer in a glycerin matrix. Element analyses were determined with a Yanaco CHN corder MT-3. DSC data were obtained using a Shimadzu DSC-50 differential calorimeter.

Synthesis of Y(tmtaa)(Htmtaa)·2THF complex

H_2tmtaa (0.688 g, 2.0 mmol) and THF (16 cm^3) were added into a 50 cm^3 flask with a rubber cap. The mixture was stirred at 0°C for 30 min. After that, *n*-butyllithium in hexane (2.5 cm^3 of 1.59 M, 3.98 mmol) was added dropwise slowly. When stirred at 0°C for 30 min, a clear red solution was formed. A saturated THF solution (20.4 cm^3) of $YCl_3(THF)_3$ (0.412 g, 1.0 mmol) was added dropwise slowly. After the reaction solution was kept at 0°C for 12 h, yellow crystals were deposited. The crystalline product was collected by filtration and washed three times with cold THF; yield 0.311 g (33.9%). Anal. calc. for $C_{52}H_{61}N_8O_2Y$: C, 68.4; H, 6.6; N, 12.0. Found: C, 67.8; H, 6.6; N, 11.7%. UV-Vis (benzene, nm) 379 ($\log\varepsilon = 4.49$), 410 ($\log\varepsilon = 4.17$). IR (KBr, cm^{-1}) 3000 (w), 2960 (w), 2925 (w), 2810 (w), 1676 (m), 1624 (w), 1551 (s), 1465 (s), 1456 (s), 1420 (s), 1390 (s), 1360 (w), 1272 (s), 1188 (s), 1114 (w), 1040 (m), 1020 (m), 923 (w), 795 (m), 740 (s). FBA-MS: $m/z = 775$ [$(M+1)^+$]. Crystals for X-ray analysis were obtained by dissolving the complex in dry THF solution. After this solution is filtered, the filtrate was cooled to 0°C for 2 h and then hexane was layered carefully. After for 24 h, the yellow and blocklike crystals had formed.

X-ray crystallography

The yellow crystals were selected from the products and were mounted on glass fibres. X-ray data were collected on a Siemens P4 four circle diffractometer by means of an ω–2θ scan and MoK_α radiation at room temperature. The cell parameters and an orientation matrix for data collection were obtained from the least squares method for the diffraction data from 25 reflections. The three check reflections measured with every 100 reflections showed no decay in intensity. The data were corrected by a Lorentz and Polarization factor and an empirical absorption correction. The structure was determined by a standard heavy atomic method and refined by the full-matrix least-squares methods. All nonhydrogen atoms of the complex were refined anisotropically. Since the THF molecules in the structure keep as uncoordinated solvent molecules, the THF molecules have high vibration states and so the second THF molecule was finally treated as a rigid group and was refined as an individual isotropic thermal parameter. A summary of the crystal data, the experimented detail and the refinement results are listed in Table 2.

RESULTS AND DISCUSSION

Syntheses and characterization of Y(tmtaa)(Htmtaa)·2THF

Reaction of the H_2tmtaa in THF solution with 2 equivalent of LiC_4H_9 in hexane gave a clear red solution and so Li_2tmtaa was produced. When the Li_2tmtaa reacted with 1/2 or 1 eq. of $YCl_3(THF)_3$, the yellow crystals, Y(tmtaa)(Htmtaa)·2THF, were crystallized out from the reaction solution. The three reactions may occur in the solution as follows:

$$H_2\text{tmtaa} + n\text{-}LiC_4H_9 \xrightarrow{THF} Li_2\text{tmtaa}$$

$$Li_2\text{tmtaa} + YCl_3 \xrightarrow{THF} LiY(\text{tmtaa})_2$$

$$LiY(\text{tmtaa})_2 \longrightarrow Y(\text{tmtaa})(\text{Htmtaa})$$

Though all reaction operations were performed in a dry box under an argon atmosphere, there were trace amounts of water in the reaction solution and so the water reacted with the $LiY(tmtaa)_2$ to produce the Y(tmtaa)(Htmtaa). Since the coordination number of yttrium(III) in $LiY(tmtaa)_2$ and Y(tmtaa)(Htmtaa) is eight, the solubility of them in the THF solution is different. Y(tmtaa)(Htmtaa) has a lower solubility than that of $LiY(tmtaa)_2$ and is easy to separate from the reaction solution. Consequently, Y(tmtaa)(Htmtaa)·2THF were obtained from the reaction solution.

The complex was characterized by UV, IR, mass and NMR spectra as well as DSC measurement. IR bands of H_2tmtaa at 1620 (s), 1600 (m), 1554 (s) and 1512 (s) cm^{-1} are assigned to C=N and C=C stretching modes [29–31]. After formation of the complex, the IR bands shifted to lower frequency and the bands appeared at 1551 (s), 1465 (s), 1456 (s) and 1390 (s) cm^{-1}. The UV-Vis spectra of the complex was mea-

sured at room temperature in benzene solutions. Two absorption peaks appear at 379 nm ($\log \varepsilon = 4.49$) and 410 nm ($\log \varepsilon = 4.17$). Comparison with a maximum absorption band (348 nm) of H_2tmtaa shows a 31 nm shift to a longer wavelength for complex formation. The crystalline complex is stable in dry air, but decomposes easily in a moist condition. The DSC data under a nitrogen atmosphere show that the complex loses two THF of crystallization at 93°C and then the complex decomposes at 399.5°C. This is in agreement with the TG result (percent mass loss: $W_{\text{calc.}} = 15.67\%$, $W_{\text{found}} = 15.7\%$).

A molecular ion peak of the complex, $[M+1]^+$, appeared at m/z 775 in the FBA mass spectra. The base peak is m/z 431 which corresponds to $[Y(tmtaa)]^+$. Consistent with diamagnetism, Y(tmtaa)(Htmtaa)·2THF gave well-resolved ^{1}H NMR spectra. Chemical shift assignments were made on the basis of comparison with H_2tmtaa. ^{1}H NMR data and its assignments for Y(tmtaa)(Htmtaa)·2THF are compiled in Table 1. The methine proton signals of two kinds appear at about 4.68 ppm because of two different macrocyclic skeletons, namely tmtaa and Htmtaa. The amine proton signal appears at 13.9 ppm and is a singlet, having no proton which couples it. The methine signal and the amine signal in the integrated rate = 2:1 spell out the complex and so the complex has two kinds of the macrocyclic skeletons. The methine proton signal, the methyl proton signal and the aromatic proton signal are little shifted on the formation of the yttrium(III) complex. On the other hand, the amine proton signal is shifted by 0.8 ppm to a lower field. This is mainly attributed to the placement of the methine, methyl and aromatic proton groups further from the positive change of the yttrium(III) ion which offers the inductive effect.

Crystal structure of the complex

The perspective view of the molecular unit is shown in Fig. 1. The selected bond lengths and the selected bond angles are given in Table 3. Though the quality of the crystal data is not very good, the results of crystal structure of the complex are in agreement with those of UV, IR, mass and NMR spectra of the complex. Figure 1 shows that the structure unit of the crystal consists of one complex molecule and two THF molecules. Because of steric interaction between the methyl groups and the benzene rings, H_2tmtaa and its transition metal complexes have a markedly nonplanar saddle shape [6]. In the complex, the Y(III) is coordinated through 8 N atoms from the two saddle shaped ligands, macrocyclic dianion, tmtaa and macrocyclic anion, Htmtaa, to form an octacoordinated sandwich complex.

The dianionic tmtaa coordinates to the central ion as two delocalized conjugated π-electron systems. On the other hand, the anionic Htmtaa coordinates to the central ion as a delocalized conjugated system and as a nonconjugated system. The position of the amine hydrogen (N–H) in the complex seems to be fixed. This may be demonstrated by the markedly longer bond length of Y–N(8) [2.66(2) Å]. The average atomic deviation from the plane of the nonconjugated 2,4-pentanediiminate chelate ring is 0.11 Å and is much larger than that of the conjugated 2,4-pentanediiminate chelate rings. In the complex, the two conjugated 2,4-pentanediiminate chelate rings of tmtaa and one conjugated 2,4-pentanediiminate chelate ring of Htmtaa are coplanar and the average atomic deviations from the planes are 0.05, 0.03 and 0.01 Å, respectively. This is shown in Fig. 2.

The average bond lengths of Y–N for tmtaa and Htmtaa are 2.40(2) and 2.47(2) Å, respectively. The longest bond length of Y–N is 2.66(2) Å and the shortest bond length is 2.34(2) Å. These parameters may be compared with those of the structurally characterized rare earth tmtaa complexes [24, 25], $[Li(THF)][Ce(tmtaa)_2]\cdot THF$ and $[K(THF)_3][Sm_2(tmtaa)_2]\cdot 4THF$, in which average bond lengths of Ce–N (A ring and B ring) and Sm–N are 2.48 Å (A ring), 2.65 Å (B ring) and 2.35 Å, respectively. The four nitrogens of tmtaa and Htmtaa are almost coplanar in the complex. The average atomic deviation from the planes (defined by nonhydrogen atoms) is 0.02 Å for tmtaa and 0.03 Å for Htmtaa, respectively. The two saddle shaped ligands are rotated by nearly 90° relative to one another and two corresponding mean 4 N planes are almost parallel to each other. The dihedral angles are only 2°. In the complex, the central ion lies at 1.44(2) Å away from the 4 N mean plane for tmtaa and at 1.51(2) Å out of the 4 N mean plane of Htmtaa. The distance is shorter than that of $[Li(THF)][Ce(tmtaa)_2]\cdot THF$ [1.53 Å (A ring) and 1.65 Å (B ring)], but is longer than that of $[K(THF)_3][Sm_2(tmtaa)_2]\cdot 4THF$ (1.23 Å).

Table 1. ^{1}H—NMR data for H_2tmtaa and Y(tmtaa)(Htmtaa)·2THF[a]

Complex	Amine (-N–H)	Aromatic	Methine (-CH═)	Methyl (-CH_3)
H_2tmtaa	13.10(s)	6.80(m)	4.69(s)	1.88(s)
Y(tmtaa)(Htmtaa)·2THF	13.90(s)	6.89(m)	4.69(s), 4.68(s)	1.88(s)

[a] Chemical shifts are given in ppm for TMS. Measured in benzene-d_6.Multiplicity of a proton signal is given parentheses after δ-value: s: singlet; m: multiple.

Table 2. Crystallographic data for Y(tmtaa)(Htmtaa)·2THF

Chemical formula	$[Y(C_{22}H_{22}N_4)(C_{22}H_{23}N_4)]\cdot 2THF$
Temperature (K)	293(2)
Wavelength (Å)	0.71073
Crystal system	monoclinic
Space group	C2
Unit cell dimensions	a = 17.470(3) Å, $\alpha = 90^\circ$, b = 16.081(3) Å, $\beta = 94.81(3)^\circ$, c = 16.166(3) Å, $\gamma = 90^\circ$
Volume (Å^3)	4526(2)
Z	4
Density (calculated) (Mg/m^3)	1.349
Absorption coefficient (mm^{-1})	1.340
Crystal size (mm)	$0.30 \times 0.32 \times 0.36$
θ Range for data collection	1.72 to 25.00°
Limiting indices	$-1 \ll h \ll 20$ $-1 \ll k \ll 19$, $-19 \ll l \ll 19$
Reflections collected	5079
Independent reflections	4451 ($R_{int} = 0.0311$)
Maximum and minimum transmission	0.62666 and 0.57701
Refinement method	Full-matrix least-squares on F^2
Data/restraint/parameters	4353/27/533
Goodness-of-fit on F^2	0.812
Final R indices [$I > 2\sigma$]	$R_1 = 0.0728$, $wR_2 = 0.1388$
Absolute structure parameter	−0.05(2)
Largest diff. peak and hole (e Å^{-3})	0.941 and −0.738

$R_1 = \Sigma \| F_0 | - | F_c \| / \Sigma | F_0 |$ $\quad wR_2 = \{\Sigma[w(F^2_0 - F^2_c)^2] / \Sigma[w(F^2_0)^2]\}^{1/2}$.

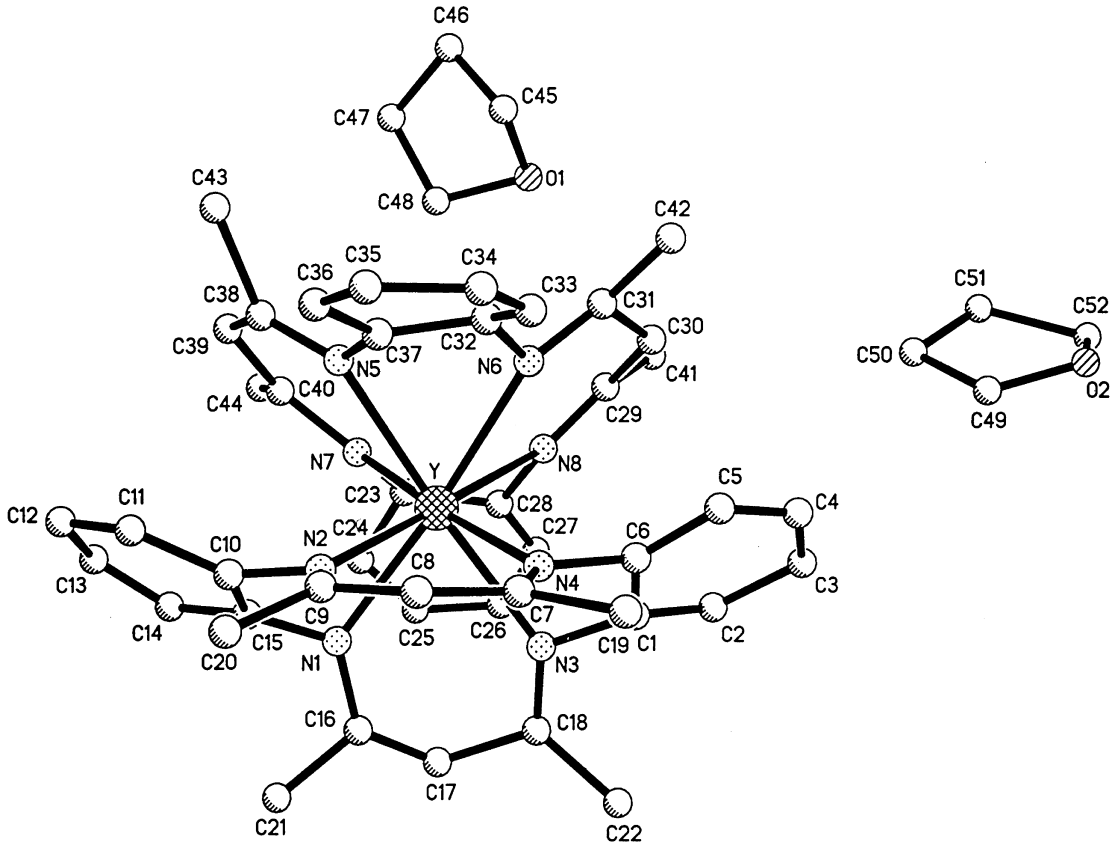

Fig. 1. The perspective view of Y(tmtaa)(Htmtaa)·2THF.

Table 3. Selected bond lengths (Å) and selected bond angles (°)

Y–N(1)	2.36(2)	Y–N(2)	2.36(2)
Y–N(3)	2.46(2)	Y–N(4)	2.43(2)
Y–N(5)	2.45(2)	Y–N(6)	2.43(2)
Y–N(7)	2.34(2)	Y–N(8)	2.66(2)
N(1)–C(16)	1.38(3)	N(1)–C(15)	1.34(3)
N(2)–C(9)	1.23(2)	N(2)–C(10)	1.35(3)
N(3)–C(18)	1.30(4)	N(3)–C(1)	1.45(3)
N(4)–C(7)	1.34(3)	N(4)–C(6)	1.52(3)
N(1)–Y–N(2)	63.8 (7)	N(1)–Y–N(7)	76.6 (7)
N(2)–Y–N(2)	112.2 (8)	N(1)–Y–N(4)	106.4 (7)
N(2)–Y–N(4)	72.8 (5)	N(7)–Y–N(4)	175.0 (8)
N(1)–Y–N(5)	111.4 (7)	N(2)–Y–N(5)	75.3 (7)
N(7)–Y–N(5)	71.2 (7)	N(4)–Y–N(5)	110.8 (6)
N(1)–Y–N(6)	173.7 (8)	N(2)–Y–N(6)	110.6 (7)
N(7)–Y–N(6)	104.1 (7)	N(4)–Y–N(6)	73.4 (7)
N(5)–Y–N(6)	63.5 (5)	N(1)–Y–N(3)	72.3 (5)
N(2)–Y–N(3)	105.6 (8)	N(7)–Y–N(3)	111.8 (8)
N(4)–Y–N(3)	66.0 (7)	N(5)–Y–N(3)	176.0 (9)
N(6)–Y–N(3)	112.7 (9)	N(1)–Y–N(8)	114.9 (7)
N(2)–Y–N(8)	178.0 (9)	N(7)–Y–N(8)	65.9 (5)
N(4)–Y–N(8)	109.1 (8)	N(5)–Y–N(8)	104.3 (7)
N(6)–Y–N(8)	70.6 (7)	N(3)–Y–N(8)	75.1 (7)

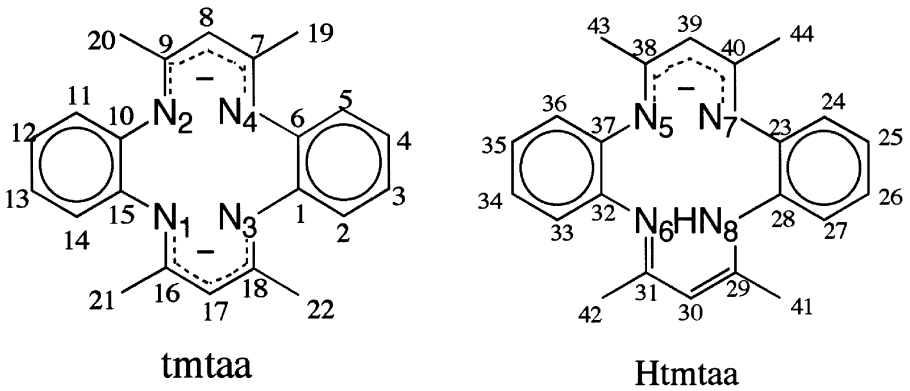

Fig. 2. The coordination models of tmtaa and Htmtaa in the complex.

Since H_2tmtaa has a property similar to phthalocyanine (H_2Pc), Y(tmtaa)(Htmtaa) has a structurally characterization similar to $LuHPc_2$ [32, 33]. Both complexes are coordinated through 8 N atoms from a dianionic ligand and an anionic ligand to form octacoordinated sandwich complexes. The electron-delocalized capability of tmtaa is different from that of Pc. Pc is a delocalized 16-membered ring with a full electron and HPc also is a delocalized system with a full electron and so the position of N–H could not be located in $LuHPc_2$. On the other hand, Htmtaa and tmtaa are nondelocalized 14-membered rings and the position of N–H could be located in the complex. Though the two ligands are rotated by nearly 90° to one another for formation of the complex, the interaction between the methyl groups and the benzene rings of the two ligands is very strong and causes the angles to change largely between the benzene planes and the 4 N atom planes. Some important angles between selected planes are listed in Table 4.

Acknowledgements—We thank the Changchun Institute of Applied Chemistry of P. R. China for X-ray structure determination. We are grateful to the Center for Instrumental Analysis, Kyushu Institute of Technology for elemental analyses, mass spectra and NMR spectra. Further details of the crystal structure determination can be ordered from the Cambridge Crystallographic Data Centre under deposition number 102943.

Table 4. Some important angles (°) between selected planes for the complex and H_2tmtaa

Defining planes N(1), N(2), N(3), N(4)	Defining planes N(5), N(6), N(7), N(8) and	Complex		Ligand[a]
		tmtaa	Htmtaa	H_2tmtaa
C(1), C(2), C(3), C(4), C(5), C(6)	C(32), C(33), C(34), C(35), C(36), C(37)	17.3	15.9	24.1
C(10), C(11), C(12), C(13), C(14), C(15)	C(23), C(24), C(25), C(26), C(27), C(28)	38.0	18.3	25.1
N(1), C(16), C(17), C(18), N(3)	N(5), C(38), C(39), C(40), N(7)	37.0	37.3	36.5
N(2), C(7), C(8), C(9), N(6)	N(8), (29), C(30), C(31), N(6)	34.1	33.8	32.0

[a] See Ref. [6].

REFERENCES

1. Jaeger, E. G., *Z. Anorg. Chem.*, 1968, **364,** 177.
2. Neves, D. R. and Dabrowiak, J.C., *Inorg. Chem.*, 1968, **15,** 129.
3. Bryan, P. S. and Dabrowiak, J.C., *Inorg. Chem.*, 1975, **14,** 296.
4. Weiss, M. C. and Goedken, V.L., *Inorg. Chem.*, 1979, **18,** 274.
5. Tsutsui, M., Bobsein, R. L., Cash, G. and Pettersen, R., *Inorg. Chem.*, 1979, **18,** 758.
6. Goedken, V. L., Plutg, J. J., Peng, Sh.M. and Bursten, B., *J. Am. Chem. Soc.*, 1976, **98,** 8014.
7. Weiss, M. C., Bursten, B., Peng, Sh.M. and Goedken, V.L., *J. Am. Chem. Soc.*, 1976, **98,** 8021.
8. Mandon, D., Giraudon, J. M., Toupet, L., Sala-Pala, J. and Guerchais, J.E., *J. Am. Chem. Soc.*, 1987, **109,** 3490.
9. Giraudon, J. M., Sala-Pala, J., Guerchais, J. E. and Toupet, L., *Inorg. Chem.*, 1992, **31,** 2676.
10. Giraudon, J. M., Sala-Pala, J., Guerchais, J. E. and Toupet, L., *Inorg. Chem.*, 1991, **30,** 891.
11. Cotton, F. A. and Czuchajowska, J., *Polyhedron*, 1990, **9,** 1221.
12. Cotton, F. A. and Czuchajowska, J., *Polyhedron*, 1990, **9,** 1217.
13. Cotton, F. A. and Czuchajowska, J., *Polyhedron*, 1990, **9,** 2553.
14. Cotton, F. A., Czuchajowska, J. and Feng, X.-J., *Inorg. Chem.*, 1990, **29,** 4329.
15. Ciurli, S., Floriani, C., Chiesi-Villa, A. and Guastini, C., *J. Chem. Soc. Chem. Commun.*, 1986, 1401.
16. Floriani, C., Ciurli, S., Chiesi-Villa, A. and Guastini, C., *Angew. Chem. Int. Ed. Engl.*, 1987, **26,** 70.
17. Giannini, L., Solari, E., Floriani, C., Chiesi-Villa, A. and Rizzoli, C., *Angew. Chem. Int. Ed. Engl.*, 1994, **33,** 2204.
18. Kajiwara, T., Murao, R. and Ito, T., *J. Chem. Soc. Dalton Trans.*, 1997, 2537.
19. Sakata, K., Koyanagi, K. and Hashimoto, M., *J. Heterocyclic Chem.*, 1995, **32,** 329.
20. Sakata, K. and Itoh, M., *J. Heterocyclic Chem.*, 1992, **29,** 921.
21. Sakata, K., Saitoh, Y., Kawakami, K., Nakamura, N. and Hashimoto, M., *Synth. React. Inorg. Met.-Org. Chem.*, 1995, **25,** 1279.
22. Sakata, K., Shimoda, M. and Hashimoto, M., *J. Heterocyclic Chem.*, 1996, **33,** 1593.
23. Sakata, K., Ueno, A., Jibuta, T. and Hashimoto, M., *Synth. React. Inorg. Met.-Org. Chem.*, 1993, **23,** 1107.
24. Magull, J. and Simon, A., *Z. Anorg. Chem.*, 1992, **615,** 77.
25. Magull, J. and Simon, A., *Z. Anorg. Chem.*, 1992, **615,** 81.
26. Goedken, V. L. and Molin-Case, J., *J. Chem. Soc. Chem. Commun.* 1992, 337.
27. Sakata, K., Yamaura, F. and Hashimato, M., *Synth. React. Inorg. Met.-Org. Chem.*, 1990, **20,** 1043.
28. Manzer, L. E., *Inorg. Synth.*, 1982, **21,** 135.
29. Olszanski, D. J. and Melson, G.A., *Inorg. Chim. Acta*, 1977, **23,** L4.
30. Willey, G. R. and Rudd, M.D., *Polyhedron*, 1992, **21,** 2805.
31. Sakata, K., Hashimoto, M., Hamada, T. and Matsuno, S., *Polyhedron*, 1996, **15,** 967.
32. Moussavi, M., De Cian, A., Fischer, J. and Weiss, R., *Inorg. Chem.*, 1988, **27,** 1287.
33. De Cian, A., Moussavi, M., Fischer, J. and Weiss, R., *Inorg. Chem.*, 1985, **24,** 3162.

Pergamon

Polyhedron Vol. 17, Nos. 25, 26, pp. 4457–4464, 1998
© 1998 Elsevier Science Ltd
All rights reserved. Printed in Great Britain
PII: SS0277-5387(98)00254-X
0277–5387/98 $19.00+0.00

Synthesis and characterisation of cobalt and nickel compounds with phosphinothiol ligands. Crystal and molecular structures of $[Co\{2\text{-}(Ph_2P)\text{-}6\text{-}(Me_3Si)C_6H_3S)\}_3]$, $[Ni\{2\text{-}(Ph_2P)\text{-}6\text{-}(Me_3Si)C_6H_3S)\}_2]$ and $[Co\{2\text{-}(Ph_2PO)\text{-}6\text{-}(Me_3Si)C_6H_3S\}_2]$

P. Pérez-Lourido,[a] J. Romero,[a,*] J. A. García-Vázquez,[a], A. Sousa,[a] J. Zubieta[b] and K. Maresca[b]

[a]Departamento de Química Inorganica, Universidad de Santiago de Compostela, 15706 Santiago de Compostela, Spain

[b]Department of Chemistry, Syracuse University, Syracuse, NY 13244, U.S.A.

(Received 24 April 1998; accepted 18 June 1998)

Abstract—The electrochemical oxidation of anodic metal (cobalt or nickel) in an acetonitrile solution of phosphinothiol ligands, 2-$(Ph_2P)C_6H_4SH$, 2-(Ph_2P)-6-$(SiMe_3)C_6H_3SH$, 2-(Ph_2PO)-6-$(SiMe_3)C_6H_3SH$, affords $[Co\{2\text{-}(Ph_2P)C_6H_4S)\}_3]$ **1**, $[Ni\{2\text{-}(Ph_2P)C_6H_4S\}_2]$ **2**, $[Co\{2\text{-}(Ph_2P)\text{-}6\text{-}(SiMe_3)C_6H_3S\}_3]$ **3**, $[Ni\{2\text{-}(Ph_2P)\text{-}6\text{-}(SiMe_3)C_6H_3S\}_2]$ **4**, $[Co\{2\text{-}(Ph_2PO)\text{-}6\text{-}(SiMe_3)C_6H_3S\}_2]$ **5**, $[Co\{2\text{-}(Ph_2PO)\text{-}6\text{-}(SiMe_3)C_6H_3S\}_3]$ **6** and $[Ni\{2\text{-}(Ph_2PO)\text{-}6\text{-}(SiMe_3)C_6H_3S\}_2]$ **7**. All compounds have been characterised by microanalysis, IR, UV-visible, FAB and NMR spectroscopic studies and compounds **3**, **4** and **5** by single-crystal X-ray diffraction. © 1998 Elsevier Science Ltd. All rights reserved

Keywords: electrochemical synthesis; crystals structures; cobalt and nickel complexes; phosphinothiol complexes

INTRODUCTION

Interest in the coordination chemistry of metal–sulfur complexes arises from their potential relevance to active sites in metallo-enzymes and also from their ability to adopt various nuclearities and significant structural complexity [1–4]. These features are the result of the tendency of thiolate ligands to bridge metal centres to give polymeric species. Such association phenomena can be controlled by introducing coligands. In this context, the synthesis and characterisation of mixed complexes containing both thiolate and additional donors, such as tertiary phosphines, have been objects of extensive studies [5]. However, ligands containing both phosphorus and sulfur as donor atoms have received far less attention. In the last decade, compounds containing arenophosphinothiolate ligands have been reported by Dilworth and Zubieta, mainly with heavier transition metals, such as molybdenum [6], technetium and rhenium [7], rhodium [8] and iridium [9].

As a result of our continuing interest in the chemistry of monomeric and low molecularity thiolate complexes, we now describe the synthesis of cobalt and nickel compounds with aromatic phosphinothiol ligands, using an electrochemical procedure, where the metal is the anode of a cell containing the ligand in an acetonitrile solution. This method has been successfully used for the synthesis of cobalt and nickel thiolate compounds [10]; and also for metallic compounds with other ligands having weak acid groups,

* Author to whom correspondence should be addressed.

such as heterocyclic thiones [11–14]. Although the compounds [Ni{2-(Ph_2P)C_6H_4S}$_2$] and [Ni{2-(Ph_2PO)-6-($SiMe_3$)C_6H_3S}$_2$] have been previously prepared by nonelectrochemical methods and their structures described [15], the other compounds reported in this article have not been reported previously.

EXPERIMENTAL

All manipulations were carried out under an inert atmosphere of dry nitrogen. Cobalt and nickel (Aldrich Chemie) were used as plates (*ca.* 2×2 cm). Ligands were synthesised using slight modifications of the standard literature procedure [16].

Electrochemical synthesis

The electrochemical method used in the synthesis of the complexes was similar to that described by Tuck [17]. The foil anode was suspended from a platinum wire and the cathode was also a platinum wire. The ligand was dissolved in acetonitrile and about 10 mg of tetramethylammonium perchlorate was added to the solution. Applied voltages of 10–20 V allowed sufficient current flow for smooth dissolution of the metal. During electrolysis, nitrogen was bubbled through the solution to provide an inert atmosphere and to stir the solution phase. The cell can be summarised as $Pt_{(-)}/CH_3CN + RP–SH/M_{(+)}$, where RP–SH represents the ligand and M is either Co or Ni.

[Co{2-(PPh_2)C_6H_4S}$_3$], ***1***. Electrochemical oxidation of a cobalt anode in a solution of 2-diphenylphosphinobenzenethiol, 2-(Ph_2P)C_6H_4SH, (0.230 g, 0.782 mmol) in acetonitrile (50 cm^3), at 16 V and 10 mA for two h caused 21 mg of cobalt to be dissolved, $E_f = 0.48$ mol F^{-1}. During the electrolysis hydrogen was evolved at the cathode and at the end of the electrolysis green crystalline needles appeared at the bottom of the vessel. The solid was filtered, washed with acetonitrile and ether and dried under vacuum, (0.20 g, 83%). Anal. Calc. for $C_{54}H_{42}CoP_3S_3$: C, 69.1; H, 4.5; S, 10.2. Found: C, 68.8; H, 4.6; S, 9.8% IR (KBr, cm^{-1}): 1571(m), 1482(m), 1433(s), 1416(m), 1241(s), 1091(m), 738(s), 692(s), 525(s). FAB (*m*/*z*): 939, $[Co(R–PS)_3]^+$; 645, $[Co(R–PS)_2]^+$; 294, $[RP–S]^+$. ^1H NMR ($CDCl_3$ ppm): δ 8.0–6.1 (m, 42 H). ^{31}P NMR ($CDCl_3$, ppm): δ 40.6, 38.8 and 37.0.

[Ni{2-(PPh_2)C_5H_4S}$_2$], ***2***. A similar experiment (12 V, 10 mA, 2 h) with nickel as anode and 0.220 g (0.748 mmol) of 2-(Ph_2P)C_6H_4SH in 50 cm^3 of acetonitrile, dissolved 23 mg of nickel, $E_f = 0.52$ mol F^{-1}. As the reaction proceeds, the solution colour changed from colourless to dark green. At the end of the electrolysis the green crystals deposited in the cell were recovered, washed with cool acetonitrile and diethyl ether, dried under vacuum and identified as **2** (0.17 g, 70%). Anal. Calc. for $C_{36}H_{28}NiP_2S_2$: C, 67.0; H, 4.3; S, 9.9. Found: C, 66.7; H, 4.3; S, 9.4%. IR (KBr, cm^{-1}): 1568(m), 1481(m), 1437(s), 1423(m), 1244(s), 1096(m), 740(s), 693(s), 530(s). FAB (*m*/*z*): 644, $[Ni(R–PS)_2]^+$; 352, $[Ni(R–PS)]^+$; 294, $[RP–S]^+$. ^1H ($CDCl_3$, ppm): δ 7.9–6.7(m, 28 H). ^{31}P NMR ($CDCl_3$, ppm): δ 54.0.

[Co{2-(Ph_2P)-6-(Me_3Si)C_6H_3S}$_3$], ***3***. A solution of acetonitrile (50 cm^3) containing 2-diphenylphosphino-6-trimethylsilylbenzenethiol (0.307 g, 0.839 mmol) was electrolyzed at 10 mA during 1.5 h and 17 mg of cobalt metal were dissolved from the anode, $E_f = 0.51$ mol F^{-1}. Dark blue crystals of **3**, suitable for X-ray studies, were obtained and the end of the reaction. They were recovered by filtration, washed with acetonitrile and dried (0.42 g, 88%) and identified by elemental analysis. Anal. Calc. for $C_{63}H_{66}CoP_3S_3Si_3$: C, 66.0; H, 5.7; S, 8,3. Found: C, 65.5; H, 5.9; S, 8.0% IR(KBr, cm^{-1}): 1554(m), 1483(m), 1434(m), 1355(s), 1245(m), 1086(m), 852(s), 746(s), 692(s), 530(s). FAB (*m*/*z*): 1153, $[Co(R–PS)_3]^+$; 789, $[Co(R–PS)_2]^+$; 365, $[RP–S]^+$. ^1H NMR ($CDCl_3$, ppm): δ 7.7–5.9 (m, 39H), 0.10(s, 9H), 0.30 (s, 9H), 0.50(s, 9H). ^{31}P NMR ($CDCl_3$, ppm): δ 45.0, 43.0 and 39.0.

[Ni{2-(Ph_2P)-6-(Me_3Si)C_6H_3S}$_2$], ***4***. A similar experiment (6 V, 10 mA, 2.0 h) with 0.29 g (0.792 mmol) of the ligand 2-(Ph_2PO)-6-(Me_3Si)C_6H_3SH in 50 cm^3 of acetonitrile, dissolved 21 mg of nickel, $E_f = 0.48$ mol F^{-1}. Green crystals, suitable for X-ray studies, were obtained directly from the cell. The solid was collected, washed with cool acetonitrile, diethyl ether and dried under vacuum (0.27 g, 86%). Anal. Calc. for $C_{42}H_{44}NiP_2S_2Si_2$: C, 63.9; H, 5.8; S, 8.1. Found: C, 63.7; H, 5.7; S, 7.8%. IR(KBr, cm^{-1}): 1555(m), 1482(m), 1433(m), 1359(s), 1243(m), 1098(m), 852(s), 746(m), 690(m), 540(s).). FAB (*m*/*z*): 789, $[Ni(R–PS)_2]^+$; 424, $[Ni(R–PS)]^+$; 365, $[RP–S]^+$. ^1H RMN ($CDCl_3$, ppm): δ 7.9–6.9(m, 26 H), 0.25(s, 18H). ^{31}P NMR($CDCl_3$, ppm): δ 52.5.

[Co{2-(Ph_2PO)-6-(Me_3Si)C_6H_3S}$_2$], ***5*** *and* [Co{2-(Ph_2PO)-6-(Me_3Si)C_6H_3S}$_3$], ***6***. The electrochemical oxidation of cobalt in a solution of 2-(Ph_2PO)-6-(Me_3Si)C_6H_3SH (0.428 g 1.12 mmol) in acetonitrile (60 ml) for 3 h at 10 V and 10 mA resulted in the loss of 32 mg of cobalt from the anode, $E_f = 0.50$ mol F^{-1}. During the electrolysis a small amount of a red crystalline compound, **5**, was recovered in the cell as a minor product. This compound has been characterised as [Co{2-(Ph_2PO)-6-(Me_3Si)C_6H_3S}$_2$]. Anal. Calc. for $C_{42}H_{44}P_2O_2S_2Si_2Co$: C, 61.4; H, 5.4; S, 7.8. Found: C, 61.0; H, 5.3; S, 7.7%. Concentration of the solution yielded dark blue crystals (0.35 g, 76%) of **6**. (Anal. Calc. for $C_{63}H_{66}P_3O_3S_3Si_3Co$: C, 62.9; H, 5.5; S, 8.0. Found: C, 62.5; H, 5.4; S, 7.9%, IR(KBr, cm^{-1}): 1554(m), 1437(s), 1352(s), 1243(m), 1127(s), 1062(s), 852(s), 750(s), 691(m), 558(s). FAB (*m*/*z*): 1201, $[Co(R–PS)_3]^+$; 821, $[Co(R–PS)_2]^+$; 382, $[RP–S]^+$. ^1H NMR ($CDCl_3$, ppm): δ 8.0–6.5(m, 39H), 0.35(s, 27H). ^{31}P($CDCl_3$, ppm): δ 41.7 ppm.

[Ni{2-(Ph_2PO)-6-(Me_3Si)C_6H_3S}$_2$], ***7***. Electrolysis of an acetonitrile solution (50 cm^3) containing 2-(Ph_2PO)-6-(Me_3Si)C_6H_3SH (0.214 g, 0.56 mmol) using

10 mA electric current for 1.5 h caused the dissolution of 16 mg of nickel ($E_f = 0.49$ mol F^{-1}). Concentration of the final solution produced green crystals (0.17 g, 74%) of **7**. Anal. Calc. for $C_{42}H_{44}P_2O_2S_2Si_2Ni$: C, 61.4; H, 5.4; S, 7.8. Found: C, 61.0; H, 5.3; S, 7.7%. IR(KBr, cm^{-1}): 1556(m), 1437(s), 1352(s), 1244(m), 1129(s), 1067(s), 854(s), 749(s), 692(m), 555(s).). FAB (m/z): 819, $[Ni(R–PS)_2]^+$; 439, $[Ni(R–PS)]^+$; 382, $[RP–S]^+$. ^1H NMR ($CDCl_3$, ppm): δ 8.6–6.4(m, 26H), 0.5 (s, 18H). $^{31}P(CDCl_3$, ppm): δ 58.2 ppm.

Instrumentation

Elemental analysis were performed on a Carlo-Erba EA microanalyser. IR spectra were recorded in KBr mulls on a Bruker IFS 66 V spectrophotometer. FAB mass spectra were recorded on a Kratos-MS-50T connected to a DS90 data system, using 3-nitrobenzyl alcohol (3-NBA) a matrix material. ^1H and ^{31}P NMR spectra were recorded on a Bruker AMX 300 MHz instrument, using in all cases $CDCl_3$ as solvent; ^1H NMR chemical shifts were determined against TMS as internal standard and ^{31}P NMR against 85% H_3PO_4. Solid-state electronic spectra were recorded on a Shimadzu UV 3101 PC.

X-ray crystallography

Compound **3** was studied on a Siemens Smart diffractometer, **4** on a CAD-4 system and **5** on a Rigaku AFC6S diffractometer. Data collection was carried out under ambient conditions, using graphite monocromated Mo Kα for all compounds. The crystal parameters and other experimental details of the data collection are summarized in Table 2. A complete description of the details of the crystallographic methods is given in Table 1. The structures were solved by direct methods and refined by a full matrix least squares procedure. Neutral atom scattering factors were taken from Cromer and Waber [18] and anomalous dispersion were taking from Cromer [19]. All calculation were performed using SHELXTL PLUS (PC version) [20] for **3** and **5** and using DECMicroVAX 3500 computer for **4**. No anomalies were encountered in the refinements of any of the structures. The crystal parameters and other experimental details of data collection and refinement are summarized in Table 1. Atomic positions, a full list of bond lengths, angles and other crystallographic data have been deposited as supplementary publication No. CCDC 102069–102071. Copies can be obtained through Cambridge crystallographic data centre, Union Road, Cambridge.

RESULTS AND DISCUSSION

The analytical data show that the electrochemical procedure described can be satisfactorily used, in good yield, for the synthesis of complexes of cobalt and nickel with phosphinothiol ligands and the method represents a simple alternative to other standard chemical procedures.

The nickel compounds have general formulae $[Ni(RP–S)_2]$ where RP–S stands for the monoanion of the RP–SH ligand. The electrochemical efficiency value, E_f, defined as the amount of metal dissolved per Faraday of charge, was always close to 0.5 mol F^{-1}. This fact and the evolution of hydrogen at the cathode are compatible with the following reaction mechanisms

$$\text{cathode: } 2\,RP-SH + 2e^- \rightarrow 2\,RP-S^- + H_2$$

$$\text{anode: } Ni + 2\,RP-S^- \rightarrow [Ni(RP-S)_2] + 2e^-.$$

Values of E_f close to 0.5 mol F^{-1} were found in the synthesis of cobalt complexes and are indicative of a similar anodic oxidation mechanism. However, the ddformulation of these compounds is $[Co(RP–S)_3]$. This observation suggests an additional oxidation in solution of Co(II) to Co(III). This behaviour has been previously observed in the synthesis of other cobalt complexes via an electrochemical procedure [21]. When the ligand used was 2-(Ph_2PO)-6-($SiMe_3$) C_6H_3SH, in addition to the analogous Co(III) compound, a small amount of crystals of $[Co\{2\text{-}Ph_2P(O)\text{-}6\text{-}(Me_3Si)C_6H_3S\}_2]$ could be isolated as a minor product.

Structure of $[Co\{2\text{-}(Ph_2P)\text{-}6\text{-}(Me_3Si)C_6H_3S\}_3]$, ***3***

Figure 1 shows the molecular structure of **3** together with the atom labelling scheme. Selected bond distances and angles are given in Table 2. The compound consists of discrete molecules with the metal coordinated to three monoanionic bidentate ligands, bonded to the cobalt through their phosphorus and sulfur atoms. The environment around the metal can be described as $[CoP_3S_3]$ slightly distorted octahedral geometry; all the dihedral angles between the coordination planes defined by four donors atoms are close to 90°. Angles defined by two *trans* donor atoms and the metal atom are the range 167.67(7)–177.39(7)° and the angles determined by cobalt atom and two *cis* donor atoms are close to 90°, even those corresponding to five membered chelating rings exhibit values of 86.49(6), 88.37(6) and 81.72(6)°. These values are larger than those found in other trischelate metal complexes containing this ligand.

The arrangement of the three sulfur and phosphorous atoms in **3**, is such that the compound can be described as the *meridional* isomer. This is the disposition found in $[Tc\{2\text{-}(Ph_2P)C_6H_4S\}_3]$, $[Re\{2\text{-}(Ph_2P)C_6H_4S\}_3]$ [7] and $[Ir\{2\text{-}(Ph_2P)C_6H_4S\}_3]$ [9]. ^1H and ^{31}P NMR data (*vide infra*) show that this arrangement is maintained in solution.

The Co–S bond distances are in the range 2.245(2)–2.335(2) Å, with the longer one corresponding to the

Table 1. Crystal data, data collection and structure refinement for compounds (**3**), (**4**) and (**5**)

	(**3**)	(**4**)	(**5**)
Crystal data			
Empirical formula	$C_{63}H_{66}CoP_3S_3Si_3$	$C_{42}H_{44}NiP_2S_2Si_2$	$C_{42}H_{44}CoO_2P_2S_2Si_2$
Formula weight	1155.45	789.72	821.94
Crystal size (mm)	$0.15\times0.12\times0.10$	$0.17\times0.15\times0.10$	$40\times0.40\times0.40$
Crystal system	monoclinic	monoclinic	monoclinic
Space group	$P2_1/n$	$P2_1/c$	Cc
Unit cell dimensions (Å)	$a=20.3177(12)$	13.262(3)	17.8803(2)
(Å)	$b=12.5633(7)$	12.690(3)	16.7345(3)
(Å)	$c=25.825(2)$	12.873(3)	29.1871(6)
(°)	$\beta=109.578(1)$	108.96(3)	92.183(1)
Volume (Å^3)	6211.0(6)	2048.9(8)	8727.0(3)
Z	4	2	8
Dc (g/cm^3)	1.236	1.280	1.251
Absorption coefficient (mm^{-1})	0.549	0.740	0.650
$F(000)$	2424	828	3432
Data collection			
Radiation	Mo Kα(0.71073 Å)		
Temperature (K)	293(2)	293(2)	298(2)
θ range (°)	1.11–28.32	1.62–22.47	1.40–28.34
Limiting indices	$-27<h<14$	$-14<h<12$	$-23<h<23$
	$-16<k<16$	$-13<k<0$	$-22<k<22$
	$-33<l<34$	$0<l<13$	$-14<l<38$
Reflections collected	36811	2971	26385
Independent reflections	14523 (rint = 0.070)	790 (rint = 0.0168)	13663 (rint = 0.0381)
Solution and refinement			
System used	full-matrix least squares on F^2		
Data/restrains/parameters	14523/0/653	790/0/224	13661/2/919
R	0.1003	0.0345	0.0503
R_w	0.1553	0.0345	0.068
Goodness-of-fit on F^2	1.381	1.153	1.118
Largest difference peak (e Å^{-3})	1.755	0.220	0.258
Largest difference hole (e Å^{-3})	−0.339	−0.211	−0.264

cobalt–sulfur bond *trans* to a phosphorous atom, suggesting some *trans* influence of the phosphorus. This effect has been also observed in other complexes, such as [Ir(2-(Ph_2P)C_6H_4S)$_3$]. Nevertheless, the average value for the Co–S bond distances, 2.286(2) Å, is comparable to the value of 2.27 Å reported for Co–S bond distances in [Co(III)–S_6] octahedral complexes [22] or 2.297(4) Å in the octahedral cation [Co(SC_6H_5)$_2$(phen)$_2$]$^+$ [10]. The Co–P bond distances are also different, with longer bond distances associated with atoms *trans* to one another. This may be again due to the *trans* influence of two mutually *trans* positioned phosphine donor atoms. The average value, 2.278(2) Å, is in the range of other octahedral Co(III) complexes containing tertiary phosphine as donors [23] (and references cited therein).

Structure of [Ni{2-(Ph_2P)-6-(Me_3Si)C_6H_3S}$_2$], ***4***

The molecular structure of [Ni{2-(Ph_2P)-6-(Me_3Si)C_6H_3S}$_2$] is shown in Fig. 2, together with the atomic numbering scheme adopted. Selected bond distances and angles are given in Table 3. The structure shows the nickel atom, located at a crystallographic inversion centre and coordinated to two thiolato sulfur atoms and to two phosphorous atoms of two symmetry related moieties. The arrangement is strictly planar to within experimental accuracy, with the sulfur atoms in a *trans* disposition; bond angles between the adjacent atoms are very close to the theoretical 90° limit. The structure of this molecule is similar to that of [Ni{2-(Ph_2P)C_6H_4S}$_2$] which exhibits the same environment for the metal, but distinct from that of [Ni{2-(Ph_2PO)-6-($SiMe_3$)C_6H_3S}$_2$] which possesses planar S_2O_2 environment around the metal, in which the two thiolate sulfur atoms adopt a *cis* disposition [15]. The Ni–S bond distance, 2.151(3) Å, is similar to the value found in [Ni{2-(Ph_2P)C_6H_4S}$_2$], 2.180(1) Å and also in the range 2.149–2.179 Å described for Ni(II) square planar complexes with five ring chelating ligands and sulfur thiolate donor atoms [15]. In addition, the Ni–P bond distance, 2.172(3) Å, is marginally shorter than the value of 2.181(2) Å found

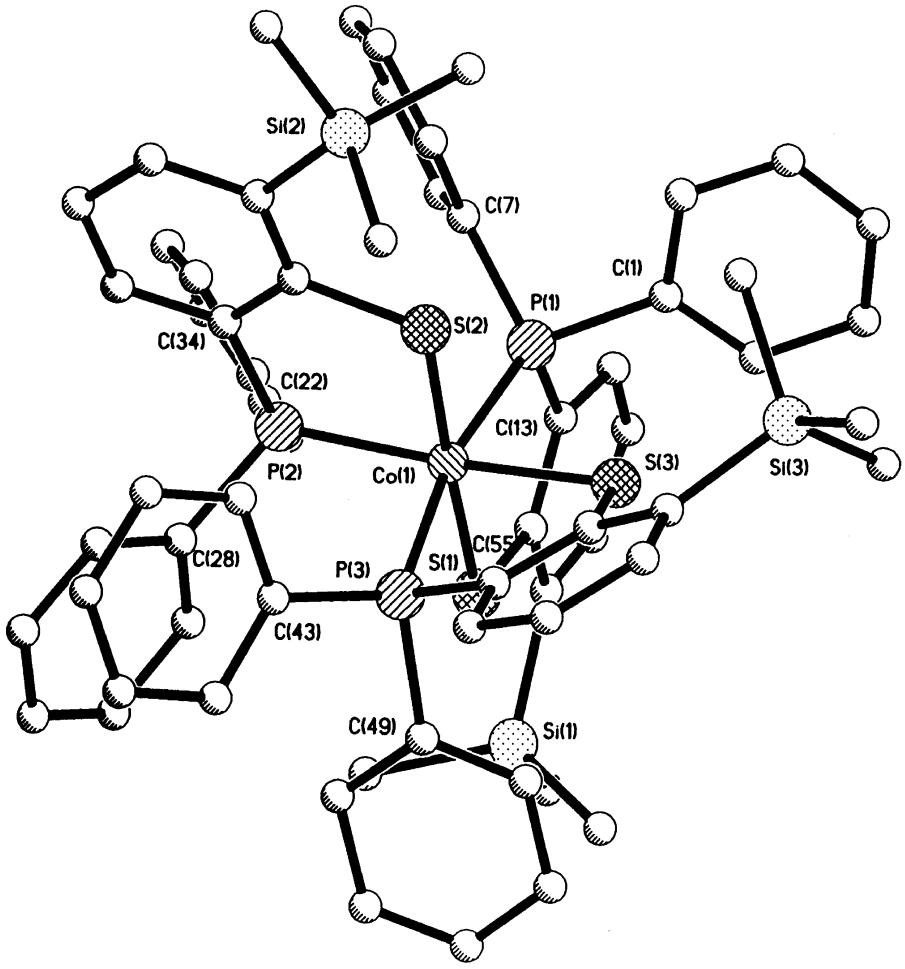

Fig. 1. The molecular structure of [Co{2-(Ph_2P)-6-(Me_3Si)C_6H_3S}$_3$].

Table 2. Selected bond lengths (Å) and angles (°) for [Co{2-(Ph_2P)-6-(Me_3Si}C_6H_3S}$_3$] **3**

Co(1)–S(2)	2.245(2)	Co(1)–P(2)	2.260(2)
Co(1)–P(1)	2.271(2)	Co(1)–S(1)	2.277(2)
Co(1)–P(3)	2.302(2)	Co(1)–S(3)	2.335(2)
S(1)–C(2)	1.757(6)	S(2)–C(23)	1.765(6)
S(3)–C(44)	1.762(6)	P(1)–C(13)	1.832(6)
P(1)–C(7)	1.843(6)	P(1)–C(1)	1.804(6)
P(2)–C(34)	1.843(6)	P(2)–C(28)	1.842(6)
P(2)–C(22)	1.820(6)	P(3)–C(55)	1.839(6)
P(3)–C(49)	1.827(6)	P(3)–C(43)	1.817(6)

S(2)–Co(1)–P(2)	88.37(6)	S(2)–Co(1)–P(1)	91.17(6)
P(2)–Co(1)–P(1)	95.68(6)	S(2)–Co(1)–S(1)	177.39(6)
P(2)–Co(1)–S(1)	93.00(6)	P(1)–Co(1)–S(1)	86.49(6)
S(2)–Co(1)–P(3)	91.35(6)	P(2)–Co(1)–P(3)	96.45(6)
P(1)–Co(1)–P(3)	167.67(7)	S(1)–Co(1)–P(3)	90.70(6)
S(2)–Co(1)–S(3)	83.43(6)	P(2)–Co(1)–S(3)	171.54(7)
P(1)–Co(1)–S(3)	86.58(6)	S(1)–Co(1)–S(3)	95.27(6)
P(3)–Co(1)–S(3)	81.72(6)		

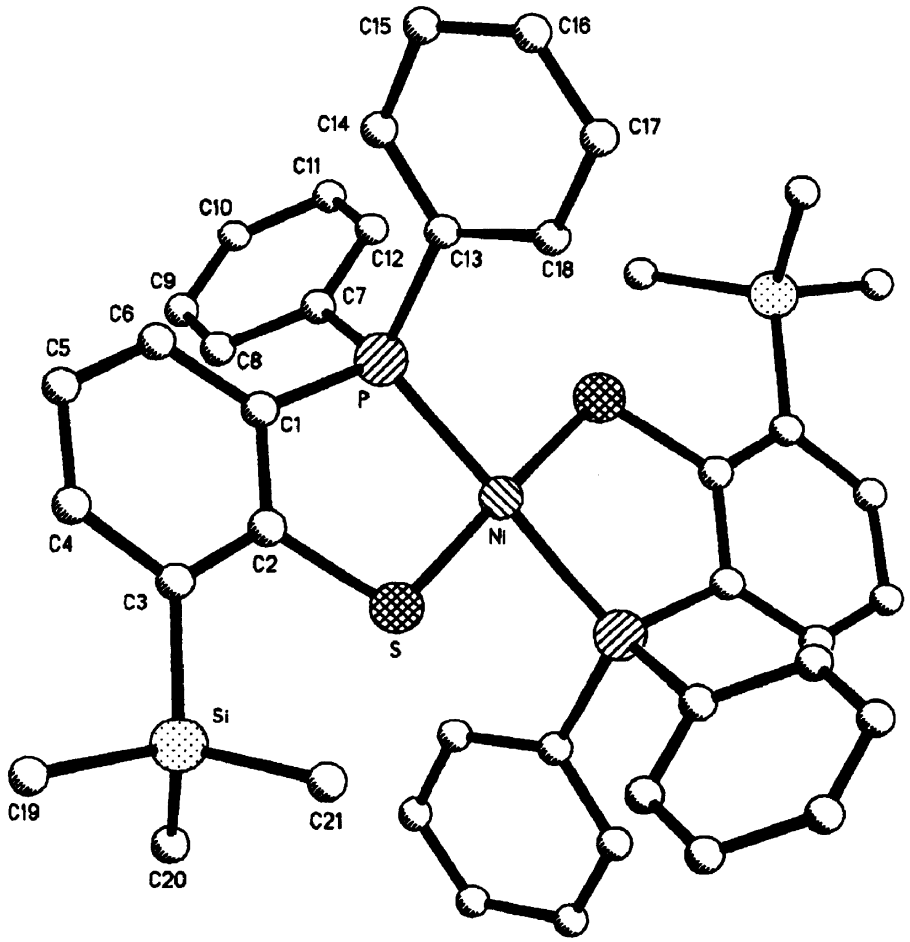

Fig. 2. The molecular structure of [Ni{2-(Ph_2P)-6-(Me_3Si)C_6H_3S}$_2$].

in the mentioned complex. These structural considerations reveal that the introduction of a trialkylsilyl group to the ligand has a negligible influence on the structural parameters of the compound.

Structure of [Co{2-(Ph_2PO)-6-(Me_3S)C_6H_3S}$_2$], **5**

The crystal structure of **5** shows the presence of two independent but structurally similar, molecules in the

Table 3. Selected bond lengths (Å) and angles (°) for [Ni{2-(Ph_2P)-6-(Me_3Si)C_6H_3S}$_2$]. **4**

Ni–S	2.151(3)	Ni–S†1	2.151(3)
Ni–P†1	2.172(3)	Ni–P	2.172(3)
S–C(2)	1.770(11)	P–C(1)	1.792(11)
P–C(7)	1.809(10)	P–C(13)	1.832(11)
S–Ni–S†1	180.0	S–Ni–P†1	90.96(12)
S†1–Ni–P†1	89.04(12)	S–Ni–P	89.04(12)
S†1–Ni–P	90.9(12)	P†1–Ni–P	180.0
C(2)–S–Ni	109.2(4)	C(1)–P–Ni	107.8(4)
C(2)–C(1)–P	116.9(9)	C(2)–S–Ni	109.2(4)
C(1)–C(2)–S	117.0(9)		

Symmetry transformations used to generate equivalent atoms: $^{\dagger}1-x+1, -y+1, -z+1$.

asymmetric unit. The structure of one, with the atom labelling is given in Fig. 3. Selected bond distances and angles with the estimated standard deviations are given in Table 4. The compound consists of discrete molecules, with the cobalt atom tetracoordinated to two thiolate sulfur atoms and two oxygen atoms of two ligands, such that the environment around the central atom can be described as $[CoO_2S_2]$ distorted tetrahedral, with bond angles, 99.46(9) and 98.80(10)°, significantly distorted with respect to the tetrahedral value.

The average values for the Co–S bond lengths for both molecules, 2.2838(14) Å, are normal and similar to that in Co(II) complexes with the same geometry and coordination number. Thus, these values are comparable to those found for the tetrahedral anion $[Co(SC_6H_5)_4]^{2-}$, average value 2.328 Å [24, 25], or in $[Co(SC_{10}H_{13})_3CH_3CN]^-$, average value 2.28 Å [26]. Similarly, the Co–O bond distances, average 1.974 Å, are in the range for those found in tetrahedral complexes containing triphenylphosfineoxide as ligand, for instance 1.971 Å (average value) in $[CoCl_2(OPMe_3)_2]$ [27] and 1.928 Å (average value) in $[CoCl_2\{OP(CH_2Ph)_3\}_2]$ [28].

Bond distances and angles in the coordinated ligand are similar to those found for the free ligand [29]. Thus the average value for the P–O bond distance in the complex, 1.518(3) Å, is slightly higher than the 1.493(3) Å value found in the free ligand. This lengthening can be attributed to the weakening of the P═O bond, by coordination to the metal.

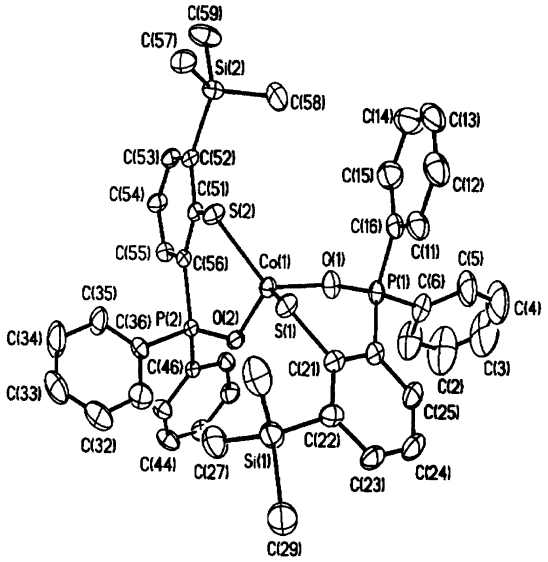

Fig. 3. The molecular structure of $[Co\{2\text{-}(Ph_2PO)\text{-}6\text{-}(Me_3Si)C_6H_3S\}_2]$.

Spectroscopic studies

The IR spectra of the ligands exhibit a band in the 2400–2550 cm^{-1} range attributed to ν(S–H). This band is absent in the spectra of the complexes, indicating that the ligand is in the anionic thiolate form in all complexes. The complexes also show bands in the 1500–1580 cm^{-1} region, characteristic of aromatic ring vibrations, as well as bands in the 1100–1000 cm^{-1} region attributable to ν(P–C). The trimethylsilyl derivatives show in addition a very strong band around 840–850 cm^{-1} assignable to the n(Si–C) mode. Compounds **5**, **6** and **7** show a very strong band at 1130 cm^{-1} characteristic of ν(P–O).

The FAB mass spectra of all compounds show the molecular ion with appropriate isotope distributions. In many cases, ions formed by loss of one ligand from the initial complex are also observed, as well as a peak attributed to the free ligand.

The magnetic moments of the Co(III) complexes show that these complexes are diamagnetic, as

Table 4. Selected bond lengths (Å) and angles (°) for $[Co\{2\text{-}(Ph_2PO)\text{-}6\text{-}(Me_3Si)C_6H_3S\}_2]$. **5**

Co(1)–O(1)	1.978(4)	Co(1)–O(2)	1.961(3)
Co(2)–O(3)	1.975(3)	Co(2)–O(4)	1.983(3)
Co(1)–S(1)	2.2826(14)	Co(1)–S(2)	2.2720(14)
Co(2)–S(3)	2.2761(14)	Co(2)–S(4)	2.3045(14)
S(1)–C(21)	1.772(5)	S(2)–C(51)	1.768(4)
S(3)–C(61)	1.775(4)	S(4)–C(111)	1.771(5)
P(1)–O(1)	1.516(3)	P(2)–O(2)	1.520(3)
P(3)–O(3)	1.521(3)	P(4)–O(4)	1.517(3)

O(2)–Co(1)–O(1)	103.3(2)	O(2)–Co(1)–S(2)	99.74(9)
O(1)–Co(1)–S(2)	126.38(1)	O(2)–Co(1)–S(1)	124.67(1)
O(1)–Co(1)–S(1)	99.19(10)	S(2)–Co(1)–S(1)	106.15(5)
O(3)–Co(2)–O(4)	108.5(2)	O(3)–Co(2)–S(3)	99.13(10)
O(4)–Co(2)–S(3)	124.18(1)	O(3)–Co(2)–S(4)	120.39(1)
O(4)–Co(2)–S(4)	98.47(10)	S(3)–Co(2)–S(4)	107.89(5)

expected for low spin d^6 octahedral complexes. The solid state electronic spectra of these complexes show two bands near 16,000 and 25,000 cm^{-1}. The first band is due to $^1T_{1g} \leftarrow {}^1A_{1g}$ transition and the second to $^1T_{2g} \leftarrow {}^1A_{1g}$ transition [30]. The nickel complexes are also diamagnetic, compatible with the square planar coordination around the metal. The solid-state electronic spectra of these complexes show two bands at *ca*. 16,000–17,000 and 22,000–24,000 cm^{-1}, which can be attributed to the $^1B_{1g} \leftarrow {}^1A_{1g}$ and $^1E_{1g} \leftarrow {}^1A_{1g}$ transitions, characteristic of nickel compounds in a square-planar environment [30].

The diamagnetic nature of these complexes (except compound **5**) allowed their study by in solution. In no instance do the ^1H NMR spectra show the thiol -SH signal of the free ligand around 4.1 ppm, proving that the ligand is in the monoanionic form in all complexes. The spectra also show multiplets over 8.0–6.5 ppm characteristic of the phenyl groups. The ^1H of $[Co\{2\text{-}(Ph_2P)\text{-}6\text{-}(Me_3Si)C_6H_3S\}_3]$ shows the presence of three nonequivalent trimethylsilyl groups, at 0.10, 0.30 and 0.50 ppm, indicating that the *meridional* conformation of the ligands found in the solid state is maintained in solution. This is corroborated by the presence of three signals in the ^{31}P NMR spectra at 39, 43 and 45 ppm corresponding to the nonequivalent phosphorus in the *meridional* conformation. By contrast, the ^1H NMR of $[Co\{2\text{-}(Ph_2PO)\text{-}6\text{-}(Me_3Si)C_6H_3S\}_3]$ shows only a singlet at 0.35 ppm, attributable to the $-SiMe_3$ groups, indicating that the ligands in this complex are equivalent and therefore that the compound has a *facial* arrangement of the ligands in solution. The ^{31}P NMR of this compound shows only one signal at 41.6 ppm, as expected for this ligand arrangement.

Acknowledgements—We thank the Xunta de Galicia (Xuga-20316B96) for financial support.

REFERENCES

1. Raper, E. S., *Coord. Chem. Rev*., 1996, **153,** 199.
2. Raper, E. S., *Coord. Chem. Rev*., 1997, **165,** 475.
3. Krebs, B. and Henkel, G., *Angew. Chem. Int. Ed. Engl*., 1991, **30,** 769.
4. Dance, I. G., *Polyhedron*, 1986, **5,** 1037.
5. Castro, R., Romero, J., García-Vázquez, J. A., Sousa, A., Chang, Y. D. and Zubieta, J., *Inorg. Chim. Acta*, 1996, **345,** 119.
6. Block, E., Kang, H., Ofori-Okai, G. and Zubieta, J., *Inorg. Chim. Acta*, 1989, **166,** 155.
7. Dilworth, J. R., Hutson, A. J., Morton, S., Harman, M., Hursthouse, M. B., Zubieta, J., Archer, C. M. and Kelly, J. D., *Polyhedron*, 1992, **11,** 2151.
8. Dilworth, J. R., Zheng, S. and Lu, S., Wu, Q., *Trans. Met. Chem*., 1992, **17,** 364.
9. Dilworth, J. R., Lu, C., Miller, J. R. and Zheng, Y., *J. Chem. Soc. Dalton Trans*., 1995, 1957.
10. Chadha, R. K., Kumar, R., Romero, J. and Tuck, D. G., *Can. J. Chem*., 1988, **66,** 2151.
11. Castro, R., García-Vázquez, J. A., Romero, J., Sousa, A., Pritchard, R. and McAulife, C. A., *J. Chem. Soc. Dalton Trans*., 1994, 1115.
12. Castro, J. A., Romero, J., García-Vázquez, J. A., Castiñeiras, A., Sousa, A. and Zubieta, J., *Polyhedron*, 1995, **14,** 2841.
13. Tallón, J., García-Vázquez, J. A., Romero, J., Louro, M. S., Sousa, A., Chem, Q., Chang, Y. and Zubieta, J., *Polyhedron*, 1995, **14,** 2309.
14. Pérez-Lourido, P. A., García-Vázquez, J. A., Romero, J., Louro, M. L., Sousa, A., Chem, Q., Chang, Y. and Zubieta, J., *J. Chem. Soc. Dalton Trans*., 1996, 2047.
15. Block, E., Ofori-Okai, G., Kang, H. and Zubieta, J., *Inorg. Chim. Acta*, 1991, **188,** 7.
16. Block, E., Ofori-Okai, G. and Zubieta, J., *J. Am. Chem. Soc*., 1989, **111,** 2327.
17. Habeeb, J. J., Tuck, D. G. and Walters, F. H., *J. Coord. Chem*., 1978, **8,** 27.
18. Cromer, D. T., Waber, J. T., *International Tables for X-ray Crystallography*, Vol. IV, Table 2.2A. The Kynoch Press, Birmingham, 1974.
19. Cromer, D. T., *International Tables for X-ray Crystallography*, Vol. IV, Table 2.3.1. The Kynoch Press, Birmingham, 1974. .
20. Sheldrick, G. M., *SHELXTL-PLUS program package* (*PC Version*) *for the determination of crystal structures*, Release 4.0. Siemens Analytical X-ray Instruments, Madison WI, 1990.
21. Castro, J. A., Romero, J., García-Vázquez, L. A., Durán, M. L., Sousa, A., Castellano, E. E., Zukerman-Schepector, J., *Polyhedron*, 1992, **11,** 235.
22. Shannon, R. D., In *Structure and bonding in crystals*, Vol. 2, Chap. 16, ed. M. O'Keeffe and A. Navrotsky, Academic Press, New York, 1981.
23. Kasiwabara, K., Kita, M., Masuda, H., Kurachi, S. and Oliba, S., *Bull. Chem. Soc. Jpn*., 1995, **68,** 883.
24. Coucouvanis, D., Swenson, D., Baenzinger, N. C., Murphy, C., Holah, D. G., Sfarnas, N., Simopoulos, A. and Kostikas, A., *J. Am. Chem. Soc*., 1981, **103,** 3350.
25. Hagen, K. S. and Holm, R. H., *Inorg. Chem*., 1984, **23,** 418.
26. Koch, S. A., Fikar, R., Millar, M. and O'Sullivan, T., *Inorg. Chem*., 1984, **23,** 121.
27. Menu, M.-J., Simard, M., Beauchamp, A., König, H., Dartiguenave, M., Dartiguenave, Y. and Klein, H., *Acta Cryst. C*, 1989, **45,** 1697.
28. De Almeida Santos, R. H. and Mascarenhas, Y., *J. Coord. Chem*., 1979, **9,** 59.
29. Pérez-Lourido, P., Romero, J., García-Vázquez, J. A., Sousa, A., Zubieta, J. and Maresca, K., unpublishied results.
30. Lever, A. B. P., *Inorganic Electronic Spectroscopy*, 2nd edn., Elsevier, Amsterdam. 1984.

Pergamon

Polyhedron Vol. 17, Nos. 25, 26, pp. 4465–4473, 1998
© 1998 Elsevier Science Ltd
All rights reserved. Printed in Great Britain
0277–5387/98 $19.00+0.00

PII: S0277–5387(98)00253–8

Synthesis and conformational studies of palladium(II) complexes containing $[Ph_2P(O)NP(E)Ph_2]^-$ (E = S or Se)

Alexandra M. Z. Slawin, Martin B. Smith and J. Derek Woollins*

Department of Chemistry, Loughborough University, Loughborough, Leics LE11 3TU, U.K.

(Received 29 April 1998; accepted 18 June 1998)

Abstract—The ligands $[Ph_2P(O)NP(E)Ph_2]^-$ (E = S **I**; E = Se **II**) can readily be complexed to a range of palladium(II) starting materials affording new six-membered Pd–O–P–N–P–E palladacycles. Hence ligand substitution reaction of the chloride complexes $[PdCl_2(bipy)]$ (bipy = 2,2′-bipyridine), $[\{Pd(\mu\text{-}Cl)(L–L)\}_2]$ (HL–L = $C_9H_{13}N$ or $C_{12}H_{13}N$), $[\{Pd(\mu\text{-}Cl)Cl(PMe_2Ph)\}_2]$ or $[PdCl_2(PR_3)_2]$ [$PR_3 = PPh_3$; $2PR_3 = Ph_2PCH_2CH_2PPh_2$ or *cis*-$Ph_2PCH=CHPPh_2$] with either **I** (or **II**) in thf or CH_3OH gave $[Pd\{Ph_2P(O)NP(E)Ph_2\text{-}O,E\}(bipy)]PF_6$, $[Pd\{Ph_2P(O)NP(E)Ph_2\text{-}O,E\}(L–L)]$, $[Pd\{Ph_2P(O)NP(E)Ph_2\text{-}O,E\}Cl(PMe_2Ph)]$ or $[Pd\{Ph_2P(O)NP(E)Ph_2\text{-}O,E\}(PR_3)_2]PF_6$ in good yields. All compounds described have been characterised by a combination of multinuclear NMR [$^{31}P\{^1H\}$ and ^1H] and IR spectroscopy and microanalysis. The molecular structures of five complexes containing the selenium ligand **II** have been determined by single-crystal X-ray crystallography. Three different ring conformations were observed, a pseudo-butterfly, hinge and in the case of all three PR_3 complexes, pseudo-boat conformations. Within the Pd–O–P–N–P–Se rings there is evidence for π-electron delocalisation. © 1998 Elsevier Science Ltd. All rights reserved

Keywords: metallacycles; palladium; ligands; X-ray

INTRODUCTION

Over the last few years the co-ordination chemistry of the monoanionic ligands $[R_2P(E)NP(E)R_2]^-$ (R = alkyl, aryl, alkoxy, aryloxy; E = O, S, Se) has been the subject of great interest due principally to its close analogy to acetylacetonate (hereafter abbreviated acac) [1–34]. Whereas metal complexes of acac (and its derivatives) have found important applications in diverse areas such as catalysis, in organic synthesis, as medicinal based drugs, CVD precursors and in liquid crystals, metal complexes of $[R_2P(E)NP(E)R_2]^-$ have found only limited use as selective metal extraction agents [30] and NMR shift reagents (Ref [10] and references cited therein). Recently the tetranuclear Ag(I) cluster $[Ag\{Ph_2P(O)NP(O)Ph_2\}]_4.2EtOH$ has been shown to be an olefin epoxidation catalyst [9].

In common with acac, the principal co-ordination mode of $[R_2P(E)NP(E)R_2]^-$ is that of chelation through both E donor atoms although the propensity to adopt a range of other different bonding modes has been reported [6–9, 27, 31, 32, 34]. One particularly interesting feature that has emerged from the extensive studies concerning the co-ordination chemistry of $[R_2P(E)NP(E)R_2]^-$ is the ability of the M–E–P–N–P–E chelate to exist in different ring conformations. An initial report from this laboratory revealed that by modifying the exocyclic substituents (Ph vs OPh) bound to phosphorus in $[R_2P(S)NP(S)R_2]^-$ the Pt–S–P–N–P–S ring conformation in $[Pt\{R_2P(S)NP(S)R_2\text{-}S,S'\}(PR'_3)_2]PF_6$ (R = Ph or OPh; R′ = Me or Et) is significantly altered [24]. Silvestru and co-workers [23] found that in the manganese(I) complex $[Mn(CO)_4\{Ph_2P(S)NP(S)Ph_2\text{-}S,S'\}]$ the unit cell contains two independent monomeric molecules in which both Mn–S–P–N–P–S rings adopt dissimilar geometries. In 1996 we reported [17] an unusual homoleptic complex *cis*-$[Pd\{Ph_2P(O)NP(Se)Ph_2\text{-}O,Se\}_2]$ which, from X-ray crystallographic studies, revealed that both six-membered Pd–O–P–N–P–Se metallacycles assume disparate ring conformations (pseudo-boat and chair-like geometries) *within* the co-ordination sphere of the molecule.

* Author to whom correspondence should be addressed. E-mail: j.d.woollins@lboro.ac.uk

Since the mixed ligands $[Ph_2P(O)NP(E)Ph_2]^-$ (E = S or Se) have been very poorly studied [13, 17] we report here the synthesis and characterisation of some new palladium(II) complexes of the type *cis*-$[PdL_2\{Ph_2P(O)NP(E)Ph_2\text{-}O,E\}]$. Five crystal structure determinations have been performed on complexes bearing different *trans* ancillary ligands and furthermore reveal that the six-membered Pd–O–P–N–P–Se metallacycles can adopt a range of different ring conformations.

EXPERIMENTAL

General

All reactions were carried out in air using distilled solvents. The potassium salts of $[Ph_2P(O)NP(E)Ph_2]^-$ (E = S or Se) [17] and the metal complexes $[\{Pd(\mu\text{-}Cl)Cl(PMe_2Ph)\}_2]$ [35] and $[\{Pd(\mu\text{-}Cl)(L\text{–}L)\}_2]$ [L–L = dimethylbenzylamine ($C_9H_{12}N$) and *N*,*N*-dimethyl-1-naphthylamine ($C_{12}H_{12}N$)] [36] were prepared according to previous published procedures. The palladium(II) compounds $[PdCl_2(PR_3)_2]$ [$PR_3 = PPh_3$; $2PR_3 = Ph_2PCH_2CH_2PPh_2$ or *cis*-$Ph_2PCH{=}CHPPh_2$] were synthesised by stoichiometric addition of the appropriate PR_3 to [$PdCl_2$(cod)] (cod = cycloocta-1,5-diene) in dichloromethane. [$PdCl_2$(bipy)] was purchased from Aldrich Chemical Co. and used without further purification.

Infrared spectra were recorded as KBr pellets in the range 4000–200 cm^{-1} on a Perkin-Elmer System 2000 Fourier-transform spectrometer. $^{31}P\{^1H\}$ NMR spectra (36.2 MHz) were recorded on a JEOL FX90Q spectrometer with chemical shifts (δ) in ppm (± 0.1) to high frequency of 85% H_3PO_4 and coupling constants (J) in Hz (± 3). All NMR spectra were measured in $CDCl_3$ unless otherwise stated. Elemental analyses (Perkin-Elmer 2400 CHN Elemental Analyzer) were performed by the Loughborough University Analytical Service within the Department of Chemistry.

Palladium salts were provided on loan by Johnson Matthey.

Preparations

$[Pd\{Ph_2P(O)NP(S)Ph_2\text{-}O,S\}(bipy)]PF_6$, **1** To the solids [$PdCl_2$(bipy)] (0.054 g, 0.162 mmol) and $K[Ph_2P(O)NP(S)Ph_2]$ (0.076 g, 0.161 mmol) was added CH_3OH (2 cm^3). The solids dissolved to give an orange solution and after stirring for *ca.* 2 h a yellow suspension formed. To this was added $[NH_4][PF_6]$ (0.067 g, 0.411 mmol, 2.54 equivs.) in CH_3OH (*ca.* 0.5 cm^3) and the mixture stirred for 10 min. The solid **1** was isolated by suction filtration, washed with CH_3OH (*ca.* 1 cm^3) and dried *in vacuo*. Yield: 0.119 g, 87%. Compound **1** could be recrystallised from CH_2Cl_2/Et_2O.

In a similar manner $[Pd\{Ph_2P(O)NP(Se)Ph_2\text{-}O,Se\}(bipy)]PF_6$ **2** was prepared in 88% yield.

$[Pd\{Ph_2P(O)NP(S)Ph_2\text{-}O,S\}(C_9H_{12}N)]$, **3**. To a solution of $[\{Pd(\mu\text{-}Cl)(C_9H_{12}N)\}_2]$ (0.040 g, 0.0724 mmol) in thf (5 cm^3) was added solid $K[Ph_2P(O)NP(S)Ph_2]$ (0.072 g, 0.153 mmol) in one portion. After stirring for *ca.* 30 min, the solvent was evaporated to dryness *in vacuo*. The residue was dissolved in CH_2Cl_2 (2 cm^3), filtered through a small Celite pad and addition of petroleum ether (b.p. 60–80°C, *ca.* 15 cm^3) gave a pale yellow solid **3**. The product was collected by suction filtration and dried *in vacuo*. Yield: 0.084 g, 86%.

Using similar experimental conditions the following compounds were prepared: $[Pd\{Ph_2P(O)NP(Se)Ph_2\text{-}O,Se\}(C_9H_{12}N)]$ **4** (92%), $[Pd\{Ph_2P(O)NP(S)Ph_2\text{-}O,S\}(C_{12}H_{12}N)]$ **5** (96%) and $[Pd\{Ph_2P(O)NP(Se)Ph_2\text{-}O,Se\}(C_{12}H_{12}N)]$ **6** (89%). Slow diffusion of petroleum ether (b.p. 60–80°C) into a CH_2Cl_2 solution of **6** over the course of *ca.* 7 d gave crystals suitable for X-ray crystallography.

$[Pd\{Ph_2P(O)NP(S)Ph_2\text{-}O,S\}Cl(PMe_2Ph)]$, **7**. To a solution of $[\{Pd(\mu\text{-}Cl)Cl(PMe_2Ph)\}_2]$ (0.042 g, 0.067 mmol) in thf (5 cm^3) was added solid $K[Ph_2P(O)NP(S)Ph_2]$ (0.065 g, 0.138 mmol) in one portion. After stirring for *ca.* 30 min, the solvent was evaporated to dryness *in vacuo*. The residue was dissolved in CH_2Cl_2 (2 cm^3), filtered through a small Celite pad and addition of petroleum ether (b.p. 60–80°C, 20 cm^3) gave a yellow solid. The product was collected by suction filtration and dried *in vacuo*. Yield: 0.088 g, 93%.

In a similar manner $[Pd\{Ph_2P(O)NP(Se)Ph_2\text{-}O,Se\}Cl(PMe_2Ph)]$, **8**, was prepared in 70% yield. Slow diffusion of petroleum ether (b.p. 60–80°C) into a $CDCl_3$ solution of **8** over the course of *ca.* 5 d gave crystals suitable for X-ray crystallography.

$[Pd\{Ph_2P(O)NP(Se)Ph_2\text{-}O,Se\}(Ph_2PCH_2CH_2PPh_2)][PF_6]$, **12**. The solids $[PdCl_2(Ph_2PCH_2CH_2PPh_2)]$ (0.048 g, 0.0834 mmol) and $K[Ph_2P(O)NP(Se)Ph_2]$ (0.047 g, 0.091 mmol) were suspended in CH_3OH (2 cm^3). After stirring for 2 h the yellow solution was treated with a methanolic solution of $[NH_4][PF_6]$ (0.032 g, 0.196 mmol, 2.35 equivs.) whereupon a yellow precipitate formed immediately. The mixture was stirred for *ca.* 10 min and the product **12** collected by suction filtration and dried *in vacuo*. Yield: 0.082 g, 87%.

The following cationic compounds were synthesised using a similar method: $[Pd\{Ph_2P(O)NP(S)Ph_2\text{-}O,S\}(PPh_3)_2][PF_6]$ **9** (94%), $[Pd\{Ph_2P(O)NP(Se)Ph_2\text{-}O,Se\}(PPh_3)_2][PF_6]$ **10** (94%), $[Pd\{Ph_2P(O)NP(S)Ph_2\text{-}O,S\}(Ph_2PCH_2CH_2PPh_2)][PF_6]$ **11** (90%), $[Pd\{Ph_2P(O)NP(S)Ph_2\text{-}O,S\}(cis\text{-}Ph_2PCH{=}CHPPh_2)][PF_6]$ **13** (79%) and $[Pd\{Ph_2P(O)NP(Se)Ph_2\text{-}O,Se\}(cis\text{-}Ph_2PCH{=}CHPPh_2)][PF_6]$ **14** (92%). Slow diffusion of diethyl ether into either $CDCl_3$ (or CH_2Cl_2) solutions of **10**, **12** or **14** over the course of several days gave crystals suitable for X-ray crystallography.

Microanalytical and selected spectroscopic data for compounds **1**–**14** are given in Tables 2 and 3.

Table 1. Details of the X-ray data collections and refinements for compounds **6**, **8**, **10**, **12** and **14**

Compound	**6**	**8**	**10**	**12**	**14**
Empirical formula	$C_{37}H_{34}Cl_2N_2OP_2PdSe$	$C_{32}H_{31}ClNOP_3PdSe$	$C_{60}H_{50}F_6NOP_5PdSe$	$C_{50}H_{44}F_6NOP_5PdSe$	$C_{52}H_{42}NOP_5F_6PdSe$
Crystal colour, habit	pale yellow, block	yellow/orange, plate	yellow, plate	yellow, plate	yellow, plate
Crystal dimensions (mm)	$0.20 \times 0.20 \times 0.12$	$0.10 \times 0.13 \times 0.13$	$0.03 \times 0.10 \times 0.20$	$0.06 \times 0.10 \times 0.15$	$0.06 \times 0.10 \times 0.15$
Crystal system	triclinic	triclinic	monoclinic	triclinic	orthorhombic
Space group	P-1	P-1	$P2_1/n$	P-1	$P2_12_12$
Lattice cell parameters					
a (Å)	11.658(2)	11.681(1)	11.891(3)	13.594(3)	15.433(3)
b (Å)	14.729(1)	12.7794(8)	17.161(6)	17.447(2)	29.404(5)
c (Å)	11.548(1)	10.7800(9)	27.861(4)	11.221(2)	11.201(4)
α (°)	108.497(7)	98.983(6)		91.83(1)	
β (°)	103.16(1)	101.008(8)	101.85(2)	107.46(2)	
γ (°)	75.62(1)	89.681(7)		103.74(1)	
Volume (Å^3)	1797(4)	1560(2)	5564(2)	2451(9)	5083(2)
Z value	2	2	4	2	4
Formula weight	840.9	759.34	1255.28	1129.12	1151.13
Density$_{calc}$ (g/cm^3)	1.55	1.62	1.50	1.53	1.50
Absorption coefficient (mm^{-1})	7.78	8.58	5.43	5.96	5.76
$2\theta_{max}$ (°)	120.1	120.2	120.1	120.3	120.1
$F(000)$	844	760	2536	1136	2312
Measured reflections	5654	4906	9093	7672	4283
Independent reflections	5349	4642	8623	7315	
Observed reflections [$I > 2.0\sigma(I)$]	3882	3369	2677	4684	2116
Reflection/parameter ratio	8.94:1	9.31:1	7.12:1	7.98:1	6.74:1
Min./max. transmission	0.37, 1.00	0.92, 1.00	0.66, 1.00	0.57, 1.00	0.68, 1.00
Weighting scheme, p[a]	0.003	0.004	0.002	0.004	0.006
No. of variables	434	362	376	587	314
Final R, R_w	0.048, 0.047	0.039, 0.041	0.053, 0.047	0.044, 0.037	0.080, 0.079
Maximum Δ/σ	3.30	0.01	0.00	0.05	0.97
Largest difference peak/hole (e Å^{-3})	0.70, −0.89	0.58, −0.60	0.61, −0.43	0.47, −0.65	0.79, −0.58

[a] The weighting scheme is as defined in Ref.[39].

Table 2. Microanalytical data (calculated values in parentheses) for compounds **1**–**14**

Compound	Analysis (%)		
	C	H	N
1	48.10 (48.60)	3.25 (3.35)	5.00 (5.00)
2	45.35 (46.05)	3.00 (3.20)	4.80 (4.75)
3	58.45 (58.90)	4.55 (4.80)	3.90 (4.15)
4	55.10 (55.05)	4.25 (4.50)	3.85 (3.90)
5	59.95 (60.95)	4.25 (4.55)	3.45 (3.95)
6	56.65 (57.20)	4.25 (4.25)	3.30 (3.70)
7	53.70 (53.95)	4.00 (4.40)	1.90 (1.95)
8	50.15 (50.60)	3.75 (4.10)	1.90 (1.85)
9	59.05 (59.65)	4.00 (4.20)	1.10 (1.15)
10	57.35 (57.40)	3.90 (4.00)	1.05 (1.10)
11	55.10 (55.50)	3.95 (4.10)	1.20 (1.30)
12	53.00 (53.20)	3.90 (3.95)	1.15 (1.25)
13	55.45 (55.60)	3.80 (3.95)	1.20 (1.30)
14	52.65 (53.25)	3.65 (3.75)	1.10 (1.25)

X-ray crystallography

The crystal structures of complexes **6**, **8**, **10**, **12** and **14** were determined using a Rigaku AFC7S diffractometer with graphite-monochromated (Cu–Kα) radiation and ω-scans. Details of the data collections and refinements are given in Table 1. Empirical absorption corrections (DIFABS [37]) were applied. Psi-scans proved unsatisfactory and DIFABS gave generally superior results. The structures were solved by the heavy-atom method [38]. In **14** poor crystal quality and the presence of an unidentified solvent fragment precluded complete refinement of the structure. The Pd, Se, P, N and O atoms were refined anisotropically whilst the C and F atoms were refined isotropically with the phenyl rings being refined as rigid bodies. All of the non-hydrogen atoms in the other structures were refined anisotropically. The C–H atoms were idealised and fixed (C–H, 0.95 Å). No additional constraints or restraints were applied. Refinement was by full-matrix least-squares methods based on *F*. Calculations were performed using TEXSAN [39].

Table 3. Selected spectroscopic data for compounds **1**–**14**

Compound	$\delta(P_O)$	$\delta(P_E)$[a]	$\delta(PR_3)$	^1J(PSe)	J(PP)	IR ν(PE)[a]
I[b]	13.9	35.3			3.3	
II[b]	12.9	23.6		664	2.2	
1[c]	40.8[d]	36.6				579
2[c]	42.3[e]	23.1		470		544
3[f]	26.5	33.6			4.4	581
4[g]	26.5	17.7		510	2.2	562
5[h]	27.4	33.4			3.8	583
6[i]	27.5	17.8		511	2.8	560
7[j]	30.0	30.0	10.5[k]			574[l]
8[m]	30.8	15.1	8.8[k]	484		555[n]
9	30.3[o]	32.6	38.9, 30.3			572
10	34.0[o]	18.6	36.7, 26.0	493		558
11	30.8[o]	31.7	67.9, 66.1			579
12	32.1	17.9	67.1, 62.9	492	8.5	557
13	32.5[o]	31.6	74.3, 71.4			576
14	32.8	18.9	72.0, 70.2	479		562

[a] E = S or Se.
[b] Taken from Ref.[17].
[c] Recorded in CD_2Cl_2.
[d] ^{1}H NMR: δ 8.99–5.31 (arom. H).
[e] ^{1}H NMR: δ 9.04–5.31 (arom. H).
[f] ^{1}H NMR: δ 8.01–6.87 (arom. H); 3.86 (CH_2); 2.65 (NCH_3).
[g] ^{1}H NMR: δ 7.98–6.83 (arom. H); 3.87 (CH_2); 2.63 (NCH_3).
[h] ^{1}H NMR: δ 8.02–7.21 (arom. H); 3.24 (NCH_3).
[i] ^{1}H NMR: δ 7.95–7.06 (arom. H); 3.15 (NCH_3).
[j] ^{1}H NMR: δ 7.92–7.30 (arom. H); 1.65 [^2J(PH) 12.3, (PCH_3)].
[k] $PR_3 = PMe_2Ph$.
[l] ν(PdCl) = 306.
[m] ^{1}H NMR: δ 7.94–7.30 (arom. H); 1.70 ^2J(PH) 12.5, (PCH_3)].
[n] ν(PdCl) = 308.
[o] Tentative assignment only.

RESULTS AND DISCUSSION

O,E-Chelate complexes of $[Ph_2P(O)NP(E)Ph_2]^-$ (*E = S or Se*)

We previously reported the synthesis of the mixed ligands $K[Ph_2P(O)NP(E)Ph_2]$ (E = S **I**; E = Se **II**) from the monooxidised compound $Ph_2P(O)NHPPh_2$ and elemental sulfur (or selenium) followed by deprotonation with base [17].

The stoichiometric reaction of $[PdCl_2(bipy)]$ (bipy = 2,2′-bipyridine) and one equivalent of either **I** (or **II**) in CH_3OH, followed by addition of a methanolic solution of $[NH_4][PF_6]$, gave the cationic complexes $[Pd\{Ph_2P(O)NP(E)Ph_2\text{-}O,E\}(bipy)]PF_6$ (E = S **1**; E = Se **2**) (Scheme 1). Analytical and spectroscopic data are given in Tables 2 and 3 and are broadly as expected. The $^{31}P\{^1H\}$ NMR spectra of **1** and **2** show, in both cases, two singlet resonances [*J*(PP) coupling not resolved] corresponding to P_O and P_E of the chelating $[Ph_2P(O)NP(E)Ph_2]^-$. In addition, the ^1J(PSe) coupling constant of 470 Hz for **2** is of similar magnitude to that reported for *cis*-$[Pd\{Ph_2P(O)NP(Se)Ph_2\text{-}O,Se\}_2]$ [^1J(PSe) 492 Hz] [17]. Treatment of **I** (or **II**) with the chloro bridged binuclear compounds $[\{Pd(\mu\text{-}Cl)(L\text{–}L)\}_2]$ (L–L = $C_9H_{12}N$ or $C_{12}H_{12}N$) or $[\{Pd(\mu\text{-}Cl)Cl(PMe_2Ph)\}_2]$ gave the neutral complexes $[Pd\{Ph_2P(O)NP(E)Ph_2\text{-}O,E\}(L\text{–}L)]$ (E = S, L–L = $C_9H_{12}N$ **3**; E = Se, L–L = $C_9H_{12}N$ **4**; E = S, L–L = $C_{12}H_{12}N$ **5**; E = Se, L–L = $C_{12}H_{12}N$ **6**) and $[Pd\{Ph_2P(O)NP(E)Ph_2\text{-}O,E\}Cl(PMe_2Ph)]$ (E = S **7**; E = Se **8**) in respectable yields (70–96%). Compounds **3**–**8** were characterised by a combination of $^{31}P\{^1H\}$, ^1H and IR spectroscopy (Table 3) and microanalysis (Table 2). In particular, $\delta(P_O)$ for **3**–**8** is shifted to lower frequency (*ca.* 10–15 ppm) with respect to **1** and **2** and to higher frequency (*ca.* 10–15 ppm) with respect to **I** and **II**. The $^{31}P\{^1H\}$ and ^1H NMR spectra of **3**–**8** (recorded in $CDCl_3$) confirm that, in all cases, only one isomer is present in solution (either the geometric isomer **A** or **B**). X-ray crystallogaphic studies on compounds **6** and **8** (*vide infra*) unambiguously demonstrate that isomer **A** (E *trans* to X where X = N, Cl) is exclusively formed. The formation of one isomer has also been observed in the related cyclopalladated complexes $[Pd\{Ph_2P(O)NPPh_2\text{-}O,P\}(L\text{–}L)]$ (L–L = $C_9H_{12}N$, $C_{10}H_8N$, $C_{12}H_{12}N$) (P *trans* to N) [40] but in contrast, both isomers of $[Pt\{Ph_2P(O)NPPh_2\text{-}O,P\}Cl(PMe_2Ph)]$ have been independently synthesised and fully characterised [41]. Furthermore in the complexes $[Pd\{Ph_2P(S)NP(Se)Ph_2\text{-}S,Se\}(L\text{–}L)]$ (L–L = $C_9H_{12}N$,

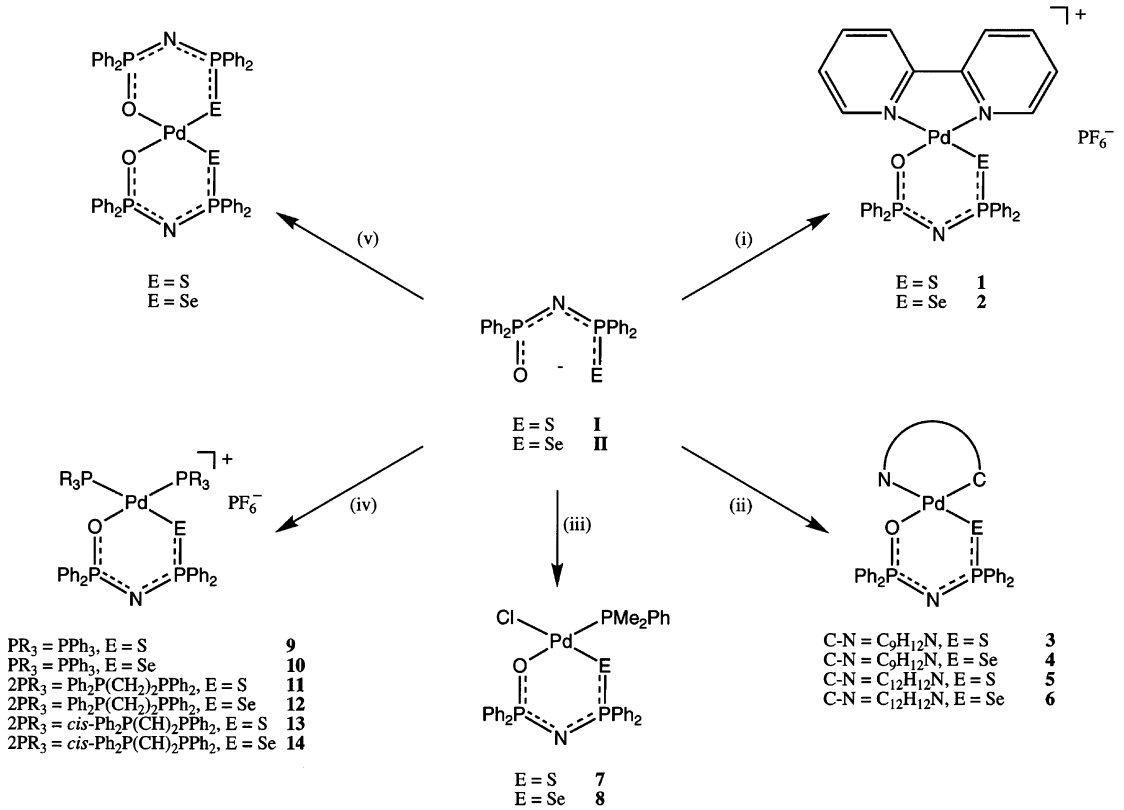

Scheme 1. (i) $[PdCl_2(bipy)]$, $[NH_4][PF_6]$, (ii) $[\{Pd(\mu\text{-}Cl)(L\text{-}L)\}_2]$ (L-L = $C_9H_{12}N$ or $C_{12}H_{12}N$), (iii) $[\{Pd(\mu\text{-}Cl)Cl(PMe_2Ph)\}_2]$, (iv) $[PdCl_2(PR_3)_2]$ ($PR_3 = PPh_3$; $2PR_3 = Ph_2PCH_2CH_2PPh_2$, *cis*-$Ph_2PCH{=}CHPPh_2$), $[NH_4][PF_6]$ and (v) $[PdCl_2(cod)]$ (cod = cycloocta-1,5-diene).

A **B**

O-E = $OPPh_2NPPh_2S$, $OPPh_2NPPh_2Se$
X,Y = $C_9H_{12}N$, $C_{12}H_{12}N$, Cl/PMe_2Ph

Isomers A and B

$C_{12}H_{12}N$) containing different "soft" donor centres, both isomers were detected in $CDCl_3$ solution in *ca.* 5:1 ratio ($^{31}P\{^1H\}$ evidence) [42].

We have also prepared several square-planar palladium(II) complexes with one chelating $[Ph_2P(O)NP(E)Ph_2\text{-}O,E]^-$ and several different tertiary phosphine ligands. Hence replacement of both chloride ligands in $[PdCl_2(PR_3)_2]$ [$PR_3 = PPh_3$; $2PR_3 = Ph_2PCH_2CH_2PPh_2$, *cis*-$Ph_2PCH{=}CHPPh_2$] with one equivalent of **I** (or **II**) in CH_3OH presumably affords the cations $[Pd\{Ph_2P(O)NP(E)Ph_2\text{-}O,E\}(PR_3)_2]Cl$. The cationic compounds were most conveniently obtained as their hexafluorophosphate salts by metathesis with $[NH_4][PF_6]$ in CH_3OH. In this manner we have isolated $[Pd\{Ph_2P(O)NP(E)Ph_2\text{-}O,E\}(PR_3)_2][PF_6]$ (E = S, $PR_3 = PPh_3$ **9**; E = Se, $PR_3 = PPh_3$ **10**; E = S, $2PR_3 = Ph_2PCH_2CH_2PPh_2$ **11**; E = Se, $2PR_3 = Ph_2PCH_2CH_2PPh_2$ **12**; E = S, $2PR_3$ = *cis*-$Ph_2PCH{=}CHPPh_2$ **13**; E = Se, $2PR_3$ = *cis*-$Ph_2PCH{=}CHPPh_2$ **14** (Scheme 1) in good yields. The *in situ* reaction between $[PdCl_2(Ph_2PCH_2CH_2PPh_2)]$ and **I** (1:1 ratio) in CH_3OH gave exclusively $[Pd\{Ph_2P(O)NP(S)Ph_2\text{-}O,S\}(Ph_2PCH_2CH_2PPh_2)]Cl$ verified by $^{31}P\{^1H\}$ NMR spectroscopy. We have also been able to liberate $[Ph_2P(O)NP(S)Ph_2]^-$ (^{31}P NMR evidence) by treatment of **11** with concentrated HCl [affording the parent acid $Ph_2P(O)NHP(S)Ph_2$] or by the addition of one equivalent of $Ph_2PCH_2CH_2PPh_2$ [giving $[Ph_2P(O)NP(S)Ph_2]^-$ and the dication $[Pd(Ph_2PCH_2CH_2PPh_2)_2]^{2+}$]. Compounds **9**–**14** were characterised by $^{31}P\{^1H\}$ NMR and IR (Table 3 for data). Typically the $^{31}P\{^1H\}$ NMR data reveal that $\delta(P_S)$ for **9**, **11** and **13** is observed at *ca.* 32 ppm whilst for **10**, **12** and **14** $\delta(P_{Se})$ is around 18 ppm with $^1J(PSe)$ *ca.* 490 Hz. Moreover the two inequivalent phosphorus centres of the co-ordinated tertiary phosphines in **9**–**14** have similar $\delta(P)$ to those observed in $[PdCl_2(PR_3)_2]$. Consistent with $[Ph_2P(O)NP(E)Ph_2\text{-}O,E]^-$ chelate formation was the absence of ν(PdCl) absorptions and the presence of ν(PE) absorptions which in the latter case, could not accurately be assigned with confidence.

Crystal structure determinations of complexes **6**, **8**, **10**, **12** and **14**

The structures of **6**, **8**, **10**, **12** and **14** (Table 4, Figs 1–5) have some common features. Thus all five complexes display the expected square planar geometry (Table 5 gives the maximum deviation from the ML_4 co-ordination plane). The Pd–P bond lengths reflect the nature of the *trans* ligand. Thus in **10**, **12** and **14** Pd(1)–P(4) (*trans* to selenium) is larger than Pd(1)–P(3) (*trans* to oxygen) suggesting that the Se atom is a poorer σ donor/better π acceptor than the O atom. The Pd–Se bond lengths vary [2.406(1)–2.521(1) Å] also as a consequence of the *trans* ligand. The phosphine ligands *trans* to Se give the largest Pd–Se bonds whilst N and Cl give the shortest Pd–Se distances which are not distinguishable from each other. Interestingly the Pd–Se bond lengths in *cis*-$[Pd\{Ph_2P(O)NP(Se)Ph\text{-}O,Se\}_2]$, with *cis* O donors, (Table 4 and Fig. 6) are much shorter than any of those reported here. The Pd–O distances are in the range 2.083(4)–2.129(5) Å [c.f. 2.075(3) and 2.085(3) Å for *cis*-$[Pd\{Ph_2P(O)NP(Se)Ph\text{-}O,Se\}_2]$ [17]] and as anticipated are less sensitive to the identity of the *trans* atom. Within the Pd–O–P–N–P–Se metallacycle the bond lengths are consistent with a fair degree of delocalisation.

The conformation of the Pd–O–P–N–P–Se rings vary somewhat in the various structures. Compound **6** has a unique conformation and the ring is best described as consisting of two planar fragments Pd(1)–Se(1)–P(1)–N(1) and Pd(1)–O(1)–P(2)–N(1) which are inclined by 36° with respect to each other. This difference in geometry is noticeable in the Pd(1)–Se(1)–P(1) angle for **6** [104.68(7)°] which lies well outside the range observed in the other structures including *cis*-$[Pd\{Ph_2P(O)NP(Se)Ph\text{-}O,Se\}_2]$ [93.46(6)–101.5(4)°]. The conformation in **6** can be described as pseudo-butterfly and to the best of our knowledge has not been observed before in ME_2P_2N systems. Compound **8** has a ring conformation which, though rare, is similar to that observed in some previous examples [17,

Table 4. Selected bond lengths (Å) and angles (°) for compounds **6**, **8**, **10**, **12** and **14**

	6	**8**	**10**	**12**	**14**	[Pd{$Ph_2P(O)NP(Se)Ph_2$-*O*,*Se*}$_2$][a]	
Pd(1)–Se(1)	2.406(1)	2.409(1)	2.457(2)	2.521(1)	2.493(4)	2.381(7)	2.383(8)
Se(1)–P(1)	2.182(2)	2.186(2)	2.195(4)	2.192(2)	2.176(7)	2.201(1)	2.198(2)
P(1)–N(1)	1.574(6)	1.580(5)	1.572(10)	1.574(5)	1.653(19)	1.586(4)	1.577(4)
N(1)–P(2)	1.604(6)	1.594(5)	1.601(11)	1.598(5)	1.559(19)	1.603(4)	1.584(4)
P(2)–O(1)	1.531(6)	1.520(4)	1.537(9)	1.536(4)	1.555(19)	1.519(3)	1.524(3)
O(1)–Pd(1)	2.129(5)	2.117(4)	2.104(9)	2.083(4)	2.110(16)	2.085(3)	2.075(3)
Pd(1)–C(32)	1.965(8)						
Pd(1)–N(2)	2.087(7)						
Pd(1)–P(3)		2.211(2)	2.254(4)	2.219(2)	2.224(8)		
Pd(1)–Cl(1)		2.336(2)					
Pd(1)–P(4)			2.354(4)	2.266(2)	2.251(8)		
Pd(1)–Se(1)–P(1)	104.68(7)	95.36(6)	98.6(1)	93.46(6)	97.8(2)	101.5(4)	96.6(1)
Se(1)–P(1)–N(1)	118.2(3)	118.0(2)	116.6(5)	116.5(2)	115.6(8)	115.8(1)	116.8(2)
P(1)–N(1)–P(2)	126.4(4)	131.6(3)	125.8(7)	123.0(3)	124.8(12)	123.7(2)	132.1(3)
N(1)–P(2)–O(1)	118.1(3)	118.1(3)	117.1(6)	117.0(3)	115.8(10)	117.4(2)	118.2(2)
P(2)–O(1)–Pd(1)	130.0(3)	125.2(3)	134.0(5)	125.0(2)	121.3(10)	124.3(2)	123.6(2)
O(1)–Pd(1)–Se(1)	99.4(2)	92.0(1)	96.1(2)	98.7(1)	100.3(5)	99.8(1)	91.6(1)
C(32)–Pd(1)–Se(1)	90.9(2)						
C(32)–Pd(1)–N(2)	84.1(3)						
N(2)–Pd(1)–O(1)	85.7(2)						
P(3)–Pd(1)–Se(1)		92.39(6)	86.5(1)	92.06(6)	87.9(2)		
P(3)–Pd(1)–Cl(1)		87.51(7)					
Cl(1)–Pd(1)–O(1)		89.0(1)					
P(3)–Pd(1)–P(4)			94.9(1)	84.86(7)	85.7(3)		
P(4)–Pd(1)–O(1)			82.6(3)	84.7(1)	85.8(5)		
O(1)–Pd(1)–O(2)						85.8(1)	
Se(1)–Pd(1)–Se(2)						82.8(1)	

[a] Taken from Ref.[17].

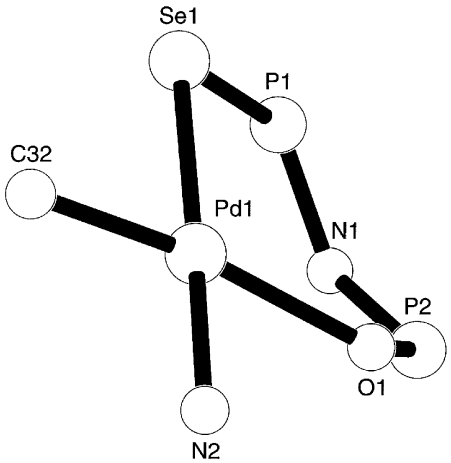

Fig. 1. Core geometry in [Pd{$Ph_2P(O)NP(Se)Ph_2$-*O*,*Se*}($C_{12}H_{12}N$)], **6**.

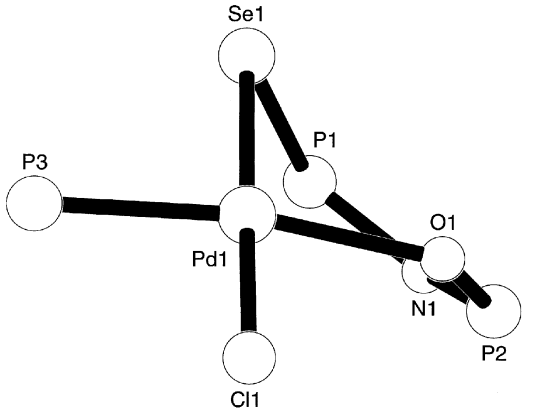

Fig. 2. Core geometry in [Pd{$Ph_2P(O)NP(Se)Ph_2$-*O*,*Se*}Cl(PMe_2Ph)], **8**.

24] with the six-membered ring being hinged about the O(1)...Se(1) vector (hinge angle 60°) and the O(1)–P(1)–N(1)–P(2)–Se(1) atoms forming an approximate planar array [maximum deviation of this mean plane is 0.27 Å for O(1)]. Compounds **10**, **12** and **14** have quite closely related ring conformations which can be most readily described as pseudo-boat with Se(1) at the prow and P(2) at the stern of the "boat". The Pd(1)...P(1) hinge angle in **10**, **12** and **14** are very similar (*ca.* 40°) but there are some differences in the hinge angle at O(1)...N(1) (Table 5). It appears that the smallest O(1)...N(1) hinge angle is

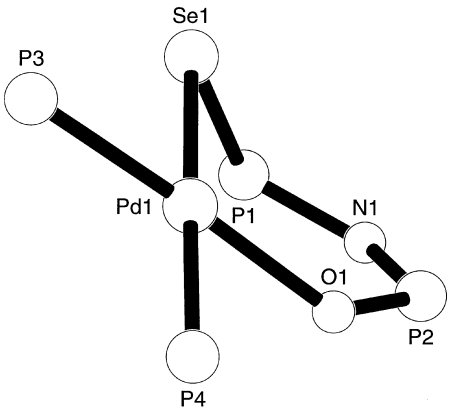

Fig. 3. Core geometry in [Pd{$Ph_2P(O)NP(Se)Ph_2$-*O*,*Se*}$(PPh_3)_2$][PF_6], **10**.

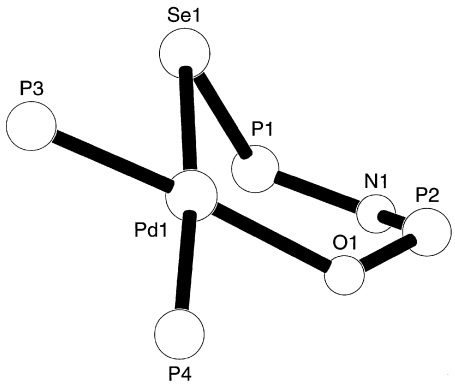

Fig. 4. Core geometry in [Pd{$Ph_2P(O)NP(Se)Ph_2$-*O*,*Se*}$(Ph_2PCH_2CH_2PPh_2)$][PF_6], **12**.

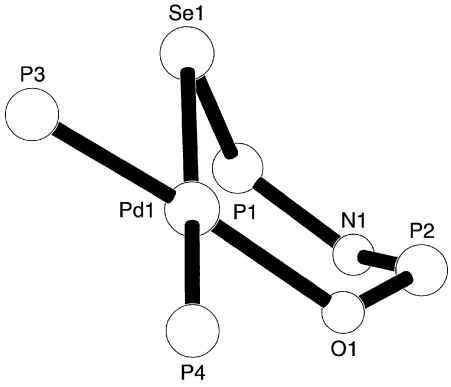

Fig. 5. Core geometry in [Pd{$Ph_2P(O)NP(Se)Ph_2$-*O*,*Se*}(*cis*-$Ph_2PCH=CHPPh_2$)][PF_6], **14**.

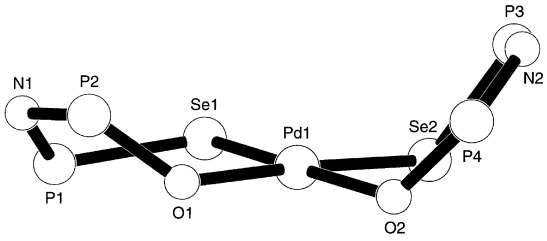

Fig. 6. Core geometry in *cis*-[Pd{$Ph_2P(O)NP(Se)Ph_2$-*O*,*Se*}$_2$] (taken from Ref. [17]).

for the bulkiest phosphine (PPh_3) and this is further reflected in the O(1)–Pd(1)–Se(1) angle which increases in the order **10** < **12** < **14** in parallel with the change in hinge angle.

Overall then, it appears that the $PdSeOP_2N$ ring is able to adopt a range of geometries and the nature of the *trans* ligand does influence the geometry within the metallacycle.

CONCLUDING REMARKS

We have shown that a range of new palladium(II) complexes with a chelating anionic [$Ph_2P(O)NP(E)Ph_2$]$^-$ (E = S or Se) ligand are ammenable and have been fully characterised. Furthermore from X-ray structure studies it is apparent that the Pd–O–P–N–P–Se six-membered chelate ring is flexible and can take up a range of conformations. Further work into the generality of these observations would be useful.

Acknowledgements—We are grateful to the EPSRC for support and to Johnson Matthey for loans of precious metals.

Table 5. Planarity and conformational details in the X-ray structures of **6**, **8**, **10**, **12** and **14**

	6	**8**	**10**	**12**	**14**
ML_4 co-ordination plane (max. deviation) (Å)	0.16 [N(2)]	0.29 [O(1)]	0.02 [O(1)]	0.14 [P(4)]	0.17 [P(4)]
Pd(1)–Se(1)–P(1)–N(1)/Pd(1)–O(1)–P(2)–N(1) hinge angle (°)	36	–	–	–	–
Pd(1)–Se(1)–O(1)/Se(1)–P(1)–N(1)–P(2)–O(1) hinge angle (°)	–	60	–	–	–
Pd(1)–P(1)–N(1)–O(1) (max. deviation) (Å)	–	–	0.23 [N(1)]	0.21 [N(1)]	0.05 [N(1)]
Pd(1)–Se(1)–P(1)/Pd(1)–O(1)–N(1)–P(1) hinge angle (°)	–	–	40	43	40
Pd(1)–O(1)–N(1)–P(1)/O(1)–P(2)–N(1) hinge angle (°)	–	–	25	40	48

REFERENCES

1. Kräuter, G., Sunny, S. K., Rees, W. S. Jr, *Polyhedron*, 1998, **17,** 391.
2. Silvestru, C., Rösler, R., Drake, J. E., Yang, J., Espinosa-Pérez, G. and Haiduc, I., *J. Chem. Soc. Dalton Trans.*, 1998, 73.
3. García-Montalvo, V., Novosad, J., Kilian, P., Woollins, J. D., Slawin, A. M. Z., García y García, P., López-Cardoso, M., Espinosa-Pérez, G. and Cea-Olivares, R., *J. Chem. Soc. Dalton Trans.*, 1997, 1025.
4. Papadimitriou, C., Veltsistas, P., Novosad, J., Cea-Olivares, R., Toscano, A., García y García, P., López-Cardosa, M., Slawin, A. M. Z. and Woollins, J. D., *Polyhedron*, 1997, **16,** 2727.
5. Abram, U., Schulz Lang, E., Abram, S., Wegmann, J., Dilworth, J. R., Kirmse, R. and Woollins, J. D., *J. Chem. Soc. Dalton Trans.*, 1997, 623.
6. Geissinger, M. and Magull, J., *Z. Anorg. Allg. Chem.*, 1997, **623,** 755.
7. Ho, E. N.-M. and Wong, W.-T., *J. Chem. Soc. Dalton Trans.*, 1997, 915.
8. Yang, J., Drake, J. E., Hernandez-Ortega, S., Rösler, R. and Silvestru, C., *Polyhedron*, 1997, **16,** 4061.
9. Rudler, H., Denise, B., Gregorio, J. R. and Vaissermann, J., *Chem. Commun.*, 1997, 2299.
10. Barkaoui, L., Charrouf, M., Rager, M.-N., Denise, B., Platzer, N. and Rudler, H., *Bull. Soc. Chim. Fr.*, 1997, **134,** 167.
11. García-Montalvo, V., Cea-Olivares, R., Williams, D. J. and Espinosa-Pérez, G., *Inorg. Chem.*, 1996, **35,** 3948.
12. García-Montalvo, V., Cea-Olivares, R. and Espinosa-Pérez, G., *Polyhedron*, 1996, **15,** 829.
13. Rösler, R., Drake, J. E., Silvestru, C., Yang, J. and Haiduc, I., *J. Chem. Soc. Dalton Trans.*, 1996, 391.
14. Cea-Olivares, R., García-Montalvo, V., Novosad, J., Woollins, J. D., Toscano, R. A. and Espinosa-Pérez, G., *Chem. Ber.*, 1996, **129,** 919.
15. Woollins, J. D., *J. Chem. Soc. Dalton Trans.*, 1996, 2893.
16. Cupertino, D., Keyte, R., Slawin, A. M. Z., Williams, D. J. and Woollins, J. D., *Inorg. Chem.*, 1996, **35,** 2695.
17. Slawin, A. M. Z., Smith, M. B. and Woollins, J. D., *J. Chem. Soc. Dalton Trans.*, 1996, 3659.
18. Browning, C. S., Farrar, D. H. and Frankel, D. C., *Inorg. Chim. Acta*, 1996, **241,** 111.
19. Williams, D. J., Slawin, A. M. Z., Phillips, J. R. and Woollins, J. D., *Polyhedron*, 1996, **15,** 3175.
20. Bhattacharyya, P., Novosad, J., Phillips, J., Slawin, A. M. Z., Williams, D. J. and Woollins, J. D., *J. Chem. Soc. Dalton Trans.*, 1995, 1607.
21. Silvestru, C., Rösler, R., Haiduc, I., Cea-Olivares, R. and Espinosa-Pérez, G., *Inorg. Chem.*, 1995, **34,** 3352.
22. Bhattacharyya, P., Slawin, A. M. Z., Williams, D. J. and Woollins, J. D., *J. Chem. Soc. Dalton Trans.*, 1995, 2489.
23. Zúñiga-Villarreal, N., Silvestru, C., Reyes Lezama, M., Hernández-Ortega, S. and Alvarez Toledano, C., *J. Organomet. Chem.*, 1995, **496,** 169.
24. Phillips, J. R., Slawin, A. M. Z., White, A. J. P., Williams, D. J. and Woollins, J. D., *J. Chem. Soc. Dalton Trans.*, 1995, 2467.
25. Bock, H., Schödel, H., Havlas, Z. and Herrmann, E., *Angew. Chem. Int. Ed. Engl.*, 1995, **34,** 1355.
26. Haiduc, I., Cea-Olivares, R., Toscano, R. A. and Silvestru, C., *Polyhedron*, 1995, **14,** 1067.
27. Slawin, A. M. Z., Ward, J., Williams, D. J. and Woollins, J. D., *J. Chem. Soc. Chem. Commun.*, 1994, 421.
28. Rossi, R., Marchi, A., Marvelli, L., Magon, L., Peruzzini, M., Casellato, U. and Graziani, R., *J. Chem. Soc. Dalton Trans.*, 1993, 723.
29. Haiduc, I., Silvestru, C., Roesky, H. W., Schmidt, H.-G. and Noltemeyer, M., *Polyhedron*, 1993, **12,** 69.
30. Navrátil, O., Herrmann, E., Grossmann, G. and Teply, J., *Collect. Czech. Chem. Commun.*, 1990, **55,** 364.
31. Zak, P. Z., Fofana, M., Kamenicek, J. and Gloweiak, T., *Acta Cryst. C*, 1989, **45,** 1686.
32. Laguna, A., Laguna, M., Rojo, A. and Fraile, M. N., *J. Organomet. Chem.*, 1986, **315,** 269.
33. Chen, H. W., Paparizos, C., Fackler, J. P. Jr, *Inorg. Chim. Acta*, 1985, **96,** 137.
34. Richter, H., Fluck, E. and Schwarz, W., *Z. Naturforsch. B*, 1980, **35,** 578.
35. Chatt, J., *J. Chem. Soc.*, 1951, 652.
36. Cope, A. C. and Friedrich, E. C., *J. Am. Chem. Soc.*, 1968, **90,** 909.
37. Walker, N. G. and Stuart, D., DIFABS, *Acta Cryst. A*, 1983, **39,** 158.
38. Beurskens, P. T., Admiraal, G., Beurskens, G., Bosman, W. P., Garcia-Granda, S., Gould, R. O., Smits, J. M. M. and Smykalla, C., *DIRDIF* 92-*PATTY. The DIRDIF Program System*. Technical Report of the Crystallography Laboratory, University of Nijmegen, 1992.
39. *TEXSAN*, *Crystal Structure Analysis Package*. Molecular Structure Corporation, The Woodlands, TX, 1985 and 1992.
40. Slawin, A. M. Z., Smith, M. B. and Woollins, J. D., *J. Chem. Soc. Dalton Trans.*, 1996, 1283.
41. Slawin, A. M. Z., Smith, M. B. and Woollins, J. D., *J. Chem. Soc. Dalton Trans.*, 1996, 4567.
42. Bhattacharyya, P., Slawin, A. M. Z. and Smith, M. B., *J. Chem. Soc. Dalton Trans.*, 1998, 2467.

Pergamon

Polyhedron Vol. 17, Nos. 25, 26, pp. 4475–4486, 1998
© 1998 Elsevier Science Ltd
All rights reserved. Printed in Great Britain
PII: S0277–5387(98)00254–X
0277–5387/98 $19.00+0.00

Syntheses and structures of diorgano(halo- or pseudohalo-) (1,3-dithiole-2-thione-4,5-dithiolato)-stannates (1-), [Q] [$R_2SnX(dmit)$] (Q = onium cation; X = halide or pseudohalide)

John H. Aupers,[a] Zahid H. Chohan,[b] Philip J. Cox,[c]
Solange M. S. V. Doidge-Harrison,[d] Alan Howie.[b] Abdullah Khan,[b]
Gavin M. Spencer[b] and James L. Wardell[b]†

[a]Rose Cottage, Middle Assendon, Henley-on-Thames, Oxon, RG9 6AU, U.K.

[b]Department of Chemistry, University of Aberdeen, Meston Walk, Old Aberdeen, AB24 3UE, U.K.

[c]School of Pharmacy, The Robert Gordon University, Schoolhill, Aberdeen, AB10 1FR U.K.

[d]School of Applied Sciences, The Robert Gordon University, St. Andrews St., Aberdeen, AB25 1HG, U.K.

(Received 5 May 1998; accepted 22 June 1998)

Abstract—Ionic compounds, [Q] [$R_2SnX(dmit)$] [dmit = 1,3-dithiole-2-thione-dithiolate; Q = 1,4-dimethylpyridinium or tetraalkylammonium; R = Ph or alkyl; X = Cl, Br, I, NCS, NCSe, or N_3] have been obtained by (a) from R_2SnX_2 and $[Q]_2[Zn(dmit)_2]$ in the presence of excess QX, (b) from halide exchange reactions in acetone solution between [Q] [$R_2SnCl(dmit)$] and a halide or pseudohalide source, or (c) by addition of QX to [$R_2Sn(dmit)$]. Crystal structure determinations of [NEt_4] [$Ph_2SnI(dmit)$] and [1,4-Me_2pyridiniuml [$Ph_2SnBr(dmit)$] as well as of the mixed halides, [1,4-Me_2pyridinium] [$Ph_2SnCl_nI_{1-n}(dmit)$] ($n = 0.57$, 0.42 or 0.22), indicated that the tin atoms have distorted trigonal bipyramidal geometries in the anions, with the X ligand and a dithiolato atom in the axial sites. The $[R_2SnX(dmit)]^-$ anions remain essentially intact in organic solvents, but lose X^- on extraction with H_2O to give the neutral species, $R_2Sn(dmit)$. © 1998 Elsevier Science Ltd. All rights reserved

Keywords: stannates; crystal structures; organotin; dithiolates.

INTRODUCTION

Complexes of the 1,3-dithiole-2-thione-4,5-dithiolato ligand, (**1**, dmit, $C_3S_5^{2-}$) attracted considerable attention in recent years [1]. While much of the interest has centred on transition metal compounds, main group metal complexes have not been neglected and indeed have featured in a number of synthetic and structural studies [2–5].

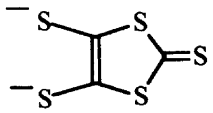

(1)

While *bis*(1,3-dithiole-2-thione-4,5-dithiolato)zincate salts, $[Q]_2[Zn(dmit)_2]$, as precursors of other metal dmit complexes, are clearly of general importance [2], tin dmit complexes have arguably enticed more structural study than those of any other main group metal [3]. *Mono*-, *bis*- and *tris*-dmit complexes, e.g [$R_2Sn(dmit)$]. (**2**: R = alkyl or aryl) [3], [Q] [$RSn(dmit)_2$] (**3**) [3], $[Q]_2[SnX_2(dmit)_2]$ (**4**: X = I or Br) [3] and $[Q]_2[Sn(dmit)_3]$ (**5**) [3], can be obtained, with the synthesis and

†Author to whom correspondence should be addressed.

structural details for **2–4** being fully reported. Some limited information on the ionic species, [Q] [$R_2SnX(dmit)$] (**6**: Q = onium cation; X = halide), [3] has been provided in earlier communications; we now wish to report more fully on **6**.

RESULTS AND DISCUSSION

Synthesis

The syntheses of [Q] [$R_2SnX(dmit)$] (**6**: R = unfunctionalised alkyl or aryl group) have been achieved in three ways: (a) from a reaction between R_2SnX_2 and [Q] [$Zn(dmit)_2$] in the presence of an excess QX, (b) from halide exchange reactions in acetone solution between [Q] [$R_2SnCl(dmit)$] and either NaX or QX, or (c) by addition of QX to [$R_2Sn(dmit)$], see Scheme 1.

Tables 1 and 2 list the compounds, **6**, with analytical, melting point and selected IR and NMR spectral data. The work-up of all products involved the minimum use of aqueous extractions to reduce the risks of loss of QX from [Q] [$R_2SnX(dmit)$] to give polymeric [$R_2Sn(dmit)$], (reaction d in Scheme 1 [3a]. The use of R_2SnX_2 with functionalised R groups able to complex intramolecularly to tin, such as $R'O_2CCH_2CH_2$, led directly to [$R_2Sn(dmit)$] species on reactions with $[Q]_2[Zn(dmit)_2]$ [3a].

The halide (or pseudohalide) exchange reactions

Table 1. Analytical and physical data for [Q][$R_2SnX(dmit)$]

Compound	Preparative method[a], (Yield, %)	m.p. (°C), recryst. solvent	Colour	Analysis. %, (calcd/(found)(%)) C	H	N
[NBu_4] [$Me_2Sn(dmit)Cl$]	a; (71)	115 $Pr^iOH/CHCl_3$	deep- orange	40.5	6.8	2.3
				(40.3)	(6.8)	(2.2)
[NBu_4] [$Me_2Sn(dmit)I$]	b	109–111 MeOH	red–brown			
[NEt_4] [$Bu_2Sn(dmit)Br$]	c		orange			
[NEt_4] [$Ph_2Sn(dmit)Cl$]	a; (79)	157–158 MeOH	orange	43.5	4.5	2.2
				(43.6)	(4.6)	(2.3)
[NBu_4] [$Ph_2Sn(dmit)Cl$]	a, (61)	101–103 Me_2CO/EtOH	orange	49.8	6.2	
				(49.3)	(6.5)	
[1,4-Me_2pyr] [$Ph_2Sn(dmit)Cl$]	a; (78)	140–142 MeOH	orange	43.1	3.3	2.3
				(43.0)	(3.2)	(2.2)
[$FcCH_2NMe_3$] [$Ph_2Sn(dmit)Cl$]	a; (78)	197–200	orange–red			
[methylviologen]	c; (54)	125–127 CH_2Cl_2/Me_2CO	black	42.2	2.9	2.3
[$Ph_2Sn(dmit)Cl]_2$				(42.1)	(2.8)	(2.2)
[PPh_3Et] [$Ph_2SnCl(dmit)$]	a;	114–116 MeOH/Pr^iOH	red–orange			
[NEt_4] [$Ph_2Sn(dmit)Br$]	b; (83)	74–77 MeOH	yellow–orange	40.7	4.5	2.1
				(41.1)	(4.6)	(2.2)
	c; (40)	77–9		(40.5)	(4.3)	(1.9)
[NBu_4] [$Ph_2Sn(dmit)Br$]	c; (78)	119–122 $CHCl_3$/petrol	orange			
[1,4-Me_2pyr] [$Ph_2Sn(dmit)Br$]	b; (79)	139-140 MeOH/Me_2CO	orange	40.2	3.1	2.1
				(40.2)	(3.0)	(2.1)
[NEt_4] [$Ph_2Sn(dmit)I$]	c; (79)	134–136 MeOH	orange	38.0	4.2	1.9
				(38.0)	(4.2)	(1.6)
[NBu_4] [$Ph_2Sn(dmit)I$]	b	115–117 $CHCl_3$/EtOH	yellow/ orange			
[1,4-Me_2pyr] [$Ph_2Sn(dmit)I$]	c	134–136 MeOH/petrol	orange	38.1	2.7	2.0
				(37.5)	(2.9)	(2.0)
[NEt_4] [$Ph_2Sn(dmit)NCS$]	b; (84)	129–30 MeOH	orange	43.8	4.6	4.3
				(43.7)	(4.3)	(4.2)
[1,4-Me_2pyr] [$Ph_2Sn(dmit)NCS$]	b; (77)	134–135 MeOH/Me_2CO	orange	43.5	3.2	4.4
				(43.0)	(3.1)	(4.2)
[NEt_4] [$Ph_2Sn(dmit)NCSe$]	b; (78)	109–10 MeOH/Me_2CO	orange	40.9	4.3	3.7
				(40.9)	(4.3)	(4.0)
[1,4-Me_2pyr] [$Ph_2Sn(dmit)NCSe$]	b; (87)	137–138 Me_2CO/petrol	orange	40.5	3.0	4.1
				(39.7)	(2.9)	(3.8)
[1,4-Me_2pyr]	b	130–134 MeOH/petrol	orange	39.9	3.0	2.1[b]
[$Ph_2SnCl_{0.22}I_{0.78}(dmit)$]				(38.7)	(2.7)	(2.0)

[a]For preparative methods a, b and c, see Section 2.1

[b]I found 14.3%, calc. 14.5%.

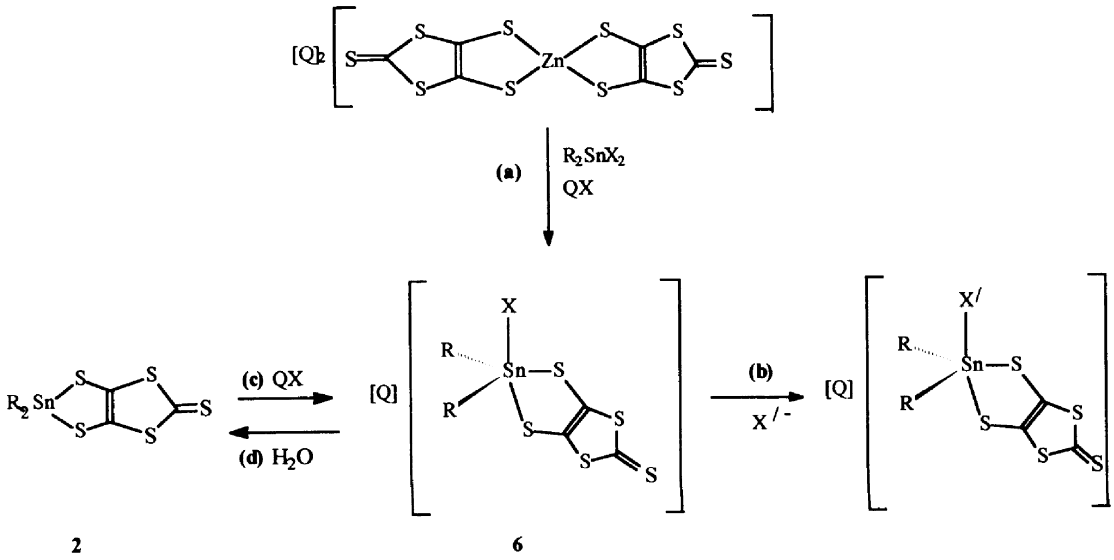

Scheme 1.

Table 2. spectral data for [Q] [$R_2Sn(dmit)X$]

Compound	IR(KBr, cm^{-1})	$\delta^{13}C(CD_3COCD_3)$		$\delta^{119}Sn(CD_3COCD_3)$
	C═S	C═C	C═S	
[NBu_4] [$Me_2SnCl(dmit)$][a]	1057, 1032	131.7 [125.3, 138.7][b]	207.9 [208.6][b]	−24.7($CDCl_3$) [−33.2][b]
[NBu_4] [$Me_2SnI(dmit)$]	1055,1034		208.6	−7.8
[NEt_4] [$Bu_2SnBr(dmit)$]				−36.1
[NEt_4] [$Ph_2SnCl(dmit)$]	1063,1036			−143.2
[NBu_4] [$Ph_2SnCl(dmit)$]	1055,1036		207.7	−135.5
[1,4-Me_2pyr] [$Ph_2SnCl(dmit)$]	1055		208.1	−145.1
[$FcCH_2NMe_3$] [$Ph_2SnCl(dmit)$]	1055	129.7	208.6	−145.8, −146.3 ($CDCl_3$)
[methylviologen] [$Ph_2SnCl(dmit)$]	1055, 1036		208.1	−144.2
[PPh_3Et] [$Ph_2SnCl(dmit)$]	1053, 1032			
[NEt_4] [$Ph_2SnBr(dmit)$]	1061, 1036	131.2	208.3	−149.6
[NBu_4] [$Ph_2SnBr(dmit)$]	1057, 1036	131.5	206.2	−150.4
[1,4-Me_2pyr] [$Ph_2SnBr(dmit)$]	1055			−149.8
[NEt_4] [$Ph_2SnI(dmit)$]	1061, 1035	130.7	207.9	−158.2
[NBu_4] [$Ph_2SnI(dmit)$]			207.2	−136.8
[1,4-Me_2pyr] [$Ph_2SnIdmit)$]	1053, 1032	131.2	207.8	−160.3
[1,4-Me_2pyr] [$Ph_2SnI_{0.58}Cl_{0.42}(dmit)$]	1055			−152.6
[NEt_4] [$Ph_2Sn(NCS)(dmit)$]	1055, 1036, 2047 (NCS)		208.5	−162.9
[1,4-Me_2pyr] [$Ph_2Sn(NCS)(dmit)$]	1055, 2046 (NCS)	129.7	208.5	−163.3
[NEt_4] [$Ph_2Sn(NCSe)(dmit)$]	1055, 1035, 2051 (NCSe)			−148.4
[1,4-Me_2pyr] [$Ph_2Sn(NCSe)(dmit)$]	1065, 2051 (NCSe)			−149.1
[1,4-Me_2pyr] [$Ph_2SnN_3(dmit)$]	1062,1037, 2104 (N_3)			

[a] δ^1H(Me 1.16 ($J^{119,117}Sn–^1H = 74.2, 71.0$ Hz); $\delta^{13}C$(Me) 13.1 ($J^{119,117}Sn–^{13}C = 569, 547$ Hz).
[b] solid state values.

(reaction b in Scheme) proceeded readily in Me_2CO solution for most [Q] [R_2SnCl(dmit)] complexes, using NaX or QX (X = Br, I, NCS or NCSe) in moderate excess (i.e. 2 to 4 mole equivalents): with these excesses, halide exchanges were generally complete. However, for the NaI/[1,4-Me_2pyridinium] [Ph_2SnCl(dmit)] exchange reaction, a larger excess of NaI was required to drive the exchange to near completion. Products with mixed chloride/iodide contents, [1,4-Me_2pyridinium] [$Ph_2SnCl_nI_{1-n}$(dmit)], could be isolated from incomplete exchanges. Examples of such mixed halide products had I:Cl mol ratios of 0.43: 0.57; 0.58: 0.42 and 0.78: 0.22, as deduced from X-ray and elemental analyses, e.g. iodine analysis in the three mixed chloride/iodide complexes were 8.2, 11.4 and 14.3%, compared to calculated values of 8.4, 11.1 and 14.5%, for [1,4-Me_2pyridinium] [$Ph_2SnCl_nI_{1-n}$(dmit)] with $n = 0.43$, 0.57 and 0.78, respectively.

A simple exchange reaction was not obtained between [NEt_4] [Ph_2SnCl(dmit)] and a large excess of NH_4F (mol ratio 1:22) in MeOH; the product isolated analysed for the fluorine bridged dinuclear species, [NEt_4] [Ph_2(dmit)SnFSn(dmit)Ph_2].

Organotin-dmit complexes undergo ready disproportionation reactions in solution, with products showing suitable losses and gains of organic and dmit groups. *Tris*(dmit)stannate salts, $[Q]_2[Sn(dmit)_3]$, are ubiquitous materials, appearing as unwanted coproducts in various tin-dmit preparations and solutions, e.g. crystals of $[NEt_4]_2[Sn(dmit)_3]$ were deposited, albeit in a low yield, from a dilute solution of analytically pure [NEt_4] [Ph_2Sn(NCSe)(dmit)] in MeOH. The isolation of a product bearing a greater number of organic groups than the original organotin compound is a strong indication of a disproportionation reaction; such an example is [NEt_4] [$Ph_3Sn(NCS)_2$], isolated [6] as a minor product, from a reaction mixture containing Na_2(dmit), $Ph_2Sn(NCS)_2$ and [NEt_4]Br. Disproportionations of diorganotin compounds, R_3SnX, to di- and tetra-organotin species, are also well-established processes, especially for compounds with chelating X groups [7].

Holmes *et al*. reported the isolation of $[NEt_4]_2[Sn(o\text{-}SC_6H_4O)_3]$, (**7**), from solutions of [NEt_4, $SnF(o\text{-}SC_6H_4O)_2$] in organic solvents [8]; rather than disproportionation, Holmes *et al*. suspected hydrolysis was responsible for the formation of **7** and suggested the intermediacy of $[NEt_4]_2[Sn(HO)_2(o\text{-}SC_6H_4O)_2]$ [8]. Hydrolysis of carbon–tin bonds was also invoked for the formation of [NEt_4] [Na] $[Sn(mnt)_3]$, from $PhSnCl_3$, Na_2(mnt) and NEt_4Cl in Me_2CO solution (mnt = 1,2-dicyanoethylene-1,2-dithiolate)] [9] and for the preparation of $[Sn(catecholato_3]^{2-}$ in the reaction of [PhSn(O)OH] with catechol in the presence [8] of NEt_3 and $Me_2C(OMe)_2$. However, our experience with the dmit complexes suggests that disproportionations are more probable causes of the unexpected products than are hydrolyses. The mobility of dmit group between tin centres has been additionally shown in exchange reactions between R_2SnX_2 and R'_2Sn(dmit) [3a].

A limited number of other [Q] [R_2SnX(dithiolate)] complexes have been previously reported; these include [NEt_4] [Ph_2SnCl(3,4-toluenedithiolate)], prepared by addition of NEt_4Cl to Ph_2Sn(3,4-toluenedithiolate) [10a, 10b] and [Ph_4As] [Me_2SnX(mnt)], from[11] Me_2SnX_2 (X = Cl, Br or I), Na_2(mnt) and $[Ph_4As]NO_3$ [11].

Crystal structure determinations

In addition to the previously reported structures of [NBu_4] [Me_2SnCl(dmit)] [3f] and [1,4-Me_2pyridinium] [Ph_2Sn(NCS)(dmit)] [3g], the crystal structures of the single halide species, [NEt_4] [Ph_2SnI(dmit)] and [1,4-Me_2pyridinium] [Ph_2SnBr(dmit)] have been determined.

Unfortunately, suitable crystals of the bridged fluoride complex, [NEt_4] [(dmit)Ph_2SnFSnPh_2(dmit)] could not be obtained for an X-ray diffraction study.

As well as those of the single halide species, the structures of the mixed halide species, [1,4-Me_2 pyridinium] [$Ph_2SnCl_nI_{1-n}$(dmit)] ($n = 0.57$, 0.42 and 0.22) have been determined. The structure of [1,4-Me_2pyridinium] [$Ph_2SnC_{0.57}I_{0.43}$(dmit)] was solved with a *R* factor of 0.049; although much less satisfactory *R* values (*ca.* 0.10) were obtained for the other mixed I/Cl species, the data is sufficient to allow useful comparisons to be made with those of the other compounds. The mixed halide species can be considered to be solid solutions, obtained by crystallisation from solutions containing both halides, with structures in which an axial site in the trigonal bipyramidal array is randomly occupied by either of the different halide ligands. In the cases of the [1,4-Me_2pyridinium] [$Ph_2SnCl_nI_{1-n}$(dmit)] ($n = 0.57$ and 0.42), the positions of both ligands, as well as their occupancy factors, could be resolved. However. only a single site could be determined for the halides in [1,4-Me_2pyridinium] [$Ph_2SnCl_{0.22}I_{0.78}$(dmit)].

Selected bond lengths and angles in these ionic compounds, including data for the previously published [NBu_4] [Me_2SnCl(dmit)] [3f] and [1,4-Me_2pyridinium] [Ph_2Sn(NCS)(dmit)] [3g] are listed in Table 3. Figs 1– provide the atom arrangements in [1,4-Me_2 pyridinium] [Ph_2SnBr(dmit)], [NEt_4] [Ph_2SnI(dmit)], [1,4-Me_2pyridinium] [$Ph_2SnCl_{0.57}I_{0.43}$(dmit)] and [1,4-Me_2pyridinium] [$Ph_2SnCl_{0.42}I_{0.58}$(dMit)], respectively. The atom numbering system used for [1,4-Me_2 pyridinium] [$Ph_2SnCl_{0.22}I_{0.78}$(dmit)] is the same as that used for [1,4-Me_2pyridinium] [$Ph_2SnCl_{0.42}I_{0.58}$(dmit)] although for the latter only a single halide site was determined.

There are no interactions between the cations and anions of the [Q] [R_2SnX(dmit)] species, however, in general there are S–S contacts between anions just within the sum of the van der Waals radii (3.67 Å) [8]. In all cases, the structures of the anions are basically

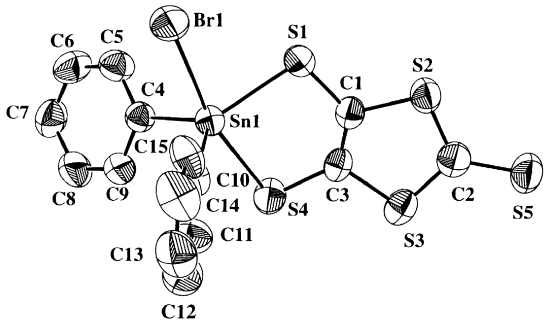

Fig. 1. The atom arrangement in the anion of [1,4-Me_2-pyridinium] [Ph_2SnBr(dmit)]. Displacement ellipsoids are shown at the 50% probability level.

trigonal bipyramidal with some distortions towards rectangular pyramidal structures. In the distorted trigonal bipyramidal anions of each compound, a thiolato sulfur and the halide or thiocyanate ligand occupy the axial sites, with the S_{ax}–Sn–X angle in the narrow range of 162.1(1) to 167.9(7)°; the equatorial atoms in each case being the other thiolato sulfur and the two carbon atoms of the organic groups. There is a particularly narrow range of values for the equatorial Sn–S_{eq} bond lengths [2.439(7) to 2.454(5) Å]; a much greater variation is found for the Sn–S_{ax} bond lengths [2.551(4) to 2.662(3) Å]. The dithiolato bite angles, S_{ax}–Sn–S_{eq}, vary over the range 84.5(1) to 86.37(3)°. The bond angles and lengths within the dmit moiety vary little in the various ionic complexes; the average geometric parameters of the dmit units are provided in Fig. 5.

The Sn–Cl, Sn–Br, Sn–I and Sn–N(CS) bond lengths in [1,4-Me_2pyridinium] [Ph_2Sn(NCS)(dmit)], [NBu_4] [Me_2SnCl(dmit)], [1,4-Me_2pyridinium, Ph_2SnBr(dmit)] and [NEt_4] [Ph_2SnI(dmit)] are 2.261(3), 2.556(3), 2.7139(10) and 2.985(2) Å, respectively; these values are *ca.* 5, 7, 7 and 9% longer, respectively, than the appropriate sums of the covalent bond radii [12] of 2.15, 2.39, 2.54 and 2.73 Å. Very few compounds of a similar nature have been reported. The Sn–Cl bond length in [NBu_4] [Me_2SnCl(dmit)] is similar to that determined of 2.556(3) Å in the trigonal bipyramidal anion of [NEt_4] [Ph_2SnCl(3,4-toluenedithiolate] [10a]. The Sn–I bond length, 3.225(1) Å, in [PPh_4, Me_2SnI(*o*-OC_6H_4S)] is considerably longer than the Sn–I bond length in [NEt_4] [Ph_2SnI(dmit)], however the anions in [PPh_4] [Me_2SnI(*o*-SC_6H_4O)] are linked via Sn–O bridges into centrosymmetric dimers[13] to give six coordinate tin centres [13].

The Sn–Cl and Sn–I bond lengths, determined for the mixed halide complexes, [1,4-Me_2pyridinium] [$Ph_2SnCl_nI_{1-n}$(dmit)], are 2.62(2) and 2.873(9) Å for

Table 3. Selected bond lengths (Å) and angles (°) for [Q] [R_2SnX(dmit)]

Q	Bu_4N [3f]	$C_7H_{10}N$	Et_4N	$C_7H_{10}N$ [3g]	$C_7H_{10}N$	$C_7H_{10}N$	$C_7H_{10}N$
R	Me	Ph	Ph	Ph	Ph	Ph	Ph
X	Cl	Br	I	NCS	Cl(0.57)[g] I(0.43)	Cl(0.42) I(0.58)	Cl(0.22) I(0.72)
S(eq)	S2	S1	S1	S2	S9	S1	S1
S(ax)	S1	S4	S5	S1	S3	S2	S2
C(A)	C5	C4	C11	C7	C17	C9	C9
C(B)	C4	C10	C21	C1	C11	C15	C15
X	Cl	Br	I	N	Cl or I	Cl or I	Cl/I
Sn–X	2.556(3)	2.7139(10)	2.985(2)	2.261(3)	2.873(8)[a], 2.62(2)[b]	2.859(13)[a], 2.724(3)[b]	2.926(3)
Sn–C(A)	2.131(10)	2.153(5)	2.14(1)	2.137(4)	2.142(5)	2.16(2)	2.12(2)
Sn–C(B)	2.132(11)	2.168(5)	2.18(1)	2.139(4)	2.147(6)	2.20(3)	2.18(3)
Sn–S(eq)	2.451(3)	2.453(2)	2.454(5)	2.4399(10)	2.448(2)	2.439(7)	2.444(7)
Sn–S(ax)	2.662(3)	2.596(2)	2.551(4)	2.5917(10)	2.590(2)	2.592(8)	2.593(8)
X–Sn–S(ax)	167.3(1)	165.79(4)	162.1(1)	164.58(8)	164.9(1)[a], 167.8(4)[b]	1643(3)[a], 167.9(7)[b]	165.0(2)
X–Sn–C(A)	91.2(4)	92.34(13)	89.6(3)	88.75(12)	92.8(2)[a], 91.3(4)[b]	92.9(8)[a], 97.3(10)[b]	92.0(6)
X–Sn–C(B)	92.5(4)	95.3(2)	95.7(3)	91.45(13)	95.9(2)[a], 94.3(4)[b]	98.0(10)[a], 90.6(11)[b]	94.7(8)
X–Sn–S(eq)	83.1(1)	80.24(4)	78.4(1)	78.53(8)	79.5(1)[a], 82.5(4)[b]	79.7(3)[a], 82.3(7)[b]	80.1(2)
C(A)–Sn–C(B)	120.9(6)	116.6(2)	110.5(3)	119.36(13)	116.3(2)	115.0(9)	117.1(9)
C(A)–Sn–S(eq)	120.8(4)	123.79(13)	127.0(3)	121.91(10)	123.7(1)	124.1(7)	123.2(6)
C(B)–Sn–S(eq)	118.2(4)	119.50(14)	121.9(3)	117.42(10)	120.0(1)	120.9(7)	119.5(7)
C(A)–Sn–S(ax)	93.0(4)	92.20(13)	93.7(3)	96.71(10)	92.3(2)	90.9(7)	92.8(6)
C(B)–Sn–S(ax)	95.6(4)	94.7(2)	99.5(4)	98.33(10)	94.5(2)	94.1(10)	95.8(9)
S(eq)–Sn–S(ax)	84.5(1)	86.04(5)	85.6(2)	86.37(3)	85.83(6)	85.7(2)	85.4(2)

[a]X = I.
[b]X = Cl.

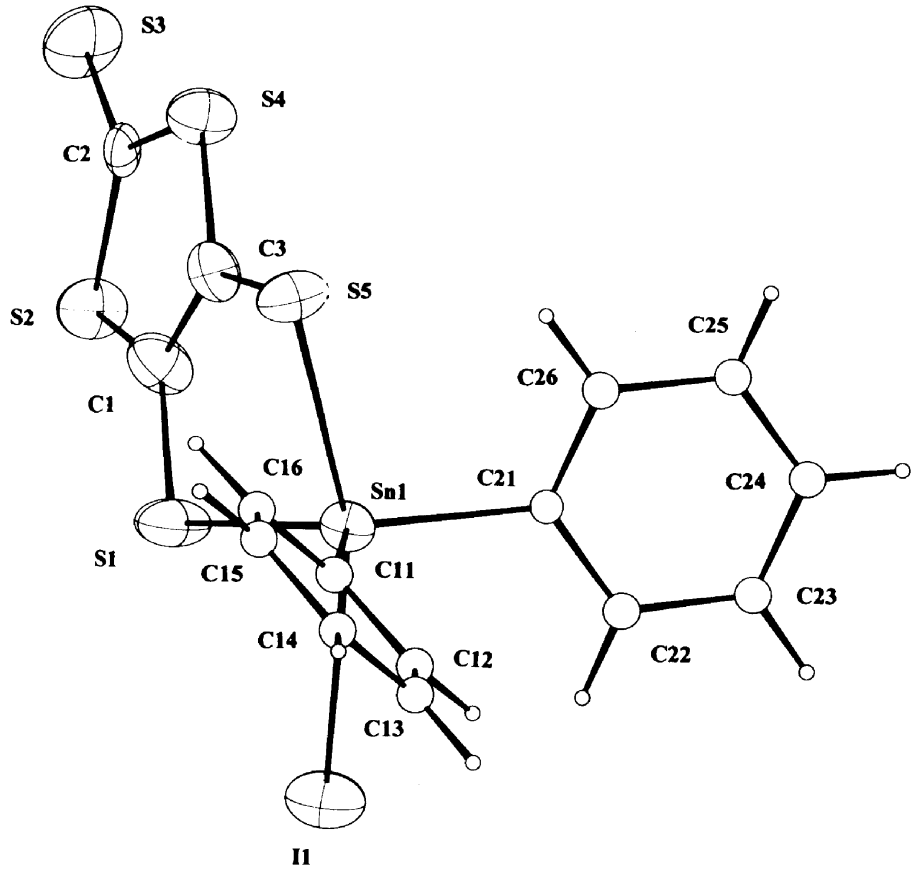

Fig. 2. The atom arrangement in the anion of $[NEt_4]$ $[Ph_2SnI(dmit)]$. Displacement ellipsoids are shown at the 50% probability level.

$n = 0.57$ and 2.724(3) and 2.859(13) Å for $n = 0.42$, i.e. the Sn–Cl and Sn–I bond lengths are longer and shorter respectively, than values determined for single halide complexes. As already indicated, only an average tin–halide bond length [2.926(3) Å] could be extracted from the X-ray data for [1,4-Me_2pyridinium] $[Ph_2SnCl_{0.22}I_{0.78}(dmit)]$. Yoon and Parkin have clearly demonstrated that bond lengths obtained from disordered structures can be incorrect, when judged against values in pure compounds [14]. Our results are in agreement with the conclusion of Yoon and Parkin, that while satisfactory refinement of a disordered structure be taken as evidence for the nature of the disorder and therefore a good indication of the molecular structure, attempts to extract the true bond lengths from such a structure must be treated with caution.

Spectra

All isolated compounds are orange to red–brown in colour: λ_{max} in Me_2CO solution for [Q] $[R_2SnX(dmit)]$ (e.g. Q = NEt_4, NBu_4or PPh_3Et; R = Me or Ph; X = Cl or Br) is 455 ± 5 mμ, compared to values of 433 ± 5 mμ for the corresponding iodides. The asymmetry of the C=C unit in the dmit group, as established by X-ray crystallography, is observed in the solid state ^{13}C NMR spectra, $\delta^{13}C(C{=}C)$ values for [1,4-Me_2 pyridinium] $[Ph_2SnI(dmit)]$ being 127.7 and 136.4 ppm and for $[NBu_4]$ $[Me_2SnCl(dmit)]$ 125.3 and 138.7 ppm. In solution, the ethylenic carbons of each anion are equivalent, with $\delta^{13}C$ values in the range 130.5 ± 0.8 ppm. The $\delta^{13}C(C{=}S)$ values are grouped around 207 ppm; the solid state $\delta^{13}C(C{=}S)$ value for [1,4-Me_2pyridinium] $[Ph_2SnI(dmit)]$ is 205.2 ppm. In the IR spectra in KBr discs, the $\nu(C{=}S)$ values are in the ranges 1055–1065 and 1032–1035 cm^{-1}.

Acetone was generally used as the NMR solvent in order to obtain reasonable concentrations. Such a coordinating solvent could influence the structure of the anions; however, essentially the same $\delta^{119}Sn$ values for $[FcCH_2NMe_3]$ $[Ph_2SnCl(dmit)]$ were obtained in Me_2CO and $CDCl_3$ solutions suggest that this is not the case, at least not for this complex. The $\delta^{119}Sn$ values could also be effected by dissociation, as shown in eq. (1) a process readily realised in aqueous systems (cf. step d in Scheme).

$$[Q]^+[R_2SnX(dmit)]^- = [Q]^+X^- + R_2Sn(dmit). \qquad (1)$$

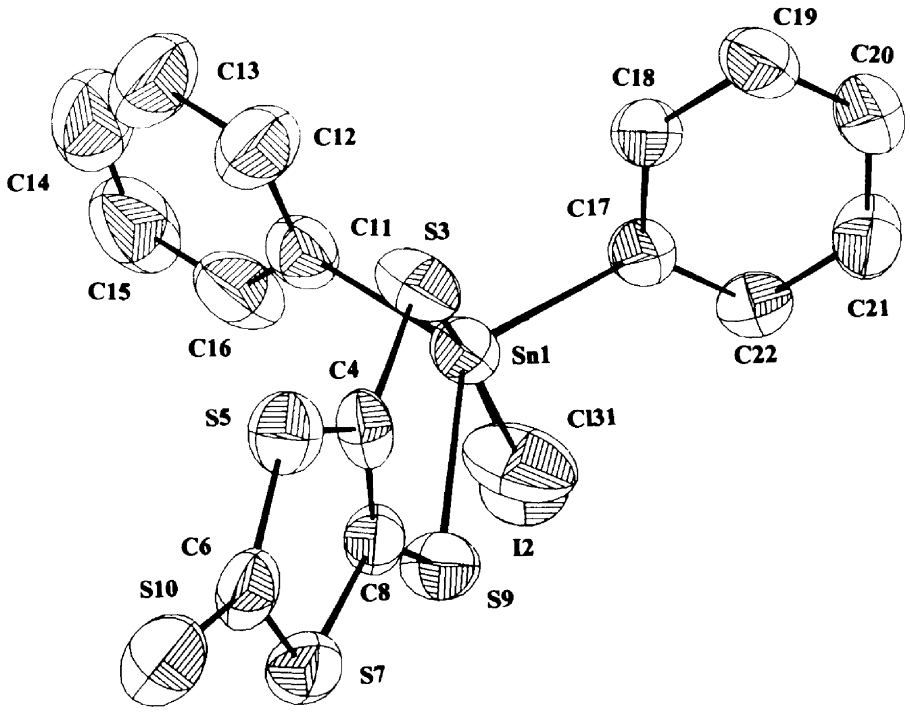

Fig. 3. The atom arrangement in the anion of [1,4-Me_2-pyridinium] [$Ph_2SnCl_{0.57}I_{0.43}$(dmit)]. Displacement ellipsoids are shown at the 50% probability level.

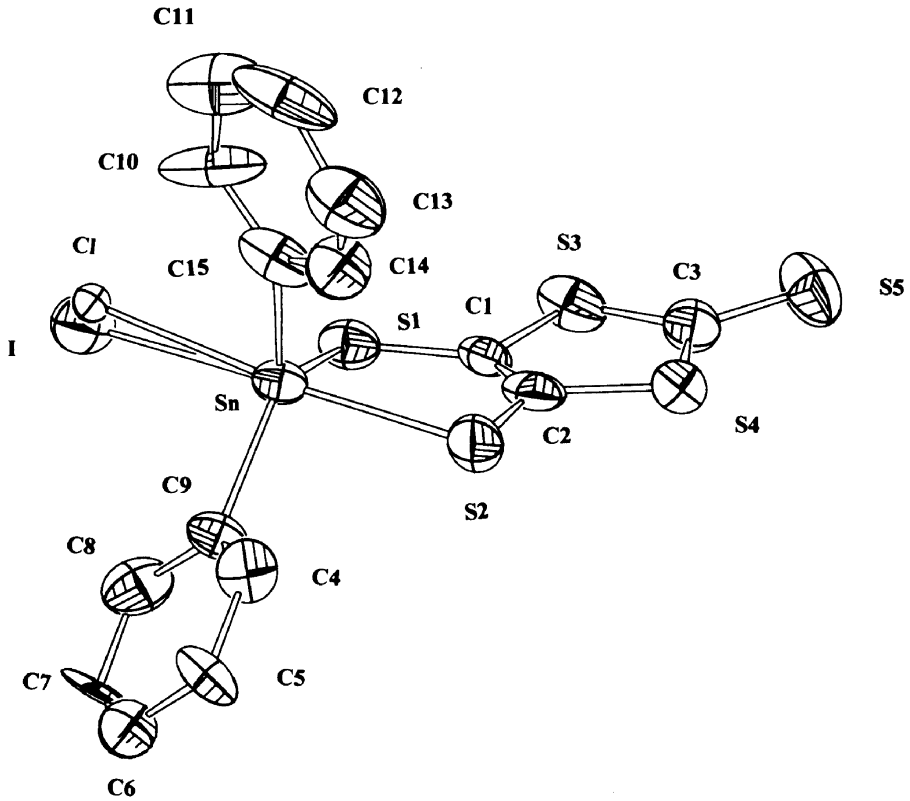

Fig. 4. The atom arrangement in the anion of [1,4-Me_2-pyridinium] [$Ph_2SnCl_{0.42}I_{0.58}$(dmit)]. Displacement ellipsoids are shown at the 40% probability level.

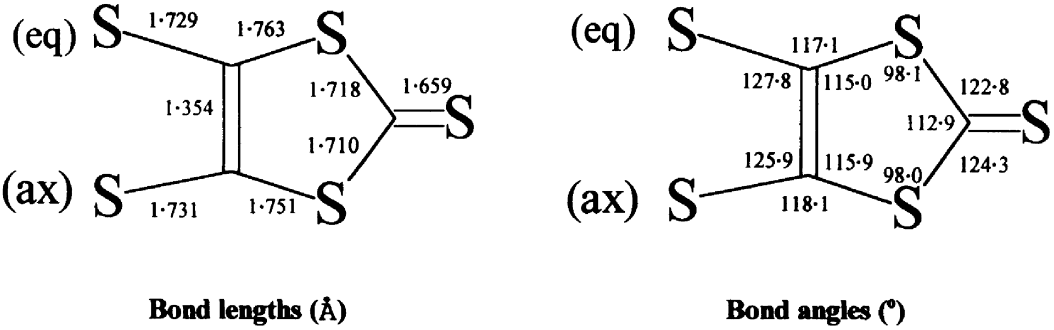

Fig. 5. The average geometric parameters within the dmit units in [Q] [$R_2SnX(dmit)$].

The δ^{119}Sn values in Me_2CO solution for [Q] [$R_2SnX(dmit)$] and $R_2Sn(dmit)$ show considerable differences; e.g. δ^{119}Sn for $Ph_2Sn(dmit)$ is -25 ppm, compared to the values for [Q] [$Ph_2SnCl(dmit)$] of -143.2, -145.1, -146.3, -144.2 and -135.5 for Q = NEt_4, 1,4-Me_2-pyridinium, $FcCH_2NMe_3$, methylviologen (2[Q]) and NBu_4, respectively. Significant differences in δ^{119}Sn values are also realised between the pairs $Me_2Sn(dmit)$/[Q] [$Me_2SnX(dmit)$] and $Bu_2Sn(dmit)$/[Q] [$Bu_2SnX(dmit)$]; δ^{119}Sn for $Me_2Sn(dmit)$ and $Bu_2Sn(dmit)$ Me_2CO-d_6 are 135.2 and 161.5 ppm, respectively [3a].

Only a single δ^{119}Sn value was observed for each solution of [Q] [$R_2SnX(dmit)$] suggesting either a single tin species was present in solution, or a rapid equilibrium process was at hand. The δ^{119}Sn values for [Q] [$R_2SnX(dmit)$] do not vary with changes in concentration or Q. This suggests that dissociations, as shown in eq. (1), can be generally ignored; furthermore, the cations and anions must be essentially independent in solution. Exception could be some NBu_4 salts, e.g. of [$Ph_2SnX(dmit)$]$^-$ (X = Cl or I) which do show lower field values than do salts of other cations, Q^+. Of interest, the mixed halide compounds, [1,4-Me_2pyridinium] [$Ph_2SnCl_nI_{1-n}(dmit)$], exhibit a single δ^{119}Sn value between those expected for the simple chloride and iodide. The similarity in the solid state and $CDCl_3$ solution δ^{119}Sn values for [NBu_4] [$Me_2SnCl(dmit)$], -33.2 and -24.7 ppm, respectively, also points to no change in structure on dissolution.

The average δ^{119}Sn values for [$Ph_2SnX(dmit)$]$^-$ vary slightly in the sequence Cl, NCSe, Br, I and NCS; -144.6, -148.3, -149.9, -159.3 and -163.3 ppm, respectively. These values indicate that the X group has little influence on the tin centres in the [$Ph_2SnX(dmit)$]$^-$ anions. The J(^{119,117}Sn–^{13}C) values for the *ipso* aryl carbon in the [$Ph_2SnX(dmit)$]$^-$ anions also show little variation with X, being *ca.* 800 Hz.

Reactions

The complexes, [Q, $R_2SnX(dmit)$] can act as dmit sources, as shown by the reactions with iodine, to give the dmit dimer, C_6S_{10} and with 2-$O_2NC_6H_4SCl$ (see equations 2 and 3).

EXPERIMENTAL

Melting points were measured using a Kofler hot-stage microscope and are uncorrected. NMR spectra were obtained on a Bruker 250 MHz instrument. Ten second pulse delays were utilised in the acquisition of

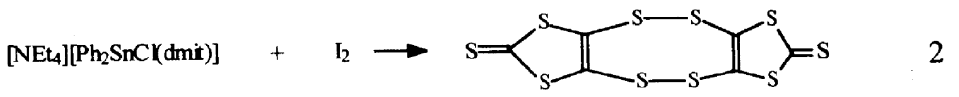

2

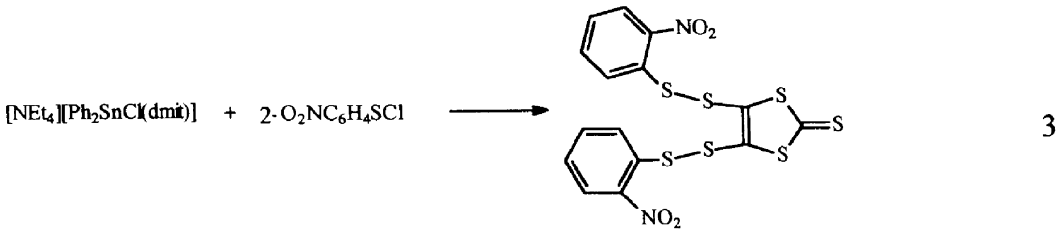

3

the ^{13}C NMR spectra of the dmit compounds. IR spectra were recorded on Phillips Analytical PU900 and Nicolet 205 Fourier-transform instruments. Solid state NMR spectra were obtained by the EPSRC service at the University of Durham.

Zincate salts, $[Q]_2[Zn(dmit)_2]$, [Q = NEt_4, NBu_4, 1,4-dimethylpyridinium or ferrocenylmethyl(trimethyl) ammonium] [15] and $R_2Sn(dmit)$ (R = Me or Ph) were prepared by published routes [3a]. Onium salts were commercial samples, except 1,4-dimethylpyridinium iodide, which was obtained from 4-methylpyridine and methyl iodide.

Preparation of [Q] [$R_2SnX(dmit)$] complexes

The [Q] [$R_2SnX(dmit)$] complexes were produced by three reactions: (a) from reaction between R_2SnX_2 and $[Q]_2[Zn(dmit)_2]$ in the presence of excess QX; (b) from halide exchange reactions in acetone solution between [Q, $R_2SnCl(dmit)$] and either NaX, KX or QX; or (c) by addition of QX to [$R_2Sn(dmit)$]. Each of these routes is illustrated below. Melting points, solvents used for recrystallisation, colours, yields, analyses and selected spectral data for [Q] [$R_2SnX(dmit)$] complexes are listed in Tables 1 and 2.

Reaction (*a*); *preparation of* [NEt_4] [$Ph_2SnCl(dmit)$]

A solution of Ph_2SnCl_2 (5.0 g, 14.5 mmol) in MeOH (10 ml) was added to a solution of [NEt_4] $[Zn(dmit)_2]$ (5.22 g, 7.27 mmol) in Me_2CO (50 ml). After stirring the reaction mixture for 30 min, it was filtered and the volume of the filtrate was reduced to *ca*. 25 ml. Orange coloured crystals were formed. These were collected and washed successively with a little water and petrol (40–60°C). The title compound was recrystallised from MeOH.

Reaction (*b*); *preparation of* [1,4-Me_2-pyridinium] [$Ph_2Sn(NCSe)(dmit)$]

A solution of KSeCN (0.72 g, 5.0 mmol) in MeOH (10 ml) was added to a solution of [1,4-Me_2 pyridinium] [$Ph_2SnCl(dmit)$] (1.53 g, 2.5 mmol) in Me_2CO (50 ml). The reaction mixture darkened in colour on reaction and a precipitate of KCl formed. The reaction mixture was filtered and the filtrate was rotary evaporated to leave an orange coloured solid residue. This was washed successively with a little water, propan-2-ol and petrol (40–60°C) and was recrystallised from Me_2CO/petrol (40–60°C).

Reaction (*c*); *preparation of* [NEt_4] [$Ph_2SnNCS(dmit)$]

The compound [$Ph_2Sn(dmit)$] (0.47 g, 1 mmol) was mixed with NEt_4Br (0.21 g, 1 mmol) and an excess of $NaSCN.2H_2O$ (0.46 g, 4 mmol) in MeOH (20 ml) and agitated on an ultrasonic bath for 2 h. The reaction mixture was filtered and the solid recrystallised from MeOH/Me_2CO to give orange needles.

Preparation of [methylviologen, $Ph_2SnCl(dmit)]_2$

A solution of $Ph_2Sn(dmit)$ (0.75 g, 1.6 mmol) and methylviologen dichloridehydrate (0.45 g, 1.8 mmol) in Me_2CO (75 ml) was agitated in an ultrasonic bath for 15 min. The reaction mixture was filtered and the filtrate evaporated under vacuum. The solid residue was recrystallised from CH_2Cl_2/Me_2CO as black crystals.

General NMR spectral data for [Q] [$Ph_2SnX(dmit)$] complexes in Me_2CO-d_6 solutions are as follows:

[NEt_4]$^+$: ^1H NMR (Me_2CO-d_6, 250 MHz): δ: 1.34 ± 0.02 [12H, tt, J 7.3 and 1.9 Hz), 3.40 ± 0.03 [8H, q, J 7.3 Hz] ^{13}C NMR (Me_2CO-d_6, 63 MHz): δ: 7.7 [Me], 52.9 [CH_2, J 6.2 Hz]

[NBu_4]$^+$: ^1H NMR (Me_2CO-d_6, 250 MHz): δ: 0.93 ± 0.02 [12H, t, J 7.3 Hz], 1.31 ± 0.03 [8H, m, CH_2CH_2Sn], 1.56 ± 0.03 [8H, m, $CH_2CH_2CH_2Sn$], 3.16 ± 0.03 [8H, t, J 7.3 Hz, CH_2N] ^{13}C NMR(Me_2CO-d_6, 63 MHz): δ: 13.5, 19.2, 23.1 and 57.5.

[1,4-Me_2pyridinium]$^+$: ^1H NMR (Me_2CO-d_6, 250 MHz): δ: 2.69 ± 0.02 [3H, s, Me–C], 4.51 ± 0.03 [3H, s, Me–N], 7.41 ± 0.03 [2H, d, J 7 Hz] and 8.02 ± 0.055 [2H, d, J 8 Hz] (aryl). ^{13}C NMR (Me_2CO-d_6, 63 MHz): δ: 21.9 [Me–C], 48.3 [Me–N], 129.3 [$C_3 + C_5$], 145.3 [$C_2 + C_6$], 160.2 [C_4].

[$Ph_2SnX(dmit)$]$^-$: ^1H NMR (Me_2CO-d_6, 250 MHz): δ: 7.42 ± 0.04 [6H, m, *m*-+*p*-H], 8.06 ± 0.06 [4H, m, *o*-H] ^{13}C NMR (Me_2CO-d_6, 63 MHz): δ: 129.3 ± 0.03[J ^{119}Sn–^{13}C 83 Hz, C*m*], 130.0 ± 0.3 [$J^{119}Sn$–^{13}C 17 Hz, C_p], 136.9 ± 0.5 $J^{119}Sn$–^{13}C 61 ± 1 Hz, C_o], 148.0 ± 0.5 [$J^{119}Sn$–^{13}C 800 ± 10 Hz, C_i], 130–131 [C=Cl, 208.2 ± 0.5 [C=S].

Reaction between [NEt_4] [$Ph_2SnCl(dmit)$] *and ammonium fluoride*; *formation of* [NEt_4, $\{Ph_2Sn(dmit)\}_2F$]

A solution of [NEt_4, $Ph_2SnCl(dmit)$] (0.634 g, 1.00 mmol) and NH_4F (0.80 g, 22 mmol) in MeOH (75 ml) was stirred for 10 min. The solution was concentrated under vacuum and cooled to yield an orange coloured solid, which was recrystallised from MeOH/Me_2CO; m.p. 195°C (dec.).

IR (KBr, cm^{-1}); 3045, 2984, 2982, 1478, 1431, 1425, 1390, 1061, 1046, 1029, 997, 893, 727, 694.

^1H NMR (250 MHz, Me_2CO-d_6): δ: 1.41 (12H, tt, J 7.2 and 1.9 Hz, Me), 3.51 (8H, q, J 7.2 Hz, CH_2), 7.41 (12H, m, *m*-H + *p*-H), 7.82 (8H, m, *o*-H).

Found: C, 42.0; H, 3.7; N, 1.5. $C_{38}H_{40}FNS_{10}Sn_2$ requires: C, 42.0; H, 3.7; N, 1.3%.

Reaction of [NEt_4] [$Ph_2SnCl(dmit)$] *with o-nitrobenzenesulfenyl chloride*; *preparation of* 4,5-*bis*(*o-nitrobenzenethiolato*)-1,3-*dithiole*-2-*thione*

Solutions of [NEt_4] [$Ph_2SnCl(dmit)$] (0.317 g, 0.500 mmol) in MeOH (10 ml) and *o*-nitro-

benzenesulfenyl chloride (0.190 g, 1.00 mmol) in MeOH (10 ml) were mixed and stirred for 10 min. A yellow precipitate formed, which was collected, washed with MeOH and recrystallised from EtOH; yield 0.097 g, 66%, m.p. 158–160°C.

IR (KBr, cm^{-1}): 3094, 1590, 1568, 1510, 1451, 1334, 1307, 1105, 1065, 1040, 1022, 853, 785, 737.

UV–VIS (Me_2CO, mμ): 367.

Found: C, 35.1; H, 1.7; N, 5.4. $C_{15}H_8N_2O_4S_7$ requires: C, 35.7; H, 1.6; N, 5.6%.

Reaction of [NEt_4] [Ph_2SnCl(dmit)] *with iodine*; *preparation of* $(dmit)_2MeOH$

To a stirred suspension of [NEt_4] [Ph_2SnCl(dmit)] (0.317 g, 0.500 mmol) in MeOH (10 ml) was added a solution of I_2 (0.127 g, 0.500 mmol) in MeOH (10 ml). The solution was filtered and the solid was collected and dried under vacuum; m.p. 155–158°C.

IR (KBr, cm^{-1}): 1061.

Found: C, 19.5; H, 0.6; S, 75.3. $C_7H_4OS_{10}$ requires: C, 19.8; H, 1.0; S, 75.5%.

Treatment of [NEt_4] [Ph_2SnCl(dmit)] *with water*; *preparation of* [Ph_2Sn(dmit)]

A solution of [NEt_4] [Ph_2SnCl(dmit)] (0.513 g, 0.809 mmol) in Me_2CO (10 ml) was shaken with H_2O (30 ml). Addition of petrol (b.p. 40–60°C, 20 ml) led to the formation of an orange solid. This was collected, refluxed for 1 h in H_2O/MeOH (2:1), filtered and dried under vacuum at 100°C; m.p. 204–206°C (Ref.[3a]; value 206–207°C). NMR and IR spectra were identical with those of an authentic sample.

Crystal structure determinations

[1,4-Me_2pyridinium] [Ph_2SnBr(dmit)]. The unit cell and intensity data were collected on a Delft Instruments FAST diffractometer using the routines ENDEX, REFINE and MADONL in the madness programme [16] and processed using ABSMAD [17]; detailed procedures have been described [18]. Absence of crystal decay in the X-ray beam was confirmed by checking equivalent reflections at the beginning and end of data collection, which lasted ca. 8 h. The structure was solved with SIR92 [19] and refined with SHELXL97 [20]. Attempts to solve the structure in the super group $C222_1$ with $a = 15.395$, $b = 34.746$ and $c = 9.479$ Å were unsuccessful. Crystal data and structure refinement details are listed in Table 4. The Sn, Br, S and C atoms were refined with anisotropic thermal displacement parameters. The hydrogen atoms were allowed to ride on their attached atoms with common isotropic temperature factors which converged at 0.010 $Å^2$. Molecular diagrams were obtained by the program ZORTEP [21].

The cation is disordered with an inversion centre in the middle of the ring. The asymmetric unit of the monoclinic cell contains the anion and two half cations, C(16)–C(19) and C(20)–C(23). See Fig. 1; the remaining atom positions in the cation are generated by the inversion centre. The positions 17 and 21 are each shared by a carbon and nitrogen atom constrained to have identical population parameters (0.5) and identical thermal parameters.

[NEt_4] [Ph_2SnI(dmit)]. The data were collected on a CAD-4 instrument. The structure was refined by full matrix least squares. All nonhydrogen atoms, except the phenyl and ethyl carbons, were refined anisotropicially. Restraints were applied to the refinement of the phenyl and tetraethylammonium groups. The hydrogen atoms were placed in calculated positions with C–H = 1.00 Å. The first phasing model was obtained and the structure completed using SIR92 [19]. Structure refinement used CRYSTALS-PC [22]. Computations were performed on a Viglen Genie P590 Pentium PC with CRYSTALS-PC running under the Salford Software Services memory manager DBROS. Crystal data and structure refinement details are listed in Table 4.

[1,4-Me_2pyridinium] [$Ph_2SnCl_{0.57}I_{0.43}$(dmit)]. The structure was solved using direct methods, SIR92 [19], followed by CRYSTALS-PC [22] for Fourier and least squares refinement. A difference Fourier synthesis yielded a peak, which was identified as Cl. This was added to the cell contents and the I and Cl occupancies refined as a limited pair. The hydrogen atoms were placed in calculated positions with C–H = 1.00 Å.

Restraints were applied to the refinement of the cation, which were on two inversion centres and the phenyl groups which were regulised before refinement. Computations were performed on a Viglen Genie P590 Pentium PC with CRYSTALS-PC running under the Salford Software Services memory manager DBROS. Crystal data and structure refinement details are listed in Table 4.

[1,4-Me_2pyridinium] [$Ph_2SnI_{0.78}Cl_{0.22}$(dmit)] *and* [1,4-Me_2pyridinium] [$Ph_2SnI_{0.58}Cl_{0.42}$(dmit)]. Cell dimensions were determined using 14 reflections at 8.5–8.7° in θ for [1,4-Me_2pyridinium] [$Ph_2SnI_{0.78}Cl_{0.22}$(dmit)] and at 8.6–9.1° in θ for [1,4-Me_2 pyridinium] [$Ph_2SnI_{0.58}Cl_{0.42}$(dmit)].

Data collection and cell refinement employed Nicolet P3 software [23]. Data collection used 2θ scan rates of 5.33 ($I_p < 150$) to 58.6 ($I_p > 2500$)°min^{-1}, where I_p was the prescan intensity. Scan widths were 2.4 to 2.7° 2θ. Refinement was by full matrix least squares. The asymmetric unit consists of a single anion in one of the 4*e* general positions of $P2_1/c$ and half of each of the two independent cations in the centrosymmetric 2*b* and 2*c* sites respectively. The cations are therefore disordered in terms of the position of the nitrogen atoms and all their constituent atoms were treated as C. In the final stages of refinement, the site occupancy factors of I and Cl were refined to give the best values of *R*.

The disorder of the cations and the partial occu-

Table 4. Crystal data and structure refinement for [Q, $R_2SnX(dmit)$]

Q	1,4-Me_2pyr	Et_4N	1,4-Me_2pyr	1,4-Me_2pyr	1,4-Me_2pyr
R	Ph	Ph	Ph	Ph	Ph
X	Br	I	$Cl_{0.57}/I_{0.43}$	$Cl_{0.42}/I_{0.58}$	$Cl_{0.22}/I_{0.78}$
Empirical formula	$C_{22}H_{20}BrNS_5Sn$	$C_{23}H_{30}INS_5Sn$	$C_{22}H_{20}Cl_{0.57}I_{0.43}NS_5Sn$	$C_{22}H_{20}Cl_{0.42}I_{0.58}NS_5Sn$	$C_{22}H_{20}Cl_{0.22}I_{0.78}NS_5Sn$
Formula wt	657.29	726.40	652.00	665.71	684.00
Temperature (K)	293(2)	298(2)	293	298	298
Wavelength (Å)	0.71073	0.71073	0.71073	0.71073	0.71073
Crystal system	monoclinic	monoclinic	monoclinic	monoclinic	monoclinic
Space group	$P2_1/n$	$P2_1/c$	$P2_1/c$	$P2_1/c$	$P2_1/c$
Unit cell dimensions					
a (Å)	19.002(5)	16.614(5)	15.362(6)	15.354(11)	15.49(2)
b (Å)	9.479(5)	9.6722(12)	9.497(2)	9.504(5)	9.620(10)
c (Å)	15.395(5)	18.8005(6)	18.917(7)	19.960(12)	19.10(2)
β (°)	113.90(5)	97.64(4)	113.60(3)	113.79(6)	114.03(10)
Volume ($Å^3$)	2535.2(17)	2994.3	2524.5	2532(3)	2598(6)
Z	4	4	4	4	4
Density (calc.) (mg/m^3)	1.722	1.611	1.72	1.727	1.800
Absorption coefficient (mm^{-1})	3.007	2.223	2.01	2.08	2.56
$F(000)$	1296	1428	1285.9	1307.5	1336.3
Crystal size (mm)	$0.215 \times 0.072 \times 0.11$			$0.44 \times 0.42 \times 0.06$	$0.6 \times 0.2 \times 0.1$
Colour	orange	orange	orange	orange	orange
Theta range for data coll[n] (°)	2.20–25.02	0 to 23.7	1. 17 to 23.99	max. 25	max 25
Index ranges					
h	$-20 \le h \le 19$	$-22 \le h \le 21$	$-16 \le h \le 16$	$-16 \le h \le 16$	$-15 \le h \le 15$
k	$-10 \le k \le 10$	$0 \le k \le 13$	$0 \le k \le 10$	$0 \le k \le 11$	$0 \le k \le 10$
l	$0 \le l \le 17$	$0 \le l \le 25$	$0 \le l \le 21$	$0 \le l \le 22$	$0 \le l \le 21$
Reflections collected	7116	15349	4410	4966	5056
Independent reflections	4032	7529	3958	3528	3739
Observed reflections	2857 [$I > 2\sigma(I)$]	1237 [$I > 3\sigma(I)$]	2906 [$I > 3\sigma(I)$]	1854 [$F > 4\sigma(F)$]	2110 [$F > 4\sigma(F)$]
R_{int}	0.0745	0.10	0.034	0.059	0.086
Refinement method	Full-matrix l.s.	Full-matrix l.s.	Full-matrix l.s.	Full-matrix l.s.	Full-matrix l.s.
Number of parameters	273	180	281	276	272
Goodness-of-fit (S)	1.025	1.126	1.147		
Final R indices	$R1 = 0.0471$; [$I > 2\sigma(I)$] $wR2 = 0.1043$	$R = 0.047$, $wR = 0.048$	$R = 0.049$, $wR = 0.054$	$R = 0.100$, $Rw = 0.107$	$R = 0.101$, $Rw = 0.107$
R indices (all data)	$R1 = 0.0668$, $wR2 = 0.1109$				
Final weighting scheme	a	b	c	$w = 1[\sigma^2(F) + 0.011072\,F^2)$	$w = 1/\sigma^2(F) + 0.005119\,F^2)$
Residual diffraction	1.289 (at Sn), −0.469	1.25, −0.92	0.95, −0.72	2.02, −1.78	1.71, −1.47

[a] $w = 1/[\sigma^2(F_0^2) + (0.0713\,P)^2]$ where $P = (F_0^2 + 2F_c^2)/3$. [b] $W = w[1 - \Delta F/6\sigma(F)^2]^2$ where w is calculated using a three term Chebychev series with coefficients: 12.7, −7.63 and 8.76 [28].
[c] $W = w[1 - \Delta F/6\sigma(F)^2]^2$ where w is calculated using a three term Chebychev series with coefficients: 5.94, −1.39 and 4.57 [28].

pancy of the halide sites, taken with the marginal quality of the crystals as evidenced by the poorly determined unit cells are all considered to be contributory factors to the relatively high R values for both compounds. No attempt was made to position or refine H. All computations were performed on the SUN SpARCserver (UNIX operating system) of the Computing Centre of Aberdeen University, SHELXS86 [24] and SHELX76 [25] were used for structure solution and refinement, respectively. Molecular graphics used are: PLOTAID [26] and ORTEX [27]. Crystal data and structure refinement details are listed in Table 4.

Acknowledgements—The authors acknowledge the financial support for A. K. (from the EU) and for Z.H.C. (from the Islamia University, Pakistan): the uses of the EPSRC X-ray crystallography service at the University of Wales, Cardiff and the EPSRC solid state NMR service at the University of Durham are also gratefully acknowledged.

REFERENCES

1a. Olk, R. M., Dietzsch, W., Kirmse, R. and Hoyer, E., *Coord. Chem. Rev.*,, 1992, **117,** 99.
1b. Cassoux, P., Valade, L., Koyabashi, H., Clarke, R. A. and Underhill, A. E., *Coord. Chem. Rev.*, 1991, **110,** 115.
2. Chohan, Z. H., Howie, R. A., Wardell, J. L., Wilkens, R., Doidge-Harrison, S. M. S. V., *Polyhedron*, 1997, **16,** 2689.
3a. Doidge-Harrison, S. M. S. V., Irvine, J. T. S., Khan, A., Spencer, G. M. and Wardell, J. L., *J. Organomet. Chem.*, 1996, **516,** 199.
3b. Doidge-Harrison, S. M. S. V., Howie, R. A., Irvine, J. T. S., Spencer, G. M. and Wardell, J. L., *J. Organomet. Chem.*, 1992, **463,** 23.
3c. Doidge-Harrison, S. M. S. V., Howie, R. A., Irvine, J. T. S. and Wardell, J.L., *Polyhedron*, 1992, **11,** 2223.
3d. Spencer, G. M., Ph.D thesis, University of Aberdeen, 1994.
3e. Buchanan, H., Howie, R. A., Khan, A., Spencer, G. M., Wardell, J. L. and Aupers, J. H., *J. Chem. Soc. Dalton Trans.*, 1966, 541.
3f. Doidge-Harrison, S. M. S. V., Howie, R. A., Irvine, J. T. S., Spencer, G. M. and Wardell, J. L., *J. Organomet. Chem.*, 1991, **414,** C5.
3g. Khan, A., Ferguson, G., Low, J. N. and Wardell, J. L., *Acta Cryst. Sect C.*, 1998, in press.
4a. Doidge-Harrison, S. M. S. V., Irvine, J. T. S., Spencer, G. M., Wardell, J. L. and Wei, M., Valle, G., *Inorg. Chem.*, 1995, **34,** 4581.
4b. Wardell, J. L., Spencer, G. M. and Aupers, J. H., *Polyhedron*, 1996, **15,** 2701.
4c. Howie, R. A., Low, I. N., Spencer, G. M. and Wardell, J. L., *Polyhedron*, 1997, **16,** 2563.
5. Doidge-Harrison, S. M. S. V., Irvine, J. T. S., Spencer, G. M., Wardell, J. L., Ganis, P., Valle, G. and Tagliavini, G., *Polyhedron*, 1996, **15,** 1807.
6. Cox, P. J. and Wardell, J. L., *Acta Cryst.*, 1996, **C52,** 317.
7. Blunden, S. J., Harston, P., Hill, R. and Wardell, J. L., *Appl. Organomet. Chem.*, 1990, **4,** 383.
8. Holmes, R. R., Shafleezad, S., Chandrasekar, V., Sau, A. C., Holmes, J. M. and Day, R. O., *J. Am. Chem. Soc.*, 1988, **110,** 1168.
9a. Day, R. O., Holtnes, R. R., Shafleezad, S., Chandrasekar, V. and Holtnes, J. M., *J. Am. Chem. Soc.*, 1988, **110,** 5377.
9b. Breitschneider, E. S. and Allen, C. W., *J. Organomet. Chem.*, 1972, **38,** 43.
10a. Sau, A. C., Day, R. O. and Holmes, R. R., *Inorg. Chem.*, 1981, **20,** 3076.
10b. Sau, A. C., Holmes, R. R., Molloy, K. C. and Zuckerman, J. J., *Inorg. Chem.*, 1982, **21,** 1421.
11. Bretschneider, E. S. and Allen, C. W., *Inorg. Chem.*, 1973, **12,** 623.
12. Bondi, A., *J. Phys. Chem.*, 1964, **68,** 441.
13. Vollano, J. F., Day, R. O. and Holmes, R. R., *Organometallics*, 1984, **3,** 751.
14. Yoon, K. and Parkin, G., *Inorg. Chem.*, 1992, **31,** 1656.
15. Valade, L., Legros, J. P., Bousseau, M. and Garbauskas, M., *J. Chem. Soc. Dalton Trans.*, 1985, 783.
16. Pflugrath, J. W. and Messerschmidt, A. *MADNES. Version* 11 *September*, 1989. Distributed by Delfts Instruments, Delft.
17. Karaulov, A. I. *ABSMAD. Program for FAST Data processing*. University of Wales. Cardiff. 1992.
18. Darr, J. A., Drake, S. R., Hursthouse, M. B. and Malik, K. M. A., *Inorg. Chem.*, 1993, **32,** 5704.
19. Altomare, A., Burla, M. C., Camalli, M., Cascarano, G., Giacovazzo, C., Guagliardi, A. and Polidori, G., *J. Appl. Cryst.*, 1994, **27,** 435.
20. Sheldrick, G. M., SHELXL97, The Shelx home page. 1997. http://linux.uni-ac.gwdg.de/SHELX/.
21. Zsolnai. L., *ZORTEP. An interactive ORTEP Program*. University of Heidelberg, 1995.
22. Watkins, D. J., Prout, C. K., Carruthers, J. R. and Betteridge. P. W., *CRYSTALS Issue* 10. 1996, Chemical Crystallography Laboratory, University of Oxford, Oxford.
23. *Nicolet P3/R3 Data Collection Operators Manual*. Nicolet XRD Corporation, Cupertino, CA 95014, 1980.
24. Sheldrick, G. M., *Acta Cryst.*, 1990, **A46,** 467.
25. Sheldrick, G. M., SHELX76. *Program for Crystal Structure Determination.* University of Cambridge, 1976.
26. Cradwick, P. D. G., PLOTAID. *A Fortran Program for the Preparation of Molecular Drawings*. Macaulay Land Use Research Institute, Aberdeen, 1970.
27. McArdle, P., *J. Appl. Cryst.*, 1994, **27,** 438.
28. Carruthers, J. R. and Watkins, D. J., *Acta Cryst. A.*, 1979, **35,** 698.

Pergamon

Polyhedron Vol. 17, Nos. 25, 26, pp. 4487–4496, 1998
© 1998 Elsevier Science Ltd
All rights reserved. Printed in Great Britain
PII: S0277-5387(98)00255-1
0277–5387/98 $19.00+0.00

Tin(IV) and organotin(IV) complexes containing mono or bidentate N-donor ligands. V. Imidazole and imidazoline-2-thione derivatives: synthesis and spectroscopic characterization. Comparison with other imidazole tin(IV) complexes

Claudio Pettinari,* Maura Pellei, Carlo Santini, Ivan Natali, Federica Accorroni and Adriana Lorenzotti

Dipartimento di Scienze Chimiche, Università degli Studi di Camerino, via S. Agostino 1, 62032 Camerino, Macerata, Italy

(Received 13 May 1998; accepted 22 June 1998)

Abstract—The reactions of imidazole (L^1), benzimidazole (L^2), 2-phenylimidazole (L^3), 1-acetylimidazole (L^4), imidazoline-2(1,3*H*)-thione (L^5) and 1-methyl-imidazoline-2(3*H*)-thione (L^6) with R_nSnCl_{4-n} (R = Me, Bu^n or Ph; $n = 1$, 2 or 3) were investigated. Twenty-seven novel adducts were obtained and characterized by analytical (elemental analysis, conductivity and vaporimetric molecular weight measurements) and spectral (IR, far IR, ^{1}H and ^{119}Sn NMR) data. The ligands L^1, L^2, L^3 and L^4 behave in the monodentate N-donor fashion, whereas L^5 and L^6 behave as monodentate S-donor molecules. Breaking of the N–CO bonds and protonation of imidazolate moiety occurred when the donor L^4 reacts with organotin acceptors in not rigorously anhydrous conditions. The behavior of the adducts in acetone and chlorinated solvents is also discussed. Comparison was made with related organotin(IV) complexes of imidazoles. © 1998 Elsevier Science Ltd. All rights reserved

Keywords: tin(IV) and organotin(IV) complexes; ligands; imidazole; imidazoline-2-thione derivatives

INTRODUCTION

Imidazole-type heterocycles represent an important class of ligands in coordination chemistry: the imidazole ring is an essential component of many biological systems such as proteins, nucleic acids and the vitamin B_{12} coenzyme.

Expanding the earlier studies carried out with mercury(II) [1] and copper(I) [2], we have recently initiated a systematic study of tin(IV) and organotin(IV) compounds of imidazoles, in order to evaluate the bonding ability of imidazoles, which is important for understanding the effect of these N-donor ligands on the physico–chemical properties of metal complexes.

To investigate the influence of the nature of the tin(IV) acceptors and of the substituents on the azole ring, we previously investigated the interaction of 1-benzyl- [3], 4-phenyl- [4], 4-methyl-, 2-methyl-, 2-isopropyl- [5] and 1-methyl-imidazole [6] with R_nSnX_{4-n} acceptors (R = Me, Et, Bu^n and Ph; $n = 1$, 2 or 3; X = Cl, Br, I, NO_3, ClO_4, NCS and BPh_4). The reactivity of these imidazoles towards organotin(IV) acceptors depends not only on the electronic and steric features of the groups bonded to tin, but also on the position of the alkylic or arylic substituent in the imidazole moiety and on the nature of the counterion: the ligand/metal ratio can range from 1:1, as in [(1-methylimidazole)$(C_6H_5)_3$SnCl] and to 4:1, as in [(4-methylimidazole)$_4(CH_3)_2$Sn]$(BPh_4)_2$. NMR data, molecular weight measurements and X-ray crystal and

* Author to whom correspondence should be addressed. E-mail: pettinar@camserv.unicam.it.

molecular structure determinations indicate that the bonding interaction between the imidazole donors and R_nSnX_{4-n} generally increases with the decreasing of *n*.

With the aim to complete our systematic study on tin(IV) and organotin(IV) complexes of imidazoles we report here the synthesis, spectroscopic characterization (IR and ^{1}H NMR data) and behavior in solution (conductivity and molecular weight measurements) of new adducts between organotin(IV) acceptors and the ligands in Fig. 1, i.e. imidazole (L^1), benzimidazole (L^2), 2-phenylimidazole (L^3), 1-acetylimidazole (L^4), imidazoline-2(1,3*H*)-thione (L^5) and 1-methyl-imidazoline-2(3*H*)-thione (L^6).

EXPERIMENTAL

General methods

The organotin(IV) halides were purchased from Alfa (Karlsruhe) and Aldrich (Milwaukee) and used as received. The ligands imidazole (L^1), benzimidazole (L^2), 2-phenylimidazole (L^3), 1-acetylimidazole (L^4), imidazoline-2(1,3*H*)-thione (L^5), 1-methyl-imidazoline-2(3*H*)-thione (L^6) were obtained from Aldrich and were crystallized from diethyl ether/petroleum ether (1:2). Solvent evaporations were always carried out *in vacuo* (water aspirator). The samples for microanalysis were dried *in vacuo* to constant weight (20°C, approx. 0.1 Torr). Elemental analyses (C, H, N, S) were performed in house with a Carlo–Erba model 1106 instrument.

IR spectra were recorded from 4000 to 100 cm^{-1} with a Perkin-Elmer System 2000 FT-IR instrument. ^{1}H and ^{119}Sn NMR spectra were recorded on a VXR-300 Varian spectrometer operating at room temperature (300 MHz for ^{1}H and 111.9 MHz for ^{119}Sn). The chemical shifts are reported in ppm from $SiMe_4$ (^{1}H calibration by internal deuterium solvent lock) and $SnMe_4$ (^{119}Sn).

Melting points were taken on an IA 8100 Electrothermal instrument. The electrical conductance of the solutions was measured with a Crison CDTM 522 conductimeter at room temperature. The osmometric measurements were carried out at 40°C, over a range of concentrations, with a Knauer KNA0280 vapor pressure osmometer calibrated with benzil. The solvent was Baker Analyzed Spectrophotometric grade chloroform. The results were reproducible to $\pm 2\%$.

Syntheses

All experiments were carried out under a dinitrogen atmosphere. Hydrocarbon solvents were dried by distillation from sodium–potassium, dichloromethane from calcium hydride and tetrahydrofuran from $LiAlH_4$. All solvents were outgassed with dry dinitrogen prior to use.

[*Trimethylbis*(*imidazole*)*tin*(*IV*)]*chloride* (***I***). To a stirred refrigerated (0°C) petroleum ether/diethyl ether (10/1) solution (100 cm^3) of imidazole (L^1) (272 mg, 4.0 mmol), $(CH_3)_3SnCl$ (398 mg, 2.0 mmol) was added under N_2 stream. The mixture was stored at 0°C and stirred for 12 h. The solution was stored in freezer overnight. A colorless precipitate was formed, which was separated from the solution, washed with diethyl ether (3×20 cm^3), dried *in vacuo* to constant weight (20°C, approx. 0.1 Torr) and shown to be com-

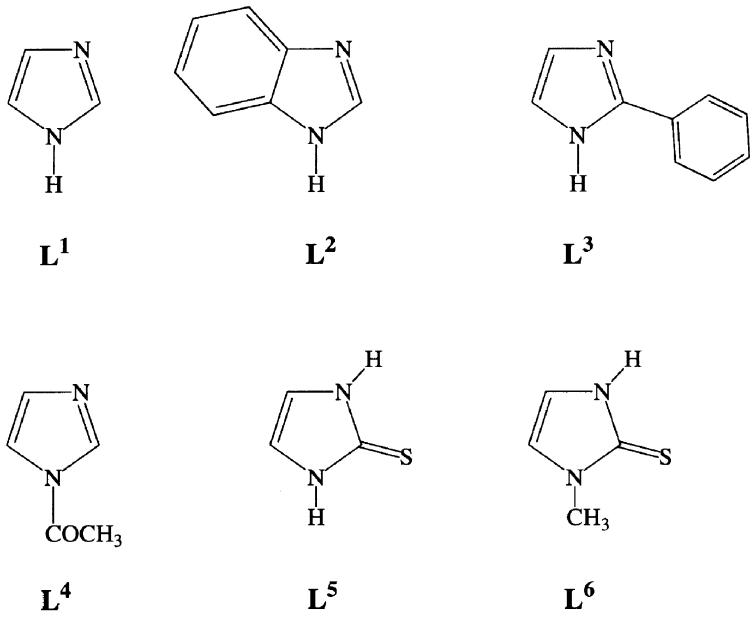

Fig. 1. Ligands employed in this work.

pound **1**. Yield: 70%, m.p. 54–56°C (Found: C, 32.4; H, 5.2; N, 16.6. Calc. for $C_9H_{17}ClN_4Sn$: C, 32.2; H, 5.1; N, 16.7%). NMR (Acetone-d_6): ^{1}H, δ 10.8 (br, 2H, N–*H*), 7.82 (s, 2H, 2-C*H*), 7.13 (s, 4H, 4-, 5-C*H*), 0.66 [$|^2J(^{119}Sn–H)| = 70.8$ Hz, $|^2J(^{117}Sn–H)| = 67.8$ Hz, s, 9H, SnCH_3]; ^{119}Sn, δ −83.5 ppm. IR: 3162 w, 3100 w [ν(C–H)], 549 s [ν(Sn–C)]. Λ (acetone, 25°C, 1.1×10^{-3} M): $1.4\,\Omega^{-1}\,cm^2\,mol^{-1}$.

[*Triphenylbis*(*imidazole*)*tin*(*IV*)]*chloride* (***2***). To a stirred refrigerated (0°C) diethyl ether solution (100 cm^3) of imidazole (L^1) (272 mg, 4.0 mmol), $(C_6H_5)_3SnCl$ (385 mg, 1.0 mmol) was added under N_2 stream. The mixture was stored at 0°C and stirred for 12 h. A white precipitate was formed, which was filtered off, washed with diethyl ether (3×20 cm^3), dried *in vacuo* to constant weight (20°C, *ca.* 0.1 Torr) and shown to be compound **2**. Yield: 39%, m.p. 155–157°C (Found: C, 55.0; H, 4.2; N, 10.4. Calc. for $C_{24}H_{23}ClN_4Sn$: C, 55.3; H, 4.4; N, 10.7%). NMR (Acetone-d_6): ^{1}H, δ 7.84 [$|^2J(^{119}Sn–H)| = 69.0$ Hz, $|^2J(^{117}Sn–H)| = 66.3$ Hz, d, 2H, Sn-*o*-C_6H_5)], 7.81 [$|^2J(^{119}Sn–H)| = 67.1$ Hz, $|^2J(^{117}Sn–H)| = 64.2$ Hz, d, 2H, Sn-*o*-C_6H_5)], 7.52 (s, 2H, 2-C*H*), 7.43 (m, 6H, Sn-*m*-, Sn-*p*-C_6H_5), 6.97 (s, 4H, 4-, 5-C*H*); ^{119}Sn, δ −225 ppm. IR: 3131 w, 3049 w [ν(C–H)], 463 s, 453 s [δ(Ph)], 290 m [ν(Sn–C)]. Λ (acetone, 25°C, 1.0×10^{-3} M): $2.6\,\Omega^{-1}\,cm^2\,mol^{-1}$.

[*Trichloromethylbis*(*imidazole*)*tin*(*IV*)]·H_2O (***3***). To a stirred diethyl ether/ethanol (1/1) solution (100 cm^3) of imidazole (L^1) (272 mg, 4.0 mmol), $(CH_3)SnCl_3$ (240 mg, 1.0 mmol) was added at room temperature. The mixture was stirred for 12 h. The solvent was removed with a rotary evaporator and diethyl ether/petroleum ether 1:1 were added until an oil was formed, which was separated from the solution. The oily residue was washed with diethyl ether/petroleum ether 1:1 (3×20 cm^3), dried *in vacuo* to constant weight (20°C, *ca.* 0.1 Torr) and shown to be compound **3**. Yield: 75% (Found: C, 21.6; H, 3.5; N, 14.6. Calc. for $C_7H_{13}Cl_3N_4OSn$: C, 21.3; H, 3.3; N, 14.2%). NMR (CD_3OD): ^{1}H, δ 8.71 s (2H, 2-C*H*), 7.50 s (4H, 4- and 5-C*H*), 1.21 s, 3H, SnCH_3]. IR: 3400 br [ν(O–H)], 3140 w, 3103 w [ν(C–H)], 569 sh br [ν(Sn–C)], 287 m, 275 m [ν(Sn–Cl)]. Λ (acetone, 25°C, 1.0×10^{-3} M): $19.7\,\Omega^{-1}\,cm^2\,mol^{-1}$.

[*Trichlorobutylbis*(*imidazole*)*tin*(*IV*)] (***4***). To a stirred diethyl ether solution (100 cm^3) of imidazole (L^1) (272 mg, 4.0 mmol), $(C_4H_9)SnCl_3$ (564 mg, 2.0 mmol) was added at room temperature. A colorless precipitate was formed immediately, which was filtered off after 6 h, washed with diethyl ether (3×20 cm^3), dried *in vacuo* to constant weight (20°C, *ca.* 0.1 Torr) and shown to be compound **4**. Yield: 95%, m.p. 93–95°C (Found: C, 28.7; H, 4.2; N, 13.3. Calc. for $C_{10}H_{17}Cl_3N_4Sn$: C, 28.7; H, 4.1; N, 13.4%). NMR (Acetone-d_6): ^{1}H, δ 12.2 (br, 2H, N–*H*), 8.70 (br, 2H, 2-C*H*), 7.50 (br, 4H, 4- and 5-C*H*), 1.6–1.8 (m, 4H, Sn–C_4H_9), 1.32 (ps, 2H, Sn–C_4H_9), 0.85 (t, 3H, Sn–C_4H_9). IR: 3126 m, 3047 w [ν(C–H)], 618 m [ν(Sn–C)], 284 m, 274 m [ν(Sn–Cl)]. Λ (acetone, 25°C, 1.1×10^{-3} M): $24.3\,\Omega^{-1}\,cm^2\,mol^{-1}$.

[*Trichlorophenylbis*(*imidazole*)*tin*(*IV*)] (***5***). Compound **5** was prepared similarly to compound **4**. Yield: 47%, m.p. 128–132°C (Found: C, 33.0; H, 3.2; N, 12.6. Calc. for $C_{12}H_{13}Cl_3N_4Sn$: C, 32.9; H, 3.0; N, 12.8%). NMR (Acetone-d_6): ^{1}H, δ 12.3 (br, 2H, N–*H*), 8.74, 8.67 (br, 2H, 2-C*H*), 7.54 (br, 4H, 4- and 5-C*H*), 8.2, 7.9, 7.8, 7.5, 7.3 (m, 5H, Sn–C_6H_5). IR: 3134 w [ν(C–H)], 462 m [δ(Ph)], 318 br, 310 m, 286 m, 270 m, 260 m [ν(Sn–C) and ν(Sn–Cl)]. Λ (acetone, 25°C, 1.1×10^{-3} M): $41.0\,\Omega^{-1}\,cm^2\,mol^{-1}$.

[*Chlorotriphenyl*(*benzimidazole*)*tin*(*IV*)] (***6***). To a stirred diethyl ether solution (100 cm^3) of benzimidazole (L^2) (236 mg, 2.0 mmol), $(C_6H_5)_3SnCl$ (385 mg, 1.0 mmol) in dichloromethane (20 cm^3) was added at 40°C. A colorless precipitate was formed immediately, which was filtered off after 6 h, washed with diethyl ether (3×20 cm^3), dried *in vacuo* to constant weight (20°C, *ca.* 0.1 Torr) and shown to be compound **6**. Yield: 40%, m.p. 149–152°C (Found: C, 59.5; H, 4.4; N, 5.8. Calc. for $C_{25}H_{21}ClN_4Sn$: C, 59.6; H, 4.2; N, 5.6%). NMR (Acetone-d_6): ^{1}H, δ 8.06 (s, 1H, 2-C*H*), 7.83 [$|^2J(^{119}Sn–H)| = 65.0$ Hz, d, 6H, Sn-*o*-C_6H_5)], 7.40–7.55 (m, 11H, Sn-*m*-, Sn-*p*-C_6H_5 and 4- and 7-C*H*), 7.17 (m, 2H, 5- and 6-C*H*). IR: 3360 br [ν(N–H)], 3157 w, 3129 w [ν(C–H)], 455 s, 426 s, 422 sh [δ(Ph)], 290 m [ν(Sn–C)], 226 s [ν(Sn–Cl)]. Λ (acetone, 25°C, 0.9×10^{-3} M): $1.3\,\Omega^{-1}\,cm^2\,mol^{-1}$.

[*Dichlorodimethylbis*(*benzimidazole*)*tin*(*IV*)] (***7***). To a stirred dichloromethane solution (100 cm^3) of benzimidazole (L^2) (473 mg, 4.0 mmol), $(CH_3)_2SnCl_2$ (220 mg, 1.0 mmol) was added at room temperature. A colorless precipitate was formed immediately, which was filtered off after 6 h, washed with dichloromethane (3×20 cm^3), dried *in vacuo* to constant weight (20°C, *ca.* 0.1 Torr) and shown to be compound **7**. Yield: 98%, m.p. 171–174°C (Found: C, 42.2; H, 4.0; N, 12.2. Calc. for $C_{16}H_{18}Cl_2N_4Sn$: C, 42.1; H, 4.0; N, 12.3%). NMR (Acetone-d_6): ^{1}H, δ 11.1 (br, 2H, N–*H*), 8.77 (s, 2H, 2-C*H*), 7.82 (m, 4H, 4- and 7-C*H*), 7.39 (m, 4H, 5- and 6-C*H*), 1.22 [$|^2J(^{119}Sn–H)| = 92.1$ Hz, $|^2J(^{117}Sn–H)| = 87.9$ Hz, s, 6H, SnCH_3]; ^{119}Sn, δ −147.2 ppm. IR: 3150 br [ν(N–H)], 3134 w [ν(C–H)], 573 s [ν(Sn–C)], 435 s, 422 s [δ(Ph)], 228 s [ν(Sn–Cl)]. Λ (acetone, 25°C, 0.9×10^{-3} M): $35.8\,\Omega^{-1}\,cm^2\,mol^{-1}$.

[*Dichlorodiphenylbis*(*benzimidazole*)*tin*(*IV*)] (***8***). To a stirred dichloromethane/diethyl ether (2/1) solution (100 cm^3) of benzimidazole (L^2) (473 mg, 4.0 mmol), $(C_6H_5)_2SnCl_2$ (344 mg, 1.0 mmol) was added at room temperature. A pale brown precipitate was formed immediately, which was filtered off after 6 h, washed with diethyl ether (3×20 cm^3), dried *in vacuo* to constant weight (20°C, *ca.* 0.1 Torr) and shown to be compound **8**. Yield: 89%, m.p. 162–164°C (Found: C, 53.6; H, 3.9; N, 9.9. Calc. for $C_{26}H_{22}Cl_2N_4Sn$: C, 53.8; H, 3.8; N, 9.7%). NMR (Acetone-d_6): ^{1}H, δ 10.0 (br, 2H, N–*H*), 8.41 (s, 2H, 2-C*H*), 7.98 [$|^2J(^{119}Sn–H)| = 108.4$ Hz, $|^2J(^{117}Sn–H)| = 107.7$, d, 4H, Sn-*o*-

C_6H_5)], 7.67, 7.24 (m, 10H, Sn-*m*-, Sn-*p*-C_6H_5 and 4-, 5-, 6- and 7-C*H*). IR: 3150 br [ν(N–H)], 3127 w [ν(C–H)], 463 s, 458 s, 432 s, 424 s [δ(Ph)], 293 s [ν(Sn–C)], 244 s, 234 s [ν(Sn–Cl)]. Λ (acetone, 25°C, 0.9×10^{-3} M): 19.9 Ω^{-1} cm^2 mol^{-1}.

[*Trichloromethylbis*(*benzimidazole*)*tin*(*IV*)] (***9***). Compound **9** was prepared similarly to compound **7**. Yield: 84%, m.p. 280°C dec. (Found: C, 38.0; H, 3.1; N, 11.6. Calc. for $C_{15}H_{15}Cl_3N_4Sn$: C, 37.8; H, 3.2; N, 11.8%). NMR (Acetone-d_6): ^{1}H, δ 8.95 (br, 2H, 2-C*H*), 7.90 (m, 4H, 4- and 7-C*H*), 7.30 (m, 4H, 5- and 6-C*H*), 1.46 [$|^2J(^{119}Sn–H)| = 131.4$ Hz, $|^2J(^{117}Sn–H)| = 121.2$ Hz, s, 3H, SnCH_3]. IR: 3340 m, 3278 br [ν(N–H)], 3139 w [ν(C–H)], 592 s, 546 m, 533 m [ν(Sn–C)], 439 s, 420 s [δ(Ph)], 304 s, 295 s [ν(Sn–Cl)]. Λ (acetone, 25°C, 1.0×10^{-3} M): 44.1 Ω^{-1} cm^2 mol^{-1}.

[*Trichlorobutylbis*(*benzimidazole*)*tin*(*IV*)] (***10***). Compound **10** was prepared similarly to compound **8**. Yield: 75%, m.p. 158–160°C (Found: C, 41.7; H, 4.1; N, 10.5. Calc. for $C_{18}H_{21}Cl_3N_4Sn$: C, 41.7; H, 4.1; N, 10.8%). NMR (Acetone-d_6): ^{1}H, δ 9.68 (s, 2H, 2-C*H*), 8.02 (m, 4H, 4- and 7-C*H*), 7.69 (m, 4H, 5- and 6-C*H*), 1.8–2.2 (m, 4H, Sn–C_4H_9), 1.47 (ps, 2H, Sn–C_4H_9), 0.93 (t, 3H, Sn–C_4H_9). IR: 3200 br [ν(N–H)], 3085 w [ν(C–H)], 597 s [ν(Sn–C)], 419 s, 403 s [δ(Ph)], 291 s, 251 s, 230 s [ν(Sn–Cl)]. Λ (acetone, 25°C, 1.3×10^{-3} M): 76.4 Ω^{-1} cm^2 mol^{-1}.

[*Trichlorophenylbis*(*benzimidazole*)*tin*(*IV*)] (***11***). Compound **11** was prepared similarly to compound **8**. Yield: 80%, m.p. 121–124°C (Found: C, 44.5; H, 3.1; N, 10.5. Calc. for $C_{20}H_{17}Cl_3N_4Sn$: C, 44.6; H, 3.2; N, 10.4%). NMR (Acetone-d_6): ^{1}H, δ 12.5 (br, 2H, N–*H*), 8.95 (br, 2H, 2-C*H*), 7.96 (br, 2H, Sn-*o*-C_6H_5), 7.72, 7.26 (br, 7H, Sn-*m*-, Sn-*p*-C_6H_5 and 4-, 5-, 6- and 7-C*H*). IR: 3278 br [ν(N–H)], 3134 w [ν(C–H)], 455 s, 437 s, 420 s, 408 s [δ(Ph)], 285 m [ν(Sn–C)], 266 sh, 257 br, 250 br, 236 s [ν(Sn–Cl)]. Λ (acetone, 25°C, 0.8×10^{-3} M): 30.5 Ω^{-1} cm^2 mol^{-1}.

[*Dichlorodimethylbis*(2-*phenylimidazole*)*tin*(*IV*)] (***12***). To a stirred dichloromethane/diethyl ether (2/1) solution (100 cm^3) of 2-phenylimidazole (L^3) (577 mg, 4.0 mmol), $(CH_3)_2SnCl_2$ (439 mg, 2.0 mmol) was added at room temperature. A colorless precipitate was formed immediately, which was filtered off after 6 h, washed with diethyl ether (3×20 cm^3), dried *in vacuo* to constant weight (20°C, *ca.* 0.1 Torr) and shown to be compound **12**. Yield: 52%, m.p. 130–132°C (Found: C, 47.4; H, 4.4; N, 10.9. Calc. for $C_{20}H_{22}Cl_2N_4Sn$: C, 47.3; H, 4.4; N, 11.0%). NMR ($CDCl_3$): ^{1}H, δ 8.22 (d, 4H, *o*-C_6H_5), 7.41 (t, 2H, *p*-C_6H_5), 7.31 (t, 4H, *m*-C_6H_5), 7.24 (s, 4H, 4- and 5-C*H*), 1.25 [$|^2J(^{119}Sn–H)| = 71.7$ Hz, $|^2J(^{117}Sn–H)| = 69.0$ Hz, s, 6H, SnCH_3]. IR: 3140 br [ν(N–H)], 3110 w, 3048 w [ν(C–H)], 575 m [ν(Sn–C)], 438 s [δ(Ph)], 233 s br [ν(Sn–Cl)]. Λ (acetone, 25°C, 1.1×10^{-3} M): 67.3 Ω^{-1} cm^2 mol^{-1}.

[*Dichlorodibutylbis*(2-*phenylimidazole*)*tin*(*IV*)] (***13***). To a stirred ethanol/diethyl ether (2/1) solution (100 cm^3) of 2-phenylimidazole (L^3) (577 mg, 4.0 mmol), $(C_4H_9)_2SnCl_2$ (304 mg, 1.0 mmol) was added at room temperature. A colorless precipitate was formed immediately, which was filtered off after 6 h, washed with diethyl ether (3×20 cm^3), dried *in vacuo* to constant weight (20°C, *ca.* 0.1 Torr) and shown to be compound **13**. Yield: 93%, m.p. 109–111°C (Found: C, 53.0; H, 6.0; N, 10.0. Calc. for $C_{26}H_{34}Cl_2N_4Sn$: C, 52.7; H, 5.8; N, 9.5%). NMR ($CDCl_3$): ^{1}H, δ 10.6 (br, 2H, N*H*), 7.96 (d, 4H, *o*-C_6H_5), 7.27 (m, 6H, *m*- and *p*-C_6H_5), 7.11 (s, 4H, 4- and 5-C*H*), 1.8 (m, 4H, Sn–C_4H_9), 1.39 (ps, 2H, Sn–C_4H_9), 0.93 (t, 3H, Sn–C_4H_9). IR: 3400 br [ν(N–H)], 3155 w [ν(C–H)] 600 v br [ν(Sn–C)], 445 m, 418 m [δ(Ph)], 230 m [ν(Sn–Cl)]. Λ (acetone, 25°C, 1.3×10^{-3} M): 23.4 Ω^{-1} cm^2 mol^{-1}.

[*Dichlorodiphenylbis*(2-*phenylimidazole*)*tin*(*IV*)] (***14***). To a stirred dichloromethane/methanol (1/1) solution (100 cm^3) of 2-phenylimidazole (L^3) (577 mg, 4.0 mmol), $(C_6H_5)_2SnCl_2$ (688 mg, 2.0 mmol) was added at 40°C. A colorless precipitate was formed immediately, which was filtered off after 6 h, washed with diethyl ether (3×20 cm^3), dried *in vacuo* to constant weight (20°C, *ca.* 0.1 Torr) and shown to be compound **14**. Yield: 54%, m.p. 171–173°C (Found: C, 57.2; H, 4.3; N, 8.7. Calc. for $C_{30}H_{26}Cl_2N_4Sn$: C, 57.0; H, 4.2; N, 8.9%). NMR ($CDCl_3$): ^{1}H, δ 7.0–8.0 (m br, 24H, Sn–C_6H_5, 2-C_6H_5, 4- and 5-C*H*). IR: 3350 br [ν(N–H)], 3061 w, 3039 w [ν(C–H)], 455 s, 444 m [δ(Ph)], 278 m, 269 s [ν(Sn–C)], 226 m [ν(Sn–Cl)]. Λ not available in acetone due to poor solubility.

[*Trichloromethylbis*(2-*phenylimidazole*)*tin*(*IV*)] (***15***). Compound **15** was prepared similarly to compound **12**. Yield: 70%, m.p. 135–138°C dec. (Found: C, 43.0; H, 3.7; N, 10.8. Calc. for $C_{19}H_{19}Cl_3N_4Sn$: C, 43.2; H, 3.6; N, 10.6%). NMR (Acetone-d_6): ^{1}H, δ 8.8 (br, 2H, N–*H*), 8.17 (d, 4H, *o*-C_6H_5), 7.60–7.72 (m, 10H, *m*-C_6H_5, *p*-C_6H_5, 4- and 5-C*H*), 1.41 [$|^2J(^{119}Sn–H)| = 117.5$ Hz, $|^2J(^{117}Sn–H)| = 113.0$ Hz, s, 3H, SnCH_3]. IR: 3150 br [ν(N–H)], 3103 w [ν(C–H)], 527 s [ν(Sn–C)], 442 s [δ(Ph)], 317 s, 300 sh, 288 m [ν(Sn–Cl)]. Λ (acetone, 25°C, 0.8×10^{-3} M): 95.0 Ω^{-1} cm^2 mol^{-1}.

[*Trichlorobutylbis*(2-*phenylimidazole*)*tin*(*IV*)] (***16***). To a stirred dichloromethane solution (100 cm^3) of 2-phenylimidazole (L^3) (577 mg, 4.0 mmol), $(C_4H_9)SnCl_3$ (564 mg, 2.0 mmol) was added at room temperature. The mixture was stirred for 24 h; the solvent was removed with a rotary evaporator and diethyl ether was added. A colorless precipitate was formed immediately, which was filtered off, washed with diethyl ether (3×20 cm^3), dried *in vacuo* to constant weight (20°C, *ca.* 0.1 Torr) and shown to be compound **16**. Yield: 90%, m.p. 109–112°C (Found: C, 47.4; H, 4.2; N, 10.0. Calc. for $C_{22}H_{25}Cl_3N_4Sn$: C, 47.3; H, 4.4; N, 9.8%). NMR ($CDCl_3$): ^{1}H, δ 13.9 (br, 2H, N*H*), 8.11 (d, 4H, *o*-C_6H_5), 7.20–7.50 (m, 10H, *m*-C_6H_5, *p*-C_6H_5, 4- and 5-C*H*), 2.45 (m, 2H, Sn–C_4H_9), 1.96 (m, 2H, Sn–C_4H_9), 1.51 (ps, 2H, Sn–C_4H_9), 0.97 (t, 3H, Sn–C_4H_9); ^{119}Sn, δ −269.1 ppm. IR: 3150 br [ν(N–H)], 3085 w [ν(C–H)], 616 m [ν(Sn–C)], 457 w, 441 w, 422 w [δ(Ph)], 316 s, 303 sh [ν(Sn–

Cl)]. Λ (acetone, 25°C, 1.0×10^{-3} M): 88.9 Ω^{-1} cm^2 mol^{-1}.

[*Trichlorophenylbis*(2-*phenylimidazole*)*tin*(*IV*)] (***17***). Compound **17** was prepared similarly to compound **12**. Yield: 65%, m.p. 128–130°C dec. (Found: C, 48.6; H, 3.4; N, 9.6. Calc. for $C_{24}H_{21}Cl_3N_4Sn$: C, 48.8; H, 3.6; N, 9.5%). NMR (Acetone-d_6): ^{1}H, δ 8.30 (d, 2H, Sn–C_6H_5), 8.19 (d, 4H, 2-C_6H_5) 7.71, 7.61, 7.33 (m, 13H, 2-C_6H_5, Sn–C_6H_5, 4- and 5-C*H*). IR: 3300 br [ν(N–H)], 3106 w [ν(C–H)], 458 s [δ(Ph)], 290 m [ν(Sn–C)], 323 m, 315 m, 303 m [ν(Sn–Cl)]. Λ (acetone, 25°C, 1.0×10^{-3} M): 85.4 Ω^{-1} cm^2 mol^{-1}.

Dichlorodimethylbis(1-*acetylimidazole*)*tin*(*IV*)] (***18***). Compound **18** was obtained similarly to compound **2**. The oily residue obtained was washed with diethyl ether (3×20 cm^3) and shown to be compound **18**. Yield: 90%. (Found: C, 32.5; H, 4.3; N, 12.4. Calc. for $C_{12}H_{18}Cl_2N_4O_2Sn$: C, 32.8; H, 4.1; N, 12.7%). NMR ($CDCl_3$): ^{1}H, δ 8.25 (br, 2H, 2-C*H*), 7.52 (br, 2H, 4- or 5-C*H*), 7.17 (br, 2H, 4- or 5-C*H*), 2.63 (s, 6H, N–CH_3), 1.23 [$|^2J(^{119}Sn–H)| = 75.9$ Hz, $|^2J(^{117}Sn–H)| = 72.3$ Hz, s, 6H, SnCH_3]. IR: 3170 w, 3147 w [ν(C–H)], 1747 s br [ν(C=O)], 564 s [ν(Sn–C)], 244 s, 217 m [ν(Sn–Cl)]. Λ (acetone, 25°C, 1.0×10^{-3} M): 0.9 Ω^{-1} cm^2 mol^{-1}.

Dichlorodiphenylbis(1-*acetylimidazole*)*tin*(*IV*)]·H_2O(***19***). Compound **19** was obtained similarly to compound **2**. The colorless precipitate formed was filtered after 24 h, washed with diethyl ether (3×30 cm^3), dried *in vacuo* to constant weight (20°C, *ca.* 0.1 Torr) and shown to be compound **19**. Yield: 95%, m.p. 140–144°C (Found: C, 43.8; H, 4.3; N, 9.5. Calc. for $C_{22}H_{26}Cl_2N_4O_4Sn$: C, 44.0; H, 4.4; N, 9.3%). NMR ($CDCl_3$): ^{1}H, δ 8.19 (br, 2H, 2-C*H*), 7.79 [$|^2J(^{119}Sn–H)| = 132$ Hz, $|^2J(^{117}Sn–H)| = 121$ Hz, m, 4H, Sn–C_6H_5], 7.51 (m br, 8H, Sn–C_6H_5, 4- or 5-C*H*), 7.13 (br, 2H, 4- or 5-C*H*), 2.60 (s, 6H, N–CH_3). IR: 3200–2800 br [ν(O–H)], 3170 w, [ν(C–H)], 1752 s br [ν(C=O)], 295 m [ν(Sn–C)], 264 sh, 256 s, 230 s [ν(Sn–Cl)]. Λ (acetone, 25°C, 1.2×10^{-3} M): 15.0 Ω^{-1} cm^2 mol^{-1}.

[*Dichlorodiphenylbis*(*imidazoline*-2(1,3H)-*thione*)*tin* (*IV*)] (***20***). To a stirred diethyl ether solution (40 cm^3) of $(C_6H_5)_2SnCl_2$ (344 mg, 1.0 mmol), imidazoline-2-thione (L^5) (200 mg, 2.0 mmol) was added at room temperature. A colorless precipitate was formed immediately, which was filtered off after 24 h, washed with diethyl ether (3×20 cm^3), dried *in vacuo* to constant weight (20°C, *ca.* 0.1 Torr) and shown to be compound **20**. Yield: 92%, m.p. 213–214°C (Found: C, 39.6; H, 3.5; N, 10.2; S, 11.6. Calc. for $C_{18}H_{18}Cl_2N_4S_2Sn$: C, 39.7; H, 3.3; N, 10.3; S, 11.8%). NMR (Acetone-d_6): ^{1}H, δ 8.12 [$|^2J(^{119}Sn–H)| = 97.2$ Hz, $|^2J(^{117}Sn–H)| = 87.1$ Hz, d, 4H, Sn-*o*-C_6H_5)], 7.3–7.6 (m, 6H, Sn-*o*-C_6H_5), 7.10 (s, 4H, 4- and 5-C*H*). IR: 3220 br [ν(N–H)], 3050 w [ν(C–H)], 1077 s, 1060 m [ν(C–S)], 460 s [δ(Ph)], 289 m, 278 m [ν(Sn–C)], 238 m, 225 s [ν(Sn–Cl)]. Λ (acetone, 25°C, 1.0×10^{-3} M): 2.0 Ω^{-1} cm^2 mol^{-1}.

[*Trichlorophenylbis*(*imidazoline*-2(1,3H)-*thione*)*tin* (*IV*)] (***21***). Compound **21** was prepared similarly to compound **20**. Yield: 79%, m.p. 291–293°C (Found: C, 29.0; H, 2.9; N, 11.0; S, 12.5. Calc. for $C_{12}H_{13}Cl_3N_4S_2Sn$: C, 28.7; H, 2.6; N, 11.1; S, 12.8%). NMR (Acetone-d_6): ^{1}H, δ 10.6 (br, 4H, N-*H*), 8.06 [$|^2J(^{119}Sn–H)| = 135.8$ Hz, $|^2J(^{117}Sn–H)| = 117.4$ Hz, d, 2H, Sn-*o*-C_6H_5)], 7.3–7.4 (m, 3H, Sn–C_6H_5), 7.28 (s, 4H, 4- and 5-C*H*). IR: 3250 br [ν(N–H)], 3120 w [ν(C–H)], 1124 w, 1102 w, 1076 m [ν(C–S)], 457 s [δ(Ph)], 301 w, 289 w [ν(Sn–C)], 255 br [ν(Sn–Cl)]. Λ (acetone, 25°C, 1.0×10^{-3} M): 6.5 Ω^{-1} cm^2 mol^{-1}.

[*Trichlorobutylbis*(*imidazoline*-2(1,3H)-*thione*)*tin* (*IV*)] (***22***). Compound **22** was prepared similarly to compound **20**. Yield: 39%, m.p. 118–121°C (Found: C, 25.0; H, 3.3; N, 11.7; S, 13.3. Calc. for $C_{10}H_{17}Cl_3N_4S_2Sn$: C, 24.9; H, 3.5; N, 11.6; S, 13.3%). NMR (Acetone-d_6): ^{1}H, δ 9.2 (br, 4H, N-*H*), 7.23 (s, 4H, 4- and 5-C*H*), 0.91 t, 1.44 ps, 1.76–1.88 m, 2.02–2.08 m (9H, Sn–C_4H_9); ^{119}Sn, δ −330.6 ppm. IR: 3170 w, [ν(C–H)], 1083 m, 1073 m [ν(C–S)], 501 m [ν(Sn–C)], 268 s [ν(Sn–Cl)]. Λ (acetone, 25°C, 1.0×10^{-3} M): 14.0 Ω^{-1} cm^2 mol^{-1}.

[*Dichlorodimethyl*(1-*methyl*-*imidazoline*-2(3*H*)-*thione*)*tin*(*IV*)] (***23***). Compound **23** was prepared similarly to compound **20**. Yield: 95%, m.p. 122–125°C (Found: C, 22.0; H, 3.8; N, 8.6; S, 9.5. Calc. for $C_6H_{12}Cl_2N_2SSn$: C, 21.6; H, 3.6; N, 8.4; S, 9.6%). NMR (Acetone-d_6): ^{1}H, δ 11.8 (br, 1H, N-*H*), 6.98, 6.87 (2d, 2H, 4- and 5-C*H*), 3.51 (s, 3H, N–CH_3), 1.22 [$|^2J(^{119}Sn–H)| = 85.9$ Hz, $|^2J(^{117}Sn–H)| = 82.8$ Hz, s, 6H, Sn–CH_3). ^{119}Sn, δ −13.7 ppm. IR: 3125 w, 3085 w [ν(C–H)], 1165 s, 1109 s [ν(C–S)], 566 s [ν(Sn–C)], 240 s br [ν(Sn–Cl)]. Λ (acetone, 25°C, 0.9×10^{-3} M): 4.9 Ω^{-1} cm^2 mol^{-1}.

[*Dichlorodiphenylbis*(1-*methyl*-*imidazoline*-2(3*H*)-*thione*)*tin*(*IV*)] (***24***). Compound **24** was prepared similarly to compound **20**. Yield: 82%, m.p. 153–155°C (Found: C, 41.7; H, 4.0; N, 9.8; S, 10.9. Calc. for $C_{20}H_{22}Cl_2N_4S_2Sn$: C, 42.0; H, 3.9; N, 9.8; S, 11.2%). NMR ($CDCl_3$): ^{1}H, δ 7.90 [$|^2J(Sn–H)| = 88.9$ Hz, m, 10H, Sn–C_6H_5)], 6.74, 6.72 (2d, 4H, 4- and 5-C*H*), 3.61 (s, 3H, N–CH_3); ^{119}Sn, δ −232.1 ppm. IR: 3125 w [ν(C–H)], 1096 m, 1084 m, 1060 m [ν(C–S)], 461 s [δ(Ph)], 283 s [ν(Sn–C)], 227 s, 222 s [ν(Sn–Cl)]. Λ (acetone, 25°C, 1.0×10^{-3} M): 10.5 Ω^{-1} cm^2 mol^{-1}.

[*Trichloromethylbis*(1-*methyl*-*imidazoline*-2(3*H*)-*thione*)*tin*(*IV*)]·H_2O (***25***). Compound **25** was prepared similarly to compound **20**. Yield: 40%, m.p. 80°C dec. (Found: C, 21.9; H, 3.3; N, 11.7; S, 13.5. Calc. for $C_9H_{17}Cl_3N_4OS_2Sn$: C, 22.2; H, 3.5; N, 11.5; S, 13.2%). NMR (Acetone-d_6): ^{1}H, δ 7.35, 7.28 (2 s br, 4H, 4- and 5-C*H*), 3.76 (s br, 6H, N–CH_3), 1.4–2.2 (br, 3H, Sn–CH_3). IR: 3200 br [ν(N–H) and ν(O–H)], 3125 w [ν(C–H)], 1160 m, 1099 m [ν(C–S)], 514 m [ν(Sn–C)], 295 s [ν(Sn–Cl)]. Λ (acetone, 25°C, 1.0×10^{-3} M): 15.0 Ω^{-1} cm^2 mol^{-1}.

[*Trichlorophenylbis*(1-*methyl*-*imidazoline*-2(3*H*)-*thione*)*tin*(*IV*)] (***26***). Compound **26** was prepared similarly to compound **20**. Yield: 92%, m.p. 80–83°C (Found: C, 30.3; H, 3.4; N, 9.9; S, 11.4. Calc. for

$C_{14}H_{19}Cl_3N_4OS_2Sn$: C, 30.7; H, 3.5; N, 10.2; S, 11.7%). NMR (Acetone-d_6): ^{1}H, δ 8.1–8.2, 7.4–7.6 (m, 5H, Sn–C_6H_5), 7.28, 7.35 (2d, 4H, 4- and 5-C*H*), 3.73 (s, 6H, N–CH_3); ^{119}Sn, δ −236.9, −330.3 ppm. IR: 3100 w [ν(C–H)], 1160 m, 1098 m [ν(C–S)], 456 s [δ(Ph)], 290 br [ν(Sn–C)], 262 br [ν(Sn–Cl)]. Λ (acetone, 25°C, 1.0×10^{-3} M): 15.8 Ω^{-1} cm^2 mol^{-1}.

[*Trichlorobutylbis*(1-*methyl-imidazoline*-2(3*H*)-*thione*)*tin*(*IV*)] (**27**). To a stirred diethyl ether solution (100 cm^3) of $(C_4H_9)SnCl_3$ (0.303 mg, 1.0 mmol) 1-methylimidazoline-2(3H)-thione (0.228 g, 2.0 mmol) was added at room temperature. The oily residue formed was separated from the solution and dissolved in dichloromethane (10 cm^3). To the clear solution diethyl ether was added (20 cm^3) and the colorless precipitate formed was filtered, washed with diethyl ether, dried *in vacuo* to constant weight (20°C, *ca.* 0.1 Torr) and shown to be compound **27**. Yield: 45%, m.p. 95–98°C (Found: C, 28.4; H, 4.3; N, 11.0; S, 12.7. Calc. for $C_{12}H_{21}Cl_3N_4S_2Sn$: C, 28.2; H, 4.1; N, 11.0; S, 12.6%). NMR ($CDCl_3$): ^{1}H, δ 7.00, 6.91 (2d, 4H, 4- and 5-C*H*), 3.72 (s, 6H, N–CH_3), 0.93 t, 1.45 ps, 1.80–1.96 m, 2.28 t (9H, Sn–C_4H_9); ^{119}Sn, δ −251.8 ppm. IR: 3154 w, 3125 w [ν(C–H)], 1133 m, 1096 m [ν(C–S)], 520 s, 512 sh [ν(Sn–C)], 276 s [ν(Sn–Cl)]. Λ (acetone, 25°C, 1.0×10^{-3} M): 4.6 Ω^{-1} cm^2 mol^{-1}.

RESULTS AND DISCUSSION

Synthesis, reactivity and properties of the organotin(IV) complexes

Interaction between R_nSnCl_{4-n} (R = Me, Bu^n or Ph; n = 1, 2 or 3) compounds and an excess of imidazole (L^1), benzimidazole (L^2) and 2-phenylimidazole (L^3) in organic solvents (alcohols, dichloromethane, diethyl ether or petroleum ether) at 0°C or at room temperature gave the compounds **1**–**17** in accordance with eq. (1):

$$x(L) + (R_nSnCl_{4-n}) \xrightarrow{\text{Solvent}} \underset{\mathbf{1–17}}{[(L)_x(R_nSnCl_{4-n})]\cdot zH_2O}. \quad (1)$$

No.	Ligand, L	R	x	n	z
1	L^1	Me	2	3	0
2	L^1	Ph	2	3	0
3	L^1	Me	2	1	1
4	L^1	Bu^n	2	1	0
5	L^1	Ph	2	1	0
6	L^2	Ph	1	3	0
7	L^2	Me	2	2	0
8	L^2	Ph	2	2	0
9	L^2	Me	2	1	0
10	L^2	Bu^n	2	1	0
11	L^2	Ph	2	1	0
12	L^3	Me	2	2	0
13	L^3	Bu^n	2	2	0
14	L^3	Ph	2	2	0
15	L^3	Me	2	1	0
16	L^3	Bu^n	2	1	0
17	L^3	Ph	2	1	0

In the same conditions no adduct was obtained from the interaction between L^1 and Bu$^n{}_3$SnCl, between L^2 and Me_3SnCl, Bu$^n{}_3$SnCl or Bu$^n{}_2$SnCl$_2$, and finally between L^3 and R_3SnCl (R = Me, Bu^n or Ph) or Me_2SnCl_2. On the other hand, even if different reaction conditions with respect to literature reports [7–10] were employed, from the interaction between L^1 and R_2SnCl_2 analogous 2:1 complexes were afforded.

With the exception of the derivative **6** (for which a ligand to metal ratio of 1:1 was observed) 2:1 adducts were obtained from the interaction between L^1 or L^2 and triorganotin(IV) acceptors. This fact further indicates the possibility of obtaining 2:1 adducts with triorganotin(IV) chlorides when imidazole type donors able to involve the halide group in a hydrogen bonding network were employed [4].

Interaction between R_2SnCl_2 (R = Me or Ph) and excess 1-acetylimidazole L^4 in diethyl ether produces the derivatives $[(L^4)_2(Me_2SnCl_2)]$ **18** and $[(L^4)_2(Ph_2SnCl_2)]\cdot H_2O$ **19**. Whereas L^4 reacts with other organotin acceptors yielding neutral adducts of unsubstituted imidazole L^1 upon hydrolysis of the N(1)–$COCH_3$ bond. The presence of a small quantity of water in the solvent is sufficient for the attack of the N(1)–C bond and formation of the donor L^1 which immediately coordinates the organotin acceptor. If rigorously anhydrous conditions were employed, no product afforded.

The reaction between imidazoline-2(1,3*H*)-thione (L^5) or 1-methyl-imidazoline-2(3*H*)-thione (L^6) and R_nSnCl_{4-n} acceptors (R = Me, Bu^n or Ph; n = 1, 2 or 3) was carried out in diethyl ether or diethyl ether/dichloromethane solutions from which compounds **20**–**27** were isolated as insoluble or sparingly soluble precipitates, in accordance with eq. (2) (see Table):

$$x(L) + (R_nSnCl_{4-n})\cdot zH_2O \xrightarrow{\text{Solvent}} \underset{\mathbf{20–27}}{[(L)_x(R_nSnCl_{4-n})]\cdot zH_2O}. \quad (2)$$

No.	Ligand, L	R	x	n	z
20	L^5	Ph	2	2	0
21	L^5	Ph	2	1	0
22	L^5	Bu^n	2	1	0
23	L^6	Me	1	2	0
24	L^6	Ph	2	2	0
25	L^6	Me	2	1	1
26	L^6	Ph	2	1	0
27	L^6	Bu^n	2	1	0

With the exception of the derivative **23** $[(L^6)(CH_3)_2SnCl_2]$ (for which a ligand to metal ratio

Table 1. Compounds obtained from various imidazoles and organotin(IV)chloride acceptors

	Organotin(IV) acceptor[b]									
Ligand[a]	Me_3SnCl	Me_2SnCl_2	$MeSnCl_3$	Bu_3SnCl	Bu_2SnCl_2	$BuSnCl_3$	Ph_3SnCl	Ph_2SnCl_2	$PhSnCl_3$	Ref.
L^1	2:1	2:1[c]	2:1	no reaction	2:1[d]	2:1	2:1	2:1[e]	2:1	This work
L^2	no reaction	2:1	2:1	no reaction	no reaction	2:1	1:1	2:1	2:1	This work
L^3	no reaction	no reaction	2:1	no reaction	2:1	2:1	no reaction	2:1	2:1	This work
L^4	N–CO break.	2:1	N–CO break.	N–CO break.	N–CO break.	N–CO break.	no reaction	2:1 (+1)	N–CO break.	This work
L^5	no reaction	2:1[f]	1:1,[f] 2:1[f]	no reaction	no reaction	2:1	no reaction	2:1	2:1	This work
L^6	no reaction	1:1	1:1,[f] 2:1 (+1)	no reaction	no reaction	1:1,[f] 2:1	1:1 anionic[g]	2:1	2:1	This work
L^7	1:1	2:1	2:1	no reaction	2:1	2:1	1:1	2:1 (+1)	2:1	[3]
L^8	2:1[h]	2:1	2:1	no reaction	2:1	3:2	2:1	2:1	3:2 (+1)	[4]
L^9	1:1	2:1[i]	2:1	1:1 (+1)	2:1 (+1)	2:1	1:1[l]	2:1	2:1	[6]
L^{10}	2:1	2:1	2:1 (+6)	2:1	2:1	3:1	1:1 (+1/3)	2:1 (+1)	3:1	[5]
L^{11}	2:1 (+1)	2:1	no reaction	no reaction	no reaction	2:1 (+2)	no reaction	no reaction	2:1 (+3)	[5]
L^{12}	1:1	2:1 (+1)	no reaction	no reaction	no reaction	no reaction	1:1	1:1 (+1)	no reaction	[5]
L^{13}	not inv.	2:1[m]	not inv.	not inv.	not inv.	not inv.	not inv	not inv.	not inv.	[28]
L^{14}	not inv.	1:1[n]	1:1[o]	not inv.	not inv.	not inv.	not inv.	1:1	not inv.	[29]

[a] L^1 = imidazole; L^2 = benzimidazole, L^3 = 2-phenylimidazole, L^4 = 1-acetylimidazole, L^5 = imidazoline-2(1,3*H*)-thione, L^6 = 1-methyl-imidazoline-2(3*H*)-thione, L^7 = 1-benzylimidazole, L^8 = 4-phenylimidazole, L^9 = 1-methylimidazole, L^{10} = 4-methylimidazole, L^{11} = 2-methylimidazole, L^{12} = 2-isopropylimidazole, L^{13} = 2-chloroimidazole, L^{14} = 1-methyl-2-(methylsulfinyl)imidazole.

[b] Molecules of water in parentheses (); not. inv. = not investigated; N–CO break. = breaking of the N(1)–$COCH_3$ bond. [c] *Trans*-octahedral from Ref. [8].

[d] From Ref. [9]. [e] From Ref. [10]. [f] s From Ref. [11]. [g] From Ref. [30]. [h] Distorted bipyramid trigonal from Ref. [4]. [i] *Trans*-octahedral from Ref. [31].

[l] Distorted bipyramid trigonal from Ref. [6]. [m] *Trans*-octahedral from Ref. [28]. [n] Bipyramid trigonal from Ref. [29]. [o] Distorted octahedral from Ref. [29].

of 1:1 was found), all the derivatives obtained show a ligand to metal ratio of 2:1.

No adduct was obtained from the interaction of L^5 or L^6 and R_3SnCl or $Bu^n_2SnCl_2$.

From the interaction of L^5 with Me_nSnCl_{4-n} ($n=1$ or 2) analogous compounds to those reported in literature afforded [11].

It is interesting to observe that in diethyl ether from the reaction between L^6 and $RSnCl_3$ ($R=Bu^n$ or Me) a 2:1 adduct was obtained, whereas in dichloromethane a 1:1 adduct was previously synthesized [11].

All the diorgano- and triorgano-tin(IV) derivatives are moderately soluble in chlorinated solvents, acetone and DMSO, and generally insoluble in diethyl ether, ethanol and water. The monoorganotin(IV) adducts are generally less soluble in all the solvents commonly used. These compounds are stable also when exposed to moisture for a long time, whereas upon prolonged standing at 120°C, or in acetone and chloroform solutions, organotin(IV) oxides and hydroxides are often recovered.

The triorganotin(IV) adducts **1** and **2** are often unstable not only in solution but also in the solid state and when they exposed to moisture for many hours, they decompose in accordance with the following equation:

$$2[L_2R_3Sn]Cl \rightleftharpoons [(L)_2R_2SnCl_2] + R_4Sn + 2L. \quad (3)$$

The decomposition (3) is established by the presence in the ^{119}Sn NMR spectrum of compounds **1** and **2**, previously exposed to moisture for 2 days, of the signals due to $[(L)_2R_2SnCl_2]$ and R_4Sn species.

IR data

By comparison with the data reported for other organotin(IV) complexes containing N-donor ligands, we suggest the following assignments for adducts **1**–**27**.

Ligand absorptions In the 3200–2950 cm^{-1} region, the ligands exhibit weak bands typical of C–H stretching due to a pseudoaromatic ring, and in the region 1600–1500 cm^{-1} some more intense absorptions due to the ring breathing mode [12]. These bands do not shift markedly upon coordination to tin, suggesting a weak influence of the complexation on the absorptions within the donor.

In the 2800–2600 cm^{-1} region the ligands exhibit a broad band typical of N–H stretching. In the tin(IV) and organotin(IV) adducts this band shifts in the 3400–3100 cm^{-1} region suggesting an important influence of the coordination to tin. The position and the broadening of the N–H stretching band are consistent with the presence of a hydrogen bond between the N–H moiety and the halide groups [4, 13, 14].

Sn–C stretching frequencies. In the trimethyltin(IV) derivative **1** a strong absorption is observed at *ca.* 549 cm^{-1}. It is due to $\nu_{(asym)}$ Sn–C stretching vibration and is consistent with an essentially trigonal pyramidal arrangement of methyl groups (C_{3v}) [15–18]. In the derivatives **2** and **6** the $\nu_{(asym)}$ Sn–C stretching vibration is found at *ca.* 290 cm^{-1}: a trigonal pyramidal arrangement of aryl groups is likely.

Only a single Sn–C stretching vibration was observed in the spectra of the diorganotin(IV) derivatives **7**, **8**, **12**, **13**, **15**, **18**, **19**, **23** and **24** in accordance with a *trans*-octahedral configuration of the two alkyl groups [19, 20]. In the spectrum of derivatives **14** and **20** two medium or strong absorptions in the range 290–270 cm^{-1} were found. In this case the presence of the *cis*–isomer is likely.

Sn-halide stretching frequencies. In the triorganotin(IV) derivative **6**, we observed the tin–chloride stretching frequency as medium absorption at 226 cm^{-1}. This indicates the non-ionic nature of this compound. The absorption is markedly shifted with respect to that indicated for the starting triorganotin(IV) chloride [21].

In the other triorganotin(IV) derivatives **1** and **2** the tin–chloride stretching frequency is absent. On the basis of previous reports [22] on triorganotin(IV) complexes and in accordance with the X-ray crystal structure determination of [bis(4-phenylimidazole)trimethyltin(IV)]chloride [4] we have hypothesized an ionic formulation of the type $[(L)_2R_3Sn]^+[Cl]^-$.

The tin(IV) chloride stretching frequencies in the di- and tri-halidetin(IV) derivatives fall as strong or medium broad bands in the range 220–320 cm^{-1}. These bands are lowered by 90–130 cm^{-1} with respect to those found in the starting tin(IV) reagents [23].

Behavior in solution

The conductivity measurements were carried out in acetone solution for all the soluble compounds whereas the molecular weight determinations were performed in chloroform solution only on selected sufficiently soluble and stable adducts.

The conductivity data show that triorganotin(IV) halide adduct **1**, **2** and **6** are not electrolytes in acetone and dissociate in $CHCl_3$ solution to a large extent (r = ratio between the vaporimetric molecular weight and formula weight lying in the range 0.30–0.55), in accordance with eq. (4), which indicates ligand loss in solution.

$$(L)_xR_3SnCl \rightleftharpoons (L)_{x-1}R_3SnCl + L \rightleftharpoons R_3SnCl + xL. \quad (4)$$

The conductance values for the diorganotin adducts of L^1, L^2, L^4, L^5 and L^6 are in the range 2.0–36 $\Omega^{-1}\,cm^{-2}\,mol^{-1}$ and also suggest a not electrolytic nature in acetone. The vaporimetric molecular weight determinations indicate extensive dissociation in chloroform solution for the soluble adducts. Some of the trichlorotin(IV) adducts and derivatives con-

taining the donor L^3 are partly ionized. The conductivity values for these complexes are in the range 44–95 $\Omega^{-1}\,cm^{-2}\,mol^{-1}$: they are lower with respect to those reported for 1:1 electrolytes in this solvent (the typical 1:1 electrolyte tetra-*n*-butylammonium bromide has a specific conductivity of 137 $\Omega^{-1}\,cm^2\,mol^{-1}$) in accordance with a partial ionic dissociation, but they are also greater with respect to those found in analogous imidazole organotin(IV) adducts [3–6].

^{1}H *NMR data*

The ^{1}H NMR spectra of the donors and of the organotin(IV) complexes **1**–**27** were recorded in $CDCl_3$ or in acetone-d_6 due to poor solubility in the former solvent.

The spectrum of the trimethyltin(IV) complex **1** indicates a nearly complete dissociation into the starting reagents. In fact, the Δ value (difference in chemical shift for the same type of proton in the free base and in its organotin(IV) complexes) is in the range 0.04–0.01 ppm and the tin–proton coupling constants are of the same order of magnitude as those reported for the starting triorganotin(IV) acceptors [24].

Instead, in the spectra of the triphenyltin(IV) complexes **2** and **6**, the signals of the ligand are displaced upfield and the Δ value is in the range (−0.26)–(−0.06) ppm. This peculiarity can be explained by considering the shielding effect exerted on H2, H4 and H5 protons by aromatic protons of the phenyl rings linked to tin(IV).

In the spectra of the mono- and di-organotin(IV) complexes of L^1, L^2, L^3 and L^4, the signals of the ligands are generally displaced to lower field. The deshielding observed is attenuated at a position remote from the metal. The Δ observed is likely due to a σ-charge donation from the N-donor to tin(IV) acceptor and is evidence of the existence of the complexes in solution. The Δ is greater for the trihalo- with respect to for dihalo-tin(IV) adducts in accordance with a stronger Sn–N bonding interaction in the former compounds.

The magnitudes of the tin(IV)–proton coupling constants for these diorganotin(IV) complexes are different from those reported in literature for the starting tetracoordinate diorganotin(IV) halides [25], but they are smaller with respect to that indicated for hexacoordinate undissociated organotin(IV) complexes containing N-donor ligands [26, 27]: this suggests a partial dissociation of our complexes in acetone or in chloroform solution in accordance with the data derived from molecular weight measurements.

The ^{1}H NMR spectra of the diorganotin(IV) adducts of 1-methyl-imidazoline-2(3*H*)thione (L^5) and imidazoline-2(1,3*H*)-thione (L^6) exhibit Δ values in the range 0.001–0.02 suggesting a nearly complete dissociation into starting reagents.

^{119}Sn *NMR data*

The ^{119}Sn NMR data are reported in acetone-d_6 for only some adducts, because the quality of the spectra is sometimes poor owing to the low solubility. The ^{119}Sn NMR chemical shift of compounds is comparable with that of the corresponding organotin(IV) acceptor in the same solvent [24] and clearly indicate that these adducts are extensively dissociated in acetone solution. Whereas the $\delta(^{119}Sn)$ chemical shifts for derivatives of imidazoline-2(1,3*H*)-thione (L^5) and 1-methyl-imidazoline-2(3*H*)thione (L^6) are sensibly different from those reported for the corresponding Lewis acid: also on the basis of literature data [24] and vaporimetric molecular weight determinations we suggest that these complexes are not completely dissociated in acetone solution.

Comparison with other imidazole organotin(IV) adducts

Table 1 shows a summary of the interactions of imidazoles with some organotin(IV) derivatives [3–11, 28–31].

In the adducts reported the ligand to metal ratio *n* goes from 1:1, for example in $[(L^2)Ph_3SnCl]$, to 3:1 in $[(L^{10})_3PhSnCl_3]$. When the ratio is 3:2, as in $[(L^8)_3(BuSnCl_3)_2]$, a dinuclear structure with the bridging chloride group is likely.

The solubility of the adducts reported in Table 1 is limited to a few polar solvent, such as acetone, *N*,*N*-dimethylformamide or DMSO. The adducts of L^7, L^8, L^9 and L^{10} are generally also soluble in chlorinated solvents due to the presence of methyl and aryl substituents in the azole ring. The derivatives of L^5 and L^6 show appreciable solubility also in water.

In no cases was the imidazole ring metallated or did basic salts result, whereas only in the interaction between 1-acetylimidazole (L^4) and organotin(IV) acceptors did breaking of the N(1)–C bond and coordination of the unsubstituted imidazole L^1 formed occur.

In most of cases mono and di-organotin(IV) chlorides adducts containing N-donor imidazole ligands have a perfect octahedral environment with all-*trans* coordination.

The triorganotin adducts prefer a distorted trigonal bipyramid geometry with the organic groups always in equatorial positions. If the imidazole was able to involve a chloride group in a hydrogen bonding network, a 2:1 adduct was obtained, whereas if the imidazole possess an alkyl or an aryl group in the N(1) position only 1:1 adducts were obtained. The reaction between imidazoles and tributyltin(IV)chloride was often unsuccessful, no simple adduct but intractable material being formed with the exception of derivatives $[(L^9)Bu_3SnCl](H_2O)$ and $[(L^{10})_2Bu_3Sn]Cl$, likely obtained owing to the greater basicity of these donors with respect to those so far employed.

The donating ability of this family of ligands can be correlated to the ratio *n* and to the stability of the complexes in solution. On the basis of this systematic study L^1, L^9 and L^{10} seem to be the better donors (L^{10} is the only able to give a 3:1 ligand to metal ratio) also due to the minor dissociation of the organotin(IV) complexes in chloroform and acetone solution. L^3, L^{11} and L^{12} are weaker donors probably due to the steric hindrance of phenyl, methyl and isopropyl group, respectively, in the C(2) position, whereas the lower donating ability of L^5 and L^6 is due to the fact that they coordinate throughout the S-atom, which has a lower affinity for the organotin(IV) acceptors with respect to the N-atom. With the latter donors, it is also possible to obtain a 1:1 adduct not only with triorgano- but also with di- and mono-organotin(IV) acceptors.

1:1 adducts are also obtained if the donor is able to coordinate in a bidentate fashion as 1-methyl-2-(methylsulfinyl)imidazole (L^{14}).

If hydroxideorganotin(IV) acceptors were used, substitution of the OH group and coordination of the deprotonated ligand occurred as in [Ph_3Sn(2-mercapto-1-methylimidazolato)tin(IV) [30].

Various degrees of hydration were found from 1/3 in [(L^{10})Ph_3SnCl]·1/3H_2O to 6 in [(L^{10})$MeSnCl_3$]·6H_2O.

Acknowledgements—We would like thank the MURST and the University of Camerino for financial help.

REFERENCES

1. Leonesi, D., Lorenzotti, A., Cingolani, A. and Bonati, F., *Gazz. Chim. Ital.*, 1981, **111,** 483.
2. Pettinari, C., Marchetti, F., Polimante, R., Cingolani, A., Portalone, G. and Colapietro, M., *Inorg. Chim. Acta*, 1996, **249,** 215.
3. Pettinari, C., Marchetti, F., Cingolani, A. and Bartolini, S., *Polyhedron*, 1996, **15,** 1263.
4. Pettinari, C., Marchetti, F., Pellei, M., Cingolani, A., Barba, L. and Cassetta, A., *J. Organomet. Chem.*, 1996, **515,** 119.
5. Pettinari, C., Pellei, M., Marchetti, F., Santini, C. and Miliani, M., *Polyhedron*, 1998, **17,** 561.
6. Pettinari, C., Pellei, M., Miliani, M., Cingolani, A., Cassetta, A., Barba, L., Pifferi, A. and Rivarola, E., *J. Organomet. Chem.*, 1998, **553,** 345.
7. Alberte, A., Sánchez González, A., García, E., Casas, J. S., Sordo, J. and Castellano, E. E., *J. Organomet. Chem.*, 1988, **338,** 187.
8. García Martínes, E., Sánchez González, A., Macías, A., Castano, M. V., Casas, J. S. and Sordo, J., *J. Organomet. Chem.*, 1990, **385,** 329.
9. Sánchez González, A., Casas, J. S., Sordo, J. and Valle, G., *J. Organomet. Chem.*, 1992, **435,** 29.
10. Casas, J. S., Castellano, E. E., García Barros, F. J., Sánchez, A., Sánchez González, A., Sordo, J., Zukerman-Schpector, J., *J. Organomet. Chem.*, 1996, **519,** 209.
11. Kovala-Demertzi, D., Tauridou, P., Russo, U. and Gielen, M., *Inorg. Chim. Acta*, 1995, **239,** 177.
12. Nieuwpoort, G., Vos, J. G. and Groeneveld, W. L., *Inorg. Chim. Acta*, 1978, **29,** 117.
13. Graziani, R., Casellato, U., Ettorre, R. and Plazzogna, G., *J. Chem. Soc., Dalton Trans.*, 1982, 805.
14. Valle, G., Ettorre, R., Peruzzo, V. and Plazzogna, G., *J. Organomet. Chem.*, 1987, **326,** 169.
15. Poller, R. C., *The Chemistry of Organotin Compounds*. Logos, London, 1970.
16. Newman, W. P., *The Organic Chemistry of Tin*. Wiley Interscience, New York, 1970.
17. Ho, B. W. K. and ZucKerman, J. J., *Inorg. Chem.*, 1973, **12,** 1552.
18. Huber, F., Vornefeld, M., Ruisi, G. and Barbieri, R., *Appl. Organomet. Chem.*, 1993, **7,** 243.
19. Edgell, W. F. and Ward, C. H., *J. Mol. Spectrosc.*, 1962, **8,** 343.
20. Sandhu, J. K., Kaur, G., Holecek, J. and Licka, A., *J. Organomet. Chem.*, 1988, **345,** 51.
21. Nakagawa, I. and Walter, J. L., *J. Chem. Phys.*, 1969, **51,** 1389.
22. Basu Baul, T. S., Dey, D., Mishra, D. D., Basaiawmoit, W. L. and Rivarola, E., *J. Organomet. Chem.*, 1993, **447,** 9.
23. Clark, R. J. H., Davies, A. G. and Puddephatt, R. J., *J. Chem. Soc.* (*A*) 1968, 1828.
24. Wrackmeyer, B., *Ann. Rep. NMR Spectrosc.*, 1985, **16,** 73.
25. Harrison, P. G., Investigating tin using spectroscopy, in: *Chemistry of Tin*, ed. P. G. Harrison. Chapman and Hall, London, 1989, Ch. 3, pp. 61–115.
26. Honnick, W. D., Hughes, M. C., Schaeffer, C. D. Jr. and Zuckerman, J. J., *Inorg. Chem.*, 1976, **15,** 1391 and references cited therein.
27. Lockart, T. P. and Manders, W. F., *Inorg. Chem.*, 1986, **25,** 892.
28. Casellato, U., Graziani, R., Sánchez González, A., *Acta Cryst. C*, 1992, **48,** 2125.
29. de Sousa, G. F., Filgueiras, C. A. L., Darensbourg, M. Y. and Reibenspies, J. H., *Inorg. Chem.*, 1992, **31,** 3044.
30. Casas, J. S., Castiñeiras, A., García Martínez, E., Sánchez González, A., Sánchez, A. and Sordo, J., *Polyhedron*, 1997, **16,** 795.
31. Bardi, R., Piazzesi, A., Ettorre, R. and Plazzogna, G., *J. Organomet. Chem.*, 1984, **270,** 171.

Pergamon

Polyhedron Vol. 17, Nos. 25, 26, pp. 4497–4506, 1998
© 1998 Elsevier Science Ltd
All rights reserved. Printed in Great Britain
PII: SS0277-5387(98)00256-3
0277–5387/98 $19.00+0.00

Tetraaryl-methane analogues in group 14—V. Distortion of tetrahedral geometry in terms of through-space π–π and π–σ interactions and NMR sagging in terms of π–σ* charge transfer

Michael Charissé[a], Andrea Zickgraf[a], Heike Stenger[a], Elmar Bräu[a], Cristelle Desmarquet[a], Martin Dräger[a,*], Silke Gerstmann[b], Dainis Dakternieks[b,*] and James Hook[c]

[a]Institut für Anorganische Chemie und Analytische Chemie der Johannes Gutenberg-Universität, D-55099 Mainz, Germany

[b]School of Biological and Chemical Sciences, Faculty of Science and Technology, Deakin University, Geelong, Vic. 3217, Australia

[c]NMR Facility, The University of New South Wales, Sydney, NSW 2052, Australia

(Received 24 February 1998; accepted 23 June 1998)

Abstract—44 members of the compound series $Ph_{4-n}MR_n$ (M = Si, Ge, Sn, Pb; R = *o*-, *m*-, *p*-Tol; *n* = 0–4) were synthesized (15 new compounds). The crystal structures of $Ph_3Sn(o\text{-Tol})$ and $PhSn(o\text{-Tol})_3$ were determined and compared to 16 known structures. Subject to the distance *d*(M–C), an interplay between through-space π–π repulsion and π–σ attraction leads to either elongated or compressed tetrahedral geometry. ^{29}Si-, ^{119}Sn- and ^{207}Pb-NMR chemical shifts were determined in solution and in the solid state. ^{73}Ge chemical shifts were measured only in solution. An upfield or downfield sagging of the chemical shifts along each series is rationalized in terms of a π–σ* charge transfer which is constrained by torsion of the aromatic groups. © 1998 Elsevier Science Ltd. All rights reserved

Keywords: silicon; germanium; tin; lead; through-space interaction; heteronuclear NMR in solution and solid state; π–σ* charge transfer.

INTRODUCTION

As part of ongoing studies about tetraarylmethane analogues [1–4], the series of compounds $Ph_{4-n}M(p\text{-Tol})_n$ (M = Si, Ge, Sn, Pb; *n* = 0–4) was synthesized and investigated using X-ray diffraction and NMR spectroscopy [1]. The structural finding of elongated tetrahedra for M = Si and Ge and compressed tetrahedra for M = Sn and Pb (see Ref. [5]) was rationalized by means of an interplay between π–σ attractions and π–π repulsions of the aromatic groups [1, 6, 7]. The sagging effect (see Refs. [8–10]) observed in the solution state ^{29}Si-, ^{119}Sn- and ^{207}Pb-NMR chemical shifts was rationalized by means of a π–σ* charge transfer from the aromatic groups into the LUMO associated mostly with the hetero atom M [1].

In this paper the subject is extended synthetically to the groups *o*- and *m*-tolyl [four series of compounds $Ph_{4-n}MR_n$, (**1**–**4**)]. In addition to the 16 crystal structures known previously [1–4], the structures of $Ph_3Sn(o\text{-Tol})$ and $PhSn(o\text{-Tol})_3$ were determined. Heteronuclear NMR chemical shifts in solution and also in the solid state were determined for all compounds of series eq. (1), eq. (3) and eq. (4). In addition, ^{73}Ge-NMR chemical shifts for the five compounds of series eq. (2) in solution are given [11–16]. Semi-empirical MO calculations have been done to support the concept of a π–σ* charge transfer. As will be seen from

* Author to whom correspondence should be addressed. Tel.: +49-6131-395757; Fax: +49-6131-395380.

the results, these exhaustive calculations concluded to be altogether unrewarding and fruitless.

$$Ph_{4-n}SiR_n \quad R = o-Tol, m-Tol, p-Tol \quad n = 0\text{–}4. \tag{1}$$

$$Ph_{4-n}GeR_n \quad R = p-Tol \quad n = 0\text{–}4. \tag{2}$$

$$Ph_{4-n}SnR_n \quad R = o-Tol, m-Tol, p-Tol \quad n = 0\text{–}4. \tag{3}$$

$$Ph_{4-n}PbR_n \quad R = o-Tol, m-Tol, p-Tol \quad n = 0\text{–}4. \tag{4}$$

RESULTS AND DISCUSSION

Structural results

Figure 1 shows the molecular structures of $Ph_3Sn(o\text{-Tol})$ and of $PhSn(o\text{-Tol})_3$. Relevant bond lengths and angles are listed in Table 1. Both molecules possess crystallographically a S_4 symmetry, i.e. the ortho methyl groups exhibit a statistical disorder. One of the four possible ordered arrangements is given in Fig. 1, respectively.

As outlined for tetraaryls with phenyl and *p*-tolyl substitution [1], the tetrahedra with M = C, Si, Ge are elongated (two bond angles less and four bond angles greater than 109.5°) whereas the tetrahedra with M = Sn, Pb are compressed (two bond angles greater and four bond angles less than 109.5°). This result is valid also for the cases of *o*-tolyl and *m*-tolyl substitution. Figure 2 gives a plot of d(M–C) vs the twofold angle Φ(C–M–C)–[2x] for all 18 cases $Ph_{4-n}MR_n$, which have been investigated by X-ray crystallography. At $d(M\text{–}C) = 2.06$ Å (cubic fit curve) an overall repulsion between the aromatic groups transforms into an overall attraction. For short M–C distances the through-space π–π repulsion predominates; for long M–C distances the through-space π–σ attraction prevails.

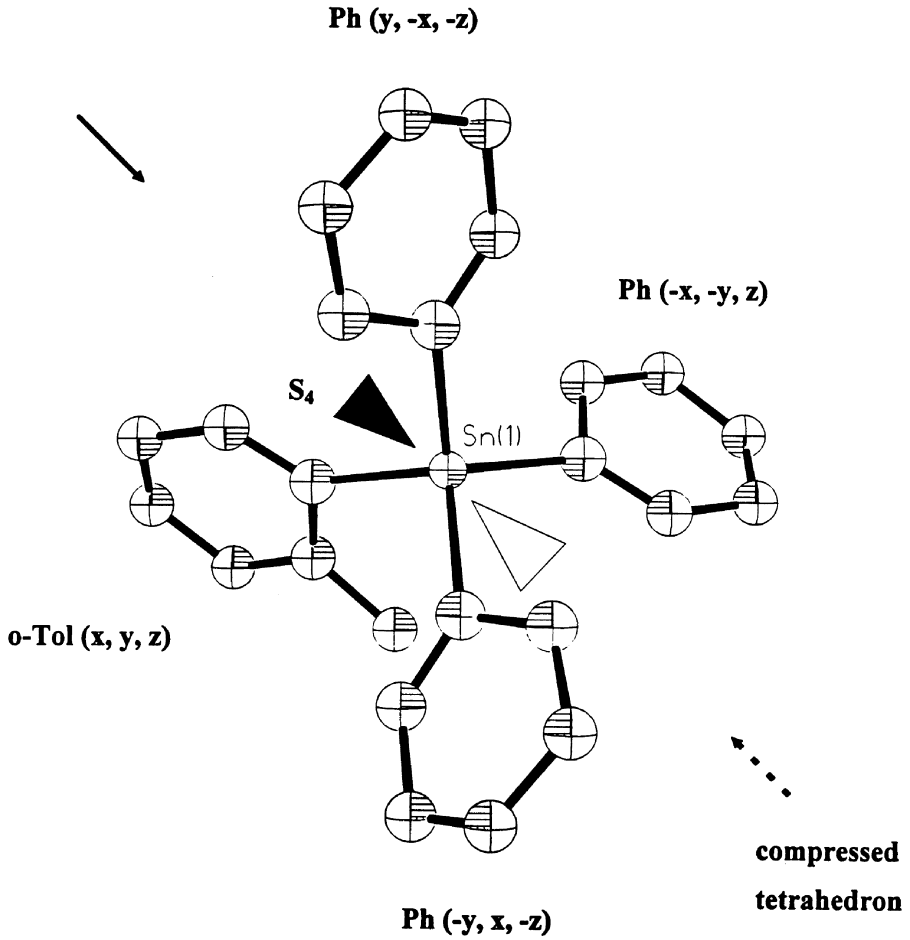

Fig. 1. Ortep drawings of $Ph_3Sn(o\text{-Tol})$ (top) and of $PhSn(o\text{-Tol})_3$ (continued). Only one of the four possible ordered arrangements is given, respectively. Thermal ellipsoids are at the 20% probability level; hydrogen atoms are omitted for better clarity. The molecules are compressed along the outlined pseudo S_4 axes. The group identifications include the symmetry operators of the space group $P\bar{4}2_1c$.

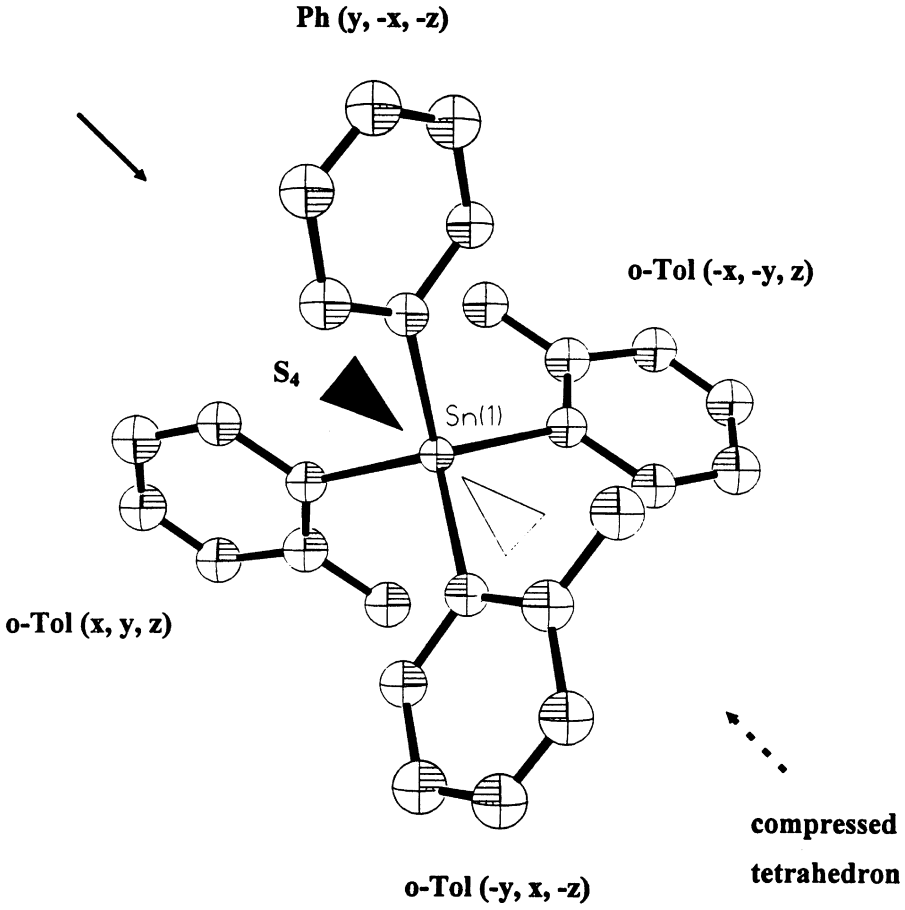

Fig. 1. *Continued.*

Table 1. Bond lengths (Å) and bond angles (°) of $Ph_3Sn(o\text{-Tol})$ and $PhSn(o\text{-Tol})_3$ and of Ph_4Sn and $Sn(o\text{-Tol})_4$[a] for comparison (all compounds crystallize in the space group $P\bar{4}2_1c$)

Compound	Distance Sn–C(1)	Two-fold angle C(1)–Sn–C(1a) $\Phi(C\text{–}Sn\text{–}C)_{2\times}$	Four-fold angle C(1)–Sn–C(1b) $\Phi(C\text{–}Sn\text{–}C)_{4\times}$
Ph_4Sn	2.139(4)	111.2(2)	108.6(1)
$Ph_3Sn(o\text{-Tol})$	2.09(4)	111(2)	109(1)
$PhSn(o\text{-Tol})_3$	2.157(8)	112.8(4)	107.8(4)
$Sn(o\text{-Tol})_4$	2.152(5)	112.6(3)	107.9(1)

[a] See Ref. [17].

NMR chemical shifts

Table 2 gives the heteronuclear NMR chemical shifts for the homoleptic and heteroleptic tetraaryls $Ph_{4-n}MR_n$ in $CDCl_3$ solution. The series eq. (2) is the first systematic investigation of ^{73}Ge-NMR chemical shifts, which has been described (Figure 3) [11–16]. Table 3 gives the solid state ^{29}Si, ^{119}Sn and ^{207}Pb chemical shifts of the compounds of the series eqs. (1, 3–4). Figure 4 shows exemplarily for M = Sn the six sequences of $\delta(^{119}Sn)$ in the solution (top) and in the solid (bottom) state. The values are connected by cubic fit curves.

With regard to the aliphatic compounds Me_4M,

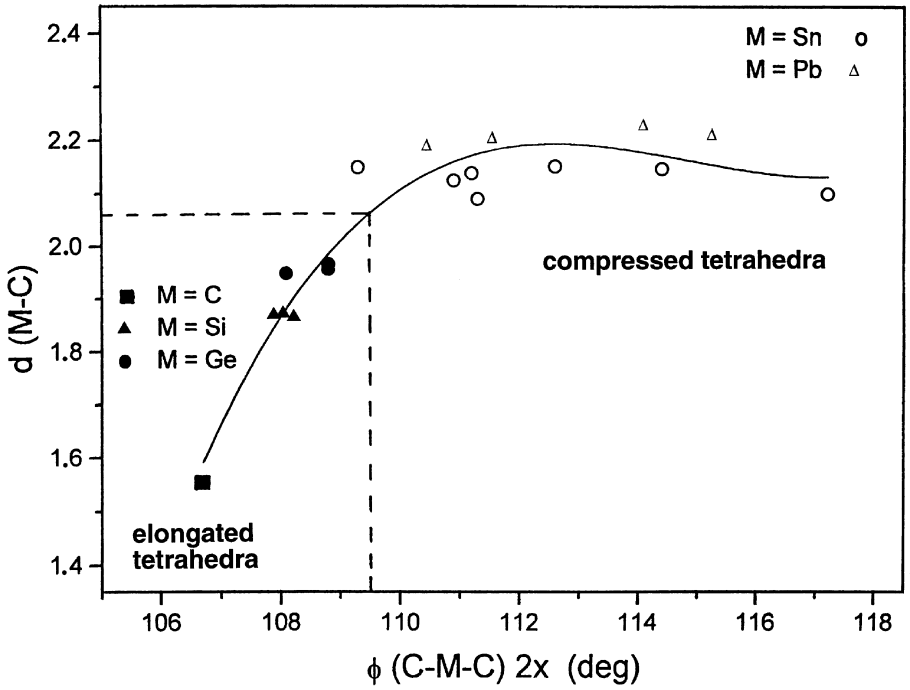

Fig. 2. Plot of the bond distances d(M–C) (Å) vs the two-fold bond angle ⟡(C–M–C)-2× (°) for 18 compounds $Ph_{4-n}MR_n$ (M = C, Si, Ge, Sn, Pb; R = *o*-, *m*-, *p*-Tol; n = 0–4) in relation to the distortion of the tetrahedra around M. Data from Ref. [1–4] and references cited therein. Cubic fit curve (change of distortion at 2.06 Å).

Table 2. Solution-state ^{29}Si-, ^{73}Ge-, ^{119}Sn- and ^{207}Pb- NMR chemical shifts (ppm[a]) for the series $Ph_{4-n}MR_n$ eqs. (1–4)

M	R	Ph_4M	Ph_3MR	Ph_2MR_2	$PhMR_3$	MR_4
Si	*o*-Tol	−13.98	−14.39	−13.90	−13.42	−12.52
	m-Tol		−14.25	−14.24	−14.23	−14.34
	p-Tol		−14.29	−14.36	−14.42	−14.55
Ge	*p*-Tol	−32.90	−32.49	−31.71	−30.77	−31.24
Sn	*o*-Tol	−128.1	−126.7	−124.7	−121.7	−124.5
	m-Tol		−130.2	−130.1	−130.0	−129.8
	p-Tol		−129.1	−127.7	−126.1	−124.6
Pb	*o*-Tol	−179.0	−170.4	−161.2	−152.9	−166.7
	m-Tol		−181.5	−180.9	−180.3	−179.5
	p-Tol		−179.5	−176.3	−174.0	−171.3

[a] Solvent $CDCl_3$; relative to the external standards $Me_4Si/Ge/Sn/Pb$, respectively, ambient temperature.

the chemical shifts $\delta(^{29}Si/^{73}Ge/^{119}Sn/^{207}Pb)$ of the homoleptic members Ph_4M and $MTol_4$ are all upfield and this shielding had been explained by a π(aromatic)→σ^*(M) charge transfer[1] [1]. Between the homoleptic end members Ph_4Sn and SnR_4, a sagging pattern [8–10] holds. The sagging effect is different for the solution and for the solid state. Furthermore, the effect changes from the (*o*-Tol) to the (*m*-Tol) to the (*p*-Tol) series. A possible explanation may be that π–σ^* charge transfer depends on the torsion of the aromatic groups about the M–C_{ipso} axis. In solution the torsion angles easily arrange themselves, such as, to optimize the energetic interactions among

[1] A seeming exception is Ph_4C with $\delta(^{13}C) = +65.0$ ppm (Me_4C + 28.0 ppm). The central carbon atom has four short distances (cf. Figure 2) to the deshielding side-on position of the aromatic ring current [1].

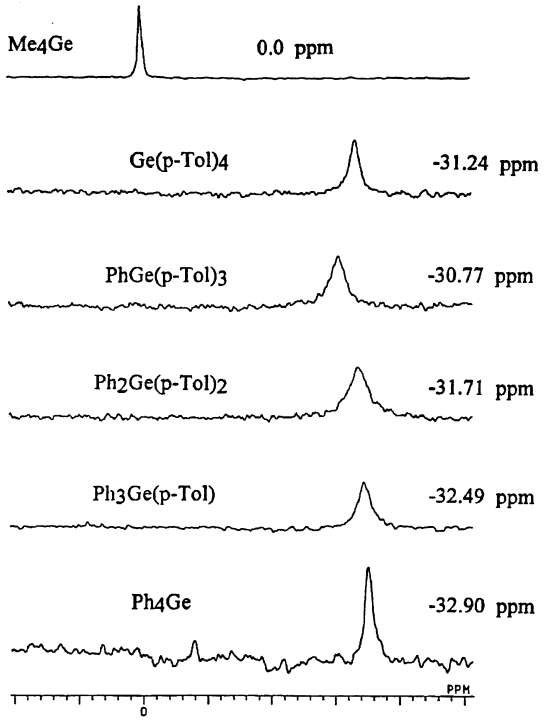

Fig. 3. ^{73}Ge-NMR spectra for the series compounds $Ph_{4-n}Ge(p\text{-Tol})_n$ in $CDCl_3$ solution. Chemical shifts are given with reference to Me_4Ge.

the four aromatic groups whereas in the solid state the torsion angles are constrained by the crystal packing [7]. In solution, the sterically undemanding groups *m*-tolyl and *p*-tolyl lead to an upfield sagging (excess of charge, with regard to a linear course). On the other hand, the sterically crowded *o*-tolyl group leads to a distinct downfield sagging (shortage of charge).

In accordance with the similar molecular forms of the compounds with M = Sn and Pb (see Section structural results), the three solution state $\delta(^{207}Pb)$ sagging curves are nearly identical to those of $\delta(^{119}Sn)$ (Table 2 and Fig. 4). Also the three solid state $\delta(^{207}Pb)$ sagging curves show a close correspondence to those of $\delta(^{119}Sn)$. Similar torsions of the aromatic groups and similar crystal structures can be assumed.

In solution the $\delta(^{73}Ge)$ and $\delta(^{29}Si)$ sagging curves show similar trends to those described for $\delta(^{119}Sn)$ and $\delta(^{207}Pb)$. The shortage of charge (downfield shift) is enhanced for the case of the sterically very demanding *o*-tolyl group at Si. However the known solid state structures of the Si series are different and this fact manifests itself in sagging curves definitely different from those of Fig. 4.

Semi-empirical MO calculations

To support the concept of a π–σ^* charge transfer, semi-empirical MO calculations at the PM3 level (MOPAC 6.0 program package, parameter set: [18, 19] (all 44 compounds $Ph_{4-n}MR_n$, molecular geometries optimized starting from the known crystal structures) and at the Extended Hückel level [20] ($PhSn(o\text{-Tol})_3$, fixed geometry of the structure determination) were performed. The results are similar for all compounds. On the basis of the main coefficients, the energetic sequences of the MO's are in the order eq. (5). With regard to this order, a definite higher transition probability is needed for the assumed π–σ^* charge transfer (high energy gap) than for a π–π^* charge transfer (low energy gap) [21] (A quantitative correspondence between the PM3 energy differences and the energies of the experimental UV bands between 240 and 270 nm does not exist.)

$$(\text{several } \pi - \text{HOMO's}) \rightarrow (\text{several } \pi^* - \text{LUMO's}) \rightarrow (\text{four } \sigma^* - \text{LUMO's}). \quad (5)$$

Table 3. Solid-state ^{29}Si-, ^{119}Sn-, and ^{207}Pb-NMR chemical shifts (ppm[a]) for the series $Ph_{4-n}MR_n$ eqs. (1, 3–4)

M	R	Ph_4M	Ph_3MR	Ph_2MR_2	$PhMR_3$	MR_4
Si	*o*-Tol	−14.07	−14.08	−17.01[b]	−14.79	−13.37
	m-Tol		−12.81	−13.26	−12.65	−12.03
	p-Tol		−14.60	−13.75	−13.48	−13.31
Sn	*o*-Tol	−121.1	−123.1	−122.1	−123.6	−127.4
	m-Tol		−120.2	−115.2	−111.4	−107.5
	p-Tol		−119.9	−117.7	−118.8	−118.8
Pb	*o*-Tol	−146.7	−146.9	−151.1	−150.2	−159.5
	m-Tol		−147.8	−146.4	−128.0	−119.3
	p-Tol		−145.9	−142.0	−150.0	−148.8

[a] Conditions as given in Section 3.
[b] Additional trace signal at −14.7 ppm.

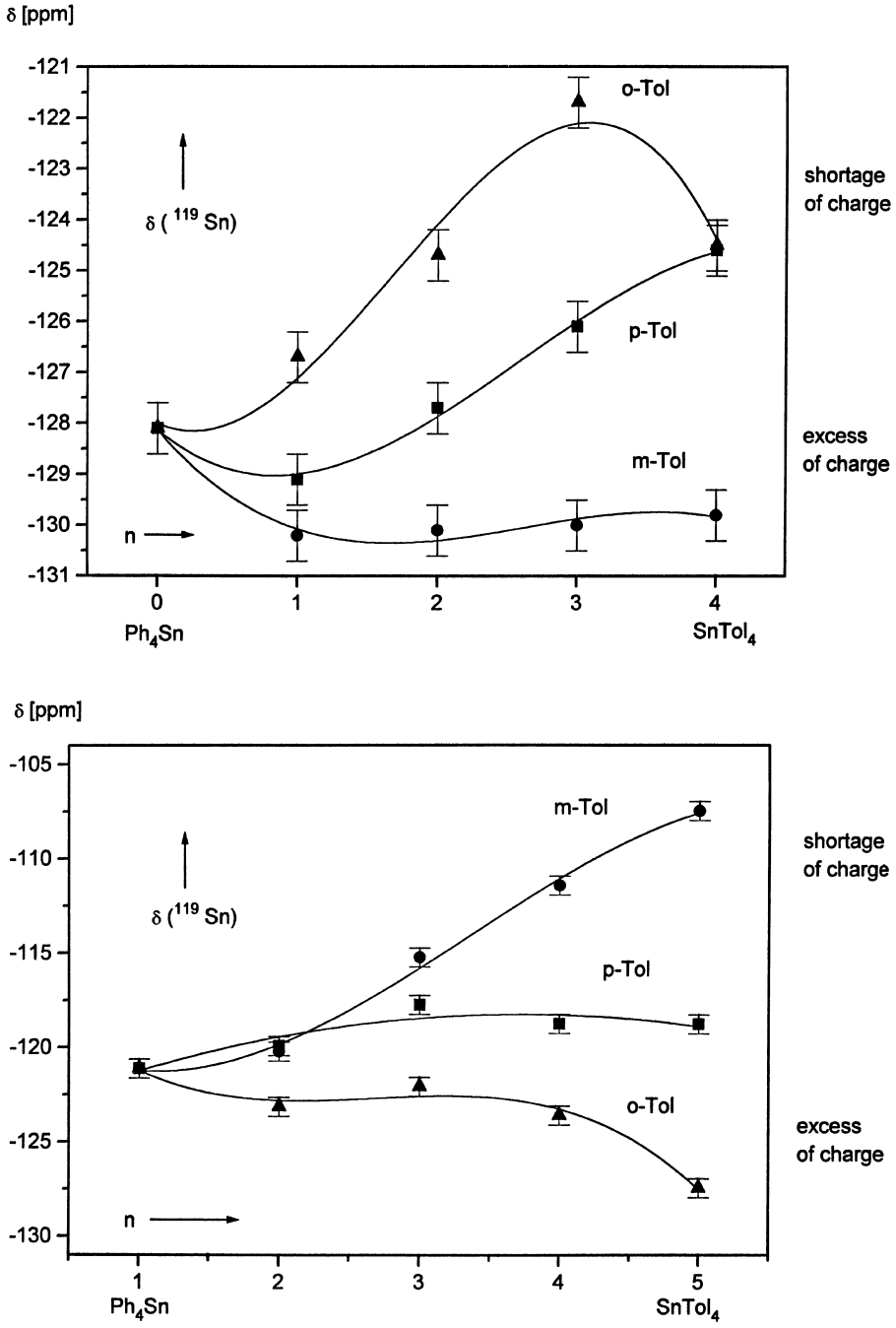

Fig. 4. Course of ^{119}Sn-NMR chemical shifts vs n for the series of compounds $Ph_{4-n}SnR_n$ (R = *o*-, *m*-, *p*-Tol; n = 0–4) in $CDCl_3$ solution (top) and in the solid state (bottom). Cubic fit curves.

In detail, all PM3 calculations result in the energetic σ^*–LUMO sequences eq. (6). With regard to the NMR behavior of eqs. (1–4), no definite order or correlation exist with E(σ^*–LUMO) or with its difference to the π–HOMO, apart from the fact that the MO sequences are most disturbed if the group (*o*-Tol) is involved.

$$E(\mathrm{Si}) > E(\mathrm{Pb}) > E(\mathrm{Sn}) > E(\mathrm{Ge}). \quad (6)$$

In fact, it can be concluded that semi-empirical calculations have to lower a sophistication, to be of any purpose in discussing the postulated π–σ^* charge transfer.

EXPERIMENTAL

Synthesis

The 14 homoleptic compounds and the 12 heteroleptic *p*-tolyl compounds were prepared by literature methods [1–4]. For previous work on the *o*-tolyl substituted silicon compounds, see Ref. [22–25]. The mixed ortho- and meta-substituted tin and lead compounds $Ph_{4-n}M(o\text{-}, m\text{-Tol})_n$ ($n = 1$–3; M = Sn, Pb) were synthesized via a Grignard reaction with the corresponding halides $Ph_{4-n}MX_n$ (X = Cl, Br, I). Compounds of the series $Ph_{4-n}SiM(m\text{-Tol})_n$ ($n = 1$–3) were obtained by reaction of $Ph_{4-n}SiCl_n$ with Li(*m*-Tol). A representative detailed procedure follows for the compound $PhGe(p\text{-Tol})_3$, which had been described in Ref. [1] as contaminated with $Ge_2(p\text{-Tol})_6$. To 15.6 mmol of (*p*-Tol)Li in 50 ml ether is slowly added, at ambient temperature 1.02 g (4 mmol) of freshly distilled $PhGeCl_3$, dissolved in 50 ml ether. After 1 h under reflux, the ether is distilled off and substituted continuously by toluene. After further stirring for 4 h under reflux and for 20 h at ambient temperature, the solution is hydrolyzed by slow addition of 1 M HCl. The organic layer is dried with Na_2SO_4, the solvent distilled off and methanol added. The crude product is separated by filtration, washed with cold methanol and recrystallized from methanol/toluene (3:1). Table 4 summarizes the results obtained in this study.

Melting points were determined in glass capillaries in a Kofler melting block. Elemental analyses (C and H) were obtained from the Institut für Organische Chemie, Universität Mainz, with a Perkin-Elmer CHN-Analyser 240.

Crystal structure determinations

Colorless single crystals of $Ph_3Sn(o\text{-Tol})$ and $PhSn(o\text{-Tol})_3$ were obtained by slow evaporation of a $CDCl_3$ solution. As previously [1–4], the crystals of the heteroleptic compounds were all of a poor quality. An inspection by means of Weissenberg exposures was essential. Both eventually chosen crystals had a low diffraction power. A summary of crystal data, intensity data collections and refinements, is given in Table 5. The crystals were fixed with glue and sealed in thin-walled glass capillaries. The experimental densities were determined by flotation in an aqueous polytungstate solution. Integrated intensities were collected on an Enraf-Nonius CAD4 diffractometer.

Both compounds crystallize in the same tetragonal space group $P\bar{4}2_1c$ as their homoleptic end members (see the first footnote of Table 5). Trials of refinement in a monoclinic setting resulted in distinctly worse geometries and esd's. The space group symmetry requires a S_4 symmetry for both molecules, i.e. the ortho-methyl groups are statistically disordered (site occupations 0.25 and 0.75, respectively). On account of the small number of reflections of significant intensity, only the Sn atom was given anisotropic thermal parameters, the C atoms were handled isotropically. The hydrogen atoms were calculated as riding on their carbon atoms. For calculations and drawings local versions of SHELX-76 and ORTEP were used. Tables listing details of crystal data and structure determinations, full sets of parameters (Sn, C and H), all bond lengths and angles and torsion angles and labelled plots have been deposited at the Cambridge Crystallographic Data Centre as supplementary material.

Solution state NMR

^{29}Si-, ^{119}Sn- and ^{207}Pb-NMR spectra were recorded on a Bruker WP 80/DS instrument (digital resolution 0.5 Hz) at 15.92 MHz (^{29}Si), 29.88 MHz (^{119}Sn) and 16.74 MHz (^{207}Pb). Solution state ^{73}Ge-NMR spectra were recorded on a Jeol JNM-GX 270 spectrometer (frequency 9.3 MHz, sweep width 2000 Hz, acquisition time 2 s, scans 1500). The chemical shifts are relative to the external standards Me_4Si, Me_4Ge, Me_4Sn and Me_4Pb. Solutions of 100–400 mg of compound/3 mL of $CDCl_3$ were used.

Solid state NMR

^{29}Si-, ^{119}Sn- and ^{207}Pb-NMR spectra were measured on a Bruker MSL-300S spectrometer operating at 59.641, 111.922 and 62.55 MHz, respectively. Samples of 300 mg of the organosilicon and lead compounds were packed into 7 mm zirconia rotors and spun at the magic-angle, at speeds of 2.5 kHz. The organotin compounds (*ca.* 100 mg) were measured in 4 mm zirconia rotors at 5 kHz. Spectra were obtained with broad-band double air-bearing cross-polarization Bruker WB–BL probes, at ambient temperature (295 K) from single contact cross-polarization (CP) experiments.

Solid state ^{29}Si-NMR: spectral width, 20 kHz; pulse width, 5.5 μs (90°) ^1H pulse; contact time, 1 ms; recycle time, 20 s; chemical shifts with respect to kaolinite ($\delta(^{29}Si) = -91.5$ ppm (Q^3 connected Si) [26, 27]; set up of the CP conditions and use as an external standard. Solid state ^{119}Sn-NMR: spectral width, 33 kHz; pulse width, 4.0 μs (90°) ^1H pulse; contact time, 10 ms; recycle time, 10 s; chemical shifts with respect to $Sn(c\text{-Hex})_4$ ($\delta(^{119}Sn) = -97.4$ ppm [28]; set up of the CP conditions and use as an external standard. Acquisition of 128 scans was sufficient to obtain spectra with a satisfactory signal to noise ratio. Solid state ^{207}Pb-NMR: spectral width, 62.5 kHz; pulse width, 3.5–4.0 μs (90°) ^1H pulse; contact time, 5–20 ms; recycle time, 30 s; chemical shifts with respect to $Pb(p\text{-Tol})_4$ ($\delta(^{207}Pb) = -148.8$ ppm [29, 30]; set up of the CP conditions and use as an external standard). Acquisition of 64–128 scans was sufficient to obtain spectra with a satisfactory signal to noise ratio.

Table 4. Experimental data and analytical results for the series $Ph_{4-n}MR_n$

Products	Preparation[a] initial compounds solvent; T [time (h)]	Recryst. from	Yield (%)	M.P. (°C) (lit.)	Formula M_r	Elemental analysis (%) C_{obs} (C_{calc})	H_{obs} (H_{calc})
$Ph_3Si(o\text{-Tol})$	$Ph_3SiCl/(o\text{-Tol})Li$ ether; RT (15)	EtOH/toluene	38	175–180 (186–187[b])	$C_{25}H_{22}Si$ 350.54	85.43 (85.66)	6.28 (6.33)
$Ph_2Si(o\text{-Tol})_2$	$Ph_2SiCl_2/(o\text{-Tol})Li$ ether; RT (15)+refl. (2)	toluene/PE(1:5)[c]	14	172 (174[b])	$C_{26}H_{24}Si$ 364.56	85.10 (85.66)	6.61 (6.64)
$PhSi(o\text{-Tol})_3$	$(o\text{-Tol})_3SiCl/PhLi$ ether; refl. (50)	EtOH/toluene	48	186–190 (195[b])	$C_{27}H_{26}Si$ 378.59	85.45 (85.66)	6.85 (6.92)
$Si(o\text{-Tol})_4$	$(o\text{-Tol})_3SiCl/(o\text{-Tol})Li$ ether; refl. (48)+neat (6[d])	toluene/PE(1:4)[e]	10	218–224[e] (228[e])	$C_{28}H_{28}Si$ 392.62	85.45 (85.66)	7.21 (7.19)
$Ph_3Si(m\text{-Tol})$	$Ph_3SiCl/(m\text{-Tol})Li$ ether; RT (15)+refl. (1)	EtOH/toluene	51	143	$C_{25}H_{22}Si$ 350.54	85.25 (85.66)	6.38 (6.33)
$Ph_2Si(m\text{-Tol})_2$	$Ph_2SiCl_2/(m\text{-Tol})Li$ ether; RT (15)+refl. (1)	EtOH/toluene	37	116	$C_{26}H_{24}Si$ 364.56	84.97 (85.66)	6.09 (6.64)
$PhSi(m\text{-Tol})_3$	$PhSiCl_3/(m\text{-Tol})Li$ ether; RT (15)+refl. (1)	EtOH/toluene	55	126	$C_{27}H_{26}Si$ 378.59	85.74 (85.66)	6.93 (6.92)
$PhGe(p\text{-Tol})_3$	$PhGeCl_3/(p\text{-Tol})Li$ ether; RT (20)+refl. (4)	MeOH/toluene	65	181–182 (106–107[f])	$C_{27}H_{26}Ge$ 423.09	76.53 (76.56)	6.40 (6.19)
$Ph_3Sn(o\text{-Tol})$	$Ph_3SnCl/(o\text{-Tol})MgBr$ THF; RT (1)+refl. (17)	EtOH/toluene	85	162–163	$C_{25}H_{22}Sn$ 441.14	67.88 (68.07)	5.11 (5.03)
$Ph_2Sn(o\text{-Tol})_2$	$Ph_2SnCl_2/(o\text{-Tol})MgBr$ THF; RT (1)+refl. (15)	EtOH/toluene	50	148–149	$C_{26}H_{24}Sn$ 455.17	68.57 (68.61)	5.41 (5.31)
$PhSn(o\text{-Tol})_3$	$PhSnCl_3/(o\text{-Tol})MgBr$ THF; RT (10)+refl. (10)	EtOH/toluene	94	166–167	$C_{27}H_{26}Sn$ 469.19	68.95 (69.12)	5.62 (5.59)
$Ph_3Sn(m\text{-Tol})$	$Ph_3SnCl/(m\text{-Tol})MgBr$ THF; RT (10)+refl. (10)	EtOH/toluene	80	122–123	$C_{25}H_{22}Sn$ 441.14	67.98 (68.07)	4.98 (5.03)
$Ph_2Sn(m\text{-Tol})_2$	$Ph_2SnCl_2/(m\text{-Tol})MgBr$ THF; RT (10)+refl. (10)	EtOH	85	91–92	$C_{26}H_{24}Sn$ 455.17	68.52 (68.61)	5.57 (5.31)
$PhSn(m\text{-Tol})_3$	$PhSnCl_3/(m\text{-Tol})MgBr$ THF; RT (10)+refl. (10)	EtOH/toluene	63	106	$C_{27}H_{26}Sn$ 469.19	68.84 (69.12)	5.43 (5.59)
$Ph_3Pb(o\text{-Tol})$	$Ph_3PbI/(o\text{-Tol})MgBr$ ether; RT (4)+refl. (12)	EtOH/toluene	57	171–175	$C_{25}H_{22}Pb$ 529.65	55.67 (56.69)	4.19 (4.19)
$Ph_2Pb(o\text{-Tol})_2$	$Ph_2PbI_2/(o\text{-Tol})MgBr$ ether; RT (2)+refl. (14)	EtOH	27	136–137	$C_{26}H_{24}Pb$ 543.68	57.29 (57.44)	4.37 (4.45)
$PhPb(o\text{-Tol})_3$	$(o\text{-Tol})_3PbBr/PhMgBr$ ether; RT (3)+refl. (14)	EtOH/toluene	65	151–153	$C_{27}H_{26}Pb$ 557.70	58.20 (58.15)	4.69 (4.70)
$Ph_3Pb(m\text{-Tol})$	$Ph_3PbCl/(m\text{-Tol})MgBr$ THF; RT (48)+refl. (10)	EtOH/toluene	27	145	$C_{25}H_{22}Pb$ 529.65	56.20 (56.69)	4.38 (4.19)
$Ph_2Pb(m\text{-Tol})_2$	$Ph_2PbI_2/(m\text{-Tol})MgBr$ THF; RT (2)+refl. (12)	EtOH	90	95	$C_{26}H_{24}Pb$ 543.68	57.30 (57.44)	4.35 (4.45)
$PhPb(m\text{-Tol})_3$	$(m\text{-Tol})_3PbCl/PhMgBr$ THF; RT (72)+refl. (10)	EtOH	31	106	$C_{27}H_{26}Pb$ 557.70	58.00 (58.15)	4.64 (4.70)

[a] Abbreviations: RT is the ambient temperature, refl. the refluxing solvent.

[b] Ref. [22].

[c] Chromatographic purification on silica gel.

[d] 150°C.

[e] Chromatographic separation on silica gel, four fractions (1:5:6:12). Fraction 1 (m.p. 160–170°C), 2 (m.p. 218–224°C, pure $Si(o\text{-Tol})_4$), 3 (colorless oil), 4 (colorless oil of high viscosity). Ref. [23] describes five stereoisomers: m.p. 145 (detail), 228 (detail), 270, 300 and 344°C. Ref. [24]: m.p. 228–230°C.

[f] Compound contaminated with $Ge_2(p\text{-Tol})_6$.

Table 5. Summary of crystal data, intensity data collection (Mo radiation, ambient temperature) and refinement for $Ph_3Sn(o\text{-Tol})$ and $PhSn(o\text{-Tol})_3$

	$Ph_3Sn(o\text{-Tol})$	$PhSn(o\text{-Tol})_3$
Cryst. syst., space group	tetragonal, $P\bar{4}2_1c$	tetragonal, $P\bar{4}2_1c$
Unit cell dimen.: a, c (Å)[a]	12.002(3), 7.204(4)	12.032(1), 7.853(2)
V (Å^3), Z, $F(000)$	1038(2), 2, 444	1136(1), 2, 476
D_{calcd}, D_{exptl} (g cm^{-3})	1.411, 1.407	1.372, 1.372
$\sin\theta_{max}/0.71069$ (Å^{-1})	0.595	0.704
Refl.: meas., indep. (int.R)	3696, 767(0.102)	3664, 1340(0.026)
Refl.: used, limit	273, $I>1\,\sigma(I)$	682, $I>1\,\sigma(I)$
Variab., ratio refl./var.	36, 7.6	35, 19.5
Final R	0.0915	0.0542

[a] Ph_4Sn: $a=12.058(1)$, $c=6.581(1)$ Å, $V=957$ Å^3; $Sn(o\text{-Tol})_4$: $a=12.021(1)$, $c=8.054(1)$ Å, $V=1164$ Å^3 (see Ref. [17]).

Acknowledgements—We gratefully acknowledge financial support from the Deutsche Forschungsgemeinschaft, Bonn, Germany and the Fonds der Chemischen Industrie, Frankfurt/Main, Germany. C. D. thanks the European Community for a grant under the Erasmus scheme.

REFERENCES

1. Part 4: Charissé, M., Mathiasch, B., Dräger, M. and Russo, U., *Polyhedron*, 1995, **14,** 2429.
2. Charissé, M., Roller, S. and Dräger, M., *J. Organomet. Chem.*, 1992, **427,** 23.
3. Charissé, M., Gauthey, V. and Dräger, M., *J. Organomet. Chem.*, 1993, **448,** 47.
4. Schneider-Koglin, C., Mathiasch, B. and Dräger, M., *J. Organomet. Chem.*, 1994, **469,** 25.
5. Chieh, P. C., The fact that the molecules become flatter as the central atom becomes larger has been mentioned first for the homoleptic series Ph_4M (M = C, Si, Ge, Sn), *J. Chem. Soc. Dalton Trans.*, 1972, 1207.
6. Hunter, C. A. and Sanders, K. M., A π–π interaction model for porphyrins, *J. Am. Chem. Soc.*, 1990, **112,** 5525.
7. Dance, I. G. and Scudder, M. L., An attractive nonbonded phenyl–phenyl association scheme in a series of $[Ph_4P]^+$ crystal structures, *Chem. Eur. J.*, 1996, **2,** 481.
8. Harris, R. K., Kennedy, J. D. and McFarlane, W., Sagging pattern (''U'' shaped appearance) in heteronuclear chemical shifts in series of heteroleptic compounds, In *NMR and the Periodic Table*, ed. R. K. Harris and B. E. Mann. Academic Press, London, 1978, p. 314.
9. Harris, R. K., Kennedy, J. D. and McFarlane, W., In *NMR and the Periodic Table*, ed. R. K. Harris and B. E. Mann. Academic Press, London, 1978, p. 346.
10. Harris, R. K., In *The Multinuclear Approach to NMR Spectroscopy*, ed. J. B. Lambert and F. G. Riddel. Reidel Publ. Comp., Dordrecht, 1982, p. 354.
11. Harris, R. K., Kennedy, J. D. and McFarlane, W., First tabulation of ^{73}Ge NMR data, In *NMR and the Periodic Table*, ed. R. K. Harris and B. E. Mann. Academic Press, London, 1978, p. 340.
12. Kennedy, J. D. and McFarlane, W., tabulation of ^{73}Ge NMR data, In *Multinuclear NMR*, p. 310, Ed. Mason, J., Plenum Press, New York, 1987.
13. Kennedy, J. D. and McFarlane, W., In *Multinuclear NMR*, ed. J. Mason, Plenum Press, New York, 1987, p. 310.
14. Schmidbaur, H. and Rott, J., *Z. Naturforsch. B*, 1990, **45,** 961.
15. Liepins, E., Petrova, M. V., Bogoradovskii, E. T. and Zavgorodnii, V. S., *J. Organomet. Chem.*, 1991, **410,** 287.
16. Takeuchi, Y., Popelis, J., Manuel, G. and Boukherroub, R., recent ^{73}Ge NMR data, *Main Group. Met. Chem.*, 1995, **18,** 191.
17. Belsky, V. K., Simonenko, A. A., Reikhsfeld, V. O. and Saratov, I. E., *J. Organomet. Chem.*, 1983, **244,** 125.
18. Stewart, J. J. P., *J. Comput. Chem.*, 1989, **10,** 221.
19. Stewart, J. J. P., *J. Comput. Chem.*, 1991, **12,** 320.
20. Mealli, C. and Proserpio, D. M., Program CACAO (Computer Aided Composition of Atomic Orbitals), *J. Chem. Educ.*, 1990, **67,** 399.
21. π–HOMO→π*–LUMO transitions are the familiar UV bands of the tetraaryls: Gouterman, M. and Sayer, P., *J. Mol. Spectrosc.*, 1974, 53, 319.
22. Gilman, H. and Smart, G. N. R., *J. Org. Chem.*, 1950, **15,** 720.
23. Smart, G. N. R., Gilman, H. and Otto, H. W., 5 different isomers of $Si(o\text{-Tol})_4$, data for 2 isomers in detail, *J. Am. Chem. Soc.*, 1955, **77,** 5193.
24. Hutchings, M. G., Maryanoff, C. A. and Mislow, K., ^{1}H-DNMR of $Si(o\text{-Tol})_4$, *J. Am. Chem. Soc.*, 1973, **95,** 7158.
25. Hutchings, M. G., Andose, J. D. and Mislow, K., Force field calculations of tetraarylmethanes and -silanes, *J. Am. Chem. Soc.*, 1975, **97,** 4553.
26. Rocha, J. and Klinowski, J., *Angew. Chem.*, 1990, **102,** 539.
27. Rocha, J. and Klinowski, J., *Angew. Chem. Int. Ed. Engl.*, 1990, **29,** 553.

28. Harris, R. K. and Sebald, A., *Mag. Reson. Chem.*, 1987, **25,** 1058.
29. Sebald, A. and Harris, R. K., *Organometallics*, 1990, **9,** 2096.
30. Ascenso, J. R., Harris, R. K. and Granger, P., $\delta(^{207}Pb) = -135$ ppm for solid Pb(p-Tol)$_4$, *J. Organomet. Chem. C*, 1986, **301,** 23.

Pergamon

PII: S0277–5387(98)00257–5

Polyhedron Vol. 17, Nos. 25, 26, pp. 4507–4517, 1998
© 1998 Elsevier Science Ltd
All rights reserved. Printed in Great Britain
0277–5387/98 $19.00 + 0.00

XAS study of actinide solvent extraction compounds. II: $UO_2(NO_3)_2(L)_2$ (with L = tri-*iso*butylphosphate, tri-*n*-butylphosphate, trimethylphosphate and triphenylphosphate)

C. Den Auwer,[a,*,†] M. C. Charbonnel,[a] M. T. Presson,[a] C. Madic[b] and R. Guillaumont[c]

[a]CEA, DCC/DRRV, Service d'Études et de Modélisation des Procédés, ValRhô, BP 171, 30207 Bagnols-sur-Cèze, France

[b]CEA, DCC, Saclay 91191 Gif sur Yvette, France

[c]Institut de Physique Nucléaire d'Orsay, BP 6, 91406 Orsay Cedex, France

(Received 25 March 1998; accepted 23 June 1998)

Abstract—In the back-end of the nuclear fuel cycle, liquid–liquid extraction is the selected separation method. For an improved design of new extracting agent, the knowledge of the coordination polyhedra of the metal ions is important. In this paper, we investigated the coordination sphere of a series of uranyl complexes with selected organophosphorus extracting molecules: $UO_2(NO_3)_2L_2$ (with L = tri-*iso*-butylphosphate, tri-*n*-butylphosphate, trimethylphosphate and triphenylphosphate) using X-ray absorption spectroscopy. FEFF7 calculations of the EXAFS spectra corresponding to the model compound $UO_2(NO_3)_2(TiBP)_2$ (with TiBP = tri-*iso*-butylphosphate) for which the crystal structure is known led to a multiple scattering approach of the data fitting. EXAFS results show subtle U–O(P) bond distance differences between the different complexes that are discussed in terms of both electronic and steric effects of L. These results are discussed with regards to the extraction ability of L. In the same time, exploratory work has been attempted in order to evaluate U–O–P bond angle variations as a function of L using multiple photon-scattering paths. Satisfactory values have been obtained compared to the crystallographic data. © 1998 Elsevier Science Ltd. All rights reserved

Keywords: uranyl nitrate; extraction; nuclear fuel cycle; EXAFS; phosphate.

INTRODUCTION

The chemical species involved in the PUREX liquid–liquid extraction process of the back-end of the nuclear fuel cycle are still poorly identified, particularly concerning the coordination polyhedra of the complexes of actinide ions (e.g. U(VI), Pu(IV)) present in the solvent. The molecular processes underlying the macroscopic behavior of extraction must be more clearly understood for a possible improved future control of behavior of the elements to be separated in this industrial process.

The determination of structural data in a liquid medium demands probing the local order of the target element (uranium in this work) in order to determine its radial distribution function (i.e. nature, number and distances of the neighbor atoms). Coupled with other spectroscopic techniques such as infra-red, Raman and NMR spectroscopies, the information obtained by X-ray absorption spectroscopy (XAS), in conjunction with a molecular model, should contribute significantly to progress in the molecular design of new extractants.

In a previous study [1], we described the use of XAS to investigate the local order around the uranium atom within the complex $UO_2(NO_3)_2(TBP)_2$ (TBP = tributylphosphate) in solution in pure liquid TBP. Solid state compound $UO_2(NO_3)_2(TiBP)_2$

*Author to whom correspondence should be addressed.

†LURE (Laboratoire d'Utilisation du Rayonnement Electromagnétique, France) associate member.

(TiBP = tri-*iso*-butylphosphate) of known crystallographic structure was taken as a reference compound by extensive use of *ab initio* XAS calculation code FEFF7 [2]. In the present paper, we continue to investigate the series of homologous extractants of the $PO(OR)_3$ type (where R = *iso*-butyl, butyl, methyl and phenyl groups, respectively) in order to try to understand the variation in the extracting power† of the organophosphate for uranyl nitrate. Oda *et al.* have recently calculated the contribution of the alkyl groups of the phosphate in the extracting ability of $PO(OR)_3$ of the $UO_2(NO_3)_2[PO(OR)_3]_2$ complexes (with $[PO(OR)_3]$ = T*i*BP, TBP and TMP) [3, 4]. According to these authors, and on an electronic point of view, the extracting power which varies in the order T*i*BP ≈ TBP > TMP ≫ TPhP [5] might be partly explained by the differences in the electron donating ability of the alkyl groups of the organophosphate (the TPhP case is however not discussed in these works). In the present work, the coordination sphere of the uranium atom is fully described for the four complexes $UO_2(NO_3)_2[PO(OR)_3]_2$ in order to evaluate the relation, if any, between the extracting power and the complex geometry. This is achieved by means of both single and multiple scattering approaches using code FEFF7. This way, all contributions from oxygen, phosphorus and nitrogen atoms (Fig. 1) are to be identified and used in the fitting procedure using FEFFIT code [6].

EXPERIMENTAL

Synthesis

$UO_2(NO_3)_2$(T*i*BP)$_2$ and $UO_2(NO_3)_2(TBP)_2$ were prepared as described in Ref.[1].

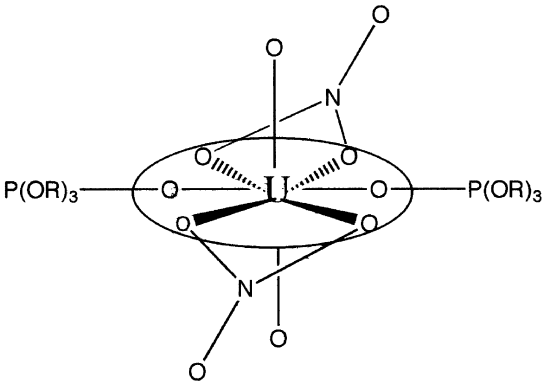

Fig. 1. Schematic representation of the uranyl equatorial plane in $UO_2(NO_3)_2L_2$ complexes where L is an organophosphorus ligand.

†Note that for TMP the U(VI) extracting power is rather low due to the high solubility of TMP in aqueous solutions and not to the peculiar weakness of the interaction between $UO_2(NO_3)_2$ and TMP.

$UO_2(NO_3)_2(TMP)_2$ solvate was prepared in an excess of TMP by dissolving 5.3 g (0.0106 mol) of $UO_2(NO_3)_2 \cdot 6H_2O$ (Prolabo grade) in 25 ml (0.21 mol) of pure TMP (Aldrich grade). Uranium(VI) concentration was determined to be 100 g/l (0.42 mol/l).

$UO_2(NO_3)_2(TPhP)_2$ was prepared from an excess of pure liquid TPhP at 60°C by dissolving 0.5 g of $UO_2(NO_3)_2 \cdot 6H_2O$ (0.0010 mol) in 2.7 g (0.008 mol) of melted TPhP (Aldrich grade). Uranium (VI) concentration was determined to be 71 g/l (0.30 mol/l). The complex remained in the liquid phase even at room temperature when introduced in the EXAFS liquid cell, but slowly crystallized for IR analysis.

IR spectroscopy

IR spectra were recorded for both liquid (on a ZnSe horizontal attenuated transmitted reflectance crystal) and solid phase (in KBr pellets) on a Nicolet Magna 560 spectrometer.

IR spectra all show the characteristic uranyl O–U–O stretching band around 940 cm^{-1} (italicized in the frequency list). Also, a sharp band due to the stretching vibration mode of the P–O–C bond appears around 1030 cm^{-1}, which is in agreement with previous studies on these phosphate ligands [1, 7]. Further structural information can be hardly deduced from these results, but the similarity of all spectra compared with that of solid $UO_2(NO_3)_2$(T*i*BP)$_2$ complex suggests the formation of the uranyl nitrate organophosphate complexes with TBP, TMP and TPhP ligands.

IR spectra (cm^{-1}):

$UO_2(NO_3)_2$(T*i*BP)$_2$: (1 mg in 80 mg of KBr pellet): 2963 (str, br), 2874 (str, br), 2552 (m), 2298 (s), 1832 (s), 1776 (s), 1729 (s), 1622 (s, br), 1533 (m, br), 1472 (m), 1385 (str), 1269 (m, br), 1172 (m), 1031 (str, br), *938* (m), 882 (m, br), 747 (m), 597 (m), 543 (m, br).

$UO_2(NO_3)_2(TBP)_2$: 2962 (str, br), 2878 (str, br), 1522 (str), 1474 (m), 1382 (w), 1278 (m), 1182 (m), 998–1030 (str, br), *937* (m), 811 (m), 747 (m).

$UO_2(NO_3)_2(TMP)_2$: 2960 (m), 2857 (m), 1635 (m), 1525 (m), 1450 (m), 1266 (str), 1185 (str), 1030 (str, br), *935* (str, s), 842 (str), 752 (m, s), 737 (m, s).

$UO_2(NO_3)_2(TPhP)_2$: (1 mg in 80 mg of Kbr pellet): 2925 (w), 1590 (m), 1529 (m), 1486 (m, s), 1384 (str, s), 1290 (m, br), 1227 (m), 1200 (m), 1184 (str, s), 1153 (m), 984 (str), *947* (str), 750 (m, br).

EXAFS spectroscopy

Data recording and data treatment. EXAFS measurements were carried out at LURE at the DCI high energy ring (1.800 GeV, $\lambda_c = 3.7$ keV) on D44 experimental hutch [8]. Transmission detection mode was used with two ionization chambers filled with argon. Spectra were taken at the uranium L_{III} edge (17166 eV) using a double crystal Si 311 monochromator.

Sample quantities were calculated in order to obtain an X-ray absorption jump close to 1 after the edge. Solid state sample (71 mg/mm^2) was dispersed in cellulose and then pressed in order to obtain a solid pellet placed in a sample holder. Liquid samples were measured in an *in house* [9] liquid cell (path length = 3 mm) at room temperature.

Data treatments were carried out using *in house* codes [10]. A straight line was used for background removal and polynomial function of order five was used to simulate the U atomic absorption. Fourier transformed (FT) window (Kaiser window with shape parameter = 2.5) was used between 3.5 and 14.5 Å^{-1}.

Data adjustment. Data adjustments were carried out using the FEFFIT code [6] that is related to the *ab initio* simulation code FEFF. Electronic parameters used to fit the spectra of the unknown compounds (electron mean free path λ, intrinsic losses, phases and amplitudes) were extracted from the simulation of solid state complex $UO_2(NO_3)_2(TiBP)_2$ at 77 K using FEFF7 code.

Adjustments were conducted in two times for each sample: (i) adjustment of the filtered single scattering contributions of the FT between 0.7 and 2.9 Å and (ii) adjustment of the total EXAFS spectrum.

Determination of global parameters, energy threshold e_0 and amplitude losses $S0^2$, was achieved by first fitting the 0.7/2.9 Å range and total spectrum on model compound $UO_2(NO_3)_2(TiBP)_2$, giving $e_0 = 2.96$ eV and $S0^2 = 1.25$. These two parameters were kept constant in all other adjustments of all other complexes.

Fitting of the 0.7/2.9 Å range was achieved by fitting both Debye–Waller factors and bond distances of the five first paths A–E (see details in the text). Debye–Waller factors of paths C and D were linked since these two paths account for the two U–O(N) contributions of the same NO_3^- ligand.

Fitting of the total EXAFS spectrum was achieved as described in details in the text (*vide infra*).

Evaluation of the goodness of the fit is given by the *r* factor (related to the statistical CHI^2 function) as fully described in Ref.[6].

RESULTS AND DISCUSSION

In order to evaluate the modifications of the uranyl nitrate coordination spheres, going from TBP to TPhP ligands, a detailed analysis of the uranium photoelectron scattering paths was undertaken. Based on our previous study of the uranium coordination sphere [1] in solid state compound $UO_2(NO_3)_2(TiBP)_2$, path enumeration was fully accomplished on this complex using FEFF7 code. According to this, quantitative adjustments of the filtered FT were carried out in two times for all four complexes.

In the first time, only single scattering paths were considered in the fit of first and second uranium coordination spheres that include all the first neighbor oxygen atoms as well as the two nitrogen atoms of the nitrate groups. In the second time, eleven single and multiple scattering paths were included to fit the total EXAFS spectra.

Uranium photoelectron scattering path enumeration of compound $UO_2(NO_3)_2(TiBP)_2$

Figure 2 shows the Fourier transform (FT) of the calculated (FEFF7) EXAFS spectrum of solid state $UO_2(NO_3)_2(TiBP)_2$ at 77 K. All the 540 scattering paths that contribute to the total EXAFS spectrum for more than 0.1% were included (path amplitudes are normalized with respect to the amplitude of the most intense path over the entire *k* range, set to 100%). However, only paths that contribute for more than 10% were isolated and presented in Fig. 2 for the seek of clarity. These eleven paths are detailed in Table 1.

Each path contributes constructively or destructively to the total EXAFS spectrum, depending on its phase. Figure 3 presents the EXAFS oscillations of each of these paths, showing the different phasors (i.e. the entity $Fi\sin(2\delta_c + \phi + 2kri)$, where *Fi* is the global path *i* amplitude, δ_c is the central atom phase-shift, ϕ the back-scatter phase-shift and *ri* the total path length) that are characteristic of both path length and atoms involved. For instance, paths C and D that both account for U–O(N) single scattering with almost the same path length are completely constructive. It is also to be noted that multiple scattering paths that involve forward scattering are particularly intense, as for example paths F and I. All multiple paths that do not include forward scattering are less than 10% intense.

The path enumeration also shows that single scattering paths that involve all the oxygen first neighbors as well as the two nitrogen atoms of the two nitrate groups can be isolated within a filter window between 0.7 and 2.9 Å (not phase-shift corrected).

Single scattering path fitting

Taking the filter window (0.7–2.9 Å) and neglecting the small part of multiple scattering paths that is included in it, a pure single scattering approach is a reasonable approximation to fit the contributions that occur in this window. The five first paths were therefore included in the fitting procedure of the filtered EXAFS spectra of compounds $UO_2(NO_3)_2(TiBP)_2$, $UO_2(NO_3)_2(TBP)_2$, $UO_2(NO_3)_2(TMP)_2$ and $UO_2(NO_3)_2(TPhP)_2$. Structural parameters (i.e. U–X (X = O, N atoms) distances and their corresponding Debye–Waller factors) that were obtained are displayed in Table 2. Best fits of the filtered EXAFS oscillations are presented in Fig. 4. In the case of $UO_2(NO_3)_2(TiBP)_2$ at 77 K, bond distances compare satisfactorily within the error of ± 0.02 Å with the U–O structural data given by X-ray diffraction at 77 K for this solid state complex [11]. It is however not surprising that path E is

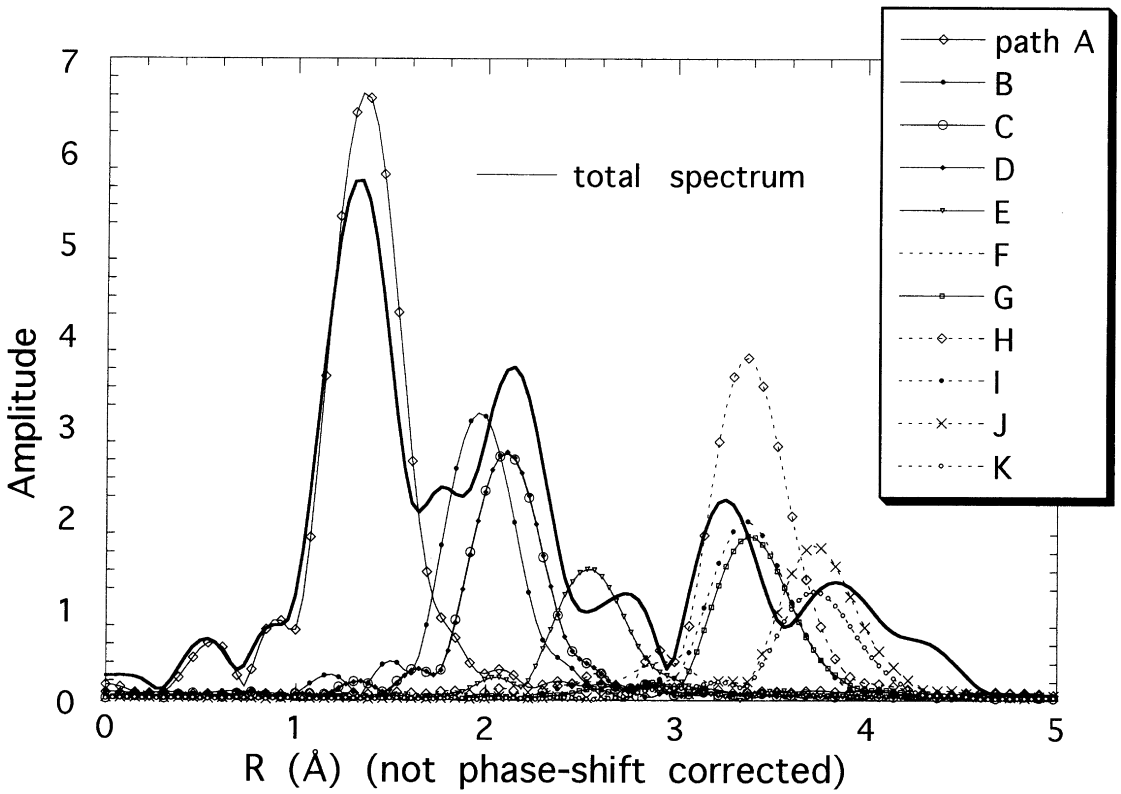

Fig. 2. Modulus of the Fourier transform (FT) of the calculated EXAFS spectrum (FEFF7) of $UO_2(NO_3)_2(T\textit{i}BP)_2$ complex. Moduli of the FTs of the main photoelectron scattering paths are also represented.

less accurately determined (within the error of $+0.04$ Å) since it does not correspond to a chemical bond between the central atom and the backscattering atom. For the solid state complex $UO_2(NO_3)_2(T\textit{i}BP)_2$ at both 77 and 298 K, all bond distances compare well. This differs from previous work results [1] that overestimated the U–O(P) bond distance r_p for this complex at room temperature. We attribute this fluctuation (-0.05 Å) to the new fitting procedure and fitting code that we used in this work, yielding to a better estimation of the energy threshold e_0 that is directly linked to the determination of the bond distances. The e_0 value taken here is equal to 17178.3 eV for all paths, whereas e_0 used in our previous study was allowed to vary for each path, being respectively equal to 17182.4 eV for U–O(UO_2^{2+}), 17194.1 eV for U–O(P) and 17189.8 eV for U–O(N). The very high discrepancy between e_0 for the U–O(P) path and the two other ones may be at the origin of r_p over-estimation in our previous work.

Considering the TBP solution complex, it was previously shown that there is no significant difference in r_p when the *iso*butyl groups in the solid state complex are replaced by the butyl ones in the liquid phase complex, both at 298 K. This result is confirmed here and the lengthening of r_p of $+0.03$ Å lies within the error bars. On the other hand, the significant shortening of r_p from $UO_2(NO_3)_2(TBP)_2$ to $UO_2(NO_3)_2(TMP)_2$ (-0.05 Å), both measured at room temperature in the liquid phase, seems to be caused by the replacement of the butyl groups by the methyl groups. Furthermore, this compares well with the X-ray diffraction measurements carried out on the TMP complex in the solid state [12]. Our assumption is that the steric hindrance of the phosphate ligand plays the main role in the structure modification. In fact, it has been shown using relativistic molecular orbital calculations that a decrease of the electronic donor effect of the alkyl group (in the order TBP > TMP) leads to a decrease of the strength of the covalent U–O(P) bond in the order TBP > TMP and thus must result in a decrease of r_p from TMP to TBP [3]. The opposite phenomenon is observed here. We think that the size of the TMP ligand allows it to approach the UO_2^{2+} coordination plane closer than the TBP ligand does, thus leading to a smaller value of r_p for TMP complex. On the contrary, the small variation of $+0.02$ Å between r_p in $UO_2(NO_3)_2(TMP)_2$ and in $UO_2(NO_3)_2(TPhP)_2$ which stays within the error bars, is not considered significant. However, it is be surprising that r_p does not increase from TMP to TPhP ligand because of the substitution of the methyl by the phenyl groups. To explain this experimental fact, two phenomena may be considered: an electronic effect due to the participation of the phenyl rings that are electron withdrawing and therefore should contribute

Table 1. Uranium photoelectron scattering path description according to FEFF7 simulation of model compound $UO_2(NO_3)_2(TiBP)_2$

Path	Description	Paths amplitude as calculated by FEFF7
A[1]		100[2]
B	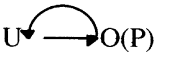	42
C	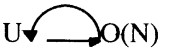	36
D	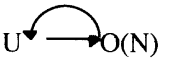	36
E	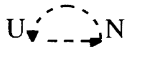	21
F	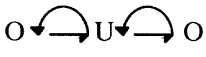	18
G	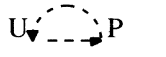	11
H		25
I	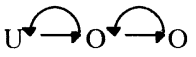	16
J	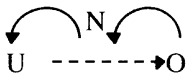	20
K	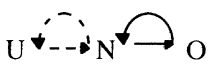	14

[1]Path legs which correspond to a chemical bond are represented by a plain line, path legs which do not correspond to a chemical bond are represented by a dashed line.

[2]Paths amplitudes are normalized with respect to the highest amplitude, set to 100%.

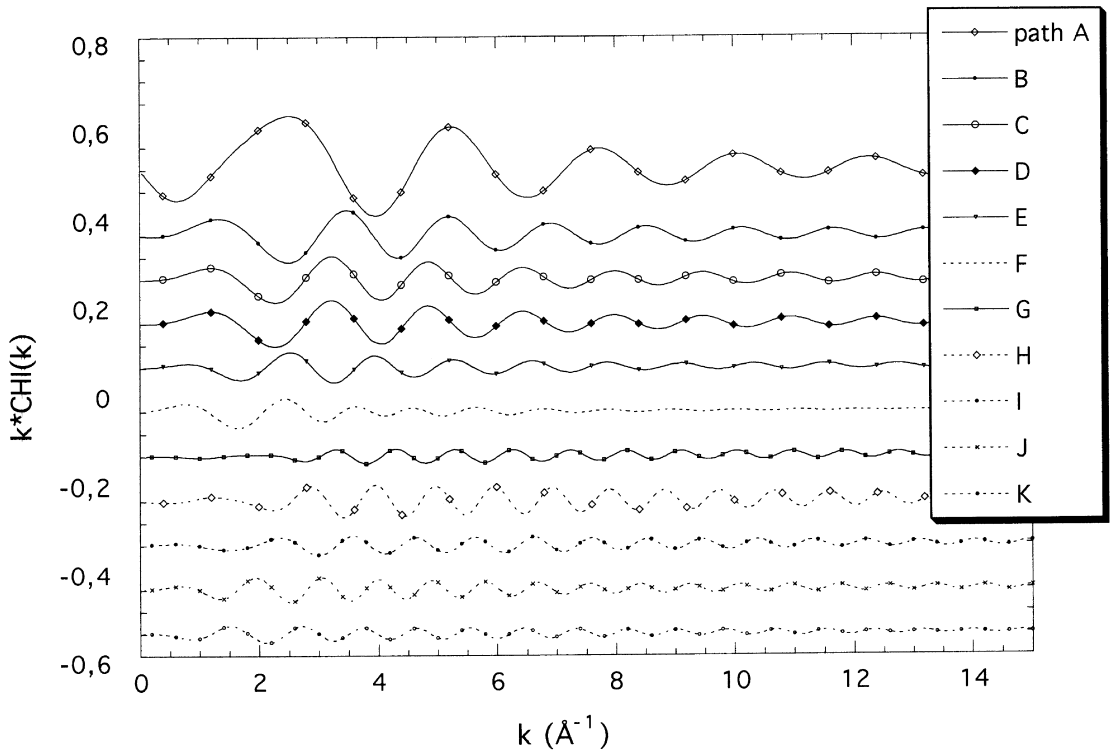

Fig. 3. EXAFS oscillations of each main scattering path. Each path, *i*, is characterized by an amplitude function *Fi* multiplied by a phasor function defined as $\sin(2\delta_c+\phi+2kri)$, where δ_c is the U atom phase-shift, ϕ the back-scatter phase-shift and *ri* the total path length.

Table 2. Best fit parameters (U to neighbor distances, *r*; Debye–Waller factors, σ) of the single scattering adjustment of the filtered EXAFS spectra of $UO_2(NO_3)_2(TiBP)_2$, $UO_2(NO_3)_2(TBP)_2$, $UO_2(NO_3)_2(TMP)_2$ and $UO_2(NO_3)_2(TPhP)_2$ complexes

Path	Crystallographic value at 77 K*	T*i*BP (solid), 77 K	T*i*BP (solid), 298 K	TBP (liquid), 298 K	TMP (liquid), 298 K	TPhP (liquid), 298 K
A: U–O	$r=1.757$ Å	$r=1.78\pm0.01$ Å, $\sigma=0.032$ Å	$r=1.78\pm0.01$ Å, $\sigma=0.045$ Å	$r=1.77\pm0.01$ Å, $\sigma=0.046$ Å	$r=1.78\pm0.01$ Å, $\sigma=0.050$ Å	$r=1.77\pm0.01$ Å, $\sigma=0.045$ Å
B: U–O(P)	$r=2.372$ Å	$r=2.37\pm0.02$ Å, $\sigma=0.064$ Å	$r=2.38\pm0.02$ Å, $\sigma=0.045$ Å	$r=2.41\pm0.01$ Å, $\sigma=0.067$ Å	$r=2.36\pm0.02$ Å, $\sigma=0.051$ Å	$r=2.39\pm0.01$ Å, $\sigma=0.040$ Å
C: U–O(N)	$r=2.509$ Å	$r=2.53\pm0.01$ Å, $\sigma=0.057$ Å	$r=2.54\pm0.01$ Å, $\sigma=0.056$ Å	$r=2.54\pm0.01$ Å, $\sigma=0.077$ Å	$r=2.53\pm0.02$ Å, $\sigma=0.086$ Å	$r=2.53\pm0.01$ Å, $\sigma=0.048$ Å
D: U–O′(N)	$r=2.510$ Å	$r=2.53\pm0.01$ Å, $\sigma=0.057$ Å	$r=2.54\pm0.01$ Å, $\sigma=0.056$ Å	$r=2.54\pm0.01$ Å, $\sigma=0.077$ Å	$r=2.53\pm0.02$ Å, $\sigma=0.086$ Å	$r=2.53\pm0.01$ Å, $\sigma=0.048$ Å
E: U · · · N	$r=2.960$ Å	$r=3.00\pm0.01$ Å, $\sigma=0.009$ Å	$r=2.98\pm0.02$ Å, $\sigma=0.036$ Å	$r=2.99\pm0.03$ Å, $\sigma=0.072$ Å	$r=2.96\pm0.08$ Å, $\sigma=0.090$ Å	$r=2.97\pm0.03$ Å, $\sigma=0.056$ Å
r factor		0.03	0.04	0.03	0.05	0.02

to weaken the bond (i.e. lengthen r_p), and a steric effect that should play the same role as TBP does compared to TMP (i.e. lengthen r_p). Our assumption is then that the phenyl groups might be stack together in a way that the steric hindrance is minimized, thus accounting for the relatively low value of r_p.

According to these results and as it might have been expected, r_p seems to be directly related to the nature of the hydrocarbon groups of the organophosphate, mainly because of steric effects of the ligand instead of electronic effects.

Using the multiple scattering paths that are particularly sensitive to bond distortions (i.e. forward scattering paths that are resonant for bond angles of 180° [13]) we further attempted to adjust the total EXAFS spectra of all complexes, allowing the dis-

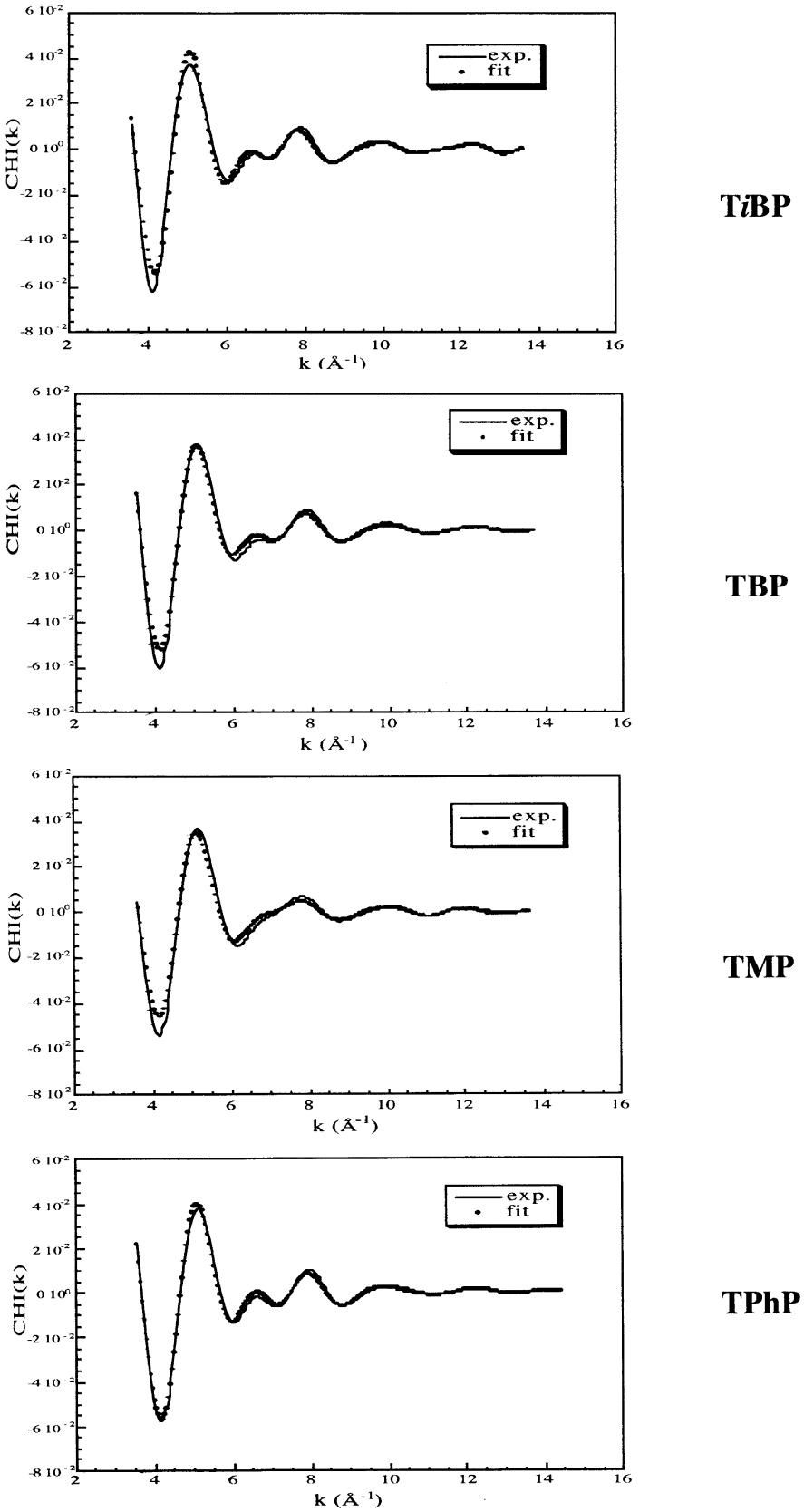

Fig. 4. Adjusted filtered EXAFS oscillations (between 0.7 and 2.9 Å) of $UO_2(NO_3)_2L_2$ complexes (L = T*i*BP, TBP, TMP, TPhP) in the single scattering approximation. All complexes are in the liquid phase (298 K) except for the solid state complex $UO_2(NO_3)_2(Ti BP)_2$ (77 K).

tortion of the U–O–P bond, if any, to vary. This is a first attempt for further bond distortion estimation in series of related compounds.

Multiple scattering approach

Further analysis of the five spectra was carried out by fitting the crude total EXAFS spectra considering the eleven paths A–K that have been defined before. In the fitting procedure, both Debye–Waller factors and bond distances of the first five paths were fixed equal to the values determined in the first adjustment of paths A–E.

In these adjustments, we took into account the distortions of the U–O–P bond that might occur when varying the hydrocarbon parts of the phosphate ligand. Forward scattering paths H and I are then of particular interest since they are the most sensitive of all eleven paths to any modifications of the U–O–P bond geometry.

In order to first test the sensitivity of the total EXAFS spectra of the organophosphate complexes to the U–O–P bond distortions (distortions considered are of two kinds: bond length elongation and bond angle variation), total EXAFS spectrum reconstruction was carried out using the eleven paths calculated from the simulation of model structure of $UO_2(NO_3)_2(TiBP)_2$ with FEFF7. Within two sets of calculations, paths H and I were both modified in order to simulate with calculated EXAFS spectra (i) bond length elongations of r_p and (ii) bond angle modifications of the U–O–P bond characterized by the δ angle, all other parameters being unchanged. The two parameters δ and r_p are identified as shown below and compared to the corresponding crystallographic values: $r_p = 2.37$ Å and $\delta = 164^\circ$ of $UO_2(NO_3)_2(TiBP)_2$ at 77 K.

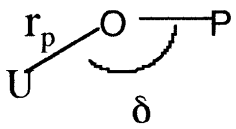

Figure 5 presents the two simulation sets and shows the influence of δ and r_p on the beating at 10 $Å^{-1}$ in the reconstructed EXAFS spectrum. Both parameter values affect the same region of the EXAFS spectrum. However, in the fitting of the experimental spectra, r_p is fixed to the value determined in the fitting of the filtered single scattering contributions (r_p is fixed by the fit of path B).

In the fitting procedure of the five experimental spectra, bond distances of paths F–K were linked and fitted according to the description of Table 3. Modification of δ in paths H and I was also taken into account by scaling the specific amplitudes $f_H(k, \delta)$ and $f_I(k, \delta)$ of these two paths by a constant factor F (all other amplitudes of all other paths being unchanged with regard to FEFF7 calculations). In order to determine the scaling factors $F_H(\delta)$ and $F_I(\delta)$, molecular models of $UO_2(NO_3)_2(TiBP)_2$ with different values of δ were generated using INSIGHT II molecular modeling system from MSI and their EXAFS spectra were simulated by FEFF7. For each δ value, $f_H(k, \delta)$ and $f_I(k, \delta)$ were plotted against k and curve fitted at 8 $Å^{-1}$ in order to get $F_H(\delta)$ and $F_I(\delta)$ for which δ was included in the fit as a free parameter. Debye–Waller factors of paths F–K were found to be highly linked with the value of δ. To avoid this influence of Debye–Waller values on δ, Debye–Waller factors of multiple scattering paths were fitted, given they were all kept equal to each other. While this is a fairly crude approximation, we have found however that adjusting the six different factors leads to unrealistic instabilities on the fit result. In all cases, oscillation amplitude below 5 $Å^{-1}$ (delimited by the vertical line in Fig. 6) is poorly adjusted, mainly because of poor estimation of the amplitude parameters by FEFF7 at low k values. This is however not affecting the fit results since the number of uranium neighbors N is not adjusted here.

Table 4 gives the best fit parameters that were obtained. The value found for $UO_2(NO_3)_2(TiBP)_2$ at 77 K, $\delta = 156^\circ$, agrees within 5% error with the crystallographic value: 164°. This is a very satisfactory agreement showing that both the number of paths considered here and the fitting approximations can account for simulating the experimental EXAFS spectra. Precision on the δ value is however to be taken

Table 3. Fitting conditions and links used for the adjustment of all A–K scattering paths

Path	Bond distance r	Deby–Waller factor (σ)
A–E	fixed	fixed
F	fixed = 2*r_A	
G	fitted = function(δ)	
H	fitted, linked with G path	fitted $\sigma_F = \sigma_G = \sigma_H = \sigma_I = \sigma_J = \sigma_K$
I	fixed = r_B	
J	fixed = r_E	
K	fixed = r_B	

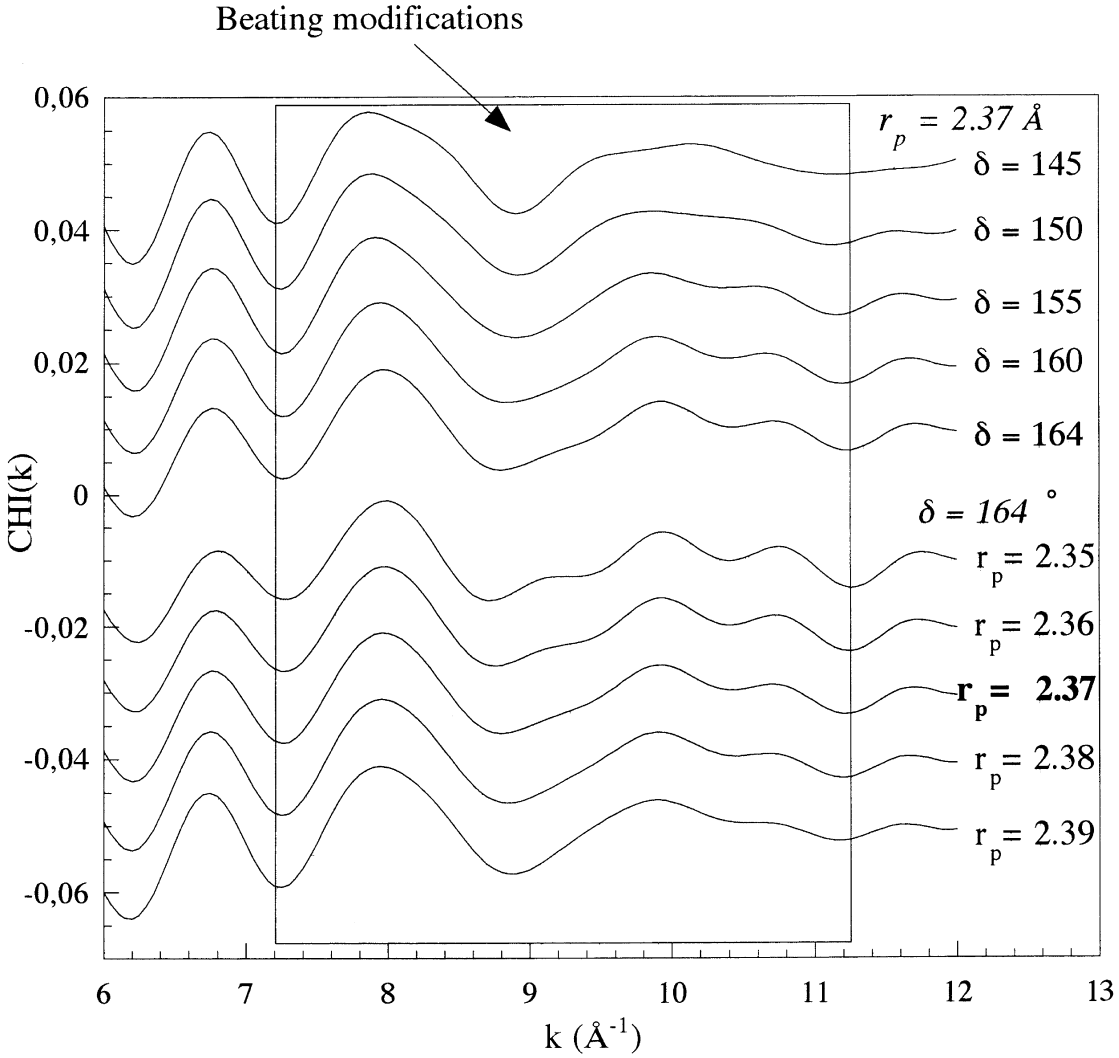

Fig. 5. Simulated EXAFS oscillations (FEFF7) based on solid state model complex $UO_2(NO_3)_2(TiBP)_2$. In the first simulation set, the U–O–P bond angle, δ, is varied and the U–O(P) bond length, r_p, is set to the crystallographic value 2.37 Å. In the second simulation set, the U–O–P bond angle, δ, is set to the crystallographic value (264°) and the U–O(P) bond length, r_p, is varied.

Table 4. Best fit parameters of the total EXAFS spectra adjustment of $UO_2(NO_3)_2(TiBP)_2$, $UO_2(NO_3)_2(TBP)_2$, $UO_2(NO_3)_2(TMP)_2$ and $UO_2(NO_3)_2(TPhP)_2$ complexes (all structural parameters that are not presented here are those given in Table 2)

Complex	δ value (°)	σ (Å)	r factor
$UO_2(NO_3)_2(TiBP)_2$ at 77 K	156 ± 3	0.053	0.06
$UO_2(NO_3)_2(TiBP)_2$ at 298 K	157 ± 3	0.058	0.06
$UO_2(NO_3)_2(TBP)_2$ at 298 K	172 ± 10	0.066	0.04
$UO_2(NO_3)_2(TMP)_2$ at 298 K	161 ± 7	0.089	0.08
$UO_2(NO_3)_2(TPhP)_2$ at 298 K	142 ± 5	0.067	0.06

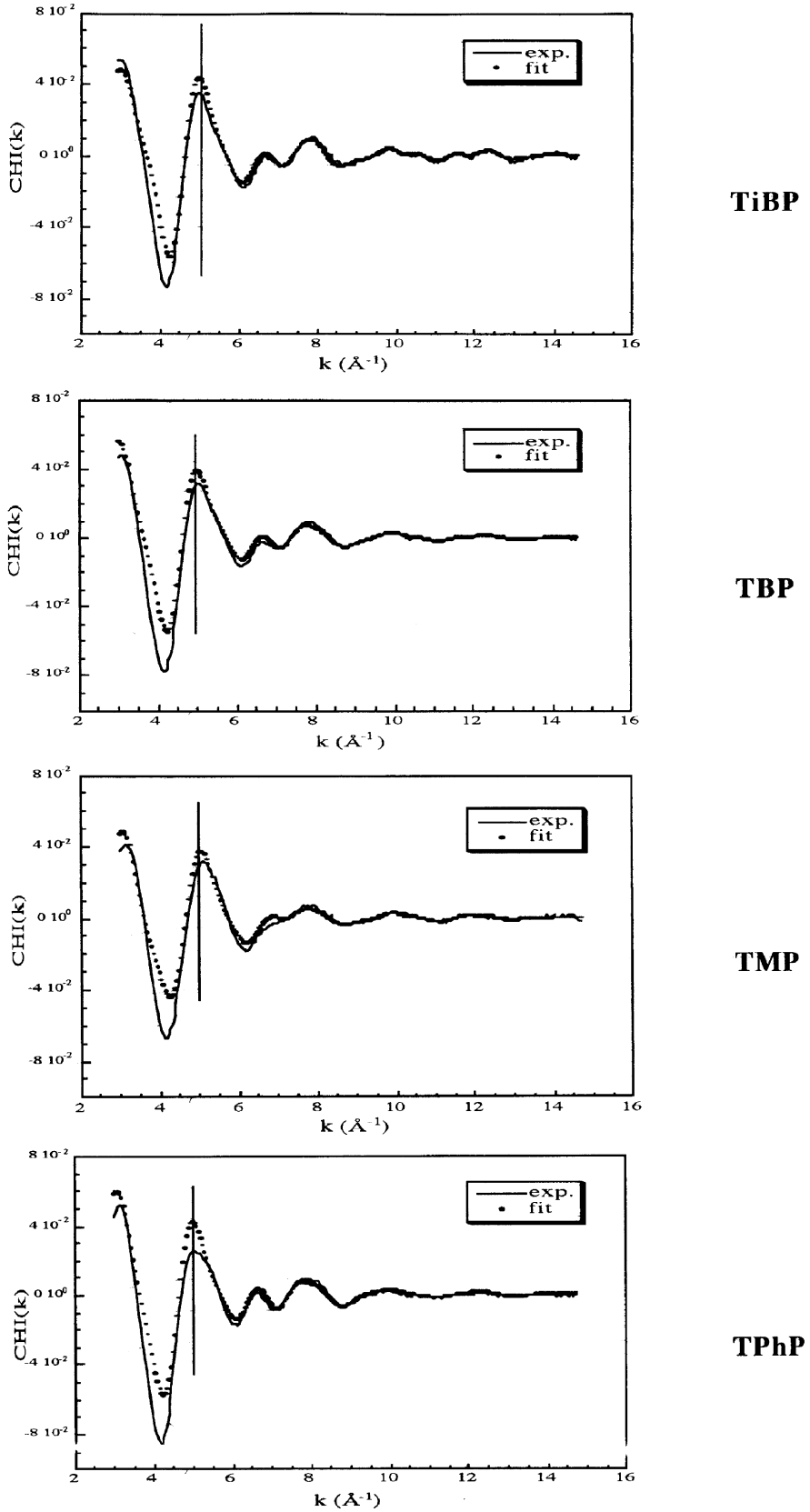

Fig. 6. Adjusted total EXAFS oscillations of $UO_2(NO_3)_2L_2$ complexes (L = T*i*BP, TBP, TMP, TPhP) in the single multiple scattering approximation. All complexes are in the liquid phase (298 K) except for the solid state complex $UO_2(NO_3)_2(Ti BP)_2$ (77 K).

very carefully since the evaluation of many parameters used in the model (as the Debye–Waller factors, the amplitude losses, amplitude of the multiple scattering paths to be taken into account as a function of δ and r_p) have still to be improved.

All δ values, except for the TPhP ligand, agree within 5% with the T*i*BP complex crystallographic value. It is striking that the δ_{TPhP} value is significantly smaller than the other δ values. This might be related to our assumption concerning the peculiar arrangement of the phenyl groups, as described above.

In light of these results (i.e. in the complexes $UO_2(NO_3)_2L_2$, r_p ranks in the order $L = TBP > TMP \approx TPhP$), a simple correlation between the extraction affinities of L for $UO_2(NO_3)_3$ (in the order $L = TBP > TMP \gg TPhP$) and shortest r_p distances is not established. More than electronic interactions between U and O phosphoryl atoms, steric hindrance as well as lipophilicity of L should be taken into account. It is therefore still not clear why L = TPhP is such a poor extractant molecule compared to TBP.

CONCLUSIONS

The results presented here are related to the characterization of uranyl nitrate coordination sphere when complexed by organophosphorus ligands. When varying the nature of the hydrocarbon groups of the organophosphate, a modification of the U–O(P) bond length r_p is observed. Decrease of r_p for the liquid phase complexes at room temperature is in the order $TBP > TMP \approx TPhP$. In all cases, this variation is attributed to a decrease of the steric hindrance of the hydrocarbon groups that allows a better approach of the ligand coordinating atom in the uranyl coordination plane.

Furthermore, tentative work using a multiple scattering approach was undertaken in order to adjust the total EXAFS spectra and accounting for U–O(P) bond distortions. Satisfactory fitting results were obtained, showing the validity of the approximations used. Not only U–O(P) bond distances were determined, but our model was able to evaluate satisfactorily U–O–P bond angles. Improvement of the method should include in the future better estimation of the Debye–Waller factors for multiple scattering paths. We believe that a major part of the uncertainties in bond angle evaluations may be caused by this poor estimation of these factors.

Our study is part of major efforts in understanding the structure–properties relationship in the field of solvent extraction. This type of approach of structure–affinity relationship was recently studied by Rabbe *et al*. [14] in the case of the uranyl nitrate extraction by monoamide extractants.

Acknowledgements—The authors are grateful to Dr J.-P. Dognon for his help in molecular modeling simulations.

REFERENCES

1. Den Auwer, C., Lecouteux, C., Charbonnel, M. C., Madic, C. and Guillaumont, R., *Polyhedron*, 1997, **16,** 2233.
2. Hudson, E. A., Rehr, J. J. and Bucher, J. J., *Phys. Rev. B*, 1995, **52,** 13815.
3. Oda, Y., Funasaka, H. and Adachi, H., in Proceedings of the GLOBAL Conference, Yokohama (Japan), 5–10 October 1997, p. 1478.
4. Oda, Y., Nakamura, Y. and Funasaka, H., in Proceedings of the 6th CEA/PNC Meeting on Partitioning, Tokai-Works, PNC (Japan), 8–10 July 1996.
5. Populus, P., unpublished results, CEA/DCC/DRRV/SEMP, 1993.
6. Newville, M., in FEFFIT notice, FEFFIT version 2.32, 1995.
7. Mortimer, F. S., *Spectrochim. Acta*, 1957, **9,** 270.
8. Sainctavit, P., Spectroscopie d'absorption X de chalcogénures de structures blende ou chalcopyrite et de complexes fer-soufre dans les verres silicates. Thèse de Doctorat, Université Paris VII, Paris, 1989.
9. Villain, F., Briois, V., Castro, I., Helary, C. and Verdaguer, M., *Anal. Chem.*, 1993, **65,** 2545.
10. Michalowicz, A., Logiciels pour la chimie: EXAFS pour le Mac. Société Française de Chimie, Paris, 1991.
11. Burns, J. H. and Brown, G. M., *Acta Cryst.*, 1985, **C41,** 1446.
12. Agostini, G. and Giacometti, G., *Inorg. Chim. Acta*, 1982, **62,** 237.
13. O'Day, P. A., Rehr, J. J., Zabinsky, S. I. and Brown, G. E. Jr., *J. Am. Chem. Soc.*, 1994, **116,** 2938.
14. Rabbe, C., Madic, C., Godard, A., Solv. Extract. Ion-Exchange, 1998, accepted for publication.

Pergamon

Polyhedron Vol. 17, Nos. 25, 26, pp. 4519–4524, 1998
© 1998 Elsevier Science Ltd
All rights reserved. Printed in Great Britain
PII: S0277–5387(98)00258–7
0277–5387/98 $19.00+0.00

The first metal–dmit polymer with 3D supramolecular networks. Synthesis and crystal structure of $[(Et_4N)_2\{Ag_4(dmit)_3\}\cdot DMF]_\infty$ (dmit = 1,3-dithiole-2-thione-4,5-dithiolate)

Tianlu Sheng, Xintao Wu,* Quanming Wang, Xiancheng Gao and Ping Lin

State Key Laboratory of Structural Chemistry, Fujian Institute of Research on the Structure of Matter, the Chinese Academy of Sciences, Fuzhou, Fujian 350002, People's Republic of China

(Received 11 March 1998; accepted 24 June 1998)

Abstract—The first metal–dmit polymeric complex, $[(Et_4N)_2\{Ag_4(dmit)_3\}\cdot DMF]_\infty$, has been synthesized and structurally characterized. The crystal of the complex is monoclinic with space group C2/c, $a=32.078(4)$, $b=11.791(2)$, $c=29.409(4)$ Å, $\beta=124.14(1)^\circ$, $V=9206.8$, $Z=8$, $R=0.053$, $R_w=0.061$. In the complex, the S · · · S contacts exist both intra- and inter-molecularly, through the intermolecular S · · · S contacts shorter than 3.7 Å the two-dimensional polymeric anions form a three-dimensional unique supramolecular networks.
© 1998 Elsevier Science Ltd. All rights reserved

Keywords: metal-dmit polymer; silver atoms; ligands

INTRODUCTION

The supramolecular chemistry has been one of the important research fields of chemists [1,2] due to the goals of developing advanced materials. Intermolecular interactions such as hydrogen bonding, S · · · S contacts and π–π stacking are efficient organizing forces in supramolecular architecture and the design of new solid-state materials for a number of applications. Some of the metal–dmit complexes with S · · · S contacts were reported to exhibit conductivities and even superconductivities [3–5]. Recently, it has been shown that intermolecular interactions in transition metal bis(dithiolate) complexes of this type are also important for the assembly of molecular ferromagnets [6]. A large number of metal–dmit complexes have been synthesized and structurally characterized, however, no polymeric compound with dmit has been reported.

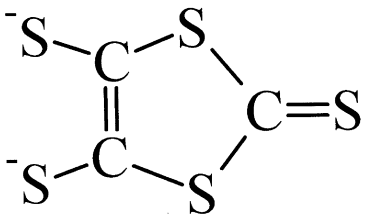

We report here the crystal structure and electrical properties of the metal–dmit complex $[(Et_4N)_2\{Ag_4(dmit)_3\}\cdot DMF]_\infty$ **1**, which is the first example of polymeric compounds with dmit.

EXPERIMENTAL

All procedures for preparation of the title complex were carried out under nitrogen atmosphere using standard Schlenk techniques. The chemicals used in the experiment were of A.R. grade and were used without purification. 4,5-Bis(benzoylthio)-1,3-dithiole-2-thione was prepared following the detailed procedure described by Steimecke [7]. Elemental analysis was performed by the Elemental Analysis Laboratory

* Author to whom correspondence should be addressed. E-mail: wxt@ms.fjirsm.ac.cn

in our institute. The UV–VIS spectra and IR spectra of the complex were recorded on a Schimadyzu UV-3000 and a Perkin Elmer 577 spectrometer. Electrical resistivity was measured by a conventional two-probe method with compacted pellets.

Preparation of $[(Et_4N)_2\{Ag_4(dmit)_3 \cdot DMF]_\infty$

0.408 g (1.0 mmol) of 4,5-bis(benzoylthio)-1,3-dithiole-2-thione was dissolved in a methanol (30 ml) solution containing 0.046 g (2 mmol) of sodium metal. To the resulting purple solution of $Na_2[C_3S_5]$ was added under stirring 10 ml of concentrate ammonia solution containing 0.085 g (0.5 mmol) of $AgNO_3$. After being stirred for a while at room temperature, to the reaction mixture was added 25 ml of methanol solution with an excess amount of Et_4NBr (0.53 g, 2.5 mmol), precipitating immediately the red product. The red precipitate was collected by filtration and re-dissolved in 10 ml of DMF, then it was filtered after stirring for several minutes, and the filtrate was diffused by gaseous Et_2O and EtOH solvent at room temperature for several weeks to yield the deep-red crystals of the complex. Yield: 0.06 g (35.5%). The crystals are insoluble in CH_3CN, CH_3COCH_3 or CH_2Cl_2. Its X-ray quality crystals were obtained after many experiments. Anal. calcd. for $C_{28}H_{47}N_3OS_{15}Ag_4$: S, 35.52%; C, 24.84%; H, 3.50%; N, 3.10%. Found: S, 35.26%. C, 25.70%; H, 3.50%; N, 3.12%.

IR (KBr pallet, cm^{-1}): 460(s), 527(s), 661(s), 783(s), 866(s), 903(s), 983(s), 997(s), 1035(vs), 1056(vs), 1099(w), 1171(vs). UV–VIS (DMF, λ_{max}, nm) (ε, $dm^3\,cm^{-1}\,mol^{-1}$): 290 (3.28×10^4), 450 (2.99×10^4).

Crystal structure determination

Crystallographic data for the complex are given in Table 1. The intensity data were collected at room temperature on an Enraf–Nonius CAD4 diffractometer. The radiation used was monochromatized MoKα with graphite. The crystal chosen for data collection had dimensions $0.10 \times 0.15 \times 0.25$ mm. The unit cell parameters were determined by least-squares refined with 25 reflections in the $10.94^\circ \leq \theta \leq 12.52^\circ$. Intensity data were collected in the range $3^\circ \leq 2\theta \leq 50^\circ$ by the ω–2θ scan technique. A total of 8545 reflections were collected, of which 7931 were unique and 4453 observed, $I > 5.0\sigma(I)$. Intensities were corrected for Lorentz and polarization effects, and DIFABS [8] empirical absorption correction was applied. The structure was solved by the direct method using MULTAN [9], from which four Ag atoms were obtained. The rest of non-hydrogen atoms were obtained from subsequent difference Fourier map. The non-hydrogen atoms in the anion were refined anisotropically, and other non-hydrogen atoms were refined isotropically, whereas the positions of the hydrogen atoms calculated in ideal positions and their isotropical thermal parameters were fixed. Non-hydrogen scattering factors were taken from Cromer and Waber [10]. All calculations were performed on a

Table 1. Crystal data and some experimental details for **1**

Empirical formula	$C_{28}H_{47}Ag_4N_3OS_{15}$
Formula weight	1354.15
Lattice parameters	
a (Å)	32.078(4)
b (Å)	11.791(2)
c (Å)	29.409(4)
β (deg)	124.14(1)
V (Å^3)	9206.8
Space group	C2/c (No. 15)
Z value	8
D_{calc} ($g\,cm^{-3}$)	1.95
$F(000)$	5376
μ (Mo K$_\alpha$) (cm^{-1})	23.5
Diffractometer	Enraf–Nonius CAD4
Radiation	Mo K$_\alpha$ ($\lambda = 0.71073$ Å)
T (K)	298
2θ(max)	50°
No. observations ($I > 5.0\sigma(I)$)	4453
No. of variables	339
Residuals: R[a]	0.053
Maximum shift in final cycle	0.001
Largest peak in final difference map (e Å^{-1})	1.42

[a] $R = \Sigma\|\|F_o| - |F_c\|\|/\Sigma|F_o|$.

COMPAQ PL4/50 computer using the MolEN program package [11].

RESULTS AND DISCUSSION

$[Ag_4(dmit)_3]_n^{2n-}$ is shown in Fig. 1. Selected bond lengths and bond angles for the complex are given in Tables 2 and 3, respectively. It is revealed that **1** consists of $[Ag_4(dmit)_3]$ repeating units and the dmit acts as a bridging and chelating ligand with coordination to silver atoms. In the repeating unit, the four silver atoms are in a distorted tetrahedral arrangement, and the tetrahedral metal frame is held together by three dmit ligands. It is noted that in **1** the sulfur atom of the thiocarbonyl group is able to coordinate and it does so by Ag(1) and Ag(4) atoms to form a two-dimensional structure polymer. In the anion of **1**, Ag(2) and Ag(3) have a distorted trigonal-planar sulfur coordination, with S–Ag–S angles of 89.2(2) to

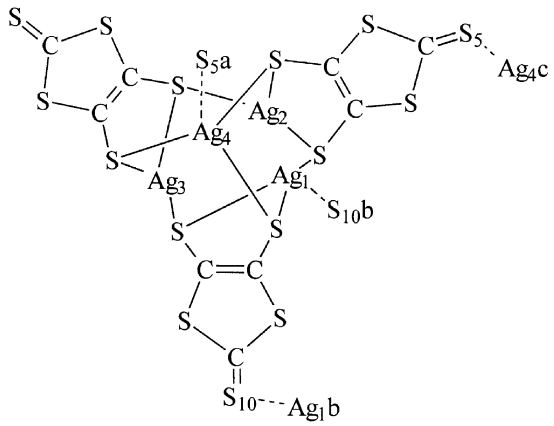

Fig. 1. X-ray structure of **1** with atom numbering scheme (dashed lines indicate S · · · S contacts shorter than 3.7 Å).

Table 2. Selected bond lengths (Å)

Atom	Atom	Distance	Atom	Atom	Distance
Ag(1)	S(1)	2.501(3)	S(8)	C(4)	1.76(1)
Ag(1)	S(6)	2.576(4)	S(8)	C(6)	1.70(1)
Ag(1)	S(7)	2.557(4)	S(9)	C(5)	1.75(1)
Ag(1)	S(10b)	2.797(1)	S(9)	C(6)	1.69(2)
Ag(2)	S(2)	2.552(4)	S(10)	C(6)	1.68(1)
Ag(2)	S(11)	2.417(3)	S(11)	C(7)	1.72(1)
Ag(3)	S(6)	2.439(2)	S(12)	C(8)	1.74(2)
Ag(3)	S(11)	2.600(4)	S(13)	C(7)	1.76(2)
Ag(3)	S(12)	2.527(4)	S(13)	C(9)	1.71(2)
Ag(4)	S(2)	2.610(4)	S(14)	C(8)	1.75(1)
Ag(4)	S(7)	2.516(2)	S(14)	C(9)	1.70(1)
Ag(4)	S(12)	2.586(4)	S(15)	C(9)	1.67(1)
Ag(4)	S(5a)	2.733(1)	C(1)	C(2)	1.37(2)
S(1)	C(1)	1.74(1)	C(4)	C(5)	1.32(2)
S(2)	C(2)	1.73(1)	C(7)	C(8)	1.35(2)
S(3)	C(1)	1.74(1)	Ag(1)	Ag(2)	3.027(2)
S(3)	C(3)	1.72(1)	Ag(1)	Ag(3)	3.305(2)
S(4)	C(2)	1.76(1)	Ag(1)	Ag(4)	3.187(1)
S(4)	C(3)	1.72(1)	Ag(2)	Ag(3)	2.914(2)
S(5)	C(3)	1.65(1)	Ag(2)	Ag(4)	3.053(2)
S(6)	C(4)	1.76(2)	Ag(3)	Ag(4)	3.218(1)
S(7)	C(5)	1.73(2)			
S(3)	S(2c)	3.605(1)	S(8)	S(13d)	3.696(1)
S(3)	S(4c)	3.552(1)	S(8)	S(15d)	3.644(1)
S(5)	S(12c)	3.656(2)	S(11)	S(11d)	3.653(3)

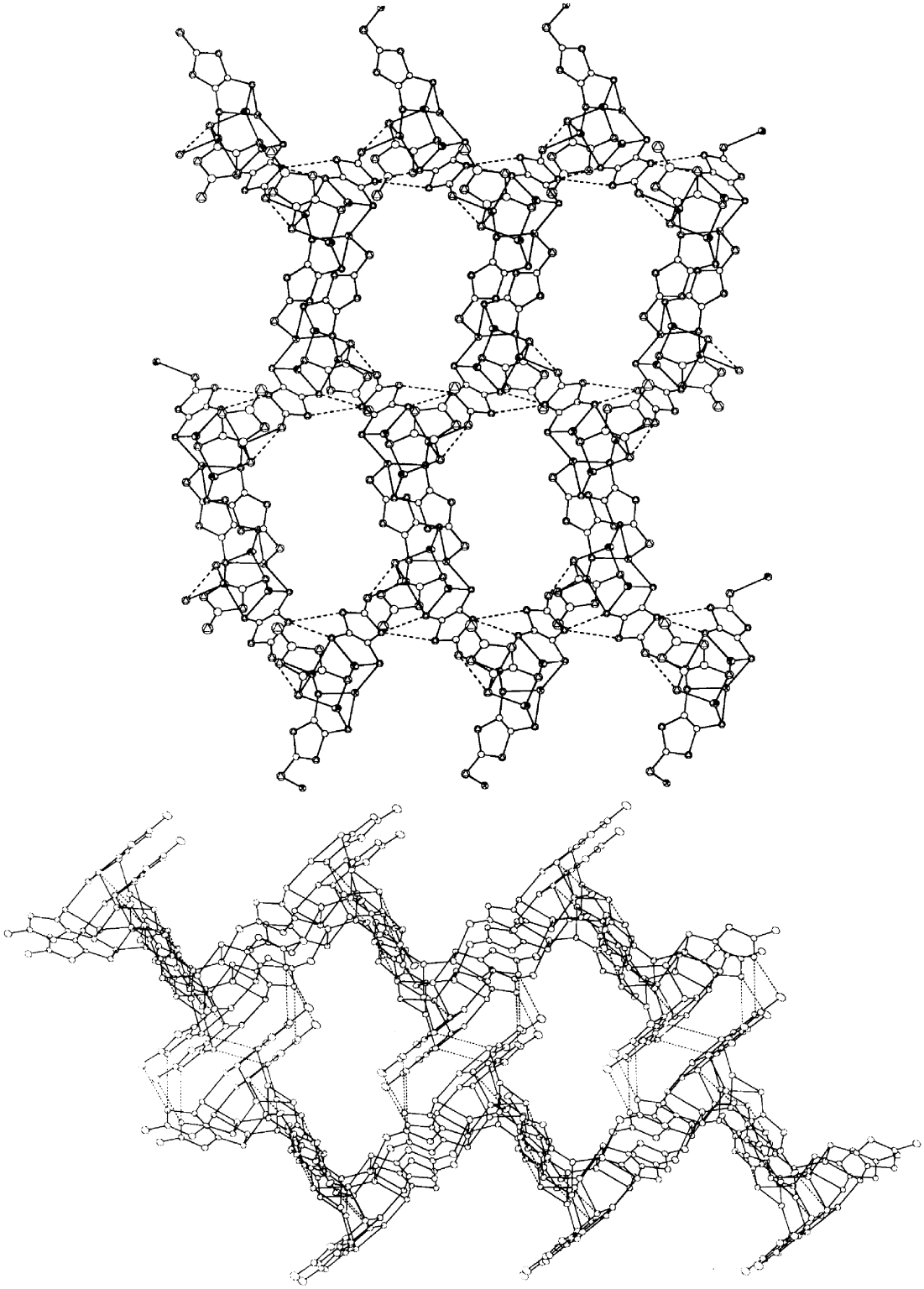

Fig. 2. (a) The two-dimensional sheet structure of **1** viewed down the *a* axis; (b) the crystal packing of **1** viewed down the *b* axis (the Et_4N^+ cations and DMF solvent molecules are omitted for clarity, dashed lines indicate S · · · S contacts shorter than 3.7 Å).

147.2(1)° and 87.4(1) to 146.4(1)°, whereas Ag(1) and Ag(4) have a distorted tetrahedral sulfur coordination, with S–Ag–S angles of 88.1(1) to 133.4(1)° and 86.8(1) to 121.00(9)°, respectively. The Ag–S bond distances in the repeating unit of **1** range from 2.417(3) to 2.600(4) Å, and are comparable to those in $[Ph_4N]_2[Ag_4(SCH_2C_6H_4\ CH_2S)_3]\cdot 6MeOH$ [12], whereas those between the two repeating units (Ag(1)–S(10b), 2.797(1) Å, Ag(4)–S(5a), 2.733(1) Å) are relatively longer, but shorter than the related Ag–S bond length of 2.812(4) and 2.841(1)–2.920(1) Å reported in the literature [13,14]. In the three dmit ligands, the bond-lengths of S–C bonds have an average value of 1.72(2) Å, and the bond lengths of C–C bonds have an average value of 1.34(8) Å, which are similar to those of other dmit complexes.

The S · · · S contacts in **1** exist both intra- and inter-molecularly. The intramolecular S · · · S contacts are 3.605(1), 3.552(1) and 3.656(2) Å, respectively. Also, there are three different intermolecular S · · · S contacts of 3.644(1), 3.653(3) and 3.696(1) Å between the two-dimensional polymeric anions (as shown in Fig. 2), through which the anions form a three-dimensional supramolecular network (as shown in Fig. 3).

Electronic absorption spectra of the complex have been obtained. The UV–visible spectrum of the complex in DMF has a characteristic absorption band at 450 nm ($\varepsilon = 2.99\times10^4\,dm^3\,cm^{-1}\,mol^{-1}$). The absorption band is ascribed to the π–π^* transition of the dmit ligand. The similar absorption bands of the π–π^* transition are also observed in the $[Au(dmit)_2]^-$ complex (468 nm in acetonitrile) [15], while the bands for Na_2dmit (514 nm in methanol), $[Zn(dmit)_2]^{2-}$ (530 nm in acetonitrile) and $[Cu(dmit)_2]^{2-}$ (540 nm in acetonitrile) [16] occur at somewhat longer wavelengths.

Table 3. Selected bond angles (°)

Atom	Atom	Atom	Angle	Atom	Atom	Atom	Angle
S(1)	Ag(1)	S(6)	132.9(2)	Ag(2)	S(11)	C(7)	101.1(5)
S(1)	Ag(1)	S(7)	133.4(1)	Ag(3)	S(11)	C(7)	96.2(4)
S(6)	Ag(1)	S(7)	88.1(1)	Ag(3)	S(12)	Ag(4)	78.0(2)
S(1)	Ag(1)	S(10b)	97.6(2)	Ag(3)	S(12)	C(8)	97.7(5)
S(6)	Ag(1)	S(10b)	98.7(1)	Ag(4)	S(12)	C(8)	99.4(64
S(7)	Ag(1)	S(10b)	96.1(1)	C(7)	S(13)	C(9)	98.8(6)
S(1)	Ag(2)	S(2)	89.2(2)	C(8)	S(14)	C(9)	98.3(7)
S(1)	Ag(2)	S(11)	147.2(1)	S(1)	C(1)	S(3)	115.9(6)
S(2)	Ag(2)	S(11)	123.1(1)	S(1)	C(1)	C(2)	128(1)
S(6)	Ag(3)	S(11)	146.4(1)	S(3)	C(1)	C(2)	117(2)
S(6)	Ag(3)	S(12)	122.4(2)	S(2)	C(2)	S(4)	116.8(7)
S(11)	Ag(3)	S(12)	87.4(1)	S(2)	C(2)	C(1)	130(2)
S(2)	Ag(4)	S(7)	117.8(2)	S(4)	C(2)	C(1)	113(1)
S(2)	Ag(4)	S(12)	121.00(9)	S(3)	C(3)	S(4)	111.5(8)
S(7)	Ag(4)	S(12)	117.4(1)	S(3)	C(3)	S(5)	124.4(6)
S(2)	Ag(4)	S(5a)	96.2(2)	S(4)	C(3)	S(5)	124.0(8)
S(7)	Ag(4)	S(5a)	106.8(1)	S(6)	C(4)	S(8)	114.1(7)
S(12)	Ag(4)	S(5a)	86.8(1)	S(6)	C(4)	C(5)	130(2)
Ag(1)	S(1)	Ag(2)	74.9(1)	S(8)	C(4)	C(5)	115.8(9)
Ag(1)	S(1)	C(1)	101.6(4)	S(7)	C(5)	S(9)	114.5(7)
Ag(2)	S(1)	C(1)	97.6(3)	S(7)	C(5)	C(4)	130(1)
Ag(2)	S(2)	Ag(4)	72.5(2)	S(9)	C(S)	C(4)	115(2)
Ag(2)	S(2)	C(2)	95.4(5)	S(8)	C(6)	S(9)	112.9(7)
Ag(4)	S(2)	C(2)	113.2(4)	S(8)	C(6)	S(10)	123.8(9)
C(1)	S(3)	C(3)	98.8(6)	S(9)	C(6)	S(10)	123.3(7)
C(2)	S(4)	C(3)	99.7(7)	S(11)	C(7)	S(13)	116.3(7)
Ag(1)	S(6)	Ag(3)	82.4(2)	S(11)	C(7)	C(8)	129.7(9)
Ag(1)	S(6)	C(4)	94.2(5)	S(13)	C(7)	C(8)	114(1)
Ag(3)	S(6)	C(4)	104.9(3)	S(12)	C(8)	S(14)	115.2(8)
Ag(1)	S(7)	Ag(4)	77.82(8)	S(12)	C(8)	C(7)	129(2)
Ag(1)	S(7)	C(5)	95.1(4)	S(14)	C(8)	C(7)	116.0(8)
Ag(4)	S(7)	C(5)	107.9(4)	S(13)	C(9)	S(14)	112.9(7)
C(4)	S(8)	C(6)	97.7(6)	S(13)	C(9)	S(15)	123.8(8)
C(5)	S(9)	C(6)	98.5(6)	S(14)	C(9)	S(15)	123(2)
Ag(2)	S(11)	Ag(3)	70.91(7)				

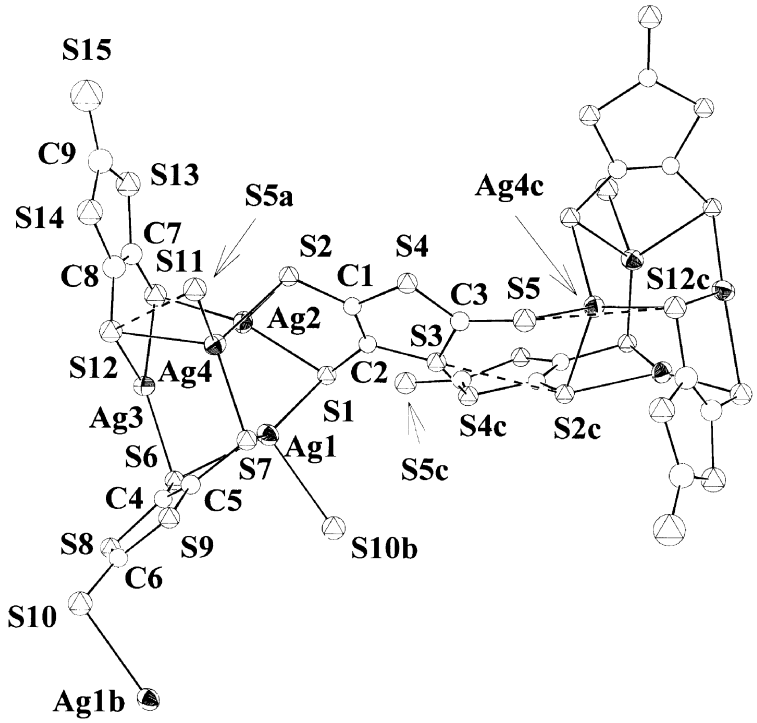

Fig. 3.

Acknowledgements—This research was supported by the State Key Laboratory of Structural Chemistry, Fujian Institute of Research on the Structure of Matter, the Chinese Academy of Sciences, the National Science Foundation of China, and Science Foundation of CAS and Fujian Province.

REFERENCES

1. Lehn, J.-M., *Angew. Chem. Int. Ed. Engl.*, 1990, **29,** 1304.
2. Lehn, J.-M., *Supramolecular Chemistry*. VCH, Weinheim, 1995.
3. Cassoux, P., Valade, L., Kobayashi, H., Kobayashi, A., Lark, R. A. and Underhill, A. E., *Coord. Chem. Rev.*, 1991, **110,** 115.
4. Olk, R. M., Olk, B., Dietzsch, K. R. and Hoyer, E., *Coord. Chem. Rev.*, 1992, **117,** 99.
5. Svenstrup, N. and Becher, J., Synthesis, 1995, 215.
6. Coomber, A. T., Beljonne, D., Friend, R. H., Bredas, J. L., Charlton, A., Robertson, N., Underhill, A. E. and Kurmoo, M., *P. Day. Nature*, 1996, **380,** 144.
7. Steimecke, G., Sieler, H.-J., Kirmse, R. and Hoyer, E., *Phosphorus and Sulfur*, 1979, **7,** 49.
8. Walker, N. G. and Stuart, D., *Acta Crystallogr. Sect. A*, 1983, **39,** 158.
9. Main, P., MULTAN, 1983, Version 3.1.0, Program for the Automatic Solution of Crystal Structures from X-ray Diffraction Data by Multiple Starting Point Tangent Formula. University of York, England.
10. Cromer, D. T. and Waber, J. T., *International Tables for X-ray Crystallography*, Vol. IV, Tables 2.2A and 2.3.1. Kynoch Press, Birmingham, 1974 (present distributor Kluwer Academic Publishers, Dordrecht).
11. MolEN, *An Interactive Structure Solution Procedure*. Enraf–Nonius, Delft.
12. Henkel, G. and Bets, P., Krebs, B., *Angew. Chem. Int. Ed. Engl.*, 1987, **26,** 145.
13. Du, S.-W. and Wu, X.-T., *J. Coord. Chem.*, 1993, **30,** 183.
14. Dai, J., Kuroda-Sowa, T., Munakata, M., Maekawa, M., Suenaga, Y. and Ohno, Y., J. Chem. Soc. Dalton Trans., 1997, 2363.
15. Matsubayashi, G. and Yokozawa, A., J. Chem. Soc. Dalton Trans., 1990, 3535.
16. Matsubayashi, G., Takahash, K. and Tanaka, T., J. Chem. Soc. Dalton Trans., 1988, 967.

Pergamon

Polyhedron Vol. 17, Nos. 25, 26, pp. 4525–4533, 1998
© 1998 Elsevier Science Ltd
All rights reserved. Printed in Great Britain
PII: S0277–5387(98)00259–9
0277–5387/98 $19.00+0.00

Metal(II)-promoted hydrolysis of pyridine-2-carbonitrile to pyridine-2-carboxylic acid. The structure of [Cu(pyridine-2-carboxylate)$_2$]·2H$_2$O

P. Segl'a,*[a] M. Jamnický,[b] M. Koman,[a] J. Šima[a] and T. Glowiak[c]

[a]Department of Inorganic Chemistry, Slovak Technical University, 812 37 Bratislava, Slovak Republic

[b]Department of Ceramics, Glass and Cements, Slovak Technical University, 812 37 Bratislava, Slovak Republic

[c]Institute of Chemistry, University of Wrocław, F. Joliot-Curie 14, 50 383 Wrocław, Poland

(Received 3 March 1998; accepted 24 June 1998)

Abstract—Pyridine-2-carbonitrile (2-CNpy) undergoes Cu(II) or Co(II)-promoted hydrolysis to pyridine-2-carboxamide (piaH) and/or pyridine-2-carboxylic acid (pycH). The pathway of pycH formation depends on the presence of 2-amino-2-hydroxymethyl-1,3-propanediol (AL^1) and on the central atom. In the absence of AL^1, Co(II) or Cu(II) ions mediate piaH formation under mild reaction conditions in the first hydrolytic step. Cu(II) ions assist in piaH transformation to pycH by subsequent reflux. In the presence of AL^1 and Co(II), a Co(II) complex containing pyoxaL^1 (2-(2-pyridinyl)-4,4-bis(hydroxymethyl)-2-oxazoline) is formed in the first stage; subsequent decomposition of pyoxaL^1 under the reflux yields pycH. Under similar conditions, no solid Cu(II) complex with pyoxaL^1 can be isolated, but a Cu(II) complex with coordinated pyc$^-$ anions precipitates from the reaction mixture. The synthesis, spectral and magnetic properties of the complexes [Co(H$_2$O)$_2$(piaH)$_2$]Cl$_2$, [Co(H$_2$O)$_2$(pyc)$_2$]·2H$_2$O, [Cu(H$_2$O)$_2$(piaH)$_2$]Cl$_2$, [Cu(pyc)$_2$] and [Cu(pyc)$_2$]·2H$_2$O, including the structure determination of the latter one, are described. © 1998 Elsevier Science Ltd. All rights reserved

Keywords: pyridine-2-carbonitrile; hydrolysis; copper(II) complexes; cobalt(II) complexes; crystal structure.

INTRODUCTION

Organic nitriles can coordinate to transition metal ions via their nitrile group (three bonding modes have been described so far; for a review see [1]) or by another donor atom of the organic moiety. In the chemistry of pyridinecarbonitriles, the former mode is typical for pyridine-2-carbonitrile (further denoted as 2-CNpy) while the latter for pyridine-3-carbonitrile and pyridine-4-carbonitrile. It should be pointed out, however, that the coordination of 2-CNpy through the pyridine nitrogen cannot be excluded, at least for kinetically inert complexes [2].

Either mode of 2-CNpy coordination to electron-withdrawing transition metal ions results in enhanced electrophilicity of the nitrile carbon, thus making it susceptible to nucleophiles such as OH$^-$, H$_2$O, ROH, and R–NH$_2$ [1,3].

As it has previously been observed [4–7], the reaction of 2-CNpy with some metal(II) salts in aqueous or alcoholic solutions leads to formation of solid complexes containing pyridine-2-carboxamide (piaH) and *O*-alkylpyridine-2-carboximidate (*O*-Rpii), respectively. It is worth mentioning that a similar metal(II) promoted hydrolysis of the nitrile group to amide was observed in the systems containing 2-carbonitrile-1,10-phenanthroline instead of 2-CNpy [8] for which, based on a kinetic analysis, the authors showed that its mechanism involved an external attack of a non-coordinated OH$^-$ ion to the nitrile group of coordinated ligand.

* Author to whom correspondence should be addressed.

In the presence of amino alcohols (AL^1–AL^3 in Scheme 1) and 2-CNpy, Ni(II) salts yield solid complexes containing 2-pyridinyl-2-oxazolines (pyoxaL^1-pyoxaL^3) [9] under mild reaction conditions both in water and alcohols. However, Cu(II) and most Co(II) complexes containing oxazolines could be prepared only from ethanolic solution. For example, solid complexes $[CoX_2(pyoxaL^1)_2]$ (X = Cl, Br or NCS) and $[CuX(pyoxaL^1)_2]X \cdot 0.5H_2O$ (X = Cl or Br) have been prepared by the reaction of 2-CNpy with AL^1 in ethanolic solutions of the corresponding Co(II) and Cu(II) salts. Also, solid complexes containing different hydrolytic products of 2-CNpy [10] have been isolated from aqueous solutions. The complexes were not, however, characterized in more detail.

In this paper the results on the hydrolytic reactions of 2-CNpy in the presence or absence of AL^1 in aqueous solutions of copper(II) and cobalt(II) salts are given. The course of the reactions was monitored by a solution IR study. Moreover, the synthesis and characterization of the solid pyc^- or piaH-containing complexes isolated from the above mentioned aqueous solutions are also described. The X-ray molecular and crystal structure of one of the products, $[Cu(pyc)_2] \cdot 2H_2O$, is presented. The paper summarizes results obtained within the study of metal(II)-facilitated hydrolysis of 2-CNpy and offers general conclusions relating to this field.

2. EXPERIMENTAL

2.1. *Chemical reagents*

All the chemicals used were of reagent grade. Solid pyridine-2-carbonitrile (2-CNpy) was purified by distillation under reduced pressure. 2-Amino-2-hydroxymethyl-1,3-propanediol (AL^1) was used without further purification. Water was double distilled prior to use. The other chemicals were used as received.

2.2. *Analysis and physical measurements*

Copper, cobalt and nickel were determined by EDTA titration; carbon, hydrogen and nitrogen by microanalytical methods (Carlo Erba Instruments EA 1108) with maximum deviations (in %): M, ±0.2; C, ±0.4; H, ±0.3; and N, ±0.2. The water content in hydrates was determined by thermogravimetry. The yields of products are related to the metal contents in reacting mixtures.

Magnetic moments were measured with a Gouy balance for the powdered solid at 293 K. Electronic spectra of the powdered samples in nujol mulls and diffuse reflectance spectra in MgO were recorded at room temperature on a Specord M 40 and a Magna 750 spectrophotometer, respectively. Magnetic moments, electronic and IR spectral data of solid complexes are gathered in Table 1.

Measurements of IR spectra (in solid state and aqueous solution) as well as pH measurements of the aqueous solutions are described elsewhere [9].

2.3. *X-ray structure determination*

Data collection and cell refinement were carried out using KUMA (1991) KM4 diffractometer software [11]. Intensity data were corrected for Lorentz and polarization effects. The structure was solved by standard heavy atom procedures with SHELX86 [12], and subsequent Fourier synthesis using SHELXL93 [13]. Anisotropic thermal parameters were refined for all non-hydrogen atoms. Geometrical analysis was performed using SHELXL93 [13]. The structures were drawn using ORTEP [14]. The final refined parameters are summarized in Table 2. Selected bond lengths and angles are collected in Table 3.

Supplementary material including non-hydrogen and hydrogen atomic coordinates ($\times 10^4$), anisotropic displacement parameters for non-hydrogen atoms ($Å^2 \times 10^3$) have been deposited at the Cambridge Crystallographic Data Centre. Observed and calculated structural factors are available from P. S.

2.4. *Preparation of complexes*

Copper(II) complexes

$[Cu(H_2O)_2(piaH)_2]Cl_2$ (**I**) and $[Cu(pyc)_2]$ (**II**). 50 cm^3

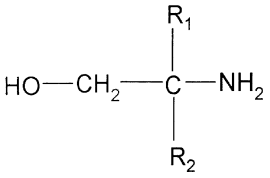

AL^1: $R_1 = R_2 = CH_2OH$
AL^2: $R_1 = CH_2OH$, $R_2 = CH_3$
AL^3: $R_1 = R_2 = CH_3$

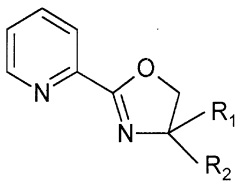

pyoxaL^1: $R_1 = R_2 = CH_2OH$
pyoxaL^2: $R_1 = CH_2OH$, $R_2 = CH_3$
pyoxaL^3: $R_1 = R_2 = CH_3$

Scheme 1. Structures and abbreviations of ligands.

Table 1. Magnetic moments, electronic spectral data, characteristic IR bands and stereochemistry of solid complexes containing pyridine-2-carboxamide (piaH) or pyridine-2-carboxylic acid (pycH)

No.	Complex	μ_{ef} (B.M.)	Electronic spectra[a], maxima of absorption band (cm^{-1})			Infrared spectra[a]		Stereo-chemistry[c]
						ν_a(CXO)[b]	ν_s(CXO)[b]	
I	$[Cu(H_2O)_2(piaH)_2]Cl_2$	1.90		15100		1663vs	1440s	O
II	$[Cu(pyc)_2]$	1.98		16800br	27000sh	1637s	1343s	S
III	$[Cu(pyc)_2]\cdot 2H_2O$	1.96		17000br	27000sh	1644s	1348s	S
IV	$[Co(H_2O)_2(piaH)_2]Cl_2$	4.90	8850		20500 21500	1657vs	1434s	O
V	$[Co(H_2O)_2(pyc)_2]\cdot 2H_2O$	4.79	8700		18800 19800 22100	1622s	1383s	O

[a]vs, very strong; s, strong; sh, shoulder; br, broad.
[b]For complexes **I** and **IV** is X = N and for complexes **II**, **III** and **V** is X = O.
[c]O, octahedral; S, square-planar.

Table 2. Crystal data and structure refinement for $[Cu(pyc)_2]\cdot 2H_2O$ (complex **III**)

Crystal data	
Empirical formula	$C_{12}H_{12}CuN_2O_6$
Formula weight	343.78
Crystal size (mm)	$0.50\times 0.30\times 0.20$
Crystal system	triclinic
Space group	$P\bar{1}$
Z	1
Unit cell dimensions	$a = 5.172(1)$ Å, $\alpha = 74.92(3)^\circ$ $b = 7.654(2)$ Å, $\beta = 84.22(3)^\circ$ $c = 9.175(2)$ Å, $\gamma = 71.69(3)^\circ$
Volume (Å^3)	332.9(1)
Density (calc.) ($Mg\,m^{-3}$)	1.715
$F(000)$	175
Linear absorption coefficient (μ) (mm^{-1})	2.622
Data collection	
Diffractometer	KUMA KM 4
Radiation type	Cu Kα $\lambda = 1.54180$ Å
Temperature (K)	293(2)
Θ range for data collection (°)	4.99–81.34
Index ranges	h −6–3, k −9–9, l −11–11
Number of data collected	2408
Independent reflections	1362 ($R_{int} = 0.0525$)
Absorption correction	no
Solution and refinement	
Refinement method	full-matrix, least-squares on F
Data/restraints/parameters	1307/0/98
Goodness-of-fit on F^2	0.897
Final R indices ($I > 2\sigma(I)$)	$R_1 = 0.0429$, $wR_2 = 0.1011$
R indices (all data)	$R_1 = 0.0488$, $wR_2 = 0.1279$
Extinction coefficient	0.019(4)
Largest diff. peak and hole (e Å^{-3})	0.910/−0.675

of an aqueous solution of copper(II) chloride dihydrate (10 mmol) was mixed with 2-CNpy (20 or 40 mmol). The resulting solution was left to slowly evaporate at room temperature. Pale blue crystals of **I** started to crystallize from the reaction solution after several hours. The crystals were filtered off, washed with ethanol and finally dried *in vacuo* (yield 80%).

Complex **II** was deposited as a blue solid when the

Table 3. Selected bond lengths (Å) and angles (°) for $[Cu(pyc)_2] \cdot 2H_2O$ (complex **III**)

Cu–O(1)	1.941(2)	Cu–N	1.979(2)
O(1)–C(6)	1.289(2)	O(2)–C(6)	1.239(3)
N–C(1)	1.343(3)	N–C(5)	1.340(3)
C(1)–C(2)	1.383(3)	C(1)–C(6)	1.510(2)
C(2)–C(3)	1.394(3)	C(3)–C(4)	1.374(4)
C(4)–C(5)	1.389(4)		
O(1)–Cu–N	82.9(1)	O(1)#1–Cu–N	97.1(1)
C(6)–O(1)–Cu	115.9(1)	C(1)–N–C(5)	119.6(2)
C(1)–N–Cu	112.2(1)	C(5)–N–Cu	128.1(2)
N–C(1)–C(2)	122.3(2)	N–C(1)–C(6)	114.6(2)
C(2)–C(1)–C(6)	123.1(2)	C(1)–C(2)–C(3)	118.1(2)
C(4)–C(3)–C(2)	119.3(2)	C(3)–C(4)–C(5)	119.7(2)
N–C(5)–C(4)	120.9(2)	O(2)–C(6)–O(1)	126.3(2)
O(2)–C(6)–C(1)	119.8(2)	O(1)–C(6)–C(1)	113.9(2)

Symmetry transformations used to generate equivalent atoms: #1 $-x, -y, -z$.

above reaction mixture was refluxed for up to 20 h. The crystals were separated from the cool solution by filtration, washed with ethanol and dried *in vacuo* (yield 95%).

In addition to the above method, the complex $[Cu(H_2O)_2(piaH)_2]Cl_2$ was prepared directly from piaH and $CuCl_2$ [15]. No hydrolysis of piaH to pycH was also observed.

$[Cu(pyc)_2] \cdot 2H_2O$ (**III**). Method A. 20 mmol of 2-amino-1,3-propanediol (AL^1) was dissolved in 50 cm^3 of an aqueous solution of $CuCl_2$ (10 mmol). 2-CNpy (20 mmol) was then added to the system and the resulting solution was left to slowly evaporate at room temperature. A mixture of solid complexes containing piaH or pyc^- ligands was deposited after several days. Upon adjusting pH of the above resulting solution to 3.5, complex **I** was precipitated within 15 min. When an aqueous solution of 2-CNpy, AL^1 and $CuCl_2$ was refluxed for 32 h and then cooled down, the only compound, formed in 95% yield, was pure blue violet solid complex **III**. A well-shaped crystal of **III** was used for structure determination.

Method B. An aqueous solution (50 cm^3) of 10 mmol of $[CuCl(pyoxaL^1)_2]Cl \cdot 0.5H_2O$ [10] was left to slowly evaporate at room temperature. From the concentrated solution, complex **III** deposited upon several days standing (yield 95%).

Cobalt(II) complexes

$[Co(H_2O)_2(piaH)_2]Cl_2$ (**IV**) *and* $[Co(H_2O)_2(pyc)_2] \cdot 2H_2O$ (**V**). When 50 cm^3 of an aqueous solution of cobalt(II) chloride hexahydrate (10 mmol) was mixed with 2-CNpy (20 or 40 mmol), orange complex **IV** started to crystallize after several days. The crystals were filtered off, washed with ethanol and finally dried *in vacuo* (yield 80%). Contrary to its Cu(II) analogue (complex **I**), complex **IV** did not convert to the pyc-ligand containing complex even after 20 h reflux of the above reaction mixture, i.e. pure complex **IV** was isolated again as the only product in 75% yield. Compound **IV** was also prepared directly from $CoCl_2$ and piaH [15, 16] with no piaH hydrolysis observed.

The complex $[Co(H_2O)_2(pyc)_2] \cdot 2H_2O$ (**V**) was formed by 30 h reflux of a 50 cm^3 aqueous solution of 2-CNpy (20 mmol), AL^1 (20 mmol) and $CoCl_2$ (10 mmol). Orange crystals of **V** were filtered off and washed with ethanol (yield 80%). Complex **V** can also be synthesized by 30 h reflux of 10 mmol $[CoCl_2(pyoxaL^1)_2]$ [10] in water in a similar way as complex **III** in about 85% yield.

3. RESULTS AND DISCUSSION

3.1. *Stereochemistry of solid complexes*

The values of magnetic moments, electronic and IR spectral data for the studied complexes are listed in Table 1. The spectral and magnetic properties of complexes $[M(H_2O)_2(piaH)_2]Cl_2$ (**I** and **IV**) are identical to those prepared directly from piaH [15, 16] and consistent with their monomeric, hexacoordinated structure with two *N*,*O*-chelating piaH ligands and two water molecules present in the primary coordination sphere. The mode of piaH coordination has been proved by a single-crystal X-ray analysis of complex **I** [17].

The IR spectra of complex **III** show broad bands located in the region from 3100 to 3600 cm^{-1} attributable to the water molecules. Both copper(II) complexes **II** and **III** exhibit (Table 1) a band of the asymmetric stretch $\nu_a(COO^-)$ at 1637 and 1644 cm^{-1} together with a band of the symmetric stretch $\nu_s(COO^-)$ at 1343 and 1348 cm^{-1}, respectively. The

difference $\nu_a(COO^-)-\nu_s(COO^-)$, being 294 and 296 cm^{-1} for complexes **II** and **III**, respectively, can be taken as a proof of unidentate coordination of the carboxylato group to the central atom [18]. The IR spectra of all complexes **I**–**V** provide an evidence of organic ligands coordination through the 2-pyridinyl ring nitrogen [19].

In general, room temperature magnetic measurements and spectral data do not provide sufficient information for a definite determination of the stereochemistry of Cu(II) complexes [20] and this relates also to complexes **II** and **III** previously prepared from pycH [21, 22, 23]. To eliminate the question on stereochemistry of **II** and **III**, an X-ray single-crystal analysis of complex **III** (the one with better evolved crystals) was performed.

The spectral and magnetic properties of $[Co(pyc)_2(H_2O)_2]\cdot 2H_2O$ (**V**) are identical to those given in [24] for a compound of the same composition synthesized directly with pycH. Moreover, the X-ray crystal study of **V** [25, 26] has revealed that the primary coordination sphere of this monomeric octahedral complex consists of two anions of pyridine-2-carboxylic acid (as *N*,*O*-coordinated chelates) and two molecules of water.

3.2. *Crystal structure description of complex* **III**

The crystal structure of $[Cu(pyc)_2]\cdot 2H_2O$ (**III**) consists of discrete $Cu(pyc)_2$ molecules and water molecules occupying lattice sites (Fig. 1). The $Cu(pyc)_2$ molecule, as a whole, is nearly planar. The Cu(II) atom has centrosymmetric square-planar coordination with *trans* positioned oxygen and nitrogen donor atoms of two *N*,*O*-chelating pyc^- ligands. The interatomic distances Cu–O(1) and Cu–N are 1.941(2) and 1.979(2) Å, respectively, and are consistent with the values reported for other copper(II) complexes [27]. The packing of $Cu(pyc)_2$ moieties in the crystal structure is shown in Fig. 1. The molecules $Cu(pyc)_2$ form parallel planes. There are weak interactions between copper atoms of one plane and O(2) atoms of neighboring planes (Cu · · · O(2aa) = 2.814(4) Å). The molecules of water are not coordinated to the central atom, they are bonded to O(2) atoms of pyc^- ligands by hydrogen bonds (O(2) · · · H(2) = 1.954(5) Å; O(3)–H(2) · · · O(2) = 172.1(6)°).

The similarity of the IR spectra for **II** and **III** (Table 1) led us to the conclusion of the square planar coordination of the central Cu(II) atom just like in **II**.

3.3. *IR spectra of aqueous solutions*

Owing to the known characteristic IR spectral features of 2-CNpy and the products of its transformation, the course of the reactions occurring in the investigated systems at various conditions can cosily be followed. The assignment of solid state and solution IR spectral bands in Fig. 2 to free and coordinated ligands is supported by the literature and our previous data [9,10,18].

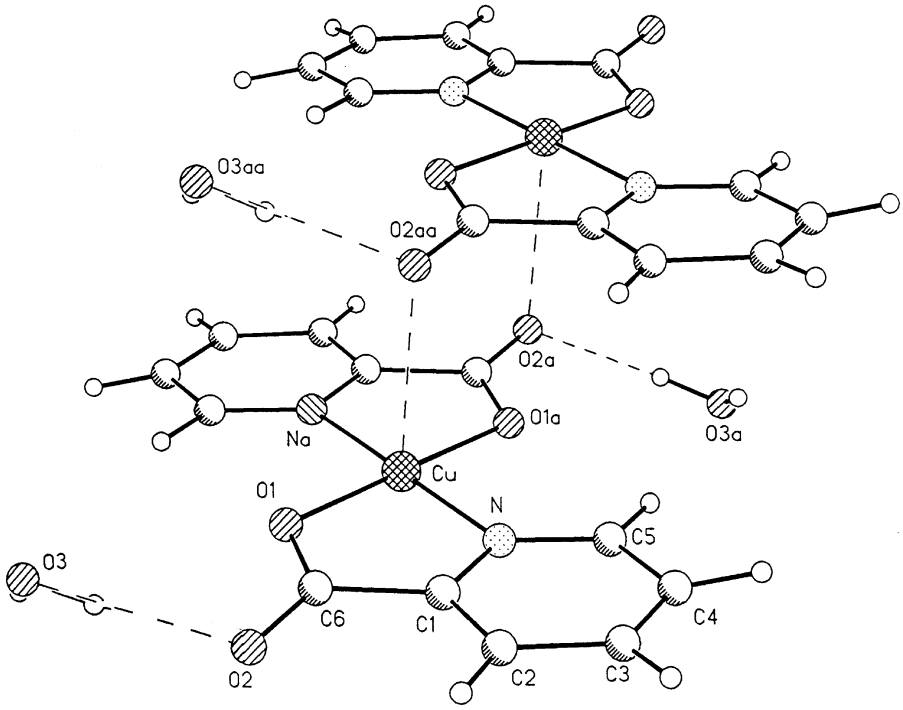

Fig. 1. Packing of $Cu(pyc)_2$ and H_2O in the crystal structure of $[Cu(pyc)_2]\cdot 2H_2O$ (complex **III**).

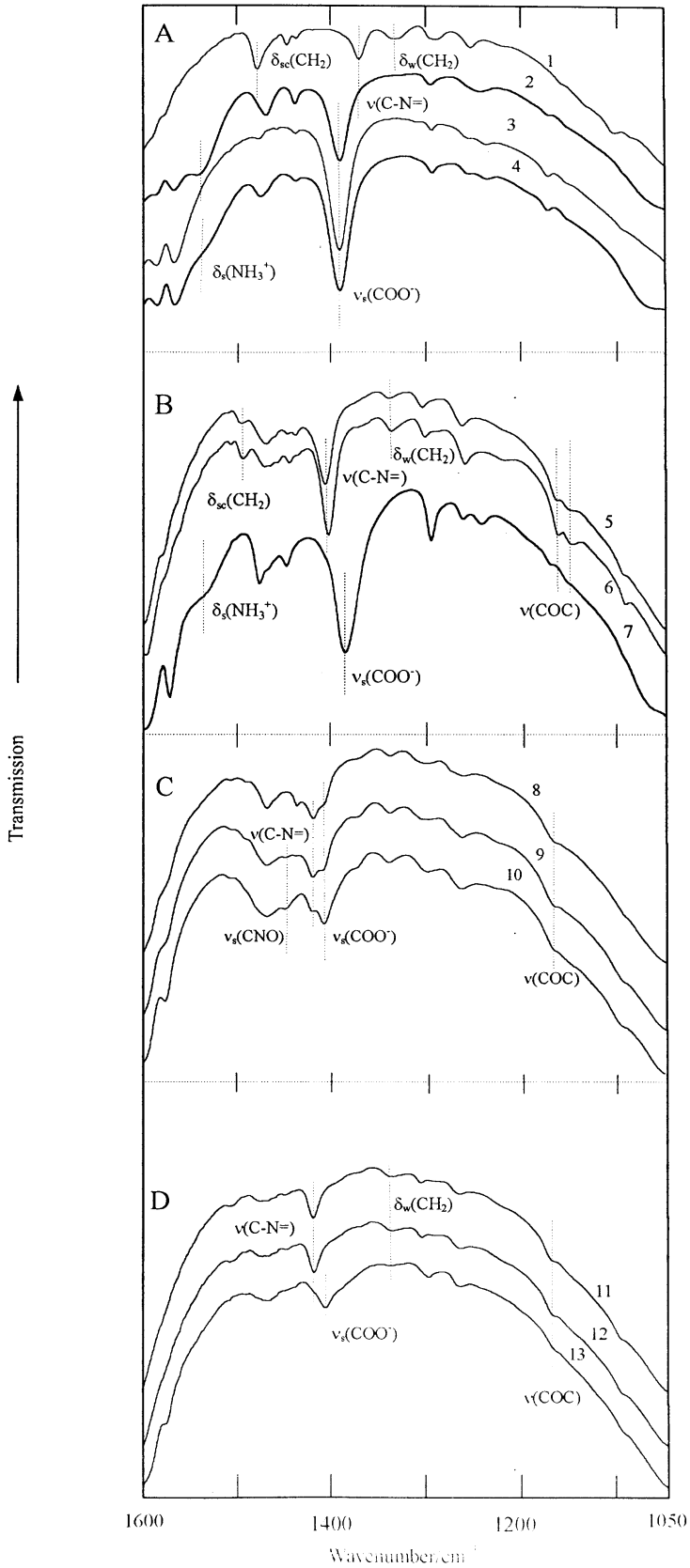

Fig. 2. IR spectra of aqueous solutions. Numbers in the figure represent spectrum numbers in Table 4. For assignment and denotation of vibrations see Table 1 and our papers [9, 10].

A kinetic study of the reaction of 2-CNpy with AL^1 in aqueous solutions of Ni(II) by means of electronic spectroscopy has been presented partly in [28]. Some new mechanistic information of this reaction was obtained from a solution IR study [9]. The IR spectra of pyoxaL^1 and its solid complexes of Ni(II), Co(II) and Cu(II) have been published, too [9, 10].

In this paper the results on the hydrolytic reactions of 2-CNpy in the presence or absence of AL^1 in aqueous solutions of copper(II) and cobalt(II) salts are given. Changes in solution IR spectra in the region from 1050 to 1600 cm^{-1} are for some of the studied systems illustrated in Fig. 2. The curves 1, 3, 5, 6, and 8–13 represent the spectra of solutions prepared at room temperature, thick solid curves 2, 4 and 7 were obtained after several-hours reflux of the solutions. The composition of the starting solutions, the time and temperature used in preparing the measured solutions, as well as the dominant components observed in the IR spectra are given in Table 4.

The spectra of pyoxaL^1 itself and its decomposition products in aqueous solution are illustrated in Fig. 2(A) [9]. Uncoordinated pyoxaL^1 (curve 1) is quite stable at room temperature for a long time. Under reflux it undergoes, however, a gradual hydrolysis to pycH, AL^1 and its protonated form AL^1H (spectrum 2). Curve 3 represents a solution IR spectrum of uncoordinated pycH, curve 4 relates to a aqueous solution of the 1:1 molar mixture of pycH and AL^1.

The room temperature IR spectra of aqueous solutions of 2-CNpy and AL^1 in the absence of metal(II) salts [9] showed that the rate of pyoxaL^1 formation is very low in comparison with that observed in the metal(II) salts containing systems.

Formation of the Co(II) complexes was indicated by significant spectral changes (Fig. 2(B)). Moreover, the IR spectrum of none of the systems related to Fig. 2(B) exhibits the strong band due to $\nu(C{\equiv}N)$ of 2-CNpy at 2246 cm^{-1}. At the same time, the pH values of the measured solutions depend strongly on the reaction time (see Table 4). In agreement with these spectral and pH changes we have concluded that a nucleophilic reaction on 2-CNpy takes place at room temperature yielding a Co(II) complex with pyoxaL^1 (spectrum 6 has not changed during several days). This conclusion is also confirmed by a comparison of the uncoordinated pyoxaL^1 spectrum (curve 1) with those of the Co(II) solutions containing pyoxaL^1 (spectra 5 and 6). However, in the presence of Co(II), pyoxaL^1 gradually hydrolyses when being refluxed for 30 h leading thus to the solution containing mainly pycH, AL^1 and its cationic form AL^1H (spectrum 7).

Unlike the solutions containing Co(II) ions, the presence of Cu(II) gives rise to different spectral changes (Fig. 2(C)). Stemming from the IR spectra evolution we have concluded that a nucleophilic reaction on the nitrile group proceeds in such solutions at room temperature (spectrum 8) and Cu(II) complexes with both pyoxaL^1 and pyc^- ligands are formed. Simultaneously, however, decomposition of pyoxaL^1 to pyc^- proceeds (spectrum 9) and after 24 h Cu(II) complexes with pyc^- ligand become dominant species in solutions (spectrum 10). Moreover, bands at 1445 cm^{-1} in spectra 9 and 10 are assigned to the

Table 4. Composition of aqueous solution

Spectrum No.	Starting solution[a]	Reaction temperature[b]	Reaction time	pH	Dominant species[c]
1	pyoxaL^1	r.t.	5 min	7.0	pyoxaL^1
2	pyoxaL^1	reflux	50 h	6.8	pyc, AL^1, AL^1H
3	pycH	r.t.	5 min	7–10	pyc
4	pyc + AL^1	reflux	50 h	6.8	pyc, AL^1, AL^1H
5	2-CNpy + AL^1 + $CoCl_2$	r.t.	5 min	8.3	complex of pyoxaL^1
6	2-CNpy + AL^1 + $CoCl_2$	r.t.	120 min	9.3	complex of pyoxaL^1
7	2-CNpy + AL^1 + $CoCl_2$	reflux	30 h	6.8	AL^1, AL^1H, complex of pyc
8	2-CNpy + AL^1 + $CuCl_2$	r.t.	5 min	6.9	complex of pyoxaL^1 and pyc
9	2-CNpy + AL^1 + $CuCl_2$	r.t.	120 min	7.8	complex of pyoxaL^1, pyc and pia
10	2-CNpy + AL^1 + $CuCl_2$	r.t.	24 h	8.3	complex of pyc, pia and pyoxaL^1
11	$[CuCl(pyoxaL^1)_2]$-$Cl \cdot 0.5H_2O$	r.t.	5 min	7.4	complex of pyoxaL^1
12	$[CuCl(pyoxaL^1)_2]$-$Cl \cdot 0.5H_2O$	r.t.	120 min	7.1	complex of pyoxaL^1
13	$[CuCl(pyoxaL^1)_2]$-$Cl \cdot 0.5H_2O$	r.t.	48 h	5.6	complex of pyc and pyoxaL^1

[a] Solutions 1–10: the concentrations of organic compounds and MCl_2 were 0.50 and 0.25 M, respectively; solutions 11–13: the concentration of complex $[CuCl(pyoxaL^1)_2]Cl \cdot 0.5H_2O$ was 0.25 M.

[b] r.t. = room temperature.

[c] Species observed in IR spectra.

symmetric valence vibration of the CNO group of pyridine-2-carboxamide (Table 1) which has appeared in the solution, too. PyoxaL[1] is present in solution after 24 h only in a small amount.

Curve 11 in Fig. 2(D) represents the IR spectrum of an aqueous solution of $[CuCl(pyoxaL^1)_2]Cl \cdot 0.5H_2O$ [10]. The spectral changes (curves 12 and 13) confirm a gradual room temperature hydrolysis of the coordinated pyoxaL[1] directly to pyc^-. Contrary to the solutions which are represented by spectra 9 and 10, no formation of piaH was observed in the solutions 12 and 13.

3.4. *Reactions of pyridine-2-carbonitrile and formation of pyridine-2-carboxylic acid*

The reactions of 2-CNpy and pyoxaL[1] in aqueous solutions of Co(II) and Cu(II) salts under our experimental conditions are outlined in Scheme 2 (see also Section 2, Fig. 2 and Table 4). Moreover, the solid complexes of Co(II) and Cu(II) containing pyoxaL[1] have been prepared by the reaction of 2-CNpy with AL[1] [10]. For the sake of mutual comparability, Ni(II) complexes are included in Scheme 2, too.

All three transition metals M(II) mediate a pyoxaL[1] formation from 2-CNpy and AL[1]. The process is, however, solvent and starting salt dependent. Solid Ni(II) complexes with pyoxaL[1] are formed both in water (reaction 8) and ethanol [9] regardless the counter anions. Halide complexes of Co(II) with pyoxaL[1] are formed only in ethanol (reaction 1) while pyoxaL[1] formation in water (reaction 8) was observed when starting with $Co(ClO_4)_2$ or $Co(NCS)_2$ [10]. Solid Cu(II)–pyoxaL[1] complexes [10] can be synthesized only in ethanolic solution (reaction 1). Some of these reactions can take place also in the presence of other amino alcohols (denoted in Scheme 1 as AL[2] and AL[3]) but the present paper is focused mainly to the influence of AL[1] on addition reaction products of 2-CNpy. However, in this paper the results on the hydrolytic reactions of 2-CNpy in the presence or absence of AL[1] in aqueous solutions of copper(II) and cobalt(II) salts are described in detail.

4. CONCLUSIONS

The main conclusions of this paper can be summarized as follows.

1. The reaction of 2-CNpy with water or hydroxide ion in aqueous solution of metal(II) salts leads to the solid complexes containing piaH (reaction 3). The hydrolysis of piaH to pycH (reaction 4) was

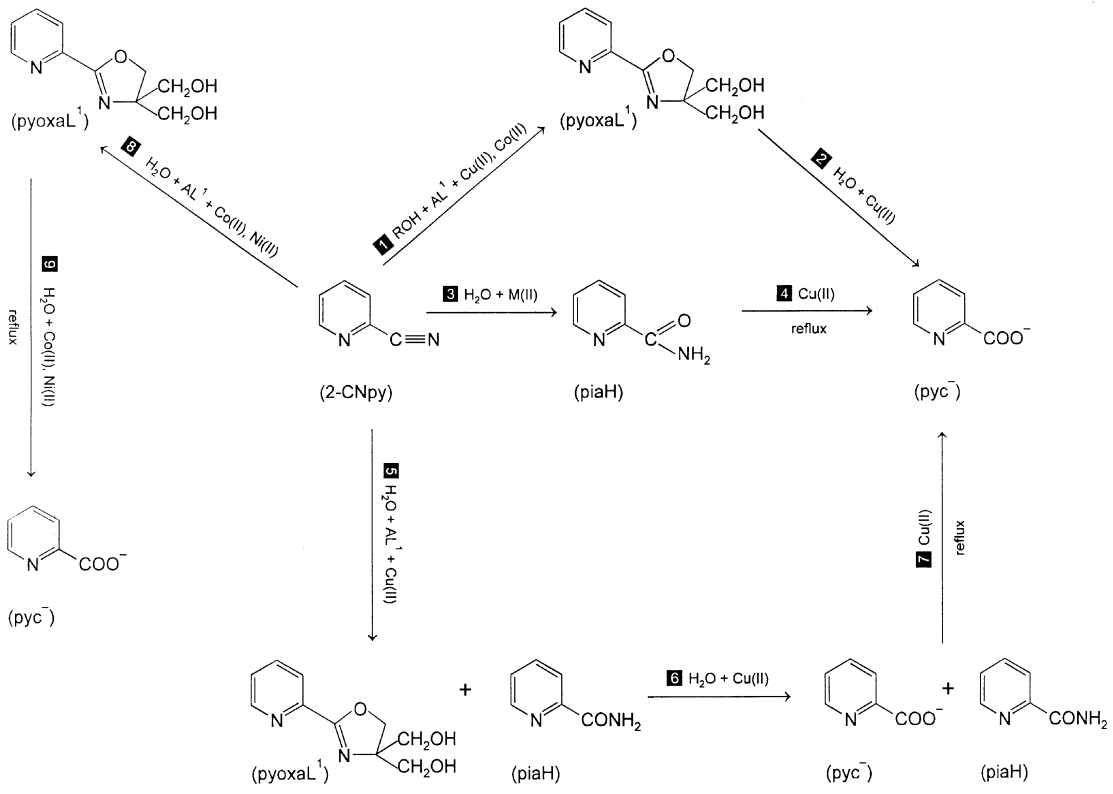

Scheme 2. Formation of Cu(II), Ni(II) and Co(II) complexes containing different reaction products of pyridine-2-carbonitrile (2-CNpy).

observed only in refluxed solutions containing Cu(II).

2. The reaction of 2-CNpy with AL^1 in aqueous solution of Cu(II) salts at room temperature (reaction 5) leads to the fast formation of Cu(II) complexes containing pyoxaL^1. These complexes behave as intermediates and undergo a gradual decomposition to pyridine-2-carboxylic acid (reaction 6) already at room temperature. Simultaneously the nucleophilic attack of water or hydroxide on the nitrile group of coordinated 2-CNpy leads to the formation of copper complex with pyridine-2-carboxamide which is fully stable at room temperature in solution. This sequence of reaction steps is supported by a kinetic analysis of analogous systems containing 2-carbonitrile-1,10-phenanthroline instead of 2-CNpy, described in [8]. From that solution a mixture of solid complexes containing piaH or pyc^- ligands deposited after several days (see Section 2). When an aqueous reaction mixture of 2-CNpy, AL^1 and $CuCl_2$ is refluxed for a long time, well-shaped crystals of product **III** appeared (reaction 7).
3. Upon a reflux of aqueous solutions of $[CoCl_2(pyoxaL^1)_2]$ (reaction 9) a gradual hydrolysis of the pyoxaL^1 ligand to pycH and AL^1 is observed and complex $[Co(H_2O)_2(pyc)_2]\cdot 2H_2O$ is isolated. That complex can also be prepared by refluxing an aqueous solution of 2-CNpy, AL^1 and $CoCl_2$ for up 30 h.
4. The pure $[Cu(pyc)_2]\cdot 2H_2O$ was also prepared at room temperature directly from $[CuCl(pyoxaL^1)_2]Cl\cdot 0.5H_2O$ [9] via its decomposition in water (reaction 2).
5. Now the crystal and molecular structure of complex **III** fully confirms the conversion of the 2-CNpy to the coordinated pyc^- anions in aqueous solutions of $CuCl_2$. This complex is square-planar with two *N*,*O*-coordinated pyc^- ligands and two uncoordinated molecules of water. The same arrangement of donor atoms bonded to the central atom Cu(II) is supposed for complex **II**.

REFERENCES

1. Michelin, R. A., Mozzon, M. and Bertani, R., *Coord. Chem. Rev.*, 1996, **147,** 299.
2. Walton, R. A., *J. Inorg. Nucl. Chem.*, 1966, **28,** 2229.
3. Belokon, Y. N., Tararov, V. I., Savel'eva, T. F., Vitt, S. V., Paskonova, E. A., Dotdyaev, S. Ch., Borisov, Y. A., Struchkov, Y. T., Batasanov, A. S. and Belikov, V. M., *Inorg. Chem.*, 1988, **27,** 4046.
4. Segl'a, P. and Jamnický, M., *Inorg. Chim. Acta*, 1988, **146,** 93.
5. Jamnický, M., Segl'a, P. and Koman, M., *Polyhedron*, 1995, **14,** 1837.
6. Barnard, P. F. B., *J. Chem. Soc. A*, 1969, 2140.
7. Byers, P., Drew, M. G. B., Hudson, M. J., Isaacs, N. S., Upadhaya, A. and Madic, Ch., *Polyhedron*, 1994, **13,** 345.
8. Breslow, R., Fairweather, R. and Keana, J., *J. Am. Chem. Soc.*, 1967, **89,** 2135.
9. Segl'a, P. and Jamnický, M., *Inorg. Chim. Acta*, 1993, **205,** 221.
10. Segl'a, P., Jamnický, M., Koman, M. and Gloweiak, T., *Polyhedron*, 1998, **17,** 2765.
11. Kuma, 1991. *Kuma KM*4 *User's Guide*, Version 3.1. Kuma Diffraction, Wrocław.
12. Sheldrick, G. M., SHELXS-86. *Crystallographic Computing*, Vol. 3. Oxford University Press, 1985, pp. 175–189.
13. Sheldrick, G. M., SHELXL-93. *Program for Refinement of Crystal Structure*. University of Göttingen, Germany, 1994.
14. Johnson, C. K., ORTEP. *Report ORNL* – 3794. Oak Ridge National Laboratory, TN, 1965.
15. Sekizaki, M. and Yamasaki, K., *Spectrochim. Acta*, 1969, **25A,** 475.
16. Sekizaki, M., Tanase, M. and Yamasaki, K., *Bull. Chem. Soc. Jpn.*, 1969, **42,** 399.
17. Brown, D. H., MacSween, D. R., Mercer, M. and Sharp, D. W. A., *J. Chem. Soc. A*, 1971, 1574.
18. Nakamoto, K., *Infrared and Raman Spectra of Inorganic and Coordination Componds*. Wiley, New York, 1986, p. 232.
19. Rao, C. N. R., *Chemical Applications of Infrared Spectroscopy*. Academic Press, New York, 1963, p. 317.
20. Lever, A. B. P., *Inorganic Electronic Spectroscopy*, 2nd edn. Elsevier, Amsterdam, 1984, p. 559.
21. Kleinstein, A. and Webb, G. A., *J. Inorg. Nucl. Chem.*, 1971, **33,** 405.
22. Gillard, R. D. and Laurie, S. H., *J. Chem. Soc. A*, 1968, 2588.
23. D'Ascenzo, G. and Wendlandt, W. W., *Anal. Chim. Acta*, 1970, **50,** 79.
24. Ellis, V. M., Vagg, R. S. and Watton, E. C., *J. Inorg. Nucl. Chem.*, 1974, **36,** 1031.
25. Chang, S. C., Ma, J. K. H., Wang, J. T. and Li, N. C., *J. Coord. Chem.*, 1972, **2,** 31.
26. Lumme, P., Viertola, M. and Lundgren, G., *Suom. Kemistil. B*, 1969, **42,** 270.
27. Melník, M., Kabešová, M., Dunaj-Jurčo, M. and Holloway, C. E., *J. Coord. Chem.*, 1997, **41,** 35.
28. Segl'a, P., Elias, H. and Geiser, C., Proc. 12th Conf. Coord. Chem., Smolenice – Bratislava, 1989, p. 315.

Pergamon

Polyhedron Vol. 17, Nos. 25, 26, pp. 4535–4541, 1998
© 1998 Elsevier Science Ltd
All rights reserved. Printed in Great Britain
PII: S0277–5387(98)00260–5
0277–5387/98 $19.00+0.00

Electrochemistry of the bis(1,4,7-triazacyclodecane) cobalt(III) complex and its role in the catalytic reduction of hydrogen

Refat Abdel-Hamid,† Hussein M. El-Sagher, A. M. Abdel-Mawgoud and Aywan Nafady

Department of Chemistry, Faculty of Science, Sohag, Egypt

(Received 11 March 1998; accepted 25 June 1998)

Abstract—The electrochemistry of the bis(1,4,7-triazacyclodecane) cobalt(III) complex at a mercury electrode, HMDE, in aqueous Britton–Robinson buffer solutions was investigated using cyclic voltammetry, double-potential-step chronoamperometry and chronocoulometry. The cyclic voltammetric data were analyzed by digital simulation to confirm and to measure the heterogeneous and homogeneous parameters for the suggested electrode mechanism. Generally, the complex is electrochemically reduced giving rise to two cyclic voltammetric waves. The first wave is a diffusion-controlled reversible wave. It is assigned to the stable Co(III)/Co(II) redox couple. The second one is found to be irreversible and corresponding to a reduction of Co(II) to Co(I) species. The monovalent cobalt, highly unstable, is rapidly protonated, and then forms cobalt hydride. The hydride decomposes to hydrogen molecules and regenerates Co(II) species following a disproportionation pathway. The overall reduction mechanism is concluded to be an EECC kinetics. © 1998 Elsevier Science Ltd. All rights reserved

Keywords: macrocycles; cobalt complexes; cyclic voltammetry; chronoamperometry; reduction; simulation; catalytic.

INTRODUCTION

Metal complexes of polyazamacrocyclic ligands have received recently great attention due to their variety of functions [1–7]. Stabilization of unusual oxidation states of coordinated metal ions and catalytic activity are the most interesting. These ligands can form complexes with various transition metals, of which the structures are similar to those of the active sites of enzymes. Electrochemical studies of transition metal complexes of tetraazamacrocylics have appeared in connection with investigations of their catalytic properties [8–13]. However, to date, no detailed studies were reported on the electrochemical behavior of triazamacrocyclic complexes. Therefore, it is important to study the electrochemical reduction behavior of this type of complexes. This has been done to learn more about the properties and electrochemical reactivity of some water soluble triazamacrocyclic complexes.

In the present investigation, the electrochemical reduction mechanism of the bis(1,4,7-triazacyclodecane) cobalt(III) complex, $[Co([10]aneN_3)_2](NO_3)_3$, has been studied on a hanging mercury drop electrode, HMDE, in aqueous Britton–Robinson universal buffer solutions using different electrochemical techniques, *viz*., cyclic voltammetry, chronoamperometry and chronocoulometry, controlled potential coulometry and digital simulation. The mechanism of the electrode reaction is fully characterized and discussed.

EXPERIMENTAL

1,4,7-triazacyclodecane was synthesized according to the Koyama and Yoshino method [14] modified by Richman and Atkins [15]. The required product was extracted as a viscous yellow oil with chloroform. The elemental analytical and ^{1}H NMR spectral data of the final product were consistent with its structure.

The bis(1,4,7-triazacyclodecane) cobalt(III) com-

†Corresponding author. E-mail: science@sohag.jwnet.cun.eg

plex was synthesized on addition of the ligand solution to an air bubbled ethanolic solution of cobalt nitrate. The solution mixture was warmed and allowed to evaporate slowly to give small yellow crystals. The crystals were filtered off, washed with ether and recrystallized from an ethanol–water mixture. The elemental analytical and ^{1}H NMR spectral data of the complex were consistent with its structure.

A stock solution of fresh 5.0 mM bis(1,4,7-triazacyclodecane) cobalt(III) complex in triple-distilled water was prepared, kept in an inert nitrogen atmosphere and diluted as required. Britton–Robinson universal buffer solutions were prepared from analytical grade chemicals.

The cell and the instruments used for cyclic voltammetry and double potential step chronocoulometry were described elsewhere [16]. The electrochemical system was interfaced with an IBM value point 433 DX/DP computer. The data were captured, stored and manipulated with EG&G M270/500 software. Positive feed back was used for compensation of the solution resistance. For all experiments an Ag/Ag^+ electrode was used as reference electrode. The hanging mercury drop electrode, HMDE, in hanging drop mode was used throughout. The electrode area is 1.66×10^{-4} cm^2. All measurements were obtained at 298 K. Solutions were deaerated by purging with pure nitrogen before measurements and a blanket of nitrogen was maintained above the working solution.

The electrode reaction mechanism was confirmed and homogeneous and heterogeneous parameters of the electrode reaction were determined on analyzing the cyclic voltammetric data making use of CVSIM and CVFIT simulation softwares [17].

RESULTS AND DISCUSSION

Cyclic voltammograms of bis(1,4,7-triazacyclodecane) cobalt(III) complex, $[Co([10]aneN_3)_2](NO_3)_3$, are recorded in aqueous Britton–Robinson universal buffer solutions over a pH range from 2.70 to 10.30 using a hanging mercury drop electrode vs Ag/Ag^+. A representative illustration is given in Fig. 1. Generally, on the negative going potential scan, two reduction waves are observed, whereas on the reverse scan, one wave is seen at less negative potentials. On limiting the potential scan to the first reduction wave, switching the potential at -1.05 V, the wave appears to be reversible. At low pH, 2.70, the second cv wave is ill-defined and it is difficult to be evaluated quantitatively due to the incipient hydrogen evolution.

Analysis of the voltammetric data for the first cv wave indicates that the anodic to cathodic peak separation, $\Delta E_p = E_{pa} - E_{pc}$, has a larger value than what would be expected for a reversible one-electron transfer process [18] and varies with scan rate, cf. Table 1. This suggests that the electrode reaction is not perfectly Nernstian. On the other hand, the unit ratio of anodic to cathodic currents, i_{pa}/i_{pc}, constancy of the peak width, $E_{pc} - E_{pc/2}$, and the peak current function, $i_{pc}/v^{1/2}$, with variation of the potential scan rate, v, indicate that the electrode reaction corresponds to a reversible one electron transfer process. Thus, taking into account the electrochemical inactivity of the

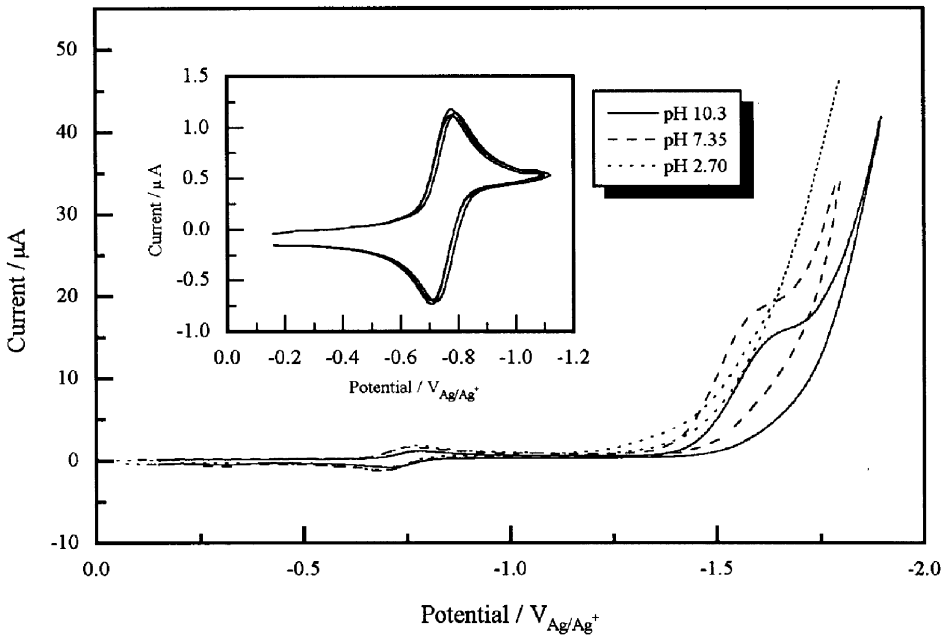

Fig. 1. Cyclic voltammograms of 4×10^{-4} mol dm^{-3} bis(1,4,7-triazacyclodecane) cobalt(III) complex at different pHs.

Table 1. Cyclic voltammetric data for the first cv wave of 5.0 mM $[Co([10]aneN_3)_2]^{3+}$ at pH 2.70 in aqueous universal buffer solution as a function of scan rate

v (mV/s)	$-E_{pc}$ (V)	i_{pc} (μA)	$-E_{pa}$ (V)	i_{pa} (μA)	ΔE_p (mV)	$E_{pc}-E_{pc/2}$ (MV)	i_{pa}/i_{pc}	$i_{pc}/v^{1/2}$ ($\mu A\,V^{-1/2}\,s^{1/2}$)
100	0.764	9.417	0.701	9.60	89	63	1.086	29.801
200	0.769	12.71	0.705	13.10	98	64	1.100	28.425
300	0.773	15.64	0.708	16.10	104	65	1.081	28.592
400	0.775	18.17	0.710	18.59	108	65	1.105	28.653
500	0.778	20.21	0.712	20.79	115	66	1.102	28.578
600	0.782	22.13	0.715	22.91	119	67	1.093	28.590
800	0.785	25.91	0.717	25.62	126	68	1.067	28.975
1000	0.788	28.25	0.718	28.86	133	70	1.094	28.250

ligand, 1,4,7-triazacyclodecane, the electrode reaction is attributed to the Co(III)/Co(II) redox couple. The one electron nature of the couple is confirmed coulometrically at a constant potential of -0.78 V. Furthermore, the peak current, i_{pc}, increases with the potential scan rate and from the log–log relationship, $\log i$–$\log v$, a straight line is obtained with a slope of 0.49 and correlation coefficient of 0.999. This is an indication of the diffusion-controlled nature of the first cv wave [19]. Thus, this wave can be used as internal standard for a reversible one-electron transfer process.

Upon increasing the pH of the solution, the peak potential and the peak current of the first cv wave do not change, while the peak potential of the second one shifts to more negative potential and its peak current decreases. This indicates that the hydrogen ions play a certain role in the electrochemical reduction process along the second cv wave. Comparing the peak current for the second wave at certain pH and scan rate with that for the first cv wave it is evident that it is always higher than what would be expected for a diffusion-controlled one electron-transfer process. Therefore, the second cv wave corresponds to either a multielectronic process or a charge-transfer coupled with a kinetic catalytic process. This leads to an electroactive species which is easily reduced at the same peak potential, thereby producing an increase in the observed current.

For the second cv wave, the peak current, i_{pc}, increases upon increasing the scan rate as shown in Fig. 2. Plotting of $\log i_{pc}$ vs $\log v$ relations gives straight lines with slopes of 0.38 and 0.23 at pH 7.35 and 10.30, respectively. This reveals that the second cv wave is complicated with a kinetic process. Moreover, the current function, $i_{pc}/v^{1/2}$, decreases upon increasing the scan rate. This supports the above suggestion that the electrode reaction is due to a reversible electron-transfer process coupled with a catalytic chemical reaction, i.e., $E_{rev.}C_{cat.}$ mechanism.

Upon scanning the cyclic voltammograms of the subject complex at different initial times, a steadily increase in the peak current for the second cv wave with time is observed until at a certain time of 180 s, it levels off. This implies an adsorption of Co(II) species on the HMDE surface. Furthermore, the peak current depends on the initial adsorption potential, E_i, cf. Fig. 3. Obviously, the peak current increases on increasing the adsorption potential cathodically, revealing an adsorption of the positively charged divalent cobalt complex species, $[Co(II)([10]aneN_3)_2]^{2+}$. Adsorption of the positively charged cobalt(H) species on the mercury electrode has also been proposed earlier [20, 21, 22]. Upon increasing the adsorption potentials to more negative values than -1.0 V, a decrease in the peak current is observed, indicating that the adsorption is inhibited and the divalent cobalt species is reduced once transported from the bulk of the solution to the reaction layer.

It is well known that cobalt macrocyclic complexes catalyze the hydrogen evolution [20–22]. Thus, the second cv wave can be attributed to a catalytic reduction of hydrogen ions. It is interpreted as follows: initially, adsorption of the cobalt(II) species on the electrode surface, then reduction into the monovalent cobalt species on uptaking of an electron occurs. The highly unstable Co(I) reacts with protons to form cobalt hydride, as a result of its powerful nucleophilicity. According to the hydrogen evolution mechanism proposed earlier [20], two possible pathways from the decomposition of the cobalt hydride are suggested. These are the proton attack on/or the disproportionation of the hydride, Eqs (1) and (2) (see below), respectively.

The Co(III) formed in the first pathway will be reduced to Co(II) at the electrode or in solution by the Co(I) species. In the second pathway, the disproportionation of the hydride, the Co(II) species is regenerated,

$$\text{Co(III)–H}^- + \text{H}^+ \longrightarrow \text{H}_2 + \text{Co(III)}, \qquad (1)$$

$$\text{Co(III)–H}^- \longrightarrow \tfrac{1}{2}\text{H}_2 + \text{Co(II)}. \qquad (2)$$

To justify which pathway is favored at the given conditions, the electromotive force and the equilibrium constants of the reactions taking place must

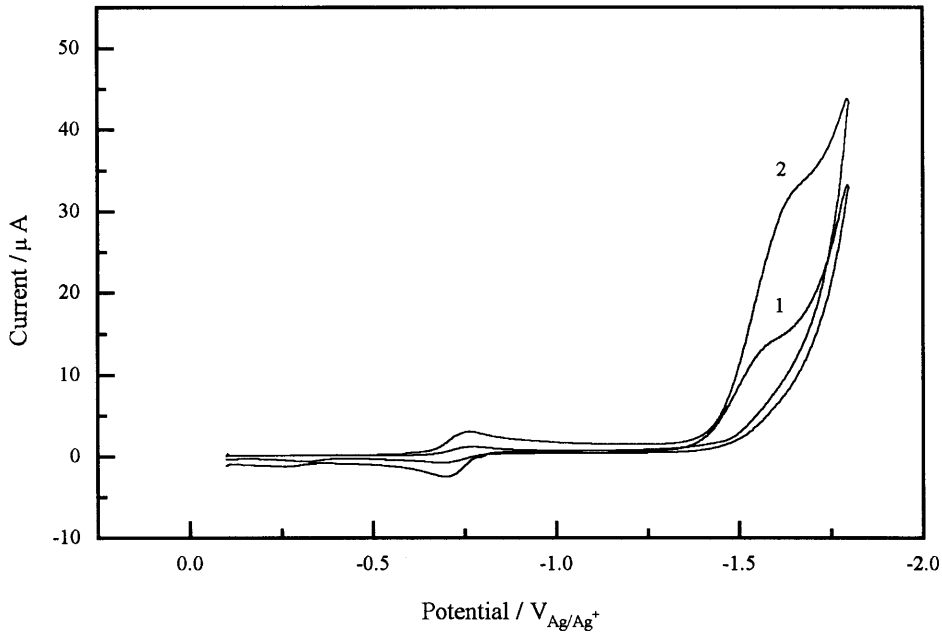

Fig. 2. Cyclic voltammograms of 4×10^{-4} mol dm^{-3} bis(1,4,7-triazacyclodecane) cobalt(III) complex at scan rates of 100 and 1000 mV s^{-1}.

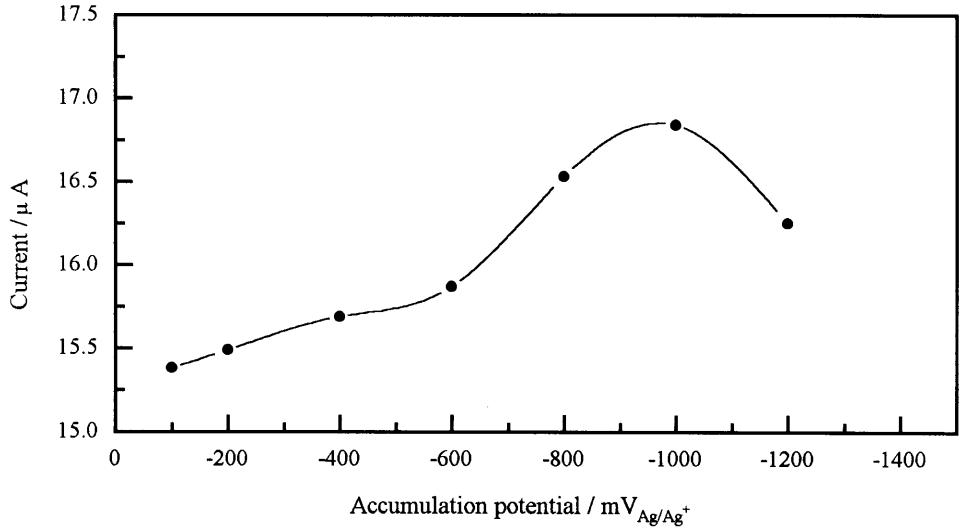

Fig. 3. Dependence of peak current on the accumulation potential of the bis(1,4,7-triazacyclodecane) cobalt(III) complex at pH 7.35.

be computed. For the first pathway, the hydrogen evolution proceeds via the following reactions:

$$\begin{aligned} &\tfrac{1}{2}\mathrm{Co(I)} + \mathrm{H^+} \rightleftarrows \tfrac{1}{2}\mathrm{Co(III)} + \tfrac{1}{2}\mathrm{H_2}, \\ &\tfrac{1}{2}\mathrm{Co(III)} + \tfrac{1}{2}\mathrm{e^-} \rightleftarrows \tfrac{1}{2}\mathrm{Co(II)}, \\ &\tfrac{1}{2}\mathrm{Co(II)} + \tfrac{1}{2}\mathrm{e^-} \rightleftarrows \tfrac{1}{2}\mathrm{dCo(I)}. \end{aligned} \quad (3)$$

The electromotive force for reaction (3) is estimated using

$$E(3) = E(\mathrm{H^+/H_2}) - \tfrac{1}{2}E(\mathrm{Co(III)/Co(II)}) - \tfrac{1}{2}E(\mathrm{Co(II)/Co(I)}). \quad (4)$$

For the second pathway, the following reactions will take place:

$$\mathrm{Co(I)} + \mathrm{H^+} \rightleftarrows \mathrm{CO(II)} + \tfrac{1}{2}\mathrm{H_2}, \quad \mathrm{Co(II)} + \mathrm{e^-} \rightleftarrows \mathrm{CO(I)} \quad (5)$$

and the electromotive force is given by

$$E(5) = E(H^+/H_2) - E(Co(II)/Co(I)). \quad (6)$$

In order to estimate the electromotive forces, $E(3)$ and $E(5)$, and the corresponding equilibrium constants, $K(3)$ and $K(5)$, for reactions (3) and (5), the standard electrode potentials for the Co(III)/Co(II) and Co(II)/Co(I) couples need to be calculated. This is performed by digital simulation analysis of the cyclic voltammograms. Digital simulation analysis is based on the suggestion that the electrode reaction proceeds following an EECC kinetics, according to the Scheme.

To establish the simulated voltammograms, the heterogeneous electron transfer reactions are assumed to be fast with k^s values of 1.0 cm/s, $\alpha = 0.5$ and the diffusion coefficients for all species are identical. Several simulations were performed by varying the input parameters, the rate of heterogeneous and homogeneous reactions, the charge-transfer coefficients and the standard electrode potentials, until a good visual fit between the experimental and simulated cyclic voltammograms is obtained. CVFIT program is used to confirm the obtained digital simulation results, through a quantitative comparison of the experimental and simulated voltammograms. The obtained digitally simulated parameters of the complete voltammogram are used as inputs to be fitted in order to obtain the best correct values. The parameters obtained for the subject triazamacrocyclic cobalt are illustrated in Table 2. A satisfactorily fit between the experimental and simulated cyclic voltammograms is recorded in Fig. 4.

Examination of the simulated E^0 values in Table 2 indicates that E^0 of the couple Co(III)/Co(II), -0.733 V, is more positive than those, -1.541 and -1.563 V, of the two pathways of the couple Co(II)/Co(I), respectively. The electromotive forces, $E(3)$ for the proton-attack pathway and $E(5)$ for the disproportionation pathway, are calculated to be $+0.926$ and $+1.319$ V, respectively. This implies that reaction (5) has a much greater driving force than reaction (3). At low pH, however, reaction (3) may be kinetically favored, it proceeds spontaneously. This condition will be satisfied so long as $E(3) > 0$. From eq. (1), the condition can be represented numerically as follows:

$$E(Co(III)/Co(II)) + E(Co(II)/Co(I)) < 2E(H^+/H_2).$$

Since $E(H^+/H_2) = -0.222$ V on the Ag/Ag^+ scale,

$$E(Co(III)/Co(II)) + E(Co(II)/Co(I)) = -0.733 + (-1.563) = -2.296\ V,$$

which is much lower than $2E(H^+/H_2)$, -0.444 V.

Furthermore, the equilibrium constants of these pathways are computed to be $K(3) = 4.49 \times 10^{15}$ and $K(5) = 1.97 \times 10^{22}$, respectively. Thus, it is evident that the decomposition of cobalt hydride is most likely to follow the disproportionation pathway, reaction (5), since the values of $E(5)$ and $K(5)$ are much higher than the corresponding values for reaction (3). Therefore, the catalytic action of the bis(1,4,7-triazacyclodecane) cobalt(III) complex for hydrogen evolution can be formulated as in the Scheme.

It is worth to mention that the decrease in the catalytic reduction current upon increasing the pH of the medium confirms its catalytic nature. However, the

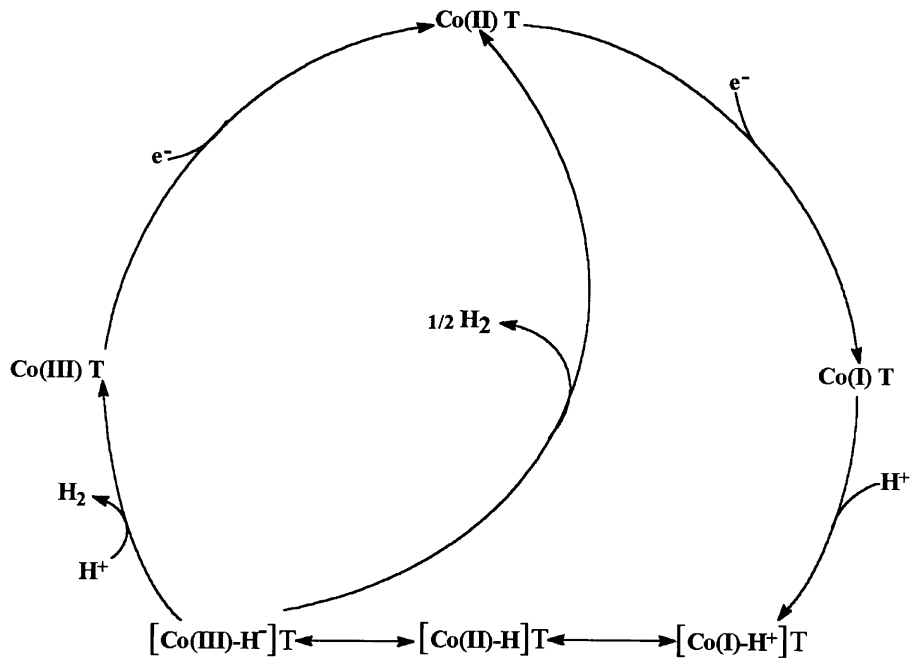

Scheme 1. Cobalt triazamacrocyclic, T, catalysis of H_2 through the EECC mechanism.

Table 2. Simulation/fitting data for the bis(1,4,7-triazacyclodecane) cobalt(III) complex, electrochemical parameters at a scan rate of 200 mV/s at pH 7.35, E^0(Co(III)/Co(II)) = -733 ± 1 mV, $k^s = (0.99 \pm 0.06)$ cm/s and $\alpha = 0.48 \pm 0.06$

Reaction pathway	$-E^0$ (mV) (Co(II)/Co(I))	k^s ($\times 10^{-3}$ cm/s)	α	k_f^1 ($M^{-1}s^{-1}$)	k_f^2 ($M^{-1}s^{-1}$)	k_b^1 ($M^{-1}s^{-1}$)	k_b^2 ($M^{-1}s^{-1}$)
Proton attack	1563 ± 1	4.97 ± 0.16	0.36	1023 ± 21	384 ± 4.1	0.001	0.001
	(1562.6)	(4.9)		(1022.7)	(383.5)	(0.001)	(0.001)
Disproportionation	1541 ± 1	12 ± 0.20	0.42	1023 ± 21	1717 ± 18	0.001	0.001
	(1540.3)	(12.4)		(1022.5)	(1720)	(0.001)	(0.001)

*Data between parentheses are simulated data. 1 and 2 refer to formation and decomposition of the hydride, respectively.

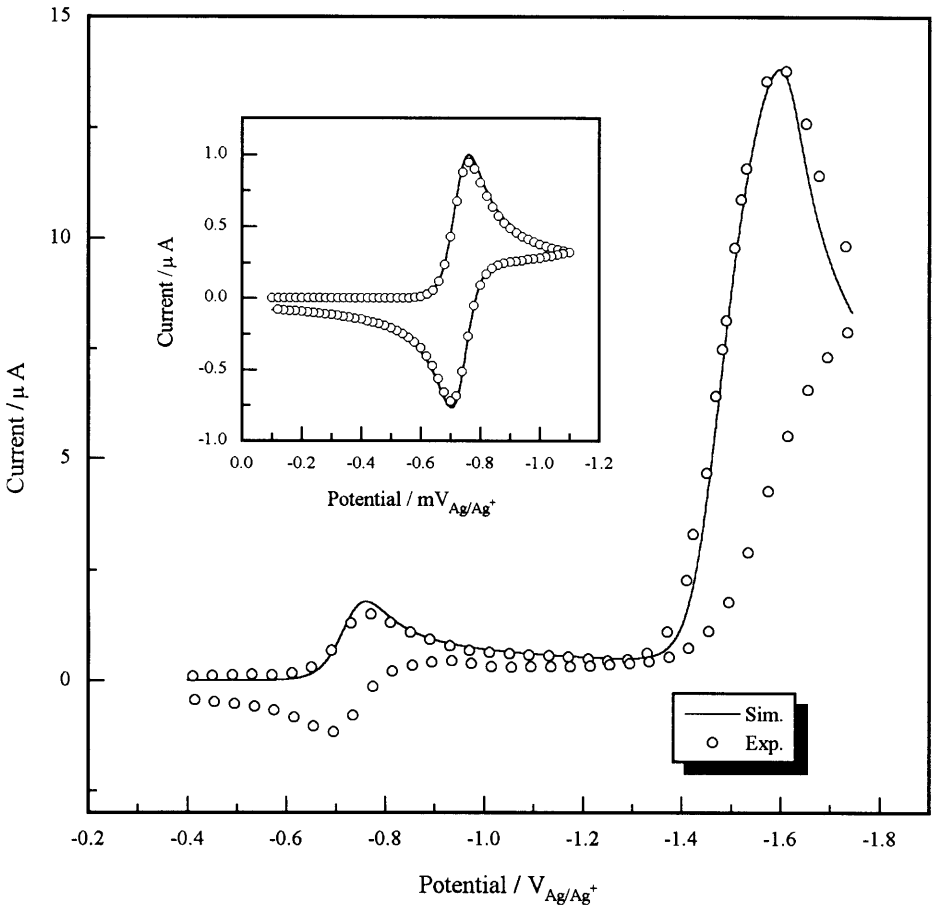

Fig. 4. Simulated/fitted cyclic voltammogram and the experimental one of the bis(1,4,7-triazacyclodecane) cobalt(III) complex for the disproportionation pathway at pH 7.35.

process is not simple. On plotting the logarithm of the catalytic current of the second cv wave as a function of pH, a straight line is obtained with a slope of 0.14, compared to an expected value of unity for the rate-limiting Co(I) protonation or proton attack on cobalt hydride reactions. This shallow response is attributed to the adsorption of the divalent cobalt complex species at the electrode surface.

In Britton–Robinson aqueous buffer solution of pH 7.35 at a hanging mercury drop electrode, chronoamperograms of 4.0×10^{-4} mol dm^{-3} bis(1,4,7-triazacyclodecane) cobalt(III) complex are recorded. The electrode potential was changed from an initial value of -0.30 V, in which the complex is electrochemically inactive, to a final potential of -0.95 V, where the desired electrode reaction takes place and the cathodic current is determined solely by diffusion. Then at switching time, τ, the potential was suddenly

returned back to its initial value. The obtained chronoamperograms were analyzed using the Cottrell equation, eq. (7). Straight lines are obtained upon plotting the cathodic current, $i(t<\tau)$ vs $t^{-1/2}$, with correlation coefficient of 0.999 at different duration times. This reveals that the reduction of the subject complex along the first cv wave is diffusion controlled. From the slopes of these straight lines the mean value of diffusion coefficient of bis(1,4,7-triazacyclodecane) cobalt(III) complex is calculated. It is found to be $(3.944 \pm 0.004) \times 10^{-6}\,\mathrm{cm^2/s}$.

On changing the electrode potential from $-1.0\,\mathrm{V}$ to $-1.60\,\mathrm{V}$ and suddenly returning back to $-1.0\,\mathrm{V}$, after a duration time τ, the chronoamperograms for the second cv wave are obtained. Upon integrating the current response, the corresponding chronocoulograms are obtained and analyzed according to the Anson equations [23], eqs (8) and (9) respectively. Straight lines are obtained for the Q_f vs $t^{1/2}$ and Q_r vs θ plots.

$$i(t<\tau) = \frac{nFAD^{1/2}{}_0C_0^*}{\pi^{1/2}t^{1/2}}, \tag{7}$$

$$Q(t<\tau) = \frac{2nFAD^{1/2}{}_0C_0}{\pi^{1/2}}t^{1/2} + Q_{dl} + nFA\Gamma_0, \tag{8}$$

$$Q_r(t) = \frac{2nFAD^{1/2}{}_0C_0}{\pi^{1/2}}\theta + Q_{dl}, \tag{9}$$

where $Q(t<\tau)$ is the amount of charge passed along the cathodic step at time t since the application of the potential step, C_0 and D_0 are the concentration and diffusion coefficient of the reactants, respectively, A is the surface electrode area, n and F have their usual significance, $Q_r(t) = Q(\tau) - Q(t>\tau)$, Q_{dl} is the charge consumed by the electrode–electrolyte double-layer capacitance, Γ_0 is the excess surface of the adsorbate and $\theta = \tau^{1/2} + (t-\tau)^{1/2} - t^{1/2}$.

The observed intercept of the cathodic step generally has a greater value than the anodic one. This is a strong evidence for the adsorption of the reactant, the divalent cobalt species, along the second cv wave. Furthermore, the amount of the adsorbate expressed as the surface excess, Γ_0, is determined from the difference in the intercepts of the forward and the reverse Anson' plots, eqs (8) and (9), which is simply $nFA\Gamma_0$. This difference cancels Q_{dl} and leaves only the net Faradaic charge due to adsorbate. The charge obtained for $4.0 \times 10^{-4}\,\mathrm{mol\,dm^{-3}}$ subject cobalt complex is found to be $2.25\,\mathrm{nC/cm^2}$. This value is equivalent to surface excess of $1.40 \times 10^{-10}\,\mathrm{mol/cm^2}$.

REFERENCES

1. Curtis, N. F., in: Melson, G. A. (Ed.), *Coordination Chemistry of Macrocyclic Compounds*, ed. G. A. Melson. Plenum Press, New York, 1979, p. 223.
2. Kimura, E., Kodama, M. and Yatsunaini, T., *J. Am. Chem. Soc.*, 1982, **104,** 4255.
3. Pearce, D. J. and Pletcher, D., *J. Electroanal. Chem.*, 1986, **197,** 317.
4. Balazs, G. B. and Anson, F. C., *J. Electroanal. Chem.*, 1992, **322,** 325.
5. Pang, D. and Wang, Z., Cha, C., *J. Electroanal. Chem.*, 1992, **325,** 219.
6. Matsuoka, S., Yamamoto, K., Ogata, T., Kusaba, M., Nakashima, N., Fojita, E. and Yanagida, S., *J. Am. Chem. Soc.*, 1993, **115,** 601.
7. Webb, R. L., Mino, M. L., Blinn, E. L. and Pinkerton, A. A., *Inorg. Chem.*, 1993, **32,** 1396.
8. Geiger, T. and Anson, F. C., *J. Am. Chem. Soc.*, 1981, **103,** 7489.
9. Beley, M., Collill, J.-P., Ruppert, R. and Sauvage, J.-P., *J. Am. Chem. Soc.*, 1986, **108,** 7461.
10. Taniguchi, I., Nakashima, N., Matsushita, K. and Yasukouchi, K., *J. Electroanal. Chem.*, 1987, **224,** 199.
11. Collin, J. P. and Sauvage, J. P., *Coord. Chem. Rev.*, 1989, **93,** 245.
12. Taniguchi, I., Shimpuka, T., Yasukouchi, K. and Ohtaki, H., *J. Chem. Soc. Chem. Commun.*, 1990, 915.
13. Fujihira, M. and Hirata, Y., Sugn, K., *J. Electroanal. Chem.*, 1990, **292,** 199.
14. Koyama, H. and Yoshino, T., *Bull. Chem. Soc. Jpn.*, 1972, **45,** 481.
15. Richinan, J. E. and Atkins, T. J., *J. Am. Chem. Soc.*, 1974, **96,** 2268.
16. Abdel-Hamide, R., *J. Chem. Soc. Perkin Trans.* 2, 1996, 691.
17. *Gosser, D. K. Jr. and Zhang, F., Talanta*, 1991, **38,** 715.
18. Nicholson, R. S. and Shain, I., *Anal. Chem.*, 1964, **36,** 706.
19. Gosser, D. K., Jr., *Cyclic Voltammetry – Simulation and Analysis of Reaction Mechanisms*. VCH Publishers, New York, 1993.
20. Kellett, R. M. and Spiro, T. G., *Inorg. Chem.*, 1985, **24,** 1373.
21. Jin, W. and Liu, K., *J. Electroanal. Chem.*, 1987, **216,** 181.
22. Taniguchi, I., Nakashima, N., Matsushita, K. and Yasukouchi, K., *J. Electroanal. Chem.*, 1987, **224,** 199.
23. Anson, F. C., *Anal. Chem.*, 1966, **38,** 54.

Pergamon

Polyhedron Vol. 17, Nos. 25, 26, pp. 4543–4551, 1998
© 1998 Elsevier Science Ltd
All rights reserved. Printed in Great Britain
PII: S0277–5387(98)00287–3
0277–5387/98 $19.00+0.00

Potentiometric, spectrophotometric and ES–mass spectroscopic studies of the formation of binary and ternary species between Cu^{2+}, a pyrazole bridged N_2S-bismacrocycle and exogenous ligands

Harald Weller,[a] Thomas A. Kaden[a,]* and Gérard Hopfgartner[b]

[a]Institute of Inorganic Chemistry, Spitalstrasse 51, CH-4056 Basel, Switzerland

[b]Hoffmann-LaRoche, Pharma Division, Grenzacherstrasse, CH-4070 Basel, Switzerland

(Received 6 April 1998; accepted 25 June 1998)

Abstract—The protonation and stability constants of the binary Cu^{2+} complexes with 1,1′-[(1H-pyrazole-3,5-diyl)bis(methylene)]bis(octahydro-1H-1,4-triazonine) were determined by potentiometric titrations at 25° and $I=0.5$ M (KNO_3). The results show that a series of mononuclear [Cu(LHn)] ($n=1, 0, -1, -2$) and dinuclear species [Cu_2(LHm)] ($m=0, -1, -2, -3$) are formed. Structures are proposed for them based on their absorption spectra and results previously obtained from X-ray diffraction studies. Complex $[Cu_2(LH_{-1})]^{3+}$, in which the pyrazole bridging group is deprotonated, is especially interesting since it is able to bind exogenous ligands Z such as N_3^-, pyrazole and 1H,1′H-4,4′-methanediyl-bis-pyrazole (bispyr) to give ternary species $[Cu_2(LH_{-1})Z]$ and $[[Cu_2(LH_{-1})]_2Z]$, the stabilities of which have been measured by spectrophotometric titrations. In the case of bispyr the existence of the tetranuclear complex $[[Cu_2(LH_{-1})]_2(bispyr)]^{2+}$ has been proven by ES–MS. © 1998 Elsevier Science Ltd. All rights reserved

Keywords: binary Cu^{2+} complexes; 1,1′-[(1H-pyrazole-3,5-diyl)bis(methylene)]bis(octahydro-1H-1,4-triazonine)

INTRODUCTION

Bismacrocyclic ligands, in which two macrocyclic rings are connected by a carbon chain, form dinuclear metal complexes [1–15]. The metal–metal interaction can be controlled in these systems by the length of the linking chain, which in this respect has also the function of a spacer. If the distance is short as in the case of an ethylene chain, strong interactions are observed. For example in the case of dinuclear Cu^{2+} complexes strong antiferromagnetic coupling has been determined from the temperature dependence of the magnetic susceptibility [16, 17], or spin–spin coupling can be observed by ESR spectroscopy [17], or the stepwise oxidation–reduction of the metal centres are found by cyclic voltammetry or differential pulse polarography at potentials which differ by more than the statistical value [17, 18]. If the distance between the two metal centers is larger than a few carbon atoms the metal ions do not interact any more and behave as two independent units [17, 19].

In many of the structures determined by X-ray diffraction studies the conformation of these dinuclear complexes is *anti*, which allows to minimize the electrostatic repulsion of the two positively charged metal centers [17, 20]. However, if an exogenous bridging ligand is also present the *syn* (ear-muff) arrangement is found [21]. Another way to induce the *syn* arrangement is to introduce a bridging group into the chain, which connects the two macrocycles [22, 23].

We have previously shown by X-ray studies that ligands of typ **1**–**3** are always found in the *syn*-conformation and that additional exogenous ligands easily can bind to complete the coordination sphere of the metal ions [16]. It was therefore interesting to study

*Author to whom correspondence should be addressed. Tel.: +41-61-267-1006; Fax: +41-61-267-1020; E-mail: kaden@ubaclu.unibas.ch

the complexation equilibria of one of these systems consisting of Cu^{2+}, ligand **2** and exogenous donors in order to gain a better understanding of their stability in water.

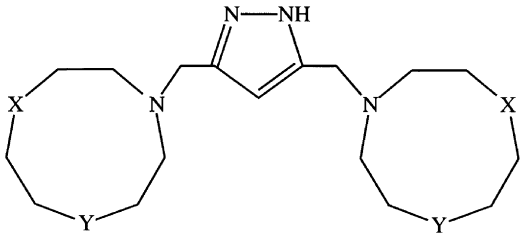

1 X = Y = NH, **2** X = NH, Y =S, **3** X = Y = S

EXPERIMENTAL

Compounds 4,4′-[(1H-pyrazole-3,5-diyl)bis(methylene)]-bis[octahydro-1,4,7-thiazonine] [16] and 1H,1′H-4,4′-methanediyl-bis-pyrazole [24] have been prepared according to the literature and identified by ^{1}H-NMR and ^{13}C-NMR.

Potentiometric titrations

Automatic titrator, as described previously [25], at $25 \pm 0.1^{\circ}$ and $I = 0.5$ M (KNO_3). Typical concentrations: $[L] = 2.51 \times 10^{-3}$ M with $[Cu^{2+}] = 0$, or 2.27×10^{-3} M, or 4.55×10^{-3} M. The equilibration of the Cu^{2+}/ligand titrations was relatively slow, so that the waiting time between the 0.4 M NaOH additions was kept at 480 s and the pH tolerance at 0.002 pH units. Calibration of the electrode and determination of the proton activity coefficient α_H and of pK_W was performed as described [25]. The evaluation of the protonation and stability constants was done with the program TITFIT [26], in which the global constants β_{mlh} are defined by eqn (1), where a_H is the proton activity.

$$\beta_{mlh} = \frac{[M_m L_l H_h]}{[M]^m [L]^l a^h{}_H} \quad (1)$$

Spectrophotometric titrations

Automatic setup as described in [27], using 1 cm quartz cuvettes and working at $25 \pm 0.1^{\circ}$ and $I = 0.5$ M (KNO_3). To determine the stability constants of the ternary complexes, 2.2–2.4 ml of a 6.0×10^{-4} M buffered solution. (4.0×10^{-2} M lutidine-3-sulfonic acid adjusted with 0.1 M NaOH to pH 5.5) of the dinuclear Cu^{2+} complex was titrated with 1.0×10^{-2}–2.5×10^{-2} M bridging ligand, which was added in 3–10 μl aliquots up to 0.06–0.3 ml. Equilibrium was fast, so that the waiting time between the additions was kept at 60 or 120 s. The calculations were done with the program SPECFIT [28].

Electrospray–ionisation–MS

Pneumatically-assisted electrospray (ES–MS) mass spectra were recorded on an *API III* tandem mass spectrometer (PE Sciex, Concord, Canada) by infusion at 5–10 μl/min. The single MS spectra were recorded under low up-front declustering or collision-induced dissociation (up-front CID) conditions, typically $\Delta V = 0$–30 V between the orifice and the first quadrupole of the mass spectrometer [29, 30]. Determination of the total charge of the complexes (z) was made by using the isotopic pattern. Solutions of the dinuclear Cu^{2+} complex (2.5×10^{-4} M) in CH_3CN (1.0 ml) were treated with different solutions of 1H,1′H-4,4′-methanediyl-bis-pyrazole (bispyr) in CH_3CN (1.0 ml) in decreasing concentrations (2.50×10^{-4}, 1.25×10^{-4}, 0.63×10^{-4}, or 0 M) containing 3 equivalents of N-ethyl-diisopropylamine as base.

UV–VIS spectra were measured on a Perkin Elmer, Lamda 9 Spectrophotometer in 1 cm cuvettes. Solutions of Cu^{2+} (2.3×10^{-3} or 4.6×10^{-3} M) and ligand (2.5×10^{-3} M) were adjusted to pH values at which the 1:1 and 2:1 species are dominant: pH 2.8 for $[Cu(LH)]^{3+}$, pH = 8.8 for $[CuL]^{2+}$, and pH = 10.8 for $[Cu(LH_{-1})]^{+}$, pH = 4.1 for $[Cu_2(LH_{-1})]^{3+}$, and pH = 8.1 for $[Cu_2(LH_{-2})]^{2+}$.

RESULTS AND DISCUSSION

From pH titrations of ligand **2** the pK_H values were determined (Table 1). The highest two pK_H cor-

Table 1. Protonation constants of **2** and of its Cu^{2+} complexes (at 25° and $I = 0.5$ M (KNO_3)) as well as spectral properties (λ_{max} and ε) of the Cu^{2+} complexes

Species	pK_H[a]	λ_{max} (ε)[b]
LH_3^{3+}	2.19 (1)	–
LH_2^{2+}	10.05 (1)	–
LH^{+}	10.72 (2)	–
$[Cu(LH)]^{3+}$	6.33 (4)	637 (116)
$[Cu(L)]^{2+}$	10.12 (4)	612 (114)
$[Cu(LH_{-1})]^{+}$	10.76 (2)	602 (123)
$[Cu(LH_{-2})]$		[c]
$[Cu_2(L)]^{4+}$	2.41 (1)	[c]
$[Cu_2(LH_{-1})]^{3+}$	6.59 (1)	627 (232)
$[Cu_2(LH_{-2})]^{2+}$	11.71 (1)	612 (221)
$[Cu_2(LH_{-3})]^{+}$		[c]

[a]Mean value and standard deviation between four batches.
[b]λ_{max} in nm and ε in $M^{-1}\,cm^{-1}$.
[c]Cannot be determined.

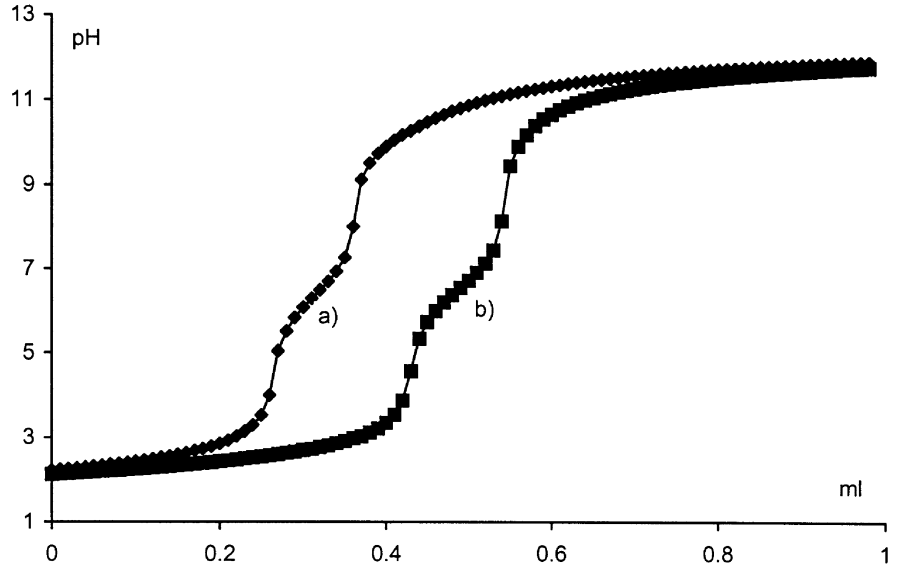

Fig. 1. Titration curves of **2** in the presence of (a) 0.9 and (b) 1.8 equivalents Cu^{2+}. ◆, ■ experimental points, — calculated curves (σ (ml) = 1.3×10^{-3}).

respond to the protonation of one nitrogen of each N_2S ring and the ΔpK_H of 0.67, very close to the statistical factor, indicates that the protonation sites are relatively independent from each other. The third and low pK_H is due to the strong electrostatic repulsion when a further proton is bound to one of the N_2S rings.

Titrations of **2** in the presence of 0.9 or 1.8 equivalents of Cu^{2+} (Fig. 1) allow in a batch calculation, in which both titration curves are fitted at the same time with one model, to calculate the stability constants of the mononuclear species $[Cu(LH)]^{3+}$, $[Cu(L)]^{2+}$, $[Cu(LH_{-1})]^{+}$ and $[Cu(LH_{-2})]$ as well as of the dinuclear complexes $[Cu_2(L)]^{4+}$, $[Cu_2(LH_{-1})]^{3+}$, $[Cu_2(LH)_{-2})]^{2+}$, and $[Cu_2(LH)_{-3})]^{+}$. The absolute stability of these species could not be determined, since $[Cu(LH)]^{3+}$ is already fully formed at low pH. To describe the system we therefore use the pK_H values (eqn (2)) connecting the protonated species and their conjugate bases (Table 1).

$$Cu(LH_n) \rightleftharpoons Cu(LH_{n-1}) + H^+;$$

$$K_n = [Cu(LH_{n-1})] \cdot [H^+]/[Cu(LH_n)] \qquad (2)$$

The species distribution (Fig. 2) for $[L] = 2.5 \times 10^{-3}$ M and $[Cu^{2+}] = 2.3 \times 10^{-3}$ M shows that $[(CuLH)]^{3+}$

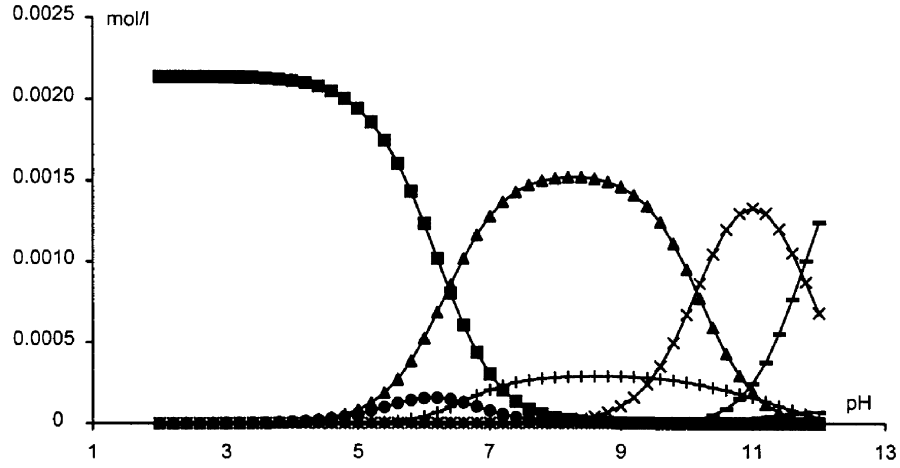

Fig. 2. Species distribution of the complexes of **2** with 0.9 equivalents Cu^{2+} ($[L] = 2.5 \times 10^{-3}$ M, $[M] = 2.3 \times 10^{-3}$ M). ■ $[Cu(LH)]^{3+}$, ▲ $[CuL]^{2+}$, × $[Cu(LH_{-1})]^{+}$, — $[Cu(LH_{-2})]$, ● $[Cu_2(LH_{-1})]^{3+}$, + $[Cu_2(LH_{-2})]^{2+}$.

dominates at pH below 6, whereas the main species between pH 6 and 11 are $[CuL]^{2+}$ and $[Cu(LH_{-1})]^{+}$ $[Cu(LH_{-2})]$. exists in measurable concentrations only above pH 11.

$[Cu(LH)]^{3+}$ (**4**) is the complex in which the Cu^{2+} ion is bound by one of the N_2S-rings, the proton being located on a nitrogen of the second ring not involved in coordination of the metal ion (see Scheme 1).

The subsequent three deprotonation steps to $[CuL]^{2+}$, $[Cu(LH_{-1})]^{+}$ and $[Cu(LH_{-2})]$ stem from the

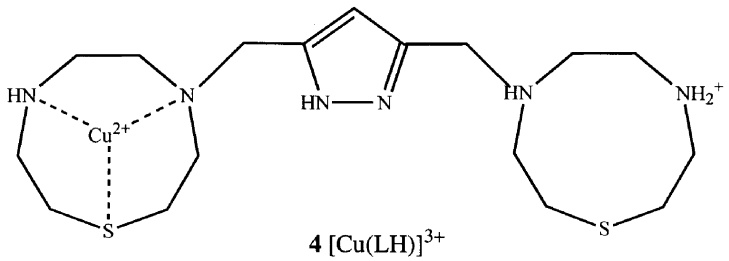

4 $[Cu(LH)]^{3+}$

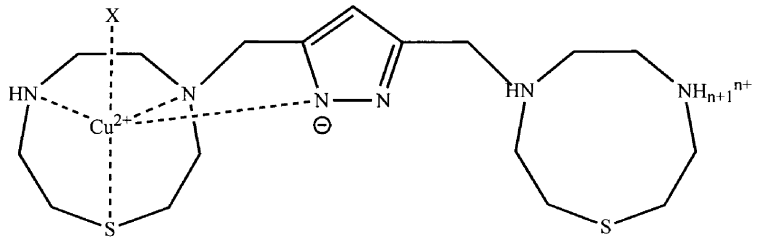

5 $[Cu(L)]^{2+}$ $X = H_2O$, n = 1

6 $[Cu(LH_{-1})]^{+}$ $X = OH^{-}$, n = 1 or $X = H_2O$, n = 0

7 $[Cu(LH_{-2})]$ $X = OH^{-}$, n = 0

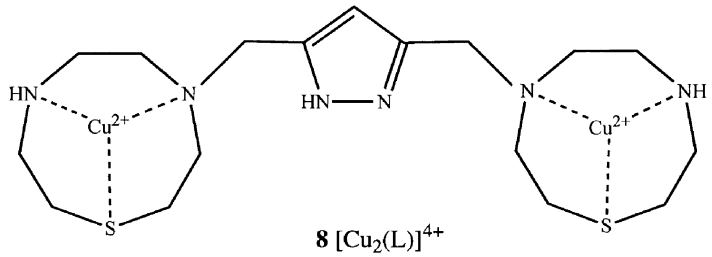

8 $[Cu_2(L)]^{4+}$

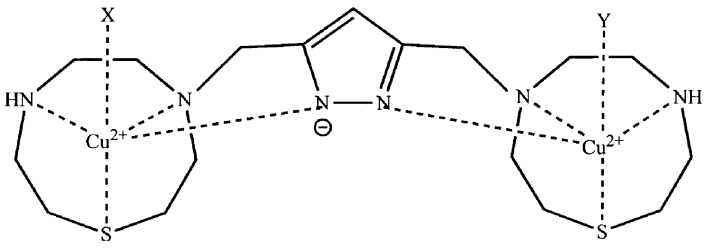

9 $[Cu_2(LH_{-1})]^{3+}$ $X = Y = H_2O$

10 $[Cu_2(LH_{-2})]^{2+}$ $X = OH^{-}$; $Y = H_2O$

11 $[Cu_2(LH_{-3})]^{+}$ $X = Y = OH^{-}$

Scheme 1.

neutralization and concomitant coordination of the pyrazole group, from the formation of a hydroxo species and from the deprotonation of the ammonium group of the N_2S ring. Whereas the structure of the final product (**7**) is clear, the exact sequence of the proton neutralizations is more difficult to determine. The shift of the absorption maximum from 637 nm for $[Cu(LH)]^{3+}$ to 612 nm for $[CuL]^{2+}$ (Table 1) is a clear indication that it is in this step that the pyrazole becomes deprotonated and through coordination of the pyrazolide group an increase of ligand field strength takes place. So the structure of $[CuL]^{2+}$ must be **5**. The exact sequence of the other two deprotonation steps is even more difficult to determine since they occur very close to each other and the spectrum of the final product cannot be measured and used for comparison purpose (structures **6** and **7**, Scheme 1).

Ligand **2** was specifically designed to form dinuclear complexes and indeed several of them have been isolated and characterized in the solid state by X-ray diffraction [16]. In aqueous solution we also find such species, which differ in their protonation degree. For example in a mixture with $[L]=2.5\times10^{-3}$ M and $[Cu^{2+}]=4.6\times10^{-3}$ M $[Cu_2L]^{4+}$ is formed already at very low pH and deprotonates with $pK_H=2.41$ to give $[Cu_2(LH_{-1})]^{3+}$ (Fig. 3). The structure of $[Cu_2L]^{4+}$ (**8**) can be described by two Cu^{2+} symmetrically coordinated by the two macrocyclic rings, whereas that of $[Cu_2(LH_{-1})]^{3+}$ (**9**) with a maximum at 627 nm contains in addition the pyrazolide bridging group as it was found in the solid state structures [16]. Further deprotonation to $[Cu_2(LH_{-2})]^{2+}$ (**10**) and $[Cu_2(LH_{-3})]^{+}$ (**11**) gives the mono- and dihydroxo moieties.

Since the X-ray studies showed that $[Cu_2(LH_{-1})]^{3+}$ is able to bind exogenous bridging ligands [16], it was interesting to study this reaction in solution. By spectrophotometric titrations (Fig. 4) one can follow the formation of the ternary species as indicated in eqs (3) and (4).

$$[Cu_2(LH_{-1})]^{3+}+Z \rightleftharpoons [Cu_2(LH_{-1})Z];\quad K_1 \quad (3)$$

$$2[Cu_2(LH_{-1})]^{3+}+Z \rightleftharpoons [[Cu_2(LH_{-1})]_2Z];\quad K_2 \quad (4)$$

As bridging ligands N_3^-, pyrazole (pyr), and 1H,1′H-4,4′-methanediyl-bis-pyrazole (bispyr) were used. The results obtained by fitting the titration with the program SPECFIT (Table 2) are interesting since they show that N_3^- and bispyr can form 1:1 and 2:1 species (Fig. 5), whereas pyr is, as expected, only able to give a 1:1 complex. It must be pointed out, that the stability constants for these ternary complexes are conditional constants obtained at pH = 5.5, at which $[Cu_2(LH_{-1})]^{3+}$ is the dominant binary moiety. A change in pH will modify not only the species distribution but in the case of pyr and bispyr, also the concentration of the deprotonated form of the exogenous ligand.

Table 2. Conditional stability constants (pH = 5.5) for the formation of the ternary complexes with N_3^-, pyr and bispyr according to Eqs (2) and (3) at 25° and $I=0.5$ M KNO_3

	N_3^-	pyr	bispyr
$\log K_1$	4.22(5)	3.85(3)	3.85[a]
$\log K_2$	7.27(6)	–	7.65(5)

[a]Kept fixed during the fitting procedure.

To confirm these findings we have studied the ternary system with bispyr also by ES–MS. By mixing $[Cu_2(LH_{-1})]^{3+}$ and bispyr in different ratio in the presence of a base one can see how the dinuclear and tetranuclear species are indeed formed (Fig. 6).

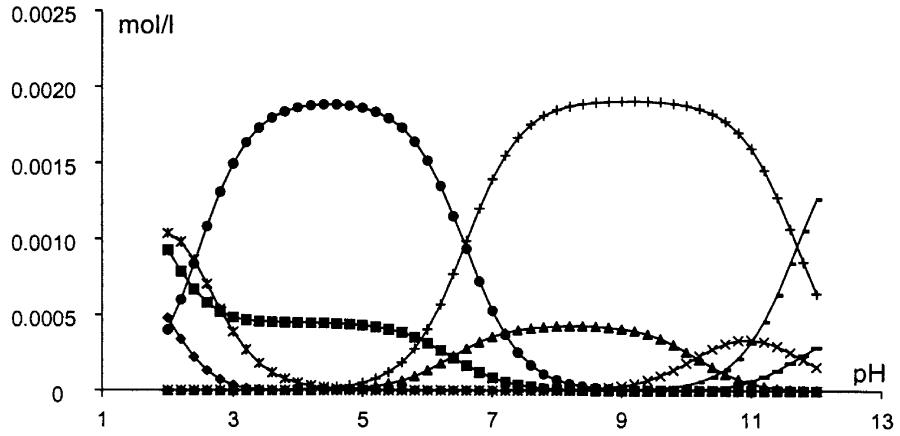

Fig. 3. Species distribution of the complexes of **2** with 1.8 equivalents Cu^{2+} ($[L]=2.5\times10^{-3}$ M, $[M]=4.5\times10^{-3}$ M). ◆ Cu^{2+}, ■ $[Cu(LH)]^{3+}$, ▲ $[CuL]^{2+}$, × $[CuLH_{-1})]^{+}$, — $[Cu(LH_{-2})]$, * $[Cu_2(L)]^{4+}$, ● $[Cu_2(LH_{-1})]^{3+}$, + $[Cu_2(LH_{-2})]^{2+}$.

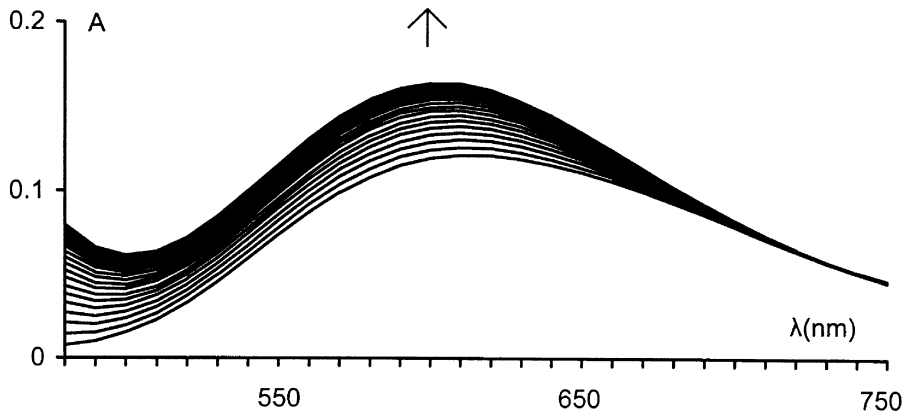

Fig. 4. Spectrophotometric titrations of $[Cu_2(LH_{-1})]^{3+}$ (6×10^{-4} M) with increasing amounts of 1H,1′H-4,4′-methanediyl-bis-pyrazole (bispyr) at pH 5.5.

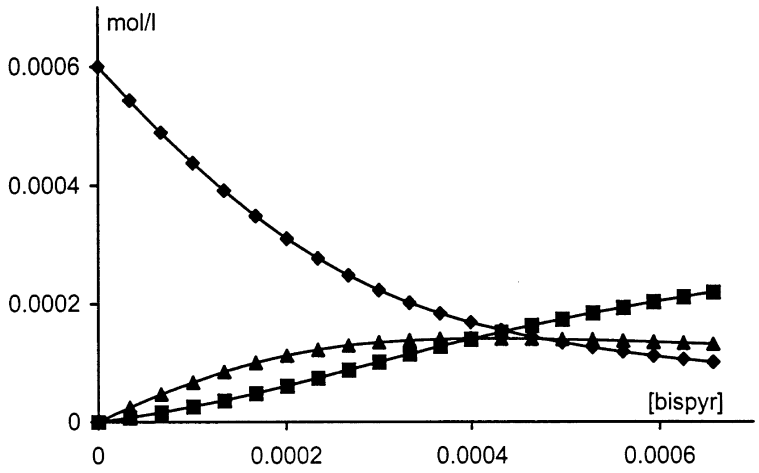

Fig. 5. Concentrations of the ternary species as a function of the 1H,1′H-4,4′-methanediyl-bis-pyrazole (bispyr) concentration. ◆ $[Cu_2(LH_{-1})]^{3+}$, ■ $[Cu_2(LH_{-1})bispyr]^{2+}$, ▲ $[[(Cu_2(LH_{-1})]_2bispyr]^{4+}$.

The ES–MS at a ratio (1:0) shows the presence of several doubly charged ions (m/z 264.1, 277.1), which may correspond to solvent cluster ions of the complex $[Cu_2(LH_{-1})]^{3+}$. The addition of small amounts of bispyr results in the appearance of the ions at m/z 292.2 and 329.0 corresponding to a quadruple and doubly charged species. At a ratio of 2:1 those two ions become predominant. The isotopic distribution of the ion at m/z 292.2 is in good agreement with a complex corresponding to $[[Cu_2(LH_{-1})]_2bispyr]^{4+}$ while the ion at m/z 329.0 fits with the complex $[Cu_2(LH_{-1})bispyr]^{2+}$. Electrospray ionization reflects generally qualitatively the species present in solution [29, 30]. The intensity of the ions observed in the spectra is strongly charge and compound dependent especially when working at such high concentration. Therefore the signal intensities can not be used quantitatively. However, at a 1:1 ratio $[Cu_2(LH_{-1})bispyr]^{2+}$ is almost exclusively observed. For the structures of these two complexes we propose Structures **12** and **13** (Scheme 2).

The species **13** is an interesting moiety which self-assembles from seven species by mixing four equivalents Cu^{2+}, two equivalents **2** and one equivalent bispyr and enough base to deprotonate the pyrazole rings.

In conclusion we can say that ligand **2** consisting of two macrocyclic units bridged by a pyrazole moiety gives a series of mononuclear $[Cu(LHn)]$ ($n = 1, 0, -1$) and dinuclear $[Cu_2(LHm)]$ ($m = 0, -1, -2, -3$) species in solution, which have been characterized. As in the structures previously found in the solid state,

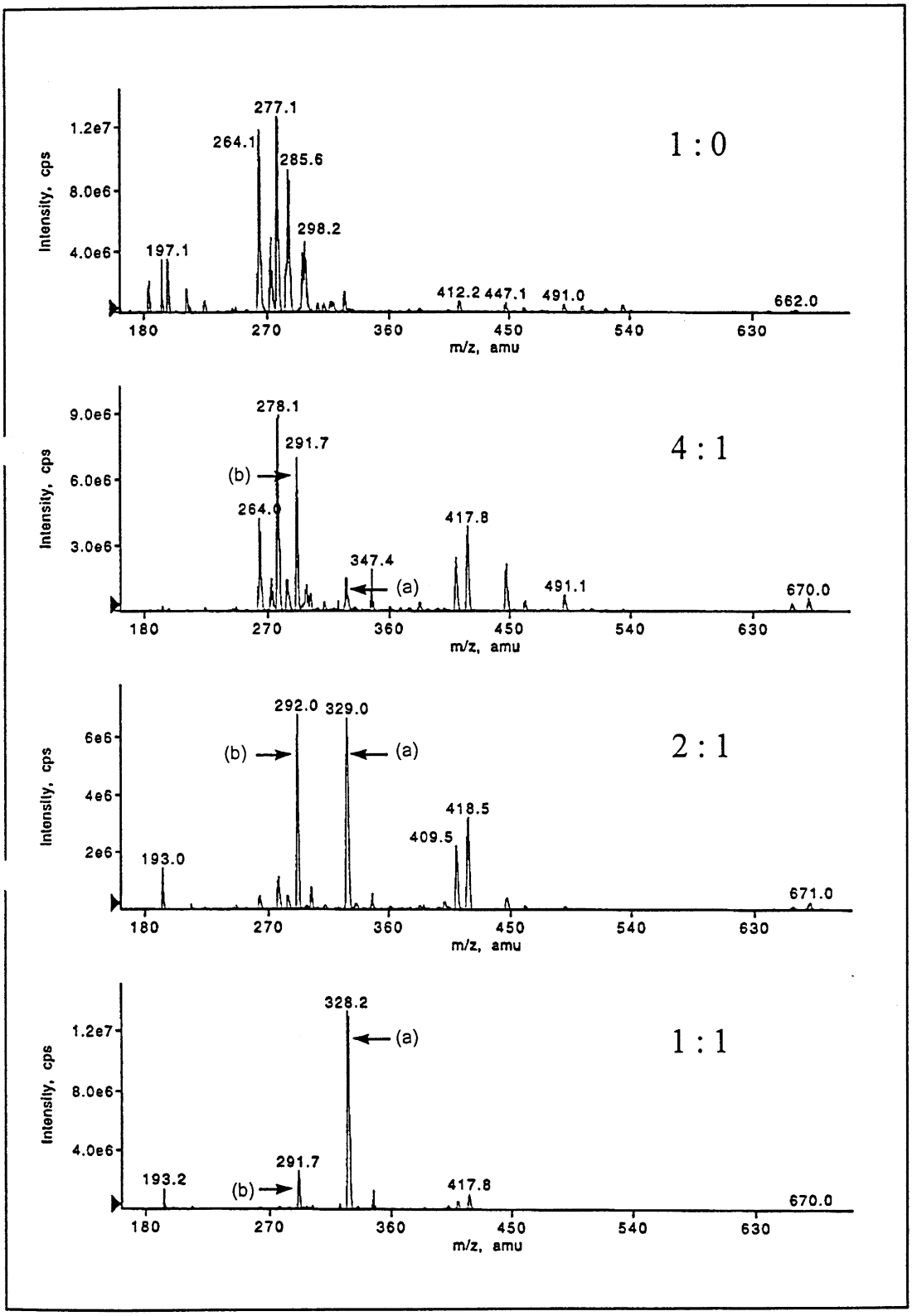

Fig. 6. ES–MS of the complex $[Cu_2(LH_{-1})]^{3+}$ in presence of different amounts of bispyr, showing the formation of $[(Cu_2(LH_{-1})]_2bispyr]^{4+}$ (a) and $[Cu_2(LH_{-1})bispyr]^{2+}$ (b).

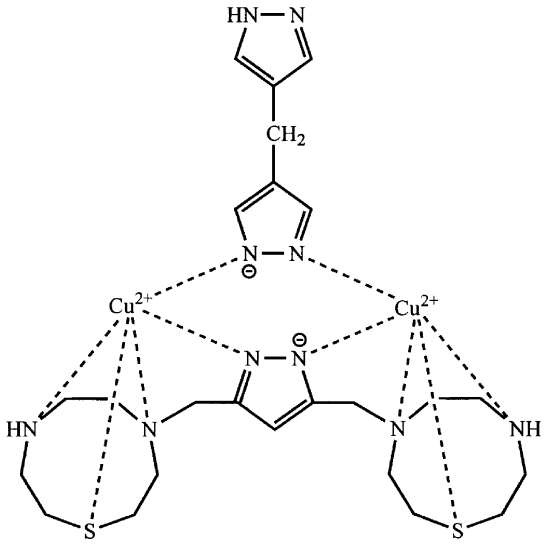

12 $[Cu_2(LH_{-1})bispyr]^{2+}$

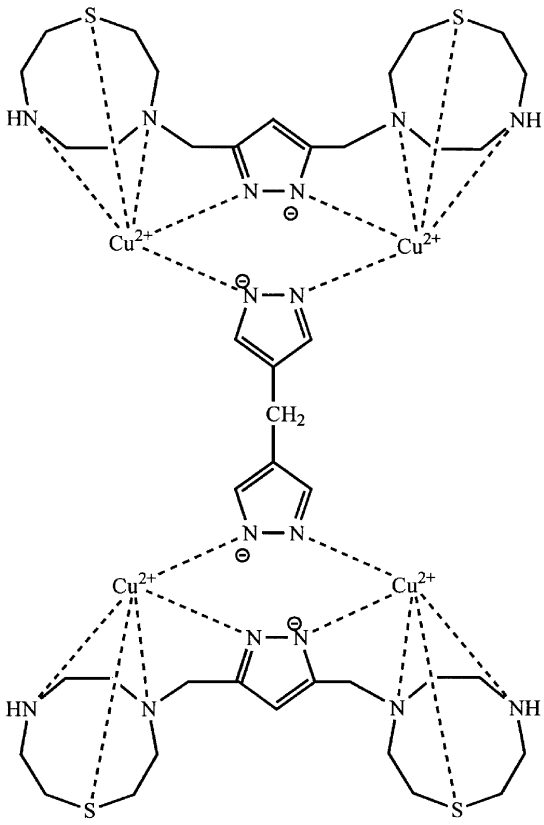

13 $[[Cu_2(LH_{-1})]_2bispyr]^{4+}$

Scheme 2.

also in solution $[Cu_2(LH_{-1})]^{3+}$ is able to coordinate exogenous ligands such as N_3^-, pyr and bispyr, the latter one giving an interesting tetranuclear species as confirmed by ES–MS experiments.

Acknowledgements—This work was supported by the Swiss National Foundation (Project Nr. 20-45408.95) and in part by COST-D1 through the Bundesamt für Bildung und Wissenschaft.

REFERENCES

1. Kaden, Th. A., in *Transition Metals in Supramolecular Chemistry*, Eds. L. Fabrizzi and A. Poggi. Kluwer, Dordrecht, 1994, p. 211.
2. Murase, L., Hamada, K. and Ueno, S., Kida, S., *Synth. React. Inorg. Met. Org.*, 1983, **13,** 191.
3. Ciampolini, M., Micheloni, M., Nardi, N., Vizza, F., Buttafava, A., Fabbrizzi, L. and Perotti, A., *J. Chem. Soc. Chem. Commun.*, 1984, **00,** 998.
4. Murase, I. and Ueno, S., Kida, S., *Inorg. Chim. Acta*, 1986, **111,** 57.
5. Barefield, E. K., Foster, K. A., Freeman, G. M. and Hodges, K. D., *Inorg. Chem.*, 1986, **25,** 4662.
6. Wieghardt, K., Tolksdorf, I. and Hermann, W., *Inorg. Chem.*, 1985, **24,** 1230.
7. Weisman, G. R., Vachon, D. J., Johnson, V. B. and Gronbeck, D. A., *J. Chem. Soc. Chem. Commun.*, 1987, 886.
8. Bourgoin, M., Wong, K. H., Hui, J. Y. and Smid, J., *J. Am. Chem. Soc.*, 1975, **97,** 3475.
9. McAuley, A., Subramanian, S. and Whitcombe, T. W., *J. Chem. Soc. Chem. Commun.*, 1987, 539.
10. Bernhardt, P. V., Comba, P., Gahan, L. R. and Lawrance, G. A., *Aust. J. Chem.*, 1990, **43,** 2035.
11. Barefield, E. K., Chueng, D., van Derveer, D. G. and Wagner, F., *J. Chem. Soc. Chem. Commun.*, 1981, 302.
12. Fabbrizzi, L., Forlini, F., Perotti, A. and Seghi, B., *Inorg. Chem.*, 1984, **23,** 807.
13. Fabbrizzi, L., Montagna, L., Poggi, A., Kaden, T. A. and Siegfried, L. C., *J. Chem. Soc. Dalton Trans.*, 1987, 2631.
14. Kimura, E., Kuramoto, Y., Koike, T., Fujikoka, H. and Kodama, M., *J. Org. Chem.*, 1990, **55,** 42.
15. Fabbrizzi, L., Montagna, L., Poggi, A., Kaden, Th. A. and Siegfried, L. C., *Inorg. Chem.*, 1986, **25,** 2672.
16. Weller, H., Siegfried, L., Neuburger, M., Zehnder, M. and Kaden, Th. A., *Helv. Chim. Acta*, 1997, **80,** 2315.
17. Urfer, A. and Kaden, Th. A., *Helv. Chim. Acta*, 1994, **77,** 23.
18. Haidar, R., Ipek, M., DasGupta, B., Yousaf, M. and Zompa, L. J., *Inorg. Chem.*, 1997, **36,** 3125.
19. Schneider, R., Riesen, A. and Kaden, Th. A., *Helv. Chim. Acta*, 1986, **69,** 53.
20. Ciampolini, M., Fabbrizzi, L., Perotti, A., Poggi, A., Seghi, B. and Zanobini, F., *Inorg. Chem.*, 1987, **26,** 3527.
21. Burk, P. L., Osborn, J. A. and Youinou, M. T., *J. Am. Chem. Soc.*, 1981, **103,** 1273.
22. Tandon, S., Thompson, L. K., Bridson, J. N., Mckee, V. and Downard, A. J., *Inorg. Chem.*, 1992, **31,** 4635.
23. Behle, L., Neuburger, M., Zehnder, M. and Kaden, Th. A., *Helv. Chim. Acta*, 1995, **78,** 693.
24. Trofimenko, S., *J. Am. Chem. Soc.*, 1979, **92,** 5118.

25. Gampp, H., Maeder, M., Zuberbühler, A. D. and Kaden, Th. A., *Talanta*, 1980, **27,** 573.
26. Zuberbühler, A. D. and Kaden, Th. A., *Talanta*, 1982, **29,** 201.
27. Hänisch, G., Kaden, Th. A. and Zuberbühler, A. D., *Talanta*, 1979, **26,** 563.
28. Gampp, H., Maeder, M., Meyer, Ch. and Zuberbühler, A. D., *Talanta*, 1985, **32,** 257.
29. Hopfgartner, G., Piguet, C. and Henion, J. D., *J. Am. Soc. Mass Spectrom.*, 1994, **5,** 748.
30. Piguet, C., Bernardelli, G. and Hopfgartner, G., *Chem. Rev.*, 1997, **97,** 2005.

Pergamon

Polyhedron Vol. 17, Nos. 25, 26, pp. 4553–4566, 1998
© 1998 Elsevier Science Ltd
All rights reserved. Printed in Great Britain
PII: S0277–5387(98)00261–7
0277–5387/98 $19.00+0.00

Thermal and photochemical reactions of copper(II) dithiocarbamate mixed-ligand complexes with chloroalkanes

B. G. Jeliazkova,† M. A. Doicheva and K. Miltchovska

Department of Chemistry, Sofia University, 1, James Bourchier ave., 1164 Sofia, Bulgaria

(Received 5 May 1998; accepted 25 June 1998)

Abstract—Thermal and/or photochemical conversion of a series of copper(II) complexes containing mixed dithiocarbamato–alcohol ligands, $Cu^{II}(Et_2dtc)^+ \ldots Y^-$ ($Y = ClO_4^-$, NO_3^-), into $Cu^{II}(Et_2dtc)Cl$ in chloroalkane/alcohol solutions, where chloroalkane = CCl_4, $CHCl_3$ or CH_2Cl_2 and alcohol = MeOH, EtOH or *i*-BuOH, proceeds in chloroalkanes. Both reactions follow a similar pathway which is more effective the stronger the acceptor properties of chloroalkanes and the weaker the coordinating abilities of alcohols are. A detailed reaction mechanism is proposed which well fits the experimental results obtained by EPR and UV–VIS spectra and quantum yields. © 1998 Elsevier Science Ltd. All rights reserved

Keywords: CT photochemistry; copper(II) dithiocarbamate mixed-ligand complexes

INTRODUCTION

In recent communications [1, 2] we have described the photochemical properties of a series of copper(II) diethyldithiocarbamate mixed-ligand complexes, $Cu^{II}(Et_2dtc)X$, where X represents Cl^-, ClO_4^- or NO_3^-, studied in acetone, $CHCl_3$/*i*-PrOH (1:1), and CCl_4/*i*-PrOH (1:1) solutions. The complexes are characterized by their strongly allowed ligand-to-metal charge-transfer (LMCT) transition in the visible region of the spectrum at about 400 nm ($\lg \varepsilon = 3.7$) [1]. The reaction from the LMCT state is reduction of Cu(II) to Cu(I) proceeding via an intramolecular electron transfer from an equatorially bound S atom of the ligand to copper(II). Photo-irradiation of $Cu^{II}(Et_2dtc)^+ \ldots NO_3^-$ and $Cu^{II}(Et_2dtc)^+ \ldots ClO_4^-$ in the CT band in chloroalkane/*i*-propanol (1:1) solutions gives rise to $Cu^{II}(Et_2dtc)Cl$ as an intermediate product as seen by the appearance of its characteristic EPR spectrum [1] where the high field copper hyperfine line with $m_I = -3/2$ splits into four shf lines, implying interaction of the Cu(II) unpaired electron with one $^{35,37}Cl$ nucleus and thus proving that one Cl^- ion is covalently bound in the plane of the complex.

In CCl_4/*i*-propanol (1:1) solutions both $Cu^{II}(Et_2dtc)^+ \ldots NO_3^-$ and $Cu^{II}(Et_2dtc)^+ \ldots ClO_4^-$ undergo thermal conversion to $Cu^{II}(Et_2dtc)Cl$. The steps involved in this conversion could be better understood if we consider the abilities of CCl_4 and $CHCl_3$ to form adducts with $Cu^{II}(Et_2dtc)X$ complexes [2].

Although our previous studies [1, 2] have shown that both the photolytic and thermal reactions of $Cu^{II}(Et_2dtc)X$ occur by a Cu–S bond cleavage, the details of the reactions occurring before and subsequent to it were unclear. In order to clarify the role of chloroalkanes in the thermal reactions of $Cu^{II}(Et_2dtc)X$ and of its primary photo-products, and to correlate their behavior with the nature of the protic solvent of the mixture, it seemed necessary to perform a systematic study varying the solvents and looking for their effect on product formation and $Cu^{II}(Et_2dtc)X$ disappearance both in the thermal and photolytic pathways.

EXPERIMENTAL

Starting materials

The ligands and the p.a. grade metal salts were obtained from Fluka and used without further purification. To remove crystal water copper salts were treated as described before [1]. The solvents were used after distillation.

†Author to whom correspondence should be addressed.

Preparation of the coordination compounds

Mixed-ligand complexes $Cu^{II}(Et_2dtc)X$ ($X = Cl^-$, ClO_4^-, NO_3^-) are insoluble in neat CH_2Cl_2, $CHCl_3$ or CCl_4, but dissolve in mixtures of chloroalkanes and alcohols. Therefore, they were obtained according to the reactions [1]:

$$Cu(Et_2dtc)_2 + CuCl_2 = 2Cu^{II}(Et_2dtc)Cl, \quad (1)$$

$$Cu(Et_2dtc)_2 + CuY_2 = 2Cu^{II}(Et_2dtc)^+ \ldots Y^- \quad (2)$$

$$(Y = ClO_4^-, NO_3^-),$$

by mixing of chloroalkane solutions of $Cu(Et_2dtc)_2$ with alcohol solutions of the corresponding copper(II) salt as described before [1, 2]. The parent bis(diethyldithiocarbamato) copper(II) complex, used in the preparation, was obtained by a standard literature method [3]. The initial concentrations of its chloroalkane solutions were determined spectrophotometrically from the value of the molar absorptivity coefficient of the visible CT-band. The alcohol solutions of the corresponding copper(II) salts were titrated with EDTA before use. The solutions in this paper were not deaerated since it was found earlier [1] that deaeration was not a significant factor.

Instrumentation

The EPR spectra were taken on an X-band Bruker ER 420 spectrometer using 100 kHz modulation of the magnetic field. The electronic absorption spectra were recorded on a Specord UV–VIS (Carl-Zeiss, Jena) spectrophotometer using quartz cells to record in the 250–750 nm region.

Kinetic study

The thermal conversion of $Cu^{II}(Et_2dtc)^+ \ldots Y^-$ ($Y = ClO_4^-, NO_3^-$) to $Cu^{II}(Et_2dtc)Cl$ has been monitored by EPR spectroscopy. For this purpose EPR spectra of CCl_4/alcohol (1:1) solutions were recorded at different time intervals after their preparation on keeping the sample probe at fixed position in the EPR spectrometer cavity and room temperature. Since the time required to obtain a spectrum was small compared to their half-lives, EPR data provided satisfactory results for compounds formed or consumed in the reaction stages. By extrapolation to zero time, the observed changes in the signal intensities of the starting complexes were related to changes in their actual concentrations. The concentration of the product was determined with the use of freshly prepared $Cu^{II}(Et_2dtc)Cl$ reference solutions in the appropriate solvent mixtures. For all reactions CCl_4 and ROH were in pseudo-first-order excess over the Cu(II) complexes (ca. 10^{-4}–10^{-3} mol dm^{-3}).

Irradiation and quantum yields

Photolysis experiments were performed with the full spectrum of a 250 W medium-pressure mercury lamp or through a 406 nm solution filter [4] as previously described [5]. For quantum yield determination the complex concentrations were such as to have essentially complete light absorption. No correction was made for internal filter effects. The incident light intensity was determined before and after each photolysis by a ferrioxalate actinometric method [4]. At least three determinations of quantum yields were made for each complex. Photolyses of all complexes were carried out at 25 ± 1°C. To correct for possible thermal reactions, UV–VIS and EPR spectra were obtained immediately after photolyses and compared with the spectrum of an aliquot kept in the dark. Thermal corrections were not significant for any of the complexes in CH_2Cl_2/ROH or $CHCl_3$/ROH solvent mixtures. UV–VIS photolysis was studied on freshly prepared CCl_4/ROH solutions.

RESULTS AND DISCUSSION

EPR spectra

The EPR measurements were carried out at room temperature under the same conditions as those of the photolytic experiments. The Hamiltonian parameters calculated from the spectra obtained for ligand and metal concentrations of 1×10^{-3} mol dm^{-3} at 293 K are listed in Table 1. Typical EPR spectra are given in Fig. 1.

The results of Table 1 provide a systematic basis for identifying the coordination of alcohol in the *xy* plane of the complex. It is seen from Table 1 that the EPR parameters of all $Cu^{II}(Et_2dtc)^+ \ldots Y^-$ complexes obtained in chloroalkane/alcohol solvent mixtures do not vary with the chloroalkane or the anion Y^- and depend on the nature of the alcohol. Therefore, it seems that besides the bi-dentate dtc ligand, the coordination plane of $Cu^{II}(Et_2dtc)^+ \ldots Y^-$ is comprised of two alcohol molecules yielding the chromophore $Cu^{II}S_2(solv)_2$ and that of $Cu^{II}(Et_2dtc)Cl$ consists of a chloride ion, and an alcohol molecule in the chromophore $Cu^{II}S_2Cl \cdot solv$ (Table 1).

Only the hyperfine lines of $Cu^{II}(Et_2dtc)^+ \ldots Y^-$ are seen in the EPR spectra obtained in all chloroalkane/ROH solutions (spectra 1–3 in Fig. 1(a)) indicating a quantitative ligand exchange between $Cu(Et_2dtc)_2$ and CuY_2 to yield exclusively $Cu^{II}(Et_2dtc)^+ \ldots Y^-$ by reaction (2) and the same is valid for $Cu^{II}(Et_2dtc)Cl$ obtained by reaction (1) in chloroalkane/*i*-BuOH (1:1) (spectrum 3 in Fig. 1(b)) and in chloroalkane/*i*-PrOH (1:1) as seen before [1, 2]. When *i*-BuOH (resp. *i*-PrOH) as solvent is replaced by MeOH (or EtOH) the EPR spectra of $Cu^{II}(Et_2dtc)Cl$ (1 and 2 in Fig. 1(b)) reveal the superposition of a spectrum that is due to the bis-solvated $Cu^{II}(Et_2dtc)^+$ species on that of

Table 1. EPR parameters of the mixed-ligand complexes $Cu^{II}(Et_2dtc)^+ \ldots ClO_4^-$, $Cu^{II}(Et_2dtc)^+ \ldots NO_3^-$, the equilibrium mono-$Cu^{II}(Et_2dtc)Cl$ and bis-solvated $Cu^{II}(Et_2dtc)^+$ species appearing in chloroalkane/ROH (1:1) solutions of $Cu^{II}(Et_2dtc)Cl$ and the products of $Cu^{II}(Et_2dtc)^+ \ldots Y^-$ ($Y = ClO_4$, NO_3) photolysis in chloroalkane/ROH (1:1) and thermal[a] reaction in CCl_4/ROH (1:1), 300 K

		$Cu(Et_2dtc)^+ \ldots ClO_4^-$		$Cu(Et_2dtc)^+ \ldots NO_3$		$Cu(Et_2dtc)^+$		$Cu(Et_2dtc)Cl$			Product of $Cu(Et_2dtc)^+ \ldots ClO_4^-$			Product of $Cu(Et_2dtc)^+ \ldots NO_3^-$		
Solvent		$g_0 \pm$ 0.001	$^{Cu}A_0 \pm$ 1 G	$g_0 \pm$ 0.001	$^{Cu}A_0 \pm$ 1 G	$g_0 \pm$ 0.001	$^{Cu}A_0 \pm$ 1 G	$g_0 \pm$ 0.001	$^{Cu}A_0 \pm$ 1 G	$^{Cl}A_0 \pm$ 0.5 G	$g_0 \pm$ 0.001	$^{Cu}A_0 \pm$ 1 G	$^{Cl}A_0 \pm$ 0.5 G	$g_0 \pm$ 0.001	$^{Cu}A_0 \pm$ 1 G	$^{Cl}A_0 \pm$ 0.5 G
MeOH	CH_2Cl_2	2.090	68	2.089	68	2.089	68	2.074	74	*	2.074	73	*	2.075	73	*
	$CHCl_3$	2.089	68	2.089	68	2.089	68	2.075	75	*	2.075	74	*	2.074	74	*
	CCl_4	2.090	68	2.090	68	2.088	68	2.076	75	*	2.074	73	*	2.074	73	*
	CCl_4 [a]										2.075	73	*	2.074	74	*
EtOH	CH_2Cl_2	2.089	72	2.088	71	2.089	72	2.074	75	7.6	2.074	74	7.6	2.074	74	7.8
	$CHCl_3$	2.090	72	2.090	72	2.089	72	2.074	75	7.7	2.075	74	7.7	2.075	74	7.9
	CCl_4	2.090	72	2.090	72	2.088	71	2.075	74	7.8	2.076	74	7.7	2.076	74	7.7
	CCl_4 [a]										2.076	74	7.6	2.076	74	7.8
i-BuOH	CH_2Cl_2	2.084	75	2.084	75			2.074	74	7.7	2.073	74	7.7	2.074	74	7.8
	$CHCl_3$	2.085	74	2.084	74			2.074	75	7.9	2.074	75	7.8	2.073	75	7.6
	CCl_4	2.087	73	2.086	74			2.075	74	7.8	2.075	74	7.9	2.075	74	7.8
	CCl_4 [a]										20.75	74	7.8	2.075	74	7.7

*^{35}Cl shfs is not well resolved because of the high polarity of the solvent.

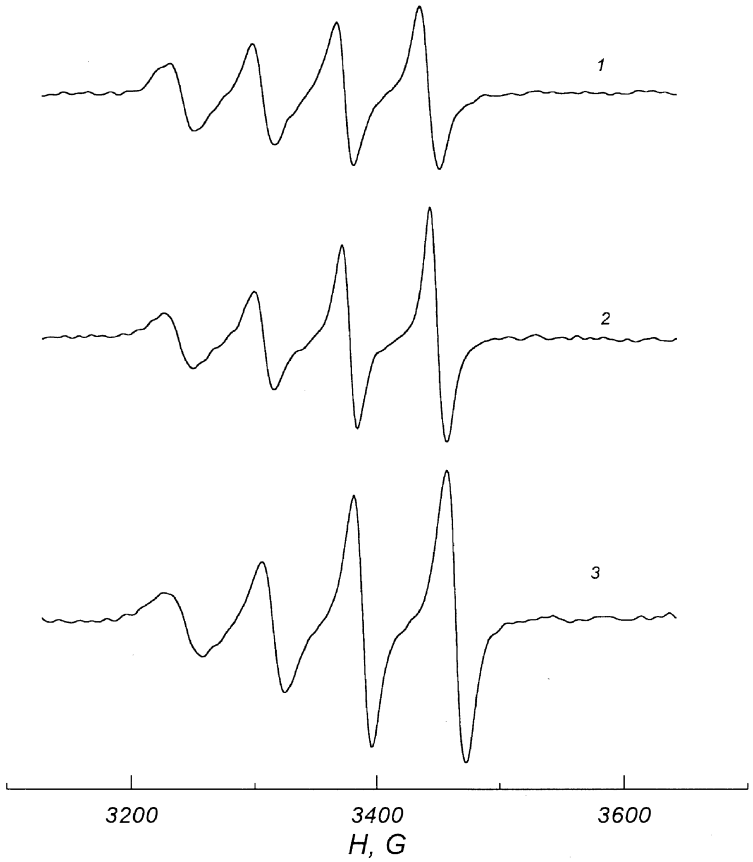

Fig. 1. EPR spectra of equimolar (1×10^{-3} mol dm^{-3}) mixtures of (a) $Cu(Et_2dtc)_2$ in CH_2Cl_2 and $Cu(ClO_4)_2$ in MeOH (1), EtOH (2), *i*-BuOH (3).

$Cu^{II}(Et_2dtc)Cl$ (see Table 1) suggesting the following equilibrium between the mono- and bis-solvated form of the complex in these solvents:

$$Cu^{II}(Et_2dtc)Cl \rightleftharpoons Cu^{II}(Et_2dtc)^+ \ldots Cl^- . \qquad (3)$$

Therefore, in chloroalkane/MeOH (1:1) solutions $Cu^{II}(Et_2dtc)Cl$ is partly converted into a bis-solvated form and MeOH has replaced chloride ion as an equatorial ligand. The same is observed with EtOH, but the relative intensities of the signals of both species in spectrum 2 (Fig. 1(b)) suggests higher amounts of $Cu^{II}(Et_2dtc)Cl$ and lower $Cu^{II}(Et_2dtc)^+$ concentration compared to spectrum 1 (Fig. 1(b)) which is in accordance with the weaker coordinating ability of EtOH compared to MeOH in the following order of nucleophilicity [6]:

$$MeOH > EtOH > i\text{-}PrOH > H_2O > t\text{-}BuOH.$$

UV spectra

In addition to the visible LMCT band, the ultraviolet spectra of the mixed-ligand complexes $Cu^{II}(Et_2dtc)X$ are dominated by two main absorptions in the region 260–300 nm ascribed to intraligand dtc transitions [7], which are not observed in CCl_4 because of the strong absorption of this solvent in UV.

Thermal reactions

The electronic absorption and EPR spectra of all mixed-ligand complexes are quite stable in CH_2Cl_2/ROH or $CHCl_3$/ROH (1:1) solutions and show no decomposition for times < 120 h. Opposite to them, the obtained absorption and EPR spectra reveal thermal decomposition of all mixed-ligand complexes in CCl_4/ROH (1:1) with more complicated changes for $Cu^{II}(Et_2dtc)^+ \ldots Y^-$ than for $Cu^{II}(Et_2dtc)Cl$. Fig. 2 illustrates the absorbance vs time profiles obtained at 25°C at the CT band of the appropriate mixed-ligand complex in CCl_4/MeOH (1:1) solution. The kinetic runs show a slow decrease in the CT absorbances and an increase of the 282 nm absorption at larger reaction times due to the appearance of tetraethylthiuramdisulphide [8, 9] (Et_4tds) as the final product. Because of the UV–VIS spectral similarities of $Cu^{II}(Et_2dtc)Cl$, $Cu^{II}(Et_2dtc)^+ \ldots NO_3^-$ and $Cu^{II}(Et_2dtc)^+ \ldots ClO_4^-$, the kinetic curves in Fig. 2 are not very informative and they are additionally

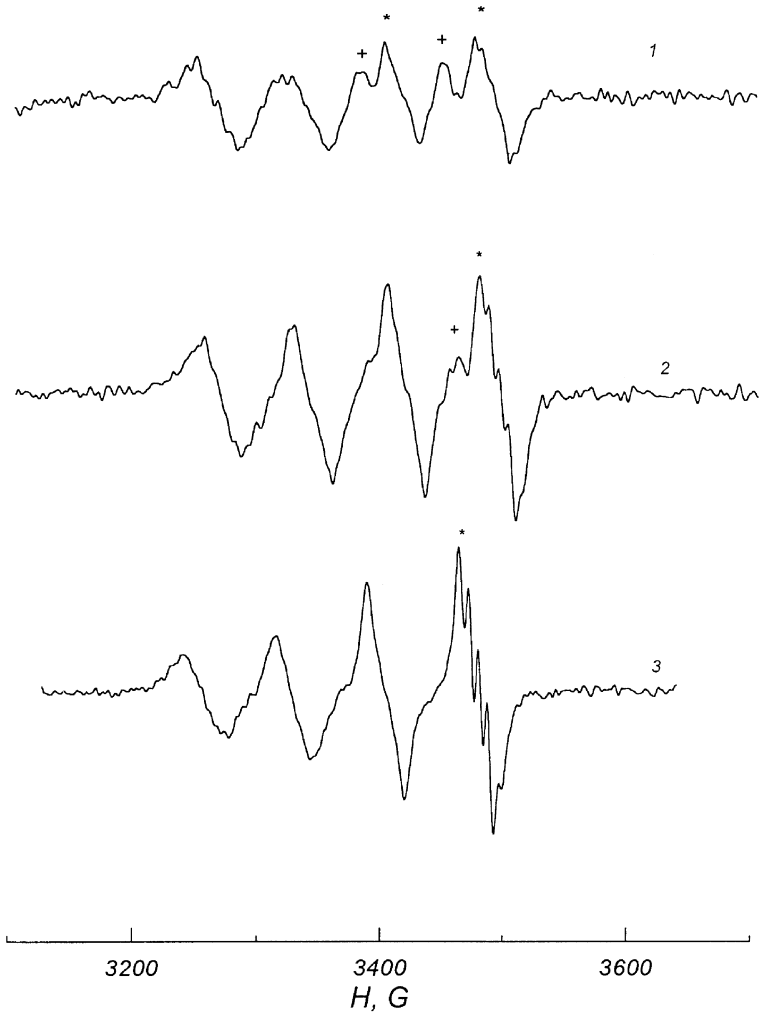

Fig. 1. (b) $Cu(Et_2dtc)_2$ in CH_2Cl_2 and $CuCl_2$ in MeOH (1), EtOH (2), *i*-BuOH (3). EPR lines marked * and + correspond to $Cu^{II}(Et_2dtc)Cl$ and $Cu^{II}(Et_2dtc)^+$ species, respectively.

complicated in CCl_4/MeOH and CCl_4/EtOH (1:1) solutions by the equilibrium reaction (3). For this reason EPR spectra were recorded at different time intervals after preparation of all CCl_4/ROH (1:1) solutions in an attempt to obtain more information about the occurrence of different kinetic steps.

A relevant representation of the EPR spectral changes obtained in the thermal reactions occurring after mixing of equimolar quantities of $Cu(Et_2dtc)_2$ in CCl_4 with *i*-BuOH solution of $Cu(ClO_4)_2$ (a) or MeOH solution of $Cu(NO_3)_2$ (b) is depicted in Fig. 3. The observed EPR spectral changes confirm the conversion of the bis-solvated $Cu^{II}(Et_2dtc)^+$ species into a chloride coordinated monosolvated $Cu^{II}(Et_2dtc)Cl$ form. This conclusion is also supported by the similarities between the values of g and A of the independently obtained (see Section 2) sample of $Cu^{II}(Et_2dtc)Cl$ and the product of $Cu^{II}(Et_2dtc)^+ \ldots NO_3^-$ thermolysis taking place in CCl_4/ROH solvent systems (Table 1). Once obtained the chromophore $Cu^{II}S_2Cl \cdot solv$ is retained in all CCl_4/alcohol (1:1) solutions and thermal decomposition of $Cu^{II}(Et_2dtc)Cl$ to $CuCl_2$ and Et_4tds proceeds much slower.

Determination of rate constants

The observed EPR behavior was used for a kinetic study. It was easy to follow by this method in CCl_4/MeOH (1:1), CCl_4/EtOH (1:1) and CCl_4/*i*-BuOH (1:1) as the starting $Cu^{II}(Et_2dtc)^+ \ldots Y^-$ complexes and the product $Cu^{II}(Et_2dtc)Cl$ had different EPR parameters and the reaction proceeded at a convenient rate at 25°C. Figure 4 shows the concentration vs time profiles derived from the EPR data for the major species detected by EPR on keeping CCl_4/*i*-BuOH (1:1) solution of $Cu^{II}(Et_2dtc)^+ \ldots ClO_4^-$(a) and CCl_4/MeOH (1:1) solution of $Cu^{II}(Et_2dtc)^+ \ldots NO_3^-$ (b) for several hours in the dark. A strong decrease

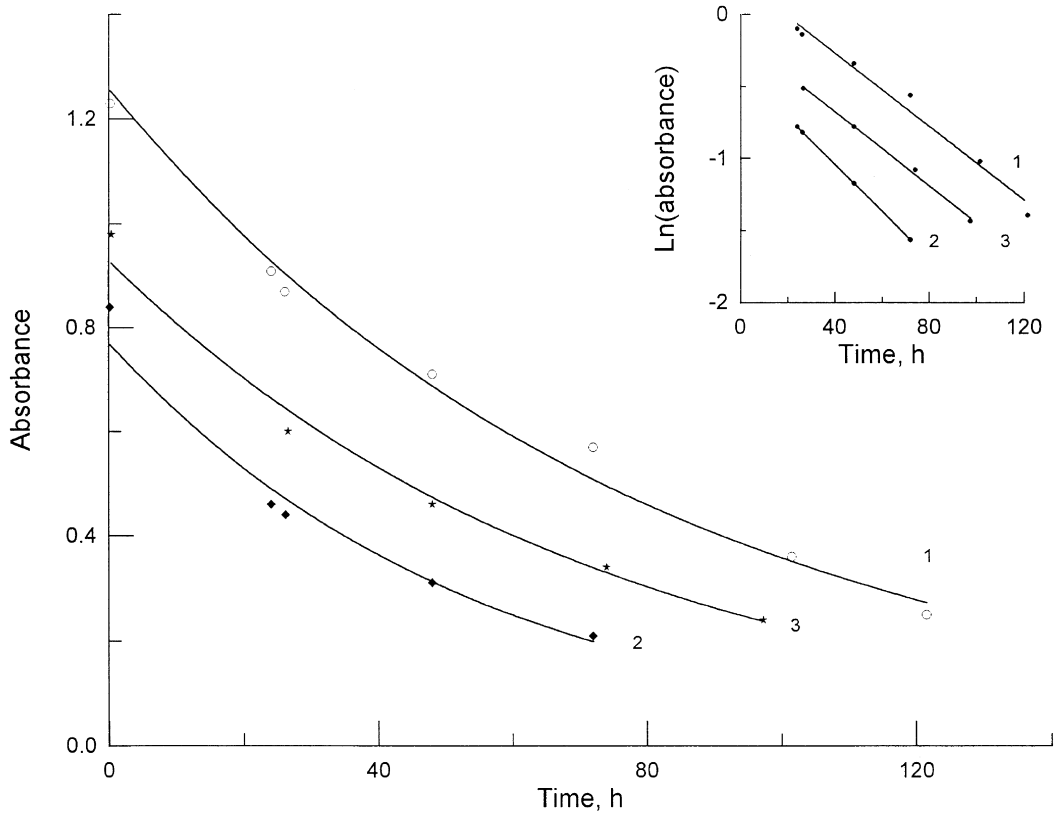

Fig. 2. Absorbance vs time profiles obtained at 25°C at the CT band of $Cu^{II}(Et_2dtc)^+ \ldots ClO_4^-$ (1), $Cu^{II}(Et_2dtc)^+ \ldots NO_3^-$ (2) and $Cu^{II}(Et_2dtc)Cl$ (3) in CCl_4/MeOH (1:1). Insets: The corresponding plots of ln(A) vs time.

in EPR intensity is observed during the reaction associated with the disappearance of the original $Cu^{II}(Et_2dtc)^+ \ldots Y^-$ complexes at 25°C illustrated by kinetic curves (1) in Fig. 4(a, b). The plots obtained in CCl_4/*i*-BuOH (1:1) showed that practically all $Cu^{II}(Et_2dtc)^+ \ldots Y^-$ had reacted in this solvent yielding $Cu^{II}(Et_2dtc)Cl$ (Fig. 4(a)). In CCl_4/MeOH (1:1) (Fig. 4(b)) and CCl_4/EtOH (1:1) the EPR signal intensity of the original $Cu^{II}(Et_2dtc)^+ \ldots Y^-$ complex was decreasing to a definite value corresponding to its equilibrium concentration maintained by reaction (3).

The strongly descending curves (1) of the starting $Cu^{II}(Et_2dtc)^+ \ldots Y^-$ complexes were analyzed by the least squares method to give the results of k_1 in Table 2. This step was first order in the concentration of the starting complex as plots of ln(concentration) vs time (insets 1 in Fig. 4(a, b)) were linear to more than 50% reaction completion and the obtained values of k_1 followed the order of the hydrogen donating power of solvents *i*-BuOH > EtOH > MeOH [10].

The kinetic analysis of the changes of $Cu^{II}(Et_2dtc)Cl$ concentration given with curves (2) in Fig. 4(a, b) indicated that in all CCl_4/ROH (1:1) solvent mixtures it appeared after induction periods at different time depending on ROH. It seemed that $Cu^{II}(Et_2dtc)Cl$ was yielded in a reaction of an EPR silent intermediate

Table 2. Rate constants ($k \times 10^4\,s^{-1}$) of the room temperature reaction of $Cu^{II}(Et_2dtc)^+ \ldots Y^-$ (Y = ClO_4, NO_3) with CCl_4 under pseudo-first-order conditions in CCl_4/ROH (1:1)

Solvent	$Cu(Et_2dtc)^+ \ldots ClO_4^-$		$Cu(Et_2dtc)^+ \ldots NO_3^-$	
	k_1	k_2	k_1	k_2
CCl_4/MeOH	2.0	1.1	2.0	1.4
CCl_4/EtOH	2.4	1.3	2.1	1.2
CCl_4/*i*-BuOH	5.0	1.5	3.0	1.4

(A) and kinetic curves (2) were complicated by the existence of at least two steps with similar rate constants. The values of the rate constant k_2 with respect to $Cu^{II}(Et_2dtc)Cl$ concentration were calculated by the least squares method from the slope of the linear plots between ln(concentration) and time, obtained after the inflection point of curves (2) and given as insets 2 in Fig. 4(a, b). Although there were few experimental points, satisfactory fits were obtained to give approximate values of the rate constant k_2 corresponding to the formation of $Cu^{II}(Et_2dtc)Cl$ in a first-order reaction of A. The

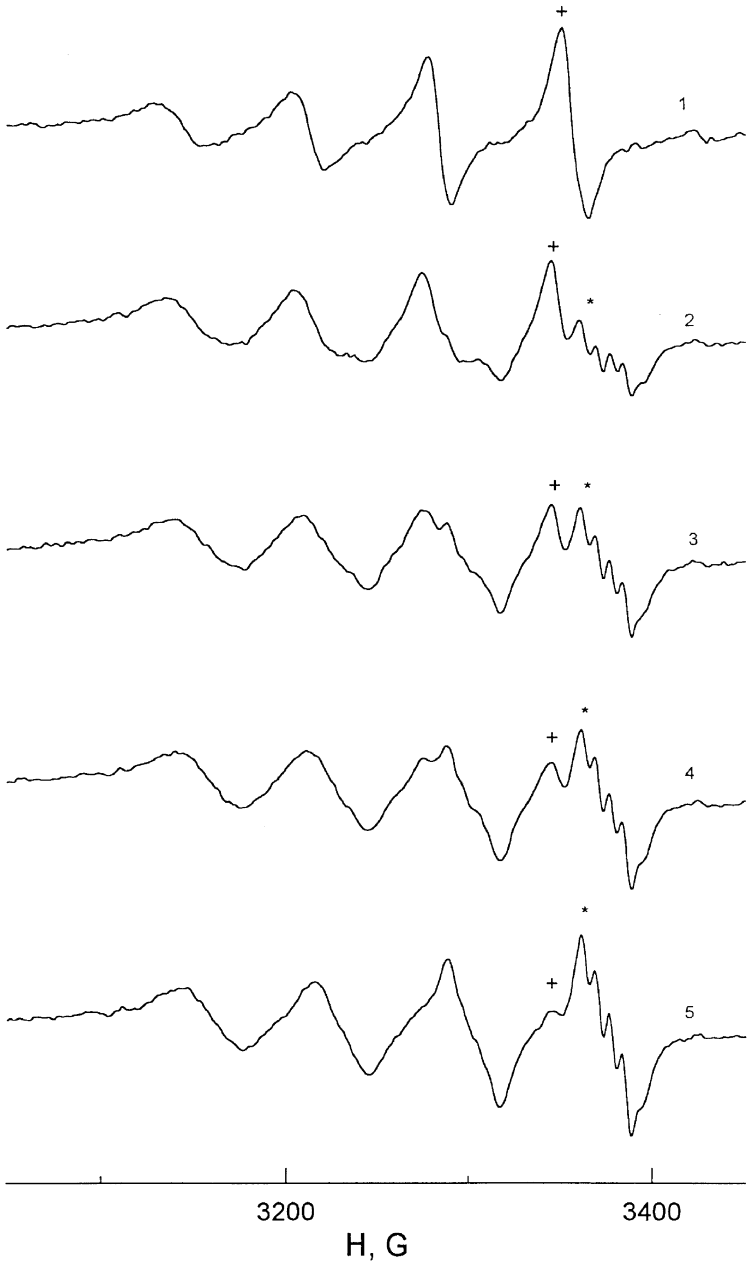

Fig. 3. EPR spectral changes obtained after mixing of equal volumes of $Cu(Et_2dtc)_2$ solution in CCl_4 (1×10^{-3} mol dm^{-3}) with 1×10^{-3} mol dm^{-3} solutions of (a) $Cu(ClO_4)_2$ in *i*-BuOH (spectra taken at 5–110 min) and (b) $Cu(NO_3)_2$ in MeOH (spectra taken 5–220 min), 25°C. EPR lines marked + and * are measured to obtain the respective curves 1 and 2 in Fig. 4.

results obtained in different solvent mixtures did not vary as seen in Table 2. On the ground of the simple rate law for this step (eqn (4)),

$$\frac{d[Cu(Et_2dtc)Cl]}{dt}=k_2[A], \qquad (4)$$

graphical differentiation of the experimental plots (2) in Fig. 4(a, b) gave the kinetic curves (3) of formation and disappearance of A.

Further conversion of $Cu^{II}(Et_2dtc)Cl$ proceeded in a slow step at the end of the reaction with very small changes in EPR occurring during large intervals compared to the scale of the intensity vs time profiles, thus this step was neglected in the EPR study. The value $k_{obs}=4\times10^{-6}$ s^{-1} about the rate constant of $Cu^{II}(Et_2dtc)Cl$ conversion was calculated by the least squares method from the slopes of the linear plots between ln(A) and time (the insets in Fig. 2) at larger reaction times.

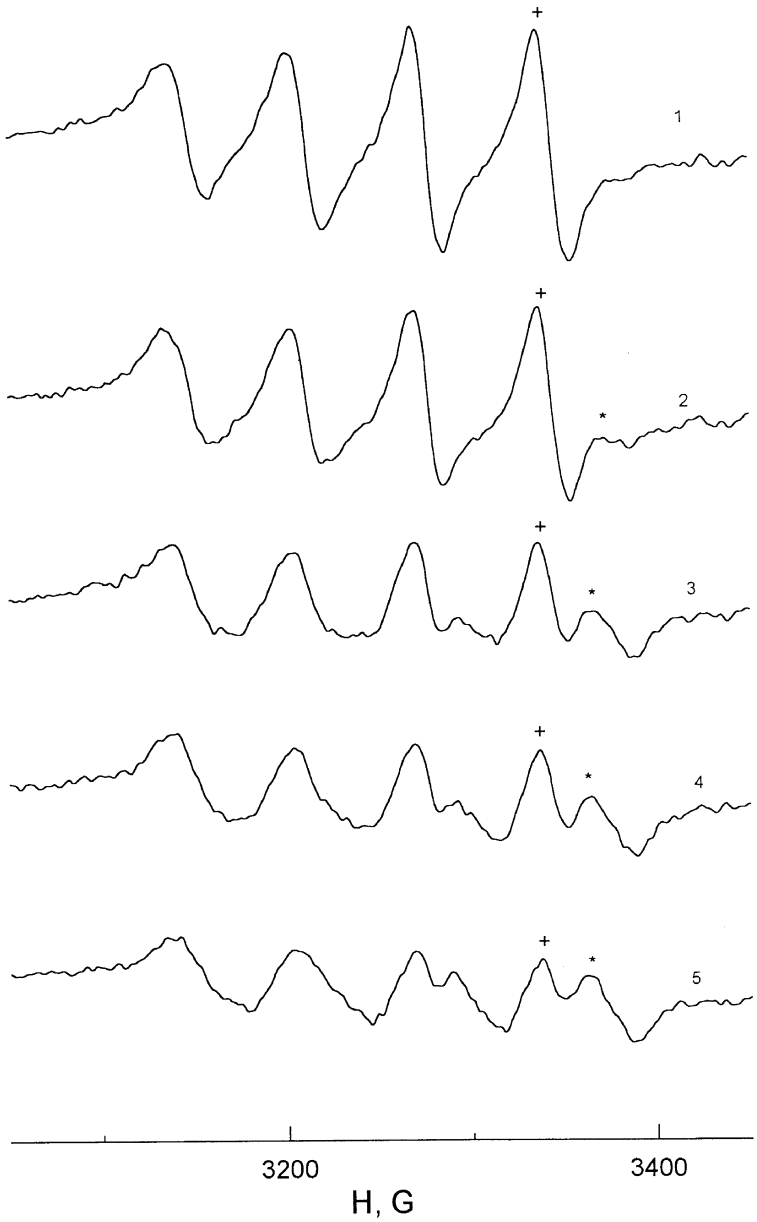

Fig. 3—*continued.*

Mechanism of the thermal reaction

Based on the observed EPR behavior the formation of $Cu^{II}(Et_2dtc)Cl$ from $Cu^{II}(Et_2dtc)^+ \ldots Y^-$ can be reasonably assumed to occur in two steps with apparent rate constants, the first involving the formation of an EPR silent intermediate. Since ligand substitution reactions of copper are typically rapid [11], it was likely to suppose that the formation of the mixed-ligand complex $Cu^{II}(Et_2dtc)Cl$ would involve two steps of electron transfer with the rate constants k_1 and k_2 involving consecutive reduction and oxidation of the metal ion. Considering the ability of CCl_4 to form associate **I** with $Cu^{II}(Et_2dtc)^+ \ldots Y^-$ we could accept that a homolytic cleavage of a Cu–S bond in **I** proceeds as the first step initiated by the close approach and coordination of the acceptor CCl_4 molecule to the S atom, which is the donor center of the chromophore $Cu^{II}S_2(solv)_2$.

There are two possible mechanistic routes after this initial step of electron transfer. The first takes into account that the homolytic cleavage of the Cu–S bond in $Cu^{II}(Et_2dtc)^+$ facilitates the breaking of the remaining Cu–S bond to give Cu(I) and the free $Et_2dtc\cdot$ radical of the ligand which may either give Et_4tds (reaction (5)) or abstract a hydrogen atom from the solvent [12] (reaction (6)) to give Et_2dtcH which itself then undergoes reaction (7),

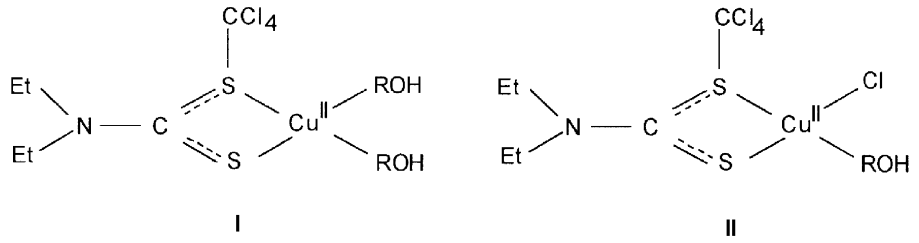

Structure 1.

$$2Et_2dtc^{\cdot} = Et_4tds, \quad (5)$$

$$Et_2dtc^{\cdot} + ROH = Et_2dtcH + RO^{\cdot}, \quad (6)$$

$$Et_2dtcH + Cu(I) = Cu^{I}(Et_2dtc) + H^{+}. \quad (7)$$

The proposed complex of Cu(I) can then be oxidized to Cu(II) in a second step of electron transfer. Several oxidants are present in these solutions that could react with $Cu^{I}(Et_2dtc)$. The oxidant present in highest concentration is CCl_4 reacting spontaneously [13] with Cu(I) compounds to give compounds of Cu(II),

$$Cu^{I}(Et_2dtc) + CCl_4 = Cu^{II}(Et_2dtc)Cl + CCl_3^{\cdot}. \quad (8)$$

The free $CCl_3^{\cdot}$ radical is converted to $CHCl_3$,

$$CCl_3^{\cdot} + ROH = CHCl_3 + RO^{\cdot} \quad (9)$$

and $RO^{\cdot}$ undergoes secondary reactions [14].

Parallel oxidation of Cu(I) by CCl_4,

$$Cu(I) + CCl_4 = Cu^{II}Cl^{+} + CCl_3^{\cdot} \quad (10)$$

would proceed much slower than reactions (6) and (7).

Another potentially oxidizing species in solutions open to the air is dissolved dioxygen and Et_4tds, the latter giving $Cu(Et_2dtc)_2$ with both Cu(I) and Cu(II) according to eqn (11)eqn (12) respectively [8],

$$Et_4tds + Cu(I) \rightarrow Cu(Et_2dtc)_2, \quad (11)$$

$$Et_4tds + Cu(II) \rightarrow Cu(Et_2dtc)_2. \quad (12)$$

However, the effect of these oxidants is minor, because of the low Et_4tds concentration and the previously observed independence of photolysis on aeration [1].

The second possible mechanism also involves an initial step of electron transfer. The close proximity of the chlorine atom from the associated CCl_4 molecule to Cu^{I} in **I** then may result in a rapid Cl atom transfer from CCl_4 to Cu in the transition state to produce $Et_2dtc^{\cdot}$, $Cu^{II}Cl$ and reduced CCl_4. This scheme may play a small part in the conversion but does not adequately explain the induction period of $Cu^{II}(Et_2dtc)Cl$ formation since reaction (13) should also be rapid,

$$Cu^{II}Cl + Et_2dtcH = Cu^{II}(Et_2dtc)Cl + H^{+}. \quad (13)$$

The first scheme appears to be a general mechanism for the thermal conversion involving related chloroalkane associates of $Cu^{II}(Et_2dtc)^{+} \ldots Y^{-}$ and $Cu^{II}(Et_2dtc)Cl$. The reaction of $Cu^{II}(Et_2dtc)^{+} \ldots Y^{-}$ with CCl_4 is much faster than that between $Cu^{II}(Et_2dtc)^{+} \ldots Y^{-}$ and $CHCl_3$ (or CH_2Cl_2). The significantly different acceptor properties of CCl_4 and $CHCl_3$ (or CH_2Cl_2) and their different C–Cl bond dissociation energies [15, 16] are expected to contribute to the observed rate difference through enthalpy terms.

Similar to **I**, the homolytic Cu–S bond cleavage in **II**, initiated by the coordinated CCl_4 molecule, proceeds with the breaking of the remaining Cu–S bond to give the free $Et_2dtc^{\cdot}$ radical of the ligand, as well as Cu(I) and chloride ion connected in the following equilibrium:

$$Cu(I) + Cl^{-} \rightleftharpoons CuCl. \quad (14)$$

Therefore, reactions of CuCl should also be considered,

$$Et_2dtcH + CuCl = Cu^{I}(Et_2dtc) + H^{+} + Cl^{-}, \quad (15)$$

$$CuCl + CCl_4 = CuCl_2 + CCl_3^{\cdot} \quad (16)$$

the first being much faster than the second. Reactions (5) and (16) give the final Et_4tds and $CuCl_2$ products of thermolysis.

Continuous photolysis

All investigated complexes undergo photodecomposition upon irradiation with UV and visible light <420 nm. EPR data in Fig. 5(a) which are typical of all chloroalkane/*i*-BuOH (1:1) solutions show that the initial EPR spectrum of $Cu^{II}(Et_2dtc)^{+} \ldots ClO_4^{-}$ is completely converted into the $Cu^{II}(Et_2dtc)Cl$ EPR spectrum which also fades on further irradiation following the reduction of Cu(II) to Cu(I).

Contrary to chloroalkane/*i*-BuOH (1:1), when CH_2Cl_2/EtOH (1:1) (Fig. 5(b)) or CH_2Cl_2/MeOH (1:1) solutions are used for the irradiation of 1×10^{-3} M $Cu^{II}(Et_2dtc)^{+} \ldots Y^{-}$, the intensity of the initial EPR spectrum is gradually decreasing, but only an extremely low intensity intermediate EPR signal of $Cu^{II}(Et_2dtc)Cl$ appears as a result. The hindered formation of the intermediate $Cu^{II}(Et_2dtc)Cl$ complex in these solvent mixtures could be explained with the low

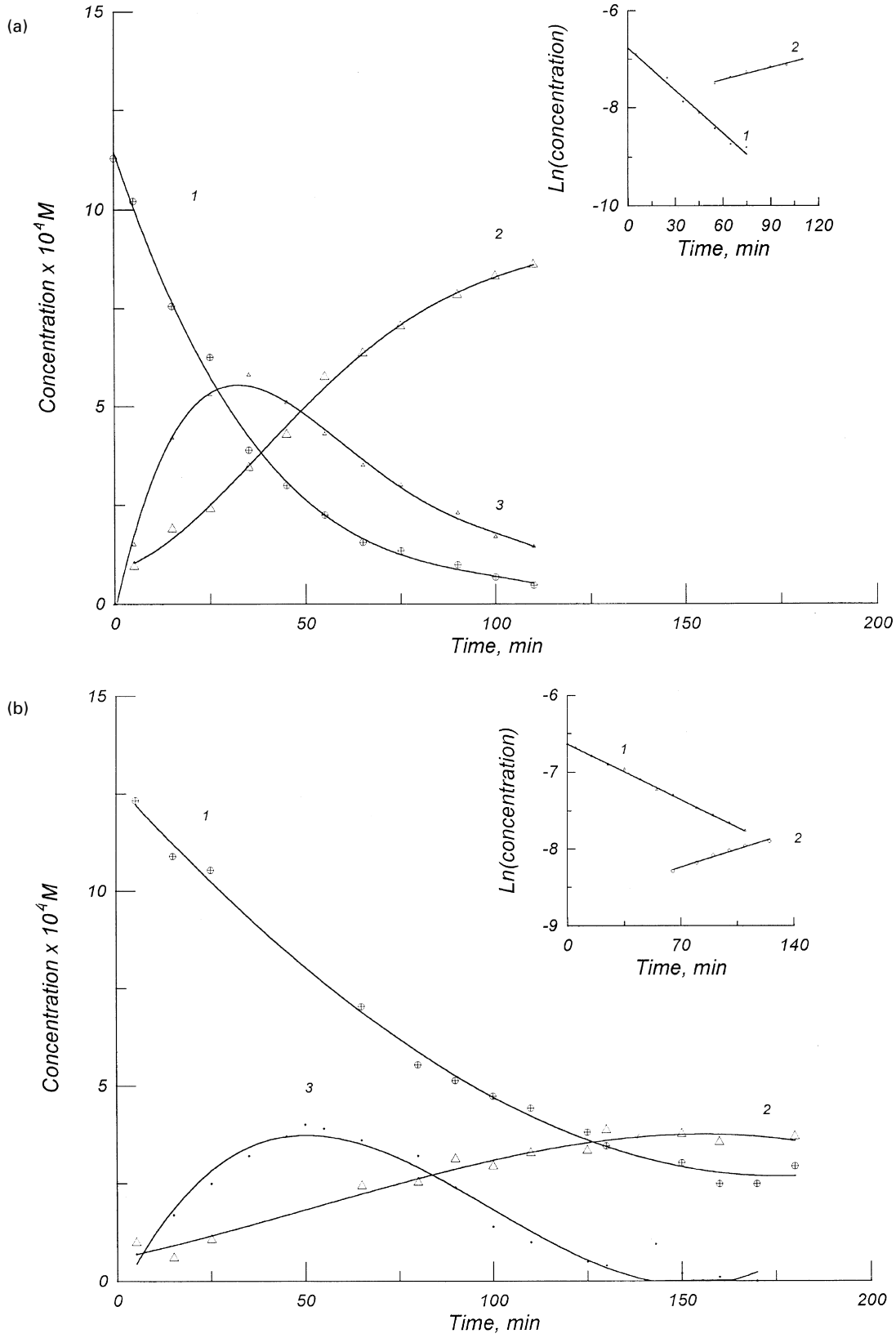

Fig. 4. Concentration vs time profiles derived from the EPR data for the major species detected after mixing of equal volumes of $Cu(Et_2dtc)_2$ solution in CCl_4 (1×10^{-3} mol dm^{-3}) with 1×10^{-3} mol dm^{-3} solutions of $Cu(ClO_4)_2$ in *i*-BuOH (a) and $Cu(NO_3)_2$ in MeOH (b), 25°C. (1) $Cu^{II}(Et_2dtc)^+ \ldots Y^-$; (2) $Cu^{II}(Et_2dtc)Cl$; (3) EPR silent intermediate. Insets: The corresponding plots of ln(conc.) vs time.

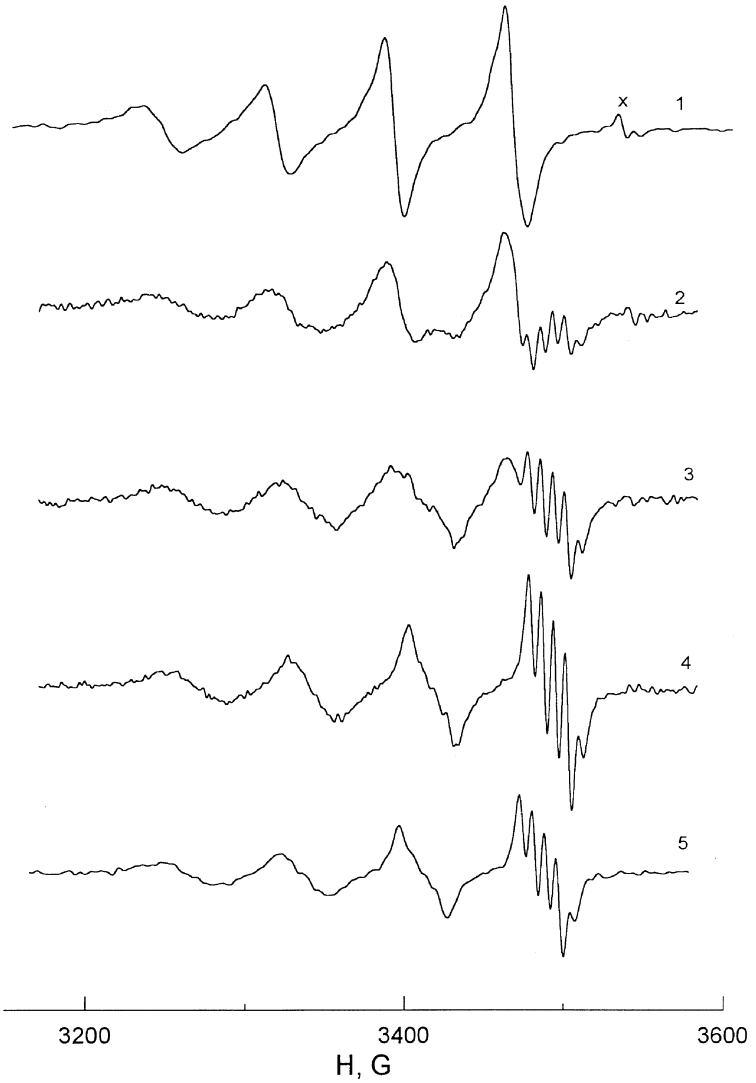

Fig. 5. EPR spectra taken after consecutive UV irradiations of (a) 1×10^{-3} M $CHCl_3$/*i*-BuOH (1:1) solution of $Cu^{II}(Et_2dtc)^+ \ldots ClO_4^-$ for 0 s (1), 15 s (2), 30 s (3), 65 s (4), and 90 s (5); and (b) 1×10^{-3} M CH_2Cl_2/EtOH (1:1) solution of $Cu^{II}(Et_2dtc)^+ \ldots NO_3^-$ for 0 s (1), 20 s (2), 40 s (3) and 50 s (4). Signals marked × are due to the parent $Cu(Et_2dtc)_2$.

concentration of the released chloride taking part in equilibrium (3).

Typical UV–VIS spectral changes (Fig. 6) observed in all chloroalkane/alcohol (1:1) solutions of $Cu^{II}(Et_2dtc)^+ \ldots Y^-$ complexes show the decay of their CT band in the time course of photolysis after the first 5–10 s of increasing. Longer irradiation leads to the formation of a new band at 282 nm due to the absorption of Et_4tds, which is the final reaction product. The appearance of Et_4tds is consistent with the formation of the free $Et_2dtc^{\cdot}$ radical as the primary photo-product.

Quantum yields of photolysis

The absorbance of the CT band at about 402 nm was observed to decrease linearly after the first 15–20 min of increasing [1] upon CT-irradiation ($\lambda_{irr} = 406$ nm), indicating that the photolytic process followed zero-order kinetics. This allowed us to calculate the photo-reduction quantum yields (ϕ_{red} = moles of Cu(II) complex per minute per mole of photons absorbed per minute) for all Cu(II) complexes examined.

Table 3 shows the quantum yields for the photolytic reactions studied upon CT irradiation at 406 nm. It seems that the three complexes display essentially the same quantum yields of electron transfer which is the main reaction neglecting the transformations of the primary photoproducts. However, this conclusion appears to be incorrect when we consider the observed conversion of $Cu^{II}(Et_2dtc)^+ \ldots Y^-$ to $Cu^{II}(Et_2dtc)Cl$ which replaces the initial 397 nm LMCT band with a similar band at 402 nm and maintains practically the

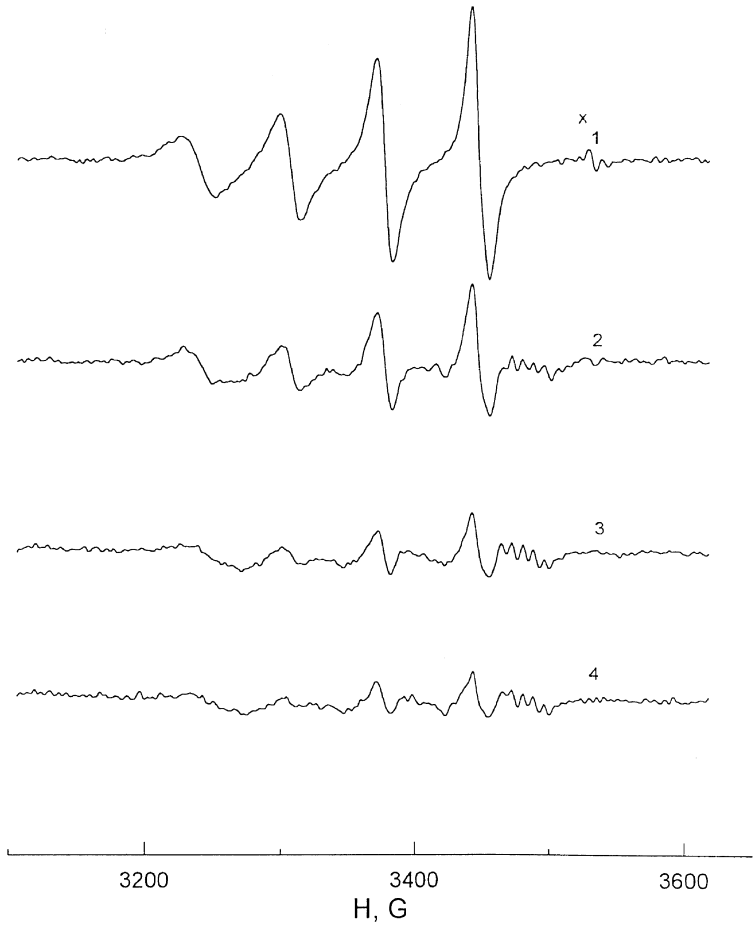

Fig. 5—*continued.*

same measured absorbance values at the early stages of photolysis. Therefore, the equal ϕ_{red} values obtained by the linear decrease of the CT band intensity upon 406 nm irradiation of all solutions correspond to $Cu^{II}(Et_2dtc)Cl$ photolysis proceeding within associate **II**, which is the main reaction at this stage. It is obvious that the primary photochemical act taking place within associate **I** at the early stages of photolysis to give $Cu^{II}(Et_2dtc)Cl$ is more effective.

On the other hand, quantum yields in Table 3 appreciably depend on the solvent composition and the ϕ_{red} values increase with decreasing coordinating abilities of ROH and increasing acceptor properties of chloroalkanes.

Mechanism of photolysis

The reaction from the LMCT excited states of both **I** and **II** is reduction of Cu(II) to Cu(I) proceeding via an intramolecular electron transfer from an equatorially bound S atom of the ligand to copper(II). The homolytic photo-cleavage of Cu–S bond in the LMCT excited state facilitates the breaking of the remaining Cu–S bond to give the same products as the thermal reaction. The primary photochemical act taking place within associate **II** is more effective the stronger the acceptor properties of chloroalkane and the weaker the coordinating abilities of alcohol.

CONCLUSIONS

The conversion of $Cu^{II}(Et_2dtc)^+ \ldots Y^-$ ($Y = ClO_4^-$, NO_3^-) to $Cu^{II}(Et_2dtc)Cl$ on photolysis in halocarbon/alcohol solvent mixtures proceeds within its associate with the halocarbon. The photolysis is proposed to occur from the LMCT excited state giving free dtc$^\bullet$ radical and Cu(I). The quantum efficiency of photolysis is attributed to the extent of charge-transfer contribution, acceptor properties of halocarbon and hydrogen atom donating ability of alcohol. Thermal reaction of $Cu^{II}(Et_2dtc)^+ \ldots Y^-$ species in CCl_4/alcohol solvent mixtures to $Cu^{II}(Et_2dtc)Cl$ follows a similar pathway.

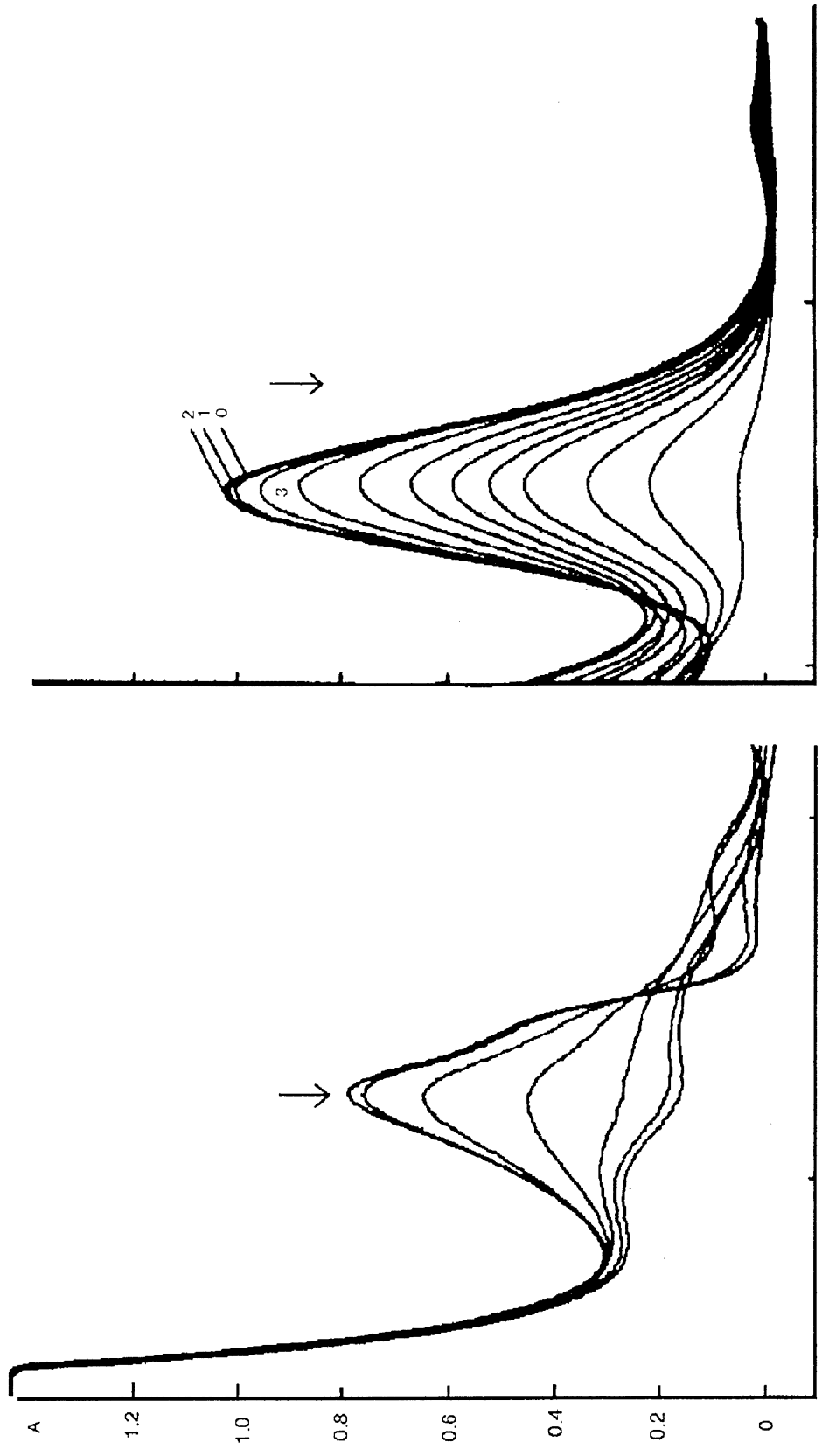

Fig. 6. UV–VIS absorption spectra taken after consecutive UV-irradiations for 0–40 min of 1.6×10^{-4} M solution of $Cu^{II}(Et_2dtc)^+ \ldots NO_3^-$ in CH_2Cl_2/MeOH (1:1).

Table 3. Quantum yields ($\phi_{red} \times 10^2$) of $Cu^{II}(Et_2dtc)X$ photolysis in chloroalkane/ROH (1:1) (X = Cl, ClO_4, NO_3), $\lambda_{irr} = 406$ nm

	Solvent	$Cu(Et_2dtc)Cl$	$Cu(Et_2dtc)^+ \ldots ClO_4^-$	$Cu(Et_2dtc)^+ \ldots NO_3^-$
MeOH	CH_2Cl_2	0.06	0.04	0.04
	$CHCl_3$	0.31	0.29	0.25
	CCl_4	0.44	0.60	0.45
EtOH	CH_2Cl_2	0.11	0.12	0.10
	$CHCl_3$	0.25	0.23	0.24
	CCl_4	0.65	0.83	0.66
i-BuOH	CH_2Cl_2	0.17	0.14	0.12
	$CHCl_3$	0.43	0.43	0.30
	CCl_4	0.83	0.96	0.82

Acknowledgements—The financial support from the National Foundation "Scientific Research" (Projects X-313 and X-623) is gratefully acknowledged.

REFERENCES

1. Jeliazkova, B. G. and Doicheva, M. A., *Polyhedron*, 1996, **15,** 1277.
2. Jeliazkova, B. G., Doicheva, M. A. and Tosheva, L. B., *Appl. Magn. Res.*, 1996, **10,** 151.
3. Jeliazkova, B. G. and Yordanov, N. D., *Inorg. Chim. Acta*, 1993, **203,** 201.
4. Calvert, J. C. and Pitts, J. N., *Photochemistry*. Wiley, New York, 1976, pp. 728, 797.
5. Jeliazkova, B. G. and Panajotova, J. K., *Z. Naturforsch.*, 1995, **50b,** 524.
6. Robbins, R. J., Yang, L. L.-N., Anderson, G. B. and Falvey, D. E., *J. Am. Chem. Soc.*, 1995, **117,** 6544 and references therein.
7. Oktaves, D., Stefanec, J., Siles, B., Beinrohr, E., Konecny, V. and Garay, J., *Coll. Czech. Chem. Commun.*, 1982, **47,** 2867.
8. Thorn, G. D. and Ludwig, R. A., *The Dithiocarbamates and Related Compounds*. Elsevier, New York, 1962, pp. 148–149.
9. Koch, H. P., *J. Chem. Soc.*, 1949, 401.
10. Chow, Y. L. and Buono-Core, G. E., *J. Am. Chem. Soc.*, 1986, **108,** 1234.
11. Margerumm, D. W., Cayley, G. R., Weatherburn, D. C. and Pagenkopf, G. K., in *Coordination Chemistry*, Vol. 2, ed. A. E. Martell. American Chemical Society, Washington, DC, 1978, pp. 1–220, and references therein.
12. Cherton, J.-C., Bertin, S., Basselier, J.-I. and Piat, R., *Bull. Soc. Chim. France*, 1983, 241.
13. Asscher, M. and Vofsi, D., *J. Chem. Soc. B*, 1968, 947.
14. Bartocci, C., Maldotti, A., Varani, G., Battioni, P., Carassiti, V. and Mansuy, D., *Inorg. Chem.*, 1991, **30,** 1255.
15. Calvert, J. C. and Pitts, J. N., *Photochemistry*. Wiley, New York, 1976, pp. 824.
16. Goldfinger, P. and Martens, G., *J. Chem. Soc.*, 1961, 2220.

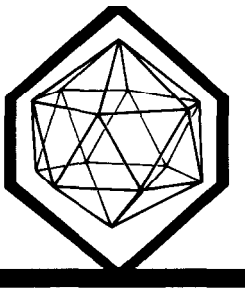

POLYHEDRON

The International Journal for Inorganic and Organometallic Chemistry

Founding Editor: Sir Geoffrey Wilkinson

Executive Editors:
The Americas
M H Chisholm, *Department of Chemistry, Indiana University, Bloomington, IN 47405, U.S.A.*
Fax: +1 812 855 7148;
e-mail: chisholm@copper.ucs.indiana.edu

Rest of the World
C **E Housecroft,** *Institutfir Anorganische Chemie, Spitalstrasse 51, CH-4056 Basel, Switzerland*
Fax: +41 61 267 1014;
e-mail: housecroft@ubaclu.unibas.ch

Editorial Board:
E W Abel, *University of Exeter*
R D Adams, *University of South Carolina*
D C Bradley, *University of London*
E Carmona, *Universidad de Sevilla*
E C Constable, *University of Base1*
F A Cotton, *Texas A & M University*
D Coucouvanis, *University of Michigan*
A H Cowley, *University of Texas at Austin*
I G Dance, *University of New South Wales*
J R Dilworth, *University of Essex*
W J Evans, *University of California at Irvine*
R D Gillard, *University of Wales, Cardiff*
M L H Green, *University of Oxford*
N N **Greenwood,** *University of Leeds*
R H Holm, *Harvard University*
M B Hursthouse, *University of Wales, Cardiff*
F Mathey, *Polytechnique CNRS-SNPE*
W McFarlane, *University of Newcastle upon Tyne*
J A Osborn, *Université Louis Pasteur*
R J Puddephatt, *University of Western Ontario*
H W Roesky, *Universitat Gottingen*
E Sinn, *University of Hull*
F G A Stone, *Baylor University*
P Stoppioni, *Università Degli Studi di Firenze*
A G Sykes, *University of Newcastle upon Tyne*
K Wade, *University of Durham*
A Yamamoto, *Waseda University*

Polyhedron Reports and Polyhedron Symposia-in-Print
Editors:
M H Chisholm, *Indiana University*
J D Woollins, *Loughborough University*

Publishing and Advertising Offices: Elsevier Science Ltd, The Boulevard, Langford Lane, Kidlington, Oxford OX5 IGB, U.K. Tel: +44 (0) 1865 843000, Fax: +44 (0) 1865 843010.

Frequency: Published semi-monthly

Subscription Information
Annual Institutional Subscription Rates 1998: Europe, The CIS and Japan 7384.00 Dutch Guilders. All other countries US$ 4244.00. Associated Personal Subscription Rates are available on request for those whose institutions are library subscribers. Dutch Guilder prices exclude VAT. Non-VAT registered customers in the European Community will be charged the appropriate VAT in addition to the price listed. Prices include postage and insurance and are subject to change without notice.

Any enquiry relating to subscriptions should be sent to:

The Americas: Elsevier Science Customer Support Department, P.O. Box 945, New York, NY 10010, U.S.A. [Tel: (+1) 212-633-3730 / 1-888 4ES-INFO. Fax: (+I) 212-633-3680. E-mail: usinfo-f@elsevier.com]. **Japan:** Elsevier Science Customer Support Department, 9-15 Higashi-Azabu I-chome, Minato-ku, Tokyo 106, Japan [Tel: (+3) 5561-5033. Fax: (+3) 5561-5047. E-mail: info@elsevier.co.jp]. **Asia Pacific (*excluding* Japan):** Elsevier Science (Singapore) Pte Ltd, No. 1 Temasek Avenue, 17-01 Millennia Tower, Singapore 039 192 [Tel: (+65) 434-3727. Fax: (+65) 337-2230. E-mail: asiainfo@elsevier.com.sg]. **Rest of the World:** Elsevier Science Customer Service Department, P.O. Box 211, 1001 AE Amsterdam, The Netherlands [Tel: (+31) 20-485-3757. Fax: (+31) 20-485-3432. E-mail: nlinfo-f@elsevier.nl].

© 1997 Elsevier Science Ltd

PERIODICALS POSTAGE PAID AT RAHWAY, NEW JERSEY AND ADDITIONAL ENTRY POINTS. **Polyhedron (ISSN 0277-5387)** is published 24 **issues per year** (2 **issues per month)** by Elsevier Science Ltd, The Boulevard, Langford Lane, Kidlington, Oxford OX5 1GB, U.K. The annual subscription in the U.S.A. is $4244. **Polyhedron** is distributed by Mercury Airfreight International Ltd, 10 Camptown Road, Irvington, New Jersey 0711 l-l 105. POSTMASTER: Please send address corrections to **Polyhedron,** c/o Elsevier Science Regional Sales Office, Customer Support Department, 655 Avenue of the Americas, New York, NY 10010.